 © 1982 The Chemical Society of Japan Bull. Chem. Soc. Jpn., 55, 1—3 (1982)

The Effect of Propyl Cellosolve on Water Structure Estimated from Ultrasonic Data

Sadakatsu NISHIKAWA,* Yoshihisa YAMASHITA, and Mitsuo MASHIMA

Department of Chemistry, Faculty of Science and Engineering, Saga University, Saga 840

(Received March 16, 1981)

Ultrasonic absorption and velocity have been measured in aqueous solution of Propyl Cellosolve (ethylene glycol monopropyl ether) in the frequency range of 7.5 to 220 MHz at 25 °C. A single relaxational process has been found and the mechanism has been attributed to the solute-solvent interaction, AB↔A+B. The rate constants obtained are $k_{12}=9.6\times10^{7}$ s^{-1} for the forward and $k_{21}=1.3\times10^{8}$ M^{-1} s^{-1} for the backward reaction. The effect of the solute on the water structure has been found to act slightly as the water structure promoter and the results have been discussed comparing with those of Butyl Cellosolve solution.

In the previous paper, we have been reporting ultrasonic properties of aqueous solutions of some alcohols.[1,2] The characteristic properties of the aqueous solutions are the observations of the Peak Sound Absorption and Peak Sound Velocity Concentrations. Depending upon the structure of the solute molecules, one or two relaxational absorptions have been found. One excess absorption which is due to the solute-solvent interaction is observed in most of the solutions of nonelectrolytes with a hydroxy group. The other excess absorption is only observed in the solutions in which the solute has a relatively large hydrophobic group, and the cause has been attributed to the perturbation of the equilibrium between the monomer and aggregate of the solute. In these respects, we have extended our dynamic studies of nonelectrolyte solutions by the ultrasonic method to ethers, one of which has been reported.[3] In this paper, we present the detail results of the ultrasonic properties in aqueous solution of Propyl Cellosolve. The result will be compared with that of Butyl Cellosolve solutions.

Experimental

Propyl Cellosolve (ethylene glycol monopropyl ether) was distilled once and the purity was more than 99.8%. Ultrasonic pulse method[4] was used to measure the absorption coefficient in the frequency range of 7.5 to 220 MHz. Sound velocity was measured at 2.5 MHz by a interferometer. A pycnometer of about 2.2 cm^3 was used to measure density of solutions. All the measurements were done at 25 °C.

Results and Discussion

The ultrasonic absorptions in aqueous solutions of Propyl Cellosolve are all characteristic of a single relaxation in the concentration range of 1.9 to 5.6 M in which the excess absorptions have been observed. The excess absorption, A, the background absorption, B, and the relaxation frequency, f_r, were determined so as to obtain the best fit of the experimental data to the single relaxational equation (Eq. 1), using a least mean square method by HITACHI Basic Master MB-6890 microcomputer.

$$\alpha/f^2 = A/[1+(f/f_r)^2] + B, \quad (1)$$

where α is the absorption coefficient. Figure 1 shows the representative absorption spectra. In Table 1, these parameters are listed as a function of the concentration along with the values of the sound velocity and the density. The sound velocity goes through a maximum at the concentration of around 2.0 M, at which the excess absorption appears and increases up to 3.0 M. Subsequently, it decreases gradually.

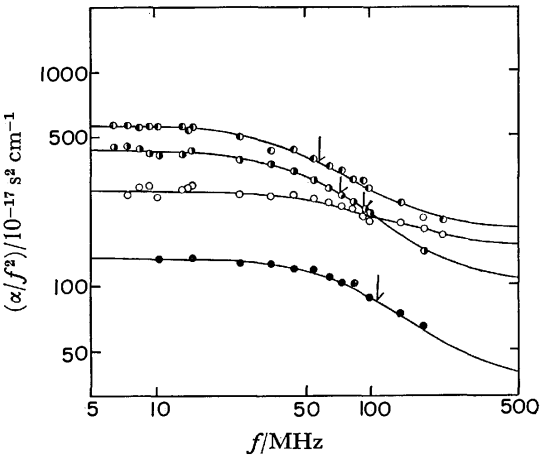

Fig. 1. Representative ultrasonic absorption spectra in aqueous solution of Propyl Cellosolve at 25 °C. The arrows show the positions of the relaxation frequencies. ●: 1.91 M, ◑: 2.69 M, ◐: 3.36 M, ○: 5.60 M.

Table 1. Ultrasonic parameters for aqueous solution of propyl cellosolve at 25 °C

C_a	f_r	A	B	ρ	c
M[a]	MHz	10^{-17} s^2 cm^{-2}		g cm^{-3}	m s^{-1}
1.91	108	99.4	34.8	0.9929	1610
2.39	55.5	249	117	0.9920	1605
2.69	73.0	333	101	0.9908	1586
2.96	79.0	416	93.2	0.9891	1560
3.00	70.0	408	145	0.9886	1558
3.36	58.9	381	184	0.9858	1540
3.99	67.0	320	187	0.9803	1517
5.60	93.0	129	151	0.9627	1466

a) 1 M=1 mol dm^{-3}.

In order to interpret the excess absorption mechanism, we use the model which has been proposed for aqueous solutions of alcohols because the ultrasonic properties are very similar to those of alcohol solutions.[1,2] It is assumed that liquid water consists of two different states, that is, the hydrogen bonded and the nonhydrogen bonded water. Only the latter molecules may associate with the interaction with Propyl

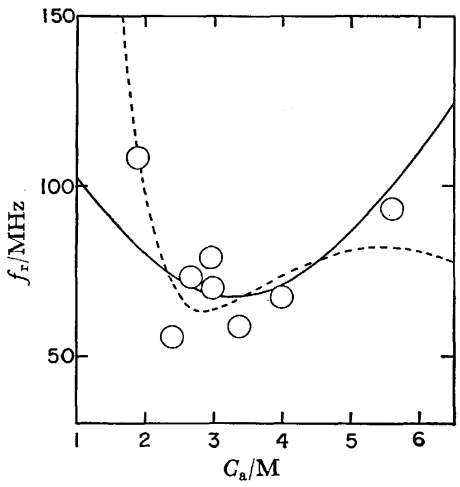

Fig. 2. Concentration dependence of the relaxation frequency for aqueous solution of Propyl Cellosolve. Solid line was calculated for the mechanism AB⟷A+B, and dashed one was for AB_2⟷A+2B mechanism.

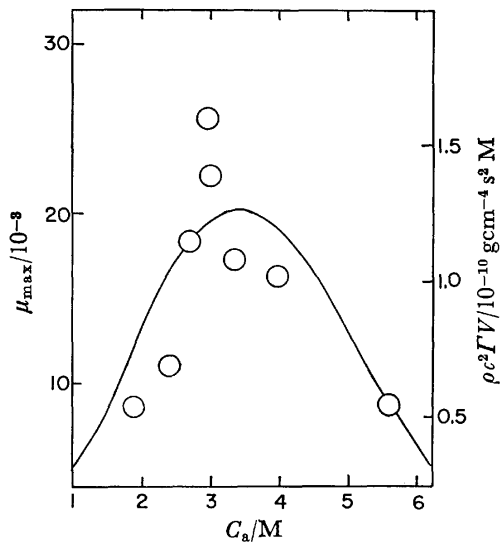

Fig. 3. The plots of μ_{max} and $\rho c^2\Gamma V$ as a function of Propyl Cellosolve concentration.

Cellosolve molecules.

$$AB_m \underset{k_{21}}{\overset{k_{12}}{\rightleftarrows}} A + mB, \qquad (2)$$
$$C_1 \qquad C_2 \quad C_3$$

where A is the solute, B the monomer of liquid water, AB_m the complex and C_i the equilibrium concentration of each component. It has been shown in the previous studies[1-3] that the 1:1 complex is the most reliable. The relation between relaxation frequency and the concentration for the above reaction is given by the next equation.

$$2\pi f_r = k_{21}[(C_a-\beta C_w+K_{12})^2 + 4\beta C_w K_{12}]^{1/2}, \qquad (3)$$

where β is the mole fraction of the water monomer, C_a the analytical concentration of Propyl Cellosolve, C_w that of water and $K_{12}=k_{12}/k_{21}$. The rate constant, k_{21}, was determined so as to minimize the error defined by $r=0.675[\Sigma(p_i-\bar{k}_{21})^2/7]^{1/2}$ where $p_i=2\pi f_{ri}/[(C_{ai}-\beta C_{wi}+K_{12})^2+4\beta C_{wi}\bar{K}_{12}]^{1/2}$, and $\bar{k}_{21}$ is the most probable value of k_{21}, assuming the appropriate β value (the relation[1] between β and K_{12} is derived from the condition that the relaxation frequency goes through a minimum at 3.5 M). Figure 2 shows the plots of the experimental relaxation frequencies, f_r, and the calculated values (solid line). We have also tested the case of $m=2$, that is, the case in which two water molecules interact with a Propyl Cellosolve molecule. The relaxation frequency for this mechanism is expressed as

$$2\pi f_r = k_{21}(4C_2C_3+C_3^2) + k_{12}. \qquad (4)$$

Assuming appropriate values of β and K_{12} because no simple relation between β and K_{12} is held, contrary to that for 1:1 complex formation, each equilibrium concentration was calculated with the relations of $C_a=C_1+C_2$, $\beta C_w=2C_1+C_3$, and $K_{12}=C_2C_3^2/C_1$ and the ratio, k_{12}/k_{21} was determined from the slope and intercept of the plots of $2\pi f_r$ *vs.* $(4C_2C_3+C_3^2)$ so as to get the same value as that of assumed K_{12} and so as that the excess absorption went through a maximum.

In the range of $\beta=0.13$ to 0.17, it may be possible to obtain the parameters of β and K_{12} which seem to satisfy the above conditions. One of the results is shown in Fig. 2 by a dashed line which has been determined when $\beta=0.150$ and $K=0.715$. However, the errors of the rate constants are too large ($k_{12}=(5.7\pm1.3)\times10^7$ s^{-1} and $k_{21}=(4.2\pm10.2)\times10^7$ M^{-2} s^{-1}), and the concentration dependence of the calculated relaxation frequency exhibits a minimum and a maximum as is seen in Fig. 2. The mechanism due to the interaction between plural water molecules and one solute may not be considered as the cause of the observed excess absoprtion from the following reasons. First, even if the calculated curve for the case of $m=2$ in Fig. 2 seems to fit to the experimental relaxation frequency, reasonable rate constants were not obtained. Propyl Cellosolve may not be special or exceptional in the ultrasonic properties compared with various alcohols and ethers reported so far because the relaxation frequencies in other solute solutions only go through a minimum.[1,2,3,5] Second is the fact that the observed absorption data is fairly well expressed by a single relaxational equation, and it seems to be unplausible that many water molecules bind the solute at a fixed characteristic time.

Another parameter determined from the ultrasonic absorption measurement is the maximum excess absorption per wave length, μ_{max} which is related to the volume and enthalpy change of the reaction. It is a good approximation that μ_{max} is proportional to $\rho c^2\Gamma V$, where ρ is the density, c the sound velocity and $\Gamma=(1/C_1+1/C_2+1/C_3-1/C_T)^{-1}(1/V)$.[3] The comparison between the μ_{max} and $\rho c^2\Gamma V$ may be used to make sure if the cause of the absorption is due to the perturbation of the equilibrium expressed by Eq. 2. The solid curve in Fig. 3 represents the calculated $\rho c^2\Gamma V$ and the circles are the experimental values of the μ_{max}. These plots confirms that the excess absorption mechanism is associated with the solute-solvent interaction. In Table 2, the rate and thermodynamic constants obtained in this study are given

Table 2. Rate and thermodynamic constants determined from ultrasonic data

	k_{12} / 10^7 M^{-1} s^{-1}	k_{21} / 10^8 s^{-1}	β	Reference
Pure water			0.26	6
Propyl Cellosolve	9.6±1.3	1.3±0.2	0.10	This work
Butyl Cellosolve	4.2±0.7	1.7±0.3	0.029	3

along with those of Butyl Cellosolve[3] and pure water.[6]

The mole fraction of water monomer in the aqueous solution of Propyl Cellosolve is smaller than that in pure water, but is larger than that in Butyl Cellosolve solution. This means that Propyl Cellosolve acts as the structure promoter for liquid water. However, the effect is not so large, comparing with that of Butyl Cellosolve. This may be because of the smaller hydrophobic group of Propyl Cellosolve than that of Butyl Cellosolve. Though the excess absorption due to the aggregation reaction is observed in the Butyl Cellosolve solution, it is not found in the Propyl Cellosolve solution. Propyl Cellosolve molecule may not have enough hydrophobicity to form the aggregate in aqueous media. Aggregation by hydrogen bonding may be possible, but the rate for this process seems to be beyond our time scale.[7]

References

1) S. Nishikawa, M. Mashima, and T. Yasunaga, *Bull. Chem. Soc. Jpn.*, **48**, 661 (1975).
2) S. Nishikawa, M. Maekawa, M. Mashima, and T. Yasunaga, *Bull. Chem. Soc. Jpn.*, **48**, 2353 (1975).
3) S. Nishikawa, M. Tanaka, and M. Mashima, *J. Phys. Chem.*, **85**, 686 (1981).
4) N. Tatsumoto, *J. Chem. Phys.*, **47**, 4561 (1967).
5) S. Nishikawa and M. Mashima, *J. Chem. Soc., Faraday Trans. 1*, in press.
6) T. A. Litovitz and E. H. Carnevale, *J. Appl. Phys.*, **26**, 816 (1955).
7) K. Oda, R. Hayakawa, and Y. Wada, *Jpn. Appl. Phys.*, **14**, 1113 (1975); **15**, 1009 (1976).

The Crystal and Molecular Structure of Diaqua(tetraphenylporphinato)-cobalt(III) Perchlorate

Hideki MASUDA,* Tooru TAGA, Kenji OSAKI, Hiroshi SUGIMOTO,† and Masayasu MORI†

Faculty of Pharmaceutical Sciences, Kyoto University, Shimoadachi-cho, Yoshida, Sakyo-ku, Kyoto 606

† *Faculty of Science, Osaka City University, Sugimoto-cho, Sumiyoshi-ku, Osaka 558*

(Received December 26, 1980)

The crystal structure of diaqua(meso-tetraphenylporphinato)cobalt(III) perchlorate, $[Co^{III}(tpp)(H_2O)_2]ClO_4$, has been determined by the X-ray method. The compound crystallizes in the monoclinic space group $P2_1/c$ with four molecules in a unit cell of dimensions, $a=13.93(4)$ Å, $b=23.46(2)$ Å, $c=17.35(6)$ Å, and $\beta=129.4(2)°$. The Co(III) ion lies on the mean plane of the porphinato core, and is coordinated by the four porphinato nitrogen atoms and the two water oxygen atoms. The average Co–N distance is 1.964(4) Å, and the average Co–O(water) distance is 1.936(5) Å. The porphyrin plane is significantly ruffled and has an approximate S_4-$\bar{4}$ symmetry. The perchlorate anion is not bound directly to the cobalt(III) ion, and links the two adjacent $[Co^{III}(tpp)(H_2O)_2]^+$ cations by the hydrogen bonds with the aqua ligand oxygen atoms.

The structures of cobalt complexes with porphyrin have been of special interest because of their biological relevance to the hemoproteins[1] and vitamin B_{12} chemistry.[2] The stereochemistry of the cobalt porphinato complexes in the solid state has been reviewed by Scheidt,[1b] in which he states that the cobalt(III) derivatives are all low-spin complexes ($S=0$). Some cobalt complexes, however, have a paramagnetic nature in solution; chloro(tetraphenylporphinato)cobalt(III) complex, $[Co^{III}(tpp)Cl]$, shows a reversible paramagnetism with temperature in the inert solution,[3a] although it is the diamagnetic five coordinate complex in the solid state.[3b] Similar temperature dependence of magnetic conversion has been reported for several Co(III) complexes.[4] This paramagnetic state differs from that caused by the spin-state exchange of the metal ion as observed in the Co(II), Fe(III), or Ni(II) complexes,[5] and is considered to be arisen from the π-cation radical of the six-coordinated low-spin cobalt(III) complex, which is formed in the thermal equilibrium state.[3c].

We have, so far, studied on the structures and chemicophysical properties of several perchlorate metalloporphyrins[6] and found that diaqua(tetraphenylporphinato)cobalt(III) perchlorate, $[Co^{III}(tpp)(H_2O)_2]ClO_4$, shows the same magnetic behavior in the inert solution as observed in $[Co^{III}(tpp)Cl]$; the ^{1}H-NMR spectra of $[Co^{III}(tpp)(H_2O)_2]ClO_4$ in chloroform or benzene give the slight low-field shift and the line broadening of signals, while those spectra in the polar solvents exhibit diamagnetic properties.[6b] Thus the structure of this complex is of interest in relation to the anomalous magnetic properties. In this paper, the crystal structure of $[Co^{III}(tpp)(H_2O)_2]ClO_4$ is described, and the structural characteristics about the Co(III) ion will be discussed in comparison with those of the other metalloporphyrins.

Experimental

$[Co^{III}(tpp)(H_2O)_2]ClO_4$ was prepared by air-oxidation of $[Co^{II}(tpp)]$ in methanol containing hydroperchloric acid.[6b] Dark-violet, needle-like crystals were obtained by recrystallization using 10:1 mixture of benzene and acetone. A crystal with dimensions of 0.5 mm × 0.2 mm × 0.2 mm was used for the diffractometer experiment. Preliminary photographic examination established a monoclinic unit cell containing four chemical units of $[Co^{III}(tpp)(H_2O)_2]ClO_4 \cdot (CH_3)_2C{=}O \cdot 3/2H_2O$. The systematic absences led to the space group $P2_1/c$. The least-squares refinement of setting angles of 20 reflections, measured on a Rigaku AFC-5 diffractometer using Mo $K\alpha$ radiation ($\bar{\lambda}=0.71073$ Å), led to the cell constants: $a=13.93(4)$ Å, $b=23.46(2)$ Å, $c=17.35(6)$ Å, and $\beta=129.4(2)°$. The calculated density of 1.35 g cm^{-3} agrees with the observed density of 1.33 g cm^{-3} by the floatation method in calcium chloride solutions.

Intensity data of 6953 reflections in the range $2\theta<50°$ were collected by the use of ω-2θ scanning technique, the scanning rate being 5° in ω per minute. During the course of data collection, three reflections were monitored every 60 reflections. The intensity data were converted to the F_o data in the usual manner. Absorption correction was not applied ($\mu=5.08$ cm^{-1} for Mo $K\alpha$). The standard deviations were estimated by counting statics. A total number of 4380 independent reflections with $F_o>3\sigma(F_o)$ were retained as observed, and employed in solving and refining the structure.

The structure was solved by the heavy-atom method and refined by the block-diagonal least-squares method. The locations of the crystal water and acetone molecules were determined by the difference Fourier syntheses. The hydrogen atoms were placed at the theoretically calculated positions (C–H=1.00 Å). After several cycles of refinement, the hydrogen atoms of the aqua ligand were revealed on the difference Fourier map. The further refinement was carried to convergence with the weighting scheme of $w=1/\sigma(F_o)^2$ including the hydrogen atoms in the structure factor calculation. The final R value was 0.077. Atomic scattering factors were obtained from the International Table for X-Ray Crystallography IV.[7] All computations were performed on a FACOM M-190 computer in the Data Processing Center of Kyoto University by using the program system KPAX.

Results and Discussion

The atomic parameters are listed in Table 1.[8] The structure of $[Co^{III}(tpp)(H_2O)_2]^+$ cation is shown in Fig. 1, and the crystal structure in Fig. 2. The atomic numbering scheme is given in Figs. 1 and 3.

Bond distances and bond angles are listed in Table 2. The average bond distances and bond angles for the four crystallographically nonequivalent pyrrole rings

TABLE 1. POSITIONAL AND THERMAL PARAMETERS FOR THE ATOMS OF $[Co^{III}(tpp)(H_2O)_2]ClO_4 \cdot (CH_3)_2C{=}O \cdot 3/2H_2O$

Estimated standard deviations in the least significant figure(s) are give in parentheses. B_{eq} is the equivalent isotropic temperature factor defined by Hamilton.[9]

Atom	x	y	z	B_{eq}/Å^2	Atom	x	y	z	B_{eq}/Å^2
Co	0.2840(1)	0.3064(1)	0.1576(1)	3.07	C_7	0.5275(7)	0.1368(3)	0.2226(5)	3.84
N_1	0.1109(5)	0.3291(2)	0.0529(4)	3.38	C_8	0.5734(8)	0.1170(3)	0.1755(6)	4.74
N_2	0.2650(5)	0.2444(2)	0.0725(4)	3.64	C_9	0.6365(8)	0.0656(3)	0.2028(6)	5.24
N_3	0.4583(5)	0.2849(2)	0.2606(4)	3.33	C_{10}	0.6550(8)	0.0336(3)	0.2771(6)	5.24
N_4	0.3045(5)	0.3673(2)	0.2452(4)	3.37	C_{11}	0.6138(8)	0.0524(4)	0.3255(6)	5.47
C_{1A}	0.0446(6)	0.3685(3)	0.0619(5)	3.71	C_{12}	0.5497(8)	0.1038(4)	0.2988(6)	5.17
C_{1B}	−0.0754(7)	0.3781(3)	−0.0343(6)	4.33	C_{13}	0.6440(7)	0.3998(3)	0.4583(5)	4.03
C_{1C}	−0.0792(7)	0.3449(3)	−0.0995(5)	4.17	C_{14}	0.6630(8)	0.4551(3)	0.4442(6)	5.00
C_{1D}	0.0334(6)	0.3135(3)	−0.0465(5)	3.82	C_{15}	0.7689(8)	0.4850(4)	0.5192(7)	5.92
C_{1M}	0.0596(6)	0.2699(3)	−0.0860(5)	3.77	C_{16}	0.8572(8)	0.4602(4)	0.6101(6)	5.94
C_{2A}	0.1655(7)	0.2366(3)	−0.0281(5)	3.91	C_{17}	0.8377(8)	0.4059(4)	0.6265(6)	5.92
C_{2B}	0.1819(7)	0.1834(3)	−0.0593(5)	4.64	C_{18}	0.2328(8)	0.3760(3)	0.5524(6)	5.01
C_{2C}	0.2874(7)	0.1590(3)	0.0208(6)	4.60	C_{19}	−0.0014(7)	0.4381(3)	0.1427(6)	4.24
C_{2D}	0.3411(7)	0.1979(3)	0.1029(5)	3.87	C_{20}	−0.0785(9)	0.4196(4)	0.1623(8)	6.90
C_{2M}	0.4574(7)	0.1914(3)	0.1949(5)	3.75	C_{21}	−0.1651(10)	0.4559(5)	0.1498(10)	8.87
C_{3A}	0.5150(6)	0.2364(3)	0.2637(5)	3.39	C_{22}	−0.1741(9)	0.5115(4)	0.1208(8)	7.65
C_{3B}	0.6469(7)	0.2390(3)	0.3444(5)	3.86	C_{23}	−0.0953(9)	0.5298(4)	0.1055(8)	6.59
C_{3C}	0.6698(7)	0.2906(3)	0.3876(5)	4.05	C_{24}	−0.0086(8)	0.4940(4)	0.1160(7)	5.47
C_{3D}	0.5528(6)	0.3185(3)	0.3393(5)	3.54	Cl	0.4016(3)	0.1661(1)	0.4395(2)	7.62
C_{3M}	0.5332(7)	0.3669(3)	0.3740(5)	3.67	O_1	0.4244(9)	0.2006(5)	0.3898(7)	13.86
C_{4A}	0.4149(6)	0.3852(3)	0.3336(5)	3.34	O_2	0.2770(8)	0.1553(5)	0.3911(8)	13.60
C_{4B}	0.3864(7)	0.4248(3)	0.3805(5)	4.15	O_3	0·4478(10)	0.1919(5)	0.5316(8)	14.45
C_{4C}	0.2637(7)	0.4300(3)	0.3221(6)	3.93	O_4	0.4723(13)	0.1173(6)	0.4689(11)	18.78
C_{4D}	0.2106(7)	0.3959(3)	0.2347(5)	3.48	C_{A1}	0.0604(13)	0.1255(6)	0.0628(10)	10.36
C_{4M}	0.0869(7)	0.3979(3)	0.1482(6)	3.84	C_{A2}	−0.0378(16)	0.1028(6)	−0.0350(13)	14.13
C_1	−0.0368(7)	0.2545(3)	−0.1934(5)	4.06	C_{A3}	0.1639(16)	0.0927(7)	0.1473(13)	13.12
C_2	−0.1522(8)	0.2343(4)	−0.2291(6)	5.40	O_A	0.0564(8)	0.1780(3)	0.0744(6)	10.08
C_3	−0.2405(8)	0.2176(4)	−0.3279(7)	6.43	O_{w1}	0.3299(5)	0.3591(2)	0.0997(4)	4.32
C_4	−0.2136(9)	0.2200(4)	−0.3913(6)	6.58	O_{w2}	0.2308(5)	0.2567(2)	0.2129(4)	4.10
C_5	−0.0999(9)	0.2388(4)	−0.3579(6)	5.75	O_{w3}	0.5515(14)	0.4162(7)	0.1923(10)	20.82
C_6	−0.0114(8)	0.2563(4)	−0.2595(6)	4.97	O_{w4}	0.5335(25)	0.4900(13)	0.0734(20)	18.86

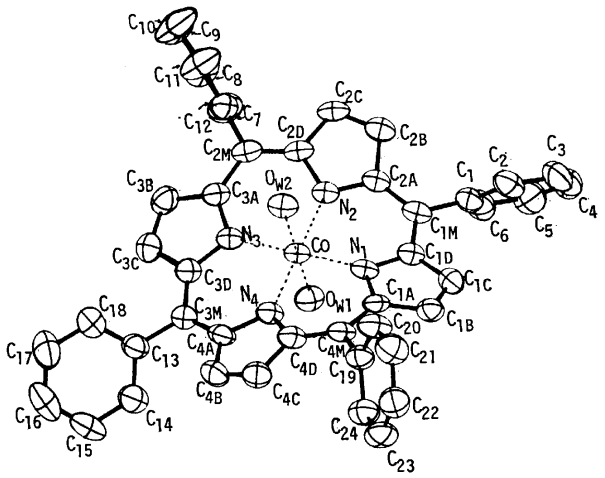

Fig. 1. Computer-drawn perspective model of $[Co^{III}(tpp)(H_2O)_2]^+$.

are given in Fig. 4. The cobalt(III) ion occupies the center of the octahedron formed by the four porphinato nitrogen atoms and the two aqua oxygen atoms, and it lies on the mean plane of the porphinato core; the displacement is 0.004 Å out of the plane defined by the four nitrogen atoms toward the O_{w2} atom and 0.006 Å out of the porphinato mean plane.

The average axial Co(III)–OH_2 bond distance of 1.936(5) Å is comparable with the sum of ionic radii of Co(III) (0.53 Å) and 0 (1.40 Å),[10] and close to the Co(III)–OCH_3 distance, 1.92 Å, observed in $[Co^{III}(OCH_3)(tpp)(py)]$.[11] The average Co–N distance of 1.964(6) Å is within the range of reported distances (1.958—1.982 Å).[1b] The Co(III)–N and Co(III)–O distance are in good agreement with those of the low-spin Co(III) ion in which d_{z^2} and $d_{x^2-y^2}$ orbitals are vacant.[1b]

Deviations of atoms from the least-squares plane of the porphinato core are given in Fig. 5. The porphinato core has a ruffled conformation with an approximate S_4-$\bar{4}$ symmetry. The four pyrrole rings are all swiveled about the metal-nitrogen bond; the dihedral angles between the pyrrole ring and the porphinato mean plane are 14, 16, 18 and 16°. Similar conformations have been observed in Ni- and Co-

TABLE 2. BOND DISTANCES AND ANGLES FOR $[Co^{III}(tpp)(H_2O)_2]ClO_4 \cdot (CH_3)_2C{=}O$
Estimated standard deviations are in parentheses.

(a) Bond distances (l/Å)

$Co-N_1$	1.959(9)	$C_{3A}-C_{3B}$	1.440(11)	$C_{3M}-C_{13}$	1.500(10)	C_3-C_4	1.370(21)
$Co-N_2$	1.967(7)	$C_{3C}-C_{3D}$	1.433(12)	$C_{4M}-C_{19}$	1.504(14)	C_4-C_5	1.369(18)
$Co-N_3$	1.958(9)	$C_{4A}-C_{4B}$	1.447(14)	C_1-C_2	1.388(15)	C_9-C_{10}	1.367(15)
$Co-N_4$	1.970(7)	$C_{4C}-C_{4D}$	1.436(12)	C_1-C_6	1.399(18)	$C_{10}-C_{11}$	1.357(19)
$Co-O_{w1}$	1.939(8)	$C_{1B}-C_{1C}$	1.346(15)	C_7-C_8	1.398(18)	$C_{15}-C_{16}$	1.370(12)
$Co-O_{w2}$	1.932(8)	$C_{2B}-C_{2C}$	1.351(10)	C_7-C_{12}	1.387(14)	$C_{16}-C_{17}$	1.370(14)
N_1-C_{1A}	1.384(12)	$C_{3B}-C_{3C}$	1.351(10)	$C_{13}-C_{14}$	1.377(11)	$C_{21}-C_{22}$	1.375(16)
N_1-C_{1D}	1.382(10)	$C_{4B}-C_{4C}$	1.328(12)	$C_{13}-C_{18}$	1.394(11)	$C_{22}-C_{23}$	1.352(22)
N_2-C_{2A}	1.389(9)	$C_{1M}-C_{1D}$	1.402(13)	$C_{19}-C_{20}$	1.386(20)	$Cl-O_1$	1.359(15)
N_2-C_{2D}	1.372(10)	$C_{1M}-C_{2A}$	1.383(10)	$C_{19}-C_{24}$	1.373(12)	$Cl-O_2$	1.390(12)
N_3-C_{3A}	1.367(10)	$C_{2M}-C_{2D}$	1.383(10)	C_2-C_3	1.388(13)	$Cl-O_3$	1.424(14)
N_3-C_{3D}	1.392(8)	$C_{2M}-C_{3A}$	1.403(10)	C_5-C_6	1.389(12)	$Cl-O_4$	1.380(15)
N_4-C_{4A}	1.378(9)	$C_{3M}-C_{3D}$	1.391(12)	C_8-C_9	1.387(11)	$C_{A1}-O_A$	1.255(16)
N_4-C_{4D}	1.375(13)	$C_{3M}-C_{4A}$	1.387(13)	$C_{11}-C_{12}$	1.393(13)	$C_{A1}-C_{A2}$	1.445(20)
$C_{1A}-C_{1B}$	1.445(10)	$C_{4M}-C_{4D}$	1.393(10)	$C_{14}-C_{15}$	1.387(11)	$C_{A1}-C_{A3}$	1.462(19)
$C_{1C}-C_{1D}$	1.420(11)	$C_{4M}-C_{1A}$	1.394(13)	$C_{17}-C_{18}$	1.377(11)		
$C_{2A}-C_{2B}$	1.435(12)	$C_{1M}-C_1$	1.493(11)	$C_{20}-C_{21}$	1.377(20)		
$C_{2C}-C_{2D}$	1.438(12)	$C_{2M}-C_7$	1.493(11)	$C_{23}-C_{24}$	1.385(18)		

(b) Bond angles (ϕ/°)

N_1-Co-N_2	90.3(3)	$N_1-C_{1D}-C_{1C}$	109.7(8)	$C_{3M}-C_{3D}-C_{3C}$	125.6(6)	$C_5-C_6-C_1$	120.6(11)
N_2-Co-N_3	89.6(3)	$N_2-C_{2A}-C_{2B}$	108.5(6)	$C_{3M}-C_{4A}-C_{4B}$	125.2(6)	$C_7-C_8-C_9$	121.0(10)
N_3-Co-N_4	89.7(3)	$N_2-C_{2D}-C_{2C}$	109.6(6)	$C_{4M}-C_{4D}-C_{4C}$	125.1(9)	$C_{11}-C_{12}-C_7$	120.6(12)
N_4-Co-N_1	90.5(3)	$N_3-C_{3A}-C_{3B}$	110.6(6)	$C_{1D}-C_{1M}-C_{2A}$	123.1(7)	$C_{13}-C_{14}-C_{15}$	121.3(7)
N_1-Co-N_3	178.5(3)	$N_3-C_{3D}-C_{3C}$	109.4(7)	$C_{2D}-C_{2M}-C_{3A}$	121.2(7)	$C_{17}-C_{18}-C_{13}$	121.1(8)
N_2-Co-N_4	178.8(2)	$N_4-C_{4A}-C_{4B}$	108.1(7)	$C_{3D}-C_{3M}-C_{4A}$	122.0(6)	$C_{19}-C_{20}-C_{21}$	120.4(11)
N_1-Co-O_{w1}	87.9(3)	$N_4-C_{4D}-C_{4C}$	108.8(6)	$C_{4D}-C_{4M}-C_{1A}$	122.1(9)	$C_{23}-C_{24}-C_{19}$	119.6(12)
N_2-Co-O_{w1}	90.8(3)	$C_{1A}-C_{1B}-C_{1C}$	106.3(8)	$C_{1D}-C_{1M}-C_1$	118.7(6)	$C_2-C_3-C_4$	120.0(11)
N_3-Co-O_{w1}	90.7(3)	$C_{1B}-C_{1C}-C_{1D}$	108.5(6)	$C_{2A}-C_{1M}-C_1$	118.0(8)	$C_4-C_5-C_6$	120.1(13)
N_4-Co-O_{w1}	90.2(3)	$C_{2A}-C_{2B}-C_{2C}$	108.1(7)	$C_{2D}-C_{2M}-C_7$	120.9(6)	$C_8-C_9-C_{10}$	119.9(12)
N_1-Co-O_{w2}	89.5(3)	$C_{2B}-C_{2C}-C_{2D}$	107.0(7)	$C_{3A}-C_{2M}-C_7$	117.9(6)	$C_{10}-C_{11}-C_{12}$	120.6(10)
N_2-Co-O_{w2}	90.9(3)	$C_{3A}-C_{3B}-C_{3C}$	106.5(7)	$C_{3D}-C_{3M}-C_{13}$	118.6(8)	$C_{14}-C_{15}-C_{16}$	120.5(9)
N_3-Co-O_{w2}	92.0(3)	$C_{3B}-C_{3C}-C_{3D}$	107.7(6)	$C_{4A}-C_{3M}-C_{13}$	119.4(8)	$C_{16}-C_{17}-C_{18}$	120.9(7)
N_4-Co-O_{w2}	88.2(3)	$C_{4A}-C_{4B}-C_{4C}$	108.0(7)	$C_{4D}-C_{4M}-C_{19}$	119.5(8)	$C_{20}-C_{21}-C_{22}$	120.8(16)
$O_{w1}-Co-O_{w2}$	176.8(3)	$C_{4B}-C_{4C}-C_{4D}$	107.8(10)	$C_{1A}-C_{4M}-C_{19}$	118.1(6)	$C_{22}-C_{23}-C_{24}$	122.0(10)
$Co-N_1-C_{1A}$	126.4(5)	$N_1-C_{1A}-C_{4M}$	126.5(6)	$C_{1M}-C_1-C_2$	120.6(10)	$C_3-C_4-C_5$	120.4(8)
$Co-N_1-C_{1D}$	127.7(6)	$N_1-C_{1D}-C_{1M}$	124.3(6)	$C_{1M}-C_1-C_6$	121.4(9)	$C_9-C_{10}-C_{11}$	120.3(8)
$Co-N_2-C_{2A}$	126.3(5)	$N_2-C_{2A}-C_{1M}$	126.3(8)	$C_{2M}-C_7-C_8$	123.0(8)	$C_{15}-C_{16}-C_{17}$	118.9(7)
$Co-N_2-C_{2D}$	126.6(5)	$N_2-C_{2D}-C_{2M}$	125.8(7)	$C_{2M}-C_7-C_{12}$	119.4(10)	$C_{21}-C_{22}-C_{23}$	118.4(12)
$Co-N_3-C_{3A}$	127.0(4)	$N_3-C_{3A}-C_{2M}$	126.1(6)	$C_{3M}-C_{13}-C_{14}$	120.4(6)	O_1-Cl-O_2	115.5(7)
$Co-N_3-C_{3D}$	127.0(5)	$N_3-C_{3D}-C_{3M}$	124.3(7)	$C_{3M}-C_{13}-C_{18}$	122.3(7)	O_1-Cl-O_3	109.7(8)
$Co-N_4-C_{4A}$	126.3(6)	$N_4-C_{4A}-C_{3M}$	126.6(8)	$C_{4M}-C_{19}-C_{20}$	121.2(8)	O_1-Cl-O_4	109.2(12)
$Co-N_4-C_{4D}$	126.3(4)	$N_4-C_{4D}-C_{4M}$	125.5(8)	$C_{4M}-C_{19}-C_{24}$	120.1(11)	O_2-Cl-O_3	104.9(9)
$C_{1A}-N_1-C_{1D}$	105.6(6)	$C_{4M}-C_{1A}-C_{1B}$	123.6(8)	$C_2-C_1-C_6$	117.9(7)	O_2-Cl-O_4	113.4(9)
$C_{2A}-N_2-C_{2D}$	106.8(6)	$C_{1M}-C_{1D}-C_{1C}$	125.8(6)	$C_8-C_7-C_{12}$	117.6(8)	O_3-Cl-O_4	103.3(9)
$C_{3A}-N_3-C_{3D}$	105.7(6)	$C_{1M}-C_{2A}-C_{2B}$	124.7(6)	$C_{14}-C_{13}-C_{18}$	117.3(6)	$O_A-C_{A1}-C_{A2}$	116.4(11)
$C_{4A}-N_4-C_{4D}$	107.1(7)	$C_{2M}-C_{2D}-C_{2C}$	124.4(8)	$C_{20}-C_{19}-C_{24}$	118.7(10)	$O_A-C_{A1}-C_{A3}$	118.2(11)
$N_1-C_{1A}-C_{1B}$	109.8(8)	$C_{2M}-C_{3A}-C_{3B}$	123.2(8)	$C_1-C_2-C_3$	121.0(12)	$C_{A2}-C_{A1}-C_{A3}$	125.4(13)

porphyrins.[12,13c] As compared with these complexes, the lengthening of the metal–N bond accompanied by increasing the C_A–N–C_A angle and decreasing the N–C_A–C_B angle seems to relieve the ruffling. The phenyl rings attached to C_M are tilted from the core plane, because of repulsions between the hydrogen atoms. The dihedral angles of each phenyl ring with the porphinato mean plane are 59, 65, 60, and 81°; their average value being 66°. As seen in Fig. 6, these angles have a linear relationship for the C_M–C_P bond distances; the C_M–C_P bond distance of 1.498(5) Å is very close to the value of 1.497(3) Å observed for the central C–C bond of planar biphenyl molecule.[14] Thus, the C_M–C_P bond has a little π-conjugation character, in spite of the steric hindrance. Although the π-conjugate system of the porphinato

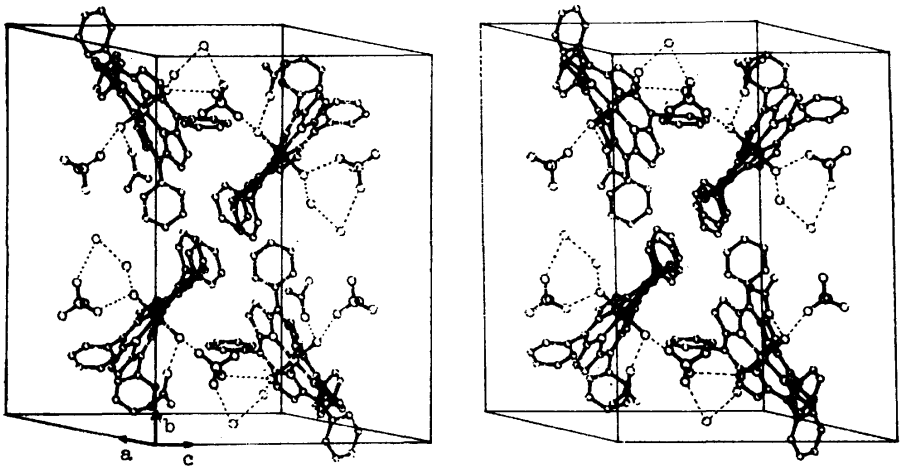

Fig. 2. Stereoscopic view of the contents in the unit cell of $[Co^{III}(tpp)(H_2O)_2]ClO_4 \cdot (CH_3)_2C{=}O \cdot 3/2H_2O$ crystal.

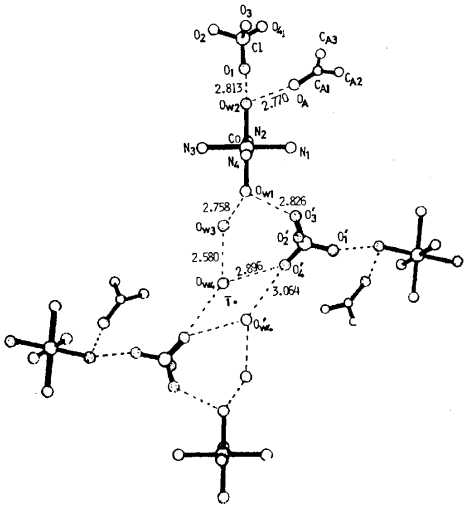

Fig. 3. Hydrogen-bonding scheme among the $[Co^{III}(tpp)(H_2O)_2]^+$ cations, the perchlorate anions, the water molecules, and the acetone molecules. The dotted lines represent hydrogen bonds. The tetraphenylporphine atoms other than the nitrogen atoms are omitted for clarity.

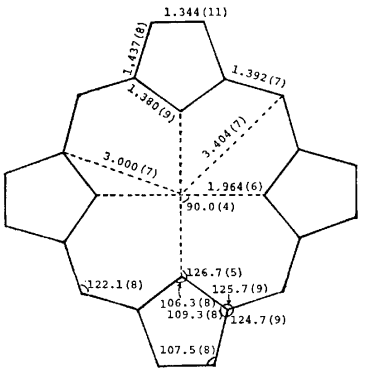

Fig. 4. Average bond distances (l/Å) and angles (ϕ/°) for the porphine skeleton of the $Co^{III}(tpp)^+$ cation (a) and for the peripheral phenyl groups (b).

core might be weakened because of its ruffled conformation, the π-conjugate system may be slightly delocalized over the phenyl rings through the C_M–C_P bond.

The crystal structure consists of the discrete $[Co^{III}(tpp)(H_2O)_2]^+$ cations, the perchlorate anions, the acetone molecules, and the water molecules other than the aqua ligands. As shown in Fig. 3, the aqua ligand O_{w1} atom forms the two hydrogen bonds with the perchlorate O_3 and water O_{w3} atoms, while the ligand O_{w2} atom forms the two hydrogen bonds with the perchlorate O_1 and acetone O_A atoms. Thus, the two $[Co^{III}(tpp)(H_2O)_2]^+$ cations are linked together by the perchlorate anion through the $O_{w1}\cdots O_3$ and $O_{w2}\cdots O_1$ hydrogen bonds. The water O_{w4} atom occupies the two positions with the half occupancy near the inversion center. This oxygen atom is hydrogen-bond to the two adjacent perchlorate anions and the water O_{w3} atom. The perchlorate O_1 atom exists near the porphinato nitrogen N_3 atom at 3.241 Å and the Co(III) atom at 4.026 Å, and it seems to have weak interactions with the central Co(III) atom because of their interorbital overlapping between the π-orbital of Co–N bond and the σ-orbital of O_1 atom. This crystal structure may, therefore, suggest that the perchlorate anion, bound directly to the Co(III) atom in the inert solvent, might be replaced by the water molecule in the crystallization process, since the water molecule acts as a little stronger ligand for the Co(III) ion than the perchlorate anion. The diamagnetic properties of $[Co^{III}(tpp)(H_2O)_2]ClO_4$ in ethanol or pyridine are considered to be caused by the strong coordination of the polar solvent molecules as the fifth and/or sixth axial ligands.

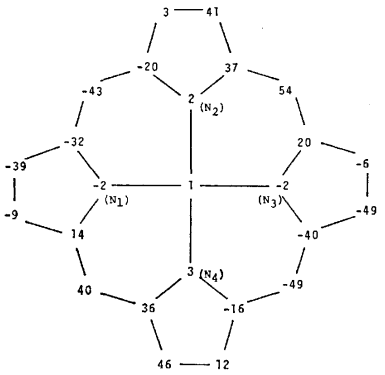

Fig. 5. Ruffling of the porphinato core. Perpendicular distances of the atoms from the porphinato mean plane are in a unit of 0.01 Å.

The authors wish to thank Professor Nobuo Morimoto and Dr. Katsutoshi Tomita, Faculty of Science in Kyoto University, for the use of the Rigaku AFC-5 diffractometer.

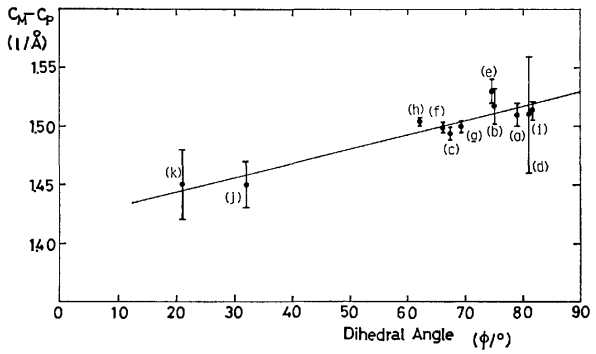

Fig. 6. The C_M–C_P bond distances (l/Å) *vs.* the dihedral angles (ϕ/°) of the phenyl groups for the porphinato mean plane. Seven Co^{III}(tpp) complexes[3b,11,13a–d] and four metal-free porphyrins (three tpp compounds[13e,f,15] and one tetrapyridylporphyrin compound[15]), as shown below, are plotted:
(a): Ref. 13a, (b): Ref. 3b, (c): Ref. 13b, (d): Ref. 11, (e): Ref. 13c, (f): this work, (g): Ref. 13d, (h): Ref. 13e, (i): Ref. 13f, (j): Ref. 15, and (k): Ref. 15.

References

1) a) E. B. Fleischer, *Acc. Chem. Res.*, **3**, 105 (1969); b) W. R. Scheidt, *ibid.*, **10**, 339 (1977); c) J. L. Hoard, "Porphyrins and Metalloporphyrins," ed by K. M. Smith, Elsevier, Amsterdam (1975), p. 317; d) J. L. Hoard, *Ann. N.Y. Acad. Sci.*, **206**, 18 (1973).

2) J. M. Pratt, "The Inorganic Chemistry of Vitamin B_{12}," Academic Press, New York (1972).

3) a) K. Yamamoto, J. Uzawa, and T. Chijimatsu, *Chem. Lett.*, **1979**, 89; b) T. Sakurai, K. Yamamoto, H. Naito, and N. Nakamoto, *Bull. Chem. Soc. Jpn.*, **49**, 3042 (1976); c) K. Yamamoto, M. Kohno, and H. Ohya-Nishiguchi, *Chem. Lett.*, **1981**, 255.

4) a) M. Gerloch, B. M. Higson, and E. D. McKenjie, *J. Chem. Soc., Chem. Commun.*, **1971**, 1149; b) C. R. Ollis, D. Y. Jeter, and W. E. Hatfield, *J. Am. Chem. Soc.*, **93**, 547 (1971).

5) L. Sacconi, *Pure Appl. Chem.*, **27**, 161 (1971).

6) a) H. Masuda, T. Taga, K. Osaki, H. Sugimoto, Z. Yoshida, and H. Ogoshi, *Inorg. Chem.*, **19**, 950 (1980); b) H. Sugimoto, M. Nagano, Z. Yoshida, and H. Sugimoto, *Chem. Lett.*, **1980**, 521; c) H. Ogoshi, H. Sugimoto, and Z. Yoshida, *Biochim. Biophys. Acta*, **621**, 19 (1980).

7) "International Tables for X-Ray Crystallography," ed by J. A. Ibers and W. C. Hamilton, Kynoch Press, Birmingham, England (1974), Vol. IV, p. 99.

8) The anisotropic thermal parameters and complete lists of the $|F_o|$ and $|F_c|$ values are deposited as Document No. 8203 at the Office of the Editor of the Bulletin of the Chemical Society of Japan.

9) W. C. Hamilton, *Acta Crystallogr.*, **12**, 609 (1959).

10) A. F. Wells, "Structural Inorganic Chemistry," Oxford University Press, New York, N. Y. (1975), p. 259.

11) C. Riche, A. Chiaroni, M. Perree-Fauvet, and A. Goudemer, *Acta Crystallogr., Sect. B*, **34**, 1868 (1978).

12) D. L. Cullen and E. F. Meyer, Jr., *J. Am. Chem. Soc.*, **96**, 2095 (1974).

13) a) J. W. Lauher and J. A. Ibers, *J. Am. Chem. Soc.*, **96**, 4447 (1974); b) W. R. Scheidt, J. A. Cunningham, and J. L. Hoard, *ibid.*, **95**, 8289 (1973); c) T. Sakurai, K. Yamamoto, N. Seino, and M. Katsura, *Acta Crystallogr., Sect. B*, **31**, 2514 (1975); d) J. A. Kaduk and W. R. Scheidt, *Inorg. Chem.*, **13**, 1875 (1974); e) S. J. Silvers and A. Tulinsky, *J. Am. Chem. Soc.*, **89**, 3331 (1967); **86**, 927 (1964); f) M. J. Hamor, T. A. Hamor, and J. L. Hoard, *ibid.*, **86**, 1938 (1964).

14) G. B. Robertson, *Nature*, **191**, 593 (1961).

15) a) E. B. Fleischer and A. L. Stone, *J. Chem. Soc., Chem. Commun.*, **1967**, 332; b) A. L. Stone and E. B. Fleischer, *J. Am. Chem. Soc.*, **90**, 2735 (1968).

Microwave Spectra of *cis*- and *trans*-1-Chloro-1,2-difluoroethylene

Teruhiko OGATA

Faculty of Liberal Arts, Shizuoka University, Ohya, Shizuoka 422

(Received January 5, 1981)

The microwave spectra of the ^{35}Cl and ^{37}Cl isotope species of *cis*- and *trans*-HFC=CFCl have been studied in the 8—50 GHz region. The rotational constants and the Cl quadrupole coupling constants in MHz are obtained and listed. The quadrupole coupling constants and the structures obtained for *cis*- and *trans*-HFC=CFCl are consistent with the results of other haloethylenes.

	cis-HFC=CF^{35}Cl	*cis*-HFC=CF^{37}Cl	*trans*-HFC=CF^{35}Cl	*trans*-HFC=CF^{37}Cl
A	9 126.182(10)	9 091.714(18)	5 336.381(8)	5 232.441(10)
B	2 461.037(5)	2 397.536(9)	3 516.721(9)	3 469.251(15)
C	1 936.689(4)	1 895.643(14)	2 117.416(5)	2 083.794(9)
χ_{aa}	−67.67(20)	−53.62(30)	9.78(10)	4.72(20)
χ_{bb}	30.05(20)	23.83(50)	−45.41(10)	−32.54(20)
χ_{cc}	37.62(20)	29.79(50)	35.63(10)	27.82(20)

The microwave spectra and Cl nuclear quadrupole coupling constants have been measured for several substituted ethylenes.[1-6] Substitutional change in the quadrupole coupling constants along the carbon-chlorine bond shows that the numerical values of the coupling constant increase as the number of substituted halogen atoms increases and that fluorine has a greater effect than chlorine.

On the other hand, complete structures for several haloethylenes have been determined by microwave spectroscopy.[1,7-9] The halogen substitution effect on the structure shows that the carbon-carbon double bond and carbon-halogen bond lengths decrease as the number of substituted halogen atoms increases and that fluorine has a greater effect than chlorione.

The present work was initiated to see if the nuclear quadrupole coupling constant and the molecular structure in *cis*- and *trans*-1-chloro-1,2-difluoroethylene are consistent with previous results on haloethylenes.

Experimental

The sample of HFC=CFCl was prepared by two different methods. The first method of preparation utilized an elimination reaction of hydrogen chloride as follows:

$$HFClC\text{-}CHFCl \xrightarrow[(EtOH)]{KOH} HFC{=}CFCl + HCl.$$

Because of competing side reactions the over-all yield was low. The doublet peak of *cis*- and *trans*-HFC=CFCl and some other peaks were observed by a vapor-phase chromatograph.

The second method of preparation was by photochemical reaction of hydrogen bromide with 1,2-dichloro-1,2-difluoroethylene followed by dehalogenation of the adduct as detailed by Birchall *et al.*[10]

$$FClC{=}CFCl + HBr \xrightarrow{h\nu} HFClC\text{-}CFClBr$$

$$HFClC\text{-}CFClBr + Zn \longrightarrow HFC{=}CFCl + ZnClBr$$

The product was shown to be a *cis-trans* mixture of almost equal amount by gas chromatography (resolved easily at room temperature on a 3 m column of Silicone DC-200(20%) and steric acid(5%) on celite). The infrared spectrum was identical to that of Birchall *et al.*[10] Separation of *cis-trans* isomers has been performed by gas chromatography at about −30 °C, the former and the latter peaks on the run were identified as *trans*- and *cis*-isomer, respectively.

The microwave spectrum was investigated in the frequency region from 8 to 50 GHz by using a conventional 100 kHz Stark modulation spectrometer. All measurements were made at the temperature of Dry Ice. The frequency measurements were performed automatically under the control of a microcomputer.[11] The microwave frequency measured by a counter YHP 5340A is processed by a microcomputer YHP 9825A. When a microwave frequency coincides with the marker frequency, the computer triggers a relay actuator YHP 59306A, which actuates a marker pen on the recorder.

Results and Disscusion

Microwave Spectra. A preliminary estimate of the molecular structure for *cis*-HFC=CFCl and *trans*-HFC=CFCl indicate that the dipole moments would lie along the b axis for the *cis*-isomer and between the a and b axes for the *trans*-isomer; spectra exhibiting b-type and both a- and b-type selection rules should be observed, respectively. Nearly all of the Q- and R-branch transitions were predicted to be multiplets due to the coupling of the over-all rotation angular momentum and the nuclear spin angular momentum for both isomers in the ^{35}Cl and ^{37}Cl isotopic species. Each Q-branch transition exhibits a characteristic quartet pattern ($\Delta F = \pm 1$ transitions being weak), and the splitting between the first and second components

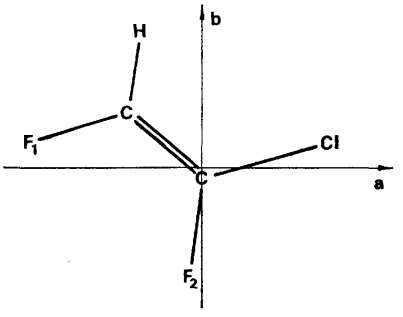

Fig. 1. Molecular structure of *cis*-HFC=CFCl.

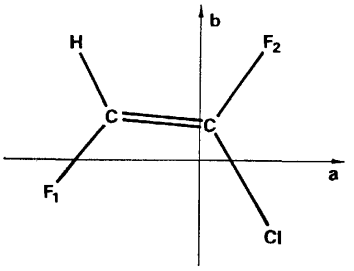

Fig. 2. Molecular structure of *trans*-HFC=CFCl.

equals that of the third and fourth components. The ratio $(\nu_C-\nu_B)/(\nu_D-\nu_A)$ (where ν_t is the frequency of the ith component of the quartet) depends only on Casimir's function. This ratio could be used to determine the J level for transitions exhibiting the characteristic Q-branch quadrupole splitting pattern.

The spectrum of *cis*-HFC=CFCl was found to be broad and moderately strong. A search was made for Q-branch transitions for the ^{35}Cl isotope in the 33—50 GHz region. Assignment was obtained by plotting $(A-C)/2$ *vs.* κ for the various Q-branch transitions. This information together with assumption of planarity, $I_c-I_a-I_b\approx 0$, give the approximate rotational constants. The measurements of R-branch transitions gave the complete assignments which were confirmed by their hyperfine structures. The final values of the rotational constants were fitted by using a least squares criterion to the rotational Hamiltonian involving a centrifugal distortion effect. In this case, when the planarity conditions are applied, only four centrifugal distortion coefficients are independent, *e.g.* τ_{aaaa}, τ_{bbbb}, τ_{aabb}, and τ_{abab}. The results are listed in Table 1. The experimental and calculated frequencies are given in Table 2. The assignment for *cis*-HFC=CF^{37}Cl was made in a manner similar to the ^{35}Cl species. The rotational constants and centrifugal distortion coefficients are listed in Table 1, and the experimental and calculated values of the transition frequency are given in Table 2.

The spectrum of *trans*-HFC=CFCl was found to be sharper and a little weaker than that of the *cis*-isomer. A search was made for Q-branch transitions for the ^{35}Cl isotope in the 8—18 GHz region and an assignment was obtained in the same way as for *cis*-HFC=CFCl. The rotational constants and centrifugal distortion coefficients are listed in Table 3, and the experimental and calculated frequencies are given in Table 4, together with the corresponding values for *trans*-HFC=CF^{37}Cl.

Nuclear Quadrupole Coupling. The Cl nuclear quadrupole interaction in 1-chloro-1,2-difluoroethylene is given by[12]

$$E_Q/h = 2\chi_{J_\tau}\cdot Y(I,J,F)/J(J+1),$$

where $Y(I,J,F)$ is Casimir's function. χ_{J_τ} is the quadrupole coupling constant (or splitting factor) for the rotational level which is given by first-order theory in terms of the diagonal elements in the χ_{J_τ} tensor in the principal inertial axis system as

$$\chi_{J_\tau} = \langle \boldsymbol{P}_a^2\rangle\chi_{aa} + \langle \boldsymbol{P}_b^2\rangle\chi_{bb} + \langle \boldsymbol{P}_c^2\rangle\chi_{cc},$$

where $\boldsymbol{P}_a^2$, $\boldsymbol{P}_b^2$, and $\boldsymbol{P}_c^2$ are the squares of the rotational angular momentum in the principal inertial-axis system. The values of $\langle \boldsymbol{P}_a^2\rangle$, $\langle \boldsymbol{P}_b^2\rangle$, and $\langle \boldsymbol{P}_c^2\rangle$ used in this work were calculated on HITAC M-200H computers at the Institute for Molecular Science and at Tokyo University.

Table 1. Rotational constants and centrifugal distortion coefficients for *cis*-1-chloro-1,2-difluroethylene[a]

	cis-HFC=CF^{35}Cl	*cis*-HFC=CF^{37}Cl
A	9 126.182(10) MHz	9 091.714(18) MHz
B	2 461.037(5)	2 397.536(9)
C	1 936.689(4)	1 895.643(14)
τ_{aaaa}	−0.0891(31)	−0.0915(61)
τ_{bbbb}	−0.00086(30)	−0.00006(77)
τ_{aabb}	0.0098(27)	0.0153(81)
τ_{abab}	−0.0097(19)	−0.0143(60)
I_a	55.376 u·Å^2	55.586 u·Å^2
I_b	205.351	210.790
I_c	260.948	266.599
Δ[b]	0.221	0.223

a) Standard deviations for last figures in parentheses.
b) $\Delta=I_c-I_a-I_b$.

The χ_{aa} and χ_{bb} components of quadrupole coupling tensor were determined from the transitions with relatively large hyperfine splitting. The χ_{cc} element was then determined from the Laplace equation $\chi_{aa}+\chi_{bb}+\chi_{cc}=0$. The results are listed in Table 5. From the observed splittings and the tabulated values of the Casimir's functions, the values ν_0 for an unperturbed transitions are easily calculated and are listed in Table 2 and Table 4. Using the results in Table 5, the quadrupole splitting in all measured transitions in both *cis*- and *trans*-HFC=CFCl was computed and compared with the experimental values. These values are also listed in Tables 2 and 4.

The diagonalized χ tensors for *cis*- and *trans*-HFC=CFCl were calculated by using the molecular structures obtained later with the assumption that the z axis coincides with the C–Cl internuclear line. θ_{az}, the angle between the a and z axes, for *cis*-HFC=CF^{35}Cl is 16.03°. It is very insensitive to the structural parameters because the C–Cl bond lies almost along a-axis. The result for *cis*-HFC=CF^{35}Cl is listed in Table 5 together with that of *cis*-HFC=CF^{37}Cl. In the same way, the diagonal χ tensor for *trans*-HFC=CF^{35}Cl was calculated, with $\theta_{az}=59.29°$, and listed in Table 5 together with the corresponding values of ^{37}Cl species. The values of $\chi_{zz}=-76.46$ MHz and $\chi_{zz}=-75.57$ MHz for *cis*- and *trans*-HFC=CF^{35}Cl, respectively, are consistent with those of other haloethylenes such as, placed in order of increasing number of substituted halogen atoms, −70.16, −70.7, −77.9, −73.42, −73.7, −77.40, and −89.14(−73.7) MHz for H_2C=CHCl,[1] *cis*-HClC=CHCl,[7] H_2C=CCl_2,[7] H_2C=CFCl,[5] *cis*-HFC=CHCl,[4] F_2C=CHCl,[6] and F_2C=CFCl,[5] respectively.

Molecular Structure. In order to determine the molecular structure the bond lengths were estimated by assuming a systematic shortening caused by halogen substitution which is well established in the r_s struc-

TABLE 2. OBSERVED AND CALCULATED SPECTRA OF *cis*-HFC=CFCl (MHz)

Transition	F[a]	*cis*-HFC=CF^{35}Cl				*cis*-HFC=CF^{37}Cl			
		ν(exptl)[d]	ν_0(exptl)	($\nu-\nu_0$) (exptl)	ν(calcd) $-\nu_0$(exptl)	ν(exptl)[d]	ν_0(exptl)	($\nu-\nu_0$) (exptl)	ν(calcd) $-\nu_0$(exptl)
$0_{00}\rightarrow1_{11}$	3/2[c]	11 055.34	11 662.82	−7.48	−7.48	10 981.33	10 987.33	−6.00	−5.95
	3/2	11 061.32		−1.50	−1.47	10 986.21		−1.12	−1.18
	3/2[b]	11 068.81		5.99	6.04	10 992.08		4.75	4.91
$1_{01}\rightarrow2_{12}$	1/2	14 919.32	14 936.21	−16.89	−16.90	14 765.39	14 778.62	−13.23	−13.40
	5/2[b]	14 926.09		−10.12	−10.09	e)			−8.00
	1/2[b]	14 928.63		−7.58	−7.48	e)			−5.96
	5/2	14 935.56		−0.68	−0.68	14 778.00		−0.62	−0.54
	3/2	14 943.10		6.89	6.84	14 784.01		5.39	5.41
	3/2[b]	14 949.67		13.46	13.55	14 789.23		10.61	10.73
$2_{20}\rightarrow3_{31}$	7/2	e)	47 816.62		−2.19	47 591.25	47 592.93	−1.68	−1.67
	1/2	47 816.61		−0.01	0.05	47 593.00		0.07	0.10
	5/2	47 818.71		2.09	2.02	47 594.72		1.79	1.66
	3/2	47 820.98		4.36	4.25	47 596.27		3.34	3.43
$2_{21}\rightarrow3_{30}$	7/2					47 619.44	47 621.17	−1.73	−1.82
	1/2					47 621.21		0.04	−0.07
	5/2					47 622.95		1.78	1.59
	3/2					47 624.62		3.45	3.39
$3_{12}\rightarrow4_{23}$	3/2	36 790.92	36 795.46	−4.54	−4.62	36 494.74	36 498.45	−3.71	−3.73
	9/2	36 794.03		−1.43	−1.51	36 497.22		−1.23	−1.26
	5/2	36 795.86		0.40	0.36	36 498.69		0.24	0.22
	7/2	36 798.97		3.51	3.46	36 501.11		2.66	2.69
$3_{13}\rightarrow4_{22}$	3/2	40 373.88	40 380.10	−6.22	−6.16	39 906.13	39 911.02	−4.83	−4.85
	9/2	40 377.95		−2.15	−2.11	39 909.25		−1.77	−1.64
	5/2	40 380·95		0.85	0.87	39 911.72		0.70	0.71
	7/2	40 385.03		4.93	4.92	39 914.92		3.90	3.92
$4_{22}\rightarrow4_{31}$	5/2					34 410.14	34 417.52	−7.38	−7.14
	11/2					34 413.89		−3.63	−3.64
	7/2					34 420.47		2.95	2.83
	9/2					34 423.80		6.28	6.32
$4_{23}\rightarrow4_{32}$	5/2	34 723.65	34 732.74	−9.09	−9.09	34 806.14	34 814.43	−7.29	−7.20
	11/2	34 728.10		−4.64	−4.63	34 809.69		−3.74	−3.67
	7/2	34 736.36		3.62	3.64	34 816.30		2.87	2.88
	9/2	34 740.86		8.12	8.10	34 819.85		6.42	6.42
$4_{14}\rightarrow5_{05}$	7/2	16 748.62	16 749.96	−1.34	−1.33				
	9/2	16 749.20		−0.76	−0.79				
	5/2	16 750.39		0.43	0.47				
	11/2	16 751.00		1.04	1.02				
$4_{13}\rightarrow5_{24}$	5/2	40 138.28	40 141.11	−2.83	−2.88				
	11/2	40 140.13		−0.98	−1.01				
	7/2	40 141.60		0.49	0.43				
	9/2	40 143.33		2.22	2.28				
$4_{14}\rightarrow5_{23}$	5/2	46 379.97	46 384.35	−4.38	−4.33				
	11/2	46 382.60		−1.75	−1.75				
	7/2	46 385.46		1.11	1.09				
	9/2	46 388.08		3.73	3.67				
$5_{23}\rightarrow5_{32}$	7/2	33 906.87	33 912.42	−5.55	−5.57	34 055.91	34 060.35	−4.44	−4.38
	13/2	33 909.20		−3.22	−3.23	34 057.80		−2.55	−2.53
	9/2	33 915.17		2.75	2.72	34 062.48		2.13	2.19
	11/2	33 917.56		5.14	5.06	34 064.42		4.07	4.04
$5_{24}\rightarrow5_{33}$	7/2	34 884.56	34 890.20	−5.64	−5.63	34 953.27	34 957.73	−4.46	−4.46
	13/2	34 886.88		−3.32	−3.23	34 955.12		−2.61	−2.56
	9/2	34 892.95		2.75	2.89	34 959.87		2.14	2.29
	11/2	34 895.53		5.33	5.29	34 961.89		4.16	4.19

TABLE 2. (Continued)

Transition	F[a]	*cis*-HFC=CF^{35}Cl				*cis*-HFC=CF^{37}Cl			
		ν(exptl)[d]	ν_0(exptl)	$(\nu-\nu_0)$ (exptl)	ν(calcd) $-\nu_0$(exptl)	ν(exptl)[d]	ν_0(exptl)	$(\nu-\nu_0)$ (exptl)	ν(calcd) $-\nu_0$(exptl)
$5_{14}\rightarrow6_{25}$	7/2	43 234.12	43 235.97	−1.85	−1.90	42 828.29	42 829.82	−1.53	−1.44
	13/2	43 235.31		−0.66	−0.72	42 829.27		−0.55	−0.51
	9/2	43 236.36		0.39	0.31	42 830.08		0.26	0.32
	11/2	43 237.45		1.48	1.49	42 831.05		1.23	1.25
$6_{06}\rightarrow6_{15}$	9/2	13 896.60	13 898.14	−1.54	−1.52				
	15/2	13 897.14		−1.00	−0.95				
	11/2	13 899.04		0.90	0.88				
	13/2	13 899.61		1.47	1.45				
$6_{15}\rightarrow6_{24}$	9/2	17 498.39	17 500.33	−1.94	−1.89	17 603.56	17 605.10	−1.54	−1.48
	15/2	17 499.10		−1.23	−1.16	17 604.10		−1.00	−0.90
	11/2	17 501.46		1.13	1.17	17 606.00		0.90	0.94
	13/2	17 502.14		1.81	1.89	17 606.55		1.45	1.51
$6_{25}\rightarrow6_{34}$	9/2	35 155.19	35 159.08	−3.89	−3.88	35 201.55	35 204.59	−3.04	−3.13
	15/2	35 156.60		−2.48	−2.43	35 202.61		−1.98	−1.98
	11/2	35 161.29		2.21	2.35	35 206.33		1.74	1.73
	13/2	35 162.78		3.70	3.71	35 207.50		2.91	2.87
$6_{25}\rightarrow7_{16}$	13/2, 11/2	16 614.72	16 616.24	−1.52	−1.63, −1.40				
	15/2, 9/2	16 617.73		1.49	1.43, 1.66				
$6_{15}\rightarrow7_{26}$	9/2	46 097.50	46 098.74	−1.24	−1.19				
	15/2	46 098.30		−0.44	−0.40				
	11/2	46 098.96		0.22	0.31				
	13/2	46 099.81		1.07	1.10				
$7_{07}\rightarrow7_{16}$	11/2	16 695.79	16 697.12	−1.33	−1.38				
	17/2	16 696.18		−0.94	−0.94				
	13/2	16 697.95		0.83	0.78				
	15/2	16 698.42		1.30	1.22				
$7_{16}\rightarrow7_{25}$	11/2	17 309.90	17.311.27	−1.37	−1.37				
	17/2	17 310.29		−0.98	−0.91				
	13/2	17 312.21		0.94	0.89				
	15/2	17 312.53		1.26	1.35				
$7_{26}\rightarrow7_{35}$	11/2	35 571.34	35 574.25	−2.91	−2.88	35 584.16	35 586.41	−2.25	−2.33
	17/2	35 572.35		−1.90	−1.94	35 584.87		−1.54	−1.58
	13/2	35 576.05		1.80	1.77	35 587.87		1.46	1.36
	15/2	35 577.00		2.75	2.72	35 588.54		2.13	2.11
$8_{17}\rightarrow8_{26}$	13/2	17 528.37	17 529.44	−1.07	−1.04				
	19/2	17 528.67		−0.77	−0.72				
	15/2	17 530.15		0.71	0.74				
	17/2	17 530.47		1.03	1.06				
$8_{27}\rightarrow8_{36}$	13/2	36 167.88	36 170.10	−2.22	−2.23				
	19/2	36 168.54		−1.56	−1.57				
	15/2	36 171.57		1.47	1.45				
	17/2	36 172.27		2.17	2.11				
$9_{36}\rightarrow9_{45}$	15/2, 21/2					47 647.53	47 649.19	−1.66	−1.74, −1.25
	17/2					47 650.46		1.27	1.32
	19/2					47 651.00		1.81	1.81
$10_{37}\rightarrow10_{46}$	17/2, 23/2					47 068.91	47 070.16	−1.25	−1.47, −1.12
	19/2, 21/2					47 071.36		1.20	1.00, 1.36

a) $\Delta F=\Delta J$. b) $\Delta F=\Delta J-1$. c) $\Delta F=\Delta J-2$. d) ±0.1 MHz. e) Overlaps with other line.

TABLE 4. OBSERVED AND CALCULATED SPECTRA OF *trans*-HFC=CFCl (MHz)

Transition	F[a]	*trans*-HFC=CF^{35}Cl				*trans*-HFC=CF^{37}Cl			
		ν(exptl)[c]	ν_0(exptl)	$(\nu-\nu_0)$ (exptl)	ν(calcd) $-\nu_0$(exptl)	ν(exptl)[c]	ν_0(exptl)	$(\nu-\nu_0)$ (exptl)	ν(calcd) $-\nu_0$(exptl)
$1_{10}\rightarrow2_{21}$	3/2	18 117.64	18 126.55	−8.91	−8.91	17 774.71	17 781.09	−6.38	−6.41
	3/2[b]	18 119.42		−7.13	−7.17	17 775.46		−5.63	−5.58
	5/2[b]	18 126.61		0.06	0.00	d)			0.55
	5/2	18 129.01		2.46	2.44	17 782.75		1.66	1.70
	1/2	18 135.45		8.90	8.87	17 788.12		7.03	6.98
	1/2[b]	18 137.93		11.38	11.31	17 789.27		8.18	8.09
$2_{12}\rightarrow3_{03}$	1/2	14 117.88	14 120.75	−2.87	−2.89	13 916.66	13 918.68	−2.02	−1.98
	3/2	14 119.16		−1.57	−1.51	13 917.43		−1.25	−1.23
	7/2	14 120.75		0.00	−0.04	13 918.77		0.09	0.09
	5/2	14 122.13		1.38	1.35	13 919.53		0.85	0.84
$2_{12}\rightarrow3_{13}$	1/2	14 503.60	14 505.53	−1.93	−1.89	14 280.72	14 282.30	−1.58	−1.55
	3/2	14 504.38		−1.15	−1.14	14 281.51		−0.79	−0.83
	5/2	14 505.45		−0.08	−0.03	14 282.14		−0.16	−0.16
	7/2	14 507.17		0.64	0.71	14.282.88		0.58	0.56
$2_{02}\rightarrow3_{03}$	5/2	15 090.78	15 093.71	−2.93	−2.95	14 849.18	14 851.31	−2.13	−2.18
	3/2	15 092.19		−1.52	−1.49	14 850.03		−1.28	−1.27
	7/2	15 095.37		1.66	1.71	14 852.68		1.37	1.25
	1/2	15 096.86		3.15	3.17	14 853.42		2.11	2.16
$2_{02}\rightarrow3_{13}$	5/2	15 474.26	15 478.61	−4.35	−4.45	15 211.71	15 214.85	−3.14	−3.09
	3/2	15 476.83		−1.78	−1.99	15 213.34		−1.51	−1.50
	7/2	15 480.88		2.27	2.34	15 216.57		1.72	1.81
	1/2	15 483.34		4.73	4.80	15 218.22		3.37	3.40
$2_{21}\rightarrow3_{22}$	1/2	16 899.89	16 902.36	−2.47	−2.44	16 657.88	16 659.09	−1.21	−1.14
	7/2	16 901.71		−0.65	−0.69	16 658.75		−0.34	−0.32
	3/2	16 902.36		0.00	0.01	16 659.18		0.09	0.01
	5/2	16 904.09		1.73	1.76	16 659.90		0.81	0.83
$4_{23}\rightarrow4_{32}$	5/2	14 133.43	14 135.04	−1.61	−1.63				
	11/2	14 134.15		−0.89	−0.83				
	7/2	14 135.74		0.70	0.65				
	9/2	14 136.46		1.42	1.45				
$4_{14}\rightarrow4_{23}$	5/2	15 191.93	15 199.41	−1.48	−7.46				
	11/2	15 195.64		−3.77	−3.79				
	7/2	15 202.37		2.96	3.02				
	9/2	15 206.09		6.68	6.68				
$4_{31}\rightarrow4_{40}$	9/2	16 079.65	16 084.44	−4.79	−4.89				
	7/2	16 082.30		−2.14	−2.17				
	11/2	16 087.20		2.76	2.86				
	5/2	16 089.80		5.36	5.57				
$4_{32}\rightarrow4_{41}$	9/2	16 987.10	16 989.63	−2.53	−2.56				
	7/2	16 988.49		−1.14	−1.16				
	11/2	16 991.07		1.44	1.44				
	5/2	16 992.46		2.83	2.84				
$5_{32}\rightarrow5_{41}$	11/2	14 577.04	14 581.66	−4.62	−4.66				
	9/2	14 579.15		−2.51	−2.53				
	13/2	14 584.57		2.91	2.88				
	7/2	14 586.65		4.99	5.01				
$5_{33}\rightarrow5_{42}$	11/2	17 343.26	17 344.04	−0.78	−0.82	16 912.60	16 912.79	−0.19	−0.26
	9/2	17 343.59		−0.45	−0.45				−0.11
	13/2	17 344.57		0.53	0.51	16 913.00		0.21	0.26
	7/2	17 344.87		0.83	0.89				0.40
$6_{15}\rightarrow6_{24}$	9/2	15 901.45	15 908.40	−6.95	−6.94	15 744.69	15 749.87	−5.18	−5.14
	15/2	15 904.04		−4.36	−4.36	15 746.62		−3.25	−3.22
	11/2	15 912.36		3.96	4.00	15 752.82		−2.95	2.98
	13/2	15 914.96		6.56	6.58	15 754.75		4.88	4.90

TABLE 4. (Continued)

Transition	F[a]	*trans*-HFC=CF^{35}Cl				*trans*-HFC=CF^{37}Cl			
		ν(exptl)[c]	ν_0(exptl)	$(\nu-\nu_0)$ (exptl)	ν(calcd) $-\nu_0$(exptl)	ν(exptl)[c]	ν_0(exptl)	$(\nu-\nu_0)$ (exptl)	ν(calcd) $-\nu_0$(exptl)
$6_{34}\rightarrow6_{43}$	9/2					17 910.25	17 910.75	−0.50	−0.75
	15/2								−0.50
	11/2					17 911.20		0.45	0.32
	13/2								0.57
$7_{43}\rightarrow7_{52}$	15/2					17 844.61	17 847.10	−2.49	−2.52
	13/2					17 845.47		−1.63	−1.66
	17/2					17 848.84		1.74	1.71
	11/2					17 849.70		2.60	2.57
$8_{44}\rightarrow8_{53}$	17/2	16 198.71	16 201.63	−2.92	−2.96	15 641.33	15 643.29	−1.96	−1.95
	15/2	16 199.55		−2.08	−2.05	15 641.88		−1.41	−1.34
	19/2	16 203.80		2.17	2.12	15 644.74		1.45	1.47
	13/2	16 204.64		3.01	3.03	15 645.35		2.06	2.08
$8_{36}\rightarrow8_{35}$	13/2	17 655.05	17 660.99	−5.94	−6.01	17 577.82	17 582.23	−4.41	−4.34
	19/2	17 656·80		−4.19	−4.24	17 579.19		−3.04	−3.04
	15/2	17 664.97		3.98	3.93	17 585.12		2.89	2.93
	17/2	17 666.71		5.72	5.71	17 586.48		4.25	4.23
$8_{26}\rightarrow8_{35}$	13/2					18 209.48	18 213.36	−3.88	−3.87
	19/2					18 210.59		−2.77	−2.73
	15/2					18 215.82		2.45	2.51
	17/2					18 216.98		3.62	3.36
$9_{45}\rightarrow9_{54}$	19/2	14 683.19	14 684.45	−1.26	−1.25	14 244.30	14 244.99	−0.69	−0.72
	17/2	14 683.55		−0.90	−0.89				−0.51
	21/2	14 685.39		0.94	0.97	14 245.70		0.71	0.60
	15/2	14 685.73		1.28	1.32				0.81
$9_{36}\rightarrow9_{45}$	15/2	15 684.13	15 687.45	−3.32	−3.29	15 558.84	15 561.40	−2.56	−2.51
	21/2	15 685.05		−2.40	−2.39	15 559.55		−1.85	−1.83
	17/2	15 689.78		2.33	−2.36	15 563.17		1.77	1.79
	19/2	15 690.66		3.21	3.26	15 563.88		2.48	2.48
$10_{46}\rightarrow10_{55}$	17/2	15 024.89	15 025.56	−0.67	−0.75	14 744.10	14 744.71	−0.61	−0.74
	23/2				−0.56				−0.56
	19/2	15 026.21		0.65	0.57	14 745.30		0.59	0.49
	21/2				0.76				0.67
$11_{57}\rightarrow11_{56}$	19/2	14 001.67	14 006.30	−4.63	−4.64				
	25/2	14 002.75		−3.55	−3.57				
	21/2	14 009.78		3.48	3.48				
	23/2	14 010.82		4.52	4.54				
$11_{56}\rightarrow11_{65}$	23/2	17 600.72	17 602.11	−1.39	−1.40	17 028.20	17 028.99	−0.79	−0.90
	21/2	17 600.98		−1.13	−1.06				−0.69
	25/2	17 603.25		1.14	1.17	17 029.80		0.81	0.69
	19/2	17 603.55		1.44	1.51				0.90
$11_{47}\rightarrow11_{56}$	19/2	17 748.64	17 751.17	−2.53	−2.53	17 612.91	17 614.89	−1.98	−1.96
	25/2	17 749.22		−1.95	−1.95	17 613.39		−1.50	−1.51
	21/2	17 753.05		1.88	1.90	17 616.36		1.47	1.47
	23/2	17 753.65		2.48	2.48	17 616.82		1.93	1.92
$12_{57}\rightarrow12_{66}$	21/2	17 405.20	17 405.47	−0.27	−0.35	17 041.70	17 042.04	−0.34	−0.37
	27/2				−0.29				−0.29
	23/2	17 405.73		0.26	0.18	17 042.36		0.32	0.30
	25/2				0.25				0.38
$13_{68}\rightarrow13_{67}$	23/2	14 696.33	14 700.41	−4.08	−4.15				
	29/2	14 697.15		−3.26	−3.32				
	25/2	14 703.61		3.20	3.24				
	27/2	14 704.42		4.01	4.08				

a) $\Delta F=\Delta J$. b) $\Delta F=\Delta J-1$. c) ±0.1 MHz. d) Overlaps with other line.

Table 3. Rotational constants and centrifugal distortion coefficients for *trans*-1-chloro-1,2-difluoroethylene[a]

	trans-HFC=CF^{35}Cl	*trans*-HFC=CF^{37}Cl
A	5 336.381(8) MHz	5 232.441(10) MHz
B	3 516.721(9)	3 469.251(15)
C	2 117.416(5)	2 083.794(9)
τ_{aaaa}	−0.0122(13)	−0.0139(14)
τ_{bbbb}	−0.0082(14)	−0.0091(26)
τ_{aabb}	0.0146(55)	0.0144(99)
τ_{abab}	−0.0095(21)	−0.0085(37)
I_a	94.704 u·Å^2	96.585 u·Å^2
I_b	143.707	145.673
I_c	238.676	242.527
Δ[b]	0.265	0.269

a) Standard deviations for last figures in parentheses. b) $\Delta=I_c-I_a-I_b$.

tures of haloethylenes. The C–Cl bond lengths of 1.726, 1.717, and 1.718 Å determined for H_2C=CHCl,[1] HCl=CHCl,[7] and H_2C=CCl_2,[7] respectively, show a systematic shortening and suggest about 1.710 Å for the C–Cl bond in HFC=CFCl. Similarly, the C–F bond lenghts of 1.349, 1.335, and 1.323 Å for H_2C=CHF,[8] HFC=CHF,[9] and H_2C=CF_2,[9] respectively, suggest about 1.328 and 1.322 Å for the C–F and C–F′ bonds in HFC=CF′Cl, respectively. The C=C bond lengths of 1.332, 1.320, 1.338, 1.329, 1.324, and 1.315 Å for H_2C=CHCl,[1] HClC=CHCl,[7] H_2C=CCl_2,[7] H_2C=CHF,[8] HFC=CHF,[9] and H_2C=CF_2,[9] respectively, present a more confused situation. The C=C bond lengths in H_2C=CCl_2 and H_2C=CF_2, however, seem to have a large effect from zero point vibration because a carbon atom in either molecules lies very close to the center of mass.[7] From the rest of the molecules, the estimation of about 1.318 Å was made for the C=C bond length in HFC=CFCl.

Table 5. Quadrupole coupling constants for *cis*- and *trans*-1-chloro-1,2-difluoroethylene (MHz)

	cis-HFC=CFCl		*trans*-HFC=CFCl	
	^{35}Cl	^{37}Cl	^{35}Cl	^{37}Cl
	Principal-axis system			
χ_{aa}	−67.67(20)	−53.62(30)	9.78(10)	4.72(20)
χ_{bb}	30.05(20)	23.83(50)	−45.41(10)	−32.54(20)
χ_{cc}	37.62(20)	29.79(50)	35.63(10)	27.82(20)
	C–Cl bond-axis system[a]			
χ_{zz}	−76.46	−60.19	−75.57	−59.68
χ_{xx}	38.84	30.40	39.94	31.86
χ_{yy}	37.62	29.79	35.63	27.82
η_{bond}[b]	−0.0160	−0.0101	−0.0570	−0.0677

a) Z is coincident with the C–Cl bond axis and x is in the plane of the molecule. b) $\eta_{bond}=(\chi_{xx}-\chi_{yy})/\chi_{zz}$.

Table 6. Plausible structural parameters of *cis*-HFC=CFCl

r(C–H)	1.080 Å
r(C–F_1)	1.328
r(C=C)	1.318
r(C–Cl)	1.710
r(C–F_2)	1.322
∠H–C=C	122.1°
∠F_1–C=C	121.9
∠C=C–Cl	123.4
∠C=C–F_2	123.3
Calculated moments of inertia	
^{35}Cl I_a	55.396 u·Å^2
I_b	205.383
I_c	260.779
^{37}Cl I_a	55.622
I_b	210.784
I_c	266.406

Table 7. Plausible structural parameters of *trans*-HFC=CFCl

	Set I	Set II	Set III
r(C–H)	1.080 Å	1.080 Å	1.080 Å
r(C–F_1)	1.328	1.324	1.323
r(C=C)	1.318	1.319	1.316
r(C–F_2)	1.322	1.322	1.320
r(C–Cl)	1.710	1.712	1.712
∠H–C=C	119.7°	120.0°	120.0°
∠F_1–C=C	123.9	123.3	122.9
∠C=C–F_2	122.7	122.1	120.8
∠C=C–Cl	122.9	123.5	124.5
θ_{az}	62.36	61.16	59.27
	Calculated Moments of inertia		
^{35}Cl I_a	94.639 u·Å^2	94.685 u·Å^2	94.671 u·Å^2
I_b	143.820	143.746	143.740
I_c	238.460	238.432	238.410
^{37}Cl I_a	96.625	96.616	96.510
I_b	145.655	145.663	145.791
I_c	242.280	142.278	242.301

By assuming the bond lengths estimated above, the bond angles in *cis*-HFC=CFCl were fitted so as to give the observed moments of inertia of both Cl isotopic species. The result is shown in Table 6 together with the calculated moments of inertia. The structural parameters obtained are consistent with those of other haloethylenes.

The same treatment was made for *trans*-HFC=CFCl. The θ_{az}, however, was found to be very sensitive to the structural parameters and a small deviation in θ_{az} gives an unlealistic value for the diagonal χ tensor. Therefore, three sets of structural parameters which have various θ_{az} were tentatively calculated, as shown in Table 7, by keeping the bond lengths close to the estimated values. The parameters of Set I and Set II, however, lead to $\chi_{zz}=-66.26$ MHz and $\chi_{zz}=-69.43$ MHz, respectively, and besides $\chi_{xx}<\chi_{yy}$, which does not seem possible. On the other hand, Set III gives reasonable values for the χ tensor as discussed before and is very probable for the structure of *trans*-HFC=CFCl.

I would like to thank Drs. C. Matsumura and H. Takeo of the National Chemical Laboratory for Industry for their helpful discussions and for the measurements of the microwave spectrum, and Professor E. Hirota and Dr. Y. Endo of the Institute for Molecular Science for a use of microwave spectrometer. I would also like to thank Dr. J. M. Birchall of Manchester University for providing a copy of the infrared spectrum of 1-chloro-1,2-difluoroethylene. Thanks are also due to Dr. A. P. Cox for critical reading of the manuscript and helpful suggestions.

References

1) D. Kivelson, E. B. Wilson, and D. R. Lide, *J. Chem. Phys.*, **32**, 205 (1960).
2) W. H. Flygare and J. A. Howe, *J. Chem. Phys.*, **36**, 440 (1962).
3) S. Sekino and T. Nishikawa., *J. Phys. Soc. Jpn.*, **12**, 43 (1957).
4) J. A. Howe, *J. Chem. Phys.*, **34**, 1247 (1961).
5) R. G. Stone and W. H. Flygare, *J. Mol. Spectrosc.*, **32**, 233 (1969); Krishnaji & Suresh Chandra, *Indian J. Pure Appl. Phys.*, **8**, 634 (1970).
6) R. G. Stone and W. H. Flygare, *J. Chem. Phys.*, **49**, 1943 (1968).
7) H. Takeo, M. Sugie, and C. Matsumura, to be published.
8) D. R. Lide and D. Christensen, *Spectrochim. Acta*, **17**, 665 (1961).
9) V. W. Laurie and D. T. Pence, *J. Chem. Phys.*, **38**, 2693 (1963).
10) J. M. Birchall, R. N. Haszeldine, and A. R. Parkinson, *J. Chem. Soc.*, **1961**, 2204.
11) T. Ogata, *Reports of Faculty of Liberal Arts, Shizuoka University*, **16**, 13 (1980).
12) W. Gordy and R. L. Cook, "Microwave Molecular Spectra," ed by W. West, Interscience Publishers, New York, N. Y. (1970).

 © 1982 The Chemical Society of Japan Bull. Chem. Soc. Jpn., 55, 17—22 (1982)

Photoelectrochemical Studies of MoS_2 Electrode by Rotating Ring-disk Electrode Technique

Akira Fujishima,* Yoshikazu Noguchi, Kenichi Honda, and Boon H. Loo†

Department of Synthetic Chemistry, Faculty of Engineering, The University of Tokyo, Hongo, Bunkyo-ku, Tokyo 113

† *Materials Research Laboratory, SRI International, Menlo Park, California 94025, U. S. A.*

(Received February 4, 1981)

Photoelectrochemical processes at both n- and p-type MoS_2 electrodes were studied by rotating ring-disk electrode technique. In comparison with other semiconductor photoelectrodes such as CdS, ZnO, and TiO_2, the competitive oxidations of various reducing agents at n-MoS_2 electrode were not clearly dependent on their redox potentials. The MoS_2 photoanode was particularly stabilized in I^- solutions, and this was attributed to the specific adsorption of I^- ions on the electrode surface. Two step waves were observed in the photocurrent-potential curves of MoS_2 photoanode in I^- solutions. The first wave was controlled by the diffusion of I^- ions from the bulk solution to the electrode surface, and the second wave at more anodic potential was dependent on the formation of the photogenerated holes.

There are about sixty kinds of transition metal dichalcogenides, and approximately 70% of them have two dimensional layer structures. This layer structure exerts great influence on the solid state properties of these dichalcogenides, in particular, the intercalation processes which have been investigated to achieve superconduction[1] and high current density batteries.[2]

Tributsch and his coworkers were the first to investigate the photoelectrochemical reactions at some layer-type semiconductor electrodes (MoS_2,[3,4] $MoSe_2$,[5,6] and WSe_2[7]). These layer type semiconductors are attractive materials for solar energy conversion because they have small bandgaps and an expected higher stability against photocorrosion, since their main photoelectrochemical reactions are based on holes from d-bands belonging to the non-bonding orbitals of the transition metals. Photoanodes using transition metal dichalcogenide semiconductor materials in photoelectrochemical cells have been reported by several groups.[3-23] Molybdenum dichalcogenide photoanodes were especially stabilized by I^-.[3-6] Electrochemical photocells based on n-WSe_2/I^- and n-$MoSe_2$/I^- systems have been reported recently to have solar conversion efficiencies of 10.2 and 9.4%, respectively.[23]

In this study we investigated in detail the photoelectrochemical processes which occurred at n-type and p-type MoS_2 electrodes by rotating ring-disk electrode (RRDE) technique, which is very useful to measure electrochemical products. Competitive reactions of I^- and other redox agents were studied to provide insights on the corrosion and stabilization processes.

Experimental

The MoS_2 single crystals (n- and p-type) used in the present study were produced naturally in Japan. The crystal was cleaved between layers and shaped into a disk of diameter 5.0 mm. Ohmic contact with a conducting wire was made by rubbing In–Ga alloy on one side of the crystal. The MoS_2 disk was then mounted on a Teflon holder using an epoxy resin with a Pt ring 7.0 mm in inner diameter and 9.0 mm in outer diameter. The MoS_2 (001) face exposed to the electrolyte was etched in 5 M HCl (1 M=1 mol dm^{-3}) for 30 s, and then rinsed with distilled water. The ring-disk electrode was set in a RRDE measurement system (Nikko Keisoku). The potentials of the disk and ring electrodes were controlled independently by means of a dual-potentiostat (Nikko Keisoku). The light source was a 250 W high pressure Hg lamp and the wavelength of illuminating light was selected with a V-Y44 (440 nm) cutoff filter (Toshiba Kasei). The rotation speed of the RRDE was set at 1000 min^{-1}. All chemicals used were of reagent grade. The experimental detail of the RRDE measurements was described elsewhere.[24]

Results and Discussion

Photoelectrochemical Reactions at an n-MoS_2 Electrode. The anodic reactions at an illuminated n-MoS_2 electrode in an inert electrolyte involved the following processes:[3]

$$MoS_2 + 8H_2O + 18h^+ \longrightarrow Mo(VI) + 2SO_4^{2-} + 16H^+, \quad (1)$$

$$MoS_2 + 4h^+ \longrightarrow Mo(IV) + 2S, \quad (2)$$

$$MoS_2 + 2H_2O + 4h^+ \longrightarrow MoS_2 + O_2 + 4H^+. \quad (3)$$

We performed quantitative analysis on all possible reaction products and found that Reaction 1 was the predominant process (Table 1), which agreed with Tributsch's results.[3] Our SEM experiments showed that elemental sulfur was present on the electrode surface in all cases. This suggests Reaction 2 always occurs to some extent in an inert electrolyte. Both Reactions 1 and 2 lead to the dissolution of the photoanode. Reaction 3 occurs in a smaller extent, however, it is the main focus of interest since water is splitted without degradation of the photoanode. Photocorrosion of MoS_2 electrode will be suppressed if Reactions 1 and 2 are suppressed.

Perhaps the photoanodic reactions at an n-MoS_2 electrode are analogous to those occuring at a pyrite (FeS_2) electrode, which has been investigated in detail by Biegler and Swift.[25] The anodic reactions at a pyrite electrode are composed of two processes which lead to formation of sulphate and elemental sulfur.

Flatband Potential of n-MoS_2 Electrode. We measured the flatband potential of n-MoS_2 electrode in 0.2 M Na_2SO_4 solution with variation in pH by impedance measurements. The flatband potential was

Table 1. Results of quantitative analysis of molybdenum ions and pH change

	Solution	Charge flowed Q	Amount of Mo[a] mg	Number of electrons or holes	pH change
Light (all wavelengths)	0.1 M KCl 150 ml	43.04	2.23	19.19	5.35→2.90
Monochromatic light (540 nm)	0.1 M KCl 150 ml	51.81	2.35	21.92	5.35→2.80
Monochromatic light (580 nm)	0.1 M KCl 100 ml	4.11	0.284	14.39	5.35→3.78

a) Colorimetric analysis of thiocyanate.

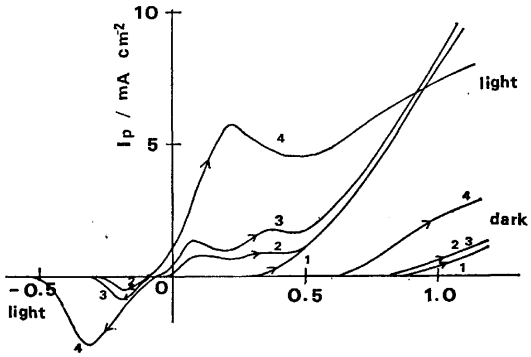

Fig. 1. Current-potential curves of n-MoS_2 electrode in 0.2 M Na_2SO_4 solutions with various concentrations of I^- ions.
1: 0 M, 2: 5×10^{-3} M, 3: 10^{-2} M, 4: 10^{-1} M.

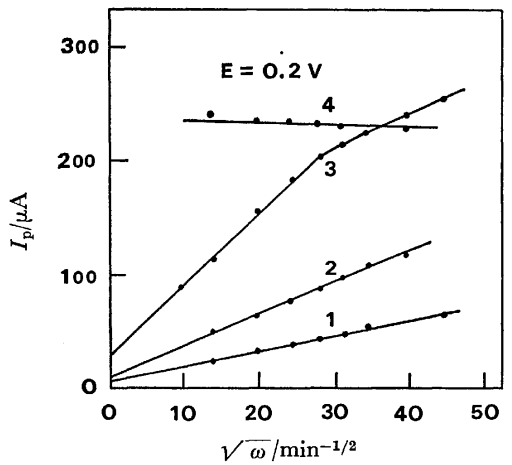

Fig. 2. Dependence of photocurrent at n-MoS_2 electrode on the rotating speed in 0.2 M Na_2SO_4 solutions with different concentrations of I^- ions.
1: 10^{-3} M, 2: 5×10^{-3} M, 3: 10^{-2} M, 4: 5×10^{-2} M.

found to be 0.15±0.05 V *vs.* SCE. This value agreed with those reported by others, 0.10 to 0.20 V in 1 M KCl aqueous electrolyte[6] and 0.30 V in CH_3CN.[17] Analogous to the behavior for CdS, the flatband potential of n-MoS_2 was found to be independent of the pH of the electrolyte. However, since the main photoanodic process of MoS_2 involved the reaction with water (Reaction 1 above), the onset of the photocurrent was influenced slightly by the variation of pH.

The donor concentration N_D of MoS_2 calculated by Mott-Schottky relationship was 1.3×10^{18} cm^{-3} (the dielectric constant of MoS_2: $\varepsilon=7$—8[26]). As the MoS_2 crystal used in the present study was a natural product, it might contain Si, Al, or Fe *etc.* as impurities.[27] Assuming much of the light was efficiently absorbed in the space charge region and using the relationship[28] $N_D=1.1\times10^{16}\times\Delta v\times a^2$, the voltage drop in the space charge layer Δv was 1.5 V, N_D being calculated donor density and a the absorption coefficient in the order of 10^{15} cm^{-1}.[27] This large drop in potential in the space charge region probably accounted for the slow rise in the photocurrent (see Fig. 1 curve 1).

The Behavior of n-MoS_2 Electrode in an I^--containing Electrolyte. Iodide ion effectively suppresses the anodic dissolution of n-MoS_2 and n-$MoSe_2$, and shifts the flatband potentials of the electrodes to more negative potentials.[5] Figure 1 shows the current-potential curves of MoS_2 photoanode in 0.2 M Na_2SO_4 solution containing different concentrations of I^- ions. The onset of the photocurrent was shifted to more negative potential as the I^- concentration increased. This shift in the onset of the photocurrent was due to a shift in the flatband potential. This behavior was quite similar to the two-step or three-step wave photocurrent observed at a CdS photoanode in a solution containing S^{2-}, SO_3^{2-}, or $S_2O_3^{2-}$ ions.[29,30] In our previous study of CdS–S^{2-} system,[29] we reported that the first wave was controlled by the diffusion of S^{2-} from the solution to the electrode surface and the second wave depended on the formation of the photoholes in the valence band.

We believed also the first wave (hereby referred to as region A) of the photocurrent-potential curve of n-MoS_2 in I^- solutions was due to the photo-oxidation of I^- ions, and was controlled by the diffusion of I^- ions from the solution to the electrode surface, and the second wave at more anodic potential (region B) was due to both the photo-oxidation of I^- ions and the photocorrosion of the electrode material, and would be dependent on the formation of the photogenerated holes in the valence band. To test our hypothesis, we studied the dependence of photocurrents on both the rotation speed and the illumination intensity. Figure 2 shows the photocurrent at region A was proportional to the square root of the rotation speed, this indicated that the rate-determining step was the diffusion of I^- from the solution to the electrode surface. Photocurrent at region B was found to be linearly dependent on the light intensity, irrespective of the I^- concentrations (Fig. 3(B)), this showed that the magnitude of the photocurrent at region B was determined by the amount of the photogenerated holes.

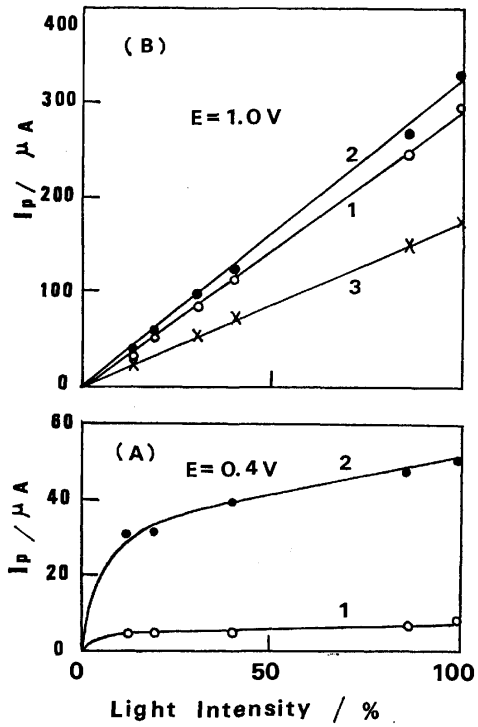

Fig. 3. Dependence of the photocurrent at n-MoS_2 electrode on the illumination intensity in 0.2 M Na_2SO_4 solutions with different concentrations of I^- ions at two different potentials. The rotation speed was 0 min^{-1}.
1: 10^{-3} M, 2: 10^{-2} M, 3: 10^{-1} M.

At region A, when I^- concentration was low ($<10^{-2}$ M) such that the duffusion process of I^- ions was important, the photocurrent was nearly independent of the light intensity (Fig. 3(A)).

Figure 4 shows the current-potential curves of Pt ring/n-MoS_2 disk RRDE. The potential of Pt ring (E_R) was held at 0 V *vs.* SCE to detect the current (I_R) due to the reduction of I_2 which was produced at the MoS_2 disk electrode. In the absence of I^-, no ring current could be observed (upper portion of Fig. 4, curve 1). This indicated that the current at the MoS_2 disk in the presence or absence of light (lower portion of Fig. 4, curve 1) was due to the dissolution of the MoS_2 electrode. Ring current was observed in the presence of I^- ions. At low E_D (<0.4 V), $-I_R/I_D$ was 0.2 which was the same as the collection efficiency of the present RRDE assembly. This meant at $E_D<0.4$ V, all of the photogenerated holes at the MoS_2 disk was totally consumed by the I^- ions, that is, the MoS_2 photoanode was 100% stabilized. At more anodic potentials, $-I_R/I_D$ was smaller than 0.2, and was significantly less than 0.2 at a lower I^- concentration. The ratio $-I_R/I_D$ describes the competitive hole capture by the I^- ions in solution (the stabilization process) and hole capture by surface atoms of the MoS_2 electrode (the corrosion process).

Figure 5 shows the ratio of the competitive hole capture by I^- ions to that by MoS_2 as a function of the I^- concentration. At $E=0.3$ V (in the region A referred to above), the ratio was 1 and was independent of the I^- concentration, since the photocurrent

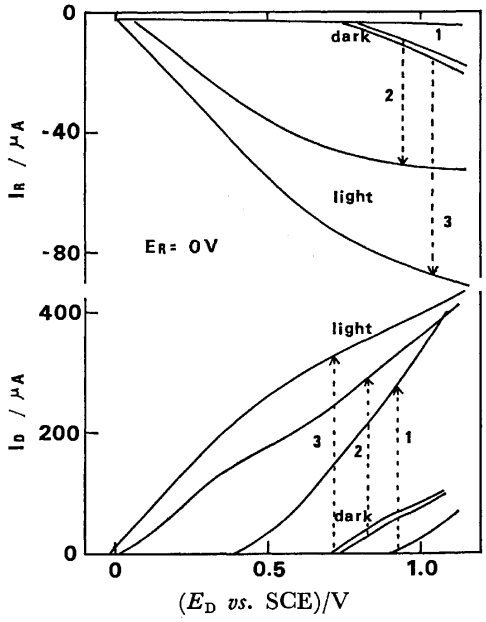

Fig. 4. I_R-E_D, I_D-E_D curves of Pt ring/n-MoS_2 disk electrode in 0.2 M Na_2SO_4 solutions with different concentrations of I^- ions. The rotation speed was 1000 min^{-1} and the scan rate was 30 s/V.
1: 0 M, 2: 2×10^{-3} M, 3: 10^{-2} M.

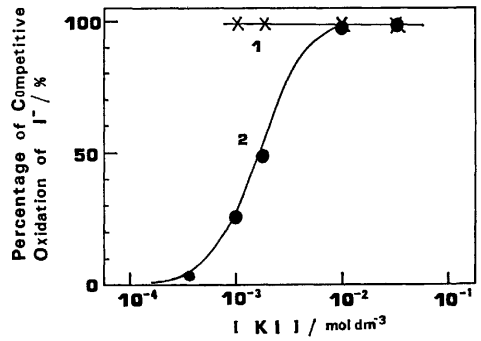

Fig. 5. Dependence of percentage of competitive reaction at n-MoS_2 electrode on concentration of I^- at two different potentials, and at constant light intensity, and rotation speed.
1: E=0.3 V, 2: 1.2 V.

was entirely due to the photo-oxidation of I^-. At more anodic potential (1.2 V), the photocurrent was due to the competitive hole capture by I^- and hole capture by MoS_2, thus the higher the I^- concentration, the larger was the ratio. Hole capture by the I^- ions was 100% when the I^- concentration was 10^{-2} M or higher.

The specific effect of I^- at the MoS_2 photoanode is similar to that of S^{2-} at the CdS photoanode.[24,32] The stabilization of the photoanode in I^- solutions may be attributed to the strong specific adsorption of I^- on the MoS_2 electrode surface, and the adsorption sites may act as surface states which participated in charge transfer.

Competitive Oxidations of Various Reducing Agents at n-MoS_2 Electrode. We reported earlier that, in the case of CdS,[24] ZnO,[31] and TiO_2,[32] the ratio of the competitive reaction increased as the redox

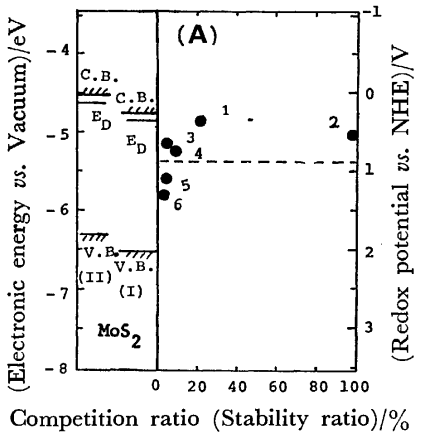

Fig. 6(A). Correlation between the energy diagram of MoS_2 and dependences of competitive ratios on redox potentials of reducing agents (0.01 M) at pH=6.
(I): Without I^-, (II): with I^-.
1: $Fe(CN)_6^{3-/4-}$, 2: I^-/I_2, 3: H_2Q/Q, 4: $Fe^{2+/3+}$, 5: Br^-/Br_2, 6: Cl^-/Cl_2.
---: Oxidation potential of water.

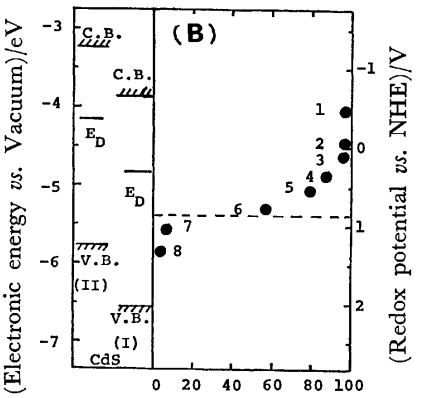

Fig. 6(B). Correlation between the energy diagram of CdS and dependences of competitive ratios on redox potentials of reducing agents (0.01 M) at pH=6.
(I): Without S^{2-}, (II): with S^{2-}.
1: S^{2-}/S, 2: $S_2O_3^{2-}/S_4O_6^{2-}$, 3: $SO_3^{2-}/S_2O_6^{2-}$, 4: $Fe(CN)_6^{4-/3-}$, 5: I^-/I_2, 6: $Fe^{2+/3+}$, 7: Br^-/Br_2, 8: Cl^-/Cl_2.
----: Oxidation potential of water.

potential of the reducing agent became more negative. Figure 6(A) shows the ratios of the competitive reactions of various reducing agents at the n-MoS_2 electrode as a function of their redox potentials, as compared to that at the CdS electrode (Fig. 6(B)). The oxidation potentials E_D of MoS_2 and CdS were derived from the thermodynamic data. The ratios of the competitive oxidation of the various reducing agents except I^- at the n-MoS_2 electrode were very small, indicating that these reducing agents were not suitable for the stabilization of the MoS_2 photoanode. Additionally, the competitive oxidations of the reducing agents were not clearly dependent on their redox potentials.

Photoanodic Reactions at n-MoS_2 Electrode in a Non-aqueous Solvent. We also investigated the photo-

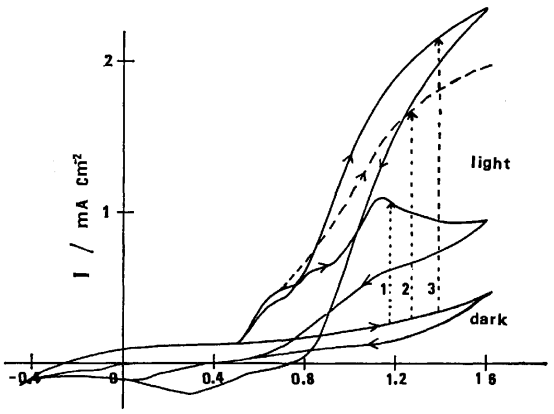

Fig. 7. *I-E* curves of n-MoS_2 in CH_3CN+0.1 M $NaClO_4$. The sweep rate was 10 s/V.
1: 1.4×10^{-3} M $I^-+1.4\times10^{-3}$ M H_2Q, no stirring,
2: 1.4×10^{-3} M $I^-+1.4\times10^{-3}$ M H_2Q, stirring, 3: 1.4×10^{-3} M I^-+10^{-2} M H_2Q, no stirring.

anodic reactions at the n-MoS_2 electrode in a non-aqueous solvent CH_3CN containing I^- and H_2Q (hydroquinine). In the presence of equal concentrations of I^- and H_2Q, some peaks could be observed (Fig. 7, curve 1), which were not seen in CH_3CN containing I^- and H_2Q individually. When excess H_2Q was added, the photocurrent increased (curve 3). These results indicated that both I^- and H_2Q contributed equally to the photoanodic reactions at MoS_2 in CH_3CN. This is in a marked contrast to the results in an aqueous electrolyte (Fig. 6(A)). Schneemeyer and Wrighton[17] also reported that Cl^- ions could be efficiently photo-oxidized at n-MoS_2 in CH_3CN.

Photoelectrochemical Reactions at p-MoS_2 Electrode. We confirmed that the cathodic reaction at the p-MoS_2 electrode was the following process,

$$2H^+ + 2e^- \longrightarrow H_2, \quad (4)$$

and the onset of the photocurrent was shifted to a more negative potential with an increase in the pH. This was because the hydrogen overvoltage was heightened, *i.e.*, $E_{onset}=-0.2$ V *vs.* SCE(in 0.5 M H_2SO_4), -0.5 V (in 0.1 M KCl), and -0.8 V (in 1 M NaOH). The onset of the photocurrent was more negative than the flatband potential. This indicates that the recombination of photogenerated electron-hole pair occurs at the small cathodic band bending.

Figure 8 shows the current-potential curves of Pt ring/p-MoS_2 disk RRDE with Fe^{3+} as the oxidizing agent. The Pt ring potential (E_R) was held at 1.0 V *vs.* SCE to detect the oxidation current (I_R) of the Fe^{2+} ions produced at the MoS_2 disk electrode. In the absence of Fe^{3+} ions, no ring current could be observed (lower portion of Fig. 8, curve 1). This indicated that the current at the MoS_2 disk in the presence or absence of light (upper portion of Fig. 8, curve 1) was due to the process (4). In the presence of the Fe^{3+} ions, the onset of the photocurrent was shifted to a more positive potential and a ring current could be observed (curves 2 and 3). Shifts in the onset of the photocurrent could also be observed with the addition of other oxidizing agents such as quinone and $Fe(CN)_6^{3-}$. This phenomenon seems to be the

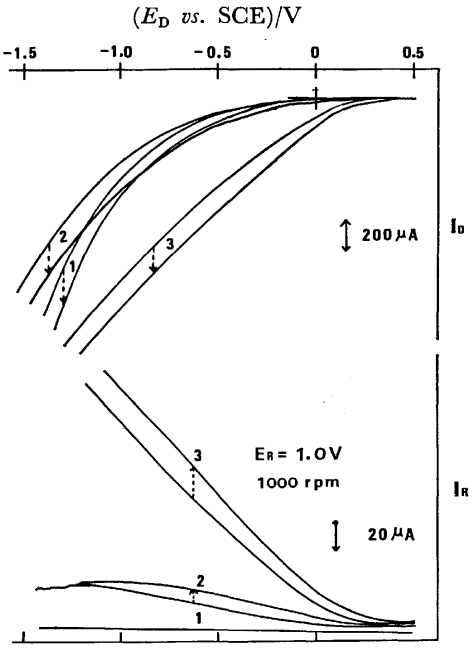

Fig. 8. I_R-E_D, I_D-E_D curves of Pt ring/p-MoS_2 disk electrode in 0.5 M H_2SO_4 solutions with different concentrations of Fe^{3+} ions. The rotation speed was 1000 min^{-1}.
1: 0 M, 2: 5×10^{-3} M, 3: 10^{-1} M.

same as in the case of n-MoS_2 electrode in I^- solutions. However, in the case of p-MoS_2, its flatband potential is not changed by the addition of oxidizing agents, for the photocurrent at the potential more positive than −0.2 V may be resulted from the process that the electron transfer from MoS_2 to Fe^{3+} is faster than the recombination of an electron-hole pair.

Figure 9 shows the ratio of the competitive electron capture by the Fe^{3+} ions to that by the H^+ ions as a function of the Fe^{3+} concentration. At E=0 V, the ratio was 1 and was independent of the Fe^{3+} concentration. This revealed that the photocurrent at 0 V was entirely due to the reduction of Fe^{3+} ions. At more cathodic potential (−0.8 V), the photocurrent was due to the competitive reduction of the Fe^{3+} ions and the hydrogen formation reaction, thus the higher the Fe^{3+} concentration, the more the hydrogen formation reaction was suppressed, and thus the larger was the ratio. Again, electron capture by the Fe^{3+} ions was 100% when the Fe^{3+} concentration was 10^{-2} or higher.

Conclusion

The MoS_2 photoanode was remarkably stabilized in I^- solutions. This effect may be attributed to the specific adsorption of I^- ions on the electrode surface, and the adsorption sites may act as surface states which participated in charge transfer. The ratios of the competitive oxidation of other reducing agents studied were very small (less than 20% hole capture), and hence they were not suitable for the stabilization of the MoS_2 photoanode. The competitive oxidations of the reducing agents were not clearly dependent on their redox potential. This was in a sharp contrast

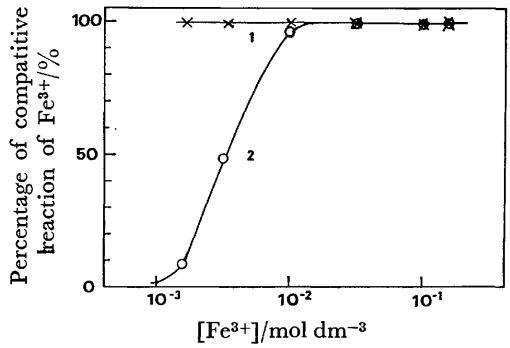

Fig. 9. Dependence of the percentage of competitive reaction of Fe^{3+} at the p-MoS_2 electrode on Fe^{3+} at two different potentials, and at constant light intensity and rotation speed.
1: E=0 V, 2: E=−0.8 V.

to that at a CdS photoanode. The cathodic reaction at the p-MoS_2 electrode was the hydrogen formation process. The onset of the photocurrent shifted in the presence of oxidizing agents. This fact may be resulted from the process that the electron transfer across the semiconductor-solution interface is faster than the recombination of an electron-hole pair.

References

1) J. A. Woollam and R. B. Somoano, *Phys. Rev. B*, **13**, 3843 (1976).
2) D. W. Murphy and F. A. Trumbore, *J. Cryst. Growth*, **39**, 185 (1977).
3) H. Tributsch and J. C. Bennett, *J. Electroanal. Chem.*, **81**, 97 (1977).
4) H. Tributsch, *Ber. Bunsenges. Phys. Chem.*, **81**, 361 (1977).
5) H. Tributsch, *J. Electrochem. Soc.*, **125**, 1086 (1978).
6) J. Gobrecht, H. Tributsch, and H. Gerischer, *J. Electrochem. Soc.*, **125**, 2085 (1978).
7) J. Gobrecht, H. Gerischer, and H. Tributsch, *Ber. Bunsenges. Phys. Chem.*, **82**, 1331 (1978).
8) S. M. Ahmed and H. Gerischer, *Electrochim. Acta*, **24**, 705 (1979).
9) W. Kautek, H. Gerischer, and H. Tributsch, *Ber. Bunsenges. Phys. Chem.*, **83**, 1000 (1979).
10) H. Tributsch, H. Gerischer, C. Clemen, and E. Bucher, *Ber. Bunsenges. Phys. Chem.*, **83**, 655 (1979).
11) W. Kautek and H. Gerischer, *Ber. Bunsenges. Phys. Chem.*, **84**, 645 (1980).
12) W. Kautek, H. Gerischer and H. Tributsch, *J. Electrochem. Soc.*, **127**, 247 (1980).
13) H. J. Lewerenz, A. Heller, and F. J. DiSalvo, *J. Am. Chem. Soc.*, **102**, 1877 (1980).
14) S. Menezes, F. J. DiSalvo, and B. Miller, *J. Electrochem. Soc.*, **127**, 1751 (1980).
15) L. F. Schneemeyer and M. S. Wrighton, *J. Am. Chem. Soc.*, **102**, 6496 (1979).
16) C. P. Kubiak, L. F. Schneemeyer, and M. S. Wrighton, *J. Am. Chem. Soc.*, **102**, 6898 (1980).
17) L. F. Schneemeyer and M. S. Wrighton, *J. Am. Chem. Soc.*, **102**, 6964 (1980).
18) L. F. Schneemeyer, M. S. Wrighton, A. Stacy, and M. J. Sienko, *Appl. Phys. Lett.*, **36**, 701 (1980).
19) F. R. Fan, H. S. White, B. Wheeler, and A. J. Bard, *J. Electrochem. Soc.*, **127**, 518 (1980).
20) F. R. Fan, H. S. White, B. Wheeler, and A. J. Bard,

J. Am. Chem. Soc., **102**, 5142 (1980).
21) D. Canfield and B. A. Parkinson, *J. Am. Chem. Soc.*, **103**, 1279 (1981).
22) B. A. Parkinson, T. E. Furtak, D. Canfield, K. Kam, and G. Kline, *Discuss. Faraday Soc.*, **70**, 233 (1980).
23) G. Kline, K. Kam, D. Canfield, and B. A. Parkinson, *Solar Energy Mat.*, **4**, 301 (1981).
24) T. Inoue, T. Watanabe, A. Fujishima, and K. Honda, *J. Electrochem. Soc.*, **124**, 719 (1977).
25) T. Biegler and D. A. Swift, *Electrochim. Acta*, **24**, 415 (1979).
26) J. Lagrenaudie, *J. Phys. Radium*, **15**, 299 (1954).
27) R. F. Frindt and A. D. Yoffe, *Proc. R. Soc. London, Ser. A*, **273**, 69 (1962).
28) A. J. Bard, *J. Photochem.*, **10**, 59 (1979).
29) T. Inoue, T. Watanabe, A. Fujishima, and K. Honda, *Bull. Chem. Soc. Jpn.*, **52**, 1243 (1979).
30) H. Minoura and M. Tsuiki, *Electrochim. Acta*, **23**, 1377 (1978).
31) T. Inoue, A. Fujishima, and K. Honda, *Bull. Chem. Soc. Jpn.*, **52**, 3217 (1979).
32) A. Fujishima, T. Inoue, and K. Honda, *J. Am. Chem. Soc.*, **101**, 5582 (1979).

Analysis of the Excess Gibbs Energies of Binary Mixtures Using Non-randomness Factors Determined from Excess Volume Data

Masanao KATO

Department of Chemistry, Faculty of Science, Tohoku University, Sendai 980

(Received March 28, 1981)

An analytical equation for the excess Gibbs energies of mixtures was derived on the basis of the non-random two-liquid model, which was applied to the derivation of an analytical equation for excess volumes proposed by the present author. The derived equation involves new adjustable parameters of intermolecular interaction. The validity of the equation was examined for 13 binary mixtures by using the non-randomness factors determined from the excess volume data, and it was shown that the calculated excess Gibbs energies were in good agreement with the observed values. The sequence of the values of the interaction parameters seems to be reasonable.

Recently, the present author found that the excess volumes of multi-component mixtures could be analyzed by an equation containing non-randomness factors as adjustable parameters, and showed that sufficient agreements were obtained between the calculated and the observed values of the excess volumes of binary and ternary mixtures.[1,2] The non randomness factors can be considered to represent the non-ideality of the molecular rearrangement of the component molecules in the vicinity of a given molecule. On the other hand, the excess Gibbs energies of multi-component mixtures have also been analyzed by an equation containing the parameters analogous to the non-randomness factor.[3–6] These parameters have been assessed to be very useful in representing the excess Gibbs energies of mixtures and widely utilized in chemical engineering. As the parameter in the equation for excess Gibbs energy is considered to have physical meanings similar to that for the excess volume, it is expected that the non-randomness factors determined from the excess-volume data can be applied to represent the excess Gibbs energies of the mixtures.

From the considerations above, the purpose of this study is to examine the applicability of the non-randomness factors in the excess-volume equation to the representation of excess Gibbs energies. The non-randomness factors at 298.15 K were determined from the excess-volume data previously reported.[1,2] On the other hand, the data for the excess Gibbs energies at the same temperature are not utilized. As the temperature dependence of the non-randomness factors was not entirely well-defined, the excess Gibbs energies at 298.15 K were measured from the vapor pressures of the mixtures.

Experimental

All the materials were guaranteed reagents of commercial origin and were purified by the distillation of 80 theoretical plates. The middle portions were collected and provided for measurements. The observed values of density, vapor pressure, and refractive index of the purified reagents were in good agreement with the literature values.[7,8]

The vapor-pressure measurements were carried out at 298.15±0.001 K by means of an apparatus constructed at our laboratory.[9,10]

The compositions of the liquid and the vapor phases were individually determined from refractive indexes measured by means of an Abbe refractometer for the methanol+benzene, ethanol+*m*-xylene, ethanol+benzene, ethanol+cyclohexane, acetone+cyclohexane, and benzene+cyclohexane mixtures. The compositions of the 1,2-dichloroethane+benzene and 1,2-dichloroethane+cyclohexane mixtures were determined from density measurements made by means of a pycnometer, while those of ethanol+acetone mixtures were determined from their ultra-violet spectra. The accuracy was ±0.02 for the mole fractions determined from the refractive-index and density measurements, and ±0.05 for those from spectrometry.

Results and Discussion

The excess Gibbs energies, g^E/RT, were calculated from Eq. 1:

$$g^E/RT = \sum_i x_i \ln \gamma_i, \tag{1}$$

while the activity coefficient, γ_i, of the i-th component was determined from Eq. 2:

$$\ln \gamma_i = \ln \frac{py_i}{x_i p_i^*} + \frac{(B_{ii}-v_i^*)(p-p_i^*)}{RT} + \frac{(1-y_i)p\delta}{RT}, \tag{2}$$

where

$$\delta = 2B_{ij} - B_{ii} - B_{jj}. \tag{3}$$

In Eqs. 1 to 3, x_i denotes the mole fraction of the liquid phase; R, the gas constant; T, the temperature; p, the total pressure; y_i, the mole fraction of the vapor phase; p_i^*, the vapor pressure of the pure i component; B_{ii}, the virial coefficient of the i component; B_{ij}, the cross-virial coefficient between the i and j components, and v_i^*, the molar volume of the pure i component. The virial coefficients were calculated from the empirical equation reported by O'Connell and Prausnitz.[11]

The observed vapor pressures of mixtures and the excess Gibbs energies are summarized in Table 1 as a function of the liquid-phase composition. The excess Gibbs energy for each mixtures was fitted with Eq. 4 according to the ordinary method:

$$g^E/RT = x_1x_2 \sum_{r=0}^{4} A_r(x_1-x_2)^r, \tag{4}$$

where x_1 and x_2 are the mole fractions of the first and second components respectively. The values of the A_r coefficients, as determined by the least-squares procedure, are summarized in Table 2, along with the values of σ_g, the standard deviation between the experimental and calculated values of g^E/RT.

TABLE 1. OBSERVED EXCESS GIBBS ENERGIES AT 298.15 K

x_1	y_1	$\frac{p}{\text{mmHg}}$ [a]	g^E/RT	x_1	y_1	$\frac{p}{\text{mmHg}}$ [a]	g^E/RT
Methanol(1)+benzene(2)				0.461	0.340	138.64	0.550
0.063	0.334	170.74	0.352	0.584	0.350	137.66	0.523
0.223	0.371	181.00	0.529	0.653	0.357	136.21	0.481
0.415	0.399	182.48	0.538	0.737	0.378	133.36	0.417
0.527	0.419	181.79	0.476	0.784	0.385	129.78	0.347
0.608	0.443	179.60	0.410	0.842	0.421	122.78	0.257
0.678	0.467	176.59	0.338	0.897	0.475	111.17	0.180
0.787	0.525	168.84	0.206	Acetone(1)+cyclohexane(2)			
0.837	0.581	161.92	0.146	0.120	0.543	192.52	0.175
0.882	0.645	154.22	0.090	0.204	0.654	228.22	0.242
0.958	0.818	138.39	0.017	0.366	0.682	248.29	0.402
Ethanol(1)+acetone(2)				0.501	0.703	255.06	0.434
0.128	0.047	211.76	0.033	0.660	0.730	259.77	0.396
0.234	0.082	202.45	0.081	0.703	0.719	259.53	0.370
0.360	0.134	188.35	0.125	0.899	0.829	255.30	0.165
0.527	0.176	169.00	0.090	0.949	0.882	247.82	0.087
0.558	0.203	159.59	0.088	Benzene(1)+cyclohexane(2)			
0.595	0.217	157.76	0.097	0.098	0.141	102.17	0.040
0.663	0.268	139.39	0.061	0.227	0.276	106.29	0.086
0.800	0.381	118.94	0.061	0.322	0.362	108.04	0.107
0.925	0.650	83.73	0.039	0.439	0.462	109.12	0.123
Ethanol(1)+*m*-xylene(2)				0.528	0.519	109.26	0.128
0.033	0.731	31.98	0.146	0.613	0.579	108.72	0.123
0.133	0.821	45.87	0.320	0.773	0.714	105.92	0.095
0.260	0.849	50.30	0.421	0.828	0.763	104.07	0.076
0.277	0.859	50.77	0.398	0.930	0.887	99.55	0.037
0.362	0.862	52.25	0.466	1,2-Dichloroethane(1)+benzene(2)			
0.562	0.877	54.01	0.465	0.107	0.096	92.29	-0.006_8
0.630	0.886	54.67	0.430	0.267	0.226	90.45	-0.000_9
0.652	0.891	54.94	0.412	0.348	0.305	89.25	0.001_4
0.778	0.910	56.70	0.319	0.455	0.422	87.86	0.007_8
0.842	0.916	57.49	0.258	0.573	0.527	85.94	0.006_0
Ethanol(1)+benzene(2)				0.654	0.609	84.92	0.009_2
0.090	0.253	120.41	0.195	0.765	0.730	82.74	0.005_5
0.208	0.291	124.36	0.352	0.841	0.807	81.52	0.004_3
0.324	0.305	124.40	0.424	0.914	0.890	80.40	0.005_1
0.461	0.326	123.37	0.443	1,2-Dichloroethane(1)+cyclohexane(2)			
0.545	0.340	122.52	0.427	0.123	0.220	111.19	0.125
0.660	0.375	117.50	0.362	0.199	0.297	115.51	0.185
0.750	0.409	112.92	0.292	0.304	0.366	118.58	0.250
0.917	0.632	85.60	0.117	0.382	0.405	119.33	0.281
0.959	0.766	73.38	0.058	0.501	0.454	119.32	0.303
Ethanol(1)+cyclohexane(2)				0.634	0.511	116.74	0.284
0.068	0.293	134.71	0.196	0.716	0.562	113.16	0.251
0.188	0.332	139.06	0.395	0.850	0.645	105.89	0.160
0.248	0.332	139.23	0.461	0.870	0.689	101.34	0.136
0.315	0.332	139.35	0.512	0.946	0.807	91.47	0.059
0.330	0.336	139.30	0.520				

a) 1 mmHg≈133.322 Pa.

Derivation of an Equation for the Excess Gibbs Energy. An equation for the excess Gibbs energy including the non-randomness factor is derived under two restrictions. The first restriction is to use the same model of mixture as that employed in the derivation of the equation for excess volumes,[1,2] that is, the non-random two-liquid (NRTL) model.[4] The second is that the equation for the excess volume must be obtained by the differentiation of the equation for the excess Gibbs energy with respect to the pressure.

The interaction free energy of the i-th component

Table 2. Coefficients for least-squares fit of data obtained by the use of Eq. 4

Mixture	A_0	A_1	A_2	A_3	A_4	$10^3\sigma_g$
Methanol + benzene	1.9803	0.9172	−0.1072	2.5855	2.3907	10.380
Ethanol + acetone	0.4170	0.4311	0.0129	−1.0139	−0.1766	8.033
Ethanol + *m*-xylene	1.9485	0.2379	−0.7455	0.4752	3.1598	9.835
Ethanol + benzene	1.7508	0.4637	0.1710	0.1096	0.1941	1.930
Ethanol + cyclohexane	2.1926	0.2416	0.3789	0.5267	0.0121	4.481
Acetone + cyclohexane	1.7666	−0.1813	−0.5875	0.0969	0.7584	8.568
Benzene + cyclohexane	0.5077	−0.0427	0.0190	−0.0228	−0.0347	1.015
1,2-Dichloroethane + benzene	0.0303	−0.0271	−0.0996	−0.0739	0.0565	1.367
1,2-Dichloroethane + cyclohexane	1.2076	−0.0796	0.0222	0.0626	−0.1099	1.721

Table 3. Interaction free-energy parameters, $g_{ij}-g_{jj}$, and non-randomness factors, Λ_{ij}, of binary mixtures at 298.15 K

Mixture	Λ_{21}	Λ_{12}	$\frac{g_{21}-g_{11}}{RT}$	$\frac{g_{12}-g_{22}}{RT}$	Data source
Water + 1-butoxyethanol	2.375	3.623	1.147	−0.071	Ref. 13
Methanol + 1-butanol	2.451	1.592	0.253	−0.194	Ref. 14
Methanol + benzene	0.225	0.161	5.606	−0.595	This work
Ethanol + acetone	2.653	2.942	0.094	0.166	This work
Ethanol + toluene	0.164	0.352	0.753	0.429	Ref. 15
Ethanol + *m*-xylene	0.199	0.799	1.876	1.392	This work
Ethanol + benzene	0.159	0.701	2.645	1.171	This work
Ethanol + cyclohexane	0.199	0.313	3.634	1.732	This work
Acetone + cyclohexane	0.141	0.825	−0.021	1.873	This work
Benzene + *m*-xylene	1.060	0.945	0.023	0.023	Ref. 16
Benzene + cyclohexane	3.754	2.450	0.157	0.169	This work
1,2-Dichloroethane + benzene	0.479	0.181	−0.022	0.088	This work
1,2-Dichloroethane + cyclohexane	6.345	2.028	0.239	0.555	This work

with the j-th component is denoted as g_{ij} (equals to g_{ji}). The local mole fraction of the j-th component in the vicinity of a given molecule of the i-th component is denoted as x_{ji}. Provided that the non-randomness factor, Λ_{ij}, is defined as a function of the local mole fractions, x_{ii} and x_{ji}, and the overall mole fractions of the mixture, x_i and x_j, as follows:

$$\frac{x_{ji}}{x_{ii}} = \Lambda_{ji}\frac{x_j}{x_i}. \tag{5}$$

We obtain the equation for the excess Gibbs energies of multi-component mixtures by means of a procedure similar to the derivation of the equation for the excess volume of multi-component mixtures:[2]

$$g^E/RT = \sum_{i=1}^{n} x_i\left[\frac{\sum_j (g_{ji}-g_{ii})x_j\Lambda_{ji}}{RT\sum_k x_k\Lambda_{ki}}\right], \tag{6}$$

$$(\Lambda_{ii}=\Lambda_{jj}=1)$$

where n denotes the number of components.

Equation 6 is in the same form as the NRTL equation well-known in chemical engineering.[4] In the NRTL equation, the non-randomness factor is defined as a function of the interaction free energy. It should be noticed that the derivation descrived above leads to the same equation. It is considered that, in the NRTL equation, the number of parameters is reduced by regarding the non-randomness factor as a function of the interaction free energy. When the Boltzmann distribution is assumed to hold in the local composition, the local mole fraction should be represented as a function of the interaction potential between molecules, as has been described by Guggenheim in his text.[12] Based on his description, the non-randomness factor is defined as follows:

$$\Lambda_{ij} = \exp\left(-\frac{w_{ij}-w_{jj}}{zRT}\right), \tag{7}$$

where w_{ij} is the interaction potential between the i and j components, and z, the coordination number of the pseudo-lattice of mixture. If both the interaction potential and the coordination number are assumed to be independent of the pressure and the temperature, the equation for the excess volume is obtained by differentiating Eq. 6 with respect to the pressure:[2]

$$v^E = \sum_{i=1}^{n} x_i\left[\frac{\sum_j (v_{ji}-v_{ii})x_j\Lambda_{ji}}{\sum_k x_k\Lambda_{ki}}\right]. \tag{8}$$

Comparison of the Calculated g^E Values with Those Observed. The values of the non-randomness factors were determined from the excess volume data,[1,2] as the values of the non-randomness factors could be obtained more accurately. The $g_{ij}-g_{jj}$ values were determined from the excess-Gibbs-energy data by an algebraic calculation of Eq. 6. The values thus obtained are listed in Table 3. The observed and the

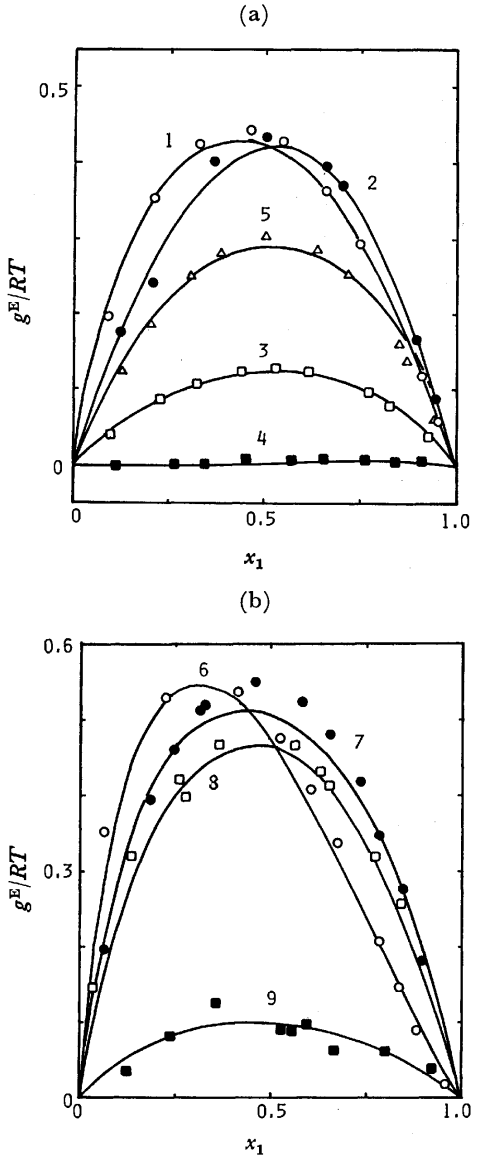

Fig. 1. Observed and calculated excess Gibbs energy of nine binary mixtures at 298.15 K. Solid lines indicate the values calculated from Eq. 6. a): 1 and ○ is ethanol(1)+benzene(2), 2 and ●, acetone (1)+cyclohexane(2), 3 and □, benzene(1)+cyclohexane(2), 4 and ■, 1,2-dichloroethane(1)+benzene (2), and 5 and △, 1,2-dichloroethane(1)+cyclohexane(2) mixtures. b): 6 and ○ is methanol(1)+benzene(2), 7 and ●, ethanol(1)+cyclohexane(2), 8 and □, ethanol(1)+*m*-xylene(2), and 9 and ■, ethanol(1)+acetone(2) mixtures.

calculated excess Gibbs energies were in good agreement, as is shown in Fig. 1.

In Fig. 2, a qualitative diagram of the interaction free-energy parameters is shown. This diagram was constructed from the values of $g_{ij}-g_{jj}$ given in Table 3. The component on the left-hand side of the diagram was established as a standard component; next, the interaction free-energy level between unlike components was calculated from the $g_{ij}-g_{jj}$ values, and finally that for the pure state of the second component was calculated from the $g_{ji}-g_{ii}$ value, where g_{ji} equals g_{ij}. In the mixtures containing ethanol, the

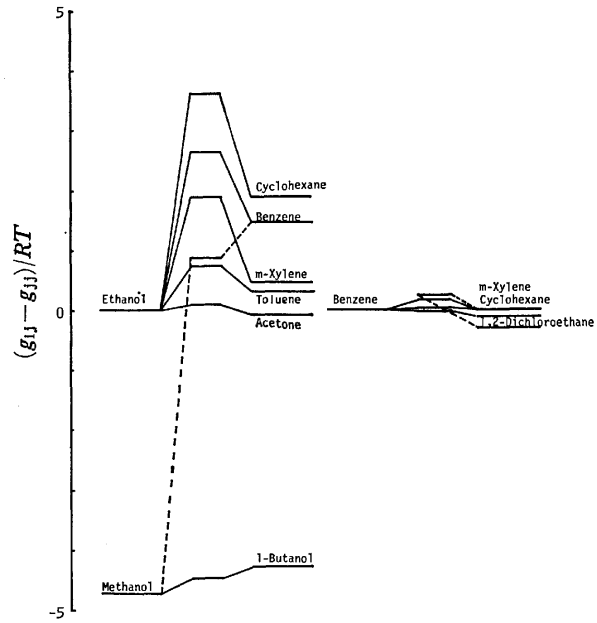

Fig. 2. The interaction free energy diagram in some binary mixtures at 298.15 K.

sequence of the interaction free-energy parameters was as follows: ethanol–acetone≈ethanol–ethanol<ethanol–toluene<ethanol–*m*-xylene<ethanol–benzene<ethanol–cyclohexane. It is likely that the hydrogen-bonding interaction or associative interaction between ethanol and acetone forms the lowest energy level among the mixtures selected. The negative values of the interaction potential parameters, $w_{ij}-w_{jj}$, of the ethanol+acetone mixture, which were calculated from the non-randomness factors by using Eq. 7, support the associative interaction. The interaction between ethanol and cyclohexane is the highest energy level, and the interaction is expected to be accompanied by the destruction of the hydrogen bond of ethanol. Ethanol is considered to interact with benzene through OH-π interaction. Toluene and *m*-xylene are expected interact slightly more strong with ethanol than benzene is, because they are slightly polar molecules (the dipole moment of toluene is 0.31 Debye, and that of *m*-xylene is 0.30 Debye, at 20 to 60 °C.[7]).

For methanol mixtures, the interaction free-energy level of methanol with benzene is much higher than that with 1-butanol. The interaction of methanol with 1-butanol is a result of the hydrogen bonding, and that with benzene is the OH-π interaction.

In the benzene+*m*-xylene, benzene+cyclohexane, 1,2-dichloroethane+benzene, and 1,2-dichloroethane+cyclohexane mixtures, the interaction free-energy parameters are relatively smaller than in ethanol mixtures. The interaction in 1,2-dichloroethane+cyclohexane is indicated by a broken line on the right-hand side in Fig. 2. Particularly, the excess Gibbs energies of the benzene+*m*-xylene and 1,2-dichloroethane+benzene mixtures are nearly zero; that is, they are almost ideal mixtures. The interaction free-energy parameters of these benzene mixtures are very small. However, the excess-volume curves of these mixtures show appreciable positive deviations from

ideal behavior. The v^E values of equimolar mixtures are 0.3 $cm^3 mol^{-1}$ for the benzene+*m*-xylene mixture and 0.2 $cm^3 mol^{-1}$ for the 1,2-dichloroethane+benzene mixture.[2] These results seem to suggest that the volumes of central molecules surrounded by different component molecules differ from those of molecules surrounded by the same component molecules, in spite of almost the same magnitude of interaction free-energy parameters between like and unlike molecular pairs.

Interaction free-energy diagrams of the non-polar or slightly polar mixtures show small free-energy gaps, as is shown in Fig. 2. When the ethanol-ethanol interaction is chosen as the standard energy level, however, a different feature appears. The interaction of ethanol molecules in pure ethanol differs remarkably from that in mixtures with non-polar or slightly polar molecules. As has been described above, the interaction of ethanol with a non-polar molecule is accompanied by a destruction of the hydrogen bonding. On the other hand, the interaction in mixtures of two non-polar substances, such as the benzene+*m*-xylene mixture, is considered not to differ essentially between pure and mixed states. It may be deduced from the above reason that the combination of the diagrams of the hydrogen bonding and the non-polar mixtures gives an inconsistent feature of interaction free energy. This fact may show the limitation of the applicability of Eq. 6.

References

1) M. Kato and N. Suzuki, *Bull. Chem. Soc. Jpn.*, **51**, 1020 (1978).
2) M. Kato, *Bull. Chem. Soc. Jpn.*, **53**, 1937 (1980).
3) G. M. Wilson and G. Scatchard, *J. Am. Chem. Soc.*, **86**, 127 (1964).
4) H. Renon and J. M. Prausnitz, *AIChE J.*, **14**, 135 (1968).
5) T. Tuboka and T. Katayama, *J. Chem. Eng. Jpn.*, **8**, 181 (1975).
6) D. S. Abrams and J. M. Prausnitz, *AIChE J.*, **21**, 116 (1975).
7) J. A. Riddick and W. B. Bunger, "Organic Solvents," 3rd ed, J. Wiley and Sons, New York (1970).
8) D. Radulescu and M. Alexa, *Bull. Soc. Chim. Romania*, **20A**, 89 (1938).
9) M. Inoue, K. Azumi, and N. Suzuki, *Ind. Eng. Chem., Fundam.*, **14**, 312 (1975).
10) M. Kato, *Ind. Eng. Chem., Fundam.*, **19**, 253 (1980).
11) J. P. O'Connell and J. M. Prausnitz, *Ind. Eng. Chem., Process Res. Dev.*, **6**, 245 (1967).
12) E. A. Guggenheim, "Mixtures," Oxford University Press (1952).
13) G. Scatchard and G. M. Wilson, *J. Am. Chem. Soc.*, **80**, 133 (1964).
14) J. Polák, S. Murakami, V. T. Lam, H. D. Pflug, and G. C. Benson, *Can. J. Chem.*, **48**, 2457 (1970).
15) S. C. P. Hwa and W. T. Ziegler, *J. Phys. Chem.*, **70**, 2572 (1966).
16) J. Singh, H. D. Pflug, and G. C. Benson, *J. Phys. Chem.*, **72**, 1939 (1968).

A Reinvestigation of Small-angle Electron Scattering by CS_2 and CCl_4 Molecules†

Makoto NAGASHIMA,†† Shigehiro KONAKA, and Masao KIMURA*
Department of Chemistry, Faculty of Science, Hokkaido University, Sapporo 060
(Received March 30, 1981)

A small-angle electron-diffraction unit (*Jpn. J. Appl. Phys.*, **11**, 1199 (1972)) has been improved by enlarging the scattering chamber and installing a new nozzle system and a better counting unit. The intensities of 50 keV electrons scattered by CS_2 and CCl_4 molecules have been measured with a $\approx 1\%$ precision in the s-range from 1 to 11.5 $Å^{-1}$. Theoretical intensities have been calculated for the independent-atom model by taking into account the intramolecular double-scattering effect, and those intensities have been compared with the experimental intensities. The oscillatory feature appearing in the difference function, $\Delta\sigma(s)=s^4(I_{\text{expt}}-I_{\text{IAM}})$, of CCl_4 has been ascribed mainly to the deformation of the one-electron density in chlorine atoms by chemical binding.

A small-angle electron-diffraction unit equipped with a scintillation counting device was used by the present authors and their collaborators to measure the total (elastic plus inelastic) intensities of electrons scattered by gas molecules.[1–3] An observed decrease in the total scattered intensity from the theoretical value for the independent-atom model (IAM) was interpreted as the effect of chemical-bond formation. However, the qualities of the above data were limited mainly by the counting loss due to the poor resolving time of the counting system and by the uncertainties associated with the correction for the delocalization of the sample gas. The purpose of the present study is to offer refined data on the total scattered intensities for CS_2 and CCl_4 by improving these weaknesses.

Intramolecular multiple scattering is known to decrease the small-angle intensities and to produce a characteristic oscillation depending on the molecular geometry.[4–9] In the previous studies of CS_2 and CCl_4,[2] the effect of the intramolecular multiple scattering was concluded to be negligible by calculating the two-atom double-scattering cross-section for CCl_4 using the formula proposed by Bonham and Peixoto[4] and by comparing it with the single-scattering cross-section. Since then, the theory of multiple scattering has further advanced.[6,8,9] At the present stage, therefore, it seems necessary to reexamine the validity of the conclusion that multiple scattering was negligible by utilizing recent theories. In the present study, the multiple-scattering cross-sections have been calculated for CS_2 and CCl_4 and incuded in the IAM intensities, which were then used for extracting the net chemical-binding effect from the experimental data.

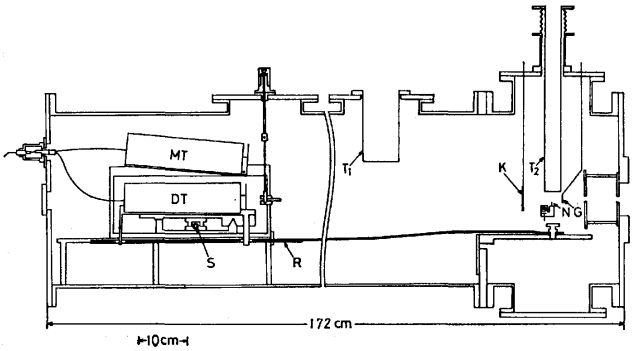

Fig. 1. Cross-sectional view of the scattering chamber. The sample chamber on the right-hand side was remodelled in this work. N, nozzle; T_1, T_2, cold traps; K, phosphorescent screen; G, gold-foil for adjusting the nozzle position; DT, detector; MT, monitor; R, arm; S, screw. Ref. 1 should be referred for the other details.

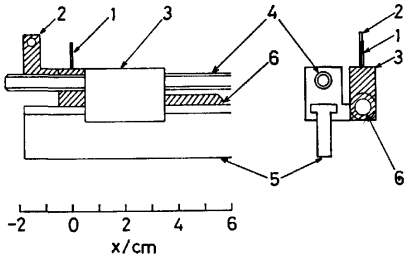

Fig. 2. Front and side view of the nozzle system. 1, Nozzle; 2, gold-foil holder; 3, nozzle-base; 4, screw; 5, a base for sliding the nozzle-base; 6, inlet of the sample gas.

Improvements of the Apparatus

The main improvements are as follows: (1) the enlargement of the scattering chamber for rarefying delocalized sample gas near the scattering center, (2) the employment of a new nozzle system, and (3) the introduction of a counting system with a shorter resolving time.

Figure 1 shows a cross-sectional view of the sample chamber. The inner diameter of the chamber, 347 mm, is about five times as large as that of the old one. The two camera lengths, 1168 and 815 mm, cover a wider range of scattering angles. A cylindrical mu-metal case placed close to the inside wall of the whole chamber shields the inside from the terrestrial magnetism. The residual magnetic field inside the case is less than 10 mG.

The construction of the nozzle system is shown in Fig. 2. The nozzle is made of non-magnetic stainless steel (SUS304). The inner and outer diameters are 0.2 and 0.6 mm respectively, and the length is 10 mm. The nozzle can be shifted in a plane perpen-

† Throughout this paper 1 Å=10^{-10} m and 1 Torr≈133.322 Pa are used.

†† Present address: Japan IBM Co., Ltd., Kusatsu 525.

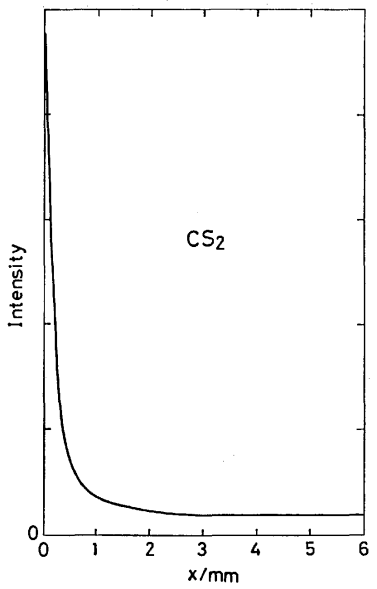

Fig. 3. Plot of the intensity of electrons scattered by carbon disulfide *versus* the nozzle position, x. The nozzle was moved along the x-direction shown in Fig. 2. The ordinate scale is arbitrary.

dicular to the incident electron beam. The interval between the nozzle tip and the incident electron beam was chosen to be about 0.5 mm. When the nozzle tip approaches the beam, the ratio of the background scattering to the main one decreases, but the reflection of scattered electrons by the nozzle increases.

Figure 3 shows the change in the intensity of electrons scattered by the sample gas when the nozzle is shifted on a horizontal plane in the direction perpendicular to the incident electron beam. Scarcely any change was found when the nozzle was placed more than 3 mm from the incident electron beam. In order to exclude a contribution corresponding to the tail of this curve, the background scattering was measured by shifting the nozzle by 5 mm and was subtracted from the scattering measured with the nozzle placed at its original position. The proportion of the background scattering to the total one varied with the molecular species as well as with the sample pressure. In the present measurement for CCl_4, the ratio was about 5% at s-values greater than 5 $Å^{-1}$, but it increased gradually with a decrease in the s-values, rising to 14—18% at $s=1$ $Å^{-1}$.

Previously, an extra nozzle for the background measurement was placed between the nozzle and the detector, about 30 cm from the nozzle and close to the wall of the diffraction chamber. With this arrangement, however, the distribution of gas injected from the extra nozzle will not reproduce successfully that of gas in the sample measurement, particularly in the neighborhood of the nozzle. In fact, systematic discrepancies of about 3% or more had previously been observed between the scattered intensities measured on both sides of the primary electron beam.[2] In the refined data, such discrepancies were reduced to about 1% or less and had no systematic feature. This refinement was achieved by enlarging the scattering chamber and by using the new nozzle system. Thus, the background correction could be made more accurately than in the previous study, and consequently, more reliable data were obtained.

The old counting system used for the detector was replaced by a new one composed of a preamplifier (ORTEC 9301), a pulse-height analyzer (9302), and a counter (770). This replacement improved the resolving time of the counting system from 3.6 μs to about 10 ns and made the statistical error in the present study one order of magnitude lower than in the previous study. After all, the limits of error for the final data could be reduced to about one-third of the estimated errors in the previous study.**

Measurement of Scattered Intensities

The ultimate vacuum pressure was about 3×10^{-6} Torr, while the pressure during the measurement on the sample gas was 1×10^{-5} Torr. By using gold foil, the product of the camera length and the electron wavelength*** and the central position of the electron beam were determined with precisions of 0.05% and 0.02 mm respectively. No change in the position or wavelength of the electron beam was detected during a continuous measurement for four hours. The beam current was about 0.05 μA, and it changed monotonously by 13% during four hours. The accelerating voltage was about 50 kV. The camera length was 815 mm, and the range of s covered by the present measurement was from 1 to 11.5 $Å^{-1}$. The room temperature was about 20 °C. Spectroscopic-grade reagents of the Merck Co., with the minimum assays of 99.9 and 99.7% for CS_2 and CCl_4 respectively, were used without further purification.

The counting rate in the present measurement was about 50 times that in the previous measurement. The counting-loss correction was made by using the following equation:

$$n = n'(1+n'\tau),$$

where n' is the apparent counting rate and τ is the resolving time.

The scannings were performed first for the sample gas. After the last data on the sample gas, $I_G^M(s_0)$, had been taken at the turning point s_0, the nozzle was shifted quickly by 5 mm to observe $I_B^M(s_0)$, and then the background measurement was performed. The scattered intensities were calculated as follows:

$$I_{\text{expt}}(s) = C\left\{\frac{I_G^D(s)}{I_G^M(s)}I_G^M(s_0) - \frac{I_B^D(s)}{I_B^M(s)}I_B^M(s_0)\right\}, \quad (1)$$

where the superscripts D and M denote the intensities measured by the detector and the monitor respectively, and where the first and second terms in the brackets are the intensities observed on the sample and the background respectively. The normalization constant, C, was determined by comparison with the theoretical intensities to be described in the next section.

** The errors listed in Table 1 of Ref. 2 were the standard errors, not the limits of error.

*** The lattice constant of 4.078 Å was used.

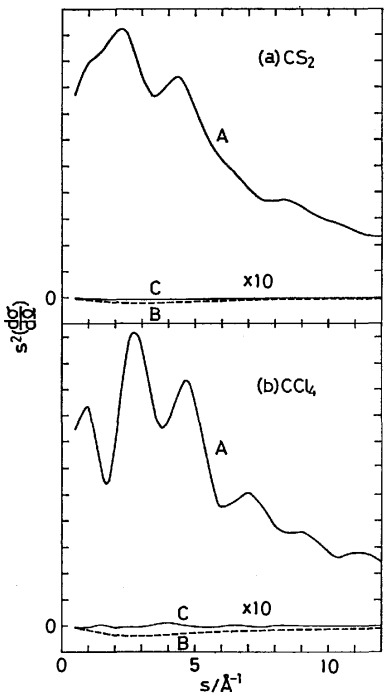

Fig. 4. Comparison of single and double scattering terms. Curves A, B, and C show $s^2\left(\frac{d\sigma}{d\Omega}\right)_{MB}$, $s^2\left(\frac{d\sigma}{d\Omega}\right)_{12}$, and $s^2\left(\frac{d\sigma}{d\Omega}\right)_{123}$, respectively. The ordinate scale is arbitrary.

Calculation of the IAM Intensities

According to the Glauber approximation,[5,6] the first-order multiple-scattering correction of the elastically scattered intensity is given by the sum of $\left(\frac{d\sigma}{d\Omega}\right)_{12}$ and $\left(\frac{d\sigma}{d\Omega}\right)_{123}$, which are two-atom and three-atom double-scattering terms respectively.

The three-atom double-scattering term was calculated by the use of the analytical expression given by Bartell.[6] It has been comfirmed by Kohl and Arvedson[8,9] that Bartell's expression reproduces very well the result of an exact numerical calculation for $s<\approx 20$ Å^{-1}. The two-atom double-scattering term was calculated according to the following formula:[10]

$$\left(\frac{d\sigma}{d\Omega}\right)_{12} = -\mathrm{Im}\sum_{i\neq j}\sum \frac{1}{ka_{ij}^2}[|f_i(s)|^2 f_j(0) + |f_j(s)|^2 f_i(0)] + \mathrm{Im}\sum_{i\neq j}\sum \frac{1}{ka_{ij}^4}[\alpha_{ij}(s) + \alpha_{ji}(s)], \quad (2)$$

where a_{ij} is the distance between i and j atoms; k, the propagation number $(2\pi/\lambda)$ of the incident electrons; $f_i(s)$, the complex scattering factor, and

$$\alpha_{ij}(s) = f_i^*(s)\left[f_j(0)\left(f_i'(s)\frac{\cos\theta}{s} + f_i''(s)\frac{\cos^2(\theta/2)}{s}\right) + 2f_i(s)\lim_{s\to 0}\frac{f_j'(s)}{2s}\right]. \quad (3)$$

The two terms in the first brackets on the right-hand side of Eq. 2 are the formulas given by Yates[5] and by Bonham and Peixoto[4] on the basis of the Glauber and second Born approximations respectively, while the terms in the second brackets are corrections derived on the basis of the second Born approximation.[10] The contribution of these correction terms to $(d\sigma/d\Omega)_{12}$ was less than 5% for CS_2 and CCl_4. The numerical values were obtained by using the scattering factors[11] based on the RHFS wave functions, the structural parameters[12,13] and the parallel and perpendicular mean amplitudes[12,14] taken from the literature. Figure 4 compares the results multiplied by s^2 with $s^2\left(\frac{d\sigma}{d\Omega}\right)_{MB}$, which is the total intensity given by the modified first Born approximation. The $\left(\frac{d\sigma}{d\Omega}\right)_{MB}$ is written as:

$$\left(\frac{d\sigma}{d\Omega}\right)_{MB} = \sum_i [|f_i(s)|^2 + (2/as^2)^2 S_i] + 2\mathrm{Re}\sum_{i<j}\sum f_i^*(s) f_j(s)\frac{\sin(sa_{ij})}{sa_{ij}}\exp\left(-\frac{1}{2}s^2 l_{ij}^2\right), \quad (4)$$

where a is the relativistic Bohr radius, and l_{ij}, the mean amplitude. The inelastic scattering factors, S_i, were taken from the literature.[11] The anharmonicity correction was omitted because it was negligible in

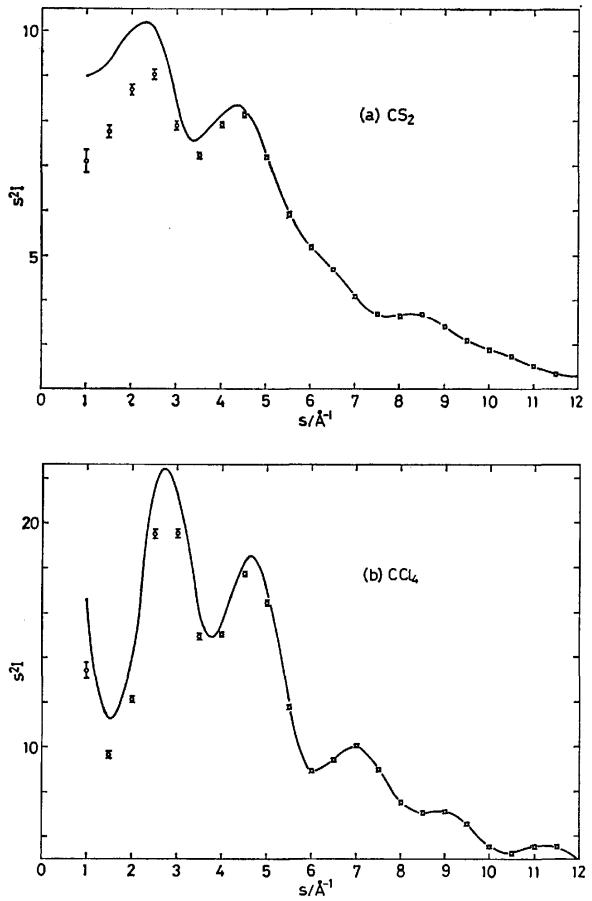

Fig. 5. Comparison between the experimental and theoretical (IAM) s^2I intensities, (a) CS_2, (b) CCl_4. —: Theoretical intensity, ○: experimental intensity, the vertical bar of experimental intensity shows the limit of experimental error.

TABLE 1. EXPERIMENTAL AND THEORETICAL (IAM) SCATTERED INTENSITIES FOR CS_2 AND CCl_4 AT 50 kV

s/Å^{-1}	CS_2			CCl_4		
	I_{exptl}[a]	ε/I_{exptl}[b]	I_{IAM}	I_{exptl}[a]	ε/I_{exptl}[b]	I_{IAM}
1.0	7.113×10^{0}	3.5%	8.981×10^{0}	1.344×10^{1}	2.5%	1.659×10^{1}
1.5	3.453	1.5	4.143	4.293×10^{0}	1.5	5.008×10^{0}
2.0	2.174	1.0	2.510	3.037	1.0	3.448
2.5	1.445	1.0	1.606	3.126	1.1	3.472
3.0	8.783×10^{-1}	1.1	9.387×10^{-1}	2.176	0.8	2.349
3.5	5.921	0.6	6.219	1.220	1.0	1.291
4.0	4.955	0.6	5.082	9.409×10^{-1}	0.4	9.693×10^{-1}
4.5	4.032	0.6	4.089	8.781	0.5	9.015
5.0	2.878	0.9	2.894	6.594	0.7	6.750
5.5	1.958	0.7	1.974	3.897	0.9	3.948
6.0	1.446	0.7	1.458	2.486	0.5	2.497
6.5	1.108	0.7	1.116	2.221	0.7	2.238
7.0	8.337×10^{-2}	0.7	8.382×10^{-2}	2.052	0.4	2.074
7.5	6.567	0.7	6.572	1.600	0.5	1.608
8.0	5.698	0.7	5.741	1.173	0.5	1.172
8.5	5.099	0.8	5.098	9.768×10^{-2}	0.5	9.784×10^{-2}
9.0	4.231	1.2	4.249	8.810	0.5	8.825
9.5	3.437	0.8	3.436	7.276	0.5	7.250
10.0	2.886	0.9	2.894	5.591	0.5	5.575
10.5	2.501	0.9	2.488	4.769	0.6	4.769
11.0	2.094	1.0	2.094	4.580	0.6	4.589
11.5	1.786×10^{-2}	1.0	1.783×10^{-2}	4.186×10^{-2}	0.6	4.182×10^{-2}

a) Normalized to I_{IAM} at s=9—11.5. b) The symbol ε denotes the estimated limits of error of I_{exptl}. The relative errors, ε/I_{exptl}, are shown in percentage units.

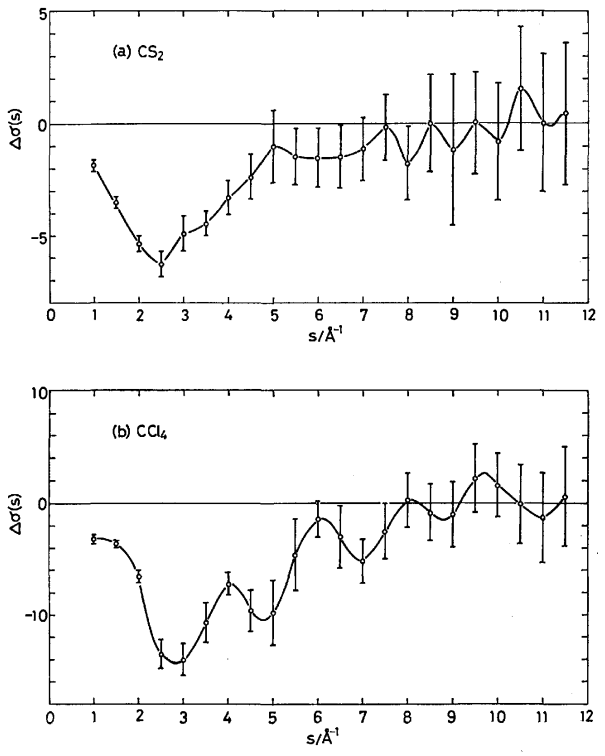

Fig. 6. Plots of $\Delta\sigma(s)$ for CS_2 (a) and CCl_4 (b). The vertical bar shows the limit of experimental error.

the s-range covered by the present work. As may be seen in Fig. 4, the double-scattering terms are insignificant for CS_2 and CCl_4, although such terms cannot be ignored for every molecule. In the present study, the I_{IAM} values defined by $(a/2)^2[(d\sigma/d\Omega)_{MB}+(d\sigma/d\Omega)_{12}+(d\sigma/d\Omega)_{123}]$ were employed; they are listed in Table 1.

Results and Discussion

The experimental intensites were normalized to I_{IAM} at s-values from 9 to 12 Å^{-1}. Four runs of measurements were performed for each sample. The experimental errors were estimated from the reproducibility of the data and the uncertainties in the s-values. Table 1 lists the experimental intensities, I_{exptl}, and the estimated limits of error. The values of s^2I_{exptl} are compared with those of s^2I_{IAM} in Fig. 5.

Figure 6 shows the $\Delta\sigma(s)$ defined by $s^4(I_{exptl}-I_{IAM})$. As in the previous work,[2] a significant oscillation is found in the $\Delta\sigma$ of CCl_4, while the oscillation in that of CS_2 is within the range of experimental error. As has been shown elsewhere,[15] the following integral relationship holds between the $\Delta\sigma$ and one-electron and two-electron deformation densities, $\Delta\rho$ and $\Delta\rho_c$.

$$\Delta j(r') = \frac{2}{\pi}\int_0^\infty ds\Delta\sigma(s)sr'\sin(sr')$$
$$= -2\sum_i(r')^2Z_i\langle\int d\Omega_{r'}\Delta\rho(\boldsymbol{r}'+\boldsymbol{r}_i)\rangle_{vlb}$$
$$+ (r')^2\langle\int d\Omega_{r'}\Delta\rho_c(\boldsymbol{r}')\rangle_{vlb}. \quad (5)$$

Here, the notations follow those given in Ref. 15. Errors in $\Delta j(r')$ were also calculated from the ex-

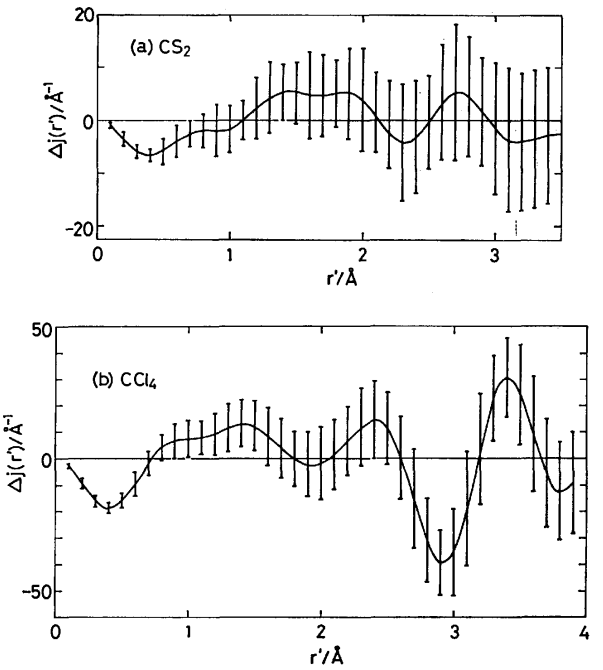

Fig. 7. Plot of $\Delta j(r')$ for CS_2 (a) and CCl_4 (b). The vertical bar corresponds to the limit of experimental error of $\Delta\sigma(s)$.

perimental errors by assuming the propagation-law of error,**** The contribution to the integral from the s-region beyond 9 $Å^{-1}$ was neglected. The results are shown in Fig. 7. The second term of Eq. 5 can be expected to be smaller than the first one.[16,17] The significant negative portion in the $\Delta j(r')$ of CS_2 at r' values of less than 1 Å corresponds to an increase in the one-electron density in the bonding region. No other conclusion can be drawn for CS_2 because of the large experimental errors. The $\Delta j(r')$ of CCl_4 has a significant valley at $\approx$2.9 Å. The position of the minimum is consistent with the Cl–Cl distance, 2.885 Å, within the range of experimental error. This valley can be ascribed to an increase in the one-electron density around chlorine atoms. This is consistent with the large electronegativity of chlorine. The other significant valley found in the small r'-region is due to an increase in the one-electron density in the C–Cl bonds. The significant positive portion at $\approx$3.4 Å can be related to the change in the distribution of the lone-pair electrons of chlorine.

In a previous paper,[2] we analysed the experimental results by the use of Tavard's energy relation. Since the relativistic atomic wave functions are used in the present study, Tavard's relation can be written as:

$$\Delta E + E_1 = E_b + E^*_{corr}, \quad (6)$$

where

$$\Delta E = \int_0^\infty \Delta\sigma(s)ds.$$

In this equation, E_b is the binding energy of the molecule, E_1 is one-half of the lowering of the potential energy of the IAM molecule from that of the separated atoms, and E^*_{corr} denotes the sum of the correlation energies for all the atoms without the contribution from the K-shell. The exclusion of the K-shell contribution is necessary because of the normalization at comparatively small s-values.[2] The contribution to the integral from the s-region beyond 9 $Å^{-1}$ was assumed to be zero. The values of $\Delta E+E_1$ are -2.0 ± 0.6 and -4.5 ± 1.4 au for CS_2 and CCl_4 respectively. These values are in good agreement with the previously reported values, -2.0 ± 0.6 and -4.1 ± 1.5 au.[2] It should be noted that the uncertainties, ε, in the present results denote the limits of error, while those quoted in the previous paper were the estimated standard errors. The present $\Delta E+E_1$ values are consistent with the calculated values of $E_b+E^*_{corr}$, -1.69 and -3.28 au for CS_2 and CCl_4 respectively.[2]

The authors wish to thank Dr. Koichi Tamagawa and Mr. Yorihiko Sasaki for their help in the calculation and Mr. Masahiko Tanisaka and his co-workers in the Workshop of the Faculty of Science for their help in the construction of the sample chamber and the nozzle system. The numerical computations were carried out on a HITAC M180 of the Hokkaido University Computing Center.

**** The program was written by Dr. Kazuyoshi Fujita, to whom the authors' thanks are due.

References

1) S. Konaka, *Jpn. J. Appl. Phys.*, **11**, 1199 (1972).
2) M. Nagashima, S. Konaka, T. Iijima, and M. Kimura, *Bull. Chem. Soc. Jpn.*, **46**, 3348 (1973).
3) M. Kimura, S. Konaka, K. Kashiwabara, and M. Nagashima, *Chem. Phys. Lett.*, **18**, 540 (1973).
4) R. A. Bonham and E. M. A. Peixoto, *J. Chem. Phys.*, **56**, 2377 (1972), and the references cited therein.
5) A. C. Yates, *J. Chem. Phys.*, **57**, 1686 (1972).
6) L. S. Bartell, *J. Chem. Phys.*, **63**, 3750 (1975), and the references cited therein.
7) S. Hayashi and K. Kuchitsu, *Chem. Phys. Lett.*, **41**, 575 (1976).
8) B. R. Miller and L. S. Bartell, *J. Chem. Phys.*, **72**, 800 (1980).
9) D. A. Kohl and M. M. Arvedson, *J. Chem. Phys.*, **72**, 1915, 1922 (1980).
10) S. Konaka, S. Sampei, K. Tamagawa, and M. Kimura, 41th National Meeting of the Chemical Society of Japan, Osaka, April 1980.
11) R. A. Bonham and L. Schäfer, "International Tables for X-Ray Crystallography," ed by J. A. Ibers and W. C. Hamilton, Kynoch Press, Birmingham (1974), Vol. 4.
12) CS_2: Y. Morino and T. Iijima, *Bull. Chem. Soc. Jpn.*, **35**, 1661 (1962).
13) The r_a(C–Cl) distance of 1.766$_4$ Å was used for CCl_4; K. Suzuki, Y. Todo, and M. Kimura, 35th National Meeting of the Chemical Society of Japan, Sapporo, August 1976.
14) CCl_4: S. J. Cyvin, J. Brunvoll, B. N. Cyvin, and E. Meisingseth, *Bull. Chem. Soc. Chim. Belg.*, **73**, 5 (1964).
15) Y. Sasaki, S. Konaka, and M. Kimura, *Bull. Chem. Soc. Jpn.*, **53**, 2461 (1980). In Eq. 6, $\Delta j(r')$ stands for $\frac{2}{\pi}(r')^2\Delta J_T^{ED}(2,r')$.
16) J. Epstein and R. F. Stewart, *J. Chem. Phys.*, **66**, 4057 (1977).
17) Y. Sasaki, S. Konaka, T. Iijima, and M. Kimura, *Int. J. Quant. Chem.*, to be published.

The Ammonolysis of Trichloroethylene to Glycine

Masami INOUE* and Saburo ENOMOTO

Faculty of Pharmaceutical Sciences, Toyama Medical and Pharmaceutical University, Sugitani, Toyama 930-01

(Received April 13, 1981)

Glycine was obtained by the ammonolysis of trichloroethylene with aqueous ammonia. Various alkalines, such as alkaline metal hydroxides, carbonates, and hydrogencarbonates, accelerated the reaction; the yield of glycine was 40—70% after a 4 h reaction at 180 °C. Our results on the effect of alkalines indicate that ammonolysis proceeded sequentially *via* the formation of aminoacetonitrile. A good yield of the intermediate compound, aminoacetonitrile, was obtained by heating trichloroethylene at 70 °C with anhydrous ammonia under reaction conditions.

Glycine and its derivatives are widely used in the pharmaceutical industry as materials for drugs and food additives. In the synthesis of glycine, the ammonolysis of chloroacetic acid, the Strecker reaction, and the hydrolysis of hydantoin are performed. As the Strecker reaction involves the hydrolysis of aminoacetonitrile, several method have been developed for the synthesis of aminoacetonitrile, *e.g.*, the ammonolysis of chloroacetonitrile[1] and hydroxyacetonitrile.[2] The use of cyanides as a raw material is now considered impractical by the chemical industry because it requires the laborious removal of cyanide ions from the waste solution.

We ourselves have previously reported that tetrachloroethanes and trichloroethylene, which are commercially used nonflammable solvents, readily react with aqueous ammonia to yield glycine selectively; the yield can be increased by adding various alkalines.[3] In our continuing investigations of the mechanism of ammonolysis, we obtained aminoacetonitrile, a possible intermediate compound, in a good yield with anhydrous ammonia under mild reaction conditions. We wish now to present details of the ammonolysis of trichloroethylene and the effect of alkalines.

Experimental

Ammonolysis of Trichloroethylene with Aqueous Ammonia. A mixture consisting of 20 ml of aqueous ammonia, 1 ml (11.15 mmol) of trichloroethylene, and alkaline catalysts was placed in a stainless steel autoclave (100 ml volume; SUS 32). The autoclave was then heated under a nitrogen atmosphere(30 kg/cm^2), and the mixture was stirred magnetically. After the reaction, glycine was analyzed by means of an amino-acid analyzer(KLA-5, Hitachi, Ltd.) using a Type #2661 column (10 mm i.d., ×250 mm in length).

Ammonolysis of Trichloroethylene with Anhydrous Ammonia. A test tube (30 mm i.d., ×150 mm in length) containing 1 ml of trichloroethylene and 10 ml of liquid ammonia, trapped by cooling with liquid nitrogen, was placed into the autoclave immediately after the introduction of the materials. The autoclave was then heated at 70 °C for 20 h under the conditions described above. Then, the unreacted ammonia was evaporated at room temperature, and the reaction products were diluted with distilled water. The aminoacetonitrile thus formed was analyzed using the above amino-acid analyzer and a Type #2663 column (6 mm i.d., ×70 mm in length).

TABLE 1. AMMONOLYSIS OF CHLOROETHANES AND TRICHLOROETHYLENE WITH AQUEOUS AMMONIA

Compound (mmol)	Yield/mmol
1,1-Dichloroethane(11.86)	0
1,2-Dichloroethane(12.66)	0
1,1,1-Trichloroethane(10.03)	0
1,1,2-Trichloroethane(10.80)	0
1,1,1,2-Tetrachloroethane(9.18)	1.54
1,1,2,2-Tetrachloroethane(9.50)	1.97
1,1,2,2-Tetrabromoethane(4.46)	1.82
Pentachloroethane(8.34)	0
Hexachloroethane(4.22)	0
Trichloroethylene(11.15)	3.05

14% Aq ammonia 20 ml, N_2 30 kg/cm^2, 180 °C for 2 h.

Results and Discussion

Ammonolysis of Trichloroethylene with Aqueous Ammonia. The ammonolyses of various halogenoethanes were carried out as is shown in Table 1. Tetrachloroethanes yield glycine exclusively; from 1,1,1,2- and 1,1,2,2-tetrachloroethanes, 16.3 and 21.2% glycine were yielded respectively when they were treated at 180 °C for 2 h with 14% aqueous ammonia. The ammonolysis was similar with trichloroethylene; the glycine yield was 27.4%. The dehydrochlorination of tetrachloroethane to trichloroethylene in an aqueous ammonia solution is a known process.[4] On the basis of these observations, we examined the ammonolysis of trichloroethylene to glycine under various conditions. As is shown in Fig. 1, the glycine yield increased with an increase in the ammonia concentrations; saturation was reached at 15% aqueous ammonia. The addition of Na_2CO_3 increased the yield almost two-fold, irrespective of the ammonia concentration used. Fig. 2 shows the effect of the reaction temperature on the glycine yield. In the presence of Na_2CO_3, ammonolysis took place from 80 °C; the maximum yield (*ca.* 60%) was obtained at 180 °C for 2 h. In the absence of Na_2CO_3, the yields were poor throughout the temperature range examined. The observations that apparently all trichloroethylene was consumed upon 180 °C, 2-h heating with aqueous ammonia, and that the glycine yield was remarkably increased by the addition of Na_2CO_3 to the reaction solution, suggests the formation of a precursor of glycine.

Judging from the comparison of glycine yields from chloroacetic acid, glycinamide, and aminoacetonitrile

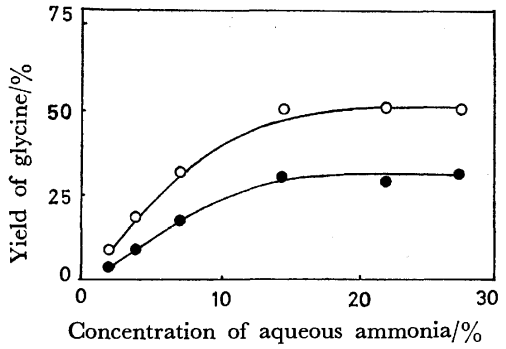

Fig. 1. Effect of the ammonia concentration on the ammonolysis of trichloroethylene to glycine.
Trichloroethylene 11.15 mmol, N_2 30 kg/cm², 180 °C for 2 h.
●: Ammonolysis in aq ammonia (20 ml), ○: ammonolysis in aq ammonia (20 ml)+Na_2CO_3 (1 g).

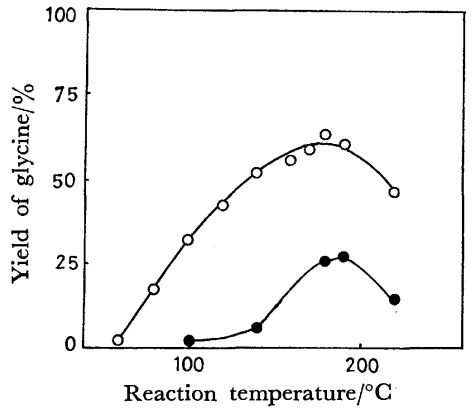

Fig. 2. Effect of the reaction temperature on the ammonolysis of trichloroethylene to glycine.
Trichloroethylene 11.15 mmol, N_2 30 kg/cm², 180 °C for 2 h.
●: Ammonolysis in 28% aq ammonia (20 ml), ○: ammonolysis in 28% aq ammonia (30 ml)+Na_2CO_3 (5 g).

in the presence and absence of Na_2CO_3 in 7% aqueous ammonia, aminoacetonitrile has been thought to be the most likely intermediate compound for this reaction.[3] As is shown in Table 2, the same tendency was observed in 28% aqueous ammonia. The glycine yields from glycinamide and chloroacetic acid were strikingly higher than from trichloroethylene. On the other hand, aminoacetonitrile gave a glycine yield similar to that in the ammonolysis of trichloroethylene. In fact, the initial step is a rapid intermediate formation process; about 90% of trichloroethylene was consumed in a reaction at 180 °C for 30 min in 28% aqueous ammonia. However, from trichloroethylene, we obtained glycine in a 15.0% yield, together with a small amount of aminoacetonitrile (3.7%). The other was a methanol-soluble resinous product (0.5 g) supposed to originate from aminoacetonitrile, since the same product was obtained by heating aminoacetonitrile in aqueous ammonia. The polymer was not hydrolyzed to glycine when treated with Na_2CO_3 and NaOH. On the other hand, there was no detectable formation of chloroacetic acid. Therefore, it

Table 2. Hydrolysis and ammonolysis of possible intermediates in the presence and absence of various alkalines

Compound (mmol)	Alkaline(mmol)	Yield/mmol
$ClCH_2COOH$(10.58)[a]	None	5.65
$ClCH_2COOH$(10.58)[a]	Na_2CO_3(9.4)	7.18
$NH_2CH_2CONH_2 \cdot HCl$(9.13)[a]	None	4.89
$NH_2CH_2CONH_2 \cdot HCl$(9.13)[a]	Na_2CO_3(9.4)	7.36
$NH_2CH_2CN \cdot H_2SO_4$(10.82)[a]	None	2.85
$NH_2CH_2CN \cdot H_2SO_4$(10.82)[a]	Na_2CO_3(14.1)	6.97
$NH_2CH_2CN \cdot H_2SO_4$(10.82)[b]	NaOH(35.0)	8.80
$NH_2CH_2CN \cdot H_2SO_4$(10.82)[b]	Na_2CO_3(17.5)	7.31
$NH_2CH_2CN \cdot H_2SO_4$(10.82)[b]	$NaHCO_3$(35.0)	6.63

28% Aq ammonia 20 ml, N_2 30 kg/cm², 180 °C for a) 4 h and b) 2 h.

Table 3. Ammonolysis of trichloroethylene in the presence of various alkalines

Alkaline (mmol)	28% Aq ammonia (ml)	Yield/mmol
None	20	3.13
LiOH(35.0)	20	4.62
NaOH(35.0)	20	4.01
KOH(35.0)	20	3.55
Li_2CO_3(17.5)	20	6.03
Na_2CO_3(17.5)	20	5.60
K_2CO_3(17.5)	20	5.35
$NaHCO_3$(35.0)	20	6.59
$NaHCO_3$(35.0)	40	6.93
$NaHCO_3$(35.0)	60	7.98
$KHCO_3$(35.0)	20	6.33

Trichloroethylene 11.15 mmol, N_2 30 kg/cm², 180 °C for 4 h.

is considered that, in aqueous ammonia, the ammonolysis to aminoacetonitrile proceeds faster than in the second step of the hydrolysis to glycine, and that aminoacetonitrile, once formed, is then polymerized to an undesirable product. In the presence of alkalines, the hydrolysis is also accelerated. The effectiveness of alkalines may be attributable to their catalytic action on the hydrolysis of the intermediate compound, such as aminoacetonitrile. The change from aminoacetonitrile to glycine has been achieved by using $Ba(OH)_2$.[5]

The use of different types of alkalines significantly affected the glycine yield (Table 3). The effect of alkaline metal compounds on the yields was on the order of: hydrogencarbonates > carbonates > hydroxides. The most effective catalyst was $NaHCO_3$; the yield reached 71.6% at 180 °C for 4 h at a 1:88 molar ratio of trichloroethylene to ammonia. The tendencies observed in the series of alkaline catalysts could not be recognized from their activity in the hydrolysis of aminoacetonitrile, because the glycine yields obtained in the hydrolysis of aminoacetonitrile were in the reverse order: $NaOH > Na_2CO_3 > NaHCO_3$. Since the decomposition of glycine in the presence of NaOH and Na_2CO_3 is essentially negligible under our reaction conditions at 180 °C, the difference in yield may be due to other factors; possibly, a facile abstraction of halogen atoms from trichloroethylene by strong alkalines results in the formation of polymerized prod-

Table 4. Composition of products in the ammonolysis of trichloroethylene

Concentration of ammonia	Products		
	Glycine (mmol)	Iminodiacetic acid (mmol)	Nitrilotriacetic acid (mmol)
7%	3.17	0.24	0.04
28%	7.45	0.18	0.05

Trichloroethylene 11.15 mmol, aq ammonia 30 ml, Na_2CO_3 1.9 g, N_2 30 kg/cm², 180 °C for 4 h.

Table 5. Ammonolysis of trichloroethylene with anhydrous ammonia

Alkaline (mmol)	Temp °C	Time h	Yield mmol
None	50	20	1.47
None	70	20	4.77
None	70	20	6.81
NaOH(35.0)	70	20	1.97
Na_2CO_3(17.5)	70	20	5.16

Trichloroethylene 11.15 mmol, liquid ammonia 10 ml.

ucts.

Reaction Products and Mechanism. In the ammonolysis of trichloroethylene, glycine is the only amino-acid species detected by means of an amino-acid analyzer. However, the elementary analysis of the reaction products obtained with 7% aqueous ammonia gave a nitrogen atomic ratio lower than that of glycine. For example, trichloroethylene (11.15 mmol) was heated at 180 °C for 4 h with 7% or 28% aqueous ammonia (30 ml) in the presence of Na_2CO_3 (1.9 g). Then, unreacted ammonia was removed by evaporation, and the amino-acid species were separated from NH_4Cl by treatment with an anion-exchange-resin (IRA-400, Roam & Haas Co.), followed by a cation-exchange-resin (IR-120B): (A) with 7% aqueous ammonia, yield, 0.4 g, Found: C, 30.68; H, 6.18; N, 16.26%; Calcd for $C_2H_5NO_2$: C, 32.00; H, 6.71; N, 18.66%; and (B) with 28% aqueous ammonia, yield, 0.6 g; Found: C, 31.78; H, 6.52; N, 18.04%. These results suggest the formation of undesired amino acids, *e.g.*, *N*-substituted amino acids, in addition to glycine.

High-power liquid chromatography, using a Shodex OHpak M-614 column (6 mm i.d., ×250 mm in length; Showa Denko K.K.) and 0.002 M H_3PO_4 as the eluent, identified glycine, iminodiacetic acid, and nitrilotriacetic acid by means of their retention times (Table 4). The ratios of these by-products to glycine was higher in the case of ammonolysis using 7% rather than 28% aqueous ammonia. Therefore, the amount of undesirable side products, such as iminodiacetic and nitrilotriacetic acid, can be decreased by increasing the molar ratio of ammonia to trichloroethylene.

Based on the present findings, we suggest that the reaction path for ammonolysis is:

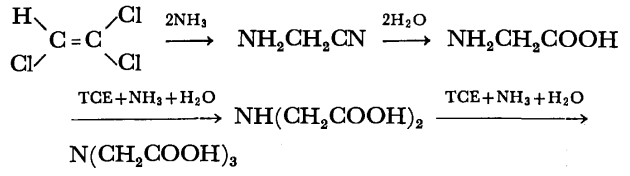

TCE: trichloroethylene.

On the basis of the proposed mechanism, we expected that aminoacetonitrile could be obtained by treating trichloroethylene with ammonia under mild reaction conditions. When trichloroethylene was heated in 28% aqueous ammonia at 80 °C for 24 h, almost all the trichloroethylene was recovered, while aminoacetonitrile and glycine were obtained only in 1.8% and 0.1% yields respectively. The aminoacetonitrile yield increased with increase in the ammonia concentration; in ammonia–water (7:3) media, aminoacetonitrile (30.7% yield) and a trace amount of glycine were obtained at 70 °C for 20 h. Anhydrous ammonia gave high yields (Table 5). At temperatures from 50 °C in the presence of excess ammonia (the volume of liquid ammonia was 10 times that of trichloroethylene), ammonolysis occurred, yielding aminoacetonitrile selectively. A yield of 61% was obtained at 70 °C for 30 h. At higher temperatures, the product decomposed, resulting in brown products. Due to the observed effect of alkalines in aqueous ammonia, we added NaOH of Na_2CO_3 to the system. The presence of NaOH induced the formation of a water-insoluble black polymer. The yield decreased far below that obtained in non-catalyzed reactions. On the other hand, the addition of Na_2CO_3 had little effect on the yield. Therefore, the difference in the catalytic activities of strong and weak alkalines in aqueous ammonia may be explicable in terms of instability of trichloroethylene with strong alkalines.

The authors wish to express their thanks to Dr. Shunichi Hirokami for his valuable Discussions.

References

1) O. W. Bauer and J. W. Teter, U. S. Patent 2443292 (1948); *Chem. Abstr.*, **42**, 7322 (1948).
2) G. A. Menge, *J. Am. Chem. Soc.*, **56**, 2197 (1934); N. Mihara, O. Furuya, and K. Wada, Ger. Offen. 2343599 (1973); *Chem. Abstr.*, **83**, 10874 (1973).
3) M. Inoue and S. Enomoto, *Chem. Lett.*, **1978** 1231.
4) Comp. d'Alais, *Chem. Z.*, **1922**, IV, 154.
5) W. K. Anslow and H. King, *Org. Synth.*, Coll. Vol. I, 298 (1941).

Application of On-line Impedance Measurement Using Fast Fourier Transform to Electrochemical Systems

Tetsuya OSAKA* and Katsuhiko NAOI

Department of Applied Chemistry, School of Science and Engineering, Waseda University, Okubo, Shinjuku-ku, Tokyo 160

(Received April 15, 1981)

An on-line impedance measuring system based on the fast Fourier transform algorithm was constructed by application of only commercially available interfaces and the FORTRAN language available for an OKITAC System 50/10. A modification of the sampling system is effective for reducing two kinds of errors: the aliasing effect is greatly reduced because of the Nyquist frequency being doubled; the leakage effect is diminished because of the truncation interval being adjusted properly. The above modification enables us to acquire high-accuracy data with quite a small number of averagings processed during one measurement, that is, errors may greatly be reduced and the measurement time to get frequency spectra may be made extremely shorter. The modified impedance measurement using the FFT algorithm is applicable to electrochemical systems proceeding not only at a mercury electrode–solution interface but also at a solid electrode–solution interface.

Impedance (or admittance) methods, providing a powerful means for electrochemical analysis, have been made applicable to practical uses through the use of a.c. bridges and phase-sensitive devices with a support by analog cross-correlation techniques. Recently much effort has been devoted to developing automatic operation devices in order to improve accuracy and satisfy a necessity for simultaneous handling of many data points. A great deal of development has been made in impedance measurements by the introduction of the so-called Fourier and Hadamard transformation which have the multiplex advantage. Smith *et al.*[1] applied the multiplex technique using the FFT (fast Fourier transform) algorithm[2] to the electrochemical field and later Schwall *et al.*[3] extended the system so as to cover a wide frequency range from 10 Hz to 125 kHz. Multiplex techniques with construction of a pseudo-random noise spectrometer[4] using the Fourier transform algorithm and with establishment of a new digital signal processing method using the Hadamard transformation algorithm[5] have also been applied to the field of dielectric dispersion measurements. De Levie *et al.*[6] used a similar multiplex technique with sinusoidal wave collection signals in a biomembrane research and recently improved the impedance method in use in the electrochemical field by applying the digital synchronous detection using the Hadamard transformation algorithm.[7]

In this communication, we will try to take out the essential multiplex advantage by means of the modified FFT impedance measurement and to make it possible to acquire high accuracy from a short time measurement with a small number of averagings; we will also describe a simple system which can be composed only of commercially available interfaces without cumbersome hardware construction and which can be operated with the FORTRAN language available for the OKITAC System 50/10; finally, the system composed will be applied not only to mercury electrode–solution systems but also to solid electrode–solution systems.

Principle of Method

Every impedance method using various small-amplitude excitations essentially contains equivalent information as indicated in terms of mathematical transformation. The principle of this method in use in electrochemistry has been introduced.[1,8] The admittance $Y(\omega)$ of a linear or shift-invariant system is completely given by a cross-power spectrum between the excitation and response of the system as follows:

$$Y(\omega) = i(\omega)/e(\omega) = i(\omega)e^*(\omega)/e(\omega)e^*(\omega),$$

where $e(\omega)$, $e^*(\omega)$, and $i(\omega)$ are a frequency domain spectrum of the applied potential, that of its complex conjugate, and that of faradaic current, respectively. This property of $Y(\omega)$ enables us to measure all frequency components simultaneously and to reduce the Fourier transformation to a demultiplexing process. Though in principle any excitation waveforms contain the same information, cross-power spectra in practical systems have to be obtained in a finite time, which requires the most suitable excitation waveform signal to be chosen. Therefore, the present system was designated to utilize the periodic pseudo-noise, which had been studied by Smith *et al.*[1] and Husimi *et al.*[4]

Instrumentation

Hardware Arrangement. The impedance measurement scheme was implemented on an OKITAC System 50/10 minicomputer (memory cycle time 0.65 μs, 75 kB) by using a floppy-disk-oriented system equipped with DMA interface cards. The maximum sampling rate of the system is 20 μs. The schematic diagram for the system is shown in Fig. 1. Programs and data are stored on floppy disks and output data may be displayed on an interfaced oscilloscope or X-Y plotter. Low pass filters are set up for three cut-off frequencies of 2.5, 7, and 12 kHz. The frequency range is restricted mainly by both the noise-applying rate $\Delta t'(f_{max}=(2\Delta t')^{-1})$ and the potentiostat response. The low pass filters (LPF) were built up by our laboratory (40 dB Butterworth) or by Fuso-Seisakusho (80 dB Butterworth), for cutting out the aliasing effect and smoothing computer-synthesized noises. The high pass filters (HPF), which were built

TABLE 1. RELATIONSHIP OF SAMPLING RATE WITH FREQUENCY LIMITS (MAXIMUM AND MINIMUM) AND MEASUREMENT DURATION IN THE CASE OF 1024-POINT (2^{10}) PSEUDO-NOISE

	Sampling rate $\Delta t/\mu s$	Noise-applying rate $\Delta t'/\mu s$	$f_{min}=(N\Delta t')^{-1}$ Hz	$f_{max}=(2\Delta t')^{-1}$ Hz	Measurement time $f_{min}^{-1}\times 3$/ms
System 1[a)]	20	80	12.2	6250	245.8
	50	200	4.9	2500	614.4
	250	1000	1.0	500	3072.0
System 2[b)]	20	40	24.4	12500	122.9
	50	100	9.8	5000	307.2
	250	500	2.0	1000	1536.0

a) System 1 means the system consisting of simultaneous sampling process of excitation $e(t)$ and response $i(t)$ (where the excitation and response are alternatively sampled with $\Delta t/\mu s$ interval and corrected with software technique). b) System 2 means the system consisting of separate sampling process of excitation $e(t)$ and response $i(t)$ (where the excitation is stored before measuring response).

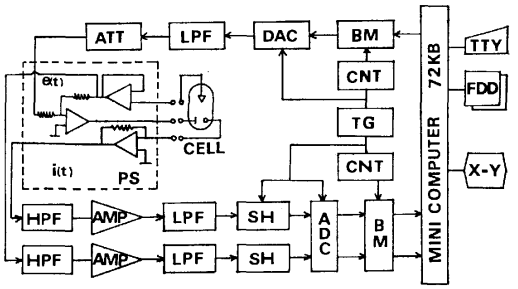

Fig. 1. Block diagram of FFT impedance instrument. Minicomputer: OKITAC system 50/10, DAC: digital-to-analog converter(12 bit), ADC: analog-to-digital converter(12 bit), TTY: teletypewriter, FDD: floppy disk drive assembly, X-Y: X-Y plotter, TG: timing generator, CNT: controller, BM: buffer memory, SH: sample and hold amplifier, LPF: low pass filter (cut off frequency 2.5, 7, 12 kHz), HPF: high pass filter (cut off frequency 1 Hz), ATT: attenuator, AMP: amplifier, PS: potentiostat.

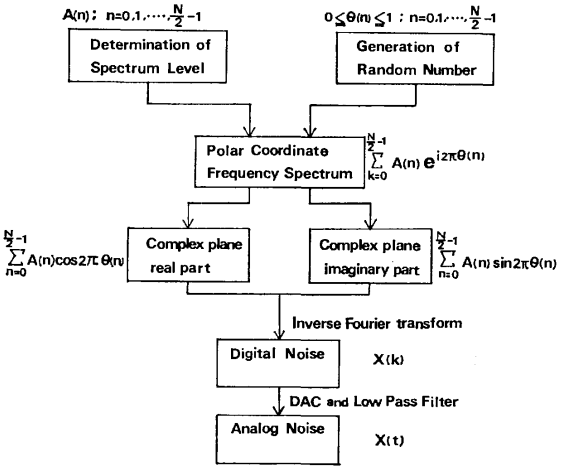

Fig. 2. Procedure for computerized digital wave form generation. $A(n)$: Amplitude array in frequency domain, $\theta(n)$: phase array in frequency domain, $\chi(k)$: digital time domain array, $\chi(t)$: analog time domain array.

by Fuso-Seisakusho, cut out dc and frequency components lower than 1 Hz. The potentiostat with high response (home built or Fuso-Seisakusho HOPATS-3)† was used instead of a dual-potentiostat as used by Smith *et al.*[1)]

Generation of Pseudo-noise. Pseudo-noises generated by the minicomputer are subject to a synthesis as shown in Fig. 2. First, twenty frequency components are selected so as to avoid higher-harmonics (especially the second-harmonics). The phase component array is loaded with random numbers between 0 and 2π. The amplitudes of the selected frequency components are set as constant non-zero levels and those of the others as zero in order for all the frequency components to be at the same excitation energy. The "complex plane" frequency-domain array with 2048 points, which has been transformed from the "polar coordinate" frequency spectrum, is converted into the time-domain digital waveform with 1024 points by use of the inverse FFT. Real and imaginary components of the complex plane are to be set as even and odd functions, respectively, in order that time domain results may become of real function. The analog pseudo-noise thus arranged is applied ten times to the measuring cell to produce a periodic noise and steady-state response. Typical examples of frequency limits and measurement-time durations, as calculated from sampling rates, are listed in Table 1. Three kinds of sampling rates, *e.g.*, 20, 50, and 250 μs, lead to arrangement of three frequency ranges as shown in Table 1, thus allowing three frequency range measurements to provide high accuracy on wide frequency measurements. Since the measurement-time duration is equal to three times the reciprocal of f_{min} ($f_{min}=(N\Delta t')^{-1}$), the measurement time is dependent on the minimum frequency value.

Measuring System. The data acquisition and calculation processes for the transfer function are shown in Fig. 3. Two alternative sampling systems, Systems 1 and 2, are adopted. System 1, designed to perform simultaneous sampling of excitation $e(t)$ and response $i(t)$, samples both data alternately at $\Delta t/\mu s$ intervals and corrects them by the software technique based on the equation $Y(\omega)=Y'(\omega)e^{-i\omega\tau}$ (where Y, Y', and τ are the admittance of real response, that of delayed response, and the delay time Δt of sampling,

† The response rate is 2 μs under the conditions of 1:1 gain and 1 kΩ resistor.

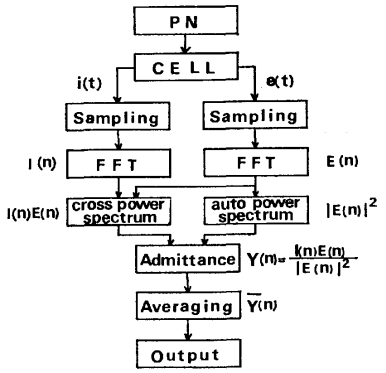

Fig. 3. Data acquisition and calculation processes for transfer function.

repectively). System 2, designed to store the excitation *e(t)* before response *i(t)* is measured, samples data of *e(t)* and *i(t)* separately. System 2 has two advantages over System 1: it can measure higher frequencies because it has its maximum frequency (f_{max}) doubled; it requires such a memory capacity as decreased to two thirds of that of System 1. We usually used System 2 because of these advantages. Data are acquired with 2048 points to be transformed into the frequency domain by means of the FFT. The transfer function of the measuring cell is calculated as admittance after the cross-power and auto-power spectra have been calculated. Final data of admittance are obtained after sampling and averaging which has been made of the last three waveform cycles of the ten-time-applied waveform signals. A remarkable feature of this sampling process is that the pseudo-noise output signal consisting of 1024 points is sampled at a doubled sampling rate (*viz.*, the noise is sampled with 2048 points). Since this sampling system causes the Nyquist frequency to be increased, errors due to the aliasing effect may be depressed (*cf.* Figs. 4 and 5). The leakage effect also may be made ineffective by adequate selection of the truncation interval which is equal to a multiple of the period. Thus, shorter-time measurement for frequency spectra may be realized by means of averaging the last three waveform signal responses.

Experimental

Polarographic measurements were performed on a Metrohm hanging mercury drop electrode (HMDE) with a surface area of 2.38×10^{-2} cm². Solutions for polarographic experiments on HMDE was purified with active charcoal after being prepared with reagent chemicals and triply-distilled water. For solid electrode–solution systems, smooth platinum (9.01×10^{-2} cm²) and gold (9.20×10^{-2} cm²) wire electrodes were used as working electrodes. To bring the solid-electrode surface into a reproducible condition, the working electrodes were cleaned with concentrated nitric acid and pretreated by allowing the electrode potentials to be scanned between the states of hydrogen and oxygen evolutions at 10 V s^{-1} for several tens of minutes. The silver–silver chloride or mercury–mercurous sulfate electrode was used as the reference electrode and the potentials were registered relative to the saturated calomel electrode (SCE). Experiments were performed in a purified nitrogen atmosphere at 25 °C.

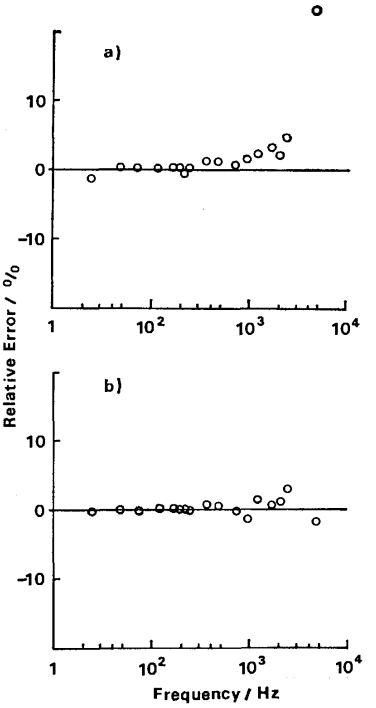

Fig. 4. Relative errors of power spectrum for System 2 using the same duration of sampling rate and noise-applying rate ($\Delta t=\Delta t'=120$ μs).
a): Relative error of power spectrum before passing LPF, b): relative error of power spectrum after passing LPF.

Results and Discussion

Dummy Cell Results. Figures 4(a) and (b) show typical data on relative errors for power spectra of pseudo-noise in the case where sampling rate is equal to the noise-applying rate ($\Delta t=\Delta t'=120$ μs); Figures 4(a) and (b) correspond to before- and after-passage through the low pass filter. Since the Nyquist frequency is *ca.* 4.2 kHz for this sampling rate, the aliasing effect at the high frequency edge is clearly observed as shown in Fig. 4(a). The aliasing effect at the high frequency edge can be cut out by the low pass filter as shown in Fig. 4(b); however, relative errors of several percents are still recognized. In the case of Fig. 5 where the sampling rate is twice as high as the noise-applying rate ($\Delta t=60$ μs, $\Delta t'=120$ μs), the Nyquist frequency is made doubled to 8.3 kHz and the aliasing effect cannot be recognized even in the absence of low pass filter as seen from Fig. 5(a). The relative errors for Fig. 5(a), which are less than 0.1%, are almost equal to those obtainable after the smoothing by means of low pass filter has been applied as seen from Fig. 5(b). Therefore, the sampling system described above is obviously effective for reducing relative errors, making it feasible to reduce the apparent measurement time. A comparison with respect to transfer function between theoretical and experimental values for a typical dummy cell shown in the figure is illustrated by use of the complex impedance representation, Z_{cell}, in Fig. 6. The experimental

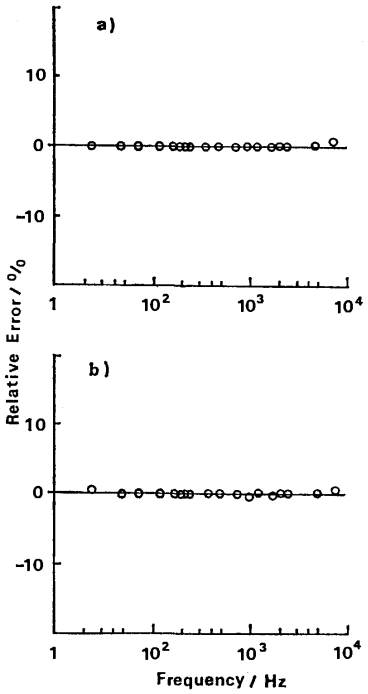

Fig. 5. Relative errors of power spectrum for System 2 using doubled sampling rate as compared with noise-applying rate (Δt=60 μs, $\Delta t'$=120 μs).
a): Relative error of power spectrum before passing LPF, b): relative error of power spectrum after passing LPF.

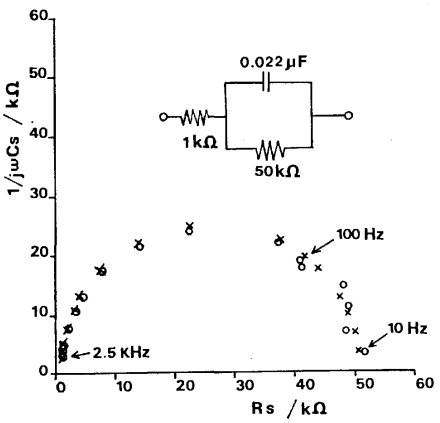

Fig. 6. Theoretical and experimental complex impedance representation of dummy cell shown in the figure.
×: Theoretical data, ○: experimental data.

data for the range from 10 Hz to 2.5 kHz are in fair agreement with the theoretical values at higher frequencies than 100 Hz. The data obtained at lower than 100 Hz, especially around 50 Hz, show some deviation from the theoretical data, which results from the line frequency interference.

Electrochemical Cell Results. An electrochemical system of a cadmium-ion reduction at an HMDE-acidified $ZnSO_4$ solution interface, which is the same system as Schwall *et al.*[3a,9] studied, was examined to obtain higher rate constants. The voltammogram for cadmium-ion reduction shown in Fig. 7(a) gives the maximum value of cot Φ (shown as $(\cot\Phi)_p$) at −0.557 V (SCE). Faradaic impedance representations as Z_k, after subtraction of solution resistance and double layer capacity, and plots of $(\cot\Phi)_p$ *vs.* $\omega^{1/2}$ at −0.557 V (SCE) are shown in Figs. 7(b) and (c). The slope for $(\cot\Phi)_p$ *vs.* $\omega^{1/2}$ plots yields the standard rate constant $k_c^\circ = 4.34\times10^{-2}$ cm s^{-1}, with the aid of the transfer coefficient α=0.35 given by Schwall *et al.*[3a,9] Though the value of k_c° obtained here is as small as half the values 8.7×10^{-2} and 8.5×10^{-2} cm s^{-1} obtained by Schwall *et al.*[3a,9] with and without scanning, respectively, our value may be considered to be in a reasonable range if data of other workers[10] are referred to.

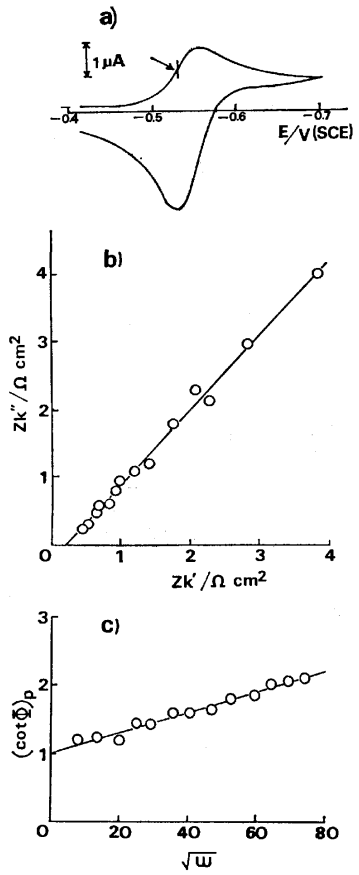

Fig. 7. Experimental results for cadmium ion reduction reaction on HMDE in 1.0 M zinc sulfate +0.18 M sulfuric acid (Cd^{2+} concentration=10^{-3} M), where M means mol dm^{-3}.
a): Single voltammogram of cadmium ion reduction, v=0.020 V s^{-1}, b): complex kinetic impedance representation of cadmium ion reduction at E=−0.557 V(SCE), c): relation between $(\cot\Phi)_p$ and $\omega^{1/2}$ of cadmium ion reduction at E=−0.557 V(SCE).

An electrochemical system of an adsorbed-hydrogen reaction at a platinum–sulfuric acid solution interface was examined as one of typical examples of solid electrode–solution systems. Figures 8(a) and (b) show typical cyclic voltammograms for reference and complex capacitance representations as $Y\omega^{-1}$ for the adsorbed-hydrogen region. The characteristic of complex capacitance representations is similar to that specified by one of the authors[11] using a phase-sensitive apparatus. The results are in accord with the equivalent circuit shown in the figure, previously proposed.[11]

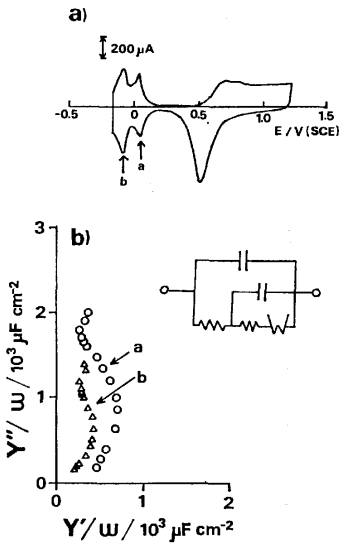

Fig. 8. Experimental results for adsorbed hydrogen reaction on platinum electrode in 0.5 M sulfuric acid.
a): Cyclic voltammogram of platinum electrode, v= 0.10 V s^{-1}, b): complex capacitance representation, $Y\omega^{-1}$, of adsorbed hydrogen reaction at 0.000 V (a) and −0.134 V(SCE) (b).

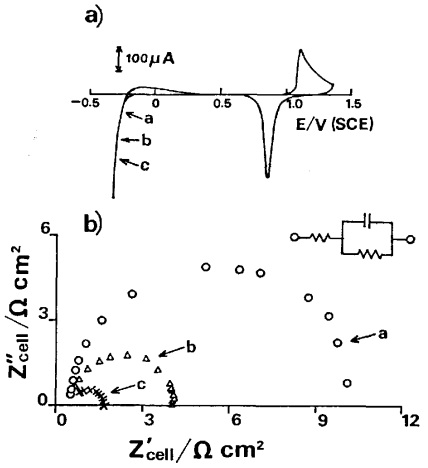

Fig. 9. Experimental results for hydrogen evolution reaction on gold electrode in 0.5 M sulfuric acid.
a): Cyclic voltammogram of gold electrode, v=0.10 V s^{-1}, b): complex impedance representation, Z_{cell}, of hydrogen evolution reaction at −0.374 V (a), −0.404 V (b), and −0.424 V(SCE) (c).

Another typical example of solid electrode-solution system, a hydrogen evolution reaction at a gold electrode–sulfuric acid solution interface, was also examined, data obtained being shown in Figs. 9(a) and (b). Figure 9(a) shows a typical cyclic voltammogram on a gold electrode and Figure 9(b) the complex cell impedance representation as Z_{cell} for the hydrogen evolution region. The characteristic of the complex cell impedance representation is of semicircle and in accord with the simple equivalent circuit shown in the figure, proposed by Masui and Ohashi.[12]

Therefore, the FFT impedance method described in the text may be concluded to be applicable to electrochemical systems proceeding not only at the mercury electrode–solution interface but also at the solid electrode–solution interface. Moreover, transient behaviors with time dependence, *e.g.*, variation in surface conditions with oxide formation, can be characterized by this method because of its short measurement time applicable.

The authors would like to thank Professor Emeritus Dr. Tadashi Yoshida, Waseda University, for his encouragement throughout this research, and Dr. Kazuhiko Nitadori, Systems Laboratory, OKI Electric Industry Company Ltd., for his valuable advice and discussion. T.O. would be greatful to Professor Dr. de Levie, Georgetown University, for calling his interest to the FFT impedance measurement. This work was partially supported by a Grant-in-Aid for Scientific Research from the Ministry of Education, Science and Culture.

References

1) D. E. Smith, *Crit. Rev. Anal. Chem.*, **2**, 247 (1971); S. C. Creason, J. W. Hayes, and D. E. Smith, *J. Electroanal. Chem.*, **47**, 9 (1973); S. C. Creason and D. E. Smith, *Anal. Chem.*, **45**, 2401 (1973).

2) E. O. Brigham, "The Fast Fourier Transform," Prentice-Hall, Inc., Englewood Cliffs, N. J. (1974).

3) a) R. J. Schwall, A. M. Bond, R. J. Loyd, J. G. Larsen, and D. E. Smith, *Anal. Chem.*, **49**, 1797 (1977); b) R. J. Schwall, A. M. Bond, and D. E. Smith, *ibid.*, **49**, 1805 (1977).

4) Y. Husimi and A. Wada, *Rev. Sci. Instrum.*, **47**, 213 (1976); H. Nakamura, Y. Husimi, and A. Wada, *J. Chem. Soc., Faraday Trans. 2*, **73**, 1178 (1977).

5) R. Hayakawa and Y. Wada, *IEE Conf. Publ.*, **177**, 396 (1979).

6) R. de Levie, J. W. Thomas, and K. M. Abbey, *J. Electroanal. Chem.*, **62**, 111 (1975).

7) P. F. Seeling and R. de Levie, *Anal. Chem.*, **52**, 1506 (1980).

8) "Computers in Chemistry and Instrumentation," ed by A. A. Pilla, J. S. Mattson, H. B. Mark, Jr., and H. D. Macdonald, Jr., Marcel Dekker (1972), Vol. 2, Chap. 6.

9) A. M. Bond, R. J. Schwall, and D. E. Smith, *J. Electroanal. Chem.*, **85**, 231 (1977).

10) S. Toshima, Y. Okinaka, and H. Okaniwa, *Denki Kagaku*, **31**, 854 (1963); J. K. Frishmann and A. Timnick, *Anal. Chem.*, **39**, 507 (1967); E. D. Moorhead and G. M. Frame, *J. Phys. Chem.*, **72**, 3684 (1968).

11) T. Osaka, Y. Sawada, T. Yoshida, and K. Nihei, *J. Electrochem. Soc.*, **123**, 1339 (1976).

12) M. Masui and K. Ohashi, Ex. Abstr. of the 47th Conf. Electrochem. Soc. Jpn., 1980, p. 102.

 © 1982 The Chemical Society of Japan Bull. Chem. Soc. Jpn., 55, 41—44 (1982)

Kinetics and Mechanism of 1,4-Cycloaddition between Tetracyanoethylene and Styrenes. III. Effects of Solvent Polarity and Temperature

Yasuhiro Uosaki, Masaru Nakahara,* and Jiro Osugi

Department of Chemistry, Faculty of Science, Kyoto University, Oiwake-cho, Kitashirakawa, Sakyo-ku, Kyoto 606

(Received April 24, 1981)

Experimental evaluation was made of rate constants for foward and backward steps of 1,4-cycloaddition between TCNE and α-methylstyrene and of constants for their complex formations in 1,2-dichloroethane, dichloromethane, chloroform, and carbon tetrachloride at a few temperatures around 25 °C. Kirkwood's dipole model for solvation is applied to analyzing kinetic data obtained. The dipole moment of the transition state is estimated to be 8.5±0.5 Debye, which is larger than either that of the complex (assumed as 1 Debye) or that of the cycloadduct (6±1 Debye). Major cause for the high dipole moment of the transition state is breakdown of the high molecular symmetry of TCNE and minor one is a certain contribution of a zwitterionic structure. The activation entropy for the cycloreversion is negative and in the range of −21 to −48 J K^{-1} mol^{-1}, corresponding to the high polarity of the transition state.

When a strong piezochromism was discovered in dichloromethane solution of tetracyanoethylene (TCNE) and styrene half a decade ago, marked solvent and temperature effects on the rate of color change in the solution were noticed in a qualitative manner.[1] Although the phenomenon was first ascribed to formation of a zwitterion because of the large solvent effect on the reaction, later structural studies on species found led to identification of 1,4-cycloadduct.[2,3] Kinetics and mechanism of the 1,4-cycloaddition were investigated with respect to α- and para-substituent effects in Parts I and II of the present series; large substituent effects were found, suggesting a participation of a polar transition state for the 1,4-cycloaddition.[4,5] The aim of the present paper is to elucidate in a quantitative way how much polar the rate-determining state is or whether or not it is similar in polarity to a zwitterion. Applying Kirkwood's dipole model for solvation[6] to kinetic data obtained in several solvents at various temperatures, it is made clear that although the transition state is polar, it is not so much polar as a zwitterion.

Experimental

α-Methylstyrene and TCNE were purified in the same way as in a previous paper.[3] The solvents, 1,2-dichloroethane, dichloromethane, chloroform, and carbon tetrachloride, were purified by the standard method and distilled over CaH_2 before use.

Two pycnometers of the Lipkin-Davison type (about 5 cm^3) were employed for measuring densities of 1,2-dichloroethane solutions of α-methylstyrene and of TCNE. They were calibrated by using distilled water for which very accurate density data are available.[7] Temperature was controlled to ±0.01 °C at 25 °C in density measurements, while it was kept to ±0.1 °C in spectrophotometric measurements of reaction rate. Concentrations of α-methylstyrene and TCNE solutions were in the ranges of 0.1 to 0.3 and 0.04 to 0.05 mol dm^{-3}, respectively. Partial molal volumes of the donor and the acceptor varied little with concentration within experimental error. The other apparatus and procedures in the present work are the same as those in Part I of this series.[4]

Analyses in the following section require some physical properties of the solvents listed in Table 1 where α is the thermal expansivity,[8] ε the dielectric constant,[9] and q equal to $(\varepsilon-1)/(2\varepsilon+1)$.

Table 1. Properties of the used solvents at 25 °C

Solvent	α[a] / 10^{-3} K^{-1}	ε[b]	q	dq/dT[c] / 10^{-4} K^{-1}
$ClCH_2CH_2Cl$	1.17[d]	10.36	0.431	3.7
CH_2Cl_2	1.37	8.93	0.421	2.5
$CHCl_3$	1.26	4.72	0.356	4.7
CCl_4	1.27	2.23	0.225	2.0

a) From Ref. 8. b) From Ref. 9. c) Estimated from the values of ε at 20 and 25 °C. d) Estimated from the densities at 25 and 30 °C.

Results and Discussion

Formation Constant of EDA Complex. α-Methylstyrene and TCNE form an EDA complex in solution. The formation constant (K_c) is defined as

$$K_c = [EDA]/([D][A]), \quad (1)$$

where EDA, D, and A denote the EDA complex, the donor, and the acceptor, respectively, and the brackets [ ] indicate the concentration of each species. The formation constant can be determined spectrophotometrically from the Scott equation under the condition of $[D]_0 \gg [A]_0$, as explained in detail elsewhere.[4] Values of K_c obtained in several solvents at various temperatures are summarized in Table 2, which includes also the wavelength (λ_{max}) of the maximum absorption for the first charge-transfer band and the molar absorption coefficient (ε_{max}) at λ_{max} utilized in the K_c determination. The higher the solvent polarity, the smaller the formation constant at any temperature. This trend is common to weak EDA complexes.[10] As a matter of fact, the complex studied here has been clarified to be weak from another criterion in a previous work.[4] Dipole moments of EDA complexes between TCNE and similar aromatic donors are reported to be approximately 1 Debye (Debye/C m$=3.33\times10^{-30}$).[11] This kind of trend for weak complexes is usually interpreted in terms of desolvation of the donor and/or acceptor during the complex formation.[10] In the present case, desolvation of TCNE seems important for the following rea-

Table 2. Formation constants of the EDA complex in several solvents at various temperatures and relevant spectroscopic and thermodynamic parameters

Solvent	λ_{max} / nm	ε_{max} / mol^{-1} dm^3 cm^{-1}	K_c/mol^{-1} dm^3 15 °C	20 °C	25 °C	30 °C	ΔH_c / kJ mol^{-1}	ΔS_c / J K^{-1} mol^{-1}
$ClCH_2CH_2Cl$	492	3330	0.092	0.088	0.084		−7.4	−45
CH_2Cl_2	495	2050	0.192	0.184	0.176		−7.2	−39
$CHCl_3$	504	1760	0.473	0.460	0.436		−6.7	−29
CCl_4	499	1510		1.49	1.39	1.31	−10.5	−32

son. Although TCNE itself has no dipole moment because of its high molecular symmetry, its CN groups have so large a bond dipole moment that they can interact strongly with polar solvent molecules. The role of higher moments like the quadrupole and octapole in TCNE is well reflected by strong dependences of its solubility[12] and heat of dissolution[13–15] on solvent polarity.

The enthalpy change (ΔH_c) and entropy change (ΔS_c) for the complex formation are obtained from the thermodynamic equations

$$\left(\frac{\partial \ln K_c}{\partial(1/T)}\right)_P = -\frac{\Delta H_c}{R} - \alpha T^2, \tag{2}$$

and

$$\Delta S_c = \frac{\Delta H_c + RT \ln K_c}{T}, \tag{3}$$

where T is the temperature, R the gas constant, and α the thermal expansivity of the solvent; values of these quantities in the temperature range studied here are given in Table 2. The negative sign of ΔH_c and ΔS_c is reasonable for the association reaction. The absolute value of ΔH_c also indicates that the complex is weak, and its decrease, though somewhat irregular, with increasing solvent polarity is compatible with the increase in solvation of TCNE mentioned above. However, the increase in magnitude of ΔS_c with increasing solvent polarity cannot be explained in terms of solvation, because the entropy loss due to the molecular association is canceled to some extent by the entropy gain due to liberation (desolvation) of polar solvent molecules on one side of the molecular plane of TCNE.

Reaction Rates and Activation Parameters. The 1,4-cycloaddition proceeds according to the scheme

$$D + A \overset{K_c}{\rightleftharpoons} \text{EDA Complex} \overset{k_1}{\underset{k_{-1}}{\rightleftharpoons}} P, \tag{4}$$

where k_1 and k_{-1} are the rate constants for the forward and backward cycloaddition processes, respectively, and P denotes the cycloaddition product.[5] The pseudo-first-order rate constant k_{obsd} for Reaction 4 is expressed as

$$k_{obsd} = \frac{k_1 K_c [D]_0}{1 + K_c [D]_0} + k_{-1}, \tag{5}$$

where $[D]_0$ denotes the initial concentration of the donor. The reaction is followed by observing the absorbance of the product at 325 nm,[3] and the value of k_{obsd} is determined from the Guggenheim plot. Figure 1 shows plots of k_{obsd} *vs.* $K_c[D]_0/(1+K_c[D]_0)$ in 1,2-dichloroethane at three different temperatures.

Table 3. Rate and formation constants of the 1,4-cycloaddition in several solvents at various temperatures

Solvent	Temperature/°C 15	20	25	30
	$10^2 k_1$/s^{-1}			
$ClCH_2CH_2Cl$	6.64	8.58	12.4	—
CH_2Cl_2	3.46	4.77	6.13	—
$CHCl_3$	1.61	2.06	2.68	—
CCl_4	—	0.091	0.130	0.210
	$10^3 k_{-1}$/s^{-1}			
$ClCH_2CH_2Cl$	3.89	6.50	10.7	—
CH_2Cl_2	3.39	5.78	9.90	—
$CHCl_3$	2.29	3.93	6.50	—
CCl_4	—	0.457	0.861	1.48
	K_1			
$ClCH_2CH_2Cl$	17.1	13.2	11.6	—
	17.9[a]	13.8[a]	10.8[a]	—
CH_2Cl_2	10.2	8.25	6.19	—
	9.97[a]	7.90[a]	6.21[a]	—
$CHCl_3$	7.03	5.24	4.12	—
	6.64[a]	5.28[a]	4.29[a]	—
CCl_4	—	1.99	1.51	1.42

a) Determined from equilibrium measurements.

Plots like these provides k_1 and k_{-1} as a slope and an intercept, respectively. Rate constants obtained in the four solvents by applying the least-squares method to plots like those in Fig. 1 are given in Table 3, together with adduct formation constants given by

$$K_1 = \frac{k_1}{k_{-1}} = \frac{[P]}{[EDA]}. \tag{6}$$

When all the steps involved in Reaction 4 are at equilibrium, we can get K_1 independently by the method described in detail elsewhere (see Eq. 11 in Ref. 4). As seen in Table 3, the kinetically and thermodynamically determined values of K_1 are in good agreement. The activation enthalpies (ΔH_1^* for k_1 and ΔH_{-1}^* for k_{-1}) and entropies (ΔS_1^* and ΔS_{-1}^*) are obtained from the Eyring equation[16]

$$R \ln \frac{hk}{k_B T} = -\frac{\Delta G^*}{T} = -\frac{\Delta H^*}{T} + \Delta S^*, \tag{7}$$

where h, k_B, and k are the Planck constant, the Boltzmann constant, and the rate constant (k_1 or k_{-1}), respectively. The activation parameters thus obtained are listed in Table 4; they will be discussed below.

TABLE 4. ACTIVATION PARAMETERS FOR THE 1,4-CYCLOADDITION IN SEVERAL SOLVENTS

Solvent	ΔH_1^* / kJ mol^{-1}	ΔH_{-1}^* / kJ mol^{-1}	ΔS_1^* / J K^{-1} mol^{-1}	ΔS_{-1}^* / J K^{-1} mol^{-1}
$ClCH_2CH_2Cl$	42	70	−121	−48
CH_2Cl_2	38	74	−139	−35
$CHCl_3$	34	72	−161	−45
CCl_4	59	84	−101	−21

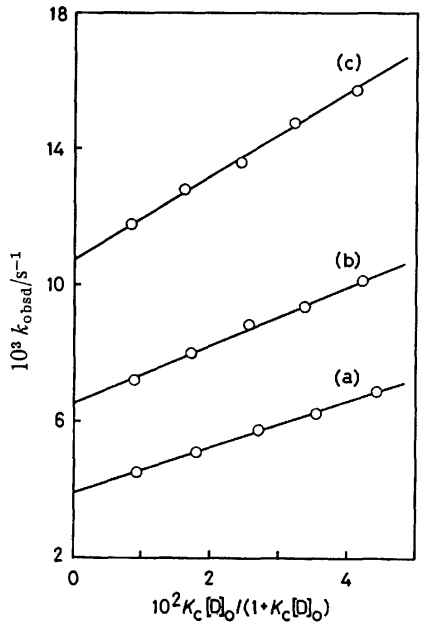

Fig. 1. Plots of k_{obsd} *vs.* $K_c[D]_0/(1+K_c[D]_0)$ in 1,2-dichloroethane.
(a): 15 °C, (b): 20 °C, (c): 25 °C.

Dipole Moments of the Transition State and Product. The dipole moment of the transition state can be determined by applying Kirkwood's dipole model for solvation to the kinetic data in Table 3.[6] Kirkwood's model leads to the equations

$$\Delta G_1^* = (\Delta G_1^*)_\phi - Lq\left(\frac{\mu_*^2}{r_*^3} - \frac{\mu_{EDA}^2}{r_{EDA}^3}\right), \quad (8)$$

and

$$\Delta G_{-1}^* = (\Delta G_{-1}^*)_\phi - Lq\left(\frac{\mu_*^2}{r_*^3} - \frac{\mu_P^2}{r_P^3}\right), \quad (9)$$

where

$$q = \frac{\varepsilon - 1}{2\varepsilon + 1}. \quad (10)$$

Here, ΔG_1^* and ΔG_{-1}^* are the activation free energies relating to the rate constants k_1 and k_{-1} through Eq. 7, respectively; $(\Delta G^*)_\phi$ denotes the activation free energy which is not explicitly given by Kirkwood's model (*i.e.*, a term associated with activation free energy in the hypothetical gas phase and with solvations due to van der Waals interactions, *etc.*); L is the Avogadro constant; r_*, r_{EDA}, and r_p are the radii of the transition state, the EDA complex, and the adduct, respectively (spherical symmetry is assumed here); and μ denotes the dipole moment for the species indicated.

Plots of ΔG_1^* and ΔG_{-1}^* against q in Table 1 are

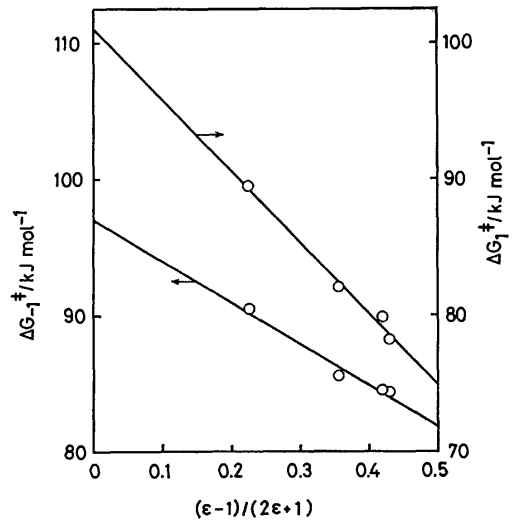

Fig. 2. Plots of ΔG_1^* and ΔG_{-1}^* *vs.* $(\varepsilon-1)/(2\varepsilon+1)$ at 25 °C.

shown in Fig. 2; they are linear as expected. If μ_{EDA} is taken to be 1 Debye and r_{EDA} and $r_* \approx r_p$ are approximated to 4.6 and 4.4 Å based on measured partial molal volumes,[17,18] respectively, the slopes in Fig. 2 corresponding to Eqs. 8 and 9 provide 8.5±0.5 and 6±1 Debye as μ_* and μ_p, respectively. Alternatively, the dipole moment of the adduct can roughly be estimated from the vector sum of dipole moments of the cyano and methyl groups; the estimated dipole moment is 7—8 Debye.[19] The fairly good agreement indicates that the present analysis is reasonable. Since the dipole moment of α-methylstyrene is 0.76 Debye,[20] we have the following polarity profile for Reaction 4:

$$\underset{0.8}{D + A} \rightleftharpoons \underset{1}{EDA\ Complex} \rightleftharpoons \underset{8.5}{TS} \rightleftharpoons \underset{6\ Debye}{P}, \quad (11)$$

where TS denotes the transition state. Although these absolute values have uncertainties as indicated above, their differences are more reliable. There is a large difference between the EDA complex and the transition state and a small difference between the adduct and the transition state. This corresponds to the fact that the forward reaction depends on solvent polarity more strongly than the backward one (see Table 3). The found polarity difference of 2.5 Debye for the backward step is very important since it suggests that a zwitterionic structure contributes to the transition state to some extent (see Fig. 1 in Ref. 5). The conclusion that the transition state is more polar than the cycloadduct, is strongly supported by the negative activation volume for the same step as determined by rapid-reaction techniques at high pressures.[21,22] A much larger dipole moment of 14 Debye is reported

for the transition state in the 1,2-cycloaddition of TCNE to *trans*-anethole where a zwitterionic intermediate is considered to exist.[23,24] Major factor for the high polarity of the transition state studied here is breakdown of the molecular symmetry of TCNE in the transition state. The symmetry breakdown is also responsible for the relatively large dipole moment for the adduct where the CN bond dipoles are not fully canceled. The large difference of 7.7 Debye between the reactants and the transition state clearly explains why the formation reaction ($k_f=K_c k_1$) has a large negative reaction constant, $\rho=-5.5\pm0.2$, for para-substituted styrenes.[5]

Effect of Solvent Polarity on Activation Entropies. To get insight into the mechanism of the cycloaddition, the cycloreversion process which is unimolecular is most important and thus, mainly the activation entropy for this process is discussed here. The negative values of $\Delta S^{\neq}_{-1}$ (-21 to -48 J mol^{-1}) correspond to the negative activation volume for the process mentioned above, and tell us that the transition state is more polar than the adduct. More negative values of $\Delta S^{\neq}_{-1}$ in the range of -40 to -100 J K^{-1} mol^{-1} have been reported for 1,2-cycloadditions in various solvents where a zwitterionic intermediate is considered to exist.[25]

By differentiating Eq. 9 with respect to temperature and neglecting temperature dependences of μ's and r's, we get the equation

$$\Delta S^{\neq}_{-1} = (\Delta S^{\neq}_{-1})_{\phi} + L\left(\frac{\mu^2_{\neq}}{r^3_{\neq}} - \frac{\mu^2_{P}}{r^3_{P}}\right)\frac{dq}{dT}. \qquad (12)$$

Inserting $\Delta S^{\neq}_{-1}$ in Table 4, dq/dT in Table 1, and the corresponding slope in Fig. 2 into Eq. 12, we obtain -20 to -40 J K^{-1} mol^{-1} as $(\Delta S^{\neq}_{-1})_{\phi}$. These negative values indicate that some solvations not explicitly represented by Kirkwood's dipole model play a role, because $(\Delta S^{\neq}_{-1})_{\phi}$ in the hypothetical gas phase is expected to be somewhat positive from the bond loosening involved in the transition state. If we plot $\Delta S^{\neq}_{-1}$ in Table 4 against dq/dT in Table 1, the slope obtained gives a larger dipole moment for the transition state. However, the differentiated form of Kirkwood's relation (Eq. 12) is no doubt less reliable than Eq. 9. Thus, the solvent effect on $\Delta S^{\neq}_{-1}$ can qualitatively be understood in terms of Kirkwood's dipole model. Influences of solvent polarity on $\Delta S^{\neq}_{1}$, $\Delta H^{\neq}_{1}$, and $\Delta H^{\neq}_{-1}$ may be explained in a similar manner.

Some other thermodynamic quantities relating to the reaction are to be mentioned in brief. The reaction enthalpy ($\Delta H_1=\Delta H^{\neq}_1-\Delta H^{\neq}_{-1}$) and entropy ($\Delta S_1=\Delta S^{\neq}_1-\Delta S^{\neq}_{-1}$) for the cycloaddition from the complex are in the ranges of -25 to -38 kJ mol^{-1} and -70 to -116 J K^{-1} mol^{-1}, respectively. Neither is unusual, telling us that the adduct is stabler and more rigid than the complex. In the literature, the activation entropy, $\Delta S^{\neq}_1=\Delta S_c+\Delta S^{\neq}_1$, from reactants is compiled for many other 1,4-cycloadditions where TCNE is involved.[26] The present values are in the range of -133 to -190 J K^{-1} mol^{-1}, comparable with those in the literature (-120 to -200 J K^{-1} mol^{-1}).

References

1) M. Nakahara, Y. Tsuda, M. Sasaki, and J. Osugi, *Chem. Lett.*, **1976**, 731.
2) M. Nakahara, Y. Uosaki, M. Sasaki, and J. Osugi, *Rev. Phys. Chem. Jpn.*, **47**, 119 (1977).
3) M. Nakahara, Y. Uosaki, M. Sasaki, and J. Osugi, *Bull. Chem. Soc. Jpn.*, **53**, 3395 (1980).
4) Y. Uosaki, M. Nakahara, and J. Osugi, *Bull. Chem. Soc. Jpn.*, **54**, 2569 (1981).
5) Y. Uosaki, M. Nakahara, and J. Osugi, *Bull. Chem. Soc. Jpn.*, **54**, 3681 (1981).
6) J. G. Kirkwood, *J. Chem. Phys.*, **2**, 351 (1934).
7) G. S. Kell, *J. Chem. Eng. Data*, **12**, 66 (1967).
8) J. A. Riddick and W. B. Bunger, "Organic Solvents," in "Techniques of Chemistry," 3rd ed, ed by A. Weissberger Wiley-Interscience, New York (1970).
9) M. H. Abraham, "Progress in Physical Organic Chemistry," ed by A. Streitwieser, Jr., and R. W. Taft, Interscience, New York (1974), Vol. 11, p. 1.
10) R. Foster, "Organic Charge-transfer Complexes," Academic Press, London (1969).
11) N. Kulevski, "Molecular Association," ed by R. Foster, Academic Press, London (1975), Vol. 1, Chap. 2.
12) M. Lotfi and R. M. G. Roberts, *Tetrahedron*, **35**, 2137 (1979).
13) F. E. Rogers, *J. Phys. Chem.*, **75**, 1734 (1971).
14) A. I. Konovalov, V. D. Kiselev, A. N. Ustyugov, and N. G. Gess, *Zh. Org. Khim.*, **12**, 2541 (1976).
15) B. N. Solomonov, I. S. Antipin, and A. I. Konovalov, *Zh. Org. Khim.*, **13**, 2491 (1977).
16) S. Glasstone, K. J. Laidler, and H. Eyring, "Theory of Rate Processes," McGraw-Hill, New York (1941).
17) Y. Uosaki, M. Nakahara, M. Sasaki, and J. Osugi, *Chem. Lett.*, **1979**, 727.
18) The radius r is calculated from the partial molal volume V by; $r=\{3V/(4\pi N)\}^{1/3}$. Values of V for D, A, and P in 1,2-dichloroethane are 132.5 ± 0.3, 107.0 ± 1.0, and *ca.* 210[17] cm^3 mol^{-1}, respectively.
19) The dipole moments of CN and CH_3 groups are 3.5—4 and 0.3 Debye, respectively.[8]
20) M. Charton, *J. Org. Chem.*, **30**, 552 (1965).
21) J. Osugi, M. Sasaki, H. Tsuzuki, Y. Uosaki, and M. Nakahara, "High-pressure Science and Technology," ed by K. D. Timmerhaus and M. S. Barber, Plenum (1979), Vol. 1, p. 651.
22) H. Tsuzuki, Y. Uosaki, M. Nakahara, M. Sasaki, and J. Osugi, *Bull. Chem. Soc. Jpn.*, submitted.
23) R. Huisgen, *Acc. Chem. Res.*, **10**, 117 (1977).
24) The reported dipole moment is based on kinetic data for $k_f=K_c k_1$. As pointed out in the text, however, not only k_1 but also K_c depend on solvent polarity. Since K_c decreases with increasing solvent polarity, a value larger than 14 Debye is to be obtained.
25) B. N. Solomonov, I. S. Antipin, A. I. Konovalov, and V. B. Novikov, *Zh. Org. Khim.*, **15**, 2466 (1979).
26) J. Sauer and R. Sustmann, *Angew. Chem. Int. Ed. Engl.*, **19**, 779 (1980).

The Crystal and Molecular Structure of (Acetylacetonato)-(diacetylmethyl)(diethylamine)palladium(II)

Takahiro KUROKAWA,† Kunio MIKI, Nobuo TANAKA,†† and Nobutami KASAI*

Department of Applied Chemistry, Faculty of Engineering, Osaka University, Yamadaoka, Suita, Osaka 565

(Received April 30, 1981)

The molecular structure of $[Pd(acac)_2(NHEt_2)]$ was determined by means of X-ray diffraction. The crystal belongs to the monoclinic system: $a=14.166(1)$, $b=8.209(1)$, $c=14.764(2)$ Å, $\beta=100.75(1)°$, space group $P2_1/n$, with $Z=4$. The structure was solved by the heavy-atom method and refined anisotropically by the least-squares procedure; $R=0.067$ for 3149 non-zero reflections. The geometry around the Pd atom is square-planar: one of the two (acac) ligands coordinates to the Pd atom by O,O'-chelation, and the other, by σ-bonding of the γ-carbon atom, while the diethylamine occupies the fourth coordination site. A weak intramolecular N–H···O hydrogen bond [2.962(10) Å] is observed.

With relation to the reactions shown below,[1] the molecular structures of $[Pd(acac)_2]$[2] (**1**) and $[\{Pd(acac)(NHEt_2)_2\}^+(acac)^-]$[3] (**3**) have been determined. This paper will deal with the molecular structure of $[Pd(acac)_2(NHEt_2)]$ (**2**).

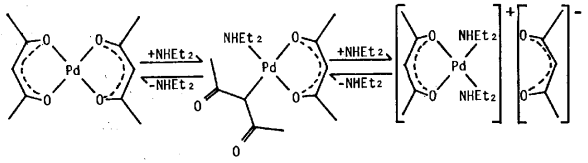

1 **2** **3**

Experimental

Yellow platelet crystals of $[Pd(acac)_2(NHEt_2)]$ were provided by Professor Seichi Okeya and Professor Shinichi Kawaguchi. A toluene–hexane mixture was used for the recrystallization. Efforts to cut out a crystal of a size suitable for an X-ray experiment was unsuccessful. A rather large crystal with dimensions of *ca.* $0.5\times0.18\times0.4$ mm was, therefore, used for the X-ray experiments, though it may limit the accuracy of the results.

Crystal Data: $C_{14}H_{25}NO_4Pd$, *F.W.* 377.8, monoclinic, $a=14.166(1)$, $b=8.209(1)$, $c=14.764(2)$ Å, $\beta=100.75(1)°$, $V=1686.7(3)$ Å^3, space group $P2_1/n$(No. 14), $D_m=1.46$(flotation), $D_c=1.488$ g cm^{-3}, $Z=4$.

The unit-cell dimensions were determined by the least-squares fit of 2θ values of 18 strong reflections measured precisely on a Rigaku automated four-circle diffractometer. The intensity data were collected using graphite-monochromatized Mo $K\alpha$ radiation on the diffractometer. The θ-2θ scan technique was applied. The scan width was $\Delta2\theta=(2.0+0.7\tan\theta)°$, and the scan rate was 4° min^{-1}. Backgrounds were measured for 7.5 s before and after the measurement of each peak. The intensity measurements were repeated up to three times for weak reflections. A total of 3694(3149 non-zero) reflections were measured up to $2\theta=54°$. Usual Lp corrections were made, but absorption corrections were ignored [μ(Mo $K\alpha$)$=10.7$ cm^{-1}].

Structure Solution and Refinement

The structure was solved by using Patterson and Fourier methods. The block-diagonal least-squares refinement (*HBLS* V)[4] with isotropic temperature factors reduced R to 0.096. The final R value was 0.066 ($R_w=0.089$) for non-zero reflections, allowing anisotropic thermal parameters for all the non-hydrogen atoms. The hydrogen atoms, except H(3) and H(6), could not be located reasonably, so they were not included in the refinement. The weighting schemes used at the final stage were $w=\{\sigma_{cs}^2(F_o)+0.0011\cdot|F_o|+0.0726|F_o|^2\}^{-1}$ for $|F_o|>0$ and $w=0$ for $|F_o|=0$, where σ_{cs} is the standard deviations obtained by the counting statistics. The final atomic positional and thermal parameters are given in Table 1.†††

TABLE 1. FRACTIONAL ATOMIC COORDINATES, WITH ESTIMATED STANDARD DEVIATIONS IN PARENTHESES

(a) Non-hydrogen atoms with equivalent temperature factors.[10]

Atom	x	y	z	B_{eq}/Å^2
Pd	0.51248(4)	0.54100(7)	0.29614(4)	3.79
O(1)	0.5847(4)	0.3299(7)	0.3182(4)	4.5
C(1)	0.6748(6)	0.3223(10)	0.3506(5)	4.0
C(2)	0.7125(6)	0.1471(11)	0.3639(7)	5.3
C(3)	0.7371(6)	0.4508(10)	0.3739(6)	4.4
C(4)	0.7166(5)	0.6164(10)	0.3658(5)	3.9
C(5)	0.7971(6)	0.7384(11)	0.3941(6)	5.0
O(2)	0.6351(4)	0.6771(6)	0.3379(4)	4.2
C(6)	0.3905(6)	0.3986(10)	0.2532(6)	4.3
C(7)	0.3675(6)	0.4181(10)	0.1523(6)	4.5
O(3)	0.3125(6)	0.5180(9)	0.1125(5)	6.2
C(8)	0.4190(8)	0.2983(15)	0.0978(7)	7.2
C(9)	0.3185(6)	0.4470(11)	0.3088(6)	5.0
O(4)	0.2621(5)	0.5581(9)	0.2875(5)	6.2
C(10)	0.3253(9)	0.3491(15)	0.3998(7)	7.4
N	0.4344(5)	0.7538(8)	0.2746(5)	4.6
C(11)	0.4715(9)	0.8697(17)	0.2115(9)	8.3
C(12)	0.4834(11)	0.8080(18)	0.1248(9)	9.5
C(13)	0.4411(10)	0.8539(14)	0.3613(10)	8.2
C(14)	0.4162(11)	0.775(2)	0.4377(9)	9.8

(b) Hydrogen atoms with isotropic temperature factors.

Atom	x	y	z	B/Å^2
H(3)	0.795(5)	0.420(9)	0.395(5)	1.4(14)
H(6)	0.412(6)	0.299(10)	0.272(5)	2.2(16)

† Present address: Hitachi Computer Consultant Co., Ltd., 23-15 Minami-ooi 6-chome, Shinagawa-ku, Tokyo 140.

†† Present address: Institute for Protein Research, Osaka University, Yamadaoka, Suita, Osaka 565.

††† Tables of observed and calculated structure factors and anisotropic thermal parameters are kept at the Chemical Society of Japan. Document No. 8201.

TABLE 2. LEAST-SQUARES PLANES AND DIHEDRAL ANGLES

The equation of the plane is of the form $AX+BY+CZ+D=0$, where X, Y, Z, and D are measured in Å units; $X=ax+cz\cos\beta$, $Y=by$, and $Z=cz\sin\beta$.

1) Coordination plane.
$0.3393X+0.0252Y-0.9404Z+1.7443=0$.

	Pd	O(1)	O(2)	C(6)	N
Δ[a]	0.003	−0.014	0.012	0.014	−0.014

2) O,O'-Chelated acac ligand.
$0.3628X+0.0031Y-0.9319Z+1.6150=0$.

	O(1)	C(1)	C(2)	C(3)	C(4)	C(5)	O(2)	Pd[b]	H(3)[b]
Δ[a]	0.009	0.002	−0.001	−0.013	0.004	0.008	−0.010	−0.004	−0.003

Dihedral angles between 1) and 2) planes[ϕ/°]. 1.9(2)

a) Deviation of atoms from the plane [l/Å]. b) Not included in the least-squares plane calculation.

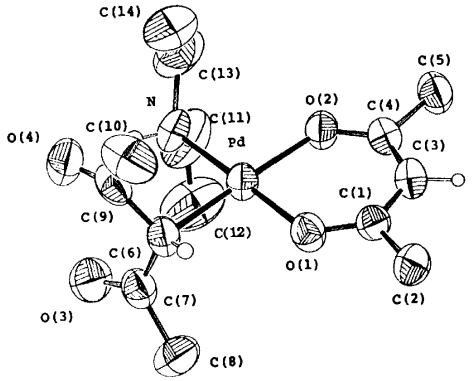

Fig. 1. Perspective view of the molecule. Non-hydrogen atoms are represented by thermal ellipsoids at 50% probability levels.

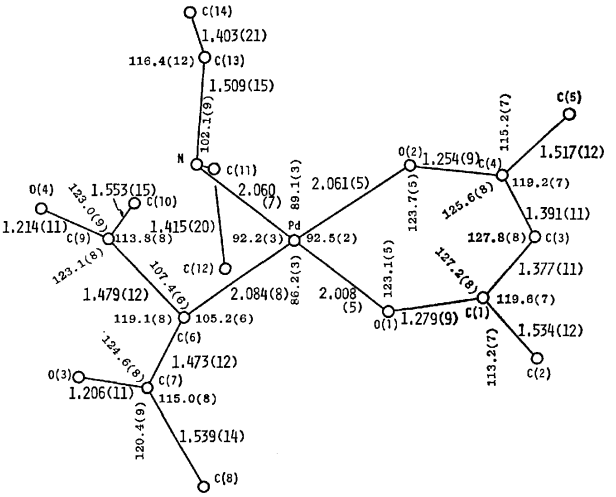

Fig. 2. Bond lengths [l/Å] and bond angles [ϕ/°] with estimated standard deviations in parentheses. The followings are bond lengths and bond angles which could not be shown in the figure.

Pd-N-C(11)	113.3(7),	C(6)-H(6)	0.90(8),
Pd-N-C(13)	112.5(7),	Pd-C(6)-H(6)	102(5),
N-C(11)-C(12)	116.8(11),	C(7)-C(6)-H(6)	114(5),
C(3)-H(3)	0.86(7),	C(9)-C(6)-H(6)	108(5).
C(1)-C(3)-H(3)	113(5),		
C(4)-C(3)-H(3)	119(5),		

The atomic scattering factors were taken from the International Tables for X-Ray Crystallography, Vol. IV.[5] The computations were done on an ACOS Series 77 NEAC System 700 computer at the Crystallographic Research Center, Institute for Protein Research, Osaka University.

Results and Discussion

A perspective view (*ORTEP* II)[6] of the molecule is shown in Fig. 1, while the bond lengths and bond angles are given in Fig. 2. The geometry around the Pd atom is square-planar: one of the two (acac) ligands coordinates to the Pd atom by the O,O'-chelation, and the other, by σ-bonding of the γ-carbon atom, while the diethylamine occupies the fourth coordination site.

The two Pd–O lengths are unequal, Pd–O(1)= 2.008(5) and Pd–O(2)=2.061(5) Å. The *trans*-influence is observed. The former is equal to the Pd–O length *trans* to the diethylamine [2.000(3) Å],[7] and the latter, to that *trans* to the acetylacetonyl ligand [2.06(1) Å].[8]

The planarity of the acetylacetonato ligand is good (Table 2). This plane is approximately parallel to the coordination plane (Fig. 1.), the dihedral angle between these planes being 1.9(2)°. The bond lengths and bond angles in the acetylacetonato ligand in the present complex are normal, like those in $Pd(acac)_2$[2] or $[\{Pd(acac)(NHEt_2)_2\}^+(acac)^-]$.[3]

The diacetylmethyl ligand is approximately perpendicular to the coordination plane. The bond angles around the γ-carbon atom are considerably distorted. The C(7)–C(6)–C(9) angle [119.1(8)°] is larger than the tetrahedral angle, whereas the Pd–C(6)–C(7) angle [105.2(6)°] is slightly smaller. The C_β–C_γ and C_β=O bond lengths and C_β–C_γ–C_β bond angles are normal compared with the corresponding values in $[(PPh_3)Pd(acac)_2]$,[7] $[Me_3Pt(acac)(bipy)]$,[8] and $[K^+\cdot\{Pt(acac)_2Cl\}^-]$.[9] The two carbonyl groups are parallel in $[K^+\cdot\{Pt(acac)_2Cl\}^-]$ and in the present complex, whereas they are not parallel in $[(PPh_3)Pd(acac)_2]$. In the pottasium salt, the dihedral angle between the two C_α–C_β–C_γ moieties is 9.5°, while in the present complex it is 27.4(3)°. It was suggested that interactions between two carbonyl oxygen atoms and the K^+ cation in the crystalline state affect the parallel position of the two carbonyl groups and the small dihedral angle. In the present complex,

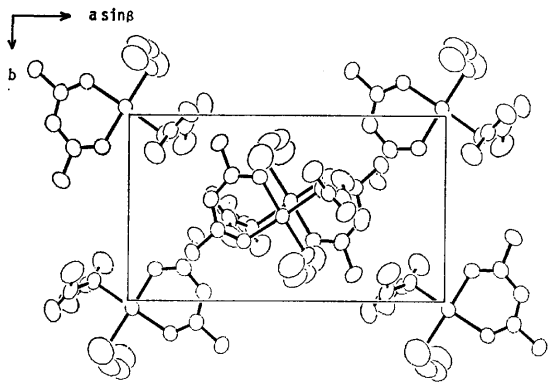

Fig. 3. Crystal structure projected along the c axis.

a weak intramolecular hydrogen bond, N–H···O(4) [2.958(10) Å], and a rather close N–H···O(3) contact [3.304(10) Å] between the two carbonyl groups and the N–H of the diethylamine ligand are observed.

The diethylamine ligand is also approximately perpendicular to the coordination plane. The two N–C bond lengths are equal [1.494(15) and 1.509(15) Å], comparable with those in $[\{Pd(acac)(NHEt_2)_2\}^+(acac)^-]$ [1.497(5) and 1.498(5) Å]. The two methyl groups are in a stable *trans* conformation.

The crystal structure projected along the c axis is shown in Fig. 3. The intermolecular atomic contacts are usual van der Waals distances, the closest being $C(10)(x,y,z)\cdots O(3)(0.5-x, -0.5+y, 0.5-z)$ [3.331(14) Å].

The authors wish to express their deep thanks to Professor Shinichi Kawaguchi, Osaka City University, and Professor Seichi Okeya, Wakayama University, for their valuable discussions and the supply of crystals.

References

1) S. Okeya, H. Sazaki, Y. Nakamura, and S. Kawaguchi, 36th National Meeting of the Chemical Society of Japan, Osaka, April 1977, Abstr. 3E05.

2) M. Sato, K. Miki, Y. Kai, N. Tanaka, N. Yasuoka, and N. Kasai, unpublished data.

3) H. Kotake, T. Sei, K. Miki, N. Yasuoka, and N. Kasai, *Bull. Chem. Soc. Jpn.*, **53**, 10 (1980).

4) T. Ashida, "The Universal Crystallographic Computing System-Osaka," The Computation Center, Osaka University (1973), p. 55.

5) "International Tables for X-Ray Crystallography," Kynoch Press, Birmingham (1974), Vol. IV, p. 71.

6) C. K. Johnson, *ORTEP* II, Report ORNL-5138, Oak Ridge National Laboratory, Tennessee (1976).

7) M. Horike, Y. Kai, N. Yasuoka, and N. Kasai, *J. Organomet. Chem.*, **72**, 441 (1974).

8) A. G. Swallow and M. R. Truter, *Proc. R. Soc. London, Ser. A*, **266**, 527 (1966).

9) R. Mason and G. Robertson, *J. Chem. Soc., A*, **1969**, 485.

10) W. C. Hamilton, *Acta Crystallogr.*, **12**, 609 (1959).

Preparation of Surfactant-free Polystyrene Latices with High Surface Charge and Electrical Double Layer on Their Surfaces

Kunio FURUSAWA

Department of Chemistry, The University of Tsukuba, Sakura-Mura, Ibaraki 305

(Received April 27, 1981)

Polystyrene latices with a wide range of surface charges were prepared in the absolute absence of conventional emulsifiers by controlling the concentration of potassium peroxodisulfate as an initiator and allowing the polymerization to proceed at a relatively high pH to suppress the Kolthoff reaction; $KHCO_3$ or K_2HPO_4 buffer was used to keep the polymerizing system near neutral pH. Conductometric titrations with different bases (NaOH and $Ba(OH)_2$) on latices show that the Stern layer charge increases with an increase in the surface charge of latices (σ_0) and at about the same rate as σ_0 does, leading to a virtually constant diffuse layer charge.

In recent years, monodisperse polystyrene latices have been recommended as a model dispersion for studying a number of fundamental phenomena in the field of colloid science.[1] Main reasons for this recommendation are the high monodispersity of particles and the well-defined composition of surface charge.[2] In considering behaviors of polystyrene latices, it is particularly important whether they have been prepared in the presence or in the absence of emulsifier. If no emulsifiers have been used in the preparation, the surface charge is made up of chemically bound polar groups originating from the initiator used in the polymerization.[3] In the presence of emulsifier, however, besides covalently linked polar groups, adsorbed ionic groups from the emulsifier can contribute to the surface charge. According to Stone-Masui and Wattilon,[4] adsorbed emulsifiers cannot easily be eliminated from the latex surface.

In this study, efforts were first concentrated on preparing monodisperse polystyrene latices with a wide range of surface charge in the absolute absence of conventional emulsifiers and then a study was made on the structure of electrical double layers on their surfaces.

For usual surfactant-free polystyrene latices prepared with potassium peroxodisulfate as an initiator,[3] the surface charge is made up of sulfonato groups originating from the initiator. Therefore, to increase the surface charge, the number of sulfonato groups on the final particle should be made maximal.[5] This can be achieved by choosing relatively high concentrations of potassium peroxodisulfate and allowing the polymerization to proceed at neutral pH in the presence of a buffer agent; the latter condition is to suppress the Kolthoff reaction[6] leading to generation of hydroxyl radicals.

It has been established that, in the neighborhood of a charged particle, there is an ionic atmosphere which is composed of two kinds of layers with different ion distributions, the Stern layer and the Gouy diffuse layer. The present study on the structure of electrical double layers is based on analyses of titration curves of latices. Since the conductivity of a latex suspension is determined by the number and distribution of counter ions in the double layer, conductometric titration curves obtained with various bases can be expected to provide direct information on the structure of electrical double layers. Here, a lot of titrations were carried out by using NaOH and $Ba(OH)_2$ on latices with a wide range of surface charge, and the relation between the surface charge and the double layer structure was discussed on the basis of analyses of titration curves.

Experimental

Materials. The styrene monomer was purified three times by vacuum distillation and the initiator, $K_2S_2O_8$, was recrystallized from water and dried in a desiccator. All the other chemicals were of analytical grade and used without further purification. The water was doubly distilled with an all-pyrex apparatus.

Preparation of Polystyrene Latices. Surfactant-free polystyrene latices were prepared with a modification of the method described by Kotera *et al.*[3] The modification is related to how to agitate the polymerizing system and how to control the pH during the polymerization. In a glass bottle of 250 cm^3, a mixture of 20 cm^3 styrene monomer and 175 cm^3 water or solution of KCl, $KHCO_3$, and K_2HPO_4 in water was purged with argon gas at 70 °C, after which 5 cm^3 of a $K_2S_2O_8$ solution was added. Immediately the bottle had a glass stopper applied, was attached to a wheel designed to rotate at a speed of 50 min^{-1} in a water bath thermostated at 70 °C, and subjected to rotation for 24 h for polymerization. Additional data on the polymerization conditions are given in Table 1.

The average particle size of each sample was determined by measuring the diameter of particles on an electron micrograph equipped with a projection scope.

Titration Experiments. Latex samples were treated with extensively purified Dowex ion-exchange resins according to the method described by Van den Hul and Vanderhoff[7] for converting all charged groups on the latex surface into the H^+ form. After the ion-exchange process, about 40 cm^3 of the latex was titrated under an argon atmosphere with two bases, NaOH and $Ba(OH)_2$ solutions, both potentiometrically and conductometrically, in the same vessel at 25 °C. In these titrations, it was necessary to adjust the solid content at 3—4% w/w, because large experimental errors were produced at lower than 3% w/w and because titration patterns were distorted at higher than 4% w/w due to surface conductivity at the latex-solution interface, as was also found by Wright and James.[8] Potentiometric titrations were performed with a Horiba pH meter (Model F-5) equipped with a glass electrode and conductometric ones with a Philips conductivity meter PW-9501 equipped with a Philips conductivity cell (PR-9515).

Determination of Coagulation Concentrations. Coagulation concentrations, C_{cfc}, of latex samples for KCl were determined by a static method. In a glass-stoppered tube 1.0 cm^3 latex of *ca.* 0.5% w/w was mixed with one of 4.0 cm^3 KCl solutions of various concentrations and the mixture

Table 1. Preparation and characterization of polystyrene latices with a wide range of surface charge

Sample	Preparation conditions			Characterization		
	$K_2S_2O_8$ concn / 10^{-4} M	Electrolyte concn / 10^{-2} M	Final pH	Radius / nm	Spec. area / m^2/g	Surface charge / $\mu C/cm^2$
1	2	3	4	5	6	7
N-1	3.71	—	3.2	212	13.5	1.1
N-2	19.07	—	2.6	260	11.0	3.5
N-3	34.21	—	2.3	290	9.9	4.1
		KCl				
K-1	19.2	0.2_7	2.6_5	350	8.5	3.2
K-2	19.2	1.0	2.6_6	528	6.4	3.5
K-3	37.1	0.5	2.6_2	381	7.9	4.3
		$KHCO_3$				
C-1	18.5	1.0	7.6	255	11.2	4.5
C-2	27.7	1.0	7.5	290	9.9	6.9
C-3	37.4	0.5	6.2	280	10.2	7.4
		K_2HPO_4				
P-1	29.3	0.5	7.4	325	8.7	8.1
P-2	36.9	0.5	7.8	300	9.6	8.7

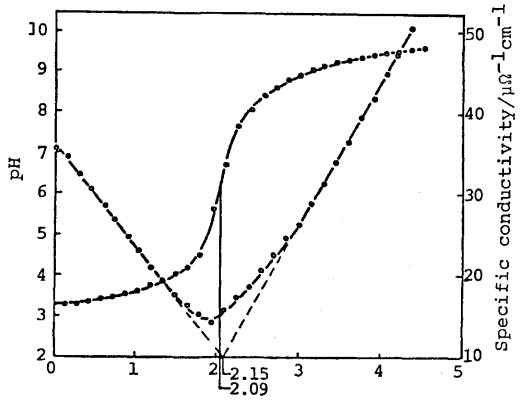

Fig. 1. Conductometric and potentiometric titration curves of latex C-3 after ion exchange.

was kept at 25 °C in a water bath. After an elapse of 20 h for equilibration the transmission coefficient of the supernatant was measured against water using an Atago spectrophotometer (440-S) at wavelength 550 nm. Transmission coefficients were plotted against the KCl concentration. Extrapolation of the linear part of the curve to the horizontal yields a KCl concentration that is taken by us as the coagulation concentration.

Results and Discussion

Preparation and Characterization of Polystyrene Latices. Some examples of results on the preparation and characterization of surfactant-free latices are shown in Table 1. Columns (5) and (6) in this table give average particle sizes determined by electron microscopy. The presence of KCl in the polymerizing system leads to larger particles; compare N-2 with K-1 or K-2. It is seen that in the absence of added electrolyte an increase in the initiator ($K_2S_2O_8$) leads to larger particles. Addition of $KHCO_3$ or K_2HPO_4, however, does not alter the radius significantly; compare N-2 with C-1 or N-3 with P-2. Size distributions are kept very narrow, with $D_w/D_n<1.01$.

The surface charge in column (7) was obtained by titration in an argon atmosphere with bases. As the example in Fig. 1 shows, both the equivalent points determined by the potentiometric and conductometric titrations are in good agreement, and the titration curves show no indication of presence of surface groups other than strong acid groups. These groups are certainly $-OSO_3^-$ groups originating from $K_2S_2O_8$.[2] Such titration curves, however, were observed only for fresh samples; for those latices left long after preparation, there were two break points on the titration curve, which suggests that surface sulfonate groups will be hydrolyzed gradually into hydroxyl or carboxyl groups during storage, with rates dependent on the conditions for storage. In each series the surface charge (σ_0) increases with increasing $K_2S_2O_8$ concentration. This tendency may be predicted from the mechanism of emulsion polymerization. Buffering the system during polymerization leads to higher values of σ_0; compare N-series with C- or P-series. As mentioned before, this is attributed to suppression of the Kolthoff reaction. The highest surface charge attained after ion exchange is 8.7 $\mu C/cm^2$. In the absence of specific adsorption it would lead to diffuse double layer potentials of 190 mV and 80 mV in 10^{-3} or 10^{-1} M† (1-1) electrolytes, respectively. However, due to specific adsorption in the Stern layer, lower values for ζ-potentials will almost certainly be found from electrokinetic study.

Double Layer Structure and Stability. The present study on the structure of electrical double layers at the polymer-solution interface is based on analysis of titration curves. The titration was carried out only for samples within a few weeks after preparation. Figure 2 shows an example of conductometric titration curves obtained by using two bases. In the case using NaOH, both the descending and ascending legs of the titration curve are linear, and the curve has

† 1 M=1 mol dm^{-3}.

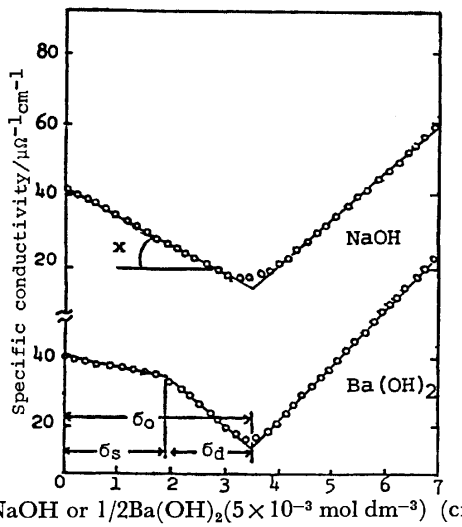

Fig. 2. Conductometric titration curves conducted using NaOH and $Ba(OH)_2$ for latex K-1.
x: Slope of the descending leg of the titration curve, σ_0: surface charge, σ_s: Stern-layer charge, σ_d: diffuse-layer charge.

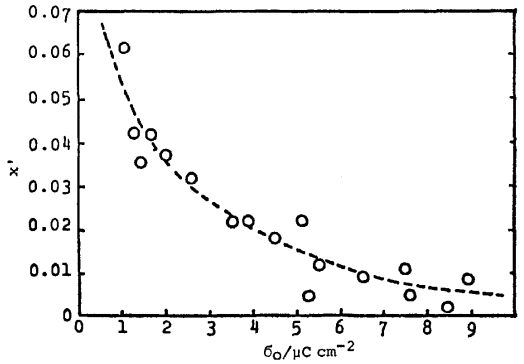

Fig. 3. Relation between the corrected slope of titration curve(x') and the surface charge(σ_0) of polystyrene latices.

a shape typical of the titration of a strong acid with a strong base. This results from equal preference of strong acid surface groups for Na^+ and H^+ ions. However, the negative slope of the descending leg is much smaller than that for a strong acid in solution; it depends on the amount of the surface charges of latex due to the limited mobility of counter ions in the double layer. Usually, the electrical conductivity of a system depends on the product of the number of mobile ions and their mobility. Therefore, the descending slope in the present system is influenced by the following three factors: (a) total surface area, (b) the amount of surface charges, and (c) the degree of binding of counter ions to the surface, which depends on the structure of the electrical double layer. If factors (a) and (b) can be controlled, the residual slope (x') gives the contribution from factor (c), which provides useful information on the structure of electrical double layer. Figure 3 shows a plot of slopes obtained by the above process against surface-charge density (σ_0) as determined from equivalent points for the same titration curves. The slope (x'), in which the dimension of x is related to the scale for

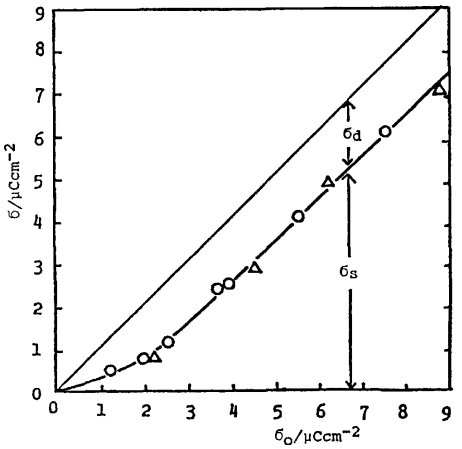

Fig. 4. Charge distribution in the Stern layer(σ_s) and the diffuse layer(σ_d) as a function of the surface charge(σ_0). △: Data reported by W. Norde.

the titration curve, decreases rapidly with an increases in σ_0, and the value for the highest surface-charge latex is about one-sixth that of the lowest one. This indicates that the higher the surface charge, the more tightly are the counter ions held on the surface.

The lower conductometric titration curve in Fig. 2 shows a result obtained using $Ba(OH)_2$, in which an inflection point is found on the descending leg. According to Van den Hul and Vanderhoff,[2] the occurrence of the inflection point is connected with fixation of counter ions in the Stern layer. Counter ions condensed closely to surface sulfonato groups are exchanged preferentially for Ba^{2+}, and then dissociated ions in the diffuse double layer are exchanged. Counter ions in the diffuse double layer contribute effectively to the conductivity through their high mobility.

Using this concept, we can determine the number of counter ions located in the Stern layer and in the diffuse layer from the position of the inflection point on the descending leg. Figure 4 shows a result derived on the basis of inflection points, which gives charge distributions in the Stern layer (σ_s) and in the diffuse double layer (σ_d) as a function of surface charge (σ_0). It is obvious that, at high σ_0 values, σ_s increases at about the same rate as σ_0, leading to a virtually constant value of σ_d.

A similar result has been reported by W. Norde[9] for polystyrene latices prepared by the same method as ours, his result being included in Fig. 4. He calculated σ_d from ζ-potentials for latices of various surface charges using the Gouy-Chapman equation. In this case, ζ-potential was derived following the method of Wiersema[10] from electrophoretic mobilities in a 0.01 M KNO_3 solution. As can be seen from Fig. 4, his data are located on the same line as ours, which suggests that the region given by the inflection point of the conductometric titration curve corresponds to the slipping plane of the electrophoresis in 0.01 M KNO_3.

According to the Derjaguin-Landau-Verway-Overbeek (DLVO) theory,[11] coagulation concentration, C_{cfc}, serves as a means for quantifying the sta-

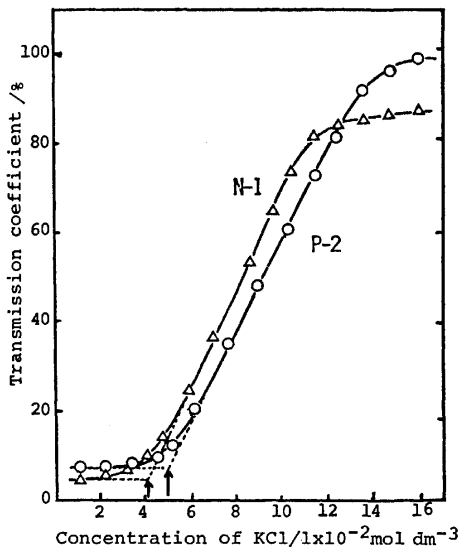

Fig. 5. Transmission coefficient *vs.* concentration of KCl plots for latex N-1(△) and latex P-2(○). The arrow indicates the derived coagulation concentration.

TABLE 2. COAGULATION CONCENTRATION OF KCl FOR THE LATICES WITH A DIFFERENT SURFACE CHARGE

Sample	Surface charge	Coagulation concn
	μC/cm²	10^{-2} M
N-1	1.1	4.02
K-1	3.2	4.35
C-2	6.9	4.71
P-2	8.7	4.97

bility of an electrostatically stabilized dispersion. Figure 5 shows an example plot of transmission coefficient *vs.* concentration of KCl. Values of C_{cfc} for latices with different surface charges are given in Table 2. It is seen that C_{cfc} increases with increasing surface charge, as expected from the DVLO theory, but C_{cfc} for the highest surface-charge latex (P-2) is not much different from C_{cfc} for the lowest-charge latex (N-1).

At any rate, it can be concluded that conductometric titration curves of polystyrene latices furnish important knowledge regarding the structure of electric double layers. From these analyses and coagulation experiments, it is realized that colloidal stability depends on the potential at the Stern layer over which the diffuse double-layer charge is distributed, because C_{cfc} is not much dependent on the surface charge of latex samples.

The author thanks Professor J. Lyklema and Dr. W. Norde, Agricultural University, Wageningen, The Netherlands, and Mr. H. Kawai, Tokyo Kyoiku University, Tokyo, Japan, for their advice and cooperation.

References

1) *E.g.*, W. Norde and J. Lyklema, *J. Colloid Interface Sci.*, **66**, 257 (1978); 285 (1978).
2) H. J. Van den Hul and J. W. Vanderhoff, *J. Electroanal. Chem.*, **37**, 161 (1972).
3) A. Kotera, K. Furusawa, and Y. Takeda, *Kolloid Z. Z. Polym.*, **239**, 677 (1970).
4) J. Stone-Masui and A. Watillon, *J. Colloid Interface Sci.*, **52**, 479 (1975).
5) K. Furusawa, W. Norde, and J. Lyklema, *Kolloid Z. Z. Polym.*, **250**, 908 (1972).
6) I. M. Kolthoff and I. K. Miller, *J. Am. Chem. Soc.*, **73**, 3055 (1956).
7) Van den Hul and J. W. Vanderhoff, *J. Colloid Interface Sci.*, **28**, 336 (1968).
8) M. H. Wright and A. H. James, *Kolloid Z. Z. Polym.*, **251**, 745 (1973).
9) W. Norde, Thesis, Agricultual Univ., Wageningen, The Netherlands (1976).
10) P. H. Wiersema, A. L. Loeb, and J. Th. G. Overbeek, *J. Colloid Interface Sci.*, **22**, 78 (1966).
11) E. J. Verwey and J. Th. G. Overbeek, "The Theory of the Stability of Lyophobic Colloids," Elsevier Publ. Co., Amsterdam (1948).

Further Studies of the Rate Constant for Chemical Excitation of OH in Shock Waves

Tohru KOIKE* and Kihei MORINAGA

Department of Chemistry, National Defense Academy, Hashirimizu, Yokosuka 239

(Received April 30, 1981)

Electronically excited $OH(^2\Sigma)$ is formed both by chemical and thermal excitations in the H_2-O_2 reaction. The $OH(^2\Sigma)$ emission in the partial equilibrium region of the reaction was measured in 1250—3450 K incident shock waves for a mixture, $H_2/O_2/Ar=2/2/96$, at starting pressures, 6—30 Torr. The correlation factor between the emission intensity and the concentration of $OH(^2\Sigma)$ was derived in the temperature region above 2800 K where the thermal excitation of $OH(^2\Sigma)$ is dominant. The factor was utilized to estimate the concentration of chemically excited $OH(^2\Sigma)$ and the rate constant of the reaction $O+H+M=OH(^2\Sigma)+M$ was determined as $10^{13.92\pm0.17}\exp[-(8.3\pm1.2)\ \mathrm{kcal}/RT)]$ ($\mathrm{cm^6\ mol^{-2}\ s^{-1}}$).

The UV emission of $OH(^2\Sigma)$, hereafter OH*, in the H_2-O_2 reaction has been studied in detail by many researchers in discharge flow systems,[1] in flames,[2] and in shock waves.[3-5] The origin of OH* in a relatively low temperature region is attributed to the chemical excitation of $O+H+M=OH^*+M$,[3,4] while, in a high temperature region, thermally excited OH* is more dominant than chemically excited.[4] The transition from chemical to thermal excitation has been observed to occur around 2300 K.[4]

The following reaction scheme represents the growth and decay of OH* in the low temperature region.[3-5]

$$O + H + M = OH^* + M \qquad (a)$$

$$OH^* + M' = OH + M' \qquad (b)$$

$$OH^* = OH + h\nu \qquad (c)$$

The reverse reaction (—b) is equivalent to the thermal excitation and it is left out in the low temperature region. The reverse reaction (—c) is self-absorption and it can be disregarded in the present experiment.[4] Since it is expected that $k_b > k_{-a}$ and $k_b[M'] > k_c$ under the present experimental conditions as discussed before,[4,5] the OH* formed is quenched mainly by reaction (b). Then, the steady state assumption for OH* leads to the following expression for OH* in the low temperature region.[4,5]

$$[OH^*]_{ch} = k_a[O][H][M]/k_b[M'] \qquad (1)$$

OH* is formed by the thermal excitation as well as by the chemical excitation as above, and the thermally excited [OH*] is expressed by the partition of OH and OH* as:

$$[OH^*]_{th} = [OH](f_{OH^*}/f_{OH})\exp(-93.4\ \mathrm{kcal}/RT), \qquad (2)$$

where the f's are partition functions of OH and OH*. The value of 93.4 kcal corresponds to the energy difference between the two states of $^2\Sigma(v=0)$ and $^2\Pi(v=0)$. Since the value of [OH] can be estimated by computer modeling with an appropriate reaction mechanism, the value of $[OH^*]_{th}$ is obtainable.

The UV emission intensity I due to the reaction (c) is related to [OH*] as:

$$I = C\,k_c[OH^*], \qquad (3)$$

where C is a correlation factor for the detecting system. In the preceding paper,[5] the dependence of $\log I$ on $10^4/T$ was analysed by computer modeling and a tentative value of k_a was reported. We mentioned in that paper that a more precise value of k_a could be obtained by absolute measurement of the emission intensity I in the low temperature region, though the method is not free from the correlation factor of a standard radiant bulb.

In the present paper, the value of $[OH^*]_{th}$ is correlated with the emission intensity I, and the constancy of $[OH^*]_{th}/I$ at high temperatures is demonstrated. The emission intensity I in the low temperature region, where the chemical excitation is predominant, is analysed to obtain more credible k_a values using the correlation factor so derived.

Experimental

The experiments were done in incident shock waves. The shock tube used in the previous work[5] was rebuilt and reinstrumented to improve the evacuation and the optics. The evacuation of the test section was less than 10^{-4} Torr (1 Torr≈133.322 Pa) before each run. A photomultiplier (Hamamatsu-TV, 7696) having S-11 response combined with a monochromator (Jarrell-Ash, JE-25, dispersion=3.3 nm/mm) was used to measure the OH* emission intensity. The wavelength of the monochromator was centered at 306.4 nm with entrance and exit slits having 1 and 2 mm width, respectively.

The gases used to prepare the test gas, $H_2/O_2/Ar=2/2/96$, were 99.99999% pure H_2, 99.999% pure O_2 and 99.999% pure Ar; all of them were from Nippon Sanso Co.

Results and Discussion

Even in the high temperature region, the oscillogram trace of the emission intensity resembles that shown in the previous paper[5] having a plateau height of I in the partial equilibrium.

The partial equilibrium $[OH^*]_{th}$ was evaluated by using a reliable partial equilibrium value of modeled [OH] and the ratio of the partition functions, f_{OH^*}/f_{OH}, in Eq. 2. The reaction mechanism adopted for the computer modeling is identical with that in the previous work.[5] The modeled [OH] along with the other species concentrations for the later discussion are shown in Fig. 1. The partition functions were evaluated using the molecular constants of OH and OH* reported.[6] If the thermal excitation is really predominant in the high temperature region, the above $[OH^*]_{th}$ divided by the emission intensity I should be constant. In Fig. 2, the values of $[OH^*]_{th}/I$ are plotted against T. Though the data are scattered,

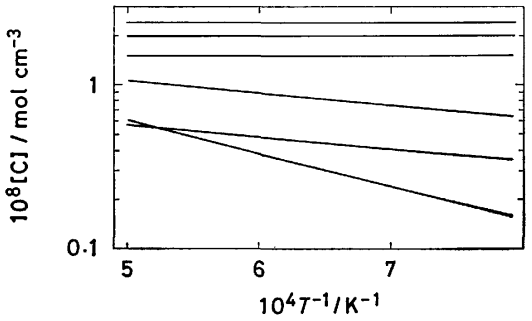

Fig. 1. Temperature variation of the modeled concentrations in the partial equilibrium (P_1=10 Torr). The species are, from top to bottom on the right hand side, H_2O, O_2, H, O, H_2, and OH.

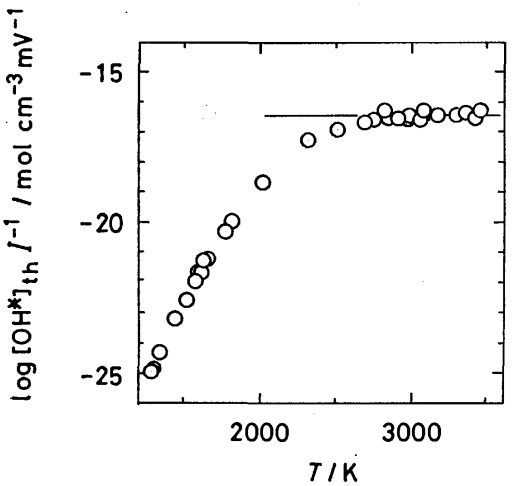

Fig. 2. Temperature variation of $[OH^*]_{th}/I$. The line shows an average value for $[OH^*]_{th}/I$ above 2800 K.

the constancy is adequate above 2800 K, and the value of $[OH^*]/I$ or C k_c in Eq. 3 was evaluated as:

$$[OH^*]/I = (3.0\pm1.0) \times 10^{-17} \text{ (mol cm}^{-3}\text{ mV}^{-1}\text{)}.$$

Because of the temperature variation of the rotational population in the $^2\Sigma(v=0)$ state, it is expected that each of the intensity maxima of six branches moves in or out of the wavelength range of 303.1—309.7 nm and, due to this effect, there might be a possibility not to hold the constancy of $[OH^*]/I$ in the temperature range. Such a temperature effect on the emission intensity could be seen by comparing following J_{max} values at different temperatures. In contrast with the vibrational and the electronic populations, the number of molecules does not simply decrease with increasing rotational quantum number. First it increases to a maximum and then decreases, and the rotational quantum number at which the number of molecules shows a maximum is given by:[6]

$$J_{max} = 0.5896 \times \sqrt{T/B} - 1/2,$$

where B=rotational constant (17.355 cm^{-1} for OH*). Since the J_{max} values increase with temperature, only the J_{max} values at the lowest and the highest ends of the temperature range need be examined. The J_{max} values evaluated are 7.0 and 7.8 at 2800 K and 3450 K, respectively. According to the spectra reported for the $^2\Sigma^+ - ^2\Pi$ transition of OH,[7] it is possible to assign each rotational transition to one of the emission lines as follows. J=7 and 8 of three branches, P_1, P_2, and Q_2 are out of the wavelength range. The J values in Q_1 branch are at the end of the wavelength range longer than 309.0 nm. As for R_1 and R_2 branches, the J values are almost at the center of the wavelength range. Thus, none of the intensity maxima of the six branches are expected to move in or out of the wavelength range in this temperature range of 2800—3450 K.

Table 1. Quenching cross section, σ, between OH* and M′ and calculated k_b value

M′	σ/Å^2	$(k_b/T^{0.5})$/cm^3 mol^{-1} s^{-1}
Ar	0.059[9]	1.5×10^{10}
H_2	6.9[9]	4.5×10^{12}
O_2	10[a]	2.6×10^{12}
H_2O	57[b]	1.7×10^{13}
H	22[9]	2.0×10^{13}
O	5[c]	1.5×10^{12}

a) H. P. Hooymayers and C. Th. Alkemade, *J. Quant. Spectrosc. Radiat. Transfer*, **7**, 495 (1967). b) M. Kaneko, Y. Mori, and I. Tanaka, *J. Chem. Phys.*, **48**, 4468 (1968). c) Assumed.

The rate constant k_c is the reciprocal of the radiative life time of OH*, which is reported to change slightly depending on the value of the rotational quantum number of the $^2\Sigma$ state.[8] In this study, such dependence of the k_c value, as well as the temperature dependence, was assumed to be negligible. Therefore, the above value of $[OH^*]/I$ could be used in the lower temperature region to obtain the chemically excited [OH*] by observing I.

Once the chemically excited [OH*] is determined, unknown parameters to evaluate the k_a value from Eq. 1 are the concentrations of H, O, M, M′, and the k_b value. The partial equilibrium concentrations of H and O are shown in Fig. 1. The third body M of the reaction (a) was assumed to be all of the species in the reaction region having the same efficiency, *i.e.*, [M]=density. The quenching partner M′ considered are shown in Table 1 along with the k_b value. The k_b values were evaluated by collision theory using the collision cross sections of M′ reported elsewhere. OH was not considered as a collision partner, since it is reported that OH has negligible quenching effect on OH*.[9]

Besides the above physical quenchings for OH*, the possibility of chemical quenchings such as $OH^*+H=H_2+O$ and $OH^*+H_2=H_2O+H$ are to be considered. The rate constant for the former reaction has been discussed in detail[9] and is elucidated to be small compared with the physical quenching of H. The rate constant for the latter reaction can be assumed to be equal to the frequency factor of the ground state reaction of $OH+H_2=H_2O+H$. If the frequency factor of 5.25×10^{13} in the H_2-O_2 reaction mechanism in Ref. 5 is adopted, the chemical quenching of OH* by H_2 is about 1/3 of the physical quench-

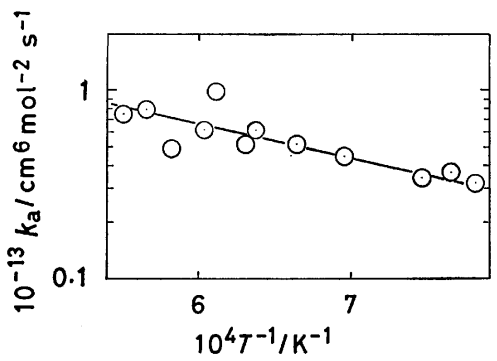

Fig. 3. Arrhenius plots for k_a.
The line shows the least squares fit for the data points.

ing by the same partner at 1500 K. Since the cross sections of the other species are larger than that of H_2, the physical quenchings are more effective than the chemical quenchings. Thus, no chemical quenchings were considered in this study.

The Arrhenius plot of k_a thus evaluated is shown in Fig. 3. The least squares fitting gave the following expression for the k_a value with one standard error.

$$k_a = 10^{13.92\pm0.17}\exp[-(8.3\pm1.2)\text{kcal}/RT)](\text{cm}^6\,\text{mol}^{-2}\,\text{s}^{-1})$$

(1 kcal=4.184 kJ)

Schiff *et al.*[1] obtained the rate constant for the chemical excitation of OH* in the course of chemiluminescence studies in a discharge flow system at pressures of 0.4—4 Torr and 300 K. They assumed the bimolecular reaction of ground state O and H to form OH* and estimated the rate constant at $(3\pm1)\times10^{-21}$ cm^3 molecule^{-1} s^{-1}. If the figure is converted to the termolecular rate constant assuming O+H+M=OH*+M, it is given as $(8.4\pm2.4)\times(10^{10}$—$10^{11})$ cm^6 mol^{-2} s^{-1}, which is 3 to 4 powers of 10 larger than our value extrapolated to 300 K. In a general discussion of Schiff's paper, Gardiner[10] remarked that the absolute intensity measurement for the chemiluminescence of OH* in the shock heated H_2-O_2 reaction done in his laboratory gave the bimolecular rate constant of 1.0×10^{-18} cm^3 molecule^{-1} s^{-1} at 1500 K. If the termolecular reaction is assumed, the figure is 3.3×10^{11} cm^6 mol^{-2} s^{-1}, which is about 10 times less than the value determined in this study. His value was derived by assuming only H_2O and O_2 to be the physical quenchers of OH*. If all of the quenchers are taken into account as was done in this study, his value should be compatible to the present value.

References

1) S. Ticktin, G. Spindler, and H. I. Schiff, *Discuss. Faraday Soc.*, **44**, 218 (1967).
2) M. G. Davis, W. K. McGregor, and A. A. Mason, *J. Chem. Phys.*, **61**, 1352 (1974).
3) D. Gutman, R. W. Lutz, N. F. Jacobs, E. A. Hardwidge, and G. L. Schott, *J. Chem. Phys.*, **48**, 5689 (1968).
4) W. C. Gardiner, Jr., K. Morinaga, D. L. Ripley, and T. Takeyama, *Phys. Fluids Supplement*, **I**, 120 (1969).
5) T. Koike and K. Morinaga, *Bull. Chem. Soc. Jpn.*, **49**, 1457 (1976).
6) G. Herzberg, "Molecular Spectra and Molecular Structure," D. Van Nostrand, N. J. (1967), Vol. 1.
7) G. H. Dieke and H. M. Crosswhite, "The Ultra Violet Bands of OH Fundamental Data," Bumblebee Series, The Johns Hopkins University (1948), Report No. 87; A. M. Bass and H. P. Broida, "Spectrophotometric Atlas of the $^2\Sigma^+$—$^2\Pi$ Transition of OH," N.B.S. Circ., (1953), No. 541.
8) K. R. German, *J. Chem. Rhys.*, **62**, 2584 (1975).
9) K. H. Becker, D. Haaks, and T. Tatarczyk, *Chem. Phys. Lett.*, **25**, 564 (1974).
10) W. C. Gardiner, *Discuss. Faraday Soc.*, **44**, 238 (1967).

 © 1982 The Chemical Society of Japan Bull. Chem. Soc. Jpn., 55, 55—58 (1982)

The Interaction of the Tris(2,2′-bipyridine)ruthenium(II) Ion with Poly(*p*-styrenesulfonate)

Yoshimi KURIMURA,* Hiroshi YOKOTA, Kiyotaka SHIGEHARA,† and Eishun TSUCHIDA†

Department of Chemistry, Ibaraki University, Mito, Ibaraki 310

† *Department of Polymer Chemistry, Waseda University, Shinjuku-ku, Tokyo 160*

(Received May 2, 1981)

The interactions of tris(2,2′-bipyridine)ruthenium(II)($[Ru(bpy)_3]^{2+}$) with some polyanions have been studied by means of cation-exchange resins and the luminescence of $[Ru(bpy)_3]^{2+}$. In an aqueous solution of $[Ru(bpy)_3]^{2+}$ in the presence of sodium poly(*p*-styrenesulfonate)(PSS), the adsorbability of $[Ru(bpy)_3]^{2+}$ on the cation-exchange resins is strongly suppressed by the binding of $[Ru(bpy)_3]^{2+}$ to the polyanion. The relative luminescence intensity of $[Ru(bpy)_3]^{2+}$ in an aqueous solution is enhanced by the addition of PSS. With the addition of sodium chloride to an $[Ru(bpy)_3]^{2+}$/PSS solution, the interaction is impeded by the shielding of the electrostatic potential in the polymer domains by the counter ions. A cooperative interaction between PSS and $[Ru(bpy)_3]^{2+}$ is postulated with a view to accounting for the results. A chemical application of the interaction is demonstrated.

The luminescence behavior of $[Ru(bpy)_3]^{2+}$ and its analogous compounds has been well studied using several experimental techniques.[1–8] Meisel and Matheson[9] suggested that the luminescence from the lowest excited state of $[Ru(bpy)_3]^{2+}$, $[*Ru(bpy)_3]^{2+}$, is efficiently quenched by low concentrations of Cu^{2+} ions when poly(vinyl sulfate)(PVS) is present in the solution. The quenching reaction occurs nearly exclusively in the PVS solution. The efficient quenching results from the Cu^{2+} and $[Ru(bpy)_3]^{2+}$ residing in the potential field of the same polymer. They demonstrated a possible utilization of this system in solar-energy conversion and storage systems. The effect of PVS on the luminescence spectrum of $[Ru(bpy)_3]^{2+}$ was also studied by Meisel and Matheson.[9] However, little change in the emission spectrum from $[*Ru(bpy)_3]^{2+}$ was seen when PVS was added to an aqueous solution. This fact indicates that PVS does not affect the energy level of $[*Ru(bpy)_3]^{2+}$ in an aqueous solution.[9]

The results of the luminescence study of $[Ru(bpy)_3]^{2+}$ in an aqueous solution of sodium dodecyl sulfate[3] show that the emission maximum shifts a little to a longer wavelength in a negatively charged micellar solution, although the emission intensity is nearly the same in both micellar solution and pure water. It has been suggested that the micellar effect on the emission spectrum is caused by the hydrocarbon chains and not by the charged sulfonato groups on the surfactant molecules.[10]

The effect of hydrophobic interaction between a polyion and a metal-complex ion has been little studied. In the present study, the interaction between PSS and $[Ru(bpy)_3]^{2+}$, both of which have hydrophobic and charged moieties, has been investigated by means of ion-exchange resins and the luminescence spectrum of $[Ru(bpy)_3]^{2+}$.

Experimental

Materials. Tris(2,2′-bipyridine)ruthenium(II) chloride hexahydrate, $[Ru(bpy)_3]Cl_2 \cdot 6H_2O$,[11] and tris(1,10-phenanthroline)cobalt(III) chloride octahydrate, $[Co(phen)_3]Cl_2 \cdot 8H_2O$,[12] were prepared and purified by the methods described elsewhere. The other inorganic reagents were of a reagent-grade purity and were used without further purification. $CuSO_4 \cdot 5H_2O$ was used for the preparation of the stock solution of Cu^{2+}. Poly(*p*-styrenesulfonic acid) was prepared by the radical polymerization of *p*-styrenesulfonic acid. Freshly distilled *p*-styrenesulfonic acid was used for the polymerization. *p*-Styrenesulfonic acid was dissolved in 50 cm^3 of dimethyl sulfoxide at a total concentration of 2 mol dm^{-3}. To the solution in a 100-cm^3 flask were added a 1.0×10^{-3} mol portion of azobisisobutyronitrile; the flask was shielded after three freeze-evacuation cycles, and then the mixture was kept at 60 °C for 5 h. The resulting polymer was collected by precipitation from diethyl ether. The white powder was dissolved in aqueous dilute hydroxide and dialyzed in water for 50 h. Sodium poly(*p*-styrene sulfonate), PSS, was obtained by the evaporation of the dialyzed solution under reduced pressure. The specific-viscosity number of the PSS in 0.1 mol dm^{-3} KCl solution was 0.51 dl g^{-1} at 25 °C. Sodium poly(vinyl sulfate)-(PVS)($\overline{M}n$ 2×10^5: $\overline{M}n$ is number-average molecular weight) was prepared by the established method.[13] Poly(acrylic acid)($\overline{M}n$ 4×10^5) and poly(methacrylic acid)($\overline{M}n$ 5×10^5) were prepared by the $K_2S_2O_8$–$Na_2S_2O_3$-initiated radical polymerization of acrylic acid and methacrylic acid, respectively, in water at 30 °C. Sodium salts of poly(acrylic acid)-(PAA) and poly(methacrylic acid)(PMA) were prepared by the dialysis of the corresponding poly acid in dilute hydroxide for 50 h. The dialyzed solutions were evaporated under reduced pressure. These poly acid salts were obtained as a white powder. The concentrations of the polyions are represented by those of the monomer units.

Column-exchange Chromatography. A 2-cm^3 portion of aqueous polyelectrolyte or benzenesulfonate, BS, if necessary, sodium chloride were poured onto a water-jacketed column of cation-exchange resins (Dowex 50 W X-8, 100—200 mesh, the H form, 1 cm × 5 cm); then, an aliquot of water was passed through the column with 0.8 cm^3 min^{-1} at 25 °C. The concentrations of $[Ru(bpy)_3]^{2+}$ and $[Co(phen)_3]^{2+}$ were determined spectrophotometrically using a Hitachi Model 320 spectrophotometer, while that of Cu^{2+} was determined by means of the atomic absorption spectra using a Hitachi Model 170-40 atomic absorption spectrometer.

Luminescence Study. Oxygen was removed from the sample solutions by bubbling a nitrogen gas which had been purified by passing it through an acidic solution of

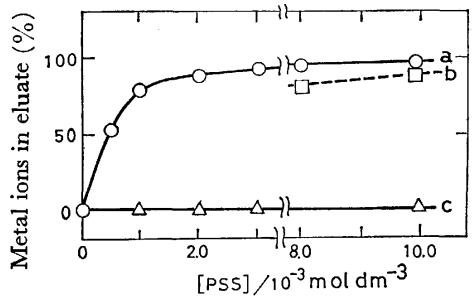

Fig. 1. Plots of the percentage of the metal ions in eluant *vs.* concentration of PSS in aqueous solution at 25 °C.
a: 1.0×10^{-4} mol dm^{-3} $[Ru(bpy)_3]^{2+}$, b: 1.0×10^{-4} mol dm^{-3} $[Co(phen)_3]^{2+}$, c: 1.0×10^{-4} mol dm^{-3} Cu^{2+}.

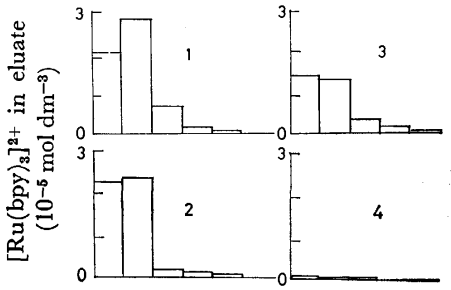

Fig. 2. Cation-exchange column chromatograms of 1.0×10^{-4} mol dm^{-3} $[Ru(bpy)_3]^{2+}$/3.0×10^{-3} mol dm^{-3} PSS/NaCl at 25 °C.
[NaCl]/mol dm^{-3}: 1; 0, 2; 1.0×10^{-4}, 3; 1.0×10^{-3}, 4; 1.0×10^{-2}.

chromium(II) sulfate for 30 min. Luminescence measurements were made in a 1 cm × 1 cm quartz cell on a Shimadzu RF-500 spectrofluorometer. The temperatures of the samples were adjusted at 25±0.1 °C by means of a thermostated cell holder. The excitation wavelength for $[Ru(bpy)_3]^{2+}$ was 455 nm. A PRA Model 3000-nanosecond fluorometer was used for the determination of the excited state lifetime of $[Ru(bpy)_3]^{2+}$.

Results and Discussion

Studies of the Effect of Polyions by Means of Ion-exchange Resins. The complex cation of $[Ru(bpy)_3]^{2+}$ and $[Co(phen)_3]^{2+}$ and the aquacopper(II) ion, Cu^{2+}, are strongly adsorbed on the cation-exchange resins. The adsorbed $[Ru(bpy)_3]^{2+}$ and $[Co(phen)_3]^{2+}$ ions were hardly eluted with water, dil HCl, and dil NaCl solutions. With the addition of PSS to an aqueous solution of $[Ru(bpy)_3]^{2+}$, however, some interesting effects upon the adsorbability of the metal ions were observed.

In $[Ru(bpy)_3]^{2+}$/PSS, a part or all of the $[Ru(bpy)_3]^{2+}$ passes through the column of the cation-exchange resins: the amount of the adsorbed $[Ru(bpy)_3]^{2+}$ is dependent on the PSS concentration, as is shown in Fig. 1. In the lower concentration region of PSS, the ratio of the amounts of $[Ru(bpy)_3]^{2+}$ in the eluate to the total amounts of $[Ru(bpy)_3]^{2+}$ in the initial solution increased with the increase in the PSS concentration. In the presence of a large amount of PSS (*ca.* 0.1 mol dm^{-3}) in the original solution, the $[Ru(bpy)_3]^{2+}$ ions were completely passed through the column.

In the $[Ru(bpy)_3]^{2+}$/PSS/NaCl systems, the total amount of $[Ru(bpy)_3]^{2+}$ in the eluate decreased with the increase in the NaCl concentration (Figs. 2 and 3). On the other hand, the adsorbability of $[Ru(bpy)_3]^{2+}$ on the resins was unaffected in the presence of a large amount of polyanions, such as PVS, PMA, and PAA and the monomer analogue such as benzenesulfonate.

A similar effect was observed in the $[Co(phen)_3]^{2+}$/PSS system (Fig. 1b). Unfortunately, the precipitate was formed by the addition of PSS to the $[Co(phen)_3]^{2+}$ solution when the PSS concentration was lower than about 6×10^{-3} mol dm^{-3}. The adsorbability of Cu^{2+} on the resins was, however, unaffected in the presence of PSS (Fig. 1c).

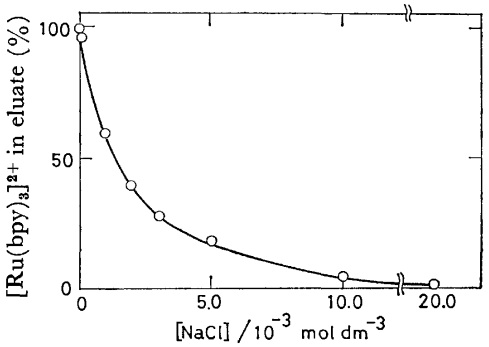

Fig. 3. Plots of the ratio of $[Ru(bpy)_3]^{2+}$ in eluate *vs.* concentration of NaCl at 25 °C.
$[Ru(bpy)_3^{2+}]=1.0\times10^{-4}$ mol dm^{-3}, $[PSS]=3.0\times10^{-3}$ mol dm^{-3}.

The decrease in the adsorbabilities of $[Ru(bpy)_3]^{2+}$ and $[Co(phen)_3]^{2+}$ on the cation-exchange resins on the addition of PSS seems to indicate that the attractive interactions between PSS and $[Ru(bpy)_3]^{2+}$ or $[Co(phen)_3]^{2+}$ are sufficiently large to prevent the cation-exchange reaction between the hydrogen ions on the resins and the metal-complex ions in the solution. In the $[Ru(bpy)_3]^{2+}$/PSS and $[Co(phen)_3]^{2+}$/PSS systems, it is considered that the hydrophobic interaction between the complex ion and the polyanion contributes to the adsorbabilities of the metal-complex ions on the resins since few changes in the adsorbabilities of $[Ru(bpy)_3]^{2+}$ and $[Co(phen)_3]^{2+}$ were observed in the presence of PVS, PAA, PMA, or BS. It may be concluded that a strong interaction between $[Ru(bpy)_3]^{2+}$ and PVS, PAA, PMA, or BS would not occur, since these polyelectrolytes have no hydrophobic moieties such as a phenyl ring on the polymer chains. Intimate multi-site bindings between the pendant phenyl rings, which are bound to the polymer backbone with a high density, and the metal-complex ion may be necessary for such a strong interaction, as has been seen in the cases of the $[Ru(bpy)_3]^{2+}$/PSS and $[Co(phen)_3]^{2+}$/PSS systems, since no change in the adsorbability was observed in the $[Ru(bpy)_3]^{2+}$/BS and $[Co(phen)_3]^{2+}$/BS systems.

The results seem to indicate that the $[Ru(bpy)_3]^{2+}$ and $[Co(phen)_3]^{2+}$ ions are concentrated in the polymer domains as a result of the electrostatic attraction,

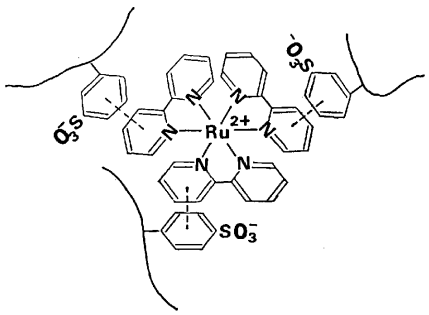

Fig. 4. Proposed structure of PSS bound $[Ru(bpy)_3]^{2+}$ by cooperative interaction.

and that, furthermore, the complex ions are bound tightly to the pendant phenyl groups of PSS by the hydrophobic interaction. The bipyridine rings of $[Ru(bpy)_3]^{2+}$ and the phenanthroline rings of $[Co(phen)_3]^{2+}$ would form intimate bindings to the pendant phenyl groups of PSS by means of hydrophobic interaction with the aid of the electrostatic force. A schematic representation of such coopertive interaction is postulated in Fig. 4. The molecular motion of the complex ions in the domains would be fairly much restricted by such interaction, and hardly none of the complex ions tightly bound to the polyanion chains should be adsorbed on the cation-exchange resins.

In the $[Ru(bpy)_3]^{2+}$/PSS/NaCl system the increase in the adsorbability of $[Ru(bpy)_3]^{2+}$ on the resins with the addition of NaCl can be explained by the fact that the $[Ru(bpy)_3]^{2+}$ ions are successively excluded from the polymer domains with increase in the concentration of the simple salt. The shielding of the potential field of the polyion domains by the counter ions reduces the electrostatic attraction for the complex ions. In the higher concentration region of NaCl, $[Ru(bpy)_3]^{2+}$ in the domains would be completely excluded from the domains. Thus, the $[Ru(bpy)_3]^{2+}$ ions are well adsorbed on the resins.

Effect of PSS on the Luminescence of $[Ru(bpy)_3]^{2+}$. The luminescence spectrum from $[*Ru(bpy)_3]^{2+}$ in an aqueous solution was greatly affected in the presence of PSS: the luminescence intensity at the luminescence maximum increased with the increase in the concentration of PSS (Figs. 5 and 6), while the absorption band in the visible region was not affected. A little change in the luminescence maximum is seen in the presence of PSS (Fig. 5): the luminescence peak of $[Ru(bpy)_3]^{2+}$ in the presence of 4.0×10^{-4} mol dm^{-3} PSS shifts to a wavelength longer by about 4 nm than that in the absence of PSS.

The variation in the relative luminescence intensity with the concentration of the polyion is given in Fig. 6. In the concentration region of PSS lower than about 2×10^{-4} mol dm^{-3}, where $[PSS]/[Ru(bpy)_3]^{2+}<10$, the relative intensity increases sharply on the addition of the polyion. However, no noticeable change in the CTTL and luminescence bands was observed in the presence of a large amount of PAA, PMA, or BS. Similar results have been reported in the luminescence study of $[Ru(bpy)_3]^{2+}$ in an aqueous PVS solution.[2] These facts seem to indicate that

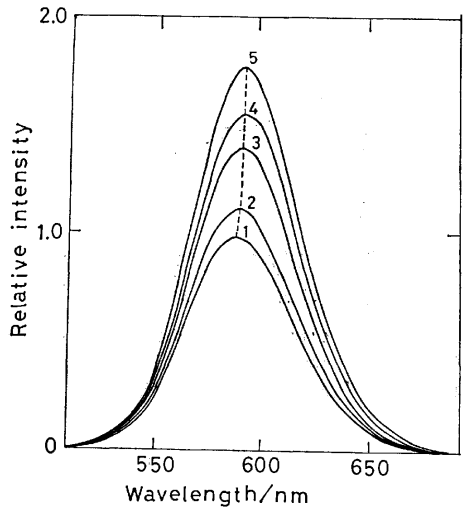

Fig. 5. Luminescence spectra of $[Ru(bpy)_3]^{2+}$ in PSS solution at 25 °C.
$[Ru(bpy)_3^{2+}]=2.0\times10^{-5}$ mol dm^{-3}, [PSS]/mol dm^{-3}: 1; 0, 2; 2.5×10^{-5}, 3; 5.0×10^{-5}, 4; 1.0×10^{-4}, 5; 4.0×10^{-4}.

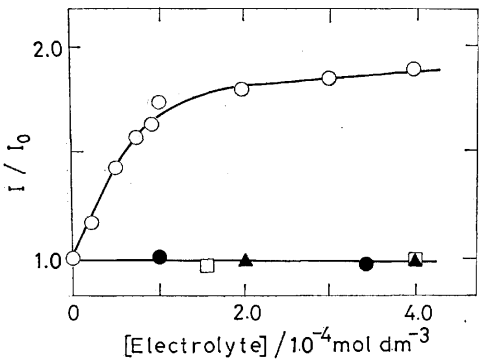

Fig. 6. Dependence of the luminescence intensity on the concentration of electrolyte at 25 °C.
$[Ru(bpy)_3^{2+}]=2.0\times10^{-5}$ mol dm^{-3}, ○: PSS, ●: BS, ▲: PAA, □: PMA.

such electrolytes as PAA, PMA, and BS do not affect the energy levels of $[Ru(bpy)_3]^{2+}$ and that no quenching or quenching reversal of the luminescence by these electrolytes occurs. These facts also suggest that the luminescence spectrum of $[Ru(bpy)_3]^{2+}$ is little affected by binding to the polyanions attributable to only the electrostatic force.

The dependence of the luminescence intensity on the concentration of urea in $[Ru(bpy)_3]^{2+}$/PSS is shown in Fig. 7. The luminescence intensity decreases with an increase in the concentration of urea. This may be due to the reduction of the hydrophobic interaction by the addition of urea. It may be concluded from the results that the enhancement of the luminescence intensity is brought about as a result of a cooperative interaction, which is also suggested by the results of the column-exchange chromatography. An intimate site binding due to the hydrophobic interaction would cause a sharp increase in the luminescence intensity upon the addition of PSS, presumably as a result of the restriction of the molecular motion of the $[Ru(bpy)_3]^{2+}$ bound to the polymer chains.

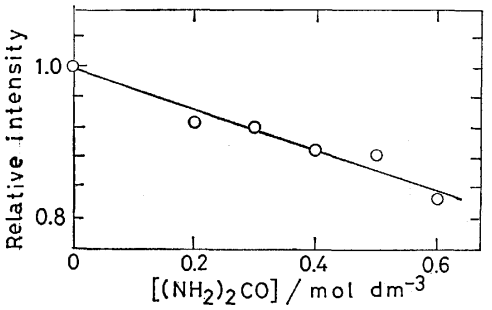

Fig. 7. Effect of urea on the luminescence intensity of $[Ru(bpy)_3]^{2+}$ in aqueous PSS solution at 25 °C. $[Ru(bpy)_3^{2+}]=2.0\times10^{-5}$ mol dm^{-3}, $[PSS]=2.0\times10^{-4}$ mol dm^{-3}.

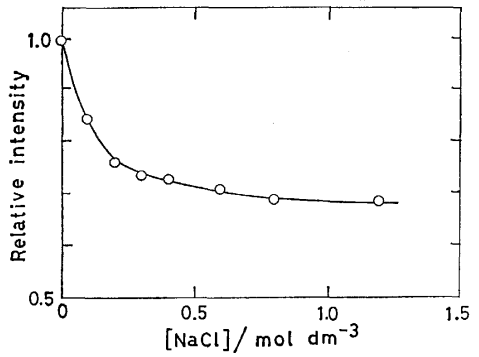

Fig. 8. Effect of sodium chloride on the luminescence intensity of $[Ru(bpy)_3]^{2+}$ in aqueous solutions at 25 °C. $[Ru(bpy)_3^{2+}]=2.0\times10^{-5}$ mol dm^{-3}, $[PSS]=2.0\times10^{-4}$ mol dm^{-3}.

Consequently, the lifetime of the lowest excited state of $[Ru(bpy)_3]^{2+}$ in the presence of 2.0×10^{-4} mol dm^{-3} PSS was longer than that in the absence of PSS: the excited-state lifetime in the presence and absence of PSS were 590±4 nsec and 450±2 nsec respectively at 28 °C.

The effect of sodium chloride on the luminescence of $[Ru(bpy)_3]^{2+}$ in an aqueous PSS solution is shown in Fig. 8. This figure shows that the luminescence intensity decreases with an increase in the salt concentration. Na^+ ions start to displace the $[Ru(bpy)_3]^{2+}$ out of the polymer domains in the higher-concentration region of sodium chloride: therefore, the luminescence intensity should be decreased with the concentration of the salt.

Application of the Cooperative Effect. In an aqueous solution of $[Ru(bpy)_3]^{2+}$ containing an excess of PSS, the $[Ru(bpy)_3]^{2+}$ ions bound to PSS should be hardly replaced by the hydrogen ions. Then, a simple application of the cooperative effect, *e.g.*, the separation of $[Ru(bpy)_3]^{2+}$ from Cu^{2+}, was tested by means of ion-exchange chromatography. To a 2-cm^3 portion of an aqueous solution containing 5.0×10^{-4} mol dm^{-3} $[Ru(bpy)_3]^{2+}$ and 5.0×10^{-4} mol dm^{-3} Cu^{2+} were added 2.0 cm^3 of 5.0×10^{-2} mol dm^{-3} PSS. The solution was poured into the column of the cation-exchange resins. Then, a 100-cm^3 portion of water was passed through the column. The Cu^{2+} ions were completely adsorbed on the resins, whereas more than 99.3% of all the $[Ru(bpy)_3]^{2+}$ ions passed through the column. The adsorbed Cu^{2+} ions could be eluted with dilute hydrochloric acid; more than 99% of the Cu^{2+} ions were recovered with 50 ml of 6 M HCl.

It is considered that the polymer domains with high local densities of negatively charged groups and the hydrophobic groups can usefully be employed as a reaction field in which the complex cations with a hydrophobic nature are concentrated and tightly bound to the polymer chains.

The authers wish to thank Dr. Akira Yamada and Dr. Masao Kaneko for their helpful discussion. The authers also indebted to Mr. Kiyomi Takato for assistance with some of the quenching studies and Mr. Yoshihiro Yamaguchi for the measurements of the lifetimes at Daini Seikosha Co.

References

1) F. Bolleta, M. Maestri, and V. Balzani, *J. Phys. Chem.*, **80**, 2499 (1976).
2) F. E. Lytle and M. Hercules, *J. Am. Chem. Soc.*, **91**, 253 (1969).
3) G. D. Hager and G. A. Crosby, *J. Am. Chem. Soc.*, **97**, 7031 (1975).
4) G. D. Hager, R. J. Watts, and G. A. Crosby, *J. Am. Chem. Soc.*, **97**, 7037 (1975).
5) J. N. Dames and J. W. Addington, *J. Am. Chem. Soc.*, **98**, 5800 (1976).
6) I. Fujita and H. Kobayashi, *J. Chem. Phys.*, **59**, 2902 (1973).
7) K. W. Hipps and G. A. Crosby, *J. Am. Chem. Soc.*, **97**, 7042 (1975).
8) J. Van Houten and R. J. Watts, *J. Am. Chem. Soc.*, **98**, 4853 (1976).
9) D. Meisel and M. S. Matheson, *J. Am. Chem. Soc.*, **99**, 6577 (1977).
10) D. Meisel, M. S. Matheson, and J. Rabani, *J. Am. Chem. Soc.*, **100**, 117 (1978).
11) R. A. Palmer and T. S. Piper, *Inorg. Chem.*, **5**, 864 (1966).
12) K. Yamazaki, *Bull. Chem. Soc. Jpn.*, **13**, 390 (1937).
13) D. Breslow and A. Kunter, *J. Polym Sci.*, **A 1, 7**, 295 (1958).

 © 1982 The Chemical Society of Japan Bull. Chem. Soc. Jpn., 55, 59—62 (1982)

The Crystal and Molecular Structure of Pikromycin

Akio Furusaki,* Takeshi Matsumoto, Kimio Furuhata,† and Haruo Ogura†

Department of Chemistry, Faculty of Science, Hokkaido University, Kita-ku, Sapporo 060

† *School of Pharmaceutical Sciences, Kitasato University, Shirokane, Minato-ku, Tokyo 108*

(Received May 19, 1981)

The detailed molecular geometry of pikromycin ($C_{28}H_{47}NO_8$) has been examined by means of X-ray crystal analysis. The crystals are orthorhombic, with four molecules in a unit cell with dimensions of $a=11.295$, $b=25.734$, and $c=10.509$ Å; the space group is $P2_12_12_1$. 2259 unique intensity data were collected on a four-circle diffractometer with graphite-monochromated Cu $K\alpha$ radiation. The structure was solved by the Monte Carlo direct method, using the 30 strongest reflections as the starting set; the 215th random phase set led to the correct solution. The R value reached 0.056 by block-diagonal least-squares refinements. The conformation of the fourteen-membered macrolide ring is considerably different from that of (*p*-bromobenzoyl)pikromycin in the solid state; *e.g.*, the C=C and C=O conjugated double bonds are cisoid in pikromycin, while they are transoid in the derivative. The molecules are held together through two kinds of intermolecular hydrogen bonds, forming a three-dimensional hydrogen-bonded structure.

Pikromycin (**1a**) is an antibiotic isolated from *Streptomyces flavochromogenese*, and is active against gram-positive bacteria.[1] The structure of **1a** was determined as **1b** by chemical and spectroscopic studies,[2] and by an X-ray study of kromycin.[3] An X-ray analysis of (*p*-bromobenzoyl)pikromycin (**2**) further revealed that the conformation of the fourteen-membered macrolide ring resembles the "diamond" conformation model (diamond model D) shown in Fig. 1.[4] It was later suggested from NMR and CD experiments that the macro-ring conformation of **1a** in the solid state might differ from this conformation of **2**.[5] Therefore, in order to obtain exact and detailed information about the molecular conformation of **1a** itself, we have now undertaken an X-ray crystal analysis.

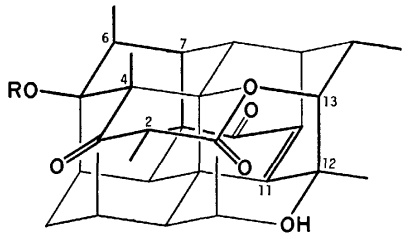

Fig. 1. Diamond model D applied to (*p*-bromobenzoyl)-pikromycin. The thick lines denote the bonds in the molecule.

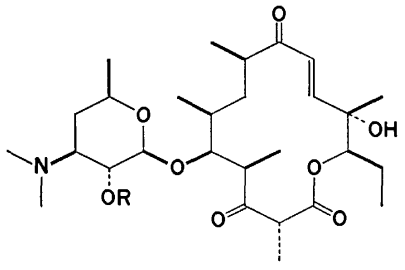

1b: R = H

2: R = p-BrC$_6$H$_4$CO

Experimental

Colorless single crystals of **1a** were grown from a methanol solution. The sample used for the X-ray measurement had dimensions of about $0.2\times0.2\times0.4$ mm^3. The crystal data are summarized in Table 1. The cell dimensions and diffraction intensities were measured on a Rigaku automatic, four-circle diffractometer with graphite-monochromated Cu $K\alpha$ radiation ($\lambda=1.5418$ Å). The θ-2θ continuous-scan technique was applied at a θ scan rate of 2° min^{-1}; the background was measured for 10 s at each end of the scan range. Three standard reflections, measured at intervals of every 50 reflections, showed no significant decrease in intensity during the course of data collection. The intensities were corrected for the Lorentz and polarization factors, but not for the absorption or the extinction effect. In the range of 2θ values up to 125°, 2259 independent structure factors above the $\sigma(F)$ level were selected for the structure determination.

Structure Determination

Since it had already been reported that an attempt to solve the present structure with the MULTAN program[6] had been unsuccessful,[4] we tried the Monte Carlo direct method.[7] The 30 strongest reflections were chosen as the starting set. In order to extend the tentative-phase set derived from random numbers, 15 cycles of the tangent procedure were performed using 520 $|E|$ values above 1.30. As the 215th phase set showed a low R_K value of 0.297 ($R_K=\Sigma||E_o|-k|E_c||/\Sigma|E_o|$), 6 additional cycles of the tangent procedure were carried out using 617 $|E|$ values above 1.20; the R_K value thereupon dropped to 0.280. An E-map based on 586 phases revealed the locations of all the 37 non-hydrogen atoms.

The structure thus obtained was refined by the block-diagonal least-squares method with anisotropic

Table 1. The crystal data

$C_{28}H_{47}NO_8$	Mol wt 525.68
Crystal system	Orthorhombic
Space group	$P2_12_12_1$
Cell dimensions	$a=11.295(1)$ Å
	$b=25.734(3)$ Å
	$c=10.509(1)$ Å
V	3054.6 Å^3
Z	4
D_c	1.143 g cm^{-3}
μ(Cu $K\alpha$)	6.41 cm^{-1}

Table 2. The final atomic parameters and estimated standard deviations
The atomic coordinates are multiplied by 10^4.

Atom	x	y	z	B_{eq}[a)]/Å^2	Atom	x	y	z	B_{eq}[a)]/Å^2
O(1)	2395 (2)	2282 (1)	3195 (2)	3.13	C(11)	2747 (4)	1845 (1)	5718 (4)	3.36
O(2)	4152 (2)	2623 (1)	3717 (3)	4.93	C(12)	2207 (3)	1553 (1)	4613 (4)	3.01
O(3)	3464 (2)	3859 (1)	4186 (3)	3.97	C(13)	2780 (3)	1745 (1)	3376 (4)	2.89
O(4)	668 (2)	4056 (1)	6659 (2)	2.95	C(14)	2399 (4)	1459 (1)	2165 (4)	3.52
O(5)	3914 (3)	2288 (1)	7802 (3)	6.64	C(15)	3276 (4)	1553 (2)	1067 (5)	5.08
O(6)	2605 (2)	1021 (1)	4734 (2)	3.62	C(16)	3285 (5)	3392 (2)	1791 (4)	6.33
O(7)	907 (2)	4401 (1)	8643 (3)	3.50	C(17)	644 (4)	3954 (2)	4015 (4)	4.07
O(8)	−867 (3)	4869 (1)	5954 (3)	4.97	C(18)	3347 (4)	3824 (2)	7875 (4)	4.51
N	−1903 (3)	5485 (1)	8041 (3)	3.37	C(19)	1237 (5)	2439 (2)	9231 (4)	5.85
C(1)	3162 (4)	2669 (1)	3354 (4)	3.13	C(20)	874 (4)	1575 (2)	4577 (4)	4.19
C(2)	2574 (4)	3183 (1)	2953 (4)	3.19	C(21)	652 (3)	4525 (1)	7335 (4)	2.79
C(3)	2615 (4)	3577 (1)	4033 (4)	2.89	C(22)	−599 (4)	4744 (1)	7231 (4)	3.22
C(4)	1505 (3)	3636 (1)	4843 (4)	2.63	C(23)	−714 (4)	5236 (1)	8045 (4)	2.88
C(5)	1785 (3)	3898 (1)	6113 (4)	2.96	C(24)	−349 (4)	5093 (2)	9416 (4)	3.56
C(6)	2485 (4)	3525 (1)	7012 (4)	3.47	C(25)	881 (4)	4857 (1)	9434 (4)	3.74
C(7)	1613 (4)	3192 (2)	7788 (4)	3.71	C(26)	1227 (5)	4669 (2)	10758 (4)	6.08
C(8)	2179 (4)	2735 (2)	8508 (4)	3.87	C(27)	−2887 (4)	5117 (2)	8086 (4)	4.60
C(9)	2867 (4)	2380 (2)	7635 (4)	4.48	C(28)	−2043 (4)	5850 (2)	6975 (4)	5.39
C(10)	2211 (4)	2137 (1)	6542 (4)	3.68					

a) $B_{eq}=8\pi^2(u_1^2+u_2^2+u_3^2)/3$, where u_i is the root-mean-square deviation in the ith principal axis of the thermal ellipsoid.

temperature factors. After all the 47 hydrogen atoms had been located in a difference Fourier map, further least-squares refinements were repeated including the hydrogen atoms with isotropic temperature factors. In this refinement, the following weighting scheme was used:

$$w = 1/\{\sigma(F)^2 \exp(AX^2+BY^2+CXY+DX+EY)\},$$

where $X=|F_o|$ and $Y=\sin\theta/\lambda$. The A, B, C, D, and E coefficients are constants which were determined from the $(\Delta F)^2$ values; $A=0.3052\times10^{-4}$, $B=-5.563$, $C=0.04688$, $D=-0.01148$, and $E=2.250$. The final R value was 0.056. The final atomic parameters are listed in Table 2. The tables of the anisotropic thermal parameters and hydrogen parameters, and the F_o-F_c table are kept at the Chemical Society of Japan (Document No. 8204).

The calculations were done on a HITAC M-200H computer at the Hokkaido University Computing Center, using our own programs. The atomic scattering factors were taken from the International Tables.[8)]

Results and Discussion

Molecular Structure. The molecular skeleton of **1a** obtained is illustrated in Fig. 2; it corresponds exactly to the **1b** structure. The bond distances and angles and the torsion angles are given in Tables 3 and 4 respectively.

As will be seen from Figs. 1 and 2, the macro-ring conformation of **1a** is considerably different from that of **2**; *e.g.*, very great differences of 159, 143, and 176° can be seen for the torsion angles about the C(5)–C(6), C(8)–C(9), and C(9)–C(10) bonds respectively. Of these, the difference for the last bond corresponds

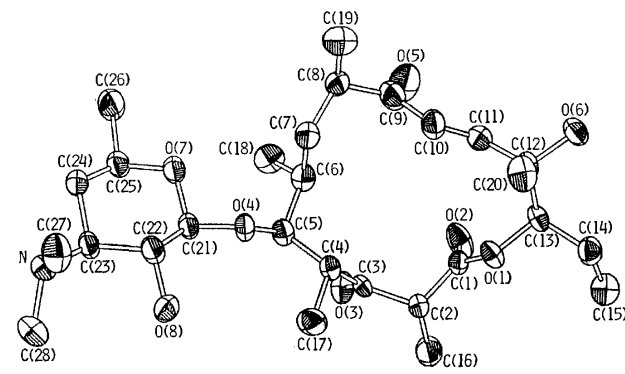

Fig. 2. A perspective view of the pikromycin molecule. Each non-hydrogen atom is represented as a thermal ellipsoid enclosing a 50% probability.

to the fact that, while the C(10)=C(11) and C(9)=O(5) conjugated double bonds are transoid for **2**, they are cisoid for **1a**. Notwithstanding the incorporation in the macrolide ring, the ester part keeps the geometry characteristic of secondary alcohol esters, *i.e.*, the synperiplanar configuration of the C(13)–O(1)–C(1)–O(2) part and the eclipsed conformation of the H–C(13)–O(1)–C(1) part.

When the macro ring is viewed along the normal of its mean plane, it looks like a somewhat-deformed right trapezoid with the four corners at the C(2), C(5), C(8), and C(12) atoms (see Fig. 2). For the cisoid configuration of the C(10)=C(11) and C(9)=O(5) bonds, the C(8)–C(9)–C(10)–C(11)–C(12) zigzag chain can form one side of such a polygon. Since the torsion angles about the C(4)–C(5), C(5)–C(6), C(7)–C(8), and C(8)–C(9) bonds do not much deviate from −60°, the C(5)–C(6)–C(7)–C(8) side makes nearly right angles with the C(2)–C(3)–C(4)–C(5) and

TABLE 3. THE BOND DISTANCES (l/Å) AND ANGLES (ϕ/°), WITH THEIR STANDARD DEVIATIONS
The standard deviations given in parentheses refer to the last decimal position.

C(1)-C(2)	1.541(5)	C(23)-N	1.488(5)	C(10)-C(11)-C(12)	127.8(4)
C(1)-O(1)	1.328(4)	C(24)-C(25)	1.517(6)	C(11)-C(12)-C(13)	108.7(3)
C(1)-O(2)	1.187(5)	C(25)-C(26)	1.525(6)	C(11)-C(12)-C(20)	113.8(3)
C(2)-C(3)	1.522(5)	C(25)-O(7)	1.437(5)	C(11)-C(12)-O(6)	106.1(3)
C(2)-C(16)	1.558(6)	C(27)-N	1.460(5)	C(13)-C(12)-C(20)	112.8(3)
C(3)-C(4)	1.523(5)	C(28)-N	1.472(5)	C(13)-C(12)-O(6)	104.3(3)
C(3)-O(3)	1.212(5)	C(2)-C(1)-O(1)	109.2(3)	C(20)-C(12)-O(6)	110.5(3)
C(4)-C(5)	1.529(5)	C(2)-C(1)-O(2)	125.3(3)	C(12)-C(13)-C(14)	115.5(3)
C(4)-C(17)	1.540(6)	O(1)-C(1)-O(2)	125.5(3)	C(12)-C(13)-O(1)	106.8(3)
C(5)-C(6)	1.562(5)	C(1)-C(2)-C(3)	110.9(3)	C(14)-C(13)-O(1)	105.3(3)
C(5)-O(4)	1.443(5)	C(1)-C(2)-C(16)	106.8(3)	C(13)-C(14)-C(15)	111.5(3)
C(6)-C(7)	1.540(6)	C(3)-C(2)-C(16)	109.8(3)	C(22)-C(21)-O(4)	107.1(3)
C(6)-C(18)	1.537(6)	C(2)-C(3)-C(4)	117.2(3)	C(22)-C(21)-O(7)	109.6(3)
C(7)-C(8)	1.537(6)	C(2)-C(3)-O(3)	121.3(4)	O(4)-C(21)-O(7)	106.9(3)
C(8)-C(9)	1.510(6)	C(4)-C(3)-O(3)	121.3(3)	C(21)-C(22)-C(23)	110.1(3)
C(8)-C(19)	1.514(6)	C(3)-C(4)-C(5)	111.2(3)	C(21)-C(22)-O(8)	110.5(3)
C(9)-C(10)	1.503(6)	C(3)-C(4)-C(17)	104.8(3)	C(23)-C(22)-O(8)	108.9(3)
C(9)-O(5)	1.219(5)	C(5)-C(4)-C(17)	112.9(3)	C(22)-C(23)-C(24)	107.5(3)
C(10)-C(11)	1.298(6)	C(4)-C(5)-C(6)	111.2(3)	C(22)-C(23)-N	115.4(3)
C(11)-C(12)	1.512(6)	C(4)-C(5)-O(4)	106.9(3)	C(24)-C(23)-N	110.2(3)
C(12)-C(13)	1.534(6)	C(6)-C(5)-O(4)	112.1(3)	C(23)-C(24)-C(25)	110.6(3)
C(12)-C(20)	1.507(6)	C(5)-C(6)-C(7)	109.8(3)	C(24)-C(25)-C(26)	111.9(4)
C(12)-O(6)	1.445(4)	C(5)-C(6)-C(18)	111.8(3)	C(24)-C(25)-O(7)	109.8(3)
C(13)-C(14)	1.531(6)	C(7)-C(6)-C(18)	111.8(3)	C(26)-C(25)-O(7)	105.3(3)
C(13)-O(1)	1.463(4)	C(6)-C(7)-C(8)	114.9(4)	C(1)-O(1)-C(13)	119.9(3)
C(14)-C(15)	1.540(6)	C(7)-C(8)-C(9)	112.2(3)	C(5)-O(4)-C(21)	117.1(3)
C(21)-C(22)	1.525(5)	C(7)-C(8)-C(19)	109.9(4)	C(21)-O(7)-C(25)	111.5(3)
C(21)-O(4)	1.401(4)	C(9)-C(8)-C(19)	111.3(3)	C(23)-N-C(27)	114.2(3)
C(21)-O(7)	1.440(5)	C(8)-C(9)-C(10)	117.5(4)	C(23)-N-C(28)	111.9(3)
C(22)-C(23)	1.534(5)	C(8)-C(9)-O(5)	122.0(4)	C(27)-N-C(28)	110.9(3)
C(22)-O(8)	1.413(5)	C(10)-C(9)-O(5)	120.5(4)		
C(23)-C(24)	1.543(6)	C(9)-C(10)-C(11)	121.4(4)		

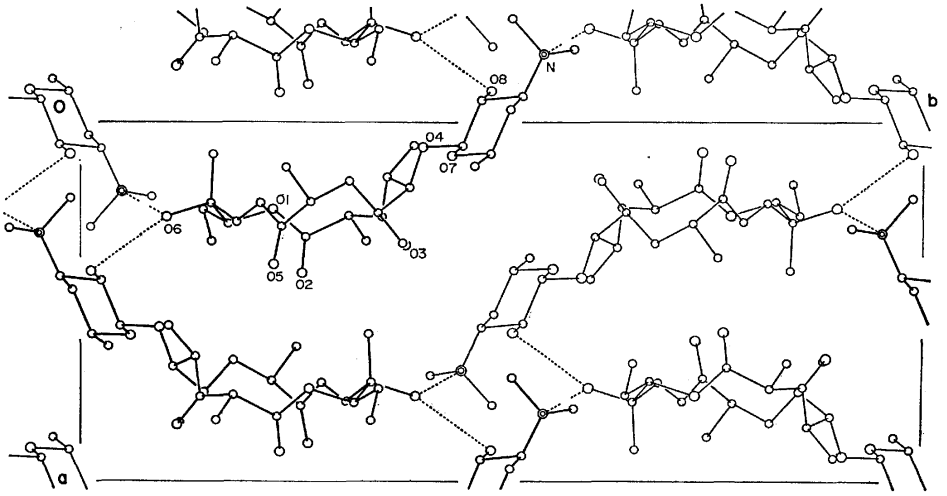

Fig. 3. The crystal structure viewed along the c axis.

C(8)–C(9)–C(10)–C(11)–C(12) sides; consequently, the latter two are nearly parallel. Because of the existence of the ester group having the special geometry mentioned above, the C(12)–C(13)–O(1)–C(1)–C(2) side deviates considerably from a straight line. The reason why the present macro ring does not take a rectangular form is probably that the planar ester part would occupy exactly one corner of the rectangle as long as the C(10)=C(11) and C(9)=O(5) bonds maintain the cisoid configuration.

The C(1)=O(2), C(3)=O(3), and C(9)=O(5) carbonyl groups protrude from the mean plane of the

Table 4. The torsion angles (ϕ/°)

O(1)-C(1)-C(2)-C(3)	124.1	C(10)-C(11)-C(12)-C(13)	120.4
O(1)-C(1)-C(2)-C(16)	−116.3	C(10)-C(11)-C(12)-C(20)	−6.2
O(2)-C(1)-C(2)-C(3)	−57.6	C(10)-C(11)-C(12)-O(6)	−127.9
O(2)-C(1)-C(2)-C(16)	62.0	C(11)-C(12)-C(13)-C(14)	175.6
C(2)-C(1)-O(1)-C(13)	173.3	C(11)-C(12)-C(13)-O(1)	−67.7
O(2)-C(1)-O(1)-C(13)	−5.0	C(20)-C(12)-C(13)-C(14)	−57.3
C(1)-C(2)-C(3)-C(4)	−98.6	C(20)-C(12)-C(13)-O(1)	59.5
C(1)-C(2)-C(3)-O(3)	86.5	O(6)-C(12)-C(13)-C(14)	62.7
C(16)-C(2)-C(3)-C(4)	143.7	O(6)-C(12)-C(13)-O(1)	179.4
C(16)-C(2)-C(3)-O(3)	−31.3	C(12)-C(13)-C(14)-C(15)	−162.2
C(2)-C(3)-C(4)-C(5)	161.4	O(1)-C(13)-C(14)-C(15)	80.3
C(2)-C(3)-C(4)-C(17)	−76.3	C(12)-C(13)-O(1)-C(1)	108.7
O(3)-C(3)-C(4)-C(5)	−23.6	C(14)-C(13)-O(1)-C(1)	−128.0
O(3)-C(3)-C(4)-C(17)	98.6	O(4)-C(21)-C(22)-C(23)	175.2
C(3)-C(4)-C(5)-C(6)	−71.9	O(4)-C(21)-C(22)-O(8)	−64.4
C(3)-C(4)-C(5)-O(4)	165.5	O(7)-C(21)-C(22)-C(23)	59.6
C(17)-C(4)-C(5)-C(6)	170.6	O(7)-C(21)-C(22)-O(8)	179.9
C(17)-C(4)-C(5)-O(4)	48.1	C(22)-C(21)-O(4)-C(5)	151.9
C(4)-C(5)-C(6)-C(7)	−87.5	O(7)-C(21)-O(4)-C(5)	−90.6
C(4)-C(5)-C(6)-C(18)	147.9	C(22)-C(21)-O(7)-C(25)	−62.7
O(4)-C(5)-C(6)-C(7)	32.0	O(4)-C(21)-O(7)-C(25)	−178.5
O(4)-C(5)-C(6)-C(18)	−92.6	C(21)-C(22)-C(23)-C(24)	−55.6
C(4)-C(5)-O(4)-C(21)	−144.0	C(21)-C(22)-C(23)-N	−179.1
C(6)-C(5)-O(4)-C(21)	94.1	O(8)-C(22)-C(23)-C(24)	−176.9
C(5)-C(6)-C(7)-C(8)	168.3	O(8)-C(22)-C(23)-N	59.6
C(18)-C(6)-C(7)-C(8)	−67.1	C(22)-C(23)-C(24)-C(25)	55.4
C(6)-C(7)-C(8)-C(9)	−55.8	N-C(23)-C(24)-C(25)	−178.0
C(6)-C(7)-C(8)-C(19)	180.0	C(22)-C(23)-N-C(27)	40.3
C(7)-C(8)-C(9)-C(10)	−57.8	C(22)-C(23)-N-C(28)	−86.7
C(7)-C(8)-C(9)-O(5)	122.7	C(24)-C(23)-N-C(27)	−81.7
C(19)-C(8)-C(9)-C(10)	65.7	C(24)-C(23)-N-C(28)	151.2
C(19)-C(8)-C(9)-O(5)	−113.8	C(23)-C(24)-C(25)-C(26)	−175.2
C(8)-C(9)-C(10)-C(11)	177.2	C(23)-C(24)-C(25)-O(7)	−58.6
O(5)-C(9)-C(10)-C(11)	−3.3	C(24)-C(25)-O(7)-C(21)	62.2
C(9)-C(10)-C(11)-C(12)	176.7	C(26)-C(25)-O(7)-C(21)	−177.2

macro ring to the same side, while the C(20)H_3 methyl group is axially placed on the opposite side of this plane. Each of the remaining seven groups attached to the macro ring is equatorially or isoclinally oriented outside the macro ring. The pyranose ring in the D-desosamine moiety has a chair form; all the four atomic groups on this ring occupy the equatorial positions.

Crystal Structure. The molecular arrangement viewed along the c axis is shown in Fig. 3. The macro rings are nearly parallel to the (100) plane, and are arranged on the two-fold screw axis penetrating them approximately perpendicularly. The crystal contains two kinds of intermolecular hydrogen bonds, O(6)–H···N′ and O(8)–H···O(6″); the O···N and O···O distances are 2.829(4) and 2.958(4) Å respectively.** The molecules are connected by these hydrogen bonds, forming a three-dimensional hydrogen-bonded structure.

** The N′ and O(6″) positions are obtained from the N and O(6) coordinates by the symmetry operations, $(-x, -1/2+y, 3/2-z)$ and $(-1/2+x, 1/2-y, 1-z)$, respectively.

References

1) T. Hata, Y. Sano, H. Tatsuta, R. Sugawara, A. Matsumae, and K. Kanamori, *J. Antibiot., Ser. A*, **8**, 9 (1955).
2) R. W. Rickards, R. M. Smith, and J. Majer, *J. Chem. Soc., Chem. Commun.*, **1968**, 1049; H, Muxfeldt, S. Schrader, P. Hansen, and H. Brockmann, *J. Am. Chem. Soc.*, **90**, 4748 (1968).
3) R. E. Hughes, H. Muxfeldt, C. Tsai, and J. J. Stezowski, *J. Am. Chem. Soc.*, **92**, 5267 (1970); C. Tsai, J. J. Stezowski, and R. E. Hughes, *ibid.*, **93**, 7286 (1971).
4) K. Furuhata, H. Ogura, Y. Harada, and Y. Iitaka, *Chem. Pharm. Bull.*, **25**, 2385 (1977).
5) H. Ogura, K. Furuhata, H. Kuwano, and M. Suzuki, *Tetrahedron*, **37**, Suppl. No. 1, 165 (1981).
6) G. Germain, P. Main, and M. M. Woolfson, *Acta Crystallogr., Sect. A*, **27**, 368 (1971).
7) A. Furusaki, *Acta Crystallogr., Sect. A*, **35**, 220 (1979).
8) "International Tables for X-Ray Crystallography," The Kynoch Press, Birmingham (1974), Vol. IV.

Bifunctional Oxidation of Ammonia with Metal Oxide–Pt/Al_2O_3 Mechanical Mixtures

Yukio Kosaki,* Akira Miyamoto, and Yuichi Murakami

Department of Synthetic Chemistry, Faculty of Engineering, Nagoya University, Furo-cho, Chikusa-ku, Nagoya 464

(Received May 21, 1981)

Selectivity to N_2 in the reaction of NH_3 with metal oxides has been markedly increased by the addition of Pt/Al_2O_3 to the metal oxides, whereas the activity of the metal oxides has not been changed. The metal oxides on their own have oxidized NH_3 to NO, NO_2, and N_2O as well as N_2, and furthermore, the selectivities in the reaction with metal oxides have depended markedly on the reaction temperature and inlet concentration of NH_3 in the pulse. In the oxidation of NH_3 with metal oxide–Pt/Al_2O_3 mechanical mixtures, N_2 has been selectively produced irrespective of the reaction temperature and the inlet concentration of NH_3 in the pulse. The activity of the mixtures has been shown, on the other hand, to be the same as that of the metal oxides. All of the experimental data have been explained in terms of the following scheme: In the oxidation of NH_3 with metal oxide–Pt/Al_2O_3 mixtures, NH_3 is at first oxidized by metal oxides to form NO_x(NO, NO_2, and N_2O) and N_2, then the NO_x components is transfered through the gas phase from the metal oxides to Pt particles on Al_2O_3, and finally the NO_x components react with NH_3 on Pt particles to form N_2 selectively.

Attention is focused on reactions on multi-component solid catalysts, because of their interesting catalyses which cannot be obtained for reactions on individual components. Synergistic effects appearing in their catalyses provide an important subject of investigation in heterogeneous catalytic chemistry. In other words, it is highly desirable to find new types of synergistic effects for various kinds of multi-components' catalysts and various types of reactions, and to reveal their mechanisms. Much research has been done on the synergistic effects involved in the multi-components' metal oxide catalysts, multi-components' precious metal catalysts (or alloy catalysts), and supported precious metal–metal oxide mixed catalysts. Furthermore, it has been suggested that these synergistic effects are brought about by various mechanisms including (i) the dispersion of the primary component, (ii) the control of the oxidation state or the electronic state of the primary component, (iii) the formation of a new active site by the chemical interaction of individual components, and (iv) the cooperation of different kinds of active sites by the transfer of intermediate species or reactive species from one component to another through the gas phase, surface, or bulk.[1] However, the synergistic effects appearing in the reactions on precious metal–metal oxide mixed catalysts have been not well investigated except the bifunctional catalyses involved in the reactions of hydrocarbons on Pt/Al_2O_3,[2] Pt/SiO_2–Al_2O_3,[3] and Pt–WO_3[4] catalysts, and the oxidation of H_2 with precious metal–metal oxide mixtures.[5] The precious metal–metal oxide catalysts have received increasing attention as catalysts for the automotive exhaust gas control,[6–11] selective oxidations of hydrocarbons,[12,13] and steam reforming reactions.[14,15]

In the present study, the synergistic effect in the oxidation of NH_3 with metal oxide–Pt/Al_2O_3 mixed catalysts was investigated using the pulse reaction technique. The oxidation of NH_3 was used as a test reaction for the following reasons: (i) The selective oxidation of NH_3 to N_2 is highly desirable from the environmental point of view. (ii) Since the mechanism of the oxidation of NH_3 is markedly different from that of hydrocarbons or H_2,[16] the metal oxide–Pt/Al_2O_3 is expected to show interesting synergistic effects which are significantly different from those in the oxidations of hydrocarbons or H_2. The enhanced activity of metal oxide caused by the addition of precious metal is considered to be brought about by the "hydrogen spillover" for the oxidation of H_2,[5] and by the migration of oxygen through the oxide lattice to react with hydrocarbon or hydrocarbon residues adsorbed at sites on or near precious metal additives for the oxidation of hydrocarbons.[17] Metal oxide–Pt/Al_2O_3 mixed catalysts were used for the following reasons: (i) Pt is one of the least active metals for the decomposition of NH_3. This would make it possible to propose a detailed mechanism of the synergistic effect in the oxidation of NH_3. Although a mixture of a metal oxide and a precious metal such as Ru or Rh—highly active for the decomposition of NH_3[18]—may cause an interesting synergistic effect, this system would be too complex, as a first step of investigation, to reveal a detailed mechanism of the synergistic effect. (ii) For the metal oxide–Pt/Al_2O_3 mechanical mixtures, most of the Pt particles can be considered to be separated from the metal oxides by Al_2O_3. Therefore, the migration of oxygen from the metal oxide to Pt particles on Al_2O_3 is not expected to proceed rapidly. The hydrogen spillover from Pt to the metal oxide, on the other hand, can proceed readily in the mixtures.[5] Pulse reaction technique was used for the following reasons: (i) It is considered that this technique is effective for the investigation of the behaviour of reactions on multi-components' catalysts. (ii) Since catalytic oxidations usually proceed by the redox mechanism, the stoichiometric oxidation of the reactant with the preoxidized catalyst often gives important information about their mechanisms. The stoichiometric reaction—in this study, the oxidation of NH_3 with the metal oxide–Pt/Al_2O_3 mixed catalysts—can be more easily investigated using the pulse reaction technique than using the flow reaction technique.

Experimental

Catalysts and Reagents. The method of preparation of metal oxides has been described previously.[16] Pt/Al_2O_3

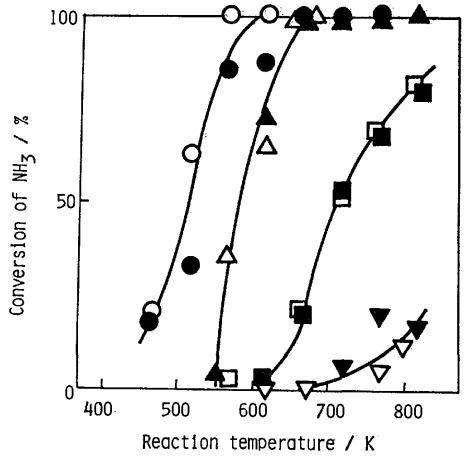

Fig. 1. Conversion of NH_3 in the oxidation of NH_3 with metal oxide–Pt/Al_2O_3 mixtures and with metal oxides.
Pluse size: 18.2 cm^3; concentration of NH_3 in pulse: 2.65%. Carrier gas (He) flow rate: 86 $cm^3\ min^{-1}$.
●: MnO_2–Pt/Al_2O_3, ○: MnO_2, ▲: V_2O_5–Pt/Al_2O_3, △: V_2O_5, ■: Co_3O_4–Pt/Al_2O_3, □: Co_3O_4, ▼: Fe_2O_3–Pt/Al_2O_3, ▽: Fe_2O_3.

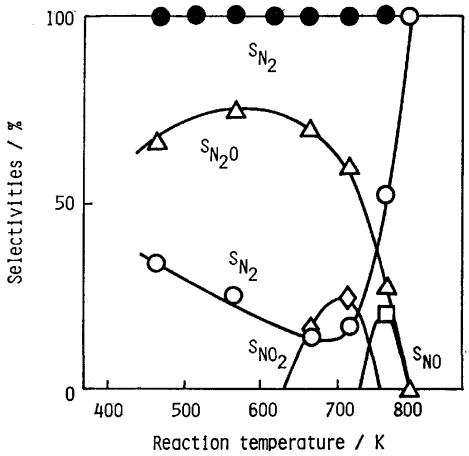

Fig. 2. Selectivities in the oxidation of NH_3 with MnO_2 and with MnO_2–Pt/Al_2O_3 mixture.
Pulse size: 18.2 cm^3; concentration of NH_3 in pulse: 2.65%. Carrier gas (He) flow rate: 86 $cm^3\ min^{-1}$.
○, ●: Selectivity to N_2, △: selectivity to N_2O, □: selectivity to NO, ◇: selectivity to NO_2.
Open symbols: MnO_2, closed symbol: MnO_2–Pt/Al_2O_3 mixture.

(Pt loading of 0.5 wt%) was purchased from Nippon Engelhard. Unless otherwise specified, a metal oxide–Pt/Al_2O_3 mechanical mixture was prepared by mixing a powder of both components in an agate mortar for 20 min without water (this mixture is hereafter referred to as *Mixing* if it is necessary to discriminate it from other mixtures with different states of mixing). The weights of samples were 0.1 g for a metal oxide and 0.2 g (0.1 g of a metal oxide and 0.1 g of Pt/Al_2O_3) for a metal oxide–Pt/Al_2O_3 mixture. The weight of metal oxide (0.1 g) was common for both samples. The metal oxides and the mixtures were then pressed and granulated to be used as samples. The size of the sample granules ranged from 0.3 mm to 0.6 mm. Commercial ammonia (99.9% purity) and hydrogen (99.99% purity) were used as reactants without further purification.

Apparatus and Procedures. Experiments were conducted using a pulse apparatus. The reactant and product components were analyzed by gas chromatography with thermal conductivity detectors at room temperature. Columns used were tetraethylenepentamine on Difron for NH_3, silica gel for N_2O, and Molecular Sieve type 13X for H_2, N_2, and NO and they were connected in the intermediate cell system.[19] The confirmation of NO_2 as a product was made with the phenol disulfonic acid method. Helium or argon as carrier gas was purified with titanium metal sponge heated at 1023 K. Pulses of ammonia at various concentrations were supplied to the reactor by a 6-way valve.

Results and Discussion

Activity of Metal Oxide–Pt/Al_2O_3 Mixtures for the Oxidation of Ammonia. The Pt/Al_2O_3 catalyst was inactive for the decomposition of NH_3 under the experimental condition in the present work. On the other hand, the metal oxides have been shown to be active for the reaction with NH_3.[20] The conversion of NH_3 (X_{NH_3}) in the oxidation of NH_3 with various metal oxides is shown in Fig. 1 together with that in the reaction with the metal oxide–Pt/Al_2O_3 mixtures. It should be noted in Fig. 1 that the conversion of NH_3 in the oxidation of NH_3 with a metal oxide–Pt/Al_2O_3 mixture is almost the same as that with the metal oxide, indicating that no synergistic effect exists in the activity of the mixtures for the oxidation of NH_3.

Selectivity in the Oxidation of Ammonia with Metal Oxide–Pt/Al_2O_3 Mixtures. Oxidation of NH_3 with the metal oxides forms various products, such as N_2, N_2O, NO, and NO_2, depending on the reaction temperature and concentration of NH_3 in the pulse.[20] The selectivities to these products in the oxidation of NH_3 with the metal oxide–Pt/Al_2O_3 mixtures and the metal oxides are shown in Figs. 2 and 3. S_{NO}, S_{NO_2}, S_{N_2O}, and S_{N_2} represent the selectivities to NO, NO_2, N_2O, and N_2, respectively. Figure 2 shows the selectivities for MnO_2 and MnO_2–Pt/Al_2O_3 mixture at various temperatures. In the oxidation of NH_3 with MnO_2, N_2, N_2O, NO, and NO_2 were all produced, although the selectivities to individual products varied markedly with reaction temperature. On the other hand, in the oxidation of NH_3 with MnO_2–Pt/Al_2O_3 mixture, only N_2 was obtained as a product irrespective of the reaction temperature indicated in Fig. 2. Similarly, N_2 was selectively produced in the oxidation of NH_3 with V_2O_5–Pt/Al_2O_3 and Co_3O_4–Pt/Al_2O_3 mixtures irrespective of the reaction temperature. In the oxidation of NH_3 with V_2O_5 or Co_3O_4 alone, N_2, N_2O, and NO were produced and the selectivities to these products varied with reaction temperature. The most remarkable feature of the synergistic effect on the oxidation of NH_3 with the metal oxide–Pt/Al_2O_3 mixtures can be seen in the selectivities at various concentrations of NH_3 in the pulse. As shown in Fig. 3, in the oxidation of NH_3 with Co_3O_4 at 793 K, the conversion of NH_3 (X_{NH_3}) was 100% and all of NO, N_2O, and N_2 were formed irrespective of the inlet concentration of NH_3. Also, as the concentration of NH_3 in the pulse decreased, the selectivity

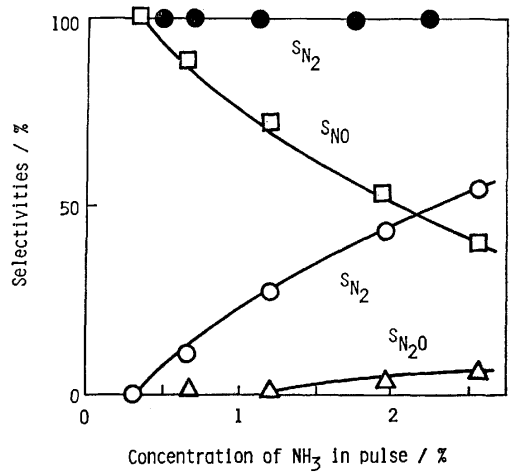

Fig. 3. Selectivities in the oxidation of NH_3 by Co_3O_4 and Co_3O_4–Pt/Al_2O_3 mixture with various concentrations of NH_3 in pluse.
Reaction temperature: 793 K; pulse size: 7.4 cm^3. Carrier gas (He) flow rate: 116 cm^3 min^{-1}.
○, ●: Selectivity to N_2, △: selectivity to N_2O, □: selectivity to NO.
Open symbols: Co_3O_4; closed symbol: Co_3O_4–Pt/Al_2O_3 mixture.

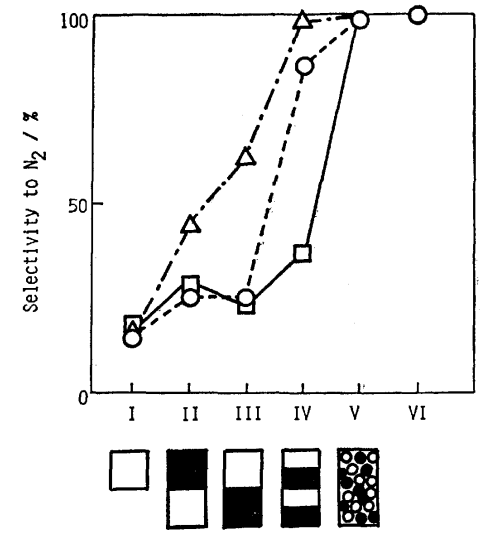

Fig. 4. Effect of the degree of mixing on the selectivity to N_2 in the oxidation of NH_3 with MnO_2–Pt/Al_2O_3.
Reaction temperature: □; 623 K, ○; 673 K, △; 723 K. Pulse size: 18.2 cm^3; concentration of NH_3 in pulse: 2.65%.
Carrier gas (He) flow rate: 86 cm^3 min^{-1}.
I: MnO_2, II: Pt/Al_2O_3 (upper layer)+MnO_2 (lower layer), III: MnO_2 (upper layer)+Pt/Al_2O_3 (lower layer), IV: MnO_2 (lst layer)+Pt/Al_2O_3 (2nd layer)+MnO_2 (3rd layer)+Pt/Al_2O_3 (4th layer), V: Roughly mixed sample of MnO_2 particles (0.3—0.6 mm) and Pt/Al_2O_3 particles (0.3—0.6 mm), VI: Throughly mixed sample in agate mortar.

to NO (S_{NO}) increased to 100%, whereas, the selectivities to N_2O (S_{N_2O}) and N_2 (S_{N_2}) decreased to 0%. This means that when the inlet concentration of NH_3 is low, NH_3 is oxidized almost selectively to NO by Co_3O_4. On the other hand, in the oxidation of NH_3 with Co_3O_4–Pt/Al_2O_3 mixture, the selectivity of the reaction was completely changed; N_2 was selectively formed even if the inlet concentration of NH_3 in the pulse was low. Similar phenomena were also observed for the MnO_2–Pt/Al_2O_3 and V_2O_5–Pt/Al_2O_3 mixtures. Thus, it can be said that the selectivity of the oxidation of NH_3 with the metal oxides was significantly changed by the mixing of Pt/Al_2O_3 with the metal oxides; N_2 was selectively produced irrespective of the concentration of NH_3 in pulse.

Oxidation of NH_3 by MnO_2–Pt/Al_2O_3 Mixtures under Various States of Mixing. Since, according to the previous studies,[4,21,22] the degree of mixing of a precious metal and a metal oxide can give a significant effect on the synergy between both components, it seems interesting to investigate the effect of the degree of mixing on the oxidation of NH_3 with the metal oxide–Pt/Al_2O_3 mixtures. The results for the mixtures of MnO_2 and Pt/Al_2O_3 are indicated in Fig. 4. In accordance with the data shown in Fig. 1, the conversion of NH_3 in the reactions with these mixtures was almost the same as that with MnO_2 for all kinds of mixtures. The mixing of MnO_2 and Pt/Al_2O_3 is considered to become closer as the number of state increases, *i.e.* from Mixture II to Mixture VI. As shown in Fig. 4, the selectivity of the reaction of NH_3 with the mixtures has varied significantly with the degree of mixing of both components. That is, both Mixtures V and VI have oxidized NH_3 selectively to N_2 at any of the temperatures indicated in Fig. 4. Mixture IV, which is coarser than Mixtures V and VI, also showed significant synergistic effect at 673 and 723 K. Mixtures II and III, the coarsest mixtures, exhibited little synergistic effect in the selectivity. It is worth noting in Fig. 4 that the incomplete mixing of Pt/Al_2O_3 particles (0.3—0.6 mm) with MnO_2 particles (0.3—0.6 mm), *i.e.* Mixture V (this is hereafter denoted as *Shaking*), was sufficient to oxidize NH_3 selectively to N_2, and furthermore very rough mixing, *e.g.* Mixture IV, exhibited a significant synergistic effect in the selectivity. Similar data to those shown in Fig. 4 were also obtained for V_2O_5–Pt/Al_2O_3 mixtures with various states of mixing (Table 1).

Contribution of Hydrogen Spillover or Migration of Oxygen to the Synergistic Effect. The hydrogen spillover plays an essential role in the oxidation of H_2 with the metal oxide–precious metal mixtures.[5] It is considered that the hydrogen spillover plays no role in the synergistic effect in the selectivity of the oxidation of NH_3 with the metal oxide–Pt/Al_2O_3 mixtures on the basis of the following reasons: In Table 1, the results of the oxidations of H_2 and NH_3 are shown for various samples, such as V_2O_5, Pt/Al_2O_3, V_2O_5–Pt/Al_2O_3(*Shaking*), and V_2O_5–Pt/Al_2O_3(*Mixing*).[23] X_{H_2} is the conversion of H_2 in the oxidation of H_2 with the samples, and it can be used as a measure of the extent of the hydrogen spillover. The inlet concentration of H_2 was nearly 1.5 times that of NH_3, which corresponds to the ratio of the number of hydrogen atoms in NH_3 to that in H_2. As shown in Table 1, the oxidation of H_2 takes place readily for V_2O_5–Pt/Al_2O_3(*Mixing*), whereas it hardly proceeds for

Table 1. Results of the NH_3 pulse reaction and the hydrogen spillover at 823 K

Sample	The reaction of H_2 with sample[a,b]	The reaction of NH_3 with sample[c,d]			
	X_{H_2}/%	X_{NH_3}/%	S_{N_2}/%	S_{N_2O}/%	S_{NO}/%
V_2O_5	3	100	83	2	15
Pt/Al_2O_3	0	4	100	0	0
V_2O_5-Pt/Al_2O_3 (*Shaking*)	6	100	100	0	0
V_2O_5-Pt/Al_2O_3 (*Mixing*)	100	100	100	0	0

Pulse size: 18.2 cm^3.
a) Concentration of H_2 in pulse: 3.7%. b) Carrier gas (Ar) flow rate: 86 $cm^3\ min^{-1}$. c) Concentration of NH_3 in pulse: 2.65%. d) Carrier gas (He) flow rate: 86 $cm^3\ min^{-1}$.
X_{H_2} and X_{NH_3} are the conversions of H_2 and NH_3, respectively. S_{N_2}, S_{N_2O}, and S_{NO} are the selectivities to N_2, N_2O, and NO, respectively.

V_2O_5–Pt/Al_2O_3(*Shaking*). This means that the hydrogen spillover cannot take place for V_2O_5–Pt/Al_2O_3 (*Shaking*) but it can take place readily for V_2O_5–Pt/Al_2O_3(*Mixing*). If the hydrogen spillover played a significant role in the oxidation of NH_3 with the metal oxide–Pt/Al_2O_3 mixtures, the selectivity of the reaction should differ considerably between V_2O_5–Pt/Al_2O_3(*Shaking*) and V_2O_5–Pt/Al_2O_3(*Mixing*). The selectivity to N_2 for V_2O_5–Pt/Al_2O_3(*Shaking*), however, was the same as that for V_2O_5–Pt/Al_2O_3(*Mixing*) and reached 100%; neither N_2O nor NO was produced for both V_2O_5–Pt/Al_2O_3(*Shaking*) and V_2O_5–Pt/Al_2O_3 (*Mixing*), in contrast to the products' distribution for V_2O_5. Furthermore, a considerable synergistic effect was observed for the Mixture IV in Fig. 4 in the selectivity of the oxidation of NH_3, while the hydrogen spillover did not take place for the mixture.

Moreover, it has been suggested that, in the oxidation of hydrocarbons with V_2O_5–precious metal systems, the migration of oxygen through the bulk oxide takes place so as to react with hydrocarbons at or near the metal additives; thereby the reaction is much enhanced by the addition of precious metals to V_2O_5.[17] Similarly, if the migration of oxygen through the bulk oxide to Pt particles takes place easily in the oxidation of NH_3 with the metal oxide–Pt/Al_2O_3 mixtures, the reaction has to be much enhanced by the addition of Pt/Al_2O_3 to the metal oxides because of the high activity of Pt/Al_2O_3 for the oxidation of NH_3 with oxygen. The migration of oxygen from the metal oxides to Pt particles on Al_2O_3, however, hardly occurs in the metal oxide–Pt/Al_2O_3 mixtures, since most of the Pt particles are expected to be separated from the particles of the metal oxide by Al_2O_3 in the metal oxide–Pt/Al_2O_3 mixtures. This inference is in accord with the experimental data; the activity of the metal oxide–Pt/Al_2O_3 mixtures for the oxidation of NH_3 is almost the same as that of the metal oxides as shown in Fig. 1. Consequently it is noted that neither the hydrogen spillover from Pt to metal oxides nor the migration of oxygen from metal oxides to Pt plays a significant role in the oxidation of NH_3 with metal oxide–Pt/Al_2O_3 mixtures.

Recently, Il'chenko[24] reported that the addition of $Pt/BaSO_4$ to metal oxides substantially increases the activity of the metal oxides for the oxidation of NH_3, while the selectivity in the reaction slightly changes. This is in marked contrast to the present results for the metal oxide–Pt/Al_2O_3 mixtures. Since Pt particles in the metal oxide–$Pt/BaSO_4$ mixtures are considered to be in contact with the grains of the metal oxide,[24] the difference may be brought about by the migration of adsorbed ammonia activated on Pt to the metal oxides or by the migration of oxygen of the metal oxides to Pt in the oxidation of NH_3 with the metal oxide–$Pt/BaSO_4$ mixtures. According to our preliminary experiments on the oxidation of NH_3 with V_2O_5–Pt black mixtures and V_2O_5–Pt mixtures supported on Al_2O_3, in fact, the activity of the metal oxide for the oxidation of NH_3 was significantly enhanced by the presence of Pt contacting with the metal oxide. The details of the results will be reported in a subsequent paper with additional data to reveal the mechanism.

It should be noted here that such mechanisms of the synergistic effects as (i) the dispersion of the primary component, (ii) the control of the oxidation state or the electronic state of the primary component, or (ii) the formation of a new active site by the chemical interaction of individual components are not important in the oxidation of NH_3 with the metal oxide–Pt/Al_2O_3 mixtures. This is because most of the Pt particles are not in contact with the metal oxides for the mixtures and a considerable synergistic effect appears even for the reaction with the V_2O_5–Pt/Al_2O_3 (*Shaking*) and the Mixture IV shown in Fig. 4.

Mechanism of the Synergistic Effect in the Oxidation of NH_3 with Metal Oxide–Pt/Al_2O_3 Mixtures. NO has been regarded to play an important role as an intermediate in the catalytic oxidation of NH_3.[18,25,26] In the preceding work,[20] it has been found that the oxidation of NH_3 with the metal oxides proceeds by a similar scheme as follows:

$$NH_3 \xrightarrow[\text{I}]{\text{lattice oxygen}} NO \xrightarrow[\text{II}]{NH_3} N_2,\ N_2O, \qquad (1)$$

where NH_3 is first oxidized by the lattice oxygen of a metal oxide to NO (Step I), which then reacts with NH_3 (the NO–NH_3 reaction) to form N_2 and N_2O (Step II). The NO–NH_3 reaction (Step II) takes place catalytically. According to this scheme, the activity in the oxidation of NH_3 with a metal oxide is determined by Step I, whereas the selectivity is limited by the relative rate of Step II to that of Step I.

This scheme is now applied to the oxidation of NH_3 with the metal oxide–Pt/Al_2O_3 mixtures in

Table 2. Relation between NO/NH_3 ratio and the selectivities of $NO-NH_3$ reaction on Pt/Al_2O_3 catalyst at 773 K

NO/NH_3 ratio	X_{NO}/%	X_{NH_3}/%	S_{N_2}/%	S_{N_2O}/%
0.49	100	61	100	0
0.53	98	77	97	3
0.73	97	85	96	4

Catalyst weight: 0.1 g. Concentration of NO in pulse: 2.0%. Pulse size: 18.2 cm^3. Carrier gas (He) flow rate: 86 $cm^3\ min^{-1}$.
X_{NO} and X_{NH_3} are the conversions of NO and NH_3, respectively. S_{N_2} and S_{N_2O} are the selectivities to N_2 and N_2O, respectively.

order to interpret the synergistic effect involved in the oxidation of NH_3 with the metal oxide–Pt/Al_2O_3 mixtures. According to the scheme, the activity of the sample is limited by Step I. Since Pt/Al_2O_3 is not active for the decomposition of NH_3, the agreement of the conversion of NH_3 for a metal oxide–Pt/Al_2O_3 mixture with that for the metal oxide means that the activity of the metal oxide for the oxidation of NH_3 is not enhanced by its mixing with Pt/Al_2O_3. In accordance with the above-mentioned discussion either the hydrogen spillover or the migration of oxygen hardly takes place in the oxidation of NH_3 with the mixtures. The activity of the metal oxide–Pt/Al_2O_3 mixtures for the oxidation of NH_3 is therefore determined only by that of the metal oxides. On the other hand, the selectivity of the reaction is determined, according to this scheme, by the rate of the $NO-NH_3$ reaction (Step II), since the rate of Step I is not changed by the addition of Pt/Al_2O_3 to the metal oxides. The metal oxides employed in this study were all active for the $NO-NH_3$ reaction. However, the activity of the metal oxides is considered insufficient to form N_2 selectively, since considerable amounts of NO, N_2O, and NO_2 were produced in the oxidation of NH_3 with the metal oxides, especially when the inlet concentration of NH_3 was decreased as shown in Fig. 3. As it is well known, Pt/Al_2O_3 catalyst is highly active for the $NO-NH_3$ reaction,[27,28] indicating that the activity of the metal oxide–Pt/Al_2O_3 mixtures for the $NO-NH_3$ reaction is much higher than that of the metal oxides. Furthermore, as shown in Table 2, the selectivity to N_2 in the $NO-NH_3$ reaction on Pt/Al_2O_3 catalyst increased as the ratio of the concentration of NO to that of NH_3 decreased, and attained 100% when the NO/NH_3 ratio was smaller than 0.5. Thus, if it can be assumed that the NO/NH_3 ratio is small enough under the condition of the oxidation of NH_3 with metal oxide–Pt/Al_2O_3 mixtures, the high selectivity to N_2 can be explained in terms of the scheme of Reaction 1. This assumption seems to be valid, since the activity of Pt/Al_2O_3 catalyst for the $NO-NH_3$ reaction has been shown to be very high and, therefore, the concentration of NO can be considered to be kept at a low level under the reaction condition.

Since most of the Pt particles in the mixtures are separated from the metal oxides by Al_2O_3, the NO

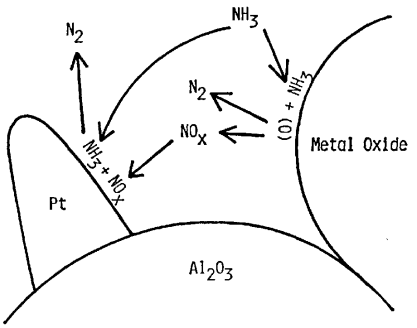

Fig. 5. Mechanism of the oxidation of NH_3 with a metal oxide–Pt/Al_2O_3 mixture.

produced by the oxidation of NH_3 should transfer from the metal oxides to Pt particles in order to react with NH_3 on Pt to form N_2 selectively. The migration of NO on the surface of Al_2O_3, however, does not seem to take place, since the migration of either oxygen or hydrogen cannot occur in the oxidations of NH_3 and H_2 with V_2O_5–Pt/Al_2O_3(*Shaking*). Consequently the migration of adsorbed NO species, which is heavier than hydrogen or oxygen, cannot be expected. Therefore, NO is considered to transfer from the metal oxides to Pt through the gas phase.

Taking into consideration that both N_2O and NO_2 can also react with NH_3 on Pt/Al_2O_3 catalyst to form N_2, the scheme shown in Fig. 5 can be proposed for the reaction of NH_3 with the metal oxide–Pt/Al_2O_3 mixtures. That is, in the oxidation of NH_3 with the metal oxide–Pt/Al_2O_3 mixtures, NH_3 is, at first, oxidized by the metal oxides to form NO_x (NO, NO_2, and N_2O) and N_2 (Step I), then NO_x components transfer through the gas phase from the metal oxides to the Pt particles on Al_2O_3, and finally NO_x components react readily with NH_3 on Pt to form N_2 selectively (Step II). The significantly high selectivity to N_2 for the incomplete mixtures, such as Mixtures IV and V in Fig. 4 and V_2O_5–Pt/Al_2O_3(*Shaking*) in Table 1, can be understood in terms of the scheme shown in Fig. 5, since the gas-phase transfer can proceed more readily than the surface migration because of the absence of the activation energy in the transfer through the gas phase.[29] It should be emphasized that the rate of the gas-phase transfer of NO_x components is much faster than the rate of Step I. This assures the selective oxidation of NH_3 to N_2 with the metal oxide–Pt/Al_2O_3 mixtures even under conditions where the yield of NO is 100% in the oxidation of NH_3 with the metal oxides (Fig. 3).

It is interesting to investigate whether metal oxide–Pt/Al_2O_3 mixtures are also effective for the selective oxidation of NH_3 to N_2 by gaseous O_2. According to our preliminary continuous flow experiments under the dilute gas condition, the yield of NO and NO_2 in the oxidation of NH_3 with gaseous O_2 on Pt/Al_2O_3 was significantly decreased by the addition of MoO_3 or WO_3 to Pt/Al_2O_3. Details of the results and mechanisms will be reported in a subsequent paper.

As mentioned above, the synergistic effect in the oxidation of NH_3 differs considerably from that of the oxidation of hydrocarbons. The difference in the

synergistic effect may be due to the difference in the schemes of both reactions, especially in the activity of deep oxidation products. In the oxidation of NH_3, the deep oxidation products, such as NO and NO_2, are produced first and then they react with NH_3 to form the mild oxidation products, such as N_2 and N_2O, while, in the oxidation of hydrocarbons, the deep oxidation products, such as CO and CO_2, do not convert to the mild oxidation products.

Conclusion

The selective oxidation of NH_3 to N_2 with the metal oxide–Pt/Al_2O_3 mixtures has been found to involve two kinds of active sites—one is the site on the metal oxide for the oxidation of NH_3 to NO_x and N_2, and the other is the site on Pt metal for the reaction of NO_x with NH_3 to form N_2. Although these two kinds of active sites are considerably separated from each other, a rapid gas-phase transfer of the reactive intermediate (NO_x) from the metal oxide to Pt assures cooperation between both sites. In other words, this kind of synergistic effect can take place even if the different kinds of active sites are considerably separated from one another. A heterogeneous catalytic reaction usually involves two or more steps; furthermore, reactive intermediates sometimes desorb from the surface to the gas phase during the reaction. Therefore, the mechanism described in this study could be applied to various types of catalytic reactions and give important suggestion on the design of multi-component catalysts.

References

1) Y. Murakami, *Shokubai*, **21**, 349 (1979).
2) K. Ohki and A. Ozaki, *Kogyo Kagaku Zasshi*, **70**, 684 (1967).
3) S. G. Hingin, S. W. Weller, and G. A. Mills, *J. Phys. Chem.*, **62**, 244 (1958).
4) R. L. Burnett and T. R. Hughes, *J. Catal.*, **31**, 55 (1973).
5) P. A. Sermon and G. C. Bond, *Catal. Rev.*, **8**, 211 (1973).
6) H. S. Gandhi, A. G. Piken, M. Shelef, and R. G. Delosh, *SAE paper* 760201 (1976).
7) H. Ohara, Y. Miura, and Y. Fujitani, *Preprints of Meeting of Society of Automotive Engineers of Japan*, **1978**, 629.
8) H. C. Yao and M. Shelef, *J. Catal.*, **44**, 392 (1976).
9) H. S. Gandhi, H. C. Yao, Y. K. Steipein, and J. T. Kummer, *Proc. 2nd Chem. Congr. North Am. Contitent, San Francisco*, **1980**, No. 150.
10) L. L. Hegedus, J. C. Summers, J. C. Schlatter, and K. Baron, *J. Catal.*, **56**, 321 (1979).
11) J. C. Schlatter and P. J. Mitchell, *Ind. Eng. Chem., Prod. Res. Dev.*, **19**, 288 (1980).
12) L. Forni and G. Terzoni, *Ind. Eng. Chem., Process Res. Dev.*, **16**, 288 (1977).
13) A. B. Evnin, J. A. Rabo, and P. H. Kasai, *J. Catal.*, **30**, 109 (1973).
14) K. Takami, A. Igarashi, and Y. Ogino, *Bull. Jpn. Petrol. Inst.*, **18**, 127 (1976).
15) Y. Kato, *Nippon Kagaku Kaishi*, **1980**, 792.
16) Y. Murakami, Y. Kosaki, M. Motokawa, Y. Ooyabu, and A. Miyamoto, *Nippon Kagaku Kaishi*, **1977**, 612.
17) A. W. Naumann and A. S. Behan Jr., *J. Catal.*, **39**, 432 (1975).
18) T. P. Kobylinski, B. W. Taylor, *J. Catal.*, **33**, 376 (1974).
19) Y. Murakami, *Bull. Chem. Soc. Jpn.*, **32**, 316 (1959).
20) Y. Kosaki, A. Miyamoto, and Y. Murakami, *Bull. Chem. Soc. Jpn.*, **52**, 617 (1979).
21) P. B. Weisz, *Proc. 2nd Int. Congr. Catalysis, Paris*, **1960**, 937.
22) G. C. Bond, M. J. Fuller, and L. R. Molloy, *Proc. 6th Int. Congr. Catalysis, London*, **1976**, 356.
23) V_2O_5 was used as the metal oxide for the investigation of the contribution of the hydrogen spillover or migration of oxygen to the synergistic effect. This is because V_2O_5 alone is inactive for the reaction with H_2 while MnO_2 and Co_3O_4 are very active for this reaction.
24) N. I. Il'chenko, *Kinet. Katal.*, **17**, 386 (1976).
25) H. S. Gandhi and M. Shelef, *J. Catal.*, **40**, 312 (1975).
26) T. Pignet and L. D. Schmidt, *J. Catal.*, **40**, 212 (1975).
27) K. Otto, M. Shelef, and J. T. Kummer, *J. Phys. Chem.*, **74**, 2690 (1970).
28) G. L. Bauerle, S. C. Wu, and K. Nobe, *Ind. Eng. Chem., Prod. Res. Dev.*, **14**, 123 (1975).
29) Selectivity to N_2 at 723 K in the oxidation of NH_3 with Mixture II was slightly higher than that with MnO_2 alone (Fig. 4). This may be due to the adhesion of a part of MnO_2 to the inner wall of the reactor above the Pt/Al_2O_3–MnO_2 interface of Mixture II, which causes the synergistic effect by the scheme shown in Fig. 5.

Electric Linear Dichroism Study of Sodium Poly(*p*-styrenesulfonate) and Its 9-Aminoacridinium Complex in Aqueous Solutions

Koichiro MATSUDA and Kiwamu YAMAOKA*

Faculty of Science, Hiroshima University, Higashisenda-machi, Naka-ku, Hiroshima 730

(Received May 25, 1981)

Electric linear dichroism (ELD) of sodium poly(*p*-styrenesulfonate) (NaPSS) and its 9-aminoacridinium (AA) complex at a mixing ratio of polymer residue-to-dye of 6.14 was studied in aqueous solutions at 20 °C. ELD signals were measured in the electric field strength range 0—*ca.* 19 kV/cm at the absorption peak wavelengths; they showed a saturating trend at extremely high fields. The average angles between the orientation axis of NaPSS and the transition moments of chromophores were estimated to be 60° at 224.5 nm and 57° at 262 nm for the side chain phenyl group and 50° at 404 nm for the bound AA by using theoretical orientation functions derived for mono- and polydisperse systems. The ELD spectra were measured at fixed field strengths; 275—215 nm for NaPSS and 440—282 nm for NaPSS–AA. The reduced dichroism of NaPSS remained nearly constant throughout the 262 nm band but steadily changed below 224 nm in the 224.5 nm band, indicating that another band exists in the far UV region. The ELD spectrum of the NaPSS–AA complex revealed that the two electronic ^1L_a and ^1L_b transition moments of the bound AA are tilted at different angles to the orientation axis of the NaPSS backbone.

The mechanism of electric field orientation of polyelectrolytes in aqueous solution is an interesting problem. Many studies on electric dipole moments of the synthetic polyelectrolytes in aqueous solutions have been carried out by the electric birefringence method.[1–11] A number of stiff or semi-flexible charged polyions are now known to be orientable by external electric fields. For example, Yamaoka and Ueda[11] recently reported reversing-pulse electric birefringence of poly(*p*-styrenesulfonate) (PSS) with various cationic counterions in aqueous solutions, attributing the orientation of PSS to the translational mobility of the counterions on the polymer surface. The electric linear dichroism (ELD) method is another powerful electrooptical technique for obtaining information on the relative disposition of the intrinsic and/or extrinsic chromophore in polyelectrolytes. However, few studies have been reported on the ELD of synthetic polyelectrolytes and their complexes with small chromophoric ligands in aqueous solutions. Soda and Yoshioka[12] investigated the ELD of Crystal Violet and Malachite Green bound to KPSS in aqueous solution, in order to clarify the metachromatic behavior of these dyes. Recently, Tricot *et al.*[13] reported the ELD of poly(*N*-alkyl-4-vinylpyridinium bromide) in aqueous solution, determining the angle between the orientation axis of the polymer backbone and the pyridinium ring.

In order to determine the conformation of polyelectrolytes and the dye complexes, the effects of the polydispersity of polymer length, the flexibility of backbone, and the transition moment direction of chromophore must be considered. In this work, the wavelength dependence of the reduced dichroism of the sodium salt of PSS (NaPSS) and its 9-aminoacridinium (AA) complex in aqueous solution was examined at 20 °C in the UV and visible absorption regions. The electric field dependence of the reduced dichroism was examined at the absorption peak wavelengths. The aims of this work are to clarify the conformations of both the phenyl ring and the bound AA relative to the molecular orientation axis of NaPSS. The limiting reduced dichroism $(\Delta A/A)_s$ was estimated by comparing the field strength dependence of reduced dichroism with theoretical orientation functions of two different types under due consideration of the polydispersity of polymer length. From this result, the angles for the transition moments of the phenyl ring and the bound AA relative to the orientation axis were obtained.

Experimental

Materials. Sodium poly(*p*-styrenesulfonate) (NaPSS) was the same sample that was used previously.[11,14,15] The original sample in the potassium salt was kindly given by Professor Koshiro Yoshioka of the University of Tokyo. The intrinsic viscosity of NaPSS in 0.1 M NaCl (1 M=1 mol dm^{-3}) was 0.9 cm^3 g^{-1}. From this value, the weight-average molecular weight (M_w) was determined to be 2.8×10^5.[16] The cationic dye, 9-aminoacridinium chloride (AA), was described in previous papers.[11,17–19]

Preparation of Sample Solutions. The freeze-dried NaPSS sample was dried under reduced pressure at 78 °C for 10 h. It was then dissolved in redistilled water. The residue concentration of NaPSS was determined by weighing the dried sample as anhydride. The concentration of AA was determined by using the molar absorption coefficient, ε, of 1.03×10^4 M^{-1} cm^{-1} at 401 nm.[18] The NaPSS–AA solution, which contained neither extra neutral salt nor buffer salt, was prepared by adding the dye solution to the NaPSS solution at a molar mixing ratio of polymer residue-to-dye (P/D) of 6.14. The final concentration of AA was 108 μM.

Absorption Measurements. The UV and visible absorption spectra were measured on a Hitachi EPS-3T spectrophotometer at 20 °C with 2 cm- and 1 cm-long quartz cells.

Measurements of Electric Linear Dichroism. The electric linear dichroism apparatus was constructed in our laboratory. Its design construction, and performance were described in detail elsewhere.[20] The measuring cell unit consists of a Kel-F "Kerr" cell and a water-jacketed cell holder. The optical path lengths of the cell were 2 cm (electrode gap 0.33 cm) and 1 cm (electrode gap 0.207 cm). An R106UH photomultiplier (Hamamatsu TV Co.) was used, and the linear response of the tube was confirmed.[20] The half-intensity band width was kept narrower than 1.5 nm through-

out. Both the parallel dichroism ($\Delta A_{//}/A$) and the perpendicular dichroism ($\Delta A_{\perp}/A$) were separately measured at 20 °C. The steady-state dichroism signal was obtained by varying both the voltage of a single square-wave pulse between 0.37 and 3.88 kV and the pulse duration between *ca.* 80 and 350 μs. External electric pulses were always applied to the NaPSS and NaPSS–AA solutions at least twice, but no degradation or irreversible change of dichroism signal was detected.

Data Analysis. The procedure for the dichroism data acquisition has been described in detail elsewhere.[20-22] The reduced dichroism ($\Delta A/A$) was calculated from $\Delta A_{//}/A$ and $\Delta A_{\perp}/A$ with the following expressions:

$$\frac{\Delta A_{//}}{A} = \frac{A_{//}^{E}-A}{A} = -\frac{1}{A}\log\left(1+\frac{\Delta I_{//}}{I_{//,0}}\right), \quad (1)$$

$$\frac{\Delta A_{\perp}}{A} = \frac{A_{\perp}^{E}-A}{A} = -\frac{1}{A}\log\left(1+\frac{\Delta I_{\perp}}{I_{\perp,0}}\right), \quad (2)$$

$$\frac{\Delta A}{A} = \frac{A_{//}^{E}-A_{\perp}^{E}}{A} = \frac{\Delta A_{//}-\Delta A_{\perp}}{A}, \quad (3)$$

where $\Delta A_{//}$ is the change in absorbances of the monochromatic light polarized parallel to the electric field direction in the presence ($A_{//}^{E}$) and the absence (A) of the externally applied pulse field, $\Delta A_{\perp}$ is the corresponding change for the perpendicularly polarized light, $\Delta I_{//}(=I_{//,E}-I_{//,0})$ is the change in transmitted intensities of light polarized parallel to the field direction in the presence ($I_{//,E}$) and the absence ($I_{//,0}$) of the pulse field, and $\Delta I_{\perp}$ is the corresponding change for the perpendicularly polarized light. If there is no electrochromism involved, the following relation should hold:[23]

$$\frac{\Delta A_{//}}{A} = -2\frac{\Delta A_{\perp}}{A} \text{ or } A = \frac{1}{3}(A_{//}^{E}+2A_{\perp}^{E}). \quad (4)$$

In this work, the validity of Eq. 4 was confirmed for NaPSS (the residue concentration of polymer, C_p=3.31 mM) below *ca.* 19 kV/cm, and both for NaPSS (C_p=0.133 mM) and for NaPSS–AA (P/D=6.14) below *ca.* 14 kV/cm.

Results

Electric Field Dependence of NaPSS and NaPSS–AA Complex. Figure 1 shows typical ELD signals of NaPSS (left) and NaPSS–AA complex (right) and applied electric pulse signals. The sign of dichroism (ΔA in Eq. 3) is negative for NaPSS in the 275—215 nm region, but it is positive for NaPSS–AA in the 440—282 nm region. Figure 2 shows the field strength dependence of the reduced dichroism ($\Delta A/A$) of NaPSS and NaPSS–AA. Values of $\Delta A/A$ were measured at the respective absorption band maxima over a wide field strength range (0—*ca.* 19 kV/cm). The similarities and differences between NaPSS at 224.5 nm (C_p=0.133 mM), NaPSS at 262 nm (C_p=3.31 mM), and NaPSS–AA at 404 nm (C_p=0.663 mM) may be summarized as follows: (1) The sign of $\Delta A/A$ is *negative* for the two NaPSS systems, but it is *positive* for NaPSS–AA system throughout the respective absorption regions, (2) the electric field dependence of $\Delta A/A$ shows a saturating trend at high fields in all cases, and (3) no electrochromic effect was observed; Eq. 4 holds for all three systems, unless the applied electric field strength is extremely large. The Kerr-law behavior was not directly observed in this work because of low signal-to-noise ratios at weak field strengths, but the Kerr law had been confirmed to hold for the same NaPSS and NaPSS–AA systems

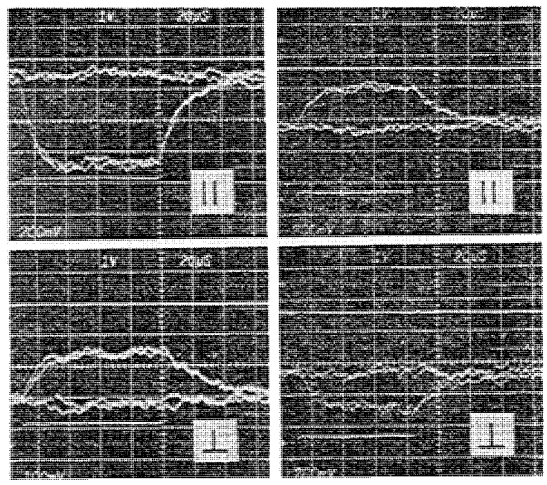

Fig. 1. Photographs of dichroism signals of NaPSS (left) and NaPSS–AA (right) and of applied pulsed electric fields at 20 °C and at 224.5 nm (left) and 404 nm (right). The parallel dichroism (//) is in the upper half and the perpendicular dichroism (⊥) is in the lower half. Electric field strengths in kV/cm are 18.8 (left) and 11.8 (right). Sweep time is 20 μs/division in all cases. Each photograph was a superposition of two displays.

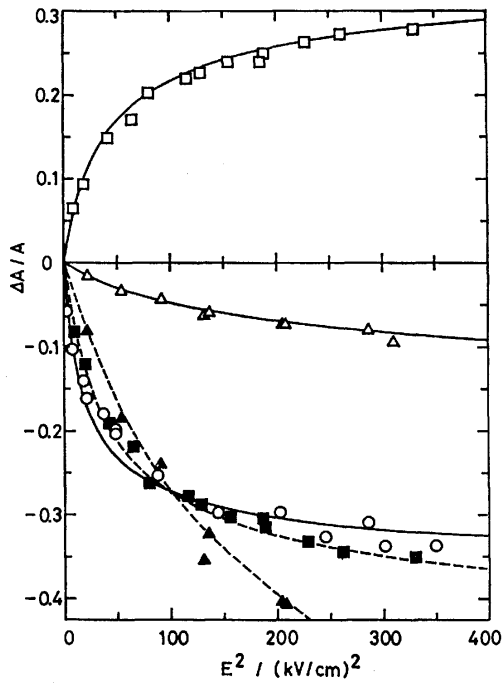

Fig. 2. Dependence of the reduced dichroism ($\Delta A/A$) of NaPSS at 224.5 nm (○) and 262 nm (△) and of NaPSS–AA at 404 nm (□) on the square of electric field strength, E^2. Open symbols were experimentally determined and solid curves were calculated by using the theoretical orientation function $\Phi(\beta,\gamma=0)$. Values of reduced dichroism of NaPSS at 262 nm were multiplied by 5.64 (--▲--▲--), and those of NaPSS–AA at 404 nm were multiplied by −1.26 (--■--■--).

TABLE 1. THE TRANSITION MOMENTS, THE MOLAR ABSORPTION COEFFICIENTS, ε_{max} IN $mol^{-1}\ dm^3\ cm^{-1}$, AND THE PEAK POSITIONS, λ_{max} IN nm, OF BENZENE, SODIUM *p*-TOLUENESULFONATE, NaPSS, AND NaPSS-AA

Benzene[a]			Sodium *p*-toluenesulfonate[b]		NaPSS		NaPSS-AA		
λ_{max}	ε_{max}	Transition moment	λ_{max}	ε_{max}	λ_{max}	ε_{max}	λ_{max}	ε_{max}	Transition moment
203	7.4×10^3	$^1B_{1u}$	220	1.01×10^4	224.5	9.54×10^3	315	1.63×10^3	^1L_b
255	2.2×10^2	$^1B_{2u}$	261.5	3.71×10^2	262	4.68×10^2	404	6.64×10^3	^1L_a

a) Ref. 30. b) Values measured in water at 20 °C.

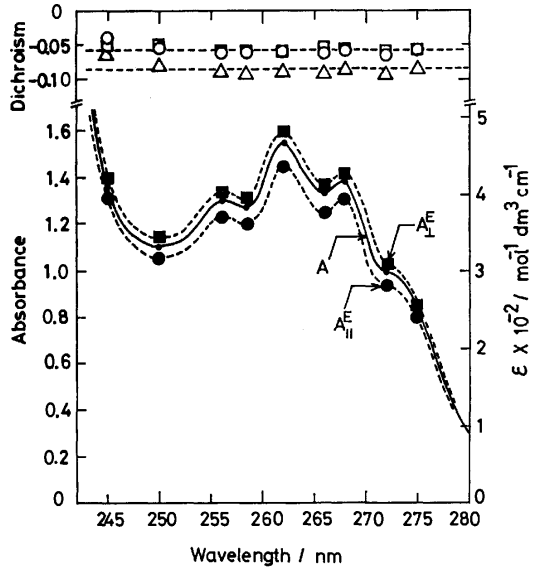

Fig. 3. Linear dichroic spectra of NaPSS in aqueous solution (C_p=3.31 mM) at 20 °C. Electric field strength=17.1 kV/cm. The lower half: Solid curve is the isotropic spectrum A in the absence of external electric field. The spectrum A_{calcd} (—•—) was calculated from the relation $A_{calcd}=(A^E_{//}+2A^E_{\perp})/3$. $A^E_{//}$ (●) and $A^E_{\perp}$(■) were calculated from Eq. 1 and Eq. 2, respectively. The upper half: The specific parallel dichroism is $\Delta A_{//}/A$ (○) and the reduced dichroism is $\Delta A/A$ (△), together with the specific perpendicular dichroism $\Delta A_{\perp}/A$ multiplied by −2 (□), in order to indicate that the relation $\Delta A_{//}/A=-2\Delta A_{\perp}/A$ holds in this case.

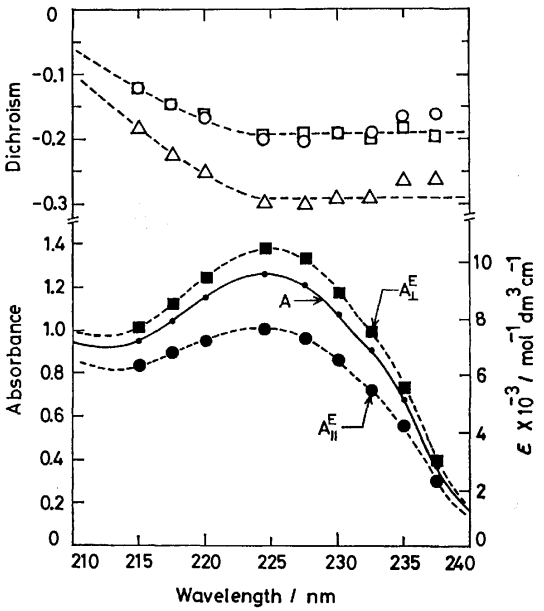

Fig. 4. Linear dichroic spectra of NaPSS in aqueous solution (C_p=0.133 mM) at 20 °C. Electric field strength=12.0 kV/cm. All notations and symbols are the same as in Fig. 3.

below *ca.* 1.2 kV/cm by an electric birefringence study.[11]

The reduced dichroism at a given electric field strength and given wavelength is the product of the orientation factor and the optical factor, which is, for example, equal to $3(3\cos^2\theta-1)/2$ for an axially symmetric molecule (*cf.* Eq. 5). If differences of the $\Delta A/A$ *vs.* E^2 curves for three systems in Fig. 2 are merely due to the optical factor, these curves should be superimposed upon one another by multiplying the observed $\Delta A/A$ by appropriate constants. In order to verify this possibility, the normalization of the three curves was attempted by multiplying the curve of NaPSS (open triangles) by 5.64 and the curve of NaPSS-AA (open squares) by −1.26 at a selected field strength (E^2=100 (kV/cm)^2). In Fig. 2, these normalized curves are represented by dashed lines with closed symbols; they do not coincide with the solid curve (open circles) of NaPSS at 224.5 nm, to which the normalization was tried. This discrepancy should be ascribed not only to the difference of the optical factor but also to the difference of the orientation factor between the above three systems. Thus, the average degree of molecular orientation by a given externally applied field differs for each, suggesting a difference in the electric moments for the three polymer systems.

Wavelength Dependence of Dichroic Spectra of NaPSS in the 275—215 nm Region. Figures 3 and 4 show absorption spectra of two NaPSS solutions in the presence ($A^E_{//}$ and $A^E_{\perp}$) and in the absence (A) of applied electric field in the lower half, and the parallel dichroism (circles), the perpendicular dichroism multiplied by −2 (squares), and the reduced dichroism (triangles) in the upper half, respectively. The isotropic spectrum of NaPSS (C_p=3.31 mM) in Fig. 3 was characterized by peaks at 268 nm (ε=418), 262 nm (468), and 256 nm (394), and by a shoulder near 272 nm (300). These values are consistent within 3.8% with those of Soda and Yoshioka,[12] but they are slightly larger than the data of Boyd.[24] The reduced dichroism is negative and constant in the 275—255 nm. Both $\Delta A_{//}/A$ and $-2\Delta A_{\perp}/A$ agree with each other within experimental uncertainty. By using values of $A^E_{//}$ and $A^E_{\perp}$, the isotropic absorbance

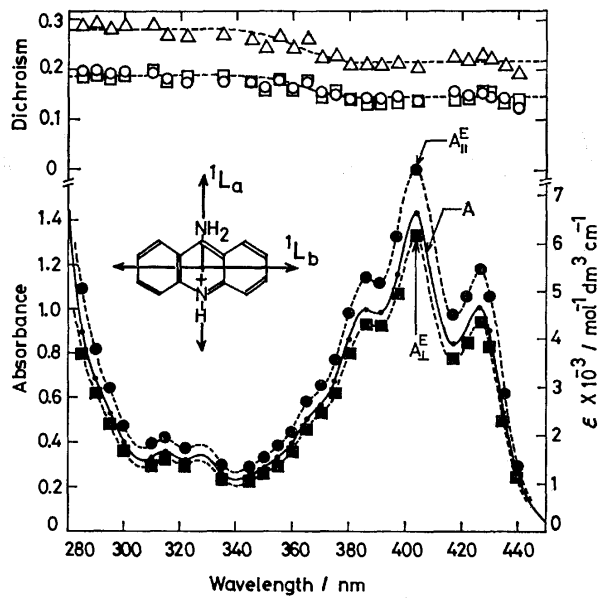

Fig. 5. Linear dichroic spectra of NaPSS–AA in aqueous solutions at a P/D value of 6.14 and at a constant field strength of 11.6 kV/cm. Symbols are all the same as in Fig. 3.

was calculated (A_{calcd}, dots) with Eq. 4. The agreement of A_{calcd} with the observed spectrum (solid curve) indicates that no detectable electrochromism is involved for the NaPSS (C_p=3.31 mM) solution.

Because of a large difference in ε between the 262 nm and 224.5 nm bands, the NaPSS solution was diluted about 25-fold (*cf.* Table 1). The isotropic spectrum of NaPSS (C_p=0.133 mM) in Fig. 4 was characterized by a peak at 224.5 nm ($\varepsilon=9.54\times10^3$) and a weak shoulder near 233 nm (6.58×10^3). The peak value was lower than Boyd's value by 10% at 224.0 nm and at 25 °C.[24] The reduced dichroism was negative throughout the 240—215 nm region. Both $\Delta A_{//}/A$ and $-2\Delta A_{\perp}/A$ agree with each other, indicating no electrochromism. The dichroic spectrum is constant only in the 240—224 nm region, increasing gradually below 224 nm, which is probably due to the influence of some higher-energy absorption bands of NaPSS in the far UV region.[25]

Wavelength Dependence of Dichroic Spectrum of NaPSS–AA Complex in the 440—280 nm Region. Figure 5 shows absorption spectra of an NaPSS–AA solution in the presence ($A^E_{//}$ and $A^E_{\perp}$) and in the absence (A) of applied electric field in the lower half, and the parallel dichroism (circles), the perpendicular dichroism multiplied by −2 (squares), and the reduced dichroism (triangles) in the upper half. The isotropic spectrum is characterized by the ^1L_a band [three peaks at 426 nm ($\varepsilon=4.68\times10^3$), 404 nm ($6.64\times10^3$), 386 nm ($4.62\times10^3$), and a weak shoulder near 370 nm (2.55×10^3)], the ^1L_b band [two weak peaks at 328 nm ($\varepsilon=1.61\times10^3$) and 315 nm ($1.63\times10^3$)], and a shoulder near 290 nm (3.16×10^3).[15] The reduced dichroism indicates that (1) its sign is always positive in the visible and near UV regions, (2) two different transitions are present (one with $\Delta A/A$ of 0.22±0.02 in the 440—370 nm region and the other with $\Delta A/A$ of 0.27±0.02 in the 335—282 nm region), (3) no electrochromism is involved, *i.e.*, $\Delta A_{//}/A=-2\Delta A_{\perp}/A$ within experimental uncertainty.

Discussion

Theoretical Orientation Functions for Monodisperse and Polydisperse Systems. The synthetic polyelectrolyte may be in a very extended form in salt-free aqueous solution at a low polymer-concentration, as a result of electrostatic repulsion between the charged side groups.[6,13] Under these conditions, the electro-optical properties of such a polyelectrolyte may be estimated, to a good approximation, with the aid of theoretical expressions for rod-like molecules (*vide post*). In order to know the highest possible reduced dichroism at infinitely high field, $(\Delta A/A)_s$, and the orientation behavior of NaPSS and NaPSS–AA complex, the field strength dependence of steady-state dichroism signals should be compared with a suitable theoretical orientation function. If the polyelectrolyte with identical chromophores in a solution can be regarded as a relatively stiff chain of axial symmetry, the reduced dichroism $\Delta A/A$ for a monodisperse system may be given as[23]

$$\frac{\Delta A}{A}=\frac{3}{2}(3\cos^2\theta-1)\Phi, \tag{5}$$

where A is the absorbance of the same solution in the absence of external electric field, $(3\cos^2\theta-1)$ is the optical term as stated before, and Φ is the orientation function.

The "classical" orientation function, $\Phi(\beta,\gamma)$, for a dipolar molecule with the permanent dipole moment (μ) and/or the polarizability anisotropy ($\Delta\alpha$) has been derived by O'Konski *et al.* (Eq. 14 of Ref. 1). The variables, β and γ, are the interaction energy terms and are given as $\beta=\mu E/kT$ and $\gamma=\Delta\alpha E^2/2kT$ (≥0), where k is the Boltzmann constant and T is the absolute temperature. In the strict sense, the O'Konski-Yoshioka-Orttung or the classical function, $\Phi(\beta,\gamma)$, was derived for the nonionic polymer in solution. Nevertheless, it has been used successfully in many cases, which include aqueous solutions of polyelectrolyte.[1,6,8,11,22] Hence, we also use $\Phi(\beta,\gamma)$ for interpreting the data of NaPSS and NaPSS–AA systems on a qualified, empirical basis. For the ionized polymer system, an orientation function, $\Phi(\kappa)$, was derived by Kikuchi and Yoshioka under consideration of ion-atmosphere polarization (Eq. 8 of Ref. 26).[26] The variable κ is given as $\kappa=ZelE/2kT$, where n is the number of condensed counterions per polyion, Z is the valence of counterion, e is the elementary charge, and l is the contour length of polyion. As Kikuchi and Yoshioka have pointed out,[6] the field strength dependence of the molecular orientation of synthetic polyelectrolyte may be related not only to the flexibility of the polyelectrolyte chain but also to the polydispersity of molecular weights. In order to explain the field strength dependence of a poly(*N*-butyl-4-vinylpridinium bromide) solution, Tricot *et al.*[8] used an orientation function with three different electric polarizabilities. Any synthetic polyelectrolyte sample

should not be the sum of a few discrete species of different molecular weights, but it should have an almost continuous molecular weight distribution. Therefore, we extend both $\Phi(\beta,\gamma)$ and $\Phi(\kappa)$ at first in such a way as to include this distribution.

Since the Schulz-Zimm function,[27,28] $f_w(M)$, has been used often for the molecular weight distribution of synthetic polymer samples, we also utilize it to describe a polydisperse NaPSS sample:

$$f_w(M) = y^{k+1}M^k e^{-yM}/\Gamma(k+1) \quad (6)$$

$$M_n = \frac{k}{y}, \quad M_w = \frac{k+1}{y}, \quad \text{and} \quad \frac{M_w}{M_n} = \frac{k+1}{k}, \quad (7)$$

where M is the molecular weight of a polymer species, M_w and M_n are the weight- and the number-average molecular weights, respectively. The conformation of polyionic NaPSS is probably in a very extended form in a dilute solution,[6,11] the molecular weight M of a particular NaPSS molecule may be equated to $m_0 l$, where l is the length of the NaPSS molecule and m_0 is the molecular weight per unit length. In this case, the ratio M_w/M_n may be equated to the ratio of weight-average length to number-average length l_w/l_n. The relation between $f_w(l)$ and $f_n(l)$, the latter of which is the distribution function for the number of molecules with the contour length l, is given as follows:

$$f_n(l) = \frac{k}{m_0 l y} f_w(l). \quad (8)$$

In the insert of Fig. 6, $f_n(l)$ is plotted against l with a value of 340 nm for l_w, which corresponds to the M_w of 2.8×10^5 daltons for NaPSS, as determined from the viscosity data, and with a value of 1.3 for l_w/l_n ($=M_w/M_n$), which was estimated for the present sample from the data of Nagasawa *et al.*[16,29] For the polydisperse system in which the limiting reduced dichroism, $3(3\cos^2\theta-1)/2$, is independent of molecular species (this is the reasonable assumption for a polymer molecule in which the number of identical chromophores is proportional to its length), Eq. 5 may be expressed in terms of the sum of the individual dichroism of the component species for which the length distribution function is defined by $f_n(l)$:

$$\frac{\Delta A}{A} = \frac{3}{2}(3\cos^2\theta-1)\int_{L_1}^{L_2} l f_n(l)\Phi dl \Big/ \int_{L_1}^{L_2} l f_n(l) dl$$
$$\equiv \frac{3}{2}(3\cos^2\theta-1)\langle\Phi\rangle_w = \left(\frac{\Delta A}{A}\right)_s \langle\Phi\rangle_w, \quad (9)$$

where $\langle\Phi\rangle_w$ is the weight-average orientation function, Φ corresponds to $\Phi(\beta,\gamma)$ or $\Phi(\kappa)$ for a monodisperse system, and $(\Delta A/A)_s$ is the limiting reduced dichroism. Both L_1 and L_2 are the lower and upper limits of l. At limiting high field strength, $\langle\Phi\rangle_w$ approaches unity; hence, $(\Delta A/A)_s = 3(3\cos^2\theta-1)/2$.

In Fig. 6(a), the field strength dependence of the weight-averaged Kikuchi-Yoshioka orientation function $\langle\Phi(\kappa)\rangle_w$ is plotted against $n\kappa_w^2/3$, where κ_w is the weight-average value equal to $Zel_wE/2kT$. The parameter n (1, 5, 10, and 50) is the number of condensed counterions on the polyion surface. Dashed curves represent $\Phi(\kappa)$ for the corresponding monodisperse system. In Fig. 6(b), the field strength dependence

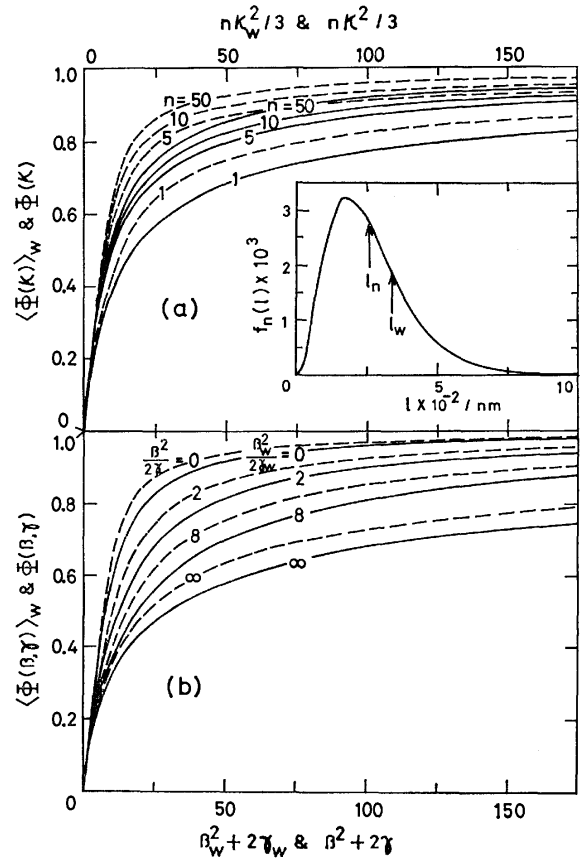

Fig. 6. The Kikuchi-Yoshioka orientation function $\Phi(\kappa)$ and the "classical" orientation function $\Phi(\beta,\gamma)$ for monodisperse and polydisperse systems. In (a), $\langle\Phi(\kappa)\rangle_w$ (——) is plotted against $n\kappa_w^2/3$ for $n=1$, 5, 10, and 50. In (b), $\langle\Phi(\beta,\gamma)\rangle_w$ (——) is plotted against $\beta_w^2+2\gamma_w$ for $\beta_w^2/2\gamma_w=0$, 2, 8, and ∞. The insert shows the Schulz-Zimm length distribution function $f_n(l)$ with the parameter l_w/l_n of 1.3, which was used for calculating both $\langle\Phi(\kappa)\rangle_w$ and $\langle\Phi(\beta,\gamma)\rangle_w$. In (a) and (b), dashed curves (----) are the respective orientation functions $\Phi(\kappa)$ and $\Phi(\beta,\gamma)$ calculated for a monodisperse system ($l_w/l_n=1.0$). The integal limits L_1 and L_2 are set at 12 and 1200 nm.

of the weight-average classical orientation function $\langle\Phi(\beta,\gamma)\rangle_w$ is plotted against $\beta_w^2+2\gamma_w$, where β_w and γ_w are values of $\mu_0 l_w E/kT$ and of $\Delta\alpha_0 l_w E^2/2kT$. Here, μ_0 and $\Delta\alpha_0$ are the permanent dipole moment and the polarizability anisotropy per unit length, respectively. Values of $\beta_w^2/2\gamma_w$ are a measure of relative contributions of those electric moments to field orientation, corresponding to the pure induced moment (0), the mixed dipole moment (2 and 8), and the permanent dipole moment (∞) orientation. Dashed curves represent $\Phi(\beta,\gamma)$ for the corresponding monodisperse system. In Fig. 6, the orientation factor (the average degree of orientation of polyions in solution) for the monodisperse system is larger than for the polydisperse system at a given field strength, except in the low field strength region.

Curve-fitting Method. Several curve fitting methods[1,6,8,22] have been used to obtain values of the intrinsic optical factor and the electric dipole moment. As shown in Fig. 7(a), the field strength dependence

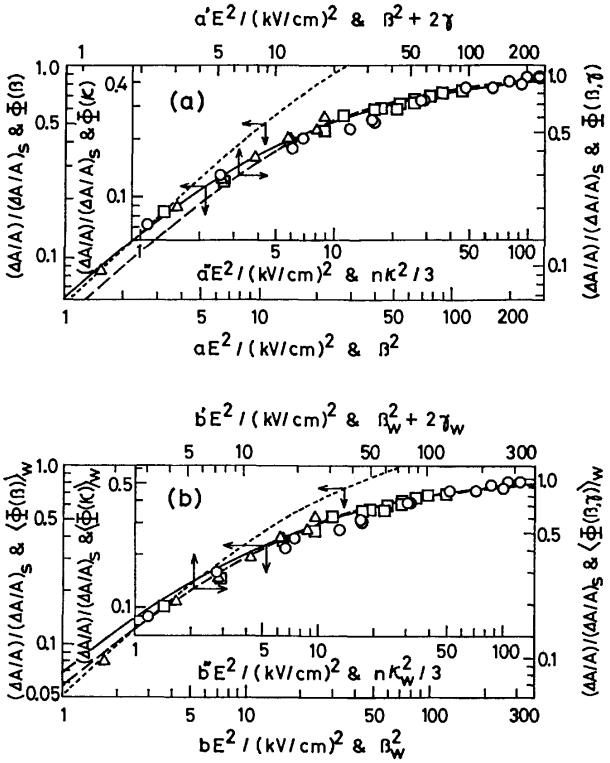

Fig. 7. Comparison of experimental values of reduced dichroism for NaPSS at 224.5 nm (○) and at 262 nm (△) and for NaPSS–AA at 404 nm (□) with theoretical orientation functions (a) for the monodisperse system and (b) for the polydisperse system. In (a), three sets of the double logarithmic plots are shown: $(\Delta A/A)/(\Delta A/A)_s$ against aE^2, $a'E^2$, $a''E^2$; $\Phi(\beta)$ against β^2 (——); $\Phi(\beta,\gamma)$ against $\beta^2+2\gamma$ (----); $\Phi(\kappa)$ against $n\kappa^2/3$ (……). The observed dichroism $\Delta A/A$ for each of NaPSS and NaPSS–AA was normalized by dividing it by the limiting value $(\Delta A/A)_s$ given in Table 2, in order to compare three sets of experimental points (○, △, and □) with a given theoretical orientation function $\Phi(\beta)$, $\Phi(\beta,\gamma)$, or $\Phi(\kappa)$ on each of three coordinates. The factors a, a', and a'' are: $a=0.806$ (○), 0.0704 (△), and 0.339 (□); $a'=0.661$ (○), 0.0577 (△), and 0.278 (□); $a''=0.140$ (□). In (b); three sets of the double logarithmic plots are shown: $(\Delta A/A)/(\Delta A/A)_s$ against bE^2, $b'E^2$, and $b''E^2$; $\langle\Phi(\beta)\rangle_w$ against β_w^2 (——); $\langle\Phi(\beta,\gamma)\rangle_w$ against $\beta_w^2+2\gamma_w$ (----); $\langle\Phi(\kappa)\rangle_w$ against $n\kappa_w^2/3$ (……). $b=0.799$ (○), 0.0610 (△), and 0.384 (□); $b'=0.769$ (○), 0.0588 (△), and 0.370 (□); $b''=0.151$ (□). Both $\Phi(\kappa)$ and $\langle\Phi(\kappa)\rangle_w$ with the n value of 1 are applicable only to the case of NaPSS–AA (□). Symblos and experimental conditions in (a) and (b) are the same as in Fig. 2.

of observed reduced dichroism of NaPSS at 224.5 and 262 nm and NaPSS–AA at 404 nm was compared with theoretical orientation functions by assuming a monodisperse system. The experimental points fit the permanent dipole moment orientation $\Phi(\beta)$ (solid curve) over a wide range of field strength. A mixed-dipole moment orientation function $\Phi(\beta,\gamma)$ with $\beta^2/2\gamma$ of 8 (dashed curve) is also plotted, but it disagrees with the experimental points except for the high field region. Although the orientation function $\Phi(\kappa)$, in which ion-atmosphere polarization is considered, seems to be the most reasonable one for the salt-free NaPSS and NaPSS–AA solutions, it fits the experimental points only in the low field strength region (dotted curve). This discrepancy may be partly due to the neglect of the effect of counterion repulsion and partly due to the polydispersity of polymer length.

In order to test the effect of polymer lengths, the field strength dependence of reduced dichroism for NaPSS and NaPSS–AA systems is compared, in Fig. 7(b), with the orientation functions which take into account the polydispersity with the length distribution function $f_n(l)$ (Fig. 6). Experimental points fit a mixed-dipole moment orientation function $\langle\Phi(\beta,\gamma)\rangle_w$ with a $\beta_w^2/2\gamma_w$ of 8 rather than the pure permanent dipole moment orientation function $\langle\Phi(\beta)\rangle_w$. On the other hand, the experimental points fit $\langle\Phi(\kappa)\rangle_w$ only in the low field strength region; $\langle\Phi(\kappa)\rangle_w$ is definitely closer to the experimental points than $\Phi(\kappa)$. At present, the best (but not necessarily unique) values of $\beta^2/2\gamma$ and $\beta_w^2/2\gamma_w$ together with those of $(\Delta A/A)_s$ were obtained by this curve fitting method and are given in Table 2. It is difficult to select either of them as the more reasonable. In order to obtain the exact value of $\beta_w^2/2\gamma_w$, the form of the length distribution function for the NaPSS sample must be known. It should be noted that the values of the limiting reduced dichroism $(\Delta A/A)_s$ are not appreciably different when they are obtained from the two best fitted orientation functions, $\Phi(\beta)$ and $\langle\Phi(\beta,\gamma)\rangle_w$. This is because both of the two functions approach unity at the limiting high field strength.

Wavelength Dependence of Reduced Dichroism of NaPSS and NaPSS–AA Complex. By comparing values of ε in Table 1 between NaPSS, sodium *p*-toluenesulfonate, and benzene,[30] the longest-wavelength band of NaPSS in the 280—245 nm region is reasonably assigned to the transition polarized in the direction bisecting the 1- and 4-carbon atoms of a phenyl plane (the $^1B_{2u}$ band), while the short-wavelength band in the 245—215 nm region is the transition polarized perpendicular to the long axis in the phenyl plane (the $^1B_{1u}$ band). The reduced dichroic spectra could not be determined at a single polymer concentration for these two bands (Figs. 3 and 4), because the $^1B_{1u}$ band absorbs light much more strongly than the $^1B_{2u}$ band. If the effect of dilution is negligibly small, the difference in $(\Delta A/A)_s$ values for these bands is interpreted as being due to the different tilt angles of the mutually perpendicular transition moments in the phenyl ring relative to the orientation axis of the NaPSS backbone. These angles are given in Table 2. The increase in $\Delta A/A$ values below 224 nm is not explained by the $^1B_{1u}$ transition moment alone, because a single transition moment should give rise to a constant reduced dichroism inside an absorption band. This result probably indicates the presence of another transition moment in the far UV region.[25]

The absorption bands of NaPSS–AA arise from the electronic transition moments of the AA molecule (^1L_a- and ^1L_b-bands), the directions of which are shown in Fig. 5.[15,31,32] They are mutually perpen-

Table 2. Electrooptical parameters of NaPSS and NaPSS-AA in aqueous solutions at 20 °C

	$\frac{\lambda}{\text{nm}}$	$\left(\frac{\Delta A}{A}\right)_s$	$\lvert\theta\rvert$	$\frac{l_w}{l_n}$	$\frac{\beta_w^2}{2\gamma_w}$	$\frac{E^2}{(\text{kV/cm})^2}$ [a]	$\frac{\langle\mu\rangle_w}{\text{D}}$ [b,c]	$\frac{\langle\Delta\alpha\rangle_w}{\text{cm}^3}$ [b,c]
NaPSS	224.5	−0.39	60°	1.0	∞	12.4	1.1×10^4	—
(C_p=0.133 mM)		−0.36	60°	1.3	8	13.0	1.0×10^4	3.1×10^{-16}
NaPSS	262	−0.17	57°	1.0	∞	142	3.2×10^3	—
(C_p=3.31 mM)		−0.18	57°	1.3	8	170	2.8×10^3	2.3×10^{-17}
NaPSS-AA	404	0.38	50°	1.0	∞	29.5	7.1×10^3	—
(C_p=0.663 mM)	315	0.49	48°					
	404	0.34	50°	1.3	8	27.0	7.0×10^3	1.5×10^{-16}
	315	0.44	49°					

a) The square of field strength at $\beta^2+2\gamma=10$ or $\beta_w^2+2\gamma_w=10$. b) When polydispersity is taken into account, the weight-average quantities become $\langle\mu\rangle_w$ and $\langle\Delta\alpha\rangle_w$, which are equated to $\mu_0 l_w$ and $\Delta\alpha_0 l_w$, respectively. c) 1 D=3.336×10^{-30} C m and 1 cm^3=1.113×10^{-16} F m^2.

dicular in the dye plane and are widely separated. Since the bound fraction of AA has been estimated to be more than 99% in the NaPSS–AA solution at a *P/D* of 6.14,[15] the amount of unbound AA in the present solution should be negligibly small. Therefore, the observed dichroic spectra in Fig. 5 can be considered to be the dichroic spectra of the bound AA. If the flexibility of the NaPSS chain is neglected at a low polymer concentration (C_p=0.663 mM), the average angle θ between the transition moment ^1L_a and the orientation axis of the NaPSS–AA complex is *ca.* 50°. The average angle for the ^1L_b band at 315 nm was calculated to be *ca.* 48°. Although the difference of the angles for the ^1L_a and ^1L_b bands is very small, it is definitely beyond the experimental error. The fact that the reduced dichroism of 0.22± 0.02 in the 440—370 nm region differs from that of 0.27±0.02 in the 335—282 nm region may be interpreted as follows: the angles of these transition moments of the bound AA differ from each other relative to the orientation axis of NaPSS–AA (provided that the number and the direction of the transition moments remain unaltered when the dye is bound to the NaPSS site). It should be noted that these angles are still only apparent, since more than one bound AA species may be present on the NaPSS surface.[15,18]

Apparent Dipole Moments of NaPSS and NaPSS–AA Complex. In the preceding section, the experimental points fit $\Phi(\beta,\gamma=0)$ and $\langle\Phi(\beta,\gamma)\rangle_w$ (with a $\beta_w^2/2\gamma_w$ of 8) curves better than $\Phi(\kappa)$ and $\langle\Phi(\kappa)\rangle_w$, over a wide range of field strength. On the other hand, it has been shown by reversing-pulse electric birefringence that both NaPSS and NaPSS–AA possess no appreciable intrinsic permanent dipole moment.[11] Hence, we term μ the pseudo-permanent dipole moment and retain it, until a more complete orientation function is derived for conducting polyelectrolytes. These values are given in Table 2. With an increase in concentrations of NaPSS, the pseudo-permanent dipole moment decreases in the order: NaPSS (C_p=0.133 mM) > NaPSS–AA (C_p= 0.663 mM) > NaPSS (C_p=3.31 mM). This result is qualitatively consistent with the concentration dependence of the specific Kerr constant, as observed by Kikuchi and Yoshioka for KPSS.[6] Thus, the dipole moment of NaPSS depends strongly on the concentration, indicating that, as the ionized sulfonate groups increase, the chain stiffness and, hence, the persistence length also increase.

Conclusion

The field strength dependence of reduced dichroism signals of NaPSS and NaPSS–AA in aqueous solutions can be described by the "classical" permanent dipole orientation function $\Phi(\beta)$ for the monodisperse system and also by the mixed-dipole orientation function $\langle\Phi(\beta,\gamma)\rangle_w$ for the polydisperse system. However, the seemingly more realistic orientation functions $\Phi(\kappa)$ and $\langle\Phi(\kappa)\rangle_w$, based on ion-atmosphere polarization, fit the dichroism data of NaPSS and NaPSS–AA only in the low field range. The necessity for an improved expression for the orientation function of charged, flexible polyelectrolytes is apparent. Such an orientation function must contain the effects of counterion repulsion, the flexibility, and the polydispersity of polymer chain. The reduced dichroism at limiting high field, estimated with different theoretical orientation functions, is almost identical. The wavelength dependence of reduced dichroism of NaPSS indicates that the UV band is composed not only of the $^1B_{1u}$ and $^1B_{2u}$ transitions but also of another higher-energy transition in the far UV region. The absorption spectrum of NaPSS–AA is composed of both the ^1L_a and ^1L_b in-plane transitions, whose average angles are slightly, but definitely, different from each other relative to the orientation axis of the NaPSS backbone.

References

1) C. T. O'Konski, K. Yoshioka, and W. H. Orttung, *J. Phys. Chem.*, **63**, 1558 (1959).
2) H. Nakayama and K. Yoshioka, *Nippon Kagaku Zasshi*, **85**, 177 (1964).
3) H. Nakayama and K. Yoshioka, *J. Polym. Sci., Part A*, **3**, 813 (1965).
4) K. Yoshioka and C. T. O'Konski, *Biopolymers*, **4**, 499 (1966).
5) K. Yoshioka and C. T. O'Konski, *J. Polym. Sci., Part A-2*, **6**, 421 (1968).
6) K. Kikuchi and K. Yoshioka, *J. Phys. Chem.*, **77**,

2101 (1973).
7) M. Tricot and C. Houssier, "Polyelectrolytes," ed by K. C. Frisch, D. Klempner, A. V. Patsis, Technomic Publishing Co., Westport, Conn. (1976), pp. 43—90.
8) M. Tricot, C. Houssier, and V. Desreux, *Eur. Polym. J.*, **12**, 575 (1976).
9) M. Shirai, "Molecular Electro-Optics Part 2," ed by C. T. O'Konski, Marcel Dekker Inc., New York (1978), pp. 685—711.
10) M. Tricot, C. Houssier, and V. Desreux, and F. V. D. Touw, *Biophys. Chem.*, **8**, 221 (1978).
11) K. Yamaoka and K. Ueda, *J. Phys. Chem.*, **84**, 1422 (1980).
12) T. Soda and K. Yoshioka, *Nippon Kagaku Zasshi*, **86**, 1019 (1965).
13) M. Tricot, C. Houssier, and V. Desreux, *Biophys. Chem.*, **3**, 291 (1975).
14) K. Yamaoka and M. Takatsuki, *Bull. Chem. Soc. Jpn.*, **51**, 3182 (1978).
15) K. Yamaoka, M. Takatsuki, and K. Nakata, *Bull. Chem. Soc. Jpn.*, **53**, 3165 (1980).
16) A. Takahashi, T. Kato, and M. Nagasawa, *J. Phys. Chem.*, **71**, 2001 (1967).
17) K. Yamaoka, *Biopolymers*, **11**, 2537 (1972).
18) M. Takatsuki, *Bull. Chem. Soc. Jpn.*, **53**, 1922 (1980).
19) K. Yamaoka and M. Takatsuki, *Bull. Chem. Soc. Jpn.*, **54**, 923 (1981).
20) K. Yamaoka and K. Matsuda, *J. Sci. Hiroshima Univ., Ser. A*, **43**, 185 (1980).
21) K. Yamaoka and E. Charney, *Macromolecules*, **6**, 66 (1973).
22) K. Yamaoka and K. Matsuda, *Macromolecules*, **14**, 595 (1981).
23) K. Yamaoka and E. Charney, *J. Am. Chem. Soc.*, **94**, 8963 (1972).
24) G. E. Boyd, "Polyelectrolytes," ed by E. Sélégny, Reidel Publishing Co., Dordrecht (1974), pp. 135—155.
25) K. Yamaoka and M. Asato, 29th Annual Meeting of the Society of Polymer Science, Japan, Kyoto, May 1980, Abstr. p. 460.
26) K. Kikuchi and K. Yoshioka, *Biopolymers*, **15**, 583 (1976).
27) G. V. Schulz, *Z. Phys. Chem.*, **B43**, 25 (1939).
28) B. H. Zimm, *J. Chem. Phys.*, **16**, 1099 (1948).
29) A. Takahashi, N. Kato, and M. Nagasawa, *J. Phys. Chem.*, **74**, 944 (1970).
30) H. H. Jaffé and M. Orchin, "Theory and Applications of Ultraviolet Spectroscopy," John Wiley and Sons, New York (1966), p. 299.
31) H. Kokubun, *Z. Elektrochem.*, **62**, 599 (1958).
32) J. Yoshino, T. Hoshi, T. Masamoto, H. Inoue, and K. Ota, *Nippon Kagaku Zasshi*, **12**, 2227 (1972).

 © 1982 The Chemical Society of Japan Bull. Chem. Soc. Jpn., 55, 77—84 (1982)

Construction of an Adiabatic Calorimeter Workable under Constant High-pressure†

Masaharu OGUNI, Kazuo WATANABE,** Takasuke MATSUO, Hiroshi SUGA,* and Syûzô SEKI***

Department of Chemistry and Chemical Thermodynamics Laboratory, Faculty of Science, Osaka University, Toyonaka, Osaka 560

(Received May 26, 1981)

An adiabatic high-pressure calorimeter was constructed. The calorimeter cell was devised for minimization of the cell mass relative to the volume of the sample chamber. The pressure in the cell was controlled by joining the cell with a transmitting tube to a stabilized high-pressure system. The adiabatic conditions were achieved by temperature control of the transmitting tube as well as of adiabatic shields inside the cryostat. Procedures for the precise pressure control and for the determination of the molar volume and heat capacity with the correction for the mass transfer of pressure-transmitting liquid in a series of measurement were discussed. The apparatus is capable of measurement under constant pressure up to 110 MPa and over the temperature range from 100 to 370 K. The results on liquid 3-methylpentane which was used as the pressure medium proved satisfactory performance of this new-type calorimeter.

Temperature and pressure are among the most fundamental parameters in specifying the thermodynamic state of substances. Various physicochemical phenomena are most profitably studied by detailed and accurate measurement of the heat capacity, volume expansivity, and compressibility as functions of both temperature and pressure. These properties under ordinary pressure have hitherto been measured with high precision and accuracy in a wide temperature range. Although volume measurements for liquids have been extended to high pressures,[1-3] few quantitative measurements of heat capacity under pressure have been reported so far. Development of such measurements is naturally expected to contribute, to a great extent, to further understanding of the behaviors of substances at ordinary pressure as well as under pressure. Among these interesting behaviors are the pressure dependences of characters of phase transitions and the details around multiple points.

The heat capacity of a condensed matter is usually measured under constant pressure because of the difficulty in keeping the volume of the specimen constant. An adiabatic calorimeter is known to give the most reliable data at the atmospheric pressure. High pressure makes it difficult to satisfy some of the conditions favorable for the adiabatic calorimetry through the requisite of placing the specimen under pressure. A fundamental problem originates from increase of the mass of the calorimeter cell. The increase of the mass of the cell necessarily results in decrease in the ratio of the sample heat capacity to the total observed heat capacity vitiating certainty of the measurement. This situation leads to two calorimetric principles applied for construction of the calorimeter, a non-adiabatic or adiabatic method, depending on the pressure range to be covered.

Non-adiabatic methods, d.c. pulse or a.c. calorimeters, are applied to the measurements in the higher pressure than about 1 GPa.[4-7] The adiabatic method, employed in the relatively low pressure range up to $\approx$1 GPa, follows the principle of the adiabatic calorimetry under the ordinary pressure. Two types of apparatuses can be devised depending upon the choice whether the pressurized specimen is isolated from the surroundings or it communicates with an external pressure reservoir. The former condition is realized in a clamp-bomb calorimeter; the high pressure is generated and clamped outside the cryostat beforehand using a screw, and then the measurement is performed with the conventional adiabatic calorimeter as is done just at ordinary pressure.[8-11] Amitin *et al.* adopted this type of apparatus for the measurements on NH_4Cl crystal.[9] The pressure applied to the sample in such a calorimeter changes with the temperature. Especially when the sample undergoes a phase transition, the change should be drastic around that temperature, resulting in quite a complicated thermodynamic path in the p-T plane followed by the specimen in a series of measurement. The latter alternative is achieved by joining the calorimeter cell to the outside pressure-control system with a pressure-transmitting tube. In such a calorimeter, transfer of a part of the pressure medium out of or into the cell is inevitable as the temperature of the cell changes. Mil'ner reported the result on NH_4Br at 35 MPa with an apparatus of this type.[12] He employed argon gas as the pressure medium, which restricted the practical pressure range to the low region in view of the danger associated.

In this paper, we report the detail of a high-pressure adiabatic calorimeter and the results on liquid 3-methylpentane obtained with it. Features of the present calorimeter are as follows; (1) it is capable of heat capacity measurement in the temperature region from 100 to 370 K and the pressure range up to 110 MPa, (2) operates under adiabatic condition, (3) operates under stabilized hydrostatic pressure, and (4) enables to measure the volume (and therefore expansivity and compressibility) simultaneously. Heat of compression can also be derived by taking an extra procedure.

† Contribution No. 23 from Chemical Thermodynamics Laboratory.

** Present address: Kanzaki Paper Mfg. Co. Ltd., 1-11, Jôkôji-machi, Amagasaki 660.

*** Present address: Department of Chemistry, School of Science, Kwansei Gakuin University, Nishinomiya 662.

Construction of Apparatus

Method of Calorimetry. Any high-pressure calorimetry is carried out at the sacrifice of some favorable conditions which are met in adiabatic calorimetry under ordinary pressure. The present calorimeter permits pressure medium to flow into or out of the cell so as to keep the pressure constant. The effect of transfer of a mass of the medium is to be corrected for later using dilatometric data. Heat capacity value obtained experimentally corresponds exactly to C_p on account of self-evident thermodynamic path in a series of measurement.

The whole apparatus consists of a calorimeter cell, a circuit for energy supply and its measurement, a temperature-measuring system, an adiabatic-control system, and a high-pressure system. Most of the parts excepting the temperature- and energy-measuring systems were installed in a room, the temperature of which was kept constant at (30.0±0.1) °C.

The calorimeter cell is equipped with a platinum resistance thermometer and a heating element. The temperature measurement of the cell was performed with a precision a.c. double bridge (AΣ*A* Inc. Model H8). The electric energy supplied to the cell was measured by using a digital voltmeter and a digital clock. An adiabatic condition of the calorimeter cell was realized by evacuating space inside the cryostat and by temperature-controlling the shields and high-pressure tube within the cryostat. The pressure in the cell was controlled by connecting the cell with the transmitting tube to the high-pressure system which consists of pressure generation, pressure transmission, pressure gauge, pressure control and dilatometry subsystems. Liquid 3-methylpentane was used as the pressure medium, because it was known to undergo neither crystallization nor glass transition down to liquid nitrogen temperature.

Calorimeter Cell. A calorimeter cell must have the strength enough to withstand the applied pressure. The requirement causes the mass of, and therefore the heat capacity of, the high-pressure cell to increase with increase of the maximum pressure to which the measurement is intended. For this reason, inaccuracy of an adiabatic calorimetry originates primarily from smallness of the heat capacity of the sample compared with that of the empty cell.

The present calorimeter cell was so designed as to maximize the volume of the sample space for the given mass of the cell material. Figure 1 shows the sectional drawing of the calorimeter cell and the annexed pressure-transmitting tube made of stainless steel. The sample vessel (D), vessel gland (M), and a packing washer (J) were made of a copper-beryllium alloy which had reasonably high thermal conductance and good mechanical properties necessary for the calorimeter cell. They were machined out from the material annealed at 315 °C for 2.5 h for the purpose of increasing the mechanical strength. A spherical shape of the vessel is one of particular devices for minimization of the mass of the empty cell and maximization of the space of the sample

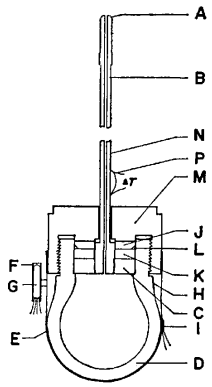

Fig. 1. Sectional drawing of the calorimeter cell.
(A): Cone-shaped connection part, (B): pressure-transmitting tube, (C): high-pressure plug, (D): sample vessel, (E): vessel cover, (F): copper sheath, (G): platinum resistance thermometer, (H): cell heater, (I): thermocouple for temperature control of inner shield, (J): copper-beryllium packing washer, (K): Teflon and indium packings, (L): copper extrusion ring, (M): vessel gland, (N): tube heater, (P): thermocouple for temperature control of tube B.

chamber. A sawtooth type of screw between the vessel and the gland was devised to minimize the thickness of the cylindrical part of the gland to the limit compatible with the mechanical strength required. Sealing of the cell was based on Bridgman's principle that the pressure exerting on the indium and teflon packing is larger than the medium pressure. A pressure transmitting tube (B), whose bottom area is unsupported, was screwed into a plug (C) made of stainless steel. An annealed-copper extrusion ring (L) served to prevent the teflon and indium from flowing outside. Heater wire (H) was wound outside the sample vessel. A thin vessel cover (E), made of copper, was installed to intercept heat leak by radiation from the heater as well as to fix thermocouple (I) and a copper sheath which held the platinum thermometer. This cover was gold-plated for reduction of radiative heat leak between the cell and its surroundings. The volume of the sample chamber was 24.522 cm^3 at 19 °C and the mass of the empty cell *ca.* 550 g. The whole cell was attached to or detached from the high-pressure system through a cone connector (A).

Cryostat and Adiabatic-control System. Adiabatic control requires minimization of the heat leak between the calorimeter cell and its surroundings. The minimization was achieved by evacuation of the space inside the cryostat (10^{-4} Pa) and by temperature regulation of the shields and the pressure tube. Figure 2 is a sectional illustration of the cryostat. The shields referred to as inner (B and D) and outer (F), and block (H) were made of copper for its high thermal conductivity. The high-pressure tube and the block were soldered to each other so as to aid their thermal contact. The electrical wires were twisted pair-wise to reduce inductive interference among them. The temperature control system utilizes the temperature difference signals ΔT_1 from the chromel-constantan thermocouples to regulate the current passing through

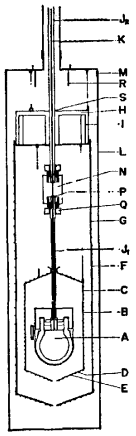

Fig. 2. Schematic diagram of the cryostat.
(A): Calorimeter cell, (B): inner-side shield, (C): side heater, (D): inner-bottom shield, (E): bottom heater, (F): outer shield, (G): outer heater, (H): block, (I): block heater, (J): tube heater, (K): pressure transmitting tube, (L): brass jacket, (M): Wood's alloy joint, (N): coupling, (P): cone connector, (Q): coupling gland, (R): thermal anchor for leads, (S): high-melting solder.

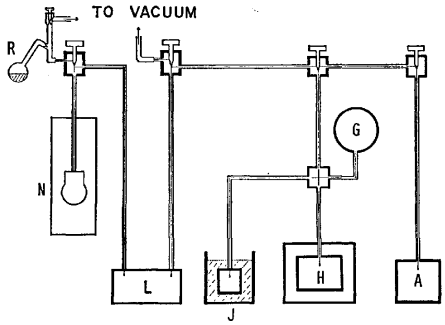

Fig. 3. Schematic drawing of the high-pressure system.
(A): Pressure generator, (G): Heise pressure-gauge, (H): oil reservoir, (J): manganin pressure-gauge, (L): dilatometer, (N): calorimeter cell, (R): glass bulb.

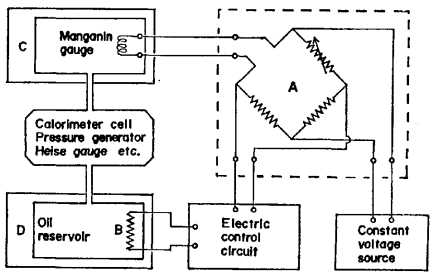

Fig. 4. Block diagram of the pressure control system.
(A): Wheatstone bridge, (B): oil heater, (C): water bath, (D): air bath.

the corresponding heater. Heat leak between the cell and the inner shield (B) and through the high-pressure tube (J_1) affected most severely the experimental results. Five pairs of thermocouple were installed between the cell and the shield. The stainless-steel pressure tube was made as slender as is compatible with the required strength, and temperature-regulated by use of PID control circuit. The bottom and the other part of the inner shield were temperature controlled separately for better temperature-homogeneity within the inner shield. The temperature of the outer shield, block, and upper pressure tube (J_2) were held at several Kelvin below that of the cell. The whole cryostat was immersed into liquid nitrogen.

High-pressure System. The high-pressure system consisted of subsystems for generation, transmission, measurement and control of the pressure, including a dilatometer in it. The whole system is schematically depicted in Fig. 3. Two liquids separated by at the dilatometer were employed as pressure media in the lines; the lines on the pressure generation side (right-hand side in the figure) of the dilatometer (L) were filled with liquid kerosene through pumping at the pressure generator (A), while the lines on the cryostat side (left-hand side) with liquid 3-methylpentane. The pressure was read from the scale of Heise gauge (G). The whole system was installed in a room controlled at (30.0±0.1) °C.

The pressure control subsystem keeps the pressure constant by cancelling pressure change which is induced by the change of the cell temperature during the heat capacity measurement. Detail of the subsystem is illustrated in Fig. 4. The pressure was controlled by adjusting the temperature of the kerosene reservoir. Change of the pressure was monitored as a change in the manganin coil resistance which constituted one arm of a Wheatstone bridge, and this electrical signal was used to regulate the current passing through the heater (B) in the reservoir. The pressure to be set up was selected by changing the variable resistance of the Wheatstone bridge. Adoption of this method enabled to control the pressure automatically within 0.1 MPa in the whole temperature range measured. The coiled manganin wire was left strain-free in a vessel (J). The resistance was measured with the method of three terminals in order to allow for the lead resistance. The whole vessel was immersed in an oil bath (C) controlled at constant temperature of (35.0±0.1) °C.

The sectional drawing of the kerosene reservoir is shown in Fig. 5. The method of unsupported area was made use of for sealing. The electrode was fixed and insulated in the same way as in the manganin gauge by using Teflon as the packing material. A high-pressure tube (P) was fixed by screwing into the plug (C) and by tightly sealing with the Araldite resin. Heater wire (D) was glued on vanes (E) with Araldite. The volume of the kerosene chamber is ≈250 cm^3 which was *ca.* 10 times larger than that of the sample chamber of the calorimeter cell. The whole vessel was installed in an air bath, the temperature of which was always kept lower by *ca.* 10 °C than that of the kerosene chamber.

Charge of liquid 3-methylpentane into the high-pressure lines was carried out by using a vacuum line as shown in Fig. 3. The liquid was first poured into the glass bulb (R) and then the bulb was connected with a joint to the vacuum line. After repeated degassing of the liquid and evacuation of the calorim-

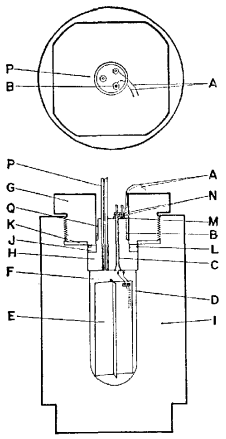

Fig. 5. Schematic diagram of the kerosene reservoir. (A): Heater lead, (B): electrode, (C): Teflon insulator and packing, (D): heater, (E): vane, (F): oil chamber, (G): gland bolt, (H): high-pressure plug, (I): body, (J): Teflon packing, (K): stainless packing washer, (L): copper extruding ring, (M): insulator, (N): nut, (P): high-pressure tube, (Q): self-extractor bolt.

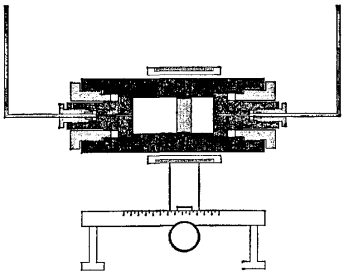

Fig. 6. Sectional drawing of the dilatometer.

eter cell and the dilatometer, the liquid was transferred into the high-pressure system by vacuum distillation at ≈50 °C.

Dilatometer. The present calorimeter permits the pressure medium to flow into or out of the cell for keeping the pressure constant. Calculation of the sample heat capacity from the apparent one requires the mass of the medium contained in the cell to be determined as a function of temperature. The dilatometer gives such data as well as essential information on the temperature dependence of the sample volume. A stainless-steel cylinder and Permalloy core constituted the dilatometer as shown in Fig. 6. The inner diameter of the cylinder was (2.000±0.010) cm. The core with very high magnetic susceptibility moved by pressure difference less than 0.1 MPa. The two pressure media (kerosene and 3-methylpentane) were separated by the core and an O-ring fitted up around it.

Expansion or contraction of the sample associated with the change of the temperature at the cell induced movement of the position of the core inside the cylinder. The position was detected by a combined apparatus of a cathetometer equipped with a differential transformer and a lock-in amplifier. The position of the transformer was read to 0.001 cm corresponding to 0.003 cm^3 in the error of volume measurement. The certainty was good enough for the temperature dependence of the mass of 3-methylpentane in the cell to be used in computing the heat capacity values.

Energy Supply and Temperature Measurement. Energy supply and temperature measurement were carried out by use of the apparatus already constructed.[13] A Minco thermometer of 469.740 Ω at 273.15 K was used as the temperature sensor of the calorimeter cell. The detailed procedure for determination of the temperature and the total input energy was given in the article reported before.[13]

Determination of the Volume and the Heat Capacity. Total heat capacity C consists of contributions from the pressure medium in the cell, mC_1, the empty cell, C_b, and the sample, C_s;

$$C = mC_1 + C_b + C_s. \tag{1}$$

One analyses the change of state induced by a heating experiment as follows. Let $T-\Delta T$ and $m+\Delta m$ designate the temperature and the mass of the pressure medium in the initial state, and $T+\Delta T$ and $m-\Delta m$ those in the final state. Here T and m are those in the intermediate of the initial and final states. The specific heat capacity of the medium is then approximated as C_1+at, where C_1 is the specific heat capacity at T, t the temperature difference from T, and a the differential coefficient of the heat capacity by temperature. Since the input energy causes the temperature increase of the materials constituting the calorimeter cell, the total input energy ΔH is written as follows;

$$\Delta H = 2\Delta T(C_s+C_b) + \int_{-\Delta T}^{\Delta T}\left(m-\frac{t}{\Delta T}\Delta m\right)(C_1+at)\mathrm{d}t$$
$$= 2\Delta T(C_s+C_b) + 2\Delta T m C_1 - \frac{2}{3}(\Delta T)^2 a\Delta m. \tag{2}$$

The apparent heat capacity C_e is expressed from this as follows;

$$C_e = \frac{\Delta H}{2\Delta T} = C_s + C_b + mC_1 - \frac{a\Delta T\Delta m}{3}. \tag{3}$$

The total heat capacity under constant pressure with the liquid medium of m is given by

$$C_p = C_s + C_b + mC_1, \tag{4}$$

and consequently

$$C_p = C_e + \frac{a\Delta T\Delta m}{3}. \tag{5}$$

The correction given by the second term of the right-hand side is estimated in order of magnitude in the case where the cell contains only the pressure medium 3-methylpentane. The following relations then hold for a typical measurement in which $2\Delta T \approx 2$ K and $T > 100$ K;

$$a\Delta T \lesssim 10^{-2} C_1, \tag{6}$$

$$\Delta m \lesssim 10^{-2} m, \tag{7}$$

because the volume expansivity is $\approx 10^{-3}$. It follows that the correction is smaller than $10^{-4} mC_1$ to be neglected to a good approximation in the determination of C_p. Thus the heat capacity under constant pressure is given by

$$C_p = C_e. \tag{8}$$

But the amount of the pressure-transmitting liquid,

m, at the midpoint of the initial and the final temperatures changes with temperature and pressure and is to be determined from dilatometric data.

The heat capacity of the evacuated cell $C_b(T)$ was measured and assumed to depend only on the temperature. This assumption was tested as follows. The effect of pressure on the heat capacity of the copper-beryllium alloy could be assessed from the equation

$$\left(\frac{\partial C}{\partial p}\right)_T = -T\left(\frac{\partial^2 V}{\partial T^2}\right)_p. \quad (9)$$

With the volume expansivity *vs.* temperature data around 200 K of copper similar to the copper-beryllium alloy, the estimate shows $(\partial C_b/\partial p)_T/C_b \simeq 10^{-5}$ MPa^{-1} for the cell, indicating that the influence is negligible within the error of measurement in the low pressure range ($\approx 10^2$ MPa).

The amount of pressure medium in the cell, m, naturally depends upon the volume of the cell. The volume $V_c(T, p)$ was given by

$$V_c(T,p)/\mathrm{cm}^3 = \{0.987740+3.5\times10^{-5}(T/\mathrm{K}) + 2.5\times10^{-8}(T/\mathrm{K})^2\} \times \{24.520+2.3\times10^{-4}(p/\mathrm{MPa})\}. \quad (10)$$

The volume was first calibrated, using water, to be 24.522 cm^3 at 19.0 °C and an atmospheric pressure. The temperature dependence, the former factor in Eq. 10, was determined assuming that the expansion coefficient α was given by a linear function of temperature, $\alpha=4\times10^{-5}+5\times10^{-6}\{(T/\mathrm{K})-100.0\}$, with the values 4×10^{-5} K^{-1} at 100 K and 5×10^{-5} K^{-1} at 300 K. The pressure coefficient in the latter factor, on the other hand, was estimated at 30 °C by measuring first the pressure dependence of the molar volume of 3-methylpentane, and then the pressure dependence of the volume of 3-methylpentane inside the cell.

The molar volume and the molar heat capacity of 3-methylpentane are derived from calorimetric and dilatometric data as follows. Let $\rho_0(p)$ and $m_0(p)$ be the density and mass of the liquid contained in the cell, respectively, at 30 °C (=303 K) and some constant pressure p. Decreasing the temperature of the cell from 303 K to T displaces the core in the dilatometer toward the cell by l. The mass of the pressure medium in the cell is then given by the expression

$$m(T,p) = m_0(p) + \pi r^2 l \rho_0(p), \quad (11)$$

where r is the inner radius of the dilatometer. The density is accordingly

$$\rho(T,p) = \{m_0(p)+\pi r^2 l\rho_0(p)\}/V_c(T,p). \quad (12)$$

From this, the molar volume is given by the expression

$$V_c(T,p) = M/\rho(T,p), \quad (13)$$

and the molar heat capacity

$$C_i'(T,p) = M\{Q/\Delta T - C_b(T)\}/m(T,p). \quad (14)$$

Here M represents molar mass of 3-methylpentane, and $Q/\Delta T$ the apparent experimental heat capacity at T. Volume expansivity and compressibility can be calculated through thermodynamic relations.

The similar procedure in the case where the sample replaces greater part of the medium in the cell is shown in the following. Using the same notations of $\rho_0(p)$, $m_0(p)$, $m(T,p)$, and l as described above, one obtains the same relation as Eq. (11). Therefore the molar volume of the sample is expressed by

$$V_s(T,p) = \frac{M_s}{m_s}\left[V_c(T,p) - \frac{m_0(p)+\pi r^2 l\rho_0(p)}{\rho(T,p)}\right], \quad (15)$$

where $\rho(T,p)$ is the density of pressure medium derived in Eq. 12. The molar heat capacity has the expression

$$C_s(T,p) = \frac{M_s}{m_s}\left[\frac{Q}{\Delta T} - C_b(T) - \frac{m(T,p)}{M}C_i'(T,p)\right], \quad (16)$$

where m_s is the mass of the sample and M_s its molar mass. Here $m(T,p)$ is not equal to that given by Eq. 11, but is to be derived from dilatometric data using the values of the sample density and $V_c(T,p)$ at a certain temperature and pressure.

In fact, the temperature of the tube immediately above the cell (*i.e.*, the part between a coupling and the cell) changes with the same time-dependence as that of the temperature of the cell for the adiabatic temperature control of the cell. The effect of this temperature change at the tube on the displacement of the core position should be corrected for in the processing of dilatometric data. Let $Y_0(p)$ and $Y(p)$ denote the readings of the core position at 30 °C and T, respectively. The volume inside of the tube the temperature of which changes according to the change in the temperature of the cell being taken 0.1 π cm^3, the reading after above correction, $Y_1(p)$, is derived from the equation

$$Y_1(p)/\mathrm{cm} = Y(p)/\mathrm{cm} + 0.1\left[\frac{\rho(T,p)-\rho_0(p)}{\rho_0(p)}\right]. \quad (17)$$

The amount of the pressure medium in the cell at T is therefore given by

$$n(T,p) = n_0(p) + \frac{[Y_1(p)-Y_0(p)]\pi\rho_0(p)}{M}, \quad (18)$$

assuming the amount at 30 °C is $n_0(p)$. This correction was applied to the processing of data in both the cases with and without the sample in addition to the pressure medium in the cell. In the former case, the application for the molar volume of the sample material gives,

$$V_s(T,p) = \frac{M_s}{m_s}\left\{V_c(T,p) - \frac{[n_0M+(Y_1(p)-Y_0(p)\pi\rho_0(p)]}{\rho(T,p)}\right\}. \quad (19)$$

Results on 3-Methylpentane

Experimental. All the space inside and outside of the cell was evacuated after connection of the cell into the high-pressure system. Heat capacity of the empty cell was measured under that vacuum condition in the temperature range from 80 to 370 K.

The molar volume and heat capacity of liquid 3-methylpentane were measured in the following procedure. The reagent, purchased from Nakarai Chemical Co., was first introduced into a glass bulb (R in Fig. 3) and degassed carefully. The sample was then transferred into the high-pressure system and

Table 1. Pressure dependence of relative volume of 3-methylpentane at 30 °C

P / MPa	$V(P)/V(101\ \text{kPa})$	P / MPa	$V(P)/V(101\ \text{kPa})$
0.101	1.0000	66	0.9305
3	0.9954	69	0.9282
6	0.9910	72	0.9258
9	0.9869	75	0.9235
12	0.9831	78	0.9213
15	0.9795	81	0.9190
18	0.9760	84	0.9169
21	0.9726	87	0.9147
24	0.9693	90	0.9126
27	0.9661	93	0.9106
30	0.9630	96	0.9086
33	0.9600	99	0.9066
36	0.9571	102	0.9047
39	0.9541	105	0.9027
42	0.9513	108	0.9009
45	0.9485	111	0.8990
48	0.9458	114	0.8972
51	0.9431	117	0.8954
54	0.9405	120	0.8937
57	0.9380	123	0.8920
60	0.9354	126	0.8903
63	0.9330	129	0.8886
		132	0.8870

Table 2. Molar volume of 3-methylpentane

T / K	$V(101\ \text{kPa})$ / cm³ mol⁻¹	$V(108.0\ \text{MPa})$ / cm³ mol⁻¹
100	104.4	
110	105.5	
120	106.6	102.6
130	107.8	103.4
140	108.9	104.2
150	110.1	105.1
160	111.2	105.9
170	112.4	106.8
180	113.6	107.6
190	114.9	108.5
200	116.1	109.3
210	117.4	110.2
220	118.7	111.0
230	120.1	111.8
240	121.5	112.7
250	122.9	113.6
260	124.4	114.5
270	126.0	115.4
280	127.5	116.3
290	129.1	117.2
300	130.9	118.2

the cell by vacuum distillation. The core of the dilatometer was brought toward the pressure generator at the room temperature to allow for the contraction of the liquid by pressure increase and/or temperature decrease. The value of molar volume at 20 °C and an atmospheric pressure was taken from a

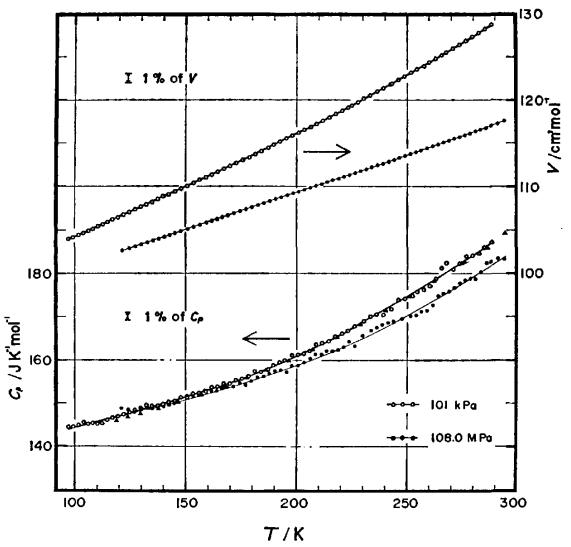

Fig. 7. Molar volume and molar heat capacity of 3-methylpentane.
○: 0.101 MPa, ●: 108.0 MPa.

reference.[14] The ratio of the molar volume at each pressure to that at 0.101 MPa was first measured at 30 °C and is collected in Table 1. The heat capacity was measured at 0.101 MPa and at 108.0 MPa in the heating direction from 100 to 300 K.

Results. The results of molar volume and heat capacity of liquid 3-methylpentane at the atmospheric pressure (0.101 MPa) and 108.0 MPa are shown in Fig. 7 and collected in Tables 2 and 3. The heat capacity at 0.101 MPa was previously measured by Finke and Messerly using a conventional adiabatic calorimeter (Δ in the figure).[16] The present value above 160 K was in good agreement with that and larger by 0.5—1 J K^{-1} mol^{-1} between 120 K and 160 K. The discrepancy in the low temperature region is approximately 0.5%. The relatively large scattering of the heat capacity data is due to the adverse situation that the sample accounted for about one tenth of the total observed heat capacity.

Comparison between the molar heat capacities at 0.101 MPa and at 108.0 MPa shows that the former values is larger by *ca.* 6 J K^{-1} mol^{-1} than the latter one around room temperature, while it is almost the same as the latter below 130 K. Self-consistency between this pressure dependence of the heat capacity and temperature dependence of the molar volume in the present experiment is checked using a thermodynamic relation (9). The second order differential coefficient of the volume with the temperature was derived from the volume data smoothed against temperature, and the average value between those at two pressures was employed in the calculation. At 280 K, the difference between the heat capacities at 0.101 MPa and at 108.0 MPa was calculated with the relation to be -7.2 J K^{-1} mol^{-1}, which should be compared with -6 J K^{-1} mol^{-1}. At 130 K, it was -1.3 J K^{-1} mol^{-1} to be compared with ≈ 0 J K^{-1} mol^{-1}. The consideration on the error included in the derivation of second-order differential coefficients of volume would make such a discrepancy as *ca.* 1 J K^{-1} mol^{-1} insignificant,

Table 3. Molar heat capacity of 3-methylpentane

T/K	C_p/J K^{-1} mol^{-1}	T/K	C_p/J K^{-1} mol^{-1}	T/K	C_p/J K^{-1} mol^{-1}	T/K	C_p/J K^{-1} mol^{-1}
		184.11	157.2	282.39	184.6	203.43	159.4
p=101 kPa		186.92	157.6	285.30	185.8	206.06	160.4
97.16	144.4	189.70	158.8	288.19	187.1	208.62	161.4
99.43	144.4	192.48	159.5			211.17	161.4
101.87	144.6	195.24	160.0	p=108.0 MPa		213.71	162.2
103.67	145.5	197.98	161.2	121.21	148.8	216.24	162.1
106.05	145.1	200.72	161.3	124.42	148.4	218.76	162.4
108.19	145.4	203.43	161.5	127.28	148.1	221.28	163.0
110.31	145.1	206.15	162.1	129.99	148.5	223.78	164.3
112.53	145.3	208.88	163.6	132.67	148.8	226.28	163.3
114.82	146.0	211.65	163.9	135.22	148.7	228.77	164.0
117.09	146.2	214.60	164.3	137.75	149.4	231.31	167.3
117.15	146.6	217.53	165.4	140.26	149.2	233.82	166.8
119.46	146.9	220.37	166.0	142.74	149.5	236.36	167.5
122.07	147.4	223.20	166.7	145.20	149.9	238.89	168.1
124.68	147.9	224.79	166.0	147.87	151.2	241.41	168.6
127.29	148.4	227.59	169.3	150.70	151.6	243.93	168.9
129.87	148.7	230.42	168.9	153.50	151.6	246.45	168.5
132.42	149.4	233.30	170.0	156.29	151.8	248.96	170.3
134.95	149.2	236.17	170.1	159.05	152.8	251.45	170.1
137.45	149.3	239.19	170.4	161.80	151.7	253.95	170.3
139.94	149.6	242.29	171.6	161.57	152.9	256.43	171.2
142.41	150.1	243.09	170.6	163.96	152.8	259.05	171.5
145.07	150.3	245.94	173.9	166.33	153.4	261.51	172.7
147.92	151.1	248.77	174.1	168.89	153.6	263.97	174.9
150.74	151.2	251.61	174.5	171.63	153.8	266.42	175.4
153.54	152.2	254.43	175.7	174.35	154.6	268.88	175.9
156.32	152.2	257.25	176.1	177.06	154.2	271.32	176.7
159.08	152.6	260.05	177.1	179.75	155.1	273.75	177.8
161.82	153.6	262.85	178.7	182.43	156.0	276.18	178.5
164.54	153.7	265.64	181.2	185.10	156.2	278.60	178.8
167.25	154.5	268.42	180.8	187.75	156.9	281.01	178.8
169.96	154.4	267.77	182.3	190.41	157.5	283.42	180.3
172.75	155.2	270.72	180.9	193.04	157.7	285.87	182.5
175.61	155.6	273.66	182.2	195.65	157.3	288.22	182.7
178.46	156.1	276.59	183.9	198.25	158.7	291.06	183.6
181.30	157.3	279.50	184.1	200.85	158.8		

Accordingly, the results of volume and heat capacity would be concluded to be consistent each other.

These facts indicate that the present calorimeter has an excellent ability to give information of volume and heat capacity at constant pressure simultaneously in the temperature region at least from 100 to 300 K and up to 110 MPa. The imprecision and inaccuracy of heat capacity datum are estimated to be 0.5% and 1%, respectively, in comparison with the previous data which were claimed to have 0.2% inaccuracy at an atmospheric pressure.[16]

Concluding Remarks

A new type of high-pressure calorimeter was constructed in the present work which operated under constant pressure up to 110 MPa.[15] The results of heat capacities on liquid 3-methylpentane proved that this calorimeter has a satisfactory accuracy. This apparatus also enabled us to measure the temperature and pressure dependences of volume at the same time. This feature should be stressed in view of the facts that any physicochemical phenomenon could be understood through the observation of several kinds of properties.

Many kinds of interesting problems in phase transitions will be studied in relation to two thermodynamic parameters, pressure and temperature. One of the examples will be described in the subsequent paper on NH_4Br and ND_4Br crystals. Another interesting use of this calorimeter will be the application to studies on glass transition phenomena. Detailed enthalpy relaxation can be followed only under adiabatic condition and volume relaxation under constant pressure.

The work to extend the pressure range up to 250 MPa is under way.

The authors would like to express sincere thanks to the late Professor Naoto Kawai, Drs. Akifumi Onodera, and Kaichi Suito at Faculty of Engineering Science, Osaka University for their valuable suggestions in the design of the calorimeter cell and kind instruction on many high-pressure techniques.

References

1) A. Quanch and R. Simha, *J. Appl. Phys.*, **42**, 4592 (1971).
2) M. S. Benson, P. S. Snyder, and J. Winnick, *J. Chem. Thermodyn.*, **3**, 891 (1971).
3) R. Landau and A. Wurflinger, *Rev. Sci. Instrum.*, **51**, 533 (1980).
4) G. Jura and W. A. Stark, Jr., *Rev. Sci. Instrum.*, **40**, 656 (1969).
5) P. Anderson and G. Bäckström, *J. Appl. Phys.*, **44**, 2601 (1973).
6) A. Bonilla and C. W. Garland, *J. Phys. Chem. Solids*, **35**, 871 (1974).
7) G. B. Kasting, K. J. Lushington, and C. W. Garland, *Phys. Rev. B*, **22**, 321 (1980).
8) D. B. McWhan and J. P. Remeika, *Phys. Rev. B*, **7**, 3079 (1973).
9) E. B. Amitin, Yu A. Kovalevskaya, E. G. Levedeva, and I. E. Paukov, *High Temp.-High Pressures*, **7**, 269 (1975).
10) E. B. Amitin, E. G. Lebedeva, and I. E. Paukov, *Fiz. Tverd. Tela.*, **18**, 614 (1976).
11) J. P. Berton, B. Cornut, J. Odin, J. Paureau, and J. Peyrard, *Cryogenics*, **19**, 543 (1979).
12) G. A. Mil'ner, *Fiz. Tverd. Tela.*, **16**, 1564 (1974).
13) M. Tatsumi, T. Matsuo, H. Suga, and S. Seki, *Bull. Chem. Soc. Jpn.*, **48**, 3060 (1975).
14) F. D. Rossini, K. S. Pitzer, R. L. Arnette, R. M. Mraun, and G. C. Pimentel, "Selected Values of Physical and Thermodynamic Properties of Hydrocarbons and Related Compounds," Published for the American Petroleum Institute by Carnegie Press, Carnegie Institute of Technology, Pittsburgh, Pennsylvania (1953), p. 37.
15) Very recently, a similar type of calorimeter was reported by M. A. Anisimov, V. M. Zaprudskii, G. A. Mil'ner, and E. I. Ponomarenko in *Zh. Eksp. Teor. Fiz.*, **80**, 787 (1981) and in *Chem. Abstr.*, **94**, 128537p (1981).
16) H. L. Finke and J. F. Messerly, *J. Chem. Thermodyn.*, **5**, 247 (1973).

Direct Observation of the Rate for Cis→Trans and Trans→Cis Photoisomerization of Stilbene with Picosecond Laser Photolysis

Minoru SUMITANI and Keitaro YOSHIHARA*

Institute for Molecular Science, Myodaiji, Okazaki 444

(Received June 29, 1981)

The rates for direct cis→trans and trans→cis photoisomerizations of stilbene in solution were measured with a newly developed monitor light source for picosecond laser photolysis in the UV region. The rate constant of the trans→cis isomerization is 1.2×10^{10} s^{-1} in hexane at 295 K. The fluorescence decay rate constant of the S_1 state of *trans*-stilbene has the same value. Thus, the decay of the S_1 state is the rate limiting step and the lifetime of an intermediate perpendicular state (^1p) has to be very short. The cis→trans isomerization is very fast and the half life of the excited *cis*-isomer is less than a few picosecond. These observations strongly indicate that the isomerization reaction proceeds through the potential surface of the singlet excited states.

Great attention has been paid to the mechanistic investigation of the cis-trans photoisomerization of olefinic compounds. Stilbene was chosen as one of the most prototypical molecules and studied in detail.[1] Several mechanisms have been proposed in the last decades. Earlier workers considered that the molecule in the excited state could rotate freely about the central double bond making *cis*- and *trans*-stilbenes interchangeable. Lewis *et al.*, however, pointed out that the fluorescence of *trans*-stilbene was not observed when the non-fluorescent *cis*-isomer was excited.[2] They proposed some energy dissipating levels among these excited states. Later, Förster suggested a mechanism according to which the isomerization proceeds through the lowest triplet state of each isomer.[3] This mechanism was supported by the analysis of the absorption spectrum of stilbene which seemed to indicate that the $S_1(^1B_u)$ state had a barrier high enough to make the state inaccesible for the photoisomerization.[4] However, this triplet mechanism failed to explain why azulene quenched the singlet excited state efficiently by energy transfer and reduced the efficiency of isomerization as well. Thus Saltiel proposed a singlet mechanism.[5] If stilbene is excited directly into the excited singlet state, it rotates about the central double bond to a perpendicular singlet intermediate (^1p), from which both isomers are formed.

From a theoretical point of view, Orlandi and Siebrand pointed out that the second excited singlet state $S_2(^1A_g)$ played an important role in the photoconversion of stilbene.[6] This S_2 level, which is characterized by a double electron excitation, is strongly stabilized, if the molecule rotates about the central double bond. The optical excitation to the lowest singlet state is followed by a non-adiabatic crossing to the S_2 potential surface, which has an energy minimum at the perpendicular (^1p) state, and then by a deactivation onto the ground potential surface.

Because of the inherently fast nature of the reaction, several works were made with time-resolved measurements.[7] The fluorescence lifetime and its temperature dependence,[8–12] the dynamics of the $S_n\leftarrow S_1$ absorption,[13–16] and the two-photon absorption[17,18] of stilbene were studied recently in order to investigate the photophysical and photochemical properties of its excited state. A few workers claimed to have observed a two-compornent decay of the excited singlet state by measuring either the fluorescence decay[8,9] or transient absorptions.[13,14] They ascribed these observations to the equilibration between the S_1 and ^1p states before deactivation to the ground state. On the other hand, we and others observed only a single exponential decay of the S_1 state by measuring the fluorescence decay,[10,11] and the $S_n\leftarrow S_1$ absorption.[15,16] No other transient absorption was observable except the $S_n\leftarrow S_1$ absorption of stilbene. Very recently we measured the time course of the cis→trans isomerization by the laser-induced fluorescence method with a picosecond double pulse, and pointed out that the ^1p state has a very short lifetime of less than a few picosecond.[19]

Laser-flash spectroscopy is a powerful method for studying the time course of photochemical reactions. In the picosecond range, several methods have been used for generating and detecting the monitoring light. A picosecond continuum light,[20] a flash lamp,[21,22] and a laser-induced dye emission[15] were combined with a vidicon camera, a photodiode array, or a picosecond streak camera. The picosecond continuum light has been used most widely, because it covers a rather wide spectral region and does not cause problems due to time jitter. However, it also has disadvantages, because it requires many laser shots in order to study the time profiles of transient species. Besides, it is usually difficult to generate UV light. The flash lamp technique has a large time jitter even with especially designed electric circuits. Using the laser-induced dye emission it is difficult to generate UV light. We developed a new simple method which does not require any special techniques using a jitter-free laser-induced Xe flash lamp and a streak camera. The spectrum of the monitoring light is continuous from the UV to the near IR region. By this method the time- and the wavelength-dependence of a transient can be resolved by one laser shot.

In this paper, we report the direct measurement of the reaction rates of both cis→trans and trans→cis isomerizations of stilbene with picosecond flash photolyses. We will show that the rate of trans→cis isomerization is limited by the S_1 lifetime of *trans*-stilbene and also that the rate of cis→trans isomerization is very high and the lifetime of the ^1p state is very short.

Experimental

The experimental set-up is shown in Fig. 1. The actinic light source of the photolysis system was the fourth harmonic

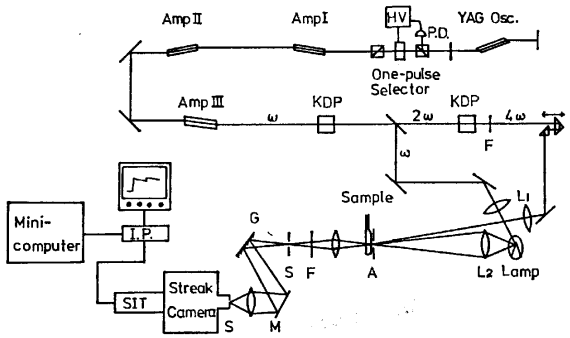

Fig. 1. Schematic diagram of apparatus employed for picosecond photolysis in the UV region.

(266 nm, ≈2 mJ) of a passively mode-locked Nd:YAG laser. A single pulse of the YAG laser was selected from the pulse train by a Pockels cell and was amplified in three stages with YAG amplifiers. The pulse width (FWHM) of the fourth harmonic was 11 ps. It was measured with a Hamamatsu streak camera/microcomputer system (C979 and C1000).

The analytic light was generated by focussing the fundamental laser beam onto the electrode of a high pressure Xe flash lamp (Xenon N722C). The break down occurred at the focal point of the laser beam at the electrode surface. An intense light emitted from this point was used as a monitoring light. No voltage was supplied on the electrodes. By this technique, the monitoring light was synchronized accurately with the actinic laser flash without any time jitter. The spectrum was similar to the Xe lamp and was continuous from the UV to the near IR region. The actinic laser and the monitoring light were focussed through an aperture onto the sample cell with lenses L_1 and L_2 (*cf.* Fig. 1), respectively. The monitoring light passed through the sample cell and a monochromator was detected by a streak camera.[23] The time delay between the start of the monitoring light and the actinic light was about 200 ps. The monochromator consisted of a Bausch & Lomb grating, G, (300 grooves/mm, 300 nm blaze wavelength), a mirror, M, and a pair of slits, S. We kept the wavelength resolution of the monochromator and the time resolution of the streak camera low in order to obtain a better signal/noise ratio. The wavelength resolution was about 10 nm at 254 nm and 313 nm. This was checked with a low pressure Hg lamp. The time resolution of this system was about 30 ps.

trans-Stilbene was purified by zone-refining and sublimation in the dark. *cis*-Stilbene was purified by means of high-speed liquid chromatography (Waters model 440). The content of *trans*-stilbene in the *cis*-isomer was less than one part in 500. The concentration of *cis*- or *trans*-stilbene was 1×10^{-4} M (1 M=1 mol dm^{-3}) in hexane.

Results

Figure 2 shows the UV absorption spectra of *cis*- and *trans*-stilbenes.[24] The molar extinction coefficients of *cis*- and *trans*-stilbenes above 240 nm are markedly different from each other except for the isosbestic point around 266 nm. By inducing the trans→cis or cis→trans isomerization the transmission of the monitoring light was, therefore, expected to change strongly by the formation of the reaction products.

Figure 3 shows the observed time-dependent transmission change after excitation of *cis*- or *trans*-stilbene

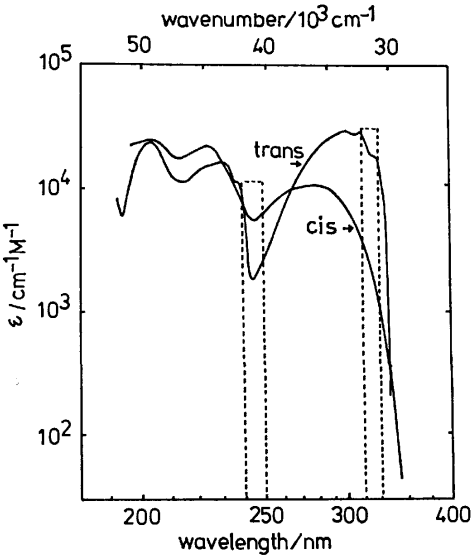

Fig. 2. UV absorption spectra of *cis*- and *trans*-stilbenes reproduced from 22. The transmission change was observed in two broken line regions.

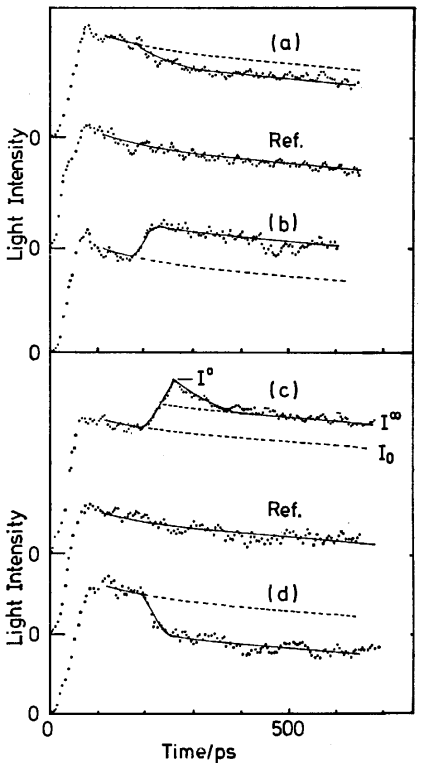

Fig. 3. Time dependent transmission change; (a) and (b) were observed at 240—250 nm upon excitation of solutions of *trans*-stilbene (a) and *cis*-stilbene (b) respectively. (c) and (d) were observed at 310—320 nm when solutions of *trans*-stilbene (c) and *cis*-stilbene (d) were excited respectively. Broken curves represent the reference light profile (ref.) at each wavelength region. The data represent the average of 5—10 shots.

by a picosecond laser flash. At 240—250 nm the molar extinction coefficient of *cis*-stilbene is larger than that of *trans*-stilbene (Fig. 2). Therefore, the transmission will decrease if trans→cis and increase

if cis→trans isomerization occurs. Flashing a solution of *trans*-stilbene one observes a decrease in the transmission which reaches a final value after about 80 ps (Fig. 3(a)). For the cis→trans isomerization (Fig. 3(b)), the transmission increases rapidly within the resolution time of the apparatus by flashing a solution of *cis*-stilbene.

The opposite transmission changes should be observed in the 310—320 nm wavelength region, because in this case the molar extinction coefficient of *trans*-stilbene is larger than that of *cis*-stilbene (Fig. 2). Indeed, when *cis*-stilbene is excited and the cis→trans isomerization takes place, the transmission decreases (Fig. 3(d)), and it increases due to the trans→cis isomerization when *trans*-stilbene is excited (Fig. 3(c)). Since in the 310—320 nm region the molar extinction coefficient is about 10 times greater than that in the 240—250 nm region (*cf.* Fig. 2) ground state depletion becomes important and causes a more complicated time behaviour of the transmission change compared with that observed in the 240—250 nm region.

Discussion

When stilbene is excited with a 266 nm laser flash, the excited singlet state is populated, from which the isomerization takes place with a characteristic rate constant. The most probable mechanism of the cis-trans photoisomerization of stilbene is shown in Scheme 1:

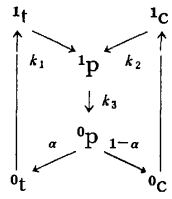

Scheme 1.

where t is the trans and c the cis isomer, 1 and 0 denote the excited singlet state and the ground state, respectively, p is the perpendicular state of stilbene, and the k's are rate constants. The change of transmission with time, $\Delta(I/I_0)$, is represented as follows:

$$\Delta(I/I_0) = 10^{-(\varepsilon_s(-\Delta c)+\varepsilon_t[^0t]+\varepsilon_c[^0c])l} \quad (1)$$

$$[^0t] = \alpha k_3 \frac{k\Delta c}{k_3-k}\left(\frac{e^{-k_3t}}{k_3}-\frac{e^{-kt}}{k}\right)+\alpha\Delta c$$

$$[^0c] = (1-\alpha)k_3\frac{k\Delta c}{k_3-k}\left(\frac{e^{-k_3t}}{k_3}-\frac{e^{-kt}}{k}\right)+(1-\alpha)\Delta c$$

$$k = k_1 \text{ or } k_2$$

where ε_t and ε_c are the molar extinction coefficients of *trans*- and *cis*-stilbene, respectively, l is the optical path length, I_0 is the reference light intensity, ε_s is the extinction coefficient of the starting material (cis or trans isomer), and Δc is the concentration of the excited singlet state of stilbene at $t=0$. From both excited singlet states of *trans*- and *cis*-stilbenes an intermediate state, ^{1}p, is produced in which the two phenyl rings are perpendicular to each other. With a characteristic branching factor α the ^{1}p state decays into

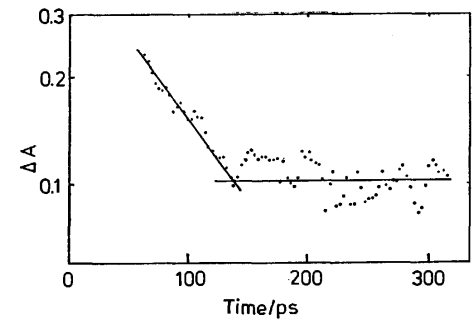

Fig. 4. Logarithmic plot of absorbance change (ΔA) taken from Fig. 3(c).

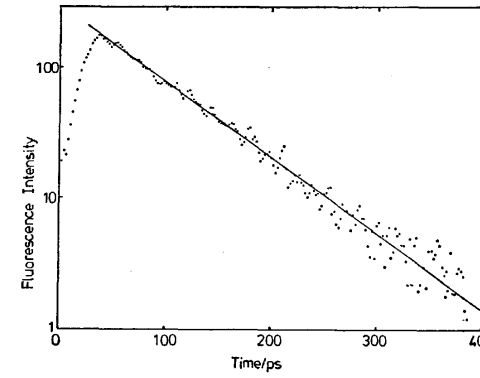

Fig. 5. Logarithmic plot of a fluorescence decay curve of *trans*-stilbene in hexane at 295 K.

^{0}t and ^{0}c. The factor α determines mainly the isomerization quantum yields ϕ_t and ϕ_c.

Trans→cis Isomerization. The lifetime of the lowest excited singlet state of *trans*-stilbene is about 75 ps, and the lifetime of the ^{1}p state is very short (less than a few picoseconds[19]), *i.e.* $k_1 \ll k_3$ and from Eq. 1, we obtain a simpler expression (2) for the absorbance change

$$\Delta A = \log(\Delta(I_0/I)) = [\varepsilon_t(-\Delta c)+\varepsilon_t\Delta c\alpha(1-e^{-k_1t}) + \varepsilon_c\Delta c(1-\alpha)(1-e^{-k_1t})]l. \quad (2)$$

In the wavelength region 240—250 nm, the molar extinction coefficient of *trans*-stilbene is smaller than that of *cis*-stilbene. Therefore, one can neglect the terms containing $\varepsilon_t\Delta cl$ and $\varepsilon_t\Delta c\alpha l$, because these are smaller than $\varepsilon_c\Delta c(1-\alpha)l$. Then we obtain Eq. 3 for the absorbance change caused by the formation of the cis isomer:

$$\Delta A = \varepsilon_c\Delta c(1-\alpha)(1-e^{-k_1t})l. \quad (3)$$

In this equation, the change of absorbance with time depends only on the rate constant k_1 of the trans→cis isomerization. In agreement with this the observed rise time was 85±10 ps (*cf.* Fig. 3(a)).

At 310—320 nm, the molar extinction coefficient of *trans*-stilbene is very large ($\approx 3\times10^4$ cm^{-1} M^{-1}) (*cf.* Fig. 2), thus the ground-state depletion contributes significantly to the observed transmission change. For this reason, the observed rise of the transmission is very fast, followed by a slower decrease to a constant value. A logarithmic plot of the latter transmission change shows that it decays exponentially with a lifetime of 85±10 ps (Fig. 4), which corresponds to

the decay of the excited singlet state of *trans*-stilbene (Fig. 5). The constant part of the depletion did not recover even 5000 ps after the laser excitation. It is due to an increase in concentration of the cis isomer which has a much smaller molar extinction coefficient than *trans*-stilbene.

The absorbance change at $t=0$ caused by the excitation of *trans*-stilbene (*cf.* Eq. 2) is given by

$$\Delta A^0 = \varepsilon_t(-\Delta c)l, \tag{4}$$

provided there is no $S_n \leftarrow S_1$ absorption in this region. After infinite time, the (permanent) decrease caused by the formation of *cis*-stilbene is

$$\Delta A^\infty = \varepsilon_t(-\Delta c\alpha)l. \tag{5}$$

In Eq. 5, we neglected the term containing $\varepsilon_c\Delta c(1-\alpha)l$, because its value is one order of magnitude smaller than the one containing $\varepsilon_t\Delta c\alpha l$ in this wavelength region. Combining Eqs. 4 and 5, we obtain Eq. 6 for the branching ratio $(1-\alpha)/\alpha$:

$$\frac{\Delta A^0-\Delta A^\infty}{\Delta A^\infty} = \frac{1-\alpha}{\alpha}. \tag{6}$$

The fluorescence process was neglected in the derivation, because of the small fluorescence quantum yield ($\phi_f=0.038$[25]). From the analysis of Fig. 4, we obtained for $\Delta A^0=0.23$ and for $\Delta A^\infty=0.10$ and the corrected branching ratio yielded $(1-\alpha)/\alpha\approx 1.3$. This ratio is also determined by a photostationary method as $(1-\alpha)/\alpha=1.4$.[1,26] These two values are in good agreement.

The fluorescence lifetime of *trans*-stilbene at room temperature was 75±5 ps in hexane as shown in Fig. 5. The observed absorbance change is caused by the isomerization of trans→cis reaction with a rise time of 85±10 ps. These observations lead us to the conclusion that the photoisomerization of *trans*-stilbene is determined by the lifetime of the excited singlet state of *trans*-stilbene. Therefore, the lifetime of the perpendicular singlet state (^{1}p), which is considered as the reaction intermediate, must be very short. The above observations are consistent with the other results in the investigations of stilbene: i) In picosecond flash experiments one observes only the $S_n \leftarrow S_1$ absorption of *cis*- or *trans*-stilbene.[15,16] ii) The fluorescence decay of *trans*-stilbene shows strictly first order kinetics between 77 K and 333 K.[10,11] In the theoretical analysis of the potential surface,[27] the perpendicular state has nearly the same energy as the S_1 state of *trans*-stilbene and the energy barrier between the excited singlet state of *trans*-stilbene and the ^{1}p state is about 14 kJ/mol. Therefore, it may be energetically possible that an equilibrium exists between these two states. However, judging from a single exponential decay of the fluorescence of *trans*-stilbene, no equilibrium between S_1 of *trans*-stilbene and the perpendicular state ^{1}p exists. This means that the lifetime of ^{1}p must be very short. iii) The fluorescence lifetime and the fluorescence quantum yield increase exactly with the same factor when the temperature is lowered from 330 K to 77 K. Moreover, in the same temperature range the trans→cis isomerization quantum yield decreases correspondingly.[10] That is to say, the isomerization is an activated process and the fluorescence lifetime becomes shorter by the increasing rate of the chemical reaction. iv) The activation energy determined from the temperature dependence of the isomerization reaction (10.5 kJ/mol[28]) is in good agreement with that calculated from the temperature dependence of the fluorescence quantum yield[4,28] and the fluorescence lifetime.[10]

Cis→trans Isomerization. The risetime of the transmission change is very fast for the cis→trans isomerization at both wavelength regions (Figs. 3(b) and (d)). The lifetime of the excited singlet state of *cis*-stilbene was observed to be 7 ps.[14] If the isomerization rate is limited by the lifetime of the excited singlet state of *cis*-stilbene, the observed risetime of the formation of *trans*-stilbene is limited by the time resolution of our flash apparatus. We already reported the rate constant of the cis→trans reaction determined by the laser-induced fluorescence method with a picosecond double pulse.[19] This isomerization rate constant was greater than 10^{11} s^{-1}. Therefore, it may be concluded that the decay of the excited singlet state of *cis*-stilbene is the rate determining step in the cis→trans isomerization reaction.

Thus the isomerization process of stilbene in solution can be described as follows: By excitation of stilbene into a higher vibrational state of the $S_1(^1B_u)$ state, the excess energy dissipated to the surrounding solvent by the vibrational relaxation. Then rotation about the central double bond with transfer to the $S_2(^1A_g)$ perpendicular state takes place. This process is the rate determining step. In the case of the trans→cis isomerization it has an activation energy of 14 kJ/mol. No energy barrier has ever been observed for the isomerization of *cis*-stilbene. The optical excitation probably leads to the maximum of the potential surface, since the ground state of *cis*-stilbene is already twisted considerably (≈40°) about the central double bond by steric hindrance.[29] After excitation a quick rotation occurs from the strongly mixed state between S_1(cis) and S_2 to the S_2(perpendicular) state across a perhaps very low energy barrier. The perpendicular state interacts strongly with the ground perpendicular $S_0(^1A_g)$ state, so that the internal conversion is very rapid. Finally the vibrational relaxation of the perpendicular $S_0(^1A_g)$ state to the cis or trans configuration takes place (α in Scheme 1).

We are indebted to Dr. K. H. Grellmann (Max-Planck-Institut für Biophysikalische Chemie and IMS) for valuable discussions.

References

1) J. Saltiel, J. D'Agostino, E. D. Megarity, L. Metts, K. R. Neuberger, M. Wrighton, and O. C. Zafiriou, *Org. Photochem.*, **3**, 1 (1973).
2) G. N. Lewis, T. T. Magel, and D. Lipkin, *J. Am. Chem. Soc.*, **62**, 2973 (1940).
3) Th. Förster, *Z. Electrochem.*, **56**, 716 (1952).
4) H. Dyck and D. S. McClure, *J. Chem. Phys.*, **36**, 2326 (1962).
5) J. Saltiel, E. D. Megarity, and K. G. Kneipp, *J. Am. Chem. Soc.*, **88**, 2386 (1966).

6) G. Orlandi and W. Siebrand, *Chem. Phys. Lett.*, **30**, 352 (1975).
7) R. M. Hochstrasser, *Pure Appl. Chem.*, **52**, 2683 (1980).
8) D. S. J. Birch and J. B. Birks, *Chem. Phys. Lett.*, **38**, 432 (1976).
9) J. R. Taylor, M. C. Adams, and W. Sibbett, *Appl. Phys. Lett.*, **35**, 590 (1979).
10) M. Sumitani, N. Nakashima, K. Yoshihara, and S. Nagakura, *Chem. Phys. Lett.*, **51**, 183 (1977).
11) F. Heisel, J. A. Miehe, and B. Sipp, *Chem. Phys. Lett.*, **61**, 115 (1979).
12) F. E. Doany, B. I. Greene, Y. Liang, D. K. Negus, and R. M. Hochstrasser, "Picosecond Phenomena II," ed by, R. M. Hochstrasser, W. Kaiser, and C. V. Shank, Springer-Verlag (1980).
13) E. Heumann, W. Triebel, R. Uhlmann, and B. Wilhelmi, *Chem. Phys. Lett.*, **45** 425 (1977).
14) O. Teschke, E. P. Ippen, and G. R. Holtom, *Chem. Phys. Lett.*, **52**, 233 (1977).
15) K. Yoshihara, A. Namiki, M. Sumitani, and N. Nakashima, *J. Chem. Phys.*, **71**, 2892 (1979).
16) B. I. Greene, R. M. Hochstrasser, and R. B. Weisman, *Chem. Phys. Lett.*, **62**, 427 (1979).
17) Th. M. Strachelek, Th. A. Pazoha, W. M. McClain, and R. P. Drucker, *J. Chem. Phys.*, **66** 4540 (1977).
18) K. Fuke, S. Sakamoto, M. Ueda, and M. Itoh, *Chem. Phys. Lett.*, **74**, 546 (1980).
19) M. Sumitani, N. Nakashima, and K. Yoshihara, *Chem. Phys. Lett.*, **68**, 255 (1979).
20) G. E. Busch, R. P. Jones, and P. M. Rentzepis, *Chem. Phys. Lett.*, **18**, 178 (1973).
21) A. Müller and G. R. Willenbring, *Ber. Bunsenges. Phys. Chem.*, **78**, 1153 (1974).
22) Y. Wang, M. K. Crawford, M. J. McAuliffe, and K. B. Eisenthal, *Chem. Phys. Lett.*, **74**, 160 (1980).
23) Y. Takagi, M. Sumitani, and K. Yoshihara, *Rev. Sci. Instrum.*, **52**, (1981), in press.
24) UV Atlas of Organic Compounds (D10/75, D10/76), Verlag Chemie, Weinheim; Butterworths, London.
25) G. Bartocci and U. Mazzucato, *Chem. Phys. Lett.*, **47**, 541 (1977).
26) G. S. Hammond, J. Saltiel, A. A. Lamola, N. J. Turro, J. S. Bradshaw, D. O. Cowan, R. C. Counsell, V. Vogt, and C. Dalton, *J. Am. Chem. Soc.*, **86**, 3197 (1964).
27) G. Orlandi, P. Palmieri, and G. Poggi, *J. Am. Chem. Soc.*, **101**, 3492 (1979).
28) S. Malkin and E. Fischer, *J. Phys. Chem.*, **68**, 1153 (1964).
29) M. Trætteberg and E. B. Frantsen, *J. Mol. Struct.*, **26**, 69 (1975).

The Extraction of Bivalent Transition Metals from Aqueous Chloride Solutions by Long-chain Alkyl Quaternary Ammonium Carboxylates

Taichi SATO* and Masahiro YAMAMOTO

Department of Applied Chemistry, Faculty of Engineering, Shizuoka University, Johoku, Hamamatsu 432

(Received January 13, 1981)

The extraction of bivalent manganese, cobalt, nickel, and copper from aqueous chloride solutions by long-chain alkyl quaternary ammonium carboxylates, prepared by combination of trioctylmethylammonium chloride ($R_3R'NCl$) and carboxylic (octanoic, decanoic, and lauric) acids ($R''COOH$) in benzene, has been investigated under different conditions. The organic phases are examined by spectrophotometry and infrared spectral measurement. The mechanism of the extraction is discussed on the basis of the results obtained. The extraction efficiency follows the order $Cu > Co \simeq Ni > Mn$, and the extraction process is expressed as $M^{2+}(aq) + 2Cl^-(aq) + 3R_3R'NR''COO(org) \rightleftarrows (R_3R'N)[M(R''COO)_3](org) + 2R_3R'NCl(org)$, in which M=Mn, Co, Ni, and Cu. The extracted species of bivalent manganese, cobalt, nickel, and copper exist as the complex $(R_3R'N)[M(R''COO)_3]$ in an octahedral arrangement.

The extraction of metals from acid solutions by high molecular weight amines has been reported by a number of investigators, but there are few observations on the extraction of metals from aqueous solution in the vicinity of neutral range. Although carboxylic acids are a possible group of reagents to extract the metals in the vicinity of neutral range,[1] their extraction efficiencies depend remarkably on the pH of the aqueous phase. Accordingly the mixed ionic solvent system consisting of long-chain alkyl quaternary ammonium carboxylates is considered of effective for such extraction. This system has been mainly applied to the extraction of magnesium,[2-4] but observations on the extraction of other metals are limited. We have been studying the extraction systems with long-chain alkyl quaternary ammonium compounds,[5] and the present study extends the work to the extraction of bivalent manganese, cobalt, nickel, and copper from aqueous chloride solutions by alkyl quaternary ammonium carboxylates.

Experimental

Reagent. The alkyl quaternary ammonium carboxylates were prepared by mixing calculated amounts (equal volumes of solutions in 0.5 mol dm^{-3} each) of trioctylmethylammonium chloride (General Mills, $R_3R'NCl$, Aliquat-336) and carboxylic acids (octanoic, decanoic, and lauric acids represented as $C_nH_{2n+1}COOH$ with $n=7$, 9, and 11, respectively or $R''COOH$), and treated with an excess amount of sodium hydroxide, and then washed thoroughly with distilled water to remove sodium and chloride ions. The resulting materials ($R_3R'NR''COO \cdot 5H_2O$) which exhibit the properties illustrated in Table 1 are diluted with benzene. The aqueous solution of nickel (II) chloride was prepared by dissolving nickel chloride hydrate ($NiCl_2 \cdot 6H_2O$) in water and its pH value was adjusted by adding perchloric acid. The aqueous solutions of other bivalent metals were similarly prepared by dissolving their salts ($MnCl_2 \cdot 4H_2O$, $CoCl_2 \cdot 6H_2O$, $CuCl_2 \cdot 2H_2O$) in water. The used reagents were of analytical grade.

Extraction and Analytical Procedures. The procedure for obtaining distribution coefficient (the ratio of the equilibrium concentration of metal in the organic phase to that in the aqueous phase), E_a^0, was described previously:[6] equal volumes (15 cm^{-3}) of the organic and aqueous phases were shaken for 10 min, and then the metal in the organic phase was stripped with 1 mol dm^{-3} hydrochloric acid. All experiments were carried out at 20 °C except the examination on temperature-dependence of distribution coefficient. The concentration of nickel was determined by edta titration using Cu–PAN (1-(2-pyridylazo)-2-naphthol) as an indicator.[7] Following indicators were used for the determination of other metals by edta titration: BT (Eriochrome Black T) for manganese;[8] XO (Xylenol Orange) for cobalt;[9] PAN for copper.[10] The concentration of chloride in the organic phase was determined by Volhard's method, and the water content of the organic phase by Karl-Fischer titration. The complexes freed from benzene were prepared by drying the metal saturated organic phase *in vacuo* at 50 °C.

Spectrophotometry and Infrared Spectral Measurement. The absorption spectra were obtained on a Shimadzu Model QV-50 spectrophotometer, using matched 1.00 cm fused silica cells, and the infrared spectra on a JASCO Model IRA-1 grating infrared spectrophotometer for measurement at 4000—650 cm^{-1}, and Model IR-F for measurement at 700—200 cm^{-1}, using a capillary film between thallium halide or polyethylene plates.

Results and Discussion

Extraction Isotherm. When nickel(II) is extracted with trioctylmethylammonium laurate from aqueous nickel chloride solution of 1 g dm^{-3} at varying pH values, the distribution coefficient steeply rises with increasing pH in the range of pH 2—3, and then becomes almost constant at $pH > \approx 3$, as shown in Fig. 1. The lowering in the distribution coefficient at low pH arises from the decrease of the available extractant, caused by the extraction of acid from aqueous solution. This interpretation is supported by the fact that hydrochloric acid is extracted by quaternary compound according to the reaction:

$$H^+(a) + Cl^-(a) + R_3R'NR''COO(o) \rightleftharpoons R_3R'NCl(o) + R''COOH(o), \quad (1)$$

in which (a) and (o) mean aqueous and organic phases, respectively. In order to elucidate further the reaction between a benzene solution of quaternary compound and aqueous hydrochloric acid solution, the variation of $[Cl]_{org}$ with $[HCl]_{initial\ aq}$ was examined by the extraction of aqueous solutions containing hydrochloric acid in the absence of nickel chloride with 0.2 mol dm^{-3} quaternary ammonium laurate. The chloride concentration in the organic phase revealed a constant

Table 1. Properties of trioctylmethylammonium carboxylate

Property		Trioctylmethylammonium carboxylate			Aliquat-336
		Octanoate	Decanoate	Laurate	
Molecular weight[a]		607	660	679	442
Appearance at room temperature		Viscous liquid	Viscous liquid	Viscous liquid	Viscous liquid
Colour		Yellowish brown	Light brown	Light yellow	Yellowish brown
Specific gravity at 20 °C		0.884	0.885	0.894	0.884
Refractive index at 20 °C		1.4594	1.4593	1.4592	1.4733
Viscosity at 20 °C, cp		1585	1590	1636	2550
Solubility[b] in	Benzene	>100	>100	>100	>100
	Kerosene	>100	>100	>100	<2
	Cyclohexane	>100	>100	>100	>100
	2-Propanol	>100	>100	>100	>100
	Carbon tetrachloride	>100	>100	>100	>100
	Water	<1	<1	<1	<1

a) Apparent molecular weight determined by using benzene on a Hitachi Model 115 isothermal molecular weight apparatus. b) Solubility in grams per solvent in 100 g.

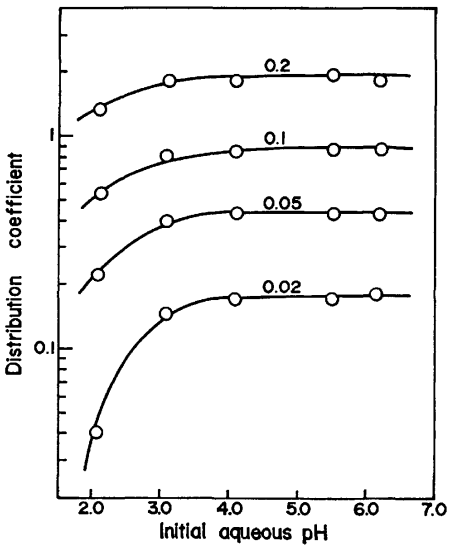

Fig. 1. Extraction of nickel chloride from aqueous solutions containing perchloric acid by trioctylmethylammonium laurate in benzene (numbers on curves are quaternary compound concentrations, mol dm^{-3}).

value of 0.02 mol dm^{-3} at the aqueous hydrochloric acid concentration above 0.02 mol dm^{-3} (Fig. 2). Additionally, the infrared spectra of the organic phase showed the formation of carboxylate supporting the reaction in Eq. 1. In addition, as the similar results are obtained in the extraction of perchloric acid with the quaternary compound, the reaction analogous to Eq. 1 holds in the extraction of perchloric acid, as well. Accordingly the quaternary compound is favorably utilized to extract metals from nearly neutral aqueous solutions at pH 5—8, since its compound is easily decomposed by acid.

In the extraction of aqueous solution containing nickel chloride at a constant pH of 5.5 with 0.01 mol dm^{-3} quaternary compound, the molar ratios of $[R_3R'NR''COO]_{org}$ and $[Cl]_{org}$ to $[Ni]_{org}$ plotted as a function of $[Ni]_{initial\ aq}$ approach the limiting values of 3 and 2, respectively, indicating the composition of the organic phase in the molar ratio of

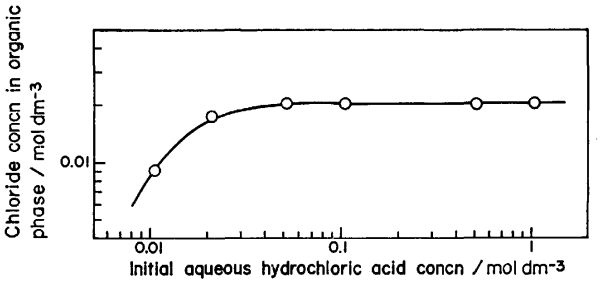

Fig. 2. Variation of the chloride concentration in the organic phase with initial aqueous hydrochloric acid concentration for the extraction of hydrochloric acid by 0.02 mol dm^{-3} trioctylmethylammonium laurate in benzene.

nickel/chlorine/quaternary compound=1:2:3. However, when the initial aqueous nickel concentration increases above 10 g dm^{-3}, the latter molar ratio becomes over 2, because the hydrochloric acid arising from the hydrolysis of nickel chloride in the aqueous phase is extracted into the organic solution. This stoichiometry corresponds to the result obtained by the continuous variation method. In the extraction at a constant $[Cl]_{aq}$ of 0.1 mol dm^{-3}, the variation of $[Ni]_{org}$ as a function of the molar fraction of $[Ni]_{initial\ aq}/([Ni]_{initial\ aq}+[R_3R'NR''COO]_{org})$ at a fixed concentration of 0.1 mol dm^{-3} gives a maximum at the molar ratio of $[Ni]_{initial\ aq}$ to $[R_3R'NR''COO]_{org}$ of 1:3. Accordingly the extraction of nickel chloride from aqueous solutions by trioctylmethylammonium compound is expressed by the equilibrium equation:

$$Ni^{2+}(a) + 2Cl^-(a) + 3R_3R'NR''COO(o) \rightleftharpoons (R_3R'N)[Ni(R''COO)_3](o) + 2R_3R'NCl(o). \quad (2)$$

This is also supported by the dependence of distribution coefficient on the concentrations of extractant and aqueous chloride. Equation 2 leads to the relationship:

$$K = [(R_3R'N)[Ni(R''COO)_3]]_{org}[R_3R'NCl]^2_{org}/[Ni^{2+}]_{aq}[Cl^-]^2_{aq}[R_3R'NR''COO]^3_{org}, \quad (3)$$

in which K is the equilibrium constant. If we assume that $E^0_d=[Ni]_{org}/[Ni]_{aq}$, $[Cl^-]_{aq}=2[Ni]_{aq}$, and $[R_3R'NCl]_{org}=2[Ni]_{org}$, the following relation is derived:

$$K = E_a^0[R_3R'NCl]_{org}^3/[Cl^-]_{aq}^2[R_3R'NR''COO]_{org}^3 \quad (4)$$

$$= E_a^{0\,3}/[R_3R'NR''COO]_{org}^3. \quad (5)$$

Thus Eqs. 4 and 5 should be satisfied by

$$\log\{E_a^0[R_3R'NCl]_{org}^3/[R_3R'NR''COO]_{org}^3\} = \log K + 2\log[Cl^-]_{aq} \quad (6)$$

and

$$\log E_a^0 = (1/3)\log K + \log[R_3R'NR''COO]_{org}. \quad (7)$$

In the extraction of nickel chloride from aqueous solutions containing perchloric acid, the log-log plots of E_a^0 *vs.* the free quaternary compound concentration, $[R_3R'NR''COO]_{org}$, give straight lines with the slopes of 1.0 and 1.1 for the initial aqueous acidities of 0 and 0.01 mol dm^{-3}, respectively, suggesting a first-power dependence of the distribution coefficient on the solvent concentration. For the extraction of nickel chloride from aqueous solutions containing lithium chloride, the distribution coefficient rises with increasing the initial aqueous lithium chloride concentration (Table 2). However, when the extraction of aqueous lithium chloride solutions in the absence of nickel chloride is examined as in the case of acid extraction (Fig. 2), the increase of $[Cl]_{org}$ is slight with increasing the aqueous lithium chloride concentration (Table 2). Therefore, in the extraction of nickel chloride from aqueous solutions containing lithium chloride, the increase of the distribution coefficient with the initial aqueous lithium chloride concentration is attributed to the salting-out effect of lithium chloride. In this extraction, the log-log plots of $E_a^0[R_3R'NCl]^2_{org}/[R_3R'NR''COO]^3_{org}$ *vs.* $[Cl^-]_{aq}$ suggest a second-power dependence of the distribution coefficient on the aqueous chloride concentration.

The result for the extraction of bivalent manganese, cobalt, and copper from aqueous solutions containing their chlorides at 1 g dm^{-3} with trioctylmethylammonium laurate in the absence of perchloric acid are shown in Table 3, compared with that for nickel (II). Although the extraction efficiency is in the order Cu>Co≃Ni>Mn, the log-log plots of E_a^0 *vs.* $[R_3R'NR''COO]_{org}$ for bivalent manganese, cobalt, and copper give straight lines with the slope of approximately unity, suggesting that their equilibria are indicated by the expression similar to Eq. 2 in the extraction of nickel(II). These facts are also supported by the variation in the stoichiometric composition of their organic phases as a function of the initial aqueous metal concentrations, and, in addition, by the continuous variation method for the metal concentrations in their organic phases. Hence it is presumed that the extraction of bivalent transition metals from aqueous chloride solutions by quaternary compound proceeds in the following expression:

$$M^{2+}(a) + 2Cl^-(a) + 3R_3R'NR''COO(o) \rightleftharpoons (R_3R'N)[M(R''COO)_3](o) + 2R_3R'NCl(o), \quad (8)$$

where M=Mn, Co, Ni, and Cu.

Temperature Effect. The extraction of aqueous solution (pH 5.5) containing nickel chloride at 1 g dm^{-3} with 0.02 mol dm^{-3} trioctylmethylammonium laurate at the temperature 10—50 °C gives the result that the distribution coefficient is little influenced by varying the temperature. When the similar experiments were carried out for the extraction of bivalent manganese, cobalt, and copper, the effect of temperature on the distribution coefficients was small (Fig. 3). From the thermodynamic values (the change in free energy, enthalpy, and entropy) for Eq. 8 estimated together with the equilibrium constants at 20 °C (Table 4), the order Cu>Co≃Ni>Mn corresponds to the increase in the free energy change and/or the decrease in the equilibrium constant, although the individual change in enthalpy or entropy does not indicate a reciprocal relation with the extraction efficiency. The equilibrium constants calculated by Eq. 7 agree with those indicated in Table 4. Especially the order of the extraction efficiency depends presumably on the variation in the equilibrium constants with different metal ions.

Infrared and Absorption Spectra. The infrared

TABLE 2. EXTRACTION OF AQUEOUS SOLUTIONS CONTAINING LITHIUM CHLORIDE IN THE ABSENCE OR THE PRESENCE OF NICKEL CHLORIDE AT 1 g dm^{-3} WITH TRIOCTYLMETHYLAMMONIUM LAURATE IN BENZENE

Initial aq [LiCl]/mol dm^{-3}	$[Cl]_{org} \times 10^3$/mol dm^{-3} a)	E_a^0
0.01	0.657	0.178
0.02	0.750	0.269
0.05	0.938	0.385
0.1	1.31	0.495
0.2	1.78	0.645
0.5	3.10	1.03
1.0	4.40	1.36

a) The extraction in the absence of nickel chloride.

TABLE 3. EXTRACTION OF BIVALENT MANGANESE, COBALT, NICKEL, AND COPPER FROM AQUEOUS SOLUTIONS CONTAINING THEIR CHLORIDES AT 1 g dm^{-3} WITH TRIOCTYLMETHYLAMMONIUM LAURATE IN BENZENE

$[R_3R'NR''COO]$ mol dm^{-3}	Distribution coefficient, E_a^0			
	Mn	Co	Ni	Cu
0.01	0.0575	0.0912	0.0908	0.579
0.02	0.140	0.204	0.175	1.92
0.05	0.325	0.450	0.451	12.4
0.1	0.637	0.941	0.938	42.3
0.2	1.24	1.93	1.99	118

TABLE 4. THERMODYNAMIC VALUES[a] ESTIMATED FROM THE TEMPERATURE-DEPENDENCE OF DISTRIBUTION COEFFICIENTS FOR BIVALENT TRANSITION METALS, COMPARED WITH THE EQUILIBRIUM CONSTANTS

Metal	ΔG kJ mol^{-1}	ΔH kJ mol^{-1}	ΔS J K^{-1} mol^{-1}	K b)
Mn	−15.65	−5.06	36.11	6.2×10^2
Co	−18.62	14.48	113.0	2.1×10^3
Ni	−17.66	0	60.25	1.4×10^3
Cu	−43.85	−25.10	64.02	6.6×10^7

a) ΔG, ΔH, and ΔS represent the changes in free energy, enthalpy and entropy, respectively. b) K denotes the equilibrium constant at 20 °C for Eq. 8.

TABLE 5. INFRARED SPECTRAL DATA FOR THE ORGANIC EXTRACTS FROM AQUEOUS SOLUTIONS CONTAINING CHLORIDES OF MANGNESE, COBALT, NICKEL, AND COPPER WITH 0.01 mol dm^{-3} TRIOCTYLMETHYLAMMONIUM LAURATE IN BENZENE

$R_3R'NCl$	$R_3R'NR''COO$	Frequency/cm^{-1} Organic extract					Probable assignment
		Mn(II) 10[b]	Co(II) 10	Ni(II) 1	Ni(II) 20	Cu(II) 1	
3420 (mb)[a]	3320 (mb)	3380 (mb)	3380 (mb)	3370 (mb)	3400 (mb)	3360 (mb)	OH stretching
2920 (s) 2860 (ms)	2920 (s) 2860 (ms)	2920 (s) 2860 (ms)	2920 (s) 2860 (ms)	2920 (s) 2860 (ms)	2920 (s) 2860 (ms)	2920 (s) 2860 (ms)	CH stretching
		2600 (sh)	2600 (sh)		2600 (sh)	2600 (sh)	OH stretching
		1720 (sh)	1720 (sh)		1720 (w)	1720 (w)	CO stretching
1625 (wb)	1650 (sh)	1640 (w)	1640 (sh)	1640 ((sh)	1640 (sh)	1640 (sh)	OH bending
	1560 (m)	1560 (m)	1560 (m)	1560 (m)	1560 (m)	1560 (m)	CO stretching
1465 (m)	1465 (m)	1465 (m)	1465 (m)	1465 (m)	1465 (m)	1465 (m)	CH_3 degenerate bending, CH_2 scissoring
					1425 (m)	1410 (m)	CO stretching, OH bending
1375 (m)	1380 (m)	1380 (m)	1380 (m)	1380 (m)	1380 (m)	1380 (m)	CO stretching, CH_3 sym. bending and/or
					1180 (w)		CO stretching, OH bending
725 (w)	725 (w)	725 (w)	725 (w)	725 (w)	725 (w)	725 (w)	CH_2 rocking

a) s=Strong, ms=medium strong, m=medium, w=weak, b=broad, sh=shoulder. b) This represents initial aqueous metal chloride concentration, g dm^{-3}.

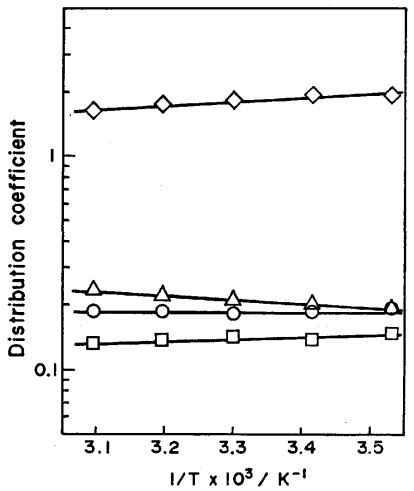

Fig. 3. Temperature-dependence of distribution coefficient for the extraction of bivalent transition metals from aqueous solutions containing their chlorides at 1 g dm^{-3} by 0.02 mol dm^{-3} trioctylmethylammonium laurate in benzene (□, △, ○, and ◇ represent the extractions of manganese, cobalt, nickel, and copper, respectively).

spectra of the organic extracts from the extraction of aqueous nickel chloride solutions at trioctylmethylammonium laurate were compared with that of the quaternary ammonium compound. The frequencies and possible band assignments are given in Table 5. In the infrared spectrum of carboxylic acid, the C–O stretching bands appear at 1710 and 1400—1200 cm^{-1}.[11] However, the quaternary compound shows the similar bands at 1560 and 1380 cm^{-1}, indicating that the extractant exists in the organic phase as a carboxylate,[12] $R_3R'NR''COO \cdot 5H_2O$. As for the infrared spectra of the organic nickel(II) extracts, the C–O stretching modes appear at the same frequencies as those of the quaternary compound. However, the relative intensity relation between the absorption band at 1465 cm^{-1} (the CH_3 degenerate bending and CH_2 scissoring) and the band at 1380 cm^{-1} (the C–O stretching vibration superposed on the CH_3 symmetrical bending absorption) becomes converse in comparison with that for the quaternary compound, in which the former band is slightly stronger than the latter one. For the nickel(II) complex, the latter band is more intense than the former one because the carboxylate group is coordinated to nickel ion as a bidentate ligand.[12,13] At higher loading, the C–O stretching bands appear at 1720, 1425, and 1180 cm^{-1}; this is ascribed to the presence of carboxylic acid formed by the combination of a part of extractant with the hydrochloric acid which results from the hydrolysis of nickel chloride in the aqueous phase at high concentrations. Further, the absorption due to the Ni–Cl vibration is not observed in far-infrared region, indicating that the chloride ion in the organic phase is not coordinated to nickel ion. Similar infrared results are also observed for the extraction of aqueous solutions containing chlorides of manganese, cobalt, and copper (Table 5).

In addition, the absorption spectra of the organic solutions from the extraction of manganese, cobalt, nickel, and copper chlorides with the quaternary compound are illustrated in Fig. 4. The spectrum of the organic nickel(II) species reveals the characteristic feature of a six-coordinated complex ion,[14] showing absorption bands at 25000, 14700, 13300, and 8300 cm^{-1} which are ascribed to three spin-allowed transitions from the ground state $^3A_{2g}(F)$ to the states

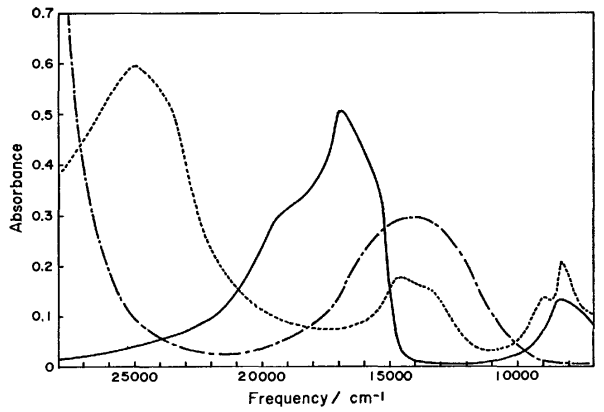

Fig. 4. Absorption spectra of the organic solutions from the extraction of aqueous solution containing chlorides of cobalt, nickel and copper at 100, 100, and 20 g dm^{-3}, respectively, with 0.05 mol dm^{-3} trioctylmethylammonium laurate in benzene (continuous, broken and chain lines represent the organic solutions of cobalt, nickel, and copper, respectively).

$^3T_{1g}(P)$, $^3T_{1g}(F)$, and $^3T_{2g}(F)$, respectively. The ligand field parameters for the complex $(R_3R'N)[Ni(R''COO)_3]$ are calculated by using the matrix elements determined by Tanabe and Sugano:[15] $B=950\ cm^{-1}$ and $10\,D_q=8550\ cm^{-1}$. The difference between the calculated value of $10\,D_q$ and the observed one (8300 cm^{-1}) may be attributed to the assignment of the absorption at 8300 cm^{-1} to the transition to $^3T_{2g}(F)$, although two absorptions appear at 8200 and 8300 cm^{-1}. This is because the state $^2T_{2g}(F)$ should be split into two states ^3E and $^3A_1$, if the symmetry of the complex is lowered from O_h to D_3.[16] Further the factor β is estimated to be 0.88, implying relative low covalent bond character in the nickel(II) complex. The spectrum of the organic cobalt(II) species exhibits the typical absorption of a six-coordinated complex at 19230, 16950, and 8260 cm^{-1}, transitions from $^4T_{1g}(F)$ to $^4T_{1g}(P)$, $^4A_{2g}(F)$, and $^3T_{2g}(F)$, respectively. Accordingly the calculated value of 10 D_q (9500 cm^{-1}) in the cobalt(II) complex is close to the value of $10\,D_q$ (9300 cm^{-1}) in the aqua ion $[Co(H_2O)_6]^{2+}$.[14] For the organic extract of copper(II) complex, the value of $10\,D_q=13990\ cm^{-1}$ resembles that in the hexaaquacopper(II) species. In contrast, the organic manganese(II) extract reveals a strong charge-transfer absorption at 34000—20000 cm^{-1}, covering the weak absorption due to the spin-forbidden transitions.

Therefore, the extracted species of bivalent manganese, cobalt, nickel, and copper exist as the octahedral complex $(R_3R'N)[M(R''COO)_3]$.

Effect of Carboxylic Acid. In the extraction of solution (at pH 5.5) containing nickel chloride at 1 g dm^{-3} by quaternary ammonium compounds with octanoic, decanoic, and lauric acids, the plots of the distribution coefficient *vs.* the free quaternary compound concentration gave a straight line with the slope of nearly unity for respective carboxylates (Fig. 5). From this the effect of the different kinds of carboxylic acid on the extraction efficiency is not remarkable, although their efficiencies increase in the

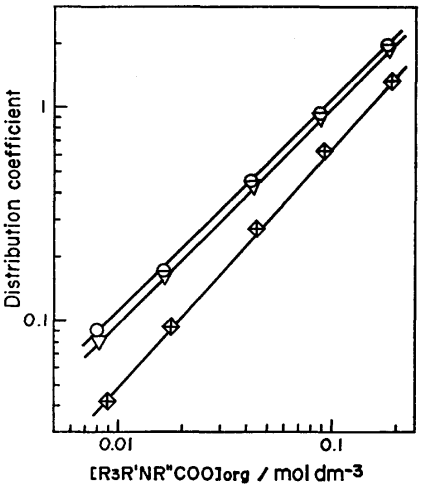

Fig. 5. Log-log plots of distribution coefficient *vs.* free alkylammonium carboxylate concentration for the extraction of aqueous solution containing nickel chloride by quaternary compounds (⊕, ▽, and ○ represent quaternary compounds with octanoic, decanoic, and lauric acids).

order of octanoic, decanoic, and lauric acids. Thus the extraction mechanism of nickel by quaternary compounds is supposed to be almost the same for each carboxylate (Eq. 2). Similar results are obtained for the extraction of bivalent manganese, cobalt, and copper by quaternary compound, as well.

References

1) E. G. Miller, *Talanta*, **21**, 685 (1974).
2) J. C. Davis and R. R. Grinstead, *J. Phys. Chem.*, **74**, 147 (1970).
3) C. Hanson and S. L. N. Murthy, "Proc. Int. Solvent Extraction Conf., Lyon, 1974," ed by Soc. Chem. Ind., London (1974), Vol. 1, p. 779.
4) C. Hanson, M. A. Hughes, and S. L. N. Murthy, *J. Inorg. Nucl. Chem.*, **37**, 191 (1975).
5) *E.g.*, T. Sato and H. Watanabe, *Anal. Chim. Acta*, **49**, 463 (1970); T. Sato, *J. Inorg. Nucl. Chem.*, **34**, 3835 (1972); T. Sato, S. Kotani, and M. L. Good, *ibid.*, *Chem.*, **35**, 2547 (1973); **36**, 451 (1974); T. Sato, H. Watanabe, and S. Kikuchi, *J. Appl. Chem. Biotechnol.*, **25**, 63 (1975); T. Sato, H. Watanabe, S. Kotani, and M. L. Good, *Anal. Chim. Acta*, **84**, 397 (1976).
6) T. Sato, *J. Inorg. Nucl. Chem.*, **24**, 1265 (1962).
7) H. Flaschka and H. Abdine, *Chemist-Analyst*, **45**, 58 (1956).
8) H. Flaschka, *Chemist-Analyst*, **42**, 56 (1953).
9) J. Kinnunen and B. Wennerstrand, *Chemist-Analyst*, **46**, 92 (1957).
10) K. L. Cheng and R. H. Bray, *Anal. Chem.*, **27**, 782 (1955); K. L. Cheng, *Anal. Chem.*, **30**, 243 (1958).
11) L. J. Bellamy, "The Infra-red Spectra of Complex Molecules," John Wiley, New York (1958), p. 161.
12) K. Nakamoto, "Infrared and Raman Spectra of Inorganic and Coordination Compounds," 3rd ed, Wiley-Interscience, New York (1978), p. 230.
13) S. D. Robinson and M. F. Uttley, *J. Chem. Soc.*, 1912 (1973).
14) *E.g.*, N. S. Gill and R. S. Nyholm, *J. Chem. Soc.*, 3977 (1959).
15) Y. Tanabe and S. Sugano, *J. Phys. Soc. Jpn.*, **9**, 753, 766 (1954).
16) T. S. Piper and R. L. Carlin, *J. Chem. Phys.*, **35**, 1809 (1960).

 © 1982 The Chemical Society of Japan Bull. Chem. Soc. Jpn., 55, 95—100 (1982)

Recovery of Heavy Metals with Calcium Silicon Alloy. II. Recovery of Copper(II) Ions

Shuzo TOKUNAGA

National Chemical Laboratory for Industry, Yatabe, Ibaraki 305

(Received January 20, 1981)

In the 20.0-matom dm^{-3} Cu(II) solution of an initial pH of 4.0, more than 99% of it was removed by addition of calcium silicon alloy in *ca.* 5 min, and the pH decreased to below 2. The X-ray diffraction pattern of the solid reaction product indicated that the Cu(II) removal took place through reduction to metallic Cu. In the 1.0-matom dm^{-3} Cu(II) solution, the pH increased from 4.0 to above 9.0 in 30 min, which consequently maintained high removal for a long time. In the constant pH runs, relation of the equivalents of Ca and Si dissolved against that of Cu(II) ions removed showed that not only the Ca moiety but also the Si moiety participated in the reduction of Cu(II) ions. It is desirable to control pH value at 3.0 or higher, or to separate the solid phase from the liquid phase in the first 30—60 min in order to avoid excess dissolution of calcium silicon alloy and to attain high Cu(II) removal. Copper(I) oxide was formed in a solution of pH above *ca.* 5, which was in contact with the air. In a HNO_3 solution, the removal decreased considerably. Sodium nitrate also caused strong interference with the removal which can be prevented by acidifying the solution with HCl to pH *ca.* 1. When Hg(II) or Cr(VI) ions are present, the Cu(II) removal tends to decrease depending on the amount of calcium silicon alloy added.

In the previous study,[1] calcium silicon alloy proved to be effective for reducing metal ions such as Cd(II), Sn(II), Pb(II), Cu(II), Ag(I), and Hg(II) ions to the elemental state. Fe(III) and Cr(VI) ions were reduced to Fe(II) and Cr(III), respectively. The solubility of calcium silicon alloy is insignificant at pH 3—8, making its use as a reductant possible in aqueous solutions without causing excess dissolution. The reduction of Hg(II) ions with the alloy was studied in detail previously.[2] The purpose of the present paper is to study in detail the recovery of copper(II) ions with calcium silicon alloy and to find the optimum conditions for recovering them in metallic powder which is more advantageous for further utilization than copper(I) compounds.

Experimental

Materials. The same calcium silicon alloy as used previously[1] was used. All other chemicals were of reagent grade. As Cu(II) solution copper(II) chloride was used.

Analysis. Analyses of Cu, Cd, Pb, Fe, Hg, Cr, Ca, and Si were made as reported previously.[1]

X-Ray Powder Diffraction. The X-ray powder diffraction pattern of a solid product was obtained with a Model 2025 Diffractometer (Rigaku Corporation) with Ni-filtered Cu $K\alpha$ radiation. Quantitative determination of copper(I) oxide was carried out by preparing a calibration curve with standard mixtures of copper(I) oxide and copper metal powder, and with the diffraction peaks at 2.47 and 2.08 Å, respectively.

Recovery of Copper(II) Ions without pH Control. A 2.0 dm^3 of 20.0- or 1.0-matom dm^{-3} Cu(II) solution was prepared in a beaker and the pH was adjusted to 4.0 with HCl. The beaker was placed in a 20 °C thermostat, and its opening was covered with a film of polyethylene which had a short rift for addition of calcium silicon alloy and for sampling. Six grams of calcium silicon alloy was added, and the solution was stirred continuously with a magnetic stirrer. Then an aliquot was taken at intervals and filtered through a membrane filter (Millipore, WH) as quickly as possible. Analysis was made on the filtrate for Cu, Ca, and Si, and the pH was determined. Selected samples of the solid product obtained from the 20.0-matom dm^{-3} Cu(II) run were washed with a small amount of water and dried in a vacuum drying oven at *ca.* 60 °C for 2 d, and then analyzed by the X-ray powder diffraction method.

Recovery of Copper (II) Ions at Constant pH. To a 2.0 dm^3 of 30.0-, 20.0-, 10.0-, 5.0-, or 1.0-matom dm^{-3} Cu(II) solution was added 6.0 g of calcium silicon alloy. The pH was maintained constant at 4.0 by automatically adding either NaOH or HCl solution with a Model HSM-10A pH Stat (Toa Electronics Ltd.). Furthermore the pH of a 1.0-matom dm^{-3} Cu(II) solution was controlled at 6.0, 4.0, 3.0, or 2.0 with HCl. The same procedure was followed as above.

Air Oxidation of Metallic Copper. A 20.0-matom dm^{-3} Cu(II) solution of an initial pH of 4.0 was treated in the same way as above without covering the opening of the beaker with a polyethylene film.

Interferences on the Reduction of Copper(II) Ions. Interference from Acids. A 100 cm^3 of 1.0-matom dm^{-3} Cu(II) solution was prepared in a 100-cm^3 Erlenmeyer flask whose acidity was adjusted with HCl, HNO_3, H_2SO_4, or $HClO_4$ to pH *ca.* 3, *ca.* 1, and 1.0 mol dm^{-3} acid. To the solution was added 0.3 g of calcium silicon alloy and the opening of the flask was sealed with "Parafilm." The solution was stirred with a magnetic stirrer in a 20 °C thermostat, and filtered through a membrane filter 30 min after the addition of calcium silicon alloy. Determination was made for Cu, Ca, Si, and pH on the filtrate.

Interference from Sodium Salts. A 100 cm^3 of 1.0-matom dm^{-3} Cu(II) solution was prepared in a 100-cm^3 flask which contained NaCl, $NaNO_3$, Na_2SO_4, or $NaClO_4$ in the concentration of 0.1, 1.0, 10.0, or 100.0 mmol dm^{-3}. The pH was adjusted to *ca.* 3 with HCl. Then the sample solution was treated in the same way as above.

Interference from Metal Ions. A 100 cm^3 of 1.0-matom dm^{-3} Cu(II) solution was prepared, which contained $CdCl_2$, $PbCl_2$, $FeCl_3$, $HgCl_2$, or K_2CrO_4 in the concentration of 0.1, 1.0, 5.0, or 20.0 mmol dm^{-3}. The pH was adjusted to *ca.* 3 with HCl. As the reference, a 100 cm^3 of metal mixture solution was prepared containing 1.0 mmol dm^{-3} of $CuCl_2$ and each 1.0, 5.0, or 10.0 mmol dm^{-3} of $CdCl_2$, $PbCl_2$, $FeCl_3$, and $HgCl_2$. The sample solution was treated in the same way as above.

Results and Discussion

Recovery of Copper(II) Ions without pH Control.

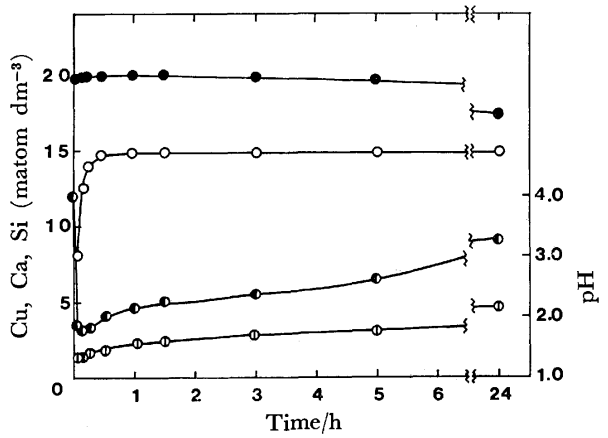

Fig. 1. Recovery of Cu(II) ions at an initial pH of 4.0. 20.0-matom dm^{-3} Cu(II) solution.
●: Cu(II) removed, matom dm^{-3}, ○: Ca dissolved, matom dm^{-3}, ⊕: Si dissolved, matom dm^{-3}, ◐: pH.

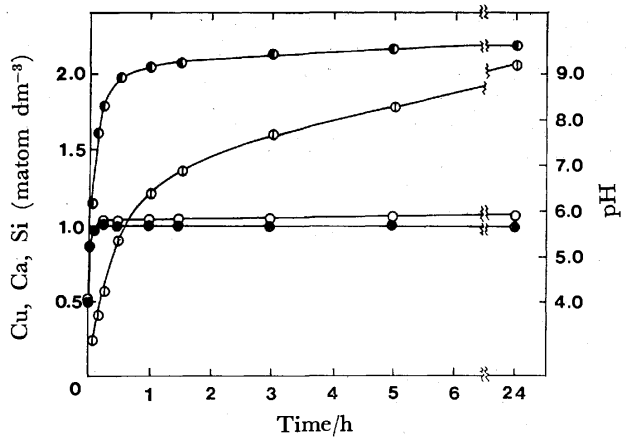

Fig. 2. Recovery of Cu(II) ions at an initial pH of 4.0. 1.0-matom dm^{-3} Cu(II) solution.
●: Cu(II) removed, matom dm^{-3}, ○: Ca dissolved, matom dm^{-3}, ⊕: Si dissolved, matom dm^{-3}, ◐: pH.

The efficiency of calcium silicon alloy for recovering Cu(II) ions was studied by determining removal rates of Cu(II) ions, dissolution rates of the Ca and Si moieties from the alloy, and the variation of pH, and by using the X-ray diffraction patterns of the obtained solid product. The pH of the Cu(II) solutions was initially adjusted to 4.0. The results are given in Figs. 1 and 2.

In the 20.0-matom dm^{-3} Cu(II) solution, the removal rate of Cu(II) ions was so great at the initial stage of the reaction that more than 99% removal was attained in *ca.* 5 min, the remaining Cu(II) concentration being lower than *ca.* 0.03 matom dm^{-3}. With the Cu(II) removal, the pH decreased remarkably from 4.0 to below 2.0, and then increased slowly. Such a great decrease in pH was observed for solutions of more concentrated than *ca.* 5-matom dm^{-3} Cu(II). The X-ray diffraction analysis showed that all of the solid products recovered on the membrane filter contained only metallic Cu as the copper component, indicating that Cu(II) ions were removed through reduction to metallic Cu. The dissolution of Ca and Si increased in accordance with the Cu(II) removal at the initial stage of the reaction, and thereafter the former reaction terminated in *ca.* 30 min, whereas the latter reaction continued to increase slowly with time. Although excess calcium silicon alloy was present in the solution, the Cu(II) concentration in the solution began to increase after *ca.* 3 h, indicating dissolution of deposited Cu again into solution. In this case, the amount of Ca dissolved was *ca.* 15 matom dm^{-3}, amounting to *ca.* 64% of the Ca moiety initially present. The Ca dissolution seems to take place from the surface of the alloy, the Ca moiety remaining just inside the alloy particles, and it was made inactive by being surrounded by silicates and the Si moiety. The reduction of Cu(II) ions by the Si moiety seems to be slower than the dissolution of metallic Cu.

In the 1.0-matom dm^{-3} Cu(II) solution (Fig. 2), the removal rate of Cu(II) ions was also great at the initial stage of the reaction, and the Cu(II) concentration was held below 0.001 matom dm^{-3}. The removal rate in percentage was slightly smaller than that for the 20.0-matom dm^{-3} Cu(II) solution. In contrast to the 20.0-matom dm^{-3} run, the pH increased considerably to above 9.0 in 30 min, which acted to depress dissolution of deposited metallic Cu, and consequently high Cu(II) removal was maintained for as long as 24 h. The amount of Ca dissolved increased with that of Cu(II) removed, their equivalents showing a good agreement. The increase in pH seems to depress excess Ca dissolution. On the other hand, the Si dissolution increased linearly independent of the Cu(II) removal, exceeding the dissolved Ca moles after *ca.* 40 min. It can be concluded that Cu(II) ions are removed by being reduced to the metal mainly with the Ca moiety.

Recovery of Copper(II) Ions at a Constant pH. The pH of the sample solution tends to vary considerably during the reaction, decreasing for Cu(II) concentrations higher than *ca.* 5 matom dm^{-3}, and increasing for lower Cu(II) concentrations. Similar experiments were carried out keeping the pH constant in order to study the reaction in detail without the effects of the pH variation.

Effects of initial Cu(II) concentrations on the reaction were studied with 30.0-, 20.0-, 10.0-, 5.0-, and 1.0-matom dm^{-3} Cu(II) solutions of pH 4.0, where the dissolution of the alloy is insignificant in a metal-free solution(blank).[1] Since the pH decreased at the initial stage of the reaction (*ca.* 5 min) for Cu(II) concentrations higher than 5 matom dm^{-3}, 1—4 mol dm^{-3} NaOH solution was added to control the pH. The results are given in Table 1 (Runs 1 to 5). In all the runs more than 99% removal was attained in as soon as 15 min, showing a very high removal efficiency. The removal rate (%) in the first 5 min was greater for higher initial Cu(II) concentrations. All the X-ray diffraction patterns of the solid products obtained from the 30.0—5.0-matom dm^{-3} runs showed that only metallic Cu was contained as the copper component. Thus, it can be concluded that the Cu(II) removal takes place through reduction to metallic Cu. Though the solid products obtained from the 1.0-matom dm^{-3} Cu(II) run failed to give X-ray diffraction pattern of copper compounds due to their

Table 1. Recovery of copper(II) ions at constant pH

Run	Initial Cu(II) (matom dm^{-3})	pH		Time/min 5	15	30	60	90	180	300	420
1	30	4.0	Cu[a)]	30.0	30.0	30.0	30.0	30.0	30.0	30.0	30.0
			Ca[b)]	14.0	14.4	14.8	14.9	15.1	15.2	15.3	15.2
			Si[c)]	2.0	2.2	2.3	2.6	2.9	3.1	3.3	3.6
2	20	4.0	Cu	20.0	20.0	20.0	20.0	20.0	20.0	20.0	20.0
			Ca	11.5	11.7	11.9	12.0	12.1	12.0	12.0	12.0
			Si	1.4	1.4	1.5	1.6	1.7	2.0	2.4	2.8
3	10	4.0	Cu	9.9	10.0	10.0	10.0	10.0	10.0	10.0	10.0
			Ca	6.6	6.7	6.9	7.2	7.5	8.2	8.8	9.1
			Si	0.6	0.7	0.8	0.9	1.1	1.4	1.9	2.1
4	5.0	4.0	Cu	4.6	5.0	5.0	5.0	5.0	5.0	5.0	5.0
			Ca	4.0	4.2	4.3	4.6	4.8	5.3	5.9	6.3
			Si	0.3	0.3	0.4	0.5	0.6	0.8	1.1	1.4
5	1.0	4.0	Cu	0.84	0.99	1.00	1.00	1.00	0.98	0.97	0.96
			Ca	0.89	1.09	1.12	1.53	1.83	2.54	3.22	3.86
			Si	0.04	0.10	0.16	0.21	0.27	0.45	0.63	0.82
6	1.0	6.0	Cu	0.74	0.98	1.00	1.00	1.00	1.00	0.99	0.98
			Ca	0.80	1.04	1.25	1.53	1.76	2.21	2.95	3.33
			Si	0.05	0.12	0.25	0.41	0.59	0.98	1.39	1.72
7	1.0	3.0	Cu	0.95	1.00	1.00	1.00	0.99	0.98	0.95	0.90
			Ca	1.07	1.23	1.34	1.63	1.95	2.75	3.72	4.56
			Si	0.07	0.12	0.18	0.26	0.33	0.57	0.92	1.37
8	1.0	2.0	Cu	0.98	1.00	1.00	1.00	0.95	0.65	0.15	0.04
			Ca	2.53	5.83	6.95	7.17	7.18	7.22	7.19	7.23
			Si	0.14	0.34	0.58	1.38	1.54	2.37	3.24	3.93

a) Cu(II) removal, matom dm^{-3}. b) Ca dissolution, matom dm^{-3}. c) Si dissolution, matom dm^{-3}.

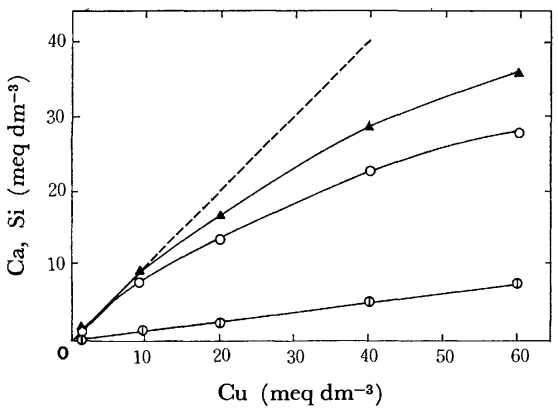

Fig. 3. Relation between equivalent of Cu(II) ions removed and those of Ca and Si dissolved.
○: Ca dissolved, meq dm^{-3}, ⊕: Si dissolved, meq dm^{-3}, ▲: Ca+Si dissolved, meq dm^{-3}.

low contents, metallic Cu seems to be present in them.

The dissolution of Ca and Si took place in accordance with the Cu(II) removal. In the 30.0- and 20.0-matom dm^{-3} solutions, the amount of Ca dissolved reached a plateau several min after the Cu(II) removal had completed, where greater part (*ca.* 50—60%) of the Ca moiety initially contained in the alloy dissolved. The Si dissolution amounted to, at most, less than 5% of the initial Si moiety, increasing linearly even after the completion of Cu(II) removal. For the stoichiometrical discussion, the equivalents of Ca and Si dissolved and their sum are plotted against that of Cu(II) ions removed (Fig. 3), where the values at 5 min after the alloy addition are used, since the Ca and Si dissolutions tend to increase even after the completion of Cu(II) removal. The Ca dissolution showed a relation not linear to the Cu(II) removal, but it is undoubtful that the Ca moiety mainly acted to reduce Cu(II) ions. The Si dissolution showed a direct proportionality to the Cu(II) removal, indicating that not only the Ca moiety but also the Si moiety participated in the reduction, but the extent of its participation was much smaller than that of the former. The ratios of the sum of the equivalents of Ca and Si dissolved to that of Cu(II) ions removed were close to unity at 1.0 and 5.0 matom dm^{-3}, well accounting for the Cu(II) removal. At higher Cu(II) concentrations, however, the ratios became smaller, the reason of which is not clear yet.

Then, the effects of pH on the reaction were studied with 1.0-matom dm^{-3} Cu(II) solutions whose pH was controlled at 6.0, 4.0, 3.0, and 2.0 (Table 1, Runs 5 to 8). The removal rate of Cu(II) ions at the initial stage of the reaction was appreciably greater at lower pH, showing that an acid condition favors the reduction of Cu(II) ions. But the dissolution of deposited metallic Cu became more significant in stronger acid solutions, the Cu(II) removal decreasing down to almost zero after 3 h at pH 2.0. Furthermore the

Table 2. Effects of acids on recovery of Cu(II) ions

Acid	Acidity[a]		Cu(II) removal (%)	Ca diss. (matom dm^{-3})	Si diss. (matom dm^{-3})
	Initial	Final			
HCl	4.1	9.0	99.9	1.4	0.4
	2.9	3.9	99.8	1.7	0.2
	2.0	3.5	99.9	6.0	0.7
	1.0	1.1	99.4	9.7	1.3
	[1.0]	—	97.5	10.4	1.5
HNO_3	3.1	3.3	16.8	0.4	0
	1.2	1.2	1.1	0.4	0
	[1.0]	—	2.1	0.7	0.1
H_2SO_4	3.0	3.7	99.8	1.0	0.2
	1.2	1.3	99.7	7.9	0.9
	[1.0]	—	99.8	8.5	1.3
$HClO_4$	3.0	3.7	99.8	1.0	0.2
	1.0	1.0	99.7	9.0	1.0
	[1.0]	—	99.7	9.7	1.4

a) Figures in parentheses are expressed in mol dm^{-3}, and others in pH unit.

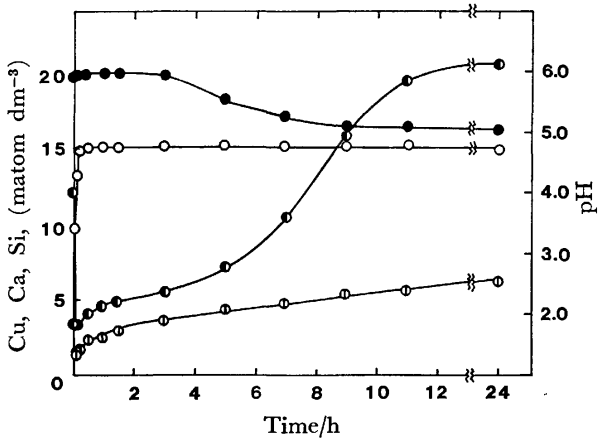

Fig. 4. Recovery of Cu(II) ions at an initial pH of 4.0 under the air. 20.0-matom dm^{-3} Cu(II) solution. ●: Cu(II) removed, matom dm^{-3}, ○: Ca dissolved, matom dm^{-3}, ⓘ: Si dissolved, matom dm^{-3}, ◐: pH.

dissolution of Ca and Si was much greater in such a strong acid condition. In the pH 6.0—3.0 runs, the equivalents of Ca dissolution at the initial stage well accounted for that of Cu(II) removal, increasing linearly with time after the completion of Cu(II) removal. It is, therefore, desirable to control pH value at 3.0 or higher, or to separate the solid phase from the solution in the first 30—60 min in order to avoid excess dissolution of the alloy and to establish complete Cu(II) removal.

Air Oxidation of Metallic Copper. When a solid product containing metallic Cu had been dried, copper was stable to the air for a long time, but when a wet product was placed in the air, formation of copper(I) oxide was recognized by its X-ray diffraction pattern, its intensity becoming significant with time. This indicates that metallic Cu is subject to air oxidation under a wet condition. When the product had been dried under reduced pressure as quickly as possible, the oxidation did not take place. Thus the air oxidation can be avoided in this way. Then the conditions were examined to cause the air oxidation of metallic Cu by making a similar experiment in the air, *i.e.* without a polyethylene film in the opening of a beaker. The result is shown in Fig. 4, and compared with that of the above-mentioned run with the solution isolated from the air (Fig. 1). The Ca dissolution showed a similar tendency with that of the above run. On the other hand, the Si dissolution was slightly greater. More than 99% Cu(II) removal was maintained for *ca.* 3 h. Thereafter the Cu(II) concentration in the solution began to increase with an increase in pH. At that time the solid product contained only metallic Cu as the copper component, indicating the reaction $Cu+1/2\ O_2+H_2O=Cu^{2+}+2\ OH^-$. After *ca.* 9 h the pH rose above *ca.* 5, and the increase in the Cu(II) concentration ceased. Then formation of copper(I) oxide was recognized in the solid product, and its content increased with time, indicating progress of its air oxidation. After 24 h metallic Cu in the solid phase changed entirely into copper(I) oxide. In another run in the air at pH 4.0, no appreciable amount of copper(I) oxide was found, and high Cu(II) removal was held for a long time. Therefore, it is found that deposited metallic Cu is stable for *ca.* 3 h in the air, and that its air oxidation is made insignificant by separating the solid product from the solution in a short time even if the reaction is carried out in the air. Thus the air oxidation yields Cu(II) ions when the pH is below *ca.* 5, decreasing the Cu(II) removal, and yields copper(I) oxide at pH higher than 5.

Interferences on the Reduction of Copper(II) Ions. For the actual calcium silicon alloy process, effects of commonly used acids and salts on the reduction of Cu(II) ions were studied, and those of metal ions as well, which are reduced to the lower oxidation state with the alloy. The results obtained in 30 min after addition of the alloy were discussed, when the removal was complete and the dissolution of deposited

Table 3. Effects of sodium salts on recovery of Cu(II) ions

Sodium salt	(mmol dm^{-3})	pH Initial	pH Final	Cu(II) removal (%)	Ca diss. (matom dm^{-3})	Si diss. (matom dm^{-3})
NaCl	0.1	3.1	3.8	98.9	1.1	0.2
	1.0	3.0	5.7	99.1	1.2	0.2
	10.0	3.0	6.4	99.1	1.1	0.2
	100.0	3.0	7.6	99.8	1.2	0.3
$NaNO_3$	0.1	3.0	3.2	90.1	0.9	0.2
	1.0	2.9	4.8	37.6	0.6	0.1
	10.0	3.0	3.9	5.9	0.2	0
	10.0	1.0	1.0	99.5	8.1	1.0
	100.0	3.0	3.9	3.9	0.2	0
	100.0	1.0	1.0	11.1	0.7	0.2
Na_2SO_4	0.1	3.0	4.4	99.9	1.0	0.1
	1.0	3.0	4.1	99.8	1.1	0.2
	10.0	3.1	3.7	83.1	1.1	0.2
	100.0	3.0	3.4	79.3	1.2	0.2
	100.0	1.0	1.0	99.6	7.6	1.3
$NaClO_4$	0.1	3.0	4.5	99.8	1.0	0.2
	1.0	3.0	4.0	99.5	1.0	0.2
	10.0	3.1	4.3	99.7	1.1	0.2
	100.0	3.0	5.4	99.9	1.4	0.3

Table 4. Effects of metal ions on recovery of Cu(II) ions

Metal salt	(mmol dm^{-3})	pH Initial	pH Final	Cu(II) removal (%)	Metal removal (%)	Ca diss. (matom dm^{-3})	Si diss. (matom dm^{-3})
$CdCl_2$	0.1	3.0	3.7	99.6	0.8	1.0	0.2
	1.0	3.1	3.7	98.8	0.6	1.1	0.2
	3.0	2.9	3.7	98.7	8.2	1.2	0.2
	10.0	2.8	3.3	99.3	27.3	3.2	0.4
	20.0	3.0	2.1	99.0	16.6	3.8	0.5
$PbCl_2$	0.1	3.0	3.5	99.3	96.5	1.1	0.2
	1.0	3.0	3.5	99.4	94.1	1.9	0.3
	3.0	3.0	3.8	99.5	96.0	3.6	0.4
	10.0	3.0	2.1	99.0	96.1	7.6	1.5
	16.0	3.0	2.2	97.6	94.4	11.3	1.8
$FeCl_3$	0.1	3.0	4.1	99.3	0.3	1.0	0.2
	1.0	2.9	3.7	98.9	19.2	1.2	0.2
	3.0	2.9	3.3	99.2	8.8	1.9	0.4
	10.0	1.7	1.8	99.0	1.4	8.9	1.4
	20.0	2.0	2.0	98.7	0.1	12.4	2.2
$HgCl_2$	0.1	3.0	3.3	99.9	99.3	1.1	0.3
	1.0	3.0	4.5	98.4	99.8	2.0	0.3
	3.0	3.0	4.4	98.8	98.9	3.7	0.6
	10.0	3.1	2.0	98.4	99.0	8.6	1.7
	20.0	3.0	1.8	92.2	98.6	13.7	2.6
K_2CrO_4	0.1	2.7	3.6	98.1	10.3	0.9	0.2
	1.0	2.1	2.8	76.3	43.4	2.8	0.4
	10.0	2.1	5.0	44.7	31.5	6.7	1.3
Mixture[a)]	1.0	2.0	2.3	99.6	b)	6.1	1.0
	5.0	1.8	1.7	98.9	c)	13.8	2.4
	10.0	1.9	1.7	96.8	d)	18.3	2.9

a) A mixture of $CdCl_2$, $PbCl_2$, $FeCl_3$, and $HgCl_2$ solutions was added to a 1.0-matom dm^{-3} Cu(II) solution so that each metal concentration was kept at 1.0, 5.0, or 10.0 matom dm^{-3}. b) Cd 60.0%, Pb 97.5%, Fe 0.8%, and Hg 99.9%. c) Cd 1.1%, Pb 64.3%, Fe 1.4%, and Hg 99.3%. d) Cd 0.3%, Pb 16.2%, Fe 0.6%, and Hg 98.4%.

metallic Cu was insignificant. Since the pH tends to increase during the reaction in the 1.0-matom dm^{-3} solution and hydrolysis of Cu(II) ions occurs from pH *ca.* 5.5, the initial pH was adjusted to 3 excluding the runs for examining acid effects. The sample solutions whose final pH exceeded 6 were acidified to pH *ca.* 3 with HCl and the pH was maintained for a minute before filtration and copper determination. The results are given in Tables 2, 3, and 4.

Of the acids examined here, HNO_3 strongly decreased Cu(II) removal even in small amount. This remarkable interference seems to be related to very low solubility of calcium silicon alloy in HNO_3 solution, possibly due to passivation by a film of silica formed on the solid surface. In the recovery of Hg(II) ions this effect was not so strong,[2] and the reduction rate of Hg(II) ions is greater than that of the film formation. In the HCl, H_2SO_4, and $HClO_4$ solutions, satisfactorily high Cu(II) removal was attained regardless of the acid concentration, because the amount of the alloy added was much greater, in equivalent, than that of Cu(II) ions present in solution. In solutions of high Cu(II) concentrations, the removal percentage will decrease with increasing acid concentration because of significant Ca dissolution. In comparison with the HCl solution, Ca dissolution was smaller in the H_2SO_4 or $HClO_4$ solution, and thus the alloy can be used more effectively for the recovery of Cu(II) ions.

Sodium salts of the conjugate bases of the above-mentioned acids were added to 1.0-matom dm^{-3} Cu(II) solutions with varying their concentration from 0.1 to 100 times the Cu(II) concentration. Effects of sodium salts can be considered to be as of the conjugate base ions. Similarly to the above runs in HNO_3, the interference from nitrate ions was significant, becoming appreciable from *ca.* 1 mmol dm^{-3}. Consequently the dissolution of Ca and Si decreased with increasing the salt concentration. When the pH of the 10.0-mmol dm^{-3} $NaNO_3$ solution decreased to 1.0 with HCl, the interference from nitrate ions can be prevented and high Cu(II) removal was attained. The Cu(II) removal, however, did not increase appreciably in the 100.0-mmol dm^{-3} $NaNO_3$ solution even when the pH decreased. The interference from sulfate ions became appreciable from 10.0 mmol dm^{-3}, and also can be prevented by decreasing pH to 1.0. NaCl and $NaClO_4$ did not decrease the Cu(II) removal at any concentration, but the dissolution of Ca and Si increased at high salt concentrations accompanying with an increase in pH.

Effects of metal ions on the reduction of Cu(II) ions are related to their reducibility, and the relative amount of the alloy added to that of the metal ions to be reduced. Since Cd(II) ions are least reducible with the alloy, it gave no appreciable effect on the Cu(II) removal, and thus the Cd(II) removal was low. Pb(II) ions, with lower standard electrode potential than Cu(II) ions, did not affect the Cu(II) removal either, and it was removed with high percentages. High Cu(II) removal was attained in the Fe(III) ion solutions. As shown previously,[1] Fe(III) ions are reduced to Fe(II) ions with the alloy, and the Fe(III) removal seems to be due to hydrolysis. Cu(II) removal decreased with increasing Hg(II) concentration, and Hg(II) ions, one of the most reducible ions, were removed with higher percentages than Cu(II) ions. Dichromate ions, having the highest standard electrode potential among the metal ions examined here, strongly suppressed the Cu(II) removal, whereas the dichromate removal was not so high, since they are efficiently reduced only in strong acid solutions and removed as Cr_2O_3(hydrated) and $CaCrO_4$.[1] Finally mixtures of Cd(II), Pb(II), Fe(III), and Hg(II) ions with various concentrations were added to a 1.0-matom dm^{-3} Cu(II) solution. In the 1.0-matom dm^{-3} metal solution, the highest removal was attained for each metal except for Fe(III). In the 5.0- and 10.0- matom dm^{-3} metal solutions, removal of the respective metal ions was in the order of increasing standard electrode potential. Thus when the concentration of a metal ion to be reduced increases in comparison to that of added calcium silicon alloy, its removal is strongly dependent on its standard electrode potentials, *i.e.* its reducibility.

References

1) S. Tokunaga, K. Uematsu, and Y. Nagawa, *Bull. Chem. Soc. Jpn.*, **54**, 733 (1981).
2) S. Tokunaga and K. Uematsu, *Nippon Kagaku Kaishi*, **1978**, 619.

Separation of Selenide Constituents from Selenide Samples Containing Elemental Selenium

Yuzo TAMARI,* Keizo HIRAKI,† and Yasuharu NISHIKAWA†

Department of Chemistry, Faculty of Science, Konan University, Higashinada-ku, Kobe 658

† *Department of Chemistry, Faculty of Science and Technology, Kinki University, Kowakae, Higashiosaka 577*

(Received January 31, 1981)

The valence state analysis to determine selenide in mixtures of selenide, elemental selenium, selenite, and selenate compounds was devised by the selective volatilization of selenium as its hydride. As the optimum conditions of the reaction, 6 M (this unit is defined to 1 M=1 mol dm^{-3} as below.) hydrochloric acid solution was dropped into the mixture and the hydrogen selenide gas generated was absorbed in a solution of sodium hydroxide and hydrogen peroxide. The optimal reaction temperature was found to be 170 °C for 40 min using nitrogen as the carrier gas. Utilizing this method, the fluctuation of the oxidation state of selenium was observed during the storage of zinc selenide samples.

The oxidation state of selenium in the lithosphere, hydrosphere, and atmosphere, selenium is mainly classified into the following species; sexivalent, quadrivalent, elemental, minus bivalent, and organically complexed species such as selenate, selenite or selenium dioxide, red amorphous or gray metallic selenium,[1] selenide, and selenomethyonine,[2] respectively.

Although numerous methods for the total analysis of selenium in rock, soil, and sediment samples have been devised. The analysis of the oxidation state of selenium in powdered solid samples has rarely been reported. A method to separate the high valent species of selenium (sexivalent and quadrivalent) from the low valent species (elemental and minus bivalent) in sediment samples was deviced by Terada *et al.*[3] Utilizing a chemical leaching method,[4] the high and low valent species of selenium in marine core sediments with its core depth were analysed by Tamari.[5]

In this work, the reaction conditions in order to determine selenium after separating selenide constituents as the gas of hydrogen selenide from the powdered samples containing elemental selenium, selenite, and selenate were investigated in detail. This study establishes the optimum conditions for the generation of the hydride and its subsequent trapping in absorbents.

Experimental

Reagents and Apparatus. Standard samples of selenide were prepared as follows. Selenide standard was prepared by mixing 0.02 g of zinc selenide powder with 1 g of silica powder in an agate mill for 10 min, and the mixture homogenized by quartering four times.[6] After this preparation, total selenium content of the selenide standard was determined to be 10.04±0.95 μg/mg.[7] Approximately 10 mg of this standard was used for experiments.

Silica powder was used to dilute the selenide standard. Fine quarts powder to pass through the sieve of 100 mesh size was taken in a beaker, and boiled with the solution of 6 M hydrochloric acid. The powder was filtered with a membrane filter (pore size: 3 μ) and rinsed with water, then dried at 110 °C.

The apparatus designed for the generation of hydrogen selenide and the collection of its hydride, is shown in Fig. 1. As can be seen in this figure, a funnel and two traps were connected to a reactor.

All chemicals used were analytical reagent grade; the other reagents and apparatus have been reported by Tamari *et al.*[8]

Recommended Procedure. About 10 mg of a sample was placed in the reactor (see Fig. 1), and 20 cm^3 of 6 M hydrochloric acid solution were added to the funnel. The mixed solution of 2.5 cm^3 of 0.1 M sodium hydroxide and 7.5 cm^3 of 30% hydrogen peroxide were placed in the trap vessels. The reactor connected to the funnel and the traps was set in the hole of an aluminium-block adjusted to 170 °C with a hot-plate. The hydrochloric acid solution was dropped into the reactor using a carrier gas of nitrogen. The hydrogen selenide generated was carried with the gas into the absorbent solution. This reaction was subjected to heating for 40 min at 170 °C. After the reaction, the reactor and the traps were disconnected, and each of the traps to which 1 cm^3 of 30% hydrogen peroxide was added was heated on a hot-plate for a few minutes in order to oxidize the selenide. Then, 1 cm^3 of concd nitric acid was added to each vessel from its tube, and the solution was boiled for a few minutes to oxidize to selenate. After cooling, the solution in each trap was placed in a 100 cm^3 or 250 cm^3 measuring flask, and diluted to the mark with water. The solution in the reactor was filtered with a membrane filter (pore size: 3 μ) and the filtrate was diluted with water to 100 cm^3 or 250 cm^3. To the aliquots of the solution, 0.5 cm^3 of 70% perchloric acid solution was added and evaporated until the perchloric acid vapor appeared. Selenium in the sample solution was completely reduced to selenite by boiling for 3 min after the addition of 2 cm^3 of 6 M hydrochloric acid solution. The selenite solution prepared was determined by fluorometry with 2,3-diaminonaphthalene.[8]

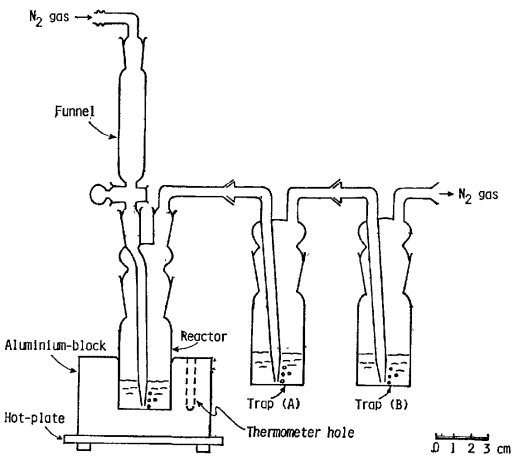

Fig. 1. Apparatus to generate and collect hydrogen selenide.

Table 1. Effect of acid concentration on the generation of hydrogen selenide

Hydrochloric acid (M)	Found selenium[a] (μg)	Ratio of selenium/%[b]		
		Reactor	Trap (A)	Trap (B)
2	85.4	25	75	0
6	91.2	1	99	0
9	100	30	70	0
12	121	37	63	0

a) Total amounts of selenium found in the reactor and traps. b) Percentage ratio of amounts of selenium found in the reactor and traps.

Table 2. Effect of reaction temperature

Reaction temp °C	Found selenium (μg)	Ratio of selenium/%		
		Reactor	Trap (A)	Trap (B)
43—49	73.3	16	84	0
99—103	70.6	27	72	1
170	43.5	7	91	2

Results and Discussion

All experiments were carried out in order to consider the optimum conditions of the reactions based on the generation of hydrogen selenide and its absorption into solutions.

Effect of Carrier Gas. Using air as a carrier gas instead of nitrogen, a considerable amount of selenium remained in the reactor, and red condensates were observed on the wall of the tube between the reactor and the trap (A). The condensate could be red amorphous selenium generated by oxidation of the hydride to elemental selenium. Accordingly the use of nitrogen gas was recommended as the carrier.

Effect of the Concentration of Hydrochloric Acid. Solutions of 2, 6, 9, and 12 M hydrochloric acid were examined. Each 20 cm^3 of the solution was added to the reactor from the funnel under the conditions of the reaction at 170 °C for 40 min and the addition of the solution mixed 19 cm^3 of 0.1 M sodium hydroxide with 1 cm^3 of 30% hydrogen peroxide to each trap. As shown in Table 1, no selenium was found in the trap (B), and the best concentration of the acid solution was considered to be 6 M hydrochloric acid from the results of the data of the recovery of hydrogen selenide in the trap (A).

Effect of Reaction Temperature. The reaction temperature for the generation of hydrogen selenide was examined under the conditions of addition of 6 M hydrochloric acid solution and the same reaction system as described above. Table 2 gives the results of the examination. Since the highest percentage of selenium was found in the trap (A) when the temperature attained 170 °C, this temperature was applied to the experiments below.

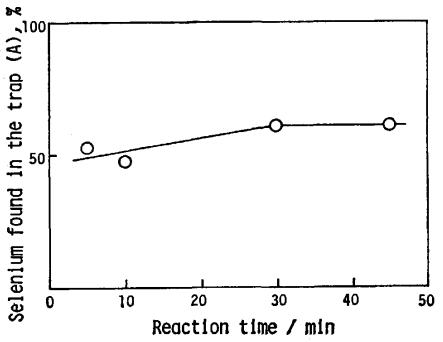

Fig. 2. Effect of reaction time on the generation of hydrogen selenide.

In the case of selenide samples containing selenite and selenate, selenate was reduced to selenite by boiling with the solution of 6 M hydrochloric acid, and the subsequent selenite may be volatilized as selenium tetrachloride above *ca.* 200 °C.[1] In this work therefore it is important to keep the reaction temperature at 170 °C to avoid the volatilization of selenium.

Effect of the Chemical Composition of the Absorbent. Sodium hydroxide solution is generally considered to be an effective absorbent for trapping of hydrogen selenide as well as hydrogen sulfide. However hydrogen selenide can be changed to a more stable chemical form as a red colored precipitate by oxidizing the hydride to avoid the revolatilization of the hydride in the trap. Hence the solutions of hydrogen peroxide and nitric acid were tested for efficiency as oxidant and absorbant of the hydride.

In the chemical system of sodium hydroxide solution containing hydrogen peroxide, the recovery percentage of selenium in the traps was fairly good, whereas in the system of nitric acid solution containing hydrogen peroxide it was relatively low because of the revolatilization of hydrogen selenide due to the acid solution. Futhermore in the latter system, selenium was absorbed into the solution in both the trap (A) and the trap (B). Therefore the fomer system was used for the experiment of hydrogen selenide as an absorbent. Table 3 lists the results of the chem-

Table 3. Effect of the chemical composition of absorbent

Chemical composion of absorbent		Found selenium (μg)	Ratio of selenium/%		
0.1 M NaOH (cm^3)	30% H_2O_2 (cm^3)		Reactor	Trap (A)	Trap (B)
19	1	91.2	1	99	0
15	5	87.2	12	88	0
10	10	108	8	92	0
5	15	107	3	97	0
0	20	87.3	7	93	0

Table 4. Recovery of hydrogen selenide in the recommended procedure

Selenide standard		Selenium found in the trap (A) (%)	Selenium recovery (%)
Taken (mg)	Added (μg)		
11.4	114	90.3	79.2
10.0	100	76.7	76.7
10.9	109	99.4	91.2
12.0	120	104	86.7
10.4	104	81.2	78.1
			Average±standard deviation 82.4±6.3
Elemental selenium added (μg) 1000		0	100
Selenium(IV) added (μg) 100		3	97

ical composition of the absorbent in the system for trapping the hydride. As can be seen in Table 3, no selenium was found in the trap (B) in each absorbent solution, and the solution obtained by mixing 19 cm^3 of 0.1 M sodium hydroxide with 1 cm^3 of 30% hydrogen peroxide was selected as the best absorbent. This was based not only on the results representing the highest value in the trap (A) but also consideration of the post-preparation for the fluorometric determination of selenium with 2,3-diaminonaphthalene.[8]

Effect of Reaction Time. The effect of the reaction time on the generation of hydrogen selenide was investigated under the optimum conditions described above. As is shown in Fig. 2, the constant percentage of selenium in the trap (A) was obtained by reacting for more than 30 min. Hence the reaction for 40 min was undertaken for all the experiments.

Recovery of Hydrogen Selenide in the Recommended Procedure. In the optimum conditions of the reaction for the generation of hydrogen selenide and its trapping in the absorbent, *i.e.*, in the recommended procedure, the experiments for the recovery of selenium were carried out. It can be seen from Table 4 that the selenium recovered was 82.4±6.3%. From the consideration of the homogeneity of selenium in the selenide standard, 10.01±0.95 μg/mg, it was indicated that the coefficient variation of the former value, 7.9%, was included in the latter case, 9.5%. This method was applied to the samples involving the other oxidation state of selenium; 100 μg of selenite and 1 mg of elemental selenium were used for the experiment. As is seen from the results, neither selenite nor elemental selenium was volatilized, and little selenium was found in the trap (A).

Since the proposed method is useful for the determination of selenide, the method will be applied to the samples of the selenium compounds as the valence state analysis of selenide. The authors will report later on the application of this method to the samples.

References

1) T. Thitani, "Muki Kagaku," Sangyo-tosho Co., Ltd., Tokyo (1964), p. 1001.
2) A. J. Barak and S. C. Swanberg, *J. Chromatogr.*, **31**, 282 (1967).
3) K. Terada, T. Ooba, and T. Kiba, *Talanta*, **22**, 41 (1975).
4) Y. Tamari, K. Hiraki, and Y. Nishikawa, *Chikyu Kagaku*, **12**, 37 (1978).
5) Y. Tamari, The Doctoral Dissertation of Kinki Univ. (1978), p. 33.
6) Y. Tamari, *Radioisotopes*, **28**, 3 (1979).
7) K. Hiraki, Y. Tamari, Y. Nishikawa, and T. Shigematsu, *Bull. Inst. Chem. Res., Kyoto Univ.*, **58**, 228 (1980).
8) Y. Tamari, K. Hiraki, and Y. Nishikawa, *Bunseki Kagaku*, **28**, 164 (1979).

Kinetics of Thermal Pyridine Dissociation of Ni(*N*-arylsalicylideneaminato)$_2$-(pyridine)$_2$ in Solid Phase

Kikuo MIYOKAWA,* Hidenori HIRASHIMA, and Isao MASUDA

Department of Chemistry, Faculty of Science, Fukuoka University, Nanakuma, Nishi-ku, Fukuoka 814-01

(Received February 16, 1981)

The kinetics of the thermal pyridine dissociation reactions of Ni[*N*-(R-C_6H_4)salam]$_2$py$_2$, where R=H(**1**), *p*-F(**2**), *p*-CH_3O(**3**), *p*-CH_3(**4**), *p*-Cl(**5**), and *p*-Br(**6**), in solid phase, were analyzed by the isothermal weight-loss measurements. On pyrolysis, these pyridine adducts with an octahedral coordination geometry of Ni(II) liberated pyridine to leave products with the formula Ni[*N*-(R-C_6H_4)salam]$_2$. The product obtained from **2** was the diamagnetic monomer, those from **4**—**6** were paramagnetic polymers with μ_{eff}=(3.11—3.30) μ_B, and that from **3** was paramagnetic with an intermediary moment of μ_{eff}=1.45 μ_B. Reaction mechanisms were different depending on the nature of R: **2** followed the contracting disk equation with E =163 kJ/mol; **3**—**6** followed the contracting disk equation in the initial period of the reaction (the E_a values were 97 for **3**, 134 for **4**, 173 for **5**, and 172 kJ/mol for **6**) and then all except **3** followed Jandar's equation, in the subsequent period. These E_a values were considered to reflect the bond stability between the central Ni(II) ion and the axial pyridine ligands; these values increased with an increase in the electron-withdrawing property of R. The pyridine dissociation reaction may give rise to the complexes of the monomeric square-planar or to those of the associated, polymeric octahedral structure. Which result occurs does not depend only on the tendency of the central Ni(II) ion to accept, at the apical positions, the coordinate bond from the adjacent molecules.

Extensive investigations on bis(*N*-substituted salicylideneaminato)nickel(II) complexes have revealed that, in non-donor solvents, these complexes exist as a mixture of square-planar, tetrahedral, dimeric square-bipyramidal, and polymeric octahedral species.[1] The di- or polymeric species is thought to arise from the association of the planar species through the coordination bonding of the phenolato oxygen atoms in the complex molecule with the central Ni(II) ion of the adjacent molecules at the apical positions.[2] Thus, the association seems to be related to the Lewis base accepting ability of the central Ni(II) ion. However, the diversity of the solute species makes it difficult to evaluate the Lewis acidity of Ni(II) ions in these complexes, in solution.[3]

In order to estimate the Lewis acidity of the Ni(II) ion, the series of the complexes bis[*N*-(*p*-substituted aryl)salicylideneaminato]bis(pyridine)Ni(II), abbreviated as Ni[*N*-(R-C_6H_4)salam]$_2$py$_2$, have been subjected to a kinetic study of the thermal pyridine liberation reaction in solid phase.

Experimental

Materials. The parent complexes Ni[*N*-(R-C_6H_4)-salam]$_2$ were prepared by the published procedure.[4,5] Their bis(pyridine) adducts were isolated as previously described.[6] The adducts were identified by the nickel and pyridine analyses.

Measurements. TG and DSC curves were recorded on a Rigaku Denki Thermal Analyzer Model 8002 and isothermal weight-loss curves on a Sinku Riko micro-DTA apparatus Model TGD-3000-RH. These measurements were carried out under a constant flow of nitrogen, 100 ml/min. No influence from the variation of the nitrogen flow rate (in the range from 50 to 150 ml/min) was observed. Other physicochemical data were obtained as previously reported.[6]

Results and Discussion

The effective magnetic moments of the bis(pyridine) adducts and the products obtained after the adducts were heated up to 200 °C to eliminate pyridine, are compared with those of the parent Ni[*N*-(R-C_6H_4)-salam]$_2$ complexes in Table 1. The reflectance spectral data are also shown in Table 1. Parent complex **2**, as well as **1**, is diamagnetic, corresponding to the singlet state of Ni(II), and the spectrum exhibits an absorption maximum at 16.1×10^3 cm^{-1}; this is ascribed to the square-planar crystal field band, $^1A_{1g}\rightarrow{}^1A_{2g}$ transition of Ni(II).[7] On the other hand, the new parent complexes **3** and **6** are paramagnetic and these paramagnetisms correspond to the triplet state of Ni(II). Moreover, their spectra comprise two peaks with the maxima around 10.0 and 16.5×10^3

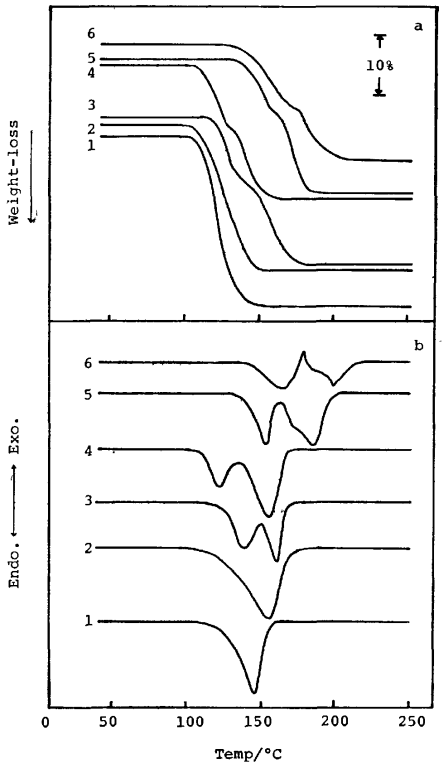

Fig. 1. TG(a) and DSC(b) curves of pyridine adducts; heating rate 10 °C/min. The numbers correspond to those given in Table 1.

Table 1. Magnetic, electronic spectral, and thermal data on the parent complexes Ni[*N*-(R-C_6H_4)salam]$_2$ and their bis(pyridine) adducts Ni[*N*-(R-C_6H_4)salam]$_2$py$_2$

No.	R	Parent complex				Bis(pyridine) adduct	Pyridine-liberated product	
		μ_{eff}[a] / μ_B		ν_{max}[b] / 10^3 cm^{-1}	t_m / °C	μ_{eff}[a] / μ_B	μ_{eff}[a] / μ_B	t_m[c] / °C
1	H	dia[d]	(dia)[e]	16.3	276	3.09 (2.9)[f]	dia	276
2	*p*-F	dia	(dia)[e]	16.1	271	3.16	dia	272
3	*p*-CH_3O	3.40		10.1, 16.5	266	3.14	1.45	264
4	*p*-CH_3	3.30	(3.28)[e]	10.3, 16.5	275	3.17	3.30	280
5	*p*-Cl	3.31	(3.34)[e]	10.2, 16.6	287	3.31	3.28	287
6	*p*-Br	3.36		10.0, 16.5	291	3.15	3.11	297

a) Effective magnetic moment. b) Powder reflectance. c) DSC-peak maximum temperature due to melting. d) dia: Diamagnetic. e) Ref. 5. f) Ref. 4.

cm^{-1}; these are respectively ascribed to the $^3A_{2g} \rightarrow {}^3T_{2g}$ and the $^3A_{2g} \rightarrow {}^3T_{1g}(F)$ transitions of Ni(II) in the octahedral crystal field.[7] The magnetic and the spectral characteristics indicate the coordination structure of the parent complexes to be square planar for **1** and **2** and octahedral for **3**—**6**.

In Fig. 1, the TG and DSC curves of the pyridine adducts are reproduced. The TG curves show that all the adducts investigated lose 2 mol of pyridine per mole of the adduct in the range (100—200) °C. Adduct **2**, like **1**,[6] shows one endothermic DSC peak and a weight-loss of 2 mol pyridine per mole of the adduct on one stage in the TG curve. But adducts **3**—**6** show two endothermic DSC peaks and, in the corresponding TG curves, they show the loss of 2 mol pyridine per mole of the adduct through two stages. Up to the break point temperature in the TG curve, the weight-loss amounts to *ca.* 40—60% of the total pyridine loss. This fact implies that in the cases of adducts **3**—**6** pyridine is liberated in two steps and hence that the formation of mono(pyridine) adduct may be expected. However, pyrolysis of these adducts at 120 °C, apparently lower than their first DSC peak temperatures, only resulted in leaving a product with the formula Ni[*N*-(R-C_6H_4)salam]$_2$. Dakternieks *et al.* have reported that the mono(pyridine) adducts of Ni(*N*-*n*-Bu-salam)$_2$ and Ni(*N*-*n*-Bu-5-Cl-salam)$_2$ are formed along with their bis(pyridine) adducts in the toluene solution containing pyridine, though the TG curves of these bis(pyridine) adducts show a smooth continuous weight-loss, indicating no evidence for the formation of a five-coordinated intermediate.[3]

As seen in Table 1, the products obtained by eliminating pyridine show either dia- or paramagnetism, in accord with the respective parent complexes, excluding product **3** which shows an intermediary magnetic moment. Product **3** is thought to be composed of both paramagnetic and diamagnetic species. It is noticed that for the diamagnetic monomeric product **1**[6] and **2**, their X-ray powder diffraction patterns were coincident with those of the respective parent complexes, while for the paramagnetic polymeric products **4**—**6**, the X-ray patterns did not agree with those of the respective parent complexes. Clark and

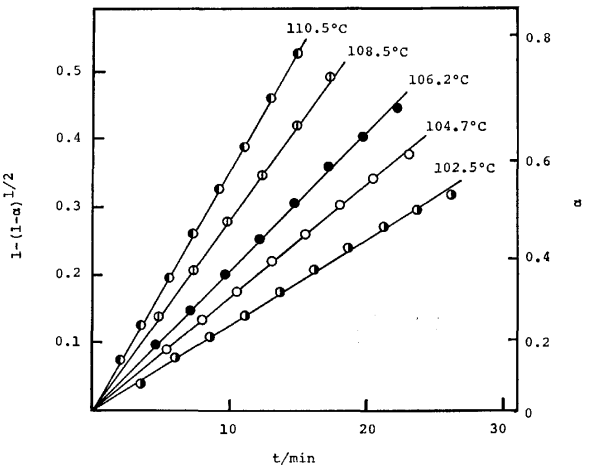

Fig. 2. Contracting disk rate plots for the pyridine liberation reaction of Ni[*N*-(*p*-F-C_6H_4)salam]$_2$py$_2$ (**2**).

O'Brien noted that for polymeric Ni(*N*-CH_3-5-Cl-salam)$_2$ the X-ray pattern of the sample obtained from the solution is not completely identical to that obtained by heating the monomeric modification in solid phase.[8]

The pyridine liberation process of adduct **1** has already been reported to follow the first order equation (Eq. 1) through α=0—0.70[6]

$$-\ln(1-\alpha) = kt, \quad (1)$$

where α, k, and t are the molar fraction of the adduct which liberated pyridine, the rate constant, and the reaction time, respectively. Adduct **2** differs from **1**; its pyridine liberation process is found to fit the contracting disk equation (Eq. 2) through α=0—0.65, as shown in Fig. 2:

$$1-(1-\alpha)^{1/2} = kt. \quad (2)$$

This fact may be interpreted by assuming that the reaction rate is determined by the reaction occurring at the phase boundary.[9]

The pyridine liberation process for adducts **3**—**6** were somewhat complicated in comparison with those for the above two cases. As is exemplified in Fig. 3 with the rate plots for **4**, the reaction mechanism appears to be altered with the progression of the pyridine dissociation reaction. The rate plots indicate

Table 2. Kinetic data of pyridine liberation reactions of Ni[*N*-(R-C_6H_4)salam]$_2$py$_2$

No.	R	α[a]	Reaction[b] scheme	$k/10^{-3}$ min^{-1} (Temp/°C)	E_a/kJ mol^{-1}
1	H[c]	0—0.70	A	6.68 (86.8), 9.37 (88.8), 12.3 (90.6), 17.3 (93.0)	167±4
2	*p*-F	0—0.65	B	12.8 (102.5), 17.0 (104.7), 20.8 (106.2), 28.2 (108.5) 38.8 (110.5)	163±4
3	*p*-CH_3O	0—0.45	B	3.06 (89.5), 3.53 (91.8), 5.30 (96.4), 7.77 (100.5)	97±5
4	*p*-CH_3	0—0.35	B	1.57 (106.8), 2.08 (110.8), 4.98 (118.5), 10.4 (124.8)	134±8
		0.35—0.75	C	0.84 (106.8), 1.75 (110.8), 3.66 (118.5), 10.1 (124.8)	159±14
5	*p*-Cl	0—0.30	B	4.17 (123.4), 5.84 (126.8), 10.8 (131.7), 20.1 (135.6)	173±12
		0.30—0.70	C	0.61 (123.4), 1.13 (126.8), 1.45 (131.7), 3.76 (135.6)	183±35
6	*p*-Br	0—0.30	B	5.00 (132.7), 5.87 (133.4), 21.7 (145.0), 30.8 (147.0)	172±7
		0.30—0.70	C	1.21 (132.7), 1.32 (133.4), 3.35 (145.0), 5.08 (147.0)	131±13

a) α: Molar fraction of the adduct liberated pyridine. b) A: $-\ln(1-\alpha)=kt$, B: $1-(1-\alpha)^{1/2}=kt$, C: $[1-(1-\alpha)^{1/3}]^2=kt$. c) Ref. 6.

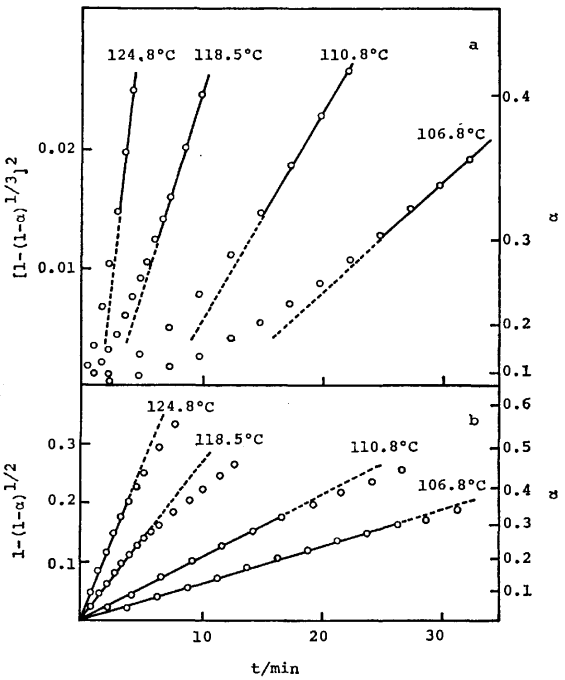

Fig. 3. Jandar's rate plots(a) and contracting disk rate plots(b) for pyridine liberation reaction of Ni[*N*-(*p*-CH_3-C_6H_4)salam]$_2$py$_2$ (**4**).

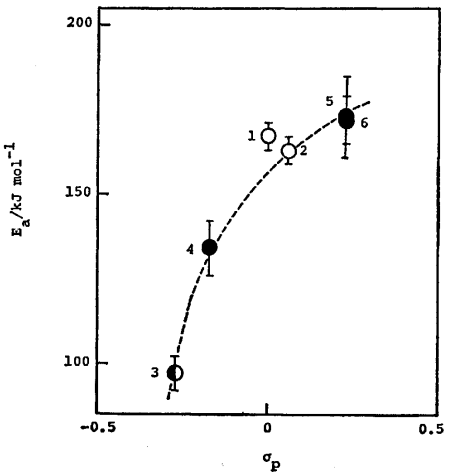

Fig. 4. Plots of activation energy, E_a *vs.* Hammett's σ_p value.
The numbers correspond to those in Tables 1 and 2. ○: Monomeric product, ●: polymeric product, ◐: (monomeric+polymeric) product.

that, in the initial period during α=0—0.35, the reaction progresses according to the contracting disk equation, as was observed for adduct **2**; however, in the subsequent period of α=0.35—0.75, it follows Jandar's equation (Eq. 3):[10]

$$[1-(1-\alpha)^{1/3}]^2 = kt. \quad (3)$$

Thus, these two processes of pyridine liberation would cause the apparent doubling observed in the TG and DSC curves of adducts **3**—**6**, as described above. The fact that the reaction follows Jandar's equation could be interpreted as meaning that the reaction is strongly influenced by the diffusion process of the liberated pyridine. For adducts **4**—**6**, which form the octahedral polymeric products upon pyrolysis, we think that as the pyridine dissociation proceeds, it becomes difficult for the free pyridine molecule to diffuse through the close product layer consisting of the polymeric species. An attempt to describe the isotherms for adduct **3** in the above subsequent period was unsuccessful.

The kinetic data are summarized in Table 2. With respect to the reactions described by Eq. 2, the values of the activation energy, E_a, are plotted against Hammett's substitution constant σ_p of R[11] in Fig. 4; the plots indicate that the E_a value increases with an increase in the electron-withdrawing property of R. As to the reaction described by Eq. 1, the E_a value does not deviate from this relation. No relation like the above was found for the reactions following Eq. 3. The electron-withdrawal through R is expected to stabilize the bonding of Ni(II) toward the axial pyridine ligands, as it may increase the Lewis acidity of the Ni(II) ion. Hence, the E_a values for the reactions following Eqs. 1 and 2 are considered to reflect mostly the bond stability between Ni(II) ion and the axial pyridine. From the solution equilibrium data on the pyridine adduct formation of Cu(*N*-R-salam)$_2$, which includes the Schiff bases with substituted aryl groups, Ewert *et al.*[12] have concluded that the electron-withdrawal by the substituent R on

the aryl ring is transmitted *via* N atom, thus decreasing the electron-density on Cu(II) ion.

Furthermore, Fig. 4 indicates that whether pyridine dissociation reaction gives rise to a square-planar monomer or to an associated octahedral polymer is not determined only by the E_a values; that is, the association of monomeric square-planar Ni(II) complexes forming the octahedral polymeric complexes is not affected solely by the Lewis acidity of the central Ni(II) ion. Though the basicity of the phenolato O atom should be taken into account in a discussion of the present association, the results of Ewert *et al.*[12] suggest that the substitution on aryl ring will exert its electronic effect on Ni(II) ion predominatly *via* N atom. Another factor would be a steric effect caused by substitution. Tsuchiya *et al.* have reported that "deaquation" of [Ni(diamine)$(H_2O)_2$]X_2 (diamine=*N*,*N*′-diethyl-, *N*,*N*′-dimethyl-, and *N*,*N*-diethylethylenediamine; X=anion) gives either octahedral [Ni(diamine)$_2X_2$] or square-planar [Ni(diamine)$_2$]X_2 depending on the steric effects arising from the *N*-substituents.[13] As far as the present complexes are concerned, the rather more bulky R seems to favor the associated form.

References

1) R. H. Holm, G. W. Everett, and A. Chakravorty, *Progr. Inorg. Chem.*, **7**, 83 (1966).
2) C. H. Harris, S. L. Lenzer, and R. L. Martin, *Aust. J. Chem.*, **11**, 331 (1958); R. H. Holm, *J. Am. Chem. Soc.*, **83**, 4683 (1961).
3) D. R. Dakternieks, D. P. Gordon, L. F. Lindoy, and G. M. Mockler, *Inorg. Chim. Acta*, **7**, 467 (1973).
4) F. Basolo and W. R. Matoush, *J. Am. Chem. Soc.*, **75**, 5663 (1953).
5) R. H. Holm and K. Swaminathan, *Inorg. Chem.*, **2**, 181 (1963).
6) K. Miyokawa, H. Hirashima, and I. Masuda, *Bull. Chem. Soc. Jpn.*, **54**, 3361 (1981).
7) A. B. P. Lever, "Inorganic Electronic Spectroscopy," Elsevier, Amsterdam (1968), p. 333.
8) H. C. Clark and J. O'Brien, *Can. J. Chem.*, **39**, 1030 (1961).
9) "Chemistry of Solid States," ed by W. E. Garner, Butterworth, London (1955), p. 184.
10) W. Jandar, *Z. Anorg. Chem.*, **163**, 1 (1927).
11) H. H. Jaffe, *Chem. Rev.*, **53**, 191 (1953).
12) A. Ewert, K. J. Wannowius, and H. Elias, *Inorg. Chem.*, **17**, 1691 (1978).
13) R. Tsuchiya, A. Uehara, A. Izumi, and S. Joba, 30th Nat. Conf. on Coordination Chemistry of Japan, Tokyo, Oct 1980, Abstr. No. 1B15.

Preparation and Characterization of Dichlorobis(*N*-alkylsalicylideneaminato)manganese(IV) Complexes

Takayuki MATSUSHITA,* Yoshihisa HIRATA, and Toshiyuki SHONO

Department of Applied Chemistry, Faculty of Engineering, Osaka University, Yamadaoka, Suita, Osaka 565

(Received February 23, 1981)

The chlorobis(*N*-alkylsalicylideneaminato)manganese(III) complexes, $Mn^{III}(N\text{-Rsai})_2Cl$, react with hydrogen chloride to give the corresponding dichloromanganese(IV) complexes, $Mn^{IV}(N\text{-Rsai})_2Cl_2$, as deep green crystals; R can be *n*-C_3H_7, *n*-C_4H_9, *i*-C_4H_9, *n*-C_6H_{13}, *c*-C_6H_{11}, *n*-C_8H_{17}, *n*-$C_{12}H_{25}$, *n*-$C_{18}H_{37}$, $CH_2C_6H_5$, or $CH_2CH_2C_6H_5$. These complexes were characterized by the magnetic susceptibilities, electronic spectra, infrared spectra, and cyclic voltammograms. The complexes (R=*n*-$C_{12}H_{25}$ and *n*-$C_{18}H_{37}$) are found to be stable toward water in the solid state. A *trans*, six-coordinate configuration is proposed for these Mn(IV) complexes on the basis of the infrared spectra.

Manganese-(III) and -(IV) complexes are of interest in connection with the biological redox systems involving manganese ions, such as the oxygen evolution process of photosystem II in green plants and the disproportionation of superoxide ion, O_2^-, by the manganese-containing superoxide dismutases.[1] In these systems the involvement of various oxidation states: Mn(II), Mn(III), and/or Mn(IV) have been proposed.[2–5] However, very few Mn(IV) complexes have been isolated and characterized so far, because Mn(IV) ion is very unstable toward water.[6,7] We have previously reported on the dichloromanganese-(IV) complexes with the Schiff bases derived from substituted salicylaldehydes with diamines or butylamine.[7] These Mn(IV) complexes are unstable toward moisture even in the solid state and decompose to the reduced manganese complexes. This may be caused because the coordinated chlorine atoms are displaced by water molecules. Thus we have aimed to obtain Mn(IV) complexes which are stable toward water.

In this paper we describe the preparation and characterization of a series of dichloromanganese(IV) complexes with the bidentate Schiff bases derived from salicylaldehyde and primary monoamines (Fig. 1). The reactivity of the Mn(IV) complexes toward water decreased as the chain length of the alkyl groups increased.

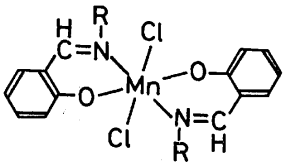

R	L	R	L
n-C_3H_7	*N*-Prsai	*n*-C_8H_{17}	*N*-Octsai
n-C_4H_9	*N*-Busai	*n*-$C_{12}H_{25}$	*N*-Dodsai
i-C_4H_9	*N*-*i*-Busai	*n*-$C_{18}H_{37}$	*N*-Octdsai
n-C_6H_{13}	*N*-Hxsai	$CH_2C_6H_5$	*N*-Bzsai
c-C_6H_{11}	*N*-*c*-Hxsai	$CH_2CH_2C_6H_5$	*N*-PEsai

Fig. 1. Manganese(IV) Schiff base complexes, $Mn(N\text{-Rsai})_2Cl_2$.

Experimental

Preparation of Mn(III) Complexes, Mn(N-Rsai)$_2$Cl. All the Mn(III) Schiff base complexes were obtained by a modification of the method described previously.[7]

Chlorobis(N-hexylsalicylideneaminato)manganese(III), Mn(N-Hxsai)$_2$Cl. The tetrahydrofuran (THF) solution (50 cm^3) containing salicylaldehyde (2.44 g) and hexylamine (2.02 g) was refluxed for 1 h. The solvent was evaporated under reduced pressure. The resulting yellow oily residue was dissolved in a mixture of dichloromethane (30 cm^3) and methanol (30 cm^3). Manganese(III) acetate dihydrate (2.68 g) and lithium chloride (0.63 g) were added to the solution. The mixture was refluxed for 1 h. The solvent was evaporated under reduced pressure to yield olive-green solids. They were collected on a glass filter, washed with 2-propanol and ether, and then dried *in vacuo*. They were recrystallized from dichloromethane. The yield was 3.2 g.

The other Mn(III) complexes were prepared in a similar manner. These complexes are soluble in dichloromethane, acetone, and acetonitrile. The analytical data are given in Table 1, together with the magnetic moments determined at room temperature.

Preparation of Mn(IV) Complexes. Dichlorobis(N-hexylsalicylideneaminato)manganese(IV), Mn(N-Hxsai)$_2$Cl$_2$. To a mixed solution of dichloromethane (20 cm^3) and 2-propanol (50 cm^3) containing $Mn^{III}(N\text{-Hxsai})_2Cl$ (1.0 g), a 2-propanol solution of HCl (1.5 molar folds over the complex) was added drop by drop with stirring at room temperature. The solution changed from greenish-brown to deep green with precipitation of deep green crystals. The mixture was cooled to 0 °C and allowed to stand for 3 h. The crystals precipitated were collected on a glass filter, washed with 2-propanol and ether, and then dried *in vacuo*. The yield was *ca.* 0.4 g. Further purification was not carried out.

The other Mn(IV) complexes (Fig. 1) were obtained in a similar manner. The analytical data are given in Table 2, together with the magnetic moments determined at room temperature. All the complexes are soluble in dichloromethane and the solutions show no noticeable change for an hour if kept isolated from contact with moisture. The complexes with R=Pr, Bu, *i*-Bu, Hx, *c*-Hx, Oct, Dod, Bz, and PE are soluble in acetone and acetonitrile; the complex with R=Octd is slightly soluble in the above solvents. All the complexes are soluble in coordinating solvents such as dimethyl sulfoxide and pyridine, but the solutions change rapidly from deep green to yellow-brown. The complexes with R=Dod and Octd have been found to be unreactive toward water in the solid state.

Reagents. All reagents were of reagent grade. Solvents were purified by refluxing over sodium (ether), calcium oxide (2-propanol), and calcium chloride (dichloromethane, acetone), and then distilled. Acetonitrile was distilled twice

Table 1. Elemental analyses and magnetic moments of manganeses(III) complexes

Complex	Found (%)				Calcd (%)				μ_{eff}[a]
	C	H	N	Mn	C	H	N	Mn	BM
Mn(*N*-Prsai)$_2$Cl	57.68	5.84	6.41	13.12	57.91	5.85	6.75	13.24	4.86
Mn(*N*-Busai)$_2$Cl	58.80	6.32	6.21	12.53	59.67	6.37	6.33	12.40	5.03
Mn(*N*-*i*-Busai)$_2$Cl	59.39	6.28	6.28	12.63	59.67	6.37	6.33	12.40	4.87
Mn(*N*-Hxsai)$_2$Cl	63.21	7.28	5.47	10.82	62.59	7.27	5.61	11.01	5.00
Mn(*N*-*c*-Hxsai)$_2$Cl·(H$_2$O)$_{0.5}$	61.50	6.59	5.61	11.28	61.96	6.60	5.55	10.90	4.89
Mn(*N*-Octsai)$_2$Cl	64.59	8.15	4.98	9·89	64.91	7.99	5.05	9.90	4.93
Mn(*N*-Dodsai)$_2$Cl	67.84	9.52	4.14	7.96	68.40	9.06	4.20	8.23	4.98
Mn(*N*-Octdsai)$_2$Cl	71.04	10.50	3.27	6.38	71.82	10.13	3.35	6.57	4.92
Mn(*N*-Bzsai)$_2$Cl	65.33	5.16	5.38	10.73	65.83	4.73	5.48	10.75	4.26
Mn(*N*-PEsai)$_2$Cl	66.88	5.21	5.20	10.20	66.86	5.24	5.20	10.19	4.85

a) Measured at room temperature.

Table 2. Elemental analyses and magnetic moments of manganese(IV) complexes

Complex	Found (%)					Calcd (%)					μ_{eff}[a]
	C	H	N	Cl	Mn	C	H	N	Cl	Mn	BM
Mn(*N*-Prsai)$_2$Cl$_2$	53.15	5.34	6.17	15.76	12.50	53.35	5.37	6.22	15.75	12.20	3.96
Mn(*N*-Busai)$_2$Cl$_2$	55.12	5.95	5.80	15.35	11.32	55.24	5.90	5.86	14.82	11.49	4.06
Mn(*N*-*i*-Busai)$_2$Cl$_2$	55.18	5.89	5.83	14.50	11.70	55.24	5.90	5.86	14.82	11.49	3.84
Mn(*N*-Hxsai)$_2$Cl$_2$	58.33	6.93	5.21	13.50	10.15	58.43	6.79	5.24	13.27	10.28	4.09
Mn(*N*-*c*-Hxsai)$_2$Cl$_2$	59.28	6.36	5.14	12.48	10.05	58.88	6.08	5.28	13.37	10.36	4.07
Mn(*N*-Octsai)$_2$Cl$_2$	60.90	7.53	4.64	11.20	9.31	61.02	7.51	4.74	12.01	9.30	3.92
Mn(*N*-Dodsai)$_2$Cl$_2$	64.90	8.70	3.95	9.90	8.02	64.95	8.61	3.99	10.09	7.82	3.93
Mn(*N*-Octdsai)$_2$Cl$_2$	68.75	9.55	3.19	8.90	6.07	68.94	9.72	3.22	8.14	6.31	4.08
Mn(*N*-Bzsai)$_2$Cl$_2$·CH$_2$Cl$_2$	55.35	4.25	4.39	21.01	8.53	55.18	4.87	4.82	22.46	8.70	3.99
Mn(*N*-PEsai)$_2$Cl$_2$	62.85	4.87	4.82	12.13	9.19	62.73	4.91	4.88	12.34	9.56	3.95

a) Measured at room temperature.

from diphosphorus pentaoxide before use.

Measurements. The UV and VIS absorption spectra were obtained from a Hitachi 340 recording spectrophotometer. The IR spectra were recorded on a Hitachi EPI-215 and a Hitachi EPI-L grating spectrophotometer for the 4000 to 650 cm^{-1} and the 700 to 250 cm^{-1} regions, respectively. The magnetic susceptibilities were measured by the Gouy method at room temperature. The cyclic voltammograms were made with a Yanagimoto P-8 polarograph connected with a Yanagimoto P8-PT potentiostat. A platinum wire and a platinum spiral were used as a working and an auxiliary electrode, respectively. An aqueous saturated calomel electrode was used as a reference electrode; this was inserted in an aqueous solution of 1 M (1 M= 1 mol dm^{-3}) KCl, which was connected with an agar salt bridge to a solution under investigation *via* an acetonitrile solution containing 0.1 M electrolyte. Tetrabutylammonium perchlorate was used as a supporting electrolyte.

Results and Discussion

The analytical data for the Mn(III) and Mn(IV) complexes are in agreement with the empirical formulas of MnL_2Cl and MnL_2Cl_2, respectively; here L denotes monoanion of *N*-alkylsalicylideneamines (Tables 1 and 2).

In general, most of the Mn(IV) compounds are not stable and are thus readily hydrolysed and reduced. The dichloromanganese(IV) complexes such as Mn^{IV}(salen)Cl_2 obtained previously are unstable in a moist air even in the solid state, where salen denotes dianion of *N*,*N*′-disalicylideneethylenediamine. Therefore many difficulties arose in the syntheses of these complexes. In this study we prepared a series of dichloromanganese(IV) Schiff base complexes (Fig. 1) in order to obtain water-resistant Mn(IV) complexes. This idea is based on the hope that the long chain alkyl groups such as *n*-$C_{12}H_{25}$ and *n*-$C_{18}H_{37}$ may protect against the attack of water molecules on the central manganese atom of the complex. Figure 2 shows the absorption spectral changes on the addition of water to an acetone solution of Mn(*N*-*c*-Hxsai)$_2$Cl$_2$. The intensity of the characteristic absorption band at 600 nm for the Mn(IV) complex decreased with time. The final absorption spectrum is almost the same as that of Mn^{III}(*N*-*c*-Hxsai)$_2$Cl in a mixture of acetone and water, indicating that water resulted in the reduction of the Mn(IV) complex. Figure 3 shows the time courses of the absorbances in the characteristic absorption bands for the complexes: Mn(*N*-Prsai)$_2$Cl$_2$, Mn(*N*-*c*-Hxsai)$_2$Cl$_2$, Mn(*N*-Octsai)$_2$Cl$_2$, and Mn(*N*-Dodsai)$_2$Cl$_2$, when water was added to these acetone solutions. It is apparent that their reactivity with water depends on the alkyl groups and decreases in the order of R= Dod<Oct<Pr<*c*-Hx. The most rapid change in absorbance observed for Mn(*N*-*c*-Hxsai)$_2$Cl$_2$ may be

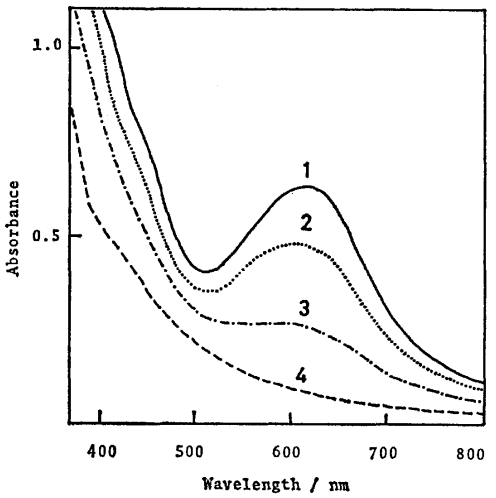

Fig. 2. Spectral changes on the addition of water (0.05 cm³) to an acetone solution of 1.6×10^{-4} M $Mn^{IV}(N\text{-}c\text{-Hxsai})_2Cl_2$ (5 cm³).
1: No addition, 2: 7.5 min after addition of water, 3: 17.5 min, 4: 42.5 min. Cell length: 1 cm.

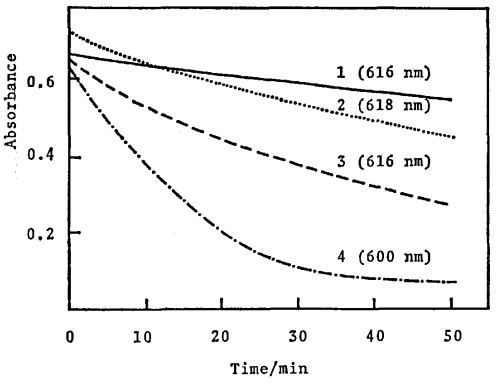

Fig. 3. Time courses of absorbances at absorption maxima of acetone solutions of Mn(IV) complexes (1.6×10^{-4} M, 5 cm³) caused by the addition of water (0.05 cm³).
1: $Mn(N\text{-Dodsai})_2Cl_2$, 2: $Mn(N\text{-Octsai})_2Cl_2$, 3: $Mn(N\text{-Prsai})_2Cl_2$, 4: $Mn(N\text{-}c\text{-Hxsai})_2Cl_2$. Cell length: 1 cm.

caused by the instability of the complex due to steric hindrance of the cyclohexyl group. In the case of $Mn(N\text{-Octdsai})_2Cl_2$, such spectral changes could not be measured owing to its solubility restriction in acetone. However, this complex may be more water-resistant than the others investigated here, because that it showed no significant change on washing with water.

Magnetic Properties. The magnetic moments of the Mn(III) complexes fall within the range of 4.85 to 5.03 BM, with the exception of $Mn(N\text{-Bzsai})_2Cl$ (Table 1). This indicates that these complexes may have a d^4 high-spin electron configuration. The low value (4.26 BM) observed for the above complex may be caused by magnetic exchange interactions due to the formation of a binuclear complex in the solid state like Fe(salen)Cl.[8] Further investigation on the complex was not made in this work. On the other hand, the magnetic moments of the Mn(IV) complexes fall within the range of 3.84 to 4.08 BM; such moments are consistent with the spin-only value expected for a complex with a d^3 high-spin electron configuration.

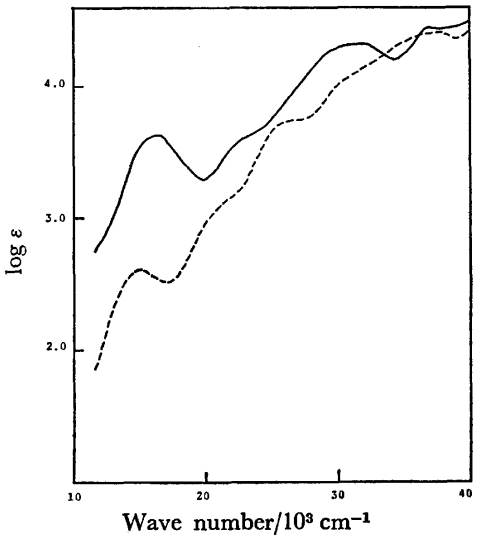

Fig. 4. Electronic spectra in dichloromethane.
——: $Mn^{IV}(N\text{-Octsai})_2Cl_2$, ----: $Mn^{III}(N\text{-Octsai})_2Cl$.

Electionic Spectra. Figure 4 shows the electronic spectra of the complexes $Mn^{III}(N\text{-Octsai})_2Cl$ and $Mn^{IV}(N\text{-Octsai})_2Cl_2$ in dichloromethane. In the Mn(III) complex, three absorption bands were observed in the visible region: at 15200, 21300 sh, and 26300 cm^{-1}. On the other hand, the electronic spectrum of the Mn(IV) complex shows an intense absorption band at 16000 cm^{-1} ($\log\varepsilon=3.62$). The frequencies of the absorption maxima for the Mn(III) and Mn(IV) complexes are summarized in Table 3. It is apparent from the Table that the alkyl groups of the Schiff base ligands have little effect on the frequencies for either Mn(III) or Mn(IV) complexes. These results suggest that the Mn(III) and Mn(IV) complex pairs may have similar configurations.

Recently, Boucher *et al.* have reported the absorption spectra of Mn^{III}(X-salen)Cl[9] and Mn^{III}(acacen)Cl[10] in noncoordinating solvents; here X-salen and acacen denote dianions of *N,N'*-di(substituted salicylidene)ethylenediamine and *N,N'*-bis(2-acetyl-1-methylethylidene)ethylenediamine, respectively. The X-ray structural analysis of the latter complex has revealed that its coordination polyhedron approximates an idealized C_{4v} symmetry.[10] They have assigned the three absorption bands observed for Mn(acacen)Cl in chloroform as follows; the band at 16400 cm^{-1} ($\log\varepsilon=2.31$) to $d_{xy}\rightarrow d_{x^2-y^2}$, the band at 22400 cm^{-1} (3.23) to $d_{xy}\rightarrow\pi^*$ (azomethine) involving $d_{yz},d_{zx}\rightarrow d_{x^2-y^2}$ as a lower energy shoulder, and the band at 26200 cm^{-1} (3.81) to $d_{yz},d_{xz}\rightarrow\pi^*$ (azomethine). The absorption spectra of the present Mn(III) complexes are similar to that of the above complex, suggesting that these Mn(III) complexes may have a five-coordinate structure ($\approx C_{4v}$) in dichloromethane. Therefore, the absorption bands near 15200 cm^{-1} can be safely assigned to the ligand field transition due to $d_{xy}\rightarrow d_{x^2-y^2}$.

Table 3. Spectroscopic data for mangnese(III) and manganese(IV) complexes

R	$Mn^{III}(N\text{-Rsai})_2Cl$					$Mn^{IV}(N\text{-Rsai})_2Cl$				
	$\frac{\nu_{max}}{10^3\ cm^{-1}}$ (log ε)[a]				$\frac{\nu(Mn-Cl)}{cm^{-1}}$	$\frac{\nu_{max}}{10^3\ cm^{-1}}$ (log ε)[a]				$\frac{\nu(Mn-Cl)}{cm^{-1}}$
Pr	15.1	(2.59)	21.3 sh	26.3 (3.74)	299	16.1	(3.63)	23.7 sh	31.2 (4.33)	351
Bu	15.2	(2.62)	21.3 sh	26.5 (3.74)	315	16.1	(3.66)	23.6 sh	31.3 (4.36)	347
i-Bu	15.2	(2.64)	21.3 sh	26.5 (3.75)	327	15.9	(3.63)	23.5 sh	31.4 (4.33)	354
Hx	15.2	(2.48)	21.3 sh	26.7 (3.67)	314	16.1	(3.62)	23.5 sh	31.6 (4.40)	348
c-Hx	15.2	(2.54)	21.3 sh	25.9 (3.71)	317	16.6	(3.55)	23.5 sh	31.8 (4.31)	351
Oct	15.2	(2.60)	21.3 sh	26.3 (3.73)	317	16.0	(3.62)	23.6 sh	31.3 (4.32)	348
Dod	15.1	(2.62)	21.3 sh	26.5 (3.75)	321	16.1	(3.59)	23.6 sh	31.6 (4.44)	348
Octd	15.2	(2.61)	21.3 sh	26.5 (3.74)	322	16.2	(3.53)	23.6 sh	31.6 (4.35)	348
Bz	15.1	(2.64)	21.3 sh	26.3 (3.73)	318	16.2	(3.55)	22.7 sh	31.6 (4.30)	350
PE	15.1	(2.60)	21.3 sh	26.3 (3.75)	305	16.1	(3.53)	22.4 sh	31.4 (4.26)	347

a) Measured in dichloromethane.

Previously we have observed intense absorption bands around 16000 cm^{-1} (log $\varepsilon \approx 3.5$) for the complexes Mn^{IV}(X-salen)Cl_2 and $Mn^{IV}(N\text{-Bu-X-sai})_2Cl_2$ and have assigned them to the charge transfer transition due to Cl to Mn on the basis of the intensity. Thus the intense absorption bands near 16000 cm^{-1} observed for the present Mn(IV) complexes can be assigned to the same transition. The ligand field transitions which are expected for a complex with a d^3 high-spin configuration may be obscured by the intense charge transfer band. Therefore, the absorption bands near 23600 cm^{-1} cannot be easily assigned.

Infrared Spectra. The IR spectra of the Mn(IV) complexes are almost the same as those of the corresponding Mn(III) complexes in the 4000 to 500 cm^{-1} region, indicating that the Schiff base ligands coordinate with manganese ions by the same fashion in both complexes. However, in the 500 to 250 cm^{-1} region, the IR spectra of the Mn(III) and Mn(IV) complexes differ markedly, especially in the region sensitive to the ν(Mn–Cl). The absorption bands observed at 310 cm^{-1} for $Mn(N\text{-Prsai})_2Cl$[11], at 290 cm^{-1} for Mn(acac)Cl,[12] and at 279 cm^{-1} for Mn(acacen)Cl[10] have been assigned to the ν(Mn–Cl); here acac denotes the monoanion of acetylacetone. In the present Mn(III) complexes, strong bands were observed around 310 cm^{-1}; these may be assigned to the ν(Mn–Cl). The band positions are listed in Table 3. On the other hand, the IR spectra of the Mn(IV) complexes showed strong bands around 350 cm^{-1}. The absorption band observed at 358 cm^{-1} for $K_2Mn^{IV}Cl_6$ has been assigned to the ν(Mn–Cl).[13] It is expected that the band due to the ν(Mn–Cl) may be shifted to higher frequencies on going from Mn(III) to Mn(IV), since the Mn(III) complexes have a five-coordinate structure, while the Mn(IV) complexes have a six-coordinate structure. The absorption bands observed around 350 cm^{-1} for the Mn(IV) complexes are assigned to the ν(Mn–Cl). The band positions are listed in Table 3. In the previous paper we have pointed out that the dichloromanganese(IV) complexes with the bidentate Schiff base ligands may have a *cis*- or *trans*-octahedral configuration; with the com-

Table 4. Reduction potentials for manganese(IV) complexes

Complex	$E_{p/2}$ *vs.* SCE[a] / V	
	$Mn^{IV}\rightarrow Mn^{III}$	$Mn^{III}\rightarrow Mn^{II}$
$Mn(N\text{-Prsai})_2Cl_2$	0.84	−0.12 (−0.18)[b]
$Mn(N\text{-Busai})_2Cl_2$	0.84	−0.17 (−0.13)
$Mn(N\text{-}i\text{-Busai})_2Cl_2$	0.81	−0.18 (−0.15)
$Mn(N\text{-Hxsai})_2Cl_2$	0.82	−0.12 (−0.15)
$Mn(N\text{-}c\text{-Hxsai})_2Cl_2$	0.75	−0.21 (−0.15)
$Mn(N\text{-Octsai})_2Cl_2$	0.83	−0.12 (−0.16)
$Mn(N\text{-Dodsai})_2Cl_2$[c]	0.79	−0.17 (−0.15)
$Mn(N\text{-Octdsai})_2Cl_2$[c]	0.75	−0.11 (−0.16)
$Mn(N\text{-Bzsai})_2Cl_2\cdot CH_2Cl_2$	0.87	−0.05 (−0.12)
$Mn(N\text{-PEsai})_2Cl_2$	0.84	−0.11 (−0.13)

a) Measured in acetonitrile containing 0.1 M Bu_4NClO_4 at 25 °C. b) Half-peak potentials for the corresponding manganese(III) complexes. c) Measured in acetonitrile–dichloromethane (2/1 volume ratio).

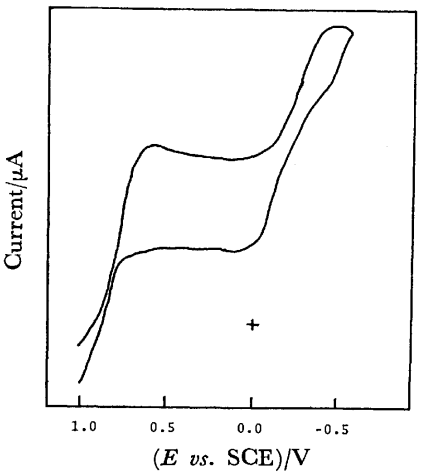

Fig. 5. Current-potential curve of $Mn^{IV}(N\text{-}i\text{-Busai})_2Cl_2$ measured in acetonitrile at 25 °C. Scan rate was 0.06 V s^{-1}.

plexes in which two chlorine atoms coordinate with manganese ion in a *cis*-form two absorption bands due to the ν(Mn–Cl) would be observed, while there is only one band in a *trans*-form. In the present Mn(IV) complexes, one strong band assignable to the ν(Mn–Cl) was observed, suggesting that two chlorine atoms may coordinate with manganese ion in a *trans*-form.

The coordination features of the bidentate Schiff base ligands cannot be determined from the available data. However, the structures of the Ni(II) complexes with the *N*-alkylsalicylideneamines have been investigated extensively and explained as follows. The complexes with *n*-alkyl groups have a *trans*-planar configuration. If the alkyl chain is branched at the β-carbon, as in the Ni(*N*-*i*-Busai)$_2$, the steric situation is very similar to the *n*-alkyl case and no tetrahedral form is observed.[14] In the present work, attempts to isolate Mn^{IV}(*N*-Rsai)$_2Cl_2$ (R=*i*-C_3H_7 and *s*-C_4H_9) were unsuccessful, perhaps because of the instability due to the steric hindrance of these groups. These results suggest that the present Mn(IV) complexes are in a *trans*, six-coordinate configuration, as shown in Fig. 1, but the Schiff base ligands may deviate from planarity to varying degrees.

Electrochemical Properties. The current-potential curve of the complex Mn^{IV}(*N*-*i*-Busai)$_2Cl_2$, is shown in Fig. 5. Two-step cathodic waves with a similar wave height were observed at the half-peak potentials of +0.81 and −0.18 V(*vs.* SCE); these can be assigned to the reductions of Mn(IV) to Mn(III) and Mn(III) to Mn(II), respectively. The reduction potentials for the Mn(IV) complexes are given in Table 4, together with those for the Mn(III) complexes. The potentials for both reductions are not much affected by the alkyl groups of the Schiff base ligands. These results are consistent with the spectroscopic data.

References

1) G. D. Lawrence and D. T. Sawyer, *Coord. Chem. Rev.*, **27**, 173 (1978).
2) K. Sauer, *Acc. Chem. Res.*, **13**, 249 (1980).
3) G. M. Cheniae, *Ann. Rev. Plant Physiol.*, **21**, 467 (1970).
4) M. E. McAdam, R. A. Fox, F. Lavelle, and E. M. Fielden, *Biochem. J.*, **165**, 71 (1977).
5) W. M. Coleman and L. T. Taylor, *Coord. Chem. Rev.*, **32**, 1 (1980).
6) W. Levason and C. A. McAuliffe, *Coord. Chem. Rev.*, **7**, 353 (1972).
7) T. Matsushita, H. Kono, and T. Shono, *Bull. Chem. Soc. Jpn.*, **54**, 2646 (1981); and the references cited therein.
8) M. Gerloch and F. E. Mabbs, *J. Chem. Soc., A*, **1967**, 1900.
9) a) L. J. Boucher and M. O. Farrell, *J. Inorg. Nucl. Chem.*, **35**, 3731 (1973); b) L. J. Boucher, *ibid.*, **36**, 531 (1974).
10) L. J. Boucher and V. W. Day, *Inorg. Chem.*, **16**, 1360 (1977).
11) A. van den Bergen, K. S. Murray, M. J. O'Connor, and B. O. West, *Aust. J. Chem.*, **22**, 39 (1969).
12) K. Isobe and S. Kawaguchi, *Bull. Chem. Soc. Jpn.*, **48**, 250 (1975).
13) D. M. Adams and D. M. Morris, *J. Chem. Soc., A*, **1968**, 694.
14) R. H. Holm, G. W. Everett, Jr., and A. Chakravorty, *Prog. Inorg. Chem.*, **7**, 83 (1966).

 © 1982 The Chemical Society of Japan Bull. Chem. Soc. Jpn., 55, 113—116 (1982)

The Preparation of Ti_5S_8

Masanobu SAEKI* and Mitsuko ONODA

National Institute for Research in Inorganic Materials, 1-1, Namiki, Sakura-mura, Niihari-gun, Ibaraki 305

(Received April 15, 1981)

Ti_5S_8 (12R type), which had never been prepared in a pure state, was obtained as a single phase by the chemical-transport method. The conditions for the preparation were determined experimentally. The existence range of the phase was examined for composition and temperature.

Several phases have been reported in the TiS–TiS_2 composition range, namely, TiS (2H), Ti_8S_9 (9R), Ti_4S_5 (10H), Ti_3S_4 (21R), Ti_2S_3 (4H), Ti_5S_8 (12R), and TiS_2 (2H). (The designations in parenthesis indicate the structures in the Ramsdell notation.) Of these, the TiS phase is of the NiAs-type, while TiS_2 is of the CdI_2-type, structure. Both have a hexagonal close packed of sulfur. However, the intermediate phases have complex structures involving both the hexagonal and cubic packing of sulfur and varying stacking sequences, with a specific titanium-to-sulfur ratio. Titanium atoms are situated in the octahedral holes of the sulfur packing.

In spite of many reports on titanium sulfide, its phase diagram has not yet been established because of the variation in experimental data reported by many investigators, as has been pointed out by Jeannin[1] or Kjekshus and Pearson.[2] Furthermore, Tronc and Huber[3] reported that, at the composition of $Ti_{1.18}S_2$, there are many structures with different periods in the c-direction, *e.g.*, polytypism. These observations have indeed indicated that the titanium–sulfur system is complicated.

The existence of Ti_5S_8 has been reported by Jeannin,[4] Flink *et al.*,[5] and Tronc and Huber,[3] although it was not prepared by any of them as a single phase. They obtained it as a mixture with other structures, like Ti_2S_3 (4H type). We ourselves were not able to prepare Ti_5S_8 from the respective elements sealed in an evacuated silica tube. However, Ti_5S_8 was obtained as a single phase by the chemical-transport method when iodine was used as the transport agent. The aim of this paper is to describe the experimental conditions needed to obtain Ti_5S_8 as a single phase.

The preparation conditions of Ti_5S_8 will first be described, and then procedure for the identification of the obtained Ti_5S_8. Finally, the range of composition and temperature of Ti_5S_8 will be shown.

Results

Preparation Conditions. The preparation of Ti_5S_8 was performed according to the following procedure. The titanium sulfide (1.5 g), the composition and structure of which will be described later, and the iodine (0.15 g) were sealed in an evacuated silica tube 150 mm in length and 12 mm inner diameter. The tube was held in a horizontal resistance furnace, where the high-temperature end was set at 600 °C and the low-temperature end at 500 °C. The titanium sulfide was transported from the low- to the high-temperature side. The transported titanium sulfide was then deposited as plate-shaped, grey-black crystals.

To prepare Ti_5S_8 in a pure form by chemical transport, several important factors had to be ascertained: (1) the preparation temperature of the starting material, (2) the composition of the starting material, (3) the transport temperature, and (4) the iodine concentration. The specimen obtained by chemical transport was influenced by the following factors.

The Effect of the Preparation Temperature of the Starting Material. The synthesis of the titanium sulfide used as the starting material was carried out according to the following procedure. Titanium metal powder (purity, 99.0%) and sulfur (purity, 99.9999%) were mixed together in a calculated ratio; the mixture was then allowed to react for a few days at 350 °C, after which the temperature was raised to 500—900 °C. With respect to the composition in the range from $Ti_{1.38}S_2$ to $Ti_{1.16}S_2$, at 500 °C the structure of the specimen was of the 2H type; at 600—700 °C, a disordered stacking of the sulfur layers was detected, and above 800 °C the 4H type was the result. The 2H type specimen prepared at 500 °C might have been heterogeneous because of the incomplete reaction.

By using the 2H type as the starting material, the transport was found to take place, but when the starting materials prepared at a temperatures above 600 °C were used, transport did not occur. The reason for this was not clear. However, it can be seen from Table 1 that whether or not the transport take place is dependent on the crystal structure of the starting material.

The Effect of the Composition of the Starting Material. How the transport was influenced by the composition of the starting material was then examined. The curve in Fig. 1 shows the transport rate *versus* the composition of the starting material. As can be seen

Table 1. Relation of the preparation temperature of the starting material and average transport rate

Iodine concentration: 5.96 mg cm^{-3}, transport time: 144 h, composition of the starting material: $Ti_{1.21}S_2$, temperature: 500 °C (low-temperature end)→600 °C (high-temperature end).

Temp/°C	Structure	Transport rate/mg h^{-1}
500	TiS_2(2H) type	0.8
600	Random	Negligibly small
700	Random	Negligibly small
800	Ti_2S_3(4H) type	0
900	Ti_2S_3(4H) type	0

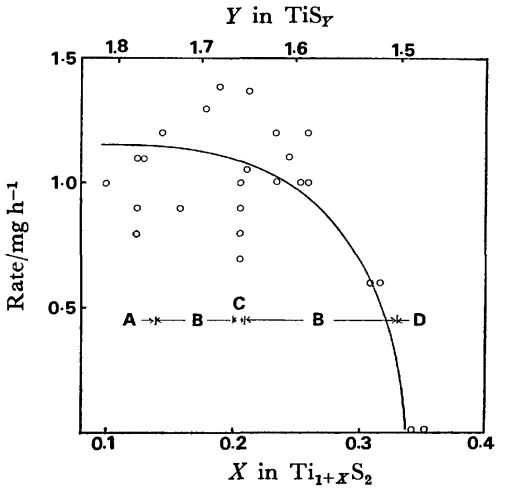

Fig. 1. Average transport rate versus composition of the starting material. (Iodine concentration: 5.96 mg cm^{-3}, transport time: 144 h, temperature: 500 °C(low temperature side)→600 °C(high temperature side)).
A: Phase with disordered stacking of sulfur layers, B: mixed phase of Ti_2S_3 and Ti_5S_8, C: single phase of Ti_5S_8, D: no transport took place.

TABLE 2. RELATION OF THE TRANSPORT TEMPERATURE AND TRANSPORTED CRYSTALS

Iodine concentration: 5.96 mg cm^{-3}, transport time: 144 h, composition of the starting material: $Ti_{1.21}S_2$.

Temp/°C	Transported crystal
400→500	—
500→600	Ti_5S_8
600→700	$Ti_5S_8+Ti_2S_3$
700→800	$Ti_5S_8+Ti_2S_3$

from this figure, the titanium sulfide was not transported by using a starting material whose composition was poorer in sulfur than $Ti_{1.33}S_2$. The transported crystals were composed of a mixed phase consisting of Ti_2S_3 and Ti_5S_8 when $Ti_{1.33}S_2$–$Ti_{1.22}S_2$ was used as the starting material. A single phase of Ti_5S_8 resulted when $Ti_{1.21}S_2$ was used. A mixed phase of Ti_2S_3 and Ti_5S_8 resulted when $Ti_{1.19}S_2$–$Ti_{1.14}S_2$ was used and a phase with disordered stacking of sulfur layers when a specimen richer in sulfur than $Ti_{1.13}S_2$ was used.

Therefore, Ti_5S_8 in a pure form was obtained by using a starting material whose composition was $Ti_{1.21}S_2$. The sulfur content of the transported crystals was always found to be smaller than that of the starting materials.

The Effect of the Transported Temperature. The transport was carried out at various temperatures in order to determine the most suitable temperature conditions. As can be seen in Table 2, Ti_5S_8 was obtained in a pure form only at the temperature of 500 °C (low temperature side)→600 °C (high temperature side). At any temperature above this, the transported crystals were found to be two phases consisting of Ti_5S_8 and Ti_2S_3. From the observation of the electron diffractometry, it was found that the needle-shaped crystal was Ti_2S_3, and the plate-shaped one, Ti_5S_8.

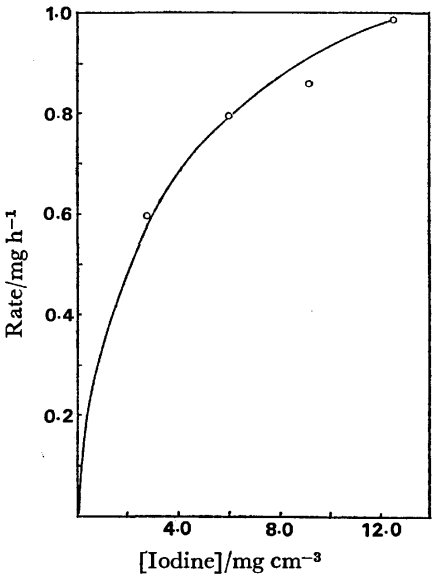

Fig. 2. Average transport rate versus iodine concentration. (Transport time: 144 h, composition of the starting material: $Ti_{1.21}S_2$, temperature: 500 °C (low temperature side)→600 °C (high temperature side)).

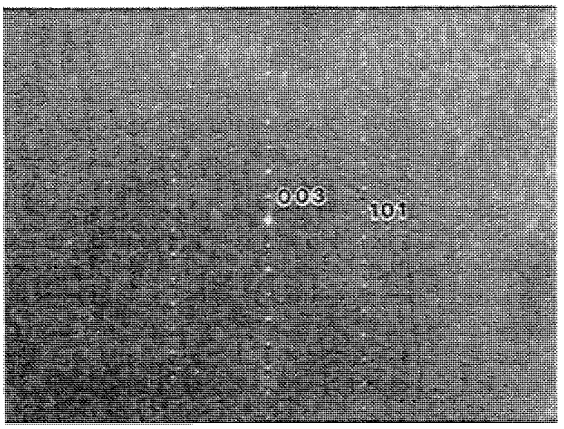

Fig. 3. Electron diffraction photograph of Ti_5S_8 obtained by the chemical transport method.

On the contrary, the transport was found no longer to take place at temperature below 500 °C (low temperature end)—600 °C (high temperature end).

The Effect of the Iodine Concentration. In order to determine the most suitable conditions, the transport was carried out at various iodine concentrations. The results are shown in Fig. 2, where the transport rate increases with the increase in the iodine concentration. Crystals with stacking faults were produced at concentrations of more than 12 mg cm^{-3}.

Identification by Means of Electron and X-Ray Diffractometry. Figure 3 shows an electron diffraction pattern taken from a crystal fragment obtained by grinding a transported crystal. The incident beam was directed parallel with the [010] direction. The distance of the repeating unit along the c-axis in the hexagonal setting was found to be 34 Å, containing 12 layers. The systematic absence, $-h+k+l=3n$, in-

Table 3. Indices, calculated, and observed *d*-spaces and intensities

h	*k*	*l*	d_{calcd}	d_{obsd}	I_{calcd}	I_{obsd}
0	0	6	5.709	5.719	64	*247
1	0	−2	2.928	2.929	21	26
0	0	12		2.857		*9
1	0	4	2.808	2.811	16	12
1	0	−5	2.727	2.728	51	44
1	0	7	2.540	2.542	98	94
1	0	−8	2.442	2.443	62	68
1	0	10	2.245	2.246	100	100
1	0	−11	2.150	2.151	9	12
1	0	13	1.972	1.973	7	6
0	0	18	1.903	1.904	3	*15
1	0	−14	1.889	1.889	54	50
1	0	16	1.737	1.737	19	18
1	1	0	1.716	1.717	87	*59
1	0	17	1.668	1.668	21	26
1	1	6	1.643	1.639	10	9
1	0	19	1.541	1.541	6	9
1	0	20	1.484		4	
2	0	2	1.481			
2	0	−4	1.464		2	
2	0	5	1.452		5	
0	0	24	1.427	1.428	14	*65
2	0	−7	1.422	1.418	12	9
2	0	8	1.404	1.403	8	9
1	0	22	1.379		2	
2	0	−10	1.363	1.363	15	21
2	0	11	1.341		2	
2	0	−13	1.244		1	
1	1	18	1.274	1.274	4	6
2	0	14	1.270	1.270	11	6

* Indicates the indices affected by the preferred orientation.

dicates the rhombohedral symmetry of the structure. Therefore, the structure of this crystal may be referred to as a 12R type using Ramsdell notation, this is consistent with the structure of Ti_5S_8 as described by Flink *et al.*,[5] and Tronc and Huber.[3]

The powder X-ray diffraction pattern of the Ti_5S_8 sample (composition, $Ti_{1.31}S_2$) obtained by crushing the transported crystals was taken by the counter-diffractometer technique using Ni-filtered Cu $K\alpha$ radiation. The pattern was indexed on the basis of the hexagonal cell (a=3.431 and c=34.25 Å), where the systematic absence, $-h+k+l\neq 3n$, is consistent with the case of the electron diffraction. Powder X-ray diffraction intensities were calculated for the structure model by Tronc *et al.*[6] for the composition of $Ti_{1.31}S_2$ (Ti_5S_8 phase) with an overall temperature factor of B=1.0. The intensities, calculated and observed, are listed in Table 3. These do not agree with each other for the 00*l* and 110 peaks because of the preferred orientation in the sample. The reliability factor R, defined by $R=\Sigma|I_{obsd}-I_{calcd}|/\Sigma|I_{obsd}|$, was 0.39; this was excessive. However, the R-value estimated by eliminating the 00*l* and 110 peaks, which were affected by the preferred orientation, was 0.14. Therefore, this specimen was identified as Ti_5S_8 (12R type), as has previously been reported by Tronc *et al.*[6]

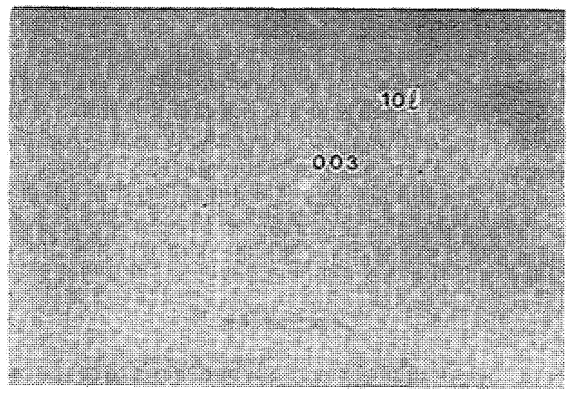

Fig. 4. Electron diffraction photograph of the specimen annealed at 1200 °C.

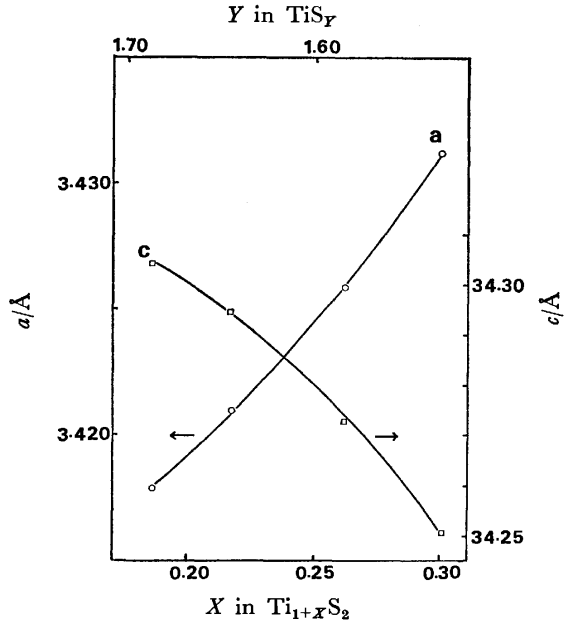

Fig. 5. Relation of the lattice constants and composition.

The information obtained from X-ray and electron diffractometry showed that the specimen prepared by the method described above was indeed a pure single phase and did not contain any other phases, like Ti_2S_3 (4H type) or TiS_2 (2H type).

Range of the Temperature and Composition in Which Ti_5S_8 Can Exist. The range of temperature and composition in which Ti_5S_8 can exist was also examined. At first, Ti_5S_8 (composition $Ti_{1.23}S_2$) was kept in evacuated tubes at 800, 900, 1000, 1100, and 1200 °C for 3 d. Disorder in sulfur stacking at 1100 °C and 1200 °C was found, although no change was detected in the specimens annealed below 1000 °C. Figure 4 is an electron-diffraction photograph of the specimen annealed at 1200 °C. In this figure, the diffusion for $h-k=3n\pm1$ shows disorder caused by sulfur stacking.[7] At 1100 °C, Ti_5S_8 began to change to another structure, but the rate of the transformation was so slow that a stable structure could not be ascertained at this temperature.

The composition range where the Ti_5S_8 phase could exist was examined through the sulfurization or desulufurization in the atmosphere of the H_2–H_2S mixture at 900 °C. After being quenched from 900 °C to room temperature, the specimens were examined by means of X-ray diffractometry. The lattice constants are shown in Fig. 5. From this experiment, it was found that Ti_5S_8 can exist in compositions from at least $Ti_{1.31}S_2$ to $Ti_{1.16}S_2$ at 900 °C.

Conclusion

From the results presented above, it can be concluded that: (1) Ti_5S_8 in a pure form can be prepared by the chemical transport method under the following conditions: transport agent; iodine (6—9 mg cm^{-3}), starting material; titanium sulfide (composition $Ti_{1.21}S_2$) prepared at 500 °C, transport temperature; 500 °C (low temperature end)→600 °C (high temperature end), and (2) Ti_5S_8 can exist over a large composition range at 900 °C.

The authors wish to thank Professor Mitsuoki Nakahira of the Okayama College of Science and Dr. Isao Kawada of our Institute for their helpful discussions.

References

1) Y. P. Jeannin, "Problems of Nonstoichiometry," ed by A. Rabenau, North-Holland, Amsterdam (1970), p. 77.
2) A. Kjekshus and W. B. Pearson, "Progress in Solid State Chemistry," ed by H. Reiss, Oxford (1964), Vol. 1, p. 83.
3) E. Tronc and M. Huber, *J. Phys. Chem. Solids*, **34**, 2045 (1973).
4) Y. P. Jeannin, *Ann. Chim.*, **7**, 57 (1962).
5) E. Flink, G. A. Wiegers and F. Jellinek, *Rec. Trav. Chim. Pays-Bas*, **85**, 869 (1966).
6) E. Tronc, R. Moret, J. J. Legendre, and M. Huber, *Acta Crystallogr., Sect. B*, **31**, 2800 (1975).
7) M. Onoda and I. Kawada, *Acta Crystallogr., Sect. A*, **36**, 134 (1980).

Gas-chromatographic Measurements of Dinitrogen Oxide in Air

Hisafumi Muramatsu, Michio Hirota,* and Yukio Makino
Meteorological Research Institute, 1-1 Nagamine, Yatabe-machi, Tsukuba-gun, Ibaraki 305
(Received April 17, 1981)

To obtain an average tropospheric mixing ratio of dinitrogen oxide over Japan, 90 air samples were collected by aircraft at altitudes up to 7 km from Autumn, 1978, to Spring, 1979, and were analysed by the GC-ECD method. The mean volume-mixing ratio of N_2O was 0.31_0 ppm, and the standard deviation was 0.01_4 ppm. These results show that the tropospheric N_2O is well mixed and that its mixing ratio is higher than 0.30 ppm.

The natural dinitrogen oxide is produced by the nitrification of the ammonium ion as well as the denitrification of nitrates through microbiological activity in soil and water.[1-6]

Though some sinks of N_2O have been proposed,[6-8] the atmospheric N_2O is rather unreactive in the troposphere and is transferred to nitrogen monoxide mainly by Reaction (1) in the stratosphere:[9]

$$\begin{aligned} N_2O + O(^1D) &\longrightarrow N_2 + O_2 \\ &\longrightarrow 2NO. \end{aligned} \quad (1)$$

The NO is strongly related to the stratospheric ozone (O_3) by Reaction (2); *i.e.*, an increase in NO leads to a depletion of the stratospheric O_3:[10-13]

$$\begin{aligned} NO + O_3 &\longrightarrow NO_2 + O_2 \\ NO_2 + O &\longrightarrow NO + O_2 \\ \text{net}\quad O_3 + O &\longrightarrow 2O_2. \end{aligned} \quad (2)$$

To know the behavior of the N_2O in the atmosphere, from the ground surface[8,14-26] through the troposphere[14,17,20,26-32] to the stratosphere,[14,17,27,30-37] and also in the sea and over the sea surface[17,29,38-43] is important in understanding the global nitrogen cycle[1,2,44] and the stratospheric O_3 chemistry.[10-13]

In a previous study,[45] several measurements of the atmospheric N_2O were performed at the Meteorological Research Institute, Koenji, Tokyo, by the gas chromatographic (GC) method, using a thermal conductivity detector (TCD); the error of the measurement was estimated to be about ±7%. It has been shown, however, that an electron-capture detector (ECD) has an increased sensitivity for N_2O at elevated temperatures[46] and needs an air sample of only a few millilitres, while the N_2O must be preconcentrated from about 30 l of air when a TCD is used.[14,15,19,38,39,47]

To obtain an average tropospheric mixing ratio of N_2O over Japan, air samples obtained by aircraft from Autumn, 1978, to Spring, 1979, have been analysed by the GC-ECD method.

Experimental

Sampling of Air. Three aircraft, an Aerocommander 685, a Piper Seneca, and a Cessna 404, were used for the air sampling. On the aircraft, the air was sampled through a silicone rubber tube or a *tylon* tube (1 m×8 mm i.d.) in stainless steel cylinders (Whitey, 0.3, 0.5, and 1.0 l) by means of two air pumps connected in series up to the pressure of 3.5—4.0 kg/cm². Before use, the cylinders were evacuated by means of an oil rotary pump and heated to 200 °C for several hours. DK shut-off valves (Whitey) were used for these cylinders. The N_2O concentration was constant for more than 40 d (<±2.0%) in the cylinder.

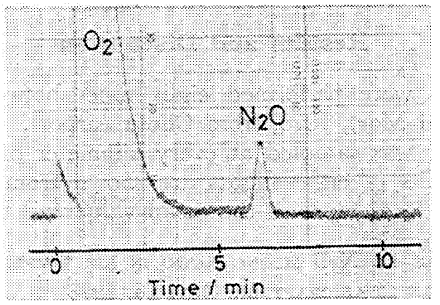

Fig. 1. The typical chromatogram of N_2O. Standing current: 2.0 nA, pulse frequency: 2.5 kHz, detector temperature: 300 °C, sample air: 2 ml. N_2O was 0.34 ppm.

Gas-chromatographic Analysis. GC measurements were performed using a Shimadzu Gas Chromatograph GC-6AM equipped with an ECD (10 mci ^{63}Ni, 300 °C). Nitrogen gas (99.9995%) passed through the tube filled with molecular sieve 5A (1/16 in. pellets) was used as the carrier gas at a flow rate of 40 ml/min. The sample air was transferred to a 2-ml gas sampler (Shimadzu, MGS-4) and then introduced into a glass column (3 m×3 mm i.d.) filled with 30—60 mesh molecular sieve 5A.† The peak of N_2O appeared 5 min after that of oxygen gas at the column temperature of 245 °C.

The reference gas of 1 ppm N_2O was prepared by diluting 15 μl of pure N_2O (>98%, Showa Denko) in 15 l of air, which was measured by means of a gas meter and passed through a tube (30 cm×3 cm i.d.) containing silica gel and three U-shaped tubes (8 mm i.d.) containing drierite, ascarite, and molecular sieve 5A (1/16 in. pellets, 0 °C) respectively. A 15 μl portion of N_2O was measured by means of a gas-tight syringe (SGE, 100A-RN-GSG). The molecular sieve tube was heated to 350 °C for 3 h before use. The air purified by this method was also used as a zero gas. The error in repeated measurements of single reference gas was less than ±0.9%. The concentrations of five reference gases made in 20-l *tedlar* bags over a period of a week were in good agreement with each other; *i.e.*, the standard deviation was 1.7%.

A typical chromatogram of N_2O is shown in Fig. 1. The peak heights of N_2O were proportional to the quantities of N_2O from 0.39 ng to 3.9 ng, which corresponded to 0.1 ppm and 1 ppm of N_2O in 2 ml of air respectively. The error in repeated peak-height measurements for 0.3 ppm of N_2O was about ±2%. The total error in the measurements of N_2O was estimated as about ±4%.

† Porapak Q and QS and Porasil B and C were also suitable for the analysis of N_2O.[29]

In the present study, measurements were performed as follows; the reference gas was first measured, and then the sample air was measured two times, and finally the reference gas was measured again. The volume-mixing ratio of N_2O in the sample air was calculated from the ratio of the two mean values of the sample air and the reference gas. The average difference between two measurements of 90 air samples was ±2%. The detection limit in this method was about 0.01 ppm of N_2O in 2 ml of air.

The temperature of the ECD was controlled in a range of ±2 °C. No effect of this temperature variation could be detected on the chromatogram.

Results and Discussion

Flights were performed eight times between Oct., 1978, and Mar., 1979, from Chofu Airport. In many cases, air was sampled at every kilometer of altitude. The results of eight flights are shown from Table 1 to Table 8, along with the mean value and the stand-

TABLE 1. N_2O MIXING RATIO IN AIR SAMPLED BY AIRCRAFT ON OCT. 26, 1978

Altitude km	Location[a)]	Volume-mixing ratio of N_2O/ppm
1	Yokohama	0.31_2
2	Yokosuka	0.32_3
3	Takeyama	0.29_6
4	Enoshima	0.34_5
6	Enoshima	0.32_2
7	Oiso	0.29_9
7	Miyakejima	0.30_8
4	Niijima	0.33_3[c)]
3		0.35_1[c)]
2	Jogashima	0.33_1[c)]
1		0.33_5[c)]
1		0.32_6[c)]
0	Chofu[b)]	0.33_5[c)]
	Mean	0.31_5
	SD	0.01_6

a) When the location is not shown, the air was sampled between the former and the latter locations. It is the same in Tables 2—8. b) Air was sampled just before landing. c) Air was sampled in a 5-l *tedlar* bag. These values were not included in the calculation of the mean value and the SD.

TABLE 2. N_2O MIXING RATIO IN AIR SAMPLED BY AIRCRAFT ON DEC. 7, 1978

Altitude km	Location	Volume-mixing ratio of N_2O/ppm
0.5		0.35_8
0.5	Zushi	0.31_8
0.5	Niijima	0.32_6
0.5	Mikurajima	0.30_3
1·5	Mikurajima	0.31_5
1.7	Niijima	0.32_0
1.5	Jogashima	0.32_5
	Mean	0.32_4
	SD	0.01_2

TABLE 3. N_2O MIXING RATIO IN AIR SAMPLED BY AIRCRAFT ON DEC. 12, 1978.

Altitude km	Location	Volume-mixing ratio of N_2O/ppm
0.5	Fujisawa	0.31_1
1	Fujisawa	0.30_7
2	Fujisawa	0.32_6
3	Fujisawa	0.33_8
4	Fujisawa	0.32_4
5	Fujisawa	0.32_0
6	Fujisawa	0.33_6
7	Fujisawa	0.32_2
7	Oshima	0.30_9
0	Chofu	0.33_1
	Mean	0.32_2
	SD	0.01_0

TABLE 4. N_2O MIXING RATIO IN AIR SAMPLED BY AIRCRAFT ON JAN. 19, 1979

Altitude km	Location	Volume-mixing ratio of N_2O/ppm
1	Iruma	0.29_0
3	Higashimatsuyama	0.28_8
5	Fujioka	0.30_1
7	Harunasan	0.28_9
7	Kashiwazaki	0.29_8
6	Kashiwazaki	0.29_0
5	Kashiwazaki	0.31_0
4	Kashiwazaki	0.30_7
3	Nagaoka	0.29_8
2	Nagaoka	0.30_3
3	Harunasan	0.30_6
2	Gyoda	0.28_7
	Mean	0.29_7
	SD	0.00_8

TABLE 5. N_2O MIXING RATIO IN AIR SAMPLED BY AIRCRAFT ON FEB. 2, 1979

Altitude km	Location	Volume-mixing ratio of N_2O/ppm
3	Enoshima	0.29_8
3	Oshima	0.30_1
3	Niijima	0.30_4
3	Mikurajima	0.30_4
3		0.31_7
3	Hachijojima	0.32_2
1		0.31_9
1	Mikurajima	0.32_7
1	Miyakejima	0.31_3
1	Oshima	0.30_4
1		0.30_5
1	Kamakura	0.31_7
	Mean	0.31_1
	SD	0.00_9

Table 6. N_2O mixing ratio in air sampled by aircraft on Feb. 9, 1979

Altitude km	Location	Volume-mixing ratio of N_2O/ppm
2.5	Enoshima	0.28_9
2.5	Oshima	0.29_9
2.5	Shimoda	0.29_0
2.5	Omaezaki	0.28_0
2.5		0.29_5
2.5	Toba	0.29_8
0.75	Toba	0.30_1
0.75		0.30_3
0.75	Omaezaki	0.30_7
0.75	Irozaki	0.29_7
0.75	Oshima	0.31_7
0.75	Enoshima	0.30_3
	Mean	0.29_8
	SD	0.00_9

Table 7. N_2O mixing ratio in air sampled by aircraft on Feb. 16, 1979

Altitude km	Location	Volume-mixing ratio of N_2O/ppm
1	Eda	0.30_6
2	Yokohama	0.31_1
3	Enoshima	0.29_9
4		0.31_1
5		0.29_9
6	Oshima	0.31_0
7		0.30_2
6		0.30_9
4	Mikurajima	0.29_6
3	Miyakejima	0.30_5
2	Miyakejima	0.29_3
2		0.31_1
1	Mikurajima	0.31_0
1	Miyakejima	0.29_9
1	Niijima	0.31_4
1	Oshima	0.30_9
1	Enoshima	0.31_1
1	Eda	0.31_2
	Mean	0.30_6
	SD	0.00_6

ard deviation (SD) for each flight. The air samples taken on Dec. 7 and Dec. 12, 1978, and Jan. 19, Feb. 2, Feb. 9, and Mar. 27, 1979, were each measured for single reference gas respectively. The mean values of each altitude are shown in Fig. 2, along with the SDs(——). The number of samples at each altitude is also shown in Fig. 2. The value at 1.5 km was that of a constant-level flight on Dec. 7, 1978. The values at 2.5 km and 0.75 km were also those of constant-level flights on Feb. 9, 1979.

The mean value of the total of 90 samples was 0.31_0 ppm, and the SD was 0.01_4 ppm (4.4%). The mean value of 48 samples, for which the difference between two measurements was less than ±2%, was 0.31_2 ppm, and the SD was 0.01_3 ppm (4.2%). These results show that the tropospheric N_2O is well mixed from the ground surface to the altitude of 7 km, and that its mixing ratio is higher than 0.30 ppm.[1,17,21,26,32] The latter has also been shown in the measurements of the surface air in Japan,[23,25] though the results in Refs. 19 and 24 were very low (0.25 ppm).†† The mixing ratio of N_2O in the air over the sea surface is rather low (<0.29 ppm)[38,39,41-43] except for the values of the Caribbean Sea[40] and the NE Pacific Ocean.[17] This has been considered due to systematic errors among the analytical procedures.[42]

In a previous study, the mixing ratios of N_2O in the air over the ground surface were very scattered from 0.25 ppm to 0.45 ppm.[45] This wide distribution, which was also observed by Katou *et al.*,[19] has not

Table 8. N_2O mixing ratio in air sampled by aircraft on Mar. 23, 1979

Altitude km	Location	Volume-mixing ratio of N_2O/ppm
1	Kokubunji	0.31_8
2	Kawagoe	0.32_7
3	Omiya	0.31_4
4		0.31_8
5	Koga	0.31_9
6		0.31_9
7.5	Iwaki	0.32_1
7		0.33_0
6		0.33_0
5	Yamatsuri	0.30_8
4		0.31_3
3	Tochigi	0.31_5
	Mean	0.31_9
	SD	0.00_7

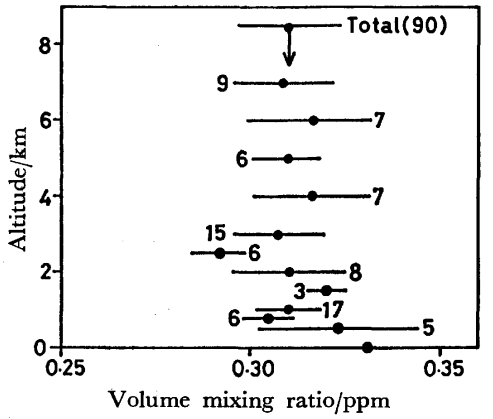

Fig. 2. The mean vertical distribution of N_2O.
●: Mean value at the same altitude, —: Its SD. The number of samples at the same altitude is also shown. a) The value of 1.7 km on Dec. 7, 1978 is included in the mean value of 1.5 km. b) The value of 7.5 km on Mar. 23, 1979 is included in the mean value of 7.0 km. c) The value of the ground surface is that at Chofu Airport.

†† The cause of this discrepancy is now under investigation.

TABLE 9. N_2O MIXING RATIO IN AIR SAMPLED BY AIRCRAFT AND MEASURED BY THE GC-TCD METHOD

Date (1978)	Altitude km	Location	Volume-mixing ratio of N_2O/ppm
Feb. 2	7	Sagami Bay	0.32_2
	4	Sagami Bay	0.34_4
	2	Sagami Bay	0.29_3
Mar. 3	7	Hayama	0.32_0
	4	Miyakejima	0.34_0
	1	Oshima-Hatsushima	0.30_2
Oct. 26	3	Oshima	0.30_2
	1	Enoshima	0.32_4
		Mean	0.31_8
		SD	0.01_9

been observed in the measurements made by the GC-ECD method. The same results have been observed in the measurements made by a GC-MS method.[24] Values such as 0.45 ppm are too high to be explained by the effect of the exhaust gas of automobiles.[25] The error in the direct preconcentration of N_2O from the outdoor air must have been much larger than the estimated one (±3%).

The SD of the sample measurements was nearly equal to the error in the measuring technique. This would imply that the tropospheric mixing ratio of N_2O is more uniform than the results of the present study indicate and that the tropospheric lifetime of N_2O is quite long.[26]

Before the ECD was equipped with, from 20 l to 30 l of air was sampled in *tedlar* or *aflon* bags. The N_2O in the sample air in these bags was preconcentrated on molecular sieve 5A (−72 °C) and then analysed by the same GC-TCD method as was adopted in the previous study.[45] The concentration of N_2O in these bags was constant for at least a week.††† The results of 8 air samples, which are shown in Table 9, were considered to be in agreement with the results obtained by the GC-ECD method.

We would like to thank Dr. Masao Misaki, Mr. Yoshio Toyama, Mr. Izuo Kanazawa, and Mrs. Miwako Ikegami for their collaboration in the air sampling by aircraft.

References

1) J. Hahn and C. Junge, *Z. Naturforsch., Teil A*, **32**, 190 (1977).
2) D. R. Bates and P. B. Hays, *Planet. Space Sci.*, **154** 189 (1967).
3) J. M. Bremner and A. M. Blackmer, *Science*, **199** 295 (1978).
4) D. J. McKenney, D. L. Wade, and W. I. Findlay, *Geophys. Res. Lett.*, **5**, 777 (1978).
5) A. D. Matthais, A. M. Blackmer, and J. M. Bremner, *Geophys. Res. Lett.*, **6**, 441 (1979).
6) C. C. Delwiche, *Pure Appl. Geophys.*, **116**, 414 (1978).
7) R. E. Rebbert and P. Ausloos, *Geophys. Res. Lett.*, **5**, 761 (1978).
8) K. A. Brice, A. E. J. Eggleton, and S. A. Penkett, *Nature*, **268**, 127 (1977).
9) M. B. McElroy and J. C. McConnel, *J. Atmos. Sci.*, **28**, 1095 (1971).
10) P. J. Crutzen, *Quart. J. Roy. Met. Soc.*, **96**, 320 (1970).
11) H. Johnston, *Science*, **173**, 517 (1971).
12) CIAP Monograph, DOT-TST-75-51 (1975).
13) P. J. Crutzen and D. H. Enhalt, *Ambio*, **6**, 112 (1977).
14) K. Schütz, C. Junge, R. Beck, and B. Albrecht, *J. Geophys. Res.*, **75**, 2230 (1970).
15) M. D. LaHue, H. D. Axelrod, and J. P. Lodge, Jr., *Anal. Chem.*, **43**, 1113 (1971).
16) H. B. Singh, L. Salas, H. Shigeishi, and A. Crawford, *Atmos. Environ.*, **11**, 819 (1977).
17) D. Pierotti and R. A. Rasmussen, *J. Geophys. Res.*, **82**, 5823 (1977).
18) Y. S. Chang, J. H. Shaw, J. G. Calvert, and W. M. Uselman, *J. Quant. Spectrosc. Radiat. Transfer*, **18**, 589 (1977).
19) T. Katou, Y. Hanai, and M. Mimura, *Bull. Inst. Environ. Sci. Tech., Yokohama National Univ.*, **3**, 5 (1977).
20) P. D. Goldan, W. C. Kuster, D. L. Albritton, and A. L. Schmeltekopf, *J. Geophys. Res.*, **83**, 935 (1978).
21) R. J. Cicerone, J. D. Shetter, D. H. Stedman, T. J. Kelly, and S. C. Liu, *J. Geophys. Res.*, **83**, 3042 (1978).
22) Th. R. Thijsse, *Atmos. Environ.*, **12**, 2001 (1978).
23) S. Araki, S. Suzuki, M. Yamada, H. Suzuki, and T. Hobo, *J. Chromatogr. Sci.*, **16**, 249 (1978).
24) Y. Hanai, T. Katou, and T. Arai, *Bull. Inst. Environ. Sci. Tech., Yokohama National Univ.*, **5**, 35 (1979).
25) T. Hiraki, M. Tamaki, and H. Watanabe, *Report Environ. Sci. Inst. Hyogo Prefecture*, No. 12, 1 (1980).
26) C. R. Roy, *J. Geophys. Res.*, **84**, 3711 (1979).
27) A. Goldan, D. G. Murcray, F. H. Murcray, and W. J. Williams, *J. Opt. Soc. Am.*, **63**, 843 (1973).
28) D. H. Ehhalt, N. Roper, and H. E. Moore, *J. Geophys. Res.*, **80**, 1653 (1975).
29) R. A. Rasmussen, J. Kransec, and D. Pierotti, *Geophys. Res. Lett.*, **3**, 615 (1976).
30) A. L. Schmeltekopf, D. L. Albritton, P. J. Crutzen, P. D. Goldan, W. J. Harrop, W. R. Henderson, J. R. McAfee, M. McFarland, H. I. Schiff, T. L. Thompson, D. J. Hofmann, and N. T. Kjome, *J. Atmos. Sci.*, **34**, 729 (1977).
31) P. Fabian, R. Borchers, K. H. Weiler, U. Schmidt, A. Volz, D. H. Ehhalt, W. Seiler, and F. Müller, *J. Geophys. Res.*, **84**, 3149 (1979).
32) P. D. Goldan, W. C. Kuster, D. L. Albritton, and A. L. Schmeltekopf, *J. Geophys. Res.*, **85**, 413 (1980).
33) A. L. Schmeltekopf, P. H. Goldan, W. R. Henderson, W. J. Harrop, T. L. Thompson, F. C. Fehsenfeld, H. I. Schiff, P. J. Crutzen, I. S. A. Isaksen, and E. E. Ferguson, *Geophys. Res. Lett.*, **2**, 393 (1975).
34) D. H. Ehhalt, L. E. Heidt, R. H. Lueb, and E. A. Martell, *J. Atmos. Sci.*, **32**, 163 (1975).
35) C. C. Gallagher and R. V. Pieri, *J. Atmos. Sci.*, **34**, 1481 (1977).
36) J. F. Vedder, B. J. Tyson, P. B. Brewer, C. A. Boitnott, and E. C. Y. Inn, *Geophys. Res. Lett.*, **5**, 33 (1978).
37) B. Y. Tyson, J. F. Vedder, J. C. Arvesen, and R. B. Brewer, *Geophys. Res. Lett.*, **5**, 369 (1978).
38) J. Hahn, *Anal. Chem.*, **44**, 1889 (1972).
39) J. Hahn, *Tellus*, **26**, 160 (1974).
40) T. Yoshinari, *Marine Chem.*, **4**, 189 (1976).
41) Y. Cohen, *Anal. Chem.*, **49**, 1238 (1977).
42) Y. Cohen and L. I. Gorden, *J. Geophys. Res.*, **84**, 347 (1979).
43) J. W. Elkins, *Anal. Chem.*, **52**, 263 (1980).
44) M. B. McElroy, J. W. Elkins, S. C. Wofsy, and Y. L. Yung, *Rev. Geophys. Space Phys.*, **14**, 143 (1976).
45) M. Hirota, *Bull. Chem. Soc. Jpn.*, **51**, 3075 (1978).
46) W. E. Wentworth, E. Chen, and R. Freeman, *J. Chem. Phys.*, **55**, 2075 (1971).
47) R. Bock and K. Schütz, *Z. Anal. Chem.*, **237**, 321 (1968).

††† This was ascertained by the GC-ECD method.

Partition Coefficients of Chlorobenzenes in Heptane-Water and Heptane-Acetonitrile Systems

Nobuo SUZUKI,* Toshinobu YOSHIDA, and Hitoshi WATARAI
Department of Chemistry, Faculty of Science, Tohoku University, Sendai 980
(Received May 6, 1981)

Partition coefficients (K_D) of benzene and 11 chloro derivatives of benzene were determined at 25 °C in two liquid-liquid partition systems: heptane/water and heptane/acetonitrile. Increase of K_D with increase of the numbers of Cl atoms in the solute is discussed in terms of surface and cohesive energies. The small difference in K_D of the isomers whose Cl atom numbers are 2, 3, or 4 was correlated with a difference in the dipole moment of the solute.

The liquid-liquid partition coefficient is utilized in measuring various solution properties: for example, transfer activity coefficient of non-electrolyte,[1] solvent effect on catalytic reaction,[2] capacity ratio in liquid chromatography,[3] and toxicity of drugs.[4] Accumulation of precise partition coefficient data is important for practical uses as well for an elucidation of the factors which influence their values. Hansch *et al.* investigated the regularity in the partition coefficients of various organic compounds. They proposed a substitution constant, π, for a variety of groups, by analogy to the Hammet σ constant.[4] Additivity of corresponding values for the components makes it possible to predict the partition coefficient of a certain compound. The additive-constitutive property is useful for practical purposes, but gives only a little insight into the nature of the solute-solute interaction.

Recently, we reported the importance of cavity formation in the partition of non-electrolytes.[5-7] In the present study, the partition equilibrium of a series of chlorobenzenes between heptane and water or acetonitrile was investigated. Chlorobenzenes are considered to be representative compounds of chlorinated organic compounds. The behavior of these compounds in the environment has recently become important. Acetonitrile was chosen to examine a difference from water in solvent effect. The partition coeffcients will be discussed in connection with the cavity formation energy in the partition systems.

Experimental

Chemicals. Monochlorobenzene (Wako G.R.) and o-dichlorobenzene (Tokyo Kasei G.R.) were washed with dilute alkaline solution, dried, and fractionally distilled under ambient pressure. *m*-Dichlorobenzene and 1,2,4-trichlorobenzene (Tokyo Kasei G.R.) were washed with dilute alkaline solution, dried, and distilled under reduced pressure. *p*-Dichlorobenzene, 1,2,3-trichlorobenzene, 1,3,5-trichlorobenzene, tetrachlorobenzene, pentachlorobenzene and hexachlorobenzene, which were all purchased from Tokyo Kasei, were purified by vacuum sublimation. Purity of the reagents was checked by GLC or mp measurement. Benzene was of spectral grade (Dotite) and used without further purification. Heptane (Kanto G.R.) was stirred with 30% fumic sulfuric acid over-night, washed with water and dilute sodium hydroxide solution, dried with sodium hydroxide and fractionally distilled. Acetonitrile (Wako G.R.) was dried with molecular sieves 3A and calcium hydride, distilled on phosphorus pentaoxide, and then redistilled on calcium hydride. Purity of the organic solvent was checked by UV spectra. Redistilled water was used throughout the experiment.

Partition Measurement. Heptane–Water System: Heptane solution of chlorobenzene of known concentration was agitated with water for 15 min by a mechanical shaker in a thermostated room at 25±1 °C. After centrifugation at 3000 rpm, an aliquot of aqueous phase was pipetted out for analysis. For benzene, monochlorobenzene, and dichlorobenzene systems, this aqueous phase was used for direct photometric determination. For trichlorobenzene and tetrachlorobenzene with quite high partition coefficients, the equilibrated aqueous phase was removed and agitated with a small volume of fresh heptane in order to re-extract and concentrate the solute dissolved in the aqueous phase. The second heptane phase was used for the photometric determination. Photometric measurement was made at 254 nm for benzene and at 220 nm for the others. The recovery in the re-extraction process was satisfactorily quantitative. The partition coefficient was calculated from this equation:

$$K_D = \frac{C_{o,init}V_o - C_aV_a}{C_aV_o}, \quad (1)$$

where $C_{o,init}$ is an initial concentration in heptane, C_a an observed concentration in aqueous phase, and V_a and V_o are volumes of aqueous and organic phases. The ratio of V_a/V_o is 1 or 10, corresponding to the magnitude of the partition coefficient. The partition coefficients of pentachlorobenzene and hexachlorobenzene were measured by means of GLC equipped with a electron capture detector.[8] The partition coefficient for every system showed no dependency on initial concentration of the solutes in the range of 0.05—0.2 mol dm^{-3}.

Heptane–Acetonitrile System: A 5-cm^3 portion of 0.003 mol dm^{-3} chlorobenzene in heptane was agitated with 5 cm^3 of acetonitrile under the same experimental conditions as used in the heptane/water system. Absorbance of the heptane phase was measured at the absorption maximum wavelength for each substance (250—300 nm). The partition coefficient was calculated by this equation:

$$K_D = \frac{A_o}{A_{o,init} - A_o}, \quad (2)$$

where $A_{o,init}$ and A_o are the absorbances of heptane solutions before and after equilibration, respectively. The acetonitrile and heptane used for partition experiments were saturated with each other prior to use. Spectrophotometry was carried out by Hitachi 356 and JASCO UVIDEC-2 spectrophotometers.

Results

In Table 1, the observed partition coefficients for the two partition systems are listed, along with the

Table 1. Partition coefficients (k_D) of chlorinated benzenes at 25 °C

No.	Solute	Abs. coeff. at 220 nm	Hep/H_2O $K_D \times 10^{-3}$	Hep/AN K_D
1	Benzene	138[a,e]	0.195	0.75
2	Chlorobenzene	4100[a]	0.838	0.83
3	*o*-Dichlorobenzene	6280[a]	2.34	0.87
4	*m*-Dichlorobenzene	6620[a]	3.41	1.15
5	*p*-Dichlorobenzene	9190[b]	3.41	1.04
6	1,2,3-Trichlorobenzene	9770[b]	10.4	1.20
7	1,2,4-Trichlorobenzene	8930[b]	13.7	1.53
8	1,3,5-Trichlorobenzene	10100[b]	25.1	2.57
9	1,2,3,4-Tetrachlorobenzene	15000[b]	35.1	1.74
10	1,2,4,5-Tetrachlorobenzene	15300[b]	45.7	2.46
11	Pentachlorobenzene	20900[c]	129[f]	2.76
12	Hexachlorobenzene	57100[d]	538[f]	4.19

a) 10% ethanol. b) Hepane. c) 40% ethanol. d) Ethanol. e) 254 nm. f) Determined by GLC.

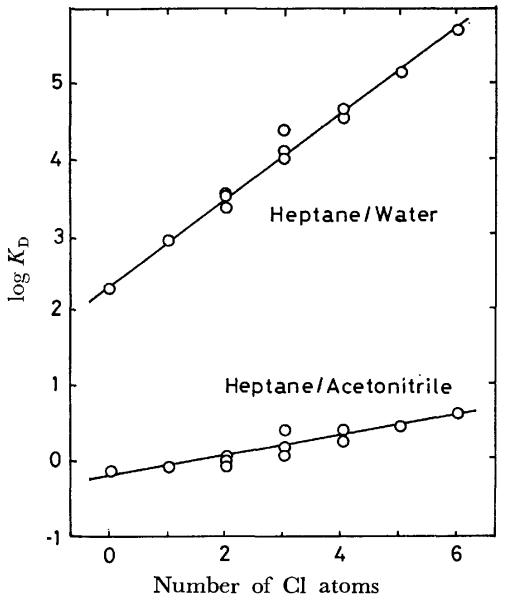

Fig. 1. Correlation between the partition coefficient and the number of chlorine atoms.

spectral data used for photometric determination. It is clearly observed that the K_D values for the heptane/water system are much larger than those for the acetonitrile system and that the values of both systems increase with an increase of number of Cl atoms in chlorobenzene. Figure 1 shows a linear relationship between log K_D and the number of Cl atoms, n. For the two partition systems, these experimental equations were obtained:

$$\left.\begin{aligned} \log K_D &= 0.566n + 2.37 \quad \text{for Heptane–}H_2O \\ \log K_D &= 0.132n - 0.203 \quad \text{for Heptane–Acetonitrile} \end{aligned}\right\}. \quad (3)$$

Increase of Cl atoms will cause an increase in molar volume and in molar surface area, as well as in the cohesive energy density of the compound. Hence, the influences of the molar surface area and the solubility parameter, defined as (cohesive energy density)$^{1/2}$, of chlorobenzene on the partition coefficient should be discussed.

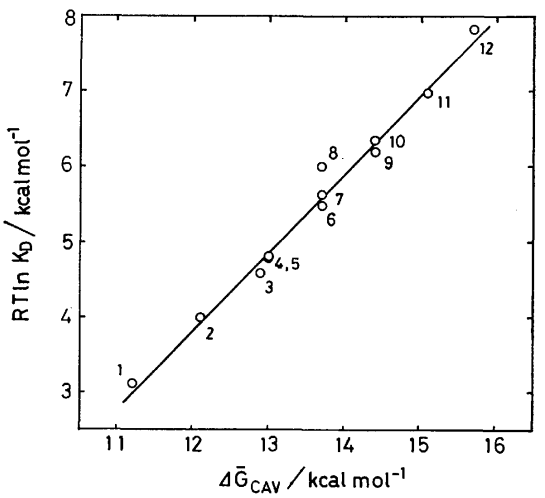

Fig. 2. Correlation between the partition coefficient and the cavity formation energy in heptane–water system. Numbers in this figure correspond to those in Table 1.

Discussion

Contribution of Surface Work. Chemical potential of solute in dilute solution is considered to be governed by two kinds of solute-solvent interaction energies, *i.e.*, a formation energy of cavity to acommodate the solute molecule and an interaction energy between the solute introduced into the cavity and the solvent molecule surrounding the solute molecule. Then, the free energy governing the partition equilibrium is represented by

$$RT \ln K_D = \Delta\bar{G}_{cav} + \Delta\bar{G}_{int}, \quad (4)$$

where $\Delta\bar{G}_{cav}$ and $\Delta\bar{G}_{int}$ correspond to free energy contributions from cavity formation and interaction accompanying the transfer of solute from organic phase into aqueous phase.

The cavity formation energy can be estimated from the molecular surface area of solute and the surface tension of bulk solvent. Sinanoglu has reported the next equation for the calculation of cavity formation energy:[9]

$$\bar{G}_{cav} = \kappa^e(\phi) 9.76\, V^{2/3}\gamma\left\{1-(1-\eta)\left(\frac{\partial \ln\gamma}{\partial \ln T}\right)+\frac{2}{3}\alpha T\right\}, \quad (5)$$

$$\eta = \frac{\kappa^s(\phi)}{\kappa^e(\phi)} = \frac{1+\phi^{2/3}(\kappa^s-1)}{1+\phi^{2/3}(\kappa^e-1)},$$

where V is molar volume of solute (cm^3 mol^{-1}), γ surface tension of solvent, α thermal expansion coefficient of solvent, ϕ molar volume ratio of solvent to solute, and κ^s and κ^e are microscopic cavity factors for surface energy and surface entropy.[10] According to Eq. 5, the cavity energy difference, $\Delta\bar{G}_{cav}$, was calculated for heptane–water system using κ^s=0.542 and 1.235, and κ^e=0.687 and 1.277 for heptane and water, respectively.[10] A correlation between RT ln K_D and $\Delta\bar{G}_{cav}$ is shown in Fig. 2. For the heptane–

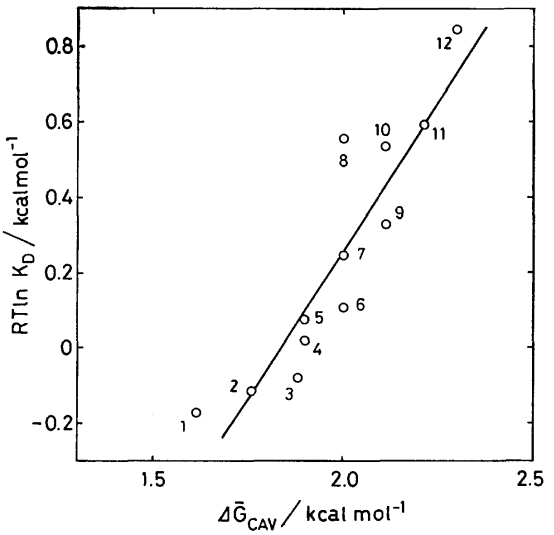

Fig. 3. Correlation between the partition coefficient and the cavity formation energy in heptane–acetonitrile system.
Numbers in this figure correspond to those in Table 1.

acetonitrile system, $\Delta\bar{G}_{cav}$ was calculated using approximated value of $\kappa^e=\kappa^s=1.0$ for acetonitrile.[9] A correlation with $RT\ln K_D$ is shown in Fig. 3. The linear relations appearing in Figs. 2 and 3 strongly suggest that the order of magnitude of the partition coefficient is governed by the cavity formation energy.

Contribution of Cohesive Work. The contributions of molar volume and of cohesive energy density of solute to the partition coefficient are accounted for by solubility parameter theory.[11] The next equation has been proposed for the partition coefficient by Suzuki *et al.*:[12]

$$\log K_D = \frac{V}{2.303RT}(\delta_a+\delta_o'-2\delta)(\delta_a-\delta_o), \quad (6)$$

$$\delta_o' = \delta_o + \frac{RT(V_o^{-1}-V_a^{-1})}{(\delta_a-\delta_o)},$$

where molar volume, V, V_o, and V_a, and solubility parameters δ, δ_o, and δ_a refer to those of solute, organic phase, and aqueous phase, respectively. This relation was successfully applied to the partition of several metal chelate compounds.[13]

Equation 6 was applied to the results of the heptane–water system. The molar volumes of chlorobenzenes were taken from the literature or estimated from the linear relationship between the molar volume and number of Cl atoms. The solubility parameters for chloro derivatives of benzene, except chlorobenzene and *o*-dichlorobenzene, were estimated from the additivity rule of group contributions in solubility parameter proposed by Renick and Lin.[14] The solubility parameter of water calculated from thermodynamic properties is 23.4 $cal^{1/2}\,cm^{-3/2}$ (conversion factor: 1 $cal^{1/2}\,cm^{-3/2}=2.0455\,J^{1/2}\,cm^{-3/2}$), but for practical use 17.15 $cal^{1/2}\,cm^{-3/2}$ is recommended by Suzuki *et al.* from their extensive study on solvent extraction of β-diketones and its metal chelates.[15] The $\log K_D$ value for chlorobenzene calculated using 17.15 $cal^{1/2}\,cm^{-3/2}$, however, decreases with increase of Cl atoms and disagrees with the observed value, *e.g.*, the calculated $\log K_D$'s are 2.50 for benzene and −0.29 for hexachlorobenzene. The same treatment, estimation of K_D according to Eq. 6, was applied to the heptane–acetonitrile system. In this system, the mutual solubility of two solvents cannot be neglected, hence the small changes in solubility parameter and molar volume of two solvent phases were corrected for by employing the solubility data reported previously.[2] The calculated results in heptane–acetonitrile did not show good agreement with the observed one, *e.g.*, the calculated $\log K_D$'s are −0.28 for benzene and −2.26 for hexachlorobenzene. When δ_a was treated as an adjustable parameter, the value of δ_a calculated introducing the observed $\log K_D$ into Eq. 6 varied from 17.4 for the benzene system to 20.9 for the hexachlorobenzene system. The value is related δ and V by the next equation:

$$\delta_a = 1.70\delta + 1.77 = 1.03V + 6.42. \quad (7)$$

The calculated values seem to be reasonable so long as the calculated δ_a value is between $\delta_v=6.4$ $cal^{1/2}\,cm^{-3/2}$ and $(\delta_v^2+\delta_r^2)^{1/2}=23.4$ $cal^{1/2}\,cm^{-3/2}$. Here δ_v and δ_r refer to the solubility parameters defined as (internal pressure)$^{1/2}$ and {(cohesive energy density) − (internal pressure)}$^{1/2}$. These reflect the physical interaction (repulsion, dispersion, and weak dipole-dipole interaction) and chemical interaction (hydrogen bonding), respectively.[16] However, in the heptane–acetonitrile system, the solubility parameters of acetonitrile calculated from the observed partition coefficient (12.4 $cal^{1/2}\,cm^{-3/2}$ for benzene system and 16.2 $cal^{1/2}\,cm^{-3/2}$ for hexachlorobenzene system) are larger than the solubility parameter calculated from the heat of vaporization (11.9 $cal^{1/2}\,cm^{-3/2}$). This suggests that the uncertainty of the solubility parameter of polar phase is not the only source of the discrepancy between the calculated and the observed partition coefficients. As another important source, the deviation from the simple geometric mean assumption should be examined. The deviation is taken into account by introducing a coefficient, l_{12}, into the activity equation derived from the regular solution theory:[11]

$$RT\ln a_2 = RT\left[\ln\phi_2+\ln\phi_1\left(1-\frac{V_2}{V_1}\right)\right] + V_2\phi_1^2[(\delta_1-\delta_2)^2+2l_{12}\delta_1\delta_2], \quad (8)$$

where a is activity, ϕ volume fraction, and subscript 1 and 2 refer to solvent and solute, respectively. Using the above expression, the partition coefficient Eq. 6 can be revised as:

$$\log K_D = \frac{V}{2.303RT}(\delta_a+\delta_o'-2q\delta)(\delta_a-\delta_o), \quad (9)$$

$$q = 1 - \frac{l_a\delta_a-l_o\delta_o}{\delta_a-\delta_o}.$$

Here q is equal to one if the strict geometric mean relation of $l_a=l_o=1$ or the apparent relation of $l_a\delta_a=l_o\delta_o$ holds, and otherwise q is different from one. The values of q are calculated using the observed $\log K_D$ and the available parameters for heptane–water and heptane–acetonitrile systems. The results

Table 2. Physical properties and parameters of the chlorobenzenes

No.	Solute	Chlorine number	Molar volume[a]	Dipole moment[c]	Solubility parameter	q value[e]	
						Hep/H_2O[f]	Hep/AN
1	Benzene	0	89.4	0	9.2,[d] 9.2	0.98	0.97
2	Chlorobenzene	1	102	1.54	9.5,[d] 9.6	0.95	0.92
3	*o*-Dichlorobenzene	2	113	2.26	10.0,[d] 10.0	0.90	0.87
4	*m*-Dichlorobenzene	2	115	1.38	9.8	0.92	0.87
5	*p*-Dichlorobenzene	2	115	0	9.8	0.92	0.88
6	1,2,3-Trichlorobenzene	3	125	2.33	10.3	0.87	0.83
7	1,2,4-Trichlorobenzene	3	125	1.26	10.3	0.86	0.81
8	1,3,5-Trichlorobenzene	3	125[b]	0.28	10.3	0.85	0.78
9	1,2,3,4-Tetrachlorobenzene	4	136[b]	1.92	10.5	0.84	0.79
10	1,2,4,5-Tetrachlorobenzene	4	136[b]	0.73	10.5	0.84	0.77
11	Pentachlorobenzene	5	146[b]	0.88	10.9	0.80	0.74
12	Hexachlorobenzene	6	156[b]	0.21	11.2	0.77	0.71

a) $cm^3\ mol^{-1}$. b) Estimated value from the relationship between molar volume and chlorine number. c) Debye. d) Calculated from the heat of vaporization. e) See Eq. 9 in the text. f) $\delta_a = 17.15\ cal^{1/2}\ cm^{-3/2}$ was used in the calculation. (Conversion factor: $1\ cal^{1/2}\ cm^{-3/2} = 2.0455\ J^{1/2}\ cm^{-3/2}$).

are listed in Table 2. The values of q are 2—30% smaller than 1.0, a result which is easily expected in simple geometric mean assumption as in Eq. 6, and decrease with increases of number of Cl atoms of solutes. This also suggests that the deviation becomes larger for larger molecule. An evaluation of l_a and l_o is difficult at the present stage, but it is probable that l_o is negative for a system composed of a large-sized solute and small-sized solvent.[11]

Equation 9 can be rearranged:

$$\log K_D = \frac{V}{2.303RT}(\delta_a^2 - \delta_o^2) + RT\left(\frac{1}{V_o} - \frac{1}{V_a}\right) - \frac{2\delta Vq}{2.303RT}(\delta_a - \delta_o). \quad (10)$$

Comparing Eq. 10 with Eq. 4, the first and the second terms in Eq. 10 are considered to refer to cavity energy and interaction energy respectively in the framework of the regular solution theory. The cavity, in this case, corresponds to the solute taking $\delta=0$ and V. Since the second term is laways negative because $\delta_a > \delta_o'$ the increase of $\log K_D$ with increase of V, observed in this study, confirmes a predominance of the cavity energy contribution.

Comparison among the Partition Coefficient of Isomers. As the partition coefficients of isomers (Cl=2,3, and 4) are compared, a slight difference among them is observed. A principal difference in physical properties of these solutes will be the difference in dipole moment, which is listed in Table 2 for each chlorobenzene.

Beveridge *et al.* derived the next equation for an electrostatic interaction energy:[17]

$$\bar{G}_{es} = -14.39\frac{\mu^2}{a^3}D\left(1+\frac{D}{3}\right) \quad (\text{kcal mol}^{-1}) \quad (11)$$

$$D = \frac{3(\varepsilon-1)}{2\varepsilon+2},$$

where ε is the dielectric constant of the solvent, μ (Debye) the dipole moment of the solute, and a(Å) the radius of solute cavity. The difference in the electrostatic interaction energy between solute–heptane and solute–water or solute–acetonitrile was calculated and compared with the partition coefficient of the solute. Figure 4 shows the correlation of the differences in $\log K_D$ between isomeric compounds of $\mu=0$ and $\mu\neq0$ with the calculated electrostatic energy difference. It is concluded from Fig. 4 that $\log K_D$ for the chlorobenzene of large dipole moment is smaller than that for a smaller dipole moment solute.

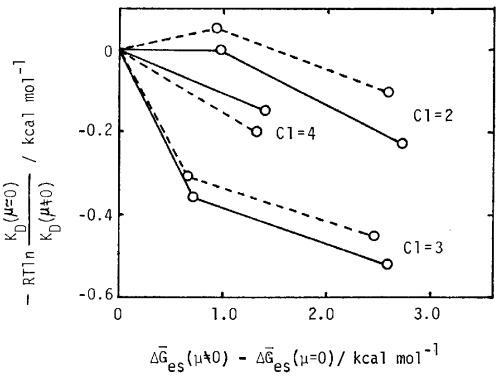

Fig. 4. Correlation between the difference in partition free energy of the isomers and the difference in electrostatic interaction energy, where $\Delta\bar{G}_{es} = \bar{G}_{es,dod} - \bar{G}_{es,polar}$.
——: Heptane–H_2O, – – –: Heptane–AN.

As a conclusion, we suggest that the partition coefficients of chlorobenzene is governed primarily by cavity formation and the difference of partition coefficient in isomers can be understood by taking into account the electrostatic interaction. More extensive study of the partition coefficient of halobenzenes is in progress, including an application of the Scaled Particle theory.[8]

References

1) H. Watarai and N. Suzuki, *J. Inorg. Nucl. Chem.*, **38**, 1683 (1976).

2) H. Watarai and N. Suzuki, *Bull. Chem. Soc. Jpn.* **52**, 2778 (1979).
3) T. Hanai, *Chromatographia*, **12**(2), 77 (1979).
4) A. Leo, C. Hansch, and D. Elkins, *Chem. Rev.*, **71**, 525 (1971).
5) H. Watarai and N. Suzuki, *Chem. Lett.*, **1977**, 321.
6) H. Watarai, M. Murakami, and N. Suzuki, *Bull. Chem. Soc. Jpn.*, **52**, 937 (1979).
7) H. Watarai and N. Suzuki, *Bull. Chem. Soc. Jpn.*, **53**, 1848 (1980).
8) H. Watarai, M. Tanaka, and N. Suzuki, *Anal. Chem.*, in press.
9) O. Sinanoglu in "Molecular Associations in Biology," ed by B. Pullman, Academic Press, New York (1968), p. 427.
10) T. Haliciglu and O. Sinanoglu, *Ann. N.Y. Acad. Sci.*, **158**, 308 (1969).
11) J. H. Hildebrand, J. M. Prausnitz, and R. L. Scott, "Regular and Related Solutions," Van Nostrand-Reinhold, New York, N.Y. (1970).
12) T. Wakahayashi, S. Oki, T. Omori, and N. Suzuki, *J. Inorg. Nucl. Chem.*, **26**, 2255 (1964).
13) N. Suzuki and K. Akiba, *J. Inorg. Nucl. Chem.*, **33**, 1169 (1971); K. Akiba, N. Suzuki, and T. Kanno, *Anal. Chim. Acta*, **58**, 379 (1972).
14) A. E. Reineck and K. F. Lin, *J. Paint Technol.*, **40**, 611 (1968).
15) H. Irving, "Ion Exchange and Solvent Extraction," ed by J. A. Marinsky and Y. Marcus, Marcel Dekker, (1974) Vol. 6, p. 139.
16) E. B. Bagley, T. P. Nelson, and J. M. Scigliano, *J. Paint Technol.*, **43**, 35 (1971).
17) D. L. Beveridge, M. M. Kelly, and R. J. Radna, *J. Am. Chem. Soc.*, **96**, 3769 (1974).

Structure and Properties of Diaquabis(ethylthioacetato)copper(II), $[Cu(C_4H_7SO_2)_2(H_2O)_2]$

Takashi Ogawa, Mamoru Shimoi, and Akira Ouchi*

Department of Chemistry, College of General Education, The University of Tokyo, Komaba 3-8-1, Meguro-ku, Tokyo 153

(Received May 7, 1981)

The crystal and molecular structure of the title complex has been determined by the X-ray diffraction method. The crystal was triclinic, space group $P\bar{1}$, $a=7.554(1)$, $b=9.001(1)$, $c=5.345(1)$ Å, $\alpha=104.83(1)$, $\beta=99.20(1)$, $\gamma=71.02(1)°$, $Z=1$, $D_x=1.684(1)$, $D_m=1.69(1)$ Mg m^{-3}, μ(Mo $K\alpha$)=2.03 mm^{-1}, and the final R value was 0.030 for 1818 reflections. The molecular arrangement has a center of symmetry and has a slightly distorted octahedral configuration around the central copper(II) atom; each ethylthioacetato ligand forms a chelate ring by coordinating through a sulfur atom and a carboxyl oxygen atom, and two water molecules are also coordinated to the central metal. The solid complex is deep green, different from the diaquabis(alkylthioacetato)copper(II) complexes of the higher alkyl groups (number of C≥3), and it is likely due to the CT band caused by the strong copper–sulfur bond in the complex.

The coordination compounds of copper(II) with sulfur containing ligands are now studied very actively in relation to the model compounds of copper proteins. The (alkylthio)acetic acids** are coordinated to the central metal atom through a sulfide sulfur atom, however, their sulfur-metal bonding is not always stable. The authors have already reported the syntheses and properties[1–5] as well as the structures[6–8] of some metal alkylthioacetates. In the case of copper (II) complexes, the formation of the strong metal-sulfur bond is expected to be due to the relatively soft character of the copper(II) atom, and also to the observed relatively high stabilities of the complexes. Moreover, they are divided into three groups according to their colors; pale blue ones (the majority of them), deep green ones (the methylthio- and ethylthioacetates), and the violet isomer of the isopropylthioacetate. The complexes of each color seems to possess characteristic structures, and we had already begun to clarify their structure by the X-ray technique, and by spectroscopic methods. The structure of the violet isomer was already elucidated.[7] This paper presents the structure of a deep green complex. Although the X-ray diffraction technique was not yet applied to the pale blue complexes, due to the difficulty in obtaining the appropriate crystals, the comparison of the visible, infrared, and electron paramagnetic resonance spectroscopic data of these alkylthioacetate complexes, suggested some relations between their structures and their spectral properties.

Experimental

Synthesis of Diaquabis(ethylthioacetato)copper(II); $[Cu(C_2H_5SCH_2CO_2)_2(H_2O)_2]$. The ligand was obtained by the condensation reaction between ethyl iodide and mercaptoacetic acid in alkaline aqueous medium as shown by Larsson.[9] The copper(II) complex was obtained by reaction between the freshly obtained copper(II) hydroxide and the free acid ligand. The pure crystals were obtained when the concentrated aqueous solution of the complex was kept overnight at ambient temperature. Analyses of the complex: Found: Cu, 18.66; C, 28.66; H, 5.41%. Calcd for $CuC_8H_{18}S_2O_6$: Cu, 18.80; C, 28.44; H, 5.37%.

X-Ray Measurement. The crystals obtained were deep-green in color, and were stable in air. The crystal used for the X-ray diffraction study was reshaped into a sphere ($\phi=0.4$ mm). The crystallographic data are as follows: $CuC_8H_{18}S_2O_6$, F.W.=337.89, triclinic, space group $P\bar{1}$, $a=7.554(1)$, $b=9.001(1)$, $c=5.345(1)$ Å, $\alpha=104.83(1)$, $\beta=99.20(1)$, $\gamma=71.02(1)°$, $Z=1$, $D_x=1.684(1)$, $D_m=1.69(1)$ Mg m^{-3}, μ(Mo $K\alpha$)=2.03 mm^{-1}. The reflections within the range of $2\theta<60°$ were collected on a Philips 1100 automated four-circle diffractometer, using Mo $K\alpha$ radiation (0.7107 Å), applying the (ω-2θ) scan technique. The 1818 independent reflections with $|F_o|>3\sigma(|F_o|)$ were used for the structure refinement. The intensities were corrected for Lorentz and polarization factors, but no correction was made for absorption and extinction.

All the calculations were carried out on a HITAC M-200H computer at the Computer Center of The University of Tokyo using the local version of UNICS program.[10] The atomic scattering factors were taken from the tables.[11]

Structure Determination. The structure was solved by the heavy-atom method. The position of the copper atom was fixed at the origin. The position of the sulfur atom was deduced from a three dimensional Patterson map, and the other non-hydrogen atoms were successively located by Fourier syntheses; their positions and their parameters were refined by a repeated block-diagonal least squares method. Then the positions of all hydrogen atoms were obtained from a difference Fourier synthesis, and were also refined. In the last cycle of the refinement with anisotropic temperature factors for all non-hydrogen atoms, all the parameter shifts were less than one-third of the corresponding standard deviations. The final R value was 0.030.[12]

Other Measurements. The infrared spectra of the samples were obtained by means of a JASCO infrared spectrophotometer type 403G, using Nujol and hexachloro-1,3-butadiene mulls.

The visible absorption spectra of the samples were obtained on a Hitachi 124 spectrophotometer, and the reflectance spectra on the same instrument with the appropriate attachment, using magnesium oxide as the reference substance.

The electron paramagnetic resonance spectra of the solid sample were measured on a JEOL PE3X electron paramagnetic resonance spectrometer, at room temperature, using 2,2-diphenyl-1-picrylhydrazyl (DPPH) as the standard for the determination of the g-values.

** For the simplicity, hereafter, the parentheses in the name of this type of compounds are neglected.

Table 1. Final atomic coprdinates ($\times 10^4$ for non-hydrogen atomics, and $\times 10^3$ for hydrogen atoms) and isotropic temperature factors (B/Å^2) with estimated standard deviations in parentheses

	x	y	z	B_{eq}[a)]
Cu	0	0	0	1.9
S	357(1)	2360.2(4)	3022(1)	2.0
O(1)	1826(1)	214(1)	−1885(2)	2.2
O(2)	3923(2)	1382(2)	−2184(3)	3.4
O(W)	−2492	1400(2)	−2885(2)	2.7
C(1)	2782(2)	1217(2)	−962(3)	2.1
C(2)	2513(2)	2192(2)	1795(3)	2.6
C(3)	−1300(2)	4006(2)	1712(3)	2.7
C(4)	−3209(3)	4323(3)	2679(4)	3.8
				B_{iso}
H(W1)	−326(4)	125(3)	−284(5)	4.7(6)
H(W2)	−218(4)	69(4)	−457(5)	5.7(7)
H(21)	348(2)	174(2)	300(4)	2.1(3)
H(22)	229(4)	344(3)	212(6)	4.9(6)
H(31)	−125(3)	358(3)	−9(4)	2.7(4)
H(32)	−79(4)	500(3)	257(6)	5.1(6)
H(41)	−376(3)	339(3)	192(5)	3.4(4)
H(42)	−315(4)	421(4)	444(6)	4.8(6)
H(43)	−398(4)	549(4)	234(6)	5.4(6)

a) The equivalent isotropic temperature factors for non-hydrogen atoms were computed using the following expression: $B_{eq} = 4/3(B_{11}a^2 + B_{22}b^2 + B_{33}c^2 + B_{12}ab\cos\gamma + B_{13}ac\cos\beta + B_{23}bc\cos\alpha)$. The B_{ij}'s are defined by: $\exp[-(h^2B_{11} + k^2B_{22} + l^2B_{33} + 2klB_{23} + 2hlB_{13} + 2hkB_{12})]$.

Table 2. Interatomic distances (l/Å) and bond angles (ϕ/°) with estimated standard deviations in parentheses

Cu-S	2.381(1)	O(2)-C(1)	1.227(2)
Cu-O(1)	1.916(2)	C(1)-C(2)	1.517(2)
Cu-O(W)	2.457(1)	C(3)-C(4)	1.524(3)
S-C(2)	1.798(2)	O(W)···O(2^{i})	2.798(2)
S-C(3)	1.815(2)	O(1)···O(W^{ii})	2.841(2)
O(1)-C(1)	1.289(2)		
S-Cu-O(1)	86.49(4)	Cu-O(1)-C(1)	122.82(10)
S-Cu-O(W)	96.29(3)	O(1)-C(1)-O(2)	123.0(2)
O(1)-Cu-O(W)	88.97(5)	O(1)-C(1)-C(2)	117.9(2)
Cu-S-C(2)	92.63(6)	O(2)-C(1)-C(2)	119.1(2)
Cu-S-C(3)	104.27(5)	S-C(2)-C(1)	115.07(12)
C(2)-S-C(3)	102.13(8)	S-C(3)-C(4)	108.0(2)
O(W)···O(1^{ii})-Cu^{ii}	124.34(5)		
O(W)···O(2^{i})-C(1^{i})	153.37(12)		
Cu-O(W)···O(1^{ii})	108.71(4)		
O(2^{i})···O(W)···O(1^{ii})	106.22(5)		
Cu-O(W)···O(2^{i})	113.28(6)		

Key to symmetry operations. i: $x-1.0, y, z$; ii: $-x, -y, -1.0-z$.

Results and Discussion

The final atomic parameters are listed in Table 1,[13] the interatomic distances and the bond angles in Table 2. A perspective drawing of the complex

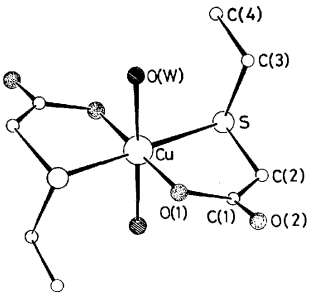

Fig. 1. A perspective drawing of the title compound with the numbering scheme of atoms.

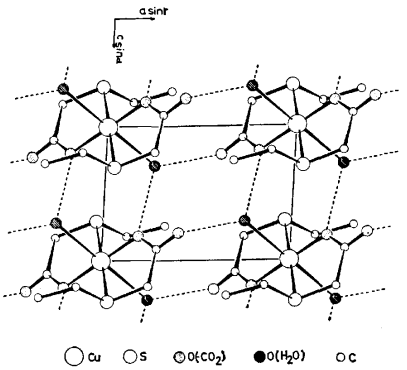

Fig. 2. Crystal packing diagram projected along b.

and the numbering scheme of atoms are shown in Fig. 1, and a projection of the structure along b in Fig. 2. The crystal consists of discrete molecules of $[Cu(C_2H_5SCH_2CO_2)_2(H_2O)_2]$ except for weak hydrogen bondings. The molecule has a center of symmetry, occupied by a copper atom. As shown in Fig. 1, and in Table 2, the central metal in this complex is in a deformed octahedral environment, elongated to both of the oxygen atoms of the coordinated waters. The ethylthioacetato ligand forms a five-membered chelate ring, being coordinated through a sulfur atom and a carboxyl oxygen atom. As shown in the previous paper,[2] the value of the magnetic moment of this complex shows no interaction between copper atoms.

The Cu–S distance is 2.381(1) Å, which is a little longer than that in the violet isomer of bis(isopropylthioacetato)copper(II) dihydrate,[7] but shorter than that of the diaquabis(methylthioacetato)cobalt(II) (2.531(1) Å).[8] The structures of some copper(II) complexes of the aliphatic ligands containing sulfide sulfur, where the sulfur atom is coordinated with the central metal, were already clarified by X-ray method.[14–22] The observed Cu–S distances for them are about 2.3—2.4 Å, and the Cu–S distance of this complex seems to be a normal one; not weak, nor very strong.

The Cu–O(1) (where O(1) is the carboxyl oxygen) is 1.916(2) Å. On the other hand, the Cu–O(W) (where O(W) is the coordinated water oxygen) is 2.457(1) Å, which is much longer than the former one. Therefore, the octahedron around the copper (II) atom was elongated to the direction of this O(W)–Cu–O(W′) axis. As the C(1)–O(1), 1.289(2) Å, is

Table 3. Infrared spectra of some metal alkylthioacetates (cm^{-1})

Complexes	ν(OH)	ν_{as}(COO)[a]	ν_s(COO) and others	Color
$Cu(MeSA)_2(H_2O)_2$	3300	1616	1441 1409 1370	dark green
$Cu(EtSA)_2(H_2O)_2$	3450 3370	1616	1409 1370	dark green
$Cu(nPrSA)_2(H_2O)_2$	3100	1593	1454 1399 1371	pale blue
$Cu(nBuSA)_2(H_2O)_2$	3100	1594	1463 1405 1376	pale blue
$Cu(iPrSA)_2 \cdot 2H_2O$	3380 3270	1592	1460 1387 1366	violet
$Co(MeSA)_2(H_2O)_2$	3180 3100	1615	1433 1391 1368	red

HMeSA: Methylthioacetic acid, HEtSA: ethylthioacetic acid, HnPrSA: propylthioacetic acid, HiPrSA: isopropylthioacetic acid, HnBuSA: butylthioacetic acid. a) Only the strongest peaks are shown.

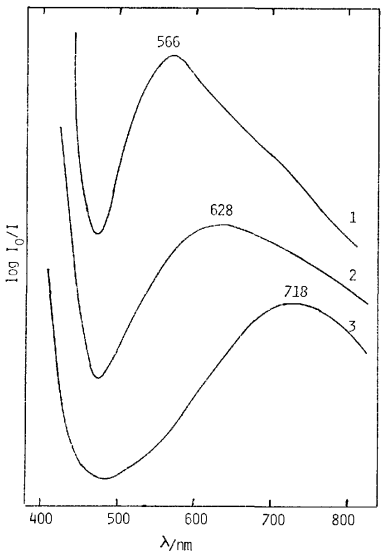

Fig. 3. Reflectance spectra of the complexes.
1: Bis(isopropylthioacetato)copper(II) dihydrate (violet isomer), 2: diaquabis(ethylthioacetato)copper(II), 3: diaquabis(propylthioacetato)copper(II).

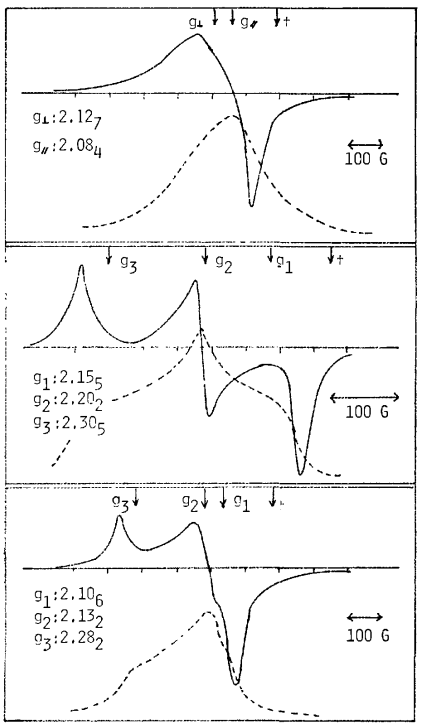

Fig. 4. Electron paramagnetic resonance spectra of the complexes.
1: Bis(isopropylthioacetato)copper(II) dihydrate (violet isomer), 2: diaquabis(ethylthioacetato)copper(II), 3: diaquabis(propylthioacetato)copper(II), †: DPPH standard. Broken lines show the integral curves of the spectra.
1 G=1×10^{-4} T.

longer than C(1)–O(2), 1.227(2) Å, the carboxyl group of the ligand seems to be the covalently bonded in the chelate.

The coordinated water molecule forms hydrogen bonds both with the O(1) atom of a complex adjacent in c-axis direction, and with the O(2) atom of the adjacent complex in a-axis direction.

Some infrared spectral data for the copper(II) ethylthioacetate together with some related complexes, are shown in Table 3.

The ν(O–H) band of methylthio- and ethylthioacetates appears at about 3300—3450 cm^{-1}, while the corresponding band of the hydrated copper(II) propylthio-, and butylthioacetates appears in the lower wave number region. (Although it is not shown in the table, the higher homolog of the alkylthioacetates also have the lower wave number ν(O–H) band.) The band of the violet isomer of the isopropylthioacetate appears in the intermediate region of them. Therefore, the grouping of the complexes in color, deep-green, pale-blue, and violet, corresponds with the grouping by the wave numbers of the ν(O–H) band. The lower wave number of the band was observed also in the spectra of diaquabis(methylthioacetato)cobalt(II), where the Co–O(W) (where O(W) is the oxygen atom of the coordinated water), is 2.066 (3) Å, and it is much shorter than that of Cu–O(W) in the present complex, even considering the difference of the radii of cobalt(II) and copper(II). On the other hand, there is no clear relation between the colors and the wave numbers of the ν_{as}(COO) and ν_s(COO) bands.

The reflectance spectra of the three types of complexes, ethylthio-, propylthio-, and isopropylthioacetates of copper(II) are shown in Fig. 3. As is shown in the figure, the pale blue complex, the propylthioacetate, has a d-d band at about 718 nm. On the other hand, the isopropylthioacetate (violet isomer), as well as the present ethylthioacetate show a broad band at 500—700 nm. Although the exact analysis of the absorption pattern has not yet been carried out, at least, it is likely that a band stronger than the common d-d one overlaps the latter one in these

two cases. The ovelapping band seems to have the maximum in the 500—600 nm region, which is shorter than that of the pure d-d band. Probably this band is due to a $p\pi$-$p\pi$ back donation from copper to sulfur, as the Cu–S bands of these complexes are short enough. On the other hand, this kind of charge transfer band does not exist in the spectra of the pale blue complexes, and therefore, their Cu–S bonds are expected to be longer than the deeper colored ones.

The electron paramagnetic resonance spectra of the complexes in the powdered solid state at room temperature are shown in Fig. 4, together with their integral curves. From these results, it can be seen that diaquabis(ethylthioacetato)copper(II) as well as diaquabis(propylthioacetato)copper(II) has three different axes like copper(II) chloride dihydrate.[23] Although the features of their spectral patterns are different from each other, their integral curves resemble each other. Therefore, the difference is likely to be a quantitative one concerning their g-values, only. On the other hand, bis(isopropylthioacetato)copper(II) dihydrate has only two kinds of axes, $g_{//}$ and $g_{\perp}$, like copper(II) sulfate pentahydrate,[23] and the structure is expected to be different from the other copper(II) alkylthioacetates. Therefore, the pale-blue copper(II) alkylthioacetates are expected to have a coordination structure similar to that of the green ones.

The authors wish to thank Professor Yoichi Iitaka of the Faculty of Pharmaceutical Sciences, The University of Tokyo, for the measurement of the intensities. The measurements of electron paramagnetic resonance spectra by Professor Ryo Hirasawa of our College are gratefully acknowledged. We are also deeply obliged to Professor Kunio Nakano, Faculty of Science, Rikkyo University, concerning the integration of the EPR spectral curves and the analysis of the data.

References

1) A. Ouchi, Y. Ohashi, T. Takeuchi, and Y. Yoshino, *Bull. Chem. Soc. Jpn.*, **43**, 1088 (1970).
2) Y. Ohashi, T. Takeuchi, A. Ouchi, and Y. Yoshino, *Bull. Chem. Soc. Jpn.*, **43**, 2845 (1970).
3) A. Ouchi, T. Takeuchi, and Y. Ohashi, *Bull. Chem. Soc. Jpn.*, **44**, 731 (1971).
4) A. Ouchi, T. Takeuchi, and Y. Ohashi, *Bull. Chem. Soc. Jpn.*, **44**, 3461 (1971).
5) A. Ouchi, H. Honda, and S. Kitazima, *J. Inorg. Nucl. Chem.*, **37**, 2599 (1975).
6) M. Shimoi, F. Ebina, A. Ouchi, Y. Yoshino, and T. Takeuchi, *J. Chem. Soc., Chem. Commun.*, **1979**, 1132.
7) T. Ogawa, M. Shimoi, and A. Ouchi, *Acta Crystallogr.*, **36**, 3114 (1980).
8) A. Ouchi, M. Shimoi, T. Takeuchi, and H. Saito, *Bull. Chem. Soc. Jpn.*, **54**, 2290 (1981).
9) E. Larsson, *Ber.*, **63**, 1347 (1930).
10) "The Universal Crystallographic Computation Program System (UNICS)," ed by T. Sakurai, Crystallographic Society of Japan, Tokyo (1967).
11) "International Tables for X-Ray Crystallography," Kynoch Press, Birmingham, U.K. (1974), Vol. IV.
12) $R=\Sigma||F_o|-|F_c||/\Sigma|F_o|$.
13) The anisotropic thermal parameters of non-hydrogen atoms, mean isotropic thermal parameters of hydrogen atoms, and the final F_o-F_c table are kept at the Chemical Society of Japan as Document No. 8205
14) A. Mangia, M. Nardelli, G. Pelizzi, and C. Pelizzi, *J. Cryst. Mol. Struct.*, **1**, 139 (1971).
15) B. Cohen, C. C. Ou, R. A. Lalancette, W. Borowski, J. A. Potenza, and H. J. Schugar, *Inorg. Chem.*, **18**, 217 (1979).
16) C. C. Ou, V. M. Miskowski, R. A. Lalancette, J. A. Potenza, and H. J. Schugar, *Inorg. Chem.*, **15**, 3157 (1976).
17) G. R. Brubaker, J. N. Brown, M. K. Yoo, R. A. Kinsey, T. M. Kutchan, and E. A. Mottel, *Inorg. Chem.*, **18**, 299 (1979).
18) Y. Agunus, R. Louis, and R. Weiss, *J. Am. Chem. Soc.*, **101**, 3381 (1979).
19) J. Coetzer, *Acta Crystallogr., Sect. B*, **26**, 1414 (1970).
20) M. R. Udupa and B. Krebs, *Inorg. Chim. Acta*, **34**, 249 (1979).
21) M. R. Udupa and B. Krebs, *Inorg. Chim. Acta*, **39**, 267 (1980).
22) J. F. Richardson and N. C. Payne, *Inorg. Chem.*, **17**, 2111 (1978).
23) F. K. Kneubühl, *J. Chem. Phys.*, **33**, 1074 (1960).

The Reduction of Cobalt(III) Complexes by Ascorbic Acid. II.[1] The Kinetics and Mechanisms of the Reactions of Diaqua and Aquahydroxo Macrocyclic N_4 Complexes

Keiichi Tsukahara,* Tatsuo Izumitani, and Yasuo Yamamoto
Department of Chemistry, Faculty of Science, Shimane University, Nishikawatsu-cho, Matsue 690
(Received June 3, 1981)

The kinetics of the reductions of several macrocyclic N_4 cobalt(III) complexes by L-ascorbic acid (H_2A) have been studied at 25.0 °C, at an ionic strength of 0.10 mol dm^{-3} ($LiClO_4$), and over the pH range from 1.64 to 3.47. The second-order rate constants in dm^3 mol^{-1} s^{-1} are 3.4 ± 0.6 (Me_6[14]4,11-dieneN$_4$),† $(4.2\pm0.2)\times10$ (Me_4[14]tetraeneN$_4$), and $(4.2\pm0.1)\times10$ (*ms*-Me_6[14]aneN$_4$) for the reactions of $[Co(N_4)(H_2O)_2]^{3+}$ with HA^- ions and $(1.1\pm0.1)\times10^2$ (Me_6[14]4,11-dieneN$_4$), $(1.3\pm0.1)\times10^3$ (Me_4[14]tetraeneN$_4$), $(5.5\pm0.1)\times10$ (*ms*-Me_6[14]aneN$_4$), and $(2.9\pm0.6)\times10$ ([14]aneN$_4$) for the reactions of $[Co(OH)(N_4)(H_2O)]^{2+}$ with HA^- ions. The mechanisms of these reactions are discussed, and it is concluded that the lack of saturation of macrocyclic ligands facilitates the electron-transfer reaction between cobalt(III) and ascorbic acid.

L-Ascorbic acid plays a significant role in biological redox systems.[2] Kinetic studies of the ascorbate reductions of metal complexes may be useful in understanding the role of ascorbic acid.

The reactions of metal complexes with ascorbic acid, as with the other organic reducing agents, are classified into three categories:[3] (i) outer-sphere electron transfer, (ii) inner-sphere electron transfer, which occurs subsequent to the substitution of a ligand for ascorbate, and (iii) a bridging mechanism in which ascorbate is bound at a ligand of the complex prior to electron transfer.

In a previous paper we reported the outer-sphere electron-transfer reactions of cobalt(III) complexes ligating 1,10-phenanthroline or 2,2′-bipyridine with ascorbic acid.[1] Cobalt(III) tetraazamacrocyclic and porphyrin complexes have a soft character, and it is expected that ascorbic acid, which is a π donor, interacts with these complexes; consequently, Mechanism (ii) or Mechanism (iii) may be possible. In this paper we will report on the ascorbate reductions of diaqua and aquahydroxo cobalt(III) complexes containing tetraazamacrocycles, Me_4[14]tetraeneN$_4$, Me_6-[14]4,11-dieneN$_4$, *ms*-Me_6[14]aneN$_4$, and [14]aneN$_4$ (Fig. 1), whose cobalt(II) complexes are low-spin species in an aqueous solution.

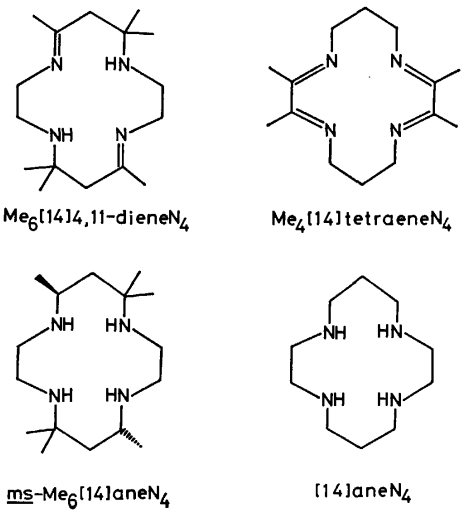

Fig. 1. Structures of tetraazamaclocycles (N_4).

Experimental

Reagents. The complexes, $[Co(Me_6[14]4,11\text{-}dieneN_4)(H_2O)_2](ClO_4)_3$,[4] $[Co(Me_4[14]tetraeneN_4)(H_2O)_2](ClO_4)_3\cdot2.5H_2O$,[5] $[Co(ms\text{-}Me_6[14]aneN_4)(H_2O)_2](ClO_4)_3$,[4,6] and $[Co([14]aneN_4)(H_2O)_2](ClO_4)_3$,[7] were prepared as reported in the literature. All the complexes are *trans* isomers. The L-ascorbic acid and sodium L-ascorbate were supplied by Wako Pure Chemical Industries. The $LiClO_4\cdot3H_2O$ was obtained according to the procedure reported previously.[8] All the solutions used for the measurements were prepared using water obtained by the distillation of alkaline permanganate solutions. A solution of ascorbic acid was freshly prepared under a nitrogen atmosphere which had been scrubbed twice with alkaline potassium pyrogallate.

Kinetic Measurements. All the measurements were made under a nitrogen atmosphere. The reaction was initiated by injecting a solution of ascorbic acid into a solution containing the required amounts of a complex and lithium perchlorate. The change in the absorbance with the time was followed with a Hitachi 200-20 spectrophotometer. The wavelengths used for the measurements were 320 nm ($[Co(ms\text{-}Me_6[14]aneN_4)(H_2O)_2]^{3+}$), 340 nm ($[Co(Me_6[14]4,11\text{-}dieneN_4)(H_2O)_2]^{3+}$), 500 nm ($[Co([14]aneN_4)(H_2O)_2]^{3+}$), and 540 nm ($[Co(Me_4[14]tetraeneN_4)(H_2O)_2]^{3+}$). In order to ensure a pseudo-first order condition, ascorbic acid was used in at least a twentyfold excess over the cobalt(III) complexes. In an aqueous solution of $[Co(Me_6[14]4,11\text{-}dieneN_4)(H_2O)_2]^{3+}$ ions[9] or $[Co(Me_4[14]tetraeneN_4)(H_2O)_2]^{3+}$ ions, a dimerization was gradually observed. In order to minimize this dimerization, the concentrations of the complexes were restricted below 4×10^{-4} mol dm^{-3} and the solution was used within 20 min after preparation.

The temperature was controlled at 25.0 ± 0.1 °C, and the ionic strength (I) was adjusted to 0.10 mol dm^{-3} with lithium perchlorate. The pH of the solution was adjusted with sodium ascorbate or perchloric acid and was measured on a Hitachi-Horiba F-7 pH meter with a 3.33 mol dm^{-3} NaCl solution as a junction. The hydrogen-ion concentrations were computed from the pH, using a value of 0.83 for the activity coefficient of H^+.[10]

† Abbreviations: Me_6[14]4,11-dieneN$_4$ = 5,7,7,12,14,14-hexamethyl-1,4,8,11-tetraazacyclotetradeca-4,11-diene, Me_4-[14]tetraeneN$_4$ = 2,3,9,10-tetramethyl-1,4,8,11-tetraazacyclotetradeca-1,3,8,10-tetraene, *ms*-Me_6[14]aneN$_4$ = *meso*-5,7,7,12,14,14-hexamethyl-1,4,8,11-tetraazacyclotetradecane, [14]aneN$_4$ = 1,4,8,11-tetraazacyclotetradecane.

Stoichiometric Determinations. The stoichiometry of the reaction of $[Co(Me_6[14]4,11\text{-}dieneN_4)(H_2O)_2]^{3+}$ with ascorbic acid was determined spectrophotometrically. The reaction was initiated by mixing solutions of the complex and of ascorbic acid under a nitrogen atmosphere ($[Co(III)]_0 = 1.20\times10^{-2}$ mol dm^{-3} and $[H_2A]_0 = (0.136\text{–}1.32)\times10^{-2}$ mol dm^{-3}). Then the reaction was monitored with a Shimadzu UV 140-02 spectrophotometer until no spectral changes were observed. After the hydrogen-ion concentrations of the solutions had been adjusted to 0.10 mol dm^{-3} with perchloric acid under a nitrogen atmosphere, the absorbance at 445 nm (absorption maximum of Co(II) complex) was recorded.

Acid-dissociation Constants. The acid-dissociation constants of the diaqua ligands of $[Co(Me_6[14]4,11\text{-}dieneN_4)(H_2O)_2]^{3+}$ were determined by pH titrations with a standard sodium hydroxide solution at 25 °C and $I=0.1$ mol dm^{-3} ($LiClO_4$) under a nitrogen atmosphere. The pK values thus obtained were 3.93 ± 0.02 and 8.6 ± 0.1, compared with the literature values of 4.02 ± 0.01 and 8.2 ± 0.1 at 25 °C and $I=1.0$ mol dm^{-3} ($NaClO_4$).[11] The acid-dissociation constants of the diaqua ligands of the other complexes and of ascorbic acid were used of the literature values for the analysis of the rate constants without any correction of the ionic strength: the pK values at 25 °C are 3.5 ± 0.1 and 6.5 ± 0.1 ($I=0.50$ mol dm^{-3}) for $[Co(Me_4[14]tetraeneN_4)(H_2O)_2]^{3+}$,[12] 2.7 ± 0.05 and 6.4 ± 0.05 ($I=1.0$ mol dm^{-3}) for $[Co(ms\text{-}Me_6[14]aneN_4)(H_2O)_2]^{3+}$,[11] 2.9 ± 0.1 and 7.2 ± 0.1 ($I=0.50$ mol dm^{-3}) for $[Co([14]aneN_4)(H_2O)_2]^{3+}$,[13] and 4.04 and 11.3 ($I=0.10$ mol dm^{-3}) for H_2A.[14]

Results

The Reactions of $[Co(Me_6[14]4,11\text{-}dieneN_4)(H_2O)_2]^{3+}$, $[Co(Me_4[14]tetraeneN_4)(H_2O)_2]^{3+}$, and $[Co(ms\text{-}Me_6[14]aneN_4)(H_2O)_2]^{3+}$ with Ascorbic Acid. Spectrophotometric titrations confirm to the following stoichiometry for the reaction of $[Co(Me_6[14]4,11\text{-}dieneN_4)(H_2O)_2]^{3+}$ with ascorbic acid ($[Co(III)]/[H_2A]=1.96\pm0.04$):

$$2Co(III) + H_2A = 2Co(II) + \text{dehydroascorbic acid}. \quad (1)$$

The spectral changes observed during the reaction of $[Co(Me_6[14]4,11\text{-}dieneN_4)(H_2O)_2]^{3+}$ with ascorbic acid gave three isosbestic points over the range from 370 to 650 nm (Fig. 2). The spectrum at infinity corresponds to that of $[Co^{II}(Me_6[14]4,11\text{-}dieneN_4)(H_2O)_2]^{2+}$.[15] In the reactions of $[Co(Me_4[14]tetraeneN_4)(H_2O)_2]^{3+}$ and $[Co(ms\text{-}Me_6[14]aneN_4)(H_2O)_2]^{3+}$, the spectra at infinity also agree with those of the corresponding cobalt(II) complexes.[15,16]

The kinetics of the title reactions were studied in various concentrations of ascorbic acid ($(0.380\text{–}2.10)\times10^{-2}$ mol dm^{-3}), cobalt(III) ($(1.42\text{–}3.41)\times10^{-4}$ mol dm^{-3}), and hydrogen ions (4.08×10^{-4}–1.19×10^{-2} mol dm^{-3}). The plots of $-\ln(A_t - A_\infty)$ *vs.* time were linear for at least 90% completion (A_t and A_∞ represent the absorbance at time t and infinity respectively). The observed first-order rate constants (k_{obsd}) obtained from the slope of this straight line were also linearly dependent on the initial concentrations of ascorbic acid (Fig. 3). Thus, the rate law was described as follows:

$$-\frac{1}{2}d[Co(III)]/dt = k[Co(III)][H_2A]_0. \quad (2)$$

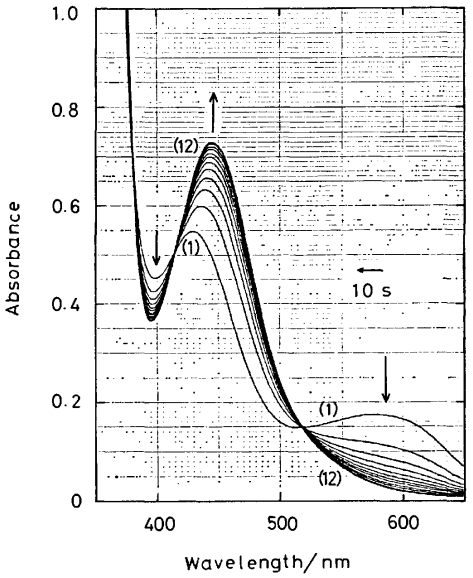

Fig. 2. Spectral changes during the reaction of $[Co(Me_6[14]4,11\text{-}dieneN_4)(H_2O)_2]^{3+}$ with ascorbic acid at $[H_2A]_0=1.00\times10^{-1}$ mol dm^{-3}, $[Co(III)]_0=8.40\times10^{-3}$ mol dm^{-3}, pH=2.60, 25.0 °C, and $I=0.50$ mol dm^{-3}: (1) 15 s; (2) 3 min; (3) 5 min 40 s; (4) 8 min 20 s; (5) 11 min 10 s; (6) 14 min; (7) 17 min; (8) 20 min; (9) 25 min; (10) 30 min; (11) 40 min; (12) 50 min after the reaction. The times given are for the start of scan at 650 nm.

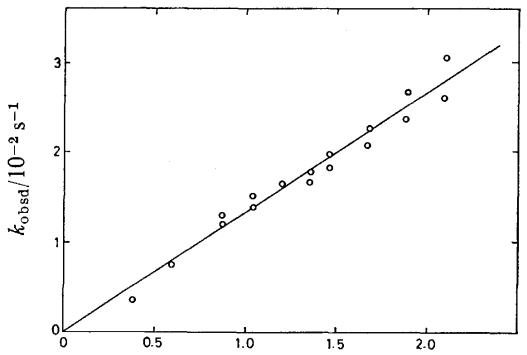

Fig. 3. Plots of k_{obsd} *vs.* $[H_2A]_0$ for the $[Co(Me_6[14]4,11\text{-}dieneN_4)(H_2O)_2]^{3+}$–ascorbic acid system at $[Co(III)]_0=2.34\times10^{-4}$ mol dm^{-3}, pH=3.12, 25.0 °C, and $I=0.10$ mol dm^{-3} ($LiClO_4$).

The second-order rate constants obtained from $k_{obsd}/[H_2A]_0$ increased with a decrease in the acidity (Fig. 4). The dependence of k on the hydrogen-ion concentrations may be explained by Scheme 1, considering that cobalt(III) complexes are not reduced by H_2A species.[1] The above mechanism leads to Eq. 3 for the second-order rate constant:

$$k = \{k_1K_{a1} + (k_0K_{a1}K_{a2} + k_1^{OH}K_1K_{a1})[H^+]^{-1} + k_0^{OH}K_1K_{a1}K_{a2} + k_1^{(OH)_2}K_1K_2K_{a1})[H^+]^{-2} + k_0^{(OH)_2}K_1K_2K_{a1}K_{a2}[H^+]^{-3}\}/\alpha(H)\beta(H)[H^+], \quad (3)$$

where the symbols are abbreviated as in Scheme 1 and where $\alpha(H)=1+K_{a1}[H^+]^{-1}+K_{a1}K_{a2}[H^+]^{-2}$ and $\beta(H)=1+K_1[H^+]^{-1}+K_1K_2[H^+]^{-2}$. The plots of the values of $k\alpha(H)\beta(H)[H^+]$ *vs.* $[H^+]^{-1}$ gave a straight

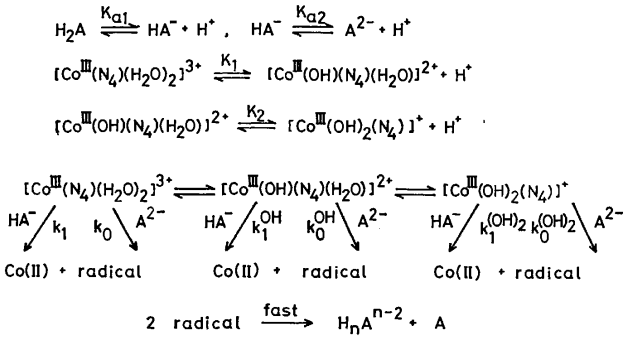

Scheme 1.

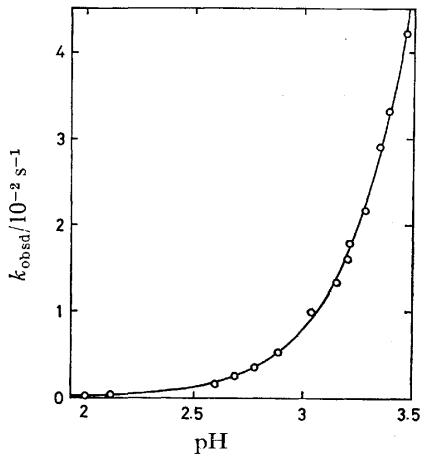

Fig. 4. Plots of k_{obsd} *vs.* pH for the $[Co(Me_6[14]4,11\text{-dieneN}_4)(H_2O)_2]^{3+}$–ascorbic acid system at $[H_2A]_0 = 1.00\times10^{-2}$ mol dm^{-3}, $[Co(III)]_0 = (2.30—3.41)\times10^{-4}$ mol dm^{-3}, 25.0 °C, and $I=0.10$ mol dm^{-3} ($LiClO_4$).

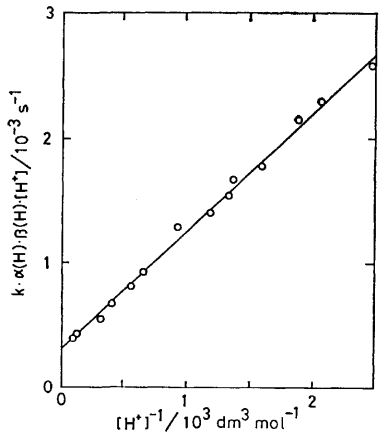

Fig. 5. Plots of $k\alpha(H)\beta(H)[H^+]$ *vs.* $[H^+]^{-1}$ for the $[Co(Me_6[14]4,11\text{-dieneN}_4)(H_2O)_2]^{3+}$–ascorbic acid system.

line (Fig. 5), showing that the k_0^{OH}, $k_1^{(OH)_2}$, and $k_0^{(OH)_2}$ paths do not contribute under the present experimental conditions. The values of k_1K_{a1} and of $(k_0K_{a1}K_{a2}+k_1^{OH}K_1K_{a1})$ are obtained from the intercept and the slope of this straight line respectively. In order to be comparable to the k_1^{OH} term, k_0 must exceed 10^{10} dm^3 mol^{-1} s^{-1}, which is in excess of the highest previously reported second-order rate constants. Therefore, the k_0 term does not contribute to the

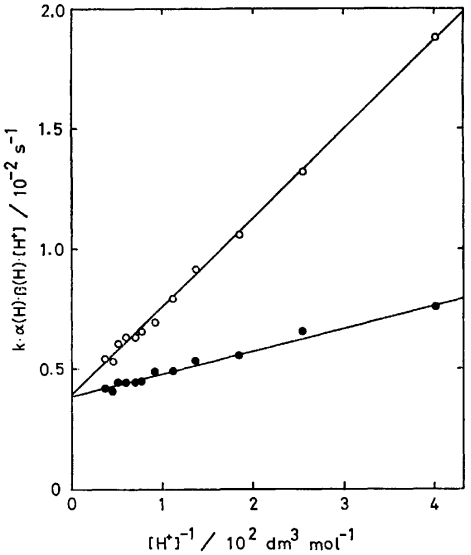

Fig. 6. Plots of $k\alpha(H)\beta(H)[H^+]$ *vs.* $[H^+]^{-1}$ for the $[Co(Me_4[14]tetraeneN_4)(H_2O)_2]^{3+}$ and $[Co(ms\text{-}Me_6[14]aneN_4)(H_2O)_2]^{3+}$–ascorbic acid system at $[H_2A]_0 = 1.00\times10^{-2}$ mol dm^{-3}, 25.0 °C, and $I=0.10$ mol dm^{-3} ($LiClO_4$).
○: $[Co(Me_4[14]tetraeneN_4)(H_2O)_2]^{3+}$ ($[Co(III)]_0 = (1.42—2.00)\times10^{-4}$ mol dm^{-3}), ●: $[Co(ms\text{-}Me_6[14]aneN_4)(H_2O)_2]^{3+}$ ($[Co(III)]_0 = (3.06—3.43)\times10^{-4}$ mol dm^{-3})

Table 1. Second-order rate constants of the reactions of $[Co(N_4)(H_2O)_2]^{3+}$ with ascorbic acid at 25.0 °C and $I=0.10$ mol dm^{-3} ($LiClO_4$)

N_4	k_1 / dm^3 mol^{-1} s^{-1}	k_1^{OH} / dm^3 mol^{-1} s^{-1}
$Me_4[14]tetraeneN_4$	$(4.2\pm0.2)\times10$	$(1.3\pm0.1)\times10^3$
$Me_6[14]4,11\text{-dieneN}_4$	3.4 ± 0.6	$(1.1\pm0.1)\times10^2$
$ms\text{-}Me_6[14]aneN_4$	$(4.2\pm0.1)\times10$	$(5.5\pm0.1)\times10$
$[14]aneN_4$	≈0	$(2.9\pm0.6)\times10$

present reaction ($k_0K_{a1}K_{a2} \ll k_1^{OH}K_1K_{a1}$). The second-order rate constants, k_1 and k_1^{OH}, were obtained by the use of the values of K_1, K_{a1}, and K_{a2}. The same analysis was also employed for the $Me_4[14]tetraeneN_4$ and the $ms\text{-}Me_6[14]aneN_4$ systems (Fig. 6). The values of k_1 and k_1^{OH} are listed in Table 1.

The Reactions of $[Co([14]aneN_4)(H_2O)_2]^{3+}$ with Ascorbic Acid. Figure 7 shows an example of the change in the absorbance at 500 nm against the time and of the consecutive reaction treatment for the evaluation of the pseudo-first-order rate constants, k_1^{obsd} and k_2^{obsd}, for the first and second stages of the title reaction.[17] The absorption spectra at infinity in the second stage at pH>3 show those of the $[Co^{II}([14]aneN_4)(H_2O)_2]^{2+}$ ion, but not at pH<2. The situation for the biphasic kinetics under the pseudo-first-order conditions can be represented by the following sequence:

$$A \xrightarrow{k_1^{obsd}} B \xrightarrow{k_2^{obsd}} C. \quad (4)$$

Equation 5 describes the change in the absorbance with the time, where ε_A, ε_B, and ε_C are the molar ab-

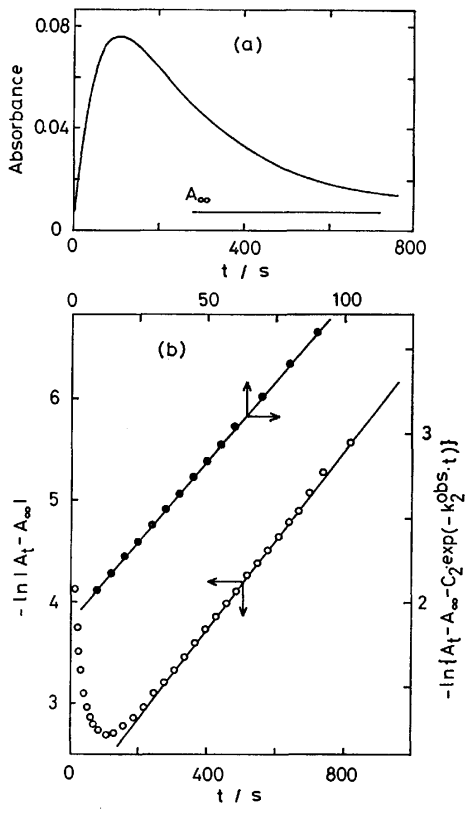

Fig. 7. Reaction of $[Co([14]aneN_4)(H_2O)_2]^{3+}$ with ascorbic acid at $[H_2A]_0=1.04\times10^{-2}$ mol dm^{-3}, $[Co(III)]_0=1.70\times10^{-4}$ mol dm^{-3}, pH=3.14, 25.0 °C, and $I=0.10$ mol dm^{-3} ($LiClO_4$) followed at 500 nm: (a) absorbance-time profile; (b) resolution of the kinetic data into its two component exponentials.

sorption coefficients of the species and where $[A]_0$ is the initial concentration of A:

$$A_t - A_\infty = C_1 \exp(-k_1^{obsd}t) + C_2 \exp(-k_2^{obsd}t), \quad (5)$$

$$C_1 = \frac{[A]_0\{k_1^{obsd}(\varepsilon_A-\varepsilon_B)-k_2^{obsd}(\varepsilon_A-\varepsilon_C)\}}{k_1^{obsd}-k_2^{obsd}}, \quad (6)$$

$$C_2 = \frac{[A]_0 k_1^{obsd}(\varepsilon_B-\varepsilon_C)}{k_1^{obsd}-k_2^{obsd}}. \quad (7)$$

The second-stage rate constant, k_2^{obsd}, is given by the slope of the linear portion observed by means of a plot of $-\ln(A_t-A_\infty)$ *vs.* t:

$$-\ln(A_t-A_\infty) = k_2^{obsd}t - \ln C_2. \quad (8)$$

A plot of the left-hand side of Eq. 9 against the time gives the first-stage rate constant, k_1^{obsd}, as a slope:

$$-\ln\{A_t-A_\infty-C_2\exp(-k_2^{obsd}t)\} = k_1^{obsd}t - \ln C_1. \quad (9)$$

The values of k_1^{obsd} and k_2^{obsd} at various concentrations of ascorbic acid and hydrogen ions are listed in Table 2. It is found that $k_1^{obsd}=a[H_2A]_0$ and that $k_2^{obsd}=b+c[H_2A]_0$, where the constants a, b, and c depend on the hydrogen-ion concentrations.

The reaction products were examined by the use of an SP-Sephadex C-25 column (Na^+ form). The reaction was initiated by mixing solutions of $[Co([14]aneN_4)(H_2O)_2]^{3+}$ ($(1.0-2.0)\times10^{-2}$ mol dm^{-3}) and of H_2A (1.0×10^{-2} mol dm^{-3}) at pH 4 and 25.0 °C under a nitrogen gas, an argon gas, or air. The reaction was monitored with a Hitachi 200-20 spectrophotometer. The first increase in absorption was observed over the range from 400 to 700 nm in each case ($\lambda_{max}\approx440$ nm and $\lambda_{sh}\approx550$ nm); thereafter, the absorbance decreased. After the first-stage reaction had been completed, the solution was poured into a Sephadex column and three species were separated with a 0.1 mol dm^{-3} $NaClO_4$ solution–violet, violet, and brown from the bottom to the top of the column. The first violet band turned green when treated with a 0.2 mol dm^{-3} $HClO_4$ solution, and the green species may have a 2+ charge (λ_{max} 620±5 nm, λ_{max} 525±5 nm, and λ_{sh} 420 nm). It has not yet been identified. The second violet band also turned green when treated with a 0.2 mol dm^{-3} $HClO_4$ solution; the green species was identified as $[Co([14]aneN_4)(H_2O)_2]^{3+}$. The last brown species have a 4+ charge and changed to $[Co([14]aneN_4)(H_2O)_2]^{3+}$ when treated with a 0.4 mol dm^{-3} $HClO_4$ solution. The brown species was identified as $[\{(H_2O)Co([14]aneN_4)\}_2O_2]^{4+}$.[18] A $[Co^{II}([14]aneN_4)(H_2O)_2]^{2+}$ ion is very sensitive to a trace of oxygen;[18-20] therefore, it is concluded that the biphasic behavior in the present system is ascribable to a trace of oxygen in a nitrogen or an argon gas. Accordingly, the present reaction is considered to be represented as follows:

$$[Co([14]aneN_4)(H_2O)_2]^{3+} \text{ or } [Co(OH)([14]aneN_4)(H_2O)]^{2+} + HA^- \longrightarrow [Co([14]aneN_4)(H_2O)_2]^{2+} + HA\cdot \quad (10)$$

$$2[Co([14]aneN_4)(H_2O)_2]^{2+} + O_2 \longrightarrow [\{(H_2O)Co([14]aneN_4)\}_2O_2]^{4+} \quad (11)$$

($k=4\times10^9$ dm^6 mol^{-2} s^{-1} at 25 °C[20])

$$[\{(H_2O)Co([14]aneN_4)\}_2O_2]^{4+} + HA^- \xrightarrow{\text{reduction}} \quad (12a)$$

$$[\{(H_2O)Co([14]aneN_4)\}_2O_2]^{4+} + H^+ \xrightarrow{\text{decomposition}} \quad (12b)$$

The first-stage reaction (Eq. 10) was only analyzed in detail on the basis of Scheme 1. The plot of $k\alpha(H)\beta(H)[H^+]$ *vs.* $[H^+]^{-1}$ ($k=k_1^{obsd}/[H_2A]_0$) gave a straight line, with an intercept of nearly zero (Fig.

Table 2. Observed rate constants of the first and the second stages for the $[Co([14]aneN_4)(H_2O)_2]^{3+}$-ascorbic acid system at 25.0 °C and $I=0.10$ mol dm^{-3} ($LiClO_4$)

$[Co(III)]_0$ / 10^{-4} mol dm^{-3}	$[H_2A]_0$ / 10^{-2} mol dm^{-3}	pH	k_1^{obsd} / 10^{-3} s^{-1}	k_2^{obsd} / 10^{-3} s^{-1}
3.01	1.00	2.34	0.940	0.630
3.01	1.00	2.48	2.09	0.640
4.04	1.00	2.68	3.55	0.900
1.82	1.00	2.89	5.05	1.39
1.67	1.00	3.00	7.30	1.74
1.74	1.00	3.15	16.0	2.11
1.50	1.00	3.28	24.4	1.91
1.82	0.594	3.14	5.30	1.36
1.91	0.872	3.14	8.10	1.88
1.70	1.04	3.14	9.50	2.20
1.74	1.20	3.14	12.2	2.38
1.60	1.36	3.14	11.9	2.48
1.78	1.68	3.14	15.8	3.40

Table 3. Second-order rate constants of the reductions of $[Co(N_4)(H_2O)_2]^{3+}$ and $[Co(OH)(N_4)(H_2O)]^{2+}$

Oxidant	Rate contant/dm³ mol⁻¹ s⁻¹ Reductant		
	HA^- a)	$[Ru(NH_3)_6]^{2+}$ b)	$[V(H_2O)_6]^{2+}$ b)
$[Co(Me_4[14]tetraeneN_4)(H_2O)_2]^{3+}$	4.2×10	1.9×10^4	1.0×10^3
$[Co(OH)(Me_4[14]tetraeneN_4)(H_2O)]^{2+}$	1.3×10^3	—	—
$[Co(Me_6[14]4,11\text{-}dieneN_4)(H_2O)_2]^{3+}$	3.4	8×10^2	2.4×10^2
$[Co(OH)(Me_6[14]4,11\text{-}dieneN_4)(H_2O)]^{2+}$	1.1×10^2	1.0×10^2	8.5×10^2
$[Co(ms\text{-}Me_6[14]aneN_4)(H_2O)_2]^{3+}$	4.2×10	3.0×10^3	1.8×10^3
$[Co(OH)(ms\text{-}Me_6[14]aneN_4)(H_2O)]^{2+}$	5.5×10	5×10^2	8.5×10^3
$[Co([14]aneN_4)(H_2O)_2]^{3+}$	—	—	—
$[Co(OH)([14]aneN_4)(H_2O)]^{2+}$	2.9×10	—	—

a) 25 °C and $I=0.10$ mol dm^{-3}; this work. b) 25 °C and $I=1.0$ mol dm^{-3}; Refs. 5 and 9.

Table 4. Comparison between the observed rate constants and the calculated ones from the Marcus cross relationships for the reactions of $[Co(N_4)(H_2O)_2]^{3+}$ with HA^- ions at 25 °C and $I=0.10$ mol dm^{-3} a)

N_4	E°_{22} b) / V	k_{22} / dm³ mol⁻¹ s⁻¹	k_{12}(calcd) / dm³ mol⁻¹ s⁻¹	k_{12}(obsd)/k_{12}(calcd)
$Me_4[14]tetraeneN_4$	0.56 d)	6×10^{-2} e)	2.7	16
$Me_6[14]4,11\text{-}dieneN_4$	0.56 d)	3×10^{-5} e)	0.065	52
$ms\text{-}Me_6[14]aneN_4$	0.54 f)	$\approx10^{-3}$ g)	≈0.2	≈200
$[14]aneN_4$	0.44 h)	7.8×10^{-4} i)	0.021	—

a) $E^\circ_{11}(HA\cdot/HA^-)=0.88$ V and $\Delta G^*_{11}=17$ kJ mol^{-1}; Ref. 23. b) The redox potential for the $[Co(N_4)(H_2O)_2]^{3+/2+}$ couple. c) The rate constant of the self-exchange reaction for the $[Co(N_4)(H_2O)_2]^{3+/2+}$ couple. d) Ref. 24. e) Ref. 25. f) The mean value between 0.49 V in Ref. 19 and 0.59 V in Ref. 9. g) Estimated value from the $[V(H_2O)_6]^{2+}$ reduction. h) Ref. 19. i) Ref. 20.

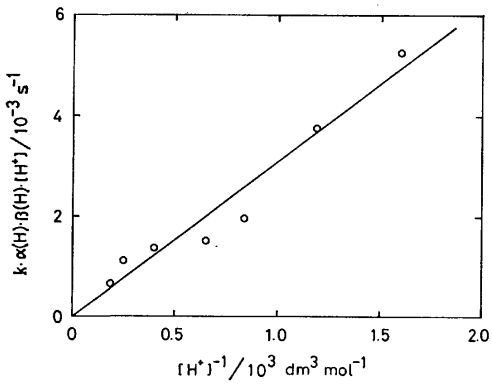

Fig. 8. Plots of $k\alpha(H)\beta(H)[H^+]$ *vs.* $[H^+]^{-1}$ for the first-stage reaction of $[Co([14]aneN_4)(H_2O)_2]^{3+}$ with ascorbic acid at $[H_2A]_0=1.00\times10^{-2}$ mol dm^{-3}, $[Co(III)]_0=(1.50—4.04)\times10^{-4}$ mol dm^{-3}, 25.0 °C, and $I=0.10$ mol dm^{-3} ($LiClO_4$).

8). The second-order rate constant, k_1^{OH}, is obtained from the slope of this straight line.

Discussion

The rate constants of the reactions of $[Co(N_4)(H_2O)_2]^{3+}$ and $[Co(OH)(N_4)(H_2O)]^{2+}$ with HA^- ions are summarized in Table 3, along with the data for the other reducing agents.

The Reactions of the $[Co(N_4)(H_2O)_2]^{3+}$ *Ions.* The trend in the relative rates of the reactions is Me_4-tetraeneN$_4$ ≃ *ms*-Me_6[14]aneN$_4$ > Me_6[14]4,11-dieneN$_4$ ≫ [14]aneN$_4$, similar to that for a $[Ru(NH_3)_6]^{2+}$ or $[V(H_2O)_6]^{2+}$ reduction, which proceeds by means of an outer-sphere mechanism.[5,9] As the water-exchange reactions of the $[Co(N_4)(H_2O)_2]^{3+}$ species may be very slow,[21] the water molecules of the $[Co(N_4)(H_2O)_2]^{3+}$ ions may not be replaced by the HA^- ions prior to electron transfer. Therefore, the reactions of the diaqua complexes are considered to proceed by an outer-sphere electron-transfer mechanism.

The rate constants of the reactions of $[Co(N_4)(H_2O)_2]^{3+}$ with HA^- are calculated on the basis of the Marcus cross relationships[22] in the way reported previously:[1]

$$\Delta G^*_{12} = \lambda(1+\Delta G^{\circ\prime}_{12}/\lambda)^2/4, \quad (13)$$

$$k_{12} = Z\exp(-\Delta G^*_{12}/RT), \quad (14)$$

$$\lambda = 2(\Delta G^*_{11}+\Delta G^*_{22}), \quad (15)$$

where Z is the collision frequency in solution (10^{11} dm³ mol^{-1} s^{-1}), where ΔG^*_{11} and ΔG^*_{22} refer to the self-exchange reactions of the reagents, and where $\Delta G^{\circ\prime}_{12}$ is the free-energy change in the reactions. The calculated rate constants are listed in Table 4. All the observed rate constants exceed the calculated ones by a factor of 10—10^2. This may be ascribable, at least in part, to the work terms neglected or to the small effect of the bond-length changes from Co^{III}–OH_2 to Co^{II}–OH_2.[25] The latter is considered to be a significant factor in the self-exchange reaction of the cobalt(III)/(II) couple.[25]

The Reactions of the $[Co(OH)(N_4)(H_2O)]^{2+}$ *Ions.*

The rate constants of these reactions tend to decrease in the following order: $Me_4[14]tetraeneN_4$ > $Me_6[14]4,11\text{-}dieneN_4$ > *ms*-$Me_6[14]aneN_4$ > $[14]aneN_4$; the ratios of k_1^{OH}/k_1 are 31 for $Me_4[14]tetraeneN_4$, 32 for $Me_6[14]4,11\text{-}dieneN_4$, 1.3 for *ms*-$Me_6[14]aneN_4$, and $\gg 29$ for $[14]aneN_4$. These results are in contrast to those of typical outer-sphere electron-transfer reactions; for example, $k_1 > k_1^{OH}$ for a cobalt(III) porphyrin–dithionite system.[26] It is suggested that the reactions of $[Co(OH)(N_4)(H_2O)]^{2+}$ with HA^- proceed *via* an OH-bridged mechanism:

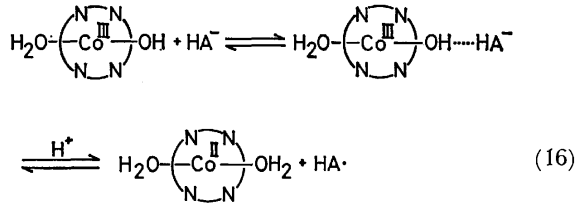

(16)

The trend in the relative rate of this reaction corresponds to the extent of the lack of saturation of the macrocyclic ligands. As the polarizability of the central cobalt(III) ion is expected to be enhanced with an increase in the extent of electronic delocalization between the cobalt(III) ion and the macrocyclic ligand, an electron of ascorbic acid, which is a π-donor, may be more easily transferred to the cobalt (III) moiety, which has an unsaturated ligand. The small difference in reactivity between $Me_6[14]4,11\text{-}dieneN_4$ and *ms*-$Me_6[14]aneN_4$ is probably due to the steric hindrance of methyl groups.

These reactivities can also be explained by an alternative pathway which is a substitution-limited inner-sphere mechanism:

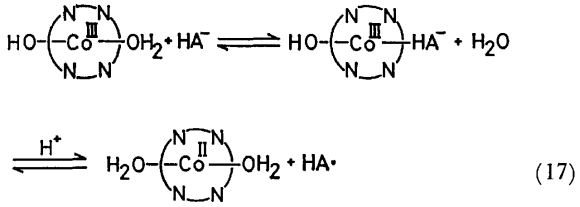

(17)

It is expected that the OH^- ligand accelerates the dissociation of the water molecule in the trans position; in fact, the dissociation of the water molecule of $[Co(OH)([14]aneN_4)(H_2O)]^{2+}$ is not slow ($k_d = (1.4\pm0.3)\times10^{-2}\ s^{-1}$ at 25 °C and I=0.1 mol dm^{-3} [21]). Studies of the kinetics of the water displacement of these macrocyclic complexes are in progress in order to establish the mechanism of the reactions of $[Co(OH)(N_4)(H_2O)]^{2+}$ with ascorbic acid.

References

1) Part I: K. Tsukahara and Y. Yamamoto, *Bull. Chem. Soc. Jpn.*, **54**, 2642 (1981).
2) S. Lewin, "Vitamin C: Its Molecular Biology and Medical Potential," Academic Press, London (1976).
3) D. Pinnel and R. B. Jordan, *Inorg. Chem.*, **18**, 3191 (1979).
4) N. Sadasivan, J. A. Kernohan, and J. F, Endicott, *Inorg. Chem.*, **6**, 770 (1967).
5) D. P. Rillema, J. F. Endicott, and R. C. Patel, *J. Am. Chem. Soc.*, **94**, 394 (1972).
6) P. O. Whimp and N. F. Curtis, *J. Chem. Soc., A*, **1966**, 867.
7) C. K. Poon and M. L. Tobe, *J. Chem. Soc., A*, **1968**, 1549.
8) H. Ogino, K. Tsukahara, and N. Tanaka, *Inorg. Chem.*, **18**, 1271, 3290 (1979).
9) M. P. Liteplo and J. F. Endicott, *Inorg. Chem.*, **10**, 1420 (1971).
10) J. Kielland, *J. Am. Chem. Soc.*, **59**, 1675 (1937).
11) J. A. Kernohan and J. F. Endicott, *Inorg. Chem.*, **9**, 1504 (1970).
12) D. P. Rillema, J. F. Endicott, and J. R. Barber, *J. Am. Chem. Soc.*, **95**, 6987 (1973).
13) C. K. Poon and M. L. Tobe, *Inorg. Chem.*, **7**, 2398 (1968).
14) M. M. Taqui Khan and A. E. Martell, *J. Am. Chem. Soc.*, **89**, 4176 (1967).
15) J. F. Endicott, J. Lilie, J. M. Kuszaj, B. S. Ramaswamy, W. G. Schmonsees, M. G. Simic, M. D. Glick, and D. P. Rillema, *J. Am. Chem. Soc.*, **99**, 429 (1977).
16) D. P. Rillema, J. F. Endicott, and E. Papaconstantinou, *Inorg. Chem.*, **10**, 1739 (1971).
17) R. G. Wilkins, "The Study of Kinetics and Mechanism of Reactions of Transition Metal Complexes," Allyn and Bacon, Boston (1974), p. 20.
18) B. Bosnich, C. K. Poon, and M. L. Tobe, *Inorg. Chem.*, **5**, 1514 (1966).
19) R. A. Heckman and J. H. Espenson, *Inorg. Chem.*, **18**, 38 (1979).
20) C. -L. Wong, J. A. Switzer, K. P. Balakrishnan, and J. F. Endicott, *J. Am. Chem. Soc.*, **102**, 5511 (1980).
21) K. Tsukahara, H. Oshita, Y. Emoto, and Y. Yamamoto, unpublished results.
22) R. A. Marcus, *Ann. Rev. Phys. Chem.*, **15**, 155 (1964).
23) E. Pelizzetti, E. Mentasti, and E. Pramauro, *Inorg. Chem.*, **15**, 2898 (1976); E. Pelizzetti, E. Mentasti, and C. Baiocchi, *J. Phys. Chem.*, **80**, 2979 (1976); E. Pelizzetti, E. Mentasti, and E. Pramauro, *Inorg. Chem.*, **17**, 1181 (1978).
24) E. L. Yee, R. J. Cave, K. L. Guyer, P. D. Tyma, and M. J. Weaver, *J. Am. Chem. Soc.*, **101**, 1131 (1979).
25) J. F. Endicott and B. Durham, "Coordination Chemistry of Macrocyclic Compounds," ed by G. A. Melson, Plenum Press, New York and London (1979), p. 393.
26) R. F. Pasternack, M. A. Cobb, and N. Sutin, *Inorg. Chem.*, **14**, 866 (1975).

Paramagnetic Cobalt(III) Complexes with Organic Ligands. VII.[1] The Isolation and Properties of Paramagnetic Tetraammine-(5-nitrososalicylato)cobalt(III) Complexes

Yoshihisa YAMAMOTO,* Hiroko KUDO, Masayasu MORI,† and Hidetaka KONNO††

Faculty of Pharmaceutical Sciences, Higashi Nippon Gakuen University, Ishikari-Tobetsu, Hokkaido 061-02

† *Faculty of Science, Osaka City University, Sumiyoshiku, Osaka 558*

†† *Faculty of Engineering, Hokkaido University, Sapporo 060*

(Received June 8, 1981)

The title paramagnetic complexes, $[Co(5\text{-}NOsal)(NH_3)_4]X_2 \cdot nH_2O$ (X_2=Cl(NO_3), $Cl_2 \cdot HCl$, and Cl_2), all brown in color, have been isolated and characterized by analytical, spectroscopic, and magnetic methods. The effective magnetic moments of the complexes are 1.6—1.8 BM, and the absorption spectra have two peaks, at 387 and 518 nm. In the XPS of the complex, the cobalt 2p peaks have satellites, and the peak of the nitrogen 1s could be deconvoluted to that of NH_3 nitrogen at 400.2 eV and to that of NO nitrogen at 402.2 eV. This binding energy of the NO nitrogen of the complex is different from that (405.6 eV) of the NO_2 nitrogen of the green Paramagnetic tetraammine(5-nitrosalicylato)cobalt(III) complexes, $[Co(5\text{-}NO_2sal)(NH_3)_4]X_2$, and establishes the difference between these two series of complexes.

In previous papers, we reported several green paramagnetic amine(5-nitrosalicylato)cobalt(III) complexes,[2-7] $[Co(5\text{-}NO_2sal)L]^{2+}$ (L: $(NH_3)_4$, $(en)_2$, $(bpy)_2$, trien), which are prepared from 60% nitric acid and the corresponding diamagnetic amine(salicylato)cobalt(III) complexes, $[Co(sal)L]Cl \cdot nH_2O$.[8,9] Gillard *et al.*[10,11] claimed, however, that the green compounds prepared in this way contain the 5-nitrososalicylato ligand rather than the 5-nitrosalicylato ligand, and the problem has so far remained unsolved. We have, though, recently been able to exclude this latter possibility by isolating a true tetraammine-(5-nitrososalicylato)cobalt(III) complexes as $[Co(5\text{-}NOsal)(NH_3)_4]X_2$, which is brown, paramagnetic, and is clearly distinguished from the green paramagnetic tetraammine(5-nitrosalicylato)cobalt(III) complexes, $[Co(5\text{-}NO_2sal)(NH_3)_4]X_2$, especially by the N ls peaks in the X-ray photoelectron spectra.

Results and Discussion

By the digestion of ammoniacal cobalt(III) chloride with 5-nitrososalicylic acid and the subsequent treatment of the precipitated substance with 60% nitric acid, brown complexes with the constitution $[Co(5\text{-}NOsal)(NH_3)_4]X_2 \cdot nH_2O$ (**1**) (X_2=Cl·(NO_3)·$2H_2O$ (**1a**), $Cl_2 \cdot H_2O \cdot HCl$ (**1b**), and $Cl_2 \cdot H_2O$ (**1c**); *cf.* Experimental sections) were obtained. They are soluble in water, nitric acid, and hydrochloric acid, but are insoluble in most organic solvents. The magnetic susceptibility obeyed the Curie-Weiss law, with effective magnetic moments of 1.6—1.8 BM, suggesting the presence of one unpaired electron.

The formula conforms to the quadrivalence of cobalt, while the rocking frequency of ligand ammonia was observed at around 830 cm^{-1} in the IR spectrum, which is within the range of those of Co(III) ammine complexes.[12,14] This, like the behavior to be described below, is similar to that of the green paramagnetic tetraammine(5-nitrosalicylato)cobalt(III) complex,[5] $[Co(5\text{-}NO_2sal)(NH_3)_4]X_2$ (**2**), reported previously. Thus, in both complexes, only the proton signals of the ammine ligands appeared in the ^1H NMR spectra in 65% DNO_3, and no proton signals of the substituted salicylato ligand were observable. The ^{13}C NMR spectrum did not show the expected signals because of paramagnetism. Also, the cobalt 2p peaks of XPS of **1** have satellites and have a somewhat greater FWHM (2.6 eV for Co $2p_{3/2}$ at 220 K), as is shown in Fig. 1, and some carbon atoms (estimated to be 17.8% of the total carbon in **1** and 22.2% thereof in **2**)[7] have a higher ls binding energy (289 eV, sh), as is shown in Fig. 2. This behavior[7] suggests that, in **1** also, the unpaired electron spends its time partly on the cobalt atom and partly on the ring of the substituted salicylato ligand.

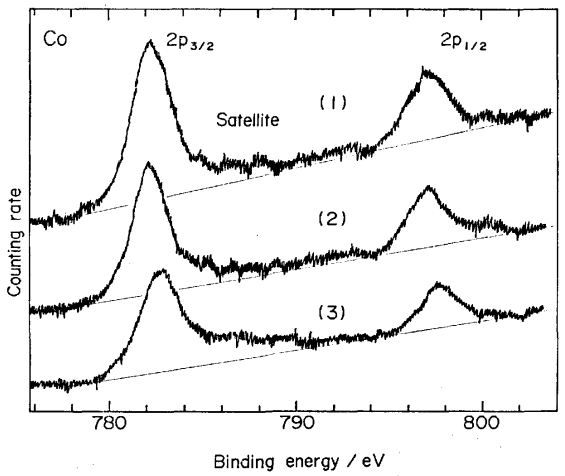

Fig. 1. The XPS in the Co_{2p} region at 220 K of **1b**, **2**, and **3** complexes.
(1): $[Co(5\text{-}NOsal)(NH_3)_4]Cl_2 \cdot H_2O \cdot HCl$, (2): $[Co(5\text{-}NO_2sal)(NH_3)_4]Cl(NO_3) \cdot 3H_2O$, (3): $[Co(5\text{-}NOsal)(NH_3)_4]Cl$.

A clear distinction between **1** and **2** was found in the XPS N ls spectra (Fig. 3): in the former, the N ls peak could be deconvoluted to that of NH_3 at 399.5 and 400.2 eV and an NO N ls peak at 402.0 eV, whereas in the latter, deconvolution gave an NH_3 N ls peak at 400.2 eV and an NO_2 N ls peak at 405.6 eV. In the ^1H NMR spectra, the proton signals of the coor-

Table 1. Some physical properties of complexes **1**—**3** and related ligands

	Absorption bands	^{1}H-NMR spectra NH_3 [-OOC, NO(2), -O]	XPS (eV) at 220 K					Magnetic moment	IR spectra
			C 1s	N 1s	O 1s	Co $2p_{3/2}$	Co $2p_{1/2}$		$\rho_r(NH_3)_r$
	λ/nm ε	δ/ppm						μ_{eff}/BM	cm^{-1}
1a	345 (9200) [a] 388 (10100) 520 (3500)	2.70 s (3H) [b] 3.63 s (3H) 3.86 s (3H)	285.6 max 289.0 sh	400.2 NH_3 402.0 NO	532.7 max FWHM 3.3	782.2 FWHM 2.6 satellites medium	797.0	1.60[i]	825
1b	342 (8800) [a] 387 (10300) 518 (3700)	2.70 s (3H) [b] 3.62 s (6H) 3.86 s (3H)	285.6 max 289.0 sh	399.5 400.2 NH_3 402.0 NO	532.7 max FWHM 3.3	782.2 FWHM 2.6 satellites medium	797.0	1.80	838
1c	346 (8300) [a] 385 (8600) 522 (3000)	2.70 s (3H) [b] 3.63 s (9H)	285.6 max 288.4 sh	399.3 400.4 NH_3 402.2 NO	532.8 max FWHM 2.9	782.6 FWHM 2.6 satellites medium	797.6	1.71	830
2	450 (3700) 660 (12400)	3.76 s (6H) 3.30 s (6H)	285.4 max 288.6 sh	400.2 NH_3 405.6 NO_2 407.2 NO_3	532.4 max FWHM 3.1	782.2 FWHM 2.4 satellites medium	797.0	1.70	840
3	356 (8500) [c]	2.79 s (6H) [d] 3.46 s (6H) [6.6— 7.8m (3H)]	285.1 max	399.8 400.5 NH_3 402.2 NO	532.8 max FWHM 3.1	782.6 FWHM 2.7 satellites strong	797.6	2.84	825
L_a[g]	348[e] 710	[6.96 d (1H) [f] 7.67dd(1H) 8.65 d (1H)]	285.1 max 289.0 sh	401.6 NO	533.2 max FWHM 3.0				
L_b[h]	320[e]	[7.06 d (1H) [f] 8.32dd(1H) 8.70 d (1H)]	285.1 max 289.0 sh	405.8 NO_2	533.0 max FWHM 2.9				

sh: Shoulder. Solvent: a) 60% HNO_3. b) 65% DNO_3. c) 1.8 mol dm^{-3} H_2SO_4. d) 11 mol dm^{-3} D_2SO_4. e) MeOH. f) MeOH-d_4. Standard: Internal DSS for NMR. The maximum of Cl $2p_{3/2}$ has been taken to be at 198.2 eV for XPS. g) L_a: 5-Nitrososalicylic acid. h) L_b: 5-Nitrosalicylic acid. i) The values obtained varied to some extent and always lower than 1.73 BM. It thus seemed difficult to obtain this chloride nitrate salt in a pure state.

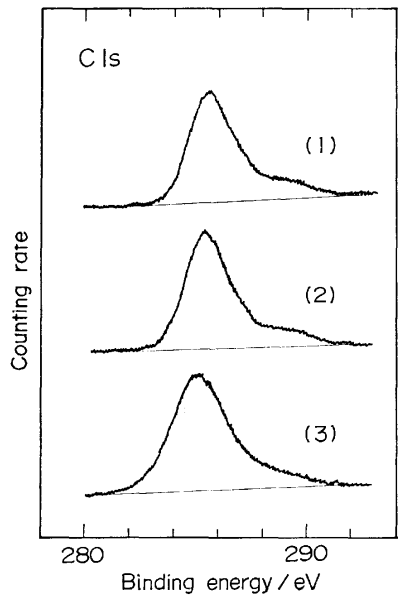

Fig. 2. The XPS in the C_{1s} region at 220 K of **1b**, **2**, and **3** complexes.
(1): $[Co(5\text{-}NOsal)(NH_3)_4]Cl_2 \cdot H_2O \cdot HCl$, (2): $[Co(5\text{-}NO_2sal)(NH_3)_4]Cl(NO_3) \cdot 3H_2O$, (3): $[Co(5\text{-}NOsal)(NH_3)_4]Cl$.

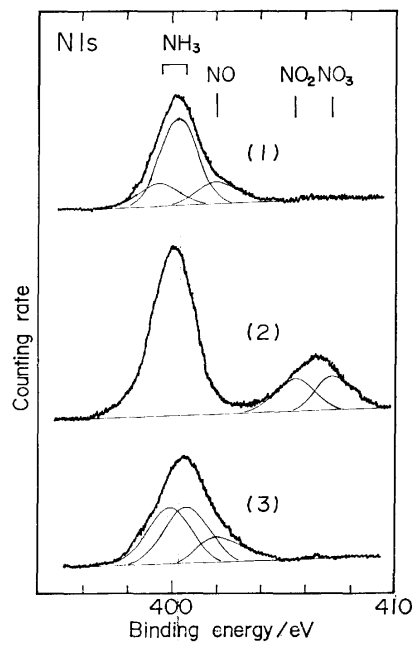

Fig. 3. The XPS in the N_{1s} region at 220 K of **1b**, **2**, and **3** complexes.
(1): $[Co(5\text{-}NOsal)(NH_3)_4]Cl_2 \cdot H_2O \cdot HCl$, (2): $[Co(5\text{-}NO_2sal)(NH_3)_4]Cl(NO_3) \cdot 3H_2O$, (3): $[Co(5\text{-}NOsal)(NH_3)_4]Cl$.

dinated ammine ligands of **1** split into three with the intensity ratio of 1:2:1, while those of **2**[5] split into two with the intensity ratio of 2:2. The chemical shift (δNH_3 at 2.7 ppm) of ammine protons in a position trans[5] to the carboxyl oxygen of the 5-nitrososalicylato ligand in **1** was at a higher field than that (3.76 ppm) of **2**. Another point of difference was found in the visible and UV absorption spectra reflecting their color differences.[2]

Paramagnetic tetraammine(5-nitrososalicylato)cobalt(III) complexes of another type, $[Co(5\text{-}NOsal)(NH_3)_4]Cl$ (**3**), has been isolated from the reaction mixture as a much less soluble minor component (*cf.* Experimental section). The formula shows that this compound has an oxidation state less by unity than that of the **1** complexes; it was at first thought to be a simple Co(III) complex. However, the measurement of the magnetic susceptibility of the complex in a solid state from 77.4 K—r.t. gave an effective magnetic moment of 2.84 BM, suggesting the presence of two unpaired electrons, and the cobalt 2p peaks of the XPS have strong satellites, as is shown in Fig. 1. Thus, the compound can be regarded as a sort of biradical complex, two electrons being accomodated in a molecular orbital formed from the ligand orbital and the Co-e_g orbital. The ^1H NMR spectrum of **3** in 11 mol dm^{-3} D_2SO_4 at room temperature showed two singlets of ammine ligands and a multiplet of the 5-nitrososalicylato ligand in the integral ratio of 6:6:3, as is shown in Table 1. The appearance of the latter seems to suggest the absence of any appreciable spin density on the 5-nitrososalicylato ligand in solution, making a marked contrast to the behavior of **1** and **2**. An ESR study which is now going on is expected to give further information as to the electronic state of the complex.

The data of various physicochemical measurements of **1**—**3** are collected in Table 1.

Experimental

Measurements. The NMR spectra were recorded with an FX-60 apparatus (JEOL) for ^{13}C NMR and with an R-40 apparatus (Hitachi) for ^1H NMR. The IR spectra were recorded on potassium bromide disks with an IR-27G apparatus (Shimadzu). The visible absorption spectra were recorded with a Shimadzu MPS-5000 recording spectrophotometer. The magnetic susceptibilities were measured by the Faraday's method using a magnetic balance (Shimadzu) from liq. N_2 to r.t. The XPS were obtained by irradiating the compounds with Mg $K\alpha$ X-rays (120 W) in a vacuum at a pressure of less than 3×10^{-7} Pa and at around 220 K.[7] The instrument used was a VG ESCA 3 electron spectrometer.

Preparation of 5-Nitrososalicyclic Acid. 5-Nitrososalicyclic acid of a green color was prepared by Gulinov's method.[15] The absorption spectrum of 5-nitrososalicylic acid in methanol has three peaks, at 268, 348, and 710 nm. The ^1H NMR spectrum of 5-nitrososalicylic acid in methanol-d_4 is different from that of 5-nitrosalicylic acid, as is shown in Table 1.

*Preparation of Complex. Tetraammine(5-nitrososalicylato)cobalt(III) Chloride Nitrate Dihydrate (**1a**).* A 28% ammonia solution (9.6 cm^3) was added to an aqueous solution (12.0 cm^3) of $CoCl_2 \cdot 6H_2O$ (5.71 g, 24.00 mmol). After the mixture has been stirred at room temperature, about 6.4 cm^3 of a 20% hydrogen peroxide solution was slowly added to the solution. 5-Nitrososalicylic acid (4 g, 24.00 mmol) was then added to the solution at 50 °C, and the mixture was concentrated at 60 °C. The precipitate (**A**) thus obtained was filtered off, washed with water, and dried. Yield: 6.88 g. Four cubic centimeters of 60% nitric acid were added to 2 g of **A**. Heat was evolved. The cooled

solution was filtered with a glass filter (G 4), and the filtrate was added to ethanol. The brown substance thus separated out was filtered with a glass filter (G 3), washed with ethanol, and dried in a vacuum desiccator. This complex is slightly unstable in nitric acid. Yield: 1.1 g. Found: C, 19.95; H, 4.73; Cl, 8.37%. Calcd for $CoC_7H_{19}N_6O_9Cl$ (MW 425.65) C, 19.75; H, 4.50; Cl, 8.33%. Dec≈172 °C.

*Tetraammine(5-nitrososalicylato)cobalt(III) Dichloride Hydrate Hydrogen Chloride (**1b**).* Two milliliters of 36% hydrochloric acid were added to 1 g (2.35 mmol) of the above complex (**1a**), the brown solution was filtered with a glass filter (G 4), and the filtrate was added to ethanol. The brown complex thus precipitated was filtered with a glass filter (G 3), washed with ethanol, and dried in a silica gel desiccator. Yield: 0.65 g. (66.2%) Found: C, 19.86; H, 4.55; Cl, 24.23%. Calcd for $CoC_7H_{18}N_5O_5Cl_3$ (MW 417.54) C, 20.13; H, 4.35; Cl, 25.47%. Dec≈182 °C.

*Tetraammine(5-nitrososalicylato)cobalt(III) Dichloride Hydrate (**1c**).* This complex was formed when Complex **1b** was dried in a vaccum desiccator over potassium hydroxide. Found: C, 22.49; H, 4.34; Cl, 19.78%. Calcd for $CoC_7H_{17}N_5O_5Cl_2$ (MW 381.08) C, 22.06; H, 4.50; Cl, 18.61%. Dec. ≈180 °C.

*Tetraammine(5-nitrososalicylato)cobalt(III) Monochloride (**3**).* Five and two-tenths grams of A were extracted with 100 cm^3 of water at 50 °C. The brown extract was concentrated in a rotary evaporator at 45 °C. The solution was cooled, and the **3** complex thus precipitated was filtered and dried. It was then recrystallized from water. Yield: 0.10 g. Found: C, 25.70; H, 4.58; Cl, 12.50%. Calcd for $CoC_7H_{15}N_5O_4Cl$ (MW 327.61) C, 25.66; H, 4.62; Cl, 10.82%. Dec 160—163 °C.

References

1) a) Part VI: Ref. 7; b) Presented at the 43rd National Meeting of the Chemical Society of Japan, Tokyo, April, 1981.
2) Y. Yamamoto, K. Ito, H. Yoneda, and M. Mori, *Bull. Chem. Soc. Jpn.*, **40**, 2580 (1967).
3) Y. Yamamoto, M. Mori, H. Yoneda, S. Misumi, and K. Ito, *Bull. Chem. Soc. Jpn.*, **42**, 984 (1969).
4) Y. Yamamoto, *Bull. Chem. Soc. Jpn.*, **42**, 999 (1969).
5) Y. Yamamoto, *Bull. Chem. Soc. Jpn.*, **51**, 2894 (1978).
6) Y. Yamamoto, E. Toyota, and N. Mitsudera, *Bull. Chem. Soc. Jpn.*, **53**, 3517 (1980).
7) Y. Yamamoto, M. Mori and H. Konno, *Bull. Chem. Soc. Jpn.*, **54**, 1995 (1981).
8) G. T. Morgan and J. D. M. Smith, *J. Chem. Soc.*, **1922**, 1956.
9) G. T. Morgan and J. D. M. Smith, *J. Chem. Soc.*, **1924**, 1924.
10) K. Garbett and R. D. Gillard, *Chem. Commun.*, **1967**, 694.
11) K. Garbett and R. D. Gillard, *J. Chem. Soc., A*, **1968**, 979.
12) K. Nakamoto, "Infrared Spectra of Inorganic and Coordination Compounds," Wiley-Interscience, New York (1970), p. 150.
13) J. K. Wilmshurst, *Can. J. Chem.*, **38**, 467 (1960).
14) G. F. Svatos, D. M. Sweeny, S. Mizushima, C. Curran, and J. V. Quagliano, *J. Am. Chem. Soc.*, **79**, 3313 (1957).
15) V. G. Gulinov, *J. Chem. Ind. (Moscow)*, **4**, 909 (1927), **5**, 225 (1928); *Chem. Abstr.*, **22**, 3648 (1928).

 © 1982 The Chemical Society of Japan Bull. Chem. Soc. Jpn., 55, 140—148 (1982) [Vol. 55, No. 1

Cobalt(III) Complexes with Tripodlike Quadridentate Ligands. II.[1] Preparations, Absorption Spectra and Circular Dichroism of (Amino carboxylato or 1,2-diamine)[*N*,*N*-bis(2-aminoethyl)-glycinato]cobalt(III) Complexes

Keiji Akamatsu,* Takashi Komorita, and Yoichi Shimura

Department of Chemistry, Faculty of Science, Osaka University, Toyonaka, Osaka 560

(Received June 13, 1981)

Four glycinato, six L-alaninato, and three (*R*)-propylenediamine cobalt(III) complexes of a tripodlike quadridentate ligand, *N*,*N*-bis(2-aminoethyl)glycinate have been prepared. The geometrical configurations are assigned on the basis of their absorption and circular dichroism spectra, ^{1}H-NMR spectra, the elution behavior in ion-exchanger column chromatography, and the optical resolution of chiral isomers. The absolute configurations of the chiral complexes are tentatively assigned and the characteristics of the tripodlike ligand are discussed.

A tripodlike quadridentate ligand *i*-dtma[2] can take two different configurations in six-coordinate metal complexes (Fig. 1). The left configuration with a plane of symmetry and the right one without it are called *s*-type (symmetrical) and *u*-type (unsymmetrical), respectively. An *s*-type configuration is achiral, while a *u*-type chiral. A complex with a tripodlike ligand of *s*-type configuration can also become chiral when unsymmetrical (such as *meso*-2,4-pentanediamine or *meso*-2,3-butanediamine) or asymmetric (such as L-alaninate or (*R*)-propylenediamine) bidentate ligands occupy the remaining two coordination sites. Only *s*-type configuration is possible for some typical tripodlike ligands, ata^{3-} and tren. It was pointed out in the previous paper[1] concerning the ata and tren cobalt(III) complexes with chiral bidentate (L-amino carboxylate or 1,2-diamine) that the CD spectra in the first and second d-d absorption band region for these complexes were considerably different in pattern and/or intensity from those for the corresponding bis- or tris(bidentate) or tetrakis(unidentate) complexes with the same L-amino carboxylate or 1,2-diamine. The differences were attributed to a new source of optical activity, which was called the "quasi-enantiomeric" effect, because this mainly determined the CD patterns in the first and second d-d band region: the CD patterns in the region are helpful in determining the coordination modes of the residual bidentate ligands, especially, those of L-amino carboxylates.

A further problem arises on the complexes of *u*-type structure which are chiral regardless of the residual ligands. Absolute configurations of cobalt(III) complexes with multidentate ligands have generally been correlated with that of a simple tris(bidentate) complex, for example, $[Co(en)_3]^{3+}$, by use of the ring-pairing-method.[3] Meanwhile, the method cannot be applied to *u*-type isomers of the complexes with tripodlike ligands such as aeida and *i*-dtma, because these isomers lack the ring-pairing chirality. Furthermore, the available data are too limited to derive any empirical rule, though Koine *et al.* have reported some L- or D-alada[4] and *β*-alada[5] complexes with amino carboxylate.

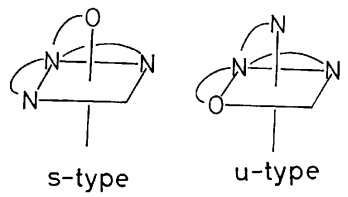

Fig. 1. Two different coordination modes of *i*-dtma ligand.

In the present paper the isomers of *i*-dtma cobalt(III) complexes with amino carboxylate or 1,2-diamine are reported.

Experimental

Preparations. *(1)* *[Co(gly)(i-dtma)]*$^+$: Two grams of *fac(N)*-[CoCl(*i*-dtma)(H_2O)]Cl·H_2O[6] was dissolved in 10 cm^3 of water, and to this violet solution was added a solution of glycine (1 g) neutralized with an equimolar amount of NaOH. The mixture was mechanically stirred at 70 °C for 2 h. The resulting red solution was poured onto a cation-exchanger column (SP-Sephadex C-25, Na^+ form) and the adsorbed complex was eluted with a 0.2 M NaCl aqueous solution (1 M=1 mol dm^{-3}). Two bands appeared; a red-orange and a purple one in this order. The second band contained mainly $[Co(i\text{-dtma})(H_2O)_2]^{2+}$. To the first eluate which had been evaporated to a small volume below 40 °C on a rotary evaporator was added a small amount of methanol to precipitate NaCl, which was filtered off with suction, as much sodium chloride as possible was removed by repetition of the procedure.

The resulting red-orange solution was then loaded on a strongly acidic cation exchanger column (Dowex 50w-x8, 2.6×40 cm, 200—400 mesh, Na^+ form) and eluted with a NaH_2PO_4–Na_2HPO_4 buffer of pH 6.8 ($NaH_2PO_4\cdot 2H_2O$, 25 g and $Na_2HPO_4\cdot 12H_2O$, 14 g per 1 dm^3 of solution). The adsorbed band had split into four well-resolved bands, which were eluted out in the following order; yellow-orange, orange, purple, and red-orange one. These are called G-1, G-2, G-3, and G-4, respectively. Each of the four fractions was treated with 44 g of $CaCl_2\cdot 2H_2O$ and 14 g of NaOH for every 1 dm^3 of eluate to convert the phosphate salts into the corresponding chloride salts. After removal of $Ca_3(PO_4)_2$ by filtration, the filtrate was evaporated to a small volume and to this was added methanol to precipitate NaCl, which was then filtered off. The procedure was repeated to remove as much sodium chloride as possible. Sodium perchlorate was added to the concentrated solution almost free from NaCl and the solution was kept standing in a refrigerator. After a few days, deposited crystals were collected with suction and recrystallized from warm water,

washed with methanol and ether and dried in air. Found for G-1: C, 23.17; H, 4.85; N, 13.64%. Calcd for [Co(gly)(*i*-dtma)]$ClO_4 \cdot H_2O$: C, 23.39; H, 4.92; N, 13.65%. Found for G-2: C, 24.24; H, 4.65; N, 14.18%. Calcd for [Co(gly)(*i*-dtma)]ClO_4: C, 24.47; H, 4.63; N, 14.27%. Found for G-3: C, 24.36; H, 4.61; N, 14.29%. Calcd for [Co(gly)(*i*-dtma)]ClO_4: C, 24.47; H, 4.63; N, 14.27%. Found for G-4: C, 24.33; H, 4.72; N, 14.20%. Calcd for [Co(gly)(*i*-dtma)]ClO_4: C, 24.47; H, 4.62; N, 14.27%.

(2) Optical Resolution of G-2: The orange isomer (G-2) of [Co(gly)(*i*-dtma)]ClO_4 (0.72 g; 1.8×10^{-3} mol) was dissolved in 10 cm^3 of warm water and converted into the chloride with a Dowex anion-exchanger column (1-x8, 100—200 mesh, Cl^- form). To the eluate was added $(+)_{589}$-Na[$Co(NO_2)_3$(edma)](vide post) (0.31 g; 0.91×10^{-3} mol) with stirring at 40 °C, and the mixture was kept standing overnight in a refrigerator. The pale orange powder deposited was filtered and washed with a small amount of water. The less-soluble diastereomer was recrystallized from warm water, washed with water, and then with methanol and ether and dried in air. Found: C, 22.56; H, 4.78; N, 19.82%. Calcd for [Co(gly)(*i*-dtma)][$Co(NO_2)_3$(edma)]·$1.5H_2O$: C, 22.72; H, 4.78; N, 19.88%.

A solution of the diastereomer in warm water was poured onto a Sephadex column (C-25, Na^+ form) and after being washed with water the adsorbed band was eluted with an aqueous $NaClO_4$ solution. The eluate was evaporated almost to dryness and a small amount of methanol was added to the residue. The $(-)_{589}$-perchlorate salt deposited was recrystallized from water. Found: C, 24.27; H, 4.60; N, 13.99%. Calcd for $(-)_{589}$-[Co(gly)(*i*-dtma)]ClO_4: C, 24.47; H. 4.63; N, 14.27%. $[M]_{589} = -520°$.

(3) [Co(L-ala)(i-dtma)]$^+$: A solution containing the desired products was prepared by the same method as that for the glycinato analogs using L-alanine instead of glycine. The red-orange solution (free from bivalent complex cations) was loaded on a Dowex cation-exchanger column (50w-x8, 200—400 mesh, Na^+ form). When eluted with the NaH_2PO_4–Na_2HPO_4 buffer described in (1), the adsorbed band separated into six, which are named A-1, A-2-a, A-2-b, A-3-a, A-3-b, and A-4 in the elution order. The eluted phosphate salts were converted into the corresponding chloride in the following way: each of the six fractions was diluted with triple volumes of water and then passed through a Dowex cation-exchanger column (50w-x8, 200—400 mesh, Na^+ form). The band on the column was washed with water and eluted with an aqueous NaCl solution. After removal of NaCl by the method previously mentioned, the desired complexes were obtained as perchlorate salts by adding $NaClO_4$ to the concentrated solution and recrystallized from warm water. The crystallization of A-3-a was not carried out because of the low yield and the high solubility in water of the isomer. Found for A-1: C, 26.05; H, 5.13; N, 13.76%. Calcd for [Co(L-ala)(*i*-dtma)]ClO_4·$0.5H_2O$: C, 26,00; H, 5.10; N, 13.48%. Found for A-2-a: C. 26.78; H, 5.04; N, 13.94%. Calcd for [Co(L-ala)(*i*-dtma)]ClO_4: C, 26.58; H, 4.93; N, 13.78%. Found for A-2-b: C, 26.82; H, 5.00; N, 13.95%. Calcd for [Co(L-ala)(*i*-dtma)]ClO_4: C, 26.58; H, 4.93; N, 13.78%. Found for A-3-b: C, 25.03; H, 5.33; N, 12.95%. Calcd for [Co(L-ala)(*i*-dtma)]ClO_4·$1.5H_2O$: C, 24.92; H, 5.36; N, 12.92%. Found for A-4: C, 26.05; H, 5.18; N, 13.30%. Calcd for [Co(L-ala)(*i*-dtma)]ClO_4·$0.5H_2O$: C, 26.00; H, 5.10; N, 13.48%.

(4) [Co(i-dtma)((R)-pn)]$^{2+}$: One gram of *fac(N)*-[CoCl(*i*-dtma)(H_2O)]Cl·H_2O[6] was suspended in 60 cm^3 of DMF (*N,N*-dimethylformamide). (*R*)-Propylenediamine (0.5 g) was added dropwise to this blue suspension with stirring and the mechanical stirring was continued for 2 h at 60 °C in a water bath. The orange powder formed was filtered, washed with methanol and ether and air-dried. A solution of this powder in 15 cm^3 of water was poured onto a cation-exchanger column (SP-Sephadex C-25, 2.6 cm × 50 cm, Na^+ form). When the adsorbed band was eluted with a NaH_2PO_4–Na_2HPO_4 buffer solution ($NaH_2PO_4 \cdot 2H_2O$, 12.5 g and $Na_2HPO_4 \cdot 12H_2O$, 7 g per 1 dm^3 of solution), it split into two orange bands. These are called P-1 and P-2 in the elution order, respectively. Each fraction was diluted with the same volume of water, passed through a Sephadex column (SP-Sephadex C-25) and then the column was washed with water to remove phosphate salts. The P-2 band concentrated on the column was eluted with an aqueous $NaClO_4$ solution. The eluate was evaporated almost to dryness below 40 °C on a rotary evaporator and to this residue was added ethanol to precipitate the perchlorate salt of P-2, which was filtered off, washed with methanol and dried in air. Found for P-2; C, 21.48; H, 5.04; N, 13.94%. Calcd for [Co(*i*-dtma)((*R*)-pn)]$(ClO_4)_2 \cdot 0.5H_2O \cdot 0.53NaClO_4$: C, 21.52; H, 5.03; N, 13.95%.

Although P-1 did not split completely, both ends of the band revealed nearly enantiomeric CD spectra. Two isomers, P-1-a and -b, were separated from the P-1 band by means of fractional crystallizations; the P-1 band was treated in the same way as that for P-2, described above, using NaCl instead of $NaClO_4$ as the eluting agent. The eluate was evaporated amost to dryness and to the residue was added methanol to remove NaCl. The deposited P-1-a including NaCl was filtered and recrystallized from warm water. The filtrate containing P-1-b was then evaporated to dryness and from the residue P-1-b was extracted into methanol. The chloride salt of P-1-a was converted into the chloride perchlorate by adding $NaClO_4$ to the solution and that of P-1-b into the perchlorate by use of a column chromatographic method similar to that in (2). Found for P-1-a: C, 24.97; H, 5.62; N, 16.40%. Calcd for [Co(*i*-dtma)((*R*)-pn)]Cl(ClO_4): C, 25.24; H, 5.66; N, 16.36%. Found for P-1-b: C, 21.88; H, 4.98; N, 14.04%. Calcd for [Co(*i*-dtma)((*R*)-pn)]$(ClO_4)_2 \cdot 0.25H_2O$: C, 21.76; H, 4.98; N, 14.10%.

(5) [Co(i-dtma)(en)]$^{2+}$: This complex was prepared with a method similar to that for the corresponding (*R*)-pn complex. Two isomers (E-1 and E-2 in the elution order) were isolated as perchlorates. Found for E-1: C, 20.05; H, 4.60; N, 14.91%. Calcd for [Co(*i*-dtma)(en)]$(ClO_4)_2$: C, 20.09; H, 4.65; N, 14.65%. Found for E-2: C, 19.82; H, 4.73; N, 14.45%. Calcd for [Co(*i*-dtma)(en)]$(ClO_4)_2 \cdot 0.5H_2O$: C, 19.72; H, 4.77; N, 14.38%.

(6) Optical Resolution of E-1: An aqueous solution of E-1, [Co(*i*-dtma)(en)]$(ClO_4)_2$ (1.3 g; 2.7×10^{-3} mol) was passed through an anion-exchanger column (Dowex 1-x8, 50—100 mesh, Cl^- form). To the eluate concentrated to 20 cm^3 on a rotary evaporator was added silver antimony tartrate (2.1 g; 2.8×10^{-3} mol) with stirring at 60 °C. After 10 min the precipitated silver chloride was filtered off and the filtrate was cooled in an ice bath with scratching the beaker to induce crystallization. The orange crystals deposited were collected by filtration, recrystallized from warm water, washed with a small amount of water, with methanol and ether and dried in air. Found: C, 22.62; H, 3.59; N, 8.29%. Calcd for [Co(*i*-dtma)(en)][Sb_2(tart)$_2$]·$2H_2O$: C, 22.58; H, 3.56; N, 8.23%.

The less-soluble diastereomer was converted into $(-)_{589}$-perchlorate salt by use of the same method as that in (2). Found: C, 20.22; H, 4.63; N, 14.73%. Calcd for $(-)_{589}$-

$[Co(i\text{-dtma})(en)](ClO_4)_2$: C, 20.09; H, 4.65; N, 14.65%. $[M]_{589}=-850°$.

(7) Preparation and Optical Resolution of $[Co(NO_2)_3(edma)]^-$: The racemate, $Na[Co(NO_2)_3(edma)]\cdot 3H_2O$, was isolated in the course of the preparation for $Na[Co(NO_2)_2(aeida)]\cdot 2H_2O$[7] by a usual column chromatographic method. Found: C, 12.34; H, 3.79; N, 18.01%. Calcd for $Na[Co(NO_2)_3(edma)]\cdot 3H_2O$: C, 12.28; H, 3.87; N, 17.91%.

The optical resolution was carried out as follows: one and four tenths gram of $Na[Co(NO_2)_3(edma)]\cdot 3H_2O$ (3.6×10^{-3} mol) was dissolved in 50 cm^3 of water at 50 °C, and to this solution was added $(-)_{589}$-$[Co(ox)(en)_2]Cl\cdot H_2O$ (0.6 g; 2.3×10^{-3} mol). Mechanical stirring was continued for 10 min after orange crystals began to deposite. While the reaction mixture was still warm, crystals of the diastereomer were collected on a glass filter, recrystallized from warm water, washed with a small amount of water and then with methanol and ether and dried in air. Found: C, 19.59; H, 4.74; N, 20.50%. Calcd for $[Co(NO_2)_3(edma)][Co(ox)(en)]\cdot 2H_2O$: C, 19.45; H, 4.74; N, 20.42%.

The less-soluble diastereomer was converted into the $(+)_{589}$-sodium salt by passing through a cation-exchanger column (Na^+ form) and evaporating the eluate on a rotary evaporator. Found: C, 14.39; H, 2.89; N, 20.58%. Calcd for $(+)_{589}$-$Na[Co(NO_2)_3(edma)]$: C, 14.25; H, 2.70; N, 20.78%. $[M]_{589}=+475°$.

Measurements. The visible and ultraviolet absorption spectra were measured with a Shimadzu UV-200 spectrophotometer in aqueous solutions. The CD spectra were recorded on a JASCO MOE-1 spectropolarimeter and the ^{1}H-NMR spectra were obtained in deuterium oxide (D_2O) on a Varian XL-100-15 spectrometer using DSS (sodium 2,2-dimethyl-2-silapentane-5-sulfonate) as an internal standard.

Results and Discussion

Four isomers are possible for a [Co(am)(*i*-dtma)]-type complex (Fig. 2). As both ends are indistinguishable in free ethylenediamine, only two isomers, *s*-α (or *s*-β) and *u*-α (or *u*-β), are possible for the complex containing en instead of gly$^-$. The upper two (*s*-type) have a plane of symmetry in the absence of a substituent group on the chelate ring, while the lower two (*u*-type) have none of the plane of symmetry even for the glycinato and ethylenediamine complexes and are optically resolvable. Accordingly, the en complex has one achiral isomer and a pair of enantiomers, the glycinato complex two achiral ones and two pairs of enantiomers, and the L-alaninato and (*R*)-pn complexes six chiral ones.

Amino Carboxylato Complexes with i-*dtma*: Several attempts were made under different conditions to prepare the glycinato and L-alaninato complexes; temperature and time in the substitution reaction were varied and activated charcoal was added or not. As for the reaction temperature and time, the condition described in the experimental section is suitable to prepare all the four and six isomers for the glycinato and L-alaninato complexes, respectively. Though, in the presence of activated charcoal, the complete substitution took place at low temperature in short time and none of the bivalent complex cation $[Co(i\text{-dtma})(H_2O)_2]^{2+}$ was detected, only two isomers (G-1 and G-2) of the four for the glycinato and only three (A-1, A-2-a, and-b)

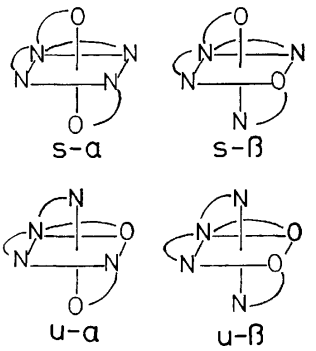

Fig. 2. Four geometrical isomers of [Co(am)(*i*-dtma)]-type complex (am=amino carboxylate).

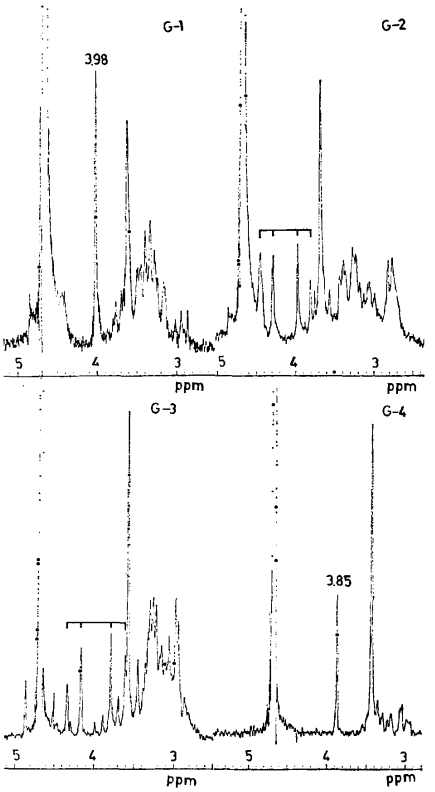

Fig. 3. ^{1}H-NMR spectra of isomers of [Co(gly)(*i*-dtma)]$^+$.

of the six for the L-alaninato complex were formed.

All isomers of the glycinato and L-alaninato complexes were ultimately isolated as crystals except for one isomer of the L-alaninato complex, A-3-a. Isomers, G-1, G-2, G-3, and G-4 were found from their absorption spectra to correspond to A-1, A-2, A-3, and A-4, respectively. A-2 and A-3 were separated into the respective pairs of the diastereomers on an ion-exchanger column. These facts indicate that G-1, G-4, A-1, and A-4 have either structure *s*-α or *s*-β and G-2, G-3, A-2, and A-3 either *u*-α or *u*-β. The two isomers, *s*-α and *s*-β are also distinguishable from *u*-α and *u*-β by means of ^{1}H-NMR spectra.

Figures 3 and 4 show the ^{1}H-NMR spectra of the gly and the en isomers. The isomers, G-1, G-4, and E-2, show a singlet due to the methylene protons of the acetate group in *i*-dtma (3.98 ppm for G-1; 3.85

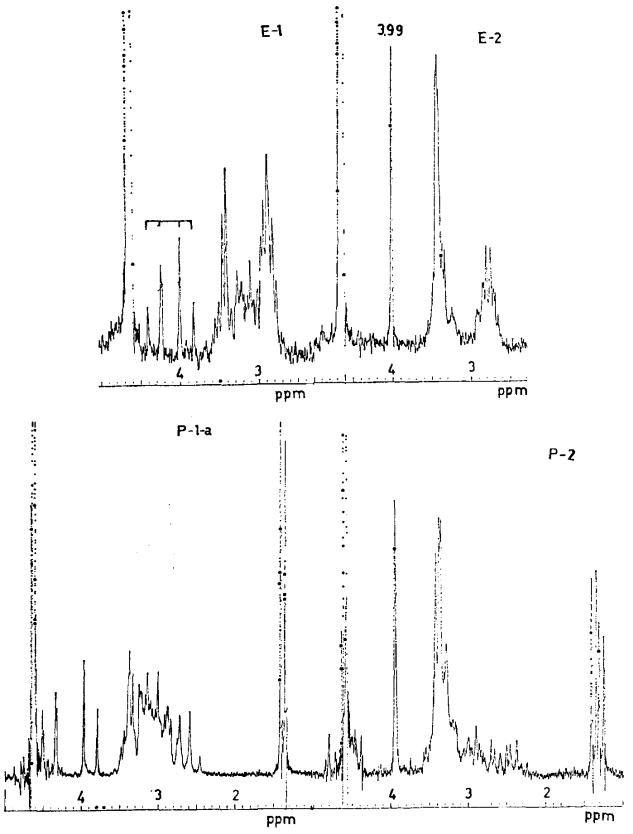

Fig. 4. ^{1}H-NMR spectra of isomers of [Co(en)(*i*-dtma)]$^{2+}$ and [Co((*R*)-pn)(*i*-dtma)]$^{2+}$.

ppm for G-4; and 3.99 ppm for E-2), while the other isomers and AB quartet due to the relevant protons with the coupling constants of 17—19 Hz (4.45, 4.28, 3.97, and 3.79 ppm for G-2; 4.31, 4.13, 3.76, and 3.57 ppm for G-3; and 4.40, 4.22, 3.99, and 3.82 ppm for E-1). The gly complex has another acetate group, not the constituent of *i*-dtma but that of glycine. The methylene protons should also show a singlet for G-1 and G-4 and an AB quartet for G-2 and G-3, and can be assigned to the signals at 3.4—3.6 ppm, though it is difficult to distinguish them from the signals of the ethylene protons of *i*-dtma.

With regard to the complexes of CoN_4O_2 chromophore, the splitting of the first spin-allowed d-d absorption band is larger for a *trans*(*O*) isomer than for a *cis*(*O*). G-1 and A-1 which show the splitting (Figs. 5 and 6) are assigned to (structure) *s*-α, and therefore, G-4 and A-4 to *s*-β. It is difficult to distinguish G-2 and A-2 from G-3 and A-3 by means of their absorption and ^{1}H-NMR spectra. G-2 and G-3 have only one kind of chirality, which is due to chiral arrangement of the tripodlike *i*-dtma ligand. On the other hand, A-2 and A-3 have two kinds of chiralities, one being the same as in G-2 and G-3 and the other a vicinal chirality of the L-alaninate ligand. In the previous paper of this series,[1] it has been shown that the vicinal chirality is such [Co(am)(tripod)]-type complexes consists of two factors, one being asymmetric carbon of the am$^-$ ligand, the other quasi-enantiomeric chirality due to the geometrical configurations. The observed CD pattern is mainly

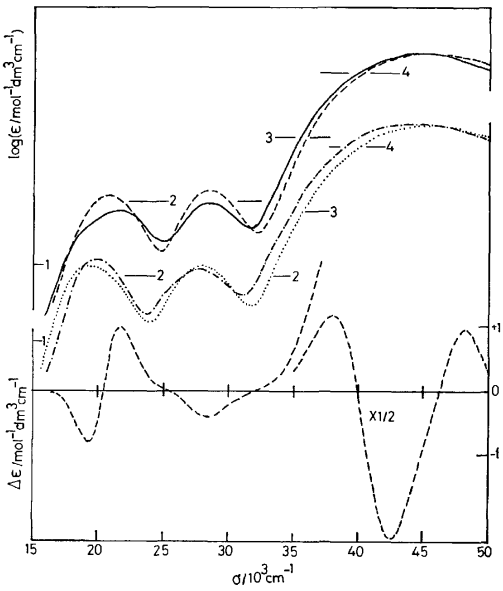

Fig. 5. Absorption and CD curves of four isomers of [Co(gly)(*i*-dtma)]$^+$: G-1 (——), G-2 (----), G-3 (·····), and G-4 (—·—).

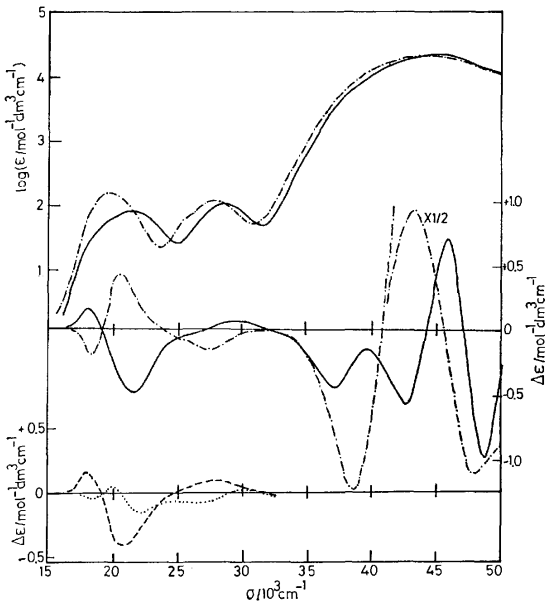

Fig. 6. Absorption and CD curves of A-1 (——) and A-4 (—·—) isomers of [Co(L-ala)(*i*-dtma)]$^+$. Calculated CD curves for asymmetric carbon (·····) and quasi-enantiomeric (----) effects are also shown.

determined by the quasi-enantiomeric effect. The CD contribution of the quasi-enantiomeric effect of [Co(L-ala)(tripod)]-type complexes in the first d-d transition band region is (+) and (—) from the longer wavelength for *s*-α isomers, and (—) and (+) for *s*-β ones, the pattern being almost unaffected by the geometry of chromophores. On the assumption that contributions from the chiral arrangement of *i*-dtma and from the vicinal effect are additive, calculated vicinal CD curves of 1/2{CD[A-2-a]+CD[A-2-b]} and 1/2{CD[A-3-a]+CD[A-3-b]} are shown together with the original CD of the isomers in Figs. 7 and 8. The calculated vicinal curves show the patterns (+) and (—)

Table 1. Absorption data of [Co(A-B)(*i*-dtma)]-type complexes (A-B=gly, L-ala, en, and (*R*)-pn)
Wave numbers and log ε values (in parentheses) are given in 10^3 cm^{-1} and mol^{-1} dm^3 cm^{-1}, respectively.

Complex	d-d Transition band		Ultraviolet band
	1st	2nd	
(G-1)-[Co(gly)(*i*-dtma)]$^+$	18.5 sh(1.5) 21.51 (1.85)	28.45 (1.97)	45.25 (4.31)
(G-2)-[Co(gly)(*i*-dtma)]$^+$	20.77 (2.08)	28.45 (2.16)	45.66 (4.29)
(G-3)-[Co(gly)(*i*-dtma)]$^+$	19.27 (2.13)	26 sh (1.9) 27.89 (2.13)	45.05 (4.31)
(G-4)-[Co(gly)(*i*-dtma)]$^+$	19.80 (2.24)	25.5 sh(1.8) 27.70 (2.08)	44.54 (4.34)
(A-1)-[Co(L-ala)(*i*-dtma)]$^+$	18.5 sh(1.5) 21.46 (1.89)	28.53 (2.00)	44.84 (4.34)
(A-2-a)-[Co(L-ala)(*i*-dtma)]$^+$	20.83 (2.10)	28.49 (2.17)	45.66 (4.31)
(A-2-b)[Co(L-ala)(*i*-dtma)]$^+$	20.88 (2.12)	28.49 (2.17)	45.35 (4.33)
(A-3-b)-[Co(L-ala)(*i*-dtma)]$^+$	19.19 (2.12)	26 sh 27.93 (2.12)	44.94 (4.30)
(A-4)-[Co(L-ala)(*i*-dtma)]$^+$	19.84 (2.18)	25.5 sh(1.8) 27.86 (2.05)	44.35 (4.31)
(E-1)-[Co(*i*-dtma)(en)]$^{2+}$	20.53 (2.08)	28.94 (2.12)	45.15 (4.29)
(E-2)-[Co(*i*-dtma)(en)]$^{2+}$	20.83 (2.00)	28.99 (2.05)	44.84 (4.32)
(P-1-a)-[Co(*i*-dtma)((*R*)-pn)]$^{2+}$	20.58 (2.07)	28.94 (2.11)	45.15 (4.27)
(P-1-b)-[Co(*i*-dtma)((*R*)-pn)]$^{2+}$	20.58 (2.08)	28.88 (2.10)	45.25 (4.25)
(P-2)-[Co(*i*-dtma)((*R*)-pn)]$^{2+}$	20.88 (1.99)	28.94 (2.05)	44.69 (4.32)
$(+)_{589}$-[$Co(NO_2)_3$(edma)]$^-$	22.22 (2.50)		30.08 (3.93) 39.60 (4.45) 49.02 (4.33)

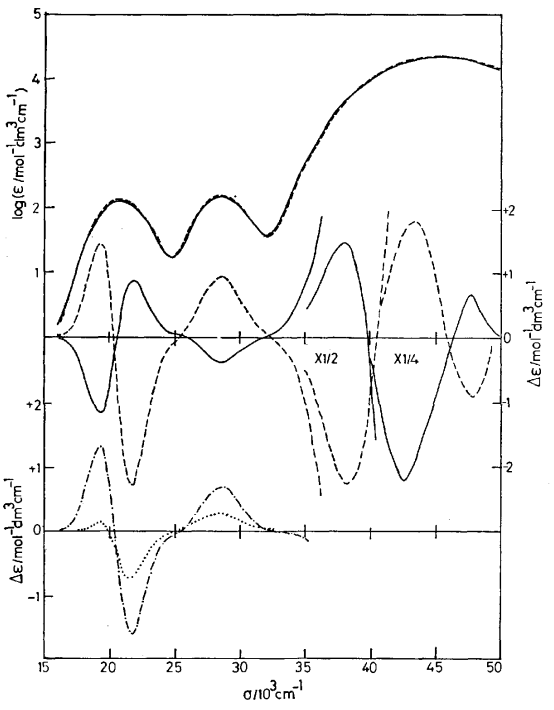

Fig. 7. Absorption and CD curves of A-2-a (——) and A-2-b (----) isomers of [Co(L-ala)(*i*-dtma)]$^+$. Two calculated CD curves of the vicinal (·····) and arrangement (—·—) effects are also shown.

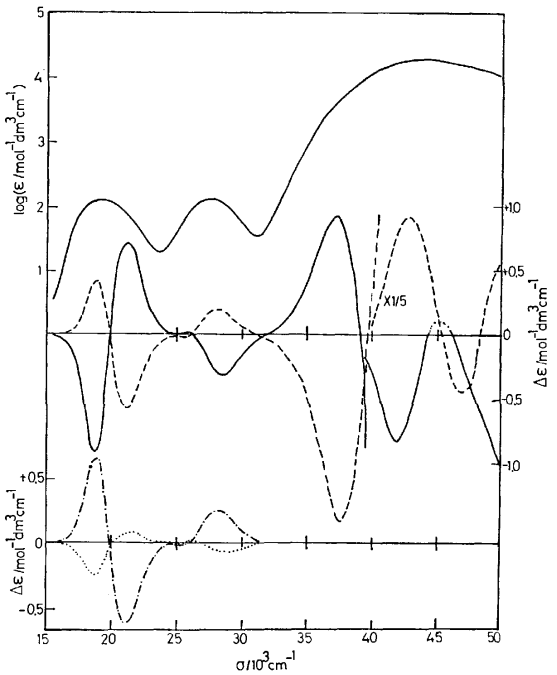

Fig. 8. Absorption and CD curves of A-3-a (----) and A-3-b (——) isomers of [Co(L-ala)(*i*-dtma)]$^+$. Two calculated CD curves of the vicinal (·····) and arrangement (—·—) effects are also shown.

for A-2, and (−) and (+) for A-3, respectively, in the first d-d absorption band region. These results lead one to the assignment that A-2 (and G-2) has structure *u*-α and A-3 (and G-3) *u*-β. Therefore, all the four and six isomers obtained for the glycinato and L-alaninato complexes, respectively, are assigned to have the following geometrical structures: G-1 and A-1 are *s*-α, G-2 and A-2 (a and b) are *u*-α, G-3 and A-3 (a and b) are *u*-β, and G-4 and A-4 are *s*-β. Without activated charcoal, the substitution reaction of [CoCl(*i*-dtma)(H_2O)]$^+$ with an amino carboxylate

TABLE 2. CD DATA OF [Co(A-B)(*i*-dtma)]-TYPE COMPLEXES (A-B=gly, L-ala, en, AND (*R*)-pn)
Wave numbers and $\Delta\varepsilon$ values (in parentheses) are given in $10^3\,cm^{-1}$ and $mol^{-1}\,dm^3\,cm^{-1}$, respectively.

Complex	d-d Transition band		Ultraviolet band
	1 st	2 nd	
$(-)_{589}$-(G-2)-[Co(gly)(*i*-dtma)]$^+$	19.31 (−0.787) 21.74 (+1.00)	28.41 (−0.395)	38.02 (+2.30) 42.55 (−4.60) 48.08 (+1.88)
(A-1)-[Co(L-ala)(*i*-dtma)]$^+$	18.12 (+0.158) 21.57 (−0.489)	29.28 (+0.062)	36.90 (−0.448) 42.55 (−0.581) 45.66 (+0.715)
(A-2-a)-[Co(L-ala)(*i*-dtma)]$^+$	19.38 (−1.20) 21.88 (+0.867)	28.57 (−0.401)	38.02 (+2.90) 42.55 (−9.02) 47.62 (+2.64)
(A-2-b)-[Co(L-ala)(*i*-dtma)]$^+$	19.38 (+1.44) 21.74 (−2.32)	28.65 (+0.917)	38.17 (−4.60) 43.29 (+7.12) 47.85 (−3.80)
(A-3-a)-[Co(L-ala)(*i*-dtma)]$^+$ [a]	18.89 (+0.415) 21.10 (−0.577)	25.64 (−0.017) 28.09 (+0.189)	37.59 (−1.47) 43.01 (+4.53) 47.06 (−2.28)
(A-3-b)-[Co(L-ala)(*i*-dtma)]$^+$	18.83 (−0.906) 21.16 (+0.701)	25.84 (+0.016) 28.53 (−0.315)	37.31 (+0.913) 41.84 (−4.18)
(A-4)-[Co(L-ala)(*i*-dtma)]$^+$	18.45 (−0.205) 20.55 (+0.422)	25.2 (−0.083) 27.59 (−0.163)	38.48 (−1.24) 43.29 (+1.88) 47.6 (−2.2)
$(-)_{589}$-(E-1)-[Co(*i*-dtma)(en)]$^{2+}$	19.53 (−1.16) 22.17 (+0.72)	26 sh 29.15 (−0.310)	37.74 (+2.22) 43.96 (−6.43)
(P-1-a)-[Co(*i*-dtma)((*R*)-pn)]$^{2+}$	19.65 (+1.14) 22.22 (−0.587)	26.46 (−0.096) 29.15 (+0.216)	37.12 (−1.79) 44.24 (+9.74)
(P-1-b)-[Co(*i*-dtma)((*R*)-pn)]$^{2+}$	19.49 (−1.20) 22.10 (+0.905)	29.03 (−0.456)	38.76 (+3.11) 44.05 (−1.43)
(P-2)-[Co(*i*-dtma)((*R*)-pn)]$^{2+}$	19.98 (−0.173) 22.27 (+0.300)	26.88 (−0.073) 29.24 (−0.053)	43.48 (+4.17)
$(+)_{589}$-[Co$(NO_2)_3$(edma)]$^-$	20.64 (+1.095) 23.42 (−0.822)		26 sh 29.76 (+1.49) 36.90 (−6.03) 42.55 (+19.4)

a) The $\Delta\varepsilon$ values were determined on assumption that the absorption spectrum of A-3-a is identical with that of A-3-b.

gave a mixture of the four isomers, whose formation ratios decreased in the following order; *u*-α, *u*-β, *s*-α, and *s*-β. Activated charcoal caused the formation of only *s*-α and *u*-α isomers, for which the nitrogen donor atom of the amino carboxylate is located at the trans position of the tertiary amine of *i*-dtma, with a preponderant yield of *u*-α.

The absorption spectra of the amino carboxylato complexes studied in the present work are rather distinct from those of usual tris-bidentate complexes with the same CoN_4O_2 chromophore. The color of G-1, *trans*(*O*), is yellow-orange, while that of *trans*(*O*)-[Co(gly)$_2$(en)]$^+$ is red. This can be explained by the fact that the intensity ratio of the split components of the first d-d absorption band is reversed between the two complexes: $18.5\times10^3\,cm^{-1}$ (sh, log ε=1.5) and 21.5 (1.85) for G-1 and 18.9 (1.94) and 22 (sh, 1.6) for *trans*(*O*)-[Co(gly)$_2$(en)]$^+$ [8]. As for the other three *cis*(*O*) isomers, the absorption maxima due to d-d transitions are generally at lower energies than those of C_1- and C_2-*cis*(*O*)-[Co(gly)$_2$(en)]$^+$ with the order of increasing energies; G-3 (*u*-β), G-4 (*s*-β), and G-2 (*u*-α) (Fig. 5). G-4 and A-4 show a trend of splitting in the second d-d transition band region (see also Table 1).

A-1 and A-4 are mutually quasi-enantiomeric isomers[1] and the CD spectra are approximately enantiomeric in the d-d transition band region but similar in the charge-transfer transition region (Fig. 6 and Table 2). On the basis of the same assumption as for the ata and tren complexes that the "quasi-enantiomeric" contribution, CD[*trans*]=−CD[*cis*], and the "asymmetric carbon" contribution, CD[S], are additive, the individual CD curves calculated from the observed CD curves of A-1 and A-4 are shown in Fig. 6. The CD[*trans*](=1/2{CD[A-1]−CD[A-4]}) curve showed a pattern similar to those of the corresponding ata and tren complexes:[1] two (+ and −) components in the first and one (+) component in the second d-d transition band region, respectively, while the pattern of CD[S] contribution for the *i*-dtma complex, 1/2{CD[A-1]+CD[A-4]} also resembled that of the vicinal CD for *trans*(*O*)-[Co(L-ala)$_2$-(en)]$^+$ [8] in the first d-d transition band region.

Isomers A-2-a and -b as well as A-3-a and -b are a pair of the diastereomers, which reveal approximately enantiomeric CD spectra over the whole range of wave numbers (Figs. 7 and 8). These CD curves consist of two contributions from the vicinal effect of the L-alaninate ligand and from the chiral arrange-

ment of *i*-dtma ligand. The contributions were separated into two, those of the chiral arrangement of the *i*-dtma; 1/2{CD[A-2-b]−CD[A-2-a]} for A-2 and 1/2{CD[A-3-a]−CD[A-3-b]} for A-3 and those of the vicinal; 1/2{CD[A-2-b]+CD[A-2-a]} for A-2 and 1/2-{CD[a-3-a]+CD[A-3-b]} for A-3, respectively, which are also shown in Figs. 7 and 8. The patterns of the former contributions are similar to that of $(+)_{589}$-(G-2)-[Co(gly)(*i*-dtma)]$^+$ which shows three (−, + and −) components in the d-d transition band region. Those of the latter contributions in the d-d transition band region are approximately enantiomeric, which means that A-2 and A-3 have the quasi-enantiomeric configurations in regard to the L-alaninate ligand. Both contributions of A-2 in the d-d transition band region are twice larger than those of A-3. For both A-2 and A-3 the CD contributions of chiral arrangement of *i*-dtma are larger than those of the vicinal; that is, the patterns of the observed CD for these *u*-type complexes are mainly determined by the chiral arrangement of the *i*-dtma ligand.

1,2-Diamine Complex with i-*dtma*: On preparing the 1,2-diamine complexes, the substitution reaction in an aqueous solution on a steam bath with activated charcoal[6] yielded a brown product (probably, organic compound) and a tris-bidentate complex besides the desired complex. However, none of the brown product and a rather small amount of the tris-diamine complex were formed when DMF was used as solvent. The main product was isomer E-1 or P-1, irrespective of the solvent, DMF or water.

Both the possible two isomers (E-1 and -2) were isolated for the en complex and the chiral isomer (E-1) was optically resolved. Six chiral isomers, four of which are two pairs of diastereomers, are possible for the (*R*)-pn complex but only three (P-1-a and -b and P-2) were isolated. It is found from their absorption spectra that P-1 and P-2 are analogous to E-1 and E-2, respectively. On the basis of the ^{1}H-NMR spectra (Fig. 4) E-1 is assigned to *u*-type, and E-2 to *s*-type. The optical resolution of E-1 confirms this assignment. The ^{1}H-NMR spectrum of P-2 (*s*-type) shows two doublets (1.40 and 1.34; 1.30 and 1.24 ppm) due to the methyl protons of the (*R*)-pn, while that of P-1-a one methyl doublet (1.38 and 1.32 ppm) and an AB quartet (4.53, 4.34, 3.97, and 3.79 ppm) due to the acetate methylene protons of *i*-dtma (Fig. 4). It is concluded from these results that P-2 is a mixture of the two *s*-type isomers, *s*-α and *s*-β, and that P-1-a comprises only one isomer of structure *u*-α or *u*-β.

The (*i*-dtma)(1,2-diamine) complexes have a CoN_5O chromophore. Figures 9, 10, and 11 show the electronic absorption and CD spectra of the en and (*R*)-pn complexes. The isomers of *u*-type, E-1 and P-1, have the absorption maxima at the energies slightly higher than *s*-type, E-2 and P-2 (Table 1). This suggests that the *i*-dtma ligand has different average ligand-field strengths in the different configurations; the strength of the *i*-dtma coordinating to the central metal facially with the three nitrogen atoms of *u*-type is smaller than that of the same ligand with *meridional*-(*N*)-coordination of *s*-type. The same argument seems

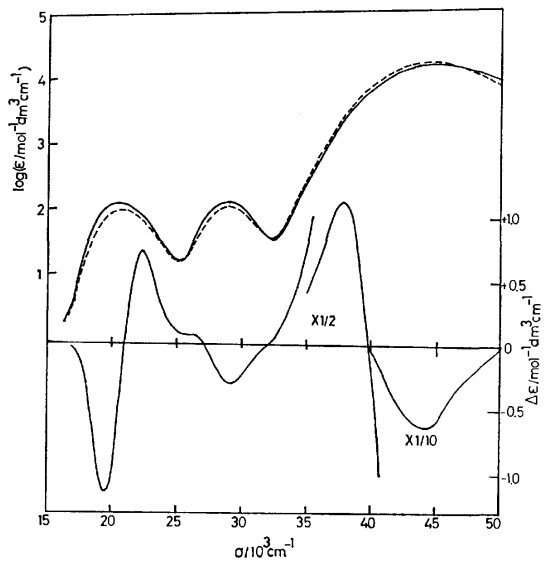

Fig. 9. Absorption and CD curves of E-1 (——) and E-2 (----) isomers of [Co(*i*-dtma)(en)]$^{2+}$.

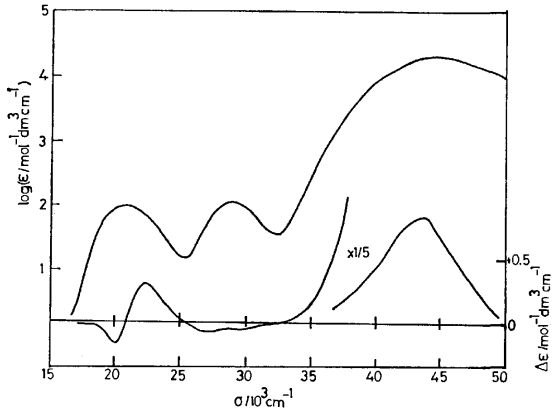

Fig. 10. Absorption and CD curves of P-2 isomer of [Co(*i*-dtma)((*R*)-pn)]$^{2+}$.

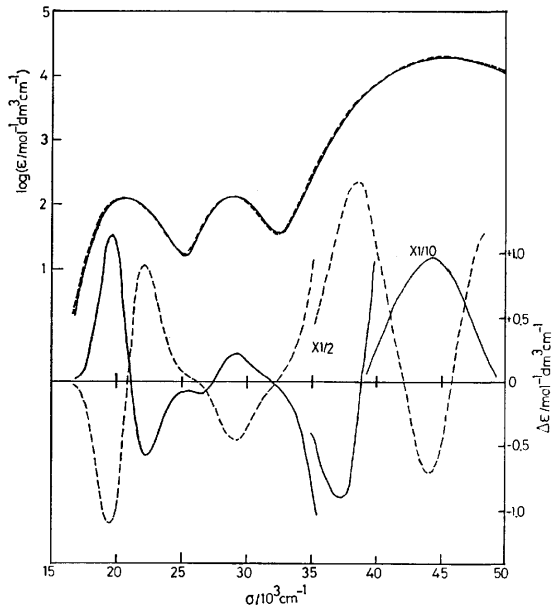

Fig. 11. Absorption and CD curves of P-1-a (——) and P-1-b (----) isomers of [Co(*i*-dtma)((*R*)-pn)]$^{2+}$.

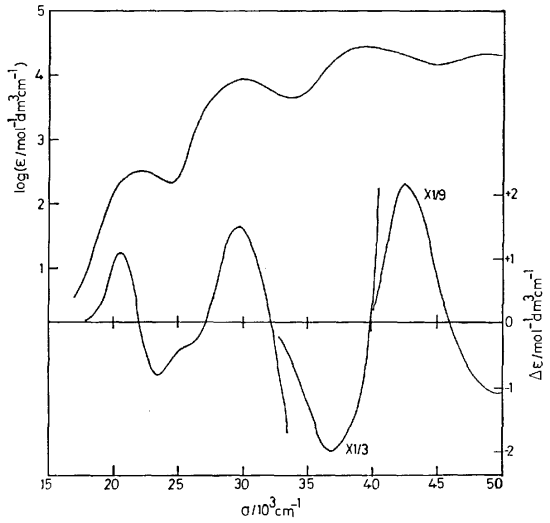

Fig. 12. Absorption and CD curves of $(+)_{589}$-isomer of $[Co(NO_2)_3(edma)]^-$.

to hold for the other complexes, [Co(*i*-dtma)(A-A)] (A-A=CO_3^{2-} [9], ox^{2-}, and $acac^-$[6]). For the *i*-dtma complexes, the molar extinction coefficients of the *u*-type *fac*(*N*) isomers are generally larger than those of the *s*-type *mer*(*N*) isomers.

[Co(NO$_2$)$_3$(edma)]$^-$: Two geometrical isomers, *mer*-*(NO$_2$)* and *fac(NO$_2$)*, are possible for the edma complex. Though both isomers should be optically resolvable, the sources of their optical activities may be quite different from each other; for *mer*(*NO$_2$*) isomer the contribution from the asymmetric nitrogen atom in edma, while for *fac*(*NO$_2$*) isomer two contributions from the asymmetric nitrogen and from the chiral arrangement of the edma ligand. It has been known that the active *mer*-$[Co(dien)_2]^{3+}$ (dien=diethylenetriamine) completely racemizes within 5 min in an aqueous solution at pH 10, though it is stable in an acidic solution at 20 °C.[10] Figure 12 shows the absorption and CD spectra of $(+)_{589}$-$[Co(NO_2)_3$-(edma)]$^-$. The fact that the CD spectrum was little affected in a LiOH solution (pH 10) at room temperature for 12 h indicates that the obtained isomer is *fac(NO$_2$)*.

Absolute Configurations: The ring-pairing method cannot be applied to the absolute configurations of the *u*-type complexes. The absolute configurations for the isomers are tentatively predicted as follows. Isomers, A-2-a and A-3-b, should have the same absolute configurations as $(-)_{589}$-(G-2)-[Co(gly)(*i*-dtma)]$^+$ (Fig. 7) in regard to *i*-dtma. The isomers of the L-alaninato complex were separated on an ion-exchanger column by eluting with a NaH_2PO_4–Na_2HPO_4 buffer. Figure 13 shows four absolute configurations of the diastereomers, where **N** signifies an amino group which can associate with phosphate species. The upper two isomers have three **N**'s in facial arrangement while the lower two have three **N**'s in meridional arrangement. The facial arrangement of the three amino group is preferable to the meridional arrangement for the association.[11] The formation of such an ion pair will decrease the average positive charge on the cationic

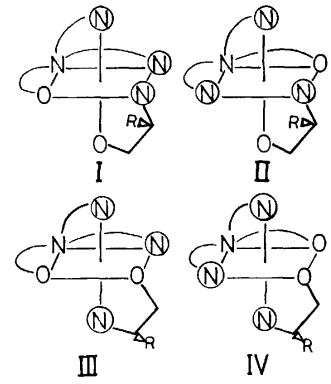

Fig. 13. Absolute configurations of four diastereomers of [Co(L-ala)(*i*-dtma)]$^+$ with u-type structure, where R=CH_3.

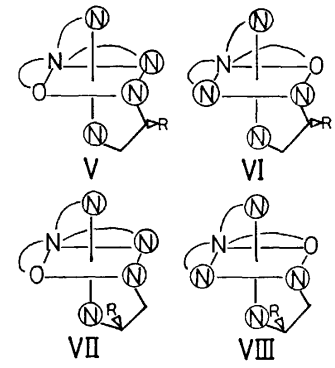

Fig. 14. Absolute configurations of four diastereomers of [Co(*i*-dtma)((*R*)-pn)]$^{2+}$ with *u*-type structure, where R=CH_3.

species and facilitate the elution of the complex. Hence it is predicted that *fac*(**N**) isomers, (I and II), should be eluted faster than *mer*(**N**), (III and IV). The *fac*(**N**) and the *mer*(**N**) isomers correspond to the structure *u*-*α* and *u*-*β*, respectively. In *fac*(**N**) isomers, isomer I should be eluted faster than II, because the methyl substituent of II will make the ion pair less stable than that of I. As for *mer*(**N**) isomers which may form an ion pair with phosphate anions not so firmly as the *fac*(**N**) isomers, the phosphate will yet prefer isomer IV to III, the former having a methyl substituent directed far from the plane of three **N**'s. Thus, the A-2-a, -b, A-3-a, and -b isomers are assigned to I, II, IV, and III, respectively, and the absolute configuration of $(-)_{589}$-[Co-(gly)(*i*-dtma)]$^+$ (G-2) to I.

From the CD spectra the P-1-b should have the same absolute configuration of *i*-dtma as that of $(-)_{589}$-[Co(*i*-dtma)(en)]$^{2+}$ (Fig. 9) and also those of A-2-a, A-3-b, and $(-)_{589}$-(G-2)-[Co(gly)(*i*-dtma)]$^+$ (Figs. 4, 6, and 7), because the CD contribution from the *u*-type configurational effect of *i*-dtma is expected to be larger than that from the so-called "vicinal" effect of (*R*)-pn and to show the same pattern as that of L-alaninato complex in the first and second d-d transition band region. Thus the absolute configurations of P-1-a and -b may be assigned to (VI or VII) and (V or VIII), respectively.

References

1) Part I of this series: K. Akamatsu, T. Komorita, and Y. Shimura, *Bull. Chem. Soc. Jpn.*, **54**, 3000 (1981).

2) Abbreviations of ligands: acac$^-$=acetylacetonate, aeida^{2-}=*N*-(2-aminoethyl)iminodiacetate, L-ala$^-$=L-alaninate, *β*-alada^{3-}=*N*,*N*-bis(carboxylatomethyl)-*β*-alaninate, ata^{3-}=nitrilotriacetate, *i*-dtma$^-$=*N*,*N*-bis(2-aminoethyl)glycinate, edma$^-$=ethylenediamine-*N*-acetate, gly$^-$=glycinate, ox^{2-}=oxalate, (*R*)-pn=(*R*)-propylenediamine, tren=tris(2-aminoethyl)amine.

3) B. E. Douglas, R. A. Haines, and J. G. Brushmiller, *Inorg. Chem.*, **2**, 1194 (1963).

4) N. Koine, N, Sakota, J. Hidaka, and Y. Shimura, *Bull. Chem. Soc. Jpn.*, **43**, 1737 (1970).

5) N. Koine, N. Sakota, J. Hidaka, and Y. Shimura, *Inorg. Chem.*, **12**, 859 (1973).

6) K. Kuroda, Y. Mori, H. Matsunaga, K. Kunigita, and K. Watanabe, *Bull. Chem. Soc. Jpn.*, **48**, 234 (1975).

7) K. Kuroda, S. Ohtsuka, and N. Matsumoto, *Bull. Chem. Soc. Jpn.*, **48**, 1055 (1975).

8) N. Matsuoka, J. Hidaka, and Y. Shimura, *Bull. Chem. Soc. Jpn.*, **40**, 1868 (1967); **45**, 2491 (1972); **48**, 458 (1975).

9) S. Nakashima and M. Shibata, *Bull. Chem. Soc. Jpn.*, **47**, 2069 (1974).

10) F. R. Keene, G. H. Searle, Y. Yoshikawa, and K. Yamasaki, *J. Chem. Soc., Chem. Commun.*, **1970**, 784.

11) F. R. Keene and G. H. Searle, *Inorg. Chem.*, **13**, 2173 (1974).

Preparation, and Structural and Spectroscopic Characterization of Cobalt(III) Phosphine Complexes of the Type, $[Co(CN)_{4-2n}(acac)_n(P)_2]^{(n-1)+}$ (acac=Acetylacetonate Ion, n=0,1,2, and P=$P(CH_3)_x(C_6H_5)_{3-x}$, x=0,1,2,3)

Kazuo KASHIWABARA, Katsuaki KATOH, Tomoji OHISHI, Junnosuke FUJITA,* and Muraji SHIBATA**

Department of Chemistry, Faculty of Science, Nagoya University, Chikusa-ku, Nagoya 464

*** Department of Chemistry, Faculty of Science, Kanazawa University, Kanazawa 920*

(Received June 15, 1981)

A series of the complexes, $[Co(CN)_{4-2n}(acac)_n(P)_2]^{(n-1)+}$ (acac=acetylacetonate ion, P=$P(CH_3)_x(C_6H_5)_{3-x}$) and several related complexes were prepared. For $[Co(acac)_2(P)_2]^+$, the $P(CH_3)_3$ and $P(CH_3)(C_6H_5)_2$ complexes afford only the *cis* and the *trans* isomers, respectively, while the $P(CH_3)_2(C_6H_5)$ complex forms both *cis* and *trans* isomers. No $P(C_6H_5)_3$ ligand gave the bis(acac)-type complex. The *trans* isomers show a strong absorption band in the region of the first absorption band, which is assumed to involve charge transfer transitions between the cobalt(III) ion and a phosphine, while the *cis* isomers give usual absorption spectra, exhibiting the first d-d absorption band of medium intensity. The methyl and phenyl groups on a phosphorus atom in both *cis* and *trans* isomers show triplet signals in the ^1H and ^{13}C NMR spectra due to virtual coupling. A *trans*(P,P) configuration was assigned to all the complexes of $[Co(CN)_2(acac)(P)_2]$ on the basis of the NMR and electronic spectra. For $[Co(CN)_4(P)_2]^-$, a *trans* configuration was assigned from the electronic spectra.

Little work has been reported for cobalt(III) complexes containing unidentate phosphines,[1] except for those of organo cobalt(III)- and bis(dimethylglyoximato)cobalt(III)-type, the latter type of which has been studied extensively as a model compound of Vitamin B_{12}.[2,3] In previous papers,[4,5] one of the present authors (M.S.) prepared several cobalt(III) complexes containing triphenylphosphine. Very recently we succeeded in isolating a pair of geometrical isomers of the bis(acetylacetonato)bis(dimethylphenylphosphine)cobalt(III) complex, and clarified some chemical and spectroscopic properties.[6] The difference in electronic spectra between the isomers was quite remarkable. In this paper, we extended the study to complexes of the type, $[Co(CN)_{4-2n}(acac)_n(P)_2]^{n-1}$ (acac=acetylacetonate ion, n=0,1,2) containing a series of phosphines, $P(CH_3)_x(C_6H_5)_{3-x}$ (x=0,1,2,3). Cyanide and acetylacetonate ions appear to afford fairly stable cobalt(III) complexes with unidentate phosphine ligands. Chemical properties such as stability and geometrical isomerism of those complexes would depend on the kinds of not only phosphine ligands, but also other ligands coexisting in a complex.

Experimental

The phosphine ligands were prepared according to the methods reported,[7] and handled under nitrogen atmosphere until they formed cobalt(III) complexes. Solvents were dried in the usual way and degassed in a stream of nitrogen. Absorption, and ^1H and ^{13}C NMR spectra were recorded on a Hitachi 323 spectrophotometer, and JEOL JNM-PMX 60 and JNM-FX 100 spectrometers, respectively.

trans-$[Co(acac)_2(PMePh_2)_2]PF_6$ *and* trans-$[Co(acac)_2(H_2O)(PMePh_2)]PF_6$. Methyldiphenylphosphine ($PMePh_2$) (0.9 g, 4.5 mmol) was added to a mixture of $[Co(acac)_3]$ (0.7 g, 2 mmol) and a small amount of active charcoal in ethanol (60 cm^3). The mixture was stirred at 25 °C for a day, and filtered. The dark red brown filtrate was diluted to 4 dm^3 with a mixture of water and ethanol (2:1). The solution was poured onto a small column of SP-Sephadex C-25 (ϕ2 cm×3 cm) in the Na^+ form. After the column had been thoroughly washed with a mixture of water and ethanol (2:1), the product adsorbed was eluted with a 0.05 mol/dm^3 NaCl solution in a mixture of water and ethanol (2:1). The eluate gave a red brown precipitate on addition of $NaPF_6$. The precipitate was filtered and dissolved in a small amount of CH_2Cl_2. The solution was mixed with ethanol and stored in a refrigerator to give red brown crystals of *trans*-$[Co(acac)_2(PMePh_2)_2]PF_6$. Yield: 35%. The corresponding *cis* complex was not yielded.

A methanol solution (*ca.* 30 cm^3) of *trans*-$[Co(acac)_2(PMePh_2)_2]PF_6$ (*ca.* 50 mg) was allowed to stand for a while at room temperature, and then chromatographed by use of a column of Sephadex LH-20 (ϕ2.7 cm×50 cm). By elution with methanol, the band was separated into two, the first blue-green and the second red brown (the starting complex) bands. The effluent of the first band was concentrated to a small volume under reduced pressure. The concentrate was mixed with a small amount of water and allowed to stand at room temperature to yield blue-green crystals of *trans*-$[Co(acac)_2(H_2O)(PMePh_2)]PF_6$.

cis- *and* trans-$[Co(acac)_2(PMe_2Ph)_2]PF_6$, *and* trans-$[Co(acac)_2(H_2O)(PMe_2Ph)]PF_6$. These complexes were prepared by modifiing the method reported previously.[6] A mixture of $[Co(acac)_3]$ (0.7 g, 2 mmol), PMe_2Ph (0.55 g, 4 mmol), and a small amount of active charcoal in ethanol (60 cm^3) was stirred at room temperature for 2 h, and filtered. The red brown filtrate was diluted with water to 3 dm^3. The solution was poured onto a small column (ϕ 2.7 cm×3 cm) of SP-Sephadex C-25, and then the column was washed with water. The Sephadex adsorbed the product was charged on the top of an SP-Sephadex C-25 column (ϕ 2.7 cm×50 cm). By elution with an aqueous 0.02 mol/dm^3 NaCl solution, the column showed two bands. The fraction of the first blue-violet band was concentrated to a small volume under reduced pressure. The concentrate gave a blue-violet precipitate on addition of $NaPF_6$. The precipitate was dissolved in a mixture of methanol and water (5:1). The solution was allowed to stand at room temperature to give blue-violet crystals of *trans*-$[Co(acac)_2(H_2O)(PMe_2Ph)PF_6$. Yield: *ca.* 15%. The effluent of the second red brown band gave red brown crystals of *cis*-$[Co(acac)_2(PMe_2Ph)_2]PF_6$ by the same method as the above. Yield: *ca.* 50%.

The *trans*-$[Co(acac)_2(PMe_2Ph)_2]PF_6$ complex was obtained by adding a slight excess of PMe_2Ph to an ethanol solu-

tion of *trans*-$[Co(acac)_2(H_2O)(PMe_2Ph)]PF_6$, red orange crystals being deposited in *ca.* 15 min. Yield: 80%.

cis-$[Co(acac)_2(PMe_3)_2]PF_6$. Red crystals of this complex were obtained by a method similar to that for the PMe_2Ph complex, using PMe_3 instead of PMe_2Ph. Yield: 50%. The formation of the corresponding *trans* isomer and the aqua complex was not observed in column chromatography.

$[Co(acac)_2(Ph_2PCH_2CH_2PPh_2)]PF_6$. This complex was prepared by the method reported previously.[8]

$[Co(acac)_2(Me_2PCH_2CH_2PMe_2)]PF_6$. A methanol solution (100 cm^3) containing $[Co(acac)_3]$ (0.25 g, 0.7 mmol) and 1,2-bis(dimethylphosphino)ethane (0.1 g, 0.7 mmol) was stirred at room temperature for 20 h. A mixture of diethyl ether and water (400 cm^3, 1:3) was added to the resulting orange solution in order to extract the unreacted free diphosphine into the diethyl ether. The diethyl ether layer was separated off, and the aqueous solution was diluted ten times with water. The solution was chromatographed by a method similar to that for the PMe_2Ph complex. The first orange eluate was evaporated to dryness under reduced pressure, and the residue was extracted with chloroform. The extract was evaporated to dryness, and the residue was again dissolved in water. Red crystals of the complex were obtained on addition of $NaPF_6$. Yield: *ca.* 20%.

trans(P,P)-$[Co(CN)_2(acac)(PPh_3)_2]$. This complex was prepared by the method reported previously.[4]

trans(P,P)-$[Co(CN)_2(acac)(PMePh_2)_2]$. A mixture of $K[Co(CN)_2(acac)_2]$[9] (0.7 g, 2 mmol) and $PMePh_2$ (0.8 g, 4 mmol) in ethanol (60 cm^3) was stirred at 30 °C for 6 h. The resulting orange yellow solution was concentrated under reduced pressure to *ca.* 15 cm^3. An orange precipitate of the crude complex was obtained on standing, which was filtered. The filtrate was chromatographed by use of an alumina column (ϕ 4 cm × 50 cm) and a mixture of hexane and ethanol (1:10). The orange yellow eluate was concentrated to a small volume. The concentrate was rechromatographed by use of a Sephadex LH-20 column (ϕ 3 cm × 60 cm) and a mixture of hexane and ethanol (5:1). Another crop of the complex was obtained by evaporating the eluate to dryness under reduced pressure. The combined first and second crops were recrystallized from a mixture of dichloromethane and ethanol (4:1). Yield: *ca.* 55%.

trans(P,P)-$[Co(CN)_2(acac)(PMe_2Ph)_2]$. This complex was prepared by a method similar to that for the $PMePh_2$ complex, using PMe_2Ph instead of $PMePh_2$. The eluate which was obtained by rechromatography with a Sephadex LH-20 column was concentrated to a small volume under reduced pressure. The concentrate was mixed with a small amount of water and allowed to stand, yielding orange yellow crystals of the complex. Yield: *ca.* 25%.

trans(P,P)-$[Co(CN)_2(acac)(PMe_3)_2]$ *and* cis-$[Co(CN)(acac)_2(PMe_3)]$. A mixture of $K[Co(CN)_2(acac)_2]$ (0.7 g, 2 mmol) and PMe_3 (0.2 g, 2.6 mmol) in methanol (100 cm^3) was stirred for 20 h at room temperature. The resulting orange solution was chromatographed by using an alumina column (ϕ2 cm × 30 cm) and methanol. The eluate was concentrated to a small volume under reduced pressure. The concentrate was rechromatographed by use of a Sephadex LH-20 column (ϕ2 cm × 50 cm) and a mixture of hexane and ethanol (10:1). Each eluate of the first red and the second orange bands was evaporated to dryness, and the residue was dissolved in a small amount of chloroform. The chloroform solutions obtained from the first and the second eluates gave crystals of red *cis*-$[Co(CN)(acac)_2(PMe_3)]$ and orange *trans*(P,P)-$[Co(CN)_2(acac)(PMe_3)_2]$, respectively, on addition of hexane. Yield: *ca.* 7% for each complex.

cis-$[Co(CN)_2(acac)(Ph_2PCH_2CH_2PPh_2)]$. A mixture of $K[Co(CN)_2(acac)_2]$ (0.2 g, 0.6 mmol) and $Ph_2PCH_2CH_2PPh_2$ (0.25 g, 0.6 mmol) in methanol (100 cm^3) was stirred at 55 °C for 4 h. The resulting orange solution was evaporated to dryness, and the residue was extracted with hot benzene. The extract afforded orange crystals of the complex on standing at room temperature. Yield: 50%.

trans(P,P)-$K[Co(CN)_4(PPh_3)_2]$. The previous method[5] was modified. A mixture of PPh_3 (5.2 g, 20 mmol) and $K_3[Co(CN)_5I]$[10] (4.3 g, 10 mmol) in glacial acetic acid (70 cm^3) was stirred at 75 °C for 6 h, and filtered. The yellow filtrate was mixed with water (500 cm^3) and stored in a refrigerator to yield a yellow precipitate. It was filtered, washed with benzene in order to remove free PPh_3, and then dissolved in a mixture of dichloromethane and methanol (1:1). The solution was chromatographed by use of a Sephadex LH-20 column (ϕ1.5 cm × 30 cm) and a mixture of dichloromethane and methanol (1:1). The first main yellow eluate was concentrated to a small volume under reduced pressure. The concentrate was mixed with a small amount of water and stored in a refrigerator to yield orange crystals of the complex. Yield: 15%.

trans(P,P)-$Na[Co(CN)_4(PMePh_2)_2]$. The method of Maki and Ohshima[11] for the PPh_3 complex was modified. A suspension of $Na_5[Co(SO_3)_2(CN)_4]3H_2O$[12] (1.2 g, 3.5 mmol) and $PMePh_2$ (1.1 g, 5.5 mmol) in glacial acetic acid (40 cm^3) was stirred at 75 °C for 7 h. The resulting orange yellow solution was evaporated to dryness under reduced pressure. The residue was extracted with methanol, and the extract was evaporated to dryness. The residue was again extracted with methanol. The extract was concentrated to *ca.* 20 cm^3 under reduced pressure to yield a yellow precipitate. It was filtered and dissolved in methanol. The methanol solution was chromatographed by use of a Sephadex LH-20 column (ϕ1.5 cm × 30 cm) and methanol. The first main yellow eluate was concentrated to a small volume. The concentrate was mixed with a small amount of water and stored in a refrigerator to give orange crystals of the complex. Yield: 10%. The complex can also be prepared from $K_3[Co(CN)_5I]$ and $PMePh_2$ by a method similar to that for the PPh_3 complex.

trans(P,P)-$K[Co(CN)_4(PMe_2Ph)_2]$. A mixture of PMe_2Ph (2.2 g, 16 mmol) and $K_3[Co(CN)_5I]$ (3.4 g, 8 mmol) in a mixture (60 cm^3) of dioxane and water (5:2) was stirred at 50 °C for 4 h, and filtered. The filtrate was evaporated to dryness under reduced pressure. The residue was extracted with a mixture of methanol and dichloromethane (3:1). The extract was chromatographed by use of a Sephadex LH-20 column (ϕ 1.5 cm × 30 cm) and a mixture of methanol and dichloromethane (3:1). The first main yellow eluate was concentrated to a small volume. The concentrate was mixed with a small amount of ethanol and stored in a refrigerator to yield yellow crystals of the complex. Yield: 10%.

$K[Co(CN)_4(Ph_2PCH_2CH_2PPh_2)]$. A mixture of $K_3[Co(CN)_5I]$ (4.3 g, 10 mmol) and $Ph_2PCH_2CH_2PPh_2$ (4.0 g, 10 mmol) in a mixture (100 cm^3) of dioxane and water (7:3) was stirred at 75 °C for 7 h, and filtered. The filtrate was evaporated to dryness under reduced pressure, and the residue was extracted with methanol. The extract was evaporated to dryness, and the residue was again extracted with methanol. The extract was chromatographed by use of a Sephadex LH-20 column (ϕ 1.5 cm × 30 cm) and methanol. The second main yellow eluate was concentrated to a small volume under reduced pressure. The concentrate was mixed with a small amount of ethanol and stored

Table 1. Elemental analyses and absorption spectral data

Complex	C (%) Found(Calcd)	H (%) Found(Calcd)	N (%) Found(Calcd)	$\tilde{\nu}/10^3$ cm^{-1} (log ε)	Solvent
trans-$[Co(acac)_2(PMePh_2)_2]PF_6$	53.53(53.88)	4.96(5.02)	—	21.5(4.13)	a)
trans-$[Co(acac)_2(PMe_2Ph)_2]PF_6$	46.03(46.03)	5.22(5.35)	—	22.8(4.13)	a)
cis-$[Co(acac)_2(PMe_2Ph)_2]PF_6$	45.75(46.03)	5.03(5.33)	—	18.4(2.49), 21.3(2.6)*	b)
cis-$[Co(acac)_2(PMe_3)_2]PF_6$	34.66(34.67)	5.77(5.82)	—	18.8(2.40) 22.6(2.6)*	b)
$[Co(acac)_2(Ph_2PCH_2CH_2PPh_2)]PF_6$	54.10(54.01)	4.91(4.78)	—	20.2(2.99)	b)
$[Co(acac)_2(Me_2PCH_2CH_2PMe_2)]PF_6$	34.56(34.80)	5.67(5.48)	—	19.3(2.4),* 23.4(2.9)*	b)
trans-$[Co(acac)_2(H_2O)(PMePh_2)]PF_6$	44.37(44.53)	4.81(4.71)	—	16.6(2.51)	b)
trans-$[Co(acac)_2(H_2O)(PMe_2Ph)]PF_6\cdot 0.5H_2O$	38.14(38.11)	4.99(4.99)	—	17.4(2.53)	b)
cis-$[Co(acac)_2(CN)(PMe_3)]$	46.83(46.55)	6.64(6.58)	3.59(3.88)	19.4(2.2),* 23.5(2.7)*	b)
trans(P,P)-$[Co(CN)_2(acac)(PPh_3)_2]$	69.86(70.30)	5.45(5.08)	3.75(3.81)	20.9(3.58)	a)
trans(P,P)-$[Co(CN)_2(acac)(PMePh_2)_2]$	64.63(64.91)	5.52(5.46)	4.29(4.59)	22.3(3.57)	b)
trans(P,P)-$[Co(CN)_2(acac)(PMe_2Ph)_2]\cdot H_2O$	55.21(54.77)	6.22(6.20)	5.74(5.55)	23.7(3.55)	b)
trans(P,P)-$[Co(CN)_2(acac)(PMe_3)_2]$	43.07(43.10)	6.76(6.96)	7.35(7.73)	24.5(3.26)	b)
cis-$[Co(CN)_2(acac)(Ph_2PCH_2CH_2PPh_2)]$	65.10(65.14)	5.00(5.13)	4.44(4.60)	23.4(3.12)	b)
trans-$K[Co(CN)_4(PPh_3)_2]\cdot 0.5H_2O$	66.15(65.30)	4.74(4.30)	7.48(7.62)	26.5(3.3)*	b)
trans-$Na[Co(CN)_4(PMePh_2)_2]\cdot 4H_2O$	54.12(54.14)	5.07(5.14)	8.53(8.42)	28.6(3.3)*	b)
trans-$K[Co(CN)_4(PMe_2Ph)_2]\cdot 2.5H_2O$	46.15(45.89)	4.94(5.20)	10.78(10.70)	29.2(3.25)	b)
$K[Co(CN)_4(Ph_2PCH_2CH_2PPh_2)]\cdot 0.5H_2O$	58.94(59.11)	3.98(4.13)	9.08(9.19)	29.6(2.92)	b)

*: Shoulder. a) CH_2Cl_2. b) CH_3OH.

Table 2. ^{1}H NMR spectral data, δ (J/Hz)[a)]

Complex	acac		P-CH_3	Solvent
	-CH_3	-CH		
trans-$[Co(acac)_2(PMePh_2)_2]PF_6$	1.52	4.47	2.10(t, 8.0)	b)
trans-$[Co(acac)_2(PMe_2Ph)_2]PF_6$	1.71	4.94	1.71(t, 8.3)	c)
cis-$[Co(acac)_2(PMe_2Ph)_2]PF_6$	1.91	5.43	1.35(t, 13.4)	b)
	2.04		1.41(t, 14.1)	
cis-$[Co(acac)_2(PMe_3)_2]PF_6$	1.83	5.48	m	b)
	2.17			
$[Co(acac)_2(Ph_2PCH_2CH_2PPh_2)]PF_6$	1.64	4.93	—	b)
	1.88			
$[Co(acac)_2(Me_2PCH_2CH_2PMe_2)]PF_6$	1.76	5.42	m	b)
	2.18			
cis-$[Co(CN)(acac)_2(PMe_3)]$	1.82	5.42	1.56(d, 13.2)	b)
	1.88	5.50		
	2.11			
	2.30			
trans(P,P)-$[Co(CN)_2(acac)(PPh_3)_2]$	1.07	4.58	—	b)
trans(P,P)-$[Co(CN)_2(acac)(PMePh_2)_2]$	1.12	4.71	2.41(t, 8.4)	b)
trans(P,P)-$[Co(CN)_2(acac)(PMe_2Ph)_2]\cdot H_2O$	1.18	4.68	2.06(t, 8.4)	b)
trans(P,P)-$[Co(CN)_2(acac)(PMe_3)_2]$	1.90	5.28	1.67(t, 8.0)	b)
cis-$[Co(CN)_2(acac)(Ph_2PCH_2CH_2PPh_2)]$	1.11	4.96	—	b)
	1.93			
trans-$Na[Co(CN)_4(PMePh_2)_2]\cdot 4H_2O$	—	—	2.41(t, 9.0)	d)
trans-$K[Co(CN)_4(PMe_2Ph)_2]\cdot 2.5H_2O$	—	—	2.06(t, 9.0)	e)

a) J refers to the interval of two outer peaks of a triplet, and d: doublet, m: multiplet. b) $CDCl_3$. c) CD_2Cl_2. d) CD_3OD. e) D_2O.

in a refrigerator to yield yellow crystals of the complex. Yield: 20%.

Analytical data of the complexes are given in Table 1.

Results and Discussion

The $[Co(acac)_2(P)_2]^+$ *Complexes.* In a previous paper,[6)] we have prepared *cis*- and *trans*-$[Co(acac)_2(PMe_2Ph)_2]^+$ and *trans*-$[Co(acac)_2(H_2O)(PMe_2Ph)]^+$

TABLE 3. ^{13}C NMR SPECTRAL DATA FOR PHOSPHINE LIGANDS, δ (J/Hz)[a]

Complex	P-CH_3	P-C_6H_5 P-C_1	*o*-C	*m*-C	*p*-C	Solvent
trans-$[Co(acac)_2(PMePh_2)_2]PF_6$	7.4(24.4)	128.3(39.1)	132.5(9.8)	128.9(8.5)	131.4	c)
trans-$[Co(acac)_2(PMe_2Ph)_2]PF_6$	9.1(24.4)	131.7(40.4)	131.3(9.7)	129.4(9.9)	131.5	d)
cis-$[Co(acac)_2(PMe_2Ph)_2]PF_6$	9.6(29.0) 10.6(29.3)	131.3(45.1)	130.9(8.6)	129.6(9.8)	131.9	d)
cis-$[Co(acac)_2(PMe_3)_2]PF_6$	11.9(29.3)	—	—	—	—	c)
cis-$[Co(CN)(acac)_2(PMe_3)]$	12.2(30.5)[b]	—	—	—	—	c)
trans(P,P)-$[Co(CN)_2(acac)(PPh_3)_2]$	—	129.9(41.6)	135.3(9.8)	128.3(9.8)	130.7	c)
trans(P,P)-$[Co(CN)_2(acac)(PMePh_2)_2]$	15.7(34.2)	130.7(43.9)	133.8(9.8)	128.5(9.8)	130.7	c)
trans(P,P)-$[Co(CN)_2(acac)(PMe_2Ph)_2]\cdot H_2O$	12.4(32.5)	132.3(40.8)	130.9(9.1)	128.3(8.8)	130.1	c)
trans(P,P)-$[Co(CN)_2(acac)(PMe_3)_2]$	13.4(29.3)	—	—	—	—	c)
trans-$Na[Co(CN)_4(PMePh_2)_2]\cdot 4H_2O$	18.6(35.2)	134.9(50.0)	134.5(9.8)	129.0(9.8)	131.7	e)
trans-$K[Co(CN)_4(PMe_2Ph)_2]\cdot 2.5H_2O$	17.1(36.1)	137.1(47.9)	131.8(8.8)	129.4(9.8)	131.4	e)

a) J refers to the interval of two outer peaks of a triplet. b) Doublet. c) $CDCl_3$. d) CD_2Cl_2. e) CD_3OD.

by a reaction of $[Co(acac)_3]$ with PMe_2Ph in ethanol in the presence of active charcoal. The geometrical configurations of these complexes can be easily assigned on the basis of the ^1H and ^{13}C NMR spectra (Tables 2 and 3). The bis(PMe_2Ph) complexes isolated as hexafluorophosphate are insoluble in water, but soluble in common organic solvents such as ethanol or dichloromethane. The *cis* isomer is quite stable in such solvents. The corresponding *trans* isomer is stable in dichloromethane, but hydrolyzes in ethanol (not anhydrous) to afford *trans*-$[Co(acac)_2(H_2O)(PMe_2Ph)]^+$ which is stable to further hydrolysis. The hydrolysis is depressed in the presence of excess PMe_2Ph Thus the *trans* bis(PMe_2Ph) isomer in hydrous ethanol gives the following equilibrium:

$$trans\text{-}[Co(acac)_2(PMe_2Ph)_2]^+ + H_2O \rightleftharpoons trans\text{-}[Co(acac)_2(H_2O)(PMe_2Ph)]^+ + PMe_2Ph$$

The *trans* bis(PMe_2Ph) isomer in ethanol slowly isomerizes to the *cis* isomer on addition of active charcoal, attaining an equilibrium between the two isomers. In fact the *cis* isomer also isomerizes to the *trans* isomer under the same conditions, the *cis* isomer being predominant at equilibrium at room temperature as indicated by the preparative experiment.

The $PMePh_2$ and PMe_3 ligands used in this study give only *trans*-$[Co(acac)_2(PMePh_2)_2]^+$ and *cis*-$[Co(acac)_2(PMe_3)_2]^+$, respectively under similar experimental conditions to that for the PMe_2Ph complex. The *trans*-$[Co(acac)_2(H_2O)(PMePh_2)]^+$ complex was derived from the *trans* bisphosphine complex by hydrolysis. These experimental results including those of the PMe_2Ph complex suggest that the $[Co(acac)_2(P)_2]^+$-type complex is stabilized in the *cis* isomer, unless there is steric hindrance between two phosphine ligands in the *cis* positions. The preponderance of *cis* coordination of phosphine ligands will be brought about by the strong *trans* effect of a phosphine ligand.[13] The $PMePh_2$ ligand might be too bulky to occupy *cis* positions in the bis(acac)cobalt(III) complex. No PPh_3 reacted with $[Co(acac)_3]$ in ethanol in the presence of active charcoal. On raising the reaction temperature reduction of Co(III) took place.

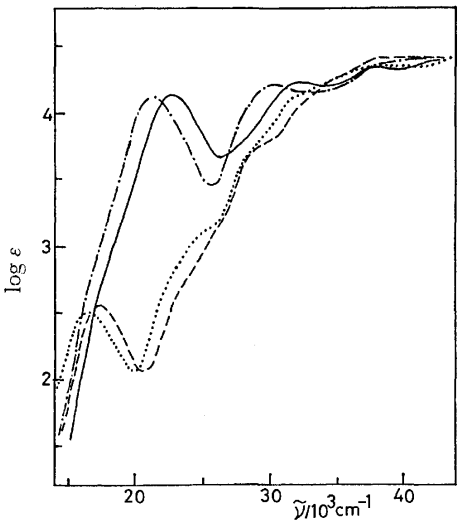

Fig. 1. Absorption spectra of *trans*-$[Co(acac)_2(PMe_2Ph)_2]^+$ (——), *trans*-$[Co(acac)_2(PMePh_2)_2]^+$ (—·—), *trans*-$[Co(acac)_2(H_2O)(PMe_2Ph)]^+$ (----), and *trans*-$[Co(acac)_2(H_2O)(PMePh_2)]^+$ (·····).

The absorption spectra of *trans*-$[Co(acac)_2(P)_2]^+$ and *trans*-$[Co(acac)_2(H_2O)(P)]^+$ ($P=PMePh_2$, PMe_2Ph) are compared in Fig. 1. The spectra of the *trans* bisphosphine complexes differ markedky from those of the aqua complexes; the formers show a very strong band around 22000 cm^{-1}. The *cis*-$[Co(acac)_2(P)_2]^+$ ($P=PMe_2Ph$, PMe_3) complexes exhibit no such strong bands in this region (Fig. 2). The strong bands of the *trans* bisphosphine complexes can be assigned to a charge transfer transition between the Co(III)–phosphine because of the strong intensity. The bands have a shoulder in the low energy side, which can be assigned to a part of the first d-d band. The aqua complexes show clearly the first d-d band, and the spectra resemble that of *trans*-$[Co(acac)_2(NH_3)_2]^+$ which gives the first d-d band at 18500 cm^{-1} (log $\varepsilon=1.89$).[14] The *cis*-$[Co(acac)_2(P)_2]^+$ ($P=PMe_2Ph$, PMe_3) complexes give a band at *ca.* 18500 cm^{-1} and a shoulder at *ca.* 22000 cm^{-1}. They can be assigned to two split components of the first d-d band. The Me_2-

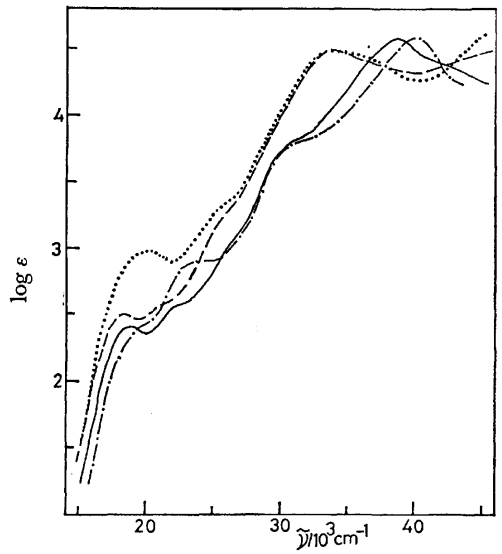

Fig. 2. Absorption spectra of *cis*-$[Co(acac)_2(PMe_3)_2]^+$ (——), *cis*-$[Co(acac)_2(PMe_2Ph)_2]^+$ (----), $[Co(acac)_2(Me_2PCH_2CH_2PMe_2)]^+$ (—·—), and $[Co(acac)_2(Ph_2PCH_2CH_2PPh_2)]^+$ (·····).

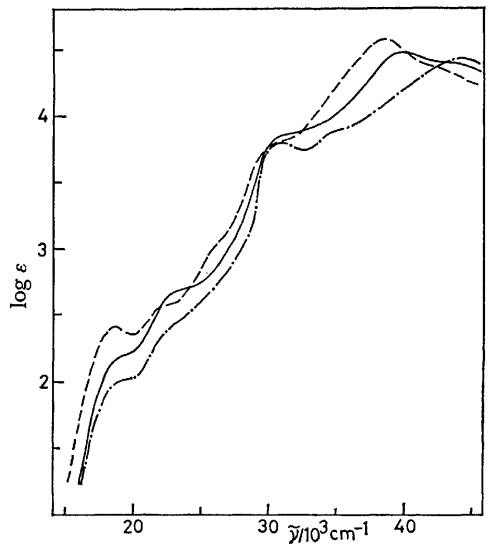

Fig. 3. Absorption spectra of *cis*-$[Co(acac)_2(PMe_3)_2]^+$ (----), *cis*-$[Co(CN)(acac)_2(PMe_3)]$ (——), and *cis*-$[Co(CN)_2(acac)_2]^-$ (—·—).

$PCH_2CH_2PMe_2$ complex also shows two components of the first d-d band, although the spectral pattern is somewhat different from that of the above bisphosphine complexes. The $Ph_2PCH_2CH_2PPh_2$ complex gives a broad, fairly strong single d-d band at 20200 cm^{-1}, but the band splits into two components (19400 and 20600 cm^{-1}) at 173 K.[8] A similar splitting spectral pattern in the first d-d band region has been observed for *cis*-$[Co(CN)_2(acac)_2]^-$[4] (Fig. 3) and *cis*-$[Co(CN)_2(C_2O_4)_2]^{3-}$.[15] In the ultraviolet region, all the complexes show complicated spectra due to absorptions arising from intramolecular transitions of the ligands and charge transfer transitions between the cobalt(III) ion and the ligands. In the complexes of each type including other cyano complexes studied here, both d-d and charge transfer bands are shifted remarkably depending on the kind of phosphine ligands. The shift occurs to the high energy side in the following order of ligands; $PPh_3 < PMePh_2 < PMe_2Ph \approx Ph_2PCH_2CH_2PPh_2 < PMe_3 < Me_2PCH_2CH_2PMe_2$. This order agrees with the decreasing order of the cone angles (θ(degree), steric effect) of phosphines given by Tolman;[16] $PPh_3(145) > PMePh_2(136) > Ph_2PCH_2CH_2PPh_2(125) \geq PMe_2Ph(122) > PMe_3(118) > Me_2PCH_2CH_2PMe_2(107)$. It also agrees with the decreasing order of the substituent additivity values ($\Sigma\chi_i$ (cm^{-1}), electronic effect) given by the same author;[16] $PPh_3(12.9) > PMePh_2(11.2) > PMe_2Ph(9.5) > PMe_3(7.8)$.

Figure 3 shows the absorption spectra of *cis*-$[Co(CN)_n(acac)_2(PMe_3)_{2-n}]^{(n-1)+}$ (n=0,1,2). By replacing the PMe_3 ligand by a cyanide ion, the first absorption band remains almost unshifted, but decreases the intensity. The band or shoulder around 30000 cm^{-1} can be assigned to a transition between the Co(III)–acac. The bands at 38800 cm^{-1} and 39900 cm^{-1} of the bisphosphine and the monocyano complexes, respectively, can be assigned to a transition between the Co(III)–PMe_3.

The ^1H NMR spectral data for the methyl and methine parts of the complexes are summarized in Table 2. Except for the *cis*-$[Co(acac)_2(PMe_2Ph)_2]^+$ complex, the methine protons of acac of the bis(acac) complexes with the phosphine ligand having a phenyl group resonate at a remarkably high field (4.47—4.94 ppm) as compared with those of the complexes with the trialkylphosphine ligand (5.42—5.50 ppm). A phenyl ring of the phosphine ligand in the former complexes comes over an acetylacetonate ring so that the methine proton should be shielded by the phenyl ring to cause the high field shift.[8] The methine proton of *cis*-$[Co(acac)_2(PMe_2Ph)_2]^+$ shows no such high field shift. The two PMe_2Ph ligands in this complex would be prohibited to rotate freely around the Co–P bond, and the conformation with the two phenyl rings stacking each other seems to be stable from studies with molecular models. When the complex has such a conformation, the methyl group(s) of the phosphine is placed over the acetylacetonate ring, and the resonance value of the methine proton would be similar to that in the PMe_3 complex. The P–CH_3 groups in $[Co(acac)_2(P)_2]^+$ (P=PMe_2Ph, $PMePh_2$) give triplet signals due to so-called virtual coupling, although those of the trialkylphosphine complexes become multiplets. The *cis* PMe_2Ph complex exhibits two kinds of the P–CH_3 signals, indicating the *cis*, chiral structure. The carbons of the methyl and phenyl groups on phosphorus except for the *p*-carbon also show triplet signals in the ^{13}C NMR spectra of both *cis* and *trans* bisphosphine complexes (Table 3). The spectral assignment was made according to the reference.[8] Thus there exists virtual coupling in both *cis* and *trans* bisphosphine complexes. In planar complexes, such virtual coupling is, in general, observed for only a *trans* isomer.[17] For some octahedral complexes of the *cis* type, however, the coupling has been reported to be remarkable.[18] Virtual coupling as a diagnosis for the *trans* arrangement of two phosphorus donor atoms seems to be limited to only planar complexes.

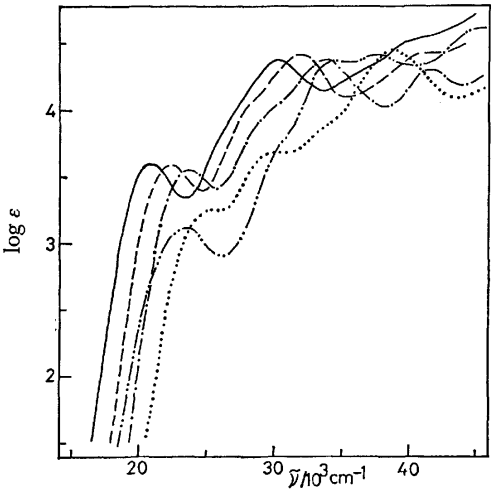

Fig. 4. Absorption spectra of *trans*(P,P)-[Co(CN)$_2$(acac)(PPh$_3$)$_2$] (——), *trans*(P,P)-[Co(CN)$_2$(acac)(PMePh$_2$)$_2$] (----), *trans*(P,P)-[Co(CN)$_2$(acac)(PMe$_2$Ph)$_2$] (—·—), *trans*(P,P)-[Co(CN)$_2$(acac)(PMe$_3$)$_2$] (·····), and *cis*-[Co(CN)$_2$(acac)(Ph$_2$PCH$_2$CH$_2$PPh$_2$)] (—··—).

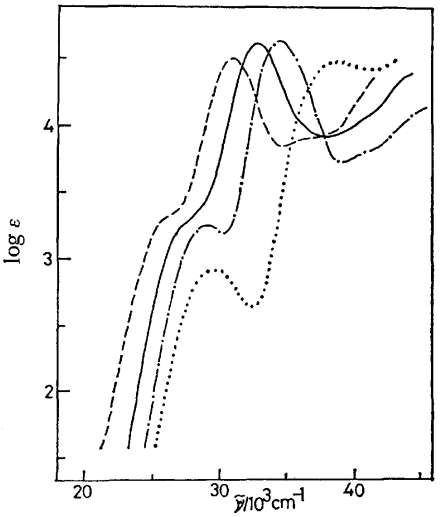

Fig. 5. Absorption spectra of *trans*-[Co(CN)$_4$(PPh$_3$)$_2$]$^-$ (----), *trans*-[Co(CN)$_4$(PMePh$_2$)$_2$]$^-$ (——), *trans*-[Co(CN)$_4$(PMe$_2$Ph)$_2$]$^-$ (—·—), and [Co(CN)$_4$(Ph$_2$PCH$_2$CH$_2$PPh$_2$)]$^-$ (·····).

The [Co(CN)$_2$(acac)(P)$_2$] Complexes. The [Co(CN)$_2$(acac)(P)$_2$]-type complex has three possible geometrical isomers, *trans*(P,P), *trans*(C,C), and *trans*(P,C) isomers. In this study, the reactions between *cis*-[Co(CN)$_2$(acac)$_2$]$^-$ and P(CH$_3$)$_n$(C$_6$H$_5$)$_{3-n}$ (n=0,1,2, or 3) afforded only one isomer for each phosphine ligand. All the complexes isolated can be assigned to either a *trans*(P,P) or a *trans*(C,C) configuration from the ^{1}H and ^{13}C NMR spectra (Tables 2 and 3). In addition the remarkable high field shift of the methine proton signals of acac in the complexes containing a phenylphosphine derivative as compared with that of the PMe$_3$ complex strongly suggests that the complexes have one or two phosphine ligands at the coordination sites perpendicular to the acetylacetonate ring. Thus the bisphosphine complexes except for the PMe$_3$ complex can be assigned to the *trans*(P,P) isomers. This assignment is supported by absorption spectra of those complexes. The complexes show the strong first d-d band as compared with that of the corresponding Ph$_2$PCH$_2$CH$_2$PPh$_2$ complex which is easily assigned to the *cis* isomer by appearance of two kinds of the methyl signals of acac in the ^{1}H NMR spectrum (Fig. 4). The bisphosphine complexes of a *cis*(P,P) type would show the first d-d band weaker than that of the Ph$_2$PCH$_2$CH$_2$PPh$_2$ complex by analogy with spectra of the [Co(acac)$_2$(P)$_2$]$^+$-type complexes as stated previously. The PMe$_3$ complex shows the weaker first d-d band than those of the other three bisphosphine complexes, but it is still stronger than that of the Ph$_2$PCH$_2$CH$_2$PPh$_2$ complex, suggesting the *trans*(P,P) isomer.

The preference of the *trans*(P,P) configuration in the [Co(CN)$_2$(acac)(P)$_2$]-type complex would result from the stronger *trans* effect of a cyanide ion than that of a phosphine. In general, ligands which exhibit a strong *trans* effect tend to avoid the *trans* positions to each other.[13] Hence the *trans*(C,C) and *trans*(P,C) configurations will be less favorable than the *trans*(P,P) configuration. Further, the bulkiness of phosphine ligands would still facilitate the *trans*(P,P) configuration.

The [Co(CN)$_4$(P)$_2$]$^-$ Complexes. There are two possible geometrical isomers, *cis* and *trans*, for the [Co(CN)$_4$(P)$_2$]-type complex. In this study, only one isomer was obtained for each of the bisphosphine complexes of this type. For the structural assignment of the bisphosphine complexes, no NMR spectra give useful information. However, the complexes show absorption spectra similar to one another, indicating the same geometrical configuration, although the spectra shift remarkably depending on the kind of the phosphine ligands (Fig. 5). In addition, the complexes exhibit a strong band or shoulder in the first d-d band region, the intensities of which are much stronger than that of the corresponding band of [Co(CN)$_4$(Ph$_2$PCH$_2$CH$_2$PPh$_2$)]$^-$. Thus the bisphosphine complexes can be assigned to the *trans*(P,P) configuration on the same consideration as that described for the other phosphine complexes. The reason for the preference of the *trans*(P,P) configuration in the [Co(CN)$_4$(P)$_2$]$^-$-type complex is not clear. When the strength of the *trans* effect of cyanide and phosphine ligands is taken into account, the *cis*(P,P) configuration would be more favorable than the *trans*-(P,P) one as stated previously. There might be a factor that stabilizes the planar-type coordination of four cyanide ligands in the complexes concerned.

This work was partly supported by the Kurata Research Grant of the Kurata Foundation. The authors wish to thank Dr. T. Ito of Institute for Molecular Science for obtaining ^{13}C NMR spectra.

References

1) "Transition Metal Complexes Containing Phosphorus, Arsenic and Antimony Ligands," ed by C. A. McAuliffe, Macmillan Press, London (1973); C. A. McAuliffe and W. Levason, "Phosphine, Arsine and Stibine Complexes of the Transition Elements," Elsevier, Amsterdam (1979).

2) G. N. Schrauzer and J. Kohnle, *Chem. Ber.*, **97**, 3056 (1964).
3) W. C. Trogler and L. G. Marzilli, *Inorg. Chem.*, **14**, 2942 (1975); R. C. Stewart and L. G. Marzilli, *ibid.*, **16**, 424 (1977).
4) H. Nishikawa, K. Konya, and M. Shibata, *Bull. Chem. Soc. Jpn.*, **41**, 1492 (1968).
5) K. Watanabe, H. Nishikawa, and M. Shibata, *Bull. Chem. Soc. Jpn.*, **42**, 1150 (1969).
6) K. Kashiwabara, K. Katoh, J. Fujita, H. Nishikawa, and M. Shibata, *Chem. Lett.*, **1981**, 575.
7) L. Maier, "Organic Phosphorus Compounds," ed by L. Maier and G. M. Kosolapott, Wiley, New York (1972), Vol. 1, p. 1.
8) K. Kashiwabara, I. Kinoshita, T. Ito, and J. Fujita, *Bull. Chem. Soc. Jpn.*, **54**, 725 (1981).
9) L. J. Boucher, C. G. Coe, and D. R. Herring, *Inorg. Chim. Acta*, **11**, 123 (1974).
10) A. W. Adamson, A. Chiang, and E. Zinato, *J. Am. Chem. Soc.*, **91**, 5467 (1969).
11) N. Maki and K. Ohshima, *Bull. Chem. Soc. Jpn.*, **43**, 3970 (1970).
12) L. Cambi and E. Paglia, *Gazz. Chim. Ital.*, **88**, 691 (1970); H. H. Chen, M. S. Taso, R. W. Garer, P. H. Tewari, and W. K. Wilmarth, *Inorg. Chem.*, **5**, 1913 (1966).
13) For example, F. Basolo and R. G. Pearson, "Mechanism of Inorganic Reactions," John Wiley & Sons, New York (1967), Chap. 5.
14) R. D. Archer and B. P. Cotsoradis, *Inorg. Chem.*, **4**, 1584 (1965).
15) S. Fujinami and M. Shibata, *Bull. Chem. Soc. Jpn.*, **46**, 3443 (1973).
16) C. A. Tolman, *Chem. Rev.*, **77**, 183 (1978).
17) J. M. Jenkins and B. L. Shaw, *J. Chem. Soc., A*, **1966**, 770.
18) G. M. Bancraft and E. T. Libbey, *Can. J. Chem.*, **51**, 1482 (1973).

The Solvent Extration of Amino Acids with Crown Ether[1)]

Hideyuki Noguchi,* Hiroyoshi Nakamura, Masatoshi Nagamatsu, and Masaki Yoshio

Faculty of Science and Engineering, Saga University, Saga 840

(Received July 3, 1981)

Protonated amino acids were extracted with crown ether and Metanil Yellow anion into 1,2-dichloroethane. The overall extraction constants (K_{ex}) for the 1:1:1 complex, AHLIn, of 18-crown-6 (L) with protonated amino acid (AH^+), and the Metanil Yellow anion (In^-) between 1,2-dichloroethane and water have been determined at 25.0 °C. The values of the extraction constants (log K_{ex}) were found to be 5.2, 6.2, 6.4, 6.3, 5.5, 6.2, and 5.5 for L-α-alanine, L-valine, L-leucine, L-phenylalanine, β-alanine, L-lysine, and aspartic acid respectively at 25.0 °C. The dependence of the varieties of crown ether on the extractability of L-leucine has been investigated. The highest extractability was obtained when water-soluble crown ether was used.

The solvent extraction of cationic metal ions with crown ether (L) has been widely carried out,[2)] the results indicate the dependence of the extractability on the cavity size of crown ether. Very few studies of the solvent extraction of organic species with crown ether have, however, been done. This work has been carried out in order to study the extraction of some organic species, amino acids, with crown ether. It is well known that the ammonium ion and protonated amine make a relatively stable complex with crown ether. A small difference in stability constant between primary and secondary amine complexes with crown ether has been observed.[3)] The present authors have previously indicated that the selectivity of crown ether for various type of amines can be improved by using the solvent-extraction method.[4)] Most amino acids include the $-NH_2$ group, its protonated form being able to complex with crown ether.

Therefore, the solvent extraction of amino acids (A) with crown ether as Metanil Yellow salt (AH^+LIn^-) has been attempted in this work. Metanil Yellow (In^-) was selected as the counter anion because of its larger dissociation constant and because it has its absorption in the visible region for spectrophotometric analysis.

Experimental

Reagents. 18-Crown-6 was synthesized by Gokel's method[5)] and recrystallized twice from acetonitrile. The acetonitrile was removed under a high vacuum (0.5 mmHg†) over a 5-h period. Crown ether shows no significant hydroxyl or cyano vibration in the 3500 and 2000 cm^{-1} infrared region. "Dibenzo-18-crown-6" was synthesized by the method of Pedersen[6)] and recrystallized from benzene. The polyether thus obtained showed a melting point and an infrared spectrum identical with those of an authentic sample. "Dicyclohexyl-18-crown-6" and the other crown ethers were obtained from the Nisso Co. and were used without further purification. The 1,2-dichloroethane and other reagents were of an analytical or special grade, and were used without purification.

Extraction Procedures. A typical extraction procedure was as follows: 25 ml of an aqueous solution containing 4×10^{-4} M (1 M=1 mol/dm^3) L-leucine and 6×10^{-5}—2.4×10^{-4} M Metanil Yellow was shaken with 10 ml of 1,2-dichloroethane containing 2×10^{-3}—1.6×10^{-2} M crown ether when 18-crown-6 was used. After equilibrium had been reached, the absorbance in the organic phase was measured at 404 nm with a Hitachi 124 spectrophotometer in a 10 mm cell.

HIn, HLIn, and AHLIn contribute to the absorbance in the organic phase at 404 nm. HIn, however, did not show the absorbance in the pH range from 2 to 4. Therefore, the absorbance of AHLIn can be corrected by the blank test, which is related to that of HLIn. The constant pH value of 2.8±0.1 was selected in order to produce a precipitate at the phase boundary in the pH range lower than 2.

† 1 mmHg≈133.322 Pa.

Results and Discussion

When a protonated amino acid (AH^+) forms a complex with a crown ether, the complex can be extracted as an ion-pair with a large anion (In^-); the distribution ratio of amino acid, D, in the pH range 2—4 can be written as:

$$D = \frac{[AHLIn]_{org}}{[A]+[AH^+]}. \quad (1)$$

Here, K_{ex} is the overall extraction constant for the complex:

$$K_{ex} = \frac{[AHLIn]_{org}}{[AH^+][L]_{org}[In^-]}. \quad (2)$$

Combining these two equations gives the following equation:

$$D = K_{ex}[L]_{org}[In^-]\left(1+\frac{K}{[H^+]}\right)^{-1}, \quad (3)$$

where K is the dissociation constant of protonated amino acid.

Under the condition of a constant pH, the distribution ratio as a function of the concentration of the crown ether in the organic phase at 25.0 °C showed a straight line with a slope of 1, while that as a function of the Metanil Yellow also showed a straight line with a slope of 1, as is shown in Figs. 1 and 2. These results show that the 1,2-dichloroethane extracts is a 1:1:1 complex composed of crown ether, amino acid, and Metanil Yellow. From Figs. 1 and 2, the values of log K_{ex} are found to be 5.2, 6.2, 6.4, 6.3, 5.5, 6.2, and 5.5 for L-α-alanine, L-valine, L-leucine, L-phenylalanine, β-alanine, L-lysine, and L-aspartic acid respectively at 25.0 °C. As was seen in the previous paper,[4)] the value of K_{ex} depends greatly on the number of hydrogen atoms available for hydrogen bonding with crown ether. In this case, the difference in K_{ex} is very small, because all of the amino acids investigated have the same number

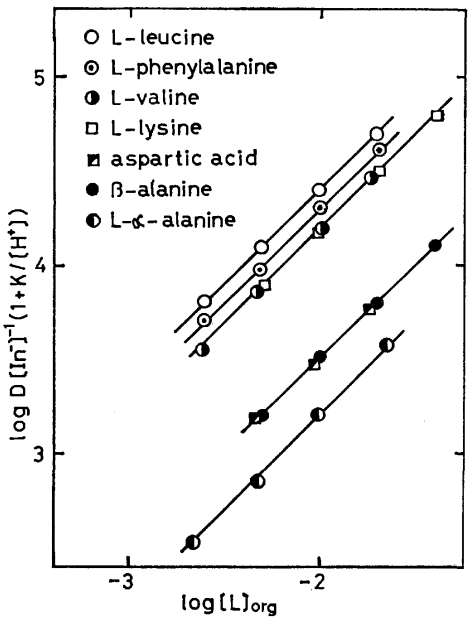

Fig. 1. Plots of $\log D\,[In^-]^{-1}\,(1+K/[H^+])$ *vs.* $\log [L]_{org}$ for amino acids at 25.0 °C.

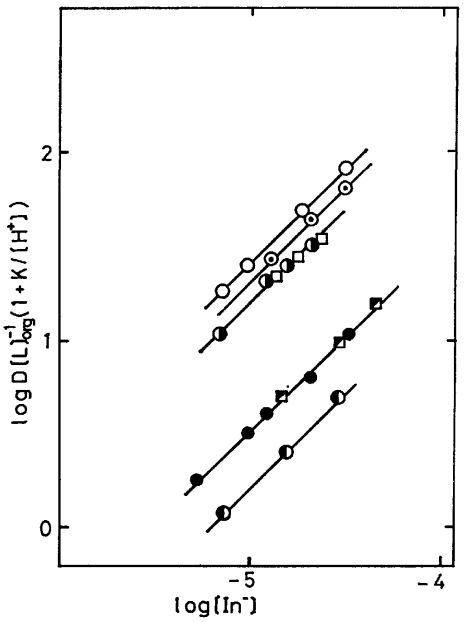

Fig. 2. Plots of $\log D\,[L]_{org}^{-1}\,(1+K/[H^+])$ *vs.* $\log [In^-]$ for amino acids at 25.0 °C.

of hydrogen atoms, $-NH_3^+$. The small difference in K_{ex} may be due to the effect of the size of the amino acids, which was also shown in the previous paper.[4]

The dependence of the varieties of crown ether on the extractability of amino acid, L-leucine, was also investigated. The extractability of L-leucine decreased in the following order: 18-crown-6>"dicyclohexyl-18-crown-6">"dibenzo-18-crown-6".

18-Crown-6, which is very soluble in water, gives rise to the most enhanced extractability, indicating that extractability is increased with an increase in the solubility of crown ether in water when the ring size of crown ether is the same.

Table 1. Extraction constants and related values of L-leucine at 25 °C

	$\log K_{ex}$	$K_{d,L}$	K_{dAHLIn}/K_{AHLIn}[a]
18-Crown-6	6.4	1.1	2.8×10^6
"Dicyclohexyl-18-crown-6"	6.1	760	9.6×10^8
"Dibenzo-18-crown-6"	4.5	3200	1.0×10^8

a) Values calculated from K_{ex} and $K_{d,L}$ using Eq. 4.

The overall extraction constant could be written as follows:

$$K_{ex} = \frac{K_{d,AHLIn}K_{AHLIn}}{K_{d,L}}, \quad (4)$$

where $K_{d,L}=[L]_{org}/[L]$, $K_{d,AHL\,In}=[AHL\,In]_{org}/[AHL\text{-}In]$, and $K_{AHL\,In}=[AHLIn]/[AH^+][L][In^-]$. The overall extraction constants (25.0 °C) obtained are shown in Table 1.

Table 1 also shows the values of $K_{d,L}$ and $K_{d,AHL\,In}$ $K_{AHL\,In}$, which were calculated from the values of K_{ex} and $K_{d,L}$.

Equation 4 shows that the trend for K_{ex} reflects $K_{AHL\,In}$ and the distribution coefficients of the AHLIn and L species. It is well known that the hydrophobic species are extracted more easily than the hydrophilic species. The values of $K_{d,AHL\,In}$ $K_{AHL\,In}$ increase with an increase in the hydrophobic nature of crown ether, which may reflect the extractability of the compound, AHLIn. However, the effect of $K_{d,L}$ on the extractability is much greater than that of the last term in Table 1.

The extraction of L-leucine with crown ether having a bigger pore size than 18-crown-6 was also investigated. The same trend of extractability was obtained: "dicyclohexyl-24-crown-8">"dibenzo-24-crown-8". The extractability of L-leucine with the 18-membered crown ethers is much greater than with the 24-membered.

Thus, the distribution coefficient of the crown ether, $K_{d,L}$ in Eq. 4 is the most important factor in determining the magnitude of K_{ex} for amino acid. Thus, a soluble crown ether in water, such as 18-crown-6, may be considered a promising reagent for the separation and extraction of amino acids.

References

1) Application of Crown Ether to Chemical Analysis. IV.

2) T. Sekine, H. Wakabayashi, and Y. Hasegawa, *Bull. Chem. Soc. Jpn.*, **51**, 645 (1978); T. Sekine, K. Shioda, and Y. Hasegawa, *J. Inorg. Nucl. Chem.*, **41**, 571 (1979); H. Sumiyoshi, K. Nakahara, and K. Ueno, *Talanta*, **24**, 763 (1977); T. Iwachido, M. Kimura, and K. Tōei, *Chem. Lett.*, **1976** 1101; A. Sadakane, T. Iwachido, and K. Tōei, *Bull. Chem. Soc. Jpn.*, **48**, 60 (1975); Y. Takeda and H. Katō, *ibid.*, **52**, 1027 (1979); Y. Takeda and H. Gotō, *ibid.*, **52**, 1920 (1979); Y. Takeda, *ibid.*, **52**, 2501 (1979); P. R. Danesi, H. Meider-Gorican, R. Chiarizia, and G. Scibona, *J. Inorg. Nucl. Chem.*, **37**, 1479 (1975); Y. Marcus and L. E. Aser,

J. Phys. Chem., **82**, 1246 (1978).

3) J. L. Roberts, R. E. McClintock, Y. El-Omrani, and J. W. Larson, *J. Chem. Eng. Data*, **24**, 79 (1979); R. M. Izatt, N. E. Izatt, B. E. Rossiter, J. J. Christensen, and B. E. Haymores, *Science*, **199**, 995 (1978); H. K. Frensdorff, *J. Am. Chem. Soc.*, **93**, 600 (1971); R. M. Izatt, D. P. Nelson, J. H. Rytting, and J. J. Christensen, *ibid.*, **93**, 1619 (1971).

4) H. Noguchi, M. Yoshio, K. Kawahara, H. Nakamura, and M. Nagamatsu, *Anal. Lett.*, **13A**, 271 (1980).

5) G. W. Gokel and D. J. Cram, *J. Org. Chem.*, **39**, 2445 (1974).

6) C. J. Pedersen, *J. Am. Chem. Soc.*, **89**, 7017 (1967).

 © 1982 The Chemical Society of Japan Bull. Chem. Soc. Jpn., 55, 159—166 (1982)

Attractive Interactions between Carbonyls and Groups Bearing Lone-pair Electrons in Triptycene Systems[1]

Michinori Ōki,* Giichi Izumi, Gaku Yamamoto, and Nobuo Nakamura

Department of Chemistry, Faculty of Science, The University of Tokyo, Bunkyo-ku, Tokyo 113

(Received February 2, 1981)

Compounds which carry a methoxyl or a chloro group in 1-position and a substituted carbonylmethyl group in 9-position of the triptycene system have been prepared to examine populations of rotamers by ^{1}H NMR spectra. The methoxy compounds favored the $\pm sc$ conformations, whereas the *ap* conformations were relatively favored in the chloro compounds. The results indicate that there are attractive interactions between the carbonyls and a methoxyl or a chloro group and are discussed from the electron-accepting ability of the carbonyl group and the electron-donating ability of the methoxyl and the chloro groups. An aldehyde group was apparently less able to interact with electron-donors than a ketone. This apparent anomaly was discussed from the intramolecular dipolar interactions.

Some five years ago, we encountered an unusual phenomenon that in a triptycene system a charge-transfer type interaction can occur between a phenyl and a dimethoxybenzo group, of which the former is acting as an electron-acceptor.[2] It is not unusual to observe that a benzene derivative carrying strongly electronegative group(s) does act as an electron-acceptor; usually, benzene and its alkyl derivatives are considered to be an electron-donor. This unusual phenomenon may be considered to appear in the situation that two substituents located in the 1 and 9 positions of the triptycene skeleton are so close to each other that a weak, otherwise not-detectable interaction is made observable. This consideration aroused our interest in extending our work to find potential, weak interactions which are theoretically feasible but have not yet been observed experimentally.

Carbonyl groups are known to possess low-lying π^* orbitals[3] which should facilitate interactions with easily ionizable electrons. Indeed, nitrogen-carbonyl interactions in medium-sized rings are well-documented.[4] Bürgi *et al.*[5] performed X-ray crystallographic studies of such compounds and suggested a pyramidal, rather than planar, configuration for the carbonyl group. Oxygen-carbonyl interactions, though much weaker, are also known.[6] Although our system will not permit us to adopt a variety of electron donating groups because of difficulties in syntheses, yet it allows us at least to vary peri-substituents to some extent. This method of approach will enable us to explore possibilities of interactions involving less electron-donating systems, especially when a strongly electron-accepting group such as the carbonyl group is present in the bridgehead position. In addition, a variety of carbonyl moieties may be introduced into the bridgehead position. This introduction will afford information about the electron-accepting ability of various carbonyl derivatives and is intriguing in that the information made available so far is confined to ketones niteracting with nitrogen or oxygen atoms. Thus, we planned to introduce formyl, acetyl, methoxycarbonyl, and cyano groups as carbonyl modifications into the bridgehead position and methoxyl and chloro groups into the *peri*-position.

Syntheses of the compounds examined were carried out in essentially four ways. When appropriate 9-(substituted methyl)anthracenes were available, they were treated with tetrachlorobenzyne (Eq. 1).

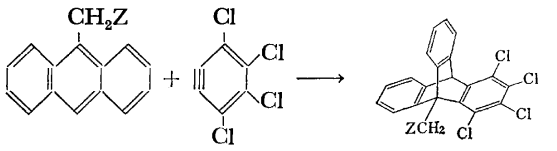

(1)

1 Z=COOCH$_3$
2 Z=CN

In the syntheses of 1,4-dimethoxytriptycene derivatives, the anthracenes were treated with *p*-benzoquinone to afford Diels-Alder adducts (**3**) which were enolized by a base and were methylated with dimethyl sulfate (Eq. 2).

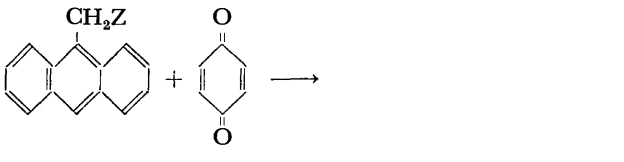

(2)

3

4 Z=C(CH$_3$)=CH$_2$
5 Z=CN
6 Z=COOCH$_3$
7 Z=C≡CCH$_3$

Some of the carbonyl derivatives were prepared by ozonolysis of the corresponding olefins (Eq. 3).

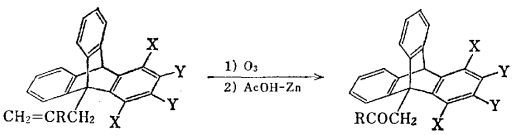

(3)

8 X=OCH$_3$, Y=R=H
9 X=OCH$_3$, Y=H, R=CH$_3$
10 X=Y=Cl, R=H
12 X=CH$_3$, Y=R=H
13 X=Y=H, R=CH$_3$

9-(Acetylmethyl)-1,2,3,4-tetrachlorotriptycene (**11**) was prepared from the corresponding aldehyde (**10**) by a Grignard reaction followed by oxidation (Eq. 4). The similar treatment of the methoxy derivative has failed to give the expected ketone because of cyclization.[7]

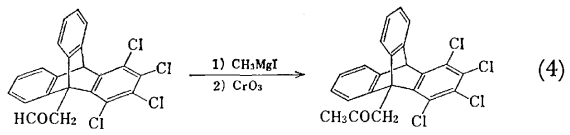

(4)

10 **11**

Detection of *ap* and ±*sc* isomers owes to the fact that, if the internal rotation about the C_9–C_{subst} bond is frozen on the NMR time scale, the methylene protons in the bridgehead give an AB quartet signal for the ±*sc* and a singlet for the *ap* in its proton NMR spectrum. The triptycene derivatives usually showed a broad signal due to the methylene protons in the 9-position at room temperature and the signal split into a set of AB quartet and a singlet in typical cases at low temperatures.

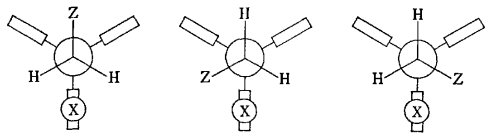

ap-form −*sc*-form +*sc*-form

Experimental

9-(Formylmethyl)-1,4-dimethoxytriptycene (8). To a solution of 1.6 g of 9-allyl-1,4-dimethoxytriptycene[7] in 80 mL of dichloromethane was introduced ozone at −78 °C until the solution changed to faint blue. The solvent was removed below 30 °C and the residue was heated with 1.5 g of zinc dust, 30 mL of acetic acid, and 5 mL of water for 1 h. The acetic acid was removed and the residue was extracted with dichloromethane. Recrystallization of the product from benzene–hexane afforded the desired compound as crystals, mp 252—253 °C, in 91% yield. Found: C, 81.02; H, 5.57%. Calcd for $C_{24}H_{20}O_3$: C, 80.88; H, 5.65%. ^{1}H NMR ($CDCl_3$, δ): 3.63 (3H, s), 3.81 (3H, s), 3.60—4.60 (2H, br. m), 5.96 (1H, s), 6.54 (2H, s), 6.90—7.60 (8H, m), 9.96 (1H, t, J=1.8 Hz).

9-(Formylmethyl)-1,2,3,4-tetrachlorotriptycene (10), mp 223—224 °C, was similarly prepared from 9-allyl-1,2,3,4-tetrachlorotriptycene[8] in 92% yield. Found: C, 60.71; H, 2.69; Cl, 32.10%. Calcd for $C_{22}H_{12}OCl_4$: C, 60.89; H, 2.79; Cl, 32.66%. ^{1}H NMR ($CDCl_3$, δ): 3.50—5.00 (2H, br. m), 6.11 (1H, s), 6.90—7.80 (8H, m), 9.40—10.5 (1H, br. m).

9-(Formylmethyl)-1,4-dimethyltriptycene (12), mp 227—228.5 °C, was similarly prepared by ozonation of 9-allyl-1,4-dimethyltriptycene.[8] Found: C, 88.99; H, 5.96%. Calcd for $C_{24}H_{20}O$: C, 88.86; H, 6.21%. ^{1}H NMR ($CDCl_3$, δ): 2.46 (6H, s), 4.14 (2H, d, J=2 Hz), 5.69 (1H, s), 6.58 (1H, d, J=8 Hz), 6.62 (1H, J=8 Hz), 6.80—7.50 (8H, m), 9.92 (1H, t, J=2 Hz).

1,4-Dimethoxy-9-(2-methyl-2-propenyl)triptycene (4). A mixture of 2 g (82 mmol) of magnesium, 2 mL of 2-methyl-2-propenyl chloride, 5 mL of tetrahydrofuran, and a small amount of iodine was allowed to react. After the initial reaction subsided, 50 mL of tetrahydrofuran was added. To the mixture, 10 mL of 2-methyl-2-propenyl chloride in 50 mL of tetrahydrofuran was added in 3 h at room temperature. Anthrone (5 g or 26 mmol) was added to the mixture in small portions and the mixture was sitrred for 1 h. The mixture was treated with water and then with concentrated hydrochloric acid. The mixture formed two layers. The tetrahydrofuran layer was separated, dried over calcium chloride, and concentrated. The product was chromatographed on silica gel, hexane being used as an eluent. 9-(2-Methyl-2-propenyl)anthracene was obtained in 75% yield. ^{1}H NMR ($CDCl_3$, δ): 1.94 (3H, s), 4.26 (3H, apparent s), 4.78 (1H, br. s), 7.30—8.25 (8H, m), 8.35 (1H, s).

The anthracene (1.5 g) and 0.8 g of *p*-benzoquinone in 20 mL of toluene were heated under reflux under a nitrogen atmosphere for 3 h and allowed to stand for 24 h. A Diels-Alder adduct which crystallized out from the mixture was collected and dissolved in 50 mL of dioxane. The solution was treated with 0.5 g of sodium hydroxide in 10 mL of water and dimethyl sulfate was added until an intense color faded. The process was repeated a few times until the coloration could not be observed on addition of alkaline solutions. The mixture was poured into water and the resulted solid was collected. It was recrystallized from benzene–hexane, mp 199.5—200.5 °C. The yield was 81%. Found: C, 84.84; H, 6.40%. Calcd for $C_{26}H_{24}O_2$: C, 84.75; H, 6.56%. ^{1}H NMR ($CDCl_3$, δ): 2.10 (3H, s), 3.62 (3H, s), 3.78 (3H, s), *ca.* 3.75 (2H), 4.21 (1H, br. s), 4.90 (1H, br. s), 5.89 (1H, s), 6.48 (2H, s), 6.80—7.50 (8H, m).

9-(Acetylmethyl)-1,4-dimethoxytriptycene (9). A solution of 1,4-dimethoxy-9-(2-methyl-2-propenyl)triptycene in dichloromethane was ozonized as above and the resulted ozonide was decomposed in the presence of zinc dust to give the product, mp 289.0—289.8 °C, in 73% yield. Found: C, 81.21; H, 5.87%. Calcd for $C_{25}H_{22}O_3$: C, 81.06; H, 5.98%. ^{1}H NMR ($CDCl_3$, δ): 2.47 (3H, s), 3.80 (3H, s), 3.60—4.70 (2H, br. m), 5.90 (1H, s), 6.51 (2H, s), 6.80—7.30 (8H, m). At −30 °C, the broad signal at *ca.* δ 4 became a distinct quartet, δ's being 4.60 and 3.81 and J being 17 Hz.

9-(Acetylmethyl)triptycene (13), mp 217—218 °C, was similarly prepared from 9-(2-methyl-2-propenyl)triptycene by ozonation. Found: C, 89.06; H, 5.97%. Calcd for $C_{23}H_{18}O$: C, 89.00; H, 5.85%. ^{1}H NMR ($CDCl_3$, δ): 2.55 (3H, s), 4.09 (2H, s) 5.49 (1H, s), 6.80—7.50 (12H, m).

9-(Cyanomethyl)-1,4-dimethoxytriptycene (5), mp 273—274 °C, was prepared as above: 9-(cyanomethyl)anthracene[9] and *p*-benzo quinone were allowed to react and the product was methylated. The yield was 78%. Found: C, 81.54; H, 5.28; N, 4.26%. Calcd for $C_{24}H_{19}NO_2$: C, 81.57; H, 5.42; N, 3.96%. ^{1}H NMR ($CDCl_3$, δ): 3.80 (6H, s), 4.18 (2H, br. s), 5.92 (1H, s), 6.58 (2H, s), 6.90—7.70 (8H, m).

9-(Methoxycarbonylmethyl)-1,4-dimethoxytriptycene (6). 9-(Methoxycarbonylmethyl)anthracene was prepared from the corresponding carboxylic acid[10] by the usual esterification. An adduct between 9-(methoxycarbonylmethyl)anthracene and *p*-benzoquinone was prepared as above and converted to the triptycene derivative, mp 223.8—224.8 °C. The yield was 85%. Found: C, 77.98; H, 5.72%. Calcd for $C_{25}H_{22}O_4$: C, 77.70; H, 5.74%. ^{1}H NMR ($CDCl_3$, δ): 3.62 (3H, s), 3.78 (3H, s), 3.80 (3H, s), 3.40—4.40 (2H, br. m), 6.53 (2H, s), 6.80—7.60 (8H, m).

9-(2-Butynyl)-1,4-dimethoxytriptycene (7). To a solution of 2.8 g (32 mmol) of 1-chloro-2-butyne and 5.6 g (29 mmol) of anthrone in 150 mL of ethanol, was added a solution of 1.7 g (30 mmol) of potassium hydroxide in 30 mL of methanol in 3 h under a nitrogen atmosphere. The mixture was stirred for an additional hour after the addition. The solvent was evaporated and the residue was taken up in dichloromethane. The solution was washed with water and evaporated. The residue was taken up in 100 mL of methanol and to the solution was added 0.7 g of sodium borohydride in 30 mL of methanol. The solvent was evaporated and the residue was shaken with dichloro-

methane and dilute hydrochloric acid. The organic layer was evaporated and the residue was chromatographed on a silica-gel column. The crude anthracene derivative thus obtained was treated with *p*-benzoquinone and then converted to the triptycene derivative. The desired compound was obtained by recrystallization from benzene–hexane in 42% yield based on 1-chloro-2-butyne. Mp 253.0—253.3 °C. Found: C, 85.14; H, 5.89%. Calcd for $C_{26}H_{22}O_2$: C, 85.22, H, 6.05%. ^{1}H NMR ($CDCl_3$, δ): 1.73 (3H, t, J=2.5 Hz), 3.69 (3H, s), 3.75 (3H, s), 4.13 (2H, br. q, J=2.5 Hz), 5.89 (1H, s), 6.80—8.00 (8H, m).

9-(Acetylmethyl)-1,2,3,4-tetrachlorotriptycene (11). To a Grignard solution prepared by adding methyl iodide in ether until 0.5 g (21 mmol) of magnesium disappaered, was added 0.9 g (21 mmol) of 9-(formylmethyl)-1,2,3,4-tetrachlorotriptycene in 20 mL of dichloromethane in 20 min. After further 10 min, the mixture was decomposed with dilute hydrochloric acid. The organic layer gave 93% 9-(2-hydroxypropyl)-1,2,3,4-tetrachlorotriptycene, mp 232—234 °C. High resolution MS (observed M^+): 447.9933, 449.9917, 451.9940, and 453.9963. $C_{23}H_{16}OCl_4$ requires 447.9956, 449.9927, 451.9897, and 453.9868. The relative intensities of the peaks agreed well with those calculated from the natural abundance of ^{35}Cl and ^{37}Cl. ^{1}H NMR ($CDCl_3$, δ): 1.69 (1H, br. s), 1.77 (3H, d, J=6.51 Hz), 3.81 (2H, m), 4.31 (1H, m), 6.03 (1H, s), 7.00—7.76 (7H, m), 8.49 (1H, m).

The hydroxylic compound (0.5 g) in 30 mL of acetone–dichloromethane (2:1) was oxidized at 0 °C by mixing with 0.42 g of chromium(VI) oxide, 0.2 mL of sulfuric acid, and 0.2 mL of water for 2 h. The solvent was evaporated and the mixture was extracted with dichloromethane. The organic layer was washed with water and evaporated. The residue was recrystallized from tetrahydrofuran–hexane to afford a pure sample, mp 276—277 °C, in 95% yield. Found: C, 61.82; H, 2.94; Cl, 31.51%. Calcd for $C_{23}H_{14}OCl_4$: C, 61.64; H, 3.15; Cl, 31.64%. ^{1}H NMR ($CDCl_3$, δ): 2.56 (3H, s), 3.40—5.10 (2H, br. q), 6.01 (1H, s), 6.80—7.70 (8H, m).

9-(Methoxycarbonylmethyl)-1,2,3,4-tetrachlorotriptycene (1). To a boiling solution of 0.73 g of 9-(methoxycarbonylmethyl)-anthracene and 0.8 mL of isopentyl nitrite in 10 mL of dichlomethane, was added a solution of 0.85 g of tetrachloroanthranilic acid[11] in 5 mL of acetone in 1.5 h. The mixture was heated for further 1 h and filtered while hot to remove an acridone derivative. The solvent was evaporated and the residue was chromatographed to give a mixture of a 1,4-adduct and the desired 9,10-adduct. Since the solubility of the desired product in carbon tetrachloride was very low, the solvent could be used for separation. Recrystallization from tetrahydrofuran–hexane gave a pure sample, mp 247.3—248.0 °C, in 8% yield. Found: C, 59.25; H, 2.95%. Calcd for $C_{23}H_{14}O_2Cl_4$: C, 59.52; H, 3.04%. ^{1}H NMR ($CDCl_3$, δ): 3.81 (3H, s), 3.5—5.2 (2H, br. m), 6.05 (1H, s), 7.00—7.80 (8H, m).

9-(Cyanomethyl)-1,2,3,4-tetrachlorotriptycene (2), mp >300 °C, was prepared similarly from 9-(cyanomethyl)anthracene and tetrachlorobenzyne. Found: C, 61.58; H, 2.39; N, 3.51; Cl, 32.56%. Calcd for $C_{22}H_{11}NCl_4$: C, 61.29; H, 2.57; N, 3.25; Cl, 32.89%. ^{1}H NMR ($CDCl_3$, δ): 4.48 (2H, br. s), 6.09 (1H, s), 7.00—7.80 (8H, s).

9-(2-Hydroxypropyl)-1,4-dimethoxytriptycene. 9-(Formylmethyl)-1,4-dimethoxytriptycene was treated with a Grignard solution prepared from magnesium and methyl iodide in ether. The reaction gave 9-(2-hydroxypropyl)-1,4-dimethoxytriptycene, mp 224—225 °C. Found: C, 80.69; H, 6.31%. Calcd for $C_{25}H_{24}O_3$: C, 80.62; H, 6.49%. ^{1}H NMR ($CDCl_3$, δ): 1.50 (3H, d, J=7 Hz), 2.55 (1H, m), 3.45 (2H, d, J=7 Hz), 3.70 (3H, s), 3.77 (3H, s), 4.65 (1H, m), 5.89 (1H, s), 6.90—8.15 (8H, m).

Table 1. $\pm sc/ap$ ratios of 1,4-dimethoxytriptycene derivatives

Compound	9-Substituent	$\pm sc/ap$	Observed temp/°C
9	CH_2COCH_3	≥10	−30
6	CH_2COOCH_3	≥10	−30
8	CH_2CHO	≥10	−45
5	CH_2CN	1.5	−50
7	$CH_2C{\equiv}CCH_3$	0.1	−60

Table 2. $\pm sc/ap$ ratios of 1,2,3,4-tetrachlorotriptycene derivatives

Compound	9-Substituent	$\pm sc/ap$	Observed temp/°C
11	CH_2COCH_3	≥10	−20
1	CH_2COOCH_3	6	−40
10	CH_2CHO	1.1	−20
2	CH_2CN	0	−40

Spectral Measurements and Population Determinations. ^{1}H NMR spectra were obtained on a Hitachi R 20B spectrometer, operating at 60 MHz and equipped with a temperature variation accessory, and ^{13}C NMR spectra on a JEOL FX-60 spectrometer operating at 15 MHz. Low temperatures were calibrated by the chemical shift difference of methanol protons. Infrared spectra were obtained on a JASCO DS-402G spectrometer with a CaF_2 cell of 0.05 mm thickness. All the spectra were obtained as solution in chloroform or chloroform-*d* unless otherwise stated. Populations of rotamers were obtained by integration of the methylene signals (an AB quartet and a singlet) in the ^{1}H NMR spectra. Where proton signals, other than those of the 9-CH_2, which are split for the respective rotamers at low temperatures are available, those were used to obtain the population ratios, because they give usually clearer results. Examples are formyl protons of **8** and **10**, and dimethoxybenzo protons of **5**.

X-Ray Crystallography. Crystals of 9-(formylmethyl)-1,4-dimethyltriptycene (**12**) suitable for the X-ray diffraction study were grown from hexane–benzene. A crystal of 0.4 mm × 0.4 mm × 0.2 mm size was mounted on a Rigaku Automatic Structure Analysis System RASA-II and data were obtained with graphite-monochromated Cu $K\alpha$ radiation. A total of 3576 independent reflections were observed up to 135° in 2θ, and 2575 of the total was judged effective ($F \geq 2\sigma$). The crystal was orthorhombic with space group *Pbca*, having the following crystal data: a=15.374(4), b=9.801(2), c=23.112(3), Z=8, D_x=1.24 g cm^{-3}. The structure was solved by the direct method with the use of the MULTAN program. The final R factor was 7.0% including hydrogens.

Results and Discussion

Population ratios obtained by integrating ^{1}H NMR signals due to the $\pm sc$ and the ap forms are listed in Tables 1 and 2.

The data in Table 1 suggest that, if an electron-accepting group is an aldehyde, a ketone, or an ester and an electron-donor is a methoxyl group, the ap

form is not detectable. Since the steric effect is expected to disfavor the $\pm sc$ form, as discussed later, the results indicate that there exists a strong attractive interaction between those carbonyl groups and a methoxyl group in proximity.

In contrast, if the electron-accepting group is a nitrile, the population ratio $\pm sc/ap$ is greatly decreased. Since the $\pm sc/ap$ ratio is 2.0 from the statistical stand point, the value of 1.5 may be argued that there is no attractive interaction between a cyano and a methoxyl group. It is especially so, if one takes into account a fact that 9-ethyl-1,4-dimethoxytriptycene, in which no attractive interaction is apparent, is reported to give $\pm sc/ap$ ratio of 0.7.[12] In order to diagnose the presence or absence of the attractive interactions in the nitrile (**2**), we have used a model compound. Since the carbon atom in the cyano group is triply bonded to a nitrogen, an acetylenic bond may be used as a model for the cyano group: an acetylene group is sterically of a similar size with a cyano group but the electron-accepting ability is far less than the cyano. As is seen in Table 1, the $\pm sc/ap$ ratio of 9-(2-butynyl)-1,4-dimethoxytriptycene (**7**) is only 0.1. Thus we conclude that there is an attractive interaction, although weak, between a cyano and a methoxyl group in this system. Since the steric effect disfavors the $\pm sc$ form, the observed value becomes less than the statistical, reflecting the weakness of the interaction.

As to a model for other compounds, an allyl group may be used as a model for a formylmethyl group: the steric sizes of these two groups are similar as far as we discuss the steric interactions between those and the methoxyl group in 1 position, because the main effect is given by CH= groups in both cases, and the electronic interaction should be minimal between the methoxyl group and the vinyl group. The population ratio $\pm sc/ap$ of 9-allyl-1,4-dimethoxytriptycene was 0.7 to indicate that the interaction between the formyl and the methoxyl group in compound **8** is fairly strong.

The data in Table 2 are indicative of several interesting points. The most apparent phenomenon is that the $\pm sc/ap$ ratios are greatly diminished relative to the methoxy derivatives, although the existence of an attractive interaction is certain. ^{13}C NMR data obtained with $CDCl_3$ solutions were in accord with the indication by the ^1H NMR spectra (chemical shifts given from TMS): **1** showed a broad singlet for the methylene carbon at 34 ppm and two singlets at 170.6 and 171.7 ppm for the carbonyl carbon at −50 °C, whereas **10** gave two singlets both for methylene (41.0 and 42.4 ppm) and for carbonyl (200.7 and 202.4 ppm) carbons. Being a weak electron-acceptor, the cyano group of **2** does not make it possible to show a sign of existence of the $\pm sc$ isomer. A similar phenomenon was found in more congested systems.[13] The results are in conformity with the expectation from the ionization potentials of 1,4-dimethoxybenzene[14] and 1,2,3,4-tetrachlorobenzene,[15] the former being lower than the latter.

Since we are looking at the population ratios as the results of combination of electronic, steric and other effects, we may not forget the steric effect. The chloro group is known to be a little larger than the methoxyl group, if the steric effect is given by the oxygen atom only in the latter. Therefore, the steric effect of the chloro group disfavors the $\pm sc$ form as well, relative to the methoxyl group. The critical case is the formyl compound (**10**), since its population ratio is lower than the statistical value: there remains a problem whether we should conclude that the attractive interaction is apparent in this compound. We used 9-(formylmethyl)-1,4-dimethyltriptycene (**12**) as a model compound which has a substituent of a similar size in the peri-position, yet the electronic effect between the formyl and the substituent in the peri-position is negligible: a methyl group is known to be a little larger than a chloro group but the difference is not large. The results show that **12** exists as the *ap* form exclusively. From these, we conclude that there is an attractive interaction between the chloro and the formyl group in this system.

Table 3. Carbonyl stretching absorptions

Compound	*peri*-Substituent	Bridgehead Substituent	$\nu_{C=O}/cm^{-1}$
10	Cl	CH_2CHO	1725
1	Cl	CH_2COOCH_3	1731, 1754
11	Cl	CH_2COCH_3	1741
8	OCH_3	CH_2CHO	1720
6	OCH_3	CH_2COOCH_3	1722, 1751
9	OCH_3	CH_2COCH_3	1742
13	H	CH_2COCH_3	1732

The third and the most striking feature of the data in Table 2 is the fact that the apparent strength of the interaction between the formyl and the chloro groups is weaker than those involving a methoxycarbonyl or an acetyl group. This is rather astonishing since, in ordinary organic reactions, aldehydes are more reactive and are consequently considered to be more electrophilic than ketones and esters. There must be reasons causing this anomalous phenomenon.

When the molecules like the aldehydes (**8**, **10**, and **12**), the ketones (**9** and **11**), and the esters (**1** and **6**) are considered, the stereoisomerism about the C_{CO}–C_α bond is possible in addition to that about the C_9–C_{subst} bond. The possible conformations of the carbonyl moiety are depicted in the following scheme, the $\pm sc$ conformations being taken as examples. Indeed, the rotational isomerism of the esters of a similar system has been found by ^1H NMR and IR spectra.[16] In order to obtain information about the conformation of the carbonyl moieties, the infrared spectra were examined. The results are shown in Table 3.

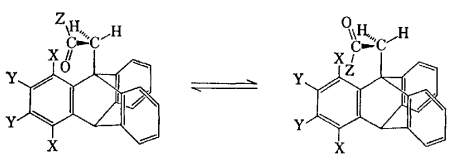

O-inside *O*-outside

A peculiarity is immediately singled out from the

Table 4. Atomic positional parameters ($\times 10^4$) with estimated standard deviations in parentheses and anisotropic temperature factors ($\times 10^4$)[a)]

Atom	x	y	z	B_{11}	B_{22}	B_{33}	B_{12}	B_{13}	B_{23}
C(1)	4490 (2)	2928 (4)	2528 (1)	47	92	14	−1	0	6
C(2)	3840 (3)	3392 (4)	2914 (1)	58	115	12	−3	4	5
C(3)	3125 (3)	4111 (4)	2733 (2)	49	124	17	−2	8	−4
C(4)	2994 (2)	4409 (4)	2143 (1)	39	90	16	1	5	−2
C(4a)	3621 (2)	3944 (3)	1762 (1)	32	67	14	−4	1	2
C(5)	4428 (2)	6136 (3)	639 (1)	41	83	13	−2	−1	3
C(6)	5237 (2)	6721 (4)	529 (1)	48	94	13	−11	2	6
C(7)	5985 (2)	6092 (4)	725 (2)	38	124	16	−19	2	4
C(8)	5949 (2)	4851 (4)	1024 (1)	32	109	14	−5	0	1
C(8a)	5143 (2)	4247 (3)	1119 (1)	33	84	10	−2	1	0
C(9)	4970 (2)	2869 (3)	1421 (1)	31	80	12	6	0	4
C(9a)	4369 (2)	3229 (3)	1941 (1)	35	70	12	−3	1	2
C(10)	3566 (2)	4172 (3)	1109 (1)	28	75	13	0	0	3
C(10a)	4388 (2)	4911 (3)	939 (1)	33	73	10	−2	0	−1
C(11)	3639 (2)	2771 (3)	836 (1)	31	76	12	−4	3	2
C(12)	4373 (2)	2058 (3)	1009 (1)	35	75	12	−4	4	3
C(13)	4494 (2)	731 (4)	807 (2)	44	85	18	4	6	−1
C(14)	3893 (3)	167 (4)	418 (2)	57	90	20	−15	8	−9
C(15)	3178 (3)	904 (4)	239 (2)	46	113	17	−25	3	−5
C(16)	3037 (2)	2211 (4)	453 (1)	37	96	13	−17	1	1
C(17)	5248 (3)	2149 (5)	2793 (2)	71	189	14	36	−2	16
C(18)	2207 (3)	5207 (5)	1957 (2)	51	164	24	33	9	−2
C(19)	5819 (2)	2104 (4)	1547 (2)	34	110	17	15	0	7
C(20)	6332 (2)	1822 (4)	985 (2)	28	111	46	19	5	−10
O	6937 (2)	1136 (5)	982 (2)	70	367	43	43	12	−1

a) The form of the anisotropic temperature factor is: $T=\exp(-B_{11}h^2-B_{22}k^2-B_{33}l^2-2B_{12}hk-2B_{13}hl-2B_{23}kl)$.

data in Table 3. Whereas the esters show two absorptions, other carbonyls give only one absorption. Although it is clear that there are two conformations, *O*-inside and *O*-outside, for the esters from the analogy of the similar system,[16] it is not apparent that other carbonyls exist in a single conformation. Especially because there is only one band in spite of the fact that at least there are two conformations concerning the rotation about the C_9–C_{subst} bond, there is a possibility that the infrared spectra cannot distinguish the rotamers which are actually present. The infrared spectra do suggest, however, that the data in Table 3 are anomalous in that the aldehydes show absorptions due to the C=O stretching at lower frequencies than those of ketones. This is the opposite of normal trends[17] and the anomaly is caused because the ketones absorb at abnormally high frequencies.

There may be various reasons for raising frequencies of C=O stretching vibrations. The most commonly encountered reason is the syn-parallel arrangement of two strong dipoles. For example, 2-halocyclohexanone is known to show C=O stretching absorptions at higher frequencies when the halogen is equatorial.[18] This kind of effect is considered to be stronger if the conformation is $\pm sc$ than the case of ap conformation in the systems examined here because the distance between the two parallel dipoles, C–Cl and C=O, is smaller in the former. Thus if the diople interaction is the cause for the IR results, the ketones should take *O*-inside conformations and the aldehydes *O*-outside conformations. Another possible cause is the steric effect. 2,6-Di-*t*-butylphenols are known to show abnormally high frequencies for the O–H stretching vibration[19] and the shift to the high frequency is attributed to the steric effect of the *t*-butyl groups. Schleyer *et al.* used this interpretation for the assignment of the two O–H stretching absorptions of cyclohexanol derivatives.[20] Birdcage compounds are known to show ν_{C-H} absorptions at abnormally high frequencies[21] and bicyclo[3.3.1]nonane systems show high C–H stretching absorptions as well.[22] If it is the *O*-inside conformation, the carbonyl stretching vibration will absorb at higher frequencies, as judged from the analogous phenomena presented above. Then the ketones take *O*-inside conformations and the aldehyde *O*-outside conformations, if the steric effect is the cause.

These discussions lead to a prediction that, if we can see the real conformation of these compounds and if the carbonyl absorptions correspond to one conformation, we can see the real reason for the phenomenon. Consideration of the steric effect gives, although not definite, a clue for judging the probability of the two possible causes. The reason for the existence of the two conformers, *O*-inside and *O*-outside, of the esters in the literature[16] is the similar bulkinesses of a methoxyl and an oxo group of the ester moiety. If the bulkiness of one side of a plane is much different from the other side, a conformation, in which the bulkier side is outside of the triptycene skeleton, is favored to a great extent relative to another which

Table 5. Bond lengths and bond angles involving nonhydrogen atoms of **12** with estimated standard deviations in parentheses

	Bond lengths(l/Å)		
C(1)-C(2)	1.4147 (52)	C(8a)-C(10a)	1.3895 (47)
C(1)-C(9a)	1.4015 (44)	C(9)-C(9a)	1.5556 (42)
C(1)-C(17)	1.5207 (58)	C(9)-C(12)	1.5443 (43)
C(2)-C(3)	1.3712 (56)	C(9)-C(19)	1.5335 (46)
C(3)-C(4)	1.4079 (49)	C(10)-C(10a)	1.5075 (44)
C(4)-C(4a)	1.3833 (46)	C(10)-C(11)	1.5143 (45)
C(4)-C(18)	1.5031 (56)	C(11)-C(12)	1.3980 (45)
C(4a)-C(9a)	1.4094 (44)	C(11)-C(16)	1.3821 (45)
C(4a)-C(10)	1.5295 (43)	C(12)-C(13)	1.3947 (47)
C(5)-C(6)	1.3939 (50)	C(13)-C(14)	1.4027 (54)
C(5)-C(10a)	1.3874 (45)	C(14)-C(15)	1.3791 (56)
C(6)-C(7)	1.3807 (52)	C(15)-C(16)	1.3909 (53)
C(7)-C(8)	1.3996 (52)	C(19)-C(20)	1.5448 (59)
C(8)-C(8a)	1.3895 (47)	C(20)-O	1.1475 (57)
C(8a)-C(9)	1.5443 (43)		
	Bond angles(ϕ/°)		
C(2)-C(1)-C(9a)	116.7 (0.3)	C(12)-C(9)-C(19)	111.9 (0.3)
C(2)-C(1)-C(17)	116.7 (0.3)	C(1)-C(9a)-C(4a)	119.8 (0.3)
C(9a)-C(1)-C(17)	126.6 (0.3)	C(1)-C(9a)-C(9)	128.4 (0.3)
C(1)-C(2)-C(3)	126.6 (0.3)	C(4a)-C(9a)-C(9)	111.8 (0.3)
C(2)-C(3)-C(4)	122.6 (0.3)	C(4a)-C(10)-C(10a)	106.3 (0.2)
C(3)-C(4)-C(4a)	116.6 (0.3)	C(4a)-C(10)-C(11)	106.0 (0.2)
C(4a)-C(4)-C(18)	123.4 (0.3)	C(10a)-C(10)-C(11)	105.9 (0.2)
C(4)-C(4a)-C(9a)	123.1 (0.3)	C(5)-C(10a)-C(8a)	121.0 (0.3)
C(4)-C(4a)-C(10)	122.8 (0.3)	C(5)-C(10a)-C(10)	125.6 (0.3)
C(9a)-C(4a)-C(10)	114.0 (0.3)	C(8a)-C(10a)-C(10)	113.3 (0.3)
C(6)-C(5)-C(10a)	119.2 (0.3)	C(10)-C(11)-C(12)	112.7 (0.3)
C(5)-C(6)-C(7)	119.9 (0.3)	C(10)-C(11)-C(16)	125.7 (0.3)
C(6)-C(7)-C(8)	121.1 (0.3)	C(12)-C(11)-C(16)	121.5 (0.3)
C(7)-C(8)-C(8a)	118.9 (0.3)	C(9)-C(12)-C(11)	113.9 (0.3)
C(8)-C(8a)-C(9)	126.7 (0.3)	C(9)-C(12)-C(13)	127.3 (0.3)
C(8)-C(8a)-C(10a)	119.7 (0.3)	C(11)-C(12)-C(13)	118.7 (0.3)
C(9)-C(8a)-C(10a)	113.5 (0.3)	C(12)-C(13)-C(14)	119.5 (0.3)
C(8a)-C(9)-C(9a)	104.7 (0.2)	C(13)-C(14)-C(15)	120.8 (0.3)
C(8a)-C(9)-C(12)	105.9 (0.2)	C(14)-C(15)-C(16)	120.0 (0.3)
C(8a)-C(9)-C(19)	111.5 (0.3)	C(11)-C(16)-C(15)	119.4 (0.3)
C(9a)-C(9)-C(12)	103.9 (0.2)	C(9)-C(19)-C(20)	111.3 (0.3)
C(9a)-C(9)-C(19)	118.0 (0.3)	C(19)-C(20)-O	121.6 (0.5)

has the bulkier group inside.[23] Since the sizes of a hydrogen and an oxo group in a formyl group are different to a large extent, the formyl group in compounds **8**, **10**, and **12** will take an *O*-outside conformation. Similar consideration suggests that the acetyl group in compounds **9**, **11**, and **13** will take *O*-inside conformations. Thus the steric effect hypothesis is more likely than the dipole interaction hypothesis.

If the charge-transfer type interaction is responsible to the observed population ratios, the interacting carbonyl groups are expected to have elongated C=O bond, thus shifting the carbonyl stretching frequencies to the low side. The fact that the C=O stretching absorption of compound **8** is at a little lower frequency than that of compound **10** may be taken as an indication of this effect, but we failed to obseve any bifurcation of absorptions in the ordinary measurements. The tetrachloroaldehyde (**10**) was shown to exist as a mixture of almost 1:1 *ap* and ±*sc* conformations. Therefore this compound was considered to have the highest possibility of showing two bands in the $\nu_{C=O}$ region. A detailed study of this compound did show two absorptions at 1725 and 1720 cm^{-1}, the latter being a shoulder. This fact suggests that the carbonyls in these compounds absorb at similar frequencies if their types, aldehydes or ketones, are given, irrespective to the presence or absence of the interaction. Alternatively, the interaction is not so strong as to cause a large shift in C=O stretching vibrations in these compounds.

The final and strongest support to the conformation of the ketones and the aldehydes can be obtained by X-ray crystallography. Accordingly X-ray-diffraction study was carried out on crystals of 9-(acetylmethyl)-1,2,3,4-tetrachlorotriptycene (**11**)[24] and 9-(formylmethyl)-1,4-dimethyltriptycene (**12**). The details of

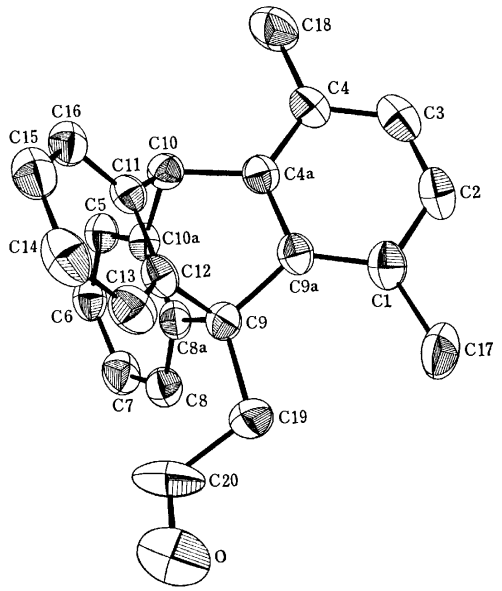

Fig. 1. An ORTEP diagram of 1,4-dimethyl-9-(formylmethyl)triptycene.

the results of the former will be described elsewhere but it is clear that the acetyl group takes an *O*-inside conformation both in $\pm sc$ and *ap* forms of **11**. The results of the X-ray structural determination of compound **12** are shown in Tables 4 and 5 and in Fig. 1, where carbon atoms are numbered, as shown in the figure for the convenience of discussion.

The feature of the structure of **12** is that the formyl group takes the *O*-outside conformation among others which follow. The steric strain caused by the substituents in 1- and 9- positions is released by deformation of the molecule throughout, as was the case of 9-*t*-butyl-1,2,3,4-tetrachlorotriptycene.[25] Although $\angle$C(4a)–C(4)–C(18) is widened from the normal value due to the steric effect of C(10), the angle is smaller than $\angle$C(9a)–C(1)–C(17). The 9-substituent is tilted against C(17) as well to relieve the steric strain. Consequently, $\angle$C(19)–C(9)–C(9a) is considerably widened. It is interesting to note also that the trigonal pyramid, of which apex is C(9) and base atoms are C(9a), C(8a), and C(12), has a smaller apex angle than that composed of an apex of C(10) and a base of C(4a), C(10a), and C(11). This may be attributed to the steric effect caused by the two substituents. The steric strain is also eased by widening angles, which are made by the bonds connecting C(9) (and C(10) to a lesser extent) and aromatic rings, and the aromatic C–C's which are outside of the triptycene skeleton. Finally the lengths of the bonds connecting C(9) with aromatic carbons are definitely longer than those connecting C(10) with aromatic carbons, although the degree of elongation is much less than those in 9-*t*-butyl-1,2,3,4-tetrachlorotriptycene. The dihedral angles made by benzene rings are as follows: $\phi(C_{8a}$–C_9–$C_{12})=121.0°$, $\phi(C_{9a}$–C_9–$C_{12})=119.4°$, $\phi(C_{8a}$–C_9–$C_{9a})=119.5°$. The hydrogen of the aldehyde group, being small, does not seem to affect the dihedral angle, in contrast to the case of 9-(acetylmethyl)-1,2,3,4-tetrachlorotriptycene.[24] Although we do neither have any piece of evidence that the structure in the solid state is retained in solutions, nor that the structure is common in all compounds of the same type, we may conclude, from pieces of evidence given by various sources discussed above, that the aldehydes take *O*-outside conformations and the ketones *O*-inside conformations.

After establishing the conformations of the aldehydes and the ketones, we may now discuss the cause for the unexpected stability of the $\pm sc$ conformation of ketone **11**. In the ketone, if the acetyl group takes the *O*-inside conformation, we realize that the bond dipoles of the C=O and the C–Cl in the *peri*-position are anti-parallel in the $\pm sc$ conformation. In contrast, the bond dipoles of the C=O in the aldehyde (**10**) and the C–Cl in the *peri*-position are syn-parallel. These arrangements of the dipoles will make the $\pm sc$ conformation of **10** less stable in nonpolar solvents and that of **11** favorable in the same solvents: the relative arrangements of the bond dipoles are the same in *ap* conformations as well, but the long distance will diminish the interaction probably due to the solvent intervention. Although the charge-transfer itself is of polar nature, this polar effect is very small on the populations, probably because of the weakness of the interaction. In conclusion, the apparently unusual phenomenon that the acetyl group stabilizes $\pm sc$ conformations more than the formyl group is mainly caused by the dipolar interaction within the molecules. The methoxycarbonyl compound (**1**) may be in the same category with ketone **11** because it can take the *O*-inside conformation.

Further support for the above discussion should be obtained by examining the population ratios in solvents of different polarity. Thus population ratios of compounds **5** and **10** were examined in mixed solvents. The examination of the populations of the ketones and others was abandoned because the populations were lop-sided. The results are shown in Table 6.

It may be difficult to compare the polarities of rotamers of compound **5** but we can assume that the group dipoles of the cyano and the methoxyl in the *ap* conformation is close to syn-parallel, because the methoxyl group is within the plane of the benzo-bridge and the methyl of the methoxyl group will be away from the bridgehead substituent: this conformation of the methoxyl group is probable if one considers the steric effect. Thus the *ap* form will be more polar than the $\pm sc$ form. The population ratios in solvents of different polarity agree with these considerations. The behaviors of the chloro-aldehyde (**10**) are in accord with expectation as well. Being more polar than the *ap* form, the $\pm sc$ conformation is favored in the more polar solvents.

Finally we wished to obtain thermodynamic parameters of the compounds examined. Unfortunately, however, it was not possible for many compounds to do so because of the lop-sided population of one isomer. The only compound we could examine its populations at various temperatures was 9-(formylmethyl)-1,2,3,4-tetrachlorotriptycene (**10**). The $\pm sc/ap$ ratios of this compound were 1.1 at 0, -20, and -50 °C: the populations were temperature independent. The

Table 6. $\pm sc/ap$ ratios of triptycenes in various solvents

Compound	Substituents 9-	Substituents *peri*-	$\pm sc/ap$	Temperature °C	Solvent (vol/vol)
10	CH_2CHO	Cl	1.1	−20	$CDCl_3$
			1.5	−25	$CDCl_3$-$(CD_3)_2CO$ (2 : 3)
			1.7	−25	$CDCl_3$-CD_3CN (7 : 10)
5	CH_2CN	OCH_3	1.5	−50	$CDCl_3$
			1.3	−45	$CDCl_3$-$(CD_3)_2CO$ (5 : 6)
			1.2	−45	$CDCl_3$-CD_3CN (5 : 7)

ΔH and ΔS were obtained as 0.0 kcal/mol (1 kcal= 4.18 J) and +1.0 e.u.

In conclusion we wish to point out that, for the first time, we have demonstrated that attractive interactions can be detected experimentally between carbonyl moieties, like cyano, formyl, and methoxycarbonyl, and a chloro or a methoxyl group. It is especially noteworthy because the presence of the interaction between ketones and oxygen was questionable by means[26,27] other than X-ray crystallography.[6,28] This finding is possible because two groups in *peri*- and bridgehead positions are well within the sum of van der Waals radii.[25] Therefore this triptycene system is considered very good in revealing an interaction experimentally which is not otherwise possible to do so because of its weakness. We wish to search other weak interactions with the use of this system in the future. Nitrogen carbonyl interactions were studied by X-ray crystallography and treated as an incipient transition state for the addition of a nucleophile to a ketone.[29] This work extends the possibility of studying the transition state of other systems. This aspect of the present work may have further extension.

We wish to thank Mr. Toshihiko Hori of Rigaku Denki Co., who performed the X-ray crystallography. We also wish to express our thanks to the Ministry of Education, Science and Culture for a Grant-in-Aid for Scientific Research from which a part of the cost was defrayed.

References

1) A preliminary note has been published: M. Ōki, G. Izumi, G. Yamamoto, and N. Nakamura, *Chem. Lett.*, **1980**, 213.
2) F. Suzuki and M. Ōki, *Tetrahedron Lett.*, **1974**, 2845; *Bull. Chem. Soc. Jpn.*, **48**, 596 (1975).
3) O. Eisenstein, J. M. Lefour, and C. Minot, *Tetrahedron Lett.*, **1976**, 1681.
4) N. J. Leonard, *Rec. Chem. Prog.*, **17**, 243 (1956).
5) H. B. Bürgi, J. D. Dunitz, and E. Shefter, *J. Am. Chem. Soc.*, **95**, 5005 (1973).
6) M. Kaftory and J. D. Dunitz, *Acta Crystallogr., Sect. B*, **30**, 1517 (1974).
7) G. Izumi, S. Hatakeyama, N. Nakamura, and M. Ōki, *Bull. Chem. Soc. Jpn.*, **54**, 258 (1981).
8) S. Hatakeyama, T. Mitsuhashi, and M. Ōki, *Bull. Chem. Soc. Jpn.*, **53**, 731 (1980).
9) F. Mayer, W. Schäfer, and J. Rosenbach, *Arch. Pharm.* **267**, 571 (1929).
10) F. H. C. Stewart, *Aust. J. Chem.*, **13**, 479 (1960).
11) V. Villiger and L. Blangey, *Ber.*, **42**, 3549 (1909).
12) H. Nakanishi and O. Yamamoto, *Bull. Chem. Soc. Jpn.*, **51**, 1777 (1978).
13) S. Otsuka, T. Mitsuhashi, and M. Ōki, *Bull. Chem. Soc. Jpn.*, **52**, 3663 (1979).
14) M. Klessinger, P. Asmus, and U. Kraatz, *Tetrahedron*, **31**, 517 (1975).
15) D. G. Streets and G. P. Ceasar, *Mol. Phys.*, **26**, 1037 (1973).
16) S. Otsuka, H. Kihara, T. Mitsuhashi, and M. Ōki, *Chem. Lett.*, **1978**, 475; *Bull. Chem. Soc. Jpn.*, **52**, 3667 (1979).
17) L. J. Bellamy, "The Infrared Spectra of Complex Molecules," Mathuen & Co., London (1958), p. 155.
18) R. N. Jones, D. A. Ramsay, F. Herling, and K. Dobriner, *J. Am. Chem. Soc.*, **74**, 2828 (1952); J. Allinger and N. L. Allinger, *Tetrahedron*, **2**, 64 (1958); N. L. Allinger, J. Allinger, L. A. Freiberg, R. T. Czaja, and N. A. LeBel, *J. Am. Chem. Soc.*, **82**, 5876 (1960).
19) L. A. Cohen and W. M. Jones, *J. Am. Chem. Soc.*, **85**, 3402 (1963).
20) L. Joris, P. von R. Schleyer, and E. Osawa, *Tetrahedron*, **24**, 4759 (1968).
21) L. DeVries, and P. R. Ryason, *J. Org. Chem.*, **26**, 621 (1961); D. Kivelson, S. Winstein, P. Bruck, and R. L. Hansen, *J. Am. Chem. Soc.*, **83**, 2938 (1961).
22) G. Eglinton, J. Martin, and W. Parker, *J. Chem. Soc.*, **1965**, 1243; E. D. Weil, K. J. Smith, and R. J. Gruber, *J. Org. Chem.*, **31**, 1669 (1966).
23) G. Yamanoto and M. Ōki, *Chem. Lett.*, **1979**, 1255; *Bull. Chem. Soc. Jpn.*, **54**, 481 (1981).
24) N. Nogami, Ph. D. Thesis, The University of Tokyo (1978).
25) M. Mikami, K. Toriumi, M. Konno, and Y. Saito, *Acta Crystallogr., Sect. B*, **31**, 2474 (1975).
26) N. J. Leonard, T. W. Milligan, and T. L. Brown, *J. Am. Chem. Soc.*, **82**, 4075 (1960).
27) T. T. Nakashima and G. E. Maciel, *Org. Magn. Reson.*, **4**, 321 (1972).
28) M. Kaftory and J. D. Dunitz, *Acta Crystallogr., Sect. B*, **31**, 2917 (1975).
29) H. B. Bürgi, J. D. Dunitz, J. M. Lehn, and G. Wipff, *Tetrahedron*, **30**, 1563 (1974).

 © 1982 The Chemical Society of Japan Bull. Chem. Soc. Jpn., 55, 167—170 (1982)

Stereochemistry of Friedel-Crafts Reaction of Benzene with Optically Active 2-Methyloxetane

Masahito Segi, Masaki Takebe, Shinji Masuda,** Tadashi Nakajima, and Sohei Suga*

Department of Industrial Chemistry, Faculty of Technology, Kanazawa University, Kodatsuno, Kanazawa 920

*** Ashikaga Institute of Technology, Omae-cho, Ashikaga 326*

(Received March 2, 1981)

The Friedel-Crafts alkylation of benzene with (+)-2-methyloxetane in the presence of Lewis acids ($AlCl_3$, $SnCl_4$, and $TiCl_4$) gave 3-phenyl-1-butanol with 20—60% inversion of configuration at the reaction center and a mixture of 4-chloro-2-butanol and 3-chloro-1-butanol in optically active form as the by-products. These by-products were formed by the attack of the chlorine atom in Lewis acid. The stereochemical course of the reaction to 3-chloro-1-butanol varied with the kind of catalyst, *i.e.*, inversion with $AlCl_3$ or $TiCl_4$ and retention with $SnCl_4$. The addition of nitromethane to the reaction system promoted the retentive ring-opening to 3-chloro-1-butanol.

Although the entire field of Friedel-Crafts chemistry has been reviewed in great detail,[1] the stereochemical view has been limited because of the long-standing acceptance of the free carbonium ion mechanism in the aromatic alkylation.[2] Some examples of Friedel-Crafts reactions with extensive stereochemical integrity have appeared during this decade. Brauman and his co-workers reported that the alkylation of benzene with (+)-γ-valerolactone[3] or (+)-2-methyltetrahydrofuran[4] proceeded with some inversion (47 or 35%) of configuration, and concluded that the stereospecificity was due to the cyclic nature of the alkylating reagent or the enforced proximity of ion-pairs produced from the ring opening. Previous studies in our laboratory demonstrated that optically active oxiranes reacted with benzene in the presence of Lewis acid to give the corresponding 2-phenyl-1-propanols with complete inversion of configuration.[5]

The difference in the degree of stereospecificity between the above reactions with five- and with three-membered ether prompted us to study the stereochemistry of the similar alkylation with oxetane. There have been few reports on the reaction of oxetane in the presence of Lewis acid,[6] but no stereochemical information is obtained even in the ring-opening of oxetane.

This paper describes the alkylation of benzene with (+)-2-methyloxetane in the presence of Lewis acid and the stereochemistry of the ring-opening reaction.

Results and Discussion

Treatment of (+)-2-methyloxetane (**1**) with Lewis acid in benzene below 0 °C gave 3-phenyl-1-butanol (**2**) as the alkylated product, and a mixture of 4-chloro-2-butanol (**3**) and 3-chloro-1-butanol (**4**). No 4-phenyl-2-butanol was obtained under these conditions. The structures of **2**, **3**, and **4** were identified by IR and NMR spectroscopy, and by comparison of the retention time of gas chromatography (GLC) with those of authentic samples. The yield and isomer distribution were determined by GLC analysis. The results under various conditions are summarized in Tables 1 and 2.

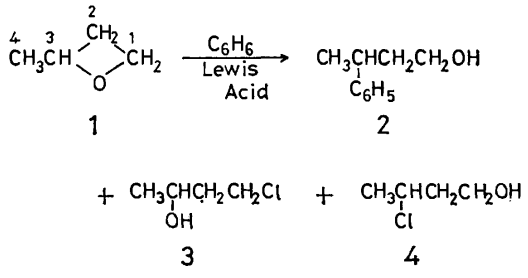

(+)-2-Methyloxetane (**1**) has S configuration, since it was prepared from (*S*)-(+)-ethyl-3-hydroxybutanoate by a series of chemical interconversions not affecting bonds to the asymmetric center, as mentioned in the experimental section. The absolute configurations of (−)-**2**, (+)-**3**, and (+)-**4** have been established to be R,[7] S,[8] and S,[9] respectively. Accordingly, it is apparent that the alkylation of benzene with (+)-**1** to (−)-**2** and the ring-opening reaction of the oxetane (formation of **4**) by aluminium chloride proceeded with inversion of configuration at the reaction center. Aluminium chloride at first coordinates with the oxygen atom of oxetane, which would result in appreciable polarization of the C_3–O bond, and then benzene attacks the C_3 atom from the back-side of the C_3–O bond.

In the case of $AlCl_3$ catalyst, as shown in Table 1, the alkylation exhibited less stereospecificity than that using propylene oxide[5a] or γ-valerolactone.[3] The optical yield of **2** increased slightly with decreasing reaction temperature. The following interpretations can be given for the less stereospecificity in the formation of **2** from **1**: first, the racemization *via* a carbonium ion intermediate and, secondly, the apparent racemization owing to the competitions between two reactions (path a and b in Scheme 1) which result in the alkylated products having the opposite configuration. Accordingly, the two-step reaction mechanism *via* (*R*)-**4** becomes significant along with the direct substitution. In fact, (*S*)-**4** reacted with benzene in the presence of $AlCl_3$ to give (*R*)-**2** with 46% inversion of configuration.[10]

When $SnCl_4$ or $TiCl_4$ was used as a catalyst, the alkylation of benzene exhibited a moderate stereospecificity with 62 and 55% optical yield, respectively. This seems to mean that the racemization mechanism through carbonium ion was depressed because of the weaker catalytic ability of $SnCl_4$ compared with that

Table 1. Friedel-crafts reaction of benzene with (+)-2-methyloxetane (**1**)[a]

Run	$[\alpha]_D$[b] of **1** °	Lewis acid	Temp °C	Time h	3-Phenyl-1-butanol (**2**) Yield[c] %	$[\alpha]_D$[d] °	Optical yield[e] %
1	+33.0	$AlCl_3$	0	0.5	62.4	−8.7	19.5
2	+33.0	$AlCl_3$	−10	0.5	36.7	−8.7	19.5
3	+33.0	$AlCl_3$	−20	0.5	5.9	−10.8	24.2
4	+33.0	$AlCl_3$	−30	2.0	8.3	−13.5	30.3
5	+33.5	$AlCl_3$-CH_3NO_2	0	2.5	7.7	−10.1	22.3
6	+31.2	$SnCl_4$	0	4.0	13.5	−26.3	62.3
7	+32.8	$SnCl_4$	−10	5.0	11.9	−27.7	62.4
8	+33.5	$SnCl_4$-CH_3NO_2	0	2.5	22.7	−18.9	41.7
9	+31.2	$TiCl_4$	0	2.5	22.9	−23.3	55.2

a) Molar ratio: (+)-**1**: Lewis acid:C_6H_6:CS_2 (or CH_3NO_2)=1:1.2:16:10(16); max$[\alpha]_D$ of *S*-(+)-**1** is +33.5°. b) Measured in chloroform (*c* 5.0). c) Based on (+)-**1** used. Determined by GLC. d) Measured in ethanol (*c* 2.4—5.0). e) Calculated from the maximum rotations of (+)-**1** and (−)-**2**. Max$[\alpha]_D$ of *R*-(−)-**2** is −45.3°.[19]

Table 2. The isomer distribution and the specific rotations of chlorobutanols (**3** and **4**) as by-products

Run	Yield[a] %	Isomer ratio[a]/% **3** : **4**	$CH_3CH(OH)CH_2CH_2Cl$ (**3**) $[\alpha]_D$[b] °	Optical yield[c] %	$CH_3CHClCH_2CH_2OH$ (**4**) $[\alpha]_D$[b] °	Optical yield[c] %
1	2.7	69 : 31	—	—	—	—
2	2.5	45 : 55	—	—	—	—
3	6.2	63 : 37	+44.0	100	−49.0	91.6
4	7.4	64 : 36	+44.0	100	−53.0	99.1
5	48.3	1 : 99	—	—	+9.6	17.7
6	32.7	8 : 92	+41.4	100	+15.2	28.0
7	30.0	4 : 96	—	—	+19.3	35.5
8	44.3	0 : 100	—	—	+17.3	31.9
9	27.8	22 : 78	+46.9	100	−20.0	39.5

a) Determined by GLC. b) Measured in chloroform (*c* 1.3—5.0). c) Calculated from the maximum rotations of (+)-**1** and (+)-**3** or (−)-**4**. Max$[\alpha]_D$ of *S*-(+)-**3** is +44.7°[20] and max$[\alpha]_D$ of *R*-(−)-**4** is −54.3°.

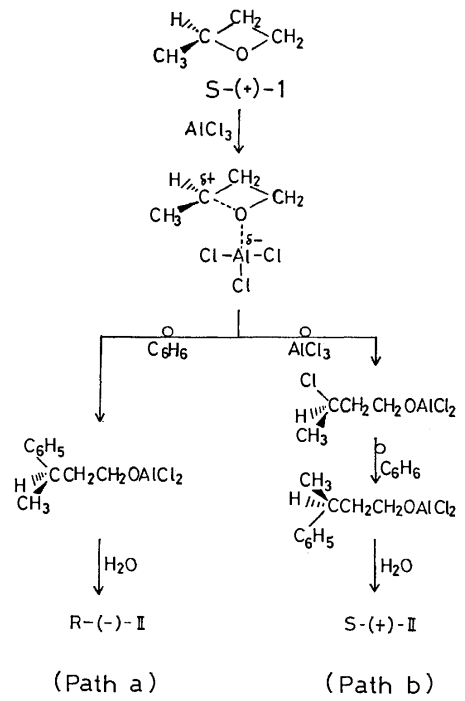

Scheme 1.

of $AlCl_3$. Furthermore, benzene did not react with 3-chloro-1-butanol in the presence of $SnCl_4$ or $TiCl_4$, so that path b in Scheme 1 should be excluded. In order to examine the possibility of racemization of the product during the reaction, (+)-**2** was treated with these Lewis acids in benzene under the same conditions as those of the alkylation. The specific rotation of this compound remained almost unchanged before and after the treatment (Table 3). Thus, it turns out that the optical yield in the presence of $SnCl_4$ or $TiCl_4$ shows a net stereospecificity in this alkylation (Table 1).

Chlorobutanol isomers (**3** and **4**), which were by-products, were separated by preparative GLC and their specific rotations were determined. As shown in Table 2, the ring-opening reaction toward **4** involves two opposite stereochemical courses: inversion with $AlCl_3$ or $TiCl_4$ and retention with $SnCl_4$. It is interesting that the formation of **4** took place with complete inversion in the presence of $AlCl_3$, despite the less stereospecificity in the alkylation (runs 1—4 in Table 1). On the other hand, the retentive ring-opening in the presence of $SnCl_4$ was observed. This retentive result was not observed in the reaction with three-membered ring oxiranes.[5] This result could be

Table 3. Treatment of (+)-3-phenyl-1-butanol (**2**) or (−)-3-chloro-1-butanol (**4**) with lewis acid in benzene[a]

Run	Substrate	Lewis acid	Temp °C	Time h	Specific rotation[b]/° Before reaction	After reaction
10	(+)-**2**	$SnCl_4$	0	4.0	+6.9	+6.9
11	(+)-**2**	$TiCl_4$	0	3.0	+6.9	+6.8
12	(−)-**4**	$SnCl_4$	20	4.5	−54.0	−53.5
13	(−)-**4**	$TiCl_4$	0	2.5	−52.1	−53.0

a) Molar ratio: (+)-**2** or (−)-**4**: Lewis acid: C_6H_6:CS_2=1:1.2:16:10. b) Measured in ethanol.

Table 4. Ring-opening reaction of (+)-2-methyloxetane (**1**) with lewis acid or hydrochloric acid[a]

Run	$[\alpha]_D$[b] of **1** °	Acid	Temp °C	Time h	Yield[c] %	Isomer ratio[c]/% **3** : **4**	$CH_3CH(OH)CH_2$-CH_2Cl (**3**) $[\alpha]_D$[b] °	O.Y.[d] %	$CH_3CHClCH_2CH_2$-OH (**4**) $[\alpha]_D$[b] °	O.Y.[d] %
14	+33.0	concd HCl	0	1.0	50.7	81 : 19	+44.1	100	−46.7	86.0
15	+32.2	$AlCl_3$	0	2.5	48.8	10 : 90	+46.3	100	−17.4	33.3
16	+33.5	$SnCl_4$	0	4.0	67.0	5 : 95	—	—	−25.0	46.0

a) Molar ratio: (+)-**1**: Lewis acid (or HCl):CS_2=1:1.2:18. b) Measured in chloroform (c 5.0). c) Determined by GLC. d) Optical yield.

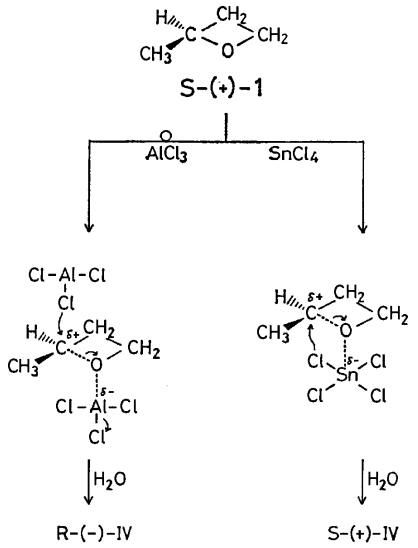

Scheme 2.

explained by considering that the conformation of the transition state fits a steric requirement which gives rise to the internal attack of the chlorine atom on the secondary carbon (Scheme 2). The configuration of 4-chloro-2-butanol (**3**) was completely retained. This shows that the successive racemization of the starting oxetane did not occur in all reactions. Further, the ring-opening of (+)-**1** with $SnCl_4$ yielded regioselectively **4** with C_3–O bond cleavage (runs 6 and 7 in Table 2).

In connection with the reaction under Friedel-Crafts condition, we examined the ring-opening reaction of (+)-**1** with aqueous hydrogen chloride or Lewis acids in CS_2 solvent. The results are presented in Table 4. The direction of ring-opening with Lewis acid differed from that with aqueous hydrogen chloride. This result is similar to that of the ring-opening reaction of propylene oxide with acids.[5a] Under Lewis acid catalyst both the C_1 and the C_3 atom adjacent to oxygen atom of **1** would develop a cationic nature to a certain extent by coordination of the Lewis acid, but especially the C_3 atom would be further stabilized because of an electron-releasing effect or a hyperconjugation of a methyl group.[11] Thus, it seems that the nucleophilic attack of the chlorine atom should take place at the C_3 atom preferentially.

Finally, some interesting results were obtained when nitromethane was added in a reaction system. $AlCl_3$–CH_3NO_2 catalyst had no influence on the stereochemistry of alkylated product, but promoted the retentive reaction of **1** to **4**, as in the case of $SnCl_4$ catalyst. The high regioselective ring-opening with C_3–O bond cleavage was observed. Similar results have been observed in the reaction of oxiranes, in which $AlCl_3$–CH_3NO_2 1:1 addition compound[12] in solution was concluded to be important for the retentive reaction and the direction of ring-opening.[13] This consideration may explain the result in the case of oxetane.

Experimental

The optical rotations were measured on a JASCO DIP-SL polarimeter with use of a 0.1 dm tube. The IR and ^{1}H-NMR spectra were recorded on a JASCO DS-301 spectrometer and a JEOL PS-100 spectrometer, respectively. Chemical shifts are given in ppm downfield from internal TMS. GLC analyses were carried out on a 2 m column of 10% Carbowax 20 M on Diasolid L with a Shimadzu GC-3A instrument.

Benzene was washed with concentrated sulfuric acid and distilled after drying on sodium ribbon. Carbon disulfide and nitromethane were dried over phosphorus pentachloride and distilled prior to use. Commercial grade aluminium chloride was purified by sublimation under a nitrogen gas stream. Commercial grade tin(IV) chloride and titanium (IV) chloride were used without further purification.

Substrate. (+)-2-Methyloxetane (1): Ethyl acetoacetate was reduced microbiologically by the reductase of baking yeast to (+)-ethyl-3-hydroxybutanoate,[14] bp 78—81 °C/17 mmHg,† $[\alpha]_D$ +36.5° (*c* 5.5, $CHCl_3$) [Lit,[14] $[\alpha]_D$ +38.5° (*c* 1.0, $CHCl_3$)], yield 73%. The hydroxybutanoate was heated under reflux with lithium aluminium hydride in THF for 30 hours and converted to (+)-1,3-butanediol, bp 108 °C/17 mmHg, $[\alpha]_D$ +32.3° (*c* 5.0, EtOH) [Lit,[15] $[\alpha]_D$ −29.6° (*c* 10, EtOH)], yield 89%. The treatment of (+)-1,3-butanediol and acetyl chloride gave a mixture of 1-chloro-3-acetoxybutane and 3-chloro-1-acetoxybutane.[16] This mixture was converted to (+)-**1** with concentrated alkali solution according to the procedure of Searles,[17] bp 60 °C, $[\alpha]_D$ +33.5° (*c* 5.0, $CHCl_3$) (Lit,[18] $[\alpha]_D$ +20.2°], yield 25%. (+)-**1** obtained in this manner seems optically pure. NMR (CCl_4, 10%): δ 1.33 (d, J=6.4Hz, 3H, $-CH_3$), 1.91—2.83 (m, 2H, $-CH_2-$), 4.19—4.63 (m, 2H, $-CH_2O-$), and 4.66—5.03 ppm (sex, J=7.2 Hz, 1H, $-CH=$).

Reaction of (+)-2-Methyloxetane (1) with Benzene in the Presence of Lewis Acid. The following example shows a typical experimental procedure. To a stirred mixture of dry benzene (18 ml) containing tin(IV) chloride (4.3 g, 16.6 mmol) and carbon disulfide (7 ml), cooled in an ice bath, a mixture of (+)-**1** (1.0 g, 13.9 mmol), benzene (2 ml), and carbon disulfide (1 ml) was added at a rate sufficient to maintain the reaction temperature. After an additional 4.0 h at 0 °C, the reaction was quenched with cooled 5% hydrochloric acid (40 ml). The organic layer was neutralized with 5% sodium hydrogencarbonate and then dried over anhydrous sodium sulfate. The yield of alkylated product was determined by GLC. After the removal of solvent, the residue was fractionated *in vacuo* to give chlorobutanol isomers (bp 70 °C/17 mmHg) and 3-phenyl-1-butanol (**2**) (bp 125 °C/17 mmHg). The water layer was extracted five times with 20 ml portions of ether. The combined organic layers were washed with water and dried over anhydrous sodium sulfate. After the removal of solvent, the residue was distilled *in vacuo* to give chlorobutanols (**3** and **4**), bp 70 °C/17 mmHg. The isomers could be separated by preparative GLC. The results are summarized in Tables 1 and 2.

Ring-opening Reaction of (+)-2-Methyloxetane (1) with Lewis Acid or Hydrochloric Acid. To a cooled and stirred mixture of carbon disulfide (12 ml) and Lewis acid or concentrated hydrochloric acid (16.6 mmol) was added a solution of (+)-**1** (1.0 g, 13.9 mmol) in carbon disulfide (2 ml) at 0 °C. The reaction mixture was worked up as mentioned above. The results are summarized in Table 4.

† 1 mmHg≈133.322 Pa.

References

1) G. A. Olah, "Friedel-Crafts and Related Reactions," Interscience Publisher, New York (1963); "Friedel-Crafts Chemistry," John Wiley and Sons, New York (1973).
2) H. Hart, "Friedel-Crafts and Related Reactions," ed by G. A. Olah, Interscience Publisher, New York (1963), Vol. 1, p. 999.
3) J. I. Brauman and A. J. Pandell, *J. Am. Chem. Soc.*, **89**, 5421 (1967).
4) J. I. Brauman and A. Solladie-Cavallo, *Chem. Commun.*, **1968**, 1124.
5) a) T. Nakajima, S. Suga, T. Sugita, and K. Ichikawa, *Bull. Chem. Soc. Jpn.*, **40**, 2980 (1967); *Tetrahedron*, **25**, 1807 (1969). b) T. Nakajima, Y. Nakamoto, and S. Suga, *Bull. Chem. Soc. Jpn.*, **48**, 960 (1975).
6) Y. Nakamoto, T. Nakajima, and S. Suga, *Kogyo Kagaku Zasshi*, **72**, 2594 (1969); P. O. I. Virtanen, S. Peltonen, and J. Hyyppa, *Acta Chem. Scand.*, **27**, 3944 (1973).
7) K. Imano and S. Mitsui, *Nippon Kagaku Zasshi*, **85**, 497 (1964).
8) (*S*)-2-Methyloxetane reacted with aqueous hydrogen chloride in CS_2 solvent to give the dextrorotatory chloride (**3**), which retains the configuration of the asymmetric center because of C_1–O bond cleavage, as shown in Table 4.
9) K. Freudenberg and W. Lwowski, *Ann. Chem.*, **597**, 141 (1955).
10) T. Nakajima, S. Masuda, S. Nakashima, T. Kondo, Y. Nakamoto, and S. Suga, *Bull. Chem. Soc. Jpn.*, **52**, 2377 (1979).
11) D. Swern, G. N. Billen, and H. B. Knight, *J. Am. Chem. Soc.*, **71**, 1152 (1949); R. E. Parker and N. S. Isaacs, *Chem. Rev.*, **59**, 737 (1959).
12) L. Schmering, *Ind. Eng. Chem.*, **40**, 2072 (1948).
13) M. Inoue, T. Sugita, Y. Kiso, and K. Ichikawa, *Bull. Chem. Soc. Jpn.*, **49**, 1063 (1976).
14) D. D. Ridley and M. Stralow, *J. Chem. Soc., Chem. Commun.*, **1975**, 400.
15) S. Murakami, T. Harada, and A. Tai, *Bull. Chem. Soc. Jpn.*, **53**, 1356 (1980).
16) R. I. Meltzer and J. A. King, *J. Am. Chem. Soc.*, **75**, 1355 (1953).
17) S. Searles, Jr., K. A. Pollart, and F. Block, *J. Am. Chem. Soc.*, **79**, 952 (1957).
18) M. Bartok and A. S. Gilde, *Acta Phys. Chem.*, **9**, 25 (1963).
19) V. Prelog and H. Scherrer, *Helv. Chem. Acta*, **42**, 2227 (1959).
20) The maximum rotation of **3** was calculated based on +20.2° of **1** (optical purity 60.3%) obtained by cyclization of (+)-**3** ($[\alpha]_D$ +26.98°) without a racemization. See Ref. 19.

Studies on the Polymerization of Acrolein Oxime. XVI.† Structure of 8-Hydroxy-1,4,5,7-tetramethyl-6,8-diazabicyclo[3.2.1]oct-6-ene 6-Oxide

Tadatoshi Ota,* Seizo Masuda, Hitoshi Tanaka, and Masaru Kido**

Department of Applied Chemistry, Faculty of Engineering, Tokushima University, Minamijosanjima-cho, Tokushima 770

** *Ōtsuka Pharmaceutical Co. Ltd., Tokushima Factory, Laboratories of Natural Products Chemistry, Kawauchi-cho, Tokushima 771-01*

(Received March 16, 1981)

The thermal oligomerization of 3-methyl-3-buten-2-one oxime leads to crystalline nitrone derivatives, 8-hydroxy-1,4,5,7-tetramethyl-6,8-diazabicyclo[3.2.1]oct-6-ene 6-oxide. Its crystal structure has been determined by X-ray diffraction. The space group is $P2_1/n$ with $a=9.459(3)$, $b=10.335(3)$, $c=11.352(4)$ Å, $\beta=105.50(2)°$, and $Z=4$.

α,β-Unsaturated aldehyde and ketone oximes which have a vinylic double bond conjugated with a C=N double bond are heated to give oligomers. For example, heating of acrylaldehyde oxime leads to an amorphous oligomer with a molecular weight of *ca.* 2000.[1] Methacrylaldehyde oxime is easily converted into the crystalline trimer, 2,4,7-trimethylperhydroisoxazolo[2,3-*a*]pyridine-2,7-dicarbaldehyde dioxime, on heating at 80 °C, but no dimer can be isolated.[2] In the course of the study of the polymerization of 3-methyl-3-buten-2-one oxime (MIKOM), it was found that MIKOM gives preferentially the cyclic dimer, 8-hydroxy-1,4,5,7-tetramethyl-6,8-diazabicyclo[3.2.1]-oct-6-ene 6-oxide (**1**). The most plausible reaction mechanism has been reported in the preceding paper;[3] *i.e.*, the Diels-Alder reaction must occur first, followed by the Michael addition. Since colorless needle-like crystals of **1** were obtained, the three-dimensional structure of this cyclic dimer was determined by X-ray analysis.

Experimental

Materials and Oligomerization. 3-Methyl-3-buten-2-one was prepared according to the procedure of White,[4] and then treated with aqueous hydroxylamine hydrochloride to give MIKOM in a 40% yield. Oligomerization of MIKOM was carried out at 80 °C for 375 h in an ampoule. The colorless solution gradually turns yellow with time. After unreacted MIKOM had been removed by distillation under reduced pressure, the residue was treated with a large amount of ether to precipitate the dimer. Yield 12%, IR (KBr): 3150 (OH), 1601 (C=N). Found: C, 60.85; H, 9.33; N, 14.42%. Calcd for $C_{10}H_{18}N_2O_2$: C, 60.58; H, 9.15; N, 14.12%. Recrystallization of the dimer from methanol solution gave colorless needle-like crystals. Mp, 147 °C.

Mass and NMR Measurements. The mass spectra were measured on a Shimadzu LKB-9000 mass spectrometer, equipped with a gaschromatographic inlet system. The ionizing potential was 70 eV, and the ionizing current was 60 μA. The ^{13}C-NMR spectra were obtained with a Hitachi R-42 FT apparatus (22.6 MHz), using DMSO-d_6 as the solvent and the internal standard.

X-Ray Measurements. A crystal of 0.2 mm × 0.2 mm × 0.3 mm in dimensions was used for data collection on a Syntex R-3 automated four-circle diffractometer with graphite-monochromated Mo $K\alpha$ radiation. The accurate unit-cell dimensions were determined by least-squares calculation. The crystal data are summarized in Table 1.

Table 1. Crystal data

$C_{10}H_{18}N_2O_2$,	M.W. = 198.27
Space group	$P2_1/n$
a/Å 9.459(3)	U/Å^3 1069(1)
b/Å 10.335(3)	$Z=4$
c/Å 11.352(4)	D_x/g cm^{-3} 1.23
β/° 105.50(2)	μ(Mo $K\alpha$)/cm^{-1} 0.9

All reflections within the range of $3° \leqq 2\theta \leqq 60°$ were collected by the use of the ω scan mode at a scan speed varying with intensities.[5] The intensities of three reference reflections were measured periodically; they showed no significant fluctuation during the course of data collection. A total of 3563 independent reflections were collected, among which 1586 reflections with $I \geqq 1.96\sigma(I)$ were used for structure refinement. The intensities were corrected for Lorentz and polarization effects, but not for absorption.

Structure Determination and Refinement. The structure was solved by the direct method and the atomic parameters were refined by the block-diagonal least-squares method. The final R-value for 710 reflections of $F_o \geqq 5$ was 0.083. In the least-squares procedure, the function minimized was $\Sigma w(|F_o| - |F_c|)^2$, where $w=1$ for 710 reflections of $F_o \geqq 5$ and $w=0$ for the others. The computer programs used were MULTAN program[6] modified for the Syntex R-3 diffractometer. All the calculations were carried out on a NOVA computer connected to the diffractometer. The atomic scattering factors were taken from "International Tables for X-Ray Crystallography."[7] The final atomic parameters are given in Table 2. The $F_o - F_c$ table and anisotropic temperature factor table are kept as Document No. 8202 at the Chemical Society of Japan.

Results and Discussion

The bond distances and bond angles are listed in Tables 3 and 4, respectively. The N(6)–C(7)–C(12) and C(7)–N(6)–O(14) angles agree fairly well with those expected from the sp^2 hybrid orbital. Considerable deviations of the N(6)–C(7)–C(1) and C(7)–N(6)–C(5) angles from the theoretical values for the sp^2 orbital may be ascribed to the highly-strained ring system. Figure 1 shows the perspective drawing of the molecule and the numbering scheme. It is a bicyclic compound having three rings; the seven-

† Part XV: T. Ota, S. Masuda, and H. Tanaka, *Chem. Lett.*, **1981**, 411.

Table 2. Atomic co-ordinates, multiplied by 10^4 foe non-hydrogen atoms and by 10^3 for hydrogen atoms

Atoms	x	y	z	Atoms	x	y	z
O(13)	12490 (4)	2570 (4)	4367 (3)	H(21)	1079 (6)	−104 (5)	203 (5)
O(14)	9092 (5)	3139 (3)	1572 (3)	H(22)	1138 (6)	−88 (5)	372 (5)
N(6)	11477 (6)	1458 (4)	4071 (4)	H(31)	877 (5)	2 (5)	166 (5)
N(8)	10023 (5)	2342 (4)	2239 (4)	H(32)	875 (6)	−105 (5)	274 (5)
C(1)	11752 (7)	807 (5)	2993 (5)	H(4)	921 (6)	63 (5)	448 (5)
C(2)	10894 (8)	−476 (5)	2887 (6)	H(91)	1419 (6)	132 (5)	309 (5)
C(3)	9248 (7)	−225 (5)	2682 (6)	H(92)	1337 (5)	−12 (5)	240 (5)
C(4)	8925 (7)	877 (5)	3469 (5)	H(93)	1393 (5)	13 (5)	407 (5)
C(5)	10019 (7)	2012 (5)	3547 (4)	H(101)	672 (6)	43 (5)	290 (5)
C(7)	11056 (6)	1651 (5)	1945 (5)	H(102)	709 (6)	146 (5)	203 (5)
C(9)	13396 (8)	560 (7)	3159 (7)	H(103)	693 (6)	212 (5)	363 (5)
C(10)	7290 (8)	1262 (6)	3002 (6)	H(111)	970 (6)	304 (5)	512 (5)
C(11)	9644 (8)	3187 (6)	4204 (5)	H(112)	903 (6)	360 (5)	383 (5)
C(12)	11232 (9)	1688 (6)	685 (6)	H(113)	1046 (5)	392 (5)	426 (5)
				H(121)	1085 (6)	234 (5)	34 (5)
				H(122)	1216 (9)	123 (8)	71 (8)
				H(123)	1046 (7)	106 (6)	14 (7)
				HO(13)	1380 (7)	229 (6)	520 (6)

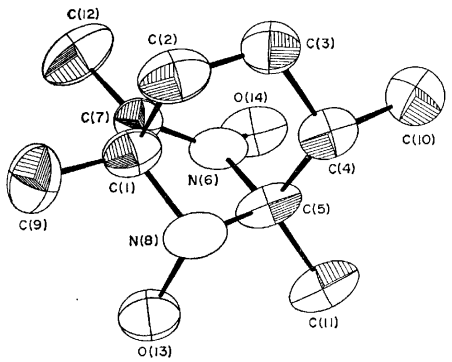

Fig. 1. A perspective drawing of **1** and the numbering scheme.

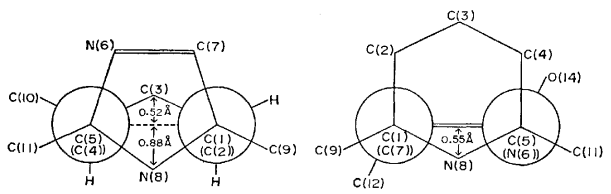

Fig. 2. Schematic drawings of the chair and half-chair forms.

membered, six-membered, and five-membered rings have a boat, chair, and half-chair comformations, respectively. All the methyl groups on the six-membered ring are equatorial, and the five-membered ring is joined to the six-membered ring through two axial–type bonds. The six- and five-membered rings are at an angle of 72.58°, *i.e.*, almost perpendicular to each other. C(1), C(2), C(4), and C(5) atoms in the six-membered ring, and C(1), N(6), C(5), and C(7) atoms in the five-membered ring are almost on a plane, respectively. The schematic drawings of the chair and half-chair forms are given in Fig. 2,

Table 3. Bond distances

Bond	Distances (l/Å)	Bond	Distances (l/Å)
N(8)-O(13)	1.455 (6)	N(6)-O(14)	1.293 (6)
N(8)-C(1)	1.492 (7)	N(8)-C(5)	1.454 (8)
N(6)-C(5)	1.524 (6)	N(6)-C(7)	1.323 (7)
C(1)-C(2)	1.542 (8)	C(1)-C(7)	1.481 (8)
C(1)-C(9)	1.537 (10)	C(2)-C(3)	1.534 (11)
C(3)-C(4)	1.528 (8)	C(4)-C(5)	1.522 (8)
C(4)-C(10)	1.547 (10)	C(5)-C(11)	1.516 (8)
C(7)-C(12)	1.483 (9)		

Table 4. Bond angles

Bond	Angle (ϕ/°)	Bond	Angle (ϕ/°)
O(13)-N(8)-C(1)	107.7 (4)	O(13)-N(8)-C(5)	107.4 (4)
C(1)-N(8)-C(5)	101.2 (4)	O(14)-N(6)-C(5)	122.3 (4)
O(14)-N(6)-C(7)	129.0 (5)	C(5)-N(6)-C(7)	108.7 (4)
N(8)-C(1)-C(2)	105.3 (5)	N(8)-C(1)-C(7)	104.2 (5)
N(8)-C(1)-C(9)	111.7 (5)	C(2)-C(1)-C(7)	109.4 (5)
C(2)-C(1)-C(9)	111.2 (5)	C(7)-C(1)-C(9)	114.5 (5)
C(1)-C(2)-C(3)	111.0 (5)	C(2)-C(3)-C(4)	113.0 (5)
C(3)-C(4)-C(5)	111.2 (5)	C(3)-C(4)-C(10)	109.2 (5)
C(5)-C(4)-C(10)	114.6 (5)	N(8)-C(5)-N(6)	103.5 (4)
N(8)-C(5)-C(4)	106.6 (4)	N(8)-C(5)-C(11)	114.9 (5)
N(6)-C(5)-C(4)	106.8 (4)	N(6)-C(5)-C(11)	111.2 (5)
C(4)-C(5)-C(11)	113.1 (5)	N(6)-C(7)-C(1)	108.3 (5)
N(6)-C(7)-C(12)	120.7 (5)	C(1)-C(7)-C(12)	130.5 (5)

using Newman's projection formula.

Figure 3 shows the crystal structure viewed along the b-axis. Only oxygen atoms take part in the hydrogen bond; O(13) forms a intermolecular hydrogen bond with O(14), the O(13)···O(14) distance being 2.659(5) Å.

Figure 4 shows the mass spectrum of **1**, which is

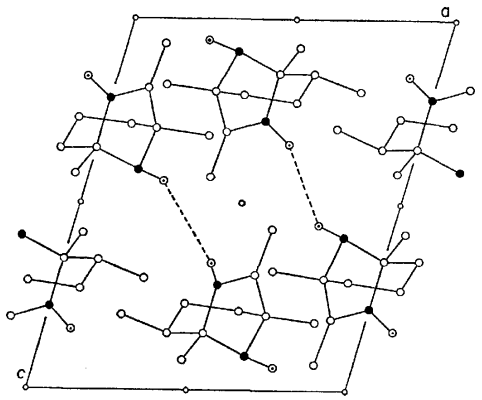

Fig. 3. The projection of the crystal structure along the b-axis.
○: Carbon, ●: nitrogen, ⊙: oxygen.

characterized by the appearance of peaks *m/e* 198 (M^+), 181, and 124, and can be satisfactorily explained on the basis of the following fragmentation pattern.[5]

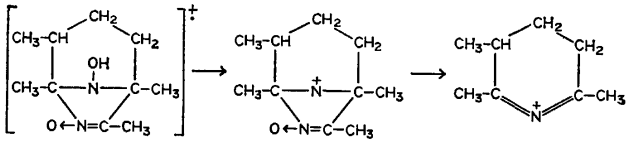

As can be expected from the structure, ^{13}C-NMR spectrum of **1**, shown in Fig. 5, shows four quartet (δ=9.24, 14.06, 16.02, and 18.94), two triplet (δ=27.73 and 32.70), one doublet (δ=36.51), and three singlet peaks (δ=71.88, 98.97, and 142.88). The quartet, triplet, and doublet peaks correspond to the methyl, methylene, and methyne carbons, respectively, and it can be presumed that the singlet peaks at 71.88, 98.97, and 142.88 ppm are assigned to the tertiary carbons linked by N–C<, $\overset{N}{N}$>C<, and $\overset{\ominus}{O}\!>\!\overset{\oplus}{N}$=C< bonds, respectively.

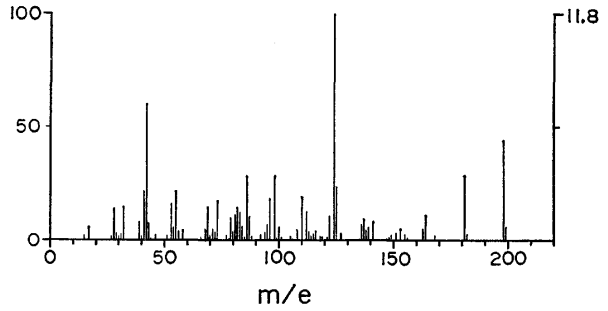

Fig. 4. Mass spectrum of **1**.

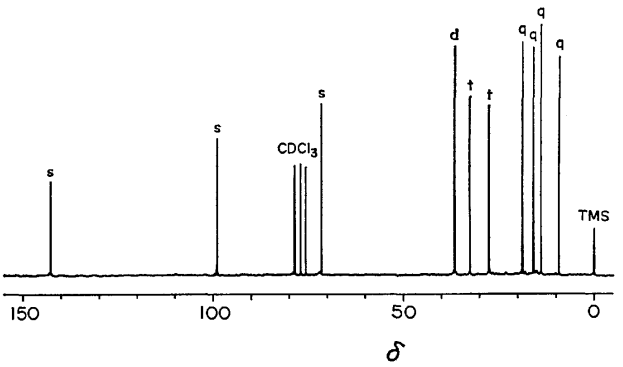

Fig. 5. ^{13}C-NMR spectrum of **1**.

References

1) S. Masuda and T. Ota, *Polym. J.*, **9**, 459 (1977).
2) T. Ota, E. Matsushima, and S. Masuda, *Polym. J.*, **11**, 909 (1979).
3) T. Ota, S. Masuda, and T. Tanaka, *Chem. Lett.*, **1981**, 411.
4) T. White, *J. Chem. Soc.*, **1943**, 238.
5) T. Ota, S. Masuda, and M. Kido, *Bull. Chem. Soc. Jpn.*, **53**, 3240 (1980).
6) G. Germain, P. Main, and M. M. Woolfson, *Acta Crystallogr., Sect. A*, **27**, 368 (1971).
7) "International Tables for X-Ray Crystallography," Kynoch Press, Birmingham (1974), Vol. IV, p. 71.

Studies on 2-Aziridinecarboxylic Acid. V.[1] Formation of Dehydroamino Acid Containing Peptides *via* the Isomerization by NaI of 2-Aziridinecarboxylic Acid Containing Peptides

Kenji Okawa,* Kiichiro Nakajima, Takumi Tanaka, and Masahiro Neya
Department of Chemistry, Faculty of Science, Kwansei Gakuin University, Nishinomiya 662

(Received March 25, 1981)

The 2-aziridinecarboxylic acid residue in peptides was isomerized with NaI in an acetone solution into the corresponding dehydroalanine or dehydro-2-aminobutyric acid derivatives, but not into the corresponding 2-oxazoline derivatives.

The isomerization of 1-acyl-2-aziridines into 2-aryl- or 2-alkyl-2-oxazolines by various nucleophiles has been investigated, and its mechanisms(Scheme 1) has been

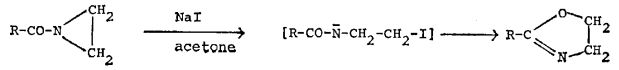

Scheme 1.

proposed.[2] The isomerization of the 2-aziridinecarboxylic acid(Azyline, Azy) residue in peptides was investigated next. Two types of Azy-peptides, *e.g.* 1-acyl-2-aziridinecarboxylic acid(**1**, **2**) and 1-acyl-3-methyl-2-aziridinecarboxylic acid peptides(**3**, **4**), were synthesized according to the procedure described in the previous paper,[3] as is summarized in Table 1.

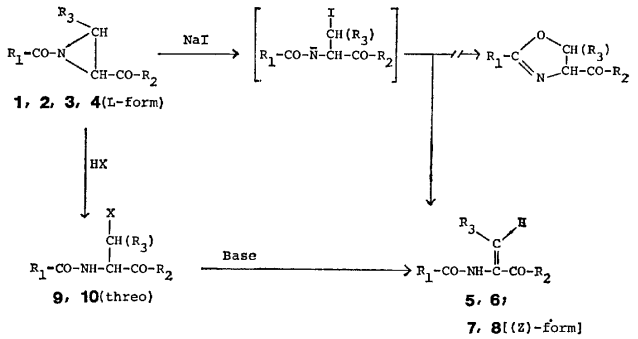

Scheme 2.

The treatment of 1-acyl-2-aziridinecarboxylic acid(**1**, **2**) and the 1-acyl-3-methyl-2-aziridinecarboxylic acid (**3**, **4**) derivatives with NaI in an acetone solution afforded dehydroalanine(⊿Ala) (**5**, **6**) peptides and dehydro-2-aminobutyric acid(⊿Aba) (**7**, **8**) peptides in high yields without any concomitant formation of 2-oxazoline derivatives, as is shown in Scheme 2, the results are summarized in Table 2. The dehydroamino acid function of these products was readily characterized by the presence of vinyl protons in the NMR spectra, as is summarized in Table 3.

In the next approach, we tried to clarify the reaction mechanism of the isomerization of Azy residues and the structure of dehydro-2-aminobutyric acid derivatives. The treatment of 1-acyl-3-methyl-2-aziridinecarboxylic acid(**4**) and 1-acyl-2-aziridinecarboxylic acid peptide(**3**) with hydrogen halide readily afforded L-*threo*-2-amino-3-halogenobutyric acid(**9**, **10**) and β-halogenoalanine derivative(**11**) respectively. These derivatives can be considered as the corresponding intermediates in the isomerization reaction of Azy residues with NaI. The subsequent treatment of these derivatives(**9**, **10**) with a tertiary amine as a base gave the corresponding dehydroamino acid peptide(**8**), which were identical with the products obtained by the isomerization of the Azy peptides with NaI in an acetone solution. The results of the dehydrogen halide reaction are also summarized in Table 2.

Based on the above data, the mechanism of the isomerization of the Azy residue upon NaI treatment was thought to be the *trans*-E_2-elimination of a 2-amino-3-iodobutyric acid intermediate, followed by the direct elimination of an α-hydrogen atom. The NMR data of the dehydro-2-aminobutyric acid derivatives indicated that both the isomerization of Azy and the dehydrogen halide reaction of L-*threo*-2-amino-3-halogenobutyric acid [Thr(Cl) or Thr(I)] derivatives occurred *via* the stereospecific *trans*-E_2-elimination reaction. Thus, only dehydro-2-aminobutyric acid derivatives of the (*Z*)-geometory were prepared.

Experimental

Uncorrected melting points are reported. The homogeneity of the products was checked by thin-layer chromatography on silica-gel plates. The optical rotations were determined at the D line on a Perkin-Elmer 141 polarimeter. The NMR spectra were obtained with a Hitachi R-20B High-resolution NMR Spectrometer, the chemical shifts being obtained using TMS as the internal reference.

All the Azy peptides used in this study were synthesized by the method described in the literature;[3] their properties and yields are summarized in Table 1.

Z-Gly-ΔAla-Gly-OBzl(5). Via *the Isomerization of Azy*: A solution of Z-Gly-L-Azy-Gly-OBzl(**1**) (200 mg, 0.47 mmol) and NaI (282 mg, 1.88 mmol) in acetone (5 ml) was refluxed for 2 h. After the solvent has been removed *in vacuo*, the residue was extracted with ethyl acetate. The ethyl acetate solution was washed with water, dried over Na_2SO_4, and then concentrated *in vacuo*. The residue was crystallized from hexane; 154 mg (78.2%); mp 134—135 °C. NMR(DMSO-d_6) δ: 5.55 (1H m, $=CH_2$), 6.20 (1H m, $=CH_2$), 9.08 (1H bs, -NH-C=). Found: C, 61.53; H, 5.50; N, 10.04%. Calcd for $C_{22}H_{23}O_6N_3 \cdot 1/2H_2O$: C, 60.82; H, 5.57; N, 9.63%.

Z-L-Ala-ΔAla-Gly-OBzl(6). Via *the Isomerization of Azy*: A solution of Z-L-Ala-L-Azy-Gly-OBzl(**2**) (200 mg, 0.46 mmol) and NaI (273 mg, 1.82 mmol) in acetone (5 ml) was refluxed for 7 h. Then the reaction mixture was worked-up as has been described above. The product was crystallized from ethyl acetate–hexane; 142 mg (71.2%); mp 128—131 °C, $[\alpha]_D^{25}$ −8.8 (*c* 1.0, DMF). NMR (DMSO-d_6) δ: 5.49 (1H m, $=CH_2$), 6.38 (1H d, J=2.0 Hz, $=CH_2$), 8.50

Table 1. Properties and yields of Azy peptides

Azy peptide	Yield/%[a]	Mp/°C	$[\alpha]_D^{23}$
Z-Gly-L-Azy-Gly-OBzl (**1**)	92.3	118—119	−52.5 (*c* 1.0, MeOH)
Z-L-Ala-L-Azy-Gly-OBzl (**2**)	83.0	128—128.5	−71.2 (*c* 1.0, $CHCl_3$)
Z-Gly-3-MeAzy-Gly-OBzl (**3**)	89.0	123.5—124.5	−58.2 (*c* 1.0, AcOEt)
Z-L-Ala-3-MeAzy-Gly-OBzl (**4**)	87.5	110—111	−59.7 (*c* 1.0, $CHCl_3$)

a) Coupled by the DCC method between Z-amino acid and Azy peptides.

Table 2. Properties and yields of dehydroamino acid derivatives

Peptide	Reagent	Product	React. time/h	Yield/%	Mp/°C	$[\alpha]_D^{23}$ (*c* 1.0, DMF)
Z-Gly-L-Azy-Gly-OBzl (**1**)	NaI	5	2[a]	78	134—135	—
Z-L-Ala-L-Azy-Gly-OBzl (**2**)	NaI	6	7[a]	71	128—131	−8.8
Z-Gly-3-MeAzy-Gly-OBzl (**3**)	NaI	7	5[a]	78	102—104	—
Z-L-Ala-3-MeAzy-Gly-OBzl (**4**)	NaI	8	2[a]	92	141—143	−8.7
Z-L-Ala-L-Thr(Cl)-Gly-OBzl (**9**)[d]	Dabco[c]	8	12	100	139—141	−9.0
Z-L-Ala-L-Thr(I)-Gly-OBzl (**10**)[e]	Dabco[c]	8	20[b]	92	141—142	−8.0

a) The reaction was carried out under refluxing in an acetone solution. b) 20 min. c) Dabco: 1,4-diazabicyclo-[2.2.2]octane. d) L-Thr(Cl): L-*threo*-2-amino-3-chlorobutyric acid. e) L-Thr(I): L-*threo*-2-amino-3-iodobutyric acid.

Table 3. NMR data of dehydroamino acid derivatives

Dehydroamino acid Peptide	NMR (δ, DMSO-d_6) =CH_2		-CH_3	-NH-
Z-Gly-⊿Ala-Gly-OBzl (**5**)[a]	5.55 (m)	6.20 (m)	—	9.08 (bs)
Z-L-Ala-⊿Ala-Gly-OBzl (**6**)[a]	5.49 (m)	6.38 (d)	—	8.50 (bs)
Z-Gly-⊿Aba-Gly-OBzl (**7**)[b]	—	6.42 (q)	1.61 (d)	9.01 (bs)
Z-L-Ala-⊿Aba-Gly-Obzl (**8**)[b]	—	6.44 (q)	1.60 (d)	9.08 (bs)

a) ⊿Ala: Dehydroalanine. b) ⊿Aba: (*Z*)-dehydro-2-aminobutyric acid.

(1H bs, -NH-CH=). Found: C, 62.76; H, 5.82; N, 9.70%. Calcd for $C_{23}H_{25}O_6N_3$: C, 62.86; H, 5.73; N, 9.56%.

Z-Gly-(Z)-ΔAba-Gly-OBzl (7). Via *the Isomerization of Azy*: A solution of Z-Gly-3-MeAzy-Gly-OBzl (**3**) (150 mg, 0.34 mmol) and NaI (205 mg, 1.36 mmol) in acetone (5 ml) was refluxed for 5 h. Then the reaction mixture was worked up as has been described above. The product was crystallized from ethyl acetate–hexane; 117 mg (78%); mp 102—104 °C. NMR (DMSO-d_6) δ: 1.61 (3H d, J= 7.0 Hz, =$CHCH_3$), 6.42 (1H q, J=7.0 Hz, =CH-), 9.01 (1H bs, -NH-C=). Found: C, 61.94; H, 6.04; N, 9.73%. Calcd for $C_{23}H_{25}O_6N_3 \cdot 1/2H_2O$: C, 61.60; H, 5.84; N, 9.37%.

Z-L-Ala-(Z)-ΔAba-Gly-OBzl (8). Via *the Isomerization of Azy*: A solution of Z-L-Ala-3-MeAzy-Gly-OBzl (**4**) (150 mg, 0.33 mmol) and NaI (200 mg, 1.32 mmol) in acetone (5 ml) was refluxed for 2 h. Then the reaction mixture was worked up as has been described above. The product was crystallized from ethyl acetate–hexane; 139.6 mg (92.4%); mp 141—143 °C, $[\alpha]_D^{23}$ −8.7 (*c* 1.0, DMF). NMR (DMSO-d_6) δ: 1.60 (3H d, J=7.0 Hz, =$CHCH_3$), 6.44 (1H q, J=7.0 Hz, =CH-), 9.08 (1H bs, -NH-C=). Found: C, 63.25; H, 5.93; N, 9.01%. Calcd for $C_{24}H_{27}O_6N_3$: C, 63.56; H, 6.00; N, 9.27%.

Via *the β-Elimination of β-Halogeno Derivative*: *i*) A solution of Z-L-Ala-L-Thr(Cl)-Gly-OBzl (**9**) (150 mg, 0.3 mmol) and 1,4-diazabicyclo[2.2.2]octane (Dabco, 67 mg, 0.6 mmol) in ethyl acetate was stirred overnight at room temperature, and then water was added to the reaction mixture. The ethyl acetate solution was dried over Na_2SO_4 and concentrated *in vacuo*. The residue was crystallized from ethyl acetate–ether–hexane; 136 mg (100%); mp 139—141 °C, $[\alpha]_D^{25}$ −9.0 (*c* 1.1, DMF).

ii) A solution of Z-L-Ala-L-Thr(I)-Gly-OBzl (**10**) (174 mg, 0.3 mmol) and Dabco (67 mg, 0.6 mmol) in ethyl acetate (10 ml) was stirred for 20 min at room temperature. The product was obtained as has been described above; 125 mg (91.9%); mp 141—142 °C, $[\alpha]_D^{25}$ −8.0 (*c* 1.0, DMF). The NMR data of these products were identical to those of the product (**8**) obtained *via* the isomerization of Azy.

Z-L-Ala-L-Thr(Cl)-Gly-OBzl (9): To a solution of Z-L-Ala-3-MeAzy-Gly-OBzl (**4**) (454 mg, 1 mmol) in acetone (10 ml) was added 1 M hydrochloric acid† (1 ml, 1 mmol) at 0 °C. After the reaction mixture had then been allowed to stand at 0 °C for 2 h, the precipitated crystals were filtered off, washed with water, and recrystallized from $CHCl_3$–ether; 478 mg (97.6%); mp 138—141 °C, $[\alpha]_D^{24}$ −1.8 (*c* 1.1, DMF). Found: C, 56.90; H, 5.51; N, 7.90; Cl, 6.70%. Calcd for $C_{24}H_{30}O_7N_3Cl$: C, 56.75; H, 5.95; N, 8.27; Cl, 6.98%.

Z-L-Ala-L-Thr(I)-Gly-OBzl (10): To a solution of Z-L-Ala-3-MeAzy-Gly-OBzl (**4**) (454 mg, 1 mmol) in acetone (10 ml) was added 1 M hydriodic acid (1 ml, 1 mmol) at 0 °C. After the reaction mixture had been allowed to stand at 0 °C for 30 min, water was added; then the precipitated crystals were filtered off, washed with water, and recrystallized from $CHCl_3$–ether; 567 mg (97.5%); mp 136—138 °C, $[\alpha]_D^{24}$ −10.4 (*c* 1.0, DMF). Found: C, 48.39; H, 4.83; N, 6.97; I, 20.86%. Calcd for $C_{24}H_{30}O_7N_3I$: C, 48.09; H, 5.04; N, 7.01; I, 21.17%.

Z-Gly-L-Ser(Cl)-Gly-OBzl (11): To a solution of Z-

† 1 M=1 mol dm^{-3}.

Gly–L-Azy–Gly–OBzl (**1**) (425 mg, 1 mmol) in acetone (10 ml) was added 1 M hydrochloric acid (1 ml, 1 mmol) at 0 °C. After the reaction mixture had been allowed to stand at 0 °C for 1 h, water was added; then the precipitated crystals were filtered off, washed with water, and recrystallized from $CHCl_3$–ether–hexane; 522 mg (100%); mp 143—145 °C, $[\alpha]_D^{24}$ −9.0 (*c* 1.0, DMF). Found: C, 55.39; H, 4.83; N, 8.97; Cl, 7.86%. Calcd for $C_{22}H_{24}O_6N_3Cl$: C, 55.52; H, 5.08; N, 8.83; Cl, 7.45%.

References

1) Part IV: T. Tanaka, K. Nakajima, and K. Okawa, *Bull. Chem. Soc. Jpn.*, **53**, 1352 (1980). The abbreviations of the IUPAC–IUB commission (*J. Biol. Chem.*, **247**, 977 (1972)) are used. Z: benzyloxycarbonyl, OBzl: benzyl ester, "Azyline" is used as name of an L-2-aziridinecarboxylic acid, "Azy" being its abbreviation. 3-MeAzy: (2*S*,3*S*)-3-methyl-2-aziridinecarboxylic acid, *Δ*Ala: dehydroalanine, *Δ*Aba: dehydro-2-aminobutyric acid, Thr(Cl): *threo*-2-amino-3-chlorobutyric acid, Thr(I): *threo*-2-amino-3-iodobutyric acid, Ser(Cl): 2-amino-3-chloropropionic acid.

2) H. W. Heine, M. E. Fetter, and E. M. Nicholson, *J. Am. Chem. Soc.*, **81**, 2202 (1959); H, W. Heine, *Angew. Chem. Int. Ed. Engl.*, **1**, 528 (1962).

3) K. Okawa, K. Nakajima, T. Tanaka, and Y. Kawana, *Chem. Lett.*, **1975**, 591.

 © 1982 The Chemical Society of Japan Bull. Chem. Soc. Jpn., 55, 177—181 (1982)

Chemistry of 1,3-Glycol Derivatives. IV. Mechanism of the Solvolyses of 2,4-Pentanediol Derivatives and the Reactions of the Proposed Intermediate Acetoxonium Ions with Carbanions and Hydride

Osamu Itoh, Naoki Iwakoshi, Toshihide Saitoh, Hiroaki Katano, Yoshiki Fujisawa, Yoshinori Hasegawa, Toshio Sugita,* and Katsuhiko Ichikawa

Department of Hydrocarbon Chemistry, Faculty of Engineering, Kyoto University, Sakyo-ku, Kyoto 606

(Received April 8, 1981)

Regio- and stereochemical studies of the solvolyses of various kinds of 2,4-pentanediol derivatives, including 2-acetoxy-4-tosylates, cyclic orthoformates and orthoacetates, have been done and the previously proposed mechanism has been partially revised. The reactions of the proposed intermediate acetoxonium ions with carbanions and with a hydride ion have also been studied.

In a previous paper,[1] some of us reported that the hydrolyses of *threo*- and *erythro*-3-acetoxy-1-methylbutyl chlorides or tosylates proceeded with inversion of configuration, while the acetolyses of the same substrates proceeded with retention of configuration; we proposed a mechanism involving a formation of a cyclic acetoxonium ion (1,3-dioxan-2-ylium ion). Further studies with the related substrates, however, have shown that a part of the proposed mechanism should be modified. This paper describes these additional results, together with the chemical behavior of the above acetoxonium ion towards several kinds of carbanions and a hydride ion.

Hydrolyses of *erythro*- and *threo*-3-acetoxy-1,2,2-trimethylbutyl tosylates (*erythro*- and *threo*-**3**) proceeded with almost complete inversion of configuration. Refluxing of *erythro*-**3** (0.45 M, 1 M=1 mol dm^{-3}) solution in ethanol–water (98:2) containing potassium acetate (0.45 M) gave a product consisting of *threo*-4-acetoxy-3,3-dimethyl-2-pentanol (*threo*-**2**, 98%), its *erythro* isomer (*erythro*-**2**, trace), and *meso*-3,3-dimethyl-2,4-pentanediol diacetate (**1**-diacetate, 2%). Under the same conditions, *threo*-**3** gave a product consisting of *erythro*-**2** (90%), *threo*-**2** (trace), and *dl*-**1**-diacetate (10%).

Acetolyses of **3** proceeded with retention of configuration, although the specificities were lower than those in the hydrolyses. *erythro*-**3** gave *meso*- and *dl*-**1**-diacetates in a ratio of 75:25, while *threo*-**3** gave a mixture of *meso*- and *dl*-**1**-diacetates and unidentified products in a ratio of 35:50:15.

These stereochemical results are qualitatively the same as the previous results with unsubstituted 2,4-pentanediol derivatives, supporting the mechanism proposed previously. However, the results of the hydrolyses of the cyclic orthoformates of 1,3-butanediol and 2-methyl-2,4-pentanediol, which should proceed through the same intermediates as those of **3**, have shown that the substitution with hydroxyl groups occurred at the more substituted carbons and that the proposed mechanism should thus be partially modified.

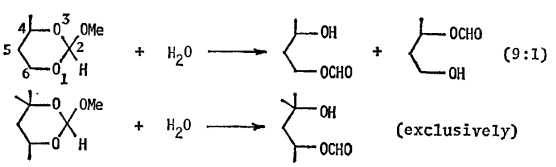

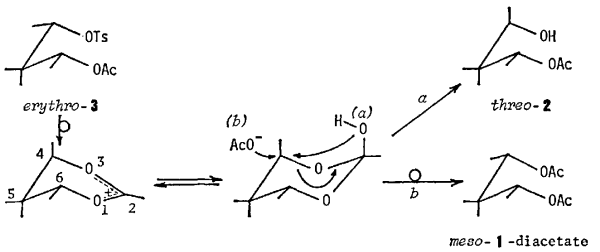

Scheme 1. Mechanism of hydrolysis of *erythro*-**3**.

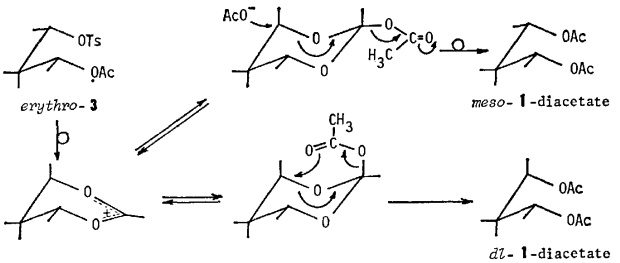

Scheme 2. Mechanism of acetolysis of *erythro*-**3**.

The previous mechanism assumed the heterolytic bond breaking of C^2–C^3 in the cyclic intermediate in Scheme 1. Instead, the bond breaking of C^4–O^3 or C^6–O^1 is more plausible, since the methyl substitution at C^4 or C^6 will make the latter type of breaking easier. Although the final decision requires a tracer experiment with isotopic oxygen, the revised mechanism can explain the results obtained so far.

As was proposed previously, the stereochemistry of the hydrolysis and acetolysis are determined by the relative rates of S_Ni and S_N2 reactions in the cyclic intermediate.

In the case of hydrolysis (Scheme 1), a cyclic intermediate with an axial hydroxyl group at C^2 can be formed preferentially because the antiparallel attack of a nucleophile to the dioxocarbonium ion will be preferred,[2] and the axial hydroxy compound thus formed is also more stable than the equatorial isomer because of the anomeric effect of hydroxyl oxygen.[3] This intermediate leads to the formation of the inversion product. In the case of acetolysis (Scheme 2), the steric hindrance of acetoxyl group against the anomeric effect prevents the formation of the intermediate with the axial acetoxyl group at C^2 and results in the formation of the one with the equatorial acetoxyl group. In the latter type of intermediate, the bond reconstruction by S_Ni path does not proceed.

As a result, the S_N2 attack of acetate ion becomes predominant and results in the formation of the retention product through double inversion.

The lower specificity observed in the acetolysis of the present substrate **3** than in the previous case without two methyl groups at C^3 can be explained by the slower S_N2 attack of acetate ion due to the steric hindrance.

The nature of the by-products appears to support the mechanism also. The minor products in the hydrolysis of **3** included the diacetate with retention of configuration, showing that the S_N2 attacks of acetate ion are operative also in this case, although the extent was small. Why the acetolysis of *threo*-**3** gave a considerable amount of unidentified products, while *erythro*-**3** gave no such products, is discussed later.

The solvolysis of cyclic orthoacetate (**1**-OA), which is expected to proceed through the formation of the same intermediate, should give the same results as those of **3**. This presumption was confirmed by the following experiments. Reaction of *meso*-**1**-OA with 80% aqueous ethanol gave *erythro*-**2**, while *dl*-**1**-OA gave *threo*-**2**. The yields were almost quantitative and no other products could be detected. Reaction of *dl*-**1**-OA with acetic acid gave a mixture of *meso*-**1** diacetate (75%) and *dl*-**1** diacetate (25%), while *meso*-**1**-OA gave a mixture of *meso*-**1** diacetate (35%), *dl*-**1** diacetate (50%) and unidentified products (15%).

The above-mentioned considerations have been extended to the case of 1,1-bis(1-hydroxyethyl)cyclopropane which is formally formed by combining the two methyl carbons attached to C^3 of **1** to form a cyclopropane ring. Hydrolyses of the orthoacetates of *meso*- and *dl*-isomers gave the *erythro*- and *threo*-diol monoacetates with excellent yields, respectively, showing that the reactions proceeded with retention of configuration as in the case of **3**, and that the solvolyses do not involve the formation of cyclopropylcarbinyl type cation, since no rearrangement products could be detected.

For reference, several kinds of cyclic orthoformates and orthoacetates of 1,3-diols and their acetoxonium ion salts were prepared; these are listed in Table 1. The preparation of the acetoxonium salt from 1,3-propanediol was unsuccessful. The salts were very sensitive to atmospheric moisture. The crystalline salt from *meso*-**1** was much more unstable than that from *dl*-**1** and decomposed, giving colored materials, within several hours after isolation. This instability of the former may be the reason why the acetolyses of *meso*-**1**-OA and *threo*-**3** gave considerable amounts of unidentified products in contrast with the clean-cut results of the other isomers.

The following results show clearly that the solvolyses of **3** and cyclic **1**-OA proceed through the same intermediate. Addition of $BF_3 \cdot OEt_2$ to an ether solution of **1**-OA formed a crystalline salt of the acetoxonium ion. The same salt was obtained by the addition of $AgBF_4$ to a dichloromethane solution of **3** (see Scheme 3).[4] The identity was confirmed by NMR spectra.

Acetoxonium ion is a stable carbonium ion. No trial of trapping this carbonium ion with an anionic

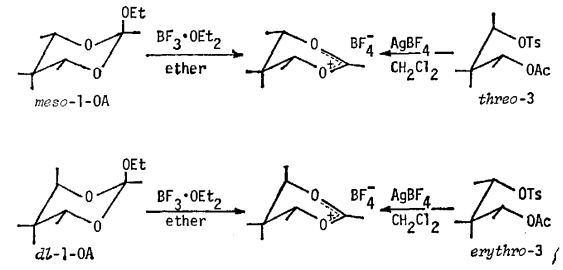

Scheme 3. Preparation of acetoxonium ion from cyclic orthoester and acetoxytosylate.

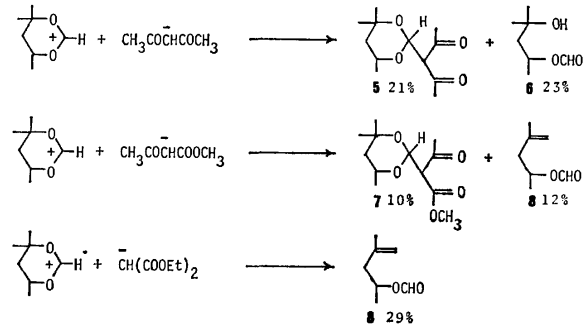

Scheme 4. Reactions of acetoxonium ions with carbanions.

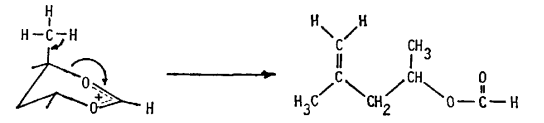

Scheme 5.

species of carbanion or with a hydride ion has been reported. Using the crystalline salt obtained above, these reactions have been examined.

For experimental convenience, the salts obtained from the orthoformate (**4**-OF) and the orthoacetate (**4**-OA) of 2-methyl-2,4-pentanediol were used as the substrate. The experimental difficulty was the purification of the acetoxonium salts. The removal of the excess $BF_3 \cdot OEt_2$, which was added to precipitate the salts from ether solutions of **4**-OA and **4**-OF, was essential to obtain the products, since BF_3 reacted with the active methylene compounds to form inactive addition products. Repeated washing with ether was required. To avoid the effects of atmospheric moisture, the weights of the starting salts before washing were used as the bases of the yield calculations; therefore, the yields are only qualitative. The results are shown in Scheme 4.

The reaction of the salt from **4**-OF with sodium salt of 2,4-pentanedione in refluxing ether for 4—5 h gave a condensation product, 2-(1-acetyl-2-oxopropyl)-4,4,6-trimethyl-1,3-dioxane (**5**), and the hydrolysis product of the acetoxonium salt, 3-hydroxy-1,3-dimethylbutyl formate (**6**). By the reaction with sodium salt of methyl acetoacetate, the expected product of 2-(1-methoxycarbonyl-2-oxopropyl)-4,4,6-trimethyl-1,3-dioxane (**7**) was obtained, together with 1,3-dimethyl-3-butenyl formate (**8**). The reaction with sodium salt of diethyl malonate gave only **8** but no condensation product.

TABLE 1. NMR DATA OF ORTHOESTERS AND THE CORRESPONDING ACETOXONIUM SALTS[a)]

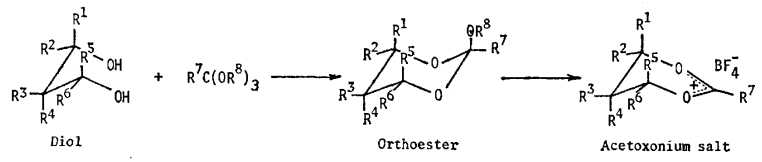

	R^1	R^2	R^3	R^4	R^5	R^6	R^7	R^8	Solvent
dl-**1**-OA	H	CH_3	CH_3	CH_3	CH_3	H	CH_3	CH_2CH_3	
	4.00(q)	1.08(d)	[0.78(s)	0.91(s)][b)]	1.21(s)	3.55(q)	1.45(s)	3.55(q), 1.20(t)	$CDCl_3$
Salt	5.37(q)	1.78(d)	1.28(s)		1.78(s)	5.37(q)	2.95(s)		$C_6H_5NO_2$
meso-**1**-OA	H	CH_3	CH_3	CH_3	H	CH_3	CH_3	CH_2CH_3	
	3.93(q)	1.08(d)	[0.73(s),	0.86(s)][b)]	3.93(q)	1.08(s)	1.46(s)	3.50(q), 1.24(t)	$CDCl_3$
Salt	5.45(q)	1.65(d)	[1.16(s),	1.22(s)][b)]	5.45(q)	1.65(s)	2.91(s)		$C_6H_5NO_2$
9-OA	H	H	$-CH_2CH_2-$		H	H	CH_3	CH_2CH_3	
	4.46(d)	2.93(d)	[0.31(m),	0.63(m)][b)]	4.46(d)	2.93(d)	1.52(s)	3.54(q), 1.26(t)	$CDCl_3$
Salt	5.20(s)		1.32(s)		5.20(s)		2.91(s)		$C_6H_5NO_2$
dl-**10**-OA	H	CH_3	$-CH_2CH_2-$		CH_3	H	CH_3	CH_2CH_3	
	4.46(q)	0.91(d)	[0.23—0.69(m)][b)]		1.28(d)	3.51(q)	1.47(s)	3.51(q), 1.28(t)	$CDCl_3$
Salt	Too unstable								
meso-**10**-OA	H	CH_3	$-CH_2CH_2-$		H	H	CH_3	CH_2CH_3	
	4.71(q)	0.89(d)	[0.27(m),	0.68(m)][b)]	4.71(q)	0.89(d)	1.51(s)	3.55(q), 1.29(t)	$CDCl_3$
Salt	Too unstable								
11-OF[c)]	CH_3	CH_3	H	H	H	CH_3	H	CH_3	
	1.2—1.4		1.54(m)		4.0	1.2—1.4	5.39(s)	3.33(s)	$CDCl_3$
					4.32		5.45(s)	3.47(s)	
Salt	[1.91(s),	1.98(s)][b)]	2.90(m)		5.73(m)	1.79(s)	d)		$C_6H_5NO_2$
11-OA[c)]	CH_3	CH_3	H	H	H	CH_3	CH_3	CH_2CH_3	
	[1.45(s),	1.75(s)][b)]	1.45—1.75(m)		4.57(m)	1.45—1.75	1.75(s)	3.62(q), 1.45(t)	$CDCl_3$
Salt	[1.91(s),	1.98(s)][b)]	2.68—2.86(m)		5.90(m)	1·79(d)	2.90(s)		$C_6H_5NO_2$
12-OF	CH_3	CH_3	CH_3	CH_3	CH_3	CH_3	H	CH_3	
	[1.28(s),	1.42(s)][b)]	[0.87(s),	1.07(s)][b)]	[1.28(s),	1.42(s)][b)]	5.46(s)	3.36(s)	$CDCl_3$
Salt	1.75(s)		1.19(s)		1.75(s)		d)		$C_6H_5NO_2$

Diol 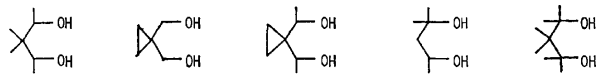

a) The chemical shifts are given in δ from TMS. b) Discrimination of axial and equatorial was unsuccessful. c) A mixture of *cis*- and *trans*-isomers. d) Hidden in a solvent region.

Table 2. Analytical data of orthoesters

			Calcd (%)	Found (%)
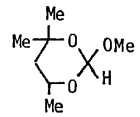	**11**-OF	$C_8H_{16}O_3$ bp 64 °C/ 11 mmHg	C, 59.96; H, 10.07	C, 59.87; H, 9.93
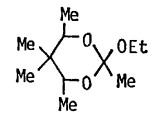	**1**-OA	$C_{11}H_{22}O_3$ *cis*, bp 88—90 °C/19.5 mmHg *trans*, bp 84—85 °C/14.8 mmHg	C, 65.97; H, 10.96	C, 65.52; H, 11.25 C, 65.60; H, 10.71
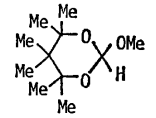	**12**-OF	bp 126 °C/13 mmHg	Too unstable to analyze	
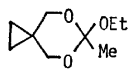	**9**-OA	$C_9H_{16}O_3$ bp 98—99 °C/39 mmHg	C, 62.82; H, 9.66	C, 62.76; H, 9.36
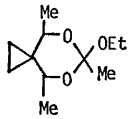	**10**-OA	$C_{11}H_{20}O_3$ *cis*, bp 90 °C/13 mmHg *trans*, bp 95—97 °C/13 mmHg	C, 65.97; H, 10.07	C, 65.83; H, 10.09 C, 66.19; H, 9.93

These results show that the condensation and the deprotonation proceeded in parallel and that the preferences depend on the reagents. The deprotonation could proceed as depicted in Scheme 5. This was consistent with the fact that the less bulky carbanions gave the condensation products and deprotonation was preferred in the case of more bulky carbanions.

The salt from **4**-OA was also treated with the carbanion, but no condensation nor deprotonation could be observed even after prolonged reaction times. The reason why the reactions did not proceed is still unclear.[5]

A trapping of the carbonium ion with hydride ion was examined by a reaction of 6-methyl-5,7-dioxaspiro-[2.5]octan-6-ylium salt with sodium borohydride. The reaction in DMF gave the same acetal (**9**-OA) as that prepared by the acetallisation of the corresponding diol (**9**).

Experimental

The IR spectra were recorded on a Hitachi EPI-G2 apparatus. The NMR spectra were taken on a Varian HR-220 apparatus at 220 MHz in $CDCl_3$ unless otherwise noted, with TMS as an internal standard.

Materials. 1,3-Propanediol, 1,3-butanediol, and 2-methyl-2,4-pentanediol were commercially available and distilled before use. Preparations of the diols containing cyclopropane rings were reported previously.[1,6]

*Preparations of Stereoisomers of **1**, **2**, and **3**.* By a reaction of 2,4-pentanedione (261 g) with methyl iodide (452 g) in acetone (600 ml) containing potassium carbonate (356 g) under reflux for 6.5 h and the usual work-up, 3-methyl-2,4-pentanedione, bp 65.0—65.5 °C/20 mmHg,† was obtained in a yield of 83%. The product (223 g) was again methylated by refluxing with methyl iodide (331 g) in acetone (600 ml) containing potassium carbonate (300 g) for 30 h. After the usual work-up, 3,3-dimethyl-2,4-pentanedione, bp 58.0—58.5 °C/12 mmHg, was obtained in a yield of 82%.

† 1 mmHg ≈ 133.322 Pa.

Into this dione (99 g) solution in ethanol (150 g), sodium borohydride (47 g) solution in water (150 g) containing sodium hydroxide (0.8 g) was added slowly under cooling in an ice-bath. After standing overnight, the solution was neutralized with hydrochloric acid. After removal of inorganic crystals, the diol layer was separated from the water layer. The latter was extracted with chloroform, and the chloroform solution was combined with the diol layer. After adding glycerol (100 ml), the solution was distilled to give 3,3-dimethyl-2,4-pentanediol (80 g). As in the case of 2,4-pentanediol,[1] the reaction of the diol with thionyl chloride gave cyclic sulfite. Distillation gave the *cis*-form, bp 63—64 °C/4.5 mmHg, and the *trans*-form, bp 78—78.5 °C/4.5 mmHg, but the complete separation was difficult even with a high reflux ratio. In contrast, a recrystallization worked well, since the *cis*-isomer was solid, while the *trans*-form was liquid. Recrystallization from petroleum ether at −18 °C gave pure *cis*-isomer, mp 32—32.5 °C. Alkaline hydrolyses of the *cis*- and *trans*-isomers with 20% aqueous sodium hydroxide gave *meso*-**1** (bp 118 °C/16 mmHg; NMR δ= 0.70 (s, 3H), 0.87 (s, 3H), 1.14 (d, 6H, J=6.8), and 3.78 (q, 2H)) and *dl*-**1** (bp 115 °C/16 mmHg; NMR δ=0.87 (s, 6H), 1.16 (d, 6H), and 3.79 (2H)).

The structures of the diols were confirmed by NMR analyses of the corresponding cyclic acetals of benzaldehyde, which were prepared as in the reported case of 2,4-pentanediol.[1] Acetal of *meso*-**1**: bp 122—123 °C/8 mmHg; NMR δ=0.78 (s, 3H), 1.00 (s, 3H), 1.20 (d, 6H), 3.67 (q, 2H) and 5.52 (s, 1H). Found: C, 76.04; H, 9.01%. Calcd for $C_{14}H_{20}O_2$: C, 76.32; H, 9.15%. Acetal of *dl*-**1**: NMR δ=0.75 (s, 3H), 1.14 (d, 3H), 1.24 (s, 3H), 1.41 (d, 3H), 3.81 (q, 1H), 5.85 (s, 1H) and 5.90 (q, 1H). Found: C, 76.26; H, 9.36%. Calcd for $C_{14}H_{20}O_2$: C, 76.32; H, 9.15%.

According to the method reported previously,[1,6] the diols were converted to the cyclic orthoacetates (see Tables 1 and 2). *meso*-**1**-OA (8.8 g) was stirred into a water (5 g)–ethanol (20 g) mixture at room temperature for 1 h. After removal of ethanol, the reaction mixture was extracted with ether, washed with saturated aqueous sodium chloride solution, dried over sodium sulfate, and then distilled to give *erythro*-**2** (6.7 g), bp 79—80 °C/4.5 mmHg. GLC analy-

sis showed that the purity was more than 99%. NMR δ=0.81 (s, 3H), 0.92 (s, 3H), 1.12 (d, 3H), 1.16 (d, 3H), 2.02 (s, 3H), 3.68 (q, 1H), 4.93 (q, 1H); IR $\nu_{C=O}$ 1740, 1720 (sh); ν_{C-O} 1270, 1255 cm^{-1}. Found: C, 62.10; H, 10.56%. Calcd for $C_9H_{18}O_3$: C, 62.04; H, 10.41%. Similarly, *dl*-**1**-OA gave *threo*-**2** in a yield of 90%, bp 84.0—84.5 °C/5.6 mmHg; NMR δ=0.81 (s, 3H), 0.85 (s, 3H), 1.10 (d, 3H), 1.18 (d, 3H), 2.05 (s, 3H), 3.56 (q, 1H), 5.00 (q, 1H); IR $\nu_{C=O}$ 1725, 1710; ν_{C-O} 1265, 1250 cm^{-1}. Found: C, 62.08; H, 10.57%. Calcd for $C_9H_{18}O_3$: C, 62.04; H, 10.41%.

Into an anhydrous pyridine (25 ml) solution of *erythro*-**2** (6 g), *p*-toluenesulfonyl chloride (6.84 g) was added. After the mixture was kept in a refrigerator for 3 d, crystalline pyridine hydrochloride was filtered off. The filtrate was treated with ice–water and then the pH of the solution was adjusted to 5 by addition of cold hydrochloric acid. The solution was extracted with ether. After drying over K_2CO_3–Na_2SO_4, the ether was removed. To the residue, petroleum ether (70 ml) was added. After filtration, the filtrate was kept in a refrigerator to give crystals (9.4 g). After recrystallization from petroleum ether, pure *erythro*-**3** was obtained, mp 72.0—72.5 °C; NMR δ=0.83 (s, 3H), 0.88 (s, 3H), 1.09 (d, 3H), 1.23 (d, 3H), 2.04 (s, 3H), 2.45 (s, 3H), 4.62 (q, 1H), 4.80 (q, 1H), 7.36 (d, 2H), 7.81 (d, 2H). Found: C, 58.66; H, 7.65; S, 9.92%. Calcd for $C_{16}H_{24}O_5S$: C, 58.51; H, 7.37; S, 9.76%. *threo*-**3** was prepared by the same procedure, mp 59.5—60.0 °C; NMR δ= 0.82 (s, 3H), 0.87 (s, 3H), 1.14 (d, 3H), 1.26 (d, 3H), 2.04 (s, 3H), 2.43 (s, 3H), 4.77 (q, 1H), 4.79 (q, 1H), 7.31 (d, 2H), 7.78 (d, 2H). Found: C, 58.39; H, 7.15; S, 9.72%. Calcd for $C_{16}H_{24}O_5S$: C, 58.51; H, 7.37; S, 9.76%.

Solvolyses of **3**. The reaction procedure was analogous to that previously reported.[1] The product ratios were determined by GLC (EGSS-X 1 m column) using 1-methylnaphthalene as an internal standard.

Hydrolyses of Orthoformates of 1,3-Butanediol and 2-Methyl-2,4-pentanediol. The primary hydrolysis products of these substrates are hydroxy formates which are readily hydrolyzed further to glycols. In order to determine the primary products, the following procedure was used. Orthoformate of 2-methyl-2,4-pentanediol (24 g) was stirred into a mixture of carbon tetrachloride (100 ml) and water (20 ml) at room temperature for 4 h. The carbon tetrachloride layer was distilled after evaporation of the solvent to give 3-hydroxy-1,3-dimethylbutyl formate in a yield of 50%, bp 88.5—91.5 °C/10 mmHg; NMR δ=1.23 (s, 3H), 1.79 (m, 2H), 2.23 (s, 1H), 5.20 (m, 1H), and 8.0 (s, 1H). Found: C, 58.01; H, 9.63%. Calcd for $C_7H_{14}O_3$: C, 57.51; H, 9.65%. The rather low yield was due to the hydrolysis to the diol. The hydrolysis of orthoformate of 1,3-butanediol did not proceed at room temperature and required refluxing for 1 h. The product was obtained from the water layer by distillation, bp 99.5—101 °C/18 mmHg. This was a mixture of 3-hydroxybutyl formate and 3-hydroxy-1-methylpropyl formate in a ratio of 9:1. The ratio was determined by NMR. NMR of the former: δ=1.20 (d, 3H), 1.70 (m, 2H), 2.46 (s, 1H), 3.50—4.43 (m, 2H), and 8.0 (s, 1H). NMR of the latter: δ=1.30 (d, 3H), 1.70 (m, 2H), 2.46 (s, 1H), 3.50—4.43 (m, 2H), 5.20 (1H), and 8.0 (s, 1H).

Authentic Samples of meso- *and* dl-*1 Diacetates.* According to the conventional method, the diacetates were prepared by the reactions of the diols with acetyl chloride (6 mole equivalent) in pyridine. *meso*-**1**-diacetate, bp 114.0—114.5 °C/18.5 mmHg; NMR δ=0.89 (s, 3H), 0.94 (s, 3H), 1.15 (d, 6H), 2.08 (s, 3H), and 4.95 (q, 2H); IR $\nu_{C=O}$ 1735, 1730; ν_{C-O} 1260, 1235 cm^{-1}. Found: C, 61.14; H, 9.30%. Calcd for $C_{11}H_{20}O_4$: C, 61.09; H, 9.32%. *dl*-**1**-diacetate, bp 106—107 °C/15.5 mmHg; NMR δ=0.91 (s, 6H), 1.16 (d, 6H), 2.03 (s, 6H), and 4.91 (q, 2H). Found: C, 60.93; H, 9.36%. Calcd for $C_{11}H_{20}O_4$: C, 61.09; H, 9.32%.

Preparation of Acetoxonium Salts. The following example shows the typical experimental procedure. Into a *meso*-**1**-OA (1.1 g) solution in dry ether (5 ml), $BF_3 \cdot OEt_2$ (1.2 g) was added slowly. After allowing the mixture to stand for 24 h at room temperature, crystals of the salt had been formed. The crystals were separated by filtration using a sintered glass filter, dissolved in dry nitrobenzene and subjected to NMR measurement. The crystals were very sensitive to atmospheric moisture and not stable enough to allow us to perform elemental analyses and IR measurements.

Reactions of Acetoxonium Ion with Carbanions. To a solution of 4-OF (16 g) in dry ether (100 ml) was added $BF_3 \cdot OEt_2$ (21 g). The resulting crystals were ground in ether and washed three times with dry ether. The crystals and sodium acetylacetonate (12 g) were added to ether (200 ml) and refluxed for 4 h. After filtering the inorganic crystals formed, the reaction mixture was distilled to give 3-hydroxy-1,3-dimethylbutyl formate, bp 79.5—80 °C/13 mmHg, 3.4 g; and **5**, bp 126—133 °C/13 mmHg, 4.7 g; NMR δ=0.89 (d, 3H), 0.93 (s, 3H), 0.98 (m, 2H), 1.03 (s, 3H), 1.78 (s, 6H), 3.07 (d, 1H), 3.04 (t, 1H), and 4.21 (d, 1H); IR $\nu_{C=O}$ 1725, 1710 cm^{-1}. Found: C, 62.87; H, 8.52%. Calcd for $C_{12}H_{20}O_4$: C, 63.16; H, 8.77%.

Similarly, the reaction with the sodium salt of methyl acetoacetate gave **8**, bp 64—65 °C/60 mmHg; NMR δ= 1.30 (d, 3H), 1.91 (s, 3H), 2.25 (s, 3H), 2.32 (q, 1H), 5.11 (d, 2H), 5.45 (s, 1H); and **7**, bp 92—93 °C/2 mmHg; NMR δ=0.92—1.08 (11H), 1.35 (s, 3H), 2.00 (s, 3H), 3.30 (m, 1H), 3.06 (m, 1H), 4.41 (s, 1H). Found: C, 59.74; H, 8.34%. Calcd for $C_{12}H_{20}O_5$: C, 59.02; H, 8.25%.

References

1) O. Itoh, Y. Ichikawa, H. Katano, and K. Ichikawa, *Bull. Chem. Soc. Jpn.*, **49**, 1353 (1976).

2) E. L. Eliel and F. W. Nader, *J. Am. Chem. Soc.*, **92**, 584 (1970).

3) E. L. Eliel, *Acc. Chem. Res.*, **3**, 1 (1970).

4) For the preparations of acetoxonium salts, see H. Meerwein and K. Wunderlich, *Angew. Chem.*, **69**, 481 (1957); H. Meerwein, K. Bodenbenner, P. Borner, F. Kunert, and K. Wunderlich, *Justus Liebigs Ann. Chem.*, **632**, 38 (1968); C. U. Pittman, Jr., S. P. McManus, and J. W. Larsen, *Chem. Rev.*, **72**, 357 (1972); G. Schneider, *Tetrahedron Lett.*, **1966**, 5921; and references cited therein.

5) In the case of the acetoxonium ion from **4**-OA, the referee, to whom the authors' thanks are due, suggested that the deprotonation might occur at the 2-methyl group giving 2-methylene-4,4,6-trimethyl-1,3-dioxane, which would decompose in the subsequent reaction. This sequence of reaction looked like a plausible one, but none of the products expected from these reactions could be detected by GLC analysis of the reaction mixture.

6) O. Itoh, Y. Kohmura, Y. Ichikawa, M. Umezu, T. Okita, and K. Ichikawa, *Bull. Chem. Soc. Jpn.*, **53**, 146 (1980).

Flash Pyrolysis of Selenides. Syntheses of Bibenzyls, Olefins, and Related Compounds

Hiroyuki HIGUCHI, Tetsuo OTSUBO,† Fumio OGURA,† Hachiro YAMAGUCHI,† Yoshiteru SAKATA, and Soichi MISUMI*

The Institute of Scientific and Industrial Research, Osaka University, Suita, Osaka 565

† *Department of Applied Chemistry, Faculty of Engineering, Hiroshima University, Sendamachi, Hiroshima 730*

(Received April 11, 1981)

Pyrolyses of a series of selenides and diselenides were studied. Selenides and diselenides bound with an active methylene group like benzyl gave a variety of substituted bibenzyls and related ethane derivatives in high yields. Other diselenides were easily caused to cleave to give various aromatic and aliphatic olefins in good yields together with elemental selenium. Lepidopterene, [2.2]paracyclophane, and benzocyclobutene were prepared by thermal cleavage of their corresponding phenylselenomethyl-substituted compounds as an application of the pyrolysis concerned.

Formation of carbon-carbon bond by sulfur extrusion is of importance as a synthetic method. For example, pyrolysis of cyclic sulfones made a significant contribution to the remarkable development of cyclophane chemistry.[1] In contrast, little attention has been paid to selenium extrusion of organoselenium compounds, partly because high oxidation states of selenium are usually unstable. Recently Chu and Lewicki[2] reported that bis(diphenylmethyl) diselenide thermally decomposed with loss of elemental selenium to give 1,1,2,2-tetraphenylethane. Couture *et al.*[3] studied pyrolysis of bis(9-anthrylmethyl) selenide and diselenide to 1,2-di(9-anthryl)ethane. We found that on gas-phase pyrolysis, dibenzyl selenide **1** gave bibenzyl in a high yield, in contrast to no reaction occurring with dibenzyl sulfide.[4] Several pieces of information on such labile C–Se bonds stimulated us to initiate an extensive study on thermal behaviors of various organoselenium compounds. Here we report on thermal decomposition of mono- and diselenides **2**—**13** and some applications to synthesis of related compounds.[5]

Results and Discussion

Selenides **2**—**13** were prepared by the conventional methods described in the experimental part. Selenium extrusion on them was carried out by the flash vacuum pyrolysis which had successfully been used for dibenzyl selenide **1**.[4] The reaction of **1** is capable of proceeding above 400 °C with the optimal yield at 600 °C under 20 mmHg (1 mmHg≈133.322 Pa). The best results obtained in the present study with almost the same conditions are summarized in Table 1. As seen from this table, pyrolysis products are significantly dependent on characters of selenium bonds, which are classified into four groups as follows:

1. Selenides **4**, **7**, and **9** were recovered because they possess no readily cleavable bonds. In spite of being highly susceptible to homolysis to phenylseleno radical, diphenyl diselenide **2** was exceptionally unreactive. Probably the fragment radical favors recombination to the original molecule over fragmentation.
2. Selenides **1** and **5**, both having labile bilateral bonds of selenium, readily underwent selenium extrusion to form C–C bonds.
3. Pyrolysis of benzyl phenyl selenide **3** gave a mixture of bibenzyl and diphenyl diselenide **2** in high yields. These two products were formed apparently by individual dimerizations of benzyl and phenylseleno radicals which had been generated by homolytic cleavage of the benzyl-Se bond of **3**.

$$\underset{\mathbf{3}}{PhCH_2SePh} \xrightarrow{\Delta} Ph\dot{C}H_2 + \dot{S}ePh$$

$$\longrightarrow PhCH_2CH_2Ph + \underset{\mathbf{2}}{PhSeSePh}$$

Table 1. Pyrolyses of organoselenides **1**—**13** at 600 °C under 20 mmHg

Selenide		Product (Yield/%)
$PhCH_2SeCH_2Ph$	**1**	$PhCH_2CH_2Ph$(80)+Se[b]
PhSeSePh	**2**	Recovery
$PhCH_2SePh$	**3**[a]	$PhCH_2CH_2Ph$(92)+PhSeSePh(98)
$PhCH_2CH_2SePh$	**4**	Recovery
$PhCH_2SeSeCH_2Ph$	**5**	$PhCH_2CH_2Ph$(96)+Se[b]
$PhCH_2SeCH_2CH_2Ph$	**6**	$PhCH{=}CH_2$(96)+$PhCH_2CH_2Ph$(37)+$PhCH_3$(48)+Se[b]
$PhCH_2CH_2SeCH_2CH_2Ph$	**7**	Recovery
$PhCH_2CH_2SeSeCH_2CH_2Ph$	**8**	$PhCH{=}CH_2$(95)+Se[b]
n-$C_6H_{13}Se$-*n*-C_6H_{13}	**9**	Recovery
n-$C_6H_{13}SeSe$-*n*-C_6H_{13}	**10**	$C_4H_9CH{=}CH_2$(90)+$C_{12}H_{26}$(7)+Se[b]
$PhSeCH_2CH{=}CH_2$	**11**	$CH_2{=}CHCH_2CH_2CH{=}CH_2$(67)+PhSeSePh(88)
$PhSeCH_2CN$	**12**	$NCCH_2CH_2CN$(87)+PhSeSePh(90)
$PhSeCH_2COCH_3$	**13**[a]	$CH_3COCH_2CH_2COCH_3$(52)+PhSeSePh(93)

a) Pyrolytic temperature, 650 °C. b) Almost quantitative yield.

Table 2. Yield and properties of $ArCH_2SePh$

Ar	Yield %	Mp °C	NMR data $CDCl_3$, δ	MS *m/e* M^+	Found (%)	Calcd (%)
p-$CH_3C_6H_4$	95	29—31 (30—31) [a]	2.30(s, CH_3), 4.08(s, CH_2), 7.08 (bs, ArH), 7.25—7.40(m, Ph)	262	C, 64.14 H, 5.31	64.37 5.36
p-ClC_6H_4	86	57.5—58.5	4.03(s, CH_2), 7.10, 7.17(A_2B_2m, ArH), 7.25—7.42(m, Ph)	282, 284	C, 55.16 H, 3.84 Cl, 12.72	55.41 3.91 12.61
o-ClC_6H_4	91	Oil	4.15(s, CH_2), 7.06—7.49(m, ArH, Ph)	282, 284	C, 55.52 H, 4.05 Cl, 12.64	55.41 3.91 12.61
p-BrC_6H_4	87	61—62	4.01(s, CH_2), 7.04, 7.45(A_2B_2m, ArH), 7.25—7.42(m, Ph)	326, 328	C, 47.62 H, 3.46 Br, 24.51	47.85 3.37 24.54
p-$NO_2C_6H_4$	67	59.5—60	4.09(s, CH_2), 7.22, 8.05(A_2B_2m, ArH), 7.26—7.37(m, Ph)	293	C, 53.23 H, 3.75 N, 4.79	53.42 3.77 4.79
p-$CH_3OC_6H_4$	90	74—75 (75—76) [a]	3.77(s, CH_3), 4.07(s, CH_2), 6.78, 7.11(A_2B_2m, ArH), 7.24—7.41(m, Ph)	278	C, 60.47 H, 5.26	60.65 5.05
p-$CH_3O_2CC_6H_4$	77	62.5—63	3.87(s, CH_3), 4.09(s, CH_2), 7.21, 7.88(A_2B_2m, ArH), 7.25—7.38(m, Ph)	306	C, 59.08 H, 4.68	59.01 4.59
p-NCC_6H_4	76	72—72.5	4.05(s, CH_2), 7.21, 7.47(A_2B_2m, ArH), 7.24—7.41(m, Ph)	273	C, 61.48 H, 4.14 N, 5.13	61.76 4.04 5.15
1-Naphthyl	83	Oil	4.54(s, CH_2), 7.21—8.08(m, ArH, Ph)	298	C, 68.41 H, 4.83	68.69 4.72
4-CH_3-1-Naphthyl	93	66—68	2.63(s, CH_3), 4.52(s, CH_2), 7.24—8.08(m, ArH, Ph)	312	C, 69.45 H, 5.23	69.45 5.44
2-Thienyl	88	Oil	4.29(s, CH_2), 6.79—7.51(m, ArH, Ph)	254	C, 51.99 H, 3.97	52.17 3.95
2-Pyridyl	78	Oil	4.22(s, CH_2), 7.15—7.47(m, ArH, Ph)	249	C, 58.23 H, 4.53 N, 5.78	58.06 4.43 5.65

a) Ref. 19.

Allyl phenyl selenide **11**, phenylselenoacetonitrile **12**, and phenylselenoacetone **13** underwent analogous cleavages to give biallyl, succinonitrile, and 2,5-hexanedione, respectively, together with diphenyl diselenide.

4. Diphenethyl diselenide **8** was caused to cleave to yield styrene and elemental selenium but no 1,4-diphenylbutane, as expected on the simple selenium extrusion sequence. Dihexyl diselenide **10** showed a similar behavior in yielding 1-hexene with a minute amount of dodecane. Pyrolyses of dioctyl diselenide **14** and dioctyl disulfide **15** were examined for comparison of reactivities between both the organochalcogen compounds. 1-Octene was obtained in a high yield (93%) from **14**, while in a low yield (18%) from **15**.

$$\underset{\mathbf{14}}{C_8H_{17}SeSeC_8H_{17}} \xrightarrow{\Delta} \underset{93\%}{C_6H_{13}CH{=}CH_2} \xleftarrow{\Delta} \underset{18\%}{\underset{\mathbf{15}}{C_8H_{17}SSC_8H_{17}}}$$

Benzyl phenethyl selenide **6** is particularly interesting, for it can combine with functional groups of types 3 and 4 specified above. In fact, it gave four products, bibenzyl, styrene, toluene, and elemental selenium, in a high total yield. As seen from the scheme, the formation of a considerable amount of toluene indicates that part of benzyl radicals are possibly quenched by H· radicals derived from phenethylseleno radicals.

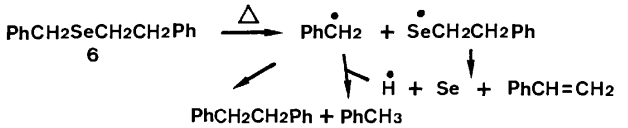

In the case of sulfur derivatives, on the other hand, benzyl phenethyl sulfide failed to undergo any pyrolytic reactions, while its sulfone **16** decomposed to give a mixture of bibenzyl, styrene, and 1,3-diphenylpropane. The pyrolysis of **6** and **16** indicates that the pyrolytic mechanism of selenide is somewhat different from that of sulfone. Analogous pyrolytic reactions were observed with polyfunctional compounds **17**, **18**, and **19** which yield polyolefins.

$$\underset{\mathbf{16}}{PhCH_2SO_2CH_2CH_2Ph} \xrightarrow{\Delta} \underset{56\%}{PhCH_2CH_2Ph} + \underset{34\%}{PhCH{=}CH_2} + \underset{28\%}{PhCH_2CH_2CH_2Ph} + SO_2$$

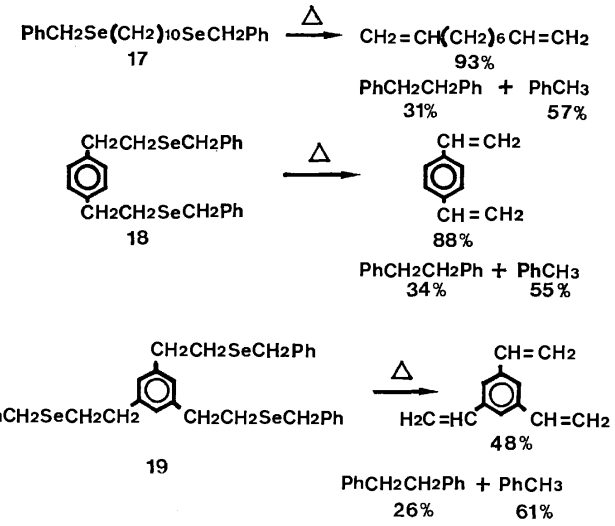

Of many synthetic methods for bibenzyls the most convenient ones utilize the Grignard reaction and the Wurtz reaction on benzyl halides. However, some functional groups have a reactivity so variable with reaction conditions as to make it difficult to synthesize their related bibenzyls by these methods. Extrusion reactions of dibenzyl sulfone,[6] dibenzyl oxalate,[7] and dibenzyl selenide[4] have been useful for preparation of some bibenzyls. Benzyl phenyl selenide **3** also can be utilized as a starting material for synthesis of bibenzyls. Thus, pyrolyses of derivatives of **3**, which are readily prepared by treatment of the corresponding benzyl halides with benzeneselenolate (Table 2), gave various bibenzyls and 1,2-diarylethanes in high yields (Table 3). It is noticeable that diphenyl diselenide **2** concomitantly formed in such reactions is reusable to generate benzeneselenolate. Accordingly, the present method surpasses the extrusion methods with regard to yield and wide applicability, as described below. Vapor pressures of sulfones, oxalates, and selenides with bifunctional polar groups are very low and hence they are often subject to undesirable decomposition before being vaporized for extrusion. For example, 4,4′-dimethoxybibenzyl could be obtained by the present method, but not by pyrolysis of its corresponding dibenzyl oxalate.[7]

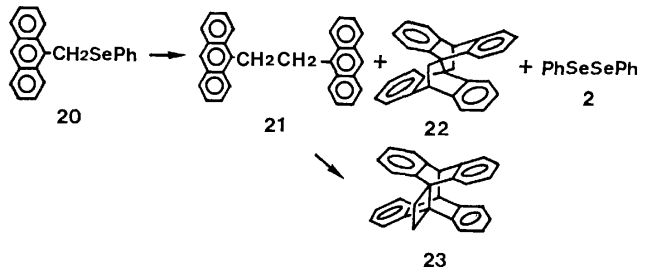

A flash vacuum pyrolysis of 9-anthrylmethyl phenyl selenide **20** gave 1,2-di(9-anthryl)ethane **21** as expected (see Table 4). On the other hand, a thermal reaction of **20** in solid state or in toluene solution at 150—170 °C provided in a high yield a unique structure compound, lepidopterene **22** which had previously been synthesized by reaction of 9-(chloromethyl)-anthracene with methylmagnesium iodide[8] or photolysis of 9-anthrylmethyl sulfide or selenide.[3] The yields of **22** by the present method are much higher than those by the previous methods. Photolysis of **20** also led to **22** as well as a photodimer biplanene **23**. In every case, diphenyl diselenide **2** was a concomitant product with almost a quantitative yield.

The ring contraction accompanying the extrusion of sulfur dioxide from cyclic sulfones is very suitable for synthesis of cyclic hydrocarbons. For example, a heating of cyclic disulfone **24** gave [2.2]paracyclophane **25** in 15—18% yield.[9] In contrast, no synthesis of cyclophanes by organoselenium has yet been known, because no cyclic selenides have so far been made available.[10] One may expect that heating of 1,4-bis(phenylselenomethyl)benzene **27** would generate, with elimination of diphenyl diselenide **2**, biradical **28** which, in equilibrium with quinodimethane **29**, is dimerized to form [2.2]paracyclophane **25**.[11] In fact, acyclic diselenide **27** was readily prepared in 85% yield from 1,4-bis(chloromethyl)benzene **26** and gave [2.2]paracyclophane **25** (23% yield) and diphenyl di-

Table 3. Pyrolyses of $ArCH_2SePh$ to $ArCH_2CH_2Ar$

Ar	Yield/% of $ArCH_2CH_2Ar$	Mp/°C of $ArCH_2CH_2Ar$(lit)
p-$CH_3C_6H_4$	87	80—81(81—81.5)[a]
p-ClC_6H_4	73	98—99(100—101)[b]
o-ClC_6H_4	72	57—58.5(59—61)[b]
p-BrC_6H_4	83	113—114(112—114)[b]
p-$NO_2C_6H_4$	73	177—178.5(179—180)[c]
p-$CH_3OC_6H_4$	66	124—125(126.4—126.8)[a]
p-$CH_3O_2CC_6H_4$	90	120—121(119)[e]
p-NCC_6H_4	73	197.5—198(198)[d]
1-Naphthyl	76	161—162(163.5—164.5)[f]
4-CH_3-1-Naphthyl	90	157—158(154—155)[i]
2-Thienyl	92	64—64.5(64—65)[g]
2-Pyridyl	68	48.5—50(49.5—50.5)[h]

a) G. H. Coleman, W. H. Holst, and R. D. Maxwell, *J. Am. Chem. Soc.*, **58**, 2310 (1936). b) W. S. Trahanovsky, C. C. Ong, and J. A. Lawson, *J. Am. Chem. Soc.*, **90**, 2839 (1968). c) W. Leppert, *Ber.*, **9**, 15 (1876). d) P. Kattwinkel and R. Wolffenstein, *Ber.*, **34**, 2423 (1901). e) C. Fischer and R. Wolffenstein, *Ber.*, **37**, 3216 (1904). f) E. A. Chandross and C. J. Dempster, *J. Am. Chem. Soc.*, **92**, 3586 (1970). g) F. F. Blicke and J. H. Burckhalter, *J. Am. Chem. Soc.*, **64**, 477 (1964). h) P. G. Campbell and P. C. Teague, *J. Am. Chem. Soc.*, **76**, 1371 (1954). i) Ref. 6.

Table 4. Thermal and photochemical reactions of 9-AnthCH_2SePh **20**

System(Conditions)	**2**	**21**	**22**	**23**
Flash vacuum pyrolysis(600 °C, 20 mmHg)	94	91	0	0
Pyrolysis in sealed tube(150 °C, 5 min)	96	14	82	0
Pyrolysis in toluene(170 °C, 735 min)[a]	95	24	68	0
Photolysis in benzene(r. t., 4 h)[b]	95	0	66	25

a) In a sealed tube, a second order reaction with a_0 9×10^{-3} mol dm^{-3} and $\tau_{1/2}=8$ min. b) Wtih a high pressure mercury lamp in nitrogen.

Table 5. Flash vacuum pyrolysis of 1,2-bis(phenylselenomethyl)benzene **34**

Conditions	Yield/%					
	2	**31**	**33**	**34**	**35**	**36**
600 °C, 3 mmHg	10	0	5	83	0	0
600 °C, 8 mmHg	42	13	40	34	0	0
600 °C, 20 mmHg	47	38	7	0	16	8

selenide **2** (69%) on pyrolysis at 650 °C under 7 mmHg.

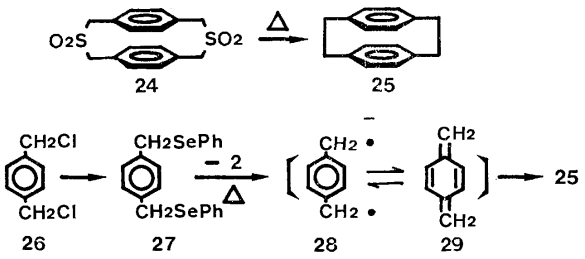

In connection with the formation of bibenzyl from dibenzyl selenide, it is expected that pyrolysis of 2,11-diselena[3.3]orthocyclophane **30** would give 1,2:5,6-dibenzo-1,5-cyclooctadiene. However, **30** gave 1,3-dihydro-2-benzoselenophene **31**[14] in 92% yield instead of 1,2:5,6-dibenzo-1,5-cyclooctadiene. Selenophene **31** is thermally stable in contrast to the fact that similarly constructed compounds **32a**[12] and **32b**[13] can easily afford 1,2-dihydrobenzocyclobutene **33** on pyrolysis. On the other hand, **33** was obtained by pyrolysis of 1,2-bis(phenylselenomethyl)benzene **34**. As shown in Table 5, the reaction conditions available are critical and the products are dependent on the vacuum pressure of the pyrolytic system. The best yield (40%) of **33** was attained under 8 mmHg. Under higher vacuum (3 mmHg), most of **34** was recovered and under lower vacuum (20 mmHg) other products, 1,3-dihydro-2-benzoselenophene **31**, anthracene **35**, and 9,10-dihydroanthracene **36**, were favored. In the present stage, the formation mechanism for **35** and **36** is equivocal.

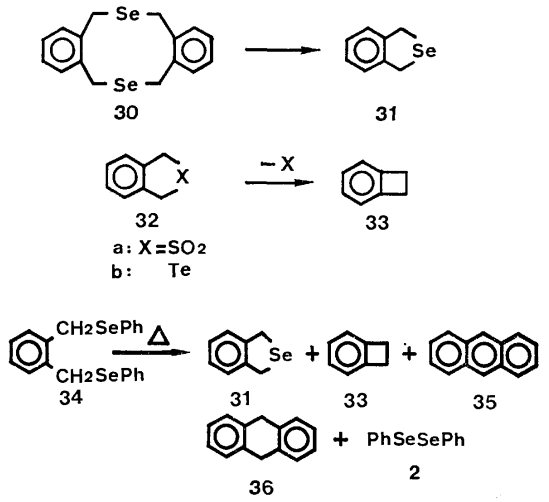

In conclusion, pyrolyses of organoseleniums are capable of providing a new method for the preparation of olefins, bibenzyls, and related compounds.

Experimental

Melting points were not corrected. All the solvents were of reagent grade. NMR spectra were recorded on a JEOL FX-100 (100 MHz) spectrometer using deuterochloroform as the solvent and tetramethylsilane as the internal standard. MS spectra were recorded on a Hitachi RMU-7 spectrometer (70 eV) using the direct injection technique. MS spectra of organoseleniums are characteristic of isotope patterns with respect to selenium atoms and description of molecular ion peaks is based on ^{80}Se only. IR spectra were recorded on a Hitachi EPI-G2 spectrometer for neat or nujol mull.

*General Synthetic Method of Selenides **3**, **4**, **6**, **7**, **9**, **11**, **12**, **13**, **20**, and Bis- and Tris-selenides **17**, **18**, **19**, **27**, and **34**.* Alkyl phenyl selenides **3**, **4**, **11**, **12**, **13**, **20**, **27**, and **34** were prepared by treatment of their corresponding alkyl halides with sodium benzeneselenolate which had been generated by reduction of diphenyl diselenide **2**[15] or phenyl selenocyanate[16] with sodium borohydride. The substitutional derivatives of **3** shown in Table 2 were prepared in the same way. The other selenides were similarly prepared by using phenethyl selenocyanate[17] for **6** and **7**, hexyl selenocyanate[18] for **9**, and benzyl selenocyanate[4] for **17**, **18**, and **19** as precursors for the above selenolates.

The general procedure will be illustrated below by using the synthesis of benzyl phenyl selenide **3** as an example. Sodium borohydride (0.32 g, 8.4 mmol) was carefully added with ice-cooling to a solution of phenyl selenocyanate (1.5 g, 8.2 mmol) in ethanol (50 ml), with nitrogen being bubbled through the solution. After the solution was allowed to stand at room temperature, a solution of benzyl chloride (1.1 g, 8.6 mmol) in ethanol (20 ml) was added dropwise over a period of 30 min. The mixture was refluxed for 5 h and cooled to room temperature. Water (100 ml) and benzene (200 ml) were successively added. The organic layer was separated, washed with saturated aq sodium chloride solution, and dried over anhyd magnesium sulfate. After evaporation, the residue was chromatographed on silica gel (Wako gel C-200) with hexane and a recrystallization of the first eluate from benzene–hexane gave colorless plates of **3** in 92% yield: mp 33.5—34 °C (lit,[19] 34—35 °C); NMR δ=4.08 (s, CH_2), 7.19 (bs, ArH), and 7.23—7.41 (m, SePhH); MS, *m/e*, 248 (M^+).

4: yield 95%; colorless oil; NMR δ=3.02, 3.12 (A_2B_2m, CH_2), and 7.02—7.47 (m, ArH); MS, *m/e*, 262 (M^+). Found: C, 64.23; H, 5.47%. Calcd for $C_{14}H_{14}Se$: C, 64.36; H, 5.36%.

6: yield 95%; colorless oil; NMR δ=2.70, 2.81 (A_2B_2m, CH_2CH_2), 3.72 (s, CH_2), and 7.21 (m, ArH); MS, *m/e*, 276 (M^+). Found: C, 65.21; H, 5.89%. Calcd for $C_{15}H_{16}Se$: C, 65.46; H, 5.82%.

7: yield 83%; pale yellow oil; NMR δ=2.81, 2.91 (A_2B_2m, CH_2), and 7.20 (m, ArH); MS, *m/e*, 290 (M^+). Found: C, 66.28; H, 6.28%. Calcd for $C_{16}H_{18}Se$: C, 66.44; H, 6.23%.

9: yield 88%; pale yellow oil; NMR δ=0.89 (t, CH_3), 1.32—1.66 (m, CH_2), and 2.55 (t, $SeCH_2$); MS, *m/e*, 250 (M^+). Found: C, 57.68; H, 10.64%. Calcd for $C_{12}H_{26}Se$: C, 57.83; H, 10.44%.

11:[20] yield 93%; pale yellow oil; NMR δ=3.50 (d, CH_2), 4.87, 5.02, 5.88 (ABXm, $CH{=}CH_2$), and 7.23—7.49 (m, ArH); MS, *m/e*, 198 (M^+); IR 1630 cm^{-1} ($\nu_{C=C}$).

12: yield 94%; colorless oil; NMR δ=3.34 (s, CH_2) and

7.34—7.65 (m, ArH); MS, *m/e*, 197 (M^+); IR 2250 cm^{-1} ($\nu_{C\equiv N}$). Found: C, 48.79; H, 3.62; N, 7.30%. Calcd for C_8H_7NSe: C, 48.98; H, 3.57; N, 7.14%.

13: yield 94%; pale yellow oil; NMR δ=2.25 (s, CH_3), 3.57 (s, CH_2), and 7.27—7.51 (m, ArH); MS ,*m/e*, 214 (M^+); IR 1715 cm^{-1} ($\nu_{C=O}$). Found: C, 50.58; H, 4.90%. Calcd for $C_9H_{10}OSe$: C, 50.70; H, 4.69%.

17: yield 89%; colorless oil; NMR δ=1.24, 1.56 (m, CH_2), 2.49 (t, $SeCH_2$), 3.76 (s, $PhCH_2$), and 7.26 (m, ArH); MS, *m/e*, 482 (M^+). Found: C, 59.73; H, 7.11%. Calcd for $C_{24}H_{34}Se_2$: C, 60.00; H, 7.08%.

18: yield 87%; colorless oil; NMR δ=2.73, 2.80 (A_2B_2m, CH_2CH_2), 3.74 (s, CH_2Se), 7.04 (s, ArH), and 7.25 (m, ArH); MS, *m/e*, 474 (M^+). Found: C, 60.95; H, 5.57%. Calcd for $C_{24}H_{26}Se_2$: C, 61.02; H, 5.51%.

19: yield 78%; colorless oil; NMR δ=2.72, 2.82 (A_2B_2m, CH_2CH_2), 3.75 (s, CH_2Se), 6.75 (s, ArH), and 7.26 (m, ArH); MS, *m/e*, 672 (M^+). Found: C, 58.94; H, 5.33%. Calcd for $C_{33}H_{36}Se_3$: C, 59.19; H, 5.38%.

20: yield 94%; pale yellow prisms from hexane–benzene; mp 124.5—126.0 °C; NMR δ=5.15 (s, CH_2), 7.25, 7.46 (m, PhH), 7.94, 8.22 (m, AnthH), and 8.37 (s, AnthH); MS, *m/e*, 348 (M^+). Found: C, 72.75; H, 4.58%. Calcd for $C_{21}H_{16}Se$: C, 72.62; H, 4.61%.

27: yield 85%; colorless plates from hexane–benzene; mp 137—138 °C; NMR δ=4.06 (s, CH_2), 7.06 (s, ArH), and 7.25—7.42 (m, PhH); MS, *m/e*, 418 (M^+). Found: C, 57.53; H, 4.34%. Calcd for $C_{20}H_{18}Se_2$: C, 57.69; H, 4.33%.

34: yield 87%; colorless plates from hexane–benzene; mp 30.5—31.5 °C; NMR δ=4.18 (s, CH_2), 7.05 (s, ArH), and 7.23—7.43 (m, PhH); MS, *m/e*, 418 (M^+). Found: C, 57.96; H, 4.44%. Calcd for $C_{20}H_{18}Se_2$: C, 57.69; H, 4.33%.

*General Synthetic Method of Diselenides **5**, **8**, **10**, and **14**.* Diselenides **5**, **8**, **10**, and **14** were prepared by alkaline hydrolysis of benzyl selenocyanate,[4] phenethyl selenocyanate,[17] hexyl selenocyanate,[18] and octyl selenocyanate,[21] respectively. The general procedure will be illustrated below by using the synthesis of dibenzyl diselenide **5** as an example.

A solution of benzyl selenocyanate (3.88 g, 19.8 mmol) in methanol (30 ml) was added dropwise to methanol (30 ml) containing potassium hydroxide (0.6 g, 23.2 mmol) at room temperature. After stirring for 3 h, water (100 ml) and benzene (200 ml) were added. The organic layer was separated, washed with saturated aq sodium chloride solution, and dried over anhyd magnesium sulfate. After evaporation, the residue was chromatographed on silica gel (Wako gel C-200) with hexane and a recrystallization of the first eluate gave **5** in 95% yield: pale yellow needles from hexane–benzene; mp 91—92 °C (lit,[22] 92—93 °C); NMR δ=3.84 (s, CH_2) and 7.25 (bs, ArH); MS, *m/e*, 342 (M^+). Found: C, 49.64; H, 4.22%. Calcd for $C_{14}H_{14}Se_2$: C, 49.41; H, 4.11%.

8: yield 98%; colorless oil; NMR δ=3.03, 3.11 (A_2B_2m, CH_2), and 7.22 (m, ArH); MS, *m/e*, 370 (M^+). Found: C, 52.42; H, 5.12%. Calcd for $C_{16}H_{18}Se_2$: C, 52.17; H, 4.89%.

10: yield 96%; pale yellow oil; NMR δ=0.89 (t, CH_3), 1.34—1.73 (m, CH_2), and 2.29 (t, CH_2Se); MS, *m/e*, 330 (M^+). Found: C, 43.76; H, 7.97%. Calcd for $C_{12}H_{26}Se_2$: C, 43.90; H, 7.93%.

14: yield 97%; colorless oil; NMR δ=0.88 (t, CH_3), 1.30—1.76 (m, CH_2), and 2.91 (t, CH_2Se); MS, *m/e*, 386 (M^+). Found: C, 50.00; H, 9.07%. Calcd for $C_{16}H_{34}Se_2$: C, 50.00; H, 8.85%.

Dioctyl disulfide **15** was prepared according to the procedure of Yiannios and Karabinos.[23] Benzyl phenethyl sulfide and sulfone **16** were prepared according to the procedure of Böhme *et al.*[24]

*2,11-Diselena[3.3]orthocyclophane **30** and 1,3-Dihydro-2-benzoselenophene **31**.* A solution of 1,2-bis(bromomethyl)benzene (2.3 g, 8.0 mmol) in benzene (30 ml) and a solution of sodium selenide (1.12 g, 8.9 mmol) in 60% ethanol (100 ml) were added simultaneously and dropwise to a stirred ethanol (150 ml) at room temperature under a nitrogen atmosphere. The addition took 1.5 h. After an additional stirring for 2 h, benzene (300 ml) was added and the mixture was washed with saturated aq NaCl solution and dried over anhyd $MgSO_4$. After evaporation of the solvent, the residue was triturated with 1:1 benzene–hexane and the insoluble solid was recrystallized from dichloromethane–benzene to give colorless needles of **30** in 25% yield: mp 201—202 °C; NMR δ=3.66 (s, CH_2), 7.21, and 7.29 (A_2B_2m, ArH); MS, *m/e*, 368 (M^+). Found: C, 52.74; H, 4.37%. Calcd for $C_{16}H_{16}Se_2$: C, 52.46; H, 4.37%.

The benzene–hexane solution was chromatographed on silica gel (Wako gel C-100) with hexane to give a minute amount of **31** from the first eluate: mp 31—33 °C. The spectral data of this specimen were identical with those of product **31** obtained by pyrolysis of **30**. **31**: NMR δ=4.30 (s, CH_2), 7.14, and 7.20 (A_2B_2m, ArH); MS, *m/e*, 184 (M^+); mol wt 191 (vapor pressure osmometry, CH_2Cl_2). Found: C, 52.60; H, 4.29%. Calcd for C_8H_8Se: C, 52.46; H, 4.37%.

General Method for Flash Vacuum Pyrolysis. A Pyrex tube closed at one end, 40 cm long and 1 cm in diameter, was used for pyrolysis. The sample (50—300 mg) of organoselenium was placed at the closed end of the tube. The other open end was connected to a vacuum system and cooled with Dry Ice or liq. nitrogen. The middle part was enclosed within an electric furnace (25 cm long) preheated at 600 °C. After heating for *ca.* 2 min, the sample part was slidden into the furnace. Pyrolysis immediately occurred and the pyrolysates condensed at the cool part. The organic products were extracted with dichloromethane and isolated by preparative gel-permeation liquid chromatography (Nihon Bunseki Kogyo LC-08) with chloroform as eluent. All of them were identified by comparison of their melting points and spectral data with those of authentic samples or reported data.[25]

*Pyrolysis of 9-Anthrylmethyl Phenyl Selenide **20**.* *a) In Solid State*: Selenide **20** (20 mg) was heated in an oil bath at 150 °C for 5 min. A gel-permeation liquid chromatography of the pyrolysates gave 1,2-di(9-anthryl)ethane **21** (1.3 mg, 14%), lepidopterene **22** (7.8 mg, 82%), and diphenyl diselenide **2** (9.2 mg, 96%), successively.

21: pale yellow plates from toluene; mp 318.5—320.5 °C (lit,[8] 320 °C); NMR δ=4.07 (s, CH_2), 7.53, 8.03, and 8.39 (m, ArH); MS, *m/e*, 382 (M^+).

22: colorless columns from toluene; mp 298—299 °C (lit,[8] 298 °C); NMR δ=2.89 (d, J=3 Hz, CH_2), 4.63 (t, J=3 Hz, CH), 6.76, 6.81, 6.98, and 7.30 (m, ArH).

b) In Solution: Selenide **20** (20 mg) was placed in an NMR tube and dissolved in 0.7 ml of toluene-d_8. The tube was degassed by the freeze-pump-thaw method and sealed. The reaction at 170 °C was followed by NMR measurement. After *ca.* 12 h, the signals of **20** completely disappeared. A gel-permeation liquid chromatography of the products gave **21** (2.2 mg, 24%), **22** (6.5 mg, 68%), and **2** (95%).

*Photolysis of 9-Anthrylmethyl Phenyl Selenide **20**.* Selenide **20** (20 mg) was dissolved in benzene (20 ml) and irradiated with a high pressure mercury lamp in a nitrogen atmosphere. After evaporation, a gel-permeation liquid chro-

matography of the residue gave **22** (6.4 mg, 66%), biplanene **23** (2.3 mg, 25%), and **2** (9.1 mg, 95%).

23: colorless columns from benzene–toluene; mp 329 °C dec (lit,[8] 320 °C); NMR δ=3.01 (s, CH_2), 4.5 (s, CH), and 6.82—7.13 (m, ArH); MS, *m/e*, 382 (M^+).

References

1) F. Vögtle and L. Rossa, *Angew. Chem. Int. Ed. Engl.*, **18**, 515 (1979) and references cited therein.
2) J. Y. C. Chu and J. W. Lewicki, *J. Org. Chem.*, **42**, 2491 (1977).
3) A. Couture, A. Lablache-Combier, R. Lapouyade, and G. Félix, *J. Chem. Res. (S)*, **1979**, 258.
4) T. Otsubo, F. Ogura, H. Yamaguchi, H. Higuchi, and S. Misumi, *Synth. Commun.*, **10**, 595 (1980).
5) A part of this work was preliminarily reported: H. Higuchi, Y. Sakata, S. Misumi, T. Otsubo, F. Ogura, and H. Yamaguchi, *Chem. Lett.*, **1981**, 627.
6) E. C. Leonard, Jr., *J. Org. Chem.*, **27**, 1921 (1962).
7) W. S. Trahanovsky, C. C. Ong, and J. A. Lawson, *J. Am. Chem. Soc.*, **90**, 2839 (1968).
8) G. Felix, R. Lapouyade, A. Castellan, H. Bouas-Laurent, J. Gaultier, and C. Hauw, *Tetrahedron Lett.*, **1975**, 409.
9) F. Vögtle, P. Fornell, and W. Löhr, *Chem. Ind.*, **1979**, 416.
10) R. H. Mitchell, *Can. J. Chem.*, **54**, 238 (1976); **58**, 1398 (1980).
11) D. J. Williams, J. M. Pearson, and M. Levy, *J. Am. Chem. Soc.*, **92**, 1436 (1970); L. A. Errede and W. A. Pearson, *ibid.*, **83**, 954 (1961); L. A. Errede and B. F. Landrum, *ibid.*, **79**, 4952 (1957).
12) M. P. Cava and A. A. Deana, *J. Am. Chem. Soc.*, **81**, 4266 (1959).
13) E. Cuthbertson and D. D. MacNicol, *Tetrahedron Lett.*, **1975**, 1893.
14) N. N. Magdesieva and V. A. Vdoulin, *Khim. Geterotsikl. Soedin.*, **8**, 24 (1972); *Chem. Abstr.*, **76**, 153481 (1972); *cf.*, L. E. Saris and M. P. Cava, *J. Am. Chem. Soc.*, **98**, 867 (1976).
15) K. B. Sharpless and M. W. Young, *J. Org. Chem.*, **40**, 947 (1975).
16) O. Behaghel and H. Seibert, *Ber.*, **65**, 812 (1932).
17) A. Drory, *Ber.*, **24**, 2563 (1891).
18) W. E. Weaver and M. W. Whaley, *J. Am. Chem. Soc.*, **68**, 2115 (1946).
19) I. I. Lapkin, N. V. Bogoslovskii, and N. I. Zenkova, *Zh. Obshch. Khim.*, **41**, 2452 (1971).
20) E. G. Kataev, L. M. Kataev, and G. A. Chmutova, *Zh. Org. Khim.*, **2**, 2244 (1966).
21) S. Morimoto, *Nippon Kagaku Zasshi*, **75**, 557 (1954).
22) E. Bulka, K. D. Ahlers, and E. Tucék, *Chem. Ber.*, **100**, 1459 (1967).
23) C. N. Yiannois and J. V. Karabinos, *J. Org. Chem.*, **28**, 3246 (1963).
24) H. Böhme, H. Bezzenberger, and H. D. Stachel, *Justus Liebigs Ann. Chem.*, **602**, 1 (1957).
25) The spectral data of the familiar compounds are given by Aldrich Library; C. J. Pauchert, "The Aldrich Library of Infrared Spectra," by Aldrich Chem. Co., Inc. (1970); C. J. Pauchert and J. R. Campbell, "The Aldrich Library of NMR Spectra," by Aldrich Chem. Co., Inc. (1974).

Mechanisms of Enzymatic *S*-Oxygenation of Thioanisole Derivatives and *O*-Demethylation of Anisole Derivatives Promoted by Both Microsomes and a Reconstituted System with Purified Cytochrome P-450

Yoshihito WATANABE, Shigeru OAE,* and Takashi IYANAGI**

Department of Chemistry, The University of Tsukuba, Niihari-gun, Sakura-mura, Ibaraki 305

*** Division of Biochemistry, School of Medicine, The University of Tsukuba, Niihari-gun, Sakura-mura, Ibaraki 305*

(Received April 13, 1981)

Oxygenations of thioanisole derivatives have been shown to be promoted with phenobarbital induced rabbit liver microsomes. In order to understand the mechanistic details of the oxygenations, a kinetic study on the *S*-oxygenation promoted by a reconstituted system with purified cytochrome P-450 has been carried out. Log-(V_{max}) were correlated with the one electron oxidation potentials of the sulfides (E_p). The oxygenation is considered to proceed *via* one electron transfer from the sulfides to the iron-bound "oxenoid" intermediate of the enzyme. A similar *O*-demethylation of anisoles has been investigated. In the oxidative *O*-demethylation of *p*-methoxy-d_3-anisole with rabbit liver microsomes, an intramolecular kinetic isotope effect of 3.4 was observed. Meanwhile, a large isotope effect of 5.1 was observed in the competitive *O*-demethylation of *p*-dimethoxybenzene and *p*-di(methoxy-d_3)benzene. In order to clarify the oxidation pathway of *O*-demethylation with the enzymatic system of cytochrome P-450, the rates of the *O*-demethylation of *p*-substituted anisoles have been measured. Unlike the enzymatic oxygenation of sulfides, there was no correlation between the rates of *O*-demethylation reaction and one electron oxidation potentials of anisoles. These observations suggest that the *O*-demethylation of anisoles proceeds *via* the initial hydrogen abstraction with the iron-bound "oxenoid" intermediate of the cytochrome P-450.

Oxidative *O*-demethylation of methyl ethers catalyzed by the hepatic microsomal cytochrome P-450 system, requiring NADPH and O_2, is one of typical oxidation reactions by mono-oxygenases,[1,2] and numerous substrates have been considered to be demethylated *via* forming the corresponding hemiacetal intermediates (Eq. 1).[3] This reaction involves the

$$\text{R-O-CH}_3 \xrightarrow{\text{enzyme}} [\text{R-O-CH}_2\text{-OH}] \xrightarrow{\text{non-enzyme}} \text{R-OH} + \text{HCHO} \quad (1)$$

initial removal of α-hydrogen and subsequent recombination of the resulting intermediate ((B) in Eq. 2) with the iron-bound "oxenoid" intermediate ($(FeOH)^{III}$) before collapsing to afford the hemiacetal intermediate. Since all the subsequent steps which involve highly reactive intermediates after the initial hydrogen removal would be quite fast, the initial hydrogen removal is presumed to be the rate-determining step of the overall reaction of demethylation. However, the removal of α-hydrogen could proceed *via* a different mechanistic route, as shown below.

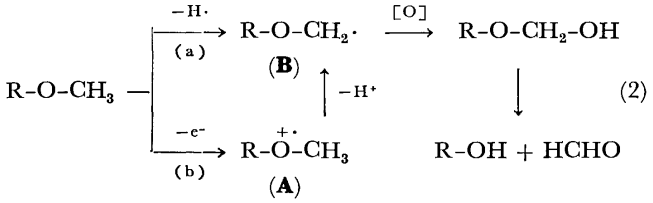

(2)

If the direct hydrogen-removal (a) is the actual path, one would find a relatively large kinetic isotope effect of α-hydrogen, whereas a small secondary kinetic isotope effect, k_H/k_D, would be observed when the proton removal takes place after the rate-determining electron transfer to form the cation radical (**A**). Thus, the kinetic isotope effect was studied to diagnose the mechanistic pathway of enzymatic demethylations and oxygenations.

In the *O*-demethylation of *o*-nitroanisole,[4] *p*-methoxy-acetanilide,[5] and *p*-dimethoxybenzene[5] and their methyl-d_3 derivatives, mediated by rat liver microsomes, the kinetic isotope effects, *i.e.* k_H/k_D of *ca.* 2 have been observed, whereas in the mono-*O*-demethylation of *p*-methoxy-d_3-anisole a large primary isotope effect ($k_H/k_D=10$)[5] was observed by the intramolecularly competitive reaction. In the *O*-dealkylation o propyl *p*-nitrophenyl ether, however, a rather small kinetic isotope effect ($k_H/k_D=1.1$) was observed during the metabolism with the rat and guinea pig hepatic enzyme systems.[6]

Recently, Hamilton and others postulated an iron-bound "oxenoid" intermediate as the active component species of mono-oxygenases.[7–13] This iron-bound "oxenoid" intermediate has been postulated to be analogous to the Compound I of peroxidase[10,13] and this postulate has been supported by extensive investigation with a few enzyme-model systems.[14,15] In other enzymatic oxidations of hydrocarbons, several *in vitro* measurements of the primary isotope effect give rather low values, such as $k_H/k_D \approx 2.0$.[16–20] In these experiments, kinetic isotope effects, k_H/k_D, were obtained by comparison of the reactivities of the deuterated and the undeuterated substrates, in separate kinetic runs. However, the enzymatic oxidation reaction consists of several succesive steps and hence the measured isotope effects are the summation of some steps of the overall enzymatic oxidation reaction. In order to avoid the complication of the kinetic treatment due to the different pre-oxygenation processes such as an electron transfer reduction of the cytochrome P-450-substrate complex and to estimate the real kinetic isotope effect of the enzymatic hydroxylation of hydrocarbons, it is desirable to measure the kinetic isotope effect of an intramolecularly competitive reaction.

Both Hjelmeland *et al.*[21] and Groves *et al.*[22] ob-

tained large values of $k_H/k_D \doteqdot 11$ for intramolecular isotope effects, using compounds which have both deuterated and undeuterated methylene groups in one molecule in the oxygenation of benzylic carbon and aliphatic carbon. These results suggest that the rate-determining step of the oxygenation is the hydrogen abstraction from hydrocarbons with the iron-bound "oxenoid" intermediate.[22]

Recently we have reported a few typical examples of enzymatic oxygenation of divalent sulfur compounds to the corresponding monoxides by both liver microsomes and its purified cytochrome P-450 system[23,24] and postulated that the oxygenation of sulfides by cytochrome P-450 involves the formation of sulfenium radical as a key intermediate.[25] Since the iron-bound "oxenoid" intermediate is considered to be a higher valent iron-oxo species and hence it would be highly electron deficient, the *S*-oxygenation of sulfur compounds would be initiated by an electron transfer from a divalent sulfide to the iron-bound "oxenoid" intermediate.[26] Meanwhile, we have also shown in the oxygenation of sulfides with a Fenton system[27] that *S*-oxygenation reaction involves generation of a cation radical of the sulfide. These observations on the oxygenation of sulfides suggest that even in the *O*-demethylation of anisole derivatives, the two mechanistic pathways shown in Eq. 2 are conceivable; i) the path (a), direct hydrogen abstraction and subsequent hydroxylation of methyl group (mechanism a), ii) the path (b), one electron transfer process prior to hydroxylation similar to the concurrent *S*-oxygenation and *S*-dealkylation.[25]

This paper gives kinetic evidence to support the one electron transfer mechanism for the *S*-oxygenation of *p*-substituted thioanisoles and to rule out the one electron transfer mechanism for the *O*-demethylation of *p*-substituted anisoles.

Results

Kinetic Experiment on The S-*Oxygenation of* p-*Substituted Thioanisole Derivatives.* When a 40—600 μM of methanolic solution of thioanisole (**1c**) was aerobically incubated in the reconstituted system, containing both purified cytochrome P-450 and NADPH-cytochrome P-450 reductase, oxidation of NADPH was observed. The addition of thioanisole (**1c**) induced a sudden increase of the rate of the NADPH consumption. Similar results were obtained in the oxidation of all the other sulfides (**1a**—**e**). Since a small amount of NADPH consumption was found to be devoured by the substrates even with a complete reconstituted system minus cytochrome P-450, the rates of the oxygenation were calculated by subtracting the rates of these undesired side reactions from the overall rates of NADPH consumption.

The V_{max} and K_m parameters of the oxygenation of sulfides by the reconstituted cytochrome P-450 system calculated from the Lineweaver-Burk plots are listed in Table 1, which also lists the effects of *p*-substituents in the oxygenation of thioanisole derivatives. Except *p*-chlorothioanisole (**1d**), the rate of oxygenation of the sulfide was found to decrease by the electron-withdrawing substituent while V_{max} value of the oxygenation increased by the electron-donating substituent.

Table 1. Kinetics of oxidation of NADPH in the reconstituted system with purified cytochrome P-450

Substrate	K_m (μM)	V_{max}[a] (μM/min)	V_{max}[a] (nmol/min/nmol P-450)	Binding type
1a	63	20	18	I
b	77	19	17	I
c	110	15	14	I
d	135	23	25	I
e	31	12	11	—[b]
3a	39	5.8	5.3	I
b	130	5.7	5.1	I
c	40	6.0	5.4	I
d	75	6.8	6.2	I
e	54	6.5	5.9	—[b]

a) The oxidation of substrate was monitored by the consumption of NADPH. b) **1e** and **3e** have so large absorbances in the region (350—500 nm) that the difference spectra cannot be observed.

Table 2. Comparison of one electron oxidation potential with both Hammett σ^+ and σ

Substrate	E_p *vs.* SCE[a] (V)	Substrate	E_p	σ^+	σ
1a	1.26	**3a**	1.47	−0.78	−0.27
b	1.41	**b**	1.76	−0.17	−0.17
c	1.53	**c**	1.83	0	0
d	1.55	**d**	2.17	0.23	0.23
e	1.85	**e**	2.36	0.79	0.71

a) Oxidation potentials were measured in 0.1 M of n-Bu_4NClO_4/CH_3CN.

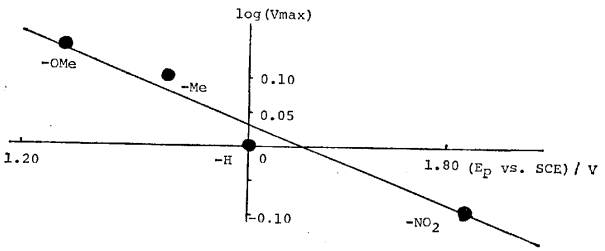

Fig. 1. Relationship between log (V_{max}) and E_p of *p*-substituted phenyl methyl sulfides.

In order to examine the possible relationship between the V_{max}'s of the oxygenation and one electron oxidation potentials of sulfides (**1a**—**e**), the cyclic voltammograms of the sulfides were obtained in acetonitrile (Table 2).

The V_{max} values in Table 1 were found to be correlated better with Hammett σ^+-values rather than σ-values ($\rho^+ = -0.16$), and the one electron oxidation potentials of the sulfides (except **1d**) are also correlated linearly with log(V_{max})'s of the enzymatic oxygenation of the sulfides (Figs. 1 and 2). E_p's (one electron oxidation potential) of the sulfides are con-

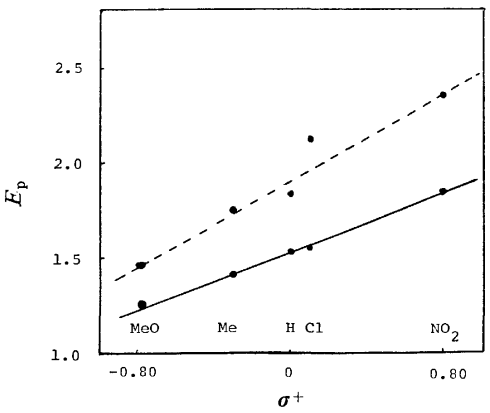

Fig. 2. Correlation between one electron oxidation potentials and Hammett σ^+-values.
----: Ether (**3**), ——sulfide (**1**).

TABLE 3. MICROSOMAL OXIDATION OF SULFIDE (**1**) AND ETHER (**2**)

Substrate	Product	(μmol)[c]	(nmol/min/nmol P-450)
1a[a]	**2a**	9.1	1.4
b	**b**	9.0	1.4
c	**c**	8.2	1.3
d	**d**	11.6	1.8
e	**e**	3.3	0.5
3a[b]	HCHO	34.0	5.3
b		17.7	2.8
c		22.5	3.5
d		21.3	3.3
e		24.4	3.8

Microsomal oxidation of sulfides and ethers were carried out for 20 min. a) $100 \times K_m$ (see Table 1) of sulfides were incubated in the oxidation. b) 250 μmol of ethers were incubated (see Experimental). c) In the oxidation of sulfides the corresponding sulfoxides were analyzed by GLC, and in the case of ethers yields of formaldehyde were determined by using Nash reagent.

sidered to correspond to the first oxidation peak potentials instead of $E_{1/2}$, due to the irreversible nature of the cyclic voltammograms.[28]

Incidentally, all the sulfides were found to be typical compounds of type I[29] having a maximum at 385—390 nm and a minimum at about 420 nm from the substrate-induced difference spectrum.

A methanolic solution of thioanisole (**1c**, 260 μmol, $100 \times K_m$) was added into a phosphate buffer (0.2 M, pH 7.4) containing both NADPH generating system and rabbit liver microsomes (see Experimental) and the incubation was carried out at 37 °C for 20 min with stirring. The oxygenation was stopped by adding 20 ml of acetone and 5 ml of trichloroacetic acid (0.5 M)† into the solution. After centrifugation of the reaction mixture, the supernatant solution was extracted with chloroform and the chloroform solution was dried over anhydrous magnesium sulfate. The product analysis was performed by GLC, and the sulfoxide (**2c**) was obtained as the sole product in

† 1 M=1 mol dm^{-3}.

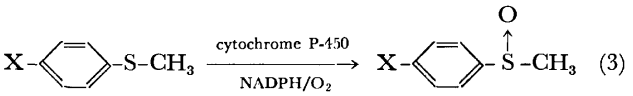

1 **2**

X: a, MeO b, Me c, H d, Cl e, NO_2

the microsomal oxygenation. Similar results were obtained with all the sulfides used (**1a—e**) (Table 3).

Kinetic Experiment on The O-Demethylation of p-*Substituted Anisole Derivatives.* Rates of the *O*-demethylation of *p*-substituted anisoles (**3a—e**) were measured according to the method described in the *S*-oxygenation. The K_m and V_{max} values of oxygenation of anisole derivatives (**3a—e**) in Table 1 show clearly that all the substrates have similar V_{max}'s values. Unlike the *S*-oxygenation or *S*-dealkylation, $\log(V_{max})$'s of enzymatic oxidations of the ethers cannot be correlated with either Hammett σ-values, σ^+-values or with one electron oxidation potentials (Fig. 3).

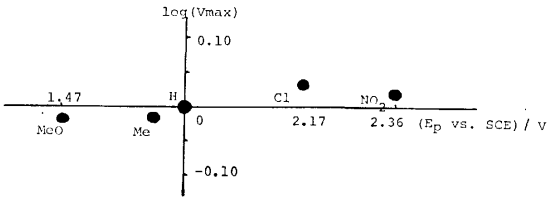

Fig. 3. Relationship between $\log(V_{max})$ and oxidation potential of *p*-substituted anisols.

On the other hand, one electron oxidation potentials of ethers (**3a—e**) in acetonitrile were correlated linearly with Hammett σ^+-values (Table 2 and Fig. 2).

The oxygenation of ethers (**3a—e**) by the reconstituted system of purified cytochrome P-450 gave *p*-substituted phenols (**4a—e**) and formadehyde. Oxygenation of anisole derivatives (**3a—e**) by the micro-

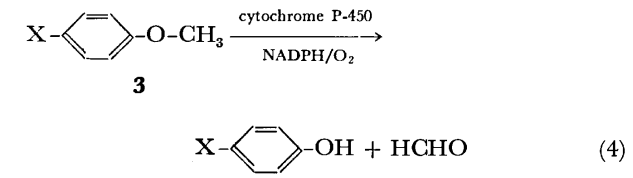

3

X: a, MeO b, Me c, H d, Cl e, NO_2

somal system were also performed similarly. After aerobical incubation, microsomal protein was removed from the mixture and formaldehyde formed was assayed using the Nash reagent,[30] and the extract was acidified with 2 M HCl and extracted with chloroform to obtain the other products such as phenols. The residure was analyzed by GLC and TLC. Only *p*-substituted phenols were obtained as the sole oxygenation product. In Table 3, the amounts of formaldehyde generated in the enzymatic reactions are listed.

O-Demethylation of p-*Substituted Anisoles and Its Methyl-d_3 Analogues.* When *p*-substituted anisole (**3**, 250 μmol) was aerobically incubated with the microsomes for 20 min, *O*-demethylation takes place as described in Table 3. Similarly, its methyl-d_3 analogue (**3**-d_3) was also oxygenated by the microsomes to give for-

Table 4. Intermolecular isotope effect by deuterium substitution on the metabolism of anisole by rabbit liver microsomes

Substrate		HCHO (μmol)	k_H/k_D[a]
Cl-C$_6$H$_4$-O-CH$_3$	**3d**	21.3	
Cl-C$_6$H$_4$-O-CD$_3$	**3d**-d_3	19.5	1.1
CH$_3$O-C$_6$H$_4$-OCH$_3$	**3a**	34.0	
CH$_3$O-C$_6$H$_4$-OCD$_3$	**3a**-d_3	32.1	1.1
CD$_3$O-C$_6$H$_4$-OCD$_3$	**3a**-d_6	15.9	2.1

a) $k_H/k_D = [HCHO]_H/[HCHO]_D$.

maldehyde and *p*-substituted phenol (**4**). (Table 4) This kinetic isotope effect, between deuterated and undeuterated anisoles, was 1.1 by the comparison of the amounts of formaldehyde. In the oxygenation of *p*-di(methoxy-d_3)benzene (**3a**-d_6), the kinetic isotope effect of 2.1 was observed.

When a solution of *p*-methoxy-d_3-anisole (**3a**-d_3) was incubated with the microsomes for three different periods (20, 60, and 90 min), the ^{1}H-FT-NMR spectrum of the mixture of **4a** and **4a**-d_3 was measured at 20—40 pulses. Since the chemical shifts of aromatic ring protons of **4a** and **4a**-d_3 appear at 6.78 ppm (δ-value, 4H,s) while that of methoxyl protons of **4a** is found at 3.76 ppm (3H, s) in $CDCl_3$, the ratio of the two products **4a** and **4a**-d_3 at three periods is given by Eq. 5.

$$[\mathbf{4a}]/[\mathbf{4a}\text{-}d_3] = \frac{[\text{methoxyl proton}]/3}{[(\text{aromatic ring proton}) - 4/3(\text{methoxyl proton})]/4} \quad (5)$$

From the intensities of the two singlet peaks of ethers, the ratios (*e.g.* **4a**:**4a**-d_3=23:77) were obtained (Table 5). From the ratio between **4a** and **4a**-d_3, the genuine kinetic isotope effect (k_H/k_D=3.4) for the *O*-demethylation was estimated.

A mixture of *p*-dimethoxybenzene (**3a**) and *p*-di(methoxy-d_3)benzene (**3a**-d_6) (1:1) was incubated with the microsomes for 20 min. In the intermolecularly competitive reaction, a kinetic isotope effect of 5.1 was obtained from ^{1}H-FT-NMR. (Table 6).

Discussion

We have recently reported a few examples of the enzymatic oxygenation of divalent sulfur compounds to the corresponding monooxides by both rabbit liver microsomes and a reconstituted system with the purified cytochrome P-450.[23,24] We have also shown

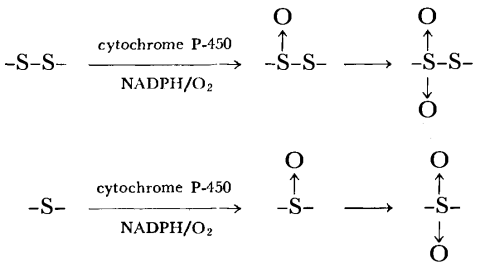

(6)

that sulfides are good substrates for the oxygenation with cytochrome P-450 enzyme and are readily oxidized to the corresponding sulfoxides and even further to sulfones,[25] or undergo *S*-dealkylation, indicating clearly that there are two reaction pathways in the enzymatic oxygenation of sulfides;[26] one is the *S*-dealkylation of sulfides to give thiols (or further oxidized disulfides) and aldehydes while the other is the ordinary *S*-oxygenation, as illustrated in Eq. 7. These two types of reactions appear to take place simultaneously while the acidity of α-hydrogen of alkyl

Table 5. Intramolecular isotope effect of deuterium substitution of *p*-dimethoxybenzene by the rabbit liver microsomes

CH$_3$O-C$_6$H$_4$-OCD$_3$ **3a**-d_3	CH$_3$O-C$_6$H$_4$-OH **4a**	CD$_3$O-C$_6$H$_4$-OH **4a**-d_3	k_H/k_D
Incubation time/min	Product ratio[a]		
20	23 : 77		3.4
60	23 : 77		3.4
90	24 : 76		3.2

a) Product ratio was measured by ^{1}H-FT-NMR spectrum.

Table 6. Competitive *O*-demethylation of *p*-dimethoxybenzene (**3a**-d_6 and **3a**) by rabbit liver microsomes

Substrates	Products	CD$_3$O-C$_6$H$_4$-OH **4a**-d_3	CH$_3$O-C$_6$H$_4$-OH **4a**	k_H/k_D
CD$_3$O-C$_6$H$_4$-OCD$_3$ **3a**-d_6[a]				
CH$_3$O-C$_6$H$_4$-OCH$_3$ **3a**[a]		84 : 16[b]		5.1

a) The mixture of **3a** (108 μmol) and **3a**-d_6 (108 μmol) was incubated for 20 min. b) Product ratio was determined by ^{1}H-FT-NMR spectrum.

sulfides and the stability of α-sulfenyl radicals seem to play important roles in determining the mode of the enzymatic oxygenation of sulfides, similar to the

$$R\text{-}S\text{-}CH_2R' \xrightarrow[NADPH/O_2]{\text{cytchrome P-450}} \begin{cases} \rightarrow R\text{-}\overset{\overset{O}{\uparrow}}{S}\text{-}CH_2R' \quad (S\text{-oxygenation}) \\ \rightarrow 1/2\ R\text{-}S\text{-}S\text{-}R + OHCR' \quad (S\text{-dealkylation}) \end{cases} \tag{7}$$

R=aryl, R′=alkyl.

N-oxygenation and *N*-dealkylation of tertiary amines with enzymatic and biomimetic model systems.[31,32] In the reaction of alkyl sulfides with hydroxyl radical generated by the Fenton's reagent,[27] a similar mode of oxidation reaction was observed. The initial step of this reaction is known to be the generation of sulfenium radical intermediate[33] (Eq. 8). Thus the similar mode of reaction and of products distribution suggests strongly that the enzymatic oxygenation of sulfide with cytochrome P-450 involves the formation of the cation radical intermediate.[25]

In order to confirm that the enzymatic oxygenation also proceeds through one electron transfer process, a kinetic study on the *S*-oxygenation promoted by the reconstituted system with purified cytochrome P-450 was performed by following the disappearence of the UV absorption of NADPH, since we had already shown that the rates of oxidation of NADPH in the

$$R\text{-}S\text{-}CH_2R' + \cdot OH \rightarrow \underset{\text{sulfenium radical}}{[R\text{-}\overset{+\cdot}{S}\text{-}CH_2R']} \begin{cases} \xrightarrow{\cdot OH} R\text{-}\overset{\overset{O}{\uparrow}}{S}\text{-}CH_2R' \\ \xrightarrow{-H^+} R\text{-}S\text{-}\dot{C}HR' \end{cases} \tag{8}$$

$$\xrightarrow{\cdot OH} R\text{-}S\text{-}\underset{|}{\overset{OH}{C}}HR' \longrightarrow R\text{-}SH\ (+OHCR')$$

$$\longrightarrow 1/2\ R\text{-}S\text{-}S\text{-}R$$

R=aryl, R′=Ph, CN, COPh *etc.*

reconstituted system with cytochrome P-450 are proportional to that of the generation of the sulfoxide.[23] Fine correlations between $\log(V_{max})$'s of the oxygenation of sulfides (**1a**—**e**) except (**1d**)[34] and both one electron oxidation potentials and Hammett σ^+-values are illustrated in Table 1 and Fig. 1. While the rates of the oxidation of these sulfides with hydrogen peroxide are correlated nicely with Hammett σ-values ($\rho=-1.17$),[35] V_{max}'s in Table 1 are correlated better with σ^+-values than σ-values ($\rho^+=-0.16$). These data cannot be explained on the basis of the simple nucleophilic attack of divalent sulfur atom of the sulfide on the electrophilic center of the iron-bound "oxenoid" intermediate, unlike the oxidation of sulfides with hydrogen peroxide. The good correlation between one electron oxidation potentials and the oxygenation rates of sulfides mediated by cytochrome P-450 system suggests clearly that the *S*-oxygenation is initiated by one electron transfer from the divalent sulfide to the iron-bound "oxenoid" intermediate of cytochrome P-450, as shown below.

$$Ar\text{-}S\text{-}CH_3 \xrightarrow{\text{cytochrome P-450 } (FeO)^{3+}} Ar\text{-}\overset{+\cdot}{S}\text{-}CH_3 + (FeO)^{2+}$$

$$\longrightarrow Ar\text{-}\overset{\overset{O}{\uparrow}}{S}\text{-}CH_3 + \text{cyt. P-450 } Fe^{3+} \tag{9}$$

The relatively small substituent effect on the V_{max} can be rationalized in term of the extremely facile nature of the one electron transfer process because of the highly electron-demanding character of the iron-bound "oxenoid" intermediate.[36]

In the enzymatic oxidative *N*-demethylation of tertiary amines, similar cation radical intermediates have been considered to be involved and the oxidation of aminopyrine by horseradish peroxidase has also been suggested to involve the cation radical intermediate on the basis of the ESR spectroscopic studies.[37] Our kinetic data on the *S*-oxygenation are in keeping with the mechanism of the *N*-demethylation promoted by horseradish peroxidase in the generation of cation radical intermediate of the substrate.

Lewis and Ho carried out photochemical oxidation of *N*-methyl-*N*-methyl-d_3-*t*-butylamine and estimated the kinetic isotope effect (k_H/k_D) of 2.2 on the basis of the amount of CD_2O and CH_2O formed in the reaction.[38] The isotope effect, 2.2 they found in the photochemical oxidation of the tertiary amine, is believed to result from the deprotonation process going from the aminium radical to the α-amino alkyl radical. Meanwhile, in the enzymatic oxidation of tertiary amines (*N*-demethylation), kinetic isotope effects of similar magnitude, *i.e.*, 1.6—2.0 were observed by Miwa *et al.*[39] The isotope effects of a similar size in both chemical and enzymatic oxidations of tertiary amines suggest that one electron transfer process described above is also taking place in the enzymatic system. The enzymatic *N*-demethylation promoted by the rat liver microsomal cytochrome P-450 also involves the similar formation of an aminium radical intermediate prior to give an α-amino alkyl radical, which reacts subsequently with iron-bound "oxenoid" intermediate, eventually affording the *N*-monodemethylated amine and formaldehyde.

Alkyl ethers, such as anisole derivatives having a nucleophilic hetero atom, also have an isoelectronic structure of alkyl sulfides and tertiary amines. However, since the ether-oxygen is highly electronegative, one-electron transfer from the ether oxygen cannot be so facile unlike tertiary amines or sulfides. Therefore a process involving direct α-hydrogen abstraction and subsequent hydroxylation as shown in Eq. 2 (a) is more conceivable.

$$R\text{-}\ddot{S}\text{-}R', \qquad R\text{-}\overset{R''}{\underset{|}{N}}\text{-}R', \qquad R\text{-}\ddot{O}\text{-}R'$$

In order to clarify the oxidation pathway of *O*-demethylation with the enzymatic system of cytochrome P-450, a kinetic study of the *O*-demethylation of *p*-substituted anisoles (**3a**—**e**) was performed.

Unlike the enzymatic oxygenation of sulfides, there

was no correlation between the rates of oxidation of NADPH and one electron oxidation potentials of anisoles. The effect of *p*-substituent in anisoles (**3**) on one electron oxidation potential is higher than that of thioanisoles (**1**); namely, the difference between the oxidation potentials of *p*-nitroanisole (**3e**) and *p*-methoxyanisole (**3a**) is 0.89 (V *vs.* SCE) while it is 0.59 (V *vs.* SCE) between those of thioanisole derivatives (**1a**) and (**1e**) (Table 2 and Fig. 2).

These results strongly suggest that the cation radical mechanism in Eq. 2 (b) is not acceptable.

In the electrochemical oxidation of several benzyl ethers, carried out by Mayeda *et al*,[40] however, they postulated a mechanistic pathway containing a cation radical intermediate (Eq. 10).

$$\mathrm{R\text{-}\ddot{O}\text{-}CH_2Ph} \xrightarrow{-e^-} \mathrm{R\text{-}\overset{+\cdot}{O}\text{-}CH_2Ph} \xrightarrow[ii)\ -e^-]{i)\ -H^+} \mathrm{R\text{-}\ddot{O}\text{-}\overset{+}{C}HPh} \xrightarrow{H_2O} \mathrm{R\text{-}O\text{-}\underset{OH}{\underset{|}{C}}HPh} \longrightarrow \mathrm{R\text{-}OH + OHCPh} \quad (10)$$

Recently, the mechanism of the anodic cleavage of benzyl ethers was examined by Boyd *et al.*[41] using benzyl benzyl-α,α-d_2 ether. When it was oxidized by electrochemically, an intramolecular primary kinetic isotope effect of 1.9 was observed. This kinetic isotope effect was interpreted to be due to the deprotonation process *via* the cation radical intermediate of the ether (Eq. 10).

In the enzymatic oxygenation of several substrates leading to the hydroxylation and/or *O*-demethylation, small kinetic isotope effects were observed.[4,16-20] For example, in the *O*-demethylation of *p*-chloroanisoles (**3d**, **3d**-d_3) the value of 1.1 for k_H/k_D was obtained (Table 4). Generally the observed intermolecular isotope effect was small.

If one electron transfer from the oxygen atom of an ether to the iron-bound "oxenoid" intermediate of cytochrome P-450 takes place at the rate-determining step, the kinetic isotope effect would be around unity, when a mixture of *p*-dimethoxybenzene (**3a**) and *p*-di(methoxy-d_3)benzene (**3a**-d_6) is aerobically incubated with a microsomal cytochrome P-450 system, since ethers **3a** and **3a**-d_6 would have roughly the same one electron oxidation potential. The subsequent deprotonation from the cation radical of ether (Eq. 2 (b)) would be fast and irreversible. Meanwhile a kinetic isotope effect of ≈ 2 is expected to be obtained in the internal competitive enzymatic oxygenation of *p*-methoxy-d_3-anisole (**3a**-d_3) as in the electrochemical oxidation of benzyl benzyl-α,α-d_2 ether.[41]

However, a large isotope effect of 5.1 was observed in the competitive *O*-demethylations of *p*-dimethoxybenzene (**3a**) and *p*-di(methoxy-d_3)benzene (**3a**-d_6), and the kinetic isotope effect of 3.4 was observed in the oxidative *O*-demethylation of *p*-methoxy-d_3-anisole (**3a**-d_3) with rabbit liver microsomes (Tables 5 and 6). Recently, even a large kinetic isotope effect of 10 was reported in the oxidative *O*-demethylation of ether (**3a**-d_3) with the rat liver microsomes by Foster *et al.*[5]

All these large values of isotope effects and the kinetic result found on the enzymatic *O*-demethylation of anisoles support the hydroxylation to involve initial α-hydrogen abstraction and subsequent hydroxylation as illustrated in Eq. 2 (a), although we cannot rule out completely an alternative mechanism involving a direct insertion of active oxygen (oxene) into methoxy C–H bond.[42]

Experimental

Reagents. The following compounds were obtained from the commercial sources as indicated below; NADPH, $NADP^+$, D-glucose 6-phosphate (G6P), and D-glucose 6-phosphate dehydrogenase (G6P-DH), Oriental Yeast. *p*-Substituted thiophenols, methyl iodide, dimethyl disulfide, and triethylbenzylammonium chloride, Wako Chemicals. *p*-Substituted phenols and *p*-substituted anisoles, Tokyo Chemicals Co. Ltd. Methyl-d_3 iodide (min. 99.5%), Merck.

Organic Synthesis. *p*-Methyl- and *p*-chlorothioanisole (**1b**, **1d**) were obtained by treating *p*-methyl- and *p*-chlorothiophenol with methyl iodide in the presence of sodium hydroxide in good yield,[43,44] and isolated upon SiO_2-column chromatography (Merck Kieselgel 60, benzene as an eluent). *p*-Methoxythioanisole (**1a**) was prepared by the reaction of anisole and *S*-methyl methanethiosulfinate as described in a recent work by Oae *et al.*[45] *p*-Nitrothioanisole (**1e**) was synthesized by treatment of *p*-nitroaniline and dimethyl disulfide with *t*-butyl thionitrate.[46] Both **1a** and **1e** were purified through SiO_2-column chromatography. ^1H NMR (δ-values in $CDCl_3$, ppm); *p*-$MeOC_6H_4$–SMe,[45] 2.4 (3H, s), 3.75 (3H, s), 6.86 (2H, d J=9.0), 7.29 (2H, d J=9.0). *p*-MeC_6H_4–SMe,[47] 2.28 (3H, s), 2.41 (3H, s), 7.12 (4H, brs). *p*-ClC_6H_4–SMe,[48] 2.41 (3H, s), 7.03 (2H, d J=8.7), 7.12 (2H, d J=8.7). *p*-$NO_2C_6H_4$–SMe,[46] 2.55 (3H, s), 7.25 (2H, d J=9.4), 8.15 (2H, d J=9.4).

All the sulfoxides (**2**) used as authentic samples were synthesized by oxidation of the corresponding sulfides (**1**) with hydrogen peroxide[49] (in acetic acid) or *m*-chloroperbenzoic acid[50] (in dichloromethane), and were isolated through Al_2O_3-column chromatography (Wako, Alumina activated 200 mesh, AcOEt:$CHCl_3$=4:1 as eluent). ^1H NMR (δ-values in $CDCl_3$); *p*-$MeOC_6H_4$–$\underset{\downarrow}{\underset{O}{S}}$Me,[51] 2.70 (3H, s), 3.85 (3H, s), 7.01 (2H, d J=9.0), 7.60 (2H, d J=9.0). *p*-MeC_6H_4–$\underset{\downarrow}{\underset{O}{S}}$Me,[51] 2.4 (3H, s), 7.27 (2H, d J=8.6), 7.54 (2H, d J=8.6). C_6H_5–$\underset{\downarrow}{\underset{O}{S}}$Me,[52] 2.64 (3H, s), 7.4—7.6 (5H, m). *p*-ClC_6H_4–$\underset{\downarrow}{\underset{O}{S}}$Me,[53] 2.64 (3H, s), 7.39 (2H, d J=8.9), 7.44 (2H, d J=8.9). *p*-$NO_2C_6H_4$–$\underset{\downarrow}{\underset{O}{S}}$Me,[54] 2.8 (3H, s), 7.84 (2H, d J=9.0), 8.40 (2H, d J=9.0).

All the deuterated anisoles (**3a**-d_3, **3a**-d_6, and **3d**-d_3) were prepared by the reaction of the corresponding phenols (**4**) with methyl-d_3 iodide (min. 99.5%) and sodium hydroxide using a phase transfer catalyst (triethylbenzylammonium chloride) described by McKillop.[55] ^1H NMR (δ-values in $CDCl_3$) and *m/e*; *p*-$CD_3OC_6H_4OCH_3$,[5] 3.80 (3H, s), 6.80 (4H, s). *m/e*, 141 (M^+, 100%), 138 (0%). *p*-$CD_3OC_6H_4$-OCD_3,[5] 6.80 (4H, s). *m/e*, 144 (M^+, 100%), 141, 138 (0%). *p*-$CD_3OC_6H_4Cl$, 6.76 (2H, d J=9.0), 7.18 (2H, d J=9.0). *m/e*, 147 (M^+, ^{37}Cl 35%), 145 (M^+, ^{35}Cl 100%), 144, 142 (0%).

All the substrates were distilled or recrystallized prior to use. ^{1}H NMR spectra described above were recorded on a Perkin Elmer Hitachi R-20 (60 MHz) and mass spectra were recorded on a Hitachi RMU-6MG Mass Spectrometer.

Preparation of Microsomes, Purified Cytochrome P-450 and NADPH-Cytochrome P-450 Reductase. The liver microsomes (cytochrome p-450, 2.45 nmol/mg protein) were obtained from male rabbits (2—3 kg) pretreated with sodium phenobarbital (50 mg/kg of body weight, each day for 5 d) according to the procedure reported earlier,[23] while the purified cytochrome P-450 was obtained by the method of Imai and Sato.[56] NADPH-cytochrome P-450 reductase was purified by the method of Iyanagi *et al.*[57]

Enzyme Assay. The standard reaction mixture for assaying the *S*-oxygenation and the *O*-demethylation activities were made to contain 76—250 μmol of the substrates, the hepatic microsomes (130 mg protein), the NADPH generating system [30 μmol of $NADP^+$, 300 μmol of G6P (2 Na salt) and 36 units of G6P-DH], and phosphate buffer (pH 7.4, 0.2 M) in a final volume of 20 ml. The reaction mixture without G6P-DH was incubated for 5 min at 36 °C with stirring to dissolve the substrates, prior to the addition of G6P-DH into the mixture. After incubating the reaction mixture for 20 min at 36 °C under air, the reaction was stopped by adding 10 ml of acetone and 0.5 M of trichloroacetic acid (to pH 3) (or 5 ml of 15% zinc sulfate and 5 ml of saturated barium hydroxide) into the mixture which was cooled for 10 min at 0 °C to precipitate the protein. After centrifugation (3000 min^{-1}) of the mixture for 15 min, the supernatant was separated, neutralized by addition of aqueous KOH solution, and then was extracted 4 times with chloroform. The chloroform layer was dried over anhydrous magnesium sulfate and concentrated under reduced pressure. The residue was diluted to 1 ml with acetone and analyzed by gas chromatography (GLC: Hitachi 163 Gas Chromatography, 1 m glass column, 10% SE-30) and thin layer chromatography (TLC: Merck, Kieselgel 60-GF_{254}, and Aluminiumoxid GF-254, 60/E). The oxidation products were isolated by preparative TLC (chloroform was used as an eluent), and identified by comparison with authentic samples. Formaldehyde was measured by the Nash reagent.[30]

Kinetic Conditions of Oxidation of Both Sulfides and Ethers with Reconstituted System Containing Purified Cytochrome P-450. The reconstituted system (1.1 nmol of cytochrome P-*450* and 1.7 nmol of NADPH-cytochrome P-450 reductase) was allowed to stand at room temperature for 10 min in UV micro-cell, and then was diluted by 0.1 M phosphate buffer (pH 7.7) containing 100 nmol of NADPH and 6.6×10^{-3}% of detergent (Emalgen 913; KAO-ATLAS Chemicals) to 1 ml. After measuring the natural consumption of NADPH by following the absorbance at 340 nm due to NADPH, a methanolic solution of the substrate (2—30 μl, 20 mM) was added into the UV micro-cell and the mixture was aerobically incubated to initiate the reaction. The rate of oxygenation of the sulfide or ether was monitored at several time intervals by following the consumption of NADPH.

Measurement of the Difference Spectra Caused by Addition of Substrates to the Purified Cytochrome P-450. Cytochrome P-450 (1.1—10 μM in 0.2 M of phosphate buffer containing 20% glycerol) was placed into a 10 mm cuvette for spectrometric recording. The substrate was dissolved in methanol (0.5—30 μl), into which was added the sample solution. The same amount of methanol was placed in the reference cuvette for spectroscopic comparison.

Analytic Procedure. The amount of protein in the microsomes was determined by Lowry's method,[58] using bovin serum albumin. The concentration of cytochrome P-450 was determined by comparison with the carbon monoxide-difference spectrum of the dithionite-treated liver microsomes. The absorbance between 450 and 490 nm ($\Delta A_{450-490}$) was used for calculation of cytochrome P-450 content (ε, 91 $mM^{-1}\,cm^{-1}$).[59,60] The concentration of the purified cytochrome P-450 was determined by measuring the absorption of the oxidized form ($\Delta A_{418-500}$), which has a molar extinction coefficient of 107 $mM^{-1}\,cm^{-1}$.[56] (UV: JASCO UVIDEC-1 and Hitachi Model 200-20 Spectrophotometer).

The ratio of *p*-methoxyphenol (**4a**) to *p*-methoxy-d_3-phenol (**4a**-d_3) was calculated from the intensities of methoxyl and aromatic ring protons which were recorded on ^{1}H-FT-NMR spectroscopy. (JEOL FX-100). ^{1}H NMR (δ-values in $CDCl_3$); *p*-$CH_3OC_6H_4OH$, 3.76 (3H, s), 6.78 (4H, s). *p*-$CD_3OC_6H_4OH$, 6.78 (4H, s).

Measurement of Cyclic Voltammograms. Cyclic voltammograms of substrates were obtained in 0.1 M *n*-Bu_4NClO_4/CH_3CN. (scan rate; 300, 150, and 50 mV/s) (HOKUTO DENKO Ltd., POTENTIOSTAT/GALVANOSTAT HA-301)

References

1) B. B. Brodie, J. R. Gillette, and B. N. La Du, *Ann. Rev. Biochem.*, **27**, 427 (1958).
2) A. H. Conney, *Pharmacol. Rev.*, **19**, 317 (1967).
3) Hemiacetal intermediate is readily hydrolyzed under the reaction conditions.
4) C. Mitoma, D. M. Yasuda, J. Tagg, and M. Tanabe, *Biochem. Biophys. Acta*, **136**, 566 (1967).
5) A. B. Foster, M. Jarman, J. D. Stevens, P. Thomas, and J. H. Westwood, *Chem. -Biol. Interact.* **9**, 327 (1974).
6) C. Mitoma, R. L. Dehn, and M. Tanabe, *Biochem. Biophys. Acta*, **237**, 21 (1971).
7) G. R. Schonbaum and S. Lo, *J. Biol. Chem.*, **247**, 3353 (1972).
8) G. D. Nordblom, R. E. White, and M. J. Coon, *Arch. Biochem. Biophys.*, **175**, 524 (1976).
9) E. G. Hrycay, J. Gustafsson, M. Ingelman-Sundberg, and L. Ernster, *Biochem. Biophys. Res. Commun.*, **66**, 209 (1975).
10) L. P. Hager, D. L. Doubek, R. M. Silverstein, J. H. Hargis, and J. C. Martin, *J. Am. Chem. Soc.*, **94**, 4364 (1972).
11) V. Ullrich, H. H. Ruf, and P. Weude, *Croat. Chem. Acta*, **49**, 213 (1977).
12) D. M. Jerina, J. W. Daly, B. Witkop, P. Zaltzman-Nirenberg, and S. Udenfriend, *Biochem.*, **9**, 147 (1970).
13) G. A. Hamilton, "Molecular Mechanisms of Oxygen Activations," ed by O. Hayaishi, Academic Press, New York (1974), p. 405.
14) C. K. Chang and Ming Shang Kuo, *J. Am. Chem. Soc.*, **101**, 3413 (1979).
15) J. T. Groves, T. E. Nemo, and R. S. Myers, *J. Am. Chem. Soc.*, **101**, 1032 (1979).
16) M. Tanabe, D. Yasuda, J. Tagg, and C. Mitoma, *Biochem. Pharmacol.*, **16**, 2230 (1967).
17) C. Elison, H. W. Elliott, M. Look, and H. Rapoport, *J. Med. Chem.*, **6**, 237 (1963).
18) R. E. McMahon, H. R. Sullivan, J. C. Craig, and W. E. Pereira. Jr., *Arch. Biochem. Biophys.*, **132**, 575 (1969).
19) M. Tanabe, D. Yasuda, S. Levalley, and C. Mitoma, *Life Sci.*, **8**, 1123 (1969).
20) I. Björkhem, *Eur. J. Biochem.*, **18**, 299 (1971).
21) L. M. Hjelmeland, L. Aronow, and J. R. Trudell, *Biochem. Biophys. Res. Commun.*, **76**, 541 (1977).

22) J. T. Groves and G. A. McClusky, *Biochem. Biophys. Res. Commun.*, **81**, 154 (1978).
23) D. Fukushima, Y. H. Kim, T. Iyanagi, and S. Oae, *J. Biochem.*, **83**, 1019 (1978).
24) T. Takata, M. Yamazaki, K. Fujimori, Y. H. Kim, S. Oae, and T. Iyanagi, *Chem. Lett.*, **1980**, 1441.
25) Y. Watanabe, T. Numata, T. Iyanagi, and S. Oae, *Bull. Chem. Soc. Jpn.*, **54**, 1163 (1981).
26) Y. Watanabe, T. Iyanagi, and S. Oae, *Tetrahedron Lett.*, **21**, 3865 (1980).
27) C. Walling, *Acc. Chem. Res.*, **8**, 125 (1975).
28) T. Sato and K. Torizuka, *J. Chem. Soc., Perkin Trans. 2*, **1978**, 1199.
29) S. Horie, "Cytochrome P-450," ed by R. Sato and T. Omura, Kodansha Ltd., Tokyo (1978), p. 73.
30) T. Nash, *Biochem. J.*, **55**, 416 (1953).
31) D. H. Rosenblatt, L. A. Hull, D. C. Deluca, G. T. Davis, R. C. Weglein, and H. K. R. Williams, *J. Am. Chem. Soc.*, **89**, 1158 and 1163 (1967).
32) C. A. Audeh and J. R. Lindsay-Smith, *J. Chem. Soc., B*, **1970**, 1280.
33) G. C. Gilbert, D. K. C. Hodgeman, and R. O. C. Norman, *J. Chem. Soc., Perkin Trans. 2*, **1973**, 1784; G. C. Gilbert, J. P. Larkin, and R. O. C. Norman, *ibid.*, **1973**, 272.
34) Some uncertain special interaction between iron-bound "oxenoid" intermediate and **1d** may be involved.
35) G. Modena and L. Mariola, *Gazz. Chim. Ital.*, **87**, 1306 (1957).
36) V. Ullrich and W. Doppel, "The Enzymes," ed by P. D. Boyer, Academic Press, New York (1975), Vol. 12, p. 284.
37) B. W. Griffin and P. L. Ting, *Biochemistry*, **17**, 2206 (1978).
38) F. D. Lewis and Tong-Ing Ho, *J. Am. Chem. Soc.*, **102**, 1751 (1980).
39) G. T. Miwa, W. A. Garland, B. J. Hodshon, A. Y. H. Lu, and D. B. Northlop, *J. Biol. Chem.*, **255**, 6049 (1980).
40) E. A. Mayeda, L. L. Miller, and J. F. Wolf, *J. Am. Chem. Soc.*, **94**, 6812 (1972).
41) J. W. Boyd, P. W. Schmalzl, and L. L. Miller, *J. Am. Chem. Soc.*, **102**, 3856 (1980).
42) J. E. Tomaszewski, D. M. Jerina, and J. W. Daly, *Biochemistry*, **14**, 2024 (1975).
43) W. Tagaki, "Organic Chemistry of Sulfur," ed by S. Oae, Plenum Press, New York (1978), Chap. 6.
44) R. B. Wagner and H. D. Zook, "Synthetic Organic Chemistry," John Wiley & Sons, New York (1953), p. 787.
45) N. Furukawa, T. Morishita, T. Akasaka, and S. Oae, *Tetrahedron Lett.*, **1979**, 3973.
46) S. Oae, K. Shinhama, and Y. H. Kim, *Bull. Chem. Soc. Jpn.*, **53**, 2023 (1980).
47) H. Gilman and F. J. Wedd, *J. Am. Chem. Soc.*, **71**, 4062 (1949).
48) L. N. Nikolenko and V. A. Koptyung, *Zh. Obshch. Khim.*, **25**, 1757 (1955).
49) L. I. Denisova and V. A. Batyakina, *Kim.- Farm. Zh.*, **4**, 9 (1970).
50) C. G. Overberg and W. Cumminus, *J. Am. Chem. Soc.*, **75**, 4250 (1953).
51) N. J. Leonard and C. R. Cohnson, *J. Org. Chem.*, **27**, 282 (1962).
52) C. C. Price and J. Hydock, *J. Am. Chem. Soc.*, **74**, 1943 (1952).
53) F. G. Bordwell and B. M. Pitt, *J. Am. Chem. Soc.*, **79**, 572 (1955).
54) F. G. Bordwell and P. J. Boutan, *J. Am. Chem. Soc.*, **79**, 717 (1957).
55) A. McKillop, J.-C. Flaud, and R. P. Hug, *Tetrahedron*, **30**, 1379 (1974).
56) Y. Imai and R. Sato, *Biochem. Biophys. Res. Commun.*, **60**, 8 (1973).
57) T. Iyanagi, F. K. Anan, Y. Imai, and H. S. Mason, *Biochemistry*, **17**, 2224 (1978).
58) O. H. Lowry, N. J. Rosenbrough, A. L. Farr, and R. J. Randall, *J. Biol. Chem.*, **193**, 265 (1951).
59) S. P. Colowick and N. O. Kaplan, "Method in Enzymology," ed by S. Fisher and L. Packer, Academic Press, New York (1978), Vol. 52, p. 215.
60) T. Omura and R. Sato, *J. Biol. Chem.*, **239**, 2370 (1964).

Reduction by a Model of NAD(P)H. 36. First and Direct Evidence for the Multi-step Mechanism

Shinro YASUI, Kaoru NAKAMURA, Atsuyoshi OHNO,* and Shinzaburo OKA
Institute for Chemical Research, Kyoto University, Uji, Kyoto 611

(Received April 16, 1981)

Reductions of thiobenzophenone derivatives with a model compound of NAD(P)H, 1-benzyl-1,4-dihydronicotinamide (BNAH) or *N*-(α-methylbenzyl)-1-propyl-2,4-dimethyl-1,4-dihydronicotinamide (Me_2PNPH), in a solvent containing an *O*-deuterated alcohol afforded products partially deuterated at their methine positions. The deuterium content depends both on the character of substituents in the substrate and on the polarity of solvent. In contrast, no incorporation of deuterium into the product was observed in the reduction of thiopivalophenone with BNAH or Me_2PNPH under the same conditions. These results can be accounted for in terms of an electron transfer followed by a proton transfer from the model to substrate. This is the first and direct evidence for the ion radical-pair intermediacy for reductions by model compounds of NAD(P)H.

Although many investigators have studied the mechanism of reductions with model compounds of NAD(P)H, several points are still ambiguous. Of these, the mechanism of transfer of a "net hydride" from a model compound to substrate has frequently been subjected to discussion. In 1957, Abeles *et al.*[1] examined reductions of thiobenzophenone derivatives with 1-benzyl-1,4-dihydronicotinamide (BNAH) and concluded that a hydride would transfer directly from a model to substrate. On the other hand, a multi-step mechanism including at least one intermediate was proposed by Steffens and Chipman[2] in order to explain a discrepancy between kinetic isotope effect and isotopic ratio in products found in a reduction of α,α,α-trifluoroacetophenone with 1-substituted 1,4-dihydronicotinamide-4-*d*. They suggested that the intermediate in this reaction would be a non-covalent charge-transfer complex generated through an electron transfer from the dihydropyridine derivative to the substrate. Thereafter, such discrepancies have been reported for reductions of substituted α,α,α-trifluoroacetophenones,[3] 1,10-phenanthroline-2-carbaldehyde,[4] *N*-methylacridinium ion,[5,6] and 2-acylisoquinolines.[7] We detected radical species on ESR spectra for reductions of benzil[8] and thiobenzophenone[9] with BNAH. These facts strongly support existence of an ion radical-pair intermediate in reduction with model compounds of NAD(P)H.

The spectroscopic detection of an ion radical, however, cannot necessarily be an unambiguous proof for its intermediacy. One can argue that at least part of hydrogen atoms incorporated in products should come from solvents or some sources other than NAD(P)H-models, if an ion radical-pair is an intermediate in the reduction. The fact that no such observations have yet been reported may be taken to be an indication that the spectroscopically detected ion radicals might be abortive species. On the other hand, one can also propose that hydrogen transfer between reactive ion radicals might take place so fast within a cage of solvent that no incorporation of hydrogen might be brought about from the solvent into product. The latter argument necessarily predicts that out-of-cage reactions may be detected chemically when one employs such substrates as are capable of affording relatively unreactive ion radical-pairs as intermediates. Thus, we tried for such reduction systems and found that a hydrogen atom from solvent is incorporated into products in some reductions of certain thiocarbonyl compounds.

In this paper we report that reductions of *p*-chlorothiobenzophenone (**1a**), thiobenzophenone (**1b**), *p,p'*-dimethoxythiobenzophenone (**1c**), or *o*-hydroxythiobenzophenone (**1d**) with BNAH or N-(α-methylbenzyl)-1-propyl-2,4-dimethyl-1,4-dihydronicotinamide (Me_2PNPH) afford products whose methine protons partially originate from the solvent and that the hydrogen atom at the 4-position of the model compound transfers directly to thiopivalophenone (**2**). Contrary to the conclusion by Abeles *et al.*,[1] this result clearly indicates an existence of intermediate in the reductions.

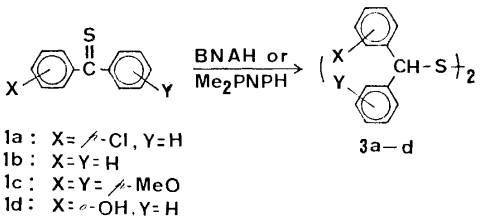

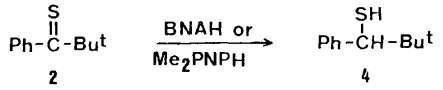

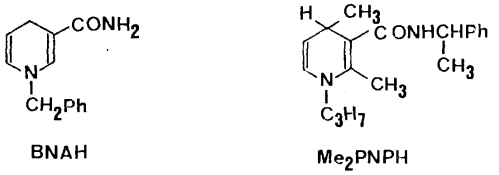

Results

One of substrates **1** was allowed to react with BNAH in a DMSO–methanol mixture at room temperature in the dark under a nitrogen atmosphere. For each run, after usual work-up, the product was isolated and assigned by NMR and mass spectrometries to the corresponding dibenzhydryl disulfide derivatives (**3**). No other products except the pyridinium salt were detected on TLC, indicating quantitative forma-

Table 1. Reaction with BNAH[a]

S[b]	Q_S[c] mmol	Q_{BNAH}[d] mmol	Reaction time	Solvent[e]	C_D/%[f] NMR	C_D/%[f] MS
1a	0.15	0.17	3 d	DMSO(1)-CD_3OD(0.5)	84	—
	0.13	0.13[g]	5 d	DMSO(1)-CH_3OH(0.5)	<10	—
	0.31	0.33	4 d	CH_2Cl_2(1)-CD_3OD(1)	<35	—
1b	0.30	0.28	0.5 h	CD_3OD(1)	31	32
	0.30	0.28	24 h	DMSO(1)-CD_3OD(0.5)	38	32
	0.15	0.16[g]	24 h	DMSO(0.5)-CH_3OH(0.25)	43	—
	0.31	0.37	20 h	MeCN(0.5)-CD_3OD(0.5)	43	48
	0.30	0.28	24 h[h]	DMF(0.5)-CD_3OD(0.5)	38	36
	0.31	0.37	20 h	$PhCH_3$(1)-CD_3OD(0.5)	31	—
	0.31	0.36	41 h	CD_3CN(2)	0	
1c	0.20	0.24	6 d	DMSO(1)-CD_3OD(0.5)	15	15
	0.16	0.17[g]	6 d	DMSO(1)-CH_3OH(0.5)	36	41
	0.21	0.23	5 d	DMF(1)-CD_3OD(0.5)	12	—
	0.21	0.23	7 d	$PhCH_3$(1)-CD_3OD(2)	6	6
1d	0.65	0.67	15 h	DMSO(1)-CD_3OD(0.5)	0	0
	0.55	0.55	19 h	C_2H_5OD(2.5)	0	0
	0.30	0.34[g]	23 h	DMSO(1)-CH_3OH(0.5)	≈100	≈100
2	0.26	0.28	2.5 h	DMSO(1)-CD_3OD(0.5)	0	0
	0.13	0.14[g]	4 h	DMSO(0.5)-CH_3OH(0.25)	≈100	≈100

a) At room temperature under a nitrogen atmosphere in the dark. b) S stands for substrate. c) Q_S is the quantity of S used. d) Q_{BNAH} is the quantity of BNAH used. e) The figures in parentheses indicate quantities in cm^3. f) C_D is the D content in a product. g) Reaction with BNAH-4,4-d_2.[10] h) At 273 K.

Table 2. Reaction with Me_2PNPH[a]

S[b]	Q_S[c] mmol	Q_M[d] mmol	Reaction time	Solvent[e]	C_D/%[f]
1a	0.15	0.18	29 h	DMSO(1)-CD_3OD(0.5)	>89
1b	0.32	0.39	33 h	DMSO(1)-CD_3OD(0.5)	92
1c	0.20	0.23	2 d	DMSO(1)-CD_3OD(0.5)	43
	0.18	0.21	2 d	DMSO(1)-C_2H_5OD(0.5)	35
1d	0.35	0.41	23 h	DMSO(2)-CD_3OD(1)	34
	0.18	0.21	41 h	DMSO(1)-C_2H_5OD(0.5)	59
2	0.16	0.18	4 d	DMSO(1)-CD_3OD(0.5)	0

a) At room temperature under a nitrogen atmosphere in the dark. b) S stands for substrate. c) Q_S is the quantity of S used. d) Q_M is the quantity of Me_2PNPH used. e) The figures in parentheses indicate quantities in cm^3. f) C_D is the D content in a product measured on NMR.

tion of **3**. In contrast, reaction of **2** with BNAH or Me_2PNPH afforded 1-phenyl-2,2-dimethyl-1-propanethiol (**4**) quantitatively.

When the reduction was carried out in a DMSO–methanol-d_4 mixture, the isolated product contained a deuterium atom in its methine position except in the case with **1d**. It is apparent that this deuterium atom originates from the solvent. Analyses by NMR and mass spectrometries gave deuterium contents 84%, 35±3%, and 15%, for **3a**, **3b**, and **3c**, respectively. Solvent effect also was examined by carrying out the reduction in several solvent systems containing methanol-d_4 or other deuterated compounds. Reductions of **1d** in DMSO–methanol-d_4 or ethanol-*O*-*d* and of **2** in DMSO–methanol-d_4 gave no deuterated products. On the other hand, reductions of these substrates with BNAH-4,4-d_2 afforded products having wholly deuterated methine groups. Results obtained are summarized in Table 1 together with those for reductions under other conditions.

A more dramatic hydrogen-incorporation from solvent into product was seen in reductions with Me_2PNPH in DMSO–methanol-d_4 or DMSO–ethanol-*O*-*d*. Even **1d** afforded a considerably deuterated product. Results obtained are listed in Table 2.

Discussion

In the reaction course leading to product **3** it is sure that **1** will be reduced by the model compound in the first stage (Eq. 1) to afford, as the primary reduction product, a thiolate anion (**5**) or thiyl radical (**6**), which will then dimerize to yield **3** during work-up or *in situ* (Eq. 2).[1,9] On the other hand, **2** is known to be reduced with the model compound to a thiolate anion (**7**),[11] which is protonated upon the

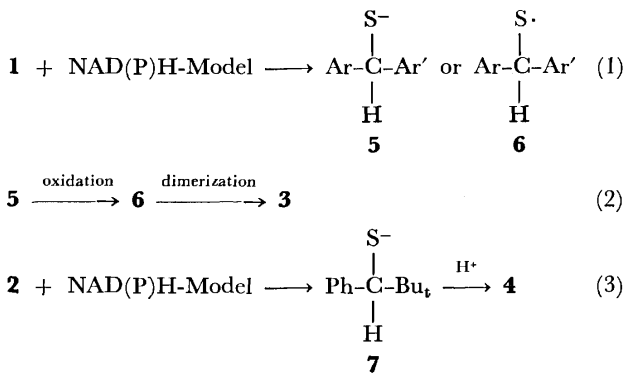

sulfur atom during work-up (Eq. 3). Here, we should recall the fact that the hydrogen on the methine position of **3** does not exchange with any hydrogens from solvents even under basic conditions.[12] Moreover, the dimerization of **5** or **6** to **3** is not likely to be accompanied by hydrogen exchange. Therefore, there is no doubt that in any cases the incorporation of hydrogen from solvent into product does occur during the first reduction step, Eq. 1, which implies involvement of at least one intermediate in this reduction step.

That the hydrogen picked up from the solvent has entered the product as a proton is obvious from the fact that no deuterium is incorporated into the product in the reduction in DMSO–acetonitrile-d_3, whereas deuterium is incorporated into the product when the reduction is carried out in ethanol-*O*-*d*. Thus, the intermediate which undergoes the out-of-cage reaction should be anionic in character. The anionic character of the intermediate is further confirmed by the following evidence. Table 1 indicates that the deuterium incorporation becomes deeper as the substituent on substrate becomes more electron-withdrawing and the solvent becomes more polar. The reduction with Me_2PNPH, as listed in Table 2, results in a deeper deuterium incorporation than that with BNAH. Me_2PNPH has two methyl groups on its dihydropyridine ring and a methylbenzyl moiety on its carbamoyl group, so that the electron-releasing power of Me_2PNPH is stronger than that of BNAH.[13] On the other hand, the presence of the 4-methyl group and less abundant reacting hydrogens makes Me_2PNPH less reactive toward proton releasing than BNAH. Consequently, the intermediate in the reduction with Me_2PNPH has more chance to escape from the solvent cage than the one in the reduction with BNAH; note that even **3d** contains deuterium from the solvent in a considerable amount.

The above discussion has revealed that the intermediate should be an anion radical, in agreement with previous evidence from kinetic,[3,11,14,15] ESR,[8,9,16] and several other studies.[5,17–19]

An anomaly with reaction of **1d** has been recognized[1] that the reduction of **1d** with BNAH takes place faster than expected from the simple electronic substituent effect. This phenomenon was interpreted in terms of general acid catalysis by *o*-hydroxyl proton on the basis of the "hydride transfer" mechanism. However, with the idea of "multi-step" mechanism,

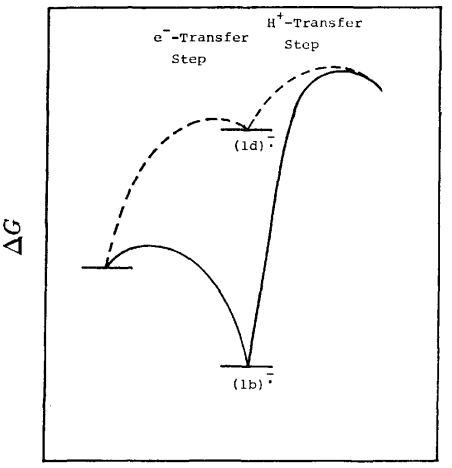

Fig. 1. Schematic illustration of energy diagrams for the reduction of thiobenzophenone (——) and *o*-hydroxythiobenzophenone (----).

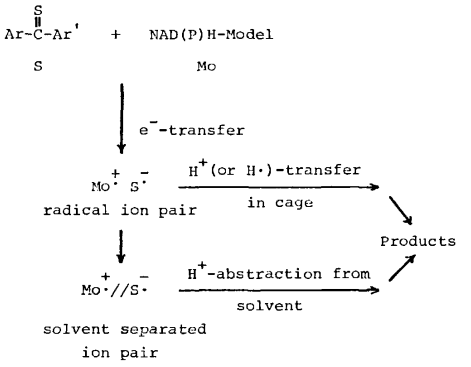

Scheme 1.

this phenomenon may be accounted for in terms of the stability of the intermediate anion radical. Reduction of **1b** and some other substrates is retarded by the presence of bivalent metal ion.[11,19] The retardation is due to an extraordinary stability of the cation-radical intermediate; a stable cation radical necessarily requires high transition energy for proton-accepting reaction.[3,6,19] In **1d**, the hydroxyl proton chelates on the thiocarbonyl sulfur by hydrogen bonding, which can be recognized by its abnormal low-field shift of proton (δ=12.7 in $CDCl_3$) in NMR spectrum and by its low-frequency shifts of ν_{OH} (3430 cm^{-1}) and $\nu_{C=S}$ (1228 cm^{-1})(in 2.5% CCl_4) in IR spectrum. Thus, the thiocarbonyl group in **1d** is different in character from the one in **1b**. The electron-accepting power of the former thiocarbonyl group is, therefore, weaker than that of the latter, and the initial electron-transfer process requires more energy for **1d** than for **1b**. In other words, the energy barrier for the proton-transfer process is less for **1d** than for **1b**, resulting in more opportunity for **1d** than for **1b** to undergo the in-cage reaction. Figure 1 visualizes energy diagrams for the reduction schematically. As mentioned above, Me_2PNPH is more electron-releasing but less proton-releasing than BNAH. Therefore, the energy diagram for the reduction with Me_2PNPH may be represented by a full line (**1b**-like relationship)

in Fig. 1. Since anion radical from **2** is the least stable of all, it has no chance to escape from the solvent cage to pick up a proton from the solvent even in the reduction with Me_2PNPH.

In conclusion, the reduction of a substrate by models of NAD(P)H proceeds *via* an intermediate of ion radical-pair. The anion radical can pick up a proton from the solvent when it has life-time long enough to escape from the solvent cage as shown in Scheme 1. Thus, "direct transfer of a hydrogen from a model to a substrate" is valid only for those substrates which will afford unstable anion radicals.

In enzymic reactions, a substrate is kept in a pocket of enzyme, and it has no chance to escape from the pocket into the bulk of solvent. It should also be kept in mind that all substrates susceptible to reduction by NAD(P)H-dependent dehydrogenases are such as afford unstable intermediates. Therefore, it is reasonable that "direct transfer of a hydrogen" is observed in all enzymic reactions.

Experimental

Materials. *p*-Chlorothiobenzophenone (**1a**), thiobenzophenone (**1b**), *p,p'*-dimethoxythiobenzophenone (**1c**), and *o*-hydroxythiobenzophenone (**1d**) were prepared from their corresponding ketones according to literature procedures,[1] and were purified by column chromatography using Florisil and carbon tetrachloride eluent (for **1a** and **1d**) or with recrystallization from ethanol (for **1b** and **1c**). Preparations of 1-benzyl-1,4-dihydronicotinamide (BNAH),[20] BNAH-4,4-d_2,[11,21] *N*-(α-methylbenzyl)-1-propyl-2,4-dimethyl-1,4-dihydronicotinamide (Me_2PNPH),[22] and thiopivalophenone (**2**)[23,24] were described previously. Spectral data of each material were satisfactory. The deuterium content of BNAH-4,4-d_2 was 99.0±1.0%. Each non-deuterated solvent was distilled and dried according to the usual method before use. Deuterated solvents were commercially available (Commissariat a l'Energie Atomique).

Product Analysis. In a vessel equipped with a Silicone-rubber stopper, a mixture of **1** or **2** and a model compound in an appropriate solvent was stirred under a nitrogen atmosphere in the dark. When the reaction was complete (on TLC), water was added to the mixture and the product was extracted three times with dichloromethane. The organic layer was washed twice with water, dried over anhydrous sodium sulfate, and concentrated *in vacuo*. The resulting residue was purified by HPLC using silica gel and benzene eluent (for **1a** and **1d**), with recrystallization from ethanol (for **1b** and **1c**), or by column chromatography using silica gel and hexane eluent (for **2**). Identification of isolated product was based on NMR (JASCO JNM-FX 100 FT NMR Spectrometer), MS (Hewlett-Packard 18947A GC/MS), and IR (Hitachi EPI-S-2 Spectrometer) spectra. Deuterium contents for products from reactions in deuterated solvent were estimated through comparison with those of authentic samples obtained from corresponding reactions in non-deuterated solvent.

References

1) R. H. Abeles, R. F. Hutton, and F. H. Westheimer, *J. Am. Chem. Soc.*, **79**, 712 (1957).
2) J. J. Steffens and D. M. Chipman, *J. Am. Chem. Soc.*, **93**, 6694 (1971).
3) A. Ohno, H. Yamamoto, and S. Oka, *J. Am. Chem. Soc.*, **103**, 2041 (1981).
4) D. J. Creighton, J. Hajdu, and D. S. Sigman, *J. Am. Chem. Soc.*, **98**, 4619 (1976).
5) J. Hajdu and D. S. Sigman, *J. Am. Chem. Soc.*, **98**, 6060 (1976).
6) A. Ohno, T. Shio, H. Yamamoto, and S. Oka, *J. Am. Chem. Soc.*, **103**, 2045 (1981).
7) A. Ohno, S. Yasui, and S. Oka, *Bull. Chem. Soc. Jpn.*, **53**, 2651 (1980).
8) Y. Ohnishi and A. Ohno, *Chem. Lett.*, **1976**, 697.
9) A. Ohno and N. Kito, *Chem. Lett.*, **1972**, 369.
10) Discrepancy between deuterium content in the product from the reduction in deuterated solvent and that from the reduction with BNAH-4,4-d_2 in non-deuterated solvent is a reasonable result from kinetic deuterium isotope effect of 3—5.
11) A. Ohno, S. Yasui, K. Nakamura, and S. Oka, *Bull. Chem. Soc. Jpn.*, **51**, 290 (1978).
12) A. Ohno and N. Kito, *Int. J. Sulfur Chem.*, **1**, 26 (1971).
13) Me_2PNPH can reduce *p*-methoxy-α,α,α-trifluoroacetophenone without a catalyst, whereas BNAH cannot. See, A. Ohno, J. Nakai, K. Nakamura, T. Goto, and S. Oka, *Bull. Chem. Soc. Jpn.*, **54**, 3486 (1981).
14) A. Ohno, H. Yamamoto, T. Okamoto, S. Oka, and Y. Ohnishi, *Bull. Chem. Soc. Jpn.*, **50**, 2385 (1977).
15) A. Ohno, S. Yasui, R. A. Gase, S. Oka, and U. K. Pandit, *Bioorg. Chem.*, **9**, 199 (1980).
16) A. Ohno, H. Yamamoto, and S. Oka, *Bull. Chem. Soc. Jpn.*, **54**, 3489 (1981).
17) A. Ohno, T. Kimura, H. Yamamoto, S. G. Kim, S. Oka, and Y. Ohnishi, *Bull. Chem. Soc. Jpn.*, **50**, 1535 (1977).
18) T. Okamoto, A. Ohno, and S. Oka, *J. Chem. Soc., Chem. Commun.*, **1977**, 181.
19) A. Ohno, S. Yasui, H. Yamamoto, S. Oka, and Y. Ohnishi, *Bull. Chem. Soc. Jpn.*, **51**, 294 (1978).
20) D. Mauzeral and F. H. Westheimer, *J. Am. Chem. Soc.*, **77**, 2261 (1955).
21) K. Nakamura, A. Ohno, S. Yasui, and S. Oka, *Tetrahedron Lett.*, **1978**, 4815.
22) A. Ohno, M. Ikeguchi, T. Kimura, and S. Oka, *J. Am. Chem. Soc.*, **101**, 7036 (1979).
23) A. Ohno, K. Nakamura, N. Nakazima, and S. Oka, *Bull. Chem. Soc. Jpn.*, **48**, 2403 (1975).
24) J. M. Beiner, D. Lecadet, D. Paquer, A. Thuillier, and J. Vialle, *Bull. Soc. Chim. Fr.*, **1973**, 1979.

Studies on Heteropentalenes. IV.[1] Heteroannelations to Pyrrolo-[2,1-*b*]benzothiazole and Pyrrolo[2,1-*b*]thiazoles

Noritaka ABE,* Tarozaemon NISHIWAKI, Toshimasa OMORI, and Emiko HARADA

Department of Chemistry, Faculty of Sciences, Yamaguchi University, Yamaguchi 753

(Received May 6, 1981)

2,3-Dibenzoylpyrrolo[2,1-*b*]benzothiazole (**2**) and 6,7-dibenzoylpyrrolo[2,1-*b*]thiazoles (**5a—b**) have been synthesized by utilizing the cycloaddition reactions of imidazo[2,1-*b*]benzothiazole and imidazo[2,1-*b*]thiazoles, respectively, with dibenzoylacetylene followed by the elimination of a nitrile from each of the cycloadducts. Heteroannelations to **2** and **5** have been achieved by their reactions with hydrazine, aminoacetonitrile, ethyl glycinate, and phosphorus pentasulfide. The annelations by the second and third reagents proceed fairly regioselectively. Facile dimerizations of thieno[3′,4′:3,4]pyrrolo[2,1-*b*]benzothiazole and thieno[3′,4′:3,4]-pyrrolo[2,1-*b*]thiazoles to be produced by the reactions with the last reagent are also described.

We have recently disclosed that the cycloadditions of imidazo[2,1-*b*]benzothiazole (**1a**) and imidazo[2,1-*b*]thiazoles (**4a—c**), respectively, with dimethyl acetylenedicarboxylate (DMAD),[2] but not with methyl propiolate,[1] are accompanied by the elimination of a nitrile from the adduct to form pyrrolo[2,1-*b*]benzothiazole and pyrrolo[2,1-*b*]thiazole ring systems. It is now reported that the reactions of dibenzoylacetylene (DBA) with the above heteropentalenes are similar to those of DMAD and that the products thereof, like other 1,2-dibenzoly-substituted aromatics,[3–7] readily undergo heteroannelations.

2,3-Dibenzoylpyrrolo[2,1-*b*]benzothiazole (**2**) and 6,7-dibenzoylpyrrolo[2,1-b]thiazoles (**5a—b**) were obtained in moderate to good yields from the reactions of **1a—b** and **4a—c**, respectively, with DBA in xylene. Their structures were proved by elemental analyses, and ^{1}H NMR and IR spectral data, the latter of which, in common with the spectra of diaryl ketones, possessed a ν(C=O) band at 1630—1650 cm^{-1}. Reactions of **2** and **5a**, respectively, with hydrazine gave 1,4-diphenylpyridazino[4′,5′:3,4]pyrrolo[2,1-*b*]benzothiazole (**3**) and 3-methyl-6,9-diphenylthiazolo[3′,2′:1,2]pyrrolo[3,4-*d*]pyridine (**6**) in exellent yields.

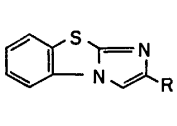

1a: R=Me
1b: R=Ph

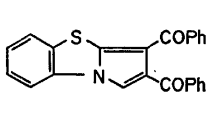

2

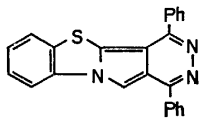

3

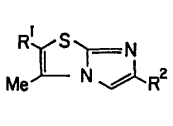

4a: R^1=H, R^2=Ph
4b: R^1=H, R^2=t-Bu
4c: R^1=CO$_2$Et, R^2=Ph

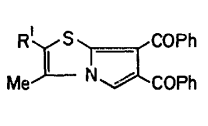

5a: R^1=H
5b: R^1=CO$_2$Et

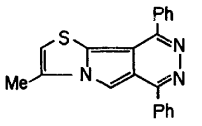

6

When **2** was heated under reflux with cyanomethylammonium hydrogensulfate in 1-butanol, a fluorescent yellow 5:1 mixture of **7a** and **8a** was obtained in almost quantitative yield, among which **7a** could be isolated by careful fractional crystallizations; separation of the products from the above mixture by means of chromatography was not successful and resulted in gradual discoloration on contact with silica gel or alumina. The structure of **7a** was assigned as 1,4-diphenylpyrido[3′,4′:3,4]pyrrolo[2,1-*b*]benzothiazole-3-carbonitrile on the basis of elemental analyses and spectral data. Whilst the ^{1}H NMR spectrum of **7a** displays a 1H singlet at δ 7.93 assignable to a H-5 proton, the spectrum of the above mixture has an additional singlet at δ 8.30 which we assign to an H-5 proton of **8a**. The H-5 proton of **7a** appears at higher field than that of **8a**; shielding by 4-Ph of **7a** will most probably result from the steric repulsion with the 3-CN group.

Likewise, **2** yielded **7b** upon reaction with ethyl glycinate hydrochloride, whose ^{1}H NMR spectrum exhibited an ester methyl singlet at δ 0.97, its higher field shift compared to that of common ethyl esters being also attributed to the shielding effect of the 4-Ph. The material before recrystallizations had a broad range of mp (140—152 °C), and its ^{1}H NMR spectral peaks were not satisfactorily integrated. Although there was only a singlet around δ 8.0, we tentatively conclude from the foregoing observations that **8b** may have been formed in addition to **7b** in the reaction.

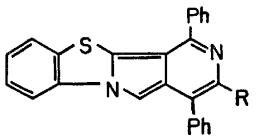

7a: R = CN
7b: R = CO$_2$Et

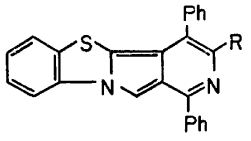

8a: R = CN
8b: R = CO$_2$Et

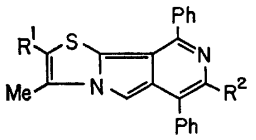

9a: R^1=H, R^2=CN
9b: R^1=CO$_2$Et, R^2=CN
9c: R^1=H, R^2=CO$_2$Et
9d: R^1=R^2=CO$_2$Et

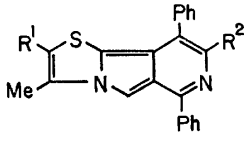

10a: R^1=H, R^2=CN
10b: R^1=CO$_2$Et, R^2=CN
10c: R^1=H, R^2=CO$_2$Et
10d: R^1=R^2=CO$_2$Et

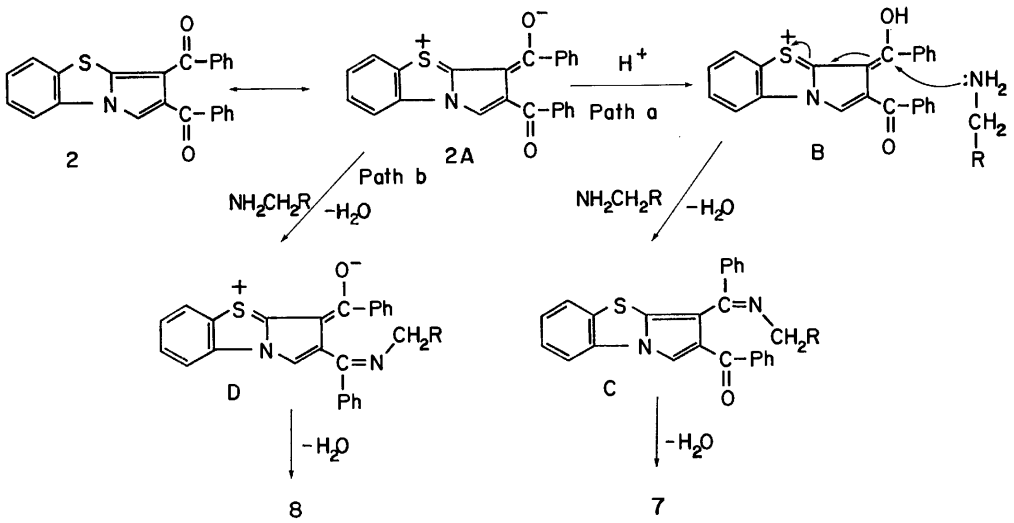

Scheme 1.

The reaction of **5a** with cyanomethylammonium hydrogensulfate gave a 6:1 mixture of 3-methyl-6,9-diphenylthiazolo[3′,2′:1,2]pyrrolo[3,4-*c*]pyridine-7-carbonitrile (**9a**) and its isomer (**10a**), as evidenced by the presence of two singlets at δ 7.93 and 8.47 in the ^{1}H NMR spectrum of the product before recrystallizations. However, the H-9 proton of each of **10b—d** was not discerned probably due to the overlap with aromatic protons in each of the ^{1}H NMR spectra of the products derived from **5b** and aminoacetonitrile or from **5a—b** and ethyl glycinate.

It may be concluded that heterocyclizations of **2** or **5** are fairly regioselective. Plausible mechanisms leading to **7** or **9** are shown in Scheme 1. Preferential attack of a proton on the carbonyl group at C-3 takes place by virtue of conjugation involving the sulfur 3d orbital (**2A**) to give an intermediate **B**, which undergoes a nucleophilic attack by an amine to form a Schiff base **C** followed by loss of water to produce **7** (Path a). Alternatively, if the amine directly attacks the carbonyl group at C-2 of **2A**, dehydration of a Schiff base **D** thereby produced would lead to **8** (Path b). Under the acidic conditions, the Path a is obviously favored and, in fact, when the reaction was effected in the presence of a base (NaOEt or DBU), an inseparable mixture of products was obtained.

Annelation of thiophene ring to **2** was achieved by its reaction in short period with phosphorus pentasulfide in pyridine followed by the rapid quenching of the reaction mixture with water. 1,3-Diphenylthieno[3′,4′:3,4]pyrrolo[2,1-*b*]benzothiazole (**11**) thus

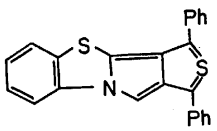

11

prepared, though not analyzed because of its hygroscopic property, showed an M^+ ion at *m/e* 381 (rel intensity 63%, base peak *m/e* 175) and M^{2+} ion at *m/e* 190.5 (6%), and had a λ_{max} absorption at 620 nm (log ε 2.11). IR and ^{1}H NMR spectra of **11** are also in keeping with the structure proposed.[8] The compound **11**, when heated in acetone or xylene, readily changed to a dimer **12**,[8,9] which is independently obtained from the reaction of **2** with phosphorus pentasulfide in boiling xylene. It has an M^+ ion at *m/e* 762 in its mass spectrum and displays a 2H singlet at δ 5.78 and a multiplet at δ 7.25—8.25 corresponding to 28 aromatic protons in its ^{1}H NMR spectrum. The reactions of **5a** and **5b**, respectively, with phosphorus pentasulfide in pyridine produced dimers alone, whose ^{1}H NMR spectra were very simple in keeping with their symmetrical structures.

Experimental

Melting points were uncorrected. IR spectra were recorded for Nujol mulls and ^{1}H NMR spectra with either of a Hitachi R-24B spectrometer at 60 MHz or a JEOL FX-100 spectrometer at 100 MHz (Me_4Si as internal standard). Mass spectra were determined with a Hitachi M-80 instrument by means of electron impact or field desorption ionization methods. Chromatography was performed on Kieselgel 60. Yields are based on consumed starting materials. Imidazo[2,1-*b*]benzothiazole (**1a**) and imidazo[2,1-*b*]thiazoles (**4a—c**) were prepared as described in the previous paper[2] and imidazo[2,1-*b*]benzothiazole (**1b**) was prepared according to the literature.[10]

*Reactions of **1a—b** and **4a—c** with DBA. General Procedure*: A mixture of **1** or **4** (0.005 mol) and DBA (0.015 mol) in xylene (30 ml) was heated under reflux for 5—24 h and then evaporated to dryness under reduced pressure. The residue was chromatographed with benzene. Thus, **1a** and **1b** gave **2** (47 and 81% yield respectively), **4a** and **4b** gave **5a** (47 and 52% yield, respectively), and **4c** gave **5b** (90% yield), respectively.

2: Colorless prisms (from EtOH), mp 209—210 °C, λ_{max} (EtOH) 250 nm (log ε 4.49), 285^{sh} (4.21), 335 (4.06). IR 1640 and 1630 cm^{-1} (C=O). ^{1}H NMR ($CDCl_3$) δ= 7.1—8.0 (14H, m, phenyl and H-5,6,7,8), 7.95 (1H, s, H-1). Found: C, 75.34; H, 3.98; N, 3.82; S, 8.58%. Calcd for $C_{24}H_{15}NO_2S$: C, 75.57; H, 3.96; N, 3.67; S, 8.40%.

5a: Colorless prisms (from EtOH), mp 137—138 °C,

λ_{max} ($CHCl_3$) 254 nm (log ε 4.49), 344 (4.08). IR 1650 and 1640 cm^{-1} (C=O). ^1H NMR ($CDCl_3$) δ=2.74 (3H, d, J=1 Hz, Me), 6.62 (1H, q, J=1 Hz, H-2), 7.0—7.7 (10H, m, phenyl), 7.47 (1H, s, H-5). Found: C, 73.27; H, 4.25; N, 4.20; S, 9.21%. Calcd for $C_{21}H_{15}NO_2S$: C, 73.02; H, 4.38; N, 4.06; S, 9.28%.

5b: Colorless needles (from EtOH), mp 157—158 °C, λ_{max} (EtOH) 252^{sh} nm (log ε 4.42), 262 (4.42), 335 (4.11). IR 1710 and 1640 cm^{-1} (C=O). ^1H NMR ($CDCl_3$) δ= 1.45 (3H, t, J=7 Hz, Me), 2.85 (3H, s, Me), 4.45 (2H, q, J=7 Hz, CH_2), 7.1—7.75 (10H, m, phenyl), 7.60 (1H, s, H-5). Found: C, 68.94; H, 4.56; N, 3.36; S, 7.83%. Calcd for $C_{24}H_{19}NO_4S$: C, 69.05; H, 4.59; N, 3.36; S, 7.68%.

Reaction of ***2*** *with Hydrazine Hydrate.* A mixture of **2** (0.20 g) and 100% hydrazine hydrate (10 ml) in EtOH (30 ml) was heated under reflux for 2 h and then diluted with water to precipitate pyridazine **3** (0.189 g, 96% yield).

3: Yellow needles (from aq EtOH), mp 252—253 °C, λ_{max} ($CHCl_3$) 272 nm (log ε 4.62), 403 (3.87). IR 700 cm^{-1} (phenyl). ^1H NMR (DMSO-d_6) δ=7.4—8.2 (12H, m, phenyl and H-7,8), 8.4—8.6 (2H, m, H-6,9), 8.97 (1H, s, H-11). Found: C, 76.56; H, 3.79; N, 11.07; S, 8.63%. Calcd for $C_{24}H_{15}N_3S$: C, 76.37; H, 4.01; N, 11.13; S, 8.49%.

Reaction of ***5a*** *with Hydrazine Hydrate.* **6a** was prepared in 91% yield by the reaction of **5a** (0.20 g) and 100% hydrazine hydrate (10 ml) in EtOH (10 ml) as described for **2**.

6a: Yellow needles (from aq EtOH), mp 220—222 °C, λ_{max} ($CHCl_3$) 272 nm (log ε 4.53), 400 (3.92). IR 700 cm^{-1} (phenyl). ^1H NMR (DMSO-d_6) δ=2.62 (3H, d, J= 0.5 Hz, Me), 7.38 (1H, q, J=0.5 Hz, H-2), 7.4—7.7 (6H, m, phenyl), 7.8—8.25 (4H, m, phenyl) 8.25 (1H, s, H-5). Found: C, 73.73; H, 4.35; N, 12.31; S, 9.36%. Calcd for $C_{21}H_{15}N_3S$: C, 73.87; H, 4.43; N, 12.31; S, 9.39%.

Reactions of ***2*** *and* ***5*** *with Cyanomethylammonium Hydrogensulfate.* A mixture of **2** (0.20 g) and cyanomethylammonium hydrogensulfate (0.807 g) in 1-butanol (10 ml) was heated under reflux for 6 h and poured into water. The mixture was extracted with $CHCl_3$, washed with dil HCl followed by water, and dried (Na_2SO_4). The extracts were evaporated to dryness and the residue was triturated with ligroine to give a mixture (0.205 g, 97% yield) of **7a** and **8a**, from which **7a** (0.120 g, 57% yield) was obtained by careful fractional crystallizations from EtOH.

7a: Yellow needles (from EtOH), mp 180 °C (dec), λ_{max} ($CHCl_3$) 275 nm (log ε 4.46), 326 (4.08), 420 (3.59), 430^{sh} (3.54). IR 2200 cm^{-1} (CN). ^1H NMR ($CDCl_3$) δ= 7.2—8.1 (14H, m, phenyl and H-7,8,9,10), 7.93 (1H, s, H-5). Found: C, 77.83; H, 3.98; N, 10.17; S, 7.75%. Calcd for $C_{26}H_{15}N_3S$: C, 77.78; H, 3.77; N, 10.47; S, 7.99%.

Similarly, **5a** gave a mixture (97% yield) of **9a** and **10a** and **5b** a mixture (84% yield) of **9b** and **10b**. **9a** and **9b**, respectively, were isolated by recrystallizations of the mixture from EtOH.

9a: Yellow needles, mp 242—243 °C, λ_{max} ($CHCl_3$) 285 nm (log ε 4.45), 324 (3.81), 416 (3.86), 430^{sh} (3.80). IR 2200 cm^{-1} (CN). ^1H NMR (DMSO-d_6) δ=2.59 (3H, d, J=1 Hz, Me), 7.45 (1H, q, J=1 Hz, H-2), 7.6—8.1 (10H, m, phenyl), 7.93 (1H, s, H-5). Found: C, 75.69; H, 4.07; N, 11.35; S, 8.86%. Calcd for $C_{23}H_{15}N_3S$: C, 75.59; H, 4.14; N, 11.50; S, 8.77%.

9b: Yellow needles, mp 250—253 °C, λ_{max} ($CHCl_3$), 268^{sh} nm (log ε 4.52), 288 (4.57), 325^{sh} (3.99), 420^{sh} (3.68), 439 (3.78), 461 (3.66). IR 2200 (CN) and 1710 cm^{-1} (C=O). ^1H NMR ($CDCl_3$) δ=1.39 (3H, t, J=7 Hz, Me), 2.88 (3H, s, Me), 4.38 (2H, q, J=7 Hz, CH_2), 7.4—7.8 (11H, m, phenyl and H-5), 7.85—8.0 (2H, m, phenyl). Found: C, 71.29; H, 4.66; N, 9.63; S, 7.54%. Calcd for $C_{26}H_{19}N_3O_2S$: C, 71.38; H, 4.38; N, 9.60; S, 7.33%.

Reactions of ***2*** *and* ***5*** *with Ethyl Glycinate Hydrochloride.* A mixture of **2** (0.20 g) and ethyl glycinate hydrochloride (0.731 g) in 1-butanol (10 ml) was heated under reflux for 24 h and then poured into water. The organic matter was extracted with ether, and washed with dil HCl followed by water. The dried (Na_2SO_4) extracts were evaporated to dryness. Trituration of the residue with ligroine afforded a mixture (0.220 g, 94% yield) of **7b** and **8b**, from which **7b** (0.138 g, 59% yield) was obtained by careful fractional crystallizations from ligroine.

7b: Yellow needles (from ligroine), mp 149—150 °C, λ_{max} ($CHCl_3$) 280 nm (log ε 4.59), 320^{sh} (4.11), 415 (3.82), 428^{sh} (3.78). IR 1720 cm^{-1} (C=O). ^1H NMR ($CDCl_3$) δ=0.98 (3H, t, J=7 Hz, Me), 4.14 (2H, q, J=7 Hz, CH_2), 7.1—7.7 (12H, m, phenyl and H-7,8,9,10), 7.50 (1H, s, H-5), 7.8—8.05 (2H, m, phenyl). Found: C, 71.81; H, 4.55; N, 5.59; S, 6.92%; M^+, m/e 448. Calcd for $C_{28}H_{20}N_2O_2S \cdot H_2O$: C, 72.08; H, 4.75; N, 6.00; S, 6.89%. M, 448.

Similarly, **5a** gave a mixture (96% yield) of **9c** and **10c** and **5b** a mixture (76% yield) of **9d** and **10d**, respectively. **9c** and **9d**, respectively, were isolated by recrystallizations of the mixture from ligroine.

9c: Yellow needles (from ligroine), mp 145—148 °C (dec), λ_{max} ($CHCl_3$) 260 nm (log ε 4.33), 315^{sh} (3.88), 410 (3.25). IR 1720 cm^{-1} (C=O). ^1H NMR ($CDCl_3$) δ=0.97 (3H, t, J=7 Hz, Me), 2.17 (3H, bs, Me), 4.07 (2H, q, J= 7 Hz, CH_2), 6.83 (1H, bs, H-2), 7.1—7.6 (8H, m, phenyl), 7.37 (1H, s, H-5), 7.8—8.05 (2H, m, phenyl). Found: C, 69.52; H, 5.13; N, 6.59; S, 7.09%; M^+, m/e 412. Calcd for $C_{25}H_{20}N_2O_2S \cdot H_2O$: C, 69.68; H, 5.15; N, 6.50; S, 7.45%; M, 412.

9d: Yellow needles (from ligroine), mp 92—93 °C, λ_{max} ($CHCl_3$) 265 nm (log ε 4.39), 283^{sh} (4.37), 330^{sh} (3.98), 425^{sh} (3.38), 441 (3.41), 463 (3.31). IR 1720 and 1710 cm^{-1} (C=O). ^1H NMR ($CDCl_3$) δ=0.97 (3H, t, J=7 Hz, Me), 1.27 (3H, t, J=7 Hz, Me), 2.57 (3H, s, Me), 4.10 (2H, q, J=7 Hz, CH_2), 4.27 (2H, q, J=7 Hz, CH_2), 7.1—7.8 (11H, m, phenyl and H-5). Found: C, 66.89; H, 5.14; N, 5.61; S, 6.25%; M^+, m/e 484. Calcd for $C_{28}H_{24}N_2O_4S \cdot H_2O$: C, 66.92; H, 5.21; N, 5.57; S, 6.38%. M, 484.

Reaction of ***2*** *with Phosphorus Pentasulfide. (a)*: A mixture of **2** (0.40 g) and phosphorus pentasulfide (1.17 g) in pyridine (5 ml) was heated under reflux for 10 min under nitrogen and then poured into ice–water (200 ml) containing acetic acid (5 ml) to give green precipitates. They were collected by filtration and recrystallized for several times from pyridine–petroleum ether to give **11** (0.075 g, 19% yield).

11: Hygroscopic green amorphous crystals, mp 120—122 °C (dec), λ_{max} (pyridine) 415^{sh} nm (log ε 2.40), 620 (2.11). IR 760 and 690 cm^{-1} (phenyl). ^1H NMR (pyridine-d_5) δ=7.0—8.2 (15H, m). M^+, m/e 381. Calcd for $C_{24}H_{15}NS_2$: M, 381.

(b): A mixture of **2** (0.10 g) and phosphorus pentasulfide (0.058 g) in xylene (30 ml) was heated under reflux for 50 min under nitrogen and then evaporated to dryness under reduced pressure. The residue was chromatographed with benzene–$CHCl_3$ to give **12** (0.051 g, 51% yield).

12: Yellow needles (from EtOH–$CHCl_3$), mp 182—183 °C, λ_{max} ($CHCl_3$) 287 nm (log ε 4.49). IR 775, 760, and 690 cm^{-1} (phenyl). ^1H NMR (CF_3CO_2D) δ=5.78 (2H, s), 7.25—8.25 (28H, m). Found: C, 75.30; H, 3.81; N, 3.73; S, 17.02%; M^+, m/e 762. Calcd for $C_{48}H_{30}N_2S_4$: C, 75.56; H, 3.96; H, 3.67; S, 16.81%; M, 762.

Dimerization of ***11***. A mixture of **11** (0.40 g) in xylene

(or acetone, 50 ml) was heated under reflux for 1 h under nitrogen and then evaporated to dryness under reduced pressure. The residue was chromatographed with benzene–$CHCl_3$ to give **12** (0.348 g, 87% yield).

*Reaction of **5a** with Phosphorus Pentasulfide.* A mixture of **5a** (0.40 g) and phosphorus pentasulfide (1.288 g) in pyridine (5 ml) was heated under reflux for 10 min under nitrogen and then poured into ice–water. Precipitates were collected by filtration, further heated in xylene under reflux for 1 h, and collected by filtration. Recrystallization from MeOH–$CHCl_3$ gave dimer **13a** (0.230 g, 57.5% yield).

13a: Yellow needles, mp 158—159.5 °C, λ_{max} ($CHCl_3$) 302 nm ($\log \varepsilon$ 4.41), IR 755 and 680 cm^{-1} (phenyl). ^1H NMR (CF_3CO_2D) δ=2.72 (6H, s), 5.57 (2H, s), 7.2—7.8 (22H, m). Found: C, 73.35; H, 4.62; N, 4.01; S, 18.21%; M^+, *m/e* 690. Calcd for $C_{42}H_{30}N_2S_4$: C, 73.43; H, 4.40; N, 4.09; S, 18.09%; M, 690.

*Reaction of **5b** with Phosphorus Pentasulfide.* A mixture of **5b** (0.40 g) and phosphorus pentasulfide (0.319 g) in pyridine (5 ml) was heated under reflux for 1 h under nitrogen and then poured into ice–water (200 ml) containing acetic acid 5 ml). Precipitates were collected by filtration, dried, and chromatographed with benzene–$CHCl_3$ to give dimer **13b** (0.262 g, 66% yield).

13b: Colorless micro needles (from benzene–$CHCl_3$), mp 256—257 °C, λ_{max} ($CHCl_3$) 285 nm ($\log \varepsilon$ 4.40). IR 1715 (C=O) and 770 and 700 cm^{-1} (phenyl). ^1H NMR δ=1.53 (6H, t, J=7 Hz), 2.68 (6H, s), 4.61 (4H, q, J=7 Hz), 6.37 (2H, s), 7.15—7.55 (20H, m). Found: C, 69.04; H, 4.41; N, 3.33; S, 15.20%; M^+, *m/e* 834. Calcd for $C_{48}H_{38}N_2O_4S_4$: C, 69.03; H, 4.59; N, 3.36; S, 15.20%; M, 834.

We thank Dr. Masafumi Yasunami, Tohoku University, for NMR spectral determinations.

References

1) Part III: N, Abe and T. Nishiwaki, *Heterocycles*, **16**, 537 (1981).

2) N. Abe, T. Nishiwaki, and N. Komoto, *Bull. Chem. Soc. Jpn.*, **53**, 3308 (1980).

3) M. P. Cava and M. V. Lakshmikantham, *Acc. Chem. Res.*, **8**, 139 (1975).

4) K. T. Potts, H. P. Youzwak, and S. J. Zurawel, Jr., *J. Org. Chem.*, **45**, 90 (1980) and previous papers for this group.

5) P. J. Garratt and S. B. Neoh, *J. Org. Chem.*, **40**, 970 (1975).

6) H. Gotthardt, F. Reiter, R. Gleiter, and R. Bartezko, *Chem. Ber.*, **112**, 260 (1979).

7) S. Mataka, K. Takahashi, and M. Tashiro, *Synthesis*, **1979**, 689; **1980**, 842; S, Mataka, K. Takahashi, Y. Tsuda, and M. Tashiro, *Heterocycles.*, **14**, 789 (1980).

8) To obtain a further confirmative evidence for the structures of **11** and its dimer, each of them was allowed to react with a reactive acetylene (*e.g.* dimethyl acetylenedicarboxylate or dibenzoylacetylene). Unfortunately, an extremely complex mixture was formed from which no product was isolated.

9) Either of the structures **12A** or **12B** appears plausible from the spectral data at hand.

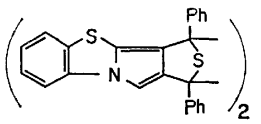

12A

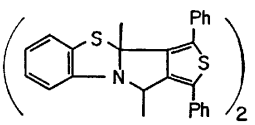

12B

10) L. Pentimalli and A. M. Guerra, *Gazz. Chim. Ital.*, **97**, 1286 (1967).

 © 1982 The Chemical Society of Japan Bull. Chem. Soc. Jpn., 55, 204—207 (1982) [Vol. 55, No. 1

Phosphinyl- and Phosphinothioylamino Acids and Peptides. VI. The Protection of the Hydroxyl Function in the Tyrosine Side-chain by the Dimethylphosphinothioyl Group

Masaaki UEKI* and Toshiyuki INAZU

Department of Applied Chemistry, Science University of Tokyo, 1-3 Kagurazaka, Shinjuku-ku, Tokyo 162

(Received May 12, 1981)

The use of the dimethylphosphinothioyl(Mpt) group for the protection of the hydroxyl function in the tyrosine side-chain was studied. *N,O*-Bis(Mpt)tyrosine was obtained directly by a Schotten-Baumann-type reaction of Mpt–Cl with tyrosine. The *O*-Mpt group was stable under acidic conditions, and it could be removed easily by alkaline hydrolysis or ester-exchange reaction. The usefulness of this new protecting group for the peptide synthesis was shown in the solid-phase synthesis of [D-Ala^2, L-Leu^5]-enkephalin(H–L-Tyr–D-Ala–Gly–L-Phe–L-Leu–OH) and its *N*-allyl derivative.

In the previous papers from our laboratory it was reported that a series of phosphinothioyl groups, such as diphenylphosphinothioyl(Ppt) and dimethylphosphinothioyl(Mpt), was useful as acid-labile amino-protecting groups for amino acids.[1–5] In accordance with the well-known acid lability of the phosphorus-nitrogen bond, these protecting groups could be removed by such mild HCl reagents as 0.2 M(1 M= 1 mol dm^{-3}) HCl in dichloromethane containing 0.2 M of triphenylphosphine(TPP). Since phosphinothioyl chlorides produced by cleavage do not react with the aromatic rings of tryptophan and tyrosine, the phosphinothioylamino acids have been successfully utilized for the synthesis of tryptophan homooligomers[6] and enkephalins.[7] When these groups are introduced into such other functional groups as hydroxyl and mercapto groups, they can be expected to become alkali-labile protecting groups according to the nature of the P–O and P–S bonds. As the first example of this line of investigation, the protection of the hydroxyl function in the tyrosine side-chain was attempted.

Tyrosine is a key amino acid in many biologically active peptides, such as enkephalin,[8,9] angiotensin II,[10] and gastrin.[11] A strategy which uses no side-chain protecting group for the tyrosine OH function has been recommended for the synthesis of a luteinizing hormone-releasing hormone,[12] and our previous syntheses of [L-Leu^5]-enkephalin and its analog were performed according to this strategy. However, the OH function of tyrosine should be protected for the synthesis of larger peptides. Benzyl ether-type protecting groups have been widely used, although the undesirable rearrangement to 3-benzyltyrosine during deprotection by acid[13] is one of the most hazardous side-reactions in peptide synthesis. In this report we would like to propose a new type of protecting group which would enable the direct alkylation of tyrosyl peptides.

Results and Discussion

A reaction of dimethylphosphinothioyl chloride (Mpt–Cl) with ethyl L-tyrosinate(H–L-Tyr–OEt) in the presence of triethylamine (TEA) gave a mixture of *N*-mono- and *N,O*-bis(Mpt)-L-tyrosine ethyl esters (**1** and **2**), which could then be separated by silica-gel column chromatography. When **2** was treated for 3 h with 0.2 M HCl in dichloromethane containing 0.1 M of TPP at room temperature, the *N*-Mpt group was removed selectively to give ethyl *O*-Mpt-L-tyrosinate hydrochloride(**3**) quantitatively. On the other hand, when the mixture of **1** and **2** was hydrolyzed by 1 M aqueous sodium hydroxide solution, *N*-Mpt-L-tyrosine was obtained in a 65% yield.[5] These results clearly show that the *O*-Mpt group was, unlike the acid-labile *N*-Mpt group, stable under acidic conditions and removable under basic conditions.

$$\text{H-L-Tyr-OEt} \xrightarrow[\text{CHCl}_3]{\text{2Mpt-Cl+2TEA}} \underset{(\mathbf{1})}{\text{Mpt-L-Tyr(Mpt)-OEt}} + \underset{(\mathbf{2})}{\text{Mpt-L-Tyr(Mpt)-OEt}}$$

$$\mathbf{2} \xrightarrow{\text{HCl}} \underset{(\mathbf{3})}{\text{HCl·H-L-Tyr(Mpt)-OEt}}$$

In order to determine the utility of the *O*-Mpt derivative of tyrosine, the alkali-lability of the *O*-Mpt group was examined more precisely by means of the pH-controlled alkaline hydrolysis of **2**. At pH 10.3, the cleavage of the *O*-Mpt group was still slow, and 90% of the **2** was recovered after a reaction period of 8 h at room temperature. This result was utilized for the preparation of *N,O*-bis(Mpt)tyrosine(**4**), a key derivative for the synthesis of tyrosine peptides, as will be described below.

With an increase in the pH value, the hydrolysis rate of the *O*-Mpt group became much faster. In these experiments, the reaction products were analyzed by means of high-performance liquid chromatography (HPLC); the results are shown in Fig. 1. At pH 11.9, the *O*-Mpt was removed rapidly, while the carboxylate ester bond was almost unaffected.

$$\mathbf{2} \xrightarrow[\text{rapid}]{\text{OH}^-} \text{Mpt-L-Tyr-OEt} \xrightarrow[\text{slow}]{\text{OH}^-} \text{Mpt-L-Tyr-O}^- \quad (\text{pH } 11.9)$$

Then, various kinds of basic reagents were examined in order to determine the most proper conditions for the removal of the *O*-Mpt group. The results are summarized in Table 1. It should be noted that the reagents with nucleophilic oxygen were clearly

Table 1. Time required for the removal of the *N*-Mpt or *O*-Mpt group from **2**

Reagent[a]	Time[b]	
	N-Mpt of **2**[c]	*O*-Mpt of **2**[c]
0.2 M HCl/0.2 M TPP/CH_2Cl_2	15 min	Stable for 24 h
1 M HCl/CH_3CO_2H	15 min	Stable for 24 h
HBr/CH_3CO_2H	5 min	Stable for 24 h
CF_3CO_2H	60 min	Stable for 24 h
1 M NaOH:CH_3OH(1:1)	Stable for 24 h	5 min
Tesser's base[14]	Stable for 24 h[d]	5 min[d]
1 M TEA/CH_3OH(RT)	Stable for 48 h	Incomplete for 48 h (66%)[e]
1 M TEA/CH_3OH(reflux)	Stable for 12 h	12 h
1 M TEA/C_2H_5OH(RT)	Stable for 48 h	Incomplete for 48 h (7%)[e]
1 M TEA/C_2H_5OH(reflux)	Stable for 12 h	Incomplete for 12 h (13%)[e]
20% NH_2NH_2/CH_3OH[f]	Stable for 48 h	24 h

a) The reagents were used in 4 cm^3 portions. b) Detected by TLC. c) The **2** was used in 0.2 mmol portions. d) The **2** was used in a 0.1 mmol portion. e) Isolated yield. f) The reagent was used in a 2 cm^3 portion.

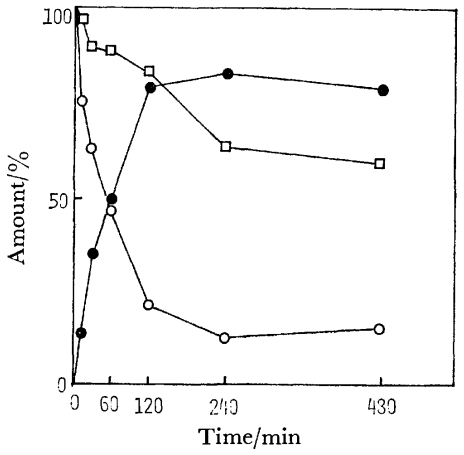

Fig. 1. Alkaline hydrolysis of **2** at constant pH.
□: Decrease of **2** at pH 10.9, ○: decrease of **2** at pH 11.9, ●: increase of **1** at pH 11.9.

preferrable to those with nucleophilic nitrogen.

In order to confirm the usefulness of the *O*-Mpt group for the synthesis of tyrosine-containing peptides, the solid-phase syntheses of [D-Ala^2, L-Leu^5]-enkephalin(**5**) and its *N*-allyl derivative were attempted. The synthetic scheme is outlined in Fig. 2.

The procedures of solid-phase synthesis were the same as those previously described.[5] All the amino acids were incorporated as Mpt derivatives except for glycine, which was coupled as its diethylphosphinothioyl (Ept) derivative. *N,O*-Bis(Mpt)-L-tyrosine(**4**) was obtained directly from tyrosine by a Schotten-Baumann-type reaction. When tyrosine was allowed to react with 3 equiv. of Mpt–Cl with special care to keep the pH of the reaction mixture in the range between 9.0 and 10.0, **4** was obtained in a 51% yield

$$\text{H-L-Tyr-O}^- \xrightarrow[\text{pH 9.0—10.0}]{\text{3Mpt-Cl + OH}^-} \xrightarrow{\text{H}^+} \text{Mpt-L-Tyr-OH} \quad (4)$$

(51% as DCHA salt)

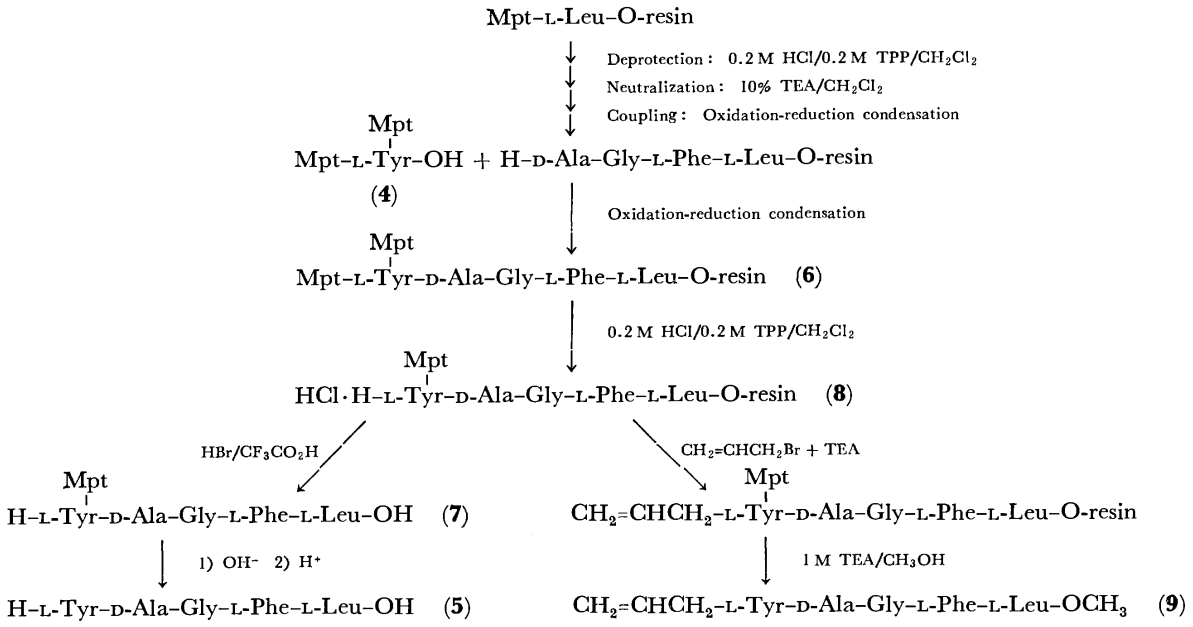

Fig. 2. Synthetic scheme for [D-Ala^2, L-Leu^5]-enkephalin and its *N*-allyl derivative.

as its dicyclohexylamine(DCHA) salt. All the couplings were mediated with the oxidation-reduction condensation method,[15] using tris(*p*-methoxyphenyl)-phosphine and 2,2'-dithiodipyridine. After the coupling of **4**, the *N*-Mpt group of *N*,*O*-bis(Mpt)pentapeptide resin(**6**) was selectively removed by the use of 0.2 M HCl solution in dichloromethane containing 0.2 M of TPP. Then, *O*-Mpt-[D-Ala^2, L-Leu^5]-enkephalin(**7**) was cleaved from the resin support by the use of HBr in trifluoroacetic acid. Pure **7** was obtained in a 53% yield as colorless crystals by purifying it by means of preparative thin-layer chromatography and successive gel chromatography on Sephadex LH-20. The removal of the *O*-Mpt group was performed by treating it with 1 M aqueous sodium hydroxide solution(1.1 equiv.) in methanol at room temperature overnight. Purification in a manner similar to that in **7** gave pure **5** in a 94% yield. Both **5** and **7** were homogeneous on thin-layer chromatography, and **7** gave satisfactory amino-acid ratios.

The biological activity of the **5** synthesized was measured by Professor Tetsuo Oka of Tokai University and found to be identical with that of an authentic sample by Mouse vas Deference assay and Guinea Pig Ileum assay.

For *N*-allylation, **8** was neutralized and further treated with 50 equiv. of allyl bromide in chloroform in the presence of TEA at room temperature for 12 h and then washed. The same treatments were repeated twice more. After thorough washing, the crude *N*-allylpentapeptide methyl ester(**9**) was cleaved from the resin support by transesterification with 1 M TEA in methanol, accompanied by the simultaneous removal of the *O*-Mpt group. After usual purification, pure **9** was obtained in a 38% yield, calculated from Mpt-L-Leu-resin. The structure of **9** was ascertained by NMR, MS, and amino-acid analysis. The acid hydrolyzate of **9** gave appropriate amino-acid ratios except for *N*-allyltyrosine, the amount of which could not be determined because of its low color value.[16]

N-Allyl-[L-Leu^5]-enkephalin is an interesting derivative of enkephalin because it shows partial agonistic and antagonistic activities,[17] but the synthesis of selectively alkylated tyrosyl peptides was not easy. This new method will be a useful route for these compounds. The syntheses of various kinds of alkylated derivatives of enkephalins are now in progress. The biological activity of these compounds will be reported by Professor Oka elsewhere.

Experimental

Thin-layer chromatography (TLC) was performed on silica-gel plates (Merck $60F_{254}$) in the following solvent systems: diethyl ether (R_f^1), chloroform–methanol–acetic acid (95:5:3, R_f^2), 1-butanol–acetic acid–water (4:1:1, R_f^3), chloroform–methanol–aqueous ammonia (60:30:5, R_f^4) and chloroform–methanol (9:1, R_f^5). The products were detected on TLC plates using ultraviolet light, iodine vapor, ninhydrin, and the Pauly reagent.

N,O-Bis(dimethylphosphinothioyl)-L-tyrosine Ethyl Ester (2) and N-Dimethylphosphinothioyl-L-tyrosine Ethyl Ester (1) (Mpt-L-Tyr(Mpt)-OEt and Mpt-L-Tyr-OEt). A solution of Mpt–Cl (25.71 g, 0.2 mol) in 50 cm^3 of chloroform was added to a suspension of H-L-Tyr-OEt·HCl (24.57 g, 0.1 mol) in 150 cm^3 of chloroform and 42 cm^3 (0.3 mol) of TEA at 0 °C. After having been stirred overnight at room temperature, the solution was evaporated *in vacuo*. The residue was dissolved in ethyl acetate. The solution was washed successively with water, an ice-cold 5% citric acid solution, water, a 5% sodium hydrogencarbonate solution, water, and a saturated sodium chloride solution, dried over anhydrous sodium sulfate, and evaporated. The oily residue was dissolved in dichloromethane and placed in a silica-gel column (3 cm × 50 cm). Elution with 600 cm^3 of dichloromethane gave **2** as colorless crystals; 26.11 g (66%). Mp 79—82 °C; $[\alpha]_D^{25}$ −12.5° (*c* 1, ethanol); R_f^1 0.37, R_f^2 0.69. Found: C, 45.43; H, 6.41; N, 3.69; P, 16.06%. Calcd for $C_{15}H_{25}NO_3P_2S_2$: C, 45.79; H, 6.40; N, 3.56; P, 15.75%. Further elution with the same solvent (about 3 dm^3) gave **1** as colorless crystals; 2.82 g (9%). Mp 68—69 °C; $[\alpha]_D^{25}$ −15.0° (*c* 1, ethanol); R_f^1 0.55, R_f^2 0.48. Found: C, 51.76; H, 6.77; N, 4.47; P, 10.32%. Calcd for $C_{13}H_{20}NO_3PS$: C, 51.81; H, 6.69; N, 4.65; P, 10.28%.

O-Dimethylphosphinothioyl-L-tyrosine Ethyl Ester Hydrochloride (H-L-Tyr(Mpt)-OEt·HCl) (3). Compound **2** (0.74 g, 2 mmol) was treated with 0.2 M HCl in dichloromethane containing 0.1 M of TPP. After having been kept standing at room temperature overnight, the solution was evaporated. The residue was distributed between water and diethyl ether, and the organic layer was extracted with 1 M hydrochloric acid several times. The combined aqueous layer and extracts were evaporated and dried over sodium hydroxide pellets *in vacuo*. The solid residue was washed with diethyl ether to give the product, 0.68 g (100%), which was then recrystallized from ethanol–diethyl ether to give pure **3** as colorless crystals; 0.56 g (83%). Mp 154—156.5 °C; $[\alpha]_D^{25}$ −15.0° (*c* 1, ethanol); R_f^2 0.17, R_f^3 0.62. Found: C, 45.40; H, 6.37; N, 4.25; P, 8.51%. Calcd for $C_{13}H_{21}NO_3PSCl\cdot 1/2H_2O$: C, 45.02; H, 6.68; N, 4.04; P, 8.93%.

N,O-Bis(dimethylphosphinothioyl)-L-tyrosine Dicyclohexylamine Salt (Mpt-L-Tyr(Mpt)-OH·DCHA) (4). L-Tyr (5.44 g, 30 mmol) was dissolved in 1 M sodium hydroxide solution (60 cm^3), and then Mpt–Cl (11.56 g, 90 mmol) in diethyl ether (30 cm^3) was added, drop by drop, at 0 °C. While the mixture was being stirred vigorously, 1 M sodium hydroxide solution was added carefully at a rate chosen so as to maintain the pH of the solution between 9.0 and 10.0 until no drop in the pH was observed. Then the solution was extracted twice with ethyl acetate. The aqueous layer was acidified with solid citric acid to pH 3—4 at 0 °C and was then extracted with ethyl acetate several times. The organic layer was washed with water, dried over anhydrous sodium sulfate, and evaporated *in vacuo*. The oily residue was dissolved in 40 cm^3 of ethyl acetate and treated with DCHA (6 cm^3, 30 mmol). DCHA salt was collected by filtration, washed with ethyl acetate and diethyl ether, and dried. Recrystallization from ethanol gave **4** as colorless crystals; 8.32 g (51%). Mp 169—170 °C; $[\alpha]_D^{25}$ −15.0° (*c* 1, ethanol); R_f^2 0.44, R_f^3 0.81. Found: C, 55.09; H, 8.00; N, 4.66%. Calcd for $C_{25}H_{44}N_2O_3P_2S_2$: C, 54.92; H, 8.11; N, 5.11%.

Solid-phase Synthesis of H-L-Tyr(Mpt)-D-Ala-Gly-L-Phe-L-Leu-OH (7). Mpt-L-Leu-resin was prepared from chloromethyl resin by the method of Gisin,[18] and the amount of esterified Leu was obtained as 0.33 mmol/g by means of amino-acid analysis. Mpt-L-Leu-resin (1 g) was placed in a reaction vessel of a Beckman Model 990 peptide synthesizer, after which synthesis was carried out according to the previously reported schedule,[5] using **4** at the final acylating step. After the final deprotection of the *N*-ter-

minal Mpt group, the *O*-Mpt-pentapeptide resin (**8**) was washed thoroughly with dichloromethane, ethanol, and diethyl ether, and dried *in vacuo*. The *O*-Mpt-pentapeptide was removed from the resin by anhydrous hydrogen bromide in trifluoroacetic acid (TFA) in the presence of 50 equiv. of anisole. The filtrate and TFA washings were combined and evaporated *in vacuo*. The residue was dried over sodium hydroxide pellets *in vacuo* and triturated with diethyl ether to yield the white solid. This crude peptide was then submitted to preparative silica-gel thin-layer chromatography using the chloroform–methanol–acetic acid (85:25:20) solvent system. The desired band (R_f=0.7—0.8) was eluted with methanol and evaporated *in vacuo*. The residue was again dissolved in a small volume of methanol and placed in a Sephadex LH-20 column (2×100 cm) monitored by means of UV absorbancy at 260 nm. The methanol eluate (flow rate 0.8 cm³/min) was collected as fractions of 4 cm³ each. The fractions (Nos. 34—43) containing a single component were collected and evaporated *in vacuo* to give **7** as colorless crystals; 0.116 g (53%). Mp 159—163 °C (dec); $[\alpha]_D^{25}$ −10° (*c* 1, methanol); R_f[3] 0.68, R_f[4] 0.66. Found: C, 55.15; H, 6.77; N, 10.24%. Calcd for $C_{31}H_{44}N_5O_7PS\cdot CH_3OH$: C, 55.40; H, 6.97; N, 10.09%. Amino-acid ratios in hydrolyzate obtained by the use of 6 M HCl at 110 °C for 24 h: $Tyr_{0.70}$, $Ala_{0.99}$, $Gly_{1.02}$, $Phe_{0.99}$, $Leu_{1.00}$. The low value for Tyr is attributable to the difficulty of the acid hydrolysis of *O*-Mpt–Tyr.

[D-*Ala*², L-*Leu*⁵]-*enkephalin* (***5***). Compound **7** (0.020 g, 0.03 mmol) was dissolved in 1 cm³ of methanol. To this solution, 0.1 cm³ of a 1 M aqueous sodium hydroxide solution was added at 0 °C. After having been stirred overnight, the solution was neutralized and evaporated *in vacuo*. The residue was placed in a Sephadex LH-20 column (2× 100 cm), and the desired fractions were collected to yield **5** as colorless crystals (0.0179 g, 94%). Mp 182—184 °C (lit,[5] 182—184 °C); $[\alpha]_D^{25}$ −20° (*c* 0.1, methanol) (lit,[5] −25.0° (*c* 0.1, methanol)); R_f[4] 0.50 (lit,[5] 0.49). Amino-acid ratios in hydrolyzate obtained by the use of 6 M HCl at 110 °C for 24 h: $Tyr_{0.97}$, $Ala_{1.02}$, $Gly_{0.99}$, $Phe_{0.99}$, $Leu_{1.02}$.

N-*Allyl*-[D-*Ala*², L-*Leu*⁵]-*enkephalin Methyl Ester* (***9***). Compound **8** synthesized from Mpt-L-Leu-resin (0.5 g, Leu content: 0.30 mmol/g) as has been described above, was used. After neutralization, the resin was treated by the following steps: (1) washing three times with chloroform, (2) allylation with 50 equiv. of allyl bromide and TEA in chloroform for 12 h, (3) washing three times with chloroform, (4) repetition of step (2) and (3) twice more, (5) washing two times with *N*,*N*-dimethylformamide, (6) washing two times with ethanol, followed by drying *in vacuo* over phosphorus pentaoxide. For the removal from resin, the peptide resin was refluxed in methanol containing 1 M of TEA for 12 h and then filtered. The same procedure was repeated, after which all the filtrates and methanol washings were collected and evaporated. The residue was distributed between water and ethyl acetate, and the organic layer was extracted with 1 M hydrochloric acid three times. The aqueous layer was neutralized with solid sodium hydrogencarbonate at 0 °C and then extracted with ethyl acetate three times. The collected extracts were washed with water and dried over anhydrous sodium sulfate. The solution was evaporated *in vacuo*, and the residue was purified by means of preparative thin-layer chromatography using the chloroform–methanol (95:5) solvent system. The desired band (R_f=0.2—0.3) was eluted with methanol and evaporated *in vacuo*. The residue was dissolved in methanol again, placed in a Sephadex LH-20 column (2×100 cm), and eluted with methanol (flow rate 0.75 cm³/min). The desired fractions (Nos. 37—42; 4.5 cm³/fraction) were collected to yield **9** as colorless crystals (0.0723 g, 38% from Mpt-L-Leu-resin): Mp 155—156 °C; NMR (CD_3OD) δ=0.97 (6H, d), 1.27 (3H, d), 3.70 (3H, s), 4.97—5.77 (3H, m), 6.73, 7.04 (4H, m), and 7.28 (5H, s); MS (70 eV), *m/e* (relative intensity), 623 (M^+, 2), 515 (22), 176 (100), 120 (65), 107 (19), 91 (13), and 77 (5). R_f[3] 0.75, R_f[5] 0.52. Amino-acid ratios in hydrolyzate obtained by the use of 12 M HCl–propionic acid at 130 °C for 2 h: $Ala_{0.94}$, $Gly_{1.05}$, $Phe_{0.97}$, $Leu_{1.04}$. *N*-Allyl-Tyr was detected, but not measured because of its low color value.

The authors wish to thank Professor Tetsuo Oka (Tokai University) for the bilogical-activity measurement.

References

1) M. Ueki and S. Ikeda, *Chem. Lett.*, **1976**, 827.
2) M. Ueki and S. Ikeda, "Peptide Chemistry 1976: Proceedings of the 14th Symposium on Peptide Chemistry," ed by T. Nakajima, Protein Research Foundation, Osaka (1977), p. 1.
3) M. Ueki, S. Ikeda, and F. Tonegawa, "Peptides: Proceedings of the 5th American Peptide Symposium," ed by M. Goodman and J. Meienhofer, John Wiley and Sons, New York (1977), p. 546.
4) S. Ikeda, F. Tonegawa, E. Shikano, K. Shinozaki, and M. Ueki, *Bull. Chem. Soc. Jpn.*, **52**, 1431 (1979).
5) M. Ueki, T. Inazu, and S. Ikeda, *Bull. Chem. Soc. Jpn.*, **52**, 2424 (1979).
6) M. Ueki and S. Ikeda, *Chem. Lett.*, **1977**, 869.
7) S. Ikeda, T. Inazu, M. Minoura, and M. Ueki, "Peptide Chemistry 1978: Proceedings of the 16th Symposium on Peptide Chemistry," ed by N. Izumiya, Protein Research Foundation, Osaka (1979), p. 41.
8) J. M. Hambrook, B. A. Morgan, M. J. Range, and C. F. C. Smith, *Nature*, **262**, 782 (1976).
9) J. S. Morley, *Ann. Rev. Pharmacol. Toxicol.*, **20**, 81 (1980).
10) M. P. Printz, G. Nemethy, and H. Beich, *Nature (London), New Biol.*, **237**, 135 (1972).
11) R. A. Gregory and H. J. Tracy, *Lancet*, **2**, 797 (1972).
12) D. H. Coy and N. Branyas, *Int. J. Pept. Protein Res.*, **14**, 339 (1979).
13) B. W. Erickson and R. B. Merrifield, *J. Am. Chem. Soc.*, **95**, 3750 (1973).
14) C. Chang, M. Waki, M. Ahmad, J. Meienhofer, E. O. Lundell, and J. D. Haug, *Int. J. Pept. Protein Res.*, **15**, 59 (1980).
15) T. Mukaiyama, R. Matsueda, and M. Suzuki, *Tetrahedron Lett.*, **1970**, 1901.
16) C. B. Pert, D. L. Bowie, A. Pert, J. L. Morell, and E. Gross, *Nature*, **269**, 73 (1977).
17) E. F. Hahn, J. Fishman, Y. Shiwaku, F. F. Foldes, H. Nagashima, and D. Duncalf, *Res. Commun. Chem. Pathol. Pharmacol.*, **18**, 1 (1977).
18) B. F. Gisin, *Helv. Chim. Acta*, **56**, 1476 (1973).

Synthesis of *dl*-3-Hydroxycuparene by a Claisen Rearrangement of Allyl Aryl Ether

Yoshinobu INOUYE,* Satoru INOMATA, Yasumasa ISHIHARA, and Hiroshi KAKISAWA
Department of Chemistry, The University of Tsukuba, Sakura-mura, Niihari-gun, Ibaraki 305
(Received May 14, 1981)

The Claisen rearrangement of 1-methyl-2-[(3-methylphenoxy)methyl]cyclopentene in *N,N*-dimethylformamide gave 5-methyl-2-(1-methyl-2-methylenecyclopentyl)phenol(**5**) *via* its trimethylsilyl ether. The methylation of **5**, followed by a Simmons-Smith reaction and by the catalytic hydrogenolysis, afforded 3-hydroxycuparene.

Claisen rearrangement[1] is one of the most attractive synthetic methods in natural-product chemistry because a new C–C bond can be created at the relatively hindered site of a molecule, where such intermolecular reactions as alkylation or acylation are frequently unsuccessful because of their steric demands. Several successes have been reported.[2] Most of them, however, have utilized the thermal reorganization of allyl vinyl ethers to γ,δ-unsaturated aldehydes or their variants.

We wish to report here the synthesis of hydroxycuparene *via* *o*-*t*-alkylphenol **5**, which is itself obtained by means of the Claisen rearrangement[3] of allyl aryl ether **4**.[4] This hydroxycuparene is expected to be a valuable intermediate for the synthesis of various cuparene derivatives found in the organisms.

6-Oxoheptanal, prepared from 1-methylcyclohexene, was cyclized with piperidinium acetate[5] to give 2-methyl-1-cyclopentenecarbaldehyde (**1**), which was then reduced with sodium borohydride to the corresponding alcohol **2**. The conversion of **2** into chloride **3** was problematic, however, because **3** was very unstable and, when isolated, immediately changed into unidentifiable green materials. Moreover, **3** was volatile, and an extraction procedure was undesirable. On this account, the alcohol **2** was treated with hexachloroacetone–triphenylphosphine,[6] after which the chloride **3** was isolated by flash distillation from the reaction mixture into a cooled (−70 °C) receiver containing small pieces of galvinoxyl. The immediate treatment of **3** with *m*-cresol in the presence of potassium carbonate gave 1-methyl-2-[(3-methylphenoxy)-methyl]cyclopentene (**4**), though the yield was low (18%). The structure of **4** was confirmed by the presence of an aromatic methyl at 2.37 ppm and an olefinic methyl at 1.82 ppm, together with the –O–CH_2–C= group at 4.49 ppm in the NMR spectrum of **4**.

The Claisen rearrangement of simple allyl aryl ethers has been extensively investigated by Schmid *et al.*;[7] they showed that *N,N*-dimethylformamide (DMF) was the most effective solvent in giving an ortho-rearranged phenol.

When **4** was heated in DMF at 195 °C, the rearrangement occurred slowly in the anticipated direction to afford 5-methyl-2-(1-methyl-2-methylenecyclopentyl)phenol (**5**); however, a prolonged heating caused the gradual isomerization of **5** into the cyclic ether **6**. Thus, **5** could not be isolated in a pure form. The trapping of the initially rearranged phenol **5** as a trimethylsilyl derivative was successively performed when the reaction was carried out in the presence of *N*-trimethylsilyldiethylamine (TMSDEA). The GC analysis of the crude products showed the absence of any material other than **7**. On the other hand, *N,O*-bis(trimethylsilyl)acetamide (BSA) was undesirable because the decomposition of BSA at a high temperature accelerated the isomerization of **5** into **6** (see Experimental). The pure **5** was obtained in a 71% yield from **4** by the treatment of **7** with benzyltrimethylammonium fluoride[8] and by subsequent chromatography on neutral alumina. The structures of **5** and **6** were confirmed by their spectroscopic properties. Besides three aromatic protons which are located in a 2,5-dialkylphenol, two methyl groups at 1.38 and 2.18 ppm, and one exocyclic methylene group at 4.82 and 4.98 ppm as broad singlets are recognized in the NMR spectrum of **5**. On the other hand, in **6** three methyl groups appear, at 1.25, 1.30, and 2.20 ppm, while the signals due to the exocyclic methylene protons in **5** vanish completely. The chemical

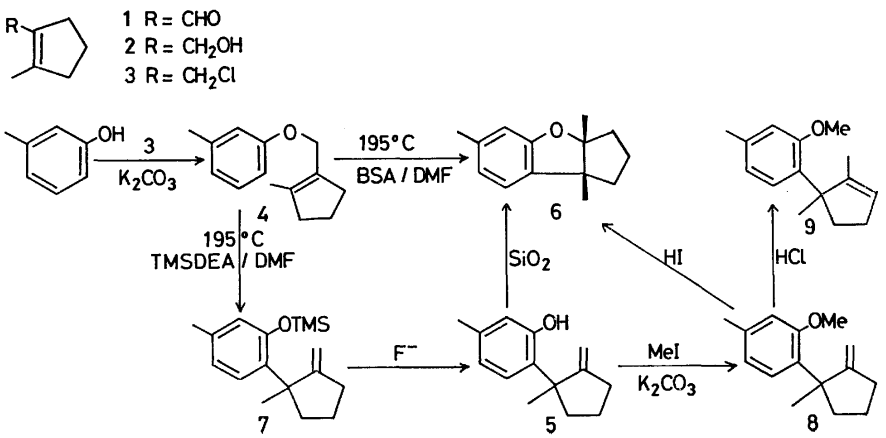

shifts of 1.25 and 1.30 ppm of the two methyl groups on the ring juncture show the *cis*-relationship of these groups in comparison with those of aplysin (1.25 and 1.30 ppm).[9]

As **5** was sensitive toward acid, the phenolic hydroxyl group was protected by methylation. Attempted hydrohalogenations of the exocyclic methylene group in **8** were unsucessful; the treatment of **8** with potassium iodide/85% phosphoric acid[10] or hydrogen iodide/carbon tetrachloride gave **6** exclusively, while the action of hydrogen chloride/ether on **8** converted it into the endocyclic olefin **9**.

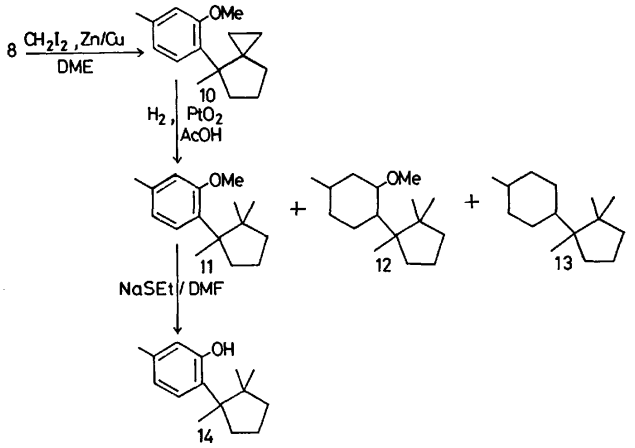

The Simmons-Smith reaction of **8** in the presence of 1,2-dimethoxyethane (DME) afforded the cyclopropane derivative **10**, which was then subjected to a careful catalytic hydrogenolysis (PtO_2 in acetic acid, 1.5 atom, 15 min) to give 3-hyrdoxycuparene methyl ether **11** in a crystalline form, together with a small amount of the octahydro compound **12** and the deoxy compound **13**.

The ether **11** was treated with sodium ethanethiolate in DMF to give oily *dl*-3-hydroxycuparene (**14**); the chemical shifts of four methyl signals (0.71, 1.13, 1.35, and 2.19 ppm) and the signal pattern of an aromatic region [6.29(br.s), 6.49(br.d, J=8 Hz), and 7.01 (d, J=8 Hz)] in the NMR spectrum of **14** are quite different from those reported for isomeric 2-hydroxycuparene.[11]

Experimental

All the melting points are uncorrected. The IR spectra were recorded with a Hitachi 215 grating spectrophotometer. The NMR spectra were measured with Hitachi H-60 and JEOL MH-100 spectrophotometers, using TMS as the internal standard. The mass spectra were obtained with a Hitachi RMU-6MG mass analyzer. The gas chromatograms were taken on a Shimadzu 3B-F analyzer, using a glass column (3 mϕ × 1.7 m, 5% OV-1). The flash chromatographies were performed using Wakogel C-300 as the adsorbent.

6-Oxoheptanal. 1-Methylcyclohexene (29.5 g) was dissolved in 1400 ml of water–dioxane (2:5) in a 3-liter three-necked flask equipped with a mechanical stirrer and a nitrogen-inlet tube. $NaIO_4$ (177 g) was added, and the mixture was cooled to 0 °C. After the system had been flushed with nitrogen, a solution of 1 g of OsO_4 in 100 ml of water was added; the whole was then allowed to warm to room temperature. After 15 hours' stirring under nitrogen, white precipitates were removed by filtration, and the filtrate was extracted with ether. The subsequent removal of the solvent gave an oil, which was then purified by distillation to afford 17.8 g (43%) of 6-oxoheptanal as a slight yellow oil; bp 57—58 °C/0.7 mmHg (1 mmHg ≈ 133.322 Pa) (Lit,[12]: bp 91—96 °C/4 mmHg): δ ($CDCl_3$): 1.46—1.76 (m, 4H), 2.14 (s, 3H), 2.22—2.68 (m, 4H), and 9.76 (t, 1H, J=1.5 Hz).

(2-Methyl-1-cyclopentenyl)methanol (2). 6-Oxoheptanal (8.49 g) was dissolved in 350 ml of dry benzene in a 1-liter three-necked flask equipped with a mechanical stirrer and a condenser. Traces of hydroquinone and a solution of dry piperidine (2.5 ml)–acetic acid (1.5 ml) in dry benzene (20 ml) were added, after which the mixture was stirred under nitrogen for 9 h at 60 °C. Water (300 ml) was then added, and the products were taken up in ether. The organic layer was washed with water and brine, and dried over Na_2SO_4. The subsequent evaporation of the solvent gave 6.89 g of crude 2-methyl-1-cyclopentenecarbaldehyde (**1**); ν ($CHCl_3$): 1660 cm^{-1}; δ ($CDCl_3$): 1.64—2.00 (m, 2H), 2.08 (s, 3H), 2.36—2.68 (m, 4H), and 9.84 (s, 1H).

The crude aldehyde **1** (6.89 g) was dissolved in 200 ml of methanol. After cooling to 0 °C, 4.13-g portions of $NaBH_4$ were gradually added; stirring was then continued for 80 min at 0 °C. Water was added, and the products were extracted with ether. The organic layer was washed with water and brine. After concentrating *in vacuo*, the oil which remained was purified by distillation to afford 3.77 g (51%) of **2** as a colorless oil; bp 42—43 °C/10 mmHg; ν ($CHCl_3$): 3600, 3400br, and 990 cm^{-1}; δ ($CDCl_3$): 1.70 (s, 3H), 1.75—2.10 (m, 2H), 2.10—2.68 (m, 4H), 2.88 (br.s, 1H), and 4.15 (br.s, 2H).

Elementray analysis was performed on its *p*-nitrobenzoate derivative; mp 71—72 °C; ν (KBr): 1720 and 1520 cm^{-1}. Found: C, 64.39; H, 5.81; N, 5.46%. Calcd for $C_{14}H_{15}NO_5$: C, 64.35; H, 5.78; N, 5.36%.

1-Methyl-2-[(3-methylphenoxy)methyl]cyclopentene (4). The alcohol **2** (736 mg) was mixed with 5 ml of hexachloroacetone[6] in a three-necked flask equipped with a thermomether and a distillor connected to a trap cooled with a Dry Ice–acetone bath. Traces of galvinoxyl were then added to the flask and the trap. Triphenylphosphine (5.2 g) was stirred in small portions into the mixture, during which the temperature of the content was controlled below 10 °C. The mixture was then allowed to warm to room temperature, and stirring was continued for a further 4 h. Crude 1-chloromethyl-2-methylcyclopentene (**3**) was flashly distilled (room temperature/0.2—0.3 mmHg) into the trap; *m/e* of **3**: 132 (11%, M^++2), 130 (33%, M^+), and 95 (100%, M^+−Cl). The chloride **3** was quite unstable and changed into a green material in the absence of galvinoxyl. Thus, the crude **3** was used immediately in the subsequent reaction.

A mixture of 0.75 ml of *m*-cresol and 1.05 g of K_2CO_3 in 5 ml of dry acetone was placed in a flask under nitrogen. A solution of **3** in 2 ml of acetone was then added into the above flask. The whole was then stirred at room temperature for 48 h. The reaction mixture was poured into water, and the products were taken up in ether. The organic layer was washed with 1 M (1 M = 1 mol dm^{-3}) NaOH and water, and dried over Na_2SO_4. After concentrating *in vacuo*, the residual oil was chromatographed on alumina (15 g) with hexane to give crude **4** (348 mg). A pure sample was obtained by repeated flash chromatographies (3 times, 1.0 ϕ, hexane) to give 239 mg (18%) of **4**; Kugelrohr dist: bath temp 80—83 °C/0.3 mmHg; ν (CCl_4): 1590, 1580,

1480, 1250br, and 1150 cm^{-1}; δ (CCl_4): 1.82 (br. s, 3H), 2.37 (s, 3H), 4.49 (s, 2H), and 6.5—7.3 (m, 4H). Found: C, 82.89; H, 9.04%. Calcd for $C_{14}H_{18}O$: C, 83.12; H, 8.96%.

Claisen Rearrangement[7] *of* **4**. *A)*: A mixture of 68 mg of **4**, 0.01 ml of BSA, and 0.25 ml of dry DMF was sealed in a test tube under argon. The tube was heated for 19 h at 195 °C. The whole was then poured into water, and the products were extracted with ether. The organic layer was washed with water and brine, dried, and concentrated *in vacuo* to give crude **6** (51 mg), which was subsequently purified by chromatography on silica gel with hexane–ethyl acetate (1:1) to give pure **6**; Kugelrohr dist: bath temp 50—65 °C/0.3 mmHg; ν ($CHCl_3$): 1640, 1615, 1590, 1490, 1110, and 945 cm^{-1}; δ ($CDCl_3$, 100 MHz): 1.25 (s, 3H), 1.30 (s, 3H), 2.20 (s, 3H), 6.24 (br.s, 1H), 6.57 (br.d, 1H, J=7 Hz), and 6.63 (d, 1H, J=7 Hz); *m/e*: 202 (67%, M^+) and 187 (100%). Found: C, 83.01; H, 9.09%. Calcd for $C_{14}H_{18}O$: C, 83.12; H, 8.96%.

B): A mixture of 225 mg of **4**, 0.5 ml of freshly distilled TMSDEA, and 4 ml of dry DMF was placed in a sealed tube under argon. The tube was heated for 30 h at 195 °C. The reaction mixture was then worked up as in A) to give crude **7**; *m/e*: 274 (M^+) and 259 (base). The GC analysis (140 °C) showed **7** was a single product. Crude **7** was treated with benzyltrimethylammonium fluoride[5] (20 mg) in 5 ml of THF for 4 h, and the products subsequently obtained by evaporating the solvent were chromatographed on neutral alumina (activity grade III, 10 g) with hexane to give **5** (159 mg, 71%). Some (20 mg) of the **4** was recovered from the earlier fractions.

An analytical sample of **5** was obtained by Kugelrohr dist: bath temp 67—70 °C/0.05 mmHg; ν (CCl_4): 3480, 1620, 1240, 1160, and 895 cm^{-1}; δ (CCl_4, 100 MHz): 1.38 (s, 3H), 2.18 (s, 3H), 4.82 (br.s, 1H), 4.98 (br.s, 1H), 5.32 (br.s, 1H), 6.42 (br.s, 1H), 6.49 (br.d, 1H, J=8 Hz), and 6.98 (d, 1H, J=8 Hz). Found: C, 83.00; H, 8.99%. Calcd for $C_{14}H_{18}O$: C, 83.12; H, 8.96%.

*1-(2-Methoxy-4-methylphenyl)-1-methyl-2-methylenecyclopentane (**8**).* To a stirred mixture of 159 mg of **5** and 2 ml of methyl iodide in 5 ml of acetone, 1 g of K_2CO_3 was added, after which the whole was stirred at room temperature for 43 h. The solids were removed by filtration, and the filtrate was evaporated to give an oil, which was chromatographed on silica gel (5 g). From the hexane eluates, 141 mg (83%) of methyl ether **8** was obtained. Kugelrohr distillation gave a pure sample; bath temp 70—75 °C/0.05 mmHg; ν (CCl_4): 1645, 1600, 1250, 1170, 895, and 880 cm^{-1}; δ (CCl_4, 100 MHz): 1.38 (s, 3H), 2.22 (s, 3H), 3.66 (s, 3H), 4.54 (br.s, 1H), 4.82 (br.s, 1H), 6.46 (br.s, 1H), 6.46 (br. d, 1H, J=8 Hz), and 7.00 (d, 1H, J=8 Hz). Found: C, 83.29; H, 9.32%. Calcd for $C_{15}H_{20}O$: C, 83.28; H, 9.31%.

Attempted Hydrohalogenation of **8**. *With KI–85% H_3PO_4*:[10] A mixture of 15 mg of **8**, 35 mg of KI, and 0.5 ml of 85% H_3PO_4 was heated at 80 °C for 3 h. The products were taken up in ether to give **6**.

With HI–CCl_4. Through a cooled (0 °C) solution of 12 mg of **8** in 1.5 ml of CCl_4 there was passed a dry HI gas, prepared from I_2 and tetralin, for 2 h. The product was found to be **6**.

With HCl–Ether. A dry HCl gas was passed through a solution of 11 mg of **8** in 2 ml of anhydrous ether at 0 °C, and then the mixture was allowed to warm to room temperature. A work-up as usual gave 8.5 mg (77%) of **9** by chromatography on silica gel (hexane). Kugelrohr dist: bath temp 40—50 °C/0.03 mmHg; ν (CCl_4): 1605, 1250, 1185, 1165, 1060, and 1035 cm^{-1}; δ (CCl_4, 100 MHz): 1.37 (s, 3H), 1.51 (br.s, 3H), 2.24 (s, 3H), 3.68 (s, 3H), 5.28 (m, 1H), 6.44 (br.d, 1H, J=8 Hz), 6.46 (br.s, 1H), and 6.75 (d, 1H, J=8 Hz). Found: C, 83.09; H, 9.34%. Calcd for $C_{15}H_{20}O$: C, 83.28; H, 9.31%.

*4-(2-Methoxy-4-methylphenyl)-4-methylspiro[2.4]heptane (**10**).* To a suspension of 280 mg (4.3 mmol) of a freshly prepared Zn–Cu couple in 5 ml of dry ether, 0.35 ml (4.3 mmol) of diiodomethane was added, after which the mixture was irradiated with IR lamp for 2 min. The whole was stirred at 40 °C for 1.5 h, after which 0.45 ml (4.3 mmol) of DME was added. A solution of 95 mg (0.43 mmol) of **8** in 3 ml of ether was then added, and the mixture was stirred at that temperature for 48 h. After the removal of the precipitates, the filtrate was washed with water and brine, dried, and evaporated to give an oil. The oil was subjected to flash chromatography with hexane to afford **10** (44 mg, 44%).

Kugelrohr dist: bath temp 75—80 °C/0.04 mmHg; ν (CCl_4): 3075, 1610, 1250, and 1170 cm^{-1}; δ (CCl_4, 100 MHz): 0.0—0.8 (m, 4H), 1.09 (s, 3H), 1.2—2.0 (m, 5H), 2.23 (s, 3H), 2.4—2.7 (m, 1H), 3.71 (s, 3H), 6.46 (br.s, 1H), 6.47 (br.d, 1H, J=8 Hz), and 7.13 (d, 1H, J=8 Hz); *m/e*: 230 (35%, M^+), 215 (64%), and 202 (100%). Found: C, 83.38; H, 9.46%. Calcd for $C_{16}H_{22}O$: C, 83.43; H, 9.63%.

*1-(2-Methoxy-4-methylphenyl)-1,2,2-trimethylcyclopentane (**11**).* A solution of 54 mg of **10** in 10 ml of acetic acid was shaken with 50 mg of PtO_2 under a hydrogen atmosphere (1.5 atm) for 15 min. The catalysts were then removed by filtration, and the filtrate was evaporated to give an oil (49 mg; GC showed the presence of four compounds, **10**:**11**:**12**:**13**=1.5:7.0:2.5:1.0). Repeated flash chromatographies with hexane separated the components:

11: mp 44—45 °C (from pentane, −78 °C); ν (CCl_4): 1615, 1255, 1060, and 1040 cm^{-1}; δ (CCl_4, 100 MHz): 0.64 (s, 3H), 1.10 (s, 3H), 1.29 (s, 3H), 2.24 (s, 3H), 3.71 (s, 3H), 6.45 (br.s, 1H), 6.48 (br.d, 1H, J=9 Hz), and 6.96 (d, 1H, J=9 Hz); *m/e*: 232 (67%, M^+), 217 (22%), 175 (41%), 162 (63%), and 149 (100%). Found: C, 82.97; H, 10.54%. Calcd for $C_{16}H_{24}O$: C, 82.70; H, 10.41%.

12: Kugelrohr dist: bath temp 50—60 °C/0.5 mmHg; ν (CCl_4): 1120 and 1095 cm^{-1}; δ (CCl_4, 100 MHz): 0.87 (s, 3H), 0.93 (s, 3H), 0.97 (s, 3H), 1.08 (br.d, 3H, J=7 Hz), and 3.18 (s, 3H); *m/e*: 238 (7%, M^+), 206 (53%,) 149 (78%), and 82 (100%). Found: C, 81.15; H, 12.63%. Calcd for $C_{16}H_{30}O$: C, 80.60; H, 12.68%.

13: oil; ν (CCl_4): 1460br and 1375 cm^{-1}; *m/e*: 208 (20%, M^+) and 124 (100%).

*5-Methyl-2-(1,2,2-trimethylcyclopentyl)phenol (**14**,3-hydroxycuparene).* A solution of 11 mg of the ether **11** in 0.5 ml of DMF in the presence of 25 equivalents of NaSEt was heated at 160 °C for 3 h. The mixture was then poured into dil hydrochloric acid, and the products were extracted with ether. The ether was dried over Na_2SO_4 and evaporated to give an oil. The oil was purified by flash chromatography with hexane to give phenol **14** (8 mg, 70%). Kugelrohr dist: bath temp 85—90 °C/0.04 mmHg; ν (CCl_4): 3630sh, 3600, 1620, 1290, and 1140 cm^{-1}; δ (CCl_4, 100 MHz): 0.71 (s, 3H), 1.13 (s, 3H), 1.35 (s, 3H), 2.19 (s, 3H), 4.42 (s, 1H), 6.29 (br.s, 1H), 6.49 (br.d, 1H, J=8 Hz), and 7.01 (d, 1H, J=8 Hz); *m/e*: 218 (50%, M^+), 203 (10%), 161 (30%), 148 (100%), and 135 (56%). Found: C, 82.34; H, 10.25%. Calcd for $C_{15}H_{22}O$: C, 82.51; H, 10.15%.

References

1) D. S. Tarbell, *Org. React.*, **2**, 1 (1944); S. J. Rhoads and N. R. Raulins, *ibid.*, **22**, 1 (1975).

2) See recent review: S. F. Martin, *Tetrahedron*, **36**, 419 (1980).

3) For other syntheses of cupane framework; see H. N. S. Rao, N. P. Damodaran, and S. Dev, *Tetrahedron Lett.*, **1968**, 2213; P. T. Lansbury, E. J. Nienhouse, D. J. Scharf, and F. R. Hilfiber, *J. Am. Chem. Soc.*, **92**, 5649 (1970); P. Leriverend, *Bull. Soc. Chim. Fr.*, **1973**, 3498; O. P. Vig, R. K. Parti, K. C. Gupta, and M. S. Bhatia, *Indian J. Chem.*, **11**, 981 (1973); R. B. Mane and G. S. K. Rao, *ibid.*, **12**, 932 (1974); P. de Mayo and R. Suan, *J. Chem. Soc., Perkin Trans. 1*, **1974**, 2559; A. Casares and L. A. Maldonado, *Synth. Commun.*, **6**, 11 (1976); M. T. Reetz, J. Westermann, and R. Steinbach, *J. Chem. Soc., Chem. Commun.*, **1981**, 237.

4) A similar Claisen rearrangement of 3-(4-methoxyphenoxy)cyclopentene into a trichothecane skeleton has been reported: W. K. Anderson, E. J. LaVoie, and G. E. Lee, *J. Org. Chem.*, **42**, 1045 (1977).

5) K. Yoshihara, T. Sakai, and T. Sakan, *Chem. Lett.*, **1978**, 433.

6) R. M. Magid, O. S. Fruchey, W. L. Johonson, and T. G. Allen, *J. Org. Chem.*, **44**, 359 (1979).

7) J. Borgulya, H.-J. Hansen, R. Barner, and H. Schmid, *Helv. Chim. Acta*, **46**, 2444 (1963); F. Scheinmann, R. Barner, and H. Schmid, *ibid.*, **51**, 1603 (1968).

8) I. Kuwajima and E. Nakamura, *J. Am. Chem. Soc.*, **97**, 3257 (1975).

9) S. Yamamura and Y. Hirata, *Tetrahedron*, **19**, 1485 (1963).

10) H. Stone and H. Shechter, *Org. Synth.*, Coll. Vol. IV, 543 (1963).

11) A. Matsuo, M. Nakayama, and S. Hayashi, *Chem. Lett.*, **1972**, 341.

12) B. G. Kovalev, N. P. Dormidontova, E. M. Al'tmark, and A. A. Schamshurin, *Probl. Poluch. Poluprod. Prom. Org. Sin., Akad. Nauk SSSR, Otd. Obshch. Tekh. Khim.*, **1967**, 53; *Chem. Abstr.*, **68**, 113993y (1968).

Cobalt(II)-substituted Horseshoe Crab Hemocyanins

Shinnichiro Suzuki,* Jun Kino, and Akitsugu Nakahara
Institute of Chemistry, College of General Education, Osaka University, Toyonaka, Osaka 560
(Received May 27, 1981)

The horseshoe crab Co(II) hemocyanins were prepared by dialyses of *Tachypleus tridentatus*, *Tachypleus gigas*, *Limulus polyphemus*, and *Carcinoscorpius rotundicauda* apohemocyanins against Tris–HCl buffer (pH 8.0) containing Co(II) ion. The amounts of Co(II) introduced into apohemocyanins reached almost 100% of the total sites for copper ion in native hemocyanins. However, all the four Co(II) hemocyanins did not take up oxygen molecule at all. The extremely similar spectral data for the four species revealed that there is no essential difference in the structure of the respective active sites. Both the two Co(II) ions at an active site are in the high spin state and in an distorted tetrahedral geometry, having no such ligating groups as cysteinyl or methionyl sulfur, but at least three nitrogenous ligands, probably histidine imidazoles. On the basis of these data, the environment of active site in native horseshoe crab hemocyanin is discussed.

Hemocyanins(Hc) are known as respiratory proteins for arthropods and molluscs, binding one oxygen molecule per two adjacent copper atoms that constitute an active site unit.[1–4] The deoxy forms containing Cu(I) are colorless and diamagnetic. The deep blue color of the oxy form stems from the absorption band at 570—580 nm, of which the extinction coefficient (ε_{Cu}) was estimated to be *ca.* 500 M^{-1} cm^{-1}.† Resonance Raman studies of oxyhemocyanins established that the O–O stretching band for bound dioxygen is observed at 744—749 cm^{-1}, which is characteristic of peroxide, implying complete transfer of two electrons from each Cu(I) to O_2 on binding of an oxygen molecule (Cu(II) O_2^{2-} Cu(II)).[5,6] The oxyHc is not detectably paramagnetic, indicating that the copper(II) ions are arranged as an antiferromagnetically coupled pair.[7,8] A broad resonance Raman band was recently observed at 1075 cm^{-1}, which is plausibly assigned to the singlet→triplet transition of coupled Cu(II) ions.[9]

Various approaches have hitherto been carried out by many investigators to shed light on the structure and properties of the active site of hemocyanins. Mason and his coworkers prepared methemocyanin by treating *C. magister* hemocyanin with H_2O_2,[10] and reported that the resulting products of H_2O_2-oxidation consist of 80—95% of diamagnetic species, small amount of ESR-detectable Cu(II) and some unreacted native hemocyanin. The active site of the diamagnetic species was assumed to contain spin coupled binuclear Cu(II) cluster which is interpreted in terms of a relaxation of superexchange through one or more bridging ligands such as tyrosine, histidine, serine, or cysteine.

Recently a model for the oxygen binding site of hemocyanin was proposed, based on extended X-ray absorption fine structure studies.[11] The coordination number of copper was proposed as five for oxyHc (three imidazoles, O_2, and the putative extra bridging ligand) and three for deoxyHc (three imidazoles, presumably in a trigonal-like arrangement). This suggests that two ligand groups are detached from each copper upon deoxygenation. The Cu–Cu distance was estimated to be 0.37 nm for oxyHc and 0.34 nm for deoxyHc.

Solomon *et al.* prepared a series of active site derivatives of mollusc and arthropod hemocynains, namely half-apo, met-apo, half-met, ESR-detectable met, ESR-silent met forms.[12] Based on their spectroscopic data, they described that the binuclear copper site in oxyHc contains an endogenous ligand bridge together with the exogenous μ-peroxide bridge between the equatorial planes of two tetragonal coppers. They also pointed out that the active sites in both phyla are quite similar, although the active site of arthropod is distorted from that of mollusc as is indicated by their CD-spectral differences.

We recently prepared a cobalt(II)-substituted Hc in order to disclose the environment of the active site of squid Hc.[13] Substitution of Co(II) ion for a native metal ion in metalloproteins has been an effective approach to the understanding of the structure of metal-site because of intensive and distinct visible absorption and magnetic circular dichroism (MCD) spectra given by Co(II) ion,[14] as clearly demonstrated through the studies of carbonic anhydrase, carboxypeptidase A, thermolysin, plastocyanin *etc.* The amount of Co(II) introduced into *S. lessoniana* apoHc reached 47% of the total sites for Cu in native form, being estimated as nearly complete formation of the half-apoCo(II) hemocyanin. The visible absorption and MCD spectra indicated that the Co(II) is in the tetrahedral geometry (high-spin state), and some histidine imidazoles are coordinated around Co(II). The binding of the imidazole ligands was also considered from the superhyperfine structure in the ESR spectrum of the purple hemocyanin formed on addition of ethylene glycol to oxyhemocyanin.[15–17]

This paper describes the preparation and the spectroscopic studies of Co(II)-substituted hemocyanins of all the four horseshoe crabs found in the world.

Experimental

Materials. Hemocyanins of the horseshoe crabs, *Tachypleus tridentatus*, *Tachypleus gigas*, *Limulus polyphemus*, and *Carcinoscorpius rotundicauda* were supplied by Professor K. Sekiguchi of the University of Tsukuba. These were purified from the respective hemolymphs according to the method of Omura *et al.*[18] The dark blue pellets of pure hemocyanins were dissolved in 50 mM Tris–HCl buffer (pH 8.0)†† and

† In this paper 1 M=1 mol dm^{-3}.

†† Tris: tris(hydroxymethyl)aminomethane.

Tabke 1. Electronic and CD absorption spectra of oxyhemocyanins

Hemocyanins	UV and VIS[a] λ_{max}/nm (ε_{Cu})	CD[a] λ_{max}/nm ($\Delta\varepsilon_{Cu}$)
T. tridentatus	340 (9320), 577 (514)	341 (−11.5), 495 (+0.752), 610 (+0.813)
T. gigas	340 (10300), 578 (500)	341 (−13.3), 495 (+0.886), 610 (+0.960)
C. rotundicauda	340 (11000), 577 (550)	341 (−14), 495 (+0.95), 610 (+1.0)
L. polyphemus	340 (10600), 578 (557)	341 (−14.0), 495 (+0.941), 610 (+1.05)

a) 50 mM Tris-HCl buffer (pH 8.0).

kept in a refrigerator at 4 °C except when the spectra were recorded. The purity of hemocyanin was checked by the ratio of the absorption coefficient at 280 nm to that at 340 nm. The ratios of the four horseshoe crab hemocyanins were in the range of 4.1—4.3.

Preparation of Co(II)-substituted Hemocyanin. First, apoHc was prepared by dialysis of oxyHc against pH 8.0 Tris-HCl buffer (50 mM) which contained 10 mM KCN at 4 °C for 3 d. The copper ion was completely removed from the active site of protein. The Co(II)-Hc was prepared by dialysis of the apoHc against the Tris-HCl buffer which contained about 1 mM $CoCl_2$ at 4 °C for 2 d under nitrogen. When a denatured protein was deposited by Co(II) ion, the dialysis bag was washed against Co(II)-free buffer to remove excess Co(II) ion bound to the protein until the turbid protein became transparent. After treating the apoHc with Co(II) ion, the Co(II)-Hc was dialyzed against Tris-HCl buffer of 2 l. Further the excess of Co(II) ion contained in the resulting crude sample was removed by treating with Chelex 100 resin (50% by volume, pre-equilibrated with the Tris-HCl buffer). The concentration of Co(II) in the final product was determined to be 85—100% of the total sites for Cu in native Hc by employing the method of standard addition, using an atomic absorption spectrophotometer (Nippon Jarrell-Ash AA-1 spectrometer).

In order to examine whether or not the Co(II) exists at the active site of Hc, reconstitution of holoHc was carried out by treating the Co(II)-Hc with $[Cu(CH_3CN)_4]ClO_4$ according to the method of Konings *et al.*[19] The introduction of Cu ion into Co(II)-Hc was observed to be inhibited by the substituted Co(II) ion. The recovery of oxyHc from Co(II)-Hc was thus limited to only 20% of that from apoHc. The extent of recovery of oxyHc was evaluated on the basis of CD intensity at 440 nm where oxyHc exhibited a maximum intensity, while Co(II)-Hc gave actually no CD absorption.

Instruments. The absorption, CD, and ESR spectra were recorded with a Hitachi 323 spectrophotometer, a JASCO J-500C circular dichroism spectrometer, and a JEOL JES-FE1X ESR spectrometer, respectively. The MCD spectra were recorded at 11500 G††† with a JASCO J-500C spectrometer equipped with an electromagnet. The measurements of spectra were carried out at 15—20 °C except for the ESR spectra which were recorded at 77 K.

Results and Discussion

Four Horseshoe Crab Oxyhemocyanins, and Effects of Addition of Ethylene Glycol to Them. The electronic absorption and CD spectra of oxyHc (*T. tridentatus*) are represented in Fig. 1. Other than the characteristic protein band at near 280 nm, two bands were

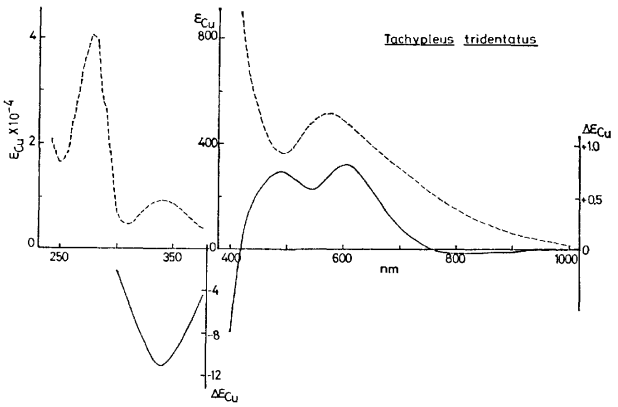

Fig. 1. Electronic absorption spectra (----) and CD spectra (——) of *T. tridentatus* oxyhemocyanin. Conditions: hemocyanin, 0.59 mM; 50 mM Tris-HCl buffer (pH 8.0). ε_{Cu}(M^{-1} cm^{-1}) and $\Delta\varepsilon_{Cu}$(M^{-1} cm^{-1}) are expressed per mol of Cu.

recorded in the near ultraviolet (340 nm), and visible (near 580 nm) regions. These two bands were absent in deoxy- and apo-Hc's. The electronic absorption band at 340 nm has been interpreted as arising from peroxide to copper charge transfer. However, the absorption band at 580 nm, which is responsible for the blue color is still controversial as to whether it should be assigned as peroxide to copper charge transfer[5,12] or as d-d transitions based on Cu(II).[20]

T. tridentatus Hc exhibited three CD bands in the visible region, namely two positive bands at 495 and 610 nm as observed in other arthropod oxyHc,[21] and a weak negative band at around 800 nm. On the other hand, molluscan oxyhemocyanins such as squid (*S. lessoniana*) oxyHc have three CD bands in the visible region; a positive band at 450 nm, a negative band at 570 nm and a positive band at around 710 nm.[21] Oxyhemocyanins of both the phyla display an intensive negative CD band at around 340 nm. The spectral data for the four horseshoe crab oxyhemocyanins bear a strong resemblance to each other as listed in Table 1. From these data it may be considered that the ligating groups and the coordination geometries around the Cu(II) ions are actually the same for the four hemocyanins.

It has been known that oxyhemocyanins exhibit no ESR signal on account of the spin-coupling of the two Cu(II) ions at the active site. However, addition of ethylene glycol (83 v/v% of the total volume) to the buffer solutions of the oxy forms produces a state containing ESR-detectable metHc. The X-band

††† 1 G=1×10^{-4} T.

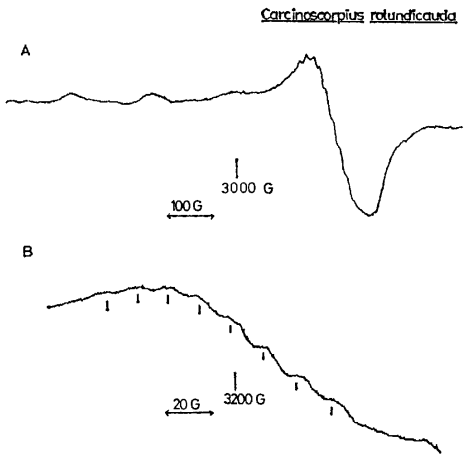

Fig. 2. (A) ESR spectrum of *C. rotundicauda* oxyhemocyanin treated with ethylene glycol (83 v/v%). $g_{//}$ 2.27, $A_{//}$ 178 G, $g_{\perp}$ 2.05. (B) Nitrogen nuclear superhyperfine structure of spectrum (A). Condition: hemocyanin, 0.25 mM.

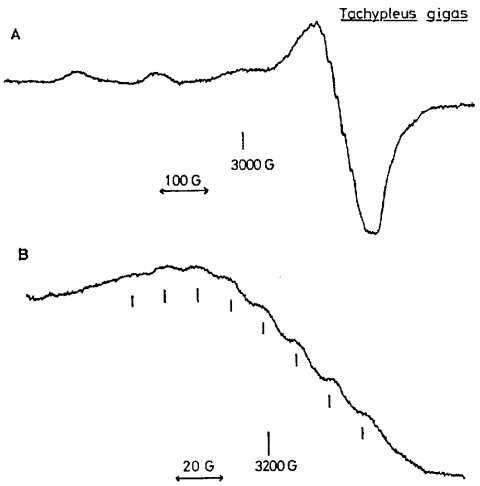

Fig. 3. (A) ESR spectrum of *T. gigas* oxyhemocyanin treated with ethylene glycol (83 v/v%). $g_{//}$ 2.27, $A_{//}$ 176 G, $g_{\perp}$ 2.05. (B) Nitrogen nuclear superhyperfine structure of spectrum (A). Condition: hemocyanin, 0.54 mM.

ESR spectra of *C. rotundicauda* and *T. gigas* are illustrated in Figs. 2 and 3, respectively. The periods between the preparations of the samples and the measurements of ESR spectra were 40 h at 4 °C. The amounts of ESR-active copper in the two samples were estimated to be *ca.* 20% of the total copper in the respective native Hc. The spectrum in Fig. 2A exhibited a signal at $g_{//}$=2.27 with spacings ($A_{//}$) between successive peaks of 178 G. The ESR parameters ($g_{//}$=2.27, $A_{//}$=176 G, $g_{\perp}$=2.05) of the spectrum in Fig. 3A are quite similar to those of *C. rotundicauda*. These values indicate that the Cu(II) ion has a tetragonal geometry. The patterns of the ESR spectra also suggested that there is no magnetic dipole-dipole interaction between the two coppers at the active sites. In other words, the ESR-active copper was supposed to be in a monomeric Cu(II) complex. The spin Hamiltonian parameters of these horseshoe crab hemocyanins were similar to those of

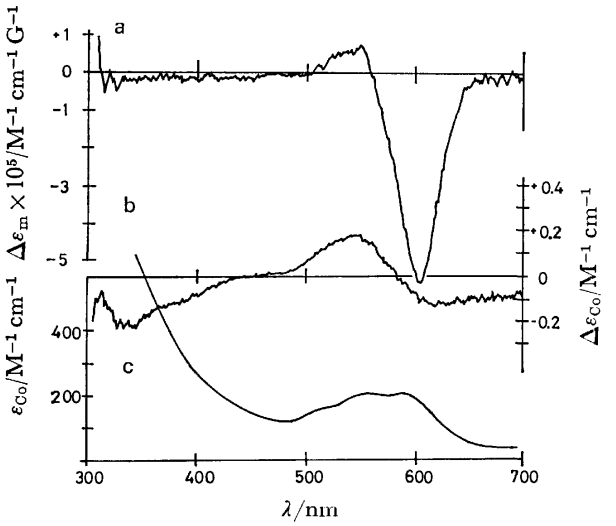

Fig. 4. MCD (a), CD (b), and electronic absorption (c) spectra of *T. gigas* Co(II) hemocyanin. Conditions: hemocyanin, 0.37 mM; 50 mM Tris–HCl buffer (pH 8.0). ε_{Co}, $\Delta\varepsilon_{Co}$, and $\Delta\varepsilon_m$ are expressed per mol of Co(II).

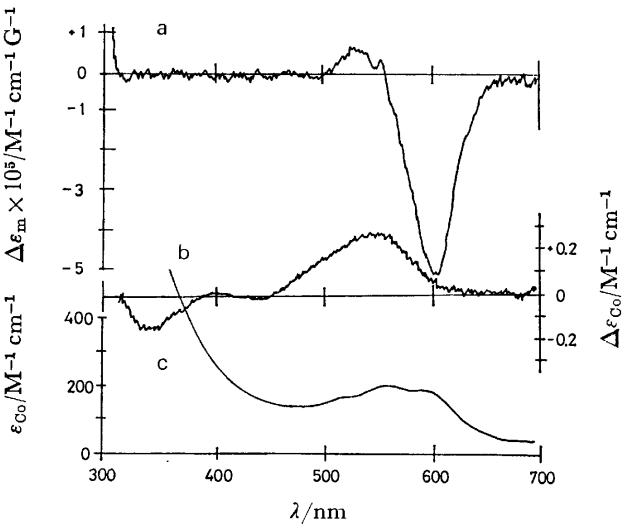

Fig. 5. MCD (a), CD (b), and electronic absorption (c) spectra of *L. polyphemus* Co(II) hemocyanin. Conditions: hemocyanin, 0.34 mM; 50 mM Tris–HCl buffer (pH 8.0).

the squid Hc treated with ethylene glycol (80 v/v%), where the values of $g_{//}$, $g_{\perp}$, and $A_{//}$ were 2.261, 2.059, and 173.8 G, respectively.[16] Further it is noteworthy that at least eight superhyperfine lines due to nitrogens with spacing (A_N) of about 14 G were observed in the region of $g_{\perp}$ (Figs. 2B and 3B), suggesting that at least three nitrogenous ligands are coordinated around Cu(II). The same kind of ESR signals and the superhyperfine structure were also observed for the other two hemocyanins (*T. tridentatus* and *L. polyphemus*) upon addition of ethylene glycol.

Preparation and Spectral Properties of Co(II)-substituted Horseshoe Crab Hemocyanins. We have already succeeded in preparing Co(II) substituted squid hemocyanin.[13] By employing the same procedure, Co(II) hemocyanins of the four horseshoe crabs were prepared. All the Co(II) hemocyanins were pink-violet.

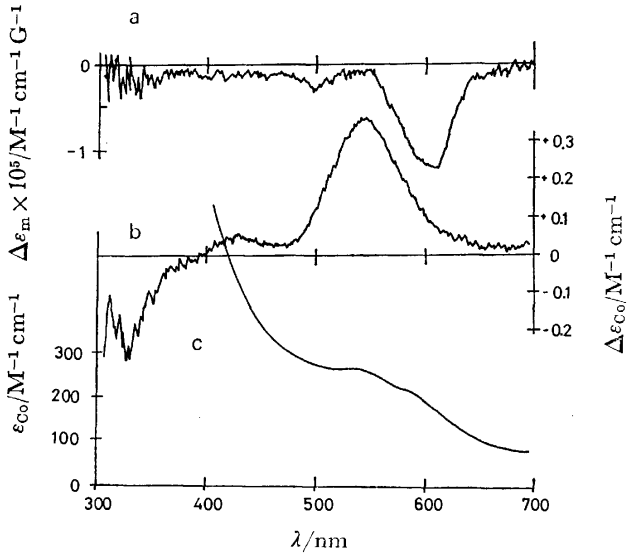

Fig. 6. MCD (a), CD (b), and electronic absorption (c) spectra of aged *T. gigas* Co(II) hemocyanin. Conditions: hemocyanin, 0.55 mM, 50 mM Tris–HCl buffer (pH 8.0). The period between the preparation and the measurement was 20 d at 4 °C.

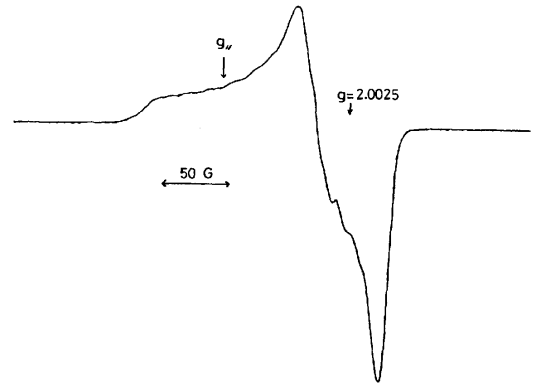

Fig. 7. ESR spectrum of mixture of *T. gigas* Co(II) hemocyanin and cyanide. Conditions: hemocyanin (Co(II), 5.5 mM) plus cyanide(22 mM); 50 mM Tris–HCl buffer (pH 8.0); 77 K.

The absorption, CD, and MCD spectra of *T. gigas* and *L. polyphemus* Co(II) hemocyanins measured at room temperature are represented in Figs. 4 and 5, which display that all the spectra of the two species are remarkably similar to each other. The appearance of CD band at 500—600 nm is indicative of the binding of Co(II) ion with the protein. The absorption and MCD bands of the Co(II)-chromophore at 500—650 nm are attributed to the d-d transition ($^4A_2(F) \rightarrow {}^4T_1(P)$) arising from a tetrahedral Co(II) in the high spin state. In general, Co(II) complexes with tetrahedral geometry are known to show a negative MCD band at a longer wavelength region and one or two weaker positive bands at a shorter wavelength region.[14] The patterns of MCD spectra in Figs. 4 and 5 further reveal that there is no MCD band arising from S→Co(II) charge transfer transition[22-24] in the range of 300—400 nm, suggesting that there is no thiol-coordination of cysteinyl residue around Co(II).[14,25] Cysteinyl sulfur (also probably methionyl sulfur) might not be a ligating atom around the two copper ions in native horseshoe crab hemocyanins. The negative CD band at around 350 nm is not assigned to charge transfer transition of the Co(II)-chromophore because of the absence of MCD band in the range of 300—400 nm. It is suggested at present that the negative CD band might be attributed to the protein structure and/or the amino acid residues (*e.g.* disulfide group) in the protein.

The active sites of the four horseshoe crab hemocyanins were almost completely filled with Co(II) ion, being contrasted to the case of the squid hemocyanin, from which the half-filled Co(II)–Hc was obtained, as already communicated.[13] However, the horseshoe crab Co(II) hemocyanins did not take up oxygen molecule either. With storage at 4 °C for several weeks pink-violet Co(II) hemocyanins turned light brown. This may be due to a kind of aging of hemocyanins, and is visuallized through absorption, CD, and MCD spectra of *T. gigas* Co(II)–Hc as illustrated in Figs. 4 and 6. Comparative inspection of these Figures apparently indicates that the intensity of the ultraviolet absorption band increased significantly and patterns of CD and MCD spectra changed considerably with aging of Co(II)–Hc. The change in 500—600 nm MCD band suggests that the distorted tetrahedral geometry of Co(II) center is converted into another geometry, probably to a five- or six-coordinate structure. It was also confirmed that the oxidation state of Co ion in Co(II)–Hc does not change with aging of the sample. This was proved through an ESR study of aged Co(II)–Hc (*vide infra*).

At liquid nitrogen temperature (77 K) we could not observe the ESR peak for the high spin Co(II) center in the hemocyanin because of the extremely broadening and low amplitude of signal. Addition of one-equivalent cyanide to Co(II) ion gave no ESR-signal either. However, the ESR signal was observed at $g=2$, upon addition of above 2-equivalent cyanide, as shown in Fig. 7 (*T. gigas* Co(II) hemocyanin). The signal did not increase any more with further addition of cyanide, whereas the signal ultimately disappeared by allowing the sample to stand for a day at 4 °C. The ESR signal having the spin Hamiltonian parameters of $g_{//}=2.06$, $A_{//}^{Co}=16$ G, and $A_{\perp}=11$ G,[26] is suggestive of the formation of 1:1 O_2:low spin Co(II) complex with CN^- donor groups and probably endogenous ligands. The characteristic feature of ESR spectrum ($g_{//}>g_{\perp}\simeq 2.00$) closely resembles those of various monomeric Co(II)–dioxygen complexes in literatures.[27-31] The result of evaluation according to the method of Hoffman *et al.* indicated that above 90% of unpaired spin density resides on the dioxygen moiety and below 10% resides on Co(II) ion.[27] The aged *T. gigas* Co(II)–Hc also quantitatively afforded the 1:1 dioxygen adduct with the addition of above 2-equivalent cyanide. This finding implies that no oxidation of the cobalt ion (from Co(II) to Co(III)) took place in the course of the aging.

Metal Binding Site of Hemocyanin. The ESR spectra of oxyhemocyanins treated with ethylene glycol are considered from g and A values to be characteristic

of many square-planar or tetragonally-distorted octahedral Cu(II) complexes with small ligands (Figs. 2 and 3). The copper nuclear hyperfine splitting constants, $A_{//}$, were 176—178 G. These values are more compatible with those observed for Type II copper proteins (150 to 190 G[32,33]) than those for Type I copper proteins (30 to 100 G[32]). The spin Hamiltonian parameters of these denatured hemocyanins are remarkably similar to that of $[Cu(imidazole)_4]^{2+}$ complex ($g_{//}=2.26$, $A_{//}=179$ G, $g_{\perp}=2.05$ at pH 8). The superhyperfine structures on the $g_{\perp}$ region are probably attributable imidazole nitrogens of histidine residues judging from the spacing of about 14 G. The seven or nine superhyperfine lines are theoretically an indicative of coordination of three or four equivalent nitrogens around Cu(II), respectively. In Figs. 2B and 3B, eight nitrogen superhyperfine lines are observed. Thus the present findings do not permit us to conclude which of $(N)_3$- or $(N)_4$-coordination is valid. However, on the basis of these superhyperfine structures, we can actually understand that copper ions at the active site in all horseshoe crab hemocyanins are surrounded by at least three nitrogens, probably histidine imidazoles.

Contrary to the case of squid Co(II)–Hc,[13] the amount of Co(II) introduced into horseshoe crab apohemocyanins essentially reached 100% of the total sites for copper. In the light of the absorption and MCD spectra illustrated in Figs. 4 and 5, coordination geometries around the two Co(II) ions at the active site were proved to be tetrahedral and almost equal to each other. Horseshoe crab Co(II) hemocyanins did not take up molecular oxygen either, although they have two adjacent Co(II) ions contrary to the case of squid Hc. This may be understood by taking into account the structural restriction of the Co(II)-binding site that favors the tetrahedral but not the octahedral geometry which enables binding of dioxygen as exhibited by many Co(II)–dioxygen complexes of low molecular weights.[29,34] The previous experimental results of squid Co(II)–Hc revealed that at least one of the two adjacent copper sites in deoxyhemocyanin provides copper with a tetrahedral-like environment, where some histidine–imidazoles are arranged as ligating groups. In the case of horseshoe crab hemocyanins, the environment of the two adjacent metal sites in deoxy form is considered to be a little more seriously distorted from tetrahedral geometry than that of the active site of squid deoxyhemocyanin, as displayed by the broad splitting of the spin allowed transition ($^4A_2(F)\rightarrow{}^4T_1(P)$) band. The amino acid residues around the metal sites in deoxy-form might be at least three histidyl imidazoles in the light of the ESR measurements of oxyhemocyanins treated with ethylene glycol. Furthermore the fourth coordination site of tetrahedral Co(II) might be occupied by a water molecule.

Recently Spiro *et al.* described a trigonal-like geometry of Cu(I) center bound by three imidazoles in deoxyhemocyanin.[9] Their conclusion does not necessarily contradict our present data, since the Cu(I) sites in deoxy form are supposed to undergo a geometrical rearrangement from a trigonal-like coordination geometry into a tetrahedral-like geometry upon substitution of Co(II) for Cu(I). Thus the active site of native oxyhemocyanin is considered as constituted from a pair of five-coordinate Cu(II) ions (distorted trigonal bipyramidal or square pyramidal geometries) which are bridged by the bound O_2^{2-} and by a putative extra bridging ligand. Although the existence of a bridging protein ligand such as tyrosine phenol was proposed by many investigators,[9,20,35] based on ESR-silent character of metHc, there has been no direct evidence for the presence of phenolate residue.[36] From the spectral investigations (MCD) of the Co(II)–substituted hemocyanins, possibility of presence of tyrosine bridge still remains unknown.

We should like to thank Prof. Koichi Sekiguchi and Dr. Hiroaki Sugita of the University of Tsukuba for providing the horseshoe crab hemocyanins and for their helpful discussions, and Prof. Seizo Misumi of Kyushu Sangyo University for measurements of CD and MCD spectra and for valuable discussion. The kindly suggestions by Dr. Wasuke Mori of this College of General Education are also acknowledged. This work was supported by a Grant-in-Aid for special Project Research No. 56109009 from the Ministry of Education, Science and Culture of Japan.

References

1) A. C. Redfield, T. Coolidge, and H. Montgomery, *J. Biol. Chem.*, **76**, 197 (1928).
2) R. Lontie and R. Witters, "Biochemistry of Copper," ed by J. Peisach, P. Aisen, and W. E. Blumberg, Academic Press, New York (1966), pp. 455—463.
3) R. Lontie and R. Witters, "Inorganic Biochemistry," ed by G. L. Eichhorn, Elsevier, Amsterdam (1973), Vol. 1, pp. 344—358.
4) R. Lontie, "Structure and Function of Haemocyanin," ed by J. V. Bannister, Springer-Verlag, Berlin (1977), pp. 150—155.
5) T. B. Freedman, J. S. Loehr, and T. M. Loehr, *J. Am. Chem. Soc.*, **98**, 2809 (1976).
6) T. J. Thamann, J. S. Loehr, and T. M. Loehr, *J. Am. Chem. Soc.*, **99**, 4187 (1977).
7) T. H. Moss, D. C. Gould, A. Efrenberg, J. S. Loehr, and H. S. Mason, *Biochemistry*, **12**, 2444 (1973).
8) E. I. Solomon, D. M. Dooly, R. H. Wang, H. B. Gray, M. Cerdonio, F. Mogno, and G. L. Romani, *J. Am. Chem. Soc.*, **98**, 1029 (1976).
9) J. A. Larrabee and T. G. Spiro, *J. Am. Chem. Soc.*, **102**, 4217 (1980).
10) N. Makino, H. van der Deen, P. McMahill, D. C. Gould, C. Simo, and H. S. Mason, *Biochim. Biophys. Acta*, **532**, 315 (1978).
11) J. M. Brown, L. Powers, B. Kincaid, J. A. Larrabee, and T. G. Spiro, *J. Am. Chem. Soc.*, **102**, 4210 (1980).
12) R. S. Himmelwright, N. C. Eickman, C. D. LuBien, and E. I. Solomon, *J. Am. Chem. Soc.*, **102**, 5378 (1980).
13) S. Suzuki, W. Mori, J. Kino, Y. Nakao, and A. Nakahara, *J. Biochem.*, **88**, 1207 (1980).
14) B. L. Vallee and B. Holmquist, "Methods for Determining Metal Ion Environments in Proteins: Structure and Function of Metalloproteins," ed by D. W. Darnall and R. G. Wilkins, Elsevier/North-Holland, New York (1980), pp. 27—74.

15) W. Mori, S. Suzuki, M. Kimura, O. Yamauchi, and A. Nakahara, *J. Inorg. Biochem.*, **12**, 179 (1980).
16) W. Mori, S. Suzuki, M. Kimura, Y. Sugiura, and A. Nakahara, *J. Inorg. Biochem.*, **13**, 89 (1980).
17) A. Nakahara, W. Mori, S. Suzuki, and M. Kimura, "Biomimetic Chemistry," ed by D. Dolphin, C. McKenna, Y. Murakami, and I. Tabushi, American Chemical Society, Washington D. C. (1980), pp. 341—350.
18) T. Omura, T. Fujita, F. Yamada, and S. Yamamoto, *J. Biochem.*, **50**, 400 (1961).
19) W. N. Konings, R. Van Driel, E. F. J. Van Bruggen, and M. Gruber, *Biochim. Biophys. Acta*, **194**, 55 (1969).
20) A. R. Amundsen, Whelan, and B. Bosnich, *J. Am. Chem. Soc.*, **99**, 6730 (1977).
21) K. W. Nickerson and K. E. Van Holde, *Comp. Biochem. Physiol.*, **39B**, 855 (1971).
22) L. Morpurgo, A. Finazzi Agró, G. Rotilio, and B. Mondovi, *Eur. J. Biochem.*, **64**, 453 (1976).
23) D. R. McMillin, R. C. Rosenberg, and H. B. Gray, *Proc. Natl. Acad. Sci. U.S.A.*, **71**, 4760 (1974).
24) J. S. Thompson, T. Sorrell, T. J. Marks, and J. A. Ibers, *J. Am. Chem. Soc.*, **101**, 4193 (1979).
25) M. Vašák, *J. Am. Chem. Soc.*, **102**, 3953 (1980).
26) The $g_{\perp}$ value which is larger than the g value of 2.0025 (Li-TCNQ marker) could not be evaluated accurately.
27) B. M. Hoffman, D. L. Diemente, and F. Basolo, *J. Am. Chem. Soc.*, **92**, 61 (1970).
28) J. S. Taylor and J. E. Coleman, *J. Biol. Chem.*, **246**, 7058 (1971).
29) R. D. Jones, D. A. Summerville, and F. Basolo, *Chem. Rev.*, **79**, 139 (1979).
30) K. Ishizu, J. Hirai, M. Kodama, and E. Kimura, *Chem. Lett.*, **1979**, 1045.
31) Y. Sugiura, *J. Am. Chem. Soc.*, **102**, 5216 (1980).
32) J. Peisach and W. E. Blumberg, *Arch. Biochem. Biophys.*, **165**, 691 (1974).
33) S. Suzuki, T. Sakurai, A. Nakahara, O. Oda, T. Manabe, and T. Okuyama, *FEBS Lett.*, **116**, 17 (1980).
34) W. P. Schaefer, B. T. Huie, M. G. Kurilla, and S. E. Ealick, *Inorg. Chem.*, **19**, 340 (1980).
35) N. C. Eickman, R. S. Himmelwright, and E. I. Solomon, *Proc. Natl. Acad. Sci. U.S.A.*, **76**, 2094 (1979).
36) J. Kino, S. Suzuki, and A. Nakahara, *Inorg. Chim. Acta*, **56**, L33 (1981).

A New Type of P-C and C-C Bond Cleavage Reactions in α-Trimethylsilyloxy-β-oxo Phosphonates and α-Ethoxy-β-oxo Phosphonates. The Synthesis of Unsymmetrical α-Hydroxy Ketones Utilizing 1:1 Carbonyl Adducts of Diethyl Trimethylsilyl Phosphite with Benzaldehyde

Mitsuo SEKINE, Masashi NAKAJIMA, and Tsujiaki HATA*

Department of Life Chemistry, Tokyo Institute of Technology, Nagatsuta, Midori-ku, Yokohama 227

(Received April 10, 1981)

α-Lithiated diethyl α-(trimethylsilyloxy)benzylphosphonate underwent facile acylation with various acylating agents to afford the corresponding α-acylated products in good yields. On treatment of the α-acylated products with 1 M† NaOH–EtOH (1:1, v/v) the P–C bond was cleaved with elimination of diethyl phosphate to give α-hydroxy ketones predominantly. On the other hand, when diethyl α-acyl-α-ethoxybenzylphosphonates were treated under the same conditions, they were rather stable and recovered. However, the prolonged alkaline treatment or the use of 4 M NaOH–EtOH (1:1, v/v) resulted in the C–C bond cleavage giving carboxylic acids and diethyl α-ethoxybenzylphosphonate in quantitative yields, respectively. The mechanisms of the above two reactions were proposed and discussed in connection with the Perkow reaction and related reactions.

Our recent studies on the unsymmetrical ketone synthesis,[2,3] using 1:1 carbonyl adducts of diethyl trimethylsilyl phosphite with aldehydes, have shown that α-alkylated α-trimethylsilyloxy phosphonates were converted by one-step treatment with dilute sodium hydroxide solution to carbonyl compounds with elimination of diethyl phosphonate ion. The simultaneous

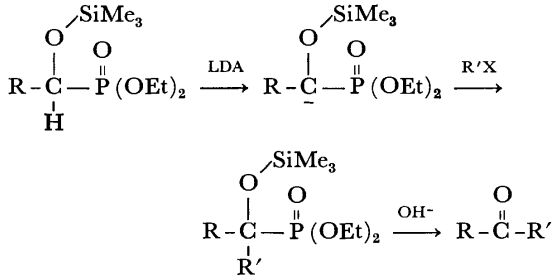

removal of the trimethylsilyl group and the tervalent phosphoryl group was considered to be the result of the neighboring participation of α-phosphoryl group where hydroxide ion attacked the phosphoryl center followed by intramolecular migration of the trimethylsilyl group from the α-oxygen to the phosphoryl oxygen so that trimethylsilanol could be eliminated.[2] Thus, it is now recognized that α-lithiated 1-(trimethylsilyloxy)alkylphosphonates can serve as a new type of acyl anion equivalents.

In this paper, we wish to report acylation of diethyl α-(trimethylsilyloxy)benzylphosphonate (**1**), conversion of the acylated products to α-hydroxy ketones, and also a novel type of C–C bond cleavage reactions in connection with the α-hydroxy ketone formation. A preliminary report of this work has already appeared.[5]

Table 1. Preparation of diethyl α-trimethylsilyloxy-α-acylbenzylphosphonates (**2**) from diethyl 1-(trimethylsilyloxy)benzylphosphonate (**1**)

Acylating agent	Acylated product	R	Yield of **2** / %
$C_6H_5C(O)Cl$	**2a**	C_6H_5	81
$4\text{-}ClC_6H_4C(O)Cl$	**2b**	$4\text{-}ClC_6H_4$	88
$4\text{-}MeOC_6H_4C(O)Cl$	**2c**	$4\text{-}MeOC_6H_4$	83
$CH_3C(O)Cl$	**2d**	CH_3	39
$[CH_3C(O)]_2O$	**2d**	CH_3	68
$[(CH_3)_2CHC(O)]_2O$	**2e**	$(CH_3)_2CH$	74
$[CH_3(CH_2)_2C(O)]O$	**2f**	$CH_3(CH_2)_2$	71

Results and Discussion

In order to obtain α-diketones from α-acylated α-(trimethylsilyloxy)benzylphosphonates in a manner similar to that described in the synthesis of unsymmetrical ketones,[2,3] we examined the acylation of **1** and the alkaline treatment of the acylated products (**2**) which would be expected to give α-diketones. Acylation of lithiated **1** with various acylating agents is summarized

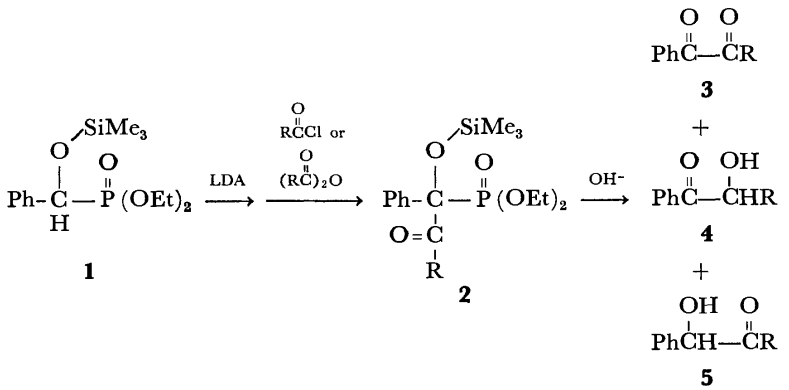

† 1 M=1 mol dm^{-3}.

Table 2. Alkaline treatment of acylated products **2**

Phosphonate	Time/min	Products	
		Yield of **3**/%	Yields of **4** and **5**/%[a]
2a	5	8	77 (**4a**)
2b	5	10	72 (**4b**)
2c	30	4	88 (**5c**)
2d	5	0	66 (**4d**:**5d**=1:2.8)
2e	10	0	83 (**4e**:**5e**=1:1.3)
2f	10	0	66 (**4f**:**5f**=1:2)

a) The ratio of **4** and **5** was determined by NMR spectra.

in Table 1. As in the case of the α-alkylation of lithiated **1**,[2,3] the acylation was also satisfactory. In the α-acylation of **1** with aliphatic acylating agents, acid anhydrides were found to be superior to acyl chlorides. The acylated products **2** were treated with 1 M NaOH–EtOH (1:1, v/v) under the same conditions as in the case of the unsymmetrical ketone synthesis. However, the alkaline treatment of **2a** resulted in the formation of benzil in only 8% yield. The main product in this reaction was found to be benzoin (**4a**) which was isolated in 77% yield. Similar results were obtained in the case of **2b** and **2c**. Especially, in the case of **2d**—**f**, α-hydroxy ketones were exclusively obtained. As shown in Table 1, the formation of **4** and/or **5** depends on the substituent of R. Under the alkaline conditions where α-hydroxy ketones were obtained, initially formed α-hydroxy ketones might be in equilibrium between the following two possible enediol enolates. In the case of **2b**, the equilibrium

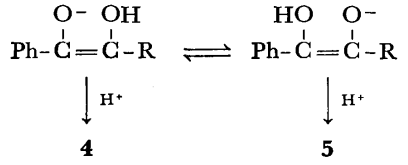

lies so far to the left because *p*-chlorophenyl group, an electron-withdrawing group, stabilizes the anion of the left compound through the double bond so that **4b** was exclusively obtained. Contrary to this result, the alkaline treatment of **2c** gave **5c** owing to the resonance effect of *p*-methoxyphenyl group as the electron-donating group.

If R is alkyl groups as in the case of the alkaline treatment of **2d**—**f**, the equilibrium lies to the right. Consequently, **5** was obtained predominantly over **4**. The ratio of **5**/**4** decreased in the order of methyl, isopropyl, butyl. This order, however, was reverse to that expected from the electronic effect of the alkyl substituents. Although the reason is not clear, in these cases probably the steric effects in the the protonation of the endiol enolates might be more important factor than the electronic environment.

There might be two possible mechanisms for the predominant formation of α-hydroxy ketones. One of them is the mechanism involving an initial attack of hydroxide ion on the phosphorus followed by P–C bond cleavage with concomitant formation of enolate ion (see Path A in Scheme 1).[6] The other mechanism is as follows: The trimethylsilyl group was first eliminated according to a mechanism similar to that described in the case of the alkaline treatment of α-alkylated 1-(trimethylsilyloxy)alkylphosphonates[2,3] and the resulting α-hydroxy β-oxo phosphonate (**6**) is deprotonated followed by phosphoryl migration from carbon to oxygen and the subsequent hydrolysis of the resulting enediol phosphate (**7**) (see Path B in Scheme 1). The latter is closely related to the mechanisms of the Perkow reaction[7] and the Kukhtin-Ramirez oxyphosphorane formation[8] which are thought to proceed *via* an initial attack of the phosphorus on the carbonyl carbon followed by phosphoryl rearrangement.[9,10] In the present α-hydroxy ketone formation, the latter mechanism (Path B) was indirectly supported by the following experiment: Treatment of **2a** with a catalytic amount of *p*-toluenesulfonic acid in methanol–water (1:1, v/v) under reflux for 2 h gave diethyl α-benzoyl-α-hydroxybenzylphosphonate (**6**) in 66% yield. On treatment of **6** with 1 M NaOH–EtOH under the same conditions as with the alkaline treatment of **2a**, **3a**, and **4a** were obtained in 67 and 11% yields, respectively. The ratio of **3a** to **4a** was quite similar to that obtained from **2a**.

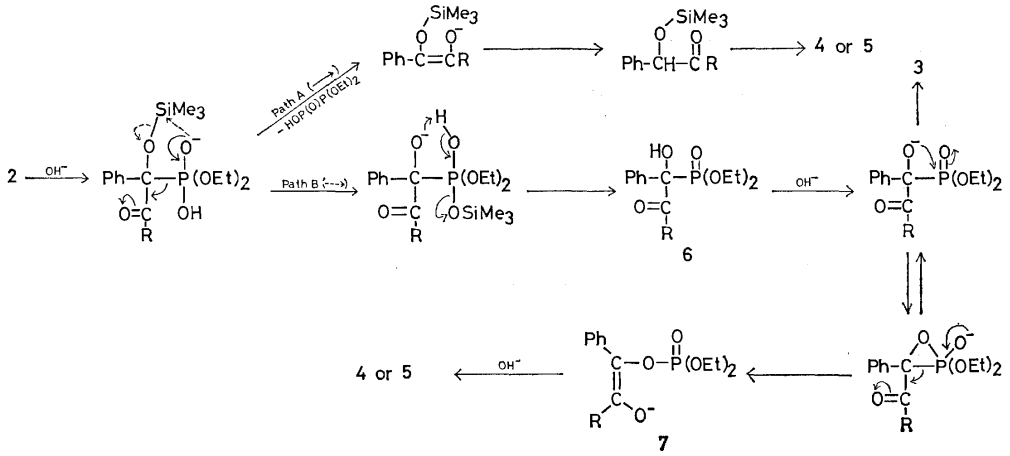

Scheme 1.

$$\mathbf{2a} \xrightarrow{H^+} \mathbf{6} \xrightarrow{OH^-} \mathbf{3a} + \mathbf{4a}$$

In connection with the mechanism *via* Path B, Kukhtin[11] reported a similar type of phosphoryl rearrangement in the alkaline treatment of the 1:1 carbonyl adduct of diethyl phosphonate with biacetyl.

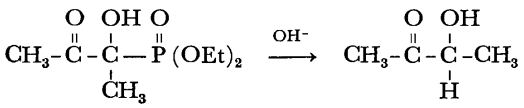

Moreover, α-hydroxy-β,β,β-trichloro phosphonates were known to undergo phosphoryl rearrangement on treatment with alkali leading to the corresponding enol phosphates.[12]

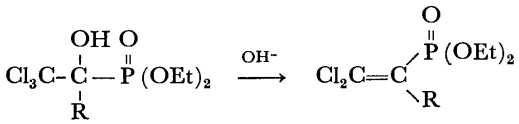

In order to ascertain the mechanism *via* Path B, we prepared α-alkoxybenzylphosphonate (**8**) substituted with an ethoxy group in place of the trimethylsilyloxy group according to the following equation.

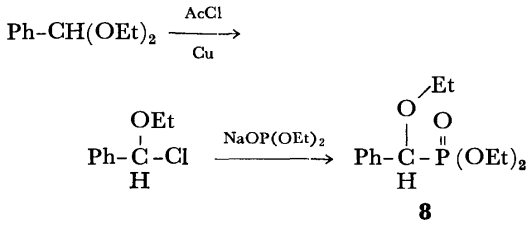

The acylation of **8** with acyl chlorides or acid anhydrides was essentially almost the same as that of **1**. The results are summarized in Table 3.

We considered that, if the α-hydroxy ketone formation from **2** was attributed to Path A, the alkaline treatment of the acylated products (**9**) would give α-ethoxy ketones (**10**). On the other hand, if Path B was the real process, **9** would be recovered unchanged since the ethyl group could not be migrated to the phosphoryl oxygen under these conditions owing to the stable Et–O bond. Therefore, we examined the hydrolysis of **9a** under the same alkaline conditions as described in the alkaline treatment of **2a**. When **9a** was treated with 1 M NaOH–EtOH (1:1, v/v) for 5 min, no reaction took place and 96% of **9a** was recovered. Similar results were obtained also in the case of **9b**—**d**. These results are summarized in Table 4. From these results, we concluded that **4** or **5** was formed *via* Path B.

Table 3. Acylation of diethyl α-ethoxybenzylphosphonates (**8**)

Acylating agent	Acylated product R		Yield of **9** %
$C_6H_5C(O)Cl$	**9a**	C_6H_5	81
$4\text{-}ClC_6H_4C(O)Cl$	**9b**	$4\text{-}ClC_6H_4$	63
$4\text{-}MeOC_6H_4C(O)Cl$	**9c**	$4\text{-}MeOC_6H_4$	81
$CH_3C(O)Cl$	**9d**	CH_3	61

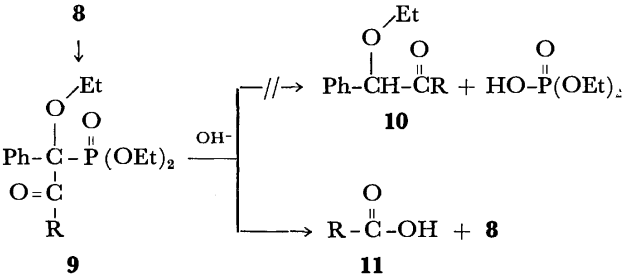

C–C Bond Cleavage of **9**. In connection with the above alkaline treatment of **9**, we found a new type of C–C bond cleavage reactions. When the alkaline treatment of **9a** was prolonged or more concentrated sodium hydroxide solution was employed, some reaction occurred. However, the reaction observed was not P–C bond but C–C bond cleavage reaction. When **9a** was treated with 1 M NaOH–EtOH (1:1, v/v) for 5 h, benzoic acid and **8** were obtained in quantitative yields, respectively. The above C–C bond cleavage reaction is regarded as a

Table 4. Alkaline treatment of acylated products **9**

Phosphonate	Conditions[a]		Yields/% of products		Recovery of **9** %
	Alkali	Time	**8**	**11**	
9a	1 M NaOH-EtOH	5 min	0	0	96
	1 M NaOH-EtOH	5 h	quant.	quant.	0
	4 M NaOH-EtOH	5 min	62	63	31
	4 M NaOH-EtOH	30 min	quant.	quant.	0
	2 M HCl, 60 °C	1 h	0	0	98
9b	1 M NaOH-EtOH	5 min	33	33	62
	1 M NaOH-EtOH	1 h	95	90	0
9c	1 M NaOH-EtOH	5 min	0	0	99
	1 M NaOH-EtOH	30 min	10	10	90
	1 M NaOH-EtOH	24 h	99	92	0
9d	1 M NaOH-EtOH	5 min	0	0	96
	1 M NaOH-EtOH	5 h	b)	quant.	0

a) The ratio of NaOH and EtOH was 1:1 (v/v) and the reaction was carried out at room temperature. b) No efforts to isolate acetic acid were made.

similar type of "acid degradation" to that in acetoacetate synthesis.[13] The conditions and results of the alkaline treatment of **9a—d** are summarized in Table 4. Table 4 implies that the reaction rate of the C–C bond cleavage is increased by an electron-withdrawing group substituted at the *p*-position of the benzoyl group and retarded by an electron-donating group. Although a numerous examples have appeared of C–C bond cleavage reactions in acetoacetate synthesis, the present type of fragmentation has not been reported in the chemistry of β-oxo phosphonates to our knowledge. This is substantially because alkoxycarbonyl groups in acetoacetates can stabilize α-carbanions more effectively than dialkoxyphosphoryl groups so that the C–C bond cleavage of acetoacetate derivatives takes place easily.

In order to study the effect of α-substituents of phosphonates in the C–C bond cleavage reaction, the following three compounds were treated with alkali: As a consequence, α-unsubstituted benzoylmethylphosphonate (**12**), α-monoalkylated and dialkylated benzoylmethylphosphonates (**13**) and (**14**) were found to

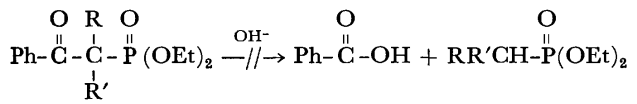

12: R=R′=H
13: R=H, R′=CH_3
14: R=R′=CH_3

be quite stable under the alkaline conditions where the fission of the C–C bond of **9** took place. The facile cleavage of the C–C bond of **9** might be due to both ethoxy and phenyl substituents which could stabilize the α-carbanion (**15**) of **8** and hence assist the fission of the C–C linkage at the stage of the transition state.

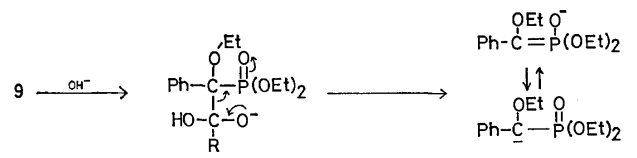

15

Conclusion. It is noted that the α-carbanion of diethyl α-(trimethylsilyloxy)benzylphosphonate can serve as the benzyl anion equivalent when it was allowed to react with acylating agents followed by the successive alkaline treatment. The α-hydroxy ketone synthesis has proved to involve a phosphoryl rearrangement where the phosphoryl group was eliminated as diethyl phosphate. This is in contrast to the unsymmetrical ketone synthesis from the same carbanion where the phosphoryl group was removed as diethyl phosphonate.

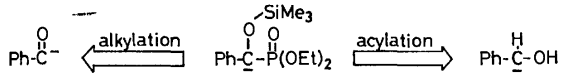

In summary, the compounds having both benzoyl and diethoxyphosphoryl groups on a quarternary carbon undergo C–C bond cleavage reactions with alkali, while the P–C bond cleavage occurs especially when a hydroxyl group is substituted on the quarternary carbon. The ease of the former cleavage reaction depended on the substituents on the quarternary carbon.

Experimental

Melting points and boiling points were uncorrected. IR spectra were recorded on a Hitachi 124 spectrophotometer. ^1H NMR spectra were recorded on a Hitachi R-24B spectrometer. Tetrahydrofuran (THF) was purified by distillation from NaOH pellets followed by redistillation from sodium ribbon and used finally after distillation from benzophenone ketyl. All lithiation and acylation reactions were carried out under argon atmosphere. Lithium diisopropylamide (LDA) was prepared by treatment of diisopropylamine with one equivalent of butyllithium (1.8 M solution in hexane) in THF at −78 °C for 30 min under argon atmosphere.

*General Procedure for Acylation of Lithiated Diethyl α-Trimethylsilyloxybenzylphosphonate (**1**).* To a cooled solution (−78 °C) of LDA (3.3 mmol) in THF (10 ml) was added dropwise diethyl α-trimethylsilyloxybenzylphosphonate (**1**) (928 mg, 3.0 mmol). The mixture was stirred for 0.5 h and then an appropriate acylating agent (3.3 mmol) was added at −78 °C. After being stirred for 0.5 h, the resulting mixture was warmed to room temperature and poured into a mixture of 1 M NH_4Cl (20 ml) and CH_2Cl_2 (20 ml) with vigorous stirring. The organic layer and further extracts with CH_2Cl_2 (3×20 ml) were combined, dried over Na_2SO_4, and evaporated *in vacuo*. The residual oil was chromatographed on silica gel with hexane–ether to afford the corresponding **2**.

*Diethyl α-Trimethylsilyloxy-α-benzoylbenzylphosphonate (**2a**).* The structure of this compound was confirmed by direct comparison with an authentic sample prepared previously.[14]

*Diethyl α-Trimethylsilyloxy-α-(4-chlorobenzoyl)benzylphosphonate (**2b**).* Mp 49—52 °C; NMR (CCl_4) δ 0.12(9H, s, Me_3Si), 1.20(3H, t, $J_{H-H}=J_{H-P}=7$ Hz, one of CH_3C–O), 1.24(3H, t, $J_{H-H}=J_{H-P}=7$ Hz, one of CH_3C–O), 3.76—4.42(4H, m, CH_2O), 7.15(2H, d, $J_{H-H}=8.5$ Hz, ArH), 7.25(3H, m, ArH), 7.52(2H, m, ArH), 7.72(2H, d, $J_{H-H}=8.5$ Hz, ArH).

Found: C, 55.68; H, 6.12%. Calcd for $C_{21}H_{28}O_5ClPSi$: C, 55.44; H, 6.20%.

*Diethyl α-Trimethylsilyloxy-α-(4-methoxybenzoyl)benzylphosphonate (**2c**).* Mp 92—98 °C; IR(NaCl) 968, 1027, 1055, 1146, 1192, 1255 (νP=O), 1320, 1516, 1579, 1604, 1672 (C=O), 2800, 2900, and 3065 cm^{-1}; NMR(CCl_4) δ 0.14(9H, s, Me_3Si), 1.19(3H, t, $J_{H-H}=J_{H-P}=7$ Hz, one of CH_3C–O), 1.23(3H, t, $J_{H-H}=J_{H-P}=7$ Hz, one of CH_3C–O), 3.68(3H, s, CH_3O), 4.02(4H, m, CH_2O), 6.67(2H, d, $J_{H-H}=10$ Hz, ArH), 7.25(3H, m, ArH), 7.58(2H, m, ArH), 7.78(2H, d, $J_{H-H}=10$ Hz, ArH).

Found: C, 59.09; H, 6.85%. Calcd for $C_{22}H_{31}O_6PSi$: C, 58.65; H, 6.94%.

*Diethyl α-Trimethylsilyloxy-α-acetylbenzylphosphonate (**2d**).* Oily substance: NMR(CCl_4) δ 0.20(9H, s, Me_3Si), 1.16 (3H, t, $J_{H-H}=J_{H-P}=7$ Hz, one of CH_3C–O), 1.25(3H, t, $J_{H-H}=J_{H-P}=7$ Hz, one of CH_3C–O), 2.22(3H, s, $CH_3C(O)$), 3.73—4.32(4H, m, CH_2O), 7.30(3H, m, ArH), 7.65(2H, m, ArH).

Found: C, 53.65; H, 7.81%. Calcd for $C_{16}H_{27}O_5PSi$: C, 53.61; H, 7.59%.

*Diethyl 1-Trimethylsilyloxy-3-methyl-2-oxo-1-phenylbutylphosphonate (**2e**).* Oily substance: NMR(CCl_4) δ 0.20(9H, s, Me_3Si), 0.70(3H, d, $J_{H-H}=7$ Hz, one of $(CH_3)_2C$), 0.99 (3H, d, $J_{H-H}=7$ Hz, one of $(CH_3)_2C$), 1.16(3H, t, $J_{H-H}=$

7 Hz, one of CH_3C–O), 1.28(3H, t, J_{H-H}=7 Hz, one of CH_3C–O), 3.42(1H, m, CH), 3.70—4.33(4H, m, CH_2O), 7.25(3H, m, ArH), 7.70(2H, m, ArH).

Found: C, 55.96; H, 8.21%. Calcd for $C_{18}H_{31}O_5PSi$: C, 55.94; 8.09%.

*Diethyl 1-Trimethylsilyloxy-2-oxo-1-phenylpentylphosphonate (**2f**).* Oily substance: NMR(CCl_4) δ 0.20(9H, s, Me_3Si), 0.80(3H, t, J_{H-H}=7 Hz, CH_3C), 1.14(3H, t, J_{H-H}=7 Hz, one of CH_3C–O), 1.24(3H, J_{H-H}=7 Hz, one of CH_3C–O), 1.50(2H, m, $CH_2CC(O)$), 2.57(2H, m, $CH_2C(O)$), 3.70—4.30(4H, m, CH_2O), 7.25(3H, m, ArH), 7.61(2H, m, ArH).

Found: C, 55.45; H, 7.92%. Calcd for $C_{18}H_{31}O_5PSi$: C, 55.94; H, 8.09%.

*Conversion of Acylated Compounds (**2**) into Acyloins (**4** and **5**) under Alkaline Conditions.* An appropriate acylated compound **2** was dissolved in ethanol (20 ml) at room temperature. To the solution was added 1 M sodium hydroxide (20 ml). The resulting solution was stirred at room temperature until **2** had disappeared and then poured into a mixture of 1 M NH_4Cl (20 ml) and CH_2Cl_2 (20 ml) with stirring. The organic layer was collected, combined with further extracts with CH_2Cl_2 (3×20 ml), dried over Na_2SO_4, and evaporated to dryness. The residual oil was chromatographed on silica gel with hexane–ether to afford the corresponding **4** and **5** as listed Table 2.

*Diethyl α-Benzoyl-α-hydroxybenzylphosphonate (**6**).* To a solution of **2a** (1.846 g, 4.39 mmol) in methanol–water (1:1, v/v, 30 ml) was added a catalytic amount of *p*-toluenesulfonic acid monohydrate (50 mg). The solution was refluxed for 2 h and diluted with water (30 ml) after cooling. The aqueous solution was extracted with CH_2Cl_2 (4×30 ml) and the organic layers were combined, dried over Na_2SO_4, and evaporated *in vacuo* to dryness. The residue was chromatographed on silica gel with hexane–ether to afford **6** (1.014 g, 66%): Mp 76—78 °C; NMR($CDCl_3$) δ 1.15(3H, t, J_{H-H}=J_{H-P}=7 Hz, one of CH_3C–O), 1.27(3H, t, J_{H-H}=J_{H-P}=7 Hz, one of CH_3C–O), 3.67—4.40(6H, m, CH_2O and CH_2Cl), 3.85(1H, s, OH), 7.27(3H, m, ArH), 7.48 (2H, m, ArH).

Found: C, 61.17; H, 6.29%. Calcd for $C_{18}H_{21}O_5P\cdot 1/4H_2O$: C, 61.27; H, 6.14%.

*Diethyl α-Ethoxybenzylphosphonate (**8**).*[15] Diethyl phosphonate (7.95 g, 57.6 mmol) was added dropwise to sodium (1.50 g, 65.2 mmol) in dry ether (25 ml) at 10 °C. After evolution of hydrogen gas ceased, the mixture was refluxed for an additional 5 h and cooled in an ice bath to 0 °C. To the cooled solution was added dropwise α-chlorobenzyl ethyl ether (10.2 g, 59.8 mmol) and the mixture was stirred at room temperature for 1 h. The resulting solution was poured into a mixture of 1 M NH_4Cl (30 ml) and CH_2Cl_2 (30 ml). The organic phase was collected and the aqueous layer was further extracted with CH_2Cl_2 (3×30 ml). The extracts were combined, dried over Na_2SO_4, evaporated *in vacuo*, and chromatographed on silica gel with hexane–ether to afford **8** (10.7 g, 68%): Bp 121—136 °C/0.49—0.53 mmHg; IR(NaCl) 960, 1023, 1050, 1094, 1160, 1254 (νP=O), 1388, 1450, 1490, 2900, and 2960 cm^{-1}; NMR (CCl_4) δ 1.14(3H, t, J_{H-H}=J_{H-P}=7 Hz, one of CH_3C–O), 3.46(2H, q, J_{H-H}=7 Hz, CH_2O–C), 3.67—4.21(4H, m, CH_2O–P), 4.45(1H, d, J_{H-P}=15.5 Hz, CH), 7.27(5H, m, ArH).

Found: C, 57.16; H, 7.99%. Calcd for $C_{13}H_{21}O_4P$: C, 57.35; H, 7.7%.

*General Procedure for Acylation of Diethyl α-Ethoxybenzylphosphonate (**8**).* To a cooled (−78 °C) solution of LDA (8.8 mmol) in dry THF (20 ml) was added **8** (2.18 g, 8 mmol). After stirring at −78 °C for 0.5 h, an appropriate acyl chloride (9.6 mmol) was added dropwise to the mixture. The usual work-up described in the case of acylation of **1** afforded the corresponding **9**.

*Diethyl α-Ethoxy-α-benzoylbenzylphosphonate (**9a**).* Oily substance: IR(NaCl) 965, 1045, 1100, 1162, 1182, 1240 (νP=O), 1260, 1392, 1448, 1485, 1597, 1680, 2915, 2970, and 3020 cm^{-1}; NMR(CCl_4) δ 1.07(3H, t, J_{H-H}=7 Hz, CH_3C–O–C), 1.22(3H, t, J_{H-H}=J_{H-P}=7 Hz, one of CH_3C–O), 1.26(3H, t, J_{H-H}=J_{H-P}=7 Hz, one of CH_3C–O), 3.05—3.65(1H, m, one of CH_2–O–C), 3.72—4.45(5H, m, one of CH_2–O–C and CH_2O–P), 7.25(5H, m, ArH), 7.25(3H, m, ArH), 7.67—7.90(2H, m, ArH).

Found: C, 63.48; H, 6.83%. Calcd for $C_{20}H_{24}O_5ClP$: C, 63.82; H, 6.70%.

*Diethyl α-Ethoxy-α-(4-chlorobenzoyl)benzylphosphonate (**9b**).* Oily substance: NMR(CCl_4) δ 0.98—1.40(9H, m, CH_3), 3.06—4.58(6H, m, CH_2), 7.05—7.60(5H, m, ArH), 7.18 (2H, d, J_{H-H}=9 Hz, ArH), 7.75(2H, d, J_{H-H}=9 Hz, ArH).

Found: C, 58.36; H, 6.17; Cl, 9.06%. Calcd for $C_{20}H_{24}O_5ClP$: C, 58.47; H, 5.89; Cl, 8.63%.

*Diethyl α-Ethoxy-α-(4-methoxybenzoyl)benzylphosphonate (**9c**).* Oily substance: NMR(CCl_4) δ 0.99—1.04(9H, m, CH_3), 3.10—4.48(6H, m, CH_2), 3.75(3H, s, CH_3O), 6.65(2H, d, J_{H-H}=9 Hz, ArH), 7.00—7.57(5H, m, ArH), 7.87(2H, d, J_{H-H}=9 Hz, ArH).

Found: C, 61.88; H, 6.73%. Calcd for $C_{21}H_{27}O_6P$: C, 62.06; H, 6.70%.

*Diethyl α-Ethoxy-α-acetylbenzylphosphonate (**9d**).* Oily substance: NMR(CCl_4) δ 1.07—1.63(9H, m, CH_3), 2.01 (3H, s, $CH_3C(O)$), 3.23—4.30(6H, m, CH_2), 7.03—7.60 (5H, m, ArH).

Found: C, 57.12; H, 7.32%. Calcd for $C_{15}H_{23}O_5P$: C, 57.32; H, 7.37%.

*Reaction of Diethyl α-Ethoxy-α-acylbenzylphosphonate (**9**) with Alkali.* An appropriate diethyl 1-ethoxy-2-oxobenzylphosphonate (**9**) (2 mmol) was dissolved in ethanol (20 ml) and 20 ml of 1 M NaOH was added at once with stirring. The reaction conditions are summarized in Table 4. After the reaction was complete, the mixture was poured into a mixture of 1 M NH_4Cl (30 ml) and CH_2Cl_2 (30 ml) put in a separatory funnel. The organic phase was collected and the aqueous layer was extracted with CH_2Cl_2 (2×30 ml). The extracts were combined, dried over Na_2SO_4, evaporated *in vacuo*, and chromatographed on silica gel with hexane–ether to afford **8** and/or the starting material **9**. The aqueous layer was acidified to pH 1.0 by concd HCl and then extracted with CH_2Cl_2 (3×20 ml). The extracts were combined and dried over Na_2SO_4. Removal of the solvent gave a carboxylic acid. The structures of the products were confirmed by comparison with authentic samples.

*Preparation of Diethyl 1-Benzoylethylphosphonate (**13**) and Diethyl 1-Benzoyl-1-methylethylphosphonate (**14**).* To a suspension of sodium hydride (50%, 144 mg, 3 mmol) in dry THF (6 ml) was added diethyl benzoylmethylphosphonate (587 mg, 2.3 mmol) at room temperature. After stirring for 18 h, the resulting homogeneous solution was treated with 1 M NH_4Cl (20 ml) and extracted with CH_2Cl_2 (3×20 ml). The extracts were combined, dried over Na_2SO_4, evaporated, and chromatographed on silica gel with benzene–ethyl acetate to afford **13**[16] (260 mg, 42%) and **14** (228 mg, 35%): NMR($CDCl_3$) δ 1.29(6H, t, J_{H-H}=7 Hz, CH_3C–O), 1.68(6H, d, J_{H-P}=17 Hz, CH_3C–P), 4.08(2H, t, J_{H-H}=J_{H-P}=7 Hz, one of CH_2O), 4.19(2H, t, J_{H-H}=J_{H-P}=7

† 1 mmHg≈133.322Pa.

Hz, one of CH_2O), 7.42(3H, m, ArH), 7.97(2H, m, ArH).

Found: C, 59.08; H, 7.43%. Calcd for $C_{14}H_{21}O_4P$: C, 59.15; H, 7.45%.

Stability of ***12***, ***13***, *and* ***14*** *under Alkaline Conditions.* Compound **12**, **13**, or **14** (0.5 mmol) was dissolved in ethanol (5 ml) and 5 ml of 1 M NaOH was added. TLC after 1 h showed that these compounds were stable under these conditions and remained as single spots.

References

1) This Paper participates as Part XVII in the series of Silyl Phosphites. Part XVI: M. Sekine, M. Nakajima, and T. Hata, *J. Org. Chem.*, **46**, 4030 (1981). Part XV: M. Sekine, K. Okimoto, K. Yamada, and T. Hata, *ibid.*, **46**, 2097 (1981).

2) T. Hata, A. Hashizume, M. Nakajima, and M. Sekine, *Tetrahedron Lett.*, **1978**, 363.

3) M. Sekine, M. Nakajima, A. Kume, and T. Hata, *Tetrahedron Lett.*, **1979**, 4475.

4) For comprehensive reviews see D. Seyferth, "New Applications of Organometallic Reagents in Organic Synthesis," Elsevier Scientific Pub. Co., Amsterdam (1976); O. W. Lever, Jr., *Tetrahedron*, **32**, 1943 (1976); D. Seebach, *Angew. Chem. Intern. Ed.*, **18**, 239 (1979).

5) T. Hata, A. Hashizume, M. Nakajima, and M. Sekine, *Chem. Lett.*, **1979**, 519.

6) J. B. Conant and A. A. Cook, *J. Am. Chem. Soc.*, **42**, 830 (1920); J. B. Conant and B. B. Coyne, *ibid.*, **44**, 2530 (1922); J. B. Conant and E. L. Jackson, *ibid.*, **46**, 1003 (1924); J. A. Maynard and J. M. Swan, *Aust. J. Chem.*, **16**, 596 (1963); J. Rebek, F. Gauina, and C. Navarro, *Tetrahedron Lett.*, **1977**, 3021.

7) For a comprehensive review see F. W. Lichtenthaler, *Chem. Rev.*, **61**, 607 (1961).

8) For comprehensive reviews see F. Ramirez, "Organo-Phosphorus Compounds," IUPAC, Butterworths, London (1964), p. 337; F. Ramirez, *Acc. Chem. Rev.*, **1**, 168 (1968); F. Ramirez, *Synthesis*, **1974**, 90.

9) I. J. Borowitz, S. Firstenberg, G. B. Borowitz, and D. Schuessler, *J. Am. Chem. Soc.*, **94**, 1623 (1972); J. Konecny, R. Dousse, and J. Rosales, *Helv. Chim. Acta*, **55**, 3048 (1972); E. M. Gaydou, G. Juono, and R. Freze, *Bull. Soc. Chim. Fr.*, **1973**, 2284; E. M. Gaydou and J. O. Bianchini, *Can. J. Chem.*, **54**, 3626 (1976).

10) Y. Ogata and M. Yamashita, *J. Am. Chem. Soc.*, **82**, 4670 (1970).

11) V. A. Kukhtin, V. S. Abramov, and K. M. Orekhova, *Dokl. Akad. Nauk SSSR*, **128**, 1198 (1959); *Chem. Abstr.*, **54**, 7536 (1960).

12) I. S. Bengelsdorf, *J. Org. Chem.*, **21**, 475 (1956).

13) C. S. Marvel and F. D. Hager, *Org. Synth.*, Coll. Vol. I, 248 (1941); N. L. Drake and R. W. Riemenschneider, *J. Am. Chem. Soc.*, **52**, 5005 (1930).

14) M. Sekine, M. Nakajima, and T. Hata, submitted to *J. Org. Chem.*

15) W. Grell and H. Machleidt, *Justus Liebigs Ann. Chem.*, **699**, 153 (1966).

16) B. A. Arbuzov, V. S. Vinogradova, N. A. Polezhaeva, and A. K. Shamsutdinova, *Izv. Akad. Nauk SSSR, Ser. Khim.*, **1963**, 1380; *Chem. Abstr.*, **59**, 15306 (1963).

Silyl Phosphites. XVIII. Versatile Utility of α-(Trimethylsilyloxy)-alkylphosphonates as Key Intermediates for Transformation of Aldehydes into Several Carbonyl Derivatives[1)]

Mitsuo SEKINE, Masashi NAKAJIMA, Akiko KUME, Akio HASHIZUME, and Tsujiaki HATA*

Department of Life Chemistry, Tokyo Institute of Technology, Nagatsuta, Midori-ku, Yokohama 227

(Received May 28, 1981)

Carbonyl addition compounds of diethyl trimethylsilyl phosphite (DTMSP) with aldehydes were converted, by treatment with lithium diisopropylamide (LDA) followed by the successive alkylation and alkaline hydrolysis, to carbonyl derivatives involving aldehydes, unsymmetrical ketones, β,γ-unsaturated ketones, and carboxylic acids. β-Substituted carboxylic esters and γ-substituted lactones were prepared by use of the carbonyl addition compounds of DTMSP with α,β-unsaturated aldehydes.

Since Corey and Seebach[2)] introduced acyl anion equivalents by use of 1,3-dithianes in 1965, a number of reagents belonging to this category have appeared in the literature and have proved to be useful key intermediates in modern organic synthesis. A few years ago, Seebach advocated the concept of "Umpolung."[3k)] These studies in this field have recently been reviewed.[3)]

In this paper, we wish to report versatile utility of the carbonyl addition products of DTMSP with aldehydes in detail.[4)]

In connection with our study, several related reactions have recently been reported.[5)]

Results and Discussion

It is well known that the carbon-phosphorus bond of dialkyl α-hydroxy phosphonates is readily cleaved under alkaline conditions to give carbonyl compounds and dialkyl phosphonates.[6)] This reaction pattern

$$R^1R^2\overset{OH}{\overset{|}{C}}\text{-P(O)(OR}^3)_2 \xrightarrow{OH^-} R^1\text{-}\overset{O}{\overset{\|}{C}}\text{-}R^2 + \text{H-P(O)(OR}^3)_2$$

led us to study alkylation of the carbonyl addition compounds obtained by the reaction of silyl phosphites with aldehydes, since the formation of unsymmetrical ketones were expected on treatment of the α-alkylated products with acid followed by alkali.

$$R^1\text{-}\overset{OSiMe_3}{\overset{|}{C}}\text{H—P(O)(OR}^3)_2 \xrightarrow{R^2X}$$

1—7

$$R^1\text{-}\overset{OSiMe_3}{\overset{|}{C}}(R^2)\text{—P(O)(OR}^3)_2 \xrightarrow{H^+} \xrightarrow{OH^-} R^1\text{-}\overset{O}{\overset{\|}{C}}\text{-}R^2$$

1: R^1=Ph **5**: R^1=*i*-Pr
2: R^1=H **6**: R^1=*n*-C_7H_{15}
3: R^1=Me **7**: R^1=$PhCH_2$
4: R^1=Et

It was found that metalation of diethyl α-(trimethylsilyloxy)benzylphosphonate (**1**) with LDA in THF proceeded quite easily to afford relatively stable α-carbanion species which reacted with alkyl halides to give the alkylated products (**18—30**) in good yields. However, in the case of addition compounds (**2—4**) of DTMSP with aliphatic aldehydes, the lithiation of **2—4** caused the Wittig rearrangement[7)] (or the anti-Brook rearrangement[8)]) of trimethylsilyl group.

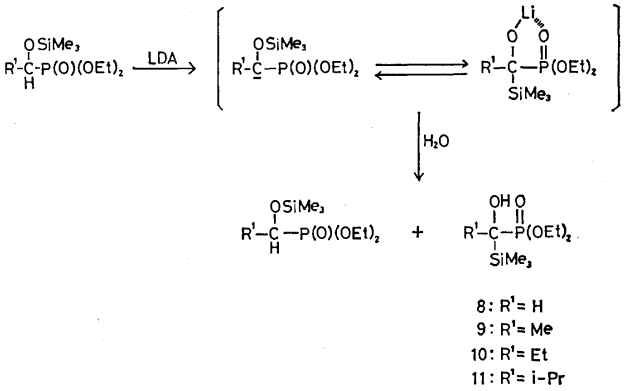

Scheme 1.

The product distributions of **2—4**/**8—10** after quenching with 1 M† NH_4Cl at −78 °C or at room temperature are summarized in Table 1. Table 1 implies that the equilibrium between the carbanion and the oxido ion is affected by both the alkyl substituent and the temperature. The ratio of the carbanion to the oxido ion grows up with a rise in temperature and also with an increase in the bulkiness of the α-substituent. The equilibrium between **4** and **10** in 1,2-dimethoxyethane (DME) is in favor of **10** as compared with THF (see Table 1). The above-mentioned facile Wittig rearrangement of the trimethylsilyl group can be explained as follows; the *O*-lithio derivatives (oxido ion) can be stabilized by an intramolecular chelation with the neighboring group of $P(O)(OEt)_2$. The Wittig rearrangement of this type has been known little.[9)] Only one example has been reported by West where benzyl trimethylsilyl ether underwent the Wittig rearrangement under special conditions using an excess amount of strong lithiating agents such as *t*-butyllithium.[9a)]

Hünig[10a—e)] reported that synthesis of aromatic ketones utilizing the addition compounds of aldehydes with trimethylsilyl cyanide. In connection with the Wittig rearrangement of α-trimethylsilyloxy phosphonates mentioned above, alkylation of 2-(trimethylsilyloxy)propionitrile (**12**) was conducted. However, all attempts to obtain the alkylated products (**13**) were unsuccessful. It is likely that the lithiated intermediate decomposes *via* the Wittig rearrangement to an acylsilane and cyanide ion which in turn react

† 1 M = 1 mol dm^{-3}.

Table 1. Product distributions of α-trimethylsilyloxy phosphonates (**2**—**5**) and α-hydroxy-α-trimethylsilyl phosphonates (**8**—**11**)

Phosphonate		**2**		**3**		**4**				**5**	
Condition for lithiation	solv.	THF		THF		THF	THF	DME		THF	
	time/h	0.5		0.5		0.5	5	1		0.5	
Temp[a]		−78 °C	r.t.	−78 °C	r.t.	−78 °C	r.t.	−78 °C	−78 °C	−78 °C	r.t.
Product (%)	**2**	0	0	**3**	0	22	**4**	45	40	45	22	**5**	85	35
	8	87	78	**9**	91	42	**10**	37	0	31	58	**11**	0	0

a) Temperature at which the lithiation mixture was quenched with 1 M NH_4Cl.

Table 2. Elemental analyses and spectral data of **8**—**10**

Compound	Molecular formula	Found (%)	Calcd (%)	IR(NaCl) $\tilde{\nu}$/cm^{-1}	^{1}H-NMR(CCl_4) δ
8	$C_8H_{21}O_4PSi$	C: 40.12 H: 8.56	39.98 8.81	1035, 1100, 1215(νP=O), 1250, 1370, 1392, 1445, 2890, 2970, 3290(OH)	0.12(9H, s, Me_3Si), 1.37(6H, t, J=7 Hz, CH_3), 3.55(1H, dd, J=6 Hz, J=14 Hz, CHP), 3.80—4.38(4H, m, CH_2-O), 5.10 (1H, d, J=6 Hz, OH)
9	$C_9H_{23}O_4PSi$	C: 42.91 H: 9.53	42.50 9.11	1030, 1055, 1104, 1170, 1222(νP=O), 1252, 1370, 1394, 1448, 2890, 2965, 3280(OH)	0.11(9H, s, Me_3Si), 1.31(6H, t, J=7 Hz, CH_3), 1.39(3H, d, J=19.2 Hz, CH_3CP), 3.80—4.38(4H, m, CH_2-O), 4.38(1H, br. OH)
10	$C_{10}H_{25}O_4PSi$	C: 44.51 H: 9.56	44.76 9.39	1027, 1057, 1228(νP=O), 1248, 1380, 1442, 2910, 2966, 3290(OH)	0.11(9H, s, Me_3Si), 1.01(3H, t, J=7 Hz, CH_3), 1.29(6H, t, J=7 Hz, CH_3), 1.30—2.23(2H, m, CH_2C), 3.80—4.43(5H, m, CH_2-O and OH)

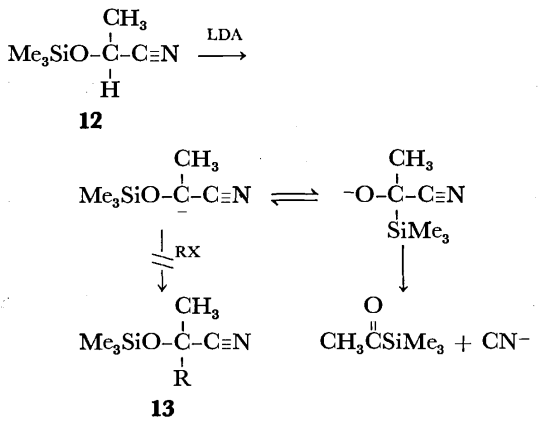

12

13

to give a complex mixture. In this respect, the utility of α-trimethylsilyloxy phosphonates should be emphasized since α-oxido phosphonates do not decompose owing to the stable chelation as shown in Scheme 1 and exist in equilibrium with the reactive carbanion species so that the alkylation proceeds under certain conditions. In this sense, it is interesting that Stork[11] and other groups[12—14] reported the usefulness of anions of protected cyanohydrins as acyl carbanion equivalents which were also stabilized through intramolecular chelations.

In order to avoid the Wittig rearrangement of α-trimethylsilyloxy phosphonates, we attempted the preparation of diphenyl α-trimethylsilyloxy phosphonates (**14**) substituted by an electron-withdrawing group such as $P(O)(OPh)_2$ group in place of diethoxyphosphinyl group. However, diphenyl trimethylsilyl phosphite (**15**) could not be prepared as a pure material. We failed also to prepare the corresponding carbonyl addition compound (**14**) by the *in situ* reaction of diphenyl phosphonate with propionaldehyde in the presence of sodium followed by trimethylsilylation. On the other hand, trimethylsilyl diphenylphosphinite (**16**) could be prepared according to the reported procedure.[15] The phosphinite (**16**) underwent facile addition reaction with propionaldehyde to afford the corresponding adduct (**17**). However, this adduct was

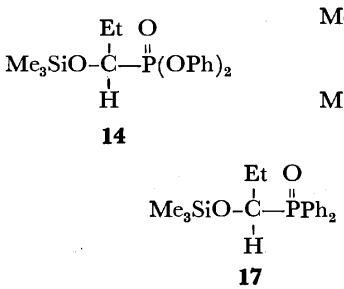

14

$Me_3SiOP(OPh)_2$

15

$Me_3SiOPPh_2$

16

17

found to be rather unstable compared with **4**. During the isolation of **17** by means of silica gel column chromatography, its decomposition to α-hydroxypropylphosphinite was observed to a considerable extent. Moreover, the lithiation of **17** led to a complex mixture.

From the above results, we finally chose the diethyl esters **1**—**7** as the precursors of acyl anion equivalents for transformation of aldehydes to ketones. The alkylation of **1** was satisfactory and a variety of alkyl halides could be employed. Since Table 1 suggested that at higher temperatures the equilibrium between the α-carbanion and the α-oxido ion was in favor of the former, the alkylation of **2**—**6** was carried out by

Table 3. Alkylation of α-trimethylsilyloxy phosphonates (**1**—**7**)

Phospho-nate	Conditions for lithiation Solvent	Time/h	LDA(equiv.)	Conditions for alkylation RX (equiv.)	Temp/°C	Time/h	Product	Compd No.	Yield/%
1	THF	0.5	(1.15)	MeI (1.15)	−78	0.5	Me-C(OSiMe$_3$)(Ph)-P(O)(OEt)$_2$	**18**	90
1	THF	0.5	(1.15)	EtI (1.2)	−78	0.7	Et-C(OSiMe$_3$)(Ph)-P(O)(OEt)$_2$	**19**	87
1	THF	0.5	(1.15)	*n*-PrI (1.25)	−78	1.3	*n*-Pr-C(OSiMe$_3$)(Ph)-P(O)(OEt)$_2$	**20**	81
1	THF	0.5	(1.15)	*n*-BuI (1.3)	−78	0.8	*n*-Bu-C(OSiMe$_3$)(Ph)-P(O)(OEt)$_2$	**21**	84
1	THF	0.5	(1.15)	*i*-PrI (1.35)	−78→r.t.	24	*i*-Pr-C(OSiMe$_3$)(Ph)-P(O)(OEt)$_2$	**22**	80
1	THF	0.5	(1.15)	$PhCH_2Br$ (1.15)	−78	0.5	Ph-C(OSiMe$_3$)(Ph)-P(O)(OEt)$_2$	**23**	85
1	THF	0.5	(1.1)	$PhCH_2CH_2Br$ (1.15)	−78→r.t.	5	Ph-C(OSiMe$_3$)(Ph)-P(O)(OEt)$_2$	**24**	67
1	THF	0.5	(1.1)	Br (1.25)	−78	1.3	C(OSiMe$_3$)(Ph)-P(O)(OEt)$_2$	**25**	88
1	THF	0.5	(1.2)	Br (1.25)	−78	0.7	C(OSiMe$_3$)(Ph)-P(O)(OEt)$_2$	**26**	67
1	THF	0.5	(1.2)	Br (1.25)	−78	1.0	C(OSiMe$_3$)(Ph)-P(O)(OEt)$_2$	**27**	68
1	THF	0.5	(1.1)	Me-S-S-Me (1.05)	−78	0.8	CH_3S-C(OSiMe$_3$)(Ph)-P(O)(OEt)$_2$	**28**	69
1	THF	0.5	(1.1)	Ph-S-S-Ph (1.2)	−78	0.5	PhS-C(OSiMe$_3$)(Ph)-P(O)(OEt)$_2$	**29**	81
1	THF	0.5	(1.1)	Me_3SiCl (1.2)	−78→r.t.	20	Me_3Si-C(OSiMe$_3$)(Ph)-P(O)(OEt)$_2$	**30**	71
2	THF	0.5	(1.05)	MeI (1.05)	−78→r.t.	12	**3**		86
2	THF	0.5	(1.1)	EtI (1.2)	−78→r.t.	1.0	**4**		77
2	THF	0.7	(1.1)	$PhCH_2Br$ (1.15)	−78→r.t.	12	Ph-C(OSiMe$_3$)-P(O)(OEt)$_2$	**31**	80

Table 3. (Continued)

Phosphonate	Conditions for lithiation Solvent	Time/h	LDA(equiv.)	Conditions for alkylation RX (equiv.)	Temp/°C	Time/h	Product	Compd No.	Yield/%
2	THF	0.5	(1.1)	$PhCH_2CH_2I$ (1.2)	−78→r.t.	3	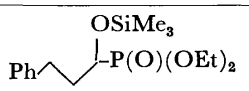	**32**	48
2	THF	0.8	(1.1)	*n*-BuI (1.15)	−78→r.t.	4	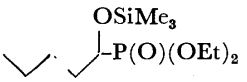	**33**	41
3	THF	0.5	(1.1)	MeI (1.2)	−78→r.t.	3	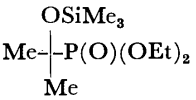	**34**	95
3	THF	0.5	(1.15)	$PhCH_2Br$ (1.15)	−78→r.t.	12	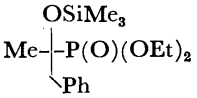	**35**	76
3	THF	0.7	(1.15)	$PhCH_2CH_2Br$ (1.15)	−78→r.t.	1.0	—		0
4	THF	5	(1.2)	MeI (1.2)	−78→r.t.	1.5	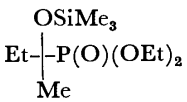	**36**	84
4	THF	5	(1.15)	$PhCH_2Br$ (1.15)	−78→r.t.	3	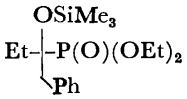	**37**	58
5	THF	15	(1.2)	MeI (1.2)	−78→r.t.	3	74% of **5** was recovered		0
5	DME	1	(1.1)	MeI (1.1)	−78→r.t.	1.5	63% of **5** was recovered		0
6	DME	1	(1.0)	MeI (1.05)	−78→r.t.	1.5	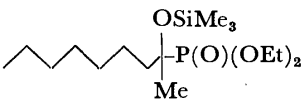	**38**	86
6	DME	1	(1.1)	$PhCH_2Br$ (1.1)	−78→r.t.	1.3	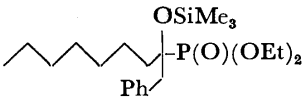	**39**	29
6	DME	1	(1.1)	*n*-BuI (1.1)	−78→r.t.	2.5	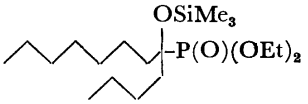	**40**	13
7	THF	0.5	(1.15)	MeI (1.2)	−78→r.t.	0.8	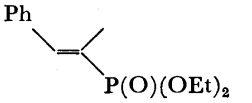	**41**	57
7	THF	0.5	(1.1)	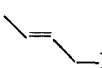 (1.05)	−78→r.t.	4	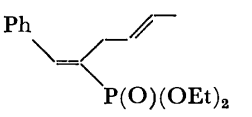	**42**	19
7	THF	1	(1.2)	H_2O (3.7)	−78	3 min	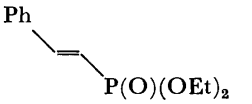	**43**	41

TABLE 4. ELEMENTAL ANALYSES AND ^{1}H-NMR DATA OF α-ALKYLATED PHOSPHONATES (**18**—**43**)

Compound	Molecular formula	Found (%)	Calcd (%)	^{1}H-NMR δ
18	$C_{15}H_{27}O_4PSi$[25]			($CDCl_3$) 0.27(9H, s, Me_3Si), 1.30(3H, t, J=7 Hz, CH_3), 1.38 (3H, t, J=7 Hz, CH_3), 2.05(3H, d, J=16 Hz, CH_3CP), 4.10 (4H, m, CH_2-O), 7.40(3H, m, ArH), 7.61(2H, m, ArH)
19	$C_{16}H_{29}O_4PSi$	C: 55.51 H: 8.57	55.79 8.49	(CCl_4) 0.28(9H, s, Me_3Si), 0.72(3H, t, J=7 Hz, CH_3), 1.08 (3H, t, J=7 Hz, CH_3C-O), 1.30(3H, t, J=7 Hz, CH_3C-O), 2.29(2H, m, CH_2CP), 3.29—4.32(4H, m, CH_2OP), 7.17—7.41 (3H, m, ArH), 7.41—7.85(2H, m, ArH)
20	$C_{17}H_{31}O_4PSi$	C: 56.93 H: 8.78	56.96 8.78	($CDCl_3$) 0.27(9H, s, Me_3Si), 0.06—1.47(11H, m, CH_3CH_2 and CH_3C-O), 1.98—2.48(2H, m, CH_2CP), 3.30—4.30(4H, m, CH_2-O), 7.05—7.34(3H, m, ArH), 7.34—7.63(2H, m, ArH)
21	$C_{18}H_{33}O_4PSi$	C: 58.36 H: 9.07	58.03 8.93	($CDCl_3$) 0.27(9H, s, Me_3Si), 0.67—1.50(13H, m, $CH_3CH_2CH_2C$ and CH_3C-O), 2.27(2H, m, CH_2CP), 3.33—4.38(4H, m, CH_2-O), 7.30(3H, m, ArH), 7.98(2H, m, ArH)
22	$C_{17}H_{31}O_4PSi$	C: 56.56 H: 8.72	56.96 8.72	($CDCl_3$) 0.25(9H, s, Me_3Si), 0.77(3H, d, J=7 Hz, CH_3), 0.98 (3H, d, J=7 Hz, CH_3), 0.92(3H, t, J=7 Hz, CH_3C-O), 1.31 (3H, t, J=7 Hz, CH_3), 2.18—2.85(1H, m, CH), 3.00—4.32 (4H, m, CH_2-O), 7.08—7.31(3H, m, CH), 7.31—7.64(2H, m, ArH)
23	$C_{22}H_{33}O_4PSi$	C: 63.15 H: 8.14	62.83 7.91	($CDCl_3$) 0.25(9H, s, Me_3Si), 0.96(3H, t, J=7 Hz, CH_3), 1.18 (3H, t, J=7 Hz, CH_3), 1.83—2.80(4H, m, CH_2CH_2), 3.08—4.25(4H, m, CH_2-O), 6.98(5H, s, ArH), 6.77—7.63(5H, m, ArH)
24	$C_{21}H_{31}O_4PSi$	C: 61.64 H: 7.87	62.04 7.69	($CDCl_3$) 0.19(9H, s, Me_3Si), 1.05(3H, t, J=7 Hz, CH_3), 1.31 (3H, t, J=7 Hz, CH_3), 3.30—4.34(6H, m, CH_2Ph and CH_2-O), 6.90(5H, s, ArH), 6.95—7.29(3H, m, ArH), 7.29—7.62 (2H, m, ArH)
25	$C_{17}H_{29}O_4PSi$	C: 57.00 H: 8.24	57.28 8.20	($CDCl_3$) 0.28(9H, s, Me_3Si), 1.10 and 1.29(3H and 3H, t and t, J=7 Hz, CH_3C-O), 3.08(2H, dd, J=7 Hz, J=7 Hz, CH_2CP), 3.38—4.37(4H, m, CH_2O), 4.86—5.26(2H, m, CH_2=C), 5.28 —5.80(1H, m, C=CH), 7.30(3H, m, ArH), 7.58(2H, m, ArH)
26	$C_{18}H_{31}O_4PSi$	C: 58.84 H: 8.35	58.35 8.43	($CDCl_3$) 0.21(9H, s, Me_3Si), 1.06 and 1.23(3H and 3H, t and t, J=7 Hz, CH_3), 1.50(3H, d, J=5 Hz, CH_3-C=C), 2.95(2H, m, CH_2CP), 3.30—4.27(4H, m, CH_2-O), 4.77—5.63(2H, m, CH=CH), 7.20(3H, m, ArH), 7.47(2H, m, ArH)
27	$C_{24}H_{41}O_4PSi$	C: 63.42 H: 9.01	63.68 9.13	($CDCl_3$) 0.25(9H, s, Me_3Si), 1.10(3H, t, J=7 Hz, CH_3), 1.32 (3H, t, J=7 Hz, CH_3), 1.60(9H, s, CH_3-C=C), 1.95(4H, b, CH_2CH_2), 3.05(2H, dd, J=7 Hz, J=7 Hz, CH_2CP), 3.40—4.40 (4H, m, CH_2-O), 4.98(2H, m, C=CH), 7.28(3H, m, ArH), 7.52 (2H, m, ArH)
28	$C_{15}H_{27}O_4PSSi$	C: 49.36 H: 7.46 S: 8.74	49.70 7.51 8.84	($CDCl_3$) 0.27(9H, s, Me_3Si), 1.15 and 1.27(3H and 3H, t and t, J=7 Hz, CH_3), 2.03(3H, s, CH_3S), 3.60—4.33(4H, m, CH_2-O), 7.13—7.37(3H, m, ArH), 7.50—7.75(2H, m, ArH)
29	$C_{20}H_{29}O_4PSSi$	C: 56.42 H: 7.03 S: 7.72	56.58 6.88 7.55	($CDCl_3$) 0.33(9H, s, Me_3Si), 1.11 and 1.30(3H and 3H, t and t, J=7 Hz, CH_3), 3.47—4.37(4H, m, CH_2-O), 6.99(5H, s, ArH), 6.80—7.70(5H, m, ArH)
30	$C_{17}H_{30}O_4PSi$	C: 52.48 H: 8.40	52.55 8.56	(CCl_4) 0.05(9H, s, Me_3Si), 0.23(9H, s, Me_3Si), 1.05 and 1.36 (3H and 3H, t and t, J=7 Hz, CH_3) 3.36—4.50(4H, m, CH_2-O), 7.10—7.80(5H, m, ArH)
31	$C_{15}H_{27}O_4PSi$[26]			(CCl_4) 0.17(9H, s, Me_3Si), 1.33(6H, t, J=7 Hz, CH_3), 2.37—3.37(2H, m, CH_2CP), 3.73—4.37(5H, m, CH and CH_2-O), 7.17 (5H, s, ArH)
32	$C_{16}H_{29}O_4PSi$	C: 55.72 H: 8.60	55.79 8.49	(CCl_4) 0.15(9H, s, Me_3Si), 1.28(6H, t, J=7 Hz, CH_3), 1.50—2.20(2H, m, CH_2CP), 2.20—3.09(2H, m, CH_2CCP), 3.33—4.32 (5H, m, CH and CH_2-O), 7.10(5H, m, ArH)

Table 4. (Continued)

Compound	Molecular formula	Found (%)	Calcd (%)	^{1}H-NMR δ
33	$C_{12}H_{29}O_4PSi$	C: 48.71 H: 9.82	48.62 9.86	(CCl_4) 0.17(9H, s, Me_3Si), 0.91(3H, t, J=7 Hz, CH_3), 1.28(6H, t, J=7 Hz), CH_3), 1.05—1.90(6H, m, (CH_2),) 3.50—3.88(1H, m, CH), 3.70—4·28(4H, m, CH_2-O)
34	$C_{10}H_{25}O_4PSi$	C: 44.70 H: 9.40	44.76 9.39	(CCl_4) 0.15(9H, s, Me_3Si), 1.30(6H, t, CH_3), 1.37(6H, d, J= 14.5 Hz, CH_3CP), 3.79—4.32(4H, m, CH_2-O)
35	$C_{16}H_{29}O_4PSi$	C: 55.96 H: 8.52	55.79 8.49	(CCl_4) 0.16(9H, s, Me_3Si), 1.18(3H, d, J=14 Hz, CH_3CP), 1.18(6H, t, J=7 Hz, CH_3), 2.74(2H, m, CH_2CP), 3.94(4H, m, CH_2-O), 7.01(5H, s, ArH)
36	$C_{11}H_{27}O_4PSi$[22]			(CCl_4) 0.13(9H, s, Me_3Si), 0.91(3H, J=7.2 Hz, CH_3) 1.30(6H, t, J=7 Hz, CH_3), 1.34(3H, d, J=16 Hz, CH_3CP), 1.40—2.00 (2H, m, CH_2CP), 4.08(4H, m, CH_2-O)
37	$C_{17}H_{31}O_4PSi$	C: 56.47 H: 8.87	56.96 8.72	(CCl_4) 0.12(9H, s, Me_3Si), 0.89(3H, t, J=6.5 Hz, CH_3), 1.05 (3H, t, J=7 Hz, CH_3), 1.12(3H, t, J=7 Hz, CH_3), 1.65(2H, m, CH_2C), 2.80(1H, d, J=12 Hz, one of CH_2Ph), 2.82(1H, d, J=10 Hz, one of CH_2Ph), 3.85(4H, m, CH_2-O), 6.99(5H, s, ArH)
38	$C_{16}H_{37}O_4PSi$	C: 54.07 H: 11.02	54.51 10.58	(CCl_4) 0.19(9H, s, Me_3Si), 0.89(3H, t, J=5.8 Hz, terminal CH_3), 1.10—1.95(21H, m, $(CH_2)_6$ and CH_3 and CH_3CP), 4.00 (4H, m, CH_2-O)
39	$C_{22}H_{41}O_4PSi$	C: 61.33 H: 9.73	61.65 9.64	($CDCl_3$) 0.15(9H, s, Me_3Si), 0.60—1.77(21H, m, CH_3C-O and heptyl), 2.82(2H, d, J=10 Hz, CH_2Ph), 3.83(4H, m, CH_2-O), 6.96(5H, s, ArH)
40	$C_{19}H_{43}O_4PSi$	C: 58.13 H: 11.19	57.83 10.98	(CCl_4) 0.18(9H, s, Me_3Si), 0.70—2.05(30H, m, heptyl and butyl and CH_3C-O), 3.77—4.30(4H, m, CH_2-O)
41	$C_{13}H_{15}O_3P$	C: 61.51 H: 7.72	61.41 7.53	(CCl_4) 1.31(6H, t, J=7 Hz, CH_3), 1.98(3H, dd, J=14.5 Hz, J=1.2 Hz, C=CCH_3), 3.78—4.28(4H, m, CH_2-O), 7.21(5H, s, ArH), 7.28(1H, dd, J=24 Hz, J=1.2 Hz, CH=C)
42	$C_{16}H_{23}O_3P(\frac{1}{4}H_2O)$	C: 64.44 H: 7.90	64.31 7.93	(CCl_4) 1.30(6H, t, J=7 Hz, CH_3), 1.65(3H, m, C-CCH_3), 3.07 (2H, d, J=19 Hz, C=CCH), 3.98(4H, m, CH_2-O), 5.41(2H, m, CH=CH), 7.21(5H, s, ArH), 7.32(1H, d, J=25 Hz, CH=CP)
43	$C_{12}H_{17}O_3P$[27]			(CCl_4) 1.29(6H, t, J=7Hz, CH_3), 4.01(4H, m, CH_2-O), 6.10 (1H, dd, J=17 Hz, J=17 Hz, C=CHP), 7.33(1H, dd, J=22 Hz, J=17 Hz, PhCH=), 7.30(5H, m, ArH)

raising the temperature from −78 °C to room temperature. Consequently, the alkylated products **3**, **4**, and **31**—**40** were obtained in good yields. When the alkylation was performed at −78 °C, the alkylated product was not obtained and the Wittig rearrangement product was recovered. In the case of the alkylation of **7** having a relatively acidic β-proton, (*E*)-1-alkenylphosphonates were obtained as the main products (**41**—**43**). These conditions and results are summarized in Table 3. The conversion of the α-alkylated products into carbonyl compounds is illustrated in the following scheme. Acid treatment of

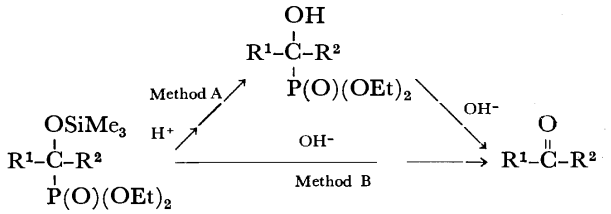

the alkylated products gave quantitatively α-hydroxy phosphonates, which in turn were treated with dilute sodium hydroxide solution to give the carbonyl compounds. The alkylated α-silyloxy phosphonates were converted also directly to ketones by the alkaline treatment as reported in a previous communication.[4a] These results are summarized in Table 5. In the case of the preparation of β,γ-unsaturated ketones, Method A was found to be essential. When Method B was employed, considerable amounts of isomers of α,β-unsaturated ketones were formed. However, the conversion of **31** into aldehyde under the conditions of Method A or Method B led to the aldol condensation product as the main product. It is generally recognized that adducts of aldehydes with nucleophiles, such as alcohols, sodium sulfite, and hydrogen cyanide, are more stable than those of ketones under neutral or alkaline conditions.[16] The aldol condensation product seems to be formed predominantly owing to the relatively slow cleavage of P–C bond in the α-hydroxy phosphonates initially formed by alkali. In fact, when **31** was treated with 0.5 M NaOH–EtOH (1:1, v/v)

TABLE 5. CONVERSION OF THE α-ALKYLATED α-TRIMETHYLSILYLOXY PHOSPHONATES TO CARBONYL COMPOUNDS

Phosphonate	Method	(time)	Product		Yield/%
18	A	{H+: 30 min, OH−: 20 min}		**44**	90
	B	20 min			86
19	A	{H+: 90 min, OH−: 5 min}		**45**	90
20	A	{H+: 3.5 h, OH−: 10 min}	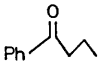	**46**	81
	B	20 min			88
21	A	{H+: 40 min, OH−: 60 min}	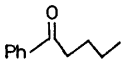	**47**	94
20	B	2.5 h		**48**	83
23	B	30 min	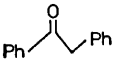	**49**	95
24	A	{H+: 90 min, OH−: 10 min}	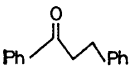	**50**	93
	B	30 min			94
25	A	{H+: 4 h, OH−: a)}	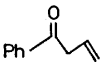	**1**	36
26	A	{H+: 5 h, OH−: 30 s}	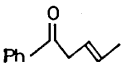	**52**	96
27	A	{H+: 60 min, OH−: 30 s}	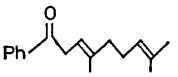	**53**	80
35	B	30 min	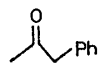	**54**	82
37	A	{H+: 30 min, OH−: 4 min}	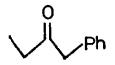	**55**	75
38	B	30 min		**56**	85
28	B	15 min	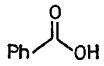	**57**	69
29	B	30 min	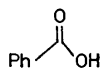	**58**	90
30	B	45 min		**59**	91

a) See Experimental.

and the reaction was quenched quickly after 1 min, diethyl 1-hydroxy-3-phenylpropylphosphonate (**60**) was isolated in quantitative yield. When **60** was further treated with the same alkali, the aldol condensation product was obtained as the main product. Therefore, our efforts were focussed on the P–C bond cleavage of **31** under milder conditions where the aldol condensation could be avoided. Thus, various conditions were tested in order to obtain aldehydes selectively. Finally, it was found that 3-phenylpropionaldehyde (**61**) could be obtained from **60** in 71% yield by employing the conditions of dilute sodium hydrogencarbonate in aqueous methanol under reflux for 2 h. In a similar manner, octanal (**62**) was obtained in 80% yield from **5**.

Synthesis of β-Alkylated Esters and Lactones. In order to extend the utility of 1:1 carbonyl adducts of DTMSP, we examined alkylation of 1,2-addition products obtained from DTMSP and α,β-unsaturated aldehydes.

The reaction of DTMSP with α,β-unsaturated aldehydes provided predominantly 1,2-carbonyl addition compounds (**64**—**66**).[4a] In the case of acrylaldehyde, 1,4-addition product (**67**), however, was formed along with the 1,2-carbonyl adduct (**63**). These products could not be separated by distillation or column chromatography. In order to separate **63** from the mixture, it was first treated with acid for removal of the trimethylsilyl group and the resulting α-hydroxy phosphonate (**68**) was obtained by column chromatography. This material was further trimethylsilylated by treatment with *N,N*-diethyltrimethylsilylamine to afford **63**.

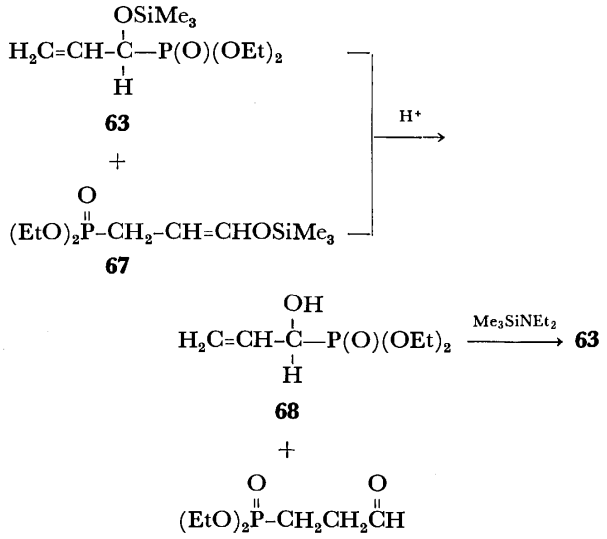

It was found that the alkylation of these 1,2-addition products occurred at the γ-position to give (*E*)-1-(trimethylsilyloxy)-1-alkenylphosphonates (**69**), while deuteration of the lithio derivatives gave α-deuterated 1-trimethylsilyloxy phosphonates exclusively. These results are of interest since Hünig[10e] reported that the 1,2-adducts of trimethylsilyl cyanide with unsaturated aldehydes were transformed to α-alkylated products exclusively on treatment with LDA followed by alkyl halides. Stork[11] also described that a similar alkylation of protected cyanohydrins of α,β-unsaturated aldehydes resulted in the exclusive for-

Table 6. Preparation of β-substituted esters (**71**—**84**)

Phosphonate	Conditions for alkylation R′X(eqiuv.)[a]	Conditions for esterification R″OH	Product	Compd No.	Yield/%
66	MeI (1.15) −78 °C, 1 h	EtOH 78 °C, 1 h	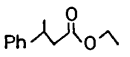	**71**	63
	MeI (5.5) −78 °C→r.t. 3 h	EtOH 78 °C, 1 h			76
	n-PrI (1.15) −78 °C, 30 min	EtOH 78 °C, 2 h	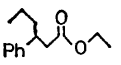	**72**	76
	i-PrI (1.1) −78 °C→r.t. 3 h	EtOH 78 °C, 2.5 h	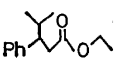	**73**	84
	$PhCH_2Br$ (1.15) −78 °C, 30 min	EtOH 78 °C, 2.5 h	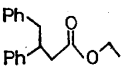	**74**	89
	allyl-Br (1.1) −78 °C→r.t. 40 min	EtOH 78 °C, 2.5 h	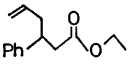	**75**	81
	$PhCH_2CH_2Br$ (1.1) −78 °C→r.t. 4.5 h	EtOH 78 °C, 2.5 h	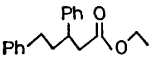	**76**	69
	Me_3SiCl (1.15) −78 °C→r.t. 5 h	EtOH 78 °C, 2 h	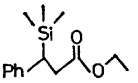	**77**	49
	Me_3SiBr (1.1) −78 °C→r.t. 2 h	EtOH 78 °C, 4 h			52
65	$PhCH_2Br$ (1.2) −78 °C, 40 min	EtOH 78 °C, 2.5 h	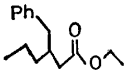	**78**	51
	n-BuI (1.15) −78 °C, 30 min	$PhCH_2CH_2OH$ (5 ml) 80 °C, 3 h	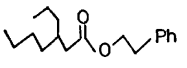	**79**	45
	n-BuI (1.1) −78 °C, 30 min	*n*-BuOH 80 °C, 3 h	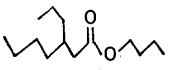	**80**	52
64	$PhCH_2Br$ (1.1) −78 °C, 1 h	EtOH 78 °C, 6 h	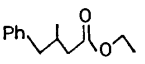	**81**	75
	$PhCH_2CH_2Br$ (1.05) −78 °C, 1 h	EtOH 78 °C, 6 h	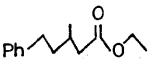	**82**	44
63	$PhCH_2Br$ (1.1) −78 °C, 1 h	EtOH 78 °C, 6 h	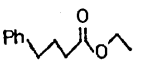	**83**	11
	n-BuI (1.2) −78 °C, 1 h	EtOH 78 °C, 6 h	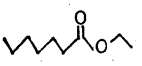	**84**	5

a) The amount of LDA employed was almost the same as that of alkyl halide in each experiment.

TABLE 7. ELEMENTAL ANALYSES AND ^{1}H-NMR DATA OF β-SUBSTITUTED ESTERS (**71**—**84**)

Compound	Molecular formula	Found (%)	Calcd (%)	^{1}H-NMR(CCl_4) δ
71	$C_{12}H_{16}O_2$[28]			1.10(3H, t, J=7 Hz, CH_3), 1.27(3H, d, J=8 Hz, CH_3CPh), 2.45 (2H, d, J=8 Hz, $CH_2(C=O)$), 2.91—3.53(1H, m, CH), 3.97(2H, q, J=7 Hz, CH_2-O), 7.12(5H, s, ArH)
72	$C_{14}H_{20}O_2$	C: 76.75 H: 9.21	76.33 9.15	0.87(3H, t, CH_3), 1.10(3H, t, J=7 Hz, CH_3), 1.00—1.85(4H, m, CH_2CH_2), 2.50(2H, d, J=7.5 Hz, $CH_2(C=O)$), 2.82—3.35(1H, m, CH), 3.95(2H, q, CH_2-O), 7.10(5H, s, ArH)
73	$C_{14}H_{20}O_2$	C: 76.18 H: 9.09	76.33 9.15	0.73 and 0.93(3H and 3H, dd, J=6.5 Hz, $(CH_3)_2C$), 1.00(3H, t, J=7 Hz, CH_3), 1.40—2.20(1H, m, CH), 2.33—3.04(3H, m, CH-$CH_2(C=O)$), 3.87(2H, q, J=7 Hz, CH_2-O), 7.10(5H, s, ArH)
74	$C_{18}H_{20}O_2$	C: 80.52 H: 7.60	80.56 7.51	1.00(3H, t, J=7 Hz, CH_3), 2.50(2H, d, J=6.5 Hz, $CH_2(C=O)$), 2.83(2H, d, J=7.5 Hz, CH_2Ph), 3.10—3.60(1H, m, CH), 3.88 (2H, q, CH_2-O), 7.00(5H, s, ArH), 7.05(5H, s, ArH)
75	$C_{14}H_{18}O_2$	C: 77.19 H: 8.31	77.03 8.31	1.07(3H, *t*, J=7 Hz, CH_3), 2.50(2H, t, J=7 Hz, $C=C$-CH_2), 2.50 (2H, d, J=6 Hz, $CH_2(C=O)$), 2.80—3.40(1H, m, CH), 3.93(2H, q, J=7 Hz, CH_2-O), 4.70—5.10(2H, m, $CH_2=C$)
76	$C_{19}H_{22}O_2$[29]			1.04(3H, t, J=7 Hz, CH_3), 1.65—2.10(2H, m, $PhCCH_2$), 2.23—2.58(4H, m, $PhCH_2$ and $CH_2(C=O)$), 2.80—3.40(1H, m, CH), 3.90(2H, q, J=7 Hz, CH_2-O), 7.03(5H, s, ArH), 7.13(5H, s, ArH)
77	$C_{14}H_{22}O_2Si$[30]			0.09(9H, s, Me_3Si), 1.16(3H, t, J=7 Hz, CH_3), 2.76(2H, s, CH_2-$(C=O)$), 2.79(1H, b, CH), 4.25(2H, q, J=7 Hz, CH_2-O), 7.09 (5H, m, ArH)
78	$C_{15}H_{22}O_2$	C: 76.58 H: 9.43	76.88 9.46	0.87(3H, t, J=5.5 Hz, CH_3), 1.21(3H, t, J=7 Hz, CH_3C-O), 1.30(4H, b, CH_2CH_2), 2.20(2H, s, $CH_2(C=O)$), 2.21(1H, m, CH), 2.57(2H, m, $PhCH_2$), 4.03(2H, q, J=7 Hz, CH_2-O), 7.11(5H, s, ArH)[a]
79	$C_{18}H_{28}O_2$	C: 78.50 H: 10.07	78.21 10.21	0.88(6H, m, CH_3), 1.25(10H, m, $(CH_2)_3$ and CH_2CH_2), 1.50—1.10(1H, m, CH), 2.12(2H, d, J=5 Hz, $CH_2(C=O)$), 2.85(2H, t, CH_2Ph), 4.20(2H, t, CH_2-O), 7.15(5H, s, ArH)
80	$C_{14}H_{28}O_2$	C: 73.09 H: 12.14	73.62 12.36	2.15(1H, d, J=5 Hz, one of $CH_2(C=O)$), 2.17(1H, d, J=7 Hz, one of CH_2Ph), 4.03(2H, t, J=6 Hz, CH_2-O)
81	$C_{13}H_{18}O_2$[31]			0.80—1.00(3H, m, CH_3), 1.28(3H, *t*, J=7 Hz, CH_3), 1.87—2.90 (5H, m, $PhCH_2$ and $CH_2(C=O)$ and CH), 4.03(2H, q, J=7 Hz, CH_2-O), 7.10(5H, s, ArH)
82	$C_{14}H_{20}O_2$[32]			0.97(3H, d, J=6 Hz, CH_3), 1.18(3H, t, J=7 Hz, CH_3), 1.36—1.83(2H, m, $PhCCH_2$), 1.83—2.28(3H, m, $CH_2(C=O)$ and CH), 2.56(2H, t, J=7.5 Hz, $PhCH_2$)
83	$C_{12}H_{16}O_2$[33]			1.25(3H, t, J=7 Hz, CH_3), 1.70—2.43(4H, m, $CH_2CH_2(C=O)$), 2.65(2H, m, $PhCH_2$, J=7 Hz), 4.07(2H, q, CH_2-O), 7.15(5H, s, ArH)
84	$C_9H_{18}O_2$[34]			0.53—1.43(14H, m, pentyl and CH_3), 2.20(2H, dd, J=9.4 Hz, J=8 Hz, $CH_2(CO)$), 4.06(2H, q, CH_2-O)

a) In this case, $CDCl_3$ was used as the solvent.

mation of α-alkylated products. Our results are in contrast to their two reports. The results of the highly regioselective γ-alkylation in the present reaction might be due to steric hindrance of the neighboring phosphoryl group. The (*E*)-1-(trimethylsilyloxy)-1-alkenylphosphonate **69** were sensitive toward moisture during work-up and tend to decompose gradually into acylphosphonates (**70**). Acylphosphonates are known to be labile toward moisture and decompose into carboxylic acids and dialkyl phosphonates.[17] It has been reported that reactions of acylphosphonates with nucleophiles such as alcohols,[18] amines,[18c,19] and carbanions[20] gave acylated products. Because of the instability of the alkylated products, the reaction mixture was further treated with alcohols in the presence of *p*-toluenesulfonic acid, whereupon the alkylated products were successfully converted *via* acylphosphonates to β-alkyl-substituted esters (**71**—**84**). These results

were summarized in Table 6.

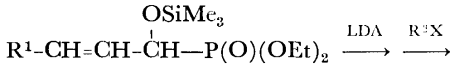

63—66

63: $R^1=H$ **65**: $R^1=n$-Pr
64: $R^1=Me$ **66**: $R^1=Ph$

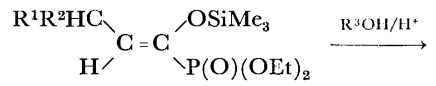

69a: $R^1=Ph$, $R^2=Me$
69b: $R^1=Ph$, $R^2=CH_2Ph$
69c: $R^1=n$-Pr, $R^2=CH_2Ph$

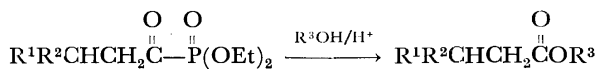

70 **71—84**

In a similar manner, benzoylation of the lithio derivative of **66** followed by treatment with alcohols under alkaline or acidic conditions or with aqueous sodium hydroxide solution gave the products depicted in the following scheme.

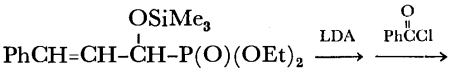

66

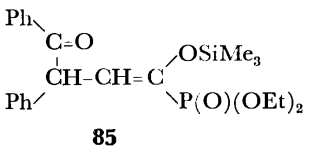

85

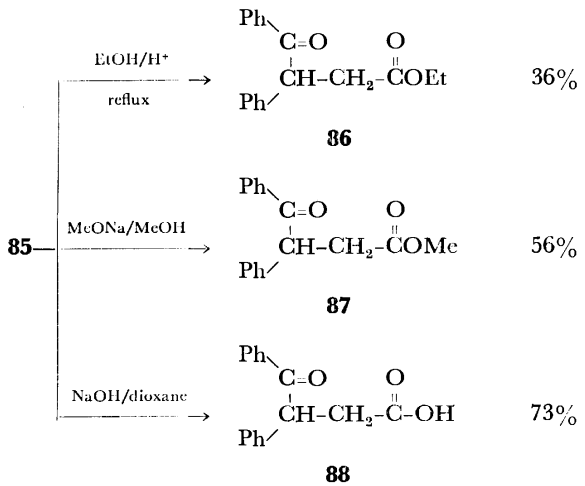

86 **87** **88**

Next, we examined the lactonization in term of intramolecular acylation utilizing the promising feature of acylphosphonate intermediates as acylating species. By treatment of the lithiated derivatives of **64—66** with aldehydes, 4-hydroxy-1-trimethylsilyloxy-1-alkenylphosphonates (**89**) could be expected to be formed. These phosphonates were also expected to be converted by acid treatment into 4-hydroxy-1-oxoalkylphosphonates (**90**), which would be cyclized under such acidic conditions to give lactones. Thus, several lactones (**91—95**) were obtained by one-pot reaction in good yields. These results are summarized in Table 8. Evans has recently reported a similar type of lactonization utilizing 1:1 carbonyl addition products of triethylsilyl *N,N,N′,N′*-tetramethylphosphorodiamidite with α,β-unsaturated aldehydes in which tetrabutylammonium fluoride was used for the removal of the trimethylsilyl group and for the cyclization.[21]

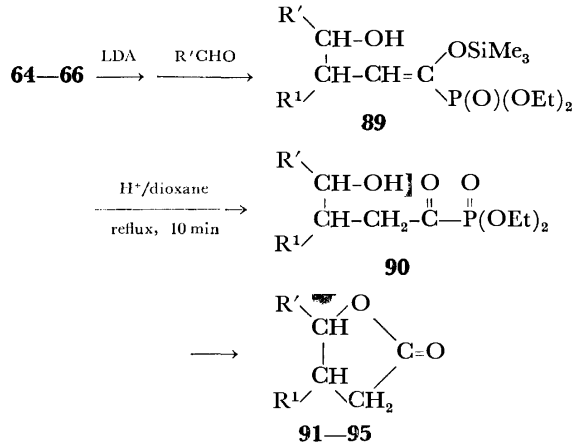

89 **90** **91—95**

In conclusion, it is noted that 1:1 carbonyl adducts of aldehydes with DTMSP could be used widely as the precursors of acyl anion equivalents and homoenolates.

Experimental

NMR spectra were measured at 60 MHz on a Hitachi R 24-B spectrometer. IR spectra were recorded on a Hitachi Model EPI-G3 spectrophotometer.

Materials. Tetrahydrofuran (THF) and 1,2-dimethoxyethane (DME) were distilled over potassium hydroxide after reflux for 6 h, redistilled over sodium wire after reflux for 6 h, and finally purified by distillation from benzophenone ketyl. Alkyl halides, acyl halides, carbonyl compounds, and other reagents were purified by distillation or recrystallization before use. Diethyl trimethylsilyl phosphite (DTMSP) was prepared according to the method previously reported.[1] Butyllithium (2—3 M) in hexane, kindly gifted from Sankyo Kasei Co., was used after titration.

All lithiation, alkylation, and acylation reactions were carried out under argon atmosphere.

Diethyl α-(Trimethylsilyloxy)benzylphosphonate (1).
Method A: To a solution of DTMSP (6.18 g, 29.4 mmol) in dry benzene (5 ml) was added dropwise benzaldehyde (3.21 g, 30.2 mmol) with continuous stirring. The mixture was stirred at room temperature for 6 h. After removal of the benzene *in vacuo*, distillation gave **1** (8.49 g, 91%): Bp 118—123 °C/0.08 mmHg† (lit,[22] 124—125 °C/1.0—1.5 mmHg); NMR($CDCl_3$) δ 0.25(9H, s, Me_3Si), 1.37(6H, t, $J=7$ Hz, CH_3), 4.18(4H, m, CH_2), 5.15(1H, d, $J=14$ Hz, CHP), 7.50(5H, m, ArH). Found: C, 53.38; H, 8.07%. Calcd for $C_{14}H_{25}O_4PSi$: C, 53.14; H, 7.96%.

Method B: Diethyl phosphonate (6.61 g, 47.9 mmol) was added dropwise to sodium (1.18 g, 51.3 mmol) in dry ether (50 ml). Exothermic reaction took place with evolution of hydrogen gas and a white precipitate was formed gradually. After 3 h benzaldehyde (4.82 g, 45.4 mmol) was added. The precipitate was dissolved at once and the solution turned bright brown. Then, chlorotrimethylsilane (5.11 g, 47.0 mmol) was added, and a precipitate appeared. After removal of the ether, distillation without separation of the precipitate gave **1** (9.64 g, 67%).

Diethyl Trimethylsilyloxymethylphosphonate (2). Diethyl

† 1 mmHg≈133.322 Pa.

Table 8. Preparation of lactones (**91**—**95**) from **64**—**66**

Adduct	Aldehyde or ketone[a)]	Time/min	Product	Compd No.	Yield/% (*trans*/*cis*)[b)]
64	PhCHO	40	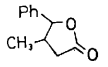	**91**	51 (75/25)
65	PhCHO	60	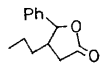	**92**	54 (75/25)
66	PhCHO	40	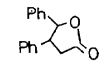	**93**	78 (85/15) (59%, TBAF)
66	*i*-C_3H_7CHO	40	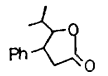	**94**	80 (60/40)
66	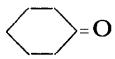	40	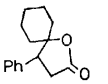	**95**	33

a) In these reactions 1.2 equiv. of aldehyde or ketone was employed. b) The ratio of *trans*/*cis* was calculated on the base of the NMR spectra of **91**—**94** (see Table 9).

Table 9. ^1H NMR data of lactones (**91**—**95**)

Compound	^1H NMR($CDCl_3$) δ
91	0.60(3H, d, J=7 Hz, *trans* CH_3), 1.03(3H, m *cis* CH_3), 1.90—2.97(3H, m, CH_2 and CHC-O), 4.80(1H, d, J=8 Hz, *cis* CH-O), 5.46(1H, d, *trans* CH-O), 7.20(5H, m, Ph)
92	1.43—0.53(7H, m, $CH_3(CH_2)_2$), 2.50(3H, m, CH_2 and CH-O), 4.93(d, J=7 Hz, *cis* CH-O), 5.53 (1H, d, J=7 Hz, *trans* CH-O), 7.23(5H, m, Ph).
93	2.90(2H, m, CH_2), 3.50(1H, m, CHC-O), 5.35(1H, d, J=8 Hz, *trans* CH-O), 5.73(1H, d, J= 7 Hz, *cis* CH-O), 7.17(10H, s, Ph)
94	0.93(6H, m, CH_3), 1.87(1H, m, $CH(CH_2)_2$), 2.70(2H, d, J=7 Hz, *cis* CH_2), 2.85(2H, d, J=7 Hz, *trans* CH_2), 3.43(1H, m, CHC-O), 4.27(1H, d, J=7 Hz, *trans* CH-O), 4.37(1H, d, J=7 Hz, *cis* CH-O), 7.27(5H, s, Ph)
95	0.50—2.33(10H, m, $(CH_2)_5$), 2.89(2H, m, $CH_2C(O)$), 3.43(1H, m, CH), 7.13(5H, s, Ph)

phosphonate (6.02 g, 43.6 mmol) was added to sodium (1.2 g, 52.2 mmol) in dry ether (20 ml). After stirring for 2 h, paraformaldehyde (1.50 g, 50.0 mmol) in dry ether (10 ml) was added. A white precipitate appeared at once but it was dissolved on addition of chlorotrimethylsilane (5.85 g, 53.8 mmol). The mixture was stirred at room temperature for 6 h. After removal of the solvent distillation gave **2** (7.20 g, 69%): Bp 72—75 °C/0.6 mmHg (lit,[23] 113 °C/9 mmHg); NMR ($CDCl_3$) δ 0.13(9H, s, Me_3Si), 1.30(6H, t, J=7 Hz, CH_3), 3.75(2H, d, J=9 Hz, CH_2P), 3.80—4.32(4H, m, CH_2O). Found: C, 40.04; H, 8.66%. Calcd for $C_8H_{21}O_4PSi$: C, 39.98; H, 8.81%.

*Diethyl 1-(Trimethylsilyloxy)ethylphosphonate (**3**).* To a solution of DTMSP (11.0 g, 52.3 mmol) in dry benzene (20 ml) was introduced acetaldehyde (90 mmol) which was generated from paraaldehyde by heating with a catalytic amount of *p*-toluenesulfonic acid (TsOH). After standing for 4 h, the solvent was removed *in vacuo* and distillation afforded **3** (11.7 g, 88%): Bp 62—63 °C/0.4 mmHg (lit,[22] 82 °C/1 mmHg); NMR(CCl_4) δ 0.15(9H, s, Me_3Si), 1.29 (6H, t, J=7 Hz, CH_3C-O), 1.33(3H, dd, J=7 Hz, J=16.5 Hz, CH_3CP), 3.78—4.22(5H, m, CH_2O and CHP).

*Diethyl 1-(Trimethylsilyloxy)propylphosphonate (**4**).* To a solution of DTMSP (5.66 g, 26.9 mmol) in dry benzene (10 ml) was added dropwise propionaldehyde (1.74 g, 30.0 mmol) at room temperature. After being stirred for 6 h, the solution was concentrated *in vacuo* and the residual oil was distilled to give **4** (5.30 g, 72%): Bp 80—82 °C/1 mmHg; IR(NaCl) 968, 1030, 1060, 1117, 1170, 1230, 1255 (νP=O), 1394, 1448, 1460, 2970 cm^{-1}; NMR(CCl_4) δ 0.15 (9H, s, Me_3Si), 0.99 (3H, t, J=7 Hz, CH_3CC), 1.34(6H, t, J=7 Hz, CH_3C-O), 1.10—1.85(2H, m, CCH_2C), 3.51—3.80(1H, m, CHP), 3.80—4.35(4H, m, CH_2O). Found: C, 44.44; H, 9.81%. Calcd for $C_{10}H_{25}O_4PSi$: C, 44.76; H, 9.39%.

*Diethyl 1-Trimethylsilyloxy-2-methylpropylphosphonate (**5**).* To a solution of DTMSP (7.58 g, 36.0 mmol) in dry benzene (15 ml) was added isobutyraldehyde (2.80 g, 38.8 mmol) dropwise at room temperature. The mixture was stirred for 6 h. The usual work-up as described before gave **5** (8.65 g, 83%): Bp 69—72 °C/0.35 mmHg; NMR(CCl_4) δ 0.14 (9H, s, Me_3Si), 0.97(6H, d, J=7.3 Hz, $(CH_3)_2C$), 1.31

(6H, t, J=7 Hz, CH_3C–O), 1.62—2.40(1H, m, CHCP), 3.59(1H, dd, J=7.5 Hz, J=4.5 Hz, CHP), 3.78—4.31(4H, m, CH_2O). Found: C, 46.75; H, 9.64%. Calcd for $C_{11}H_{27}O_4PSi$: C, 46.78; H, 9.64%.

*Diethyl 1-(Trimethylsilyloxy)octylphosphonate (**6**).* To a solution of DTMSP (18.3 g, 87.1 mmol) in dry benzene (10 ml) was added dropwise octanal (9.67 g, 75.4 mmol) at room temperature. After stirring for 3 h, the solvent was removed and distillation of the residual oil gave **6** (23.1 g, 91%): Bp 104—105 °C/0.04 mmHg: NMR(CCl_4) δ 0.15 (9H, s, Me_3Si), 0.92(3H, t, J=4.5 Hz, terminal CH_3), 1.32(6H, t, J=7 Hz, CH_3C–O), 1.31(12H, m, $(CH_2)_6$), 3.73(1H, m, CHP), 3.75—4.35(4H, m, CH_2O). Found: C, 52.85; H, 10.55%. Calcd for $C_{15}H_{35}O_4PSi$: C, 53.22; H, 10.42%.

*General Procedure for the Synthesis of Diethyl 1-Hydroxy-1-(trimethylsilyl)alkylphosphonates (**8—10**). The Wittig Rearrangement of Diethyl 1-(Trimethylsilyloxy)alkylphosphonates (**2—4**).* To a cold solution (−78 °C) of diisopropylamine (0.5 ml, 3.58 mmol) in dry THF (10 ml) or DME (10 ml) was added butyllithium (3.58 mmol) in hexane. After 0.5 h, an appropriate 1-trimethylsilyloxyphosphonate (**2—5**) was added. The mixture was stirred at −78 °C for the time given in Table 1, and then or after warming to room temperature the resulting solution was poured into a vigorously stirred mixture of 1 M NH_4Cl (20 ml) and CH_2Cl_2 (20 ml). The CH_2Cl_2 layer was collected and the aqueous layer was further extracted with CH_2Cl_2 (3×10 ml). The organic extracts were combined, dried over Na_2SO_4, and concentrated *in vacuo*. The residue was chromatographed on silica gel (hexane–ether) to give a 1-hydroxy-1-(trimethylsilyl)alkylphosphonate (**8**, **9**, or **10**) and the starting phosphonate. The physical properties of the new compounds **8—10** are listed in Table 2.

*Trimethylsilyl Diphenylphosphinite (**16**).*[15] A mixture of diphenylphosphine oxide (10.5 g, 52 mmol) and *N*,*N*-diethyltrimethylsilylamine (9.08 g, 62.5 mmol) was stirred at room temperature for 4 h under slightly reduced pressure. Distillation gave **16** (12.8 g, 89%): Bp 110 °C/0.8 mmHg. This compound was identified with an authentic sample reported by Issleib by comparison with its physical data.[15]

*[1-(Trimethylsilyloxy)propyl]diphenylphosphine Oxide (**17**).* To a solution of propionaldehyde (1.17 g, 20.2 mmol) in dry benzene (10 ml) was added **16** (5.41 g, 19.7 mmol). The exothermic reaction took place. After the mixture was stirred at room temperature for 3 h, the solvent was removed *in vacuo*. The residue was chromatographed on silica gel (hexane–ether) to give **17** (2.5 g, 38%) as a crude material and (1-hydroxypropyl)diphenylphosphine oxide (1.98 g, 39%). While the former was too sensitive toward moisture to be purified, the latter was well characterized by its NMR spectrum and elemental analysis: NMR($CDCl_3$) δ 0.99(3H, t, J=7 Hz, CH_3), 1.65(2H, m, CH_2), 4.21(1H, m, CHP), 5.14(1H, s, OH), 7.32(6H, s, ArH), 7.70(4H, m, ArH). Found: C, 68.90; H, 6.80%. Calcd for $C_{15}H_{17}O_2P$: C, 69.22; H, 6.59%.

*General Procedure for Alkylation of α-Lithiated 1-(Trimethylsilyloxy)alkylphosphonates (**1—7**).* To a cooled solution (−78 °C) of diisopropylamine in dry THF was added an equimolar amount of butyllithium in hexane. After 0.5 h an appropriate phosphonate was added. The lithiation time was listed in Table 3. Then an alkyl halide or a disulfide was added to the mixture. The reaction time was also shown in Table 3. The mixture was poured into a vigorously stirred mixture of 1 M NH_4Cl and CH_2Cl_2. The organic layer was collected and the aqueous layer was further extracted with CH_2Cl_2 three times. The organic extracts were combined, dried over Na_2SO_4, evaporated *in vacuo* to dryness, and chromatographed on silica gel (hexane–ether) to give an α-alkylated phosphonate as listed in Table 3. The amounts of the reagents used are listed in Table 3. All new compounds were characterized by their NMR spectra and elemental analyses. The previously known compounds were identified by comparison with their NMR spectra. These data are listed in Table 4.

General Procedure for Transformation of 1-(Trimethylsilyloxy)-alkylphosphonates into Carbonyl Compounds. Method A: An appropriate alkylated phosphonate (2 mmol) was dissolved in a mixture of methanol (10 ml) and water (1 ml) and then a catalytic amount (30 mg) of *p*-toluenesulfonic acid was added. The mixture was refluxed for the time given in Table 5. The mixture was first treated with a mixture of CH_2Cl_2 (25 ml) and water (25 ml). The organic layer was collected and the aqueous layer was further extracted with CH_2Cl_2 (3×10 ml). The organic extracts were combined, dried over Na_2SO_4, and evaporated *in vacuo* to afford a crude 1-hydroxyalkylphosphonate derivative. It was further treated with a mixture of EtOH (30 ml) and 1 M NaOH (30 ml). After the time given in Table 5, the mixture was extracted with CH_2Cl_2 (3×10 ml). The extracts were combined, dried over Na_2SO_4, evaporated *in uacuo*, and chromatographed on silica gel to give a pure carbonyl compound.

In the following cases, special conditions were employed: 1) Diethyl 1-trimethylsilyloxy-1-phenylbutylphosphonate (**20**) was treated with 2 M HCl (2.5 ml) in MeOH instead of TsOH and the reaction was carried out at room temperature. 2) Allyl phenyl ketone was obtained by treatment of the detrimethylsilylated intermediate with a large excess amount of Na_2CO_3 (1 g) in a mixture of CH_2Cl_2 (20 ml) and EtOH (10 ml) at room temperature for 3 d or by treatment with a catalytic amount of tetrabutylammonium hydroxide for 1 min in a heterogeneous mixture of ether (20 ml) and 1 M NaOH (20 ml). According to the former treatment allyl phenyl ketone was obtained in 36% yield along with (*E*)-1-phenyl-2-buten-1-one (10%) and the latter gave the ketone in 36% yield.

Diethyl 1-Hydroxy-1-phenyl-3-butenylphosphonate(Purified Intermediate). Mp 71—73 °C; NMR($CDCl_3$) δ 1.15 and 1.19 (3H and 3H, t and t, J=7 Hz, CH_3C–O), 2.96(2H, dd, J=J=7 Hz, $C{=}CCH_2$), 3.63—4.30(4H, m, CH_2O), 4.53 (1H, s, OH), 4.80—5.17(2H, m, $CH_2{=}C$), 5.26—5.90(1H, m, $C{=}CH$), 7.13(3H, m, ArH), 7.45(2H, m, ArH). Found: C, 59.34; H, 7.33%. Calcd for $C_{14}H_{21}O_4P$: C, 59.15; H, 7.45%.

Method B: To a solution of an alkylated phosphonate (2—3 mmol) in ethanol (30 ml) was added 1 M NaOH (30 ml). The solution was stirred for the period as shown in Table 5. The mixture was poured into a mixture of CH_2Cl_2 (20 ml) and 1 M NH_4Cl (20 ml). The organic layer was collected, and the aqueous layer was further extracted with CH_2Cl_2 (3×50 ml). The CH_2Cl_2 extracts were combined, dried over Na_2SO_4, concentrated, and chromatographed on silica gel (hexane–ether) to give a carbonyl compound.

*Diethyl 1-Trimethylsilyloxy-2-propenylphosphonate (**63**).* To a solution of acrylaldehyde(1.17 g, 20.8 mmol) in dry benzene (5 ml) was added DTMSP (4.46 g, 21.2 mmol) with stirring on an ice bath. After stirring at room temperature for 6 h the solvent was removed, and distillation gave a mixture (4.90 g, Bp 105 °C/1.25 mmHg) of **63** and **67**. The mixture (32 g) was treated with $TsOH{\cdot}H_2O$ (1 g) in MeOH (500 ml) and H_2O (20 ml) under reflux for 3 h. After extraction with CH_2Cl_2 (4×100 ml) and drying

over Na_2SO_4, and removal of the solvent, the residue was chromatographed on silica gel (hexane–ether) to give a detrimethylsilylated phosphonate of **63** (14.3 g, 38%). The α-hydroxy phosphonate (14 g) was further treated with *N,N*-diethyltrimethylsilylamine (16.5 ml) at 50 °C under slightly reduced pressure for 3 h. Then, the mixture was evaporated *in vacuo* and chromatographed on silica gel (hexane–ether) to give **63**: NMR(CCl_4) δ 0.15(9H, s, Me_3Si), 1.29(6H, t, J=7 Hz, CH_3C–O), 4.05(4H, m, CH_2O), 4.33(1H, m, CHP), 4.98—5.50(2H, m, CH_2=C), 5.69—6.27(1H, m, C=CH). This product was used further for alkylation without purification.

*Diethyl 1-Trimethylsilyloxy-2-butenylphosphonate (**64**).* To a solution of *trans*-2-butenal (1.54 g, 21.9 mmol) in dry benzene (5 ml) was added DTMSP (4.71 g, 22.4 mmol). The reaction mixture was stirred at room temperature for 6 h. After removal of the benzene *in vacuo*, distillation gave **64** (4.45 g, 72%): Bp 110—113 °C/1.8 mmHg; NMR($CDCl_3$) δ 0.15(9H, s, Me_3Si), 1.30(6H, t, J=7 Hz, CH_3C–O), 1.57—1.81(3H, m, CH_3C=C), 3.80—4.53(5H, m, CH_2–O and CHP), 5.62(2H, m, CH=CH). Found: C, 46.87; H, 9.49%. Calcd for $C_{11}H_{25}O_4PSi$: C, 47.12; H, 8.99%.

*Diethyl 1-Trimethylsilyloxy-2-hexenylphosphonate (**65**).* To a solution of *trans*-hexenal (9.95 g, 101 mmol) in dry benzene (10 ml) was added DTMSP (19.52 g, 92.8 mmol) with stirring on an ice bath. Then the mixture was stirred at room temperature for 8 h. After removal of the solvent *in vacuo*, distillation gave **65** (21.6 g, 73%): Bp 90—100 °C/0.15—0.20 mmHg; NMR(CCl_4) δ 0.20(9H, s, Me_3Si), 0.95(3H, t, terminal CH_3), 1.33(6H, t, J=7 Hz, O–C–CH_3), 1.40(2H, m, CH_2CC=C), 1.80—2.30(2H, b, CH_2C=C), 3.80—4.33(4H, m, CH_2–O), 4.25—4.50(1H, m, CHP), 5.50—5.77(2H, m, CH=CH). Found: C, 50.48; H, 9.95%. Calcd for $C_{13}H_{29}O_4PSi$: C, 50.63; H, 9.48%.

*Diethyl 1-Trimethylsilyloxy-3-phenyl-2-propenylphosphonate (**66**).* To a solution of cinnamaldehyde (3.82 g, 28.9 mmol) in dry benzene (5 ml) was added dropwise DTMSP (6.27 g, 29.8 mmol) with stirring at room temperature. The mixture was further stirred at room temperature for 6 h. After removal of the solvent, distillation of the residual oil gave **66** (6.94 g, 70%): Bp 134—137 °C/0.10 mmHg; NMR(CCl_4) δ 0.19(9H, s, Me_3Si), 1.29(6H, t, J=7 Hz, CH_3C–O), 3.78—4.33(4H, m, CH_2O), 4.50(1H, dd, J=16, J=5.5 Hz, CHP), 5.97—6.80(2H, m, CH=CH), 7.23(5H, m, Ph). Found: C, 55.97; H, 8.18%. Calcd for $C_{16}H_{27}O_4PSi$: C, 56.12; H, 7.95%.

*Lithiation and Deuteration of **63**.* To a cooled (−78 °C) solution of LDA(3.58 mmol) in dry THF (10 ml) was added 805 mg (3.02 mmol) of **66**, whereupon the solution turned orange yellow. After 0.5 h, CD_3OD (0.2 ml) was added and the solution was treated with 1 M ammonium chloride (20 ml). The mixture was extracted with CH_2Cl_2 (4× 20 ml). The organic extracts were combined, concentrated to dryness, and chromatographed on silica gel (hexane–ether) to give deuterated diethyl 1-hydroxy-2-propenylphosphonate (169 mg, 29%) and deuterated **63** (68 mg, 8%).

*Lithiation and Deuteration of **64**.* Deuterated diethyl 1-hydroxy-2-butenylphosphonate (557 mg, 78%) and deuterated **64** (110 mg, 12%) were obtained from **64** (952 mg, 3.40 mmol), LDA (3.58 mmol) in dry THF (10 ml), and CH_3OD (0.5 ml).

*Lithiation and Deuteration of **65**.* The deuterated **65** (587 mg, 84%) was similarly obtained from **65** (905 mg, 2.94 mmol), LDA (3.58 mmol) in dry THF (10 ml), and CH_3OD (0.5 ml).

*Lithiation and Deuteration of **66**.* Deuterated 1-hydroxy-3-phenyl-2-propenylphosphonate (169 mg, 29%) and deuterated **66** (68 mg, 8%) were similarly obtained from **66** (970 mg, 2.83 mmol), LDA (3.19 mmol) in dry THF (10 ml), and CD_3OD (0.2 ml).

*Preparation of **85**.* To a solution of 4 mmol of LDA in THF (15 ml) at −78°C was added **66** (1.23 g, 3.6 mmol) and the solution was stirred for 30 min. Benzoyl chloride (607 mg, 4.32 mmol) was added and the mixture was warmed gradually to room temperature. After being stirred at room temperature for 30 min, the solution was poured into a stirred heterogeneous mixture of 1 M NH_4Cl (10 ml) and CH_2Cl_2 (10 ml). The CH_2Cl_2 layer was collected and the aqueous solution was further extracted with CH_2Cl_2 (3× 10 ml). The organic extracts were combined, dried over Na_2SO_4, and evaporated to give the crude **85**, which was used without purification for further transformations into **86—88**.

*Esterification of **85**. Under Acidic Conditions*: The crude **85** was dissolved in dry ethanol (20 ml) and TsOH·H_2O (5 mg) was added. After being refluxed for 2 h, the mixture was poured into a stirred mixture of 1 M NaOH (20 ml) and CH_2Cl_2 (20 ml). The organic layer was collected, combined with further CH_2Cl_2 extracts (3×10 ml), dried over Na_2SO_4, evaporated, and chromatographed on silica gel (hexane–ether) to give **86** (362 mg, 36%): NMR($CDCl_3$) δ 7.90 and 7.17(10H, m, ArH), 5.07(1H, dd, J=9 Hz, J=6 Hz, CHPh), 4.00(2H, m, CH_2O), 3.36(1H, dd, J=16 Hz, J=9 Hz, $CH^aC(=O)O$), 2.63(1H, dd, J=16 Hz, J=6 Hz, $CH^bC(=O)O$), 1.10(3H, t, CH_3).

Under Alkaline Conditions. The crude **85** was prepared from **66** (1.86 g, 5.38 mmol) and was treated with sodium methoxide prepared from sodium (143 mg, 6.2 mmol) in dry methanol (20 ml). The solution turned reddish brown. After being stirred for 30 min, the mixture was poured into a mixture of 1 M NH_4Cl (20 ml) and CH_2Cl_2 (20 ml). The usual work-up gave **87** (813 mg, 56%).

*Synthesis of **88**.* The crude **85** was prepared from **66** (1.48 g, 4.32 mmol), dissolved in dioxane (30 ml), treated with 1 M NaOH (30 ml). After being stirred for 15 min, the solution was treated with a mixture of 1 M NH_4Cl (20 ml) and CH_2Cl_2 (20 ml). Dilute hydrochloric acid was added until the aqueous layer had been acidified to pH 1. The aqueous layer was extracted with CH_2Cl_2 (4× 20 ml). The usual work-up gave **88** (802 mg, 73%). The products **86—88** were identified with the authentic samples by comparison with their spectral data.

General Procedure for the Synthesis of Lactones. To a THF solution of 3.3 mmol of LDA at −78 °C was added 3 mmol of an appropriate phosphonate (**64—66**). The mixture was stirred at −78 °C for the time given in Table 8 and warmed gradually to room temperature. The mixture was poured into a stirred mixture of 1 M NH_4Cl (20 ml) and CH_2Cl_2 (20 ml). The CH_2Cl_2 layer was collected and the aqueous layer was extracted with CH_2Cl_2 (3×20 ml). The combined CH_2Cl_2 extracts were dried over Na_2SO_4, evaporated, and dissolved in dioxane (10 ml). To the solution was added 571 mg (3 mmol) of TsOH·H_2O, and the mixture was refluxed in the presence of molecular sieves 3A for 10 min. After cooling to room temperature, the solution was diluted with water (20 ml) and extracted with CH_2Cl_2 (3×20 ml). The combined extracts were dried over Na_2SO_4, evaporated, and chromatographed on silica gel (hexane–ether) to give a lactone given in Table 8. All of the products were identified by comparison with their spectral data with authentic samples previously reported.[21,24–26]

*Diethyl 1-Trimethylsilyloxy-3-phenyl-1-butenylphosphonate (**69a**).* To a cooled (−78 °C) solution of LDA (3.31 mmol) in dry THF (10 ml) was added **66** (1048 mg, 3.06 mmol),

the solution turned bright brown. After 0.5 h methyl iodide (515 mg, 3.63 mmol) was added. The solution turned yellow. Then the mixture was gradually warmed to room temperature. After 3 h, the solution was quenched with 1 M NH_4Cl, extracted with CH_2Cl_2 (3×25 ml) and dried over Na_2SO_4. After removal of the solvent, chromatography on silica gel afforded **69a** (473 mg, 43%) as a crude material: NMR(CCl_4) δ 0.18(9H, s, Me_3Si), 1.25 and 1.28(3H and 3H, t and t, J=7 Hz, CH_3C–O), 2.35—3.33(1H, m, CH), 3.98 (4H, m, CH_2O), 5.92(1H, dd, J=J=10 Hz, CH=C–P), 7.13(5H, s, Ph).

*Diethyl 1-Trimethylsilyloxy-3,4-diphenyl-1-butenylphosphonate (**69b**).* To a cooled (−78 °C) mixture of **66** (1594 mg, 4.66 mmol) and LDA (5.45 mmol) in dry THF (10 ml) was added benzyl bromide (984 mg, 5.75 mmol). After stirring at −78 °C for 0.5 h, the usual work-up gave **69b** (1305 mg, 69%) as a crude material: NMR(CCl_4) δ 0.07 (9H, s, Me_3Si), 1.19(6H, t, J=7 Hz, CH_3C–O), 2.90(1H, d, J=8.1 Hz, one of CH_2Ph), 2.91(1H, d, J=6.6 Hz, one of CH_2Ph), 2.40—3.20(1H, m, CH), 5.97(1H, dd, J=J= 10 Hz, CH=C), 7.00(5H, s, Ph), 7.07(5H, s, Ph).

*Diethyl 1-Trimethylsilyloxy-3-benzyl-1-hexenylphosphonate (**69c**).* To a cooled (−78 °C) solution of **65** (1051 mg, 3.29 mmol) and LDA (3.58 mmol) in 10 ml of dry THF was added benzyl bromide (0.420 ml, 3.54 mmol). After stirring at −78 °C for 0.5 h, the usual work-up gave **69c** (755 mg, 58%) as a crude material: IR(NaCl): 1045, 1260(P=O), 1370, 1394, 1606, 1635, 1696, 1728, 2920, 2955, 3015 cm^{-1}; NMR(CCl_4) δ 0.13 (9H, s, Me_3Si), 0.90(3H, t, J=6 Hz, CH_3CC), 1.30(10H, m, CH_2CH_2 and CH_3C–O), 2.75(3H, m, $PhCH_2$ and CH), 3.98(4H, m, CH_2O), 5.50(1H, dd, J=J=9.5 Hz, CH=C), 7.15(5H, s, Ph).

General Procedure for the Synthesis of β-Substituted Carboxylates. To a cooled solution of diisopropylamine (1.12±0.09 equiv.) in dry THF was added an equimolar amount of butyllithium in hexane. After 0.5 h an appropriate phosphonate (3.0 mmol) was added. After stirring at −78 °C for 0.5 h, alkyl halide (1.12±0.09 equiv.) was added. The reaction time and the temperature were given in Table 6. The mixture was poured into a mixture of CH_2Cl_2 (20 ml) and 1 M NH_4Cl (20 ml) with vigorous stirring. The CH_2Cl_2 layer was collected and the aqueous layer was further extracted with CH_2Cl_2 (3×20 ml). The organic extracts were combined, dried over Na_2SO_4, and concentrated *in vacuo*. The residual oil was dissolved into ethanol (30 ml) without further purification and a catalytic amount of TsOH was added. The reaction time and the temperature were given in Table 6. The resulted solution was diluted with water and extracted with CH_2Cl_2 (3×20 ml). The combined organic layers were dried over Na_2SO_4, concentrated to dryness, and chromatographed on silica gel (hexane–ether) gave a β-substituted carboxylate. The data of the NMR spectra and elemental analyses for all new compounds are summarized in Table 7. The previously known products are characterized by their NMR spectra.

References

1) Part XVII: M. Sekine, M. Nakajima, T. Hata, *Bull. Chem. Soc. Jpn.*, **55**, 218 (1982); Part XVI: M. Sekine, M. Nakajima, and T. Hata, *J. Org. Chem.*, **46**, 4030 (1981); Part XV: M. Sekine, K. Okimoto, K. Yamada, and T. Hata, *ibid.*, **46**, 2097 (1981).

2) E. J. Corey and D. Seebach, *Angew. Chem., Int. Ed. Engl.*, **4**, 1075, 1077 (1965).

3) a) D. Seebach, *Angew. Chem., Int. Ed. Engl.*, **8**, 639 (1969); b) D. Seebach, *Synthesis*, **1**, 17 (1969); c) D. Seebach and M. Kolb, *Chem. & Ind.*, **1974**, 687; d) D. A. Evans and G. C. Andrews, *Acc. Chem. Res.*, **7**, 147 (1974); e) S. S. Washburne, *J. Organomet. Chem.*, **83**, 155 (1974); f) D. Seebach and D. Enders, *Angew. Chem., Int. Ed. Engl.*, **14**, 15 (1975); g) O. W. Lever, Jr., *Tetrahedron*, **32**, 1943 (1976); h) S. S. Washburne, *J. Organomet. Chem.*, **123**, 1 (1976); i) D. Seebach, K. Geiss, M. Kold, and A. K. Beck, "Modern Synthetic Methods," Chemiker-Verband, Zürich (1976), p. 173; j) P. F. Hudrlik, "New Applications of Organometallic Reactions in Organic Synthesis," ed by D. Seyferth, Elsevier, Amsterdam (1976), pp. 127—160; k) B. Gröbel and D. Seebach, *Synthesis*, **1977**, 357; l) D. Seebach, E. W. Colvin, F. Lehr, and T. Weller, *Chimia*, **33**, 1 (1979); m) D. Seebach, *Angew. Chem., Int. Ed. Engl.*, **18**, 239 (1979).

4) Our preliminary communications have already been reported: a) T. Hata, A. Hashizume, M. Nakajima, and M. Sekine, *Tetrahedron Lett.*, **1977**, 363; b) T. Hata, M. Nakajima, and M. Sekine, *ibid.*, **1979**, 2047; c) M. Sekine, M. Nakajima, A. Kume, and T. Hata, *ibid.*, **1979**, 4479.

5) a) P. Savignac, A. Breque, and F. Mathey, *Synth. Commun.*, **9**, 287, 487 (1979); b) R. E. Koenigkramer and H. Zimmer, *Tetrahedron Lett.*, **1980**, 1017; c) R. E. Koenigkramer and H. Zimmer, *J. Org. Chem.*, **45**, 3994 (1980).

6) a) V. S. Abramov, L. P. Semenova, and L. G. Semenova, *Dokl. Alad. Nauk SSSR*, **84**, 281 (1952); *Chem. Abstr.*, **47**, 3227 (1953); b) L. D. Freedman and G. O. Doak, *Chem. Rev.*, **57**, 479 (1957); c) I. Shahak and E. D. Bergmann, *Isr. J. Chem.*, **4**, 225 (1966); d) L. H. Horner and H. Roder, *Chem. Ber.*, **103**, 2984 (1970); e) G. M. Kosolapoff and L. Maier, "Organic Phosphorus Compounds," Wiley, New York (1976), Vol. 7, p. 30.

7) a) G. Wittig and L. Löhmann, *Justus Liebigs Ann. Chem.*, **550**, 260 (1942); b) D. L. Dalvymple, T. L. Kruger, and W. N. White, "The Chemistry of the Ether Linkage," ed by S. Patai, Interscience, New York (1967), p. 617; c) U. Schöllkopf, *Angew. Chem. Int. Ed. Engl*, **9**, 763 (1970).

8) A. G. Brook, *Acc. Chem. Res.*, **7**, 77 (1974) and references cited therein.

9) a) R. West, R. Lose, H. F. Stewart, and A. Wright, *J. Am. Chem. Soc.*, **93**, 282 (1971); b) A. Wright, D. Ling, P. Boudjouk, and R. West, *ibid.*, **94**, 4784 (1972).

10) a) K. Deuchert, U. Hertenstein, and S. Hünig, *Synthesis*, **1973**, 777; b) S. Hünig and G. Wehner, *ibid.*, **1975**, 180; c) G. Wehner and S. Hünig, *ibid.*, **1975**, 391; d) U. Hertenstein and S. Hünig, *Angew. Chem. Int. Ed. Engl.*, **14**, 179 (1975). e) U. Hertenstein, S. Hünig, and M. Öller, *Synthesis*, **1976**, 416.

11) a) G. Stork and L. Maldonado, *J. Am. Chem. Soc.*, **93**, 5286 (1971); b) G. Stork and L. Maldonado, *ibid.*, **96**, 5272 (1974).

12) A. Kalir and D. Balderman, *Synthesis*, **1973**, 358.

13) M. Hamana, T. Endo, and S. Saeki, *Tetrahedron Lett.*, **1975**, 903.

14) R. M. Jacobson, G. P. Lahm, and J. W. Clader, *J. Org. Chem.*, **45**, 395 (1980).

15) K. Issleib and B. Walther, *Angew. Chem. Int. Ed. Engl.*, **6**, 88 (1967).

16) Y. Ogata and A. Kawasaki, "The Chemistry of the Carbonyl Group," ed by S. Patai, Interscience, New York (1970), Vol. 2, pp. 1—69.

17) a) B. Ackerman, T. A. Jordan, C. R. Eddy, and D. Swern, *J. Am. Chem. Soc.*, **78**, 4444 (1956); b) K. D. Berlin and H. A. Taylor, *J. Am. Chem. Soc.*, **86**, 3862 (1964); c) W. Jugelt, S. Andreae, and G. Schubert, *J. Prakt. Chem.*, **1971**, 83; d) R. Kluger and J. Chin, *J. Am. Chem. Soc.*, **100**, 7382 (1978); e) R. Kluger, D. C. Pike, and J. Chin, *Can.*

J. Chem., **56**, 1792 (1978); f) K. S. Narayanan and K. D. Berlin, *J. Am. Chem. Soc.*, **101**, 109 (1979).

18) a) M. I. Kabachnik and P. A. Rossiiskaya, *Izu. Akad. Nauk SSSR, Ser. Khim.*, **1945**, 597; *Chem. Abstr.*, **41**, 88 (1945); b) K. Terauchi and H. Sakurai, *Bull. Chem. Soc. Jpn.*, **43**, 883 (1970); c) A. P. Pashinkin, T. K. Gazizov, and A. N. Pudovik, *Zh. Obshch. Khim.*, **40**, 28 (1970); *Chem. Abstr.*, **72**, 100827 (1970).

19) M. Soroka and P. Mastalerz, *Zh. Obshch. Khim.*, **44**, 463 (1974); *Chem. Abstr.*, **80**, 121058 (1974).

20) a) I. Shahak and E. D. Bergmann, *Isr. J. Chem.*, **4**, 225 (1966); b) I. Shahak, *Tetrahedron Lett.*, **1966**, 2201; c) G. M. Baranov, V. V. Perekalin, M. V. Ponamarenko, and I. A. Orlovskii, *Khim. Primen. Forsfororg. Soedin., Tr. Konf.*, 4th, **1969**, 228; d) O. G. Plantema, H. de Konig, and H. O. Huisman, *Tetrahedron Lett.*, **1975**, 2945; e) M. Sekine, M. Satoh, H. Yamagata, and T. Hata, *J. Org. Chem.*, **45**, 4162 (1980).

21) D. A. Evans, J. M. Takacs, and K. M. Hurst, *J. Am. Chem. Soc.*, **101**, 371 (1979).

22) Z. S. Novikova, S. N. Mashoshina, T. Sapozhnikova, and I. F. Lupsenko, *Zh. Obshch. Khim.*, **41**, 2622 (1971).

23) N. F. Orlov, V. P. Nileshkevich, and E. S. Andronov, *Zh. Obshch. Khim.*, **35**, 2193 (1965).

24) E. I. Heiba, R. M. Dessau, and W. J. Koehl, Jr., *J. Am. Chem. Soc.*, **90**, 5905 (1968).

25) J. B. Bush, Jr., and H. Finkbeiner, *J. Am. Chem. Soc.*, **90**, 5903 (1968).

26) M. Tokuda, Y. Yokoyama, T. Taguchi, A. Suzuki, and M. Itoh, *J. Org. Chem.*, **37**, 1859 (1972).

Protection of Phosphonate Function by Means of Ethoxycarbonyl Group. A New Method for Generation of Reactive Silyl Phosphite Intermediates

Mitsuo SEKINE, Hiroyuki MORI, and Tsujiaki HATA*

Department of Life Chemistry, Tokyo Institute of Technology, Nagatsuta, Midori-ku, Yokohama 227

(Received June 12, 1981)

Nucleoside ethoxycarbonylphosphonates were prepared by condensation of appropriately protected nucleosides with ethoxycarbonylphosphonic acid. They were easily converted by treatment with 1 M NaOH followed by trimethylsilylation to highly reactive bis(trimethylsilyl) nucleoside phosphite intermediates which were allowed *in situ* to react with water, diphenyl disulfide, 2,2′-dipyridyl disulfide, and aldehydes to afford the corresponding nucleoside phosphonates, nucleoside *S*-phenyl phosphorothioates, nucleoside phosphates, and nucleoside α-hydroxy phosphonates in good yields, respectively. The nucleoside phosphonates were further converted to nucleosides under mild acidic conditions. Thus, the ethoxycarbonyl group proved to serve as a versatile protecting group for not only H–P(O) but also HO–P(O) and hydroxyl groups of sugars.

Nucleoside phosphonates (**1**) have been shown as versatile synthetic intermediates in nucleotide chemistry. For example, **1** could be converted to highly reactive "nucleoside bis(trimethylsilyl) phosphites (**2**)" having tervalent form by simple trimethylsilylation. Fixation of phosphonates in the tervalent form has proved to be quite useful for the synthesis of various phosphate and phosphonate derivatives.[2-11] The trimethylsilyl group of the silylated products was readily removed by addition of water or alcohols. The above feature enhances the synthetic value of **2**. Thus, the preparation of **1** as the starting materials for the synthesis of **2** has become of more importance in nucleotide chemistry. However, the preparative method of **1**, *i.e.*, the introduction of a hydroxyphosphinyl group [H(HO)P(O)–] into nucleoside hydroxyl groups has been extremely limited,[12-17] because **1** is unstable under weakly acidic conditions (for example, 80% acetic acid[12]) though it is quite stable under alkaline conditions. The H–P(O) group of **1** is also sensitive to oxidizing agents,[12,17,18] halogenating agents,[19-23] and condensing agents.[24]

In order to overcome the problems owing to the instability of the hydroxyphosphinyl group, an appropriate masking group is required. We feel that, in this case, the protection of the H–P(O) function should be designed not in reactive phosphite form but in nonreactive phosphonate form.

Warren[25] described an interesting study on decarboxylation of carboxyphosphonic acid (**3**) to give phosphonic acid (**4**) under relatively drastic condi-

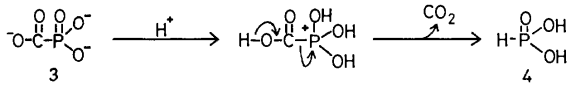

3 **4**

tions using strong acids. This fact suggests that the H–P(O) group of **1** can be protected by alkoxycarbonyl groups such as ethoxycarbonyl group. Therefore, our attention has been paid to the P–C bond cleavage of **3** with elimination of carbon dioxide under milder conditions than those reported by Warren.

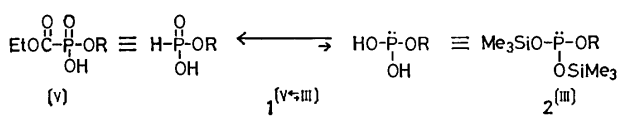

(V) **1** (V+III) **2** (III)

Consequently, we found a unique method for the decarboxylation of **3** *via* trimethylsilylation. When the pyridinium salt of **3** was treated with trimethylsilyl chloride and triethylamine (3.3 equiv. each) in tetrahydrofuran at room temperature for 30 min and then water was added, phosphonic acid was isolated as barium salt in 96% yield. When the reaction mixture was distilled without addition of water, tris(trimethylsilyl) phosphite (TMSP) was obtained in 81% yield. The mechanism of formation of TMSP might involve intramolecular rearrangement of one trimethylsilyl group *via* a five-membered ring transition state from a fully trimethylsilylated intermediate (**5**). Furthermore, the formation of TMSP was supported by the fact that treatment of the reaction mixture with diphenyl disulfide and benzaldehyde gave *S*-phenyl phosphorothioate (**6**) and α-hydroxybenzylphosphonic acid (**7**)

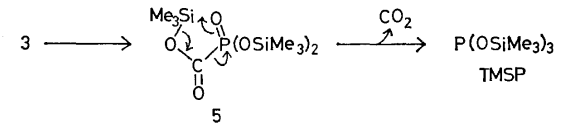

5

in 95 and 35% (quant. on TLC) yields, respectively. These results led us to study the protection of the H–P(O) group of **1** with ethoxycarbonyl group. Pyridinium ethoxycarbonylphosphonate (**8**) was prepared starting from TMSP and ethyl chloroformate according to the following equation. When com-

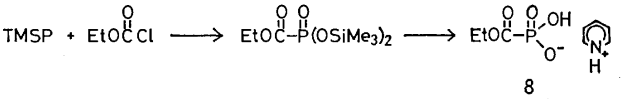

8

pound **8** was condensed with 2′,3′-*O*-isopropylideneuridine (**10**) in the presence of 1-(*p*-toluenesulfonyl)-1*H*-1,2,4-triazole[26] at r.t. overnight, 2′,3′-*O*-isopropylideneuridine 5′-(ethoxycarbonyl)phosphonate (**11**) was obtained in 84% yield by paper chromatography. It was found that the ethoxycarbonyl group of **11** was quite stable under acidic conditions required for removal of the isopropylidene group. Accordingly, treatment of **11** with 60% formic acid at r.t. for 2 h gave **12** in 93% yield. The ethoxycarbonyl group was found to be stable toward agents such as iodine, *N*-bromosuccimide,[27] and 2,4,6-triisopropylbenzenesulfonyl chloride.[24,28]

Compound **12** was treated with 1 M NaOH at r.t. for 5 min followed by neutralization with DIAION

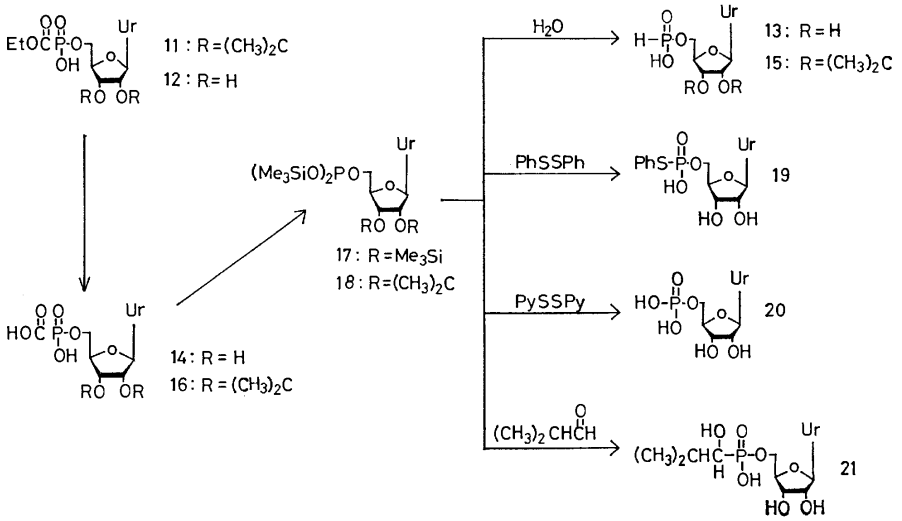

SK 1B (pyridinium form). After the mixture was evaporated to dryness, the residual syrup was successively treated with *N,O*-bis(trimethylsilyl)acetamide (BSA) in pyridine at r.t. for 3 h. By treatment of the mixture with water, uridine 5′-phosphonate (**13**) was obtained in 92% yield. In this reaction, the first intermediate **14** was clearly detected as a single spot on TLC and electrophoresis. The intermediate **14** was characterized by its NMR spectrum. However, attempts to purify **14** by chromatographical methods were unsuccessful because **14** decomposed to **13** and uridine during the chromatography. In a similar manner, **11** was converted to 2′,3′-*O*-isopropylidene 5′-phosphonate (**15**) in 86% yield *via* intermediate **16**. It should be emphasized that the "*in situ*" treatment of **14** with BSA gave rapid and simultaneous generation of a silyl phosphite intermediate (**17**). The presence of **17** was confirmed by the subsequent reaction with diphenyl disulfide, which gave *S*-phenyl uridine 5′-phosphorothioate (**19**)[2] in 94% yield. Furthermore, the use of 2,2′-dipyridyl disulfide[3] in place of diphenyl disulfide gave uridine 5′-phosphate (**20**) in 95% yield. In addition, a new type of nucleotide derivative, uridine 5′-(1-hydroxy-2-methylpropyl)phosphonate (**21**), could be obtained in 84% yield through the reaction of the intermediate **19** with isobutyraldehyde at r.t. for 3 h. Moreover, it was found that the phosphonate group was removed from **13** by treatment with 80% acetic acid at 100 °C for 2 h[12] to give uridine in 90% yield.

Conclusion. In contrast with the fixation of **1** in the tervalent form **2** by the silylation described previously,[2] nucleoside ethoxycarbonylphosphonates can serve as the synthetic equivalents of **1** fixed perfectly in the phosphonate form **3**. It is significant that H–P(O) group can be fixed rigidly in the phosphonate form by the introduction of the (ethoxycarbonyl)hydroxyphosphinyl group. No study has appeared on protection of the H–P(O) group. From this point of view, the present work is the first example in phosphorus chemistry. It is also noteworthy that nucleoside derivatives having the (ethoxycarbonyl)hydroxyphosphinyl group can be converted under the varied conditions to nucleoside bis(trimethylsilyl) phosphites, nucleoside phosphonates, nucleoside phosphates, and nucleosides. From the different point of view, it can be said that the ethoxycarbonyl or (ethoxycarbonyl)hydroxyphosphinyl group can serve as a versatile protecting group for H–P(O), HO–P(O), or HO–R.

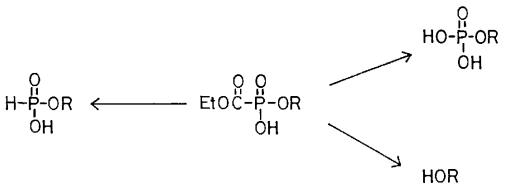

Experimental

Melting points and boiling points are uncorrected. ^{1}H NMR spectra were recorded at 60 MHz on a Hitachi R 24-B spectrometer using DSS and benzene (δ 7.24) as internal standards in D_2O and $CDCl_3$, respectively. IR spectra were measured on a Hitachi Model EPI-G3 spectrometer. ^{31}P NMR spectra were obtained on a JEOL PS-100 FT spectrometer at 40.50 MHz using 85% H_3PO_4 as an external standard. UV spectra were recorded with a Hitachi 124 spectrophotometer.

Paper chromatography was performed by descending technique with Toyo Roshi No. 51 and Whatman 3 MM papers. The solvent systems used were Solvent I: ethanol–1 M ammonium acetate (pH 7.5) (7:3, v/v); Solvent II: 1-butanol–water (84:16, v/v); Solvent III: 2-propanol–concentrated aqueous ammonia–water (6:1:3, v/v/v). Solvent IV: 2-propanol–concentrated aqueous ammonia–water (7:1:2, v/v/v). Paper electrophoresis was carried out by using Buffer I (0.05 M phosphate, pH 8.0) at 1200 V for 1.5 h. The Rm values relative to **13** were described. Estimation of the yields of products was carried out spectrophotometrically by using the ε value (10.1×10^3) of uridine at pH 7.0 after elution of the spots from paper chromatograms.

Phosphorus-containing spots were detected on TLC or paper by spraying Hanes-Isherwood reagent[29] followed by irradiation of UV.

Pyridine was distilled over *p*-toluenesulfonyl chloride and stored over calcium hydride. Tetrahydrofuran (THF) was distilled over $LiAlH_4$ and stored over sodium wire. Trimethylsilyl chloride was purchased from Nihon Silicon

Shokai Ltd. and distilled over calcium hydride before use. *N,O*-Bis(trimethylsilyl)acetamide (BSA) was purchased from Tokyo Kasai Ltd. and distilled before use.

Preparation of Tris(trimethylsilyl) Phosphite. An aqueous solution (100 ml) of trisodium carboxyphosphonate (2.83 g, 9.43 mmol) was passed through a column of DIAION SK 1B (pyridinium salt) (3×20 cm). The column was washed with 500 ml of pyridine–water (1:4, v/v). The eluents were combined, evaporated *in vacuo*, coevaporated with dry pyridine several times, and dissolved in dry THF (30 ml). Triethylamine (4.4 ml, 31.1 mmol) and trimethylsilyl chloride (3.9 ml, 31.1 mmol) were added and the mixture was vigorously stirred at room temperature. After 2 h, dry ether (15 ml) was added. The resulting precipitate was removed by filtration and washed with dry ether (10 ml). The filtrate and washings were combined, evaporated *in vacuo*, and the residue was distilled to give TMSP (2.27 g, 81%): Bp 76—77 °C/10 mmHg (lit,[30] 90—92/20 mmHg); ^{31}P NMR ($CDCl_3$) −113.2 ppm.

The same experiment was performed until washing with dry ether had been done. The residual liquid was treated with methanol (50 ml) and the solution was evaporated to dryness. The residue was dissolved in water (50 ml) and 9.5 ml of 1 M barium acetate aqueous solution was added. To the resulting solution was added with stirring ethanol (250 ml). The resulting precipitate was collected by filtration, washed with ethanol (50 ml) and ether (30 ml) and dried *in vacuo* over P_4O_{10} at 100 °C to give barium phosphonate **5** (1.98 g, 96%). This product was identified with the authentic sample by its IR spectra and paper chromatography (Solvent II).

*S-Phenyl Phosphorothioate (**6**).*[2] Trisodium carboxyphosphonate (90 mg, 0.3 mmol) was converted to the pyridinium salt as described in the above experiment. The salt was rendered anhydrous by repeated coevaporation with dry pyridine and dissolved in dry THF (5 ml). Diphenyl disulfide (71.9 mg, 0.33 mmol) was added and the mixture was treated with trimethylsilyl chloride (0.23 ml, 2 mmol) and triethylamine (0.25 ml, 2 mmol) at room temperature for 1 h. The reaction mixture was diluted with pyridine by using a measuring flask to 10.0 ml. A one-tenth of the solution was chromatographed on Whatman 3 MM paper (Solvent III) to give **6** (95%): R_f 0.42; $UV_{max}^{pH\ 7.0}$ 248 nm (ε=6560), $UV_{min}^{pH\ 7.0}$ 235 nm.

*α-Hydroxybenzylphosphonic Acid (**7**).* Trisodium carboxyphosphonate (900 mg, 3 mmol) was converted to the pyridinium salt as described before. The salt was rendered anhydrous by repeated coevaporation with dry pyridine and dissolved in dry THF (3 ml). To the solution was added successively benzaldehyde (318 mg, 3 mmol), triethylamine (2.52 ml, 18 mmol), and trimethylsilyl chloride (2.27 ml, 18 mmol). After the mixture was stirred at room temperature for 1 h, a white precipitate of triethylamine hydrochloride was removed by filtration. Ethanol (10 ml) was added to the filtrate. The resulting solution was concentrated to a small volume and hexane (100 ml) was added to the concentrated solution. A precipitate was collected by filtration, washed with hexane (20 ml), and dried over P_4O_{10} *in vacuo* to afford **7** (197 mg, 38%): Mp 171—174 °C (lit,[9] 179—180 °C). Found: C, 44.65; H, 4.84%. Calcd for $C_7H_9O_4P$: C, 44.69; H, 4.83%.

*2′,3′-O-Isopropylideneuridine 5′-(Ethoxycarbonyl)phosphonate (**11**).* An aqueous solution (100 ml) of anilinium ethoxycarbonylphosphonate[11] (296.6 mg, 1.2 mmol) was passed through a column (1×5 cm) of DIAION SK 1B (pyridinium salt). The column was washed with pyridine–water (1:5, v/v, 200 ml). The combined eluents were concentrated to a small volume and diluted with pyridine by using a measuring flask to 20 ml. From the measuring flask, 6.67 ml (0.75 mmol) of the standard solution was taken and 2′,3′-*O*-isopropylideneuridine (142 mg, 0.5 mmol) was added. The mixture was rendered anhydrous by repeated coevaporation with dry pyridine and dissolved in dry pyridine (2.5 ml). 1-(*p*-Toluenesulfonyl)-1*H*-1,2,4-triazole (227 mg, 1 mmol) was added. After being stirred at room temperature for 16 h, the mixture was quenched by addition of water and chromatographed on Whatman 3 MM papers (Solvent I). A band of R_f 0.90 was cut and eluted with water (1 l). The eluent was concentrated and applied to Whatman 3 MM papers. Rechromatography was performed by using Solvent II. A band of R_f 0.37 was cut and eluted with water (500 ml) to give the ammonium salt of **11** (4240 OD, 84%): R_m 0.92 (Buffer I); $UV_{max}^{pH\ 7.0}$ 262 nm, $UV_{min}^{pH\ 7.0}$ 232 nm; NMR (D_2O) δ 1.10 (t, 3H, J=7 Hz, CH_2CH_3), 1.18 (s, 3H, CH_3), 1.43 (s, 3H, CH_3), 3.53 (m, 2H, 5′-H), 4.04 (t, 2H, J=7 Hz, CH_2–CH_3), 4.47 (m, 1H, 4′-H), 4.85 (m, 2H, 2′- and 3′-H), 5.66 (d, 1H, J=8.2 Hz, 6-H), 5.72 (s, 1H, 1′-H), 7.61 (d, 1H, J=8.2 Hz, 5-H).

*Uridine 5′-(Ethoxycarbonyl)phosphonate (**12**).* The ammonium salt of **11** (0.062 mmol) was dissolved in 60% formic acid (30 ml). The solution was kept at room temperature for 2 h. The solvent was removed *in vacuo* and the residue was chromatographed on Whatman 3 MM paper (Solvent II). A band of R_f 0.11 was cut and eluted with water (200 ml) and water–ethanol (3:1, v/v, 300 ml) to give the ammonium salt of **12** (576 OD, 93%): $UV_{max}^{pH\ 7.0}$ 262 nm, $UV_{min}^{pH\ 7.0}$ 230 nm; NMR (D_2O) δ 1.11 (t, 3H, J_{H-H}=7 Hz, CH_3), 3.90—4.38 (m, 5H, 2′, 3′, 4′, 5′-H), 5.72 (d, 1H, J_{H-H}=8.2 Hz, 6-H), 5.80 (s, 1H, 1′-H), 7.70 (d, 1H, J=8.2 Hz, 5-H).

*Alkaline Hydrolysis of **12**.* The ammonium salt of **12** (0.05 mmol) was treated with 1 M NaOH (0.8 ml) at room temperature. After being kept for 5 min, the solution was neutralized with DIAION SK 1B (NH_4^+ form). The resin was filtered and washed with water (20 ml). The filtrate and washings were combined and evaporated *in vacuo* to give the diammonium salt of **14**. Its analyses using paper electrophoresis and TLC showed a homogeneous spot: R_f 0.12 (Solvent I), 0.01 (Solvent II); R_m 1.40 (Buffer I); NMR (D_2O) δ 3.85—4.32 (m, 5H, 2′,3′,4′-H and 5′-H), 5.74 (d, 1H, J_{H-H}=8.2 Hz, 6-H), 5.78 (d, 1H, J_{H-H}=3.8 Hz, 1′-H), 7.84 (d, 1H, J_{H-H}=8.2 Hz, 5-H).

*Uridine 5′-Phosphonate (**13**).* The diammonium salt of **14** (0.01 mmol) was rendered anhydrous by repeated coevaporation with dry pyridine and dissolved in dry pyridine (0.5 ml). BSA (0.2 ml) was added and the mixture was stirred at room temperature for 30 min. Water (0.5 ml) was added and the resulting solution was kept for 1 h. The solution was applied to Whatman 3 MM papers. Chromatography using Solvent IV was performed. A band of R_f 0.36 was cut and eluted with water (200 ml) to give the ammonium salt of **13** (93 OD, 92%): This product was identified with the authentic sample by comparison with its R_f and R_m values and UV spectrum.

*S-Phenyl Uridine 5′-Phosphorothioate (**19**).* The diammonium salt of **14** (0.01 mmol) was rendered anhydrous as described in the above experiment. The dried material was mixed with diphenyl disulfide (2.6 mg, 0.012 mmol) and dissolved in dry pyridine (0.5 ml). BSA (0.2 ml) was added and the solution was kept at room temperature for 30 min. Water (0.5 ml) was added and the mixture was kept at room temperature for 1 h. Paper chromatography on Whatman 3 MM papers using Solvent IV gave a band of **19** (R_f 0.52, 100 OD, 94%): R_m (Buffer I); $UV_{max}^{pH\ 7.0}$ 244,

260 nm, $UV_{min}^{pH\ 7.0}$ 231, 251 nm. This compound was identified with the authentic sample obtained by the reaction of **15** with diphenyl disulfide in the presence of triethylamine and trimethylsilyl chloride in pyridine followed by treatment with 80% acetic acid.

*Uridine 5'-Phosphate (**20**).* The above mentioned reaction was done by using 2,2'-dipyridyl disulfide (2.7 mg, 0.012 mmol) in place of diphenyl disulfide. The usual work-up gave **20** (96 OD, 95%): R_f 0.10 (Solvent IV). $UV_{max}^{pH\ 7.0}$ 261 nm, $UV_{min}^{pH\ 7.0}$ 230 nm. The compound was identified with the authentic sample.

*Uridine 5'-(1-Hydroxy-2-methylpropyl)phosphonate (**21**).* The ammonium salt of **12** (0.038 mmol) was converted to **14** according to the method described before. Compound **14** was rendered anhydrous by repeated coevaporation with dry pyridine and dissolved in dry THF (1 ml). BSA (0.114 ml) was added and the mixture was kept at room temperature for 20 min. Then, isobutyraldehyde (0.066 ml) was added and the mixture was stirred for 3 h. The solution was applied to Whatman 3 MM papers and chromatographed using Solvent IV. A band of R_f 0.39 was cut and eluted with water (100 ml) to give the ammonium salt of **21** (323 OD, 84%): $UV_{max}^{pH\ 7.0}$ 262 nm, $UV_{min}^{pH\ 7.0}$ 231 nm; NMR (D_2O) δ 0.84 (d, 6H, J_{H-H}=6.4 Hz, $(CH_3)_2C$), 1.88 (m, 1H, CHCP), 3.42 (dd, 1H, J_{H-H}=5.4 Hz, J_{P-H}=8.9 Hz, CHP), 3.73—4.29 (m, 6H, 2',3',4'-H and 5'-H), 5.72 (d, 1H, J_{H-H}=8.4 Hz, 6-H), 5.76 (s, 1H, 1'-H), 7.80 (d, 1H, J_{H-H}=8.4 Hz, 5-H).

*2',3'-O-Isopropylideneuridine 5'-Phosphonate (**15**).* The ammonium salt of **11** (0.1 mmol) was dissolved in 1 M NaOH (1 ml). After being kept at room temperature for 5 min, the solution was neutralized with DIAION SK 1B (pyridinium salt). The resin was washed with water (20 ml). The eluent was concentrated and diluted with pyridine–H_2O (2:1, v/v) to 10 ml. The analysis by paper electrophoresis and TLC showed that **16** [R_m 1.44 (Buffer I); R_f 0.36 (Solvent I)] was obtained. The solution was evaporated and rendered anhydrous by repeated coevaporation with dry pyridine. The residue was dissolved in dry THF (1 ml) and triethylamine (0.084 ml, 0.6 mmol) and trimethylsilyl chloride (0.076 ml, 0.6 mmol) were added. After being kept at room temperature for 5 min, the solution was analyzed by paper electrophoresis, which showed that **15** [R_f 0.76 (Solvent III): R_m 0.95 (Buffer I); $UV_{max}^{pH\ 7.0}$ 262 nm, $UV_{min}^{pH\ 7.0}$ 231 nm] was obtained in 86% yield.

*Removal of Phosphonate Group from **13**.* Compound **13** (0.05 mmol) was dissolved in 80% acetic acid (100 ml). The solution was heated at 100 °C for 2 h and then cooled to room temperature. After the solvent was removed *in vacuo*, the residue was chromatographed on Whatman 3 MM paper (Solvent IV) to give a band of R_f 0.75 which was eluted with water and identified with the authentic sample of uridine. The yield was spectrophotometrically estimated to be 90%.

References

1) This paper participates as Part XIX in the series of silyl phosphites. Part XVIII: M. Sekine, M. Nakajima, A. Kume, A. Hashizume, and T. Hata, *Bull. Chem. Soc. Jpn.*, **55**, 224 (1982).
2) T. Hata and M. Sekine, *J. Am. Chem. Soc.*, **96**, 7363 (1974).
3) T. Hata and M. Sekine, *Tetrahedron Lett.*, **1974**, 3943.
4) M. Sekine and T. Hata, *Tetrahedron Lett.*, **1975**, 1711.
5) T. Hata, M. Sekine, and N. Kagawa, *Chem. Lett.*, **1975**, 635.
6) A. F. Rosenthal, L. A. Vogas, Y. A. Isaacson, and R. Bittman, *Tetrahedron Lett.*, **1975**, 977.
7) T. Hata, I. Yamamoto, and M. Sekine, *Chem. Lett.*, **1976**, 601.
8) D. E. Gibbs, *Tetrahedron Lett.*, **1977**, 679.
9) M. Sekine, I. Yamamoto, A. Hashizume, and T. Hata, *Chem. Lett.*, **1977**, 485.
10) M. Sekine, K. Okimoto, and T. Hata, *J. Am. Chem. Soc.*, **100**, 1001 (1978).
11) M. Sekine and T. Hata, *Chem. Commun.*, **1978**, 285.
12) J. A. Schofield and A. R. Todd., *J. Chem. Soc.*, **1961**, 2316.
13) A. M. Michelson, "The Chemistry of Nucleosides and Nucleotides" Academic Press, London (1963).
14) A. Holy and F. Sorm, *Collect. Czech. Chem. Commun.*, **31**, 1544 (1966).
15) A. Holy and F. Sorm, *Collect. Czech. Chem. Commun.*, **31**, 1562 (1966).
16) H. Pischel and A. Holy, *Collect. Czech. Chem. Commun.*, **35**, 3584 (1970), and references therein.
17) M. Yoshikawa, M. Sakuraba, and K. Kusashio, *Bull. Chem. Soc. Jpn.*, **43**, 456 (1970).
18) D. M. Brown and P. R. Hammond., *J. Chem. Soc.*, **1960**, 4229, 4232.
19) A. J. Kirby, *Chem. Ind.*, **1963**, 1877.
20) N. S. Corby, G. W. Kenner, and A. R. Todd., *J. Chem. Soc., C*, **1952**, 3669.
21) G. W. Kenner, A. R. Todd, and F. J. Weymouth, *J. Chem. Soc.*, **1952**, 3675.
22) T. Mukaiyama, H. Koba, and K. Kodera, *Bull. Chem. Soc. Jpn.*, **39**, 2721 (1966).
23) G. M. Blackburn, J. S. Cohen, and A. R. Todd., *J. Chem. Soc., (C)*, **1966**, 240.
24) M. Sekine, H. Mori, and T. Hata, *Tetrahedron Lett.*, **1979**, 1145.
25) S. Warren and M. R. Williams, *J. Chem. Soc., B*, **1971**, 618.
26) N. Katagiri, K. Itakura, and S. A. Narang, *J. Am. Chem. Soc.*, **97**, 7332 (1971).
27) In this case, 5-bromination of the uracil part occurred but the ethoxycarbonyl group itself remained intact.
28) R. Lohrmann and H. G. Khorana, *J. Am. Chem. Soc.*, **88**, 829 (1966).
29) C. A. Hanes and F. A. Isherwood, *Nature*, **164**, 1107 (1949).
30) M. Sekine, K. Okimoto, K. Yamada, and T. Hata, *J. Org. Chem.*, **46**, 2097 (1981).

 © 1982 The Chemical Society of Japan Bull. Chem. Soc. Jpn., 55, 243—246 (1982)

Synthesis and Reactions of *o*-Naphthothioquinone Methides

Renji Okazaki,* Kazuhiko Sunagawa, Mitsuharu Kotera,
Kyung-Tae Kang, and Naoki Inamoto

Department of Chemistry, Faculty of Science, The University of Tokyo, Hongo, Bunkyo-ku, Tokyo 113

(Received June 5, 1981)

Photochemical reactions of naphtho[1,2-*c*][1,2]dithiole-3-thione (**7**), naphtho[2,1-*c*][1,2]dithiole-1-thione (**10**), and naphtho[2,3-*c*][1,2]dithiole-3-thione (**16**) with cyclohexene and 2,3-dimethyl-2-butene afford the corresponding naphthothioquinone methides. The thioquinone methide from **7** exists only as a monomeric form and is the first isolable *o*-thioquinone methide, while that from **16** exists as a dimer of [4+4] type in the solid state although the chemical behavior suggests the presence of a monomeric form in solution to a very minor extent. In the case of the thioquinone methide from **10**, there exists an equilibrium between a monomer and a dimer of [4+2] type. Some cycloadditions of these thioquinone methides are also described.

In a previous report,[1] we described the photochemical formation of *o*-benzothioquinone methides (**2**) from benzo-1,2-dithiole-3-thione (**1**) and olefins and their some reactions. The deep blue thioquinone methide **2** is equilibrated with colorless dimer **3**, thus representing a unique thermochromic system.

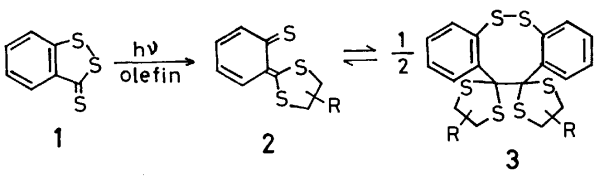

The pure monomeric *o*-thioquinone methide **2**, however, could not be obtained although its existence in solution was established by spectroscopic data and chemical reactions.

The study described in this paper was initiated in the hope that (i) three isomers (*i.e.* **4**, **5**, and **6**), are possible for the naphtho analog of **2** and comparison of them would shed light on the detailed properties of the *o*-thioquinone methide, (ii) **4** and **5** are reasonably expected to be more stable than **2** and hence they might be isolated as monomer.[2]

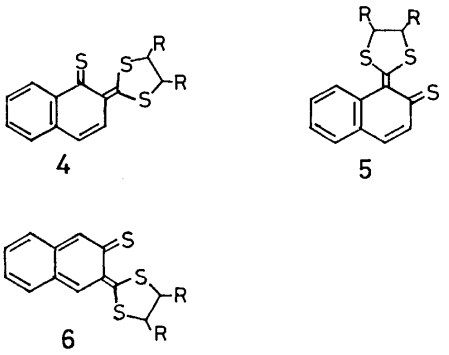

Results and Discussion

Photoreaction of Naphtho[1,2-c][1,2]dithiole-3-thione (7) with Cyclohexene. Irradiation of **7** in the presence of cyclohexene afforded thioquinone methide **4** (RR= $(CH_2)_4$ hereafter in this paper unless otherwise noted) as deep purple cyrstals in a quantitative yield. The monomeric nature of **4** was established by molecular weight determination (Found 319; Calcd 316.5) and by electronic spectrum (λ_{max} 323 (ε 24300), 353 (10800), 392 (sh, 2540), and 540 nm (11800)), which showed no concentration dependence. This is the first example of isolation of stable *o*-thioquinone methide. Reaction of **4** with *N*-phenylmaleimide gave 1:1-adduct **8** in 83% yield.

Photoreaction of **7** with 2,3-dimethyl-2-butene also

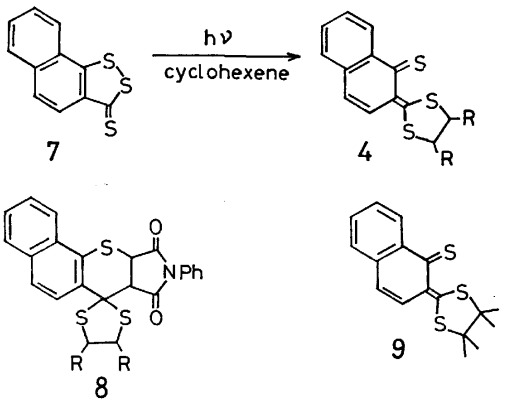

gave deep violet thioquinone methide **9** in a quantitative yield. Here also, there was no evidence which indicated the presence of a dimeric form; the NMR spectrum showed only two resonances due to the methyl group with the intensity ratio of 1:1.[3]

Photoreaction of Naphtho[2,1-c][1,2]dithiole-1-thione (10) with Cyclohexene. Irradiation of **10** with cyclohexene led to a deep red solution, the thin layer chromatography (TLC) of which showed the presence of a single product together with a small amount of the starting **10**. The addition of *N*-phenylmaleimide to the reaction mixture affords 1:1-adduct **12** (54%), the structure of the red compound thus being established as **5**. Purification of the reaction mixture by

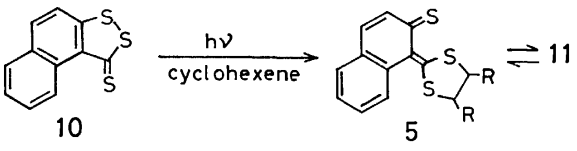

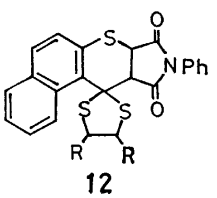

dry column chromatography (DCC) to remove **10**, however, resulted in the formation of a yellow crystalline compound **11** besides the red compound **5** (total yield 95%).

A sample rich in the yellow compound **11** could also be obtained by heating the solution of the red compound **5** at about 60 °C and subsequent cooling. Therefore, attempts to obtain pure **5** by TLC or recrystallization always formed the yellow compound, thus precluding us to get a completely pure specimen of **5**. However, almost pure **5** was obtained by TLC purification and a strong absorption at longer wavelength (496 nm (ε *ca.* 5000)) in the electronic spectrum is consistent with the monomeric structure. The yellow compound **11** free from **5** was obtained by purification with TLC, and was identified as a dimer of **5** on the basis of molecular weight determination (Found 666; Calcd 633) and its reversion to **5** by heating. When the benzene solution of **11** and *N*-phenylmaleimide was heated at about 60 °C, **12** was formed in 64% yield. The structure of the dimer **11** was established as [4+2] adduct **13** or **14** in the following way. The visible absorption at 450 nm (ε 9540) eliminates the possibility of [4+4] dimer, [2+2] dimer other than **15**, and [4+2] dimer other than **13** and **14**, since the [4+4] dimer has only naphthalene chromophore and the dimers of the latter two types have a conjugated thione system which would show an n-π^* absorption around 570 nm.[4] The NMR spectrum with intensity ratio of the aromatic to the olefinic protons of 10:2 rules out the structure **15**. Although we can not determine which of **13** or **14** is correct, the head-to-head structure in **3** suggests that the [4+2] dimer probably has the disulfide structure **13**.

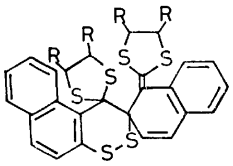

13

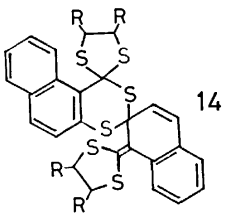

14

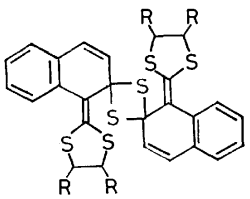

15

*Photoreaction of Naphtho[2,3-c][1,2]dithiole-3-thione (**16**) with Cyclohexene.* Irradiation of **16** in the presence of cyclohexene afforded **17a** (61%) and **18** (RR=$(CH_2)_4$, R′=H) (3.8%) as white and yellow crystals, respectively.

The compound **17a** was found to be [4+4] dimer of naphthothioquinone methide **6a** (RR=$(CH_2)_4$, R′=H), on the basis of molecular weight determination (Found 629; Calcd 632) and the spectral and analytical data. The UV (λ_{max} 243 (sh, ε 18300), 339 (2340), and 374 nm (sh, 488)) and NMR spectra indicated only the presence of naphthalene and cyclohexane rings, thus [4+4] adducts **19a** (RR=$(CH_2)_4$, R′=H) and **20a** (RR=$(CH_2)_4$, R′=H) remaining as possible structures for the photoproduct **17a** to the exclusion of [4+2] and [2+2] adducts.

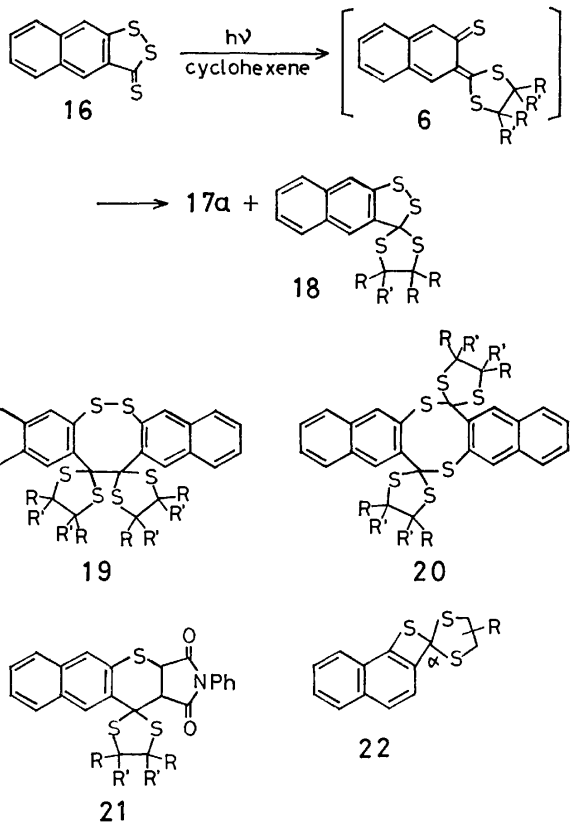

Desulfurization with Raney nickel resulted in the formation of 1,2-di(2-naphthyl)ethane (4.6%) along with 2-methylnaphthalene (29.8%), suggesting that the dimer is of head-to-head type **19** as in the case of the benzo counterpart.[1] The dimer **17a** reacts with *N*-phenylmaleimide in benzene at room temperature for a month or at 80 °C for 1 h to afford white crystals **21** which is derived from the monomer **6a**.

This fact shows that **19a** is dissociated to the monomer **6a** in solution to a very minor extent in spite of the absence of any color due to the monomer **6a** even upon heating at 80 °C.

In order to observe the monomeric naphthothioquinone methide,[5] a similar photoreaction of **16** with 2,3-dimethyl-2-butene in dichloromethane was carried out at −78 °C, but the color due to monomer **6b** (R=R′=CH_3) was not observed, suggesting that *o*-thioquinone methide of this type is too unstable to be observed even at such a low temperature. This photoreaction in benzene at about 0 °C afforded a dimer **19b** (R=R′=CH_3) in 81%.

Since irradiation of **19a** afforded **18** (75%), the formation of **18** in the photoreaction of **16** with cyclohexene described above is due to a secondary photodecomposition of **19a**. The compound **18** reacted with triphenylphosphine to give **19a** and triphenylphosphine sulfide, indicating that such a 1,2-dithiole as **18** is a good precursor of the *o*-thioquinone methide,

which has been demonstrated in our recent report.[6]

Comparison of the Stability of the Three Isomeric Naphthothioquinone methides **4**, **5**, *and* **6**. The above results indicate that the stability of monomeric naphthothioquinone methides **4**, **5**, and **6** is in the order of **4**>**5**>**6**. The instability of **6** compared with **4** and **5** is reasonable in view of the loss of aromaticity in the former structure.[7] The lower stability of **5** than **4** is probably attributed to the steric interaction of the dithiolane ring with the peri hydrogen; dimerization would reduce such an interaction to some extent. The difference in structure of the dimer between benzo **2** and naphtho system **5** (*i.e.* [4+4] *vs.* [4+2]) may also be due to strong steric interaction between the dithiolane ring and the aromatic ring in [4+4] adduct of the latter. The isolation of **4** and **5** suggests that an isomeric naphthothiete structure like **22** is rendered less stable than the corresponding *o*-thioquinone methide structure by the presence of two sulfur atoms on the α carbon. Some benzothietes have recently been reported to be stable isolable compounds.[8]

Experimental

All the melting points were not corrected. NMR spectra were recorded with a Hitachi R-20B or R-24 spectrometer using tetramethylsilane as an internal standard. Electronic spectra were recorded on a Hitachi EPS-3 spectrophotometer. IR spectra were taken with a Hitachi EPI-G2 spectrometer. Mass spectra were measured with a Hitachi RMU-6L spectrometer (beam energy 70 eV). High pressure liquid chromatography was done with a Hitachi 634 liquid chromatograph (column: Hitachi 3010). Molecular weight were measured with a Hitachi 117 Molecular Weight Apparatus (vapor pressure osmometry in benzene at 40 °C). All the photoreactions were carried out using Pyrex-filtered light (100 W medium pressure mercury lamp) while nitrogen was being bubbled through the reaction solution during the reaction. Thin layer (TLC), preparative layer (PLC), and dry column chromatography (DCC) were performed with silica gel.

*Photoreaction of Naphtho[1,2-c][1,2]dithiole-3-thione (***7***) with Cyclohexene.* The dithiolethione **7**[9] (534 mg, 2.3 mmol) and cyclohexene (7 cm³) were dissolved in 70 cm³ of benzene and the solution was irradiated for 90 min. The evaporation of the solvent gave the thioquinone methide **4** (713.6 mg, *ca.* 100%): mp 153.8—155.3 °C (from ethanol); NMR ($CDCl_3$): δ=1.1—2.3 (8H, m), 3.7—4.2 (2H, m), 7.05 (1H, B part of AB quartet, J=10 Hz), 7.42—7.53 (4H in total, m), 7.68 (1H, A part of AB quartet, J=10 Hz), and 8.8—9.0 (1H, m); UV (CH_2Cl_2): 323 (ε 24300), 353 (10800), 392 (sh, 2540), and 540 nm (11800); molecular weight, Found: 319; Calcd for $C_{17}H_{16}S_3$: 316. Found: C, 64.21; H, 4.97; S, 29.92%. Calcd for $C_{17}H_{16}S_3$: C, 64.51; H, 5.10; S, 30.39%.

Reaction of **4** *with* N-*Phenylmaleimide.* The thioquinone methide **4** (55 mg, 0.17 mmol) and *N*-phenylmaleimide (36 mg, 0.24 mmol) were dissolved in 16 cm³ of benzene and the solution was allowed to stand for 1 d at room temperature. The evaporation of the solvent and PLC (CH_2Cl_2) of the residue gave **8** (71.1 mg, 83%): mp 235.0—237.0 °C (dec) (from ethanol); NMR ($CDCl_3$): δ=1.1—2.2 (8H, m), 3.6—4.0 (2H, m), 4.53 (2H, s), 6.7—8.0 (9H, m), and 8.2—8.6 (2H, m); IR (KBr): 1710 cm^{-1} (C=O); MS: *m/e* (rel intensity) 489 (M^+, 14) and 234 (100). Found: C, 66.29; H, 4.76; N, 2.98; S, 19.39%. Calcd for $C_{27}H_{23}NO_2S_3$: C, 66.23; H, 4.74; N, 2.86; S, 19.64%.

*Photoreaction of Naphtho[2,1-c][1,2]dithiole-1-thione (***10***) with Cyclohexene.* The dithiolethione **10**[9] (350 mg, 1.5 mmol) and cyclohexene (7 cm³) were dissolved in 70 cm³ of benzene and the solution was irradiated for 45 min. After the irradiation, the color of the solution turned deep red. The TLC of the reaction mixture showed a single product, **5**. The solution was evaporated and DCC (CCl_4) of the residue gave a mixture of **5** and **11** (450.5 mg, 95%), as indicated by TLC.

Pure **11** free from **5** was obtained by TLC (CH_2Cl_2) and subsequent recrystallization from ethanol and dichloromethane at −78 °C, and **5** which contained a small amount of **11** was obtained by TLC (CH_2Cl_2): **5**; NMR ($CDCl_3$): δ=1.0—2.5 (8H, m), 3.2—4.2 (2H, m), 7.3—8.2 (5H, m), and 8.3—8.6 (1H, m); UV (CH_2Cl_2): 235 (ε 23900), 263 (17800), 295 (12100), 327 (7160), 392 (sh, 3170), 412 (4440), and 496 nm (4630); **11**; mp 119.0—121.0 °C (from CH_2Cl_2 and ethanol); NMR ($CDCl_3$): δ=1.0—2.5 (16H, m), 3.5—4.2 (4H, m), 6.82 (1H, B part of AB quartet, J=9 Hz), 7.2—8.1 (11H in total, m), and 7.55 (1H, A part of AB quartet, J=9 Hz); UV (CH_2Cl_2): 263 (ε 19400), 354 (sh, 4650), and 450 nm (9540); molecular weight, Found: 666; Calcd: 632. Found: C, 63.91; H, 5.15; S, 30.28%. Calcd for $C_{34}H_{32}S_6$: C, 64.51; H, 5.10; S. 30.39%.

Reaction of **5** *and* **11** *with* N-*Phenylmaleimide.* The thioquinone methide **5** (26.6 mg, 0.08 mmol) and *N*-phenylmaleimide (19.5 mg, 0.11 mmol) were dissolved in 20 cm³ of benzene and the solution was kept at 63 °C for 8.5 h under nitrogen atmosphere. The solvent was evaporated and the residue was subjected to PLC (benzene) to give **12** (22.1 mg, 54%). A benzene solution of **11** (91.5 mg, 0.14 mmol) and *N*-phenylmaleimide (63.9 mg, 0.37 mmol) was kept at 63 °C under nitrogen atmosphere for 8.5 h. The solvent was evaporated and the residue was subjected to PLC (benzene) to give **12** (90.5 mg, 64%): mp 238.0—239.5 °C (dec) (from ethanol); NMR ($CDCl_3$): δ=1.0—2.5 (8H, m), 3.8—4.2 (2H, m), 4.62 (AB q, 2H, J=9 Hz), and 6.8—8.0 (11H, m); IR (KBr): 1720 cm^{-1} (C=O). Found: C, 65.87; H, 4.69; N, 3.08%. Calcd for $C_{27}H_{23}NO_2S_3$: C, 66.23; H, 4.74; N, 2.86%.

*Photoreaction of Naphtho[2,3-c][1,2]dithiole-3-thione (***16***) with Cyclohexene.* The dithiolethione **16**[10] (1.02 g, 4.4 mmol) and 14 cm³ of cyclohexene were dissolved in 200 cm³ of benzene and the solution was irradiated for 100 min. The solution was concentrated to afford white crystals of **19a** (531 mg), which contained one molecule of benzene as solvent of crystallization. The filtrate was subjected to DCC (CH_2Cl_2–CCl_4 1:9) to give **18** (27.9 mg, 3.8%) and **19a** (463 mg), which contained one molecule of CCl_4 as solvent of crystallization. The total yield of **19a** was 994 mg (61%). It was recrystallized from CH_2Cl_2 and the crystals contained one molecule of CH_2Cl_2 as solvent of crystallization: **19a**; mp 200.0—201.0 °C (dec) (from CH_2Cl_2); NMR (in C_6D_6 at 80 °C): δ=1.65 (16H, s), 4.47 (4H, s), 6.7—7.4 (8H, m), 8.15 (1H, bs), 8.26 (1H, bs), 8.38 (1H, bs), and 8.47 (1H, bs); (in CS_2 at 50 °C): δ=1.3—2.3 (16H, m), 3.0—4.5 (4H, m), 7.0—7.7 (8H, m), 7.7—7.9 (2H, m), 7.98 (1H, bs), and 8.07 (1H, bs): UV (CH_2Cl_2): 243 (sh, ε 18300), 339 (2340), and 374 nm (sh, 488); molecular weight, Found: 629; Calcd: 632. Found: C, 58.74; H, 4.99; S, 26.92; Cl, 10.08%. Calcd for $C_{35}H_{34}S_6Cl_2$: C, 58.55; H, 4.77; S, 26.80; Cl, 9.88%. **18**; mp 139—145 °C (from ethanol); NMR ($CDCl_3$): δ=1.2—2.5 (8H, m); 3.8—4.3 (2H, m), 7.2—8.0 (4H, m), 7.70 (1H, s), and 7.99 (1H, s); UV (CH_2Cl_2): 258 (ε 22000), 285 (sh, 13000),

and 342 nm (2750); molecular weight, Found: 355; Calcd: 348; MS: *m/e* (rel intensity) 348 (M^+, 36) and 266 (100). Found: C, 58.58; H, 4.63; S, 36.79%. Calcd for $C_{17}H_{16}S_4$: C, 58.37; H, 4.48; S, 36.63%.

*Photoreaction of **16** with 2,3-Dimethyl-2-butene.* The dithiolethione **16** (1 g, 4.3 mmol) and 5 cm^3 of 2,3-dimethyl-2-butene were dissolved in 80 cm^3 of benzene and the solution was irradiated for 20 min. The solvent was removed and DCC (CCl_4–CH_2Cl_2 5:1) of the residue gave yellow crystals **19b**. The product contained one molecule of CCl_4 as solvent of crystallization. The yield was 1.52 g (81%). The pure product free from CCl_4 was obtained by recrystallization from CS_2 and ethanol: **19b**; mp 172.0—173.5 °C (dec) (from CS_2 and ethanol); NMR ($CDCl_3$): δ=1.22 (6H, bs), 1.35 (6H, bs), 1.66 (6H, bs), 1.78 (6H, bs), 7.1—7.7 (8H, m), 7.87 (2H, s), and 8.28 (2H, s). Found: C, 63.75; H, 5.61; S, 30.28%. Calcd for $C_{34}H_{36}S_6$: C, 64.10; H, 5.70; S. 30.20%.

*Reaction of **19a** with N-Phenylmaleimide.* The dimer **19a** (22.4 mg, 0.06 mmol) and *N*-phenylmaleimide (12.5 mg, 0.07 mmol) were dissolved in 16 cm^3 of benzene and the solution was allowed to stand for 17 d at room temperature. After removal of the solvent, PLC (hexane–ether 1:1) of the residue gave **21** (33 mg, 94%). *N*-Phenylmaleimide (44.4 mg, 0.26 mmol) and **19a** (33 mg, 0.09 mmol) were dissolved in 20 cm^3 of benzene and the solution was refluxed for 1 h. The solvent was evaporated and the residue was recrystallized from benzene to give white crystals **21** (42.2 mg, 83%): mp 258.0—259.5 °C (dec) (from CH_2Cl_2); NMR ($CDCl_3$): δ=1.0—2.3 (8H, m), 3.5—4.4 (2H, m), 4.70 (2H, s), 6.7—7.0 (3H, m), 7.0—8.2 (7H, m), 8.70 (1H, s); NMR (DMSO-d_6): δ=1.2—2.1 (8H, m), 3.8—4.3 (2H, m), 4.70 (2H, s), 6.5—6.9 (3H, m), 7.2—8.1 (7H, m), and 8.68 (1H, s); IR (KBr): 1716 cm^{-1} (C=O); MS: *m/e* (rel intensity) 489 (M^+, 6) and 234 (100). Found: C, 66.30; H, 4.68; N, 2.93%. Calcd for $C_{27}H_{23}NO_2S_3$: C, 66.23; H, 4.74; N, 2.86%.

*Desulfurization of **19a** by Raney Nickel.* Under nitrogen atmosphere at 30 °C, **19a** (206 mg, 0.29 mmol) was added to Raney Ni (W-4), prepared from 20 g of Raney Ni alloy, in 100 cm^3 of benzene and the mixture was kept stirring for 45 min. After **19a** was consumed, the mixture was refluxed for 30 min. Raney Ni was removed by filtration and 1,2-di(2-naphthyl)ethane and 2-methylnaphthalene were analyzed for the filtrate with high pressure liquid chromatography by comparison with authentic samples (solvent: NH_3–MeOH 1:10 for 1,2-di(2-naphthyl)ethane; NH_3–MeOH 1:19 for 2-methylnaphthalene). The yields of 1,2-di(2-naphthyl)ethane and 2-methylnaphthalene were 4.6 and 29.8%, respectively. 1,2-Di(2-naphthyl)ethane was prepared by bromination (*N*-bromosuccinimide) of 2-methylnaphthalene followed by coupling with magnesium; mp 194—194.3 °C ($CHCl_3$).

*Photolysis of **19a**.* A benzene solution (50 cm^3) of **19a** (50 mg, 0.14 mmol) was irradiated for 100 min. The solvent was evaporated and the residue was subjected to PLC (benzene) to give **18** (17.8 mg, 75%). The spectral data of **18** were in agreement with those obtained in the photoreaction of **16** with cyclohexene.

*Desulfurization of **18** with Triphenylphosphine.* Triphenylphosphine (116 mg, 0.44 mmol) and **18** (128 mg, 0.37 mmol) were dissolved in 30 cm^3 of benzene and the solution was allowed to stand for 1 d at room temperature. The solvent was removed and PLC (benzene–hexane 1:1) of the residue gave **19a** and triphenylphosphine sulfide quantitatively.

*Photoreaction of **16** with Olefins at −78 °C.* The dithiolethione **16** (29 mg, 0.12 mmol) and 0.5 cm^3 of cyclohexene were dissolved in 5 cm^3 of dichloromethane and the solution was irradiated at −78 °C for 90 min, but the color derived from **6** was not observed. Dichloromethane solution (5 cm^3) of **16** (5 mg, 0.02 mmol) and 2,3-dimethyl-2-butene (0.5 cm^3) was irradiated for 30 min under the same conditions. However, the color of **6** was not observed.

References

1) R. Okazaki, K. Sunagawa, K.-T. Kang, and N. Inamoto, *Bull. Chem. Soc. Jpn.*, **52**, 496 (1979); see also, P. de Mayo and H. Y. Ng., *Can. J. Chem.*, **55**, 3763 (1977).

2) A part of work described in this paper was published in a preliminary form. R. Okazaki, K. Sunagawa, M. Kotera, and N. Inamoto, *Tetrahedron Lett.*, **1976**, 3815.

3) The dimeric photoproducts of **1**[1] and **16** (*i.e.* **19b**) with 2,3-dimethyl-2-butene show four different methyl signals in their NMR spectra.

4) D. H. R. Barton, L. S. L. Choi, R. H. Hesse, M. M. Pechet, and C. Wilshire, *J. Chem. Soc., Perkin Trans. 1*, **1979**, 1166.

5) The results obtained for the benzothioquinone methide **2** indicate that the equilibrium between the monomer and the dimer is most favorable for the monomer in the case of the thioquinone methide obtained from 2,3-dimethyl-2-butene.[1] Therefore, we expected that the low temperature photolysis with 2,3-dimethyl-2-butene might give a chance to observe a deep blue (or purple) color expected for a monomer.

6) K.-T. Kang, R. Okazaki, and N. Inamoto, *Bull. Chem. Soc. Jpn.*, **52**, 3640 (1979).

7) G. T. Gleicher, D. D. Newkirk, and J. C. Arnold, *J. Am. Chem. Soc.*, **95**, 2526 (1973).

8) W. J. M. van Tilborg and R. Plomp, *Rec. Trav. Chim. Pays-Bas*, **96**, 282 (1977); E. Voigt and H. Meier, *Chem. Ber.*, **110**, 2242 (1977).

9) L. Legrand, *Bull. Soc. Chim. Fr.*, **1959**, 1599.

10) L. Legrand, Y. Mollier, and N. Lozac'h, *Bull. Soc. Chim. Fr.*, **1953**, 327.

Ring Opening of Oxiranes by Trimethylsilyl Trifluoromethanesulfonate†

Sizuaki MURATA, Masaaki SUZUKI, and Ryoji NOYORI*
Department of Chemistry, Nagoya University, Chikusa-ku, Nagoya 464

(Received July 29, 1981)

Trimethylsilyl trifluoromethanesulfonate promotes ring opening reactions of oxirane derivatives. The reaction course is highly affected by the structures and substitution pattern of the substrates. Tetra-, tri-, and 2,2-disubstituted oxiranes and simple cycloalkene oxides are converted to the corresponding allylic alcohol trimethylsilyl ethers. The overall transformation is interpreted in terms of trans addition of the silyl trifluoromethanesulfonate to the oxirane ring followed by base-promoted anti elimination of a trifluoromethanesulfonic acid element. 2,3-Dialkyl- or monoalkyloxiranes isomerize to the corresponding ketones and aldehydes, respectively. (*Z*)-Cyclooctene oxide undergoes the transannular reaction to give *endo-cis*-2-trimethylsiloxybicyclo[3.3.0]octane. The reaction of 6-methyl-5-hepten-2-one oxide produces 2,2,6-trimethyl-3-trimethylsiloxy-3,4-dihydro-2*H*-pyran. 1,2-Methyl migration takes place in the reaction of (*E*)-3α-*t*-butyldimethylsiloxy-5α-pregnene 17α,20-oxide to afford 3α-*t*-butyldimethylsiloxy-17β-methyl-17α-[1-(trimethylsiloxy)ethyl]-18-nor-5α-androst-13(14)-ene. α-Pinene oxide gives *trans*-carveol trimethylsilyl ether.

Trimethylsilyl trifluoromethanesulfonate (triflate) (**1**)[1,2] is known as a powerful reagent for the silylation of various active hydrogen compounds such as alcohols, carbonyl compounds, imines, nitriles, *etc.*[3] The efficiency is based on the strong tendency of the trimethylsilyl moiety to coordinate to hetero atoms, particularly an oxygen atom, in the organic substrates. We have been intrigued by the reaction with oxiranes which possess a basic oxygen atom.[4] The strained oxonium salts of type **3**, formed from **1** and oxiranes (**2**), are anticipated to undergo a variety of unique transformations depending on the structures of the substrates and reaction conditions. This paper describes the silyl triflate promoted reactions of a series of oxirane substrates.

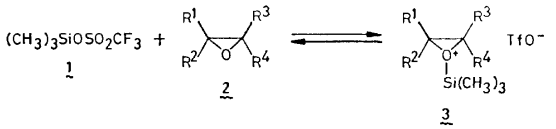

Results and Discussion

Conversion of Oxiranes to Allyl Trimethylsilyl Ethers.[5] Certain classes of oxiranes (**4**) were converted smoothly to the allyl trimethylsilyl ethers of type **5** by the treatment with **1** and a nitrogen base in aromatic hydrocarbon media. The trimethylsilyl group of **5** was easily removed by exposure to dilute hydrochloric acid or potassium fluoride in methanol to give the allylic alcohol **6**. Simple cycloalkene oxides were con-

verted to the allyl silyl ethers by exposure to a 1:1 mixture of **1** and 1,8-diazabicyclo[5.4.0]undec-7-ene (DBU) in benzene at ambient temperature (method A). Tetra-, tri-, and 2,2-dialkylated oxiranes are even more reactive and the ring opening reaction has been usually accomplished by the treatment with an equimolar mixture of **1** and 2,6-lutidine in toluene at temperatures as low as −78 °C and then with 1.2—1.3 equiv of DBU at room temperature (method B). Some examples are given in Table 1.

Although ketonic and ester substrates are susceptible to the silylation with **1** in the presence of a nitrogen base,[3] the oxirane ring is much more reactive under these reaction conditions and is cleaved in an ordinary manner, leaving these functions intact. The chemoselective transformations of the bifunctional substrates **17** and **19** illustrate this feature (entries 8 and 9). Oxiranes containing a hydroxyl function were converted to the bis(trimethylsilyl) ethers by using 2 equiv of **1** (entries 10—12).

The overall transformation, **4**→**5**, is accomplished *via* trans addition of **1** to the oxirane ring[6] followed by anti elimination of a TfOH element away from the trimethylsiloxy group. Under the present reaction conditions, trimethylsilylammonium triflates of type **31** or **32** may serve as active species.[7] Triflate,

though is a feeble nucleophile, displaces the oxirane ring activated through coordination of a trimethylsilyl group, giving the addition product. When an unsymmetrically alkylated oxirane is used, the triflate displacement takes place preferentially at the more substituted carbon atom. This regioselection is readily understood by considering the electronic properties of the silylated oxirane structure; the alkyl substitution decreases the relative magnitude of electron density at the carbon attached to it and increases the LUMO coefficient of the same carbon, resulting in enhancement of the electrophilic reactivity.[6]

When cyclohexene oxide (**9**) was treated with **1** equiv of **1** and triethylamine in hexane at room temperature, a single, labile product **33** was produced. The ^{1}H NMR spectrum exhibited Ha and Hb signals at δ 4.46 (ddd) and 3.57 (ddd) with the vicinal coupling constant of 10 Hz, substantiating the trans stereochemistry. Treatment of **33** with DBU led to the olefinic compound **10**. The production of the allyl silyl ether **10** (not an enol silyl ether) is a consequence

† Dedicated to Professor Hitosi Nozaki on the occasion of his 60th birthday.

of anti elimination of TfOH; the two conformers, **33a** and **33b**, are possible for **33**, but only the less stable conformer **33a** can undergo the E2 elimination reaction.[8] It is worth noting that such controlling factors display a unique selectivity in the reaction of certain cyclic trisubstituted oxirane derivatives. For instance, the reaction of 1-methylcyclohexene oxide (**34**) with **1** produces the initial adduct **35**. Since the TfO group locates in an equatorial position in the stable conformer, the base-promoted anti elimination of TfOH occurs selectively in such a way to produce **36** which possesses an exocyclic methylene group.[8e,f] In a like manner, the reaction of the steroidal substrate **37** with **1** and 2,6-di-*t*-butylpyridine afforded after desilylation the alcoholic product **38** exclusively.

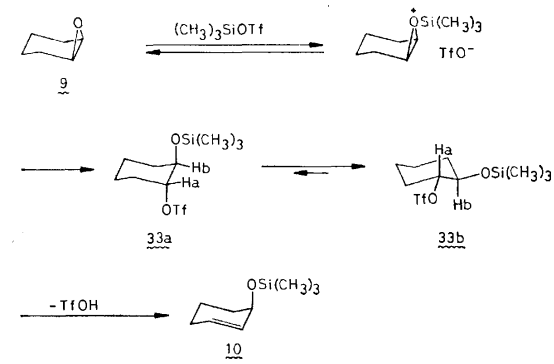

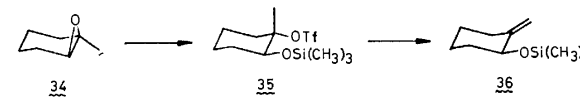

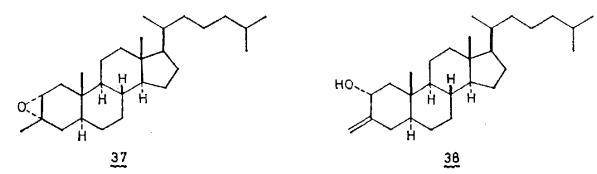

When a monocyclic oxirane is subjected to the displacement by **1**, a conformationally flexible adduct of type **39a**⇄**39b**⇄**39c** is formed. The E2 elimination reaction occurs from the most stable conformer **39a** in which the dipole repulsion is minimized, resulting in the regioselective formation of the allyl silyl ether. The stereoselective production of *E* dienes from geraniol or nerol 2,3-oxide (**23** and **25**, respectively) is interpreted in terms of the preference of the conformer **40a** over **40b**[8a-d] (entries 11 and 12).

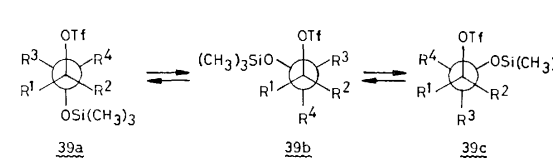

$R^1 = (CH_3)_2C{=}CHCH_2-$

$R^2 = (CH_3)_3SiOCH_2\underset{\displaystyle OSi(CH_3)_3}{\underset{|}{CH}}-$

Table 1. Conversion of oxiranes to allyl trimethylsilyl ethers

Entry	Orirane	Method	Product	Yield/%[a]
1	7	A	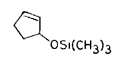 8	59[b]
2	9	A	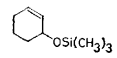 10	87
3	11	A	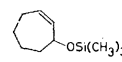 12	40, 100[c]
4	13	A	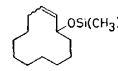 14	38
5		B	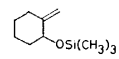	80
6	3β-Methyl-5α-cholest-2-ene 2α,3α-oxide	d)	3-Methylene-5α-cholestan-2α-ol trimethylsilyl ether	59,[e] 95[c]
7	15	B	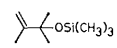 16	87[b]
8	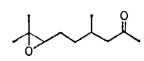 17	B	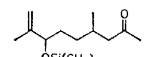 18	69
9	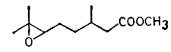 19	B	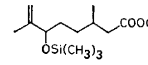 20	79
10	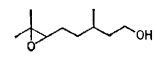 21	B	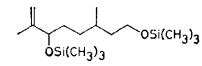 22	71
11	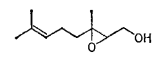 23	B	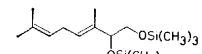 24	66
12	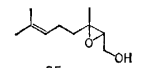 25	B	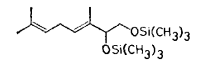 24	65
			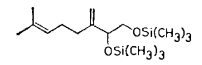 26	16
13	27	B	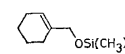 28	72
14	29	B	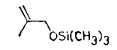 30	62[b]
15	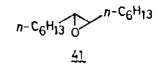 41	B[f]	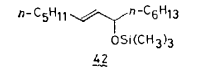 42	179[g]

a) Isolated yield. b) Determined by GLPC analysis. c) Based on consumed starting material. d) The reaction was carried out in toluene by using 2,6-di-*t*-butylpyridine as base. e) Isolated yield of desilylated product. f) The reaction was carried at 80 °C. g) A mixture of isomeric enol silyl ethers was obtained in 65% yield.

The oxirane to allylic alcohol conversion is an important operation from the synthetic point of view, and a number of effective reagents have been devised for this purpose. Oxiranes derived from five- to seven-membered cyclic olefins can be converted to the corresponding allylic alcohols by strongly basic lithium amide reagents in refluxing solvents.[9] The recently developed dialkylaluminum amides[10] and a dialkylboron triflate[11] are applicable to the reaction of *trans*-2,3-dialkylated or further alkylated oxiranes. These reagents are not utilized for the isomerization of the *cis*-2,3-dialkylated oxiranes, however. A mild, two-step procedure by the use of an organoselenium compound was also elaborated; reaction of oxiranes with sodium benzeneselenolate followed by oxidative deselenation of the addition products gives rise to the allylic alcohols.[12] Here when an unsymmetrically substituted oxirane is used, the ring opening occurs preferentially at the less substituted carbon atom, and the sense of the regioselection is opposite that observed in this work. The present procedure based on the use of the organosilicon compound **1** requires very mild reaction conditions and displays unique stereo-, regio-, and chemoselectivity. As such this method, complementary to the existing recipes, provides a useful tool in organic synthesis. It should be added that silyl iodides[13] and silyl selenides in the presence of a Lewis acid[14] behave in a similar manner in the reaction with oxiranes.

Isomerization of Oxiranes to Carbonyl Compounds. Unlike cycloalkene oxides, simple 2,3-dialkylated and monoalkylated oxiranes were inert to the standard reaction conditions. When these substrates with **1** added amines were subjected to the more forcing conditions, there were obtained the corresponding carbonyl compounds as exclusive or major products. For instance, reaction of 1-decene oxide with **1** and 2,6-lutidine in benzene at 80 °C led to decanal in 89% yield. Likewise, (*Z*)-7-tetradecene oxide was converted to 7-tetradecanone quantitatively. The reaction of the *E* isomer gave some allylic alcohol derivatives. Thus, reaction of (*E*)-7-tetradecene oxide (**41**) with **1** and 2,6-lutidine in benzene at 80 °C followed by treatment with DBU at room temperature afforded (*E*)-8-trimethylsiloxy-6-tetradecene (**42**) (17% yield) in addition to isomeric enol silyl ethers of 7-tetradecanone (65% combined yield) (Table 1, entry 15).[15] The isomerization to carbonyl compounds would proceed *via* carbocation intermediates. The oxonium species

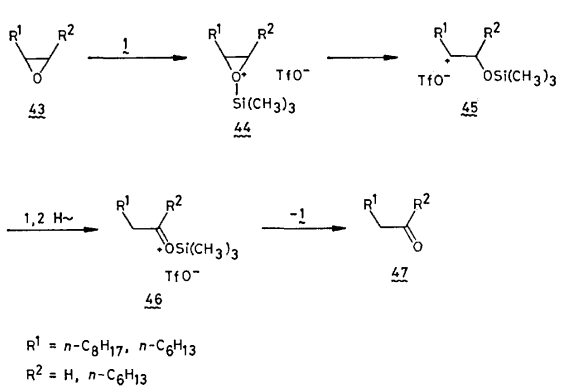

44, generated from a di- or monosubstituted oxirane **43**, is not reactive enough to suffer nucleophilic displacement by triflate anion.[5] When **44** is heated, however, it undergoes unimolecular C–O bond rupture to produce the unstable carbocation **45**,[16] which readily isomerizes to the stable carboxonium intermediate **46** *via* 1,2-hydride transfer. Subsequent desilylation gives rise to the carbonyl product **47**.

Reaction of Cyclooctene Oxide (48). In the presence of 2,6-lutidine the title reaction proceeded cleanly at room temperature to give the bicyclic compound **49** in quantitative yield. Although the mechanism has not yet been clarified, the carbene species **51** formed by base-aided α-elimination of the trimethylsilylated oxirane **50** seems to be an attractive candidate for the intermediate.[17] The lithium amide-generated carbene is known to undergo the same type of transannular reaction.[18] When reaction of **48** and **1** was conducted in the absence of any added amines, cyclooctanone was formed (87% yield), probably *via* a carbocation mechanism.

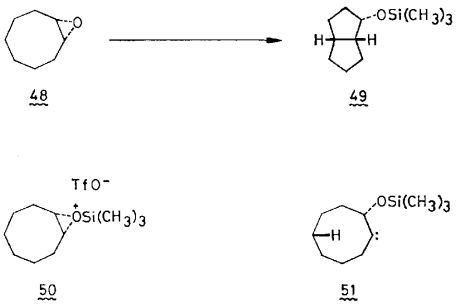

Neighboring Group Participation in the Oxirane Ring Opening. When oxirane substrates contain some nucleophilic atom or bond at a spatially suitable position, the ring opening is facilitated by electron release from such moiety.[19]

The keto oxirane **52** upon sequential treatments by a mixture of **1** and 2,6-lutidine and then by DBU underwent clean cyclization *via* carbonyl group participation to give the dihydropyran derivative **53** in 80% yield.

The carbon-carbon σ bond participation is exemplified by the reaction of the steroidal 17α,20-oxide **54** which affords after removal of the trimethylsilyl group the product **55** in 86% yield. Here the triflate attack on the silylated oxirane species is prevented by screening effect of the adjacent methyl group and, instead, this angular methyl undergoes 1,2-migration to form the rearranged product.[20]

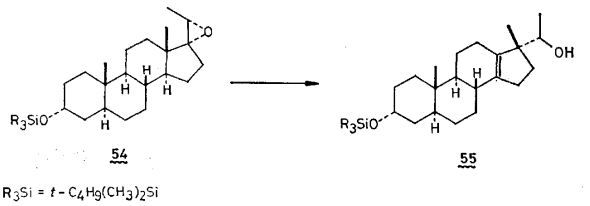

When α-pinene oxide (**55**) was exposed to a mixture of **1** and 2,6-lutidine and then DBU, there was obtained after desilylation *trans*-carveol (**57**) in 72% yield.[21] In addition, α-pinene (**58**), a deoxygenation product, was formed in 6% yield.

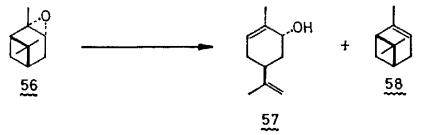

56 57 58

The recently discovered conformationally selective transannular cyclization of humulene 9,10-oxide (**59**) to the tricyclic compounds **60** and **61**[22,23] is an example of the C=C bond participation in the silyl triflate promoted ring cleavage.

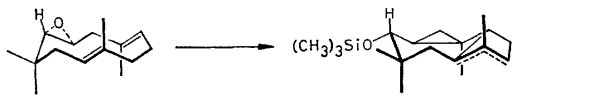

59 60 and 61 (two isomers)

Deoxygenation of Oxiranes. With certain oxirane substrates, the deoxygenation becomes a significant pathway. For example, squalene 2,3-oxide (**62**) was converted to squalene (**63**) in 70% yield by the treatment with **1** and 2,6-lutidine at −78 °C. The mechanism is unclear.[24]

62 63

Experimental

*General.*** Melting points and boiling points were uncorrected. IR spectra were recorded on a JASCO IR A-1 spectrometer in a noted phase. ^{1}H NMR spectra were determined on a Varian NV-21 or HA-100 spectrometer. Chemical shifts are reported as δ values in parts per million relative to tetramethylsilane=0. Splitting patterns are indicated as s, singlet; d, doublet; t, triplet; q, quartet; m, multiplet, and br means a broad signal. Mass spectra were determined on a JEOL D-100 spectrometer, operating with an ionization energy of 75 eV. Elemental analyses were performed at Department of Applied Chemistry, Nagoya University. All reactions using trimethylsilyl triflate (**1**) were carried out in a dried vessel under argon atmosphere. Unless otherwise stated, the organic extracts were dried by passing through a short column of anhydrous K_2CO_3. For concentration of solutions, unless otherwise stated, a vacuum (50—100 mmHg) rotary evaporator was used. Bulb-to-bulb short-path distillation was performed by using a Büchi Kugelrohrofen. The cited temperatures for these distillations refer to the maximum temperature attained by the oven during the distillation and are thus not true boiling points.

Chromatography. Silica gel 60 F_{254} precoated plates (E. Merck) at 0.25 mm thickness were used for both analytical and preparative TLC. Analytical plates were visualized by spraying with a solution of 2% $Ce(SO_4)_2$ in 5% H_2SO_4 or 2% *p*-anisaldehyde in 5% ethanolic H_2SO_4 followed by heating on a hot plate, or exposure to I_2 vapor. Column chromatography was conducted by using 70—230 mesh silica gel 60 available from E. Merck. In certain cases silica gel was used after ammonia treatment; silica gel was mixed with about 30% parts of 10% ammonia solution and then heated at 130 °C for 2 h. GLPC analyses were performed on a Hitachi 063 or 163 instrument, using nitrogen or helium as the carrier gas (9.807×10^4 Pa), respectively. A Varian 1700 instrument was used for preparative GLPC, using helium as the carrier gas (1.961×10^5 Pa).

Solvents and Materials. Trimethylsilyl triflate (**1**), prepared from chlorotrimethylsilane and trifluoromethanesulfonic acid,[2c] was distilled twice with *ca.* 1 vol% of triethylamine to remove all protic substances. Commercial oxiranes, **9**, **29**, and **48**, obtained from Tokyo Kasei Kogyo, Wako Junyaku, and Aldrich Chemical Co, respectively, were used without further purification. Oxiranes, **7**, **11**, **19**, **21**, **31**, **36**, **52**, **56**, 1-decene oxide, and (*Z*)- or (*E*)-7-tetradecene oxide were prepared from commercial alkenes by oxidation with 25% acetone solution of peracetic acid or 85% *m*-chloroperbenzoic acid in dichloromethane at 0 °C. The purities (>99%) of these oxiranes were confirmed by the ^{1}H NMR, GLPC, and TLC analises. Other oxiranes, **13**, **23**, **25**, **27**, **39**, **54**, and **62**, were prepared according to the procedures in the literatures.[10c, 25-29] DBU, 2,6-lutidine, and 2,6-di-*t*-butylpyridine were dried by distillation from CaH_2 before use. Benzene, toluene, and hexane were distilled from Na. Dichloromethane was distilled from P_2O_5. Other commercially supplied materials and solvents were used as received.

*Preparation of 4,8-Dimethyl-7-nonen-2-one Oxide (**17**).* To a 1.1 mol dm^{-3} ethereal solution of methylmagnesium bromide (70 ml, 0.077 mol) was added citronellal (10.0 g, 0.065 mol) dissolved in dry ether (50 ml) drop by drop over a period of 30 min at 0 °C. The mixture was stirred at 22 °C for 1 h and at reflux temperature for 3 h. The mixture was cooled to 0 °C and to this was added 1 mol dm^{-3} HCl (100 ml) slowly. The organic layer was separated and the aqueous layer was extracted with ether (50 ml × 2). The combined organic layers were dried over anhydrous $MgSO_4$ and concentrated. The residue was dissolved in acetone (300 ml) and to this was added a 3 M CrO_3 solution in 50% H_2SO_4 (150 ml) drop by drop at 0 °C. The mixture was poured into ice water (800 g) and extracted with ether (100 ml × 2) and benzene (100 ml × 3). The combined extracts were washed with saturated KNO_3, dried over anhydrous $MgSO_4$, and concentrated. Distillation (76—82 °C/3 mmHg) gave 4,8-dimethyl-7-nonen-2-one (7.68 g, 70%) as a colorless oil.

To a mixture of 4,8-dimethyl-7-nonen-2-one (3.00 g, 0.018 mol) thus obtained and anhydrous Na_2CO_3 (3.0 g) in dichloromethane (80 ml) was added in a dropwise manner a 2 mol dm^{-3} acetone solution of peracetic acid (11 ml, 0.022 mol) at 0 °C. After stirring at 0 °C for 4 h, the mixture was poured into water (300 ml). The organic layer was separated and the aqueous layer was extracted with dichloromethane (30 ml × 3). The combined organic layers were washed with saturated $NaHCO_3$ and twice with saturated Na_2SO_3, dried, and concentrated. Distillation (80—86 °C/1 mmHg) afforded pure **17** (2.81 g, 85%) as a colorless oil: IR (neat) 1716 cm^{-1} (C=O); NMR (CCl_4) 0.90 (3H, d, J=6.5 Hz, CH_3), 1.20 (3H, s, CH_3), 1.24 (3H, s, CH_3), 1.65—1.25 (5H, m, methylene and methine), 2.04 (3H, s, CH_3C=O), 2.27 (2H, triplet-like, J=7 Hz, CH_2C=O), and 2.51 (1H, t, J=5.2 Hz, CHO). Found:

** 1 mmHg≈133.3 Pa; 1 ml=0.001 dm^3.

C, 71.5; H, 10.7%. Calcd for $C_{11}H_{20}O_2$: C, 71.7; H, 10.9%.

*Reaction of Cyclopentene Oxide (**7**) with **1**.* To a solution of **1** (1.01 g, 4.56 mmol) in benzene (12 ml) was added a mixture of **7** (0.348 g, 4.13 mmol) and DBU (0.8 ml) in benzene (5 ml) drop by drop over a period of 5 min at 32 °C. The mixture was stirred for 19 h and then poured into 0.1 mol dm^{-3} HCl. The mixture was extracted with pentane (20 ml×3). The extracts were dried, concentrated at 200 mmHg, and chromatographed on a column of NH_3-treated silica gel, eluting with a 1:1 mixture of benzene and hexane, to afford pure **8** (0.236 g, 33%) as a colorless oil. GLPC analysis of the extracts on a column of 5% FFAP on Chromosorb W AW (3 mm×2 m) at 60 °C indicated the yield of **8** (t_R=2.3 min) to be 59%: IR (neat) 1251 cm^{-1}; NMR ($CDCl_3$) 0.14 (9H, s, CH_3Si), 2.5—1.4 (4H, m, two methylenes), 4.88 (1H, m, CHO), 5.71 (1H, br d, J=5.7 Hz, CH=), and 5.98 (1H, br d, J=5.7 Hz, CH=).

*Reaction of Cyclohexene Oxide (**9**) with **1**.* A mixture of **1** (2.26 g, 10.2 mmol), **9** (1.06 g, 10.7 mmol), and DBU (2 ml) in benzene (25 ml) was stirred at 22 °C for 20 h. The mixture was poured onto a column of NH_3-treated silica gel (15 g) and eluted by a 2:1 mixture of hexane and ether (300 ml). The eluate was cocentrated at 200 mmHg and distilled. Redistillation of the fraction boiling at 50—60 °C/50 mmHg gave pure **10** (1.51 g, 87%) as a colorless oil; IR (neat) 1250 cm^{-1}; NMR ($CDCl_3$) 0.13 (9H, s, CH_3Si), 2.1—1.2 (6H, m, methylene), 4.19 (1H, m, CHO), and 5.67 (2H, m, CH=).

*Reaction of Cyclohexene Oxide (**9**) with **1** in the Absence of DBU.* A mixture of **1** (0.225 g, 1.15 mmol), triethylamine (0.16 ml), and **9** (0.110 g, 1.12 mmol) in hexane (5 ml) was stirred at 21 °C for 10 h and then the solvent was removed at 1 mmHg. The adduct **35** (0.339 g) was obtained as a pale brown oil: NMR (CCl_4) 0.14 (9H, s, CH_3Si), 2.4—1.2 (8H, m, methylene), 3.57 (1H, ddd, J=10.0, 7.8, and 4.2 Hz, CHOSi), and 4.47 (1H, ddd, J=10.0, 7.8, and 4.0 Hz, CHOTf).

*Treatment of **35** with DBU.* The adduct **35** (0.339 g, 1.13 mmol) was mixed with DBU (0.3 ml) in benzene (5 ml) and the mixture was stirred at 21 °C for 18 h. This was then poured into water and extracted with hexane (5 ml×3). The extracts were dried and concentrated. Column chromatography on NH_3-treated silica gel, eluting with a 1:1 mixture of benzene and hexane, gave pure **10** (0.133 g, 71%).

*Reaction of Cycloheptene Oxide (**11**) with **1**.* A mixture of **1** (1.14 g, 5.01 mmol), **11** (0.506 g, 4.51 mmol), and DBU (1 ml) in benzene (15 ml) was stirred at 22 °C for 14 h. This was then poured into water and extracted with pentane (5 ml×3). The extracts were dried, concentrated, and chromatographed on a column of silica gel, eluting with a 1:1 mixture of benzene and hexane, to give **11** (0.298 g, 59%) and pure **12** (0.317 g, 40%, 100% based on consumed **11**): IR (neat) 1251 cm^{-1}; NMR ($CDCl_3$) 0.12 (9H, s, CH_3Si), 2.2—1.2 (8H, m, four methylenes), 4.38 (1H, m, CHO), and 5.68 (2H, m, CH=).

*Reaction of (E)-Cyclododecene Oxide (**13**) with **1**.* A mixture of **1** (0.502 g, 2.26 mmol), **13** (0.392 g, 2.15 mmol), and DBU (0.4 ml) in benzene (11 ml) was stirred at 27 °C for 40 h, and then to this was added a mixture of hexane (10 ml) and 0.1 mol dm^{-3} HCl (3 ml). The organic layer was separated and the aqueous layer was extracted with pentane (5 ml×6). The combined organic layers were washed with 0.1 mol dm^{-3} HCl and 5% $NaHCO_3$, dried, and concentrated. Column chromatography on silica gel, eluting with a 1:1 mixture of benzene and hexane, gave pure **14** (0.208 g, 38%): IR (neat) 1249 cm^{-1}; NMR (CCl_4) 0.12 (9H, s, CH_3Si), 2.5—1.2 (18H, m, nine methylenes), 3.94 (1H, br, CHO), and 5.28 (2H, m, CH=).

*Reaction of 2,3-Dimethyl-2-butene Oxide (**15**) with **1**.* To a solution of **1** (0.195 g, 0.88 mmol) and 2,6-lutidine (0.10 ml) in toluene (4 ml) was added **15** (0.105 g, 1.10 mmol) dissolved in toluene (1 ml) at −78 °C drop by drop over a period of 5 min. The mixture was stirred at −78 °C for 4 h, and then to this was added DBU (0.15 ml). After stirring at 15 °C for 5 h, a solution of 1-trimethylsiloxycyclohexene (0.158 g, 0.93 mmol) in hexane (2 ml) was added as the internal standard. The mixture was washed with 0.1 mol dm^{-3} HCl and dried. The GLPC analysis on a column of 3% Silicone OV-1 on Chromosorb W AW (3 mm×2 m) at 90 °C indicated the yield of **16** (t_R=4.6 min) to be 87%. Pure **16** was isolated by preparative GLPC, by using a column of 10% Silicone OV-1 on Chromosorb W AW (7 mm×3 m) at 110 °C: IR (neat) 1248 cm^{-1}; NMR (CCl_4) 0.08 (9H, s, CH_3Si), 1.33 (6H, s, CH_3), 1.76 (3H, br s, CH_3C=), 4.68 (1H, m, CH_2=), and 4.87 (1H, m, CH_2C=).

*Reaction of 4,8-Dimethyl-7-nonen-2-one Oxide (**17**) with **1**.* A mixture of **1** (0.545 g, 2.45 mmol), 2.6-lutidine (0.28 ml), and **17** (0.516 g, 2.45 mmol) in toluene (7 ml) was stirred at −78 °C for 4 h, and to this was added DBU (0.35 ml). The mixture was stirred at 20 °C for 30 min and poured into a mixture of hexane (30 ml) and water (10 ml). The mixture was extracted with hexane (5 ml×3). The extracts were washed with 0.1 mol dm^{-3} HCl and 5% $NaHCO_3$, dried, and concentrated. Column chromatography on silica gel, eluting with benzene, gave pure **18** (0.437 g, 69%) as a colorless oil: IR (neat) 1718 (C=O) and 1249 cm^{-1}; NMR (CCl_4) 0.02 (9H, s, CH_3Si), 0.86 (3H, d, J=6.1 Hz, CH_3), 1.62 (3H, br s, CH_3C=), 2.0—1.0 (5H, m, two methylenes and methine), 2.03 (3H, s, CH_3C=O), 2.18 (1H, d, J=6.5 Hz, CH_2C=O), 2.26 (1H, d, J=6.5 Hz, CH_2C=O), 3.91 (1H, t, J=6.0 Hz, CHO), 4.68 (1H, m, CH_2=), and 4.78 (1H, m, CH_2=); Ms *m/e* (rel intensity) 256 (15), 143 (100), and 73 (44). Found: C, 65.8; H, 10.8%. Calcd for $C_{14}H_{28}O_2Si$: C, 65.6; H, 11.0%.

*Reaction of Methyl Citronellate Oxide (**19**) with **1**.* A mixture of **1** (0.346 g, 1.55 mmol), 2,6-lutidine (0.18 ml), and **19** (0.306 g, 1.53 mmol) in toluene (6 ml) was stirred at −78 °C for 4 h. Then to this was added DBU (0.15 ml) at −78 °C. The mixture was stirred at 15 °C for 2 h and diluted by hexane (30 ml). The mixture was washed with 0.1 mol dm^{-3} HCl and saturated $NaHCO_3$, dried, and concentrated. Column chromatography on silica gel, eluting with a 20:1 mixture of benzene and ethyl acetate, gave pure **20** (0.330 g, 79%) as a colorless oil: IR (neat) 1742 (C=O) and 1250 cm^{-1}; NMR (CCl_4) 0.02 (9H, s, CH_3Si), 0.90 (3H, d, J=6.2 Hz, CH_3), 1.64 (3H, br s, CH_3C=), 2.3—1.0 (7H, m, three methylenes and methine), 3.61 (3H, s, CH_3O), 3.92 (1H, t, J=6.0 Hz, CHO), 4.76 (1H, m, CH_2=), and 4.81 (1H, m, CH_2=); Ms *m/e* (rel intensity) 272 (8), 257 (7), 143 (100), 73 (59), and 59 (21). Found: C, 61.7; H, 10.4%. Calcd for $C_{14}H_{28}O_3Si$: C, 61.8; H, 10.3%.

*Reaction of Citronellol Oxide (**21**) with **1**.* To a solution of **1** (0.429 g, 1.93 mmol) and 2,6-lutidine (0.22 ml) in toluene (5 ml) was added in a dropwise manner **21** (0.170 g, 0.99 mmol) dissolved in toluene (3 ml) at −78 °C. The mixture was stirred at −78 °C for 5 h and then to this was added DBU (0.3 ml). The mixture was stirred at 28 °C for 4 h, poured into 0.1 mol dm^{-3} HCl, and extracted with hexane (8 ml×4). The combined extracts were dried and

concentrated. Bulb-to-bulb distillation (120 °C/1 mmHg) gave pure **22** (0.217 g, 71%) as a colorless oil: IR (neat) 1248 cm^{-1}; NMR ($CDCl_3$) 0.10 (18H, s, CH_3Si), 0.83 (3H, d, J=6.2 Hz, CH_3), 1.7—1.0 (7H, m, three methylenes and methine), 1.70 (3H, br s, CH_3C=), 3.62 (2H, t, J=6.5 Hz, CH_2O), 4.20 (1H, t, J=6.5 Hz, CHO), 4.80 (1H, m, CH_2=), and 4.87 (1H, m, CH_2=).

*Reaction of Geraniol 2,3-Oxide (**23**) with **1**.* To a solution of **1** (0.264 g, 1.19 mmol) and 2,6-lutidine (0.14 ml) in toluene (3 ml) was added **23** (0.109 g, 0.64 mmol) dissolved in toluene (2 ml) in a dropwise manner over a period of 5 min at −78 °C. After stirring at −78 °C for 4 h, DBU (0.2 ml) was added. The mixture was stirred at 30 °C for 54 h, poured into 0.1 mol dm^{-3} HCl, and extracted with hexane (5 ml×3). The combined extracts were dried, concentrated, and chromatographed on a column of NH_3-treated silica gel, eluting with a 1:1 mixture of benzene and hexane, to give bis(trimethylsilyl) ether of (*E*)-3,7-dimethyl-3,6-octadiene-1,2-diol[10] (**24**) (0.124 g, 66%) as a colorless oil: IR (neat) 1250 cm^{-1}; NMR ($CDCl_3$) 0.09 (18H, s, CH_3Si), 1.58 (3H, s, CH_3C=), 1.72 (3H, s, CH_3C=), 2.71 (2H, t, J=7.0 Hz, =CCH_2C=), 3.48 (2H, d, J=6.3 Hz, CH_2O), 4.04 (1H, t, J=6.2 Hz, CHO), 5.11 (1H, br t, CH=), and 5.38 (1H, t, J=7.0 Hz, CH=).

*Reaction of Nerol 2,3-Oxide (**25**) with **1**.* To a mixture of **1** (0.330 g, 1.48 mmol) and 2,6-lutidine (0.17 ml) in toluene (4 ml) was added a solution of **25** (0.132 g, 0.78 mmol) in toluene (2 ml) drop by drop over a period of 10 min at −78 °C. After stirring at −78 °C for 3 h, DBU (0.25 ml) was added and the mixture was stirred at 32 °C for an additional 14 h. The reaction was quenched by pouring into 0.1 mol dm^{-3} HCl. The mixture was extracted with hexane (5 ml×3). The extracts were dried and concentrated. Column chromatography on NH_3-treated silica gel, eluting with a 1:2 mixture of benzene and hexane, afforded a 4:1 mixture of **24** and bis(trimethylsilyl) ether of 7-methyl-3-methylene-6-octene-1,2-diol[10d] (**26**) (totally 0.188 g, 81%) as a colorless oil: IR (neat) 1252 cm^{-1}; NMR (CCl_4) 0.07 and 0.09 (totally 18H, two singlets, CH_3Si), 1.55 and 1.72 (totally 8.4H, two broad singlets, CH_3C= of **24** and **26**), 2.04 (0.4H, m, CH_2C= of **26**), 2.72 (1.6H, t, J=7.0 Hz, =CCH_2C= of **24**), 3.45 (2H, m, CH_2O of **24** and **26**), 4.06 (1H, m, CHO of **24** and **26**), 4.83 (0.2H, m, CH_2= of **26**), 5.3—5.0 (1.2H, m, CH_2= of **26** and CH= of **24**), and 5.41 (0.8H, t, J=6.3 Hz, CH= of **24**).

*Reaction of Methylenecyclohexane Oxide (**27**) with **1**.* To a stirred solution of **1** (0.987 g, 4.40 mmol) and 2,6-lutidine (0.52 ml) in toluene (7 ml) was added in a dropwise manner **27** (0.490 g, 4.37 mmol) dissolved in toluene (3 ml) over a period of 5 min at −78 °C. The mixture was stirred at −78 °C for 3 h and to this was added DBU (0.52 ml). The mixture was stirred at 32 °C for 14 h, then poured into 0.1 mol dm^{-3} HCl, and extracted with hexane (5 ml×3). The combined extracts were dried and concentrated. Bulb-to-bulb distillation (150 °C/40 mmHg) gave pure **28** (0.581 g, 72%) as a colorless oil: IR (neat) 1250 cm^{-1}; NMR (CCl_4) 0.11 (9H, s, CH_3Si), 1.60 (4H, m, two methylenes), 1.98 (4H, m, CH_2C=), 3.96 (2H, s, CH_2O), and 5.62 (1H, br, CH=).

*Reaction of 2-Methylpropene Oxide (**29**) with **1**.* To a solution of **1** (0.473 g, 2.13 mmol) in toluene (7 ml) was added 2,6-lutidine (0.25 ml) at 13 °C. The mixture was cooled in a Dry Ice–acetone bath (−78 °C), and to this was added a solution of **29** (0.164 g, 2.27 mmol) in toluene (1 ml). After the mixture was stirred at −78 °C for 10 h, DBU (0.33 ml) was added. Then the cooling bath was removed and the mixture was stirred at 13 °C for 0.5 h. To this was added 1-trimethylsiloxycyclopentene (0.229 g, 1.47 mmol) as the internal standard and poured into water. The mixture was extracted with pentane (10 ml). The GLPC analysis on a column of 5% Apiezone-L on Neopak 1 A (3 mm×2 m) at 70 °C indicated the yield of **30** (t_R= 5.6 min) to be 62%. The product identification was made by coinjection with authentic sample prepared from 2-methyl-2-propen-1-ol and chlorotrimethylsilane.

*Reaction of 1-Methylcyclohexene Oxide (**34**) with **1**.* To a mixture of **1** (0.705 g, 3.17 mmol) and 2,6-lutidine (0.37 ml) in toluene (5 ml) was added **34** (0.368 g, 3.28 mmol) dissolved in toluene (2 ml) drop by drop over a period of 10 min at −78 °C. The mixture was stirred at −78 °C for an additional 2 h, and then to this was added DBU (0.55 ml). The mixture was stirred at 24 °C for 3 h, poured into 0.1 mol dm^{-3} HCl, and extracted with hexane (5 ml× 4). The extracts were washed with water, dried, concentrated, and chromatographed on a column of silica gel, eluting with a 2:3 mixture of benzene and hexane, to afford pure **36** (0.459 g, 80%) as a colorless oil: IR (neat) 1252 cm^{-1}; NMR ($CDCl_3$) 0.11 (9H, s, CH_3Si), 2.6—1.1 (8H, m, four methylenes), 4.04 (1H, m, CHO), 4.69 (1H, m, CH_2=), and 4.86 (1H, m, CH_2=).

*Reaction of 3β-Methyl-5α-cholest-2-ene 2α,3α-Oxide (**37**) with **1**.* A 0.2 M toluene solution of **1** (0.5 ml, 0.1 mmol) was cooled to −78 °C and to this was added 2,6-di-*t*-butylpyridine (0.03 ml) followed by the addition of **37** (0.020 g, 0.05 mmol) dissolved in toluene (1.5 ml). The mixture was stirred at −78 °C for 10 h and quenched by adding methanol (1 ml) and 3 drops of concd HCl. The mixture was stirred at 17 °C for 2 h, poured into water, and extracted with petroleum ether (5 ml×3). The extracts were dried and concentrated. Preparative TLC on a silica gel plate, developing with a 7:1 mixture of petroleum ether and ethyl acetate, gave pure **37** (0.008 g) and pure **38** (0.012 g, 58%, 95% based on consumed **37**) as colorless crystals: mp 112—114 °C (lit,[30] mp 113—114 °C); IR (KBr) 3640—3250 cm^{-1} (OH); NMR (CCl_4) 2.2—0.6 (45H, m, methyl, methylene, and methine), 4.13 (1H, m, CHO), 4.65 (1H, m, CH_2=), and 4.80 (1H, m, CH_2=).

*Reaction of 1-Decene Oxide with **1**.* A mixture of **1** (0.260 g, 1.17 mmol), 2,6-lutidine (0.1 ml), and 1-decene oxide (0.167 g, 1.07 mmol) in benzene (4 ml) was heated at 80 °C for 10 h. After cooling to 18 °C, the mixture was poured into water and extracted with hexane (5 ml×3). The extracts were washed with saturated $NaHCO_3$, dried, and concentrated. Bulb-to-bulb distillation (120 °C/100 mmHg) gave pure decanal (0.148 g, 89%) as a colorless oil. The identification was made by GLPC analysis on a column of 5% DEGS on Neopak 1A (3 mm×2 m) at 110 °C (t_R=6.4 min).

*Reaction of (Z)-7-Tetradecene Oxide with **1**.* A mixture of **1** (0.542 g, 2.44 mmol), 2.6-lutidine (0.19 ml), and (*Z*)-7-tetradecene oxide (0.536 g, 2.53 mmol) in benzene (5 ml) was heated at 80 °C for 10 h. After cooling to 15 °C, the mixture was poured into water and extracted with hexane (5 ml×3). The extracts were washed with saturated $NaHCO_3$, dried, and concentrated. Bulb-to-bulb distillation (100 °C/1 mmHg) gave 7-tetradecanone (0.511 g, 100%) as a colorless oil. The identification was made by GLPC analysis on a column of 5% DEGS on Nepopak 1A (3 mm× 2 m) at 150 °C (t_R=5.1 min).

*Reaction of (E)-7-Tetradecene Oxide (**41**) with **1**.* A mixture of **1** (0.270 g, 1.20 mmol), 2,6-lutidine (0.14 ml), and **41** (0.260 g, 1.22 mmol) in benzene (5 ml) was heated at 80 °C for 8 h in a sealed tube. After cooling to 13 °C, to this was added DBU (0.19 ml). The mixture was stirred

at 13 °C for 2 h and then poured into 0.1 mol dm^{-3} HCl. The mixture was extracted with hexane (10 ml×3), and the extracts were dried and concentrated. Bulb-to-bulb distillation (125 °C/0.5 mmHg) gave a mixture (0.305 g, 89%) of **42** and four isomers of 7-tetradecanone enol silyl ethers as a colorless oil: IR (neat) 1675 (C=C) and 1251 cm^{-1}; NMR (CCl_4) 0.04 (2H, s, CH_3Si), 0.14 (7H, s, CH_3Si), 0.88 (6H, br t, CH_3), 1.28 (16H, br s, eight methylenes), 1.94 (3H, br, CH_2C=), 2.26 (1H, t, CH_2C=), 3.98 (0.2H, m, CHO of **42**), 4.35 (0.2H, t, J=7.4 Hz, CH= of enol silyl ethers trans to OSi),[31] 4.47 (0.6H, t, J=7.0 Hz, CH= of enol silyl ethers cis to OSi),[31] 5.27 (0.2H, m, CH= of **42**), and 5.51 (0.2H, dd, J=14.8 and 6.3 Hz, =CCHO of **42**).

Reaction of Cyclooctene Oxide (48) with 1. To a solution of **1** (0.344 g, 1.55 mmol) and 2,6-lutidine (0.18 ml) in toluene (3 ml) was added **48** (0.205 g, 1.63 mmol) dissolved in toluene (2 ml) drop by drop over a period of 5 min at −50 °C. After 3-h reaction at −50 °C, the mixture was warmed to 26 °C and stood for 40 h. The mixture was poured into water and extracted with hexane (5 ml×4). The combined extracts were dried and concentrated. The crude products consisted of the silyl ether **49** and the desilylated alcohol. This was dissolved in 5% methanolic HCl (10 ml), stirred at 26 °C for 1 h, and concentrated. Bulb-to-bulb distillation (125 °C/20 Torr) gave pure *endo-cis*-bicyclo[3.3.0]octan-2-ol[9r] (0.203 g, 100%): IR (neat) 3650—3300 cm^{-1} (OH); NMR (CCl_4) 1.9—1.2 (10H, m, five methylenes), 2.40 (2H, m, bridgehead CH), 3.2—2.7 (1H, br, OH, exchangeable with D_2O), and 4.11 (1H, m, CHO).

Reaction of Cyclooctene Oxide (48) with 1. Formation of Cyclooctanone: A mixture of **1** (0.919 g, 4.14 mmol) and **48** (0.464 g, 3.68 mmol) in toluene (5 ml) was stirred at 0 °C for 2 h. The mixture was poured into saturated $NaHCO_3$ and extracted with hexane (7 ml×3). The combined extracts were dried and concentrated. Bulb-to-bulb distillation (120 °C/40 mmHg) gave cyclooctanone (0.403 g, 87%) as colorless crystals: mp 39—41 °C.

Reaction of 6-Methyl-5-hepten-2-one Oxide (52) with 1. To a solution of **1** (0.408 g, 1.83 mmol) and 2,6-lutidine (0.22 ml) in toluene (4 ml) was added **52** (0.242 g, 1.83 mmol) dissolved in toluene (2 ml) at −78 °C. After stirring at −78 °C for 3 h, to this was added DBU (0.28 ml), and stirring was continued at 15 °C for 1 h. The mixture was quenched by pouring into water and extracted with hexane (5 ml×3). The extracts were dried, concentrated, and chromatographed on a column of NH_3-treated silica gel, eluting with a 10:1 mixture of pentane and ether, gave pure **53** (0.314 g, 80%) as a colorless oil: IR (neat) 1684 (C=C) and 1245 cm^{-1}; NMR (CCl_4) 0.06 (9H, s, CH_3Si), 1.06 (3H, s, CH_3), 1.19 (3H, s, CH_3), 1.63 (3H, br s, CH_3C=), 1.96 (2H, m, CH_2), 4.53 (1H, dd, J=8.6 and 6.0 Hz, CHO), and 5.22 (1H, t, J=3.6 Hz, CH=). Found: C, 61.6; H, 10.4. Calcd for $C_{11}H_{22}O_2Si$: C, 61.6; H, 10.4.

Reaction of (E)-3α-t-Butyldimethylsiloxy-5α-pregnene Oxide (54) with 1. A mixture of **1** (0.075 g, 0.34 mmol), 2,6-lutidine (0.04 ml), and **54** (0.104 g, 0.24 mmol) in toluene (4 ml) was stirred at −78 °C for 4 h and then at 15 °C for 10 h. The mixture was poured into 0.1 mol dm^{-3} HCl and extracted with hexane (5 ml×3). The combined extracts were washed with saturated $NaHCO_3$, dried, and concentrated. Column chromatography on silica gel, eluting with a 10:1 mixture of benzene and ethyl acetate, gave pure **55** (0.090 g, 86%) as colorless crystals: mp 118—120 °C; IR (CCl_4) 3635 (OH) and 1253 cm^{-1}; NMR (CCl_4) 0.04 (6H, s, CH_3Si), 0.76 (3H, s, CH_3), 0.94 (9H, s, $(CH_3)_3CSi$), 1.04 (3H, s, CH_3), 2.2—1.0 (24H, m, methyl, methylene, and methine), 3.60 (1H, q, J=6.5 Hz, CHO), and 4.01 (1H, m, CHO); Ms *m/e* (rel intensity) 432 (4), 414 (7), 387 (72), 255 (25), and 75 (100). Found: C, 75.1; H, 10.9%. Calcd for $C_{27}H_{48}O_2Si$: C, 74.9; H, 11.2%.

Reaction of α-Pinene Oxide (56) with 1. To a mixture of **1** (0.483 g, 2.17 mmol) and 2,6-lutidine (0.25 ml) in toluene (5 ml) was added a solution of **56** (0.332 g, 2.18 mmol) in toluene (2 ml) at −50 °C. The mixture was stirred at −50 °C for 1 h and then to this was added DBU (0.4 ml) at −50 °C. The mixture was stirred at 26 °C for 10 h, quenched by pouring into 0.1 mol dm^{-3} HCl, and extracted with hexane (7 ml×4). The combined extracts were dried, concentrated, and chromatographed on a silica gel column, eluting with a 5:1 mixture of benzene and ethyl acetate. Careful concentration of the eluates gave α-pinene (**58**) (0.023 g, 6%) and pure **57** (0.240 g, 72%) as a colorless oil. **57**: IR (neat) 3660—3300 (OH) and 1643 cm^{-1} (C=C); NMR (CCl_4) 2.7—1.1 (6H, m, CH_2, CH, and OH, 1H was D_2O exchangeable), 1.73 (6H, br s, CH_3C=), 3.98 (1H, br, CHO), 4.62 (2H, br s, CH_2=), and 5.44 (1H, m, CH=).

Reaction of Squalene Oxide (62) with 1. A mixture of **1** (0.392 g, 1.76 mmol) 2,6-lutidine (0.15 ml), and **62** (0.512 g, 1.20 mmol) in toluene (7 ml) was stirred at −78 °C for 12 h, then poured into 0.1 mol dm^{-3} HCl, and extracted with hexane (10 ml×3). The combined extracts were dried, concentrated, and chromatographed on a silica gel column, eluting with benzene, to give pure squalene (**63**) (0.348 g, 70%) as a colorless oil.

References

1) This paper is part 12 in the series entitled "Trialkylsilyl Triflate in Organic Synthesis," Part 11: R. Noyori, S. Murata, and M. Suzuki, *Tetrahedron*, **37**, 3899 (1981).

2) a) M. Schmeißer, P. Sartori, and B. Lippsmeier, *Chem. Ber.*, **103**, 868 (1970); b) H. W. Roesky and H. H. Giere, *Z. Naturfosch., Tail B*, **25**, 773 (1970); c) H. C. Marsmann and H.-G. Horn, *Z. Naturfosch., Tail B*, **27**, 1448 (1972).

3) a) G. Simchen and W. Kober, *Synthesis*, **1976**, 259; b) H. Emde and G. Simchen, *ibid.*, **1977**, 636; c) **1977**, 867; d) H. Ahlbrecht and E.-O. Düber, *ibid.*, **1980**, 630; e) H. H. Hergott and G. Simchen, *Justus Liebigs Ann. Chem.*, **1980**, 1718; f) K. Krägeloh and G. Simchen, *Synthesis*, **1981**, 30.

4) S. Searles and M. Tamres, *J. Am. Chem. Soc.*, **73**, 3704 (1951).

5) For a preliminary account of this work, see: S. Murata, M. Suzuki, and R. Noyori, *J. Am. Chem. Soc.*, **101**, 2738 (1979).

6) a) R. E. Parker and N. S. Isaacs, *Chem. Rev.*, **59**, 737 (1959); b) J. K. Addy and R. E. Parker, *J. Chem. Soc.*, **1965**, 644; c) J. G. Buchanan and H. Z. Sable, "Selective Organic Transformations," ed by B. S. Thyagarajan, Wiley-Interscience, New York (1972), Vol. 2, pp. 1—95; d) Y. Pocker and B. P. Ronald, *J. Am. Chem. Soc.*, **100**, 3122 (1978); e) A. H. Haines, "Comprehensive Organic Chemistry," ed by J. F. Stoddart, Pergamon Press, London (1979), Vol. 1, Chap. 4.4, pp. 866—868.

7) T. J. Barton and C. R. Tully, *J. Org. Chem.*, **43**, 3649 (1978).

8) a) D. S. Bailey and W. H. Saunders, Jr., *J. Am. Chem. Soc.*, **92**, 6904 (1970); b) R. A. Bartsch, *ibid.*, **93**, 3683 (1971); c) J. K. Borchardt, J. C. Swanson, and W. H. Saunders, Jr., *ibid.*, **96**, 3918 (1974); d) F. A. Carey and R. J. Sundberg, "Advanced Organic Chemistry," Plenum Press, New York (1977), Part A, Chap. 6, pp. 286—290;

e) T. D. Nevitt and G. S. Hammond, *J. Am. Chem. Soc.*, **76**, 4124 (1954); f) N. A. Lebel, "Advances in Alicyclic Chemistry," ed by H. Hart and G. J. Karabatsos, Academic Press, New York (1971), Vol. 3, pp. 217—238.

9) a) A. C. Cope, H. H. Lee, and H. E. Petree, *J. Am. Chem. Soc.*, **80**, 2849 (1958); b) A. C. Cope, M. Brown, and H. H. Lee, *ibid.*, **80**, 2855 (1958); c) A. C. Cope, G. A. Berchtold, P. E. Peterson, and S. H. Sharman, *ibid.*, **82**, 6370 (1960); d) J. K. Crandall, *J. Org. Chem.*, **29**, 2830 (1964); e) A. C. Cope and J. K. Heeren, *J. Am. Chem. Soc.*, **87**, 3125 (1965); f) J. K. Crandall and L.-H. Chang, *J. Org. Chem.*, **32**, 435 (1967); g) **32**, 532 (1967); h) *J. Am. Chem. Soc.*, **89**, 4526 (1967); i) **89**, 4527 (1967); j) B. Rickborn and R. P. Thummel, *J. Org. Chem.*, **34**, 3583 (1969); k) R. P. Thummel and B. Rickborn, *J. Am. Chem. Soc.*, **92**, 2064 (1970); l) *J. Org. Chem.*, **36**, 1365 (1971); m) B. D. Mookherjee, R. W. Trenkle, and R. R. Patel, *ibid.*, **36**, 3266 (1971); n) M. N. Sheng, *Synthesis*, **1972**, 194; o) C. L. Kissel and B. Rickborn, *J. Org. Chem.*, **37**, 2060 (1972); p) B. M. Trost and M. J. Bogdanowicz, *J. Am. Chem. Soc.*, **95**, 5311 (1973); q) J. K. Crandall and L. C. Crawley, *Org. Synth.*, **53**, 17 (1974); r) J. K. Whitesell and P. D. White, *Synthesis*, **1975**, 602.

10) a) A. Yasuda, S. Tanaka, K. Oshima, H. Yamamoto, and H. Nozaki, *J. Am. Chem. Soc.*, **96**, 6513 (1974); b) S. Tanaka, A. Yasuda, H. Yamamoto, and H. Nozaki, *ibid.*, **97**, 3252 (1975); c) A. Yasuda, H. Yamamoto, and H. Nozaki, *Bull. Chem. Soc. Jpn.*, **52**, 1705 (1979); d) A. Yasuda, S. Tanaka, H. Yamamoto, and H. Nozaki, *ibid.*, **52**, 1752 (1979).

11) T. Inoue, T. Uchimaru, and T. Mukaiyama, *Chem. Lett.*, **1977**, 1215.

12) K. B. Sharpless and R. F. Lauer, *J. Am. Chem. Soc.*, **95**, 2697 (1973).

13) a) H. Sakurai, K. Sasaki, and A. Hosomi, *Tetrahedron Lett.*, **21**, 2329 (1980); b) G. A. Kraus and K. Frazier, *J. Org. Chem.*, **45**, 2579 (1980); c) J. N. Denis and A. Krief, *Tetrahedron Lett.*, **22**, 1429 (1981); d) M. R. Detty and M. D. Seidler, *J. Org. Chem.*, **46**, 1283 (1981).

14) N. Miyoshi, K. Kondo, S. Murai, and N. Sonoda, *Chem. Lett.*, **1979**, 909.

15) Evidently, these enol silyl ethers were formed from initially produced 7-tetradecanone. The patterns of the gas chromatogram and NMR spectra of the products were the same as those obtained by the reaction of the ketone with **1** and triethylamine.[3]

16) R. H. Nobes, W. R. Rodwell, W. J. Bouma, and L. Radom, *J. Am. Chem. Soc.*, **103**, 1913 (1981).

17) H. Perst, "Carbonium Ions," ed by G. A. Olah and P. von R. Shleyer, Wiley-Interscience, New York (1976), Vol. 5, Chap. 34, p. 2024.

18) a) A. C. Cope, M. M. Martin, and M. A. McKervey, *Quart. Rev.*, **20**, 119 (1966); b) F. J. McQuillin, "Alicyclic Chemistry," Cambridge University Press, Cambridge (1972), Chap. 3, pp. 51—57.

19) B. Capon and S. P. Mcmanus, "Neighboring Group Participation," Plenum Press, New York (1976), Vol. 1.

20) For the 1,2-rearrangement of the methyl group in steroid 17α-oxides see: a) K. Heusler and A. Wettstein, *Chem. Ber.*, **87**, 1301 (1954); b) H. L. Herzog, M. J. Gentles, A. Mitchell, E. B. Hershberg, and L. Mandell, *J. Am. Chem. Soc.*, **81**, 6478 (1959); c) E. L. Shapiro, M. Steinberg, D. Gould, M. J. Gentles, H. L. Herzog, M. Gilmore, W. Charney, E. B. Hershberg, and L. Mandell, *ibid.*, **81**, 6483 (1959); d) D. N. Kirk and M. P. Hartshorn, "Steroid Reaction Mechanisms," Elsevier, Amsterdam (1968), Chap. 8, p. 364.

21) The solvolytic cleavage of α-pinene oxide (**56**) gives *trans*-carveol (**57**) as the minor product: a) E. E. Royals and J. C. Leffingwell, *J. Org. Chem.*, **29**, 2098 (1964); b) M. P. Hartshorn, D. N. Kirk, and A. F. A. Wallis, *J. Chem. Soc.*, **1964**, 5494. On the other hand, reaction of **56** and lithium diethylamide gives *trans*-pinocarveol, an allylic alcohol, without concomitant four-membered ring fission.[9f,g]

22) H. Shirahama, K. Hayano, Y. Kanemoto, S. Misumi, T. Ohtsuka, N. Hashiba, A. Furusaki, S. Murata, R. Noyori, and T. Matsumoto, *Tetrahedron Lett.*, **21**, 4835 (1980).

23) For the conversion with $BF_3 \cdot O(C_2H_5)_2$ see: J. A. Mlotkiewicz, J. Murray-Rust, P. Murray-Rust, W. Parker, F. G. Riddall, J. S. Roberts, and A. Sattar, *Tetrahedron Lett.*, **1979**, 3887.

24) The related deoxygenation of oxiranes by use of iodotrimethylsilane was reported: J. N. Denis, R. Mangnane, M. Van Eenoo, and A. Krief, *Nouv. J. Chim.*, **3**, 705 (1979).

25) E. J. Corey and M. Chaykovsky, *Org. Synth.*, Coll. Vol. V, 755 (1973).

26) D. H. R. Barton, A. da S. Campos-Neves, and R. C. Cookson, *J. Chem. Soc.*, **1956**, 3500.

27) K. B. Sharpless and R. C. Michaelson, *J. Am. Chem. Soc.*, **95**, 6136 (1973).

28) a) A. M. Krubiner and E. P. Oliveto, *J. Org. Chem.*, **31**, 24 (1966); b) B. M. Trost and T. R. Verhoeven, *J. Am. Chem. Soc.*, **100**, 3435 (1978).

29) I. Ichiose, T. Hosogai, and T. Kato, *Synthesis*, **1978**, 605.

30) A. Nickon, J. B. DiGiorgio, and P. J. L. Daniels, *J. Org. Chem.*, **38**, 533 (1973).

31) The stereochemistry of the enol silyl ethers was determined by ^{1}H NMR; the olefinic proton signal of the *Z* isomers occurs at higher field than that of the *E* isomers. See, H. O. House, L. J. Czuba, M. Gall, and H. D. Olmstead, *J. Org. Chem.*, **34**, 2324 (1969).

Organofluorosilicates in Organic Synthesis. XVI.[1] Synthesis of Organopentafluorosilicates *via* the Diels-Alder, Ene, and Friedel-Crafts Reaction. Their Transformations to Organic Halides and Alcohols

Kohei TAMAO, Jun-ichi YOSHIDA, Munetaka AKITA, Yoshihiro SUGIHARA, Takahisa IWAHARA, and Makoto KUMADA*

Department of Synthetic Chemistry, Faculty of Engineering, Kyoto University, Yoshida, Sakyo-ku, Kyoto 606

(Received August 5, 1981)

Described herein are several representative examples of cleavage reactions of otherwise hardly accessible organopentafluorosilicates which are obtainable *via* the Diels-Alder reaction, ene reaction, and the Friedel-Crafts reaction of vinyl-, ethynyl-, or allyl-trichlorosilanes. The Diels-Alder reaction between vinyltrichlorosilane and *o*-xylylene generated *in situ* by debromination of α,α′-dibromo-*o*-xylene afforded (1,2,3,4-tetrahydro-2-naphthyl)-trichlorosilane which was converted to the corresponding silicate. The silicate reacted with NBS and MCPBA to give the respective bromide and alcohol. The Diels-Alder reaction between ethynyltrichlorosilane and methyl coumalate gave a mixture of meta and para isomers of methyl (trichlorosilyl)benzoate in the ratio of 55/45, the silicate of which reacted with NBS to give two positional isomers of methyl bromobenzoate. The electronic effect of the methoxycarbonyl group on the Si–C bond cleavage was small. The silicate derived from 4-octenyltrichlorosilane which was obtained by the ene reaction between vinyltrichlorosilane and 1-hexene afforded, upon treatment with NBS, 4-octenyl bromide in the ratio of E/Z=83/17. The sterically crowded neophylsilicate obtainable *via* the Friedel-Crafts reaction of 2-methyl-1-propenyltrichlorosilane with benzene underwent the cleavage reaction with NBS in methanol. Neophyl bromide was formed with $CuBr_2$ in a low yield, no product being formed arising from rearrangement of the neophyl radical.

The Diels-Alder reaction,[2] ene reaction,[3] and the Friedel-Crafts reaction[4] of the compounds containing silyl groups provide the useful methods for preparation of organosilanes. Since the trichlorosilyl group has strong electron-withdrawing ability, vinyltrichlorosilane and ethynyltrichlorosilane are efficient dienophiles and enophiles which readily react with various dienes and olefins to give the corresponding adducts containing the trichlorosilyl group.[2a-d] The Friedel-Crafts reaction of allylic trichlorosilanes with aromatic compounds has been known to give rise to the introduction of the aromatic ring onto the carbon β to the silicon atom. Such organotrichlorosilanes that are usually difficult to prepare by hydrosilylation of olefins or acetylenes are expected to be useful precursors of organopentafluorosilicates. Thus we have developed a new methodology involving the synthesis of organosilicates *via* the Diels-Alder reaction, ene reaction, and the Friedel-Crafts reaction followed by their characteristic reactions with electrophiles. One of the unique applications of such methodology has already been demonstrated in the previous paper,[5] where the Diels-Alder reaction between vinyltrichlorosilane and cyclopentadiene followed by hydrogenation and silicate formation gave 2-norbornylpentafluorosilicate which reacted with NBS or Br_2 to afford 2-norbornyl bromide. This paper describes several new aspects on the reactivity of organopentafluorosilicates which are otherwise hardly accessible.

Results and Discussion

Preparation and Reaction of 1,2,3,4-(Tetrahydro-2-naphthyl)pentafluorosilicates. Since *o*-xylylene (5,6-dimethylene-1,3-cyclohexadiene) is known to be a highly reactive diene which readily reacts with various dienophiles to give the 1,2,3,4-tetrahydronaphthalene derivatives,[6] we examined the Diels-Alder reaction between vinyltrichlorosilane and *o*-xylylene generated *in situ* by debromination of α,α′-dibromo-*o*-xylene. A solution of α,α′-dibromo-*o*-xylene in acetonitrile was slowly added to a mixture of zinc powder and vinyltrichlorosilane in acetonitrile at 50 °C. After work-up (1,2,3,4-tetrahydro-2-naphthyl)trichlorosilane (**1**), the Diels-Alder adduct, was isolated by distillation in 55% yield.

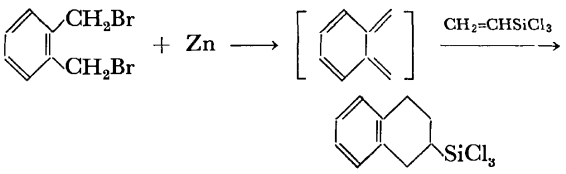

1

Acetonitrile was the most suitable among the solvents examined. The reaction in DMF, which had usually been used for debromination of α,α′-dibromo-*o*-xylene, THF, or ethyl acetate did not give the Diels-Alder adduct at all, but gave a mixture of unidentified products. Without solvent α,α′-dibromo-*o*-xylene was recovered unchanged. The reaction was also examined at three different temperatures (20 °C, 50 °C, and acetonitrile reflux), and the reaction at 50 °C gave the most satisfactory result.

(1,2,3,4-Tetrahydro-2-naphthyl)trichlorosilane could be readily converted into the corresponding silicate **2** in 97% yield on treatment with KF in ethanol. Treatment of the adduct with aqueous KF resulted in lower yield.

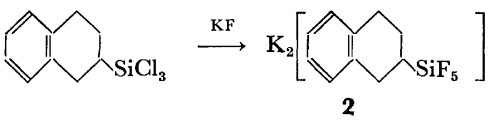

2

The silicate **2** thus obtained was found to react with NBS in dioxane to give the corresponding bromide **3** in 52% yield. The product was contaminated with a small amount of naphthalene which was considered to be formed by bromination of the benzylic

carbon of the initial product followed by the dehydrobromination. The formation of naphthalene, however, could not be retarded even in the presence of a radical inhibitor such as 2,4,6-tri-*t*-butylphenol.

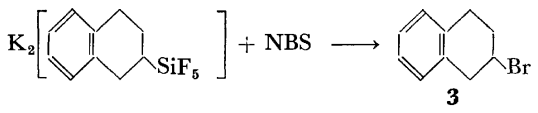

3

Silicate **2** also reacted exothermically with MCPBA[7] in DMF to give 1,2,3,4-tetrahydro-2-naphthol **4** in 65% yield. The result shows that vinyltrichlorosilane provides a vinyl alcohol equivalent in the Diels-Alder reaction. 1,2,3,4-Tetrahydro-2-naphthol is known to be an effective insect repellent with the requisite properties of low irritancy and low toxicity, and several procedures for its preparation have been reported involving hydrogenation of 2-naphthol.[8] The present procedure provides a new alternative route to this highly valuable insect repellent.

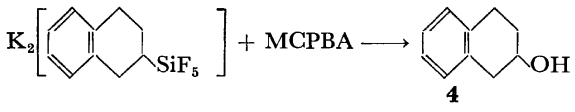

4

Preparation and Reaction of (Methoxycarbonylphenyl)pentafluorosilicate. The Diels-Alder reaction between methyl coumalate and ethynyltrichlorosilane[2c] followed by spontaneous decarboxylation afforded methyl (trichlorosilyl)benzoate **5** in 90% yield. GLC analysis of the methylated (MeMgBr in ether) product showed that both meta and para isomers were formed in the ratio of 55/45, showing a poor regioselectivity.

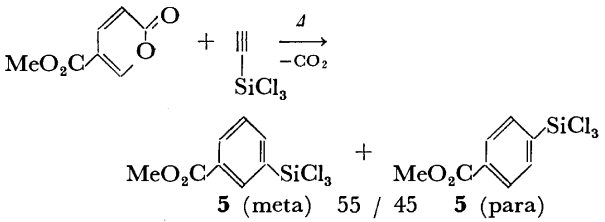

5 (meta) 55 / 45 **5** (para)

The mixture of meta- and para-trichlorosilyl derivatives was converted into the corresponding silicate **6** by treatment with KF in water in the usual manner (54% yield).

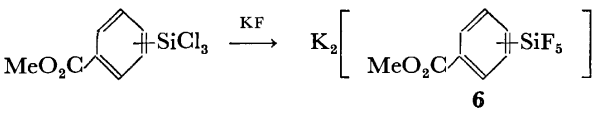

6

The silicate thus obtained was allowed to react with one equiv of NBS in methanol to give a mixture of meta and para isomers of methyl bromobenzoate **7** in the ratio of 58/42 (54% yield). The use of a half equiv of NBS did not change the product ratio significantly, implying that both the meta- and para-silicate have similar reactivities toward NBS.

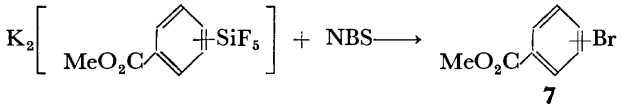

7

It should be mentioned here that the unusually low ionization potentials assignable to the π- and Si–C σ-bonding electrons, suggested by the MO calculation,[5] may screen the rather small substituent effects and level up the reactivities of the meta and para isomers.

Preparation and Reaction of 4-Octenylpentafluorosilicate. 4-Octenylpentafluorosilicate was prepared *via* the ene reaction between vinyltrichlorosilane and 1-hexene.[3] Heating a mixture of vinyltrichlorosilane and 1-hexene at 280 °C for 48 h gave 4-octenyltrichlorosilane (**8**) in 52% yield. The adduct, a mixture of the *E* and *Z* isomers (*E*/*Z*=83/17), was converted into the silicate on treatment with aqueous KF in the usual manner. 4-Octenylpentafluorosilicate (**9**) thus obtained was relatively unstable and decomposed after standing at room temperature for 1 month. IR analysis of the decomposed matters showed characteristic bands of the hexafluorosilicate. The 4-octenylsilicate reacted with NBS exothermically to give a mixture of (*E*)- and (*Z*)-4-octenyl bromide (**10**) in 36% yield in the ratio of *E*/*Z*=83/17.

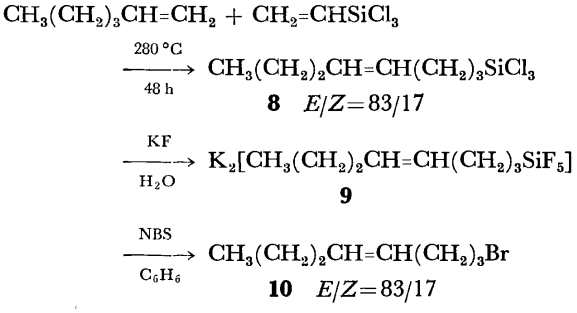

8 *E*/*Z*=83/17

9

10 *E*/*Z*=83/17

Reactions of Organopentafluorosilicates Synthesized via *the Friedel-Crafts Reaction of Allylic Trichlorosilanes.* In this study, we carried out the Friedel-Crafts reaction of allyl-, 2-methylpropenyl-, and crotyl-trichlorosilane. Of particular interest is that the method provides the most convenient route to otherwise hardly accessible (2-methyl-2-phenylpropyl)trichlorosilane (**12**) (hereafter abbreviated to neophyltrichlorosilane).

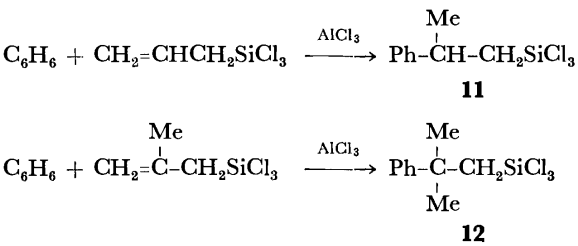

11

12

We have found that crotyltrichlorosilane gave a mixture of two positional isomers, (2- and 3-phenylbutyl)trichlorosilane, **13** and **14**. The initial product **13** isomerized thermally to the 3-phenyl isomer **14** in the presence of aluminum chloride, eventually the equilibrium mixture, **13**/**14**=9/91, being formed. Only **14** was isolated in a pure state by fractional distillation. The results show that the Cl_3Si– group, unlike the Me_3Si– group,[9] exhibits no stabilizing effect on the β-carbocation, and the γ-secondary carbocation is thermally more stable.

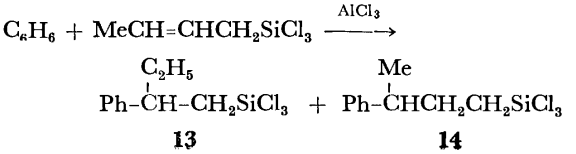

13 **14**

Table 1. Reactions of phenyl-substituted silicates with NBS or $CuBr_2$

Silicate	Reagent	Conditions	Product	Yield/%[a]
$K_2[Ph\text{-}CH(Me)CH_2SiF_5]$	NBS	Et_2O, r.t., 4 h	$Ph\text{-}CH(Me)CH_2Br$	84
		MeOH, r.t., 2 h		48
	$CuBr_2$	Et_2O, r.t., 6 h		53
$K_2[Ph\text{-}CH(Me)(CH_2)_2SiF_5]$	NBS	MeOH, r.t., 5 h	$Ph\text{-}CH(Me)(CH_2)_2Br$	71
	$CuBr_2$	Et_2O, r.t., 6 h		55
$K_2[Ph\text{-}C(Me)_2\text{-}CH_2SiF_5]$	NBS	Et_2O, r.t., 4 h	$Ph\text{-}C(Me)_2\text{-}CH_2Br$	trace[b]
		MeOH, r.t., 5 h		53
		MeOH, r.t., 20 h		62
	$CuBr_2$	Et_2O, reflux, 4 h		16[c]

a) Determined by GLC. b) $PhCMe_2CH_2SiF_3$ was formed in 76% yield. c) $PhCMe_2CH_2SiF_3$ was formed in 71% yield.

The silicates, even the sterically crowded neophyl derivative **17**, could be readily prepared in the usual manner (KF in water).

$K_2[Ph\text{-}CH(Me)(CH_2)_nSiF_5]$ $n=1$; **15** $n=2$; **16**

$K_2[Ph\text{-}C(Me)_2\text{-}CH_2SiF_5]$ **17**

The transformation of these silicates to the corresponding bromides has been examined with NBS or $CuBr_2$.[10] The results are summarized in Table 1. The reactivity of these silicates may reflect primarily the steric effect on the cleavage reactions. These three silicates were converted to the bromides in satisfactory yields. It seems interesting to note that the most crowded neophylsilicate **17** was cleaved in MeOH, but in ether dissociation of the silicate to the corresponding trifluorosilane occurred exclusively. With $CuBr_2$ silicates **15** and **16** gave the corresponding bromides in fair yields, while silicate **17** took the dissociation process predominantly, together with the formation of neophyl bromide in a low yield. As reported previously,[10] the CuX_2-cleavage of alkylsilicates may proceed through an alkyl radical intermediate, but the neophylsilicate gave no rearranged product, showing that the halogen-transfer proceeds much faster than the neophyl radical rearrangement, the rate of which has been estimated to be 10^5 s^{-1} at 100 °C.[11] This observation is consistent with the previous result on the 5-hexenylsilicate which gave no cyclization product upon treatment with $CuBr_2$; the rate of the cyclization of 5-hexenyl radical being reported to be 10^5 s^{-1} at 25 °C.[12]

$K_2[Ph\text{-}CH(Me)(CH_2)_nSiF_5]$ (**15** or **16**) + MCPBA $\xrightarrow[\text{r.t., 2h}]{\text{DMF}}$ $Ph\text{-}CH(Me)(CH_2)_n\text{-}OH$ $n=1$, 83% $n=2$, 92%

17 + MCPBA $\xrightarrow[\text{r.t., 8 h}]{\text{DMF}}$ $Ph\text{-}C(Me)_2\text{-}CH_2OH$ trace

The MCPBA-cleavage reaction was also examined. Silicates **15** and **16** reacted smoothly with MCPBA to give the corresponding alcohols in high yields. In contrast, neophylsilicate **17** was reluctant to react under the similar conditions, indicative of the importance of the steric effect also in the MCPBA cleavage.

Experimental

General. Infrared spectra were recorded on a Hitachi EPI-G3 grating infrared spectrometer. ^1H NMR spectra were determined with a JEOL JNM-MH-100 (100 MHz) spectrometer in carbon tetrachloride. Chemical shifts (δ) are recorded in ppm downfield from Me_4Si. Mass spectra were measured on a JEOL JMS-D300 mass spectrometer connected with a JEOL LGC-20K gas chromatograph, equipped with a 1 m glass column packed with OV-17 (1%) on Chromosorb B, and a JMA-2000 data processing system. Ionization voltage was 24 eV for all compounds. GLC analyses and preparative purification were performed on a Shimadzu GC-4B gas chromatograph, equipped with a 3 m column packed with 30% Silicone DC550 on Chromosorb B or Celite 545. GC peak integrals were recorded using a Shimadzu Chromatopac C-E1B integrator.

Materials. Vinyltrichlorosilane provided by Shin-etsu Chemical Co., Ltd. was purified by distillation. Ethynyltrichlorosilane[2c] allyl-, 2-methylpropenyl- and 2-butenyltrichlorosilanes[13] and methyl coumalate[14] were prepared according to the reported method. All solvents were dried in the usual manner and distilled before use. Other chemicals were used as obtained commercially.

1,2,3,4-Tetrahydro-2-naphthyltrichlorosilane (1). Vinyltrichlorosilane (161.5 g; 1.00 mol), zinc powder (90% purity, 21.8 g; 0.30 mol) and dry acetonitrile (100 ml) were placed in a three-necked flask equipped with a reflux condenser, a mechanical stirrer, and a dropping funnel. α,α'-Dibromo-*o*-xylene (26.4 g; 0.10 mol) in acetonitrile (260 ml) was added dropwise at 50 °C with stirring over a period of 19 h. After the addition was completed the reaction mixture was stirred further at 50 °C for 4 h. The solvent and excess vinyltrichlorosilane were evaporated. Pentane was added to the residue and the insoluble matters were removed by filtration. The solvent was evaporated and the residue was distilled under reduced pressure (118—127 °C/5 mmHg) to

give 20.07 g of the crude product, which was purified by fractional distillation to give 14.31 g (54% yield) of pure **1**: bp 122—127 °C/5 mmHg; mp 23.5—25.0 °C; ^{1}H NMR 1.55—1.9 (m, 2H), 2.05—2.35 (m, 1H), 2.7—3.05 (m, 4H), 7.00 (br s, 4H); MS *m/e* (%) 268 (M^++4, 4), 266 (M^++2, 14), 264 (M^+, 14), 131 (M^+-SiCl_3, 100); Found: Cl, 40.48%. Calcd for $C_{10}H_{11}Cl_3Si$: Cl, 40.04%.

1,2,3,4-Tetrahydro-2-naphthylpentafluorosilicate (2). 1,2,3,4-Tetrahydro-2-naphthyltrichlorosilane (6.94 g; 26.1 mmol) was added dropwise to a mixture of KF (37.92 g; 653 mmol) and ethanol (76 ml) at 0 °C. After the addition the mixture was stirred at room temperature overnight. The mixture was poured into 150 ml of cold water in order to dissolve an excess of KF and the resulting KCl. White powder was separated by filtration, and washed with water, ethanol, and ether. Drying under vacuum gave 8.41 g (97% yield) of potassium 1,2,3,4-tetrahydro-2-naphthylpentafluorosilicate: IR (KBr) 3060(w), 3010(w), 2900 (m), 2830(m), 1445(m), 1255(m), 1050(m), 769(s), 738(s), 650(vs), 523(s) cm^{-1}. The product was not analytically pure, but used in the subsequent reaction without further purification.

2-Bromo-1,2,3,4-tetrahydronaphthalene (3). A mixture of 1,2,3,4-tetrahydronaphthylpentafluorosilicate (997 mg; 3.0 mmol), 2,4,6-tri-*t*-butylphenol (8.6 mg), NBS (587 mg; 3.3 mmol), and dry dioxane (10 ml) was stirred at 50 °C for 16 h. Pentane was added and insoluble matters were removed by filtration. After evaporation of the solvent the residue was dissolved in pentane. The solution was washed with water and dried over Na_2SO_4. After evaporation of the solvent bulb-to-bulb distillation (200 °C/3 mmHg) of the residue gave 326 mg (52% yield) of 2-bromo-1,2,3,4-tetrahydronaphthalene which was contaminated with *ca.* 10% of naphthalene: IR (liquid film) 3070, 3020, 2945, 1580, 1495, 1450, 745 cm^{-1}; ^{1}H NMR 1.95—2.5 (m, 2H), 2.6—3.05 (m, 2H), 3.05—3.5 (m, 2H), 4.2—4.55 (m, 1H), 6.8—7.2 (m, 4H); MS *m/e* (%) 212 (M^++2, 27), 210 (M^+, 32), 131 (M^+-Br, 100); High MS 210.0055 (Calcd for $C_{10}H_{11}{}^{79}Br$, 210.0041), 212.0029 (Calcd for $C_{10}H_{11}{}^{81}Br$, 212.0021).

1,2,3,4-Tetrahydro-2-naphthol (4). A mixture of (1,2,3,4-tetrahydro-2-naphthyl)pentafluorosilicate (1.662 g; 5.0 mmol), *m*-chloroperbenzoic acid (90% pure, 1.150 g; 6.0 mmol as active oxygen), dry DMF (10 ml) was stirred at 50 °C for 14 h. Ether was added and the mixture was washed with water and aq $NaHCO_3$, and dried over Na_2SO_4. After evaporation of the solvent bulb-to-bulb distillation (150 °C/3 mmHg) of the residue gave 482 mg (65% yield) of 1,2,3,4-tetrahydro-2-naphthol: An analytical sample was purified by preparative GLC. n_D^{20} 1.5607 (lit,[8] n_D^{25} 1.5630); IR (liquid film) 3700—3100 (br. OH), 3060, 3020, 2920, 1580, 1490, 1450, 1040, 740 cm^{-1}; ^{1}H NMR 1.5—2.1 (m, 2H), 1.98 (br s, 1H), 2.5—3.15 (m, 4H), 3.85—4.15 (m, 1H), 6.92 (br s, 4H); MS *m/e* (%) 148 (M^+, 13), 130 (M^+-H_2O, 100).

Methyl (Trichlorosilyl)benzoate (5). A mixture of methyl coumalate (3.10 g; 20.1 mmol), ethynyltrichlorosilane (5.85 g; 37 mmol), and hydroquinone (50 mg) was heated at 175±5 °C (bath temperature) until the methyl coumalate was completely consumed (*ca.* 50 h). The extent of the reaction could be monitored by GLC analysis or ^{1}H NMR. After the reaction was completed the mixture was distilled under reduced pressure to give 4.9 g (90% yield) of methyl (trichlorosilyl)benzoate: bp 154—155 °C/21 mmHg; Found: Cl, 39.04%. Calcd for $C_8H_7Cl_3O_2Si$: Cl, 39.46%.

The product appeared as a single peak on GLC (Silicone DC550 or SE 30), but ^{1}H NMR showed that the product consisted of meta and para isomers. Since the ratio could not be determined by the ^{1}H NMR spectrum, an aliquot (293 mg, 1.08 mmol) of the product was methylated (MeMgBr in ether, 15 mmol, reflux, 2 h). Usual work-up and distillation gave a distillate (151 mg) boiling over the range of 190—220 °C/15 mmHg (bath temperature). GLC analysis of the distillate showed the formation of two major products (A and B) in the ratio of 55:45, together with two minor ones. Products were isolated by preparative GLC (Silicone DC550, 200 °C). Product A, having the shorter retention time, was characterized as 2-(3-trimethylsilylphenyl)-2-propanol: mp 70.5—71.0 °C (lit,[15] 62—63 °C); IR (KBr) 755, 710 cm^{-1} (1,3-disubstituted benzene); ^{1}H NMR 0.27 (s, 9H), 1.52 (s, 6H), 2.13 (br s, 1H), 7.1—7.6 (m, 4H). The other major product B was identified as the para isomer, 2-(4-trimethylsilylphenyl)-2-propanol: a liquid contaminated with some decomposition products (lit,[15] mp 52—52.5 °C); IR (liquid film) 820 cm^{-1} (1,4-disubstituted benzene); ^{1}H NMR 0.25 (s, 9H), 1.15 (s, 6H), 7.37 (s, 4H). The two minor products were collected as a mixture and characterized as the dehydrated olefinic compounds of the above two products: ^{1}H NMR 0.25 and 0.27 (total 9H), 2.15 (br s, 3H), 5.0—5.1 (m, 1H), 5.25—5.35 (m, 1H), 7.25—7.55 (m, 4H). High MS *m/e* 190.1184 (Calcd for $C_{12}H_{18}Si$, 190.1179).

(Methoxycarbonylphenyl)pentafluorosilicate (6). Methyl trichlorosilylbenzoate (2.52 g; 9.35 mmol) was added dropwise to a solution of KF (13.6 g; 234 mmol) in water (20 ml) at 0 °C with vigorous stirring. After stirring at room temperature for 5 h the mixture was filtered, washed with water, ethanol, and ether, and then dried *in vacuo*. The silicate weighed 1.76 g (54% yield): IR (KBr) 3020(w), 2970(w), 1730(s), 1710(s), 1600(w), 1440(m), 1300(s), 1265 (m), 1195(w), 1167(w), 1130(m), 1095(m), 1020(w), 847(w), 747(m), 720(w), 675(vs), 660(sh), 580(w), 557(w), 492(w), 470(w), 455(w) cm^{-1}; Found: C, 28.26; H, 2.33; F, 27.81%. Calcd for $C_8H_7F_5K_2O_2Si$: C, 28.56; H, 2.10; F, 28.24%.

Methyl Bromobenzoate (7). Reaction of $K_2[MeO_2CC_6H_4SiF_5]$ with NBS. A mixture of the silicate **6** (172 mg; 0.51 mmol), NBS (93 mg; 0.52 mmol), and methanol (5.0 ml) was stirred at room temperature for 24 h. After usual work-up GLC analysis showed a single peak, the retention time of which was the same as that of authentic methyl 4-bromobenzoate. GLC yield was 54%. The product was isolated by column chromatography on silica gel (hexane/benzene 1/1). ^{1}H NMR showed that the product was a mixture of meta and para isomers of methyl bromobenzoate: ^{1}H NMR 3.86 and 3.87 (total 3H), 7.25 (t, J=8 Hz), 7.35—7.67 (m), 7.78—7.97 (m), 8.05—8.15 (m), (total 4H). High MS *m/e* 213.9640 (calcd for $C_8H_7O_2{}^{79}Br$, 213.9630), 215.9599 (Calcd for $C_8H_7O_2{}^{81}Br$, 215.9609). The very close two signals due to the methyl protons were separated by the addition of Eu(fod)$_3$, fod=1,1,1,2,2,3,3-heptafluoro-7,7-dimethyl-4,6-octanedionato. For example, a solution of the sample (0.0338 M) containing Eu(fod)$_3$ (0.0169 M) in CCl_4 exhibited two methyl signals at δ 5.15 for the para isomer and at 4.85 for the meta isomer. In this way, the meta/para ratio of the product was determined to be 58/42.

The silicate (328 mg; 0.975 mmol) was allowed to react with a half equiv of NBS (90 mg; 0.506 mmol) in methanol (5.0 ml) at room temperature for 5 h. The insoluble precipitate was filtered and washed with ether. The organic layer and the washings were combined and analyzed by GLC which indicated that the bromide was formed in 40% yield. The ^{1}H NMR spectrum of the isolated product showed that the meta/para ratio was 57—60/43—40. The filter cake was further treated with NBS (100 mg) in methanol (5.0 ml) as above to give the bromide in 14% yield, the

meta/para ratio being 50/50.

4-Octenyltrichlorosilane (8).[3] A mixture of 1-hexene (10.10 g; 120 mmol) and vinyltrichlorosilane (10.0 g; 62 mmol) was heated in a sealed tube at 280 °C for 48 h. After the reaction, distillation of the reaction mixture gave 7.85 g (52% yield) of 4-octenyltrichlorosilane: bp 63—64 °C/7 mmHg; ^{1}H NMR 0.94 (t, J=6 Hz, 3H), 1.1—1.85 (m, 6H), 1.85—2.3 (m, 4H), 5.0—5.6 (m, 2H). GLC analysis of the product showed two peaks in a ratio of 17/83, probably due to the *Z* and *E* isomers.

4-Octenylpentafluorosilicate (9). To a solution of KF (32.0 g; 550 mmol) in deionized water (48 ml) was added dropwise 4-octenyltrichlorosilane (5.40 g; 22.0 mmol) at 0 °C. After the addition the mixture was stirred overnight at room temperature. White powder thus obtained was separated by filtration, and washed with water, ethanol, and ether. After drying under vacuum 4.64 g (68% yield) of 4-octenylpentafluorosilicate was obtained: IR (KBr) 2950 (m), 2900(m), 1460(w), 1375(w), 970(w), 745(s), 640(vs), 540(m), 445(m) cm^{-1}; Found: C, 28.02; H, 4.50; F, 28.23%. Calcd for $C_8H_{16}F_5K_2Si$: C, 30.75; H, 4.84; F, 30.40%.

1-Bromo-4-octene (10). 4-Octenylpentafluorosilicate (937 mg; 3.0 mmol) was allowed to react with NBS (587 mg; 3.3 mmol) in dry benzene (5.0 ml) at room temperature for 3 h. GLC analysis of the reaction mixture showed that two products were formed in a ratio of 17/83. The GCMS spectra of them showed the same parent peaks (*m/e*= 192 and 190), indicating that they were isomers of bromooctene. The major product was isolated by preparative GLC: n_D^{20} 1.4687; IR (liquid film) 970 cm^{-1} (*trans*-CH=CH–); ^{1}H NMR 0.90 (t, J=6 Hz, 3H), 1.15—1.6 (m, 2H), 1.7—2.35 (m, 6H), 3.36 (t, J=6 Hz, 2H), 5.1—5.6 (m, 2H). Irradiation at the methylene protons adjacent to the double bond gave AB quartet (J=16 Hz): MS *m/e* (%) 192 (M^++2, 18), 190 (M^+, 19), 150 (22), 148 (24), 111 (M^+−Br, 8), 69 (100); High MS *m/e* 190.0381 (calcd for $C_8H_{15}{}^{79}Br$, 190.0353), 192.0350 (calcd for $C_8H_{15}{}^{81}Br$, 192.0333). On the basis of these spectral data the major product was identified as (*E*)-1-bromo-4-octene. The minor product could not be isolated; it was probably the (*Z*)-1-bromo-4-octene.

Friedel-Crafts Reaction between Allylic Trichlorosilanes and Benzene. A typical procedure is given for the reaction of 2-methylpropenyltrichlorosilane. To a mixture of 27 g (0.142 mol) of 2-methylpropenyltrichlorosilane and benzene (118 g; 1.5 mol) was added 3.3 g (25 mmol) of freshly sublimed aluminum chloride at 0 °C with stirring. After stirring at 0 °C for 15 min the mixture was stirred at room temperature. A slightly exothermic reaction occurred and was completed in about 3 h. Dried sodium chloride (11.5 g) was added and the mixture was stirred at room temperature for 0.5 h and then under refluxing for another 0.5 h. The resulting black mixture was filtered quickly under suction through a filter aid (Hyfrosuper cell). The filtrate was distilled, after evaporation of benzene, to give (2-methyl-2-phenylpropyl)trichlorosilane (neophyltrichlorosilane) (**12**) as a colorless liquid boiling at mainly 99—100 °C/7 mmHg in 72% yield (29.1 g); ^{1}H NMR 1.57 (s, 6H), 2.00 (s, 2H), 7.15—7.45 (m, 5H). (Found: Cl, 39.37%).

(2-Phenylpropyl)trichlorosilane (**11**) was prepared in a similar manner: bp 98—106 °C/3 mmHg; ^{1}H NMR 1.40 (d, J=7 Hz, 3H), 1.70—1.85 (m, 2H), 3.17 (sextet, J=7 Hz, 1H), 7.0—7.3 (m, 5H). (Found: Cl, 41.54%).

Friedel-Crafts Reaction of Crotyltrichlorosilane with Benzene. To a mixture of crotyltrichlorosilane (28.4 g; 0.15 mol) and dry benzene (133 ml; 1.5 mol) was added aluminum chloride (2.2 g). An exothermic reaction started and benzene began to reflux. The reaction was controlled by intermittent cooling with a water bath. After the exothermic reaction ceased, the mixture was heated to reflux for 1 h. Sodium chloride-treatment, filtration, and distillation gave 34.9 g (87% yield) of a colorless liquid boiling over the range of 99—102 °C/4 mmHg. The fraction consisted of two isomers. Fractional distillation through a column packed with glass helices gave 11.8 g (29% yield) of (3-phenylbutyl)trichlorosilane (**14**) as the major product: bp 98—102 °C/2 mmHg; ^{1}H NMR 1.05—1.45 (m) and 1.30 (d, J=7 Hz) (total 5H), 1.7—2.0 (m, 2H), 2.70 (sextet, J=7 Hz, 1H), 7.0—7.4 (m, 5H). (Found: Cl, 39.84%). The minor product could not be isolated pure but characterized by ^{1}H NMR to be (2-phenylbutyl)trichlorosilane (**13**): ^{1}H NMR 0.78 (t, J=7 Hz, 3H), *ca.* 1.6—2.0 (m, 4H), *ca.* 2.6—3.0 (m, 1H), *ca.* 7.0—7.45 (m, 5H).

The isomer distribution was dependent upon the reaction conditions. The reaction was followed by GLC which showed the following ratios of **13**/**14**: 63/37 (0 °C, 10 min), 54/46 (0 °C, 20 min), 56/44 (0 °C, 1 h), 38/62 (r.t., 24 h), 13/87 (reflux, 1 h), 9/91 (reflux, 2 h).

Preparation of Silicates. Preparation of silicates was performed in a similar manner to that described in the previous paper[5] ($RSiCl_3$/KF=1/25, in water, 0 °C—r.t., overnight). Yield, infrared absorption bands, and analytical data are given below.

K_2[PhCHMeCH$_2$SiF$_5$] (15): 54%; IR (KBr) 3020(w), 2950(w), 2875(m), 2810(w), 1602(w), 1520(w), 1490(m), 1450(m), 1360(w), 1277(w), 1255(w), 1225(w), 1192(w), 1100(w), 1072(w), 910(w), 768(s), 740(s), 702(s), 640(br, vs), 540(m), 500(m), 482(m), 450(m) cm^{-1}; Found: C, 32.10; H, 3.40%. Calcd for $C_9H_{11}F_5K_2Si$: C, 33.73; H, 3.46%.

K_2[PhCHMeCH$_2$CH$_2$SiF$_5$] (16): 78%; IR (KBr) 3025(w), 2950(sh), 2900(s), 2840(w), 1603(w), 1520(br, w), 1492(m), 1450(m), 1370(w), 1258(w), 1215(w), 1180(w), 1150(w), 1075(w), 1032(w), 900(br, w), 785(w), 750(s), 725(s), 700(s), 645(br, vs), 550(w), 518(m), 490(w), 450(m) cm^{-1}; Found: C, 34.82; H, 3.88; F, 29.60%. Calcd for $C_{10}H_{13}F_5K_2Si$: C, 35.91; H, 3.92; F, 28.40%.

K_2[PhCMe$_2$CH$_2$SiF$_5$] (17): 63%; IR (KBr) 3050(w), 3010(w), 2970(m), 2950(m), 2925(m), 2900(m), 2875(m), 1600(w), 1580(w), 1520(br, m), 1495(m), 1440(w), 1370 (m), 1352(m), 1263(m), 1200(w), 1190(w), 1100(br, w), 1075(w), 1032(w), 860(w), 790(m), 770(m), 735(s), 717(s), 702(s), 655(vs), 630(vs), 550(m), 505(m), 445(m) cm^{-1}; Found: C, 35.19; H, 3.91; F, 27.30%. Calcd for $C_{10}H_{13}F_5K_2Si$: C, 35.91; H, 3.92; F, 28.40%.

Cleavage Reactions with NBS and $CuBr_2$. The cleavage reactions of **15**—**17** were carried out in a similar manner to that described above and previously. The reaction conditions are listed in Table 1. Products were characterized as follows.

PhCHMeCH$_2$Br: n_D^{20} 1.5488; ^{1}H NMR; 1.41 (d, J=7 Hz, 3H), 3.10 (sextet, J=7 Hz, 1H), 3.3—3.62 (m, 2H), 7.1—7.45 (m, 5H); MS *m/e* (%) 200 (M^++2, 6), 198 (M^+, 6), 105 (100), 91 (11); High MS *m/e* 198.0041 (calcd for $C_9H_{11}{}^{79}Br$; 198.0043), 200.0027 (calcd for $C_9H_{11}{}^{81}Br$; 200.0025). *PhCHMeCH$_2$CH$_2$Br*: ^{1}H NMR 1.30 (d, J=7 Hz, 3H), 2.10 (q, J=7 Hz, 2H), 2.85—3.45 (m, 3H), 7.05—7.35 (m, 5H); MS *m/e* (%) 214 (M^++2, 4), 212 (M^+, 4), 105 (100); High MS *m/e* 212.0190 (calcd for $C_{10}H_{13}{}^{79}Br$; 212.0199), 214.0202 (calcd for $C_{10}H_{13}{}^{81}Br$; 214.0182).

PhCMe$_2$CH$_2$Br: n_D^{20} 1.5458; ^{1}H NMR 1.45 (s, 6H), 3.50 (s, 2H), 7.1—7.45 (m, 5H); High MS *m/e* 212.0153 (calcd for $C_{10}H_{13}{}^{79}Br$; 212.0199), 214.0200 (calcd for $C_{10}H_{13}{}^{81}Br$; 214.0182).

The MCPBA Cleavage of 15—17. These cleavage

reactions were also performed in the same manner as described above and previously. $PhCHMeCH_2OH$ was identified by IR spectrum (*cf.* The Aldrich Library of IR Spectra, 616A) and ^1H NMR: 1.23 (d, $J=7$ Hz, 3H), 2.70—3.0 (m, 1H), 2.92 (s, 1H), 3.52 (d, $J=7$ Hz, 2H), 7.0—7.3 (m, 5H). $PhCHMeCH_2CH_2OH$: n_D^{20} 1.5185; IR (neat) 3325, 1045, 760, 700 cm^{-1}; ^1H NMR 0.90 (br s, 1H), 1.26 (d, $J=7$ Hz, 3H), 1.77 (q, $J=7$ Hz, 2H), 2.87 (sextet, $J=7$ Hz, 1H), 3.45 (dt, $J=7$ Hz and 3 Hz, 2H), 7.05—7.25 (m, 5H). (Found: C, 80.00; H, 9.67%).

We thank the Ministry of Education for the Grant-in-Aid for Scientific Research (No. 303523) and Shinetsu Chemical Co., Ltd. for support of this work.

References

1) For part XV, see K. Tamao, M. Mishima, J. Yoshida, M. Takahashi, N. Ishida, and M. Kumada, *J. Organomet. Chem.*, in press.

2) a) G. H. Wagner, D. L. Bailey, A. N. Pines, M. L. Dunham, and D. B. McIntire, *Ind. Eng. Chem.*, **45**, 367 (1953); b) H. G. Kuivila and C. R. Warner, *J. Org. Chem.*, **27**, 2845 (1964); c) R. F. Cunico, *ibid.*, **36**, 929 (1971); d) R. F. Cunico and E. M. Dexheimer, *Organomet. Chem. Synth.*, **1**, 253 (1971); e) D. Seyferth and D. L. White, *J. Organomet. Chem.*, **34**, 119 (1972); f) L. Birkofer and R. Stilke, *ibid.*, **74**, C1 (1974); g) L. Birkofer and D. Eichstaedt, *ibid.*, **145**, C29 (1979); h) D. G. Batt and B. Ganem, *Tetrahedron Lett.*, **1978**, 3323; i) M. E. Jung and B. Gaede, *Tetrahedron*, **35**, 621 (1979); j) A. Hosomi, M. Saito, and H. Sakurai, *Tetrahedron Lett.*, **21**, 355 (1980).

3) A. Laporterie, J. Dubac, and M. Lesbre, *J. Organomet. Chem.*, **101**, 187 (1975).

4) N. S. Nesmeyanov, V. M. Vdovin, E. Sh. Finkelschtein, V. D. Oppengeim, and N. A. Chekalina, *Izv. Akad. Nauk SSSR, Ser. Khim.*, **1966**, 1998.

5) K. Tamao, J. Yoshida, H. Yamamoto, T. Kakui, H. Matsumoto, M. Takahashi, A. Kurita, M. Murata, and M. Kumada, *Organometallics*, in press.

6) a) K. Alder and M. Fremery, *Tetrahedron*, **14**, 190 (1961); b) J. J. McCullough, *Acc. Chem. Res.*, **13**, 270 (1980).

7) K. Tamao, T. Kakui, and M. Kumada, *J. Am. Chem. Soc.*, **100**, 2268 (1978).

8) H. J. Dauber, B. C. McJusick, and G. P. Mueller, *J. Am. Chem. Soc.*, **70**, 4179 (1948).

9) a) A. R. Bassindale, C. Eaborn, D. R. M. Walton, and D. J. Young, *J. Organomet. Chem.*, **20**, 49 (1969); b) C. Eaborn, F. Feichtmayr, M. Horn, and J. N. Murrell, *ibid.*, **77**, 39 (1974); c) T. G. Traylor, W. Hanstein, M. J. Berwin, N. A. Clinton, and R. S. Brown, *J. Am. Chem. Soc.*, **93**, 5715 (1971); d) G. D. Hartman and T. G. Traylor, *ibid.*, **97**, 6147 (1975).

10) J. Yoshida, K. Tamao, T. Kakui, A. Kurita, M. Murata, K. Yamada, and M. Kumada, *Organometallics*, in press.

11) E. J. Hamilton, Jr., and H. Fischer, *Helv. Chim. Acta*, **56**, 795 (1973).

12) D. Lal, D. Griller, S. Husband, and K. U. Ingold, *J. Am. Chem. Soc.*, **96**, 6355 (1974).

13) N. Furuya and T. Sukawa, *J. Organomet. Chem.*, **96**, C1 (1975).

14) W. T. Caldwell, F. T. Tyson, and L. Lauer, *J. Am. Chem. Soc.*, **66**, 1479 (1944).

15) H. C. Brown, Y. Okamoto, and T. Inukai, *J. Am. Chem. Soc.*, **80**, 4964 (1958).

Configuration of Alanine Part in Natural Octopine[1)]

Kazuo Goto, Michinori Waki, Nobuo Mitsuyasu,† Yasuo Kitajima, and Nobuo Izumiya*

Laboratory of Biochemistry, Faculty of Science, Kyushu University 33, Higashi-ku, Fukuoka 812

(Received February 12, 1981)

Octopine has a structure of N^2-(1-carboxyethyl)arginine or N-(1-carboxy-4-guanidinobutyl)alanine. Configuration of the arginine part in natural octopine is determined as (*S*), whereas that of the alanine part has been assumed as (*R*). The configuration of the alanine part was concluded to be (*R*) by the present synthesis of (+)-octopine, which was identical with the natural one, by a sequence of reactions starting from (*R*)-alanine and (*R*)-2-bromo-5-acetamidopentanoic acid. The reaction of (*R*)-alanine and (*R*)-2-bromo-5-acetamidopentanoic acid in alkaline conditions gave N^2-((*R*)-1-carboxyethyl)-N^5-acetyl-(*S*)-ornithine which was converted to N^2-((*R*)-1-carboxyethyl)-(*S*)-ornithine ((*R*),(*S*)-octopinic acid) by hydrolysis with hydrochloric acid. (*R*),(*S*)-Octopinic acid gave (+)-octopine ((*R*),(*S*)-octopine) by guanidination. The reaction of (*S*)-alanine and (*R*)-2-bromo-5-acetamidopentanoic acid led to give (*S*),(*S*)-octopinic acid and subsequently (+)-isooctopine ((*S*),(*S*)-octopine).

Octopine is an unusual amino acid first isolated from octopus muscle in 1927[2)] and from crown-gall tissue.[3)] A number of imino acids structurally related to octopine have recently been found in crown-gall tumors of plants, and the use of these imino acids as markers of a possible transfer of gene from the tumor-inducing bacterium into host plant cells has sparked further interest in these compounds.[4)]

The chemical structure of octopine was established as N^2-(1-carboxyethyl)arginine or N-(1-carboxy-4-guanidinobutyl)alanine.[5,6)] The configuration of the arginine (Arg) part in natural octopine has been determined to be (*S*) by either enzymic method or synthetic approach as follows. Akasi demonstrated that natural octopine is susceptible to arginase which decomposes (*S*)-arginine, but not (*R*)-arginine.[7)] Akasi also prepared identical compound with natural octopine from (*S*)-arginine and (*S*)-2-bromopropionic acid; in this reaction the configuration of the (*S*)-Arg part is retained.[5)]

However, no definite conclusion in respect to the configuration of the alanine (Ala) part has been reached. (*R*)-Configuration of the Ala part in natural octopine has been assumed by two groups. Izumiya *et al.* assumed the (*R*)-configuration by data of optical rotatory dispersions of natural octopine and its diastereomer.[8)] They also assumed the (*R*)-configuration by occurrence of Walden inversion of (*S*)-2-bromopropionic acid from kinetic data on the reaction of (*S*)-arginine and (*S*)-2-bromopropionic acid in alkaline conditions.[8)] Biellmann *et al.* demonstrated the (*R*)-configuration by an elegant method; they prepared octopine mixture from (*R*)-alanine and 2-oxo-5-guanidinopentanoic acid by reduction with cyanoborohydride, and observed the presence of natural octopine in the octopine mixture by enzymic method.[9)] They, however, failed to separate the octopine diastereomers mentioned above, despite that they could isolate crystalline (+)-octopine corresponding to the natural one and its diastereomer in good yields after reduction of (*S*)-arginine and 2-oxopropionic acid by cyanoborohydride.[9)] Previously, Izumiya *et al.* observed a similar result that hydrogenation of a mixture of (*S*)-arginine and 2-oxopropionic acid in the presence of palladium black produced octopine, but hydrogenation of a mixture of (*R*)-alanine and 2-oxo-5-guanidinopentanoic acid did not.[8)]

This paper presents a definite conclusion for (*R*)-configuration of the Ala part by the synthesis of (+)-octopine corresponding to natural octopine starting from (*R*)-alanine and (*R*)-2-bromo-5-acetamidopentanoic acid.

Results and Discussion

Approach in Determination of Configuration of Ala Part in Natural Octopine. Two groups reported that the reaction of (*S*)-arginine and (*S*)-2-bromopropionic acid produces (+)-octopine which is confirmed to be identical with natural octopine.[5,8)] Since the configuration at an asymmetric carbon of the Arg part is in full retention, the configuration of Ala part of natural octopine should be either (*R*) or (*S*) as shown in Scheme 1. Supposed natural octopine containing (*R*)-alanine residue is designated as (+)-**1a**, and the one containing (*S*)-alanine residue as (+)-**1b**. We designed to synthesize an octopine starting from (*R*)-alanine and (*R*)-2-bromo-5-acetamidopentanoic acid ((*R*)-2-Br-5-Acpa) as shown in Scheme 2. We postulated that the configuration of the Ala part in natural octopine should be (*R*) if we would obtain (+)-octopine ((+)-**1a**) which is identical with natural one, whereas the configuration should be (*S*) if we obtain (−)-octopine ((−)-**1b**) which is an antipode of supposed natural octopine ((+)-**1b**).

Conclusion for Configuration of Ala Part in Natural Octopine. We could isolate (+)-octopine ((+)-**1a**) after a sequence of the reactions shown in Scheme 2, therefore we conclude that the configuration of the Ala part in natural octopine is (*R*). Then, we propose new nomenclature for four isomers of octopine as given in Table 1. It is also concluded that the asymmetric carbon with (*R*)-configuration in (*R*)-2-Br-5-Acpa is converted to (*S*) by Walden inversion during the formation of (*R*),(*S*)-Ac-octopinic acid.

Reaction of (R)-Alanine and (R)-2-Br-5-Acpa. The route to synthesize (*R*),(*S*)-octopine is shown in Fig. 1. Izumiya *et al.* reported that (+)-octopine and (+)-isooctopine were obtained in good yields

† Present address: Laboratory of Chemistry, College of General Education, Saga University, Saga 840.

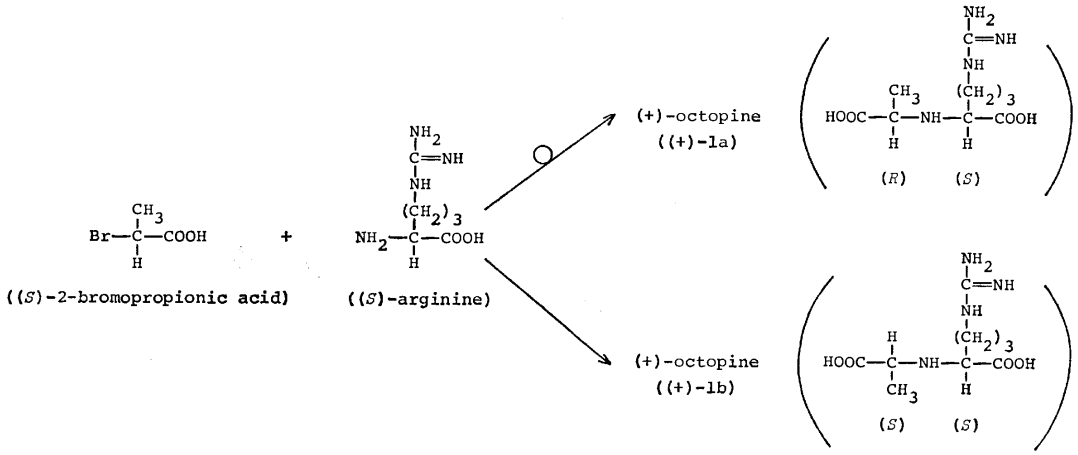

Scheme 1. Formation of (+)-octopine ((+)-**1a** or (+)-**1b**) from (*S*)-arginine and its supposed configuration.

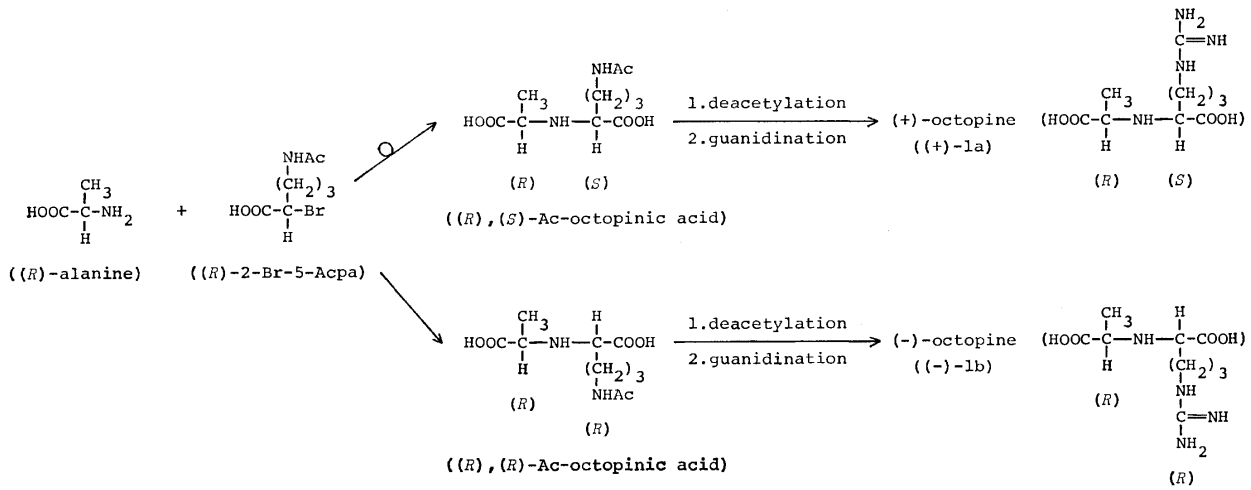

Scheme 2. Supposed formation of (+)-octopine ((+)-**1a**) or (−)-octopine ((−)-**1b**) from (*R*)-alanine.

Table 1. Configurations of isomers of octopine

Nomenclature		Configuration of		Source	$[\alpha]_D(H_2O)$
By Akasi[a] and Izumiya *et al.*[b]	By present authors	Ala part	Arg part		°
(+)-Octopine	(*R*),(*S*)-Octopine	(*R*)	(*S*)	Natural or Synthetic	+20.8
(−)-Octopine	(*S*),(*R*)-Octopine	(*S*)	(*R*)	Synthetic	−20.6[b]
(+)-Isooctopine	(*S*),(*S*)-Octopine	(*S*)	(*S*)	Synthetic	+26.7
(−)-Isooctopine	(*R*),(*R*)-Octopine	(*R*)	(*R*)	Synthetic	−26.6[b]

a) Cited from Ref. 10. b) Cited from Ref. 8.

(*ca.* 50%) from (*S*)-arginine, (*RS*)-2-bromopropionic acid, and $Ba(OH)_2$ in 1:2:2 molar ratio at 37 °C for 2 d.[8] However, the reaction of (*R*)-alanine, (*R*)-2-Br-5-Acpa, and $Ba(OH)_2$ under the same conditions gave the desired N^2-((*R*)-1-carboxyethyl)-N^5-acetyl-(*S*)-ornithine ((*R*),(*S*)-Ac-octopinic acid) in only trace amount. We assume that poor yield compared with the reaction of arginine and 2-bromopropionic acid is due to the presence of a bulky 3-acetamidopropyl group in 2-Br-5-Acpa and/or absence of basic guanidino group in alanine moiety. Then, we had to search for the conditions to give Ac-octopinic acid in fairly good yield.

In order to estimate a yield of Ac-octopinic acid and a possible occurrence of epimerization in N^5-acetylornithine part, we tried to separate (*R*),(*S*)- and (*S*),(*S*)-forms of N^2-(1-carboxyethyl)ornithine (octopinic acid) by an amino acid analyzer,[11] and found the conditions (see Experimental) to achieve the separation as shown in Fig. 2. A mixture of (*R*)-alanine, (*R*)-2-Br-5-Acpa, and $Ba(OH)_2$ was incubated for certain intervals, and a part of the mixture was refluxed with 2 M HCl, and the yield and the degree of epimerization of (*R*),(*S*)-octopinic acid in the acid hy-

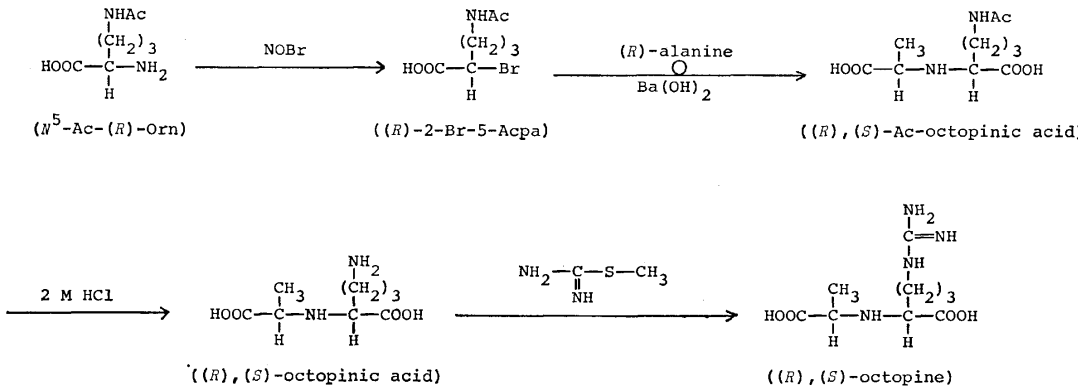

Fig. 1. Synthetic route for (*R*),(*S*)-octopine from (*R*)-alanine and (*R*)-2-Br-5-Acpa.

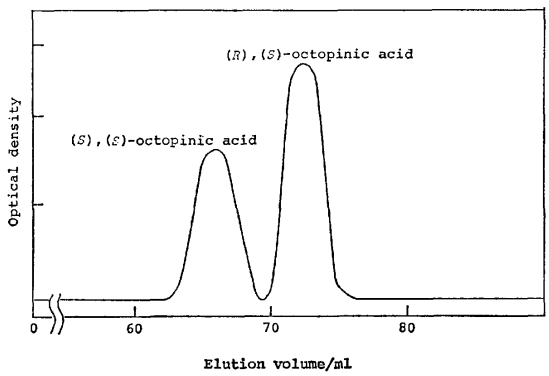

Fig. 2. Chromatogram of isomers of octopinic acid by an amino acid analyzer.

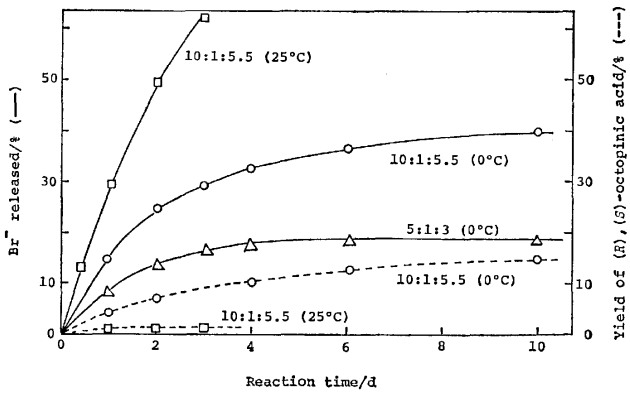

Fig. 3. Liberation of Br^- and formation of (*R*),(*S*)-Ac-octopinic acid during the reaction of (*R*)-alanine and (*R*)-2-Br-5-Acpa. Ratio of *e.g.* 10:1:5.5 means that of (*R*)-Ala:(*R*)-2-Br-5-Acpa:$Ba(OH)_2$ in molar term.

drolysate were determined by an amino acid analyzer using (*R*),(*S*)- and (*S*),(*S*)(instead of (*R*),(*R*))-forms of octopinic acid as reference substances under the conditions described above. At the same time, Br^- released during the reaction was analyzed by the Volhard titration method.

In Fig. 3, time-courses of Br^- release and (*R*),(*S*)-octopinic acid formation are given. The increase of the reaction temperature to 25 °C or 37 °C resulted in rapid liberation of Br^-, but the formation of Ac-octopinic acid was very poor. Molar ratios of the

Table 2. Effect of ratio of reactants on formation of acetyl octopinic acid[a)]

Reactant in molar ratio			Yield/% of (*R*),(*S*)-Ac-octopinic acid[b)]
(*R*)-Alanine	(*R*)-2-Br-5-Acpa	$Ba(OH)_2$	
1	2	2	1
2	1	1.5	5
5	1	3	12
10	1	5.5	15

a) The reaction was carried out at 0 °C for 10 d. b) Yields are calculated from (*R*)-2-Br-5-Acpa and estimated from (*R*),(*S*)-octopinic acid derived from (*R*),(*S*)-Ac-octopinic acid by an amino acid analyzer.

reactants gave also some influences on a yield; some of the results of the experiments are summarized in Table 2. We observed that the formation of Ac-octopinic acid was favored when the ratios of (*R*)-alanine to (*R*)-2-Br-5-Acpa were increased. Based on the above results, the favorable conditions to yield Ac-octopinic acid were settled as follows: a mixture of (*R*)-alanine, (*R*)-2-Br-5-Acpa, and $Ba(OH)_2$ in molar ratio of 10:1:5.5 is allowed to react at 0 °C for 10 d. It was observed, however, that the occurrence of possible (*R*),(*R*)-Ac-octopinic acid was 5—6% of the desired (*R*),(*S*)-isomer. We assume that the reasons of epimerization will be that (*R*)-2-Br-5-Acpa contains already some (*S*)-form and/or racemization at N^5-acetyl-(*R*)-ornithine part occurs during the reaction. Nevertheless, an undesirable (*R*),(*R*)-isomer in a small amount could be removed by recrystallization as mentioned latter.

Syntheses of (R),(S)- *and* (S),(S)-*Forms of Ac-octopinic Acid, Octopinic Acid, and Octopine.* Employing the favorable conditions mentioned above, recrystallized (*R*),(*S*)-Ac-octopinic acid was obtained from (*R*)-alanine and (*R*)-2-Br-5-Acpa in a yield of 16%. This compound still contained 3% of its possible isomer, (*R*),(*R*)-Ac-octopinic acid. However, (*R*),(*S*)-octopinic acid, obtained from the (*R*),(*S*)-Ac-octopinic acid by hydrolysis and recrystallized from water–ethanol, was free from (*R*),(*R*)-octopinic acid; the (*R*),(*R*)-isomer might be removed during the recrystallization. Alternatively, octopinic acid was also obtained from (+)-octopine ("natural octopine"), derived from (*S*)-

arginine and (*S*)-2-bromopropionic acid, with the treatment of $Ba(OH)_2$ at 80 °C. The octopinic acid obtained above showed the same properties as those of the (*R*),(*S*)-octopinic acid derived from the (*R*),(*S*)-Ac-octopinic acid (*e.g.*, melting point, R_f values on paper, and specific rotations). Finally, crystalline (*R*),(*S*)-octopine was prepared from (*R*),(*S*)-octopinic acid, derived from (*R*),(*S*)-Ac-octopinic acid, and *S*-methylisothiourea in a yield of 61%. Identity between this (*R*),(*S*)-octopine and (+)-octopine ("natural octopine") was established by comparison of chromatographies on paper and silica gel-thin layer, and specific rotations. In the same manner, (*S*),(*S*)-Ac-octopinic acid was synthesized from (*S*)-alanine and (*R*)-2-Br-5-Acpa. Subsequently, (*S*),(*S*)-forms of octopinic acid and octopine were prepared by the same procedure as for the (*R*),(*S*)-forms. Their physical properties were different from those of the corresponding octopinic acid and octopine derived from (+)-octopine ("natural octopine") or (+)-octopine itself.

Experimental

All the melting points are uncorrected. Paper chromatography was carried out on Toyo Roshi No. 52 paper with the solvent system: R_f, *n*-BuOH–AcOH–pyridine–H_2O (15:3:10:12, v/v). TLC was carried out on silica gel G (Merck) with the same solvent system as described above: R_f (TLC). Material possessing an amino group was detected by spraying with 0.2% ninhydrin solution in acetone, followed by heating at 100 °C. Material having a guanidino group was detected by spraying with an alkaline pentacyanonitrosylferrate(III)–hexacyanoferrate(III) reagent.[12] Material having blocked amino group was detected by spraying with 10% H_2SO_4, followed by heating on a hot plate. Optical rotations were measured on a Yanagimoto polarimeter OR-20. Amino acid analyses were performed with a Hitachi amino acid analyzer KLA-3B.

N^5-Acetyl-(R)-ornithine (N^5-Ac-(R)-Orn). This was prepared from (*R*)-ornithine monohydrochloride (16.9 g, 100 mmol) in the same manner as the preparation of *N^5*-Ac-(*S*)-Orn,[13] and was recrystallized from water–EtOH; yield, 15.9 g (91%); mp 233—234 °C (dec); $[\alpha]_D^{20}$ −24.6° (*c* 1, 5 M HCl); R_f 0.29. Reported value for *N^5*-Ac-(*S*)-Orn; $[\alpha]_D^{25}$ +24.0° (*c* 1, 5 M HCl).[13]

(R)-2-Bromo-5-acetamidopentanoic Acid ((R)-2-Br-5-Acpa). This was prepared from *N^5*-Ac-(*R*)-Orn (8.71 g, 50 mmol), KBr (20.9 g, 175 mmol) and sodium nitrite (5.58 g, 80 mmol) in 1.25 M H_2SO_4 (105 ml) according to the procedure of Izumiya[14]; yield of an oil, 6.43 g (54%); R_f (TLC) 0.70.

Chromatography of (R),(S)- or (S),(S)-Form of Octopinic Acid with Amino Acid Analyzer. Certain amount (5 μmol) of either (*R*),(*S*)- or (*S*),(*S*)-form of octopinic acid was dissolved in 0.2 M citrate buffer of pH 2.2, and an aliquot (0.5 μmol) of the solution was subjected to the analyzer. The following conditions were sufficient to permit the separation of two isomers; column with spherical resin, 0.9 cm × 50 cm; buffer, the standard citrate at pH 3.25; flow rate, 60 ml/h; jacket temperature, 55 °C. A chromatogram with a mixture of both isomers is shown in Fig. 2. The ratio of color intensities in the chromatogram of equimolar amount of (*R*),(*S*)-form and (*S*),(*S*)-form of octopinic acid was found to be 140:100.

Reaction of (R)- or (S)-Alanine and (R)-2-Br-5-Acpa. Determination of Bromide Ion: (*R*)- or (*S*)-Alanine, (*R*)-2-Br-5-Acpa and $Ba(OH)_2 \cdot 8H_2O$ in each specified amount were dissolved in water (20 ml). An aliquot (1 ml) of the solution was withdrawn for certain intervals, and was subjected to the Volhard titration. An amount of Br^- released was determined, the result being shown in Fig. 3.

Determination of (R),(S)- or (S),(S)-Form of Ac-octopinic Acid: An aliquot (1 ml) of the reaction mixture described above for certain intervals was put on a column (1.1 cm × 6 cm) of Dowex 50X8 (H^+ form), and the column was washed with water and eluted with 2 M NH_3 aq. The eluate was evaporated, and the residue was dissolved in 2 M HCl. After being refluxed for 2 h, the solution was evaporated, and the residue was dissolved in 0.2 M citrate buffer (pH 2.2). An aliquot was subjected to an amino acid analyzer as described previously. Yield of (*R*),(*S*)- or (*S*),(*S*)-form of Ac-octopinic acid was calculated from a peak of corresponding octopinic acid. Elution volume of unchanged alanine on the analyzer was 98 ml, and the ratio of color intensities in the chromatogram of equimolar amount of (*R*),(*S*)-octopinic acid and alanine was found to be 85:100.

(R),(S)-Ac-octopinic Acid. A solution of (*R*)-alanine (4.45 g, 50 mmol), (*R*)-2-Br-5-Acpa (1.19 g, 5 mmol), and $Ba(OH)_2 \cdot 8H_2O$ (8.68 g, 27.5 mmol) in water (50 ml) was stirred at 0 °C. After being stirred for 10 d at 0 °C, the solution was applied to a column (2.8 cm × 26 cm) of Dowex 50X8 (H^+ form), which was washed with water and eluted with 2 M NH_3 aq (300 ml). The eluate was evaporated and the residual solid was dissolved in a small amount of 0.1 M AcOH. The solution was put on a column (1.1 cm × 50 cm) of Amberlite IR-45 pre-equilibrated with 0.1 M AcOH. Elution was performed with 300 ml of 0.1 M AcOH and then 2 M AcOH (each fraction, 25-ml), fractions being monitored by TLC; the fractions 2—6 contained (*R*)-alanine. The fractions 17—21 were evaporated, and recrystallized from water–EtOH–acetone; yield, 197 mg (16% based on (*R*)-2-Br-5-Acpa); R_f (TLC) 0.36. This compound contained small amount (*ca.* 3%) of possible (*R*),(*R*)-Ac-octopinic acid, which was determined by an amino acid analyzer on an acid hydrolysate of a part of the product (197 mg).

Found: C, 46.85; H, 7.41; N, 10.46%. Calcd for $C_{10}H_{18}O_5N_2 \cdot 2/3H_2O$: C, 46.51; H, 7.55; N, 10.85%.

(S),(S)-Ac-octopinic Acid. This was prepared from (*S*)-alanine (4.45 g, 50 mmol) and (*R*)-2-Br-5-Acpa (1.19 g, 5 mmol) as described above; yield, 172 mg (14%); R_f (TLC) 0.36. This compound contained small amount (*ca.* 4%) of possible (*S*),(*R*)-Ac-octopinic acid.

Found: C, 47.92; H, 7.31; N, 11.19%. Calcd for $C_{10}H_{18}O_5N_2 \cdot 1/4H_2O$: C, 47.90; H, 7.44; N, 11.17%.

(R),(S)-Octopinic Acid. From (R),(S)-Ac-octopinic Acid: A solution of (*R*),(*S*)-Ac-octopinic acid (123 mg, 0.5 mmol) in 2 M HCl was refluxed for 2 h and evaporated. The residue dissolved in a small amount of water was put on a column (1.1 cm × 6 cm) of Dowex 50X8 (H^+ form), and the column was washed with water and eluted with 2 M NH_3 aq. The eluate was evaporated and recrystallized from water–EtOH; yield, 76 mg (74%); mp 275—277 °C (dec); $[\alpha]_D^{20}$ +19.2° (*c* 0.5, H_2O); R_f 0.11. This compound was pure (*R*),(*S*)-octopinic acid showing no contamination of possible (*R*),(*R*)-isomer.

Found: C, 45.90; H, 7.84; N, 13.23%. Calcd for $C_8H_{16}O_4N_2 \cdot 1/4H_2O$: C, 46.04; H, 7.97; N, 13.42%.

From (+)-Octopine: (+)-Octopine (246 mg, 1 mmol)[8] derived from (*S*)-arginine and (*S*)-2-bromopropionic acid was dissolved in saturated aqueous $Ba(OH)_2$ solution (100 ml) at 0 °C, and the solution was left to stand at 75—80 °C for 6 h. After removal of Ba^{++} by H_2SO_4, the filtrate was treated with a column of Dowex 50X8 as described above.

The eluate with 2 M NH_3 aq was evaporated and the residue dissolved in 0.1 M pyridine–formate buffer (pH 3.1) was put on a column (1.1 cm×40 cm) of Dowex 50X8 pre-equilibrated with the same buffer. Elution was performed with the same buffer (each fraction, 10-ml), and the fractions 10—15 were evaporated to afford crude (*R*),(*S*)-octopinic acid which contained *ca.* 1.5% possible (*R*),(*R*) (or (*S*),(*S*))-octopinic acid. Crude product was recrystallized from water–EtOH to give pure (*R*),(*S*)-octopinic acid; yield, 80 mg (39%); mp 276—278 °C (dec); $[\alpha]_D^{20}$ +19.1° (*c* 0.5, H_2O); R_f 0.11. Reported values[15] for octopinic acid derived from natural octopine: mp 270—271 °C; $[\alpha]_D^{20}$ +18.48° (*c* 0.5, H_2O).

(S),(S)-Octopinic Acid. This was prepared from (*S*),(*S*)-Ac-octopinic acid (123 mg, 0.5 mmol) as described for the preparation of (*R*),(*S*)-octopinic acid from (*R*),(*S*)-Ac-octopinic acid; yield, 73 mg (72%); mp 237 °C (dec); $[\alpha]_D^{20}$ +24.6° (*c* 0.5, H_2O); R_f 0.11.

Found: C, 45.80; H, 7.89; N, 13.28%. Calcd for $C_8H_{16}O_4N_2 \cdot 1/3H_2O$: C, 45.71; H, 7.99; N, 13.33%.

(R),(S)-Octopine. A solution of (*R*),(*S*)-octopinic acid (41 mg, 0.2 mmol), derived from (*R*),(*S*)-Ac-octopinic acid, and *S*-methylisothiourea sulfate (56 mg, 0.4 mmol) in 0.1 M NaOH (4 ml) was kept at 35 °C for 6 d, and the solution was put on a column (1.1 cm×6 cm) of Dowex 50X8 (H^+ form). The column was washed with water and eluted with 2 M NH_3 aq. The eluate was concentrated and applied to a column (1.4 cm×3 cm) of Dowex 1X2 (OH^- form), and the column was washed with water and eluted with 1 M AcOH. The eluate was evaporated, and the residue dissolved in 0.1 M pyridine–formate buffer (pH 3.1) was put on a column (0.9 cm×33 cm) of Dowex 50X8 (pyridinium form). The column was washed with the same buffer (75 ml), and eluted with 1 M pyridine. The eluate containing octopine was evaporated and recrystallized from water–EtOH–acetone; yield, 30 mg (61%); mp 280—283 °C (dec); $[\alpha]_D^{20}$ +20.8° (*c* 1, H_2O); R_f 0.15.

Found: C, 43.78; H, 7.32; N, 22.83%. Calcd for $C_9H_{18}O_4N_4$: C, 43.89; H, 7.37; N, 22.75%. Reported values[15] for natural octopine: mp 281—282 °C; $[\alpha]_D^{17}$ +20.94° (*c* 2.6, H_2O). Reported values[8] for (+)-octopine prepared from (*S*)-arginine and (*S*)-2-bromopropionic acid; mp 283—284 °C; $[\alpha]_D^{24}$ +20.8° (*c* 2, H_2O).

Identity of (*R*),(*S*)-octopine obtained from (*R*)-alanine and (*R*)-2-bromo-5-acetamidopentanoic acid, and (+)-octopine[8] prepared from (*S*)-arginine and (*S*)-2-bromopropionic acid was ascertained by co-chromatographies on paper and silica gel-thin layer with several solvent systems in addition to the same specific rotations described above.

(S),(S)-Octopine. (*S*),(*S*)-Octopinic acid (41 mg, 0.2 mmol) was treated with *S*-methylisothiourea sulfate followed by work-up as described above. The crude product was recrystallized from water–EtOH–acetone; yield 32 mg (65%); mp 263—264° (dec); $[\alpha]_D^{20}$ +26.7° (*c* 1, H_2O); R_f 0.15.

Found: C, 43.67; H, 7.48; N, 22.65%. Calcd for $C_9H_{18}O_4N_4$: C, 43.89; H, 7.37; N, 22.75%. Reported values[8] for (+)-isooctopine prepared from (*S*)-arginine and (*R*)-2-bromopropionic acid; mp 264—265 °C; $[\alpha]_D^{24}$ +26.8° (*c* 2, H_2O).

We thank Dr. N. Nishino in this laboratory for his discussion.

References

1) This work was reported: N. Izumiya, K. Goto, M. Waki, and N. Mitsuyasu, 29th National Meeting of the Chemical Society of Japan, Hiroshima, October 1973, Abstr. No. 2U18.
2) K. Morizawa, *Acta Schol. Med. Univ. Imp. Kioto*, **9**, 285 (1927).
3) A. Ménagé and G. Morel, *C. R. Acad. Sci. Paris*, **259**, 4795 (1964).
4) M. Drummond, *Nature*, **281**, 343 (1979).
5) S. Akasi, *J. Biochem. (Tokyo)*, **25**, 281 (1937).
6) E. Moore and D. W. Wilson, *J. Biol. Chem.*, **119**, 573 (1937).
7) S. Akasi, *J. Biochem. (Tokyo)*, **26**, 129 (1937).
8) N. Izumiya, R. Wade, M. Winitz, M. C. Otey, S. M. Birnbaum, R. J. Koegel, and J. P. Greenstein, *J. Am. Chem. Soc.*, **79**, 652 (1957).
9) J. F. Biellmann, G. Branlant, and L. Wallén, *Bioorg. Chem.*, **6**, 89 (1977).
10) S. Akasi, *J. Biochem. (Tokyo)*, **25**, 291 (1937).
11) (*S*),(*S*)-Form of octopinic acid was used as a reference substance instead of (*R*),(*R*)-form which is a possible epimerization product in the Ac-octopinic acid. The elution volume and color intensity of the (*S*),(*S*)-form of octopinic acid were identical with those of (*R*),(*R*)-form on the amino acid analyzer.
12) S. Makisumi, *Nippon Kagaku Zasshi*, **73**, 737 (1952).
13) J. P. Greenstein, M. Winitz, P. Gullino, S. M. Birnbaum, and M. C. Otey, *Arch. Biochem. Biophys.*, **64**, 342 (1956).
14) N. Izumiya, *Bull. Chem. Soc. Jpn.*, **26**, 53 (1953).
15) S. Akasi, *J. Biochem. (Tokyo)*, **25**, 261 (1937).

A Theoretical Study of the Resonance Raman Scattering from a Molecular System. Effects of Vibronic and Nonadiabatic Couplings

Katsumi Seo, Hirohiko Kono,† and Yuichi Fujimura*

Department of Chemistry, Faculty of Science, Tohoku University, Sendai 980

(Received March 30, 1981)

A theory of the resonance Raman scattering (RRS) from a molecular system in which the vibronic levels of the resonance state are perturbed by both the Herzberg-Teller vibronic and the nonadiabatic coupling is developed. By using the time-independent Green-function formalism, an expression for the RRS is derived in the three-electronic-state model. The RRS cross-sections obtained are classified into four types: the pure RRS cross-section, independent of the coupling mode: the vibronically induced one, the nonadiabatically induced one, and the interference term. Assuming that the molecular system consists of a totally symmetric mode characterized by a displaced harmonic oscillator, with a nontotally symmetric mode as the inducing mode, analytical expressions for the relevant RRS cross-sections of the n_s-th order vibrational transition for the totally symmetric mode are derived. Model calculations of the cross-sections indicate that, for an increasing potential displacement parameter, Δ, between the coupled states, the nonadiabatic correction to the higher-order vibrational transitions, as well as the zero-order vibrational transition, makes a significant contribution.

The mechanisms of the resonance Raman scattering (RRS) from molecules have been investigated by many authors.[1–12] It is experimentally and theoretically recognized that the intensity of the RRS is enhanced as a result of the Herzberg-Teller vibronic coupling in the resonant state and/or the nonadiabatic coupling between the resonant and other electronically excited states.[13–27] Considering a simple model for the RRS by using a nontotally symmetric vibrational mode, Mortensen[3] has shown that the excitation energy profile of the RRS derived within the conventional linear Herzberg-Teller vibronic coupling approximation consists of two identical maxima corresponding to a resonance with 0-0 and 0-1 bands, neglecting the incident-photon-frequency dependence. Zgierski[4] has investigated the effect of nonadiabatic coupling to explain the asymmetry of the 0-0 and 0-1 bands. Hassing and Mortensen[18] have claimed that the asymmetry may be explained by taking into account the interference from a displaced totally symmetric mode in the RRS of the nontotally symmetric mode. By using the third-order perturbation theory, Johnson, Nafie, and Peticolas[7] have calculated the excitation energy profile of the zero-order vibrational transition for a displaced totally symmetric mode, and have concluded that the importance of the nonadiabatic correction is minimal relative to the adiabatic contribution unless the vibronic energy level of the upper state is within a few vibrational quanta of the resonant state.

The main purpose of this paper is to develop a theory of the RRS from a molecular system in which the vibronic levels of the resonant state are perturbed by both the Herzberg-Teller vibronic and the nonadiabatic coupling, and to clarify the role of the couplings on the excitation profiles of the RRS using the adiabatic basis set. Our theory is applicable to a molecular system with any potential energy surface displacements, and includes the results obtained by Zgierski[4] and by Johnson *et al.*[7] as special cases. Their theoretical treatments are restricted to a molecular system with small potential energy surface displacements between the resonant and the ground or upper electronic states. A preliminary study of the effect of the nonadiabatic coupling on the RRS was reported in a previous paper.[28]

In theory section, on the basis of the time-independent Green-function formalism, an expression for the RRS cross-section in the weak radiation field is derived using the three-electronic-state model. The RRS cross-sections are classified in terms of its mechanisms: the pure RRS, which is irrelevant to the inducing mode; the vibronically induced RRS; the nonadiabatically induced RRS, and the RRS originating from their interference, which are further divided into three groups. The most important terms of the interference are those between the components of the RRS within the same resonant state. The interference term between the vibronically induced and nonadiabatically induced RRS contributes to the asymmetry of the vibrational transitions of the excitation profile. In displaced harmonic oscillator model section, assuming that the molecular system consists of a totally symmetric mode characterized by a displaced harmonic oscillator, with a nontotally symmetric mode as the inducing mode, analytical expressions for the relevant RRS cross-sections of the n_s-th order vibrational transition for the totally symmetric mode are derived. The RRS cross-section thus obtained is explicitly expressed as a function of two displacement parameters between the equilibrium points in the relevant state. In the final section, model calculations of the excitation-energy profiles of the RRS cross-section of the n_s-th order vibrational transitions are performed in order to compare the effects of the couplings. It is shown that, for increasing the displacement, Δ, between the two coupled states, the nonadiabatic correction to the higher-order vibrational transitions as well as the zero-order vibrational transition makes a significant contribution.

Theory

Time-independent Green-function Formalism of the RRS Cross-sections in the Three-electronic-state Model. In

† Present address: Department of Chemistry, Arizona State University, Tempe, Arizona, U.S.A.

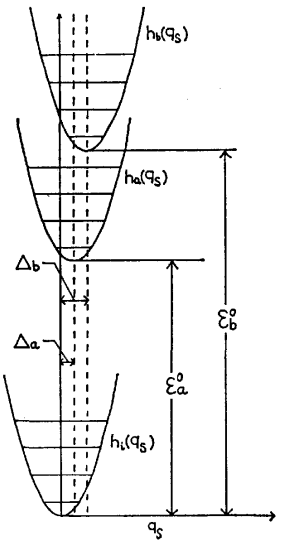

Fig. 1. Displaced harmonic potential model for three electronic state system. $h_i(q_s)$ represents the molecular Hamiltonian of a totally symmetric mode q_s in the ground state, and $h_a(q_s)$ and $h_b(q_s)$ those in the two electronic states a and b, respectively. Δ and ε^0 represent the dimensionless displacement between the equilibrium points, and the energy gap between the bottoms in the ground and relevant excited states, respectively.

a previous paper,[11] the time-independent Green-function formalism was applied to the derivation of the RRS cross-sections in the two-electronic-state model. In this section, in order to take systematically into account the effects of the vibronic and nonadiabatic couplings, we consider a typical model consisting of three electronic states. The total system of the molecular states and radiation field is assumed to be composed of an initial state, $|I\rangle = |\varepsilon_i; \{n_i\hbar\omega_i\}|$; two intermediate states, $|A\rangle = |\{\varepsilon_a\}; \{n_a\hbar\omega_a\}\rangle$ and $|B\rangle = |\{\varepsilon_b\}; \{n_b\hbar\omega_b\}\rangle$, and a final state, $|F\rangle = |\{\varepsilon_f\}; \{n_f\hbar\omega_f\}\rangle$, where ε_i denotes the lowest state in the molecular-ground state; $\{\varepsilon_a\}$ the manifold in the a-th electronically excited state, and $n\hbar\omega$, the photon energy. The energy diagram of the molecular system is shown in Fig. 1.

The time evolution of the initial state, $|I\rangle$, is expressed by:

$$|\Psi_I(t)\rangle = \exp[-i\hat{H}t/\hbar]|I\rangle \tag{1}$$

where the total Hamiltonian, $\hat{H}$, is given by:

$$\hat{H} = \hat{H}_0 + \hat{V}. \tag{2}$$

Here,

$$\hat{H}_0 = \hat{H}_m^0 + \hat{H}_r^0 \tag{2a}$$

and

$$\hat{V} = \hat{V}_{nd} + \hat{V}_{mr}, \tag{2b}$$

where $\hat{H}_m^0$ and $\hat{H}_r^0$ are the molecular Hamiltonian in the Born-Oppenheimer basis set, and the Hamiltonian for the free electromagnetic field, respectively, while $\hat{V}_{nd}$ and $\hat{V}_{mr}$ denote the nuclear kinetic energy, $\hat{T}_N$, and the molecule-radiation interaction respectively.

The transition amplitude, U_{FI}, from the initial state, I, to the final state, F, is expressed in terms of the transformation of the time-independent Green function as:

$$U_{FI}(t) = \langle F|\Psi_I(t)\rangle = \frac{1}{2\pi i}\int \exp(-iEt/\hbar)G_{FI}dE, \tag{3}$$

where G_{FI} is the matrix element of the Green-function. Equations for the relevant matrix elements of the Green-function in the present model are written as:

$$G_{FI} = \sum_A G_{FF}^0 V_{FA} G_{AI} + \sum_B G_{FF}^0 V_{FB} G_{BI}, \tag{4a}$$

$$G_{AI} = G_{AA}^0 V_{AI} G_{II} + \sum_F G_{AA}^0 V_{AF} G_{FI} + \sum_B G_{AA}^0 V_{AB} G_{BI}, \tag{4b}$$

$$G_{BI} = G_{BB}^0 V_{BI} G_{II} + \sum_F G_{BB}^0 V_{BF} G_{FI} + \sum_A G_{BB}^0 V_{BA} G_{AI}, \tag{4c}$$

and:

$$G_{II} = G_{II}^0 + \sum_A G_{II}^0 V_{IA} G_{AI} + \sum_B G_{II}^0 V_{IB} G_{BI}, \tag{4d}$$

where G^0 represents the zero-order Green-function,[11] the summations in Eqs. 4 are carried out over both the molecular vibronic states and the radiation-field variables. By substituting Eqs. 4a and 4d into Eqs. 4b and 4c, we obtain:

$$(E-E_A^0-\Lambda_{AA})G_{AI} = V_{AI}G_{II}^0 + \sum_{A'\neq A}\Lambda_{AA'}G_{A'I} + \sum_B (V_{AB}+\Lambda_{AB})G_{BI}, \tag{5a}$$

and:

$$(E-E_B^0-\Lambda_{BB})G_{BI} = V_{BI}G_{II}^0 + \sum_{B'\neq B}\Lambda_{BB'}G_{B'I} + \sum_A (V_{BA}+\Lambda_{BA})G_{AI}. \tag{5b}$$

Here, $\Lambda_{AA'}$ and Λ_{AB} represent the diagonal and off-diagonal self-energy terms respectively.[11]

In order to solve the coupled equations 5a and 5b, we substitute G_{BI}, neglecting the term involving $G_{B'I}$ in Eq. 5b, into 5a:

$$(E-E_A^0-\tilde{\Lambda}_{AA})G_{AI} = \tilde{V}_{AI}G_{II}^0 + \sum_{A'\neq A}\tilde{\Lambda}_{AA'}G_{A'I}, \tag{6}$$

where:

$$\tilde{\Lambda}_{AA'} = \Lambda_{AA'} + \sum_B (V_{AB}+\Lambda_{AB})(E-E_B^0-\Lambda_{BB})^{-1}\times(V_{BA'}+\Lambda_{BA'}), \tag{7}$$

and:

$$\tilde{V}_{AI} = V_{AI} + \sum_B (V_{AB}+\Lambda_{AB})(E-E_B^0-\Lambda_{BB})^{-1}V_{BI}. \tag{8}$$

Equation 6 can be solved by using the iterative method described in Ref. 11. By using the similar procedure described above, the decoupled equation for G_{BI} is obtained.

Substituting the decoupled equations for G_{AI} and G_{BI} into Eq. 4a, the matrix element of the Green function G_{FI} is expressed as:

$$G_{FI} = \sum_A G_{FF}^0 V_{FA}(E-E_A^0-\tilde{\Lambda}_{AA})^{-1}\tilde{V}_{AI}G_{II}^0 + \sum_B G_{FF}^0 V_{FB}(E-E_B^0-\tilde{\Lambda}_{BB})^{-1}\tilde{V}_{BI}G_{II}^0, \tag{9}$$

where the effect of the off-diagonal terms involving $\tilde{\Lambda}_{AA'}$ and $\tilde{\Lambda}_{BB'}$ were neglected. The energy-dependent

self-energy part is, at the zero-order approximation, expressed as:

$$\tilde{\Delta}_{AA} = \Delta_{AA}(E_A^0) = D_A - \frac{i\Gamma_A}{2}, \tag{10a}$$

and, in the first-order approximation, as:

$$\tilde{\Delta}_{AA} = \tilde{\Delta}_{AA}(E_A^0) = \tilde{D}_A - \frac{i\tilde{\Gamma}_A}{2}, \tag{10b}$$

where:

$$\tilde{D}_A = D_A + \sum_B \frac{(E_A^0 - E_B^0 - D_B)|V_{BA}|^2}{(E_A^0 - E_B^0 - D_B)^2 + (\Gamma_B/2)^2}, \tag{11}$$

and:

$$\tilde{\Gamma}_A = \Gamma_A + \sum_B \frac{\Gamma_B|V_{AB}|^2}{(E_A^0 - E_B^0 - D_B)^2 + (\Gamma_B/2)^2}. \tag{12}$$

Here, the level shift, D_A, and the decay width, Γ_A, of the A intermediate state are given in Ref. 11. In a case of weak nonadiabatic coupling, Eq. 10a can be used.

Neglecting the terms involving Δ_{AB} in $\tilde{V}_{AI}$ and Δ_{BA} in $\tilde{V}_{BI}$ of Eq. 9 because these terms give rise to the higher-order photon processes, and substituting Eq. 9 into Eq. 3, the transition amplitude U_{FI}, is expressed as:

$$\begin{aligned}
U_{FI}(t) = \sum_A \Bigg(& \frac{V_{FA}V_{AI}\exp(-iE_I^0t/\hbar)}{E_I^0 - E_A + i\tilde{\Gamma}_A/2} \frac{\{1-\exp[-i(E_F^0-E_I^0)t/\hbar]\}}{E_I^0 - E_F^0} \\
& + \frac{V_{FA}V_{AI}\exp[-i(E_A - i\tilde{\Gamma}_A/2)t/\hbar]}{(E_A - E_F^0 - i\tilde{\Gamma}_A/2)(E_A - E_I^0 - i\tilde{\Gamma}_A/2)} - \frac{V_{FA}V_{AI}\exp(-iE_F^0t/\hbar)}{(E_I^0 - E_A + i\tilde{\Gamma}_A/2)(E_F^0 - E_A + i\tilde{\Gamma}_A/2)} \Bigg) + \sum_B (A \to B) \\
& + \sum_A \sum_B \Bigg(\frac{V_{FB}V_{BA}V_{AI}\exp(-iE_I^0t/\hbar)}{(E_I^0 - E_A + i\tilde{\Gamma}_A/2)(E_I^0 - E_B + i\tilde{\Gamma}_B/2)} \frac{\{1-\exp[-i(E_F^0-E_I^0)t/\hbar]\}}{E_I^0 - E_F^0} \\
& + \frac{V_{FB}V_{BA}V_{AI}\exp[-i(E_B - i\tilde{\Gamma}_B/2)t/\hbar]}{(E_B - E_A - i\tilde{\Gamma}_B/2 + i\tilde{\Gamma}_A/2)(E_B - E_I^0 - i\tilde{\Gamma}_B/2)(E_B - E_F^0 - i\tilde{\Gamma}_B/2)} \\
& + \frac{V_{FB}V_{BA}V_{AI}\exp[-i(E_A - i\tilde{\Gamma}_A/2)t/\hbar]}{(E_A - E_B - i\tilde{\Gamma}_A/2 + i\tilde{\Gamma}_B/2)(E_A - E_I^0 - i\tilde{\Gamma}_A/2)(E_A - E_F^0 - i\tilde{\Gamma}_A/2)} \\
& - \frac{V_{FB}V_{BA}V_{AI}\exp(-iE_F^0t/\hbar)}{(E_I^0 - E_A + i\tilde{\Gamma}_A/2)(E_I^0 - E_B + i\tilde{\Gamma}_B/2)(E_F^0 - E_B + i\tilde{\Gamma}_B/2)} \\
& - \frac{V_{FB}V_{BA}V_{AI}\exp(-iE_F^0t/\hbar)}{(E_I^0 - E_A + i\tilde{\Gamma}_A/2)(E_F^0 - E_A + i\tilde{\Gamma}_A/2)(E_F^0 - E_B + i\tilde{\Gamma}_B/2)} \Bigg) + \sum_A \sum_B (A \rightleftarrows B),
\end{aligned} \tag{13}$$

where $E_A = E_A^0 + D_A$ and $E_B = E_B^0 + D_B$. When we use the on-the-energy-shell approximation ($E_I^0 \to E_F^0$) and the limit, $t \to \infty$, it seems that the following terms make the dominant contribution to the scattering cross-section:

$$\begin{aligned}
U_{FI}(t) = \Bigg[& \sum_A \frac{V_{FA}V_{AI}\exp(-E_I^0t/\hbar)}{E_I^0 - E_A + i\tilde{\Gamma}_A/2} + \sum_B (A \to B) \\
& + \sum_A \sum_B \frac{V_{FB}V_{BA}V_{AI}\exp(-iE_I^0t/\hbar)}{(E_I^0 - E_A + i\tilde{\Gamma}_A/2)(E_I^0 - E_B + i\tilde{\Gamma}_B/2)} \\
& + \sum_A \sum_B (A \rightleftarrows B) \Bigg] \frac{1-\exp[-i(E_F^0 - E_I^0)t/\hbar]}{E_I^0 - E_F^0}.
\end{aligned} \tag{14}$$

By using the dipole and rotating wave approximations, and after integrating over the radiation-field variables, the differential cross-section for the Raman scattering is given by:

$$\begin{aligned}
\frac{d\sigma(\omega_1)}{d\Omega} = & \frac{\omega_1(n_2+1)}{2^4\pi^2\varepsilon_0^2c^4} \sum_f \int_0^\infty d\omega_2 \omega_2^3 \\
& \times \Bigg| \sum_c \frac{\langle f|e_2\cdot\mu|c\rangle\langle c|e_1\cdot\mu|i\rangle}{\varepsilon_1 + \hbar\omega_1 - \varepsilon_c + i\tilde{\Gamma}_c/2} \\
& + \sum_{\substack{c,d \\ (c\neq d)}} \frac{\langle f|\hat{e}_2\cdot\mu|d\rangle\langle d|\hat{T}_N|c\rangle\langle c|\hat{e}_1\cdot\mu|i\rangle}{(\varepsilon_1 + \hbar\omega_1 - \varepsilon_c + i\tilde{\Gamma}_c/2)(\varepsilon_1 + \hbar\omega_1 - \varepsilon_d + i\tilde{\Gamma}_d/2)} \\
& + (\text{non-resonant terms}) \Bigg|^2 \delta\left(\frac{\varepsilon_1 - \varepsilon_f + \hbar\omega_1 - \hbar\omega_2}{\hbar}\right),
\end{aligned} \tag{15}$$

where $\hbar\omega_1$ and $\hbar\omega_2$ denote the excitation and emission energies of the photon respectively, and where the summations, c and d, are taken over the vibronic states of two electronic states, a and b. Compared with the expression for the differential cross-section derived in the one-intermediate electronic state,[11] it should be noted that, in the two-intermediate-state model, the term originating from the nonadiabatic interaction appears in Eq. 15.

Mechanisms of the RRS from Randomly Oriented Molecules. We note that the complex tensor, t, for the RRS cross-section is written as the sum of symmetric and antisymmetric tensors, $\{t\} = \{S\} + \{A\}$, where $S_{12} = 1/2(t_{12} + t_{21})$ and $A_{12} = 1/2(t_{12} - t_{21})$. Here, the suffixes 1 and 2 specify the molecular fixed Cartesian coordinates, x, y, and z. We assume that the molecules are randomly oriented. If the incident radiation is linearly polarized, and if the polarization lies on the XY plane, the RRS cross-section, $d\sigma(\omega_1)/d\Omega$, along the Z axis is given by:[29]

$$\frac{d\sigma(\omega_1)}{d\Omega} = \frac{1}{15}\left\{7\frac{d\sigma_S(\omega_1)}{d\Omega} + 5\frac{d\sigma_A(\omega_1)}{d\Omega}\right\}, \tag{16}$$

where $d\sigma_S(\omega_1)/d\Omega$ and $d\sigma_A(\omega_1)/d\Omega$ represent the symmetric and antisymmetric parts of the cross-section and are given by:

$$\frac{d\sigma_I(\omega_1)}{d\Omega} = \frac{\omega_1(n_2+1)}{2^6\pi^2\varepsilon_0^2c^4} \sum_f \int_0^\infty d\omega_2 \omega_2^3$$

$$\left|\sum_c\left(\frac{\langle f|\mu_2|c\rangle\langle c|\mu_1|i\rangle}{\varepsilon_1+\hbar\omega_1-\varepsilon_c+i\tilde{\Gamma}_c/2}\pm\frac{\langle f|\mu_1|c\rangle\langle c|\mu_2|i\rangle}{\varepsilon_1+\hbar\omega_1-\varepsilon_c+i\tilde{\Gamma}_c/2}\right)\right.$$
$$+\sum_{\substack{c,d\\(c\neq d)}}\left(\frac{\langle f|\mu_2|d\rangle\langle d|\hat{T}_N|d\rangle\langle d|\mu_1|i\rangle}{(\varepsilon_1+\hbar\omega_1-\varepsilon_c+i\tilde{\Gamma}_c/2)(\varepsilon_1+\hbar\omega_1-\varepsilon_d+i\tilde{\Gamma}_d/2)}\right.$$
$$\left.\left.\pm\frac{\langle f|\mu_1|d\rangle\langle d|\hat{T}_N|c\rangle\langle c|\mu_2|i\rangle}{(\varepsilon_1+\hbar\omega_1-\varepsilon_c+i\tilde{\Gamma}_c/2)(\varepsilon_1+\hbar\omega_1-\varepsilon_d+i\tilde{\Gamma}_d/2)}\right)\right|^2$$
$$\times\delta\left(\frac{\varepsilon_1-\varepsilon_f+\hbar\omega_1-\hbar\omega_2}{\hbar}\right), \tag{17}$$

where the + and − signs correspond to the symmetric (I=S) and antisymmetric (I=A) cross-sections respectively. In the above expression, the non-resonant terms were disregarded.

To classify the RRS into the pure RRS irrelevant to the couplings, vibronically induced, and nonadiabatically induced types, we expand the matrix element of the transition dipole and the nonadiabatic coupling matrix element as:

$$\langle f|\mu_2|a\rangle=\langle\chi_f|M_{fa}(2)|\chi_a\rangle$$
$$+\langle\chi_f|(M_{fb}(2)V_{ba}-V_{fb}M_{ba}(2))q|\chi_a\rangle+\cdots, \tag{18}$$

and:

$$\langle a|\hat{T}_N|b\rangle=\left\langle\chi_a\left|\left(\Phi_a\left|-\frac{\hbar\omega}{2}\frac{\partial^2}{\partial q^2}\right|\Phi_b\right)\right|\chi_b\right\rangle$$
$$\simeq-\hbar\omega\left\langle\chi_a\left|V_{ab}\frac{\partial}{\partial q}\right|\chi_b\right\rangle, \tag{19}$$

respectively, where $M_{fa}(2)=\langle\Phi_f|\mu_2|\Phi_a\rangle_{q=q_0}$ and where $V_{ba}=\left[\frac{\langle\Phi_b|\partial V/\partial q|\Phi_a\rangle}{\varepsilon_a-\varepsilon_b}\right]_{q=q_0}$. Here, Φ, χ, and V denote the BO electronic wave function, the nuclear wave function, and the electrostatic interaction between electron and nucleus respectively. The above matrix elements are evaluated at the equilibrium nuclear configuration (q_0) in the ground state. Restricting ourselves to the first-order variation of the nuclear coordinate, q, and disregarding the vibronic coupling between the ground (final or initial) and intermediate states because of $|\varepsilon_a(q_0)-\varepsilon_b(q_0)|<|\varepsilon_b(q_0)-\varepsilon_f(q_0)|$, the symmetric and antisymmetric cross-section of the spontaneous RRS can be written as:

$$\frac{d\sigma_I(\omega_1)}{d\Omega}=\frac{\omega_1}{2^6\pi^2\varepsilon_0^2c^4}\sum_f\int_0^\infty d\omega_2\omega_2^3\delta\left(\frac{\varepsilon_1-\varepsilon_f+\hbar\omega_1-\hbar\omega_2}{\hbar}\right)$$
$$\left|\sum_c\left(\frac{\langle\chi_f|M_{fc}(2)|\chi_c\rangle\langle\chi_c|M_{c1}(1)|\chi_1\rangle}{\varepsilon_1+\hbar\omega_1-\varepsilon_c+i\tilde{\Gamma}_c/2}\pm\frac{\langle\chi_f|M_{fc}(1)|\chi_c\rangle\langle\chi_c|M_{c1}(2)|\chi_1\rangle}{\varepsilon_1+\hbar\omega_1-\varepsilon_c+i\tilde{\Gamma}_c/2}\right)\right.$$
$$+\sum_c^{(elec)}\sum_{\substack{d\\(c\neq d)}}\left[\left\{-\frac{\langle\chi_f|M_{fc}(2)|\chi_c\rangle\langle\chi_c|V_{cd}M_{d1}(1)q|\chi_1\rangle}{\varepsilon_1+\hbar\omega_1-\varepsilon_c+i\tilde{\Gamma}_c/2}+\frac{\langle\chi_f|M_{fd}(2)V_{dc}q|\chi_c\rangle\langle\chi_c|M_{c1}(1)|\chi_1\rangle}{\varepsilon_1+\hbar\omega_1-\varepsilon_c+i\tilde{\Gamma}_c/2}\right\}\right.$$
$$\left.\pm\left\{-\frac{\langle\chi_f|M_{fc}(1)|\chi_c\rangle\langle\chi_c|V_{cd}M_{d1}(2)q|\chi_1\rangle}{\varepsilon_1+\hbar\omega_1-\varepsilon_c+i\tilde{\Gamma}_d/2}+\frac{\langle\chi_f|M_{fd}(1)V_{dc}q|\chi_c\rangle\langle\chi_c|M_{c1}(2)|\chi_1\rangle}{\varepsilon_1+\hbar\omega_1-\varepsilon_c+i\tilde{\Gamma}_c/2}\right\}\right]$$
$$-\sum_c\sum_{\substack{d\\(c\neq d)}}\left\{\hbar\omega\frac{\langle\chi_f|M_{fd}(2)|\chi_d\rangle\langle\chi_d|V_{dc}\partial/\partial q|\chi_c\rangle\langle\chi_c|M_{c1}(1)|\chi_1\rangle}{(\varepsilon_1+\hbar\omega_1-\varepsilon_c+i\tilde{\Gamma}_c/2)(\varepsilon_1+\hbar\omega_1-\varepsilon_d+i\tilde{\Gamma}_d/2)}\right.$$
$$\left.\left.\pm\hbar\omega\frac{\langle\chi_f|M_{fd}(1)|\chi_d\rangle\langle\chi_d|V_{dc}\partial/\partial q|\chi_c\rangle\langle\chi_c|M_{c1}(2)|\chi_1\rangle}{(\varepsilon_1+\hbar\omega_1-\varepsilon_c+i\tilde{\Gamma}_c/2)(\varepsilon_1+\hbar\omega_1-\varepsilon_d+i\tilde{\Gamma}_d/2)}\right\}\right|^2, \tag{20}$$

where $\sum_d^{(elec)}$ means the summation over the electronic states, a and b. Here, the first and second terms independent of q and $\partial/\partial q$ express the pure RRS; the terms involving q the vibronically induced RRS, and the terms involving $\partial/\partial q$, the nonadiabatically induced RRS.

In this paper, since we are interested in the RRS originating from the couplings between a and b electronic states, we will consider the special case in which the irreducible representations of the point group of the electronic states, Φ_a and Φ_b, at the equilibrium configuration in the ground state are different from each other: $M_{fa}(2)=0$ and $M_{b1}(1)=0$, which also means that $M_{1a}(2)=0$ and $M_{fb}(1)=0$, while the inducing mode, q, belongs to a nontotally symmetric mode. In this case, the pure RRS terms vanish and Eq. 20 is reduced to:

$$\frac{d\sigma_I(\omega_1)}{d\Omega}=\frac{\omega_1}{2^6\pi^2\varepsilon_0^2c^4}\sum_f\int_0^\infty d\omega_2\omega_2^3\delta\left(\frac{\varepsilon_1-\varepsilon_f+\hbar\omega_1-\hbar\omega_2}{\hbar}\right)$$
$$\left|\sum_a^{(vibro)}\frac{\langle\chi_f|M_{fb}(2)V_{ba}q|\chi_a\rangle\langle\chi_a|M_{a1}(1)|\chi_1\rangle}{\varepsilon_1+\hbar\omega_1-\varepsilon_a+i\tilde{\Gamma}_a/2}-\sum_b^{(vibro)}\frac{\langle\chi_f|M_{fb}(2)|\chi_b\rangle\langle\chi_b|V_{ba}qM_{a1}(1)|\chi_1\rangle}{\varepsilon_1+\hbar\omega_1-\varepsilon_b+i\tilde{\Gamma}_b/2}\right.$$
$$\pm\sum_b^{(vibro)}\frac{\langle\chi_f|M_{fa}(1)V_{ab}q|\chi_b\rangle\langle\chi_b|M_{b1}(2)|\chi_1\rangle}{\varepsilon_1+\hbar\omega_1-\varepsilon_b+i\tilde{\Gamma}_b/2}\mp\sum_a^{(vibro)}\frac{\langle\chi_f|M_{fa}(1)|\chi_a\rangle\langle\chi_a|V_{ab}qM_{b1}(2)|\chi_1\rangle}{\varepsilon_1+\hbar\omega_1-\varepsilon_a+i\tilde{\Gamma}_a/2}$$
$$-\sum_{\substack{a,b\\(a\neq b)}}^{(vibro)}\hbar\omega\left\{\frac{\langle\chi_f|M_{fb}(2)|\chi_b\rangle\langle\chi_b|V_{ba}\partial/\partial q|\chi_a\rangle\langle\chi_a|M_{a1}(1)|\chi_1\rangle}{(\varepsilon_1+\hbar\omega_1-\varepsilon_a+i\tilde{\Gamma}_a/2)(\varepsilon_1+\hbar\omega_1-\varepsilon_b+i\tilde{\Gamma}_b/2)}\right.$$
$$\left.\left.\pm\frac{\langle\chi_f|M_{fa}(1)|\chi_a\rangle\langle\chi_a|V_{ab}\partial/\partial q|\chi_b\rangle\langle\chi_b|M_{b1}(2)|\chi_1\rangle}{(\varepsilon_1+\hbar\omega_1-\varepsilon_a+i\tilde{\Gamma}_a/2)(\varepsilon_1+\hbar\omega_1-\varepsilon_b+i\tilde{\Gamma}_b/2)}\right\}\right|^2. \tag{21}$$

Utilizing the Fourier transformations, and carrying out the summations over the vibronic states in Eq. 21 by using the closure property of the states,[11] we obtain:

$$\frac{d\sigma_I(\omega_1)}{d\Omega} = \frac{d\sigma_I^{VI}(\omega_1)}{d\Omega} + \frac{d\sigma_I^{NA}(\omega_1)}{d\Omega} + \frac{d\sigma_I^{INT(VI)}(\omega_1)}{d\Omega} + \frac{d\sigma_I^{INT(NA)}(\omega_1)}{d\Omega} + \frac{d\sigma_I^{INT(VI-NA)}(\omega_1)}{d\Omega}, \quad (22)$$

where $d\sigma_I^{VI}(\omega_1)/d\Omega$ and $d\sigma_I^{NA}(\omega_1)/d\Omega$ represent the vibronically induced and nonadiabatically induced RRS cross-sections respectively; $d\sigma_I^{INT(VI)}(\omega_1)/d\Omega$ and $d\sigma_I^{INT(NA)}(\omega_1)/d\Omega$, the interference term between the vibronically induced RRS and that between the nonadiatically induced RRS respectively, and $d\sigma_I^{INT(VI-NA)}(\omega_1)/d\Omega$, the interference term between the vibronically induced and the nonadiabatically induced RRS. It should be noted that the signs specifying the symmetric and antisymmetric cross-sections are involved in the interference terms.

The vibronically induced and nonadiabatically induced cross sections are expressed as:

$$\frac{d\sigma_I^{VI}(\omega_1)}{d\Omega} = \frac{\omega_1}{2^7\pi^3\varepsilon_0^2c^4\hbar^2}|M_{gb}(2)V_{ba}M_{ag}(1)|^2 \sum_{ca,b}\int_0^\infty d\omega_2\omega_2^3\int_0^\infty d\tau'\int_0^\infty d\tau\int_{-\infty}^\infty dt \exp[-i(t-\tau+\tau')\omega_1+it\omega_2] \times\{\langle\chi_1|\exp[(i\hat{H}_c^0-\tilde{\Gamma}_c/2)\tau'/\hbar]q_n\exp(i\hat{H}_I^0t/\hbar)q_n \exp[-(i\hat{H}_c^0+\tilde{\Gamma}_c/2)\tau/\hbar]\exp[-i\hat{H}_I^0(t-\tau+\tau')/\hbar]|\chi_I\rangle + \langle\chi_I|q_n\exp[(i\hat{H}_c^0-\tilde{\Gamma}_c/2)\tau'/\hbar] \exp(i\hat{H}_I^0t/\hbar)\exp[-(i\hat{H}_c^0+\tilde{\Gamma}_c/2)\tau/\hbar]q_n \exp[-i\hat{H}_I^0(t-\tau+\tau')/\hbar]|\chi_I\rangle\}, \quad (23)$$

and:

$$\frac{d\sigma_I^{NA}(\omega_1)}{d\Omega} = \frac{\omega_1\omega_n^2}{2^7\pi^3\varepsilon_0^2c^4\hbar^2}|M_{gb}(2)V_{ba}M_{ag}(1)|^2 \sum_{\substack{c\\(c\neq d)}}\sum_d\int_0^\infty d\omega_2\omega_2^3\int_0^\infty d\tau'\int_0^\infty d\xi'\int_0^\infty d\tau\int_0^\infty d\xi\int_{-\infty}^\infty dt \exp[-i(t-\tau-\xi+\tau'+\xi')\omega_1+it\omega_2] \times\langle\chi_I|\exp[(-i\hat{H}_c^0-\tilde{\Gamma}_c/2)\tau'/\hbar](\partial/\partial q_n)^\dagger \exp[(i\hat{H}_d^0-\tilde{\Gamma}_d/2)\xi'/\hbar]\exp(i\hat{H}_I^0t/\hbar) \exp[-(i\hat{H}_d^0+\tilde{\Gamma}_d/2)\xi/\hbar]\partial/\partial q_n\exp[-(i\hat{H}_c^0+\tilde{\Gamma}_c/2)\tau/\hbar] \exp[-i\hat{H}_I^0(t-\tau-\xi+\tau'+\xi')/\hbar]\chi_I\rangle, \quad (24)$$

respectively, where n denotes a nontotally symmetric mode and $\hat{H}^0$, the relevant vibronic Hamiltonian, while the vibronic-level dependence of the decay width, $\tilde{\Gamma}$, is disregarded. Because Eqs. 23 and 24 are expressed in terms of the vibronic Hamiltonians and are independent of the summation over the intermediate vibronic levels, these equations are suitable for the investigation of the coupling effects of the RRS from a molecular system consisting of any potential energy surfaces. They can thus be used as a basis for studying the frequency change[30] and anharmonic effects of the RRS. The expressions for the interference RRS cross-sections are given in Appendix A.

Displaced Harmonic Oscillator Model

In this section, we are concerned with the derivation of analytical expressions for the vibronically induced RRS, the nonadiabatically induced RRS, and their interference RRS in the displaced harmonic oscillator model. The molecular Hamiltonians of the ground and two excited states, a and b consist of a totally symmetric mode (q_s) with a nontotally symmetric mode (q_n) as the inducing mode. These potential surfaces are assumed to be harmonic and to be displaced for the totally symmetric mode. The frequency change in the vibrationsl modes were disregarded. In terms of the Boson annihilation and creation operators, $\hat{b}$ and $\hat{b}^\dagger$, which satisfy $[\hat{b}, \hat{b}^\dagger]=1$, these Hamiltonians are expressed as:

$$\hat{H}_I^0 = \hat{h}_I(q_s) + \hat{h}_I(q_n), \quad (25a)$$

$$\hat{h}_I(q_s) = \frac{\hbar\omega_s}{2}(p_s^2+q_s^2) = \hbar\omega_s\left(\hat{b}_s^\dagger\hat{b}_s+\frac{1}{2}\right), \quad (25b)$$

$$\hat{h}_I(q_n) = \frac{\hbar\omega_n}{2}(p_n^2+q_n^2) = \hbar\omega_n\left(\hat{b}_n^\dagger\hat{b}_n+\frac{1}{2}\right), \quad (25c)$$

$$\hat{H}_a^0 = \hat{h}_I(q_s-\Delta_a) + \hat{h}_I(q_n) + \varepsilon_a^0 = \hbar\omega_s\left(\hat{b}_s^\dagger\hat{b}_s+\frac{1}{2}\right) - \frac{\hbar\omega_s\Delta_a}{\sqrt{2}}(\hat{b}_s+\hat{b}_s^\dagger) + \frac{\hbar\omega_s\Delta_a^2}{2} + \hbar\omega_n\left(\hat{b}_n^\dagger\hat{b}_n+\frac{1}{2}\right)+\varepsilon_a^0, \quad (25d)$$

and

$$\hat{H}_b^0 = \hat{h}_I(q_s-\Delta_b) + \hat{h}_I(q_n) + \varepsilon_b^0, \quad (25e)$$

where we have taken into account the potential displacement between the potential energy surfaces of the two intermediate excited states; Δ_a and Δ_b represent the dimensionless displacements between the equilibrium points in the ground and excited states, a and b respectively, and ε^0, the electronic energy gap between the bottoms in the ground and excited states.

Nonadiabatically Induced RRS. The nonadiabatically induced RRS cross-section, $d\sigma_I^{NA}(\omega_1)/d\Omega$, Eq. 24 is written as:

$$\frac{d\sigma_I^{NA}(\omega_1)}{d\Omega} = \omega_n^2k(\omega_1)\sum_{\substack{c\\(c\neq d)}}\sum_d\int_0^\infty d\omega_2\omega_2^3 \int_0^\infty d\tau'\int_0^\infty d\xi'\int_0^\infty d\tau\int_0^\infty d\xi\int_{-\infty}^\infty dt \exp\left[-i(t-\tau-\xi+\tau'+\xi')\omega_1+it\omega_2-\frac{\tilde{\Gamma}_c}{2\hbar}(\tau+\tau') -\frac{\tilde{\Gamma}_d}{2\hbar}(\xi+\xi')+\frac{i\varepsilon_c^0}{\hbar}(\tau'-\tau)+\frac{i\varepsilon_d^0}{\hbar}(\xi'-\xi)\right] f_n(\tau',\xi',\tau,\xi,t)g_s(\tau',\xi',\tau,\xi,t), \quad (26)$$

where $k(\omega_1)=\frac{\omega_1}{2^7\pi^3\varepsilon_0^2c^4\hbar^2}|M_{gb}(2)V_{ba}M_{ag}(1)|^2$,

$$f_n(\tau',\xi',\tau,\xi,t) = \left\langle 0_n\middle|\exp\left[\frac{i\hat{h}_I(q_n)\tau'}{\hbar}\right]\left(\frac{\partial}{\partial q_n}\right)^\dagger\right.$$

$$\exp\left[\frac{i\hat{h}_l(q_n)\xi'}{\hbar}\right]\exp\left[\frac{i\hat{h}_l(q_n)t}{\hbar}\right]$$
$$\exp\left[-\frac{i\hat{h}_l(q_n)\xi}{\hbar}\right]\frac{\partial}{\partial q_n}\exp\left[-\frac{i\hat{h}_l(q_n)\tau}{\hbar}\right]$$
$$\exp\left[-\frac{i\hat{h}_l(q_n)(t-\tau-\xi+\tau'+\xi')}{\hbar}\right]\Big|0_n\Big\rangle, \quad (27a)$$

and

$$g_s(\tau',\xi',\tau,\xi,t)=\Big\langle 0_s\Big|\exp\left[\frac{i\hat{h}_l(q_s-\Delta_c)\tau'}{\hbar}\right]$$
$$\exp\left[\frac{i\hat{h}_l(q_s-\Delta_d)\xi'}{\hbar}\right]\exp\left[\frac{i\hat{h}_l(q_s)t}{\hbar}\right]$$
$$\exp\left[-\frac{i\hat{h}_l(q_s-\Delta_d)\xi'}{\hbar}\right]\exp\left[-\frac{i\hat{h}_l(q_s-\Delta_c)\tau}{\hbar}\right]$$
$$\exp\left[-\frac{i\hat{h}_l(q_s)}{\hbar}(t-\tau-\xi+\tau'+\xi')\right]\Big|0_s\Big\rangle. \quad (27)$$

By using the Feynman-disentangle and Boson-operator techniques, the generating functions for the nontotally symmetric and totally symmetric modes, $f_n(\tau',\xi',\tau,\xi,t)$ and $g_s(\tau',\xi',\tau,\xi,t)$, can be evaluated as:

$$f_n(\tau',\xi',\tau,\xi,t)=\frac{1}{2}\exp\left[i\omega_n(\xi'-\xi+t)\right], \quad (28)$$

and:

$$g_s(\tau',\xi',\tau,\xi,t)=\exp\left[\frac{\Delta_c^2}{2}\{\exp(i\omega_s\tau')-1\}\right.$$
$$+\frac{\Delta_c^2}{2}\{\exp(-i\omega_s\tau)-1\}+\frac{\Delta_d^2}{2}\{\exp(i\omega_s\xi')-1\}$$
$$\left.+\frac{\Delta_d^2}{2}\{\exp(-i\omega_s\xi)-1\}\right]\exp\left[\lambda_c^*(\tau')\lambda_c^*(\xi')\right.$$
$$+\lambda_c(\tau)\lambda_c(\xi)+\exp(i\omega_s t)\{\lambda_c^*(\tau')\exp(i\omega_s\xi')+\lambda_d^*(\xi')\}$$
$$\left.\{\lambda_c(\tau)\exp(-i\omega_s\xi)+\lambda_d(\xi)\}\right], \quad (28)$$

where

$$\lambda_c(\tau)=\frac{\Delta_c}{\sqrt{2}}\{1-\exp(-i\omega_s\tau)\}. \quad (29)$$

The $\frac{\partial}{\partial q_n}=\frac{1}{2}(\hat{b}_n-\hat{b}_n^\dagger)$ relation was used. A derivation of Eq. 28 is given in detail in Appendix B. Expanding the last term in Eq. 28, the generating function for the totally symmetric mode, $g_s(\tau',\xi',\tau,\xi,t)$, is written as:

$$g_s(\tau',\xi',\tau,\xi,t)=\sum_{n_s=0}^{\infty}\frac{1}{n_s!}\{\lambda_c^*(\tau')\exp(i\omega_s\xi')+\lambda_d^*(\xi')\}^{n_s}$$
$$\{\lambda_c(\tau)\exp(-i\omega_s\xi)+\lambda_d(\xi)\}^{n_s}\exp\left[\frac{\Delta_c^2}{2}\{\exp(i\omega_s\tau')-1\}\right.$$
$$+\frac{\Delta_c^2}{2}\{\exp(-i\omega_s\tau)-1\}+\frac{\Delta_d^2}{2}\{\exp(-i\omega_s\xi)-1\}$$
$$\left.+\lambda_c^*(\tau')\lambda_d^*(\xi')+\lambda_c(\tau)\lambda_d(\xi)+in_s\omega_s t\right]. \quad (30)$$

By substituting Eqs. 28 and 30 into Eq. 26 and by integrating over t, we obtain:

$$\frac{d\sigma_I^{NA}(\omega_1)}{d\Omega}=k(\omega_1)\sum_c\sum_{d\,(c\neq d)}\sum_{n_s=0}^{\infty}\frac{\pi\omega_n^2}{n_s!}\int_0^\infty d\omega_2\omega_2^3$$
$$\left|\int_0^\infty d\tau\int_0^\infty d\xi\{\lambda_c(\tau)\exp(-i\omega_s\xi)+\lambda_c(\xi)\}^{n_s}\right.$$
$$\exp\left[i\tau\left(\omega_1-\frac{\varepsilon_c^0}{\hbar}+\frac{i\tilde{\Gamma}_c}{2\hbar}\right)+\frac{\Delta_c^2}{2}\{\exp(-i\omega_s\tau)-1\}\right.$$
$$+i\xi\left(\omega_1-\frac{\varepsilon_d^0}{\hbar}-\omega_n+\frac{i\tilde{\Gamma}_d}{2\hbar}\right)+\frac{\Delta_d^2}{2}\{\exp(-i\omega_s\xi)-1\}$$
$$\left.\left.+\lambda_c(\tau)\lambda_d(\xi)\right]\right|^2\delta(\omega_1-\omega_2-\omega_n-n_s\omega_s). \quad (31)$$

Integrating over ω_2, using the binomial and Taylor expansions, and finally integrating over τ and ξ, we obtain an analytical expression for the nonadiabatically induced RRS cross-section as:

$$\frac{d\sigma_I^{NA}(\omega_1)}{d\Omega}=\pi\omega_m^2k(\omega_1)\sum_c\sum_{d\,(c\neq d)}\sum_{n_s=0}^{\infty}\frac{(\omega_1-\omega_n-n_s\omega_s)^3}{n_s!}$$
$$\left|\sum_{l=0}^{n_s}\binom{n_s}{l}\left(\frac{\Delta_c}{\sqrt{2}}\right)\left(\frac{\Delta_d}{\sqrt{2}}\right)^{n_s-l}\sum_{m=0}^{\infty}\frac{1}{m!}\left(\frac{\Delta_c\Delta_d}{2}\right)^m\right.$$
$$\sum_{p=0}^{l}\binom{l}{p}(-1)^p\sum_{r=0}^{m}\binom{m}{r}(-1)^r$$
$$\sum_{t=0}^{\infty}\frac{S_{10,ct}}{\omega_1-\varepsilon_c^0/\hbar-(p+r+t)\omega_s+i\tilde{\Gamma}_c/(2\hbar)}$$
$$\sum_{q=0}^{n_s-l}\binom{n_s-l}{q}(-1)^q\sum_{s=0}^{m}\binom{m}{s}(-1)^s$$
$$\left.\sum_{u=0}^{\infty}\frac{S_{10,du}}{\omega_1-\varepsilon_d^0/\hbar-\omega_n-(l+q+s+u)\omega_s+i\tilde{\Gamma}_d/2\hbar}\right|^2, \quad (32)$$

where $S_{10,ct}$ is the optical Franck-Condon factor between the lowest level in the ground state and the t-th vibrational level in the excited state c; it is given by $S_{10,ct}=\left(\frac{\Delta_c^2}{2}\right)^t e^{-\frac{\Delta_c^2}{2}}/t!$. Eq. 32 is the desired analytical expression for the RRS cross-section originating from the nonadiabatic coupling between the two excited states a and b; it consists of the n_s-th order vibrational transition for a totally symmetric mode. In Ref. 28, the results have been given without a detailed derivation.

Vibronically Induced RRS. An analytical expression for the RRS cross-section originating from the vibronic coupling has been derived in Ref. 26.

Interference Terms. In Theory section, the interference RRS cross-sections have been classified into three groups. Because the significant terms are those between the components of the RRS within the same resonant state, and because the interference between the components of the resonant and other excited states can be safely disregarded, the expressions for the RRS cross-section due to the interference are written as:

a): Interference between the components of the vibronically induced RRS:

$$\frac{d\sigma_I^{INT(VI)}(w_1)}{d\Omega}\simeq\pm2\pi k(\omega_1)$$
$$\sum_c\sum_{n_s=0}^{\infty}\frac{(\omega_1-\omega_n-n_s\omega_s)^3}{n_s!}(\Delta_c^2/2)^{n_s}$$
$$\mathrm{Re}\left\{\sum_{j=0}^{n_s}\sum_{j'=0}^{n_s}\binom{n_s}{j}\binom{n_s}{j'}(-1)^{j+j'}\right.$$

$$\sum_{k=0}^{\infty}\sum_{k'=0}^{\infty}\frac{S_{\mathrm{I0,ck}}}{\omega_1-\varepsilon_c^0/\hbar-(j+k)\omega_s-\mathrm{i}\tilde{\Gamma}_c/2\hbar}\frac{S_{\mathrm{I0,ck'}}}{\omega_1-\varepsilon_c^0/\hbar-\omega_n-(j'+k')\omega_s+\mathrm{i}\tilde{\Gamma}_c/2\hbar}\Bigg\}, \quad (33)$$

and:

b): Interference between the components of the vibronically and the nonadiabatically induced RRS:

$$\frac{\mathrm{d}\sigma_I^{\mathrm{INT(VI-NA)}}(\omega_1)}{\mathrm{d}\Omega}=2\pi\omega_n k(\omega_1)\sum_{\substack{c\\(c\neq d)}}\sum_{d}\sum_{n_s=0}^{\infty}\frac{(\omega_1-\omega_n-n_s\omega_s)^3}{n_s!}\left(\frac{\Delta_c}{\sqrt{2}}\right)^{n_s}\mathrm{Re}\Bigg\{\sum_{j=0}^{n_s}\binom{n_s}{j}(-1)^j\sum_{k=0}^{\infty}\frac{S_{\mathrm{I0,ck}}}{\omega_1-\varepsilon_c^0/\hbar-(j+k)\omega_s-\mathrm{i}\tilde{\Gamma}_c/2\hbar}\sum_{l=0}^{n_s}\binom{n_s}{l}\left(\frac{\Delta_c}{\sqrt{2}}\right)\left(\frac{\Delta_d}{\sqrt{2}}\right)^{n_s-l}\sum_{m=0}^{\infty}\frac{1}{m!}\left(\frac{\Delta_c\Delta_d}{2}\right)^m\sum_{p=0}^{l}\binom{l}{p}(-1)^p\sum_{r=0}^{m}\binom{m}{r}(-1)^r\sum_{t=0}^{\infty}\frac{S_{\mathrm{I0,ct}}}{\omega_1-\varepsilon_c^0/\hbar-(p+r+t)\omega_s+\mathrm{i}\tilde{\Gamma}_c/2\hbar}\sum_{q=0}^{n_s-l}\binom{n_s-l}{q}(-1)^q\sum_{s=0}^{m}\binom{m}{s}(-1)^s\sum_{u=0}^{\infty}\frac{S_{\mathrm{I0,du}}}{\omega_1-\varepsilon_d^0/\hbar-\omega_n-(l+q+s+u)\omega_s+\mathrm{i}\tilde{\Gamma}_d/2\hbar}-\sum_{j=0}^{n_s}\binom{n_s}{j}(-1)^j\sum_{k=0}^{\infty}\frac{S_{\mathrm{I0,ck}}}{\omega_1-\varepsilon_c^0/\hbar-\omega_n-(j+k)\omega_s-\mathrm{i}\tilde{\Gamma}_c/2\hbar}\sum_{l=0}^{ns}\binom{n_s}{l}\left(\frac{\Delta_d}{\sqrt{2}}\right)\left(\frac{\Delta_c}{\sqrt{2}}\right)^{n_s-l}\sum_{m=0}^{\infty}\frac{1}{m!}\left(\frac{\Delta_c\Delta_d}{2}\right)^m\sum_{q=0}^{n_s-l}\binom{n_s-l}{q}(-1)^q\sum_{s=0}^{m}\binom{m}{s}(-1)^s\sum_{u=0}^{\infty}\frac{S_{\mathrm{I0,cu}}}{\omega_1-\varepsilon_c^0/\hbar-\omega_n-(l+q+s+u)\omega_s+\mathrm{i}\tilde{\Gamma}_c/2\hbar}\sum_{p=0}^{l}\binom{l}{p}(-1)^p\sum_{r=0}^{m}\binom{m}{r}(-1)^r\sum_{t=0}^{\infty}\frac{S_{\mathrm{I0,dt}}}{\omega_1-\varepsilon_d^0/\hbar-(p+r+t)\omega_s+\mathrm{i}\tilde{\Gamma}_d/2\hbar}\Bigg\}. \quad (34)$$

Discussion

In Theory Section, using the Born-Oppenheimer basis set, the RRS cross-section has been formulated. It is shown that the cross-section can be classified into four terms. In this paper, one is called pure RRS, while the others are the vibronically induced and the nonadiabatically induced RRS, and their interferences. The pure RRS, independent of the inducing mode, corresponds to Albrecht's A term,[31] and the vibronically induced RRS, to the B term. The RRS cross-section corresponding to the C term was disregarded because this term makes a negligibly small contribution to the Raman scattering in the resonance region.

In Fig. 2, the excitation profiles of the RRS within the weak coupling limits are analyzed. The spectra on the low- and high-frequency sides reflect the RRS

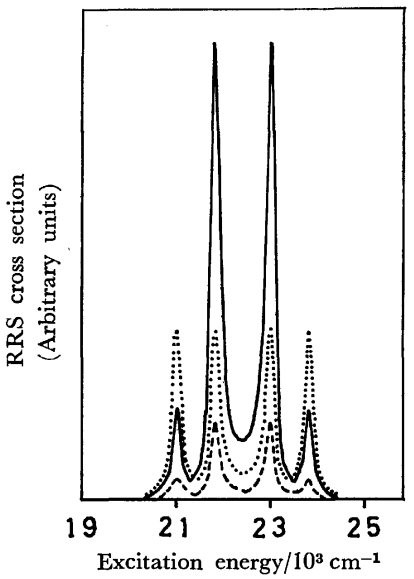

Fig. 2. Excitation profiles of the RRS in the case of $\Delta_a=0$ and $\Delta_b=0$. The dotted, broken, and solid lines represent the excitation profile of the vibronically induced RRS, that of the nonadiabatically induced RRS, and that of the RRS with both the vibronic and nonadiabatic couplings including the interference terms, respectively. The molecular parameters used are $\varepsilon_0^a=21000\ \mathrm{cm^{-1}}$, $\varepsilon_0^b=23000\ \mathrm{cm^{-1}}$, $\omega_n=800\ \mathrm{cm^{-1}}$, and $\tilde{\Gamma}_a=\tilde{\Gamma}_b=200\ \mathrm{cm^{-1}}$. The profiles were plotted neglecting the constants involving the transition moments.

from the *a* and *b* electronic states respectively, and they have a mirror symmetry with respect to the plane intersecting the center because the same potential energy surfaces and the same decay widths in the two excited states are assumed. The molecular parameters used are $\varepsilon_a^0=21000\ \mathrm{cm^{-1}}$, $\varepsilon_b^0=23000\ \mathrm{cm^{-1}}$, $\omega_n=800\ \mathrm{cm^{-1}}$, $\tilde{\Gamma}_a=\tilde{\Gamma}_b=200\ \mathrm{cm^{-1}}$, and $\Delta_a=\Delta_b=0$. The dotted, broken, and solid lines represent the excitation profile of the vibronically induced RRS, that of the nonadiabatically induced RRS, and that of the RRS with both the vibronic and nonadiabatic couplings, including the interference terms respectively.

For the vibronically induced RRS, two bands, 0-0 and 0-1, sometimes called Mortensen's doublet, appear on the low- and high-frequency sides of the excitation profile. It is recognized that the RRS from the molecular system with small potential displacements is expressed by the succession of absorption from the ground to the resonance state and emission from the resonance state to the ground state.[11] For the 0-0 and 0-1 bands, the inducing mode operates in the course of the emission and absorption processes respectively. It can easily be seen that the intensities of the two bands are equal, for they have the same energy-denominator dependence of the polarizability.

As a result of the nonadiabatic coupling between the resonant and other excited states, two bands, 0-0 and 0-1, appear in the excitation profile as well. The band intensity of the nonadiabatically induced RRS is inversely proportional to the square of the

energy difference between the relevant states; from Eq. 32, the intensities of the 0-0 and 0-1 bands in the case of the resonance with the lower excited state, a denoted by $I_{0\text{-}0}^{\mathrm{NA(a)}}$ and $I_{0\text{-}1}^{\mathrm{NA(a)}}$, are given by:

$$I_{0\text{-}0}^{\mathrm{NA(a)}} \propto \left| \frac{\tilde{\Gamma}_a}{2}(\varepsilon_a^0 - \varepsilon_b^0 - \hbar\omega_n + i\tilde{\Gamma}_b/2) \right|^{-2}, \tag{35a}$$

and:

$$I_{0\text{-}1}^{\mathrm{NA(a)}} \propto \left| \frac{\tilde{\Gamma}_a}{2}(\varepsilon_a^0 - \varepsilon_b^0 + \hbar\omega_n + i\tilde{\Gamma}_b/2) \right|^{-2}, \tag{35b}$$

respectively, from which we obtain the relation:

$$I_{0\text{-}0}^{\mathrm{NA(a)}} < I_{0\text{-}1}^{\mathrm{NA(a)}}. \tag{36}$$

Similarly, for the case of the resonance with the upper state b, we obtain:

$$I_{0\text{-}0}^{\mathrm{NA(b)}} \propto \left| \frac{\tilde{\Gamma}_b}{2}(\varepsilon_b^0 - \varepsilon_a^0 - \hbar\omega_n + i\tilde{\Gamma}_a/2) \right|^{-2}, \tag{37a}$$

$$I_{0\text{-}1}^{\mathrm{NA(b)}} \propto \left| \frac{\Gamma_b}{2}(\varepsilon_b^0 - \varepsilon_a^0 + \hbar\omega_n + i\tilde{\Gamma}_a/2) \right|^{-2}, \tag{37b}$$

and then:

$$I_{0\text{-}0}^{\mathrm{NA(b)}} > I_{0\text{-}1}^{\mathrm{NA(b)}}$$

As is shown in Fig. 2, the asymmetry of the 0-0 and 0-1 bands originates from the interference between the vibronically induced RRS and nonadiabatically induced one. The main contribution of the interference comes from Eq. 34. In the cases of the small displacement, Eq. 34 can be expressed as:

$$\frac{d\sigma_I^{\mathrm{INT(VI-NA)}}(\omega_1)}{d\Omega} \simeq 2\pi\omega_n(\omega_1-\omega_n)^3 \sum_c \sum_{d\,(c\neq d)} \left\{ \frac{\omega_1 - \varepsilon_d^0/\hbar - \omega_n}{[(\omega_1-\varepsilon_c^0/\hbar)^2+(\tilde{\Gamma}_c/2\hbar)^2][(\omega_1-\varepsilon_d^0/\hbar-\omega_n)^2+(\tilde{\Gamma}_d/2\hbar)^2]} - \frac{\omega_1-\varepsilon_d^0/\hbar}{[(\omega_1-\varepsilon_c^0/\hbar)^2+(\tilde{\Gamma}_c/2\hbar)^2][(\omega_1-\varepsilon_d^0/\hbar)^2+(\tilde{\Gamma}_d/2\hbar)^2]} \right\}. \tag{38}$$

This expression indicates that, for the resonance with the lower excited state, a, the interference term between the vibronically induced RRS and the nonadiabatically induced one decreases the 0-0 band intensity and increases the 0-1 band intensity. On the other hand, for the resonance with the higher excited state, b, this term interferes, constructively near the 0-0 band and destructively near the 0-1 band. Eq. 33, representing the interference between the vibronically induced RRS, does not contribute to the asymmetry of the excitation profile, but makes an important contribution to the depolarization ratio.[26]

Let us now focus our attention on the effects of the RRS on the molecular parameters. In the displaced harmonic oscillator model, analytical expressions for the n_s-th order vibrational transitions of the RRS cross-sections have been derived; these cross-sections are expressed in terms of the molecular parameters, such as the dimensionless potential displacements, the molecular vibrational frequencies, the decay widths, and the electronic energy gaps. Using the analytical expressions, we have performed model calculations of the excitation profiles of the n_s-th order vibrational transitions.

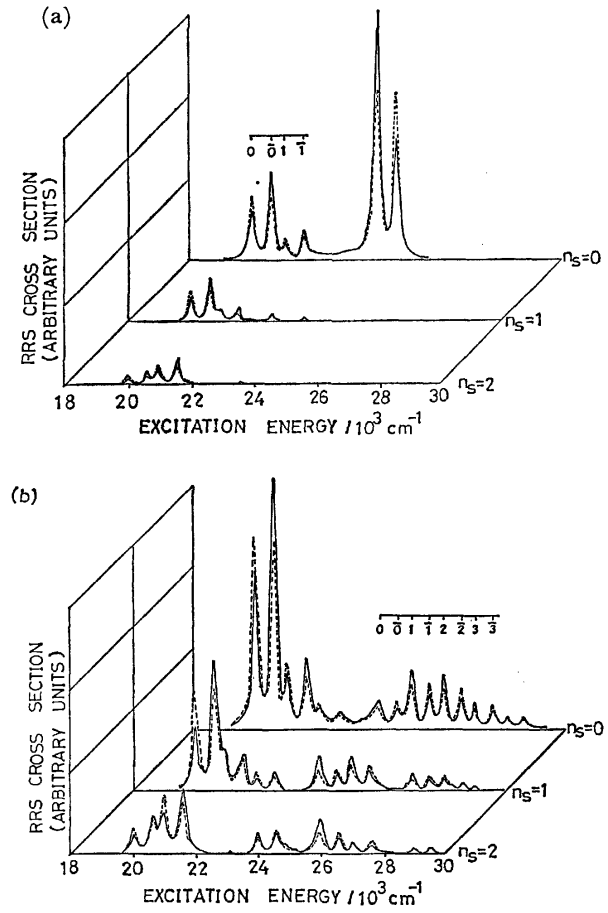

Fig. 3. The dimensionless displacements Δ_a and Δ_b dependence of the excitation profiles of the n_s-th order vibrational transition. The progressions of the totally symmetric vibration built upon one quantum of the coupling mode are monitored. The following parameters are used: $\varepsilon_a^0=20000\ \mathrm{cm^{-1}}$; $\varepsilon_b^0=24000\ \mathrm{cm^{-1}}$; $\omega_n=600\ \mathrm{cm^{-1}}$ and $\omega_s=1000\ \mathrm{cm^{-1}}$; $\tilde{\Gamma}_a=\tilde{\Gamma}_b=200\ \mathrm{cm^{-1}}$; $\Delta_b=0.1$, and 1.0 in Figs. 3a and 3b, respectively, and $\Delta_a=1.0$. The ordinate is shown without $k(\omega_1)$. The broken line represents the excitation profile without the nonadiabatic coupling, and the solid line the whole excitation profile with both the nonadiabatic and vibronic couplings including the interference terms. The band peaks which appear in the zero order vibrational transition ($n_s=0$) of the excited state, a in Fig. 3a and those of the excited state, b in Fig. 3b are indicated by the vibrational quantum number of the displaced oscillator excited in the resonant states. The band peaks with the wavy line above the number represent the one quantum excitation of the inducing mode in addition to the excitation of the displaced oscillator.

It should be noted that the expressions derived in this paper are applicable to the RRS of the molecular system with any displacement. In Figs. 3, the effects of the dimensionless displacements, Δ_a and Δ_b, are shown. The excitation profiles of the first order, $n_s=1$ and the second order, $n_s=2$, vibrational transitions, in addition to the zero-order transition, are plotted. The progressions of the totally symmetric vibrational mode built upon one quantum of the inducing mode were monitored. The broken line represents the

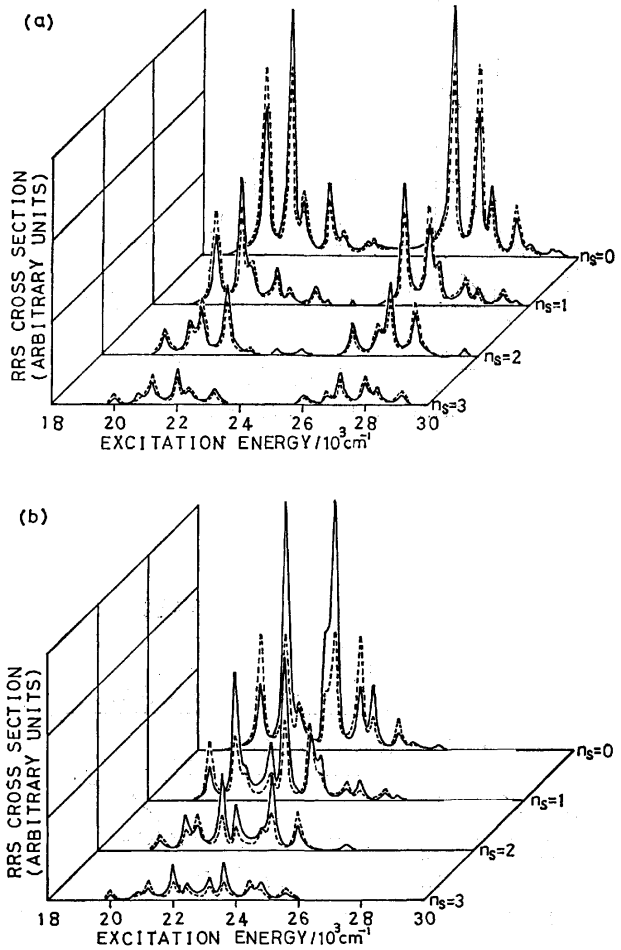

Fig. 4. The electronic gap dependence of the excitation profiles of the n_s-th order vibrational transition. The following molecular parameters are used: $\omega_n = 800\ \mathrm{cm^{-1}}$ and $\omega_s = 1200\ \mathrm{cm^{-1}}$; $\Delta_a = \Delta_b = 1.0$; $\varepsilon_b^0 = 26000\ \mathrm{cm^{-1}}$, and $22400\ \mathrm{cm^{-1}}$ in Figs. 4a and 4b, respectively. The others are the same as those in Fig. 3.

excitation profile without the nonadiabatic coupling, and the solid line, that with both the nonadiabatic and vibronic couplings. The displacements used are $\Delta_a = 1.0$, and $\Delta_b = 0.1$ and 2.0 in Figs. 3a and 3b respectively. The other parameters are $\varepsilon_a^0 = 20000\ \mathrm{cm^{-1}}$, $\varepsilon_b^0 = 24000\ \mathrm{cm^{-1}}$, $\omega_n = 600\ \mathrm{cm^{-1}}$, $\omega_s = 1000\ \mathrm{cm^{-1}}$, and $\tilde{\Gamma}_a = \tilde{\Gamma}_b = 200\ \mathrm{cm^{-1}}$. In Figs. 3a and 3b, the band peaks which appear in the zero-order vibrational transitions of the excited states, *a* and *b*, are indicated by the vibrational quantum number of the respective displaced oscillator excited in the resonant states. The band peaks with the wavy line above the number represent the one-quantum excitation of the inducing mode in addition to the excitation of the displaced oscillator. It can be seen that, as the displacements increase, the first- and second-order vibrational transitions, as well as the zero-order transition, appear in the excitation profiles. The nonadiabatic coupling makes significant contributions not only to the latter transition, but also to the former transitions.

In Figs. 4, the electronic-energy-gap dependence of the RRS is shown as a function of the incident photon frequency, ω_1. The progressions for the totally symmetric vibration of $\omega_s = 1200\ \mathrm{cm^{-1}}$, built upon one quantum of the inducing mode of $\omega_n = 800\ \mathrm{cm^{-1}}$, are monitored. In these figures, $\Delta_a = \Delta_b = 1.0$ was assumed. The electronic-energy-gaps, ε_b^0 are taken to be $26000\ \mathrm{cm^{-1}}$ and $22400\ \mathrm{cm^{-1}}$ in Figs. 4a, and 4b respectively. The others are the same as those in Figs. 3. The Figures 4 indicate that the nonadiabatic coupling plays an important role, as the two excited states exist close to each other. The nonadiabatic coupling effect on the higher-order vibrational transitions is qualitively similar that on the zero-order transition.

In the model calculations shown in Figs. 3 and 4, the effects of the potential displacements and those of the electronic-energy gap between two excited states are examined, the other parameters being fixed. In order to apply the theoretical results developed in this paper to analyzing the observed excitation profiles of the RRS, such molecular parameters as the decay widths, $\tilde{\Gamma}_a$ and $\tilde{\Gamma}_b$, should be properly chosen.[32]

In summary, in this paper, we have developed a theory of the RRS from two electronically excited states coupled by a nontotally symmetric mode. The vibronic and nonadiabatic coupling effects on the RRS cross-sections have been examined. The RRS cross-sections have been classified into four groups according to the mechanisms: one is the RRS independent of the inducing mode, while the others are the vibronically induced and the nonadiabatically induced RRS, and their interference terms. Assuming a model system with two vibrational modes, the inducing mode, and a totally symmetric mode characterized by a displaced harmonic oscillator, analytical expressions for the RRS cross-sections have been derived. The expressions consisting of the n_s-th order vibrational transition of the totally symmetric mode are explicitly formulated as a function of the two displacement parameters between the equilibrium points in the ground state and in the two excited states, and are applicable to the system with any potential displacement.

We are grateful to Professor Takeshi Nakajima for his stimulating discussions and for his encouragement during the course of this work. One of us (Y. F.) wishes also to thank Professor Sheng. H. Lin for his gracious hospitality.

References

1) J. Tang and A. C. Albrecht, "Raman Spectroscopy," ed by H. A. Szymanski, Plenum, New York (1970), Vol. 2, p. 33.
2) L. A. Nafie, P. Stein, and W. L. Peticolas, *Chem. Phys. Lett.*, **12**, 131 (1971).
3) O. S. Mortensen, *Chem. Phys. Lett.*, **30**, 406 (1975).
4) M. Z. Zgierski, *Chem. Phys. Lett.*, **36**, 390 (1975).
5) M. Mingardi and W. Siebrand, *J. Chem. Phys.*, **62**, 1074 (1975).
6) A. R. Gregory, W. H. Henneker, W. Siebrand, and M. Z. Zgierski, *J. Chem. Phys.*, **63**, 5475 (1975).
7) B. Johnson, L. A. Nafie, and W. L. Peticolas, *Chem. Phys.*, **19**, 303 (1977).
8) H. K. Hong, *J. Chem. Phys.*, **67**, 801 (1977).

9) J. A. Shelnutt, L. D. Cheung, R. C. C. Chang, N. T. Yu, and R. H. Felton, *J. Chem. Phys.*, **66**, 3387 (1977).
10) M. Z. Zgierski, *Acta Phys. Pol.* A, **53**, 243 (1978).
11) Y. Fujimura and S. H. Lin, *J. Chem. Phys.*, **70**, 247 (1979).
12) K. Ohno, *Chem. Phys. Lett.*, **69**, 495 (1980).
13) M. Ito, I. Suzuka, Y. Udagawa, N. Mikami, and K. Kaya, *Chem. Phys. Lett.*, **16**, 211 (1972).
14) G. J. Small and E. S. Yeung, *Chem. Phys.*, **9**, 379 (1975).
15) G. J. Small, *J. Chem. Phys.*, **62**, 4661 (1975).
16) M. Garozzo and F. Galluzzi, *J. Chem. Phys.*, **64**, 1720 (1976).
17) P. Stein, V. Miskowski, W. H. Woodruff, J. P. Griffin, K. G. Werner, B. P. Gaber, and T. G. Spiro, *J. Chem. Phys.*, **64**, 2159 (1976).
18) S. Hassing and O. S. Mortensen, *Chem. Phys. Lett.*, **47**, 115 (1977).
19) H. K. Hong and C. W. Jacobsen, *Chem. Phys. Lett.*, **47**, 457 (1977).
20) S. Muramatsu, K. Nasu, M. Takahashi, and K. Kaya, *Chem. Phys. Lett.*, **50**, 284 (1977).
21) T. G. Spiro and P. Stein, *Ann. Rev. Phys. Chem.*, **28**, 501 (1977).
22) H. K. Hong and C. W. Jacobsen, *J. Chem. Phys.*, **68**, 1170 (1978).
23) L. D. Cheung, N. T. Yu, and R. H. Felton, *Chem. Phys. Lett.*, **55**, 527 (1978).
24) J. A. Shelnutt and D. C. O; Shea, *J. Chem. Phys.*, **69**, 5361 (1978).
25) W. H. Henneker, A. P. Penner, W. Siebrand, and M. Z. Zgierski, *J. Chem. Phys.*, **69**, 1704 (1978).
26) Y. Fujimura and S. H. Lin, *Chem. Phys. Lett.*, **63**, 199 (1979).
27) L. D. Ziegler and A. C. Albrecht, *J. Chem. Phys.*, **70**, 2644 (1979).
28) K. Seo, H. Kono, and Y. Fujimura, *Chem. Phys. Lett.*, **74**, 549 (1980).
29) M. M. Sushchinskii, "Raman Spectra of Molecules and Crystals," Keter, New York (1972).
30) Y. Fujimura, K. Seo, and J. Shiraishi, *Chem. Phys. Lett.*, **83**, 568 (1981).
31) A. C. Albrecht, *J. Chem. Phys.*, **34**, 1476 (1961).
32) In this paper, the effects of transverse relaxation are disregarded. They can, however, theoretically be taken into account by using the method of the density matrix. (See Y. Fujimura and S. H. Lin, *J. Chem. Phys.*, **71**, 3733 (1979), and Y. Fujimura, H. Kono, T. Nakajima, and S. H. Lin, *ibid.*, **75**, 99 (1981).)

Appendix A: Expressions for the Interference RRS Cross-sections

The interference term between the vibronically induced RRS is given by:

$$\frac{d\sigma_I^{INT(VI)}(\omega_1)}{d\Omega} = k(\omega_1)\int_0^\infty d\omega_2\omega_2^3\int_0^\infty d\tau'\int_0^\infty d\tau\int_0^\infty dt$$
$$\exp[-i(t-\tau+\tau')\omega_1+it\omega_2]$$
$$\{\sum_c[\pm\langle\chi_1|\alpha_c^*(\tau')q_n\beta_1(t)\alpha_c(\tau)q_n\beta_1(t-\tau+\tau')|\chi_1\rangle$$
$$\pm\langle\chi_1|q_n\alpha_c^*(\tau')\beta_1^*(t)q_n\alpha_d(\tau)\beta_1(t-\tau+\tau')|\chi_1\rangle$$
$$+\sum_{\substack{c\\(c\neq d)}}\sum_d[\mp\langle\chi_1|\alpha_c^*(\tau')q_n\beta_1^*(t)q_n\alpha_d(\tau)\beta_1(t-\tau+\tau')|\chi_1\rangle$$
$$-\langle\chi_1|\alpha_c^*(\tau')q_n\beta_1^*(t)\alpha_d(\tau)q_n\beta_1(t-\tau+\tau')|\chi_1\rangle$$
$$-\langle\chi_1|q_n\alpha_d^*(\tau')\beta_1^*(t)q_n\alpha_1(\tau)\beta_1(t-\tau+\tau')|\chi_1\rangle$$
$$\mp\langle\chi_1|q_n\alpha_c^*(\tau')\beta_1^*(t)\alpha_d(\tau)q_n\beta_1(t-\tau+\tau')|\chi_1\rangle]\}, \quad (A.1)$$

where

$$k(\omega_1) = \omega_1|M_{gb}(2)V_{ba}M_{ag}(1)|^2/(2^7\pi^3\varepsilon_0^2c^4\hbar^2),$$
$$\alpha_c(\tau) = \exp[-(i\hat{H}_c^0-\tilde{\Gamma}_c/2)\tau/\hbar],$$

and

$$\beta_1(t) = \exp[-i\hat{H}_1^0t/\hbar].$$

The interference term between the nonadiabatically induced RRS is given by:

$$\frac{d\sigma_I^{INT(NA)}(\omega_1)}{d\Omega} = \mp\omega_n^2k(\omega_1)\sum_{\substack{c\\(c\neq d)}}\sum_d$$
$$\int_0^\infty d\omega_2\omega_2^3\int_0^\infty d\tau'\int_0^\infty d\xi'\int_0^\infty d\tau\int_0^\infty d\xi\int_{-\infty}^\infty dt$$
$$\exp[-i(t-\tau-\xi+\tau'+\xi')\omega_1+it\omega_2]$$
$$\langle\chi_1|\alpha_c^*(\tau')(\partial/\partial q_n)^\dagger\alpha_c^*(\xi')\beta_1^*(t)\alpha_c(\tau)$$
$$(\partial/\partial q_n)\alpha_d(\xi)\beta_1(t-\tau-\xi+\tau'+\xi')|\chi_1\rangle. \quad (A.2)$$

The interference term between the vibronically induced and the nonadiabatically induced RRS is given by:

$$\frac{d\sigma_I^{INT(VI-NA)}(\omega_1)}{d\Omega} = \omega_nk(\omega_1)\sum_{\substack{c\\(c\neq d)}}\sum_d$$
$$\int_0^\infty d\omega_2\omega_2^3\int_0^\infty d\tau'\int_0^\infty d\tau\int_0^\infty d\xi\int_{-\infty}^\infty dt$$
$$\{\exp[-i(t-\tau-\xi+\tau')\omega_1+it\omega_2]$$
$$[\langle\chi_1|\alpha_c^*(\tau')q_n\beta_1(t)\alpha_d(\xi)(i\partial/\partial q_n)\alpha_c(\tau)$$
$$\beta_1(t-\tau-\xi+\tau')|\chi_1\rangle$$
$$\mp\langle\chi_1|\alpha_c^*(\tau')q_n\beta_1^*(t)\alpha_c(\tau)(i\partial/\partial q_n)\alpha_d(\xi)\beta_i(t-\tau-\xi+\tau')$$
$$|\chi_1\rangle\pm\langle\chi_1|q_n\alpha_c^*(\tau')\beta_1^*(t)\alpha_d(\xi)(i\partial/\partial q_n)\alpha_c(\tau)$$
$$\beta_1(t-\tau-\xi+\tau')|\chi_1\rangle-\langle\chi_1|q_n\alpha_c^*(\tau')\beta_1^*(t)\alpha_c(\tau)(i\partial/\partial q_n)$$
$$\alpha_d(\xi)\beta_1(t-\tau-\xi+\tau')|\chi_1\rangle]+$$
$$\exp[-i(t-\tau+\tau'+\xi)\omega_1+it\omega_2][\langle\chi_1|\alpha_c^*(\tau')(i\partial/\partial q_n)^\dagger$$
$$\alpha_d^*(\xi')\beta_1^*(t)q_n\alpha_c(\tau)\beta_1(t-\tau+\tau'+\xi)|\chi_1\rangle$$
$$\mp\langle\chi_1|\alpha_d^*(\xi)(i\partial/\partial q_n)^\dagger\alpha_c^*(\tau')\beta_1^*(t)q_n\alpha_c(\tau)\beta_1(t-\tau+\tau'+\xi)$$
$$|\chi_1\rangle\pm\langle\chi_1|\alpha_c^*(\tau')(i\partial/\partial q_n)^\dagger\alpha_d^*(\xi)\beta_1^*(t)\alpha_c(\tau)q_n\beta_1$$
$$(t-\tau+\tau'+\xi)|\chi_1\rangle-\langle\chi_1|\alpha_d^*(\xi)(i\partial/\partial q_n)^\dagger$$
$$\alpha_c^*(\tau')\beta_1^*(t)\alpha_c(\tau)q_n\beta_1(t-\tau+\tau'+\xi)|\chi_1\rangle]\}. \quad (A.3)$$

Appendix B: Derivation of Eq. 28

In this appendix, we will present a brief derivation of Eq. 28 by utilizing the Boson operator algebra. By using this relation:[11]

$$\exp\left[\frac{i\hat{h}_1(q_s-\Delta_c)\tau'}{\hbar}\right] = \exp\left[\frac{\Delta_c^2}{2}\{\exp(i\omega_s\tau')-1\}\right]$$
$$\exp\left(\frac{i\hat{h}_1\tau'}{\hbar}\right)\exp[-\lambda_c(\tau')\hat{b}_s^\dagger]\exp[\lambda_c^*(\tau')\hat{b}_s], \quad (B.1)$$

where $\lambda_c(\tau')=\frac{\Delta_c}{\sqrt{2}}[1-\exp(-i\omega_s\tau')]$, Eq. 27 is expressed as:

$$g_s(\tau',\xi',\tau,\xi,t) = \exp\left[\frac{\Delta_c^2}{2}\{\exp(i\omega_s\tau')-1\}\right.$$
$$+\frac{\Delta_c^2}{2}\{\exp(-i\omega_s\tau)-1\}+\frac{\Delta_d^2}{2}\{\exp(i\omega_s\xi')-1\}$$
$$\left.+\frac{\Delta_d^2}{2}\{\exp(-i\omega_s\xi)-1\}\right]\langle 0_s|\exp_*(i\omega_s\tau\hat{b}_s^\dagger\hat{b}_s)$$

$$\exp[-\lambda_c(\tau')\hat{b}_s^\dagger]\exp[\lambda_c^*(\tau')\hat{b}_s]\exp[i\omega_s\xi\hat{b}_s^\dagger\hat{b}_s]$$
$$\exp[-\lambda_d(\xi')\hat{b}_s^\dagger]\exp[\lambda_d^*(\xi')\hat{b}_s]\exp[i\omega_s t\hat{b}_s^\dagger\hat{b}_s]$$
$$\exp[\lambda_d(\xi)\hat{b}_s^\dagger]\exp[-\lambda_d^*(\xi)\hat{b}_s]\exp[-i\omega_s\xi\hat{b}_s^\dagger\hat{b}_s]$$
$$\exp[\lambda_c(\tau)\hat{b}_s^\dagger]\exp[-\lambda_c^*(\tau)\hat{b}_s]\exp[-i\omega_s\tau\hat{b}_s^\dagger\hat{b}_s]$$
$$\exp[-i\omega_s(t-\tau-\xi+\tau'+\xi')\hat{b}_s^\dagger\hat{b}_s]|0\rangle. \qquad (B.2)$$

By using the Boson operator algebra,[11] Eq. (B.2) is expressed as:

$$g_s(\tau',\xi',\tau,\xi,t) = \exp\left[\frac{\Delta_c^2}{2}\{\exp(i\omega_s\lambda')-1\}\right.$$
$$+\frac{\Delta_c^2}{2}\{\exp(-i\omega_s\tau)-1\}+\frac{\Delta_d^2}{2}\{\exp(i\omega_s\xi')-1\}$$
$$+\frac{\Delta_d^2}{2}\{\exp(-i\omega_s\xi)-1\}+\lambda_c^*(\tau')\lambda_d^*(\xi')$$
$$+\lambda_c(\tau)\lambda_d(\xi)+\lambda_d^*(\xi')\lambda_d(\xi)\exp(i\omega_s t)$$
$$+\lambda_c(\tau)\lambda_d^*(\xi')\exp(-i\omega_s\xi+i\omega_s t)$$
$$+\lambda_c^*(\tau')\lambda_d(\xi)\exp(i\omega_s\xi+i\omega_s t)$$
$$\left.+\lambda_c^*(\tau')\lambda_c(\tau)\exp(i\omega_s\xi'-i\omega_s\xi+i\omega_s t)\right]. \qquad (B.3)$$

This expression is equivalent to Eq. 28.

 © 1982 The Chemical Society of Japan Bull. Chem. Soc. Jpn., 55, 277—281 (1982)

A Displaced Harmonic Oscillator Model for the Time-resolved Emission Spectra

Yuichi FUJIMURA,* Kenji SATO,† and Takeshi NAKAJIMA

Department of Chemistry, Faculty of Science, Tohoku University, Sendai 980

(Received March 30, 1981)

In a displaced harmonic oscillator model for an energy-accepting mode, analytical expressions for the time-resolved emission intensity distribution are derived for both the allowed and vibronically induced electronic transitions. In the case of the vibronically induced transition, the inducing mode as well as the accepting mode is assumed to undergo a collisional vibrational relaxation. A linear vibrational quantum-number-dependence of the electronic and collisional vibrational relaxation constants is assumed. Model calculations of the time-resolved emission-intensity distribution for a molecular system are performed using the expressions derived. The calculated time-resolved emission spectra of benzene in the vapor phase after an excitation to a single vibronic level semi-quantitatively account for the experimental results.

It is well known that time-resolved spectroscopy plays an important role in elucidating the dynamics as well as the static behavior of vibronically excited molecules. The time-resolved emission spectra have been reported by several authors. Hochstrasser and Wessel[1] have observed the time-resolved fluorescence of anthracene in mixed crystals of low temperatures. Werkhoven *et al.*[2] have investigated the vibrational redistribution effects by analyzing the time-resolved emission spectrum of the isolated pyrene molecule. Swords and Phillips[3] have observed the nano-second time-resolved emission of benzene in order to study the collisional processes.

The purpose of this paper is to develop a theory for the time-resolved emission of a molecular system. The time-resolved emission intensity distribution is expressed as the emission intensity weighted by the time-dependent population of the single vibronic level in the excited state. In other words, the observed intensity distribution is governed by both the Franck-Condon factor and the kinetics of the excited state. The time-dependence of the population is determined by solving the kinetic equation in the excited state in which the vibronic level undergoes the electronic relaxation, the collisional vibrational relaxation, and/or the vibrational redistribution among the vibrational modes.

A similar time-dependent theory has been proposed for analyzing the time-resolved absorption spectra of electronically excited molecules.[4-6] Fleming *et al.*[7] have developed a theory for the time-resolved emission spectra of molecules in which the single vibronic emission-intensity distribution of the δ-function form is adopted. A master-equation approach to the time-dependent luminescence during the vibrational relaxation has been used by Seshadri and Kenkre.[8]

In Theory section, analytical expressions for the time-resolved emission-intensity distribution are given for both the allowed and vibronically induced electronic transitions in the displaced harmonic oscillator model for an accepting mode. Both Lorentzian and Gaussian single vibronic level intensity distributions are assumed. It is assumed that the electronic and vibrational relaxation constants are linear functions of the vibrational quantum number. This assumption is valid for a molecular system with low excited vibronic levels. In the case of the vibronically induced transition, the inducing mode as well as the accepting mode is assumed to undergo a collisional deactivation. In discussion, model calculations of the time-resolved emission intensity distribution are performed. A non-exponential fluorescence decay can be predicted if the rate of vibrational relaxation is fast compared with those of the radiation and electronic relaxations. For the vibronically induced transition, a fast fluorescence decay can be expected upon the excitation to the vibronic level of the inducing mode.

Theory

We will consider an electronic transition, $a \leftarrow b$, of a molecular system. The time-resolved emission-intensity distribution, $P_{ab}(\nu, t)$, as a function of the optical frequency, ν, and time, t, is given by:[7]

$$P_{ab}(\nu, t) = \sum_{\{v\}} \sum_{\{v'\}} I_{a\{v\},b\{v'\}}(\nu) \chi_{b\{v'\}}(t), \quad (1)$$

where $I_{a\{v\},v\{b'\}}(\nu)$ represents the intensity of the emission from a single vibronic level of the b electronic state, $b\{v'\}$, to that of the ground state $a\{v\}$, and $\chi_{b\{v'\}}(t) = \prod_j \chi_{bv'_j}(t)$, the population of the molecule in the single vibronic level, $b\{v'\}$, at time t.

The $\chi_{bv'}(t)$ population, depends on the dynamical behavior in the electronic state, such as the electronic and/or vibrational relaxations. χ satisfies the following equation for the molecular system undergoing the electronic and vibrational relaxations after the optical transition:

$$\frac{d\chi_{bv'}(t)}{dt} = C_{bv'}(t) - K_{bv',bv'}\chi_{bv'}(t) - \sum_{v''} R_{bv'bv''}\chi_{bv''}(t), \quad (2)$$

where K is a diagonal matrix element involving the radiative and nonradiative decay constants; R represents the vibrational relaxation matrix in the electronic state b, and $C_{bv}(t)$ is a function related to the optical excitation. Equation 2 can be solved by using i) the diagonalization method of the matrix[9] or ii) the generating-function method.[10] In this paper, we use the generating-function method. Assuming, for the rates of vibrational and nonradiative relaxations, linear dependences on the vibrational quantum num-

† Present address: The Institute for Molecular Science, Okazaki, Aichi 444.

bers of the vibronic levels, *i.e.* $k_v^{c\prime}=v'k^c$ and $k_v^{n\prime}=k+v'k^n$ respectively, with the effect of the radiative decay being included as the k parameter, the solution of Eq. 2 is given by:[4,5]

$$\chi_{bv'}(t)=\frac{v_0'!}{v'!(v_0'-v')!}\left\{\frac{k^c}{k^c+k^n}[1-\exp\{-(k^c+k^n)t\}]\right\}^{v_0'-v'}\exp[-kt-v'(k^c+k^n)t], \tag{3}$$

where an optical exitation to a single vibronic level, bv_0', at $t=0$ has been assumed.

Two types of emission, dipole-allowed transitions and vibronically induced transitions, are taken into account of in this paper.

Dipole-allowed Transition. In the case of the Lorentzian single-vibronic-level-intensity distribution, the intensity from the vibronic level, bv', to av is given by:

$$I_{av,bv'}(\nu)=\frac{4\pi\nu^3}{3\hbar c^3}|M_{ab}^0|^2|\langle\theta_{av}|\theta_{bv'}\rangle|^2\frac{\Gamma_{av,bv'}}{(\omega_{bv',av}-\nu)^2+\Gamma_{av,bv'}^2}, \tag{4}$$

where M_{ab}^0, θ, $\Gamma_{ab,bv'}$, and $\omega_{bv',av}$ represent the electronic transition moment evaluated at the equilibrium nuclear configuration in the initial electronic state, the nuclear wave function, the damping constant, and the energy gap between two single-vibronic levels, bv' and av, respectively. Using the transformation:

$$\frac{a}{x^2+a^2}=\frac{1}{2}\int_{-\infty}^{\infty}d\tau\exp[-i\chi\tau-a|\tau|], \tag{5}$$

and summing over the vibronic level, v, in the electronic state, a, Eq. 4 can be expressed as:

$$\begin{aligned}I_{a,bv'}(\nu)&=\sum_v I_{av,bv'}(\nu)\\&=\frac{2\pi\nu^3}{3\hbar c^3}|M_{ab}^0|^2\int_{-\infty}^{\infty}d\tau\exp[i\nu\tau-\Gamma_{ab}|\tau|]\\&\quad\langle\theta_{bv'}|\exp[-i\hat{H}_b\tau/\hbar]\exp[i\hat{H}_a\tau/\hbar]|\theta_{bv'}\rangle,\end{aligned} \tag{6}$$

where $\hat{H}_a$ and $\hat{H}_b$ represent the nuclear Hamiltonian in the electronic states, a and b, respectively; the vibronic-level dependence of the damping constant is neglected *i.e.*, $\Gamma_{ab}\simeq\Gamma_{av,bv'}$.

In the displaced-harmonic-oscillator model (the other modes are assumed to be common in the electronic states a and b),

$$\hat{H}_b=\frac{\hbar\omega}{2}\{p^2+(q-\Delta)^2\}+\omega_{ba}, \tag{7a}$$

and

$$\hat{H}_a=\frac{\hbar\omega}{2}(p^2+q^2), \tag{7b}$$

where ω and Δ are the frequency and the displacement of the vibrational mode respectively, with ω_{ba} the electronic energy difference between two states, b and a. Equation 6 can be expressed as:

$$\begin{aligned}I_{a,bv'}(\nu)&=\frac{2\pi\nu^3}{3\hbar c^3}|M_{ab}^0|^2\exp\left(-\frac{\Delta^2}{2}\right)\int_{-\infty}^{\infty}d\tau\\&\quad\exp\left[i\tau(\nu-\omega_{ba})-\Gamma_{ab}|\tau|+\frac{\Delta^2}{2}e^{i\omega\tau}\right]\\&\quad\sum_{n=0}^{v'}\frac{v'!(\Delta^2/2)^n}{(v'-n)!(n!)^2}(\cos\omega\tau-1)^n.\end{aligned} \tag{8}$$

Substituting Eqs. 3 and 8 into Eq. 1, and summing over v', the time-resolved emission intensity for the allowed transition can be expressed as:

$$\begin{aligned}P_{ab}(\nu,t)&=\frac{4\pi\nu^3}{3\hbar c^3}|M_{ab}^0|^2\exp\left(-\frac{\Delta^2}{2}\right)\exp(-kt)\\&\quad\sum_{l=0}^{\infty}\sum_{n=0}^{v_0'}\sum_{r=0}^{2n}\frac{v_0'!(2n)!\left(\frac{\Delta^2}{2}\right)^{l+n}}{l!(n!)^2(v_0'-n)!(2n-r)!r!}\\&\quad\exp[-n(k^c+k^n)t]\left\{\frac{k^c}{k^c+k^n}+\frac{k^n}{k^c+k^n}\right.\\&\quad\left.\exp[-(k^c+k^n)t]\right\}^{v_0'-n}\frac{\Gamma_{ab}}{\{\nu-\omega_{ba}+\omega(l+n-r)\}^2+\Gamma_{ab}^2}.\end{aligned} \tag{9}$$

By assuming the homogeneous broadening, the Lorentzian band shape has so far been used. In the case of an inhomogeneous broadening, the band shape is usually expressed by a Gaussian form. After the Fourier transformation, the band-shape function, $A(x)$, is given by:

$$A(x)=\frac{1}{2\sqrt{\pi a}}\int_{-\infty}^{\infty}\exp\left[-i\chi\tau-\frac{\tau^2}{4a}\right]d\tau, \tag{10}$$

where $a=\ln 2/\tilde{\Gamma}^2$, in which $\tilde{\Gamma}$ is the half width at the half-maximum. In this case, the time-resolved emission-intensity distribution can be formulated by using a method similar to that described above. The result is written as:

$$\begin{aligned}P_{ab}(\nu,t)&=\frac{4\pi\nu^3}{3\hbar c^3}|M_{ab}^0|^2\exp\left(-\frac{\Delta^2}{2}\right)\exp(-kt)\\&\quad\sum_{l=0}^{\infty}\sum_{n=0}^{v_0'}\sum_{r=0}^{2n}\frac{v_0'!(2n)!\left(\frac{\Delta^2}{2}\right)^{l+n}}{l!(n!)^2(v_0'-n)!(2n-r)!r!}\exp[-n(k^c+k^n)t]\\&\quad\left\{\frac{k^c}{k^c+k^n}+\frac{k^n}{k^c+k^n}\exp[-(k^c+k^n)t]\right\}^{v_0'-n}\\&\quad\exp[-a\{\nu-\omega_{ba}+\omega(l+n-r)\}^2].\end{aligned} \tag{11}$$

Vibronically Induced Transition. The emission intensity from the single vibronic level, $bv_d'v_i'$, to av_dv_i is given by:

$$\begin{aligned}I_{bv_d'v_i',av_dv_i}(\nu)&=\frac{4\pi\nu^3}{3\hbar c^3}\left(\frac{\partial M_{ab}}{\partial q_i}\right)_{q_i=0}|\langle\theta_{av_i}|q_i|\theta_{bv_i'}\rangle|^2\\&\quad|\langle\theta_{av_d}|\theta_{bv_d'}\rangle|^2\frac{\Gamma_{ab}}{(\omega_{bv_d'v_i',av_dv_i}-\nu)^2+\Gamma_{av}^2},\end{aligned} \tag{12}$$

where i and d specify the inducing and accepting modes respectively; the Lorentzian band shape has been assumed. In Eq. 12, one inducing mode and one accepting mode were assumed (*i.e.*, the other modes are disregarded), and the v_i-dependence of the damping constant was neglected.

We will consider a model system in which the accepting and inducing modes consist of a displaced harmonic oscillator and a harmonic oscillator with no frequency change and no displacement respectively. After summing over the vibronic levels, v_i and v_d, Eq. 12 can be expressed as:

$$\begin{aligned}I_{a,bv_d'v_i'}(\nu)&=C(\nu)\exp\left(-\frac{\Delta^2}{2}\right)\int_{-\infty}^{\infty}d\tau\\&\quad\exp\left[-i(\nu-\omega_{ba})\tau-\Gamma_{ab}|\tau|+\frac{\Delta^2}{2}\exp(i\omega\tau)\right]\end{aligned}$$

$$\{(1+v_i')\exp(-i\omega_i\tau)+v_i'\exp(i\omega_i\tau)\}$$
$$\sum_{n=0}^{v_d'}\frac{v_d'!\Delta^{2n}}{(v_d'-n)!(n!)^2}(\cos\omega\tau-1)^n, \quad (13)$$

where ω_i represents the frequency of the inducing mode; the constant, $C(v)$, is given by:

$$C(v)=v^3\left(\frac{\partial M_{ab}}{\partial q_i}\right)_{q_i=0}\Big/3\hbar c^3\beta_i \text{ in which } \beta_i=(\omega_i/\hbar)^{1/2}.$$

The time-resolved emission intensity in a case in which the molecular system is excited to a singlet vibronic level $bv_{d0}'v_{i0}'$ at $t=0$ can be expressed as:

$$P_{ab}(v,t)=C(v)\exp\left(-\frac{\Delta^2}{2}\right)\exp(-kt)$$
$$\sum_{l=0}^{\infty}\sum_{n_d=0}^{v_{d0}'}\sum_{n_i=0}^{v_{i0}'}\sum_{r=0}^{n_d2}\frac{v_{i0}'}{n_i!(v_{i0}'-n_i)!}$$
$$\left[\frac{k_i^c}{k_i^c+k_i^n}\{1-\exp[-(k_i^c+k_i^n)t]\}\right]^{v_{i0}'-n_i}$$
$$\exp[-n_i(k_i^c+k_i^n)t-n_d(k^n+k^c)t]$$
$$\frac{(-1)^r v_{i0}'!(2n_d)!\left(\frac{\Delta^2}{2}\right)^{l+n_i}}{l!(n_d!)^2(v_{d0}'-n_i)!(2n_d-r)!r!}$$
$$\left\{\frac{k^c}{k^c+k^n}+\frac{k^n}{k^c+k^n}\exp[-(k^c+k^n)t]\right\}^{v_{d0}'-n_d}$$
$$\left[(n_i+1)\frac{\Gamma_{ab}}{\{v-\omega_{ba}+\omega(l+n_d-r)+\omega_i\}^2+\Gamma_{ab}^2}\right.$$
$$\left.+n_i\frac{\Gamma_{ab}}{\{v-\omega_{ba}+\omega(l+n_d-r)-\omega_i\}^2+\Gamma_{ab}^2}\right], \quad (14)$$

where a linear dependence of the relaxation constants on the vibrational quantum number of the inducing mode as well as the accepting mode has been assumed; $k_{v_i'}^c=v_i'k_i^c$, $k_{v_i'}^n=k_i^0+v_i'k_i^n$; and $k\equiv k+k_i^0$. The time-resolved emission-intensity distribution in which the vibronic band shape is expressed by the Gaussian form can easily be derived.

Model Calculations and Discussion

Figures 1 and 2 show the time-dependence of the emission spectra calculated by using Eq. 9 in the case of $v=\omega_{ba}$. The ordinate expresses the emission intensity relative to that at $t=0$. The excitation to the first vibronic level, $v_0'=1$, from the lowest level in the ground state is assumed. Figures 1 and 2 correspond to the slow and fast vibrational-relaxation cases respectively. The parameters used for Figs. 1 and 2 are $k=10^8\ s^{-1}$, $k^c=2\times10^7\ s^{-1}$. $k^n=4\times10^7\ s^{-1}$, and $\Delta=0.14$, and $k=2\times10^7\ s^{-1}$, $k^c=10^8\ s^{-1}$, $k^n=4\times10^7\ s^{-1}$, and $\Delta=0.14$, respectively. In Fig. 1, a single exponential decay is shown, while in Fig. 2, a nonexponential time-dependence is seen. The appearance of the nonexponential decay can be qualitatively explained by examining Eq. 9. For simplicity, we consider the weak coupling limit to be where $\Delta\to0$. Then, in the case of v near ω_{ba}, Eq. 9 for $v_0'=1$ can be expressed as:

$$P(v,t)\propto\left\{\frac{k^c}{k^c+k^n}\exp(-kt)+\frac{k^n}{k^c+k^n}\exp[-(k+k^n+k^c)t]\right\}\frac{\Gamma}{(v-\omega_{ba})^2+\Gamma^2}. \quad (15)$$

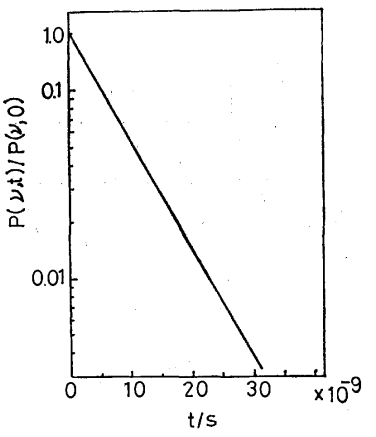

Fig. 1. Time-dependence of the emission intensity in the case of the slow collisional vibrational relaxation. The intensity relative to that at $t=0$ is plotted by using Eq. 9 for $v=\omega_{ba}$. The excitation to the first vibronic level $v_0'=1$ from the lowest level in the ground state is assumed. The parameters used are $k=10^8\ s^{-1}$, $k^c=2\times10^7\ s^{-1}$, $k^n=4\times10^7\ s^{-1}$, and $\Delta=0.14$.

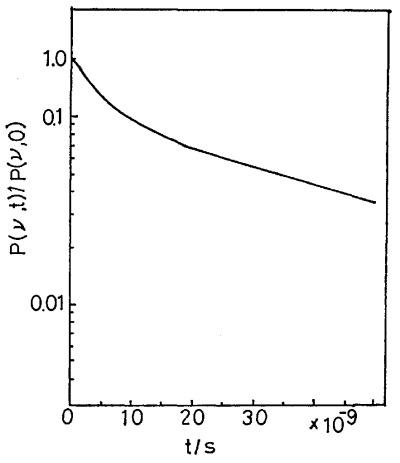

Fig. 2. Time-dependence of the emission intensity in the case of the fast collisional vibrational relaxation. The excitation and emission monitoring conditions are the same in Fig. 1. The parameters used are $k=2\times10^7\ s^{-1}$ and $k^c=10^8\ s^{-1}$, and the other parameters are the same in Fig. 1. When $k<k^c$ and $k^n\approx k^c$, the bi-exponential decay of fluorescence may be observed as shown in this figure.

Equation 15 indicates that, when $k\gg k^c+k^n$ (or $k^c\gtrless k^n$), $P(v,t)$ obeys a single exponential decay, while when $k\ll k^c+k^n$ and $k^n\approx k^c$, a bi-exponential fluorescence decay can be expected.

Figures 3 and 4 show model calculations of the time-resolved emission-intensity distribution as a function of the frequency for a model system corresponding to a vibronically induced optical transition such as $^1A_{1g}\leftarrow{}^1B_{2u}$ of benzene. The emission intensity distribution relative to its maximum value, $\tilde{P}(\omega_0,t)$, is plotted by using Eq. 14. In Figs. 3 and 4, the intensity distribution is plotted in the case of the excitation to a vibronic level with $v_{d0}'=1$ and $v_{i0}'=0$, and with $v_{d0}'=v_{i0}'=1$, respectively. The parameters used are $\omega=993\ cm^{-1}$, $k^n=3.67\times10^6\ s^{-1}$, and $\Delta=$

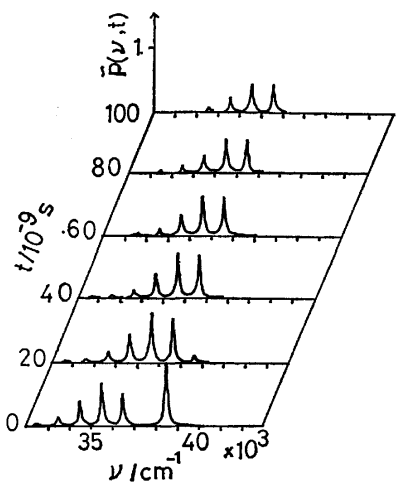

Fig. 3. Calculated time-resolved emission intensity distribution for a model system corresponding to a vibronically induced optical transition. The emission intensity distribution relative to its maximum value, $\tilde{P}(\nu,t)=P(\nu,t)/P(\nu,t)_{max}$ is plotted by using Eq. 12. The excitation to the vibronic level $v'_{a0}=1$ and $v'_{i0}=0$ is assumed. The parameters used are $\omega_{ab}=38090$ cm^{-1}, $\omega=993$ cm^{-1}, $\omega_i=522$ cm^{-1}, $\Delta=1.43$, $k^n=3.67\times10^6$ s^{-1}, $k_i^n=1.35\times10^6$ s^{-1}, $k=7.8\times10^6$ s^{-1}, and $\Gamma_{ab}=75$ cm^{-1}.

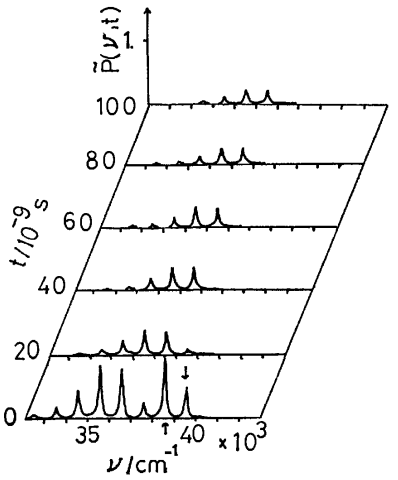

Fig. 4. Calculated time-resolved emission intensity distribution. The excitation to the vibronic level with $v'_{a0}=1$ and $v'_{i0}=1$ is assumed. The parameters used are the same in Fig. 3. The downward and upward arrows indicate the origins of the progressions, $6_0^1 1_n^1$ and $6_2^1 1_n^1$, respectively.

1.43[11] for the accepting mode (ν_1); $\omega_i=522$ cm^{-1} [12] and $k_i^n=1.35\times10^6$ s^{-1} for the inducing mode (ν_6), and $k=7.8\times10^6$ s^{-1},[13] $\omega_{ab}=38090$ cm^{-1}, and $\Gamma_{ab}=75$ cm^{-1}. These parameters are taken from the calculated and experimental data for the $^1A_{1g}\leftarrow{}^1B_{2u}$ transition of benzene. The collisional vibrational-relaxation constants, which depend on pressure, are assumed to be $k^c=0.1\times10^9$ s^{-1} and $k_i^c=0.2\times10^9$ s^{-1}. In Fig. 3, the diffuse spectrum as a function of the emission frequency at $t=0$ is shown, and we can see no band peak corresponding to the $1\leftarrow1$ vibronic transition for the accepting mode near 37600 cm^{-1}. This can be explained by the vanishingly small Franck-Condon

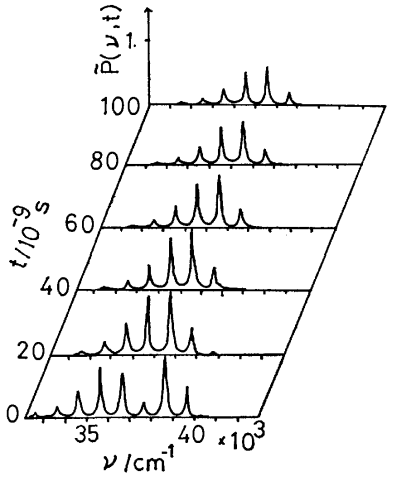

Fig. 5. Calculated time-resolved emission intensity distribution in the case of no collisional vibrational and electronic relaxations relevant to the inducing mode. The excitation to the vibronic level with $v'_{a0}=1$ and $v'_{i0}=1$ is assumed. The parameters used are the same in Fig. 3 except for $k_i^c=k_i^n=0$.

overlap for $\Delta^2/2\simeq1$. It is shown that the intensity decay in Fig. 4 is faster than that in Fig. 3. This is qualitatively due to the fact that, in the case of the one-vibrational quantum excitation of the inducing mode, not only are there two emission-decay paths, but also there are a collisional vibrational relaxation and a nonradiative decay path involving the inducing mode compared with the case of the zero-quantum excitation.

It is shown in Fig. 4 that the emission spectrum at $t=0$ consists of two progressions, $6_0^1 1_n^1$ and $6_2^1 1_n^1$, where n=0, 1,$\cdots$(their origins are indicated by downward and upward arrows respectively), while after time enough to reach the steady state, the emission-intensity distribution consists of one progression, $6_1^0 1_n^0$. These spectral features have been observed by Blondeau and Stockburger[15] and by Swords and Phillips.[3] Blondeau and Stockburger have also studied the resonance flourescence spectra of benzene in the vapor phase, and have compared them with the fluorescence spectra from a Boltzmann distributed vibrational levels in the first excited state; the resonance fluorescence from the $6^1 1^1$ level consists of two progressions, $6_0^1 1_n^1$ and $6_2^1 1_n^1$; the main progression in the equilibrated fluorescence by the 253.7 nm excitation is $6_1^0 1_n^1$. The time-resolved fluorescence spectra of benzene in the gas phase have been reported by Swords and Phillips.[3] In the time-resolved fluorescence spectra observed at $t=70$ ns after the excitation at 257.25 nm in which two major transitions, $6_1^0 1_0^1 16_0^2$ and $6_0^1 16_1^3$, are involved, the bands related to the inducing mode decrease, while those belonging to the $6_1^0 1_n^0$ progression increase, in intensity compared with those observed at $t=20$ ns.

In Fig. 5, the relative emission-intensity distribution in the case of no collisional vibrational and electronic relaxations related to the inducing mode, $k_i^c=k_i^n=0$, is shown. The emission-intensity distribution is plotted by using Eq. 14. The other parameters used are the same as in Fig. 4. We can see that the vi-

bronic-intensity distribution in Fig. 5 after a long time is different from that in Fig. 4. In Fig. 5, the band peak at about 38600 cm^{-1}, which corresponds to the 0←1 transition for the inducing mode, still remains because of the absence of any relaxation for the mode.

Finally, we should mention the value of the damping constant. The damping constant is expressed by a sum of two terms: $\Gamma_{ab}=1/2(\Gamma_{aa}+\Gamma_{bb})+\Gamma^{(d)}_{ab,at}$,[16] where Γ_{aa} and Γ_{bb} are the population-decay constants of the a and b states respectively, and where $\Gamma^{(d)}_{ab,ab}$ denotes the pure dephasing constant originating from elastic interaction processes between molecules and heat bath. A value of Γ_{ab} close to that observed in nanosecond time-resolved emission spectroscopy[3] has been used in this paper. In other words, the value does not always represent the real damping constant, for there are no corrections for the optical detection or for the inhomogeneous broadening.

References

1) R. M. Hochstrasser and J. E. Wessel, *Chem. Phys.*, **6**, 19 (1974).
2) C. J. Werkhoven, T. Deinum, J. Langelaar, R. P. H. Rettschnick, and J. D. W. Van Voorst, *Chem. Phys. Lett.*, **30**, 504 (1975).
3) M. D. Swords and D. Phillips, *Chem. Phys. Lett.*, **43**, 228 (1976).
4) G. R. Fleming, O. L. J. Gijeman, and S. H. Lin, *J. Chem. Soc., Faraday Trans. 2*, **70**, 1074 (1974).
5) Y. Fujimura, S. H. Lin, H. Schröder, H. J. Neusser, and E. W. Schlag, *Chem. Phys.*, **43**, 205 (1979).
6) Y. Fujimura, T. Nakajima, S. H. Lin, and E. W. Schlag, *Chem. Phys. Lett.*, **67**, 299 (1979).
7) G. R. Fleming, O. L. J. Gijeman, K. F. Freed, and S. H. Lin, *J. Chem. Soc., Faraday Trans. 2*, **71**, 773 (1975).
8) V. Seshadri and V. M. Kenkre, *Phys. Rev. A*, **17**, 223 (1978).
9) S. H. Lin, *J. Chem. Phys.*, **56**, 4155 (1972).
10) E. W. Montroll and K. E. Shuler, *J. Chem. Phys.*, **26**, 454 (1957).
11) Y. Fujimura and T. Nakajima, *Chem. Phys. Lett.*, **14**, 104 (1971).
12) C. S. Parmenter, *Adv. Chem. Phys.*, **22**, 365 (1972).
13) K. G. Spears and S. A. Rice, *J. Chem. Phys.*, **55**, 5561 (1971).
14) F. M. Garforth, and C. K. Ingold, *J. Chem. Soc.*, **1948**, 417.
15) J. M. Blondeau and M. Stockburger, *Ber. Bunsenges. Phys. Chem.*, **75**, 450 (1971).
16) S. H. Lin, "Radiationless Transitions," Academic Press, New York (1980), p. 363.

Effect of 1,4-Dioxane on the Structure of Aqueous *t*-Butyl Alcohol. Sound Velocity Studies

Neriyanuri MANOHARA MURTHY and Saraswatula Venkata SUBRAHMANYAM*

Department of Physics, SVU Autonomous Post-Graduate Center, Anantapur 515003, India

(Received December 19, 1980)

The structure of aqueous *t*-butyl alcohol in the water rich region is known to be more structured than pure water. 1,4-dioxane is known to be a weakly hydrophobic solute. The effect of 1,4-dioxane on the structure of aqueous *t*-butyl alcohol has been studied by fixing the temperature of sound velocity maximum in the ternary solution from the experimentally determined ultrasonic velocity data at different temperatures. The structural contribution to the shift in the temperature of sound velocity maximum of the aqueous *t*-butyl alcohol solution due to the addition of 1,4-dioxane, $[\Delta T_{str.}]_{exptl}$, has been found to be positive having the nature of variation similar to that of the effect of 1,4-dioxane on pure water, when the concentration (X_s) of *t*-butyl alcohol is 0.0075. But, for aqueous *t*-butyl alcohol solutions having $X_s=0.0025$ and $X_s=0.0046$, $[\Delta T_{str.}]_{exptl}$, has been found to be negative reaching maximum values around $X_2=0.0045$ and there after decreasing with a tendency to become positive at higher concentrations of 1,4-dioxane. These results have been explained in the light of structure breaking and formation of dioxane complexes in the ternary solutions.

The hydrophobic nature of *t*-butyl alcohol has been established beyond doubt[1–16] whereas controversial views exist on the structural propensity of 1,4-dioxane.[17–27] Our earlier studies on the effect of *t*-butyl alcohol[28,29] and 1,4-dioxane[30] on the temperature of sound velocity maximum (TVM) and adiabatic compressibility minimum (TACM) indicated both the solutes to enhance the ordered structure of water when present in small amounts. In our earlier work,[31] we have carried out the TVM studies on ternary systems namely water+glycerol+1-butanol and water+pyridine+1-butanol and found to be useful in delineating the temperature dependence of structural propensity of 1-butanol. In continuation of TVM studies in probing the structure of ternary systems, we have taken up the studies on the effect of 1,4-dioxane on the temperature of sound velocity maximum of aqueous mixtures of *t*-butyl alcohol of different concentrations and the results are reported in this paper. Our interest in these studies is to see how a structure promoter (1,4-dioxane) influences the aqueous binary solution structure containing a structure promoter (*t*-butyl alcohol).

Experimental

Triple distilled degassed water was used to prepare stock solutions of aqueous *t*-butyl alcohol. This stock solution was used to prepare ternary solution of 1,4-dioxane of desired concentration. The concentration of 1,4-dioxane in the ternary solution was calculated by considering aqueous binary stock solution as a cosolvent of effective molecular weight M_{12} given by $X_wM_w+X_sM_s$ where M_w,M_s and X_w,X_s represent the molecular weights and mole fractions respectively of water and *t*-butyl alcohol. AR grade *t*-butyl alcohol and 1,4-dioxane were used after necessary purification following the procedure given by Weissberger.[32] Ultrasonic velocity in the solutions was determined using a single crystal variable path interferometer working at 3 MHz with an accuracy of ±0.003%, the details of which were discussed elsewhere.[28]

Results

Diffraction corrected ultrasonic velocity as a function of temperature at different concentrations of 1,4-dioxane in aqueous *t*-butyl alcohol ($M_{12}=18.1556$, $X_s=0.0025$; $M_{12}=18.2735$, $X=0.0046$, and $M_{12}=18.4884$, $X_s=0.0075$) are presented graphically in Figs. 1—3.

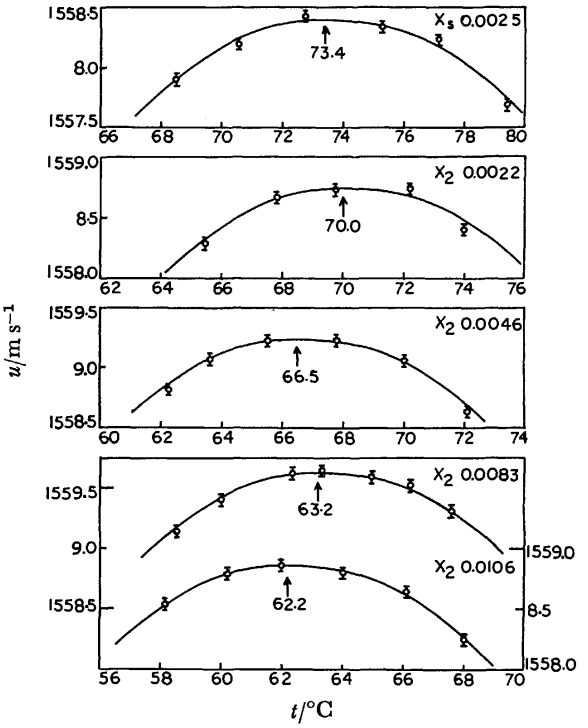

Fig. 1. Ultrasonic velocity *versus* temperature in aqueous solutions of *t*-butyl alcohol ($X_s=0.0025$) at different mole fractions of 1,4-dioxane.

The TVM in the ternary solution was fixed using the template of the velocity-temperature curve for pure water with an accuracy of ±0.2 °C as described earlier.[31]

Discussion

The shift in the temperature of sound velocity maximum of aqueous *t*-butyl alcohol due to the addition of 1,4-dioxane may be given by

$$\Delta T = (T_{\text{exptl}})_{\text{ternary soln}} - (T_{\text{exptl}})_{\text{binary soln}} \quad (1)$$

ΔT arises due to two effects namely dilution effect and structural effect which may be separated by considering the expressions representing the temperature dependence of velocity in aqueous *t*-butyl alcohol and 1,4-dioxane. The structural contribution to the shift in the temperature of sound velocity maximum in the ternary solution can be calculated using the following expressions that may be obtained on the same lines as that for pure water.[29]

$$[\Delta T_{\text{str.}}]_{\text{exptl}} = T_{\text{exptl}} - T_{\text{id.}} \quad (2)$$

where

$$T_{\text{id.}} = T_{\text{binary soln}} - \left(\frac{\phi_2}{\phi_{12}}\right)^2\left(\frac{W_{12}}{W_2}\right)\frac{2\beta}{\alpha}\left(\frac{u_{12}}{u_2}\right)^3. \quad (3)$$

In the above expression ϕ_{12}, ϕ_2 and W_{12}, W_2 represent the volume fractions and weight fractions of aqueous *t*-butyl alcohol and 1,4-dioxane respectively in the terary solution. α represents the temperature coefficient of sound velocity in 1,4-dioxane and u_{12} and u_2 the velocities in the aqueous *t*-butyl alcohol and 1,4-dioxane respectively. For 1,4-dioxane u_2 is given by

$$u_2 = u_2^0 - \alpha t, \quad (4)$$

where u_2^0 and α are 1452.42 ms^{-1} and 4.33 ms^{-1} $°C^{-1}$ respectively and t represents the temperature in °C. u_{12} may be written as

$$u_{12} = u_{12}^0 - \beta(T-t)^2. \quad (5)$$

The values of u_{12}, β, and T for aqueous *t*-butyl alcohol for different X_s are given in Table 1.

In all cases $T_{\text{id.}}$ was calculated using the method of successive approximations. Table 2 gives the values of T_{exptl}, $T_{\text{id.}}$, and $[\Delta T_{\text{str.}}]_{\text{exptl}}$ at different concentrations of 1,4-dioxane. The variation of $[\Delta T_{\text{str.}}]_{\text{exptl}}$ *versus* mole fraction X_2 of 1,4-dioxane in different aqueous *t*-butyl alcohol solutions are shown graphically in Fig. 4 along with the $[\Delta T_{\text{str.}}]_{\text{exptl}}$ *versus* X_2 of

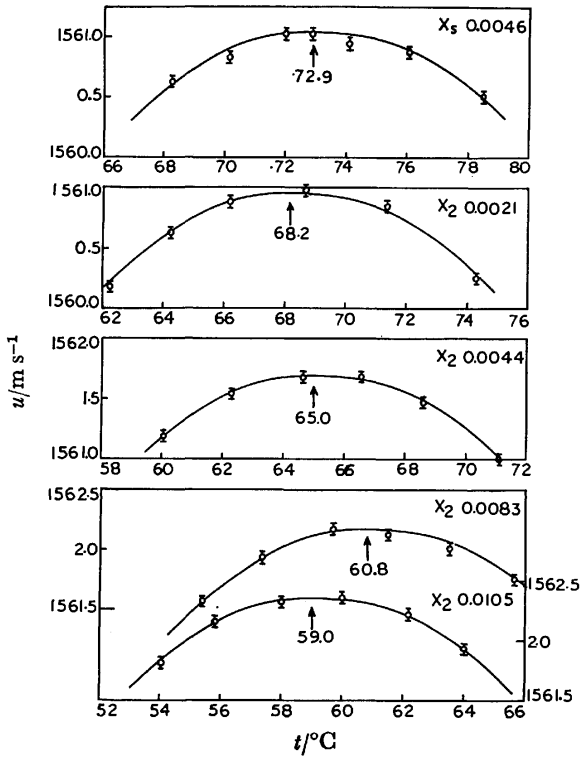

Fig. 2. Ultrasonic velocity *versus* temperature in aqueous solutions of *t*-butyl alcohol (X_s=0.0046) at different mole fractions of 1,4-dioxane.

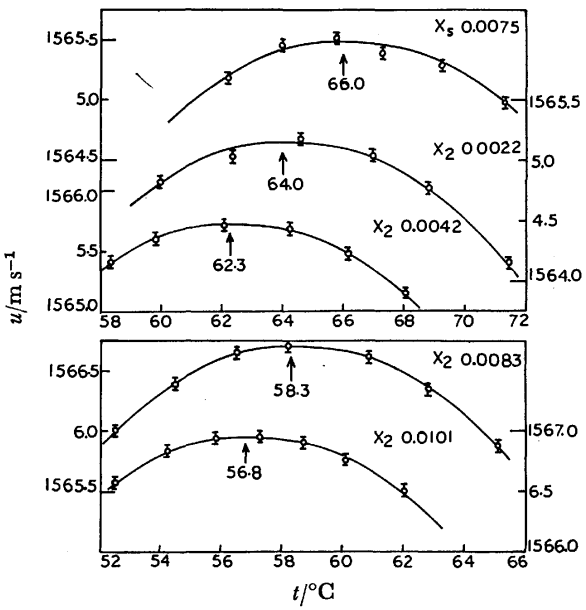

Fig. 3. Ultrasonic velocity *versus* temperature in aqueous solutions of *t*-butyl alcohol (X_s=0.0075) at different mole fractions of 1,4-dioxane.

Table 1. Values of u_{12}^0, β, and T for aqueous *t*-butyl alcohol

X_s	u_{12}^0 / ms^{-1}	β / ms^{-1} °C^{-2}	T / °C
0.0000	1557.00	0.0245	74.0
0.0025	1558.44	0.0217	73.6
0.0046	1561.02	0.0196	73.0
0.0075	1565.48	0.0190	66.1

Table 2. $T_{\text{id.}}$, T_{exptl}, and $[\Delta T_{\text{str.}}]_{\text{exptl}}$ at different mole fractions X_2 of 1,4-dioxane in binary aqueous mixtures of *t*-butyl alcohol

W_2	X_2	$T_{\text{id.}}$ / °C	T_{exptl} / °C	$[\Delta T_{\text{str.}}]_{\text{exptl}}$ / °C
		X_s=0.0025		
0.0106	0.0022	70.9	70.0	−0.9
0.0220	0.0046	68.1	66.5	−1.6
0.0392	0.0083	63.5	63.2	−0.3
0.0495	0.0106	62.0	62.2	+0.2
		X_s=0.0046		
0.0100	0.0021	70.3	68.2	−2.0
0.0210	0.0044	67.5	65.0	−2.4
0.0387	0.0083	63.0	60.8	−2.1
0.0485	0.0105	60.5	59.0	−1.5
		X_s=0.0075		
0.0104	0.0022	63.4	64.0	+0.6
0.0197	0.0042	61.0	62.3	+1.3
0.0385	0.0083	56.4	58.3	+1.9
0.0465	0.0101	54.5	56.8	+2.3

1,4-dioxane in pure water taken from literature.[30] From the figure it is clear that the structural contribution to the shift in TVM of aqueous *t*-butyl alcohol is negative for the binary mixtures in which X_s= 0.0025 and 0.0046 reaching maximum values around $X_2 \simeq 0.0045$ and thereafter decreases with a tendency to become positive at higher concentrations of 1,4-dioxane. But, when the mole fraction of *t*-butyl alcohol in the aqueous *t*-butyl alcohol is 0.0075,

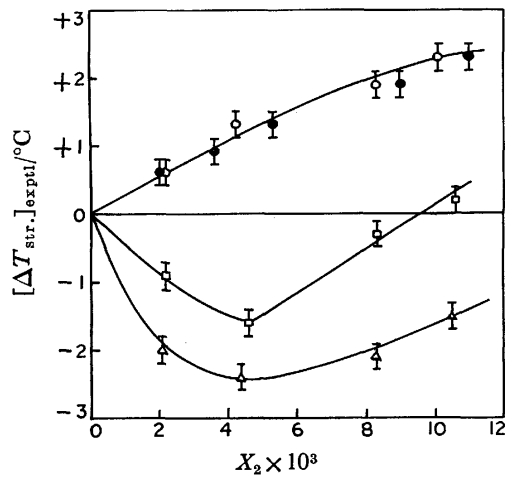

Fig. 4. $\Delta T_{str.\ exptl}$ *versus* mole fraction X_2 of 1,4-dioxane in different solvents.

: Aqueous *t*-butyl alcohol X_s=0.0025, TVM 73.6 °C, : Aqueous *t*-butyl alcohol X_s=0.0046, TVM 73.0 °C, : Aqueous *t*-butyl alcohol X_s=0.0075, TVM 66.1 °C, : Pure water, TVM 74 °C.

$[\Delta T_{str.}]_{exptl}$ is positive increasing with increase in the concentration of 1,4-dioxane and is quite similar to the structural contribution to the shift in TVM of water, not only with respect to sign but even with respect to the magnitude of the structural shift. These results indicate that the structural propensity of 1,4-dioxane remains the same whether the solvent is pure water or aqueous *t*-butyl alcohol in which X_s=0.0075. But, the negative values of the structural shifts when X_s=0.0025 or 0.0046 point out the existence of a complex behavior. It is worthwhile to note here that the structural contribution to the shift in TVM of pure water due to the addition of *t*-butyl alcohol[29] reaches maximum around $X_s \simeq 0.0046$. Beyond this the structural shift decreases with increasing concentration of *t*-butyl alcohol. Hence it may be concluded that when $X_s \simeq 0.0046$ the rate of collapse of the hydrogen bonded clusters due to the addition of 1,4-dioxane may be more than the rate at which water molecules become organized into clusters around 1,4-dioxane molecules leading to the negative values of the structural shifts. But as the concentration of 1,4-dioxane increases, the rate of cluster formation around 1,4-dioxane molecules due to the hydrophobic nature of its methylene groups overtakes the rate of disintegration of the hydrogen bonded clusters. This situation is reflected in the tendency of $[\Delta T_{str.}]_{exptl}$ to become positive as the concentration of 1,4-dioxane increases. When X_s=0.0075, the time average of the structure of aqueous *t*-butyl alcohol resembles that of pure water and free water molecules try to form clusters around 1,4-dioxane and positive structural shifts may be thought of as due to the ordering of water structure owing to the formation of hydrates of dioxane as reported in literature.[18,19,33]

TABLE 3. COMPARISON OF THE SHIFTS PRODUCED IN THE TVM OF WATER DUE TO THE ADDITION OF ORGANIC SOLUTES WITH THE OBSERVED SHIFT IN THE TERNARY SOLUTION, TREATING AQUEOUS BINARY SOLUTIONS AS AQUEOUS

X_D	X_B	$(\Delta T)_{X_D}$ / °C	$(\Delta T)_{X_B}$ / °C	$\Delta T_{calcd} = (\Delta T)_{X_D} + (\Delta T)_{X_B}$ / °C	$\Delta T_{obsd} = T_w - T_{T\ soln}$ / °C
		Water + *t*-Butyl alcohol + 1,4-Dioxane			
		X_s=0.0025			
0.0022	0.00247	1.75±0.4	0.65±0.4	2.40±0.8	4.0±0.4
0.0046	0.00246	3.65±0.4	0.65±0.4	4.30±0.8	7.5±0.4
0.0083	0.00245	6.60±0.4	0.65±0.4	7.25±0.8	10.8±0.4
0.0106	0.00245	8.40±0.4	9.05±0.8	9.05±0.8	11.8±0.4
		X_s=0.0046			
0.0021	0.00459	1.65±0.4	1.2±0.4	2.85±0.8	5.8±0.4
0.0044	0.00458	3.50±0.4	1.2±0.4	4.70±0.8	9.0±0.4
0.0083	0.00456	6.60±0.4	1.2±0.4	7.80±0.8	13.2±0.4
0.0105	0.00455	8.35±0.4	1.2±0.4	9.55±0.8	15.0±0.4
		X_s=0.0075			
0.0022	0.00748	1.75±0.4	8.00±0.4	9.75±0.8	10.0±0.4
0.0042	0.00747	3.35±0.4	7.95±0.4	11.30±0.8	11.7±0.4
0.0083	0.00743	6.60±0.4	7.90±0.4	14.50±0.8	15.7±0.4
0.0101	0.00742	8.05±0.4	7.85±0.4	15.90±0.8	17.2±0.4

X_D: Mole fraction of 1,4-dioxane when aqueous *t*-butyl alcohol is treated as cosolvent of effective molecular weight $M_{B,W}$. X_B: Mole fraction of *t*-butyl alcohol when aqueous 1,4-dioxane is treated as cosolvent of effective molecular weight $M_{D,W}$.

The structural shifts have been evaluated based on the assumption that aqueous *t*-butyl alcohol as seen by 1,4-dioxane is aqueous implying that the cosolvent (aqueous *t*-butyl alcohol) solute (1,4-dioxane) interactions are similar to that of pure solvent (water) and solute. This is true only if the interactions between 1,4-dioxane and *t*-butyl alcohol are negligible when compared with the interaction of 1,4-dioxane with aqueous nature of the solution structure. Even though the parabolic nature of velocity *versus* temperature profile of ternary solutions, as is evident from Figs. 1—3, support the validity of the above contention; we have calculated the shift in TVM of water due to the addition of the two organic solutes (independently) namely 1,4-dioxane and *t*-butyl alcohol to water, ΔT_{calcd}, and a comparison is made with the observed shift, ΔT_{obsd}, (74 °C-T_{exptl} in the ternary solution) to see whether the shift ΔT is additive with respect to them. Our earlier data[30,31] on TVM of aqueous 1,4-dioxane and *t*-butyl alcohol are taken for the evaluation of the shifts corresponding to the concentrations of these solutes in the ternary systems. The shift in TVM of water corresponding to the concentrations of the present study are obtained by least square fitting of the data.[30,31] As per the data presented in Table 3, the agreement between the calculated and observed shifts is quite good in the case of ternary system for which X_s=0.0075. But when X_s=0.0025 or 0.0046 the observed shifts and calculated shifts differ significantly. This disparity may be attributed to the hindrance caused by *t*-butyl alcohol molecules in the formation of hydrates of dioxane or to some enhancement in the structural propensity of both *t*-butyl alcohol and 1,4-dioxane due to the presence of each over the other in destabilizing the three dimensional structure of water. The agreement between the observed and calculated shifts when X_s= 0.0075 clearly indicates that the structure of aqueous *t*-butyl alcohol as seen by 1,4-dioxane is the same as that of pure water. In other words the structural propensity of 1,4-dioxane is unaffected by the presence of *t*-butyl alcohol when its mole fraction is 0.0075. This behavior may be due to the fact that for aqueous *t*-butyl alcohol in which X_s=0.0075, further addition of *t*-butyl alcohol or 1,4-dioxane destabilize the hydrogen bonded clusters and the monomers so formed take part readily in the formation of hydrates of dioxane leading to a positive sign for the structural shifts.

References

1) F. Franks and M. J. Quickendon, *Chem. Commun.*, **1968**, 388.
2) D. N. Glew, H. D. Mak, and N. S. Rath, *Chem. Commun.*, **1968**, 264.
3) E. K. Baumgartner and G. J. Atkinson, *J. Phys. Chem.*, **75**, 2336 (1971).
4) M. J. Blandamer, D. E. Clerke, N. J. Hidden, and M. C. R. Symons, *Trans. Faraday Soc.*, **64**, 2691 (1968).
5) F. Franks and H. T. Smith, *Trans. Faraday Soc.*, **64**, 2962 (1968).
6) G. Wada and S. Umeda, *Bull. Chem. Soc. Jpn.*, **35**, 646 (1962).
7) A. Arnand, L. Avalikian, and J. P. Morel, *J. Chem. Phys.*, **69**, 45 (1972).
8) H. Endo and O. Nomoto, *Bull. Chem. Soc. Jpn.*, **46**, 3004 (1973).
9) N. Manohara Murthy and S. V. Subrahmanyam, *Indian J. Pure Appl. Phys.*, **15**, 485 (1977).
10) K. Tamura, N. Maekawa, and T. Yasunaga, *J. Phys. Chem.*, **81**, 2122 (1977).
11) C. DeVisser, G. Perron, and J. E. Desnoyers, *Can. J. Chem.*, **55**, 856 (1977).
12) R. Kingston and M. C. R. Symons, *J. Chem. Soc., Faraday Trans. 2*, **69**, 978 (1973).
13) D. Oakenfull and D. E. Fenwick, *J. Chem. Soc., Faraday Trans. 1*, **75**, 636 (1979).
14) R. K. Mohanty, T. S. Sharma, S. Subramaniyan, and J. C. Ahluwalia, *Trans. Faraday Soc.*, **67**, 305 (1971).
15) G. L. Bertrand and L. E. Smith, *J. Phys. Chem.*, **74**, 4171 (1970).
16) E. M. Arnett and D. R. Mckelvey, *J. Am. Chem. Soc.*, **87**, 1393 (1965).
17) G. N. Malcolm and J. C. Rowlinson, *Trans. Faraday Soc.*, **53**, 921 (1957).
18) J. R. Goates and R. Sullivan, *J. Phys. Chem.*, **62**, 188 (1958).
19) J. A. Geddes, *J. Am. Chem. Soc.*, **55**, 2264 (1936).
20) C. J. Clement, *J. Chem. Soc., A*, **45**, 458 (1969).
21) O. Kiyohara, G. Perron, and J. E. Desnoyers, *Can. J. Chem.*, **53**, 2591 (1975).
22) A. Fratello and J. P. Luongo, *J. Am. Chem. Soc.*, **85**, 3073 (1963).
23) A. R. Toarky, H. A. Rizk, and Y. M. Girgis, *J. Phys. Chem.*, **65**, 40 (1961).
24) R. K. Mohanty and J. C. Ahluwalia, *J. Solution Chem.*, **1**, 531 (1972).
25) K. Arakawa and N. Takenaka, *Bull. Chem. Soc. Jpn.*, **42**, 5 (1969).
26) R. L. Kay and T. L. Broadwater, *Electrochim. Acta*, **16**, 667 (1971).
27) G. Wada and S. Umeda, *Bull. Chem. Soc. Jpn.*, **35**, 1797 (1962).
28) S. V. Subrahmanyam and N. Manohara Murthy, *J. Solution Chem.*, **4**, 347 (1975).
29) N. Manohara Murthy and S. V. Subrahmanyam, *Bull. Chem. Soc. Jpn.*, **50**, 2589 (1977).
30) N. Manohara Murthy and S. V. Subrahmanyam, *Can. J. Chem.*, **56** 2412 (1978).
31) N. Manohara Murthy and S. V. Subrahmanyam, *Bull. Chem. Soc. Jpn.*, **53**, 1728 (1980).
32) A. Weissberger, "Physical Methods of Organic Chemistry," 2nd ed, Interscience, New York (1955), Vol. VII.
33) G. G. Hammes and W. Knoche, *J. Chem. Phys.*, **45**, 4041 (1964).

Electroreduction of 4-(2-Thienyl)quinazoline in Acetonitrile

T. Priyamvada Devi, Chatty Kalidas, and
Chitoor Sivaramakrishnan Venkatachalam*
Department of Chemistry, Indian Institute of Technology, Madras-600 036, India
(Received February 6, 1981)

The electroreduction of 4-(2-thienyl)quinazoline (4-TQ) in acetonitrile solutions gave a single two-electron well-defined polarographic wave. The well-defined wave was found to be diffusion-controlled and irreversible on the basis of the usual criteria. Based on the controlled-potential electrolysis and cyclic voltammetric experiments, a disproportionation reaction mechanism is suggested for 4-TQ reduction in acetonitrile.

4-(2-Thienyl)quinazoline (4-TQ) possesses some biologically-active properties. It is found to be an analgesic, antiinflammatory, and antipyretic.[1,2] During our detailed electrochemical investigations on the reduction of this compound in amphiprotic[3] (methanol–water mixtures) and dipolar aprotic (*N*,*N*-dimethylformamide)[4,5] media, very interesting results have been obtained. In continuation of this work, we present here the results obtained on the electrochemical behaviour of 4-TQ in acetonitrile.

Experimental

4-(2-Thienyl)quinazoline was prepared according to the literature procedure and its purity tested by mp (65 °C), TLC, IR, and mass spectrometry.[6,7] AR(BDH) tetrabutylammonium iodide (TBAI) was used as supporting electrolyte without further purification. Acetonitrile (S. Merck) was dried by keeping it over heated anhydrous sodium sulfate for a day with intermittent shaking and the clear supernatant liquid was then distilled using all glass assembly in the presence of silver nitrate.[8] The middle fraction boiling at 82 °C was collected and stored in glass vessel painted black.[9] The purified sample had a water content of 0.04% (Karl Fischer titration). The measured specific conductance of the purified acetonitrile sample ($6.0\times10^{-8}\,\Omega^{-1}$ at 25 °C) was found to be in agreement with the reported value.[10] In the present investigation, the purification method outlined above was found to be satisfactory as shown by the absence of polarographic reduction waves in the region of potentials studied. However, in certain cases where the supporting electrolyte polarograms showed appreciable residual currents, a pre-electrolysis[11] of the distilled sample was necessary and it was carried out at a potential which is slightly positive to the decomposition potential of the supporting electrolyte.

The polarographic measurements using a three electrode system were similar to those described previously.[3] The dropping mercury electrode (d.m.e.) used in acetonitrile solution containing 0.1 M TBAI (1 M=1 mol dm^{-3}) supporting electrolyte at 55 cm height of the mercury column (height uncorrected for back pressure) had the following capillary characteristics under open circuit conditions: 'm'= 0.6885 mg s^{-1}; 't'=7.1 s. The details of the cyclic voltammetric (CVM) experiments for 4-TQ reduction using hanging mercury drop electrode (HMDE) and the analysis of cyclic voltammograms for obtaining the kinetic parameters of the electrode process have been described previously.[4] All the measurements were carried out at 25 °C.

Results and Discussion

The d.c. and a.c. polarograms of 4-TQ (1.0×10^{-3} M) obtained in acetonitrile solution containing 0.1 M TBAI supporting electrolyte are shown in Fig. 1 and the corresponding polarographic data are presented in Table 1. It is seen from Fig. 1 that 4-TQ gives a single well-defined d.c. wave and the a.c. polarogram shows a single peak corresponding to the d.c. step. The well-defined wave was found to be diffusion-controlled as indicated by the linearity in the plots passing through the origin of (i) limiting currents *versus* concentration of 4-TQ and (ii) limiting

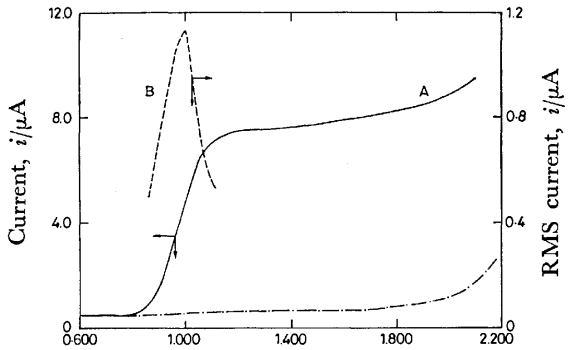

Fig. 1. D.c. Polarogram (A) and a.c. polarogram (B) of 4-TQ (1×10^{-3} M) in acetonitrile containing 0.1 M TBAI.

Table 1. Polarographic data for 4-TQ reduction in acetonitrile solutions

Concentration of 4-TQ $\times10^{-3}$ / M	Limiting current i_l/μA[a]	Half-wave potential, ($-E_{1/2}$ *vs.* silver wire electrode)/V	$-(E_{3/4}-E_{1/4})$/V	Summit potential, ($-E_s$ *vs.* silver wire electrode)/V	Diffusion current constant, I_d[b]	$-dE/d\log\frac{(i_d-i)}{i}$
0.2	1.47	0.960	0.120	0.980	7.24	0.120
0.4	2.95	0.960	0.100	0.980	7.26	0.103
0.6	4.11	0.955	0.100	0.970	6.74	0.108
0.8	5.70	0.945	0.100	0.960	7.01	0.110
1.0	7.14	0.940	0.110	0.960	7.03	0.108

a) Average current. b) Corrected for the change in drop time of the d.m.e. with applied potential.

currents *versus* square root of the height of the mercury column. A slope of 0.50 in the (log i_l—log h) linear plot further confirmed the diffusion-controlled nature of the wave in acetonitrile solutions. The larger values of ($E_{3/4}$—$E_{1/4}$) and the slopes of the logarithmic plots[—E *vs.* log (i_d—i)/i] for different concentrations of 4-TQ indicate irreversible nature of the wave (Table 1). This is further supported by the dependence of half-wave potential on the concentration of 4-TQ. The product of the average corrected diffusion current constant (I_d) and square root of the viscosity of acetonitrile ('η'=0.350 cP), $I_d\eta^{1/2}$ for 4-TQ reduction was calculated to be 4.17. This value is in good agreement with 4.20 reported by Wasa and Elving[12] for a two-electron reduction in acetonitrile.

The total number of electrons (n_{app}) involved in 4-TQ reduction in acetonitrile at the limiting region of the polarographic wave (—1.300 V *vs.* silver wire electrode) was calculated from microscale controlled-potential electrolysis (CPE) experiments[3] and found to be 1.97, 2.03, and 2.00 (accuracy ±0.04), respectively, for three separate experiments. Macroscale CPE experiments were not carried out due to volatility of acetonitrile.

Cyclic voltammograms of 4-TQ obtained at different sweep rates in acetonitrile solutions in the presence of 0.1 M TBAI supporting electrolyte are shown in Fig. 2. The CVM data are presented in Table 2. The cyclic voltammograms show two cathodic peaks in the forward scan and one anodic peak during the reverse scan. The first cathodic peak potential corresponds to the d.c. polarographic step and the anodic peak corresponds to the first cathodic peak. At lower sweep rates (less than 0.05 V s^{-1}, for example, at 0.008 V s^{-1}), the second cathodic and the first anodic peaks are absent and these peaks once again appear with increase in sweep rate (Fig. 2). Although a single well-defined two-electron wave is obtained in acetonitrile a *small* EPR signal observed[13] when 4-TQ in acetonitrile solution was electrolysed at the limiting region of the wave (—1.300 V *vs.* silver wire electrode) indicates single electron addition in the first step. The neutral radical of 4-TQ formed during the reduction undergoes a *fast* disproportionation (secondary) reaction[4] and the average disproportionation rate constant (k_d) in acetonitrile solution was calculated to be (2.14±0.38)×10^{-2} M^{-1} s^{-1} (Table 3). The presence of a fast second-order reaction following the first charge-transfer step is expected

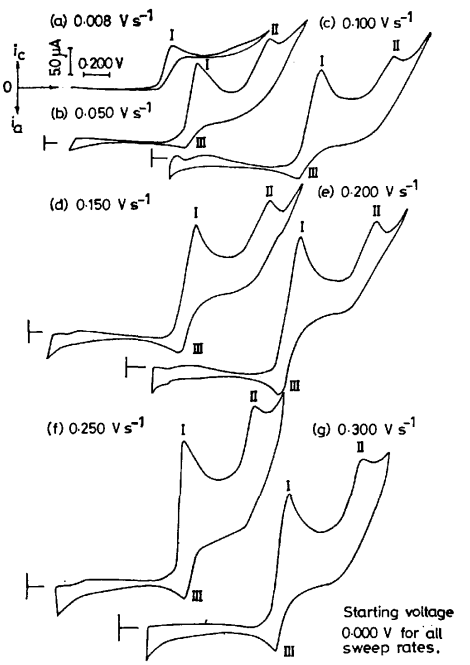

Fig. 2. Cyclic voltammograms for 4-TQ (1.0×10^{-3} M) reduction in acetonitrile containing 0.1 M TBAI at different sweep rates.

Table 2. Cyclic voltammetric data for 4-TQ (1.0×10^{-3} M) reduction in acetonitrile solutions

Sweep rate, v/V s^{-1}	Peak	i_p/μA[a]	Peak potential, (—E_p *vs.* silver wire electrode)/V	$i_p v^{-1/2} C_{ox}^{-1}$ [b]	($E_{p/2}$—E_p)/V
0.050	I	13.75	0.995	61.49	0.065
	II	7.50	1.490	—	—
	III	10.00	0.895	—	—
0.100	I	17.50	1.000	55.34	0.065
	II	8.50	1.495	—	—
	III	14.50	0.900	—	—
0.150	I	20.00	1.000	53.64	0.070
	II	10.25	1.150	—	—
	III	17.25	0.900	—	—
0.200	I	23.75	1.000	53.11	0.070
	II	11.75	1.500	—	—
	III	20.75	0.900	—	—
0.250	I	25.00	1.000	50.00	0.070
	II	12.25	1.510	—	—
	III	22.25	0.905	—	—
0.300	I	25.75	1.005	47.00	0.075
	II	12.75	1.520	—	—
	III	21.25	0.985	—	—

a) Cathodic peak current. b) Current function.

Table 3. Heterogeneous charge-transfer and homogeneous disproportionation rate constants (k_s and k_d, respectively) from cyclic voltammetry

Sweep rate, v/V s^{-1}	E_p [a]	$k_s \times 10^2$ [b] / cm s^{-1}	i_p^a/i_p^c	$\tau=(E_\lambda$ [c] $-E_{1/2})/v$	$-\log k_f C_{ox}\tau$	$k_d \times 10^2$ [d] / M^{-1} s^{-1}
0.050	0.100	0.44	0.727	14.80	0.75	1.60
0.100	0.100	0.63	0.829	7.40	1.01	1.75
0.150	0.100	0.77	0.863	4.93	1.14	2.00
0.200	0.100	0.89	0.874	3.70	1.18	2.40
0.250	0.095	1.02	0.890	2.96	1.25	2.50
0.300	0.120	0.69	0.903	2.47	1.32	2.60
		Average: 0.74±0.18			Average: 2.14±0.38	

a) Difference between the anodic and cathodic peak potentials. b) $k_s=\Psi v^{1/2}/28.8$ cm s^{-1}.[18] c) E_λ is switching potential. d) $k_d=k_f C_{ox}\tau/C_{ox}\tau$ M^{-1} s^{-1}.[19]

to cause a shift in $E_{1/2}$ to positive values with increase in concentration of 4-TQ[14] (Table 1). A comparison of disproportionation rate constants in DMF[4] and acetonitrile solutions shows that in acetonitrile, the disproportionation reaction is about forty times faster than in DMF solutions. The observation of a single two-electron wave obtained under polarographic conditions is thus clear on the basis of a fast disproportionation reaction[15] in acetonitrile.

Mechanism for 4-TQ Reduction (CEC-type) in Acetonitrile. Based on the polarographic and CPE experiments, the following mechanism is suggested for 4-TQ reduction in acetonitrile solution:

$$\text{4-TQ} + H^+ \rightleftharpoons [\text{4-TQH}]^+ \text{ (fast)},$$

$$[\text{4-TQH}]^+ + e \rightleftharpoons [\text{4-TQH}]^\cdot \text{ (first electron-transfer)},$$

$$2[\text{4-TQH}]^\cdot \longrightarrow \text{4-TQH}_2 + \text{4-TQ} \text{ ("fast" homogeneous disproportionation)}.$$

However, it may be pointed out that 4-TQ obtained in the fast homogeneous disproportionation step may undergo again single-electron reduction to give the final dihydro-4-TQ product *via* the free radical formation step. It is quite likely that the formation of the dihydro-4-TQ from 4-TQ radical also takes place through the uptake of a proton and an electron. The pre-protonation of 4-TQ in the suggested mechanism (prior to electron-transfer step) is brought out by the trace amount of water (proton donor) present in acetonitrile[16] and this has been further evidenced by the correlation of EPR results with theoretical Hückel molecular orbital (HMO) calculations.[5] It is also known that acetonitrile solvent itself could donate protons[17] according to the equilibrium, $H_3C-C\equiv N \rightleftharpoons H_2C^{(-)}-C\equiv N+H^{(+)}$, since the conjugate base of acetonitrile is a resonance stabilised species. Mann also refers to the abstraction of protons from tetraalkylammonium ions.[16]

It may be mentioned here that the mechanism suggested for 4-TQ reduction in acetonitrile solutions is similar that encountered in DMF solutions.[4]

References

1) A. Albert, R. Goldaire, and J. Phillips, *J. Chem. Soc.*, **1948**, 2240.
2) A. Albert and J. Phillips, *J. Chem. Soc.*, **1956**, 1294.
3) G. Antony, T. Priyamvada Devi, M. Srinivasan, and C. S. Venkatachalam, *Trans. S. A. E. S. T.*, **14**, 213 (1979).
4) T. Priyamvada Devi, C. Kalidas, and C. S. Venkatachalam, *J. Electroanal. Chem.*, **113**, 285 (1980).
5) T. Priyamvada Devi, M. S. Gopinathan, and C. S. Venkatachalam, *Electrochim. Acta*, **25**, 1173 (1980).
6) M. Srinivasan and J. B. Rampal, *Tetrahedron Lett.*, **1973**, 2883.
7) M. Srinivasan and J. B. Rampal, *J. Sul. Phos.*, **2**, 105 (1976).
8) E. S. Jayadevappa, *Ind. J. Chem.*, **7**, 1146 (1969).
9) W. S. Muney and J. F. Coetzee, *J. Phys. Chem.*, **66**, 89 (1962).
10) O. Hans, *Chem. Abstr.*, **73**, 120668 (1970).
11) J. N. Butler, "Advances in Electrochemistry and Electrochemical Engineering," ed by P. Delahay and C. W. Tobias, Interscience, New York (1970), Vol. 7, p. 158.
12) T. Wasa and P. J. Elving, *J. Electroanal. Chem.*, **91**, 249 (1978).
13) T. Priyamvada Devi, Ph. D. Thesis, Indian Institute of Technology, Madras, 1980.
14) J. Koutecky and V. Hanus, *Collect. Czech. Chem. Commun.*, **20**, 124 (1955).
15) H. L. Strauss, T. J. Katz, and G. K. Fraenkel, *J. Am. Chem. Soc.*, **85**, 2360 (1980).
16) C. K. Mann and K. K. Barnes, "Electrochemical Reactions in Non-aqueous Systems," Marcel Dekker, New York (1970), Chap. 1.
17) J. E. Harriman and A. H. Maki, *J. Chem. Phys.*, **39**, 778 (1963).
18) R. S. Nicholson, *Anal. Chem.*, **37**, 1351 (1965).
19) M. L. Ohmstead and R. S. Nicholson, *Anal. Chem.*, **41**, 862 (1969).

 © 1982 The Chemical Society of Japan Bull. Chem. Soc. Jpn., 55, 289—292 (1982)

Kinetics and Mechanism of the Oxidation of (Substituted Phenylthio)acetic Acids by Chloramine T

Chockalingam SRINIVASAN* and Kasi PITCHUMANI
School of Chemistry, Madurai Kamaraj University, Madurai 625 021, India
(Received February 20, 1981)

The kinetics of oxidation of (phenylthio)acetic acid and several (para-substituted phenylthio)acetic acids by chloramine T has been studied in alkaline medium (pH 10.06). A first-order dependence in chloramine T and (phenylthio)acetic acid and a near inverse first-order dependence in hydroxide ion has been observed. The oxidation rate considerably decreases with increase of pH. The reaction exhibits positive salt effect and added *p*-toluenesulfonamide increases the rate. The oxidation process has been shown to proceed *via* two paths, the major path involving *N*-chloro-*p*-toluenesulfonamide as the main oxidizing species and the other involving hypochlorite ion. Studies with (para-substituted phenylthio)acetic acids show an excellent correlation of the rate constants with σ constants. The reaction exhibits a reaction constant ρ of -2.46 at 308 K ($r=0.998$, $s=0.05$, confidence limit on $\rho \pm 0.15$). The activation parameters and isokinetic temperature have been determined.

Chloramine T (CAT) is a strong oxidant in both acidic and alkaline media. Its redox potential varies with the pH of the medium (E_{red} 1.138 V at pH 0.65 and 0.5 V at pH 12).[1] The reactions of several organic compounds[2] with CAT have been reviewed. A wide range of alkyl and aryl sulfides[2,3] yield the corresponding sulfimides and sulfoxides with CAT. Vasudeva Murthy and co-workers[4] have reported the oxidation of some acyclic sulfur compounds and also some phosphorus-sulfur compounds. However, the detailed kinetics of the reaction of several dialkyl, alkyl aryl, and diaryl sulfides with CAT (Mann-Pope reaction) were investigated in buffered water–ethanol solution by Kucsman and co-workers[5,6] and a mechanism has been proposed on the basis of kinetic measurements and product analysis. Oxidation of (phenylthio)acetic acid by sodium salt of *N*-chlorobenzenesulfonamide[7] yields (phenylsulfinyl)acetic acid. However, an abnormal reaction was encountered[8] when CAT reacted with sodium salt of (phenylthio)acetic acid, affording not the sulfimide, but the *N*-(*p*-tolylsulfonyl)benzenesulfimidic *p*-tolylsulfonylamide (**1**).

$$C_6H_5SCH_2COO^- \xrightarrow{CAT} C_6H_5-\underset{\underset{NTs}{\|}}{S}-NHTs$$

1

During the course of our detailed studies on the kinetics of oxidation of organic sulfur compounds by several oxidants, we have recently reported the kinetics of the reaction of (substituted phenylthio)acetic acids with peroxodisulfate.[9] In this paper we report the results of the kinetic investigations of the oxidation of (substituted phenylthio)acetic acids by CAT in alkaline medium.

Experimental

Materials. Chloramine T from May & Baker which was pure as found by iodometric method, was used as such and its aqueous solution was stored in black coated vessels to prevent its photochemical deterioration. (Substituted phenylthio)acetic acids were prepared by standard procedures.[9] All other reagents were of AnalaR grade. Equimolar amounts of (phenylthio)acetic acids and potassium hydroxide were dissolved and used in kinetic runs. Sodium hydrogencarbonate–sodium carbonate buffer was used to maintain the pH. Measurements of the pH were carried out using a digital pH meter (pH 5651, Electronic corporation of India Limited).

Kinetics. Kinetic studies were carried out in sodium hydrogencarbonate–sodium carbonate aqueous buffer (pH 10.06 unless mentioned otherwise) under pseudo first-order conditions with the substrate and oxidant concentrations in the ratio of 10:1. The reaction was followed by estimating the unconsumed CAT iodometrically.[10] Aliquots (5 ml) of the reaction mixture were quickly transferred at regular intervals of time to iodine flasks containing five ml of 2 M (1 M=1 mol dm^{-3}) hydrochloric acid and 10 ml of 10% aqueous solution of potassium iodide. Unconsumed CAT liberated an equivalent amount of iodine and the latter was estimated by standard sodium thiosulfate solution using starch as indicator.

Reactions were generally followed to 70—80% completion; reproducible results giving good first-order plots ($r>0.995$) were obtained for reactions run in duplicate. The kinetic constants, k_ψ, were calculated by the method of least squares using a Micro 2200 computer (Hindustan Computers Limited). The precision of k values is given in terms of 95% confidence limit calculated with 'student t'. From the k_ψ values, the second-order rate constants were obtained ($k=k_\psi/$[substrate]).

Stoichiometry. The reaction stoichiometry was found to be 1:1 by allowing an excess of CAT to react with (phenylthio)acetic acid overnight and estimating the unreacted CAT.

Product Analysis. The product of the reaction was found to be (phenylsulfinyl)acetic acid. A thin layer chromatography (silica gel) analysis of the reaction mixture developed in a solvent system of butanol–water–acetic acid (4:5:1—upper layer) gave two spots corresponding to (phenylthio)acetic acid (R_f 0.84) and (phenylsulfinyl)acetic acid (R_f 0.45) respectively. IR spectrum of the product separated from the reaction mixture shows an intense absorption band at 1050 cm^{-1} characteristic of SO stretching in (phenylsulfinyl)acetic acid and the IR spectrum is superimposable with that of an authentic sample of (phenylsulfinyl)acetic acid. The overall reaction in the oxidation is given by Eq. 2.

$$C_6H_5SCH_2COO^- + TsNCl^- + H_2O \longrightarrow C_6H_5SOCH_2COO^- + TsNH_2 + Cl^- \quad (2)$$

In an earlier work,[8] the product of the reaction between sodium salt of (phenylthio)acetic acid and CAT was found to be **1**. The authors obtained **1** (yield<10%) when a large excess of CAT was employed and also by heating the

mixture on a steam bath for 30 min. In our kinetic conditions, the substrate was taken in large excess and hence the (phenylsulfinyl)acetic acid formed did not undergo further reaction. It may be noted here that the oxidation of (phenylthio)acetic acid by sodium salt of *N*-chlorobenzenesulfonamide[7] yields the corresponding sulfoxide.

Results and Discussion

Kinetic data were obtained for all the (phenylthio)-acetic acids investigated, but as the results are similar, only those of (phenylthio)acetic acid (PTAA) are presented in detail.

The reaction exhibits a clean first-order kinetics with respect to CAT as evidenced by good first-order linear plots for the disappearance of CAT. The order with respect to PTAA is also one as demonstrated by the constant numerical values of k in Table 1 and also by the good linear plot of log k_ϕ *versus* log[PTAA] with a slope of 0.98±0.05 (r=0.999, s=0.01). Further a plot of k_ϕ *versus* [PTAA] gave a good straight line passing through the origin indicating the absence of any substrate independent path and the second-order nature of the reaction.

There is a slight increase in rate with an increase in [CAT]. Since a positive salt effect has been observed in the oxidation, the increase in rate with [CAT] has been accounted for by the reaction between the (phenylthio)acetate and hypochlorite ions. (*cf.* mechanism).

Dependence of pH. The oxidation is highly susceptible to changes in pH of the medium (Table 2). An increase in pH considerably retarded the rate. A plot of log k against pH gave a straight line (slope= −0.93±0.09, r=0.999, s=0.04) indicating a near inverse first-order dependence on hydroxide ion concentration.

Table 1. Dependence of rate on initial concentration of reactants[a]

10^3[CAT] / mol dm^{-3}	10^2[PTAA] / mol dm^{-3}	$10^5 k_\phi$[b] / s^{-1}	$10^3 k$[b] / dm^3 mol^{-1} s^{-1}
1.0	1.0	16.6±0.37	16.6±0.37
1.0	1.4	23.4±0.39	16.7±0.28
1.0	2.0	32.1±0.96	16.1±0.48
1.0	2.5	40.8±1.07	16.3±0.43
1.0	3.0	49.1±1.40	16.4±0.47
0.5	2.5	39.1±1.98	15.6±0.79
1.5	2.5	43.1±1.58	17.2±0.63
2.0	2.5	45.4±1.30	18.2±0.52
2.5	2.5	45.8±1.07	18.3±0.43

a) In aqueous buffer, at 308 K and pH=10.06. b) The error quoted in k is the 95% confidence limit of the 'student t'.

Effect of Salt Concentration. The rate constant for the oxidation of PTAA by CAT at different concentrations of sodium perchlorate and potassium chloride have been determined (Table 3). Though there is a positive salt effect, the presence of chloride ion has no specific effect on the rate of oxidation.

Effect of p-*Toluenesulfonamide.* Addition of *p*-toluenesulfonamide causes a slight increase in the rate of oxidation (Table 4).

Activation Parameters. The rate constants were determined at three temperatures for the oxidation of PTAA by CAT and the data fit the Arrhenius and Eyring equations. The activation parameters are given in Table 5 along with those for (substituted phenylthio)acetic acids. The reaction is characterized by a low enthalpy of activation and an appreciable negative entropy of activation implying that the activated complex should have an exacting specificity of orientation. Ruff and Kucsman[5] report than the enthalpy and entropy of activations are 41.0 kJ mol^{-1} and −79.1 J K^{-1} mol^{-1} for the reaction of TsNHCl (active species of CAT) with methyl phenyl sulfide.

Mechanism and Rate Law. An aqueous solution of CAT undergoes hydrolysis giving a variety of products, the relative amounts of which depend on the pH of the solution. Thus the oxidizing species

$$TsNNaCl + H_2O \rightleftharpoons TsNHCl + NaOH \quad (3)$$

$$TsNHCl + NaOH \rightleftharpoons TsNH_2 + Na^+ + ClO^- \quad (4)$$

$$2TsNHCl \rightleftharpoons TsNCl_2 + TsNH_2 \quad (5)$$

$$TsNCl_2 + NaOH \rightleftharpoons TsNHCl + Na^+ + ClO^- \quad (6)$$

of CAT are dichloramine T ($TsNCl_2$), *N*-chloro-*p*-toluenesulfonamide (TsNHCl), hypochlorite ion (ClO^-) and CAT itself. One of the above will be the main oxidizing species and their reactivities[5] should follow the order $TsNCl_2 > TsNHCl > ClO^- > CAT$.

In an alkaline medium dichloramine T does not exist (Eq. 6, the equilibrium will be more towards TsNHCl). Higuchi and Hussain[11] have already concluded that only in the pH range 6.35—6.85 the formation of dichloramine T is significant. Further, a second-order dependence of rate on CAT is predicted if dichloramine T is assumed to be the active species. The observed first-order dependence on CAT in the oxidation of PTAA clearly points out that dichloramine T is not the active oxidizing species. Since an increase in hydroxide ion concentration (or pH) decreases the rate of oxidation (Table 2 and Eq. 4), it has to be concluded that TsNHCl is the main oxidizing species of CAT in the oxidation of PTAA. This conclusion gains further support from the observation that addition of *p*-toluenesulfonamide increases the rate (Table 5). Addition of $TsNH_2$ shifts the equilibrium (4) towards the left which results in the increased formation of TsNHCl and hence

Table 2. Dependence of the reaction rate on pH[a]

pH	8.980	9.570	10.06	10.48	10.75
$10^3 k$ / dm^3 mol^{-1} s^{-1}	174±2.5	45.4±1.5	16.6±0.37	7.73±0.07	3.59±0.07

a) In aqueous buffer, at 308 K, [CAT]=0.001 M and [PTAA]=0.01 M.

the enhanced rate becomes understandable.

On the basis of the experimental data discussed earlier, the following mechanism has been suggested:

$$TsNNaCl + H_2O \underset{k_{-1}}{\overset{k_1}{\rightleftharpoons}} TsNHCl + NaOH, \quad (3)$$

$$TsNHCl + C_6H_5SCH_2COO^- \xrightarrow[\text{slow}]{k_2}$$

$$\left[TsNH^- \overset{+}{S}\overset{C_6H_5}{\underset{CH_2COO^-}{Cl}} \right], \quad (7)$$

2

$$\mathbf{2} \xrightarrow{\text{fast}} TsNH^- + \overset{+}{S}\overset{C_6H_5}{\underset{CH_2COO^-}{Cl}} \xrightarrow[\text{fast}]{H_2O}$$

$$C_6H_5SOCH_2COO^- + TsNH_2 + HCl. \quad (8)$$

Application of steady state treatment for TsNHCl with a reasonable approximation that $k_{-1}[NaOH] \gg k_2[C_6H_5SCH_2COO^-]$ yields the rate law as

$$\frac{-d[CAT]}{dt} = \frac{k_1k_2[CAT][C_6H_5SCH_2COO^-]}{k_{-1}[NaOH]} = \frac{k'[CAT][C_6H_5SCH_2COO^-]}{[NaOH]}, \quad (9)$$

where $k' = k_1 k_2/k_{-1}$. At constant[NaOH] or pH,

$$\frac{-d[CAT]}{dt} = k''[CAT][C_6H_5SCH_2COO^-]. \quad (10)$$

Thus the proposed mechanism involves the intermediate **2** formed by the reaction between (phenylthio)acetate ion and TsNHCl and the subsequent disintegration of **2** in a fast step to give the products.

The kinetic studies discussed above clearly demonstrate that under our experimental conditions, TsNHCl is the main oxidizing species of CAT. However, the following observations are not accounted for by the above mechanism: i) a small positive salt effect implying a small fraction of the reaction between ions of the same charge and ii) deviation of order in hydroxide ion concentration from −1. Hence it is proposed that a small fraction of the overall reaction proceeds *via* the formation of ClO^- (Eqs. 11 and 12). It is worth mentioning here that though the reaction is carried out under alkaline conditions, the generation of ClO^- is only small since i) ClO^- is generated from TsNHCl which is very reactive and ii) the relative order of reactivity is found[5] to be $TsNCl_2 > TsNHCl > ClO^- > TsNCl^-$.

$$C_6H_5SCH_2COO^- + ClO^- \xrightarrow[\text{slow}]{k_2'} C_6H_5SOCH_2COO^- + Cl^-, \quad (11)$$

$$C_6H_5SCH_2COO^- + ClO^- + H_2O \xrightarrow[\text{slow}]{k_2'} C_6H_5SOCH_2COO^- + HCl + OH^-, \quad (12)$$

Table 3. Effect of salt concentration on the reaotion rate[a]

Salt concentration / mol dm^{-3}	$10^3 k$ / dm^3 mol^{-1} s^{-1}	
	$NaClO_4$	KCl
0.00	16.6±0.37	16.6±0.37
0.10	19.6±0.34	18.9±0.57
0.20	22.9±0.52	20.7±0.83
0.30	27.2±1.12	21.7±0.49
0.40	31.7±0.99	22.7±0.52

a) In aqueous buffer, at 308 K, [CAT]=0.001 M, [PTAA]=0.01 M and pH=10.06.

Table 4. Influence of *p*-toluenesulfonamide on the reaction rate[a]

10^3[TSA] / mol dm^{-3}	0.00	2.00	4.00	10.0	15.0
$10^3 k$ / dm^3 mol^{-1} s^{-1}	16.6±0.37	18.0±0.26	17.8±0.47	19.0±0.34	18.9±0.79

a) In aqueous buffer at 308 K, [CAT]=0.001 M, [PTAA]=0.01 M, and pH=10.06.

Table 5. Second-order rate constants and enthalpies and entropies of activation for the oxidation of (substituted phenylthio)acetic acids by CAT[a]

Substituent	$10^3 k$ / dm^3 mol^{-1} s^{-1}			ΔH^* [b] / kJ mol^{-1}	ΔS^* [b] / J K^{-1} mol^{-1}
	303 K	308 K	313 K		
H	13.1±0.21	16.6±0.37	20.9±0.46	34.4±3.7	168±12
p-OMe	73.9±1.96	92.2±2.90	112 ±2.79	30.7±5.0	166±17
p-Me	44.9±0.77	57.9±1.22	74.0±1.12	37.0±3.2	149±11
p-Pr^i	37.4±1.02	46.0±1.78	58.2±1.04	32.5±5.1	166±17
p-Cl	4.75±0.18	6.15±0.08	8.09±0.29	39.7±5.2	159±17
p-Br	3.88±0.06	5.26±0.10	6.83±0.12	42.3±3.1	152±10
p-I	4.63±0.10	6.06±0.12	7.73±0.10	38.0±3.3	165±11
p-NO_2	0.18±0.01	0.25±0.01	0.30±0.02	36.2±7.5	160±25

a) In aqueous buffer, at [CAT]=0.001 M, [substrate]=0.01 M, and pH=10.06. b) The precision of ΔH^* and ΔS^* values were calculated using the method of Petersen *et al.*[15]

leading to the rate law

$$\frac{-\mathrm{d[CAT]}}{\mathrm{d}t} = k'''[\mathrm{CAT}][\mathrm{C_6H_5SCH_2COO^-}]. \quad (13)$$

Rate law (9) predicts an inverse first-order dependence in [NaOH] and rate law (13) suggests a zero-order dependence in [NaOH]. The net outcome of these two satisfactorily accounts for the fractional inverse order in [NaOH].

Substituent Effects. Since an analysis of the substituent effects can give more informations about the nature of the transition state and thereby the mechanism, kinetic studies were carried out with a number of (para-substituted phenylthio)acetic acids at three temperatures. The second-order rate constants and the activation parameters are presented in Table 5. The rate constants fit the simple Hammett equation at all the three temperatures. The reaction constant, ρ, at 308 K is -2.46 ($r=0.998$, $s=0.05$, confidence limit on $\rho \pm 0.15$). The marked negative value of ρ shows that electron-donating groups cause a considerable increase in the reactivity of $XC_6H_5SCH_2COO^-$ with CAT. This is consistent with a significant positive polarity of the sulfur atom in the transition state. It may be mentioned here that Ruff and Kucsman[5] observed a value of -4.25 as the reaction constant for the reaction of $XC_6H_5SCH_3$ with TsNHCl wherein a chlorosulfonium ion intermediate has been postulated and Miotti, Modena, and Sedea[12] have reported a ρ value of -3.2 for the oxidation of $XC_6H_5SCH_3$ with bromine proceeding *via* a bromosulfonium ion intermediate. Hence the large negative value obtained with (phenylthio)acetic acids justifies the assumption of the intermediate **2**. It is interesting to note here that, in contrast with the excellent correlation with σ in the reaction of (phenylthio)acetic acids with CAT, in the reactions of (phenylthio)acetic acids with peroxodisulfate[9] and peroxodiphosphate[13] (acetic acid medium) better correlations are observed only when σ^+ values are employed. This may be due to the fact that in CAT oxidations, (phenylthio)acetic acids are present as their anions in which the resonance interaction of the substituents with the reaction site would be small.

Thus the results of the oxidation of (phenylthio)-acetic acid by CAT may be interpreted as a two process reaction, the predominating path involving *N*-chloro-*p*-toluenesulfonamide as the oxidizing species and a small path involving hypochlorite ion as the oxidizing species.

From Table 5, it becomes evident that these oxidation reaction is of isoentropic type. Thus changes in rate are caused chiefly by changes in ΔH^* when ΔS^* is substantially constant. Many reaction series that follow the Hammett $\rho\sigma$ relationship falls within this category. However, the isokinetic temperature is found to be -116 K for the reaction series by the method of Exner.[14]

We thank Prof. N. Arumugam for helpful discussion, Prof. N. R. Subbaratnam for his interest in this work and CSIR, New Delhi for the award of a Senior fellowship to one of us (K.P.).

References

1) A. R. V. Murthy and V. S. Rao, *Proc. Indian Acad. Sci.*, **35A**, 69 (1952); M. C. Agarwal and S. P. Mushran, *Z. Naturforsch. Teil B*, **27**, 401 (1972).

2) M. M. Campbell and C. Johnson, *Chem. Rev.*, **78**, 65 (1978).

3) K. Tsujihara, N. Furukawa, K. Oae, and S. Oae, *Bull. Chem. Soc. Jpn.*, **42**, 2631 (1969).

4) D. K. Padma, R. A. Shaw, A. R. V. Murthy, and M. Woods, *Int. J. Sulfur Chem., A*, **1**, 243 (1971); D. K. Padma, R. A. Shaw, C. P. Thakur, A. R. V. Murthy, and M. Woods, *Phosphorus*, **2**, 81 (1972).

5) F. Ruff and A. Kucsman, *J. Chem. Soc., Perkin Trans. 2*, **1975**, 509; F. Ruff, I. Kapovits, J. Rabai, and A. Kucsman, *Tetrahedron*, **34**, 2767 (1978).

6) A. Kucsman, I. Kapovits, and B. Tanacs, *Tetrahedron*, **18**, 79 (1962).

7) A. Tanager, *Arkiv Kemi. Mineral Geol.*, **24A**, 18 (1947).

8) J. Holloway, J. Kenyon, and H. Phillips, *J. Chem. Soc.*, **1928**, 3000; S. G. Clarke, J. Kenyon, and H. Phillips, *J. Chem. Soc.*, **1927**, 188; **1930**, 1225.

9) C. Srinivasan and K. Pitchumani, *Indian J. Chem.*, **17A**, 162 (1979).

10) A. Kumar, A. K. Bose, and S. P. Mushran, *J. Indian Chem. Soc.*, **13**, 755 (1976).

11) T. Higuchi and A. Hussain, *J. Chem. Soc., B*, **1967**, 549.

12) U. Miotti, G. Modena, and L. Sedea, *J. Chem. Soc., B*, **1970**, 802.

13) In the oxidation of (phenylthio)acetic acids by peroxodiphosphate ion, a better correlation of the rate data with σ^+ ($r=0.998$, $s=0.02$ at 40 °C) has been observed.

14) O. Exner, *Nature*, **201**, 488 (1964); *Coll. Czech. Chem. Commun.*, **29**, 1094 (1964).

15) R. C. Petersen, J. H. Markgraf, and S. D. Ross, *J. Am. Chem. Soc.*, **83**, 3819 (1961).

Conductometric Study of Ion-Ion and Ion-Solvent Interactions. III.† Conductances of Silver Acetate in Acetonitrile–Water Mixtures at 25 °C

U. G. Krishnam Raju, Bangalore Sethuram, and T. Navaneeth Rao*
Department of Chemistry, Osmania University, Hyderabad-500 007, India
(Received March 7, 1981)

Conductances of the solutions of silver acetate in 10 to 90% (w/w) acetonitrile–water mixtures were measured at 25 °C. The molar conductances at infinite dilution and association constants were calculated, using the Fuoss-Hsia equation with Fernandez-Prini coefficients. There was no association in 10 and 20% acetonitrile. The log K_A *vs.* $1/D$ plot was a straight line with negative intercept in accordance with the modified Denison-Ramsey theory of ion-pair formation. Walden products were also calculated. From these results it was concluded that silver ions are preferentially solvated by acetonitrile whereas acetate ion is hydrated in acetonitrile–water mixtures.

Existing literature indicates that in aqueous solutions of alkali metal halides ion-association increases from lithium to caesium whereas in solutions of their acetates, hydroxides and fluorides a reverse trend is observed *i.e.*, ion-association increases from caesium to lithium.[1] Eventhough ion-pair formation in solutions of alkali metal halides and halides of small metal ions have been extensively investigated[2] both in aqueous and aquo-organic solvents, such studies on acetates[3] of small metal ions are sporadic. The extended Fuoss-Hsia equation[4] with Fernandez-Prini coefficients,[5] which is based on the hard spheres model can be used for the analysis of the conductance data. A number of papers have been published by Lee and Wheaton[6] and Fuoss[7] proposing different models for ion-pair formation and new conductance equations. Beronius[8] comments that these equations based on solvent separated as well as contact ion-pairs are not exceptions to the Fuoss-Hsia conductance equation as they yield identical association constants when the values are above 15. Therefore in the present investigation, the electrical conductances of silver acetate in 10, 20, 40, 60, 80, and 90% (w/w) acetonitrile–water mixtures at 25 °C were measured and analysed using the Fuoss-Hsia equation[4] with Fernandez-Prini coefficients[5] with a view to calculate the association constants. The applicability of various theories of ion-pair formation such as those of Bjerrum,[9] Fuoss,[10] Denison-Ramsey (DR),[11] and Ebeling-Kraeft-Yokoyama-Yamatera(EKYY)[12,13] has also been discussed. The Walden products were calculated and the possible ion-solvent interactions were also discussed.

Experimental

Silver acetate (Fluka:Purum) was used after repeated recrystallisations from ethanol and drying. Acetonitrile (BDH) was purified as described by Vogel[14] and had a specific conductance of less than 1.0×10^{-7} S cm^{-1}. Water with a specific conductance less than 5.0×10^{-7} S cm^{-1} was used. Due correction was made for the solvent contribution to the conductance values of all the salt solutions. All the solutions were prepared freshly just before use and protected from light by covering the reaction vessel with a thick dark cloth. The experimental arrangement was the same as reported earlier.[15] The overall accuracy of the measured molar conductances was better than ±0.05%.

† Part II: *Rev. Roum. Chim.* (Communicated).

Results and Discussion

The molar conductances of the solutions of silver acetate in 10, 20, 40, 60, 80, and 90% (w/w) acetonitrile–water mixtures at 25 °C are given in Table 1. The dielectric constants and viscosities of the solvent mixtures were taken from literature.[16]

The conductance data was analysed using the Fuoss-Hsia equation[4] with Fernandez-Prini coefficients[5]

$$\Lambda = \Lambda_0 - s(\propto c)^{1/2} + E \propto c \ln(\propto c) + J_1 \propto c - J_2(\propto c)^{3/2} - K_A \Lambda y_\pm^2 \propto c, \quad (1)$$

where the various symbols have their usual significance. The activity coefficients ($y_\pm$) were calculated by the equation

$$-\log y_\pm = A(\propto c)^{1/2}/\{1+Ba(\propto c)^{1/2}\}. \quad (2)$$

Equation 1 was solved as originally described by Justice.[17] This procedure envisages the replacement of the distance of closest approach of ions (a) by the Bjerrum critical distance (q) term. The standard deviation (σ) values were calculated from the relation

$$\sigma = \{\Sigma(\Lambda_{exp}-\Lambda_{cal})^2/(N-3)\}^{1/2}. \quad (3)$$

All these calculations were carried out on a TDC-12 computer and the results are given in Table 2.

The functional dependence of log K_A *vs.* $1/D$ was used to test the applicability of various theories of ion-pair formation. Figure 1 shows that the association constants of silver acetate in water is very high and far off from the values in the other solvent mixtures. It is observed that there is no association in 10 and 20% acetonitrile–water mixtures. Strechlow and Koepp[18] have shown that silver ions are preferentially solvated by acetonitrile molecules than water. The solubility of silver acetate is more in acetonitrile–water mixtures than in pure solvents. Further the solubility is least in pure acetonitrile. This could be due to the non-solvation of acetate ion in acetonitrile. When small amounts of acetonitrile were added to aqueous solutions of silver acetate, Ag^+ ion gets heavily solvated by acetonitrile and prevents the acetate ions from reaching the Ag^+ ions so that no association could be found in 10 and 20% acetonitrile–water

Table 1. Conductances of silver acetate in acetonitrile-water mixtures at 25 °C

$10^5 c$ / mol dm^{-3}	S cm^2 mol^{-1}	$10^5 c$ / mol dm^{-3}	S cm^2 mol^{-1}
10% Acetonitrile		20% Acetonitrile	
649.41	69.688	950.06	66.120
556.64	69.875	814.33	66.441
487.06	69.984	712.54	66.676
389.65	70.256	570.03	66.990
324.71	70.354	475.03	67.307
278.32	70.352	415.65	67.566
243.53	70.536	332.52	67.714
194.82	70.648	277.10	67.930
162.35	70.726	237.51	68.096
139.16	70.790	207.82	68.195
121.76	70.847	166.26	68.423
97.410	70.904	138.53	68.574
81.180	70.941	103.91	68.755
65.820	70.959	83.130	68.898
		71.660	69.024
40% Acetonitrile		60% Acetonitrile	
708.42	70.993	940.57	75.806
566.74	71.913	806.20	76.886
472.28	72.516	705.42	77.880
404.81	73.145	564.34	79.367
354.21	73.606	470.29	80.313
283.37	74.216	403.10	81.094
257.61	74.563	352.71	81.722
220.81	74.847	282.17	82.814
192.25	75.180	235.14	83.556
154.57	75.638	201.55	84.118
128.80	76.035	176.36	84.642
110.40	76.240	141.09	85.322
96.600	76.559	117.57	85.797
85.870	76.747	88.180	86.558
64.400	77.087	75.050	86.907
80% Acetonitrile		90% Acetonitrile	
940.20	86.643	689.95	72.300
806.20	88.584	591.39	74.140
705.42	90.206	517.46	75.869
564.34	92.659	413.97	78.669
470.29	93.617	344.98	80.631
403.10	95.886	295.69	81.883
352.71	96.989	258.73	83.009
282.17	98.819	206.99	84.899
235.14	100.05	172.49	86.297
201.55	101.12	147.85	87.289
176.36	102.10	129.37	88.219
141.09	103.14	103.49	89.398
117.57	104.16	86.240	90.330
88.160	105.41	67.080	91.630
75.050	106.97	54.880	92.212

mixtures. At higher percentages of acetonitrile, the decrease in the dielectric constant dominates the solvation and hence association is observed from 40% acetonitrile onwards. Leaving the K_A value for water the rest of the values at 40, 60, 80, and 90% acetonitrile exhibit a good linear trend, (drawn as a chained line in Fig. 1) with a correlation coefficient of 0.999. The linearity of the plot suggests the applicability of either DR theory or Fuoss theory excluding Bjerrum and EKYY theories from consideration. From the slope and intercept values of the log K_A *vs.* $1/D$ plot, the relative merits of the DR and Fuoss theories can be elucidated. Both DR and Fuoss theories predict the same slope *i.e.*, $|Z_+Z_-|e^2/(2.303\,akT)=96.23$ whereas the experimentally obtained line is having a slope of 109.33 and intercept −1.1472. But DR theory predicts zero intercept and Fuoss theory predicts log $(4\pi Na^3/3000)$ as intercept. Equating the experimental slope of 109.33 to $|Z_+Z_-|e^2/(2.303\,akT)$ the average ion-size parameter (a) for silver acetate in these solvents was obtained as 2.23 Å. However, when experimentally obtained intercept was equated to $3\log a+\log(4\pi N/3000)$, the '$a$' value calculated form there had a value 3.05 Å. Thus Fuoss theory predicts contradictory and different 'a' values of 2.23 Å and 3.05 Å from the slope and intercept values respectively of the same plot for the same ion-pair studied. On the other hand the finite value of the intercept could be accommodated by the modified DR expression

$$K_A = K_A^\circ \exp(|Z_+Z_-|e^2/aDkT). \quad (4)$$

Table 2. Association parameters for silver acetate obtained using Fuoss-Hsia equation in acetonitrile-water mixtures for $a=q$ at 25 °C

Solvent	Λ_0	K_A	σ
Water[a)]	102.4	32.90	0.304
40% AN	79.75	4.347	0.054
60% AN	91.24	10.17	0.077
80% AN	113.7	25.43	0.338
90% AN	100.2	43.76	0.335

a) Ref. 20.

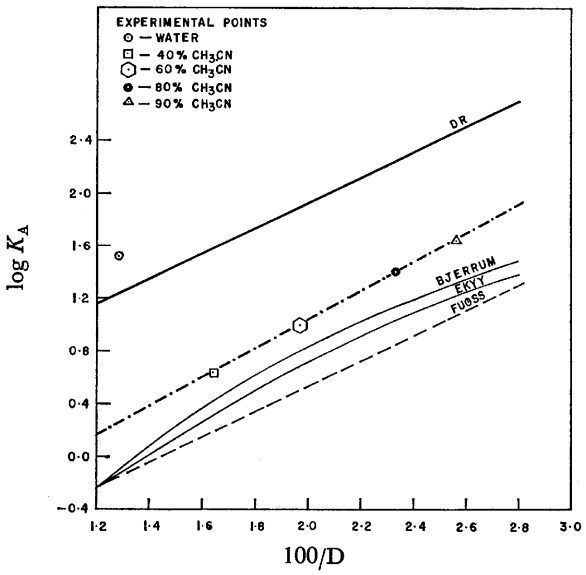

Fig. 1.

The experimental results could be fitted into this expression as

$$\log K_A = -1.1472 + 109.33/D, \quad (5)$$

$$\text{or } K_A = 0.0713 \exp(251.7/D), \quad (6)$$

and $a = 2.23$ Å.

This is slightly less (≈12%) than the crystallographic value of 2.53 Å (The ionic radius of Ag^+ is 1.26 Å and the effective radius of CH_3COO^- is 1.27 Å). Similar results are reported in the literature.[19] Bodenseh and Ramsey[19] reported that the 'a' value for tetrapropylammonium bromide obtained from the slope of the straight line of the plot of log K_A *vs.* $1/D$ was approximately 17% less than the corresponding minimum distance in the crystals. These deviations may be due to the fact that each ion in an isolated ion-pair whether in solution or in the vapour state is bound or coordinated with only one ion of opposite charge whereas in the crystalline state it will be coordinated with more than one oppositely charged ions. This explanation conforms to the fact that the smaller the number of nearest neighbours of oppositely charged associated ions in the crystal, the smaller will be the minimum distance between the oppositely charged ions in the salt. Figure 1 also shows the theoretical log K_A *vs.* $1/D$ plots corresponding to Bjerrum, Fuoss, DR, and EKYY theories using a=2.53 Å.

The ion-size parameter (a) values required by different theories to predict the experimental K_A values are compared with the 'a' values calculated from crystallographic data *i.e.*, 2.53 Å. In the solvent mixtures containing acetonitrile it is evident that the Bjerrum, EKYY, and Fuoss theories predict very low values of 'a' in the range of 1.45 to 1.88 Å which are unreasonable. The DR theory predicts meaningful 'a' values of 3.79 to 6.25 Å. In water[20] the DR theory predicts 2.04 Å which is much better than the values predicted by other theories *i.e.*, 0.61 to 0.67 Å. Getting higher 'a' values than the crystallographic value can be explained by considering the solvent separated ion-pairs.

The main effect of ion-association on ion-pair formation is either to decrease K_A due to increase in contact distance for the formation of 'solvent separated ion-pairs' (SSIP) or to increase K_A due to the formation of the additional associated species such as 'contact ion-pairs' (CIP). Earlier work[21] shows that silver acetate exists mostly as CIP in water. Whereas in acetonitrile–water mixtures the preferential solvation of Ag^+ ions by acetonitrile and CH_3COO^- ions by water suggests the formation of SSIP. The crystallographic radius of AgOAc is 2.53 Å. For this 'a' value the expected association constants are 37.64, 77.59, 174.7, and 287.7 $dm^3\,mol^{-1}$ for 40, 60, 80, and 90% (w/w) acetonitrile–water mixtures respectively. But the corresponding experimental values are 4.343, 10.17, 25.43, and 43.76 $dm^3\,mol^{-1}$. These low values of experimental association constants compared to the theoretical values indicate that there might be a large contribution of weakly bound solvent separated ion-pairs. Therefore, SSIP and CIP may be in equilibrium as shown below.

$$M^+S + S'A^- \rightleftharpoons M^+SS'A^- \text{ or } M^+SA^-S' \text{ or } SM^+S'A^-$$

$$\Downarrow\Uparrow$$

$$SM^+M^-S' \text{ or } [M^+A^-]S[M^+A^-]S'$$

By assuming perfect 'Stick' of the solvent at the surface of the ion, Walden[22] modified the Stokes law and obtained the relation

$$\lambda_0^{\pm}\eta = 0.820|Z_{\pm}|1/r_s^{\pm}, \quad (7)$$

$$\text{or } \Lambda_0\eta = 0.820(|Z_+|1/r_s^+ + |Z_-|1/r_s^-),$$

$$= \text{constant}, \quad (8)$$

where $\lambda_0^{\pm}$ is the limiting ionic conductances of hydrodynamic entity of radius $r_s^{\pm}$ and charge $Z_{\pm}$ in a medium of viscosity η. The Walden product $\Lambda_0\eta$ is expected to be constant for a given electrolyte in a series of solvents/solvent mixtures in which ion-solvent interactions are uniform. It is evident from the Walden products calculated (Table 3) that $\Lambda_0\eta$ decreases with increasing percentage of acetonitrile in acetonitrile–water mixtures indicating that the total solvation increases with increasing percentage of acetonitrile.

Table 3. Walden products and Stokes law radii for silver acetate at 25 °C

Solvent	$\Lambda_0\eta$	λ_0^+	λ_0^-	r_s^+/Å	r_s^-/Å
Water	0.9114	61.92	40.41	1.49	2.27
40% AN	0.6771	45.64	34.11	2.12	2.83
60% AN	0.6040	56.83	34.41	2.18	3.60
80% AN	0.5266	70.90	42.84	2.50	4.13
90% AN	0.3877	78.52	21.66	2.70	9.78

Interesting results could be obtained by splitting the salt conductance (Λ_0) into its ionic conductances. The limiting single ion conductances of Ag^+ ion were taken from the plot of $\lambda_0^+\eta$ *vs.* mole fraction of acetonitrile. By subtracting this from Λ_0 value, the limiting ionic conductance of acetate ion were obtained. The hydrodynamic radii of the Ag^+ and acetate ions were calculated by substituting these λ_0^+ and λ_0^- in Eq. 7 and the values thus obtained are presented in Table 3. The r_s^+ values for Ag^+ increase from 2.12 Å in 40% acetonitrile to 2.70 Å in 90% acetonitrile whereas it is only 1.49 Å in water which clearly indicates that in the acetonitrile–water mixtures Ag^+ is preferentially solvated by acetonitrile. The r_s^- values for acetate ion go on increasing from 2.27 to 9.78 Å. These odd values for acetate ion could be attributed to the unsymmetrical shape and distribution of the charge between the two oxygen atoms of the carboxylate group. This could also be the reason for the departure from the Stoke's law in the polarizable solvent. From these results one can conclude that Stoke's law may be applicable to the simple ions like Ag^+ and not to the ions in which charge is distributed.

One of the authors (UGKR) is thankful to CSIR-(New Delhi) for the award of a postdoctoral fellowship.

References

1) H. S. Harned and B. B. Owen, "The Physical Chemistry of Electrolyte Solutions," Reinhold, N. Y. (1950), pp. 369, 562, and 563.
2) L. G. Sillen and A. E. Martell, "Stability Constants of Metal-Ion Complexes, Supplement No. 1." ed by The Chemical Society, London (1971), Special Publication No. 25.
3) F. H. MacDougall and L. E. Topol, *J. Phys. Chem.*, **56**, 1090 (1952).
4) R. M. Fuoss and K. L. Hsia, *Proc. Natl. Acad. Sci. U.S.A.*, **57**, 1550 (1966); **58**, 1818 (1967).
5) R. Fernandez-Prini, *Trans. Faraday Soc.*, **65**, 3311 (1969).
6) W. H. Lee and R. J. Wheaton, *J. Chem. Soc., Faraday Trans. 2*, **74**, 743, 1456 (1978); **75**, 1128 (1979); *Acta Chem. Scand.*, **A34**, 307 (1980).
7) R. M. Fuoss, *J. Phys. Chem.*, **78**, 1383 (1974); **79**, 525 (1975); **80**, 2091 (1976); **82**, 2427 (1978); *J. Solution Chem.*, **7**, 771 (1978).
8) P. Beronius, *Acta Chem. Scand.*, **A34**, 309 (1980).
9) N. K. Bjerrum, *Danske Vidensk. Selsk.*, **7**, No. 9 (1926).
10) R. M. Fuoss, *J. Am. Chem. Soc.*, **77**, 2615 (1958).
11) J. T. Denison and J. B. Ramsey, *J. Am. Chem. Soc.*, **77**, 2615 (1955).
12) H. Falkenhagen, W. Ebeling and W. D. Kraeft, "Ionic Interactions," ed by S. Petrucci, Academic Press, N. Y. (1971), Vol. I. p. 104.
13) H. Yokoyama and H. Yamatera, *Bull. Chem. Soc. Jpn.*, **48**, 1770 (1975).
14) A. I. Vogel "A Textbook of Practical Organic Chemistry," Longmans, London (1955), p. 407.
15) J. Ananthaswamy, B. Sethuram, and T. N. Rao, *Indian J. Chem.*, **15A**, 9 (1977).
16) A. D. Aprano and R. M. Fuoss, *J. Phys. Chem.*, **73**, 400 (1969).
17) J. C. Justice, *J. Chim. Phys.*, **65**, 353 (1968); *Electrochim. Acta*, **16**, 701 (1971).
18) H. Strechlow and H. M. Koepp, *Z. Electrochem. Ber. Bunsenges. Phys. Chem.*, **62**, 373 (1958).
19) H. K. Bodenseh and J. B. Ramsey, *J. Phys. Chem.*, **69**, 543 (1965).
20) J. Ananthaswamy, B. Sethuram, and T. N. Rao, *J. Inorg. Nucl. Chem.*, **42**, 735 (1980).
21) J. Ananthaswamy, B. Sethuram, and T. N. Rao, *Bull. Chem. Soc. Jpn.*, **52**, 3076 (1979).
22) P. Walden and E. Birr, *Z. Phys. Chem.*, **153A**, 1 (1931).

 © 1982 The Chemical Society of Japan Bull. Chem. Soc. Jpn., 55, 297—300 (1982)

Studies on the Interaction between Mercury(II) Chloride and Copper(I) Halides in Solid State

Mirza Aijaz Beg* and Afaq Ahmad

Department of Chemistry, Aligarh Muslim University, Aligarh-202001, India

(Received April 5, 1981)

Kinetics and mechanism of $HgCl_2$–CuI and $HgCl_2$–CuBr reactions were studied in solid state. It has been demonstrated that $HgCl_2$ reaches CuI by surface migration and the reaction proceeds through counter diffusion of Cu^+ and Hg^{2+}. Both the reactions follow the parabolic rate law and the activation energies are 77.11 ± 3.84 and 51.08 ± 1.29 kJ/mol. While the former is a complex multi-stage reaction, the latter is a simple exchange process.

Like Ag_2HgI_4, Cu_2HgI_4 is also known to be formed from the reaction of CuI and HgI_2 in solid state[1] but neither the kinetics and mechanisms of this reaction nor the interaction of CuI with other mercury(II) halides seem to be reported. In an attempt to obtain some new solid state materials and mixed halide complexes like $AgHgClI_2$ and $AgHgCl_2I$ formed in solid state[2], we studied the reaction of $HgCl_2$ with CuI and CuBr in solid state. Though the expected mixed halides could not be detected, the information obtained on the mechanistic aspect is worth reporting. The reaction of $HgCl_2$ with CuI is multi-step, and different molar ratios of reactants give rise to different products, HgI_2 being formed as an intermediate in all cases. Contrary to the above, $HgCl_2$–CuBr reaction is a simple exchange process. Formation of several solid solutions among the reactants and products were also noted.

Experimental

Materials. $HgCl_2$ (BDH, AR Grade) was used without further purification. Copper(I) iodide and copper(I) bromide, being photosenstive, were prepared afresh for each set of experiments following the methods of Berthemot,[3] Guichard[4] and Lean and Whatmough.[5] X-Ray patterns of the products showed them to be single phase γ-CuI[6] and γ-CuBr.[7]

Cu_2HgI_4 was prepared as reported elsewhere.[8] Its X-ray pattern showed it to be single phase β-Cu_2HgI_4.[9]

Rate Measurements. The kinetics of the reactions were studied by placing mercury(II) chloride over copper(I) halides (each above 300 mesh size) in a vertically held glass tube described elsewhere[10,11] (The readability of the microscope was 0.001 cm and the average deviation of the measured values was ±0.00043 cm). Each experiment was performed in triplicate and the average of the three respective values was taken as the thickness of the product.

X-Ray Studies. Different molar mixtures of the reactants (above 300 mesh size) were mixed thoroughly in an agate mortar. One part of each mixture was heated in an air thermostat at 120 ± 0.05 °C, while the other was kept at 25 °C. Each set of mixtures was analysed, after about 60 h by Norelco Geiger Counter Diffractometer using Cu $K\alpha$ radiations with a Ni-Filter, applying 32 kV at 12 mA. The compounds present were identified by calculating the d values and comparing them with the standard values of the expected compounds.

Thermal Studies. Weighed amounts of $HgCl_2$ and CuI in molar ratios 1:4, 1:3, 1:2, and 1:1 were mixed in a Dewar flask, and the rise in temperature was noted against time. Similarly, thermal studies were carried out with different molar mixtures of $HgCl_2$ and CuBr. Same proportions of $HgCl_2$ and CuX (X is Br^- or I^-) as weighed for thermal studies were weighed separately, mixed thoroughly and pressed into tablets. Conductance of each tablet was measured by current ratio I–C bridge, applying 0.2 V and frequency 5×10^3 Hz.

Table 1. Dependence of parabolic rate constant on temperature for CuI–$HgCl_2$ reaction

Temperature °C	K/cm h^{-1}
80	4.01×10^{-9}
95	11.11×10^{-9}
110	23.33×10^{-9}
115	43.25×10^{-9}
121	80.00×10^{-9}

Table 2. Dependence of parabolic rate constant on temperature for CuBr–$HgCl_2$ reaction

Temperature °C	K/cm h^{-1}
75	0.4×10^{-7}
85	0.72×10^{-7}
96	1.11×10^{-7}
101	1.50×10^{-7}
107	1.75×10^{-7}

Results and Discussion

It is clear from Tables 3 and 4 that $HgCl_2$ reacts differently with CuBr and CuI.

CuI–$HgCl_2$ Reaction. CuI reacts with $HgCl_2$ in 4:1 molar ratio, giving Cu_2HgI_4 and CuCl.

$$4CuI + HgCl_2 \longrightarrow 2CuCl + Cu_2HgI_4 \quad (1)$$

Thermal (Fig. 1) as well as conductance (Fig. 2) measurements carried out at 25 °C provided no evidence for any sub-step in this reaction. However, the presence of HgI_2 (Table 3) in addtion to CuCl and Cu_2HgI_4 in the mixture kept at 25 °C, is indicative of the fact that HgI_2 is first formed:

$$2CuI + HgCl_2 \longrightarrow 2CuCl + HgI_2, \quad (1a)$$

which subsequently disappears giving Cu_2HgI_4 through (1b)

$$2CuI + HgI_2 \longrightarrow Cu_2HgI_4. \quad (1b)$$

Table 3. X-Ray diffraction analyses of CuI-$HgCl_2$ reaction mixtures

Molar ratio CuI : $HgCl_2$	Compounds identified in mixtures: Kept at 25 °C	Compounds identified in mixtures: Heated at 120 °C and then cooled to 25 °C
4 : 1	CuCl, Cu_2HgI_4, and HgI_2	CuCl and Cu_2HgI_4
3 : 1	CuCl, Cu_2HgI_4, and HgI_2	CuCl, Cu_2HgI_4, and HgI_2
2 : 1	CuCl, Cu_2HgI_4, and HgI_2	CuCl and HgI
1 : 1	CuCl, Cu_2HgI_4, HgI_2, and $HgCl_2$	CuCl, HgI_2, and $HgCl_2$
1 : 2	CuCl, HgI_2, and $HgCl_2$	CuCl, HgI_2, and $HgCl_2$

Table 4. X-Ray diffraction analyses of CuBr-$HgCl_2$ reaction mixtures

Molar ratio CuBr : $HgCl_2$	Compounds identified in mixtures: Kept at 25°C	Compounds identified in mixtures: Heated at 120 °C and then cooled to 25 °C
4 : 1	CuBr, CuCl, and $HgBr_2$	CuBr, CuCl, and $HgBr_2$
3 : 1	CuBr, CuCl, and $HgBr_2$	CuBr, CuCl, and $HgBr_2$
2 : 1	$HgBr_2$ and CuCl	CuCl and $HgBr_2$
1 : 1	CuCl, $HgCl_2$, CuBr, $HgBr_2$, and $HgCl_2$	CuCl and HgClBr
1 : 2	CuCl, HgClBr, $HgBr_2$, and $HgCl_2$	CuCl, HgClBr, and $HgCl_2$

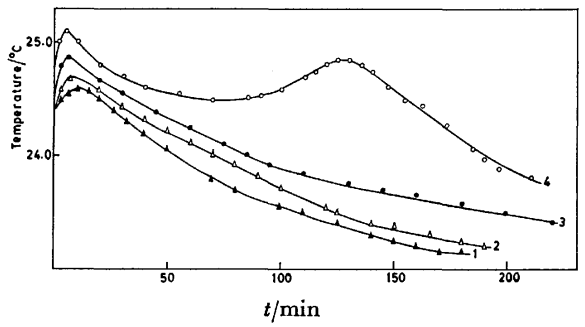

Fig. 1. Temperature rise as a function of time for CuI and $HgCl_2$ reaction.
Molar ratios (1) 4:1, (2) 3:1, (3) 2:1, (4) 1:1.

As reaction (1b) is extremely fast, disappearance of HgI_2 through (1c) looks improbable:

$$HgCl_2 + HgI_2 \longrightarrow 2HgClI. \quad (1c)$$

However, at higher temperature, reaction (1c) is known to occur appreciably, but on cooling the product HgClI decomposes immediately into its components.[12]

An equimolar mixture of HgI_2 and $HgCl_2$ kept at 25 °C did not show any evidence for the formation of HgClI even after about 6 d. Hence, the possibility that HgI_2 is consumed by $HgCl_2$ through step (1c) is completely ruled out. The overall reaction in 4:1 molar mixture of CuI and $HgCl_2$ will therefore, be as follows:

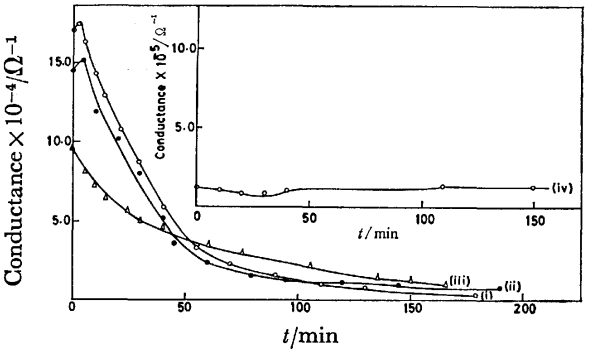

Fig. 2. Change in conductance as function of time for CuI and $HgCl_2$ reaction.
Molar ratios (i) 4:1, (ii) 3:1, (iii) 2:1, (iv) 1:1.

$$2CuI + HgCl_2 \longrightarrow 2CuCl + HgI_2 \quad \text{(Slow)}$$
$$2CuI + HgI_2 \longrightarrow Cu_2HgI_4 \quad \text{(Fast)}$$
$$4CuI + HgCl_2 \longrightarrow Cu_2HgI_4 + 2CuCl$$

The results of thermal (Fig. 1) and conductance (Fig. 2) measurements made with 3:1 molar mixture are similar to those obtained with 4:1 molar mixture. The presence of HgI_2 in 3:1 molar mixture even at higher temperature confirms the above view point and it is detected here in the end products because CuI in these mixture is not sufficient to convert whole of HgI_2 into Cu_2HgI_4. Hence, the overall reaction in 3:1 molar mixture is as follows:

$$4CuI + 2HgCl_2 \longrightarrow 2HgI_2 + 4CuCl \quad (2a)$$
$$2CuI + HgI_2 \longrightarrow Cu_2HgI_4 \quad (2b)$$
$$6CuI + 2HgCl_2 \longrightarrow Cu_2HgI_4 + HgI_2 + 4CuCl$$

The X-ray analysis of the products of 2:1 molar mixture of CuI and $HgCl_2$ heated at 120 °C and cooled to 25 °C indicated the presence of only CuCl and HgI_2.

$$2CuI + HgCl_2 \longrightarrow 2CuCl + HgI_2 \quad (3)$$

The thermal (Fig. 1) curve for 2:1 molar mixture of CuI and $HgCl_2$ has only one inflection. It thus appears that this is a simple exchange reaction. The X-ray analysis of this mixture kept at 25 °C did show the presence of Cu_2HgI_4 but the one that was heated to 120 °C and then cooled to 25 °C did not indicate the presence of Cu_2HgI_4. It is presumed that Cu_2HgI_4 is consumed at higher temperature by the excess $HgCl_2$ present in this mixture:

$$Cu_2HgI_4 + HgCl_2 \longrightarrow 2HgI_2 + 2CuCl. \quad (3a)$$

This was confirmed by heating an equimolarmixture of Cu_2HgI_4 and $HgCl_2$ at 120 °C. The X-ray analysis showed only the presence of HgI_2 and CuCl. Hence, the overall reaction sequence for 2:1 molar ratio at high temperatures is as follows:

$$2CuI + HgCl_2 \longrightarrow HgI_2 + 2CuCl \quad (3a)$$
$$2CuI + HgI_2 \longrightarrow Cu_2HgI_4 \quad (3b)$$
$$Cu_2HgI_4 + HgCl_2 \longrightarrow 2HgI_2 + 2CuCl \quad (3c)$$
$$4CuI + 2HgCl_2 \longrightarrow 2HgI_2 + 4CuCl$$

Product analysis of 1:1 molar mixture of CuI and $HgCl_2$ heated to 120 °C (Table 3) indicated that CuCl and HgI_2 are the final products. The presence

of Cu_2HgI_4 in addition to CuCl, HgI_2, and $HgCl_2$, in the 1:1 mixture kept at room temperature (25 °C) indicated that the reaction is multi-step. Thermal (Fig. 1) and conductance (Fig. 2) measurements at room temperature did show two maxima in the curves.

The first inflection in the curve may be due to the formation of HgI_2 and its subsequent elimination by excess of CuI giving Cu_2HgI_4, both the steps being fast.

$$2CuI + HgCl_2 \longrightarrow 2CuCl + HgI_2 \quad (4a)$$

$$2CuI + HgI_2 \longrightarrow Cu_2HgI_4 \quad (4b)$$

The second inflection in the curve may be due to the fact that presence of $HgCl_2$ pushes the reaction (3c) to an appreciable extent. This reaction, however, does not occur to an appreciable extent in 2:1 and other molar mixtures at the room temperature, hence the second inflection does not show up. This viewpoint is confirmed by the fact that Cu_2HgI_4 is completely consumed and is not detected even at room temperature in 1:2 mixture (Table 3).

1:1 Molar mixture of CuI and $HgCl_2$, kept at 120 °C, turns yellow after some time which on cooling to room temperature changes into red. HgClI is light yellow and stable at high temperature, and decomposes into HgI_2 and $HgCl_2$ when brought to room temperature.[12]

$$HgI_2 + HgCl_2 \xrightarrow{120°C} 2HgClI \xrightarrow{\text{cooled}} HgI_2 + HgCl_2 \quad (4d)$$

Hence, the overall reaction sequence in 1:1 molar mixture will be as follows:

$$2CuI + HgCl_2 \longrightarrow HgI_2 + 2CuCl \quad (4a)$$

$$2CuI + HgI_2 \longrightarrow Cu_2HgI_4 \quad (4b)$$

$$Cu_2HgI_4 + HgCl_2 \longrightarrow 2CuCl + 2HgI_2 \quad (3c)$$

$$2HgCl_2 + 2HgI_2 \longrightarrow 4HgClI \quad (4d)$$

$$4CuI + 4HgCl_2 \longrightarrow 2HgI_2 + 2HgCl_2 + 4CuCl \quad (4d')$$

The X-ray analysis of 1:2 molar mixtures of CuI and $HgCl_2$ (Table 3) showed the presence of CuCl, HgI_2, and $HgCl_2$. By all account, the reaction sequence occurring in this mixture is the same as that in 1:1 molar mixture.

CuBr–$HgCl_2$ Reaction. CuBr reacts with $HgCl_2$ in 2:1 molar ratio giving CuCl and $HgBr_2$ (Table 4).

$$2CuBr + HgCl_2 \longrightarrow 2CuCl + HgBe_2 \quad (5)$$

Product analysis (Table 4) suggests that the reaction sequence in 4:1 and 3:1 molar mixtures is the same as in 2:1 molar mixture. CuBr in excess over 2:1 stoichiometry is left as such. Thermal (Fig. 3) and conductance (Fig. 4) measurements also support this view.

The products obtained in 1:1 molar mixture heated at 120 °C are CuCl and HgClBr (Table 4). In addition to these, the room temperature mixture shows $HgCl_2$ and $HgBr_2$.

The occurrence of second inflection in thermal (Fig. 3) as well as in conductance (Fig. 4) curves clearly shows that this is a two step reaction. The first step in this case as well, may be the formation of $HgBr_2$ through the simple exchange reaction (5). The second inflection refers to the consecutive reaction of $HgBr_2$ with the remaining amount of $HgCl_2$

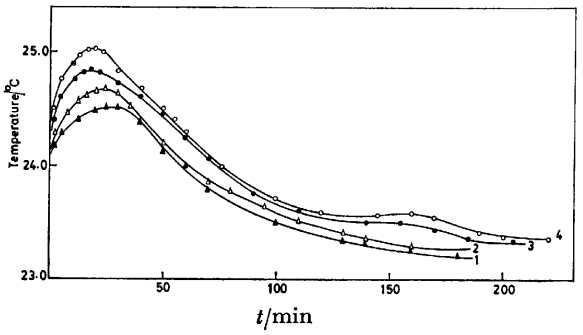

Fig. 3. Temperature rise as a function of time for CuBr–$HgCl_2$ reaction.
Molar ratios (1) 4:1, (2) 3:1, (3) 2:1, (4) 1:1.

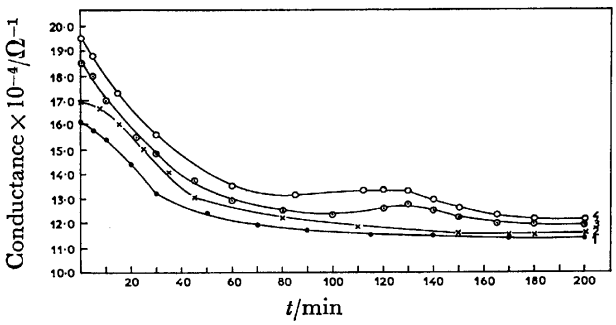

Fig. 4. Change in conductance as function of time for CuBr and $HgCl_2$ reaction. Molar ratios (1) 4:1, (2) 3:1, (3) 2:1, (4) 1:1.

in the reaction mixture giving HgClBr[12] through the much slower step:

$$HgCl_2 + HgBr_2 \longrightarrow 2HgClBr. \quad (6)$$

In case of 1:2 molar mixture, still larger proportion of $HgCl_2$ pushes reaction (6) to a still greater extent, making the second inflection slightly more pronounced. Hence, the complete reaction may be written as follows:

$$2CuBr + HgCl_2 \longrightarrow 2CuCl + HgBr_2$$

$$HgBr_2 + HgCl_2 \longrightarrow 2HgClBr$$

$$2CuBr + 2HgCl_2 \longrightarrow 2CuCl + 2HgClBr$$

Formation of HgClBr in earlier cases did not occur probably due to lesser proportion of $HgCl_2$ in the mixture.

Mechanism of Lateral Diffusion: In the kinetic experiment of the CuI–$HgCl_2$ system, soonafter the placement of $HgCl_2$ over CuI in the reaction tube, a dark brown layer appeared at the interface, which increased on CuI side with time, separating later into white and brown layers. On cooling to room temperature, the dark brown layer changed to scarlet red (Cu_2HgI_4 is dark brown above 70 °C and scarlet red below this temperature.[13] The analyses of the white and scarlet product layer at room temperature revealed them to be CuCl and β-Cu_2HgI_4. In the CuBr–$HgCl_2$ system also, the layer appearing at the interface increased on CuBr side and later separated into white and very light yellowish layers. They were analysed for CuCl and HgClBr.

The growth rate of the thickness of the product

layer in either case when reactants were in contact, follow the parabolic rate equation, $X^2=Kt$. The parabolic rate constant, K, in each case follows Arrehenius equation (Tables 1 and 2). The activation energies for the two reactions are respectively 77.11 ± 3.84 and 51.08 ± 1.29 kJ/mol.

The formation of the product on copper(I) halide side in another lateral diffusion experiment, where the reactants were placed with an air gap in between and the high vapour density of $HgCl_2$ suggest the possibility of vapour phase reaction. However, in a set of lateral diffusion experiments, the rate of product growth was found to decrease with increase in the length of the air gap. This fact and also the magnitude of activation energy[14] show that these reactions proceed through surface migration. The reaction continues *via* counter diffusion of Cu^+ and Hg^{2+} through the product layers.

Product analyses by X-ray diffraction, indicated the formation of solid solutions between CuI–CuCl, CuCl–Cu_2HgI_4, and CuBr–CuCl.

We are thankful to Dr. B. Rama Rao, Regional Research Laboratory, Hyderabad for the help in X-ray measurements and to Council of Scientific & Industrial Research, New Delhi for supporting this project.

References

1) A. T. Pinnock, *J. Soc. Chem. Indu.*, **38**, 78 (1919).
2) M. A. Beg and S. M. Ansari, *J. Solid State Chem.*, **20**, 1 (1978).
3) J. B. Berthemot, *J. Pharm.*, **14**, 614 (1830).
4) M. Guichard, *C. R. Acad. Sci.*, **144**, 1430 (1907).
5) B. Lean and W. H. Whatmough, *J. Chem. Soc.*, **73**, 148 (1898).
6) ASTM Powder Diffreaction File No. 6-0246.
7) ASTM Powder Diffreaction File No. 6-0292.
8) M. Meyer, *J. Chem. Educ.*, **20**, 145 (1943).
9) ASTM Diffraction File No. 18-0450.
10) R. P. Rastogi and B. L. Dubey, *J. Am. Chem. Soc.*, **89**, 200 (1967).
11) M. A. Beg and S. M. Ansari, *J. Solid State Chem.*, **18**, 57, (1976).
12) R. P. Rastogi, B. L. Dubey, and N. H. Singh, *J. Inorg. Nucl. Chem.*, **37**, 1167 (1976).
13) Z. Ketelaar, *Z. Krist.*, **83**, 440 (1934).
14) R. P. Rastogi, *J. Sci. Indus. Res.*, **29**, 184 (1970).

 © 1982 The Chemical Society of Japan Bull. Chem. Soc. Jpn., 55, 301—304 (1982)

The Separation of Cobalt(II), Copper(II), Zinc(II), Lead(II), and Cadmium(II) as Their 3-Methyl-1-phenyl-4-thiobenzoyl-5-pyrazolone (SBMPP) Chelates by Thin-layer Chromatography on Silica Gel

V. S. Chouhan and G. N. Rao*

Chemistry Department, Indian Institute of Technology, New Delhi 110016, India

(Received September 16, 1980)

Thin-layer chromatographic separation technique has been employed for the separation of Co(II), Ni(II), Cu(II), Zn(II), Pb(II), and Cd(II) as their 3-methyl-1-phenyl-4-thiobenzoyl-5-pyrazolone (SBMPP) chelates. Metal chelates are intensely coloured and so no additional reagent was needed for the development of spots. Silica gel G was used as an adsorbent in the form of thin layer coating (0.25 mm) on glass plates (5 cm×20 cm). The R_f values of SBMPP and metal–SBMPP chelates have been determined by the ascending method with pure solvents and various binary solvent mixtures on thin layer of silica gel. In benzene the order of R_f values is Cd(II)<Pb(II)<Zn(II)<Co(II)<SBMPP<Ni(II)=Cu(II). By employing solvents like dichloromethane, benzene, and toluene, mutual separation of metal complexes was achieved successfully. The mixed solvents are more useful for the mutual separation of chelates than the pure solvents.

Thin-layer chromatography has been employed to separate metal ions using some chelating ligands.[1] In our laboratory extensive work has been conducted on the analytical applications of acylpyrazolones[2–6] in solvent extraction, spectrophotometric estimations and gravimetric determinations. Recently the authors have reported the solvent extraction of cobalt(II), zinc(II), and europium(III) with a new chelating ligand 3-methyl-1-phenyl-4-thiobenzoyl-5-pyrazolone (SBMPP),[5,7] Preliminary results on the utility of SBMPP[8] have been also published. It has been found that 4-benzoyl-3-methyl-1-phenyl-5-pyrazolone (BMPP) is comparable to thenoyl trifluoroacetone (TTA) in the solvent extraction of metals.[9] It is reasonable to expect SBMPP to be comparable to (thiothenoyl) trifluoroacetone (STTA) as analytical reagent since these are thioderivatives of BMPP and TTA respectively. In this paper the results of our original studies on thin-layer chromatographic separation of metals as their SBMPP chelates on silica gel are reported. Honjo and Kiba[10] have earlier described the separation of transition metals as their STTA chelates by thin-layer chromatography on silica gel.

Experimental

Apparatus and Reagents. Glass chromatographic plates (5 cm×20 cm), chromatographic chamber and universal applicator (Toshniwal) were used. Sample solutions were prepared by dissolving the metal chelates in acetone. Silica gel G (BDH), incorporating 13% calcium sulphate as binder was used as adsorbent for the thin-layer chromatography.

Developing Solvents. Analar reagent grade of methanol, ethanol, 2-propanol, 1-butanol, diethyl ether, dichloromethane, chloroform, carbon tetrachloride, benzene, toluene, cyclohexane, and hexane were used. They were purified by standard methods, if necessary. It has been found that SBMPP forms stable and extractable chelates with a specific color with many metal ions.[8] Spectrophotometric methods for the estimation of cobalt(II) and nickel(II) with SBMPP have been developed.[5] Solid complexes of cobalt(II), nickel(II), copper(II), zinc(II), lead(II), and cadmium(II) with SBMPP were prepared by dissolving their respective acetates in aqueous media followed by adding requisite amounts of ethanolic solution of SBMPP. The complexes were filtered, purified by recrystallization from suitable solvents and analysed. The ligand SBMPP was prepared by passing hydrogen sulphide gas and hydrogen chloride gas through a solution of BMPP in absolute ethanol, maintaining the temperature at 0 °C. This method is similar to the one employed by Honjo and Kiba[11] for the preparation of (thiothenoyl) trifluoroacetone. Structural formulas of SBMPP and BMPP are shown in Fig. 1. Cryoscopic determination of molecular weight in benzene gave a value of 296±4 (calculated molecular weight of SBMPP is 294). Analytical data and some important characteristics like λ_{max} and ε_{max} of the ligand SBMPP and complexes of SBMPP with metals are given in Table 1.

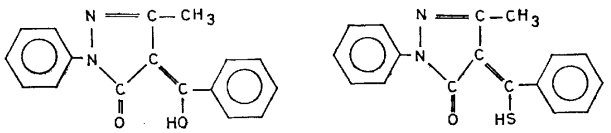

BMPP SBMPP

Fig. 1. Structural formulas of SBMPP and BMPP.

Procedure. Chromatographic plates were prepared by applying 0.25 mm thick coating of silica gel slurry with the help of universal applicator. Coated plates of the silica gel were dried for 20—30 min at 25±2 °C and then they were activated in an oven for two hours at 110 °C. The plates were stored over calcium chloride in a desiccator. With the help of a capillary tube a 5-μl portion of sample solution is spotted on the thin layer at definite intervals within about 2 cm from one end of the plate. One millimolar solutions of the metal chelates in acetone were used to prepare the sample. The spots were then air dried at room temperature (25±2 °C). The plate was placed in a chromatographic chamber containing an organic solvent or solvent mixture (20 ml), so that the plate dips into the solvent upto 1 cm below the sample spot. The solvent migrates upwards through the thin layer separating the sample into spots by ascending development. When the solvent proceeded to ≈10 cm from the sample spot the development was stopped and the plate was taken out of the chromatographic chamber. It was then exposed to air. Since the metal chelates showed characteristic colours (colours are mentioned in Table 1) no spraying with additional developing reagent was needed.

The resulting chromatogram is generally characterized

TABLE 1. ANALYTICAL DATA AND SOME CHARACTERISTICS OF SBMPP AND METAL CHELATES OF SBMPP

Compound	Colour	λ_{max} / nm	ε_{max} [a] / $L\,M^{-1}\,cm^{-1} \times 10^{-3}$	Mp θ_m/°C	Carbon [b] (%)	Hydrogen [b] (%)
SBMPP	Greenish yellow	328	4.8	80— 82	69.4C 69.5F	4.75C 4.88F
$Co(L)_3$ [c]	Reddish brown	328	9.2	188—190	65.3C 65.6F	4.16C 4.21F
$Ni(L)_2$	Brick red	330	10.2	201—204	63.3C 63.0F	4.03C 4.23F
$Cu(L)_2$	Olive brown	328	7.4	256—258	62.8C 62.9F	4.00C 4.08F
$Zn(L)_2$	Bright yellow	330	12.3	178—180	62.6C 62.4F	3.99C 4.06F
$Pb(L)_2$	Orange	330	12.9	238—242	51.4C 51.2F	3.28C 3.35F

a) Absorption spectra measured in chloroform solution against the same solvent. ε_{max} values are approximate.
b) C: Calculated, F: found. c) (L)−: Anion of SBMPP.

TABLE 2. R_f VALUES OF SBMPP AND ITS METAL CHELATES WITH VARIOUS PURE SOLVENTS ON SILICA GEL

Developing solvent	Dielectric constant	Developing length/cm	Developing time/min	Metal						
				Co	Ni	Cu	Zn	Pb	Cd	SBMPP
Methanol	32.6	12.0	20	1.0	1.0	1.0	0.98	0.97	0.98	0.98
Ethanol	24.3	9.8	30	0.97	1.0	1.0	0.98	0.98	1.0	0.98
2-Propanol	18.3	7.8	45	1.0	1.0	1.0	1.0	1.0	1.0	0.98
1-Butanol	17.1	9.0	45	0.96	0.97	0.98	0.98	0.97	0.95	0.94
Diethyl ether	4.3	9.5	25	1.0	1.0	1.0	1.0	1.0	1.0	1.0
Dichloromethane	9.08	10.2	40	0.29	0.49	0.40	0.30	0.27	0.13	0.54
Chloroform	4.8	10.3	30	1.0	1.0	1.0	1.0	1.0	1.0	1.0
Carbon tetrachloride	2.2	10.2	55	0.0	0.0	0.0	0.0	0.0	0.0	0.14
Benzene	2.3	11.4	30	0.37	0.80	0.80	0.34	0.03	0.0	0.43
Hexane	1.9	11.2	35	0.0	0.0	0.0	0.0	0.0	0.0	0.03
Cyclohexane	2.0	11.7	38	0.0	0.0	a)	0.0	0.0	a)	0.01
Toluene	2.38	9.4	15	0.21	0.58	0.59	0.22	0.04	0.0	0.28

a) Spots disappear during development. Average deviation of R_f values = 0.02.

by R_f values which are calculated from the following equation.

$$R_f = \frac{\text{Distance (cm) travelled by the substance}}{\text{Distance travelled by the solvent}}$$

Results and Discussion

The R_f value measures the velocity of movement of the spot relative to that of the solvent front. Moreover the R_f value is a measure of the interaction among solute, solvent and adsorbent and is reproducible and characteristic for each solute in a given solvent–adsorbent system under specified conditions.

Some typical results of the development of SBMPP and its metal STTA chelates with individual pure solvents on a silica gel employing the ascending method are summarised in Table 2. Metal chelates can be divided into three groups on the basis of their chromatographic behaviour. (1) Chelates which do not migrate from the sample spot (with carbon tetrachloride, cyclohexane and hexane) (2) Chelates which can be developed to moderate distances over a comparatively wide range (with toluene, benzene and dichloromethane) (3) Chelates which move upto solvent front (methanol, ethanol, chloroform, diethyl ether, and 2-propanol). The average deviation of R_f values was 0.02. The R_f values of SBMPP chelates in benzene increased in the order of Cd(II)<Pb(II)<Zn(II)<Co(III)<SBMPP<Ni(II), Cu(II). By employing solvents like dichloromethane, benzene and toluene, separation of metal complexes was obtained successfully. Representative chromatograms of SBMPP and its metal chelates in benzene and dichloromethane are shown in Fig. 2. Results indicate that the distance of the development on the chromatographic plate depends on the polarity of the solvent. Honjo and Kiba[10] reported that R_f values of STTA chelates generally increased in the order of: Cd(II)<Zn(II)<Pb(II), STTA<Hg(II)<Co(II), (III)<Cu(II)<Ni(II).

It was considered interesting to study the effect of binary mixtures of solvents in the thin layer chromatography of SBMPP and its metal chelates and some representative results are listed in Table 3. The average deviation of the R_f values is 0.02. It is seen that the mixed solvents could separate the SBMPP chelates of metals more successfully than the pure

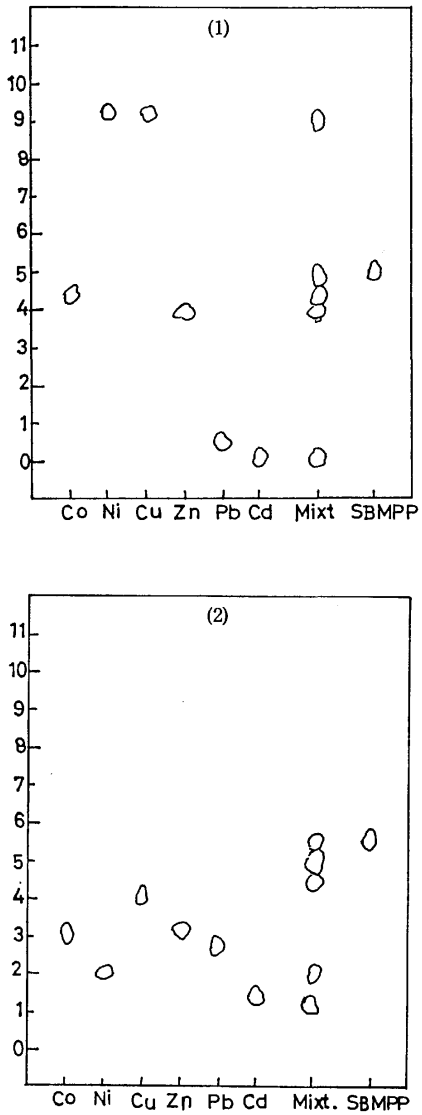

Fig. 2. Chromatogram of SBMPP and its metal chelates with single component solvent.
SBMPP, Chelate $\approx 5 \times 10^{-4}$ M; developing solvent (1) benzene (2) dichloromethane.
Y axis-migration distance (cm).

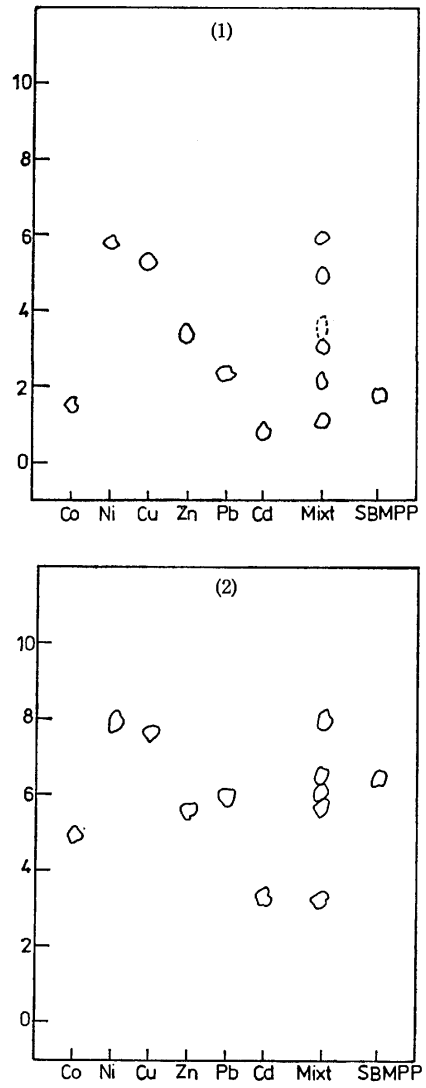

Fig. 3. Chromatogram of SBMPP and its metal chelates with binary solvent mixture.
SBMPP, Chelate $\approx 5 \times 10^{-4}$ M; developing solvent (1) benzene–carbon tetrachloride (2) toluene– chloroform.
Y axis-migration distance (cm).

TABLE 3. R_f VALUES OF SBMPP AND ITS METAL CHELATES WITH VARIOUS MIXED DEVELOPING SOLVENTS ON SILICA GEL

Developing solvent (1:1, v/v)	Developing length/cm	Developing time/min	Metal						
			Co	Ni	Cu	Zn	Pb	Cd	SBMPP
Benzene-carbon tetrachloride	9.5	32	0.15	0.60	0.55	0.34	0.24	0.07	0.17
Benzene-chloroform	8.6	20	0.73	1.0	1.0	1.0	0.21	0.11	0.24
Benzene-cyclohexane	11.0	35	0.03	0.32	0.31	0.91	0.14	0.0	0.13
Benzene-ethanol	11.7	45	1.0	1.0	1.0	1.0	1.0	1.0	1.0
Toluene-carbon tetrachloride	11.5	35	0.07	0.38	0.38	0.07	0.07	0.0	0.10
Toluene-chloroform	10.5	15	0.46	0.75	0.73	0.53	0.55	0.31	0.6
Toluene-ethanol	11.0	40	1.0	1.0	1.0	1.0	1.0	1.0	1.0
Chloroform-carbon tetrachloride	8.5	35	0.31	0.92	0.95	0.63	0.30	0.0	0.30

Average deviation of R_f values=0.02.

solvents. Some typical results are shown in Fig. 3. Among these binary solvent mixtures the pairs of benzene–carbon tetrachloride, toluene–chloroform, and chloroform–carbon tetrachloride were suitable for the separation of metal chelates. The R_f values of SBMPP chelates in benzene–carbon tetrachloride increased in the order Cd(II)<Co(III)<SBMPP<Pb(II)<Zn(II)<Cu(II)<Ni(II).

The effectiveness of binary solvent mixtures in the separation of SBMPP chelates is probably due to some demixing of mixed solvents leading to some changes in the solvent ratio. Since the adsorbability of each solvent on the silica gel is different, this may lead to better separation of the developed spots. According to Honjo and Kiba[10] binary mixtures of solvents show a similar beneficial effect in the thin layer chromatographic separation of STTA chelates of metals on silica gel.

The sequence of R_f values obtained with the SBMPP chelates differs from the acetylacetonate series,[12,13] the dithiazonate series[14,15] or the diethyldithiocarbamate.[16,17] Chelates of SBMPP are similar to those of STTA and do not form hydrates like acetylacetonate chelates of metals. Further nickel chelate of SBMPP is red and diamagnetic while that of BMPP is green dihydrate which is paramagnetic.[4,5] Cobalt(II) forms stable paramagnetic chelate with BMPP which is a dihydrate while it forms diamagnetic chelate containing three moles of ligand with SBMPP in which cobalt is present in the oxidation state three.[4] Though there are some differences, the behaviour of SBMPP chelates is closer to that of STTA chelates than others such as dithiazonates and acetylacetonates.

In conclusion it can be stated that thin layer chromatographic separation technique is useful for the separation of transition metal ions as their SBMPP chelates using certain solvents and mixtures of solvents.

The authors thank C.S.I.R. (India) for financial assistance.

References

1) E. Stahl, "Thin Layer Chromatography," 2nd ed, Springer-Verlag, Berlin, Heidelberg, New York (1969).
2) G. Nageswara Rao and H. C. Arora, *Micro Chem. J.*, **21**, 1 (1978).
3) G. N. Rao and H. C. Arora, *J. Inorg. Nucl. Chem.*, **39**, 2057 (1977).
4) H. C. Arora, Ph. D. Thesis, Indian Institute of Technology, New Delhi, India (1976).
5) V. S. Chouhan, Ph. D. Thesis, Indian Institute of Technology, New Delhi, India (1978).
6) H. C. Arora, Ch. Venkateswarlu, G. N. Rao, *Indian J. Chem.*, **19**, 500 (1980).
7) V. S. Chouhan and G. N. Rao, *J. Radio Anal. Chem.*, **52**, 199 (1979).
8) G. N. Rao and V. S. Chouhan, *Chemical Era*, **14**, 124 (1978).
9) E. B. Sandell and H. Onishi, "Photometric Determination of Traces of Metals," John Wiley and Sons, New York (1978), p. 939.
10) T. Honjo and T. Kiba, *Bull. Chem. Soc. Jpn.*, **46**, 3768 (1973).
11) T. Honjo and T. Kiba, *Bull. Chem. Soc. Jpn.*, **45**, 185 (1972).
12) J. C. Trehan, *Chromatographia.*, **2**, 17 (1969).
13) Y. Tsunoda, T. Takeuchi, and Y. Yoshino, *Nippon Kagaku Zasshi*, **85**, 275 (1964).
14) M. Hranisavljevic-Jakovljievic and I. Pejkovic-Tadie, *Microchim. Acta*, **1965**, 936.
15) T. Takeuchi and Y. Tsunoda, *Nippon Kagaku Zasshi*, **88**, 176 (1967).
16) J. Senf, *J. Chromatogr.*, **21**, 363 (1966).
17) J. Rai and V. P. Kukreja, *Chromatographia*, **3**, 41, 499 (1970).

© 1982 The Chemical Society of Japan

NOTES

Bull. Chem. Soc. Jpn., 55, 305—306 (1982)

^{14}N Nuclear Quadrupole Relaxation in *N*-Methylpiperidine

Hisao NEGITA,* Tsuneo KUBO, and Michio MAEKAWA

Department of Chemistry, Faculty of Science, Hiroshima University, Hiroshima 730

(Received March 23, 1981)

Synopsis. Two crystal modifications of *N*-methylpiperidine were found by means of the nuclear quadrupole resonance (NQR) of Nitrogen-14. From the temperature dependence of the ^{14}N spin-lattice relaxation times (T_1), it is deduced that the α-form has a lower activation energy for the reorientation of the methyl group than the β-form.

The ^{14}N nuclear quadrupole resonance (NQR) spectrum of *N*-methylpiperidine was first reported by Colligiani *et al.*[1] In the present research we have attempted to obtain further information on the dynamical properties of this compound from the ^{14}N nuclear quadrupole relaxation. The spin-lattice relaxation time (T_1) was measured by the pulse method, and the molecular motions in this compound will be discussed.

Experimental

^{14}N NQR measurements were carried out using a pulse spectrometer described previously.[2] The resonance lines were observed by means of the spin-echo signals, using a 90°—180° pulse sequence series. The spin-lattice relaxation time (T_1) was determined by the repeating-90°—180°-pulse method.[3] The pulse width of a 90° pulse was about 50 μs. The spin-echo signal was averaged by means of a Nicolet Instrument Model 527 signal averager. The temperature was controlled by the method of Abe.[4] The temperature was stabilized within ±0.1 K. The frequency was measured by means of a frequency counter, TR-5104, from the Takeda Riken Co.

N-Methylpiperidine of an extra-pure reagent grade was purchased from the Wako Pure Chemical Ind. Co. and was purified by distillation. About 20 g of the reagent was used for the measurement.

Results and Discussion

In the case of the nitrogen-14 resonance, a pair of NQR absorption lines, ν_- and ν_+, are observed, and the frequencies are expressed as follows:

$$\nu_\pm = \frac{|e^2Qq|}{4h}(3\pm\eta), \qquad (1)$$

where $|e^2Qq/h|$ and η are the quadrupole coupling constant and the asymmetry parameter respectively. Table 1 shows the results at the temperature of liquid nitrogen. The α-form, the ^{14}N NQR spectrum of which was observed by Colligiani *et al.*,[1] is obtained by cooling the compound to the temperature of liquid nitrogen. This form is transformed to the β-form at about 157 K by rapid warming, but remains the same upon slow warming and melts at about 163 K. The data for the α-form were checked again and are listed for comparison.

TABLE 1. ^{14}N NQR PARAMETERS IN α- AND β-FORMS OF *N*-METHYLPIPERIDINE

	ν_-/MHz	ν_+/MHz	$(\|e^2Qq/h\|)$MHz	η/%
α-Form	3.6898	3.7803	4.9801	3.63
β-Form	3.7674	3.8262	5.0624	2.32

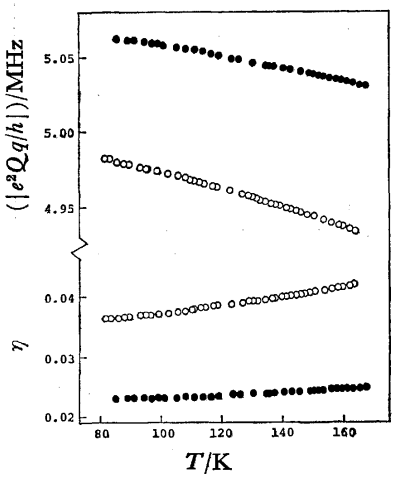

Fig. 1. The temperature dependence of the quadrupole coupling constant and asymmetry parameter in the α-form (○) and β-form (●) of *N*-methylpiperidine.

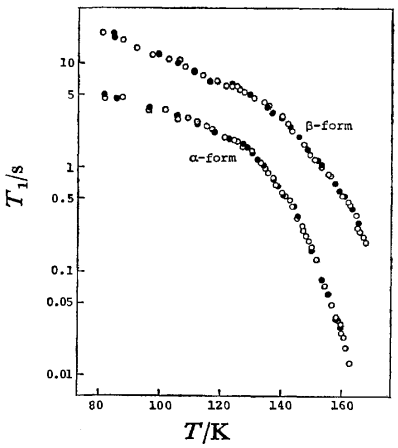

Fig. 2. The temperature dependence of the spin-lattice relaxation times in *N*-methylpiperidine. ●: ν_- line; ○: ν_+ line.

The temperature dependences of the quadrupole coupling constant and the asymmetry parameter in *N*-methylpiperidine in the temperature range from the temperature of liquid nitrogen to the melting point are shown in Fig. 1. The temperature coefficient of the quadrupole coupling constant in the α-form (denoted by the open circle) is slightly smaller than that in the β-form (denoted by the filled circle). This may indicate that the packing of the molecules in the β-form is closer than that in the α-form.

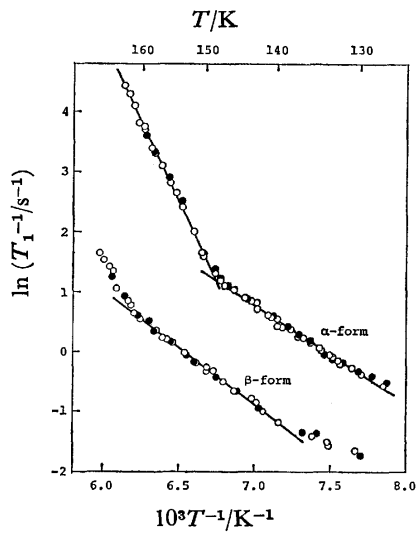

Fig. 3. $\ln(1/T_1)$ *vs.* $10^3/T$ in *N*-methylpiperidine. ●: ν_- line; ○: ν_+ line.

The temperature dependences of the spin-lattice relaxation times (T_1) for the ν_- and ν_+ lines in the α-form and β-form of *N*-methylpiperidine are shown in Fig. 2. In each form, the T_1's for both ν_- and ν_+ lines are coincident within the limits of experimental error. This suggests that the molecular motions equally contribute to T_1 for both resonance lines.

In the case of the α-form, up to 115 K the spin-lattice relaxation time decreases monotonously as the temperature rises. In this region, T_1 is determined by the torsional lattice vibration and is dominated by two indirect phonon processes, so that $1/T_1 \propto T^2$. In the temperature range from about 130 K to the melting point, T_1 drops exponentially as the temperature rises. This process can be attributed to the reorientation of the methyl group around the N–C bond. In this case, the relaxation formula is expressed as follows:

$$1/T_1 = C\tau/(1+\omega^2\tau^2), \tag{2}$$

and:

$$\tau = \tau_0 \exp(E_a/RT), \tag{3}$$

where C is a constant which describes the strength of the interaction; ω is the resonance angular frequency; τ is the correlation time of the motion, which changes according to the Arrhenius relation (Eq. 3); τ_0 is the inverse frequency factor, and E_a is the activation energy of the motion. In the low-temperature region of the T_1 minimum, where $\omega\tau \gg 1$, the following equation is obtained:

$$\ln(1/T_1) = -E_a/RT + f(\omega), \tag{4}$$

where $f(\omega)$ is a function of ω, the temperature dependence of which is negligible. In Fig. 3, the $\ln(1/T_1)$ value is plotted as a function of $1/T$. A break point is found near 150 K; T_1 values below 150 K are dominated by different molecular motions. That is, the dominant relaxation mechanism below 150 K is considered to be caused by the reorientation of the methyl group around the N–C bond, whereas that above 150 K is brought about by the reorientation of the molecule. In fitting Eq. 4 to the experimental T_1 values, the activation energies for these motions are determined to be 12.6 kJ/mol for the former motion and 51.2 kJ/mol for the latter.

The ^{14}N spin-lattice relaxation times (T_1) in *N,N'*-dimethylpiperazine were measured in the temperature range from 77 K to the melting point by Tzalmona and Kaplan.[5] T_1 drops exponentially above 200 K. It is considered that this is caused by the switching between the two chair configurations. The activation energy for this motion is calculated to be 56.5 kJ/mol. Therefore, we consider that the molecular motion with the barrier of 51.2 kJ/mol in *N*-methylpiperidine is the switching motion between the two chair configurations.

In the case of the β-form, below 130 K the spin-lattice relaxation time is determined by the torsional lattice vibration. On the other hand, in the temperature range from 140 K to the melting point (about 168 K), T_1 drops rapidly as a function of the temperature. This may be caused by the reorientation of the methyl group. In Fig. 3, the $\ln(1/T_1)$ value is plotted as a function of $1/T$. In fitting Eq. 4 to the experimental T_1 values, the activation energy for this motion is evaluated to be 15.8 kJ/mol. This value is larger than that in the α-form. This indicates that the methyl group in the β-form is slightly more suppressed than is the α-form. That is, the packing of the molecules in the α-form is less compact than that in the β-form. This is parallel to the finding of the temperature dependence of the quadrupole coupling constant.

References

1) A. Colligiani, R. Ambrosetti, and R. Angelone, *J. Chem. Phys.*, **52**, 5022 (1970).
2) H. Negita, T. Kubo, M. Maekawa, A. Ueda, and T. Okuda, *Bull. Chem. Soc. Jpn.*, **52**, 1881 (1979).
3) A. I. Andreeva, V. L. Matukhin, D. Ya. Osokin, and I. A. Safin, *Fiz. Tverd. Tela*, **15**, 3410 (1973).
4) Y. Abe, *J. Phys. Soc. Jpn.*, **18**, 1804 (1963).
5) A. Tzalmona and A. Kaplan, *J. Chem. Phys.*, **61**, 1912 (1974).

A Molybdenum Polynuclear Complex as Small Metallic Particles

Hajime OKUMURA, Tooru TAGA,† Kenji OSAKI,† and Ikuji TSUJIKAWA*

Department of Chemistry, Faculty of Science, Kyoto University, Oiwake-cho, Kitashirakawa, Sakyo-ku, Kyoto 606

† *Faculty of Pharmaceutical Sciences, Kyoto University, Shimoadachi-cho, Yoshida, Sakyo-ku, Kyoto 606*

(Received March 30, 1981)

Synopsis. The crystal structure of $(H_3O)_2[(Mo_6Cl_8)Cl_6]\cdot 6H_2O$ was determined by the X-ray method and its near-infrared absorption spectra were measured. These results can be interpreted by a view that the molybdenum nuclei of this complex are regarded as a small metallic particle.

The energy levels of conduction electrons in metal are generally regarded as continuous. However, in small metallic particles, the intervals of the energy levels are no longer small in comparison with other energies such as the thermal energy, kT and the electronic Zeeman energy, μH. It has been theoretically predicted[1] that anomalies occur in the macroscopic properties of small metallic particles, such as the electron heat capacity and the spin paramagnetic susceptibility, due to the restriction of the excitations of conduction electrons.

Some experiments have been recently performed[2] in order to detect these kinds of anomalies. The samples used in these experiments were small metallic particles prepared by the gas evaporation method and other techniques, the average diameters of which were 40—200 Å. With regard to such samples, size and shape of each particle were inhomogeneous, and only the average properties of all particles were measurable. Then the authors paied their attention to a polynuclear complex $(H_3O)_2[(Mo_6Cl_8)Cl_6]\cdot 6H_2O$ as the sample of this kind. They thought that the molybdenum nuclei of this complex could be regarded as a small metallic particle homogeneous in both size and shape, and some anomalies as small metallic particles would be detectable. In the present paper, the X-ray structure analysis and the near-infrared absorption spectra measurement for $(H_3O)_2[(Mo_6Cl_8)Cl_6]\cdot 6H_2O$ crystal are reported.

Experimental and Structure Determination

The sample was prepared by the method of Sheldon modified by Jolly.[3] Single crystals were obtained from the 6 mol dm^{-3} HCl solution by evaporating the solvent slowly. For the X-ray experiment a single crystal enclosed in a glass capillary with its mother liquor was used to prevent its efflorescence. Intensity data were collected on the Weissenberg camera with Ni-filtered Cu $K\alpha$ radiation. Crystal data are: Monoclinic, $a=17.27(11)$, $b=9.17(6)$, $c=18.55(12)$ Å, $\beta=98.0(7)°$, $Z=4$, and space group C2/c. The structure factors for 865 independent reflections were obtained. The structure was solved by the heavy atom method, refined by the full-matrix least-squares method, and the final R factor was 0.117. The positions of H atoms could not be determined. The near-infrared absorption spectra were measured on a Varian Cary 17-I spectrophotometer at 77 K and room temperature. In the measurement a quartz Dewer vessel was used. The measured data were corrected for the blank data measured in the absence of the sample.

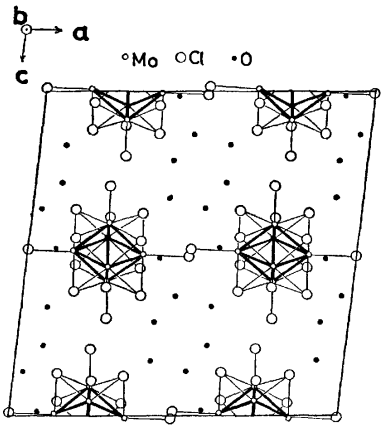

Fig. 1. The crystal structure of $(H_3O)_2[(Mo_6Cl_8)Cl_6]\cdot 6H_2O$ viewed along the b axis.

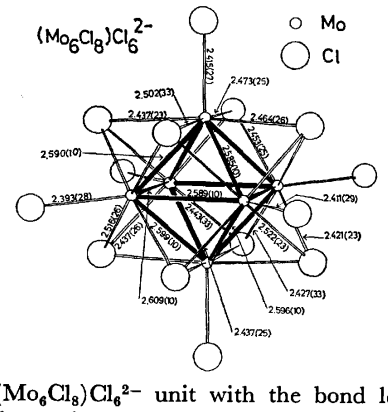

Fig. 2. $(Mo_6Cl_8)Cl_6^{2-}$ unit with the bond lengths(Å). There is an inversion center at the center of this unit. The estimated standard deviations are in parentheses.

Results and Discussion

The atomic parameters are deposited as Document No. 8212 at the Office of the Editor of the Bulletin of the Chemical Society of Japan, and Fig. 1 shows the crystal structure viewed along the b axis. The structure consists of the discrete units of $(Mo_6Cl_8)Cl_6^{2-}$ (shown in Fig. 2). In this unit, six Mo atoms form an approximate regular octahedron, and their configuration is very similar to that in bulk Mo metal, *i.e.*, b.c.c.structure. However, the distance between the neighboring Mo atoms (2.59 Å on the average) is shorter than in bulk Mo metal (2.72 Å), in other words, the Mo atoms are packed closer so that the overlap of the Mo atomic orbitals is large in this unit.

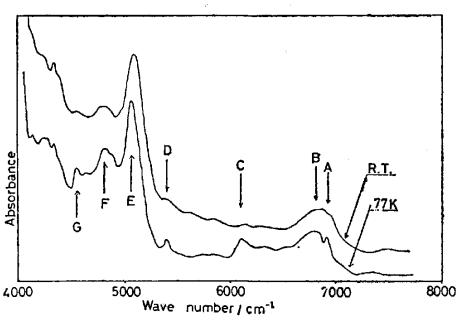

Fig. 3. The near-infrared absorption spectra of $(H_3O)_2[(Mo_6Cl_8)Cl_6]\cdot 6H_2O$ crystal at 77 K and room temperature.

Also eight Cl atoms form an approximate cube outside the Mo octahedron. The distance between Mo atoms and these 8 Cl atoms (2.46 Å on the average) agrees with the sum of the ion radii of sexivalent Mo^{6+} (0.62 Å) and Cl^- (1.81 Å), in contrast with that the Mo atoms are formally divalent in this material. Hence, the valence electrons of Mo atoms may be delocalized. These facts suggest that the feature of metallic bonding is still present even in such a small quasi-metallic system. In addition, these units are apart from one another in the crystal. It is quite possible to regard the crystalline state of this material as an aggregation of small metallic particles which are homogeneous in both size and shape.

Then the authors tried to estimate the order of the energy level interval of conduction electrons at the Fermi energy(δ), by regarding the 24 d-electrons of Mo atoms as conduction electrons and by applying the free electron model to this system. The formula $\delta=2\varepsilon_F/3N$ (ε_F: Fermi energy, N: number of electrons), which is applicable to a cube of bulk metal, was used in this estimation. The obtained order of energy level interval (about 1.0×10^{-19} $J=5.0\times10^3$ cm^{-1}) corresponded to the photon energy of the near-infrared region. Figure 3 shows the near-infrared absorption spectra measured for this crystal. The seven peaks observed are divided into two groups on the basis of their behaviors against temperature, *i.e.*, the A, C, D, F, and G peaks become broader at room temperature, while the B and E peaks do not show such temperature dependence. The latter peaks were ascertained to be attributable to the vibrational overtones of the water of crystallization. On the other hand, it is not adequate to attribute the former peaks to the molecular or lattice vibration of $(Mo_6Cl_8)Cl_6^{2-}$ unit, considering the heavy masses of the atoms which constitute this unit. In fact, the absorptions which arise from such vibrations were found in the far-infrared region.[4] Therefore, the peaks, except for B and E, should be related to various electronic transitions, where electronic levels split by low symmetry of the crystal may be involved. Also their peak positions fall satisfactorily within the range estimated above, though it remains a question that the valence electrons of molybdenum atoms in this case are assumed as free electrons. Then it is concluded that these absorption peaks may be attributed to the electronic transitions between the energy levels of conduction electrons which manifest the smallness of the system. From the standpoint of small metallic particles, the observation of such transitions is one of the evidences of energy quantization with respect to conduction electrons.

The basic concept of the authors is to regard the nuclei in a polynuclear complex as a small metallic particle. However, since the nuclei of single complex ion in the present material consist of only six molybdenum atoms, the energy level intervals of electrons are too large and the electronic states may not be well described by the Bloch functions. It is highly desired for the study of small metallic particles to synthesize complex ions which involve more metal atoms.

The authors wish to thank Dr. Hanako Kobayashi and Prof. Tsuyoshi Murao of Kyoto University for their continuous encouragement, and Prof. Tadamasa Shida of Kyoto University for his kind offer of the spectrophotometer.

References

1) R. Kubo, *J. Phys. Soc. Jpn.*, **17**, 975 (1962).
2) P. Yee and W. D. Knight, *Phys. Rev. B*, **11**, 3261 (1975).
3) W. L. Jolly, "The Synthesis and Characterization of Inorganic Compounds," Prentice-Hall, Englewood Cliffs, N. J. (1970), pp. 456—459.
4) F. A. Cotton, R. M. Wing, and R. A. Zimmerman, *Inorg. Chem.*, **6**, 11 (1967).

Nuclear Quadrupole Resonance of Chlorine-35 in Molybdenum(V) and Rhenium(III) Chlorides. Evidence for the Crystal Modifications of $MoCl_5$

Yoshio KUME*,† and Daiyu NAKAMURA

Department of Chemistry, Nagoya University, Chikusa-ku, Nagoya 464

(Received April 13, 1981)

Synopsis. The ^{35}Cl NQR frequencies were determined for molybdenum(V) and rhenium(III) chlorides at various temperatures. Two crystal modifications, showing two and three ^{35}Cl NQR frequencies, were found for the former compound. The three resonance frequencies observed for the latter compound are attributable to three chemically different chlorine atoms in the crystal.

Molybdenum(V) and rhenium(III) chlorides are known to form crystals in which polymeric units, Mo_2Cl_{10} and Re_3Cl_9, respectively, are discernible.[1,2] It is interesting to examine the temperature dependence of ^{35}Cl NQR frequencies for both compounds, because there exist both terminal and bridging chlorine atoms, which usually yield temperature dependences considerably different from each other.

Experimental

Molybdenum(V) chloride $MoCl_5$ was procured from commercial sources and was purified by means of a sublimation method similar to that described in the literature.[3] Commercial $MoCl_5$ was placed in the end of a Pyrex bulb train, and the sublimation system including the train was evacuated. When the bulb containing crude $MoCl_5$ was heated to about 130 °C, dark purple crystals were deposited in the next-neighboring bulb. The temperature of this bulb was maintained at a lower temperature than about 40 °C. After the sublimation process had finished, the bulb was sealed off at each side, with great care being taken not to heat the deposited crystals. The sample thus prepared is called $MoCl_5$ (I). When the bulb containing $MoCl_5$ (I) was heated very rapidly by a flame to the melting point of $MoCl_5$, the deposited crystals were melted without breaking the Pyrex bulb. The melted $MoCl_5$ was cooled very slowly, and black crystals with a bluish gloss were obtained. The sample obtained after melting is called $MoCl_5$ (II). Since the X-ray analysis of $MoCl_5$ was carried out with the sample prepared by melting,[1] $MoCl_5$ (II) is considered to have a dimeric structure. Commercial rhenium(III) chloride $ReCl_3$ was purified by use of a similar sublimation method. The chloride was sublimed at a temperature of about 450 °C under reduced pressure.

Chlorine NQR was observed by means of a modified Dean-type spectrometer in a frequency-modulation mode.[4]

Results and Discussion

Table 1 shows the NQR frequencies of ^{35}Cl in $MoCl_5$ and $ReCl_3$ at room, Dry Ice, and liquid-nitrogen temperatures.

The sample $MoCl_5$ (I) yielded four rather closely separated resonance frequencies at various temperatures observed. The second-highest frequency line was broad and weak, whereas other lines were moderately strong and had a relatively narrow line-width. The relative intensity of the second-highest line to that of other lines varied depending on the samples, which were different from each other in the deposit temperature in the sublimation purification process. The sample deposited at a lower temperature gave a weaker second-highest line. Furthermore, the resonance frequencies of the second-highest line determined at various temperatures agree with those reported by Brown and Kent[5] for Mo_2Cl_{10}. The sample $MoCl_5$ (II), prepared by melting, showed two widely separated broad resonance lines at liquid N_2 temperature, the higher-frequency line of which yielded a resonance frequency identical with that of the second-highest line of $MoCl_5$ (I). The lower-frequency line of the doublet, which escaped detection in the study of Brown and Kent,[5] was weaker. With increasing the tem-

TABLE 1. NQR FREQUENCIES OF ^{35}Cl IN MOLYBDENUM(V) AND RHENIUM(III) CHLORIDES

Compound	NQR frequency ν/MHz		
	27 °C	−78 °C	−196 °C
$MoCl_5$ (I)	14.224±0.01	14.346±0.01	14.471±0.01
	14.036±0.01	14.114±0.01	14.206±0.01
	13.904±0.01	13.977±0.01	14.063±0.01
$MoCl_5$ (II)	14.10 ±0.02	14.19 ±0.02	14.27 ±0.02
	(fade-out at −50 °C)	12.22 ±0.02	12.18 ±0.02
$ReCl_3$	21.772±0·003	21.843±0.003	21.921±0.003
	16.475±0.003	16.481±0.003	16.494±0.003
	15.040±0.003	15.058±0.003	15.074±0.003

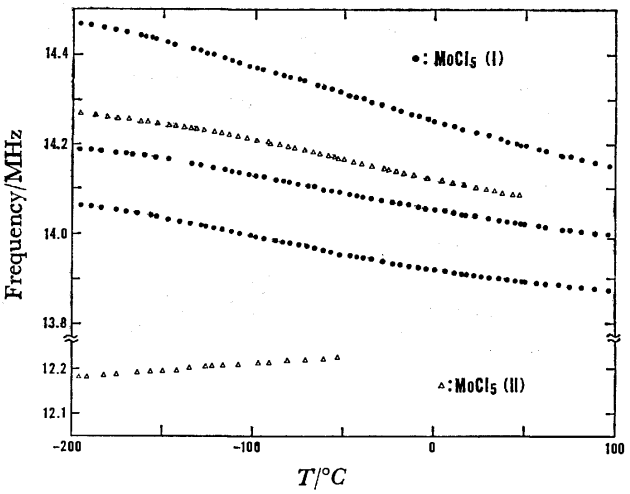

Fig. 1. Temperature dependence of ^{35}Cl NQR frequencies in $MoCl_5$ (I) prepared by sublimation and $MoCl_5$ (II) obtained by once melting $MoCl_5$ (I).

† Present address: Faculty of General Education, Azabu University, Fuchinobe 1-17-71, Sagamihara, Kanagawa 229.

perature from liquid N_2 temperature, this line showed a positive temperature coefficient, as shown in Fig. 1; it gradually became weaker until it faded out at about −50 °C. These experimental facts indicate that molybdenum(V) chloride directly crystallized by sublimation gives three ^{35}Cl NQR frequencies at various temperatures, whereas the compound once melted yields two widely separated lines. Accordingly, it is concluded that there exist two crystalline modifications in molybdenum(V) chloride: one, the crystal directly deposited from its vapor, has at least three nonequivalent chlorine atoms in the crystal, while the other is the crystal once melted and contains at least two chemically different chlorine atoms.

Three widely separated ^{35}Cl NQR frequencies were observed for rhenium(III) chloride at various temperatures studied. This indicates that there exist three chemically nonequivalent chlorine atoms in the crystal. According to the X-ray crystal analysis by Cotton and Mague,[2] crystallographically equivalent trimer units, Re_3Cl_9, exist in the crystal. In a trimer unit, there are three chemically nonequivalent chlorine atoms: terminal chlorine, **a**, asymmetric bridging chlorine, **b**, and symmetric bridging chlorine, **c**. Consequently, the present NQR results agree well with those of the X-ray analysis.

The highest-frequency line of the triplet is greatly separated from the remaining two lines. By referring to the NQR results of dimeric IIIB metal halides,[6,7] this line can be assigned to the terminal chlorine, **a**, and the lower-frequency lines, to the bridging chlorine atoms, **b** and **c**. Since the asymmetric bridging chlorine **b** forms a weak bridge bond with rhenium in the neighboring trimer, the chlorine atom may have a character of terminal chlorine to some extent. Accordingly, the middle-frequency and the lowest-frequency lines can be assigned to the bridging chlorine atoms, **b** and **c**, respectively.

The temperature coefficients, $|d\nu/dT|$, of the middle-frequency and lowest-frequency lines were very small (0.09 and 0.15 kHz K^{-1}, respectively, in the temperature range of −196—27 °C). Since bridging chlorine is usually bound more tightly than terminal chlorine, the thermally excited vibrational amplitude of the former chlorine atom is smaller than that of the latter. According to the simple Bayer-Kushida theory,[8,9] the coefficient, $|d\nu/dT|$, is proportional to the vibrational amplitude. This fact supports the above assignments of the observed resonance frequencies.

References

1) D. E. Sands and A. Zalkin, *Acta Crystallogr.*, **12**, 723 (1959).
2) F. A. Cotton and J. T. Mague, *Inorg. Chem.*, **3**, 1402 (1964).
3) L. C. Hurd and E. Brimm, *Inorg. Synth.*, Vol. I, 180 (1939); M. H. Lietzke and M. L. Holt, *ibid.*, Vol. III, 163 (1950).
4) D. Nakamura, Y. Kurita, K. Ito, and M. Kubo, *J. Am. Chem. Soc.*, **82**, 5783 (1960).
5) T. L. Brown and L. G. Kent, *J. Phys. Chem.*, **74**, 3572 (1970).
6) R. G. Barnes and S. L. Segel, *J. Chem. Phys.*, **25**, 180 (1956); S. L. Segel and R. G. Barnes, *ibid.*, **25**, 578 (1956); R. G. Barnes, S. L. Segel, P. J. Bray, and P. A. Casabella, *ibid.*, **26**, 1345 (1957); P. A. Casabella, P. J. Bray, and R. G. Barnes, *ibid.*, **30**, 1393 (1959).
7) T. Okuda, H. Terao, O. Ege, and H. Negita, *J. Chem. Phys.*, **52**, 5489 (1970).
8) H. Bayer, *Z. Phys.*, **130**, 227 (1951).
9) T. Kushida, *J. Sci. Hiroshima Univ.*, **A19**, 327 (1955).

Further Comments on the Line-broadening of the Chlorine 35 NMR Spectra and the Local Structure around a Chloride Ion in Aqueous Solutions of Non-electrolytes

Masako YUDASAKA,† Tadahi SUGAWARA, Hiizu IWAMURA, and Tsunetake FUJIYAMA*

Institute for Molecular Science, Myodaiji, Okazaki 444

† *Department of Chemistry, Faculty of Science, Tokyo Metropolitan University, Setagaya-ku, Tokyo 158*

(Received May 15, 1981)

Synopsis. The remarkable line-broadenings of the ^{35}Cl NMR spectra observed for the KCl in aqueous solutions of non-electrolytes were explained well by considering the formation of water-cages which surround the non-electrolytes. This result, in turn, suggests that the line-width measurement is a useful method for determining local structures formed in solutions.

In the previous report on the ^{35}Cl NMR spectra,[1] we have reported the remarkable line-broadening observed for the KCl in the aqueous acetone system. This result seemed important because the line-broadening cannot be observed in an aqueous solution of KCl in which a so-called "contact-ion pair" is not formed. Stimulated by this line-broadening observation, we have now extended our study of line-widths to aqueous solutions of non-electrolytes in order to establish the origin of the line-broadening.

Let us first add a supplemental finding on the aqueous solution of dimethyl sulfoxide (DMSO hereafter). The ^{35}Cl line-width in of KCl in the H_2O–DMSO system was observed for various solvent components. In this mixed solution, KCl dissociates completely or does not exist in the form of a contact-ion pair. The results and the related physical quantities are summarized in Table 1. The observed concentration-dependence of the line-width is illustrated in Fig. 1. It can be seen from the figure that the line-width is as narrow as about 5—10 Hz both in pure water and in pure DMSO, while it becomes broader in a mixed solvent. For example, the viscosity-corrected line-width[2] in a 0.5 mole fraction of an aqueous DMSO solution is almost twenty times as broad as those observed in pure solvents. A chloride ion is known to be symmetrically solvated by water molecules in an aqueous solution. As DMSO is also known to solvate a chloride ion as strongly as water does, it is natural to consider that DMSO molecules can also exist as the nearest neighbours of a chloride ion. Therefore, the water molecules which solvate a chloride ion in the aqueous solution of KCl are replaced by DMSO molecules, one by one, by adding DMSO to the aqueous solution of KCl. That is to say, the field gradient at a chloride ion increases with the increase in the DMSO concentration, this results in the line-broadening due to the increase in the DMSO concentration. In the high-concentration range of DMSO, on the other hand, a chloride ion comes to be surrounded mostly by DMSO molecules, which again increases the symmetry around the chloride ion. Therefore, the line-width will again become narrower at a very high concentration of DMSO.

Let us now turn back to the aqueous acetone solution. We wanted to know why we observed line-broadening upon adding acetone to an aqueous solution of KCl.[1] As salts like KCl and NaCl are not dissolved in pure acetone, the line-broadening cannot be ascribed to the direct interaction between acetone and a chloride ion. It has been established in our previous works[3] that, in an aqueous acetone solution, water molecules form a cage-structure by surrounding

Table 1. Chemical shifts, δ, line-width, $\Delta\nu$, and viscosity-corrected line-width, $\Delta\nu^\circ$, of ^{35}Cl NMR in the DMSO–H_2O solvent system at 62 °C

Concentration x_{DMSO}	Chemical shift[a] δ/ppm	Line-width $\Delta\nu$/Hz	Viscosity[b] η/cP	Viscosity corrected line-width $\Delta\nu^\circ$/Hz
1.000	200	9.5	0.927	10
0.100	207	38	0.930	41
0.195	212	91	1.33	68
0.432	227	112	1.52	74
0.595	239	105	1.45	72
0.798	250	67	1.29	52
0.902	256	41	1.25	33
1.000	265	4.8	1.35	3.6

a) The exact Larmor frequency was divided by the ^{35}Cl resonance frequency (7.794 MHz) and expressed in ppm. Chemical shifts relative to aqueous potassium chloride can be obtained by subtracting 200 ppm from each value. b) 1 cP = 10^{-3} Pa s.

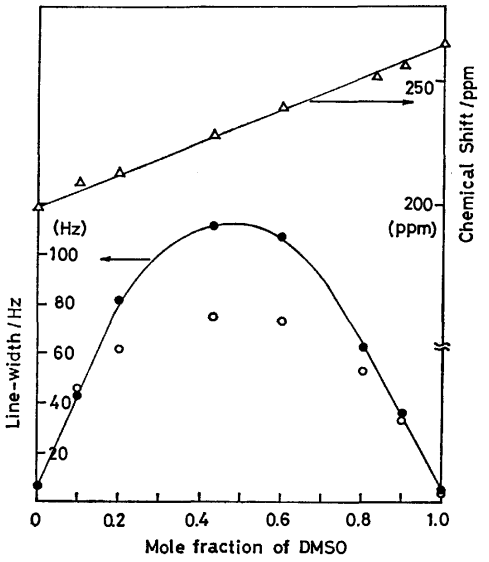

Fig. 1. Line-width and chemical shift of the ^{35}Cl NMR as a function of solvent component in DMSO–H_2O system.
△: Chemical shift, ●: observed line-width, ○: viscosity corrected line-width.

an acetone molecule. On the base of this idea, we can reasonably explain the observed line-broadening. In an aqueous acetone solution, chloride ions can exist in two ways. Some chloride ions can exist as isotropically solvated ions which can be responsible for narrower line-widths. Some other chloride ions, on the other hand, can take part in the formation of the cage which is formed by water molecules in the aqueous acetone solution. In the latter case, the local symmetry around a chloride ion is not spherical, which results in the appearance of a large field gradient at the chloride ion. Therefore, the line-width arising from this chloride ion is much broader than that of the isotropically solvated ion.

Next, let us consider the line-broadening observed in the ^{35}Cl NMR spectra of tetraethylammonium chloride (Et_4NCl hereafter) in a water solution. It has been shown in our previous report[1] that the concentration dependence of the line-width can be explained well by considering the equilibrium between two chemical species, namely, a free ion (the line-width of which is 11.6 ± 0.3 Hz) and a contact-ion pair (the line-width of which is 546 ± 194 Hz). Now we can give a more accurate image of the species referred to as a "contact-ion pair". As the outer part of an Et_4N^+ ion is composed of methyl groups which have a strong hydrophobic character, water-cage can be formed around the Et_4N^+ ion.[3] A chloride ion can exist in this solution either by dissolving in bulk water or by taking part in the formation of the cage-structure in place of a water molecule. The line-width corresponding to the former case is very narrow, because the local symmetry around the chloride ion is spherical. As the local symmetry is lowered by the asymmetric hydration in the latter case the line-width corresponding to this case can be very greatly broadended because of the large field gradient produced by the surrounding water dipoles.[4] Thus, we can conclude that the "contact-ion pair" which has been described in our previous report corresponds to the chemical species whose structure is composed of an Et_4N^+ ion surrounded by a water-cage and a chloride ion which takes part in the formation of the cage. Such a caging-in effect of fluoride ions has been ascertained by the X-ray diffraction study of the solid clathrate hydrate of tetraisopentylammonium fluoride.[5] It is of interest to add that the ^{35}Cl NMR lines corresponding to these two species are observed to be averaged single Lorentzians. This result suggests that the exchange rate between the free and in-cage species is faster than the NMR-time scale ($\approx10^{-7}$ s) and that the lifetime of the in-cage chloride ion is longer than the rotational correlation time of the chloride ion ($\approx10^{-11}$ s).[6] Incidentally, this type of line-broadening has not been observed for these aqueous solutions of KCl, NaCl, and NH_4Cl, simply because these cations cannot form water-cages in aqueous solutions. Thus, the apparent complexities observed for the concentration dependences of the line-widths can be understood by considering the local symmetry of the hydrations around chloride ions. This, in turn, suggests that the line-width measurement of the ^{35}Cl NMR spectra is a powerful and straightforward method for demonstrating cage-structure formations in aqueous solutions.

The authors wish to express their thanks to Mr. Yukihiro Yokoyama for his help in the ^{35}Cl NMR spectral measurements.

References

1) M. Yudasaka, T. Sugawara, H. Iwamura, and T. Fujiyama, *Bull. Chem. Soc. Jpn.*, **54**, 3273 (1981).

2) A viscosity-corrected line-width, $\Delta\nu^\circ$, is defined as follows using the measured line-width, $\Delta\nu$, and the viscosity, η:

$$\Delta\nu^\circ = \Delta\nu/(\eta/\eta_0),$$

where η_0 is a unit of viscosity. The validity of using a viscosity-corrected line-width for the discussion of line-broadening was confirmed as follows. The line-width of NaCl was measured in aqueous polyethylene glycol (av. MW 200, 4000, 20000). The line-width was found to be proportional to the mobility of the chloride ion as determined by conductivity measurements (R. Tamamushi, private communication) and also proportional to the viscosity of the solution, as long as the Walden product of the solution is less than 2.

3) T. Kato, M. Yudasada, and T. Fujiyama, *Bull. Chem. Soc. Jpn.*, **54**, 1632 (1981).

4) The line-broadening due to the asymmetric hydration has already been pointed out: H. Wennerström, B. Lindman, and S. Forsén, *J. Phys. Chem.*, **75**, 2936 (1971); H. G. Hertz and M. Holtz, *ibid.*, **78**, 1002 (1974).

5) D. Feil and G. A. Jeffrey, *J. Chem. Phys.*, **35**, 1231 (1959).

6) A. G. Marshall, *J. Chem. Phys.*, **52**, 2527 (1970).

Thermal Stability Enhancement of Liquid-crystal Phase by Charge-transfer Interaction in Binary Mixtures. Application of Solid-solution Model

Yôichi IIDA

Department of Chemistry, Faculty of Science, Hokkaido University, Sapporo 060

Synopsis. Phase transition in liquid crystal of binary mixture consisting of electron donor and acceptor was examined by using modified solid-solution model. The charge-transfer interaction between donor and acceptor is essential for parallel molecular arrangement in liquid crystal, resulting in thermal stability enhancement of mesophase in binary mixture.

Much attention has been paid to a great number of liquid crystals, which show intermediate state between crystalline solid and isotropic liquid.[1] Intermolecular attractions appear to be essential for producing the parallel molecular arrangement characteristic of such a state. Binary systems have been often used to achieve extended liquid crystalline temperature ranges.[2,3] Usually, the mesophase→isotropic liquid transition temperature of binary mixture varies linearly with composition. However, large deviations from such a linearity are observable, if molecular complex formation takes place between the components of the binary system. Complex formation due to electron donor-acceptor (charge-transfer) interaction may be effective for parallel molecular arrangement in liquid crystals. Park *et al.* examined nematic phase→isotropic liquid transition temperature (T_{NI}) in the binary system of *N*-(*p*-methoxybenzylidene)-*p*-*n*-butylaniline (MBBA) and 4-cyano-4′-pentylbiphenyl (CPB) and in several closely related binary mixtures, because there was a possibility of a weak charge-transfer interaction between a donor of MBBA and an acceptor of CPB.[2] As is shown in (a) of Fig. 1, the experimental relation of T_{NI} to composition of MBBA–CPB mixtures exhibits a broad curve whose maximum is located near 1:1 mole ratio, and T_{NI} of mixture is higher than the straight line joining T_{NI} of the two components ((c) of Fig. 1). In the present paper, using modified solid-solution model, we shall show that the attractive forces between donor and acceptor due to charge-transfer interaction is essential for such a thermal stability enhancement of liquid-crystal phase.

In the following, we discuss nematic phase induced by charge-transfer interaction in binary mixtures composed of rod-like donors and acceptors. Let us denote mole fractions of donors and acceptors as x_D and x_A, ($x_D+x_A=1$), respectively. The nematic→isotropic transition temperatures of pure donor and acceptor components are indicated by T_D and T_A, respectively. In general, nematic phase has a high degree of long range orientational order of the molecules, but no long range translational order. The molecules are spontaneously oriented with their long axes approximately parallel. In the present paper, we only consider how Gibbs free energy of nematic phase is influenced by the manner of mixing of donors and acceptors. For this purpose, we examine a three-dimensional lattice where molecules are oriented with their long axes parallel. It is assumed that such

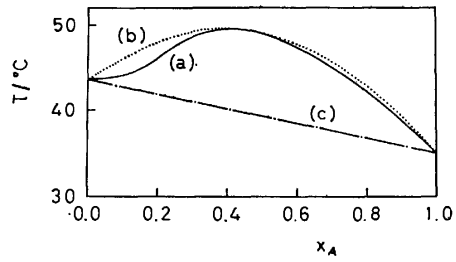

Fig. 1. Phase transition temperature of binary system of *N*-(*p*-methoxybenzylidene)-*p*-*n*-butylaniline (MBBA) and 4-cyano-4′-pentylbiphenyl (CPB). (a) indicates the experimental relation of nematic→isotropic transition temperature (T_{NI}) to mole fraction of CPB (x_A), as given by Ref. 2; (b), the theoretical relation of order→disorder transition temperature (T_c) to x_A; (c), the straight line joining T_{NI} of the two components. See text.

a lattice can be subdivided into two sublattices D and A, and that one site of D or A sublattice is surrounded by z equivalent nearest neighbor sites of A or D sublattice, respectively. Then, if the charge-transfer interaction between donor and acceptor is essential for parallel molecular arrangement to induce nematic phase, the nematic→isotropic phase transition should correspond to order→disorder phase transition for mixing of donors and acceptors. In other words, if the order of molecular arrangement of donors and acceptors remains, the system is supposed to be in nematic phase, while if the order is lost, it goes to isotropic liquid.

In order to show this situation more clearly, we take an approach of solid-solution model. Let us denote the numbers of sites of D and A sublattices as $N/2$ and $N/2$, respectively. The total number of donor and acceptor molecules in binary mixture is N, so that each site of D and A sublattices is occupied by either donor or acceptor. It is assumed that charge-transfer interaction acts in (1:1) manner between nearest neighbor donor and acceptor. In the system of pure donors ($x_D=1.00$), all the sites of D and A sublattices are occupied by donors at temperature T_D, while in the system of pure acceptors ($x_A=1.00$), by acceptors at temperature T_A. For binary mixtures, let us denote the numbers of donors and acceptors in D sublattice as $[^d_D]$ and $[^a_D]$, respectively, while the numbers of donors and acceptors in A sublattice as $[^d_A]$ and $[^a_A]$, respectively. We introduce order parameter X, ($0\leq X\leq 1$), in such a way that, if $0\leq x_D\leq 1/2$, $[^d_D]=(1/2)N\ x_D(1+X)$, $[^a_D]=(1/2)N\ (x_A-x_DX)$, $[^d_A]=(1/2)N\ x_D(1-X)$ and $[^a_A]=(1/2)N\ (x_A+x_DX)$. In other words, if $X=1$, all donors occupy sites of D sublattice, while if $X=0$, donors and acceptors occupy sites of D and A sublattices randomly. Similar expressions can be obtained in the case of $0\leq x_A\leq 1/2$. The state of $X=0$ is called disordered phase with

respect to mixing of donors and acceptors, while $X=1$, ordered phase. For order parameter X, the entropy for mixing donors and acceptors in binary mixture with composition (x_D, x_A) is then calculated as

$$S = k \ln \frac{\frac{N}{2}!}{[\frac{d}{D}]![\frac{a}{D}]!} \frac{\frac{N}{2}!}{[\frac{d}{A}]![\frac{a}{A}]!}$$
$$= -\frac{N}{2}k\{x_D(1+X)\ln x_D(1+X) + (x_A-x_DX)\ln(x_A-x_DX) + x_D(1-X)\ln x_D(1-X) + (x_A+x_DX)\ln(x_A+x_DX)\}. \quad (1)$$

Next, we examine the energy of our binary system in terms of order parameter X. We take only into consideration the intermolecular interaction energies between nearest neighbor molecules. The terms v_{DD}, v_{AA} and v_{DA} indicate the energies between a pair of donor-donor, acceptor-acceptor and donor-acceptor molecules in nearest neighbor sites, respectively. Note that v_{DD} and v_{AA} are weak stabilization energies due to van der Waals forces, while v_{DA} corresponds to stabilization energy due to charge-transfer interaction which is much stronger than v_{DD} and v_{AA}. Then, $v=(1/2)(v_{DD}+v_{AA})-v_{DA}\geq 0$. In terms of v, the energy, E, of binary mixture is given by

$$E = \frac{z}{2}N\{v_{DD}x_D^2 + 2v_{DA}x_Dx_A + v_{AA}x_A^2\} - zNx_D^2vX^2. \quad (2)$$

For binary mixture, because of strongly attractive charge-transfer interaction, the order parameter at temperature $x_DT_D+x_AT_A$ is assumed to be $X=1$. If there is no volume change, Gibbs free energy of the system is given by

$$G_o = E_o - (x_DT_D+x_AT_A)S_o, \quad (3)$$

where $E_o=zNv_{DA}x_D+(z/2)Nv_{AA}(x_A^2-x_D^2)$ and $S_o=-(Nk/2)\{2x_D\ln 2x_D+(x_A-x_D)\ln(x_A-x_D)\}$. At temperatures above $x_DT_D+x_AT_A$, we are only concerned with how Gibbs free energy is changed by the manner of mixing of donors and acceptors. For this purpose, we consider G_o at temperature $x_DT_D+x_AT_A$ as a standard. When temperature is elevated from $x_DT_D+x_AT_A$, the order parameter decreases from $X=1$, and at certain temperature $T>x_DT_D+x_AT_A$, the energy and the entropy of our system change from E_o and S_o to E and S with order parameter $1>X\geq 0$, as are given by Eqs. 2 and 1, respectively. As long as we consider the effect of mixing upon free energy change, we can only discuss the difference of Gibbs free energy, ΔG, with respect to G_o, so that we obtain, at $T\geq x_DT_D+x_AT_A$,

$$\Delta G = E - E_o - (T-x_DT_D-x_AT_A)\cdot(S-S_o). \quad (4)$$

Eq. 4 means that, if temperature increases further, the order parameter decreases progressively, and at critical temperature T_c, the system undergoes a phase transition from ordered state with $X\neq 0$ to disordered state with $X=0$. In order to examine this condition, we consider $(\partial\Delta G/\partial X)=0$. The equation to determine X is given by

$$\frac{zx_Dv}{k(T-x_DT_D-x_AT_A)}X = \frac{1}{4}\ln\left(\frac{1+X}{1-X}\cdot\frac{x_A+x_DX}{x_A-x_DX}\right). \quad (5)$$

After some manipulation of Eq. 5, the transition temperature is found to be $T_c=x_DT_D+x_AT_A+4x_Dx_AT_c^\circ$, where $T_c^\circ=zv/2k$. The magnitude of the thermal stability enhancement of ordered phase, $4x_Dx_AT_c^\circ$, above temperature $x_DT_D+x_AT_A$ is closely related to that of $v=(1/2)(v_{DD}+v_{AA})-v_{DA}\geq 0$. If $v=0$, then $T_c^\circ=0$, $T_c=x_DT_D+x_AT_A$ and we obtain no thermal stability enhancement of ordered state. However, if greater energy stabilization of v_{DA} occurs with parallel molecular arrangement of donors and acceptors, both v and T_c° increase appreciably and the stability enhancement of ordered state occurs accordingly.

Let us examine how the order→disorder phase transition for mixing of donors and acceptors corresponds to the nematic→isotropic phase transition of MBBA–CPB mixtures reported by Park *et al.*[2] If we take $T_D=43.5$ °C, $T_A=35.0$ °C, and $T_c^\circ=9.6$ °C, the order→disorder transition temperature $T_c=x_DT_D+x_AT_A+4x_Dx_AT_c^\circ$ *versus* composition is given by curve (b) of Fig. 1. This is compared with curve (a) of the experimental relation of T_{NI} to composition. In the composition range $0.4\leq x_A\leq 1.0$, both curves are found to agree quite well. The maximum temperature of T_c occurs at $x_A=0.39$, while that of T_{NI}, at $x_A=0.40$, so that the agreement of both values is very good. In the range $0.0\leq x_A\leq 0.4$, T_c is found to be somewhat higher than T_{NI}. This discrepancy implies that, in the range $0.0\leq x_A\leq 0.4$, some specific intermolecular interaction may take place in MBBA and CPB, so that our solid-solution model is not enough to describe that situation exactly. Except for this little discrepancy, the relation of T_c to composition appears to agree well with that of T_{NI} to composition. Therefore, the order→disorder transition for mixing of donors and acceptors corresponds well to the nematic→isotropic phase transition in MBBA–CPB mixtures. This means that the charge-transfer interaction between donor of MBBA and acceptor of CPB is essential for parallel molecular arrangement to induce nematic phase above temperature $x_DT_D+x_AT_A$. From the value of $T_c^\circ=9.6$ °C together with $T_c^\circ=zv/2k$, the magnitude of zv in the nematic phase of MBBA–CPB mixture is estimated to be 0.16 kJ mol^{-1}.

Finally, we have to say a few words about our solid-solution model. As was mentioned, nematic phase has a high degree of long range orientational order of the molecules but no long range translational order, whereas in solid-solution model, we consider a three-dimensional lattice where not only orientational order but also translational order are assumed. In the present paper, however, we have only discussed how Gibbs free energy of binary mixture is changed by the manner of mixing of donors and acceptors. As long as the problem is limited to such a difference in the degree of mixing, the solid-solution model is still applicable to liquid crystals where long range translational order no longer exists.

References

1) See, for example, S. Chandrasekhar, "Liquid crystals," Cambridge University Press, London, New York, New Rochelle, Melbourne, Sydney (1980).

2) J. W. Park, C. S. Bak, and M. M. Labes, *J. Am. Chem. Soc.*, **97**, 4398 (1975).

3) A. C. Griffin, R. F. Fisher, and S. J. Havens, *J. Am. Chem. Soc.*, **100**, 6329 (1978); M. Domon and J. Billard, *J. Phys. (Paris), Colloq.*, **40**, C3-413 (1979); N. K. Sharma, G. Pelzl, D. Demus, and W. Weissflog, *Z. Phys. Chem. (Leipzig)*, **261**, 579 (1980); K. Araya and Y. Matsunaga, *Bull. Chem. Soc. Jpn.*, **53**, 3079 (1980).

The Electron-donor Property of Zirconia

Kunio Esumi* and Kenjiro Meguro

Department of Applied Chemistry, Faculty of Science, Science University of Tokyo, Kagurazaka, Shinjuku-ku, Tokyo 162

(Received June 22, 1981)

Synopsis. The electron-donor property of zirconia was investigated by means of the adsorption of TCNQ. The TCNQ anion radicals were formed as a result of electron transfer to adsorbed TCNQ from the zirconia surface. The radical concentration decreased with an increase in the calcining temperatures, reached a minimum value at 700 °C, and then increased. This behavior can be explained by a change in the electron-donor site number and the strength of the electron-donor site.

The adsorption of electron acceptors on metal oxides has been investigated, in order to characterize the electron-donor properties of the metal-oxide surfaces. Flockhart *et al.*[1] attempted the adsorption of tetracyanoethylene (TCNE) for the estimation of the electron-donor properties of the alumina surface. In this respect, they associated the electron-donor sites with the unsolvated hydroxide ions and the defect centers involving oxide ions. Meguro and Esumi,[2] carrying out a study of the adsorption of electron acceptors with electron affinities ranging from 1.26 to 2.84 eV on the surface of alumina, have shown that the limit of electron transfer from the alumina surface to the electron acceptors ranged between 1.77 and 1.26 eV in the affinity of the electron acceptor. Thus, the utility of electron-acceptor adsorption for the study of the electron-donor properties of metal oxides has been established.

Zirconia is an important promoter of various dispersed catalysts. To characterize zirconia catalysts, it is necessary to study the surface properties of zirconia. Already, works involving the adsorption of gases, the heat of immersion, and infrared spectroscopy for zirconia have been reported.[3–5] The present study will discuss the electron-donor property of zirconia when 7,7,8,8-tetracyanoquinodimethan (TCNQ) adsorption is used.

Zirconia was prepared by the hydrolysis of zirconium tetrachloride, which had been dissolved in distilled water. The solution was neutralized by ammonium hydroxide, and the precipitate thus formed was washed with distilled water until free from chloride ions. The precipitate was dried for 48 h at 120 °C. The final products were then obtained by calcination in air for 2 h at temperatures between 300 and 1000 °C in an electric furnace, followed by cooling *in vacuo*. The pertinent properties of these samples are given in Table 1.

The TCNQ was supplied by Dainippon Ink Chemical Ltd., and was recrystallized from an acetonitrile solution. The acetonitrile used was of a reagent grade. The apparatus and procedure used in this study have been described elsewhere.[2]

The adsorption isotherms of TCNQ at 25 °C from a solution in acetonitrile on the surface of zirconia calcined between 300 and 1000 °C are shown in Fig. 1. All of the isotherms are convex to the concentration axes, and all follow the Langmuir plots. The half-value of the limiting amount of TCNQ adsorbed on the zirconia surfaces, as estimated from the Langmuir plots, is given in the first column of Table 2. As shown in Table 2, it can be seen that the amount of TCNQ adsorbed on the ziconia surfaces increases with an increase in the calcining temperature, reaches a maximum value at 500 °C, and then decreases.

Table 1. Pertinent properties of zirconia

Sample	Calcining temp/°C	Phase[a]	Surface area[b] m^2/g^{-1}
A	300	A[c]+T(tr)	276.9
B	500	M+T(tr)	88.1
C	700	M	60.1
D	900	M	42.8
E	1000	M	34.5

a) From X-ray analysis. b) From the nitrogen adsorption at 77 K after outgassing at 100 °C. c) A=amorphous, T=tetragonal, M=monoclinic, (tr)=trace.

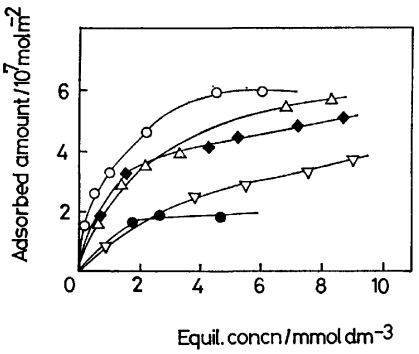

Fig. 1. Adsorption isotherm of TCNQ on zirconia (at 25 °C). Calcination temperature; ○: 300 °C, △: 500 °C, ◆: 700 °C, ▽: 900 °C, ●: 1000 °C.

When TCNQ was adsorbed from a solution in acetonitrile on the surfaces of zirconia, the zirconia surfaces developed a remarkable coloration. The color was violet in all of the samples. It has previously been reported[2,6,7] that the adsorption of electron acceptors onto metal oxides produces a surface coloration. The samples colored by the TCNQ adsorption gave unresolved ESR spectra with a *g*-value of 2.003. These spectra can be attributed to the hindered freedom of the adsorbed species, which obscures the hyperfine structure of the spectra. The spectra have been identified as being those of TCNQ anion radicals.[2]

The above results support the idea that the TCNQ anion radicals are formed as a result of electron transfer from the zirconia surfaces to the TCNQ adsorbed.

The TCNQ-radical concentration formed on the surface of zirconia is plotted against the equilibrium

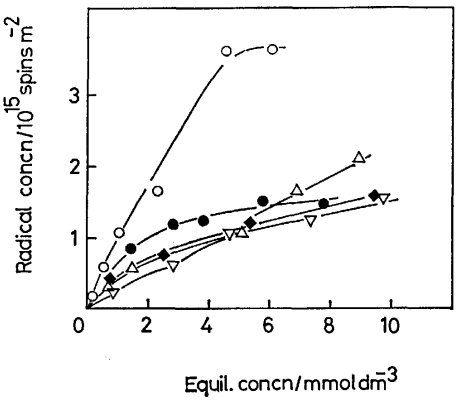

Fig. 2. Radical concentration on zirconia *vs.* equilibrium concentration of TCNQ (at 25 °C). Calcination temperature; ○: 300 °C, △: 500 °C, ◆: 700 °C, ▽: 900 °C, ●: 1000 °C.

concentration of TCNQ at 25 °C in Fig. 2. Many of the isotherms were of a Langmuir type. Therefore, to compare the TCNQ-radical concentration on the surface of zirconia as a function of the calcination temperature, the TCNQ-radical concentration corresponding to the half-value of the limiting amount of TCNQ adsorbed is employed, it is given in the second column of Table 2. It is found that the TCNQ radical concentration decreases with an increase in the calcining temperatures, reaches a minimum value at 700 °C, and then increases.

The nature of the electron-donor sites responsible for the electron-transfer process is not well understood. However, it has been proposed[5,6] that the electron-donor sites of metal oxides, such as alumina and titania, are associated with surface hydroxide ions at lower calcining temperatures and with surface oxide ions at higher temperatures. In the case of zirconia, it is also expected that the electron-donor sites are correlated with the two different sites described above. Indeed, it has been observed by infrared spectroscopy[7] that the surface of zirconia contains hydroxide ions.

The change in the TCNQ radical concentration as a function of the calcination temperatures might be interpreted as follows. At the calcining temperature of 300 °C, the electron-donor sites are surface hydroxide ions. The decrease in the TCNQ radical concentration between 300 and 700 °C corresponds to a reduction in the number of hydroxide ions on the surface. Above 900 °C, surface oxide ions play an important role as electron-donor sites.

Table 2. Data of TCNQ adsorption on zirconia

Sample	Adsorbed amount	Radical concn	Radical concn adsorbed amount
	10^{-7} mol m^{-2}	10^{4} spins m^{-2}	10^{21} spins mol^{-1}
A	3.4	10.0	3.2
B	3.6	6.8	1.9
C	2.9	5.3	1.8
D	2.5	8.5	3.4
E	1.1	6.4	5.8

The ratio of the transformation from the TCNQ adsorbed into the TCNQ radical on the surface of zirconia is important to an understanding of the strength of the electron-donor sites. That is, the larger the ratio, the stronger the electron-donor sites. This ratio can be estimated by dividing the TCNQ radical concentration by the corresponding half-value of the limiting amount of TCNQ. The values are given in the third column of Table 2. This ratio decreases with an increase in the calcining temperatures, reaches a minimum value at 700 °C, and then increases. This result suggests that, in the electron-transfer process, the surface oxide ions are much stronger electron-donor sites than the surface hydroxide ions.

References

1) B. D. Flockhart, I. R. Leith, and R. C. Pink, *Trans. Faraday Soc.*, **66**, 469 (1970).
2) K. Meguro and K. Esumi, *J. Colloid Interface Sci.*, **59**, 93 (1977).
3) H. F. Holmes, E. L. Fuller, Jr., and R. A. Ben, *J. Colloid Interface Sci.*, **47**, 365 (1974).
4) H. F. Holmes, E. L. Fuller, Jr., and R. B. Gammage, *J. Phys. Chem.*, **76**, 1497 (1972).
5) P. A. Agron, E. L. Fuller, Jr., and H. F. Holmes, *J. Colloid Interface Sci.*, **52**, 553 (1975).
6) K. Esumi and K. Meguro, *J. Jpn Soc. Colour Material.*, **48**, 544 (1975); **48**, 535 (1975).
7) A. J. Tench and R. L. Nelson, *Trans. Faraday Soc.*, **63**, 2254 (1967).

Substituent Effect on a Photo-Smiles Rearrangement by Laser Photolysis

Kenji YOKOYAMA, Junko NAKAMURA, Kiyoshi MUTAI,† and Saburo NAGAKURA*

The Institute of Physical and Chemical Research, Wako, Saitama 351

† *Department of Chemistry, College of General Education, The University of Tokyo, Meguro-ku, Tokyo 153*

(Received July 4, 1981)

Synopsis. The photo-Smiles rearrangement was studied for two homologues of *N*-[2-(4-nitrophenoxy)ethyl]-aniline by laser photolysis, an importance being attached to the effect of the alkoxyl substituent on the reactive position. The nitro group enhances the substitution at the para position, but the alkoxyl group does not play a significant role in the photosubstitution of the molecules.

The photo-Smiles reaction of *N*-[2-(4-nitrophenoxy)-ethyl]aniline (**1**) is a typical example of intramolecular nucleophilic photosubstitution.[1] In the previous study,[1] the authors demonstrated by the aid of laser photolysis that this reaction proceeds *via* an intramolecular ion radical pair and the Meisenheimer-type complex. This means that the substitution takes place through interaction between the ground state cation and anion radicals in pair. From this point of view, it is reasonable that the photosubstitution reaction is para directing with regard to the NO_2 group as is usual for the thermal nucleophilic substitution. This is also supported by the theoretical consideration that in the nitrobenzene anion radical the free valency is larger at the para position than at the other positions, that is, the NO_2 group activates the para position.[2]

Mutai *et al.*[3] studied the photo-Smiles reaction of *N*-[2-(2-methoxy-4-nitrophenoxy)ethyl]aniline (**2**) and *N*-[2-(2-methoxy-5-nitrophenoxy)ethyl]aniline (**3**) in polar solvents by analyzing their final products and reported that the substitution takes place at the para position with regard to the NO_2 group.

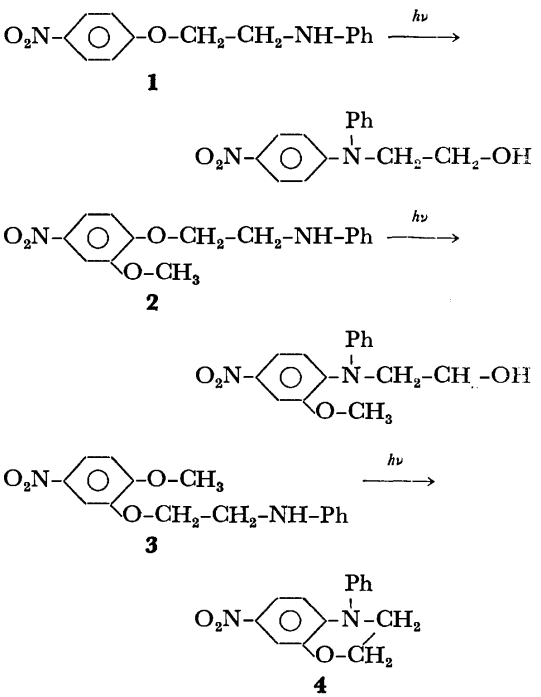

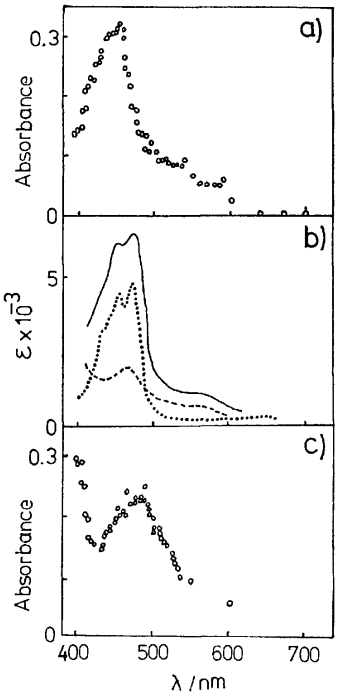

Fig. 1. a) Absorption spectrum of **a** 10 ns after the excitation. b) Broken line: absorption spectrum of the DMNB anion radical. Dotted line: absorption spectrum of the NMA cation radical. Solid line: the 1:1 superposition of the spectra of the DMNB anion and NMA cation radicals. c) $T_n \leftarrow T_1$ absorption spectrum of DMNB in the acetonitrile solution (present study).

These results indicate that NO_2 group plays a significant role in the photo-Smiles reactions. Therefore, in the present study, we have carried out the laser photolysis experiment of **2** and **3** together with **1** in acetonitrile to confirm the effect of NO_2 and CH_3O group upon the photosubstitution by elucidating their reaction mechanism directly.

1, **2**, and **3** were prepared as mentioned previously and purified by chromatography.[3] 1,2-Dimethoxy-4-nitrobenzene (DMNB) (Aldrich Chemical Co.) was purified by a sublimation and repeating recrystallizations. Acetonitrile (Wako, spectroscopic grade) was used as solvent without further purifications. Sample solutions for transient absorption measurements were degassed by repeating freeze-and-thaw cycles. The transient absorption was measured with the same apparatus as mentioned previously.[1,4]

Results and Discussion

The transient absorption of **2** was measured in the acetonitrile solution containing triethylamine (0.1 mol dm^{-3}) by the excitation with an N_2 laser at 337 nm.

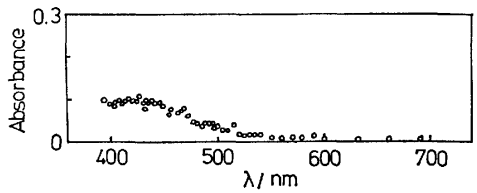

Fig. 2. Absorption spectrum of **b** 3 μs after the excitation.

It consists of two components, the faster one, **a**, and the slower one, **b**, their decay time constants being 35 ns and more than 200 μs, respectively. Figure 1a) shows the spectrum of **a**. Component **a** cannot be observed in nonpolar solvents like benzene and cyclohexane. Furthermore, the spectrum of **a** is different from $T_n \leftarrow T_1$ absorption spectrum of DMNB which is measured in the present study (see Fig. 1c)) and also from that of aniline and *N*,*N*-dimethylaniline.[5] In Fig. 1b) is shown a 1:1 superoposition of the spectrum of the DMNB anion radical[6] and that of the *N*-methylaniline (NMA) cation radical.[7] The superposition is very similar to the spectrum in Fig. 1a). Thus, **a** is assigned to an intramolecular ion radical pair, and the photosubstitution of **2** proceeds *via* the ion pair as that of **1** does.[1]

The other component, **b**, whose spectrum is shown in Fig. 2, is assigned to the relating Meisenheimer-type complex. The spectrum of **b** is not remarkably different from that of the relating complex of 1.[1] This implies that the conjugation of the CH_3O group with the residual system is not so significant for the complex. Polliff and Saunder showed that the spectra of 1,1-dimethoxy-2,6-dinitrocyclohexadienide and 1,1,4-trimethoxy-2,6-dinitrocyclohexadienide, are very similar to each other.[8]

These results mean that the photosubstitution reactions of **1** and **2** are very similar in their mechanism to each other. Particularly, the fact that the substitution takes place for **2** at the para position with regard to the NO_2 group shows that in the DMNB anion radical the NO_2 group activates the para position, but the CH_3O group does not play a significant role in activation of the benzene ring.

The acetonitrile solution of **3** shows the transient absorption with two components by the excitation with an N_2 laser. Both components of **3**, however, are different from those of **2**. The fast component of **3** rises up very fast and decays with the time constant of 1.0 μs, which is much larger than that of **2**, 35 ns. The slow component of **3** rises up with the time constant of 20 μs and does not decay within the time domain of the monitor light pulse (200 μs). Both components of **3** are not quenched by the addition of O_2 gas.

Figure 3a) and 3b) show the spectrum of the fast and slow components of **3**, respectively. The latter

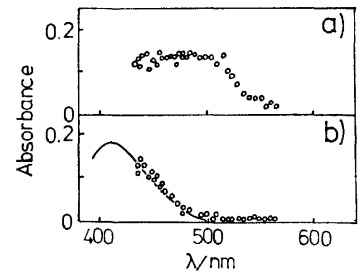

Fig. 3. Transient absorption spectrum of **3**.
a): Absorption spectrum of the fast component 10 ns after the excitation. b): Absorption spectrum of the slow component 45 μs after the excitation. Solid line; absorption spectrum of the final product, **4**.

may be assigned to that of the final product, **4**, because both spectra are very similar to each other, as shown in Fig. 3b). The assignment of the fast component is not clear so far. The built up time constant of the slow one is twenty times larger than the decay time constant of the fast one. Consequently, the fast component is not a direct precursor of the slow component. These results suggest that the reaction mechanism of **3** is different from those of **1** and **2**, that is, the para directing character with regard to the NO_2 group in **3** should not be due to the same origin as in **1** and **2**.

The present study indicates that the orientation rule should be discussed taking not only the final products but also the respective reaction mechanisms into account. Furthermore, it is shown that in **1** and **2** the para directing character is due to the activation by the NO_2 group but not the CH_3O group. The reaction mechanism of **3** should be studied further.

References

1) K. Yokoyama, R. Nakagaki, J. Nakamura, K. Mutai, and S. Nagakura, *Bull. Chem. Soc. Jpn.*, **53**, 2472 (1980).
2) S. Nagakura and J. Tanaka, *Bull. Chem. Soc. Jpn.*, **32**, 734 (1959).
3) K. Mutai, S. Kanno, and K. Kobayashi, *Tetrahedron Lett.*, **1978**, 1273; K. Mutai and K. Kobayashi, *Bull. Chem. Soc. Jpn.*, **54**, 462 (1981); K. Mutai, K. Yokoyama, S. Kanno, and K. Kobayashi, *Bull. Chem. Soc. Jpn.*, to be submitted.
4) H. Hayashi and S. Nagakura, *Bull. Chem. Soc. Jpn.*, **53**, 1519 (1980).
5) K. D. Cadogan and A. C. Albrecht, *J. Phys. Chem.*, **73**, 1868 (1969).
6) T. Shida, private communication. The molecular absorption coefficient of the DMNB anion radical is estimated to be about 2000 at 455 nm.
7) T. Shida, Y. Nosaka, and T. Kato, *J. Phys. Chem.*, **82**, 695 (1978).
8) R. J. Polliff and B. C. Saunders, *J. Chem. Soc.*, **1964**, 1132.

The Crystal Structure of *p*-Iodobenzoic Acid Investigated by X-Ray Powder Diffraction

Yoshito TAKAKI,* Arifumi KURISU, and Kazuaki NAKATA
Department of Physics, Osaka Kyoiku University, Tennoji-ku, Osaka 543
(Received July 10, 1981)

Synopsis. The crystal of the title compound is monoclinic with space group $P2_1/a$, $a=30.36(3)$, $b=6.04(1)$, $c=4.16(1)$ Å, $\beta=97.4(1)°$ and $Z=4$. The crystal structure was solved from X-ray powder diffractometer data by the packing analysis based on an ellipsoid-model and by the pattern-fitting structure refinement. The final R (profile) value was 0.168. This structure is isostructural with that of *p*-bromobenzoic acid.

In order to obtain single crystals of *p*-iodobenzoic acid suitable for X-ray intensity data collection, many attempts were made but they were all unsuccessful. Then the crystal structure was solved from X-ray powder diffractometer data using the method of pattern-fitting refinement with structural constraints.[1)]

Experimental

Crystals grown from an aqueous solution occur as very thin lamellas with the well-developed (100) plane. The intensity measurements were made on an X-ray powder diffractometer (Rigaku-Denki, Ru-200PL) with Cu $K\alpha$ radiation monochromatized by a curved graphite monochromator. A scan was made from 11 to 44° in 2θ with scanning speed of 0.25 °/min; in this angular range there are 82 contributing reflections. The background-corrected intensities were measured on the chart in steps of 0.05° (in 2θ) over the above angular range. The intensity measurements of the profile with 2θ greater than 44° were not made because a large number of diffraction peaks overlap each other considerably.

Crystal data of this compound have been reported by Toussaint.[2)] They are: monoclinic with cell dimensions, $a=30.46$, $b=6.05$, $c=4.16$ Å, $\beta=97°19'$, space group $P2_1/a$ and $Z=4$. The cell dimensions were refined by using diffraction data from a powder sample mixed with the silicon powder as internal standard. They are $a=30.36(3)$, $b=6.04(1)$, $c=4.16(1)$ Å and $\beta=97.4(1)°$.

Structure Determination

Trial structures were obtained by the packing analysis based on an ellipsoid-model[3)] which was obtained on the assumption that two planar molecules with conventional bond lengths and angles form a centrosymmetric dimer and the three orthogonal molecular axes coincide with the principal axes of the ellipsoid. The dimensions of the ellipsoid, 10.6, 3.0, and 1.8 Å, were obtained from a consideration of van der Waals radii of the atoms. The center of the ellipsoid was placed on the center of symmetry and its orientation was described by the use of Eulerian angles ϕ, θ, and ψ, where ϕ and θ are the ordinary polar-coordinate angles of the major axis L of the ellipsoid referred to the axes a and b* and ψ is the angle measuring the rotation about the axis L.

By the above method five sets of ellipsoid-packing each having quite different packing mode were obtained. After transforming the coordinates of atoms in a molecule referred to the principal axes of the ellipsoid to those referred to the crystal axes, we calculated powder intensity profiles by using the expression given below. In the structure-factor calculation, an overall temperature factor, $B=3.0$ Å^2, was used and the contribution from the H atoms was neglected. A structure having an intensity profile strikingly similar to the observed one was chosen as the starting structure for refinement; the Eulerian angles were $\phi=165$, $\theta=55$, and $\psi=150°$. The R value defined by

$$R = \sum_i |y_i(\text{obsd}) - y_i(\text{calcd})| / \sum_i y_i(\text{obsd})$$

was 0.26, where y_i is an intensity at a given point $2\theta_i$ in a profile and is expressed in the form

$$y_i = \sum_k \left[\frac{2}{3} I_k \Omega(2\theta_i, 2\theta_{k1}) + \frac{1}{3} I_k \Omega(2\theta_i, 2\theta_{k2}) \right].$$

Here summation is taken over all possible contributing reflections at $2\theta=2\theta_i$; I_k is the calculated intensity of reflection k for Cu $K\alpha$; $\Omega(2\theta_i, 2\theta_{k1})$ and $\Omega(2\theta_i, 2\theta_{k2})$ are the line shape functions for Cu $K\alpha_1$ and Cu $K\alpha_2$ respectively and are represented by Cauchy functions with full width (in 2θ) at half height of a peak, H_k, given by

$$H_k = v \tan\theta_k + w,$$

where v and w are parameters.

The pattern-fitting refinement was made by visual comparison of observed and calculated intensity profiles. The parameters varied in the refinement were: three Eulerian angles, one C–I bond distance, one temperature factor for the I atom and two for the peak shape. Note that the refinements of positional and thermal parameters for the atoms except the I atom were not made since their contributions to the structure factors can be considered to be very small as compared with that of the I atom. The final values of the parameters are: Eulerian angles, $\phi=166$, $\theta=56$, and $\psi=150°$, C–I=2.03 Å (initial value, 2.15 Å), $B=3.0$ Å^2 and peak shape parameters, $v=0.24$ and $w=0.13$. The final R value is 0.168 for

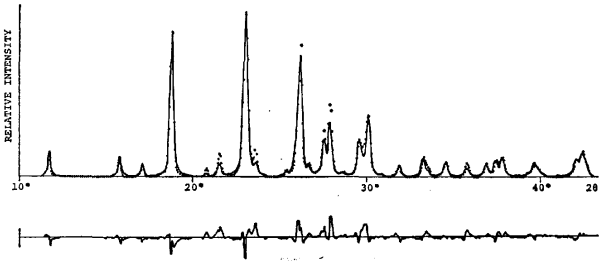

Fig. 1. Observed (dots) and calculated (full line) intensity profiles for *p*-iodobenzoic acid. The lower trace is the difference between observed and calculated profiles.

Table 1. The final fractional coordinates for non-hydrogen atoms

Atom	x	y	z
C_1	−0.0874	0.3156	0.1660
C_2	−0.0800	0.5223	0.3068
C_3	−0.1156	0.6508	0.3744
C_4	−0.1585	0.5726	0.3011
C_5	−0.1659	0.3660	0.1603
C_6	−0.1303	0.2375	0.0928
C_7	−0.0493	0.1779	0.0936
O_1	−0.0577	−0.0010	−0.0283
O_2	−0.0121	0.2459	0.1572
I	−0.2106	0.7609	0.3996

The bond lengths are C-C(benzene ring) = 1.39 Å, C_1-C_7 = 1.49 Å, C-O = 1.20 Å, C-I = 2.03 Å, and OH···O = 2.65 Å.

631 intensities from 11.5 to 43° in 2θ.

Figure 1 shows observed and calculated intensity profiles together with the differences between them. The final coordinates of non-hydrogen atoms are listed in Table 1. The structure viewed along the c axis is shown in Fig. 2. This structure is isostructural with that of *p*-bromobenzoic acid.[4]

In conclusion we may say that the use of structural constraints in the powder-pattern-fitting refinement[1,5] is certainly very useful, especially when only low-angle intensity data with highly overlapped peaks are available. Further, in such a case, it would be very important to find a starting structure very close to the final one for obtaining a stable refinement.

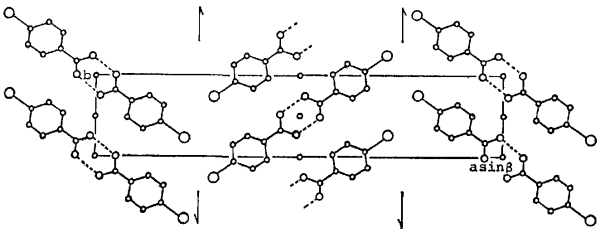

Fig. 2. The crystal structure viewed along the c axis.

The authors thank Mr. M. Setoguchi of Goverment Industrial Research Institute, Osaka, for use of the X-ray powder diffractometer. They also thank Prof. K. Sakurai for his continued interest and Mr. Y. Kubota and Mr. M. Satoh for assistance with the computing.

References

1) G. S. Pawley, G. A. Machenzie, and O. W. Dietrich, *Acta Crystallogr., Sect. A*, **33**, 142 (1977).
2) J. Toussaint, *Mém. Soc. Sci. Liège*, **12**, 1 (1952).
3) Y. Takaki and K. Nakata, *Mem. Osaka Kyoiku Univ. Ser. III*, **30**, (1981) in the press.
4) K. Ohkura, S. Kashino, and M. Haisa, *Bull. Chem. Soc. Jpn.*, **45**, 2651 (1972).
5) A. Immirzi, *Acta Crystallogr., Sect. B*, **36**, 2378 (1980).

Zero-field Splitting Tensor and Orientation of the Phosphorescent-state Benzo[*h*]quinoline in Biphenyl Host

Hiroshi Sekiya and Yasuhiko Gondo*

Department of Chemistry, Faculty of Science, Kyushu University 33, Hakozaki, Higashi-ku, Fukuoka 812

(Received July 24, 1981)

Synopsis. ESR absorption has been observed in a single-crystal solid solution of benzo[*h*]quinoline in biphenyl under UV irradiation at 120 K. The triplet-state zero-field splitting tensor and the guest orientation are reported, in comparison with the previous results on benzo[*f*]-quinoline.

In order to investigate the nature of the triplet-state wave function, it is important to determine the zero-field splitting (ZFS) principal axes, not to speak of the principal values. However, the number of compounds for which the ZFS principal axes were determined are limited.[1] The main object of this work is to determine the ZFS principal axes in the phosphorescent state of benzo[*h*]quinoline (BHQ), to be compared with those of benzo[*f*]quinoline (BFQ) reported previously.[1]

Experimental

BHQ (Nakarai GR) was treated with sulfuric acid and sodium hydroxide,[2] and then zone-refined extensively. Single-crystal samples were grown from the melts.[1]

The ESR measurements were performed as described previously,[1] except for the use of a microwave frequency of 9.15 GHz instead of 9.25 GHz. The sample crystals were cooled at 120±10 K by a flow of cold nitrogen gas, and irradiated with a 250-W high-pressure mercury lamp. Quartz wedges were used in order to rotate the static external magnetic field in the particular magnetic planes associated with one type of BHQ molecule in the crystal. We have also studied the phosphorescence spectra and decays of BHQ in biphenyl at 77 and 4.2 K, and identified the phosphorescent state, as described previously.[1]

Results and Discussion

General Remarks. Figure 1 shows the molecular axes adopted, designation of the ZFS principal axes, x, y, z, and the in-plane rotation of the ZFS tensor, θ. For the sake of convenience, the two sites in a unit cell of the biphenyl crystal are designated as sites A and B, respectively, the quartz wedges being assumed to fit site A. The main features of the biphenyl crystal have been summarized previously,[1] and there are two magnetically inequivalent orientations of the BHQ molecule at each site. Since the procedures in this work resemble the previous for BFQ,[1] the presentation will duly be brief.

ESR Spectra in the yz Plane and Tilt of the Guest Plane. Figure 2 shows the resonance fields obtained by rotating the static external magnetic field $\boldsymbol{H}$ nearly in the yz plane with the wedge of an inclination of 17.8° which gave a maximum resonance field; four wedges of inclination in the range 13.8°—19.0° were actually used, while the biphenyl crystal structure specifies the inclination of 17.7° for $\boldsymbol{H}$ to be in the M'N' plane.

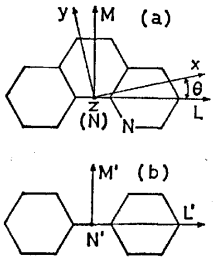

Fig. 1. Axis systems for (a) benzo[*h*]quinoline and (b) biphenyl. ZFS principal axes are denoted by x, y, and z.

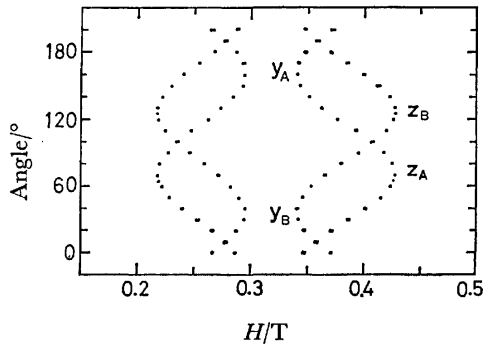

Fig. 2. Magnitude of $\boldsymbol{H}$ for resonance *vs.* rotation of $\boldsymbol{H}$ in a plane close to the yz plane.

The two patterns correspond to sites A and B, and are identical to each other except for the phase. The largest separations correspond to the z axes, while the smallest to the y axes. With very poor resolutions, eight lines could be recognized for some orientations of $\boldsymbol{H}$ between the y and z axes. This indicates the small value of θ to be discussed later on, and that the molecular planes of the two inequivalent guests at each site are parallel to each other within experimental errors. Thus, the angle of 55.0° between the fine-structure z axes may represent the dihedral angle between the planes of the A- and B-site BHQ molecules, in contrast with the corresponding angle of 69.3° for the A- and B-site biphenyl molecules.[3] The difference of 14.3° in the two angles amounts to a decrease of 7° in the tilt of the guest plane relative to the host, in coincidence with the case of BFQ in biphenyl,[1] and in a slight deviation from the tilt of 5°—6° found for phenanthrene in biphenyl.[4,5] The nitrogen-atom location essentially does not affect the tilt of the guest plane.

ESR Spectra in the xy Plane. Five wedges were used in order to rotate $\boldsymbol{H}$ in the xy plane, *i.e.*, LM plane, their dihedral angles ranging from 101.0° to 105.9°. Taking account of the yz-plane measurements, the b axis of the crystal was set at 62° on the wedge

Table 1. Observed zero-field splitting parameters[a)]

	Benzo[*h*]quinoline[b)] in biphenyl	Benzo[*f*]quinoline[c)] in biphenyl	Benzo[*h*]quinoline[d)] in ethanol	Benzo[*f*]quinoline[d)] in ethanol
D/cm^{-1}	±0.09738(2)	±0.09926(18)	+0.1011	+0.1023
E/cm^{-1}	∓0.04642(2)	∓0.04781(6)	−0.0468	−0.0477
$\|E/D\|$	0.4767	0.4817	0.463	0.466
g_{xx}	2.0016(4)	2.0024(6)		
g_{yy}	2.0023(4)	2.0018(4)		
g_{zz}	2.0018(2)	2.0018(4)		
θ/°	±0.5	±4		

a) Numbers in parentheses are estimated standard deviations in units of the last significant digit. b) This work. c) Ref. 1. d) Ref. 7.

surface as detailed previously.[1)] The wedge of a dihedral angle of 103.3° gave a maximum resonance field. The y-axis resonance-field separations are the same as those in the yz-plane measurements. In addition, the L axes of sites A and B are practically parallel to each other, since the four lines draw closer together and coalesce into one as $\boldsymbol{H}$ moves to the x axes, as it is the case for BFQ.[1)]

*ZFS Tensor, **g**-Tensor, and Hyperfine Structure.* The ZFS parameters were determined with the procedure of Hutchison and Mangum,[6)] the principal axes of the $\boldsymbol{g}$-tensor being assumed to coincide with those of the ZFS tensor. The parameters fitting the spin-Hamiltonian are given in Table 1. The D value is somewhat smaller in biphenyl than in ethanol glass,[7)] while the E value is essentially indifferent to the solvents, as it is the case for BFQ.[1,7)] The resemblance of the D and E values of BHQ to those of BFQ[1)] and phenanthrene[4)] confirms the $\pi\pi^*$ nature of the phosphorescent state in BHQ.

The two pairs of curves in the xy-plane measurements correspond to the two magnetically inequivalent orientations at site A, as exemplified in Fig. 6 of Ref. 1. From the phase difference of 1° between the two curves, we obtain a θ value of ±0.5°, in good agreement with a theoretical value of +0.2°,[8)] and in contrast with the larger value of ±4° for BFQ,[1)] as shown in Table 1.

Although the hyperfine structures could be observed for $\boldsymbol{H}$ nearly on the three ZFS principal axes, they actually are complicated owing to the low molecular symmetry and to overlapping of the signals due to the different sites. Accordingly, the hyperfine coupling constants could not be determined, as it was the case for BFQ.[1)]

The present work was partially supported by the Ito Science Foundation and by the Grants-in-Aid for Scientific Research Nos. 334026 and 347014 from the Ministry of Education, Science and Culture.

References

1) H. Sekiya, Y. Gondo, and Y. Kanda, *Bull. Chem. Soc. Jpn.*, **53**, 1201 (1980), and the references therein.
2) Y. Kanda and R. Shimada, *Spectrochim. Acta*, **15**, 211 (1959).
3) J. Trotter, *Acta Crystallogr.*, **14**, 1135 (1961); A. Hargreaves and S. H. Rizvi, *ibid.*, **15**, 365 (1962).
4) W. Brandon, R. E. Gerkin, and C. A. Hutchison, Jr., *J. Chem. Phys.*, **41**, 3717 (1964).
5) C. A. Hutchison, Jr., and V. H. McCann, *J. Chem. Phys.*, **61**, 820 (1974).
6) C. A. Hutchison, Jr., and B. W. Mangum, *J. Chem. Phys.*, **34**, 908 (1960).
7) Y. Gondo and A. H. Maki, *J. Phys. Chem.*, **72**, 3215 (1968).
8) Y. Gondo and Y. Kanda, Preprint of the 10th ESR Symposium, Osaka, October 1971, p. 84; *Bull. Chem. Soc. Jpn.*, **43**, 3943 (1970).

Kinetics of Gas Phase Addition Reactions of Trichlorosilyl Radicals. IV.[1] Relative Rates of Additions to 1-Alkenes

Takaaki DOHMARU* and Yoshio NAGATA

Radiation Center of Osaka Prefecture, Shinke-cho, Sakai, Osaka 593

(Received August 5, 1981)

Synopsis. Trichlorosilyl radical additions to a mixture of ethene, propene, 1-butene, and 1-pentene and to a mixture of propene and 2-methylpropene have been investigated. The rate of adduct formation from each olefin was obtained relative to that from propene between 403 K and 548 K. These relative rates are in good agreement with those calculated from the rate parameters obtained previously in this laboratory.

Kinetic data relating to elementary reactions of silyl radicals are quite important since reliable thermochemical or kinetic informations are now still very scarce.

Previously,[2] we obtained Arrhenius parameters for forward and reverse steps of $\cdot SiCl_3$ additions to 1-alkenes between 405 K and 524 K by a competitive method in which an addition to acetone was employed as a reference reaction. To check the reliability of these results and to obtain precise relative rates of additions to 1-alkenes, we conduct a series of experiments in which mixtures of 1-alkenes are subjected to reactions with $\cdot SiCl_3$ radicals.

Experimental

The materials were prepared, purified and checked in the way described previously.[2] Sample preparations and photolyses were performed on a conventional greaseless and mercury-free vacuum line. The full light from a 50 W medium pressure mercury arc was used. Given amounts of $HSiCl_3$ and a mixture of olefins were admitted into a quartz reaction vessel of 139 cm^3 which was heated in an electrical oven controlled to better than ± 1 K. Probably very weak photoabsorption by olefins in the ultraviolet region initiates the reactions, since $HSiCl_3$ was found almost transparent in this region. After photolyzed, the reaction mixture was allowed to diffuse to a gas sampling loop which was directly attached to a gas chromatograph with a Gow-Mac gas density detector. All the analyses were made on a 2 m column of 30% SE 30 on Chromosorb W mixed with 30% Silicone DC QF-1 on Chromosorb W (1:1 by weight). Reactant conversions were kept smaller than 5%.

Results and Discussion

Equimolar mixtures of ethene, propene, 1-butene and 1-pentene (0.267×10^{-6} mol cm^{-3} each) were photolyzed in the presence of $HSiCl_3$ (5.34×10^{-6} mol cm^{-3}). Products were $C_2H_5SiCl_3$, n-$C_3H_7SiCl_3$, n-$C_4H_9SiCl_3$, and n-$C_5H_{11}SiCl_3$; additions occur exclusively at their terminal carbons. Since it was difficult to separate i-$C_4H_9SiCl_3$ completely from n-$C_4H_9SiCl_3$ in gas chromatographic analyses, 2-methylpropene was subjected to another photolysis in which propene and 2-methylpropene (0.134×10^{-6} mol cm^{-3} each) were photolyzed with $HSiCl_3$ (5.34×10^{-6} mol cm^{-3}). In both series of photolyses, the amounts of the products were measured at various temperatures between 403 K and 548 K. The results are summarized in Table 1.

Table 1. Relative rates of additions of $HSiCl_3$ to 1-alkenes

T/K	C_2H_4	C_3H_6	Δ^1-C_4H_8	Δ^1-C_5H_{10}	i-C_4H_8
403	0.27	1	1.1	1.0	4.1
428	0.32	1	1.1	1.2	4.1
452	0.34	1	1.1	1.1	3.0
477	0.39	1	1.2	1.0	2.0
501	0.52	1	1.1	0.9	1.3
525	0.85	1	1.1	1.0	1.0
548	1.1	1	1.2	1.0	0.8

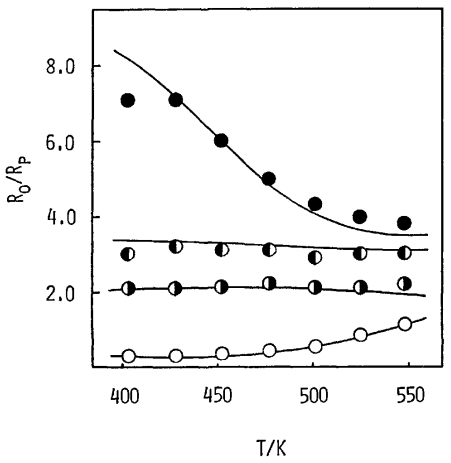

Fig. 1. Observed and calculated relative rates of addition between 403 K and 548 K.
○: C_2H_4, ◑: Δ^1-C_4H_8 (shifted by +1), ◐: Δ^1-C_5H_{10} (shifted by +2), ●: i-C_4H_8 (shifted by +3)
The solid curves represent the calculated values.

Features characteristic of the number of the alkyl substituents around the double bond are clear in Table 1. Monosubstituted ethenes (C_3H_6, Δ^1-C_4H_8, and Δ^1-C_5H_{10}) are very similar in reactivity with each other throughout the temperature range. Ethene has a small rate at low temperature but gets to the same rate as that of propene at 548 K. 2-Methylpropene behaves in a quite opposite way to ethene. It is quite interesting to note that each relative rate attains almost the same value at about 530 K.

The photolytic addition of $HSiCl_3$ to olefin is known to proceed by the following radical chain reactions.[3]

$$\cdot R + HSiCl_3 \longrightarrow RH + \cdot SiCl_3 \quad (1)$$

$$\cdot SiCl_3 + CR_1R_2{=}CH_2 \rightleftharpoons \cdot CR_1R_2CH_2SiCl_3 \quad (2, -2)$$

$$\cdot CR_1R_2CH_2SiCl_3 + HSiCl_3 \longrightarrow HCR_1R_2CH_2SiCl_3 + \cdot SiCl_3 \quad (3)$$

$\cdot R$ in Reaction 1 represents any radicals formed as a result of photoabsorption by some olefins.

The rate of the formation of the respective adduct, R_o, is derived as in Eq. 4 applying the steady state treatment of the above scheme; the conditions of long reaction chains and low conversion of reactants are satisfied in the present runs.[2]

$$R_o = \frac{k_2[\text{Olefin}][\cdot SiCl_3]}{1+(k_{-2}/k_3)[HSiCl_3]^{-1}}. \quad (4)$$

We have already obtained rate constant ratios k_2/k_5 and k_{-2}/k_3 for 1-alkenes where k_5 denotes the rate constant of the $\cdot SiCl_3$ addition to acetone.[2] Accordingly, the relative rates of adduct formations among olefins can be calculated from Eq. 4. The rates of adduct formation from the respective olefin, R_o, relative to that from propene, R_p, are compared with the calculated values at various temperatures in Fig. 1. The experimental rate ratios are in good agreement with the calculated values; the present study lends support to the rate parameters obtained previously.[2]

References

1) Part 3: T. Dohmaru and Y. Nagata, *J. Chem. Soc., Faraday Trans. 1*, in press.
2) T. Dohmaru and Y. Nagata, *J. Chem. Soc., Faraday Trans. 1*, **75**, 2617 (1979).
3) T. Dohmaru, Y. Nagata, and J. Tsurugi, *Chem. Lett.*, **1973**, 1031.

Preparation of Alkylnickel(II)-Phosphine Complexes by Reactions of $Ni(acac)_2$ with Alkylaluminums in the Presence of Tertiary Phosphine

Takakazu YAMAMOTO,* Masakatsu TAKAMATSU, and Akio YAMAMOTO
Research Laboratory of Resources Utilization, Tokyo Institute of Technology, 4259, Nagatsuta, Midori-ku, Yokohama 227

(Received May 6, 1981)

Synopsis. Four new alkylnickel(II)-phosphine complexes, $NiR_2(PR'_3)_2$ ($R=CH_3$, C_2H_5; PR'_3=triethylphosphine (PEt_3), tributylphosphine (PBu_3), 1,2-bis(diphenylphosphino)ethane(dpe)) and $Ni(CH_3)(acac)(PEtPh_2)$ ($PEtPh_2$=ethyldiphenylphosphine), have been prepared by reactions of $Ni(acac)_2$ with $AlR_2(OC_2H_5)$ in the presence of phosphine ligands.

Alkylnickel complexes are regarded as intermediates in important catalytic reactions such as isomerization and oligomerization of olefins and dienes.[1] Although several groups have been engaged in research on the preparation and chemical properties of alkylnickel complexes,[1a,2] the number of well-characterized alkylnickel complexes is still not large. We now report preparation of four new alkylnickel(II) complexes by reactions of $Ni(acac)_2$ (acac=2,4-pentanedionato) with alkylaluminums in the presence of tertiary phosphines (L).

Results and Discussion

Reactions of $Ni(acac)_2$ with $AlR_2(OEt)$ below −30 °C in the presence of phosphine ligands give NiR_2L_2, NiR(acac)L, zero-valent nickel complexes, or Ni–Al binary complexes depending on the alkylaluminum and phosphine ligand employed,

$$Ni(acac)_2 + AlR_2(OEt) + L \xrightarrow[Et_2O]{-30\,^\circ C \text{ or below}} NiR_2L_2,\ NiR(acac)L,\ NiL_4,\ \text{Ni–Al complex} \quad (1)$$

R	L	Product
Me	PEt_3	$NiMe_2(PEt_3)_2$ **1**
Et	PEt_3	Ni–Al binary complex **2**
Me	PBu_3	$NiMe_2(PBu_3)_2$ **3**
Me	dpe	$NiMe_2(dpe)$ **4**
Et	dpe	$NiEt_2(dpe)\cdot(Et_2O)_{0.5}$ **5**
Me	$PEtPh_2$	$NiMe(acac)(PEtPh_2)$ **6**
Me	$PMePh_2$	$Ni(PMePh_2)_4$ **7**
Me	$P(OEt)_3$	Ni–Al binary complex **8**
Me or Et	$P(OPh)_3$	$Ni(P(OPh)_3)_4$ **9**

Me=CH_3, Et=C_2H_5, Bu=*n*-C_4H_9, Ph=C_6H_5, acac=2,4-pentanedionato, dpe=1,2-bis(diphenylphosphino)-ethane

Among the complexes listed above, the dimethylnickel complex, **4**,[2g] and zero-valent nickel complexes, **7**[3] and **9**,[4] have been prepared by other researchers through different pathways. The comparison of the products obtained using the phosphine ligands listed above reveals that subtle differences in electronic and steric effects of the phosphine ligands exerts a pronounced influence on the course of alkylation reaction. Properties of the complexes are described below.

NiR_2L_2: Dialkylnickel(II) complexes **1**, **3**, and **5** have relatively low thermal stabilities, the thermal decomposition proceeding gradually even at room temperature in a solid, with evolution of CH_4 and C_2H_6 from the dimethyl complexes and C_2H_6 and C_2H_4 from **5**. The absence of butane in the thermolysis product of **5** contrasts with the results of thermolysis of $NiEt_2$(2,2′-bipyridine), which liberates mainly butane during the thermolysis.[2a,2c] The low thermal stabilities of the dialkyl complexes not only require the researchers to carry out the preparation and work-up below −30 °C, but also prevent characterization of the complexes by microanalysis. Thus characterization of NiR_2L_2 was performed mainly on the basis of macroanalysis of Ni, the amount of RH released on acidolysis with H_2SO_4, and spectroscopy (IR and NMR). As for **3**, we characterized it by the amount of RH released on the acidolysis and by ^1H NMR spectroscopy, due to its high instabilities. As for **1** and **5**, their chemical reactivities with active hydrogen compounds[5] and CO[6] support the proposed structures. All the dialkyl complexes are free of aluminum, as proved by qualitative analyses.

Table 1 summarizes spectroscopic data of the new complexes prepared by Reaction 1. IR spectra show signals due to R and L ligands. In the ^1H NMR spectrum, the dimethyl complexes **1** and **3** give rise to the Ni–CH_3 signal at higher magnetic field than TMS; similar results were reported for dimethylnickel complexes.[2] The triplet pattern ($J(^1H–^{31}P)=8$ Hz) of the Ni–CH_3 signal of **1** at −70 °C reveals that **1** has a *trans* configuration. The $^1H–^{31}P$ spin-spin coupling, however, is not observable at −60 °C or above, presumably due to rapid exchange between PEt_3 in **1** and free PEt_3 partly liberated from **1**. The Ni–CH_2– signal of **5** is located at higher magnetic field than the Ni–CH_2–CH_3 signal, as is found for $NiEt_2$(2,2′-bipyridine).[2b]

$NiMe(acac)(PEtPh_2)$ **6**: Complex **6** has higher thermal stabilities than the dialkylnickel complexes. The IR spectrum of **6** shows ν(C=O) bands at 1590 and 1520 cm^{-1} characteristic of a bidentate acac ligand. ^1H-NMR spectrum shows two singlets for the two CH_3 groups of the acac ligand, indicating **6** has a

Table 1. IR and NMR data of new alkylnickel(II) complexes

Complex	IR ν/cm^{-1}	^{1}H-NMR Solvent	Temp/°C	Chemical shift δ[a]
1	2970 1160 770	C_6H_6	25	−0.70(6H, s, br, Ni-CH_3) 1.04(18H, m, br, P-CH_2-CH_3) 1.52(12H, q, 7 Hz, P-CH_2-)
		Toluene-d_8	−70	−0.60(6H, t, 8 Hz, Ni-CH_3) 0.96(18H, qui, 8 Hz, P-CH_2-CH_3) 1.40(12H, m, br, P-CH_2-)
3		Pyridine	−30	−0.50(6H, s, br, Ni-CH_3) 1.0(18H, t, 6 Hz, P{$(CH_2)_3CH_3$) 1.5—1.9(36H, m, P{$(CH_2)_3$)
5	2900 2810 1430 695	Pyridine	25	0.48(4H, q, 8 Hz, Ni-CH_2-) 1.55(6H, t, 8 Hz, Ni-CH_2-CH_3) 2.2(4H, P-CH_2) 4.2(2H, O(CH_2CH_3)$_2$)
6	2950 1590 1520 1390	C_6H_6	25	−0.10(3H, s, Ni-CH_3) 0.9—1.3(3H, m, P-CH_2-CH_3) 1.60(3H, s, acac-CH_3) 1.80(3H, s, acac-CH_3) 1.7—2.1(2H, m, P-CH_2-) 5.3(1H, s, acac-CH)

a) s: Singlet, t: triplet, q: quartet, qui: quintet, m: multiplet, br: broad.

square planar structure like that known for NiEt(acac)(PPh_3)[7] and NiR(acac)(PCy_3).[8]

Binary Complexes Containing Nickel and Aluminium Components: The Ni(acac)$_2$/$AlEt_2$(OEt)/PEt_3 and Ni(acac)$_2$/$AlMe_2$(OEt)/P(OEt)$_3$ systems afford yellow crystalline complexes. The complexes contain both nickel and aluminum. Electric conductivities of solutions of the complexes reveal that they have ionic structures. Their IR spectra show characteristic bands of aluminate anion at *ca.* 650 cm^{-1}. ^{1}H NMR spectra show signals not only due to R groups and L ligands but also one due to Al-OC$\underline{H}_2$CH$_3$ group at about 3.7 ppm. These results suggest that the complexes have ionic structures like [CoR_2(2,2′-bipyridine)$_2$]$^+$-[AlR_4]$^-$, which were isolated from Co(acac)$_3$/AlR_3/2,2′-bipyridine systems.[9] The ^{1}H NMR spectrum of **8** is consistent with the structure: [NiMe(P(OEt)$_3$)$_3$]$^+$-[$AlMe_3$OEt]$^-$.

Experimental

General. Manipulation of complexes, analysis, and measurement of IR and NMR spectra were carried out as reported.[2a-2c,5-7]

Preparation of Complexes. *NiR_2L_2*: $AlMe_2$(OEt) (13 cm^3, 100 mmol) was added to a mixture of Ni(acac)$_2$ (6.0 g, 23 mmol) and PEt_3 (8.0 cm^3, 54 mmol) in Et_2O (60 cm^3) at −60 °C. Stirring the mixture at −30 °C for 10 h gave a brown homogeneous solution, which was condensed to *ca.* 20 cm^3. Cooling the solution to −78 °C gave brown needles (6.1 g, 84%). The brown needles were separated by filtration, washed repeatedly with Et_2O at −78 °C, and recrystallized from Et_2O to obtain 4.4 g (60%) of **1**. Mp 35 °C (dec). Found: Ni, 18.0%. Calcd for $NiMe_2(PEt_3)_2$: Ni, 18.1%. CH_4/**1** (acidolysis with H_2SO_4)=1.8.

Complex **3** was obtained analogously from a mixture of Ni(acac)$_2$ (5.0 g, 19 mmol), PBu_3 (9.3 cm^3, 37 mmol), and $AlMe_2$(OEt) (11 cm^3, 88 mmol); the reaction time was 5 h and the temperature was −40 °C; yield=14%. Mp 0 °C (dec): CH_4/**3** (acidolysis)=2.0.

$AlEt_2$(OEt) (24 cm^3, 150 mmol) was added to a mixture of Ni(acac)$_2$ (6.5 g, 25 mmol) and dpe (10 g, 25 mmol) in 100 cm^3 of Et_2O at −50 °C. Stirring the mixture for 10 h at −20 °C gave a yellowish orange precipitate, which was separated by filtration, washed repeatedly with Et_2O, and dried in a vacuum to obtain **5** (yield=12%). Mp 50 °C (dec). Found: Ni, 10.3%. Calcd for $NiEt_2$(dpe)-(Et_2O)$_{0.5}$: Ni, 10.6%. C_2H_6/**5** (acidolysis)=2.0.

Complex **4** was prepared analogously and characterized by comparing its NMR data with those reported in the literature.

NiMe(acac)(PEtPh$_2$) **6**: $AlMe_2$(OEt) (14 cm^3, 110 mmol) was added to a mixture of Ni(acac)$_2$ (7.3 g, 28 mmol) and $PEtPh_2$ (14 cm^3, 57 mmol) in Et_2O (60 cm^3) at −70 °C. Stirring the mixture at −40——25 °C for 10 h gave a brown solution and a yellow precipitate. After condensing the solution to *ca.* 20 cm^3, the yellow precipitate was separated by filtration, washed with Et_2O, and dried in vacuum to yield 3.5 g (35%) of **6**. Mp 80 °C (dec). Found: C, 62.1; H, 6.5; Ni, 15.2%. Calcd for NiMe(acac)($PEtPh_2$): C, 62.3; H, 7.0; Ni, 15.1%. CH_4/**6** (acidolysis)=1.0.

Ni–Al Complexes: $AlMe_2$(OEt) (5.0 cm^3, 44 mmol) was added to a mixture of Ni(acac)$_2$ (2.6 g, 10 mmol) and P(OEt)$_3$ (3.4 cm^3, 20 mmol) in Et_2O (45 cm^3) at −50 °C. Stirring the mixture at −10 °C for 10 h gave a brown hoogeneous solution, which was condensed to *ca.* 30 cm^3. Coolming the solution to −78 °C gave transparent brown prisms. After washing with a mixture of Et_2O and hexane, the complex was recrystallized from Et_2O to yield 2.0 g of **8**. ^{1}H NMR (acetone-d_6, −60 °C): δ=−0.98 (9H, s, Al-C$\underline{H}_3$), −0.90 (3H, s, Ni-CH_3), 1.18 (3H, Al-$OCH_2C\underline{H}_3$), 1.30 (27H, t, 7 Hz, P-$OCH_2C\underline{H}_3$), 3.70 (2H, q, 7 Hz, Al-O$C\underline{H}_2CH_3$), 4.20 (18H, q, 7Hz, P-O$C\underline{H}_2CH_3$). Equivalent conductivity: 35% of the equivalent conductivity of KI in acetone at −72 °C. Complex **2** was prepared analogously.

Ni(0)-Complexes: Complexes **7** and **9** were prepared under similar conditions to those adopted to prepare **1**—**6** and **8**. They were characterized by elemental analysis.

References

1) a) P. W. Jolly and G. Wilke, "The Organic Chemistry of Nickel," Vol. 1 (1974) and Vol. 2 (1975), Academic Press, New York; b) R. F. Heck, "Organotransition Metal Chemistry," Academic Press, New York (1974); c) J. Tsuji, "Organic Synthesis by Means of Transition Metal Complexes," Springer, Berlin (1975).

2) a) A. Yamamoto, K. Morifuji, S. Ikeda, T. Saito, Y. Uchida, and A. Misono, *J. Am. Chem. Soc.*, **87**, 4652 (1965); b) T. Saito, Y. Uchida, A. Misono, A. Yamamoto, K. Morifuji, and S. Ikeda, *ibid.*, **88**, 5198 (1966); c) T. Yamamoto, A. Yamamoto, and S. Ikeda, *ibid.*, **93**, 3350 (1971); d) G. Wilke and J. Herrmann, *Angew. Chem.*, **78**, 591 (1966); e) H.-F. Klein and H. H. Karsch, *Chem. Ber.*, **106**, 2438 (1973); f) A. Yamamoto, T. Yamamoto, M. Takamatsu, T. Saruyama, and Y. Nakamura, "Organotransitionmetal Chemistry," Plenum (1975), p. 281; g) M. L. H. Green and M. J. Smith, *J. Chem. Soc., A*, **1971**, 639; h) E. A. Jeffery, *Aust. J. Chem.*, **26**, 219 (1973).

3) J. Browning, C. S. Cundy, M. Green, and F. G. A. Stone, *J. Chem. Soc., A*, **1969**, 20.

4) J. R. Olechowski, C. G. McAlister, and R. F. Clark, *Inorg. Synth.* **9**, 181 (1967).

5) T. Yamamoto, T. Kohara, and A. Yamamoto, *Bull. Chem. Soc. Jpn.*, **54**, 1720, 2010 (1981).

6) T. Yamamoto, T. Kohara, and A. Yamamoto, *Chem. Lett.*, **1976**, 1217.

7) T. Yamamoto, T. Saruyama, Y. Nakamura, and A. Yamamoto, *Bull. Chem. Soc. Jpn.*, **49**, 589 (1976).

8) P. W. Jolly, K. Jonas, C. Krüger, and Y.-H. Tsay, *J. Organometal. Chem.*, **33**, 109 (1971).

9) S. Komiya, M. Bundo, T. Yamamoto, and A. Yamamoto, *J. Organometal. Chem.*, **174**, 343 (1979).

A Voltammetric Study of the Reduction of Ruthenium(II) Complexes with Mixed Ligands

Junya WATANABE, Tetsuo SAJI,* and Shigeru AOYAGUI

Department of Electronic Chemistry, Graduate School at Nagatsuta, Tokyo Institute of Technology, Nagatsuta, Midori-ku, Yokohama 227

(Received May 25, 1981)

Synopsis. Each cyclic voltammogram for the reduction of $[Ru(bpm)_3]^{2+}$ (bpm=2,2′-bipyrimidine) and $[Ru(bpm)L_2]^{2+}$ (L=2,2′-bipyridine and dimethyl derivatives) exhibits three reversible one-electron steps. The relation between the half-wave potentials of the complexes and those of ligands suggests that the lowest redox orbital of $[Ru(bpm)L_2]^{2+}$ should be localized on a single bpm molecule.

We have previously reported cyclic voltammograms for the reduction of complexes of the $[M(II)L_3]$ and $[M(II)L_2]$ forms with Fe and Ru as M and 2,2-bipyridine (bpy) and some other polypyridines as L.[1–4] The tris(or bis) complexes had one or two sets of three (or two) nearly neighbouring reduction steps. They were all reversible one-electron steps whose half-wave potentials ($E^{red}_{1/2,C}$) were related to the reversible half-wave potentials for the first reduction steps of the ligands ($E^{red}_{1/2,L}$) by the following equation:[1]

$$E^{red}_{1/2,C} = E^{red}_{1/2,L} + \text{const.} \quad (1)$$

This finding led us to the conclusion that the excess electrons over d^6 should be added to the ligand π^*-orbitals or, strictly speaking, that the redox orbitals should be molecular orbitals to which ligand π^*-orbitals make a predominant contribution. The characteristic patterns of the cyclic voltammograms suggested, furthermore, that the redox orbitals of the tris(or bis) complexes are probably three(or two)-fold degenerate. Molecular orbital calculations of the energies of the redox orbitals led to the same conclusion.[5] The present work is an extension of these works; it deals with mixed-ligand complexes.

The $[Fe(bpm)_3(PF_6)_2]$[6] (bpm=2,2′-bipyrimidine), $[Ru(bpm)_3(PF_6)_2]$[7,8] and $[Ru(bpm)(bpy)_2(PF_6)_2]$[7,9] complexes were prepared by the literature methods, while $[Ru(bpm)L_2(PF_6)_2]$ (L=4,4′-dimethyl-2,2′-bipyridine (4-dmbpy) and 5,5′-dimethyl-2,2′-bipyridine (5-dmbpy) were prepared by a method similar to that was used for $[Ru(bpm)(bpy)_2(PF_6)_2]$. The $[Ru(4\text{-dmbpy})_3(ClO_4)_2]$ and $[Ru(5\text{-dmbpy})_3(ClO_4)_2]$ complexes were described previously.[1] Cyclic voltammograms for the reduction of these complexes were obtained on a platinum working electrode with an acetonitrile base solution containing 0.1 M (1 M= 1 mol dm^{-3}) tetrabutylammonium hexafluorophosphate (Bu_4NPF_6) at room temperature, unless otherwise noted. A $Ag/AgNO_3$(sat.) electrode was used as the reference electrode. The rate of potential sweep was 0.1 V s^{-1}.

The cyclic voltammogram of $[Ru(bpm)_3]^{2+}$ was similar to that of $[Ru(bpy)_3]^{2+}$ in exhibiting three nearly neighbouring steps. They were all reversible one-electron steps, judging from the well-defined anodic current peaks and from the separation between the cathodic peak potential and the anodic one (ΔE_p).

Table 1. Reversible half-wave potentials for the reduction of iron(II) and ruthenium(II) complexes in acetonitrile containing 0.1 Bu_4NPF_6 at room temperature

Complex	$[-E^{red}_{1/2,C}$ *vs.* $(Ag/AgNO_3)]$/V (ΔE_p/mV)		
	1st	2nd	3rd
$[Fe(bpm)_3]^{2+}$	1.41 (45) [a]	1.57 (48) [a]	1.75 (50) [a]
$[Ru(bpm)_3]^{2+}$	1.40 (60)	1.55 (60)	1.75 (63)
$[Ru(bpy)_3]^{2+}$	1.81 (60)	2.01 (65)	2.25 (60)
$[Ru(4\text{-dmbpy})_3]^{2+}$	1.94 (60)	2.13 (65)	2.37 (64)
$[Ru(5\text{-dmbpy})_3]^{2+}$	1.98 (62)	2.19 (62)	2.44 (65)
$[Ru(bpm)(bpy)_2]^{2+}$	1.51 (61)	1.95 (65)	2.14 (70)
$[Ru(bpm)(4\text{-dmbpy})_2]^{2+}$	1.52 (60)	2.05 (65)	2.26 (68)
$[Ru(bpm)(5\text{-dmbpy})_2]^{2+}$	1.53 (60)	2.12 (65)	2.36 (65)

a) At −40 °C, the $E^{red}_{1/2,C}$ values are almost unaffected by the temperature.

The ratios of the anodic to the cathodic peak currents could not be determined, however, because of the proximity of the reduction steps. A similar pattern of voltammogram was obtained for $[Fe(bpm)_3]^{2+}$ at −40 °C, but at room temperature no reversible steps were observed besides the one for the liberated ligand molecules. The cyclic voltammograms for $[Ru(bpm)(bpy)_2]^{2+}$ and methyl derivatives were quite similar. They had one remote and two nearly neighbouring reversible one-electron steps. The reversible half-wave potentials and the peak separations thus obtained are listed in Table 1. The $E^{red}_{1/2,L}$ values for the first reduction steps of bpm, bpy, 4-dmbpy, and 5-dmbpy were, respectively, −2.33, −2.71, −2.77, and −2.82 V *vs.* $Ag/AgNO_3$(sat.).

The $E^{red}_{1/2,C}$ values for the (a) first, (b) second, and (c) third reduction steps of the unmixed-ligand complexes, $[Ru(bpm)_3]^{2+}$, $[Ru(bpy)_3]^{2+}$, $[Ru(4\text{-dmbpy})_3]^{2+}$, and $[Ru(5\text{-dmbpy})_3]^{2+}$, are plotted in Fig. 1 against the $E^{red}_{1/2,L}$ values. The experimental points for each step obey Eq. 1 approximately. Consequently, we may conclude that the redox orbitals of $[Ru(bpm)_3]^{2+}$ are also three-fold degenerate ligand π^*-orbitals.

Figure 2 shows similar plots for the mixed-ligand complexes, $[Ru(bpm)(bpy)_2]^{2+}$, $[Ru(bpm)(4\text{-dmbpy})_2]^{2+}$, and $[Ru(bpm)(5\text{-dmbpy})_2]^{2+}$. A striking feature is that the $E^{red}_{1/2,C}$ values for the first steps are almost independent of the ligands. All the experimental points for the second and the third steps lie on straight lines. Their slopes are inconsistent with Eq. 1, but this is not surprising because only two of the three ligands are changed in this case.

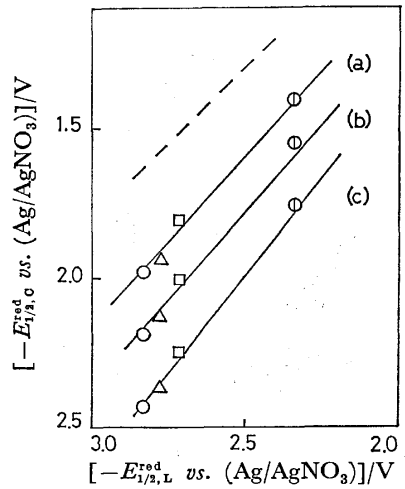

Fig. 1. Plots of $E^{1/2,c}_{red}$ for (a) $[RuL_3]^{2+}$, (b) $[RuL_3]^{+}$, and (c) $[RuL_3]$ *vs.* $E^{red}_{1/2,L}$ for L. L=(①) bpm, (□) bpy, (△) 4-dmbpy and (○) 5-dmbpy. The broken line shows the slope given by Eq. 1.

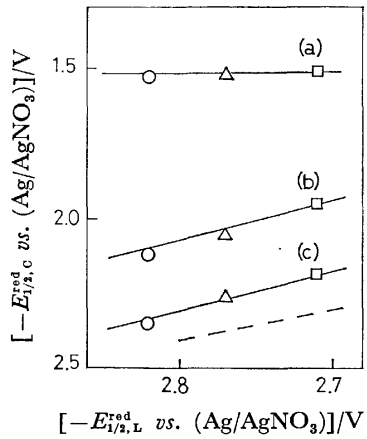

Fig. 2. Plots of $E^{1/2,c}_{red}$ for (a) $[Ru(bpm)L_2]^{2+}$, (b) $[Ru(bpm)L_2]^{+}$, and (c) $[Ru(bpm)L_2]$ *vs.* $E^{red}_{1/2,L}$ for L. L=(□) bpy, (△) 4-dmbpy and (○) 5-dmbpy. The broken line shows the slope given by Eq. 1.

The feature of Fig. 2 can be explained as follows. When we construct the MO of a $[Ru(bpm)L_2]^{2+}$ complex by the configuration interaction of the d_π atomic orbitals of the central metal and the LUMO's (lowest unoccupied molecular orbitals) of bpm and two L's, the metal orbitals are not taken into consideration.[5] Since the LUMO of bpm is lower than the LUMO's of L's by about 0.4 to 0.5 eV, it does not mix with the latter, which form two-fold degenerate orbitals. In $[Ru(bpm)_3]^{2+}$, three LUMO's of bpm can mix with each other and form three-fold degenerate orbitals, which are probably lower than the unmixed bpm orbital. This orbital order is consistent with the experimental finding that $[Ru(bpm)_3]^{2+}$ is reducible at a more positive potential than $[Ru(bpm)L_2]^{2+}$ (Table 1). When three electrons are added to $[Ru(bpm)L_2]^{2+}$, they may occupy these redox orbitals with parallel spins, because the energy of repulsion between a pair of electrons on the same MO may be much greater than the promotion energy between the lowest and the second lowest orbitals. Since the lowest orbital of $[Ru(bpm)L_2]^{2+}$ should be insensible to the small perturbation of methyl substitution applied to bpy, the $E^{red}_{1/2,c}$ values for the first steps should be invariable among the three $[Ru(bpm)L_2]^{2+}$ complexes.

In conclusion, the LUMO of $[Ru(bpm)L_2]^{2+}$ is actually localized on a single ligand bpm and is not delocalized over three ligand molecules. On the basis of the emission spectra of the mixed-ligand complexes of Rh(III) with bpy and 1,10-phenanthroline, Halper and DeArmond[10] have concluded that π^*-orbitals are localized on each ligand molecule, even when the $E^{red}_{1/2,L}$ values are almost identical. If their conclusion is right, though we are not in a position to comment on it now, it should be quite natural to get our present result.

We wish to thank Dr. Eiichi Ichikawa for his guidance in the synthesis of 2,2′-bipyrimidine.

References

1) T. Saji and S. Aoyagui, *J. Electroanal. Chem. Interfacial Electrochem.*, **58**, 401 (1975).
2) T. Saji, T. Fukai, and S. Aoyagui, *J. Electroanal. Chem. Interfacial Electrochem.*, **66**, 81 (1975).
3) T. Saji and S. Aoyagui, *Bull. Chem. Soc. Jpn.*, **49**, 1399 (1976).
4) T. Saji and S. Aoyagui, *J. Electroanal. Chem. Interfacial Electrochem.*, **110**, 329 (1980).
5) T. Saji and S. Aoyagui, *J. Electroanal. Chem. Interfacial Electrochem.*, **108**, 223 (1980).
6) D. D. Bly and M. G. Mellon, *Anal. Chem.*, **35**, 1386 (1963).
7) M. Hunziker and A. Ludi, *J. Am. Chem. Soc.*, **99**, 7370 (1977).
8) C-T. Lin, W. Bottcher, M. Chou, C. Creutz, and N. Sutin, *J. Am. Chem. Soc.*, **98**, 6536 (1976).
9) E. V. Dose and L. J. Wilson, *Inorg. Chem.*, **17**, 2660 (1978).
10) W. Halper and M. K. DeArmond, *J. Luminescence*, **5**, 225 (1972).

Pyrolytic Sulfurization Gas Chromatography. X. The Reduction of the Analysis Time by Means of High-frequency Heating

Tadashi Hara* and Fujio Okui

Department of Chemical Engineering, Faculty of Engineering, Doshisha University, Karasuma Imadegawa, Kamigyo-ku Kyoto 602

(Received May 27, 1981)

Synopsis. With the objective of reducing the analysis time in the previous PSGC method, a high-frequency induction furnace was used instead of an electric furnace. By using the present furnace, the time necessary for the pyrolytic sulfurization was reduced from 40 min to 1 min with satisfactory results.

By using pyrolytic sulfurization gas chromatography (PSGC), which was originated by the present authors, the atomic ratio between C, H, O, and N in a usual organic compound,[1] a metal organic chelate compound,[2] a polymer,[3] and an organic halogen compound[4] has been successfully and simultaneously determined. Moreover, the atomic ratio between C, H, O, N, Cl, Br, and I in an organic halogen compound has been successfully determined[5] using only one sample by a combination of gas chromatography and ion chromatography. Since the analysis by the PSGC was, however, batch-by-batch and time-consuming, a high-frequency induction furnace instead of the electric furnace used in the previous work[1-7] has been employed in order to reduce the reaction time of the pyrolytic sulfurization. The new furnace designed by the present authors consists of a work coil and an ampule holder in which an outer quartz tube is packed with granulated tungsten. By the use of the present furnace, the reaction temperature between a sample and S in a quartz ampule can be raised from the 950 °C in the previous work[1] to about 1500 °C; also, the reaction time is reduced from 40 min to 1 min. Various organic compounds were analyzed under experimental conditions similar to those used in the previous PSGC method.

Experimental

Apparatus. To subject an organic compound to the pyrolytic sulfurization, a high-frequency induction furnace (type: HFT-10S, frequency: 13.5 MHz, maximum power: 1 KW) was introduced instead of the electric furnace used in the previous work.[1] The furnace consists of a work coil and an ampule holder in which an outer quartz tube is packed with *ca.* 10 g of granulated tungsten as the heating medium. The furnace is shown in detail in Fig. 1.

Reagents. The granulated tungsten used as the heating medium was commercially available (purity: 99.9%; particle size; 10—20 mesh). The organic compounds used as standard samples were of a reagent grade for elemental analysis except for cyanoguanidine, which was of a reagent grade for a melting-point standard.

Procedure. The ampule containing a sample and S was prepared in a manner similar to that used in the previous work,[1] except that the ampule was shortened from 5 cm to 3 cm because of the furnace conditions, and placed in the ampule holder in the furnace. After replacing the contents of the furnace with helium, the ampule was treated for 1 min by high-frequency heating and then left standing for 3 min in the furnace. The ampule thus obtained was inserted into a gas sampler, and the reaction products in the ampule were analyzed by means of gas chromatography under the same conditions as in the previous work.[6]

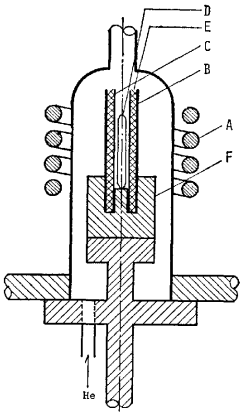

Fig. 1. High-frequency induction furnace.
A: Work coil, B: outer quartz tube (10.5 i.d., 12.5 o.d., 50 mm long), C: inner quartz tube (5.5 i.d., 6.5 o.d., 50 mm long), D: ampule containing a sample and S, E: granulated tungsten (10—20 mesh), F: ceramic support.

The atomic ratio between C, H, O, and N was calculated by the use of correction factors[6] which had been obtained from the analytical results of cyanoguanidine and sucrose by the above-mentioned procedure.

Results and Discussion

High-frequency Heating. Several kinds of granulated metals were examined as heating medium in high-frequency heating, and tungsten was found to be best. Since tungsten was easily oxidized to the oxide under the experimental conditions in the air, it was used in an atmosphere of helium, the tungsten being usable repeatedly. By using 10 g of granulated tungsten as the heating medium, an ampule containing a sample and S could be heated at about 1500 °C in a moment.

Reaction Time. The time necessary for the reaction between a sample and S in an ampule was investigated for 8-quinolinol as a standard sample; the relationship between the reaction time and the amounts of gases evolved from 1 mg of a sample is shown in Fig. 2. As can be seen from Fig. 2, the reaction between the sample and S in an ampule was completed within 40 s. The reaction products also indicated the same composition as in the previous PSGC method. In the present study, therefore, an ampule containing a sample and S was heated for 1 min by means of a high-frequency induction furnace.

Table 1. Analytical results of various organic compounds

Sample	C (wt%)			H (wt%)			O (wt%)			N (wt%)		
	Theor.	Found	Error	Theor.	Found	Error	Theor.	Found	Error	Theor.	Found	Error
8-Quinolinol	74.47	74.18	−0.29	4.86	4.93	+0.07	11.02	10.99	−0.03	9.65	9.90	+0.25
Cholesterol	83.87	84.23	+0.36	11.99	11.98	−0.01	4.14	3.79	−0.35			
Thiourea[a)]	27.26	27.08	−0.18	9.15	9.11	−0.04				63.59	63.81	+0.22
2,2-Bis(ethyl-sulfonyl)propane[a)]	51.21	51.30	+0.09	9.82	10.06	+0.24	38.97	38.64	−0.33			
Naphthalene	93.71	93.56	−0.15	6.29	6.44	+0.15						
Anthraquinone	80.76	80.53	−0.23	3.87	4.05	+0.18	15.37	15.42	+0.05			
Tris(2,4-pentane-dionato)iron(III)	60.59	60.72	+0.13	7.12	7.19	+0.07	32.29	32.09	−0.20			
Bis(2,4-pentane-dionato)-magnesium(II)	51.27	51.32	+0.05	7.75	7.77	+0.02	40.98	40.91	−0.07			

a) The sulfur atom was neglected in considering the composition of a sample, since it could not be determined.

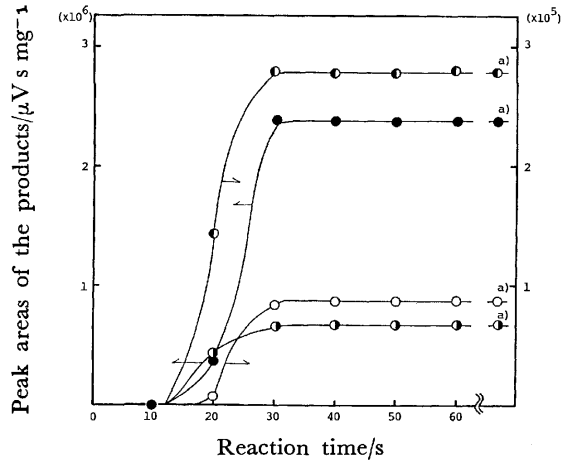

Fig. 2. Relationship between the reaction time and the amount of the reaction product.
○: N_2, ◑: H_2S, ◐: COS, ●: CS_2. a): By the previous PSGC method.

Standing Time after the Reaction. The effect on the result of the standing time of an ampule after high-frequency heating was investigated for 8-quinolinol as a standard sample. A standing time of less than 20 min had no effect on the analytical results of organic compounds analyzed by the present procedure. Therefore, the reaction products in an ampule were analyzed after leaving the ampule standing for 3 min in the furnace.

Analytical Results of Various Organic Compounds. Various organic compounds and metal organic chelate compounds were analyzed by the present procedure; the results are shown in Table 1. As can be seen from Table 1, both the precision and the accuracy were similar to those in the previous PSGC method.

From the results obtained by the present study, it can be concluded that the introduction of a high-frequency induction furnace reduces not only the reaction time between a sample and S in an ampule, but also the overall time necessary for an analysis. This will be very valuable for the further improvement of the PSGC method.

References

1) K. Tsuji, K. Fujinaga, and T. Hara, *Bull. Chem. Soc. Jpn.*, **50**, 2292 (1977).
2) T. Hara, K. Fujinaga, and T. Tsuji, *Bull. Chem. Soc. Jpn.*, **51**, 2951 (1978).
3) T. Hara, K. Fujinaga, F. Okui, and K. Negayama, *Sci. Eng. Rev. Doshisha Univ.*, **21**, 241 (1981).
4) T. Hara, K. Fujinaga, and F. Okui, *Bull. Chem. Soc. Jpn.*, **53**, 1308 (1980).
5) T. Hara, K. Fujinaga, and F. Okui, *Bull. Chem. Soc. Jpn.*, **54**, 2956 (1981).
6) T. Hara, K. Fujinaga, and T. Tsuji, *Bull. Chem. Soc. Jpn.*, **51**, 1110 (1978).
7) T. Hara, K. Fujinaga, and F. Okui, *Bull. Chem. Soc. Jpn.*, **53**, 951 (1980).

Dysprosium and Holmium Complexes of *N*-(2-Pyridyl)salicylideneamine

Megh SINGH* and K. Singh GHARIA

Department of Chemistry, University of Jodhpur, Jodhpur-342001, India

(Received January 23, 1981)

Synopsis. Dysprosium and holmium isopropoxides react with monofunctional bidentate Schiff base, *N*-(2-pyridyl)salicylideneamine, in 1:1, 1:2, and 1:3 molar ratios in benzene to yield complexes of the types $Ln(OPr^i)_2(sap)$, $Ln(OPr^i)(sap)_2$, and $Ln(sap)_3$ (where Ln=Dy or Ho and sap^- is the anion of the Schiff base sapH). Probable structures for these complexes are proposed on the basis of molecular weight and IR spectroscopic data. Reports on metal complexes derived from Schiff bases have aroused considerable interest in the field of coordination chemistry, and have been extensively studied.[1-4] A literature survey reveals that no work has been done on Dy(III) and Ho(III) complexes of heterocyclic Schiff base, *N*-(2-pyridyl)salicylideneamine. However, complexes of this Schiff base with d-transition elements[5,6] have been reported. The present paper deals with the synthesis of Dy(III) and Ho(III) complexes of *N*-(2-pyridyl)salicylideneamine and their characterization by infrared spectra.

Experimental

Dy(III) and Ho(III) isopropoxides were prepared from the respective trichlorides by sodium alkoxide method.[7] The Schiff base was prepared by usual method.[6] The reactions of Dy(III) and Ho(III) isopropoxides with the Schiff base in different molar ratios (1:1, 1:2, and 1:3) were carried out in refluxing benzene and the 2-propanol liberated in these reactions was collected azeotropically and estimated by oxidation method.[8] For brevity the reactions and their analyses have been summarized in Table 1. The lanthanoid content was determined by ignition to sesquioxide. Nitrogen was estimated by the Kjeldahl method. Molecular weights were determined in refluxing benzene by Cottrell's method.[9] IR spectra were recorded in the 4000—200 cm^{-1} range on a Perkin-Elmer 621 instrument using KBr pellets and as mulls in Nujol.

Results and Discussion

The reactions of Dy(III) and Ho(III) isopropoxides with the Schiff base in 1:1, 1:2, and 1:3 molar ratios in anhydrous benzene liberated one, two and three moles of 2-propanol respectively and resulted in the formation of the corresponding mono-, bis-, and tris-Schiff base derivatives of Dy and Ho.

Diisopropoxy-mono(Schiff base) derivatives are orange-red solids, soluble in benzene and they decompose at temperature ≈150 °C whereas monoisopropoxy-bis(Schiff base) derivatives are benzene insoluble orange coloured solids. Tris(Schiff base) derivatives are isolated as dark yellow powders, insoluble in benzene but fairly soluble in *N*,*N*-dimethylformamide.

The molecular weights of diisopropoxy-mono(Schiff base) derivatives of Dy(III) and Ho(III) in boiling benzene indicate them to be essentially trimeric involving the most probable structure of the type (I).

The products $Ln(OPr^i)(sap)_2$ were found to be insoluble in benzene. The insolubility of these derivatives in common organic solvents prevented determination of molecular weights which could have otherwise useful information about their structures. On serric grounds it can be said that this Schiff base cannot form monomeric structures. With the help of previous work on similar type of derivatives,[10-12] we suggest that these complexes may be present in dimeric form (II) where two metal octahedra are bridged through isopropoxide oxygen bridges. The probability of other structures having lanthanoid atom with more than six coordination number, however, cannot be ruled out since lanthanoids have tendency to show coordination number more than six.[13]

The tris(Schiff base) derivatives of Dy(III) and Ho(III) are also insoluble in benzene and common organic solvents. The insolubility in common noncoordinating solvents and high melting or decomposition temperature (≈260 °C) indicate their associated or polymeric nature. A polymeric structure has also

TABLE 1. REACTIONS OF DYSPROSIUM AND HOLMIUM ISOPROPOXIDES WITH SCHIFF BASE (sapH)

Reactants (Molar ratio) (g)	Refluxing time / h	Product and colour	2-Propanol in azeotrope (g) Found(Calcd)	Found(Calcd) (%) Ln	Found(Calcd) (%) N	Decomposition temp / °C
$Dy(OPr^i)_3$+sapH (1:1) 1.6626+0.9700	5	$Dy(OPr^i)_2(sap)$ Orange red	0.2896 (0.2940)	33.95 (34.00)	5.43 (5.86)	160
$Dy(OPr^i)_3$+sapH (1:2) 1.5202+1.7524	8	$Dy(OPr^i)(sap)_2$ Orange	0.5284 (0.5377)	26.17 (26.77)	9.00 (9.09)	282
$Dy(OPr^i)_3$+sapH (1:3) 1.0006+1.7512	10	$Dy(sap)_3$ Dark yellow	0.5296 (0.5309)	20.89 (21.54)	10.95 (11.14)	260
$Ho(OPr^i)_3$+sapH (1:1) 1.3458+0.7795	5	$Ho(OPr^i)_2(sap)$ Orange red	0.2368 (0.2363)	34.05 (34.33)	5.83 (5.83)	148
$Ho(OPr^i)_3$+sapH (1:2) 1.2772+1.4796	8	$Ho(OPr^i)(sap)_2$ Orange	0.4452 (0.4485)	26.59 (26.66)	8.95 (9.05)	285
$Ho(OPr^i)_3$+sapH (1:3) 1.2592+2.1880	10	$Ho(sap)_3$ Dark yellow	0.6539 (0.6633)	21.43 (21.79)	11.00 (11.10)	260

sapH=$C_{12}H_{10}N_2O$

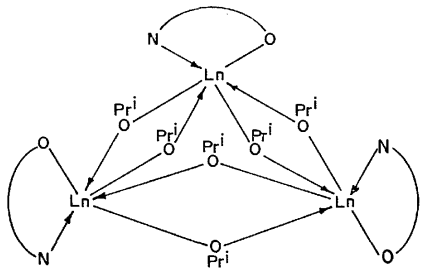

I

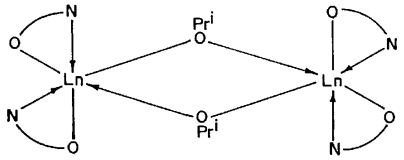

II

Ln = Dy or Ho ($\overset{O}{N}$ = anion of Schiff base SAPH.

been suggested for tris(salicylideneamino)triethylenetetramine complexes of lanthanoids on the basis of their practically insoluble nature in any available solvents.[14]

The IR spectrum of ligand exhibited a broad band around 2990—2800 cm^{-1} due to O–H stretching vibration, shifted to lower frequency as a result of intramolecular hydrogen bonding OH···N. The disappearance of this band (ν O–H) in the complexes suggests the participation of OH group of Schiff base in bound formation.

A strong band is observed at 1610 cm^{-1} in the free ligand. This is a characteristic absorption band of the azomethine (>C=N–) group. This band (ν C=N) in the spectra of all the complexes appears at almost the same position and remain unaffected on complexation. Since these bands are associated with –C=N– stretching frequencies, this is consistent with observation of Sarma and Bailar[15] that indicate coordination through the nitrogen atom of azomethine group. However, some workers have reported a shift of ν C=N frequency either to higher[16] or to lower[17] wave number on complexation.

The phenolic C–O stretching vibration in free ligand is observed at 1280 cm^{-1}. This band in complexes is slightly shifted to higher frequency ($\approx$1295 cm^{-1}) indicating the bonding of the ligand to the metal atom through phenolic oxygen. The higher ν C–O in complexes may be ascribed to delocalization of electron density from the oxygen atom to the metal resulting in greater ionic character of the C–O bond and a consequent increase in the C–O vibration frequency. A similar observation was observed by Kovacic for Cu(II) complexes of salicylidene–anilines.[18]

The mono and diisopropoxy derivatives of Schiff base show characteristic frequencies of isopropyl group at $\approx$1385, 1160, 1150, and 1000 cm^{-1}.[19] The medium strong band at $\approx$1385 and 1000 cm^{-1} may be assigned to the *gem*-dimethyl structure and bridged C–O stretching vibrations respectively. The value of C–O stretching vibration in mono- and diisopropoxy derivatives of Dy(III) and Ho(III) *ca.* $\approx$1000 cm^{-1} agrees with C–O vibration of bridging alkoxy group.[20]

The coordination of pyridine molecule to metal is known to cause an upward shift of the four principal bands of pyridine between 1600 and 1430 cm^{-1}, which corresponds to ν C=C and ν C=N vibrations.[21] In our case no appreciable shift was observed in these bands. This suggests that pyridine nitrogen is not involved in coordination.

The medium and weak bands between 700—200 cm^{-1} are observed in these complexes. These bands are assigned to ν M–O and ν M–N vibrations. No significant differences among the IR spectra were observed for the mono-, bis-, and tris-Schiff base complexes in this region. The bands at $\approx$660, 535, 505, and 460 cm^{-1} are due to metal-oxygen vibrations[22] whereas the bands observed in the region 400—200 cm^{-1} are assigned to metal-nitrogen vibrations.[23]

References

1) R. H. Holm, G. W. Everett, Jr., and A. Chakravorty, *Prog. Inorg. Chem.*, **7**, 83 (1966).
2) E. Sinn and C. M. Harris, *Coord. Chem. Rev.*, **4**, 391 (1969).
3) S. Yamada, *Coord. Chem. Rev.*, **1**, 415 (1966).
4) S. Yamada, K. Yamanouchi, and H. Kuma, *Synth. React. Inorg. Met.-org. Chem.*, **1**, 9 (1971).
5) M. K. Misra, R. C. Das, and S. K. Mohanty, *Indian J. Chem.*, **14A**, 679 (1976).
6) M. R. Mahmoud and M. T. EL Haty, *J. Inorg. Nucl. Chem.*, **42**, 349 (1980).
7) S. N. Misra, T. N. Misra, R. N. Kapoor, and R. C. Mehrotra, *Chem. Ind.*, **1963**, 120.
8) D. C. Bradley, F. M. A. Halim, and W. Wardlaw, *J. Chem. Soc.*, **1950**, 3450.
9) J. M. Wilson, R. J. Newcombe, A. R. Denaro, and R. M. W. Rickett, "Experiments in Physical Chemistry," Pergamon Press, London (1962), p. 16.
10) M. Hasan, K. Kumar, S. Dubey, and S. N. Misra, *Bull. Chem. Soc. Jpn.*, **41**, 2619 (1968).
11) S. K. Agarwal and J. P. Tandon, *J. Inorg. Nucl. Chem.*, **37**, 949 (1975).
12) P. Pfeiffer and H. Pfitzner, *J. Prakt. Chem.*, **145**, 243 (1936).
13) S. P. Sinha, *Struct. Bonding*, **25**, 69 (1976).
14) T. Isobe, S. Kida, and S. Misumi, *Bull. Chem. Soc. Jpn.*, **40**, 1862 (1967).
15) B. Sarma and J. C. Bailar, Jr., *J. Am. Chem. Soc.*, **77**, 5476 (1955).
16) D. H. Busch and J. C. Bailar, Jr., *J. Am. Chem. Soc.*, **78**, 1137 (1956).
17) E. C. Alyea, A. Malek, and P. H. Merrell, *Transition Met. Chem.*, **4**, 172 (1979).
18) J. E. Kovacic, *Spectrochim. Acta, Part A*, **23**, 183 (1967).
19) C. T. Lynch, K. S. Mazdiyasni, J. S. Smith, and W. J. Crawford, *Anal. Chem.*, **36**, 2332 (1964).
20) C. H. S. Wu, G. R. Rossman, H. B. Gray, G. S. Hammond, and H. J. Schugar, *Inorg. Chem.*, **11**, 990 (1972).
21) N. S. Gill, R. H. Nutall, D. E. Scaife, and D. W. A. Sharp, *J. Inorg. Nucl. Chem.*, **18**, 79 (1961).
22) C. Y. Liang, E. J. Schimtschek, and J. A. Trias, *J. Inorg. Nucl. Chem.*, **32**, 811 (1970).
23) J. R. Ferraro, L. J. Basile, and D. L. Kovacic, *Inorg. Chem.*, **5**, 391 (1966).

The Reaction of 2-Benzylidenetetralin-1-thione *S*-oxide with Acrylonitrile or Styrene

Haruo OHMURA, Takayuki KARAKASA,† Sadayoshi SATSUMABAYASHI,† and Shinichi MOTOKI*

Department of Chemistry, Faculty of Science, Science University of Tokyo, Kagurazaka, Shinjuku-ku, Tokyo 162

† *Nippon Dental University, Tokyo, 1-9-20, Fujimi, Chiyoda-ku, Tokyo 102*

(Received June 29, 1981)

Synopsis. The cycloaddition reaction of 2-benzylidenetetralin-1-thione *S*-oxide with acrylonitrile (or styrene) gave a mixture of 2- and 3-cyano(or phenyl)-4-phenyl-3,4,5,6-tetrahydro-2*H*-naphtho[1,2-*b*]thiopyran *S*-oxide. Pummerer reaction of these *S*-oxides resulted to afford the corresponding acetates.

α,β-Unsaturated sulfines[1] have been inaccessible compounds and their chemical properties have not been investigated. Previously, we reported the generation of α,β-unsaturated sulfine [2-benzylidenetetralin-1-thione *S*-oxide (**3**)] by the thermolysis of its dimer (**2**), and the cycloaddition reaction of **3** with norbornene.[1b] α,β-Unsaturated thiones such as the compound (**4**) are known to react with various kinds of olefins giving Diels-Alder type 1,4-cycloaddition products,[2] and we are interested in the reaction of **3** with some olefinic compounds.

When a mixture of **2** and acrylonitrile in xylene was heated to reflux, a mixture of the adducts **5a** and **6a** were obtained. They were separated and identified by the conversion into their sulfides by Pummerer reaction. Refluxing of the mixture (**5a** and **6a**) in acetic anhydride afforded two acetates **7a** and **8a**. Both **7a** and **8a** showed absorptions at 2250 cm^{-1} for cyano group and at 1760 and 1210 cm^{-1} for $OCOCH_3$ in their IR spectra. The ^1H-NMR spectrum of **7a** showed signals at δ 3.68 (dd, J=4 and 6 Hz) 3.93 (d, J=6 Hz), and 6.34 (d, J=4 Hz). These signals were readily assigned to those of the C-3, the C-4 and the C-2 protons, respectively. The proton-noise-decoupled ^{13}C-NMR spectrum of **7a** also showed three methine carbon signals at δ 37.1, 45.4, and 69.5. The structure of **7a** was further confirmed by an independent synthesis. Namely, oxidation of **10a** with *m*-chloroperbenzoic acid (mCPBA) followed by the treatment with acetic anhydride produced the acetate, which was completely identical with that obtained from **5a**. The ^1H-NMR spectrum of **8a** showed signals at δ 3.96 (m, 1H) and 2.83 (m, 2H) and the ^{13}C-NMR spectrum showed signals at δ 41.7 for the C-3, 44.4 for the C-4, and 71.9 for the C-2 carbons.

Similarly, the reaction of **3** with styrene gave a mixture of the adducts **5b** and **6b**. The Pummerer reaction of the mixture afforded two products **7b** and **9**. The IR spectrum of **7b** showed absorptions at 1760 and 1210 cm^{-1} for $OCOCH_3$. The ^1H-NMR spectrum showed signals at δ 3.69 (dd, J=4 and 6 Hz) for the C-3, 3.90 (d, J=6 Hz) for the C-4, and 6.19 (d, J=4 Hz) for the C-2 protons. The ^{13}C-NMR spectrum showed the three methine carbon signals at δ 50.8, 51.4, and 75.7. Also, **7b** was identical with the spectrum prepared by an independent synthetic route from **10b** (Scheme 2). The IR spectrum of **9** had no band in the near region of 1720 cm^{-1} for $OCOCH_3$ and the mass spectrum showed a molecular ion peak at 352. The ^1H-NMR spectrum showed signals at δ 4.31 (d, J=6 Hz) for the C-4 and 6.01 (d, J=6 Hz) for the C-3 protons. The ^{13}C-NMR spectrum showed a signal at δ 50.1 for the C-4 carbon. These data and elementary analysis

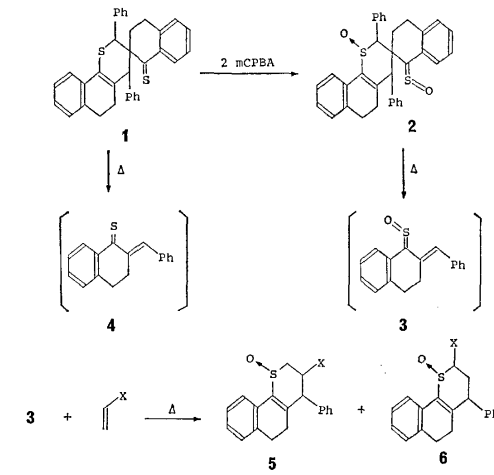

a: X=CN, b: X=Ph

Scheme 1.

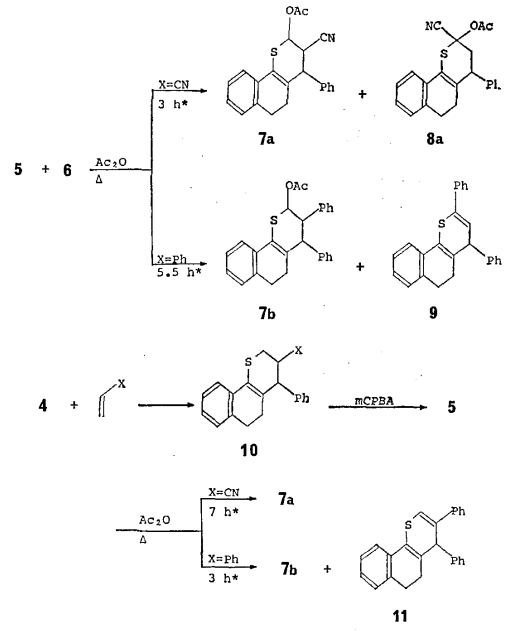

a: X=CN, b: X=Ph * Reaction time

Scheme 2.

were in agreement with the proposed structure (**9**).

The reaction of **3** with maleic anhydride gave tarry unidentified products. Butyl vinyl ether or 1-morpholinocyclohexene did not react with **3** but the thermal rearrangement of **3** to β-thioxo ketone[3] was observed in this case.

As a result, it has been found that the α,β-unsaturated sulfine **3** does not react with electron rich dienophiles and that the cycloaddition reaction of **3** is less regioselective than that of the corresponding α,β-unsaturated thione **4**.

Experimental

All the melting points are uncorrected. ^{1}H-NMR (100 MHz) and ^{13}C-NMR (25 MHz) spectra were recorded on a JEOL JNM-FX 100 spectrometer with Me_4Si as an internal standard. IR spectra were obtained on a Hitachi Model 260-10 infrared spectrometer. Mass spectral data were obtained with a Hitachi RMU-7M double-focusing mass spectrometer.

*A Typical Procedure for the Reaction of **3** with Olefins.* A suspension of **2**[2b] (0.65 g) and acrylonitrile (1.2 g) in dry xylene (6 cm^3) was refluxed for 2.5 h under a nitrogen atmosphere. The solvent was evaporated to give a mixture of **5a** and **6a** which could not be separated by crystallization or chromatography: yield 32%; colorless powder. Found: C, 75.43; H, 5.29%. Calcd for $C_{20}H_{17}NOS$: C, 75.21; H, 5.29%. A mixture of **5b** and **6b** (reaction time 1 h): yield 67%; colorless powder. Found: C, 80.84; H, 5.96%. Calcd for $C_{25}H_{22}OS$: C, 81.04; H, 5.99%.

*A Typical Procedure for the Reaction of the Sulfoxide (**5** and **6**) with Acetic Anhydride.* A suspension of a mixture of **5a** and **6a** (2.62 g) in acetic anhydride (15 cm^3) was refluxed for 3 h under a nitrogen atmosphere. The excess acetic anhydride was evaporated and the residue was chromatographed on Wakogel C-200 [eluting with benzene–hexane (1:1)]. **7a**: yield 10%; mp 190—191 °C; MS (70 eV) *m/e* 361 (43), 250 (60), 249 (100); ^{1}H-NMR ($CDCl_3$) δ 1.76 (s, 3H), 2.12—2.85 (m, 4H), 3.68 (dd, *J*=4 and 6 Hz, 1H), 3.93 (d, *J*=6 Hz, 1H), 6.34 (d, *J*=4 Hz, 1H), 7.04—7.60 (m, 9H); ^{13}C-NMR ($CDCl_3$) δ 20.4 (q), 28.0 (t), 29.9 (t), 37.1 (d), 45.4 (d). Found: C, 73.08; H, 5.21; N, 3.81; S, 8.76%. Calcd for $C_{22}H_{19}O_2NS$: C, 73.10; H, 5.30; N, 3.88; S, 8.87%.

8a: yield 12%; mp 160—161 °C; MS (70 eV) *m/e* 361 (100), 319 (68), 249 (54); ^{1}H-NMR ($CDCl_3$) δ 1.80 (s, 3H), 2.04—2.76 (m, 4H), 2.83 (m, 2H), 3.96 (m, 1H), 7.00—7.36 (m, 9H); ^{13}C-NMR ($CDCl_3$) δ 20.4 (q), 27.9 (t), 29.0 (t), 41.6 (t), 44.4 (d), 71.9 (s). Found: C, 72.75; H, 5.26; N, 3.64; S, 8.90%. Calcd for $C_{22}H_{19}O_2NS$: C, 73.10; H, 5.30; N, 3.88; S, 8.87%.

7b: yield 25%; mp 106—108 °C; MS (70 eV) *m/e* 352 (62), 275 (100); ^{1}H-NMR ($CDCl_3$) δ 2.08—2.84 (m, 4H), 4.31 (d, *J*=6 Hz, 1H), 6.01 (d, *J*=6 Hz, 1H), 6.81—7.57 (m, 14H); ^{13}C-NMR ($CDCl_3$) δ 28.1 (t), 28.7 (t), 50.1 (d). Found: C, 84.99; H, 5.62; S, 8.96%. Calcd for $C_{25}H_{20}S$: C, 85.19; H, 5.72; S, 9.09%.

9: yield 13%; mp 150—151 °C; MS (70 eV) *m/e* 412 (15), 250 (75), 249 (100); ^{1}H-NMR ($CDCl_3$) δ 1.60 (s, 3H), 2.20—2.90 (m, 4H), 3.69 (dd, *J*=4 and 6 Hz, 1H), 3.90 (d, *J*=4 Hz, 1H), 6.19 (d, *J*=6 Hz, 1H), 7.12—7.40 (m, 14H); ^{13}C-NMR ($CDCl_3$) δ 20.5 (q), 28.3 (t), 30.1 (t), 50.8 (d), 51.4 (d), 75.7 (d). Found: C, 78.46; H, 5.81; S, 7.75%. Calcd for $C_{27}H_{24}O_2S$: C, 78.61; H, 5.86; S, 7.77%.

*A Typical Procedure for the Oxidation of **10** with mCPBA.* To **10**[2b] (1.0 g) dissolved in 30 cm^3 of dichloromethane a solution of mCPBA (0.57 g in 25 cm^3 dichloromethane) was added at 0 °C under a nitrogen atmosphere in 30 min. After the addition of 30 cm^3 chloroform, the solution was washed with aqueous sodium hydrogencarbonate. The solvent was evaporated and the residue was recrystallized from chloroform–ligroine to give **5a**: yield 67%; mp 240—241 °C; MS (70 eV) *m/e* 319 (M^+, 3), 249 (37); IR (KBr) 2250 (CN), 1040—1050 (SO) cm^{-1}. Found: C, 75.23; H, 5.30; N, 4.20; S, 10.00%. Calcd for $C_{20}H_{17}NOS$: C, 75.20; H, 5.36; N, 4.39; S, 10.04%.

5b: yield 64%; mp 223—225 °C; MS (70 eV) *m/e* 370 (M^+, 4), 218 (77); IR (KBr) 1030 (SO) cm^{-1}; ^{1}H-NMR ($CDCl_3$) δ 1.92—2.84 (m, 4H), 3.24 (m, 2H), 3.84 (m, 1H), 4.36 (m, 1H), 7.00—7.32 (m, 13H), 8.03 (m, 1H). Found: C, 81.12; H, 6.01; S, 8.64%. Calcd for $C_{25}H_{22}OS$: C, 81.04; H, 5.99; S, 8.65%.

*Reaction of **5** with Acetic Anhydride.* **7a**: yield 24%. **7b**: yield 10%.

11: yield 35%; mp 97—98 °C; MS (70 eV) *m/e* 352 (34), 276 (25), 275 (100); ^{1}H-NMR ($CDCl_3$) δ 2.08—2.88 (m, 4H), 4.51 (s, 1H), 6.70 (s, 1H), 6.82—7.44 (m, 14H); ^{13}C-NMR ($CDCl_3$) δ 28.2 (t), 29.8 (t), 51.4 (d). Found: C, 85.41; H, 5.92; S, 9.12%. Calcd for $C_{25}H_{20}S$: C, 85.19; H, 5.72; S, 9.09%.

References

1) a) M. F-Neumann and J. J. Lohmann, *Tetrahedron Lett.*, **1979**, 2397; b) T. Karakasa and S. Motoki, *ibid.*, **1979**, 3961.

2) a) J. P. Pradere, G. Bouet, and H. Quiniou, *Tetrahedron Lett.*, **1972**, 3471; K. B. Lipkowitz and B. P. Mundy, *ibid.*, **1977**, 3417; K. B. Lipkowitz, S. Scarpone, B. P. Mundy, and W. G. Bornmann, *J. Org. Chem.*, **44**, 487 (1979); J. P. Guemas, A. Reliquet, F. Reliquet, and H. Quiniou, *C. R. Acad. Sci., Ser. C*, **1979**, 89; b) T. Karakasa and S. Motoki, *J. Org. Chem.*, **43**, 4147 (1978); c) T. Karakasa and S. Motoki, *ibid.*, **44**, 4151 (1979); T. Karakasa, H. Yamaguchi, and S. Motoki, *ibid.*, **45**, 927 (1980); T. Karakasa and S. Motoki, *Chem. Lett.*, **1980**, 879.

3) T. Karakasa, H. Ohmura, and S. Motoki, *Chem. Lett.*, **1980**, 825.

Electrooxidative Conversion of Aldehydes into Methyl Carboxylates

Toshiro CHIBA,* Mitsuhiro OKIMOTO, Hiroshi NAGAI, and Yoshiyuki TAKATA**
Department of Applied Chemistry, Kitami Institute of Technology, Koen-cho 165, Kitami 090
***Faculty of Engineering, Hokkaido University, Sapporo 060*

(Received January 26, 1981)

Synopsis. The electrolytic oxidation of methanolic solutions of aldehydes in the presence of sodium cyanide at a platinum anode was found to produce corresponding methyl carboxylates.

Several chemical procedures for the preparation of methyl carboxylates from aldehydes in methanolic media using peroxides,[1] ozone,[2] or manganese dioxide[3] have been reported, but only a few reports are available on the electrooxidative conversion of aldehydes into methyl carboxylates.[4]

Thus, we wish to report here the electrochemical oxidation of aldehydes[5] in methanol containing sodium cyanide, which can afford methyl benzoates in good yields.

Results and Discussion

Table 1 shows the results of the electrooxidation of several aldehydes in methanolic sodium cyanide on a macro-scale. These electrolyses were performed in a divided cell at room temperature using a platinum gauge anode under constant current conditions until almost all of the aldehyde was consumed.

Generally, aromatic aldehydes readily underwent anodic oxidation and were converted into the respective methyl benzoates. As an example of the oxidation of benzaldehyde, the ester yield at the stage where $2F$/mol of electricity passed was 62%, and by passing an excess of electricity it reached approximately 90%, according to GLC analysis. From the resulting anolyte, essentially pure methyl benzoate could be isolated by simple distillation in a yield of 80%. Chemical side reactions such as benzoin condensation rarely took place under the present conditions in spite of the reaction in the presence of sodium cyanide.

Similar results were obtained in the oxidation of substituted benzaldehydes with a methyl group or chlorine atom in an *ortho* or *para* position. The yield of their esters was hardly affected by the substituent and its position. However, *p*-methoxybenzaldehyde afforded methyl *p*-methoxybenzoate in yield less than 50% along with the nuclear cyanation product of the ester in yield *ca.* 15%.[6]

Attempted oxidation of aliphatic aldehydes by the same procedure gave only about a 40% yield of the methyl carboxylates and a considerable amount of a highly viscous liquid which may be derived from aldol condensation.

The aldehydes were more oxidizable in methanolic sodium cyanide than in a lithium perchlorate-acetonitrile electrolyte system, since benzaldehyde was oxidized at the potential of 2.3 V *vs.* SCE in lithium perchlorate-acetonitrile solution in contrast to the potential at about 1.7 V in methanolic sodium cyanide.[7] Therefore, it was assumed that the anodically oxidized species would not be the aldehyde itself, but its derivatives such as cyanohydrin.

The present reaction seems to proceed by a scheme

TABLE 1. ELECTROOXIDATIVE CONVERSION OF ALDEHYDES INTO METHYL CARBOXYLATES IN METHANOLIC SODIUM CYANIDE[a]

RCHO R	Oxidation potential *vs.* SCE[b] / V	Anode potential *vs.* SCE / V	Consumed current F/mol	Material yield[c]/%	Collected range Bp θ_b/°C (mmHg)	Reported[1] Bp θ_b/°C (mmHg)
C_6H_5-	2.30	1.6—1.8	5.6	80	82— 84(15)	96—98(24)
2-CH_3-C_6H_4-	2.26	1.8—2.0	6.2	77	97—100(18)	97(15)
4-CH_3-C_6H_4-	2.23	1.7—1.9	5.5	83	98—100(16) mp 32—33 °C	217 mp 33.2 °C
4-CH_3O-C_6H_4-	1.82	1.6—1.9	5.1	48[d]	123—140(14)[h]	256 mp 48 °C
2-Cl-C_6H_4-	2.42	1.6—1.8	6.3	73	110—115(16)	234
4-Cl-C_6H_4-	2.22	1.6—1.8	5.7	78	103—106(15) mp 42—43 °C	mp 44 °C
n-C_3H_7-	—	1.6—1.9	18.3	(44)[e,f]		
n-C_7H_{15}-	—	1.7—2.0	18.3	38[g,f]		

a) Anolyte: aldehyde(50 mmol) and NaCN(75 mmol) in 160 ml of MeOH. Constant current, 0.8 A. Temperature, *ca.* 17 °C. b) $E_{1/2}$, measured in 0.25 mol dm^{-3} $LiClO_4$-MeCN containing the aldehyde in concentration of 5×10^{-3} mol dm^{-3} with a voltage scanning rate of *ca.* 0.1 V/s at a platinum electrode. c) Based on aldehyde. d) From the residue of the distillate, nuclear cyanation product of the ester was isolated in a yield of *ca.* 15%: mp 124—125 °C, white needles from methanol; IR ν 2230 cm^{-1} (CN); MW 191 (mass). e) According to GLC. f) Undistilled viscous liquid was also obtained, but it was not further investigated. g) Isolated by column chromatography on silica gel using benzene as the eluent. h) This fraction was purified by reduistillation, bp 132—135 °C (14 mmHg), mp 45—47 °C. i) Ref. 8.

analogous to that of the oxidative conversion of aldehydes into esters with mangenese dioxide and sodium cyanide,[3] in which the initial step is the formation of cyanohydrin, followed by oxidation to acyl cyanide which can readily react with alcohol to form the ester.

In fact, a similar electrolysis of mandelonitrile gave methyl benzoate in a reasonable yield, but the ester was scarcely obtainable by anodic oxidation of benzaldehyde using sodium perchlorate or tetraethylammonium *p*-toluenesulfonate in place of sodium cyanide as the supporting electrolyte.

Apparently, the cyanide ion played an important role in this reaction; however, the exact catalytic behavior could not be recognized, because the consumption of the cyanide ion was confirmed. Consequently, an excess of more than an equivalent of sodium cyanide to the aldehyde should be used to obtain the ester effectively.

This electrolysis was not applicable to α,β-unsaturated aldehydes such as cinnamaldehyde or 2-methyl-2-pentanal under the present experimental conditions. In these cases, many unidentified miscellaneous products were formed.

Experimental

The macro-scale electrolyses were carried out in a 200 ml beaker separated from the cathode compartment by a glass filter. The anode was a cylindrical platinum gauge (4.5 cm in high, 11 cm in circumference, 55 mesh), and the cathode was a platinum coil (0.8 mmϕ, 20 cm). The cell was externally cooled with water, and the anolyte was stirred by a magnetic stirring bar.

The general procedure is as follows. A solution of benzaldehyde (50 mmol) in methanol (160 ml) containing sodium cyanide (76 mmol) was electrolyzed at a constant current of 0.8 A for 9.4 h. After completion of the reaction, the solvent was distilled off, and the residue was washed with water, followed by dual extraction with ether. The combined extracts were concentrated on a water bath, and the warm residue was vigorously shaken with a small quantity of saturated sodium hydrogensulfite solution. The oily layer was extracted with ether, and then distilled under reduced pressure after dehydration with anhydrous sodium sulfate.

Identification of products was made by infrared spectroscopy and comparison with authentic samples prepared by the usual manner.

References

1) a) A. Nishihara and I. Kubota, *J. Org. Chem.*, **33**, 2525 (1968); b) C. W. Smith and R. T. Holm, *ibid.*, **22**, 746 (1957); c) M. Kitahara, T. Mitsui, and T. Hirayama, *Rikagaku Kenkyusho Hokoku*, **38**, 81 (1962); *Chem. Abstr.*, **58**, 13788a (1963).

2) P. Sundararaman, E. C. Walker, and C. Djerassi, *Tetrahedron Lett.*, **1978**, 1627.

3) E. J. Corey, N. W. Gilman, and B. E. Ganem, *J. Am. Chem. Soc.*, **90**, 5616 (1968).

4) To the best of our knowledge, only one paper has previously showed that the anodic oxidation of benzaldehyde in methanolic sodium methoxide gives methyl benzoate; however, the yield was less than 30%: M. Tatsumi, Japan Patent, 68 14683 (1968); *Chem. Abstr.*, **71**, 70336d (1969).

5) For a review of anodic oxidation of aldehydes, see: N. L. Weinberg and H. R. Weingerg, *Chem. Rev.*, **68**, 449 (1968).

6) The same product was obtained in a poor yield in an anodic oxidation of methyl *p*-methoxybenzoate in methanolic sodium cyanide.

7) Addition of significant amounts of the aldehyde to the electrolyte brought about a remarkable increase of electrolytic current at higher cathodic potentials rather than the potential of methanolic sodium cyanide without aldehydes.

8) "Dictionary of Organic Compounds," 4th ed, ed by J. R. A. Pollack and R. Stevens, Eyre and Spottiswoode (Publishers) Ltd., Great Britain (1965).

ortho-Disubstituted *F*-Benzenes. IV. The Formation of 2-Acyl-*F*-phenyl Carboxylates from (*F*-Benzo)furans by the Oxidative Cleavage of the Furan-ring

Yoshinari INUKAI,† Takaaki SONODA, and Hiroshi KOBAYASHI*

Research Institute of Industrial Science, Kyushu University 86, Kasuga 816

(Received May 6, 1981)

Synopsis. 2,3-Diphenyl-, 2-phenyl-3-methyl-, and 2-methyl-3-phenyl(*F*-benzo)furans were oxidized with chromium trioxide in acetic acid to yield 2-benzoyl-*F*-phenyl benzoate, 2-acetyl-*F*-phenyl benzoate, and 2-benzoyl-*F*-phenyl acetate respectively, while 2-phenyl(*F*-benzo)furan was least susceptible to the same reagent, affording 1-(2-hydroxy-*F*-phenyl)-2-phenylethanedione in a poor yield. The spectral data of the products were compatible with the structure of *ortho*-disubstituted *F*-benzene.

In connection with the studies of the *ortho*-disubstituted *F*-benzenes,[1,2] we have examined the oxidative cleavage of the side-ring of (*F*-benzo)furans (**1**), which were previously described.[3] In a manner similar to that of unfluorinated analogues,[4] the (*F*-benzo)furans (**1**) were oxidatively cleaved between the 2- and 3-positions of the furan ring with chromium trioxide to give *ortho*-disubstituted *F*-benzenes. 2,3-Diphenyl-, 2-phenyl-3-methyl-, and 2-methyl-3-phenyl-(*F*-benzo)furans (**1a**—**c**) yielded 2-benzoyl-*F*-phenyl benzoate (**2a**), 2-acetyl-*F*-phenyl benzoate (**2b**), and 2-benzoyl-*F*-phenyl acetate (**2c**) respectively. The *F*-phenyl ester groups remained intact; they were not hydrolyzed in acid-reaction media. 2-Phenyl(*F*-benzo)furan (**1d**), however, behaved in a different manner upon oxidation with the same reagent. The (*F*-benzo)furan (**1d**) was cleaved at the C–O bond under similar reaction conditions to give 1-(2-hydroxy-*F*-phenyl)-2-phenylethanedione (**2d**) in a poor yield. In the meantime, approximately one-third of the starting compound was recovered unchanged. Although a considerable amount of benzoic acid was isolated from the resulting mixture, no trace was found relating to the *F*-benzo moiety, which would be present in the form of *F*-salicylic acid or salicylaldehyde.

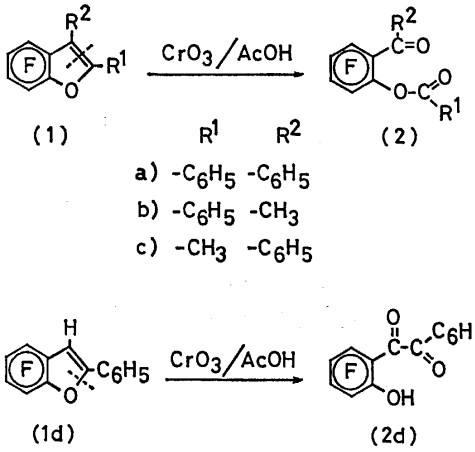

The cleavage of the furan-ring structure was proved by the disappearance of the UV band characteristic of the benzofuran moiety.[5] The ^{19}F-NMR signal of the fluorine atom at the 3-position in Compound (**2b**) was assigned by means of the long-range coupling between the fluorine and the three hydrogens on the vicinal-acetyl group. The fluorine atoms at the 3- and 6-positions in Compounds (**2a**) and (**2c**) were assigned on the basis of the fluorine chemical shifts obtained in Compound (**2b**). Those of Compound (**2d**) were tentatively assigned according to the spin-spin coupling pattern exhibited in its ^{19}F-NMR spectrum.

Experimental

General Procedure. A solution of chromium trioxide (2.9 mmol) in water (2 ml) was added to a mixture of a (*F*-benzo)furan derivative (**1a**—**c**) (1.2 mmol) and acetic acid (60 ml). The mixture was refluxed for 9 h, cooled, concentrated to a quarter of the original volume, and poured into ether. The ethereal solution was washed with water, dried over sodium sulfate, and evaporated *in vacuo*. The residue was chromatographed on a silica-gel column. The fraction eluted with hexane–dichloromethane gave a 2-acyl-*F*-phenyl carboxylate (**2a**—**c**). No fraction of the starting compound remained unchanged in the reaction mixture. The ^{1}H- and ^{19}F-NMR shifts were measured against TMS and *F*-benzene respectively as internal references.[6]

*2-Benzoyl-*F*-phenyl Benzoate (**2a**)*: Yield: 61%. Recrystallization from hexane gave colorless needles, mp 53—54 °C. IR (KBr): 1750 and 1670 cm^{-1} (C=O). ^{1}H-NMR ($CDCl_3$): δ=7.0—8.1 (m, arom.). ^{19}F-NMR ($CHCl_3$): δ=5.0 (ddd, 1F, F^4), 10.5 (ddd, 1F, F^5), 13.5 (ddd, 1F, F^6), and 22.3 (ddd, 1F, F^3), J_{4-6}=1.9, J_{3-5}=2.9, J_{3-6}=10.2, J_{5-6}=20.4, and J_{3-4}=23.4 Hz). UV (EtOH); λ_{max} (log ε); 202 (4.50) and 238 nm (4.26). Found: C, 64.09; H, 3.06%; M$^+$, 374. Calcd for $C_{20}H_{10}O_3F_4$: C, 64.18; H, 2.69%; M, 374.

*2-Acetyl-*F*-phenyl Benzoate (**2b**)*: Yield: 48%. Colorless oil. IR (neat): 1760 and 1640 cm^{-1} (C=O). ^{1}H-NMR (CCl_4): δ=2.45 (d, J=3 Hz, 3H, CH_3) and 7.2—8.2 (m, 5H, arom.). ^{19}F-NMR (CCl_4): δ=4.0 (ddd, 1F, F^4), 10.4 (ddd, 1F, F^5), 11.3 (ddd, 1F, F^6), and 21.0 (dddq, 1F, F^3), (J_{4-6}=1.0, J_{3-H}=3.4, J_{3-5}=3.9, J_{3-6}=9.7, J_{5-6}=J_{4-5}=20.4, and J_{3-4}=23.4 Hz). UV (EtOH): λ_{max} (log ε); 205 (3.10), 233 (4.27), and 277 nm (3.44). Found: C, 57.84; H, 2.67%; M$^+$, 312. Calcd for $C_{15}H_8O_3F_4$: C, 57.70; H, 2.58%; M, 312.

*2-Benzoyl-*F*-phenyl Acetate (**2c**)*: Yield; 81%. Colorless oil. IR (neat): 1790 and 1690 cm^{-1} (C–O). ^{1}H-NMR (CCl_4): δ=2.0 (s, 3H, CH_3) and 7.2—7.8 (m, 5H, arom.). ^{19}F-NMR (CCl_4): δ=8.3 (ddd, 1F, F^4), 8.9 (ddd, 1F, F^5), 14.4 (ddd, 1F, F^6), and 24.1 (ddd, 1F, F^3), J_{4-6}=1.5, J_{3-5}=2.4, J_{3-6}=10.2, J_{5-6}=J_{4-5}=20.4, and J_{3-4}=23.4 Hz). UV (EtOH): λ_{max} (log ε); 206 (4.19) and 255 nm (4.15). Found: C, 57.65; H, 2.70%; M$^+$, 280. Calcd for $C_{15}H_8O_3F_4$: C, 57.70; H, 2.58%; M, 280.

† Present address: Government Industrial Research Institute in Kyushu, Shukumachi, Tosu, Saga 841.

*Oxidation of 2-Phenyl(F-benzo)furan (**1d**).* After they had been worked-up in a similar manner, the reaction products from the (*F*-benzo)furan (**1d**) were chromatographed on a silica-gel column. The fraction eluted with hexane–dichloromethane gave 1-(2-hydroxy-*F*-phenyl)-2-phenylethanedione (**2d**), in a 3.7% yield. Mp 99—100 °C. IR (KBr): 3500 (OH), 1740 and 1660 cm^{-1} (C=O). ^{1}H-NMR ($CDCl_3$): δ=7.4—8.2 (m, 5H, arom.) and 11.4—11.8 (br.s, 1H, OH). ^{19}F-NMR ($CDCl_3$): δ=−6.1 (br.dd, 1F, F^4), 1.2 (ddd, 1F, F^6), 21.4 (ddd, 1F, F^5) and 28.7 (m, 1F, F^3), (J_{3-4}=24.5, J_{3-5}=8.5, J_{3-6}=10.0, J_{4-5}=20.0, J_{4-6}=3.5, and J_{5-6}=20.5 Hz). Found: *m/e*, 298.0275. Calcd for $C_{14}H_6O_3F_4$: 298.0296. A phenol test with iron(III) chloride in methanol gave red purple coloration. The starting substance (**1d**) (33%) and benzoic acid (13%) were isolated from the hexane- and the dichloromethane fractions respectively.

References

1) Part III: Y. Inukai, Y. Oono, T. Sonoda, and H. Kobayashi *Bull. Chem. Soc. Jpn.*, **54**, 3447 (1981).
2) According to the revised nomenclature of highly fluorinated organic compounds by J. A. Yound, *J. Chem. Document.*, **14**, 98 (1974) and *J. Fluorine Chem.*, **6**, 571 (1975).
3) Y. Inukai, T. Sonoda, and H. Kobayashi, *Bull. Chem. Soc. Jpn.*, **52**, 2657 (1979).
4) A. Wacek and F. Zeisler, *Monatsch. Chem.*, **83**, 5 (1952).
5) Note 9 in Ref. 3 and the literature cited therein.
6) ^{19}F-NMR chemical shifts are given as positive values downfield from the reference signal.

The Reactions of the 1,2-Ethanediylbis(trithiocarbonic acid) Dianion with Several Electrophilic Reagents

Shigeo TANIMOTO,* Tatsuo OIDA, Toshio KOKUBO, and Masaya OKANO
Institute for Chemical Research, Kyoto University, Uji, Kyoto 611

(Received June 17, 1981)

Synopsis. It has been found that the reaction of the 1,2-ethanediylbis(trithiocarbonic acid) dianion with haloacetic esters, chloromethyl ethers, and chloromethyl sulfides in tetrahydrofuran proceeds smoothly to afford 1,2-ethanediylbis(alkoxycarbonylmethyl trithiocarbonates), 1,2-ethanediylbis(alkoxymethyl trithiocarbonates) and bis(alkylthiomethyl) trithiocarbonates plus ethylene trithiocarbonate respectively.

We have recently reported[1] that 2,2′-[1,2-ethanediylbis(thio)]bis-1,3-dithiolane (**1**) is easily metalated with butyllithium in tetrahydrofuran to generate the 1,2-ethanediylbis(trithiocarbonic acid) dianion (**2**), with the elimination of 2 moles of ethylene; the dianion is then condensed with a variety of alkyl bromides and iodides to give 1,2-ethanediylbis(alkyl trithiocarbonates) and/or dialkyl trithiocarbonates plus ethylene trithiocarbonate (**8**). However, to the best of our knowledge, there has not been any other information concerning the synthetic utility of this anion. In this paper we would like to report the results of the reactions of **2** with several electrophilic reagents, such as haloacetic esters, chloromethyl ethers, and chloromethyl sulfides. The reaction of **2** with alkyl chlorides, studied under like conditions, did not show the formation of any products, suggesting a selectivity of **2** toward alkyl halides. Such selectivity was not observed in the reaction with haloacetic esters as the trapping agent. Bromoacetic esters undergo a condensation reaction with **2** similar to that observed with methyl iodide to afford 1,2-ethanediylbis(alkoxycarbonylmethyl trithiocarbonates) (**3**), along with a small amount of **8**. The reaction utilizing the chloro analogs, chloroacetic esters, had the same result, but the yields were somewhat lower. The results obtained by the reaction of **2** with several haloacetic esters are listed in Table 1, along with the physical data of the products.

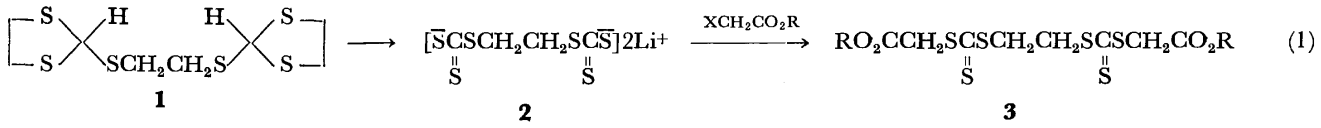

(1)

1 **2** **3**

a: X=Cl, R=CH_3, **b**: X=Cl, R=C_2H_5, **c**: X=Br, R=CH_3, **d**: X=Br, R=C_2H_5, **e**: X=Br, R=$CH_3(CH_2)_2$, **f**: X=Br, R=$CH_3(CH_2)_3$, **g**: X=Br, R=$C_6H_5CH_2$

Price and Oae[2] have pointed out that, in a certain nucleophilic substitution reaction, chloromethyl ethyl sulfide reacts about several thousand times as fast as butyl chloride; furthermore, chloromethyl ethyl ether was found to react far faster than the sulfur analog. Thus, we have investigated the reactions of **2** with chloromethyl ethers and sulfides. When some chloromethyl ethers were employed, 1,2-ethanediylbis(alkoxymethyl trithiocarbonates) (**4**) were obtained, suggesting that the ethers attack directly both of the nucleophilic ends of **2** (Eq. 2). On the other hand, when some chloromethyl sulfides were used, the products consist of an approximately equal mixture of bis(alkylthiomethyl) trithiocarbonates (**7**) and **8**, indicating that the reaction assuredly occurred acoording to Eq. 3. Thus, an obvious difference in behavior between chloromethyl ethers and sulfides was noted. In addition, it was found that the fragmentation of **2** by the intramolecular attack of its own nucleophilic end does not occur under the given conditions; that is, even if a solution of **2** in tetrahydrofuran had been stored at −5——10 °C for 5 h or more prior to the addition of haloacetic esters or chloromethyl ethers, substantially the same result was obtained. This evi-

TABLE 1. REACTION OF THE 1,2-ETHANEDIYLBIS(TRITHIOCARBONIC ACID) DIANION WITH SEVERAL HALOACETIC ESTERS

Haloacetic ester used			Eluent used for chromatography	Products[a] (yield/%)	Mp θ_m/°C (recryst. from C_6H_{14})
X	R	Moles per mol **1**			
Cl	CH_3	2.8	CH_2Cl_2/C_6H_{14}, (1:1)	**3a**(27), **8**(19)	63—65
Cl	C_2H_5	2.7	CH_2Cl_2/C_6H_{14}, (1:1)	**3b**(44), **8**(20)	55.5—57.5
Br	CH_3	2.7	CH_2Cl_2/C_6H_{14}, (1:1)	**3a**(75), **8**(15)	64—65
Br	C_2H_5	2.7	CH_2Cl_2/C_6H_{14}, (1:1)	**3b**(55), **8**(15)	56—57.5
Br	$CH_3(CH_2)_2$	2.7	CH_2Cl_2/C_6H_{14}, (1:2)	**3e**(73), **8**(<11)	46—47.5
Br	$CH_3(CH_2)_3$	2.7	CH_2Cl_2/C_6H_{14}, (1:2)	**3f**(85), **8**(4)	45—47
Br	$C_6H_5CH_2$	2.5	CH_2Cl_2/C_6H_{14}, (2:1)	**3g**(54), **8**(<6)	66.5—68

a) All **3** products gave satisfactory elemental analyses and exhibited spectral properties in accordance with the assigned structures. The ^{1}H-NMR spectra (δ values, in $CDCl_3$) are as follows: **3a**: 3.47(s, 4H), 3.52(s, 6H), 3.97(s, 4H). **3b**: 1.21(t, 6H), 3.50(s, 4H), 3.97(s, 4H), 4.00(q, 4H). **3e**: 0.89(t, 6H), 1.2—1.9(m, 4H), 3.50(s, 4H), 3.90(t, 4H), 3.97(s, 4H). **3f**: 0.82(t, 6H), 1.0—1.7(m, 8H), 3.40 (s, 4H), 3.81(t, 4H), 3.86(s, 4H). **3g**: 3.39(s, 4H), 3.91(s, 4H), 4.86(s, 4H), 6.7—7.1(m, 10H). Although a relatively small amount of **8** was observed in all runs, we were unable to find any bis(alkoxycarbonylmethyl) trithiocarbonate, which is supposed to arise simultaneously, within the limits of our detection.

dence leads us to favor the above mechanism. The products obtained by the reaction of **2** with several chloromethyl ethers and sulfides are listed in Tables 2 and 3, along with their physical data.

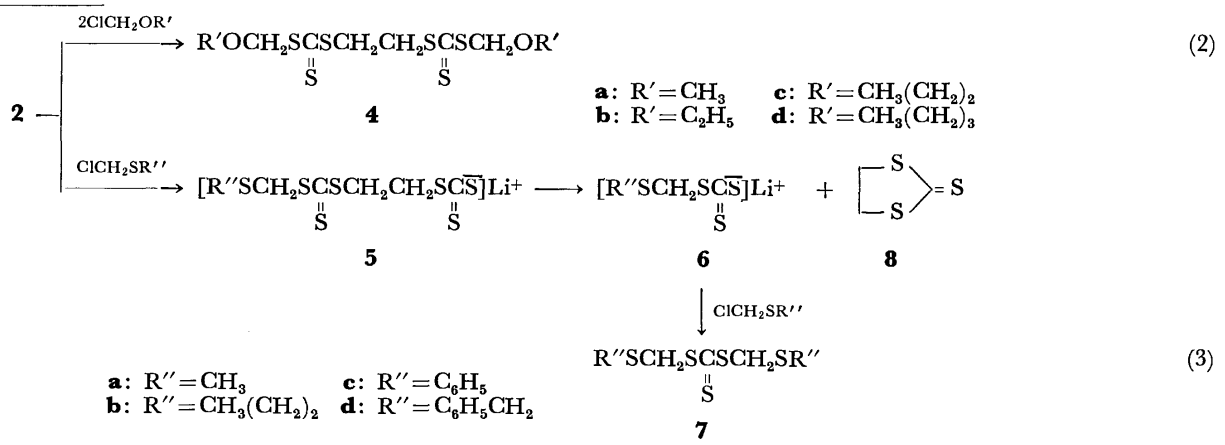

(2)

(3)

Among the products described in this report, **3** and **4** are difficult to synthesize by the other routes; moreover, the former may have great synthetic potential resulting from the presence of the two alkoxycarbonyl groups at both molecular ends.

Experimental

Reaction Summarized in Tables 1, 2, and 3. In each experiment, 2.0 g (6.6 mmol) of 2,2'-[1,2-ethanediylbis-(thio)]bis-1,3-dithiolane (**1**) was used; the mole ratio of electrophilic reagents to **1** and the eluents used for column chromatography are noted in the tables. All the reactions were carried out in the manner described in the preceeding report.[1]

References

1) S. Tanimoto, T. Oida, K. Hatanaka, and T. Sugimoto, *Tetrahedron Lett.*, **1981**, 655.
2) C. C. Price and S. Oae, "Sulfur Bonding," The Ronald Press Company, New York (1962), p. 10.
3) H. J. Renner, G. Schneider, and J. Weissflog, Ger. (East) Patent 15431; *Chem. Abstr.*, **54**, 2650 (1960).

Table 2. Reaction of the 1,2-ethanediylbis(trithiocarbonic acid) dianion with several chloromethyl ethers

Chloromethyl ether used: R'	Chloromethyl ether used: Moles per mol **1**	Eluent used for chromatography	Products[a] (yield/%)	Bp θ_b/°C(Torr)
CH_3	2.7	CH_2Cl_2/C_6H_{14}, (1:1)	**4a** (48), **8** (33)	124—129 (3)
			$CH_3OCH_2SCSCH_2OCH_3$ (11)	—[b]
C_2H_5	2.5	$C_2H_5OC_2H_5/C_6H_{14}$, (1:1)	**4b** (72), **8** (16)	137—143 (3)
$CH_3(CH_2)_2$	2.5	$C_2H_5OC_2H_5/C_6H_{14}$, (1:1)	**4c** (73), **8** (20)	152—158 (3)
$CH_3(CH_2)_3$	2.5	$C_2H_5OC_2H_5/C_6H_{14}$, (1:1)	**4d** (77), **8** (18)	162—167 (2.5)

a) The ^{1}H-NMR spectra of **4** (δ values, in $CDCl_3$) are as follows. **4a**: 3.43(s, 6H), 4.02(s, 4H), 5.53(s, 4H). **4b**: 1.20(t, 6H), 3.60(q, 4H), 4.00(s, 4H), 5.56(s, 4H). **4c**: 0.90(t, 6H), 1.2—1.9(m, 4H), 3.49(t, 4H), 3.97(s, 4H), 5.53(s, 4H). **4d**: 0.89(t, 6H), 1.1—1.8(m, 8H), 3.53(t, 4H), 3.99(s, 4H), 5.53(s, 4H). b) Mp or bp could not be determined because of the limited amounts. ^{1}H-NMR (in $CDCl_3$): δ 3.39(s, 6H), 5.52(s, 4H).

Table 3. Reaction of the 1,2-ethanediylbis(trithiocarbonic acid) dianion with several chloromethyl sulfides

Chloromethyl sulfide used: R''	Chloromethyl sulfide used: Moles per mol **1**	Eluent used for chromatography	Products[a] (yield/%)	Bp θ_b/°C(Torr)
CH_3	3.0	CH_2Cl_2/C_6H_{14}, (1:1)	**7a** (71), **8** (78)	154—158 (3), Lit,[3] mp 41 °C
$CH_3(CH_2)_2$	2.7	$C_2H_5OC_2H_5/C_6H_{14}$, (1:1)	**7b** (79), **8** (80)	174—179 (2.5)
C_6H_5	2.3	$C_2H_5OC_2H_5/C_6H_{14}$, (1:2)	**7c** (48), **8** (76)	195—198 (2.5—3)
$C_6H_5CH_2$	2.0	$C_2H_5OC_2H_5/C_6H_{14}$, (1:2)	**7d** (74), **8** (87)	223—227 (3)

a) The ^{1}H-NMR spectra of **7** (δ values, in $CDCl_3$) are as follows. **7a**: 2.17(s, 6H), 4.45(s, 4H). **7b**: 0.98(t, 6H), 1.2—2.0(m, 4H), 2.61(t, 4H), 4.46(s, 4H). **7c**: 4.70(s, 4H), 7.0—7.7(m, 10H). **7d**: 3.76(s, 4H), 4.27(s, 4H), 7.0—7.5(m, 10H).

Studies of Unusual Amino Acids and Their Peptides. XIV. The Asymmetric Hydrogenation of the Phenylhydrazone of Methyl *N*-(3,3-Dimethyl-2-oxobutanoyl)-L-valinate

Toshifumi MIYAZAWA,* Katsumi TAKASHIMA, Takashi YAMADA, Shigeru KUWATA, and (the late) Hiroshi WATANABE

Department of Chemistry, Faculty of Science, Kōnan University, Okamoto, Higashinada-ku, Kobe 658

(Received July 6, 1981)

Synopsis. The asymmetric hydrogenation of the phenylhydrazone of methyl *N*-(3,3-dimethyl-2-oxobutanoyl)-L-valinate was investigated using palladium catalysts. The configuration of the newly formed *t*-leucine moiety was found to be L.

In the previous papers,[1,2] the present authors have reported on the convenient syntheses and the optical resolution of *t*-leucine (2-amino-3,3-dimethylbutanoic acid). One of our attempts at preparing racemic *t*-leucine on a large scale consisted in the reductive cleavage of the phenylhydrazone (**1**) of 3,3-dimethyl-2-oxobutanoic acid by hydrogenation (Scheme 1).

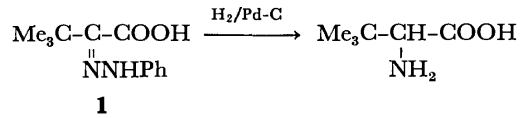

Scheme 1.

The success of this method prompted us to examine the asymmetric synthesis of this amino acid through the hydrogenation of the condensation product between the phenylhydrazone (**1**) and an amino-acid ester as the source of chirality. Methyl L-valinate was chosen in the present investigation, as in our previous study of the kinetic resolution of *t*-leucine.[3] The diastereomeric ratio of the resulting dipeptide, after conversion to the *N*-pivaloyl derivative, can easily be estimated by means of GLC analysis.[3,4]

Thus, the phenylhydrazone (**1**) was coupled with methyl L-valinate by means of the DCC[5] method. The resulting phenylhydrazone (**2**) of methyl *N*-(3,3-dimethyl-2-oxobutanoyl)-L-valinate was hydrogenated in methanol in the presence of a double molar amount of *p*-toluenesulfonic acid, using a palladium catalyst. For estimating the diastereomeric ratio of the resulting dipeptide, the crude product was pivaloylated in the usual manner.[4] The results are summarized in Table 1. The authentic samples were prepared by condensing *N*-Z-L- or *N*-Z-D-*t*-leucine with methyl L-valinate by means of the DCC method, followed by debenzyloxycarbonylation and the subsequent pivaloylation.

When palladium on carbon was used as a catalyst, the configuration of the newly formed *t*-leucine moiety was L (L-Tle–L-Val:D-Tle–L-Val=67:33). The reaction temperature, as far as we examined it, had little influence on the diastereomeric ratio. In a series of studies[6] of the asymmetric amino-acid syntheses through the hydrogenation of oximes or Schiff bases of α-keto esters or amides, Harada *et al.* postulated an intermediate substrate-catalyst complex for explaining the configurations and the optical yields of the products. According to this hypothesis, the present results could be explained by assuming the preferred conformation of the intermediate complex formed prior to hydrogenation to be as is shown in Scheme 2.[7] The choice of catalyst was found to have a significant influence on the present asymmetric hydrogenation. Thus, the use of palladium black or palladium oxide resulted in a higher optical purity of the *t*-leucine moiety than in the case of palladium on carbon.

TABLE 1. *t*-LEUCYL DIPEPTIDE PREPARED VIA THE ASYMMETRIC HYDROGENATION[a] OF THE PHENYLHYDRAZONE (**2**) OF METHYL *N*-(3,3-DIMETHYL-2-OXOBUTANOYL)-L-VALINATE

Catalyst	Temp °C	Yield[b] %	Ratio of diastereomers L-L %	D-L %
Pd-C	10	43	66	34
Pd-C	50	45	67	33
Pd-C	60	52	66	34
Pd-C	100	52	64	36
Pd black	50	44	77	23
PdO	50	48	78	22

a) Under an initial pressure of 100 kg/cm². b) Overall yield of the pivaloylated derivative isolated by preparative TLC on silica gel (see Experimental).

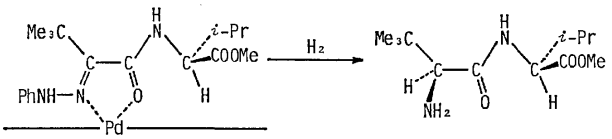

Scheme 2.

Experimental

All the melting points are uncorrected. The optical rotations were measured with a JASCO DIP-4 polarimeter. The ^{1}H NMR spectra (in $CDCl_3$) were recorded on a Hitachi R-24B spectrometer, with TMS as the internal standard. The GLC analyses were performed on a Hitachi 063 gas chromatograph equipped with a flame-ionization detector, using a column packed with 0.5% FFAP on Chromosorb G (ϕ 3 mm×2 m; column temp 150 °C; carrier gas, N_2 11 ml/min; injector temp, 250 °C). Merck Kieselgel 60 and Kieselgel GF_{254} (Type 60) were used for the column chromatography and the preparative TLC respectively.

Phenylhydrazone (2) of Methyl N-(3,3-Dimethyl-2-oxobutanoyl)-L-valinate. Into a chilled mixture of the phenylhydrazone (**1**) of 3,3-dimethyl-2-oxobutanoic acid (17.6 g), L-Val-OMe·HCl (14.1 g), and triethylamine (8.5 g) in THF (240 ml), a solution of DCC (16.5 g) in THF (40 ml) was stirred.

Stirring was continued at 0 °C for 2 h and then at room temperature overnight. After *N,N'*-dicyclohexylurea had been removed by filtration, the filtrate was evaporated under reduced pressure. The residue was dissolved in EtOAc, washed successively with water, 0.5 M HCl, water, 0.5 M $NaHCO_3$, and water, and dried over $MgSO_4$. After the removal of the solvent, the residue was chromatographed on a silica-gel column with $CHCl_3$–EtOAc (1:1). The first colored fraction gave the desired product (**2**) as pale yellow needles: yield, 20.5 g (77%); mp 110—112 °C (from MeOH aq); $[\alpha]_D^{20}$ −16.9° (*c* 1.0, MeOH). Found: C, 64.78; H, 8.35; N, 12.34%. Calcd for $C_{18}H_{27}N_3O_3$: C, 64.84; H, 8.16; N, 12.60%.

The phenylhydrazone of ethyl *N*-(3,3-dimethyl-2-oxobutanoyl)-L-valinate was prepared in the same manner as above: mp 99—100 °C (from EtOH aq); $[\alpha]_D^{20}$ −20.9° (*c* 1.0, MeOH). Found: C, 65.71; H, 8.70; N, 11.86%. Calcd for $C_{19}H_{29}N_3O_3$: C, 65.68; H, 8.41; N, 12.09%.

Hydrogenation of the Phenylhydrazone **2**. The phenylhydrazone **2** (1.00 g) and *p*-toluenesulfonic acid monohydrate (1.26 g) were dissolved in MeOH (50 ml), after which the mixture was hydrogenated overnight in the presence of a palladium catalyst (0.5 g) under the conditions shown in Table 1. The reaction mixture was freed from the catalyst and evaporated to dryness under reduced pressure. The residue was dissolved in CH_2Cl_2 (30 ml) and acylated with Piv–Cl (0.94 g) in the presence of *N,N*-diisopropylethylamine (1.86 g) in the usual manner.[4] A part of the crude product was used without purification for the GLC analysis in order to estimate the diastereomeric ratio. The *N*-pivaloyl derivative was isolated as a mixture of diastereomers by preparative TLC on silica gel using benzene–EtOAc (9:1). The results are summarized in Table 1.

Preparation of Authentic Samples. *Z-L-Tle-L-Val-OMe*: Into a chilled mixture of Z-L-Tle[1] (398 mg), L-Val-OMe·HCl (252 mg), *N*-ethylmorpholine (173 mg), and THF (3.5 ml), DCC (340 mg) was stirred. The mixture was stirred at 0 °C for 2 h and then at room temperature overnight. The usual work-up afforded white crystals; yield, 457 mg (81%). The analytical sample was obtained by recrystallization from EtOAc–Et_2O–petroleum ether: mp 71—72.5 °C; $[\alpha]_D^{25}$ −21.2° (*c* 1.0, MeOH); ^1H NMR δ=0.91 (6H, d, J=7 Hz), 1.00 (9H, s), 2.11 (1H, m), 3.67 (3H, s), 4.05 (1H, d, J=9 Hz), 4.47 (1H, dd, J=5 Hz and 8.5 Hz), 5.05 (2H, s), 5.54 (1H, bd, J=9 Hz), 6.48 (1H, bd, J=8.5 Hz), and 7.23 (5H, s). Found: C, 63.40; H, 8.16; N, 7.42%. Calcd for $C_{20}H_{30}N_2O_5$: C, 63.47; H, 7.99; N, 7.40%.

Piv-L-Tle-L-Val-OMe: A solution of Z-L-Tle-L-Val-OMe (182 mg) in MeOH (5 ml) was hydrogenated in the presence of concd HCl (53 mg), using 5% Pd-C (50 mg). The catalyst was then filtered off, and the filtrate was evaporated under reduced pressure, followed by the successive addition and the evaporation of MeOH. The residual solid (125 mg) was dissolved in CH_2Cl_2 (3 ml), and the mixture was treated with Piv–Cl (71 mg) in the presence of *N,N*-diisopropylethylamine (134 mg); yield, 125 mg (85%). The analytical sample was obtained by recrystallization from EtOAc–hexane: mp 138.5—139.5 °C; $[\alpha]_D^{25}$ −39.4° (*c* 1.0, MeOH); GLC t_R=62.3 min; ^1H NMR δ=0.90 (6H, d, J=7 Hz), 0.99 (9H, s), 1.20 (9H, s), around 2.15 (1H, m), 3.69 (3H, s), 4.23 (1H, d, J=9.5 Hz), 4.37 (1H, dd, J=5.5 Hz and 8.5 Hz), and 6.0—6.45 (2H, b). Found: C, 62.31; H, 9.83; N, 8.63%. Calcd for $C_{17}H_{32}N_2O_4$: C, 62.16; H, 9.82; N, 8.53%.

The corresponding D-L-isomer was obtained, starting from Z-D-Tle,[1] in the same manner as above.

Z-D-Tle-L-Val-OMe: mp 78—79 °C (from hexane); $[\alpha]_{25}^{D}$ −7.8°(*c* 1.0, MeOH); ^1H NMR δ=0.91 (6H, d, J=7 Hz), 1.01 (9H, s), 2.13 (1H, m), 3.65 (3H, s), 4.06 (1H, d, J=9.5 Hz), 4.49 (1H, dd, J=5 Hz and 8.5 Hz), 5.05 (2H, s), 5.65 (1H, bd, J=9.5 Hz), 6.61 (1H, bd, J=8.5 Hz), and 7.25 (5H, s). Found: C, 63.35; H, 8.04; N, 7.66%.

Piv-D-Tle-L-Val-OMe: mp 129—130 °C (from hexane); $[\alpha]_D^{25}$ +0.6° (*c* 1.0, MeOH); GLC t_R=58.3 min; ^1H NMR δ=0.94 (6H, d, J=6.5 Hz), 1.01 (9H, s), 1.21 (9H, s), 2.15 (1H, m), 3.68 (3H, s), 4.35 (1H, d, J=9 Hz), 4.45 (1H, dd, J=5 Hz and 8.5 Hz), 6.32 (1H, bd, J=9 Hz), and 6.61 (1H, bd, J=8.5 Hz). Found: C, 62.35; H, 9.75; N, 8.59%.

References

1) T. Miyazawa, K. Takashima, Y. Mitsuda, T. Yamada, S. Kuwata, and H. Watanabe, *Bull. Chem. Soc. Jpn.*, **52**, 1539 (1979).

2) T. Miyazawa, T. Nagai, T. Yamada, S. Kuwata, and H. Watanabe, *Memoirs of Kōnan University, Science Series*, No. 23 (1979), p. 51.

3) T. Miyazawa, K. Takashima, T. Yamada, S. Kuwata, and H. Watanabe, *Chem. Lett.*, **1978**, 873.

4) The asymmetric synthesis of this dipeptide sequence by the oxazolone method has been reported; E. Frauendorfer, W. Steglich, and F. Weygand, *Chem. Ber.*, **106**, 1019 (1973).

5) The following abbreviations are used throughout: DCC, dicyclohexylcarbodiimide; Z, benzyloxycarbonyl; THF, tetrahydrofuran; Piv–Cl, pivaloyl chloride; Tle, *t*-leucine; Piv, pivaloyl.

6) K. Harada, T. Munegumi, and S. Nomoto, *Tetrahedron Lett.*, **22**, 111 (1981), and the references cited therein.

7) The formation of an L-alanyl dipeptide in the catalytic hydrogenation of the benzylamine Schiff base of *N*-(2-oxopropanoyl)-L-valine methyl or isobutyl ester has been reported: K. Harada and K. Matsumoto, *J. Org. Chem.*, **32**, 1794 (1967); *Bull. Chem. Soc. Jpn.*, **44**, 1068 (1971).

Selective Hydrogenation of Cyclic Diolefins to Monoolefins Catalyzed by a Nickel Complex

Mutsuji SAKAI,* Fumiya HARADA, Yasumasa SAKAKIBARA, and Norito UCHINO
Department of Fiber Chemistry, Kyoto Technical University, Matsugasaki, Sakyo-ku, Kyoto 606
(Received July 29, 1981)

Synopsis. Cyclic diolefins were hydrogenated selectively to monoolefins with a nickel catalyst prepared from bis(acetylacetonato)nickel(II), triethyldialuminium trichloride, and triphenylphosphine at 40 °C under an atmospheric hydrogen pressure.

The hydrogenation of olefins using homogeneous Ziegler catalysts has been studied.[1] We found that the nickel catalyst prepared from bis(acetylacetonato)-nickel(II), triethyldialuminium trichloride, and triphenylphosphine (mole ratio, $Ni(acac)_2:Al_2Et_3Cl_3:PPh_3=1:10:5$) catalyzed the selective hydrogenation of conjugated diolefins.[2] In the preceding paper[3] the selective hydrogenation of 2,3-dimethyl-1,3-butadiene to monoenes with the nickel catalyst was studied kinetically. This paper reports that cyclic diolefins were hydrogenated selectively to monoolefins with the nickel catalyst under mild conditions (40 °C, 1 atm H_2).

Results and Discussion

1,4-Cyclohexadiene was hydrogenated to produce cyclohexene alone in a high yield of 81%. Trace amounts of benzene (disproportionation product) were detected in the hydrogenation. Under nitrogen 1,4-cyclohexadiene neither isomerized to 1,3-diene nor disproportionated to benzene and cyclohexene with the catalyst, remaining unchanged. On the contrary, a Ziegler-type nickel catalyst, Ni(II)–$AlEt_3$, has been reported to be active for the disproportionation.[4]

Substituted cyclic 1,4-diene, such as 1-methyl- and 1,2-dimethyl-1,4-cyclohexadiene, were hydrogenated selectively to similar extents, as shown in Table 1. In the case of 1-methyl-1,4-cyclohexadiene the hydrogenation products were 1-methyl-1-cyclohexene (yield, 67%) and a mixture of 3- and 4-methyl-1-cyclohexene (yield, 7%). Under the conditions used, however, the resulting latter two methylcyclohexenes isomerized very rapidly to thermodynamically more stable 1-methyl-1-cyclohexene. The equilibrium composition consisted of 90% of 1-methyl-1-cyclohexene and 10% of a mixture of 3- and 4-methyl isomers. Thus, the alkyl substituted 1,4-dienes may be hydrogenated selectively to the corresponding thermodynamically more stable monoolefins.

In the case of 1,3-cyclohexadiene polymerization occurred exclusively. However, 1,3-cyclohexadiene was hydrogenated selectively to cyclohexene by adding the 1,3-diene dropwise to the catalyst system. The order and rate of addition played a significant role in the hydrogenation of the 1,3-diene. 1,3-Cyclooctadiene was hydrogenated selectively without requiring its slow addition, while 1,5-cyclooctadiene isomerized quantitatively to bicyclo[3.3.0]oct-2-ene. 1,5,9-Cyclododecatriene also was hydrogenated to cyclododecene. 2,5-Norbornadiene and 4-vinyl-1-cyclohexene polymerized with the catalyst.

The nickel catalyst is thus useful for the selective hydrogenation of cyclic diolefins.

Experimental

Materials. 1-Methyl-1,4-cyclohexadiene and 1,2-dimethyl-1,4-cyclohexadiene were prepared by Birch reduction.[5] The other reagents were commercially available. Solvents were distilled over sodium and diolefins were distilled freshly before use.

Hydrogenation. To a 200 ml flask fitted with a hydrogen buret, a septum inlet, and a magnetic stirrer were added

TABLE 1. HYDROGENATION OF CYCLIC DIOLEFINS BY A NICKEL COMPLEX CATALYST
Diolefin 11 mol, $Ni(acac)_2$, 0.11 mol, $Ni:Al_2:P=1:10:5$, solvent 100 ml, temp 40 °C, H_2 1 atm.

Diolefin	Solvent	Time / h	Conv. / %	Product (Select/%)
1,4-Cyclohexadiene	Toluene	6	100	Cyclohexene(81) Cyclohexane(0)
1-Methyl-1,4-cyclohexadiene	Toluene	8	100	1-Methyl-1-cyclohexene(67) 3- and 4-Methyl-1-cyclohexene(7) 1-Methylcyclohexane(2)
1,2-Dimethyl-1,4-cyclohexadiene	Ethylbenzene	22	100	1,2-Dimethylcyclohexene(73) 1,2-Dimethylcyclohexane(0)
1,3-Cyclohexadiene	Toluene	1	99	Cyclohexene(4) Cyclohexane(0)
1,3-Cyclohexadiene	Toluene	5[a]	93	Cyclohexene(74) Cyclohexane(6)
1,3-Cyclooctadiene	Ethylbenzene	3	100	Cyclooctene(89) Cyclooctane(0)
1,5-Cyclooctadiene	Ethylbenzene	(10 min)	100	Cyclooctene(0) Cyclooctane(0) Bicyclo[3.3.0]oct-2-ene(100)
1,5,9-Cyclododecatriene	Toluene	30[b]	70	Cyclododecene(48) Cyclododecane(0)

a) 1,3-Cyclohexadiene was added dropwise over a period of 5 h. b) 50 °C.

$Ni(acac)_2$ (0.11 mmol) and PPh_3 (0.55 mmol) in toluene. After the atmosphere had been replaced with hydrogen the diolefin (11 mmol) in toluene was added. The hydrogenation reaction was started by the addition of $Al_2Et_3Cl_3$ (1.1 mmol) in toluene. The mixture became a homogeneous solution. The solution was stirred with a magnetic stirrer and kept in a thermostated bath. An aliquot (2 ml) of the solution was taken and treated with a methanol–aqueous hydrochloric acid mixture. The organic layer was separated, washed with water, and subjected to GLC analysis.

Analysis. The gas chromatographic analyses were made by a Yanagimoto G-80 apparatus using columns of bis(2-cyanoethyl) ether, poly(ethylene glycol) 20 M, and 1,2,3-tris(2-cyanoethoxy)propane.

References

1) B. R. James, "Homogeneous Hydrogenation," John Wiley & Sons, New York (1973), pp. 363—383, and references cited therein.
2) Y. Sakakibara, H. Hisaki, M. Sakai, and N. Uchino, *Nippon Kagaku Kaishi*, **1976**, 1893.
3) Y. Sakakibara, S. Yagi, M. Sakai, and N. Uchino, *Nippon Kagaku Kaishi*, **1980**, 240.
4) C. B. Hanson, *Tetrahedron Lett.*, **21**, 1581 (1980).
5) T. Yamaguchi, T. Ono, K. Nagai, and C. C. Sin, *Kogyo Kagaku Zasshi*, **73**, 727 (1970).

$SbCl_5$ Complexes of Pyridine *N*-Oxide and Trimethylamine Oxide as the Oxidizing Agent

Jiro YAMAMOTO,* Mitushige MURAKAMI, Noriaki KAMEOKA, Norio OTANI, Masahiro UMEZU, and Teruo MATSUURA†

Department of Industrial Chemistry, Faculty of Engineering, Tottori University, Tottori 680

† *Department of Synthetic Chemistry, Faculty of Engineering, Kyoto University, Kyoto 606*

(Received April 25, 1981)

Synopsis. A 1:1 complex of pyridine *N*-oxide or trimethylamine oxide with $SbCl_5$ acted as an oxidizing agent to benzyl alcohol, bezoin, furoin, and thiophenols more easily than *via* the oxides to give benzaldehyde, benzil, furil, and the corresponding disulfides respectively. The trimethylamine oxide–$SbCl_5$ also oxidized *p*-xylene to *p*-tolualdehyde under nitrogen and to *p*-toluic acid under air.

We reported previously that α-pyridone is formed in a high yield by a thermally occurring intramolecular oxygen-transfer reaction of the pyridine *N*-oxide–$SbCl_5$ (1:1) complex (Complex A), and that the thermolysis of the *N,N*-dimethylaniline *N*-oxide–$SbCl_5$ (1:1) complex gives *o*-dimethylaminophenol.[1-2] We now find that Complex A and the trimethylamine oxide–$SbCl_5$ (1:1) complex (Complex B) can oxidized such organic compounds *i.e.* as benzyl alcohol, benzoin, furoin, thiophenols and *p*-xylene more easily than their parent oxides.

Results and Discussion

Complex B was prepared by the same procedure as has been reported for Complex A[2] (98.4%). Complex B is a white and hygroscopic solid: mp 98—100 °C (in a sealed capillary tube). Found: C, 9.73; H, 2.77; N, 3.71%. Calcd for $C_3H_9NOSbCl_5$: C, 9.66; H, 2.43; N, 3.74%. ν_{max}^{KBr}, 1610 cm^{-1}, 1470 cm^{-1}, 1440 cm^{-1}, 1230 cm^{-1}, 980 cm^{-1}; $\lambda_{max}^{CHCl_3}$ 270 nm (ε: 2400).

The thermolysis of Complex B in benzyl alcohol resulted in the formation of benzaldehyde in high yields (for example, a 63% yield in 300:1 (benzyl alc.:Complex B) at room temperature for 47 h and a 84.5% yield in 100:1 (benzyl alc.:Complex B) at 160 °C for 2 h), whereas trimethylamine oxide did not oxidize benzyl alcohol under similar conditions.

Thiophenols were more easily oxidized to give the corresponding diaryl disulfides in high yields with Complexes A and B than in the cases of oxidation using pyridine *N*-oxide and trimethylamine oxide (see Table 1). The effects of the para substituents on the oxidation rate of thiophenols were in the following order; $CH_3>H>NO_2$. Benzoin and furoin were also oxidized with Complexes A and B to give benzil and furil respectively (see the table). *p*-Xylene was found to be oxidized with Complex B under aerial conditions to give *p*-toluic acid in a 35% yield, while *p*-tolualdehyde was obtained in a 27% yield under nitrogen.

The reaction of Complex A with thiophenols appears to proceed according to the following stoichiometry. Complex A may first oxidize a thiophenol

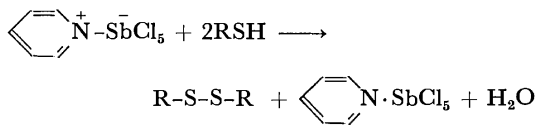

TABLE 1. THE OXIDATION OF THIOPHENOLS AND BENZOINS BY AMINE *N*-OXIDE–$SbCl_5$ (1:1) COMPLEXES

Substrates	X	Oxidants	Molar ratio (Substrates : Oxidants)	Temp/°C	Time/h	Solvents[c]	Yield/% of products[d]
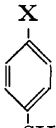	H		1 : 1	50	2	C_6H_6	No detected
		Complex A[a]	1 : 1	50	2	C_6H_6	16.7
				Room temp	20	CH_3NO_2	77.5
		$(CH_3)_3N\rightarrow O$	1 : 1	Room temp	20	CH_3NO_2	55.3
		Complex B[b]	1 : 1	Room temp	20	CH_3NO_2	84.1
	CH_3	Complex B	1 : 1	Room temp	20	CH_3NO_2	92.7
	NO_2	Complex B	1 : 1	Room temp	20	CH_3NO_2	14.2
		Complex A	1 : 2.1	40	5	CH_3NO_2	84.5
		Complex B	1 : 2.1	40	5	CH_3NO_2	66.0
		Complex A	1 : 1	40	0.5	CH_3NO_2	65.3
		Complex B	1 : 2	65	1.5	CH_3NO_2	60.5

In a typical run, a solution of thiophenol (4.3 g, 19.5 mmol) and Complex B (7.3 g, 19.5 mmol) in nitromethane (10 ml) was allowed to stand at room temperature for 20 h. The mixture was diluted with water and extracted with ether. The ethereal layer was washed with a 3% sodium hydroxide solution, water, dilute hydrochloric acid, and water successively and then dried. After the evaporation of the ether, the residue was practically distilled in a vacuum to give diphenyl disulfide (3.3 g, 77.5%). a) . b) $(CH_3)_3N$–O–$SbCl_5$. c) The dessolved oxygen in these solvents did not affect any run. d) The oxidation products were identified by a comparison of their melting points and IR spectra with those of authentic samples.

to a sulfenic acid, similar to the formation of a sulfenic acid from $R_3\overset{+}{N}OH$ and RS^- ions.[3] The sulfenic acid thus reacts with a thiophenol to give a disulfide.[4]

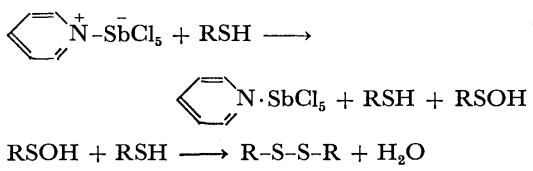

$$RSOH + RSH \longrightarrow R\text{-}S\text{-}S\text{-}R + H_2O$$

Benzaldehyde, *p*-tolualdehyde, and cinnamaldehyde resist oxidation with Complexes A and B, probably because of the formation of a stable adduct between an aldehyde and $SbCl_5$[5-6].

References

1) J. Yamamoto, Y. Nishigaki, M. Imagawa, M. Umezu, and M. Matsuura, *Chem. Lett.*, **1976**, 261.

2) J. Yamamoto, M. Imagawa, S. Yamauchi, O. Nakazawa, M. Umezu, and T. Matsuura, *Tetrahedron*, **37**, 1871 (1981).

3) D. I. Relyea, P. O. Tawney, and A. R. Williams, *J. Org. Chem.*, **27**, 474 (1962).

4) E. E. Reid, "Organic Chemistry of Bivalent Sulfur," Chemical Publishing Co., New York (1958), Vol. 1, p. 264.

5) F. Klaarges, H. Trages, and E. Muhlbauer, *Chem. Ber.*, **92**, 1819 (1959).

6) R. C. Paul, H. R. Singel, and S. L. Chadha, *J. Chem. Soc., A*, **1959**, 1819.

Reduction of Aromatic Compounds by Solvated Electrons Generated at Cathode

Ram A. Misra* and Ashok K. Yadav
Department of Chemistry, University of Rajasthan, Jaipur-302004, India
(Received January 17, 1981)

Synopsis. Phenol, anisole, and toluene can be reduced electrochemically to cyclohexanol, methoxycyclohexane, and methylcyclohexane respectively, in ethanol containing hexamethylphosphoric triamide (HMPA) at aluminium cathode. The reduction of these aromatics is believed to occur due to electrochemically generated solvated electrons.

The electrochemical reduction of benzene has been reported in variety of reaction conditions.[1-5] In some reports[4,5] it has been observed that direct electron transfer from cathode to aromatic nucleus does not take place, but the electron is introduced into the solution as solvated electrons, which may cause the reduction of benzene away from the electrode in the bulk of the solution.

$$e^-_{(cathode)} + \text{solvent} \rightleftharpoons e^-_{(solvent)}$$

The use of solvated electrons is of particular significance because the reported chemical methods involve high temperature and pressure. Furthermore, the yield of the reduced product in chemical hydrogenation depends upon a number of factors such as acid concentration, catalyst, hydrogen pressure, mode of addition and presence of water soluble quaternary ammonium compounds.[6-9] Fichter and Stocker[10] reported the reduction of phenol to cyclohexanol in 2 mol dm^{-3} sulfuric acid at platinized platinum electrode in poor yield. The use of solvated electrons in reduction of benzene has been reported by Sternberg and coworkers.[11,12] Recently Misra and Sharma[13] investigated the cathodic reduction of phenol and 2-naphthol to cyclohexanol and *trans*-2-dacalol respectively, at platinum foil in 2 mol dm^{-3} perchloric acid in good yield. In the present communication, we report the electrochemical reduction of phenol, anisole, and toluene in EtOH–HMPA (67:33). Lithium chloride was used as supporting electrolyte.

Experimental

Materials. Phenol, toluene, and anisole (all B.D.H.), lithium chloride (SISCO) and hexamethylphosphoric triamide(Fluka) were used without further purification.

Cell Assembly. A 400 ml beaker with provision to hold the cathode, porous diaphragm, thermometer, and magnetic bar, was used as electrolysis cell. Aluminium sheet was used as cathode and a carbon plate inside the diaphragm served as anode. A constant current was passed from a current regulated power supply (0-10 A/0-100 V).

Electrolysis, Work Up, and Analysis. Following is the detail of electrolysis: catholyte 125 ml, 3% lithium chloride solution in EtOH–HMPA (67:33), and 0.025 mol dm^{-3} of organic compound, anolyte 35 ml, 3% lithium chloride solution in EtOH–HMPA (67:33), current (0.3 A, current density 0.0326 A/C m^2), cell temperature (28±2 °C).

After the theoretical time corresponding to 6 F/mol, the catholyte was filtered and poured into 200 ml of water and acidified with dilute hydrochloric acid. The organic material was extracted with hexane (in case of phenol, the remain is also extracted with ether), and the organic layer was fractionally distilled to separate the reduced product and unreacted aromatic compound. The reduced product thus obtained was redistilled to get pure product. Their bp, yield, IR, and NMR data are given in Table 1.

Results and Discussion

The aromatics *viz.*, phenol, anisole, and toluene in EtOH–HMPA at aluminium cathode in a divided cell afforded the corresponding hexahydro derivatives. The cathodic potential which initiates the reduction of phenol, anisole, and toluene was −2.4, −2.10, and −2.00 V (*vs.* saturated calomel electrode) respectively. A blue colouration during the reaction indicates the formation of solvated electrons whose existence has been proved and detected by electron

Table 1. Physico-chemical and spectral characteristics of cyclohexanol, methoxycyclohexane, and methylcyclohexane

Product	Bp θ_b/°C Found (reported)	Yield %	IR[a] $\nu_{O-H/O-CH_3}$ cm^{-1}	IR[a] ν_{C-H} cm^{-1}	^1H NMR[b] δ
Cyclohexanol	160—161 (161)[c]	51.7	3450—3300 ν_{O-H}	2825, 2750	1.1—2.9 (m, 1OH; CH_2) 3.8 (s, 1H; CH) 5.4 (s, 1H; CH)
Methoxycyclohexane	134—136 (135—136)[d]	45.8	3060—3010 ν_{O-CH_3}	2825, 2750, 2725	1.0—2.9 (m, 1OH; CH_2) 3.45 (s, 1H; CH) 3.85 (s, 3H; CH_3)
Methylcyclohexane	98—101 (100)[e]	45.4	—	2950, 2920, 2850	1.0 (s, 3H; CH_3) 1.1—2.1 (m, 11H; CH_2 and CH)

a) IR were recorded on Perkin-Elmer-577 Grating IR Spectrophotometer. b) NMR were recorded on Perkin-Elmer RB 12 Spectrometer using TMS as internal Standard. c) Ref. 17(i). d) Ref. 17(ii). e) Ref. 17(iii).

spin resonance studies.[4,11] The solvated electrons formed by the reduction of metal ion followed by a dissolution step, interact with the monosubstituted benzene to give the dihydro derivative by the same mechanism reported previously.[14] Further reduction of dihydro product depends upon reaction conditions. For example, electrochemical reduction of benzene in methylamine[15] and tetralin in ethylenediamine[16] produces di- and tetra- hydro derivatives *viz.*, cyclohexadiene and cyclohexene in case of benzene, hexahydronaphthalene and octahydronaphthalene in case of tetralin. The non reducibility of benzene from olefin stage in amine solvent is due to the reason that the reduction of isolated double bond is much slower than the reduction of benzene to cyclohexadiene. But in our case fully reduced products of aromatics were isolated, indicating thereby that hydrogen evolution reaction 1 is suppressed, because HMPA is selec-

$$e^-_{cathode} + C_2H_5OH \longrightarrow C_2H_5\bar{O} + 0.5\,H_2 \quad (1)$$

tively adsorbed on the metal surface and hence preventing the decomposition of ethanol.

In addition to suppressing the hydrogen evolution at cathode, HMPA must also suppress the hydrogen evolution in solution. This is corroborated by the fact that when the reduction of phenol is carried out in absence of HMPA, the yield of cyclohexanol is very low ($\approx 5\%$). Hence it is reasonable to deduce that the reduction of phenol (also anisole and toluene) is possible if the electron and proton transfer reactions 2 and 3 are faster

$$\bar{e}_{C_2H_5OH} + R \longrightarrow R^{\cdot-} + C_2H_5OH \quad (2)$$

$$R^{\cdot-} + C_2H_5OH \longrightarrow RH^{\cdot} + C_2H_5\bar{O} \quad (3)$$

than the two competing hydrogen forming reactions 4 and 5.

$$\bar{e}_{C_2H_5OH} + \bar{e}_{C_2H_5OH} \longrightarrow H_2 + 2\,C_2H_5\bar{O} \quad (4)$$

$$\bar{e}_{C_2H_5OH} + C_2H_5OH \longrightarrow 0.5\,H_2 + C_2H_5\bar{O} \quad (5)$$

The financial support from the U. G. C., New Delhi to one of us (A. K. Y.) is gratefully acknowledged.

References

1) R. A. Benkeser and E. M. Kaiser, *J. Am. Chem. Soc.*, **85**, 2858 (1963).
2) R. A. Benkeser, E. M. Kaiser, and R. Lambert, *J. Am. Chem. Soc.*, **86**, 5272 (1964).
3) Continental Oil Co., U. S. Patent 3488266 (1967).
4) T. Osa, Yamagishi, T. Kodama, and A. Misono, Symposium on The Synthetic and Mechanistic Aspects of Electro-Organic Chemistry, U. S. Army Research Office, Durham, North Caroline, Oct., 14—16 (1968), p. 157.
5) H. W. Sternberg, R. E. Markby, I. Wender, and M. Mohilner, *J. Electrochem. Soc.*, **113**, 1060 (1966).
6) N. V. De, Fr. Patent 700067; *Chem. Abstr.*, **25**, 3358 (1931).
7) L. Brunel, *Ann. Chim. (Paris)*, **6**, 207 (1905).
8) A. A. Bag, T. P. Egupov, and D. F. Volokintin, *Org. Chem. Ind. USSR*, **2**, 141 (1936); *Chem. Abstr.*, **30**, 3439 (1936).
9) P. Sabatier and J. B. Senderens, *C. R. Acad. Sci.*, **137**, 1025 (1903).
10) F. Fichter and R. Stocker, *Ber.*, **47**, 2003 (1914); *Chem. Abstr.*, **8**, 3037 (1914).
11) H. W. Sternberg, R. E. Markby, I. Wender, and D. M. Mohilner, *J. Am. Chem. Soc.*, **89**, 186 (1967).
12) H. W. Sternberg, R. E. Markby, I. Wender, and D. M. Mohilner, *J. Am. Chem. Soc.*, **91**, 4191 (1969).
13) R. A. Misra and B. L. Sharma, *Electrochim. Acta*, **24**, 727 (1979).
14) "Physical Methods of Chemistry," ed by A. Weissberger and B. W. Rossiter, Wiley Interscience (1971), Vol. 1, Part IIB, p. 60.
15) H. W. Sternberg, R. E. Markby, and I. Wender, *J. Electrochem. Soc.*, **110**, 425 (1963).
16) H. A. Laitinen and C. J. Nyman, *J. Am. Chem. Soc.*, **70**, 3052 (1948).
17) "Dictionary of Organic Compounds," ed by I. Heilbron and H. M. Bunbury, Eyre and Spottiswoode (1953), Vol. 1, p. 637; Vol. 3, p. 343; Vol. 4, p. 514.

Cyclization of Isomeric 2-Hydrazino-4-methylbenzo[*h*]quinoline and 3-Hydrazino-1-methylbenzo[*f*]quinoline. A Reinterpretation

Marjan Kočevar, Slovenko Polanc, Branko Stanovnik,*
Franc Škerjanc, and Miha Tišler
Department of Chemistry, E. Kardelj University of Ljubljana, 61000 Ljubljana, Yugoslavia
(Received May 23, 1981)

Synopsis. Cyclization of 2-hydrazino-4-methylbenzo[*h*]quinoline and 3-hydrazino-1-methylbenzo[*f*]quinoline with formic acid occurs on nitrogen rather than carbon to give 5-methylbenzo[*h*][1,2,4]triazolo[4,3-*a*]quinoline and 11-methylbenzo[*f*][1,2,4]triazolo[4,3-*a*]quinoline and not 7-methyl-10*H*-benzo[*h*]pyrazolo[3,4-*b*]quinoline and 11-methyl-8*H*-benzo[*f*]pyrazolo[3,4-*b*]quinoline, respectively, as it has been claimed before.

During our continuous interest in the field of polycyclic polyaza heterocyclic systems of "steroid" and "helicene" type,[1–9] a report by Tiagi and Yoshi[10] has attracted our attention. Namely, it has been claimed that the reaction of 2-hydrazino-4-methylbenzo[*h*]quinoline (**1**) and 3-hydrazino-1-methylbenzo[*f*]quinoline (**5**) with formic acid gave 7-methyl-10*H*-benzo[*h*]pyrazolo[3,4-*b*]quinoline (**2**) and 11-methyl-8*H*-benzo[*f*]pyrazolo[3,4-*b*]quinoline (**6**), respectively.

There are no other examples, known in the literature, in which cyclization of hydrazino group at α-position to ring nitrogen is taking place onto carbon atom. To the contrary, according to the common experience, cyclization of hydrazino group attached at α-position to ring nitrogen is taking place onto ring nitrogen to give *s*-triazolo[4,3-*x*]azines.[11–14] Therefore, it seems, that reinterpretation of the results reported by Tiagi and Yoshi is fully justified.

When 2-hydrazino-4-methylbenzo[*h*]quinoline (**1**) was heated with formic acid as discribed by Tiagi and Yoshi,[10] a product with mp 167—168 °C (*cf.*[10] mp 204—205 °C) was obtained. Mass spectrum (M^+=251) together with elemental analysis gave molecular formula $C_{15}H_{13}ON_3$. IR absorption (1690 cm^{-1}) characteristic for a formyl group and a singlet at δ=7.63, a doublet for CH_3 group (δ=2.45) and a quartet for H-3 with a coupling constant ($J_{3\text{-H},4\text{-CH}_3}$ =1.0 Hz) characteristic for the coupling of a methyl group with an ortho proton in aromatic and heteroaromatic compounds in NMR spectrum suggest that the product is 2-(2-formylhydrazino)-4-methylbenzo[*h*]quinoline (**2**) and not the corresponding benzopyrazoloquinoline **2**, which presumably, according to the authors,[10] crystallizes with one half mole of water, in order to explain the low analysis for nitrogen.

On the other hand, the cyclization was effected by treatment of hydrazino compound **1** with triethyl orthoformate to give 5-methylbenzo[*h*][1,2,4]triazolo[4,3-*a*]quinoline (**3**), mp 299—300 °C, and not 7-methyl-10*H*-benzo[*h*]pyrazolo[3,4-*b*]quinoline (**2**) as reported by Tiagi and Yoshi.[10] That cyclization occured onto nitrogen rather than carbon is supported by the coupling of the methyl group at position 5 with 4-H ($J_{4\text{-H},5\text{-CH}_3}$=1.0 Hz) and by a long-range coupling of 1-H and 4-H ($J_{1\text{-H},4\text{-H}}$=0.9 Hz). This latter coupling is charasteristic for all 1,2,4-triazolo- and other azoloazines with bridgehead nitrogen atom.[15–17] The same tetracyclic compound was obtained also by prolonged heating of the 2-formylhydrazino compound **4**, however in lower yield.

3-Hydrazino-1-methylbenzo[*f*]quinoline (**5**) when treated with either triethyl orthoformate or formic acid gave a compound with mp 280—282 °C. Mass spectrum (M^+=233) and elemental analysis correspond to molecular formula $C_{15}H_{11}N_3$. A doublet for a methyl group ($J_{12\text{-H},11\text{-CH}_3}$=0.6 Hz) further supported by a long-range coupling between 3-H and 12-H ($J_{3\text{-H},12\text{-H}}$=0.6 Hz) are unambiguously consistent with 11-methylbenzo[*f*][1,2,4]triazolo[4,3-*a*]quinoline (**7**). On this basis, 11-methyl-8*H*-benzo[*f*]pyrazolo[3,4-*b*]quinoline (**6**) proposed by Tiagi and Yoshi[10] can be excluded. Furthermore, the compound obtained by Tiagi and Yoshi from hydrazino

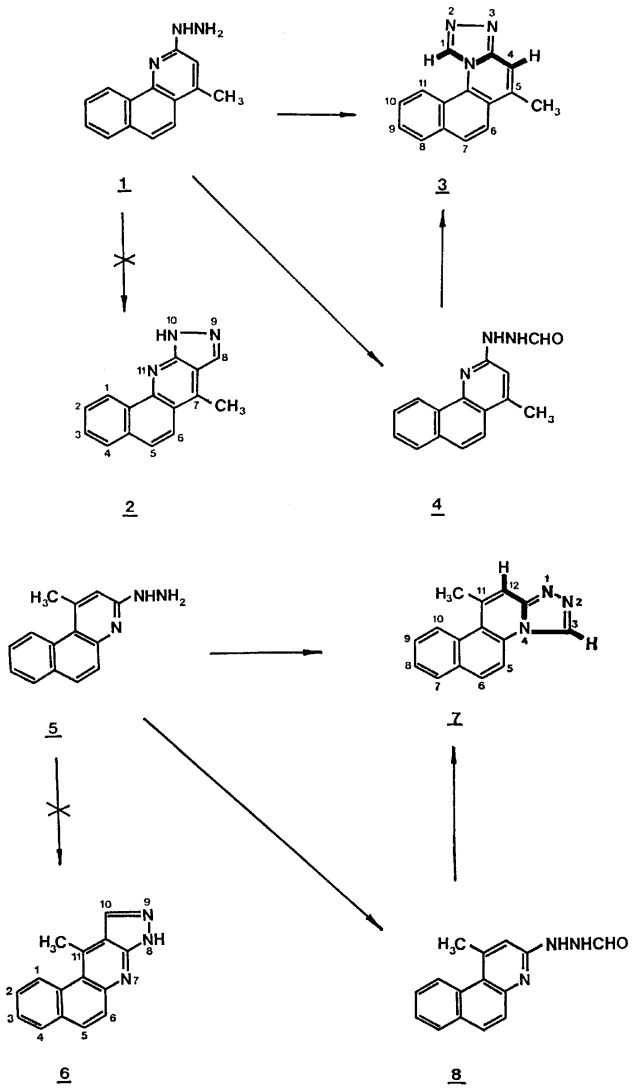

compound **5** with formic acid is most probably the corresponding 2-formylhydrazino derivative **8** since the reported analysis for nitrogen (Found: 17.28%; Calcd: N, 16.72%) fits this much better than the cyclized products **6** or **7**. However, we have not been able to isolate this intermediate under reported conditions.

An analoguous reinterpretation for the products obtained from hydrazines **1** and **5** with nitrous acid has been reported recently.[18]

Experimental

2-Hydrazino-4-methylbenzo[*h*]quinoline (**1**) and 3-hydrazino-1-methylbenzo[*f*]quinoline (**5**) were prepared according to the procedure described in the literature.[10,18] ^{1}H NMR spectra were recorded on a JEOL JNM C60-HI spectrometer, IR spectra on Perkin-Elmer 727B instrument, and mass spectra were obtained on a Hitachi-Perkin-Elmer RMU-6L instrument.

2-(Formylhydrazino)-4-methylbenzo[h]*quinoline (**4**).* 2-Hydrazino-4-methylbenzo[*h*]quinoline (**1**) (800 mg) and formic acid (98—100%, 6 ml) were heated under reflux for two hours. The mixture was evaported to dryness and methanol (20 ml) was added to dry residue, followed by addition of water (20 ml). After cooling the precipitate was collected by filtration and recrystallized from a mixture of methanol and water (4:1) to give 2-(2-formylhydrazino)-4-methylbenzo[*h*]quinoline (**4**) (620 mg, 69%), mp 167—168 °C, *m/e* 252 (M^+), NMR (d_6-DMSO, 110 °C): 9.5—9.2 (2H, br, NHNH), 8.4 (1H, m, 10-H), 7.63 (1H, s, CHO), 7.50—6.95 (5H, m, 5-H, 6-H, 7-H, 8-H, 9-H), 6.38 (1H, q, 3-H), 2.45 (3H, d, 4-CH_3); $J_{3\text{-H},4\text{-CH}_3}=1.0$ Hz). Found: C, 71.35; H, 5.52; N, 16.97%. Calcd for $C_{15}H_{13}N_3O$: C, 71.69; H, 5.21; N, 16.72%.

5-Methylbenzo[h][*1,2,4*]*triazolo*[*4,3*-a]*quinoline (**3**).*
Method A: 2-Hydrazino-4-methylbenzo[*h*]quinoline (**1**) (800 mg) and triethyl orthoformate (4 ml) were heated under reflux for 1 h. After cooling ether (16 ml) was added and precipitate collected by filtration and recrystallized from ethanol to give 5-methylbenzo[*h*][1,2,4]triazolo[4,3-*a*]quinoline (**3**), (470 mg, 56%), mp 299—300 °C, *m/e* 233 (NMR (d_6-DMSO): 9.35 (1H, d, 1-H), 8.35—8.10 (1H, m, 11-H), 7.60—7.05 (6H, m, 4-H, 6-H, 7-H, 8-H, 9-H, 10-H), 2.57 (3H, d, 5-CH_3), $J_{4\text{-H},5\text{-CH}_3}=1.0$ Hz, $J_{1\text{-H},4\text{-H}}=0.9$ Hz. Found: C, 77.26; H, 5.14; N, 18.29%. Calcd for $C_{15}H_{13}N_3$: C, 77.23; H, 4.75; N, 18.02%.

Method B: 2-Hydrazino-4-methylbenzo[*h*]quinoline (**1**) (100 mg), sodium acetate (10 mg), dioxane (1 ml) and formic acid (98-100%, 1 ml) were heated under reflux for 6 h. After evaporation to dryness methanol (1 ml) and water (1 ml) were added to the residue, and the solid collected by filtration. Recrystallization from ethanol gave **3** (48%). The compound was identical in every respect to the compound described above.

11-Methylbenzo[f][*1,2,4*]*triazolo*[*4,3*-a]*quinoline (**7**).*
Method A: 1-Methyl-3-hydrazinobenzo[*f*]quinoline (**5**) (1,0 g) and triethyl orthoformate (5 ml) were heated under reflux for 1 h. After cooling ether (20 ml) was added, precipitate collected by filtration and recrystallized from ethanol to give 11-methylbenzo[*f*][1,2,4]triazolo[4,3-*a*]quinoline (**7**), (780 mg, 79%), mp 280—282 °C, *m/e* 233 (M^+), NMR (d_6-DMSO): 9.1 (1H, d, 3-H), 8.25—8.02 (1H, m, 10-H), 7.75 (1H, d, 5-H), 7.50 (1H, d, 6-H), 7.40—6.90 (4H, m, 7-H, 8-H, 9-H, 12-H), 2.82 (3H, d, 11-CH_3), $J_{3\text{-H},12\text{-H}}=0.6$ Hz, $J_{5\text{-H},6\text{-H}}=8.0$ Hz, $J_{12\text{-H},11\text{-CH}_3}=1.0$ Hz). Found: C, 77.41; H, 4.87; N, 18.05%. Calcd for $C_{15}H_{11}N_3$: C, 77.23; H, 4.75; N, 18.02%.

Method B: 1-Methyl-3-hydrazinobenzo[*f*]quinoline (**5**) (200 mg) and formic acid (98—100%, 1.5 ml) were heated under reflux for three hours. Ethanol (5 ml) was added and the mixture evaporated to dryness. Dry residue was suspended in ether (10 ml) and the solid collected by filtration and recrystallized from ethanol to give 11-methylbenzo[*f*][1,2,4]triazolo[4,3-*a*]quinoline (**7**), (81%). The compound was identical in every respect with the compound obtained from **5** and triethyl orthoformate as described above.

References

1) B. Stanovnik and M. Tišler, *Chimia*, **22**, 141 (1968).
2) B. Stanovnik, M. Tišler, and P. Škufca, *J. Org. Chem.*, **33**, 2910 (1968).
3) J. Kobe, B. Stanovnik, and M. Tišler, *Croat Chem. Acta*, **41**, 245 (1969).
4) D. Fortuna, B. Stanovnik, and M. Tišler, *J. Org. Chem.*, **39**, 1833 (1974).
5) M. Kočevar, D. Kolman, H. Kranjc, S. Polanc, B. Porovne, B. Stanovnik, and M. Tišler, *Tetrahedron*, **32**, 725 (1976).
6) S. Gorjan, B. Klemenc, M. Starič, B. Stanovnik, and M. Tišler, *Monatsh. Chem.*, **107**, 1199 (1976).
7) B. Stanovnik and M. Tišler, *Monatsh. Chem.*, **101**, 303 (1970).
8) M. Kočevar, B. Stanovnik, and M. Tišler, *J. Heterocyclic Chem.*, **15**, 1175 (1978).
9) M. Kočevar, B. Stanovnik, and M. Tišler, *Heterocycles*, **6**, 681 (1977).
10) R. P. Tiagi and B. C. Yoshi, *Bull. Chem. Soc. Jpn.*, **45**, 2507 (1972).
11) The cyclization onto nitrogen was first reported by W. Marckwald and E. Meyer,[12] followed by many other examples. For reviews see *e.g.*[13,14]
12) W. Marckwald and E. Meyer, *Ber.*, **33**, 1885 (1900).
13) G. Maury, "Special Topics in Heterocyclic Chemistry. The Chemistry of Heterocyclic Compounds," ed by A. Weissberger and E. C. Taylor, John Wiley, New York, London (1977), Vol. 30, pp. 179—244.
14) M. Tišler and B. Stanovnik, "Condensed Pyridazines Including Cinnolines and Phthalazines," ed by R. N. Castle, John Wiley & Sons, New York, London (1973), pp. 761—1056.
15) W. W. Paudler and D. E. Dunham, *J. Heterocyclic Chem.*, **2**, 410 (1965).
16) J. Kobe, B. Stanovnik, and M. Tišler, *Tetrahedron*, **24**, 239 (1968).
17) M. Japelj, B. Stanovnik, and M. Tišler, *J. Heterocyclic Chem.*, **6**, 559 (1969).
18) C. W. Ress, D. L. R. Reeves, and R. C. Storr, *J. Chem. Soc., Perkin Trans. 1*, **1976**, 2178.

 © 1982 The Chemical Society of Japan Bull. Chem. Soc. Jpn., 55, 351—357 (1982)

Additive Effect of CF_3Cl on an Oxidation Reaction in Shock Waves. I. Study with H_2–O_2

Yoshiaki HIDAKA,* Hiroyuki KAWANO, and Masao SUGA

Department of Chemistry, Faculty of Science, Ehime University, Bunkyo-cho, Matsuyama 790

(Received January 30, 1981)

Sample gases, H_2–O_2, H_2–O_2–CF_3Cl, and CF_3Cl, highly diluted with Ar were heated behind reflected shock waves over the temperature range 1400—2200 K and an additive effect of CF_3Cl at various concentrations (0—0.5%) was studied by monitoring ultraviolet and visible emissions. At a temperature below 2200 K, C_2* and CH* species were found to be formed in the oxidation reaction of H_2 together with CF_3Cl, but hardly formed in the thermal decomposition of CF_3Cl. The addition of small and large amounts of CF_3Cl increased and decreased, respectively, the intensity of OH* emission from the H_2–O_2 mixture heated to a constant temperature. An ignition delay time at a fixed temperature above 1400 K was found to shorten with an increase in the concentration of CF_3Cl. A brief discussion is given of the mechanism for the formation of the chemiluminescent species.

The additive effect of an organic halogen compound (*e.g.*, CH_3I, CH_3Br, CH_3F, CF_3Br, CF_3Cl, or CCl_4) on a combustion reaction has been studied by measuring flammability limit,[1] burning velocity,[2-3] flame structure,[4] induction period,[5] *etc.*, and the compound has been found to generally lower the concentration of active species such as H, OH, and O, thereby inhibiting the combustion reaction. According to a study of the burning velocity in a methane oxidation,[3] however, CF_3Cl acts as an inhibitor under some conditions but as a promoter under others. This reversible action of CF_3Cl is particularly interesting, and a detailed investigation of the action seems helpful in elucidating an effect of organic halogen compounds on an oxidation reaction.

A visible emission from reaction mixtures including halogen compounds has been studied by using discharges[6,7] counterflow diffusion flame,[8] shock waves,[9,10] *etc.*, and both C_2* ($A\,^3\Pi_g$) and CH* ($A^2\Delta$) were observed in the reaction of H with CCl_4, $CHCl_3$, or CH_3Br.[6] In addition, C_2* was observed when halomethanes $CH_{2-n}X_{2+n}$ (X=Cl, Br, or I) were introduced into a stream of H produced by passing a H_2–He mixture through a 2450 MHz microwave discharge[7] and also when a decomposition reaction of CF_4 or CCl_4 occurred in a shock tube at a temperature above 4000 K.[10] At a relatively low temperature below 2200 K, however, such a C_2* formation from organic halogen compounds has not yet been reported.

From the viewpoints described above, we have examined the additive effect of CF_3Cl on the light emission from chemiluminescent species produced in the oxidation reaction of CH_4 over the temperature range 1600—2200 K by using a shock tube, and have found that the addition of CF_3Cl increases the C_2* and CH* emission intensities.[11] This previous result is not interpreted reasonably by a mechanism proposed by Gaydon,[12] and hence suggests that another mechanism should be taken into consideration. Namely, C_2* and CH* may be formed from some species produced by the decomposition of CF_3Cl in the oxidation reaction. A mixture of H_2–O_2–CF_3Cl–Ar seems most suited to check this mechanism experimentally, because no emissions of CH* and C_2* are observed in the oxidation reaction of H_2.

Our purpose of this work is to clarify the CH* and C_2* formation in H_2–O_2–CF_3Cl–Ar, and also to investigate the additive effect of CF_3Cl on the oxidation reaction of H_2.

Experimental

The apparatus and procedures employed in this work are essentially the same as in previous work.[13,14] Therefore, only a brief description will be given here. In order to record an emission spectrum, a high sensitive film (Kodak 2475) was exposed as many as 15 times by repeating runs with a reaction mixture heated at 2100 ± 50 K, but this trial was fruitless because all of the resultant emissions were extremely weak. Therefore, the spectral distribution was measurod with a system consisting of a monochromator with the half-width 25 Å (Rico-MC-20) and of a photomultiplier (Hamamatsu R-306). Wavelength dependence of the relative detection sensitivity (β) of the system was determined according to NBS data (lamp input voltage 96 V and PM H. V. 1220 V, EMI 9635QA), and the result thus obtained is shown in Fig. 1, on the basis of which the emission intensities measured at various wavelengths were corrected. The emissions at 3055, 4330, 5150, and 2400 Å were monitored with four filters, the half-widths of which were 150, 120, 110, and 200 Å, respectively. After passing through one of the interference filters located behind a quartz window of the shock tube and through two slits with widths 0.2 and 0.4 mm, three kinds of emission among the four were simultaneously monitored at various temperatures by using three photomultipliers (Hamamatsu R-306).

The computer routine used Gear-type integration of the set of differential equations describing the chemical kinetics under constant density conditions for reflected shock waves. Thermochemical properties were computed as functions of temperature using accurate polynomial representations of

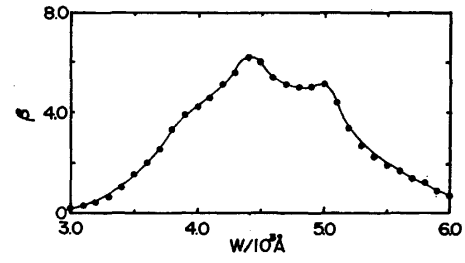

Fig. 1. The relative sensitivity (β) at different wavelengths (W) observed with the measurement system in this work.

JANAF data.[15] Reverse reactions were automatically included with rate constants calculated from the forward rate constants and equilibrium constants. All temperatures referred to in connection with data were calculated from the incident shock velocity assuming full vibrational relaxation but no chemical reaction. The computer programs used previously[16] were modified to match the Facom 230-28 system.

The gases of CF_3Cl, H_2, O_2, and Ar specified to be 99.0, 99.9, 99.9, and 99.99% pure, respectively, were obtained from commercial cylinders and were used without further purification. Table 1 summarizes the composition of the reaction gas mixtures used, each of which had the initial pressure 100±0.1 Torr (1 Torr≈133. 322 Pa).

TABLE 1. MIXTURE COMPOSITION

Mixture	H_2 (%)	O_2 (%)	CF_3Cl (%)	Ar (%)
(A)	0.50	0.25		99.25
(B)	0.50	0.25	0.05	99.20
(C)	0.50	0.25	0.10	99.15
(D)	0.50	0.25	0.17	99.08
(E)	0.50	0.25	0.25	99.00
(F)	0.50	0.25	0.35	98.90
(G)	0.50	0.25	0.50	98.75
(H)			0.50	99.50
(I)	0.50		0.50	99.00
(J)		0 25	0.50	99.25

Results and Discussion

An emission spectrum recorded with the mixture (G) at intervals of about 100 Å is illustrated in Fig. 2, which shows that strong emissions appear at 3900, 4315, 4700, 5165, and 5600 Å. According to Gaydon,[17] (1) the Swan bands of C_2* lie in the wavelength region 4365—6762 Å, (2) the outstanding heads of C_2* exist at 4737, 5165, and 5635 Å, (3) the emission bands of CH* are situated in the region 3144—4941 Å, and (4) the strong peaks of CH* appear at 3871 and 4315 Å. Therefore, the two groups (A_1 and A_2) of the strong heads at 4700, 5165, and 5600 Å and at 3900 and 4315 Å shown in Fig. 2 correspond to spectra of the electronically excited species C_2* and CH*, respectively. As may be known well, C_2* and CH* bands are characteristic of hydrocarbon-flames. To our particular interest, such bands are observed in the oxidation reaction of the H_2–O_2–CF_3Cl–Ar mixtures, too, as shown in Fig. 2, where the spectral distribution is quite similar to that in the oxidation reaction of CH_4.[11] With the mixtures of CF_3Cl–Ar (H), H_2–CF_3Cl–Ar (I), and O_2–CF_3Cl–Ar (J) heated to 1400—2200 K, on the other hand, neither CH* nor C_2* was observed. Hence, it is concluded that, even at the temperature below 2200 K, CH* and C_2* are formed in the oxidation reaction of H_2 together with CF_3Cl, but are produced in neither the thermal decomposition of CF_3Cl nor the reaction of CF_3Cl with O_2 or with H_2. This makes us infer that H, O, or OH which is the active species formed in the oxidation reaction of H_2 helps to form CH* and C_2*.

Since the intensities of emissions at 4315 Å (CH*) and 5165 Å (C_2*) are very strong and also since the emissions other than the CH* and C_2* do not exist in the vicinity of 4315 Å and 5165 Å, the emissions observed at 4330 and 5150 Å by using the interference filters are concluded to come from CH* and C_2*, respectively.

The OH* emission at 3064 Å which is generally observed in the oxidation reaction of H_2 doesn't appear in Fig. 2. This may be due to both the weak emission of OH* observed with the mixture (G) (see Fig. 3) and the low sensitivity near 3064 Å in our measurement system, as shown in Fig. 1. The emission at 3055 Å found with the filter probably comes from the electronically excited species OH* because the strong band of OH* has a main head at 3064 Å.[17] In addition, we observed the emission at 2400 Å, which may be concluded to come from the electronically excited species CF* because the CF*($A^2\Sigma^+$—$X^2\Pi$) bands extend from 2240 to 2560 Å, among which the emission at 2404 Å is particularly strong.[17]

By using one of the filters mentioned above, the emission intensities at 3055, 4330, 5150, and 2400 Å corresponding to OH*, CH*, C_2*, and CF*, respectively, were measured with the mixtures (A)—(G) in the range 1600—2200 K, and their respective maximum intensities are plotted against the concentration (C) of CF_3Cl in Figs. 3—6. In contrast to OH*, neither CH*, C_2*, nor CF* emission at any temperatures is

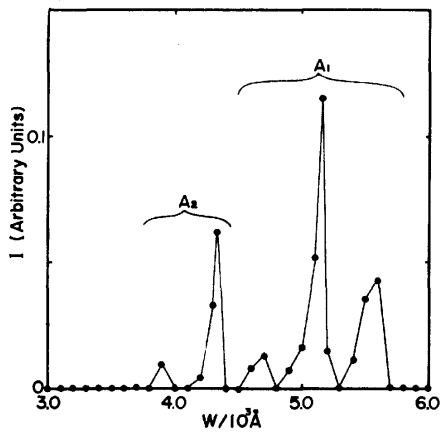

Fig. 2. The spectral distribution observed with the mixture (G) at 2100±50 K.

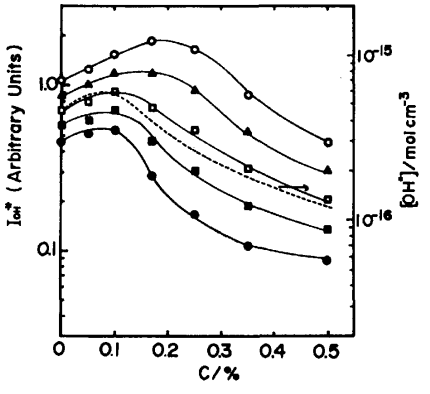

Fig. 3. A plot of the maximum intensity (I_{OH}*) of OH* emission *vs.* CF_3Cl concentration (C). ●: 1600 K, ■: 1700 K, □: 1800 K, ▲: 1900 K, ○: 2000 K, ------: computed curve.

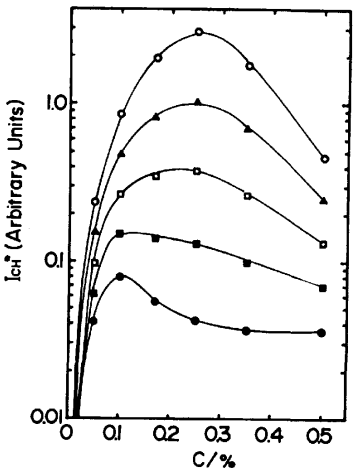

Fig. 4. A plot of the maximum intensity (I_{CH}*) of CH* emission *vs.* CF_3Cl concentration (C). ●: 1600 K, ■: 1700 K, □: 1800 K, ▲: 1900 K, ○: 2000 K.

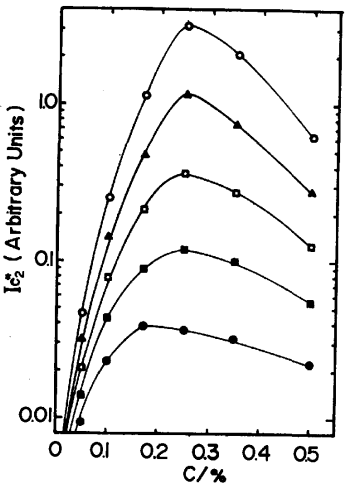

Fig. 5. A plot of the maximum intensity (I_{C_2}*) of C_2* emission *vs.* CF_3Cl concentration (C). ●: 1600 K, ■: 1700 K, □: 1800 K, ▲: 1900 K, ○: 2000 K.

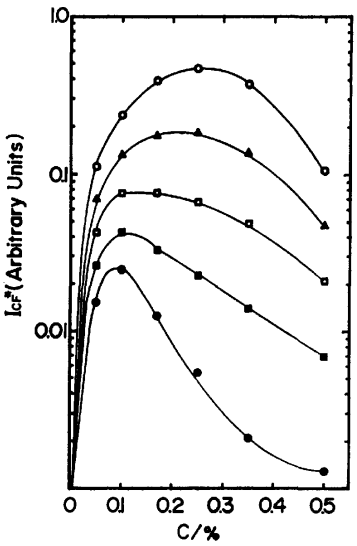

Fig. 6. A plot of the maximum intensity (I_{CF}*) of CF* emission *vs.* CF_3Cl concentration (C). ●: 1600 K, ■: 1700 K, □: 1800 K, ▲: 1900 K, ○: 2000 K.

naturally observed at C=0 %. At C>0 %, however, any of the four emission intensities at a fixed temperature increases and reaches a maximum at C=0.1—0.3 %, above which each emission intensity decreases gradually. This pattern is quite similar among the five curves at different temperatures. Especially CH* and CF* among the four species have a quite similar pattern at each temperature.

Table 2. ΔH_0° value of elementary reactions

Number	Reaction	ΔH_0°/kcal
1	$CF_3Cl+(M)=CF_3+Cl+(M)$	85
2	$Cl+H_2=HCl+H$	−1
3	$CF_3+H_2=CF_3H+H$	−1
4	$CF_3Cl+H=CF_3+HCl$	−18
5	$CF_3+H=CF_2+HF$	−49
6	$CF_2+H=CF+HF$	−14
7	$CF+H=C+HF$	−7
8	$C+CH=C_2+H$	−61
9	$CH+CH=C_2+H_2$	−85
10	$CH_2+C=C_2+H_2$	−63
11	$CF+CH=C_2+HF$	−68
12	$C+CF=C_2+F$	−14
13	$CF+CF=C_2+F_2$	79
14	$C+CF_2=C_2+F_2$	72
15	$C_2+OH=CH+CO$	−93
16	$CF+HF=CH+F_2$	147
17	$C+H_2=CH+H$	24
18	$CF+H_2=CH+HF$	17
19	$C+OH=CH+O$	21
20	$CH+F_2=CF+HF$	−147
21	$C+F_2=CF+F$	−93
22	$C+HF=CF+H$	6
23	$O+H+M=OH+M$	−102
24	$CH+O_2=OH+CO$	−160

Some of the elementary reactions that may be helpful to find a formation mechanism for the chemiluminescent species in this work are summarized in Table 2 together with respective enthalpy changes ΔH. As mentioned above, fair amounts of C_2*, CF*, and CH* are formed under our experimental condition. When the values of ΔH in Table 2 are taken into consideration, the existence of the above electronically excited species makes us infer that both C_2 and CH species must be formed in the reaction process.

Some of typical oscillograms obtained at a middle temperature (about 1850 K) are shown in Fig. 7. The emission curve of C_2* observed with each mixture was similar in shape to that of CH* or CF* emission.

The OH* emission curves thus recorded with the five mixtures heated to high temperature (2150 K) are shown in Fig. 8. The emission intensity of OH* measured with the CF_3Cl-free mixture (A) increases rather slowly up to a maximum after the ignition delay time (τ) which is the time lag between the reflected shock arrival and the onset of the rapid increase of the emission signal, and then decreases more slowly toward the base line. When a small amount of CF_3Cl is added, the emission of OH* rises rapidly to a maximum, falls quickly to some intensity, and then declines slowly

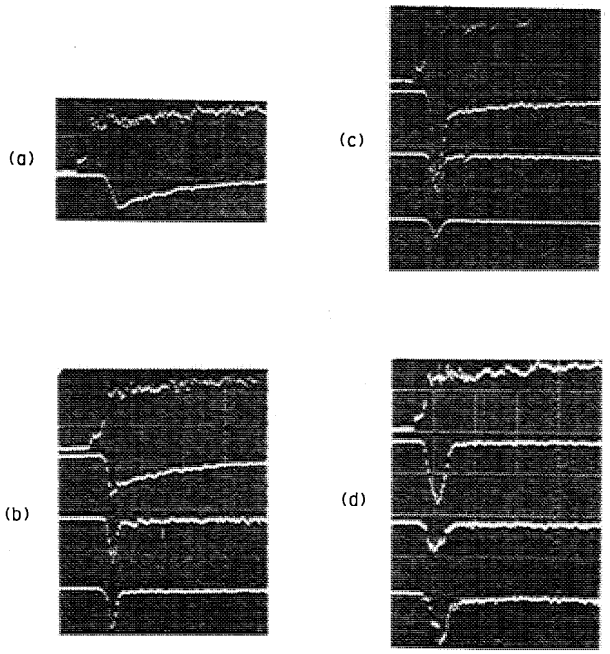

Fig. 7. Time history curves of pressure and emissions. Sweep time=100 μs/div.
Uppermost trace : pressure. Second trace : OH* emission. Third trace : CF* emission. Lowest trace : CH* emission.
(a) Mixture (A), T_5=1860 K, P_5=4.3 atm. (b) Mixture (B), T_5=1885 K, P_5=4.6 atm. (c) Mixture(C), T_5=1828 K, P_5=4.1 atm. (d) Mixture (G), T_5=1853 K, P_5=4.2 atm.

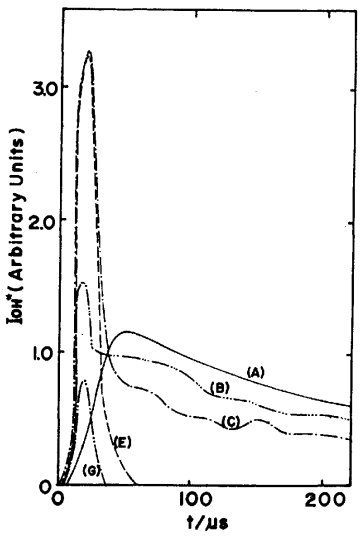

Fig. 8. Time variation of the OH* emissions at 2150± 20 K observed with the five mixtures.

toward the base line, thereby showing a spike with a shoulder, as may be seen in Figs. 7b, 7c, and 8. When CF_3Cl is added abundantly, on the other hand, OH* shows a spike with no shoulder (see Figs. 7d and 8).

OH* may be formed through the reactions (23′) and (24′) in the oxidation of hydrogen[18-21] and of hydrocarbon,[22-23] respectively.

$$O + H + M = OH^* + M \quad (23')$$

$$CH + O_2 = OH^* + CO \quad (24')$$

Compared with chemical excitation, thermal excitation below 2000 K seems to have little contribution to the OH* formation.[18] Even at a high temperature the emission intensity of OH* (I_{OH}*) observed in the hydrogen oxidation slowly decreases with time from a maximum intensity as shown in Figs. 7a and 8, and this slow decrease of OH* is considered to be a characteristic of the OH* formation through the reaction(23′). These OH* emission curves shown in Figs. 7a and 8 have a striking contrast to those previously obtained with the hydrocarbon oxidation, where I_{OH}* rapidly decreased from a maximum intensity.[11,13] This rapid decrease of OH* may be a characteristic of the OH* formation through the reaction (24′). As already described above, the addition of CF_3Cl has a strong effect upon the emission pattern and intensity of OH*. As may be seen in Figs. 7 and 8, the spike of OH* (rapid decrease of OH* emission from a maximum) appears when CF_3Cl is added. Therefore, this spike suggests that some OH* species are formed through the reaction (24′). For the OH* formation under our experimental condition, the existence of CH needs, in analogy with the C_2* formation mentioned below. Therefore, we consider the reactions for the CH formation, as mentioned below.

It is known well that the reaction $C_2H_6+M=2CH_3+M$ occurs at the temperature above 1300 K.[24] Quite similarly the dissociation reaction (1) may occur readily to produce CF_3[25] because both of the reactions are nearly identical in ΔH. In the present experiment with H_2–O_2–CF_3Cl–Ar mixture, therefore, a fairly large amount of CF_3 may be produced during the reaction process. Since the reactions (5)—(7) are exothermic, the intermediate products CF and C also may be produced quite easily. There exists a large amount of H_2 at the initial stage in the present experiment, and the ΔH values of the reactions (17), (18), and (19) are 24, 17, and 21 kcal/mol, respectively. Hence, it may be possible through the reactions, (17), (18), and (19) that CH is produced in the present experiment. By considering the reactions, as mentioned above, we have repeated computations and finally completed the mechanism and the rate-constant expressions, as shown in Table 3, which are employed in order to obtain the concentration-time relations of all the species at 1800 K. The rate constants for the OH* formation in the H_2–O_2 reaction shown in Table 3 are cited from other paper.[21] The curve calculated with it fits the experimental data best, as may be seen in Fig. 3. When the CH formation reactions (15), (17), and (19), without the reaction (18), were used for the computation, the experimental finding shown in Fig. 3 can not reasonably be explained. Therefore, CH seems to be produced through the reaction (18) in the present experiment. In the computation except the reaction (23′) or (24′) from the mechanism in Table 3, we also were capable to substantiate the characteristic time-variation for the OH* emission, as mentioned above, and found that much existence of CF_3Cl makes it difficult to form OH* through the reaction (23′). The OH* concentration variation computed at 1800 K is shown in Fig. 9. This figure interprets well the relationship, as shown in Figs. 7 and 8. Provided that CH is produced in our

Table 3. Elementary reactions and rate constant expressions[a)]

Reaction	A	n	E	Reference
$H_2+O_2=OH+OH$	1.7×10^{13}	0.0	48100	29
$H_2+M=H+H+M$	2.2×10^{12}	0.5	92600	30
$O_2+M=O+O+M$	1.8×10^{11}	0.5	95700	31
$O+H_2=OH+H$	2.2×10^{14}	0.0	13700	32
$OH+H_2=H_2O+H$	5.2×10^{13}	0.0	6500	33
$H_2+HO_2=H_2O+OH$	7.3×10^{11}	0.0	18700	34
$H+O_2=OH+O$	1.2×10^{17}	−0.91	16630	35
$H+O_2+M=HO_2+M$	2.5×10^{15}	0.0	0	36
$H+OH+M=H_2O+M$	7.5×10^{23}	−2.6	0	37
$H+HO_2=OH+OH$	2.5×10^{14}	0.0	1900	34
$H+HO_2=H_2+O_2$	2.5×10^{13}	0.0	700	34
$O+HO_2=OH+O_2$	5.0×10^{13}	0.0	1000	34
$OH+OH=H_2O+O$	5.5×10^{13}	0.0	7000	38
$OH+HO_2=H_2O+O_2$	5.0×10^{13}	0.0	1000	34
$CF_3Cl+M=CF_3+Cl+M$	2.1×10^{17}	0.0	75000	39
$CF_3Cl+H=CF_3+HCl$	4.4×10^{13}	0.0	10200	39
$H_2+Cl=HCl+H$	7.9×10^{13}	0.0	5500	40
$CF_3+H_2=CF_3H+H$	4.0×10^{11}	0.0	8800	41
$CF_3Cl+Cl=CF_3+Cl_2$	2.0×10^{14}	0.0	31300	42
$CF_3+OH=CF_2O+HF$	1.0×10^{12}	0.0	0	39
$CF_3+O=CF_2O+F$	1.0×10^{12}	0.0	0	39
$CF_3+H=CF_2+HF$	6.0×10^{12}	0.0	0	39
$H+CF_3+M=CF_3H+M$	1.2×10^{20}	−1.0	0	39
$CF_3+CF_3+M=C_2F_6+M$	7.1×10^{17}	0.5	0	43
$CF+CF_3+M=C_2F_4+M$	3.0×10^{18}	0.0	0	Assumed[b)]
$HCl+M=H+Cl+M$	6.8×10^{21}	−2.0	102000	44
$CF_2+H=CF+HF$	4.0×10^{12}	0.0	0	Assumed[b)]
$CF+H=C+HF$	1.0×10^{12}	0.0	0	Assumed[b)]
$C+CF=C_2+F$	1.0×10^{12}	0.0	0	Assumed[b)]
$CF+O=CO+F$	1.0×10^{13}	0.0	0	Assumed[b)]
$CF+H_2=CH+HF$	1.5×10^{11}	0.0	0	Assumed[b)]
$C+O_2=CO+O$	1.0×10^{13}	0.0	0	Assumed[b)]
$C_2+O_2=CO_2+C$	1.0×10^{11}	0.0	0	Assumed[b)]
$H_2+F=HF+H$	1.2×10^{14}	0.0	1700	41
$CH+O=CO+H$	1.0×10^{13}	0.0	0	Assumed[b)]
$O+H+M=OH^*+M$	5.0×10^{13}	0.0	6940	21
$CH+O_2=CO+OH^*$	6.0×10^{10}	0.0	0	45
$OH^*+M=OH+M$	2.5×10^{11}	0.5	0	46
$OH^*+H_2O=OH+H_2O$	4.1×10^{13}	0.5	0	46
$OH^*=OH+h\nu$	1.4×10^{6}	0.0	0	21

a) Rate constants in the form, $AT^n\exp(-E/RT)$, in cm, mol, cal, and K units. b) Rate constants assumed for the reaction at 1800 K.

experiment, then C_2^* is probably formed by some of the following reactions:

$$C + CH = C_2^* + H, \quad (8')$$

$$CH + CH = C_2^* + H_2, \quad (9')$$

$$CH_2 + C = C_2^* + H_2, \quad (10')$$

$$CF + CH = C_2^* + HF. \quad (11')$$

The reactions (8′)—(10′) have already been reported for the C_2^* formation in the hydrocarbon oxidation.[26-28]

The concentration of CH thus produced is less than that of CF, as shown in Fig. 10. Accordingly, assumed that the rate constants of these reactions are nearly equal, it appeared that the reaction (11′) was most important for the C_2^* formation under our experimental condition. The CH and CF concentrations calculated with mixture (G) were smaller than those calculated with mixtures (C) and (D), respectively. Hence, it may be possible to explain the relationship between maximum C_2^* intensity and CF_3Cl concentration, as shown in Fig. 5.

As already mentioned above, the endothermic reaction (18) among reactions (17)—(19) contributed to the formation of not CH* but CH in this work because none of the ΔH values (17—24 kcal/mol) is small enough to form CH*. However, the reaction (15) is strongly exothermic, and C_2 and C exist during the reaction process, as shown in Fig. 10. Consequently, it is concluded that CH* is mainly formed by

$$C_2 + OH = CH^* + CO. \quad (15')$$

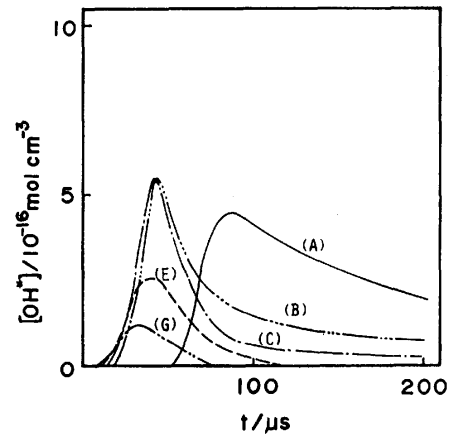

Fig. 9. OH* concentration profiles computed with mixtures (A), (B), (C), (E), and (G) using the mechanism and rate constants in Table 3.

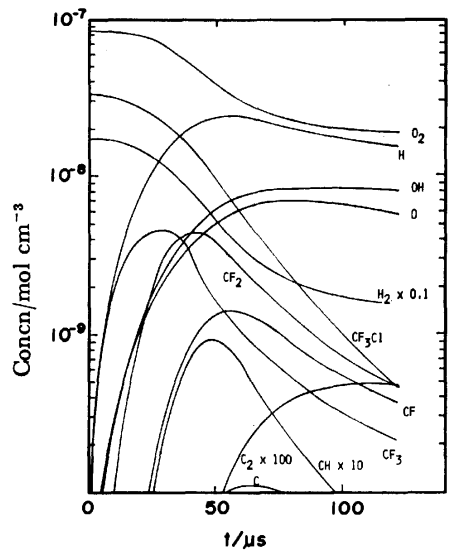

Fig. 10. Concentration profiles computed for mixture (C) at 1800 K using the mechanism and rate constants shown in Table 3.

The OH concentration calculated with mixture (G) is almost the same as that calculated with mixtures (C) and (D), but the C_2 concentration with mixture (G) is extremely smaller than that calculated with mixture (C) or (D). The relationship between maximum CH* intensity and CF_3Cl concentration, as shown in Fig. 4 may be easily interpreted. According to our computation, the increase and decrease of OH*, CH*, and C_2* concentrations owing to the addition of a small and large amounts of CF_3Cl, respectively, were also concluded to mainly come from the competition of the reactions $CF+CF_3+M=C_2F_4+M$ and $CF+H_2=CH+HF$.

Since the reaction (21) is greatly exothermic and since C and F_2 exist abundantly enough to cause the reaction (21′), the reaction (21′) is concluded to be a main process for the CF* formation.

$$C + F_2 = CF^* + F. \qquad (21')$$

Temperature dependence of the ignition delay time τ observed with OH* is shown in Fig. 11, which reveals that τ at a temperature above 1500 K decreases with

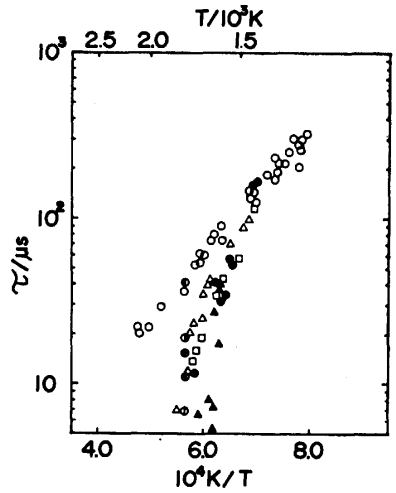

Fig. 11. Temperature dependence of the ignition delay time τ measured with the OH* emission for the mixtures (A)—(G), ○: (A), △: (B), □: (C), ●: (E), ▲: (G), and calculated at 1800 K for the mixtures (A)—(G), ◐: (A), ◑: (B), ◎: (C), ⊙: (E), ⊕: (G).

an increase in C. Fig. 11 also shows the value τ computed with mixtures (A), (B), (C), (E), and (G) at 1800 K. τ observed is in fair agreement with that simulated.

Under our experimental condition employed with the H_2–O_2–CF_3Cl–Ar mixtures, a fair amount of CF_3 and Cl may be produced through the reaction (1), as shown in Fig. 10. These intermediate products CF_3 and Cl easily generate the active species H through the reactions (2) and (3). In the oxidation reaction of the H_2–O_2–CF_3Cl–Ar mixtures, an occurrance of the reactions (1)—(3) increases the H concentration at the initial stage, thereby promoting the overall reaction rate, as shown in Fig. 11. In the H_2 oxidation over the range 1500—2200 K, therefore, CF_3Cl is concluded to act as a promoter.

The authors wish to express their thanks to Prof. Toshiaki Yokota for his kindness in measuring the relative sensitivity. The present work was partially supported by a Grant-in-Aid for Scientific Research No. 174145 from the Ministry of Education, Science and Culture.

References

1) R. F. Simmons and H. G. Wolfhard, *Trans. Faraday Soc.*, **51**, 1211 (1955).
2) W. A. Rosser, H. Wise, and J. Miller, "Symp. Combust. 7th," The Combustion Institute, Butterworths (1959), p. 175.
3) C. Halpern, *J. Res. Natl. Bur. Stand.*, **70A**, 133 (1966).
4) W. E. Wilson, "Symp. Combust. 10th," The Combustion Institute, Pittsburgh (1965), p. 47.
5) G. B. Skinner and G. H. Ringrose, *J. Chem. Phys.*, **43**, 4129 (1965).
6) A. G. Gaydon and H.G. Wolfhard, *Proc. R. Soc. London, Ser. A*, **213**, 366 (1952).
7) S. L. Arnold, G. H. Kimbell, and D. R. Snelling, *Can. J. Chem.*, **53**. 2419 (1975).
8) M. M. Ibiricu and A. G. Gaydon, *Combust. Flame*, **8**, 51 (1964).

9) J. A. Harrington, A. P. Modica, and D. R. Libby, *J. Chem. Phys.*, **44**, 3380 (1966).
10) A. R. Fairbairn, *Proc. R. Soc. London, Ser. A*, **312**, 229 (1969).
11) Y. Hidaka, H. Kawano, and M. Suga, to be published.
12) A. G. Gaydon, "The Spectroscopy of Flame," Chapman and Hall, London (1974), p. 216.
13) Y. Hidaka, T. Kataoka, and M. Suga, *Bull. Chem. Soc. Jpn.*, **47**, 2166 (1974).
14) Y. Hidaka, T. Nishi, and M. Suga, *Bull. Chem. Soc. Jpn.*, **49**, 2007 (1976).
15) H. Prophet and D. R. Stull, *JANAF Thermochemical Data 2nd Ed.*, NSRDS-NBS, **37** (1971).
16) D. B. Olson and W. C. Gardiner, Jr., *Combust. Flame*, **32**, 151 (1978).
17) A. G. Gaydon, "The Spectroscopy of Flame," Chapman and Hall, London (1974), pp. 343—349.
18) W. C. Gardiner, Jr., K. Morinaga, D. L. Ripley, and T. Takeyama., *Phys. Fluids Supplement*, **1**, 120 (1969).
19) D. Gutman, R. W. Luty, N. F. Jacobs, E. A. Hardwidge, and G. L. Schott, *J. Chem. Phys.*, **48**, 5689 (1968).
20) S. Ticktin, G. Spindler, and H.I. Schiff, *Discuss. Faraday Soc.*, **44**, 218 (1967).
21) Y. Hidaka, S. Takahashi, H. Kawano, M. Suga, and W. C. Gardiner, Jr., *J. Phys. Chem.*, in press.
22) A. G. Gaydon, "The Spectroscopy of Flame," Chapman and Hall, London (1974), p. 267.
23) R. P. Porter, A. H. Clarke, W. E. Kaskan, and W. G. Browne, "Symp. Combust. 11th," The Combustion Institute, Pittsburgh (1967), p. 907.
24) D. B. Olson, T. Tanzawa, and W. C. Gardiner, Jr., *Int. J. Chem. Kinet.*, **11**, 23 (1979).
25) D. F. Dever and E. Grunwald, *J. Am. Chem. Soc.*, **98**, 5055 (1976).
26) R. F. Ferguson, *J. Chem. Phys.*, **23**, 2085 (1955).
27) W. J. Miller and H. B. Palmer, "Symp. Combust. 9th," Academic Press, New York (1963), p. 90.
28) J. Peeters, J. F. Lambert, P. Hertoghe, and A. Van Tiggelen, "Symp. Combust. 13th," The Combustion Institute, Pittsburgh (1971), p. 321.
29) C. J. Jachimowski and W. M. Houghton, *Combust. Flame*, **17**, 25 (1971).
30) A. L. Meyerson and W. S. Watt, *J. Chem. Phys.*, **49**, 425 (1969).
31) W. S. Watt and A. L. Meyerson, *J. Chem. Phys.*, **51**, 1638 (1969).
32) G. L. Schott, R. W. Getzinger, and W. A. Seitz, *Int. J. Chem. Kinet.*, **6**, 921 (1974).
33) W. C. Gardiner, Jr., W. G. Mallard, M. Mcfarland, K. Morinaga, J. H. Owen, W. T. Rawlins, T. Takeyama, and B. F. Walker, "Symp. Combust. 14th," The Combustion Institute, Pittsburgh (1973), p. 61.
34) A. C. Lloyd, *Int. J. Chem. Kinet.*, **6**, 169 (1974).
35) G. L. Schott, *Combust. Flame*, **21**, 357 (1973).
36) R. W. Getzinger and L. S. Blair, *Combust. Flame*, **13**, 271 (1969).
37) J. B. Homer and I. R. Hurle, *Proc. R. Soc. London, Ser. A*, **314**, 585 (1970).
38) W. T. Rawlins and W. C. Gardiner, Jr., *J. Chem. Phys.*, **60**, 4676 (1974).
39) Unpublished data.
40) P. G. Ashmore and J. Chanmugam, *Trans. Faraday Soc.*, **49**, 254 (1953).
41) "Kagakubinran," ed by the Chemical Society of Japan, Maruzen, Tokyo (1980), pp. 1024—1027.
42) J. C. Amplett and E. Whittle, *Trans. Faraday Soc.*, **63**, 2695 (1967).
43) A. P. Modica and S. J. Sillers, *J. Chem. Phys.*, **48**, 3283 (1968).
44) J. A. Jacobs, N. Cohen, and R. R. Giedt, *J. Chem. Phys.*, **46**, 1958 (1967).
45) R. P. Porter, A. H. Clark, W. E. Kaskan, and W. E. Browne, "Symp. Combust. 11th," The Combustion Institute, Pittsburgh (1967), p. 907.
46) Y. Hidaka, H. Kawano, and M. Suga, to be published.

The Electron Exchange Rates of Anthracene/Anthracene Radical Anion Ion-paired with Various Tetraalkylammonium Cations

Kosaku SUGA* and Shigeru AOYAGUI

Department of Chemical Engineering, Faculty of Engineering, Tokyo Institute of Technology, O-okayama, Meguro-ku, Tokyo 152

(Received March 13, 1981)

The electron exchange reaction between anthracene and its radical anion formed by the sodium reduction of the parent molecule in 1,2-dimethoxyethane, tetrahydrofuran, and a tetrahydrofuran-1,4-dioxane mixture was studied by ESR spectroscopy in the preseuce of tetraalkylammonium cations of various kinds and amounts. Analytical equations were presented to evaluate the rate constants of two competitive electron exchange reactions between anthracene and its anion, which was ion-paired in part with a tetraalkylammonium cation and in part with a sodium cation. The experimental results obeyed the theoretical equations and, consequently, yielded the electron exchange rate constants for the ion pairs of the former type, which were unaffected by the coexistence of the ion pairs of the latter type. They were of the order of 10^8 M^{-1} s^{-1} (1 M = 1 mol dm^{-3}), a value which was one order of magnitude smaller than the rate constant for the solvent-separated ion pair of anthracene anion with sodium cation. They were smaller for tetraalkylammonium cations with longer carbon chains. These findings are discussed on the basis of the theory of Marcus.

It is a well-known fact that a solution of anthracene radical anion (A^-) formed by sodium reduction of anthracene (A) in tetrahydrofuran (THF) gives an ESR spectrum with hyperfine splittings due to ^{23}Na, besides those due to ^1H.[1,2] This specific splitting pattern is considered to be evidence for the tight ion-pairing between Na^+ and A^-. In a previous paper[2] we reported a finding that the ^{23}Na-splittings disappeared on addition of tetrabutylammonium perchlorate (Bu_4NClO_4) to this solution, and suggested that A^- formed a more stable ion pair with Bu_4N^+ than with Na^+. By using a solution of this composition, measurements were made on the electron exchange rate constants for a few redox systems of aromatic hydrocarbons and their radical anions ion-paired with Bu_4N^+. No kinetic information had been available concerning the electron transfer reaction of ion pairs, except those of alkali metal cations.

In that work, however, no regard was paid on other kinds of ion pairs coexisting with those between Bu_4N^+ and A^-. According to Hirota *et al.*[3] sodium dihydroanthrylide (NaA) in THF exists as the following chemical species: the free anion, A^-, the loose or solvent-separated ion pair, $Na^+:A^-$, and the tight ion pair, $Na^+\cdot A^-$. Conductometrically, A^- can be distinguished from the others and ESR-spectroscopically, $Na^+\cdot A^-$ can be distinguished. Consequently, there is an unfortunate possibility that our previous rate constant for the A/A^- electron exchange in the presence of Bu_4N^+ was an average of the rate constants for the reactions in which A^-, $Na^+:A^-$, $Bu_4N^+:A^-$, and $Bu_4N^+\cdot A^-$ participated. $Na^+\cdot A^-$ is excluded on the basis of the previous finding described above.

This paper presents an analytical procedure to obtain the rate constant for the electron exchange between an aromatic hydrocarbon and its anion ion-paired with a tetraalkylammonium cation in the presence of the ion pair with Na^+. It is applied to the redox systems of A/A^- ion-paired with various kinds of tetraalkylammonium cations (R_4N^+).

Experimental

Anthracene was recrystallized twice from benzene. The perchlorates of tetrabutylammonium, tetrapropylammonium (Pr_4N^+), tetraethylammonium (Et_4N^+), and tetramethylammonium (Me_4N^+) were prepared from perchloric acid and the respective tetraalkylammonium iodides (R_4NI). They were recrystallized from water and then from ethylacetate. Bu_4NI was synthesized by the usual methods from tributylamine and butyl iodide. Other iodides, including tetraamylammonium iodide (Am_4NI), were commercially obtained.

The purification of the solvents used, THF, 1,2-dimethoxyethane (DME), and 1,4-dioxane (DO) and the preparation of the test solution were performed in the same way as described previously.[4] Sodium metal was used as the reducing agent.

The electron-transfer rates at 25±2°C were determined by the conventional method based on the line broadening of ESR spectra. A JEOL Model JES-3BSX spectrometer was used.

Analytical Procedure

The following ion pairs may exist in a solution containing NaA and a large excess of R_4NClO_4: $Na^+:A^-$, $R_4N^+\cdot A^-$, $R_4N^+:A^-$, $Na^+\cdot ClO_4^-$, $Na^+:ClO_4^-$, $R_4N^+\cdot ClO_4^-$, and $R_4N^+:ClO_4^-$. Since we cannot distinguish between $R_4N^+\cdot A^-$ and $R_4N^+:A^-$, $R_4N^+\cdot ClO_4^-$ and $R_4N^+:ClO_4^-$, and $Na^+\cdot ClO_4^-$ and $Na^+:ClO_4^-$, these couples of ion pairs are denoted by the common formulae $R_4N^+A^-$, $R_4N^+ClO_4^-$, and $Na^+ClO_4^-$, respectively.

Among these ion pairs and the free ions the following equilibria are established:

$$Na^+ + A^- \overset{K_1}{\rightleftharpoons} Na^+:A^-, \quad (1)$$

$$R_4N^+ + A^- \overset{K_2}{\rightleftharpoons} R_4N^+A^-, \quad (2)$$

$$R_4N^+ + ClO_4^- \overset{K_3}{\rightleftharpoons} R_4N^+ClO_4^-, \quad (3)$$

$$Na^+ + ClO_4^- \overset{K_4}{\rightleftharpoons} Na^+ClO_4^-, \quad (4)$$

where the K's are the formation constants of the ion pairs.

When the concentration of A^- is much smaller than

that of $Na^+: A^-$, which is true of solutions of low dielectric constants, the anthracene molecules added to this solution undergo the following electron exchange reactions:

$$Na^+: A^- + A \underset{}{\overset{k_1}{\rightleftharpoons}} A + Na^+: A^-, \quad (5)$$

$$R_4N^+A^- + A \underset{}{\overset{k_2}{\rightleftharpoons}} A + R_4N^+A^-, \quad (6)$$

where k's are the electron-exchange rate constants. The values for the coupling constant and the line width of the ESR spectrum of a solution containing $Na^+: A^-$ and $R_4N^+A^-$ should be, respectively, the average values for the spectra of these ion pairs, if the following exchange reaction is sufficiently fast:

$$Na^+: A^- + R_4N^+A^- \rightleftharpoons R_4N^+A^- + Na^+: A^-. \quad (7)$$

This condition may be fulfilled, since the solution containing NaA and R_4NClO_4 gave only a single ESR spectrum similar to that of free A^-. Therefore, it is assumed after Stevenson *et al.*[5] that the observed increase in line width is equal to the weighted mean of the increases due to Reactions 5 and 6. Then the observed rate constant, k, can be expressed in terms of k_1 and k_2 as follows:

$$k = (k_1[Na^+: A^-] + k_2[R_4N^+A^-])/([Na^+: A^-] + [R_4N^+A^-])$$
$$= (k_1 + k_2K_2[R_4N^+]/K_1[Na^+])/(1 + K_2[R_4N^+]/K_1[Na^+]), \quad (8)$$

where the brackets mean the concentration in molarity.

When it is assumed that the K values are large enough for the existence of any free ions to be neglected, which may be true of solvents of low dielectric constant such as THF, DME, and DO, Eq. 8 can be rewritten as follows (see Appendix):

$$k = k_2 + (k_1 - k_2)/(1 + K_2K_4[R_4NClO_4]_0/K_1K_3[A^-]_0), \quad (9)$$

where the subscript 0 denotes the analytical concentration of the substance indicated. Equation 9 can be linearized with respect to $[R_4NClO_4]_0$ or its inverse in the following forms:

$$(k_1 - k)^{-1} = K^{-1}(k_1 - k_2)^{-1}[R_4NClO_4]_0^{-1} + (k_1 - k_2)^{-1}, \quad (10)$$

or

$$(k - k_2)^{-1} = K(k_1 - k_2)^{-1}[R_4NClO_4]_0 + (k_1 - k_2)^{-1}, \quad (11)$$

with

$$K = K_2K_4/K_1K_3[A^-]_0. \quad (12)$$

When the k_1 value is known, the k_2 value can be obtained from the intercept of a linear plot of $(k_1 - k)^{-1}$ *vs.* $[R_4NClO_4]_0^{-1}$ and the K value can be obtained from the intercept and the slope together. When k_1 is not known, measurements must be made by using a concentration $[R_4NClO_4]_0$ high enough for the relation $K[R_4NClO_4]_0 \gg 1$ to be satisfied. Then Eq. 9 can be adequately approximated by the following linear relation between k and $[R_4NClO_4]_0^{-1}$:

$$k = k_2 + (k_1 - k_2)/K[R_4NClO_4]_0. \quad (13)$$

The k_2 value is obtained from the intercept of the linear plot drawn after Eq. 13. The k_1 value can then be obtained from the intercept and the slope together.

Results and Discussion

ESR Spectra of NaA in Solutions with and without R_4N^+. The ESR spectrum of NaA in THF exhibited hyperfine splittings due to ^{23}Na, whereas that in DME did not. The ^{23}Na hyperfine coupling constant was as large as 0.15 mT for a 1:1 THF–DO mixed solution whose dielectric constant was lower than that of THF. According to Hirota *et al.*[3] the ion-pairing reaction of A^- with Na^+ and the conversion reaction between $Na^+ \cdot A^-$ and $Na^+: A^-$ are both very rapid and, consequently, the ^{23}Na hyperfine coupling constant of the ion pair is the mean value of the coupling constants for $Na^+ \cdot A^-$ and $Na^+: A^-$ or A^-.

No ^{23}Na hyperfine structure was observed in the spectra for 0.1 mM NaA solutions in THF and THF–DO when they contained more than 0.5 mM R_4NClO_4 (R=Me, Et, Pr, Bu, and Am). This result can be explained on the basis of the ion-pair concept of Hirota *et al.* in the following way: most anthracene anions in DME exist as A^- and $Na^+: A^-$; in THF and THF–DO containing no R_4N^+, a part of the anthracene anions exist as $Na^+ \cdot A^-$; in the presence of R_4N^+, however, $Na^+ \cdot A^-$ may be converted into $R_4N^+ \cdot A^-$ and $R_4N^+: A^-$. The analytical equations derived above are based on these premises.

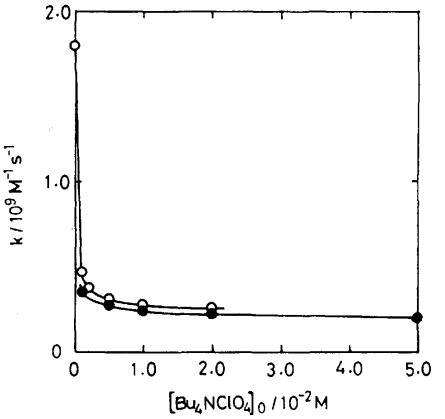

Fig. 1. Dependence of the electron-exchange rate constants for A/A^- in (○) DME and (●) THF on the concentration of added Bu_4NClO_4, $[Bu_4NClO_4]_0$.

Dependence of k on $[Bu_4NClO_4]_0$. Figure 1 shows the rate constants for the electron exchange reactions between anthracene and its radical anion in THF and DME at various Bu_4NClO_4 concentrations. The k value in DME decreases very rapidly with increasing $[Bu_4NClO_4]_0$ and then decreases gradually, approaching the value of *ca.* 2×10^8 M^{-1} s^{-1}. The k *vs.* $[Bu_4NClO_4]_0$ curve in THF also behaves in a similar way. The k value at $[Bu_4NClO_4]_0 = 0$ in DME, 1.8×10^9 M^{-1} s^{-1}, was taken from our previous paper.[4] This is regarded as the k_1 value. The same quantity in THF could not be obtained from ESR spectra, because ^{23}Na hyperfine lines due to $Na^+ \cdot A^-$ made them too complicated to be analyzed. The k *vs.* $[R_4NClO_4]_0$ curves for Pr_4NClO_4 and Et_4NClO_4 in DME are shown in Fig. 2. Because of the low solubility of these salts, the available concentration ranges were much narrower than the range for Bu_4NClO_4.

Evaluation of k_2. The $(k_1 - k)^{-1}$ *vs.* $[R_4NClO_4]_0^{-1}$ plot for Bu_4NClO_4 in DME is shown in Fig. 3. The

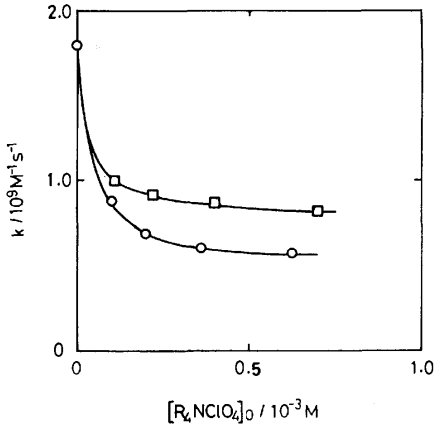

Fig. 2. Dependence of the electron-exchange rate constants for A/A^- in DME on the concentrations of (□) Et_4NClO_4 and (○) Pr_4NClO_4.

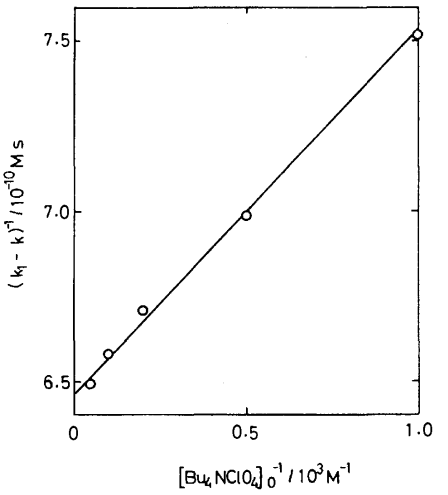

Fig. 3. $(k_1-k)^{-1}$ *vs.* $[Bu_4NClO_4]_0^{-1}$ in DME plotted after Eq. 10.

experimental points lie on a straight line in accord with the theoretical requirement of Eq. 10. The values for k_2 and K were obtained, respectively, as 2.5×10^8 M^{-1} s^{-1} and 4.8×10^3 M^{-1}.

Since the k_1 value in THF is not known, the k_2 value in this solvent was determined to be 1.8×10^8 M^{-1} s^{-1} from the intercept of the k *vs.* $[Bu_4NClO_4]_0^{-1}$ plot at $[Bu_4NClO_4]_0\rightarrow\infty$ in Fig. 4. The linearity of the experimental plot of $(k-k_2)^{-1}$ *vs.* $[Bu_4NClO_4]_0$ was excellent, as is shown in Fig. 5. On the basis of Eq. 11 the k_1 and K values were obtained, respectively, as 5×10^8 M^{-1} s^{-1} and 2.5×10^2 M^{-1}. However, it should be noted that this k_1 value was obtained at the infinite dilution of Bu_4NClO_4 at which the tight ion pair $Na^+\cdot A^-$ exists. Thus, the physical meaning of k_1 in THF is less clear than that in DME. The difference between the k_1 values in THF and DME may be caused by these circumstances, rather than the difference between the solvent properties.

The literature values for K_1 and $K_3(Bu_4N^+ClO_4^-)$ in THF at 25 °C are 2.3×10^5 M^{-1} [6] and 1.6×10^6 M^{-1}, [7] respectively. The $[A^-]_0$ value was held constant at

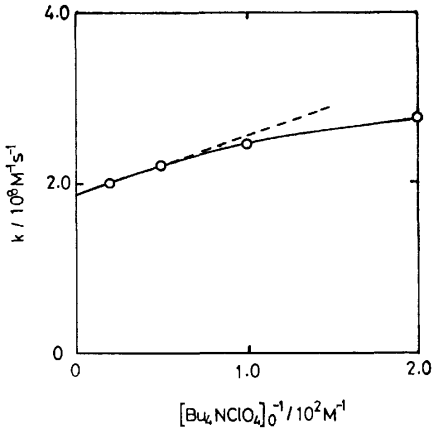

Fig. 4. *k vs.* $[Bu_4NClO_4]_0^{-1}$ in THF plotted after Eq. 13.

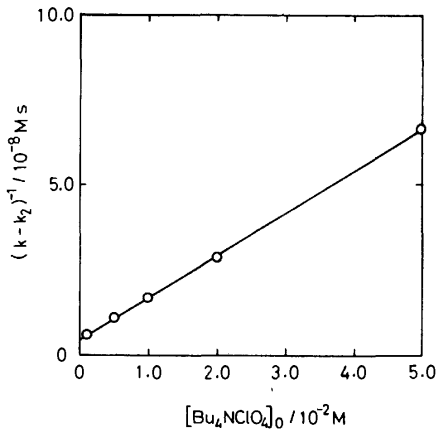

Fig. 5. $(k-k_2)^{-1}$ *vs.* $[Bu_4NClO_4]_0$ in THF plotted after Eq. 11.

about 10^{-4} M. According to Eq. 12 and the K value just obtained, the product K_2K_4 would be of the order of 10^{10} M^{-2}. Although neither K_2 nor K_4 is known, this may be a reasonable value, because most of the association constants in THF at 25 °C fall in the range of 10^4-10^6 M^{-1}. [7-9]

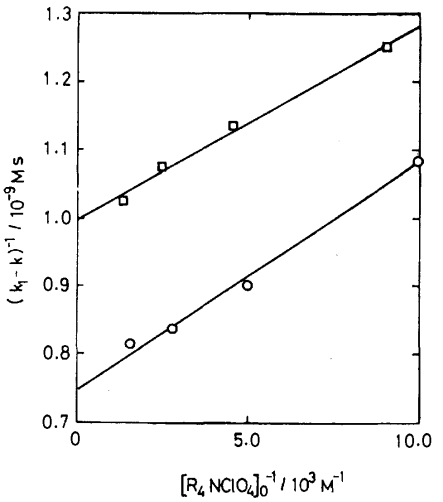

Fig. 6. $(k_1-k)^{-1}$ *vs.* (□) $[Et_4NClO_4]_0^{-1}$ and (○) $[Pr_4NClO_4]_0^{-1}$ in DME plotted after Eq. 10.

Equation 9 has been derived under the condition $[R_4NClO_4]_0 \gg [A^-]_0$. Though this condition was not fulfilled in the DME solutions of Pr_4NClO_4 and Et_4NClO_4, as seen in Fig. 2, the $(k_1-k)^{-1}$ *vs.* $[R_4NClO_4]_0$ plots in Fig. 6 exhibited the linearity required by Eq. 10 and yielded the following k_2 and K values: $k_2=4.6\times10^8$ (Pr_4NClO_4) and 8.1×10^8 (Et_4NClO_4) $M^{-1}s^{-1}$; $K=3.4\times10^4$ (Pr_4NClO_4) and 2.3×10^4 (Et_4NClO_4) M^{-1}.

These K values are compared with the value 4.8×10^3 M^{-1} for the Bu_4NClO_4 case. It may be safe to conclude that $K_2=KK_1K_3[A^-]_0/K_4$ is larger for smaller R_4N^+ ions, because K_3 may be larger for smaller ions and K_1, K_4, and $[A^-]_0$ are invariable.

Table 1. Rate constants for electron-exchange reactions between $R_4N^+A^-$ and A in different solvents

R_4NClO_4	$k_2/10^8$ $M^{-1}s^{-1}$		
	DME	THF	THF+DO (1 : 1)
Et_4NClO_4	8.1	(7.5) [b]	(6.6) [d]
Pr_4NClO_4	4.6	(4.9) [c]	(3.8) [d]
Bu_4NClO_4	2.5	1.8	(2.9) [e]
Am_4NClO_4	(1.5) [a]		

a) Obtained only with a 1 mM Am_4NI solution. b) Obtained only with a saturated solution of Et_4NClO_4 whose concentration is less than 5 mM. c) Obtained only with a 5 mM Pr_4NClO_4 solution. d) Obtained only with a saturated solution of R_4NClO_4. e) Obtained only with a 1 mM Bu_4NClO_4 solution.

The k_2 values thus obtained are summarized in Table 1. This also shows some approximate k_2 values in parentheses. Each of them was obtained at a fixed R_4NClO_4 concentration. Consequently, they should be averages of the real values for k_1 and k_2. However, the contribution of k_1 cannot be important, because k_1 and k_2 are of the same order and, furthermore, Figs. 1 and 2 suggest that anthracene anion should exist exclusively as $R_4N^+A^-$ under the given experimental conditions. In fact, the previously reported k value in THF containing 20 mM Bu_4NClO_4, 2.0×10^8 M^{-1} s^{-1},[2] is in good agreement with the k_2 value described above, 1.8×10^8 M^{-1} s^{-1}. This agreement points to the validity of the previous rate constant values obtained with no consideration of the competing reaction of Eq. 2. This may be due to the high Bu_4NClO_4 concentration which would make Na^+: A^- negligible.

Table 1 shows that $R_4N^+A^-$ undergoes a slower electron exchange than Na^+: A^-, whose k value in DME is 1.8×10^9 M^{-1} s^{-1}, and that the electron exchange rate decreases with increasing length of alkyl carbon chain. The former finding is in contrast with the finding of Campion *et al.*[10] that the rate of electron exchange between $[Fe(CN)_6]^{3-}$ and $[Fe(CN)_6]^{4-}$ in aqueous solutions is enhanced in the presence of R_4N^+ cations, whereas the latter agrees with theirs. However, it is doubtful that such a comparison makes sense. One of the reactants is uncharged in our experiments, but in theirs both reactants are highly charged and, consequently, the electrostatic repulsion between the reactants can have a serious effect on the electron exchange rate. They suggested that the ion-pairing of the reactant anions with R_4N^+ cations might reduce the effective charge on the reactants and thus might cause the enhancement in electron exchange rate. However, our experimental results show that the electrostatic effect is not the only effect of ion-pairing on the electron exchange rate.

The theories of electron transfer reaction which have been proposed so far are applicable only to reactions with the outer-sphere mechanism.[11] It is evident that the electron-transfer reaction between A and $R_4N^+A^-$ do not belong to this category of reaction. However, it may be worthwhile to extend the basic concept of nuclear rearrangement in the Marcus theory[12] to the reactions of our present concern. The intervening of R_4N^+ between A and A^- elongates their separation; the elongation may be greater for R_4N^+ with longer carbon chains. According to the theory, such a longer distance can account for the higher outer-sphere reorganization energy and, in turn, for the lower reaction rate. Furthermore, the intervening of R_4N^+ may decrease the activation entropy and, consequently, the rate constant, because the effective collision number in the electron exchange between $R_4N^+A^-$ and A may be smaller than that between A^- and A. It is probable that these effects are reflected in the observed rate constants.

Appendix

Derivation of Eq. 9. In solvents of low dielectric constants such as those used in this work, the concentrations of free ions are all negligible compared with those of the associated species. Then the following stoichiometric relations can be written among the chemical species existing in a solution containing sodium dihydroanthrylide and tetraalkylammonium perchlorate:

$$[R_4N^+A^-] + [R_4N^+ClO_4^-] = [R_4NClO_4]_0, \quad (A1)$$

$$[Na^+:A^-] + [R_4N^+A^-] = [A^-]_0, \quad (A2)$$

and

$$[Na^+ClO_4^-] = [R_4N^+A^-]. \quad (A3)$$

When $[R_4NClO_4]_0 \gg [A^-]_0$, the terms $[R_4N^+A^-]$ and $[Na^+:A^-]$ can be neglected in comparison with $[R_4N^+ClO_4^-]$ and $[R_4N^+A^-]$, respectively. Consequently the following relations are obtained:

$$[R_4NClO_4]_0 = [R_4N^+ClO_4^-] = K_3[R_4N^+][ClO_4^-], \quad (A4)$$

and

$$[A^-]_0 = [Na^+ClO_4^-] = K_4[Na^+][ClO_4^-], \quad (A5)$$

which lead to the relation

$$[R_4N^+]/[Na^+] = K_4[R_4NClO_4]_0/K_3[A^-]_0. \quad (A6)$$

Equation 9 in the text can be obtained from Eqs. 8 and A6.

References

1) A. Crowley, N. Hirota, and R. Kreilick, *J. Chem. Phys.*, **46**, 4815 (1967).

2) K. Suga and S. Aoyagui, *Bull. Chem. Soc. Jpn.*, **45**, 1375 (1972).

3) N. Hirota, R. Carraway, and W. Schook, *J. Am.*

Chem. Soc., **90**, 3611 (1968).
4) K. Suga and S. Aoyagui, *Bull. Chem. Soc. Jpn.*, **46**, 755 (1973).
5) G. R. Stevenson, R. Concepcion, and I. Ocasio, *J. Phys. Chem.*, **80**, 861 (1976).
6) P. Chang, R. V. Slates, and M. Szwarc, *J. Phys. Chem.*, **70**, 3180 (1966).
7) C. Treiner and J. C. Justice, *C. R. Acad. Sci., Ser. C*, **269**, 1364 (1969).
8) C. Carvajal, K. J. Tölle, J. Smid, and M. Szwarc, *J. Am. Chem. Soc.*, **87**, 5548 (1965).
9) D. N. Bhattacharyya, C. L. Lee, J. Smid, and M. Szwarc, *J. Phys. Chem.*, **69**, 608 (1965).
10) R. J. Campion, C. F. Deck, P. King, Jr., and A. C. Wahl, *Inorg. Chem.*, **6**, 672 (1967).
11) R. A. Marcus, *Ann. Rev. Phys. Chem.* **15** 155 (1964).
12) R. A. Marcus, *J. Chem. Phys.*, **43**, 679 (1965).

 © 1982 The Chemical Society of Japan Bull. Chem. Soc. Jpn., 55, 363—368 (1982)

Conformational Analysis of Intramolecular Excimer Formation in Dinaphthylalkanes

Shinzaburo Ito,* Masahide Yamamoto, and Yasunori Nishijima

Department of Polymer Chemistry, Kyoto University, Sakyo-ku, Kyoto 606

(Received March 23, 1981)

Intramolecular excimer formation processes were explained by the conformational energy calculated by an empirical method. Observed rate constants of excimer formation processes are closely correlated to the fraction of *tg* conformation. This indicates that intramolecular excimers are mainly formed by the internal rotation, *trans*→*gauche*, with reference to the naphthalene unit. The fraction of the *tg* conformation, which is an adjacent conformation to the excimer conformation on the conformational energy map, serves as an effective concentration of the intramolecular reaction. The small formation rate for *rac*-2,4-di(2-naphthyl)pentane is due to the unfavorable rotational mode ($g^+ \rightleftarrows g^-$) required to take the excimer conformation.

Since intramolecular excimers have been observed in various vinyl aromatic polymers and their dimer model compounds, it has become clear that the efficiency of excimer formation is greatly governed by the micro structures of molecules. Hirayama,[1] Longworth,[2] Chandross,[3] and Klöpffer[4] studied configurational requirements for the intramolecular excimer formation, and showed that the molecular structure in which two aromatic groups are separated with three carbon atoms of the methylene chain is the most favorable configuration for the intramolecular excimer formation. Their results show that the parallel sandwich arrangement of the aromatic groups is attainable with a propane chain, and that in the other type of compounds with shorter or longer chains than the propane chain, *e.g.*, ethane, butane, and pentane, two aromatic groups cannot approach each other owing to the conformational instability. This selectivity for the excimer formation in diarylalkanes is generally accepted as the $n=3$ rule.

Since we know that the intramolecular excimers are formed by the conformational relaxation after excitation of chromophores, the formation processes should be interpreted by the equilibrium conformations of the molecules and their internal rotation processes. For example, different efficiencies of the excimer formation even for the compounds holding $n=3$ rule, were reported by Hirayama,[1] and similar results were recently obtained by other workers.[5-7] These results suggest that there are some conformational factors controlling the intramolecular excimer formation besides the $n=3$ rule. But, in order to discuss the process of the intramolecular excimer formation in greater detail, quantitative data for the rate constant of the formation process are required.

In the preceding paper,[8] we reported a large difference in the efficiency of the excimer formation for the compounds satisfying the $n=3$ rule: 1,3-di(2-naphthyl)propane (1,3-DNPr), 1,3-di(2-naphthyl)butane (1,3-DNBu), *meso*-2,4-di(2-naphthyl)pentane (2,4-DNPe (*meso*)), and *rac*-2,4-di(2-naphthyl)pentane (2,4-DNPe (*rac*)). It was also shown by time-resolving measurements that the excimer formation rate constants change markedly with the molecular structures of the samples. We have tried to elucidate the internal rotation processes which lead to the intramolecular excimer formation.

In this paper, conformational energies of the four compounds mentioned above were calculated as functions of rotations about their C–C bonds, using an empirical treatment for the repulsive energies between nonbonded atoms and intrinsic torsional energies. The pathway of the internal rotation from the most stable conformation to the excimer conformation is discussed on the basis of the conformational energies. The observed rates of excimer formation are quantitatively well explained by these conformational analyses.

Procedures of the Calculation

The conformational energies of dinaphthylalkanes were calculated by using the conventional empirical method described in the preceding paper.[9] Potential energies due to the van der Waals interaction between nonbonded atoms and due to the intrinsic torsional potential energies associated with the rotation about the bonds are considered. For calculation of the van der Waals interaction, a potential function of Lennard-Jones type is used. The potential function is truncated by considering the molecule-solvent interaction according to Flory *et al.*[10,12] The total potential energy due to the van der Waals interaction is calculated as the sum over all pairs of nonbonded atoms. The intrinsic torsional potential energy for the skeletal alkane chain, $E(\phi)$, is calculated for the rotational angle ϕ, which is regarded as having a three fold periodicity:

$$E(\phi) = (E_0/2)\ (1-\cos 3\phi),$$

where E_0 is the torsional barrier energy, and is taken to be 12 kJ/mol.[11] The torsional energy for the rotation of naphthalene units, θ_i, is neglected, since the potential barrier is too low. The total potential energy is given by the sum of the potential energies due to the van der Waals interaction and the intrinsic torsional potentials.

The structural parameters used in this calculation are shown in Fig. 1. We must consider four independent angles to generate a given conformation of the dimers: two rotational angles, ϕ_1 and ϕ_2, for the chain skeleton and two rotational angles, θ_1 and θ_2, for the naphthyl groups, which are denoted as shown in Fig. 2. Angles are taken as 0 ° in the *trans* conformation. The naphthalene substituents are adopted as a reference conformation for the notation of *trans* and *gauche* conformations, in order to represent consistently the conformations of all

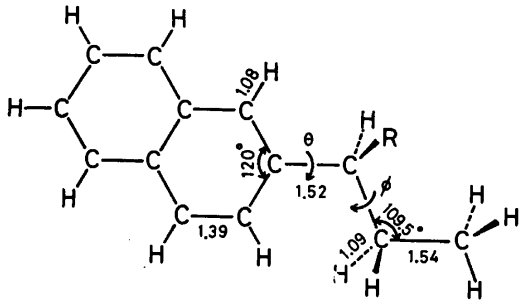

Fig. 1. Structural parameters of 1-(2-naphthyl)propane (R=H) and 2-(2-naphthyl)butane (R=CH_3).

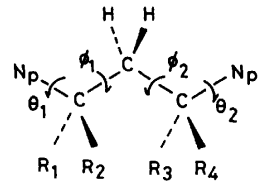

tt

Fig. 2. Dinaphthylalkanes in the *tt* conformation. 1,3-DNPr: (R_1=H, R_2=H, R_3=H, R_4=H), 1,3-DNBu: (R_1=H, R_2=H, R_3=CH_3, R_4=H), 2,4-DNPe(*meso*): (R_1=CH_3, R_2=H, R_3=CH_3, R_4=H), 2,4-DNPe(*rac*): (R_1=H, R_2=CH_3, R_3=CH_3, R_4=H). N_P=2-naphthyl.

compounds used in this study. For example, the *tt* conformation of 2,4-DNPe(*meso*), which is situated at (ϕ_1, ϕ_2)=(0°, 0°), represents the conformation in which two naphthalene units are extended at the ends of trimethylene chain as shown in Fig. 2, but this does not mean the planar zigzag conformation of the five skeletal carbon atoms.

Conformation maps should be drawn as a function of four angles: θ_1, ϕ_1, ϕ_2, and θ_2. But, in order to make the survey easier for the energy maps, they are drawn as a function of skeletal bond rotations ϕ_1 and ϕ_2. The other rotational angles, θ_1 and θ_2, are fixed on the angles to give a minimum energy at the most stable position of ϕ_1 and ϕ_2. For some specific region on the energy maps, the conformational energy is calculated as a function of all four angles, and the minimum energy was adopted. With the rotation of the skeletal angles, several stable conformations appear on the conformation maps. The fraction of i-th conformation f_i is calculated on the assumption that the distribution of conformations obeys the Boltzmann distribution including a weighting factor W_i,

$$f_i = \{W_i \exp(-E_i/RT)\}/\sum_i W_i \exp(-E_i/RT),$$

where E_i is the minimized potential energy for i-th conformation. The weighting factor is estimated by the 2-dimensional local energy maps for the rotation angles (θ_1, ϕ_1) and (θ_2, ϕ_2); here the values of one angle set are varied, holding the angles of the other set constant at the minimum position of the energy. In their local energy maps, the area surrounded by the contour which is 2.1 kJ/mol higher than the energy of each minimum is measured, and the weighting factor is calculated by $W_i=w_{1,i}\times w_{2,i}$, where $w_{1,i}$ and $w_{2,i}$ are proportional to calculated areas on the local energy maps for (θ_1, ϕ_1) and (θ_2, ϕ_2), respectively, corresponding to i-th conformation.

Conformational Energies

The calculation is carried out at first for 1-(2-naphthyl)propane (R=H in Fig. 1) and 2-(2-naphthyl)-butane (R=CH_3 in Fig. 1) which are the model compounds corresponding to the monomer units of dinaphthylalkanes. Conformational energy maps for these compounds are shown in Figs. 3 and 4, where

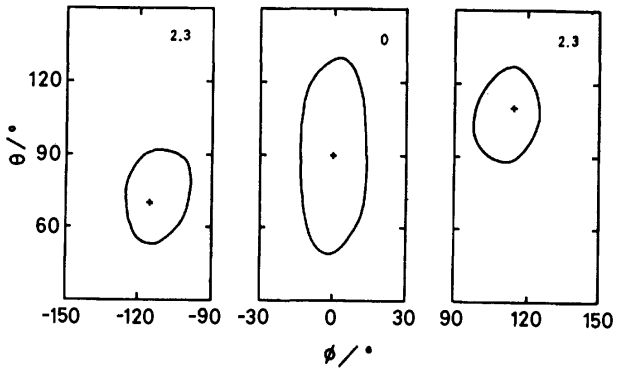

Fig. 3. Conformational energy maps of 1-(2-naphthyl)-propane. The energy minima are marked by+signs. The contour lines indicate the 2.1 kJ/mol higher energies than each minimum. Numerals in the figures show the potential energy at the minimum position in the unit of kJ/mol.

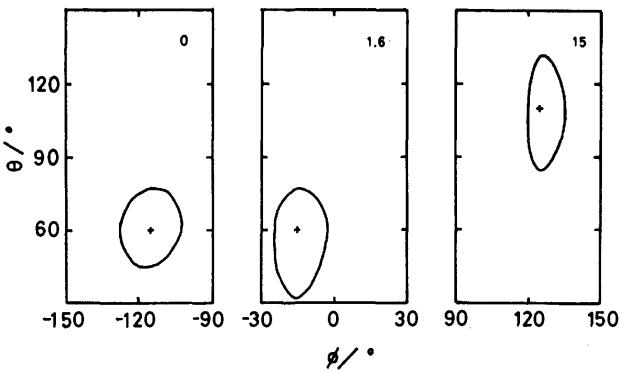

Fig. 4. Conformational energy maps of 2-(2-naphthyl)-butane.

the potential energies are calculated at intervals of 5° for each rotation angle. For 1-(2-naphthyl)propane, the potential minima are situated at (θ, ϕ)=(90°, 0°), (70°, −115°), and (110°, 115°). The potential minima for 2-(2-naphthyl)butane are found at (θ, ϕ)=(60°, −15°), (60°, −115°), and (110°, 125°). The stable conformations considerably deviate from the *trans* or *gauche* positions, owing to the repulsion between the methyl and naphthyl groups. The areas surrounded by the contour for each energy minimum differ significantly. The areas for the *trans* conformations are larger than that for *gauche* conformation; they are about 2.4 times or 1.2 times larger than the other potential

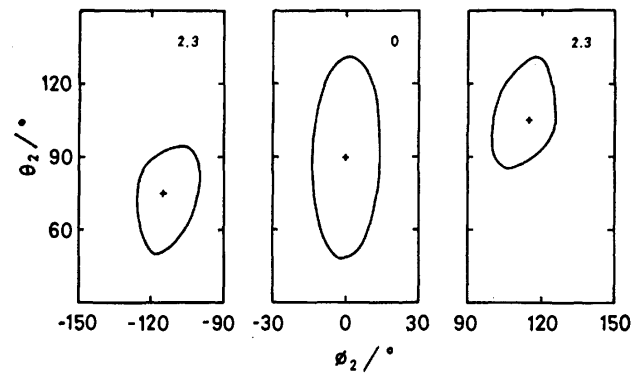

Fig. 5. Conformational energy maps of 1,3-DNPr as a function of θ_2 and ϕ_2, where θ_1 and ϕ_1 are fixed at *trans* position ($\theta_1=90°$, $\phi_1=0°$). Notations of the contour lines and numerals are the same as Fig. 3.

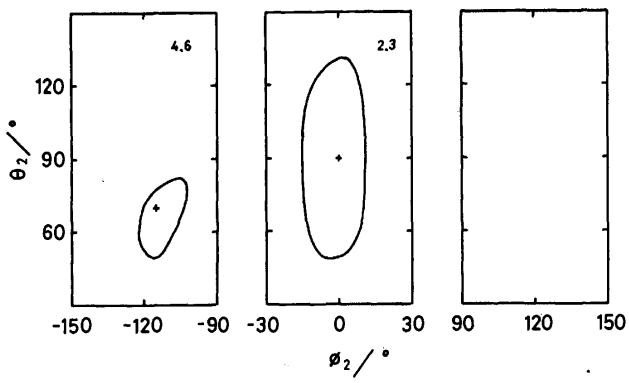

Fig. 6. Conformational energy maps of 1,3-DNPr as a function of θ_2 and ϕ_2, where θ_1 and ϕ_1 are fixed at *gauche* position ($\theta_1=70°$, $\phi_1=-115°$). Notations of the contour lines and numerals are the same as Fig. 3.

minima of 1-(2-naphthyl)propane or 2-(2-naphthyl)-butane, respectively. This must be reflected in the calculation of the fraction of each conformation. Next, the local energy maps as a function of θ_2 and ϕ_2 for the dimer compounds were calculated; in this calculations the angles θ_1 and ϕ_1 are held at the values obtained by the calculation for the monomeric model compounds. The local maps for 1,3-DNPr are shown in Figs. 5 and 6. The energy maps were calculated once more, by changing the rotational angle set to θ_1 and ϕ_1 and holding θ_2 and ϕ_2 to the minimum positions obtained on the previous maps. These procedures are repeated until the minimum position becomes consistent with that obtained on the previous map. For each stable conformation, the angles, minimized potential energy, weighting factor, and fraction of the conformation at 25 °C are listed in Tables 1, 2, and 3.

For 1,3-DNPr, the conformational energy map as a function of skeletal bond rotations, ϕ_1 and ϕ_2, is shown in Fig. 7, where the angles, θ_1 and θ_2 are fixed at $\theta_1=90°$ and $\theta_2=90°$. In this figure, a minimum position (*tt*) is marked by the symbol +, and the excimer conformations (g^+g^- and g^-g^+) are represented by the symbol ●. The most stable conformation is situated at *tt*, and is surrounded by four equivalent *tg* conformations. The potential energy of *tg* conformation is *ca.* 2.1 kJ/mol higher than that of *tt*. The minimized energy by the rotation of all angles at the important region of Fig. 7 is calculated. This result indicates that the barrier energies corresponding to the transitions of $tt \rightleftarrows tg$ and $tt \rightleftarrows g^+g^-$ ($tt \rightleftarrows g^-g^+$) are about 15 kJ/mol and 29 kJ/mol, respectively. These potential energies are caused mainly by the intrinsic torsional energies.

For 1,3-DNBu, the conformational energy map is shown in Fig. 8. The fixed angles θ_1 and θ_2 are chosen to be $\theta_1=90°$ and $\theta_2=120°$ for 1- and 3-naphthyl groups according to the result obtained from the local potential maps. The most stable conformation is found at tg^+, and metastable conformations appear at *tt*, g^-t, and g^+g^+. The barrier energy corresponding to the transition of $tt \rightleftarrows tg^+$ and $tt \rightleftarrows g^-g^+$ has the same values as that for 1,3-DNPr.

For 2,4-DNPe, conformational energy maps are shown

Table 1. Conformational energies and fractions of stable conformations in 1,3-DNPr

	θ_1/°	ϕ_1/°	ϕ_2/°	θ_2/°	W_i[a)]	E_i / kJ mol^{-1}	f_i
tt	90	0	0	90	22	0	0.57
tg^+	90	0	115	105	10	2.3	0.10
tg^-	90	0	−115	75	10	2.3	0.10
g^+t	105	115	0	90	10	2.3	0.10
g^-t	75	−115	0	90	10	2.3	0.10
g^+g^+	110	115	115	110	1	4.6	0.01
g^-g^-	70	−115	−115	70	1	4.6	0.01

a) Weighting factors are given by the areas relative to the smallest one among the conformations.

Table 2. Conformational energies and fractions of stable conformations in 1,3-DNBu

	θ_1/°	ϕ_1/°	ϕ_2/°	θ_2/°	W_i[a)]	E_i / kJ mol^{-1}	f_i
tt	90	0	15	120	5.0	1.3	0.35
tg^+	90	0	115	120	4.7	0	0.56
tg^-	90	5	−125	70	3.0	15	0.0
g^-t	70	−110	15	120	2.0	4.6	0.04
g^+g^+	110	115	115	120	1.0	2.1	0.05

a) Weighting factors are given by the areas relative to the smallest one among the conformations.

Table 3. Conformational energies and fractions of stable conformations in 2,4-DNPe

	θ_1/°	ϕ_1/°	ϕ_2/°	θ_2/°	W_i[a)]	E_i / kJ mol^{-1}	f_i
meso							
tg^+	−120	−15	115	−120	4.4	0	0.49
g^-t	−120	−115	15	−120	4.4	0	0.49
g^-g^+	−120	−105	100	−120	1.0	4.6	0.02
racemo							
tt	−60	15	15	120	1.4	4.6	0.18
g^+g^+	−60	115	115	120	1.0	0	0.82

a) Weighting factors are given by the areas relative to the smallest one among the conformations.

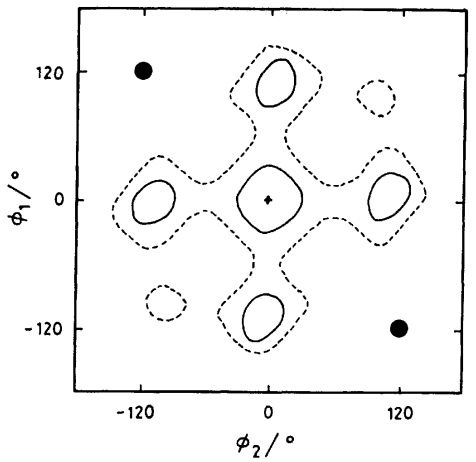

Fig. 7. Conformational energy map of 1,3-DNPr as a function of ϕ_1 and ϕ_2. The rotational angles of naphthalene units, θ_1 and θ_2 are fixed at $\theta_1=\theta_2=90°$. The most stable position and the excimer conformations are marked by the signs, + and ●, respectively. Solid lines indicate the 8.5 kJ/mol higher energy than the minimum. Broken lines show the 17 kJ/mol higher energy than the minimum.

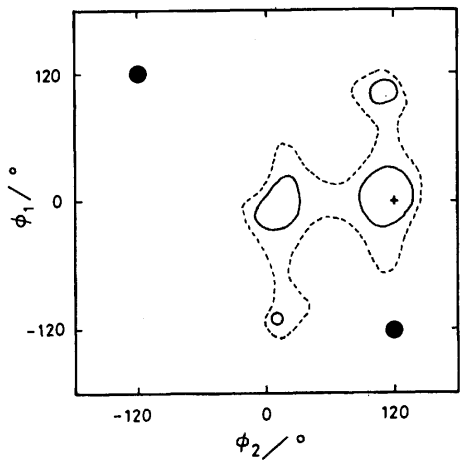

Fig. 8. Conformational energy map of 1,3-DNBu as a function of ϕ_1 and ϕ_2. The rotational angles of naphthalene units, θ_1 and θ_2 are fixed at $\theta_1=90°$, $\theta_2=120°$. Notations of the signs and lines are the same as Fig. 7.

in Fig. 9 for *meso* isomer and in Fig. 10 for *racemo* isomer. In these compounds, most of the conformations are unstable due to the steric hindrance of methyl substituents. Only two conformations are allowed: tg^+ and g^-t conformations for *meso* isomer, tt and g^+g^+ conformations for *racemo* isomer. In Fig. 9, a third potential minimum is observed besides the excimer conformation, g^-g^+, but its fraction is so small, as shown in Table 3, that it can be neglected.

Discussion

All rate constants in the photophysical kinetic scheme were reported in the previous paper. The observed excimer formation rate constant k_{21}, is shown again in Table 4. The values of k_{21} are much different for each

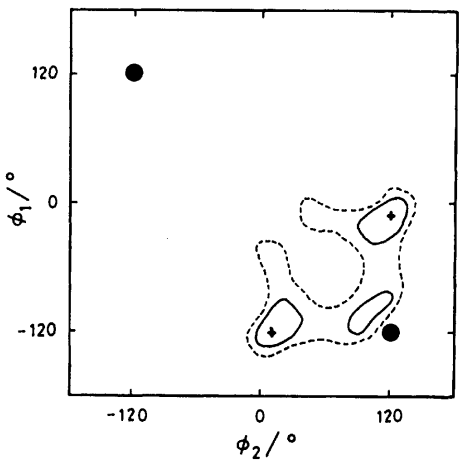

Fig. 9. Conformational energy map of 2,4-DNPe(*meso*). The rotational angles, θ_1 and θ_2 are fixed at $\theta_1=-120°$, $\theta_2=-120°$. Notations of the signs and lines are the same as Fig. 7.

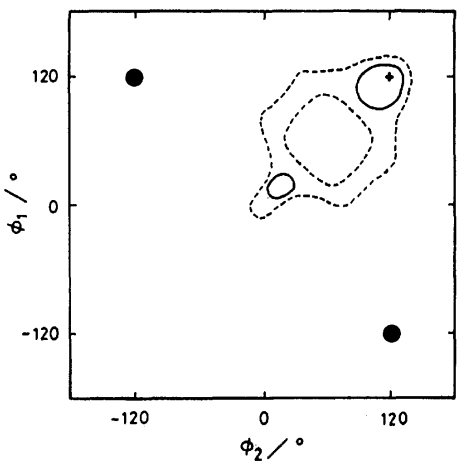

Fig. 10. Conformational energy map of 2,4-DNPe(*rac*). The rotational angles, θ_1 and θ_2 are fixed at $\theta_1=-60°$, $\theta_2=120°$. Notations of the signs and lines are the same as Fig. 7.

Table 4. Intramolecular excimer formation rate constants and their activation energies

	$k_{21}/10^7$ s^{-1}			
T/°C	1,3-DNPr	1,3-DNBu	2,4-DNPe	
			(*meso*)	(*rac*)
50	—	—	—	17
25	21	28	79	8.7
0	12	17	41	3.6
−2	4.8	7.0	17	—
−40	1.9	2.6	7.8	—
−60	0.7	1.0	3.3	—
E_a/kJ mol^{-1}	21	22	20	23

compound. In order to discuss the relationship between the excimer formation rate constants and the configuration of the compounds, it is necessary to follow the pathway of conformational changes on the potential

energy map for each compound.

In the ground state, the excimer conformation marked by ● is one of the unstable conformations, because of the steric hindrance of naphthalene units. However, in the excited state, this conformation is stabilized by the electronic interactions between two naphthalene units. The enthalpy change due to excimer formation is found to be *ca.* 19 kJ/mol for the intermolecular excimer formation in THF. This electronic interaction acts mainly in the parallel alignment of two naphthalene units.

The investigations on various dinaphthylalkanes have demonstrated the strict geometrical requirements for the attractive interaction in naphthalene chromophores.[3,13] The initial distribution of the molecular conformations at the instant of photo-excitation is the same as that in the ground state, and conformational relaxation to the excimer state occurs from the initial distribution. In the low temperature region, where the molecular motion is frozen, there is no indication of specific interaction between naphthalene chromophores. Hence, the relaxation processes will be discussed hereinafter on the assumption that there is no attractive interaction between two naphthalene units except in the excimer state.

For 1,3-DNPr, the conformational energy map shows that the *tt* position (0°, 0°) is the stable conformation where the naphthalene units are furthest apart from each other. Two excimer conformations, g^+g^- (g^-g^+), are equivalent in this compound. As for the pathway to the excimer conformations, the direct conformational changes from *tt* to g^+g^- (g^-g^+), are unfavorable, since such transitions require the co-operative motion of two rotational angles, ϕ_1 and ϕ_2; the calculated barrier energy is found to be 29 kJ/mol. This barrier comes from the intrinsic torsional potential. This value is higher than the activation energy observed for the excimer formation process: *ca.* 21 kJ/mol. Therefore, in order to reach the excimer conformations, it is necessary to pass through the *tg* conformations which are neighbors with both the stable *tt* and the excimer conformations. For the fraction of the *tg* conformation, a fairly large value is obtained: 0.4. The barrier energy for the conformational change from *tt* to *tg* is found to be 15 kJ/mol, and this value is sufficiently smaller than the observed activation energy of excimer formation. Hence, the appearance of *tg* conformations under the equilibrium, $tt \rightleftarrows tg$, contributes to the intramolecular excimer formation in 1,3-DNPr. The *tg* conformation can be considered as a precursory conformation of the intramolecular excimers.

For 1,3-DNBu, the energy map indicates that the most stable conformation is tg^+, which corresponds to the planar conformation of skeletal carbon atoms. The minimized energy for the *tt* conformation is 1.3 kJ/mol higher than that of lowest conformation *tg*, and the barrier energy for the transition from the *tt* conformation to the excimer state is the same as that of 1,3-DNPr: 29 kJ/mol. The fractions of the other conformations, except for tg^+ and *tt*, are negligibly small owing to the steric hindrance of the methyl substituent. In this compound, two excimer conformations, g^+g^- and g^-g^+ are not equivalent. The g^+g^- conformation which lies in the upper left-hand corner in Fig. 8, is unable to become an excimer site, since there is no available adjacent conformation to the excimer one. The intramolecular excimers in 1,3-DNBu, therefore, are formed at the g^-g^+ conformation. The sum of fractions for tg^+ and g^-t which are neighbors with the excimer site, is found to be 0.6. This predicts a larger excimer formation rate constant for 1,3-DNBu than that for 1,3-DNPr.

For 2,4-DNPe(*meso*), the calculation shows three potential minimum: tg^+ of lowest energy, its mirror image g^-t, and g^-g^+, which corresponds to the excimer conformation. Fractions of other conformations are rather small. The distribution is found predominantly in the tg^+ and g^-t forms, which are adjacent conformations to the excimer one, g^-g^+. There is a little fraction for the excimer conformation, g^-g^+ in the ground state. This rotational isomer was also found in the calculations of *meso*-2,4-diphenylpentane and its derivatives.[14,15] The fraction of this g^-g^+ conformation has been reported to be a few percent by NMR spectroscopy.[16] In this calculation, it was estimated to be 1—2% at 25 °C. If an appreciable fraction of 2,4-DNPe(*meso*) takes this conformation, a large component of excimer emission, rising immediately after the excitation pulse, should be observed in the time-resolving measurements. However, such a fast-rise component cannot be observed at all. Efficient intramolecular excimer formation is expected for 2,4-DNPe(*meso*), since a large portion of the molecules takes the adjacent conformations to the excimer state, g^-g^+. The other excimer conformation, g^+g^- can be neglected, because it has no available conformation for the excimer formation. Moreover, there is a steric hindrance between the two methyl substituents at this excimer state, g^+g^-.

The calculation for the three compounds: 1,3-DNPr, 1,3-DNBu, and 2,4-DNPe(*meso*), indicates that the intramolecular excimers are formed by the internal

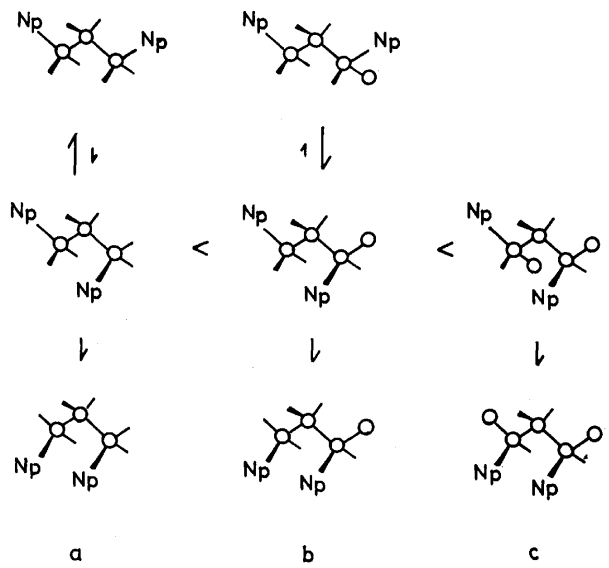

Fig. 11. Schematic illustration of excimer formation processes in dinaphthylalkanes. (a): 1,3-DNPr, (b) 1,3-DNBu, and (c) 2,4-DNPe(*meso*). N_P=2-naphthyl.

rotation, *trans*→*gauche* from the tg^+ or g^-t conformations, as shown in Fig. 11. Since the activation energies for the excimer formation processes are almost the same, the difference between the rate constants of the excimer formation is due to the frequency factors of their rate constants. These factors should be proportional to the fraction of the adjacent conformations, tg^+ and g^-t, if the intramolecular excimers are formed by the same rotational mode. Calculated fractions are 0.4 for 1,3-DNPr, 0.6 for 1,3-DNBu, and 0.98 for 2,4-DNPe(*meso*). These values are consistent with the results of excimer formation rate constants obtained experimentally: 2.1×10^8 s^{-1} for 1,3-DNPr, 2.8×10^8 s^{-1} for 1,3-DNBu, and 7.9×10^8 s^{-1} for 2,4-DNPe(*meso*). The somewhat larger value of 2,4-DNPe(*meso*) than that expected by the calculation may come from the existence of the metastable g^-g^+ conformation in the ground state, which slightly lowers the activation energy for the excimer formation process.

For 2,4-DNPe(*rac*), the situation is much different from that described above. Calculations reveal the lowest energy for the g^+g^+ form, which corresponds to the planar *trans* conformation of the skeletal five carbon atoms, and which is also a neighbor with the excimer conformation. However, the internal rotations, $g^+g^+\rightleftarrows g^+g^-$ ($g^+g^+\rightleftarrows g^-g^+$) are required for the excimer formation. This transition is a different type of rotation from that of the other three compounds. It is known that the barrier to the interconversion of *gauche* forms, $g^+\rightleftarrows g^-$ is higher than that between *t* and *g* forms; the barrier energy has been reported to be *ca.* 27 kJ/mol.[17] On the route to the excimer state, it is also possible to take the tg^+ (g^+t) conformations. But these conformations are unstable because of the steric hindrance, and the imposed energy is 13—17 kJ/mol.[16] Moreover, the *trans*→*gauche* transition to the excimer conformation ($tg^+\rightarrow g^-g^+$ or $g^+t\rightarrow g^+g^-$) becomes a $g^+\rightleftarrows g^-$ transition with reference to the methyl groups. Thus, for 2,4-DNPe(*rac*), the interconversion $g^+\rightleftarrows g^-$ is necessary in the case of either rotation in order to reach the excimer site. The small value of the formation rate constant ($8.7\times10^7\,s^{-1}$) and the somewhat higher activation energy (23 kJ/mol) obtained for this compound is not determined by the fraction of the adjacent conformation but by the different transition mode of the internal rotation.

Our calculation did not include the interaction energy in the electronically excited state. However, the rate of intramolecular excimer formation can be interpreted reasonably by this conformational analysis. The agreement between the observed rate constants and the results of calculations indicates that the formation of intramolecular excimers are determined by the internal rotation, *trans*→*gauche*, and that the fraction of the *tg* conformation, which is an adjacent conformation to the excimer one, serves as an effective concentration in the intramolecular reaction.

References

1) F. Hirayama, *J. Chem. Phys.*, **42**, 3163 (1965).
2) J. W. Longworth and F. A. Bovey, *Biopolymers*, **4**, 1115 (1966).
3) E. A. Chandross and C. J. Dempster, *J. Am. Chem. Soc.*, **92**, 3586 (1970).
4) W. Klöpffer, *Ber. Bunsenges. Phys. Chem.*, **74**, 693 (1970).
5) R. S. Davidson and T. D. Whelan, *J. Chem. Soc., Chem. Commun.*, **1977**, 361.
6) L. Bokobza, B. Jasse, and L. Monnerie, *Eur. Polym. J.*, **13**, 921 (1977).
7) M. Goldenberg, J. Emert, and H. Morawetz, *J. Am. Chem. Soc.*, **100**, 7171 (1978).
8) S. Ito, M. Yamamoto, and Y. Nishijima, *Bull. Chem. Soc. Jpn.*, **54**, 35 (1981).
9) T. Kanaya, Y. Hatano, M. Yamamoto, and Y. Nishijima, *Bull. Chem. Soc. Jpn.*, **52**, 2079 (1979).
10) D. A. Brant and P. J. Flory, *J. Am. Chem. Soc.*, **87**, 2791 (1965).
11) A. Abe, R. L. Jernigan, and P. J. Flory, *J. Am. Chem. Soc.*, **88**, 631 (1966).
12) D. Y. Yoon, P. R. Sundararajan, and P. J. Flory, *Macromolecules*, **8**, 776 (1975).
13) S. Ito, M. Yamamoto, and Y. Nishijima, *Rep. Prog. Polym. Phys. Jpn.*, **22**, 453 (1979).
14) S. Gorin and L. Monnerie, *J. Chim. Phys. Phys.-Chim. Biol.*, **67**, 869 (1970).
15) B. Froelich, B. Jasse, C. Noel, and L. Monnerie, *J. Chem. Soc., Faraday Trans. 2*, **74**, 445 (1978).
16) T. Moritani and Y. Fujiwara, *J. Chem. Phys.*, **59**, 1175 (1973).
17) J. E. Piercy and M. G. S. Rao, *J. Chem. Phys.*, **46**, 3951 (1967).

 © 1982 The Chemical Society of Japan Bull. Chem. Soc. Jpn., 55, 369—373 (1982)

Synthesis, Electrical Resistivities, and Electronic Reflection Spectra of Alkaline-earth Metal Cation-TCNQ-Crown Ether Complexes

Tsuruyoshi MATSUMOTO, Takashi NOGAMI,* Hidekazu TANAKA, and Hiroshi MIKAWA

Department of Applied Chemistry, Faculty of Engineering, Osaka University, Yamada-oka, Suita, Osaka 565

(Received May 6, 1981)

Two types of alkaline-earth metal cation–TCNQ–crown ether complexes were synthesized: one is the simple salt, expressed as $[M^{2+}(TCNQ^-)_2]_m$(crown ether)$_n$ and the other is the complex salt expressed as $[M^{2+}(TCNQ^-)_2]_m(TCNQ)_n$(crown ether)$_t$. The electrical resistivities of the complexes were measured for compacted samples and single crystals. The resistivities of the simple salts were greater than 10^5 Ω cm, so they are much less conductive than the original TCNQ salts, $M^{2+}(TCNQ^-)_2$. Most of the complex salts were more conductive than the original TCNQ salts, with the resistivities of 4—10^3 Ω cm.

The studies on the electrical conductivities of 7,7,8,8-tetracyanoquinodimethan (TCNQ) complexes have clarified that the mixed valent complex is more conductive than the other type complex which does not contain neutral TCNQ.[1] Many metal-cation TCNQ salts have been synthesized. However, most of them are simple salts, expressable as $M^{m+}(TCNQ^-)_m$.[2] Therefore, we can not expect high conductivity.[3] Even if we try to synthesize a complex salt, $M^{m+}(TCNQ^-)_m(TCNQ)_n$, from a solution by the reaction of a simple salt with neutral TCNQ, the simple salt only crystallizes out because of its poor solubility. We noticed that a series of macrocyclic polyethers called crown ethers have a specific property of accepting metal cations into their cavities and thereby of solubilizing many inorganic salts into organic solvents like benzene.[4] We thought that a simple salt solubilized by using crown ether would complex with neutral TCNQ in solution to produce complex salt. In fact, we could obtain several complex salts, as well as simple salts, in the case of alkali-metal cation–TCNQ–crown ether complexes.[5] Comparing the conductivities of the complexes thus obtained with those of the original TCNQ salts, we found comparable conductivities. This fact will be explained as follows. Although the introduction of the crown ether has a negative effect on the conductivity by the steric hindrance, the complex salt formation has a positive effect on the conductivity. Thus, compensation of the two effects resulted in the same order of magnitude of the conductivity in the case of the alkali-metal cation complex. We thought that the former negative effect could be overcome by using the multi-valent cation TCNQ salts. One metal-cation accompanies more than one TCNQ molecule in this case; this may result in a closer distance between TCNQ molecules as compared with the spacing in the alkali-metal cation complex. So we synthesized alkaline-earth metal cation–TCNQ–crown ether complexes, and measured the electrical resistivities of the compacted samples and two single crystals in expectation of achieving highly conductive materials. We also measured the electronic diffuse reflection spectra of the new complexes in order to know the electronic interaction between TCNQ molecules in the solid-state.

Experimental

Materials. Alkaline-earth metal–TCNQ salts were synthesized according to the reported procedures.[6] All the crown ethers were purchased from Nakarai Chemicals, Ltd.

Synthesis of Cation–TCNQ–Crown Ether Complexes. Simple salts, $[M^{2+}(TCNQ^-)_2]_m$(crown ether)$_n$, were synthesized by the reaction of the original $M^{2+}(TCNQ^-)_2$ with a crown ether in methanol. Complex salts, $[M^{2+}(TCNQ^-)_2]_m(TCNQ)_n$(crown ether)$_t$, were synthesized either by the reaction of a simple salt with neutral TCNQ or by the reaction of $M^{2+}(TCNQ^-)_2$, crown ether and neutral TCNQ in organic solvent. The details of the synthesis were described before.[5]

Electrical Resistivity Measurements. Electrical resistivity in the compacted sample was measured by the same procedures as described before.[5] The electrical resistivity of the single crystal was measured by a four probe method, and the temperature was regulated by type-D Cryomini refrigerator (Osaka Sanso Co., Ltd).

Electronic Diffuse Reflection Spectra. Electronic diffuse reflection spectra of the complexes were measured by a Hitachi 340 Recording Spectrophotometer. The sample was smeared onto a filter paper. The reflected light was collected by integrating over a sphere.

Results and Discussion

Isolation of Alkaline-earth Metal Cation–TCNQ–Crown Ether Complexes. The following crown ethers and TCNQ salts were used for the preparation of the complexes: 12-crown-4,15-crown-5, 18-crown-6, perhydrobenzo[*b*,*k*][1,4,7,10,13,16]hexaoxacyclooctadecane

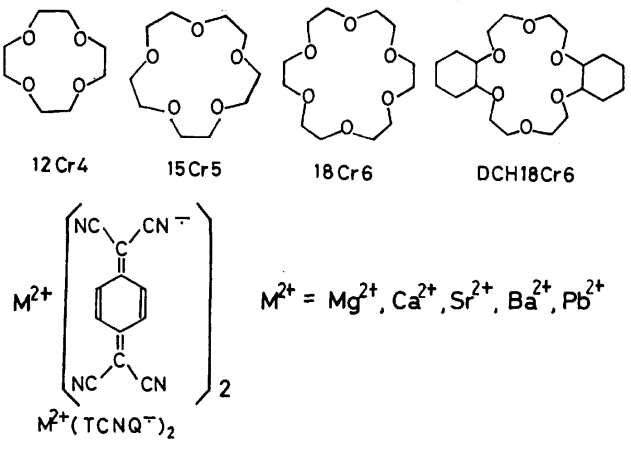

(usually called as "dicyclohexy-18-crown-6"), $Mg^{2+}(TCNQ^-)_2 6H_2O$, $Ca^{2+}(TCNQ^-)_2$, $Sr^{2+}(TCNQ^-)_2$, $Ba^{2+}(TCNQ^-)_2$, and $Pb^{2+}(TCNQ^-)_2\ 1.5H_2O$, the molecular structures of which are shown above. In the above figure, the abbreviations of Cr, and DCH mean crown ether, and bis(perhydrobenzo) component, respectively. Thus, DCH18Cr6 denotes "dicyclohexyl-18-crown-6." We have isolated two types of complexes: one is in the simple salts and expressed as $[M^{2+}(TCNQ^-)_2]_m$-(crown ether)$_n$ and the other is in the complex salt and expressed as $[M^{2+}(TCNQ^-)_2]_m$–$(TCNQ)_n$-(crown ether)$_i$. Table 1 summarizes the complexes isolated and their yields, melting points, analytical data, and appearences and colors. As expected, the stoichiometry of the simple salt has a tendency for the crown ether with a cavity comparable to or larger than the cation size to have a one-to-one stoichiometry, while the crown ether with a cavity smaller than the cation size has a two-to-one stoichiometry arising from the cation being sandwiched by crown ethers.[7] The stoichiometries of most of the complex salts are derived from the simple salts plus one molecule of neutral TCNQ. However, the complex salts, including DCH18Cr6, have two molecules of neutral TCNQ. In general, the solubility becomes low when a simple salt complexes with neutral TCNQ. Because the solubilities of DCH18Cr6 complexes are higher than those of the other crown ether complexes, the complex salt of DCH18Cr6 does not crystallize out from the solution until two molecules of neutral TCNQ complex with one simple salt. Some of the magnesium complexes contained water of crystallization. A variety of crystal colors (violet, green, yellow green, or purple) were found in the simple salts; these resulted from the

TABLE 1. ALKALINE-EARTH METAL CATION–TCNQ–CROWN ETHER COMPLEXES

Complex	Yield[a] %	Mp θ_m/°C	Found (Calcd) (%) C	H	N	Description[b]
Simple salts						
$Mg^{2+}(TCNQ^-)_2(15Cr5)_2 2H_2O$	11	169—170	58.74 (58.12)	5.59 (5.76)	12.34 (12.32)	violet plate
$Mg^{2+}(TCNQ^-)_2(18Cr6)$		239—240	62.00 (62.04)	4.57 (4.63)	16.18 (16.08)	purple needle
$Ca^{2+}(TCNQ^-)_2(12Cr4)_2$		100	59.33 (59.99)	4.98 (5.03)	14.07 (13.99)	violet needle
$Sr^{2+}(TCNQ^-)_2(15Cr5)_2$	30	242—245	56.50 (56.43)	5.21 (5.17)	11.89 (11.96)	dark green microcrystal
$Ba^{2+}(TCNQ^-)_2(15Cr5)_2$	36	249—250	53.43 (53.58)	5.09 (4.91)	11.42 (11.36)	dark green microcrystal
$Ba^{2+}(TCNQ^-)_2(18Cr6)$	33	220—221	52.73 (53.38)	4.04 (3.98)	13.70 (13.83)	violet plate
$Pb^{2+}(TCNQ^-)_2(15Cr5)_2$	35	265—270	50.05 (50.04)	4.59 (4.58)	10.66 (10.61)	yellow-green microcrystal
Complex salts						
$Mg^{2+}(TCNQ^-)_2TCNQ(12Cr4)_2$	47	>300	62.40 (63.13)	4.45 (4.48)	17.09 (16.99)	plate
$[Mg^{2+}(TCNQ^-)_2TCNQ]_2(15Cr5)_3 2H_2O$		>300	62.65 (62.16)	4.40 (4.50)	17.17 (17.05)	needle
$Ca^{2+}(TCNQ^-)_2TCNQ(12Cr4)_2$	21	240—245	62.09 (62.14)	4.31 (4.41)	17.44 (16.72)	microcrystal
$Ca^{2+}(TCNQ^-)_2TCNQ(15Cr5)_2$	41	>300	61.78 (62.14)	4.65 (4.41)	16.47 (16.72)	long thin plate
$Ca^{2+}(TCNQ^-)_2TCNQ(18Cr6)$	53	>300	61.61 (62.87)	3.98 (3.96)	17.88 (18.33)	long thin plate
$Ca^{2+}(TCNQ^-)_2(TCNQ)_2(DCH18Cr6)$	34	234—235	66.13 (66.44)	4.35 (4.26)	18.04 (18.23)	needle
$Sr^{2+}(TCNQ^-)_2TCNQ(15Cr5)_2$	59	250—257	58.92 (58.97)	4.57 (4.59)	14.97 (14.73)	needle
$Sr^{2+}(TCNQ^-)_2TCNQ(18Cr6)$	20	195—200	59.64 (59.77)	3.51 (3.76)	17.53 (17.43)	long thin plate
$Ba^{2+}(TCNQ^-)_2TCNQ(12Cr4)_2$		215—216	56.01 (56.66)	4.49 (4.02)	15.08 (15.25)	plate
$Ba^{2+}(TCNQ^-)_2TCNQ(15Cr5)_2$	53	234—235	56.48 (56.50)	4.30 (4.40)	14.34 (14.12)	violet needle
$Ba^{2+}(TCNQ^-)_2TCNQ(18Cr6)$	58	261—263	56.47 (56.84)	3.62 (3.77)	16.53 (16.57)	microcrystal
$Ba^{2+}(TCNQ^-)_2(TCNQ)_2(DCH18Cr6)$	19	235—236	60.60 (61.57)	3.81 (3.95)	17.09 (16.89)	needle
$Pb^{2+}(TCNQ^-)_2TCNQ(15Cr5)_2$	58	238—240	53.38 (53.37)	4.25 (4.16)	13.75 (13.34)	purple needle

a) Unless specified, the yield is less than 10%. b) The colors of most of the complex-salts were black.

TABLE 2. ELECTRICAL RESISTIVITIES AND ELECTRONIC REFLECTION PEAK POSITIONS OF ALKALINE-EARTH METAL CATION–TCNQ–CROWN ETHER COMPLEXES

Complex	Resistivity[b] / Ω cm	Reflection peak position/10^3 cm^{-1}				
Simple salts						
(1) Violet complex						
$Mg^{2+}(TCNQ^-)_2(15Cr5)_2 2H_2O$		11.1	17.4	24.6		
$Mg^{2+}(TCNQ^-)_2(18Cr6)$						
$Ca^{2+}(TCNQ^-)_2(12Cr4)_2$	2.1×10^5	11.9	17.3	24.2		
$Ba^{2+}(TCNQ^-)_2(18Cr6)$	9.0×10^7	11.7	17.0	24.8		
(2) Green complex						
$Sr^{2+}(TCNQ^-)_2(15Cr5)_2$	7.7×10^8	8.8	11.7	13.4	29.9	
$Ba^{2+}(TCNQ^-)_2(15Cr5)_2$	3.7×10^{10}	8.8	11.7	13.3	29.4	
$Pb^{2+}(TCNQ^-)_2(15Cr5)_2$	5.8×10^6	8.8	11.4	13.5	14.7	29.4
Complex salts[a]						
$Mg^{2+}(TCNQ^-)_2TCNQ(12Cr4)_2$	4.2×10^3					
$[Mg^{2+}(TCNQ^-)_2TCNQ]_2(15Cr5)_3 2H_2O$	86, 4[c]	12.4	17.7	24.7		
$Ca^{2+}(TCNQ^-)_2TCNQ(12Cr4)_2$	38, 10[c]	11.7	17.2	25.0		
$Ca^{2+}(TCNQ^-)_2TCNQ(15Cr5)_2$	4.5×10^2	11.9	17.3	25.7		
$Ca^{2+}(TCNQ^-)_2TCNQ(18Cr6)$	1.8×10^3					
$Ca^{2+}(TCNQ^-)_2(TCNQ)_2(DCH18Cr6)$	1.2×10^3					
$Sr^{2+}(TCNQ^-)_2TCNQ(15Cr5)_2$	6.5×10^3	11.8	16.6	25.0		
$Sr^{2+}(TCNQ^-)_2TCNQ(18Cr6)$	5.1×10^3	12.0	16.3	25.1		
$Ba^{2+}(TCNQ^-)_2TCNQ(12Cr4)_2$	6.4×10^2					
$Ba^{2+}(TCNQ^-)_2TCNQ(15Cr5)_2$	3.5×10^3	11.7	17.3	25.0		
$Ba^{2+}(TCNQ^-)_2TCNQ(18Cr6)$	4.5×10^3	11.8	12.1	17.0	24.4	
$Ba^{2+}(TCNQ^-)_2(TCNQ)_2(DCH18Cr6)$	5.9×10^2	11.8	15.2			
$Pb^{2+}(TCNQ^-)_2TCNQ(15Cr5)_2$	3.2×10^3					

a) Besides these reflection peaks, all the complex-salts have the reflection bands lower than 7×10^3 cm^{-1} ascribable to the charge-transfer transition from $TCNQ^-$ to TCNQ. b) Compacted Sample. c) Single crystal.

differences of the electronic interaction between the TCNQ anion radicals in the solid state. In other words, we can modify the interaction between TCNQ anion radicals in the solid state by introducing the crown ether. The colors of most of the complex salts were black. The melting points of the complexes thus obtained were much lower than those of the original salts, $M^{2+}(TCNQ^-)_2$, which are higher than 300 °C. This fact will result from the much weaker electrostatic attraction between metal cation and $TCNQ^-$; this results in a much smaller Madelung energy than in the cases of the original salts. Unlike the poor solubilities of the original TCNQ salts in the usual organic solvent, the solubilities of the complexes isolated here were large as expected. Their high solubilities in the organic solvents may be useful for practical applications. These complexes were stable in air for several months.

Electrical Resistivities. The electrical resistivities of the simple salts and complex salts were measured for the compressed samples at room temperature. The resistivities of the conductive salts, $Mg^{2+}(TCNQ^-)_2$-$TCNQ(15Cr5)_2 2H_2O$ and $Ca^{2+}(TCNQ^-)_2$ $TCNQ(12Cr4)_2$ were measured for single crystals. Table 2 summarizes the observed results. Table 3 shows the electrical resistivities of the original TCNQ salts, for the sake of comparison. Table 2 shows that the resistivities of the simple salts are greater than 10^5 Ω cm; these salts are thus much less conductive than the original TCNQ salts (see Table 3). On the other hand, the complex salts are much more conductive than the corresponding simple salts, with the electrical resistivities of 4—10^3 Ω cm. Thus, most of the complex salts were more conductive than the original TCNQ salts, which is in line with our expectation. The lowest resistivity (4 Ω cm) was found in $Mg^{2+}(TCNQ^-)_2$ $TCNQ(15Cr5)_2$ $2H_2O$ single crystal at room temperature. The signle crystal of $Ca^{2+}(TCNQ^-)_2$ TCNQ-$(12Cr4)_2$ showed a resistivity of 10 Ω cm at room temperature. The temperature dependence of the electrical resistivity of the former single crystal is shown in Fig. 1.[8] The change of the temperature dependence of the resistivity at 154 K may be caused by a phase transition. The activation energies were 0.06 eV and 0.02 eV at the higher and lower temperature ranges, respectively. The complex, $Ca^{2+}(TCNQ^-)_2TCNQ$-$(12Cr4)_2$, is expected to incorporate another neutral TCNQ in principle, although we could not isolate such a type of complex from the solution. However, we

TABLE 3. THE RESISTIVITIES OF DI-VALENT METAL–TCNQ COMPLEXES

Complex	Resistivities/Ω cm[a]
$Mg^{2+}(TCNQ^-)_2 6H_2O$	5×10^3
$Ca^{2+}(TCNQ^-)_2$	1×10^4
$Sr^{2+}(TCNQ^-)_2$	1×10^3
$Ba^{2+}(TCNQ^-)_2$	8×10^5
$Pb^{2+}(TCNQ^-)_2 1.5H_2O$	2×10^3

a) D. S. Acker, Waynesboro, Va., and D. C. Blomstrom, U. S. Patent 3162641 (1964).

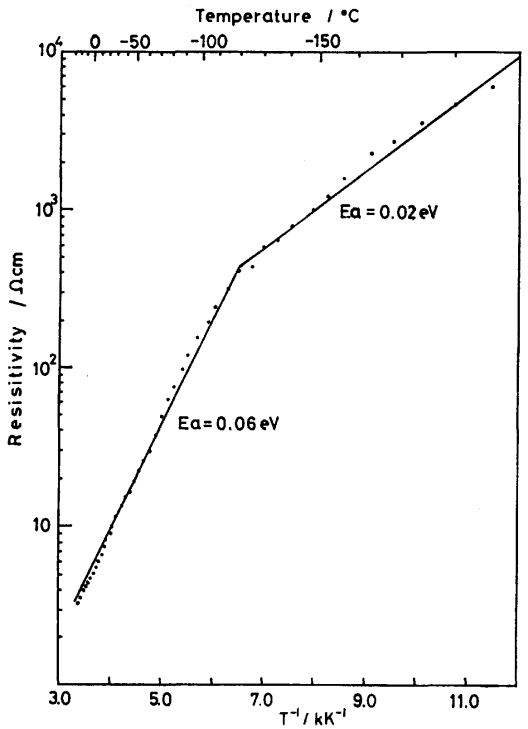

Fig. 1. Temperature dependence of the electrical resistivity of $Mg^{2+}(TCNQ^-)_2$ $TCNQ(15Cr5)_2 2H_2O$ single crystal.

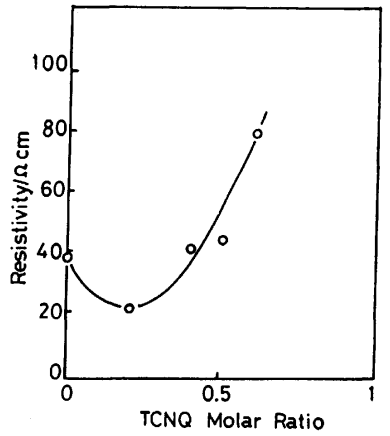

Fig. 2. The plot of the electrical resistivity against the molar fraction of neutral TCNQ added to Ca^{2+}-$(TCNQ^-)_2$ $TCNQ(12Cr4)_2$.

found that the complex salt formation occurs by simply grinding $Ca^{2+}(TCNQ^-)_2TCNQ(12Cr4)_2$ with neutral TCNQ in an agate bowl. Figure 2 shows the plot of the electrical resistivity against the molar fraction of neutral TCNQ added to Ca^{2+} $(TCNQ^-)_2$ TCNQ-$(12Cr4)_2$. This complex had a values of 38 Ω cm for the compacted sample at room temperature. As more and more neutral TCNQ was added to this complex, the resistivity of the complex first decreased down to 20 Ω cm and then increased. The increase of the conductivity in the range of less than 0.2 added TCNQ molar fraction indicates that the solid-state complex-salt formation reaction occurs simply by grinding the original salt with neutral TCNQ in an agate bowl. An analogous reaction was also found in alkali-metal cation-TCNQ–crown ether complex.[5] Thus, the solid-state reaction is characteristic of these crown ether complexes: it is not found in the original TCNQ salts. The fact that the above mentioned 12Cr4 complex is a good conductor suggests that the small crown ether may be an important factor in the high conductivity. But the order of the conductivity of the 12Cr4-complex salts does not correspond to the order of the cation size. Thus, we could not simply correlate the conductivities of the complex-salts with the cation size.[9]

Now, let us compare the electrical resistivities of the complexes isolated here with those of the alkali-metal-TCNQ–crown ether complexes. In the case of the alkali-metal cation complexes, simple salts and complex salts had resistivities of the order of 10^8—10^{14} Ω cm and 10^3—10^4 Ω cm, respectively, On the other hand, in the case of the alkaline-earth metal cation complexes, simple salts and complex salts had resistivities of the order of 10^5—10^{10} Ω cm and 10^0—10^3 Ω cm, respectively. Thus, the alkaline-earth metal cation complexes are much more conductive than the alkali-metal cation complexes both in the simple and complex salts, which is in line with our expectation.

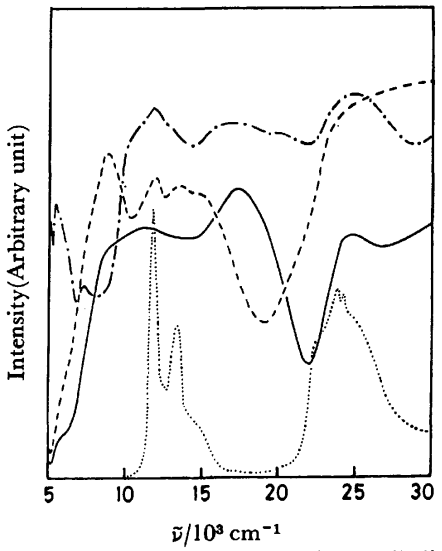

Fig. 3. Diffuse reflection spectra of the alkaline-earth metal cation–TCNQ–crown ether complexes.
——: $Ca^{2+}(TCNQ^-)_2(12Cr4)_2$, ------: $Ba^{2+}(TCNQ^-)_2$-$(15Cr5)_2$, —·—: $Ca^{2+}(TCNQ^-)_2TCNQ(12Cr4)_2$, ……: K^+TCNQ^- in acetonitrile solution.

Electronic Diffuse Reflection Spectra. Electronic diffuse reflection spectra of the complexes were measured at room temperature.[10] Figure 3 shows the spectra of $Ca^{2+}(TCNQ^-)_2(12Cr4)_2$, $Ba^{2+}(TCNQ^-)_2(15Cr5)_2$, and $Ca^{2+}(TCNQ^-)_2$ $TCNQ(12Cr4)_2$ as typical examples. This figure also shows the absorption spectra of K^+-$TCNQ^-$ in acetonitrile solution for the sake of comparison.

All the violet complexes showed two broad absorption peaks at less than 20×10^3 cm^{-1}, like $Ca^{2+}(TCNQ^-)_2$-$(12Cr4)_2$. Although the crystallographic study and polarized absorption measurements are needed for the

assignments of these absorption bands, the most probable assignment of the lowest energy band is the charge-transfer (CT) transition between TCNQ anion radicals, and that of the next band is the local excitation band within $TCNQ^-$.[11] Thus, a TCNQ dimer structure is suggested from the spectra. On the other hand, all the green complexes have the characteristic profiles at 8—15×10^3 cm^{-1} like $Ba^{2+}(TCNQ^-)_2(15Cr5)_2$. In view of the similarity of the spectrum of the green complex to that of K^+TCNQ^- in solution, one possibility is that the $TCNQ^-$ is isolated in the crystal.[12] All the complex salts gave almost the same reflection spectra as $Ca^{2+}(TCNQ^-)_2TCNQ(12Cr4)_2$. The absorption band at less than 7×10^3 cm^{-1} is ascribed to the CT transition from TCNQ anion radical to neutral TCNQ. Table 2 shows the absorption peak positions of the isolated simple and complex salts. Some relation exists between the colors of the simple salts and their resistivities: violet complexes were more conductive than the green ones in the simple salts. If $TCNQ^-$ is isolated in the green complex as discussed above, its poor conductivity can be explained by the small overlap of the π-electron could between adjacent TCNQ molecules.

We are grateful to Miss Junko Maenaka, Mr. Kazuaki Muneishi, and Miss Yuriko Sako, Faculty of Engineering, Osaka University, for the elemental analyses.

References

1) J. B. Torrance, *Acc. Chem. Res.*, **12**, 79 (1979).

2) $Cs_2(TCNQ)_3$ is the exception.

3) Cu TCNQ crystallized electrochemically was reported to be highly conductive (784 $(\Omega\,cm)^{-1}$). This complex was suggested to have the mixed valent structure. See P. Kathirgamanathan and R. Rosseinsky, *J. Chem. Soc., Chem. Commun.*, **1980**, 839.

4) "Synthetic Multidentate Macrocyclic Compounds," ed by R. Izatt and J. J. Christensen, Academic Press, New York (1978).

5) M. Morinaga, T. Nogami, Y. Kanda, and H. Mikawa, *Chem. Lett.*, **1979**, 111; M. Morinaga, T. Nogami, Y. Kanda, T. Matsumoto, K. Matsuoka, and H. Mikawa, *Bull. Chem. Soc. Jpn.*, **53**, 1221 (1980).

6) L. R. Melby, R. J. Harder, W. R. Hertler, M. Mahler, R. E. Benson, and W. E. Mochell, *J. Am. Chem. Soc.*, **84**, 3374 (1962).

7) N. S. Poonia, *J. Am. Chem. Soc.*, **96**, 1012 (1974).

8) Because of the fragility of $Ca^{2+}(TCNQ^-)_2TCNQ(12Cr4)_2$ single crystal, we could not measure the temperature dependence of its resistivity.

9) The resistivity of $Na^+TCNQ^-TCNQ(12Cr4)_2$ was found to be 1.5×10^3 Ω cm.

10) Uncorrected spectra.

11) J. Tanaka, M. Tanaka, T. Kawai, T. Takabe, and O. Maki, *Bull. Chem. Soc. Jpn.*, **49**, 2358 (1976).

12) The reflection spectrum of the green complex may be due to the isolated $TCNQ^-$ in the crystal, shifted about 3×10^3 cm^{-1} to the lower energy side by the crystal field. Another possibility is that the band at 8.85×10^3 cm^{-1} is the CT transition between $TCNQ^-$ molecules and that the bands at 10—15×10^3 cm^{-1} correspond to the isolated $TCNQ^-$.

Dual Fluorescence of Pyrazine Cooled in a Supersonic Free Jet

Naohiko MIKAMI,* Hisao IGARASHI, Koji KAYA,† and Mitsuo ITO
Department of Chemistry, Faculty of Science, Tohoku University, Sendai 980
(Received May 7, 1981)

The fluorescence excitation spectrum of the lowest excited $^1B_{3u}(n\,\pi^*)$ state of pyrazine cooled in a pulsed supersonic free jet was observed. The fluorescence decay of the isolated molecule was also measured in the free jet. The rotationally cooled pyrazine in the collision free condition exhibits extremely large fluorescence quantum yield and dominant slow fluorescence component for low lying vibronic levels. The ratio of the pre-exponential factors of the dual fluorescence decay was examined in terms of the available theory of singlet-triplet mixed state model. It was found that the number of coupled triplet levels obtained from the observed ratio is inconsistent with the calculated excess energy dependence of vibronic density in the triplet state. Remarkable rotational level dependence of the ratio of the pre-exponential factors was observed for the electronic origin, while such a rotational dependence was not found for the lifetime of the slow fluorescence.

The fluorescence decay of low pressure diazabenzene vapor such as pyrazine and pyrimidine is known to be bi-exponential, being composed of a pressure-independent fast decay and of a pressure-sensitive slow one.[1,2] The bi-exponential decay has been explained by a mixed state model proposed by Lahmani *et al.*[3] According to this model, the number of triplet levels coupled to a singlet level plays an important role in decay constant of the slow fluorescence component as well as in the fluorescence quantum yield ratio of the slow and fast components. The experimental results of vibronic energy dependence of the lifetimes and the yield ratio have been found to be in accordance with the prediction based on the model.[1,2] Recently, Baba *et al.*[4] have reported the rotational state dependence of the fluorescence quantum yields for low pressure pyrazine and pyrimidine vapor. The rotational dependence on the nonradiative rate has also been discussed theoretically.[5,6] These studies suggest that critical test of the model should be made for an isolated molecule excited to a particular ro-vibronic state. However, the experimental study under such a critical condition is quite difficult for room temperature vapor of large molecule because of spectral congestion of many rotational levels. Recently, it was shown by many workers[7-11] that the isolated molecule at very low rotational temperature is easily prepared by a supersonic free expansion of the molecule seeded in inert carrier gas. Combining the supersonic free expansion with a narrow band tunable laser, one can study dynamical behaviour of the excited molecule confined in a few ro-vironic level.

In the present study we observed the fluorescence excitation spectrum of the first singlet state of pyrazine ($^1B_{3u}$) in a supersonic free jet seeded in He carrier gas. It was found that the fluorescence quantum yield of the isolated molecule in the jet is extremely large for low-lying vibronic levels compared with the vapor value obtained by extrapolation to zero pressure. The observed lifetimes and the ratio of the pre-exponential factors of a bi-exponential decay were examined in terms of the mixed state model. A remarkable rotational state dependence of the fluorescence decay, which has been observed very recently by ter Horst *et al.*[12] was also found in the present work.

Experimental

Pulsed supersonic free jets of pyrazine seeded in He gas as a carrier were generated by a pulsed supersonic nozzle described in a previous paper.[13] Visible dye laser pumped by a frequency doubled YAG laser (Quanta-Ray), which is synchronized with the pulsed nozzle, was converted to tunable UV light by a SHG crystal (RDP or ADA), phase matching angle of the crystal being controlled by a microcomputer. Cresyle violet+rhodamine B in ethanol solution (650—635 nm) and rhodamine 640 in ethanol solution (640—610 nm) were used. Spectral resolution of the dye laser was about 0.4 and 1.5 cm^{-1} with and without an etalon, respectively. The supersonic free jet was irradiated by the UV light at 15 mm downstream from the nozzle and the fluorescence was observed from the direction perpendicular to the light beam and to the jet stream. By use of several light baffles, scattered light was reduced to the level not to be detected even at a maximum sensitivity of our detection system. The fluorescence was collected by a lens system ($f=2$) and the image of the fluorescent region in the jet was made on a field lens. Unwanted emission from the shock boundaries in the jet was removed by an adjustable mask which was inserted in front of the field lens, and the fluorescence from isentropic core of the jet was focussed on a photomultiplier (Hamamatsu R562) by a lens.

For the measurement of the fluorescence excitation spectrum, the total fluorescence was detected by the photomultiplier combined with a preamplifier (PAR #115) and a boxcar integrator (Brookdeal 9415) with 1.5 μs gate width. The fluorescence intensity was recorded on a strip chart recorder as a function of the exciting wavelength. For lifetime measurement, a sampling oscilloscope (Tektronix 564B) was used instead of the boxcar integrator. In order to ensure the temporal response of the photomultiplier, a high breeder current (≈10 mA) and a 50 Ω load resistance were used; time resolution was not more than 18 ns. In the case of the lifetime measurement, a solid etalon was inserted in the dye laser cavity to improve the spectral resolution for the excitation. The fluorescence spectra were taken by a monochomater (Nikon P-250) and a photon counting system (Ortec #9302, #9315, and #9325) in a gated mode with 3 μs gate width.

Fluorescence quantum yield of pyrazine in the supersonic jet was estimated by comparing the intensity of fluorescence of the 0-0 band excitation with the corresponding intensity of aniline in the jet. Assuming that the fluorescence quantum

† Present address: Department of Chemistry, Faculty of Science and Engineering, Keio Univeristy, Hiyoshi-machi, Kohoku-ku, Yokohama 223.

yield of aniline in the jet is the same as that in vapor at room temperature[14] and taking into account of differences of saturated vapor pressures and integrated absorption coefficients of pyrazine and aniline, the ratio of the fluorescence intensities of two molecules in the jet can be converted into a relative quantum yield of pyrazine with respect to that of aniline.

Results and Discussion

Quantum Yield Spectrum. The fluorescence excitation spectrum of the first excited $^1B_{3u}$ state of pyrazine in a supersonic free jet of helium carrier gas at 4 atm is shown in Fig. 1, together with the room temperature absorption spectrum of pyrazine vapor. The assignments of the vibronic bands were taken from Ref. 15. The band width (FWHM) of the 0-0 band in the supersonic jet was about 4 cm^{-1}, from which the rotational temperature of the molecule was estimated to be less than 5 K.

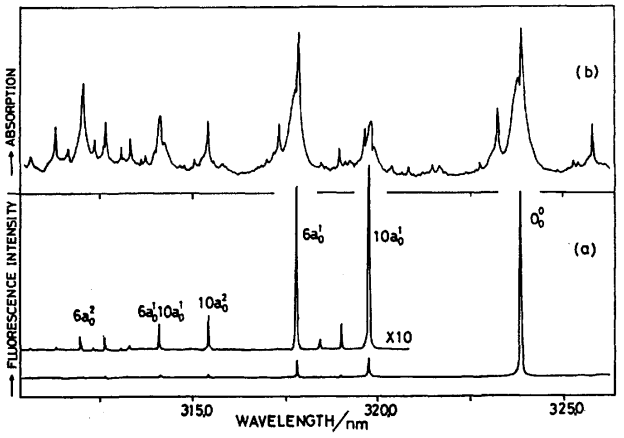

Fig. 1. (a) The excitation spectrum of pyrazine in a supersonic free jet. Saturated vapor of pyrazine at room temperature was seeded in 4 atm He carrier gas. (b) Absorption spectrum in vapor at room temperature.

As is seen from Fig. 1, the excitation spectrum in the free jet shows a rapid decrease of the band intensity with increase of the excess vibrational energy. For example, the 0-0 band is about ten times stronger than that of the $6a^1$ band, while they are comparable in the vapor spectrum. The remarkable difference between the excitation spectrum and the absorption spectrum must be ascribed to a great excitation energy dependence of the fluorescence quantum yield. Although the absorption spectrum of the supersonic jet is not available, it is reasonable to assume that integrated absorption intensities of the individual cold bands in vapor spectrum are proportional to those of the free jet. Since the main cold bands are well isolated in the vapor spectrum, the estimation of their relative integrated intensities should be made with a good accuracy. Using the fluorescence quantum yield of the zero point level obtained by the procedure described in the previous section, we have a quantum yield spectrum of the free jet, which is shown in Fig. 2. The quantum yields of the main vibronic levels are also listed in Table 1.

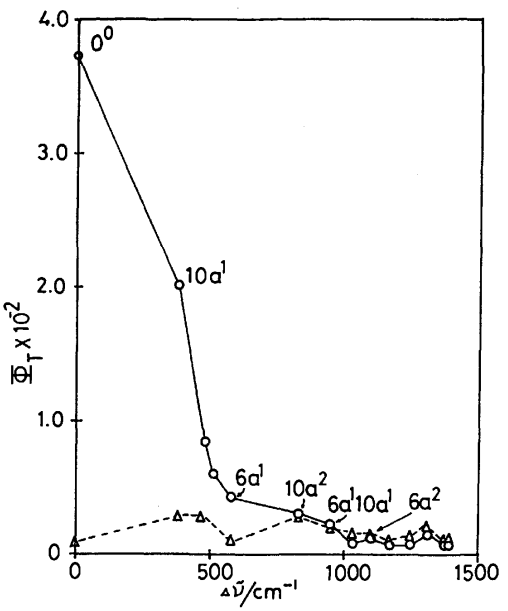

Fig. 2. Fluorescence quantum yield spectrum of pyrazine in a supersonic free jet (—○—). $\Delta\tilde{\nu}$ indicates the energy difference from the electronic origin. For comparison the quantum yield spectrum of 13.3 Pa pyrazine vapor with 2400 Pa isopentane is shown (---△---).

Table 1. Observed quantum yield and lifetime of pyrazine

Level	$\tilde{\nu}/cm^{-1}$	Φ_T[a] $\times 10^2$	τ_2[b]/ns	τ_1[c]/ps	c_1/c_2[d]
0^0	30876	3.7	455±10	130	<3
$10a^1$	31259	2 0	264±10	125	10
$6a^1$	31459	0.49	255±10	100	43
$10a^2$	31709	0.35	170±15	120	210
$6a^1 10a^1$	31821	0.29	180±15	120	240
$6a^2$	32043	0.11	200±20	95	739

a) Quantum yields of the total fluorescence in supersonic free jet. b) Lifetime of the slow fluorescence in supersonic free jet. c) Lifetime of the fast fluorescence in vapor, taken from Ref. 17. d) Ratio of the pre-exponential factors.

The quantum yield of the zero point level is 0.037, which is one order of magnitude larger than the vapor value (3×10^{-3} at 1.33 Pa in vapor phase) obtained by Frad *et al.*[1] The quantum yield of the free jet rapidly decreases with the excess vibrational energy as seen from Fig. 2 and Table 1. In Fig. 2, the quantum yield spectrum for 13.3 Pa pyrazine vapor in 2400 Pa isopentane is shown for comparison. In contrast to the case of the supersonic jet, the quantum yield is very small (1×10^{-3}) and almost constant over the excess energy region measured, although an appreciable variation is seen at the $10a^1$ level and its combinations.

Fluorescence Decay from the Vibronic Level. In our experimental condition of the supersonic free jet, translational temperature is estimated to be 0.5 K and mean collisional time will be greater than 10 μs which is the value for the hard sphere collision with helium atom. Therefore, the fluorescence which decays within

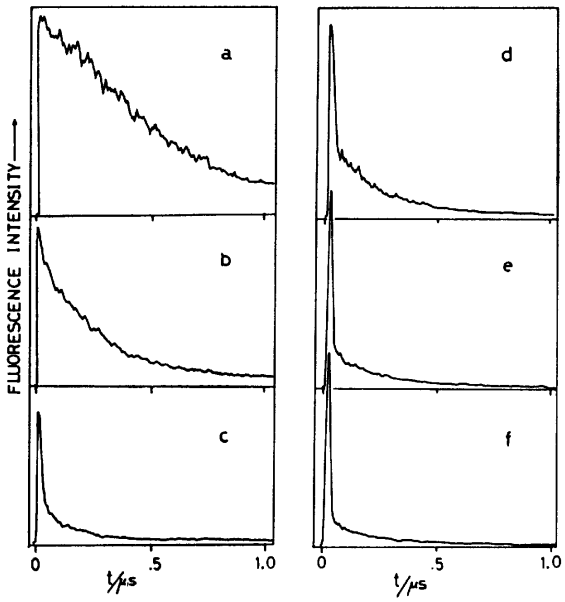

Fig. 3. Oscillogram traces of the fluorescence decay from (a) the electronic origin, (b) $6a^1$ and (c) $6a^2$ of the ultracold pyrazine seeded in 4 atm He gas. Corresponding traces of pyrazine vapor of about 6.65 Pa at room temperature are shown in (d), (e), and (f), respectively.

a time scale less than 10 μs can be regarded as being in a collision free condition.

Oscillogram traces of the fluorescence decay of the jet from several vibronic levels are shown in Fig. 3. The decay from the zero point level was approximately single exponential with lifetime of 455 ± 10 ns (see Fig. 3(a)). On going to the higher vibronic levels, the fast fluorescence component gradually shows up and increases with the excess energy from the zero point level. At a large excess energy the fast component dominates over the slow component (see Fig. 3(c)). The lifetime of the slow component decreases with increase of the excess energy and at $6a^2$ level (excess energy of 1168 cm^{-1}) it reduces to a half of the value for the zero point level (see Table 1). On the other hand, in the case of low pressure pyrazine vapor the fluorescence decay is already bi-exponential even for the zero point level as shown in Fig. 3(d). The lifetime of the slow fluorescence in vapor is about 200 ns which is shorter than the value of the jet. The different fluorescence decays between the jet and the low pressure vapor indicate that the slow fluorescence is extremely sensitive to the collisional quenching[16] which still exists in the case of vapor even at extremely low pressure regarded as collision free condition. The lifetime of the slow decay component in the free jet is summarized in Table 1.

Since our detection system is not fast enough to resolve the fast fluorescence decay, the oscillogram traces shown in Fig. 3 do not represent the real decay. Assuming a bi-exponential decay, the fluorescence intensity is given by

$$I_F(t)=I_1(t)+I_2(t)=c_1e^{-t/\tau_1}+c_2e^{-t/\tau_2}, \qquad (1)$$

where 1 and 2 refer to the fast and slow components. c_2 can be easily obtained by extrapolating the observed $I_2(t)$ into $t=0$. The difference between the oscillogram peak height at $t=0$ and the c_2 obtained is defined as A_1. Since τ_1 is known to be shorter than 10^{-9} s, the A_1 value obtained directly from the oscillogram trace is not necessarily equal to c_1. By taking a half width δ of the fast component displayed on the oscillogram trace, the integrated intensity of $I_1(t)$ will be approximately given by $A_1\delta$. On the other hand, the integrated intensity of $I_1(t)$ over a time scale greater than τ_1 can be expressed by

$$\int_0^T I_1(t)\,dt=c_1\tau_1, \qquad T\gg\tau_1. \qquad (2)$$

We have, therefore,

$$c_1=\frac{\delta}{\tau_1}\times A_1. \qquad (3)$$

δ was found to be 18 ns from a temporal resolution of our detection system. The lifetime τ_1 of the fast component reported by McDonald and Rice[17] is shown in Table 1. Since no pressure dependence of the fast decay component is observed, it is reasonable to assume that the lifetime of the fast fluorescence of the supersonic jet is the same as that of vapor. The estimated ratios†† c_1/c_2 for the individual vibronic bands are shown in the last column of Table 1.

Rotational Level Dependence of the Fluorescence Decay. The rotational level dependence of the fluorescence quantum yield has been recently reported by Baba *et al.*[4] for the zero point level of pyrazine. In order to examine the rotational level dependence, we measured the fluorescence decay from various rotational levels of the zero point vibrational level. The measurements

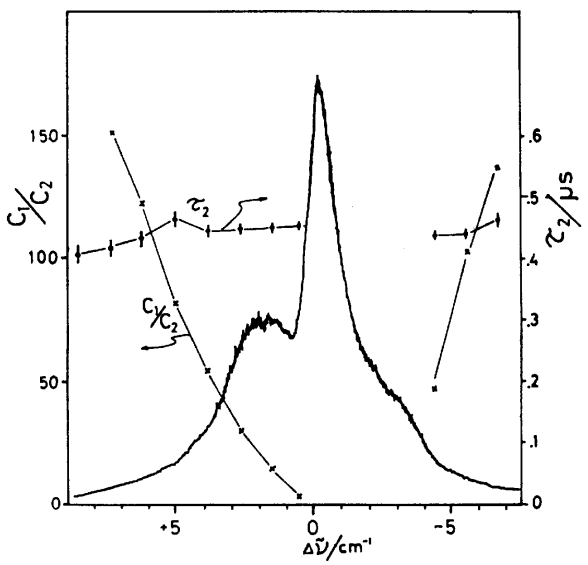

Fig. 4. Excitation spectrum of the electronic origin of pyrazine seeded in 0.05 atm He carrier gas. Lifetime τ_2 of the slow fluorescence decay (ϕ) and ratio of the pre-exponential factors c_1/c_2 ($\times$) are shown superimposedon the excitation spectrum.

†† The vapor value for $6a^1$ band at 31459 cm^{-1} (see Fig. 3(e)) was found to be about 700, which agrees with the value (10^3) obtained by Frad *et al.*[1] with the excitation at 31680 cm^{-1}.

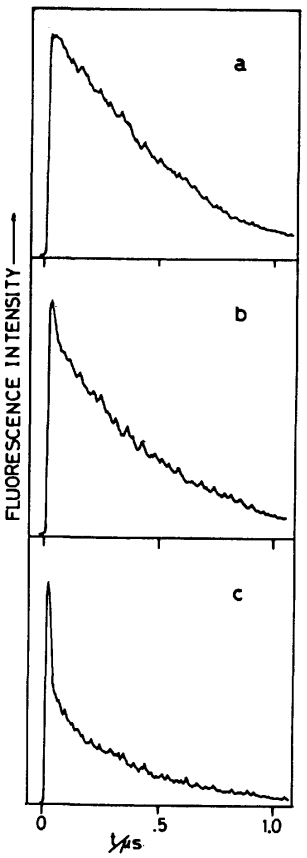

Fig. 5. Rotational dependence of the fluorescence decay from the electronic origin by the excitation of (a) $J'=\approx 1$, (b) $J'=6$—7, and (c) $J'=14$—15.

were made for the supersonic jet with a reduced stagnation pressure of helium gas. In the reduced He pressure, the rotational temperature becomes higher, so that the relatively high rotational levels can also be excited. Excitation spectrum of the 0-0 band under a stagnation pressure less than 0.05 atm of He is actually broad with a rotational envelope as shown in Fig. 4. Rotational temperature was estimated to be higher than 40 K. When the peak at 30876 cm^{-1}, which is the Q-branch head, is excited by narrow band UV light of FWHM of 0.4 cm^{-1}, a single exponential decay was obtained whose decay constant is the same as that of the jet at a high stagnation pressure (compare Fig. 5(a) and Fig. 3(a)). Tuning the pumping light to the higher energy side (R-branch) of the rotational envelope, a fast component appears prior to the slow component and the ratio of the fast to slow component increases at the far edge of the R-branch. Similar decay was observed also for the P-branch. The typical oscillogram traces are shown in Fig. 5. The results are essentially the same as those reported very recently by ter Harst *et al.*[12]

The observed lifetime of the slow fluorescence component and the ratio of the pre-exponential factors of the fast and slow components (c_1/c_2) are given in Table 2. Since the R-branch is well separated from the Q-branch, rotational quantum number J' in the excited state can be roughly assigned for the R-branch with reference to the high resolution vapor spectrum obtained by Merritt and Innes.[18] Although the onset

Table 2. Lifetimes of the slow fluorescence and the ratio of pre-exponential factors of the different rotational levels in the electronic origin

	$\Delta\tilde{\nu}/cm^{-1}$ a)	J'level	τ_2/ns c)	c_1/c_2 d)
R	+8.5	20—21	411±20	(138)
	+7.3	16—18	418±20	152
	+6.2	14—15	432±15	123
	+5.0	12—13	461±15	82
	+3.8	9—10	445±15	54
	+2.6	6— 7	450±10	30
	+1.5	3— 4	452±10	15
	+0.5	≈1	456±10	<3
P	−4.4	10—11	442±15	48
	−5.5	14—15	441±15	104
	−6.7	17—18	424±20	138

a) Energy difference from the head of the Q-branch at 30875.8 cm^{-1}. b) Estimated rotational quantum number. c) Lifetime of the slow fluorescence. d) Ratio of the pre-exponential factors, by assuming the constant lifetime (130 ps) of the fast fluorescence for the rotational levels.

of the P-branch is congested by overlapping with the Q-branch, the rotational quantum number can be also estimated for the far edge of the P-branch. The estimated J' value are given in Table 2. It is seen from Fig. 4 and Table 2 that the lifetime is almost constant for different J' values, whereas the ratio c_1/c_2 greatly increases with increase of J' value.

For the other vibronic bands such as $10a_0^1$ and $6a_0^1$, the detailed lifetime measurements over their rotational structure were not successful because of their small fluorescence quantum yields. However, we could observe increase of the fast component with increase of the rotational temperature of the jet in the broad band (≈1.5 cm^{-1} FWHM) excitation at the peak positions of these vibronic bands. This result may be interpreted as follows. At the low rotational temperature the fluorescence by the broad band excitation arises mainly from a few number of rotational levels with very low J' where the c_1/c_2 is small. With increase of the rotational temperature, the fluorescence from the higher rotational levels becomes dominant, resulting in large c_1/c_2. Thus, the rotational level dependence of these vibronic bands is concluded to be essentially the same as that of the 0-0 band. According to Baba *et al.*,[4] the change of the fluorescence quantum yield over the rotational levels of the zero point level is ascribed to change of the slow fluorescence component. Their results of the high quantum yield for the low rotational levels are, therefore, consistent with our result of dominant slow component for the low rotational levels.

Fluorescence Spectrum. In order to ensure that the slow decay component is actually the fluorescence of pyrazine, we observed the spectrum of the slow decay component in the supersonic free jet. Figure 6 shows the spectrum obtained by excitation at the head of the Q-branch of the 0-0 transition. As seen from Fig. 5(a), only the slow decay component is observed in this excitation. For comparison, the ordinary SVL fluorescence spectrum in vapor at 400 Pa of pyrazine,[15]

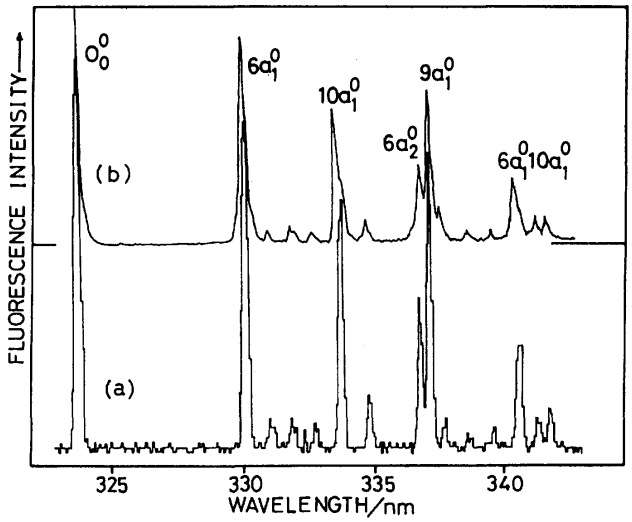

Fig. 6. (a) Fluorescence spectrum of the ultracold pyrazine in a supersonic free jet, being excited at the electronic origin. The slow fluorescence was monitored. (b) Fluorescence spectrum of 400 Pa pyrazine vapor at room temperature. The fast fluorescence was monitored.

which represents practically only the fast component, is shown in the same figure. As seen from the figure, the two spectra are idential with respect to the frequencies and relative intensities of the vibronic bands. Therefore, it is concluded that the slow decay component is really the fluorescence of the molecule.

Coupled State Density and Fluorescence Lifetime. The bi-exponential decay of the fluorescence of pyrazine has been interpreted by the model of intermediate strong coupling, where a radiative singlet state strongly interacts with non- or weakly-radiative triplet levels with a relatively large level density.[3] Consider that a single vibronic state $|S>$ in the singlet manifold interacts with N triplet levels $|T>$ through a coupling strength v_{ST}. The $|S>$ and $|T>$ levels are assumed to have total energy width γ_S and γ_T, respectively, each of which is composed of radiative and nonradiative contributions. The coupling between the zero order $|S>$ and $|T>$ levels provides $(N+1)$ quasi-stationary molecular eigen states, whose energy levels are distributed within a spectral width Δ of the exciting light. In the case of coherent excitation of these eigen states by a pulsed light, the time evolution of the wavefunction of the molecule leads to dual fluorescence with fast and slow decay as the result of coherent and incoherent superpositions of the eigen states. In the intermediate case of $|\gamma_S-\gamma_T| \ll \Delta$, the overall fluorescence decay can be approximated by a bi-exponential type given by Eq. 1. The observables in Eq. 1 can be incorporated in the following ways,[1]

$$1/\tau_1 = \frac{\gamma_S}{N} + \gamma_T + \Delta_{ST}, \tag{4}$$

$$1/\tau_2 = \frac{\gamma_S}{N} + \gamma_T, \tag{5}$$

$$c_1/c_2 = N + 1. \tag{6}$$

Since the fast fluorescence is similar to that of the large molecule case, $1/\tau_1$ is dominated by the nonradiative width Δ_{ST} which is expressed in terms of coupling v_{ST} and the density of state ρ_T in the triplet manifold as far as $v_{ST}\rho_T \gg 1$ is held. Therefore, Eq. 4 can be replaced by

$$1/\tau_1 \simeq \Delta_{ST} = 2\pi\rho_T v_{ST}^2. \tag{7}$$

Thus, the number of interacting levels N is given by

$$N = \pi\Delta_{ST}\rho_T \approx \frac{c_1}{c_2} \quad \text{for } N \gg 1, \tag{8}$$

where Eq. 6 was used. From Eqs. 7 and 8, we obtain

$$\frac{c_1}{c_2} \times \tau_1 = \pi\rho_T. \tag{9}$$

Therefore, ρ_T can be obtained for the individual vibronic levels by using c_1/c_2 and τ_1 given in Table 1. ρ_T thus obtained are plotted in Fig. 7 against the excess energy from the origin of T_1.

In order to find any correlation between the ρ_T obtained and the density of state in the triplet state, we calculated the state density of the vibrational levels ρ_T^V in T_1. The calculation of ρ_T^V was made by the method given by Haarhoff[19] by assuming the same vibrational frequencies of T_1 state as those of S_0. The result is shown by curve (b) in Fig. 7. ρ_T^V was calculated also by assuming the vibrational frequencies of S_1 for those of T_1. The calculated result is shown by curve (a) of the same figure. Since the vibrational frequency change upon the excitation from S_0 to T_1 is generally less significant than the change in the excitation to S_1,[20] the curves (a) and (b) are regarded as the maximum and minimum vibronic state densities, respectively.

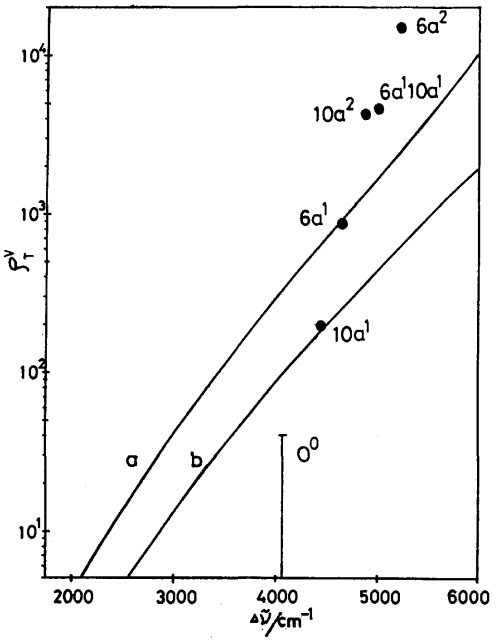

Fig. 7. The triplet state density ρ_T^V (number of levels/cm^{-1}) estimated from the N value at the vibronic levels (○) and the calculated vibronic state density ρ_T^V as a function of the excess energy $\Delta\tilde{\nu}$ from the electronic origin of the lowest triplet state. At the electronic origin 0^0 maximum value is indicated. The vibrational frequencies in the triplet state is assumed at that in the lowest excited siglet state (a) and in the ground state (b).

It is seen from Fig. 7 that the observed ρ_T value agrees with the calculated ρ_T^V for the excess energy region of around 4500 cm^{-1}. However, ρ_T is smaller than ρ_T^V for the smaller excess energy region and it is larger for the greater excess energy region. Increase of the observed ρ_T with increase of the excess energy is much rapid than expected from ρ_T^V. These facts suggest that the number of coupled triplet levles is not determined simply by the vibronic state of T_1. The disagreement between ρ_T and ρ_T^V for the larger excess energy region might be improved by taking into account of the rotational level density which is roughly two orders of magnitude larger than ρ_T^V. On the other hand, the fact that ρ_T for the lower energy region is much smaller than the calculated ρ_T^V suggests that there might be a sort of selection rule which selects the interacting levels from the vibronic or ro-vibronic levels of the triplet state.[5]

It is seen from Fig. 4 and Table 2 that the ratio c_1/c_2 exhibits a remarkable increase on going to higher J' value in the electronic origin, while the lifetime τ_2 is almost constant over the rotational quantum numberless than $J'=20$. From Eqs. 5 and 6, we have

$$\tau_2 = \frac{c_1/c_2}{\gamma_S + (c_1/c_2)\gamma_T}, \quad \text{for } N \gg 1. \tag{10}$$

A constant value of τ_2 irrespective of various values of c_1/c_2 means that τ_2 must be equal to the triplet lifetime $1/\gamma_T$. The triplet lifetime is reported to be the order of 10^{-5} s in vapor phase,[1] while $\tau_2 \simeq 450$ ns. Therefore, Eq. 10 is not supported from our experimental results. Since the change of the vibronic or ro-vibronic state density of the triplet state over a range of several wave number around the electronic origin must be very small, we expect no rotational level dependence of τ_2, as it is observed. However, the observed large rotational dependence of c_1/c_2 is hard to be explained with the mixed state model proposed by Lahmani *et al.*,[3] suggesting a need of revision of the model.

One of the author (N. M.) wishs to thank Daniel B. McDonald and Prof. S. A. Rice for providing their results. This work was suported by the Kurata Research Grant from the Kurata Foundation and by a Grant-in-Aid for Developmental Scientific Research from the Ministry of Education, Science and Culture.

References

1) A. Frad, F. Lahmani, A. Tramer, and C. Tric, *J. Chem. Phys.*, **60**, 4419 (1974).
2) K. G. Spears, and M. El-Manguch, *Chem. Phys.*, **24**, 65 (1977).
3) F. Lahmani, A. Tramer, and C. Tric, *J. Chem. Phys.*, **60**, 4431 (1974).
4) H. Baba, M. Fujita, and K. Uchida, *Chem. Phys. Lett.*, **73**, 425 (1980).
5) W. E. Howard, and E. W. Schlag, *Chem. Phys.*, **17**, 123 (1976); *ibid.*, **29**, 1 (1978).
6) F. A. Novak, and S. A. Rice, *J. Chem. Phys.*, **73**, 858 (1980).
7) S. M. Beck, D. L. Monts, M. G. Liverman, and R. E. Smalley, *J. Chem. Phys.*, **70**, 1062 (1979).
8) F. M. Behlen, N. Mikami, and S. A. Rice, *Chem. Phys. Lett.*, **60**, 364 (1979).
9) A. Amirav, U. Even, and J. Jorther, *J. Chem. Phys.*, **71**, 2319 (1979).
10) J. B. Hopkins, D. E. Powers, and R. E. Smalley, *J. Chem. Phys.*, **73**, 683 (1980).
11) J. Chaiken, T. Benson, M. Gurnick, and J. D. McDonald, *Chem. Phys. Lett.*, **61**, 195 (1979).
12) G. ter Horst, D. W. Pratt and J. Kommandeur, *J. Chem. Phys.*, **74**, 3616 (1981).
13) N. Mikami, A. Hiraya, I. Fujiwara, and M. Ito, *Chem. Phys. Lett.*, **74**, 531 (1980).
14) W. R. Ware and A. M. Garcia, *J. Chem. Phys.*, **61**, 187 (1974).
15) Y. Udagawa M. Ito, and I. Suzuka, *Chem. Phys.*, **46**, 237 (1980).
16) H. Igarashi and K. Kaya, *Bull. Chem. Soc. Jpn.*, **54**, 1928 (1981).
17) D. B. McDonald and S. A. Rice, *J. Chem. Phys.*, **74**, 4907 (1981).
18) J. A. Merritt and K. K. Innes, *Spectrochim. Acta*, **16**, 945 (1960).
19) P. C. Haarhoff, *Mol. Phys.*, **7**, 101 (1963).
20) N. Nishi, M. Kinoshita, T. Nakashima, R. Shimada, and Y. Kanda, *Mol. Phys.*, **33**,31, (1977).

The Synthesis and Luminescence Quenching of the Water-soluble Polymer-supported Tris(2,2′-bipyridine)ruthenium(II) Analogue

Yoshimi KURIMURA,* Norio SHINOZAKI, Fumio ITO, Yasuyo URATANI, Kiyotaka SHIGEHARA,† Eishun TSUCHIDA,† Masao KANEKO,†† and Akira YAMADA††

Department of Chemistry, Ibaraki University, Bunkyo, Mito, Ibaraki 310

†*Department of Polymer Chemistry, Waseda University, Shinjuku-ku, Tokyo 160*

††*Department of Polymer Chemistry, The Institute of Physical and Chemical Research, Wako, Saitama 351*

(Received May 18, 1981)

The *p*-aminostyrene-*N*-vinylpyrrolidone copolymer-supported tris(2,2′-bipyridine)ruthenium(II) analogue, $[Ru(bpy)_2(pbyCOOH)]^{2+}$ (bpy=2,2′-bipyridine and pbyCOOH=polymeric bipyridine ligand), has been prepared, and the luminescence behavior of the polymer complex has been investigated in an aqueous solution. The efficiency of the quenching of the excited state of the polymer complex with $[Fe(CN)_6]^{4-}$, $[Co(phen)_3]^{2+}$, and Cu^{2+} is compared with that of $[Ru(bpy)_3]^{2+}$. The quenching of the excited state of the polymer complex by Cu^{2+} is strongly enhanced by the effect of the polymer chains. In the polymer complex/Cu^{2+} system, the quenching by Cu^{2+} in the presence of poly(*p*-styrenesulfonate) is much more effective than in the absence of the polyion. The characteristics of the polymer complex in terms of the luminescence behavior are discussed.

Recently much attention has been paid to the photochemical property of tris(2,2′-bipyridine)ruthenium(II), $[Ru(bpy)_3]^{2+}$, and the utilization of the excited state of $[Ru(bpy)_3]^{2+}$, $*[Ru(bpy)_3]^{2+}$, in solar-energy-conversion systems has been proposed by many workers.[1-6] The photochemistry of $[Ru(bpy)_3]^{2+}$ in micellar-core and polyelectrolyte solutions,[4] and those of $[Ru(bpy)_3]^{2+}$ derivatives in aqueous solutions[3,7,8] and the exterior aqueous phase of phospholipid vesicle[9] have been studied.

For the photosensitized reactions of $[Ru(bpy)_3]^{2+}$ and the related complexes, it would be desirable to immobilize them in polymer chains in order to prevent non-productive back reactions and in order to promote efficient energy capture by the reactive species.[10] The polymer-supported bis(2,2′-bipyridine)ruthenium(II) complexes, $[Ru(bpy)_2(pvp)]^{2+}$ and $[Ru(bpy)_2(pvp)Cl]^{+}$ (pvp=poly(4-vinylpyridine)), have been synthesized.[10] However, these complexes were easily decomposed by thermal and photo-substitution reactions. Polymer-supported metal complexes with bipyridine ligands were prepared by the reaction of a polystyrene-supported bipyridine ligand with a variety of transition-metal salts by Card and Neckers.[11]

In this connection, we marked a water-soluble $[Ru(bpy)_3]^{2+}$ analogue with a polymeric ligand as a polymer-bound photosensitizer.

Experimental

Materials. The $[Ru(bpy)_3]Cl_2\cdot 6H_2O$[12] and $[Ru(bpy)_2CO_3]5H_2O$[13] were prepared by the methods previously described. The *p*-aminostyrene was prepared from 1-(*p*-aminophenyl)ethanol.[14] The *p*-aminostyrene(PAS)/*N*-vinylpyrrolidone(VPo) copolymer (**1**) was prepared by the azobisisobuthyronitrile(AIBN)-initiated radical polymerization of PAS with VPo in tetrahydrofuran. Found: C, 67.30; H, 8.19; N, 12.41%. Calcd for $(C_8H_9N)_{0.14}(C_6H_9NO)_{0.86}$: C, 67.19; H, 8.02; N, 12.77%. IR spectra (in cm^{-1}): 3350 3230 (PAS, NH_2), 2930 (VPo ring, CH), 1630 1520 (PAS, ph ring), 1290 (VPo ring, CN). The intrinsic viscosity of the **1** copolymer in an aqueous solution was 0.37 at 25 °C. 2,2′-Bipyridine-4,4′-dicarboxylic acid, $bpy(COOH)_2$, was prepared by the method of Whitten *et al.*[15] The polymeric bipyridine ligand pbpCOOH, **2**, was prepared by the following method under a nitrogen atmosphere. To 50 ml of a *N*,*N*-dimethylformamide (DMF) solution containing $bpy(COOH)_2$ (2.0 g, 0.0082 mol) and triethylamine (0.83 g, 0.0082 mol), we added ethyl chloroformate (0.89 g, 0.0082 mol). The reaction mixturewas then stirred at 0—5 °C for 1 h. To the reaction mixture we then added 20 ml of a DMF solution of the **1** copolymer (0.32 g, 4.0×10^{-4} mol units of aminostyrene). The solution was stirred at 0—5 °C for 1 h and then kept overnight at room temperature. The volume of the reaction mixture was reduced to *ca.* 20 ml and the resulting precipitate was filtered. Pale yellow powder was dissolved in small amounts of ethanol. The powder of pbyCOOH was reprecipitated twice from ethanol into ether and dried in vacuo (yield, *ca.* 1.6 g). Found: C, 66.25; H, 7.08; N, 12.72%. Calcd for $(C_{20}H_{15}N_3O_3)_{0.14}(C_6H_9NO)_{0.86}$: C, 66.43; H, 6.89; N, 12.45%. IR spectra (in cm^{-1}): 2940 (VPo ring, CH), 1660 (VPo ring, CO), 1630, 1520 sh (PAS, ph ring), 1290 (VPo ring, CN), 1200 (pendant bpy ring). The results of elemental analysis and IR measurements indicate that no appreciable amounts of free amino groups remained on the polymeric ligand; the IR peak at 3350 cm^{-1} (νNH_2) of the PAS/VPo copolymer completely disappeared in the polymeric bipyridine ligand, **2**.

The polymer-supported Ru(II) complex (**3**), which is represented by $[Ru(bpy)_2(pbyCOOH)]^{2+}$, was obtained by the reaction of **2** with $[Ru(bpy)_2CO_3]$. An ethanolic solution (50 ml) of **2** (2.0 g, 0.0020 mol) and $[Ru(bpy)_2CO_3]5H_2O$ (1.13 g, 0.0020 mol) was allowed to reflux for 10 h. After the addition of several drops of 1 M HCl (1 M=1 mol dm^{-3}), the reaction mixture was dialized in cold water for 40 h under dark. The chloride salt of the polymer complex was obtained by the evaporation of the dialyzed solution under reduced pressure and dried in vacuo. The molar fraction of the Ru (II) complex unit (x) of **3** was determined to be 0.096 ± 0.005 by means of the atomic-absorption spectrum, using $[Ru(bpy)_3]Cl_2\cdot 6H_2O$ as the standard material. The dialized solution of the polymer complex was usually kept frozen.

Luminescence and Quenching Experiments. Deoxygenated samples were used for the experiments. The pH values of the solution were adjusted by the addition of dil HCl or dil NaOH solutions. The ionic strength of the solutions was not adjusted to be constant by the addition of simple salt, since, if a large amount of the salt is added, the potential fields of the polymer domains are shielded with the counter ions. This causes a

shrinking of the polymer chains and, thus, a reduction of the polymer effect. The excitation wavelength was 465 nm. Comparison measurements were taken on the same day.

Instruments. The absorption spectra were recorded with a Hitachi 320 spectrophotometer. The infrared spectra (KBr disks) were measured using a Hitachi Model 200-10 infrared spectrophotometer. A Hitachi Model 170-40 atomic absorption spectrometer was used for the determination of ruthenium. The emission spectra were made in 1 cm × 1 cm quartz cell on a Shimadzu RF-500 spectrofluorometer at 25±0.1 °C by means of a thermostated cell holder. A PRA Model 3000 nanosecond fluorometer (Photochemical Research Associates, Inc.) was used for the determination of the excited lifetimes of the polymer complex.

Results and Discussion

The reaction of pbyCOOH with $[Ru(bpy)]_2CO_3$ (Eq. 1) was completed in about 10 h at 50 °C: the initial

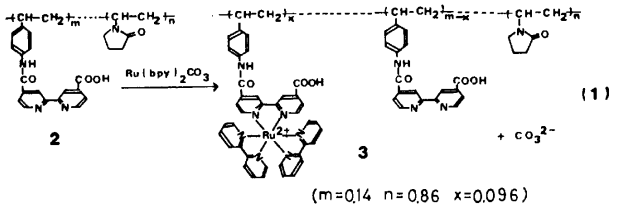

(1)

absorption maximum at *ca.* 500 nm due to $[Ru(bpy)_2CO_3]$ shifted at *ca.* 460 nm due to the ligand-substitution reaction. The absorption and emission spectra of an aqueous solution of **3** and $[Ru(bpy)_3]^{2+}$ are shown in Fig. 1. In an aqueous solution, the molar extinction coefficients of the polymer complex and $[Ru(bpy)_3]^{2+}$ at their absorption maxima are 1.48±0.05 M^{-1} (459 nm) and 1.40±0.02 M^{-1} (455 nm) respectively. No appreciable change in the absorption spectrum of the polymer complex was observed for at least 3 d at room temperature.

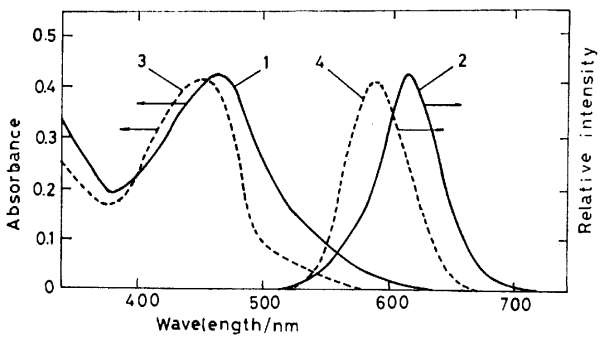

Fig. 1. Absorption and luminescence spectra of $[Ru(bpy)_2(pbyCOOH)]^{2+}$ (1 and 2) and $[Ru(bpy)_3]^{2+}$ (3 and 4) in aqueous solution at 25 °C. [Ru(II)]= 3.0×10^{-5} M.

The absorption maximum of the CTTL band of the polymer complex was dependent on the pH of the solution, whereas the molar extinction coefficient of the absorption maximum was relatively insensitive to the pH. The relative emission intensity was, however, greatly dependent on the pH, and the luminesecence

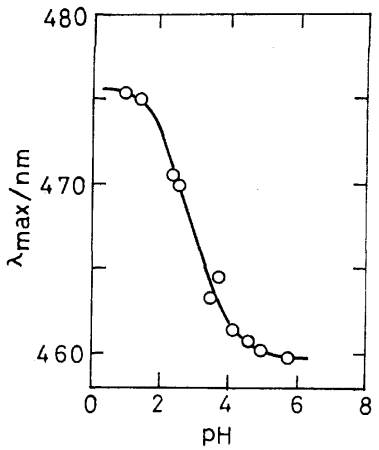

Fig. 2. Dependence of λ_{max} of $[Ru(bpy)_2(pbyCOOH)^{2+}]$ on pH at 25 °C.

maximum was not so sensitive to the pH. The pH dependence of the absorption maximum (Fig. 2) can be attributed to the acid dissociation of the -COOH on the bipyridine ring. The acid-dissociation constant of the ground state of the polymer complex, pK_a^0, was estimated to be 2.80±0.05 from the titration curve (Fig. 2).

The direct measurement of the excited-state equilibrium for $[Ru(bpy)_2(pby(COOH)_2)]^{2+}$, where bpy-$(COOH)_2$ is 2,2'-bipyridine-4,4'-dicarboxylic acid, had been accomplished by Giordano *et al.*[16] by means of luminescence titration. They demonstrated that the two acid groups of the complex behave identically and that the acid-dissociation constant of the ground state and that of the excited state were 5.50±0.05 and 8.50±0.05 respectively at 25 °C. In the present system, the pK_a^* of the polymer complex was also calculated from Eq. 2.[16]

$$pH = pK_a^* - \log\frac{\tau_p^*}{\tau_d^*}, \quad (2)$$

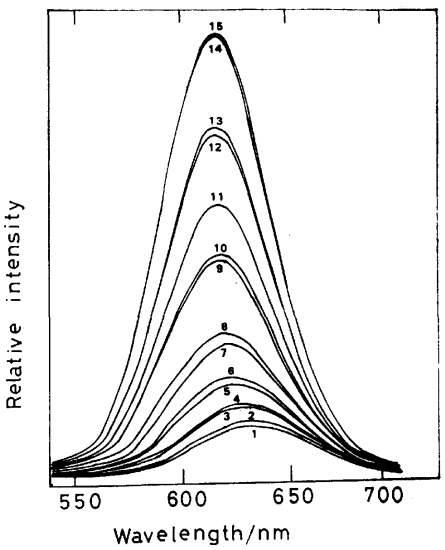

Fig. 3. Variation of the luminescence spectra of $[Ru(bpy)_2(pbyCOOH)]^{2+}$ on pH in aqueous solution at 25 °C. pH: 1, 1.26; 2, 1.64; 3, 2.18; 4, 2.63; 5, 3.27; 6, 3.29; 7, 3.49; 8, 3.54; 9, 3.90; 10, 4.08; 11, 4.18; 12, 4.58; 13, 4.89; 14, 5.83; 15, 6.13.

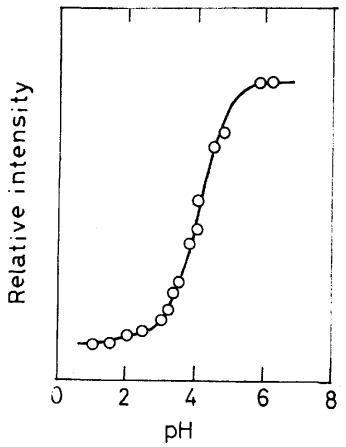

Fig. 4. Luminescence titration of $[Ru(bpy)_2(pby-COOH)]^{2+}$ in aqueous solution at 25 °C.

where the pH was taken at the inflection point in the relative intensity *vs.* the pH curve (Fig. 4) and where τ_p^* and τ_d^* are the lifetimes of the excited state of the protonated and deprotonated species of the polymer complex respectively. The effect of the pH on the luminescence spectrum and the luminescence titration curve of the polymer complex are shown in Fig. 3 and 4 respectively. For the polymer complex, the values of τ_p^* and τ_d^* were estimated to be 287 ± 0.01 ns (pH 1.4) and 359 ± 0.02 ns (pH 6.0) at 25 °C. From Eq. 4, we obtained $pK_a^*=4.30\pm0.05$. The results show that the protonated complex species is a weaker acid in the lowest excited state than in the ground state. This seems to indicate that the charge transfer from the central Ru(II) ion to the polymer ligand (Process a) is predominant.

$$[Ru^{II}(byp)_2(pbyCOOH)]^{2+} \xrightarrow{a} [Ru^{III}(bpy)_2(pb\bar{y}COOH)]^{2+}$$
$$\quad\quad\quad

TABLE 1. VALUES OF K_{SV}/M^{-1} AND $(k_q/M^{-1}\,s^{-1})$ IN AN AQUEOUS SOLUTION AT 25 °C[a,c]

	Quencher		
	$[Fe(CN)_6]^{4-}$	Cu^{2+}	$[Co(phen)_3]^{2+}$
$[Ru(bpy)_2(pbyCOOH)]^{2+}$ [d]	1.7×10^3 (5.7×10^9)	26 (8.7×10^7)	—
$[Ru(bpy)_2(pbyCOO)]^+$ [e]	3.9×10^3 (1.1×10^{10})	360 (1.0×10^9)	42 (1.2×10^8)
$[Ru(bpy)_2(pbyCOO)]^+ + PSS$ [f]	—	3.7×10^3 (1.0×10^{10})	—
$[Ru(bpy)_3]^{2+}$	1.3×10^4 (2.2×10^{10})	41 (6.8×10^7)	490 (8.2×10^8)

a) The excited-state lifetimes used for the calculations of the k_q values were 290 ns for $[Ru(pby)_2(pbyCOOH)]^{2+}$, 360 ns for $[Ru(bpy)_2(pbyCOO)]^+$, and 600 ns for $[Ru(bpy)_3]^{2+}$[b] at 25 °C. b) Ref. 18. c) The errors of the Stern-Volmer constants and k_q are within $\pm5\%$. d) pH 1.4. e) pH 6.2. f) 2.8×10^{-5} M Ru(II) and 1.0×10^{-3} M PSS.

Ru(II) complex moieties on the polymer chains because the polymer domians have a large positive-charge density.

It is noteworthy that the k_q for the reaction of the deprotonated from of the polymer complex with Cu^{2+} is considerably greater than those of $[Ru(bpy)_2(pbyCOOH)]^{2+}$ and $[Ru(bpy)_3]^{2+}$ (Fig. 6 and Table 1). The higher reactivity of $[Ru(bpy)_2(pbyCOO)]^+$ with Cu^{2+} can be partly explained in terms of the "effect of the uncoordinated ligand" on the polymer chains. In the case of the polymer complex, uncoordinated bipyridine rings exist with the mole fraction of 0.044 and a part of Cu^{2+} ions probably coordinate to the uncoordinated ligands. Therefore, a hydrid metal complex with Ru(II) and Cu^{2+} is probably formed. The excited state of the Ru(II) complex on the polymer chains probably reacts rapidly with the coordinated Cu^{2+}, which can be represented by $[Cu(pbyCOO)]^+$. In the lower pH region. the uncoordinated bipyridine would be protonated; for example, the pK of HL^+ of 4,4'-bipyridine is 4.44 at 25 °C.[19] Thus, the hybrid-metal complex should not be formed in the lower pH region. This mainly accounts for the greater k_q value in $[Ru(bpy)_2(pbyCOO])^+/Cu^{2+}$ than in $[Ru(bpy)_2(pbyCOOH)]^{2+}/Cu^{2+}$. In the higher-pH region, the interactions between carboxylate ions and amide groups on the polymer ligand and Cu^{2+} ions should also be considered. However, the details of these interactions have not yet been made clear.

On the addition of sodium poly(*p*-styrenesulfonate), PSS, to $[Ru(bpy)_2(pbyCOO)]^+/Cu^{2+}$, a further enhancement of the quenching rate was observed; the value of k_q in the presence of 1.0×10^{-3} M PSS is about ten times greater than that in the absence of PSS and about 150 times greater than k_q for the reaction of $*[Ru(bpy)_3]^{2+}$ with Cu^{2+}. The acceleration of the quenching rate in this system can be attributed to the formation of the polyion-polyion complex between PSS and $[Ru(bpy)_2(pbyCOOH)]^+$. When a large excess of PSS is present, the domains of the polyion-polyion complex should have a large negative charge density. Thus, the Cu^{2+} ions would be accumulated in the negatively charged domains. In such polyion domains, the collision frequencies between the excited state of the Ru(II)-complex moieties and the coordinated Cu^{2+} and uncoordinated Cu^{2+} should be enhanced.

We would like to thank Professor Kunihiko Mizumachi for many helpful suggestions. We are also indebted to Mr. Hiroshi Yokota and Mr. Kiyomi Takato for their assistance with some of the quenching studies and Mr. Yoshihiro Yamaguchi for the measurements of the lifetimes at the Daini Seikoshya Co.

References

1) C. Lin and N. Sutin, *J. Phys. Chem.*, **80**, 97 (1976).
2) K. Kalyanasundaram and M. Gratzel, *Angew. Chem. Int. Ed. Engl.*, **18**, 701 (1979).
3) G. Sprinstschnik, H. W. Sprintschnik, P. P. Kirsch, and D. G. Whitten, *J. Am. Chem. Soc.*, **98**, 2337 (1976).
4) D. Meisel and M. S. Matheson, *J. Am. Chem. Soc.*, **99**, 6577 (1977).
5) Y. Kurimura and R. Onimura, *Inorg. Chem.*, **19**, 3516 (1980).
6) D. Meisel, M. S. Matheson, and J. Rabani, *J. Am. Chem. Soc.*, **100**, 117 (1978).
7) K. Takizawa, M. Kajiwara, and T. Matsuo, *Chem. Lett.*, **1977**, 1199.
8) R. Memming and F. Shroppel, *Chem. Phys. Lett.*, **62**, 207 (1979).
9) W. E. Ford, J. W. Otvos, and M. Calvin, *Nature*, **274**, 507 (1978).
10) J. M. Clear, J. M. Kelly, D. C. Peper, and J. G. Vos, *Inorg. Chim. Acta*, **33**, L139 (1979).
11) R. J. Card and D. C. Neckers, *Inorg. Chem.*, **17**, 2345 (1978).
12) R. A. Palmer and T. S. Piper, *Inorg. Chem.*, **5**, 864 (1966).
13) M. Tanaka, T. Nagai, E. Miko, K. Mizumachi, and I. Ishimori, *Nippon Kagaku Kaishi*, **1979**, 1112.
14) V. G. Sinyav'kii, A. I. Turbina, and M. Ya. Romankevich, *Dopov. Akad. Nauk. Ukr. RSR*, **12**, 1622 (1962).
15) G. Sprintschnik, H. W. Sprintschnik, P. P. Kirsch, and D. G. Whitten, *J. Am. Chem. Soc.*, **99**, 4947 (1977).
16) P. J. Giordano, C. R. Bock, M. S. Wrington, L. V. Interrante, and R. F. X. Williams, *J. Am. Chem. Soc.*, **99**, 3187 (1977).
17) J. Demas and J. W. Addington, *J. Am. Chem. Soc.*, **98**, 5800 (1976).
18) G. Navon and N. Sutin, *Inorg. Chem.*, **13**, 2159 (1974).
19) K. Yamasaki and M. Yasuda, *J. Am. Chem. Soc.*, **78**, 1324 (1956).

Infrared Intensities of Bending Fundamentals in Gaseous HCCCN and DCCCN

Masakatsu UYEMURA,* Shuji DEGUCHI,† Yoshikazu NAKADA,† and Takashi ONAKA†

Department of Industrial Chemistry, Faculty of Engineering, Tokyo Institute of Polytechnics, Atsugi, Kanagawa 243-02

†*Department of Astronomy, Faculty of Science, The University of Tokyo, Hongo, Bunkyo-ku, Tokyo 113*

(Received May 21, 1981)

The infrared spectra of three bending fundamentals (ν_5, ν_6, and ν_7) of gaseous cyanoacetylene and cyanoacetylene-*d* have been measured and their integrated absorption coefficients $A(\nu_i)$ have been determined. The spectral pattern of ν_5 fundamental region in HCCCN has been interpreted by assuming the Fermi resonance between $v_5=1$ and $v_7=3$ states. On the basis of the experimental intensity data and the normal coordinate treatment, the dipole-moment derivatives with respect to the internal bending coordinates have been calculated.

Many spectral data of cyanoacetylene have been obtained from several astronomical sources, and many microwave studies have been reported.[1] Lafferty and Lovas reviewed them to obtain information applicable to radio astronomy.[2] Several infrared studies have been reported since Turrell *et al.*'s first work of HCCCN in gaseous, liquid, and crystalline states. Job and King studied the infrared spectra of gaseous HCCCN and DCCCN; they also studied the Raman spectra of liquids. The infrared, far-infrared, and Raman spectra of crystalline HCCCN and DCCCN were reported by Nolin *et al.*[3] One of the present authors studied the infrared intensities of the stretching fundamentals in gaseous and crystalline states with special interest in the intensity changes caused by the hydrogen-bond formation.[4] Recently, Mallinson and Fayt measured the high-resolution spectra of HCCCN and DCCCN in the region of 1800—6500 cm^{-1}, in order to determine the accurate band centers for all seven fundamentals and the rotational constants for three stretching fundamentals, which had not been available from microwave studies.[5] Their spectrometer, however, was uanable to cover the lower frequency region where the three bending fundamentals lie. The present study was undertaken to measure the infrared intensities of the three bending fundamentals of gaseous HCCCN and DCCCN, and thereby to obtain the information concerning the dipole-moment changes due to molecular bending motions.

Experimental

HCCCN was kindly supplied from Takeda Chemical Industries. The methods of purification and deuteration were described previously.[4]

The deuterium content in DCCCN determined from the band intensity of resudual HCCCN, was found to be 98%. Spectra of ν_5 and ν_6 fundamentals were obtained using a Perkin-Elmer model 125 spectrometer with a 5 cm path-length cell, and those of ν_7 were obtained using a Hitachi model FIS-21 single beam far-infrared spectrometer with a 10 cm path-length cell equipped with polyethylene windows. The spectral resolution of the spectrometers were from 1.1 cm^{-1} to 1.6 cm^{-1} in the ν_5 and ν_6 band regions and about 0.6 cm^{-1} in the ν_7 band region. In the measurements of ν_5 and ν_6 bands, the sample gas was first admitted to the cell, then Helium gas was added to fill it; the total pressure was about 7×10^4 Pa. The integrated absorption coefficients:

$$B(\nu_i) = \int_{\text{band}} \ln(T_0/T)\mathrm{d}\tilde{\nu} \qquad (1)$$

were obtained and plotted against to the sample pressure p at 273 K. In the case of ν_7, the spectra were recorded first with an empty cell, and then with a cell containing the sample gas; the transmittances were calculated point by point. In these measurements, the changes of recording conditions would appreciably affect the apparent spectra, so that relatively large errors would be expected to accumulate in $B(\nu_7)$ if the integration were carried out over the entire band region. Therefore, the integratation was carried out over the Q-branch region and then this value was used to obtain the integrated molar absorption coefficient $A(\nu_7)$, as described later.

Results and Discussions

Observed frequencies of the bending fundamentals, their combinations and overtones are given in Table 1, together with those reported previously.[3,5] In the ν_5 and ν_6 band regions of HCCCN and DCCCN, two sharp and strong bands were observed, accompanied by some sub-bands. The former were assigned to the Q-branch of $v_5=1\leftarrow0$ and $v_6=1\leftarrow0$ transitions. Most of the latter may be assigned to hot bands, on the basis of their intensities relative to the fundamentals and their small frequency shifts from the $v_i=1\leftarrow0$ transitions, because the bending fundamental frequencies are relatively low in these molecules. In the ν_5 band region of HCCCN, the band at 663.7 cm^{-1} was assigned to the $v_5=1\leftarrow0$ transitions, as shown above. The situation here is, however, somewhat different in that the sub-bands shift considerably from the $v_5=1\leftarrow0$ transition and the intensity of the band at 669.8 cm^{-1} seems to be appreciably larger than that expected from a hot band (Fig. 1). In order to determine the spectral origin of these sub-bands, the spectra were recorded at different temperatures. As the temperature was changed from 51 °C to −17 °C, the bands at 649.8 cm^{-1} and 676.9 cm^{-1} showed an appreciable intensity decrease, whereas the band at 669.8 cm^{-1} did not show such a change. This observation suggests that the bands at 649.8 cm^{-1} and 676.9 cm^{-1} may be attributed to hot bands, but the band at 669.8 cm^{-1} may not. At this point, it may be noted that the ν_7 fundamental lies at 222.4 cm^{-1}, and hence the $3\nu_7$ band is expected near the ν_5 fundamental. Incidentally, in the $2\nu_5$ band region, two bands were observed at 1313.1 cm^{-1} and 1340 cm^{-1}; the former is of the parallel type and is much stronger than the letter. These two bands can be assigned to $2\nu_5$ and $\nu_5+3\nu_7$ respectively, if a resonance

TABLE 1. OBSERVED FREQUENCIES OF BENDING FUNDAMENTALS, THEIR OVERTONES AND COMBINATIONS IN GASEOUS CYANOACETYLENE (cm^{-1})

	Job *et al.*[a),c)]	Mallinson *et al.*[b)]	This work[c)]
HCCCN			
$\nu_5+3\nu_7$ / $2\nu_5$	1314		1340 / 1313.1
$2\nu_6$	1010		1012
$\nu_5+\nu_7$	885		
$\nu_6+\nu_7$	720		719
			676.9[d)]
$3\nu_7$ / ν_5	663	663.209	669.8 / 663.7
			649.8[d)]
			514.6[d)]
ν_6	500	498.5	499.2
ν_7		222.402	223.5
DCCCN			
$2\nu_5$	1045		1044.6
$\nu_5+\nu_6$	1015		1015.2
$2\nu_6$			997.6
$\nu_5+\nu_7$	723		
$\nu_6+\nu_7$	702		704
			528.2[d)]
			525.2[d)]
ν_5	522	523.008	522.6
			505.5[d)]
ν_6	494	494.500	494.6
ν_7		213.000	213.0

a) Ref. 3. b) Ref. 5. Band centers which do not include the $-l^2B_v$ term. c) Frequencies of the Q-branch maxima in perpendicular bands or those of the minimum absorption between P and R branches in parallel bands. d) Hot band.

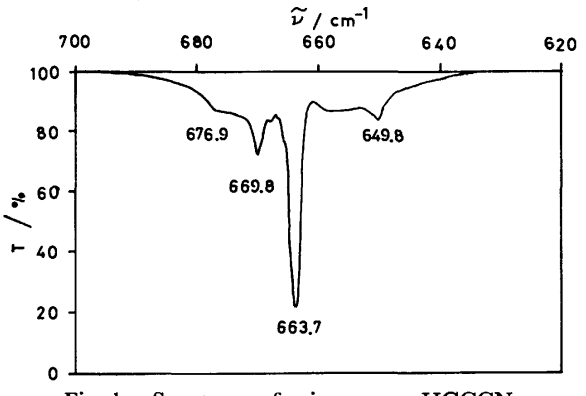

Fig. 1. Spectrum of ν_5 in gaseous HCCCN.

interaction is assumed between $v_5=2$ and $v_5=1$, $v_7=3$ states. Although the existence of the Fermi resonance between $v_5=1$ and $v_7=3$ in Π symmetry state has not been confirmed from the microwave studies,[2] and the origin of the interaction between $v_5=2$ and $v_5=1$, $v_7=3$ states is still open to discussion, the present infrared results may be best interpreted by the energy level diagram shown in Fig. 2, where the Fermi resonance between $v_5=1$ and $v_7=3$ states is taken into account. According to this energy level diagram, the large

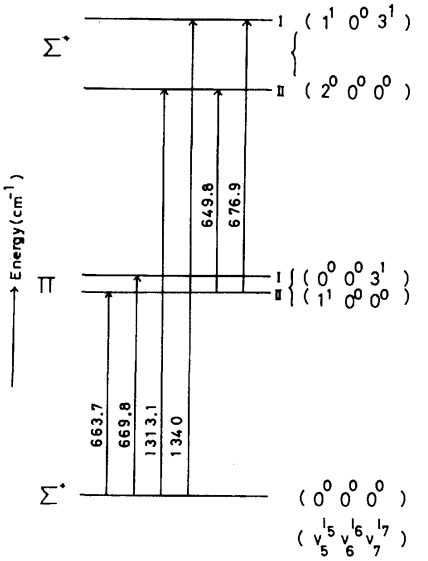

Fig. 2. Energy level diagram involving the excited states of ν_5 and ν_7 in HCCCN.

frequency shifts of the sub-bands are due to the energy splitting in the initial and final states, and the anomalous intensity of the band at 669.8 cm^{-1} is due to the intensity borrowing from ν_5 fundamental. Since the majority of the sub-bands in this region were related to the ν_5 fundamental, the integrated absorption coefficient in this region was ascribed only to the ν_5 fundamental intensity.

In the ν_6 band region of HCCCN, the band at 499.2 cm^{-1} was assigned to the Q-branch of the $v_6=1\leftarrow0$ transition; the band at 514.6 cm^{-1} was assigned to the Q-branch of the $v_6=2\leftarrow1$ transition, and the other weaker bands may be assigned to the hot bands originating from other excited states. Therefore, the observed intensities in this region were integrated to give $B(\nu_6)$.

In the case of DCCCN, ν_5 and ν_6 bands were observed to overlap and form a single band envelope. In this region, two strong bands at 522.6 cm^{-1} and 494.6 cm^{-1} were unambiguously assigned to the Q-branches of $v_5=1\leftarrow0$ and $v_6=1\leftarrow0$ transitions respectively. In addition to these bands, there appeared some bands of small frequency shifts and low intensities relative to $v_5=1\leftarrow0$ or $v_6=1\leftarrow0$ transition, and these may be assigned to a hot band. Then, the intensities in this region were integrated to give an intensity sum $B(\nu_5)+B(\nu_6)$. The method used to separate this sum into individual components will be shown in the later section. Experimental quantities, *i.e.*, $B(\nu_5)$ and $B(\nu_6)$ of HCCCN, and $B(\nu_5)+B(\nu_6)$ of DCCCN, were plotted against to sample pressure p at 273 K, as shown in Fig. 3. Then, the limiting slope at $p\rightarrow0$ was obtained to give the integrated molar absorption coefficient:

$$A(\nu_i)=\int_{\text{band}}\alpha d\tilde{\nu}. \quad (2)$$

The resultant intensity sum $A(\nu_5)+A(\nu_6)$ in DCCCN was divided by the following method. Since the Q-branch intensity of ν_5 band was close to that of ν_6, the integrated intensities were divided at the wavenumber halfway between the Q-branch maxima, and $A(\nu_5)$ and

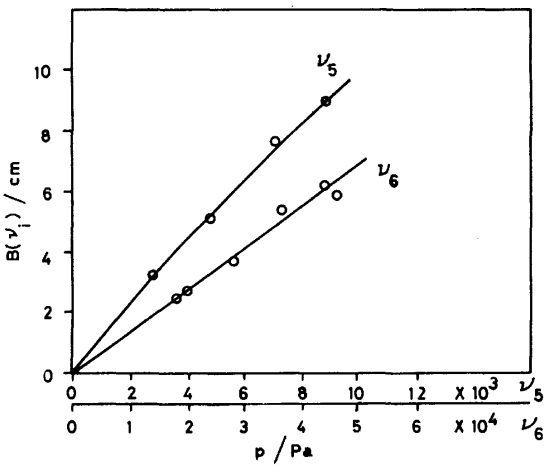

Fig. 3a. Beer's law plots for gaseous HCCCN.

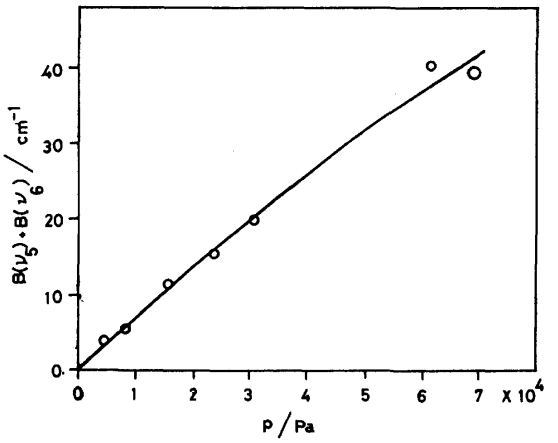

Fig. 3b. Beer's law plots for gaseous DCCCN.

$A(\nu_6)$ were assumed to be proportional to the divided areas of the higher and lower frequency sides. As for the determination of $A(\nu_7)$, the absorption coefficients were integrated over the Q-branch region of ν_6 and ν_7 bands to give $B_Q(\nu_6)$ and $B_Q(\nu_7)$. Then $A(\nu_7)$ was determined from the following expression:

$$A(\nu_7) = A(\nu_6) \times \frac{B_Q(\nu_7)}{B_Q(\nu_6)} \times \frac{p_6}{p_7} \times \frac{l_7}{l_6}, \qquad (3)$$

where l_i is the path-length of the gas cell, and p_i stands for the pressure of the sample. The integrated molar absorption coefficients obtained in this study are shown in Table 2.

TABLE 2. OBSERVED INFRARED INTENSITIES OF BENDING FUNDAMENTALS IN GASEOUS CYANOACETYLENE (km mol^{-1})

	$A(\nu_5)$	$A(\nu_6)$	$A(\nu_7)$
HCCCN	68.4	8.0	0.18
DCCCN	21.0	24.5	0.22

Now, let us consider the errors in the resultant intensities. It is well known that among the various sources of error, the relation between the spectral slit-width and the half-width of the pressure-broadened spectra is most important for the determination of $A(\nu_i)$. In the case of ν_5 and ν_6 fundamentals, the Beer's law plots are seen to be almost linear; this gives the experimental evidence that the relation between the slit-width and the half-width of the spectra was appropriate. Although the Beer's law plots was not available in the ν_7 fundamental, the relation may be regarded as close to that in ν_5 and ν_6, because the spectral slit-width and the total pressure of the gas in the measurement of ν_7 were nearly half of those in ν_5 and ν_6. It is also well known that the half-width of a spectral line is proportional to the pressure of gas when the pressure broadening is the dominant factor for the line-width. The errors in $A(\nu_i)$ may be estimated at 15% for ν_5 and ν_6, and 25% for ν_7, based on the estimation of the errors in the intensities of the stretching fundamentals in gaseous states.

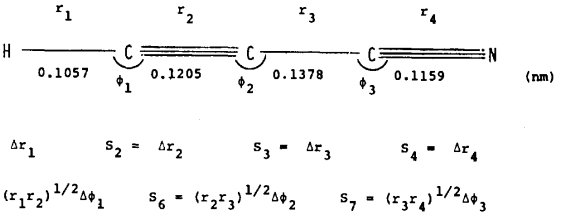

Fig. 4. Molecular structure and internal coordinates.

In order to obtain L^{-1} matrix elements which are necessary for the conversion of $(\partial\mu/\partial Q_i)$ to the dipole-moment derivatives with respect to internal coordinates $(\partial\mu/\partial S_i)$, the force constants for bending vibrations were determined by a least squares method based on the frequency data by Mallinson *et al.*[5] The force constants for stretching vibrations were determined by the same method. The molecular geometry and internal coordinates used are shown in Fig. 4. It is not practical to assume a general valence force field, because the number of the observed frequencies in HCCCN and DCCCN are limited to eight in the stretching vibration and six in the bending vibration, so that the following potential function was used;

$$\begin{aligned} 2V = {} & K_1\Delta r_1^2 + K_2\Delta r_2^2 + K_3\Delta r_3^2 + 2K(\Delta r_2\Delta r_3 + \Delta r_3\Delta r_4) \\ & + H_1 r_1 r_2 \Delta\phi_1^2 + H_2 r_2 r_3 \Delta\phi_2^2 + H_3 r_3 r_4 \Delta\phi_3^2 \\ & + 2H\sqrt{r_1 r_3}\, r_2 \Delta\phi_1\Delta\phi_2, \end{aligned} \qquad (4)$$

where K stands for the interaction between C≡C stretch and C–C stretch, and also for that between C–C stretch and C≡N stretch, whereas H stands for the interaction between HCC bend and CCC bend. When other forms of the function were assumed, the resultant force constants diverged or gave large correlation factors. The force constants, and the calculated and observed frequencies are shown in Table 3, where a fairly good agreement is obtained between them. The largest correlation factor is 0.86 for the element between K_4 and K. Then, $(\partial\mu/\partial S_j)$ were calculated by the following expression, using $(\partial\mu/\partial Q_i)$ and L^{-1} matrix elements obtained above:

$$(\partial\mu/\partial S_j) = \sum_k (\partial\mu/\partial Q_k) L_{kj}^{-1}. \qquad (5)$$

It is well known that $(\partial\mu/\partial S_j)$ derivatives obtained from Eq. 5 include some contribution due to molecular rotation, if S_j and overall rotation belong to the same symmetry species.[6,7] This is the case for the bending vibration of these molecules, so that the derivatives

Table 3a. Force constants of gaseous cyanoacetylene (10^2 N m^{-1})

	Force eonstants	(Dispersion)
K_1	5.924	(0.027)
K_2	15.93	(0.15)
K_3	6.673	(0.126)
K_4	17.21	(0.30)
K	0.607	(0.090)
H_1	0.1882	(0.0015)
H_2	0.1643	(0.0043)
H_3	0.2224	(0.0038)
H	0.0672	(0.0026)

Table 3b. Calculated frequencies of gaseous cyanoacetylene (cm^{-1})

	HCCCN		DCCCN	
	Mallinson[a]	Calculated	Mallinson[a]	Calculated
ν_1	3327.372	3332.2	2608.520	2600.3
ν_2	2273.996	2279.6	2252.155	2246.7
ν_3	2079.306	2083.1	1968.329	1967.0
ν_4	863.5	863.9	850.3	849.7
ν_5	663.209	664.2	523.008	521.8
ν_6	498.5	500.3	494.500	492.7
ν_7	222.554	222.2	213.000	213.0

a) Ref. 5. Band centers which do not include the $-l^2B_v$ term.

obtained from HCCCN and DCCCN are designated as $(\partial\mu/\partial S_j)_H$ and $(\partial\mu/\partial S_j)_D$, because the effect of the compensating rotation is different for different isotopes. In order to compare these derivatives on the same basis, a reference molecule was assumed, where the mass of hydrogen atom is supposed to be zero. Then, it can be shown that the experimental quantities $(\partial\mu/\partial S_j)_H$ and $(\partial\mu/\partial S_j)_D$ are related to $(\partial\mu/\partial S_j)_R$ in this reference molecule by the following expression:

$$(\partial\mu/\partial S_j)_R = (\partial\mu/\partial S_j)_H - (\partial\mu/\partial S_j)^{Corr}_{R.H}, \quad (6a)$$

$$(\partial\mu/\partial S_j)_R = (\partial\mu/\partial S_j)_D - (\partial\mu/\partial S_j)^{Coor}_{R.D}, \quad (6b)$$

where $(\partial\mu/\partial S_j)^{Corr}_{R.H}$ and $(\partial\mu/\partial S_j)^{Corr}_{R.D}$ stand for the rotational corrections. These correction terms can be calculated by the following expression:

$$(\partial\mu/\partial S_j)^{Corr}_{R.I} = \sum_{s=1}^{3N}(\partial\mu/\partial x_s)\sum_{n=1}^{6}(\alpha_R)_{s,n}\Big[\sum_{\substack{t=1\\ I=H.D}}^{3N}(\beta_R)_{n,t}(A_I)_{t,j}\Big], \quad (7)$$

where μ is the molecular permanent dipole-moment and A, β, and α are the matrices relating the Cartesian displacement coordinates x with the internal coordinates S and the coordinates of translation and rotation ρ:

$$x_s = \sum_{k=1}^{3N-6}(A_I)_{s,k}S_k + \sum_{n=1}^{6}(\alpha_I)_{s,n}(\rho_I)_n, \quad (8a)$$

$$S_k = \sum_{s=1}^{3N-6}B_{k,s}x_s, \quad (\rho_I)_n = \sum_{\substack{s=1\\ I=H.D}}^{3N}(\beta_I)_{n,s}x_s. \quad (8b)$$

Since the signs of $(\partial\mu/\partial Q_i)$ are not determinable experimentally, all possible sign combinations in $(\partial\mu/\partial Q_i)$ are shown in Table 4, together with the rotational correction terms. It may be seen from the table that the sign combinations $(+-+)$ and $(+--)$ with the correction term subtracted give better agreement between HCCCN and DCCCN: $(+--)$ gives the best agreement in $(\partial\mu/\partial S_5)_R$ and $(\partial\mu/\partial S_7)_R$, whereas $(+-+)$ gives the best agreement in $(\partial\mu/\partial S_6)_R$. It may be pointed out here that the observed $(\partial\mu/\partial S_6)_R$ may contain a larger error that the others, because $A(\nu_7)$ is expected to contain the largest error in the three bending fundamentals and it gives the largest contribution to $(\partial\mu/\partial S_6)_R$. Therefore, the difference of $(\partial\mu/\partial S_6)_R$ in $(+--)$ may be ascribed to the experimental error. In view of the above discussions, it seems most reasonable to take the $(+--)$ sign combination with the correction term subtracted as the most preferable one. In order to determine the direction of the rotational correction term, it is necessary to know the direction of the permanent dipole-moment μ. For this purpose, the semi-empirical SCF calculation was carried out and the dipole-moment μ was obtained to be 2.93 D, with the polarity of $\overset{+}{H}CCC\overset{-}{N}$. This polarity agrees with that expected from the generally accepted bond polarities of $\overset{+}{H}$–$\overset{-}{C}$ and $\overset{+}{C}\equiv\overset{-}{N}$. The rotational correction terms

Table 4a. Calculated values of the rotational correction term[a] (D/A)

	S_5	S_6	S_7
HCCCN	−0.11	−0.11	−0.05
DCCCN	−0.19	−0.21	−0.10

a) Calculated using $\mu=3.724$ D (Ref. 2). The positive direction of the dipole-moment change caused by atomic displacements is shown in Fig. 5.

Table 4b. Possible combinations of relative signs in $(\partial\mu/Q_5, \partial\mu/Q_6, \partial\mu/Q_7)$ (D/A)

		+++	+−+	++−	+−−
(Rotational correction term added)					
S_5	HCCCN	−0.74	−0 79	−0.71	−0.76
	DCCCN	0.02	−0.72	0.08	−0.66
S_6	HCCCN	−0.01	−0.47	0 21	−0.25
	DCCCN	0.55	−0.29	0.83	−0.01
S_7	HCCCN	−0.43	0.36	−0.25	0.54
	DCCCN	−0.90	0.39	−0.70	0.59
(Rotational correction term subtracted)					
S_5	HCCCN	−0.96	−1.01	−0.93	−0.98
	DCCCN	−0.36	−1.10	−0.30	−1.04
S_6	HCCCN	−0.23	−0.69	−0.01	−0.47
	DCCCN	0.13	−0.71	0.41	−0.43
S_7	HCCCN	−0.53	0 26	−0.35	0.44
	DCCCN	−1.10	0.19	−0.90	0.39

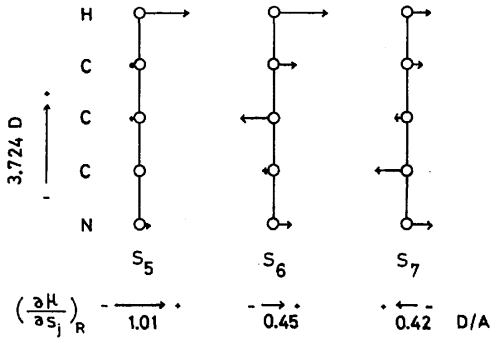

Fig. 5. Atomic displacements along internal coordinates and changes of dipole-moment.

were calculated from the dipole-moment of 3.724 D derived from the microwave studies[2] with the polarity of $\overset{+}{H}CCC\overset{-}{N}$. The experimentally determined relative signs in $(\partial\mu/\partial S_j)_R$ and $(\partial\mu/\partial S_j)^{corr}_{R,H(D)}$ then lead to the determination of the direction of each $(\partial\mu/\partial S_j)_R$. The atomic displacements along each internal coordinate and the resultant changes of the dipole-moment are shown in Fig. 5. It may be noted that $(\partial\mu/\partial S_5)_R$ of cyanoacetylene and $(\partial\mu/\partial S_2)_R$ of hydrogen cyanide have same direction and their values are close, *i.e.*, the value of $(\partial\mu/\partial S_2)_R$ in hydrogen cyanide after the rotational correction has been taken into account is 1.08 D/A. It can be seen from the B matrix elements for each internal coordinate that both dipole-moment derivatives are due to the displacement of hydrogen atoms. Therefore, the close agreement between them may be regarded as the experimental evidence of the similar nature of the H–C bond in these molecules. Though it does not seem so simple to relate the dipole-moment derivatives to each bond polarity of molecule, as in the case of $(\partial\mu/\partial S_5)_R$, the dominant part of $(\partial\mu/\partial S_7)_R$ may be due to the C≡N bond which has a high polarity of $\overset{+}{C}\equiv\overset{-}{N}$.

The authors wish to express their thanks to Professor Shiro Maeda and Professor Chiaki Hirose of Tokyo Institute of Technology for helpful discussions and encouragements. The normal coordinate calculations and the semi-empirical SCF (CNDO) calculations were carried out at the Computer Center, the University of Tokyo.

References

1) S. Deguchi, Y. Nakada, T. Onaka, and M. Uyemura, *Publ. Astron, Soc. Jpn.*, **31**, 105 (1979).
2) W. J. Lafferty and F. J. Lovas, *J. Phys. Chem. Ref. Data*, **7**, 441 (1978).
3) G. C. Turrell, W. Johns, and A. Maki, *J. Chem. Phys.*, **26**, 1544 (1957); V. A. Job and G. W. King, *Can. J. Chem.*, **41**, 3132 (1962); C. Nolin, J. Weber, and R. Savoie, *J. Raman Spectrosc.*, **5**, 21 (1976).
4) M. Uyemura and S. Maeda, *Bull. Chem. Soc. Jpn.*, **47**, 2930 (1974).
5) P. D. Mallinson and A. Fayt, *Mol. Phys.*, **32**, 473 (1976).
6) J. Overend, "Infrared Spectroscopy and Molecular Structure," ed by M. Davis, Elsevier Publ. Co., Amsterdam (1963), p. 374.
7) B. Crawford, Jr., *J. Chem. Phys.*, **20**, 977 (1952); A. D. Dickson, I. M. Mills, and B. Crawford, Jr., *ibid.*, **27**, 445 (1957).
8) M. Uyemura and S. Maeda, *Bull. Chem. Soc. Jpn.*, **45**, 1081 (1972).
9) E. B. Wilson and A. T. Wells, *J. Chem. Phys.*, **14**, 578 (1946).
10) J. A. Pople and G. A. Segal, *J. Chem. Phys.*, **43**, s 136, (1965); **44**, 3289 (1966).

 © 1982 The Chemical Society of Japan Bull. Chem. Soc. Jpn., 55, 389—393 (1982)

Hydrates of Organic Compounds. VI. Heats of Fusion and of Solution of Quaternary Ammonium Halide Clathrate Hydrates

Haruo NAKAYAMA

Department of Chemistry, Faculty of Engineering, Yokohama National University, Tokiwadai, Hodogaya-ku, Yokohama 240

(Received June 10, 1981)

The heat of solution in water of four quaternary ammonium halide clathrate hydrates, $R_4NX \cdot nH_2O$ ($R = n\text{-}C_4H_9$, X=F and Cl, $n=30$; $R = i\text{-}C_5H_{11}$, X=F and Cl, $n=39$), and the heat of dilution of their aqueous solutions were measured calorimetrically. From these results, the heat of fusion of the clathrate hydrate solid (ΔH_f) and the heat of solution of it in saturated solutions (ΔH_{sat}) were obtained. The ΔH_f was compared with a hypothetical heat of fusion of the same number of moles of ice I as the hydration number of the hydrate. The ΔH_{sat} was about 14 kJ/mol smaller than the ΔH_f in the $(n\text{-}C_4H_9)_4NX$ hydrates and about 27 kJ/mol smaller in the $(i\text{-}C_5H_{11})_4NX$ hydrates irrespective of the type of anion. Furthermore, ΔH_{sat} was calculated thermodynamically and it agreed with the calorimetrically obtained value within the experimental error.

Clathrate-like hydrates of quaternary ammonium salts, which were originally found in Kraus' laboratory in 1940[1] and were examined later in detailed structural studies by Jeffrey *et al.*,[2-4] have been known to have some unusual properties in comparison with ordinary gas hydrates. The most striking features are summarized as follows:

(1) They are easily formed by cooling their aqueous solutions at atmospheric pressure and the concentration range from which the hydrate is separated out is very wide, especially for a stable hydrate.[5] (2) Generally these hydrates are very stable, *i.e.*, they have fairly high melting points as compared to ordinary gas hydrates. Melting points at around room temperature are not unusual. (3) The formation of such a hydrate is possible for salts having a variety of anions,[2,5] but a suitable alkyl chain of the cation is almost exclusively limited to the butyl or the isopentyl group.[6]

The thermodynamic properties of aqeous tetraalkylammonium salt solutions have been extensively studied[7] and the results of these studies are often interpreted by structural modifications of water molecules around the cation from analogy with the clathrate hydrates. However little is known about the thermodynamic properties of the clathrate hydrate itself. Such thermodynamic properties as the heat of fusion and of solution of the clathrate hydrate are basic properties not only for the interpretation of the nature of the hydrogen-bonded water networks around the alkyl groups of the cation but also for an application of these hydrates as, for example, a heat reservoir utilizing the heat evolved or absorbed when their states change.

In this paper the author reports the heats of fusion and of solution in water of four clathrate hydrates, $(n\text{-}C_4H_9)_4NF \cdot 30H_2O$, $(n\text{-}C_4H_9)_4NCl \cdot 30H_2O$, $(i\text{-}C_5H_{11})_4NF \cdot 39H_2O$, and $(i\text{-}C_5H_{11})_4NCl \cdot 39H_2O$, and discusses the effect of the type of the anion and of the alkyl group of the cation on these thermal properties. In addition, the calorimetrically determined heats of solution are compared with those calculated from the data concerning both temperature dependence of the solubilities and concentration dependence of the mean molal activity coefficients.

The hydrates used in this paper are the most convenient ones for calorimetric measurement since they all have relatively high congruent melting points and each hydration number has been well determined in previous phase-diagramatic investigations.[5]

Experimental

Materials. The procedures for preparing and purifying the materials used in this experiment were the same as those in the previous work.[5,8] The concentration of the mother solution was determined by the Karl Fischer titration method for the fluoride solutions and by a standard KNCS titration method (Volhard method) for the chloride solutions.[5]

Calorimetry. A twin-type rotating-microcalorimeter manufactured by Ōyōdenki Kenkyujo (RCM-1N)[9] was used. The mixing cell was a glass cylinder of 45 mm diameter and 30 mm high. Part of it was divided into two compartments by a glass wall and a sample solution and water were loaded into each compartment from a weighed syringe fitted with a stainless steel needle.

The heats of dilution (or solution) at infinite dilution were obtained by measuring heat changes in the following two steps: sample solution (or solid)→0.07 mol kg^{-1} solution→0.005 mol kg^{-1} solution. The heat due to a further dilution from 0.005 mol kg^{-1} which was estimated to be smaller than 0.1 kJ/mol, was neglected. The heat evolved in the second stage of dilution was also small compared with that in the first stage of dilution (or solution) and was found to be 0.68 kJ/mol, 0.52 kJ/mol, 1.29 kJ/mol, and 1.14 kJ/mol for $(n\text{-}C_4H_9)_4NF$, $(n\text{-}C_4H_9)_4NCl$, $(i\text{-}C_5H_{11})_4NF$, and $(i\text{-}C_5H_{11})_4NCl$, respectively.

In this experiment the following three heats were determined for each salt. These heats and their experimental methods for measuring the heat changes in the first step of dilution (or solution) are summarized as follows:

(i) The Heat of Solution of a Clathrate Hydrate Solid in Water at Infinite Dilution (ΔH_S). A given amount of a sample solution whose concentration was equal to its congruent composition (1.850 mol kg^{-1} for the tetrabutylammonium salts and 1.423 mol kg^{-1} for the tetraisopentylammonium salts) was loaded into one of the compartments of the cell at temperatures a few degrees higher than its congurent melting point (T_C). Then the cell was gradually cooled down, with occasional shaking, until the sample solution solidified after which it was kept standing for about 4 h at a temperature a few degrees lower than the T_C in order to anneal the solid. Next the cell was loaded into the calorimeter, followed by the insertion of water into the other compartment of the cell in amounts which corresponded to a final concentration of 0.07 mol kg^{-1}. After thermal equilibrium was reached, the heat change was

measured when the solid was dissolved in the water.

(ii) The Heat of Dilution in Water of a Metastable Clathrate Hydrate Liquid at Infinite Dilution ($-\phi_{L,C}$). Since the liquid sample whose concentration was equal to its congruent composition could stay in a metastable liquid state for a long time at the measuring temperature (10 °C for the (n-$C_4H_9)_4$NCl and 25°C for the other salts) if not cooled down deliberately as in (*i*), its heat of dilution could easily be measured by mixing it with water. A given amount of a sample solution whose concentration was equal to its congruent composition was loaded into one compartment of the cell at a temperature a few degrees higher than its T_C. The cell was then loaded into the calorimeter, followed by the insertion of an adequate amount of water into the other compartment of the cell. After thermal equilibrium was attained, the heat change was measured when both liquids were mixed.

(iii) The Heat of Dilution of a Salt Solution from a Saturated Solution to an Infinitely Dilute Solution ($-\phi_{L,sat}$). The heat of dilution of a given amount of salt solution whose concentration was equal to its solubility at a measuring temperature was measured in a similar way as in (*ii*).

The three heats measured and other heats discussed in later sections are mutually interconnected by the following scheme:

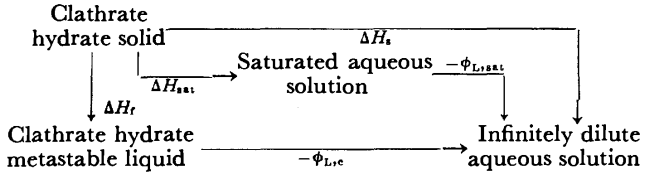

Solubility and Mean Molal Activity Coefficient Measurements.

The solubilities of the clathrate hydrate solid in water were measured by the following manner. In a glass cylinder, which was 30 mm diameter and 100 mm high and was immersed in a constant temperature bath, the solid hydrate was saturated in about 10 cm^3 water by vigorous stirring with a magnetic stirrer. Then a given amount of the saturated solution was withdrawn and analyzed. In the case of the fluoride solutions, concentration was determined by measuring the water content by the Karl Fischer titration method for the sample solution which had partially been concentrated by dehydration on P_2O_5 in a desiccator. The standard KNCS titration method (Volhard method[5]) was used for the chloride solutions.

The mean molal activity coefficients ($\gamma_\pm$) for the tetraisopentylammonium salt solutions were obtained from the isopiestic data by the conventional method.[10,11] The apparatus and procedure for the isopiestic measurements were the same as that in the previous work.[12]

Results and Discussion

(1) Fundamental Properties of the Clathrate Hydrates. Prior to the calorimetric experiments we must specify the fundamental properties of each clathrate hydrate such as the hydration number (n), the congruent melting point (T_C), and the solubility in water (m_{sat}). These values are summarized in Table 1. Although somewhat different hydration numbers are found in the literature,[2,5,8,13] we chose 30 for the (n-$C_4H_9)_4$NX hydrates and 39 for the (i-$C_5H_{11})_4$NX hydrates by reference to our previous phase-diagramatic results.[5] Therefore, the congruent compositions become 1.850 mol kg^{-1} for tetrabutylammonium halide systems and 1.423 mol kg^{-1} for the tetraisopentylammonium halide systems.

Table 1. Fundamental properties of the tetraalkylammonium halide (R_4NX) clathrate hydrates

R_4NX	Hydration number[5]	Mp θ_m[5] / °C	Solubility in water / mol kg^{-1}
(n-$C_4H_9)_4$NF	30	28.3	0.920±0.002[a]
(n-$C_4H_9)_4$NCl	30	15.0	0.561±0.003[b]
(i-$C_5H_{11})_4$NF	39	31.5	0.293±0.002[a]
(i-$C_5H_{11})_4$NCl	39	29.6	0.203±0.002[a]

a) At 25 °C. b) At 10 °C.

Calorimetric measurements were carried out at 10 °C for the (n-$C_4H_9)_4$NCl system and at 25 °C for the other three systems, taking into account each congruent melting point listed in Table 1.[5]

(2) Calorimetric Measurements. The observed ΔH_s's and ϕ_L's are summarized in Table 2. The physical meaning of these quantities has been explained in the experimental section. Listed values were averages of 4—5 determinations. The error limit attached to each value was estimated by taking into account the dispersion in each measurement as well as the errors inherent in sampling the solution and in determining its concentration.

Narten and Lindenbaum[13] have reported ΔH_s and $\phi_{L,c}$ for (n-$C_4H_9)_4$NF hydrate, which are also listed in Table 2. Their values are somewhat higher than the present values. The values of $\phi_{L,c}$ and $\phi_{L,sat}$ for (n-$C_4H_9)_4$NCl solutions which are calculated from the heats of dilution data at 25 °C (not at 10 °C) obtained by Lindenbaum[14] are also listed in Table 2. These

Table 2. The heats of solution of the tetraalkylammonium halide (R_4NX) clathrate hydrates and the relative apparent molal heat contents of the aqueous R_4NX solutions

R_4NX	Temperature / °C	ΔH_s / kJ mol^{-1}	$\phi_{L,c}$ / kJ mol^{-1}	$\phi_{L,sat}$ / kJ mol^{-1}
(n-$C_4H_9)_4$NF	25	158.6±3.7 (170.6[13])	25.8±0.5 (26.6[13])	12.6±0.2
(n-$C_4H_9)_4$NCl	10	136.2±4.0	19.5±0.4 (20.5[14])[a]	5.5±0.2 (5.2[14])[a]
(i-$C_5H_{11})_4$NF	25	223.1±5.0	32.8±1.2	6.2±0.3
(i-$C_5H_{11})_4$NCl	25	253.0±4.2	29.7±0.3	3.9±0.2

a) At 25 °C.

values are in fairly good agreement with the present data regardless of the slight difference in temperature.

The heat of fusion of clathrate hydrate solid (ΔH_f) and its heat of solution in a saturated aqueous solution (ΔH_{sat}) can be calculated by the following relations:

$$\Delta H_f = \Delta H_s + \phi_{L,c}, \quad (1)$$

$$\Delta H_{sat} = \Delta H_s + \phi_{L,sat}. \quad (2)$$

These heats are tabulated in Table 3 and discussed in the following sections.

Table 3. The heats of fusion of the tetraalkylammonium halide (R_4NX) clathrate hydrates and the heats of solution of them in saturated aqueous solutions

Hydrate	Temperature °C	ΔH_f kJ mol^{-1}	ΔH_{sat} kJ mol^{-1}
$(n\text{-}C_4H_9)_4NF\cdot 30H_2O$	25	184±4	171±4
$(n\text{-}C_4H_9)_4NCl\cdot 30H_2O$	10	156±4	142±4
$(i\text{-}C_5H_{11})_4NF\cdot 39H_2O$	25	256±5	229±5
$(i\text{-}C_5H_{11})_4NCl\cdot 39H_2O$	25	283±4	257±4

(3) The Heats of Fusion of Clathrate Hydrate Solids. The heat of fusion of a tetraalkylammonium halide clathrate hydrate may be considered to be made up by the following three terms:

$$\Delta H_f = \Delta H_c + \Delta H_e + \Delta H_h, \quad (3)$$

in which ΔH_c is the change in enthalpy of the hydrogen-bonded water networks (cages) when a clathrate hydrate solid melts, ΔH_e and ΔH_h is the change in electrostatic energy between ions and that in the energy due to additional hydration of ions, respectively. Although it is impossible to discuss each enthalpy change quantitatively, we can reasonably assume that the last two heats, ΔH_e and ΔH_h, are relatively small as compared with the first term, ΔH_c, from the following reasons: (1) The local structure of the melt is expected to be essentially similar to that of the solid state, as exemplified for $(n\text{-}C_4H_9)_4NF$ solution.[13] Thus, interionic distance will not change appreciably when the solid melts. (2) A large extent of additional hydration of the ions cannot be expected from the fact that all the ions are already surrounded by water molecules in the solid state and further that the total amount of water remains constant in the melting process.

Therefore, if we assume that the last two terms of Eq. 3 are negligible as compared with the first term and further that the first term may be approximately expressed as $n\cdot\Delta H_{f,ice}$, Eq. 3 becomes

$$\Delta H_f \simeq \Delta H_c \simeq n\cdot\Delta H_{f,ice}, \quad (4)$$

in which n is the hydration number of a clathrate hydrate, and $\Delta H_{f,ice}$ is a hypothetical molal heat of fusion of ice I at the measuring temperature. This heat of fusion is estimated to be 6.375 kJ/mol at 10 °C and 6.896 kJ/mol at 25 °C taking into account the heat capacity data.[15] Equation 4 has been proved to be fairly adequate for ordinary gas hydrates[16,17] or for some of the liquid hydrates.[18] However, it may not be so appropriate for the tetraalkylammonium salt hydrates since the central N atom of the cation and the fluoride anion (and probably also the chloride anion) replace water molecules within the lattice. This leads to the disappearance of some of the hydrogen bonds and a decrease in the number of stable orientations of the water molecules at sites neighboring the N^+ and F^- (and Cl^-) sites.[3,4,17]

Tentatively, the observed ΔH_f's (Table 3) were compared with the calculated $n\cdot\Delta H_{f,ice}$ in the form of the ratio of the two, $\Delta H_f/n\cdot\Delta H_{f,ice}$. This ratio was 0.89, 0.82, 0.95, and 1.05 for $(n\text{-}C_4H_9)_4NF$, $(n\text{-}C_4H_9)_4NCl$, $(i\text{-}C_5H_{11})_4NF$, and $(i\text{-}C_5H_{11})_4NCl$ hydrate, respectively. This result indicates that the apparent heats of fusion of the tetrabutylammonium halide hydrates are a little smaller (about 85%) than that of a hypothetical heat of fusion of ice I of the same number of moles as the hydration number of the hydrates, whereas those of the tetraisopentylammonium halide hydrates are approximately equal to the corresponding heats of fusion of ice I. The reason for this different behavior in the two series of hydrates can be explained, at least partly, by the following facts; (a) the proportion of the water molecules which are structurally affected by the presence of R_4N^+ cation and F^- anion (or Cl^- anion) is larger in the tetrabutylammonium halide hydrate than in the tetraisopentylammonium halide hydrate since the hydration number of the former is smaller than that of the latter; (b) the hydrogen-bonded water networks in the tetraisopentylammonium halide hydrate seem to be stabler than that in the tetrabutylammonium halide hydrate since the melting points of the tetraisopentylammonium halide hydrates are relatively high and are not so predominantly affected by the kind of anion.[2,5] Furthermore, even $(i\text{-}C_5H_{11})_4NI$ can form a clathrate-like hydrate.[5] Tetrabutylammonium iodide cannot form a clathrate hydrate, presumably because a stabilizing ability of water networks surrounding the butyl chain is not strong enough to overcome the lattice distortion caused by the presence of the bulky iodide anion.

(4) The Heats of Solution of the Clathrate Hydrate Solids in Saturated Aqueous Solutions. From Eqs. 1 and 2, the ΔH_{sat} can be expressed by the following relation:

$$\Delta H_{sat} = \Delta H_f - (\phi_{L,c} - \phi_{L,sat}). \quad (5)$$

The heat in the parenthesis of the right-hand side of the above equation is made up by two heats of dilution which are due to an additional hydration of ions including hydrophobic hydration. It should be noted that, from Table 2 (or 3), this quantity is about 14 kJ/mol for the tetrabutylammonium halide hydrates and about 27 kJ/mol for the tetraisopentylammonium halide hydrates irrespective of the type of the anion and further that these heats correspond roughly to about 10% of the ΔH_{sat} in each hydrate. Therefore, it may be concluded that the heat of solution of a clathrate hydrate has similar values to its heat of fusion and, in turn, the latter heat may approximately be estimated by Eq. 4. The phenomenon that the heat of solution of a solid is close to its heat of fusion is commonly found in the dissolution process of ordinary hydrated electrolytes like $CaCl_2\cdot 6H_2O$.[19]

On the other hand, the heat of solution of a hydrated electrolyte in saturated solution can be expressed by the following thermodynamic equation:[19]

$$\Delta H_{sat} = -\nu R(1-nm_{sat}/M)^2 \times (1 + (\partial \ln \gamma_{\pm}/\partial \ln m)_{sat}) \times (\partial \ln m'_{sat}/\partial(1/T)), \quad (6)$$

in which $\nu=\nu_+ + \nu_-$, R=the gas constant, n=the hydration number, m_{sat}=solubility expressed in molality, M=55.51, $\gamma_{\pm}$=mean molal activity coefficient, $m'_{sat}=m_{sat}/(1-nm_{sat}/M)$, and T=the absolute temperature. Though this equation has been applied to ordinary inorganic hydrated electrolytes and its validity has been verified in several systems,[19] it has not previously been applied to a clathrate hydrate system. Therefore, it is interesting to see to what extent the heat of solution which is calculated by Eq. 6 is compatible with that directly obtained by calorimetry (Table 3).

The values of $(\partial \ln \gamma_{\pm}/\partial \ln m)_{sat}$ for the two tetrabutylammonium halide solutions were calculated from existing data[20,21] and those for the tetraisopentylammonium halide solutions were newly obtained in this experiment from the isopiestic data. Because of the low solubilities of the two tetraisopentylammonium halide hydrates (Table 1), which are compatible with the concentration limit (about 0.1 mol kg^{-1} [10]) to which an accurate isopiestic measurement can be done, the values of $(\partial \ln \gamma_{\pm}/\partial \ln m)_{sat}$ for these two halide solutions have errors in the order of 4—5%. The temperature dependence of the solubilities of all the hydrates are shown in Fig. 1. The slopes of $\partial \ln m'_{sat}/\partial(1/T)$, which were obtained by graphical differentiation of Fig. 1, have also some uncertainties since $\ln m'_{sat}$ decreases nonlinearly with increasing $1/T$. The calculated ΔH_{sat} and all the values used for this calculation are summarized in Table 4. These calculated values of ΔH_{sat} agree within experimental error with those obtained by direct calorimetry (Table 3). It is interesting to note that, as is seen from Table 4, the approximate values of the ΔH_{sat} for the two chloride hydrates can be calculated only from the solubility *vs.* temperature data since the values $(\partial \ln \gamma_{\pm}/\partial \ln m)_{sat}$ are relatively small as compared with unity for these hydrates.

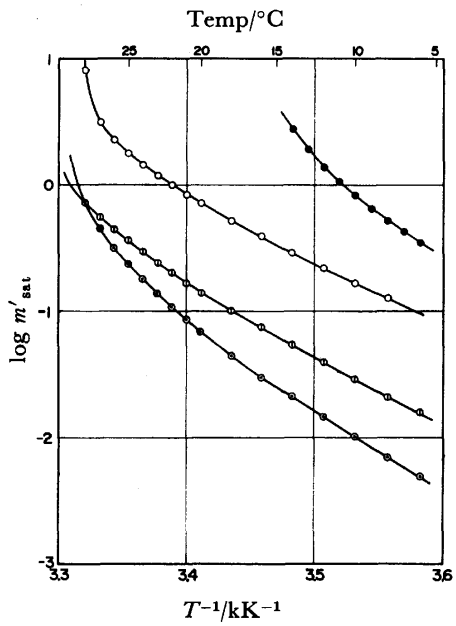

Fig. 1. Temperature dependence of the solubilities (m'_{sat}) of tetraalkylammonium halide clathrate hydrates in water:
$(n\text{-}C_4H_9)_4NF \cdot 30H_2O$ (○); $(n\text{-}C_4H_9)_4NCl \cdot 30H_2O$ (●); $(i\text{-}C_5H_{11})_4NF \cdot 39H_2O$ (◑); $(i\text{-}C_5H_{11})_4NCl \cdot 39H_2O$ (⊙).

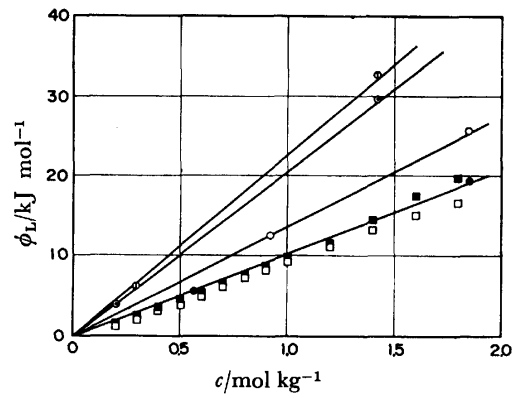

Fig. 2. Concentration dependence of the relative apparent molal heat contents (ϕ_L) of tetraalkylammonium halide solutions:
$(n\text{-}C_4H_9)_4NF$ at 25 °C (○); $(n\text{-}C_4H_9)_4NCl$ at 10 °C (●); $(i\text{-}C_5H_{11})_4NF$ at 25 °C (◑); $(i\text{-}C_5H_{11})_4NCl$ at 25 °C (⊙); $(n\text{-}C_4H_9)_4NCl$ at 25 °C taken from Ref. 14 (■); $(n\text{-}C_4H_9)_4NBr$ at 25 °C taken from Ref. 14 (□).

(5) The Relative Apparent Molal Heat Contents. In Table 2, two relative apparent molal heat contents, $\phi_{L,c}$ and $\phi_{L,sat}$, are given for each salt solution. These values are plotted against m in Fig. 2, assuming that ϕ_L is a linear function of m in the concentration range studied rather than a linear function of $\sqrt{m}$ as derived from the limiting law.[11] This assumption seems to be reasonable, at least as a first approximation, as exemplified in Fig. 2 by the data for $(n\text{-}C_4H_9)_4NCl$ and $(n\text{-}C_4H_9)_4NBr$ (at 25 °C) solutions obtained by Lindenbaum.[14] Figure 2 clearly indicates that the increase of ϕ_L with increasing m for the tetraisopentylammonium salt is more marked than that for the tetrabutylammonium salt, irrespective of the type of anion.

Table 4. The tabulation of each term in Eq. 6 and the calculation of ΔH_{sat}

Hydrate	Temp °C	$(1-nm_{sat}/M)^2$	$1+(\partial \ln \gamma_{\pm}/\partial \ln m)_{sat}$	$\partial \ln m'_{sat}/\partial(1/T)$ 10^4 K	ΔH_{sat} kJ mol^{-1}
$(n\text{-}C_4H_9)_4NF \cdot 30H_2O$	25	0.253±0.001	1.830±0.005	−2.14±0.05	165±4
$(n\text{-}C_4H_9)_4NCl \cdot 30H_2O$	10	0.486±0.003	0.931±0.005	−1.80±0.03	135±3
$(i\text{-}C_5H_{11})_4NF \cdot 39H_2O$	25	0.631±0.003	1.23 ±0.05	−1.84±0.04	237±11
$(i\text{-}C_5H_{11})_4NCl \cdot 39H_2O$	25	0.735±0.002	0.95 ±0.05	−2.27±0.05	263±15

This indicates that the structural modification of the water molecules around the isopentyl group is greater than that around the butyl group. The high stability of the tetraisopentylammonium halide hydrates has already been pointed out in section *(3)*.

References

1) D. L. Fowler, W. V. Loebenstein, D. B. Pall, and C. A. Kraus, *J. Am. Chem. Soc.*, **62**, 1140 (1940).
2) R. McMullan and G. A. Jeffrey, *J. Chem. Phys.*, **31**, 1231 (1959).
3) R. K. McMullan, M. Bonamico, and G. A. Jeffrey, *J. Chem. Phys.*, **39**, 3295 (1963).
4) D. Feil and G. A. Jeffrey, *J. Chem. Phys.*, **35**, 1863 (1961).
5) H. Nakayama, *Bull. Chem. Soc. Jpn.*, **54**, 3717 (1981).
6) H. Nakayama and K. Watanabe, *Bull. Chem. Soc. Jpn.*, **49**, 1254 (1976).
7) W.-Y. Wen, "Water and Aqueous Solutions," ed by R. A. Horne, John Wiley and Sons, Inc., New York (1971), Chap. 15.
8) H. Nakayama, *Bull. Chem. Soc. Jpn.*, **52**, 52 (1979).
9) H. Nakayama and K. Shinoda, *J. Chem. Thermodyn.*, **3**, 401 (1971).
10) R. A. Robinson and R. H. Stokes, "Electrolyte Solutions," 2nd ed, Butterworths, London (1970), Chap. 8.
11) H. S. Harned and B. B. Owen, "The Physical Chemistry of Electrolytic Solutions," Reinhold Publishing Corporation, New York (1958), Chap. 9.
12) H. Nakayama, *Bull. Chem. Soc. Jpn.*, **45**, 1371 (1972).
13) A. H. Narten and S. Lindenbaum, *J. Chem. Phys.*, **51**, 1108 (1969).
14) S. Lindenbaum, *J. Phys. Chem.*, **70**, 814 (1966).
15) H. F. Stimso, *Am. J. Phys.*, **23**, 614 (1955); D. Eisenberg and W. Kauzmann, "The Structure and Properties of Water," Oxford Univ. Press, London (1969).
16) R. de Forcrand, *Compt. Rend.*, **134**, 835 (1902).
17) D. W. Davidson, "Water," ed by F. Franks, Plenum Press (1973), Vol. 2, Chap. 3.
18) H. Nakayama and M. Tahara, *Bull. Chem. Soc. Jpn.*, **46**, 2965 (1973).
19) H. Nakayama, *Bull. Chem. Soc. Jpn.*, **44**, 1709 (1971); *Bull. of the Faculty of Engineering, Yokohama National University*, **19**, 29 (1970).
20) S. Lindenbaum and G. E. Boyd, *J. Phys. Chem.*, **68**, 911 (1964).
21) W.-Y. Wen, S. Saito, and C. Lee, *J. Phys. Chem.*, **70**, 1244 (1966).

Catalytic Properties of Perovskite-type Mixed Oxides, $La_{1-x}Sr_xCoO_3$

Teiji NAKAMURA, Makoto MISONO,* and Yukio YONEDA

Department of Synthetic Chemistry, Faculty of Engineering, The University of Tokyo, Hongo, Bunkyo-ku, Tokyo 113

(Received June 8, 1981)

The reactivity and related properties of oxygen both in the bulk and on the surface has been investigated for perovskite-type mixed oxides ($La_{1-x}Sr_xCoO_3$), in regard to the effects of Sr^{2+}-substitution and calcination temperature. The reducibility and the readiness of oxygen desorption increased with the Sr^{2+} content, x, but the reoxidation became slower with x. These results have been explained on the basis of the change in the chemical potential of lattice oxygen. The diffusivity of oxygen in the bulk and the ability to activate the oxygen molecule also increased with x. Oxygen vacancies in the bulk and on the surface, which tended to increase with x, are likely responsible for these reactions. The release of oxygen from the bulk became more difficult as the calcination temperature increased, in conformity with the trend of the catalytic activity.

For the design of catalysts, it is very helpful to know the relationships between the solid state chemistry of catalysts and the catalytic properties, that is, the structure-property relationships. It is, therefore, desirable to study catalyst materials of which the structure is well defined and for which the surface or bulk properties can be continuously or stepwise changed without affecting the fundamental structure of the catalyst.

Perovskite-type mixed oxides (ABO_3) are typical examples suitable for this purpose, since their structures have been satisfactorily clarified and their electronic properties can be modified in various ways by the substitution of the constituting elements.[1] For example, the oxidation state of the B-site ion and the number of oxygen defects can be controlled by introducing a divalent ion in the A-site. Futhermore, perovskite-type mixed oxides are important catalysts in practical processes such as oxidation,[2,3] NO elimination[4,5] and hydrogenolysis.[6] It has already been reported that the perovskite-type mixed oxides are very active in complete oxidation reactions.[7,8]

We found previously that $La_{1-x}Sr_xCoO_3$ (x=0—0.4) showed high catalytic activity for the oxidation of C_3H_8, CH_4, and CO.[8] Among them, $La_{0.8}Sr_{0.2}CoO_3$ calcined at 850 °C was the most active, and its activity was comparable with or greater than that of Pt, Pd, and Ni catalysts. However, there have been few studies on the reaction mechanism and the reactivity of oxygen species of the perovskite-type mixed oxides, in relation to the catalytic activity for oxidation reactions.

Oxygen species responsible for the oxidation reaction have been well clarified, for example, in the case of Bi_2O_3–MoO_3[9] and γ-Fe_2O_3.[10] Both are active catalysts for allyl-type oxidation of olefins, in which lattice oxygen is responsible for catalysis. Reduction and oxidation of the whole bulk of these catalysts proceed readily under the reaction conditions, by the diffusion of lattice oxygen for Bi_2O_3–MoO_3 or metal cation for γ-Fe_2O_3. The diffusion of the cation or anion appears very important for allyl-type oxidation. As for the perovskite-type mixed oxide, it is only reported in the field of electrochemistry that the oxygen diffusion in $Nd_{1-x}Sr_xCoO_3$ is more rapid than that in ordinary metal oxides.[11] In the present work we studied the reactivity and diffusivity of oxygen in $La_{1-x}Sr_xCoO_3$, in order to clarify the relationships between these properties and the catalytic action. We studied particularly the effects of Sr^{2+}-substitution and the calcination temperature on the reactivity and related properties of oxygen, both in the bulk and on the surface.

Experimental

Catalysts. The catalysts were prepared from the mixture of metal acetates as described in the previous paper.[8] Powder X-ray diffraction patterns (XRD) were recorded with an X-ray diffractometer (Rigaku Denki, Rotaflex, RU-200) using Cu Kα radiation. All the $La_{1-x}Sr_xCoO_3$ (calcined above 850°C) used in this work showed diffration peaks only of the perovskite-type structure. Some of the samples are non-stoichiometric, $La_{1-x}Sr_xCoO_{3-\lambda}$. This non-stoichiometry and slight change in XRD observed upon reduction will be discussed in the later sections.

Apparatus. Besides conventional pulse and flow reactors, a circulation system (*ca.* 250 cm^3) was used for the reactions. These were the same as described elsewhere.[8,10]

Procedures. *Pulse Reaction*: The reduction of the catalysts by CO was conducted in the pulse reactor. Prior to the reaction, the catalysts (50 mg) were heated in O_2 stream for 1 h at 300 °C. The flow rate of carrier gas (He) was 30 cm^3 min^{-1} and the size of each CO pulse was usually 0.1 cm^3. Products were analyzed by a gas chromatograph (DMS, 5 m, 0 °C, or Porapak Q, 1.5 m, 83 °C).

Isotopic Exchange and Equilibration of O-18: ^{18}O-exchange between O_2 and perovskites and ^{18}O-equilibration of O_2 in the gas phase were conducted in the closed circulation system. Prior to reaction, the samples (300 mg) were treated with pure O_2 (10 kPa) at 300 °C (with circulation and a trap kept at liquid-nitrogen temperature) and subsequently evacuated for 1 h at 300 °C. O_2 enriched in ^{18}O (70 atom%) was purchased from Japan Radioisotope Association.^{18}O-distributions in O_2 in the gas phase was analyzed by a mass spectrometer (Hitachi Co. Ltd., RMU-S) by intermittent sampling.

Temperature Programmed Desorption (TPD) of Oxygen: TPD of oxygen was carried out with a flow system using helium as a carrier gas. Prior to each run, the samples (0.5 g or 1 g) were treated in an O_2 stream for 1 h at 300 °C and cooled to room temperature in the O_2 stream. Then an He stream was substituted for an O_2 stream at room temperature. Oxygen impurity in He was removed by a molecular sieve trap kept at the temperature of liquid nitrogen. Then the temperature of the sample was raised at the constant rate of 20 °C min^{-1} and the oxygen desorbed was detected by use of a quadrupole mass spectrometer (NEVA, NAG-531).

Results

Temperature Programmed Desorption (TPD) of Oxygen. Figure 1 shows TPD of oxygen from $La_{1-x}Sr_xCoO_3$ (x=0—0.6), where the rate of desorption calculated from the O_2 concentration in the eluent gas is plotted against temperature. It is obvious in this figure that the rate and the amount of O_2 desorption increased with the Sr^{2+} content, x. Oxygen desorbed below 600 °C amounted to 5.4 $cm^3\ g^{-1}$ (1.20 $cm^3\ m^{-2}$) for x=0.6, 2.8 $cm^3\ g^{-1}$ (0.519 $cm^3\ m^{-2}$) for x=0.4, 0.6 $cm^3\ g^{-1}$ (0.14 $cm^3\ m^{-2}$) for x=0.2, and 0.07 $cm^3\ g^{-1}$ (0.028 $cm^3\ m^{-1}$) for x=0. The amounts for x=0.4 and 0.6 corresponded to several layers of oxygen. These desorptograms of x=0—0.4 were reproducible after the heat treatment in an O_2 stream at 300 °C for 1 h. In the case of x=0.6 it was not completely reversible by this treatment, indicating that the rate of re-oxidation for x=0.6 was not rapid enough. For x=0.6, an O_2-treatment longer than 2 h at 300 °C was necessary to reproduce the initial desorptogram.

Figure 2 shows TPD of oxygen from $La_{0.8}Sr_{0.2}CoO_3$ calcined at 850, 900, and 1200 °C. The amount of oxygen desorbed decreased with the calcination temperature. The shapes of the desorptograms were rather similar: The desorption rate increased sharply at 500—600 °C after initial rises at lower temperatures. However, a significant difference was found in the temperature at which the desorption curves first increased: it was about 200 °C for $La_{0.8}Sr_{0.2}CoO_3$ calcined at 850 °C, about 250 °C for 900 °C-calcined sample, and about 350 °C for a 1200 °C-calcined sample. This result demonstrates that the release of oxygen from the bulk of $La_{1-x}Sr_xCoO_3$ becomes more difficult as the calcination temperature increased, even though the catalysts had the same composition.

It is to be noted that the increase in the readiness of oxygen desorption with increasing x was also found for 1200 °C-calcined samples.

Reversible Adsorption of Oxygen. Figure 3 shows the adsorption of oxygen for x=0 and 0.2 measured in the static system (P_{O_2}=10—20 Torr**). The samples were pre-evacuated for 0.5 h at each temperature. The adsorption isotherms exhibited saturation at about 10 Torr. The amount of adsorption increased with

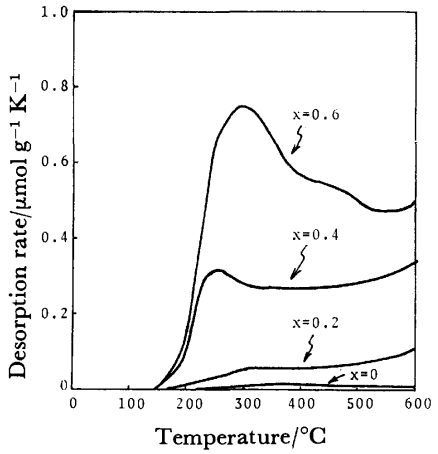

Fig. 1. TPD curves of oxygen from $La_{1-x}Sr_xCoO_3$ (x=0—0.6). Rate of temperature increase (β)=20 °C min^{-1}.

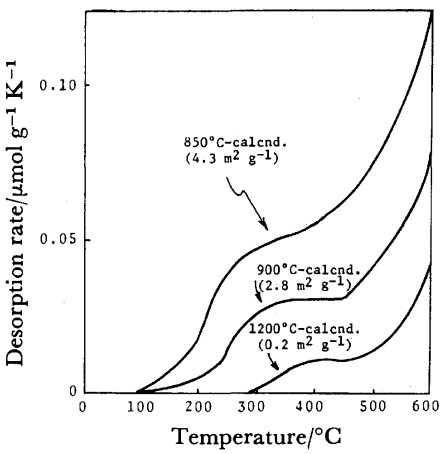

Fig. 2. TPD curves of oxygen from $La_{0.8}Sr_{0.2}CoO_3$ calcined at 850, 900, and 1200 °C. Rate of temperature increase (β)=20 °C min^{-1}.

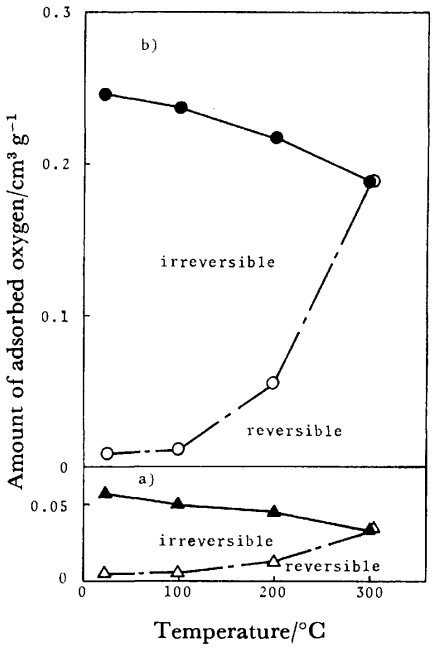

Fig. 3. Adsorption (or absorption) of oxygen by $LaCoO_3$ (a) and $La_{0.8}Sr_{0.2}CoO_3$ (b).
After the catalysts were evacuated at 300 °C for 0.5 h, O_2 was introduced at 300 °C. The solid symbols (▲, ●) at 300 °C represent the amounts of oxygen adsorbed at this stage. Then, the samples were cooled to 200, 100, and 25 °C stepwisely in the presence of O_2 (*ca.* 10 Torr). Solid symbols at each temperature express the cumulative amount of adsorbed oxygen. Open symbols (△, ○) are the amounts of oxygen which were reversibly adsorbed at each temperature. Therefore, the differences between the solid and open symbols are the irreversibly adsorbed oxygen at each temperature.

** 1 Torr≈133.3 Pa.

temperature, and the reversible adsorption of oxygen at room temperature was very small. If one assumes the value of δ to be null at room temperature, the values of δ are calculated to be 0.0049 (after 300 °C-evac.), 0.0012 (at 300 °C in O_2) for $x=0.2$, and 0.0011 (after 300 °C-evac.), 0.00046 (at 300 °C in O_2) for $x=0$.

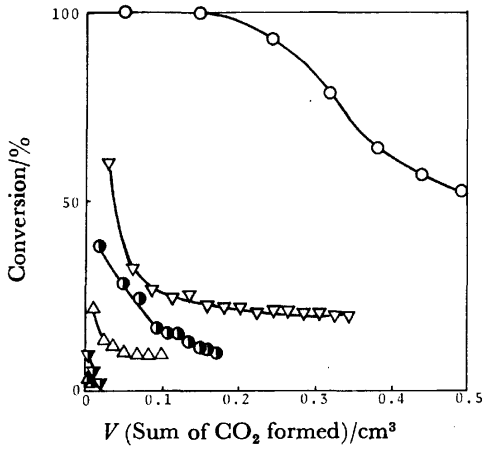

Fig. 4. Reduction by CO pulse at 200 and 300 °C.
▲: $LaCoO_3$, ◑: $La_{0.8}Sr_{0.2}CoO_3$, ▼: $La_{0.8}Ce_{0.2}CoO_3$ at 200 °C, △: $LaCoO_3$, ○: $La_{0.8}Sr_{0.2}CoO_3$, ▽: $La_{0.8}Ce_{0.2}CoO_3$ at 300 °C.
Catal. wt: 50 mg, CO pulse size: 0.1 cm³.

Reducibility of Catalysts by CO (Pulse Method). Figure 4 shows results of reduction by CO pulses at 200 and 300 °C. The ordinate indicates the conversion of each CO pulse to CO_2, and the abscissa is the sum of CO_2 formed from the pulse and the preceding pulses, which expresses the extent of the reduction of the catalysts. It is noted that $La_{0.8}Sr_{0.2}CoO_3$ was reduced more easily than $LaCoO_3$ and $La_{0.8}Ce_{0.2}CoO_3$. Even after oxygen molecules corresponding to several layers of surface were removed, the reducibility maintained a high level for $La_{0.8}Sr_{0.2}CoO_3$.

This fact indicates that the rate of oxygen supply from the bulk to the surface is very rapid in the case of $La_{0.8}Sr_{0.2}CoO_3$. Rapid diffusion of bulk oxide ion to the surface is further demonstrated by the effect of CO-pulse size on the rate of reduction (Fig. 5). CO was converted completely to CO_2 at 300 °C up to the pulse size of 0.3 cm³, while the formation of CO_2 was almost saturated at 0.1—0.2 cm³ at 150 °C. Since the oxide ion on the surface (by assuming 0.96×10^{19} atom m^{-2} for one surface layer) corresponds to 0.1 cm³ of CO_2, this result demonstrates that the rate of oxygen supply is very fast at 300 °C.

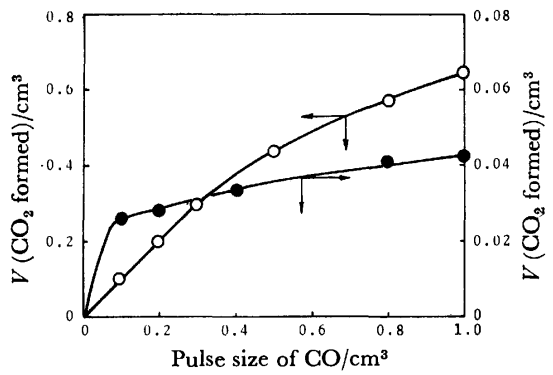

Fig. 5. Effect of pulse size on CO reduction of $La_{0.8}Sr_{0.2}CoO_3$ at 150 and 300 °C.
●: 150 °C, ○: 300 °C.

$LaCoO_3$ was much less reducible than $La_{0.8}Sr_{0.2}CoO_3$. $La_{0.8}Ce_{0.2}CoO_3$ appeared a little more reducible than $LaCoO_3$. However, the difference is small when normalized to the surface area. The conversion of the first CO pulse at 150 °C given in Table 1 demonstrates clearly the trend that the reducibility increases with the Sr^{2+} content.

TABLE 1. REDUCTION OF $La_{1-x}Sr_xCoO_3$ BY CO[a] AT 150 °C

x	Conversion/% CO→CO_2
0	1
0.2	25
0.4	77
0.6	100

a) Pulse size of CO: 0.1cm³.

Re-oxidation of the Reduced Catalysts. When O_2 was pulsed at 300 °C over $LaCoO_3$ and $La_{0.8}Sr_{0.2}CoO_3$ which had been reduced by CO pulses, these catalysts absorbed O_2 until its amount became equivalent to that removed in the preceding reduction, that is, the reduction and re-oxidation cycle was stoichiometric and reversible for these two catalysts. However, in the case of $La_{0.6}Sr_{0.4}CoO_3$ and $La_{0.4}Sr_{0.6}CoO_3$, the reduced catalysts were not fully re-oxidized by O_2 pulse at 300 °C. For example, $La_{0.4}Sr_{0.6}CoO_3$ (reduced by 3%) absorbed 74% of the stoichiometric amount of oxygen. This trend was enhanced at lower temperatures. At 150 °C $La_{0.6}Sr_{0.4}CoO_3$ (3% reduced) absorbed only 19% and $La_{0.4}Sr_{0.6}CoO_3$ (3% reduced) only 10%. The rate of re-oxidation tended to be faster when the catalyst was pre-reduced to a greater extent.

Structural Changes Accompanying the Reduction and Re-oxidation. Changes in XRD upon reduction and

TABLE 2. CHANGES IN XRD OF $La_{1-x}Sr_xCoO_3$ BY REDUCTION[a]

Distance of lattice planes/Å					
$x=0$		$x=0.2$		$x=0.6$	
i[b]	ii[c]	i[b]	ii[c]	i[b]	ii[c]
3.82	3.86	3.82	3.89	3.83	3.85
	2.77				2.77
2.71	2.74	2.71	2.74	2.71	2.72
2.68	2.71				
2.22	2.23	2.21	2.24	2.21	2.22
2.18	—	2.19	2.22		
					2.06
	1.94				1.94
1.91	1.92	1.91	1.93	1.91	1.92

a) About 5% reduced by CO at 400 °C. b) Before reduction. c) After reduction.

re-oxidation are summarized in Table 2. When the catalysts were reduced by about 5% by CO pulses at 400 °C (to $La_{1-x}Sr_xCoO_{2.85}$ if the sample was $La_{1-x}Sr_xCoO_3$ in the initial state), the diffraction peaks shifted about 0.2—0.5° (2θ) to lower angles. In addition to this shifts, new weak peaks (1.94, 2.06, 2.77 Å) appeared in the case of $LaCoO_3$ and $La_{0.4}Sr_{0.6}CoO_3$. The reduction and re-oxidation of the catalysts are reversible and the structure of the catalysts did not change significantly with reduction.

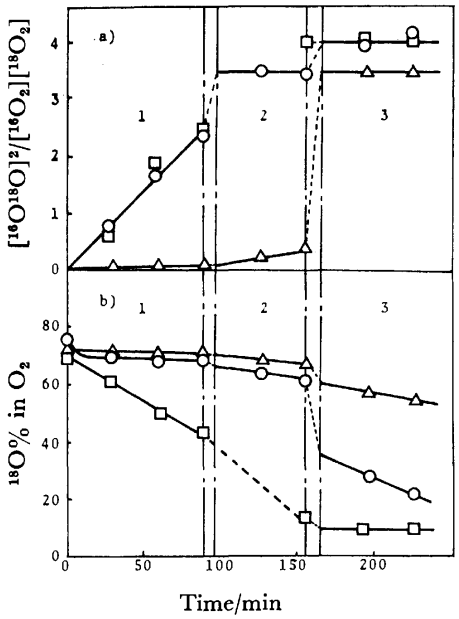

Fig. 6. Isotopic exchange of oxygen.
a): Equilibration, b) Exchange between gaseous and lattice oxygen.
React temp, 1; 150, 2; 200, 3; 300 °C.
△: $LaCoO_3$, ○: $La_{0.8}Sr_{0.2}CoO_3$, □: $La_{0.4}Sr_{0.6}CoO_3$.

Isotopic Equilibration and Exchange of Oxygen. Results of isotopic equilibration and exchange are shown in Fig. 6. The reaction was carried out at three different temperatures for each sample in a successive manner without replacing the gas mixture. The times required to increase the reaction temperature from 150 to 200 °C and 200 to 300 °C were 10 and 15 min, respectively. As shown in Fig. 6a, the isotopic equilibration over $La_{0.8}Sr_{0.2}CoO_3$ and $La_{0.4}Sr_{0.6}CoO_3$ proceeded rapidly at 150 °C, and the value of $[^{16}O^{18}O]^2/[^{16}O_2][^{18}O_2]$ was close to 4 at 200 and 300 °C, the value expected at equilibrium. On the other hand, the equilibration was slow over $LaCoO_3$ even at 200 °C. Figure 6b shows the results of isotopic exchange between lattice oxygen and gaseous oxygen. The rate of exchange on $LaCoO_3$ and $La_{0.8}Sr_{0.2}CoO_3$ was slow at 150 and 200 °C, but it became considerably more rapid at 300 °C. Over $La_{0.4}Sr_{0.6}CoO_3$ both reactions proceeded much more rapidly. In this case about 1.01 cm^3 of oxygen was absorbed just after the introduction of oxygen at 150 °C, indicating that desorption of oxygen was significant during the evacuation at 300 °C prior to the reaction. The ^{18}O-content in O_2 after 1 h at 300 °C was 8.4%. This value was not far from 6.5%, which is expected for complete mixing of lattice oxygen and gaseous oxygen.

Discussion

Structure and Stoichiometry of $La_{1-x}Sr_xCoO_3$ Catalysts. It was previously reported that $La_{1-x}Sr_xCoO_3$ formed perovskite structure when x did not exceed 0.8.[12] But according to a recent report,[13] this system forms a complete solid solution in the whole range of x. A slight distortion to rhombohedral exists in $LaCoO_3$, but it decreases gradually as the Sr^{2+} content, x, increases, and above $x=0.6$ the structure becomes cubic.[12] In spite of this distortion the crystal structures are essentially identical and there is only a small variation in the lattice constant of the pseudo cubic cell from 3.82 Å for $LaCoO_3$ to 3.84 Å for $SrCoO_3$.[14] In accordance with these results, the $La_{1-x}Sr_xCoO_3$ used in the present work all showed the perovskite structure.

When Sr^{2+} is partly substituted for La^{3+}(A-site) of $LaCoO_3$, the oxidation state of Co changes from Co^{3+} to Co^{4+}.[14] Although Co^{4+} was confirmed in $BaCoO_3$[15] $SrCoO_{3-\delta}$[16] and $La_{1-x}Sr_xCoO_{3-\delta}$,[14] it is not stable and tends to be reduced by releasing oxygen. For example, it was reported that the value of δ in $SrCoO_{3-\delta}$ is 0.26 when annealed under 50 bar*** of oxygen at 350 °C and 0.05 under 2000 bar at 300 °C.[16] Therefore, it is probable at a high x value that the charge compensation is accomplished by the formation of oxygen vacancies in addition to the Co^{4+} formation. Actually, according to Jonker *et al.*,[14] Co^{4+} is formed without the formation of oxygen vacancy for $x \leqq 0.4$, but oxygen vacancies are formed besides the Co^{4+} formation when x exceeds 0.4. It was recently confirmed with single crystals that stoichiometric $La_{1-x}Sr_xCoO_3$'s were obtained for $x \leqq 0.2$ by annealing in air.[17] Although the samples used in the present investigation were polycrystalline powders and were mostly calcined at a relatively low temperature, the content of Co^{4+} determined by chemical analysis[15,18] was 20 ± 1% for the sample with $x=0.2$, *i.e.*, $La_{0.8}Sr_{0.2}CoO_{3\pm0.005}$. The sample had been calcined at 850 °C, cooled slowly to 25 °C and then treated in oxygen at 300 °C. Final treatment is the same as the pre-treatment for the catalytic reactions. This result was in agreement with the results reported previously.[14,17] The composition was not determined for $x=0.6$, but it is probably close to $La_{0.4}Sr_{0.6}CoO_{2.925}$ (Co^{4+}: 45%), which was observed by Jonker *et al.*[14] For the single crystals of $x=0.5$, δ was estimated to be 0.077.[17] Consequently, δ of $La_{1-x}Sr_xCoO_{3-\delta}$ catalysts, which were calcined at 850 °C and treated in oxygen at 300 °C, may be close to zero for $x=0$ and 0.2, and 0.075 or slightly smaller for $x=0.6$. This trend in δ with the Sr^{2+} content is thus explained by the instability of Co^{4+}, in other words, the chemical potential of lattice oxygen at a given δ increases with the Sr^{2+} content. As discussed below, the changes with x in the readiness of desorption and reducibility of lattice oxygen are explained by this change in the chemical potential of the lattice oxygen.

*** 1 bar = 10^5 Pa.

Structural Changes during the Redox Cycle. When $La_{1-x}Sr_xCoO_{3-\delta}$ (x=0, 0.2, and 0.6) were reduced by 5% (from δ=0 to 0.15 for x=0 and 0.2, and from *ca.* 0.07 to *ca.* 0.22 for x=0.6) by CO at 400 °C, the diffraction peaks shifted to lower angles and the separation of the lattice planes, d, increased by 0.01—0.05 Å (Table 2). The ionic radius of Co^{3+} is 0.61 Å for high spin state and 0.525 Å for low spin state, while the ionic radius of Co^{4+} is 0.518 Å for $SrCoO_3$[16] and 0.476 Å for 2H-$BaCoO_3$.[19] Therefore, the increase of d on reduction may be due to the difference in the ionic radius between Co^{3+} and Co^{4+}; that is, Co^{4+} changed to Co^{3+} by the reduction. Similar increase in d with δ was reported for $SrCoO_{3-\delta}$ (δ=0.05—0.26).[16] New weak peaks were observed for x=0.6 after reduction besides the shifts of the original diffraction peaks. However, no new peaks were observed for x=0.2, although oxygen vacancies are probably less stable for x=0.2. Therefore, a possible explanation of the new peaks for x=0.6 may be as follows. A Sr-rich phase was present in the sample before reduction and a phase similar to $SrCoO_{2.5}$ was formed by reduction from this Sr-rich phase. $SrCoO_{2.5}$ has the brownmillerite structure, which is closely related to the perovskite structure and there is essentially little difference between these two structures, as discussed above.

For x=0, new weak peaks also appeared by reduction. It was reported that $La_4Co_3O_{10}$ and CoO were formed partially by reduction,[20] but the new peaks for x=0 do not agree with those expected for $La_4Co_3O_{10}$ and the diffraction peaks of CoO were not observed. Although the origin of the new peaks for x=0 is not evident, it is probable that oxygen vacancies are formed by reduction, causing crystal distortion, but it did not lead to decomposition or significant change in the structure. XRD peaks of $La_4Co_3O_{10}$+CoO were not observed for $LaCoO_3$, probably because the degree of reduction in this study (δ=0.15) was smaller than that in the literature (δ=0.26: 1.68 wt%).[20]

The starting perovskite structures were reversibly restored by re-oxidation for all reduced samples. Therefore, the fundamental structure of perovskite was presumably preserved during the redox cycle when the extent of reduction was small as in this study.

Adsorbed Oxygen and Lattice Oxygen. First, the amounts of oxygen desorbed from $La_{1-x}Sr_xCoO_3$ by TPD are compared with those from other metal oxides. CuO and Co_3O_4 are among the oxides showing large values; 1.42×10^{-1} cm^3 m^{-2} for CuO (0.17 m^2 g^{-1}) and 3.30×10^{-2} cm^3 m^{-2} for Co_3O_4 (5.7 m^2 g^{-1}) in the temperature range from 25 °C to 560 °C.[21] The amounts for $La_{1-x}Sr_xCoO_3$ were comparable with (for x=0.2) or much larger (for $x\geqq0.4$) than CuO. The amounts of desorbed oxygen correspond to the increase in δ by 0.012 for x=0.2, 0.051 for x=0.4, and 0.097 for x=0.6. If one assumes the surface oxide density to be 0.96×10^{19} atom m^{-2}, those amounts are about 0.7 surface layers for x=0.2 and several layers for x=0.6. Thus, it is obvious that most of the oxygen desorbed was not the adsorbed oxygen but came from the lattice oxygen.

Oxygen adsorbed after evacuation at a certain temperature was greater than oxygen desorbed in TPD up to the same temperature, indicating that the amount of oxygen desorbed in TPD at each temperature had not reached equilibrium. However, the amount was not very far from the equilibrium value. Therefore, although TPD is governed by the rate, it reflects closely the equilibrium properties. This is in accord with the result in Fig. 7, where the second TPD after the interruption mostly reproduced the rest of TPD conducted without the interruption.

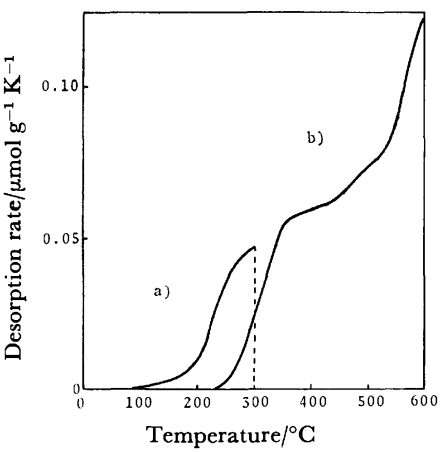

Fig. 7. TPD curues of oxygen from $La_{0.8}Sr_{0.2}CoO_3$.
a): First TPD up to 300 °C, b): second TPD after a) and cooled to room temperature.

The adsorption (and/or absorption) of oxygen at 300 °C was reversible and was saturated at about 10 Torr. When this sample (x=0.2) was cooled to room temperature in oxygen, 0.06 cm^3 g^{-1} of oxygen was adsorbed (absorbed) during the cooling process. The amount of reversible O_2 uptake at room temperature was 2.5×10^{-3} cm^3 g^{-1}, corresponding to a change in δ of 5×10^{-5}, much smaller than the oxygen desorbed in TPD. When the values of δ at 200—300 °C after evacuation (*ca.* 10^{-4} Torr) and under oxygen pressure (*ca.* 10 Torr) (both values increased with x) were plotted against P_{O_2}, difference of several orders of magnitude in the equilibrium pressure of oxygen was found at the same δ value among the samples with different x. Samples having greater x had higher equilibrium pressures of oxygen. That is to say, the chemical potential of lattice oxygen increases enormously with x. This fact confirms again that the results of TPD reflect the chemical potential of lattice oxygen.

As shown in Fig. 2, the release of oxygen from the bulk becomes more difficult for samples calcined at higher temperatures. The result reported previously that the catalytic activities of C_3H_8 oxidation over $La_{0.8}Sr_{0.2}CoO_3$ changed with the calcination temperature and showed a maximum at 850 °C[8] may be explained by the trend seen in TPD of Fig. 2.

In the reduction by CO pulse, the amount of oxygen consumed in one pulse was so large that the CO-pulse experiments reflect mainly the reactivity of lattice oxygen. The conversion of CO increased enormously with x (Table 1) similarly to the trend found with TPD. This similarity between the results of two experiments demonstrates that the reactivity of adsorbed oxygen runs parallel with that of lattice oxygen even if adsorbed

oxygen should exist. It is noted in TPD that the change from oxygen desorbed at low temperature (adsorbed oxygen or weakly bonded lattice oxygen) to oxygen desorbed at higher temperature (lattice oxygen) was continuous and a parallelism was found between the two oxygen species. Probably, it is reasonable not to distinguish between adsorbed and lattice oxygen in the present system.

There was a tendency that re-oxidation became slower on increasing Sr^{2+} substitution, contrary to the case of reduction. The easier reduction and slower re-oxidation with samples having high x mean the equilibrium pressure of oxygen is very much greater for these samples. Actually the equilibrium pressure estimated as above increased tremendously with x. This result will be discussed in more detail in the following paper.

Diffusion of Oxygen in the Bulk and Activation of Oxygen on the Surface. It is known that the diffusion of oxygen in the bulk is rapid in the perovskite-type mixed oxides.[11] We also reported that the diffusion was very rapid during the redox cycle of $La_{0.8}Sr_{0.2}CoO_3$.[22] As shown in Fig. 6b, exchange reaction between gaseous and lattice oxygen occurred under oxygen atmosphere in $La_{1-x}Sr_xCoO_3$, and ^{18}O diffused into the bulk at a considerable rate. The rates of exchange reaction at 150 °C were not so different between $x=0$ and 0.2, 0.0015 $cm^3\ g^{-1}\ min^{-1}$, but the rates at 300 °C were 0.014 $cm^3\ g^{-1}\ min^{-1}$ for $x=0$ and 0.127 $cm^3\ g^{-1}\ min^{-1}$ for $x=0.2$. Sample with $x=0.6$ exhibited a much greater value of 0.045 $cm^3\ g^{-1}\ min^{-1}$, even at 150 °C. Since equilibration was much more rapid and the equilibration usually proceeds *via* dissociation of oxygen in this temperature range, the dissociation of oxygen molecules at the surface is much more rapid than the exchange reaction. Therefore, the rate-determining step of the exchange reaction is probably not the surface reaction but the diffusion in the bulk. The acceleration of the exchange reaction by the Sr^{2+} substitution may be due to the increase in the diffusion rate of oxygen. This is reasonable, if one considers that the diffusion occurs through oxygen vacancies and the amount of the vacancy increases with the Sr^{2+} content. This rapid diffusion of oxygen was revealed also by the results of CO pulse reaction described above.

Finally, the activation of oxygen at the surface will be discussed. The rates of equilibration at 150 °C were 0.037 $cm^3\ g^{-1}\ min^{-1}$ for $x=0$ and 0.35 $cm^3\ g^{-1}\ min^{-1}$ for $x=0.2$. For $x=0.6$ it was not possible to determine the rate of equilibration because of the rapid exchange between gaseous and lattice oxygen even at 150 °C, but the rate appears greater than that for $x=0.2$. Thus, the ability to activate oxygen also increases with x. In $La_{1-x}Sr_xCoO_3$, considerable amount of oxygen vacancies are formed even under oxygen atmosphere as shown in the results of oxygen adsorption, and its amount increased with x. It can therefore be presumed that the equilibration occurs at this surface oxygen defect and the rate becomes faster when the oxygen defects at the surface increases.

Conclusion. In the perovskite-type mixed oxides, $La_{1-x}Sr_xCoO_3$, the reactivity of lattice oxygen, the desorption of oxygen and the reduction tends to become easier as the Sr^{2+} content, x, increases. This is due to the formation of unstable Co^{4+} and the high chemical potential of lattice oxygen. Unstable Co^{4+} changes to Co^{3+}, when oxygen is desorbed and oxygen vacancy is formed. As the vacancy increases, the diffusion of lattice oxygen from bulk to surface becomes easier. In this system, even in an oxygen atmosphere, oxygen vacancies are present and their amount increases with x. This is the reason why the rate of isotopic equilibration of oxygen and exchange between gaseous and lattice oxygen increased with x. Thus, easy formation of oxygen vacancies, keeping its structure unchanged, is the remarkable characteristics of the present mixed oxide system. Relationships between the present results and catalytic activity will be discussed in the following paper.

References

1) R. J. H. Voorhoeve, "Advanced Materials in Catalysis," Academic Press, New York (1977), p. 129.
2) R. J. H. Voorhoeve, J. P. Remeika, P. E. Freeland, and B.T. Mattias, *Science*, **177**, 353 (1972).
3) Y.-F. Yu Yao, *J. Catal.*, **36**, 266 (1975).
4) R. J. H. Voorhoeve, J. P. Remeika, and L. E. Trimble, "The Catalytic Chemistry of Nitrogen Oxides," Plenum Press, New York (1975), p. 215.
5) M. W. Chien, I. M. Pearson, and K. Nobe, *Ind. Eng. Chem., Prod. Res. Dev.*, **14**, 131 (1975).
6) K. Ichimura, Y. Inoue, and I. Yasumori, *Bull. Chem. Soc. Jpn.*, **53**, 3044 (1980).
7) T. Nakamura, M. Misono, and Y. Yoneda, *Shokubai*, **21**, 310 (1979).
8) T. Nakamura, M. Misono, T. Uchijima, and Y. Yoneda, *Nippon Kagaku Kaishi*, **1980**, 1679.
9) G.W. Keulks, *J. Catal.*, **19**, 232 (1970).
10) M. Misono, K. Sakata, F. Ueda, Y. Nozawa, and Y. Yoneda, *Bull. Chem. Soc. Jpn.*, **53**, 648 (1980).
11) T. Kudo, H. Obayashi, and T. Gejo, *J. Electrochem. Soc.*, **122**, 159 (1975).
12) H. Ohbayashi, T. Kudo, and T. Gejo, *Jpn. J. Appl. Phys.*, **13**, 1 (1974).
13) H. Taguchi, M. Shimada, and M. Koizumi, *Mat. Res. Bull.*, **13**, 1225 (1978).
14) G. H. Jonker and J. H. Van Santen, *Physica*, **19**, 120 (1953).
15) B. E. Gushee, L. Katz, and R. Ward, *J. Am. Chem. Soc.*, **79**, 5601 (1957).
16) H. Taguchi, M. Shimada, and M. Koizumi, *J. Solid State Chem.*, **29**, 221 (1979).
17) A. Hashimoto, J. Mizusaki, S. Yamauchi, and K. Fueki, *Preprint 19th Symp. Basic Science of Ceramics*, Nagoya, Japan, **1981**, 88.
18) H. A. Laitenen and L. W. Burdett, *Anal. Chem.*, **23**, 1268 (1951).
19) H. Taguchi, Y. Takeda, F. Kanamaru, M. Shimada, and M. Koizumi, *Acta Crystallogr., Sect. B*, **33**, 1299 (1977).
20) J. J. Janecek and G. P. Wirtz, *J. Am. Ceram. Soc.*, **61**, 242 (1978).
21) M. Iwamoto, Y. Yoda, N. Yamazoe, and T. Seiyama, *J. Phys. Chem.*, **82**, 2564 (1980).
22) K. Sakata, T. Nakamura, M. Misono, and Y. Yoneda, *Chem. Lett.*, **1979**, 273.

Catalysis by Heteropoly Compounds. III.† The Structure and Properties of 12-Heteropolyacids of Molybdenum and Tungsten ($H_3PMo_{12-x}W_xO_{40}$) and Their Salts Pertinent to Heterogeneous Catalysis

Makoto Misono,* Noritaka Mizuno, Koichi Katamura, Atsushi Kasai, Yasuo Konishi, Kanji Sakata, Toshio Okuhara, and Yukio Yoneda

Department of Synthetic Chemistry, Faculty of Engineering, The University of Tokyo, Hongo, Bunkyo-ku, Tokyo 113

(Received June 19, 1981)

The fundamental properties of 12-heteropolyacids of Mo and W, such as the structure, the surface area, the acidity, and the reduction-oxidation mechanism, have been studied in their solid state in relation to heterogeneous catalysis. The primary structure (heteropolyanion) was rather stable, but the secondary structure was very variable according to the interaction with various molecules, like water, alcohols, ketones, and pyridine. This structural characteristic is important for the understanding of the catalysis of these compounds; it may be called the "pseudo-liquid phase." The heteropolyacids were all strong protonic acids, as revealed by the interaction with pyridine. The redox cycle was reversible within a limited extent of reduction. The redox mechanism is also discussed in this paper.

Heteropoly compounds have recently attracted much attention as catalysts for various industrial processes, such as oxidation, hydration, esterification, and etheration.[1] Considerable efforts have also been devoted to them in basic studies. It is hoped that the structure of the catalyst can be defined on a molecular scale of the heteropolyanion.[2,3]

We have studied the acidic and redox properties of several heteropoly compounds in their solid state and have attempted to correlate these properties with the catalytic actions.[2] In our opinion, the "pseudo-liquid phase" hypothesis we have proposed represents one of the very important aspects of heteropolyacid catalysis.[4] These studies are, in a sense, an extension of our early efforts at the design of catalysts based on the relationships between the acidity or the oxidizing power and the catalytic activity or selectivity.[5] Possible way of catalyst design based on heteropoly acids has also been discussed before.[6]

In the present paper, we wish to report some of the fundamental properties pertinent to the heterogeneous catalysis of heteropolyacids, such as the structure, the water content, the surface area, the pore-size distribution, and the acidic and redox properties. The heteropolyacids studied are 12-heteropolyacids of Mo and W containing P as the heteroatom.

Experimental

X-Ray Diffraction Powder Pattern. The powder pattern of X-ray diffraction was recorded on an X-ray diffractometer (Rigaku Denki, Rotaflex). When heteropoly acids or their salts were very water-soluble, samples were usually pretreated in nitrogen or helium saturated with water vapor. In the case of heat-treated samples, they were quickly set on a sample holder and covered with a Mylar film.

Infrared Spectra. About a 5-mg portion of the sample was deposited on a silicon plate or pressed into a KBr disk, and the spectra were recorded in an in situ IR cell by means of an FT-IR spectrometer (JEOL JIR-10), as has been described previously.[7,8]

Other Properties. The water content and the amount of pyridine absorption were measured by the use of a quartz spring balance. The surface area and pore-size distribution were measured by means of the absorption of nitrogen. The latter was kindly measured at the Daicel Chem. Ind. Co., Ltd., by the use of a Sorptomatic 1800 apparatus (Carlo Erba), based on the BJH equation.[24]

Materials. $H_3PW_{12}O_{40}\cdot nH_2O$ (A) was prepared according to the literature.[9] $Na_2WO_4\cdot 2H_2O$ (100 g) and $Na_2HPO_4\cdot 12H_2O$ (50 g) were added to 160 ml of decationized water, and the mixture was refluxed at 80 °C with stirring. Then, 24% HCl (150 ml) was added to the solution at 80 °C. After the solution had been concentrated to a volume of 100 ml by evaporation at 50 °C, it was cooled to room temperature. $H_3PW_{12}O_{40}$ was extracted with an equal amount of diethyl ether (with slow agitation after the addition of several drops of 35% HCl). The ether was removed by keeping the etherate at 50 °C. Then it was dissolved in water and concentrated at 50 °C. Recrystallization from an aqueous solution and drying in a KOH-desiccator for 2 d formed $H_3PW_{12}O_{40}\cdot 21—22H_2O$. $H_3PW_{12}O_{40}\cdot nH_2O$ (B) was prepared by extraction with ether from a 50% aqueous solution of $H_3PW_{12}O_{40}$ obtained from the Nippon Inorganic Colour and Chemical Co., Ltd. After evacuation at room temperature, the n value was 6 for both samples.

$H_3PMo_{12}O_{40}\cdot nH_2O$(A) was prepared by extraction with ether from a 50% aqueous solution of $H_3PMo_{12}O_{40}$ obtained from the Nippon Inorganic Colour and Chemical Co., Ltd. The $H_3PMo_{12}O_{40}\cdot nH_2O$(B) was kindly donated by the Climax Molybdenum Co. (Japan), Ltd. Two samples different in source, (A) and (B), behaved very similarly, so that, unless otherwise stated, no distinction of the two samples will be made in the following description.

$H_3PW_6Mo_6O_{40}\cdot nH_2O$ was prepared as follows. $Na_2WO_4\cdot 2H_2O$ (45.1 g), $Na_2MoO_4\cdot 2H_2O$ (33.0 g) and $Na_2HPO_4\cdot 2H_2O$ (8.15 g) were dissolved in 200 ml of decationized water. The solution was kept at 80 °C for 3 h with agitation and then concentrated to 80 ml by the use of an evaporator. Then, 100 ml of 24% HCl was added (the solution was yellow). After extraction with ether at room temperature, the crystal

† Part I: *Proc. 7th Intern. Congr. Catal., Tokyo 1980*, Kodansha, Tokyo, and Elsevier, Amsterdam (1981), p. 1047; Part II: *Nippon Kagaku Kaishi*, accepted for publication.

was obtained in the same way as $H_3PMo_{12}O_{40}\cdot nH_2O$. The other $H_3PW_{12-x}Mo_xO_{40}$'s were similarly prepared.

The alkali salts were prepared by slowly adding equivalent amounts of alkali carbonates (aqueous solution) to the aqueous solutions of heteropolyacids following the methods in the literature.[10] The Na salt was obtained by removing water at 50—60 °C. The K and Cs salts were precipitated from a solution and evaporated to dryness.

Results

XRD and IR. Figure 1 shows the IR spectra and XRD of $H_3PMo_{12}O_{40}$ and some of its salts. These results were briefly reported before.[2] Figure 1 demonstrates that the pattern changed markedly depending on the kind of metal species. The XRD pattern of $H_3PMo_{12}O_{40}$ varied significantly also upon dehydration and rehydration. On the other hand, the IR spectra in the range of 600—1100 cm^{-1} characteristic of the heteropolyanion were quite similar with one another, indicating that the Keggin structure of the heteropolyanion (primary structure) remained unchanged. The changes in the secondary structures upon the dehydration of $H_3PMo_{12}O_{40}$ and its salts have recently been reported by Eguchi *et al.*[11] Their results and conclusion are in general agreement with ours. The IR band at *ca.* 1610 cm^{-1}, which is the bending mode of the water of crystallization, was observed for all salts, the intensity being smaller for K and Cs salts. The band at *ca.* 1720 cm^{-1}, which was presumably to be assigned to $H^+(H_2O)_n$, disappeared upon the salt formation.[8]

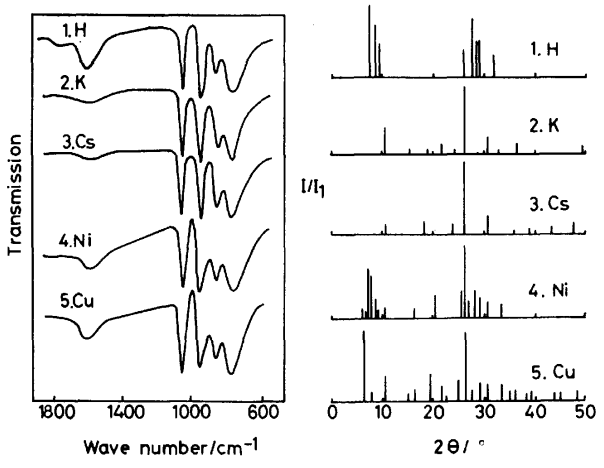

Fig. 1. IR spectra (KBr disk) and X-ray diffraction patterns of $H_3PMo_{12}O_{40}$ and its salts.

The IR spectra characteristic of the Keggin structure changed in a continuous way upon the substitution of Mo with W. The shifts in wave numbers are summarized in Table 1. In Fig. 2, the IR of $K_3PMo_6W_6O_{40}$ is compared with those of $K_3PMo_{12}O_{40}$ and $K_3PW_{12}O_{40}$ (identical XRD patterns were obtained for all of these samples). It may be seen in Fig. 2 that $PMo_6W_6O_{40}$ was not a mixture of $PMo_{12}O_{40}$ and $PW_{12}O_{40}$. Similar changes with the Mo/W ratio were also found for acid forms. However, since the bands were broader for

Table 1. Infrared bands of $K_3PMo_{12-x}W_xO_{40}$

x in $K_3PMo_{12-x}W_xO_{40}$	IR Band $\tilde{\nu}/cm^{-1}$ [a]			
	P–O	M=O	M–O–M	
0	1064	964	867	794
2	1068	968	871	802
6	1072	971	877	800
10	1079	983	887±2	811±2
12	1079	983	890	813±4

Measured by FT-IR (resolution: 4 cm^{-1}), KBr disk. a) Assignment after C. Rochioccioli-Deltcheff *et al.*, *Spectrochim. Acta, Part A*, **32**, 587 (1976).

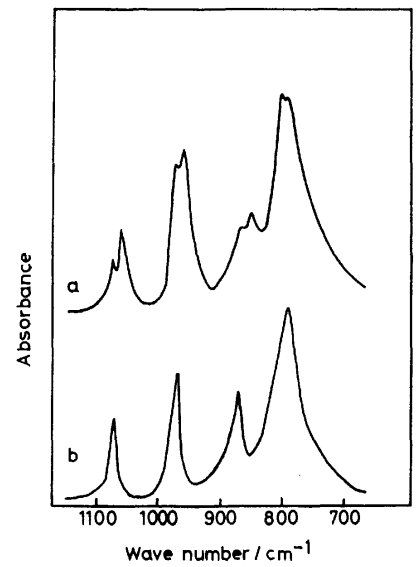

Fig. 2. IR spectra of the mixture of $K_3PMo_{12}O_{40}$ and $K_3PW_{12}O_{40}$ (a) and $K_3PMo_6W_6O_{40}$ (b) (KBr disk).

acid forms, the distinction of $PMo_6W_6O_{40}$ from the mixture of $PMo_{12}O_{40}$ and $PW_{12}O_{40}$ was not possible by IR.

Water Content, Surface Area, and Pore-size Distribution. The changes in the water content and the surface area are shown in Table 2 for $H_3PMo_{12}O_{40}$ and $H_3PW_{12}O_{40}$. The surface area and water content were measured after the samples had been heated in a dry helium stream and after evacuation, respectively, at given temperatures. As we have reported before,[7] the dehydration of $H_3PMo_{12}O_{40}$ proceeded at low temperatures, and the surface area, showing a maximum value when treated at about 100 °C, decreased upon treatment at higher temperatures. The pore-size distribution of $H_3PMo_{12}O_{40}$ (B) is given in Fig. 3a. The surface area as estimated from the pore-size distribution was close to that obtained by the BET method. In the case of $H_3PW_{12}O_{40}$, dehydration proceeded at somewhat higher temperatures, and the change in the surface area was smaller. Two samples different in source gave similar results.

The IR bands of ν_{OH} (≈3600 cm^{-1}) and δ_{H_2O} (≈1610 cm^{-1} for Mo; ≈1700 cm^{-1} for W) due to the water of crystallization disappeared upon evacuation at 25 °C for $H_3PMo_{12}O_{40}$ and at 100 °C for $H_3PW_{12}O_{40}$. The

Table 2. Water content and surface area (in parentheses) of 12-tungsto- and 12-molybdophosphoric acid after heat treatment

	Surface area ($m^2\ g^{-1}$) and Water content (molecule/anion)[a]				
	Before treatment	Temperature of heat treatment (°C)			
		25	100	200	300
$H_3PW_{12}O_{40}$					
A	10	6.0(—)	1.0(4.8)	0.8(—)	0.2(4.7)
B	21	6.0(3)	1.3(4)	1.0(8)	≈0(5.5)
$H_3PMo_{12}O_{40}$					
A	22	5(<0.1)	1.2(13)	0.8(8)	≈0(3)
B	19	≈5(<1)	1.2(14)	1 (10)	≈0(2)

a) It is assumed that heat treatment at 450°C causes $H_3PM_{12}O_{40} \rightarrow 1/2P_2O_5 + 12MoO_3 + 3/2H_2O$

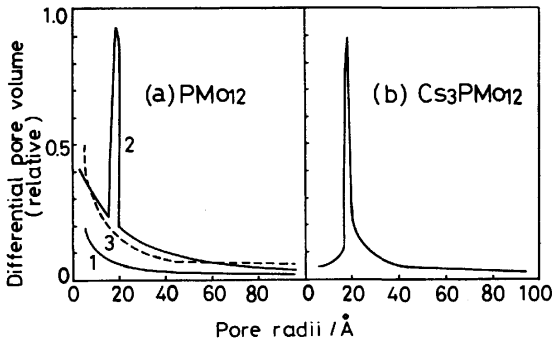

Fig. 3. Pore-size distibution.
(a) $H_3PMo_{12}O_{40}$, 1: treated at 25 °C, 2: at 110 °C, 3: at 300 °C. (b) $Cs_3PMo_{12}O_{40}$, treated at 110 °C.

bands at ≈3200 cm^{-1} of $H_3PMo_{12}O_{40}$, presumably attributable to $H^+(H_2O)_n$, remained below 200 °C, but the 1720 cm^{-1}-band became very small upon 25 °C-evacuation. The ν_{OH} band of $H_3PW_{12}O_{40}$ (3200 cm^{-1}) also decreased, but remained after the evacuation at 200—250 °C, while the bending modes of H_2O and $H^+(H_2O)_n$, which were not clearly separated into two peaks, almost disappeared upon 100 °C-evacuation. The Cs salt exhibited a very high surface area, which decreased upon heat treatment above about 300 °C. An example of the pore-size distribution is given in Fig. 3b.

The observation, by means of a microscope (×100) and a scanning-electron microscope (SEM) (×1000—5000), of the change in the appearance of $H_3PMo_{12}O_{40}$ upon heat treatment is summarized as follows. A sample was, before treatment, constituted of large lustrous particles whose surfaces were covered by fine particles *ca.* 10 μm in diameter. According to SEM, the surface of the particles was irregular (roughness in the order of 1—5 μm: probably primary particles) and had crevices of *ca.* 1 μm. After 100 °C-treatment, SEM indicated that the particles had grown (*ca.* 5 μm), possibly by experiencing partial melting. The surface had become less irregular, but the number and length of crevices (≈1 μm) had increased. After 450 °C-treatment, only aggregated fine particles (≈1 μm) were observed by SEM.

Acidic Properties. We reported previously that a considerable amount of pyridine was absorbed in the bulk of $H_3PMo_{12}O_{40}$.[8] According to the weight measurement,[2,12] $H_3PMo_{12}O_{40}$ and $H_3PW_{12}O_{40}$ absorbed several molecules of pyridine per heteropoly-anion when they were brought in contact with pyridine vapor, and after evacuation at 100—150 °C, three molecules per anion, equivalent to the number of protons, remained in the bulk. The IR spectra showed that pyridine was present exclusively in the form of the pyridinium ion, indicating the formation of pyridinium salts. Broad bands which could be assigned to the ν_{N-H} of the pyridinium ion appeared in some cases at 2500—3000 cm^{-1}, but so far we have not been able to obtain sufficient reproducibility to confirm this band, although it would be good evidence to demonstrate the uniformity of the acid strength.

The acidity was measured by means of the thermal desorption of pyridine from the pyridinium salts. The results are given in Fig. 4. Only a small amount of pyridine was desorbed by the evacuation below about 300 °C in the case of $H_3PW_{12}O_{40}$. An increase in the evacuation period from 1 h to 4 h at 300 °C changed the results little. At 350 °C, the pyridine was removed gradually. In the case of $H_3PMo_{12}O_{40}$, the removal was not significant at 250 °C, but a considerable amount was desorbed above 300 °C. Examination by means of IR revealed that this removal was accompanied by

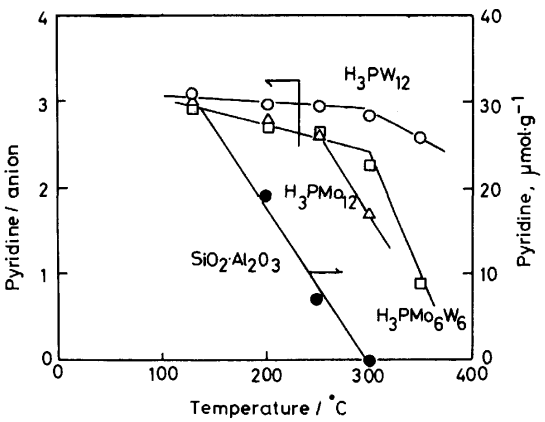

Fig. 4. Thermal desorption of pyridine.
Evacuated for 1 h at each temperature by increasing the temperature stepwise.

a partial degradation of the Keggin structure. The result for $H_3PMo_6W_6O_{40}$ was intermediate.

Redox Properties. The stoichiometry of the reduction by H_2 and re-oxidation by O_2 of $H_3PMo_{12}O_{40}$ has previously been reported.[2,4c] At 200—300 °C, reduction-oxidation by 2 electrons per polyanion proceeded reversibly in a stoichiometric manner. By this redox cycle, the intensity of the IR bands assigned to P–O (1060 cm^{-1}) and Mo–O–Mo (880 and 790 cm^{-1}) changed reversibly. However, when $H_3PMo_{12}O_{40}$ was reduced by 4 electrons per anion, the O_2-uptake was only 36% of the preceding H_2-uptake (72% of the amount required to re-oxidize to the original oxidation state). In this case, the IR spectrum after re-oxidation resembles that before reduction, but it was not identical. The sample pre-reduced by 8 electrons was re-oxidized only to 56%, and the IR spectrum after re-oxidation was significantly different. Reduction at 350 °C by 30 electrons per anion resulted in the formation of a mixture of MoO_3 and MoO_2, as revealed by XRD. Reduction by 3 electrons in the presence of water vapor was nearly reversible.

In the case of the reversible redox cycle, water (collected for 1—2 h by a trap kept at the temperature of liquid N_2) was evolved in both the reduction and re-oxidation steps. In the reduction step at 300 °C, only a half of the H_2 absorbed was collected as water. The rest was collected in the subsequent re-oxidation step, satisfying the stoichiometry, $H_2+1/2O_2\rightarrow H_2O$. As the temperature increased, the water evolved in the first step increased. The fact that only a part of the H_2 observed was collected as water in the reduction step is not likely to be the result of the incomplete desorption of water which had already been formed in this step, because only a negligible amount of water was collected by pumping after the reduction. Therefore, the water collected in the re-oxidation step was probably formed by the reaction with O_2. This idea was confirmed further by the temperature-programmed desorption (TPD) and reduction (TPR).[13] According to TPR, $H_3PW_{12}O_{40}$ was much less reducible than $H_3PMo_{12}O_{40}$.

The reduction processes of other heteropolyacids and the correlation with the catalytic activity were previously reported briefly.[2,14] The details will be reported in forthcoming papers.

Interaction of Heteropolyacids with Inorganic and Organic Molecules. Water: A large amount of water was absorbed or desorbed rapidly in the case of acid forms. When D_2O was brought into contact with $H_3PW_{12}O_{40}$ at 25 °C after evacuation, the IR bands due to the water of crystallization (δ_{H_2O}) exhibited a very rapid shift (in 1 min) from the 1700 cm^{-1}-region to 1272 cm^{-1}.[12] A similar rapid exchange was also found in the case of $H_3PMo_{12}O_{40}$. According to the absorption isotherm of water, about one molecule of water was absorbed per anion at 300 °C for $H_3PMo_{12}O_{40}$ at 10—30 Torr**.

The oxygen exchange between water vapor and the heteropoly anion was also very rapid.[15] The oxygen of the heteropoly anion in the whole bulk (except for PO_4) of $H_3PMo_{12}O_{40}$ and $Cu_{3/2}PMo_{12}O_{40}$ exchanged at 150—250 °C, as was revealed by the IR isotope shifts (10—15 cm^{-1}).

CO_2 and O_2: The ^{18}O-exchange of $H_3PMo_{12}O_{40}$ with CO_2 was much slower than with H_2O. The rate was represented by a first-order rate equation where the whole bulk oxygen atoms participate equally. The exchange with O_2 was still slower, the rate being $H_2O \gg CO_2 \gg O_2$.

Other Molecules: The rate and amount of absorption varied from molecule to molecule. The pretreatment temperature also had an influence on the rate of absorption. For example, the absorption process of acetone was as follows (as monitored by IR bands). Over $H_3PMo_{12}O_{40}$ having about 5 molecules of crystal water (pre-evacuated at 25 °C), the amount of acetone which was absorbed within 30 min at 25 °C increased linearly with the pressure of acetone. However, in the case of $H_3PMo_{12}O_{40}\cdot H_2O$, there was a critical pressure for absorption. Acetone suddenly started to be absorbed when its partial pressure reached 60 Torr. The critical pressure was also observed for acrolein.

Table 3. Absorption (and adsorption) of various molecules by $H_3PW_{12}O_{40}$ at room temperature (molecule/heteropoly anion)

Molecule	Irreversible	Total
Pyridine	6.0	>9
NH_3	3.2	4.3
2-Propanol	6.3	∞
Ethanol	6.2	∞
Methanol	2.2	∞
Benzene	0.1 (0.8)[a]	0.5
Toluene	0.04 (0.4)	0.4
1-Butene	0.2 (1.1)	0.25
Ethylene	0.03 (0.05)	0.04

a) Figures in parentheses are surface coverage.

The amounts of reversible and irreversible adsorption (or absorption) by $H_3PW_{12}O_{40}$ at 25 °C are given in Table 3. The uptake of hydrocarbons was very small. Probably adsorption took place only on the surface. In support of this idea, no change in the IR spectrum was found by contact with butene at 25 °C. On the other hand, polar molecules containing oxygen or nitrogen (O-base and N-base) were adsorbed rapidly, and 2—6 molecules per anion were retained in $H_3PW_{12}O_{40}$ after evacuation. Most of the O-bases were desorbed when evacuated at a slightly higher temperature. For example, changes upon heat treatment in the IR spectra of $H_3PMo_{12}O_{40}$ and $H_3PW_{12}O_{40}$ which had absorbed acetone are shown in Fig. 5. A large portion of the acetone observed for $H_3PMo_{12}O_{40}$ (1100—600 cm^{-1}) were changed to the reduced state after evacuation at 130 °C. When $H_3PMo_{12}O_{40}$ was evacuated at 130 °C in the absence of acetone, such a great change was not observed. In the case of $H_3PW_{12}O_{40}$ pre-evacuated at 25 °C, acetone was more easily absorbed into the bulk at a low pressure. This absorbed acetone was held in the bulk more tightly than in $H_3PMo_{12}O_{40}$. New peaks (1461, 1538, and

** 1 Torr≈133.322 Pa.

1592 cm^{-1}) began to appear at 80 °C, accompanied by a decrease in the bands corresponding to acetone. Then, these new peaks increased with the increase in the evacuation temperature up to 130 °C. Their intensities were reduced at 160 °C.

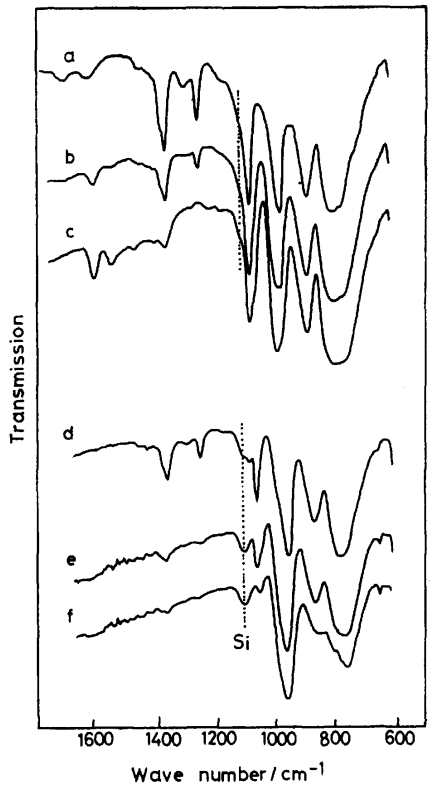

Fig. 5. Thermal desorption of acetone from $H_3PW_{12}O_{40}$ and $H_3PMo_{12}O_{40}$.
$H_3PW_{12}O_{40}$; a: Acetone (60 Torr) and evacuated at 25 °C, b: evacuated at 80 °C, c: evacuated at 130 °C. $H_3PMo_{12}O_{40}$; d: Acetone (120 Torr) and evacuated at 25 °C, e: evacuated at 80 °C, f: evacuated at 130 °C. Samples were pre-evacuated at 25 °C.

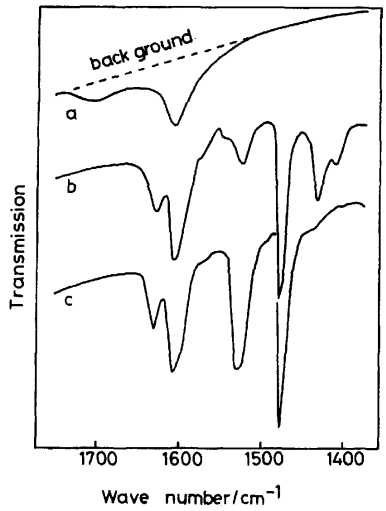

Fig. 6. IR spectral change by the interaction of $H_3PMo_{12}O_{40}$ with pyridine.
a: Evacuated for 30 s at 25° C, b: 1 h after the introduction of pyridine vapor (4 Torr), c: evaculated for 1 h at 130 °C after b.

The absorption of pyridine was followed by means of the IR, as is shown in Fig. 6. As the 1720 cm^{-1}-band and probably also the 1620 cm^{-1}-band disappeared, the 1540 cm^{-1}-band, characteristic of the pyridinium ion, appeared, together with the other bands of absorbed pyridine. Upon evacuation at 130 °C, the bands at 1400—1700 cm^{-1} became identical with that of the authentic pyridinium ion (Fig. 6c).[16] The re-addition of pyridine at 25 °C and evacuation at 130 °C reversibly changed the spectrum between b and c.

Discussion

Primary and Secondary Structure. As is shown by the IR spectra in Fig. 1, the Keggin structure is retained upon salt formation and dehydration (or rehydration). However, the XRD patterns which reflect a three-dimensional regularity vary tremendously. These facts led us to conclude that the "primary structure" (the Keggin unit) of heteropoly acids ($PMo_{12}O_{40}^{3-}$, in this case) is stable, but that the "secondary structure" (the three-dimensional arrangement of the heteropolyanion, water, and the counter cation) is subject to easy rearrangement.[2,4] We consider that a clear distinction between the primary and secondary structures is important for understanding the catalytic action of heteropoly acids. These characteristics make heteropoly acids behave like a solution, and in some cases the catalytic reactions proceed in the interstitial space of the bulk. This is the hypothesis of the "pseudo-liquid phase."[2,4] In this respect, water in the bulk and in the gas phase often plays an important role. Evidence to support the reactions in the bulk has previously been reported.[17,18]

Since the lattice constant of $H_3PW_{12}O_{40}\cdot 29H_2O$ is 23.3 Å,[19a] and since the $H_3PW_{12}O_{40}\cdot 6H_2O$ which is formed by dehydration has the lattice constant of 12.5 Å,[19b] dehydration obviously causes a shrinkage of the unit cell. Adjacent heteropolyanions come much closer when water molecules between the anions are removed. Therefore, the water of crystallization is not zeolitic in this case. The pore-size distribution also supports this idea as has been discussed before.[7] Since the size of the Keggin unit is about 10 Å or a little greater in diameter, the pore size which would be expected from the zeolitic desorption of water should be 5—7 Å in radius for 29-hydrate and 1—2 Å for 6-hydrate. This does not agree with the pore-size distribution observed. Therefore, the pore actually measured must have been formed between fine primary particles which had been shrunk by dehydration. The apparent expansion of the volume by the absorption of water, pyridine, *etc.* also supports the idea that water is not zeolitic. These molecules penetrate into the bulk by expanding the interstitial space. A similar explanation may be applied to water-soluble metal salts. The dehydration-rehydration of 0—2 hydrates probably proceeds in essentially the same way, although no direct evidence has been obtained.

In the case of water-insoluble salts, like K, Cs, and NH_4 salts, almost the same XRD patterns, which were close to the ASTM card of K or NH_4 salt (9-408, 412), were reproducibly obtained, indicating that the secondary structures of these salts are rather stable. Recently, Eguchi, Yamazoe, and Seiyama reported that water is zeolitic for these salts.[11]

Acidic and Redox Properties. The acidic properties (amount, strength, and type (Brønsted or Lewis)) of ordinary solid acids can be determined most reliably when the thermal desorption of pyridine is measured by IR spectroscopy. Therefore, the thermal desorption of pyridine (or the thermal decomposition of pyridinium salt) given in Fig. 4 reasonably reflects the acidic properties of these compounds. The amount of pyridine which remained after evacuation represents the amount of acidic protons, and the change in this amount by the evacuation temperature is related to the acid-strength distribution. Although the number of pyridine did not change by a prolonged period of evacuation, we are still uncertain whether or not these data reflect the true equilibrium. Therefore, we will discuss here only the number of acidic protons and the qualitative trend of the acid strength.

The quantity of pyridine which was not removed by 100—250 °C-evacuation agreed with the total number of protons for three heteropoly acids. Thus, uniform pyridinium salts were formed after this procedure. This uniformity enables us to estimate the number of acidic protons on or near the surface. If one assumes the surface area to be 10 $m^2\ g^{-1}$, and the number of Keggin units on the surface to be 1/100 $Å^2$, the number of the surface acidic proton becomes 50 $\mu eq\ g^{-1}$, which is comparable with the value of 30—50 $\mu eq\ g^{-1}$ of Brønsted sites for SiO_2–Al_2O_3.[21] As for the acid strength, we may conclude qualitatively that heteropolyacids are stronger than SiO_2–Al_2O_3, since the pyridinium ion on SiO_2–Al_2O_3 almost disappears upon evacuation above 300 °C, as is shown in Fig. 4. Pyridine started to be removed at about 250 °C in the case of heteropolyacids containing Mo. However, a partial degradation was indicated by the IR in this case, so that the desorption at lower temperatures does not necessarily mean that their acid strength is weaker than $H_3PW_{12}O_{40}$.

The IR spectra of pyridine absorbed changed by evacuation at 130 °C and the readdition of pyridine at 25 °C, as is shown in Fig. 5. This process was reversible, and the spectrum after evacution (Spectrum d) was identical with the authentic pyridinium salt given in the literature.[16] It was suggested that the 1540-cm^{-1}-band characteristic of the pyridinium ion becomes weak when a dimer ion is formed.[20] Therefore, the change taking place between Spectra b and c in Fig. 5 may be as follows, if one takes into account the fact that the pyridine/proton ratio was about two after evacuation at 25 °C:

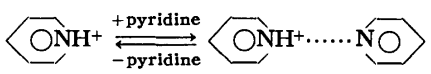

The general redox properties have already been discussed by several investigators.[2,4,13,22,23] We will discuss here only the spectral changes in the IR spectra given in Fig. 5. The spectral change in $H_3PMo_{12}O_{40}$ in the 600—1100 cm^{-1} region may be due to the reduction of $H_3PMo_{12}O_{40}$ by acetone, since it is much more reducible than $H_3PW_{12}O_{40}$ and the spectral change resembles that found upon reduction by H_2.[2,13] The new peaks which appeared at 1400—1600 cm^{-1} for $H_3PW_{12}O_{40}$ may be attributed to the mesityl oxide formed from acetone, since mesityl oxide absorbed by $H_3PW_{12}O_{40}$ gave IR bands at 1619, 1442, and 1376 cm^{-1}.

This work was supported in part by Grant-in-Aid for Special Project Research No. 520804 from the Ministry of Education, Science and Culture.

References

1) T. Ohara, *Shokubai*, **19**, 157 (1977); K. Onoue, Y. Mizutani, S. Akiyama, and Y. Izumi, *CHEMTECH*, July (1978), p. 432.

2) M. Misono, K. Sakata, Y. Yoneda, and W. Y. Lee, *Proc. 7th Intern. Congr. Catal., 1980, Tokyo*, Kodansha-Elsevier (1981), p. 1047.

3) a) S. Nakamura and H. Ichihashi, *Proc. 7th Intern. Congr. Catal., 1980, Tokyo*, Kodansha-Elsevier (1981), p. 755; b) M. Otake and T. Onoda, *ibid.*, (1981), p. 780; c) Y. Ono, T. Mori, and T. Keii, *ibid.*, (1981), p, 1414; d) H. Niiyama, Y. Saito, and E. Echigoya, *ibid.*, (1981), p. 1416; e) K. Urabe, F. Kimura, and Y. Izumi, *ibid.*, (1981), p. 1418.

4) a) M. Misono, K. Sakata, and Y. Yoneda, The CSJ/ACS Chemical Congress, Honolulu, April (1979); b) M. Misono and Y. Yoneda, 1st Japan-France Catalysis Seminar, Lyon, July (1979); c) K. Sakata, M. Misono, Y. Konishi, and Y. Yoneda, *Shokubai*, **21**, 226 (1979).

5) *E.g.*, Y. Yoneda, *Proc. 4th Intern. Congr. Catal., 1968, Moscow*, Akademi Kiado, Budapest (1971), Vol. 2, p. 449.

6) M. Misono, *Kagaku (Chemistry)*, **36**, 15 (1981).

7) M. Misono, Y. Konishi, M. Furuta, and Y. Yoneda, *Chem. Lett.*, **1978**, 709.

8) M. Furuta, K. Sakata, M. Misono, and Y. Yoneda, *Chem. Lett.*, **1979**, 31.

9) J. C. Bailar, *Inorg. Synth.*, **1**, 132 (1939).

10) G. A. Tsigdinos, *Ind. Eng. Chem., Prod. Res. Dev.*, **13**, 267 (1974).

11) K. Eguchi, N. Yamazoe, and T. Seiyama, *Nippon Kagaku Kaishi*, **1981**, 336.

12) M. Furuta, T. Okuhara, M. Misono, and Y. Yoneda, 44th Symposium on Catalysis, Fukuoka, 1979, 4R11.

13) K. Katamura, T. Nakamura, K. Sakata, M. Misono, and Y. Yoneda, *Chem. Lett.*, **1981**, 89.

14) Y. Konishi, K. Sakata, M. Misono, and Y. Yoneda, Symposium on Oxidation Reactions, Yokohama (1980), 1-2.

15) K. Sakata, M. Misono, and Y. Yoneda, *Chem. Lett.*, **1980**, 151.

16) E. P. Parry, *J. Catal.*, **2**, 371 (1963).

17) T. Okuhara, A. Kasai, M. Misono, and Y. Yoneda, *Chem. Lett.*, **1981**, 391.

18) Y. Saito, H. Niiyama, N. Yoneda, and E. Echigoya, 46th Symposium on Catalysis, Sendai 1980, 3P07.

19) a) A. J. Bradley and J. W. Illingworth, *Proc. R. Soc. London, Ser. A*, **157**, 113 (1936); b) G. M. Brown, M. R. Noe-Spiret, W. R. Busing, and H. A. Levy, *Acta Crystallogr.*, **833**, 1038 (1977).

20) R. Clements and J. L. Wood, *J. Mol. Structure*, **17**, 265 (1973).
21) T. Matsubara, J. Take, and Y. Yoneda, *Shokubai*, **20**, 202 (1978).
22) H. Niiyama, H. Tsuneki, and E. Echigoya, *Nippon Kagaku Kaishi*, **1979**, 996.
23) M. Akimoto, S. Sakamaki, and E. Echigoya, *Nippon Kagaku Kaishi*, **1981**, 203.
24) E. P. Barrett, L. G. Joyner, and P. P. Halenda, *J. Am. Chem. Soc.*, **73**, 373 (1951).

The Structure of the Cyclodextrin Complex. XI. Crystal Structure of Hexakis-(2,3,6-tri-*O*-methyl)-α-cyclodextrin-*p*-Iodoaniline Monohydrate

Kazuaki HARATA,* Kaneto UEKAMA,† Masaki OTAGIRI,† and Fumitoshi HIRAYAMA†

Research Institute for Polymers and Textiles, 1-1-4, Yatabe-Higashi, Tsukuba, Ibaraki 305

†*Faculty of Pharmaceutical Sciences, Kumamoto University, 5-1, Oe-honmachi, Kumamoto 862*

(Received June 26, 1981)

The crystal structure of hexakis(2,3,6-tri-*O*-methyl)-α-cyclodextrin–*p*-iodoaniline complex, $C_{54}H_{96}O_{30}\cdot C_6H_6NI\cdot H_2O$, was determined by the X-ray method. The crystal is monoclinic with the space group $P2_1$, $Z=2$, $a=11.440(4)$, $b=23.674(6)$, $c=13.531(3)$ Å, and $\beta=91.90(2)°$. The structure was solved by the heavy atom method combined with the rigid-body least-squares technique and refined by the block-diagonal least-squares method to the final *R*-value of 0.11 for 2186 reflections ($\sin\theta/\lambda<0.49$). Hexakis(2,3,6-tri-*O*-methyl)-α-cyclodextrin is in the shape of a truncated elliptical cone; these cones are stacked along the a axis to form a channel-type structure. The guest *p*-iodoaniline and water molecules are located in the channel. The iodophenyl group is inserted rather loosely from the base side of the truncated cone. The iodine atom is located at the center of the cavity, while the amino group outside the host cavity forms a hydrogen bond with the water molecule. The water molecule is also hydrogen bonded to the adjacent host molecule along the channel. The crystal is built up of columns of the host molecules, which are closely packed in the van der Waals contact.

The chemical modification of cyclodextrins has been investigated to improve complexing and catalytic abilities by introducing various groups into the macrocyclic ring.[1] Permethylation of cyclodextrins gives compounds which are quite interesting in their macrocyclic structure and complex formation, since permethylated cyclodextrins have no hydroxyl groups. Syntheses and some chemical and spectroscopic data have been recently reported,[2-5] but their structural features have not yet published. The crystal structure of hexakis(2,3,6-tri-*O*-methyl)-α-cyclodextrin(methyl-α-CDx)complex with *p*-iodoaniline has been investigated by the X-ray method. In this paper, the structure of the complex will be discussed mainly by comparison with the structure of α-cyclodextrin–*p*-indoaniline complex.[6]

Experimental

Methyl-α-CDx was added to a *p*-iodoaniline-saturated aqueous solution at 40 °C to prepare a 5% solution. The solution was cooled to 0 °C to dissolve methyl-α-CDx, then allowed to stand at 50 °C. Colorless rod-like crystals were obtained. Lattice parameters and intensities were measured on a Nicolet P3/F diffractometer with graphite-monochromated Cu *Kα* radiation. 2168 independent reflections with $|F_o|\geq 3\sigma(F)$ were obtained up to 90° in 2θ. No corrections were made for absorption and extinction.

Crystal Data. $C_{54}H_{96}O_{30}\cdot C_6H_6NI\cdot H_2O$, *F.W.*=1462.4, monoclinic, space group $P2_1$, $Z=2$, $a=11.440(4)$, $b=23.674(6)$, $c=13.531(3)$ Å, $\beta=91.90(2)°$, $V=3662.6$ Å^3, $D_x=1.326$, $D_m=1.31$ g cm^{-3}.

Determination and Refinement of the Structure

The structure was solved by the heavy atom method. The electron-density map calculated with iodine phases revealed that the methyl-α-CDx ring is located nearly perpendicular to the a axis. But the center of symmetry which appeared in the map made it quite difficult to estimate the position of light atoms. Therefore, the rigid-body least-squares technique was adopted to determine the orientation and disposition of each 2,3,6-tri-*O*-methylglucose residue. Non-iodine atoms in *p*-iodoaniline and water molecules were found on Fourier and difference-Fourier maps. The structure was refined

Table 1. Fractional coordinates (×10³) and isotropic temperature factors (B/Å²) of hexakis(2,3,6-tri-*O*-methyl)-α-cyclodextrin

	x	*y*	*z*	*B*/Å²		*x*	*y*	*z*	*B*/Å²
C(1,G1)	56(3)	472(2)	300(3)	7.5(1.0)	C(1,G4)	110(3)	23(2)	181(3)	6.6(0.9)
C(2,G1)	138(3)	492(2)	374(3)	6.6(0.9)	C(2,G4)	190(3)	10(1)	106(2)	6.0(0.9)
C(3,G1)	189(3)	442(1)	421(2)	5.2(0.8)	C(3,G4)	232(3)	67(1)	65(2)	4.9(0.8)
C(4,G1)	96(3)	406(1)	471(2)	5.0(0.8)	C(4,G4)	130(3)	94(1)	9(2)	5.8(0.8)
C(5,G1)	-16(3)	397(1)	393(2)	6.0(0.8)	C(5,G4)	29(3)	100(1)	80(2)	5.4(0.8)
C(6,G1)	-129(4)	373(2)	432(3)	9.9(1.3)	C(6,G4)	-84(3)	110(2)	9(3)	6.8(0.9)
C(7,G1)	197(5)	579(2)	295(4)	13.9(1.8)	C(7,G4)	289(4)	-77(2)	148(3)	9.6(1.3)
C(8,G1)	373(5)	454(2)	498(4)	12.6(1.6)	C(8,G4)	432(4)	65(2)	31(3)	9.8(1.3)
C(9,G1)	-270(6)	402(3)	562(5)	18.7(2.6)	C(9,G4)	-277(4)	123(2)	18(3)	9.7(1.3)
O(2,G1)	237(2)	521(1)	335(2)	8.7(0.7)	O(2,G4)	289(2)	-16(1)	163(2)	8.2(0.7)
O(3,G1)	267(3)	459(1)	511(2)	10.2(0.8)	O(3,G4)	318(2)	54(1)	-10(2)	8.3(0.7)
O(4,G1)	145(2)	351(1)	495(1)	5.3(0.5)	O(4,G4)	172(2)	150(1)	-13(1)	4.6(0.5)
O(5,G1)	-43(2)	447(1)	345(2)	6.2(0.6)	O(5,G4)	-1(2)	47(1)	121(1)	5.1(0.5)
O(6,G1)	-144(4)	413(2)	514(3)	16.7(1.4)	O(6,G4)	-172(2)	124(1)	77(2)	8.1(0.7)
C(1,G2)	95(3)	386(2)	-62(3)	7.2(1.0)	C(1,G5)	105(3)	109(1)	541(2)	6.0(0.8)
C(2,G2)	166(3)	436(1)	-32(2)	5.4(0.8)	C(2,G5)	197(3)	63(2)	517(3)	6.9(0.9)
C(3,G2)	194(3)	438(1)	73(2)	4.6(0.7)	C(3,G5)	222(3)	67(2)	409(3)	7.4(1.0)
C(4,G2)	85(3)	443(2)	126(3)	7.5(1.0)	C(4,G5)	116(3)	57(1)	345(2)	4.1(0.7)
C(5,G2)	2(3)	393(2)	90(3)	7.1(1.0)	C(5,G5)	20(3)	96(1)	385(2)	4.8(0.7)
C(6,G2)	-126(3)	393(2)	131(3)	7.2(1.0)	C(6,G5)	-100(3)	76(2)	342(3)	7.2(1.0)
C(7,G2)	292(4)	458(2)	-172(3)	9.7(1.3)	C(7,G5)	340(5)	38(2)	642(4)	13.4(1.7)
C(8,G2)	362(4)	478(2)	151(3)	9.3(1.2)	C(8,G5)	396(4)	48(2)	342(4)	12.0(1.5)
C(9,G2)	-295(4)	438(2)	147(3)	9.5(1.2)	C(9,G5)	-298(4)	106(2)	337(4)	11.8(1.5)
O(2,G2)	280(2)	430(1)	-81(2)	7.5(0.6)	O(2,G5)	305(3)	79(1)	580(2)	9.5(0.8)
O(3,G2)	263(2)	486(1)	98(2)	6.6(0.6)	O(3,G5)	305(2)	23(1)	392(2)	8.1(0.7)
O(4,G2)	108(2)	436(1)	231(2)	5.4(0.5)	O(4,G5)	140(2)	64(1)	250(1)	4.5(0.5)
O(5,G2)	-10(2)	394(1)	-12(2)	6.7(0.6)	O(5,G5)	7(2)	96(1)	487(2)	5.6(0.5)
O(6,G2)	-177(2)	442(1)	114(2)	7.4(0.6)	O(6,G5)	-184(2)	121(1)	370(2)	9.5(0.8)
C(1,G3)	171(3)	165(1)	-109(2)	5.8(0.8)	C(1,G6)	150(3)	339(2)	593(3)	6.7(0.9)
C(2,G3)	275(3)	204(1)	-138(2)	4.4(0.7)	C(2,G6)	260(3)	300(1)	614(2)	5.7(0.8)
C(3,G3)	263(2)	259(1)	-80(2)	4.7(0.7)	C(3,G6)	266(3)	248(2)	552(2)	6.1(0.7)
C(4,G3)	147(3)	289(1)	-100(2)	4.6(0.7)	C(4,G6)	152(3)	213(2)	575(2)	5.2(0.7)
C(5,G3)	47(3)	248(2)	-87(2)	5.3(0.7)	C(5,G6)	47(2)	250(2)	559(2)	4.7(0.6)
C(6,G3)	-63(4)	274(2)	-132(3)	9.3(1.2)	C(6,G6)	-67(4)	217(2)	593(3)	8.8(1.2)
C(7,G3)	448(4)	159(2)	-186(3)	10.2(1.3)	C(7,G6)	448(4)	333(2)	664(3)	9.1(1.2)
C(8,G3)	441(4)	313(2)	-32(3)	8.1(1.1)	C(8,G6)	433(4)	200(2)	505(3)	9.8(1.3)
C(9,G3)	-249(7)	263(4)	-159(6)	24.3(3.5)	C(9,G6)	-245(6)	234(4)	524(6)	21.9(2.9)
O(2,G3)	379(2)	177(1)	-102(2)	6.2(0.6)	O(2,G6)	361(2)	335(1)	584(2)	7.2(0.6)
O(3,G3)	356(2)	294(1)	-111(2)	8.0(0.7)	O(3,G6)	380(2)	214(1)	585(2)	8.0(0.7)
O(4,G3)	150(2)	333(1)	-31(1)	4.6(0.5)	O(4,G6)	153(2)	167(1)	507(1)	5.0(0.5)
O(5,G3)	67(2)	196(1)	-144(2)	6.1(0.6)	O(5,G6)	55(2)	301(1)	616(2)	5.5(0.5)
O(6,G3)	-154(3)	245(2)	-110(3)	16.0(1.2)	O(6,G6)	-157(3)	252(2)	573(2)	12.5(0.9)

Table 2. Fractional coordinates (×10³) and B_{eq} of *p*-iodoaniline and water

	x	*y*	*z*	B_{eq}/Å²
C(1,IA)	557(5)	272(2)	263(4)	13.1
C(2,IA)	519(8)	227(2)	217(4)	22.3
C(3,IA)	383(5)	215(2)	209(4)	13.3
C(4,IA)	306(4)	257(4)	243(4)	15.1
C(5,IA)	352(6)	307(2)	278(5)	15.8
C(6,IA)	475(8)	314(2)	282(6)	25.5
N(IA)	669(4)	276(3)	255(6)	19.6
I(IA)	114.2(0.2)	247.8(—)	238.7(0.3)	12.4
O(W)	−190(6)	200(3)	219(5)	29.4

by the block-diagonal least-squares method. Anisotropic temperature factors were used for *p*-iodoaniline and water, isotropic ones for methyl-α-CDx. The quantity minimized was $\sum w(|F_o|-|F_c|)^2$ with $w=1.0$ for all the reflections. The final *R*-value was 0.11. The atomic scattering factors were taken from "International Tables for X-Ray Crystallography."[7] The atomic parameters are given in Tables 1 and 2. Tables of observed and calculated structure factors, anisotropic temperature factors of *p*-iodoaniline and water, bond-distances, angles, and conformation angles of methyl-α-CDx are kept at The Chemical Society of Japan (Document No. 8211).

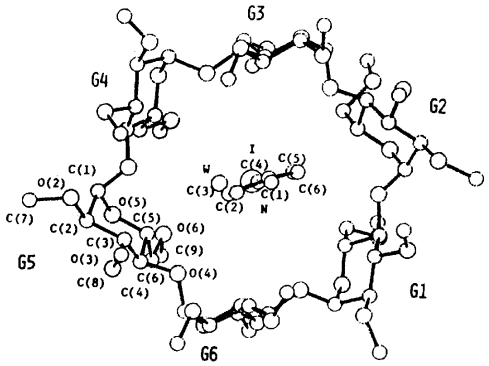

Fig. 1. Structure and numbering scheme of hexakis (2,3,-6-tri-*O*-methyl)-α-cyclodextrin–*p*-iodoaniline monohydrate. The water molecule is denoted by W.

Description and Discussion of the Structure

Outline of the Structure. The structure and numbering scheme of the methyl-α-CDx–*p*-iodoaniline complex are shown in Figs. 1 and 2. Methyl-α-CDx is in the shape of a truncated elliptical cone, and is stacked along the a axis with a head-to-tail fashion to form a channel-type structure, as shown in Fig. 3. About two-thirds of the guest *p*-indoaniline molecules are inserted from the O(2), O(3) side of methyl-α-CDx. The amino group forms a hydrogen bond with the water molecule.

Conformation of Methyl-α-CDx. Average bond distances and angles over six 2,3,6-tri-*O*-methylglucose residues are shown in Fig. 4. Geometrical data for the methyl-α-CDx ring are given in Tables 3—5. The C(6)–O(6) bonds of G1 and G2 residues are in the *gauche-gauche* conformation, the other four C(6)–O(6) bonds

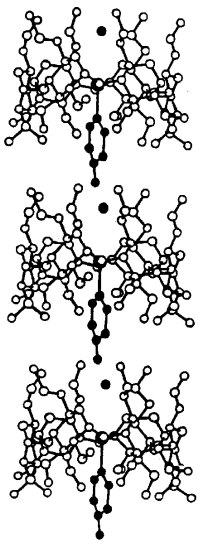

Fig. 3. A stacking feature of the complex. *p*-Iodoaniline and water are shown by black dots.

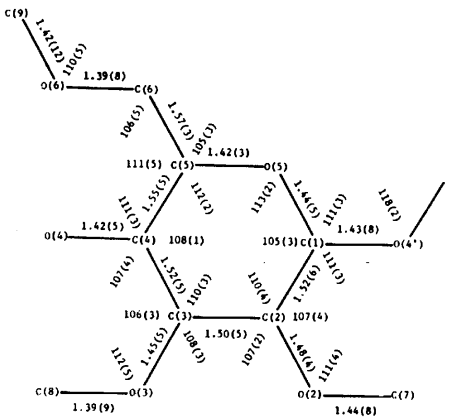

Fig. 4. Average bond distances (l/Å) and angles (ϕ/°) of hexakis(2,3,6-tri-*O*-methyl)-α-cyclodextrin over six 2,3,-6-tri-*O*-methylglucose residues. Standard deviations in parentheses were estimated according to the equation, $\sigma=[\sum_{i=1}^{6}(x_i-\bar{x}^2)/5]^{1/2}$, where x_i referes to the bond distance or angle in the *i*-th residue and $\bar{x}$ is the average value.

being in the *gauche-trans* conformation. All O(6)–C(9) bonds are *trans* to the C(5)–C(6) bond. The orientations of O(2)–C(7) and O(3)–C(8) bonds are different. All O(2)–C(7) bonds are oriented outside the methyl-α-CDx

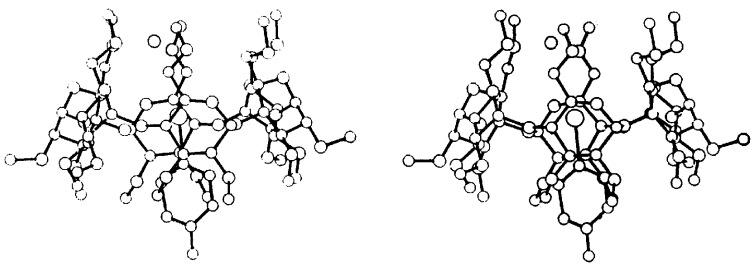

Fig. 2. A stereo-drawing of a side-view of the complex.

Table 3. Selected intramolecular distances

Distance(*l*/Å)		Distance(*l*/Å)	
I. O(4)···O(4) distances			
O(4,G1)···O(4,G2)	4.11	O(4,G5)···O(4,G6)	4.25
O(4,G1)···O(4,G6)	4.36	O(4,G1)···O(4,G4)	8.37
O(4,G2)···O(4,G3)	4.35	O(4,G2)···O(4,G5)	8.82
O(4,G3)···O(4,G4)	4.34	O(4,G3)···O(4,G6)	8.27
O(4,G4)···O(4,G5)	4.13		
II. O(2)···O(3) distances			
O(2,G1)···O(3,G2)	3.33	O(2,G3)···O(3,G4)	3.26
O(2,G6)···O(3,G1)	3.26	O(2,G4)···O(3,G5)	3.23
O(2,G2)···O(3,G3)	3.37	O(2,G5)···O(3,G6)	3.25
III. O(2)···C(8) distances			
O(2,G6)···C(8,G1)	3.04	O(2,G3)···C(8,G4)	3.25
O(2,G1)···C(8,G2)	3.08	O(2,G4)···C(8,G5)	3.07
O(2,G2)···C(8,G3)	3.38	O(2,G5)···C(8,G6)	3.39

Table 4. Least-squares plane through six O(4) atoms and deviations from the plane

The plane equation is of the $AX+BY+CZ=D$ form, where X, Y, and Z are the coordinates in Å units along the a, b, and c* axes, respectively.

$0.9979X+0.0418Y+0.0497Z=1.9499$

Deviations of atoms from the plane (*l*/Å)

O(4,G1)	0.16	O(4,G4)	0.15
O(4,G2)	−0.24	O(4,G5)	−0.24
O(4,G3)	0.08	O(4,G6)	0.08

Table 5. Torsion-angle indices and tilt-angles

Residue	φ/°	Residue	φ/°
I. Torsion-angle index[a]			
G1	160	G4	491
G2	145	G5	142
G3	151	G6	134
II. Tilt-angle[b]			
G1	24.5	G4	23.6
G2	22.6	G5	22.1
G3	3.0	G6	3.0

a) The torsion-angle index is defined as follows: $|\phi(C(1)-C(2))|+|\phi(C(2)-C(3))|+|\phi(C(5)-O(5))|+|\phi(O(5)-C(1))|-|\phi(C(3)-C(4))|-|\phi(C(4)-C(5))|$.

b) The tilt-angle is defined as the angle made by the plane through six O(4) atoms and the plane through O(4′), C(1), C(4), and O(4) of each glucose residue.

ring; the average conformation angles of C(1)–C(2)–O(2)–C(7) and C(3)–C(2)–O(2)–C(7) are 106° and −137°, respectively. On the other hand, the O(3)–C(8) bonds turn inside the methyl-α-CDx ring, giving the average C(2)–C(3)–O(3)–C(8) and C(4)–C(3)–O(3)–C(8) angles of −120° and 123°, respectively.

Methyl-α-CDx is in the shape of an elliptically distorted and truncated cone (Fig. 2). The diagonal O(4)···O(4) distances of 8.27, 8.37, and 8.82 Å are similar to those of the α-cyclodextrin-*p*-iodoaniline complex (8.16, 8.44, and 8.88 Å). The longest diagonal is found along the plane of the included *p*-iodoaniline. The O(4)···O(4) distances between adjacent 2,3,6-tri-*O*-methylglucose residues (4.11—4.36 Å) also resemble those of the α-cyclodextrin–*p*-iodoaniline complex (4.07—4.40 Å). But the torsion angle indices (134—160°) are significantly larger than those of the α-cyclodextrin complex (115—134°), suggesting that the pyranose-ring conformation is slightly different in methyl-α-CDx and α-cyclodextrin.

The deviations of O(4) atoms from their least-squares plane (Table 4) shows that these atoms are arranged in a boat form. The boat form is also observed in the α-cyclodextrin–*p*-iodoaniline complex, although the atomic deviation in the α-cyclodextrin complex is smaller than that in the methyl-α-CDx complex. Significant conformational differences between α-cyclodextrin and methyl-α-CDx are observed in O(2)···O(3) distances between the adjacent residues and tilt-angles. The O(2)···O(3) distances in methyl-α-CDx range from 3.23 to 3.37 Å. On the other hand, the corresponding distances in α-cyclodextrin are in the range 2.68—3.00 Å, indicating hydrogen-bond formation. The relatively large O(2)···O(3) distances in methyl-α-CDx are mainly ascribed to the steric hindrance between O(2) and C(8) methyl group of adjacent residue. As seen from Table 3, relatively short distances are found between O(2) and C(8) (3.04—3.39 Å). The steric hindrance also affects the tilt-angle of the 2,3,6-tri-*O*-methylglucose residues (Table 5). The G3 and G6

Table 6. Intermolecular distances less than 3.5 Å

Distance(*l*/Å)		Distance(*l*/Å)	
O(6,G4)–O(W)	2.77	C(2,G2)–O(5,G4)	3.43(c)
O(6,G5)–O(W)	2.65	C(9,G2)–O(3,G4)	3.32(c)
N(IA)–O(W)	2.49(a)	O(6,G2)–C)2,G4)	3.38(c)
C(1,IA)–O(W)	3.43(a)	O(6,G2)–O(3,G4)	3.39(c)
C(2,IA)–O(W)	3.39(a)	C(9,G1)–O(3,G5)	2.95(d)
C(7,G3)–O(3,G6)	3.47(b)	O(6,G1)–O(3,G5)	3.46(d)
O(3,G3)–C(7,G6)	3.38(b)		

Code	Symmetry operator		
None	x,	y,	z
a	$1+x$,	y,	z
b	x,	y,	$-1+z$
c	$-x$,	$1/2+y$,	$-z$
d	$-x$,	$1/2+y$,	$1-z$

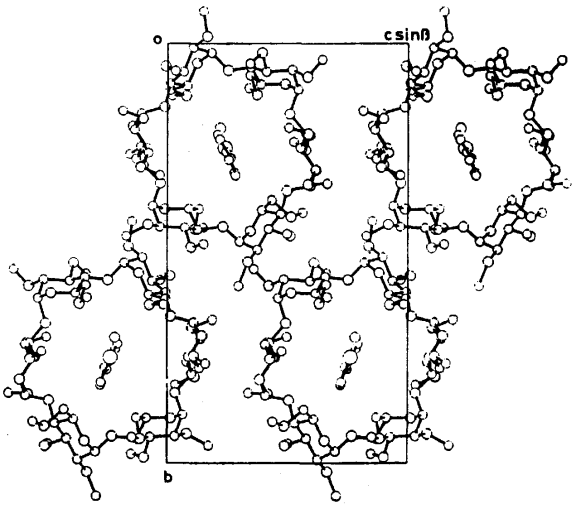

Fig. 5. Crystal structure viewed down the a axis.

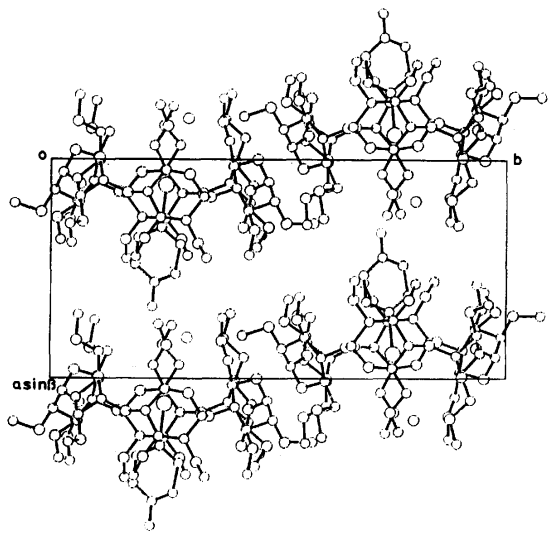

Fig. 6. Crystal structure viewed down the c axis.

residues are almost perpendicular to the O(4) plane, but the other four residues are tilted by the angles of 22.1—24.5°. In the α-cyclodextrin–*p*-iodoaniline complex, the tilt-angles are in the range from 2.1 to 15.6°, and the average value (10.8°) is smaller than that of methyl-α-CDx (16.7°). The conformation of α-cyclodextrin is held by the O(2)···O(3) hydrogen bonds. Since methyl-α-CDx forms no intramolecular hydrogen bonds, the macrocyclic conformation may be more responsible for the steric hindrance between 2,3,6-tri-*O*-methylglucose residues, host-guest interaction, and molecular packing in the crystal.

Methyl-α-CDx–Guest Interaction. *p*-Iodoaniline molecule is inserted into the methyl-α-CDx ring from the O(2), O(3) side, and about two-thirds of the molecule is included. The shortest methyl-α-CDx···guest distance is 3.87 Å, which is found between O(4,G1) and C(5,1A). Therefore, *p*-iodaniline is rather loosely bound in the methyl-α-CDx cavity. The benzene ring is nearly parallel to the C(2,G2)···C(2,G5) diagonal, along which the methyl-α-CDx is elliptically distorted. The iodine atom is located at the center of the cavity. This inclusion geometry is different from that of the α-cyclodextrin complex, in which the whole iodophenyl group is tightly included, although *p*-iodoaniline is also inserted from the O(2), O(3) side. In the methyl-α-CDx complex, the deep penetration of *p*-iodoaniline may be interrupted by the large tilt of G1, G2, G4, and G5 residues, making the O(6) side narrower. The amino group is hydrogen-bonded to a water molecule located at the O(6) side of the adjacent methyl-α-CDx. The water molecule is also hydrogen-bonded to the O(6) atoms of G4 and G5 residues, thus forming $-NH_2\cdots$ water···O(6) hydrogen-bond bridges.

Molecular Packing. Methyl-α-CDx molecules are stacked along the a axis to form a typical channel-type structure. This packing feature resembles those of the α-cyclodextrin complexes with *m*-nitroaniline[8] and benzaldehyde.[9] But, owing to the methylation of all hydroxyl groups, no hydrogen bonds can be formed between methyl-α-CDx molecules along the channel. The O(4) plane is nearly perpendicular to the channel axis (86.3°). *p*-Iodoaniline and water molecules are alternately arranged in the channel. The α-cyclodextrin–*p*-iodoaniline complex does not form a channel-type structure because the dimension of *p*-iodoaniline is large compared with the repetition unit of the channel. In contrast, the repetition unit in the methyl-α-CDx complex is larger than the size of the guest *p*-iodoaniline; thus, a water molecule is also located in the channel to fill the vacant space.

Projections of the crystal structure are shown in Figs. 5 and 6. Since the two-fold screw axis is perpendicular to the channel axis, methyl-α-CDx in the symmetry-related column are arranged upside down. The methyl-α-CDx columns are closely packed in the crystal (Fig. 5). A somewhat short contact (2.95 Å) is found between C(9,G1) and O(3,G5), but other intermolecular distances (Table 6) indicate that the methyl-α-CDx columns are in the van der Waals contact.

References

1) M. L. Bender and M. Komiyama, "Cyclodextrin Chemistry," Springer Verlag, Berlin (1978).
2) B. Casu, H. Reggiani, G. G. Gallo, and A. Vigevani, *Tetrahedron*, **24**, 803 (1968).
3) R. J. Bergeron, M. P. Meeley, and Y. Machida, *Bioorg. Chem.*, **5**, 121 (1976).
4) J. Boger, R. J. Corcoran, and J. M. Lehn, *Helv. Chim. Acta*, **61**, 2190 (1978).
5) J. Szejtli, A. Lipták, I. Jodál, P. Fügedi, P. Nánási, and A. Hesmélyi, *Starch/Starke*, **32**, 165 (1980).
6) K. Harata, *Bull. Chem. Soc. Jpn.*, **48**, 2409 (1975).
7) "International Tables for X-Ray Crystallography," Kynoch Press, Birmingham (1974), Vol. IV, pp. 72—86.
8) K. Harata, *Bull. Chem. Soc. Jpn.*, **53**, 2782 (1980).
9) K. Harata, K. Uekama, M. Otagiri, F. Hirayama, and H. Ogino, *Bull. Chem. Soc. Jpn.*, **54**, 1954 (1981).

Algorithm of Data Processing in Correlation NMR Spectroscopy

Hiroshi Ozawa* and Yoji Arata†

Computer Center, The University of Tokyo, Yayoi, Bunkyo-ku, Tokyo 113

†*Department of Chemistry, The University of Tokyo, Hongo, Bunkyo-ku, Tokyo 113*

(Received June 30, 1981)

The algorithm for data processing in correlation NMR spectroscopy has been closely checked. Procedures have been proposed by which one can obtain the spectrum free from artifacts and can carry out phase correction of the spectrum easily.

In correlation NMR spectroscopy developed by Dadok and Sprecher,[1] the steady-state spectrum is derived from the response to a linear rapid frequency scan. In previous papers,[2-8] we have described a system where a variety of capabilities were incorporated to allow additional freedom in the correlation technique. So far we have written several programs which are based on different algorithms for dealing with the rapid scan response. It has been noticed that in some cases, even when the baseline of the rapid scan response is sufficiently flat, the finally obtained spectrum is accompanied by an oscillation which is spread over the entire range of frequency. In view of this, the algorithm for data processing in correlation NMR has been closely checked. It will be shown how improper ways of data processing result in artifacts in the final steady-state spectrum. Procedures will be described by which one can obtain the spectrum free from artifacts and can make phase correction of the spectrum easily.

Data Processing of Correlation NMR Spectroscopy

It has been shown[9] that the steady-state NMR spectrum $H(f)$ can be obtained by Fourier transforming the free induction decay $h(t)$ which is given by

$$h(t) = g(t)\exp(-ibt^2/2), \tag{1}$$

where $b/2\pi$ is the sweep rate of the linear rapid frequency scan in Hz/s, and $g(t)$ is the inverse Fourier transform of the rapid scan response $G(f)$ which is observed after the phase sensitive detection of the radio frequency. It will hereafter be assumed that the rapid scan response $G(f)$ is sampled using N data points at a time interval of Δt s or at every $\Delta f = b\Delta t/2\pi$ Hz of the spectrum. The values of $G(f)$ at $s\Delta t$ s and at frequency positions of $s\Delta f$ Hz where $s=0,1,\cdots,N-1$ will be denoted by $G[s]$.

Quadrature Phase Detection. The quadrature phase detection of the rapid scan response would provide $G[s]$ expressed in complex numbers as

$$G[s] = X[s] + iY[s], \quad s=0, 1,\cdots, N-1, \tag{2}$$

where $X[s]$ and $Y[s]$ are the response in quadrature. Inverse Fourier transformation of $G[s]$ gives $g[k]$,

$$g[k] \equiv A[k] - iB[k] = (1/N)\sum_{s=0}^{N-1}(X[s] + iY[s])\exp(2\pi iks/N), \quad k=0, 1,\cdots, N-1, \tag{3}$$

where

$$A[k] = 0, \quad k = N/2 + 1, N/2 + 2,\cdots, N-1, \tag{4a}$$

$$B[0] = 0, \tag{4b}$$

$$B[k] = 0, \quad k = N/2, N/2 + 1,\cdots, N-1. \tag{4c}$$

The $N/2+1$ values of $A[k]$ and $B[k]$ ($k=0,1,\cdots, N/2$) are used to calculate the discrete values $h[k]$ ($k=0,1,\cdots, N/2$) of the free induction decay $h(t)$ at $k\delta t$ s where

$$\delta t = 1/N\Delta f = 2\pi/Nb\Delta t, \tag{5a}$$

which is given by

$$h[k] \equiv D[k] - iE[k] = (A[k] - iB[k])(\cos(b(k\delta t)^2/2) - i\sin(b(k\delta t)^2/2)), \quad k=0, 1,\cdots, N/2, \tag{6a}$$

with

$$E[0] = 0. \tag{6b}$$

The N values $H[s]$ ($s=0,1,\cdots,N-1$) which represent the steady-state spectrum $H(f)$ at $s\delta f$ Hz where

$$\delta f = 1/N\delta t = b\Delta t/2\pi = \Delta f \tag{5b}$$

can be derived by putting

$$D[k] - iE[k] = 0, \quad k = N/2 + 1, N/2 + 2,\cdots, N - 1, \tag{7}$$

and Fourier transforming $h[k]$ ($k=0,1,\cdots,N-1$) according to the following equation:

$$H[s] \equiv U[s] + iV[s] = \sum_{k=0}^{N-1}(D[k] - iE[k])\exp(-2\pi isk/N), \quad s = 0, 1,\cdots, N - 1. \tag{8}$$

The phase correction of the spectrum is performed by mixing $U[s]$ and $V[s]$,

$$U[s]' = U[s]\cos\theta + V[s]\sin\theta, \quad s = 0, 1,\cdots, N - 1, \tag{9a}$$

$$V[s]' = -U[s]\sin\theta + V[s]\cos\theta, \quad s = 0, 1,\cdots, N - 1. \tag{9b}$$

Single Phase Detection. In the case of single phase detection which is generally used, inverse Fourier analysis of the rapid scan response $X[s]$ ($s=0, 1,\cdots, N-1$) in Eq. 2 gives

$$A[k]' = (1/N)\sum_{s=0}^{N-1}X[s]\cos(2\pi ks/N), \quad k = 0, 1,\cdots, N/2, \tag{10a}$$

$$B[k]' = -(1/N)\sum_{s=0}^{N-1} X[s]\sin(2\pi ks/N),$$
$$k = 1, 2, \cdots, N/2-1, \quad (10b)$$
$$B[0]' = B[N/2]' = 0. \quad (10c)$$

It should be noted that $A[k]'$ and $B[k]'$ in Eq. 10 are related to $A[k]$ and $B[k]$ obtained by Eq. 3 as in the following:

$$A[0] = A[0]', \quad (11a)$$
$$A[k] = 2A[k]', \quad k = 1, 2, \cdots, N/2-1, \quad (11b)$$
$$A[N/2] = A[N/2]', \quad (11c)$$
$$B[0] = B[0]' = 0, \quad (11d)$$
$$B[k] = 2B[k]', \quad k = 1, 2, \cdots, N/2-1, \quad (11e)$$
$$B[N/2] = B[N/2]' = 0. \quad (11f)$$

In order to calculate the steady-state spectrum with a phase correction angle of θ, the free induction decay $h[k]$ ($k=0,1,\cdots,N/2$) is obtained by Eq. 6 after Eq. 11 is applied to $A[k]'$ and $B[k]'$ ($k=0,1,\cdots,N/2$), which is modified to $D[k]'$ ($k=0,1,\cdots,N/2$) and $E[k]'$ ($k=1,2,\cdots,N/2-1$) by the following relation:

$$D[0]' = D[0]\cos\theta, \quad (12a)$$
$$D[k]' = (1/2)(D[k]\cos\theta + E[k]\sin\theta),$$
$$k = 1, 2, \cdots, N/2-1, \quad (12b)$$
$$D[N/2]' = D[N/2]\cos\theta, \quad (12c)$$
$$E[k]' = -(1/2)(D[k]\sin\theta - E[k]\cos\theta),$$
$$k = 1, 2, \cdots, N/2-1. \quad (12d)$$

Inverse Fourier synthesis of $D[k]'$ and $E[k]'$ is then performed to give N values of the phase-corrected steady-state spectrum $U[s]'$,

$$U[s]' = D[0]' + 2\sum_{k=1}^{N/2-1}(D[k]'\cos(2\pi sk/N) - E[k]'\sin(2\pi sk/N)) + D[N/2]'\cos(\pi s),$$
$$s = 0, 1, \cdots, N-1. \quad (13)$$

Discussion

For the convenience of the following discussion, a schematic diagram of the algorithms of correlation NMR is illustrated in Fig. 1, where Procudure A and Procedure B correspond to the cases of quadrature phase and single phase detections described in the previous section, respectively.

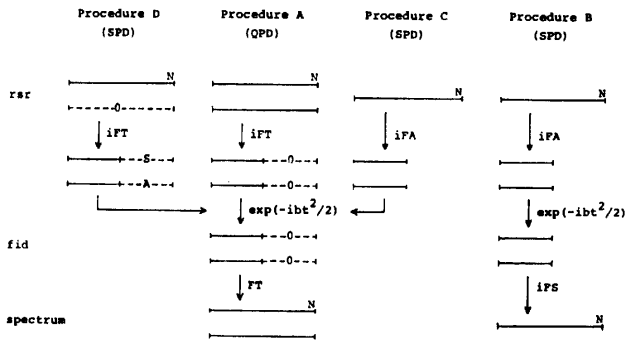

Fig. 1. Schematic diagram of the algorithms of correlation NMR spectroscopy. The symbols iFT, FT, iFA, and iFS stand for inverse Fourier transformation, Fourier transformation, inverse Fourier analysis, and inverse Fourier synthesis, respectively.

It is necessary for correct data processing in the correlation technique that the in-phase component $U[s]'$ of the spectrum becomes identical to the rapid scan response $X[s]$ when the phase correction angle θ is zero and the sweep rate b is extrapolated to zero. Procedures A and B satisfy this condition. What is important in obtaining the correct result is that $N/2+1$ points rather than $N/2$ points of the free induction decay have to be calculated by Eq. 6 before Eq. 8 or Eq. 13 is used to obtain the spectrum. Unless the $N/2+1$st point of the free induction decay is used in the calculation, an oscillation appears which is equally spread over the entire range of the spectrum. This point will also be discussed later.

In the case of single phase detection which is generally used, a most natural way in mathematical sense to obtain the spectrum is to use a combination of inverse Fourier analysis (Eq. 10) and inverse Fourier synthesis (Eq. 13) as shown in Procedure B. This procedure is equivalent to what has been given by Patt.[10] A disadvantage of Procedure B to Procedure A is that whenever one wants to change the phase of the spectrum, one has to go back to the free induction decay $D[k]'$ and $E[k]'$ by performing inverse Fourier analysis of the phase-corrected spectrum $U[s]'$, and inverse Fourier synthesize it again using the appropriate value of θ (Eqs. 12—13). When one wants to change the phase of the spectrum by mixing its in-phase and out-of-phase components (Eq. 9), Procedure A should be followed starting with the rapid scan response observed by quadrature phase detection. In this case, a combination of inverse Fourier transform (Eq. 3) and Fourier transform (Eq. 8) of complex numbers is employed to obtain the spectrum.

It should be noticed that, even when single phase detection is employed, the in-phase and out-of-phase components of the spectrum can be calculated and the phase correction of the spectrum can easily be made by mixing these components if one uses a combination of Eqs. 10—11 and Eqs. 6—9 as shown in Procedure C of Fig. 1. In this case, the free induction decay is calculated by Eq. 6 after $A[k]'$ and $B[k]'$ are modified to $A[k]$ and $B[k]$ using Eq. 11; Eps. 7—9 involving Fourier transformation of complex numbers are then used to obtain the phase-corrected spectrum.

Another way of dealing with the single phase detected rapid scan response $X[s]$ ($s=0,1,\cdots,N-1$) is to inverse Fourier transform it assuming that its imaginary part $Y[s]$ ($s=0,1,\cdots,N-1$) is all zero as shown in Procedure D of Fig. 1. This procedure is similar to the one outlined by Gupta, Ferretti, and Becker[9] without detailed discussion on the algorithm and the values of the calculated data. It can be shown that the values $A[k]'$ and $B[k]'$ obtained by the inverse Fourier transformation of $X[s]$,

$$g[k]' \equiv A[k]' - iB[k]'$$
$$= (1/N)\sum_{s=0}^{N-1} X[s]\exp(2\pi iks/N),$$
$$k = 0, 1, \cdots, N-1, \quad (14)$$

are identical to those given by Eq. 10 for $k=0,1,\cdots,N/2$

and that

$$A[k]' = A[N-k]', \quad k = N/2+1, N/2+2, \cdots, N-1, \tag{15a}$$

$$B[k]' = -B[N-k]', \quad k = N/2+1, N/2+2, \cdots, N-1. \tag{15b}$$

Therefore, after $A[k]$ and $B[k]$ ($k=0,1,\cdots,N/2$) are obtained using Eq. 11, the phase-corrected spectrum can be calculated by Eqs. 6—9 just as in the case of quadrature phase detection.

In Procedures B, C, and D, it must always be remembered that $A[k]'$ and $B[k]'$ where $k=1,2,\cdots,N/2-1$ are to be multiplied by a factor of two to obtain $A[k]$ and $B[k]$ ($k=0,1,\cdots,N/2$) according to the relation in Eq. 11 before Eq. 6 is used to calculate the free induction decay. This is closely related to the fact that the first and $N/2+1$st points of $A[k]'$ are different from others in a sense that these two points are equal in magnitude to $A[0]$ and $A[N/2]$ which would be observed when quadrature detection is employed with two detectors each of which has kept its gain exactly the same as in the case of single phase detection; as far as other points ($k=1,2,\cdots,N/2-1$) are concerned, the coefficients $A[k]$ and $B[k]$ are twice as large as $A[k]'$ and $B[k]'$. If $A[k]'$ and $B[k]'$ where $k=0,1,\cdots,N/2$ are substituted into Eq. 6 to obtain the free induction decay, an oscillation appears in the final spectrum in addition to that the magnitude of the spectrum is half as large as it should be. This oscillation is exactly the same in origin as the one observed when the $N/2+1$st point of the free induction decay is eliminated in Eq. 8 or Eq. 13. What actually happens is that the baseline level for the even-numbered points of the obtained spectrum is different from that for the odd-numbered points. Another kind of artifact which is observed when one fails to modify $A[k]'$ and $B[k]'$ is that the average value of the spectrum depends on the value of first point of the free induction decay which is calculated from the rapid scan response and on the number of sampling points. In this case, it would become impossible to compare the intensities of signals from two or more spectra simply by reading their values.

A different type of oscillation which is inherent in correlation NMR appears when the baseline of the rapid scan response is tilted. This can effectively be removed by *wing processing* which has been previously described.[6,8]

One can obtain a smoothed spectrum $U[s]'$ at $s\delta f/m = sb\Delta t/2m\pi$ Hz where $s=0,1,\cdots,mN-1$ when *zero supplement*[6,11] of the free induction decay is carried out to make it m times in length; equation 7 is replaced by

$$D[k] - iE[k] = 0, \quad k = N/2+1, N/2+2, \cdots, mN-1, \tag{16}$$

to get $h[k]$ ($k=0,1,\cdots,mN-1$), or Eq. 12c is replaced by

$$D[N/2]' = (1/2)D[N/2]\cos\theta \tag{17a}$$

and Eqs. 12a—b, 17a, and 12d are supplemented by

$$D[k]' = 0, \quad k = N/2+1, N/2+2, \cdots, mN/2, \tag{17b}$$

$$E[N/2]' = -(1/2)D[N/2]\sin\theta, \tag{17c}$$

$$E[k]' = 0, \quad k = N/2+1, N/2+2, \cdots, mN/2-1, \tag{17d}$$

to get $D[k]'$ ($k=0,1,\cdots,mN/2$) and $E[k]'$ ($k=1,2,\cdots,mN/2-1$) before Fourier transformation or inverse Fourier synthesis to obtain mN data points is made, respectively. Although the values $U[s]'$, $s=0,m,2m,\cdots,(N-1)m$, obtained by these procedures are equal to $U[s]'$, $s=0,1,2,\cdots,N-1$, which are obtained without *zero supplement*, the values of the interpolated points $U[s]'$, $s\neq 0,m,2m,\cdots,(N-1)m$, which lie near either end of the spectrum become different from what they should be even when the sweep rate b is extrapolated to zero. In this case, the method of *wing processing*[6] has also been proved useful in order to decrease the error of the interpolated values.

In the case of conventional pulse Fourier transform NMR, Fourier analysis of the free induction decay is performed to obtain the spectrum; N' points of the free induction decay is Fourier analyzed to give the in-phase and out-of-phase spectra each of which is made of $N'/2+1$ data points. On the other hand, in the case of quadrature phase detection pulse Fourier transform NMR, a set of $N'/2$ points of the free induction decay observed in quadrature is used to obtain $N'/2$ points of the in-phase and $N'/2$ points of the out-of-phase components of the spectrum. A similar procedure can be used in the case of correlation NMR. The free induction decay in Eq. 6 is modified to

$$h[k]'' \equiv D[k]'' - iE[k]'', \quad k = 0, 1, \cdots, N/2-1, \tag{18}$$

using the relation

$$D[0]'' - iE[0]'' = (D[0] + D[N/2]) - i(E[0] + E[N/2]), \tag{19a}$$

$$D[k]'' - iE[k]'' = D[k] - iE[k], \quad k = 1, 2, \cdots, N/2-1, \tag{19b}$$

and the spectrum $H[s]''$ which consists of $N/2$ data points is obtained by Fourier transforming $N/2$ data points of $h[k]''$. The values $H[s]''$, $s=0,1,2,\cdots,N/2-1$, obtained by this procedure are equal to $H[s]$, $s=0,2,4,\cdots,N-2$, obtained by Eq. 8. The phase correction of the spectrum can then be done by mixing the in-phase and out-of-phase components of $H[s]''$.

It should be noted that in quadrature phase detection pulse Fourier transform NMR, N' points of the in-phase and N' points of the out-of-phase components of the spectrum can be calculated from a set of $N'/2+1$ points of the free induction decay if one follows the procedure in Eqs. 7—9. In this case, one has to have a size of computer memory which is twice as large as what is needed to store the free induction decay. If one follows the procedure in Eqs. 12—13 involving inverse Fourier synthesis, one obtains N' points of the phase-corrected spectrum without having an additional size of memory at a sacrifice of convenience of the phase correction.

The authors wish to express their hearty gratitude to Prof. Shizuo Fujiwara for his continuous encouragement throughout the present work.

References

1) J. Dadok and R. F. Sprecher, *J. Magn. Reson.*, **13**, 243 (1974).

2) Y. Arata and H. Ozawa, *Chem. Lett.*, **1974**, 1257.
3) H. Ozawa and Y. Arata, *Chem. Lett.*, **1975**, 239.
4) Y. Arata and H. Ozawa, *J. Magn. Reson.*, **21**, 67 (1976).
5) Y. Arata, *J. Magn. Reson.*, **22**, 327 (1976).
6) H. Ozawa and Y. Arata, *Bull. Chem. Soc. Jpn.*, **49**, 1542 (1976).
7) Y. Arata, H. Ozawa, T. Ogino, and S. Fujiwara, *Pure Appl. Chem.*, **50**, 1273 (1978).
8) T. Ogino, Y. Arata, and S. Fujiwara, *J. Magn. Reson.*, **39**, 381 (1980).
9) R. K. Gupta, J. A. Ferretti, and E. D. Becker, *J. Magn. Reson.*, **13**, 275 (1974).
10) See: J. W. Cooper, "Advanced Techniques in Fourier Transform NMR," in "Transform Techniques in Chemistry," ed by P. R. Griffiths, Plenum Press, New York (1978).
11) E. Bartholdi and R. R. Ernst, *J. Magn. Reson.*, **11**, 9 (1973).

 © 1982 The Chemical Society of Japan Bull. Chem. Soc. Jpn., 55, 415—419 (1982)

Solvent Effects on the Intensities of Forbidden Bands of Molecules. Absorption Spectra of Acetone and Cyclopentanone[1]

Kenichi NAKASHIMA,† Kuniko UCHIDA-KAI, Motohiko KOYANAGI,* and Yoshiya KANDA

Department of Chemistry, Faculty of Science, Kyushu University, Hakozaki, Higashi-ku, Fukuoka 812

(Received July 13, 1981)

The near ultraviolet absorption spectra of acetone and cyclopentanone have been studied in various fluid solutions at room temperature. The intensity enhancements observed are ascribed to perturbation of dispersion forces between solute and solvent molecules. The results are parallel to those of the Ham effect in benzene. No correlation was found between the intensity increments and solvent polarities. This is at variance with the correlation that has been reported in the $S_1(L_b)$—S_0 transition spectra of pyrene and coronene.

Many investigations have been reported on solvent effects for electronically forbidden transitions of molecules[2–14] since the first finding of the "Ham bands" in the 260 nm absorption spectrum of benzene in a solid solution containing 7% CCl_4.[12] From a systematic study on the $S_1(L_b)$←S_0 absorption spectra of benzene, naphthalene, and phenanthrene in solid glasses at 83 K, Durocher and Sandorfy have suggested that the environmental perturbation causing the Ham effect of benzene is essentially the same for the others.[6] One of the authors (M. K.) has derived the formulas by which the absorption enhancements of benzene and naphthalene are closely correlated with solvent polarizabilities and solute-solvent intermolecular distances.[9]

An interesting example of solvent perturbations was demonstrated in the absorption and fluorescence spectra of pyrene and coronene in polar solvents by Nakajima.[11,15] The intensity enhancements of the origin bands in the S_1—S_0 spectra of pyrene and coronene were found closely correlative with solvent polarities rather than with solvent refractive indexes. This correlation is at variance with the Ham effect in benzene and similar effects in the other aromatic compounds.[7,10] Very recently, Nakajima also proposed that quadrupole-dipole interactions should be taken into account[15] besides dipole-dipole interactions which have been employed for the explanation of the Ham effect by Koyanagi.[9] On the other hand, Lianos and Georghiou have suggested on the basis of the IR studies that a weak complex is formed between pyrene and a certain polar solvent.[16] By studying the $S_2(L_a)$←S_0 absorption spectra in several polar solvents, we have also confirmed the validity of their suggestions.[17]

In the present work we studied the $S_1(n\pi^*)$←S_0 absorption spectra of acetone and cyclopentanone in various solvents and found that the correlation of the absorption increments with solvent properties is very similar to those in benzene and naphthalene.

Experimental

Materials and Apparatus. The solutes, acetone (Dotite Spectrosol) and cyclopentanone (a reagent from Wako Pure Chemical Industries, Ltd.), were distilled *in vacuo* after drying over anhydrous potassium carbonate and anhydrous sodium sulfate, respectively. The solvents employed were of spectroscopically pure grade (Dotite Spectrosol) except benzonitrile and perfluorohexane (GR grade reagents from Wako Chemical Industries, Ltd. and Tokyo Kasei Co. Ltd., respectively). Almost all of the solvents were thus used without further purification. The exceptions are for benzene, toluene, and benzonitrile. Since these aromatics in the atmosphere have well been known to give poor transparency below 350 nm due to formation of transient complexes with oxygen, *i.e.*, the so-called contact charge transfer complexes,[18,19] nitrogen gas was bubbled into the solvents prior to use.

Absorption spectra were observed at room temperature using a Shimadzu Multipurpose Spectrometer type MPS-50 and/or a Hitachi Perkin-Elmer 139 UV-VIS Spectrometer. Cells employed were of 1.0 cm in optical path. The other experimental conditions are similar to those given previously.[5]

Intensity Measurements. The *f*-values of the absorption spectra of two ketones were determined by means of the usual expression of the integrated absorption intensity:[20]

$$f = 4.317 \times 10^{-9} \int_{pq} \varepsilon(\tilde{\nu}) d\tilde{\nu},$$

where the integral denotes the area under a plot of molecular extinction coefficients ε in $dm^3\ mol^{-1}\ cm^{-1}$ units *versus* $\tilde{\nu}$ in cm^{-1} units. The alphabetical indexes p and q limit the wavenumber range within which the $S_1(n\pi^*)$←S_0 absorption of light in effect takes place. The substantial absorptions of acetone and cyclopentanone extend, in many cases, from 29800 to 45400 cm^{-1} and 28000 to 43500 cm^{-1}, respectively (for example, see Figs. 1—4). Unfortunately, however, several solvents showed poor transparency in the short wavelength region of the absorption spectra in question and only a part of each absorption system was measurable in these solutions. The *f*-value of each ketone in such a case was then obtained by comparing the partial absorption area in the solution with the corresponding area in cyclohexane used as a standard solvent: On an assumption that a change in the frequencies of the prominent vibrations in the spectra of the ketones is little with a change in solvents, the wavelength truncation in these solutions was carried out at an equal wavenumber position from the absorption maximum in the case of acetone and also at an equal wavenumber position from one of the prominent vibronic peaks in the case of cyclopentanone. The solvents treated in this way are $CHCl_3$, CCl_4, benzene, toluene, and benzonitrile.

Molecular Radii and Other Molecular Properties. The molecular radii employed were calculated using molecular weights and densities available for the liquid states, on an assumption that all the molecules are spherical. No correction factor was taken for the assumption of the spherical volume. The polarizability data[21] is summarized in Table 1 together with other properties of solvents.[22,23]

† Present address: Department of Food Science, Nishikyushu University, Kanzaki, Kanzaki-gun, Saga 842.

TABLE 1. SOLVENT PROPERTIES[a)]

Solvent	Mol wt	Density / 10^3 kg m^{-3}	R[b)] / Å	$\bar{\alpha}$[c)] / 10^{-31} m^3	D[d)]	n[e)]
C_6F_{14}	338[f)]	1.695[f,g)]	4.292	125.5[h)]	—	1.2514[i)]
C_6H_{14}	86.18	0.65937	3.728	118.4[h)]	1.890	1.37486
C_6H_{12}	84.16	0.7791	3.499	108.7	2.023	1.42623
CCl_4	153.8	1.63195	3.343	105	2.238	1.46030
$CHCl_3$	119.4	1.4892	3.168	82.3	4.806	1.44858[j)]
CH_2Cl_2	84.93	1.3266	2.938	64.8	9.08	1.4246
CH_3CN	41.05	0.77683[g)]	2.757	48.6	37.5	1.34411
C_6H_6	78.12	0.87865	3.279	103.2	2.284	1.50112
$C_6H_5CH_3$	92.14	0.86694	3.480	123.1[h)]	2.379[g)]	1.49693
C_6H_5CN	103.1	1.0051	3.439	124.4[h)]	25.20[g)]	1.5282

a) Data at 20 °C unless mentioned otherwise. b) Molecular radius. c) Mean molecular polarizability. d) Dielectric constant. e) Refractive index at the sodium D line. f) Taken from the catalog of Tokyo Kasei Co. Ltd. g) Data at 25 °C. h) Calculated from refractive index and molar volume. i) Taken from Ref. 7. j) Data at 15 °C.

Results and Discussion

In their electronic ground states, both acetone and cyclopentanone can be treated as a nonrigid species belonging to a point group isomorphous with C_{2v}. No matter what it may be, however, the $S_1(n\pi^*)\leftarrow S_0$ absorption transition of each molecule is considered to be essentially electric dipole forbidden.[24-26)] The very small oscillator strengths observed confirm that this is the case.

The absorption spectra of acetone and cyclopentanone were studied in various solvents at room temperature. Some representative spectra are shown in Figs. 1 and 2, respectively. The spectra of acetone do not show any prominent vibronic band, but only a broad band maximum around 36000 cm^{-1}. This broadness in the spectra is assumed to come from (i) a low energy barrier to rotation of the methyl group about the bond to the C=O chromophore (*e.g.*, ≈3.15 kJ mol^{-1} in the vapor[27)]) and (ii) active participation of several low frequency modes as has been demonstrated in the $n\pi^*$ spectra of acetones.[28)] The greater enhancement of the absorption intensity is found in solvents with the greater molecular polarizability. For example, the relative ratios of the band areas in Fig. 1 are 1.00 : 1.21 : 1.25 : 1.32 : 1.41 : 1.57 in C_6F_{14}, CH_3CN, C_6H_{12}, CH_2Cl_2, $CHCl_3$, and CCl_4, respectively. As for C_6F_{14}, it is well known that spectra in perfluoro-hydrocarbons generally give *quasi*-vapor spectra.[7,13)]

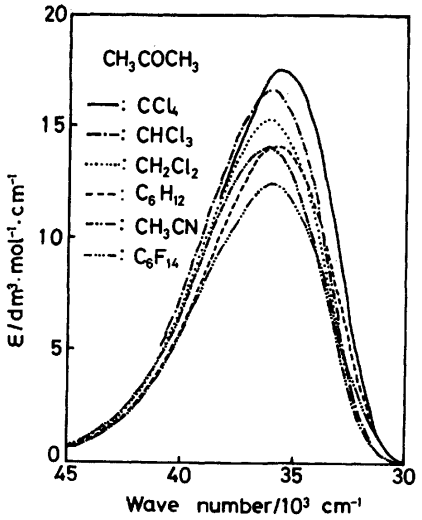

Fig. 1. The $S_1(n\pi^*)\leftarrow S_0$ absorption spectra of acetone in several solvents at 20 °C.

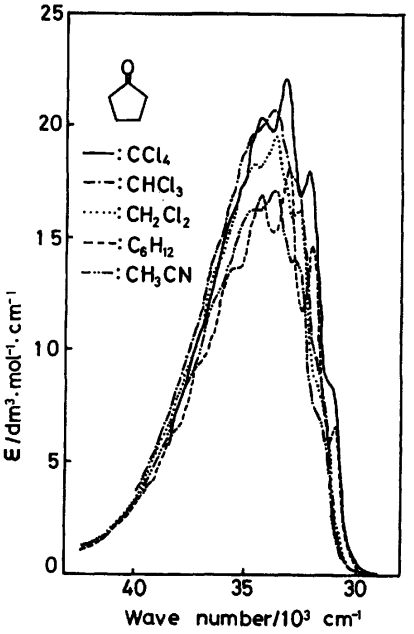

Fig. 2. The $S_1(n\pi^*)\leftarrow S_0$ absorption spectra of cyclopentanone in several solvents at 20 °C.

Another spectral aspect is found in Fig. 3 which displays the spectral behavior in a binary solvent system of CCl_4 and hexane. The intensity enhancement of the overall band system seems to almost satisfy an additivity rule between the respective solvents. This fact never supports an idea that the intensity enhancement might closely be related with some complex formation between the solute and solvent molecules.[5,17)] Similar additive properties in the spectral behaviors are also found in many other binary solvent systems employed.

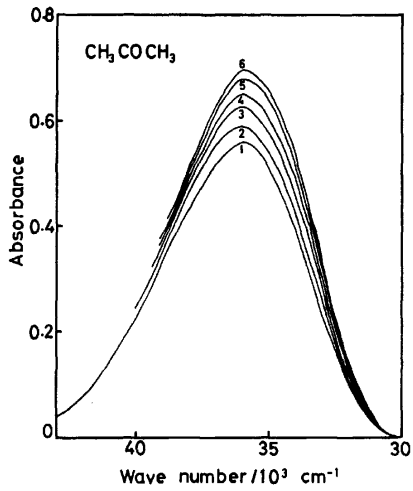

Fig. 3. The absorption spectra of acetone in CCl_4–C_6H_{14} binary mixed solutions at 20 °C. Concentration of CCl_4 in mol dm^{-3} units: (1) 0; (2) 2.1_2; (3) 4.2_4; (4) 6.3_7; (5) 8.4_9; and (6) $10._6$.

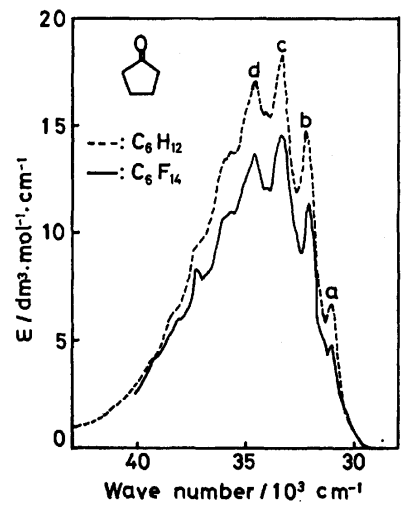

Fig. 4. The absorption spectra of cyclopentanone in cyclohexane and perfluorohexane at 20 °C.

In contrast with the acetone case mentioned above, the absorption spectra of cyclopentanone show several prominent vibrational structures in the vapor and in most fluid solutions (Fig. 2). For a further advance in discussion, the absorption spectra in cyclohexane and perfluorohexane solutions are chosen and demonstrated in Fig. 4. Here four characteristic bands are designated as *a*, *b*, *c*, and *d*. The detailed vibrational assignment of the absorption bands in the vapor and some comments on the spectra in solutions have been given by Howard-Lock and King.[29] Since one-to-one band correspondence between the spectra in fluid solutions and in the vapor is quite inferior to those in the cases of benzene and naphthalene because of great inhomogeneous broadening and participation of several intense sequence bands in the case of cyclopentanone, it is very difficult to definitely identify the origin band in the spectra of cyclopentanone in such fluid solutions. However, comparison of a very low resolution spectrum in the vapor with the spectra in solutions enables us to predict a probable location of the origin band in the solutions around the band *a* (Fig. 4).

In the vapor a cold *pseudo*-origin band of 25_0^1 due to the inversion doubling splitting along to the b_1 out-of-plane vibrational coordinate has been observed close to the undetected 0-0 band (see Ref. 30 for the vibrational notation and assignment of cyclopentanone in the ground state): The splitting has been established to be extremely small, say, less than 0.2 cm^{-1}.[29] Furthermore, there appear several sequence bands with considerable intensity in the neighborhood of the origin band. For these reasons, it is also very difficult to fully estimate the intensity contribution of the origin band in these solutions.

Despite the obscured assignment of the origin band, it is favorable to see that intensities of almost all of the "bands," *e.g.*, those of bands *a*—*d* shown in Fig. 4, are enhanced in a proportional ratio when solvents are changed from perfluorohexane to cyclohexane (see Fig. 4). This proportionality in the intensity enhancement is possibly of an apparent feature, originating mainly in the inhomogeneous broadening of these solution spectra superimposed on the vibrationally tangled band system in the spectrum of cyclopentanone. Similar intensity increments are also found to take place in the other solvent systems (see Fig. 2).

The total intensity of each solute is thus taken as a measure of the environmental effects about which some discussion will be given below. First let us apply the treatments of environmental effects given by Nakajima[11] to our ketone cases. For the explanation of the anomalous $S_1(L_b)$—S_0 spectra of pyrene in polar solvents, he has introduced a new solvent parameter f'. The parameter is rewritten as follows:

$$f' = (D-1)/(2D+1) - x(n^2-1)/(2n^2+1),$$

where D denotes the dielectric constant, n the refractive index of the solvent, and x an adjustable dimensionless parameter. Although the physical meaning of f' is not necessarily clear, his treatments with a partial success seem to give a correlation between f' and ε_p, where ε_p means the molar extinction coefficient of the $S_1 \leftarrow S_0$ absorption origin band of pyrene. In Fig. 5 the oscillator strength of cyclopentanone, f, is plotted against the

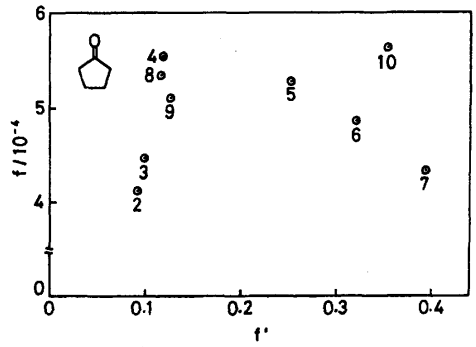

Fig. 5. Plots of the oscillator strength of cyclopentanone, f, against the solvent parameter given by Nakajima (Ref. 11), $f'=(D-1)/(2D+1)-0.5\,(n^2-1)/(2n^2+1)$. The numbering of the plots is as follows: (1) C_6F_{14}; (2) C_6H_{14}; (3) *cyclo*-C_6H_{12}; (4) CCl_4; (5) $CHCl_3$; (6) CH_2Cl_2; (7) CH_3CN; (8) C_6H_6; (9) $C_6H_5CH_3$; and (10) C_6H_5CN.

solvent parameter f' with $x=0.5$, the value which Nakajima has employed for the elucidation of the environmental effect in the S_1—S_0 spectra of pyrene. However, we could not find any straightforward correlation between f and f'. This was never improved for the other solute, acetone; no settled correlation was obtained between f and f' in the case of acetone, either. It seems thus that the Nakajima-like treatments[31] are not valid for the explanation of the environmental intensity enhancement in the $S_1(n\pi^*)\leftarrow S_0$ spectra of acetone and cyclopentanone in fluid solutions.

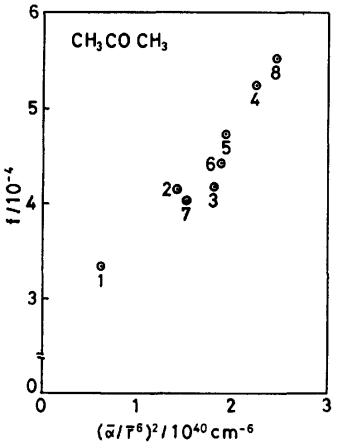

Fig. 6. A correlation diagram between the oscillator strength of acetone, f, and the squared value of the relative dispersion energy of solvents, $(\bar{\alpha}/\bar{r}^6)^2$. For the numbering of the plots, see the caption given in Fig. 5.

Next let us adopt another treatment given by one of the authors (M. K.) who has succeeded in explaining the Ham effect in terms of other solvent properties.[9] In Fig. 6 the oscillator strength of acetone, f, is plotted as a function of the squared value of a relative dispersion energy between the solute and solvent molecules, $(\bar{\alpha}/\bar{r}^6)^2$. Here $\bar{\alpha}$ denotes the mean molecular polarizability of the solvent and $\bar{r}$ the mean molecular distance between the solute and solvent molecules. Despite

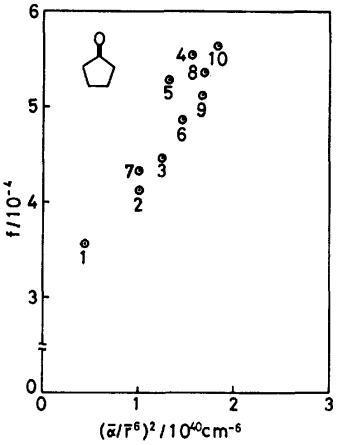

Fig. 7. A correlation diagram between the oscillator strength of cyclopentanone, f, and the squared value of the relative dispersion energy of solvents, $(\bar{\alpha}/\bar{r}^6)^2$. For the numbering of the plots, see the caption given in Fig. 5.

roughness in the approximation for $\bar{r}$, the observed oscillator strengths of acetone show an approximately linear increase with an increase in $(\bar{\alpha}/\bar{r}^6)^2$. A similar correlation is also found to hold for cyclopentanone (see Fig. 7).

With the help of the perturbation theory, we shall here give a qualitative explanation and a comment on the environmental intensification observed. Now let us take a model that one solute molecule is surrounded by n solvent molecules. The total Hamiltonian H is then given by

$$H = H_0 + H', \tag{1}$$

where H_0 is the zeroth order Hamiltonian, that is, the intramolecular terms of the free molecules, and H' is the total perturbation sum between the solute and n solvent molecules.

$$H' = \sum_a^n \sum_i \sum_j h_a(\xi_i, \eta_{aj}), \tag{2}$$

where ξ_i denotes i-th charge(electron) coordinates of the solute, η_{aj} j-th electron coordinates of a-th solvent molecule, and $\sum_i \sum_j h_a(\xi_i, \eta_{aj}) \equiv \phi_a$ represents interactions between the solute and the a-th solvent molecule. For the intermolecular interactions of neutral molecules the terms ϕ_a are generally described by a two-center expansion of reciprocal intermolecular distance r^{-1} in terms of spherical harmonics:[33]

$$\phi_a = \sum_{k=1}^{\infty} (b_{k+2}/r^{k+2}). \tag{3}$$

Here the first term in Eq. 3 represents the so-called dipole-dipole interactions. A further detailed description for them is found in Ref. 33.

If Ψ_0°, Ψ_1°, $\cdots$, Ψ_S° are the electronic wavefunctions for the free solute molecule, the k-th wavefunction of the solute in a fluid solution can be described as follows:

$$\Psi_k = \sum_j^s C_{jk}\Psi_j^\circ, \tag{4}$$

where the absolute values of coefficients, $|C_{jk}|_{j\neq k}$, are much smaller than unity and their magnitudes are evaluated by off-diagonal matrix elements, $\langle \Psi_j^\circ | H' | \Psi_k^\circ \rangle$, and energy differences between the respective states, ΔE_{jk}.

In general, environmental interactions may mix Ψ_j° with Ψ_k°. The coefficients C_{jk} will then be related to solvent properties as follows:

$$C_{jk} = \sum_{q,q'}^{X,Y,Z} \sum_{\hat{q},\hat{q}}^{x,y,z} \{A_q(\mu_{\hat{q}}/r^3) + B_{qq'} + (\mu_{\hat{q}}/r^4) + B'_{q'} \times (Q_{\hat{q}\hat{q}'}/r^4) + C_{qq'}(Q_{\hat{q}\hat{q}'}/r^5) + D_{qq'}(\alpha_{\hat{q}\hat{q}}/r^6) + \cdots\}. \tag{5}$$

Here A, B, B', C, $\cdots$ denote intramolecular integrals of the solute multiplied by appropriate proportional constants; each of the subscripts q and q' represents one component of the Cartesian coordinates (X,Y,Z) of the solute and each of $\hat{q}$ and $\hat{q}'$ one component of the Cartesian coordinates (x,y,z) of the solvent; and μ, Q, α are the dipole moment, quadrupole moment, molecular polarizability of the solvent molecule, respectively.

Here it should be noted that only a small number of the terms are effective for the intensity borrowing mechanism: This contrasts with the solvent shift

mechanism for which many terms with large matrix elements in Eq. 5 generally play an important role. In the case of a high symmetry molecule such as benzene, for example, the transition-dipole selection rule severely restricts the number of effective perturbation terms in Eq. 5. The terms D_{xx} and D_{yy} have thus been shown to be most important and predominant in the benzene 260 nm absorption case.[9] At present *a priori* we can offer no quantitative explanation for the observed intensity enhancement of acetone and cyclopentanone, because the treatments employed in an explanation of the Ham effect of benzene can not be applied to lower symmetric guest and host molecules without further revision and extention. However, *a posteriori* we may postulate, in the present cases,

$$C_{j1} \propto (\bar{\alpha}/\bar{r}^6), \tag{6}$$

where j may possibly be taken as $^1\pi\pi^*$. Supposing that the electronic transition $1 \leftrightarrow 0$ is forbidden in the free molecule, we may then relate the borrowed intensity of the transition in the fluid solutions to the squared value of C_{j1}. Thus we obtain for the intensity of the origin band:

$$I_{0-0} \propto (\bar{\alpha}/\bar{r}^6)^2. \tag{7}$$

In conclusion the intensity enhancement of the $S_1(n\pi^*) \leftarrow S_0$ absorption spectra of acetone and cyclopentanone in fluid solutions is qualitatively interpreted in terms of dispersion force interactions unless solvents have no strong chemical interactions such as hydrogen bondings and charge transfer interactions with the solute molecules.[34,35] Although we strongly believe the dispersion force interactions play a main role also in the intensifications of many other aliphatic carbonyls,[36,37] careful check must be required for further generalization.

One of the authors (K. N.) wishes to express thanks to Professor Y. Gondo for his warm hospitality and encouragements in Kyushu University. This work has in part been supported by a Grant-in-Aid for Scientific Research from the Ministry of Education, Science and Culture.

References

1) Presented in part at the 43rd National Meeting of the Chemical Society of Japan, Tokyo, April 1981, Abstr. No. 3X44. Taken partially from the Senior Thesis of K. U-K., Kyushu University, 1973.
2) S. Leach, R. Lopez-Delgado, and F. Delmas, *J. Mol. Spectrosc.*, **7**, 304 (1961).
3) J. R. Platt, *J. Mol. Spectrosc.*, **9**, 288 (1962).
4) N. S. Bayliss and N. W. Cant, *Spectrochim. Acta*, **18**, 1287 (1962).
5) M. Koyanagi and Y. Kanda, *Spectrochim. Acta*, **20**, 993 (1964).
6) G. Durocher and C. Sandorfy, *J. Mol. Spectrosc.*, **14**, 400 (1964).
7) J. W. Eastman and S. J. Rehfeld, *J. Phys. Chem.*, **74**, 1438 (1970).
8) G. W. Robinson, *J. Chem. Phys.*, **46**, 572 (1967).
9) M. Koyanagi, *J. Mol. Spectrosc.*, **25**, 273 (1968).
10) N. S. Bayliss, *J. Mol. Spectrosc.*, **31**, 406 (1969).
11) A. Nakajima, *Bull. Chem. Soc. Jpn.*, **44**, 3272 (1971).
12) J. S. Ham, *J. Chem. Phys.*, **21**, 756 (1953).
13) C. W. Lawson, F. Hirayama, and S. Lipsky, *J. Chem. Phys.*, **51**, 1590 (1969).
14) R. B. Cundall and L. C. Pereira, *Chem. Phys. Lett.*, **18**, 371 (1973).
15) A. Nakajima, *Kagaku No Ryoiki*, **33**, 394 (1979).
16) P. Lianos and S. Georghiou, *Photochem. Photobiol.*, **29**, 843 (1979); **30**, 355 (1979).
17) K. Nakashima and M. Koyanagi, *Photochem. Photobiol.*, (to be published).
18) D. F. Evans, *Proc. R. Soc. London, Ser. A*, **255**, 55 (1960).
19) H. Tsubomura and R. S. Mulliken, *J. Am. Chem. Soc.*, **82**, 5966 (1960).
20) A. L. Sklar, *Rev. Mod. Phys.*, **14**, 232 (1942).
21) Landolt-Börnstein, "Zahlenwerte und Funktionen," Springer Verlag, Berlin (1951), Vol. 1, Part 3.
22) A. Weissberger, E. S. Proskauer, J. A. Riddick, and E. E. Toops, Jr., "Organic Solvents," Technique of Organic Chemistry, Interscience Publishers, New York (1955), Vol. VII.
23) "Kagaku-binran," (Handbook of Chemistry), ed by The Chemical Society of Japan, Maruzen, Tokyo (1975).
24) J. W. Sidman, *Chem. Rev.*, **58**, 686 (1958).
25) J. H. Callomon and K. K. Innes, *J. Mol. Spectrosc.*, **10**, 166 (1963).
26) W. D. Chandler and L. Goodman, *J. Mol. Spectrosc.*, **36**, 141 (1970); **37**, 33 (1971).
27) J. D. Swalen and C. C. Costain, *J. Chem. Phys.*, **31**, 1562 (1959).
28) M. Koyanagi and L. Goodman, *Chem. Phys.*, **5**, 107 (1974) and references cited therein.
29) H. E. Howard and G. W. King, *J. Mol. Spectrosc.*, **36**, 53 (1970).
30) H. E. Howard and G. W. King, *J. Mol. Spectrosc.*, **35**, 393 (1970).
31) In Ref. 11, Nakajima has also tried to correlate ε_p with two other solvent parameters, *i.e.*, Kosower's Z-value (Ref. 32) and $(D-1)/(2D+1)$. In our cases, however, no correlation was obtained between f and each of these solvent parameters.
32) E. M. Kosower, "An Introduction to Physical Organic Chemistry," John Wiley and Sons, Inc., New York, N. Y. (1968).
33) J. O. Hirschfelder, C. F. Curtiss, and R. B. Bird, "Molecular Theory of Gases and Liquids," John Wiley and Sons, Inc., New York, N. Y. (1954), Chap. 13.
34) N. S. Bayliss and G. Wills-Johnson, *Spectrochim. Acta, Part A*, **24**, 551, 563 (1968).
35) M. Yudasaka and H. Hosoya, *Bull. Chem. Soc. Jpn.*, **51**, 1708 (1978).
36) Some interesting data of several aliphatic ketones have been reported by Bayliss and Wills-Johnson (Ref. 34). However, the data for benzene solutions are likely to contain great errors coming mainly from less transparency of the solvent below 280 nm. It is well known that the use of wide slits for such less transparency solutions leads sometimes to counterfeit bands (see also Ref. 38). Using degassed (oxygen-free) benzene and two different types of spectrometers, we carefully reexamined the absorption spectra of acetone and cyclopentanone in benzene. We thus determined the band maximum of acetone at 36.0×10^3 cm^{-1} with $\varepsilon_{max} = 19.8$ dm^3 mol^{-1} cm^{-1}, whereas Bayliss and Wills-Johnson reported $\nu_{max} = 35.45 \times 10^3$ cm^{-1} and $\varepsilon_{max} = 16.4$ dm^3 mol^{-1} cm^{-1}.
37) M. Koyanagi, unpublished.
38) E. C. Lim and V. L. Kowalski, *J. Chem. Phys.*, **36**, 1729 (1962). We also reexamined and confirmed this.

Cation Interdiffusion in Polycrystalline Fluorite-cubic MgO-ZrO_2 Solid Solution

Yoshio SAKKA, Yasumichi OISHI,* and Ken ANDO
Department of Nuclear Engineering, Kyushu University, Higashi-ku Fukuoka 812
(Received July 24, 1981)

Lattice and grain-boundary interdiffusion coefficients were calculated from the concentration distributions as determined for cation interdiffusion in polycrystalline MgO-stabilized zirconias by applying a grain-boundary enhanced diffusion model. Lattice interdiffusion coefficients in the temperature range of 1650—1990 °C were represented by $\tilde{D}=5.9\times10^{-4}\exp[-293(\mathrm{kJ/mol})/RT]\ \mathrm{cm^2/s}$. Magnesium self-diffusion coefficients were calculated from the obtained interdiffusion coefficients and the reported Zr self-diffusion coefficients. The results confirmed that interdiffusion in the fluorite-cubic solid solution is primarily controlled by the diffusivity of the faster cation.

MgO-stabilized ZrO_2 (MSZ) is a fluorite-type cubic solid solution[1] similar to CaO-stabilized ZrO_2 (CSZ). One difference is that the radius of the Mg ion is smaller than that of the Zr ion in MSZ, while that of the Ca ion is larger than that of the Zr ion in CSZ. Since MSZ exhibits high oxygen diffusivities similar to those of CSZ at high temperatures,[2] the defects in MSZ are assumed to be of the oxygen-vacancy type, as in CSZ.

During interdiffusion in oxygen-vacancy type fluorite structures, differing diffusivities of the two cations cause mass flow and electrical field effects on the cation interdiffusion, while the interchange of oxygen ions and oxygen vacancies on the simple cubic sublattice contributes only to the electrical field effect but does not necessarily contribute to the mass flow effect (since the concentration of the oxygen vacancy is equal to that of the dopant cation and therefore temperature-independent). For such conditions, an interdiffusion coefficient has been theoretically derived in terms of the self-diffusion coefficients of the constituent ions. The derived interdiffusion coefficient described satisfactorily interdiffusion in a CSZ system.[3] In the present work, a similar analysis was carried out for interdiffusion in the MSZ system to clarify the interdiffusion mechanism.

The self-diffusion coefficient of the oxygen ion in MSZ has been determined,[2] but that of the Mg ion has not. The tracer diffusion coefficient of the Zr ion in MSZ has not so far been determined but has been estimated from the Zr-Hf interdiffusion in the MgO–$(Zr+Hf)O_2$ system.[4] Since cation diffusion is enhanced by grain boundaries in polycrystalline CSZ,[5] a similar grain-boundary enhancement is assumed for the cations in polycrystalline MSZ.

In the present study, cation concentration distributions are determined after interdiffusion of polycrystalline diffusion couples, and lattice and grain-boundary interdiffusion coefficients are separately calculated. The results are compared with those of the CSZ system.[6]

Experimental

Diffusion Couples and Diffusion Annealing. Appropriate mixtures of MgO (99.7% purity) and ZrO_2 (99.69% purity) to give the compositions of $12MgO\cdot88ZrO_2$, $16MgO\cdot84ZrO_2$, and $18MgO\cdot82ZrO_2$ were isostatically pressed into a pellet of 10 mm dia. and 10 mm height with the aid of dextrin under a pressure of $6—7\times10^3\ \mathrm{kg/cm^2}$. Pressed pellets were sintered in two ways: at 1750 °C for over 12 h in air, and at 2200°C for 3 h in an Ar atmosphere. The densities of the sintered pellets ranged from 93—99% of the theoretical. The grain radii of the pellets, necessary to the present analysis, were determined using Fullman's relation.[7]

Diffusion couples were prepared by joining pellets of different compositions at 1650 °C for 10 min in a molybdenum susceptor high-frequency induction furnace. Diffusion anneals were carried out at temperatures between 1650 and 1990 °C, where a single fluorite-cubic phase is stable according to the MgO–ZrO_2 phase diagram proposed by Grain.[1] Diffusion anneals below 1730 °C were conducted in air using an SiC furnace, and those above 1823 °C using a tungsten-mesh heater furnace in an Ar atmosphere at 100 Torr. (1 Torr≈133.322 Pa).

Electron Probe Microanalysis. After diffusion annealing, each diffusion couple was sawed into halves parallel to the diffusion direction. One half was used for measuring the grain size to confirm that no grain growth occurred during diffusion annealing. The other half was employed for determining the concentration distribution by electron probe microanalysis. Mg and Zr distributions were determined at 20 μm intervals from the interface along the diffusion direction. Chemical compositions were determined from the relative intensities of the Mg $K\alpha$ and Zr $L\alpha_1$ lines by using a calibration curve previously determined from standard samples.

Because of preferential diffusion of Mg and Zr ions along grain-boundaries, the Mg and Zr distributions perpendicular to the diffusion direction were not homogeneous in the present polycrystalline samples. Thus the composition at a given diffusion distance represents an average composition obtained by scanning perpendicular to the diffusion direction.[4]

Results

The concentration distribution for grain-boundary enhanced diffusion has been described by Oishi and Ichimura as a function of the lattice and grain-boundary interdiffusion coefficients by,[6]

$$\frac{2(C-C_1)}{C_2-C_1}=\frac{M_t}{M_\infty}\exp(-my), \tag{1}$$

where

$$\frac{M_t}{M_\infty}=1-\frac{6}{\pi^2}\sum_{n=1}^{\infty}\frac{1}{n^2}\exp\left(-\frac{\tilde{D}n^2\pi^2t}{r^2}\right), \tag{2}$$

$$m=\left[\frac{4\tilde{D}}{r\delta\tilde{D}'}\sum_{n=1}^{\infty}\exp\left(-\frac{\tilde{D}n^2\pi^2t}{r^2}\right)\right]^{1/2}, \tag{3}$$

y is the diffusion distance from the interface, C the

avarage concentration at y, C_1 and C_2 the initial concentrations of the diffusion couple, M_t and M_∞ the diffusion amounts at times t and infinity, respectively, $\tilde{D}$ and $\tilde{D}'$ the lattice and grain-boundary interdiffusion coefficients, respectively, r the grain radius, and δ the grain-boundary thickness.

Equation 1 can be rewritten as Eq. 4 in a logarithmic form,

$$\ln\frac{2(C-C_1)}{C_2-C_1} = \ln\frac{M_t}{M_\infty} - my, \qquad (4)$$

showing that $\ln[2(C-C_1)/(C_2-C_1)]$ is proportional to the diffusion distance y.

An example of the MgO concentration distribution is shown in Fig. 1 for the diffusion couple of $12MgO\cdot88ZrO_2$ with 45 μm grain radius and $16MgO\cdot84ZrO_2$ with 57 μm grain radius after annealing at 1650 °C for 48 h. Also shown is the MgO concentration for the diffusion couple of $12MgO\cdot88ZrO_2$ with 49 μm grain radius and $16MgO\cdot84ZrO_2$ with 55 μm grain radius after annealing at 1823 °C for 12 h. The corresponding $\ln[2(C-C_1)/(C_2-C_1)]$ values are plotted in Fig. 2 as a function of y, where the satisfactorily linear relationships indicate that the diffusion model represented by Eq. 1 is applicable to the present interdiffusion. The solid lines in Figs. 1 and 2 represent theoretical values calculated by Eq. 1 so as to provide the best fit to the experimental results. From the slopes and intercepts of the straight lines in Fig. 2, $\tilde{D}$ and $\delta\tilde{D}'$ are separately calculated from Eqs. 2 and 3. A correction to diffusion time was made in all calculations for the period of joining the diffusion couple as well as for increasing and decreasing the temperature before and after an isothermal diffusion annealing.[6]

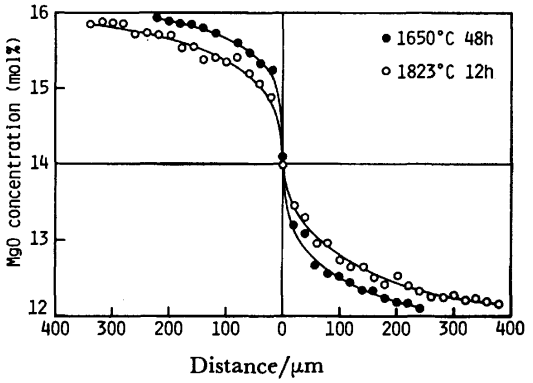

Fig. 1. Concentration distributions for the diffusion couples of $12MgO\cdot88ZrO_2$ and $16MgO\cdot84ZrO_2$.

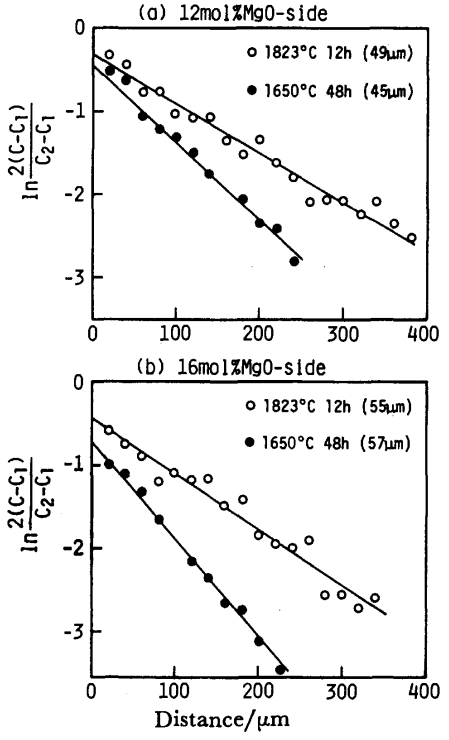

Fig. 2. Logarithmic concentration distributions for the diffusion couples of $12MgO\cdot88ZrO_2$ and $16MgO\cdot84ZrO_2$.
(a) 12 mol% MgO-side. (b) 16 mol% MgO-side.

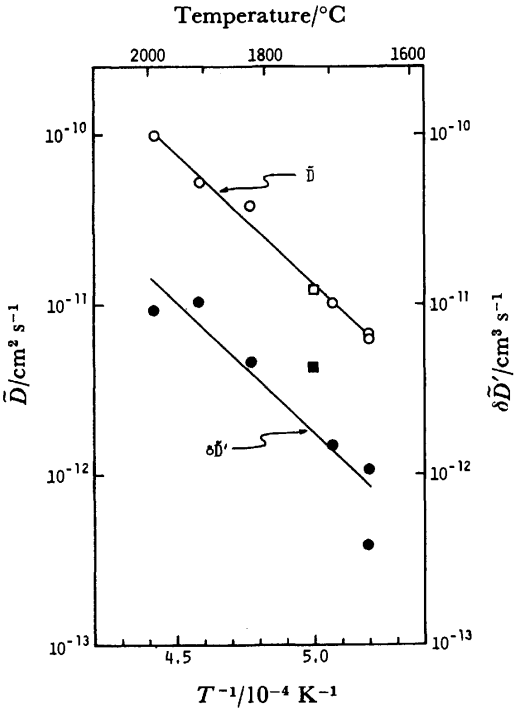

Fig. 3. Lattice interdiffusion coefficients and grain-boundary diffusion parameters for MSZ as a function of temperature. Circles denote the couple of $12MgO\cdot88ZrO_2$–$16MgO\cdot84ZrO_2$ and squares the couple of $12MgO\cdot88ZrO_2$–$18MgO\cdot82ZrO_2$.

The $\tilde{D}$ and $\delta\tilde{D}'$ thus calculated are shown in Fig. 3, where the averages of values obtained on both sides of the diffusion couples are plotted. Circles denote the couple of $12MgO\cdot88ZrO_2$–$16MgO\cdot84ZrO_2$ and squares the couple of $12MgO\cdot88ZrO_2$–$18MgO\cdot82ZrO_2$. Comparison of $\tilde{D}$ for the two diffusion couples with different combinations of MgO contents indicates no significant composition dependence. Comparison of results from diffusion anneals conducted in air (below 1730 °C) and in an Ar atmosphere (above 1823 °C) indicates no noticeable effect of the atmosphere on the results.

Values of $\tilde{D}$ and $\delta\tilde{D}'$ for the temperature range of

1650—1990 °C are described by Eqs. 5 and 6, respectively.

$$\tilde{D} = \left(5.9^{+5.8}_{-2.9}\right) \times 10^{-4} \exp[-293 \pm 11(\mathrm{kJ/mol})/RT]\ \mathrm{cm^2/s}, \quad (5)$$

$$\delta\tilde{D}' = \left(1.0^{+5.1}_{-0.8}\right) \times 10^{-4} \exp[-279 \pm 30(\mathrm{kJ/mol})/RT]\ \mathrm{cm^3/s}. \quad (6)$$

The activation energy for the grain-boundary diffusion parameter $\delta\tilde{D}'$ is close to that for lattice interdiffusion. Similar results have been also demonstrated for the CSZ system.[6]

Discussion

The calculated $\tilde{D}$ values are much smaller than the self-diffusion coefficients of the oxygen ion.[2]

The relation between the interdiffusion coefficient and the self-diffusion coefficients of the constituent ions for the fluorite-cubic solid solution has been given by Eq. 7 as,[3]

$$D = \frac{(Z_A^2C_AC_B - Z_AZ_BC_AC_B + Z_0^2C_BC_0)D_AD_0 + (Z_B^2C_AC_B - Z_AZ_BC_AC_B + Z_0^2C_AC_0)D_BD_0}{(Z_A^2C_AC_B - Z_AZ_BC_AC_B)D_A + (Z_B^2C_AC_B - Z_AZ_BC_AC_B)D_B + (Z_0^2C_AC_0 + Z_0^2C_BC_0)D_0}, \quad (7)$$

where Z is the valence, C the mole concentration, D the self-diffusion coefficient, and subscripts refer to the constituent ions. Since D_0 is much greater than D_{Zr} and D_{Mg} in the MSZ system, Eq. 7 reduces to Eq. 8.

$$D = [(Z_{Zr}^2C_{Zr}C_{Mg} - Z_{Zr}Z_{Mg}C_{Zr}C_{Mg} + Z_0^2C_{Mg}C_0)D_{Zr} + (Z_{Mg}^2C_{Zr}C_{Mg} - Z_{Zr}Z_{Mg}C_{Zr}C_{Mg} + Z_0^2C_{Zr}C_0)D_{Mg}] \times (Z_0^2C_{Zr}C_0 + Z_0^2C_{Mg}C_0)^{-1} \quad (8)$$

The Mg self-diffusion coefficients can be calculated by using Eq. 8 from known values of D and D_{Zr}. The Zr self-diffusion coefficients estimated for MSZ in the temperature range of 1680—2083 °C[4] have been represented by Eq. 9.

$$D_{Zr} = 0.033 \exp[-381(\mathrm{kJ/mol})/RT]\ \mathrm{cm^2/s}. \quad (9)$$

The D_{Mg} values calculated by Eq. 8 from D_{Zr} (Eq. 9) and $\tilde{D}$ (Eq. 5) for the average composition of the diffusion couple are represented by Eq. 10.

$$D_{Mg} = 3.7 \times 10^{-4} \exp[-285(\mathrm{kJ/mol})/RT]\mathrm{cm^2/s}. \quad (10)$$

As shown in Fig. 4, the interdiffusion coefficient is higher in magnitude and lower in activation energy than D_{Zr}, and close to the calculated value of D_{Mg} both in magnitude and in activation energy. (The D_{Zr} in MSZ is similar to the D_{Zr} in CSZ in both magnitude and activation energy.[4])

The activation energy of D_{Mg} in MSZ (285 kJ/mol) is smaller than that of D_{Ca} in CSZ (419.2 kJ/mol).[5] This difference is interpreted as due to the ionic radii of the dopant cations relative to that of the Zr ion; that is, the Mg ion in MSZ is smaller than the Ca ion in CSZ.

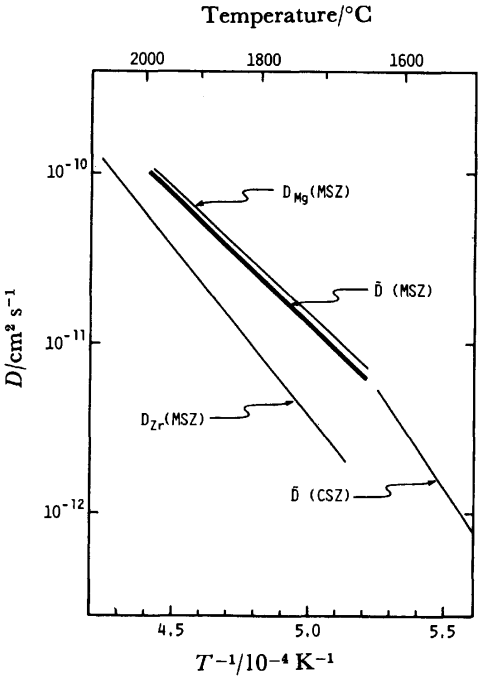

Fig. 4. Lattice interdiffusion coefficient and self-diffusion coefficients of Mg and Zr[4] ions in MSZ; lattice interdiffusion coefficient in CSZ.[6]

Since D_R (R=Mg or Ca) is greater than D_{Zr} in both MSZ and CSZ, $\tilde{D}$ tends to be close to D_R in the respective systems in accordance with Eq. 7. Consequently, the small activation energy of interdiffusion in MSZ relative to that in CSZ, as shown in Fig. 4, is attributed to the activation energy of D_{Mg} in MSZ being smaller than that of D_{Ca} in CSZ.

In summary, cation interdiffusion in MgO-stabilized zirconia is controlled primarily by the diffusivity of the faster cation (Mg), and the contribution of the high diffusivity of the oxygen ion is small.

The authors acknowledge H. S. Spacil's comments to the manuscript.

References

1) C. F. Grain, *J. Am. Ceram. Soc.*, **50**, 288 (1967).
2) Y. Oishi, K. Ando, and M. Akiyama, *Nippon Kagaku Kaishi*, **1981**, 1445.
3) Y. Oishi and Y. Sakka, *J. Nucl. Mater.*, **97**, 44 (1981).
4) Y. Oishi, Y. Sakka, and K. Ando, *J. Nucl. Mater.*, **96**, 23 (1981).
5) W. H. Rhodes and R. E. Carter, *J. Am. Ceram. Soc.*, **49**, 244 (1966).
6) Y. Oishi and H. Ichimura, *J. Chem. Phys.*, **71**, 5134 (1979).
7) R. L. Fullman, *Trans. AIME*, **197**, 447 (1953).

 © 1982 The Chemical Society of Japan Bull. Chem. Soc. Jpn., 55, 423—426 (1982)

Chemical Systems Exhibiting Complicated Temporal Oscillations

Kazutoshi IWAMOTO, Susumu KAWAUCHI, Kiyoshi SAWADA, and Manabu SENŌ*
Institute of Industrial Science, The University of Tokyo, 7-22-1 Roppongi, Minato-ku, Tokyo 106
(Received July 27, 1981)

Two model systems exhibiting complicated oscillations were proposed and analyzed. One of them is a double oscillation system, which shows alternating oscillations of large and small amplitudes and the mechanism for appearance of the double oscillations is clarified. In the other system, either large or small amplitude oscillation appears depending on the parameter values, and the transition between the large and the small amplitude oscillation is very abrupt and sensitive to the change in external constraints.

Until now, many papers concerning various kinds of behaviors of chemical systems far from equilibrium states have been reported.[1-27] These systems show occasionally some characteristic behaviors like chemical oscillations,[1,2] excitation,[3-5] wave propagation,[6-9] and so on. The well-known chemical oscillatory system is the Belousov-Zhabotinskii reaction,[14,15] in which malonic acid is oxidized by bromate ion catalyzed by some metallic ions in sulfuric acid solutions, and its reaction mechanism has been studied in detail.[16] As a model system for this reaction the Oregonator was proposed and analyzed with a computer simulation method by Field *et al.* of the University of Oregon.[5,17] Similar chemical oscillation models were proposed and analyzed by some investigators.[1-4,18,19] We also proposed a simple model which explains chemical oscillation and excitation,[4] and applied it for interpretation of some problems.[20-23] The characteristic point of the Oregonator and our model is that both of them include a subsystem having multiple steady states, some of which are stable and other are unstable.[4]

In this article, we investigate two chemical systems exhibiting temporal oscillations, one of which shows double oscillation and the other exhibits abrupt changes in the amplitude of oscillation depending on the parameter values.

The former system is obtained by some modifications of our original system[4] and it is useful to investigate the appearance of alternating large and small amplitude oscillations, which are observed in the Belousov-Zhabotinskii reaction in a well-stirred continuous flow reactor.[24,25] A chaotic behavior was also reported in this system.[24] Showalter *et al.* studied a modified Oregonator which exhibits complicated behaviors in a flow system.[26] Although their system, in which two intermediates are newly introduced to the original Oregonator, is fairly complicated, it can well explain the behaviors of the Belousov-Zhabotinskii reaction in the well-stirred continuous flow reactor. A similar model system was studied by Janz *et al.*[27] On the other hand, our system proposed in the present paper contains three intermediates and well explains the appearance of alternating large and small amplitude oscillation.

In the latter system, either large or small amplitude oscillation emerges depending on the parameter values, and the transition between the large and the small amplitude oscillation at critical values of parameters is so abrupt that the system is very sensitive to changes in the external constraints. In this case the behavior of the system at the critical point is largely affected by fluctuations in a similar way as reported already.[3,4,20-22]

Chemical System Exhibiting Double Oscillation

In a preceding paper,[4] we proposed a simple chemical system exhibiting temporal oscillations. Here, the system is modified a little as follows:

$$P + Z \xrightarrow{k_1} E + Z, \qquad \text{(R-1)}$$

$$E + X \xrightarrow{k_2} R + X, \qquad \text{(R-2)}$$

$$A + 2X + E \underset{k_4}{\overset{k_3}{\rightleftharpoons}} 3X + E, \qquad \text{(R-3)}$$

$$B + X \underset{k_6}{\overset{k_5}{\rightleftharpoons}} C, \qquad \text{(R-4)}$$

where the concentrations of A, B, C, P, and R are kept constant to maintain the total system far from an equilibrium state, E and X are intermediates, and Z is a newly introduced chemical species acting as a catalyst in the process (R-1). The chemical species Z is introduced to control the rate of the process (R-1) and for a while its concentration is assumed to be constant.

The rate equations of E and X are written as follows:

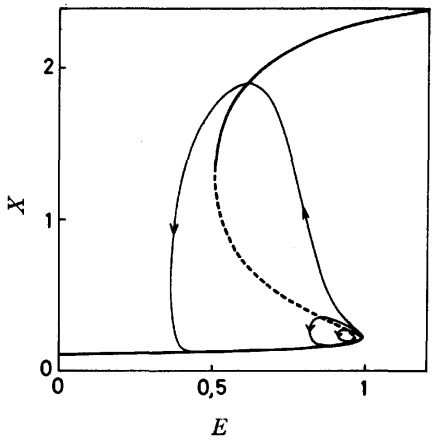

Fig. 1. Phase plane diagrams for Eqs. 3 and 4. Steady states S and S′ are stable and unstable, respectively. The closed cycle shows the trajectory of the temporal oscillation determined by Eqs. 1 and 2 for $Z=1.0$. Parameter values used are: $k_1=1.0$, $k_2=4.76$, $k_3=100.0$, $k_4=48.64$, $k_5=10.0$, $k_6=1.0$, $A=1.332$, $B=5.02$, $C=5.32$, and $P=1.13$.

$$\frac{dE}{dt} = k_1PZ - k_2EX, \quad (1)$$

$$\frac{dX}{dt} = k_3AEX^2 - k_4EX^3 - k_5BX + k_6C. \quad (2)$$

Putting the steady state conditions, $dE/dt=0$ and $dX/dt=0$, into Eqs. 1 and 2 gives

$$k_1PZ - k_2EX = 0, \quad (3)$$

$$k_3AEX^2 - k_4EX^3 - k_5BX + k_6C = 0. \quad (4)$$

By plotting Eqs. 3 and 4 on an E-X phase plane, we get Fig. 1, where two curves from Eq. 3 are shown for $Z=1.0$ and 0.8, respectively. All the parameter values used are as follows:

$k_1 = 1.0$, $k_2 = 4.76$, $k_3 = 100.0$, $k_4 = 48.64$, $k_5 = 10.0$,

$k_6 = 1.0$, $A = 1.332$, $B = 5.02$, $C = 5.32$, and $P = 1.13$.

The crossing point of the curve of Eq. 3 and that of Eq. 4 represents the steady state of the total chemical system. The steady state indicated with S′, where the value of Z is 1.0, is unstable,[4] and then an oscillatory behavior appears. Its trajectory is shown by a closed cycle in Fig. 1. When the value of Z is 0.8, the crossing point S is a stable steady state, into which the chemical system falls with time independently of the initial states.

Now, let us introduce the following processes.

$$Q \xrightarrow{k_7} Z, \quad (R\text{-}5)$$

$$Z + X \xrightarrow{k_8} D + X, \quad (R\text{-}6)$$

where the concentrations of Q and D are kept constant. Then, the concentration of Z changes according to the following equation.

$$\frac{dZ}{dt} = k_7Q - k_8XZ. \quad (5)$$

In this equation, the consuming rate of Z, k_8XZ, increases with an increasing concentration of X. When $dZ/dt>0$, that is, the production rate of Z, k_7Q, is larger than the consuming rate of Z, for the system at the state S in Fig. 1, the concentration of Z increases and in time the chemical system will transit towards an oscillatory state. On the other hand, the system in the oscillatory region takes sometimes so large X values during the oscillatory path that the consumption rate of Z increases largely beyond the production rate of Z. Then, the concentration of Z decreases again and the system approaches to the stable steady state showing a damped oscillation.

Repetition of these processes causes alternating large and small amplitude oscillations. Figure 2 shows the typical examples of temporal changes of X of the system determined by solving Eqs. 1, 2, and 5 for three values of P. The oscillating behavior changes according to the P value. These results resemble those reported by Hudson *et al.*,[25] although the flow terms are not taken into consideration in the present treatment.

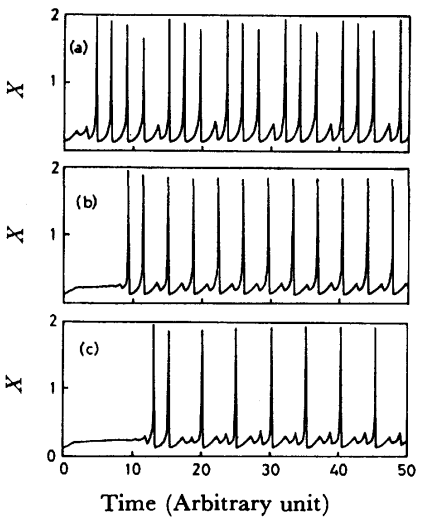

Fig. 2. Some typical behaviors of the double oscillation defined by Eqs. 1, 2, and 5. (a) $P=1.2$, (b) $P=1.13$, (c) $P=1.1$, and $Q=1.0$, $k_7=0.1$, $k_8=0.4$, and other parameter values are the same as those of Fig. 1.

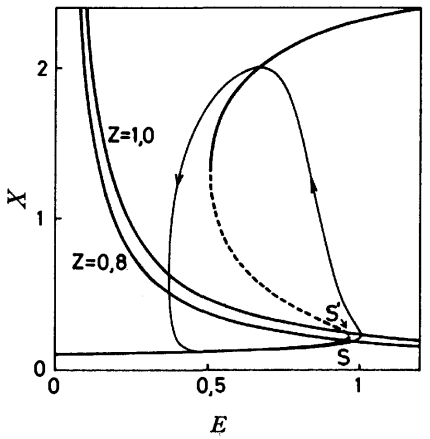

Fig. 3. Projection onto E-X phase plane of the double oscillation trajectory for $P=1.1$. The system evolves from a smallest cycle to a larger and a largest cycles, returning the original smallest amplitude oscillatory state. The parameter values are the same as those of Figs. 1 and 2.

In Fig. 3, the trajectory of oscillation in the case of $P=1.1$ is shown on the E-X phase plane. The thin line representing the trajectory shows that a phase point starts from a certain point on the smallest cycle and transits the phase space into larger cycles, returning to the original small cycle.

Chemical System Showing Abrupt Change in Amplitude

Behaviors of Chemical Reaction Model. Let us consider a system consisting of the following chemical reactions:

$$P' \xrightarrow{pk_9} E', \quad (R\text{-}7)$$

$$E' + X' \xrightarrow{pk_{10}} X' + R', \quad (R\text{-}8)$$

$$A' + 4X' + E' \underset{k_{12}}{\overset{k_{11}}{\rightleftharpoons}} 5X' + E', \quad (R\text{-}9)$$

$$B' + 2X' \underset{k_{14}}{\overset{k_{13}}{\rightleftharpoons}} 3X' + C', \quad (R\text{-}10)$$

$$D' + X' \underset{k_{16}}{\overset{k_{15}}{\rightleftharpoons}} G', \qquad \text{(R-11)}$$

where E' and X' are intermediate species. All the chemical species are represented by superscript dashes to discriminate this chemical system from the double oscillation system described in the preceding section. The concentrations of A', B', C', D', G', P', and R' are kept constant to sustain the system far from an equilibrium state.

The temporal changes of E' and X' are given by

$$\frac{dE'}{dt} = \rho k_9 P' - \rho k_{10} E' X', \qquad (6)$$

$$\frac{dX'}{dt} = k_{11} A' E' X'^4 - k_{12} E' X'^5 + k_{13} B' X'^2 - k_{14} C' X'^3 - k_{15} D' X' + k_{16} G'. \qquad (7)$$

At the steady state, where dE'/dt and dX'/dt are zero,

$$k_9 P' - k_{10} E' X' = 0, \qquad (8)$$

$$k_{11} A' E' X'^4 - k_{12} E' X'^5 + k_{13} B' X'^2 - k_{14} C' X'^3 - k_{15} D' X' + k_{16} G' = 0. \qquad (9)$$

In Fig. 4, Eqs. 8 and 9 are shown on the E-X phase plane for two different values of P'. The parameter values used are:

$A' = B' = C' = D' = G' = 1.0$, $k_9 = 1.0$, $k_{10} = 1.40 \times 10^2$, $k_{11} = 2.5 \times 10^5$, $k_{12} = 5.67 \times 10^5$, $k_{13} = 8.91 \times 10^2$, $k_{14} = 2.50 \times 10^4$, $k_{15} = 12.0$, and $k_{16} = 5.37 \times 10^{-2}$.

The crossing point of the two curves represents the steady state of this chemical system. It was clarified according to the linearized stability analysis[1] that the steady state of the chemical system for adequately small ρ values, *e.g.*, smaller than unity, is unstable when the two curves intersect in the dotted parts of the curve drawn by Eq. 9, and in this case we can expect evolution of the system into an oscillatory state.[4] The trajectories are dependent on the value of parameter ρ. The closed cycle in Fig. 4 shows approximate path of the temporal oscillation for $P' = 7.90$, where the value of ρ is selected to be 0.01. Dependence of the oscillation behaviors on the position of crossing point is shown in Fig. 5.

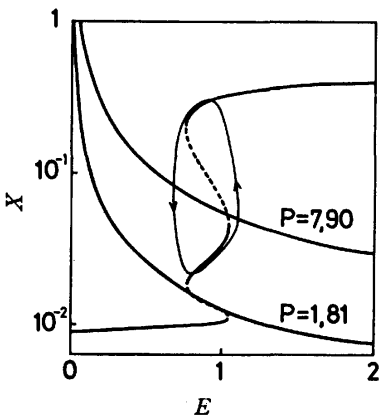

Fig. 4. Phase plane diagrams for Eqs. 8 and 9. The closed cycle is the trajectory of the temporal oscillation determined from Eqs. 6 and 7 in the case of $P' = 7.90$. Parameter values used for calculations are: $A' = B' = C' = D' = G' = 1.0$, $k_9 = 1.0$, $k_{10} = 1.40 \times 10^2$, $k_{11} = 2.5 \times 10^5$, $k_{12} = 5.67 \times 10^5$, $k_{13} = 8.91 \times 10^2$, $k_{14} = 2.50 \times 10^4$, $k_{15} = 12.0$, $k_{16} = 5.37 \times 10^{-2}$, and $\rho = 0.01$.

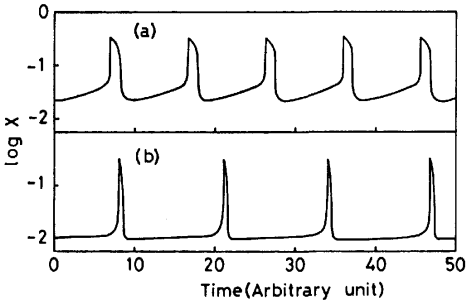

Fig. 5. Oscillatory behaviors of the chemical system. (a) $P' = 7.90$ and (b) $P' = 1.81$. Parameter values used for calculations are the same as those of Fig. 4.

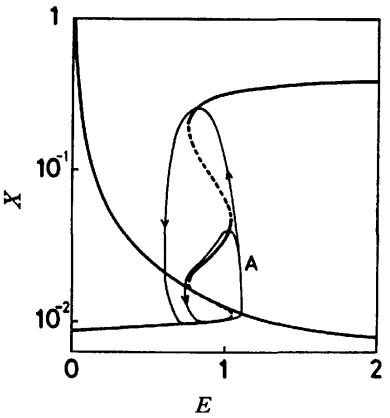

Fig. 6. Trajectories of the oscillations in the case of $P' = 1.81$. Two closed cycles show schematic courses of oscillations for two values, 0.01 and 0.02, of ρ. Point A is a junction at the two cycles. When $\rho = 0.02$, the decreasing rate of E at A is larger than that in the case of $\rho = 0.01$ and the chemical system chooses the course to the small amplitude oscillation.

Next, while the value of P' is fixed to be 1.81, changes in oscillatory behaviors according to the value of ρ is examined. It was revealed that, when ρ is 0.02, the chemical system shows an oscillation of a small amplitude and when ρ is 0.01, an oscillation of a large amplitude appears. Figure 6 shows the approximate trajectories of the chemical system for the two cases of $\rho = 0.01$ and 0.02, respectively. In the case of $\rho = 0.02$, the decreasing rate of E at the junction A at the two passes is faster than that in the case of $\rho = 0.01$ and, therefore, the chemical system chooses the course of the small cycle. Both the oscillatory behaviors are shown in Fig. 7. The larger amplitude oscillation has longer period than that of the smaller amplitude oscillation. The abrupt change in amplitude is observed between 0.019 and 0.018 of ρ value, and for ρ values larger than 0.019, the smaller amplitude oscillation appears.

The characteristic point of the present chemical system is that the amplitude of oscillations changes largely at a certain value of ρ, and we can say that this system is very sensitive to change of parameter values.

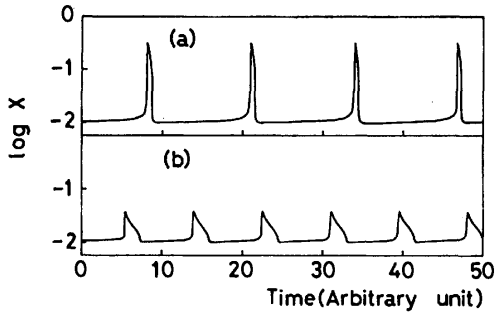

Fig. 7. Oscillatory behaviors of the chemical system for $P'=1.81$. (a) $\rho=0.01$ and (b) $\rho=0.02$. Other parameter values are the same as those of Fig. 5. The critical value of ρ, at which the amplitude changes abruptly, is between 0.018 and 0.019.

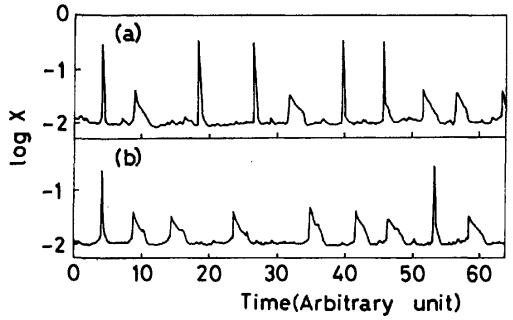

Fig. 8. Appearance of random oscillations in amplitude under the influence of fluctuation. $P'=1.81$. (a) $\rho=0.018$ and (b) $\rho=0.019$. The strengths of fluctuations are selected to be $\alpha=0$ and $\beta=0.1$ for calculations. Other parameter values are the same as those of Fig. 5.

Effects of Fluctuations on the Behaviors of the Chemical System. Since the chemical system described in this section is very sensitive to a small variation in the parameter values, it would be expected that the amplitude of oscillations of this chemical system changes randomly under the influence of fluctuation. To confirm this expectation, the following Langevin type equations representing the behaviors of the chemical system subjected to fluctuation should be examined; that is,

$$\frac{dE'}{dt} = \rho k_9 P' - \rho k_{10} E'X' + \alpha F(t), \tag{10}$$

$$\frac{dX'}{dt} = k_{11}A'E'X'^4 - k_{12}E'X'^5 + k_{13}B'X'^2 - k_{14}C'X'^3 - k_{15}D'X' + k_{16}G' + \beta H(t), \tag{11}$$

where $F(t)$ and $H(t)$ are the fluctuation terms of Gaussian type. The average values $\langle F(t)\rangle$ and $\langle H(t)\rangle$ are zero and the standard deviations are set to be 0.1. The coefficients α and β represent the strengths of fluctuations. Figure 8 illustrates typical behaviors of the chemical system under the influence of fluctuations, which were obtained by solving these equations in some cases. Certainly, random appearance of large and small amplitude oscillations is observed.

References

1) P. Glansdorff and I. Prigogine, "Thermodynamic Theory of Structure, Stability, and Fluctuations," Wiley, New York (1971).
2) G. Nicolis and I. Prigogine, "Self-organization in Nonequilibrium Systems," Wiley, New York (1977).
3) H. S. Hahn, A. Nitzan, P. Ortoleva, and J. Ross, *Proc. Natl. Acad. Sci. U.S.A.*, **71**, 4067 (1974).
4) K. Iwamoto and M. Seno, *J. Chem. Phys.*, **70**, 5851 (1979).
5) J. J. Tyson, *J. Chem. Phys.*, **66**, 905 (1977).
6) P. Ortoleva and J. Ross, *J. Chem. Phys.*, **58**, 5673 (1973).
7) P. Ortoleva and J. Ross, *J. Chem. Phys.*, **60**, 5090 (1974).
8) P. Ortoleva and J. Ross, *J. Chem. Phys.*, **63**, 3398 (1975).
9) L. M. Pismen, *J. Chem. Phys.*, **71**, 462 (1979).
10) M. Flicker and J. Ross, *J. Chem. Phys.*, **60**, 3458 (1974).
11) D. Feinn, P. Ortoleva, W. Scalf, S. Schmidt, and M. Wolff, *J. Chem. Phys.*, **69**, 27 (1978).
12) K. Showalter, *J. Chem. Phys.*, **73**, 3735 (1980).
13) C. S. Haase, J. Chadam, D. Feinn, and P. Ortoleva, *Science*, **209**, 272 (1980).
14) A. M. Zhabotinskii, *Biophysics*, **9**, 329 (1964).
15) B. P. Belousov, *Ref. Radiats. Med.*, **1958**, 145 (1959).
16) R. J. Field, E. Körös, and R. M. Noyes, *J. Am. Chem. Soc.*, **94**, 8649 (1972).
17) R. J. Field and R. M. Noyes, *J. Chem. Phys.*, **60**, 1877 (1974).
18) H. S. Hahn, P. Ortoleva, and J. Ross, *J. Theor. Biol.*, **41**, 503 (1973).
19) M. Senō, K. Iwamoto, and K. Sawada, *J. Theor. Biol.*, **72**, 577 (1978).
20) K. Iwamoto and M. Senō, *J. Chem. Phys.*, **70**, 5858 (1979).
21) K. Iwamoto and M. Senō, *J. Chem. Phys.*, **72**, 4235 (1980).
22) K. Iwamoto and M. Senō, *Bull. Chem. Soc. Jpn.*, **54**, 669 (1981).
23) K. Iwamoto and M. Senō, *J. Chem. Phys.*, **74**, 3376 (1981).
24) R. A. Schmitz, K. R. Graziani, and J. L. Hudson, *J. Chem. Phys.*, **67**, 3040 (1977).
25) J. L. Hudson, M. Hart, and D. Marinko, *J. Chem. Phys.*, **71**, 1601 (1979).
26) K. Showalter, R. M. Noyes, and K. Bar-Eli, *J. Chem. Phys.*, **69**, 2514 (1978).
27) R. D. Janz and D. J. Vanecek, *J. Chem. Phys.*, **73**, 3132 (1980).

Studies of the Cobalt(III) Complexes of 8-Amino-3,6-diazaoctanate Ion. III.[1] Preparations and Some Properties of Complexes with Chloro, Nitro, or Aqua Ligands

Kiyokatsu WATANABE

Department of Chemistry, Faculty of Science, Ehime University, Matsuyama, Ehime 790

(Received April 27, 1981)

The following new cobalt(III) complexes containing the 8-amino-3,6-diazaoctanate ion (adao)[2] have been prepared: α-[Co(adao)Cl_2], two isomers of *β-mer(N)*-[Co(adao)Cl_2], *β-fac(N)*-[Co(adao)Cl_2], α-[Co(adao)$(NO_2)_2$], two isomers of *β-mer(N)*-[Co(adao)$(NO_2)_2$], α-[Co(adao)$(H_2O)_2$]$(ClO_4)_2$, and *β-mer(N)*-[Co(adao)$(H_2O)_2$]$(ClO_4)_2$. The geometrical structures have been determined on the basis of the electronic spectra, the proton NMR spectra, and the deductions from their derivation processes.

Four geometrical isomers, α, *β-mer(N)*, *β-fac(N)*, and *trans*,[3] are possible in each [Co(adao)X_2] type complex ($X=Cl^-$, NO_2^-, or H_2O), as is shown in Fig. 1-a. When we consider the configuration of the secondary amine nitrogen atom (*s*-N) in adao, further discrimination is possible in the *β-mer(N)*, *β-fac(N)*, and *trans* isomers (Fig. 1-b). Thus, seven racemic geometrical isomers, α-(*SR,RS*), *β-mer(N)*-(*RS,SR*), *β-mer(N)*-(*RR,SS*), *β-fac(N)*-(*RS,SR*), *β-fac(N)*-(*SS,RR*), *trans*-(*RS,SR*), *trans*-(*SS,RR*),[4] are possible when two same unidentate ligands occupy the residual sites. In a previous paper,[1] the present author reported that three geometrical isomers, α, *β-mer(N)*, and *β-fac(N)*, were isolated in each [Co(adao)(O–O)] type complex ($O-O=CO_3^{2-}$, ox, and mal). Also in the [Co(adao)X_2] type, the existence of other isomers than *β-mer(N)* is to be expected. However, only the existence of *β-mer(N)* coordination mode was suggested by Schneider *et al.*[3] Furthermore, their *s*-N configurations were not decided. In order to clarify this problem, the isolation of the isomers was attempted. Thus, the author succeeded in isolating some of α, *β-mer(N)*, and *β-fac(N)* isomers for the dichloro, dinitro, and diaqua complexes.

Experimental

Preparation of Ligand. 8-Amino-3,6-diazaoctanoic acid (Hadao) was prepared by modifying the method of Schneider and Collman.[3]

Preparations of Complexes. *(1) Crude-[Co(adao)$(NO_2)_2$]*: The crude dinitro complex was isolated by modifying the Collman's method.[3]

(2) Crude-[Co(adao)Cl_2]: The crude dichloro complex was prepared by modifying the Collman's method.[3]

(3) α-*[Co(adao)Cl_2]*: The treatment of the crude-[Co(adao)Cl_2] with $HClO_4$ gave *β-mer(N)*-[Co(adao)(Cl)(H_2O)]-ClO_4. The detailed preparative procedure and the structural assignment will be described elsewhere. The resulting *β-mer(N)*-[Co(adao)(Cl)(H_2O)]ClO_4 (7.44 g) was added to 30 cm^3 of water containing Li_2CO_3 (2.22 g). The suspension was heated on a water bath at 80 °C for 4 h. After cooling, the resulting precipitate was removed by filtration. When the filtrate was concentrated on a water bath with an aid of air stream, red crystals began to deposit. After the product was cooled, the crystals were collected on a filter, and then washed with an ethanol–ether (1 : 1) mixture. The filtrate was concentrated again, and then the second precipitate was filtered off. To the remaining filtrate was added 5 cm^3 of 6 M (1 M=1 mol dm^{-3}) HCl. When the mixture was heated at about 65 °C in a water bath for 20 min, blue crystals began to appear. To the resulting product was poured 10 cm^3 of water, and the mixture was then cooled in an ice bath. The deep blue crystals precipitated were collected on a filter, and washed with water, ethanol, and ether, in turn. Yield, ≈0.3 g.

Found: C, 24.38; H, 4.97; N, 14.28%. Calcd for [Co(adao)Cl_2]=$CoC_6H_{14}N_3O_2Cl_2$: C, 24.85; H, 4.87; N, 14.49%.

(4) β-mer(N)-[Co(adao)Cl_2]: *a)*: *β-mer(N)*-[Co(adao)-Cl_2]·$2H_2O$ (violet gray); The crude dichloro complex (30 g) obtained in *(2)* was dissolved in 390 cm^3 of hot 2 M HCl (≈80 °C), and then the product was filtered. The filtrate was cooled in a refrigerator for 3 d. The crystals were collected on a filter, and washed first with ethanol, then with a mixture of ethanol and ether (1 : 1). Yield, ≈5 g.

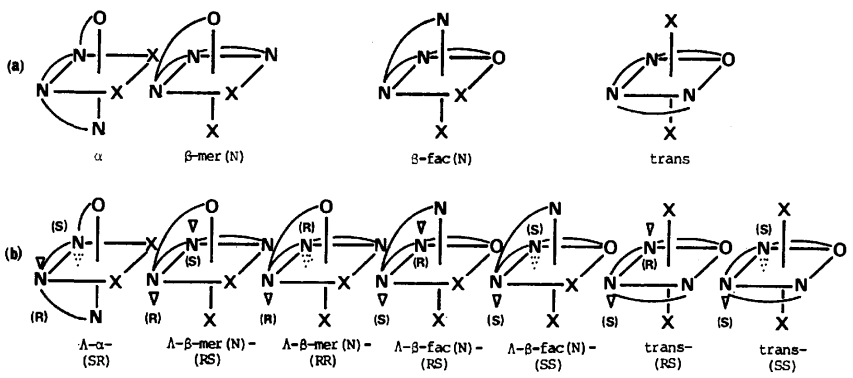

Fig. 1. The possible isomers of [Co(adao)X_2] type complex. (a): Without consideration of *s*-N configurations, (b): under consideration of *s*-N configurations.

Found: C, 22.40; H, 5.43; N, 13.18%. Calcd for [Co(adao)Cl_2]·2H_2O=$CoC_6H_{16}N_3O_4Cl_2$: C, 22.10; H, 5.56; N, 12.89%.

b): *β-mer(N)*-[Co(adao)Cl_2]·HCl·0.5H_2O (silver gray); The filtrate obtained in the previous procedure *(4-a)* was evaporated with an aid of air stream until silver gray crystals appeared. After cooling, the crystals were collected, and then washed with ethanol, a mixture of ethanol and ether (1 : 1), in turn. Yield, ≈15 g.

Found: C, 21.19; H, 4.95; N, 12.49%. Calcd for [Co(adao)Cl_2]·HCl·0.5H_2O=$CoC_6H_{16}N_3O_{2.5}Cl_3$: C, 21.48; H, 4.81; N, 12.52%.

(5) *β-fac(N)-[Co(adao)Cl_2]*: *β-fac(N)*-[Co(adao)(Cl)-(H_2O)]ClO_4·H_2O (0.26 g), of which preparative procedure will be described elsewhere, was suspended in 10 cm³ of water. To the suspension, 2 cm³ of 2 M HCl was added, and the mixture was heated until it dissolved. The resulting solution was concentrated to dryness on a water bath with an aid of air stream. After 5 cm³ of water and 2 cm³ of 2 M HCl were added to the concentrated product, the mixture was concentrated again, and then the product was allowed to stand at room temperature. The product was convered with 2 cm³ of 2 M HCl, and then this mixture was evaporated to a half of its original volume. After the violet blue crystals were collected on a filter, they were washed with ethanol, and ether in this order. Yield, ≈0.1 g.

Found: C, 24.55; H, 4.64; N, 14.46%. Calcd for [Co(adao)Cl_2]=$CoC_6H_{14}N_3O_2Cl_2$: C, 24.85; H, 4.87; N, 14.49%.

(6) *α-[Co(adao)(NO_2)$_2$]*: To a solution of silver perchlorate (3 g) in 10 cm³ of water, α-[Co(adao)Cl_2] (1.45 g) was suspended, and then the suspension was heated at 60 °C for 10 min. During the reaction, silver chloride came out. After the reaction mixture had been cooled in an ice bath, the silver chloride was filtered off. The pink red filtrate was reduced in volume to about 2 cm³ in a rotary evaporator below 40 °C, and then a small amount of 2 M NaBr solution was added until no more white crystals precipitated. After the silver bromide was removed by filtration, the filtrate was diluted to 10 cm³ with water. To the solution, sodium nitrite (0.69 g) was added, and then the mixture was heated at 65 °C for 5 min. Orange crystals appeared. They were collected, and then washed with ethanol, and with ether. Yield, ≈0.6 g.

Recrystallization was carried out by means of fractional extraction with hot water (≈80 °C). The first extract (≈50 cm³) was discarded. The crystals in the second and third extract (150 cm³ respectively) consisted of only α-dinitro isomer. Yield, ≈0.3 g.

Found: C, 22.98; H, 4.60; N, 22.94%. Calcd for [Co(adao)(NO_2)$_2$]=$CoC_6H_{14}N_5O_6$: C, 23.16; H, 4.54; N, 22.51%.

(7) *β-mer(N)-[Co(adao)(NO_2)$_2$]*: Although the *β-mer(N)*-dinitro isomer had been separated by Schneider and Collman,[3] the present author found that the following procedure gave the *β-mer(N)* isomer in a higher purity. Furthermore, it was also found that there are two *β-mer(N)* dinitro isomers, namely one sparingly soluble isomer and another soluble one.

a): The sparingly soluble isomer with an orange yellow color; Sodium nitrite (0.7 g) and *β-mer(N)*-[Co(adao)(Cl)-(H_2O)]ClO_4 (1.86 g) were added in 30 cm³ of water, and the mixture was heated at 80 °C for half an hour with stirring. During this period, a large amount of orange yellow crystals appeared. After cooling, the crystals were collected on a filter, and washed with a mixture of ethanol and ether (1 : 1). The filtrate was reserved for the isolation of soluble isomer.

Recrystallization was carried out by the fractional extraction. The orange yellow crystals (1.2 g) were extracted with four 20 cm³ portions of hot water (≈80 °C), and then 50 cm³ one. The last main extract (≈50 cm³) was cooled in an ice bath, then the orange yellow crystals were deposited. They were washed with ethanol, and with ether. Yield, ≈0.2 g.

Found: C, 23.07; H, 4.61; N, 22.28%. Calcd for [Co(adao)(NO_2)$_2$]=$CoC_6H_{14}N_5O_6$: C, 23.16; H, 4.54; N, 22.51%.

b): The soluble isomer with a yellow color; The reserved filtrate in *(7-a)* was allowed to stand at room temperature for 3 h, whereupon the yellow needles precipitated. When the yield of needles was very small, the filtrate was permitted to stand for 3 d. After filtration, the crystals were washed with an ethanol–ether (1 : 1) mixture. Yield, ≈0.1 g. They were recrystallized from 5 cm³ of hot water.

Found: C, 23.02; H, 4.62; N, 22.54%. Calcd for [Co(adao)(NO_2)$_2$]=$CoC_6H_{14}N_5O_6$: C, 23.16; H, 4.54; N, 22.51%.

(8) *α-[Co(adao)(H_2O)$_2$](ClO_4)$_2$·H_2O*: In 3 cm³ of water, α-[Co(adao)(NO_2)$_2$] (0.15 g) was suspended, and then to the suspension, 3 cm³ of 6 M $HClO_4$ was added dropwise. The mixture was heated at 80 °C about 10 min. The resulting solution with a red orange color was concentrated on a water bath under an air stream. The color of solution changed to a red one. The concentrated solution was cooled, and then filtered. After ethanol (30 cm³) was added to the filtrate, ether (150 cm³) was poured to it. When the mixture was cooled in an ice bath, pink crystals appeared. The crystals were collected on a filter, and washed with ethanol, and then stored over silica gel in a desiccator. Yield, ≈0.05 g.

Found: C, 15.53; H, 4.36; N, 8.96%. Calcd for [Co(adao)(H_2O)$_2$](ClO_4)$_2$·H_2O=$CoC_6H_{20}N_3O_{13}Cl_2$: C, 15.27; H, 4.27; N, 8.90%.

(9) *β-mer(N)-[Co(adao)(H_2O)$_2$](ClO_4)$_2$·H_2O*: *β-mer(N)*-[Co(adao)CO_3] (1.4 g), of which preparative procedure was described in the previous paper,[1] was suspended in 3 cm³ of iced cold water. To the suspension, 2 cm³ of 6 M $HClO_4$ was added slowly drop by drop under cooling in an ice bath. The product was filtered out, and then the filtrate was evaporated below 40 °C with an aid of air stream. When the red crystals began to deposit, the reaction mixture was cooled sufficiently for the complete deposition. They were filtered, and washed with a mixture of ethanol and ether (1 : 2). Yield, ≈0.4 g.

Found: C, 15.24; H, 4.23; N, 8.97%. Calcd for [Co(adao)(H_2O)$_2$](ClO_4)$_2$·H_2O=$CoC_6H_{20}N_3O_{13}Cl_2$: C, 15.27; H, 4.27; N, 8.90%.

Analyses. The carbon, hydrogen, and nitrogen in the isolated complexes were analyzed at the Microanalysis Center of Osaka University, and at the Analysis Center of the Institute for Chemical Reserch, Kyoto University.

Measurements. The absorption spectra in solution were measured with a Shimadzu UV-200 Recording Spectrophotometer using 1 cm or 10 cm silica cells. The diffuse reflectance spectra of solid samples in the range 340—750 nm were measured with a Hitachi EPU-2A Spectrophotometer equipped with a reflectance attachment (Type R-3), and MgO disks for the reference. The IR spectra were recorded with a JASCO IRA-1 Spectrophotometer by a Nujol mull method. The proton NMR spectra were recorded with a Varian XL-100 Spectrometer or a Japan Electron Optics JNM-4H-100 Spectrometer in a deuterium oxide, with *t*-butyl alcohol as the internal reference.

Results and Discussion

Preparative Remarks. The preparation routes for [Co(adao)X_2] are shown schematically in Fig. 2. Schneider and Collman[3] reported that *β-mer(N)*-

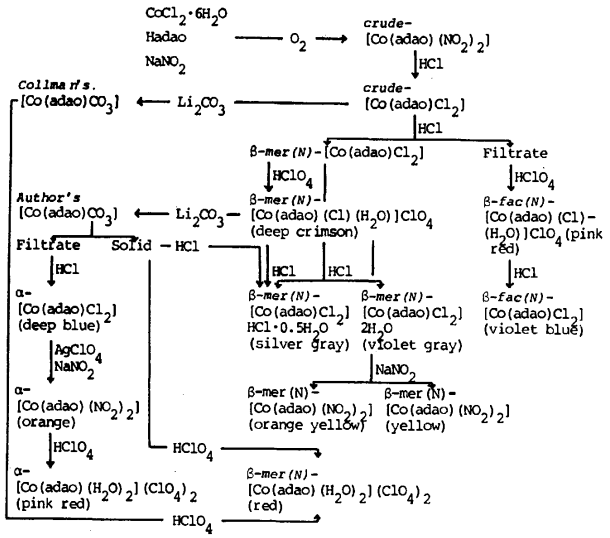

Fig. 2. The preparation scheme of $[Co(adao)X_2]$ (X= Cl^-, NO_2^-, and H_2O).

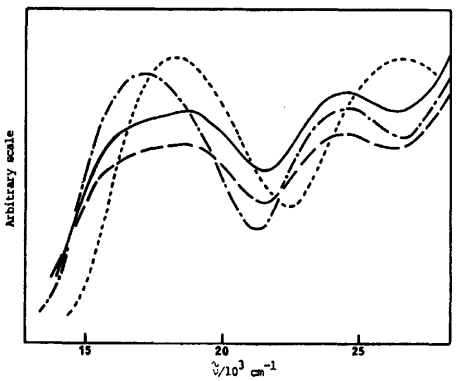

Fig. 3. The reflectance spectra of $[Co(adao)Cl_2]$.
-·-·-: α-$[Co(adao)Cl_2]$ (deep blue), ——: *β-mer(N)*-$[Co(adao)Cl_2] \cdot HCl \cdot 0.5H_2O$ (silver gray), — —: *β-mer(N)*-$[Co(adao)Cl_2] \cdot 2H_2O$ (violet gray), ------: *β-fac(N)*-$[Co(adao)Cl_2]$ (violet blue).[a]
a) in HCl solution.

$[Co(adao)(NO_2)_2]$ could be obtained by air oxidation of the suspension of $CoCl_2 \cdot 6H_2O$, $NaNO_2$, and Hadao. However, the present author found that the *β-mer(N)*-dinitro isomer prepared according to the Collman's method *(1)* was different from the *β-mer(N)*-dinitro isomer which was prepared by the present author's method *(7)*, from the differences of their absorption spectra as well as their solubilities in water. It was also found that the reaction of the author's *β-mer(N)*-dinitro isomer and $HClO_4$ gave *β-mer(N)*-$[Co(adao)(NO_2)(H_2O)]ClO_4$ with a higher yield than that of the Collman's *β-mer(N)*-dinitro isomer and $HClO_4$. These facts indicate that the Collman's *β-mer(N)*-dinitro isomer contains another complex than *β-mer(N)*-$[Co(adao)(NO_2)_2]$. On the other hand, the author's method, in which the reaction of *β-mer(N)*-$[Co(adao)(Cl)(H_2O)]ClO_4$ and $NaNO_2$ was used, gave two kinds of *β-mer(N)*-$[Co(adao)(NO_2)_2]$ in a pure state *(7-a, b)*. α-, and *β-fac(N)*-$[Co(adao)(NO_2)_2]$ have not been isolated so far. For the isolation of these dinitro isomers, each reaction of α-$[Co(adao)(H_2O)_2]^{2+}$ or *β-fac(N)*-$[Co(adao)(Cl)(H_2O)]^+$ with sodium nitrite was attempted. Although the reaction of former complex afforded α-$[Co(adao)(NO_2)_2]$*(6)*, the latter complex gave *β-fac(N)*-$[Co(adao)(Cl)(NO_2)]$ (this will be described elsewhere).

For the α-diaqua isomer, it was recognized that the aquation of α-$[Co(adao)Cl_2]$ with silver perchlorate in acidic solution gave the desired species. However, because of contamination with other salts such as silver chloride, it was difficult to isolate the α-diaqua isomer in a pure state. Hence, the preparation route using the α-dinitro isomer and $HClO_4$ was adopted for the isolation of α-$[Co(adao)(H_2O)_2](ClO_4)_2$ *(8)*.

The Structures of [Co(adao)Cl$_2$] Isomers. As may be seen in Fig. 2, four kinds of isomers of $[Co(adao)Cl_2]$, deep blue, silver gray, violet gray, and violet blue isomers, could be isolated. Among these four dichloro isomers, the silver gray and violet gray isomers are sparingly soluble in HCl, while the yield of violet blue isomer is very poor. Therefore, three reflectance spectra of the deep blue, silver gray, and violet gray isomers are shown in Fig. 3, together with the absorption

Table 1. Electronic spectral data of $[Co(adao)X_2]$

Complex	Color	I				II or SP.[a]	
		Ia		Ib			
		$\tilde{\nu}_{max}$ / cm^{-1}	ε / mol^{-1} dm^3 cm^{-1}	$\tilde{\nu}_{max}$ / cm^{-1}	ε / mol^{-1} dm^3 cm^{-1}	$\tilde{\nu}_{max}$ / cm^{-1}	ε / mol^{-1} dm^3 cm^{-1}
α-$[Co(adao)Cl_2]$[b]	Deep blue		17240			24670	
β-mer(N)-$[Co(adao)Cl_2] \cdot HCl$[b]	Silver gray	≈16100		18670		24500	
β-mer(N)-$[Co(adao)Cl_2] \cdot 2H_2O$[b]	Violet gray	≈16100		18670		24500	
β-fac(N)-$[Co(adao)Cl_2]$	Violet blue		18150	(194)		26230	(172)
α-$[Co(adao)(H_2O)_2](ClO_4)_2$	Pink red		19450	(119)		27380	(98)
β-mer(N)-$[Co(adao)(H_2O)_2](ClO_4)_2$	Red		20340	(117)		27210	(112)
α-$[Co(adao)(NO_2)_2]$	Orange		21820	(184)		30520	(4370)
β-mer(N)$[Co(adao)(NO_2)_2]$	Orange yellow		22250	(255)		30860	(3800)
β-mer(N)$[Co(adao)(NO_2)_2]$	Yellow		22370	(260)		31000	(3200)

a) Specific band due to the nitro ligand. b) Data of the reflectance spectra.

spectrum in solution for the violet blue isomer. Their electronic spectral data are summarized in Table 1. From Fig. 3, it is found that the first bands of silver gray and violet gray isomers show more pronounced splitting ($\approx$16100, 18670 cm^{-1}) than that of the deep blue one (17240 cm^{-1}). Furthermore, it is found that the deep blue and violet blue isomers show symmetrical first absorption bands, although the first band of the violet blue isomer is observed at a higher wave number (18150 cm^{-1}) than that of the deep blue one (17480 cm^{-1}). Also in their second absorption bands, the band of violet blue isomer is located at a higher wave number (26230 cm^{-1}) than that of the deep blue one (25190 cm^{-1}).

In IR spectral measurements, all dichloro isomers show a strong band at around 1650 cm^{-1}. These spectral results suggest that their adao's carboxyl groups coordinate to the central cobalt.[5,6] The IR spectral patterns assignable to the N–H stretching in the region of 3400—3100 cm^{-1} are not the same; these differences are proof for that the four dichloro isomers are different. It is further recognized that the violet blue isomer, which places the second absorption band at a higher wave number region, exhibits no peak due to the aqua ligand in any wave number region higher than 3400 cm^{-1}. This observation indicates that the violet blue isomer in the solid state is not an aquachloro complex.

Study of the ligating atoms of $[Co(adao)Cl_2]$ shows that the dichloro complex belongs to the complex of $[CoN_3OCl_2]$ type. In the case of *trans(Cl)*-$[CoCl_2(NH_3)_3(H_2O)]Cl$,[7,8] its first band splits into two components (15870, 19470 cm^{-1}).[9] When this splitting (3600 cm^{-1}) is compared with that of the silver gray $[Co(adao)Cl_2]$ (2570 cm^{-1}), the former is larger than the latter. Therefore, it is found that the silver gray isomer is not the *trans* one.

It was reported that the difference of the first d-d band splitting pattern in the Co(III) complexes mainly depends upon the symmetry of the complex.[10,11] Then, Yamatera proposed the so-called "Yamatera's rule," which predicts the d-d bands splitting pattern in the Co(III) complex.[12] It is possible to calculate the positions of the first band splitting components in the respective isomers of $[Co(adao)Cl_2]$ according to the Yamatera's rule.[12] Their predicted positions are calculated by using the following three shift parameters: $\delta(N) = +330\ cm^{-1}$ (estimated from $[Co(en)_3]^{3+}$),[13] $\delta(O) = -3800\ cm^{-1}$ (estimated from *fac*-$[Co(gly)_3]^{3+}$ and $[Co(en)_3]^{3+}$),[13] and $\delta(Cl) = -10070\ cm^{-1}$ (estimated from *trans(Cl)*-$[CoCl_2(en)_2]^+$).[14] This estimation indicates that the difference between the highest and the lowest wave number components increases in the order of $\alpha \simeq \beta\text{-}fac(N) < \beta\text{-}mer(N) < trans$.

From the comparison of this estimation and the observed absorption bands, it is found that the silver gray and violet gray isomers take the β-*mer*(*N*) coordination mode, and the deep blue and violet blue isomers, the α or β-*fac*(*N*) one. The reflectance spectral resemblance and IR spectral difference suggest that two kinds of β-*mer*(*N*)-dichloro isomers with the different *s*-N configurations were isolated. It is very difficult to decide their *s*-N configurations. However, Buckingham *et al.*[15,16] obtained two diastereoisomers of β_1-$[Co(gly)(trien)]I_2$[17] with the different *s*-N(trien) configurations. It was also found that A-β_1-$(S_N{}^aS_N{}^\delta)$-$[Co(gly)(trien)]I_2$[18] is more stable than A-β_1-$(S_N{}^aR_N{}^\delta)$-$[Co(gly)(trien)]I_2$, on the basis of their isomerization experiments and strain energy calculations. Also in β_2-$[Co(gly)(trien)]Cl_2$,[16,17] it was found that A-β_2-$(S_N{}^aS_N{}^\delta)$ isomer is more stable than the A-β_2-$(S_N{}^aR_N{}^\delta)$ one, and the former's yield is higher than the latter's. When these facts are considered, it is reasonable to assume that the *s*-N(adao) configurations of silver gray isomer with the higher yield are $(R_{N_1}{}^aS_{N_2}{}^\delta,\ S_{N_1}{}^aR_{N_2}{}^\delta)$[19] and those of violet gray with the lower yield are $(R_{N_1}{}^aR_{N_2}{}^\delta,\ S_{N_1}{}^aS_{N_2}{}^\delta)$.

It is difficult to determine the structures of the deep blue and violet blue isomers on the basis of their reflectance spectra alone. In the case of the deep blue isomer, however, the absorption spectrum of the diaqua species, which was derived from the deep blue isomer by the treatment with $AgClO_4$ in acidic solution, resembles to that of α-$[Co(adao)(H_2O)_2](ClO_4)_2$, of which structure will be decided in the later section on the basis of the proton NMR spectrum. Furthermore, the reaction of α-$[Co(adao)(H_2O)_2](ClO_4)_2$ and HCl gave mainly the deep blue isomer. Therefore, the deep blue isomer seems to take the α structure. For the violet blue isomer, decisive data for the determination of its structure were not obtained. However, because the violet blue isomer was obtained from β-*fac*(*N*)-$[Co(adao)(Cl)(H_2O)]ClO_4$ by the treatment with HCl, and the deep blue isomer takes the α structure, the violet blue isomer is assigned to the β-*fac*(*N*) structure, at present.

The Structures of $[Co(adao)(NO_2)_2]$ *Isomers.* As is shown in Fig. 2, three isomers of $[Co(adao)(NO_2)_2]$, orange, orange yellow, and yellow isomers, were isolated. The orange isomer was derived from α-$[Co(adao)Cl_2]$ by the treatment with $NaNO_2$, and the orange yellow and yellow isomers were derived from β-*mer*(*N*)-$[Co(adao)(Cl)(H_2O)]ClO_4$. Differences in solubilities were observed among the three isomers, that is, at about 20 °C, 4230 cm^3 of H_2O was required for the dissolution

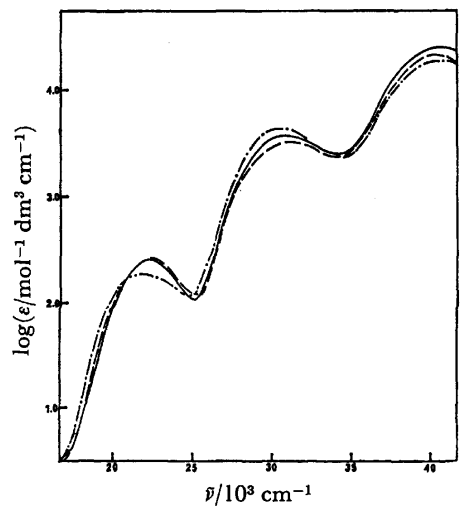

Fig. 4. The absorption spectra of $[Co(adao)(NO_2)_2]$. -·-·-: α-$[Co(adao)(NO_2)_2]$ (orange), ——: β-*mer*(*N*)-$[Co(adao)(NO_2)_2]$ (orange yellow), – – –: β-*mer*(*N*)-$[Co(adao)(NO_2)_2]$ (yellow).

of one gram orange isomer, 2500 cm^3 for the orange yellow, and 794 cm^3 for the yellow.

As is seen in Fig. 4, and Table 1, the first absorption band of orange yellow isomer is almost identical to that of the yellow one. On the other hand, the first band of orange isomer is broader than those of the other two isomers. It has been reported that the so-called nitro specific band of *trans* dinitrocobalt(III) complex is located at a lower wave number region (28570—29850 cm^{-1}) than that of the corresponding *cis* one.[10,14,20-26] Judging from the fact that the maxima of the nitro specific bands of three $[Co(adao)(NO_2)_2]$ are located at similar wave numbers (30520 cm^{-1} for the orange isomer, 30860 cm^{-1} for the orange yellow, and 31000 cm^{-1} for the yellow), the isomers are *cis*.

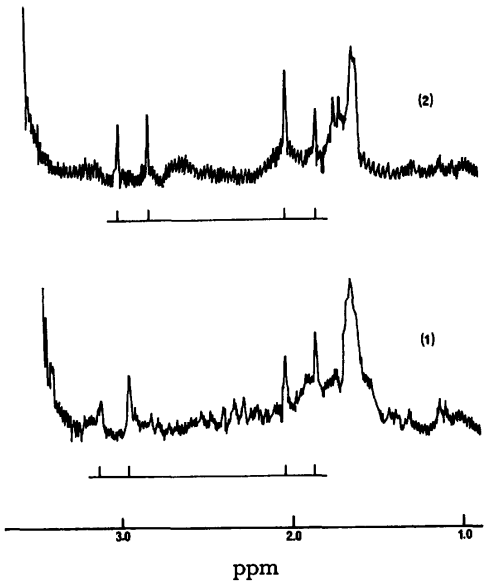

Fig. 5. The proton NMR spectra of $[Co(adao)(NO_2)_2]$. (1): *β-mer(N)*-$[Co(adao)(NO_2)_2]$ (orange yellow), (2): *β-mer(N)*-$[Co(adao)(NO_2)_2]$ (yellow).

Although the proton NMR spectrum of orange isomer could not be measured because of its low solubility in D_2O, the proton NMR spectra of orange yellow and yellow isomers were obtained, as is shown in Fig. 5. The former's NMR spectrum shows one AB quartet in the range of 1.87 to 3.13 ppm, and the latter's one, in the range of 1.85 to 3.01 ppm. As can be inferred from the coordination modes of adao in Fig. 1-a, these four coordination modes may be classified into two groups from the standpoint of the disposition of adao glycinate ring.[27] One group is composed of the isomers with an apical glycinate ring (α and *β-mer(N)*), and another, those with an equatorial ring (*β-fac(N)* and *trans*). Therefore, the proton NMR spectra of the former should be different from those of the latter at the resonances of the glycinate ring protons.

It has been reported that a considerable difference exists between the proton NMR spectra for the isomers of [Co(edda)(AA)](AA=$(NH_3)_2$, en, ox, and mal),[28-31] that is, a AB quartet appears for the apical ring (R-ring)[32] protons and an apparent singlet for the equatorial ring (G-ring)[32] protons. It has also been observed in the proton NMR spectra of edda- and ed3a-Co(III) complexes that the value of $\delta_{AB}(=\delta_A-\delta_B)$[33] for the apical ring protons is in the range of 0.7 to 1.0 ppm, while that for the equatorial ring protons is in the range of 0.0 to 0.4 ppm.[29] The proton NMR spectra of two dinitro isomers (Fig. 5) show the AB quartet pattern, and their values of δ_{AB} are 1.09 ppm for the orange yellow isomer, and 0.96 ppm for the yellow one. Therefore, the orange yellow and yellow isomers take the α or *β-mer(N)* structure. Furthermore, it was found that the reaction of orange isomer and $HClO_4$ gave α-$[Co(adao)(H_2O)_2](ClO_4)_2$, as was described in Fig. 2. From these facts, it is inferred that the orange isomer takes the α structure.

When the same shift parameters as used in the previous case of $[Co(adao)Cl_2]$ and $\delta(NO_2)=+4300$ cm^{-1} (estimated from *mer*-$[Co(NO_2)_3(NH_3)_3]$ and *cis*-$[Co(NO_2)_2(NH_3)_4]^+$),[34,35] are used for the calculation of the first band components of four possible dinitro isomers, the Yamatera' srule suggests that the predicted first band of α isomer is broader than that of *β-mer(N)*. Therefore, it is reasonable to assign the orange yellow and yellow isomers to the *β-mer(N)* structure, and the orange isomer, to the α one.

Consequently, it is certain that two kinds of *β-mer(N)* isomers were isolated also in $[Co(adao)(NO_2)_2]$. Furthermore, the difference of these *β-mer(N)* isomers is checked by the comparison of their IR spectra, which are shown in Fig. 6. For the assignment of their *s*-N configurations, it is inferred on the basis of their yields

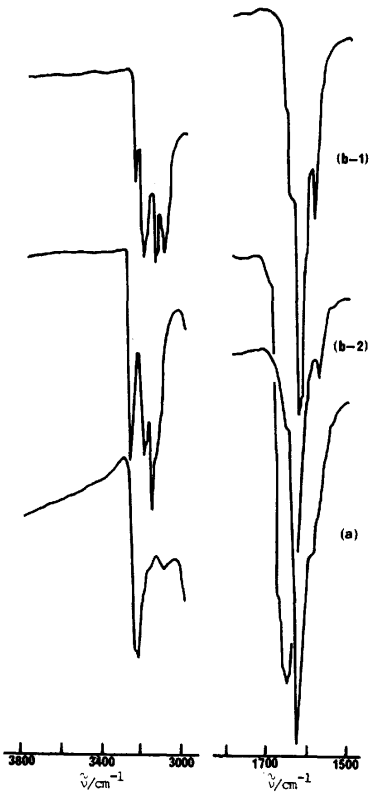

Fig. 6. The infrared spectra of $[Co(adao)(NO_2)_2]$. (a): α-$[Co(adao)(NO_2)_2]$ (orange), (b-1): *β-mer(N)*-$[Co(adao)(NO_2)_2]$ (orange yellow), (b-2): *β-mer(N)*-$[Co(adao)(NO_2)_2]$ (yellow).

that the orange yellow isomers with a higher yield adopts the ($R_{N_1}^{a}S_{N_1}^{b}$, $S_{N_1}^{a}R_{N_1}^{b}$) configuration, and the yellow isomer with a lower yield, the ($R_{N_1}^{a}R_{N_1}^{b}$, $S_{N_1}^{a}S_{N_1}^{b}$) one.

The Structures of [Co(adao)(H_2O)$_2$](ClO_4)$_2$ Isomers. Four possible geometrical isomers of the diaqua complex belonging to a type of [CoN_3O_3] may be classified into two groups, that is, the α and *β-fac(N)* isomers belong to a *fac*-[CoN_3O_3] type, and the *β-mer(N)* and *trans* isomers, to a *mer*-one. It is well known that the first band of the *mer*-type is broader than that of the *fac*-one.[36-39] In Fig. 7, the absorption spectra of the pink red and red isomers are shown, and in Table 1, their numerical data are summarized.

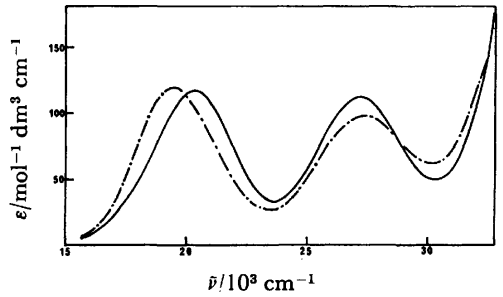

Fig. 7. The absorption spectra of [Co(adao)(H_2O)$_2$]-(ClO_4)$_2$.
-·-·-: α-[Co(adao)(H_2O)$_2$](ClO_4)$_2$ (pink red), ——: *β-mer(N)*-[Co(adao)(H_2O)$_2$](ClO_4)$_2$ (red).

As is seen in Fig. 7, the half width of first absorption band for the pink red isomer is almost identical to that for the red one. On account of this, their structures can not be distinguished by the application of the empirical rule for the first band width in a [CoN_3O_3] complex.[36-39] However, the first absorption maximum of the red isomer is located at a higher wave number than that of the pink red one. On the contrary, the second band maximum of the former is located at a lower wave number than that of the latter.

It has been found that the first band of *mer*-[$Co(NH_3)_3(H_2O)_3$]$^{3+}$ is broader than that of the *fac*-one, and that the apparent first band maximum of the *mer* isomer is located at a higher wave number than that of the *fac* one.[40,41] Furthermore, it has been reported that *mer*-[Co(dien)(H_2O)$_3$]$^{3+}$ places the first band maximum at a higher wave number than that of the corresponding *fac* one, although these isomers have not been obtained as crystalline forms.[42,43] On the basis of the different first band positions, it is found that the red isomer adopts the *β-mer(N)* or the *trans* structure, and the pink red one, the α or the *β-fac(N)* structure.

The proton NMR spectrum shows one AB quartet pattern in the range of 2.16 to 3.20 ppm for the red isomer, and in the range of 2.15 to 3.13 ppm for the pink red one. These observations suggest that the coordination mode of adao in each isolated isomer is either the α or the *β-mer(N)* one. Taking into consideration of their preparative routes (Fig. 2), it can be concluded that the red isomer is the *β-mer(N)* one, and the pink red, the α.

Summary. In the three kinds of [Co(adao)X_2] type complexes (X=Cl^-, NO_2^-, and H_2O), α and *β-mer(N)* isomers were isolated. Consequently, the previously unknown α coordination mode could be established also in [Co(adao)X_2] type complex. As to the *cis(Cl)*-[CoN_3OCl_2] type complex, the *β-fac(N)*-[Co(adao)Cl_2] besides the α- and *β-mer(N)*-[Co(adao)-Cl_2] were also detected. Furthermore, two kinds of *β-mer(N)* isomers could be isolated in the cases of [Co(adao)Cl_2] and [Co(adao)(NO_2)$_2$]. From the comparison of the yields in a pair of *β-mer(N)* isomers respectively, it is inferred that the silver gray dichloro and the orange yellow dinitro complexes, which were isolated with the higher yields, adopt the ($R_{N_1}^{a}S_{N_1}^{b}$, $S_{N_1}^{a}R_{N_1}^{b}$) configurations, while the violet gray dichloro and yellow dinitro complexes, which were isolated with the lower yields, adopt the ($R_{N_1}^{a}R_{N_1}^{b}$, $S_{N_1}^{a}S_{N_1}^{b}$) configurations.

The author is sincerely grateful to Professor Yoichi Shimura of Osaka University for the guidance of this work. He also thanks Professor Kashiro Kuroda of Ehime University for his continuing interest and encouragement during the work.

References

1) Part II of this series: K. Watanabe, *Bull. Chem. Soc. Jpn.*, **49**, 3068 (1976).
2) The following abbreviations are used for the ligands: adao, 8-amino-3,6-diazaoctanate; edda, ethylenediamine-*N*,*N'*-diacetate; ed3a, ethylenediamine-*N*, *N*, *N'*-triacetate; trien, triethylenetetramine; dien, diethylenetriamine; en, ethylenediamine; gly, glycinate; ox, oxalate; mal, malonate.
3) P. W. Schneider and J. P. Collman, *Inorg. Chem.*, **7**, 2010 (1968).
4) R. S. Cahn, C. K. Ingold, and V. Prelog, *Angew. Chem.*, **5**, 385 (1966).
5) D. H. Busch and J. C. Bailar, *J. Am. Chem. Soc.*, **75**, 4574 (1953).
6) L. J. Bellamy, "The Infrared Spectra of Complex Molecules," Mathuen, London (1964), pp. 161—177.
7) A. Werner, *Z. Anorg. Chem.*, **8**, 161 (1895); **15**, 146, 153 (1897); S. M. Jörgenesen, *ibid.*, **14**, 44, 419 (1897).
8) O. Stelling, *Ber.*, **60**, 652 (1927); O. Stelling, Z. *Phys.*, **50**, 520 (1928).
9) N. Matsuoka and Y. Shimura, provided the reflectance spectral datum.
10) M. Linhard and M. Weigel, *Z. Anorg. Chem.*, **264**, 321 (1951); **271**, 101 (1952).
11) Y. Shimura, *Bull. Chem. Soc. Jpn.*, **25**, 49 (1952).
12) H. Yamatera, *Bull. Chem. Soc. Jpn.*, **31**, 95 (1958).
13) J. Fujita and Y. Shimura, *Bull. Chem. Soc. Jpn.*, **36**, 1281 (1963).
14) Y. Shimura and R. Tsuchida, *Bull. Chem. Soc. Jpn.*, **28**, 572 (1955).
15) D. A. Buckingham, P. J. Greswell, R. J. Dellaca, M. Dwyer, G. J. Gainsford, L. G. Marzilli, I. E. Maxwell, W. T. Robinson, A. M. Sargeson, and K. R. Turnbull, *J. Am. Chem. Soc.*, **96**, 1713 (1974).
16) D. A. Buckingham, M. Dwyer, G. J. Gainsford, V. Janson, L. G. Marzilli, W. T. Robinson, A. M. Sargeson, and K. R. Turnbull, *Inorg. Chem.*, **14**, 1739 (1975).
17) The prefix β_1 refers to the isomer with the nitrogen atom of glycinate ligand *trans* to the primary amine of trien.

The prefix β_2 refers to the isomer with the nitrogen atom of glycinate ligand *trans* to the *s*-N^p(trien).[18]

18) The two kinds of *s*-N(trien) dispositions are discriminated by using the superscripts of a (angular) and p (planar): N^a or N^p.

19) The two kinds of *s*-N(adao) are discriminated by numbering as follows: O–N_1–N_2–N. Furthermore, the two *s*-N(adao) dispositions, angular and planar, are represented with the same notation as used for the *s*-N(trien) ones.[18]

20) F. Basolo, *J. Am. Chem. Soc.*, **10**, 2634 (1948).
21) Y. Shibata, *Tokyo Kagaku Kaishi*, **36**, 1243 (1915).
22) R. Tsuchida, *Bull. Chem. Soc. Jpn.*, **11**, 721 (1936).
23) F. Basolo, *J. Am. Chem. Soc.*, **72**, 4393 (1950).
24) Y. Shimura, *J. Am. Chem. Soc.*, **73**, 5079 (1951).
25) K. Yamazaki, J. Hidaka, and Y. Shimura, *Bull. Chem. Soc. Jpn.*, **49**, 3060 (1976).
26) V. M. Miskowski and H. B. Gray, *Inorg. Chem.*, **14**, 401 (1975).

27) The adao-Co(III) moiety consists of three kinds of five membered chelate rings. These are designated as the glycinate (or O terminal), central, and NH_2 terminal rings. When the glycinate and the central rings are disposed in the same plane, the glycinate ring is named as the equatorial glycinate ring. When their rings are disposed in the different plane, the glycinate ring is named as the apical glycinate ring.

28) J. I. Legg and D. W. Cook, *Inorg. Chem.*, **4**, 1576 (1965).
29) P. F. Coleman, J. I. Legg, and J. Steele, *Inorg. Chem.*, **9**, 937 (1970).
30) K. Kuroda, *Chem. Lett.*, **1972**, 197.
31) K. Kuroda, *Chem. Lett.*, **1972**, 1153.

32) These notations were described by Coleman *et al.* in the Ref. 29.

33) The value of δ_{AB} is obtained by the subtration of the chemical shift (δ_B) of H_B proton from that (δ_A) of H_A one.

34) M. Linhard and M. Weigel, *Z. Anorg. Chem.*, **267**, 113 (1951).
35) Y. Yamamoto, S. Kaizaki, and Y. Shimura, *Bull. Chem. Soc. Jpn.*, **49**, 3540 (1976).
36) Y. Shimura and R. Tsuchida, *Bull. Chem. Soc. Jpn.*, **29**, 311 (1956).
37) N. Matsuoka, Y. Shimura, and R. Tsuchida, *Nippon Kagaku Zasshi*, **82**, 1637 (1961).
38) N. Matsuoka, J. Hidaka, and Y. Shimura, *Bull. Chem. Soc. Jpn.*, **39**, 1257 (1966).
39) K. Kuroda, Y. Mori, H. Matsunaga, K. Kunigita, and K. Watanabe, *Bull. Chem. Soc. Jpn.*, **48**, 234 (1975).
40) M. Linhard and H. Siebert, *Z. Anorg. Allg. Chem.*, **364**, 24 (1969).
41) H. Siebert, *Z. Anorg. Allg. Chem.*, **389**, 22 (1972).
42) P. H. Crayton and J. A. Mattern, *J. Inorg. Nucl. Chem.*, **13**, 248 (1960).
43) S. H. Caldwell and D. A. House, *J. Inorg. Nucl. Chem.*, **31**, 811 (1969).

Fluorometric Determination of Aluminium(III) and Cadmium(II) by Solvent Extraction of the Ternary Complex Composed of Metal Ion, 8-Hydroxy-5-quinolinesulfonic Acid, and Methyltrioctylammonium Ion

Yukihiro KONDOH, Masamitsu KATAOKA, and Tomihito KAMBARA*

Department of Chemistry, Faculty of Science, Hokkaido University, Sapporo 060

(Received June 3, 1981)

A fluorometric micro determination of aluminium(III) and cadmium(II) using the formation of metal–8-hydroxy-5-quinolinesulfonic acid–capriquat (methyltrioctylammonium) ternary complex is described. These complexes are easily extracted into chloroform phase and the extract emits a strong fluorescence. Spectra of aluminium(III) and cadmium(II) ternary complexes have the excitation maximum at 396 nm and 400 nm, and emission maximum at 501 nm and 524 nm, respectively. Fluorescence intensity of the aluminium(III) and cadmium(II) ternary complexes extracted into chloroform showed the constant and maximum values in the pH range of aqueous phase from 5.3 to 8.5 and 8.1 to 8.5, respectively. The calibration curves for aluminium(III) and cadmium(II) show good proportionality in the concentration range from 0.5 to 5.0 and 1.0 to 50.0 μg, respectively. The relative standard deviation observed with four measurements was found to be 1.8% for 0.5 μg of aluminium(III) and 1.1% for 10.0 μg of cadmium(II). The effect of diverse ions is studied and a 25-fold amount of Cu(II), Ni(II), Fe(II), Fe(III) in weight gave errors, however, the interferences were easily eliminated by the addition of appropriate masking agent. In the determination of cadmium(II), an equal amount of Co(II), Ni(II), Mn(II), Fe(III) and twice amount of Al(III) gave negative errors, however, the interference of Fe(III) and Al(III) were also eliminated as above.

It has been recognized that the 8-hydroxy-5-quinolinesulfonic acid (abbreviated as H_2qs), which is well known as a derivative of oxine, forms several water soluble complexes with many metal ions, which emit strong fluorescence around 520 nm. Cadmium(II)[1] and magnesium(II),[2] were determined fluorometrically in aqueous phase by using H_2qs as the chelating agent. Kina *et al.*[3] reported that the fluorescence intensity of some metal complex is enhanced in the presence of surfactant.

We reported the photometric determination of iron(III),[4] cobalt(II),[5] and zinc(II)[6] employing the ion-pair extraction of metal–H_2qs chelate anion with Zephiramine (benzyldimethyltetradecylammonium chloride) cation. Cadmium(II) was also determined spectrophotometrically with H_2qs after separation as an ion-pair of tetraiodocadmate(II) anion with Capriquat (methyltrioctylammonium chloride, abbreviated as Cq^+-Cl^-) cation. We also reported the fluorometric determination of zinc(II) by using the formation of zinc(II)–H_2qs–Cq ternary complex.[8]

In the present paper, the fluorometric micro determination of aluminium(III) and cadmium(II) was described. The fluorescence intensity of the ternary complex composed of aluminium(III)–, as well as cadmium(II)–H_2qs–Cq in chloroform phase is proportional to the amount of metal ion in the aqueous phase.

Experimental

Reagents. *Standard Solution of Aluminium(III) and Cadmium(II)*: Aluminium(III) and cadmium(II) standard solution (Wako Pure Chemicals Co., for atomic absorption use, 1000 ppm) was applied and diluted with water as required.

1 mM H_2qs Solution:† The solution was prepared by dissolving 0.2252 g of H_2qs (Wako Pure Chemicals Co.) with 1 dm^3 of water.

7 mM Capriquat–Chloroform Solution: The solution was prepared by dissolving Dotite Capriquat (methyltrioctylammonium chloride, Dojindo Laboratories) in chloroform.

Buffer Solutions: Acetate, borate, and acetic acid–ammonia buffer solutions were prepared and adjusted to the appropriate pH values.

Organic solvents used in this study were all of analytical reagent grade. All the solutions were prepared with once deionized and then twice distilled water.

Apparatus. Fluorescence intensity was measured with a Shimadzu Digital Spectrofluorophotometer, Model RF-510, equipped with a Shimadzu recorder, U-125MU. Fused quartz cells, 10 mm × 10 mm × 45 mm, were used throughout the study.

Procedure. *Determination of Aluminium(III)*: To a sample solution containing (0.1—5.0)μg of aluminium(III) are added a 7-ml portion of 1 mM H_2qs solution and a 10-ml portion of the buffer solution (pH 6.5). The mixture is diluted to 50 ml with water and shaken with 10 ml of 6 mM Capriquat–chloroform solution for 3 min and then allowed to stand for 30 min. The organic layer is transferred into a beaker containing anhydrous sodium sulfate to remove the remaining water. Then, the fluorescence intensity of the extract is measured at 396 nm (excitation) and 501 nm (emission).

Determination of Cadmium(II): To a sample solution containing (1.0—50.0) μg of cadmium are added 8 ml of 1 mM H_2qs solution and 10 ml of borate buffer solution (pH 8.3). The mixture is diluted to 50 ml with water and shaken with 10 ml of 7 mM Capriquat–chloroform solution for 3 min and then allowed to stand for 30 min. Organic layer is separated and fluorescence intensity is measured at 400 nm (excitation) and 524 nm (emission).

Results and Discussion

Fluorescence Spectra. The fluorescence spectra of the organic extract obtained by the above procedure are given in Fig. 1. The aluminium(III)–H_2qs–Capriquat ternary complex in chloroform exhibited the excitation maximum at 396 nm and the fluorescence emission maximum at 501 nm, whereas the cadmium(II) complex showed at 400 nm and at 524 nm, respectively.

† 1 M = 1 mol dm^{-3}.

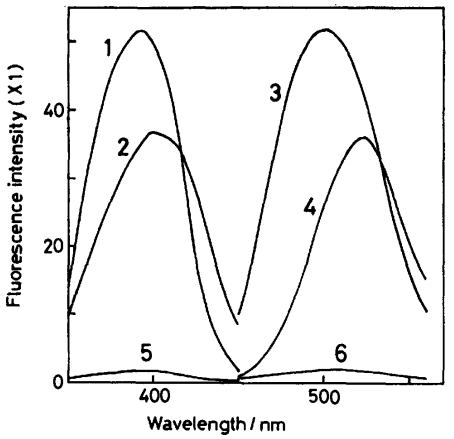

Fig. 1. Excitation and emission spectra.
Excitation spectrum of ternary complex: 1: Al(III) (λ_{Em}=501 nm), 2: Cd(II) (λ_{Em}=524 nm). Emission spectrum of ternary complex: 3: Al(III) (λ_{Ex}=396 nm), 4: Cd(II) (λ_{Ex}=400 nm), 5: excitation spectrum of reagent blank (λ_{Em}=501 nm), 6: emission spectrum of reagent blank (λ_{Ex}=524 nm).

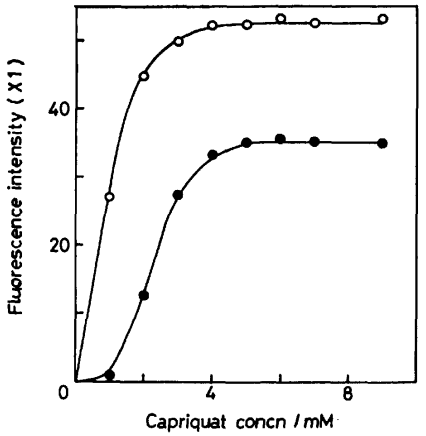

Fig. 2. Effect of Capriquat amount on the fluorescence intensity of chloroform extract.
—○—: Al(III) 5 μg/50 ml; $[H_2qs]_w$=0.2 mM; pH=7.7; λ_{Ex}=396 nm; λ_{Em}=501 nm. —●—: Cd(II) 50 μg/50 ml; $[H_2qs]_w$=0.2 mM; pH=8.3; λ_{Ex}=400 nm; λ_{Em}=524 nm.

An ion-pair of H_2qs–Capriquat was also extracted into chloroform, but showed a very weak fluorescence.

Effect of Capriquat Concentration. Effect of the Capriquat concentration on the fluorescence intensity is shown in Fig. 2. Capriquat–chloroform solutions of the various concentrations were added to the solution containing 5.0 μg of aluminium or 50.0 μg of cadmium with an excess amount of H_2qs at the optimum pH, and after extraction, the fluorescence intensity of the extract was measured. It was found that the fluorescence intensity shows a constant value for more than 4 mM of Capriquat for aluminium and 5 mM for cadmium. Thus, the concentration of Capriquat was adjusted to 6 mM for aluminium and 7 mM for cadmium.

Effect of H_2qs Amount. The effect of H_2qs concentration on the fluorescence intensity is shown in Fig. 3. The fluorescence intensity was found to be almost

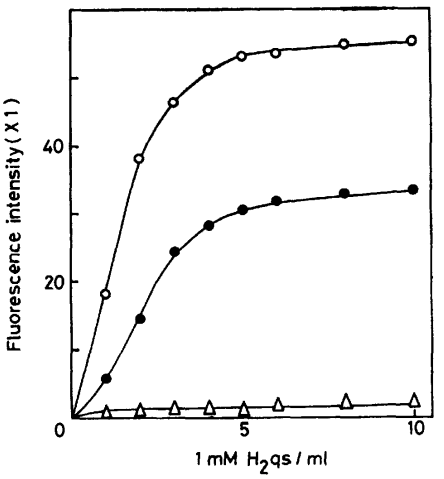

Fig. 3. Effect of H_2qs concentration on the fluorescence intensity of chloroform extract.
—○—: Al(III) 5 μg/50 ml; $[CqCl]_0$=6 mM; pH=7.7. —●—: Cd(II) 50 μg/50 ml; $[CqCl]_0$=8 mM; pH=8.3. —△—: Reagent blank.

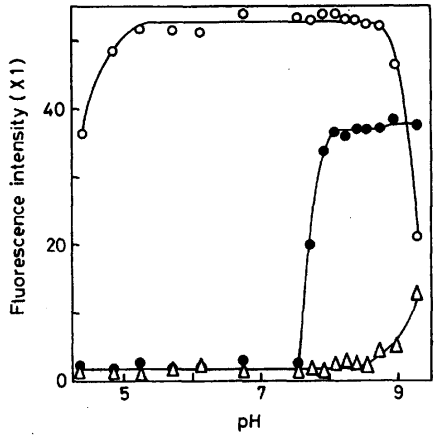

Fig. 4. Effect of pH on the fluorescence intensity o chloroform extract.
—○—: Al(III) 5 μg/50 ml; $[H_2qs]_w$=0.16 mM; $[CqCl]_0$=7 mM. —●—: Cd(II) 50 μg/50 ml; $[H_2qs]_w$=0.16 mM; $[CqCl]_0$=7 mM. —△—: Reagent blank.

Table 1. Selection of organic solvent

Organic solvent	Fluorescence intensity of ternary complex				Separation speed
	Al(III)[a]	Blank	Cd(II)[b]	Blank	
Chloroform	55.4	2.0	35.4	2.2	Fast
1,2-Dichloroethane	35.1	1.2	28.3	1.5	Fast
IBMK	28.9	1.3	31.5	1.4	Slow
Benzene	28.8	3.0	33.6	3.4	Slow
Xylene	24.3	3.5	33.2	3.6	Slow

a) Al(III) taken: 5.0 μg. b) Cd(II) taken: 50.0 μg.

constant, when more than 5 ml and 6 ml of 1 mM H_2qs solution were employed for aluminium(III) and cadmium(II), respectively. Therefore, the amount of H_2qs was kept to 7 ml for aluminium and 8 ml for cadmium.

TABLE 2. EFFECT OF DIVERSE IONS

Ion	M^{n+} added as	M^{n+} added (μg)	Al^{3+} found[a] (μg)	M^{n+} added (μg)	Cd^{2+} found[b] (μg)
Al^{3+}	$AlCl_3$	—	—	20	10.0[g]
Ba^{2+}	$BaCl_2 \cdot 2H_2O$	500	1.01	1000	9.5
Bi^{3+}	$Bi(NO_3)_3 \cdot 5H_2O$	5	0.99	20	10.4
Ca^{2+}	$CaCl_2$	500	0.97	1000	10.2
Cd^{2+}	$CdCl_2$	100	0.97	—	—
Co^{2+}	$CoSO_4 \cdot (NH_4)_2SO_4 \cdot 6H_2O$	5	0.90	10	8.6
Cr^{3+}	$CrCl_3 \cdot 6H_2O$	10	1.01	250	10.3
Cu^{2+}	$CuSO_4 \cdot 5H_2O$	25	1.00[c]	10	9.5
Fe^{2+}	$FeSO_4 \cdot (NH_4)_2SO_4 \cdot 6H_2O$	25	0.96[d]	20	9.8[d]
Fe^{3+}	$FeCl_3$	25	0.98[e]	10	7.6
Hg^{2+}	$HgSO_4$	100	1.02	100	10.0
Mg^{2+}	$MgSO_4 \cdot 7H_2O$	500	1.05	250	10.2
Mn^{2+}	$MnSO_4 \cdot 4H_2O$	500	1.05	10	8.8
Ni^{2+}	$NiSO_4 \cdot 7H_2O$	25	0.95[d]	10	8.1
Pb^{2+}	$Pb(NO_3)_2$	500	1.05	50	9.7
Sr^{2+}	$Sr(NO_3)_2$	500	0.98	1000	9.9
Zn^{2+}	$ZnSO_4 \cdot 7H_2O$	5	1.02[f]	10	25.7

a) Al(III) taken: 1.00 μg. b) Cd(II) taken: 10.0 μg. c) With thiourea. d) With ascorbic acid and phen. f) pH 5.3. g) With tiron.

Effect of pH. Effect of the pH of aqueous layer was examined. As shown in Fig. 4, the fluorescence intensity is constant over the pH range from 5.3 to 8.5 for aluminium(III) and from 8.1 to 8.5 for cadmium(II), while the observed blank value is very low. Thus, the pH was kept to 6.5 by 0.2 M acetic acid and 0.2 M ammonia for aluminium and to 8.3 by borate buffer for cadmium.

Organic Solvents. The effect of the various organic solvents on the fluorescence intensity was studied and the results were shown in Table 1. Benzene and xylene gave high blank value. Chloroform, 1,2-dichloroethane, and IBMK (isobutyl methyl ketone) gave low blank value, but the separation speed of IBMK was slow. Chloroform is adopted as the best organic slovent, because it shows the highest fluorescence intensity and the good separation was rapidly attained for both aluminium(III) and cadmium(II) complexes.

Effect of Shaking and Standing Time. A stable and constant fluorescence intensity of the extract was found with a shaking time longer than 1 min for both aluminium(III) and cadmium(II), so the shaking time was kept to 3 min. The optimum standing time was found to be 30 min for the both metal ions.

Calibration Curves. The calibration curves for aluminium(III) and cadmium(II) were obtained by the above procedures. A good proportionality between the fluorescence intensity and the concentration was observed in the concentration range from 0.1 to 2.0 μg for aluminium(III) and from 1.0 to 10.0 μg for cadmium-(II). At higher concentrations the calibration curve deviated slightly from the linearity, but the determination was feasible up to 5.0 μg for aluminium(III) and 30.0 μg for cadmium(II). The relative standard deviation observed with four measurements was found to be 1.8% for 5 μg of aluminium and 1.1% for 10.0 μg of cadmium.

Effect of Diverse Ions. The effect of sixteen cations on the determination of aluminium(III) and cadmium-(II) was studied. The results are summarized in Table 2. In the determination of 1.0 μg of aluminium(III), a 5-fold amount of cobalt(II) and 25-fold amount of copper(II), nickel(II), iron(II), and iron(III) reduced the fluorescence intensity, whereas a 5-fold amount of zinc(II) gave a positive error. However, the interferences were eliminated by the addition of thiourea for copper(II), together with 1,10-phenanthroline for nickel(II) and iron(II), and ascorbic acid with 1,10-phenanthroline for iron(III). The interference of zinc-(II) was eliminated by adjusting the pH to 5.3.

In the determination of 10.0 μg of cadmium(II), an equal amount in weight of cobalt(II), nickel(II), manganese(II), and iron(III) and a twice amount of iron(II) gave the negative errors, whereas an equal amount of zinc(II) and a twice amount of aluminium-(III) gave the positive errors. The interferences were eliminated, however, by the addition of 1,10-phenanthroline for iron(II) and tiron for aluminium(III).

References

1) D.E. Ryan, A.E. Pitts, and R.M. Cassidy, *Anal. Chim. Acta*, **34**, 491 (1966).
2) B. Klein and M. Oklander, *Clin. Chem.*, **13**, 26 (1967).
3) K. Kina, K. Tamura, and N. Ishibashi, *Bunseki Kagaku*, **23**, 1404 (1974).
4) T. Kambara, S. Matsumae, and K. Hasebe, *Bunseki Kagaku*, **19**, 462 (1970).
5) T. Kambara, and M. Sugawara, *Bull. Chem. Soc. Jpn.*, **45**, 1430 (1972).
6) K. Hasebe, H. Mori, and T. Kambara, *Nippon Kagaku Kaishi*, **12**, 2305 (1973).
7) M. Sugawara, G. Hanagata, and T. Kambara, *Bunseki Kagaku*, **27**, 683 (1978).
8) Y. Kondoh, M. Kataoka, and T. Kambara, *Bunseki Kagaku*, **30**, 109 (1981).

 © 1982 The Chemical Society of Japan Bull. Chem. Soc. Jpn., 55, 437—440 (1982)

The Vapor-phase Reaction of Aluminium Trichloride with Oxygen in the Presence of Steam and Properties of the Aluminium Oxide Formed

Yuichi Shoji, Ryoko Matsuzaki, and Yuzo Saeki*

Research Laboratory of Resources Utilization, Tokyo Institute of Technology, 4259, Nagatsuta-cho, Midori-ku, Yokohama 227

(Received July 3, 1981)

The reaction of gaseous $AlCl_3$ with oxygen containing 2—5 vol% H_2O in the temperature range of 200 to 1000 °C, and the thermal transitions of the Al_2O_3 formed under various conditions were examined. At 200 °C, only the reaction of gaseous $AlCl_3$ with H_2O occurs, regardless of the H_2O content in oxygen. Above about 400 °C, the reactions of gaseous $AlCl_3$ with both H_2O and oxygen occur, and all the $AlCl_3$ reacts at 1000 °C. The reaction with H_2O mainly occurs below about 900 °C, and the reaction with oxygen mainly occurs at 1000 °C. Regardless of the H_2O content in oxygen, the reaction product is amorphous Al_2O_3 below 600 °C, amorphous Al_2O_3 containing poorly crystallized γ-Al_2O_3 at 800 °C, γ-Al_2O_3 containing amorphous Al_2O_3 at 900 °C, and a mixture of γ-Al_2O_3 and δ-Al_2O_3 at 1000 °C. It was also observed that the Al_2O_3 formed below 800 °C included a chloride oxide of aluminium. On heating the amorphous Al_2O_3 formed by the reaction of gaseous $AlCl_3$ with oxygen containing 2—5 vol% H_2O, the amorphous $\xrightarrow{ca.\ 700\ °C}$ χ $\xrightarrow{ca.\ 800\ °C}$ κ $\xrightarrow{ca.\ 1000\ °C}$ α transition occurs; on heating the γ-Al_2O_3 formed, the γ $\xrightarrow{ca.\ 900\ °C}$ δ $\xrightarrow{ca.\ 1000\ °C}$ θ $\xrightarrow{ca.\ 1000\ °C}$ α transition occurs.

To study the chemical process for preparing fine powders of aluminium oxide(Al_2O_3) from aluminium trichloride ($AlCl_3$) by the vapor-phase reaction, the present authors have examined the reactions of $AlCl_3$ with oxygen[1] and with steam[2] in the vapor phase, as well as the properties of the Al_2O_3 formed.

Cuer *et al.*[3] have examined the oxidation of gaseous $AlCl_3$ in a hydrogen-oxygen flame. From the particle size of the Al_2O_3 formed, they estimated that during the oxidation of gaseous $AlCl_3$ with a gaseous mixture of oxygen and steam, the reaction with oxygen was predominant at higher temperatures (>2000 K) and that the reaction with steam mainly occurred at low temperature (1700 K). No report on the vapor-phase reaction of gaseous $AlCl_3$ with oxygen in the presence of steam is presently available.

In this paper, the reaction of gaseous $AlCl_3$ with oxygen containing 2—5 vol% steam in the temperature range of 200 to 1000 °C was examined. The thermal transitions of the Al_2O_3 formed under various conditions were also examined.

Experimental

The $AlCl_3$ used was prepared by the reaction of pure aluminium (Al: 99.99%) with chlorine at 400 °C.[1]

A transparent quartz reaction tube (1000 mm length) with an inner concentric tube was used. Gaseous $AlCl_3$ was formed by heating $AlCl_3$ placed in the inner tube at 150 °C, and was carried by a stream of argon (40 cm^3/min) to the reaction zone (27 mm i.d. and 250 mm length) held at a specified temperature. In the meantime, a stream of oxygen (100 cm^3/min) containing a specified amount of steam was introduced through a separate tube into the reaction zone. The mean flow-rate of the $AlCl_3$ was approximately 3.8 cm^3 Al_2Cl_6 (g)/min. The reaction was allowed to proceed for 2 h.

The total amount of chlorine (Cl_2) and hydrogen chloride (HCl) formed during the reaction was absorbed in a known amount of 0.1 M sodium hydroxide (NaOH) solution,† and was determined by neutralization titration of the excess NaOH. The Cl_2 formed by the reaction was absorbed in a potassium iodide solution and was determined by iodometry. The amount of HCl formed was determined as the difference between the total amount of Cl_2 and HCl and the amount of Cl_2.

The unreacted $AlCl_3$, which was deposited outside the reaction zone together with the reaction product, was separated by heating the mixture in an argon stream at 250 °C. The $AlCl_3$ adsorbed on Al_2O_3 formed was separated by washing the Al_2O_3 with ethanol at the boiling point with stirring.[1]

X-Ray analysis of the solid product was performed with an X-ray powder diffractometer equipped with a proportional counter, using Ni filtered Cu radiation.

Throughout this work, $AlCl_3$ and the reaction products were handled in an argon atmosphere or *in vacuo* to prevent any contamination with moisture in the air.

Results and Discussion

Reaction of Gaseous Aluminium Trichloride with Oxygen

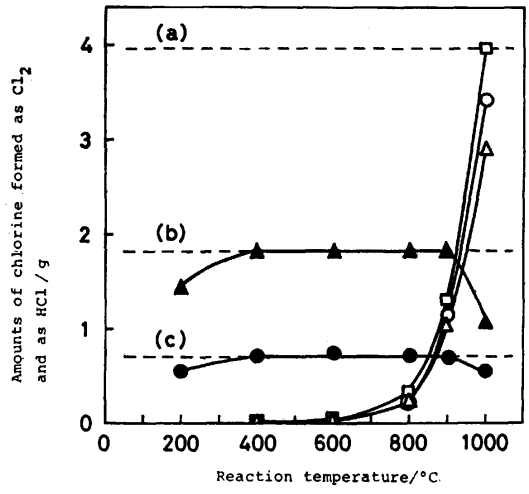

Fig. 1. Amounts of chlorine formed as Cl_2 and as HCl by the reaction of gaseous $AlCl_3$ with oxygen containing H_2O at various temperatures.
O_2+2 vol% H_2O: —○— as Cl_2, —●— as HCl. O_2+5 vol% H_2O: —△— as Cl_2, —▲— as HCl. O_2: —□— as Cl_2.

† 1 M=1 mol dm^{-3}.

in the Presence of Steam. Amounts of Cl_2 and HCl formed by the reaction of gaseous $AlCl_3$ with oxygen containing 2 or 5 vol% steam (H_2O) at various temperatures were examined. A reaction temperature above 200 °C was employed, because gaseous $AlCl_3$ was generated by heating $AlCl_3$ at 150 °C. The amounts of chlorine formed as Cl_2 and as HCl at various temperatures are shown in Fig. 1. For comparison, the amounts of Cl_2 formed by the reaction of gaseous $AlCl_3$ with oxygen at various temperatures, which have been reported in the previous paper,[1] are also shown in Fig. 1. The broken line (a) in Fig. 1 shows the calculated value of the amount of chlorine formed as Cl_2 or as HCl, based on the assumption that all the $AlCl_3$ introduced reacts with oxygen or H_2O to form Cl_2 or HCl. The broken lines (b) and (c) show the calculated values of chlorine formed as HCl, based on the assumption that all the H_2O which is contained in a stream of oxygen containing 5 or 2 vol% H_2O reacts with gaseous $AlCl_3$ to form HCl.

These results indicated that, at 200 °C, only the reaction of gaseous $AlCl_3$ with H_2O occurred, regardless of the H_2O content in oxygen. At 400—900 °C, all the H_2O introduced reacted with $AlCl_3$ and the reaction of gaseous $AlCl_3$ with oxygen also occurred. The amount of Cl_2 formed by the reaction with oxygen increased markedly with the increase in the reaction temperature above 800 °C. At 1000 °C, total amounts of chlorine formed as Cl_2 and as HCl agreed with the value shown by the broken line (a), regardless of the H_2O content in oxygen. This fact indicated that the percentage of the reacted $AlCl_3$ reached 100 at 1000 °C. It was also found that a part of the H_2O introduced did not react with gaseous $AlCl_3$ at 1000 °C. This result indicates that, during the vapor-phase reaction of $AlCl_3$ with oxygen in the presence of H_2O, the reaction of gaseous $AlCl_3$ with H_2O mainly occurs below about 900 °C and that the reaction with oxygen mainly occurs at 1000 °C.

The products formed by the reaction of gaseous $AlCl_3$ with oxygen containing 2 and 5 vol% H_2O at temperatures above 400 °C were examined by similar experiments[1,2] through X-ray analysis, thermogravimetry, and differential thermal analysis; these were employed in the examination of the reaction products of gaseous $AlCl_3$ with oxygen and with H_2O.

The results for the products formed by the reaction with oxygen containing 5 vol% H_2O show that the reaction product is amorphous Al_2O_3 at 400—600 °C, amorphous Al_2O_3 containing poorly crystallized γ-Al_2O_3 at 800 °C, γ-Al_2O_3 containing amorphous Al_2O_3 at 900 °C, and a mixture of γ-Al_2O_3 and δ-Al_2O_3 at 1000 °C. It was also observed that the Al_2O_3 formed below 800 °C included the chloride oxide of aluminium, which was found to be included in the Al_2O_3 formed by the reaction between gaseous $AlCl_3$ and H_2O below 900 °C.[2] On heating the chloride oxide, it decomposes to γ-Al_2O_3 with the evolution of gaseous $AlCl_3$ in the vicinity of 830 °C.[2] The weight losses due to the decomposition of the chloride oxide contained in the Al_2O_3 formed at 400, 600, and 800 °C were 8, 3, and 2 %, respectively.

The modification of the Al_2O_3 formed by the reaction of gaseous $AlCl_3$ with oxygen containing 2 vol% H_2O at each temperature was found to be the same as that formed by the reaction with oxygen containing 5 vol% H_2O, which was described above. Also, the Al_2O_3 formed below 800 °C included the chloride oxide mentioned above.

The modification of the Al_2O_3 formed by the reaction with oxygen containing 2—5 vol% H_2O at each temperature was found to be the same as that of the Al_2O_3 formed by the reaction with H_2O,[2] except that the Al_2O_3 formed by the reaction with H_2O at 1000 °C was γ-Al_2O_3. The Al_2O_3 formed by the reaction of gaseous $AlCl_3$ with oxygen is amorphous Al_2O_3 at 800 °C, γ-Al_2O_3 containing amorphous Al_2O_3 at 900 °C, and γ-Al_2O_3 at 1000 °C.[1] While, the Al_2O_3 formed by the reaction with oxygen containing 2—5 vol% H_2O is amorphous Al_2O_3 containing poorly crystallized γ-Al_2O_3 at 800 °C, and a mixture of γ-Al_2O_3 and δ-Al_2O_3 at 1000 °C, as described above.

The products formed by the reaction of gaseous $AlCl_3$ with oxygen containing 2—5 vol% H_2O at various temperatures were examined by electron microscopy.

The Al_2O_3 formed by the reaction with oxygen is relatively uniform, ultrafine powders with the particle diameters of the order of 1/100 μm.[1] The range of the particle sizes of the Al_2O_3 formed by the reaction with oxygen containing 5 vol% H_2O was observed to be wide, as was that of the Al_2O_3 formed by the reaction with H_2O.[2] The Al_2O_3 formed by the reaction with oxygen containing 2 vol% H_2O at 800 and 900 °C were relatively uniform, ultrafine powders, as seen from Figs. 2 (a) and (b).

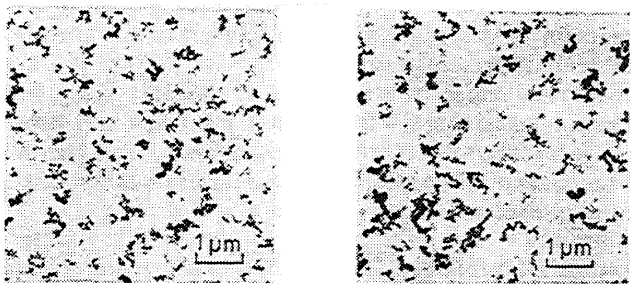

(a) 800 °C (b) 900 °C

Fig. 2. Electron micrographs of the Al_2O_3 formed by the reaction of gaseous $AlCl_3$ with oxygen containing 2 vol% H_2O at 800 and 900 °C.

Thermal Transition of the Aluminium Oxide Formed. The thermal transitions of the Al_2O_3 formed under various conditions were examined. The samples obtained by heating the Al_2O_3 at a specified temperature for 2 h both in an argon atmosphere and in the air were examined by X-ray analysis.

The results for the Al_2O_3 formed by the reaction with oxygen containing 5 vol% H_2O are shown in Table 1.

The experimental results show that on heating the amorphous Al_2O_3 formed at 400 and 600 °C both in an argon atmosphere and in the air, the amorphous $\xrightarrow{ca.700\,°C}$ χ $\xrightarrow{ca.800\,°C}$ κ $\xrightarrow{ca.1000\,°C}$ α transition occurs, re-

Table 1. Thermal transitions of Al_2O_3 formed by the reaction of gaseous $AlCl_3$ with oxygen containing 5 vol% H_2O at various temperatures

Heating temp/°C	Formation temperature of Al_2O_3 and heating atmosphere							
	400 °C		600 °C		800 °C		900 °C	1000 °C
	In argon	In air	In argon	In air	In argon	In air	In argon and air	In argon and air
600	Amorphous		Amorphous		Amorphous		γ	γ, δ
700	χ	χ	χ	χ	χ	χ	γ, χ	γ, δ
800	χ, κ, γ	χ, κ	χ, κ, γ	χ, κ	χ, κ, γ	χ, κ, γ	γ, χ, κ	γ, δ
900	χ, κ, γ	χ, κ	χ, κ, γ	χ, κ	χ, κ, γ, δ	χ, κ, γ, δ	γ, δ, κ	γ, δ
1000	κ, $\delta > \alpha$	κ, α	κ, $\delta > \alpha$	κ, α	κ, $\delta > \theta$, α	κ, δ, θ, α	δ, θ, α	δ, $\theta > \alpha$
1100	α	α	α	α	$\alpha > \theta$, δ	$\alpha > \theta$, δ	$\alpha > \theta$, δ	δ, θ, α
1200	—	—	—	—	α	α	α	α, θ
1300	—	—	—	—	—	—	—	$\alpha > \theta$

Amorphous = amorphous Al_2O_3, $\chi = \chi$-Al_2O_3,[4,5] $\kappa = \kappa$-Al_2O_3,[4,6] $\alpha = \alpha$-Al_2O_3,[7] $\gamma = \gamma$-Al_2O_3,[4,8] $\delta = \delta$-Al_2O_3,[4,9] $\theta = \theta$-Al_2O_3.[10]

gardless of the heating atmosphere. The γ-Al_2O_3 observed in the samples obtained after heating the amorphous Al_2O_3 at 800 and 900 °C in an argon atmosphere is due to the decomposition of the chloride oxide which is included in the amorphous Al_2O_3, and the δ-Al_2O_3 observed at 1000 °C is due to the thermal transition of the γ-Al_2O_3 formed.[2] The samples obtained after heating the amorphous Al_2O_3 in the air give neither diffraction line corresponding to γ-Al_2O_3 nor corresponding to δ-Al_2O_3, because the chloride oxide is oxidized in the air to amorphous Al_2O_3 which transforms in the same manner as the amorphous Al_2O_3 formed from gaseous $AlCl_3$.[2]

The results for the γ-Al_2O_3 containing amorphous Al_2O_3, formed at 900 °C, and for the mixture of γ-Al_2O_3 and δ-Al_2O_3, formed at 1000 °C, indicate that, on heating the γ-Al_2O_3, the $\gamma \xrightarrow{ca.900\,^\circ C} \delta \xrightarrow{ca.1000\,^\circ C} \theta \xrightarrow{ca.1000\,^\circ C} \alpha$ α transition occurs, regardless of the heating atmosphere. The χ-Al_2O_3 and κ-Al_2O_3 observed in the samples obtained after heating the Al_2O_3 formed at 900 °C are due to the thermal transition of amorphous Al_2O_3 which is contained in the γ-Al_2O_3.

On heating the amorphous Al_2O_3 containing poorly crystallized γ-Al_2O_3, formed at 800 °C, both the amorphous$\rightarrow\chi\rightarrow\kappa\rightarrow\alpha$ and $\gamma\rightarrow\delta\rightarrow\theta\rightarrow\alpha$ transitions occur, as is expected from the above results.

The experimental results for the Al_2O_3 formed by the reaction with oxygen containing 2 vol% H_2O at temperatures below 800 °C were similar to those for the Al_2O_3 formed by the reaction with oxygen containing 5 vol% H_2O. The results for the γ-Al_2O_3 containing amorphous Al_2O_3, formed at 900 °C, and for the mixture of γ-Al_2O_3 and δ-Al_2O_3, formed at 1000 °C, are shown in Table 2.

Table 2. Thermal transitions of Al_2O_3 formed by the reaction of gaseous $AlCl_3$ with oxygen containing 2 vol% H_2O at 900 and 1000 °C

Heating temp/°C	Formation temperature of Al_2O_3 and heating atmosphere	
	900 °C In argon and air	1000 °C In argon and air
600	γ	γ, δ
700	γ, χ	γ, δ
800	γ, χ, κ	γ, δ
900	γ, δ, χ, κ	γ, δ
1000	δ, θ, α, κ	$\delta > \theta$, α
1100	δ, θ, α	δ, $\theta > \alpha$
1200	$\alpha > \theta$	α, θ
1300	$\alpha > \theta$	α, θ

From these results, the thermal transitions of amorphous Al_2O_3 and of γ-Al_2O_3, formed by the reaction of gaseous $AlCl_3$ with oxygen containing 2 vol% H_2O, are found to be the same as those of the Al_2O_3 formed by the reaction with oxygen containing 5 vol% H_2O. In more details, the sample obtained after heating at 1300 °C the γ-Al_2O_3 containing amorphous Al_2O_3, formed by the reaction with oxygen containing 2 vol% H_2O at 900 °C, was found to be a mixture of α-Al_2O_3 and θ-Al_2O_3 (Table 2). The sample obtained after heating at 1200 °C the γ-Al_2O_3 containing amorphous Al_2O_3, formed by the reaction with oxygen containing 5 vol% H_2O at 900 °C, gave diffraction lines corresponding to α-Al_2O_3 alone (Table 1). These results can be well understood, considering the thermal transitions of γ-Al_2O_3 containing amorphous Al_2O_3, formed by the reactions of gaseous $AlCl_3$ with oxygen[1] and H_2O[2] at 900 °C.

These experimental results show that on heating the amorphous Al_2O_3 formed by the reaction of gaseous $AlCl_3$ with oxygen containing 2—5 vol% H_2O, the amorphous $\xrightarrow{ca.700\,^\circ C} \chi \xrightarrow{ca.800\,^\circ C} \kappa \xrightarrow{ca.1000\,^\circ C} \alpha$ transition occurs. On heating the γ-Al_2O_3 formed, the $\gamma \xrightarrow{ca.900\,^\circ C} \delta \xrightarrow{ca.1000\,^\circ C} \theta \xrightarrow{ca.1000\,^\circ C} \alpha$ transition occurs.

The thermal transition of the amorphous Al_2O_3 is the same as that of the amorphous Al_2O_3 formed by the reactions with oxygen[1] and with H_2O.[2] The transition temperatures of $\gamma\rightarrow\delta$, $\delta\rightarrow\theta$, and $\theta\rightarrow\alpha$ on heating the γ-Al_2O_3 are approximately 100 °C lower than those of the γ-Al_2O_3 formed by the reaction with oxygen[1] and are the same as those of the γ-Al_2O_3 formed by the reaction with H_2O.[2]

References

1) Y. Shoji, K. Tatsumi, R. Matsuzaki, and Y. Saeki, *Bull. Chem. Soc. Jpn.*, **53**, 269 (1980).

2) Y. Shoji, R. Matsuzaki, and Y. Saeki, *Bull. Chem. Soc. Jpn.*, **54**, 2652 (1981).
3) J. P. Cuer, J. Elston, and S. J. Teichner, *Bull. Soc. Chim. Fr.*, **1961**, 81, 89.
4) K. Funaki and Y. Shimizu, *Denki Kagaku*, **28**, 358 (1960).
5) JCPDS, Powder Diffraction File, 13-373.
6) ASTM, X-Ray Powder Data File, 4-878.
7) ASTM, Powder Diffraction File, 10-173.
8) JCPDS, Powder Diffraction Data Card, 29-63.
9) JCPDS, Powder Diffraction File, 16-394.
10) JCPDS, Powder Diffraction File, 11-517.

 © 1982 The Chemical Society of Japan Bull. Chem. Soc. Jpn., 55, 441—443 (1982)

Plasma Treatment of Packing Materials for Gas Chromatography. Diatomaceous Earth Coated with Squalane

Yukio YAMAMOTO,* Seiji OKA, and Koichiro HAYASHI

The Institute of Scientific and Industrial Research, Osaka University, Yamadakami, Suita, Osaka 565

(Received July 9, 1981)

Commercially obtained column packings for gas chromatography, diatomaceous earth coated with 5% squalane, were treated with argon plasma by using a radiofrequency generator. It has been shown that the plasma treatment improves the chromatographic properties, in particular, reduces the tailing of aromatic hydrocarbon peaks. The effect of the plasma treatment has been attributed to the reduction of the support adsorptivity by the formation of inert coating on the support surface.

A growing interest has been arising in the application of plasma chemistry to surface treatment of solid materials.[1-3] An attempt has been made to apply inert gas plasma to the treatment of packing materials for gas chromatography, and the results of the preliminary experiments suggested that the argon plasma treatment of the packing such as diatomaceous earth coated with Apiezon L or squalane improves its chromatographic properties.[4] The effect has been attributed to the formation of inert coating on the support surface. The surface of diatomite supports is known to be covered with reactive silanol groups which cause tailing of chromatographic peaks, and several methods are used to reduce the activity of the supports.[5] It is expected that the argon plasma treatment of packings is effective for the reduction of the support adsorptivity. In the present study the effect of the plasma treatment of diatomaceous earth coated with 5% squalane was studied in some detail.

Expermental

Column packings, 60/80 mesh Chromosorbs W and P (non-acid washed) coated with 5% squalane, were obtained from Wako Pure Chemical Industry. The reactor used for the plasma treatment is shown in Fig. 1. The packing (about 4 g) was treated on a glass plate (9 cm diameter) in a bell jar with argon plasma at a pressure of 0.20 Torr (27 Pa). The power for the reactor was supplied by a radiofrequency generator operated at 13.56 MHz and an output of 50 W. After the treatment the packing was packed with tamping and vibration into a 1 m × 3 mm i.d. stainless steel tube as well as the untreated packing. Before its use the column was conditioned overnight at 130 °C. The gas chromatography was carried out on a Hitachi gas chromatograph, Model 063, equipped with a flame ionization detector by injecting about 0.1 μl hydrocarbon mixtures. The flame ionization detector was substituted for a thermal conductivity cell detector when the retention time of oxygen was measured for determination of the adjusted retention times. The column was operated at 40 °C with a nitrogen flow of 30 ml/min. ESCA measurement of the support recovered from the packing by Soxhlet extraction was performed on a Du Pont ESCA 650 B electron spectrometer by employing a Mg $K\alpha_{1,2}$ photon source at 1253.6 eV.

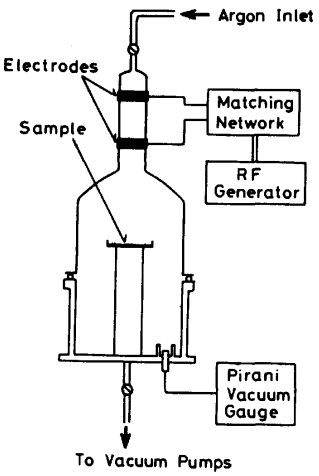

Fig. 1. Reactor used for the plasma treatment.

Results and Discussion

The effect of the argon plasma treatment of 60/80 mesh Chromosorb W (non-acid washed) coated with 5% squalane is shown in Fig. 2 where the chromatograms of a mixture of hexane, benzene, cyclohexane, heptane, toluene, ethylbenzene, and *o*- and *m*-xylenes on the untreated and 30 min treated packings are presented. It can be seen that the retention times of all the compounds and the tailings of the aromatic hydrocarbon peaks are reduced by the plasma treatment. Greater peak separation is also shown for benzene and cyclohexane on the treated packing. The changes in the adjusted retention times of the aliphatic and aromatic hydrocarbons are shown in Figs. 3 and 4, respectively, where the ratio of the adjusted retention time on the treated packing to that on the untreated packing, t'_{RO}/t'_{Rt}, is plotted against treatment time. A comparison of the figures shows that the retention times

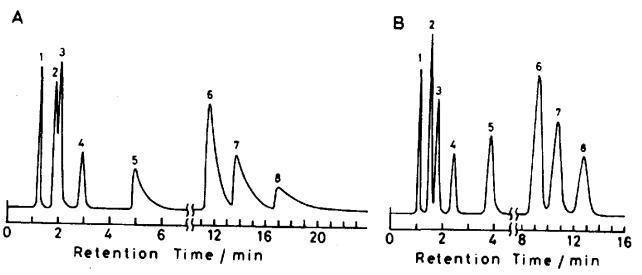

Fig. 2. Gas chromatograms on (A) untreated and (B) 30 min treated packings (Chromosorb W coated with 5% squalane) at 40 °C: the peaks are 1, hexane; 2, benzene; 3, cyclohexane; 4, heptane; 5, toluene; 6, ethylbenzene; 7, *m*-xylene; and 8, *o*-xylene.

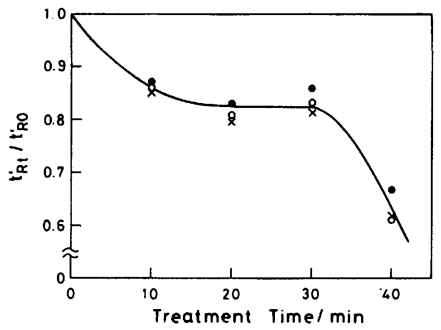

Fig. 3. Change in the adjusted retention times of aliphatic hydrocarbons: (○), hexane; (●), cyclohexane; and (×), heptane.

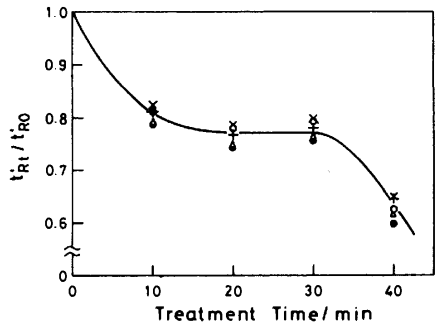

Fig. 4. Change in the adjusted retention times of aromatic hydrocarbons: (○), benzene; (●), toluene; (×), ethylbenzene; (△), *o*-xylene and (+), *m*-xylene.

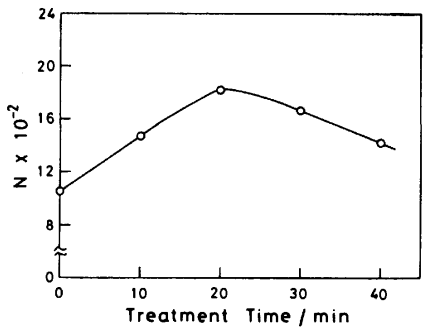

Fig. 5. Change in the number of theoretical plates (N).

of the aromatic hydrocarbons are reduced more than those of the aliphatic hydrocarbons by the plasma treatment. Figure 5 shows the change in the number of theoretical plates (N) by the plasma treatment, which was calculated from the peaks of ethylbenzene and *o*- and *m*-xylenes as $16(t_R/W_b)^2$, where t_R and W_b are the retention time and the peak width at base, respectively. The value attains maximum at around 20 min and then decreases by further treatment. The weight loss of the packing during the plasma treatment was too small to measure accurately, less than 0.4% up to a treatment time of 40 min.

In order to elucidate the modification of the packing by the plasma treatment the stationary liquids were extracted from the untreated and 20 and 40 min treated packings with tetrahydrofuran by using Soxhlet extractors and refluxing for 5 h, and then the recovered supports were dried under vacuum. The weight losses of the untreated and 20 and 40 min treated packings by the extraction were 4.9, 4.0, and 3.4%, respectively. Since the original packing has a liquid phase content of about 4.8% (5% relative to the support), the result means that the stationary liquid is almost completely extracted from the untreated packing but not from the treated packing, and the remaining component increases with increasing treatment time.

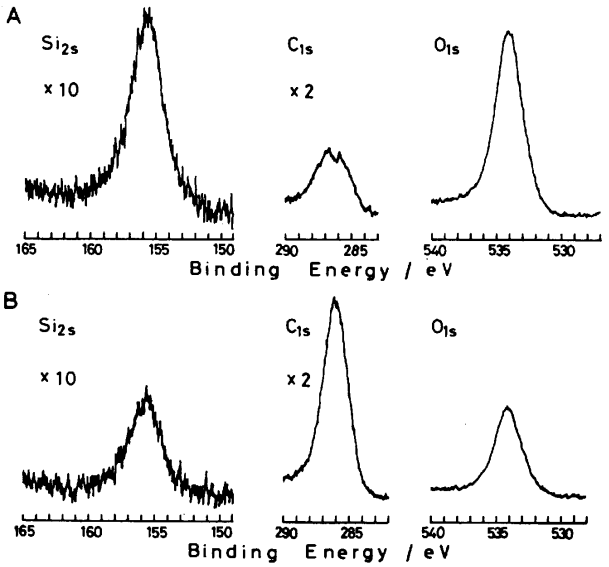

Fig. 6. ESCA Si_{2s}, C_{1s}, and O_{1s} peaks of supports recovered from (A) untreated and (B) 20 min treated packings.

ESCA measurement of the recovered supports was examined to obtain information about their surface compositions. Figure 6 shows the Si_{2S}, C_{1S}, and O_{1S} peaks of the ESCA spectra obtained for the untreated and 20 min treated packings. The C_{1S} peak is much larger for the treated sample than for the untreated sample, and the Si_{2S} and O_{1S} peaks arising from the diatomite support are reduced for the treated sample. The spectra demonstrate that the surface of the support recovered from the treated packing is covered with an organic component. On the other hand, the relative heights of the Si_{2S} and O_{1S} peaks are not affected by the plasma treatment, indicating that the surface composition of the support itself does not change.

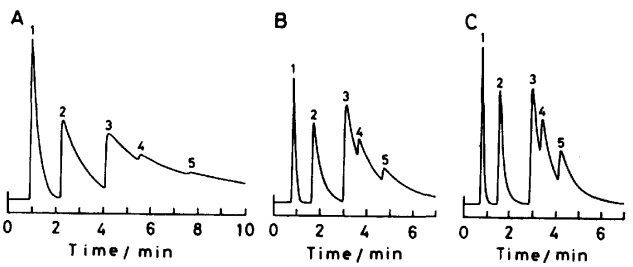

Fig. 7. Gas chromatograms on supports recovered from (A) untreated, (B) 20 min and (C) 40 min treated packings at 40 °C: The peaks are 1, benzene; 2, toluene; 3, ethylbenzene; 4, *m*-xylene; and 5, *o*-xylene.

The supports recovered from the packings were packed into the 1 m stainless steel tubes, and the columns were examined for gas chromatography. Figure 7 shows the gas chromatograms of a mixture of the aromatic hydrocarbons on the recovered supports. The retention times and tailings are reduced with increasing treatment time, suggesting that the adsorptivity of the support is reduced by the plasma treatment.

The untreated and treated packings were washed with carbon tetrachloride, and after filtration the carbon tetrachloride solutions of the stationary liquids were submitted to NMR spectrometry. There was no detectable difference in the spectra between the untreated and treated samples, and the spectra were identical with that of commercially obtained squalane. The result suggests that the soluble component of the stationary liquid of the treated packing remains unchanged.

On the basis of these results it can be considered that the plasma-induced reaction is restricted to the support surface and results in the formation of inert coating which is not extracted with tetrahydrofuran. The effect of the plasma treatment on gas chromatogram was shown to be more pronounced for the aromatic hydrocarbons than for the saturated aliphatic hydrocarbons. This is due to the fact that aromatic hydrocarbons have greater interaction with the surface silanol groups of the support than saturated aliphatic hydrocarbons.

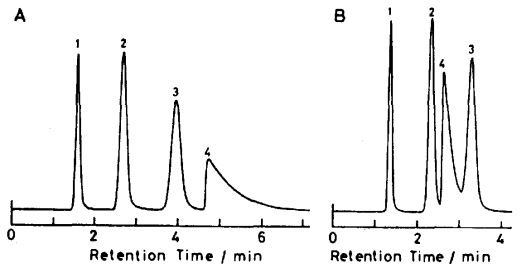

Fig. 8. Gas chromatograms on (A) untreated and (B) 20 min treated packings (Chromosorb P coated with 5% squalane) at 40 °C: the peaks are 1, hexane; 2, cyclohexane; 3, heptane; and 4, benzene.

The argon plasma treatment of the packing with another kind of support, 60/80 mesh Chromosorb P (non-acid washed) coated with 5% squalane, was examined by the same way to investigate the effect on the support adsorptivity. Figure 8 shows the gas chromatograms on the untreated and 20 min treated packings. On the untreated packing with Chromosorb P benzene is eluted later than heptane with a significant tailing, while on the untreated packing with Chromosorb W benzene is eluted faster than cyclohexane with a much smaller tailing (Fig. 2). It is known that Chromosorb P is more adsorptive than Chromosorb W because of the greater number of hydroxyl groups on the surface.[5] Therefore, the difference in the gas chromatograms between the untreated packings with Chromosorbs P and W can be explained by the great interaction of aromatic hydrocarbons compared with saturated aliphatic hydrocarbons. The result also demonstrates that the gas chromatograms are significantly affected with the support adsorptivity. On the other hand, on the treated packing with Chromosorb P benzene is eluted faster than heptane with a reduced tailing, indicating that the plasma treatment is effective for the reduction of the support adsorptivity.

Usually, the lower the column temperature, the greater is the tailing of gas chromatographic peaks. The results of the present study show that the plasma treatment makes it possible to use the packings at lower column temperature. Unfortunately, no information has been obtained about the chemical composition and formation mechanism of the insoluble component produced on the support surface. However, it seems reasonable to assume that the stationary liquid is converted to a highly crosslinked polymer on the support surface by the plasma treatment and the reaction is promoted by the reactive support surface.

This work was supported in part by Shimadzu Co. The authors wish to thank Mr. Hitoshi Yamada for his assistance in measuring the ESCA spectra.

References

1) M. Hudis, "Techniques and Applications of Plasma Chemistry," ed by J. T. Hollahan and A. T. Bell, Wiley-Interscience, New York, N. Y. (1974), p. 113.

2) H. Yasuda, *J. Macromol. Sci., Chem.*, **A10**, 383 (1976).

3) D. H. Reneker and L. H. Bolz, *J. Macromol. Sci., Chem.*, **A10**, 599 (1976).

4) Y. Yamamoto, S. Oka, and K. Hayashi, *Chem. Lett.*, **1981**, 221.

5) O. E. Schupp, III, "Gas Chromatography," ed by E. S. Perry and A. Weissberger, Interscience, New York, N. Y. (1968), p. 173.

^{197}Au-Mössbauer Spectroscopic Studies of Gold Compounds

Motomi KATADA,* Yoshio UCHIDA, Kumiko SATO, Hirotoshi SANO, Hiroshi SAKAI,† and Yutaka MAEDA†

Department of Chemistry, Faculty of Science, Tokyo Metropolitan University, Fukasawa, Setagaya-ku, Tokyo 158

†*Research Reactor Institute, Kyoto University, Kumatori-cho, Sennan-gun, Osaka 590-04*

(Received July 13, 1981)

^{197}Au Mössbauer effect measurements of mixed-valence compounds and chelates of Au(III) with ligands of 1,10-phenanthroline, 8-quinolinol, and their derivatives have been carried out. The Mössbauer data of $Cs_2Au_2Cl_6$, $Cs_2AgAuCl_6$, and [Au(phen)Cl_2]Cl show the existence of an interaction between metal atoms through Cl atoms. Although the metal-metal interaction in [Au(Hdmg)$_2$][$AuCl_2$] has been postulated by X-ray study, no such interaction was observed. Two kinds of 8-quinolinol Au(III) complexes which have *cis-trans* isomers are assigned to the compounds of the [Au(oxine)$_2$][$AuCl_4$] and [Au(oxine)Cl_2] types.

Mössbauer spectroscopy has been widely used to study the nature of chemical bonding and the structures of inorganic and organometallic compounds, especially those of iron and tin compounds.

Although the ^{197}Au Mössbauer experiment has some disadvantages, such as the short half-life (18 h) of the source nuclide and the low recoil-free fraction, which require the use of a nuclear reactor and low-temperature measurement, the application of Mössbauer spectroscopy has recently become popular as a useful physicochemical technique because the spectrum is generally unambiguous and sensitive to the nature of chemical bonding and the structures of gold compounds.[1,2]

The present work was carried out in order to elucidate the interaction between the two different gold atoms in different sites in the mixed-valence compounds, such as $Cs_2Au_2Cl_6$, [Au(Hdmg)$_2$][$AuCl_2$], and [Au(phen)Cl_2][$AuCl_4$], and in order to clarify the structure of chelate complexes of Au(III) with 1,10-phenanthroline, 8-quinolinol, and their derivatives as ligands.

Experimental

$CsAuCl_4$,[3] $Cs_2AgAuCl_6$,[3] [Au(Hdmg)$_2$][$AuCl_2$] (Hdmg=dimethylglyoximato(1-)),[4] [Au(phen)Cl_2]Cl (phen=1,10-phenanthroline),[5] [Au(phen)Cl_2]ClO_4,[5] [Au(phen)Cl_2][$AuCl_4$],[5] Au(dmp)Cl_3 (dmp=2,9-dimethyl-1,10-phenanthroline),[6] Au(dmp)Br_3,[6] [Au(oxine)$_2$][$AuCl_4$] (oxine=8-quinolinol),[7] and [Au(oxine)Cl_2][7] were prepared by the methods described in the literature. Thermal decomposition product of $CsAuCl_4$, $Cs_2Au_2Cl_6$(dec) was prepared by a method similar to that of Brauer and Sleater[8] by checking the decomposition process by TGA and DSC. Another sample of $Cs_2Au_2Cl_6$(syn) was prepared directly by heating the stoichiometric mixture of CsCl, Au, and $CsAuCl_4$ in an evacuated quartz tube at 450 °C for one week and then cooling it rapidly in water. The crystal thus obtained was annealed at 250 °C for 3 d.

[Au(5-Cl-oxine)Cl_2] (5-Cl-oxine=5-chloro-8-quinolinol) was prepared by a method similar to that used in the preparation of 8-quinolinol gold complexes.[7] The purity of the samples was checked by elemental analysis and powder X-ray diffractometry (Cu $K\alpha$ radiation).

^{197}Au Mössbauer spectroscopic measurements were carried out with a source and an absorber, both cooled to 18 K by using a constant acceleration-type spectrometer accompanied by a pure-Ge diode detector. The data were stored in a microcomputerized multichannel analyser constructed by Uehara and Maeda.[9] A ^{197}Pt source was made by irradiating a 100-mg disk of metallic Pt enriched to 98% in ^{196}Pt. The velocity scale was calibrated by taking the spectrum of an iron foil against a ^{57}Co(Pt) source, both at room temperature. The spectra were fitted with Lorentzian line shapes by using the least-squares fitting program. The precision of the Mössbauer parameters obtained is within $\pm$0.04 mm/s for single component spectra and $\pm$0.08 mm/s for double component spectra. All the isomer shift data are referred to the Au-metal resonance at 18 K.

Results and Discussion

$CsAuCl_4$, $Cs_2Au_2Cl_6$(syn), $Cs_2Au_2Cl_6$(dec), and $Cs_2AgAuCl_6$. Some typical Mössbauer spectra of $CsAuCl_4$, $Cs_2Au_2Cl_6$(syn), and $Cs_2AgAuCl_6$ are shown in Fig. 1. Table 1 summarizes the Mössbauer parameters, isomer shift (*IS*), quadrupole splitting (*QS*), and half-width (Γ_{exp}) derived from the observed spectra. The isomer shift and quadrupole splitting of $CsAuCl_4$ are similar to those of the compounds containing discrete square-planar-complex ions, $[AuCl_4]^-$.[10,11] This indicates that gold atoms are coordinated essentially in the square-planar form and that the isolated $[AuCl_4]^-$ ion exists in a solid. The complicated spectra of both the

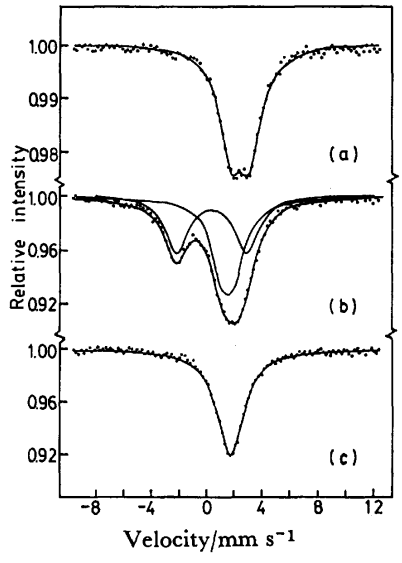

Fig. 1. Mössbauer spectra of (a) $CsAuCl_4$, (b) $Cs_2Au_2Cl_6$ (syn), and (c) $Cs_2AgAuCl_6$.

Table 1. Mössbauer data of cesium gold chlorides and cecium silver gold chloride

Compound	*IS* mm s^{-1}	*QS* mm s^{-1}	Γ_{exp} mm s^{-1}
$CsAuCl_4$	2.16	1.37	1.96
$Cs_2Au_2Cl_6$(syn)			
Au(I)	0.13	5.06	2.04
Au(III)	1.31	1.00	1.88
$Cs_2Au_2Cl_6$(dec)			
Au(I)	0.23	5.25	1.89
Au(III)	1.56	0.95	2.00
$Cs_2AgAuCl_6$	1.54	—	2.33

$Cs_2Au_2Cl_6$(dec and syn) samples suggest the presence of two or more different sites or oxidation states for the gold atom in these compounds. The crystal structure of $Cs_2Au_2Cl_6$ was determined first by Elliot and Pauling from powder X-ray diffraction data.[12]

According to their results, this compound contains complex ions of linear $[AuCl_2]^-$ and square-planar $[AuCl_4]^-$ units, and they postulated the possibility of interaction between Au(I) and Au(III) sites through Cl atoms. In recent years, however, the structure was redetermined by using single crystal data by Tindermans-v. Eijindhoven and Verschoor.[13] They pointed out that there was no interaction between Au(I) and Au (III) atoms through Cl atoms. In Fig. 1(b), the outer doublet is assigned to the Au(I), and the inner doublet to the Au(III). The slight differences in Mössbauer parameters between the two samples (syn and dec), and between ours and those reported by Faltens and Shirley,[10] may be due to the different preparation process and/or an error in the deconvolution of the spectra. In the work by Faltens and Shirley, $Cs_2Au_2Cl_6$ was prepared from an acid solution of CsCl and AuCl. The values of *IS* for Au(III) in both $Cs_2Au_2Cl_6$ (syn) and $Cs_2Au_2Cl_6$ (dec) are smaller than that of $CsAuCl_4$ and those of some compounds containing a discrete $[AuCl_4]^-$ ion. Unfortunately, Faltens and Shirley did not interpret the correlation of the Mössbauer parameters with the structures of $Cs_2Au_2Cl_6$. If the postulation of Elliot and Pauling were correct, the configuration around the Au(III) atom in the $[AuCl_4]^-$ site should be a distorted octahedron with four Cl atoms of the $[AuCl_4]^-$ ion and two additional Cl atoms from adjacent $[AuCl_2]^-$ ions, as is shown in Fig. 2. In this case, it would be impossible to form six equivalent $5d^26s6p^3$ hybrid bonds involving the promotion of two electrons. The formation of six equivalent bonds using a $5d6s6p^36d$ hybridization also seems to be unlikely from the point of view of energy. However, the formation of an octahedron elongated to the z-axis (normal to the square plane of $[AuCl_4]^-$) with six Cl atoms, may be explained by assuming that two 6p6d hybrid bonds are added to the $5d6s6p^2$ hybrid bonds which hold the four Cl atoms in square-planar form. The additional co-linear 6p6d hybrid bonds should be elongated in the direction of the z-axis because of the repulsion of the filled $5d_z$ gold orbital in the gold atom. This explanation was suggested by Sutton to interpret hexa-coordinated Au(III) ions, such as $[Au(diars)_2I_2]^+$ (diars = *o*-phenylenbis(dimethylarsine)) and $[AuBr_6]^{3-}$.[14,15] The additional electrons of the 6p6d hybrid orbital may be expected to decrease the isomer shift because of the increased shielding effect of p- and d-electrons on s-electrons.

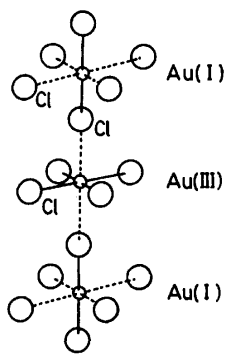

Fig. 2. Stacking arrangement of the $[AuCl_4]^-$ and $[AuCl_2]^-$ units.

The *IS* value of the Au(I) site is considerably smaller than that of the corresponding Au(I) chloride, $(C_6H_5)_4AsAuCl_2$ (*IS*=1.72 mm/s and *QS*=6.13 mm/s).[16] Au-atoms are also surrounded by six Cl atoms and form a contracted octahedron, as is shown in Fig. 2.

The additional four bonds may be formed by using $6p^26d^2$ hybridization; hence, the s-electron density decreases as a result of the increased shielding effect of p- and d-electrons, as in the case of Au(III).

The decreasing tendency of *QS* values for Au(I) and Au(III) sites also supports the hexa-coordinated structure of gold atoms. As is known in the case of covalent square-planar Au(III) compounds where Au (III) uses the $5d_{x^2-y^2}$, 6s, $6p_x$, and $6p_y$ orbitals, the occupation of these orbitals will cause a positive contribution to the electric field gradient (EFG), while a nonbonding $5d_{z^2}$ orbital will produce a negative contribution to the EFG. By assuming that the EFG of the original $[AuCl_4]^-$ site is positive, it may be concluded that the increase in electron densities along the z-axis as a result of 6p6d hybridization produces a negative contribution to the EFG, so that the total EFG becomes smaller. For linear Au(I) compounds, the z-axis is taken along the molecular axis and 6s6p hybrid orbitals of gold are used as σ-bonds. This has been confirmed experimentally for $K[Au(CN)_2]$, in which the EFG value for linear Au(I) compounds is negative.[17] Since four additional Au–Cl bonds, using the $6p^26d^2$ hybrid orbitals, produce a positive contribution to the EFG, the total EFG can be expected to decrease.

The crystal structure of $Cs_2AgAuCl_6$ is known to be the same as that of $Cs_2Au_2Cl_6$. From the discussion presented above of Mössbauer parameters of $Cs_2Au_2Cl_6$, the unresolved quadrupole splitting found on $Cs_2AgAuCl_6$ can be explained as follows: the positive and negative contributions to the EFG are almost equal, so that the effective EFG becomes zero or negligible. This result suggests that there is a strong interaction between Ag(I) and Au(III) sites through Cl atoms. The existence of such a strong interaction between the metal atoms in $Cs_2AgAuCl_6$ has also been pointed out by Yamada and Tsuchida from the dichroism measurement of this

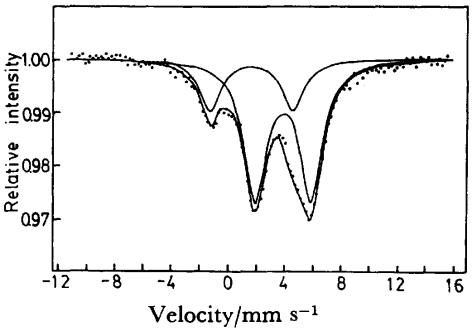

Fig. 3. Mössbauer spectrum of $[Au(Hdmg)_2][AuCl_2]$.

TABLE 2. MÖSSBAUER DATA OF $[Au(Hdmg)_2][AuCl_2]$

Compound	IS / mm s^{-1}	QS / mm s^{-1}	Γ_{exp} / mm s^{-1}
$[Au(Hdmg)_2][AuCl_2]$			
Au(I)	1.58	6.03	1.74
Au(III)	3.88	4.04	2.03

compound.[3] The present data also support their conclusion that the interaction between two metal atoms in $Cs_2AgAuCl_6$ is stronger than that in $Cs_2Au_2Cl_6$.

[Au(Hdmg)$_2$][AuCl$_2$]. The Mössbauer spectrum and the derived parameters of $[Au(Hdmg)_2][AuCl_2]$ are shown in Fig. 3 and in Table 2, respectively. Rundle determined the structure of this compound and postulated the existence of a direct interaction between the Au(I) and Au(III) atoms.[4] However, the fact that the values of *IS* and *QS* for the Au(I) site are similar to those of the isolated $[AuCl_2]^-$ ion in $[(C_6H_5)_4As][AuCl_2]$ indicates no metal-metal interaction between Au(I) and Au(III) atoms.

This result is consistent with the results of dichroism measurement obtained by Yamada and Tsuchida.[18] The values of *IS* and *QS* for Au(III) in the $[Au(Hdmg)_2]^+$ ion are larger than those of the $[AuCl_4]^-$ ion. If the $5d6s6p^2$ hybrid orbitals are used to form a square-planar form, this difference can be explained by the stronger σ-donating power of the Hdmg ligand compared to the Cl ligand, because the increased σ-donation by the ligand to the 6s orbital increases the s-electron density, and hence the isomer shift. At the same time, the EFG will increase as a result of the donation to the $6p_x$ and $6p_y$ orbitals. Therefore, the values of *IS* and *QS* depend mainly on the σ-donating character of the Hdmg ligand, which is estimated to lie between those of the N_3^- and CN^- ligands, this is consistent with the estimation based on the spectrochemical series of ligands.

[Au(phen)Cl$_2$]Cl, [Au(phen)Cl$_2$]ClO$_4$, [Au(phen)Cl$_2$][AuCl$_4$], Au(dmp)Cl$_3$, and Au(dmp)Br$_3$. The Mössbauer spectra of $[Au(phen)Cl_2]X$ (X=Cl, ClO_4, and $AuCl_4$) and $Au(dmp)Cl_3$ are shown in Fig. 4. The Mössbauer parameters of these complexes are summarized in Table 3, together with those of $Au(dmp)Br_3$. The values of *IS* and *QS* for $[Au(phen)Cl_2]Cl$, $[Au(phen)Cl_2][AuCl_4]$ and $Au(dmp)Cl_3$ are in good agreement with those reported by Takeda *et al.*[19] $[Au(phen)Cl_2]Cl$ and $Au(dmp)X_3$ (X=Cl or Br) show

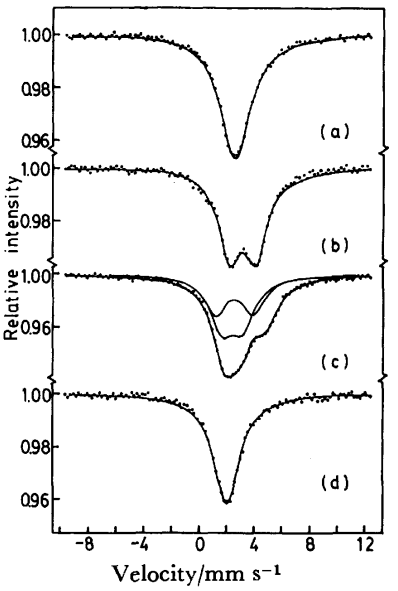

Fig. 4. Mössbauer spectra of (a) $[Au(phen)Cl_2]Cl$, (b) $[Au(phen)Cl_2]ClO_4$, (c) $[Au(phen)Cl_2][AuCl_4]$, and (d) $Au(dmp)Cl_3$.

TABLE 3. MÖSSBAUER DATA OF 1,10-PHENANTHROLINE AND 2,9-DIMETHYL-1,10-PHENANTHROLINE Au(III) COMPLEXES

Compound	IS / mm s^{-1}	QS / mm s^{-1}	Γ_{exp} / mm s^{-1}
$[Au(phen)Cl_2]Cl$	2.39	—	2.66
$[Au(phen)Cl_2]ClO_4$	3.01	1.95	2.06
$[Au(phen)Cl_2][AuCl_4]$			
$[Au(phen)Cl_2]^+$	3.33	2.74	1.97
$[AuCl_4]^-$	2.24	1.53	2.13
$Au(dmp)Cl_3$	1.87	—	2.31
$Au(dmp)Br_3$	2.07	—	2.76

spectra consisting of a single broad line with unresolved quadrupole splitting. This suggests that the structures of these complexes are different from the square-planar structure which is to be expected for a number of Au(III) chelate compounds. The smaller value of *IS* for $[Au(phen)Cl_2]Cl$, compared with those for $[Au(phen)Cl_2]ClO_4$ and $[Au(phen)Cl_2][AuCl_4]$, also supports a gold atom with a coordination number beyond four.

Harris has investigated the structure of the 1,10-phenanthroline complexes of Au(III) halides by

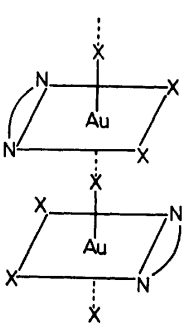

Fig. 5. Coordination of gold in $[Au(phen)X_2]X$.

conductance and spectral measurements in nonaqueous solvents.[5] From the molecular conductivities of the complexes, $[Au(phen)X_2]X$ (X=Cl or Br), he has suggested that those complexes have a polymeric structure, in which there are two elongated gold-halogen bonds normal to the square-planar $[Au(phen)X_2]^-$ ion, as is shown in Fig. 5. Two additional elongated Au–X bonds have been explained by assuming a colinear 6p6d hybrid bond. In accordance with his conclusion, the present Mössbauer results of $[Au(phen)Cl_2]Cl$ can also be explained by the consideration described in the case of $Cs_2AgAuCl_6$.

On the other hand, the quadrupole splitting is clearly observed for $[Au(phen)Cl_2]ClO_4$ and the *IS* is higher than that of $[Au(phen)Cl_2]Cl$, both indicating little or no interaction between the Au atoms in the $[Au(phen)Cl_2]^+$ ion and the counter anion, ClO_4^-. The rather complicated Mössbauer spectrum of $[Au(phen)Cl_2][AuCl_4]$ shown in Fig. 4(c) consists of two overlapped doublets. The outer doublet corresponds to the $[Au(phen)Cl_2]^+$ ion, and the inner doublet, to the $[AuCl_4]^-$ ion. Both the *IS* and *QS* of the $[Au(phen)Cl_2]^+$ ion in $[Au(phen)Cl_2][AuCl_4]$ show the highest values among a series of $[Au(phen)Cl_2]X$ salts. The Mössbauer parameters of the $[AuCl_4]^-$ ion found in $[Au(phen)Cl_2][AuCl_4]$ are similar to those of discrete $[AuCl_4]^-$ ions in other compounds previously reported by several researchers.[10,11] The results indicate that the $[Au(phen)Cl_2]^+$ cation has no effect on its counter anion $[AuCl_4]^-$, although the existence of metal-metal interaction in $[Au(phen)Cl_2][AuCl_4]$ might be expected, as in the case of Magnus's salt, $[Pt(NH_3)_4][PtCl_4]$, and similar complexes. Two complexes with chelating ligand 2,9-dimethyl-1,10-phenanthroline instead of 1,10-phenanthroline, $Au(dmp)Cl_3$ and $Au(dmp)Br_3$, were prepared, and their crystal structures were determined by Robinson and Sinn.[6] According to their results, these complexes have a five-coordinated structure, described as a distorted square-pyramidal structure or as an intermediate one between trigonal- and square-pyramidal. These structure are sterically hindered from forming the expected square-planar coordination as is found in 1,10-phenanthroline complexes. The smaller *IS* value compared with those of $[Au(phen)Cl_2]X$ (X=Cl, ClO_4, or $AuCl_4$) can be explained as follows: the structural data show that these complexes possess an approximately square-pyramidal geometry, with a weaker extra Au–N bond along the z-axis (perpendicular to the plane of the square); therefore, it is impossible to form five equivalent σ-bonds using $5d6s6p^3$ hybridization. Another possible explanation of these structures is to assume the vacant $6p_z$ orbital is used to form an extra Au–N bond, which is elongated to the z-axis due to the repulsion of the filled $5d_z^2$ orbital. The population in the $6p_z$ orbital decreases the s-electron density, and hence the isomer shift. The unresolved quadrupole splitting of these complexes can be interpreted by assuming that the magnitude of the negative contribution to the EFG nearly balances the positive contribution by the extra Au–N bond formation.

[Au(oxine)$_2$][AuCl$_4$], [Au(oxine)Cl$_2$], and [Au(5-Cl-oxine)Cl$_2$]. 8-Quinolinol complexes may be used as typical examples of the diagnosis of the structure and chemical bonding of two kinds of gold chelate complexes described with the same chemical formula. The spectra of these complexes and $[Au(5\text{-Cl-oxine})Cl_2]$ are shown in Fig. 6, while the Mössbauer parameters are summarized in Table 4.

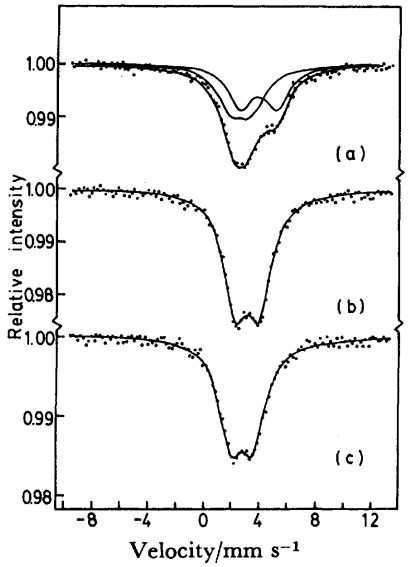

Fig. 6. Mössbauer spectra of (a) $[Au(oxine)_2][AuCl_4]$, (b) $[Au(oxine)Cl_2]$, and (c) $[Au(5\text{-Cl-oxine})Cl_2]$.

Table 4. Mössbauer data of 8-quinolinol and 5-chloro-8-quinolinol complexes

Compound	*IS* / mm s^{-1}	*QS* / mm s^{-1}	Γ_{exp} / mm s^{-1}
$[Au(oxine)_2][AuCl_4]$			
$[Au(oxine)_2]^+$	3.64	2.64	2.12
$[AuCl_4]^-$	2.43	1.49	2.39
$[Au(oxine)Cl_2]$	2.91	1.72	2.12
$[Au(5\text{-Cl-oxine})Cl_2]$	2.72	1.62	2.11

Two kinds of 8-quinolinol complexes, $[Au(oxine)_2][AuCl_4]$ have first been prepared and explained by Inazu[7] by assuming the *cis* and *trans* isomers with respect to the coordination of oxine ligands to the central gold atom, although he did not determine which was *cis*-form or *trans*-form. One is green, and the other is amber in color. The latter complex was assigned to the compound, consisting of either a *cis* or *trans* $[Au(oxine)_2]^+$ cation and an $[AuCl_4]^-$ anion, by Inazu on the basis of paper-ionophoreisis measurements. Concerning the green-colored species, an alternative stereoisomeric cation was suggested, although no experimental information on the green-colored complex was available. We prepared these complexes according to Inazu's method and obtained green and amber-colored samples. The Mössbauer spectrum of the amber-colored complex shows the existence of two kinds of gold atoms. The present result partially confirms Inazu's conclusion, in which gold exists as both cationic and anionic species in the amber-colored compound. On the other hand, our findings for the

green complex are different from the conclusion suggested by Inazu. The spectrum consisting of the doublet indicates the existence of only one kind of gold atom in its chemical state. Therefore, the formula of $[Au(oxine)Cl_2]$ instead of $[Au(oxine)_2][AuCl_4]$ may be appropriate for this compound. The possible structure should be square-planar, denoted as $[Au(oxine)Cl_2]$, in view of the Mössbauer parameters. The values of *IS* for the $[Au(oxine)_2]^+$ ion and for the $[AuCl_4]^-$ ion also support the conclusion concerning the green-colored complex, $[Au(oxine)Cl_2]$. On the other hand, the 5-chloro-8-qunolinol ligand gives no structural isomer, and only a green complex is synthesized. As may be seen from Fig. 6, the Mössbauer spectrum for the $[Au(5\text{-}Cl\text{-}oxine)Cl_2]$ consists of only one doublet, and the Mössbauer parameters are similar to those of the green-colored 8-quinolinol complex, $[Au(oxine)Cl_2]$.

This work has been carried out at the research Reactor Institute, Kyoto University. We are grateful to Assistant Professor Haruhiko Tanaka and Mr. Satoshi Oshima of Hiroshima University for their cooperation in obtaining the TGA and DSC results for $CsAuCl_4$.

References

1) H. D. Bartunik and G. Kaindl, "Mössbauer Isomer Shift," ed by G. K. Shenoy and F. D. Wagner, North-Holland, Amsterdam (1978), p. 515.

2) P. Gütlich, R. Link, and A. Trautwein, "Mössbauer Spectroscopy and Transition Metal Chemistry," Springer-Verlag, Berlin (1978), p. 201.

3) S. Yamada and R. Tsuchida, *Bull. Chem. Soc. Jpn.*, **29**, 421 (1956).

4) R. E. Rundle, *J. Am. Chem. Soc.*, **76**, 3101 (1954).

5) C. M. Harris, *J. Chem. Soc.*, **1959**, 682.

6) W. T. Robinson and E. Sinn, *J. Chem. Soc., Dalton Trans.*, **1975**, 726.

7) T. Inazu, *Bull. Chem. Soc. Jpn.*, **39**, 1065 (1966).

8) G. Brauer and G. Sleater, *J. Less-Common Metals*, **21**, 283 (1970).

9) S. Uehara and Y. Maeda, *Annu. Rep. Res. Reactor Inst. Kyoto Univ.*, **11**, 189 (1978).

10) M. O. Faltens and D. A. Shirley, *J. Chem. Phys.*, **53**, 4249 (1970).

11) H. D. Bartunik, W. Potzel, R. L. Mössbauer, and G. Kaindl, *Z. Phys.*, **240**, 1 (1970).

12) N. Elliot and L. Pauling, *J. Am. Chem. Soc.*, **60**, 1846 (1938).

13) J. C. M. Tindermans-v. Eijindhoven and G. C. Verschoor, *Mat. Res. Bull.*, **9**, 1677 (1974).

14) C. M. Harris and R. S. Nyholm, *J. Chem. Soc.*, **1957**, 63.

15) L. E. Sutton, Personal communication quated in Ref. 14.

16) P. G. Jones, A. G. Maddock, M. J. Mays, M. M. Muir, and A. F. Williams, *J. Chem. Soc., Dalton Trans.*, **1977**, 1434.

17) H. Prosser, F. E. Wagner, G. Wortmann, G. M. Kalvius, and R. Wäppling, *Hyperfine Interactions*, **1**, 25 (1975).

18) S. Yamada and R. Tsuchida, *Bull. Chem. Soc. Jpn.*, **30**, 715(1957).

19) M. Takeda, Y. Ito, T. Takano, and T. Tominaga, Abstracts 1D15 of the 29th Symp. on Co-ordination Chemistry, Hamamatsu, 1979.

 © 1982 The Chemical Society of Japan Bull. Chem. Soc. Jpn., 55, 449—452 (1982)

Thermochemical Studies on the Lanthanoid Complexes of *N,N,N',N'*-Tetramethylurea

Kozo Sone,* Kenzo Nagase,† Miuaco K. Kuya,†† and Ernesto Giesbrecht††

Department of Chemistry, Faculty of Science, Ochanomizu University, Otsuka, Bunkyo-ku, Tokyo 112

†*College of General Education, Tohoku University, Kawauchi, Sendai 980*

††*Instituto de Química, Universidade de São Paulo, C. P. 20780, São Paulo, Brazil*

(Received July 21, 1981)

The techniques of thermogravimetry (TG) and differential thermal analysis (DTA) were applied to the study of the thermal decomposition of the lanthanoid (Ln) complexes of *N,N,N',N'*-tetramethylurea (TMU), $Ln(TMU)_6X_3$ ($X=ClO_4$, PF_6, or BPh_4). In general, the ease of decomposition increases in the order of $BPh_4<ClO_4<PF_6$; in the latter two cases, the release (and, in the case of ClO_4, partial oxidation) of the coordinated TMU molecules takes place together with the decomposition of the anions, leading finally to the formation of $LnCl_3$ or LnF_3, respectively. The data were also discussed on the basis of the effects of the lanthanoid contraction.

N,N,N',N'-Tetramethylurea (TMU) is an interesting new solvent and coordinating agent. Its donor ability is expected to be quite high, but the four *N*-methyl groups protruding around its coordinating atom (*i.e.*, the C=O oxygen) bring about considerable steric hindrance for its complexation. It is expected, therefore, that stable complexes with it can be formed with large and hard cations, which have strong affinity toward oxygen-containing ligands.[1]

In fact, it has been found that the lanthanoid(III) ions, which just fulfill these conditions, can readily form numerous complexes with TMU; when the coexisting anion is a non-coordinating one (ClO_4^-, PF_6^-, or BPh_4^-), the complexes obtained are usually of the type $Ln(TMU)_6X_3$.[2-4]

We recently tried to apply the techniques of thermogravimetry (TG) and differential thermal analysis (DTA) to these complexes, to study the modes of their thermal decomposition. The obtained results will be briefly summarized and discussed.

Experimental

Preparation of Materials. The complexes studied are listed in Tables 1 and 2. They were prepared according to previously reported methods.[2-4] The complexes of La and Ce were not studied because of the strong hygroscopicity of their perchlorates.

TG-DTA Measurements. The TG and DTA measurements were made with a Shinku Riko TGD-3000 differential thermal microbalance under two conditions, *i.e.*, in static N_2 and in a vacuum (*ca.* 10^{-1} Torr≈13.3 Pa), with the heating rate of 3 °C/min. The sample amount taken in each run was *ca.* 10 mg.

Results and Discussion

Perchlorates. The general appearance of the TG-DTA curves obtained in N_2 is shown in Fig. 1, taking the case of the Nd complex as an example. Essentially similar data are obtained with other perchlorates.

The complex begins to lose a part of its TMU molecules when heated to a certain temperature t_i, and a step AB, which is usually rather dull as shown in Fig. 1, appears on the TG curve. At the end of this step, *n* molecules of TMU are lost from the complex.

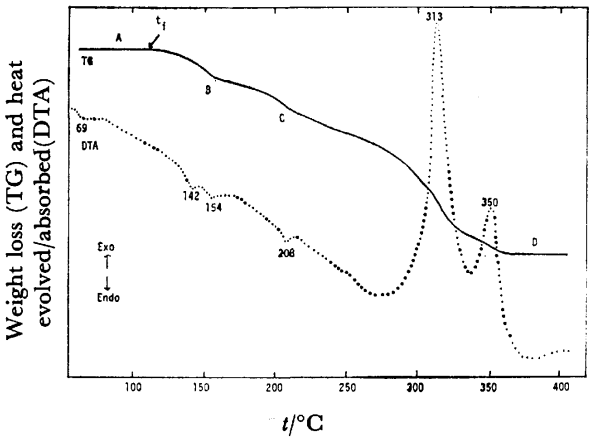

Fig. 1. TG and DTA curves of $Nd(TMU)_6(ClO_4)_3$ in N_2.

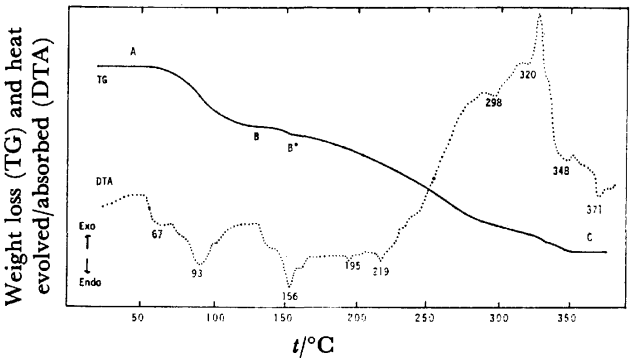

Fig. 2. TG and DTA curves of $Nd(TMU)_6(ClO_4)_3$ in a vacuum.

Then comes another step BC, which is more dull than the step AB and often is observed as a slight inflection of the TG curve, in the course of which some more TMU molecules are lost. Then comes the decomposition of the remaining complex, first gradually but more and more quickly with the rise of temperature, up to a point D, where the weight of the residue becomes nearly constant. The weight loss at D, expressed in percent of the initial weight, will be denoted with Δ.

Table 1 summarizes the values of t_i, *n*, and Δ of all the perchlorates studied, together with the values observed in a vacuum (see later). One can readily

Table 1. Values of t_1, n, and Δ for the complexes $Ln(TMU)_6(ClO_4)_3$

Ln	In N_2			In a vacuum		
	t_1	n[a]	Δ[b]	t_1	n[c]	Δ
Pr	108	1.2	79.1(78 2)	34	2.9	82.5
Nd	110	1.3	77.6(78.0)	48	2.6, 2.9	88.5
Sm	109	1.3	79.2(77.6)	63	2.3, 3.1	88.5
Eu	115	1.2	80.2(77.5)	65	2.8, 3.1	87.2
Gd	124	1.4	76.8(77 2)	57	1.6, 2.3	89.5
Tb	123	1.4	76.6(77.0)	59	1.6	90.2
Dy	124	1.3	75.8(76.8)	67	1.7	90.4
Ho	122	1.3	75.7(76.6)	66	2.1	89.6
Er	134	1.2	77.1(76.5)	73	1.4	89.2
Tm	134	1.3	76.7(76.4)	72	2.7	88.6
Yb	141	1.2	72.3(76.1)	65	2.6, 2.8	91.2
Lu	140	1.3	76.2(76.0)	70	2.7, 2.9	90.9
Y	143	1.2	82.3(82.0)	73	3.1	92.3

a) The values are only approximate owing to the dullness of the step in most cases. b) The values calculated for the complete transformation into $LnCl_3$ are shown in parentheses. c) Two inflection points are often observed at the foot of the step, as the points B and B′ in Fig. 2. The n values corresponding to each of them are given in such cases.

understand that, as to the thermal changes in N_2, there are the following relationships among these values:

1) The value of t_1 rises gradually from Pr to Lu, corresponding to the strengthening of the Ln–TMU bonds caused by the effect of the lanthanoid contraction.

2) The values of n lie in the range of 1—1.5, and do not depend remarkably on the position of Ln in the series. Nearly the same amount of TMU seems to be lost in the next step BC. Taking the dullness of these steps and their possible overlap into account, one can estimate that, in general, about 1.5 molecules of TMU are lost in the step AB, and about 3 in the two consecutive steps AB+BC.

3) The values of Δ correspond, reasonably well, to those expected when the complexes are converted completely into $LnCl_3$ at the end of their decomposition.

4) The steps AB and BC are accompanied by a few weakly endothermic peaks on the DTA curve, but the subsequent decomposition CD is accompanied by a very strong exothermic peak, with a much weaker one which appears at the high temperature end of CD.

All these relationships can now be reasonably well understood by the following picture. On heating the complex, a part of the coordinated TMU molecules are liberated endothermically in two steps which, approximately, can be formulated as follows:

$$Ln(TMU)_6(ClO_4)_3 \longrightarrow Ln(TMU)_{4.5}(ClO_4)_3 + 1.5TMU,$$

$$Ln(TMU)_{4.5}(ClO_4)_3 \longrightarrow Ln(TMU)_3(ClO_4)_3 + 1.5TMU.$$

In the course of these changes,** on the other hand, the ClO_4^- ions will come into closer contact with the Ln^{3+} ions which lost some of their bulky ligands. So they will be polarized and eventually begin to decompose by further heating:[6]

$$ClO_4^- \longrightarrow Cl^- + 4O.$$

The O atoms liberated will oxidize the TMU molecules which are still in the complex. Since the number of O atoms liberated is insufficient to oxidize them completely, there will be partial oxidation or incomplete combustion of the ligands by the anions. This will certainly be a strongly exothermic process. When this combustion is over, $LnCl_3$ is left as the final residue.

The data obtained in a vacuum*** are, in general, similar to those in N_2, but some apparent differences can be discerned.

1) The t_1 values are much lower than those in N_2, showing that the initial release of TMU is notably facilitated by evacuation. Here again there is a general rise of t_1 along the series, but there are some deviations which suggest that they are composed of three parts, Pr–Eu, Gd–Er, and Tm–Lu, corresponding to the variation of n (see below; *cf.* Fig. 3A).

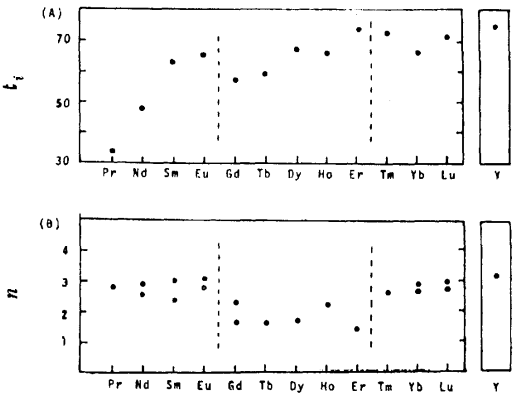

Fig. 3. t_1 and n values of $Ln(TMU)_6(ClO_4)_3$ in a vacuum plotted against the atomic number of Ln.

2) The n values are again *ca.* 1.5 for the middle-weight members of the series, Gd–Er, but are definitely larger and *ca.* 3 for the lighter and heavier members and Y. In these latter cases, the two steps AB and BC observed in N_2 are seemingly united into a single more well-defined step; one can also say that, in a vacuum, all the three TMU molecules which are lost in two steps in N_2 are driven off at once, at temperatures which are much lower than in N_2. In the case of the middle-weight members, however, the complex $Ln(TMU)_{4.5}(ClO_4)_3$ retain certain thermal stability even in a vacuum, and the release of further TMU ligands and the final decomposition occur without any clear step (*cf.* Fig. 3B).

These results can now be explained as follows: The complexes of the lighter members, with larger ionic radii of Ln^{3+}, will contain weaker Ln–TMU bonds, and

** It is highly probable that the complexes thus formed, with 4.5 and 3 molecules of TMU, respectively, are dimeric or polymeric in nature; for example, the one with 4.5 TMU can be formulated as $Ln_2(TMU)_9(ClO_4)_6$, *i.e.*, a dimer with each Ln^{3+} surrounded by three terminal and three bridging TMU ligands.[5]

*** Only TG data will be discussed here, because the DTA curves obtained in a vacuum are complicated in their appearance, and their accuracy cannot be as high as those in N_2 in principle.

it is also possible that their coordination spheres are not perfectly packed with six TMU ligands, so that the $Ln^{3+}\cdots ClO_4^-$ interaction will be stronger than in the complexes with smaller Ln^{3+} ions. These situations will favor the driving out of as many TMU molecules as possible by slight heating. In the case of the heavier members, on the other hand, the coordination spheres will be heavily crowded with TMU ligands, and their mutual repulsion will destabilize the structure, so that the driving out of many TMU molecules by heating is again favored. There is probably a "safety zone" between these two extremes, where the complexes $Ln(TMU)_{4.5}X_3$ can enjoy their thermal stability.

3) The Δ values are all much higher than those in N_2, and the differences between the two sets of values increase from Pr to Lu (*cf.* Table 1). In most cases, rather strangely, the weights of the final residues were even lower than those of the lanthanoid elements themselves in the original samples. Taking the experimental conditions (relatively low temperature, slow heating rate, *etc.*) and the nature of the samples into account, the most probable reason for this anomaly seems to be found in the formation of some volatile Ln-containing product in the course of the decomposition. Such a product will escape from the sample as soon as it is formed in a vacuum, causing the decrease of Δ as observed.**** However, we could not identify this volatile complex, mainly owing to its small quantity (at most 1 mg).

Table 2. Values of t_i and Δ for the complexes $Ln(TMU)_6X_3$, where X is PF_6 or BPh_4

Ln	X	In N_2		In a vacuum	
		t_i	Δ	t_i	Δ[a]
Sm	PF_6	73	80.5	40	82.8(83.8)
Gd	PF_6	64	80.8	43	81.1(83.4)
Dy	PF_6	79	81.2	43	81.7(83.1)
Er	PF_6	85	77.8	53	82.6(82.7)
Nd	BPh_4	176	82.0	119	86.6
Eu	BPh_4	136	82.2	131	—
Y	BPh_4	194	86.5	154	93.5

a) The values for the complete transformation into LnF_3 are shown in parentheses.

Hexafluorophosphates. The complexes $Ln(TMU)_6(PF_6)_3$ shown in Table 2 all show a single step in their TG curves, either in N_2 or in a vacuum (see Fig. 4 for an example), and the Δ values observed roughly correspond to those of LnF_3 formed by the reaction:

$$Ln(TMU)_6(PF_6)_3 \longrightarrow LnF_3 + 3PF_5 + 6TMU.$$

It can be seen that the t_i values for this single step are much lower than in the case of the perchlorates, corresponding to the high heats of formation of LnF_3 and PF_5.[7] Since PF_5 is a fairly stable molecule, only a strong endothermic peak is observed on the DTA curves, corresponding to the total disintegration of the complex.

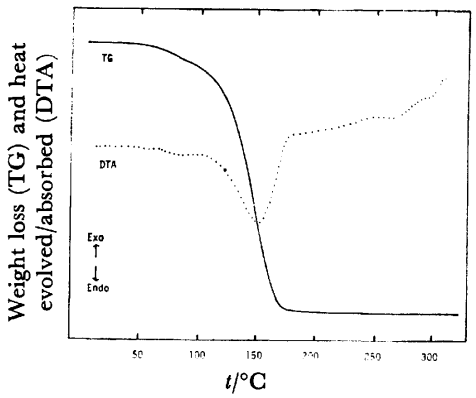

Fig. 4. TG and DTA curves of $Gd(TMU)_6(PF_6)_3$ in a vacuum. Essentially similar curves are obtained, either in N_2 or in a vacuum, with the complexes shown in Table 2. In some case it is seen that a small part of TMU is lost in advance of the main decomposition (*cf.* the small DTA peak (and weak TG shoulder) at *ca.* 85 °C and the large peak at 152 °C in this figure), but its amount is difficult to estimate.

Tetraphenylborates. On the other hand, the complexes $Ln(TMU)_6(BPh_4)_3$, also shown in Table 2, decompose only with much difficulty. Their TG curves are more or less like those of the hexafluorophosphates, composed of a single TG step and DTA peak, but their t_i values are quite high, and their Δ values are incompatible with any simple picture for their decomposition.

Although the nature of the thermal changes involved here is thus not clear as yet, the higher t_i values (or difficulty of decomposition) of these complexes can certainly be related to the inability of BPh_4^- for coordination. We can imagine that the thermal decompositions observed here are, in general, initiated by the S_N2-type attack of the anion (or a part of the anion, such as F^-), by which some TMU ligands are driven out of the coordination sphere. If this idea is essentially true, it is easy to see why the ease of decomposition increases in the following order of anions:

$$BPh_4^- < ClO_4^- < PF_6^-,$$

since BPh_4^- is a practically non-coordinating anion, and PF_6^- is easily split into F^- and PF_5, they will come before and after ClO_4^- in this series, respectively.

Thus we see that TG and DTA techniques can bring about a number of new insights into these complexes, as in the case of the Ln complexes of dimethyl sulfoxide and tetrahydrothiophene 1-oxide studied before.[8] The earlier TG-DTA data of Seminara *et al.*[9-10] on the Ln complexes of various urea derivatives, including $Gd(TMU)_3Cl_3$, may also be of interest in connection with the present study.

**** At first, it was suspected that the complexes $Ln(TMU)_3Cl_3$ may be the volatile complexes, but preliminary studies on them (Ln=Nd and Er) showed that they are not remarkably volatile in a vacuum, and lose their TMU molecules by heating (t_i: 85—90 °C) in a complicated way.

References

1) As to the general properties and solvent behaviors of TMU, *cf.* B. J. Barker and J. A. Caruso, "The Chemistry of

Nonaqueous Solvents," ed by J. J. Lagowski, Academic Press, New York (1976), Vol. 4, p. 110.

2) E. Giesbrecht and M. Kawashita, *J. Inorg. Nucl. Chem.*, **32**, 2461 (1970).

3) M. K. Kuya, S. M. Melo, and O. A. Serra, *An. Acad. Brasil. Cienc.*, **51**, 239 (1979).

4) M. K. Kuya and O. A. Serra, *J. Coord. Chem.*, **10**, 13 (1980).

5) *Cf.* also M. Perrier, R. Najjar, and G. Vicentini, *An. Acad. Brasil. Cienc.*, **42**, 439 (1970), where the data on the complex $LaCl_3 \cdot 3.5$ TMU are given and the possibility of its dimeric nature is suggested.

6) As to the thermal decomposition of perchlorates, *cf.* A. J. Downs and C. J. Adams, "Comprehensive Inorganic Chemistry," ed by J. C. Bailar, Jr., *et al.*, Pergamon Press, Oxford, (1973), Vol. 2, p. 1448.

7) *Cf.* N. V. Sidgwick, "Chemical Elements and Their Compounds," Clarendon Press, Oxford (1950), Vol. 1, p. 757, where a similar decomposition of the diazonium salts of PF_6^- is described.

8) K. Nagase, H. Yokobayashi, A. Iwase, and K. Sone, *Thermochim. Acta*, **17**, 335 (1976).

9) A. Seminara, A. Musumeci, and G. Condorelli, *Ann. Chim. (Rome)*, **59**, 978 (1969).

10) A. Seminara and G. Condorelli, *Ann. Chim. (Rome)*, **59**, 990 (1969).

 © 1982 The Chemical Society of Japan Bull. Chem. Soc. Jpn., 55, 453—454 (1982)

Stereochemistry of Bis[*N*-(2,6-diisopropylphenyl)salicylideneaminato]-cobalt(II) Complexes

Shoichiro YAMADA* and Kuniko YAMANOUCHI

Institute of Chemistry, College of General Education, Osaka University, Toyonaka, Osaka 560

(Received July 28, 1981)

The compounds bis[*N*-(2,6-diisopropylphenyl)salicylideneaminato]cobalt(II) and analogous species with substituents at the 5-position of the salicyl moiety have been synthesized. They prefer the tetra-coordinate tetrahedral geometry in non-donor solvents, while some of them are forced into planar structures in the solid state. In pyridine, exclusively predominant species are five-coordinate complexes with the base bound with the cobalt(II) ion. Monopyridine adducts, which consist of five-coordinate complexes, have been isolated as crystals.

The stereochemistry of the cobalt(II) complexes with bidentate *N*-aryl- and *N*-alkylsalicylideneaminates, abbreviated as Co(X-sal-R)$_2$, has been widely studied.[1,2] In order to investigate the steric and electronic effects of the Schiff bases on the stereochemistry of these cobalt(II) complexes, a series of bis[*N*-(2,6-dialkylphenyl)salicylideneaminato]cobalt(II) complexes were studied previously, the alkyl being methyl and ethyl.[3]

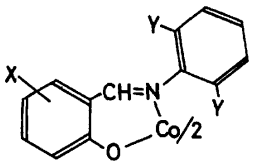

I

In the present work, cobalt(II) complexes of the type Co(X-sal-R)$_2$, for which R is 2,6-diisopropylphenyl, have been examined. It is anticipated that the steric effects arising from the substituents at the 2- and 6-positions may become more explicit in the complexes of this series, since the isopropyl group is more bulky than the methyl and ethyl groups. During this study, we have isolated for the first time the spin-paired planar cobalt(II) complexes with the *N*-arylsalicylideneaminates.

Experimental

Materials. 2,6-Diisopropylaniline was obtained commercially.

Bis[*N*-(2,6-dissopropylphenyl)salicylideneaminato]cobalt(II) and analogous species, which are abbreviated as Co(X-sal-dpp)$_2$, were synthesized in red-orange crystals in the same manner as reported previously.[2,3] They are readily soluble in chloroform, benzene, and acetone, but slightly soluble in ethanol.

Monopyridine adducts were also obtained in orange crystals as described previously.[2,3]

Analytical data of these complexes are given in Table 1.

Measurements. Electronic absorption spectra of the complexes in solution and in Nujol were recorded on a Shimadzu MPS-500 spectrophotometer. Magnetic measurements at room temperature were carried out by the Gouy method using $CoHg(SCN)_4$ as a calibrant.

TABLE 1. ANALYTICAL DATA OF BIS[*N*-(2,6-DIISOPROPYLPHENYL)SALICYLIDENEAMINATO]COBALT(II), Co(X-sal-dpp)$_2$

Compound	Calcd (%)			Found (%)			μ[a]
	H	C	N	H	C	N	BM
Co(H-sal-dpp)$_2$	7.15	73.65	4.52	7.18	73.93	4.63	4.5
Co(5-Br-sal-dpp)$_2$	5.45	58.70	3.60	5.32	58.72	3.61	2.4
Co(5-Cl-sal-dpp)$_2$	6.15	66.28	4.07	6.22	66.23	4.13	2.6
Co(5-NO_2-sal-dpp)$_2$	5.97	64.31	7.89	6.06	63.99	7.75	5.1
Co(H-sal-dpp)$_2$·py[b]	7.07	73.90	6.01	6.97	73.82	6.07	5.0
Co(5-Br-sal-dpp)$_2$·py	5.53	60.29	4.91	5.33	60.26	4.95	4.8
Co(5-Cl-sal-dpp)$_2$·py	6.17	67.27	5.47	6.15	67.27	5.46	4.9
Co(5-NO_2-sal-dpp)$_2$·py	6.01	65.47	8.88	6.13	65.44	9.15	4.8

a) At room temperature. b) py: Pyridine.

Results and Discussion

Previous extensive studies of cobalt(II) complexes with bidentate *N*-alkyl- and *N*-arylsalicylideneaminates have disclosed that all these cobalt(II) complexes are tetrahedral,[1,2] with the exception of bis(*N*-methylsalicylideneaminato)cobalt(II), which consists of binuclear molecules with the cobalt(II) ion in five-coordinate environment.[4]

In the complexes (I), the steric constraint due to the bulky substituent (R-2,6-Y_2-C_6H_3) seems to be appreciable. In view of the conformations observed in all known crystal structure analyses, the phenyl group in the complexes is expected to be essentially perpendicular to the salicylideneaminate plane.[1] The cobalt(II) complexes with R=2,6-Me_2-C_6H_3 and 2,6-Et_2-C_6H_3 prefer the tetra-coordinate tetrahedral geometry in the solid state and in non-donor solvents, although the steric constraint is not slight.[3] In the cobalt(II) complexes with R=2,6-(*i*-Pr)$_2$-C_6H_3, which is more bulky than 2,6-$Et_2C_6H_3$, there is remarkable steric constraint not only on the tetrahedral configuration but also on the planar one. However, either of the two configurations is not precluded from the steric condition alone.

The cobalt(II) complexes Co(X-sal-dpp)$_2$ (X=H, 5-Cl, 5-Br, and 5-NO_2) in chloroform show electronic spectra typical of the tetrahedral cobalt(II) complex.[2] Some of the representative spectra are shown in Fig. 1, the main absorption maxima being set out in Table 2.

In the solid state, the configuration of these cobalt(II) complexes depends upon the substituent X at the 5-position of the salicyl moiety. The cobalt(II) complex (X=H) in the solid state is concluded to have a tetrahedral configuration on the basis of the magnetic moment (4.4 BM) and an electronic spectrum with a broad d-d band consisting of double humps at about 8.2

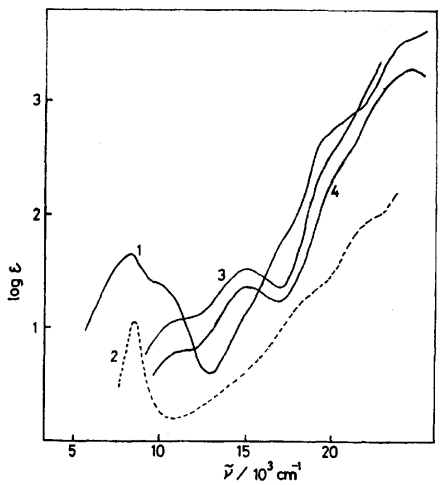

Fig. 1. Electronic absorption spectra of Co(5-Br-sal-dpp)$_2$ (curves 1—3) and Co(5-Br-sal-dpp)$_2$·py (curve 4).
1: In $CHCl_3$, 2: in Nujol (arbitrary absorbance scale), 3: in pyridine; 4: in Nujol (arbitrary absorbance scale).

and 10.7×10^3 cm^{-1}. On the contrary, the two complexes (X=5-Cl and 5-Br) in the solid state are paramagnetic with magnetic moments at room temperature of 2.6 and 2.4 BM, respectively, which lie in the range expected for the spin-paired planar cobalt(II) complex.[5] Their electronic spectra have a comparatively sharp d-d band at about 8.5 and 8.4×10^3 cm^{-1}, respectively, in agreement with the spin-paired planar structure.[6] Thus they provide new examples of spin-paired planar cobalt(II) complexes with bidentate *N*-arylsalicylideneaminates. Since the two complexes are tetrahedral in chloroform, the energy gap between the tetrahedral and the planar configurations seems to be small.

In pyridine, these cobalt(II) complexes Co(X-sal-dpp)$_2$ (X=H, 5-Cl, 5-Br, and 5-NO_2) exist exclusively as five-coordinate species with a pyridine molecule coordinated. Beer's law is found to hold good, so that no assumption of equilibria among various species with different structures is needed. The five-coordinate pyridine adducts have been isolated in crystals from the pyridine solutions, their spectra (Fig. 1 and Table 2) being in agreement with the proposed five-coordinate structure. Six-coordinate bis(pyridine)adducts have neither been detected in the solutions, nor isolated in crystals.

The complex (X=5-NO_2) in the solid state has magnetic moment of 5.1 BM, which is in the range expected for the 6-coordinate cobalt(II) complex. Its electronic spectrum (Table 2) is also typical of the 6-coordinate cobalt(II) complex. A multinuclear structure is most likely, although a definitive conclusion about the precise structure must await further studies.

Financial support of this work by the Ministry of Education, Science and Culture is gratefully acknowledged.

References

1) R. H. Holm and M. J. O'Connor, *Prog. Inorg. Chem.*, **14**, 241 (1971).
2) S. Yamada, *Coord. Chem. Rev.*, **1**, 415 (1966).
3) S. Yamada and E. Yoshida, *Bull. Chem. Soc. Jpn.*, **38**, 683 (1965); **40**, 1298, 1395, 1854 (1967); *Proc. X. ICCC*, Tokyo and Nikko (1967), p. 275; S. Yamada, E. Yoshida, and Y. Kuge, *Pcoc. IX. ICCC*, St. Moritz (1966), p. 68.
4) P. O. Orioli, O. Sacconi, and M. Di Vaira, *Chem. Commun.*, **1**, 103 (1965); *Inorg. Chem.*, **5**, 400 (1966).
5) B. N. Figgis and J. Oewis, *Prog. Inorg. Chem.*, **6**, 37 (1964).
6) H. Nishikawa and S. Yamada, *Bull. Chem. Soc. Jpn.*, **37**, 8 (1964).

TABLE 2. MAIN ABSORPTION MAXIMA OF BIS[*N*-(2,6-DIISOPROPYLPHENYL)-SALICYLIDENEAMINATO]COBALT(II), Co(X-sal-dpp)$_2$

Compound	Medium	$\tilde{\nu}/10^3$ cm^{-1} (log ε)		
Co(H-sal-dpp)$_2$	$CHCl_3$	8.2 (1.77)	10.3 (1.46) sh	
	Nujol	8.2	10.7 sh	
	py	7.3 (0.85)	11.0 (1.06)	15.1 (1.46)
Co(H-sal-dpp)$_2$·py	Nujol	7.2	11.1	15.2
Co(5-Cl-sal-dpp)$_2$	$CHCl_3$	8.3 (1.59)	10.1 (1.36) sh	
	Nujol	8.4 (sharp)		
	py	7.3 (0.85)	11.3 (1.07)	15.3 (1.52)
Co(5-Cl-sal-dpp)$_2$·py	Nujol	7.2	11.3	15.3
Co(5-Br-sal-dpp)$_2$	$CHCl_3$	8.3 (1.65)	10.2 (1.35) sh	
	Nujol	8.4 (sharp)		
	py	7.3 (0.82)	11.0 (1.05)	15.2 (1.51)
Co(5-Br-sal-dpp)$_2$·py	Nujol	7.1	11.2	15.2
Co(5-NO_2-sal-dpp)$_2$	$CHCl_3$	8.1 (1.84)	10.2 (1.60) sh	
	Nujol	9.6	16.3 sh	26.0 (CT) str
	py	7.2 (0.81)	11.4 (1.25) sh	15.2 (1.78)
Co(5-NO_2-sal-dpp)$_2$·py	Nujol	7.0	11.3	15.3

sh: Shoulder. str: Strong. CT: Charge transfer band.

An X-Ray Diffraction Study on the Structures of Bis- and Tris-(ethylenediamine)nickel(II) Complexes in Solution

Tadao FUJITA and Hitoshi OHTAKI*

Department of Electronic Chemistry, Tokyo Institute of Technology at Nagatsuta, Nagatsuta-cho, Midori-ku, Yokohama 227

(Received August 21, 1981)

The structures of nickel(II) complexes with ethylenediamine(en) in solution have been determined by means of X-ray diffraction. The measurements were performed at 25 °C for aqueous ethylenediamine solutions of nickel nitrate, the mole ratios (en/Ni) in the solutions being 3.964, 3.672, 2.071, and 1.892. In the two solutions of the higher en/Ni mole ratio, the tris(ethylenediamine)nickel(II) complex was predominant, whereas in the other solutions the bis(ethylenediamine)nickel(II) complex was contained as the main species. From the analysis of the X-ray scattering data of the solutions, it was shown that in the bis-complex four nitrogen atoms within ethylenediamine and two oxygen atoms within water molecules were octahedrally coordinated to the central nickel(II) atom, the oxygen atoms being assumed to be axially bonded. The Ni–N bond length within the bis-complex was 2.10 Å, which was almost the same as the length of the Ni–O bonds. The nonbonding Ni···C distance was 2.82(2) Å. In the tris-complex the nickel ion was coordinated with six nitrogen atoms and Ni–N and Ni···C distances were determined to be 2.202(4) Å and 2.88(1) Å, respectively. These parameter values obtained in the experiment were compared with the crystallographic data reported.

The structures of the bis- and tris(ethylenediamine)-zinc(II) and -cadmium(II) complexes have recently been reported.[1,2] In the present study, we have attempted to determine the structures of the bis- and tris(ethylenediamine)nickel(II) complexes in aqueous nitrate solutions in a series of structural studies of chelate complexes of transition metals in solution. The ground state of a nickel(II) octahedral complex is known to have the electronic configuration of $(t_{2g})^6(e_g)^2$ and thus most nickel(II) complexes have the O_h symmetry in the solid state. In a complex of the NiA_4B_2 type (A and B denote ligand atoms) in which B atoms locate along the axis of the octahedron, the symmetry of the complex may be approximated to be D_{4h}. Most of the bis-nickel(II) chelate complexes with bidentate ligands have the symmetry of this type.[3] The distortion of the symmetry of such nickel(II) complexes has been extensively investigated by means of electronic spectra and X-ray diffraction in crystal.[4]

Dorosh and Skryshevskii[5] reported the distorted octahedral structures of $Ni(OH_2)_6^{2+}$ with two different Ni–O bond lengths of 2.0—2.1 and 2.25—2.30 Å by means of X-ray diffraction in solution. However, according to a recent study the $Ni(OH_2)_6^{2+}$ complex has a regularly octahedral structure with the length of Ni–O=2.04 Å.[6]

Many works on the crystal structures of the $Ni(en)_3^{2+}$ complex with various counter anions have been carried out and showed that the $Ni(en)_3^{2+}$ complex has a regularly octahedral structure independent of the counter anions. In the $Ni(en)_3SO_4$ salt, the Ni–N bond length was found to be 2.12 Å.[7] In the structure of $Ni(en)_2(NCS)_2$, on the other hand, the equatorial Ni–N bond distance was 2.10 Å and the Ni–NCS bond length in the axial position was 2.15 Å, the latter being slightly longer than the former. Thus the structure of the $Ni(en)_2(NCS)_2$ complex is distorted octahedral.[8] The structure of the $Ni(en)_2(OH_2)_2^{2+}$ has not been investigated either in the crystalline state or in solution. In this paper, the structural determination of the bis- and tris(ethylenediamine)nickel(II) complexes has been attempted by the X-ray diffraction method in solution.

Experimental

Preparation and Analysis of Sample Solutions. Ethylenediamine was purified by the method previously reported.[1] Nickel(II) nitrate of reagent grade was purchased from Wako Pure Chemical Co., Osaka and was recrystallized twice from water. The sample solutions were prepared by dissolving nickel(II) nitrate into aqueous ethylenediamine solutions.

The concentration of nickel(II) ions in the test solutions was determined by gravimetry using dimethylglyoxime. The concentration of the nitrate ion was calculated from the stoichiometry of the nickel nitrate. The density of the test solutions was measured pycnometrically. The composition of the test solutions is given in Table 1.

Table 1. Composition of solutions A, B, C, and D (mol/dm³)

	A	B	C	D
Ni	1.476	1.356	1.717	1.787
N	13.79	13.46	10.54	10.34
C	10.84	10.75	7.113	6.762
O	42.69	42.34	50.13	50.09
H	111.0	111.4	106.1	92.27
ρ/g cm^{-3}	1.205	1.187	1.227	1.237
V/Å^3	1267	1224	967.1	929.2
en/Ni	3.672	3.964	2.071	1.892

Method of Measurements and Treatment of X-Ray Scattering Data. The method of measurements and the apparatus used were essentially the same as those in previous papers.[6,9] Mo $K\alpha$ radiation (λ=0.7107 Å) was used for the measurements over the range $1° < \theta < 70°$ (2θ is the scattering angle). The data were recorded twice over the whole angle range. Corrections and analysis of the scattering data were performed in the same ways to those previously reported.[1,2,6,9,10] Coherent and reduced intensities of the test solutions are given in Figs. 1 and 2, respectively. The radial distribution function $D(r)$ was calculated by the following equation:

$$D(r) = 4\pi r^2\rho_0 + \frac{2r}{\pi}\int_0^{s_{max}} s\cdot i(s)\cdot M(s)\cdot\sin(rs)\mathrm{d}s, \quad (1)$$

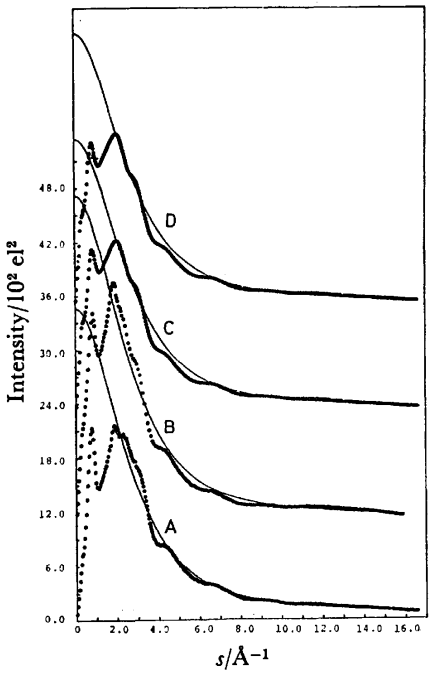

Fig. 1. Coherent scattering intensities of sample solutions A, B, C, and D. Experimentally obtained intensities I^{coh} are shown by circles and calculated values of independent scattering intensities by solid lines.

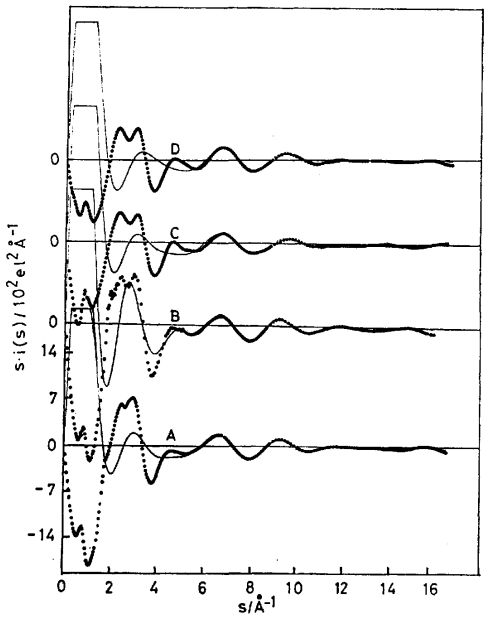

Fig. 2. The reduced intensities multiplied by s for solutions A, B, C, and D. The observed $s \cdot i(s)$ curves are shown by circles and the calculated ones by solid lines.

where ρ_0 is the average scattering density in the stoichiometric volume V of the solution per Ni atom, and s_{max} denotes the maximum s-value attained in the measurements ($s_{max}=16.7$ Å^{-1}). $M(s)$ represents the modification function[10] and the reduced intensities $i(s)$ are given by

$$i(s) = I^{coh}(s) - \sum n_i\{(f_i(s) + \Delta f_i')^2 + (\Delta f_i'')^2\}, \quad (2)$$

where n_i is the number of atom i and $f_i(s)$ denotes the scattering factor of atom i at s. $\Delta f_i'$ and $\Delta f_i''$ represent the real and imaginary parts of the anomalous dispersion, respectively.[11] The radial distribution curves $D(r)$ of the solutions were drawn after the Fourier transform of the reduced intensities which had been smoothed by the method described previously.[6]

The theoretical scattering intensities due to atom pairs of all possible combinations in the system were given as follows:

$$i_{calcd}(s) = \sum_{i}\sum_{i\neq j}\sum_{j} n_{ij}\{(f_i(s) + \Delta f_i')(f_j(s) + \Delta f_j') + (\Delta f_i'')(\Delta f_j'') \cdot \frac{\sin(r_{ij}s)}{(r_{ij}s)} \cdot \exp(-b_{ij}s^2), \quad (3)$$

where r_{ij}, b_{ij}, and n_{ij} denote the distance, the temperature factor, and the frequency factor of the atom pair i-j, respectively.

All calculations were performed with the electronic computers M-160 and M-180 by means of KURVLR program.[12]

Results and Discussion

According to the formation constants so far reported, sample solutions A and B contain the tris(ethylenediamine)nickel(II) complex as the main species and, on the other hand, sample solutions C and D contain the bis(ethylenediamine)nickel(II) complex as the predominant one.[13] Solutions A and B may contain a little amount of the bis-complex. In solutions C and D, small amounts of the mono- and tris-complexes may coexist with the bis-complex.

Solution A. From the diffraction data after corrections for absorption and polarization[9] (Fig. 1A), the $s \cdot i(s)$ curve (Fig. 2A) was obtained and then, the radial distribution function $D(r)$ was drawn by using the Fourier transformation according to Eq. 1 (Fig. 3a). A broad and small peak at about 1.0—1.3 Å in the $D(r)$ curve is composed of peaks due to the O–H bond within water, the N–H, C–H, C–C, and C–N bonds within ethylenediamine molecules and the N–O bond within nitrate ions as we have pointed out in the previous papers[1,2] (Fig. 3b). The second peak appearing at 2.2 Å is attributed to the Ni–N bond within the metal complex, the O···O pairs within nitrate ions and the C···N interactions within ethylenediamine molecules.

The third peak at about 2.9 Å may be mainly ascribed to nonbonding Ni···C and O···O interactions within the metal complex and in bulk water, respectively. The O···O interactions between nitrate ions and water molecules may contribute to some extent to this peak. In the analysis of the radial distribution curve of solution A which contains a small amount of the bis-complex, the amount of the bis-complex coexisting was assumed to be negligible at the first approach. After subtraction of the theoretical peaks of the intramolecular interactions within ethylenediamine molecules and nitrate ions, the chain line (·—·—·) was obtained as the residual curve, from which we obtained the parameter values of intramolecular interactions of the tris-complex. A successive approximation which has been described in the previous papers[1,2] was employed in order to refine the parameter values thus obtained on the assumption of the existence of the only tris-complex, but assumptions taking into account the coexistence of various amounts of the bis-complex in

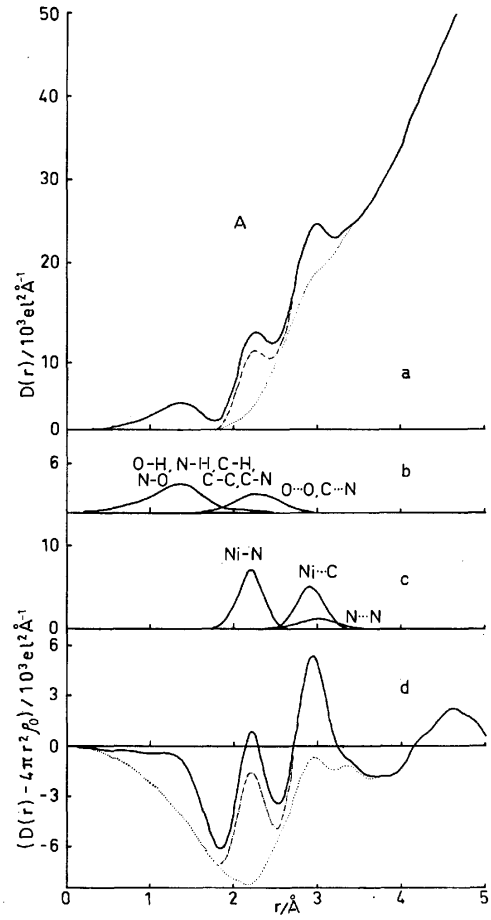

Fig. 3. (a) : $D(r)$ curve for solution A. The chain line (·–·–) shows the residual curve after subtraction of the theoretical peak shapes shown in (b) from the original radial distribution curve represented by the solid line. The dotted line shows the residual curve after subtraction of the theoretical peak shapes shown in (c) from the data represented by the chain line. (b) and (c) : The theoretical peak shapes for atom pairs. (d) : The corresponding $D(r)-4\pi r^2\rho_0$ curve to (a).

solution A did not improve the parameter values of the tris-complex. The lengths of the Ni–N bond and nonbonding Ni···C interaction were found to be 2.20 and 2.90 Å, respectively. The distance of the N···N pair was estimated to be $\sqrt{2}$ times the length of the Ni–N bond. The area under the peak at 2.20 Å corresponded to six Ni–N bonds. The temperature factors of the Ni–N and Ni···C interactions were evaluated to be 0.002—0.003 Å² and 0.005—0.007 Å², respectively. Subtraction of the peaks of all the intramolecular interactions from the original radial distribution curve led to a smooth background having no appreciable peak over the range <4 Å, expect for the peak at about 2.9 Å which was ascribed to the adjacent O···O interactions in the bulk water and hydrated nitrate ions. From the analysis of the radial distribution curve of solution A, the tris(ethylenediamine)nickel(II) complex in the solution was concluded to have an octahedral structure.

Solution B. The atomic composition in solution B was almost the same as that in solution A, and solution B was considered to contain the tris(ethylenediamine)-nickel(II) complex as the main species with a very small amount of the bis-complex. The analytical procedure of solution B was the same as that in the case of solution A. The radial distribution curve of solution B showed that the lengths of the Ni–N bond and nonbonding Ni···C interaction were 2.20 Å and 2.90 Å, respectively, which were consistent with the results obtained in solution A. The parameter values of the tris(ethylenediamine)nickel(II) complex are further refined by the least squares method by using the reduced intensity data in the high angle region of the $s\cdot i(s)$.

Solutions C and D. According to the stability constants previously reported, solutions C and D contain a small amount of the tris- and mono-complexes besides the bis-complex as the main species.[10] In the course of the analysis of the radial distribution curve

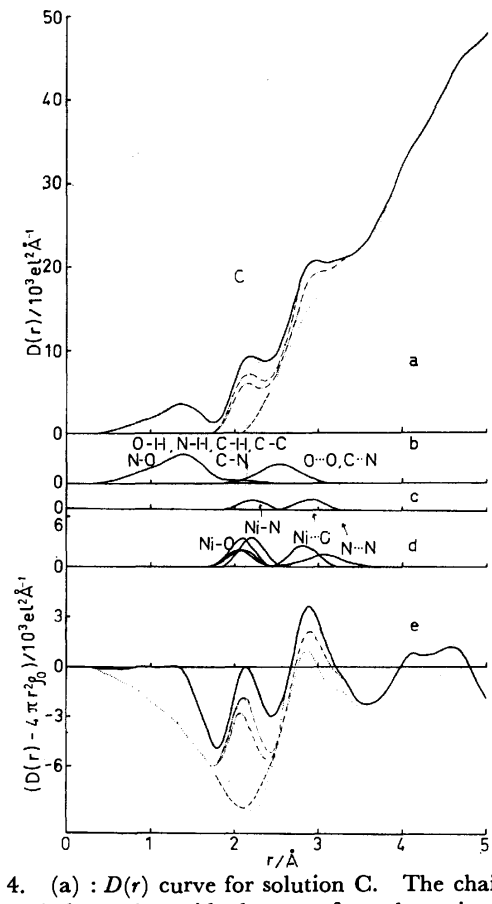

Fig. 4. (a) : $D(r)$ curve for solution C. The chain line (·–·–) shows the residual curve after subtraction of the theoretical peaks in (b). The chain line with double-dots (···–··) is obtained after further subtraction of the theoretical peak shapes due to the tris-complex in (c) from the data represented by the chain line, ·–·–. After subtraction of the theoretical peak shapes due to the biscomplex assuming that both the Ni–N and Ni–O bond distances are 2.10 Å, the dashed line is obtained as the residual curve. Assuming that the Ni–O distance is the same as that $Ni(OH_2)_6^{2+}$ and that the Ni–N distance is slightly larger than 2.10 Å, the dotted line is obtained as the residual curve. (b), (c), and (d) : The theoretical peak shapes for atom pairs. (e) : The corresponding $D(r)-4\pi r^2\rho_0$ curve to (a).

in solution C, the tris-complex was assumed to coexist with the bis-complex, whereas the formation of the mono-complex was neglected.

The analytical procedure of the radial distribution curve of solution C is as follows.

By introducing the parameter values of the tris-complex found from the analysis of solutions A and B, the parameter values of the bis(ethylenediamine)nickel(II) complex was obtained by changing the mole ratio of the bis-/tris-complexes until a smooth background curve was obtained in the residual radial distribution curve. The chain line (·-·-·) in Fig. 4 was obtained after subtraction of the peaks of the intramolecular interactions of ethylenediamine molecules and nitrate ions from the original radial distribution curve, and further subtraction of the theoretical peaks of the tris-complex from the curve led to the chain line with double-dots (·····). The curve (·····) might show the radial distribution curve due to the bis-complex. The area under the peak at 2.10 Å approximately corresponded to six Ni–N pairs. Since the bis-complex has at most four Ni–N bonds within it, the other two pairs must be Ni–O ones, because X-ray scattering due to the Ni–O bond is close to that due to the Ni–N bond as far as the bond lengths of the pairs are practically the same. Thus, we concluded that the bis-complex has four Ni–N bonds and two Ni–O bonds within the complex.

The structure of $Ni(OH_2)_6^{2+}$ in an $Ni(ClO_4)_2$ solution has been determined by X-ray diffraction method and the length of the Ni–O bond has been estimated to be 2.04 Å.[6] Bol, *et al.*[14] reported a slightly longer Ni–O bond length (2.06 Å) in a nickel(II) nitrate solution than that reported by Ohtaki *et al.*[6] However, if we assume that the Ni–O bond length within the $Ni(en)_2(OH_2)_2^{2+}$ was 2.04—2.06 Å, the theoretical radial distribution curve showed descrepancies from the experimental curve, and the radial distribution curve in solution C could be better explained by assuming the Ni–O bond distance within the bis-complex to be about 2.10 Å, which was almost the same length as the Ni–N bond. The results obtained from the studies by means of infrared[15] and electronic[16] spectroscopic analyses suggested that the bis(ethylenediamine)nickel(II) complex has two water molecules at the axial positions. Since the area under the peak at 2.10 Å corresponded to the sum of four Ni–N and two Ni–O bonds, the bis-complex was concluded to be almost regularly octahedral which contained two water molecules at the axial positions, and thus, the residual radial distribution curve of solution C was well analyzed by assuming the bond distances of the Ni–N: 2.10 Å (the frequency factor $n_{Ni-N}=4$), Ni–O : 2.10 Å ($n_{Ni-O}=2$), Ni···C : 2.87 Å ($n_{Ni...C}=4$), and N···N (or N···O)$=\sqrt{2}\times 2.10$ Å ($n_{N...N}+n_{N...O}=12$), and no appreciable peak remained on the double-dotted curve over the range <4 Å except for the broad peak at around 3.0 Å, which was attributed to the O···O interactions in bulk water and the hydrated nitrate ions.

Solution D may contain a small amount of the mono-complex and a lesser amount of the tris-complex according to the literature.[13] However, the concentration of the mono-complex is too small to be determined by the present X-ray diffraction method, and thus, the radial distribution curve of solution D could be analyzed assuming the only bis-complex existed in the solution. The essentially same procedure as that used in the analysis of the radial distribution curve of solutions A and B was employed. The parameter values of the bis-complex obtained from the analysis of the radial distribution curve of solution D were almost consistent with those obtained in solution C. The parameter values obtained by analyzing the radial distribution curves of each solution were refined by the least squares method using the intensities $s\cdot i(s)$ in the high angle region ($4\ Å^{-1}\lesssim s\lesssim 16\ Å^{-1}$).

Least Squares Refinements. The intensity data in the high angle region ($s>4\ Å^{-1}$) of the $s\cdot i(s)$ curves of solutions A, B, and C were used for the least squares refinements[17] of the structural parameters of the bis- and tris-complexes. For avoiding errors introduced by neglecting long range intermolecular interactions in the course of least squares calculations, the lowest s-value was varied from 4.5 $Å^{-1}$ to 7 $Å^{-1}$.

In the A-1 type calculation of the least squares refinement of the intensity data of solution A, the frequency factor (n) of the metal-ligand bond was floated. The frequency factors of the Ni–N and Ni···C interactions of the tris(ethylenediamine)nickel(II) complex were actually six. In the A-2 type calculation, the bond distances and temperature factors were floated, while the frequency factors of the Ni–N and Ni···C interactions were kept constant ($n=6$). The final values of the Ni–N and Ni···C distances were 2.191(3) Å and 2.876(8) Å, respectively (Table 2). The values of the Ni–N and Ni···C distances were practically independent of the type of calculations.

TABLE 2. RESULTS OF THE LEAST SQUARES REFINEMENTS OF SOLUTION A

Interaction	Parameter	A-1[b]	A-2[b]
O···O(NO_3^-)	r/Å	2.25(2)	2.24(2)
C···N (en)	r/Å	2.46(4)	2.48(3)
N···N (en)	r/Å	2.87(6)	2.92(5)
$Ni(en)_3^{2+}$			
Ni–N	r/Å	2.193(4)	2.191(3)
	b/Å^2	0.0022(3)	0.0025(2)
	n	5.99(9)	6[a]
Ni···C	r/Å	2.87(1)	2.876(8)
	b/Å^2	0.005[a]	0.005[a]
	n	6.2(1)	6[a]

a) Fixed. b) Standard deviations are given in parentheses.

By the same procedure of the least squares refinements of the intensity data of solution B, the Ni–N and Ni···C distances were found to be 2.202(4) Å and 2.88(1) Å, respectively.

In the least squares calculations of solution C, an assumption of two water molecules binding to the central nickel(II) ion within the bis(ethylenediamine)-nickel(II) complex was introduced as an initial condition which should be refined in the course of the calcula-

Table 3. Results of the least squares refinements of solution C[a)]

Interaction	Parameter	$5.0<s/Å^{-1}<16.7$	$6.0<s/Å^{-1}<16.7$
Ni–O	r/Å	2.10(1)	2.10(1)
	b/Å^2	0.0030(7)	0.0029(7)
	n	2.00(7)	2.1(1)
Ni–N	r/Å	2.102(7)	2.099(8)
	b/Å^2	0.0028(4)	0.0027(4)
	n	4.00(9)	4.2(1)
Ni···C	r/Å	2.82(2)	2.83(2)
	b/Å^2	0.0046(7)	0.0048(8)
	n	4.1(2)	4.2(2)
N···N	r/Å	3.01(5)	3.06(7)

a) The concentration of the tris-complex is assumed to be 20 mol% on the basis of the stability constants reported in the literature. Standard deviations are given in parentheses.

Table 4. Final values of the intramolecular distances (Å) within the bis- and tris-(ethylenediamine)Ni(II)complexes

	Bis-complex[a)]	Tris-complex[a)]
Ni–N	2.102(7)	2.202(4)
Ni–O	2.10(1)	—
Ni···C	2.82(2)	2.88(1)
Structure	Regular octahedron	

a) The values in parentheses are their standard deviations.

tions. The final results showed that the frequency factors of the Ni–O interaction was about two and those of the Ni–N and Ni···C interactions within the bis-complex were approximately four (Table 3). In the least squares calculations of the intensity data of solution C, various types of calculation were carried out. In one case, the frequency factors of the Ni–N or Ni···C interactions within the bis-complex were held constant at four, other parameter values being refined. In other cases, the frequency factor of the Ni–O bond was fixed at two by assuming the structures of the bis-complex, and other parameters were refined. The s_{min}-value was changed in some cases. All the calculations examined here led to almost the same values of the Ni–N and Ni–O bond lengths. The final results obtained in the calculations were summarized in Table 3, in which the bond lengths, temperature, and frequency factors were floated. The results obtained by the calculations gave almost the same results as listed in Table 3 and the distances of the Ni–N and Ni–O bonds were finally determined to be 2.10 Å. Consequently, the bis(ethylenediamine)nickel(II) complex has almost a regularly octahedral structure with four nitrogen and two oxygen atoms. The parameter values obtained in the analysis of the intensity data of solution D were almost the same as those obtained for solution C. As shown in Fig. 2, the $s\cdot i(s)$ curves calculated from the refined parameters thus obtained well fit the observed $s\cdot i(s)$ curves in the region $5\ Å^{-1}<s<16\ Å^{-1}$. The final parameter values found in this study are summarized in Table 4.

In the X-ray crystal analysis, the Ni–N bond distance within the tris(ethylenediamine)nickel(II) complex has been found to be 2.07—2.17 Å (Table 5). The Ni–N bond distance within the tris-complex in solution found in the present study is 2.20 Å, which is slightly longer than the distances found in crystals. The bis(ethylenediamine)nickel(II) complex in crystals has the Ni–N bond distances of 2.08—2.12 Å, which is almost the same as that in this study (Table 5).

The work has partially been supported by the Grant-in-Aid for Scientific Research No. 343011 from the Ministry of Education, Science and Culture.

References

1) T. Fujita, T. Yamaguchi, and H. Ohtaki, *Bull. Chem. Soc. Jpn.*, **52**, 3539 (1979).
2) T. Fujita and H. Ohtaki, *Bull. Chem. Soc. Jpn.*, **53**, 930 (1980).
3) K. Ueno, "Kireito Kagaku," Nankodo, Tokyo (1976), Vol. 2.

Table 5. The Ni–N and Ni–O distances within the bis- and tris(ethylenediamine)-nickel(II) complexes in crystal and in solution

Compound	Ni–N(Ni–O)(Å)	Author
$Ni(en)_3(NO_3)_2$	2.120	Swink and Atoji[a)]
$[Ni(en)_3]Si_2O_5\cdot 8.7H_2O$	2.066—2.171	Smolin[b)]
$Ni(en)_3SO_4$	2.124	Ul-Haque *et al.*[c)]
$[Ni(en)_3](O_2C_2H_3)_2\cdot 2H_2O$	2.104—2.139	Cramer *et al.*[d)]
$[Ni(en)_3][B(C_6H_5)_4]_2\cdot 3(CH_3)_2SO$	2.11—2.17	Cramer and Huneke[e)]
$Ni(en)_2(NCS)_2$	2.09—2.11	Brown and Lingafelter[f)]
$[Ni(en)_2(OH_2)(BF_4)]\cdot BF_4$	2.08—2.12(2.19)	Tomlinson *et al.*[g)]
$[Ni(en)(OH_2)_4](NO_3)_2$	2.08(2.10)	Komiyama and Lingafelter[h)]
$Ni(en)_3^{2+}$	2.20	This work[i)]
$Ni(en)_2(OH_2)_2^{2+}$	2.10(2.10)	This work[i)]

a) L. N. Swink and M. Atoji, *Acta Crystallogr.*, **13**, 639 (1960). b) Yu. I. Smolin, *Soviet Phys. Crystallogr.*, **15**, 23 (1970). c) M. Ul-Haque, C. N. Caughlan, and K. Emerson, *Inorg. Chem.*, **9**, 2421(1970). d) R. E. Cramer, W. Van Doorne, and J. T. Huneke, *ibid.*, **15**, 529 (1976). e) R. E. Cramer and J. T. Huneke, *ibid.*, **17**, 365 (1978). f) B. W. Brown and E. C. Lingafelter, *Acta Crystallogr.*, **16**, 753 (1963). g) A. A. G. Tomlinson, M. Bonamico, G. Dessy, V. Fares, and L. Scaramuzza, *J. Chem. Soc., Dalton Trans.*, **1972**, 1671. h) Y. Komiyama and E. C. Lingafelter, Reports Faculty Eng. Yamanashi University, **1963**, 5. i) In solution.

4) K. O. Joung, C. J. O'Conner, E. Sinn, and R. L. Carlin, *Inorg. Chem.*, **18**, 804 (1979).
5) A. K. Dorosh and A. F. Skryshevskii, *Zh. Strukt. Khim.*, **8**, 348 (1967).
6) H. Ohtaki, T. Yamaguchi, and M. Maeda, *Bull. Chem. Soc. Jpn.*, **49**, 701 (1976).
7) M. Ul-Haque, C. N. Caughlan, and K. Emerson, *Inorg. Chem.*, **9**, 2421 (1970).
8) B. W. Brown and E. C. Lingafelter, *Acta Crystallogr.*, **16**, 753 (1963).
9) H. Ohtaki and M. Maeda, *Bull. Chem. Soc. Jpn.*, **47**, 2197. (1974); H. Ohtaki, M. Maeda, and S. Ito, *ibid.*, **47**, 2217 (1974).
10) T. Yamaguchi and H. Ohtaki, *Bull. Chem. Soc. Jpn.*, **51** 3227 (1978).
11) D. T. Cromer and J. T. Waber, *Acta Crystallogr.*, **18**, 104 (1965); D. T. Cromer, *J. Chem. Phys.*, **50**, 4857 (1965); D. T. Cromer and D. Liberman, *ibid.*, **53**, 1891 (1970).
12) G. Johansson and M. Sandström, *Chem. Scripta*, **4**, 195 (1973).
13) L. G. Sillén and A. E. Martell, "Stability Constants," ed by The Chemical Society, London, Spec. Publ. No. 17 (1964) and Supplement No. 1 Spec. Publ. No. 25 (1971).
14) W. Bol, G. J. A. Gerrits, and C. L. P. van Eck, *J. Appl. Chem.*, **3**, 140 (1970).
15) R. J. H. Clark and R. E. Hester, "Advances in Infrared and Raman Spectroscopy," Heyden, London (1976), Vol. 1.
16) K. Yamasaki and H. Yamatera, "Mukikagaku Zensho: Suppl., Sakutai," Maruzen, Tokyo (1969), p. 129.
17) J. Waser and V. Schomaker, *Rev. Mod. Phys.*, **25**, 671 (1953); K. Furukawa, *Rep. Prog. Phys.*, **25**, 395 (1962); T. Yamaguchi, Doctor Thesis, Tokyo Institute of Technology (1978).

 © 1982 The Chemical Society of Japan Bull. Chem. Soc. Jpn., 55, 461—465 (1982)

A Potentiometric Study on Mixed Ligand Cadmium(II) Complexes with 2-Amino Carboxylic Acids

Haruo MATSUI* and Hitoshi OHTAKI†

Government Industrial Research Institute, Nagoya, Hirate-cho, Kita-ku, Nagoya 462
†*Department of Electronic Chemistry, Tokyo Institute of Technology at Nagatsuta, Nagatsuta-cho, Midori-ku, Yokohama 227*

(Received August 22, 1981)

Formation constants of mixed ligand cadmium(II) complexes, CdLL′, were determined in aqueous solutions containing 3 mol dm^{-3} $LiClO_4$ as a constant ionic medium at 25 °C by potentiometric titration, where the ligands HL and HL′ are 2-amino carboxylic acids such as glycine, α-alanine, 2-aminobutanoic acid, 2-aminopentanoic acid, and 2-aminohexanoic acid. Ten kinds of the mixed ligand cadmium(II) complexes were examined with the combination of five 2-amino carboxylic acids. The formation constant, $\beta_{prs}=[Cd_pL_rL_s'^{(2p-r-s)+}]/([Cd^{2+}]^p\times[L^-]^r[L'^-]^s)$, of the mixed ligand cadmium(II) complexes containing glycine as one of the ligands lie between those of the parent complexes, while the formation constants of the other complexes are larger than those of the parent complexes. No protonated mixed ligand complex has been observed. The small values of β_{111} of the Cd(gly)L complexes are due to the considerably small values of the first stepwise formation constants of the CdL^+ complexes. On the other hand, the stepwise formation constants of the CdL^+ complexes with glycinate ion are larger than the stepwise formation constants with 2-amino carboxylate ions and the second stepwise constant of the bis(glycinato)cadmium(II) complex. Interactions between the ligands through the central cadmium(II) ion are discussed. The b-values ($b=\log\{(K_{110}\cdot K_{101})/(K_{120}\cdot K_{102})\}$, where K_{1rs} denotes the stepwise formation constant of the complex $CdL_rL'_s$) of the mixed ligand cadmium(II) complexes containing glycinate ion as one of the components lie between 0.93 and 0.98, and are larger than those of the other complexes ($b=0.83$—0.90), the fact indicating that the mixed ligand glycinato complexes have larger inter-ligand interactions within the complexes than those within complexes containing other 2-amino carboxylate ions. The inter-ligand interaction may occur through the central cadmium ion within the complex.

Mixed ligand complexes of a number of metal ions with various amino acids have been extensively investigated because of their biological importance, and the role of the metal ions in the mixed ligand complexes in various reactions has been discussed. Among them, copper(II) complexes are the most extensively studied ones, and zinc(II) complexes have also drawn attentions of chemists due to their interesting behavior in catalytic reactions in biological systems. Cadmium(II) ions often show similar properties in chemical reactions to zinc(II) ions because of their similar electron configurations (d^{10} electrons).[1] However, mixed ligand amino acido complexes of cadmium(II) ion have scarecely been examined so far. Toxity of cadmium(II) ion is an important problem to be elucidated in the view-point of medical science, as well as of complex chemistry. Reactions of cadmium(II) ions with amino acids which exist in human plasma[2] and other biological tissues and organs, therefore, are worthwhile studying in connection of complex chemistry of cadmium(II) ions with biochemistry.

The aim of the present work is to determine formation constants of mixed ligand complexes of cadmium(II) ion with a series of 2-amino carboxylic acids, such as glycine, α-alanine, 2-aminobutanoic acid, 2-aminopentanoic acid and 2-aminohexanoic acid, and variations of the formation constants of the mixed ligand complexes are discussed in terms of the effect of substituted alkyl groups at the carbon atom of glycine.

The effect of the size of chelate rings of amino acids in the complexes on formation constants of various mixed ligand complexes has also been examined by using 3- and 4-amino carboxylic acids, but the complexes of cadmium(II) ions with the acids are so weak that the complexes are not practically formed.

Experimental

Reagents. The amino acids were obtained from Wako Pure Chemicals Ind., Osaka, Nakarai Chemicals Co., Kyoto, and Katayama Chemicals Ind., Osaka. Each reagent was purchased from at least two different companies and purity of the reagents was checked by paper chromatography. A reagent having better quality was chosen, and then, it is recrystallized and used after drying crystals for several hours at 90—110 °C in an electric oven. Cadmium perchlorate, lithium perchlorate and lithium hydroxide were prepared by the methods as described in previous papers.[3,4]

Apparatus. Beckman (Nos. 40495 and 40498) glass electrodes were used in combination with an Orion Digital pH Meter 801. The Kawai-type half cell[5] was used, in which an Ag–AgCl electrode was set. The Ag–AgCl electrode was prepared according to Brown.[6]

Measurements. During potentiometric titrations the total concentration of perchlorate ions was kept constant at 3 mol dm^{-3} by using lithium perchlorate. The ratio of the total concentration of ligands (the sum of the concentrations of two amino acids) to that of cadmium(II) ions (C_L^t/C_{Cd}^t) was 5 in all the cases. The total concentration of amino acids in the solution (C_L^t) was changed, but the ratio of the concentrations of each amino acid was kept 1 : 1. The method of emf measurements was essentially the same as that employed in the previous work.[3,4]

All the measurements were carried out under a nitrogen atomosphere at 25.00±0.02 °C in a liquid paraffin bath set in a room thermostated at 25.0±1.5 °C.

Results

Typical results of titration curves of the systems of cadmium(II)–amino acids are shown in Fig. 1, in which the degree of neutralization of the total amino acids in the solutions X ($=-\boldsymbol{H}/C_L^t$; $\boldsymbol{H}$ stands for the analytical

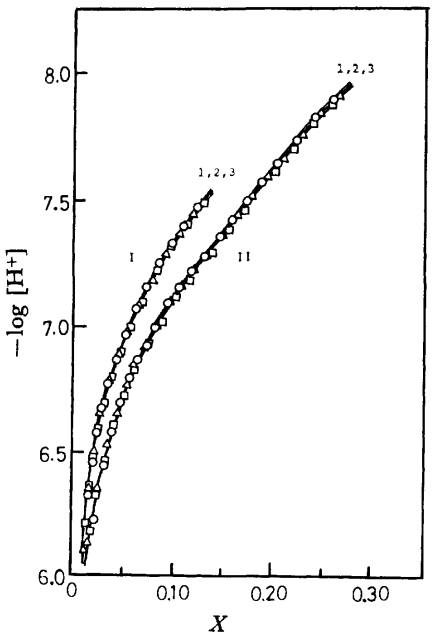

Fig. 1. Typical titration curves of cadmium(II)–amino acid mixed solutions.
Curve I (Cd(II)–2-aminobutanoic acid–2-aminopentanoic acid):
1 (○), C_{Cd}(mmol dm^{-3})=7.524, C_L(mmol dm^{-3})=18.71, C_L' (mmol dm^{-3})=18.71; 2 (△), 7.793, 19.36, 19.35; 3 (□), 7.847, 19.62, 19.59.
Curve II (Cd(II)–glycine–2-aminobutanoic acid): 1 (○), 7.571, 18.80, 18.81; 2 (△), 7.771, 19.38, 19.38; 3 (□), 8.139, 20.39, 20.37.

excess concentration of hydrogen ion) was plotted against $-\log [H^+]$. The least squares method was employed to determine the best value of the formation constant of a mixed ligand complex, CdLL', by taking into account the formation constants of the parent cadmium(II) complexes with each amino acid as the component, which had been determined by separate experiments using solutions containing cadmium(II) ions and one kind of amino acid as a ligand. The formation constants of the mixed ligand complexes $\beta_{pqrs}=[Cd_pH_qL_rL'_s]^{(2p+q-r-s)+}/([Cd^{2+}]^p[H^+]^q[L^-]^r[L'^-]^s)$ are summarized in Table 1, together with the ionization constants of the ligands (pK_1 and pK_2) and the formation constants of mono- and bis-complexes with one kind of amino acid as the ligand ($\log K_{11}$ and $\log K_{12}$). Neither the protonated complexes nor the tris(amino acido)cadmium(II) complexes have been found with reliable accuracies under the present experimental conditions. The values of K_{11} and K_{12} are refined ones which had been determined,[7] the refinement being done for eliminating titration data at higher pH regions where white precipitates sometimes appeared. The formation of hydroxo complexes of cadmium ions[8] has been taken into consideration in the course of the least squares refinement of the formation constants of the mixed ligand complexes. The calculations were carried out by using the SCOGS program[9] with an electronic computer FACOM M-160S.

The solid lines in Fig. 1 were drawn using calculated values of X (X_{calcd}) by the following equation:

$$X_{calcd} = \frac{C_L^t + K_t[H^+]^{-1} - [H^+] - \sum_p \sum_q \sum_r \sum_s q\beta_{pqrs}[Cd^{2+}]^p[H^+]^q[L^-]^r[L'^-]^s}{C_L^t}, \quad (1)$$

where K_t represents the autoprotolysis constant of water in 3 mol dm^{-3} $LiClO_4$ aqueous solution at 25 °C ($10^{-13.87}$ mol^2 dm^{-6} [10]). Under the present conditions, the values of p, q, r, and s for the mixed ligand cadmium(II) complexes are 1, 0, 1, and 1, respectively. The formation of the $CdOH^+$ ($p=1$, $q=-1$, $r=s=0$) and Cd_2OH^{3+} ($p=2$, $q=-1$, $r=s=0$) complexes[8] has been taken into account in the determination of formation constants of the mixed ligand complexes, β_{pqrs}, by using Eq. 1. Since only the 1 : 1 : 1 type mixed ligand complexes without protons ($p=1$, $q=0$, $r=1$, $s=1$) have been found in the present work, the formation constants of the mixed ligand complexes will be simply denoted as β_{1rs} (*e.g.*, β_{111} for a 1 : 1 : 1 mixed complex).

Table 1. Formation constants of cadmium(II) complexes with 2-amino carboxylic acids in 3 mol dm^{-3} $LiClO_4$ at 25 °C

		Glycine	α-Alanine	2-Amino-butanoic acid	2-Amino-pentanoic acid	2-Amino-hexanoic acid
a) Ionization constants of 2-amino carboxylic acids.						
pK_1		2.76	2.81	—	—	—
pK_2		9.68	9.72	9.73	9.75	9.76
b) Formation constants of mono- and bis(2-amino carboxylato)cadmium(II) complexes.						
$\log K_{11}$		4.01	3.69	3.64	3.72	3.74
$\log K_{12}$		3.48	3.24	3.24	3.29	3.29
c) Formation constants of mixed ligand complexes of cadmium(II) ion.[a]						
$\log \beta_{111}$	Glycine	7.49	7.47	7.34	7.41	7.43
	α-Alanine		6.93	7.13	7.15	7.24
	2-Aminobutanoic acid			6.88	7.05	7.20
	2-Aminopentanoic acid				7.01	7.31
	2-Aminohexanoic acid					7.03

a) Values underlined are $\log \beta_{120}$ or $\log \beta_{102}$ ($=\log K_{11}+\log K_{12}$). Standard deviations are ±0.02.

Protonation reactions of mono- and bis(amino acido)-cadmium(II) complexes have not been observed under the present experimental conditions.

It should be noted from the results in Table 1 that the values of pK_1 and pK_2 are increased, whereas the values of log K_{11} and log K_{12} are decreased, by introducing alkyl groups to glycine, where K_{11} and K_{12} represent the stepwise formation constants of the CdL^+ and CdL_2 complexes, respectively.

Discussion

The formation constant of a mixed ligand complex should be larger than the average value of the formation constants of the parent complexes by a statistical factor as long as the bond strength between the central metal ion and the ligands is unaffected by replacing a ligand with another one and the contribution of entropy changes in each reaction to the formation constants are the same.

In the formation of a 1 : 1 : 1 mixed ligand complex CdLL′ from the parent bis-complexes, CdL_2 and CdL'_2, the statistical factor is 4.

The formation reaction of the mixed ligand CdLL′ complex from the parent complexes can be described as follows:

$$CdL_2 + CdL'_2 = 2CdLL'. \quad (2)$$

The formation constants of the mixed ligand complex β_{111} are related to the formation constants of the parent CdL_2 and CdL'_2 complexes, β_{120} and β_{102}, respectively, by the following equation:

$$2 \log \beta_{111} = \log \beta_{120} + \log \beta_{102} + \log F_m. \quad (3)$$

F_m is 4 in the ideal case.

For most mixed ligand complexes examined here, β_{111} is larger than β_{120} and β_{102}. However, as we can see from Table 1c, the formation constants of the mixed ligand complexes containing glycinate ion as one component lie between the values of the two parent complexes, thus, $\beta_{120} > \beta_{111} > \beta_{102}$, although the relationship $\beta_{111}^2 > \beta_{120} \cdot \beta_{102}$ still holds for the complexes.

The second stepwise formation constants K_{12}^m of the mixed ligand complexes in the reaction

$$CdL^+ + L'^- = CdLL' \quad (4)$$

are calculated by using the following equation:

$$\log K_{12}^m = \log \beta_{111} - \log K_{11}. \quad (5)$$

The values of log K_{12}^m are summarized in Table 2. The values of log K_{12}^m of the Cd(gly)L complexes with various 2-amino carboxylate anions L^-

$$CdL^+ + gly^- = Cd(gly)L \quad (6)$$

are in the range of 3.69 to 3.78, which are larger than the log K_{12} value of the bis(glycinato)cadmium(II) complex. On the other hand, the log K_{12}^m values of the reaction

$$Cd(gly)^+ + L^- = Cd(gly)L \quad (7)$$

fall in the range of 3.33 to 3.46, which are comparable to the values of the other complexes given in Table 2. Therefore, we see that the small values of β_{111} of the Cd(gly)L complexes are due to the considerably small values of the first stepwise formation constants of the CdL^+ complexes compared with those of the $Cd(gly)^+$ complex (Table 1b).

The second formation constants of the mixed ligand complexes containing glycinate ion as the second entering ligand are larger than those of other complexes, and even larger than the K_{12} value of the bis(glycinato)-cadmium(II) complex. This fact implies that glycinate ion combines more favorably with a CdL^+ than with the $Cd(gly)^+$ complex. Since direct interactions between glycinate and another ligand within the CdL^+ complex may hardly be expected, interactions between the ligands through the central metal ion should be considered.

Electrons in the highest orbitals of cadmium(II) ion which is a considerably soft acid according to classification by Ahrland, *et al.*[11] and Pearson[12] may partially delocalize over the central metal ion and the ligand atoms within the complex in order to decrease the total energy of the whole complex. Although it is generally accepted that atoms of the first and second rows of the periodic table cannot be acceptors of such electrons, we think that the possibility may not be completely excluded in cases where a central atom has electrons with very large principal quantum numbers, or in other words, it has a very soft character, because energy levels of electrons of the central metal ion and ligand atoms such as oxygen and nitrogen are so different that even small delocalization of electrons of the metal ion by using a higher orbitals of the ligand atoms may decrease, to some extent, the total energy of the system.

Table 2. The second stepwise formation constants (log K_{12}^m) of the CdLL′ complexes in 3 mol dm^{-3} $LiClO_4$ at 25 °C[a]

CdL[b]	L′				
	Glycinate	Alaninate	2-Amino-butanoate	2-Amino-pentanoate	2-Amino-hexanoate
$Cd(gly)^+$	<u>3.48</u>	3.46	3.33	3.40	3.42
$Cd(ala)^+$	3.78	<u>3.24</u>	3.44	3.46	3.55
$Cd(but)^+$	3.70	3.49	<u>3.24</u>	3.41	3.56
$Cd(pen)^+$	3.69	3.43	3.33	<u>3.29</u>	3.59
$Cd(hex)^+$	3.69	3.50	3.46	3.57	<u>3.29</u>

a) Values underlined are log K_{12} of the bis(2-amino carboxylato)cadmium(II) complexes. b) Ala : Alaninate ion, but : 2-aminobutanoate ion, pen : 2-aminopentanoate ion, hex : 2-aminohexanoate ion.

This kind of electron delocalization may easily be prevented by an increase in the charge density at the ligand atoms due, for instance, to inductive effects of substituted groups within the ligand molecules.

An interpretation of the change in the K_{12}^{m} value of the Cd(gly)L complex may thus be given in the following way: the basicity of the functional groups (amino and carboxyl groups) of glycine increases by introduction of an alkyl group to the carbon atom due to its inductive effect, and therefore, the pK_1 and pK_2 values of 2-amino carboxylic acids having alkyl groups become larger than the pK_1 and pK_2 values, respectively, of glycine (see Table 1a). The introduction of the alkyl groups thus results an increase in electron densities at the nitrogen and oxygen atoms within the amino and carboxyl groups, and it may prevent electron donation from the central cadmium(II) ion. Therefore, the affinity of the amino acid anions to cadmium(II) ion decreases, as we can see from the values of K_{110} and K_{120} of the bis(amino acido)cadmium(II) complexes smaller than the corresponding values of the bis(glycinato)cadmium(II) complex (see Table 1b). The increased charge density of the cadmium(II) ion due to the decreased electron donation to the ligand atoms may result a decreased acceptability of electron pairs from the coordinated water molecules. As the result, the $H_2O\cdots CdL^+$ bonds in the solvated CdL^+ complex weaken, and the water molecules can be easily substituted with the second ligand. Since glycinate anion has the largest acceptability (*i.e.*, the smallest electron density at the ligand atoms) among the ligands examined here for the electron donation from the cadmium(II) ion, the substitution of glycinate ion with the water molecules coordinated to the cadmium(II) ion might occur most favorably to form the strongest metal-ligand bond. Thus the K_{12}^{m} value of the reaction

$$CdL(H_2O)_n^+ + gly^- = Cd(gly)L(H_2O)_{n-2} + 2H_2O \quad (8)$$

becomes larger than the K_{12} value of the following reaction:

$$Cd(gly)(H_2O)_n^+ + gly^- = Cd(gly)_2(H_2O)_{n-2} + 2H_2O. \quad (9)$$

The statistical factors $\log F_m$ defined by Eq. 3 for various mixed ligand complexes are summarized in Table 3, but no systematic trend of the values can be found.

Another relationship

$$\log \beta_{111} = \log \beta_{110} + \log \beta_{101} + \log F'_m \quad (10)$$

TABLE 3. VALUES OF $\log F_m$, F'_m, AND b IN EQS. 3, 10, AND 13, RESPECTIVELY

Exptl No.	Complex	$\log F_m$	$\log F'_m$	b
1	Cd(gly)(ala)	0.52	−0.23	0.98
2	Cd(gly)(but)	0.31	−0.31	0.93
3	Cd(gly)(pen)	0.32	−0.32	0.96
4	Cd(gly)(hex)	0.34	−0.32	0.98
5	Cd(ala)(but)	0.45	−0.20	0.85
6	Cd(ala)(pen)	0.36	−0.26	0.88
7	Cd(ala)(hex)	0.52	−0.19	0.90
8	Cd(but)(pen)	0.21	−0.31	0.83
9	Cd(but)(hex)	0.49	−0.18	0.85
10	Cd(pen)(hex)	0.58	−0.15	0.88

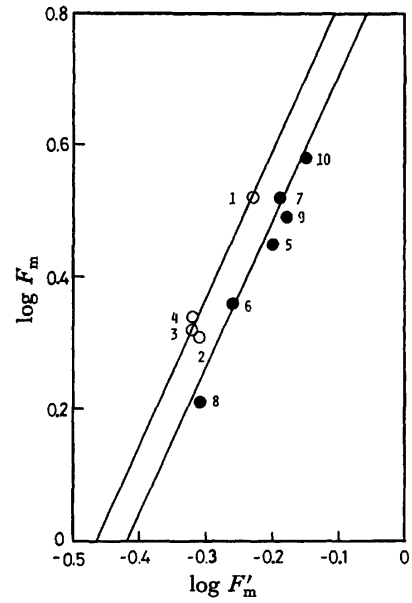

Fig. 2. The relationship between $\log F_m$ and $\log F_m'$. ○: Mixed ligand cadmium(II) complexes containing glycinate ion, ●: other mixed ligand cadmium(II) complexes. The numbers given in the figure correspond to those of the complexes in Table 3.

is obtained for the formation of the CdLL' complex from the parent CdL^+ and CdL'^+ complexes as follows:

$$CdL^+ + CdL'^+ = CdLL' + Cd^{2+}. \quad (11)$$

F'_m is 2 in the ideal case. The values of $\log F'_m$ found are summarized in Table 3. Since the following relationship holds between F_m and F'_m

$$\log F_m = 2 \log F'_m + b, \quad (12)$$

where

$$b = \log\{(K_{110}\cdot K_{101})/(K_{120}\cdot K_{102})\} \quad (13)$$

plots of $\log F_m$ against $\log F'_m$ should give straight lines as we can see in Fig. 2. The experimental points fell on the two straight lines with a slope 2. The open circles show the mixed ligand complexes containing glycinate ion and the closed circles show the complexes not containing glycinate ion. The b-values found from the plots are given in Table 3, which should be zero in the ideal case. The b-values of the mixed ligand glycinato complexes are obviously larger than those of the other complexes, the fact indicating that the inter-ligand interactions within the mixed ligand glycinato complexes are larger than those of other complexes.

The authors thank Prof. O. Yamauchi of Kanazawa University for his helpful discussion.

References

1) a) A. E. Martell and M. Calvin, "Chemistry of the Metal Chelate Compounds," Prentice-Hall, Inc., New York (1952); b) J. Bjerrum, "Metal Ammine Formation in Aqueous Solution," Hasse and Son, Copenhagen (1957).

2) P. M. May P. W. Linder, and D. R. Williams, *J. Chem. Soc., Dalton Trans.*, **1977**, 588.

3) H. Matsui, *Denki Kagaku*, **47**, 466 (1979).

4) H. Matsui and H. Ohtaki, *Bull. Chem. Soc. Jpn.*, **50**,

1472 (1977).
5) H. Tsukuda, T. Kawai, M. Maeda, and H. Ohtaki, *Bull. Chem. Soc. Jpn.*, **48**, 691 (1975).
6) A. S. Brown, *J. Am. Chem. Soc.*, **56**, 646 (1934).
7) H. Matsui, *J. Inorg. Nucl. Chem.*, **43**, 2187 (1981).
8) H. Matsui and H. Ohtaki *Bull. Chem. Soc. Jpn.*, **47**, 2603 (1974).
9) I. G. Sayce, *Talanta*, **15**, 1397 (1968).
10) T. Kawai, S. Ishiguro, and H. Ohtaki, *Bull. Chem. Soc. Jpn.*, **53**, 2221 (1980).
11) S. Ahrland, J. Chatt, and N. R. Davies, *Quart. Rev., London*, **12**, 265 (1958).
12) R. G. Pearson, *J. Am. Chem. Soc.*, **85**, 3533 (1963); *Science*, **151**, 172 (1966); *J. Chem. Educ.*, **45**, 581 (1968).

Binuclear Metal Complexes. XLII.[1] Manganese(IV) Complexes Synthesized by Oxidation of Binuclear Manganese(II) Complexes of 2-(Salicylideneamino)phenols with Tetrachloro-*o*-benzoquinone

Hisashi Ōkawa,* Masaaki Nakamura, and Sigeo Kida
Department of Chemistry, Faculty of Science, Kyushu University 33, Hakozaki, Higashi-ku, Fukuoka 812
(Received July 24, 1981)

Manganese(IV) complexes $Mn(R\text{-}R'\text{-}sap)_2$, where $H_2(R\text{-}R'\text{-}sap)$ denotes 2-(salicylideneamino)phenols with the substituent R on the salicylaldehyde ring and the R′ on the *o*-aminophenol ring, were prepared by the oxidation of binuclear manganese(II) complexes $Mn_2(R\text{-}R'\text{-}sap)_2$ with tetrachloro-*o*-benzoquinone (TCOQ). The complexes showed magnetic moments corresponding to three unpaired electrons and strong absorptions in the region $15—20\times10^3$ cm^{-1} attributable to CT transitions. Cyclic voltammograms of $Mn(R\text{-}R'\text{-}sap)_2$ showed two redox waves which can be interpreted in terms of a two-step reaction, $Mn(IV)\rightleftharpoons Mn(III)\rightleftharpoons Mn(II)$. Both redox potentials of the first and the second processes depend on the substituents R and R′, and there is a good correlation between the redox potentials and Hammett's σ-values of R and R′ to the phenolic oxygen. $Mn_2(R\text{-}R'\text{-}sap)_2$ reacts with TCOQ to give a binuclear manganese(III) complex $Mn_2(R\text{-}R'\text{-}sap)_2(tcoq)$, which decomposes in the presence of water forming $Mn(R\text{-}R'\text{-}sap)_2$.

Manganese is known to play several important roles in biological processes.[2] Among these, manganese in the photosystem-II has become particularly of interest, where manganese in higher oxidation state functions as a catalyst for oxidizing water to molecular oxygen.[3,4] The recent findings that two or more manganese ions are involved in the active center of the photosystem-II[5-7] stimulated interest in binuclear manganese complexes in higher oxidation states (Mn(III) and Mn(IV)).[8,9] On the other hand, Wang[10] proposed a mechanism of water oxidation promoted by mononuclear manganese(IV). Thus, much attention is being devoted to synthesis, redox behavior and reactivity of new manganese complexes in higher oxidation state. However, both mononuclear manganese(IV) complexes and binuclear manganese(III) and manganese(IV) complexes seem to be very limited.

Previously, we have reported synthesis, magnetism and structure of binuclear manganese(III) complexes of 3-(salicylideneamino)-1-propanols.[11,12] As a part of the continuing study on binuclear manganese complexes in higher oxidation state, we brought binuclear manganese(II) complexes of 2-(salicylideneamino)-phenols to reaction with tetrachloro-*o*-benzoquinone (TCQO), in an attempt to prepare binuclear manganese(III) complexes bridged by two phenolic oxygens in the equatorial plane and tetrachlorocatecholate moiety in the apical position. Deep colored products, however, were free from TCOQ and the metal to ligand (2-(salicylideneamino)phenols) ratio was 1 : 2, suggesting the formation of manganese(IV) complexes. In this study, we have characterized the new complexes in terms of magnetic susceptibilities, electronic spectra and cyclic voltammetry. The mechanism of formation of the manganese(IV) complexes has been discussed.

Experimental

Preparations. Ligands employed in this study are the 1 : 1 condensation products of salicylaldehyde or a substituted salicyladehyde and 2-aminophenol or a substituted 2-aminophenol. The ligands are abbreviated as $H_2(R\text{-}R'\text{-}sap)$, in

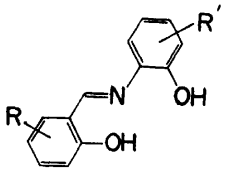

Fig. 1.

which R and R′ are the substituents on salicylaldehyde and 2-aminophenol, respectively (Fig. 1). Following ligands were used in this study: 2-(salicylideneamino)phenol (H_2(sap)), 2-(3-methoxysalicylideneamino)phenol (H_2(3-MeO-sap)), 2-(5-methylsalicylideneamino)phenol (H_2(5-Me-sap)), 2-(5-bromosalicylideneamino)phenol (H_2(5-Br-sap)), 2-(salicylideneamino)-4-chlorophenol (H_2(4′-Cl-sap)), and 2-(salicylideneamino)-5-nitrophenol (H_2(5′-NO_2-sap)). Manganese(II) complexes of $H_2(R\text{-}R'\text{-}sap)$ were prepared by the method described in the literature.[13]

Mn(sap)$_2$·1/2H$_2$O. To a suspension of $Mn_2(sap)_2$ (266 mg) in methanol (20 cm^3) was added tetrachloro-*o*-benzoquinone (TCOQ) (125 mg) under stirring. The mixture was gently refluxed for 3 h and allowed to stand overnight to give black-purple prisms. They were collected, washed with methanol, and dried over P_2O_5 *in vacuo*. The yield was 130 mg.

Found: C, 64.23; H, 3.92; N, 5.72%. Calcd for $C_{26}H_{18}N_2O_4Mn\cdot1/2H_2O$: C, 64.21; H, 3.94; N, 5.76%.

Mn(3-MeO-sap)$_2$·H$_2$O. A mixture of Mn_2 (3-MeO-sap)$_2$ (296 mg) and TCOQ (125 mg) in methanol (20 cm^3) was refluxed for 30 min to give almost black prisms. They were collected, washed with methanol, and dried over P_2O_5 *in vacuo*. The yield was 75 mg.

Found: C, 60.66; H, 4.55; N, 4.91%. Calcd for $C_{28}H_{22}N_2O_6Mn\cdot H_2O$: C, 60.55; H, 4.36; N, 5.04%.

Mn(5-Me-sap)$_2$·1/2H$_2$O. A mixture of Mn_2 (5-Me-sap)$_2$ (280 mg) and TCOQ (125 mg) in methanol (20 cm^3) was refluxed for 2 h to give a deep colored solution. To this solution was added dropwise a 1 : 1 mixture of methanol–water (1 cm^3), and stirring was continued for additional 30 min. Almost black prisms thus obtained were collected, washed with a small amount of methanol, and dried over P_2O_5 *in vacuo*. The yield was 90 mg.

Found: C, 65.11; H, 4.34; N, 5.30%. Calcd for $C_{28}H_{22}N_2O_4Mn\cdot1/2H_2O$: C, 65.40; H, 4.53; N, 5.45%.

Mn(5-Br-Sap)$_2$·H$_2$O. This complex was obtained as deep blackish green prisms (80 mg) by the reaction of Mn$_2$(5-Br-sap)$_2$ (345 mg) with TCOQ (125 mg) in methanol (30 cm^3) for 1 h at room temperature.

Found: C, 47.53; H, 2.53; N, 4.07%. Calcd for $C_{26}H_{16}N_2O_4Br_2Mn\cdot H_2O$: C, 47.81; H, 2.78; N, 4.29%.

Mn(4'-Cl-sap)$_2$·3/2H$_2$O. This complex was prepared as almost black powder (130 mg) by the reaction of Mn$_2$(4'-Cl-sap)$_2$ (620 mg) and TCOQ (250 mg) in methanol (50 cm^3) for 30 min at room temperature.

Found: C, 54.24; H, 3.09; N, 4.65%. Calcd for $C_{26}H_{16}N_2O_4Cl_2\cdot 3/2H_2O$: C, 54.47; H, 3.34; N, 4.89%.

Mn(5'-NO$_2$-sap)$_2$·2H$_2$O. This complex was obtained as deep green crystalline powder (150 mg) by the reaction of Mn$_2$(5'-NO$_2$-sap)$_2$ (620 mg) and TCOQ (250 mg) in methanol (60 cm^3) for 1 h at room temperature.

Found: C, 51.94; H, 3.09; N, 9.65%. Calcd for $C_{26}H_{16}N_4O_8Mn\cdot 2H_2O$: C, 51.93; H, 3.35; N, 9.32%.

Mn$_2$(sap)$_2$(tcoq). A mixture of Mn$_2$(sap)$_2$ (275 mg) and TCOQ (125 mg) in absolute acetonitrile (25 cm^3) was stirred for 3 h at room temperature in an atmosphere of nitrogen. The reaction was protected from the moisture by means of a VAC Inert Atmosphere and Vaccum Deposition equipment Model HE-43-2. Dark green prisms which separated were collected, washed with acetonitrile, and dried *in vacuo.*

Found: C, 49.23; H, 2.47; N, 3.83%. Calcd for $C_{32}H_{18}N_2O_6Cl_4Mn_2$: C, 49.39; H, 2.33; N, 3.60%.

Ti(sap)$_2$. H$_2$(sap)$_2$ (2.13 g) was dissolved in absolute methanol (50 cm^3), and to this solution was added TiCl$_4$ (0.95 g) dropwise under stirring. The mixture was stirred for 3 h at room temperature to give red crystals. They were collected, washed with methanol, and dried *in vacuo.*

Found: C, 66.20; H, 3.90; N, 5.90%. Calcd for $C_{26}H_{18}N_2O_4Ti$: C, 66.40; H, 3.86; N, 5.96%.

Measurements. Elemental analyses were performed at the Service Center of Elemental Analysis, Kyushu University. Electronic spectra were recorded on a Shimadzu multipurpose spectrometer Model MPS-5000 in dichloromethane or methanol. Magnetic susceptibilities were measured by the Faraday method. The apparatus was calibrated by the use of [Ni(en)$_3$]S$_2$O$_3$.[14] Diamagnetic corrections were made with Pascal's constants[15] and magnetic moments were calculated by the equation, $\mu_{eff}=2.828(\chi_A\times T)^{1/2}$. Cyclic voltammograms were recorded with a Yanagimoto voltammetric analyzer Model 1000. Measurements were made on dichloromethane solutions containing 0.1 M tetrabutylammonium perchlorate as the supporting electrolyte, using a three-electrode cell. The working electrode is glassy carbon and the auxiliary electrode is platinum coil. The saturated calomel electrode was used as the reference. All the potentials were corrected by the use of ferrocene as an internal standard (Fc$^+$/Fc: $E_{1/2}$=0.400 V *vs.* NHE[16]).

Results and Discussion

Manganese(II) complexes of H$_2$(R-R'-sap) were already synthesized,[13,17,18] whose metal to ligand ratio (1 : 1) suggests a polynuclear structure. The 1 : 1 copper(II) complexes with H$_2$(R-R'-sap) was demonstrated to be binuclear on the basis of magnetic measurements.[19] The two copper(II) ions are supposed to be bridged by the phenolic oxygen atoms of 2-aminophenol, in analogy with the result of X-ray structural analysis of the copper(II) complex for the Schiff base derived from acetylacetone and 2-aminophenol.[20] Thus, it is naturally assumed that the manganese(II) complexes of H$_2$(R-R'-sap) also possess a binuclear structure bridged by the 2-aminophenol oxygen, hence the complexes being represented as Mn$_2$(R-R'-sap)$_2$. According to Consiglio *et al.*,[13] the magnetic moments of Mn$_2$(R-R'-sap)$_2$ are temperature-dependent. For example, they reported that the moment of Mn$_2$(sap)$_2$ is 5.82 BM at room temperature and 3.89 BM at 140 K. Thus, they presumed an antiferromagnetic spin-exchange interaction operating between a pair of manganese(II) ions. Magnetic properties of Mn$_2$-(R-R'-sap)$_2$ were reexamined in this study in the temperature range 78—300 K. Our measurements revealed that all of the complexes possess a magnetic moment falling in the range 5.8—6.0 BM at room temperature and the moments are almost independent of temperature down to the liquid nitrogen temperature. Magnetic data for Mn$_2$(sap)$_2$ reported by Consiglio *et al.* can not be interpreted by the susceptibility equation for the (s=5/2)–(s=5/2) system on the basis of the Heisenberg model. We believe that Mn$_2$(R-R'-sap)$_2$ has a binuclear skeleton, 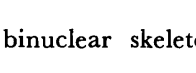 , and spin-exchange interaction between the metal ions is very weak.

Table 1. Magnetic moments (μ_{eff}) of Mn(R-R'-sap)$_2$ at room temperature

Complex	μ_{eff}/BM(T/K)
Mn(sap)$_2$·1/2H$_2$O	3.91(297.3)
Mn(3-MeO-sap)$_2$·H$_2$O	3.94(294.8)
Mn(5-Me-sap)$_2$·1/2H$_2$O	3.96(296.4)
Mn(5-Br-sap)$_2$·H$_2$O	4.03(294.9)
Mn(4'-Cl-sap)$_2$·3/2H$_2$O	4.01(298.0)
Mn(5'-NO$_2$-sap)$_2$·2H$_2$O	4.16(298.1)

Oxidation of Mn$_2$(R-R'-sap)$_2$ with TCOQ in the open atmosphere resulted in the formation of deeply colored Mn(R-R'-sap)$_2$. Magnetic moments of Mn-(R-R'-sap)$_2$ except for Mn(5'-NO$_2$-sap)$_2$·2H$_2$O fall in the range 3.91—4.03 BM (Table 1), which is in good agreement with the moments of the characterized manganese(IV) complexes.[21] Magnetic moment of Mn(5'-NO$_2$-sap)$_2$·2H$_2$O (4.16 BM) is slightly higher than the spin-only value. This may be attributed to the contamination of impurities such as manganese-(III) or manganese(II) species. It seems that Mn(sap)$_2$·1/2H$_2$O, Mn(3-MeO-sap)$_2$·H$_2$O and Mn(5-Me-sap)$_2$·1/2H$_2$O are stable in dichloromethane and in the solid state. On the other hand, Mn(5-Br-sap)$_2$·H$_2$O, Mn-(4'-Cl-sap)$_2$·3/2H$_2$O and Mn(5'-NO$_2$-sap)$_2$·2H$_2$O are unstable in dichloromethane and amorphous substance precipitates when the solutions are exposed to air for a few hours. Mn(5'-NO$_2$-sap)$_2$·2H$_2$O is particularly unstable and it gradually decomposes in the open atmosphere even in the solid state.

1,2-Naphthoquinone and 9,10-phenanthroquinone do not oxidize Mn$_2$(R-R'-sap)$_2$. This may be due to the low oxidation potentials of these quinones compared with TCOQ.[22]

Table 2. Band maxima ($\tilde{\nu}/10^3\,cm^{-1}$) and extinction coefficients (log ε) of CT bands of Mn(R-R'-sap)$_2$

Mn(sap)$_2$·1/2H$_2$O	15.38(3.32), 18.42(3.68), 19.42(3.66)
Mn(3-MeO-sap)$_2$·H$_2$O	13.50(3.38), 16.21(3.50), 18.02(3.48)
Mn(5-Me-sap)$_2$·1/2H$_2$O	15.10(3.36), 18.02(3.69), 18.87(3.69)
Mn(5-Br-sap)$_2$·H$_2$O	15.15(3.39), 17.95(3.68), 19.05(3.67)
Mn(4'-Cl-sap)$_2$·3/2H$_2$O	15.00(3.40), 18.18(3.65), 19.23(3.67)
Mn(5'-NO$_2$-sap)$_2$·2H$_2$O	14.70(3.48), 17.70(3.68), 19.42(3.81)

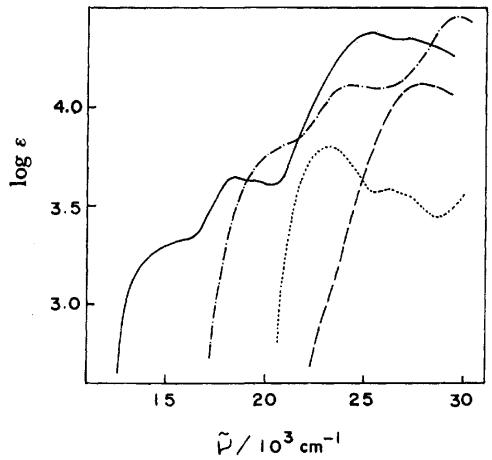

Fig. 2. Electronic spectra of (——) Mn (sap)$_2$·1/2H$_2$O, (– – –) H$_2$(sap), (------) Mn$_2$(sap)$_2$, and (–·–) Ti (sap)$_2$.

Electronic spectra of Mn(R-R'-sap)$_2$ were measured in dichloromethane. All the spectra are similar to each other. The spectrum of Mn(sap)$_2$·1/2H$_2$O is shown in Fig. 2. Figure 2 also includes the spectra of H$_2$(sap), Mn$_2$(sap)$_2$ and Ti(sap)$_2$ for comparison. The intra-ligand transition around $28\times10^3\,cm^{-1}$ of H$_2$(sap) (measured in methanol) shifts to lower frequency and its intensity decreases when it coordinates to a metal. H$_2$(sap) and Mn$_2$(sap)$_2$ do not show any strong absorption in the frequency region less than $20\times10^3\,cm^{-1}$. On the other hand, Mn(sap)$_2$·1/2H$_2$O exhibits strong absorptions at $\approx15\times10^3$ and $\approx19\times10^3\,cm^{-1}$, the latter band being composed of two components. The band maxima and the extinction coefficients of these new bands are given in Table 2. These absorptions are too strong to assign to the ligand field bands. Judging from the fact that Ti(sap)$_2$ shows a strong band around $20\times10^3\,cm^{-1}$, the 15 and $19\times10^3\,cm^{-1}$ bands of Mn(R-R'-sap)$_2$ may be assigned to the charge transfer transitions from phenolic oxygens to manganese(IV) ion. Recently, Matsushita *et al.*[23] synthesized manganese(IV) complexes Mn(R-X-sal)$_2$Cl$_2$ of *N*-alkylsalicylideneamines and assigned the strong absorption near $17\times10^3\,cm^{-1}$ (log ε=3.5) to the charge transfer transition p_π(Cl)→d_π(Mn). This band is similar to those of Mn(R-R'-sap)$_2$ in frequency and intensity, despite no chloride ion being included in Mn(R-R'-sap)$_2$.

Electrochemical properties of Mn(R-R'-sap)$_2$ were studied by means of cyclic voltammetry. All of the complexes displayed two redox waves. Cyclic voltammetric data are given in Table 3. Cyclic voltammogram of Mn(sap)$_2$·1/2H$_2$O is shown in Fig. 3. Electrochemical behaviors of Mn(R-R'-sap)$_2$ can be interpreted

Table 3. Cyclic voltammetric data of Mn(R-R'-sap)$_2$

Complex	E_{pc}	E_{pa}	ΔE_p / mV	$E_{1/2}$
Mn(sap)$_2$·1/2H$_2$O	−0.11	−0.01	100	−0.06
	−0.87	−0.65	220	−0.76
Mn(3-MeO-sap)$_2$·H$_2$O	−0.15	−0.05	100	−0.10
	−0.88	−0.69	190	−0.78
Mn(5-Me-sap)$_2$·1/2H$_2$O	−0.15	−0.04	110	−0.10
	−0.94	−0.64	300	−0.79
Mn(5-Br-sap)$_2$·H$_2$O	−0.01	+0.08	90	+0.04
	−0.73	−0.58	150	−0.66
Mn(4'-Cl-sap)$_2$·3/2H$_2$O	0.00	+0.08	80	+0.04
	−0.76	−0.55	210	−0.66
Mn(5'-NO$_2$-sap)$_2$·2H$_2$O	+0.18	+0.23	50	+0.21
	−0.53	−0.45	80	−0.49

E_{pc} and E_p are calibrated by the use of E_{Fc/Fc^+}[16] and are given in V *vs.* NHE; $E_{1/2}$ is approximated by $E_{1/2}=1/2(E_{pc}+E_{pa})$.

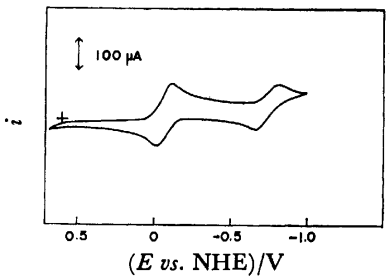

Fig. 3. Cyclic voltammogram of Mn(sap)$_2$·1/2H$_2$O.

by the following processes:

$$\text{Mn(IV)} \overset{E^1_{1/2}}{\rightleftharpoons} \text{Mn(III)} \overset{E^2_{1/2}}{\rightleftharpoons} \text{Mn(II)}.$$

The separation between the cathodic and the anodic peaks of the first process is less than 110 mV, indicating a reversible or quasi-reversible redox of this process. The potentials of the first and the second processes, $E^1_{1/2}$ and $E^2_{1/2}$, markedly depend on the substituents R and R'. Complexes containing an electron-withdrawing group, Mn(5-Br-sap)$_2$·H$_2$O, Mn(4'-Cl-sap)$_2$·3/2H$_2$O and Mn(5'-NO$_2$-sap)$_2$·2H$_2$O, possess higher redox potentials than other complexes. It is evident that an electron-withdrawing group destabilizes the oxidation state of manganese(IV). The substituents R and R' primarily alter the electron density on the phenolic oxygens. Thus, we plotted the potentials $E^1_{1/2}$ and $E^1_{1/2}$ against the Hammett σ values[24] of R and R' to the phenolic oxygen (σ_m for 5'-NO$_2$ and σ_p for 5-Me, 5-Br, and 4'-Cl). As is seen in Fig. 4, a good correlation exists between the redox potentials and the substituents of the ligand. The redox potentials of Mn(3-MeO-sap)$_2$-

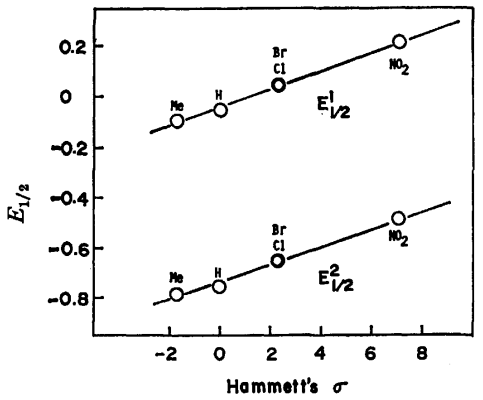

Fig. 4. Correlation between the redox potentials $E_{1/2}$ and $E_{1/2}$ and the Hammett σ values of the substituents R and R′ to the phenolic oxygen for Mn(R-R′-sap)$_2$.

H_2O are comparable to those of Mn(sap)$_2$·1/2H_2O, in spite of the prominent electron releasing ability of methoxy group. This may be interpreted in terms of the "ortho effect."[25]

It is likely that the redox potential of the first process of Mn(5′-NO_2-sap)$_2$·2H_2O (0.21 V. *vs.* NHE) is close to the potential for water oxidation and the instability of this complex must be due to its high redox potential. Similarly, relatively high potentials of Mn(5-Br-sap)$_2$-H_2O and Mn(4′-Cl-sap)$_2$·3/2H_2O ($E^1_{1/2}$=0.04 V) may be responsible for the ready decomposition of these complexes in dichloromethane.

In order to examine the formation mechanism of Mn-(R-R′-sap)$_2$, we brought Mn_2(sap)$_2$ to reaction with TCOQ in acetonitrile under nitrogen atmosphere free from moisture and obtained Mn_2(sap)$_2$(tcoq) as dark green prisms. The magnetic moment of this complex is 4.89 BM at room temperature and 4.80 BM at the

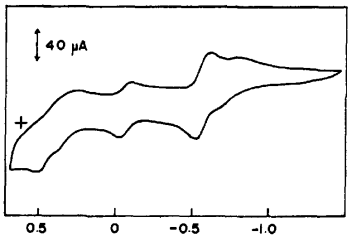

(*E vs.* NHE)/V

Fig. 5. Cyclic voltammogram of Mn_2(sap)$_2$ (tcoq).

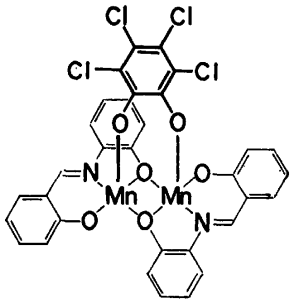

Fig. 6. A possible structure for Mn_2(sap)$_2$(tcoq).

liquid nitrogen temperature. Based on the composition and the magnetic moment, we presume that Mn_2-(sap)$_2$(tcoq) is a binuclear manganese(III) complex. Cyclic voltammogram of this complex revealed a redox wave at −0.58 V, which can be attributed to the Mn(III)⇌Mn(II) process (Fig. 5). In analogy with the molecular structure of a binuclear manganese(III) complex Mn_2(spa)$_2$(CH_3COO)$_2$ of 3-(salicylidene-amino)-1-propanol in which two mangenese(III) ions are bridged by two alcoholic oxygens and two bidentate acetate groups,[12] the most plausible structure for Mn_2(sap)$_2$(tcoq) is given in Fig. 6.

Mn_2(sap)$_2$(tcoq) is very sensitive to water. When water was added dropwise to a methanolic solution of this complex, yellow and blackish purple products were isolated. They were found to be identical with the authentic samples of Mn_2(sap)$_2$ and Mn(sap)$_2$-1/2H_2O, respectively, on the basis of IR spectra. The additional waves at −0.06 and −0.75 V found in cyclic voltammogram of Mn_2(sap)$_2$(tcoq) (Fig. 5) well correspond to the waves of Mn(sap)$_2$·1/2H_2O (Fig. 3 and Table 3). This suggests that Mn_2(sap)$_2$(tcoq) was partly decomposed by the atmospheric moisture to form Mn(sap)$_2$·1/2H_2O. On the basis of these facts, we can represent the reaction between Mn_2(R-R′-sap)$_2$ and TCOQ as follows: Mn_2(R-R′-sap)$_2$+TCOQ⟶ Mn_2 (R-R′-sap)$_2$ (tcoq) $\xrightarrow{H_2O}$ Mn(R-R′-sap)$_2$ Mn_2 (R-R′-sap)$_2$, and others.

References

1) Part XLI: M. Mikuriya, H. Okawa, and S. Kida, *Bull. Chem. Soc. Jpn.*, **54**, 2979 (1981).
2) G. D. Lawrence and D. T. Sawyer, *Coord. Chem. Rev.*, **27**, 173 (1978).
3) A. J. Bearden and R. Malkin, *Q. Rev. Biophys.*, **7**, 131 (1975).
4) K. Sauer, *Acc. Chem. Res.*, **13**, 249 (1980).
5) G. M. Cheniae and I. F. Martin, *Biochim. Biophys. Acta*, **197**, 219 (1970).
6) J. M. Olson, *Science*, **168**, 438 (1970).
7) G. Renger, *Z. Naturforsch.*, **256**, 966 (1970).
8) M. Calvin, *Rev. Pure Appl. Chem.*, **15**, 1 (1965).
9) D. T. Sawyer, M. E. Modini, L. A. Willis, T. L. Riechel, and K. D. Magers, "Bioinorganic Chemistry-II," ed by K. N. Raymond, Am. Chem. Soc., Washington (1977), p. 330.
10) J. H. Wand, *Acc. Chem. Res.*, **3**, 90 (1970).
11) N. Torihara, M. Mikuriya, H. Ōkawa, and S. Kida, *Bull. Chem. Soc. Jpn.*, **53**, 1610 (1980).
12) M. Mikuriya, N. Torihara, H. Ōkawa, and S. Kida, *Bull. Chem. Soc. Jpn.*, **54**, 1063 (1981).
13) M. Consiglio, F. Maggio, T. Pizzino, and V. Romano, *Inorg. Nucl. Chem. Lett.*, **14**, 135 (1978).
14) N. F. Curtis, *J. Chem. Soc.*, **1961**, 3147.
15) F. E. Mabbs and D. J. Machin, "Magnetism and Transition Metal Complexes," Chapman and Hall, London (1973), p. 5.
16) H. M. Koepp, H. Wendt, and H. Strehlow, *Z. Electrochem.*, **64**, 483 (1960).
17) M. Consiglio, *Inorg. Nucl. Chem. Lett.*, **16**, 227 (1978).
18) F. Magio, T. Pizzino, and V. Romano, *Inorg. Nucl. Chem. Lett.*, **10**, 1005 (1974).

19) A. P. Ginsberg, R. C. Sherwood, and E. Koubek, *J. Inorg. Nucl. Chem.*, **29**, 353 (1967).
20) G. A. Barclay and B. F. Hoskins, *J. Chem. Soc.*, **1965**, 1979.
21) A. T. Casey and S. Mitra, "Theory and Applicaption of Molecular Paramagnetism," ed by E. A. Boudreaux and L. N. Mulay, Wiley and Sons, Inc., New York (1976), p. 169.
22) S. L. Kessel, R. M. Emberson, P. G. Dubrunner, and D. N. Hendrickson, *Inorg. Chem.*, **19**, 1170 (1980).
23) T. Matsushita, M. Fujiwara, and T. Shono, *Chem. Lett.*, **1981**, 631.
24) P. R. Wells, S. Ehrenson, and R. W. Taft, "Progress in Physical Organic Chemistry," John Wiley and Sons Inc., New York (1968), Vol. 6, p. 150
25) M. Newman, "Steric Effect in Organic Chemistry," John Wiley and Sons, Inc., New York (1956), p. 648.

Binuclear Metal Complexes. XLIII.[1] Magnetic, Spectroscopic, and Electrochemical Studies on Hetero-metal Binuclear Complexes of *N,N'*-Bis(3-carboxysalicylidene)-1,1-dibenzylethylenediamine

Wakako KANDA, Masaaki NAKAMURA, Hisashi ŌKAWA,* and Sigeo KIDA

Department of Chemistry, Faculty of Science, Kyushu University 33, Hakozaki, Higashi-ku, Fukuoka 812

(Received August 24, 1981)

Copper(II)–M(II) and copper(II)–iron(III) hetero-metal binuclear complexes of *N,N'*-bis(3-carboxysalicylidene)-1,1-dibenzylethylenediamine (H_4fsadb), CuM(fsadb)·nH_2O (M=Co, Ni, Cu, Zn, Mg, Ca, Ba) and CuFe(fsadb)Cl·1.5H_2O, have been prepared and characterized. Cryomagnetic measurements (78—300 K) revealed that an antiferromagnetic spin-exchange interaction operates between the metal ions in the cases CuM(fsadb)·nH_2O (M=Co, Ni, Cu) and CuFe(fsadb)Cl·1.5H_2O, exchange integrals being evaluated on the basis of the Heisenberg model. Ligand field bands due to the copper(II) ion bound at the N_2O_2-site of CuM(fsadb)·nH_2O (M=Co, Ni, Cu, Zn, Mg) and CuFe(fsadb)Cl·1.5H_2O are in the range 1.9×10^3—21.4×10^3 cm^{-1}, while in the cases of CuCa(fsadb)·4H_2O and CuBa(fsadb)·3.5H_2O the frequencies of the bands are close to that (17.8×10^3 cm^{-1}) of the mononuclear complex Cu(H_2fsadb)·H_2O. This spectral feature has been explained in terms of the configuration of the second metal ion adjacent to the copper(II) ion: *trans*-octahedral in the cases of small metal ions (Fe(III), Co(II), Ni(II), Cu(II), Zn(II), Mg(II)) and presumably *cis*-octahedral in the cases of large metal ions (Ca(II), Ba(II)). Copper(II/I) redox potentials of the hetero-metal complexes are much low compared with that of Cu(H_2fsadb)·H_2O. This shift has been discussed in terms of the electronic effect of the carboxylate group and the covalency in the bonding between the bridging phenolic oxygen and the second metal ion.

Recently there is a growing interest in chemistry of binuclear metal complexes in connection with metalloenzymes which involve two metal ions at their active sites.[2] Particularly, the recognition that superoxide dismutase[3] and cytochrome oxidase[4] contain two kinds of metal ions has stimulated an interest in hetero-metal binuclear complexes. Electrochemical technique is one of the essential tools for bioinorganic approach to metalloenzymes and several recent papers have been devoted to the analysis of the redox behavior of binuclear copper(II) complexes[5–9] in the hope to clarify the oxido-reductive function of copper proteins. On the other hand, electrochemical investigations on hetero-metal binuclear complexes are very limited,[10] because of the difficulty in preparation and the low stability in solvents.

Previously we reported the synthesis and the magnetic properties of copper(II)–M(II),[11–14] nickel(II)–M(II),[13] and cobalt(II)–M(II)[15,16] complexes of N,N'-bis(3-carboxysalicylidene)alkanediamines, which were demonstrated to be an excellent binucleating ligand possessing coordination selectivity. However, electrochemical properties of these complexes could not be examined because of their low solubility in solvents suitable for electrochemical measurements. In this study, we have prepared copper(II)–M(II) and copper(II)–iron(III) complexes of a new binucleating ligand, *N,N'*-bis(3-carboxysalicylidene)-1,1-dibenzylethylenediamine (abbreviated as H_4fsadb) which possesses hydrophobic benzyl groups in the ethylenediamine moiety (Fig. 1). These complexes, CuM(fsadb)·nH_2O (M=Co, Ni, Cu, Zn, Mg, Ca, Ba) and CuFe(fsadb)Cl·1.5H_2O, are soluble in dichloromethane or *N,N*-dimethylformamide. Thus, we have examined the optical and electrochemical properties of the copper(II) ion bound at the N_2O_2-site varing the second metal ion at the O_4-site. We have also studied magnetic spin-exchange interaction in CuM(fsadb)·nH_2O (M=Co, Ni, Cu) and CuFe(fsadb)Cl·1.5H_2O, comparing the results with those previously reported.[11–16]

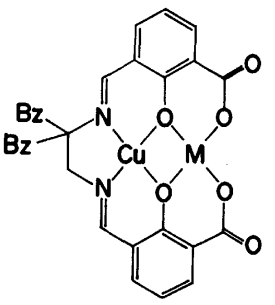

Fig. 1. The structure of hetero-metal binuclear complexes; M=Fe(III)Cl, Co(II), Ni(II), Cu(II), Zn(II), Mg(II), Ca(II), and Ba(II).

Experimental

Syntheses. 3-Formylsalicylic acid was prepared after the method of Duff and Bills.[17]

1,1-Dibenzylethylenediamine. An aqueous solution (20 cm^3) containing ammonium chloride (2.95 g), sodium cyanide (2.5 g) and ammonia water (28%, 7 cm^3) was placed in a round-bottomed flask, and to this was added an ethanolic solution (15 cm^3) of benzyl ketone (10.5 g). The flask was sealed with a rubber stopper and heated at 60 °C on a water bath for 5 hours to give an orange colored solution. The reaction mixture was shaken three times with 70 cm^3 portions of ether. The combined etherial solution was dried over sodium sulfate. Evaporation of the solvent left 2-amino-2-benzyl-3-phenylpropionitrile as pale orange solid. It was washed with a small amount of methanol and recrystallized from methanol to give colorless needles.

Found: C, 81.20; H, 7.02; N, 11.78%. Calcd for $C_{16}H_{16}N_2$: C, 81.32; H, 6.82; N, 11.85%.

This amino nitrile (15 g) was added to a suspension of $LiAlH_4$ (5 g) in absolute ether (250 cm^3). The mixture was stirred for 3 h at room temperature and then refluxed for 40 h on an oil bath. Unreacted $LiAlH_4$ was decomposed by addition of methanol–water (1: 1, 40 cm^3), while the flask was cooled by means of ice–water. The reaction mixture

was shaken with 150 cm³ portions of ether four times and the combined etherial solution was dried over sodium sulfate. On evaporating the solvent, there remained 1,1-dibenzylethylenediamine as a hygroscopic, yellow solid. It was used for the preparation of the complexes without further purification.

Cu(H₂fsadb)·H₂O. 3-Formylsalicylic acid (310 mg) and 1,1-dibenzylethylenediamine (270 mg) were dissolved in absolute methanol (40 cm³). To this solution was added a methanolic solution (20 cm³) of copper(II) acetate monohydrate (220 mg), and the mixture was refluxed for several hours to give purple crystalline solid. It was collected, washed with methanol and recrystallized from a mixture of *N,N*-dimethylformamide and water.

Found: C, 62.77; H, 4.49; N, 4.74; Cu, 12.3%. Calcd for $C_{32}H_{26}N_2O_6Cu \cdot H_2O$: C, 62.38; H, 4.55; N, 4.55; Cu, 12.24%.

CuFe(fsadb)Cl·1.5H₂O. This complex was synthesized as purplish brown prisms by reacting Cu(H₂fsadb)·H₂O (50 mg) and iron(III) chloride (14 mg) in methanol (20 cm³) in the presence of triethylamine.

Found: C, 53.68; H, 3.76; N, 3.80; Cu, 8.8; Fe, 8.2%. Calcd for $C_{32}H_{24}N_2O_6ClCuFe \cdot 1.5H_2O$: C, 53.79; H, 3.81; N, 3.92; Cu, 8.89; Fe, 7.82%.

CuCo(fsadb)·3H₂O. Cu(H₂fsadb)·H₂O (100 mg) was dissolved in a solution of lithium hydroxide monohydrate (16 mg) in methanol (40 cm³). The solution was once filtered to separate insoluble materials. To the red-colored filtrate was added a methanolic solution (10 cm³) of cobalt(II) acetate tetrahydrate (41 mg), and the mixture was heated at *ca.* 60 °C for a while. After the reaction mixture was left stand overnight, reddish orange needles which separated were collected, washed with water and dried under reduced pressure.

Found: C, 54.22; H, 4.12; N, 4.04; Co, 8.5; Cu, 8.8%. Calcd for $C_{32}H_{24}N_2O_6CoCu \cdot 3H_2O$: C, 54.20; H, 4.28; N, 3.95; Co, 8.31; Cu, 8.96%.

CuNi(fsadb)·6H₂O. This complex was obtained as reddish purple needles in the same way as that of CuCo(fsadb)·3H₂O except for using nickel(II) chloride hexahydrate (39.7 mg) instead of cobalt(II) acetate tetrahydrate.

Found: C, 50.28; H, 4.32; N, 3.59; Cu, 8.3; Ni, 8.0%. Calcd for $C_{32}H_{24}N_2O_6CuNi \cdot 6H_2O$: C, 50.38; H, 4.76; N, 3.67; Cu, 8.33; Ni, 7.69%.

CuCu(fsadb)·1.5H₂O. To a red solution of Cu(H₂fsadb)·H₂O (100 mg) and lithium hydroxide monohydrate (16 mg) in methanol (40 cm³) was added a methanolic solution (10 cm³) of copper(II) acetate monohydrate (37 mg). The mixture was heated at *ca.* 60 °C for 3 h to give pale green solid. It was collected and recrystallized from a mixture of *N,N*-dimethylformamide and water.

Found: C, 55.84; H, 4.01; N, 4.26; Cu, 18.6% Calcd for $C_{32}H_{24}N_2O_6Cu_2 \cdot 1.5H_2O$: C, 55.97; H, 3.96; N, 4.08; Cu, 18.51%.

CuZn(fsadb)·3H₂O. This complex was obtained as reddish orange needles in the same way as that of CuCo(fsadb)·3H₂O using zinc(II) chloride (22.8 mg). It was recrystallized from a chloroform–ether mixture.

Found: C, 53.34; H, 4.20; N, 3.86; Cu, 8.9%. Calcd for $C_{32}H_{24}N_2O_6CuZn \cdot 3H_2O$: C, 53.72; H, 4.23; N, 3.92; Cu, 8.88%.

CuMg(fsadb)·4H₂O. This complex was obtained as reddish pink needles in the same way as that of CuCo(fsadb)–3H₂O using magnesium(II) acetate tetrahydrate (36 mg). It was recrystallized from a chloroform–ether mixture.

Found: C, 55.75; H, 4.32; N, 3.93; Cu, 9.1%. Calcd for $C_{32}H_{24}N_2O_6CuMg \cdot 4H_2O$: C, 55.51; H, 4.66; N, 4.05; Cu, 9.18%.

CuCa(fsadb)·4H₂O. This complex was obtained as reddish pink needles by the reaction of Cu(H₂fsadb)·H₂O (100 mg) and calcium(II) chloride dihydrate (24.4 mg) in methanol (50 cm³) in the presence of lithium hydroxide monohydrate (16 mg).

Found: C, 54.34; H, 4.34; N, 4.01; Cu, 8.7%. Calcd for $C_{32}H_{24}N_2O_6CaCu \cdot 4H_2O$: C, 54.27; H, 4.55; N, 3.96; Cu, 8.97%.

CuBa(fsadb)·3.5H₂O. This complex was obtained as greenish purple needles by the reaction of Cu(H₂fsadb)·H₂O (100 mg) and barium(II) chloride dihydrate (41 mg) in the presence of lithium hydroxide monohydrate (16 mg).

Found: C, 48.20; H, 3.81; N, 3.59; Cu, 7.7%. Calcd for $C_{32}H_{24}N_2O_6BaCu \cdot 3.5H_2O$: C, 48.27; H, 3.92; N, 3.65; Cu, 7.98%.

Cu(saldb)·0.5H₂O. A mixture of salicylaldehyde (102 mg), 1,1-dibenzylethylenediamine (100 mg) and copper(II) acetate monohydrate (83 mg) in methanol (50 cm³) was heated under stirring for 3 h. The reaction mixture was allowed to stand overnight to give purple prisms, which were collected and dried *in vacuo*.

Found: C, 68.91; H, 5.60; N, 5.25; Cu, 12.3%. Calcd for $C_{30}H_{26}N_2O_2Cu \cdot 0.5H_2O$: C, 69.41; H, 5.24; N, 5.40; Cu, 12.24%.

Measurements. Elemental analyses of carbon, hydrogen, and nitrogen were carried out at the Service Center of Elemental Analysis, Kyushu University. Analyses of copper, cobalt, iron, and nickel were made with a Shimadzu Atomic Absorption-Flame Spectrometer Model AA-610S. Infrared spectra were measured with a Hitachi Infrared Spectrometer Model 215 on a KBr disk. Electronic Spectra were recorded on a Shimadzu Multipurpose Spectrophotometer Model MPS-5000 in dichloromethane or in *N,N*-dimethylformamide. Magnetic susceptibilities were measured by the Faraday method in the temperature range from liquid nitrogen temperature to room temperature. Diamagnetic correction was made using Pascal's constants.[18] Effective magnetic moments were calculated by the equation, $\mu_{eff}=2.828\times\sqrt{(\chi_M-N\alpha)T}$, where χ_M is the susceptibility per molecule. In the case of CuCu(fsadb)·1.5H₂O, the moment was calculated for one copper atom. Cyclic voltammograms were recorded with a Yanagimoto Voltammetric Analyzer Model P-1000 in dichloromethane or in *N,N*-dimethylformamide containing 0.1 M tetrabutylammonium perchlorate as the supporting electrolyte. A three-electrode cell was used for measurements, in which the working electrode is a glassy carbon, the auxiliary electrode a platinum coil, and the reference electrode a saturated calomel electrode. All the redox potentials were corrected by the use of ferrocene as an internal standard,[19] where the ferrocenium/ferrocene redox potential is assumed to be 0.400 V *vs.* NHE.[20]

Results and Discussion

Hetero-metal binuclear complexes were prepared by reacting the mononuclear copper(II) complex Cu(H₂fsadb)·H₂O with a metal ion. The formation of the hetero-metal complexes can be diagnosed by the presence of a strong band at 1550 cm⁻¹ attributable to the coordinated carboxylate group, while Cu(H₂fsadb)·H₂O exhibits a band at 1710 cm⁻¹ due to the free carboxyl group.

Magnetic susceptibilities of the complexes were measured in the temperature range 78—300 K. Magnetic moments of CuM(fsadb)·nH₂O (M=Co, Ni, Cu)

and CuFe(fsadb)Cl·1.5H_2O are temperature-dependent, indicating that a spin-exchange interaction operates between the metal ions. Magnetic properties of these complexes could be interpreted in terms of the magnetic susceptibility equations (1), (2), (3), and (4) for the (s=1/2)-(s=5/2),[21,22] (s=1/2)-(s=3/2),[13,14] (s=1/2)-(s=1),[10,13,14] and (s=1/2)-(s=1/2)[23] systems, respectively, on the basis of the Heisenberg model:

$$\chi_M = \frac{Ng^2\beta^2}{kT} \times \frac{5\exp(-6J/kT)+14}{5\exp(-6J/kT)+7} + N\alpha, \quad (1)$$

$$\chi_M = \frac{Ng^2\beta^2}{kT} \times \frac{2\exp(-4J/kT)+10}{3\exp(-4J/kT)+5} + N\alpha, \quad (2)$$

$$\chi_M = \frac{Ng^2\beta^2}{kT} \times \frac{\exp(-3J/kT)+2}{\exp(-3J/kT)+10} + N\alpha, \quad (3)$$

and

$$\chi_A = \frac{Ng^2\beta^2}{kT} \times \frac{1}{\exp(-2J/kT)+3} + N\alpha, \quad (4)$$

where χ_M and χ_A represent magnetic susceptibilities per molecule and per atom, respectively, and other symbols have their usual meanings. Best-fits of magnetic susceptibilities to the theoretical curves are shown in Figs. 2 and 3. Magnetic parameters thus determined are given in Table 1. The exchange integrals found for the present complexes are all negative, indicating antiferromagnetic spin-exchange interactions operating between the metal ions. Each integrals obtained is close to the value of corresponding hetero-metal complex of *N,N'*-bis(3-carboxysalicylidene)alkanediamine reported previously.[11-14,22] Magnetic moments of CuM(fsadb)·$n$$H_2O$ (M=Zn, Mg, Ca, Ba) fall in the range 1.83—1.88 BM at room temperature, which indicates the presence of one unpaired electron per molecule.

Conductance measurements revealed that the hetero-metal complexes are nonelectrolytes in *N,N*-dimethylformamide, suggesting the coordination of the second metal ion to the O_4-site.

Electronic spectra of the hetero-metal complexes were measured in dichloromethane. Because of the sparing solubility of CuCu(fsadb)·1.5H_2O in dichloromethane, the spectrum of this complex was measured in *N,N*-dimethylformamide. Some representatives of absorption spectra are shown in Fig. 4. Absorption maxima and

Table 1. Effective magnetic moments at room temperature and magnetic paramete rs, J, g, and $N\alpha$, of hetero-metal complexes

	μ_{eff}/BM(T/K)	J / cm^{-1}	g	$N\alpha\times10^6$ / c.g.s. mol^{-1}
CuFe(fsadb)-Cl·1.5H_2O	5.57(297.4)	−48	2.00	60
CuCo(fsadb)·3H_2O	5.11(292.5)	−30	2.50	500
CuNi(fsadb)·6H_2O	3.67(295.5)	−22	2.24	200
CuCu(fsadb)·1.5H_2O	0.78(298.5)	−305	2.10	65[a]
CuZn(fsadb)·3H_2O	1.86(295.7)			
CuMg(fsadb)·4H_2O	1.87(296.2)			
CuCa(fsadb)·4H_2O	1.88(295.4)			
CuBa(fsadb)·3.5H_2O	1.83(298.5)			

a) Data per copper atom.

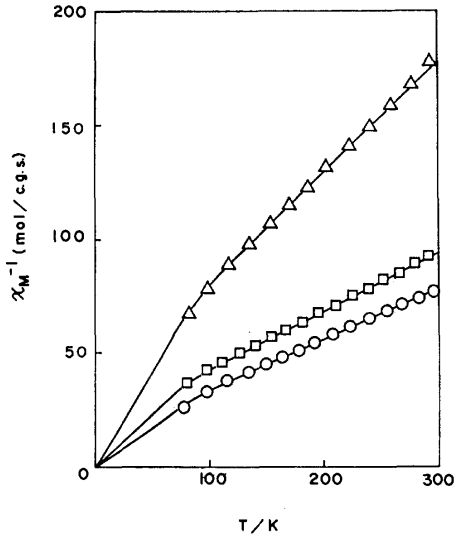

Fig. 2. Temperature variations of inverse magnetic susceptibilities for (○) CuFe(fsadb)Cl-1.5H_2O, (□) CuCo (fsadb)-3H_2O, and (△) CuNi (fsadb)-6H_2O.

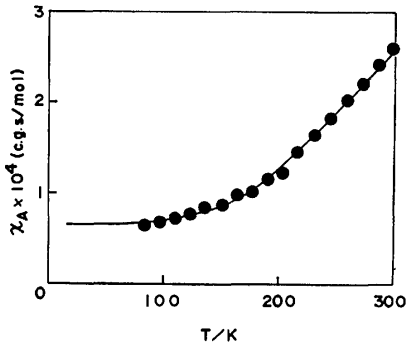

Fig. 3. Temperature variation of magnetic susceptibility for CuCu(fsadb)·1.5H_2O.

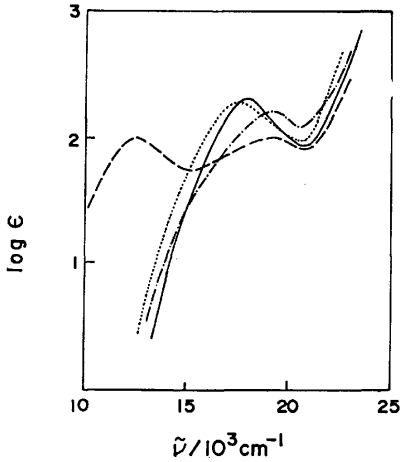

Fig. 4. Absorption spectra of (——) Cu(H_2fsadb)·H_2O (in CH_2Cl_2), (- - -) CuCu(fsadb)·1.5H_2O (in DMF), (—·—) CuMg(fsadb)·3H_2O (in CH_2Cl_2), and (·····) CuBa(fsadb)·3.5H_2O (in CH_2Cl_2).

TABLE 2. FREQUENCIES AND EXTINCTION COEFFICIENTS OF THE LIGAND FIELD BANDS OF HETERO-METAL COMPLEXES IN DICHLOROMETHANE AND IONIC RADII OF THE SECOND METAL IONS

	$\tilde{\nu}/10^3\ cm^{-1}\ (\varepsilon)$				Ionic radius[a] / Å
$Cu(H_2fsadb)\cdot H_2O$	17.8 (211)				
$CuFe(fsadb)Cl\cdot 1.5H_2O$	21.4 (1338)				0.63
$CuCo(fsadb)\cdot 3H_2O$	20.2 (198)	18.0 (151)	16.2 (72)	7.5 (9)	0.88
$CuNi(fsadb)\cdot 6H_2O$	19.0 (164)	16.5 (87)	7.8 (4)		0.84
$CuCu(fsadb)\cdot 1.5H_2O$[b]	19.0 (149)	12.6 (97)			0.76
$CuZn(fsadb)\cdot 3H_2O$	20.5 (385)				0.89
$CuMg(fsadb)\cdot 4H_2O$	19.1 (168)				0.86
$CuCa(fsadb)\cdot 4H_2O$	18.2 (210)				1.14
$CuBa(fsadb)\cdot 3.5H_2O$	17.5 (197)				1.50

a) Radius for six-coordinate metal ion except for copper(II). b) Measured in *N,N*-dimethylformamide.

TABLE 3. CATHODIC AND ANODIC PEAKS (E_{pc} AND E_{pa}), PEAK SEPARATIONS (ΔE_p) AND REDOX POTENTIALS ($E_{1/2}$)

	E_{pc} / V	E_{pa} / V	ΔE_p / mV	$E_{1/2}$ / V
$Cu(H_2fsadb)\cdot H_2O$	−0.91	−0.80	110	−0.86
	(−0.93	−0.79	140	−0.86)[a]
$CuFe(fsadb)Cl\cdot 1.5H_2O$	−1.34	−1.23	110	−1.29
	(−0.30	−0.23	70	−0.27
$CuCo(fsadb)\cdot 3H_2O$	−1.39	−1.14	250	−1.27
$CuNi(fsadb)\cdot 6H_2O$	−1.38	−1.18	200	−1.28
$CuCu(fsadb)\cdot 1.5H_2O$	(−0.84	−0.75	90	(−0.80[a]
	−1.29)	−1.18	110	−1.24)
$CuZn(fsadb)\cdot 3H_2O$	−1.36	−1.20	160	−1.29
$CuMg(fsadb)\cdot 4H_2O$	−1.38	−1.23	150	−1.31
$CuCa(fsadb)\cdot 4H_2O$	−1.63	−1.21	420	−1.42
$CuBa(fsadb)\cdot 3.5H_2O$	−1.52	−1.37	150	−1.45

a) Data obtained by the measurements in *N,N*-dimethylformamide.

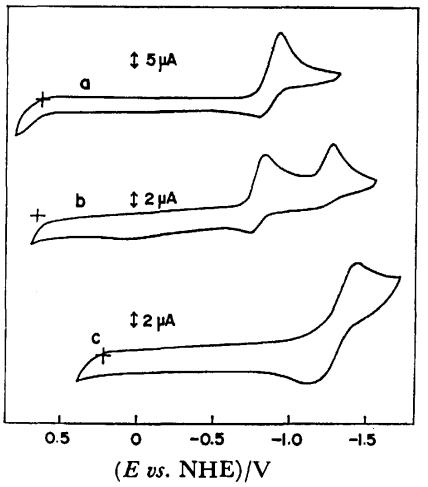

Fig. 5. Cyclic voltammograms of (a) $Cu(H_2fsadb)\cdot H_2O$ (in CH_2Cl_2), (b) $CuCu(fsadb)\cdot 1.5H_2O$ (in DMF), and (c) $CuMg(fsadb)\cdot 3H_2O$ (in CH_2Cl_2).

extinction coefficients of the ligand field bands are given in Table 2. The d-d band of $Cu(H_2fsadb)\cdot H_2O$ was observed at $17.8\times10^3\ cm^{-1}$ in dichloromethane and at $17.0\times10^3\ cm^{-1}$ in *N,N*-dimethylformamide. On the other hand, $CuCu(fsadb)\cdot 1.5H_2O$ shows two bands at 12.6×10^3 and $19.0\times10^3\ cm^{-1}$, which are assigned to the ligand field bands of the copper(II) ions bound at the O_4- and the N_2O_2-sites, respectively.[12] The spectrum of $CuCo(fsadb)\cdot 3H_2O$ is composed of the bands at 7.5×10^3, 16.2×10^3, 18.0×10^3, and $20.2\times10^3\ cm^{-1}$. The $20.2\times10^3\ cm^{-1}$ band is attributed to the $[CuN_2O_2]$ chromophore. The remaining bands can be ascribed to the $[CoO_6]$ chromophore,[14] which consists of four oxygen atoms of the ligand in the equatorial plane and of two water oxygens at apical positions. This is supported by the single-crystal X-ray analysis of $CuCo(fsaen)\cdot 3H_2O$.[24] Electronic spectrum of $CuNi(fsadb)\cdot 6H_2O$ can also be explained by the superposition of the d-d bands of the planar $[CuN_2O_2]$ and the $[NiO_6]$ chromophores. This is also supported by the X-ray analysis for $CuNi(fsaen)\cdot 3H_2O$.[25] In the cases of $CuFe(fsadb)Cl\cdot 1.5H_2O$ and $CuM(fsadb)\cdot nH_2O$ (M= Zn, Mg, Ca, Ba), no absorption was found in the region less than $18.0\times10^3\ cm^{-1}$. This is natural since high-spin iron(III) has no spin-allowed d-d transition and zinc(II), magnesium(II), calcium(II) and barium(II) ions have no ligand field band. It is likely that the second metal at the O_4-site takes a six-coordinate configuration with two water molecules.[26]

The d-d band due to the copper(II) ion in $CuFe(fsadb)Cl\cdot 1.5H_2O$ and $CuM(fsadb)\cdot nH_2O$ (M=Co, Ni, Cu, Zn, Mg) fall in the range 19.0×10^3—$21.4\times10^3\ cm^{-1}$, which is higher than $17.8\times10^3\ cm^{-1}$ of $Cu(H_2fsadb)\cdot H_2O$. Such a blue shift of the d-d band may be attributed to the increased planarity of the $[CuN_2O_2]$

chromophore on forming a binuclear complex with a second metal bridged by the phenolic oxygens.[26,27] On the other hand, the frequencies of the d-d bands of $CuCa(fsadb)\cdot 4H_2O$ and $CuBa(fsadb)\cdot 3.5H_2O$ are close to that of $Cu(H_2fsadb)\cdot H_2O$. It seems that this spectral feature is closely concerned with the configuration around the second metal ion at the O_4-site. Since iron(III), cobalt(II), nickel(II), copper(II), zinc(II) and magnesium(II) are small in size (ionic radii being less than 0.9 Å; Table 2), these metal ions can fit to the O_4-site to form a *trans*-octahedral configuration with water molecules at the apical positions.[24-26] On the other hand, calcium(II) and barium(II) are considerably large (radius being 1.14 and 1.50 Å respectively) so as to be forced to take a distorted structure such as *cis*-β-octahedral configuration when the metal ions bind at the O_4-site. This steric requirement may bring about the distortion of the CuN_2O_2 plane and hence the d-d bands of these complexes shift to a lower frequency compared with other hetero-metal binuclear complexes.

Electrochemical properties of the hetero-metal complexes were investigated by means of cyclic voltammetry in dichloromethane. In the case of $CuCu(fsadb)\cdot 1.5H_2O$ the measurement was carried out in *N,N*-dimethylformamide. Typical examples of cyclic voltammograms are shown in Fig. 5. Cathodic and anodic peaks, peak separations, and redox potentials ($E_{1/2}$) are given in Table 3. Cyclic voltammogram of $Cu(H_2fsadb)\cdot H_2O$ showed a Cu(II/I) redox wave at -0.86 V *vs.* NHE. Cyclic voltammogram of $CuCu(fsadb)\cdot 1.5H_2O$ (in *N,N*-dimethylformamide) was characterized by two redox waves at -0.80 and -1.24 V *vs.* NHE, indicating the difference in coordination environment between the two metal ions. Though the first redox potential is close to that of $Cu(H_2fsadb)\cdot H_2O$, we attributed the -0.80 V wave to the Cu(II/I) redox process of the copper at the O_4-site and the -1.24 V wave to the copper at the N_2O_2-site, on the grounds described below. Cyclic voltammogram of $CuFe(fsadb)Cl\cdot 1.5H_2O$ also reveals two redox waves at -0.27 and -1.29 V *vs.* NHE, which are tentatively assigned to the Fe(III/II) and the Cu(II/I) redox processes respectively. Only one redox wave was observed for other hetero-metal complexes at -1.28—-1.45 V *vs.* NHE. This is unambiguously attributed to the redox of the copper(II) bound at the N_2O_2-site. This adds a strong support for the electrochemical interpretations for $CuCu(fsadb)\cdot 1.5H_2O$ and $CuFe(fsadb)Cl\cdot 1.5H_2O$ described above.

It is noteworthy that the Cu(II/I) redox potentials for the hetero-metal complexes are very lower than that of $Cu(H_2fsadb)\cdot H_2O$. Recently, we have found that the reduction potential of the copper(II) ion of *N,N'*-disalicylidenealkanediaminatocopper(II) practically remains constant even when it forms a hetero-metal binuclear complex with a metal(II) halide, bridged by the phenolic oxygens.[28] Further, Gagne *et al.*[10] pointed out that the Cu(II)–M(II) complexes of a macrocycle (M=Mn, Fe, Co, Ni, Cu, Zn) show the Cu(II/I) redox at similar potentials, irrespective of second metal ions. Thus, the marked difference in the Cu(II/I) redox potential between the mononuclear and the hetero-metal binuclear complexes can not be attributed to the different coordination modes of the phenolic oxygen (simple coordination in the former and bridging in the latter). Since the peripheral substituents of the ligands are known to change the redox potential of the central metal in a striking manner,[29,30] it is likely that carboxyl and carboxylate groups differ in electronic effect on the redox potential of the copper(II) ion at the N_2O_2-site. In fact, *N,N'*-disalicylidene-1,1-dibenzylethylenediaminatocopper(II) $Cu(saldb)\cdot 0.5H_2O$, containing no carboxyl group on the ring, shows the Cu(II/I) redox wave at -1.36 V *vs.* NHE, which is more lower than that of $Cu(H_2fsadb)\cdot 1.5H_2O$ and comparable to those of the hetero-metal complexes. This implies that the electron-withdrawing effect of the carboxyl group diminishes the electron density on the phenolic oxygen and hence destabilizes the copper(II) oxidation state of $Cu(H_2fsadb)\cdot H_2O$ compared with $Cu(saldb)\cdot 0.5H_2O$. On the other hand, the electronic effect of the carboxyl group almost vanishes when it is deprotonated.[30] Thus, the substitution of a metal ion for the carboxyl protons of $Cu(H_2fsadb)\cdot H_2O$ may bring about the negative shift of the Cu(II/I) redox potential.

It is also noticed that the Cu(II/I) redox potential depends somewhat on the second metal ion. In the cases of $CuM(fsadb)\cdot nH_2O$ (M=Co, Ni, Zn, Mg) and $CuFe(fsadb)Cl\cdot 1.5H_2O$, the Cu(II/I) redox potentials fall in the range -1.27——-1.31 V *vs.* NHE, while the potentials of $CuCa(fsadb)\cdot 4H_2O$ and $CuBa(fsadb)\cdot 3.5H_2O$ are -1.42 and -1.45 V *vs.* NHE respectively. We presume that the bonding between the phenolic oxygen and calcium(II) or barium(II) ion is practically ionic. On the other hand, the bonding between the phenolic oxygen and the second metal ion of $CuM(fsadb)\cdot nH_2O$ (M=Co, Ni, Cu, Mg, Zn) and $CuFe(fsadb)Cl\cdot 1.5H_2O$ must contain some covalent character. This might result in the decrease in electron density on the phenolic oxygens and hence the positive shift of the Cu(II/I) redox potential compared with those of $CuCa(fsadb)\cdot 4H_2O$ and $CuBa(fsadb)\cdot 3.5H_2O$.

References

1) Part XLII: H. Ōkawa, M. Nakamura, and S. Kida, *Bull. Chem. Soc. Jpn.*, **55**, 466 (1982).

2) G. L. Eichhorn, "Inorganic Biochemistry," Elsevier, New York (1973), Vols. 1 and 2.

3) J. S. Richardson, K. A. Thomas, B. H. Rubin, and D. C. Richardson, *Proc. Natl. Acad. Sci. U.S.A.*, **72**, 1349 (1975).

4) G. Palmer, G. T. Babcock, and L. E. Vickery, *Proc. Natl. Acad. Sci. U. S. A.*, **73**, 2206 (1977).

5) A. W. Addison, *Inorg. Nucl. Chem. Lett.*, **12**, 899 (1976).

6) D. E. Fenton, R. R. Schroeder, and R. L. Lintvedt, *J. Am. Chem. Soc.*, **100**, 1931 (1978).

7) D. E. Fenton and R. L. Lintvedt, *J. Am. Chem. Soc.*, **100**, 6367 (1978).

8) R. R. Gagne, C. A. Koval, and T. J. Smith, *J. Am. Chem. Soc.*, **99**, 8367 (1977).

9) J. P. Gisselbrecht, M. Gross, A. H. Alberts, and J. M. Lehn, *Inorg. Chem.*, **19**, 1386 (1980).

10) R. R. Gagne and C. L. Spiro, *J. Am. Chem. Soc.*, **102**,

1443 (1980).
11) H. Ōkawa, M. Tanaka, and S. Kida, *Chem. Lett.*, **1974**, 987.
12) M. Tanaka, M. Kitaoka, H. Ōkawa, and S. Kida, *Bull. Chem. Soc. Jpn.*, **49**, 2469 (1976).
13) H. Ōkawa, Y. Nishida, M. Tanaka, and S. Kida, *Bull. Chem. Soc. Jpn.*, **50**, 127 (1977).
14) N. Torihara, H. Ōkawa, and S. Kida, *Inorg. Chim. Acta*, **26**, 97 (1976).
15) N. Torihara, H. Ōkawa, and S. Kida, *Bull. Chem. Soc. Jpn.*, **51**, 3236 (1978).
16) N. Torihara, H. Ōkawa, and S. Kida, *Chem. Lett.*, **1979**, 683.
17) J. C. Duff and E. J. Bills, *J. Chem. Soc.*, **1932**, 1987.
18) P. W. Selwood, "Magnetochemistry," Interscience, New York (1956), pp. 78, 91.
19) R. R. Gagne, C. A. Koval, and G. C. Lisensky, *Inorg. Chem.*, **19**, 2855 (1980).
20) H. M. Koepp, H. Wendt, and H. Strehlow, *Z. Electrochem.*, **64**, 483 (1960).
21) W. J. Stratton and D. H. Busch, *J. Am. Chem. Soc.*, **82**, 4833 (1960).
22) H. Ōkawa, W. Kanda, and S. Kida, *Chem. Lett.*, **1980**, 1281.
23) B. Bleaney and K. D. Bowers, *Proc. R. Soc. London, Ser. A*, **214**, 451 (1952).
24) M. Mikuriya, H. Ōkawa, S. Kida, and I. Ueda, *Bull. Chem., Soc. Jpn.*, **51**, 2920 (1978).
25) J. Galy, J. Jaud, Y. Journaux, and O. Kahn, Presented at the XXIth International Conference on Coordination Chemistry, Toulouse (1980).
26) J. P. Beale, J. A. Cummingham, and D. J. Phillips, *Inorg. Chim. Acta*, **33**, 113 (1979).
27) S. J. Gruber, C. M. Harris, and E. Sinn, *J. Inorg. Nucl. Chem.*, **30**, 1805 (1968).
28) M. Nakamura, H. Ōkawa, and S. Kida, to be published.
29) A. Giraudeau, H. J. Callot, and M. Gross, *Inorg. Chem.*, **18**, 201 (1979).
30) J. A. Streeky, D. G. Pillsbury, and D. H. Busch, *Inorg. Chem.*, **19**, 3148 (1980).
31) P. R. Wells, S. Ehrenson, and R. W. Taft, "Progress is Physical Organic Chemistry," John Wiley and Sons Inc., New York (1968), Vol. 6, p. 150.

η^3-2,4-Pentanedionato(2-) and Terminal-carbon-bonded β-Diketonato Complexes of Platinum(II)

Seichi OKEYA,*,† Yukio NAKAMURA, Shinichi KAWAGUCHI,* and Tetsu HINOMOTO††

Faculty of Science, Osaka City University, Sumiyoshi-ku, Osaka 558
†*Faculty of Education, Wakayama University, Masago-cho, Wakayama 640*
††*Japan Electron Optics Laboratories, Ltd., Akishima, Tokyo 196*

(Received August 27, 1981)

A platinum(II)complex containing a 2,4-pentanedionate dianion as a trihapto ligand [Pt(acac(2−)-C^1—C^3)-{P(p-ClC_6H_4)$_3$}$_2$] was prepared by the reaction of [Pt(acac)$_2$] with tris(p-chlorophenyl)phosphine and reacted with pyridinium perchlorate to afford [Pt(acac-C^1)(py){P(p-ClC_6H_4)$_3$}$_2$](ClO_4). A similar terminal-carbon-bonded complex of 1,1,1-trifluoro-2,4-pentanedionate monoanion with platinum(II) was also derived from [Pt(tfac(2−)-C,O)($AsPh_3$)$_2$] by the reaction with pyridinium perchlorate. These novel platinum(II) complexes were characterized mainly by IR and NMR spectroscopy.

2,4-Pentanedione and other β-dicarbonyl compounds are very popular ligands,[1] and widely used as a chelating monoanion.[2] Recently coordination chemistry of their dianions has been greatly advanced and at present seven coordination modes illustrated in Fig. 1 are known. This paper reports a platinum(II) complex of type **5** containing a trihapto 2,4-pentanedionate dianion (acac-(2−)-C^1—C^3) as well as the first examples of platinum (II) complexes containing the terminal-carbon-bonded acac and 1,1,1-trifluoro-2,4-pentanedionate (tfac) monoanions.

Experimental

Preparation. The starting chelates bis(2,4-pentanedionato)platinum(II), [Pt(acac)$_2$] and bis(1,1,1-trifluoro-2,4-pentanedionato)platinum(II), [Pt(tfac)$_2$] were prepared by the method reported recently.[12] Tris(p-chlorophenyl)phosphine was purchased and used without further purification. 1,1,1-Trifluoro-2,4-pentanedionato(2-)-C,O-bis(triphenylarsine)platinum(II), [Pt(tfac(2-)-C,O)($AsPh_3$)$_2$] was prepared by the reaction of [Pt(tfac)$_2$] with triphenylarsine.[9] Pyridinium perchlorate was prepared by adding concentrated perchloric acid dropwise to a dichlotomethane solution of pyridine kept in an ice bath and a white precipitate dried *in vacuo* was recrystallized from ethanol. Found: C, 33.29; H, 3.39; N, 7.78%. Calcd for [pyH]ClO_4=$C_5H_6O_4NCl$: C, 33.45; H, 3.37; N, 7.80%. The compound is hygroscopic.

η^3-1-Acetyl-2-oxoallylbis {tris(p-chlorophenyl)phosphine} platinum-(II), [Pt(acac(2-)-C^1—C^3){P(p-ClC_6H_4)$_3$}$_2$] (8): When tris-(p-chlorophenyl)phosphine (1.086 g, 2.97 mmol) was added to a chloroform solution (2 cm^3) of [Pt(acac)$_2$] (584 mg, 1.48 mmol) with stirring under nitrogen, color of the solution changed from yellow to red. After being left to stand for 10 h, the solvent was removed under reduced pressure to leave a red oil, which changed to a yellow solid on prolonged pumping. The product was pulverized and treated with a mixture of dichloromethane (5 cm^3) and hexane (30 cm^3). A pale yellow powder, which remained undissolved, was filtered and dissolved in dichloromethane (10 cm^3). Hexane (30 cm^3) was added to the solution and the mixture was left to stand, depositing a white crystalline solid, which was filtered, washed with small portions of methanol and diethyl ether, and dried *in vacuo*. The yield was 769 mg (49%). Dec temp 190—210 °C. Inclusion of one molecule of water and one fourth molecule of dichloromethane per metal atom was confirmed by ^{1}H NMR spectroscopy. Found: C, 46.68; H, 3.07%. Calcd for $C_{41.25}H_{32.5}O_3P_2Cl_{6.5}Pt$: C, 46.58; H, 3.08%. Recrystallization from pyridine–diethyl ether gave a white crystalline solid which contained one molecule of water and a half molecule of pyridine per metal atom. Found: C, 48.43; H, 3.38; N, 0.53%. Calcd for $C_{43.5}H_{34.5}N_{0.5}O_3P_2Cl_6$: C, 48.29; H, 3.21; N, 0.65%. The former specimen was used for spectral measurements and reaction studies.

2, 4-Pentanedionato-C^1-(pyridine) bis{tris(p-chlorophenyl) phosphine} platinum(II). Perchlorate, [Pt(acac-C^1)(py){P(p-ClC_6H_4)$_3$}$_2$]ClO_4 (9a): An acetone solution (2 cm^3) of pyridinium perchlorate (55 mg, 0.31 mmol) was added to a dichloromethane solution (1 cm^3) of **8** (126 mg, 0.118 mmol) and the mixture was heated to 40 °C with stirring for 5 min. Undissolved portion of the pyridinium salt was filtered and the filtrate was left standing overnight at ambient temperature to make the solvent evaporate spontaneously. White needles left on the wall of vessel were recrystallized from dichloromethane–hexane to afford white needles (96 mg) in a 64%

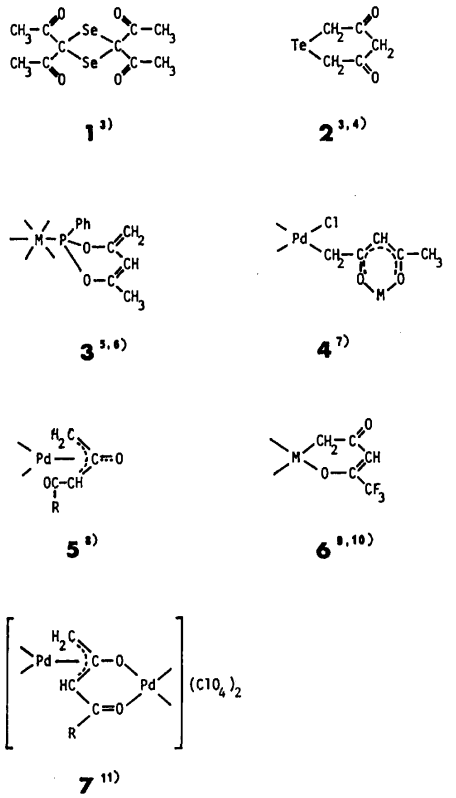

Fig. 1. Bonding modes of β-diketonate dianions in metal complexes.

yield. Dec temp 190—200 °C. Inclusion of three fourths molecule of dichloromethane as the solvent of crystallization was confirmed by ^{1}H NMR spectroscopy. Found: C, 44.31; H, 2.95; N, 1.14%. Calcd for $C_{46.75}H_{37.5}NO_6P_2Cl_{8.5}Pt$: C, 44.29; H, 2.98; N, 1.10%.

Measurements. Infrared spectra were obtained in Nujol mull with a Hitachi 295 infrared spectrophotometer. NMR spectra were recorded on JEOL FX-60Q (for ^{1}H and ^{13}C) and FX-90Q (for ^{31}P and ^{195}Pt) instruments.

Results and Discussion

Trihapto Complex of the 2,4-Pentanedionate Dianion with Platinum(II). The reaction of [Pt(acac)$_2$] with twice molar P(*p*-ClC$_6$H$_4$)$_3$ under a very mild condition gave a platinum(II) complex containing a 2,4-pentanedionate dianion as a ligand, [Pt(C$_5$H$_6$O$_2$){P(*p*-ClC$_6$H$_4$)$_3$}$_2$]·H$_2$O·S (**8**) (S = 1/4CH$_2$Cl$_2$ or 1/2py depending on the solvent of recrystallization, which could not be removed by pumping). The infrared spectra in the 1700—1500 cm^{-1} region are quite similar to those of [Pd(acac(2−)-*C*^{1}—*C*^{3})(NN)] (NN=bpy (**5a**), 4,4′-Me$_2$bpy, and phen)[8] and [Pd(acac(2−)-*C*^{1}—*C*^{3})(PP)] (PP=Ph$_2$PCH$_2$CH$_2$PPh and Ph$_2$PCH=CHPPh$_2$(**5b**)),[11]

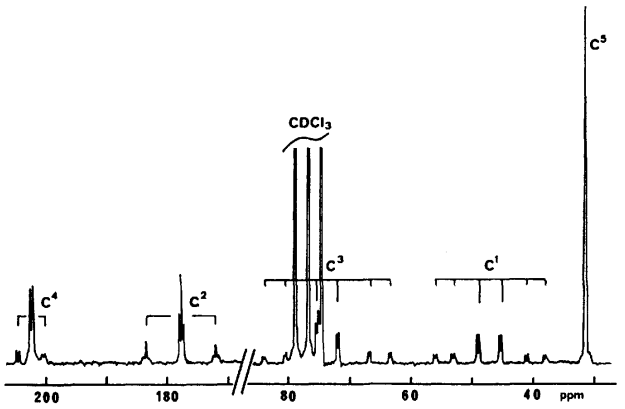

Fig. 2. ^{13}C{^{1}H}NMR spectrum at 15.0 MHz of [Pt(acac(2−)-*C*^{1}—*C*^{3}){P(*p*-ClC$_6$H$_4$)$_3$}$_2$]·H$_2$O·1/4CH$_2$Cl$_2$ (**8**) in CDCl$_3$ with Me$_4$Si as an internal reference. Signals of the phenyl carbons are omitted.

exhibiting a medium ν(C=O) band at 1650 cm^{-1} and a very strong and broad band at 1548 cm^{-1} assignable to the ν(C···O) and/or ν(C···C) vibration.

Figure 2 shows the ^{13}C{^{1}H} NMR spectrum of **8**. Assignment of the three sets of higher-field signals to the methyl, methylene, and methine carbons was made on the basis of the ^{1}H off-resonance data and listed in Table 1. Except the highest-field signal assignable to the methyl carbon, all carbons of the acac(2−) ligand couple to ^{31}P atom(s) and are flanked by the ^{195}Pt satellites. The methylene and methine carbons couple much more strongly to the ^{31}P atom situated at the *trans* position than to the *cis* ^{31}P atom, both appearing as a doublet of doublets. On the other hand, the central carbonyl carbon (C^2) resonates as a triplet, indicating that the coupling constants to both ^{31}P atoms are nearly equal in spite of their environmental nonequivalence (*vide infra*). The other carbonyl carbon (C^4) is remote from the coordination sites and weakly couples only to the *trans* ^{31}P. The fact that the J(Pt–C) values are much larger for C^1, C^2, and C^3 than for C^4 strongly supports the proposed trihapto structure, and the chemical shifts of C^1 and C^3 are well in accord with those recorded for other η-allylic systems.[13] The central carbon of the η-allyl moiety usually resonates at about 100 ppm,[13] but substitution of a proton bonded to a carbon atom with a hydroxyl group is generally known to shift the carbon resonance to 36—51 ppm lower field.[14] Now substitution with oxo anion causes downfield shift by about 80 ppm and the shielding of C^2 (177.8 ppm) nearly coincides with those of **5a** (180.5 ppm)[8] and **5b** (177.0 ppm).[11]

The ^{1}H NMR spectrum of **8** is composed of signals at 1.31 (CH$_3$), 1.97 (H$_2$O), 2.2—4.7 (CH$_2$ and CH), 5.30 (CH$_2$Cl$_2$), and 7.3 (phenyl protons) ppm with the relative intensities 3 : 2 : 3 : 0.5 : *ca.* 30 (Table 1). The signals at 1.97 and 5.30 ppm were assigned to solvents of crystallization since they increased their intensities on addition of water and dichloromethane, respectively. The signals in the 2.2—4.7-ppm region are complex because of coupling of CH$_2$ and CH protons to ^{31}P and ^{195}Pt atoms, and are divided into three groups of which two are flanked by ^{195}Pt satellites: a broad multiplet

Table 1. ^{1}H and ^{13}C{^{1}H} NMR data for complex **8** in CDCl$_3$[a]

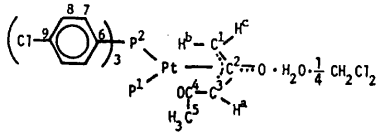

	H^a	H^b	H^c	CH$_3$	Ph	Other
δ_H	4.22	2.91	2.55	1.31	7.3	1.97(H$_2$O), 5.30(CH$_2$Cl$_2$)
J(H–H)	*ca.* 3(H^a,H^c)	*ca.* 7(H^b,H^c)				
J(Pt–H)	35	68				

	C^1	C^2	C^3	C^4	C^5	C^6	C^7	C^8	C^9
δ_C	47.2	177.8	73.8	203.1	31.4	129.3	134.9	128.8	137.7
J(P^1–C)	55	5	5	0					
J(P^2–C)	5	5	52	5		65	10	10	2
J(Pt–C)	233	168	259	48			24		

a) Chemical shift (δ) in ppm from internal Me$_4$Si and coupling constant (J) in Hz.

at 2.55 ppm (H^c), a multiplet at 2.91 ppm (H^b, J(Pt–H) =*ca.* 70 Hz), and a broad doublet at 4.22 ppm (H^a, J(Pt–H)=35 Hz). The ^{1}H NMR spectra of **5a** and related complexes are much more simpler due to lack of couplings to P and Pt atoms and were assigned unequivocally.[8] By reference to these data, the doublet at 4.22 ppm is assigned to the methine proton H^a, of which coupling to H^c demonstrates that the dangling acetyl moiety occupies the anti position of the η-allylic skeleton, making the H^a and H^c protons accord with the so-called W rule.[15]

When one drop of D_2O was added to a $CDCl_3$ solution of **8**, the signal at 1.97 ppm diminished at once and the one at 4.22 ppm decreased remarkably on stirring of the mixture overnight. The *ca.* 3 Hz coupling which had been observed for the multiplet at 2.55 ppm also disappeared on D_2O addition. These results indicate that the signal at 4.22 ppm is assigned to an exchangeable unique proton H^a. Partial decoupling of the signal at 2.55 ppm by deuteration of H^a also accords with the proposed structure. The fact that the ^{13}C signal from the methine carbon (C^3) at 73.8 ppm was remarkably diminished by the D_2O treatment also certifies that the methine proton was deuterated. As to the mechanism of methine deuteration, an intermediate containing the terminal-carbon-bonded acac ligand of keto form must be presumed.

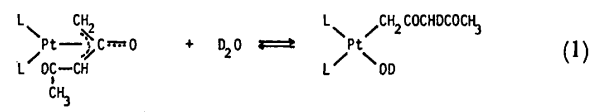

(1)

Since the terminal-carbon-bonded acac ligand contained in the stable Pt(II) complex **9a** (*vide infra*) is composed almost of the enol tautomer, the intermediate containing the unidentate keto acac presumed in Eq. 1 may be far less stable, and this situation might be the reason why the deuteration reaction is so slow.

Assignment of the multiplet signals centered at 2.55 and 2.91 ppm to the syn (H^c) and anti (H^b) protons, respectively, was made by reference to data for **5a**. The ^{1}H{^{31}P} NMR data for [Pt($C_5H_6O_2$)(PPh_3)$_2$] reported by Ito and Yamamoto[16] were also very helpful. They obtained the complex from the reaction of [Pt(acac)$_2$] with twice molar PPh_3 in refluxing THF and tentatively presumed a π-oxoallylic coordination.

Figure 3 shows the ^{31}P{^{1}H} NMR spectrum of complex **8** in $CDCl_3$. Main signals appear as an AB quartet at 18.6_3 and 19.2_8 ppm downfield from external H_3PO_4 with ^2J(P–P)=7 Hz. Both signals are flanked by ^{195}Pt satellites, ^1J(Pt–P) being $2.88_4\times10^3$ and $3.18_6\times10^3$ Hz, respectively. The spectrum indicates that the two phosphorus atoms are not equivalent but the difference in their environments is slight, since differences in the chemical shifts and ^1J(Pt–P) values are small. Unequivocal discrimination of phosphorus atoms is not easy, but the signal at 19.2_8 ppm with larger ^1J(Pt–P) value may be assigned to P^2 situated at the site *trans* to C^3, since the dangling acetyl moiety is electron attracting and the acetonyliden group will exert slightly smaller *trans* influence than the unsubstituted methylene end (C^1).

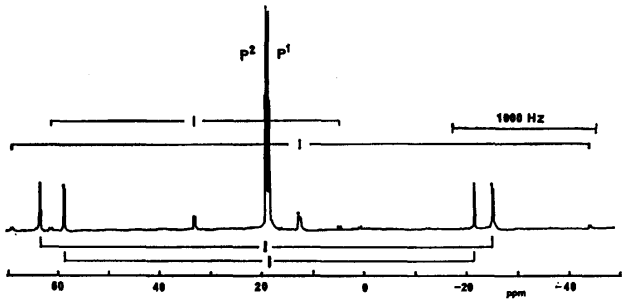

Fig. 3. ^{31}P{^{1}H}NMR spectrum at 36.3 MHz of [Pt(acac(2−)-C^1—C^3){P(p-ClC_6H_4)$_3$}$_2$]·H_2O·1/4CH_2Cl_2 (**8**) in $CDCl_3$ with H_3PO_4 as an external reference.

As is noticed in Fig. 3, the spectrum involves another AB quartet at 12.6_7 and 33.1_4 ppm with ^2J(P–P)=11 Hz, indicating contamination with a minor product which also contains two nonequivalent phosphine ligands. The ^1J(Pt–P) values are $4.06_0\times10^3$ and $2.03_4\times10^3$ Hz, respectively, of which the difference is large, suggesting a large difference in the environments of two phosphorus atoms situated at mutually *cis* positions. The pattern of the minor signals resembles closely to the ^{31}P{^{1}H} spectrum of [Pt(tfac(2−)-C,O)L_2] which contains a C,O-chelated 1,1,1-trifluoro-2,4-pentanedionate dianion with PPh_3 or P(p-ClC_6H_4)$_3$ as L (**6a**).[9] Thus the minor product is presumed to be [Pt(acac(2−)-C,O){P(p-ClC_6H_4)$_3$}$_2$] which is an isomer of **8**. Relative intensities of signals in Fig. 3 suggest that content of the minor product is less than 10% and could not be detected in ^{13}C{^{1}H} and other NMR spectra, whereas [Pd(acac(2−)-C^1—C^3)(NN)] (NN=bpy, 4,4′-Me_2bpy, and phen) contained [Pd(acac(2−)-C,O)-(NN)] in 20—25% proportions which were determined by ^{1}H NMR spectroscopy.[8] Isolation of the minor isomers has not been successful for either of the Pd(II) and Pt(II) complexes and it is not certain whether the isomerization equilibria are attained in solution or both isomers are inert, preserving the products ratio under the conditions of preparation.

The ^{195}Pt{^{1}H} NMR spectrum at 19.2 MHz of **8** in $CDCl_3$ was observed as a doublet of doublets at 3373.5 ppm upfield from external $K_2[PtCl_4]$. The coupling constants ^1J(Pt–P) to the two phosphorus atoms are $2.88_6\times10^3$ and $3.18_9\times10^3$ Hz, showing excellent agreement with the values obtained from the ^{31}P{^{1}H} NMR spectroscopy (*vide supra*).

It is surprising that the reaction of [Pt(acac)$_2$] with P(p-ClC_6H_4)$_3$ to produce **8** proceeds under a very mild condition. Comprehensive studies have been carried out on the reactions of [M(β-dik)$_2$] (M=Pd(II) and Pt(II)) with nitrogen bases[17] and tertiary phosphines.[18] The ^{1}H NMR spectroscopy revealed that the reaction of [Pt(tfac)$_2$] with twice molar PPh_3 in $CDCl_3$ produces [Pt(tfac)(PPh_3)$_2$](tfac) at first, which is then transformed into [Pt(tfac(2−)-C,O)(PPh_3)$_2$]. The tfac anion in the outer sphere seems to abstract a proton from the chelating tfac ligand, whereas the corresponding Pd(II) complex salt [Pd(tfac)(PPh_3)$_2$](tfac) is stable in solution and deprotonated only by added bases such as pyridine and its derivatives.[10] In the present case, changes of ^{1}H and ^{13}C NMR spectra during the reaction of

TABLE 2. ^1H AND $^{13}C\{^1H\}$ NMR DATA FOR COMPLEXES **9a** AND **9b** IN $CDCl_3$

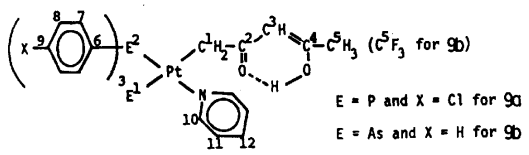

	CH_2	CH	CH_3	OH	Ring H adjacent to N	Other
9a, δ_H	2.11	4.53	1.53	15.6	8.60	7.4(ring H), 5.30(CH_2Cl_2)
J(P^1–H)	9					
J(P^2–H)	5					
J(Pt–H)	77	*ca.* 4			34	
9b, δ_H	2.71	4.91		*ca.* 15	8.67[b]	7.4(ring H), 5.30(CH_2Cl_2)
J(Pt–H)	94				40	
	C^1	C^2	C^3	C^4	C^5	Other
9a, δ_C	32.2	198.2	100.3	189.7	24.1	151.9(C^{10}), c)
J(P^1–C)	70	5				
J(Pt–C)	d)	40				
9b, δ_C	26.8	201.9	94.8	174.6q	d)	151.8(C^{10}), c)
J(Pt–C)	*ca.*500	*ca.*40				
J(F–C)				35		

a) Same as footnote a) for Table 1. Q=quartet. b) J(H–H)=5 Hz. c) Indistinguishable because of overlapping. d) Not recorded due to insufficient scans.

$[Pt(acac)_2]$ with twice molar PPh_3 in $CDCl_3$ were complex and could not be analyzed satisfactorily. However intermediate formation of $[Pt(acac)(PPh_3)_2]$-(acac) is evidenced by isolation in high yields of $[Pt(acac)(PPh_3)_2]X$ (X=BPh_4[19] and ClO_4[20]) on addition of NaX.

Deprotonation of the chelating β-diketonate ligand will produce a complex of type **3** primarily. Although such a dienediolate type bonding of acac(2–) was found for $[(\eta\text{-}C_5H_5)(CO)_2Mn\{PPh(C_5H_6O_2)\}]$[5] and $[(CO)_5M\{PPh(C_5H_6O_2)\}]$ (M=Cr and W),[6] analogous complex of transition metals has not been reported. In the present Pd(II) and Pt(II) cases, complexes of type **3** are not stable, but transformed either to the trihapto coordination or to *C,O*-chelation. The tfac(2–) ligand carrying the electron-attracting trifluoromethyl group prefers *C,O*-chelation in both Pd(II)[10] and Pt(II)[9]

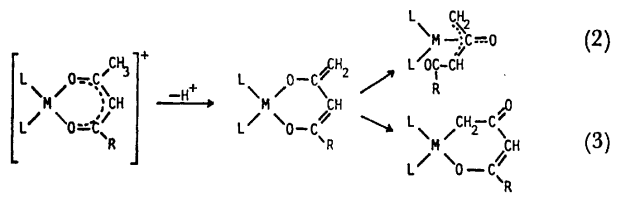

(2)

(3)

complexes, while the dianion of ethyl acetoacetate carring the electron-releasing ethoxyl group affords the trihapto Pd(II) complexes exclusively.[8] The acac(2–) ligand exhibits an intermediate behavior, producing the trihapto complexes accompanied by a small amount of *C,O*-chelate.

Terminal-carbon-bonded Complexes of the β-Diketonate Monoanions with Platinum(II). Terminal-carbon-bonded complexes of 2,4-pentanedionate[21] and 1-ethoxy-1,3-butanedionate (etac)[22] monoanions with palladium(II) were derived from the corresponding trihapto complexes $[PdCl(\eta^3\text{-}\beta\text{-dik})]_2$, where β-dik is acac[21] and etac,[23] respectively. Trihapto complexes of β-diketonate monoanions with platinum(II) have not yet been obtained and thus the terminal-carbon-bonded β-dik complexes with platinum(II) are not known either.

Now the reaction of **8** with pyridinium perchlorate in a mixture of dichloromethane and acetone gave $[Pt(acac\text{-}C^1)(py)\{P(p\text{-}ClC_6H_4)_3\}_2]\cdot 3/4CH_2Cl_2$ (**9a**), which is the first example of the terminal-carbon-bonded acac complex with platinum(II). Figure 4 shows ^1H and ^{13}C NMR spectra of **9a** in $CDCl_3$ and results of the signal analysis are listed in Table 2. The

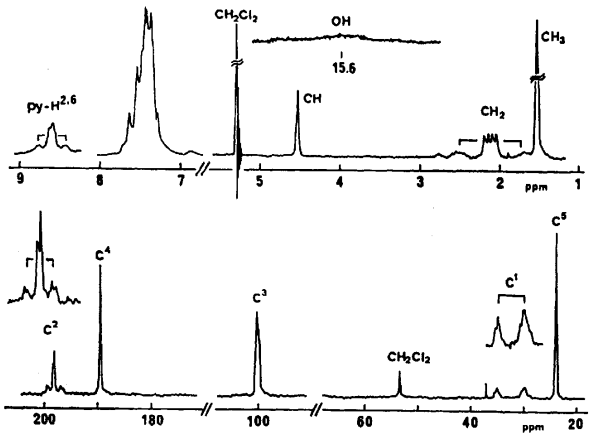

Fig. 4. ^1H and $^{13}C\{^1H\}$ NMR spectra at 100 and 15.0 MHz, respectively, of $[Pt(acac\text{-}C^1)(py)\{P(p\text{-}ClC_6H_4)_3\}_2]ClO_4\cdot 3/4CH_2Cl_2$ (**9a**) in $CDCl_3$ with Me_4Si as an internal reference. In the ^1H NMR spectrum, intensity of the ring protons except py-$H^{2,6}$ is decreased to *ca.* 1/4 and that of OH is increased about four times. In the ^{13}C NMR spectrum, signals of all ring carbons are omitted.

proton signal at 2.11 ppm appearing as a doublet of doublets flanked by ^{195}Pt satellites with a large J(Pt–H) value is assigned to the methylene group bonded to platinum(II). The signal multiplicity indicates unequivocally that **9a** has a *cis* configuration. No other methylene signal is observed, but instead a methine signal and a broad OH signal are observed, indicating that the terminal-carbon-bonded acac ligand is composed mainly of the enol tautomer. The coupling constant of the methine protons to ^{195}Pt is smaller than that in [Pt(acac)$_2$] (^4J(Pt–H) = 10.7 Hz)[24] in accordance with the unidentate state. Coordination of pyridine is demonstrated by the fact that the signal from the ring protons adjacent to nitrogen is flanked by the ^{195}Pt satellites.

It is worth noting that keto tautomer of **9a** is not detected on the ^{1}H NMR spectrum. The equilibrium quotient Q=[enol]/[keto] for [PdCl(acac-C^1)(bpy)] was reported to be 0.7 in $CDCl_3$ at 25 °C.[21] This value is smaller than 6.7 for free acacH molecules in $CDCl_3$ at 33 °C[25] and the PdCl(bpy)$^+$ moiety was considered to be electron releasing,[21] since an electron-attracting substituent on acacH increases Q, while an electron-releasing substituent exerts the opposite effect. Thus Q is 32 for tfacH and 0.43 for 3-methyl-acacH as neat liquids at 33 °C.[26] Now the Pt(py){P(p-ClC$_6$H$_4$)$_3$}$_2^{2+}$ moiety is functioning as a powerful electron-attracting substituent comparable to the trifluoromethyl group. The remarkable discrepancy in behaviors of this and PdCl(bpy)$^+$ moieties may arise from the difference in charge densities at the central metals, since Pt is coordinated with three neutral ligands of which two are π accepting, whereas Pd is bonded to a chloride anion and 2,2′-bipyridine which is a weaker π-acceptor than phosphines.[27]

The ^{13}C{^{1}H} NMR spectrum of **9a** accords well with the proposed structure. The methylene carbon bonded to the metal appears as a broad doublet in accordance with the *cis* structure, the ^2J(P^1–C) being 70 Hz and ^2J(P^2–C) indiscernibly small. Of the two signals attributable to the carbonyl carbons, the lower field one is assigned to C^2 because of its coupling both to Pt and P^1. The signal at 189.7 ppm is then ascribed to C^4.

Employment of pyridinium perchlorate was successful in preparing the cationic platinum(II) complex containing the terminal-carbon-bonded acac. The complex seems to be stabilized by coordination of pyridine at the fourth site. As the protonation site on the η^3-acac(2−) in **8** three atoms are conceivable, leading to different products (Eqs. 4—6). If a proton adds to the terminal methylene, the central-carbon-bonded complex will be resulted (Eq. 4). On the other hand, addition of a proton to the methine carbon will give rise to a complex of the terminal-carbon-bonded keto tautomer of acac (Eq. 6). Either of these two was not the case, but reaction 5 was predominant, indicating that the proton affinity is highest at the enolate oxygen atom.

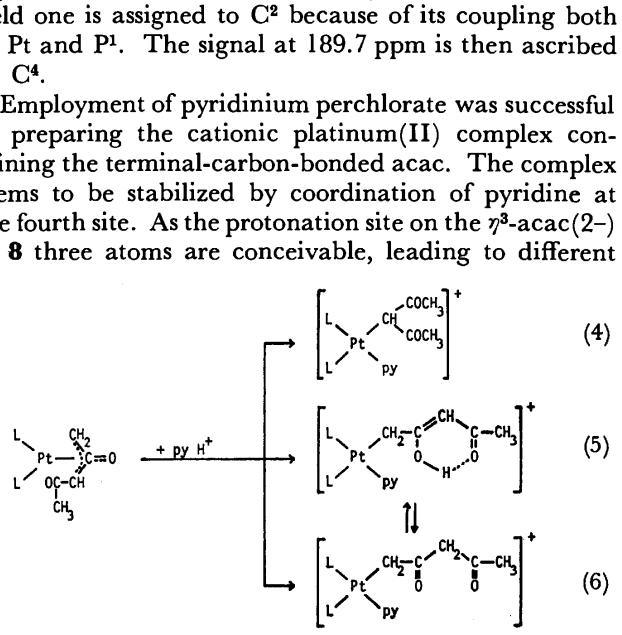

When an equimolar amount of pyridinium perchlorate was added to a solution of [Pt(tfac(2−)-C,O)(AsPh$_3$)$_2$]·1/4CH$_2$Cl$_2$[9] in $CDCl_3$, [Pt(tfac-C^1)(py)(AsPh$_3$)$_2$]ClO$_4$ (**9b**) was produced quantitatively as evidenced by ^{1}H and ^{13}C NMR spectra listed in Table 2, although its isolation was not successful. The tautomerization equilibrium of the terminal-carbon-bonded tfac in **9b** is also shifted to enol completely. Protonation did not occur at the terminal carbon, but occurred at the enolate oxygen.

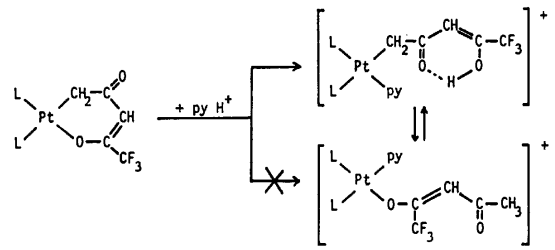

We wish to thank Mr. Junichi Gohda for elemental analyses. S. O. and S. K. are grateful to the Ministry of Education, Science and Culture for Grant-in-Aid for Scientific Research, Nos. 454196 and 243014, respectively.

References

1) R. C. Mehrotra, R. Bohra, and D. P. Gaur, "Metal β-Diketonates and Allied Derivatives," Academic Press, New York (1978).

2) J. P. Fackler, Jr., *Prog. Inorg. Chem.*, **7**, 361 (1966); K. C. Joshi and V. N. Pathak, *Coord. Chem. Rev.*, **22**, 37 (1977).

3) D. H. Dewar, J. E. Fergusson, R. P. Hentschel, C. J. Wilkins, and P. P. Williams, *J. Chem. Soc.*, **1964**, 688.

4) C. L. Raston, R. J. Secomb, and A. H. White, *J. Chem. Soc., Dalton Trans.*, **1976**, 2307; J. C. Dewan and J. Silver, *ibid.*, **1977**, 644; *J. Organomet. Chem.*, **125**, 125 (1977).

5) M=Mn: J. von Seyerl, D. Neugebauer, and G. Huttner, *Angew. Chem., Int. Ed. Engl.*, **16**, 858 (1977).

6) M=Cr, W: J. von Seyerl, D. Neugebauer, G. Huttner, C. Krüger, and Y.-H. Tsay, *Chem. Ber.*, **112**, 3637 (1979).

7) N. Yanase, Y. Nakamura, and S. Kawaguchi, *Inorg. Chem.*, **17**, 2874 (1978).

8) N. Yanase, Y. Nakamura, and S. Kawaguchi, *Inorg. Chem.*, **19**, 1575 (1980).

9) M=Pt: S. Okeya, Y. Nakamura, S. Kawaguchi, and T. Hinomoto, *Inorg. Chem.*, **20**, 1576 (1981).

10) M=Pd: N. Kanehisa, K. Miki, N. Kasai, S. Matsumoto, S. Kawaguchi, and S. Okeya, 27th Symposium on Organometallic Chemistry in Japan, Tokyo, 1980, Abstr., p. 73.

11) Y. Otani, Y. Nakamura, S. Kawaguchi, S. Okeya, and T. Hinomoto, *Chem. Lett.*, **1981**, 11.

12) S. Okeya and S. Kawaguchi, *Inorg. Synth.*, **20**, 65 (1980); S. Okeya, S. Ooi, K. Matsumoto, Y. Nakamura, and S.

Kawaguchi, *Bull. Chem. Soc. Jpn.*, **54**, 1085 (1981).
13) M. H. Chisholm and S. Godleski, *Prog. Inorg. Chem.*, **20**, 366 (1976).
14) J. D. Roberts, F. J. Weigert, J. I. Kroschwitz, and H. J. Reich, *J. Am. Chem. Soc.*, **92** 1338 (1970).
15) L. M. Jackman and S. Sternhell, "Applications of Nuclear Magnetic Resonance Spectroscopy in Organic Chemistry," 2nd ed, Pergamon Press, London (1969), p. 334.
16) T. Ito and A. Yamamoto, *J. Organomet. Chem.*, **161**, 61 (1978).
17) M=Pd(II): S. Okeya, H. Sazaki, M. Ogita, T. Takemoto, Y. Onuki, Y. Nakamura, B. K. Mohapatra, and S. Kawaguchi, *Bull. Chem. Soc. Jpn.*, **54**, 1978 (1981); M=Pt(II): S. Okeya, Y. Nakamura, and S. Kawaguchi, *ibid.*, submitted for publication.
18) S. Okeya, Y. Nakamura, and S. Kawaguchi, *Bull. Chem. Soc. Jpn.*, **54**, 3396 (1981).
19) T. Ito, T. Kiriyama, and A. Yamamoto, *Bull. Chem. Soc. Jpn.*, **49**, 3250 (1976).
20) S. Okeya, unpublished data.
21) Z. Kanda, Y. Nakamura, and S. Kawaguchi, *Inorg. Chem.*, **17**, 910 ((1978).
22) S. Baba, T. Sobata, T. Ogura, and S. Kawaguchi, *Bull. Chem. Soc. Jpn.*, **47**, 2792 (1974); M. Horike, Y. Kai, N. Yasuoka, and N. Kasai, *J. Organomet. Chem.*, **86**, 269 (1975).
23) Y. Tezuka, T. Ogura, and S. Kawaguchi, *Bull. Chem. Soc. Jpn.*, **42**, 443 (1969); K. Oda, N. Yasuoka, T. Ueki, N. Kasai, and M. Kakudo, *ibid.*, **43**, 362 (1970).
24) S. Okeya, S. Ooi, K. Matsumoto, Y. Nakamura, and S. Kawaguchi, *Bull. Chem. Soc. Jpn.*, **54**, 1085 (1981).
25) M. T. Rogers and J. L. Burdett, *Can. J. Chem.*, **43**, 1516 (1965).
26) J. L. Burdett and M. T. Rogers, *J. Am. Chem. Soc.*, **86**, 2105 (1964).
27) W. R. McWinnie and J. D. Miller, *Adv. Inorg. Chem. Radiochem.*, **12**, 135 (1969).

Dinuclear Palladium(II) Complexes Containing Anilide Anions as Bridging Ligands

Seichi OKEYA,* Hisako YOSHIMATSU, Yukio NAKAMURA,† and Shinichi KAWAGUCHI*,†

Faculty of Education, Wakayama University, Masago-cho, Wakayama 640
†*Faculty of Science, Osaka City University, Sumiyoshi-ku, Osaka 558*

(Received August 27, 1981)

The reactions of $[Pd(hfac)_2]$ with aniline and its derivatives (L) in benzene at room temperature afforded $[Pd(hfac)(hfac\text{-}C^3)L]$, $[Pd(hfac)L_2](hfac)$, and $[PdL_4](hfac)_2$ depending on the reactants mole ratio. On the other hand, the reactions of various $[Pd(\beta\text{-dik})_2]$ complexes with L in refluxing benzene (in most cases) gave rise to the anilide-bridged dinuclear complexes $[Pd(\beta\text{-dik})(L-H)]_2$, which in turn reacted with primary amines and pyridine (L′) to produce $[PdL'_2(L-H)]_2(\beta\text{-dik})_2$.

Comprehensive investigations on the reactions of bis(β-diketonato)palladium(II) and -platinum(II), $[M(\beta\text{-dik})_2]$ (**1**), with various nitrogen bases[1] and tertiary phosphines[2] have revealed that the chelating β-diketonate anions are readily converted into other bonding states, affording a series of complexes, $[M(\beta\text{-dik})_2L]$ (**2**), $[M(\beta\text{-dik})(\beta\text{-dik-}O)L]$ (**3**), $[M(\beta\text{-dik})L_2](\beta\text{-dik})$ (**4**), $[ML_4](\beta\text{-dik})_2$ (**5**), $[M(\beta\text{-dik-}O)_2L_2]$ (**6**), $[M(\beta\text{-dik})(\beta\text{-dik-}C^3)L]$ (**7**), and $[M(\beta\text{-dik-}C^3)_2L_2]$ (**8**) depending on the natures of the metal, β-dik, and Lewis base (L). Here, β-dik, β-dik-*O*, and β-dik-C^3 in the coordination sphere represent the chelating, O-unidentate, and central-carbon-bonded states, respectively, β-dik in the outer sphere acting as a counter anion.

Characteristics of β-diketones (β-dikH) in keto-enol tautomerization and acid dissociation as well as the basicities and steric requirements of Lewis bases are the most important factors influencing the preference of bonding modes. Less basic β-dik ligands are readily displaced by L to outer sphere, while the keto-favorable β-dik anions prefer the carbon bonding. Thus, 1,1,1,5,5,5-hexafluoro-2,4-pentanedione (hfacH), which exists solely as enol and is strongly acidic, has not given the carbon-bonded complexes **7** and **8**.[1,2]

This paper reports the reactions of $[Pd(\beta\text{-dik})_2]$ with aniline and its derivatives which afford complexes **7** as well as **4** and **5** at room temperature and the anilide-bridged dinuclear complexes at higher temperatures. Dialkylamide and disilylamide complexes of early transition metals are well-known[3] but those of the d^8 metals are rather scanty, and the amide-bridged dinuclear palladium(II) complexes reported in this paper are the first examples.

Experimental

Preparation of Complexes. The starting bis(β-diketonato)-palladium(II) complexes were prepared by the methods reported recently.[4] Aniline and its derivatives were used as supplied without further purification but some samples which had been stored for a good while were purified by the method analogous to that employed for purification of aniline.[5]

*Bis(aniline)(1,1,1,5,5,5-hexafluoro-2,4-pentanedionato)palladium(II) 1,1,1,5,5,5-Hexafluoro-2,4-pentanedionate–Benzene (2/1), $[Pd(hfac)(C_6H_5NH_2)_2](hfac)\cdot 1/2C_6H_6$ (**4a**)*: On addition of a benzene solution (1 cm³) of aniline (233 mg, 2.50 mmol) to a solution of $[Pd(hfac)_2]$ (**1a**) (325 mg, 0.624 mmol) in benzene (5 cm³), color of the solution changed immediately from orange yellow to red and orange crystallites began to deposit. After being left overnight, the crystals were filtered, washed with petroleum ether (bp<50 °C) and dried *in vacuo*. The product (306 mg) was recrystallized from hot benzene. The final yield of red-orange plates was 237 mg (51%). Hexane was added to the filtrate and the mixture was left to stand for a week. Yellow plates deposited were filtered, washed with a mixture (1:1 by volume) of benzene and hexane, dried *in vacuo* and characterized to be $[Pd(C_6H_5NH_2)_4](hfac)_2$ (**5a**), of which the yield was 124 mg (22%).

*$[Pd(hfac)(2,5\text{-}(CH_3)_2C_6H_3NH_2)_2](hfac)$ (**4b**)*: Hexane (1 cm³) was added to a mixture of **1a** (89 mg, 0.17 mmol) and 2,5-dimethylaniline (41 mg, 0.34 mmol) in benzene (2.5 cm³) and the solvent mixture was allowed to vaporize spontaneously to leave an orange-red crystalline solid, which was washed with petroleum ether and dried *in vacuo*. The yield was 14 mg (11%).

*$[Pd(hfac)(2,6\text{-}(CH_3)_2C_6H_3NH_2)_2](hfac)\cdot H_2O$ (**4c**) and $[Pd(hfac)(3,5\text{-}(CH_3)_2C_6H_3NH_2)_2](hfac)$ (**4d**)*: Orange crystallites of **4c** and orange-red plates of **4d** were obtained in 88 and 92% yields, respectively, by the reactions of **1a** with twice molar amounts of 2,6- and 3,5-dimethylanilines in benzene at room temperature.

*$[Pd(hfac)(2,4,6\text{-}(CH_3)_3C_6H_2NH_2)_2](hfac)\cdot H_2O$ (**4e**)*: A benzene solution (6 cm³) containing **1a** (322 mg. 0.619 mmol) and 2,4,6-trimethylaniline (168 mg, 1.24 mmol) was heated under reflux for 2.5 h and then concentrated to 1 cm³ by evaporation under reduced pressure. After being left overnight at room temperature, big orange crystals were filtered, washed with petroleum ether, and dried *in vacuo*. The yield was 339 mg (68%).

*$[Pd(hfac)(3\text{-}CF_3C_6H_4NH_2)_2](hfac)$ (**4f**)*: Hexane (0.2 cm³) was added to a benzene solution (1 cm³) containing **1a** (40 mg, 0.077 mmol) and 3-(trifluoromethyl)aniline (91 mg, 0.56 mmol) and the mixture was kept in a refrigerator to deposit orange plates (42 mg) in a 65% yield.

*Tetrakis(aniline)palladium(II) 1,1,1,5,5,5-Hexafluoro-2,4-pentanedionate, $[Pd(C_6H_5NH_2)_4](hfac)_2$ (**5a**)*: Pale yellow plates of **5a** were obtained by addition of hexane (1 cm³) to a mixture of **1a** (55 mg, 0.11 mmol) and aniline (77 mg, 0.83 mmol) in benzene (1.5 cm³). The crystals lost lattice solvent to turn opaque on being dried *in vacuo*. The yield was 68 mg (72%).

*$[Pd(2\text{-}CH_3C_6H_4NH_2)_4](hfac)_2$ (**5b**)*: When a solution (0.5 cm³) of 2-methylaniline (27 mg, 0.25 mmol) in diethyl ether was added to a solution (0.5 cm³) of **1a** (35 mg, 0.067 mmol) in the same solvent, color of the solution changed from orange to orange red, depositing yellow crystals, which were filtered, washed with diethyl ether and air-dried. The yield was 55 mg (86%). Recrystallization was performed from dichloromethane–petroleum ether.

*$[Pd(4\text{-}CH_3C_6H_4NH_2)_4](hfac)_2$ (**5c**)*: 4-Methylaniline (98 mg, 0.91 mmol) was added to a suspension of **1a** (97 mg,

0.19 mmol) in benenze (1 cm³) to result in a clear orange solution and deposit soon a pale yellow precipitate, which was filtered, washed with benzene and dried *in vacuo*. The yield was 90 mg (51%). Recrystallization from dichloromethane gave yellow plates.

[Pd(2,4-(CH₃)₂C₆H₃NH₂)₄](hfac)₂ (5d), *[Pd(2,5-(CH₃)₂C₆H₃NH₂)₄](hfac)₂ (5e)*, *and [Pd(3,5-(CH₃)₂C₆H₃NH₂)₄](hfac)₂ (5f)*: A benzene solution (2 cm³) of **1a** (74 mg, 0.14 mmol) and 2,4-dimethylaniline (66 mg, 0.54 mmol) was allowed to stand overnight to produce yellow crystals of **5d**. The yield was 91 mg (64%). When 2,5- or 3,5-dimethylaniline was used as a base, a benzene solution containing **1a** and each of these anilines in the mole ratio of 1 : 4 was left at room temperature until the solvent vaporized spontaneously to leave a yellow crystalline solid of **5e** or yellow plates of **5f** in an 85 or 57% yield, respectively.

2,6-Dimethylaniline(1,1,1,5,5,5-hexafluoro-2,4-pentanedionato)-(1,1,1,5,5,5-hexafluoro-2,4-pentanedionato-C³)palladium(II), *[Pd(hfac)(hfac-C³)(2,6-(CH₃)₂C₆H₃NH₂)] (7a)*: A benzene solution (1 cm³) of 2,6-dimethylaniline (70 mg, 0.58 mmol) was added to a benzene solution (10 cm³) of **1a** (298 mg, 0.573 mmol) and the solvent was allowed to evaporate spontaneously to leave orange-red columns, which were washed with benzene and dried *in vacuo*. The yield was 358 mg (97%). This compound is sparingly soluble in organic solvents.

[Pd(hfac)(hfac-C³)(3,5-(CH₃)₂C₆H₃NH₂)] (7b): When a benzene solution (1 cm³) of 3,5-dimethylaniline (42 mg, 0.35 mmol) was added to a benzene solution (2 cm³) of **1a** (178 mg, 0.342 mmol), color of the solution changed gradually from orange yellow to orange red and orange-red crystals began to deposit. After being left overnight the precipitate was filtered, washed with benzene and dried *in vacuo*. The yield was 92 mg (42%).

[Pd(hfac)(hfac-C³)(2,4,6-(CH₃)₃C₆H₂NH₂)] (7c): When a mixture of **1a** (509 mg, 0.978 mmol) and 2,4,6-trimethylaniline (135 mg, 0.998 mmol) in benzene (12 cm³) was heated under reflux for 2.5 h, color of the solution changed gradually from orange yellow to dark red. The solution was then concentrated to 3 cm³ by evaporation under reduced pressure. Hexane (2 cm³) was added to the concentrate and the solvent mixture was allowed to vaporize spontaneously to leave orange-red columns, which were washed with diethyl ether (5 cm³) and air-dried. The yield was 365 mg. The washings were allowed to vaporize spontaneously, leaving another crop of **7c**, which was filtered and washed with a mixture (1 : 1 by volume) of diethyl ether and petroleum ether. The total yield was 447 mg (70%).

Di-μ-anilidobis(2,4-pentanedionato)dipalladium(II), *[Pd(acac)-(C₆H₅NH)]₂ (9a)*: Aniline (98 mg, 1.05 mmol) was added to a benzene solution (5 cm³) of [Pd(acac)₂] (**1b**) (42 mg, 0.14 mmol) and the mixture was heated under reflux for 7 h. The solvent was then distilled away under reduced pressure to leave a red-brown powder, which was washed with diethyl ether and air-dried. The yield was 16 mg (39%). Very low solubility of **9a** prevented recrystallization.

[Pd(acac)(2-CH₃C₆H₄NH)]₂ (9b): A benzene solution containing **1b** and excess 2-methylaniline was refluxed for 30 min and cooled to room temperature to deposit a red-brown precipitate, which was filtered, washed with petroleum ether, and then recrystallized from hot benzene. The yield was 92%.

[Pd(acac)(2,5-(CH₃)₂C₆H₃NH)]₂ (9c): 2,5-Dimethylaniline (1.58 g, 13.0 mmol) was added to a benzene solution (5 cm³) of **1b** (405 mg, 1.33 mmol) and the mixture was refluxed for 8 h. The solvent was then distilled away under reduced pressure, leaving an orange powder behind, which was washed with petroleum ether and dried *in vacuo*. The same compound was obtained by spontaneous evaporation of the washings. The total yield of **9c** was 295 mg (68%). With an aim of recrystallization, the product was dissolved in hot dichloromethane (10 cm³) and the solution was kept in a refrigerator overnight to deposit red plates (**9c**-α; 62 mg, 13%), which were filtered, washed with diethyl ether, and air-dried. The filtrate was kept further in a refrigerator to precipitate orange needles (**9c**-β; 68 mg, 16%), which was filtered, washed with diethyl ether, and air-dried. Red plates were analysed to contain one half molecule of dichloromethane per palladium as the lattice solvent and orange needles to contain one sixth molecule of dichloromethane. Results of the elemental analysis indicate that these two compounds are isomers (*vide infra*). The α-form is more soluble than the β-form in chloroform and dichloromethane.

[Pd(acac)(2,6-(CH₃)₂C₆H₃NH)]₂ (9d), *[Pd(acac)(2-C₂H₅-C₆H₄NH)]₂ (9e)*, *[Pd(acac)(C₁₀H₇-1-NH)]₂ (9f)*, *and [Pd-(acac)(5-NH₂C₁₀H₆-1-NH)]₂ (9g)*: The reactions of **1b** with 2,6-dimethylaniline, 2-ethylaniline, 1-naphthylamine, and 1,5-naphthalenediamine were carried out in a similar way to the case of **9b** and the orange-red products were recrystallized from hot benzene, the yields being *ca.* 3, 56, 11, and 98%, respectively.

Di-μ-anilidobis(1-phenyl-1,3-butanedionato)dipalladium(II), *[Pd-(bzac)(C₆H₅NH)]₂ (9h)*: On addition of excess aniline (*ca.* 0.2 cm³) to a solution of [Pd(bzac)₂] (101 mg, 0.236 mmol) in dichloromethane (3 cm³), color of the solution changed from orange yellow to red. A small amount of petroleum ether was added to the solution and the solvent mixture was allowed to evaporate spontaneously to leave an orange residue, which was washed with diethyl ether. The yield was 80 mg (94%).

Di-μ-anilidobis(1,1,1-trifluoro-2,4-pentanedionato)dipalladium-(II), *[Pd(tfac)(C₆H₅NH)]₂ (9i)*: Excess aniline was mixed with [Pd(tfac)₂] (**1c**) (351 mg, 0.851 mmol) in dichloromethane (10 cm³) and the solvent was vaporized spontaneously to leave a red crystalline solid on the wall and a red oily substance at the bottom of the vessel. The solid was washed with methanol. The oil was dissolved in dichloromethane. Hexane was added to the solution and the mixture was cooled to deposit a red crystalline solid, which was filtered and washed with methanol. The two specimens gave the same IR spectra. After drying *in vacuo*, the total yield was 175 mg (58%). Recrystallization from *N,N*-dimethylformamide gave brown needles of **9i**. On the other hand, the combined washings were kept in a refrigerator for 6 h to precipitate orange-yellow needles of Shiff base complex, *bis(4-phenylamino-1,1,1-trifluoro-3-penten-2-onato)palladium(II)* *[Pd{N(C₆H₅)C(CH₃)CHCOCF₃}₂] (11)*, which were filtered, washed with methanol, and dried *in vacuo*. The yield of **11** was 10%. Recrystallization was performed from methanol or dichloromethane. Found: C, 47.32; H, 3.35; N, 5.03%. Calcd for $C_{22}H_{18}N_2O_2F_6Pd$: C, 46.95; H, 3.22; N, 4.98%. IR in Nujol: ν(C=O)+ν(C=C)+ν(C=N), 1616 vs, 1586 m, 1524 vs; no ν(NH) band.

[Pd(tfac)(2-CH₃C₆H₄NH)]₂ (9j), *[Pd(tfac)(4-CH₃C₆H₄-NH)]₂ (9k)*, *and [Pd(tfac)(2,6-(CH₃)₂C₆H₃NH)]₂ (9l)*: The reactions of **1c** with three times molar 2-methylaniline, equimolar 4-methylaniline, and excess 2,6-dimethylaniline in refluxing benzene for several hours followed by spontaneous evaporation of the solvent gave **9j**, **9k**, and **9l** as an orange powder, orange-yellow needles, and orange-red needles in 32, 34, and several percent yields, respectively.

[Pd(hfac)(2-CH₃C₆H₄NH)]₂ (9n): A mixture of **1a** (497 mg, 0.955 mmol) and 2-methylaniline (103 mg, 0.963 mmol) in benzene (10 cm³) was heated under reflux for 7 h and then concentrated to 2 cm³ by evaporation under reduced pressure. Hexane (several cm³) was added to the concentrate and the

mixture was left to stand for three days to deposit dark red needles, which were filtered, washed with hexane and dried *in vacuo*. The yield was 295 mg (74%).

[Pd(hfac)(C$_6$H$_5$NH)]$_2$ (9m) and [Pd(hfac)(4-CH$_3$C$_6$H$_4$NH)]$_2$ (9o): These complexes were obtained in a similar manner as above as dark red crystals in 55 and 25% yields, respectively.

Alternatively, employment of 1,8-bis(dimethylamino)-naphthalene, "proton sponge," greatly enhanced the reaction of **1a** with 4-methylaniline to form **9o**. After addition of "proton sponge" (87 mg, 0.41 mmol) to a chloroform solution (1.5 cm^3) of **1a** (207 mg, 0.398 mmol) and 4-methylaniline (43 mg, 0.40 mmol), the solvent was distilled away under reduced pressure and the residue was washed with a mixture (1 : 1 by volume) of methanol and water, and dried *in vacuo*. The yield of a red-brown powder was 148 mg (88%). The washings were vaporized under reduced pressure and the residue was recrystallized from methanol–water. Pale yellow columns (46 mg) were identified to be the naphthylammonium salt of hfac (**12**) based on the following analytical and spectroscopic data and the yield was 27%. Found: C, 54.15;

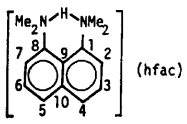

12

H, 4.80; N, 6.66%. Calcd for $C_{19}H_{20}N_2O_2F_6$: C, 54.03; H, 4.77; N, 6.63%. Dec temp (sublimation) 105—130 °C. IR in Nujol: ν(C=C)+ν(C=O) 1675 vs, 1550 vs, and 1530 s; ν(C–F) 1250 vs, 1172 vs, 1145 vs, 1123 vs. NMR in $CDCl_3$ (δ, ppm from internal Me_4Si), ^{1}H: 3.29d (12H, N–CH$_3$, J(NH–CH$_3$)=1.$_2$ Hz), 5.68s (1H, hfac-CH), *ca.* 7.8 m (6H, ring-CH), 18.6 br (1H, N–H–N); ^{13}C: 118.4 q (CF$_3$, ^1J(C–F) =292 Hz), 173.5 q (CO, ^2J(C–F)=30 Hz), 84.2 (hfac-CH, ^1J(C–H)=159 Hz), 46.6 (CH$_3$, ^1J(C–H)=140 Hz), 144.8 (C^1, C^8), 120.9 (C^2, C^7, ^1J (C–H)=159 Hz), 129.2 (C^3, C^6, ^1J (C–H)=164 Hz), 126.9 (C^4, C^5, ^1J (C–H)=160 Hz), 118.9 (C^9), 135.5 (C^{10}). (Ring-carbon assignments are tentative.)

[Pd(hfac)(2,5-(CH$_3$)$_2$C$_6$H$_3$NH)]$_2$ (9p) and [Pd(hfac)(2,6-(CH$_3$)$_2$C$_6$H$_3$NH)]$_2$ (9q): The reactions of **1a** with equimolar 2,5-dimethylaniline and 2,6-dimethylaniline were allowed to proceed in refluxing benzene for 1 and 2 h, respectively. After evaporation of the solvent, residues were treated with hexane and methanol, respectively. Dark red needles of **9p** and a dark red powder of **9q** were obtained in 68 and 60% yields, respectively. Compound **9q** was also obtained as orange-red needles in a 9% yield when **7a** was dissolved in methanol and the solution was left to stand at room temperature.

[Pd(hfac)(3,5-(CH$_3$)$_2$C$_6$H$_3$NH)]$_2$ (9r): The reaction of **1a** with equimolar 3,5-dimethylaniline in refluxing toluene for 1.5 h and work up similar to the case of **9n** gave dark red needles in a 57% yield.

[Pd(hfac)(2,4,6-(CH$_3$)$_3$C$_6$H$_2$NH)]$_2$ (9s): Compound **7c** (20 mg, 0.031 mmol) was dissolved in hot methanol (1 cm^3) and the solution was left to stand at ambient temperature to deposit orange-red plates, which were filtered, washed with hexane and dried *in vacuo*. The yield was 5 mg (36%).

[Pd(hfac)(3-CF$_3$C$_6$H$_4$NH)]$_2$ (9t): A benzene solution (5 cm^3) of **1a** (138 mg, 0.265 mmol) and 3-(trifluoromethyl)-aniline (43 mg, 0.27 mmol) was refluxed for 1.5 h and then concentrated to 1 cm^3 by evaporation under reduced pressure. Petroleum ether (several cm^3) was added to the concentrate and the mixture was left to stand for a week at room temperature to deposit a red-orange crystalline solid, which was filtered and washed with petroleum ether. The yield was 90 mg (72%). Recrystallization from dichloromethane–petroleum ether gave a mixture of red plates (α-form) and dark red column (β-form), which was filtered, washed with petroleum ether, and air-dried. Manual separation gave **9t**-α (20 mg) and **9t**-β (34 mg) in 16 and 27% yields, respectively.

[Pd(hfac)(2-NO$_2$C$_6$H$_4$NH)]$_2$ (9u): Hexane (several cm^3) was added to a benzene solution (2.5 cm^3) of **1a** (81 mg, 0.16 mmol) and 2-nitroaniline (22 mg, 0.16 mmol) and the mixture was left to stand for five days to precipitate red needles, which were filtered, washed with petroleum ether, and dried *in vacuo*. The washings were evaporated spontaneously to separate another crop. The total yield was 34 mg (48%).

[Pd(hfac)(4-NO$_2$C$_5$H$_4$NH)]$_2$ (9v): 4-Nitroaniline (39 mg 0.28 mmol) was allowed to react with **1a** (146 mg, 0.281 mmol) in refluxing dichloromethane (2 cm^3) for 3 h. The solvent was then distilled away under reduced pressure and the residue was recrystallized from dichloromethane–petroleum ether to give red plates. Another crop of red crystalline solid was also obtained by cooling the filtrate. The total yield was 85 mg (67%).

Di-μ-anilidotetrakis(propylamine)dipalladium(II) 1,1,1-Trifluoro-2,4-pentanedionate, [Pd(C$_6$H$_5$NH)(n-PrNH$_2$)$_2$]$_2$(tfac)$_2$ (10a): Complex **9i** (61 mg, 0.087 mmol) was dissolved in propylamine (0.5 cm^3) and the excess amine was allowed to evaporate spontaneously to leave a yellow crystalline solid (64 mg) in a 78% yield.

[Pd(C$_6$H$_5$NH)(py)$_2$]$_2$(tfac)$_2$·2H$_2$O (10b): Complex **9i** was dissolved in a minimum amount of pyridine and diethyl ether was added to the solution. On cooling the mixture, yellow columns appeared, which were filtered, washed with diethyl ether, and dried *in vacuo*. The yield was about 50%.

[Pd(4-CH$_3$C$_6$H$_4$NH)(4-CH$_3$C$_6$H$_4$NH$_2$)$_2$]$_2$(tfac)$_2$·1/2 C$_6$H$_6$ (10c): 4-Methylaniline (76 mg, 0.71 mmol) reacted with **1c** (81 mg, 0.20 mmol) in benzene (1.5 cm^3) at room temperature to deposit orange crystals, which were filtered, washed with hexane, and dried *in vacuo*. The yield was 73 mg (62%).

[Pd(2-CH$_3$C$_6$H$_4$NH)(2-CH$_3$C$_6$H$_4$NH$_2$)$_2$]$_2$(hfac)$_2$ (10d): A mixture of complex **9n** (123 mg, 0.146 mmol) and 2-methylaniline (93 mg, 0.87 mmol) in benzene (5 cm^3) was heated under reflux for 4.5 h and concentrated by evaporation under reduced pressure to deposit a yellow-brown crystalline solid, which was filtered, washed with petroleum ether, and dried *in vacuo*. The yield was 108 mg (58%).

[Pd(2-CH$_3$C$_6$H$_4$NH)(3,5-(CH$_3$)$_2$C$_6$H$_3$NH$_2$)$_2$]$_2$(hfac)$_2$ (10e): 3,5-Dimethylaniline (75 mg, 0.62 mmol) was added to a benzene solution (5 cm^3) of **9n** (65 mg, 0.077 mmol) and the mixture was left to stand at room temperature to deposit a yellow-brown precipitate. The solvent was removed under reduced pressure and the residue was recrystallized from dichloromethane–petroleum ether to give orange tiny crystals (46 mg) in a 45% yield.

[Pd(2-CH$_3$C$_6$H$_4$NH)(CH$_3$NH$_2$)$_2$]$_2$(hfac)$_2$ (10f): Complex **9n** was dissolved in methylamine and the excess amine was removed under reduced pressure to leave a yellow powder of **10f** in a quantitative yield.

[Pd(2-CH$_3$C$_6$H$_4$NH)(n-PrNH$_2$)$_2$]$_2$(hfac)$_2$·2H$_2$O (10g): Complex **9n** (54 mg, 0.064 mmol) was dissolved in propylamine (3 cm^3) and the excess amine was vaporized spontaneously. The residue was washed with hexane and dried *in vacuo* to give a yellow powder (31 mg) in a 44% yield. Yellow columns were obtained by recrystallization from dichloromethane–petroleum ether.

[Pd(2-CH$_3$C$_6$H$_4$NH)(py)$_2$]$_2$(hfac)$_2$ (10h): Small amounts

of diethyl ether and hexane were added to a solution of **9n** (23 mg, 0.027 mmol) in pyridine (0.1 cm^3) and the mixture was cooled to deposit a yellow precipitate, which was filtered, washed with diethyl ether, and dried *in vacuo*. Although solubilities in usual solvents are low, recrystallization was possible from dichloromethane–petroleum ether. The yield was very low (less than 10%).

[Pd (3,5-$(CH_3)_2C_6H_3NH$) (3,5$(CH_3)_2C_6H_3NH_2$)$_2$]$_2$ (hfac)$_2$ (10i): 3,5-Dimethylaniline (34 mg, 0.28 mmol) was added to a benzene solution (2 cm^3) of complex **9r** (56 mg, 0.065 mmol) and the mixture was left to stand at room temperature for three days to deposit an orange precipitate, which was filtered, washed with hexane, and dried *in vacuo*. The yield was 42 mg (48%).

Measurements. IR spectra were recorded in Nujol mull on Hitachi EPI-S2 and 295 spectrophotometers. NMR spectra were measured with JEOL-C60 HL (^1H), FX60Q (^1H and ^{13}C), and PS-100 (^{19}F) spectrometers. The molecular weight was determined in dichloromethane at room temperature by vapor pressure osmometry with an instrument manufactured by Knauer in West Berline, West Germany.

Results and Discussion

Table 1 shows the analytical data for most of the newly prepared complexes together with their decomposition temperatures, but data for twelve compounds were omitted for brevity. The reactions of [Pd(hfac)$_2$] (**1a**) with aniline and its derivatives (L) mostly in benzene at room temperature afforded [Pd(hfac)L$_2$](hfac) (**4**) and [PdL$_4$](hfac)$_2$ (**5**) when twice molar and more than

Table 1. Analytical data for newly prepared complexes, [Pd(hfac)L$_2$](hfac) (**4**), [PdL$_4$](hfac)$_2$ (**5**), [Pd(hfac)(hfac-C^3)L] (**7**), [Pd(β-dik)(L−H)]$_2$ (**9**), and [PdL'$_2$(L−H)]$_2$(β-dik)$_2$ (**10**)

Compd	Dec pt °C	Found (Calcd) (%)		
		C	H	N
4a[a]	*ca.* 96	40.29 (40.26)	2.56 (2.57)	3.93 (3.76)
4c[b]	164—165	40.13 (39.98)	3.42 (3.36)	3.75 (3.59)
4d[c]	122—123	41.06 (40.93)	3.25 (3.17)	3.70 (3.67)
4e[b]	98—100	41.61 (41.57)	3.73 (3.74)	3.31 (3.46)
5a[c]	106—110	45.77 (45.73)	3.36 (3.39)	6.51 (6.27)
5b	115—116[d]	48.51 (48.09)	4.22 (4.04)	5.98 (5.90)
5c	118—119	48.02 (48.09)	4.08 (4.04)	5.89 (5.90)
5f	134—135	50.26 (50.18)	4.68 (4.61)	5.55 (5.57)
7a	116—117[d]	33.85 (33.69)	2.10 (2.03)	2.05 (2.18)
7b	101—102	33.42 (33.69)	1.94 (2.04)	2.19 (2.18)
7c	97—100[d]	34.86 (34.80)	2.31 (2.31)	2.07 (2.14)
9a	214—218	43.95 (44.39)	4.34 (4.40)	4.64 (4.71)
9b	*ca.* 208	46.84 (46.25)	4.90 (4.85)	4.58 (4.50)
9c-α[e]	*ca.* 180	46.20 (45.87)	5.09 (5.08)	4.01 (4.04)
9c-β[f]	213—214	47.20 (47.22)	5.22 (5.20)	3.90 (4.21)
9d	*ca.* 198	48.31 (47.94)	5.31 (5.26)	4.46 (4.30)
9e	*ca.* 218	47.95 (47.94)	5.32 (5.26)	4.43 (4.30)
9f	*ca.* 190	52.53 (51.82)	4.36 (4.34)	4.02 (4.02)
9h	*ca.* 240	53.41 (53.42)	4.23 (4.20)	3.87 (3.89)
9i	*ca.* 216[d]	37.63 (37.57)	2.88 (2.87)	4.11 (3.98)
9m	*ca.* 183[d]	32.63 (32.58)	1.74 (1.74)	3.52 (3.45)
9n	*ca.* 187[d]	34.46 (34.35)	2.19 (2.16)	3.40 (3.34)
9o	*ca.* 85 (mp)	34.24 (34.35)	2.20 (2.16)	3.34 (3.34)
9p	*ca.* 165	36.03 (36.01)	2.54 (2.56)	3.13 (3.23)
9q	*ca.* 144[d]	35.89 (36.01)	2.56 (2.56)	3.24 (3.23)
9r	*ca.* 172[d]	35.85 (36.01)	2.50 (2.56)	3.40 (3.23)
9t-α	*ca.* 165[d]	30.37 (30.43)	1.19 (1.28)	2.89 (2.96)
9t-β	*ca.* 153[d]	30.53 (30.43)	1.27 (1.28)	2.91 (2.96)
9u	*ca.* 120	29.31 (29.32)	1.36 (1.34)	6.21 (6.22)
9v	*ca.* 210	29.36 (29.32)	1.36 (1.34)	6.18 (6.22)
10a	*ca.* 140	43.68 (43.46)	5.89 (6.01)	8.72 (8.94)
10b[g]	90— 95	47.99 (47.79)	4.26 (4.20)	8.01 (7.96)
10c[a]	190—195	54.91 (55.10)	5.59 (5.30)	6.86 (7.01)
10d	*ca.* 180	49.79 (49.26)	4.31 (4.29)	6.51 (6.63)
10g[g]	110—119	39.01 (38.89)	5.28 (5.26)	7.25 (7.56)
10i	*ca.* 150	51.27 (51.53)	4.94 (4.92)	5.97 (6.22)

a) Benzene solvate (one half molecule per Pd). b) Monohydrate. c) Crystals contain solvent of crystallization which is lost gradually at room temperature. Solvent-free specimens were analyzed which were obtained by pulverizing and through pumping. d) The compound sublimes at this temperature. e) Dichloromethane solvate (1/2 molecule per Pd). f) Dichloromethane solvate (1/6 molecule per Pd). g) Dihydrate.

four times molar amounts of L was used, respectively, while the equimolar reaction gave rise to [Pd(hfac)-C^3)L] (**7**). The carbon-bonded complex of hfac has never been produced by the reactions of **1a** with alkylamines, pyridines, and tertiary phosphines.[1,2b] Now the presence of type **7** complexes in the equimolar reaction mixtures of **1a** and various aniline derivatives was confirmed by the NMR assay, although isolation of the products was successful only for **7a**, **7b**, and **7c**. 2,6-Dimethyl- and 2,4,6-trimethylanilines gave type **4** and **7** complexes but do not produce **5** probably because of their large steric demands.

Refluxing of an equimolar mixture of **1a** and an aniline derivative L in benzene gave rise to dinuclear complexes [Pd(hfac)(L−H)]$_2$ (**9**) containing the bridging anilide anions (L−H). Complexes **9** were also derived spontaneously from **7** in methanol solutions. The reactions of other [Pd(β-dik)$_2$] complexes (β-dik= 2,4-pentanedionate (acac), 1-phenyl-1,3-butanedionate (bzac), and 1,1,1-trifluoro-2,4-pentanedionate (tfac) anions) with L did not give **4**, **5**, and **7**, but produced **9** exclusively. Solubilities of anilide complexes **9** in organic solvents are very low and somewhat improved by methy substitutions on thephenyl ring. The molecular weight of **9n** (842) determined in dichloromethane (0.005—0.05 mol dm^{-3}) coincides well with the value (839) calculated for the dinuclear strueture, whereas those for **9c**-β (732) and **9i** (610) observed only for very dilute solutions are far less accurate and do not coincide with but are near the calculated values, 666 and 704, respectively. The analytical results in Table 1 together with these molecular-weight data accord with the dinuclear formulation of **9**, which is also supported by the NMR data reported below.

Deprotonation of amine groups coordinated to d^8 metals is usually effected by a strong base such as potassium amide in liquid ammonia,[6] but the reaction of dichloro(2,2′-bipyridine)platinum(II) with *cis,cis*-1,3,5-triaminocyclohexane (tach) in aqueous solution was found to result in [Pt(bpy)(tach−2H)H$_2$O]Cl$_2$, an octahedral Pt(IV) complex containing the tach dianion as a terdentate ligand.[7] In the present case, the coordinated aniline seems to be deprotonated by the β-diketonate anion situated in the inner or outer sphere (*vide infra*).

Although the hfac complexes **4** and **5** containing alkylamines as L are yellow and colorless, respectively,[1a] the corresponding aniline complexes are generally reddish and complexes **9** are dark red. The dinuclear anilide complexes **9** are thermally stable and the hfac complexes except **9o** can be sublimed in accordance with the general trend that substitution of the methyl groups of acac with CF$_3$ increases volatility of the complex.[8] The anilide-bridged dinuclear structure is very stable in solution, too. Treatment of complexes **9** with pyridine or primary amines (L′) does not effect cleavage of the bridge, but displaces the chelating β-dik ligands to produce [PdL′$_2$(L−H)]$_2$(β-dik)$_2$ (**10**). A platinum(II) complex containing an anilide anion as a unidentate ligand, *trans*-[PtCl(C$_6$H$_5$NH)(PEt$_3$)$_2$] was prepared by the reaction of *trans*-[PtH(Cl)(PEt$_3$)$_2$] with phenyl azide,[9] and was treated with silver hexafluorophosphate in acetone.[10] Abstraction of the chloride ligand did not occur, but oxidative coupling of the anilide was effected to result in a benzidine complex. The ancillary ligands may strongly affect the behavior of the anilide ligand.

Recrystallization of **9c** from dichloromethane gave two kinds of crystals, red plates and orange needles, containing different numbers of solvent molecules per palladium, which are tentatively designated as α and β forms, respectively. The two specimens **9c**-α and **9c**-β exhibit different IR and NMR spectra (*vide infra*) and seem to constitute a pair of isomers. The following two stereoisomers are conceivable for the di-μ-anilide structure, although it is difficult at present to identify which of **9c**-α and **9c**-β has the syn structure. Recrystallization of **9t** from dichloromethane–petroleum ether also gave both red plates and dark red columns. The IR spectra suggest that the former has the same structure as that of **9c**-α and the latter corresponds to the β form.

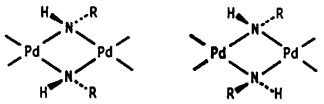

syn *anti*

When complex **9i** was prepared by the reaction of **1c** with aniline, complex **11** was obtained as a by-product and characterized by elemental analysis and IR spectroscopy. A Schiff base ligand 4-phenylamino-1,1,1-trifluoro-3-penten-2-one was prepared by Röhrscheid *et al.*[11] according to a previous method for 4-phenylamino-3-penten-2-one,[12] and the structure of *mer*-[V{N(C$_6$H$_5$)C(CH$_3$)CHCOCF$_3$}$_3$] was confirmed by ^{1}H and ^{19}F NMR spectroscopy.[11] In the present case, tfacH which was freed from **1c** by its reaction with aniline must have reacted with excess aniline to produce the Schiff base, which in turn seems to have replaced the tfac ligand in **1c** to give rise to **11**.

Infrared Spectra. Figure 1 exemplifies the characteristic IR bands of complexes **4d**, **5f**, **7b**, **9r**, and **10i**, all of which contain the hfac anion and 3,5-dimethylaniline as L and are suitable for comparing the IR spectra of complexes of different types. In general complexes **4** and **5** show two or three broad ν(NH) bands of strong to medium intensity in the 3300—3090 cm^{-1} region, while complexes **7** have sharper bands. Complexes **9** show one or two sharp bands of medium to weak intensity in the 3320—3220 cm^{-1} region, which are assigned to the ν(NH) vibration of the bridging anilide ligand. Each of the isolated α and β isomers of **9c** and **9t** shows a single ν(NH) band, of which the frequency is 20—30 cm^{-1} higher for the α form than for the β form. Then other complexes **9** exhibiting two bands in this region seem to be a mixture of both isomers. In the case of complexes **10** containing primary amines as L′, the ν(NH) band from the bridging anilide is indiscernible because of overlapping with the ν(NH) bands from L′. On the other hand, the pyridine complex **10h** shows a sharp band at 3255 cm^{-1}.

The IR bands in the 1800—1500-cm^{-1} region are useful for diagnosing the bonding mode of β-diketonate

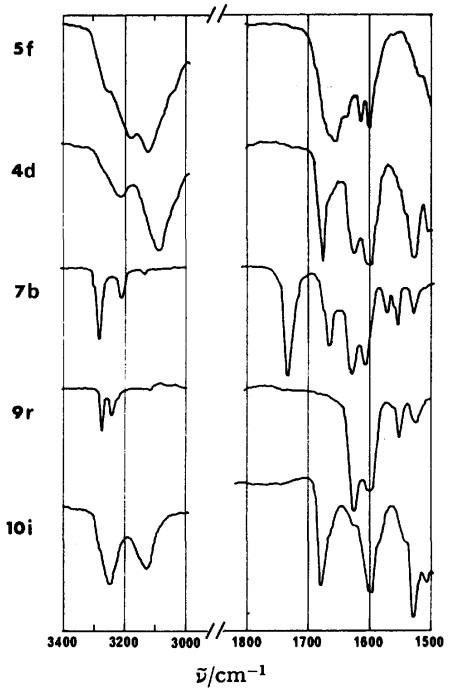

Fig. 1. IR spectra of complexes **5f**, **4d**, **7b**, **9r**, and **10i** in Nujol mull.

anions,[1,2] although aromatic ν(C=C) bands are also observed in this region. The strong absorption of **4d** at 1675 cm^{-1} and a very broad band of **5f** at 1655 cm^{-1} are assigned to the hfac anion in the outer sphere, since these bands are very close to the band exhibited by K(hfac) at 1675 cm^{-1}. Complex **4d** shows additional strong bands caused by the chelating hfac at 1625 and 1526 cm^{-1}. Besides the absorption of chelating hfac at 1628 and 1528 cm^{-1}, complex **7b** exhibits a very strong band at 1733 cm^{-1} which is characteristic of the central-carbon-bonded β-dik ligand.[1,2] The spectrum of **9r** includes the bands caused by the chelating hfac at 1626 and 1526 cm^{-1} but lacks bands in the region higher than 1626 cm^{-1}, certifying absence of hfac either carbon-bonded or situated in the outer sphere. On the other hand, the spectrum of **10i** again demonstrates the existence of hfac in the outer sphere.

NMR Spectra. Solubilities of compounds **4**, **5**, and **7** in organic solvents are generally insufficient to allow NMR measurements and ^{1}H NMR data for only a limited number of compounds were recorded (Table 2). Complexes **4** exhibit two methine signals, of which the lower-field one is assigned to CH of the chelated hfac by reference to the spectrum of [Pt(hfac)-(2-$CH_3C_6H_4NH_2$)$_2$](hfac) showing two methine signals at 5.79 and 6.03 ppm of which the latter is flanked by ^{195}Pt satellites with ^4J(Pt–H)=8 Hz.[1b] Spectra of **5** are generally broad over the whole field, but three kinds of amine-proton signals are observed inclusive of those from the corresponding **4** and free L, indicating attainment of the following equilibria.

$$\underset{\mathbf{5}}{[PdL_4](hfac)_2} \overset{K_1}{\rightleftharpoons} \underset{\mathbf{4}}{[Pd(hfac)L_2](hfac)} + 2L \qquad (1)$$

The same value of about 2×10^{-3} $mol^2\,dm^{-6}$ was obtained as K_1 at 25 °C for **5c**, **5e**, and **5f**.

Complex **7c** is not stable either in $CDCl_3$, but signals assignable to **4e** and **1a** are noticed about 1 min after dissolution and grow gradually with time to attain equilibrium (Eq. 2 with 2,4,6-$(CH_3)_3C_6H_2NH_2$ as L), K_2 being estimated as 0.25 at 25 °C. The corresponding platinum(II) complex does not undergo such a disproportionation reaction. The methine proton of the

$$2\underset{\mathbf{7}}{[Pd(hfac)(hfac\text{-}C^3)L]} \overset{K_2}{\rightleftharpoons} \underset{\mathbf{4}}{[Pd(hfac)L_2](hfac)} + \underset{\mathbf{1a}}{[Pd(hfac)_2]} \qquad (2)$$

carbon-bonded hfac in **7c** resonates at higher field than that of the chelating hfac and the ^{13}C signal of the methine carbon bonded to the metal also appears at much higher field (33.6 ppm) than that of the chelating hfac (92.0 ppm). The chemical shift of the amine protons in **7c** is also smaller by more than 1 ppm as compared with those in compounds **4** and **5**, indicating absence of the hydrogen-bonding anion in the outer sphere.[1]

Table 3 lists the ^{1}H NMR data for complexes **9**. All complexes except **9h** and **9v** exhibit two sets of signals, demonstrating that they contain stereoisomers α and β. Both the acac methyl protons and the anilide proton of **9c**-α resonate at higher field than those of **9c**-β. Thus the higher-field one of the two NH signals from each complex was assigned to the α form by reference to **9c**. Then the hfac methine signals from **9m**—**9u** were distinguished based on the area ratio to accord with that of the NH signals. In each case the hfac methine proton of the α form resonates at higher field than that of the β form, although the chemical shifts

Table 2. ^{1}H NMR data for [Pd(hfac)L_2](hfac) (**4**), [PdL_4](hfac)$_2$ (**5**), and [Pd(hfac)(hfac-C^3)L] (**7**) in $CDCl_3$ at room temperature[a]

Compd	CH of hfac[b]		L		
	Chelated	OS or C-Bonded	NH_2	CH_3[c]	Ring CH
4d	6.10	6.01	6.8	2.25(3,5)	6.82 br
4e	5.99	5.81	6.2_8	2.49(2,6), 2.16(4)	6.81
5c		5.98 br	5.8	2.20(4)	7.03 br
5e		5.90 br	5.4	2.21 br (2,5)	6.95 br
5f		5.93 br	6.1	2.16(3,5)	6.63 br
7c	6.12	5.31	4.3_4	2.18(2,4,6)	6.80

a) Chemical shift is expressed in ppm from internal Me_4Si, br: broad. b) OS abbreviates the outer sphere. c) Figures in parentheses give the positions of substitution on the phenyl ring.

TABLE 3. ^{1}H NMR DATA FOR [Pd(β-dik)(L−H)]$_2$ (**9**) IN $CDCl_3$ AT ROOM TEMPERATURE[a)]

Compd	[α]/[β]	β-Dik		Anilide (L-H)		
		CH_3	CH	NH	CH_3	Ring CH
9c-α		1.58	5.07	1.1_8	2.35, 2.42	$H^{3,4}$ 6.74, H^6 8.61
9c-β		1.65	5.07	1.3_1	2.42, 2.51	$H^{3,4}$ 6.74, H^6 8.28
9h[b)]		1.67	5.67			6—7 m
9i[c)]		1.75, 1.83	5.46	1.2		7.0 m, 7.7 m
9m	α 3—4		5.90	1.0_3		7.2 m, 7.9 m
	β 1		5.95	1.2_5		
9n	α 2		5.87	1.1_5	2.35	7.1 m, 8.7 m
	β 3		5.91	1.3_6	2.39	
9o	α *ca.* 4		5.90	0.9_8	2.22	$H^{2,6}$ 7.79 d (J=8 Hz), $H^{3,5}$ 6.99
	β 3		5.94	1.2_4		
9p	α 1		5.88	1.1_5	2.28, 2.42	$H^{3,4}$ 6.8 m, H^6 8.37
	β 2		5.92	1.3_5	2.34, 2.47	$H^{3,4}$ 6.8 m, H^6 8.47
9r	α 1		5.94	0.9_8	2.32	7.49 br, 6.79 br
	β 1		5.95	1.2_2		
9u	α 3—4		5.95	4.6_3		H^3 8.0_4 dd (J=8.2 Hz), $H^{4,5}$ 7.1—7.8 m H^6 9.01 d, br (J=8 Hz) for α H^6 9.28 dd (J=8.2 Hz) for β
	β 1		5.98	4.9_1		
9v			6.00	1.5		$H^{2,6}$, $H^{3,5}$ 8.10, 7.95 (AB quartet, J=9 Hz)

a) Same as footnote a) for Table 2, m=multiplet, d=doublet, dd=doublet of doublets. b) In C_6D_6. c) In CD_2Cl_2.

TABLE 4. $^{13}C\{^1H\}$ NMR DATA FOR COMPLEXES **9** IN $CDCl_3$ AT ROOM TEMPERATURE[a)]

Compd	β-Dik[b)]			Anilide[c)]						
	CH_3 or CF_3	CO	CH	C^1	C^2	C^3	C^4	C^5	C^6	CH_3
9c-α	25.9	185.6	100.0	149.2	128.0	129.0	122.6	135.2	125.8	18.4(2), 21.2(5)
9c-β	25.9	185.6	100.0	149.6	127.2	129.7	122.6	135.6	125.0	18.5(2), 21.2(5)
9m α	116.1	174.4	91.6	147.3	124.1	128.9	124.4			
β	[286]	[36]		d)	123.7	128.5	124.4			
9n α	116.1	174.4	91.5	145.4	d)	130.0	124.2	126.6	124.9	18.0(2)
β	[284]	[36]		146.8	d)	130.7	124.3	127.0	124.1	18.0(2)
9o α	116.2	174.4	91.5	145.2	123.5	129.5	134.0			21.0(4)
β	[284]	[36]		144.6	124.0	129.1	134.0			21.0(4)
9r α	116.2	174.4	91.6	147.0	122.1	138.3	126.2			21.0(3, 5)
β	[284]	[35]		147.5	121.6	138.6	126.2			21.0(3, 5)

a,c) Same as footnotes a) and c) for Table 2. b) Figures in brackets give the J(C–F) values in Hz. d) Indiscernible because of overlapping with other signals or low intensity.

were accidentally same for acac methine protons of **9c-α** and **9c-β**. The abundance ratio of isomers for each complex determined by the ^{1}H NMR measurements parallels the relative intensities of the ν(NH) bands in the IR spectrum.

Very recently a single crystal of [$AlMe_2$(*i*-PrNH)]$_2$ was revealed by X-ray analysis to contain two stereoisomers in the ratio of 2 : 1, of which both have four-membered $(AlN)_2$ rings.[13] The syn to anti ratio of 2 : 1 was preserved in toluene solution and changed only slightly with temperature. In the case of [AlBr(Et)-(*t*-BuNH)]$_2$, five stereoisomers are conceivable, of which two were isolated and shown to isomerize in benzene solution at room temperature to give an equilibrium mixture containing three principal isomers.[14] In the case of the present palladium(II) complexes, the stereoisomers are very inert in solution. Even when heated to 60 °C for several hours, **9c-α** in $CDCl_3$ solution showed no sign of isomerization to **9c-β**. The isomer ratios of other compounds **9** do not change with temperature either. Transformation between the syn and anti forms either by cleavage of the anilide bridge or by dissociation of the anilide proton does not occur easily, and the isomer ratio observed is not an equilibrium value in solution, but was realized under the preparative conditions.

The ^{19}F NMR spectrum of **9n** in dichloromethane at room temperature exhibits two signals at 3.36 and 3.06 ppm downfield from external CF_3COOH. The area ratio (2 : 3) coincides with the isomer ratio determined by ^{1}H NMR spectroscopy. Therefore the two ^{19}F signals are assigned to the α and β forms, respectively.

As is seen in Table 3, the NH proton of the anilide ligand in complexes **9** resonates usually in the field higher than 1.5 ppm, but that of **9u** absorbs in remarkably lower field. This exceptional behavior may stem from the hydrogen bonding of the NH group to the ortho nitro group, the NH group being retained on the same plane as the phenyl ring and suffering its anisotropic effect.

The ^{13}C NMR spectra of complexes **4**, **5**, and **7** are similar to those for corresponding β-dik complexes containing other nitrogen bases as L.[1] Therefore $^{13}C\{^1H\}$ NMR data only for the new type complexes **9** are listed in Table 4. In each case two sets of signals from the phenyl-ring carbons are observed and assigned to α and β forms based on the relative intensities to accord with the isomer ratios determined by ^1H NMR measurements. Shieldings of the β-diketonate carbons in **9** are quite similar to those of the corresponding bis-chelates **1**[4b] and chelating ligands in **4** and **7** containing alkylamines as L.[1a] Signals of the β-dik carbons do not show any difference due to the stereoisomerism, suggesting that the splitting observed for proton signals may be caused by different anisotropic effect exerted through space and not through bonds by the phenyl rings of bridging anilide ligands in the syn and anti isomers. Complexes **10** are not sufficiently soluble in usual solvents to allow NMR measurements.

Relative Stabilities of Complexes. Relative stabilities of the palladium(II) complexes **4**, **5**, and **7** containing ammonia, alkylamines, and pyridines as L were found to depend on basicities of both the nitrogen bases and β-dik anions as well as bulkiness of the former.[1a] Thus complexes **5** are favored by more basic L and less basic β-dik. Anilines are far less basic than alkylamines and pyridines, and can not displace the β-dik ligands in $[Pd(acac)_2]$ (**1b**), $[Pd(bzac)_2]$, and $[Pd(tfac)_2]$ (**1c**), reacting only with $[Pd(hfac)_2]$ (**1a**) to produce complexes **4**, **5**, and **7**. It is noteworthy that reactions between anilines and **1a** afford either **4** or **5** depending on the reactants mole ratio, whereas primary alkylamines and pyridine gave solely **5**[1a] because of higher reactivity of $[Pd(hfac)L_2](hfac)$ toward L than that of **1a** when L are these bases. 2-Nitro- and 4-nitroanilines, which are less basic than aniline, the pK_a values of conjugate acids being -0.26 and 1.11 as compared with 4.60 for aniline,[15] do not give **4** and **5**, but produce anilide complexes **9**. On the other hand, 2-methyl- and 2,4-dimethylanilines are more basic than aniline, giving **4** and **5**. It may be due to their bulkiness that 2,6-dimethyl- and 2,4,6-trimethylanilines produce **4** and **7** but do not give **5**. The central-carbon-bonded complexes **7** were supposed to be preferred by β-diketones which favor the keto form over enol.[1,16] In spite of the fact that hfacH is composed exclusively of the enol tautomer,[17] some substituted anilines give rise to complexes **7**. Besides the basicity at the central carbon atom of β-dik anion (the keto-favoring factor), some balance between basicities of L and β-dik might be important for stabilization of **7**.

Mechanism for Formation of the Anilide-bridged Complexes. Kinetic and equilibrium studies on the reactions of **1b** with alkylamines revealed that complexes of type **7** are produced not directly from **1b** but *via* **4** reversibly, and the equilibrium is favorable to **7** in dichloromethane and to **4** in methanol when diethylamine is used as L.[18] The same situation will be reallized for the present aniline complexes. Complexes **7a**—**7c** were prepared in benzene and changed spontaneously to complexes **9** in methanol. The transformation reaction might be represented by Eqs. 3 and 4.

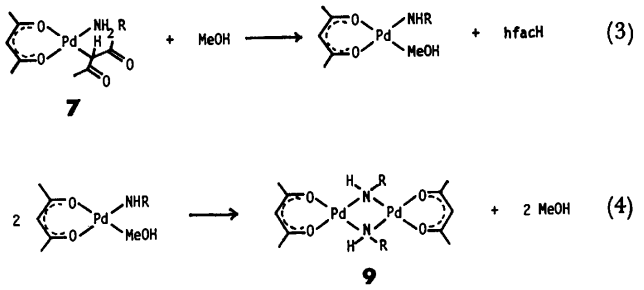

It is a characteristic feature of anilines to afford anilide complexes **9** irreversibly by the reactions with **1** on heating. The overall reaction might proceed *via* complex **4** (Eq. 5) or alternatively in a direct fashion as depicted in Eq. 6. In previous papers,[1a,19] complexes

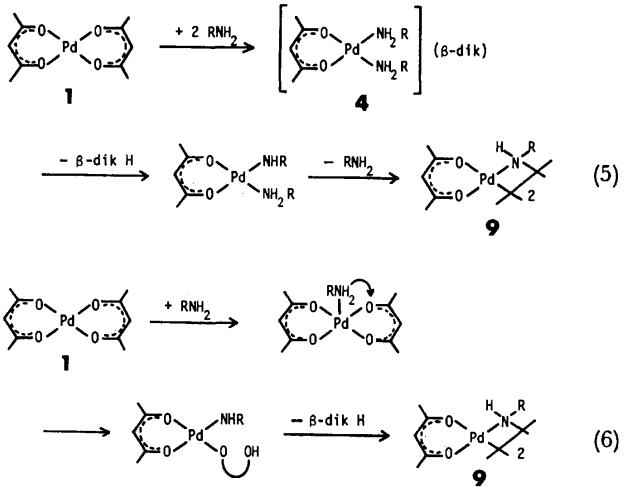

4 and **5** containing secondary and primary amines as L, respectively, were reported to catalyze the hydrogen exchange reactions between amines and chloroform. Deprotonation of the coordinated amine molecule by the β-dik anion in the outer sphere was presumed to be a key step and the rate was found to parallel the basicity of the β-dik anion. The present results that the reactions of $[Pd(\beta\text{-dik})_2]$ (β-dik=acac, bzac, and tfac) with aniline and its methyl derivatives as well as reactions of **1a** with nitroanilines do not afford complexes **4** but give rise directly to **9** seem to support reaction scheme 6.

1,8-Bis(dimethylamino)naphthalene, a powerful proton acceptor known as "proton sponge," greatly accelerates the **9**-forming reactions. An equimolar mixture of **1a** and 4-methylaniline in $CDCl_3$ promptly attains an equilibrium shown by Eq. 2, K_2 being estimated as 0.1 from ^1H NMR spectroscopy. On addition of an equimolar amount of "proton sponge" to this mixture, the reaction to form **9o** proceeds almost quantitatively at room temperature and **9o** and the hfac salt **12** were isolated in 88 and 27% yields, respectively. An equimolar mixture of **1a** and 2-nitroaniline in $CDCl_3$ showed no sign of reaction on the NMR spectra after a while at room temperature, but reacted immediately on addition of the equimolar base to result in **9u** and **12** quantitatively (based on the ^1H and ^{13}C NMR spectra), which were isolated in 60 and 48% yields, respectively.

These results demonstrate that the deprotonation of anilines is the most important step in production of **9**. In the absence of added base, basicity of the β-dik anion and acidity of the amine seem to be the most important factors to facilitate formation of the anilide complexes. Much lower acidities of alkylamines as compared with those of anilines may be the reason why alkylamines fail to afford amide complexes.

We wish to thank Mr. Junichi Gohda for elemental analyses and also Professor T. Tanaka and Dr. K. Kawakami of Osaka University for ^{19}F NMR measurements. S. O. and S. K. are grateful to the Ministry of Education, Science and Culture for Grant-in-Aid for Scientific Research, Nos. 454196 and 243014, respectively.

References

1) a) S. Okeya, H. Sazaki, M. Ogita, T. Takemoto, Y. Onuki, Y. Nakamura, B. K. Mohapatra, and S. Kawaguchi, *Bull. Chem. Soc. Jpn.*, **54**, 1978 (1981); b) S. Okeya, Y. Nakamura, and S. Kawaguchi, *ibid.*, submitted for publication.

2) a) S. Okeya, T. Miyamoto, S. Ooi, Y. Nakamura, and S. Kawaguchi, *Inorg. Chim. Acta*, **45**, L135 (1980); b) S. Okeya, Y. Nakamura, and S. Kawaguchi, *Bull. Chem. Soc. Jpn.*, **54**, 3396 (1981).

3) D. C. Bradley and M. H. Chisholm, *Acc. Chem. Res.*, **9**, 273 (1976); D. C. Bradley, *Adv. Inorg. Chem. Radiochem.*, **15**, 259 (1972).

4) a) S. Okeya and S. Kawaguchi, *Inorg. Synth.*, **20**, 65 (1980); b) S. Okeya, S. Ooi, K. Matsumoto, Y. Nakamura, and S. Kawaguchi, *Bull. Chem. Soc. Jpn.*, **54**, 1085 (1981).

5) J. A. Riddick and W. B. Bunger, "Organic Solvents," 3rd ed, Wiley-Interscience, New York (1970), p. 815.

6) G. W. Watt and J. F. Knifton, *Inorg. Chem.*, **7**, 1443 (1968); G. W. Watt, J. F. Knifton, and C. V. Senoff, *ibid.*, **8**, 2252 (1969).

7) J. E. Sarneski, A. T. McPhail, K. D. Onan, L. E. Erickson, and C. N. Reilley, *J. Am. Chem. Soc.*, **99**, 7376 (1977).

8) R. C. Mehrotra, R. Bohra, and D. P. Gaur, "Metal β-Diketonates and Allied Derivatives," Academic Press, New York (1978), p. 58.

9) W. Beck and M. Bauder, *Chem. Ber.*, **103**, 583 (1970).

10) N. W. Alcock, R. D. O'Sullivan, and A. W. Parkins, *J. Chem. Soc., Chem. Commun.*, **1980**, 1216.

11) F. Röhrscheid, R. E. Ernst, and R. H. Holm, *Inorg. Chem.*, **6**, 1607 (1967).

12) W. Koenigs and A. Mengel, *Ber.*, **37**, 1325 (1904).

13) A. Amirkhalili, P. B. Hitchcock, A. D. Jenkins, J. Z. Nyathi, and J. D. Smith, *J. Chem. Soc., Dalton Trans.*, **1981**, 377.

14) R. E. Bowen and K. Gosling, *J. Chem. Soc., Dalton Trans.*, **1974**, 964.

15) "The Chemistry of the Amino Croup," ed by S. Patai, Interscience, London (1968), p. 182.

16) T. Ito and A. Yamamoto, *J. Organomet. Chem.*, **174**, 237 (1979).

17) G. Allen and R. A. Dwek, *J. Chem. Soc., B*, **1966**, 161.

18) S. Matsumoto and S. Kawaguchi, *Bull. Chem. Soc. Jpn.*, **53**, 1577 (1980).

19) S. Okeya, Y. Nakamura, and S. Kawaguchi, *J. Chem. Soc., Chem. Commun.*, **1977**, 914.

Carbene in Rigid Matrix. XI.[1] Temperature and Matrix Effect on Phenylcarbene Processes in Ether and Amine

Hideo Tomioka,* Shinji Suzuki, and Yasuji Izawa

Department of Industrial Chemistry, Faculty of Engineering, Mie University, Tsu, Mie 514

(Received February 20, 1981)

Product distributions from reactions of phenylcarbene with diethyl or diisopropyl ether or diethylamine were found to be highly dependent on reaction temperature. As temperature decreases, the C–O displacement reaction and N–H insertion are decreased. Concomitantly, primary C–H insertion products markedly increase especially at lower matrix temperatures.

In recent years the importance of the method of generation of a carbene for its chemical behavior has become evident. Among examples which may be cited, the low temperature photolysis of aryldiazomethanes in rigid matrices has been shown[2,3] to be a unique method for looking into the triplet arylcarbene chemistry, especially in systems in which competitive singlet and triplet reactions occur. Photolysis of aryldiazomethane in olefin matrices at −196 °C, for example, results[2] in a dramatic increase in the yield of C–H insertion products at the expense of cyclopropane, which is a dominant product in a liquid phase photolytic run. A similar dramatic yield increase of C–H insertion products is also observable[3] in the photolysis of aryldiazomethanes in alcoholic matrices, whereas O–H insertion is generally a major reaction pathway of arylcarbene generated at ambient temperature. These C–H insertion products are proposed[2,3] to be formed *via* an abstraction-recombination (*a-r*) of the triplet carbene on the basis of ample spectroscopic[4] and chemical[4a] evidence for the presence of the ground-state triplet carbene in the low temperature matrix photolysis of most aryldiazomethanes at −196 °C. The method is thus expected to serve as a useful adjunct in the investigation of the relationship between the multiplicity and reaction pattern of carbene. However, since there is still some ambiguity as to the exact mechanism by which the matrix controls C–H insertion processes within itself, we have investigated temperature effects on carbene reactions with other reactive substrates involving hetero atoms, *i.e.*, ether and amine. Temperature effect studies of reactions of carbene with these substrates are intriguing in the following points in connection with results in alcohols. First, one can expect to get information on the temperature dependence of C–H insertion selectivity in both the liquid and solid phases, since C–H insertion is a major pathway[5] for these substrates; in contrast, C–H insertion scarcely proceeds[2] in reactions with alcohol, especially in the liquid phase. Second, it is quite important to examine the temperature effect on characteristic reactions[5] of the singlet carbene in these solvents, *i.e.*, the successive sequence of two reactions: the electrophilic attack on the lone pair of electrons on the hetero atom (X) to form an ylidic intermediate; and the Stevens rearrangement and/or the Hoffman type β-elimination, leading to C–X insertion and C–X displacement. The N–H insertion process of carbene will especially be informative because, unlike its reaction with alcohols[2] involving, if possible, abstraction of a hydrogen atom from the α-carbon atom, the triplet carbene may be expected to abstract[5b] hydrogen from the N–H bond in view of the bond energy and hence will take part also in the N–H insertion together with the singlet-state carbene. Thus, the present systems are expected to throw additional light not only on the applicability of the technique to looking into the triplet carbene chemistry but also on the mechanism of reactions of arylcarbene with ether or amine.

Reaction of Phenylcarbene with Ethers. A solution of phenyldiazomethane (**1**) in ether (**2**, R=H, CH_3) was irradiated at 0 °C and analysed by GC. This analysis revealed formation of the C–O displacement product (**3**), the C–O insertion product (**4**), and two C–H insertion products (**5** and **6**) (Table 1). The product distributions are found to be sensitive to the structure of ethers. Thus, either **3** or **4**, presumably resulting *via* an oxygen ylide intermediate, is formed in more suppressed yield as the ether changes from ethyl ether to isopropyl ether. This is apparently due to the steric hindrance on the accessibility to the central oxygen. A similar steric hindrance on the ylide formation has been noted with a photolysis[6] of dimethyl diazomalonate in allyl ethers, where the yield of the ylidic product decreases from 31 to 0% as the ether changes from allyl methyl ether to allyl *t*-butyl ether. Since it is quite important here to examine the exact intermediates leading to each insertion product, we have examined effects of precursor, triplet sensitizer, and singlet carbene quencher on product distributions (Table 1). First, photolysis of *cis*- and *trans*-1,2-diphenyloxiranes, a nitrogen-free precursor[7] of phenylcarbene, in ethyl ether gave a comparable result with that observed in similar photolysis of **1**. This eliminates the possible intervention of the diazomethane as an intermediate in the reaction and thus indicates involvement of free carbene. Second, product distributions were not altered by the addition of a large excess of benzophenone as a triplet sensitizer so as to assure absorption of 99% of the incident light by the sensitizer. This is often observed[8] in the arylcarbene system and can be interpreted as indicating that singlet-triplet equilibrium is faster than reactions with ether. Third, the examination of effect of 2-propanol, an efficient quencher for singlet carbene,[2,9] on the product distribution indicated that both the ylidic products and the C–H insertion products were quenched but with different degrees of efficiency. Thus, the ratio of the C–H insertion products to the ylidic products increased as the concentration of alcohol increased. This implies

Table 1. Product distribution in photolysis of **1** in ethers at 0 °C[a]

R_2O	Additive (mmol dm^{-1})	Relative yield/%[b]			
		3	**4**	**5**	**6**
Et_2O	None	13.7	18.1	68.2	Trace
	None[c]	11.3	19.3	69.4	Trace
	Ph_2CO (25)	12.5	17.3	70.2	Trace
	i-PrOH (25)[d]	8.0	12.6	65.2	Trace
	i-PrOH (75)[d]	5.9	9.6	59.2	Trace
	i-PrOH (125)[d]	4.5	8.3	54.4	Trace
i-Pr_2O	None	≈1	≈1	95.1	2.9
	None[c]	≈1	≈1	96.8	1.2

a) Irradiations were performed on a 2.5 mmol dm^{-3} solution of **1** in Pyrex tubes. b) Yields were determined by GC and normarized to 100%. Total yields (*ca.* 50—60%) did not vary appreciably under these conditions. c) Diphenyloxiranes used as a carbene precursor. d) OH insertion product, $PhCH_2OCH(CH_3)_2$, formed was included in numerator.

Table 2. Product distribution as a function of temperature. Photolysis of **1** in ethers

R_2O	*T*/°C	Relative yield/%[a]			
		3	**4**	**5**	**6**
Et_2O	0[b]	13.7	18.1	68.2	Trace
	−50[b]	6.3	5.3	84.7	3.7
	−78[b]	2.6	1.3	94.8	1.3
	−110[b]	1.9	Trace	94.2	3.9
	−150[c]	1.6	Trace	92.5	5.9
	−196[c]	1.1	Trace	89.2	9.7
	−196[c,d]	≈1	Trace	88.3	10.4
i-Pr_2O	0[b]	≈1	≈1	95.1	2.9
	−50[b]	≈1	≈1	96.5	1.5
	−78[b]	≈1	≈1	97.0	1.0
	−110[c]	Trace	Trace	66.4	33.6
	−150[c]	Trace	Trace	25.9	74.1
	−196[c]	Trace	Trace	14.6	85.4
	−196[c,d]	Trace	Trace	12.3	87.7

a) Normarized to 100%. Total yields were *ca.* 50—60%. Other minor products detected in each run were toluene, bibenzyl, stilbenes, and aldehyde azine. Control experiments ruled out the interconversion of products during irradiation. b) Liquid phase. d) Solid phase. d) Diphenyloxiranes used as a carbene precursor.

that singlet carbene takes part in the ylidic products but that not only singlet but also triplet carbenes are involved in the C–H insertion reaction.

The effect of temperature on the product distribution was next examined and the results are summerized in Table 2. Two apparent trends of temperature dependence can be seen from an inspection of Table 2. First, as the photolysis temperature was lowered, yields of the displacement product (**3**) and C–O insertion product (**4**) decreased continuously, especially in the reaction with ethyl ether, and they were almost completely suppressed at −196 °C, whereas the C–H insertion product increased. Similar phenomena have been observed[2] in the O–H/C–H insertion ratio in the

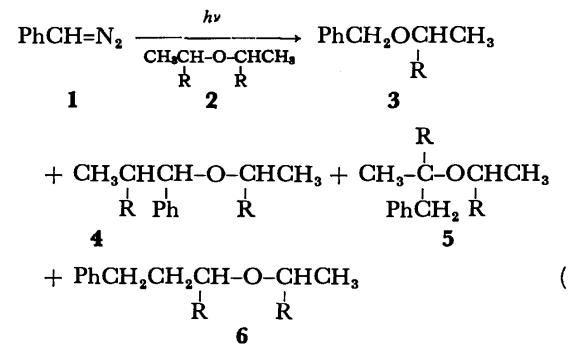

(1)

a, R = H; **b**, R = Me

reaction of phenylcarbene with alcohols as temperature is lowered. This can be interpreted as indicating that triplet reactions gain over singlet reactions since it has been demonstrated[4] that a photolysis of aryldiazomethanes in organic matrices at −196 °C results in an almost exclusive formation of triplet carbenes. Thus the present results indicate that the characteristic reaction of singlet carbene with ethers is also suppressed at lower temperature. This suggests that the process has a higher activation energy than the competitive C–H insertion process. Alternatively, the reason for suppression of **3** and **4** at lower temperature probably lies partly in the ramification of stabilization by solvation. Thus, the transition state for the formation of **3** and **4** might be more polar than that leading to the C–H insertion and hence is more stabilized by solvation. Such solvation becomes less important as temperature decreases and hence yields of **3** and **4** decrease.

One more interesting feature of the present reaction is that C–H insertion selectivity is also highly temperature dependent; the selectivity increases as temperature is lowered as far as the reaction phase is liquid, but it dramatically decreases when the reaction phase changes from liquid to solid. Similar phenomena have been observed[10] in the C–H insertion selectivity of phenylcarbene in hydrocarbons with various types of C–H bonds and can be explained in terms of competitive temperature and matrix effects. Thus, as temperature decreases, the tertiary C–H insertion gains over the primary one because the tertiary C–H insertion is favored by lower activation energy. It has been suggested that both singlet and triplet carbenes take part in the C–H insertion at least in liquid phase, but if the C–H "insertion" takes place *via* the *a-r* reaction of the triplet, apparently tertiary abstraction is favored over primary one in view of bond energy, and if, on the other hand, the concerted insertion of the singlet is assumed, the transition state (**7**) proposed[11] for the insertion predicts that tertiary insertion is favored by an electronic factor. In the matrix photolysis, however, triplet carbene is thought to be a dominant intermediate for the C–H insertion product since recent studies[4b]

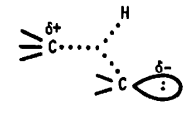

7

on decay rates of triplet arylcarbenes in various organic matrices have shown that the predominant decay pathway of the triplet is hydrogen atom tunneling to give C–H "insertion." Intervention of free carbene was again verified by the finding that the photolysis of the diphenyloxirane in rigid matrix gave a comparable trend in the product distribution. The decrease in the C–H insertion selectivity observed in rigid matrix is, however, a completely unexpected behavior for triplet carbenes since triplet carbenes have been shown[12] to be much more selective intermediates in the C–H insertion reaction than the corresponding singlet in gas- as well as liquid-phase experiments. The reason for the marked increase in the primary C–H insertion in a rigid matrix then probably lies partly in that a matrix imposes steric demand on the C–H insertion process. It is not unreasonable to assume that the size and shape provided by the host molecule and its rigidity impose severe steric hindrance on the guest molecule (PhCH:) in the accessibility to tertiary C–H bonds. A similar argument can be applied to explain that a much less dramatic change in the C–H insertion selectivity was observed even at −196 °C in the reaction with ethyl ether matrix which has less sterically-hindered secondary C–H bonds.

Reactions of Phenylcarbene with Diethylamine. Photolysis of **1** in diethylamine resulted in formation of the N–H insertion product (**8**) and two C–H insertion

$$\mathbf{1} \xrightarrow[HNEt_2]{h\nu} \underset{\mathbf{8}}{PhCH_2NEt_2} + \underset{\mathbf{9}}{\overset{PhCH_2}{\overset{|}{CH_3}}CHNH(Et)} + \underset{\mathbf{10}}{\overset{PhCH_2}{\overset{|}{CH_2}}CH_2NH(Et)} \quad (2)$$

products (**9** and **10**). Temperature dependence of the product distribution (**8**—**10**) is summerized in Table 3. From the Table, it is evident that the N–H insertion product decreases steadily concomitant with the increase in the C–H insertion product, as temperature is lowered. Accepting that triplet arylcarbene is generated also in the amine matrix, it is somewhat surprising to note that **8** is not appreciably formed even at −196 °C, because the energy for N–H bond must be less by some 3 kcal mol^{-1} than that for the α-CH bond[5b] in the amine and hence the abstraction of hydrogen by triplet carbene should occur from the N–H bond more easily than from C–H bonds especially at lower temperature,

Table 3. Product distribution as a function of temperature. Photolysis of **1** in diethylamine

T/°C	Relative yield/%[a]		
	8	**9**	**10**
0[b]	62.5	37.5	0
−50[b]	59.9	38.5	1.6
−78[c]	35.1	59.8	5.1
−110[c]	25.5	69.6	4.9
−150[c]	18.1	80.8	1.1
−196[c]	17.0	80.8	1.2

a) See footnote a in Table 2. b) Liquid phase. c) Solid phase.

resulting in the production of **8** *via a-r* mechanism. It is worth noting that, in gas-phase reactions of methyl radical with methylamine, the N–H bond is more than twice as reactive as the C–H bond.[13] Moreover, CIDNP studies of thermal (80 °C) decomposition of diphenyldiazomethane in butylamines have shown[5b] that triplet diphenylcarbene actually abstracts hydrogen from the N–H bond to form the radical pair $\overline{Ph_2CH\cdot \cdot NHR}$, which however separates to each component to give radical dimeric products at this temperature. The kinetics of the reaction have indicated,[5b] on the other hand, that the N–H insertion product is formed *via* an initial attack of the singlet carbene on nitrogen atom of the amine followed by rearrangement of the resulting ylide. The present results support this mechanism. Since the recombination of the radical pair is shown[2] to be favored in rigid media due to the increased viscosity, a decrease in the formation of **8** even in rigid amine matrix suggests that the triplet carbene generated in rigid matrix does not abstract hydrogen from the N–H bond in spite of the energetic advantage. Exact reason for this interesting phenomena is not known at present. It might partly lie in that the interaction of solvent molecules themselves comes to predominate over interactions between guest and amine molecules as temperature is lowered.[14]

Concluding Remarks. The present results have suggested that the low temperature photolysis of aryldiazomethanes in a rigid matrix is a very useful technique to suppress characteristic reactions of singlet carbene and to increase C–H insertions presumably resulting *via a-r* reaction of triplet arylcarbenes. The method has its merits in that (i) it generates the triplet arylcarbene which is usually in a rapid equilibrium with the upper-lying singlet states and hence is not populated generally in liquid phase to the extent which permits the prominent formation of the product derived from it in the sensitized experiment and (ii) it also makes the triplet arylcarbene a synthetically more useful intermediate, while the triplet arylcarbene generated in the liquid phase usually leads to a complex mixture of radical-derived products.

Experimental

The infrared, ^{1}H NMR, and GC-MS spectra were recorded on a JASCO IR-G spectrometer, a JEOL JNM-MH-100 NMR spectrometer, and a Shimadzu GC-MS 1000 spectrometer, respectively. The GC analyses performed on a Yanagimoto instrument, Model G-180, with a flame ionization detector. The following columns were used: A, 4.0 mm × 2.0 m 10% PEG 20 M on 60—80 mesh Diasolid L; B, 4.0 mm × 2.0 m 10% OV-17 on 60—80 mesh Diasolid L.

Materials. Diazomethane **1** was prepared from the corresponding tosylhydrazone immediately before use. All authentic ethers (**3**—**6**) in Eq. 1 were prepared by treatment of the corresponding aromatic alcohols with either ethyl bromide or isopropyl bromide in the presence of silver oxide according to the literature procedure.[5c] Authentic amines (**8**—**10**) were prepared by the reaction of appropriate bromide with excess diethylamine or ethylamine. Their boiling points were 101—103 °C/23 mmHg† (**8**), 103—105 °C/24 mmHg (**9**),

† 1 mmHg≈133.3 Pa.

and 117—119 °C/21 mmHg (**10**), respectively. Preparations of commercially unavailable alcohols were reported elsewhere.[2a,6] Satisfactory spectroscopic and mass spectral data have been obtained on all compounds.

Irradiations and Analyses. All irradiations were conducted using a Halos 300-W high-pressure mercury lamp with a water-cooled quartz jacket. In a typical procedure, 0.005 mmol of the diazomethane was added to 2.0 cm^3 of the appropriate solvent in Pyrex tubes. The sample was then degassed using three freeze-thaw cycles, and the sample tube was sealed in vacuum. The tube was suspended in a transparent Pyrex Dewar flask filled with coolant and irradiated until all diazomethane was destroyed. Photolysis of diphenyloxirane was carried out in quartz tubes in a transparent quartz Dewar. Control experiments ruled out the interconversion of the product during irradiations and also showed that no reaction occurred in the absence of light in the range of temperature studied.

The product identification and relative yields were conveniently determined by standard GC and/or GC-MS techniques.

This work was supported by Grant-in-Aid for Scientific Research No. 454140 from the Ministry of Education, Science and Culture and the Asahi Glass Foundation.

References

1) Part X: H. Tomioka, H. Ueda, S. Kondo, and Y. Izawa, *J. Am. Chem. Soc.*, **102**, 7817 (1980).

2) a) H. Tomioka and Y. Izawa, *J. Am. Chem. Soc.*, **99**, 6128 (1977); b) H. Tomioka, T. Inagaki, S. Nakamura, and Y. Izawa, *J. Chem. Soc., Perkin Trans. 1*, **1979**, 130; c) H. Tomioka, T. Miwa, S. Suzuki, and Y. Izawa, *Bull. Chem. Jpn.*, **53**, 753 (1980); d) Tomioka, H. Okuno, and Y. Izawa, *J. Chem. Soc., Perkin Trans. 2*, **1980**, 1636; e) H. Tomioka, S. Suzuki, and Y. Izawa, *J. Am. Chem. Soc.*, in press.

3) a) R. A. Moss and U.-H. Dolling, *J. Am. Chem. Soc.*, **93**, 954 (1971); b) R. A. Moss and M. A. Joyce, *ibid.*, **99**, 1262 (1977); c) R. A. Moss and J. K. Huselton, *ibid.*, **100**, 1314 1978); d) R. A. Moss and M. A. Joyce, *ibid.*, **100**, 4475 (1978).

4) a) A. M. Trozzolo, *Acc. Chem. Res.*, **1**, 329 (1968) and references cited therein; b) V. P. Senthilnathan and M. S. Platz, *J. Am. Chem., Soc.* **102**, 7637 (1980).

5) a) See for review, W. Kimse, "Carbene Chemistry," 2nd ed, Academic Press, New York (1971), p. 407; b) D. Bethell, J. Hayes, and A. R. Newall, *J. Chem. Soc., Perkin Trans. 2*, **1974**, 1307: c) H. Iwamura, Y. Imahashi, K. Kushida, K. Aoki, and S. Satoh, *Bull. Chem. Soc. Jpn.*, **49**, 1690 (1976); d) G. K. Agopian, D. W. Brown, and M. Jones, Jr., *Tetrahedron Lett.*, **1976**, 2931.

6) W. Ando, S. Kondo, K. Nakayama, K. Ichibori, H. Kohda, H. Yamato, I. Imai, S. Nakaido, and T. Migita, *J. Am. Chem. Soc.*, **94**, 3870 (1972).

7) A comprehensive review of carbene formation from oxiranes by cycloelimination is presented, N. R. Bertoniere and G. W. Griffin, "Carbenes," ed by M. Jones and R. A. Moss, Wiley-Interscience, New York (1973), Vol. I.

8) See for example, G. L. Closs and B. E. Rabinow, *J. Am. Chem. Soc.*, **98**, 8190 (1976).

9) J. J. Zupancic and G. B. Suchuster, *J. Am. Chem. Soc.*, **102**, 5958 (1980).

10) H. Tomioka, *J. Am. Chem. Soc.*, **99**, 6128 (1977).

11) D. Seyferth and Y.-M. Cheng, *J. Am. Chem. Soc.*, **95**, 6763 (1973).

12) a) M. Jones, Jr., W. Ando, M. E. Hendrick, A. Kulczycki, Jr., P. M. Howley, K. F. Hummel, and D. S. Malament, *J. Am. Chem. Soc.*, **94**, 7469 (1972); b) B. M. Herzog and R. W. Carr, Jr., *J. Phys. Chem.*, **70**, 1971 (1966).

13) P. Gray and J. C. J. Tynne, *Trans. Faraday Soc.*, **59**, 2275 (1963).

14) S. Hirayama, *Bull. Chem. Soc. Jpn.*, **48**, 2653 (1975).

High Pressure Organic Chemistry. V.[1] Diels-Alder Reactions of Furan with Acrylic and Maleic Esters

Hiyoshizo KOTSUKI,* Hitoshi NISHIZAWA,* Masamitsu OCHI, and Kiyoshi MATSUOKA

Department of Chemistry, Faculty of Science, Kochi University, Akebono-cho, Kochi 780

(Received February 5, 1981)

A series of Diels-Alder reactions of furan with acrylic and maleic esters has been investigated under conditions of high pressure. The approximate *endo/exo* ratios of the adducts with acrylic and maleic esters were 6 : 4 and 8 : 2 respectively. The observed isomer distributions are ascribed to the kinetic control.

In a previous paper we reported the successful Diels-Alder reaction of thiophene with maleic anhydride at 15 kbar and 100 °C, which afforded stereoselectively the *exo*-adduct.[2] In the pioneering work of Dauben and Krabbenhoft on the cycloaddition reactions of furan, it has been reported that both *endo* and *exo* isomers are obtained in approximate ratios of 1 : 1 with acrylic esters and only the *endo* isomer with dimethyl maleate.[3]

As a continuation of our investigation in this area, we were particularly interested in the stereochemical outcome of the Diels-Alder reaction at very high pressure.

Generally, steric factors play a significant role in determining the reactivity of dienophiles for high pressure reactions.[3,4] We presumed that in the Diels-Alder reaction of furan with acrylic and maleic esters, the *endo/exo* ratio would change with the variation o alkoxyl in the ester group, since the volume of the transition state for the *endo* addition is expected to be increased by crowding of R function, as shown in the Scheme 1 for the reaction of the acrylic esters. Based on this assumption, we have examined the Diels-Alder reaction of furan with several acrylic and maleic esters at very high pressure.

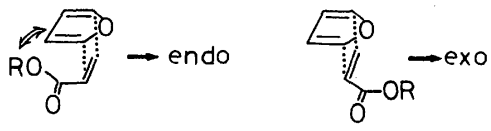

Scheme 1.

TABLE 1. DIELS-ALDER REACTION OF FURAN WITH MALEIC ESTERS

R	Temp °C	Time h	*P* kbar	Yield %[a]	*endo/exo* ratio[b]
	27	8	20	94	81 : 19
	27	8	15	90	81 : 19
a Me	27	8	10	60	82 : 18
	27	16	15	95	82 : 18
	16	6	15	46	82 : 18
	27	8	20	88	80 : 20
	27	8	15	87	81 : 19
b Et	27	8	10	58	81 : 19
	16	6	15	40	80 : 20
	27	8	20	96	84 : 16
	27	8	15	88	83 : 17
c *n*-Bu	27	8	10	43	83 : 17
	16	6	15	37	83 : 17

a) Crude yields determined from ^{1}H NMR integrals. The values are the average of three or more runs. b) The ratios were determined from ^{1}H NMR integrals.

Results and Discussion

The results are summarized in Tables 1 and 2. The

TABLE 2. DIELS-ALDER REACTION OF FURAN WITH ACRYLIC ESTERS (27 °C, 4 h)

	R	*P* kbar	Yield %[a]	*endo/exo* ratio[b]
		20	83	
a	H[c,d]	15	63	6 : 4
		10	43	
		20	79	
		15	95[e]	
b	Me[d]	15	62	6 : 4
		10	20	
		20	82	
c	Et[d]	15	58	6 : 4
		10	23	
		20	65	
d	*n*-Bu	15	55	6 : 4
		10	17	
e	CH_2CCl_3	15	75	6 : 4
f	*i*-Bu	15	55	6 : 4
g	C_6H_5	15	40	6 : 4

a) Crude yields by ^{1}H NMR except as noted. The values are the average of three or more runs. b) The ratios were determined from ^{1}H NMR integrals. c) Isolated after esterification with diazomethane. d) Isolated after evaporation. e) 60 °C, 6 h.

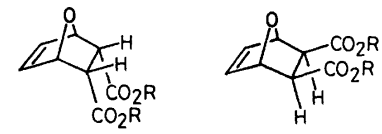

1a R=Me
b R=Et
c R=n-Bu

2a R=Me
b R=Et
c R=n-Bu

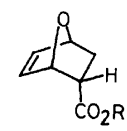

3a R=H
b R=Me
c R=Et
d R=n-Bu

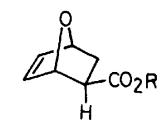

4a R=H
b R=Me
c R=Et
d R=n-Bu

Table 3. Spectral data of Diels-Alder adducts and their dihydro derivatives

Compound	IR ν_{CO}/cm^{-1}	NMR δ C_1,C_4–H	C_2,C_3–H	C_5,C_6–H	Others
1a	1740	4.97 (2H, m)	3.27 (2H, dd, J=2, 3 Hz)	6.42 (2H, br s)	3.55 (6H, s)
2a[a]	1740[b]	5.24 (2H, br s)	2.80 (2H, s)	6.47 (2H, br s)	3.68 (6H, s)
1b	1735	4.95 (2H, m)	3.24 (2H, br d, J=2 Hz)	6.39 (2H, br s)	3.98 (4H, q, J=6 Hz) 1.20 (6H, t, J=6 Hz)
1c	1740	4.95 (2H, m)	3.26 (2H, dd, J=2, 3 Hz)	6.40 (2H, br s)	3.94 (4H, t, J=6 Hz) 1.7—1.1 (8H) 0.95 (6H, t, J=6 Hz)
5a	1735	4.57 (2H, m)	3.08 (2H, m)	2.1—1.5 (4H, m)	3.60 (6H, s)
5b	1735	4.57 (2H, m)	3.06 (2H, m)	2.1—1.5 (4H, m)	4.06 (4H, q, J=7 Hz) 1.23 (6H, t, J=7 Hz)
5c	1735	4.55 (2H, m)	3.06 (2H, m)	2.1—1.1	3.97 (4H, t, J=6 Hz) 2.1—1.1 (12H) 0.94 (6H, t, J=6.5 Hz)
3b	1735	5.01 (1H, br d, J=5 Hz) 4.89(1H, br d, J=5 Hz)	2.96 (1H, quintet, J=4.5 Hz) 2.00 (1H, ddd, J=11.5, 10, 5 Hz) 1.50 (1H, dd, J=11.5, 4 Hz)	6.35 (1H, dd, J=6, 1.5 Hz) 6.13 (1H, dd, J=6, 1.5 Hz)	3.56 (3H, s)
4b	1735	5.06 (1H, br s) 4.94 (1H, d, J=4 Hz)	2.20 (1H, dd, J=8, 4 Hz) 2.09 (1H, dt, J=11, 4 Hz) 1.43 (1H, dd, J=11, 8 Hz)	6.30 (2H, br s)	3.64 (3H, s)
3c	1735	5.02 (1H, br d, J=5 Hz) 4.89 (1H, dd, J=5, 2 Hz)	2.96 (1H, quintet, J=4.5 Hz) 1.99 (1H, ddd, J=11.5, 9.5, 5 Hz) 1.51 (1H, dd, J=11.5, 4 Hz)	6.35 (1H, dd, J=6, 2 Hz) 6.13 (1H, br d, J=6 Hz)	4.01 (2H, q, J=7 Hz) 1.22 (3H, t, J=7 Hz)
4c	1735	5.02 (1H, br s) 4.91 (1H, d, J=4 Hz)	2.27 (1H, dd, J=8, 4 Hz) 2.12 (1H, dt, J=10.5, 4 Hz) 1.41 (1H, dd, J=10.5, 8 Hz)	6.26 (2H, br s)	4.10 (2H, q, J=7 Hz) 1.28 (3H, t, J=7 Hz)
3d	1735	4.97 (1H, d J=5 Hz) 4.85 (1H, dd, J=5, 2 Hz)	2.93 (1H, quintet, J=4.5 Hz) 1.96 (1H, ddd, J=11.5, 10, 5 Hz)	6.31 (1H, dd, J=6, 2 Hz) 6.08 (1H, dd, J=6, 1.5 Hz)	3.93 (2H, t, J=6 Hz) 1.7—1.2 (5H) 0.94 (3H, t, J=7 Hz)
4d	1735	5.04 (1H, br s) 4.93 (1H, d, J=4 Hz)	2.28 (1H, dd, J=8, 4 Hz) 2.10 (1H, dt, J=11, 4 Hz)	6.30 (2H, br s)	4.06(2H, t, J=6 Hz) 1.8—1.2 (5H) 0.96 (3H, t, J=7 Hz)
6b	1735	4.5 (2H, br m)	2.90 (1H, br q, J=7 Hz) 1.9—1.4	1.9—1.4 (6H)	3.57 (3H, s)
7b	1735	4.69 (1H, m) 4.53 (1H, br dd, J=5, 3 Hz)	2.46 (1H, dd, J=10, 5 Hz) 2.2—1.3	2.2—1.3 (6H)	3.63 (3H, s)

a) Measured in $CDCl_3$. b) Measured in $CHCl_3$.

isomer distributions of the reactions were analyzed by means of NMR (Table 3).[5]

The observed *endo*/*exo* ratios of the adducts with acrylic and maleic esters were approximately 6 : 4 and 8 : 2 respectively. The *endo*/*exo* ratios were not substantially affected by the change of pressure up to 20 kbar[6] nor by the variation of the alkoxyl in the ester group in the reactions with either acrylic or maleic esters.[7] To examine the possibility of equilibrium between the stereoisomers, the isolated *endo* and *exo* products with methyl acrylate and dimethyl maleate were each kept at 15 kbar for 15 h. However, no isomerization was observed by NMR measurements. These results are in accordance with the restricted retro-Diels-Alder reaction under high pressure conditions.[8] Therefore, the obtained *endo*/*exo* isomer distributions would be the results of kinetic control rather than the type of kinetic and thermodynamic pattern mentioned for the furan-

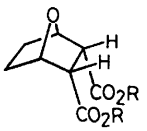

5a R = Me
b R = Et
c R = n-Bu

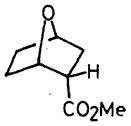

6b

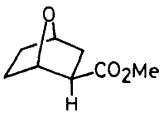

7b

Table 4. Relative rates in the Diels-Alder reactions of furan with maleic and acrylic esters at 15 kbar and 27 °C in dichloromethane

No.	Dienophile		Relative rate[a]
1		R=Me	2.76
2		Et	2.06
3		*n*-Bu	2.25
4		R=H	1.05
5		Me	1.00
6		Et	0.85
7		*n*-Bu	0.75
8		CH_2CCl_3	1.84
9		*i*-Bu	0.75
10		C_6H_5	0.41

a) Rate relative to that of reaction 5 ($k=3.77\times10^{-5}$ l mol^{-1} s^{-1}). The values are the average of three or more runs.

maleic anhydride reaction.[9] The high *endo* selectivity of maleic esters is probably due to large secondary orbital interactions.[10]

The steric effects of an alkoxyl group on the reactivity of these dienophiles were explored by a kinetic approach. All the reactions were clearly second-order at 15 kbar. The rate constant (k_2) for the reaction of furan with methyl acrylate was 3.77×10^{-5} l mol^{-1} s^{-1} at 27 °C. The relative rates are shown in Table 4. These show that the reactivity of both acrylic and maleic esters was slightly decreased by increasing the bulkiness of the alkoxyl in the ester group. The most notable decrease is in the reaction with phenyl acrylate (No. 10). The steric factors, such as expected from "rule of six,"[11] might affect the reactivity of these dienophiles. For the usual Diels-Alder reactions, *e.g.*, the reactions of cyclopentadiene with acrylic esters at atmospheric pressure, no such effects due to the variation of an alkoxyl group were observed.[12] Our findings suggest the steric effects must be more serious for high pressure reactions.

Experimental

General Methods. All boiling points and melting points are uncorrected. ^{1}H NMR spectra were obtained on a JEOL-MH-100 spectrometer using solutions in carbon tetrachloride with TMS as the internal standard; the IR spectra were recorded as films on a JASCO IRA-1, unless otherwise stated.

Table 5. Physical constants of Diels-Alder adducts and their dihydro derivatives

Compound	Mp θ_m/°C or Bp θ_b/°C(mmHg[a])	Found (Calcd) (%) C	H
2a	120—121.5	56.70 (56.60	5.75 5.70)
5a	135—140 (14)	55.75 (56.07	6.55 6.59)
5b	170—175 (15)	59.27 (59.49	7.46 7.49)
5c	148—15 (21)	64.20 (64.40	8.68 8.78)
6b	130 (23)	61.55 (61.52	7.69 7.75)
7b	130 (18)	61.64 (61.52	7.68 7.75)

a) Bath temperature. 1 mmHg=133.322 Pa.

All high pressure reactions were performed at a concentration of 3 M† of the reactants in dry dichloromethane. For a description of our high pressure equipment and of the general procedure for high pressure reactions, see Ref. 2.

Since the direct distillation of oily adducts gave a complete decomposition,[3] the elemental analyses were performed after hydrogenation and are expressed as their dihydro derivatives.

Diels-Alder Reaction of Furan with Maleic Esters. The general procedure is as follows. A CH_2Cl_2 solution (1 ml) of furan (3 mmol) and dimethyl maleate (3 mmol) was subjected to 15 kbar hydrostatic pressure for 8 h at 27 °C. After the run, the solution was concentrated to a clear, colorless liquid whose NMR spectrum indicated that the cycloadduct was obtained in a 90% yield and in an *endo*/*exo* ratio of 8 : 2. By chromatographic separation on neutral alumina (elution with hexane–ether), a pure *endo* isomer was obtained as a colorless liquid.[13] An analytical sample was obtained as a colorless liquid after hydrogenation in AcOEt on 10% Pd/C and bulb-to-bulb distillation.[3]

For a large scale preparation of the *exo* isomer, a mixture of 1 g (7 mmol) of dimethyl maleate and 0.48 g (7 mmol) of furan was subjected to 15 kbar pressure at 60 °C for 16 h *without solvent*.[14] The crude product was purified by column chromatography on neutral alumina using hexane–dichloromethane (1 : 1) as the eluent to give the *endo*-adduct **1a** (232 mg; 15.7%). Further elution with dichloromethane gave the *exo*-adduct **2a** (345 mg; 23.4%), which was recrystallized from ether or hexane–dichloromethane.

The spectral data and physical constants are given in Tables 3 and 5.

Diels-Alder Reaction of Furan with Acrylic Esters. The reaction of furan with methyl acrylate was performed as described above. A pure sample of each *endo* and *exo* isomer was obtained after column chromatography on neutral alumina (with hexane–ether, *endo* isomer was obtained from earlier fractions).[13] Analytical samples **6b** and **7b** were obtained as in the case of dimethyl maleate after hydrogenation and distillation.[3] The spectral data and physical constants are given in Tables 3 and 5.

Equilibrium Experiments. A pure sample of each *endo* and *exo*-adduct with methyl acrylate or dimethyl maleate was kept at 15 kbar and 27 °C for 15 h in dichloromethane (*ca.* 1.5 M solution). After the treatments all equilibrium mixtures were checked by NMR.

† 1 M = 1 mol dm^{-3}.

Kinetic Experiments. Kinetic measurements were made using a piston-cylinder type high pressure apparatus[2] in teh same manner as was used for the other high pressure reactions. Each kinetic solution of a diene and a dienophile in dichloromethane was transferred into a Teflon cell (0.8 cm^3) and subjected to pressure. The amount ratio of dienophile and adduct were measured by NMR at appropriate time intervals for 16 h.

Each reaction studied was clearly second-order and gave a mixture of *end-exo* isomeric products. The second-order rate constants were calculated by the usual second-order rate expression.

The authors wish to thank Professor Takashi Tokoroyama, Osaka City University, for valuable discussions and continuous encouragement. They also thanks Mr. Sachio Kitagawa for his experimental assistance.

References

1) Part IV: H. Kotsuki and H. Nishizawa, *Heterocycles*, **16**, 1287 (1981).

2) H. Kotsuki, H. Nishizawa, S. Kitagawa, M. Ochi, N. Yamasaki, K. Matsuoka, and T. Tokoroyama, *Bull. Chem. Soc. Jpn.*, **52**, 544 (1979).

3) W. G. Dauben and H. O. Krabbenhoft, *J. Am. Chem. Soc.*, **98**, 1992 (1976).

4) W. G. Dauben and H. O. Krabbenhoft, *J. Org. Chem.*, **42**, 282 (1977); W. G. Dauben, C. R. Kessel, and K. H. Takemura, *J. Am. Chem. Soc.*, **102**, 6893 (1980).

5) For the literature of NMR data, see a) W. L. Nelson and D. R. Allen, *J. Heterocycl. Chem.*, **9**, 561 (1972); b) T. A. Eggelte, H. de Koning, and H. O. Huisman, *Tetrahedron*, **29**, 2491 (1973); c) S. Iwase, T. Maeda, S. Hamanaka, and M. Ogawa, *Nippon Kagaku Kaishi*, **1975**, 1934. The isomer distributions could be also determined by GLC (OV-101) of hydrogenated samples.

6) Similar results for the pressure independency of *end/exo* ratio have appeared: K. Seguchi, A. Sera, and K. Maruyama, *Tetrahedron Lett.*, **1973**, 1585.

7) The temperature effect was briefly examined and the *endo/exo* ratio of the adduct with methyl acrylate was 6 : 4 at 60 °C for 6 h (96% yield).

8) *Cf.* S. D. Hamann, "Physico-Chemical Effects of Pressure," Butterworths, London (1957), Chap. 9; G. Jenner, *Angew. Chem.*, **87**, 186 (1975); J. Osugi *et al.*, *Kagaku Sosetsu*, **22**, Chap. 7 (1979).

9) M. W. Lee and W. C. Herndon, *J. Org. Chem.*, **43**, 518 (1978).

10) *Cf.* K. Seguchi, A. Sera, Y. Otsuki, and K. Maruyama, *Bull. Chem. Soc. Jpn.*, **48**, 3641 (1975); J. Rimmelin, G. Jenner, and P. Rimmelin, *Bull. Soc. Chim. Fr.*, **1978**, II, 461; T. Asano and W. J. le Noble, *Chem. Rev.*, **78**, 407 (1978).

11) "Steric Effects in Organic Chemistry," ed by M. S. Newman, Wiley, New York (1956), Chap. 4.

12) J. M. Mellor and C. F. Webb, *J. Chem. Soc., Perkin Trans. 2*, **1974**, 17.

13) Column or preparative thin layer chromatography on silica gel resulted in a considerable decomposition of the products. Both the *endo* and the *exo* products from maleic or acrylic esters were simply separated by using alumina columns. For the use of silica gel–$AgNO_3$, see Ref. 5a.

14) Considerable amounts of unidentified by-products were also obtained, as well as *ca.* 20% of recovered dimethyl maleate.

NMR and CD Spectral Features of Thiaheterohelicenes. Effect of Intramolecular Overlap of Aromatic Rings

Koh-ichi YAMADA,* Hisao TANAKA, Hiroko NAKAGAWA, Susumu OGASHIWA, and Hiroshi KAWAZURA

Faculty of Pharmaceutical Sciences, Josai University, Sakado, Saitama 350-02

(Received March 30, 1981)

NMR and CD spectral features of a series of thiaheterohelicenes containing alternant thiophene and benzene rings were examined as associated with their helical structures. The terminal ring protons of the thiaheterohelicenes reflected the characteristics of intramolecular overlap of aromatic rings in ^{1}H NMR spectra. With the progression of the helix a sudden chemical shift of the β proton in the end thiophene ring to the higher field occurred, in contrast to carbohelicenes in which the drift of the upfield shift of the corresponding terminal ring proton was gradually suppressed. The CD spectra of thiaheterohelicenes were quite different from those of carbohelicenes. The intensities of the α and β absorption bands weakened with the progressive annelation, whereas the intensity of the p absorption band gradually increased, accompanied by a successive increase in the anisotropy factor of the band. These facts suggest that the structures of thiaheterohelicenes differ from those of carbohelicenes in having a peculiar distortion of the helix.

It has been of interest in helicene chemistry that helicenes are powerful inherently-dissymmetric chromophores of themselves, and that they possess the possibility of interactions between overlapping aromatic rings owing to their helically shaped structures. Chiroptical properties,[1,2] NMR[3] and ESR[4,5] spectral features, and X-ray analyses[6–8] of helicenes have been widely studied, together with molecular orbital calculations.[9,10] However, these investigations have so far been limited to [9] rings, especially in the field of heterohelicenes, presumably because of difficulties in preparations and purifications of the compounds with multi-rings; thus the properties of helicenes higher than [9] rings have remained uncertain. We found high performance liquid chromatography (HPLC) very useful for purifications and optical resolutions of thiaheterohelicenes annelated with alternant thiophene and benzene rings.[11,12] The pure racemic and enantiomeric thiaheterohelicenes obtained by applying this method to the final stages of preparations enabled us to perform the present work.

We describe here the characteristics of ^{1}H NMR and circular dichroism (CD) spectra of thiaheterohelicenes ([7] to [15]), compare them with those of carbohelicenes, and discuss the effect of intramolecular overlap of aromatic rings.

Experimental

The preparations[11] and the optical resolutions[12] of thiaheterohelicenes studied have been reported in previous papers. ^{1}H NMR spectra (in $CDCl_3$) were recorded on a JEOL PFT-100 spectrometer operating at 100 MHz in the Fourier transform mode. CD spectra (in $CHCl_3$) were measured on a JASCO J-20A automatic recording spectropolarimeter at 23 °C with concentrations of 8.5×10^{-6}—6.0×10^{-5} mol dm^{-3}; the concentration was 4.25×10^{-4} mol dm^{-3} for the measurement of the α band of [13]thiaheterohelicene.

Results and Discussion

^{1}H NMR Spectral Features. In the previous communication we have assigned the ^{1}H NMR spectra of thiaheterohelicenes studied here, except for that of [15] homolog, where some ambiguity remained because of the partial overlapping of the peaks.[11] Among the protons in this series of compounds the chemical shifts of two protons in the terminal thiophene rings, giving AB or AX type quartet peaks, reflected most characteristically the effect of intramolecular overlap of the aromatic rings. Figure 1 demonstrates the changes in the chemical shifts of the terminal ring protons in the thiaheterohelicene series (A and B protons) against the number of rings, along with the changes in the carbohelicene series (X and Y protons).[13] To clarify the degree of helical turns, the abscissa indicates also the internal angles of the molecules, which were assessed by allocating 45° for a thiophene and 60° for a benzene ring.[2]

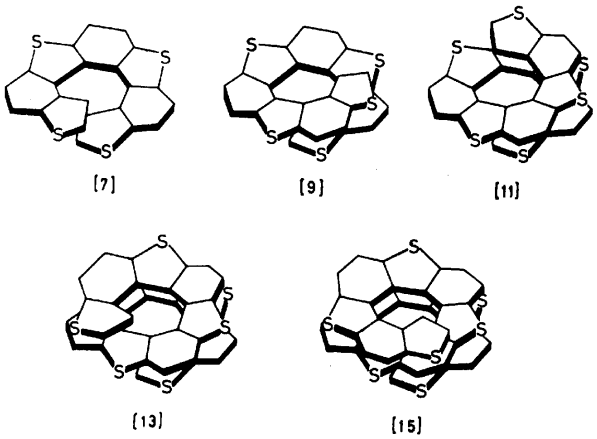

The chemical shifts of both A proton in [5]thiaheterohelicene and X proton in [4]carbohelicene likewise appeared in the lower field owing to the mutual van der Waals compressions between the continuous hydrogens.[3,14] When an overlap between the terminal rings occurs (internal angle is more than 360°), large upfield shifts of the protons appeared in both series. Molecular models suggest that A proton is located approximately above the center of the adjacent faced ring and B proton is located in the vicinity outside the helix, whereas X proton lies in the vicinity of the axis of the helix and Y proton lies above the faced ring. These situations are supported by the fact that A and Y

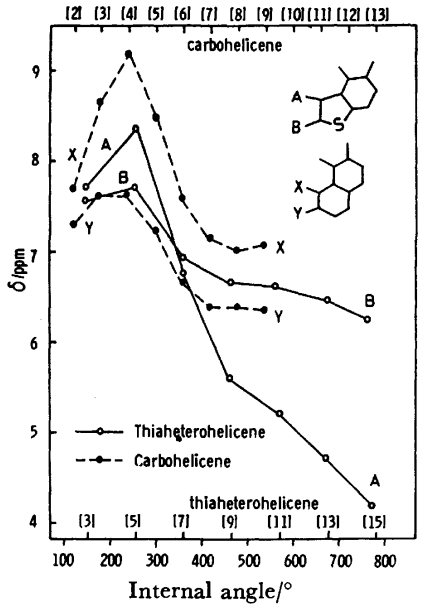

Fig. 1. Influence of the progressive overlap of aromatic rings on the chemical shifts of the terminal ring protons in thiaheterohelicenes and carbohelicenes. The data for carbohelicenes were quoted from the literature.[3]

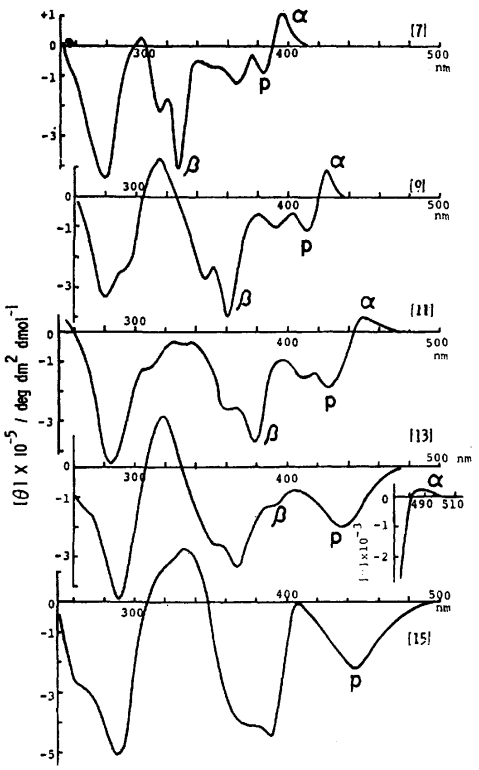

Fig. 2. CD spectra of (*M*)-(−)-thiaheterohelicenes in $CHCl_3$.

protons shifted to higher fields than B and X protons, as a consequence of the stronger diamagnetic shielding by the ring current of the faced rings.

In the carbohelicene series the drifts of upfield shifts of both X and Y protons seem almost to converge with an increase of helical turns, indicating that the diamagnetic shielding effect might become constant at the higher homologs. This is substantiated by X-ray analyses which show that the pitch of the inner helix of carbohelicenes has not varied so much with an increase of number of benzene rings ([7], [10], and [11]-carbohelicene: 3.17, 3.22, and 3.22 Å, respectively).[6] In the thiaheterohelicene series this trend holds approximately for B proton, but not for A proton, the behavior of the latter in the chemical shifts making the thiaheterohelicenes very peculiar. A few reports on the syntheses of carbohelicenes up to [14] rings have been published;[15] nevertheless, to our regret, no NMR data of the carbohelicenes are available for comparing the trends of chemical shifts.

The extents of upfield shifts by the ring current remained in the range of 0.6—1.0 ppm for X and Y and B protons; these values may be compared with those for naphthalene ([2]carbohelicene) and benzo[1,2-*b* : 4,3-*b'*]dithiophene ([3]thiaheterohelicene), which possess no diamagnetic shielding effect. On the other hand, the upfield shift of A proton went up far beyond this range; 2.1 ppm in [9]thiaheterohelicene and 3.5 ppm in [15]. It is rare that an aromatic ring proton shifts as high as about 4 ppm(δ); this is only found for those of metacyclophanes which have a great constraint in a molecule.[16] The trend of A proton shifts may imply that the proton comes closer to the adjacent faced ring with the progression of the helix, since their relative position does not alter, as molecular models suggest. In this case the degree of diamagnetic shielding may be mainly determined by the distance between the proton and the aromatic ring. In order to shorten the distance we can not make the pitches of the thiaheterohelicene helices become smaller with the progressive annelation, because this does not occur in the case of carbohelicenes, as mentioned above.

The significant structural difference between thiaheterohelicenes and carbohelicenes lies in the presence of bulky sulfur atoms. The sulfur atoms in the upper and lower decks of the molecules are relatively close to each other (refer to the Figure). The repulsive forces between the sulfur atoms may keep them as far away from each other as possible and thus bring about distortion of the molecules. This distortion compels the A proton to come closer to the faced ring. With an increase of the number of rings an accumulation of the distortions caused by the repulsions between some pairs of sulfur atoms in a molecule makes the distance smaller and smaller, resulting in the more and more upfield shift of A proton.

CD Spectral Features. In order to study the chiroptical properties of helicenes, precise optical resolutions are needed. We reported the resolutions by HPLC fitted with a silica-gel column containing a chiral charge transfer complexing agent, 2-(2,4,5,7-tetranitro-9-fluorenylideneaminooxy)propionic acid, which functions as a selector.[12] The preparative HPLC was somewhat tedious, but ensured the complete separations between enantiomers. Though CD spectra of some helicene congeners have been described, few changes of the spectra have been discussed from the standpoint of the progression of the helix.

Figure 2 shows the CD spectra of (*M*)-(−)-enantiomers of [7] to [15]thiaheterohelicenes. CD absorption

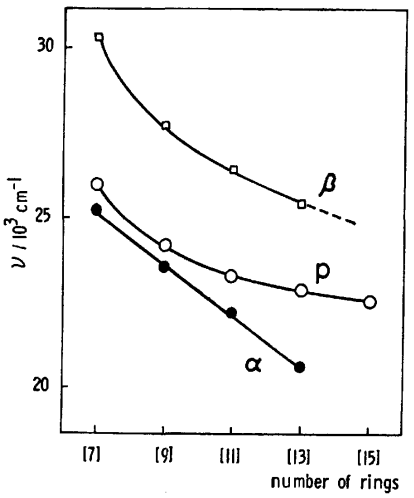

Fig. 3. Changes in transition energies of α, p, and β absorption bands of thiaheterohelicenes.

bands of thiaheterohelicenes are resolved well in comparison with those of carbohelicenes, and there is a clear difference between the spectra.[17] Band assignments to α, p, and β absorptions according to the Clar's nomenclature were tentatively made by the comparison with their UV spectra and by the supposition that the more the extension of the conjugated systems, the longer the wavelength light they absorb. The transition energies of the three longest wavelength absorptions thus assigned are illustrated in Fig. 3 for each thiaheterohelicene. The energies for p and β absorptions appear nearly to converge, but not that for α absorption which is anticipated to have the same tendency in homologs higher than [13]. It is interesting, though the reason is not clear as yet, that the convergency of the energies becomes faster in the order of p>β>α, which is contrary to that of the case in polynuclear aromatic hydrocarbons.[18]

As seen in Fig. 2, each band became successively broader, showing some variation of its intensity with an increase of the number of rings. The broadening of the bands may be ascribable to the increasing overcrowding of the molecules. The intensity of p band was gradually enhanced as the number of rings increases, while those of α and β bands were gradually diminished and finally could not be discerned in the [15] homolog. Wavelength at absorption maxima and molecular ellipticity(θ) of the three bands, together with molecular absorption coefficient(ε) and anisotropy factor(g) of p band, are tabulated in Table 1. Apparent ε values of p band decreased from [7] to [15]thiaheterohelicenes, but the absolute values of [θ], in contrast, increased, leading the absolute values of g to become greater.

As the absorption for p band is due to the transition polarized mainly along the molecular axis,[17] the increment of the intensity may be explicable in terms of the enhanced transition moments caused by an increase of helical turns along the axis. The trend of g factors may reflect the cumulatively increasing distortions with the progression of the helix, as noted in the NMR study. It turns out that the extent of molecular dissymmetry of the present thiaheterohelicene is enhanced as the number of rings increases. On the other hand, as the absorptions for α and β bands are due to the transitions polarized along the perpendicular (C_2 axis) to the molecular axis,[17] the intensities of these bands are not expected to vary significantly with the progressive annelation because molecular diameters along the C_2 axis on a molecular plane are almost the same for each thiaheterohelicene studied. In addition, the increasing overcrowding of the series of molecules may bring about the gradually broadening of the two absorption peaks, resulting in the weak intensity which makes them unobservable in [15]thiaheterohelicene.

In consequence, the configurations of thiaheterohelicenes studied are anticipated to differ considerably from those of carbohelicenes owing to the existence of bulky sulfur atoms. However, we inferred the difference on the basis of the properties only in solutions, and X-ray crystallographic analysis on the compounds may reveal such interesting results.

This work was supported by Grant-in-Aid for Scientific Research No. 447010 from the Ministry of Education, Science and Culture.

References

1) R. H. Martin, *Angew. Chem. Int. Ed. Engl.*, **13**, 649 (1974), and references cited therein.

TABLE 1. THREE LONGEST WAVELENGTH ABSORPTIONS (α, p, AND β) OF (*M*)-(−)-THIAHETEROHELICENES IN $CHCl_3$

Figures in parentheses are wavelengths (nm) at absorption maximum.

	α	β	p		
	$[\theta]\times10^{-4}$ deg dm² dmol⁻¹	$[\theta]\times10^{-4}$ deg dm² dmol⁻¹	$[\theta]\times10^{-4}$ deg dm² dmol⁻¹	$\varepsilon\times10^{-3}$ mol⁻¹ dm³ cm⁻¹	$g\times10^{3}$
[7]	11.2 (397)	−44.4 (330)	−9.6 (385)	19.0 (389)	−1.5
[9]	10.0 (426)	−39.7 (361)	−11.5 (413)	15.1 (424)	−2.3
[11]	5.8 (450)	−35.0 (379)	−18.0 (429)	8.1 (430)	−6.8
[13]	3.1×10^{-2} (485)	−12.6 (394)	−20.0 (437)	7.2 (434)	−8.4
[15]	—	—	−22.8 (443)	6.0 (440)	−11.5

2) H. Wynberg, *Acc. Chem. Res.*, **4**, 65 (1971), and references cited therein.
3) R. H. Martin, N. Defay, H. P. Figeys, M. Flammang-Barbieux, J. P. Cosyn, M. Gelbcke, and J. J. Schurter, *Tetrahedron*, **25**, 4985 (1969).
4) H. J. Fey, H. Kurreck, and W. Lubity, *Tetrahedron*, **35**, 905 (1979).
5) H. Tanaka, S. Ogashiwa, and H. Kawazura, *Chem. Lett.*, **1981**, 585.
6) G. Le Bas, A. Navaza, M. Knossow, and C. De Ranso, *Cryst. Struct. Commun.*, **5**, 713 (1976).
7) G. Le Bas, A. Navaza, Y. Mausuen, and C. De Ranso, *Cryst. Struct. Commun.*, **5**, 357 (1976).
8) T. E. M. Van den Hark and P. T. Beurskens, *Cryst. Struct. Commun.*, **5**, 247 (1976).
9) B. M. Deb and G. Kavu, *Can. J. Chem.*, **58**, 258 (1980).
10) L. D. Barron, *J. Chem. Soc., Faraday Trans. 2*, **71**, 293 (1975).
11) K. Yamada, S. Ogashiwa, H. Tanaka, H. Nakagawa, and H. Kawazura, *Chem. Lett.*, **1981**, 343.
12) H. Nakagawa, S. Ogashiwa, H. Tanaka, K. Yamada, and H. Kawazura, *Bull. Chem. Soc. Jpn.*, **54**, 1903 (1981).
13) Chemical shifts of carbohelicene protons were quoted from Ref. 3.
14) X-ray analysis on [5]thiaheterohelicene has shown that the distance between A and A′ protons is 2.06 Å, which is considerably shorter than twice the van der Waals radius of 1.2 Å for H atoms; M. Konno, Y. Saito, K. Yamada, and H. Kawazura, *Acta Crystallogr., Sect. B*, **36**, 1680 (1980).
15) R. H. Martin and M. Baes, *Tetrahedron*, **31**, 2135 (1975).
16) T. Sato, S. Akabori, S. Muto, and K. Hata, *Tetrahedron*, **24**, 5557 (1968).
17) M. B. Groen and H. Wynberg, *J. Am. Chem. Soc.*, **93**, 2968 (1971).
18) S. Basu, *Bull. Chem. Soc. Jpn.*, **54**, 319 (1981).

Selective Dimerization of Aldehydes to Esters Catalyzed by Hydridoruthenium Complexes

Takashi Ito,† Hiroshi Horino,†† Yoshitaka Koshiro, and Akio Yamamoto*

Research Laboratory of Resources Utilization, Tokyo Institute of Technology, 4259, Nagatsuta, Midori-ku, Yokohama 227

(Received April 11, 1981)

$RuH_2(PPh_3)_4$ and other hydridoruthenium complexes catalyze selective conversion of aldehydes into esters in high yields. The method is applicable to most aliphatic aldehydes as well as to aromatic aldehydes. The purity of aldehydes is critical for achieving high conversions, since the presence of carboxylic acid completely inhibits the reaction and alcohol and triphenylphosphine reduce the yields of esters. $RuH_2(PPh_3)_4$ is converted into $Ru(CO)_3(PPh_3)_2$ through the reaction indicating the occurrence of decarbonylation of aldehyde. A mechanism involving the acyl-H cleavage of aldehyde is proposed to account for the catalysis and formation of compounds accompanying the reaction. The mechanism is compared with an alternative one which comprises of consecutive insertions of two aldehyde molecules into Ru–H bond followed by β-hydrogen abstraction from an alkoxo intermediate formed. Addition of water changes the reaction course to give carboxylato carbonyl complexes $Ru(OCOR)_2(CO)_m(PPh_3)_2$ ($m=1$ and 2). Cross esterification studies showed the reactivity order of RCHO as R = Et > Me > *n*-Pr > *i*-Pr ≫ Ph.

In contrast to the much utilized aldol reaction of aldehydes another type of aldehyde dimerization converting aldehydes into esters, known as Tishchenko reaction,[1] has been much less explored. The reaction is usually catalyzed by aluminium alkoxides and somewhat detailed studies have been made concerning the structural effects of aldehydes and catalysts.[2-6] Studies have been also made concerning the catalyst systems with boric acid[7] and a system without catalyst.[8] Only a limited study,[9] however, has been made to utilize a transition metal complex for the Tishchenko reaction.

Some transition metal complexes coordinated with tertiary phosphines have been found to decarbonylate aldehydes to hydrocarbons,[10-17] *e.g.*,

$$RCHO + RhCl(PPh_3)_3 \longrightarrow RH + RhCl(CO)(PPh_3)_2 + PPh_3. \quad (1)$$

The reaction is considered to proceed by coordination of the aldehyde to rhodium, followed by oxidative addition of the aldehyde group to give an acyl intermediate which is decarbonylated.[18] Such an assumption seems reasonable in view of the known examples of aldehyde coordination to transition metal complexes[19,20] and of acyl-H bond cleavage.[21-25]

Hydrido-ruthenium complexes, particularly $RuH_2(PPh_3)_4$ (**1**) exhibit quite a variety of stoichiometric as well as catalytic reactions,[26-35] and are considered to possess yet unexploited potentiality to catalyze various reactions. Catalytic hydrogenation of aldehydes to give alcohols with molecular hydrogen[36,37] or with organic hydrogen donors[38,39] using Ru, Rh, or Ir complexes have been reported. From a system containing **1** and propionaldehyde a reportedly "intermediate" complex formulated as $Ru(EtCHO)(PPh_3)_3$ has been isolated[38] but this was later refuted as a mixture of $RuH_2(CO)(PPh_3)_3$ (**2**) and $RuH(OCOEt)(PPh_3)_3$ (**3a**).[29]

We report here the catalytic conversion of aldehydes into carboxylic esters catalyzed by **1** and related ruthenium hydride complexes. Characterization of the ruthenium complexes recovered from the reaction systems is also included with a hope to shed light on the reaction mechanism. A preliminary account of this system was made previously.[40]

Results

Reactions of Butyraldehyde with $RuH_2(PPh_3)_4$ (1). When carefully purified butyraldehyde is brought into contact with a catalytic amount of **1** *in vacuo* at room temperature, a violent, exothermic reaction starts in 2—3 min. The reaction is completed in several minutes to give a dark brown solution, the GLC analysis of which shows conversion of most butyraldehyde into butyl butyrate.

$$2\,Pr^nCHO \xrightarrow{\text{cat.}} Pr^nCOOBu^n \quad \text{cat.} = \mathbf{1} \quad (2)$$

Although the reaction is accompanied by the formation of a stoichiometric amount of 1-butanol, the reaction product is free of either aldol-condensation products or trimeric glycol ester, indicating the high selectivity of the reaction. On working up the system after completion of the reaction, the known tricarbonyl complex, $Ru(CO)_3(PPh_3)_2$[41-43] (**4**) is isolated as a sole characterizable ruthenium complex. A careful purification of aldehyde, especially rigorous exclusion of carboxylic acid and water was found essential for initiating the catalytic reaction.

The results of typical experiments are listed in Table 1. The ester forming reaction took place at −20 to +100 °C, with the highest conversion around 0 °C (compare runs 3, 10, 20, and 21). The system kept at −20 °C afforded a lower yield of ester and a dihydrido carbonyl complex, tentatively assigned to $RuH_2(CO)(PPh_3)_3$(**2**),[44] was isolated from the reaction mixture. The system is essentially inactive at −30 °C and the carboxylato complex, $RuH(OCOPr^n)(PPh_3)_3$(**3b**), was obtained on working up the system kept at −30 °C for 2 h. One

† Present address: Department of Materials Chemistry, Faculty of Engineering, Yokohama National University, Tokiwadai, Hodogaya-ku, Yokohama 240.

†† Present address: College of General Education, Tohoku University, Kawauchi, Sendai 980.

Table 1. Reaction of butyraldehyde with $RuH_2(PPh_3)_4$[a]

Run	Pr^nCHO (mmol)	$RuH_2(PPh_3)_4$ (mmol)	Pr^nCHO/Cat. (molar ratio)	Temp °C	Pr^nCOOBu^n (mmol)	Conv.[b] %
1	68.6	0.547	125	100	31.0	90
2	15.1	0.132	114	20	7.4	98
3	49.7	0.132	377	20	19.4	78
4	49.7	(0.039)[c]	291	20	20.7	83
5	49.7	(0.057)[c]	218	20	21.2	85
6	49.7	(0.043)[c]	183	20	21.7	87
7	49.7	(0.050)[c]	155	20	22.9	92
8[d]	43.6	0.145	301	20	6.0	28
9[e]	35.8	0.119	301	20	0.0	0
10	52.4	0.129	406	0	26.0	99
11[f]	56.4	0.115	490	0	25.4	90
12[g]	99.9	0 256	390	0	35.4	71
13[h]	41.5	0.060	692	0	20.4	98
14	70.1	0.088	797	0	30.7	88
15	67.8	0.034	1994	0	30.2	89
16[i]	56.1	0.138	407	0	25.4	91
17[j]	45.8	0.142	323	0	20.6	90
18[k]	55.6	0.156	356	0	27.8	100
19[l]	63.0	0.145	434	0	4.3	14
20	53.8	0.175	307	−10	25.0	93
21	61.1	0.150	407	−20	18.7	61
22	63.9	0.156	410	−30	0.2	1

a) Reactions were carried out for 2 h *in vacuo* without solvent unless otherwise stated. b) On the basis of the amount of Pr^nCHO initially used. c) $RuH_2(PPh_3)_4$ was added successively to the reaction system of run 3 after completion of each run. d) 1-Butanol (0.291 mmol) was added to the system. e) Butyric acid (0.239 mmol) was added to the system. f) Reaction was carried out under nitrogen atmosphere. g) Reaction was carried out under H_2 pressure (*ca.* 2 atm). h) Reaction was carried out for 30 min. i) Hexane (20 ml) was used as solvent. j) Toluene (20 ml) was used as solvent. k) Reaction was carried out in the presence of 6 ml of tetrahydrofuran. l) Pyridine (15 ml) was used as solvent.

Table 2. Reaction of aldehydes (RCHO) other than butyraldehyde with $RuH_2(PPh_3)_4$[a]

Run	RCHO (mmol)	$RuH_2(PPh_3)_4$ (mmol)	RCHO/Cat. (molar ratio)	Temp °C	Time h	$RCOOCH_2R$ (mmol)	Conv.[b] %
23	CH_3CHO	90.0 0.147	612	20	2/3	31.7	70
24	CH_3CHO	81.0 0.153	529	0	2/3	38.0	94
25	CH_3CHO	67.3 0.120	561	−20	2	0.0	0
26	CH_3CH_2CHO	68.5 0.250	274	20	2	17.4	51
27[c]	CH_3CH_2CHO	27.8 0.100	280	20	2	1.2	9
28	$(CH_3)_2CHCHO$	59.8 0.226	264	20	4.5	21.1	71
29	$CH_3(CH_2)_3CHO$	23.5 0.142	165	85	2	5.1	43
30	$(CH_3)_2CHCH_2CHO$	18.2 0.131	140	85	3	6.2	68
31	$CH_3(CH_2)_4CHO$	16.0 0.200	80	85	3	3.5	44
32	C_6H_5CHO	14.8 0.120	120	20	2	1.7	23

a) Reactions were carried out *in vacuo* in a glass autoclave. b) On the basis of the amount of RCHO initially used. c) PPh_3 (1.00 mmol) was added to the system.

possible reaction for the catalyst deactivation at the low temperature is the conversion of catalyst **1** into the carboxylato complex **3b** prior to the initiation of the esterification reaction. Complex **3b** was found to be inactive for the esterication reaction (*vide infra*).

For pure aldehydes, complex **1** proved to be quite active achieving *ca.* 2000 turnovers at 0 °C with the concentration of as low as 0.05 mol% (run 15). Although the catalyst is deactivated at the completion of the reaction, addition of the new crop of the catalyst to the reaction system containing remaining unreacted aldehyde initiated the catalysis (runs 3—7).

Addition of butyric acid completely inhibits the reaction (run 9) whereas the presence of two equivalents of 1-butanol per catalyst did not completely block the reaction but considerably reduced the conversion of aldehyde to ester (run 8). The reaction can be performed under nitrogen as well as in vacuum (run 11) whereas hydrogen somewhat reduced the conversion (run 12). Solvents such as hexane, toluene and tetrahydrofuran may be used provided they are appropriately purified (runs 16—18) but employment of the more coordinating solvent such as pyridine notably reduced the catalytic activity (run 19).

Complex **1** can be used for conversion of other aldehydes such as acetaldehyde, propionaldehyde,

Table 3. Cross-esterification of aldehydes catalyzed by $RuH_2(PPh_3)_4$[a]

$$R^1CHO + R^2CHO \xrightarrow{RuH_2(PPh_3)_4} \begin{cases} R^1COOCH_2R^1\ (A) \\ R^1COOCH_2R^2\ (B) \\ R^2COOCH_2R^1\ (C) \\ R^2COOCH_2R^2\ (D) \end{cases}$$

Run	R^1CHO (mmol)	R^2CHO (mmol)	$\frac{R^1CHO}{R^2CHO}$	Cat. (mmol)	Total conv. %[b]	Products (mmol) A	B	C	D	$\frac{A}{D}$
33	CH_3CHO (17.8)	CH_3CH_2CHO (18.1)	0.98	0.161	74	2.76	1.47	5.37	3.73	0.74
34	CH_3CHO (19.5)	$CH_3(CH_2)_2CHO$ (22.7)	0.86	0.088	71	7.31	3.09	1.20	3.35	2.18
35	CH_3CHO (17.8)	$(CH_3)_2CHCHO$ (22.1)	0.81	0.167	31	1.49	3.03	0.67	1.03	1.45
36	$CH_3(CH_2)_2CHO$ (11.3)	$(CH_3)_2CHCHO$ (11.0)	1.03	0.167	90	2.74	(5.06)[c]		2.22	1.23
37	C_6H_5CHO (14.8)	$CH_3(CH_2)_2CHO$ (13.6)	1.09	0.101	48	0.10	0.17	1.47	5.04	0.02
38	C_6H_5CHO (14.8)	$(CH_3)_2CHCHO$ (15.6)	0.95	0.102	44	0.13	0.43	2.42	3.72	0.04

a) Reactions were carried out *in vacuo* at room temperature. b) Total conversion (mol%)=200 [A (mmol)+B (mmol)+C (mmol)+D (mmol)]/[R^1CHO (mmol)+R^2CHO (mmol)]. c) Total amount of isobutyl butyrate and butyl isobutyrate was recorded as they were not distinguishable each other by means of GLC analysis.

Table 4. Complexes formed by the reaction of butyraldehyde with $RuH_2(PPh_3)_4$ and $RuH(OCOPr^n)(PPh_3)_3$ under various conditions[a]

Run	$RuH_2(PPh_3)_4$ (mmol)	Pr^nCHO (mmol)	H_2O (mmol)	Temp °C	Pr^nCOOBu^n (mmol)(Conv/%)	Bu^nOH (mmol)	Resulting complex (mmol)[b]
1	0.547	68.6	0	100	31.0(90)	0.10	**4** (0.31)
39	0.198	51.6	0	0	23.2(90)	trace[c]	**4** (0.16)
20	0.175	53.8	0	−10	25.0(93)	0	**2**[d]
21	0.150	61.1	0	−20	18.7(61)	trace	**2**[d]
22	0.156	63.9	0	−30	0.2(1)	trace	**3b**[d]
40[e]	0.552	66.5	5.55	0	0	trace	**3b** (0.500)
41[f]	0.83	187	2.87	110	8.4(9)	1.07[g]	**5b** (0.51)
42[f]	1.10	167	11.1	110	[d]	[d]	**5b** (0.59)
43[f]	2.22	340	16.0	110	[d]	[d]	**6b** (1.5)
44[f]	0.171[h]	59.9	0	110	0.03	trace	**5b** (0.094)
45[i]	1.84[h]	330	0	75	[d]	[d]	**6b** (1.4)

a) Reactions were carried out *in vacuo* for 2 h in a Schlenk type flask unless otherwise stated. b) **2**: $RuH_2(CO)(PPh_3)_3$; **3b**: $RuH(OCOPr^n)(PPh_3)_3$; **4**: $Ru(CO)_3(PPh_3)_2$; **5b**: $Ru(OCOPr^n)_2(CO)_2(PPh_3)$; **6b**: $Ru(OCOPr^n)_2(CO)(PPh_3)_2$. c) Other products(yield in mmol): H_2 (0.04), C_3H_6 (0.018), C_3H_8 (0.059), and CO (trace). d) The yield was not measured. e) Reactions were carried out in a Pyrex glass-autoclave. f) Reactions were carried out in a stainless steel-autoclave. g) Other products: H_2 (0.21), C_3H_6 (0.04), C_3H_8 (0.05), and CO(0.272). h) Amount of $RuH(OCOPr^n)(PPh_3)_3$ **3b**. i) Heated under reflux under N_2 atmosphere for 2 h in a Schlenk type flask.

isobutyraldehyde, valeraldehyde, isovaleraldehyde, hexanal, and benzaldehyde (Table 2). The yields are somewhat low for some aldehydes, but optimization of the reaction conditions may well enhance the yields. Considerable hindrance of the catalysis by addition of triphenylphosphine was noted (run 27). The reaction of acrylaldehyde with **1** either at 0° or at −20 °C afforded a massive brown polymeric material, which is insoluble in most organic solvents.[45]

Cross-esterification Reaction. For examining relative reactivities of aldehydes cross esterifications using about 1 : 1 binary mixtures of aldehydes have been carried out. Cross esterification of the 1 : 1 mixture of acetaldehyde and propionaldehyde, for example, catalyzed by **1** at room temperature afforded ethyl acetate (A), propyl acetate (B), ethyl propionate (C), and propyl propionate (D) in a ratio of 1.00 : 0.53 : 1.95 : 1.35. The result, indicating the higher yield of D than A as well as the higher yield of C than B, suggests that the reactivity of propionaldehyde to the esterification reaction is slightly higher than that of acetaldehyde. Similar comparison of the product distributions, using especially the ratios of A/D as the reactivity index in Table 3 in the mixed esterification reactions of various aldehydes, allows one to estimate their relative reactivities toward esterification reaction as $CH_3CH_2CHO > CH_3CHO > CH_3(CH_2)_2CHO > (CH_3)_2CHCHO \gg PhCHO$. The same order was obtained for the relative proton donor ability of each aldehyde which was estimated from the comparison of values B and C in Table 3. The similar values of the product distribution have been reported for the systems containing acetaldehyde and butyraldehyde, and benzaldehyde and butyraldehyde catalyzed by aluminium alkoxides.[2,3]

Absence of the ester exchange reaction between the product esters under the reaction conditions was confirmed by the additional experiments in which propionaldehyde and butyraldehyde, respectively, were allowed to react with **1** at 85 °C in the presence of ethyl acetate. In both cases, the resulting systems contained only propyl propionate and butyl butyrate, respectively, in addition to the added ethyl acetate and no mixed esters were detected showing the absence of the ester exchange reaction.

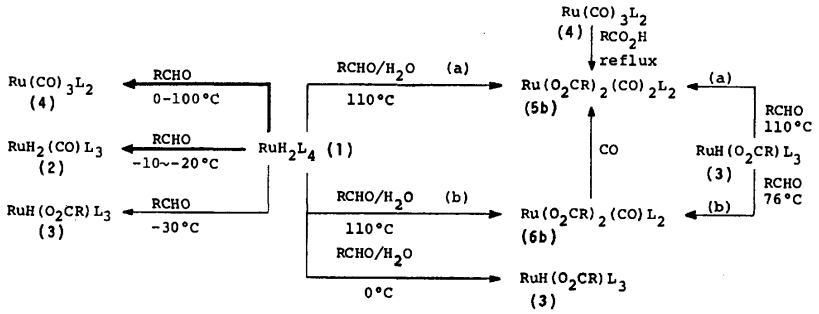

(a): Reactions were carried out *in vacuo* in a stainless steel autoclave.
(b): Reactions were carried out *in vacuo* or under N_2 in a Pyrex glass flask.
L=PPh_3, R=*n*-C_3H_7, broad arrows stand for the reactions accompanied with catalytic ester-formation reactions.

Scheme 1. Reactions of $RuH_2(PPh_3)_4$ with butyraldehyde and related reactions.

Table 5. Spectral data of some relevant carboxylato–ruthenium complexes

Complex		IR bands[a] ν(C=O) cm^{-1}	$\nu_a(CO_2)$ cm^{-1}	$\nu_s(CO_2)$ cm^{-1}	^{1}H-NMR signals[b] $\delta(CH_3)$	$\delta(\gamma\text{-}CH_2)$	$\delta(\beta\text{-}CH_2)$	^{31}P-NMR signals[b]
$RuH(OCOPr^n)(PPh_3)_3$	**3b**	2000w[c]	1520m[e]	1420m[e]	0.57 (t, 3H) δ(RuH)	1.07(hex, 2H) −17.6 (q, 1H)	1.43 (q, 2H)	43.60 (d, 2P) 77.46 (t, 1P) ^2J(PP)=27.3 Hz
$Ru(OCOPr^n)_2(CO)_2(PPh_3)_2$	**5b**	2010vs 1960vs	1610s[d] 1590s[d]	1325s[d]	0.51 (t, 6H)	1.01 (hex, 4H)	1.33 (t, 4H)	31.56 (s)
$Ru(OCOPr^n)_2(CO)(PPh_3)_2$	**6b**	1965vs	1640s[d] 1505m[e]	1315m[d] 1460m[e]	0.67 (t, 6H)	1.17 (hex, 4H)	1.49 (m, 4H)	48.15 (s)
$Ru(OCOEt)_2(CO)(PPh_3)_2$	**6a**	1960vs	1620s[d] 1510m[e]	1325m[d] 1445m[e]	0.66 (t, 6H) {0.55 (t, 3H)[f] {0.65 (t, 3H)[f]	—	1.62 (q, 4H) {1.40 (q, 2H)[f] {1.68 (q, 2H)[f]	48.22 (s)

a) KBr disc. b) In CD_2Cl_2 at room temperature unless otherwise stated. ^3J(HH)=7 Hz. ^{31}P-NMR chemical shifts are based on external H_3PO_4 reference, with downfield positive values. c) ν(Ru–H). d) CO_2 stretching bands due to a unidentate carboxylato ligand. e) CO_2 stretching bands due to a bidentate carboxylato ligand. f) The spectrum taken at −20°C.

Examination of Ruthenium Complexes Recovered from the Reaction Mixture of Aldehyde and $RuH_2(PPh_3)_4$ in the Presence or Absence of Added Water. In order to obtain insight into the mechanism of the present reaction, the ruthenium complexes recovered after completion of the reactions under various conditions were examined. The results are summarized in Table 4 and Scheme 1. As mentioned previously, tricarbonyl complex **4** was isolated from the reaction system carried out at temperatures above 0 °C where high conversions to ester was achieved (run numbers 1 and 39 in Table 4). Hydridocarbonyl complex **2** was also formed when the reaction was carried out at −10 ——20 °C (runs 20 and 21). On the other hand, wherever no esterification reaction proceeded, as in the reaction at −30 °C (run 22) or at 0 °C in the presence of water (run 40), hydridocarboxylato complex **3b** was isolated a as sole ruthenium complex. Heating the reaction mixture at 110 °C in the presence of water resulted in the formation of carboxylato-carbonyl-complexes, $Ru(OCOPr^n)_2(CO)_2(PPh_3)_2$ (**5b**) or $Ru(OCOPr^n)_2(CO)(PPh_3)_2$ (**6b**) depending on the experimental conditions (runs 41—43).

In some reaction systems listed in Table 4, examination of gaseous product revealed the formation of H_2, methane, propane and propene (runs 39 and 41).

Properties of Dicarboxylato-mono- and -dicarbonyl Complexes and Some Related Reactions. Spectroscopic data for the new carboxylato–carbonyl complexes **5b** and **6b** thus obtained are listed in Table 5. Their reactions with an excess of methyl iodide afforded methyl propionate, although their yields were less than stoichiometric amount. Complex **6b** absorbed about one mole of carbon monoxide per mole of **6b** in toluene at room temperature to give complex **5b** quantitatively. Complexes **5b** and **6b** were also obtained by the reaction between hydridocarboxylato complex **3b** and butyraldehyde in the absence of water (runs 44 and 45 in Table 4). The reaction of **4** with Pr^nCHO at 100 °C either with or without added water only resulted in the recovery of the unreacted complex. These results suggest that the ability of the ruthenium complexes to decarbonylate aldehydes decreases with increase in the number of CO ligand attached to ruthenium.

A propionato homolog of **6b**, $Ru(OCOEt)_2(CO)(PPh_3)_2$ (**6a**), was obtained by the reaction of $RuH_2(PPh_3)_4$ **1** with a slightly impure propionaldehyde at 80 °C *in vacuo*.[46] Spectral data of **6a** are included in Table 5. In the ^{1}H-NMR spectrum of **6a**, triplet and multiplet signals at room temperature assignable to the

Table 6. Catalytic activities of various transition metal complexes for conversion of aldehydes to esters[a)]

Run	Catalyst: Complex	Catalyst: mmol	RCHO[b)] (mmol)	Temp °C	Time h	$RCOOCH_2R$[c)] (mmol)	Conv. %	Gases evolved (mol/mol complex)
46	$RuH_2(PPh_3)_3$	0.30	21.5	85	3	10.5	96	
47	$RuH_2(CO)(PPh_3)_3$	0.35	20.6	90	3	8.42	77	
48	$RuHCl(PPh_3)_3$	0.11	5.8	85	1.5	1.31	45	
49	$RuHCl(CO)(PPh_3)_3$	0.19	25.1	85	2	3.72	29	
50	$RuH(-CH=CMeCOOEt)(PPh_3)_3$	0.45	36.2	85	4	18.1	98	
51	$Ru(C_2H_4)(PPh_3)_3$	0.16	16.6	90	2	7.66	91	
52	$RuCl_2(PPh_3)_3$	0.19	17.7	85	3	0	0	
53	$Ru(CO)_3(PPh_3)_2$	0.54	41.7	90	3	0	0[d)]	
54	$[RuH(PPh_3)_4]^+[PF_6]^-$	0.13	55.5	20	5	11.9	43	
55	$RhH(PPh_3)_4$	0.18	27.6	100	1.5	0.74	5.3	
56	$FeH_2(N_2)(PEtPh_2)_3$	0.18	27.7	85	1	0.066	0.48	N_2(main)+H_2 (total 1.49)
57	$CoH(N_2)(PPh_3)_3$	0.22	55.9	20	6	0.012	0.04	N_2(1.00)
58	$MoH_4(Ph_2PCH_2CH_2PPh_2)_2$	0.26	62.3	100	2	0	0[d)]	
59	$MoH_4(PMePh_2)_4$	0.31	55.3	85	1	0	0	H_2(0.96)
60	$Mo(C_2H_4)(Ph_2PCH_2CH_2PPh_2)_2$	0.23	56.7	85	1	0	0	C_2H_4(1.00)
61	$Pd(C_2H_5)_2(PMePh_2)_2$	0.50	56.9	0	4	trace	≈0	C_2H_4(0.20)+C_2H_6 (1.06)
62	$Pt(C_2H_5)(C_5H_7O_2)(PPh_3)_2$	0.17	55.6	20	6	trace	≈0	C_2H_6(0.76)

a) Reactions were carried out *in vacuo* in a Schlenk type glass flask. b) Propionaldehyde (R=C_2H_5) for runs 46—52 and butyraldehyde (R=*n*-C_3H_7) for runs 54—62. c) Propyl propionate for runs 46—52 and butyl butyrate for runs 53—62. d) Starting complex was recovered quantitatively.

ethyl groups of the propionato ligands split into a set of pairs of triplets and quartets at −20 °C indicating the existence of two unequivalent carboxylato groups in **6a**. Similarly to **6b**, complex **6a** released about a half mole of methyl propionate per mole of complex on reaction with excess methyl iodide.

Examination of the Catalytic Activities of Various Transition Metal Complexes for Conversion of Aldehydes into Esters. As shown in Table 6, most hydrido ruthenium complexes possess catalytic ability of esterification reaction among various transition metal complexes examined. That the "ethylene" complex of a composition $Ru(C_2H_4)(PPh_3)_3$ also shows the catalytic activity may be due to the presence of the hydrido species such as $RuH(o\text{-}C_6H_4PPh_2)(PPh_3)_2(C_2H_4)$ or $RuH_2(o\text{-}C_6H_4PPh_2)(CH=CH_2)(PPh_3)_n$ in solution.[28,29] The introduction of a chloride anion to the hydrido complex considerably reduced its efficiency (runs 48 and 49). Dichloro derivative and tricarbonylruthenium(0) complex were inactive, although a stoichiometric amount of 1-propanol was formed in the reaction with the former complex.

Among hydrido and alkyl transition metal complexes other than ruthenium ones examined, only hydrido rhodium complex showed a feeble activity yielding ester in more than a stoichiometric amount (run 55).

Discussion

The Mechanism of the Catalytic Reaction. Two alternative routes, shown in Schemes 2 and 3 are conceivable for the present catalytic conversion of aldehyde to ester.

In Scheme 2 aldehyde first coordinates to $RuH_2(PPh_3)_3$, formed by ligand dissociation, to give $RuH_2(RCHO)(PPh_3)_3$ followed by insertion of the carbonyl group of aldehyde into Ru–H bond (path b). The insertion of the organic carbonyl group into the metal to carbon or hydrogen bond, not unusual reaction for the main group elements such as Grignard reagent and alkyllithium, has been postulated in some reactions involving organo transition metal complexes.[47] Reductive elimination of alkoxo and hydrido ligands from intermediate A yielding RCH_2OH and the Ru(0) species, $[RuL_3]$, then follows (path c). The similar processes to paths a—c have been proposed by Imai

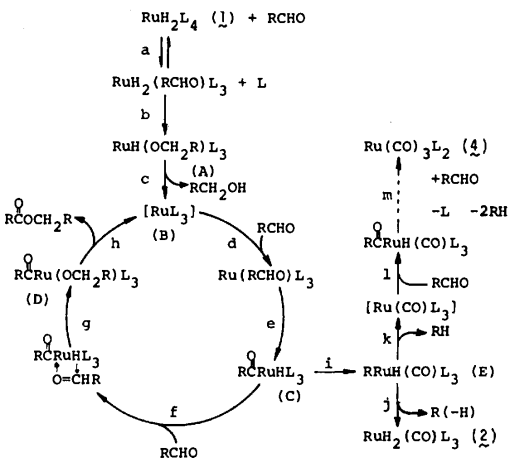

L = PPh_3, R = CH_3, CH_3CH_2, $CH_3(CH_2)_2$, etc.

Scheme 2.

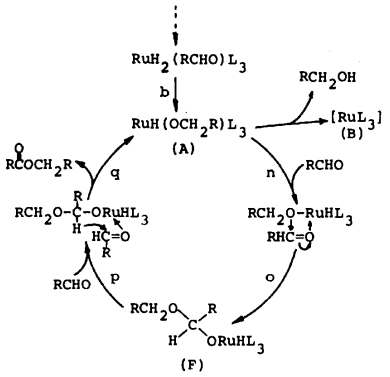

L = PPh_3; R = CH_3, CH_3CH_2, etc.

Scheme 3.

et al. for the catalytic hydrogen transfer reaction from organic hydrogen donor molecule to aldehyde by complex **1**.[38]

The second molecule of aldehyde coordinates to [RuL_3] and oxidatively adds to Ru to give hydrido acyl intermediate (path e). The oxidative addition of aldehyde involving a cleavage of aldehydic hydrogen-carbon bond has been postulated in many examples accounting for the decarbonylation from aldehyde with transition metal complexes,[10-17] and the hydridoacyl type complex corresponding to the intermediate C has been isolated in some cases.[21-25]

The third aldehyde molecule coordinates to the intermediate C and is inserted into the Ru–H bond to give an acyl-alkoxo type intermediate D, which on reductive elimination releases ester accompanied by regeneration of B. In this catalytic cycle, acyl intermediate C may isomerize *via* a decarbonylation reaction (path i) to alkyl carbonyl intermediate E, which may give hydrido carbonyl complex **2** and alkene by the β-elimination reaction (path j), or tricarbonyl complex **4** on repetition of the reductive elimination of alkane, the oxidative addition of aldehyde, and decarbonylation (paths k, l, and m). Both complexes **2** and **4** are the final products isolated in the ester formation reaction carried out at −20 °C and above 0 °C, respectively.

The mechanism of catalytic ester formation alternative to Scheme 2 is shown in Scheme 3 which is somewhat similar to those proposed for the so called Tishchenko reaction catalyzed by aluminium alkoxide.[5] In this mechanism, hydridoalkoxo intermediate A which is formed in a similar path as in Scheme 2 reacts with the second aldehyde molecule (path n) which is inserted into Ru–O bond to give another alkoxo intermediate F (path o). The following hydrogen transfer from alkoxo ligand to the third aldehyde, presumably by a β-hydrogen elimination mechanism, affords ester regenerating A. The hydrido and alkoxo ligands in A may be eventually removed as alcohol by a reductive elimination process.

It is difficult to decide which mechanism is operative in the catalytic conversion on the basis of limited information presently available. However, formation of the carbonyl complexes **2**, **4**, **5**, and **6** indicates that a decarbonylation reaction of aldehyde involving the acyl-H bond cleavage is taking place during or after the catalytic process. Assumption of the oxidative addition of aldehyde is consistent in Scheme 2, although the occurrence of the oxidative addition of aldehyde to RuL_3 (B) to give the carbonyl complexes *after* the completion of the catalytic process can not be excluded. Furthermore the high activity of hydrido ruthenium complexes is in favor of the mechanism involving aldehyde insertion into Ru–H.

The presence of a small amount of water drastically alters the reaction path (run 40 of Table 4).

The formation of the hydrido(carboxylato) complex **3** may be caused by interaction of water with **1** by a possible mechanism as shown below. Disproportionation

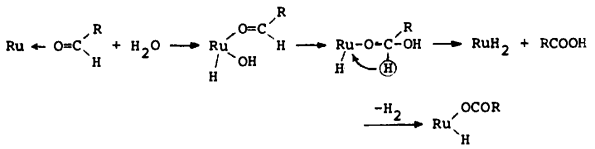

of aldehydes into alcohols and carboxylic acids in the presence of water was recently found to be catalyzed by ruthenium and rhodium complexes under neutral conditions presumably by a different mechanism.[48] The reaction of **1** with carboxylic acid is known to give **3**.[49]

Recently, catalytic dimerization of terminal epoxides to carboxylic ester by $RuCl_2(PPh_3)_3$ has been reported.[50] Although epoxides can be regarded as one of the isomeric forms of aldehyde, the mechanism of the ester formation of this system differs from that of the present study described above, since the order of reactivity, *i.e.*, aromatic epoxides >aliphatic epoxides, is opposed to that found in our system.

The Configuration of Carboxylato Complexes of Ruthenium-(II). Analogous complexes to di(butyrato)dicarbonylbis(triphenylphosphine)ruthenium **5b** was previously prepared by reaction of $Ru(CO)_3(PPh_3)_2$ with carboxylic acids RCOOH in benzene,[51] or in 2-methoxyethanol,[49,52] by treatment of RuH(OCOR)-$(PPh_3)_3$ with CO,[42] for R=H, CH_3, C_2H_5, p-ClC_6H_4, p-$NO_2C_6H_4$, and CF_3. By analogy to discussion presented for $Ru(OCOCF_3)_2(CO)_2(PPh_3)_2$,[53] complex **5b** probably has the configuration (I). However, the possibility of (II) is not completely ruled out since the $^{31}P\{^1H\}$ NMR chemical shift of **5b** (Table 5) deviates from that observed in this type of complexes where two phosphorus atoms are in mutually *trans* positions (44±0.5 ppm).[53]

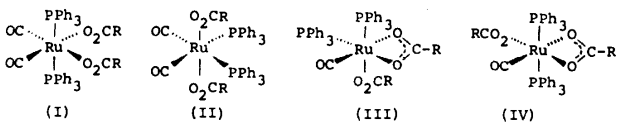

(I) (II) (III) (IV)

Dicarboxylato monocarbonyl complexes Ru-$(OCOR)_2(CO)(PPh_3)_2$ **6** have been prepared by treating $RuH_2(CO)(PPh_3)_3$ with carboxylic acid in 2-methoxyethanol (R=p-ClC_6H_4, and p-$NO_2C_6H_4$)[49] or in toluene (R=CF_3).[52] Acetato analogue has been prepared by the action of $NaOCOCH_3$ with trifluoro-

acetato complex,[54] or by the action of CO with $Ru_2O(OCOMe)_4(PPh_3)_2$.[55] According to the configurational assignment made by Dobson and Robinson,[54] complexes **6a** and **6b** may have structure III where unidentate and bidentate carboxylato ligands are exchanging in an NMR time scale above room temperature. The alternative structure IV which has been assigned for the acetato complex prepared by Wilkinson's method[55] can be ruled out for the present product because of the significant resemblance of the spectra of complexes **6a** and **6b** to those reported by Dobson and Robinson.[54] Similarly to the trifluoroacetato complex,[54] complex **6** was converted into dicarbonyl analogue **5** on treatment with carbon monoxide.

Experimental

All reactions and manipulations were carried out under dry, oxygen-free nitrogen or *in vacuo* using Schlenk-type flasks unless otherwise stated. Solvents were dried and purified in the usual manner and stored under an inert atmosphere. Commercial aldehydes were purified by a careful distillation over calcium hydride or molecular sieve 5A through the Widmer type fractionating column of 30 cm length under nitrogen. Aldehydes thus purified was stirred with calcium hydride or, more preferably to avoid the formation of aldol condensates, molecular sieve 5A for about 1 h just before the reaction and distilled at room temperature directly into the flask containing the catalyst complex *in vacuo* (*ca.* 10^{-3} mmHg, 1 mmHg≈133.3 Pa). Dihydridotetrakis(triphenylphosphine)ruthenium(II) **1** was prepared from $RuCl_3 \cdot 3H_2O$ (Nippon Engelhard) by the methods reported by Levison and Robinson[56] and Harris *et al.*[57] The other complexes used in the present study were prepared according to the reported method as follows: $RuH_2(PPh_3)_3$,[56] $RuH_2(CO)(PPh_3)_3$,[58] $RuHCl(PPh_3)_3$,[59] $RuHCl(CO)(PPh_3)_3$,[58] $RuH\{-CH=C(Me)-COOEt\}(PPh_3)_3$,[31] $Ru(C_2H_4)(PPh_3)_3$,[28] $RuCl_2(PPh_3)_3$,[60] $Ru(CO)_3(PPh_3)_2$,[58] $[RuH(PPh_3)_4]^+[PF_6]^-$,[61] $RhH(PPh_3)_4$,[56] $FeH_2N_2(PEtPh_2)_3$,[62] $CoH(N_2)(PPh_3)_3$,[63] $MoH_4(Ph_2PCH_2CH_2PPh_2)_2$,[64] $Mo(C_2H_4)(Ph_2PCH_2CH_2PPh_2)_2$,[65] $Pd(C_2H_5)_2(PMePh_2)_2$,[66] and $Pt(C_2H_5)(C_5H_7O_2)(PPh_3)_2$.[67] Hydridopropionato complex $RuH(OCOPr^n)(PPh_3)_3$ **3b** was prepared according to the method reported for the preparation of the acetato analogue $RuH(OCOMe)(PPh_3)_3$[49] with some modification.

The reaction products in the ester formation reaction was quantitatively analyzed by GLC using internal standard. GLC was performed on Shimadzu GC-3BT, GC-5AP$_3$F, and GC-6APT models using Shimadzu ITG-2A and Chromatopac-ElA integrators. SDC-410 (4m) and -550 (4m), PEG-20M (3 and 4m), TCP (3 m), and DOP (3 m) were employed as columns for the analyses of esters. Gaseous products were analyzed quantitatively by a Toepler pump and characterized by GLC using Molecular sieve 5A (for H_2, N_2, and CH_4 analyses), activated charcoal (for C_2) and Porapak Q (for C_3–C_4) as columns. Infrared spectra were recorded on a Hitachi model 295 spectrometer using KBr disks prepared under inert atmosphere. ^{1}H- and ^{31}P-NMR spectra were measured on JEOL's JNM-PS-100 and FX-100 instruments at 100 MHz for ^{1}H and 40.5 MHz for ^{31}P operated by Mr. Y. Nakamura of our Laboratory. Microanalyses were carried out on a Yanagimoto's CHN autocorder type MT-2 by Mr. T. Saito of our Laboratory.

Catalytic Ester Formation Reaction. Reactions were carried out with various aldehydes under a variety of conditions. However, since the routine procedure does not differ so much with each other, the typical process is described below for the reaction of butyraldehyde at different temperatures. Schlenk type flasks were used for the most of runs, but the use of small autoclave made of Pyrex glass or stainless steel is indispensable for reactions of acetaldehyde in order to avoid the dangerous breakage of the vessel due to the violent exothermic reaction.

The reaction can also be carried out in the atmosphere of nitrogen instead of under vacuum (run 11). This method is more convenient in a practical sense than that using vacuum line technique, but a sufficient care is necessary to control the explosive exothermic reaction.

Although the reactions were usually brought to completion in the initial several minutes, most reactions were carried out for 2 h unless otherwise stated.

a) Reactions of Butyraldehyde at 0 °C: Into the Schlenk flask containing $RuH_2(PPh_3)_4$ **1** (0.149 g, 0.129 mmol), 4.71 cm^3 (52.4 mmol) of butyraldehyde was distilled over molecular sieve 5A *in vacuo* by a trap-to-trap method. In about 2 or 3 min at 0 °C *in vacuo*, the system evolved a lot of heat causing refluxing and the initial yellow suspension was converted into a dark brown turbid solution. The rapid heat evolution is ceased in a few min. After the system was stirred in an ice-bath for 2 h, gases evolved by the reaction were analyzed to reveal the formation of H_2, propane and propene. GLC analysis of the resulting solution indicated the presence of butyl butyrate (26.0 mmol) and a small amount of 1-butanol. The reactions at 20 °C and 100 °C proceeded similarly.

For the purpose of isolating the complex formed by the reaction, the similar reaction as above was carried out in a larger scale. From the dark brown solution obtained as above from 0.630 g of **1** (0.547 mmol) and 69 mmol of Pr^nCHO, volatile matters were evaporated off *in vacuo* to leave brown solid which was washed with Et_2O and hexane to afford a brown powder. The powder was dissolved in 40 ml of toluene. The resulting brown solution was repeatedly filtered to remove traces of decomposed product such as ruthenium metal. On concentration of the filtrate *in vacuo*, a yellow precipitate came out which was filtered, washed with hexane and dried *in vacuo*. The yellow complex thus obtained was charaterized as the known $Ru(CO)_3(PPh_3)_2$ (0.217 g, yield 56%) on the basis of its IR spectrum (ν(CO) 1900 cm^{-1} vs; lit, 1900 cm^{-1} vs[58]).

b) Reactions of Butyraldehyde at −10—−20 °C: The reaction mixture prepared as *a*) from 0.173 g of $RuH_2(PPh_3)_4$ (0.150 mmol) and 61.1 mmol of Pr^nCHO, when kept at −20 °C, evolved heat in 10 min to give a dark grey, turbid solution. After stirring at −20 °C for 2 h, formation of 18.7 mmol of butyl butyrate was observed by GLC analysis together with a small amount of 1-butanol. On working up the system as *a*), about 50 mg of a white micro crystalline powder was obtained which was identified tentatively on the basis of IR spectrum as $RuH_2(CO)(PPh_3)_3$ (ν(Ru–H) 1960 sh, and ν(CO) 1935 cm^{-1} vs; lit, ν(Ru–H), 1960 m, 1898 m, and ν(CO), 1940 cm^{-1} vs[58]).

c) Reactions of Butyraldehyde at −30 °C: Stirring the yellow suspension of $RuH_2(PPh_3)_4$ (0.180 g, 0.156 mmol) in 63.9 mmol of Pr^nCHO prepared similarly to the method described in *a*) at −30 °C resulted in the color change of the system to a greenish yellow, heterogeneous mixture in 2 h without any heat evolution. No ester was detected in the system. Working up the system as *a*) yielded 0.12 g of a yellow microcrystalline powder which was identified as $RuH(OCOPr^n)(PPh_3)_2$ (yield 80%) on the basis of the comparison of the IR data with those reported for RuH-

$(OCOR)(PPh_3)_2$ where R=Me or Et[49] (ν(Ru–H) 1990 w and $\nu(CO_2)$ 1515 m and 1415 cm^{-1}).

Preparation of Dibutyratodicarbonylbis(triphenylphosphine)-ruthenium(II), $Ru(OCOPr^n)_2(CO)_2(PPh_3)_2$ 5b. Dihydrido-complex **1** $RuH_2(PPh_3)_4$ (0.96 g, 0.83 mmol) was put into a stainless steel autoclave flashed with nitrogen, then the autoclave was connected to a vacuum line and evacuated. Butyraldehyde (187 mmol) and 2.87 mmol of water were added successively *in vacuo* by means of a trap-to-trap method to the reaction vessel. The system was heated at 110 °C *in vacuo* by immersing the autoclave in an oil bath. After 2 h, the amounts of gases evolved by the reaction were measured and the resulting pale grey heterogeneous mixture was transferred to the Schlenk flask and worked up as already described. An off-white powder thus obtained was recrystallized from toluene to give pale yellow crystals of $Ru(OCOPr^n)_2(CO)_2(PPh_3)_2$ **5b** (0.22 g, yield 30%). IR and ^1H- and ^{31}P-NMR data are as listed in Table 5. Found: C, 63.9; H, 5.3%. Calcd for $C_{46}H_{44}O_6P_2Ru$: C, 64.6; H, 5.2%. The purified sample was still contaminated with a trace amount of $RuH_2(CO)(PPh_3)_2$ **2** as indicated by its IR spectrum.

Complex **5b** was also obtained by the similar reaction as above from $RuH(OCOPr^n)(PPh_3)_2$ **3b** and butyraldehyde in a stainless steel autoclave at 110 °C. The reaction was accompanied by the formation of a small amount of H_2, CO, Pr^nCOOBu^n, and Bu^nOH.

Preparation of Dibutyratocarbonylbis(triphenylphosphine)ruthenium (II), $Ru(OCOPr^n)_2(CO)(PPh_3)_2$ 6b. The similar reaction as above between 2.95 g of $RuH_2(PPh_3)_4$ **1** (2.22 mmol) and 340 mmol of Pr^nCHO in the presence of 16.1 mmol of water in a glass autoclave yielded a clear, orange solution. On cooling the solution to room temperature, pale yellow crystals deposited, which were filtered, washed with diethyl ether and hexane and dried in vacuo and identified as $Ru(OCOPr^n)_2(CO)(PPh_3)_2$ **6b** (1.21 g, yield 55%) on the basis of IR and ^1H- and ^{31}P-NMR spectra (Table 5). Found: C, 64.4; H, 5.4%; Mw, 806. Calcd for $C_{45}H_{44}O_5P_2Ru$: C, 65.3; H, 5.3%; Mw, 828. The reaction accompanied the formation of the dicarbonyl complex **5b** which was sometimes difficult to remove.

Complex **6b** was also obtained by the reaction of hydridocarboxylato complex **3b** (1.84 g, 1.64 mmol) with butyraldehyde (222 mmol) in a Pyrex glass Schlenk flask heated under reflux under nitrogen for 2 h. On working up, 1.00 g of **6b** was obtained (yield 86%).

This work was partially supported by a program sponsored by Japan Society for Promotion of Science and by the Ministry of Education, Science and Culture (Grant-in-Aid, No. 155325).

References

1) V. E. Tishchenko, *J. Russ. Phys. Chem. Soc.*, **38**, 355, 482 (1906).
2) I. Lin and A. R. Day, *J. Am. Chem. Soc.*, **74**, 5133 (1952).
3) K. Kasano and T. Takahashi, *Yuki Gosei Kagaku Kyokai Shi*, **23**, 144 (1965).
4) W. C. Child and H. Adkins, *J. Am. Chem. Soc.*, **45**, 3013 (1923); *ibid.*, **47**, 798 (1925).
5) Y. Ogata, A. Kawasaki, and I. Kishi, *Tetrahedron*, **23**, 825 (1967).
6) F. J. Villani and F. F. Nord, *J. Am. Chem. Soc.*, **68**, 1674 (1946); **69**, 2605 (1947).
7) P. R. Stapp, *J. Org. Chem.*, **38**, 1433 (1973).
8) G. K. Finch, *J. Org. Chem.*, **25**, 2219 (1960).
9) M. Yamashita, Y. Watanabe, T. Mitsudo, and Y. Takegami, *Bull. Chem. Soc. Jpn.*, **49**, 3597 (1976).
10) J. Tsuji and K. Ohno, *J. Am. Chem. Soc.*, **90**, 94 (1968).
11) K. Ohno and J. Tsuji, *J. Am. Chem. Soc.*, **90**, 99 (1968).
12) M. C. Baird, C. J. Nyman, and G. Wilkinson, *J. Chem. Soc., A*, **1968**, 348.
13) R. R. Schrock and J. A. Osborn, *J. Am. Chem. Soc.*, **93**, 2397 (1971).
14) H. M. Walborsky and L. E. Allen, *J. Am. Chem. Soc.*, **93**, 5465 (1971).
15) R. H. Prince and K. A. Raspin, *J. Chem. Soc., A*, **1969**, 612.
16) D. H. Doughty and L. H. Pignolet, *J. Am. Chem. Soc.*, **100**, 7083 (1978).
17) C. A. Tolman, S. D. Ittel, A. D. English, and J. P. Jesson, *J. Am. Chem. Soc.*, **101**, 1742 (1979).
18) See for example, J. Tsuji, "Organic Synthesis by Means of Transition Metal Complexes," Springer-Verlag, Berlin (1975).
19) D. Walther, *Z. Chem.*, **15**, 490 (1975); **17**, 348 (1977); E. Dinjus, H. Langbein, and D. Walther, *J. Organomet. Chem.*, **152**, 229 (1978).
20) K. L. Brown, G. R. Clark, C. E. L. Headford, K. Marsden, and W. R. Roper, *J. Am. Chem. Soc.*, **101**, 503 (1979).
21) A. M. Abeysekera, R. Grigg, J. Trocha-Grimshaw, and V. Viswanatha, *J. Chem. Soc., Perkin Trans. 1*, **1977**, 1395.
22) J. W. Suggs, *J. Am. Chem. Soc.*, **100**, 640 (1978).
23) T. B. Rauchfuss, *J. Am. Chem. Soc.*, **101**, 1045 (1979).
24) K. A. Azam and A. J. Deeming, *J. Chem. Soc., Chem. Commun.*, **1977**, 472.
25) R. R. Hitch, S. K. Gondal, and C. T. Sears, *Chem. Commun.*, **1971**, 777.
26) T. Ito, S. Kitazume, A. Yamamoto, and S. Ikeda, *J. Am. Chem. Soc.*, **92**, 3011 (1970).
27) S. Komiya, A. Yamamoto, and S. Ikeda, *Bull. Chem. Soc. Jpn.*, **48**, 101 (1975).
28) S. Komiya and A. Yamamoto, *J. Mol. Cat.*, **5**, 279 (1979).
29) D. J. Cole-Hamilton and G. Wilkinson, *Nouveau J. Chem.*, **1**, 141 (1977).
30) S. Komiya and A. Yamamoto, *J. Organomet. Chem.*, **87**, 333 (1975).
31) S. Komiya, T. Ito, M. Cowie, A. Yamamoto, and J. A. Ibers, *J. Am. Chem. Soc.*, **98**, 3874 (1976).
32) S. Komiya and A. Yamamoto, *Bull. Chem. Soc. Jpn.*, **49**, 2553 (1976).
33) D. J. Cole-Hamilton and G. Wilkinson, *J. Chem. Soc., Chem. Commun.*, **1977**, 59.
34) M. A. A. F. de C. T. Carrondo, B. N. Chaudret, D. J. Cole-Hamilton, A. C. Skapski, and G. Wilkinson, *J. Chem. Soc., Chem. Commun.*, **1978**, 463.
35) B. N. Chaudret, D. J. Cole-Hamilton, and G. Wilkinson, *J. Chem. Soc., Dalton Trans.*, **1978**, 1739.
36) R. S. Coffey, *Chem. Commun.*, **1967**, 923.
37) a) W. Strohmeier and H. Steigerwald, *J. Organomet. Chem.*, **129**, C43 (1977); b) W. Strohmeier and L. Weigelt, *ibid.*, **145**, 189 (1978).
38) H. Imai, T. Nishiguchi, and K. Fukuzumi, *J. Org. Chem.*, **41**, 665; 2688 (1976).
39) B. R. James and R. H. Morris, *J. Chem. Soc., Chem. Commun.*, **1978**, 929.
40) H. Horino, T. Ito, and A. Yamamoto, *Chem. Lett.*, **1978**, 17.
41) J. P. Collman and W. R. Roper, *J. Am. Chem. Soc.*, **87**, 4008 (1965).
42) D. Rose, J. D. Gilbert, R. P. Richardson, and G. Wilkinson, *J. Chem. Soc., A*, **1969**, 2610.

43) N. Ahmad, S. D. Robinson, and M. F. Uttley, *J. Chem. Soc., Dalton Trans.*, **1972**, 843.
44) P. S. Hallman, B. R. McGarvey, and G. Wilkinson, *J. Chem. Soc., A*, **1968**, 3143.
45) T. Yamamoto, S. Noda, and A. Yamamoto, *Kobunshi Kagaku*, **30**, 94 (1973).
46) The previous statement that a propionylruthenium complex was produced[40] is now considered in error made by misinterpretation of the spectral data.
47) K. Maruyama, T. Ito, and A. Yamamoto, *Bull. Chem. Soc. Jpn.*, **52**, 849 (1979), and references cited therein; G. Cahiez and J. F. Normant, *Tetrahedron Lett.*, **1977**, 3383; T. Ikariya, K. Osakada, and S. Yoshikawa, *ibid.*, **1978**, 3749; J. A. Roth and M. Orchin, *J. Organomet. Chem.*, **172**, C27 (1979).
48) J. Cook, J. E. Hamlin, A. Nutton, and P. M. Maitlis, *J. Chem. Soc., Chem. Commun.*, **1980**, 114.
49) S. D. Robinson and M. F. Uttley, *J. Chem. Soc., Dalton Trans.*, **1973**, 1912.
50) J. Blum, B. Zinger, D. Milstein, and O. Buchman, *J. Org. Chem.*, **43**, 2961 (1978).
51) B. F. G. Johnson, R. D. Johnston, J. Lewis, and I. G. Williams, *J. Chem. Soc., A*, **1971**, 689.
52) A. Dobson, S. D. Robinson, and M. F. Uttley, *J. Chem. Soc., Dalton Trans.*, **1975**, 370.
53) A. Spencer, *Inorg. Nucl. Chem. Lett.*, **12**, 661 (1976).
54) A. Dobson and S. D. Robinson, *Inorg. Chem.*, **16**, 1321 (1977).
55) A. Spencer and G. Wilkinson, *J. Chem. Soc., Dalton Trans.*, **1974**, 786.
56) J. J. Levison and S. D. Robinson, *J. Chem. Soc., A*, **1970**, 2947.
57) R. O. Harris, N. K. Hota, L. Sadavoy, and J. M. C. Yuen, *J. Organomet. Chem.*, **54**, 259 (1973).
58) N. Ahmad, J. J. Levison, S. D. Robinson, and M. F. Uttley, *Inorg. Synth.*, **15**, 45 (1974).
59) R. A. Schunn and E. R. Wonchoba. *Inorg. Synth.*, **13**, 131 (1972).
60) P. S. Hallman, T. A. Stephenson, and G. Wilkinson, *Inorg. Synth.*, **12**, 237 (1970).
61) J. R. Sanders, *J. Chem. Soc., Dalton Trans.*, **1973**, 743.
62) M. Aresta, P. Giannoccaro, M. Rossi, and A. Sacco, *Inorg. Chim. Acta*, **5**, 203 (1971).
63) A. Yamamoto, S. Kitazume, L. S. Pu, and S. Ikeda, *J. Am. Chem. Soc.*, **93**, 371 (1971).
64) P. Meakin, L. J. Guggenberger, W. G. Peet, E. L. Muetterties, and J. P. Jesson, *J. Am. Chem. Soc.*, **95**, 1467 (1973).
65) T. Ito, T. Kokubo, T. Yamamoto, A. Yamamoto, and S. Ikeda, *J. Chem. Soc., Dalton Trans.*, **1974**, 1783.
66) T. Ito, H. Tsuchiya, and A. Yamamoto, *Bull. Chem. Soc. Jpn.*, **50**, 1319 (1977).
67) T. Ito, T. Kiriyama, and A. Yamamoto, *Bull. Chem. Soc. Jpn.*, **49**, 3250 (1976).

Photoreduction of Bisviologen Compounds, Viologen-$(CH_2)_n$-Viologen, by 2-Propanol

Masaoki FURUE* and Shun-ichi NOZAKURA

Department of Macromolecular Science, Faculty of Science, Osaka University, Toyonaka, Osaka 560

(Received May 13, 1981)

In order to study the polymer effect in the photoreduction of viologen-containing polymers by 2-propanol, bisviologen compounds, V^{2+}-$(CH_2)_n$-V^{2+}, were subjected to photoreduction. The rates of photoreduction occur in the order $n=2>3>4>5>MV^{2+}$. The structure of the photoreduced species was found to be predominantly the doubly reduced species, V^+-$(CH_2)_n$-V^+, in the cases of $n=2$ and 3, and mixtures of the doubly reduced and singly reduced species, V^+-$(CH_2)_n$-V^{2+}, in the cases of $n=4$ and 5. Intramolecular dimeric association of V^+ units was observed for all the compounds except for $n=2$, where the intramolecular association was structurally inhibited. The variation of rate and structure distribution of reduced species was interpreted in terms of the local concentration effect in the photoreduction step.

Methylviologen (MV^{2+}) is known as an efficient electron transfer mediator in the conversion of light energy into chemical energy.[1-5] We are interested in the viologen-containing polymers because we expect the facilitated electron migration along the polymer chain and some possible multi-electron transfer from the reduced polymer. In the previous paper we reported the synthesis of some viologen-containing vinyl polymers and studied the polymer effect in the photoreduction by 2-propanol and in the properties of the reduced polymer.[6] It was found that the two neighboring viologen units on a polymer chain appeared to cooperate in the photoreduction and that this cooperation resulted in the increase of the rate of photoreduction and in the dimeric association of two reduced viologen units. This may be a kind of local concentration effect.

The object of the present paper is to confirm the local concentration effect by the use of model compounds **1** containing two viologen units at various polymethylene intervals. The part of the present work on compound **1b** ($n=3$) has been briefly communicated.[7]

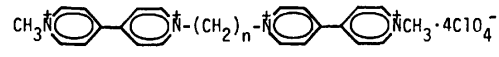

1 (a,b,c,d for $n=2,3,4$, and 5, respctively)
1′,1″-(Polymethylene)bis(1-methyl-4,4′-bipyridinium)perchlorate.

Results and Discussion

Structure of Reduced Species ($n=3$). Figure 1 shows the time profile for the photoreduction of compound **1b** ($n=3$) in an aqueous solution. A monotonous increase of the radical cation species absorbing at 360, 533, and ≈850 nm was observed. The same spectral change was observed by the treatment of **1b** ($n=3$)

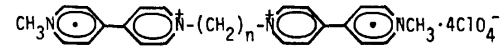

2

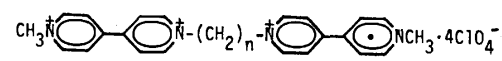

3

2: Doubly reduced form, **3**: singly reduced form (a,b,c,d for $n=2,3,4$, and 5, respectively).

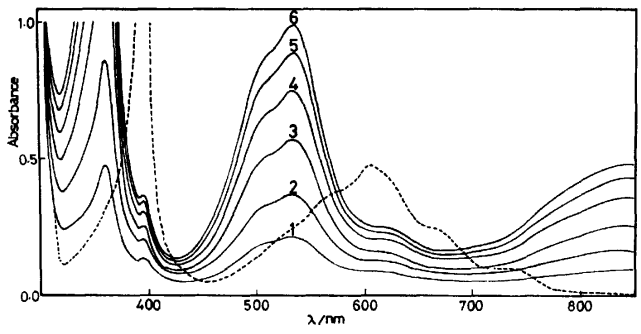

Fig. 1. Absorption spectra of photoreduced species of **1b** ($n=3$) in phosphate buffered aqueous solution (pH 5.9) containing 2-propanol (0.65 mol dm^{-3}). The concentration was [**1b**]$=5.0\times10^{-4}$ mol dm^{-3}. Irradiation time, 1: 0.5, 2: 1.0, 3: 2.0, 4: 3.0, 5: 4.0, 6: 5.0 h. Absorption spectrum of MV^+ was shown by a dotted line.

(6.5×10^{-5} mol dm^{-3}) with an excess of sodium dithionite (1.7×10^{-2} mol dm^{-3}) under anaerobic condition, where both viologen units of **1b** ($n=3$) were reduced to form the doubly reduced form **2**. As shown in Fig. 1, the spectrum obtained on photoreduction was different from that of MV^+ at ambient temperature. MV^+ has been known to exist in an equilibrium with a dimeric associated species $(MV^+)_2$, as in Eq. 1:[8,9]

$$MV^+ + MV^+ \rightleftharpoons (MV^+)_2. \quad (1)$$

The observed spectrum in the photolysis corresponds to that of the associated form, which was stable only at very low temperatures. Thus, the spectral difference between the photoreduced **1b** ($n=3$) and MV^+ in Fig. 1 can be explained by intramolecular association of the V^+ groups in the photoreduced **1b** ($n=3$). Moreover, we prepared the singly reduced form **3** ($n=3$) and confirmed that its spectrum corresponds to that of monomeric MV^+, as shown in Fig. 2. The singly reduced form **3** ($n=3$) was prepared by the electron transfer reaction from hydroxydiphenylmethyl radicals, which were generated *in situ* by the unimolecular thermolysis of benzpinacol at 60 °C in a methanol solution containing **1b** ($n=3$, Cl^- form) under an anaerobic condition. It has been known that the reduction of MV^{2+} by the hydroxydiphenylmethyl radical was very efficient.[10] The time profile for the

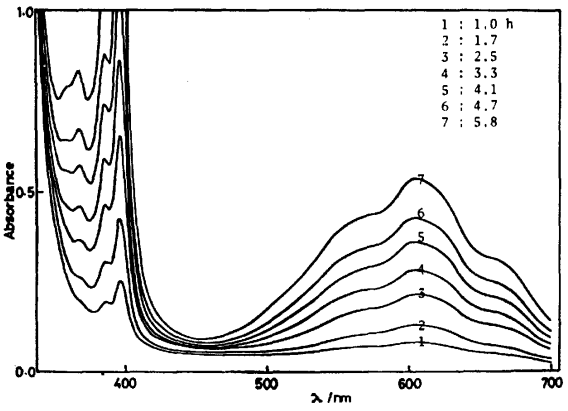

Fig. 2. Reduction of **1b** ($n=3$, Cl^- form) by hydroxyphenylmethyl radical in a methanol solution at 60°C. The concentrations were [**1b**]$=8.0\times10^{-3}$ mol dm^{-3} and [benzpinacol]$=2.0\times10^{-3}$ mol dm^{-3}.

thermal reaction (Fig. 2) showed a monotonous increase of the MV^+-type absorption of **3** ($n=3$). Thus, the photoreduced **1b** ($n=3$) has been shown to be **2** in the intramolecular associated form.

It is interesting to note that this assignment excludes the possibility of molecular complexes between the V^+ unit and the V^{2+} unit, although several examples of aromatic compounds are known to exhibit this kind of association.[11] Furthermore, in spite of the exothermicity of the dimeric association, there was no indication of an intermolecular electron transfer process which would lead to the formation of **2** ($n=3$) by the electron exchange between **3**'s ($n=3$).[12,13]

Structure of Photoreduced Species (n=*2, 4, and 5*).

The absorption spectrum of the partially photoreduced **1a** ($n=2$) shown in Fig. 3A, however, is entirely of the MV^+ type and the completely reduced species obtained with $Na_2S_2O_4$-treatment also showed the same spectrum. It is therefore reasonable to assign the structure **2a** ($n=2$) to the photoreduced **1a** ($n=2$) and to assume that **2a** ($n=2$) does not take an associated structure. Inspection of molecular models shows conformational difficulty in the association.

When **1c** ($n=4$) and **1d** ($n=5$) were completely reduced by $Na_2S_2O_4$, the spectra showed maxima at 536 and 539 nm, respectively, indicating that **2c** ($n=4$) and **2d** ($n=5$) show the intramolecular association like that in **2b** ($n=3$) (Figs. 3C and D). The spectra of the partially photoreduced specimens of **1c** ($n=4$) and **1d** ($n=5$) in Figs. 3 C and D have maxima at 540 and 603 nm in 6 : 4 ratio for $n=4$ and 5 : 5 for $n=5$. These two specimens may be concluded to be mixtures of **2** and **3**.

Rate of Photoreduction by 2-Propanol. Based upon the above interpretation of the absorption spectra, the concentrations of the singly reduced and doubly reduced species are evaluated. The observed absorbance (A) at any given wavelength is given by

$$A = \varepsilon_1 C_1 L + \varepsilon_2 C_2 L, \qquad (2)$$

where ε_1 and ε_2 are the molar extinction coefficients at the wavelength of the singly reduced and doubly reduced species, respectively, C_1 and C_2 are the corresponding concentrations, and L is the light path (1 cm). Table 1 shows λ_{max} and ε_{max} of bisviologen compounds (**1**) and doubly reduced species (**2**) together with the other ε values necessary for the estimation of C_1 and C_2. ε_2 in each case was determined from the absorption spectrum of the doubly reduced species which was produced by the treatment with an excess of $Na_2S_2O_4$. The singly reduced species was assumed to have the same extinction coefficient (ε_1) as that of MV^+. C_1 and C_2 were calculated using equation 2 from absorbance values at two different wavelengths, namely, at 603 nm and 530—540 nm. The latter wavelength is the maximum absorption of the doubly reduced species of **1b** ($n=3$), **1c** ($n=4$), and **1d** ($n=5$). In the case of **1a** ($n=2$), the photoreduced product was found to be only the doubly reduced species, as shown in Fig. 3A. ε_2 in this case is the value of **2a** ($n=2$).

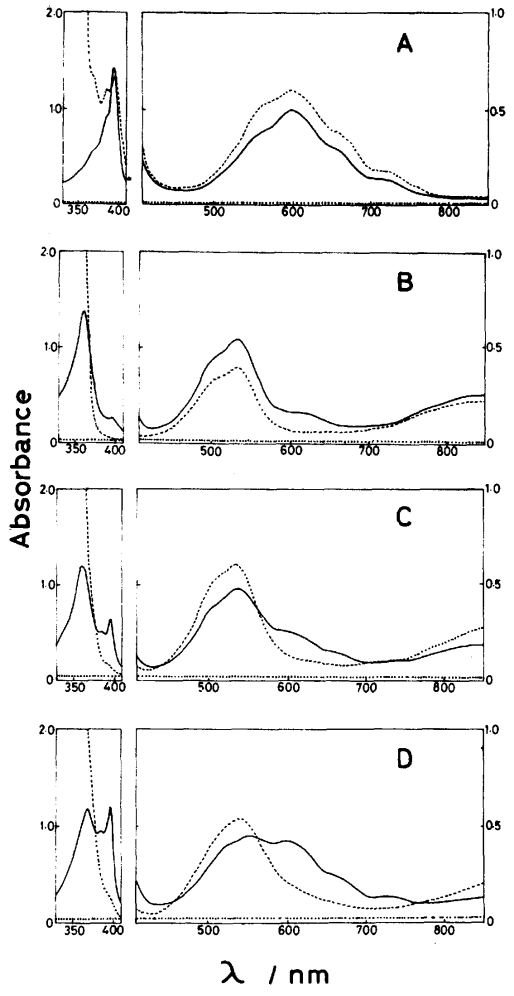

Fig. 3. Absorption spectra of radical cations of **1** partially photoreduced (——) and completely reduced with $Na_2S_2O_4$ (------) and base lines (·····) for the latter.
A: [radical ion]$=4.95\times10^{-5}$ unit mol dm^{-3}, [2a ($n=2$)] $=3.01\times10^{-5}$ mol dm^{-3}.
B: [radical ion]$=5.14\times10^{-5}$ unit mol dm^{-3}, [2b ($n=3$)] $=1.67\times10^{-5}$ mol dm^{-3}.
C: [radical ion]$=4.59\times10^{-5}$ unit mol dm^{-3}, [2c ($n=4$)] $=2.54\times10^{-5}$ mol dm^{-3}.
D: [radical ion]$=5.08\times10^{-5}$ unit mol dm^{-3}, [2d($n=5$)] $=2.43\times10^{-5}$ mol dm^{-3}.

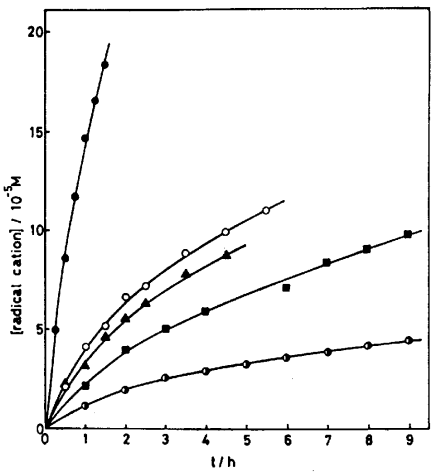

Fig. 4. Photochemical formation of radical cations from bisviologen compounds **1** and MV^{2+} in phosphate buffered aqueous solution (pH 5.9) containing 2-propanol (0.65 mol dm^{-3}). The concentrations were $[\mathbf{1}]=5.0\times10^{-4}$ mol dm^{-3} and $[MV^{2+}]=1.0\times10^{-3}$ mol dm^{-3}.
●: **1a** ($n=2$), ○: **1b** ($n=3$), ▲: **1c** ($n=4$), ■: **1d** ($n=5$), ◑: MV^{2+}.

The total amount of photoreduced species, C_1+2C_2, is plotted *versus* time in Fig. 4. Bisviologen compounds were found to show no special interunit interaction at the ground state, as shown by similar absorption maxima in Table 1. The rate curves of the photoreduction in Fig. 4, however, show marked differences. The initial rate decreased in the order $n=2>3>4>5>MV^{2+}$. This fact may be explained in terms of the local concentration effect by the following argument. The photoreduction of MV^{2+} by 2-propanol is known to proceed by the following mechanism:[10]

$$MV^{2+} \xrightarrow{h\nu} MV^{2+*}, \quad (3)$$

$$MV^{2+*} + (CH_3)_2CHOH \longrightarrow MV^{+} + (CH_3)_2CHO\cdot + H^{+}, \quad (4)$$

$$MV^{2+} + (CH_3)_2CHO\cdot \longrightarrow MV^{+} + (CH_3)_2C{=}O + H^{+}, \quad (5)$$

$$\text{Net}\quad 2MV^{2+} + (CH_3)_2CHOH \xrightarrow{h\nu} 2MV^{+} + (CH_3)_2C{=}O + 2H^{+}. \quad (6)$$

The excited viologen receives an electron from 2-propanol, leaving the alkoxyl radical. The latter in turn gives up another electron to a ground state MV^{2+}. One photon eventually results in the reduction of two MV^{2+} molecules and the oxidation of one alcohol molecule. The alkoxyl radical $(CH_3)_2CHO\cdot$, in addition to reaction 5, has another possibility of reaction 7, which is a backward electron transfer reaction. The competition between reactions 5 and 7

$$MV^{+} + (CH_3)_2CHO\cdot \longrightarrow MV^{2+} + (CH_3)_2CHO^{-} \quad (7)$$

depends on the relative local concentration of MV^{+} and MV^{2+}. In the case of bisviologen compounds, the alkoxyl radical will find nearby another viologen unit of the bisviologen compound before it diffuses out of the reaction site, and reaction 5 will take place (Scheme 1). Thus the local concentration effect will be exerted favorably on the rate of reaction in bisviologen compound- and viologen polymer-systems, compared with MV^{2+}. It is reasonable that bisviologen compounds with shorter intervening polymethylene chains have higher initial rate because of higher local concentrations of V^{2+} units.

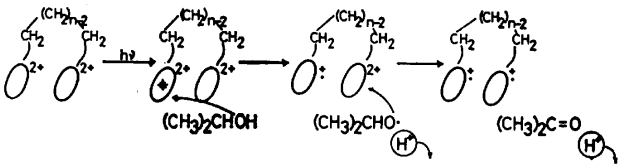

Scheme 1. Mechanism of photoreduction of bisviologen compounds ($n=2$—5) by 2-propanol.

Figure 4 shows that there was a saturation phenomenon and that the saturation appeared at an earlier stage of conversion in the compounds whose initial rate was slower. The saturation phenomenon is also explained in terms of reaction 7. When the concentration of V^{+} unit increases, the contribution of the backward reaction 7 relative to the forward reaction 5 will increase, leading to saturation in the concentration of V^{+} units. Moreover, if the local concentration effect is small, as in the case of **1d** ($n=5$) in comparison to **1a** ($n=2$), the larger contribution of reaction 7 relative to reaction 5 will result in the slower initial rate and at the same time the earlier occurrence of the saturation phenomena. The saturation phenomena in the case of MV^{2+} were explained by Ledwith in terms of the quenching reaction 8 of excited

$$MV^{2+*} + MV^{+} \longrightarrow MV^{2+} + MV^{+} \quad (8)$$

MV^{2+} with MV^{+}.[10,14] This reaction alone, however, does not explain the difference in onset of the saturation phenomena among bisviologen compounds.

Table 1. Absorption spectral data of methylviologen and bisviologen compounds[a]

Compound	1 (Bisviologen compounds)		2 (Doubly reduced species)			
	λ_{max}/nm	ε_{max}/mol^{-1} cm^{-1}	λ_{max}/nm	ε_{max}/mol^{-1} cm^{-1}	λ/nm	ε/mol^{-1} cm^{-1}
1a ($n=2$)	263	4.40×10^4	595	1.99×10^4	603	1.96×10^4
1b ($n=3$)	260	4.38×10^4	533	2.36×10^4	603	0.18×10^4
1c ($n=4$)	259	3.88×10^4	536	2.39×10^4	603	0.41×10^4
1d ($n=5$)	258	4.52×10^4	539	2.20×10^4	603	0.68×10^4
MV^{2+}	256	1.39×10^4	603	1.20×10^4	533[c]	0.53×10^4

a) Measured at 25 °C. b) Reduced with $Na_2S_2O_4$. c) ε : 0.62×10^4 mol^{-1} cm^{-1} at 539 nm and 0.53×10^4 mol^{-1} cm^{-1} at 536 nm.

Experimental

*Preparation of Bisviologen Compounds, **1a** (n=2), **1b** (n=3), **1c** (n=4), and **1d** (n=5).* 1′,1″-(Polymethylene)bis(1-methyl-4,4′-bipyridnium)perchlorate **1** was prepared according to the following general procedure.

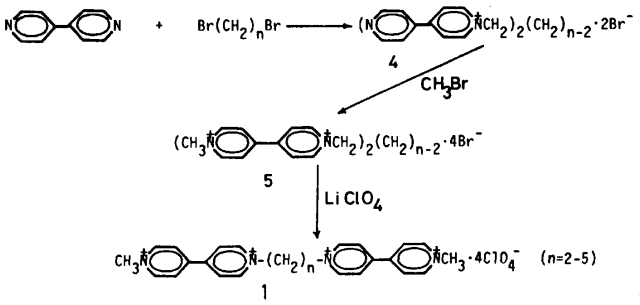

1,1′-(Polymethylene)bis(4-bipyridinium)dibromide **4** was prepared by warming a solution of 4,4′-bipyridine (25 g, 0.16 mol) in *N,N*-dimethylformamide (DMF) (200 ml) with α,ω-dibromoalkane (40 mmol) at 70 °C for 24 h. A light yellow precipitate separated out and was recrystallized from water for $n=2$ and 3 and from an acetone–methanol mixture for $n=4$ and 5. Yields of **4** were 25, 55, 50, and 64% for $n=2$, 3, 4, and 5, respectively.

Treatment of **4** (20 mmol) with an excess of methyl bromide (30 ml) in DMF (270 ml) in a glass autoclave (400 ml) at 90 °C for 24 h afforded **5** in nearly quantitative yields. **5** (4 mmol) was converted to the corresponding perchlorate **1** by the treatment with an aqueous solution (100 ml) of $LiClO_4$ (47 mmol) at room temperature. For $n=5$, 94 mmol of $LiClO_4$ was used under the same conditions. Recrystallization from water gave colorless crystals. Yields of **1** were 75, 61, 73, and 47% for **1a** ($n=2$), **1b** ($n=3$), **1c** ($n=4$), and **1d** ($n=5$), respectively.

1a. Found: C, 37.25: H, 3.49; N, 7.30; Cl, 18.43%. Calcd for $C_{24}H_{26}N_4O_{16}Cl_4$: C, 37.52; H, 3.31; N, 7.29; Cl, 18.46%.

1b. Found: C, 37.70; H, 3.71; N, 7.18; Cl, 18.01%. Calcd for $C_{25}H_{28}N_4O_{16}Cl_4$: C, 38.38, H, 3.61; N, 7.16; Cl, 18.13%.

1c. Found: C, 39.16; H, 3.90; N, 7.07; Cl, 17.91%. Calcd for $C_{26}H_{30}N_4O_{16}Cl_4$: C, 39.21; H, 3.80; N, 7.04; Cl, 17.81%.

1d. Found: C, 39.68; H, 4.11; N, 6.98; Cl, 17.41%. Calcd for $C_{27}H_{32}N_4O_{16}Cl_4$: C, 40.02; H, 3.98; N, 6.91; Cl, 17.50%.

A chloride ion type of **1** ($n=3$) was prepared by the replacement of the bromide ion of **5** with a chloride ion; this involved passing an aqueous solution of **5** through a column of anion exchange resin (Amberlite IRA 400).

Photoreaction. Light from a 300 W high pressure mercury lamp was filtered through aqueous 5% potassium hydrogen phthalate to remove light of shorter wavelength than 300 nm. A quartz cell was charged with a viologen sample in an aqueous solution of 2-propanol (0.65 mol dm^{-3}) at pH 5.9 (phosphate buffer, 1/15 mol dm^{-3}), degassed, sealed, and set in a thermostat equipped with a merry-go-round.

Measurements. Electronic absorption spectra were measured by a Hitachi Model 124 spectrophotometer with a thermostatically controlled cell compartment.

References

1) J. M. Lehn and J. P. Sauvage, *Nouv. J. Chim.*, **1**, 449 (1977).
2) B. V. Koryakin, T. S. Dzhabiev, and A. E. Shilov, *Dokl. Akad. Nauk SSSR*, **233**, 620 (1977).
3) K. Kalyanasundaram, J. Kiwi, and M. Graetzel, *Helv. Chim. Acta.*, **61**, 2720 (1978).
4) A. Moradpour, E. Amouyal, P. Keller, and H. Kagan, *Nouv. J. Chim.*, **2**, 547 (1978).
5) T. Nishijima, T. Nagamura, and T. Matsuo, *J. Polym. Sci., Polym. Lett. Ed.*, **19**. 65 (1981).
6) M. Furue, S. Yamanaka, Ly Phat, and S. Nozakura, *J. Polym. Sci., Polym. Chem. Ed.*, **19**, 2635 (1981).
7) M. Furue and S. Nozakura, *Chem. Lett.*, **1980**, 821.
8) E. M. Kosower and J. L. Cotter, *J. Am. Chem. Soc.*, **86**, 5524 (1964).
9) A. G. Evans, N. N. Dodson, and N. H. Rees, *J. Chem. Soc., Perkin Trans. 2*, **1976**, 859.
10) A. Ledwith, *Acc. Chem. Res.*, **5**, 133 (1972).
11) A. J. Bard, A. Ledwith, and H. J. Shine, *Adv. Phys. Org. Chem.*, **13**, 210 (1976).
12) A. G. Evans, J. C. Evans, and M. W. Baker, *J. Am. Chem. Soc.*, **99**, 5882 (1977).
13) A. G. Evans, J. C. Evans, and M. W. Baker, *J. Chem. Soc., Perkin Trans. 2*, **1978**, 1787.
14) A. S. Hopkins, A. Ledwith, and M. F. Stam, *J. Chem. Soc., Chem. Commun.*, **1970**, 494.

 © 1982 The Chemical Society of Japan Bull. Chem. Soc. Jpn., 55, 517—519 (1982)

The Photo-induced Radical Rearrangement of 7-Oxocholesteryl Hypoiodite in the Presence of Mercury(II) Oxide and Iodine[1]

Hiroshi SUGINOME*, ** and Fumihiro YONEBAYASHI

Department of Chemistry, Faculty of Science, Hokkaido University, Sapporo 060

(Received May 15, 1981)

7-Oxocholesteryl hypoiodite in benzene containing mercury(II) oxide and iodine underwent a photo-induced rearrangement to give 5-iodomethyl-*A*-nor-5ξ-cholestane-3,7-dione and 2-iodo-7-oxo-*A*-nor-2,3-secocholest-5-en-3-yl formate in low yields, together with cholesta-3,5-dien-7-one without any accompanying 3α,5-epoxy-6-iodo-*A*-homo-4-oxacholestanes which are common products in the reactions of cholest-5-en-3-ols. The results thus show that the introduction of an oxo group at the C-7 position results in an appreciable change in the products of the reactions of cholest-5-en-3-ols.

The mercury(II) oxide-iodine reagent has been shown to be an effective reagent for the formation of hypoiodites from alcohols.[2] A variety of hypoiodites of steroidal alcohols thus prepared undergo either heat or light-induced reactions to give products which can be explained as having originated by the homolysis of the hypoiodites.[2,3] The active species generated from mercury(II) oxide and iodine is believed to be iodine oxide, I_2O,[4] which transforms the alcohols into the hypoiodites.

In a series of previous papers, we reported the results of our investigations of the photo- and thermally-induced rearrangements of hypoiodites of cholesterol,[5] the related 5-cholesten-3-ols,[6,7] and *C*-nor-*D*-homosteroid-5-en-3β-ols[8] in the presence of mercury(II) oxide and iodine. Cholesteryl hypoiodite has been found to afford oxabicyclic compounds, 3α-5-epoxy-6β-iodo-*A*-homo-4-oxa-5α-cholestane and its 6α-isomer, accompanied by a moderate yield of 2-iodo-*A*-nor-2,3-secocholest-5-en-3-yl formate.[5] The pathways to these products, which involve the reactions of iodine oxide and intermediary radical species generated by the β-scission of the corresponding oxyl radicals, have been discussed in the previous papers.[5-8]

In this paper, we wish to report the results of the photoinduced reaction of 7-oxocholesteryl hypoiodite in the presence of mercury(II) oxide and iodine, which was undertaken in order to assess the effects of the carbonyl group adjacent to the potential allyl radical portion of the intermediate generated by the β-scission of the 3β-oxyl radical.

7-Oxocholesterol (**1**)[9] in dry benzene containing mercury(II) oxide and iodine in a Pyrex vessel was irradiated with a 100-W high-pressure mercury arc under an argon atmosphere for 8.5 h to afford a mixture of products. The preparative TLC of the mixture gave three crystalline compounds, (**2**) (4%), (**3**) (13%), and (**4**) (5%), in the order of their mobility, together with several unidentified minor products (Scheme 1). Compound **2**, carrying an iodine atom, has a molecular formula of $C_{27}H_{43}O_2I$ as determined by mass spectrometry and the elemental analysis. The chemical ionization mass spectrum gave a series of ions attributable to $M^+ + 1$, $M^+ + 29$ and $M^+ + 41$ indicative of a molecular weight of 526, while the EI mass spectrum gave the molecular ion of *m/e* 526. All the spectral results on **2** can be reconciled with the 5-iodomethyl-*A*-nor-5ξ-cholestane-3,7-dione structure. The infrared spectrum showed two bands in the carbonyl region ascribed to five- and six-membered cyclic ketones. The presence of these carbonyl groups was further confirmed by the ^{13}C NMR spectrum, which showed two signals arising from carbonyl carbons at δ 212.4 and 206.7 ppm. The ^1H NMR spectrum, which was most instructive, showed an AB quartet (τ 6.65 and 6.75 $J=10.7$ Hz) with very small outer peaks ascribable to the iodomethyl group attached to the C-5 and a one-proton doublet at τ 7.07 ($J=13.5$ Hz) ascribed to one of the protons attached to the C-6. It also showed another doublet at τ 7.91 ($J=13.5$) which was superimposed on the other protons. On irradiation at the center of doublet at τ 7.07, the doublet at τ 7.91 collapsed to a singlet while on irradiation at the center of the doublet at τ 7.91, the other doublet collapsed to a singlet. The doublet at τ 7.91 is thus ascribed to one of the protons attached to the C-6. The 10β- and 13β-methyl groups resonated at τ 8.69 and 9.35.

The spectral evidence also enabled us to formulate the structure of compound **3** as 2-iodo-7-oxo-*A*-nor-2,3-secocholest-5-en-3-yl formate. The IR spectrum showed three strong bands at 1738, 1677, and 1178 cm^{-1}. The former two are assigned to bands arising from formate and α,β-unsaturated carbonyl groups. The latter is attributed to the C–O stretching of formate. The UV spectrum showed a strong absorption maximum at 231 nm (ε; 11570) ascribable to an α,β-unsaturated carbonyl group. The NMR spectrum showed two one-proton singlets at τ 1.86 and 3.98 ascribable to the formate proton[10] and the C-6 proton. It also showed an AB quartet with the very small outer peaks (5.11 and 5.30, $J=15.0$ Hz) ascribed to the methylene protons carrying a formyloxy group and a two-proton multiplet at from τ 6.86 to 7.30 ascribed to the C-2 methylene carrying an iodine atom. The 10β- and 13β-methyl groups resonated at τ 8.77 and 9.31.

Finally, product **4** was found to be cholesta-3,5-dien-7-one[9] on the basis of its IR, UV, ^1H NMR, and mass spectra.

The foregoing results show that the introduction of an oxo group at the C-7 of cholest-5-en-3-ol results in an appreciable change in the products in this reaction. Thus, we failed to isolate the 7-oxo derivative of 3α,5-

** Present address: Organic Chemistry Laboratory, Department of Chemical Process Engineering, Faculty of Engineering, Hokkaido University, Sapporo 060.

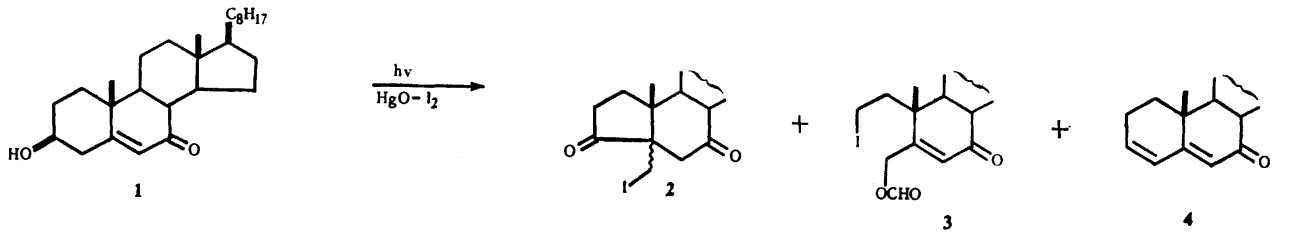

Scheme 1.

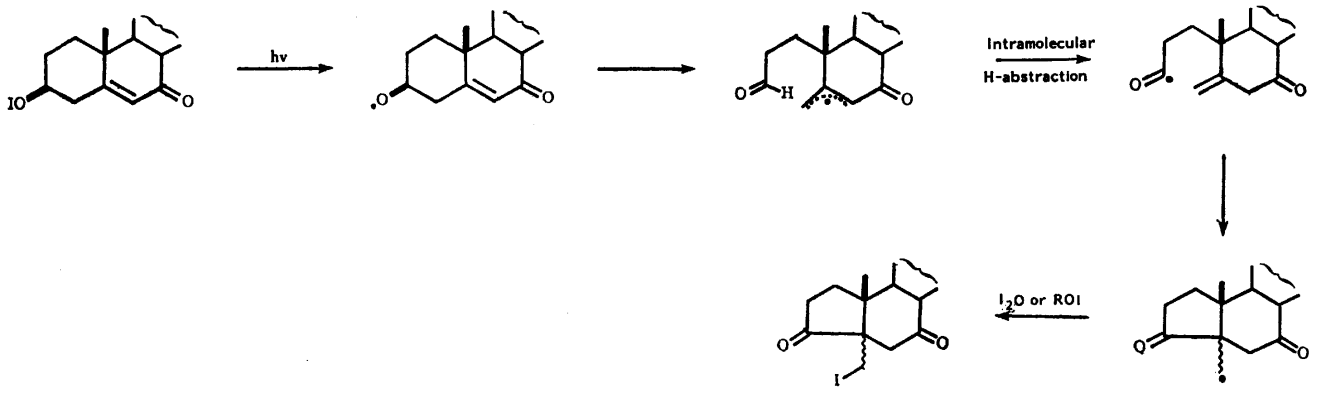

Scheme 2.

epoxy-6-iodo-*A*-homo-4-oxacholestanes, which are 7-oxo-derivatives of the products from cholesterol, from the product mixture in spite of repeated careful experiments. It is almost certain, therefore, that these oxabicyclic compounds are not formed in the present reaction.

The iodo-seco compound **3**, on the other hand, is an example of the type of products which are commonly obtained in the reaction of 5-cholesten-3β-ols.[5-8] A probable pathway by which this class of compound is formed has already been discussed in a previous paper.[5] The OI group appears to be a good leaving group, and dienone **4** may thus be formed by an ionic removal of the element of IOH.

The diketone **2** is a new type of product in this reaction. The mechanism by which this compound is formed is not clear at the present stage. One probable pathway to lead to the diketone **2**, which passes through the allyl radical intermediate and involves an intramolecular hydrogen abstraction *via* a seven-membered transition state by the C-6 center of the allyl radical to form an acyl radical which cyclizes to the five-membered ring,[11] is depicted in Scheme 2. A pathway involving the photo-rearrangement of β,γ-unsaturated ketone,[12] which can be formed from the 3β-oxyl radical, is, however, another possibility.

Experimental

For the instruments used and the general procedures, see Ref. 5. The mass spectrum was recorded by Miss Yuko Chiba in the Faculty of Agriculture with a JEOL JMS-D 300 spectrometer (70 eV).

7-Oxocholesterol. To a solution of 7-oxocholesteryl acetate[13] (2.48 g) in methanol (150 cm^3), there was added potassium hydroxide (10 g) in water (3 cm^3) and chloroform (40 cm^3). The solution was stirred for 2.5 h at room temperature. The solution was neutralized with 2 mol dm^{-3} hydrochloric acid, and a part of the solvent was removed by means of a rotary evaporater. The solution was then extracted with chloroform, and the chloroform solution was washed with water and dried over anhydrous sodium sulfate. The subsequent evaporation of the solvent gave a crude 7-oxocholesterol. Its recrystallization from diethyl ether–hexane gave pure 7-oxocholesterol (**1**); mp 172—174 °C (lit,[9] mp 157 °C). NMR, τ 9.30 (18-H), 8.81 (19-H), and 4.30 (6-H).

Irradiation of 7-Oxocholesteryl Hypoiodite in the Presence of Mercury(II) Oxide and Iodine. 7-Oxocholesterol (1 g) in benzene (145 cm^3) containing mercury(II) oxide (1.62 g) and iodine (1.91 g) in a Pyrex vessel was irradiated with a 100-W high pressure mercury arc under an argon atmosphere. The lamp was placed outside the reaction vessel. The irradiation was discontinued after 8.5 h since the decomposition of 7-oxocholesterol was nearly complete at this point. The solution was filtered, and the filtrate was worked up in a usual manner.[2] The oily product was subjected to column chromatography (Merck Kiesel gel 60, 70—230 mesh, 30 g). Elutions with benzene gave two fractions, A (836 mg) and B (34 mg). Further elutions with benzene containing an increasing amount of chloroform and with chloroform gave Fraction C (310 mg). Further elutions with chloroform containing an increasing amount of diethyl ether, diethyl ether only, and a 1 : 1 mixture of diethyl ether and acetone gave Fraction D (256 mg). Elutions with acetone, a 1 : 1 mixture of acetone and methanol, and methanol gave Fraction E (66 mg). Fraction A was a mixture, and it was subjected to preparative TLC with hexane–diethyl ether (5 : 1) to give four fractions; A^1, (7 mg), A^2 (24 mg), A^3 (171 mg), and A^4 (52 mg). Fraction A^2 was a diketone which was identical with Fraction B. Fraction A^3 was a formate **3**. Fraction A^4 was a diene **4**.

Fraction A^2 and B were combined and recrystallized from acetone to afford compound **2**, mp 188.5—190.0 °C; IR, 1739 (5-membered-ring ketone) and 1714 cm^{-1} (6-membered-ring ketone); for NMR, see text. MS, *m/e* (rel intensity) 526 (M^+, 0.7), 511(M^+-CH_3, 0.9), 399 (M^+-I, 100), 95

(24.4), 69 (19.8), 57 (25.4), 55 (22.5), and 43 (24.3). (Found; C, 61.46; H, 8.30; I, 24.17, Calcd for $C_{27}H_{43}O_2I$; C, 61.59, H, 8.23, I, 24.10%). Fraction A[3] was recrystallized from methanol to give **3**; mp 99—100 °C. (Found: C, 58.78: H, 7.90; I, 23.87. Calcd for $C_{26}H_{41}O_3I$; C, 59.08, H, 7.82; I, 24.01%); IR, 1738 (OCHO), 1738 and 1677 (α,β-unsaturated carbonyl), and 1178 cm^{-1} (OCHO): for NMR, see text; UV_{max} (C_2H_5OH), 231 (ε: 11570). Fraction A[4] was recrystallized from methanol to yield cholesta-3,5-dien-7-one, (4)[9]; mp 108—110 °C. (Lit,[9] mp 112 °C); IR 1653 cm^{-1} ($\alpha,\beta,\gamma,\delta$-unsaturated C=O); UV_{max} (C_2H_5OH) 278 (ε 26320); NMR τ 9.29 (3H, s, 18-H), 8.87 (3H, s, 19-H); 4.39 (1H, broad s, 3-H), 3.88 (1H, s, 6-H), and 3.88 (1H, broad s, superimposed on 6-H signal, 4-H).

We wish to thank Mrs. Tomoko Okayama for the measurements of the ^1H NMR spectrum and the spin-decoupling experiments. We also wish to thank the Finnigan Corporation, Sunnyvale, California, U. S. A., for the chemical-ionization mass spectrum of Compound **2**.

References

1) Photo-induced Transformations. Part 62. Part 61: H. Suginome, T. Yabe, and E. Osawa, *J. Chem. Soc., Perkin Trans. 1*, in press.

2) A. A. Petrov, *J. Gen. Chem. U.S.S.R.*, **10**, 819 (1940); *Chem. Abstr.*, **35**, 2112 (1941); M. Akhtar and D. H. R. Barton, *J. Am. Chem. Soc.*, **86**, 1528 (1964).

3) *E. g.*, H. Suginome, H. Ono, and T. Masamune, *Bull. Chem. Soc. Jpn.*, **54**, 852 (1981); for a general review see J. Kalvoda and K. Heusler, *Synthesis*, **1971**, 501.

4) M. Akhtar and S. Marsh, *J. Chem. Soc., C*, **1966**, 938; C. P. Forbes, A. Goosen, and H. A. Laue, *J. Chem. Soc., Perkin Trans. 1*, **1974**, 2346.

5) H. Suginome, A. Furusaki, K. Kato, N. Maeda, and F. Yonebayashi, *J. Chem. Soc., Perkin Trans. 1*, **1981**, 236.

6) H. Suginome and N. Maeda, *Bull. Chem. Soc. Jpn.*, **53**, 2621 (1980).

7) H. Suginome and N. Maeda, *Bull. Chem. Soc. Jpn.*, **53**, 2626 (1980).

8) H. Suginome, K. Kato, and T. Masamune, *Bull. Chem. Soc. Jpn.*, **54**, 3042 (1981).

9) J. Mauthner and W. Suida, *Monatsh. Chem.*, **17**, 579 (1896).

10) O. E. Edwards and M. Lesage, *Can. J. Chem.*, **41**, 1592 (1963); D. G. Kowalewski, *Mol. Phys.*, **8**, 93 (1964).

11) For a review, see A. L. J. Beckwith, *Tetrahedron*, **37**, 3037 (1981).

12) S. Domb, G. Bozzato, J. A. Saboz, and K. Schaffner, *Helv. Chim. Acta*, **52**, 2436 (1969); S. Domb and K. Schaffner, *ibid.*, **53**, 677 (1970).

13) A. Windaus, H. Lettre, and F. Schenck, *Ann.*, **520**, 98 (1935).

The Cyclic Voltammetry and Cathodic Reduction of Steroidal Homoallylic Nitro Esters. Dimerization *vs.* Cyclopropane Formation[1]

Takeo SATO,* Yoshihisa KOMEICHI, Shoichi KOBAYASHI, and Akira OMURA
Department of Chemistry, Tokyo Metropolitan University, Setagaya-ku, Tokyo 158
(Received May 20, 1981)

The cathodic reduction of homoallylic nitro esters was carried out in DMF–TBAP using platinum electrodes. The reaction was found to be highly dependent on the ester-leaving group: Whereas 6-nitrocholest-5-en-3β-yl acetate (**3a**) gave a 3,3′-dimer **4**, 3β-tosylate **3d** gave a cyclosteroid, 6β-nitro-3α,5-cyclo-5α-cholestane (**7**). 3β-Trifluoroacetate showed intermediate behavior and gave both **4** and **7**. Similarly, 6-nitrocholest-5-ene-3β,19-diol 3-acetate 19-tosylate gave 5β,19-cyclosteroid. The cyclic voltammetry was carried out for these and related compounds. A reversible cyclic voltammogram was recorded for **3a**, but **3d** showed no anodic peak on potential reversal. A possible electron-transfer and the following chemical-reaction mechanism was discussed.

The cathodic reactions of conjugated or homoconjugated systems in aprotic media are potentially useful as a means to induce remote reactions without reducing or protonating the electroactive group which itself is serving as the electron inlet. In this investigation we carried out the cathodic reduction of homoallylic nitro esters, such as **1**, in a steroid series. We found two

$$ROCHCH_2C{=}CNO_2$$

1, R = Ac, Ts *etc.*

types of reactions, namely, dimerization and cyclopropane-ring formation, which were highly dependent on the nature of the ester-leaving groups. The results are discussed in relation to the electrochemical parameters, as determined by cyclic voltammetry.

Results

Controlled-potential Electrolyses of Two Nitro Esters, 3a and 3d. 6-Nitrocholest-5-en-3β-yl acetate (**3a**) was obtained by the nitration reaction of cholesteryl acetate (**2a**).[2] The acylation or sulfonylation of 6-nitrocholest-5-en-3β-ol (**3**, R=H) gave benzoate **3b**, trifluoroacetate **3c**, and tosylate **3d**. For comparison, some cholesteryl esters **2a—d** were also prepared.

The cathodic reduction was carried out in a divided cell using platinum electrodes. Anhydrous DMF containing tetrabutylammonium perchlorate (TBAP, 0.1 mol dm^{-3}) was used as the reaction medium; it had been purged with nitrogen before the electrolysis. As reference, a saturated calomel electrode (SCE) was used.

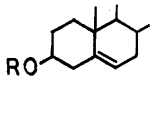

2

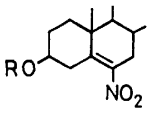

3

a, R = Ac
b, R = PhCO
c, R = CF_3CO
d, R = Ts

The controlled-potential electrolysis of the acetate **3a** supplied from a potentiostat at −1.44 V gave a precipitate after 1 F mol^{-1} of electricity had been consumed. We thus obtained a high-melting material with a molecular weight of 826 (the Rast method), for which a dimeric structure **4** (MW 829) was assigned based on the spectral evidence to be presented below. The yield of **4** was 45%.

Compound **4** showed an IR absorption at 1550 cm^{-1}, indicating the presence of a nitro group substituted on a saturated carbon. The proton NMR spectrum showed two single-proton resonances due to a vinylic proton (C-4H) at δ 5.90 as a multiplet and a proton attached to a saturated carbon carrying a nitro group (C-6H) at δ 4.67 (multiplet).

The location of the olefinic linkage and the configuration of the nitro group were determined by spectral comparison with related materials, 6β-nitrocholest-4-ene

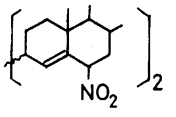

4

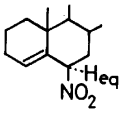

5

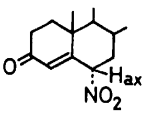

6

(**5**)[3] and 6α-nitrocholest-4-en-3-one (**6**).[4] Compound **5** showed the C-4H proton resonance at δ 5.90. The half-band width of C-5H in **4** (7.5 Hz, H_{eq}) can be compared with that of **6** (16.5 Hz, H_{ax}). The configuration at C-3 could not be determined.[5]

The use of a lead cathode instead of platinum reduced the yield of **4**. When tetrabutylammonium tetrafluoroborate (TBAF) was used as a supporting electrolyte instead of TBAP, the yield of **4** was also reduced. The addition of methanol to the reaction mixture caused intense coloration and greatly reduced the yield of **4**, indicating that a reduction of the nitro group occurred.

When the tosylate **3d** was electrolyzed at −1.45 V as above (1.5 F mol^{-1}), we obtained only a 4% yield of the dimer **4**. Instead, a new compound was formed which showed the IR maxima at 3030, 3070, and 3080 cm^{-1}, indicating the presence of a cyclopropane ring. A nitro group was assumed to be attached to a saturated carbon (1550 cm^{-1}). The proton NMR spectrum showed no vinylic proton resonance, but it did show a one-proton absorption at δ 3.87 with a half-band width of 8.3 Hz, which was attributable to an equatorial proton at C-6. Accordingly, the nitro group exists in an axial configuration. The compound showed the highest-field carbon-13 NMR resonance at δ 12.3. For comparison, compound **8**[6] showed the C-4 carbon resonance at δ 12.1. These results indicate the compound

Table 1. Controlled-current electrolyses of nitro esters **3a**—**3d**[a]

Compound	Concn/mmol dm^{-3}	Potential variation/$-$V[b]	Yield/% 4	7
3a	5.1	1.23—2.00	13.8	—
3a	25.6	1.23—2.00	29	—
3a	50.8	1.23—2.00	54	—
3b	25.4	1.54—2.00	30	—
3c	50.0	1.28—2.00	12	10
3d	39.2	1.10—2.00	2	36

a) The electrolysis was carried out at a constant current of 0.85 mA cm^{-2} in DMF–TBAP (0.1 mol dm^{-3}) using platinum elctrodes. The yields shown were obtained after 1.0—1.2 F mol^{-1} of electricity had been passed through (for **3c** 1.9 F mol^{-1}). b) Reference electrode, SCE.

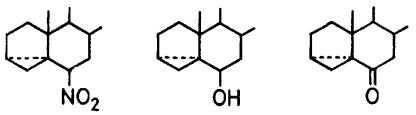

7 8 9

obtained is 6β-nitro-3α,5-cyclo-5α-cholestane (**7**). Chemical evidence for the suggested structure, including the stereochemistry of the cyclopropane ring, comes from the conversion of **7** into the known 3α,5-cyclo-5α-cholestan-6-one (**9**)[7] (see below). The yield of **7** from **3d** was 43%.

Controlled-current Electrolyses of Nitro Esters 3a—d. In order to investigate the effect of C-3 substituents on the course of the cathodic reaction, we further examined the reaction of the benzoate **3b** and the trifluoroacetate **3c**. During the controlled-potential electrolyses of these nitro esters, the current showed a wide variation. In order to avoid current-density variation during the dimerization reaction, we employed controlled-current conditions for the purposes of comparison. The compounds **3a**—**d** were reduced cathodically under the same current density of 0.85 mA cm^{-2} until 1.0—1.2 F mol^{-1} of electricity had been consumed (with **3c** 1.9 F mol^{-1}). The results are summarized in Table 1.

The concentration of the substrate had a marked effect on the yield of the intermolecular reaction product **4**. Table 1 shows several experiments carried out for **3a** using 5 to 50 mmol dm^{-3} solutions which gave yields of **4** ranging from 14 to 54%. For **3c** and **3d**, 40—50 mmol dm^{-3} solutions were used, but for the benzoate **3b** a more dilute solution had to be used because of the limited solubility. The course of the reaction appeared to be primarily determined by the leaving-group ability for the nucleophilic reactions;[8] the compound with a good leaving group such as tosylate gave a high yield of **7**. Both the acetate **3a** and the benzoate **3b** gave only a dimer ever when a dilute solution was used. The trifluoroacetate **3c** showed an intermediate behavior and gave comparable yields of **4** and **7**.

Both the dimer and cyclosteroid are stable under the present electrolytic conditions. No interconversion between **4** and **7** was observed in the control experiments, suggesting that they were formed by independent routes (see Discussion). The rest of the material was a colored matter which could not be characterized.

Cyclic Voltammetry. To obtain further insight into the structural dependence on the one-electron transfer reaction, we carried out cyclic voltammetric measurements in DMF containing 0.1 mol dm^{-3} TBAP using the cell and instruments as has been described before.[1] The measurements were carried out for related compounds, including the starting esters **2a**—**d**, **5**, **7**, and 6α-nitro-5α-cholestan-3β-yl acetate (**11**).[9]

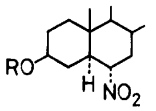

10, R = H
11, R = Ac

The results are summarized in Table 2. When an anodic peak was recorded on a potential reversal, the cathodic potential, $E^0=E_{pc}-(E_{pc}-E_{pa})/2$, was calculated. As a measure of reversibility, the current ratio, i_{pa}/i_{pc}, was also calculated. In cases where no anodic peak was recorded, the potential at which $i=0.85i_{pc}$ was taken as E^0.[10]

As the control, the CV curves of the starting cholesteryl esters **2a**—**d** were determined. None of these materials showed a cathodic peak in the potential range of 0——2 V, indicating that the ester carbonyl or sulfonyl groups were not reducible at the potentials used for the reduction of the nitro esters **3**.

Saturated nitro acetate **11** showed a cathodic potential, E^0, at -1.6 V. The β,γ-unsaturated nitro compound **5** and cyclosteroid **7** showed E_{pc}'s higher than -2.0 V and had no corresponding E_{pa}. Their cathodic potentials were estimated[10] to be -1.9 V and *ca.* -2 V respectively. Whereas compound **11**, with an equatorial nitro group, gave a quasi-reversible wave, compound **5** and **7**, with a nitro group in an axial geometry, showed no anodic wave. Figure 1 records

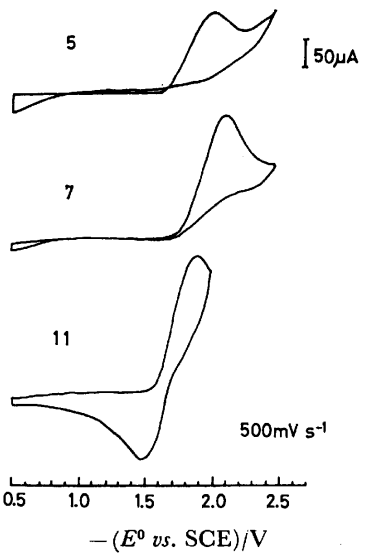

Fig. 1. Cyclic voltammograms for compounds **5**, **7**, and **11** determined in DMF using TBAP as supporting electrolyte.

TABLE 2. THE CYCLIC VOLTAMMETRY DATA FOR THE NITRO ESTERS **3a—d** AND RELATED COMPOUNDS **5**, **7**, **11**, **33a**, AND **33b**[a)]

Compound	Scan rate / mV s^{-1}	Peak potential/$-$V[b)] E_{pc}	E_{pa}	Peak pot. diff. $(E_{pa}-E_{pc})$/mV	E^0/$-$V[b)]	Current ratio i_{pa}/i_{pc}
3a	50	1.47	1.23	240	1.35	0.84
	100	1.55	1.18	370	1.36	0.83
	150	1.59	1.14	450	1.37	0.77
	250	1.63	1.10	530	1.37	0.72
	500	1.70	1.01	690	1.36	0.55
3b	250	1.50	1.21	290	1.36	0.85
	500	1.52	1.21	310	1.36	0.88
	1000	1.55	1.18	370	1.37	0.87
3c	500	1.61	1.10	510	1.36	0.55
	750	1.65	1.08	570	1.37	0.53
	1000	1.66	1.06	600	1.36	0.50
3d	50	1.49	—		1.44[c)]	
	100	1.55	—		1.48[c)]	
	150	1.63	—		1.54[c)]	
	250	1.69	—		1.58[c)]	
	500	1.74	—		1.55[c)]	
5	500	2.01	—		1.90[c)]	
7	250	2.06	—		1.96[c)]	
	500	2.10	—		2.00[c)]	
	1000	2.18	—		2.06[c)]	
11	500	1.89	1.47	420	1.68	
33a	50	1.59	1.07	520	1.33	0.68
	150	1.61	1.01	600	1.31	0.63
	250	1.63	1.00	630	1.32	0.64
	500	1.69	0.96	730	1.33	0.50
33b	50	1.46	—		1.39[c)]	
	100	1.50	—		1.44[c)]	
	150	1.53	—		1.46[c)]	
	250	1.61	—		1.53[c)]	
	500	1.66	—		1.56[c)]	

a) The cyclic voltammetry was carried out in DMF–TBAP (0.1 mol dm^{-3}) using a platinum inlay electrode (Beckman No. 39273) and platinum wire as cathode and the counter electrode respectively. b) Reference electrode, SCE. c) When no anodic peak was recorded on potential reversal, the potential at which $i=0.85\ i_{pc}$[10)] was calculated.

the voltammograms for compounds **5**, **7**, and **11**, determined at the scan rate of 500 mV s^{-1}.

The α,β-unsaturated nitro esters **3a—d** showed E_{pc} values at considerably anodic potentials. Compounds **3a**, **3b**, and **3c** showed a quasi-reversible wave with quite similar E^0's at -1.35——1.37 V. Compound **3d**, on the other hand, showed only a cathodic wave with *ca.* -1.5 V (Table 2). Figure 2 shows the CV curves for **3a** at 50 and 250 mV s^{-1} and for **3b—d** either at 250 or 500 mV s^{-1}.

At the slow scan rate of 50 mV s^{-1}, for example, **3a** showed a fairly good reversible wave with $E^0=-1.35$ V. The peak potential difference, $\Delta E_p=E_{pc}-E_{pa}$, was 240 mV, whereas the current ratio, i_{pa}/i_{pc} was 0.84. When higher scan rates were used, the peak separation increased, and, unexpectedly, the current ratio showed a decrease. These phenomena were supposed to be caused both by a limited electron-transfer rate and a coupled chemical reaction.[10)] Based on the Randles-Cevcik equation[10)] the ratio, $i_p/269\,ACv^{1/2}=D^{1/2}n^{3/2}$, was calculated; it was found to be essentially unchanged on scan-speed variation.

The benzoate **3b** showed an even more prominent reversible wave with respect both to the peak separation and the current ratio (Fig. 2, Table 2). The current ratio for these compounds showed no change at the scan rates employed.

With the tosylate **3d** no anodic wave was recorded, not even when a high speed scan was used. The anion radical formed at this potential was shown to be highly reactive and was lost by the following chemical reaction in the time scale of the CV measurements. When the CV of **3a** and **3d** was determined under the same conditions using a similar concentration of the substrates, the cathodic current of **3d** was larger than that of **3a**, suggesting that the cathodic wave for **3d** might involve a two-electron transfer, whereas those for **3a—c** were quasi-reversible one-electron transfer processes.

Discussion

Whereas the electrochemical reduction of nitro compounds in protic media provides a useful synthetic process,[11)] a similar reaction under aprotic conditions results only in a reversible electron-transfer process involving an anion radical, as is shown by cyclic voltam-

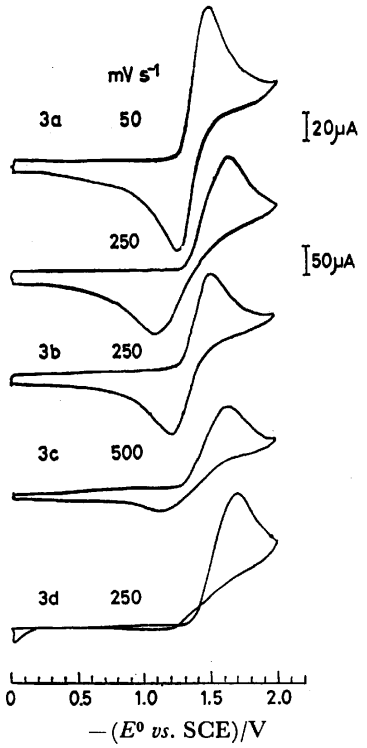

Fig. 2. Cyclic voltammograms for compounds **3a**, **3b**, **3c**, and **3d** determined in DMF using TBAP as supporting electrolyte. Current units (ordinate) for **3b**, **3c**, and **3d** are 20, 10, and 50 μA, respectively for the range shown for **3a**.

metry and ESR spectroscopy.[12,13] Accordingly, not much is known about the behavior of the anion radical in aprotic solvents. The anion radical of 2-methyl-2-nitropropiononitrile has been reported[14] to be cleaved into an alkyl radical and a nitrate ion.

The cathodic reactions of the homoallylic nitro esters **3a—d** were found to give a dimer and/or a cyclosteroid, depending on the nature of the ester group. The situation was found to be well reflected in the CV curves: those compounds that show a reversible wave tend to give the dimerization reaction product, whereas, those which fail to show an anodic wave tend to give the cyclosteroid. The time-dependent CV behavior of **3a** and **3b** suggests that the reaction involves an EC step, in which a reversible electron-transfer process is followed by the chemical reaction with the rate constant k_1. When k_1 is small and the scan rate is low,

$$O \underset{-e}{\overset{e}{\rightleftharpoons}} R \xrightarrow{k_1} P$$

the reversibility is good and the current ratio becomes nearly unity. The CV measurements carried out for related model compounds, such as **2a—d**, **5**, **7**, and **11** revealed that electrophores in these compounds could be reduced only at considerably cathodic potentials. On the other hand, **3a—d** were reduced at less cathodic potentials, indicating that the reduction occurred on an α,β-unsaturated nitro electrophore. As a result of the one-electron reduction, the electrophore is converted to an anion radical **12**, which is a resonance hybrid **13↔14**.

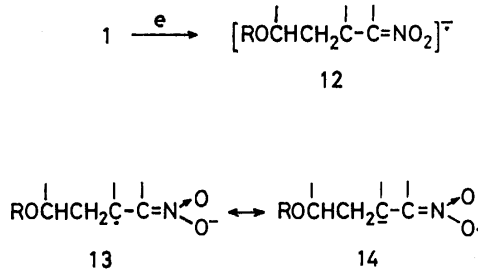

The tosylate **3d** showed no corresponding anodic peak on potential reversal, not even when the scan speed was increased by using a storage-memory technique. This indicates that the anion radical derived from **3d** is short-lived and hence possesses a high reactivity. The anion radicals equivalent to **13** and **14** can be written as **15** and **16**. The high reactivity of **16** can be expected, since a tosylate anion is an extremely good leaving group. An intramolecular nucleophilic displacement reaction gives **17**, which, on further one-electron reduction, forms an aci-anion **18**, the protonation of which gives **7** *via* **19**. The protonation of **18** appeared to occur in the isolation step, since the addition of D_2O, after the reaction was over, gave a deuterated product **20**. The mass-spectral analysis indicated the formation of **20** in up to a 60% yield by quenching the electrolysis reaction with D_2O. Before the addition of water, the reaction mixture remained colored, suggesting the stability of the aci-anion species **18**. No deuterium incorporation was observed in the control experiments in which **7** was treated with D_2O after electrolysis. The preferential formation of the thermodynamically unstable 6β-nitro compound **7** with an axial nitro group suggests that the proton attack occurs from a less hindered α-side for steric reasons.

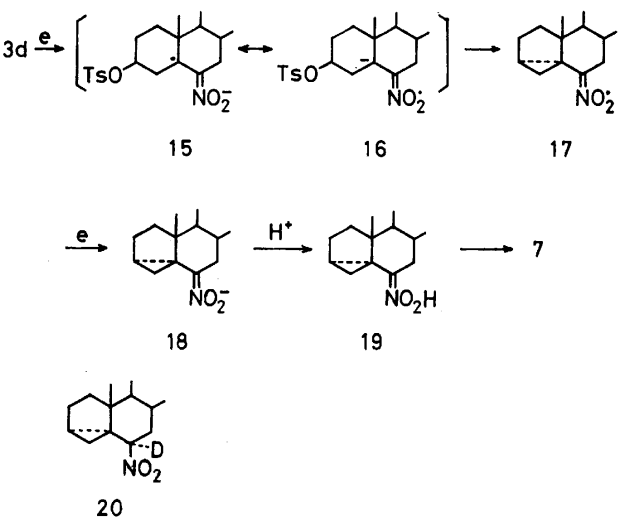

In the case of the acetate **3a** the corresponding anion radical exists as a resonance hybrid **21↔22**. Since an acetate ion is a less efficient leaving group, prototropy precedes to give **23** from **21**. The C-4 proton is sufficiently acidic, and its abstraction by the aci-anion is favored by the proximity effect.[3] The elimination of an acetate ion gives the corresponding allyl radical (**24↔25**).

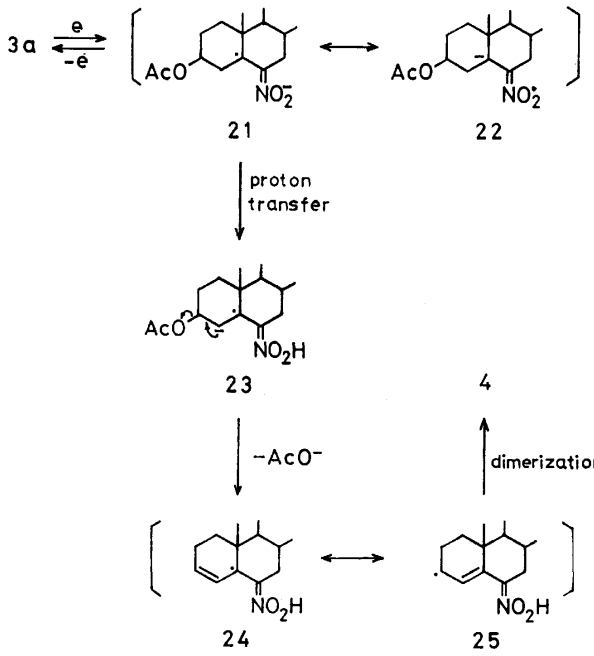

Dimerization is expected to occur on **25** to iveg **4**.

Alternatively, it is also possible to assume the isomerization of **3a** to give **26** prior to the one-electron reduction. The radical anion **23** can be derived from **26** by means of a cathodic reaction.

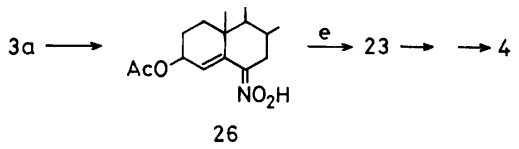

It might be possible that the dimer **4** was formed *via* the cyclosteroid **7** as an intermediate. That this is not likely is shown by the electrolysis reaction of **7**, coupled with the CV data indicating that it was reducible only at a more cathodic potential than that used for the actual electrolysis. Moreover, the controlled potential electrolysis of **7** at −1.90 V gave no trace of **4**, but instead gave the cyclosteroidal ketone **9** in a 16% yield, 72% of the starting material being recovered. Compound **9** was identical with the authentic material[7] and thus served as chemical evidence for the structure of **7**.

The ketone **9** may be formed *via* the oxime **27**. As support of this idea, we have observed that 6β-nitro-5α-cholestan-3β-ol (**10**) gives a hydroxy oxime **28** and a hydroxy ketone **29** upon controlled potential electrolysis in DMF–TBAP containing methanol at −1.70 V.[15]

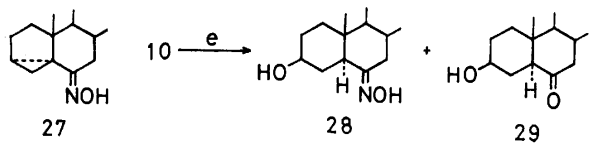

Related Reactions

The homoallylic nitro ester electrophore can be constructed in the steroidal system in another disposition. We further investigated the CV and controlled-potential electrolyses of 19-acetate **33a** and -tosylate **33b**. These were obtained by the above scheme.

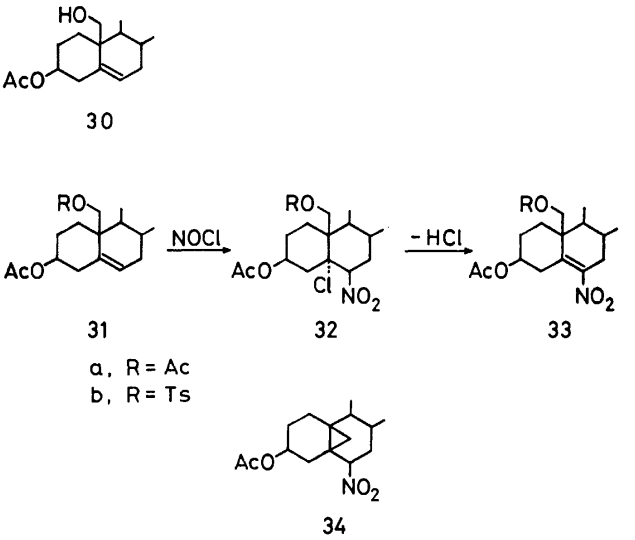

Cholest-5-ene-3β,19-diol 3-acetate (**30**)[16] was converted to 19-acetate **31a** and 19-tosylate **31b**, which were then treated with nitrosyl chloride using the method previously reported from these laboratories[17] to give two nitro chlorides **32a** and **32b**; this was followed by dehydrochlorination with pyridine.

The CV data of **33a** and **33b** are shown in Table 2. Whereas compound **33a** showed a quasi-reversible couple, $E^0 = -1.33$ V, the tosylate **33b** showed a cathodic peak at −1.5——1.7 V, but not any anodic peak, on potential reversal (Fig. 3). In view of the data found for **3a—d**, the CV results suggested that the tosylate **33b** might be highly reactive and might give the corresponding cyclosteroid. In fact, the electrolysis of **33b** carried out at −1.30 V in DMF–TBAP gave a 27% yield of 6β-nitro-5,19-cyclo-5β-cholestan-3β-ol acetate (**34**). The electricity consumed amounted to 1.7 F mol^{-1}. The structure was supported by the IR spectral data, which showed absorptions at 3070 (cyclopropane ring), 1730 (acetoxy), and 1545 cm^{-1} (nitro group on saturated carbon), and also by the NMR spectra, which showed a one-proton multiplet at δ 4.77 with a half-band width of 9 Hz. On the other

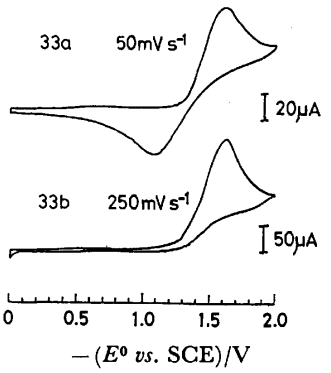

Fig. 3. Cyclic voltammograms for compounds **33a** and **33b** determined in DMF using TBAP as supporting electrolyte.

hand, no isolable compounds were obtained by similar experiments carried out for **33a**.

Experimental

6-Nitrocholest-5-en-3β-yl Acetate (3a). Cholesteryl acetate was nitrated with concd nitric acid and potassium nitrite according to the method of Shoppee *et al.*,[2] to give **3a**: mp 103.5—104.5 °C. The hydrolysis of **3a** with 60% perchloric acid in methanol gave **3** (R=H); mp 129—131 °C.[18]

6-Nitrocholest-5-en-3β-yl Benzoate (3b). A mixture of 14.6 g (27 mmol) of **3** (R=H) and 12 cm³ (54 mmol) of benzoyl chloride, in 10 cm³ of pyridine, was left to stand overnight. A subsequent usual work-up gave benzoate **3b** in an 86% yield; recrystallized from ethyl acetate: mp 191—196 °C; IR (KBr) 1510, 1710 cm⁻¹; NMR ($CDCl_3$) δ 0.72 (3H, s, C-18H), 1.18 (3H, s, C-19H), 6.35 (1H, m, $W_{1/2}$= 16.8 Hz, C-3αH), 7.35—8.15 (5H, m, ArH).

Found: C, 75.90; H, 9.37; N, 2.62%. Calcd for $C_{34}H_{49}NO_4$: C, 76.20; H, 9.22; N, 2.61%.

6-Nitrocholest-5-en-3β-yl Trifluoroacetate (3c). A mixture of 9.2 g (21 mmol) of **3** (R=H) and 11 cm³ (78 mmol) of trifluoroacetic anhydride in 80 cm³ of pyridine was left to stand overnight; recrystallization from methanol then gave 49% of **3c**: mp 110.5—111.5 °C; IR (KBr) 1510, 1780 cm⁻¹; NMR ($CDCl_3$) δ 0.69 (3H, s, C-18H), 1.18 (3H, s, C-19H), 4.87 (1H, m, $W_{1/2}$=17.4 Hz, C-3αH).

Found: C, 65.68; H, 8.14; N, 2.65%. Calcd for $C_{29}H_{44}NO_4F_3$: C, 66.00; H, 8.40; N, 2.65%.

6-Nitrocholest-5-en-3β-yl Tosylate (3d). A mixture of 15 g (31.7 mmol) of **3** (R=H), 7.5 g (39.3 mmol) of tosyl chloride, and 100 cm³ of pyridine was warmed at 50 °C for 1 h. A usual work-up subsequently gave an 88% yield of **3d** after recrystallization from acetone–methanol: mp 168—169 °C (dec); IR (KBr) 1510, 1780 cm⁻¹; NMR ($CDCl_3$) δ 0.67 (3H, s, C-18H), 1.10 (3H, s, C-19H), 2.47 (3H, s, ArMe), 4.35 (1H, m, $W_{1/2}$=16.2 Hz, C-3αH), 7.55 (4H, m, ArH).

Found: C, 69.92; H, 8.95; N, 2.31%. Calcd for $C_{34}H_{51}NO_5S$: C, 69.72; H, 8.79; N, 2.39%.

Electrolyses. Both controlled-potential and controlled-current electrolyses were carried out for **3a**—**d**. As representative examples, the controlled-potential electrolysis of **3a** and **3d** and the controlled-current electrolysis of **3d** will be described. The results of the controlled-current electrolysis are summarized in Table 2.

The cylindrical cell used for the electrolysis was equipped with a side arm for connecting the reference electrode, SCE, using two junction bridges, filled with saturated KCl and DMF–TBAP (0.1 mol dm⁻³) solutions. A ceramic thimble (o. d. 3 cm) was used as a divider and was placed on a spacer to allow stirring using a magnetic bar. A punched platinum electrode with an area of 60 cm² was used as the cathode, while a platinum wire was used as the anode. Before the electrolysis, the reaction mixture was purged with nitrogen for at least 20 min. A Hokuto potentiostat/galvanostat HA-101 apparatus (max. output 30 V, 1 A) was used, together with a Hokuto digital coulometer HF-102.

The Controlled-potential Cathodic Reduction of 3a. 6β,6'β-Dinitro-3,3'-cholesta-4,4'-diene (4): A solution of 600 mg (12.7 mmol) of **3a** in 250 cm³ of purified DMF containing TBAP (0.1 mol dm⁻³) was purged with nitrogen and electrolyzed at the controlled potential of −1.44 V. During the reaction, a solid material was separated out as a precipitate. After 1 F mol⁻¹ of electricity had been consumed, the precipitate was filtered, washed with DMF, water, and dried. Recrystallization from benzene gave colorless needles; mp 234—235 °C. The filtrate was evaporated to dryness, extracted with ether, and washed with water to eliminate TBAP. The residue was dissolved in benzene and passed through a Florisil column to give a second crop (mp 233—235 °C) of **4**; the total yield was 45%: IR (KBr) 1550, 1635 cm⁻¹; NMR ($CDCl_3$) δ 0.72 (3H, s, C-18H), 0.92 (3H, s, C-19H), 4.67 (1H, m, $W_{1/2}$=8.25 Hz, C-6αH), 5.90 (1H, m, $W_{1/2}$=4.2 Hz, C-4H); MW 829 (Rast).

Found: C, 77.81; H, 10.69; N, 3.24%. Calcd for $C_{54}H_{88}N_2O_4$: C, 78.02; H, 10.91; N, 3.37%.

The Controlled-potential/current Cathodic Reduction of 3d. A solution of 1.0 g (1.7 mmol) of **3d** in 100 cm³ of DMF–TBAP was electrolyzed at the controlled potential of −1.45 V. After 1.5 F mol⁻¹ of electricity had been consumed, the product was purified by silica-gel chromatography and eluted with hexane containing an increasing amount of benzene. Compound **7** was thus obtained in a 43% yield (mp 102—102.5 °C), after recrystallization from methanol: IR (KBr) 3080, 3030, 3007, 1550 cm⁻¹; NMR ($CDCl_3$) δ 0.73 (3H, s, C-18H), 0.94 (3H, s, C-19H), 3.87 (1H, m, $W_{1/2}$=8.25 Hz, C-6αH).

Found: C, 77.84; H, 10.77; N, 3.27%. Calcd for $C_{27}H_{45}NO_2$: C, 78.03; H, 10.91; N, 3.37%.

The controlled-current reduction of **3d** was carried out using a solution of 5.8 g (9.8 mmol) of **3d** in 250 cm³ of DMF–TBAP at the current density of 0.85 mA cm⁻². The electrolysis was continued until the potential between the working and reference electrodes reached −2.0 V and 1 F mol⁻¹ of electricity had been consumed. A 36% yield of **7** and a 2% yield of **4** were obtained.

When D_2O (1 cm³) was added after the electrolysis was over, a 6α-deuterio compound **20** was isolated. Compound **20** was characterized by means of its mass spectrum; *m/e* 370. NMR analysis showed that **20** was present in a 60% quantity together with 40% of **7**.

The Controlled-potential Reduction of 7. A solution of 430 mg (1.0 mmol) of **7** in 100 cm³ of DMF–TBAP was electrolyzed at −1.90 V. A usual work-up, followed by silica-gel chromatography and eluting with benzene–hexane (1 : 4), gave 310 mg of colorless needles; mp 101—102 °C; recrystallized from acetone–methanol. It was identical with the **10** prepared by the known route.[11] The yield was 16%.

5-Chloro-6β-nitro-5α-cholestane-3β,19-diol Diacetate (32a). Nitrosyl chloride (4.9 g, 75 mmol) was added to a solution of 3.7 g (7.6 mmol) of cholest-5-ene-3β,19-diol diacetate (**31a**) in 41 cm³ of ether at 0 °C. Then 2.9 g of potassium acetate had been added, the mixture was left to stand for 4 d in a refrigerator. Filtration and then evaporation gave a blue oil, which, after solidification, was recrystallized from acetone–methanol; mp 120.5—121.5 °C. The yield was 58%: IR (KBr) 1745, 1550 cm⁻¹; NMR ($CDCl_3$) δ 0.73 (3H, s, C-18H), 2.04 (6H, s, CH_3COO), 5.35 (1H, m, $W_{1/2}$=28.5 Hz, C-3αH).

Found: C, 65.80; H, 8.97; N, 2.39%. Calcd for $C_{31}H_{50}NO_6Cl$: C, 65.52; H, 8.87; N, 2.46%.

6-Nitrocholest-5-ene-3β,19-diol Diacetate (33a). Compound **32a** was dissolved in pyridine, warmed at 50 °C for 30 min, and then left to stand overnight. The product was recrystallized from acetone–methanol; mp 114.5—115.5 °C (69%): IR (KBr) 1740, 1520 cm⁻¹; NMR ($CDCl_3$) δ 0.73 (3H, s, C-18H), 2.03 (3H, s, CH_3COO), 2.07 (3H, s, CH_3COO), 4.32 (2H, dd, C-19H), 4.60 (1H, m, $W_{1/2}$=21 Hz, C-3αH).

Found: C, 70.15; H, 9.34; N, 2.56%. Calcd for $C_{31}H_{49}NO_6$: C, 70.02; H, 9.29; N, 2.63%.

5-Chloro-6β-nitro-5α-cholestane-3β,19-diol 3-Acetate 19-Tosylate (32b). To a solution of 2.6 g (4.3 mmol) of cholest-5-ene-3β,19-diol 3-acetate 19-tosylate (**31b**) in ether (94 cm³), were added nitrosyl chloride (2.8 g) and potassium acetate (1.7 g) at 0 °C. The product was then recrystallized from

acetone–methanol; mp 131—132 °C (47% yield): IR (KBr) 1735, 1565 cm^{-1}; NMR ($CDCl_3$) δ 0.41 (3H, s, C-18H), 2.04 (3H, s, CH_3COO), 5.32 (1H, m, C-3αH), 7.38—7.80 (4H, m, ArH).

Found: C, 63.55; H, 8.05; N, 1.88%. Calcd for $C_{36}H_{54}O_7NSCl$: C, 63.55; H, 8.00; N, 2.06%.

*6-Nitrocholest-5-ene-3β,19-diol 3-Acetate 19-Tosylate (**33b**).* The dehydrochlorination of **32b** with pyridine gave **33b**, mp 116.5—117.5 °C (85%, recrystallized from acetone–methanol): IR (KBr) 1735, 1520 cm^{-1}; NMR ($CDCl_3$) δ 0.63 (3H, s, C-18H), 1.98 (3H, s, CH_3COO), 2.44 (3H, s, ArMe), 7.35—7.79 (4H, m, ArH), 4.53 (1H, m, $W_{1/2}$=25.5 Hz, C-3αH).

Found: C, 67.43; H, 8.37; N, 2.10%. Calcd for $C_{36}H_{53}O_7NS$: C, 67.15; H, 8.29; N, 2.17%.

*Controlled-potential Reduction of **33b**.* A solution of 590 mg (0.91 mmol) of **33b** in 60 cm^3 of DMF–TBAP was electrolyzed at −1.30 V until 1.7 F mol^{-1} of electricity had been consumed. Chromatography on silica gel eluted with benzene–hexane (1 : 4) gave a 27% yield of 5β,19-cyclo-6β-nitro-5β-cholestan-3β-ol 3-acetate (**34**); mp 88—89 °C (recrystallized from methanol): IR (KBr) 1730, 1545 cm^{-1}; NMR ($CDCl_3$) δ 0.52 and 0.98 (2H, dd, J=6 Hz, cyclopropyl CH_2), 2.05 (3H, s, CH_3COO).

Found: C, 73.48; H, 10.01; N, 2.80%. Calcd for $C_{29}H_{47}O_4N$: C, 73.53; H, 10.00; N, 2.96%.

Cyclic Voltammetry. The measurements were carried out using a generator, Hokuto HB-107A and a potentiostat, Hokuto HA-101. As a cathode, a platinum inlay electrode, Beckman No. 39273, was used. Samples are dissolved in DMF containing 0.1 mol dm^{-3} of TBAP. The results are shown in Table 2 and Figs. 1—3. For high-speed scans, the output was stored in a wave-memory unit, NF Circuit Block WM-812A.

References

1) Electron-organic Chemistry VII. Part VI: K. Torizuka and T. Sato, *Bull. Chem. Soc. Jpn.*, **53**, 2411 (1980).
2) C. W. Shoppee, *J. Chem. Soc.*, **1948**, 1032.
3) J. R. Bull, E. R. H. Jones, and G. H. Meakins, *J. Chem. Soc.*, **1965**, 2611.
4) W. A. Harrison, E. R. H. Jones, and G. H. Meakins, *J. Chem. Soc.*, **1964**, 3214.
5) J. Fried and N. A. Abraham, *Tetrahedron Lett.*, **1964**, 1879.
6) W. B. Smith, D. C. Deavenport, J. A. Swanzy, and G. A. Pate, *J. Magn. Reson.*, **12**, 15 (1972).
7) R. M. Dodson and P. Riegel, *J. Org. Chem.*, **13**, 424 (1948).
8) J. March, "Advanced Organic Chemistry," McGraw-Hill Book Co. (1968), p. 294.
9) A. Hassner and C. Heathcock, *J. Org. Chem.*, **29**, 1350 (1964); J. R. Bull, E. R. H. Jones, and G. D. Meakins, *J. Chem. Soc.*, **1965**, 2601.
10) A. J. Fry, "Synthetic Organic Electrochemistry," Harper and Row Publishers (1972), p. 95.
11) M. R. Rifi, "Technique of Electroorganic Synthesis," ed by N. L. Weinberg, John Wiley and Sons (1975), Part II, Chap. VIII, p. 137.
12) W. H. Smith and A. J. Bard, *J. Am. Chem. Soc.*, **97**, 5203 (1975); V. M. Kozakova, I. G. Makarov, M. E. Kurek, and E. A. Chernyshev, *Zh. Struk. Khim.*, **9**, 525 (1968) [*Chem. Abstr.*, **69**, 9886 (1968)]; H. Watanabe, M. Aoki, H. Matsumoto, Y. Nagai, and T. Sato, *Bull. Chem. Soc. Jpn.*, **50**, 1019 (1977).
13) P. Stradyn and R. A. Gavar, "Progress in Electrochemistry of Organic Compounds," ed by A. N. Frumkin and A. B. Ershler, Plenum Press (1971), Vol. 1, Chap. 1, p. 1.
14) F. Lambert and K. Kobagaski, *J. Am. Chem. Soc.*, **82**, 5324 (1960).
15) T. Sato, Y. Komeichi, and S. Kobayashi, unpublished results.
16) J. Kalvoda, K. Hensler, H. Ueberwasser, G. Anner, and A. Wettstein, *Helv. Chim. Acta*, **46**, 1361 (1963).
17) Y. Komeichi, Y. Osawa, W. L. Duax, and A Cooper, *Steroids*, **15**, 619 (1970).
18) K. Tanabe and R. Hayashi, *Chem. Pharm. Bull.*, **10**, 1177 (1962); M. Davis, *J. Chem. Soc.*, **1964**, 2830.

 © 1982 The Chemical Society of Japan Bull. Chem. Soc. Jpn., 55, 527—533 (1982)

Collins Oxidation of Methyl (+)-13β-Abiet-8-en-18-oate and Absolute Configuration of Suaveolic Acid

Takashi MATSUMOTO,* Sachihiko IMAI,* Shuhei YUKI, Arata KATAYAMA, and Manabu FURUTANI

Department of Chemistry, Faculty of Science, Hiroshima University, Higashisenda-machi, Naka-ku, Hiroshima 730

(Received May 29, 1981)

The oxidation of methyl (+)-13β-abiet-8-en-18-oate with Collins reagent yielded nine oxidation products. Their structures were elucidated on the basis of spectroscopic and chemical data to be methyl (−)-14-hydroxy-7-oxoabieta-8,11,13-trien-18-oate (1% yield), methyl (−)-11,14-dioxoabieta-8,12-dien-18-oate (1%), methyl (+)-11-oxo-13β-abiet-8-en-18-oate (18%), methyl (−)-8α,9α-epoxy-7-oxo-13β-abietan-18-oate (2%), methyl (+)-7-oxoabieta-8,11,13-trien-18-oate (2%), methyl (+)-11,14-dihydroxy-7-oxoabieta-8,11,13-trien-18-oate (2%), methyl (+)-7,11-dioxo-13β-abiet-8-en-18-oate (17%), methyl (+)-14-oxo-13β-abiet-8-en-18-oate (**15**) (4%), and methyl (+)-7-oxo-13β-abiet-8-en-18-oate (23%) respectively. It is noteworthy that oxygenation occurs not only at the C-7 and C-11 positions but also at the C-14 position. The oxygenated products obtained in this studies could be useful intermediates for the synthesis of the oxidized diterpenoids of abietane skeleton. To exemplify this, **15** was converted to methyl suaveolate and suaveolol. Hydrolysis of the former yielded suaveolic acid, thus confirming its absolute configuration to be 4R, 5R, 10S, 13S, and 14S.

The allylic oxygenated derivatives of methyl (+)-13β-abiet-8-en-18-oate (**1**)[1] seem to be useful intermediates for the partial syntheses of naturally occurring diterpenes possessing oxygen functions at the C-7, C-11, and/or C-14 positions. For this reason we attempted the oxidation of **1** with Collins reagent, which was superior to other reagents used for allylic oxidation,[2] and obtained the products oxygenated at the C-14 position in addition to those with oxygen functions at the C-7 and C-11 positions. This result is in contrast with the previously reported oxidation of **1** with *t*-butyl chromate.[3] A compound of the former type has been successfully converted to suaveolic acid;[4] this conversion confirms its absolute configuration.

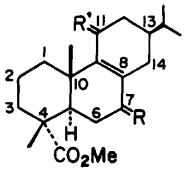

1 R=R'=H$_2$
5 R=H$_2$, R'=O
9 R=α-H·β-OH, R'=H$_2$
14 R=R'=O
16 R=O, R'=H$_2$

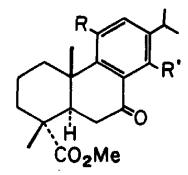

2 R=H, R'=OAc
3 R=H, R'=OH
11 R=OAc, R'=OH
12 R=R'=OH
13 R=R'=H

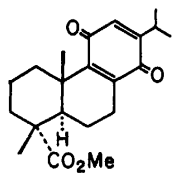

4

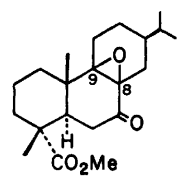

6 8α,9α-epoxy
8 8β,9β-epoxy

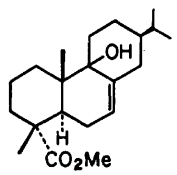

7 9α-OH
10 9β-OH

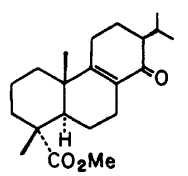

15

Collins Oxidation of Methyl (+)-13β-Abiet-8-en-18-oate (1). The oxidation of **1** was carried out with Collins reagent[5] in dichloromethane at room temperature for 24 h. The reaction mixture was carefully separated by repeated column chromatography on silica gel to give nine keto ester compounds: A (1%), B (1%), C (18%), D (2%), E (2%), F (2%), G (17%), H (4%), and I (23%), in the order of elution. The structure elucidation of these oxidation products was carried out as follows.

Compounds A and B were obtained as a mixture which could not be separated satisfactorily. Therefore the mixture was acetylated with refluxing acetic anhydride in the presence of sodium acetate and the resulting crude product was successfully separated by column chromatography on silica gel to give an acetylated A and the original ketone B. The more polar acetylated A showed the presence of an acetoxyl group at 1763 cm^{-1} in its IR spectrum and a conjugated carbonyl group at 1673 cm^{-1}. Its ^{1}H NMR spectrum indicated signals due to a pair of ortho-coupling aromatic protons at δ 7.14 and 7.37 (each 1H, d, and J= 8 Hz). Consequently, the structure of the acetylated A was determined to be methyl 14-acetoxy-7-oxoabieta-8,11,13-trien-18-oate (**2**). Hydrolysis of the acetate **2** with sodium hydrogencarbonate in refluxing aqueous methanol gave the original ketone A, methyl 14-hydroxy-7-oxoabieta-8,11,13-trien-18-oate (**3**),[6] whose ^{1}H NMR spectrum showed a reasonable signal at δ 13.08 (1H, s), indicating the presence of a hydroxyl group chelated with a conjugated carbonyl group (IR: 1622 cm^{-1}). The compound B, which was less polar than the acetate **2**, showed the presence of a *p*-quinone moiety [IR: 1640, 1597 cm^{-1}; ^{1}H NMR: δ 6.32 (1H, d, J=1 Hz); UV: λ_{max}^{EtOH} 257 nm (ε 11800), 338 (340), 420 (40)]. On the basis of these spectral data and mass spectrum [*m/e* 344 (M$^+$)] the structure of the compound B was determined to be methyl 11,14-dioxoabieta-8,12-dien-18-oate (**4**).[7]

The compound C (mp 108—110 °C; IR: 1715, 1652 cm^{-1}) was identified as methyl 11-oxo-13β-abiet-8-en-18-oate (**5**) by direct spectral comparison with an

authentic sample.[3,8]

The compound D (mp 122—123 °C, $C_{21}H_{32}O_4$) showed absorption bands at 1718 and 1695 cm^{-1} in its IR spectrum and no UV absorption band in the 220—250 nm region, indicating the presence of an ester group and a non-conjugated carbonyl group. The fourth oxygen atom should be an epoxide one. In its ^1H NMR spectrum a signal at δ 2.81 (1H, dd, J=11.5 and 8 Hz) assignable to a C-5α proton[9] suggested that the structure of the ketone D was methyl 8α,9α-epoxy-7-oxo-13β-abietan-18-oate (**6**). This structure was subsequently confirmed by transformation of **6** to the known methyl 9α-hydroxy-13β-abiet-7-en-18-oate (**7**)[10] by refluxing with hydrazine hydrate in methanol containing a small amount of acetic acid under a stream of nitrogen. For comparison, methyl 8β,9β-epoxy-7-oxo-13β-abietan-18-oate (**8**) was also synthesized by epoxidation of methyl 7β-hydroxy-13β-abiet-8-en-18-oate (**9**)[11] with *m*-chloroperbenzoic acid followed by oxidation of the resulting methyl 8β, 9β-epoxy-7β-hydroxy-13β-abietan-18-oate with Jones reagent. The epoxide **8** was then converted to methyl 9β-hydroxy-13β-abiet-7-en-18-oate (**10**) by a similar treatment with hydrazine hydrate. The ^1H NMR signals corresponding to the methyl groups at the C-4 and C-10 positions in **6**, **7**, **8**, and **10** are shown in Table 1. The chemical shifts of the C-10 methyl groups in the 9β series are more deshielded than those in 9α series; this follows from the stereochemistry of their oxygen functions. The pyridine-induced solvent shift[12] (Δ −0.21 ppm) of the C-10 methyl group in **10** also supported the conclusion that the stereochemistry of the hydroxyl group at the C-9 position was in β-configuration.

Compounds E and F were obtained as a mixture which contained one component possessing a free phenolic hydroxyl group [^1H NMR: δ 6.01 (1H, bs)]. Therefore, the mixture was acetylated with acetic anhydride in pyridine at room temperature and the resulting crude product was purified by column chromatography on silica gel to give the original E and an acetylated F. The acetylated F, mp 158.5—159.5 °C, which was less polar, showed the presence of an acetoxyl group [IR: 1757 cm^{-1}, ^1H NMR: δ 2.32 (3H, s)], an aromatic proton [^1H NMR: δ 6.95 (1H, s)], and a hydroxyl group [^1H NMR: δ 13.54 (1H, s)] chelated with a conjugated carbonyl group (IR: 1630 cm^{-1}). These spectral data suggested that the structure of the acetylated F was methyl 11-acetoxy-14-hydroxy-7-oxoabieta-8,11,13-trien-18-oate (**11**). Hydrolysis of the acetate **11** with sodium hydrogencarbonate in refluxing aqueous methanol gave the original ketone F, methyl 11,14-dihydroxy-7-oxoabieta-8,11,13-trien-18-oate (**12**), mp 233.5—234.5 °C, whose ^1H NMR spectrum showed a signal at δ 3.47 (1H, dm, J=12 Hz) assignable to C-1β proton; this supported the presence of a hydroxyl group at the C-11 position.[13] The compound E isolated from the more polar fraction was identified as methyl 7-oxoabieta-8,11,13-trien-18-oate (**13**) by direct spectral comparison with an authentic sample.[14]

Compound G (mp 87—89.5 °C; IR: 1720, 1670 cm^{-1}) was also identified as methyl 7,11-dioxo-13β-abiet-8-en-18-oate (**14**) by direct spectral comparison with an authentic sample.[3,8]

TABLE 1. CHEMICAL SHIFTS OF C_4- AND C_{10}-METHYL GROUPS OF **6**, **7**, **8**, AND **10** (δ VALUE)

	9α Series			9β Series		
	6		**7**	**8**		**10**
Solvent[a]	A	B	C	A	B	C
C_4–Me	1.18	1.30	1.39	1.15	1.30	1.37
C_{10}–Me	0.94	0.96	1.03	1.15	1.08	1.29

a) A, carbon tetrachloride; B, chloroform-*d*; C, pyridine-d_5.

Compound H showed the presence of a conjugated carbonyl group in the IR spectrum (1655 cm^{-1}) and a characteristic isopropyl group in the ^1H NMR spectrum [δ 0.79 and 0.94 (each 3H, d, and J=7 Hz)]. The IR and ^1H NMR spectra of ketone H were identical with those reported for methyl 14-oxo-13β-abiet-8-en-18-oate (**15**).[4]

Compound I (mp 111—112 °C; IR: 1725, 1652 cm^{-1}) was identified as methyl 7-oxo-13β-abiet-8-en-18-oate (**16**) by direct spectral comparison with an authentic sample.[3,8]

Thus, the structures of nine oxidation products could be elucidated. The present oxidation of **1** with Collins reagent occurred not only at the C-7 and C-11 positions, as was the case with *t*-butyl chromate, but also at the C-14 position; this latter resulted in the formation of **3**, **4**, **12**, and **15**. The latter compounds would be useful intermediate for the synthesis of 14-oxygenated abietane diterpenes as illustrated below.

The compounds, **5** and **14**, were each converted[15] to methyl 11-methoxyabieta-8,11,13-trien-18-oate (**17**).[16] Treatment of **15** with copper(II) bromide and lithium bromide in refluxing acetonitrile afforded methyl 14-hydroxyabieta-8,11,13-trien-18-oate (**18**),[17] which was then methylated with methyl iodide and sodium hydride in *N*,*N*-dimethylformamide to give methyl 14-methoxyabieta-8,11,13-trien-18-oate (**19**).[17] These compounds, **17** and **19**, seem to be useful intermediates for the syntheses of nellionol (**20**),[18] premnolal (**21**),[18,19] and the like.[18]

Absolute Configuration of Suaveolic Acid. Suaveolic acid and suaveolol have been isolated from the leaves and stems of *Hyptis suaveolens* (L) Point (Labiatae) by Manchand *et al.*[4] On the basis of chemical and spectro-

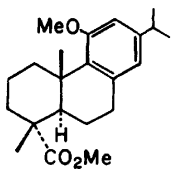

17

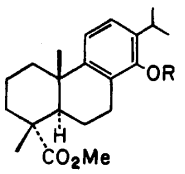

18 R=H
19 R=Me

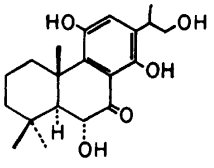

20

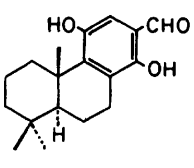

21

scopic studies, the structures of suaveolic acid and suaveolol were assigned respectively to be **22** and **23**; their relative stereochemistry were further confirmed by an X-ray structure analysis of methyl suaveolate (**24**).[4] In order to clarify the absolute configurations of these unusual[4] tricyclic diterpenes, metal hydride reductions of the 14-oxo compound **15** were carried out.

The compound **15** was reduced with sodium borohydride in refluxing tetrahydrofuran in the presence of aqueous sodium hydroxide to afford a mixture of alcohols. The mixture was then separated by column chromatography on silica gel to give four alcohols: W (24%), X (38%), Y (7.5%), and Z (15%), in the order of elution. Treatment of **15** with sodium methoxide in refluxing methanol provided an inseparable mixture of **15** and its C-13 epimer (**25**) [^{1}H NMR: δ 0.90 and 0.91 (each 3H, d, and J=6 Hz, $-CH(C\underline{H}_3)_2$)]. The ^{1}H NMR spectrum of the mixture showed these epimers were present approximately in a 2 : 1 ratio. However, when **15** was treated with aqueous sodium hydroxide in refluxing tetrahydrofuran, the starting ketone **15** was recovered. Therefore, it is clear that no epimerization at the C-13 position in **15** occurred under the above reduction conditions.

The oily alcohol W ($[\alpha]_D$+125°) showed the presence of a hydroxyl group (3620, 3460 br cm^{-1}) and an ester group (1720 cm^{-1}) in the IR spectrum. Its ^{1}H NMR spectrum showed signals at δ 0.95 and 0.98 (each 3H, d, and J=6 Hz) due to an isopropyl group and at δ 3.78 (1H, br, $W_{1/2}$=5.5 Hz) due to C-14α proton. These physical and spectral data were not identical with those of methyl suaveolate (**24**). Oxidation of the alcohol W with pyridinium chlorochromate in dichloromethane afforded the ketone **15**. The alcohol W was then acetylated with acetic anhydride in pyridine to give an oily monoacetate (**27**) ($[\alpha]_D$+181°, IR: 1713 cm^{-1}). Thus, the structure of the alcohol W was identified as methyl 14β-hydroxy-13β-abiet-8-en-18-oate (**26**).

The alcohol X (mp 102—103 °C, $[\alpha]_D$+59°; IR: 3600, 3450 br, 1720 cm^{-1}) was further characterized as its acetate (**28**) (mp 134.5—135 °C, $[\alpha]_D$−41°, IR: 1720 cm^{-1}). Oxidation of the alcohol X with pyridinium chlorochromate in dichloromethane afforded the ketone **15**. The physical and spectral data, including optical rotation of the alcohol X and **28**, were identical with those of methyl suaveolate and its acetate.

The oily alcohol Y ($[\alpha]_D$+92°; IR: 3625, 3450 br cm^{-1}) showed the presence of hydroxyl groups [^{1}H NMR: δ 3.15 and 3.44 (each 1H, d, and J=10.5 Hz, $-C\underline{H}_2OH$) and 3.77 (1H, br, $W_{1/2}$=6 Hz, $-C\underline{H}OH$)] and the absence of an ester group. Acetylation of the alcohol Y with acetic anhydride in pyridine afforded the corresponding diacetate (**30**) (mp 93—95 °C, $[\alpha]_D$+201°, IR: 1722 cm^{-1}). The physical and spectral data of the alcohol Y and **30** were different from those of suaveolol and its diacetate. Thus, the structure of the alcohol Y was identified as 13β-abiet-8-ene-14β,18-diol (**29**).

The alcohol Z (mp 180—182 °C, $[\alpha]_D$+84°; IR: 3620, 3290 br cm^{-1}) showed signals at δ 2.97 and 3.46 (each 1H, d, and J=11 Hz) due to a hydroxymethyl group and at δ 3.77 (1H, bd, J=7 Hz) due to C-14β proton in the ^{1}H NMR spectrum. Acetylation of the alcohol Z with acetic anhydride in pyridine yielded an oily diacetate (**31**) ($[\alpha]_D$−41°, IR: 1720 cm^{-1}). The physical and spectral data of the alcohol Z and **31** were identical with those of suaveolol and its diacetate.

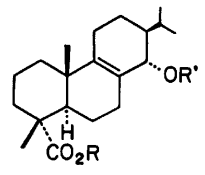

22 R=R'=H
24 R=Me, R'=H
28 R=Me, R'=Ac

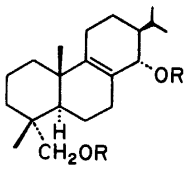

23 R=H
31 R=Ac

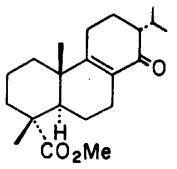

25

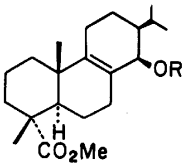

26 R=H
27 R=Ac

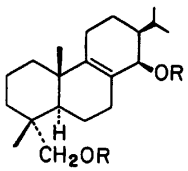

29 R=H
30 R=Ac

Subsequently, the ketone **15** was reduced with lithium aluminium hydride in refluxing ether. Chromatographic purification of the crude product gave **23** (47%) and **29** (23%).

Finally, the synthetic methyl suaveolate **24** was hydrolyzed with potassium *t*-butoxide in dimethyl sulfoxide at room temperature to give suaveolic acid **22**, mp 188—190 °C, $[\alpha]_D$+71°.

From the present study, the absolute configurations of suaveolic acid and suaveolol were conclusively assigned as 4R, 5R, 10S, 13S, and 14S.

Experimental

All melting points are uncorrected. The IR and optical rotations were measured in chloroform, and the ^{1}H NMR spectra in carbon tetrachloride at 90 MHz, with tetramethylsilane as an internal standard, unless otherwise stated. The chemical shifts are presented in terms of δ values; s: singlet, bs: broad singlet, d: doublet, bd: broad doublet, dd: double doublet, dm: doublet of multiplet, t: triplet, bt: broad triplet, m: multiplet. The low-resolution mass spectra were obtained by direct inlet (ion-source temperature 200 °C and ionizing voltage 70 eV). The column chromatography was performed using Merck silica gel (0.063 mm).

Methyl (+)-13β-Abiet-8-en-18-oate (1). A suspension of (+)-13β-abiet-8-en-18-oic acid[1] in acetone was methylated with diazomethane at room temperature for 3 h to give **1**[3] as an oil, $[\alpha]_D$ +79° (*c* 3.82), which without purification was used in the next reaction.

Oxidation of 1 with Collins Reagent. Chromium trioxide

(113.2 g) was added to a mechanically stirred solution of pyridine (188 g) in dichloromethane (2.4 l) over a period of 20 min with cooling in an ice-bath. After the mixture had been stirred at room temperature for 2 h, a solution of **1** (24.0 g) in dichloromethane (200 ml) was added over a period of 30 min. The reaction mixture was further stirred at room temperature for 24 h and then decanted from a tarry residue, which was washed with ether (3.2 l). The combined organic solution was washed successively with aqueous sodium hydrogencarbonate, dilute hydrochloric acid, and brine. The solution was concentrated to *ca.* 2 l of volume, dried over sodium sulfate, and evaporated to give a reddish brown oil (24.0 g). The crude product (48.0 g) obtained from two runs of the oxidation was chromatographed on silica gel (1.5 kg), using benzene as the eluent, to give the recovered **1** (5.66 g: 12%).

Subsequent elution with benzene gave a mixture of two ketones (1.02 g), A (**3**) and B (**4**), whose separation and purification are described later.

Further elution with benzene afforded a ketone C (8.95 g: 18%) which was recrystallized from methanol, mp 108—110 °C, $[\alpha]_D$ +104° (*c* 0.743, EtOH) [lit,[3] mp 108—109 °C, $[\alpha]_D^{25}$ +104° (EtOH)]; IR: 1715, 1652, 1608 cm^{-1}; ^1H MNR ($CDCl_3$): 0.90 (6H, bd, J=5.5 Hz, $-CH(C\underline{H}_3)_2$), 1.18 and 1.21 (each 3H and s, C_4-CH_3 and $C_{10}-CH_3$), 2.87 (1H, dm, J=13 Hz, $C_{1\beta}-H$), 3.65 (3H, s, $-CO_2CH_3$). The IR and ^1H NMR spectra of the ketone C were identical with those of methyl 11-oxo-13β-abiet-8-en-18-oate (**5**).[3,8]

Elution with ether–benzene (1 : 99) gave a fraction (1.36 g) containing a ketone D, which was further purified by column chromatography on solica gel (150 g) to afford the pure ketone D (0.84 g: 2%), methyl 8α,9α-epoxy-7-oxo-13β-abietan-18-oate (**6**). This was recrystallized from methanol to give colorless needles, mp 122—123 °C, $[\alpha]_D$ −64° (*c* 1.70); IR: 1718, 1695 cm^{-1}; ^1H NMR: 0.88 (6H, bd, J=7 Hz, $-CH(C\underline{H}_3)_2$), 0.94 (3H, s, $C_{10}-CH_3$), 1.18 (3H, s, C_4-CH_3), 2.81 (1H, dd, J=11.5 and 8 Hz, $C_{5\alpha}-H$), 3.65 (3H, s, $-CO_2CH_3$). Found: C, 72.33; H, 9.19%. Calcd for $C_{21}H_{32}O_4$: C, 72.38; H, 9.26%.

Elution with ether–benzene (1 : 99) afforded a mixture of two ketones (3.02 g), E (**13**) and F (**12**), whose separation and purification are described later.

Further elution with ether–benzene (1 : 99) gave a ketone G (8.96 g: 17%) which was recrystallized from methanol, mp 87—89.5 °C, $[\alpha]_D$ +78° (*c* 1.10) (lit,[3] mp 88—89.5 °C, $[\alpha]_D^{25}$ +87°); IR: 1720, 1670 vs cm^{-1}; ^1H NMR ($CDCl_3$): 0.94 (6H, bd, J=6 Hz, $-CH(C\underline{H}_3)_2$), 1.28 and 1.32 (each 3H and s, C_4-CH_3 and $C_{10}-CH_3$), 2.84 (1H, dm, J=12 Hz, $C_{1\beta}-H$), 3.67 (3H, s, $-CO_2CH_3$). The IR and ^1H NMR spectra of the ketone G were identical with those of methyl 7,11-dioxo-13β-abiet-8-en-18-oate (**14**).[3,8]

The next fraction (2.40 g) containing ketone H was rechromatographed on silica gel (240 g), using ether–hexane (1 : 4) as the eluent, to give the pure ketone H (1.91 g: 4%) as an oil, $[\alpha]_D$ +99° (*c* 0.985) (lit,[4] $[\alpha]_D^{25}$ +115.2°); IR: 1720, 1655, 1620 cm^{-1}; ^1H NMR ($CDCl_3$): 0.79 and 0.94 (each 3H, d, and J=7 Hz, $-CH(C\underline{H}_3)_2$), 1.11 (3H, s, $C_{10}-CH_3$), 1.21 (3H, s, C_4-CH_3), 3.66 (3H, s, $-CO_2CH_3$); UV: λ_{max}^{EtOH} 245.5 nm (ε 12700). Found: C, 75.96; H, 9.60%. Calcd for $C_{21}H_{32}O_3$: C, 75.86; H, 9.70%. The IR and ^1H NMR spectra of the ketone H were identical with those reported for methyl 14-oxo-13β-abiet-8-en-18-oate (**15**).[4]

Elution with ether–benzene (3 : 97) gave a ketone I (11.4 g: 23%) which was recrystallized from methanol; mp 111—112 °C; $[\alpha]_D$ +110° (*c* 5.54); IR: 1725, 1652, 1618 cm^{-1}; ^1H NMR: 0.95 (6H, bd, J=6 Hz, $-CH(C\underline{H}_3)_2$), 1.11 (3H, s, $C_{10}-CH_3$), 1.24 (3H, s, C_4-CH_3), 3.66 (3H, s, $-CO_2CH_3$). Found: C, 75.96; H, 9.89%. Calcd for $C_{21}H_{32}O_3$: C, 75.86; H, 9.70%. The IR and ^1H NMR spectra of the ketone I were identical with those of methyl 7-oxo-13β-abiet-8-en-18-oate (**16**).[3,8]

*Separation and Purification of the Ketones A (**3**) and B (**4**).* A part (125 mg) of the above mixture of ketones A and B was refluxed with acetic anhydride (5.5 mL) in the presence of sodium acetate (270 mg) for 5 h. After removal of the acetic anhydride *in vacuo*, the residue was mixed with brine and extracted with ether. The ether extract was washed successively with aqueous sodium hydrogencarbonate and brine, dried over sodium sulfate, and evaporated to give an oil (136 mg), which was chromatographed on silica gel (20 g). The less polar fraction eluted with ether–hexane (5 : 95) afforded the ketone B (38 mg), $[\alpha]_D$ −77° (*c* 0.575) (lit,[7] $[\alpha]_D$ −68.9°); IR: 1715, 1640, 1597 cm^{-1}; UV: λ_{max}^{EtOH} 257 nm (ε 11800), 338 (340), 420 (40); ^1H NMR ($CDCl_3$): 1.11 (6H, d, J=7 Hz, $-CH(C\underline{H}_3)_2$), 1.26 and 1.31 (each 3H and s, C_4-CH_3 and $C_{10}-CH_3$), 3.67 (3H, s, $-CO_2CH_3$), 6.32 (1H, d, J=1 Hz, $C_{12}-H$); MS (*m/e*): 344 (M^+). The IR, ^1H NMR, and low-resolution mass spectral data were identical with those reported for methyl 11,14-dioxoabieta-8,12-dien-18-oate (**4**).[7]

The more polar fraction eluted with ether–hexane (4 : 6) afforded an acetylated ketone A (37 mg), methyl 14-acetoxy-7-oxoabieta-8,11,13-trien-18-oate (**2**), which was recrystallized from hexane, mp 160—161.5 °C, $[\alpha]_D$ +19° (*c* 0.520); IR: 1763, 1725, 1673 cm^{-1}; ^1H NMR: 1.16 and 1.21 (each 3H, d, and J=7 Hz, $-CH(C\underline{H}_3)_2$), 1.25 and 1.30 (each 3H and s, C_4-CH_3 and $C_{10}-CH_3$), 2.28 (3H, s, $-OCOCH_3$), 3.62 (3H, s, $-CO_2CH_3$), 7.14 and 7.37 (each 1H, d, and J=8 Hz, $C_{11}-H$ and $C_{12}-H$); MS (*m/e*): 386 (M^+).

The acetoxy ketone (**2**) (20.5 mg) was refluxed with sodium hydrogencarbonate (17.5 mg) in 90% aqueous methanol (2.5 mL) for 1 h. After evaporation of the solvent *in vacuo*, the residue was mixed with brine, and extracted with ether. The ether extract was washed with brine, dried over sodium sulfate, and evaporated. The residue was chromatographed on silica gel (5.0 g), using benzene as the eluent, to give the original hydroxy ketone A (14.0 mg) as an oil, $[\alpha]_D$ −18° (*c* 0.560); IR 1725, 1622 cm^{-1}; ^1H NMR ($CDCl_3$): 1.21 and 1.23 (each 3H, d, and J=7 Hz, $-CH(C\underline{H}_3)_2$), 1.25 and 1.34 (each 3H and s, C_4-CH_3 and $C_{10}-CH_3$), 3.67 (3H, s, $-CO_2CH_3$), 6.77 and 7.36 (each 1H, d, and J=8 Hz, $C_{11}-H$ and $C_{12}-H$), 13.08 (1H, s, -OH); MS (*m/e*): 344 (M^+). The IR and ^1H NMR spectra of the hydroxy ketone A were identical with those reported for methyl 14-hydroxy-7-oxoabieta-8,11,13-trien-18-oate (**3**).[6]

*Methyl 9α-Hydroxy-13β-abiet-7-en-18-oate (**7**).* A mixture of **6** (45.0 mg), 80% hydrazine hydrate (0.1 ml), and acetic acid (0.03 ml) in methanol (1.57 ml) was refluxed for 30 min under a stream of nitrogen. After the solvent had been removed, the residue was extracted with ether. The ether extract was washed successively with aqueous sodium hydrogencarbonate and brine, dried over sodium sulfate, and evaporated. The residual oil was chromatographed on silica gel (5.0 g), using ether–benzene (5 : 95) as the eluent, to afford **7**[10] (7.9 mg: 18%), $[\alpha]_D$ −120° (*c* 0.395); IR: 3600, 3450 br, 1713 cm^{-1}; ^1H NMR ($CDCl_3$): 0.88 (6H, d, J=7 Hz, $-CH(C\underline{H}_3)_2$), 0.96 (3H, s, $C_{10}-CH_3$), 1.30 (3H, s, C_4-CH_3), 3.64 (3H, s, $-CO_2CH_3$), 5.41 (1H, bd, J=4 Hz, C_7-H); MS (*m/e*): 334 (M^+).

*Methyl 8β,9β-Epoxy-7-oxo-13β-abietan-18-oate (**8**).* Sodium borohydride reduction[11] of **16** afforded methyl 7β-hydroxy-13β-abiet-8-en-18-oate (**9**), mp 101—102 °C, $[\alpha]_D$ +71° (*c* 2.41, EtOH) [lit,[11] mp 100—101 °C, $[\alpha]_D^{25}$ +66° (EtOH)]; IR: 3600, 3425 br, 1720 cm^{-1}; ^1H NMR ($CDCl_3$): 0.89 (6H, d, J=6.5 Hz, $-CH(C\underline{H}_3)_2$), 1.04 (3H, s, $C_{10}-CH_3$), 1.20 (3H,

s, C_4–CH_3), 3.65 (3H, s, $-CO_2CH_3$), 4.07 (1H, bt, J=8 Hz, $C_{7\alpha}$–H).

A mixture of **9** (334 mg) and 85% *m*-chloroperbenzoic acid (406 mg) in dichloromethane (15 ml) was stirred at room temperature for 5 h and diluted with ether. The organic solution was washed successively with aqueous potassium iodide, aqueous sodium thiosulfate, aqueous sodium hydrogencarbonate, and brine. After drying over sodium sulfate, the solution was evaporated *in vacuo*. The residual oil was chromatographed on silica gel (30 g), using ether–benzene (5 : 95) as the eluent, to give methyl 8β,9β-epoxy-7β-hydroxy-13β-abietan-18-oate (165 mg); IR: 3575, 3400 br, 1718 cm^{-1}; ^1H NMR ($CDCl_3$): 0.85 (6H, d, J=6.5 Hz, $-CH(C\underline{H}_3)_2$), 1.06 (3H, s, C_{10}–CH_3), 1.16 (3H, s, C_4–CH_3), 3.67 (3H, s, $-CO_2CH_3$), 3.78 (1H, bt, J=8 Hz, $C_{7\alpha}$–H).

A solution of the above epoxy compound (165 mg) in acetone (3.3 ml) was treated with Jones reagent (2.5 M: 0.5 ml) at 0 °C for 5 min. After the usual work-up, the crude product was purified by column chromatography on silica gel (15 g), using ether–benzene (1 : 99) as the eluent, to give **8** (107 mg: 31% from **9**) as an oil, $[\alpha]_D$ +32° (*c* 2.11), IR: 1710 cm^{-1}; ^1H NMR: 0.88 (6H, bd, J=6.5 Hz, $-CH(C\underline{H}_3)_2$), 1.15 (6H, s, C_4–CH_3 and C_{10}–CH_3), 3.65 (3H, s, $-CO_2CH_3$). Found: C, 72.23; H, 9.32%. Calcd for $C_{21}H_{32}O_4$: C, 72.38; H, 9.26%.

*Methyl 9β-Hydroxy-13β-abiet-7-en-18-oate (**10**).* A mixture of **8** (56 mg) and 80% hydrazine hydrate (0.12 ml), and acetic acid (0.04 ml) in methanol (1.86 ml) was treated as described for the preparation of **7**. The crude product was chromatographed on silica gel (5.0 g), using ether–benzene (3 : 97) as the eluent, to give **10** (14 mg: 26%) as an oil, $[\alpha]_D$ −66° (*c* 0.455); IR: 3615, 3410 br, 1715 cm^{-1}; ^1H NMR ($CDCl_3$): 0.88 (6H, d, J=6.5 Hz, $-CH(C\underline{H}_3)_2$), 1.08 (3H, s, C_{10}–CH_3), 1.30 (3H, s, C_4–CH_3), 3.65 (3H, s, $-CO_2CH_3$), 5.38 (1H, bd, J=4 Hz, C_7–H); MS (*m/e*): 334 (M^+).

*Separation and Purification of the Ketones E (**13**) and F (**12**).* The mixture of the ketones (400 mg) E and F was treated with acetic anhydride (2.0 ml) in pyridine (2.0 ml) at room temperature for 2.5 h. After the usual work-up, the crude product was purified by column chromatography on silica gel (40 g), using ether–benzene (1 : 99) as the eluent, to give methyl 11-acetoxy-14-hydroxy-7-oxoabieta-8,11,13-trien-18-oate (**11**) (99 mg) which was recrystallized from methanol, mp 158.5—159.5 °C, $[\alpha]_D$ +93° (*c* 1.13); IR: 1757, 1723, 1630 cm^{-1}; ^1H NMR ($CDCl_3$): 1.23 (6H, d, J=6 Hz, $-CH(C\underline{H}_3)_2$), 1.32 and 1.34 (each 3H and s, C_4–CH_3 and C_{10}–CH_3), 2.32 (3H, s, $-OCOCH_3$), 3.69 (3H, s, $-CO_2CH_3$), 6.95 (1H, s, C_{12}–H), 13.54 (1H, s, –OH). Found: C, 68.50; H, 7.62%. Calcd for $C_{23}H_{30}O_6$: C, 68.63; H, 7.51%. Subsequent elution gave a mixture of **11** and **13** (154 mg) (*ca.* 2 : 3 ratio by ^1H NMR analysis).

Further elution afforded the original ketone E (86 mg), $[\alpha]_D$ +20° (*c* 3.91); IR: 1720, 1672, 1608 cm^{-1}; ^1H NMR: 1.25 (6H, d, J=7 Hz, $-CH(C\underline{H}_3)_2$), 1.25 and 1.31 (each 3H and s, C_4–CH_3 and C_{10}–CH_3), 3.62 (3H, s, $-CO_2CH_3$), 7.20 (1H, d, J=8.5 Hz, C_{11}–H), 7.27 (1H, dd, J=8.5 and 2 Hz, C_{12}–H), 7.76 (1H, d, J=2 Hz, C_{14}–H). The IR and ^1H NMR spectra of the ketone E were identical with those of methyl 7-oxoabieta-8,11,13-trien-18-oate (**13**).[14]

A mixture of **11** (90 mg) and sodium hydrogencarbonate (80 mg) in 90% aqueous methanol (12 ml) was refluxed for 1 h and the solvent was removed *in vacuo*. The residue was extracted with ether and the ether extract was washed with brine, dried over sodium sulfate, and evaporated. The residue was recrystallized from methanol to give methyl 11,14-dihydroxy-7-oxoabieta-8,11,13-trien-18-oate (**12**) (52 mg), mp 233.5—234.5 °C, $[\alpha]_D$ +121° (*c* 0.595); IR: 3590, 3330 br, 1720, 1630 cm^{-1}; ^1H NMR (acetone-d_6): 1.16 and 1.17 (each 3H, d, and J=7 Hz, $-CH(C\underline{H}_3)_2$), 1.33 and 1.45 (each 3H and s, C_4–CH_3 and C_{10}–CH_3), 3.47 (1H, dm, J=12 Hz, $C_{1\beta}$–H), 3.66 (3H, s, $-CO_2CH_3$), 7.05 (1H, s, C_{12}–H), 7.87 (1H, s, disappeared with D_2O, C_{11}–OH), 13.02 (1H, s, disappeared with D_2O, C_{14}–OH). Found: C, 70.07; H, 8.05%. Calcd for $C_{21}H_{28}O_5$: C, 69.97; H, 7.83%.

*Methyl 14-Hydroxyabieta-8,11,13-trien-18-oate (**18**).* A mixture of **15** (332 mg), copper(II) bromide (402 mg), and lithium bromide (78 mg) in acetonitrile (16.6 ml) was refluxed for 6.5 h and then evaporated *in vacuo*. The residue was dissolved in ether. The ether solution was washed with brine, dried over sodium sulfate, and evaporated. The crude product was chromatographed on silica gel (40 g), using ether–benzene (1 : 99) as the eluent, to give **18**[17] (190 mg: 57%) as an oil, $[\alpha]_D$ +38° (*c* 0.635); IR: 3610, 1718, 1610, 1570 cm^{-1}; ^1H NMR ($CDCl_3$): 1.22 and 1.28 (each 3H and s, C_4–CH_3 and C_{10}–CH_3), 1.23 and 1.26 (each 3H, d, and J=7 Hz, $-CH(C\underline{H}_3)_2$), 3.65 (3H, s, $-CO_2CH_3$), 4.69 (1H, bs, –OH), 6.83 and 6.99 (each 1H, d, and J=8.5 Hz, C_{11}–H and C_{12}–H). Found: C, 76.32; H, 9.10%. Calcd for $C_{21}H_{30}O_3$: C, 76.32; H, 9.15%. Further elution with ether–benzene (3 : 97) gave the recovered **15** (123 mg: 37%).

*Methyl 14-Methoxyabieta-8,11,13-trien-18-oate (**19**).* A mixture of **18** (1.18 g) and 55% sodium hydride (0.78 g) in *N,N*-dimethylformamide (39 ml) was stirred at room temperature for 45 min under a stream of nitrogen. After the addition of methyl iodide (0.30 ml), the mixture was stirred at 35—40 °C for 3 h and then some additional methyl iodide (0.30 ml) was added. The mixture was further stirred at the same temperature for 4 h, cooled, poured into a mixture of ice and dilute hydrochloric acid, and extracted with ether. The ether extract was washed with brine, dried over sodium sulfate, and evaporated. The residue was chromatographed on silica gel (100 g), using benzene as the eluent, to give **19**[17] (0.76 g: 67%) which was recrystallized from methanol, mp 102—104 °C, $[\alpha]_D$ +50° (*c* 1.82); IR: 1712 cm^{-1}; ^1H NMR ($CDCl_3$): 1.20 (6H, d, J=7 Hz, $-CH(C\underline{H}_3)_2$), 1.21 and 1.27 (each 3H and s, C_4–CH_3 and C_{10}–CH_3), 3.67 and 3.71 (each 3H and s, $-CO_2CH_3$ and $-OCH_3$), 7.04 (2H, s, C_{11}–H and C_{12}–H). Found: C, 76.71; H, 9.46%. Calcd for $C_{22}H_{32}O_3$: C, 76.70; H, 9.36%.

*Isomerization of **15**.* *a)*: A solution of **15** (67 mg) and sodium methoxide (44 mg) in absolute methanol (3.4 ml) was refluxed for 1 h. The solution was poured into dilute hydrochloric acid and extracted with ether. The ether extract was washed with brine, dried over sodium sulfate, and evaporated *in vacuo*. The residue was chromatographed on silica gel (10 g), using ether–hexane (1 : 9) as the eluent, to give an inseparable mixture (62 mg) of **15** and its C-13 epimer (**25**) (*ca.* 2 : 1 ratio by ^1H NMR analysis). ^1H NMR ($CDCl_3$) signals assigned to **25**: 0.90 and 0.91 (each 3H, d, and J=6 Hz, $-CH(C\underline{H}_3)_2$), 1.09 (3H, s, C_{10}–CH_3), 1.21 (3H, s, C_4–CH_3), 3.67 (3H, s, $-CO_2CH_3$).

b): A solution of **15** (67 mg) and 5% aqueous sodium hydroxide (0.3 ml) in tetrahydrofuran (3.4 ml) was refluxed for 10 h. The solution was poured into dilute hydrochloric acid and extracted with ether. The ether extract was washed with brine, dried over sodium sulfate, and evaporated *in vacuo* to give an oil (66 mg), whose IR and ^1H NMR spectra were identical with those of the starting **15**.

*Reduction of **15** with Sodium Borohydride.* A mixture of **15** (670 mg), sodium borohydride (1.52 g), and 5% aqueous sodium hydroxide (3.0 ml) in tetrahydrofuran (34 ml) was refluxed for 10 h. The mixture was poured into dilute hydrochloric acid and extracted with ether. The ether extract was washed with brine, dried over sodium sulfate, and evaporated *in vacuo*. The residue was chromatographed on

silica gel (65 g), using ether–benzene (3 : 97) as the eluent, to give methyl 14β-hydroxy-13β-abiet-8-en-18-oate (**26**) (159 mg: 24%) as an oil, $[\alpha]_D$ +125° (*c* 2.17); IR: 3620, 3460 br, 1720 cm^{-1}; ^1H NMR ($CDCl_3$): 0.95 and 0.98 (each 3H, d, and J=6 Hz, $-CH(C\underline{H}_3)_2$), 1.01 (3H, s, $C_{10}-CH_3$), 1.20 (3H, s, C_4-CH_3), 3.66 (3H, s, $-CO_2CH_3$), 3.78 (1H, br, $W_{1/2}$=5.5 Hz, $C_{14\alpha}-H$). Found: C, 75.68; H, 10.48%. Calcd for $C_{21}H_{34}O_3$: C, 75.40; H, 10.25%.

Further elution with ether–benzene (3 : 97) gave methyl 14α-hydroxy-13β-abiet-8-en-18-oate (**24**) (256 mg: 38%), which was recrystallized from methanol; mp 102—103 °C (after drying *in vacuo* at 40 °C for 5 h), $[\alpha]_D$ +59° (*c* 0.625) (lit,[4] mp 102—103 °C, $[\alpha]_D^{25}$ +66.7°); IR: 3600, 3450 br, 1720 cm^{-1}; ^1H NMR ($CDCl_3$): 0.83 and 0.96 (each 3H, d, and J=7 Hz, $-CH(C\underline{H}_3)_2$), 1.00 (3H, s, $C_{10}-CH_3$), 1.20 (3H, s, C_4-CH_3), 3.65 (3H, s, $-CO_2CH_3$), 3.80 (1H, bd, J=7.5 Hz, $C_{14\beta}-H$). Found: C, 75.35; H, 10.47%. Calcd for $C_{21}H_{34}O_3$: C, 75.40; H, 10.25%. The identity of **24** with natural methyl suaveolate was confirmed by mixed melting point determination and by IR and ^1H NMR spectral comparison.[20]

Elution with ether–benzene (1 : 1) afforded 13β-abiet-8-ene-14β,18-diol (**29**) (46 mg: 7.5%) as an oil; $[\alpha]_D$ +92° (*c* 0.39); IR: 3625, 3450 br cm^{-1}; ^1H NMR ($CDCl_3$): 0.81 (3H, s, C_4-CH_3), 1.03 (3H, s, $C_{10}-CH_3$), 0.95 and 0.98 (each 3H, d, and J=6 Hz, $-CH(C\underline{H}_3)_2$), 3.15 and 3.44 (each 1H, d, and J=10.5 Hz, $-C\underline{H}_2OH$), 3.77 (1H, br, $W_{1/2}$=6 Hz, $C_{14\alpha}-H$). Found: C, 78.40; H, 11.25%. Calcd for $C_{20}H_{34}O_2$: C, 78.38; H, 11.18%.

Subsequent elution with ether–benzene (1 : 1) gave 13β-abiet-8-ene-14α,18-diol (**23**) (95 mg: 15%) which was recrystallized from dichloromethane; mp 180—182 °C; $[\alpha]_D$ +84° (*c* 0.285) (lit,[4] mp 186—187 °C, $[\alpha]_D^{25}$ +81.3°); IR: 3620, 3290 br cm^{-1}; ^1H NMR ($CDCl_3$): 0.76 (3H, s, C_4-CH_3), 0.82 and 0.95 (each 3H, d, and J=6.5 Hz, $-CH(C\underline{H}_3)_2$), 1.00 (3H, s, $C_{10}-CH_3$), 2.97 and 3.46 (each 1H, d, and J=11 Hz, $-C\underline{H}_2OH$), 3.77 (1H, bd, J=7 Hz, $C_{14\beta}-H$). Found: C, 78.15; H, 11.47%. Calcd for $C_{20}H_{34}O_2$: C, 78.38; H, 11.18%. The identity of **23** with natural suaveolol was confirmed by mixed melting point determination and by IR and ^1H NMR spectral comparison.[20]

*Reduction of **15** with Lithium Aluminium Hydride.* A mixture of **15** (166 mg) and lithium aluminium hydride (57 mg) in dry ether (5.0 ml) was refluxed for 4 h with stirring. The mixture was poured into aqueous ammonium chloride solution and extracted with ether. The ether extract was washed with brine, dried over sodium sulfate, and evaporated. The residue was chromatographed on silica gel (20 g), using ether–benzene (3 : 7) as the eluent, to give an oil (35 mg: 23%). The IR and ^1H NMR spectra of the oil were superimposable with those of **29**.

Further elution with ether–benzene (1 : 1) gave a solid (72 mg: 47%). The IR and ^1H NMR spectra of the solid were identical with those of suavelol.

*Oxidation of **24** and **26** with Pyridinium Chlorochromate. a)*: A mixture of **24** (23 mg) and pyridinium chlorochromate (22 mg) in dichloromethane (1.0 ml) was stirred at room temperature for 2 h. The mixture was then decanted from a tarry residue, which was washed with ether. The combined organic solution was washed with brine, dried over sodium sulfate, and evaporated to give an oil (21 mg), whose IR and ^1H NMR spectra were identical with those of **15**.

b): A mixture of **26** (14 mg) and pyridinium chlorochromate (14 mg) in dichloromethane (1.0 ml) was treated as described in *a)* to give an oil (14 mg), which was shown to be identical with **15** by spectral comparison.

*Methyl 14β-Acetoxy-13β-abiet-8-en-18-oate (**27**).* A mixture of **26** (70 mg), acetic anhydride (1.0 ml), and pyridine (1.0 ml) was allowed to stand overnight at room temperature. After the usual work-up, the crude product was chromatographed on silica gel (10 g), using ether–hexane (1 : 9) as the eluent, to give **27** (64 mg) as an oil; $[\alpha]_D$ +181° (*c* 0.575); IR: 1713 cm^{-1}; ^1H NMR ($CDCl_3$): 0.90 (6H, d, J=6 Hz, $-CH(C\underline{H}_3)_2$), 1.02 (3H, s, $C_{10}-CH_3$), 1.19 (3H, s, C_4-CH_3), 2.03 (3H, s, $-OCOCH_3$), 3.64 (3H, s, $-CO_2CH_3$), 5.32 (1H, br, $W_{1/2}$= 5 Hz, $C_{14\alpha}-H$). Found: C, 73.97; H, 9.83%. Calcd for $C_{23}H_{36}O_4$: C, 73.67; H, 9.64%.

*Methyl 14α-Acetoxy-13β-abiet-8-en-18-oate (**28**).* The alcohol **24** (58 mg) was acetylated with acetic anhydride in pyridine, as described for the preparation of **27**. The acetate (**28**) (47 mg) was recrystallized from methanol; mp 134.5—135 °C; $[\alpha]_D$ −41° (*c* 0.245) (lit,[4] mp 132—133 °C, $[\alpha]_D^{25}$ −44.5°); IR: 1720 cm^{-1}; ^1H NMR ($CDCl_3$): 0.82 and 0.92 (each 3H, d, and J=6.5 Hz, $-CH(C\underline{H}_3)_2$), 0.99 (3H, s, $C_{10}-CH_3$), 1.19 (3H, s, C_4-CH_3), 2.06 (3H, s, $-OCOCH_3$), 3.65 (3H, s, $-CO_2CH_3$), 5.37 (1H, bd, J=8 Hz, $C_{14\beta}-H$). Found: C, 73.68; H, 9.79%. Calcd for $C_{23}H_{36}O_4$: C, 73.67; H, 9.64%.

*14β,18-Diacetoxy-13β-abiet-8-ene (**30**).* The diol **29** (68 mg) was acetylated as described for the preparation of **27**. The crude product was chromatographed on silica gel (10 g), using ether–hexane (15 : 85) as the eluent, to give **30** (64 mg), which was recrystallized from methanol; mp 93—95 °C; $[\alpha]_D$ +201° (c 1.695); IR: 1722 cm^{-1}; ^1H NMR ($CDCl_3$): 0.88 (3H, s, C_4-CH_3), 1.04 (3H, s, $C_{10}-CH_3$), 0.92 (6H, d, J=6 Hz, $-CH(C\underline{H}_3)_2$), 2.04 and 2.05 (each 3H and s, 2-$OCOCH_3$), 3.68 and 3.88 (each 1H, d, and J=11 Hz, $-C\underline{H}_2$-OAc), 5.35 (1H, br, $W_{1/2}$=5.5 Hz, $C_{14\alpha}-H$). Found: C, 74.09; H, 10.11%. Calcd for $C_{24}H_{38}O_4$: C, 73.80; H, 9.81%.

*14α,18-Diacetoxy-13β-abiet-8-ene (Suaveolol Diacetate) (**31**).* The diol **23** (71 mg) was acetylated as described for the preparation of **27**. The crude product was chromatographed on silica gel (10 g), using ether–hexane (15 : 85) as the eluent, to give **31** (71 mg) as an oil; $[\alpha]_D$ −41° (*c* 0.590) (lit,[4] $[\alpha]_D^{25}$ −39.1°); IR: 1720 cm^{-1}; ^1H NMR ($CDCl_3$): 0.83 and 0.95 (each 3H, d, and J=6.5 Hz, $-CH(C\underline{H}_3)_2$), 0.89 (3H, s, C_4-CH_3), 1.02 (3H, s, $C_{10}-CH_3$), 2.06 and 2.07 (each 3H and s, 2-$OCOCH_3$), 3.72 and 3.85 (each 1H, d, and J=11 Hz, $-C\underline{H}_2OAc$), 5.39 (1H, bd, J=8.5 Hz, $C_{14\beta}-H$). Found: C, 74.07; H, 10.09%. Calcd for $C_{24}H_{38}O_4$: C, 73.80; H, 9.81%.

*Suaveolic Acid (14α-Hydroxy-13β-abiet-8-en-18-oic Acid) (**22**).* A mixture of **24** (68 mg) and potassium *t*-butoxide (381 mg) in dimethyl sulfoxide (3.4 ml) was stirred at room temperature for 1 h. The mixture was poured into ice–water, acidified with 10% aqueous acetic acid, and extracted with ether. The ether extract was washed with brine, dried over sodium sulfate, and evaporated *in vacuo* to give a pale yellow oil (70 mg). The crude product was chromatographed on silicic acid (Mallinckrodt, CC-4, 10g), using ether–benzene (3 : 7) as the eluent, to give **22** as a solid (34 mg: 55%). It was recrystallized from hexane to give needles, mp 188—190 °C after drying at 80 °C for 2 h, $[\alpha]_D$ +71° (*c* 0.14) (lit,[4] mp 198—201 °C dec, $[\alpha]_D^{25}$ +68.2°); IR (KBr): 3390—2630, 1698 cm^{-1}; ^1H NMR ($CDCl_3$): 0.82 and 0.95 (each 3H, d, and J=7 Hz, $-CH(C\underline{H}_3)_2$), 0.99 (3H, s, $C_{10}-CH_3$), 1.19 (3H, s, C_4-CH_3), 3.83 (1H, bd, J=7.5 Hz, $C_{14\beta}-H$), 6.02 (2H, br, $-CO_2H$ and $-OH$). The IR and ^1H NMR spectra of **22** were identical with those of natural suaveolic acid.[20]

The authors are grateful to Arakawa Chemical Co. Ltd. for the generous gift of (+)-13β-abiet-8-en-18-oic acid. Thanks are also due to Dr. P. S. Manchand, Hoffmann-La Roche Inc., for kindly supplying the natural samples and their spectral data.

References

1) The corresponding acid; L. Velluz, G. Muller, A. Petit, and J. Mathieu, *Bull. Soc. Chim. Fr.*, **21**, 401 (1954). H. Murai, H. Enomoto, I. Fujita, Y. Yoshikuni, and T. Mori, Japan Kokai, 76149256 (1976); *Chem. Abstr.*, **87**, 6230t (1977). The acid (mp 183—185 °C, $[\alpha]_D$ +131° (*c* 1.67, EtOH)) used in the present study was kindly supplied by Arakawa Chemical Co. Ltd.

2) W. G. Dauben, M. Lorber, and D. S. Fullerton, *J. Org. Chem.*, **34**, 3587 (1969).

3) W. Herz and J. J. Schmid, *J. Org. Chem.*, **34**, 3464 (1969).

4) P. S. Manchand, J. D. White, J. Fayos, and J. Clardy, *J. Org. Chem.*, **39**, 2306 (1974).

5) R. Ratcliffe and R. Rodehorst, *J. Org. Chem.*, **35**, 4000 (1970).

6) A. Tahara, H. Akita, and Y. Ohtsuka, *Chem. Pharm. Bull.*, **22**, 1547 (1974).

7) J. F. Biellmann and G. Branlant, *Bull. Soc. Chim. Fr.*, **1973**, 2086.

8) According to the procedure of Herz and Schmid[3] the ester (**1**) was oxidized with *t*-butyl chromate to obtain some authentic samples.

9) W. Herz and A. L. Hall, *J. Org. Chem.*, **39**, 11 (1974).

10) W. Herz and H. J. Wahlborg, *J. Org. Chem.*, **30**, 1881 (1965).

11) W. Herz and J. J. Schmid, *J. Org. Chem.*, **34**, 3473 (1969).

12) P. V. Demarco, E. Farkas, D. Doddrell, B. L. Mylari, and E. Wenkert, *J. Am. Chem. Soc.*, **90**, 5480 (1968).

13) T. Miyase, P. Rüedi, and C. H. Eugster, *Helv. Chim. Acta*, **60**, 2770 (1977).

14) H. Erdtman and L. Malmborg, *Acta Chem. Scand.*, **24**, 2252 (1970).

15) T. Matsumoto, S. Imai, and S. Yuki, *Bull. Chem. Soc. Jpn.*, **54**, 1448 (1981).

16) Y. Ohtsuka and A. Tahara, *Chem. Pharm. Bull.*, **21**, 653 (1973).

17) A. Tahara and H. Akita, *Chem. Pharm. Bull.*, **23**, 1976 (1975).

18) C. B. Rao, T. N. Rao, and E. K. S. Vijayakumar, *Curr. Sci.*, **47**, 455 (1978); *Chem. Abstr.*, **89**, 163778m (1978). C. B. Rao, T. N. Rao, and E. K. S. Vijayakumar, *Indian J. Chem.*, **18B**, 513 (1979).

19) C. B. Rao and T. N. Rao, *Curr. Sci.*, **47**, 498 (1978); *Chem. Abstr.*, **89**, 180185 h (1978).

20) The IR and ^{1}H NMR spectra of natural methyl suaveolate, suaveolol, and suaveolic acid, kindly supplied by Dr. P. S. Manchand, were measured in our laboratory.

Carbon-Carbon Bond Formation by the Use of Chloroiodomethane as a C_1 Unit. III.[1] A Convenient Synthesis of the Mannich Base from Enol Silyl Ether by a Combination of Chloroiodomethane and *N,N,N',N'*-Tetramethylmethanediamine[2]

Sotaro MIYANO,* Hiroshi HOKARI, and Harukichi HASHIMOTO

Department of Applied Chemistry, Faculty of Engineering, Tohoku University, Aramaki-Aoba, Sendai 980

(Received June 15, 1981)

The Mannich dimethylaminomethylation of carbonyl compounds is conveniently carried out *via* enol trimethylsilyl ethers by a combination of chloroiodomethane (CH_2ClI) and *N,N,N',N'*-tetramethylmethanediamine (TMMD) in DMSO as the solvent at ambient temperature. The mechanism of the transformation is discussed on the basis of product analysis and ^1H NMR spectral studies. The reagent system CH_2ClI/TMMD also provides a convenient route to the Eschenmoser's salt ($Me_2\overset{+}{N}=CH_2,\bar{I}$).

One of the most general entrances into the α-methylene carbonyl system[3] is by deamination of α-aminomethyl carbonyl compounds, *i.e.* the Mannich base.[4] In this context, much attention has been centered in the last few years on the Mannich reaction of carbonyl substrates *via* enolates by means of preformed *N,N*-dimethylmethyleneiminium reagents, ($Me_2\overset{+}{N}=CH_2$, $\bar{X}$) (**1**),[5] among which the Eschenmoser's salt (X=I)[6] has conventionally been utilized because of its relative easiness of handling and compatibility with a variety of reaction conditions.[7]

From a practical point of view, however, operationally simple Mannich reaction which does not require separate preparation and handling of these highly reactive iminium salts may be desirable.[8]

We recently communicated briefly that the reagent system chloroiodomethane (CH_2ClI)/*N,N,N',N'*-tetramethylmethanediamine (TMMD) can serve as the *in situ* Mannich dimethylaminomethylation reagent of enol trimethylsilyl ethers under mild conditions (Eq. 1),[9] and herein we wish to report the results we have obtained in the course of this investigation and the relative experimental details.

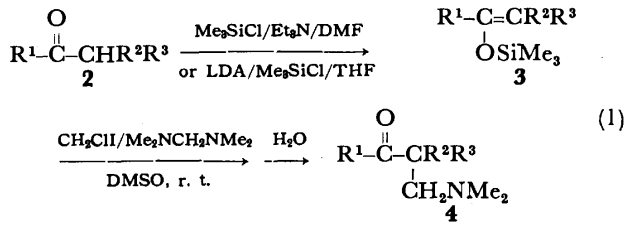

(1)

Results and Discussion

Synthesis of the Mannich Base. 3-Pentanone enol silyl ether (**3a**) was treated with 1.5 molar amounts of CH_2ClI and TMMD in DMSO; after 3-h stirring at ambient temperature, almost all of the substrate was consumed with the formation of 2-(dimethylaminomethyl)-3-pentanone (**4a**) in a 93% yield. After the usual work-up, a pure sample of the amino ketone was isolated in a 68% yield by distillation; the product was fully characterized by IR and ^1H NMR spectral studies and elemental analysis.

As the transformation seemed to be of synthetic utility because of its mildness, operational simplicity, and reasonable yield of the Mannich base, further investigations with respect to both reagent system and substrate were carried out. Among the several solvents examined, DMSO gave the best result in the reaction of cyclohexanone enol silyl ether (**3c**) with CH_2ClI/TMMD (Table 1). Both DMF and CH_2Cl_2 may also be utilized as the reaction medium, while THF and diethyl ether gave poor results. It is reported that preformed iminium salts **1** (X=Cl, I) did not work in diethyl ether for the aminomethylation of propiophenone enol silyl ether (**3b**), presumably because of the insolubility of the halide salts.[7]

As for the dihalide component, CH_2ClI seemed to be the one of choice under a given reaction conditions (3-h reaction in DMSO), while even CH_2Br_2 gave a good result when the reaction was allowed to continue for 50 h (Table 2). It is interesting that the reactivity of the dihalides was in the order of $CH_2ClI > CH_2I_2 > CH_2Br_2 > CH_2Cl_2$ as judged by the unchanged halide.

Table 1. Effect of solvent on the reaction of cyclohexanone enol silyl ether (**3c**)[a]

Solvent	Mannich base (**4c**) yield/%[b]
DMSO	83
DMF	76
CH_2Cl_2	68
THF	6.2
Et_2O	0

a) **3c**, 10 mmol; TMMD, 15 mmol; CH_2ClI, 15 mmol; solvent, 10 ml; r. t., 3 h. b) Determined by GLC using dodecane as the internal standard (Silicone GE SE-52 column).

Table 2. The Mannich reaction of cyclohexanone enol silyl ether (**3c**) with CH_2X_2/TMMD[a]

CH_2X_2	Mannich base (**4c**) yield/%
CH_2ClI	83
CH_2I_2	55
CH_2Br_2	23 (88)[b]
CH_2Cl_2	0

a) Reaction conditions like those described in Table 1. b) Reaction time, 50 h.

TABLE 3. THE MANNICH REACTION OF ENOL SILYL ETHERS WITH CH_2ClI/TMMD[a)]

	Enol silyl ether (3)	Reaction time/h	Product(s) (4, 4′, 5)	Yield/%[b)]	Bp θ_p/°C (mmHg)
a	C_2H_5–C(OTMS)=CH–CH_3	3	C_2H_5–CO–CH(CH_2NMe_2)–CH_3	68 (93)[c)]	42—43(3)
b	Ph–C(OTMS)=CH–CH_3	3	Ph–CO–CH(CH_2NMe_2)–CH_3	51	39—40(0.4)
		24		71	
c	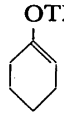	3	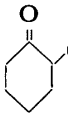	67 (83)[c)]	42—47(0.3—0.4)
d		3		65	34—35.5(0.3)
e		3	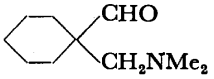	22	52—55(0.2)
		24		71	
f	n-C_5H_{11}–CH=C(OTMS)–H	3	n-C_5H_{11}–CH(CH_2NMe_2)–CHO	18	38—40(0.8)
			n-C_5H_{11}–C(=CH_2)–CHO	(12)[c)]	
		24	n-C_5H_{11}–C(=CH_2)–CHO	(42)[c)]	
g	Ph–CH=C(OTMS)–CH_3	3	Ph–CH(CH_2NMe_2)–CO–CH_3	54	65—68(0.4)
			Ph–C(=CH_2)–CO–CH_3	(22)[c)]	
h	Ph–CH=C(OTMS)–Ph	80	Ph–CH(CH_2NMe_2)–CO–Ph	67	Mp 78.2 °C
			Ph–C(=CH_2)–CO–Ph	(22)[d)]	
i	n-C_4H_9–CH=C(OTMS)–OC_2H_5	3	n-C_4H_9–CH(CH_2NMe_2)–$COOC_2H_5$	46 (66)[c)]	35—36/0.3
			n-C_4H_9–C(=CH_2)–$COOC_2H_5$	(13)[c)]	
j	$(CH_3)_3$C–C(OTMS)=CH_2	5	$(CH_3)_3$C–CO–CH(CH_2NMe_2)$_2$	36	Mp 58.5 °C
		0.5[e)]	$(CH_3)_3$C–CO–$CH_2CH_2NMe_2$	36	32(2)
			$(CH_3)_3$C–CO–CH(CH_2NMe_2)$_2$	12	
k	Ph–C(OTMS)=CH_2	3	Ph–CO–$CH_2CH_2NMe_2$	(22)[d)]	
			Ph–CO–CH(CH_2NMe_2)$_2$	58 (78)[d)]	Mp 57—58 °C

a) **3**, 15—20 mmol; **3**/CH_2ClI/TMMD≈1/1.5/1.5 (molar ratio); solvent, DMSO, 20 ml; room temp. b) Isolated yields unless otherwise noted. c) Determined by GLC. d) Determined by ^1H NMR. e) After CH_2ClI and TMMD had been stirred for 3 h, the enol silyl ether was added.

Table 3 lists the results of the Mannich reaction of various carbonyl compounds *via* enol silyl ethers with CH_2ClI/TMMD in DMSO as the solvent. It can be seen that the substrates in the Table can be divided into three categories: The first group enol silyl ethers (**3a** to **3e**) gave the corresponding mono(aminomethylation) products in fair to good yields, though **3e** required a longer reaction period in order to obtain appreciable yield. It should be noted that regioselective aminomethylation of 1-methylcyclohexanone was accomplished *via* enol silyl ether **3d**.

In the case of the second group enol silyl ethers (**3f** to **3i**), the Mannich reaction was accompanied by the formation of considerable amounts of α-methylenation products. GLC analysis showed that the reaction mixture of heptanal enol silyl ether (**3f**) (3-h reaction) contained 2-methyleneheptanal in a 12% yield based on the starting substrate. Distillation caused serious resinification of the reaction mixture, allowing the isolation of the desired Mannich base in a poor yield (18%). The exact mechanism by which the α-methylene carbonyl derivatives were formed remains to be determined, while it seems that the initially formed Mannich base released dimethylamine under

the reaction conditions.[10] Thus, upon treatment of **3f** with CH_2ClI/TMMD in DMSO for 24 h, the amount of the α-methylene aldehyde reached a 42% yield; this may be of some utility for the synthesis of α-methylene aldehydes (Eq. 2).

$$n\text{-}C_5H_{11}\text{-}CH{=}CH\text{-}OSiMe_3 \quad \textbf{3f}$$

$$\xrightarrow[\text{DMSO, r.t., 24h}]{CH_2ClI/Me_2NCH_2NMe_2} \xrightarrow{H_2O} n\text{-}C_5H_{11}\text{-}\underset{\underset{CH_2}{\|}}{C}\text{-}CHO \quad \textbf{5f} \qquad (2)$$

As was stated earlier the Mannich base itself is frequently utilized as the precursor for the α-methylene carbonyl compound, so the concurrent deamination in these transformations may not always be deteriorative to the Mannich aminomethylation.

The third group enol silyl ethers (**3j** and **3k**) which are characterized by bearing terminal methylene function gave bis(aminomethylation) products (**4'**) preferentially (Eq. 3). Even under the reaction conditions

$$\underset{Me_3SiO}{\overset{R}{\diagdown}}C{=}CH_2 \xrightarrow[\text{DMSO, r. t., 3h}]{CH_2ClI/Me_2NCH_2NMe_2} \xrightarrow{H_2O}$$

$$\textbf{3j or 3k} \quad R\text{-}\overset{O}{\overset{\|}{C}}\text{-}CH_2CH_2NMe_2 \quad \textbf{4}$$

$$+\,R\text{-}\overset{O}{\overset{\|}{C}}\text{-}CH(CH_2NMe_2)_2 \quad \textbf{4'} \qquad (3)$$

where 40% of the substrate **3k** was remained unchanged, a 57 : 43 mixture of mono- to diamino ketone was resulted (Table 4). This is a sharp contrast to the report that the preformed Mannich reagent (**1**) did not afford disubstitution products from these type of enol silyl ethers.[7] At present, we have no idea to explain these discrepancies.

*A Convenient Synthesis of the Eschenmoser's Salt (**1**, X=I) from CH_2ClI and TMMD.* In 1971, Böhme *et al.* reported that CH_2Br_2 slowly reacts with TMMD to afford **1** (X=Br)[11] (Eq. 4).

$$Me_2NCH_2NMe_2 + CH_2Br_2 \longrightarrow 2Me_2\overset{+}{N}{=}CH_2,\ Br^- \qquad (4)$$

From the results in Table 2, it seems reasonable to anticipate that CH_2ClI would react more promptly with TMMD than CH_2Br_2 to give similar iminium salt of mixed halides (**1**, X=Cl and I). Thus, upon mixing TMMD with CH_2ClI, a mild exothermic reaction set in with the formation of white precipitate. To our surprise, however, the solid was shown to be the Eschenmoser's salt (**1**, X=I), as was evidenced by elemental analysis (*vide infra*). NMR and GLC study showed the presence of CH_2Cl_2 as a reaction product in the liquid part of the reaction mixture. Then, the overall transformation may be represented as follows:

$$Me_2NCH_2NMe_2 + 2CH_2ClI \longrightarrow 2Me_2\overset{+}{N}{=}CH_2,\ \bar{I} + CH_2Cl_2. \qquad (5)$$

On the basis of the stoichiometry according to Eq. 5, an 82% yield of the iminium iodide was attained after the mixture was allowed to stand for 3 d at ambient temperature in the dark. Under the similar reaction conditions, CH_2Br_2 and CH_2I_2 did not give appreciable amounts of the corresponding precipitate.

The conventional method for the preparation of the Eschenmoser's salt requires time-consuming, two-step procedure which must be carried out under strictly anhydrous conditions.[6] Recently Bryson *et al.* reported a convenient preparation of the iodide *via* cleavage of TMMD with stoichiometric amount of trimethylsilyl iodide.[12] In our Mannich reaction, separate preparation of the iminium reagent is not required for the aminomethylation of groups 1 and 2 enol silyl ethers in Table 3, but if desired, the transformation depicted in Eq. 5 will provide another convenient route to the Eschenmoser's salt.

Mechanistic Aspects of the Mannich Reaction of Enol Silyl Ether with CH_2ClI/TMMD. The time-course of the reaction of CH_2ClI with TMMD in DMSO was followed quantitatively by GLC (Fig. 1). On the basis of the material balance on chlorine and CH_2ClI, the amount of iminium iodide and chloride species are obtainable (see Experimental part). In this regard, NMR study of the reaction in DMSO-d_6 is suggestive

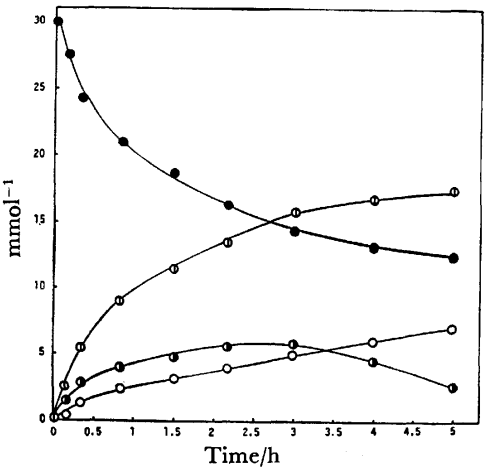

Fig. 1. Reaction of CH_2ClI with TMMD in DMSO. Reaction conditions: CH_2ClI, 30 mmol; TMMD, 30 mmol; DMSO, 20 ml; room temp. ●: CH_2ClI, ⓘ: $Me_2\overset{+}{N}{=}CH_2,\bar{I}$, ◑: $Me_2\overset{+}{N}{=}CH_2,\bar{Cl}$, ○: CH_2Cl_2.

TABLE 4. REACTION OF ACETOPHENONE ENOL SILYL ETHER (**3k**)[a]

3k (mmol)	CH_2ClI (mmol)	TMMD (mmol)	Solvent (ml)	Reacted **3k**(%)	Reacted CH_2ClI (mmol)	**4k**/**4'k** Ratio	Me_2NCH_2- Required (mmol equiv.)
16.1	24.0	27.4	DMSO 20	100	16.3	22/78	28.7
10.5	17.4	17.6	DMF 15	98	10.1	35/65	17.0
10.5	5.72	11.4	DMSO 15	61	4.64	57/43	9.2

a) Room temp, 3 h.

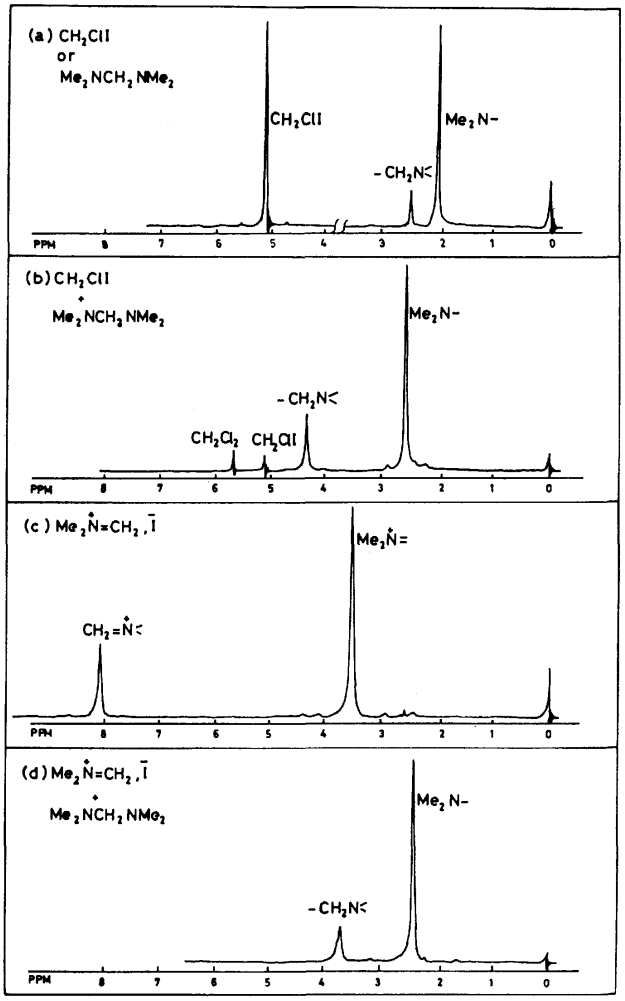

Fig. 2. NMR study of the reaction of CH_2ClI with TMMD in DMSO-d_6.
Internal standard, hexamethyldisiloxane; 35 °C.
(a) Spectrum of CH_2ClI and TMMD before mixing.
(b) A mixture of CH_2ClI (3.46 mmol) and TMMD (4.88 mmol) was stirred in DMSO-d_6 for 2 h at 35 °C.
(c) Eschenmoser's salt ($Me_2\overset{+}{N}=CH_2,\bar{I}$). (d) A mixture of $Me_2\overset{+}{N}=CH_2$, $\bar{I}$(0.146 mmol) and TMMD (0.166 mmol).

(Fig. 2). Mixing of the two components (Fig. 2-a) caused gradual decrease of CH_2ClI proton with concomitant downfield shift of the $-CH_2N<$ proton, accompanied by the formation of CH_2Cl_2 (Fig. 2-b). In some cases, depending on the relative amounts of the reagents and the solvent, a white precipitate separated from the reaction mixture. The precipitate, upon dissolution in another portion of DMSO-d_6, showed identical NMR spectrum with that of the authentic sample of the Eschenmoser's salt (Fig. 2-c). On the other hand, a mixture of the Eschenmoser's salt and TMMD showed only two signals of ^1H NMR absorption at 35 °C, which were assigned to CH_3–N and $-CH_2$–N protons, suggesting rapid exchange between iminium species and TMMD (Fig. 2-d).

These observations indicate that the reagent system CH_2ClI/TMMD contains complex iminium species, while most simply, the reaction of CH_2ClI and TMMD is depicted as follows (Eq. 6) (TMMD complexed with **6** or **1** is omitted), where plausibe intermediate species such as **6** can also serve as the Mannich reagent for the enol silyl ether present in the system.

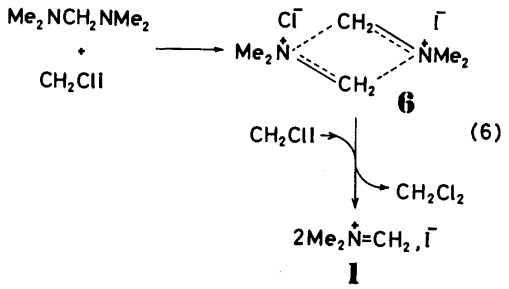

In fact, detailed inspection of the results in Table 4 indicates that up to 2 molar amounts of Me_2NCH_2- moiety could be trapped into acetophenone enol silyl ether from 1 mol of CH_2ClI and TMMD. It is well demonstrated that iminium salt (**1**) readily reacts with not only enol silyl ethers but also various enolates,[5b,13] where highly electrophilic iminium methylene attacks enolate carbon in a regiospecific manner.[7,14]

Experimental

IR spectra were obtained on a Shimadzu IR 430 spectrophotometer. NMR spectra were determined on a Hitachi R-24A instrument using hexamethyldisiloxane as an internal standard in CCl_4 unless otherwise stated. Mass spectra were recorded on a JEOL JMS-D 300 double focusing spectrometer. Analytical GLC was recorded on a Shimadzu GC 3AF with FID detector or Shimadzu 3BT with TCD detector, on a Silicone GE SE-52 on Chromosorb W(AW), Apiezon Grease L on Diasolid M, or Silicone DC 550 on Uniport C column. Preparative GLC was carried out on a Shimadzu GC 6AM using appropriate column mentioned above. Microanalyses were performed at the Microanalysis Center, Chemical Research Institute of Nonaqueous Solutions, Tohoku University.

Materials. CH_2ClI (bp 108 °C) and CH_2I_2 (bp 70 °C/12 mmHg)† were obtained *via* halogen exchange of CH_2Cl_2 with NaI, and stored over a few tin pellets in the dark.[15] CH_2Br_2 was dried over $CaCl_2$, and distilled before use (bp 94—95 °C). Commercial carbonyl compounds were dried over $MgSO_4$ and distilled before use, while 1,2-diphenylethanone (**2h**) (mp 55—56 °C) was used as purchased. TMMD (bp 83—84 °C)[16] and Et_3N (bp 90 °C) were distilled from CaH_2 after having been refluxed for several hours. Solvents were purified as usual. Purified materials were stored under positive nitrogen pressure.

Phenylacetone (2g): The method of Hass *et al.*[17] was slightly modified. A mixture of benzaldehyde (106 g, 1 mol) and nitroethane (≈85 g, ≈1.1 mol) in 50 ml of benzene was refluxed for 15 h with continuous removal of water as benzene azeotrope. Volatiles were removed *in vacuo*, and the residue was recrystallized from ethanol to give 135 g of 1-phenyl-2-nitropropene (83%), mp 64—65 °C (lit,[17] mp 65 °C). A 75 g sample of the phenylacetone, bp 74—74.2 °C/3 mmHg, was prepared from 100 g of the 1-phenyl-2-nitropropene by treatment with 250 g of Fe powder as was described in the literature.[17]

† 1 mmHg≈133.322 Pa.

Enol Silyl Ethers (3): These were prepared from the corresponding carbonyl compounds and trimethylsilyl chloride[18] by means of lithium diisopropylamide in THF (**3d**, bp 33—35 °C/1.5—1.7 mmHg; **3i**, bp 72—76 °C/6—7 mmHg), or by refluxing in Et_3N-DMF (**3a**, bp 65—70 °C/50 mmHg, $E/Z=35/65$; **3b**, bp 54—57 °C/3—4 mmHg; **3c**, bp 65—66 °C/17—18 mmHg; **3e**, bp 68—71 °C/9—10 mmHg; **3f**, bp 60—62 °C/16 mmHg, $E/Z=59/41$; **3g**, bp 87—89 °C/3 mmHg; **3h**, bp 135 °C/1.3 mmHg; **3j**, bp 58—59 °C/45—46 mmHg; **3k**, 97—99 °C/16—17 mmHg).

General Procedure for the Synthesis of the Mannich Base from Enol Silyl Ether (3) with CH_2ClI/TMMD. The reactions were conveniently carried out in a two-necked, 50 ml Schlenk tube under a nitrogen atmosphere. To a water-cooled, stirred solution of the enol silyl ether (**3**) (≈20 mmol) and CH_2ClI (≈30 mmol) was added ≈30 mmol of TMMD. After a slight exothermic reaction subsided, the mixture was stirred at room temperature. Net reaction times are specified in Table 3. At the end of the reaction, 30 ml of 2 M HCl was added, and the mixture was stirred for *ca.* 1 h. Non-basic components, which included unchanged CH_2ClI, starting carbonyl substrate or enol silyl ether, and α-methylenation product, were extracted with portions of cyclohexane. The aqueous phase was made alkaline with 10% NaOH, and extracted with CH_2Cl_2 (4×30 ml). The combined extracts were washed successively with 10% NaOH, brine, and water. After the solution had been dried over $MgSO_4$, CH_2Cl_2 was evaporated *in vacuo*, and the residue was trap-to-trap distilled under reduced pressure; after a small forerun was discarded, middle distillate was collected as the product Mannich base. Results are summarized in Tables 3 and 5.

Upon termination of the reaction of **3h**, addition of aq HCl caused separation of hydrogen halide salt of the Mannich base; the solid was separated by filtration. The Mannich base (**4h**) was liberated by treatment with aq NaOH, and taken into ether.

The cyclohexane extracts were treated as usual, concentrated to an appropriate volume, which was subjected to preparative GLC to recover the α-methylene products (**5**).

5f: NMR: δ ≈0.9 (3H, Me–), 1.1—1.6 (6H, $-(\underline{CH_2})_3-$Me), 2.0—2.5 (2H, $-CH_2-\dot{C}=C\langle$), 5.8 (1H, br) and 6.1 (1H, br) (2H for $H_2C=C\langle$), 9.4 (1H, s, –CHO). MS (70 eV), *m/e* (%): 126 (M^+, 0.53), 97 (M−CHO, 28.3), 95 (10.2), 79 (6.1), 71 (10.4), 70 (11.7). IR (liq. film): 2700, 1690, 1460, 940 cm^{-1}.

5g: NMR: δ 2.35 (3H, s, –Me), 5.7 (1H, br) and 5.9

TABLE 5. SPECTRAL AND ANALYTICAL DATA FOR THE MANNICH BASE

Mannich base	IR (liq. film) ν_{max}/cm^{-1}	NMR (CCl_4) δ	Found(%) (Calcd (%)) or MS (70 eV), *m/e* (%)
4a	2820, 2780, 1710, 1460, 1380, 1045	0.91 (3H, d, J=6.4 Hz, Me–CH⟨), 0.93 (3H, t, J=7.0 Hz, Me–CH_2–), 2.05 (6H, s, Me_2N–), 2.31 (2H, d, J=7.3 Hz, $-CH_2-N\langle$), 2.0—2.8 (3H, $-CH_2-CO-CH\langle$)	C 67.29(67.08) H 11.89(11.97) N 9.88(9.78)
4b	2830, 2770, 1680, 1460, 1235, 980	1.1 (3H, d, J=6.8 Hz, Me–CH⟨), 2.1 (6H, s, Me_2N–), 2.1—2.7 (2H, $-CH_2N\langle$), 3.5—4.0 (1H, –CH⟨), 7.2—8.1 (5H, –Ph)	C 75.55(75.35) H 8.68(8.96) N 7.06(7.32)
4c	2800, 2750, 1710, 1450, 1125, 1030	1.1—3.0 (11H), 2.04 (6H, s, Me_2N–)	MS: 110 (M−Me_2NH, 14.3), 82 (17.1), 67 (36.8), 54 (8.9)
4d	2850, 2780, 1710, 1460, 1375, 1130, 1050	0.90 (d, J=6.8 Hz) and 0.94 (d, J=6.4 Hz)(3H, Me–CH⟨), 1.5—2.1 (6H, $-(CH_2)_3-$), 2.1 (s, 6H, Me_2N–), 2.1—3.0(4H,Me–CH–CO–CH–CH_2–N⟨)	C 70.73(70.96) H 10.95(11.31) N 8.08(8.27)
4e	2750, 2700, 1720, 1450, 1265, 1045	1.0—2.0 (10H, $-(CH_2)_5-$), 2.1 (6H, s, Me_2N–), 2.27 (2H, s, $-CH_2N\langle$), 9.33 (1H, s, –CHO)	C 70.81(70.96) H 11.02(11.31) N 7.91(8.27)
4f	2800, 2770, 2720, 1715, 1460, 1375, 1265, 1160, 1040	0.9 (3H, Me–CH_2–), 1.0—1.8 (8H, $-(CH_2)_4-$), 2.1 (6H, s, Me_2N–), 2.2—2.5 (2H, $-CH_2N\langle$), 2.5—2.8 (1H, –CH⟨), 9.4 (1H, br, –CHO)	C 70.32(70.12) H 12.21(12.36) N 8.07(8.18)
4g	2840, 2780, 1710, 1465, 1360, 1160, 1030	2.0 (3H, s, Me–CO–), 2.1 (6H, s, Me_2N–), 2.2—3.2 (2H, $-CH_2N\langle$), 3.5—3.9 (1H, –CH⟨), 6.8—7.5(5H, –Ph)	MS: 191 (M^+, 0.70), 146 (M−Me_2NH, 10.5), 103 (44.2)
4h	a) 2810, 2770, 1665, 1450, 1250, 1210	2.2 (6H, s, Me_2N–), 2.4—2.8 (2H, $-CH_2N\langle$), 4.6—5.0 (1H, –CH⟨), 6.9—8.1 (10H, 2Ph–)	C 80.78(80.60) H 7.79(7.56) N 5.39(5.53)
4i	2820, 2770, 1730, 1460, 1380, 1035, 850	0.8 (3H, Me–$(CH_2)_3$–), 1.0—1.6 (9H, Me–CH_2–O–+Me–$(CH_2)_3$–), 2.1 (6H, s, Me_2N–), 1.9—2.7 (3H, –CH–CH_2–N⟨), 4.0 (2H, q, J=7.2 Hz, $-CH_2O-$)	C 65.76(65.63) H 11.61(11.52) N 6.53(6.96)
4j	2810, 2750, 1700, 1460, 1385, 1080	1.05 (9H, s, Me_3C–), 2.1 (6H, s, Me_2N–), 2.4 (4H, s, $-(CH_2)_2-$)	MS: 157 (M^+, 3.8), 72 (4.9), 59 (3.1), 58 (80.5)
4'j	a) 2820, 2750, 1690, 1460, 1365, 1275, 1195, 1035, 985	1.05 (9H, s, Me_3C–), 2.1 (12H, s, $2Me_2N$–), 2.2—2.4 (4H, 2-$CH_2N\langle$), 3.0—3.4 (1H, –CH⟨)	MS: 169 (M−Me_2NH, 8.4), 156 (M−*t*-BuH, 45.7), 154 (4.3), 138(7.2), 137 (16.0)
4k	2830, 2790, 1680, *1450, 1240*	2.12 (6H, s, Me_2N–), 2.3—3.1 (4H, $-(CH_2)_2-$), 7.1—*8.0 (5H, –Ph)*	
4'k	a) 2770, 1670, 1450, 1280, 1235	2.06 (6H, s, Me_2N–), 2.2—2.8 (4H, 2-$CH_2N\langle$), 3.4—3.9 (1H, –CH⟨), 7.1—8.0 (5H, –Ph)	C 71.52(71.76) H 9.74(9.46) N 11.83(11.95)

a) KBr disk.

(1H, br) (2H for $H_2C=C\langle$), 7.1 (5H, -Ph). MS (70 eV), *m/e* (%): 146 (M^+, 24.4), 131 (16.3), 104 (6.6), 103 (36.7), 77 (3.3).

5h: NMR: δ 5.4 (1H, s) and 5.8 (1H, s) (2H for $H_2C=C\langle$), 6.9—8.0 (10H, 2Ph-). IR (liq. film): 1670, 1440, 1215, 990 cm^{-1}.

5i: NMR: δ ≈0.9 (3H, Me-$(CH_2)_3$-), 1.2 (3H, t, J=6.8 Hz, Me-CH_2O-), 1.1—1.8 (4H, Me-$(CH_2)_2$-), 2.2 (2H, t, J=6.0 Hz, $-CH_2-C=C\langle$), 4.1 (2H, q, J=6.8 Hz, Me-CH_2O-), 5.35 (1H, br) and 5.95 (1H, br) (2H for $H_2C=C\langle$).

Reaction of Acetophenone Enol Silyl Ether (3k): The following example is illustrative. A mixture of **3k** (3.10 g, 16.1 mmol), CH_2ClI (4.24 g, 24.0 mmol), and TMMD (2.80 g, 27.4 mmol) was stirred in 20 ml of DMSO at room temperature for 3 h, and was worked up as above. The cyclohexane extract was analyzed by GLC to determine the amount of CH_2ClI and acetophenone (Table 4). Evaporation of the CH_2Cl_2 layer *in vacuo* left a 3.5 g of syrupy residue which was comprised of the monoamino (**4k**) and diamino ketone (**4'k**) as was evidenced by NMR. The relative amount of the two was estimated to be 22/78 by integration of the Me_2N-resonance (δ 2.12 for **4k** and δ 2.06 for **4'k**). The residue was dissolved in 15 ml of hot pentane, and was kept at −20 °C overnight to give 2.19 g of **4'k** as white crystals (Table 5). Distillation of the filtrate caused serious deamination of the amino ketones, while following distillates were recovered:

Phenyl Vinyl Ketone: Trace, bp 55 °C/0.7 mmHg. NMR: δ 5.7 (1H, dd, J_{cis}=10.2 Hz, J_{gem}=2.4 Hz, for $HC=C\langle$ *trans* to -CO-Ph), 6.25 (1H, dd, J_{trans}=16.8 Hz, for $HC=C\langle$ *cis* to -CO-Ph), 7.0 (1H, dd, $-CH=CH_2$), 7.1—8.0 (5H, -Ph). IR (liq. film): 1670, 1660, 1610, 1450, 1400, 1230, ≈1000—960 cm^{-1}.

4k: Trace, see Table 5.

2-Methylene-3-(dimethylamino)propiophenone: 0.74 g, bp 115—120 °C/3 mmHg. NMR: δ 2.1 (6H, s, Me_2N-), 3.1 (2H, br, $-CH_2N\langle$), 5.5 (1H, br) and 5.75 (1H, br) (2H for $H_2C=C\langle$), 7.1—8.0 (5H, -Ph). IR (liq. film): 2820, 2780, 1660, 1450, 1325, 1280, 1040, ≈1000—970, 860 cm^{-1}.

Formation of the Eschenmoser's Salt from CH_2ClI and TMMD. Under a nitrogen atmosphere, 1.18 g (11.5 mmol) of TMMD was added to a 6.0 g (34 mmol) of CH_2ClI which was chilled in an ice-water bath. The bath was removed after 3 h, and the mixture was allowed to stand at room temperature for 3 d in the dark. Precipitated white crystal was filtered under nitrogen, and was washed with CCl_4, yield, 3.50 g (18.9 mmol calculated as **1** (X=I), 82% based on TMMD). Found: C, 19.60; H, 4.58; N, 7.60; I, 69.0%. Calcd for C_3H_8IN: C, 19.48; H, 4.36; N, 7.57; I, 68.59%. NMR (DMSO-d_6): δ 8.05 (2H, br, $CH_2\overset{+}{N}=$), 3.52 (6H, br, $Me_2\overset{+}{N}=$). On heating, the precipitate colored from white to yellow (≈100 °C) and to dark-brown (≈220 °C), and melted with decomposition at *ca.* 235 °C. By the use of 1 ml of DMSO as the solvent, the yield of the precipitate was improved to 90%. Control of the temperature at the early stage of the reaction and exclusion of moisture seemed essential in order to obtain pure product.

Time-course of the Reaction of CH_2ClI with TMMD. A mixture of CH_2ClI (5.30 g, 30 mmol), TMMD (3.07 g, 30 mmol), and 1.20 g of ethylbenzene (internal standard) in 20 ml of DMSO was stirred at room temperature. Samples (*ca.* 1 ml) were withdrawn at various times through a septum cap by means of a hypodermic syringe, and quenched with aq HCl. After three extractions with cyclohexane, the combined organic phase was analyzed by GLC (Apiezon Grease L column); only CH_2Cl_2 was detected as the reaction product. Material balance on chlorine and CH_2ClI requires following equations:

$$[CH_2ClI \text{ reacted}] = [\overset{+}{Me_2N}=CH_2, \bar{I}],$$

$$[\overset{+}{Me_2N}=CH_2, \bar{Cl}] = [CH_2ClI \text{ reacted}] - 2[CH_2Cl_2],$$

where it is supposed that species which lose halide ion on hydrolysis can be represented as **1** (X=Cl or I).

Financial support of this work by a Grant-in-Aid for Scientific Research No. 585223 from the Ministry of Education, Science and Culture is gratefully acknowledged.

References

1) Part II: S. Miyano, H. Hokari, Y. Umeda, and H. Hashimoto, *Bull. Chem. Soc. Jpn.*, **53**, 770 (1980).

2) Part of this work was presented at the 42nd National Meeting of the Chemical Society of Japan, Sendai, 1980, Abstr. No. 1L13.

3) Recent review: T. Shono and Y. Matsumura, *Yuki Gosei Kagaku Kyokai Shi*, **39**, 358 (1981).

4) a) M. Tramontini, *Synthesis*, **1973**, 703; b) J. Mathieu and J. Weill-Raynal, "Formation of C-C Bonds," Georg Thieme Publ., Stuttgart (1973), Vol. 1, pp. 78—91; c) H. O. House, "Modern Synthetic Reactions," 2nd ed, W. A. Benjamin, Inc., California (1972), pp. 654—660.

5) a) "Iminium Salts in Organic Chemistry," ed by H. Böhme and H. G. Viehe, Wiley-Interscienc, New York (1976), Part 1; b) S. Murahashi, *Kagaku (Chemistry)*, **34**, 922 (1979).

6) J. Schreiber, H. Maag, N. Hashimoto, and A. Eschenmoser, *Angew. Chem.*, **83**, 355 (1971).

7) N. Holy, R. Fowler, E. Burnett, and R. Lorenz, *Tetrahedron*, **35**, 613 (1979).

8) The Mannich reaction of enol silyl ether by a combination of aminomethyl ethers and trimethylsilyl iodide catalyst has recently been reported: S. Iijima, A. Hosomi, and H. Sakurai, The 43rd National Meeting of the Chemical Society of Japan, Tokyo, 1981, Abstr. No. 1D08.

9) S. Miyano, H. Hokari, A. Mori, and H. Hashimoto, *Chem. Lett.*, **1980**, 1213.

10) *Cf.* J.-L. Gras, *Tetrahedron Lett.*, **1978**, 2111.

11) H. Böhme, M. Hilp, L. Koch, and E. Ritter, *Chem. Ber.*, **104**, 2018 (1971).

12) T. A. Bryson, G. H. Bonitz, C. J. Reichel, and R. E. Dardis, *J. Org. Chem.*, **45**, 524 (1980); See also Ref. 8.

13) a) J. L. Roberts, P. S. Borromeo, and C. D. Paulter, *Tetrahedron Lett.*, **1977**, 1621; b) S. Danishefsky, T. Kitahara, R. McKee, and P. F. Schuda, *J. Am. Chem. Soc.*, **98**, 6715 (1976); c) J. Hooz and J. N. Bridson, *ibid.*, **95**, 602 (1973).

14) S. Danishefsky, M. Prisbylla, and B. Lipisko, *Tetrahedron Lett.*, **1980**, 805.

15) S. Miyano and H. Hashimoto, *Bull. Chem. Soc. Jpn.*, **44**, 2864 (1971).

16) Though commercially available, it can easily be prepared in large quantities: D. Lednicer and C. R. Hauser, *Org. Synth.*, Coll. Vol. 5, p. 434 (1973).

17) H. B. Hass, A. G. Susie, and R. L. Herder, *J. Org. Chem.*, **15**, 8 (1950).

18) H. O. House, L. J. Czuba, M. Gall, and H. D. Olmstead, *J. Org. Chem.*, **34**, 2324 (1969).

Proton and Carbon-13 Nuclear Magnetic Resonance Studies of the Effects of Retinal on the Dynamic Structure and Stability of Lipid Bilayer

Yoshio INOUE,* Yoshito HANAFUSA, Masakazu TODA, and Riichiro CHŪJŌ
Department of Polymer Chemistry, Tokyo Institute of Technology, O-okayama, Meguro-ku, Tokyo 152
(Received June 23, 1981)

The effects of retinal and vitamin A on the dynamic structure and stability of hen egg yolk lecithin bilayers have been studied by means of carbon-13 and proton NMR spectroscopies. ^{13}C spin-lattice relaxation and paramagnetic ion permeability studies on lecithin bilayers indicate a marked decrease in flexibility of the lipid acyl chain and a breakdown of membrane impermeableness to ion by the intercalated *all-trans*- and 11-*cis*-retinal, whereas the effect of incorporated vitamin A on the fluidity of bilayers is small and its impermeableness to ion remains effective even in the presence of higher concentration of vitamin A. The experimental results are discussed in connection with the mechanism of the permeability change in photoreceptive disk membrane.

Rod outer segments are organelles in which the photon is captured by rhodopsin, the visual pigment of the retinal photoreceptor cells for black and white vision in the eye. Rhodopsin is composed of the vitamin A_1 aldehyde isomer 11-*cis*-retinal and the lipoprotein opsin, in which the former is bonded through a Schiff base linkage to the ε-amino group of a lysine residue. Upon exposure to light, rhodopsin bleaches through a series of transformations and finally releases *all-trans*-retinal from opsin into lipid medium in retina.[1] During these events the ionic permeability of the disk membrane is altered and thus the photoreception is translated into an electrical response.[2]

Much is known about bleaching process of rhodopsin,[1] while the mechanism of the translation of photoinformation to the neural system has so far remained almost an event of conjecture. The fact, which seems established, is that the absorption of a single photon by rhodopsin leads to a reduction of the sodium influx[2-4] and consequent hyperpolarization of the disk membrane.[5]

There are considerable interests in the role of membrane lipid in these photochemical events; almost half of the retina rod outer segment fragments is lipid on a weight basis and most of lipid is phospholipid.[6] Phosphatidylethanolamine (PE), phosphatidylcholine (PC), and phosphatidylserine (PS) are the major phospholipids of bovine rod outer segments, making up about 39, 40, and 13%, respectively, of the lipid phosphorus. The major fatty acids in PE and PS are 18 : 0 and 22 : 6, while PC is made up predominantly of 16 : 0 and 22 : 6, and all of the phospholipids contain high levels of polyunsaturated fatty acids.[6,7] Rhodopsin is considered to be an integral membrane protein and at least a part of the protein is embedded within the membrane interior. The interactions between rhodopsin and phospholipid including artificially reconstructed model membranes have been studied by many authors,[8-15] while those between retinal isomers and phospholipid have not been studied well. Retinal has been thought to decompose some biomembranes,[16] especially, *all-trans*- and 11-*cis*-retinal hemolyse rabbit erythrocytes.[17] Retinal isomers may, therefore, affect the arrangement of lipid membrane and *all-trans*-retinal released from rhodopsin plays significant roles in alteration of ionic permeability of plasma membrane.

By the way, the chromophore *all-trans*-retinal released from bleached pigment can be recycled with newly incorporated one *in vivo* to rhodopsin regeneration.[18] Rhodopsin regeneration is believed to occur *via* two discrete reactions: isomerization of *all-trans*-retinal to 11-*cis*-retinal and binding of 11-*cis*-retinal with opsin. *In vivo*, little free retina is found in the photoreceptor cell in contrast to the presence of retinylidene phosphatidylethanolamine.[19-21] Shichi and Somers[18,22,23] have found that phospholipid stimulates the photo-regeneration of rhodopsin from opsin and *all-trans*-retinal. The enhancement of stereoselective isomerization of retinal by an addition of phosphatidylethanolamine has been demonstrated *in vivo* experiment[24] and a series of molecular orbital calculations.[25] It was pointed out[22] that the role of phosphatidylethanolamine in retina are (i) to maintain the integrity of the visual pigment and (ii) to participate in the regenaration of rhodopsin after bleaching, although the latter role is still a matter of speculation.[7,26,27]

In this paper, the interactions between model membrane lipid and retinal and vitamin A were studied by observing the proton and carbon-13 nuclear magnetic resonance spectra. The locations of retinal compounds in the membrane and their effects on the dynamic structure and stability of membrane were investigated by measuring the carbon-13 spin-lattice relaxation time and by monitoring the ionic permeability of the membrane by proton spectra. The determinations of the position of retinals in the lipid bilayers and their effects on the membrane properties are expected to give valuable informations required for the elucidation of the visual process, including the ion permeation and rhodopsin regeneration. As pigments, we will choose *all-trans*- and 11-*cis*-retinal, and vitamin A: the former two are compounds participating in a visual cycle, and the latter one was chosen for the sake of comparison with the formers.

Hen egg yolk phosphatidylcholine (egg yolk lecithin, EYL) bilayer will be used as a model membrane of disk. Use of phosphatidylethanolamine, in spite of one of major phospholipid constituents of rod outer segment's membrane, will be excluded, since it forms Schiff base with retinal. The formation of Schiff base may shade off our purposes. Egg yolk lecithin has several advantages as a lipid membrane system for a model study of disk membrane. Needless to say phosphatidylcholine is one of major constituents of lipid of rod outer segments. The structure of EYL is,

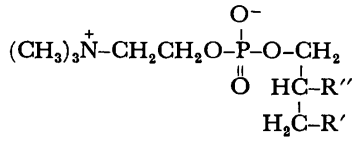

where the predominant esterified residues of fatty acids R′ are palmitic (16 : 0) and stearic (18 : 0), and those of R″ are oleic (18 : 1) and linoleic (18 : 2).[28,29] Long-chain esterified fatty acids with varying degree of unsaturation amounts to 12% are also contained in EYL. EYL thus contains high levels of polyunsaturated fatty acids like a disk phospholipid, and EYL bilayer is in the liquid crystalline states at physiological temperature corresponding to the state of disk membrane. The kinetic study of interconversion from metarhodopsin I to II in a rhodopsin recombinant indicates comparable rate of interconversion in rod outer segments membrane and rhodopsin-EYL bilayers.[30] Thus, EYL could be convinced for a pertinent model for phospholipids of rod outer segments.

Experimental

Vitamin A was purchased from Riken Vitamin Co. Ltd., Tokyo. The crystal of *all-trans*-retinal was prepared by oxidation of vitamin A with manganese dioxide in petroleum ether. The crystal of 11-*cis*-retinal was prepared by successive procedures,[31] *i.e.*, photoisomerization of *all-trans*-retinal in ethanol at 0 °C, fractionation of retinal isomers on an alumina column by eluting with petroleum ether, and seeded recrystallization at −20 °C. Details of preparation of these retinal compounds were described elsewhere.[32]

Egg yolk lecithin was isolated from fresh hen egg yolk according to the procedure of Singleton *et al.*[33] The purity of EYL was checked by thin-layer chromatography. Paramagnetic reagents, $Eu(NO_3)_3 \cdot 6H_2O$, $K_3[Fe(CN)_6]$, and $MnSO_4$ were purchased from Nakarai Chemicals, Ltd., Kyoto. Before use, $Eu(NO_3) \cdot 6H_2O$ were treated by repeated process of dissolving in deuterium oxide and freeze-drying to exchange H_2O with D_2O.

Lecithin dispersions (10% w/v) were prepared by shaking the dry EYL with 0.05 M KCl/D_2O solution (pH 5.6±0.2). The dispersions were then sonicated under cooling by ice/water until translucence (about 20 min) with an Ultrasonic Disruptor Model UR-200P (Tomy Seiko Co. Ltd., Tokyo, frequency 20 kHz, output power 200 W). The resultant vesicle solutions were thoroughly deoxygenated by bubbling argon gas, and were centrifuged (10000 min^{-1} for 1 h) to remove titanium fragment from sonicator's microtip and to remove multilayer liposomes. The vesicle solution was transfered under argon to NMR glass-tubes (5 mm for ^1H and 8 mm for ^{13}C NMR samples) and the NMR spectra were measured immediately after the preparation. Retinal compound-lipid mixed vesicle solution was prepared by first co-dissolving both components in chloroform followed by evaporating the solvent and then treating the resulting dry mixture in a similar manner as described above. KCl was not added to the sample for the proton NMR study of cationic permeability. In this case pH of sample was 7.0. The total concentrations of lipid and retinal-compounds were about 5% (w/v) for proton and 10—20% (w/v) for carbon-13 NMR samples. It has been reported that lecithin concentration over the range of 10—20% (w/v) and changes of pH from 2.5 to 8.0 did not have a significant effect on the carbon-13 relaxation time.[34] Proton and carbon-13 NMR spectra were measured using a JEOL JNM PS-100 spectrometer operating at 100 and 25 MHz, respectively. Proton spectra were measured in a continuous-wave mode. In the ^1H NMR experiment of ionic permeability, $1—2 \times 10^{-2}$ mol dm^{-3} paramagnetic compounds were added to the vesicle dispersion.

In the measurement of carbon-13 spectrum, the spectrometer was equipped with a JEOL JNM PFT-100 Fourier transform system, internal deuterium lock, noise-modulating proton-decoupler, JEOL JEC-6 computer (12K), and JEOL CM-219 IC core (8K) as an auxiliary memory device. A width of frequency domain spectra was 5000 Hz and a data file was 4096 points. The normal spectra were recorded after 1024 or 2048 pulses. The pulse sequence was repeated after a delay time at least five times greater than the largest spin-lattice relaxation time to be measured in order to avoid the effect of saturation. The duration time for 90° pulse was about 2×10^{-5} s. Chemical shifts were measured as down field shifts from external tetramethylsilane (TMS). Carbon-13 spin-lattice relaxation time (T_1) was determined by fast inversion recovery method[35] with a waiting time 5s in order to circumvent the required waiting period. T_1 values for several carbon atoms were checked by the so-called inversion recovery method[36] and were found to be in agreement with the fast inversion recovery determination within experimental error (±10% for well-resolved large peaks and ±15% for less-resolved and small peaks). The sample temperature was kept at 36±1 °C. The preparations of samples and NMR measurements were carried out in the dark. Electron micrographs of sonicated aqueous dispersions of EYL vesicle were observed on a copper sheet mesh soiled by a drop of 2% tungstophosphoric acid with a JEOL JEM-7A type electron microscopy. Ultraviolet spectra were observed on a Beckman-25 spectrometer.

Results

Electron Micrograph. Electron micrographs of sonicated dispersions of EYL indicated the presence of a distribution of vesicle sizes but the most of vesicle have a narrow range of sizes (200—300 Å in diameter). The addition of 20 mol% 11-*cis*-retinal shifted and spread the distribution of vesicle sizes (300—500 Å in diameter). The formations of multilayer or large aggregate with diameter greater than 500 Å were found to be scarce but not negligible. Thus the incorporation of retinal causes the expansion of vesicle size although most of the vesicles remained small. The structural invariableness of retinals and vitamin A before and after the sonication in an EYL dispersion was confirmed by observing ultravilet spectra. Furthermore no major differences were noted between the electron micrographs of sonicated dispersions, even the dispersions with retinals and vitamin A, observed at immediately after and 3—4 d after the preparation.

Carbon-13 Spin-lattice Relaxation Time. The ^{13}C spin-lattice relaxation times for EYL, EYL with 20 mol% incorporated *all-trans*- and 11-*cis*-retinal, and vitamin A are shown in Table 1, where the carbons are listed along the lipid backbone. Since the EYL's esterified fatty acids are heterogeneous, there is some ambiguity in the exact position of the carbon on the fatty acyl chain. Spectral assignments were followed to those made previously.[34] No detectable chemical shifts differences over the experimental error were found between EYL alone and EYL with incorporated

TABLE 1. VALUES OF ^{13}C NT_1[a,b] FOR EGG YOLK LECITHIN(EYL)-RETINALS AND -VITAMIN A BILAYERS IN 5×10^{-2} mol dm^{-3} KCl/D_2O SOLUTIONS AT 36 °C[c]

Carbon	^{13}C NT_1/s			
	EYL	EYL+20 mol% *all-trans*-Retinal	EYL+20 mol% 11-*cis*-Retinal	EYL+20 mol% Vitamin A
$-N(\underline{C}H_3)_3$	1.89	1.50 (0.80)	1.41 (0.75)	1.74 (0.92)
$\underline{C}=O$	1.8[d]	1.4[d] (0.78)	1.4[d] (0.78)	1.9[d] (1.05)
$-\underline{C}H_2CO_2-$	0.48	0.42 (0.88)	—[e]	—[e]
Main fatty acyl $(\underline{C}H_2)_n$	0.96	0.66 (0.69)	0.72 (0.75)	0.84 (0.88)
$-\underline{C}H_2-CH=CH-$	0.96	0.60 (0.62)	0.70 (0.73)	—[e]
$-CH=\underline{C}H-CH_2-CH_2-$	0.58	0.40 (0.69)	0.49 (0.84)	0.52 (0.90)
$-CH=\underline{C}H-CH_2-\underline{C}H=CH-$	0.67	0.54 (0.81)	0.66 (0.99)	0.65 (0.97)
$-CH=CH-\underline{C}H_2-CH=CH-$	1.20	0.92 (0.77)	0.70 (0.58)	0.96 (0.80)
$-\underline{C}H_2-CH_2-CH_3$	1.46	1.14 (0.78)	0.78 (0.53)	—[e]
$-\underline{C}H_2-CH_3$	3.00	2.20 (0.73)	1.80 (0.60)	2.80 (0.93)
$-\underline{C}H_3$	9.60	5.64 (0.59)	5.40 (0.56)	7.80 (0.81)

a) Here, T_1 is the spin-lattice relaxation time and N is the number of protons attached to the carbon. The measured T_1 values correspond to the underlined carbons. b) Estimated maximum error in T_1 is $\pm15\%$. c) The values shown in parentheses are the T_1 ratios of EYL-additive mixture to EYL alone. d) The values shown are T_1's. e) Not measured accurately.

retinals and vitamin A. At the concentrations employed here, resonance intensities of the retinal additives were too weak for an accurate determination of their relaxation times. The ^{13}C relaxation times for some carbon resonances of EYL also could not be measured accurately due to their low signal to noise ratios and are not included in Table 1. Since no major differences were noted between normal spectra observed at the beginning and the end of a set of inversion-recovery experiment, and between micrographs observed at immediately after and 3—4 d after the preparation of dispersion, an extent of vesicle fusion during the course of NMR experiment may be small.

The decrease in the rate of motion and in the acyl chain disorder of EYL will result in smaller NT_1 values, although an interpretation of ^{13}C T_1 value is hampered by the fact that the relaxation rate is determined by the anisotropy of molecular motion as well as the rate of motion.[37] Here N is the number of protons bonded to a given carbon atom. For dispersions of EYL alone and EYL with retinals and vitamin A in bilayers, NT_1 values increase from the glycerol carbons toward both the $N^+(CH_3)_3$ group and the terminal methyl carbon of acyl chains, indicating that there are increases in the mobility along the lipid chain in going from the glycerol carbons to the terminal methyl groups. These observations are in agreement with previous ^{13}C relaxation studies of lecithin dispersions.[34,38]

Inspection of ^{13}C T_1 values of EYL listed in Table 1 reveals that the effects of added retinals and vitamin A on T_1 values of EYL are relatively small but almost all T_1 values decrease, namely the motion of EYL molecule is slowed down by additions of retinals and vitamin A. It is noticeable that the reductions of T_1 values of acyl chain carbons are larger in EYL–retinal systems than in EYL–vitamin A system. In the former systems, the carbons of methyl terminal region of acyl chain ($-CH_2CH_2CH_3$) show especially larger T_1 reductions than the other part of EYL molecules, indicating that the retinal molecules locate rather preferentially at the acyl chain region than at the choline polar region of the lipid bilayer. Since retinal is not soluble in water alone, retinal molecule may be solubilized and incorporated into the acyl chain region of lipid bilayer by the hydrophobic interaction between retinal and lipid acyl chain.

On the other hand, the reductions of NT_1 values for EYL–vitamin A system are relatively small and not suggesting any localization of vitamin A molecule at special region in the lipid bilayer. Vitamin A may be allowed to stay near the polar hydrophilic site of lipid bilayer, exposing its hydroxyl group to aqueous medium and extending its hydrophobic part into nonpolar region of lipid bilayer.

For a comparison, ^{13}C T_1 values for EYL alone and EYL with 22 mol% *all-trans*-retinal were also measured in $CDCl_3$ solutions, where lecithin molecules exist as spherical inverted micelles. The results are shown in Table 2. As reported previously,[38] NT_1 values of the chain resonances in $CDCl_3$ are longer than those for the corresponding nuclei in bilayers in D_2O and there is a marked increase in NT_1 values from carbonyl carbon toward the terminal methyls. The NT_1 value of choline methyl resonance is similar to that of $OOC-CH_2-$ methylene carbon resonance in $CDCl_3$ solution, contrasting with the results in D_2O solution where choline methyl NT_1 value is much larger than $OOC-CH_2-$ methylene carbon value. The small NT_1 value for choline methyl groups may result from tight packing of these groups in the inverted micellar structure.[38] In $CDCl_3$ solutions, the inverted micellar structure of EYL is not perturbed by *all-trans*-retinal, since NT_1 values are not changed greatly by an addition of it. Furthermore the resonances corresponding to the retinal carbons are sharper in $CDCl_3$ solution than in D_2O solution. Thus, there isn't any specific interaction between EYL and retinal in $CDCl_3$ solution. These results also confirm that the nature of interaction between EYL and retinals and vitamin A in D_2O solution is essentially hydrophobic.

TABLE 2. VALUES OF ^{13}C T_1[a] FOR EGG YOLK LECITHIN(EYL) IN $CDCl_3$ AT 37 °C

Carbon	EYL		EYL+22 mol% *all-trans*-Retinal		T_1 Ratio[c]
	T_1/s	NT_1/s[b]	T_1/s	NT_1/s[b]	
$-N(\underline{C}H_3)_3$	0.15	0.44	0.14	0.41	0.93
$\underline{C}=O$	2.68		2.31		0.86
$-\underline{C}H_2CO_2-$	0.23	0.46	0.30	0.59	1.29
Main fatty acyl $(\underline{C}H_2)_n$	0.94	1.87	1.11	2.21	1.18
$-\underline{C}H_2-CH=CH-$	1.08	2.15	1.24	2.49	1.16
$-CH=\underline{C}H-CH_2-\underline{C}H=CH-$	1.50	1.50	1.10	1.10	0.73
$-CH=CH-\underline{C}H_2-\underline{C}H=CH-$	1.39	2.78	1.42	2.84	1.02
$-\underline{C}H_2-CH_2-CH_3$	2.53	5.06	2.77	5.54	1.09
$-\underline{C}H_2-CH_3$	3.49	6.99	3.51	7.02	1.00
$-\underline{C}H_3$	4.70	14.10	5.05	15.15	1.07

a) Here, T_1 is the spin-lattice relaxation time of the underlined carbon. Estimated maximum error in T_1 is ±10%. b) N is the number of protons attached to the carbon. c) The observed T_1 values of EYL under the coexistence of 22 mol% *all-trans*-retinal relative to those obtained for EYL alone.

^1H NMR Studies on Ionic Permeability of Bilayers. The stability and vesicular nature of the lipid has been further investigated using ^1H NMR. The ionic permeability of lipid bilayers can be correlated with the membrane fluidity as described by ^{13}C spin-lattice relaxation times. In this paper, we studied the effect of the incorporation of retinals and vitamin A on the permeability of EYL vesicles using a paramagnetically induced variation of choline methyl proton resonance. It had previously been shown for ^1H, ^{13}C, and ^{31}P NMR that an addition of paramagnetic ion to lipid bilayer systems results in broadening or shifting of resonances from nuclei near the bilayer surface.[39,40] Paramagnetic ions can hence be used to distinguish the internal and external surface of a phospholipid vesicle by selectively adding the paramagnetic ion to the interior or exterior of the vesicle. Furthermore a variation of resonances induced by paramagnetic ion can be used to study the ionic permeability of lipid bilayers. Here, we used Eu^{3+} and $Fe(CN)_6^{3-}$ ions as the shift reagents and Mn^{2+} ion as the broadening reagent.

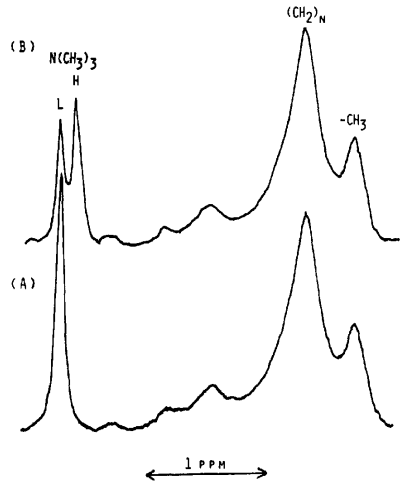

Fig. 1. 100 MHz proton NMR spectra of: (A) sonicated egg yolk lecithin vesicles (5 w/v%) in deuterium oxide solution and (B) sample A plus 10^{-2} mol dm^{-3} Eu^{3+} outside the vesicles. The spectra weretaken at 36 °C.

Figure 1 illustrates the effects of shift reagent $Eu(NO_3)_3$ as typical example. Spectral assignments are taken from those made previously.[40] Spectra A and B were obtained from the same sample without and with $Eu(NO_3)_3$. Upon addition of the $Eu(NO_3)_3$ to sample A, the choline methyl resonance splits into a doublet, while the other resonances are hardly affected. The high-field, shifted(H) and low-field, non-shifted(L) parts of the choline methyl resonance correspond to choline $N(CH_3)_3$ protons on the outside and the inside of the lecithin bilayers, respectively. The intensity ratio L : H of the non-shifted and shifted choline methyl resonance were 1 : 1.4. Assuming that the packing densities of both outside and inside layers of vesicle bilayers are equal and the thickness of the membrane is 37 Å,[40] the diameter of vesicle is estimated from the intensity ratio to be about 480 Å, which is slightly larger than that of prominent particles found by electron micrograph.

If the bilayers are permeable to Eu^{3+} and $Fe(CN)_6^{3-}$ ions, the inward-facing choline methyl groups are exposed to these ions, and the intensity of the shifted signal increases while that of the non-shifted signal correspondingly decreases with progress of ion permeation. When Mn^{2+} is added to the permeable bilayers, the resonance of only inward-facing choline methyl group may be firstly observed, but all finally disappears from ^1H NMR spectrum.

The intensity ratio of the choline methyl doublet shown in Fig. 1B remained practically constant for two days, indicating that Eu^{3+} cation is impermeable through EYL bilayers. Same impermeableness was also observed for Mn^{2+} and $Fe(CN)_6^{3-}$ ions. We have investigated the influences of incorporated retinals and vitamin A in the concentration range 5—33 mol% on the ionic permeability of EYL bilayers. It was found that an addition of vitamin A even at the concentration of 33 mol% does not disturb the impermeableness of bilayers which are effective ion barriers. Furthermore EYL vesicle containing less than 20 mol% *all-trans*- or 11-*cis*-retinal was found to form bilayers stable on the time scale of our experiments and also practically

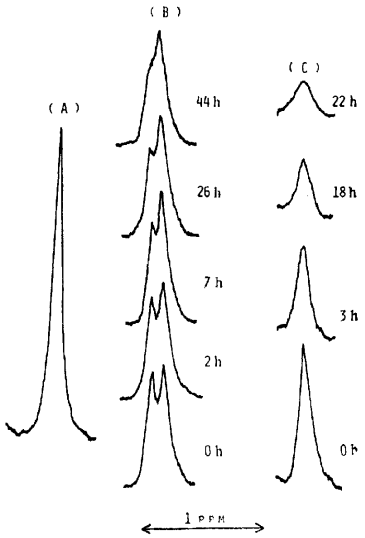

Fig. 2. Time dependence of choline methyl resonance of sonicated egg yolk lecithin vesicles (5 w/v%) with 33 mol% incorporated *all-trans*-retinal in deuterium oxide solution at 36 °C. (A) spectrum before adding the paramagnetic ions; (B) spectra of sample A just after (0 h) and 2, 7, 26, and 44 h after adding the $Eu(NO_3)_3$ (10^{-2} mol dm^{-3}); and (C) spectra of sample A just after (0 h) and 3, 18, and 22 h after adding the $MnSO_4$ (10^{-2} mol dm^{-3}).

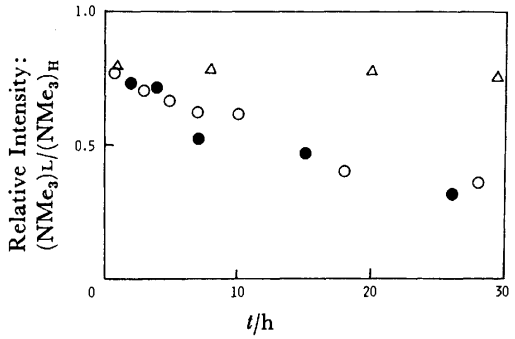

Fig. 3. Time dependence of intensity ratio of low-field(L) to high-field(H) choline methyl resonances for egg yolk lecithin(EYL) with 20 mol% incorporated *all-trans*-retinal plus 10^{-2} mol dm^{-3} Eu^{3+} (△), EYL with 33 mol% incorporated *all-trans*-retinal plus 10^{-2} mol dm^{-3} Eu^{3+} (●), and EYL with 33 mol% incorporated *all-trans*-retinal plus 2×10^{-2} mol dm^{-3} $Fe(CN)_6^{3-}$ (○).

impermeable to Eu^{3+}, $Fe(CN)_6^{3-}$, and Mn^{2+} ions.

On the contrary, less but significant ion permeation was found with the incorporation of over 20 mol% *all-trans*- and 11-*cis*-retinal to the system. Figure 2 shows the change of the choline methyl resonance with time after adding Eu^{3+} and Mn^{2+} ions to EYL dispersion with 33 mol% incorporated *all-trans*-retinal. The rate of penetration of ions across the bilayers is reflected in the rate of the spectral change. Time dependence of the intensity ratio of low-field to high-field choline methyl resonances after the addition of Eu^{3+} and $Fe(CN)_6^{3-}$ for EYL–*all-trans*-retinal systems are shown in Fig. 3. The increased amount of incorporated *all-trans*-retinal results in the increased rate of permeation of ion. Similar plots were also obtained for EYL–11-*cis*-retinal systems.

The ^1H results show that the incorporations of *all-trans*- and 11-*cis*-retinal but not vitamin A disturb the integrity of the lipid bilayers and cause the formation of a channel through which the ion is allowed to permeate.

Discussion

The results of ^1H permeability studies parallel those of ^{13}C relaxation studies. The ^{13}C and ^1H NMR studies have shown a decrease in flexibility of the lipid acyl chain and a breakdown of membrane impermeableness to ion caused by the intercalation of *all-trans*- and 11-*cis*-retinal, whereas the effect of vitamin A on the fluidity of bilayers is small and its impermeableness to ion remains effective even in the presence of higher concentration of vitamin A. From the results reported here, it is clear that retinal and vitamin A are incorporated into EYL bilayers and they expand the bilayers slightly without significant disruption of overall vesicular structure. These incorporated molecules may be situated in the bilayer orienting its polyene chain nearly parallel to the lipid acyl chain. *All-trans*- and 11-*cis*-retinal molecules stay preferentially at the acyl chain region due to the hydrophobic interaction. On a molecular level, incorporations of *all-trans*- and 11-*cis*-retinal, which have inflexible polyene chain and bulky ionone ring, stiffen the flexible chain of lipid molecules surrounding the intercalated retinal molecules and disrupt the packing of the hydrocarbon region of phospholipid bilayers. In other words, the incorporated retinal molecules obstruct the formation of stable association of lipid acyl chains, which is considered to be responsible for the impermeableness of lipid membrane to ion.[41] The significant difference was not observed between the effects of incorporated *all-trans*- and 11-*cis*-retinal on the structure and stability of bilayers.

The position of vitamin A molecule, on the other hand, may be not restricted only at the hydrocarbon region, but it can interject further into the polar hydrophilic region of the EYL bilayers than does retinal, since the former has the hydroxyl group. Vitamin A seems to be alike cholesterol, in respect that the intercalation of the latter does not cause any appreciable change in ^{13}C spin-lattice relaxation time of EYL[42] and further the incorporation of the latter is known to decrease the permeability of phospholipid bilayers to Na^+, K^+, and Cl^-.[43] The cholesterol hydroxyl, which is on the bulky steroid ring, is found at the position of the ester carbonyl of phospholipid.[44] Vitamin A hydroxyl, which attaches to the nonbulky polyene chain, is expected to penetrate as far into the hydrophilic region or parallel, at least, that occupied by the hydroxyl of incorporated cholesterol. In this situation, the effect of incorporated vitamin A molecule on the structural integrity and dynamic nature of lipid bilayers is not expected to be large, because the lipid head group and acyl chain end region near the head have essentially high ordering and low mobility and vitamin A hydroxyl is not effective to disrupt the strong electrostatic interac-

tion between lecithin head groups.

Several studies[16,17] have indicated that vitamin A as well as retinal are effective in lysis of erythrocytes. These results are not necessarily to match well with whole of our results observed here, since the erythrocytes membrane contains not only phospholipid but also lipoproteins and glycolipids. In that case, vitamin A and retinal can affect the arrangement of lipid and/or protein molecules in the membrane. It is not clear whether retinal acts on the same site on the erythrocyte membrane as vitamin A.

The experimental results described above give some suggestions meaningful in physiology; the incorporated retinal resides inside of the lipid bilayer and causes the ionic permeability change of the membrane. Hence the released *all-trans*-retinal from the photobleached pigment is suggested to be able to effect an increase in the ionic permeability of the disk membrane. Namely, it is not unreasonable to assume that *all-trans*-retinal released from photobleached pigment affects the arrangement of lipid and plays significant or at least some role in the alteration of ionic permeability of disk membrane, and in this way it participates the transmission of photosignal to the neural system. Since the chromophore 11-*cis*-retinal in the unbleached visual pigment is fixed to and surrounded by an opsin through Schiff base linkage, its ability to increase in permeability of membrane may be less important in visual process.

It is known that the thermal stability of rhodopsin, the completion of the photolytic cycle, and the regeneration of rhodopsin from opsin and retinal require the presence of a lipid membrane.[44] The experimental fact that hydrophobic retinal molecule can stay stable in the lipid bilayer in aqueous dispersion supports the idea that the isomerization of *all-trans*-retinal to 11-*cis*-form and the regeneration of rhodopsin from opsin and retinal take place in the disk membrane.

The authors thank Dr. T. Komoto of Tokyo Institute of Technology for measuring the electron micrograph. The present work was partially supported by Grant-in-Aid for Special Project Research No. 510309 from the Ministry of Education, Science and Culture.

References

1) For a review a) S. E. Ostroy, *Biochim. Biophys. Acta*, **463**, 91 (1977); b) W. L. Stone and E. A. Dratz, *Photochem. Photobiol.*, **26**, 79 (1977); c) T. Yoshizawa and Y. Shichida, *Kagaku No Ryoiki*, **32**, 159 (1978).

2) T. Tomita, *Quat. Rev. Biophys.*, **3**, 179 (1970).

3) J. I. Korenbrot and R. A. Cone, *J. Gen. Physiol.*, **60**, 20 (1972).

4) A. J. Silman, H. Ito, and T. Tomita, *Vision Res.*, **9**, 1443 (1969).

5) J. E. Brown and L. H. Pinto, *J. Physiol.*, **236**, 575 (1974).

6) N. C. Nielsen, S. Fleischer, and D. G. McConnell, *Biochim. Biophys. Acta*, **211**, 10 (1970).

7) R. E. Andreson and M. B. Maude, *Biochemistry*, **9**, 3624 (1970).

8) D. F. O'Brien, N. Zumbulyadis, F. M. Michaels, and R. A. Ott, *Proc. Natl. Acad. Sci. U.S.A.*, **74**, 5222 (1977).

9) D. F. O'Brien, L. F. Costa, and R. A. Ott, *Biochemistry*, **16**, 1295 (1977).

10) L. K. Sklar, G. P. Miljanich, S. L. Bursten, and E. A. Dratz, *J. Biol. Chem.*, **254**, 9583 (1979).

11) A. Darszon, R. J. Strasser, and M. Montal, *Biochemistry*, **18**, 5205 (1979).

12) A. Watts, I. D. Volotovski, and D. Marsh, *Biochemistry*, **18**, 5006 (1979).

13) B. J. Litman, *Photochem. Photobiol.*, **29**, 671 (1979).

14) A. J. Adams, R. L. Somers, and H. Shichi, *Photochem. Photobiol.*, **29**, 687 (1979).

15) N. Zumbulyadis and D. F. O'Brien, *Biochemistry*, **24**, 5427 (1979).

16) a) J. T. Dingle and J. A. Lucy, *Biochem. J.*, **84**, 611 (1962); b) J. T. Dingle, *ibid.*, **79**, 509 (1961).

17) K. Azuma and T. Yoshizawa, *Biochim. Biophys. Acta*, **249**, 135 (1971).

18) H. Shichi, *J. Biol. Chem.*, **246**, 6178 (1971).

19) R. P. Poincelot, P. G. Miller, R. L. Kimbel, and E. W. Abrahamson, *Nature*, **221**, 256 (1969).

20) F. J. M. Daemen and S. L. Bonting, *Nature*, **222**, 879 (1969).

21) R. E. Anderson and M. B. Maude, *Biochemistry*, **9**, 3924 (1970).

22) H. Shichi and R. L. Somers, *J. Biol. Chem.*, **249**, 6570 (1974).

23) H. Shichi and R. L. Somers, *Photockem. Photobiol.*, **22**, 187 (1975).

24) G. W. T. Groenendijk, C. W. M. Jacobs, S. L. Bonting, and F. J. M. Daemen, *Eur. J. Biochem.*, **106**, 119 (1980).

25) B. Rabinovitch, *Photochem. Photobiol.*, **29**, 567 (1979).

26) R. Hubbard, *J. Gen. Physiol.*, **39**, 935 (1955).

27) S. Amer and M. Akhtar, *Biochem. J.*, **128**, 987 (1972).

28) N. H. Tattrie, J. R. Bennett, and R. Cyr., *Can. J. Biochem.*, **46**, 819 (1968).

29) R. D. Kornberg and H. M. McConnell, *Biochemistry*, **10**, 1111 (1971).

30) M. L. Appleburg, D. M. Zuckerman, A. A. Lamola, and T. M. Jovin, *Biochemistry*, **13**, 3448 (1974).

31) P. K. Brown and G. Wald, *J. Biol. Chem.*, **222**, 865 (1956).

32) a) Y. Inoue, Y. Tokito, R. Chûjô, and Y. Miyoshi, *J. Am. Chem. Soc.*, **99**, 5592 (1977); b) Y. Inoue, Y. Tokito, S. Tomonoh, and R. Chûjô, *Bull. Chem. Soc. Jpn.*, **52**, 265 (1979).

33) W. S. Singleton, M. S. Gray, L. N. Brown, and J. L. White, *J. Am. Oil. Chem. Soc.*, **42**, 53 (1965).

34) P. E. Godici and F. R. Landsberger, *Biochemistry*, **13**, 362 (1974).

35) D. Canet, G. C. Levy, and I. R. Peat, *J. Magn. Reson.*, **18**, 199 (1975).

36) R. L. Vold, J. S. Waugh, M. P. Klein, and D. E. Phelps, *J. Chem. Phys.*, **48**, 3381 (1968).

37) G. W. Stockton, C. F. Polnaszek, A. T. Tulloch, F. Fasan, and I. C. P. Smith, *Biochemistry*, **15**, 954 (1976).

38) Y. K. Levine, N. J. M. Birdsall, A. G. Lee, and J. C. Metcalfe, *Biochemistry*, **11**, 1416 (1972).

39) S. B. Andrews, J. W. Faller, J. M. Gilliam, and R. J. Barnett, *Proc. Natl. Acad. Sci. U. S. A.*, **70**, 1814 (1973).

40) J. A. Berden, R. W. Barker, and G. K. Radda, *Biochim. Biophys. Acta*, **375**, 186 (1975).

41) H. Hauser and M. D. Barrat, *Biochem. Biophys. Res. Commun.*, **53**, 399 (1973).

42) P. E. Godici and F. R. Landsberger, *Biochemistry*, **14**, 3927 (1975).

43) D. Papahadjopoulos, S. Ni, and S. Ohki, *Biochim. Biophys. Acta*, **266**, 561 (1972).

44) W. L. Hubbell, *Acc. Chem. Res.*, **8**, 85 (1975).

Reaction of Haloazoxybenzenes with Sulfuric Acid

Ichiro SHIMAO,* Ken FUJIMORI,† and Shigeru OAE†

Department of Industrial Chemistry, Faculty of Engineering, Toyama University, Takaoka, Toyama 933
†Department of Chemistry, The University of Tsukuba, Sakura-mura, Niihari, Ibaraki 305

(Received June 27, 1981)

Treatment of 4,4′-dihaloazoxybenzenes with sulfuric acid afforded 4,4′-dihaloazobenzenes (**6**) as the major product and 5-halo-2-(*p*-halophenylazo)phenols, the Wallach rearrangement products as minor products, besides 2-halo-5-(*p*-halophenylazo)phenols, 2-halo-4-(*p*-halophenylazo)phenols, and 4-(*p*-halophenylazo)phenols as abnormal rearrangement products. The reaction of fluoro compound gave the azophenols (**3a** or **5a**) in the best yields. However, the ratio of **3a** to **5a** was found to vary with the concentration of sulfuric acid. Treatment of 4-haloazoxybenzenes with sulfuric acid gave 4-(*p*-halophenylazo)phenols and 4-haloazobenzenes (**13**) as major products together with 2-(*p*-halophenylazo)phenols and 5-halo-2-(phenylazo)phenols as minor products. Yields of reduction products **6** and **13** increased as the halosubstituent became heavier in the following sequence: F→Cl→Br→I.

In 1951, Gore and Hughes[1] reported that a treatment of 4,4′-dichloroazoxybenzene (**1b**) with concentrated sulfuric acid yielded 5-chloro-2-(*p*-chlorophenylazo)-phenol (**2b**) and 4,4′-dichloroazobenzene (**6b**). Recently, Cox and Buncel[2] reported briefly that a reaction of 4,4′-dihaloazoxybenzene (**1**) with concentrated sulfuric acid produced their corresponding 5-halo-2-(*p*-halophenylazo)phenols (**2**) together with a large amount of 4,4′-dihaloazobenzenes (**6**), except in the case of the iodo compound (**1d**).

Our recent study[3] on reactions of 4,4′-dialkylazoxybenzenes with sulfuric acid revealed that the major product was 2-alkyl-5-(*p*-alkylphenylazo)phenols and not 4,4′-dialkyl-2-hydroxyazobenzenes as early workers[1] had reported; formation of 4,4′-dialkylazobenzenes was observed as rather a minor reaction. Thus, it is anticipated that a detailed investigation of the Wallach rearrangement of various *p*-halo-substituted azoxybenzenes may provide vital information useful for understanding the nature of the Wallach hydroxyl migration as well as that of the deoxygenation which often predominates. This paper describes results of our reinvestigation and presents our new interpretation of reactions of **1** and 4-haloazoxybenzenes (**11**) with sulfuric acid.

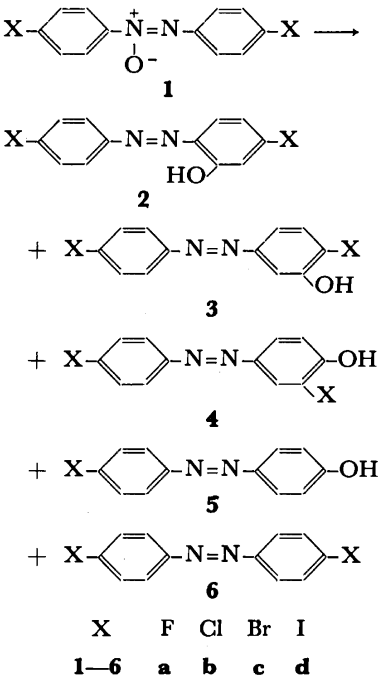

Results and Discussion

Reaction of **1** with 92% sulfuric acid gave a mixture of azophenols and **6**. **6** was separated from azophenols by column chromatography on alumina. Azophenols were separated from one another by chromatography on a deactivated silica-gel column in most cases. Some unidentified resinous materials also were formed in the reaction. The results are shown in Table 1.

In all cases, the main reaction was the reduction of **1** to give **6**; especially, **1d** gave **6d** predominantly. **1d** was reported[2] to be reduced exclusively to **6d** on treatment with sulfuric acid. However, the rearrangement product **2d** also was found to be formed, though in a small amount.

In general, azoxy group is known[1,4] to be reduced partially to azo group in reaction of azoxybenzenes with

TABLE 1. REACTION OF 4,4′-DIHALOAZOXYBENZENE (**1**) WITH SULFURIC ACID
(**1**: 0.5 g, 92% H_2SO_4: 25 cm³, temp: 50 °C, time: 30 min)

	X	Yield/%				
		2	**3**	**4**	**5**	**6**
1a	F	0.6	7.4		25	40
1b	Cl	12	3.6	2.4	0.2	59
1c	Br	11		1.5	0.2	69
1d[a]	I	1				83

a) 92% H_2SO_4: 75 cm³.

TABLE 2. REACTION OF AZOXYBENZENE WITH SULFURIC ACID
(Azoxybenzene: 0.1 g, temp: 50 °C, time: 30 min)

V[a] / cm³	Yield/%	
	Azobenzene	4-(Phenylazo)phenol
0.5	45	35
0.75	39	40
1.0	36	43
5.0	21	65
10	15	72
50	5	83

a) V is the volume of 92% H_2SO_4.

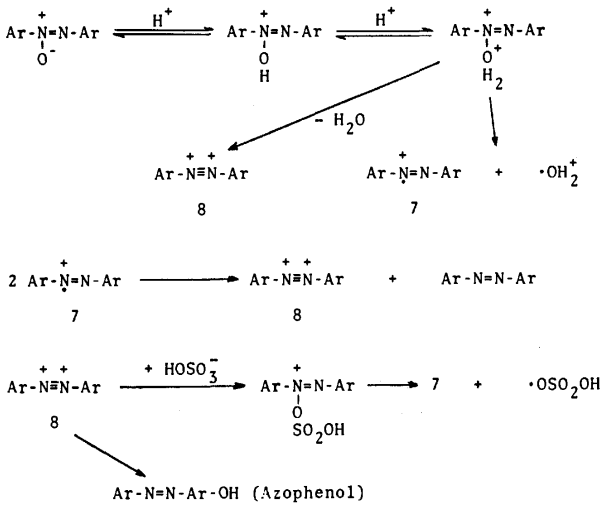

Scheme 1.

sulfuric acid. In order to understand the nature of the formation of azoarene, the reaction of azoxybenzene with 92% sulfuric acid was carried out with varying amounts of sulfuric acid used. The results are shown in Table 2. The yield of azobenzene depends clearly on the ratio of azoxybenzene to sulfuric acid. The extent of reduction decreases as the concentration of azoxybenzene decreases.

Earlier, we[5] noticed predominat reduction to azobenzene in a reaction of azoxybenzene with acetic anhydride around 190 °C, presuming the reduction to proceed *via* a radical cation species. In the present reaction, the reduction to azobenzene is presumed to proceed *via* radical cation **7** shown in Scheme 1. Diprotonation of the azoxy group followed by heterolysis of the N–O bond gives dicationic intermediate **8**, whereas homolytic fission of the N–O bond affords radical cation **7** similarly to an oxygen exchange[6] of diaryl sulfoxide in concentrated sulfuric acid. Disproportionation of **7** gives both an azo compound and dicationic intermediate **8**. This must be a bimolecular process in view of the observation that the amount of the reduction product, azobenzene, increases as the amount of sulfuric acid used decreases. One-electron reduction of **8** can also afford cation radical **7**.[7] There would be a possibility that **7** is partly reduced to give the azo compound by one-electron transfer. Of course, **8** can also formed by diprotonation and subsequent dehydration of the azoxy group.[2] The resulting $\cdot OH^+$ radical cation may be consumed in the oxidation of phenolic substance formed during the reaction to give a resinous material which would also be formed in the reduction of **7** or **8** with phenolic substance. Actually, the yield of reduced products increases under the conditions in which the yield of resinous material increases.[1]

Table 3. Reaction of 4,4′-dichloroazoxybenzene (**1b**) and thianthrene with sulfuric acid

	Yield/%	
	6b	Thianthrene *S*-oxide
1b	54	
1b+Thianthrene	70	56
Thianthrene		42

The amount of the reduction product from **1b** increased somewhat in the presence of thianthrene, a good electron transfer agent, as shown in Table 3. Since the cation radical is known to be formed when thianthrene is dissolved in concentrated sulfuric acid, eventually affording thianthrene *S*-oxide,[8] both thianthrene and its radical cation would be involved in the electron transfer to afford azoarene.

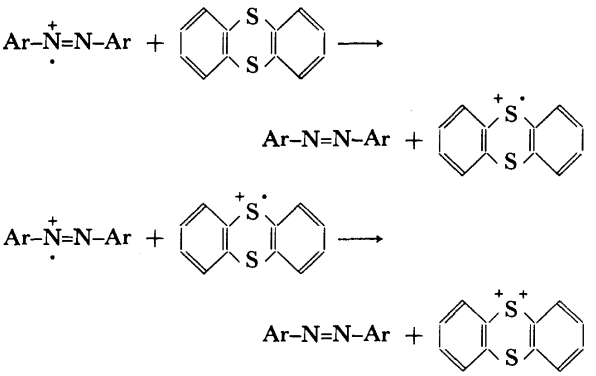

When an equimolar mixture of **1b** and 4-(phenylazo)-phenol was treated with 92% sulfuric acid, **1b** was reduced to **6b** nearly quantitatively, though with 65% of 4-(phenylazo)phenol recovered. Thus azophenol acts as a reducing agent. The azophenol would be oxidized by radical cations, such as H_2O^+ or **7**, and/or dication **8**, to form resinous material.

The amount of the reduction product, azoarene, seems to be related to the relative stability of the cation radical **7**. Within the same series in the periodic table, heavier atoms are known to stabilize the α-carbon radical to a higher extent.[9]

In the cases of **1b** and **1c**, *o*-hydroxy azo compounds, **2b** and **2c**, were obtained in substantial yields, in accordance with earlier reports.[1,3] However, **1c** gave a small amount of **4c** and **5c**, and **1b** yielded **3b**, **4b**, and **5b**. Although **3b** and **4b** were not separated from each other by column chromatography, they were partially separated by fractional crystallization described in the Experimental, while the ratio of **3b** to **4b** was determined by high-speed liquid chromatographic analysis.

The reaction of **1a** is peculiar. The yield of *o*-hydroxy azo compound, **2a**, the normal Wallach rearrangement product, was only 0.6%. Beside the reduction product, azophenol **5a** which is also a rearrangement product, was the second main product, accompanied with a comparable amount of **3a**.

These reaction products, **2**, **4**, **5**, and **6**, were identified by comparison with authentic samples, respectively, while **3b** was acetylated, and the resulting acetate was identified by comparing physical properties with those of the authentic sample obtained independently. Attempts to obtain the authentic sample of **3a** were unsuccessful. The mass spectrum of **3a** showed *m/e* values: 234 (M^+), 139 ($C_6H_4FN_2O$), 123 ($C_6H_4FN_2$), and 111 (C_6H_4F). Chemical shift of the OH proton in $CDCl_3$ was δ 5.60 ppm. A characteristic NMR absorption signal of *o*-hydroxyazobenzene (hydrogen bonded OH, δ about 13 ppm) was not observed.

Further, mp and IR spectrum of this compound are different from those of **4a** obtained by diazo-coupling reaction. Consequently, this compound was ascribed to 2-fluoro-5-(*p*-fluorophenylazo)phenol (**3a**), by analogy with the reaction of **1b**.

Shemyakin *et al.*[10] and we[11] reported independently on the basis of ^{18}O-tracer experiment that the rearrangement leading to *o*-hydroxy azo compound, **2**, is intramolecular. However, the formation of azophenols, **3** and **4**, is considered to be effected by a rearrangement similar to that in the reaction of 4,4'-dialkylazoxybenzenes described previously.[3] Either halide or an other nucleophile, *e.g.*, hydroxysulfonyloxy group or water, is shifted to the adjacent carbon atom in the intermediate (**9**) formed by nucleophilic attack on the dicationic intermediate **8**,[2,3] eventually affording **3** or **4** as shown in Scheme 2. Apparently the shift of chloride is more facile than that of fluoride, while bromide is more readily shifted than hydroxysulfonyloxy or hydroxyl group.

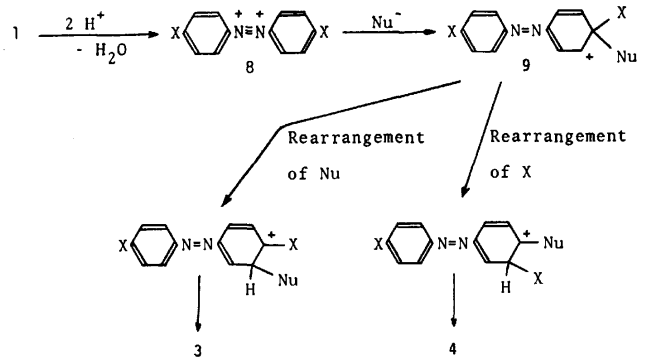

Scheme 2.

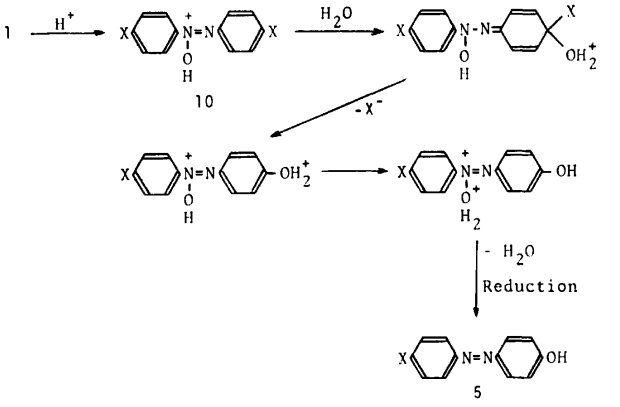

Scheme 3.

TABLE 4. REACTION OF 4,4'-DIFLUOROAZOXYBENZENE (**1a**) WITH SULFURIC ACID
(**1a**: 0.5 g, sulfuric acid: 25 cm³)

H_2SO_4 Concn %	Temp °C	Time h	Yield/% 2a	3a	5a	6a
92	25	4	0.4	8.8	18	42
92	50	0.5	0.6	7.4	25	40
92	80	1/6	0.9	6.8	27	38
85	80	1	0.6	0.6	58	15
98	25	1	1.2	30	3	43

Compound **5** may be formed by the aromatic nucleophilic substitution on the monoprotonated azoxybenzenes as shown in Scheme 3, *i.e.*, the replacement of halide by nucleophile in the intermediate (**10**). The mechanism of Wallach rearrangement appears to change with chang of concentration of sulfuric acid and structure of azoxy compound. At higher acid concentrations, the dicationic intermediate is generally considered to be formed; in some cases, at lower acid concentrations, a mechanism *via* a quinonoid intermediate formed from monoprotonated azoxybenzenes has been proposed.[2]

In the reaction of **1a**, the distribution of products changed markedly by change of reaction conditions, particularly of the concentration of sulfuric acid. Table 4 shows these results. When a concentrated sulfuric acid was used, **3a** was the main rearrangement product probably because fluoride, which is certainly not a good leaving group, is not a good nucleophile to compete in the migration. On the other hand, **5a** was formed as the major product when a dilute sulfuric acid (85%) was used.[23] The leaving of fluoride is obviously facilitated by the presence of water. In the cases of **1b** and **1c**, however, the acid concentration had little effect on the product distribution. The natures of neither chloride nor bromide ion is much changed by the small change in acid concentration.

4-Haloazoxybenzenes (**11**) were allowed to react with 92% sulfuric acid at 50 °C. The sample **11** was an equimolar mixture of α- and β-isomers. The distribution of products in the reaction of **11** with sulfuric acid are listed in Table 5.

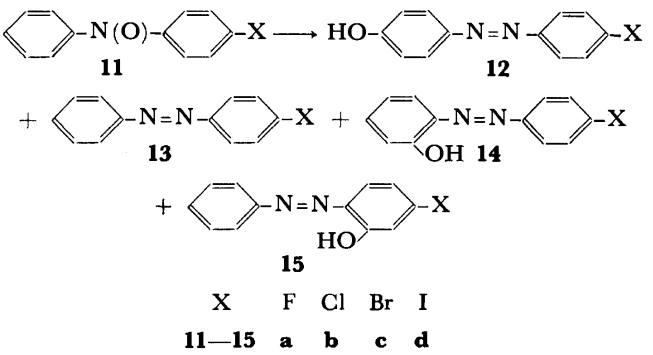

Main products were corresponding 4-(*p*-halophenylazo)phenols (**12**) and 4-haloazobenzenes (**13**), while no

TABLE 5. REACTION OF 4-HALOAZOXYBNZENES (**11**) WITH SULFURIC ACID
(**11**: 0.5 g, 92% H_2SO_4: 25 cm³, temp: 50 °C, time: 30 min)

	X	Yield/% 12	13	14	15
	H	65	20	0.3	
11a	F	54	26	0.5	0.3
11b	Cl	34	46	1.4	0.2
11c	Br	27	55	1.7	0.3
11d	I	5	72	2.0	0.3
11cα		30	56	0.14	0.35
11cβ		27	52	2.0	0.1

abnormal rearrangement product, such as 2-halo-4-(phenylazo)phenol or 2-halo-5-(phenylazo)phenol, was obtained. The *p*-halosubstituent did not allow the ipso nucleophilic attack which was observed in the reaction of 4-alkylazoxybenzenes.[12]

Hahn and Jaffe[13] reported that treatment of 4-bromoazoxybenzenes (**11c**) with sulfuric acid gave only 4-(*p*-bromophenylazo)phenol (**12c**). However, under the same reaction conditions the rearrangement product **12c** was a minor product, the major product being the reduction product, *i.e.*, azo compound **13c**. The yield of reduction product **13** was found to increase in the following sequence for substituents: H→F→Cl→Br→I. The same trend was observed in the reactions of 4,4'-dihaloazoxybenzenes. Apparently the *p*-halo substituent facilitates the formation of radical cation intermediate **7** which is stabilized by resonance interaction with the *p*-halo substituent, especially with heavy halo substituents. The radical cation is considered to give eventually the azo compound **13**, as mentioned above.

When both α- and β-isomers of **11c** and their mixture were treated separetely with 92% sulfuric acid, the two isomers and the mixture gave practically the same products (**12c** and **13c**), except the *o*-hydroxy azo compounds (**14c** and **15c**). Interconversion between α- and β-isomers, **11c**α and **11c**β, was not observed by high-speed liquid chromatographic analysis of the unchanged azoxy compound recovered at about 25% conversion of the reaction, thus supporting the mechanism that *p*-hydroxy azo compound **12** is formed *via* the dicationic intermediate, $C_6H_5N^+{\equiv}N^+C_6H_4X(p)$. The ratio of the rates of **11c**α and **11c**β, $k\alpha/k\beta$, was determined as about 0.85 from the α/β ratio of the starting material and that of the azoxy compound recovered at 60% conversion. Duffey and Hendley[14] also reported through UV spectrographic experiments that the value of $k\alpha/k\beta$ was 0.9.

In all cases, *o*-hydroxy azo compounds, **14** and **15**, also were obtained in very low yields. The ortho rearrangement to a benzene ring having a *p*-halo substituent is more difficult than that to the other rings. However, the products obtained by UV irradiation of these samples **11** consisted of nearly equal amounts of **14** and **15**.

Experimental

No melting points were corrected. IR spectra were recorded on a JASCO-IRA-1 spectrophotometer. NMR spectra were obtained with a JEOL MH-100 spectrometer using TMS as the internal standard, and mass spectra with a JEOL-OlSG spectrometer. High-speed liquid chromatographic analyses were carried out with a JASCO-FLC 150 apparatus on a 0.5 m×2.1 mm column packed with JASCODAC SV-02 (the solvent was methanol–water).

4,4'-Dihaloazobenzenes, **6a** and **6d**, were obtained from their corresponding *p*-haloanilines by oxidation with active manganese dioxide.[24] **6b** and **6c** were prepared by air oxidation of their corresponding hydrazo compounds which had been obtained by reduction of *p*-nitrohalobenzenes with zinc powder and sodium hydroxide.[24] 4-Haloazobenzenes, **13**, were prepared by condensation of nitrosobenzene with *p*-haloanilines.[24]

4,4'-Dihaloazoxybenzenes, **1a** and **1d**, and 4-haloazoxybenzenes, **11**, were prepared by oxidation of their corresponding azoarene with hydrogen peroxide.[15] Compounds **1b** and **1c** were obtained by reduction of *p*-halonitrobenzenes with D-glucose.[16] Isomeric *p*-bromoazoxybenzenes, **11c**α and **11c**β, were prepared by the well known method described in the literature.[17,18]

Reaction of 4,4'-Dihaloazoxybenzenes (1) with Sulfuric Acid. A mixture of **1** (0.5 g) and 92% sulfuric acid (25 cm^3) was heated at 50 °C for 30 min. The reaction mixture was poured into cold water and then extracted with benzene. After removal of the solvent, the residue was chromatographed on an alumina column using benzene as the eluent. The eluate gave **6** which was recrystallized from benzene or toluene.

Azophenols remaining at the top of column were extracted with ethanol–water. The extract was chromatographed on a silica gel column using benzene as the solvent.

The first fraction gave **2** which was recrystallized from hexane or benzene.

The second fraction gave **3** and/or **4**. Compound **3a** was recrystallized from hexane, mp 119—121 °C. Found: C, 61.34; H, 3.40; N, 11.83%. Calcd for $C_{12}H_8F_2N_2O$: C, 61.53; H, 3.45; N, 11.96%. IR (KBr): 3480, 1595, 1459, 1280, and 1230 cm^{-1}. In the reaction of **1b**, this fraction gave a mixture of **3b** and **4b**. High-speed liquid chromatographic analysis of the mixture showed that the ratio of **3b** to **4b** was 3 : 2. The mixture was recrystallized from benzene to yield **3b**. The mother liqour was evaporated and the resulting crystalline mass was dissolved in methanol. When the methanol solution was allowed to stand for a long time open in air, two kinds of crystals were formed. The crystals were extracted with boiling hexane for a short time and then the hexane solution was quickly separated by decantation. After removal of the solvent, the residue was recrystallized from hexane–benzene to give **4b**. Compound **3b**: mp 197—198 °C. Found: C, 54.23; H, 2.87; N, 10.52%. Calcd for $C_{12}H_8Cl_2N_2O$: C, 53.96; H, 3.02; N, 10.49%. IR (KBr): 3480, 1580, 1490, and 1410 cm^{-1}. In the case of **1c**, **4c** was obtained.

The third fraction gave **5** which was recrystallized from hexane or toluene.

Compounds **3a** and **3b** were acetylated with acetic anhydride and pyridine. Acetate of **3a**: mp 65—66 °C. Found: C, 60.71; H, 3.38; N, 10.14%. Calcd for $C_{14}H_{10}F_2N_2O_2$: C, 60.87; H, 3.65; N, 10.14%. IR (KBr): 1780 and 1495 cm^{-1}. Acetate of **3b**: mp 116.5—118 °C. The mp and IR spectra of **3b** acetate were identical with those of an authentic sample.

Reaction of 1b and Thianthrene with Sulfuric Acid. A solution of **1b** (0.267 g) and thianthrene (0.216 g) in 98% sulfuric acid (50 cm^3) was stirred at 27 °C for 3 h. The reaction mixture was poured into cold water, and then extracted with benzene. The extract was chromatographed on an alimina column using benzene as the solvent. The eluate geve a mixture of **6b** and thianthrene. **6b** was separated from thianthrene by recrystallization from acetone. The residue on the column was eluted with a mixture of ethanol, benzene, and water, and then the eluate chromatographed on a silica-gel column using benzene as the solvent. The first fraction gave **2b** in 2% yield. Treatment of the second fraction with dilute sodium hydroxide solution gave thianthrene *S*-oxide. Acidification of the mother liquor yielded a mixture of **3b** and **4b** (1%).

Reaction of 4-Haloazoxybenzene (11) with Sulfuric Acid. Compound **11** (0.5 g) was treated with 92% sulfuric acid

(25 cm^3) at 50 °C for 30 min. The reaction mixture was poured into excess cold water and then extracted with benzene. When the extract was chromatographed on an alumina column using benzene as the eluent, 4-haloazobenzene **13** was eluted out. The residue on the column was then eluted with a mixture of ethanol, benzene, and water, to give azophenols. The mixture of azophenols was chromatographed on silica gel. The first fraction was a mixture of **14** and **15** as analyzed by GLPC, while the second fraction was **12**.

In the case of **11c**, when the reaction was stopped in a few min, the unchanged azoxy compound was eluted out together with **13c** by the chromatography on alumina of the reaction mixture, and then the eluent was separated by chromatography on alumina using hexane–benzene as the solvent. The azoxy compound was analyzed by high-speed liquid chromatography.

Preparation of the Authentic Samples. 5-Halo-2-(*p*-halophenylazo)phenols (**2**) were prepared by irradiation of an ethanolic solution of **1**.[25] **2a**: mp 126—126.5 °C. Found: C, 61.40; H, 3.20; N, 11.79%. Calcd for $C_{12}H_8F_2N_2O$: C, 61.53; H, 3,45; N, 11.96%. IR (KBr): 1595 and 1495 cm^{-1}. **2b**: mp 178—180 °C. (lit,[19] 176.5 °C). **2c**: mp 182—184 °C. (lit,[19] 181.5 °C). **2d**: mp 213—215 °C. Found: C, 32.18; H, 1.60; N, 6.22%. Calcd for $C_{12}H_8I_2N_2O$: C, 32.02; H, 1.79; N, 6.23%. IR (KBr): 1590, 1460, and 1395 cm^{-1}.

2-Halo-4-(*p*-halophenylazo)phenols (**4a—4c**) and 4-(*p*-halophenylazo)phenols (**5**) were obtained by diazo-coupling of the corresponding phenols and diazonium salts.[24] **4a**: mp 153—155 °C. Found: C, 61.43; H, 3.23; N, 11.89%. Calcd for $C_{12}H_8F_2N_2O$: C, 61.53; H, 3.45; N, 11.96%. IR (KBr): 3480 and 1495 cm^{-1}. **4b**: mp 141—142 °C. Found: C, 53.77; H, 3.24; N, 10.72%. Calcd for $C_{12}H_8Cl_2N_2O$: C, 53.96; H, 3.02; N, 10.49%. IR (KBr): 3480 and 1480 cm^{-1}. **4c**: mp 158—159.5 °C. Found: C, 40.66; H, 2.26; N, 8.05%. Calcd for $C_{12}H_8Br_2N_2O$: C, 40.48; H, 2.27; N, 7.87%. IR (KBr): 3480, 1485, and 1475 cm^{-1}. **5a**: mp 157—159 °C. Found: C, 66.55; H, 4.17; N, 12.85%. Calcd for $C_{12}H_9FN_2O$: C, 66.66; H, 4.20; N, 12.96%. IR (KBr): 1585 and 1495 cm^{-1}. **5b**: mp 158—160 °C (lit,[20] 154 °C). **5c**: mp 161—163 °C (lit,[21] 162 °C). **5d**: mp 174—176 °C (lit,[22] 172 °C).

3-Acetoxy-4,4'-dichloroazobenzene (3b Acetate): 2-Chloro-5-nitrophenol was acetylated with acetic anhydride and pyridine. Recrystallization from hexane–benzene gave 2-chloro-5-nitrophenyl acetate, mp 78—79 °C. Found: C, 44.82; H, 2.55; N, 6.58%. Calcd for $C_8H_6ClNO_4$: C, 44.56; H, 2.78; N, 6.49%. IR (KBr): 1760, 1525, and 1350 cm^{-1}.

The acetate was reduced by catalytic hydrogenation to yield 3-acetoxy-4-chloroaniline which was recrystallized from hexane–benzene, mp 98—99 °C.

A solution of the amine (0.32 g) and *p*-chloronitrosobenzene (0.24 g) in acetic acid was allowed to stand for 24 h at room temperature. The reaction mixture was poured into cold water. The precipitate was filtered off and purified by chromatography on silica gel, and then recrystallized from hexane (yield 42%), mp 117—118.5 °C. Found: C, 54.25; H, 3.09; N, 9.14%. Calcd for $C_{14}H_{10}Cl_2N_2O_2$: C, 54.39; H, 3.26; N, 9.06%. IR (KBr): 1780 and 1480 cm^{-1}.

Acetate of **3c** was obtained by a similar method, mp 139—141 °C. Found: C, 42.05; H, 2.37; N, 7.27%. Calcd for $C_{14}H_{10}Br_2N_2O_2$: C, 42.24; H, 2.54; N, 7.04%. IR (KBr): 1770 cm^{-1}. The acetate was hydrolyzed by the chromatography on alumina to yield **3c**, mp 212—212.5 °C. Found: C, 40.66; H, 2.32; N, 7.92%. Calcd for $C_{12}H_8Br_2N_2O$: C, 40.48; H, 2.27; N, 7.87%. IR (KBr): 3480 and 1480 cm^{-1}.

References

1) P. H. Gore and G. K. Hughes, *Aust. J. Sci. Res.*, **4A**, 185 (1951).

2) R. A. Cox and E. Buncel, "The Chemistry of the Hydrazo, Azo and Azoxy Groups," ed by S. Patai, John Wiley and Sons, New York (1975), p. 808.

3) I. Shimao and S. Matsumura, *Bull. Chem. Soc. Jpn.*, **49**, 2294 (1976).

4) A. Lachman, *J. Am. Chem. Soc.*, **24**, 1178 (1902).

5) S. Oae, T. Maeda, and S. Kozuka, *Bull. Chem. Soc. Jpn.*, **44**, 442 (1971).

6) S. Oae and N. Kunieda, *Bull. Chem. Soc. Jpn.*, **41**, 696 (1968).

7) Concentrated sulfuric acid containing any one of 4,4'-dihaloazoxybenes gives complex but distinct ESR signals, a part of which may be ascribed to those of the cation radicals **7**, but further study is necessary to understand the nature of the ESR signals.

8) H. J. Shine and L. Piette, *J. Am. Chem. Soc.*, **84**, 4798 (1962).

9) C. C. Price and S. Oae, "Sulfur Bonding, "Ronald Press, N. Y. (1962), pp. 26—28.

10) M. M. Shemyakin, T. E. Agadzhanyan, V. M. Mainind, and R. V. Kudryantsev, *Izv. Akad. Nauk SSSR, Ser. Khim.*, **1963**, 1339; *Chem. Abstr.*, **59**, 12619b (1963).

11) S. Oae, T. Fukumoto, and M. Yamagami, *Bull. Chem. Soc. Jpn.*, **36**, 601 (1963).

12) I. Shimao and S. Matsumura, *Bull. Chem. Soc. Jpn.*, **51**, 926 (1978).

13) C. Hahn and H. H. Jaffe, *J. Am. Chem. Soc.*, **84**, 946 (1962).

14) D. Duffey and E. C. Hendley, *J. Org. Chem.*, **33**, 1918 (1968).

15) B. T. Newbold, *J. Org. Chem.*, **27**, 3919 (1962).

16) H. W. Galbraith, F. Degering, and E. F. Hitch, *J. Am. Chem. Soc.*, **73**, 1323 (1951).

17) L. C. Behr, *J. Am. Chem. Soc.*, **76**, 3672 (1954).

18) T. E. Stevens, *J. Org. Chem.*, **29**, 311 (1964); *ibid.*, **32**, 1641 (1967).

19) R. Tanikaga, *Bull. Chem. Soc. Jpn.*, **41**, 2151 (1968).

20) J. T. Hewitt, *Ber.*, **26**, 2978 (1893).

21) J. J. Fox and J. T. Hewitt, *J. Chem. Soc.*, **93**, 340 (1908).

22) F. D. Chattaway and A. B. Constable, *J. Chem. Soc.*, **105**, 128 (1914).

23) The yield of reduction product **6a** was low under this conditions, because monoprotonated azoxy compound (**10**) may preferentially undergo the nucleophilic attack and hence the formation of radical cation **7** may be depressed.

24) Y. Nomura and S. Tomoda, "Shin-jikken-kagaku-koza," ed by the Chemical Society of Japan, Maruzen, Tokyo (1978), **14**/III, pp. 1516—1534.

25) G. M. Badger and R. G. Buttery, *J. Chem. Soc.*, **1954**, 2243.

Products and Kinetic Substituent Effects in the Reactions of Diaryldiazomethanes with 2,5-Dichloro-*p*-benzoquinone

Takumi OSHIMA and Toshikazu NAGAI*

Institute of Chemistry, College of General Education, Osaka University, Toyonaka, Osaka 560

(Received May 28, 1981)

Substituted diphenyldiazomethanes[$(x\text{-}C_6H_4)_2CN_2$; x=*p*-OCH_3, *p*-CH_3, H, *p*-Cl] were found to react with 2,5-dichloro-*p*-benzoquinone at its conjugated C=C and C=O bonds to give bicyclic diones and poly(2,5-dichlorohydroquinone benzhydryl ether)s respectively, obeying the second-order kinetic law. The product ratios of the polyethers to the bicyclic diones increased from 1.1 to 8.1 with the electron-donating ability of the substituents. The individual rate constants were well correlated with the Hammett equation: $\log k_3 = -2.15 - 1.55\,\sigma$ ($r=0.996$) and $\log k_4 = -2.03 - 1.85\,(\sigma^0 + 0.515\Delta\bar{\sigma}_R^+)$ ($r=1.00$) for the bicyclic diones and polyethers processes respectively. The presence of methanol as a trapping agent stopped the polymerization completely and afforded the methanolysis product, though no essential change was found in the formation of the bicyclic dione.

In the reaction of diazomethane or diazoethane with 2,5-dichloro-*p*-benzoquinone (**2**), Eistert *et al.*[1] obtained pyrazoline derivatives formed *via* 2+3 cycloaddition toward the C=C bonds of the quinone. In contrast to **2**, tetrasubstituted quinones, such as chloranil and 2,3-dichloro-5,6-dicyanobenzoquinone (DDQ), are known to react with diazomethane at the C=O bonds, giving oxirane derivatives.[2,3] Recently, we showed that these quinones also react at the C=O bonds with aryl- and diaryldiazomethanes to give stilbenes and spirooxetanes[4] and poly(hydroquinone benzhydryl ether)s[5,6] respectively. Thus, **2** differs from chloranil or DDQ in its reaction pattern toward the diazoalkanes. However, no reactions of **2** with diaryldiazomethanes have hitherto been known. Therefore, we have carried out the reactions of diaryldiazomethanes with **2** in order to obtain further insight into the factors governing the reaction mode and also in order to compare the results with those of chloranil and DDQ reactions.

We found that **2** reacts with diaryldiazomethanes at both the C=C and C=O bonds, yielding bicyclic diones and poly(2,5-dichlorohydroquinone benzhydryl ether)s. Kinetic substituent effects in these two reaction courses were also discussed.

Results and Discussion

Product Analysis. The reactions of disubstituted diaryldiazomethanes (**1a—d**) with an equimolar amount of 2,5-dichloro-*p*-benzoquinone (**2**) were carried out in 1,2-dichloroethane at 30 °C. The **1a** with the *p,p'*-OCH_3 substituents violently decomposed, with an evolution of N_2 and the immediate deposition of white precipitates, while the **1d** with the *p,p'*-Cl substituents needed *ca.* 10 h for the complete disappearance of the diazo color. All these reactions gave considerable amounts of white precipitates. The filtrate was evaporated to dryness, followed by column chromatography

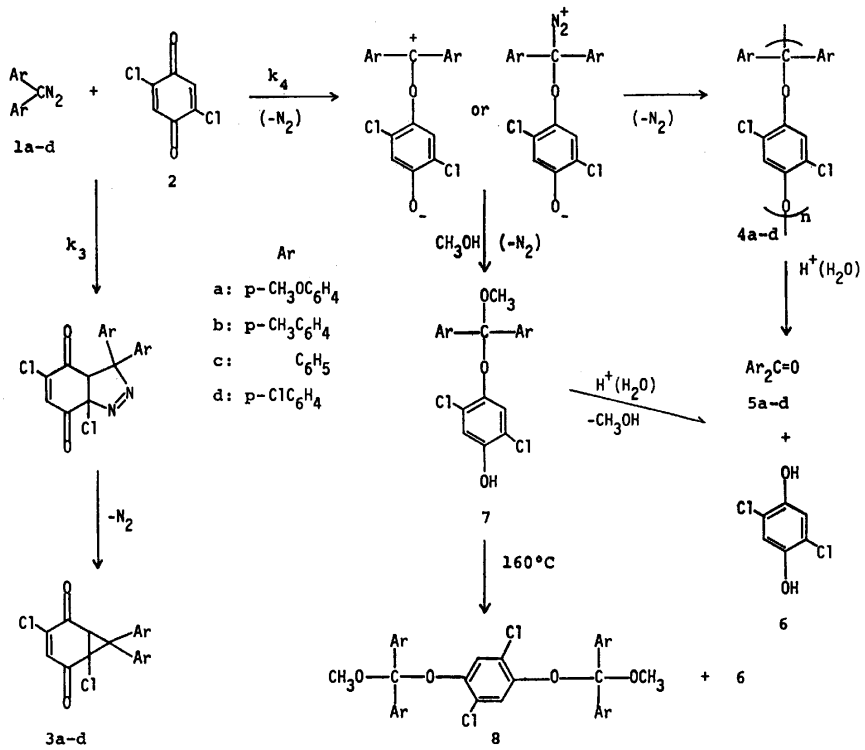

Scheme 1.

on silica gel to give bicyclic diones (**3a**—**d**) (Scheme 1). The ^{1}H NMR spectra showed the vinylic proton at the lower fields (δ, 6.60—6.65) and the cyclopropyl proton at the higher fields (3.58—3.67), in accordance with the bicyclic structure. The precipitate isolated in the reaction of **1a** was gradually hydrolyzed into almost equimolar amounts of *p,p'*-dimethoxybenzophenone (**5a**) and 2,5-dichlorohydroquinone (**6**) during the work-up. However, the precipitates for **1b**—**d** were so stable that the complete hydrolyses needed refluxing for 8—20 h in aqueous methanol containing hydrochloric acid. These hydrolyses gave almost equimolar amounts of benzophenones (**5b**—**d**) and **6**. Next, we examined the effect of methanol as an additive on the reaction features employing **1c**. No essential change was found in the yield of **3c**, but a different product, 2,5-dichloro-4-[(methoxy)diphenylmethoxy]phenol (**7**), was provided instead of the precipitate. The **7** was easily hydrolyzed into **5c** and **6** under the influence of hydrochloric acid, whereas a short-time heating slightly over its melting point (151 °C) smoothly brought about the disproportionation to yield 2,5-dichloro-1,4-bis[(methoxy)-diphenylmethoxy]benzene (**8**) and **6**.

It can be suggested that the bicyclic diones (**3a**—**d**) may be produced *via* 1,3-dipolar cycloaddition, followed by the rapid elimination of N_2 from the resulting pyrazolines, considering that methanol does not participate as an additive. With regard to the structure of white precipitates, poly(2,5-dichlorohydroquinone benzhydryl ether)s (**4a**—**d**) are conceivable from the observations that the IR spectra of the stable precipitates for the **1b**—**d** showed no carbonyl, but strong absorptions assignable to the ethereal bonds, and also that the hydrolyses gave equimolecular amounts of benzophenones and **6**. In analogy with the reactions with chloranil[5] and DDQ,[6] the formation of polyethers prompted us to suggest the operation of the same mechanism in these polymerization reactions (Scheme 1). We had previously proposed the diazonium or carbonium betaine as the intermediate in chloranil and DDQ systems.[5,6] In fact, the presence of methanol as a trapping agent stopped the polymerization completely and afforded the methanolysis product, **7**, instead of the polyether, though the 2+3 cycloaddition process leading to **3c** was little affected.

The results are summarized in Table 1. The product ratios of **4** to **3** increased in the order of **1a**>**1b**>**1c**>**1d**, with the electron-donating ability of the substituents.

Table 2. Observed second-order rate constants, k_{obsd}, and the individual rate constants, k_3 and k_4, for the process giving **3** and **4** in the reactions of **1a**—**d** with **2** in CH_2ClCH_2Cl at 30°C

Compound	$10^3 k_{obsd}$ / l mol^{-1} s^{-1}	$10^3 k_3$[a] / l mol^{-1} s^{-1}	$10^3 k_4$[a] / l mol^{-1} s^{-1}
1a	463	51.0	412
1b	81.9	24.1	57.8
1c	14.9	5.81	9.09
1d	3.24	1.54	1.70

a) The values determined by multiplying k_{obsd} by the relative yields of **3** and **4**.

A comparison of the present results with those observed in the reaction with diazomethane[1] and in the diaryldiazomethanes–chloranil[5] and –DDQ systems[6] is of some interest from the mechanistic point of view. The **2** is known to react at the C=C bonds with two moles of diazomethane to produce the pyrazoline derivative,[1] while the C=O bonds of **2** are unreactive toward diazomethane. On the other hand, the diaryldiazomethanes can react at both the C=O and the C=C bonds of **2**. In contrast to the case of **2**, the 2+3 cycloaddition process is not anticipated in the reactions of diaryldiazomethanes with chloranil[5] and DDQ,[6] where the C=O bonds selectively participate in the reactions. The lack of such bicyclic diones in the chloranil and DDQ reactions is certainly attributable to the larger steric hindrance due to the bulky Cl and/or CN substituents on either side of the C=C bonds, by which the approach of diaryldiazomethanes (even diazomethane and aryldiazomethane) to the double bonds is inhibited.

It is also noticed that the polyethers derived from **2** are more stable against solvolyses than those derived from chloranil or DDQ. In addition, the presence of methanol in the chloranil or DDQ reaction inhibited the formation of polyether, as in the present case, but the initially resulting methanolysis products like **7** further underwent a nucleophilic attack by methanol to be converted into α,α-dimethoxydiphenylmethane and the respective hydroquinones.[5,6] These chemical observations are probably the result of the stronger electron-acceptor ability of chloranil and DDQ moieties than that of **2**;[7] hence, the ethereal C–O linkage for the chloranil or DDQ reaction is much more subject to hydrolysis and methanolysis than those for the **2** reaction.

Kinetic Study. Substituent Effects: The 1,2-dichloroethane solutions of **1a**—**d** used for kinetic purposes were diluted by a factor of about 10 compared to those for the product study. Thus, the decompositions of **1a**—**d** at 30 °C could be followed spectrophotometrically over 60—70% reactions without the disturbance due to the suspension of polyethers (**4a**—**d**). The observed second-order rate constants increased with the electron-donating ability of the *p*-substituents (Table 2). From the results in Tables 1 and 2, one can easily obtain the

Table 1. Product distributions in the equimolar (5.67 mmol) reactions of diaryldiazomethanes (**1a**—**d**) and 2,5-dichloro-*p*-benzoquinone (**2**) in CH_2ClCH_2Cl at 30 °C

Compound	Additive	Reaction time / h	Yield/%[a] **3**	**4**	**7**
1a	—	1	10.5	85.1[c]	—
1b	—	1	28.0	67.3[c]	—
1c	—	2	38.1	59.7[c]	—
1c	CH_3OH[b]	2	37.6	—	58.6
1d	—	6	46.3	51.2[c]	—

a) Yield as mole percentage based on **1**. b) A five-fold molar excess was added with respect to **1c**. c) Based on the benzophenones (**5a**—**d**) obtained by the hydrolyses of **4a**—**d**.

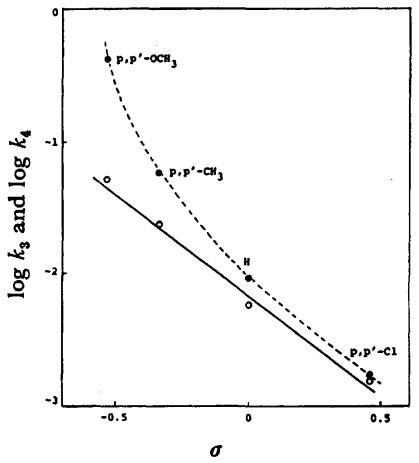

Fig. 1. The plots of log k_3 (○) and log k_4 (●) against the Hammett σ constants.

individual rate constants leading to the formations of **3a—d** and **4a—d** by multiplying the observed rate constants by the relative product ratios. The rate constants, k_3 and k_4, thus determined may also be seen in Table 2.

The dependence of the logarithmic rate constants on the Hammett σ constants[8] is shown in Fig. 1. As may easily be noticed, **3a—d** formation gave an excellent linear dependence (Eq. 1), where r, s, and n are the correlation coefficient, the standard deviation, and the data points respectively:

$$\log k_3 = -2.51 - 1.55\sigma \quad (r = 0.996,\ s = 0.0735,\ n = 4). \qquad (1)$$

However, the correlation line for the **4a—d** process displayed an upward deviation, especially in the OCH_3 substituent. The replacement of σ by the Brown σ^+ constants[9] was also unsuccessful, causing a downward deviation. Neither the σ nor σ^+ values apparently fit the correlation of the logarithmic rate constants for the **4a—d** process well. Therefore, we attempted the two-parameter Yukawa-Tsuno equation,[10] $\log k = \rho(\sigma^0 + R\Delta\bar{\sigma}_R^+)$, where σ^0, R, and $\Delta\bar{\sigma}_R^+$ are the normal substituent constants, the resonance reaction constant, and the resonance substituent constant respectively. The result of regression analysis indicates that the use of the two-parameter equation improves the correlation significantly (Eq. 2):

$$\log k_4 = -2.03 - 1.85\,(\sigma^0 + 0.515\,\Delta\bar{\sigma}_R^+) \quad (r = 1.00,\ s = 0.0105,\ n = 4). \qquad (2)$$

A comparison of the ρ values in Eqs. 1 and 2 shows a larger susceptibility of the rate of the **4a—d** process on the substituents than that of the **3a—d** process. Also, the value of R=0.515 confirms that a substantial

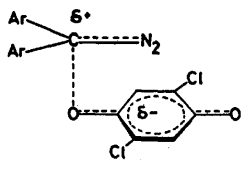

I

π-resonance stabilization of a transition state operate in the **4a—d** process. By analogy to the mechanism of the reactions of diaryldiazomethanes with chloranil and DDQ, a similar transition state such as I is likely to account for the electronic demand. On the contrary, the process leading to **3a—d** may be through the 1,3-dipolar addition mechanism, since the rate constants were well correlated with the simple Hammett equation using normal σ values† in accordance with the product analysis, where no essential change was found in the yield of the bicyclic dione, as has been mentioned above.

Experimental

The IR, NMR, and UV spectra were recorded on a Hitachi 215, a Varian EM-360, and a JASCO UVIDEC 505 spectrophotometer respectively.

Materials. The 2,5-dichloro-*p*-benzoquinone (**2**) was prepared according to the procedure described by A. R. Ling[12] and was recrystallized from ethanol; pale yellow prisms, mp 164—166 °C (lit, 161 °C).[12] The diaryldiazomethane were made by the oxidation of the corresponding hydrazones with yellow mercury(II) oxide, as has been described.[5] The physical properties of these diazoalkanes were listed in previous papers.[5,13] The 1,2-dichloroethane was dried over phosphorus pentaoxide and fractionated.

Kinetic Measurements. The values of k were determined spectrophotometrically by monitoring the decrease in the absorption of **1a—d** at the maximum wavelength (524—540 nm) in the visible region. The mean deviations were ±3% (usually two determinations). The temperature was kept at 30 °C (±0.1 °C) by means of a Haake circulator.

Reactions of Diaryldiazomethanes (1a—d) with 2 in CH_2ClCH_2Cl. The reaction of **1c** is described below as a typical example; the reactions of the other diazoalkanes were carried out similarly till the diazo color completely disappeared . To a stirred 1,2-dichloroethane solution (30 ml) of **2** (1.0 g, 5.65 mmol) was added, drop by drop, a 1,2-dichloroethane solution (10 ml) containing **1c** (1.1 g, 5.67 mmol) at 30 °C. A vigorous evolution of N_2 was observed except for the case of **1d**. After the mixture had been stirred for 2 h (1 h for **1a** and 6 h for **1d**), the white precipitate which appeared was filtered, washed with a small portion of 1,2-dichloroethane, and submitted to IR measurement. The precipitate in the case of **1a** was easily hydrolyzed into *p,p'*-dimethoxybenzophenone (**5a**) and **6** on the work-up. On the other hand, the precipitates in the cases of **1b—d** were stable enough to be hydrolyzed only in refluxing aqueous methanol containing hydrochloric acid for 8—20 h; they thus gave the corresponding benzophenones (**5b—d**) and **6**. The column chromatography (silica gel) of the hydrolyzed products gave an almost equimolar amount of **5a—d** (benzene as an eluent) and **6** (benzene–ether). These compounds were identified by a comparison of their IR spectra with those of authentic samples.[5,12] On the other hand, the filtrate parts were dried *in vacuo*, and the residues were chromatographed on silica gel. Elution with benzene gave pure bicyclic diones (**3a—d**). The structures of **3a—d** were identified by means of the IR, the NMR, and the elemental analyses.

† The rate enhancement by the electron-donating substituents can be explained in terms of the increase in the HO-(dipole)-LU (dipolarophile) interaction in the concerted 1,3-dipolar addition by a raising of the HO energy.[11]

1, 4-Dichloro-7, 7-bis(p-methoxyphenyl)bicyclo[4. 1. 0]hept-3-ene-2,5-dione (3a). Pale yellow prisms (petroleum ether–benzene); mp 148—150 °C. IR (KBr): 3055, 1693, 1509, 1243 cm^{-1}. NMR (δ, $CDCl_3$): 3.62 (1H, s, cyclopropyl H), 3.73 (3H, s, OCH_3), 3.77 (3H, s, OCH_3), 6.56 (1H, s, vinyl H), 6.8—7.5 (8H, m, aromatic H). MS: *m/e* 402 (M^+). Found: C, 62.64; H, 4.05%. Calcd for $C_{21}H_{16}Cl_2O_4$: C, 62.54; H, 4.00%.

1,4-Dichloro-7,7-di-p-tolylbicyclo[4.1.0]hept-3-ene-2,5-dione(3b). Pale yellow prisms (ether); mp 151—153 °C. IR (KBr): 3053, 1684, 1588, 1512, 1291. 1063, 995, 820 cm^{-1}. NMR (δ, $CDCl_3$): 2.27 (3H, s, CH_3), 2.30 (3H, s, CH_3), 3.62 (1H, s, cyclopropyl H), 6.60 (1H, s, vinyl H), 7.03 (4H, s, aromatic H), 7.1—7.5 (4H, m, aromatic H). MS: *m/e* 370 (M^+). Found: C, 68.16; H, 4.41%. Calcd for $C_{21}H_{16}Cl_2O_2$: C, 67.94; H, 4.34%.

1,4-Dichloro-7,7-diphenylbicyclo[4.1.0]hept-3-ene-2,5-dione(3c). Pale yellow prisms (petroleum ether–benzene); mp 179—180 °C. IR (KBr): 3052, 1703, 1689, 1597, 1295, 1062, 996, 709 cm^{-1}. NMR (δ, $CDCl_3$): 3.67 (1H, s, cyclopropyl H), 6.61 (1H, s, vinyl H), 7.0—7.6 (10H, m, aromatic H). MS: *m/e* 342 (M^+). Found: C, 66.71; H, 3.59%. Calcd for $C_{19}H_{12}Cl_2O_2$: C, 66.49; H, 3.53%.

1,4-Dichloro-7,7-bis(p-chlorophenyl)bicyclo[4.1.0]hept-3-ene-2,5-dione (3d). Pale yellow prisms (benzene); mp 209—210 °C. IR (KBr): 3051, 1701, 1677, 1584, 1485, 1087, 995, 833 cm^{-1}. NMR (δ, $CDCl_3$): 3.58 (1H, s, cyclopropyl H), 6.63 (1H, s, vinyl H), 7.1—7.3 (8H, m, aromatic H). MS: *m/e* 410 (M^+). Found: C, 55.58; H, 2.48%. Calcd for $C_{19}H_{10}Cl_4O_2$: C, 55.37; H, 2.45%.

Reaction of 1c with 2 in CH_3OH–CH_2ClCH_2Cl. To a stirred 1,2-dichloroethane solution (30 ml) of **2** (1.0 g, 5.65 mmol) was added, drop by drop, a 1,2-dichloroethane solution (10 ml) containing **1c** (1.10 g, 5.67 mmol) and a 5-fold molar excess of methanol (0.9 g) at 30 °C. In contrast to the reactions in the absence of methanol, no precipitate was found. After having been stirred for 2 h, the solvent was evaporated and the trituration of the resinous products with 3×30 ml pentane left **3c** (0.72 g, 37%). The combined pentane solution was concentrated to afford 2,5-dichloro-4-[(methoxy)diphenylmethoxy]phenol (**7**); mp 151 °C (dec) IR (KBr): 3520, 1476, 1203, 1002 cm^{-1}, NMR (δ, $CDCl_3$): 3.30 (3H, s, OCH_3), 5.17 (1H, s, OH), 7.0—7.8 (12H, m, aromatic H), MS: *m/e* 343 ($M^+ - OCH_3$), Found: C, 64.03; H, 4.13%. Calcd for $C_{20}H_{16}Cl_2O_3$: C, 64.02; H, 4.26%. The **7** was easily hydrolyzed into benzophenone and **6** under the influence of aqueous methanol saturated with hydrochloric acid. When heated at 160 °C for 2 min, however, the **7** underwent a disproportionation into 2,5-dichloro-1,4-bis[(methoxy)diphenylmethoxy]benzene (**8**) and **6**. The **8** had a mp of 269—271 °C (from benzene); IR (KBr): 1477, 1211, 1091, 991, 697 cm^{-1}, NMR (δ, $CDCl_3$): 3.20 (6H, s, OCH_3), 7.0—7.7 (22H, m, aromatic H), MS: *m/e* 539 ($M^+ - OCH_3$), Found: C, 71.55; H, 4.97; Cl, 12.60%. Calcd for $C_{34}H_{28}Cl_2O_4$: C, 71.45; H, 4.94; Cl, 12.40%.

References

1) B. Eistert, K. Pfleger, and P. Donath, *Chem. Ber.*, **105** 3915 (1972).
2) B. Eistert, H. Fink, and A. Müller, *Chem. Ber.*, **95**, 2403 (1962).
3) H. D. Becker, *J. Org. Chem.*, **34**, 1203 (1969).
4) T. Oshima and T. Nagai, *Bull. Chem. Soc. Jpn.*, **53**, 726 (1980).
5) T. Oshima and T. Nagai, *Bull. Chem. Soc. Jpn.*, **53**, 3284 (1980).
6) T. Oshima and T. Nagai, *Bull. Chem. Soc. Jpn.*, **54**, 2039 (1981).
7) G. Briegleb, *Angew. Chem.*, **76**, 326 (1964).
8) H. H. Jaffe, *Chem. Rev.*, **53**, 191 (1953); D. H. McDaniel and H. C. Brown, *J. Org. Chem.*, **23**, 420 (1958).
9) H. C. Brown and Y. Okamoto, *J. Am. Chem. Soc.*, **79**, 1913 (1957); **80**, 4979 (1958); **81**, 3323 (1959).
10) Y. Yukawa, Y. Tsuno, and M. Sawada, *Bull. Chem. Soc. Jpn.*, **39**, 2274 (1966).
11) R. Sustmann, *Tetrahedron Lett.*, **1971**, 2717.
12) A. R. Ling, *J. Chem. Soc.*, **61**, 558 (1892).
13) T. Oshima, A. Yoshioka, and T. Nagai, *J. Chem. Soc., Perkin Trans. 2*, **1978**, 1283.

 © 1982 The Chemical Society of Japan Bull. Chem. Soc. Jpn., 55, 555—560 (1982)

Kinetic Solvent Effects in the Decomposition of Diphenyldiazomethane with Chloranil and 2,5-Dichloro-*p*-benzoquinone

Takumi OSHIMA and Toshikazu NAGAI*

Institute of Chemistry, College of General Education, Osaka University, Toyonaka, Osaka 560

(Received July 21, 1981)

A kinetic study was made of the reactions of diphenyldiazomethane (DDM) with chloranil and 2,5-dichloro-*p*-benzoquinone (DCQ) at 30 °C in 20 and 22 aprotic solvents respectively (19 solvents are common). The chloranil reaction gave poly(tetrachlorohydroquinone benzhydryl ether) alone, obeying the second-order kinetic law. On the other hand, the DCQ reaction afforded bicyclic dione and poly(2,5-dichlorohydroquinone benzhydryl ether), also obeying the second-order kinetic law. All these rate constants generally increased with the solvent polarity and decreased with the solvent basicity. The kinetic solvent effects can be interpreted in terms of the effects of the polarity and the basicity of the solvents respectively to the transition and to the initial states. Thus, the multiple linear correlations of the logarithmic rate constants with a suitable function of the polarity and the basicity of the solvents are fairly successful. It was found that the basicity is more pronounced in the chloranil reaction than in the DCQ reaction, whereas the reverse can be said for the solvent polarity. These results were compared to those of the reactions of DDM with 2,3-dichloro-5,6-dicyanobenzoquinone and tetracyanoethylene.

In our previous paper,[1] we proposed an empirical basicity parameter, D_π, based on the kinetic solvent effects on the reaction of diphenyldiazomethane (DDM) with tetracyanoethylene (TCNE) as a typical π-acceptor. The D_π was found to be preferable to the conventional solvent basicity parameters, such as Kagiya's $\Delta\nu_D$[2] Kamlet-Taft's β scale,[3] and Gutmann's DN (donor number),[4] to describe the solvent effects in the kinetics of the various reactions involving π-acceptor soft acids. For example, the correlation of log k with D_π for the 2,3-dichloro-5,6-dicyanobenzoquinone (DDQ)–DDM reaction over a wide range of aprotic solvents was highly successful (r=0.977).[1] We have now extended the work to the chloranil– and 2,5-dichloro-*p*-benzoquinone (DCQ)–DDM reactions in order to examine further the application of D_π in the interpretation of the kinetic solvent effects. In this paper, we also discuss the results in comparison with those for the DDM–TCNE and DDM–DDQ systems.

Results and Discussion

The Dependence of the Rate Constants on the Properties of the Aprotic Solvents in the Reactions of Diphenyldiazomethane with Chloranil. The chloranil–DDM reaction is found to afford poly(tetrachlorohydroquinone benzhydryl ether) by way of a diazonium or carbonium betaine intermediate, **1** or **1'** (Scheme 1).[5] The second-order rate constants over a wide range of aprotic solvents are shown in Table 1, together with the D_π[1] and the solvent polarity parameters, the Kirkwood function of the dielectric constants ε, $f(\varepsilon)=(\varepsilon-1)/(2\varepsilon+1)$,[6] and Dimroth and Reichardt's E_T values.[7] An inspection of the results shows that the rates did not correlate well only with the usual solvent basicity or polarity parameter. Dipolar solvents, *e.g.*, nitro compounds and nitriles, tended to increase the rates, while the basic aromatic hydrocarbons and cyclic ethers decrease them. A preliminary correlation of log k with the conventional basicity parameters, such as $\Delta\nu_D$, the β scale, and DN, yielded worse results because of the marked deviation of the aromatic hydrocarbons: log k= $-0.0048\Delta\nu_D-1.97$ (correlation coefficient(r)=0.35, data points (n)=18), log $k=-0.198\beta-2.23$ (r=0.10, n=11), and log $k=-0.028DN-1.76$ (r=0.45, n=11). However, a plot of log k against D_π values showed a better correlation, suggesting the stabilization of the initial state as a result of the basic solvation of the chloranil molecule; log $k=-0.536D_\pi-2.23$ (r=0.826, n=20) (Fig. 1). The six nonpolar aromatic hydrocarbons and derivatives (Solv. Nos. 9, 10, 11, 18, 21, and 23) were well correlated (slope=−0.600, r=0.998), but the dipolar solvents displayed an inverted U-shaped deviation. The apparent acceleration by the dipolar solvents may be attributed to the stabilization of the transition state by the dipole-dipole interaction. The effects of the substituents on the rate supported the polar transition state with a partial positive charge on

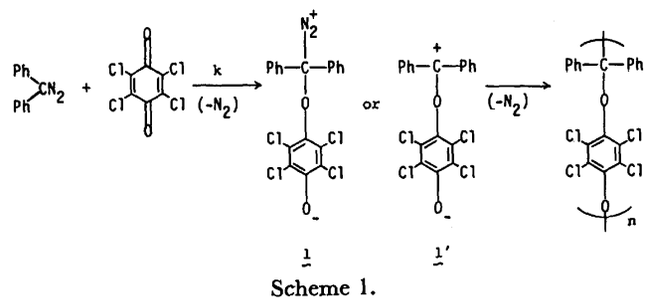

Scheme 1.

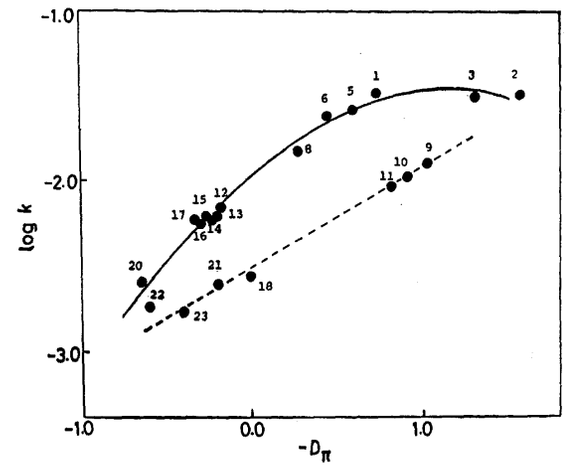

Fig. 1. Plot of log k against D_π.

Table 1. Second-order rate constants (l mol^{-1} s^{-1}) for the decompositions of diphenyldiazomethane with chloranil and 2,5-dichloro-*p*-benzoquinone in various solvents at 30 °C, with the solvent basicity and the polarity parameters

Solvent	Chloranil	2,5-Dichloro-*p*-benzoquinone				D_π[b]	E_T[c]	f(ε)[d]
	$10^3 k$	**2**/**3**[a]	$10^3 k_{obsd}$	$10^3 k_1$	$10^3 k_2$			
1 Nitromethane	32.3	0.670	15.9	6.44	9.46	−0.724	46.3	0.479
2 Chloroform	30.7	0.535	15.5	5.40	10.1	−1.56	39.1	0.359
3 1,2-Dichloroethane	30.5	0.611	14.3	5.65	9.25	−1.22	41.9	0.431
4 Dichloromethane	—	0.611	13.5	5.12	8.38	−1.30	41.1	0.420
5 Nitrobenzene	24.4	—	—	—	—	−0.583	42.0	0.479
6 Acetonitrile	23.4	0.711	13.4	5.57	7.83	−0.440	46.0	0.480
7 Benzonitrile	—	0.618	11.1	4.24	6.86	−0.398	42.0	0.471
8 Propionitrile	14.5	0.676	10.8	4.35	6.45	−0.277	43.7	0.473
9 Bromobenzene	12.1	0.681	7.26	2.94	4.32	−1.03	37.5	0.373
10 Chlorobenzene	10.1	0.685	6.32	2.57	3.75	−0.903	37.5	0.377
11 Fluorobenzene	8.90	0.690	5.56	2.27	3.29	−0.818	38.1	0.373
12 Ethyl methyl ketone	6.43	0.496	8.02	2.66	5.36	0.177	41.3	0.461
13 Methyl acetate	6.29	0.848	5.23	2.40	2.83	0.196	40.0	0.396
14 Cyclohexanone	5.69	0.501	7.01	2.34	4.67	0.243	40.8	0.460
15 Acetone	5.68	0.685	7.48	3.04	4.44	0.261	42.2	0.464
16 Ethyl acetate	5.34	0.710	4.65	1.93	2.72	0.289	38.1	0.385
17 Propyl acetate	5.30	0.697	5.26	2.16	3.10	0.337	37.5	0.385
18 Benzene	2.66	0.954	3.38	1.65	1.73	0.000	34.5	0.230
19 Tetrahydropyran	—	0.670	3.39	1.36	2.03	0.539	—	0.377
20 Tetrahydrofuran	2.43	0.634	2.37	0.919	1.45	0.639	37.5	0.407
21 Ethylbenzene	2.42	0.706	3.07	1.27	1.80	0.197	—	0.241
22 1,4-Dioxane	1.79	0.655	2.93	1.16	1.77	0.590	36.0	0.223
23 Toluene	1.65	0.864	2.46	1.14	1.32	0.394	33.9	0.239

a) The product ratios (**2**/**3**) were determined by means of high-performance liquid chromatography; the yield of **3** was taken as the amount of benzophenone after the hydrolysis of **3**. b) Relative logarithmic rate constants of the reaction of diphenyldiazomethane with TCNE in benzene as the reference solvent and in a given solvent; Ref. 1. c) Dimroth and Reichardt's E_T values; Ref. 7. d) Kirkwood function; $f(\varepsilon)=(\varepsilon-1)/(2\varepsilon+1)$; Ref. 6.

the diazo-carbon: $\log k/k_0=-1.67(\sigma^0+0.66\Delta\bar{\sigma}_R^+)+0.009$,[5] at 30 °C in THF. However, the correlation of log k with f(ε) (r=0.69) or E_T (r=0.74) was less satisfactory than that with D_π. This implies that the chloranil reaction is more dependent on the basic property (D_π) of the solvents.

To obtain a more satisfactory regression, let us examine the multiple correlation of log k with D_π values and with E_T or f(ε) as the solvent polarity parameter. The two parameter equations consisting of linear combination of D_π and E_T or f(ε) improved the correlation, as may be seen in Eq. 1 for 19 solvents and in Eq. 2 for 20 solvents:

Chloranil-DDM reaction:

$$\log k = -4.77 - 0.421 D_\pi + 0.0650 E_T \quad (r = 0.977, s = 0.0945, n = 19), \quad (1)$$

$$\log k = -3.16 - 0.450 D_\pi + 2.45 f(\varepsilon) \quad (r = 0.963, s = 0.120, n = 20). \quad (2)$$

The Kirkwood function, f(ε), appears less successful than E_T, as is shown by the values of r in Eqs. 1 and 2. A plot of log k(obsd) *vs.* log k(calcd) according to Eq. 1 is shown in Fig. 2.

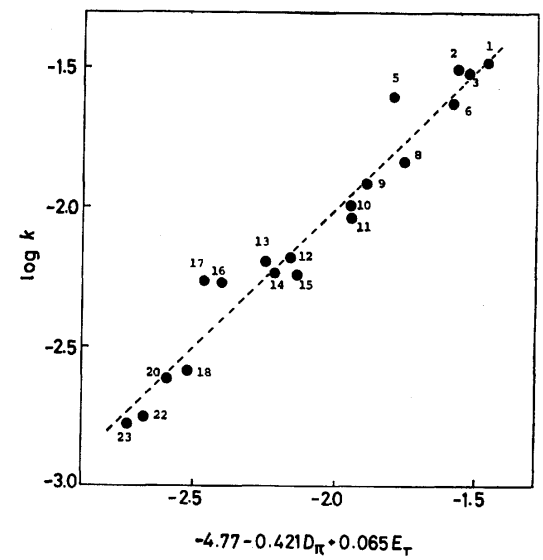

Fig. 2. Plot of log k (obsd) against log k (calcd) according to Eq. 1, for point numbers, see Table 1.

The Dependence of the Rate Constants on the Properties of the Aprotic Solvents in the Reactions of Diphenyldiazomethane with 2,5-Dichloro-p-benzoquinone (DCQ). The DCQ decomposed DDM to give two products, bicyclic dione (**2**) and poly(2,5-dichlorohydroquinone benzhydryl ether) (Scheme 2).[8] The formation of **2** may be explained as arising from the initial product, pyrazoline, followed by the loss of N_2; the polyether may then be thought to be made up by the polymerization of a diazonium or carbonium betaine intermediate, like **1** or **1'**. The participation of the betaine intermediate was evidenced by the isolation of 2,5-dichloro-4-

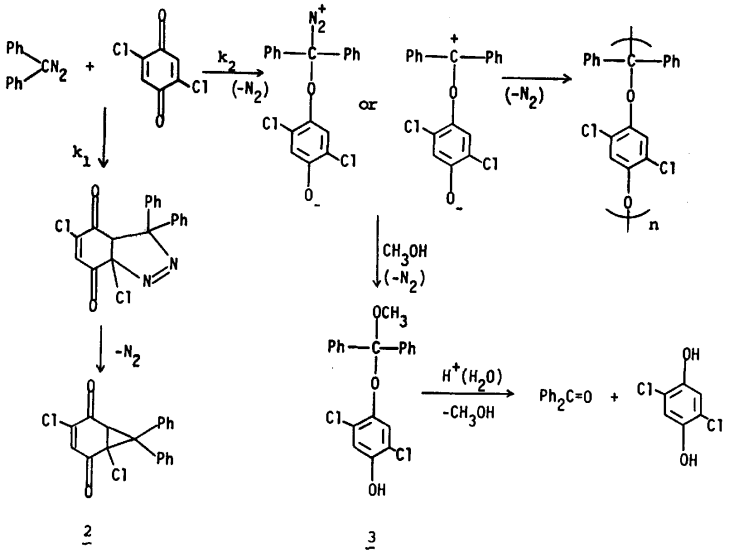

Scheme 2.

[(methoxy)diphenylmethoxy]phenol (**3**) in the reaction carried out in the presence of a trace amount of CH_3OH;[8] **3** was easily hydrolyzed into benzophenone and 2,5-dichlorohydroquinone. Thus, the yield was taken as the amount of benzophenone. However, no essential change was noticed in the observed rate constant or in the yield of **2** between the reaction in the absence and in the presence of a trace of CH_3OH as an additive, as exemplified by a 1,2-dichloroethane solution.[8] Therefore, we made product and kinetic studies of the solvents containing a 5 molar excess of CH_3OH with respect to DDM, and then the total and the relative yields of **2** and benzophenone after the hydrolysis were conveniently determined by means of high-performance liquid chromatography. The combined yields of **2** and **3** amount to more than 95% in all the solvents used. The observed second-order rate constants (k_{obsd}) were divided into the individual rate constants, k_1 and k_2, for the paths leading, respectively, to **2** and **3**, by combining them with their relative yields. The kinetic data and the relative product yields are also shown in Table 1.

An examination of the results shows that, although the variation in the rate constants with the changing solvent is considerably low, k_1 and k_2 depend on both the basicity and the polarity of the solvents, as in the case of a chloranil reaction; $\log k_1 = -1.35 + 0.584 \log k$ ($r=0.962$, $n=19$) and $\log k_2 = -1.05 + 0.644 \log k$ ($r=0.946$, $n=19$), where k is the rate constant in the chloranil-DDM reaction. For a comparison of k_1 and k_2, a similar but slightly greater dependence of k_2 on the properties of the solvents can be anticipated from the linear correlation: $\log k_2 = 0.392 + 1.08 \log k_1$ ($r=0.973$, $n=22$).

For example, a single-parameter correlation of the logarithmic rate constants with the D_π, E_T, and $f(\varepsilon)$ values is as follows: $\log k_1 = -2.65 - 0.289D_\pi$ ($r=0.769$, $n=22$), $\log k_1 = -4.87 + 0.0582E_T$ ($r=0.797$, $n=20$), $\log k_1 = -3.38 + 2.05\,f(\varepsilon)$ ($r=0.673$, $n=22$), and $\log k_2 = -2.48 - 0.311D_\pi$ ($r=0.743$, $n=22$), $\log k_2 = -5.02 + 0.0664E_T$ ($r=0.807$, $n=20$), $\log k_2 = -3.37 + 2.46\,f(\varepsilon)$ ($r=0.727$, $n=22$). A comparison of the r values of these correlations indicates that both k_1 and k_2 are more affected by the solvent polarity (E_T) than by the basicity (D_π). This trend is the opposite of that found in the chloranil reaction. Attempts to obtain more satisfactory correlations were done using two parameters, D_π and E_T or $f(\varepsilon)$. The results are shown as Eqs. 3 and 4 for $\log k_1$ and as Eqs. 5 and 6 for $\log k_2$:

DCQ–DDM reaction:

$$\log k_1 = -4.45 - 0.205D_\pi + 0.0460E_T \quad (r = 0.962,\ s = 0.0176,\ n = 20), \tag{3}$$

$$\log k_1 = -3.24 - 0.240D_\pi + 1.55f(\varepsilon) \quad (r = 0.912,\ s = 0.110,\ n = 22), \tag{4}$$

$$\log k_2 = -4.57 - 0.218D_\pi + 0.0535E_T \quad (r = 0.953,\ s = 0.090,\ n = 20), \tag{5}$$

$$\log k_2 = -3.22 - 0.249D_\pi + 1.94f(\varepsilon) \quad (r = 0.926,\ s = 0.113,\ n = 22). \tag{6}$$

As the case of the chloranil reaction, both the equations involving D_π and E_T gave better correlations than the corresponding expressions involving D_π and $f(\varepsilon)$. The superiority of the E_T paramater may be ascribed to the intrinsic combined measure of solvent polarity and acidity,[9] by which the specific solvation of the transition state with the negatively charged quinone moiety is effected. Furthermore, a comparison of the coefficients of D_π and E_T in Eqs. 3 and 5 shows that the **3** path receives more influence of the solvent polarity than does the **2** path; the absolute coefficients of D_π increased *ca.* 6%, but the corresponding values of E_T increased *ca.* 16%, in going from Eq. 3 to Eq. 5. The plots of $\log k_1$ (obsd) *vs.* $\log k_1$ (calcd) and $\log k_2$ (obsd) *vs.* $\log k_2$ (calcd), according to, respectively, Eqs. 3 and 5, are shown in Fig. 3. The greater susceptibility of the **3** path to the solvent polarity than the **2** path can be ascribed to the more-charged transition state suggested by the kinetic substituent effects: $\log k_1 = -2.15 - 1.55\sigma$ and $\log k_2 = -2.03 - 1.85$ ($\sigma^0 + 0.515\,\Delta\bar{\sigma}_R^+$).[8]

Comparison of the Kinetic Solvent Effects of the Chloranil–

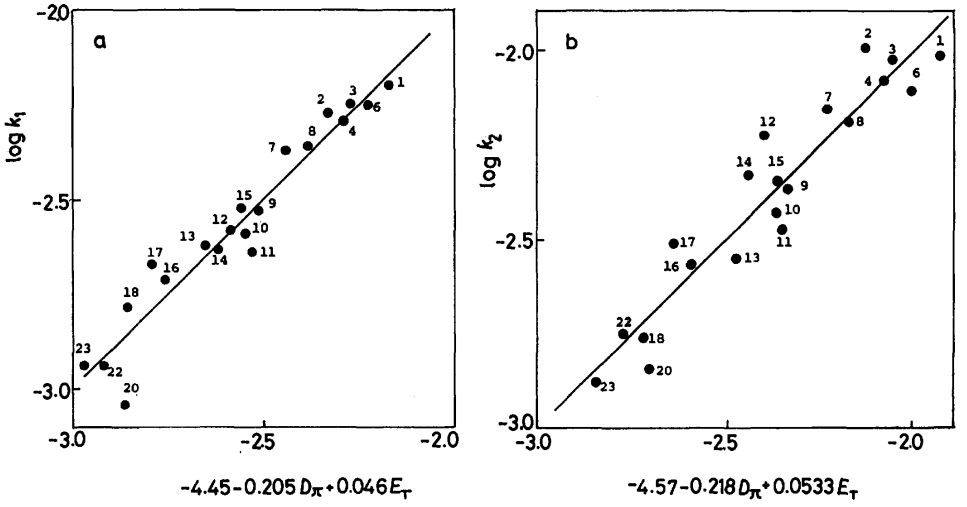

Fig. 3. a) Plot of log k_1 (obsd) *vs.* log k_1 (calcd) according to Eq. 3. b) Plot of log k_2 (obsd) *vs.* log k_2 (calcd) according to Eq. 5, for point numbers, see Table 1.

DDM and DCQ–DDM Reactions with Those of the DDQ–DDM and TCNE–DDM Reactions. We are now in a position to compare the kinetic solvent effects in the decomposition of DDM with various π-acceptor acids, *i.e.*, chloranil, DCQ, DDQ, and TCNE.

In formulating the D_π scale in 34 aprotic solvents,[1] we used the difference between the logarithmic rate constants of the TCNE–DDM reaction in benzene (as a reference solvent) and the solvent at 30 °C, so the log k can be described by this modified form:

TCNE–DDM reaction:

$$\log k = -1.01 - D_\pi, \tag{7}$$

where the intercept is log k for benzene.

This empirical parameter could successfully be applied to the kinetics of the DDQ–DDM reaction in 26 aprotic solvents at 30 °C.[1] The least-square correlation equation is as in Eq. 8:

DDQ–DDM reaction:

$$\log k = 0.623 - 1.10D_\pi \quad (r = 0.977,\ s = 0.161,\ n = 26). \tag{8}$$

A comparison of the intercepts and the slopes in Eqs. 7 and 8 indicates that the DDQ reaction is *ca.* 30 times faster in the benzene solution ($D_\pi = 0$) and depends slightly more on the solvent basicity than the TCNE reaction. On the contrary, the chloranil and DCQ reactions, both having substantially the same orders of rates, gave rates about 50 times lower in benzene and showed a less effective contribution of the D_π compared to the TCNE reaction, as may be seen in the coefficients of D_π in Eqs. 1, 3, and 5. It should also be noted that these equations are characteristic in incorporating the solvent-polarity parameter.

The solvation effects in both initial and transition states must be taken into account in order to understand the influence of the solvent on the rate. In the initial state, the basic solvation of the π-acceptor acids is the chief factor influencing the rate constants, as exemplified by the UV blue shifts and the appearance of the charge-transfer absorption of TCNE[10,11] and chloranil[12] on going to more basic solvents† (Table 2). One can easily notice the parallelism between the absolute coefficients of D_π and the electron affinity of these π-acids in the order of DDQ (1.95 eV)>TCNE (1.80)> chloranil (1.37)>DCQ (1.1).[13] This means that the extent of the basic solvation can be related to the π-acceptor ability of these acids. On the other hand, the transition states may be stabilized by the dipole-dipole interaction in the polar media, since the kinetic substituents effects of all these reactions suggest charged transition states.

Here again, let us summarize the Hammett parameters, ρ, with the correlation fashion: TCNE reaction; −2.67 (with Brown's σ^+)[14], DDQ; −2.33 (Yukawa-Tsuno equation),[15] chloranil; −1.67 (Yukawa-Tsuno equation),[5] and DCQ; −1.85 (for the path giving **3**, Yukawa-Tsuno equation) and −1.55 (for path giving **2**, with normal σ).[8] If the ρ values may be taken as a suitable estimate of the charge appearance of the transition state, the TCNE and DDQ reactions are more likely to be stabilized by the polar solvent than are the chloranil and DCQ reactions. An examination of Eqs. 1—8, however, shows that the DDQ reaction is satisfactorily correlated only with D_π, while the chloranil and DCQ reactions are well expressed by a linear combination of D_π and a polarity parameter, such as E_T and $f(\varepsilon)$. This apparent discrepancy can be easily explained by the relative significance of the stabilizations in the initial and transition states in comparison with that for the model TCNE–DDM reaction. By definition, the D_π parameter inherently reflects the influence of the solvent, not only on the initial state, but also on the transition state of the TCNE–DDM reaction. The free energies of the solvation of the initial state (ΔG_B) are, of course, greater than those of the transition state (ΔG_P), as was demonstrated earlier by the statistically better correlation of the logarithmic rate constants with the conventional basicity param-

† By contrast, the π-π^* absorption of DDM in the ultraviolet region remained essentially unchanged during such a variation of solvents, reflecting the lower solvation of DDM.[1]

Table 2. Solvent effects on the UV absorption spectra of TCNE and chloranil at 25 °C

Solvent	TCNE λ_{max}/nm (log ε)		Chloranil λ_{max}/nm (log ε)	
Chloroform	267.7(4.16)	277.6(4.15)	292.0(4.35)	374.0(2.37)
Dichloromethane	267.4(4.13)	277.7(4.09)		
Acetonitrile	262.5(4.20)	271.5(4.16)	287.0(4.32)	367.5(2.39)
Propionitrile	263.0(4.22)	272.3(4.18)		
Ethyl acetate	259.0(4.18)	270[a] (4.08)	287.0(4.27)	364.0(2.40)
Propyl acetate	258.5(4.19)	270[a] (4.09)		
Tetrahydrofuran	260.6(4.08)	270[a] (4.02) 318(3.49)[b,c]	283.5(4.23)	330[a] (3.16)[e]
1,4-Dioxane	259.5(3.98)	350(3.27)[b,c]	285.5(4.20)	330[a] (3.20)[e]
Fluorobenzene			285.5(4.12)	330[a] (3.27)[e]
Benzene		384(3.55)[b,d]	283.5(4.16) 346[b,f]	332(3.33)[b,e]
Toluene		406(3.52)[b,d]	286.5(4.19) 365[b,f]	362(3.27)[b,e]

a) Shoulder. b) Due to charge-transfer absorption. c) Values taken from Ref. 10; measured in $CHCl_3$ at 25 °C. d) Values taken from Ref. 11; measured in CH_2Cl_2 at 22 °C. e) Measured in 7.0×10^{-4} mol/l. f) Values taken from Ref. 12; measured in cyclohexane at 18—20 °C.

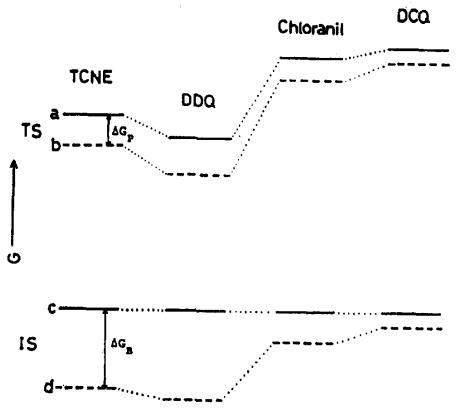

Fig. 4. Solvent effect upon reactants and transiton states, TS: transition states in nonpolar (a) and in polar (b) solvents; IS: initial states in nonbasic (c) (depicted arbitrarily in the same level) and basic (d) solvents.

eters, such as $\Delta\nu_D$, β, and DN, than those with E_T and $f(\varepsilon)$.[1] This situation is schematically shown in Fig. 4, together with the other cases of DDQ, chloranil, and DCQ reactions.

In the case of the DDQ reaction, the lack of a polarity parameter and the slightly excess sensitivity to the D_π may, therefore, be ascribed to essentially the same $\Delta G_P/\Delta G_B$ ratios, but to somewhat greater individual values, compared to the TCNE reaction. On the other hand, the incorporation of the polarity parameter in the chloranil and DCQ reactions is the result of the significant decrease in the basic solvation; therefore, the relative role of ΔG_p may be pronounced with respect to ΔG_B.

Recently, Krygowski and Fawcett proposed a similar two-parameter regression with the aid of E_T and DN, where Q is a physicochemical quantity and α and β are the regression coefficients:[9]

$$Q = Q_0 + \alpha E_T + \beta DN.$$

The application of this empirical equation to the present chloranil and DCQ reactions, however, resulted in a much worse correlation because DN is inadequate to describe the softness of aromatic solvents.

Experimental

The bicyclic dione (**2**): benzophenone ratios and the overall yields of **2** and benzophenone were determined by means of JASCO trirotor high-performance liquid chromatography (HPLC), using biphenyl as the internal standard. The HPLC analysis was carried out at room temperature using a 250 mm × 4.6 mm column packed with ODS (octadecylsilane) on silica gel; methanol–water (7 : 3 by volume); flow rate, 1 ml/min. The UV detector was calibrated at 245 nm with standard mixtures of known concentrations of benzophenone, **2**, and biphenyl. The relative retention times were as follows: benzophenone (0.53), **2** (0.68), and biphenyl (1.0).

Materials. The diphenyldiazomethane (DDM) was synthesized as has been described by Smith and Howard[16] and recrystallized from light petroleum; mp 29—30 °C. The chloranil was of commercial origin and was recrystallized twice from benzene; mp 290 °C. The 2,5-dichloro-*p*-benzoquinone (DCQ) was prepared according to the procedure described by Ling[17] and was recrystallized from ethanol; mp 164—166 °C. All the solvents were dried and purified according to the standard procedures.[18]

Kinetic Measurements. The values of k were determined spectrophotometrically as has previously been described[5,8] by the use of Hitachi 323 and JASCO UVIDEC-505 instruments. The absorption cells were thermostated at 30±0.1 °C with a Haake circulator. The mean deviations for k were ±3% (usually two determinations).

References

1) T. Oshima, S. Arikata, and T. Nagai, *J. Chem. Res.*, **1981**, (*S*) 204; (*M*) 2518.

2) T. Kagiya, Y. Sumida, and T. Inoue, *Bull. Chem. Soc. Jpn.*, **41**, 767 (1968).

3) M. J. Kamlet and R. W. Taft, *J. Am. Chem. Soc.*, **98**, 377 (1976); M. J. Kamlet, J. L. Abboud, M. E. Jones, and R.

W. Taft, *J. Chem. Soc., Perkin Trans. 2*, **1979**, 342.

4) V. Gutmann and E. Wychera, *Inorg. Nucl. Chem. Lett.*, **2**, 257 (1966); V. Gutmann and R. Schmid, *Coord. Chem. Rev.*, **12**, 263 (1974); V. Gutmann, *Electrochim. Acta*, **21**, 661 (1976).

5) T. Oshima and T. Nagai, *Bull. Chem. Soc. Jpn.*, **53**, 3284 (1980).

6) J. G. Kirkwood, *J. Chem. Phys.*, **2**, 351 (1934); K. J. Laidler and H. Eyring, *Ann. New York Acad. Sci.*, **39**, 303 (1940).

7) K. Dimroth, C. Reichardt, T. Siepmann, and R. Bohlmann, *Justus Liebigs Ann. Chem.*, **661**, 1 (1963); C. Reichardt, *Angew. Chem. Int. Ed. Engl.*, **18**, 98 (1979).

8) T. Oshima and T. Nagai, *Bull. Chem. Soc. Jpn.*, **55**, 551 (1982).

9) T. M. Krygowski and W. R. Fawcett, *J. Am. Chem. Soc.*, **97**, 2143 (1975).

10) R. Vars, L. A. Tripp, and L. W. Pickett, *J. Phys. Chem.*, **66**, 1754 (1962).

11) R. E. Merrifield and W. D. Phillips, *J. Am. Chem. Soc.*, **80**, 2778 (1958).

12) R. Foster, D. L. Hammick, and B. N. Parsons, *J. Chem. Soc.*, **1956**, 555.

13) G. Briegleb, *Angew. Chem.*, **76**, 326 (1964).

14) T. Oshima, A. Yoshioka, and T. Nagai, *J. Chem. Soc., Perkin Trans. 2*, **1978**, 1283.

15) T. Oshima and T. Nagai, *Bull. Chem. Soc. Jpn.*, **54**, 2039 (1981).

16) L. I. Smith and K. L. Howard, *Org. Synth.*, Coll. Vol. III, 351 (1955).

17) A. R. Ling, *J. Chem. Soc.*, **61**, 558 (1892).

18) J. A. Riddick and W. R. Bunger, "Techniques of Chemistry, Vol. II, Organic Solvents," 3rd ed, ed by A. Weissberger, Wiley (1970).

 © 1982 The Chemical Society of Japan Bull. Chem. Soc. Jpn., 55, 561—568 (1982)

Highly Selective Carbon-Carbon Bond Forming Reactions Mediated by Chromium(II) Reagents

Tamejiro HIYAMA,* Yoshitaka OKUDE, Keizo KIMURA, and Hitosi Nozaki

Department of Industrial Chemistry, Kyoto University, Yoshida, Sakyo-ku, Kyoto 606

(Received July 14, 1981)

A low valent chromium reagent is generated from chromium(III) chloride and a half mol of lithium aluminum hydride in tetrahydrofuran. The reagent behaves similarly to anhydrous chromium(II) chloride, which is commercially available, and reduces allylic halides to produce unisolable allylchromium species which add efficiently to aldehydes or ketones with high degree of stereo- and chemoselectivity. Particularly, high *threo* selectivity is observed in the reaction of aldehydes and 1-bromo-2-butene and is ascribed to a chair-like six-membered transition state. Simple reduction of allylic and benzylic halides produces biallyls and bibenzyls, while *gem*-dibromocyclopropanes afford the corresponding allenes in excellent yields.

Main group organoelement compounds containing lithium, magnesium, or boron have been basic reagents for carbon-carbon bond formation.[1] These are generally so reactive as to make C–C bonds indiscriminately. In contrast, highly selective reactions are accomplished recently with the aid of transition metal elements such as chromium,[2] samarium,[3] ytterbium,[3] manganese,[4] tin,[5] titanium,[6] and zirconium.[7] This article deals with the Barbier-Grignard type reaction by means of chromium reagents with the emphasis on the chemo- and stereoselectivity.

Preparation of Allylic Chromium Reagent and the Carbonyl Addition. Chromium(II) salts are widely used in organic synthesis as one-electron reducing agents.[8] These are generally prepared and used in aqueous media. Therefore, when organic halides are treated with conventional chromium(II) reagents, the intermediary organochromium species, assumed to be formed at the initial stage of the reaction, are soon attacked by the coexisting water.[9] This has been the largest limitation and the chromium(II) reagents could not be utilized for intermolecular C–C bond forming reactions. We have found that chromium(III) chloride is reduced by lithium aluminum hydride (LAH)[10] in tetrahydrofuran (THF) to form a reagent which behaves quite analogously to chromium(II) chloride. Although the identity has not been established yet, we will call it chromium(II) reagent hereafter. This allows us to work in non-aqueous solutions.

When anhydrous chromium(III) chloride[11] suspended in THF was treated with a half mol of LAH at 0 °C, exothermic reaction took place spontaneously with hydrogen evolution. The initial purple color of the reaction mixture darkened and finally turned dark brown after 10 min. The reagent thus prepared can be stored for more than a month in a refrigerator without appreciable loss of activity. Treatment of a mixture of benzaldehyde and 1-bromo-3-methyl-2-butene with this reagent produced 2,2-dimethyl-1-phenyl-3-buten-1-ol (**1**). The optimum $CrCl_3$/LAH ratio was estimated to be 2 based on the results shown in Table 1. When

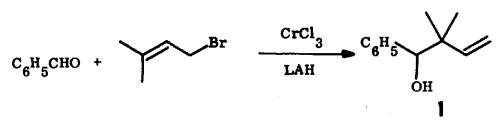

1

TABLE 1. REACTION OF BENZALDEHYDE AND 1-BROMO-3-METHYL-2-BUTENE WITH THE CHROMIUM REAGENTS GENERATED FROM VARIOUS RATIO OF CHROMIUM (III) CHLORIDE AND LITHIUM ALUMINUM HYDRIDE[a]

$CrCl_3$:	$LiAlH_4$	Yield of **1**/%
1	1	25[b]
2	1	90
4	1	48[c]
$CrCl_2$[d]		89

a) Benzaldehyde (1 mmol) and 1-bromo-3-methyl-2-butene (2 mmol) were added to the chromium reagent (4 mmol) in THF (20 cm^3) at room temperature and the reaction was stopped after 3 h. b) Benzyl alcohol was produced as a main product. c) Benzaldehyde remained as evidenced by TLC assay. d) Purchased from Research Organic/Inorganic Chemical Corp.

an equimolar amount of LAH was applied, active hydride remained unchanged and reacted with benzaldehyde competitively to produce benzyl alcohol. In the experiment with a ratio of 4, the yield of the adduct decreased to *ca.* 50%. The same transformation could be achieved by means of the commercially available anhydrous chromium(II) chloride. The results of the reaction between allylic halides (or tosylate) and aldehydes or ketones are listed in Table 2. The general features of the chromium(II) mediated Barbier-Grignard reaction are as follows:

(1) The stoichiometry says that 2 mol of the chromium reagent is required for reduction of each halide.

(2) Although stoichiometric amount of allylic halide was sufficient for aldehyde, the use of excess allylic chromium reagents gives better yields in the reaction with ketones (*vide infra*).

(3) Generally the more substituted γ-carbon of an allyl group is attached to the carbonyl carbon. However, the methylene carbon of 3-bromopropyne preferentially connected with the carbonyl carbon of nonanal to give 1-dodecyn-4-ol (run 20).[12]

(4) *N,N*-Dimethylformamide (DMF) solvent is more effective than THF and, in particular, essential for the reaction with allyl chloride or tosylate.

(5) With α,β-unsaturated aldehydes, the reaction proceeds exclusively in 1,2-fashion. Examples are seen in runs 9 and 14 (altemisia alcohol synthesis), and also in the synthesis of Ips dienol (**2**).[13]

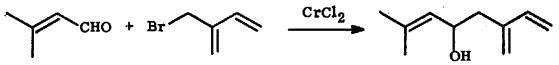

Ips dienol **2**

(6) Ketones are in general less reactive than aldehydes and required 2 mol of halides (*i.e.*, 4 mol of chromium reagent). Thus, chemospecific carbonyl addition is effected (run 17). Furthermore, the reagent discriminated 2-heptanone from 4-heptanone with the selectivity of 88 to 84%. α,β-Unsaturated ketones such as benzylideneacetophenone and 1,4-naphthoquinone do not give the corresponding adduct cleanly.

(7) Nitriles and carboxylates are not affected. Thus, selective carbonyl addition was achieved with respect to aldehydes having cyano or alkoxycarbonyl groups (runs 18 and 19).

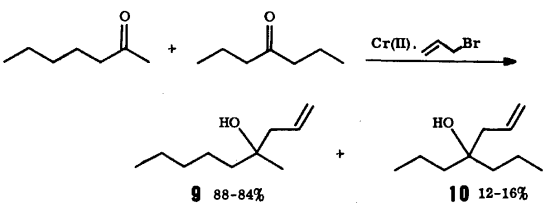

9 88-84% **10** 12-16%

(8) Allylation of 4-*t*-butylcyclohexanone resulted in the preferential formation of the axial alcohol (runs 5 and 6). Namely, equatorial attack predominates with the selectivity of 88% (for $CrCl_3$–LAH reagent) and

TABLE 2. CHROMIUM(II) MEDIATED CARBONYL ADDITION OF ALLYL HALIDES[a]

Run	Ketone or aldehyde (mg or g, mmol)	Allyl halide (mg or g, mmol)	Chromium[b] reagent (g, mmol)	Solvent (cm^3)	Reaction time/h	Product[c] (mg, or g, % yield)
1	104, 1.06	143, 1.18	A (-, 1.18)	THF (9)	2	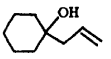 116, 78
2	129, 1.32	0.22, 1.32	B (0.32, 2.6)	THF (10)	3	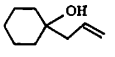 136, 74
3	94, 0.96	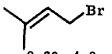 0.60, 4.0	A (-, 8.0)	DMF (16)	o.n.[d]	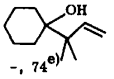 -, 74[e]
4	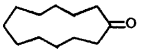 0.21, 1.13	0.27, 2.3	A (-, 4.5)	THF (8)	3	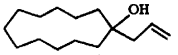 0.21, 82[f]
5	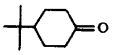 156, 1.01	0.25, 2.0	B (0.50, 4.1)	THF (12)	2.6	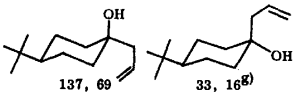 137, 69 33, 16[g]
6	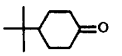 146, 0.95	0.23, 1.89	A (-, 3.8)	THF (12)	3	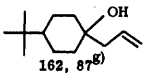 162, 87[g]
7	n-C_6H_{13}CHO 119, 1.04	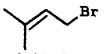 0.31, 2.1	B (0.51, 4.1)	DMF (10)	3	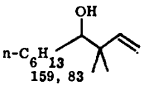 159, 83
8	81, 1.12	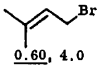 0.60, 4.0	A (-, 8.0)	DMF (13)	o.n.[d]	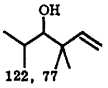 122, 77
9	91, 1.30	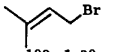 193, 1.30	A (-, 2.6)	THF (10)	2	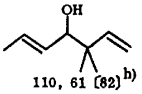 110, 61 (82)[h]
10	C_6H_5CHO 65, 0.62	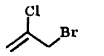 0.34, 2.2	B (0.53, 4.3)	THF (8)	3	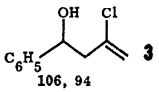 **3** 106, 94
11	C_6H_5CHO 148, 1.39	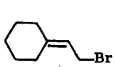 0.49, 2.6	A (-, 5.2)	THF (10)	o.n.[d]	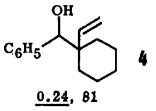 **4** 0.24, 81
12	C_6H_5CHO 90, 0.85	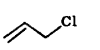 134, 1.75	B (0.43, 3.5)	DMF (10)	o.n.[d]	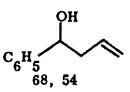 68, 54

TABLE 2. Continued.

Run	Ketone or aldehyde (mg or g, mmol)	Allyl halide (mg or g, mmol)	Chromium[b] reagent (g, mmol)	Solvent (cm³)	Reaction time/h	Product[c] (mg, or g, % yield)
13	C_6H_5CHO 106, 1.00	0.44, 2.1	B (0.51, 4.1)	DMF (9)	2,6	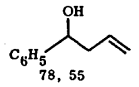 78, 55
14	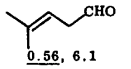 0.56, 6.1	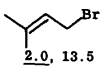 2.0, 13.5	A (-, 27)	THF (30)	3	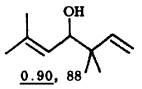 0.90, 88
15	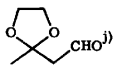 1.29, 9.9	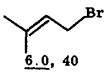 6.0, 40	A (-, 80)	DMF (110)	o.n.[d]	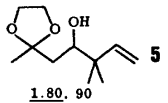 1.80, 90 **5**
16	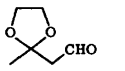 92, 0.70	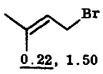 0.22, 1.50	B (0.39, 3.2)	DMF (7)	0.2	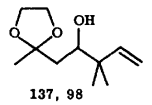 137, 98
17	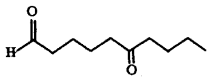 0.20, 1.19	173, 1.43	B (0.35, 2.9)	THF (10)	2.3	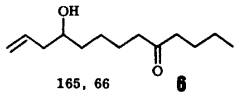 165, 66 **6**
18	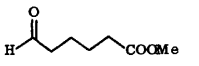 116, 0.80	117, 0.96	B (0.24, 1.93)	THF (8)	3	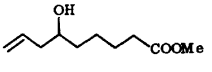 112, 75 **7**
19	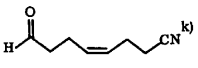 70, 0.51	0.23, 1.88	B (0.46, 3.8)	THF (8)	3	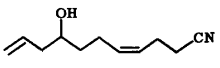 60, 66 **8**
20	$n\text{-}C_6H_{13}CHO$ 130, 1.14	0.26, 2.2	B (0.54, 4.4)	THF (10)	3	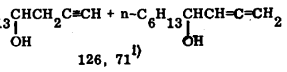 126, 71[i]
21	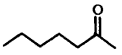 66, 0.58	0.24, 2.0	B (0.56, 4.5)	THF (7)	5.5	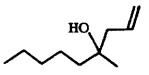 70, 78 **9**
22	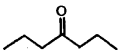 102, 0.89	0.42, 3.4	B (0.87, 7.1)	THF (11)	4.5	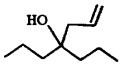 47, 33 **10**

a) All the reaction was carried out at room temperature under an argon atmosphere. b) A: $CrCl_3$–1/2$LiAlH_4$ reagent. B: $CrCl_2$ reagent. c) Unless otherwise stated products were isolated by preparative TLC or column chromatography. d) Overnight. e) Determined by GLC (PEG 20 M, 5% on Celite 545, 1.5 m, 94 °C) analysis. f) Cyclododecanone (35 mg, 17%) was recovered. g) Stereochemical assignment: *cf.* Ref. 12. The axialalcohol: TLC (SiO_2, hexane–ether 3: 1) R_f 0.27; GLC (PEG 20 M, 10%, on Celite 545, 1.5 m, 140 °C) R_t 37.4 min; ^1H NMR ($CDCl_3$) δ=0.87 (*t*-Bu), and equatorial alcohol: TLC R_f 0.16; GLC, R_t 41.8 min; ^1H NMR δ=0.79. The ratio of the axial alcohol and the equatorial alcohol was estimated by GLC. h) GLC yield. i) The ratio of the acetylene/allene was revealed to be 9.8 : 1 by GLC (Apiezon L 5%, KOH 1%, on Chromosorb WAW, 2 m, 104 °C, R_t 4.0 min and 6.0 min respectively) or 10 : 1 by ^1H NMR. j) Bp 57—60 °C (bath temp)/13 Torr. Found: C, 55.25; H,8.02%. Calcd for $C_6H_{10}O_3$: C, 55.37; ^1H, 7.75%. This material was prepared by ethylene acetalization of ethyl acetoacetate, LAH reduction, followed by oxidation with CrO_3. k) K. Lunkwitz, W. Pritzbow, and G. Schmid, *J. Prakt. Chem.*, **37**, 319 (1968). This was prepared by the Beckmann rearrangement of 8-hydroxy-4-cyclooctenone oxime (mp 104.0—104.7 °C ($CHCl_3$), Found: C, 61.85; H, 8.61; N, 9.05%. Calcd for $C_8H_{12}NO_2$: C, 61.91; H, 8.44; N, 9.08%. *Cf.* M. Ohno, N. Naruse, S. Torimitsu, and I. Terasawa, *J. Am. Chem. Soc.*, **88**, 3168 (1966).

81% (for $CrCl_2$) comparable to that of allylzinc bromide (85%), and better than the Grignard addition (49%) or allyllithium reaction (35%).[14] This is compatible with the empirical rule that the softer the metal atom of allyl metallic compounds becomes, the more important equatorial attack becomes.[14]

(9) Styrene oxide does not undergo allylation and gives instead a mixture of halohydrins. Acetal group

TABLE 3. THREO-SELECTIVE SYNTHESIS OF HOMOALLYL ALCOHOLS 1-BROMO-2-BUTENE AND ALDEHYDES[a]

Run	Aldehyde (mg, mmol)	1-Bromo-2-butene (g, mmol)	Solvent (cm^3)	Chromium[b] reagent (g, mmol)	Reaction time/h	Product (mg, % yield, *threo* : *erythro*[c])
1	PhCHO 140, 1.31	0.34, 2.5	THF (9)	A (—, 5.1)	3.5	206, 96, 100 : 0[d]
2	PhCHO 117, 1.11	0.31, 2.3	THF (7)	B (0.58, 4.7)	4	180, 100, 90 : 10[d]
3	PhCHO 106, 1.00	0.33, 2.4[e]	THF (7)	A (—, 5.0)	3	141, 87, 100 : 0[d]
4	*n*-C_3H_7CHO 74, 1.03	0.23, 1.67	THF (9)	A (—, 3.5)	7.5	78, 59, 93 : 7
5	*i*-C_3H_7CHO 80, 1.11	0.26, 1.91	THF (9)	A (—, 5.5)	3.5	78, 55, 95 : 5
6	*i*-C_3H_7CHO 61, 0.85	0.25, 1.87	THF (6.5)	B (0.40, 3.3)	3.5	88, 81, 97 : 3
7	*n*-$C_5H_{11}CHO$ 98, 0.98	0.25, 1.87	THF (8)	A (—, 4.0)	5	107, 70, 97 : 3
8	*n*-$C_5H_{11}CHO$ 124, 1.24	0.33, 2.5	THF (7)	B (0.61, 5.0)	3	188, 97, 96 : 4
9	*n*-$C_5H_{11}CHO$ 81, 0.81	0.23, 1.68	THF[f] (10)	A (—, 3.8)	1.3	110, 88, 94 : 6
10	*n*-$C_5H_{11}CHO$ 121, 1.21	0.28, 2.1	THF[g] (11)	A (—, 4.5)	4	166, 88, 95 : 5
11	PhCHO 127, 1.20	0.34, 2.5	THF[h] (8.5)	B (0.68, 5.5)	3.5	161, 83, 83 : 17[d]
12	PhCHO 98, 0.92	0.25, 1.81	DMF (7)	A (—, 3.2)	4.3	137, 92, 75 : 25[d]
13	*i*-C_3H_7CHO 78, 1.08	0.25, 1.83	DMF (9)	B (0.45, 3.7)	3	109, 78, 66 : 34
14	*n*-$C_5H_{11}CHO$ 112, 1.12	0.32, 2.4	DMF (9)	A (—, 4.4)	5	115, 77, 68 : 32
15	*t*-C_4H_9CHO 85, 0.98	0.27, 1.97	DMF (8)	A (—, 3.8)	3	88, 63, 37 : 63
16	*t*-C_4H_9CHO 81, 0.94	0.25, 1.83	THF (8)	A (—, 4.3)	3	86, 64, 35 : 65
17	$CH_3CH{=}CHCHO$ 90, 1.29	0.30, 2.2	THF (7)	B (0.56, 4.6)	3	119, 73, 83 : 17[i]

a) Chromium reagent (4 mmol) and 1-bromo-2-butene (2 mmol) were allowed to react with an aldehyde (1 mmol) at room temperature. b) A: $CrCl_3$–1/2$LiAlH_4$ reagent and mmol values are given. B: $CrCl_2$. c) The stereochemistry of the products was determined by comparing the spectral properties and retention times with those of the authentic samples (Ref. 15). d) Determined by ^1H NMR (the absorption of the methine proton H–C–OH): *threo*, δ=4.26 (d, J=6.8 Hz); *erythro*, δ=4.43 (d, J=5.8 Hz). e) *cis*-1-Bromo-2-butene was used. f) At THF refluxing temperature. g) Triphenylphosphine (1.18 g, 4.5 mmol) was added. h) Pyridine (0.86 g, 10.9 mmol, 2 equivalents of chromium) was used. i) Determined by ^{13}C NMR: *threo* (intensity)/*erythro* (intensity) δ=15.83 (94)/15.00(20), 44.32(99)/43.69(20), 115.62(99)/115.03(19).

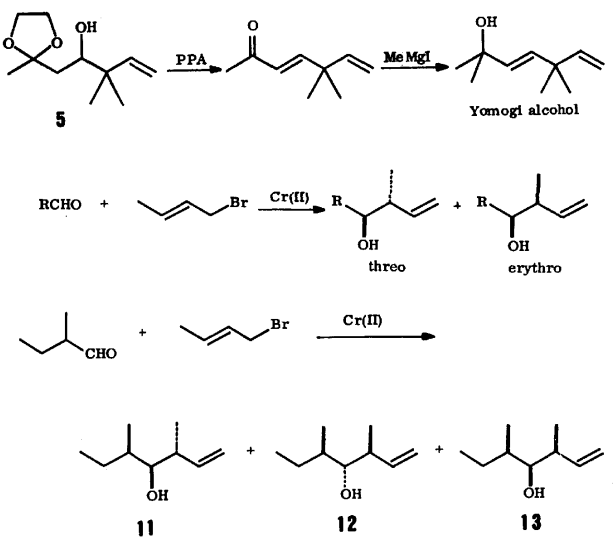

is not affected as evidenced by the reaction of 1-bromo-3-methyl-2-butene with 3,3-ethylenedioxybutanal (runs 15 and 16). The product **5** was subsequently dehydrated and deacetalized with polyphosphoric acid (PPA). Treatment of the resulting enone with methylmagnesium iodide yielded Yomogi alcohol.[15]

threo-*Selective Synthesis of Homoallyl Alcohols.* Benzaldehyde and 1-bromo-2-butene gave only one diastereomer of 2-methyl-1-phenyl-3-buten-1-ol whose stereochemistry was determined later to be *threo* by Heathcock and his coworker.[16] The *threo*-selectivity was found valid for various aldehydes as shown in Table 3 and independent both of the chromium reagents and the stereochemistry of 1-bromo-2-butenes.[17] The selectivity in THF was in general extremely high for relatively unhindered aldehydes (runs 1—11) compared with the reaction of 2-butenylmetals derived from magnesium, zinc, or cadmium.[18] In DMF the *erythro* alcohol (runs 12—14) was produced as much as 25—34%. The

only exception is seen in the reaction of a bulky aldehyde, 2,2-dimethylpropanal, which gave preferentially the *erythro* alcohol irrespective of the solvent (runs 15 and 16). As both *cis*- and *trans*-1-bromo-2-butene gave the *threo* alcohol as the sole product (runs 1, 2, and 3), the stereochemical integrity was lost completely in contrast to the reaction of 2-butenylboron and -silicon derivatives.[17]

The reaction of 2-methylbutanal with 1-bromo-2-butene under the standard conditions gave three adducts whose stereochemical assignments were based on the ^{13}C NMR spectra of the hydrogenated products. Thus, *threo* selectivity in this case turned out to be 93%, although *α-erythro* induction[16] was 69%.

The C–C bond formation with benzaldehyde and 1-bromo-2,4-hexadiene took place exclusively at the γ-position of the bromide[19] to give **14**. The stereochemistry of the major product was assumed to be the one depicted in analogy to the above results.

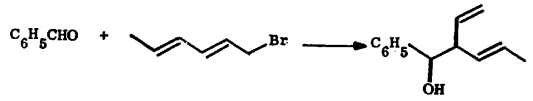

14

The *threo* selectivity observed on the relatively unhindered aldehydes is explained reasonably by a chair form transition state I wherein interaction between the methyl and R groups is most reduced.[20] As chromium-

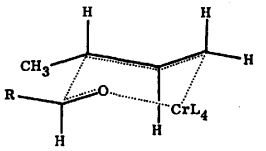

I

(III) ion has an octagonal configuration and consequently accepts six ligands,[21] these ligands will have an effect on the stereoselectivity. The low *threo*-selectivity in DMF may be attributed to the good solvating power of DMF compared with THF and consequently to the increased bulkiness around the chromium metal to disfavor the transition state I. This rationale is applicable to explaining the results of the experiment carried out in the presence of triphenylphosphine (run 10) or pyridine (run 11) which stabilizes the complex of type $RCrCl_2(ligand)_3$.[22]

Reduction of Organic Halides with the Chromium(II) Reagents. In the absence of electrophiles such as aldehydes or ketones allyl halides are dimerized under dehalogenation. For example, 1-bromo-3-methyl-2-butene gave three isomers of the coupling product (see Table 6, runs 1 and 2). Benzylic halides were transformed into the corresponding bibenzyls.[23] However, the assumed intermediate, benzylchromium, did not add across aldehydic carbonyl group. Reductive elimination of vicinal dihalides to olefins proceeded non-stereospecifically as evidenced by the transformation of *trans*-1,2-dibromocyclododecane into a mixture or

Table 4. Reduction of organic halides with the chromium(II) reagents

Run	Halide (mg or g, mmol)	Chromium reagent[a] (mmol)	Solvent (cm^3)	Time h	Product (mg or g, % yield)
1	1-Bromo-3-methyl-2-butene (1.04, 7.0)	A (23)	THF (25)	2	2,7-Dimethyl-2,6-octadiene,3,3,6-trimethyl-1,5-heptadiene, and 3,3,4,4-tetramethyl-1,5-hexadiene (0.34, 70)[b]
2	1-Bromo-3-methyl-2-butene (0.37, 2.5)	B (6.2)	THF (8)	o.n.[c]	2,7-Dimethyl-2,6-octadiene, 3,3,6-trimethyl-1,5-heptadiene, and 3,3,4,4-tetramethyl-1,5-hexadiene (174, 100)[d]
3	Benzyl bromide (0.23, 1.32)	A (2.6)	THF (9)	40	1,2-Diphenylethane (—, 49[e] [61][f])
4	(Dichloromethyl)benzene (183, 1.14)	A (4.5)	DMF (5)	3	*cis*-1,2-Diphenylethene (16, 16) and *trans*-1,2-diphenylethene (33, 32)
5	(Trichloromethyl)benzene (0.23, 1.2)	A (4.3)	DMF (7.5)	3	Diphenylethyne (45, 43)
6	*trans*-1,2-Dibromocyclododecane (0.62, 1.91)	A (3.8)	DMF (5)	o.n.[c,g]	*cis*-Cyclododecene (86, 29)[h] and *trans*-cyclododecene (121, 41)
7	2-Bromocyclododecanone (0.27, 1.05)	A (5.3)	THF (7)	3.5	Cyclododecanone (187, 96)
8	9,9-Dibromobicyclo[6.1.0]-nonane (0.33, 1.16)	A (5.8)	DMF (10)	2[i]	1,2-Cyclononadiene (—, 100)[j]
9	9,9-Dibromobicyclo[6.1.0]-nonane (0.57, 2.0)	A (10)	THF (24) DMF (2)	2[k]	1,2-Cyclononadiene(152, 63 [71][f])
10	2-Phenyl-1,1-dibromocyclopropane (0.29, 1.04)	A (5.2)	DMF (7)	4	Phenylpropadiene (75, 62)
11	*trans*-2-Methyl-3-phenyl-1,1-dibromocyclopropane (0.29, 1.00)	A (5.0)	DMF (8)	5	1-Phenyl-1,2-butadiene (76, 58)

a) A: $CrCl_3$–1/2$LiAlH_4$ reagent, B: $CrCl_2$. All the reaction was carried out at room temperature unless otherwise specified. b) The mixture of the product was purified by preparative TLC and analyzed. The ratio of these products was determined by GLC (Apiezon L, 5%, KOH 1%, on Chromosorb WAW DMS, 1.5 m, 76 °C) to be 72 : 22 : 6. c) Overnight. d) These products were isolated by distillation (Kugelrohr) and the ratio was found to be 62 : 27 : 11 by the GLC assay. e) Estimated by ^1H NMR. f) Based on the consumed starting material. g) At 90 °C. h) Starting dibromide (30 mg, 5%) was recovered. i) At 60 °C. j) GLC yield. k) At reflux temperature.

cis- and *trans*-cyclododecene. α-Bromocyclododecanone was reduced to the parent ketone quantitatively. Trapping experiment of the intermeidary chromium enolate with methyl iodide or trimethylsilyl chloride failed to give the expected product. Quenching with deuterium oxide resulted in only 38% deuterium incorporation. Therefore, hydrogen abstraction from the solvent has possibly occurred during the reaction.

A salient feature of the chromium(II) reagent is illustrated by the very smooth conversion of *gem*-dibromocyclopropanes to allenes (runs 8—11). The reaction is a key in an effective synthetic route to 1,2-dienes. In this particular transformation, the $CrCl_3$–LAH reagent was essential for clean reaction, as the commercial reagent, anhydrous chromium(II) chloride gave products contaminated with monobromocyclopropanes.

In conclusion, reduction of organic halides with the chromium(II) reagent in anhydrous media gives organochromium intermediates which react with aldehydic carbonyl carbon with high selectivity. This will provide a new tool for selective methodology of C–C bond formation.

Experimental

Distillation was carried out by use of Kugelrohr (Büchi) and boiling points were determined by measuring the bath temperature. All the temperatures are uncorrected. ^1H NMR spectra (tetramethylsilane as an internal standard) were taken in carbon tetrachloride solution on a Varian EM 390 spectrometer or EM 360 spectrometer, chemical shifts being given in ppm units. ^{13}C NMR spectra were recorded on a Varian CMR-20 spectrometer (tetramethylsilane, internal standard). IR spectra were obtained on a Shimadzu IR-27G spectrometer in neat liquid film unless otherwise stated, mass spectra on a Hitachi RMU-6L spectrometer. Chromium(III) chloride hexahydrate was dehydrated by the reported procedure.[11] Anhydrous chromium(II) chloride was purchased from Research Inorganic/Organic Chemical Corp., and all reactions as well as all operations dealing with chromium salts were carried out under an argon or a nitrogen atmosphere. LAH purchased from Metalgesellschaft A.-G., West Germany, was used directly. TLC analyses were carried out with Merck Silica Gel 60 F_{254} plates. Preparative TLC plates (20 cm × 20 cm) were prepared by use of Merck Kiesel-gel PF_{254}. Column chromatography was carried out with silica gel (Wakogel C-100) at atmospheric pressure or under pressure of $4—6 \times 10^5$ N/m^2 (Wakogel C-300). In this text 1 Torr corresponds to 133.322 N/m^2.

Preparation of the Chromium Reagent from Chromium(III) Chloride and Lithium Aluminum Hydride. A Typical Procedure. Lithium aluminum hydride (101 mg, 2.6 mmol) was added portionwise to chromium(III) chloride (0.84 g, 5.3 mmol) suspended in THF (5 cm^3) at 0 °C. Immediate gas evolution occurred with darkening of the initial purple color which finally turned dark brown. After the gas evolution had ceased the reaction mixture was stirred for 5 to 10 min at 0 °C, and the reagent was used for reaction. Replacing THF with DMF was effected by evaporation of THF under reduced pressure, introduction of argon, and addition of DMF.

Reaction of Benzaldehyde with 1-Bromo-3-methyl-2-butene. A Typical Procedure. To the chromium reagent, prepared from chromium(III) chloride (0.37 g, 2.3 mmol) and LAH (44 mg, 1.2 mmol) in THF (5 cm^3), were added benzaldehyde (92 mg, 0.86 mmol) and successively a THF (5 cm^3) solution of 1-bromo-3-methyl-2-butene (173 mg, 1.2 mmol) at room temperature. After 2 h the reaction mixture was treated with water (5 cm^3) and extracted thoroughly with ether. The ethereal solution was washed with brine, dried with sodium sulfate, and concentrated. Distillation of the residue at 105—110 °C (bath temp)/0.12 Torr gave 2,2-dimethyl-1-phenyl-3-buten-1-ol (**1**) (124 mg, 82% yield). In another experiment the yield estimated by GLC was 90%. IR 3425, 3095, 3075, 3035, 1638, 1605, 1490, 1020, 1000, 915, 730, and 702 cm^{-1}; ^1H NMR δ=0.94 (s, 3H), 0.99 (s, 3H), 1.5—1.8 (br s, OH), 4.34 (s, 1H), 4.8—6.2 (m, 3H, vinyl), and 7.26 (s, 5H); MS, *m/e* (rel intensity), 176 (M$^+$, trace), 107 (100), 82 (33), 79 (69), and 70 (64).

The reactions between various aldehydes and allylic bromides are summarized in Table 2. Physical properties of the new compounds follow.

3-Chloro-1-phenyl-3-buten-1-ol (3). Bp 88—93 °C (bath temp)/0.07 Torr; IR 3360, 3050, 3020, 1630, 1605, 1495, 1040, 883, 758, and 700 cm^{-1}; ^1H NMR δ=2.3 (br s, 1H, OH), 2.60 (two d, J=7.5 Hz, 2H), 4.91 (dd, J=7, 5 Hz, 1H), 5.10 (s, 1H), and 7.25 (s, 5H); MS *m/e* (rel intensity), 182 (M$^+$, 0.07), 107 (100), 79 (67), and 77 (33). Found: C, 65.53; H, 6.03%. Calcd for $C_{10}H_{11}ClO$: C, 65.76; H, 6.07%.

Phenyl(1-vinylcyclohexyl)methanol (4). Bp 160—162 °C (bath temp)/0.15 Torr; IR 3450, 3045, 1630, 1605, 1493, 1453, 1040, 1022, 918, 733, and 708 cm^{-1}; ^1H NMR δ=1.1—2.0 (m, 11H), 4.23 (s, 1H), 4.8—5.9 (m, 3H, vinyl), and 7.16 (s, 5H); MS *m/e* (rel intensity), 198 (M$^+-H_2O$, 0.7), 110 (98), 107 (100), 81 (86), and 67 (43). Found: C, 83.33; H, 9.59%. Calcd for $C_{15}H_{20}O$: C, 83.28; H, 9.32%.

6,6-Ethylenedioxy-3,3-dimethyl-1-hepten-4-ol (5). Bp 115—120 °C (bath temp)/4 Torr; IR 3510, 3070, 1634, 1368, 1120, 1094, 1036, and 904 cm^{-1}; ^1H NMR δ=1.00 (s, 6H), 1.28 (s, 3H), 1.57 (d, J=9 Hz, 1H), 1.67 (d, J=2 Hz, 1H), 2.95 (br s, 1H, OH), 3.43 (dd, J=9, 2 Hz, 1H), 3.92 (s, 4H), and 4.7—6.1 (m, 3H, vinyl); MS *m/e* (rel intensity), 185 (M$^+-CH_3$, 1.5), 167 (1.5), 97 (100), and 43 (59). Found: C, 65.94; H, 10.29%. Calcd for $C_{11}H_{20}O_3$: C, 65.97; H, 10.07%.

10-Hydroxy-12-tridecen-5-one (6). Bp 109—112 °C (bath temp)/0.06 Torr; IR 3425, 3080, 1705, 1640, 1128, 1000, and 916 cm^{-1}; ^1H NMR δ=0.8—1.9 (m, 14H), 2.0—2.6 (m, 6H), 3.3—3.8 (m, 1H), and 4.7—6.2 (m, 3H, vinyl); MS, *m/e* (rel intensity), 194 (M$^+-H_2O$, 2), 171 (M$^+-CH_2CH{=}CH_2$, 7), 153 (21), 135 (17), 85 (75), and 57 (100). Found: C, 73.46; H, 11.62%. Calcd for $C_{13}H_{24}O_2$: C, 73.54; H, 11.39%.

Methyl 6-Hydroxy-8-nonenoate (7). Bp 90—95 °C (bath temp)/0.04 Torr; IR 3450, 3080, 1728, 1632, 1435, 1200, 1092, 998, and 914 cm^{-1}; ^1H NMR δ=1.2—1.9 (m, 6H), 2.0—2.5 (m, 5H), 3.4—3.9 (m+s (δ=3.62), 4H), and 4.9—6.2 (m, 3H, vinyl); MS, *m/e* (rel intensity), 155 (1), 145 (M$^+-CH_2$-$CH{=}CH_2$, 12), 113 (100), 85 (24), and 67 (85). Found: C, 64.20; H, 9.91%. Calcd for $C_{10}H_{18}O_3$: C, 64.49; H, 9.74%.

*(4Z)-8-Hydroxy-*cis*-4,10-undecadienenitrile (8).* Bp 115—120 °C (bath temp)/0.06 Torr; IR 3430, 3070, 3005, 2265, 1633, 992, and 913 cm^{-1}; ^1H NMR δ=1.1—1.7 (m, 2H), 2.0—2.5 (m, 9H), 3.57 (quintet, J=6 Hz, 1H), 4.7—6.2 (m, 3H, vinyl); MS, *m/e* (rel intensity), 138 (M$^+-CH_2CH{=}CH_2$, 66), 120 (44), 110 (20), 94 (66), and 67 (100). Found: C, 73.53; H, 9.81; N, 7.88%. Calcd for $C_{11}H_{17}NO$: C, 73.70; H, 9.56; N, 7.81%.

Competitive Reaction of 2-Heptanone and 4-Heptanone. A mixture of 2-heptanone (86 mg, 0.75 mmol) and 4-heptanone (86 mg, 0.75 mmol) dissolved in THF (1.5 cm^3) was added to chromium(II) chloride (0.38 g, 3.1 mmol) suspended in THF (3 cm^3) at 0 °C. Then allyl bromide (186

mg, 1.5 mmol) dissolved in THF (3 ml) was added to the reaction mixture at room temperature in 6 min and the mixture was stirred for 3 h. Work-up and GLC analysis (PEG 20 M, 10%, on Chromosorb W, 1.5 m, 100 °C) revealed that the reaction had proceeded with 54% conversion to give 4-methyl-1-nonen-4-ol (R_t 30.0 min) and 4-propyl-1-hepten-4-ol (R_t 23.7 min) (84 : 16) in 49% yield (91% yield based on the consumed ketones). In a repeated experiment the ratio was 88 : 12.

Conversion of **5** *into Yomogi Alcohol.* A THF (5 cm³) solution of **5** (1.01 g, 5.0 mmol) was added to a THF (5 cm³) solution of PPA (105% H_3PO_4, 1.3 g) under a nitrogen atmosphere and the mixture was stirred for 1 h, then heated to reflux for 3.5 h. Work-up followed by preparative TLC (hexane–ether 3 : 1, R_f 0.74) gave (3*E*)-5,5-dimethyl-*trans*-3,6-heptadien-2-one (0.59 g, 84% yield), bp 123—127 °C (bath temp)/28 Torr. IR 1670, 1616, 1350, 1245, 974, and 908 cm⁻¹; ¹H NMR δ=1.18 (s, 6H), 2.14 (s, 3H), 4.7—6.1 (m (vinyl)+d (δ=5.87, J=16 Hz), totally 4H), and 6.60 (d, J=16 Hz, 1H); MS, *m/e* (rel intensity), 138 (M^+, 4), 123 ($M^+ - CH_3$, 26), 95 (70), 67 (35), and 43 (100). Found: C, 78.06; H, 10.36%. Calcd for $C_9H_{14}O$: C, 78.21; H, 10.21%.

To the ether (2 cm³) solution of the dienone (138 mg, 1.00 mmol) excess methylmagnesium iodide (generated from 5 mmol of each of magnesium and methyl iodide in ether (5 cm³)) and the reaction mixture was stirred at room temperature for 30 min. Work-up and distillation gave Yomogi alcohol (124 mg, 81% yield), bp 80 °C (bath temp)/1 Torr, having spectral properties consistent with the reported one.[15]

*Synthesis of Ips-dienol (***2***).* A THF (3 cm³) solution of 2-bromomethyl-1,3-butadiene (0.20 g, 1.35 mmol) was added to a mixture of chromium(II) chloride (0.26 g, 2.1 mmol) and 3-methyl-2-butenal (44 mg, 0.52 mmol) at room temperature and the whole was stirred for 3.6 h. Work-up followed by distillation at 72 °C (bath temp)/0.03 Torr gave the desired product (34 mg, 45% yield) having the correct spectra.[13]

threo-*2-Methyl-1-phenyl-3-buten-1-ol.* A THF (4 cm³) solution of *trans*-1-bromo-2-butene (0.34 g, 2.5 mmol) was added at room temperature over a period of 20 min to a mixture of benzaldehyde (140 mg, 1.31 mmol) and the chromium reagent A prepared by mixing chromium(III) chloride (0.81 g, 5.1 mmol) and LAH (96 mg, 2.5 mmol) in THF (5 cm³). The reaction mixture was stirred for 3.4 h at room temperature. Work-up and distillation at 110 °C (bath temp)/4 Torr gave the title alcohol (0.21 g, 96% yield) which proved uniform on TLC analysis (hexane–ether 3 : 1, R_f 0.35) and GLC (PEG 20 M, 5%, on Celtite 545, 1.5 m, 141 °C; or Apiezon L 5%, KOH 1%, on Chromosorb, 2 m, 140 °C).

Reaction of 2-Methylbutanal with 1-Bromo-2-butene. A THF (6 cm³) solution of 2-methylbutanal (182 mg, 2.1 mmol) and 1-bromo-2-butene (0.62 g, 4.6 mmol) was added to chromium(II) chloride (1.14 g, 9.3 mmol) suspended in THF (9 cm³) over a period of 10 min at room temperature, and the whole was stirred for 3 h. Work-up and column chromatography gave a mixture (0.27 g, 90% yield) of adducts (**11**, **12**, and **13**) with the ratio of 62 : 31 : 7 as revealed by GLC assay (PEG 20 M, 5%, on Celite 545, 1.5 m, 80 °C).

The mixture of the adduct (130 mg) in ethanol (6 cm³) was stirred under a hydrogen atmosphere in the presence of 10% palladium on charcoal for 31 h. Filtration and short column chromatography gave a stereoisomeric mixture of 3,5-dimethyl-4-heptanol. ¹³C NMR ($CDCl_3$, TMS an internal standard) spectra showed clearly two sets of chemical shifts (δ), (intensity): [11.26 (80), 11.86 (100), 12.44 (82), 15.43 (77), 24.99 (77), 27.19 (85), 36.79 (81), 37.74 (87), and 78.41 (80)] for the dihydro derivative of **11**; [11.65 (70), 16.14 (66), 23.52 (71), 37.29 (74), and 80.60 (35)] for the dihydro derivative of **12**. The minor product, the dihydro derivative of **13**, was characterized by the peaks at δ=13.90 (13), 26.46 (11), and 77.98 (7).[17a,25]

*4-Methyl-1-nonen-4-ol (***9***).* Bp 61—65 °C (bath temp)/13 Torr; ¹H NMR δ=0.9—1.6 (m, 12H), 1.13 (s, 3H, Me), 2.20 (d, J=8.1 Hz, 2H), and 5.0—6.1 (m, 3H, vinyl); IR 3390, 1642, 1155, 999, and 913 cm⁻¹. Found: C, 77.07; H, 13.06%. Calcd for $C_{10}H_{20}O$: C, 76.86; H, 12.90%.

*4-Propyl-1-hepten-4-ol (***10***).* Bp 56—59 °C (bath temp)/13 Torr; ¹H NMR δ=0.8—1.5 (m, 15H), 2.11 (d, J=7.2 Hz, 2H), 4.97 (dd, J=2.3, 15.3 Hz, 1H, CH=CH–H), 5.00 (dd, J=2.3, 9.0 Hz, 1H, CH=CH–H), and 5.5—6.0 (m, 1H, CH=CH_2); IR 3400, 1637, 1152, 989, and 919 cm⁻¹. Found: C, 76.68; H, 13.14%. Calcd for $C_{10}H_{20}O$: C, 76.86; H, 12.90%.

threo-*3-Methyl-1-nonen-4-ol.* Bp 88—91 °C (bath temp)/11 Torr; ¹H NMR δ=0.92 (t, J=7.5 Hz, 3H, terminal methyl), 1.04 (d, J=6.6 Hz, 3H, $CHCH_3$), 1.0—1.6 (m, 8H, methylenes), 1.80 (br s, 1H, OH), 2.0—2.4 (m, 1H, $CHCH_3$), 3.2—3.5 (m, 1H, CHOH), 5.01 (dd, J=2.7, 17.1 Hz, 1H, CH=CH–H), 5.18 (dd, J=2.7, 10.8 Hz, 1H, CH=CH–H), and 5.6—5.9 (m, 1H, CH=CH_2); IR 3380, 1638, 1260, 1081, 1001, and 911 cm⁻¹; MS, *m/e* (rel intensity), 141 ($M^+ - CH_3$, 2), 138 ($M^+ - H_2O$, 2), 101 (9), 83 (29), 56 (41), 55 (38), 44 (46), and 40 (100). Found: C, 76.74; H, 13.18%. Calcd for $C_{10}H_{20}O$: C, 76.86; H, 12.90%.

*1-Phenyl-2-vinyl-3-penten-1-ol (***14***).* ¹H NMR δ=1.37 (d, J=6 Hz, 0.78H), 1.62 (d, J=6 Hz, 2.22H), 1.88 (br s, 1H, OH), 2.8—3.5 (two multiplets, 1H), 4.3—4.6 (m, 1H), 4.9—6.0 (m, 5H, olefinic H), and 7.23 (s, 5H, Ph); IR 3450, 3090, 3040, 2980, 2930, 2890, 2865, 1640, 1608, 1500, 1458, 1038, 1024, 997, 968, 914, 760, 718, and 698 cm⁻¹; MS, *m/e* (rel intensity), 170 ($M^+ - H_2O$, 2), 107 (77), 91 (8), 82 (47), 79 (100), 77 (56), 67 (31), and 51 (25). *Cf.* Ref 24.

A Typical Procedure for the Reduction of 1,1-Dibromocyclopropanes. Synthesis of Phenylpropadiene: To the chromium reagent, prepared from chromium(III) chloride (0.82 g, 5.2 mmol) and LAH (99 mg, 2.6 mmol) in THF (5 cm³) and by replacing the solvent with DMF (5 cm³), a DMF (2 cm³) solution of 1,1-dibromo-2-phenylcyclopropane (0.29 g, 1.04 mmol) was added at room temperature and the mixture was stirred for 4 h. Work-up followed by distillation at 80—85 °C (bath temp)/20 Torr gave phenylpropadiene (75 mg, 62% yield): IR 1940, 850, 760, and 692 cm⁻¹; ¹H NMR δ=5.06 (d, J=7 Hz, 2H), 6.05 (t, J=7 Hz, 1H), and 7.15 (s, 5H).

References

1) E. Negishi, "Organometallics in Organic Synthesis," John Wiley and Sons, New York (1980), Vol. 1.

2) Preliminary reports: Y. Okude, S. Hirano, T. Hiyama, and H. Nozaki, *J. Am. Chem. Soc.*, **99**, 3179 (1977); Y. Okude, T. Hiyama, and H. Nozaki, *Tetrahedron Lett.*, **1977**, 3829; T. Hiyama, K. Kimura, and H. Nozaki, *ibid.*, **22**, 1037 (1981).

3) P. Girard, J. L. Namy, and H. B. Kagan, *J. Am. Chem. Soc.*, **102**, 2693 (1980).

4) G. Cahiez and J. F. Normant, *Tetrahedron Lett.*, **1977**, 3383; *Bull. Soc. Chim. Fr.*, **1977**, 570; G. Cahiez, D. Bernard, and J. F. Normant, *Synthesis*, **1977**, 130.

5) Y. Naruta, S. Ushida, and K. Maruyama, *Chem. Lett.*, **1979**, 919; T. Mukaiyama, T. Harada, and S. Shoda, *ibid.*, **1980**, 1507.

6) J. E. McMurry, M. G. Silvestri, M. P. Fleming, T. Hoz, and M. W. Grayston, *J. Org. Chem.*, **43**, 3249 (1978); J. E. McMurry, M. P. Fleming, K. L. Kees, and L. R. Krepsi, *ibid.*, **43**, 3255 (1978).

7) D. A. Evans and L. R. McGee, *Tetrahedron Lett.*, **21**,

3975 (1980); Y. Yamamoto and K. Maruyama, *ibid.*, **21**, 4607, (1980).

8) J. R. Hanson, *Synthesis*, **1974**, 1; Tse-Lok Ho, *ibid.*, **1979**, 1.

9) J. K. Kochi and P. E. Mocadlo, *J. Am. Chem. Soc.*, **88**, 4094 (1966); C. E. Castro and W. C. Kray, Jr., *ibid.*, **88**, 4447 (1966).

10) We have attempted to use *i*-Bu_2AlH, Et_3Al, metallic K, $NaH_2Al(OCH_2CH_2OMe)_2$, $NaBH_4$, BH_3SMe_2, but these reducing agents failed to reduce the chromium(III) ion effectively into the lower valent one.

11) A. R. Pray, *Inorg. Synth.*, **5**, 153 (1954).

12) P. Place, F. Delbecq, and J. Gore, *Tetrahedron Lett.*, **1978**, 3801; C. Verniere, B. Cazes, and J. Gore, *ibid.*, **22**, 103 (1981).

13) R. G. Riley, R. M. Silverstein, J. A. Katzenellenbogen, and R. S. Lenox, *J. Org. Chem.*, **39**, 1957 (1974).

14) M. Gaudemar, *Tetrahedron*, **32**, 1689 (1976).

15) W. Sucrow and W. Richter, *Chem. Ber.*, **103**, 3771 (1970) and references cited therein.

16) C. T. Buse and C. H. Heathcock, *Tetrahedron Lett.*, **1978**, 1685.

17) R. W. Hoffmann and H.-H. Zeiss, *Angew. Chem., Int. Ed. Engl.*, **18**, 306 (1978); *Angew. Chem.*, **92**, 218 (1980); H. Yatagai, Y. Yamamoto, and K. Maruyama, *J. Am. Chem. Soc.*, **102**, 4548 (1980); Y. Yamamoto, H. Yatagai, Y. Naruta, and K. Maruyama, *ibid.*, **102**, 7107 (1980); M. Yamaguchi and T. Mukaiyama, *Chem. Lett.*, **1980**, 993.

18) G. Courtois and L. Miginiac, *J. Organomet. Chem.*, **69**, 1 (1974).

19) Regioselectivity in the reaction of pentadienylmetals with electrophiles: D. Seyferth and J. Pornet, *J. Org. Chem.*, **45**, 1721 (1980); A. Hosomi, M. Saito, and H. Sakurai, *Tetrahedron Lett.*, **21**, 3783 (1980).

20) The *erythro* selective reaction of 2,2-dimethylpropanal may be understood by the anticipated severe interaction between *t*-butyl and methyl groups and accordingly by a preferred skew boat-like transition state II.

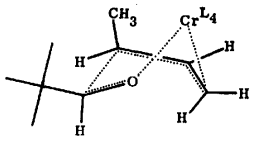

II

21) A. Segnitz, "Methoden zur Herstellung und Umwandlung von Organo-chrom-Verbindungen," in "Methoden der Organischen Chemie," ed by E. Müller (1975), XIII/7, p. 375.

22) K. Nishimura, H. Kuribayashi, A. Yamamoto, and S. Ikeda, *J. Organomet. Chem.*, **37**, 317 (1972); A. Yamamoto, Y. Kato, and T. Yamamoto, *ibid.*, **102**, 57 (1975); K. Maruyama, T. Ito, and Y. Yamamoto, *Chem. Lett.*, **1978**, 479.

23) J. Wellmann and E. Steckhan, *Synthesis*, **1978**, 901.

24) L. Miginiac-Groizeleau, P. Miginiac, and C. Prevost, *Bull. Soc. Chim. Fr.*, **1965**, 3560.

25) We thank Dr. R. W. Hoffmann for sending us the ^1H NMR data of **11**—**13** as well as the ^{13}C NMR data of each dihydro derivative.

 © 1982 The Chemical Society of Japan Bull. Chem. Soc. Jpn., 55, 569—574 (1982)

The Solvomercuration, Bromination, and Related Reactions of 1,5-Dimethyl-6-methylenetricyclo[3.2.1.0^{2,7}]oct-3-en-8-one and Its Related Compounds

Makoto NITTA,* Akihiko OMATA, and Hiroshi SUGIYAMA

Department of Chemistry, School of Science and Engineering, Waseda University, Shinjuku-ku, Tokyo 160

(Received July 20, 1981)

The solvomercuration-demercuration reactions of 1,5-dimethyl-6-methylenetricyclo[3.2.1.0^{2,7}]oct-3-en-8-one (**1**), its corresponding alcohol, and 5,8-dimethyl-9-methylenetricyclo[3.3.1.0^{2,8}]non-3-en-7-one (**2**) were investigated. In all cases, the solvent was stereospecifically incorporated on the exomethylene group, and the original tricyclic skeleton did not undergo rearrangement. Similarly, **1** and **2** underwent a stereospecific bromination on the exomethylene group by means of the reaction with pyridinium tribromide. These results suggest the stabilization of the formal cyclopropylcarbinyl cation intermediates by the adjacent acetoxymercury moiety or the bromine atom. On the other hand, the reaction of NBS–MeOH or NBS–H_2O with **1** afforded an addition product on the exomethylene group, and 1,4-addition originated from the cleavage of the cyclopropane ring, while with **2** the reaction afforded only an addition product on the exomethylene group. The difference in this reaction mode is discussed on the basis of the solvent effect and the ring strain of **1**.

The solvomercuration reaction of olefins has been widely studied and has been the subject of frequent reviews.[1-3] Mercurinium ions of Type (**A**) have been postulated as the intermediates in the electrophilic addition of mercury(II) acetate to olefins.[4-7] However, there is an oposing mechanistic interpretation that oxymercuration occurs to give an unsymmetrical open carbocation of Type (**B**).[8-10] The bromination of olefins seems also to be an atypical systems, for its cationic intermediates are not in all cases cyclic, but can also be opened carbocations.[11] Recently, Tidwell *et al.* concluded, in comparison with the rate of the acid-catalyzed hydration and addition reaction of arenesulfenyl chloride to various olefins, that the bromination of various olefins proceeds *via* bridged ion-like intermediates.[12] The high rate of the bromination of cyclopropylethylene is explained by a mechanism involving an open-ion-like rate-determining transition state. This change in mechanism is due to the great ability of the cyclopropyl group to stabilize an adjacent carbocation by resonance electron donation.

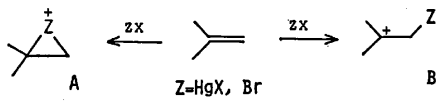

It has been elucidated that the tricyclo[3.2.1.0^{2,7}]-oct-3-en-6-yl cation (**C**) rearranges to bicyclo[3.2.1]-oct-3,6-dienyl cation (**D**) at a rate competing with solvent (MeOH) attack, as is shown by the generation of the latter cation from the *exo*-tricyclo[3.2.1.0^{2,4}]oct-6-en-3-anti diazonium ion.[13] Furthermore, the acid-catalyzed rearrangement of 1,5-dimethyl-6-methylenetricyclo[3.2.1.0^{2,7}]oct-3-en-8-one (**1**) has been investigated, and it has been elucidated that the tricyclic cation (**E**) rearranges to the bicyclic cation (**F**).[14] A consideration of the formal cation (**G**), which has a skeleton similar to those of the (**C**) and (**E**) cations, suggests that the solvomercuration or bromination reaction of compounds possessing a 6-methylenetricyclo[3.2.1.0^{2,7}]-oct-3-en-8-one or its related skeleton would seem to be of interest for several reasons. The formal cation (**G**) has an adjacent mercury moiety or bromine atom,

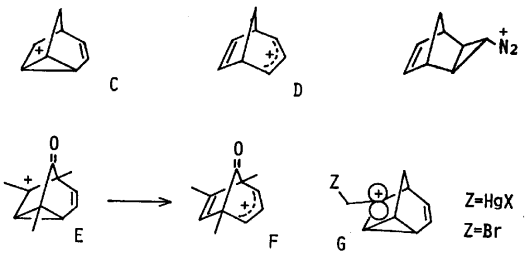

both of which can stabilize the cationic center by making mercurinium ions or bromonium ions similar to Type (**A**), and a cyclopropane ring which also can stabilize the cationic center by resonance electron donation in a bisected conformation.[15] Therefore, if the stabilizing effect of a cyclopropane to the cationic center by electron donation overcomes the formation of mercurinium ions[16] or bromonium ions, the rearrangement of (**G**) to the bicyclo[3.2.1]heptadienyl cation may compete with the solvent attack, as in the case of the behavior of the cation (**C**) or (**E**). From this point of view, the solvomercuration-demercuration, bromination, and related reactions of **1**[17] and 5,8-dimethyl-9-methylenetricyclo[3.3.1.0^{2,8}]non-3-en-7-one (**2**)[18] and their related compounds were investigated. The results will be presented in this paper.

Solvomercuration-demercuration Reaction

A solution of **1** in anhydrous methanol was treated with an equivalent amount of mercury(II) acetate. After the reaction mixture has been stirred for 30 min, it was treated with 3 mol dm^{-3} aqueous sodium hydroxide and then with sodium borohydride in 3 mol dm^{-3} aqueous sodium hydroxide, according to the reported procedure.[19] The usual workup afforded, in a 98% yield, *exo*-6-methoxy-1,5,6-trimethyltricyclo-[3.2.1.0^{2,7}]oct-3-en-8-one (**3**), the structure of which was identified by a comparison of the spectral data.[14] No *endo*-methoxy isomer was detected at all.

In order to examine the ring-size effect on the solvomercuration reaction, the reaction of **2** was carried out in a way similar to the case of **1**, and *exo*-9-methoxy-

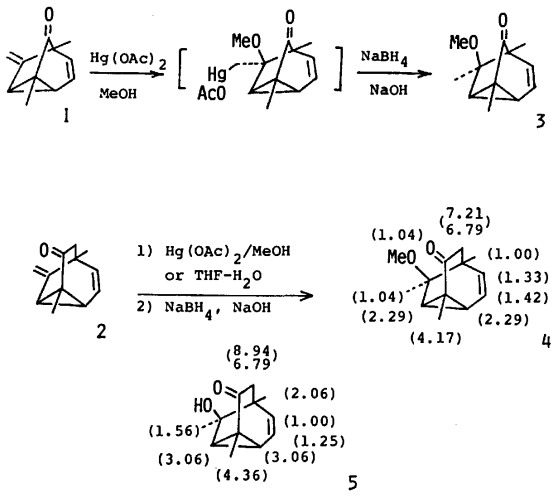

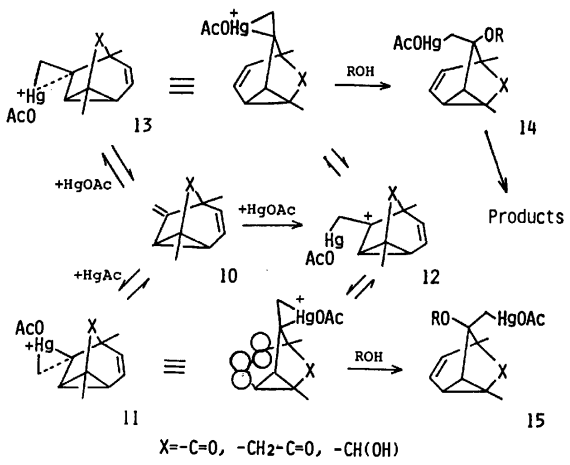

Scheme 1.

5,8,9-trimethyltricyclo[3.3.1.$0^{2,8}$]non-3-en-7-one (**4**) was thus obtained in a 93% yield. Similarly, the reaction of **2** with mercury(II) acetate in tetrahydrofuran (THF)–H_2O and a subsequent demercuration reaction afforded *exo*-9-hydroxy-5,8,9-trimethyltricyclo[3.3.1.$0^{2,8}$]non-3-en-7-one (**5**) in a 94% yield. The spectral data of **4** and **5** were consistent with the proposed structures (see Experimental). The stereochemistry of the methoxyl or the hydroxyl group of **4** or **5** was determined clearly by means of the pseudo-contact NMR spectra obtained by using $Eu(fod)_3$. The relative downfield shifts of δ's are given in parentheses in the structural formulae **4** and **5**.[21] The relatively small shifts of methoxyl and methyl at the 9-position of **4** suggest that the coordination of $Eu(fod)_3$ does not occur on methoxyl oxygen, but on the carbonyl oxygen, and that the methyl group on the 9-position is located anti to the carbonyl group. In the case of **5**, the coordination of $Eu(fod)_3$ seems to occur on the hydroxyl oxygen as well as the carbonyl oxygen. However, the relatively small shifts of the methyl group on the 9-position compared to that of the methyl group on the 8-position suggest that methyl group on the 9-position is *anti* to the carbonyl group.

Compounds **1** and **2** have an electron-withdrawing carbonyl function adjacent to the cyclopropane ring. This carbonyl group may possibly reduce the electron-donating character of the cyclopropane ring to the cationic center. Therefore, the solvomercuration-demercuration reaction of 1,5-dimethyl-6-methylenetricyclo[3.2.1.$0^{2,7}$]oct-3-en-8-*endo*-ol (**6**)[20] was investigated. When **6** was allowed to react with an equivalent amount of mercury(II) acetate in THF–H_2O (4/1) in a manner similar to that in the case of **1** or **2**, 1,5,6-trimethyltricyclo[3.2.1.$0^{2,7}$]oct-3-en-6-*exo*-,8-*endo*-diol (**7**) was obtained in a 95% yield. The spectral data of **7** are in good agreement with those of the known compounds, obtained by the sulfuric acid-catalyzed hydration of **6**.[22]

In all of the presented reactions, the solvent was

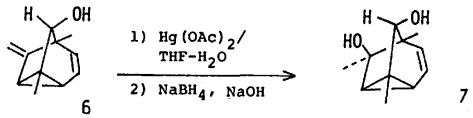

stereospecifically incorporated on the exomethylene group, and the original tricyclic skeleton did not undergo rearrangement. The ring size and the absence of the electron-withdrawing carbonyl group adjacent to the cyclopropane ring did not affect the reaction pathway. These experimental results suggest the formation of mercurinium ions such as **13**, as is shown in Scheme 1. The cationic center of a tricyclic skeleton such as that of **12** is stabilized by the formation of **13**. This fact seems to indicate that the stabilization of the cationic center of the cyclopropylcarbinyl cation by the mercury moiety adjacent to the cationic center is preferable over the resonance-electron donation of the cyclopropane ring in the present case. The initial addition of $^{+}$Hg(OAc)[23] to the exocyclic double bond seems to favor the formation of **11** over the formation of **13** because of the steric hindrance (*vide infra*). In the supposition of a *trans* addition mechanism, however, the *endo*-attack of the solvent molecule on **11** seems to be unfavorable because of the electronic repulsion of the π-electron lobe of the endocyclic double bond with the solvent molecule, as is shown in the structural formula, **11**.[22] Therefore, the mercuration-demercuration (equilibration) step or the possible short-lived intermediate of the opened cation, **12**, should participate in the present reactions, thereby causing the formation of **13**. In the mercurinium cation **13**, some stabilization by the coordination of the endocyclic double bond to the mercury atom would be expected,[24] the *trans* additions of the solvent molecule from the less hindered site then afford the products.[25]

Bromination and Related Reaction

It has been reported that the bromination of **1** with an equivalent amount of bromine in dichloromethane at −78 °C gives an unstable dibromide, **16**, which then affords tricyclic tetrabromide, **17**, by further bromination.[26] In relation to this reaction and the solvomercuration-demercuration reaction described above, the addition reactions of pyridinium tribromide (PyH-Br_3), *N*-bromosuccinimide (NBS)–H_2O, and NBS–MeOH with **1** and **2** were also investigated.

The reaction of **1** with an equivalent amount of $PyHBr_3$ in dichloromethane–carbon tetrachloride (1/1)

at 0 °C for 2 h, and the subsequent column chromatography on alumina afforded a dibromide, **18** (mp 92.9—93.5 °C) in a 77% yield. Similarly, the reaction of $PyHBr_3$ with a one-carbon-ring enlarged ketone, **2**, afforded **19** in a 55% yield. The NMR spectrum of the crude product of the reaction did not exhibit the presence of any other addition product. The dibromide **19** is an unstable oil and turns black even in the refrigerator. Therefore, a correct elemental analysis has not been obtained. However, the mass-spectral data of **18** and **19** clearly indicate that **18** and **19** are dibromides of **1** and **2** respectively. The spectral data of **18** and **19** clearly indicate that these bromides have skeletons similar to those of their starting ketones, **1** and **2** respectively, and that the bromination proceeds on the exomethylene group. The stereochemistry of the bromomethyl group of **18** and **19** was deduced from the pseudo-contact NMR spectra obtained by using $Eu(fod)_3$.[21] These results are completely different from that of **1** and molecular bromine, but are similar to the solvomercuration- demercuration reaction of **1** and **2** described above.

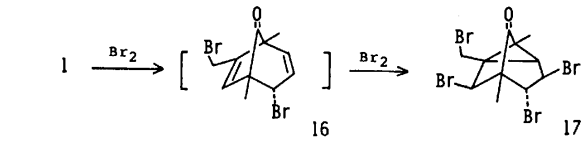

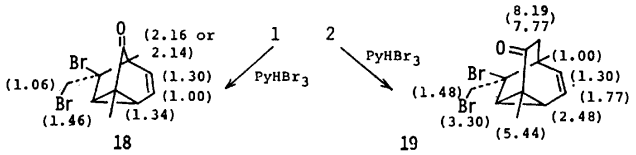

On the other hand, when **1** was allowed to react with NBS in THF–H_2O (4/1) at 25 °C for 30 min, a mixture of two products was obtained. This mixture was separated by TLC on silica gel to afford **20** and **21** in 34% and 17% yields respectively. The partial decomposition of **20** and **21** on the TLC plates causes the low yields of the products. The mass spectral data and the other spectral data indicates that **21** has a tricyclic skeleton and a bromine atom and that a hydroxyl group was incorporated on the exomethylene group. The stereochemistry of the hydroxyl group of **21** was assigned on the basis of the pseudo-contact NMR spectra.[21] Compound **20** is an unstable oil, and so a correct elemental analysis has not been made. However, satisfactory mass-spectral data were obtained. The NMR spectrum of **20** exhibited three protons of vinyl groups at δ 5.72 (dxd, J=10.2, 3.0 Hz), δ 6.26 (dxd, J=10.2, 1.8 Hz), δ 6.14 (s), in addition to two methyl groups at δ 1.25, δ 1.35, an allylic hydrogen at δ 4.07—4.21. The proton of the hydroxyl group has not been assigned distinctly. These NMR data are in accord with the proposed structure of **20**. Another structural possibility for **20** is **23**, however, **23** was discarded on the basis of the following chemical transformation. When **20** was treated with an aqueous sodium hydrogencarbonate solution in THF, **22** was obtained in a 90%

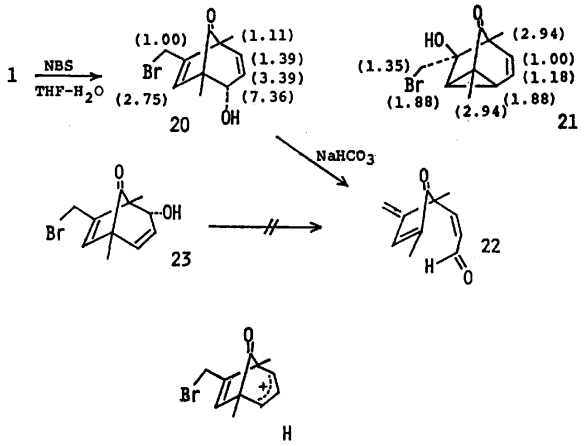

yield. The formation of **22** was considered to be the base induced Grob-type fragmentation of **20**.[7] Therefore, the structure of **20** was determined. The formation of **20** also indicates the absence of a bicyclic intermediate such as (H), from which both of **20** and **23** could be expected to be derived.

The pseudo-contact NMR spectra of **20** were obtained by using $Eu(fod)_3$.[21] The large value (7.36) of the allylic hydrogen indicates that the coordination of $Eu(fod)_3$ occurs on hydroxyl oxygen. The stereochemistry of the hydroxyl group is not elucidates here however, it must be *endo*, judging from the following experimental results.

The reaction of **1** with NBS in anhydrous methanol afforded two products, **24** and **25**, in a ratio of 9/5 and in a 90% yield. This mixture was separated by TLC on silica gel. The two compounds, **24** and **25** gradually decomposed and turns black, therefore, satisfactory elemental analyses have not been obtained. However, satisfactory mass-spectral data were obtained. The other spectral data were consistent with the proposed

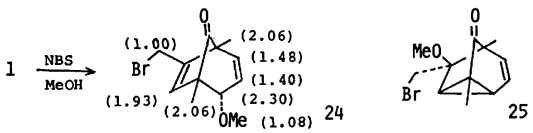

structures, **24** and **25**. The pseudo-contact NMR spectra of **24** was obtained by using $Eu(fod)_3$.[21] The small value of 1.08 for the methoxyl group suggest that coordination of $Eu(fod)_3$ occurs not on the methoxyl oxygen, but on the carbonyl oxygen. The large value of 2.30 for the allylic hydrogen suggests that the methoxyl group of **24** is located in the *endo* position. Therefore, the stereochemistry of the hydroxyl group of **20** must also be *endo* in this analogy. The orientation of the methoxyl group of **25** has not been determined directly because of the instability of **25**. However, it is probably *exo*, by analogy with the hydroxyl group of **21**.

In these reactions induced by NBS, 1,2-addition on the exomethylene group and 1,4-addition accompanying cyclopropane-ring opening took place with a stereospecific solvent incorporation. The 1,4-addition in the present case is very similar to the case of **1** with molecular bromine.[26]

On the other hand, the reaction of **2** with NBS–H_2O

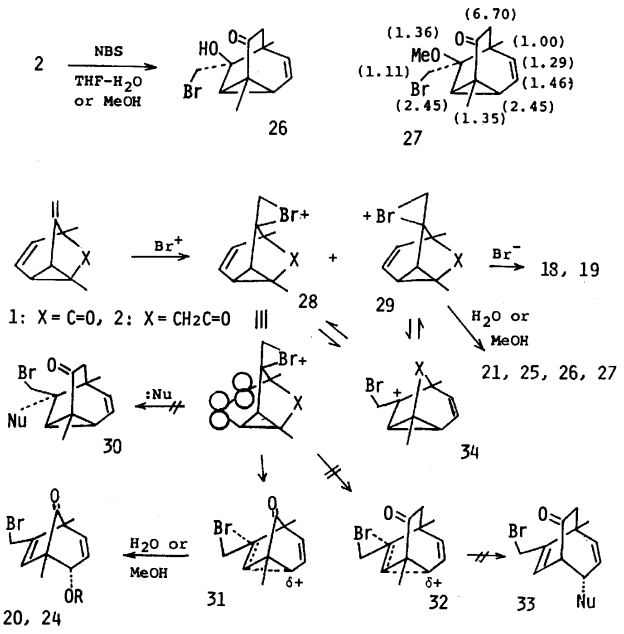

Scheme 2.

or NBS–MeOH in a similar manner to that in the case of **1** afforded only a 1,2-addition product, **26** (mp 115—117 °C) or **27**, in a 47 or 83% yield respectively, after separation by TLC on silica gel. The structures of **26** and **27** were deduced by a comparison of the spectral data (see Experimental) with those of the related compounds which had been obtained by the solvomercuration-demercuration reaction described in this paper. The stereochemistry of the hydroxyl group or the methoxyl group was assigned on the basis of the pseudo-contact NMR spectra of **27**.[21]

The plausible reaction sequences are summarized in Scheme 2. It has been indicated that the tricyclo-[3.2.1.$0^{2,7}$]oct-3-en-6-yl cation (**C**) rearranges to the bicyclo[3.2.1]octa-3,6-dienyl cation (**D**) at a rate competing with the solvent (MeOH) attack.[13] Furthermore, in the acid-catalyzed reaction of **1**, it was indicated that the cation (**E**) was rearranged to bicyclic cation (**F**).[14] In the case of the reaction of **1**, the cyclopropane-ring opening took place to afford **20**, but not **23**. Therefore, the present experimental results seem to suggest that an initial attack of $^{+}$Br on the *exo*-methylene group affords a bromonium ion, such as **28** or **29**. From the product composition of **20**/**21** or **24**/**25**, the formation of **28** seems more likely than that of **29** because of the steric effect. The *exo*-attack of the nucleophile on **29** (X=–C=O) should afford **18** and **19** or **21**, **25**, **26**, and **27**. On the other hand, the attack of the nucleophile on a bromonium ion such as **28** to afford **30** must be hindered by the π-electron lobe of the endocyclic double bond presented in the structural formula **28**. In the case of **1**, however, a transition state such as **31** may be stabilized in a polar media, such as methanol or THF–H_2O.[28] The nucleophile may then be incorporated in the cyclopropane ring from the *endo* site to afford **20** and **24**. On the other hand, the one-carbon ring-enlarged **32** should be less strained than **31**, therefore, **33** should not be obtained. This fact seems to suggest that an equilibrium between such substances as **28** and **29** may be made possible by bromination-debromination *via* **1** and **2** or by possible short-lived, opened cation, **34**. The difference between the reactions of **1** with molecular bromine and with $PyHBr_3$ is not clear at the present stage.

Consequently, the present results suggest that bromine atoms adjacent to cyclopropylcarbinyl cation centers stabilize these cationic centers, as in the case of the solvomercuration reaction described above, and that the nucleophilic attacks on them are probably affected by the stereoelectronic factor existing in the molecular framework.

Experimental

The IR spectra were recorded with a Shimadzu IR-400 spectrometer. The mass spectra were obtained with a Hitachi RMU-60 mass spectrometer. The NMR spectra were recorded on a JEOL PS-100 high resolution spectrometer. The abbreviations "s, d, dxd, t, m, and br" in the NMR spectra denote "singlet, doublet, doublets of doublet, triplet, multiplet, and broad" respectively. All of the melting points are uncorrected.

Methoxymercuration-demercuration of ***1***. To a well stirred solution of **1** (320 mg, 2 mmol) in 2 cm^3 of anhydrous methanol, was added 689 mg (2 mmol) of mercury(II) acetate. After the reaction mixture had then been stirred for 30 min, 2 cm^3 of 3 mol dm^{-3} sodium hydroxide solution was added, followed by 34 mg (2 mmol) of sodium borohydride in 2 cm^3 of 3 mol dm^{-3} aqueous sodium hydroxide. To this mixture, was added 10 cm^3 of brine and 10 cm^3 of ether. It was then filtered. The filtrate was extracted with ether, and the ether extract was dried over sodium sulfate. After the removal of the solvent *in vacuo*, 376 mg (98%) of **3** was obtained: bp 107 °C/582.8 Pa.

Methoxymercuration-demercuration of ***2***. The reaction was carried out as has been described above using 174 mg (1 mmol) of **2**, 319 mg (1 mmol) of mercury(II) acetate, and 19 mg (0.5 mmol) of sodium borohydride. The product, **4**, was obtained in a 93% yield (191 mg): IR (CCl_4), 3027—2848, 1681, 1119, 1058 cm^{-1}; NMR (CCl_4), δ 0.98 (3H, s), 1.13 (3H, s), 1.19 (3H, s), 1.68 (1H, d, J=20.7 Hz), 1.85 (2H, m), 2.58 (1H, d, J=20.7 Hz), 3.26 (3H, s), 5.43 (1H, dxd, J=9.6, 1.5 Hz), 5.76 (1H, dxd, J=9.6, 4.8 Hz).

Oxime of ***4***. A solution of **4** (35 mg, 0.17 mmol), hydroxylamine hydrochloride (24 mg, 0.3 mmol), and sodium acetate (55 mg, 0.67 mmol) in 1 cm^3 of ethanol was refluxed overnight. The reaction mixture was poured into 5 cm^3 of water and then extracted with ether. The combined organic portion was dried over sodium sulfate, filtered, and evaporated *in vacuo*. The residue was crystallized from ethanol to give 24 mg (72%) of an oxime, **8**: mp 134—135 °C; IR (CCl_4), 3516—3064, 2947, 1688, 1114, 947 cm^{-1}; NMR ($CDCl_3$), δ 1.00 (3H, s), 1.12 (3H, s), 1.30 (3H, s), 1.60—1.82 (1H, m), 1.70 (1H, d, J=6.4 Hz), 2.41 (1H, d, J=18.0 Hz), 2.56 (1H, d, J=18.0 Hz), 3.32 (3H, s), 5.42 (1H, dxd, J=9.2, 1.0 Hz), 5.79 (1H, dxd, J=9.2, 3.2 Hz), 9.36 (1H, br s); MS, *m/e* (rel intensity), 221 (M^+, 12), 115 (100). Found: C, 70.69; H, 8.69; N, 6.25%. Calcd for $C_{13}H_{19}O_2N$: C, 70.56; H, 8.65, N, 6.33%.

Hydroxymercuration-demercuration of ***2***. The reaction was carried out as has been described above using 174 mg (1 mmol) of **2**, 319 mg (1 mmol) of mercury(II) acetate, and 19 mg (0.5 mmol) of sodium borohydride. The product, **5**, was obtained in 94% (194 mg) yield: IR (CCl_4), 3450, 1678, 1098, 1045

cm^{-1}; NMR ($CDCl_3$), δ 1.03 (3H, s), 1.25 (6H, s), 1.72 (1H, d, J=8.0 Hz), 1.75—2.00 (1H, m), 2.02 (1H, d, J=18.7 Hz), 2.60 (1H, d, J=18.7 Hz), 3.10 (1H, br s), 5.47 (1H, dxd, J=9.5, 2.0 Hz), 5.75 (1H, dxd, J=9.5, 6.0 Hz). An oxime of **5** was prepared in a manner similar to that used in the case of **4**. The oxime, **9**, exhibited the following physical data: mp 213—215 °C; MS, *m/e* (rel intensity), 207 (M^+, 26), 101 (100). Found: C, 69.95; H, 8.38; N, 6.81%. Calcd for $C_{12}H_{17}O_2N$: C, 69.54; H, 8.27; N, 6.76%.

Hydroxymercuration-demercuration of ***6***. To a stirred solution of **1** (162 mg, 1 mmol) in 5 cm^3 of THF–H_2O (4/1), was added 345 mg (1 mmol) of mercury(II) acetate. After the reaction mixture had then been stirred for 30 min, 2 cm^3 of 3 mol dm^{-3} aqueous sodium hydroxide was added, followed by 17 mg (0.5 mmol) of sodium borohydride in 1 cm^3 of 3 mol dm^{-3} sodium hydroxide. To this reaction mixture, was subsequently added 10 cm^3 of brine and 10 cm^3 of ether. It was then filtered. The filtrate was extracted with ether, and the extract was dried over sodium sulfate. After the removal of the solvent *in vacuo*, 160 mg (94%) of **7** was obtained.

Reaction of ***1*** *with Pyridinium Tribromide.* To a stirred solution of pyridinium tribromide ($PyHBr_3$) (320 mg, 1 mmol) in carbon tetrachloride (3 cm^3), was added **1** (160 mg, 1 mmol) in dichloromethane (3 cm^3) at 0 °C. After this reaction mixture had then been stirred for 2 h, the precipitated pyridinium bromide was filtered off. The filtrate was concentrated under reduced pressure, and the resulting residue was chromatographed on alumina (10 g), using benzene–hexane (1/1) as the eluent, to give 246 mg (77%) of **18**: mp 92.5—93.5 °C (from CCl_4); IR (CCl_4), 1735 cm^{-1}; NMR (CCl_4), δ 1.25 (3H, s), 1.30 (3H, s), 2.10 (1H, m), 2.52 (1H, d, J=7.0 Hz), 3.57 (1H, d, J=11.0 Hz), 3.73 (1H, d, J=11.0 Hz), 5.27 (1H, dxd, J=8.0, 2.0 Hz), 6.06 (1H, dxd, J=8.0, 5.0 Hz); MS, *m/e* (rel intensity), 322 (M^+, 2), 320 (M^+, 2), 119 (100), 117 (95). Found: C, 41.14; H, 3.58%. Calcd for $C_{11}H_{12}OBr_2$: C, 41.29; H, 3.78%.

Reaction of ***2*** *with Pyridinium Tribromide.* The reaction was carried out as has been described above using 320 mg (1 mmol) of $PyHBr_3$ and 174 mg (1 mmol) of **2**. After the reaction mixture had been stirred for 2.5 h, it was worked up as described above to give 183 mg (55%) of **19**: oil, IR (film), 1690 cm^{-1}; NMR (CCl_4), δ 1.24 (3H, s), 1.27 (3H, s), 1.90—2.10 (1H, m), 2.12 (1H, d, J=18.0 Hz), 2.58 (1H, d, J=8.0 Hz), 2.74 (1H, d, J=18.0 Hz), 5.65 (1H, dxd, J=9.0, 2.0 Hz), 5.93 (1H, dxd, J=9.0, 5.0 Hz); MS, *m/e* (rel intensity), 336 (M^+, 3), 334 (M^+, 8), 332 (M^+, 4), 199 (97), 197 (100). Found: C, 44.35; H, 4.23%. Calcd for $C_{12}H_{14}OBr_2$: C, 43.15; H, 4.22%.

Reaction of ***1*** *with NBS in THF–H_2O.* To a stirred solution of **1** (160 mg, 1 mmol) in 2.5 cm^3 of THF–H_2O (4/1). was added NBS (178 mg, 1 mmol). After the reaction mixture has been stirred for 30 min, it was extracted with ether. The ether extract was dried over sodium sulfate and evaporated under reduced pressure to give 205 mg (80%) of a mixture of **20** and **21** in a ratio of 9/5, as determined by means of the NMR spectrum. This mixture was separated by TLC on silica gel, using benzene–dichloromethane (1/1) as the eluent. The first band from the TLC plates afforded 44 mg (17%) of **21**: mp 120—121 °C (from benzene); IR ($CHCl_3$), 3573, 1739 cm^{-1}; NMR ($CDCl_3$), δ 1.17 (3H, s), 1.34 (3H, s), 2.08—2.25 (2H, m), 2.25—2.60 (1H, br s), 3.61 (1H, d, J=10.8 Hz), 3.81 (1H, d, J=10.8 Hz), 5.50 (1H, dxd, J=7.8, 3.0 Hz), 6.21 (1H, dxd, J=7.8, 4.5 Hz); MS, *m/e* (rel intensity), 258 (M^+, 5), 256 (M^+, 2), 177 (100). Found: C, 51.21; H, 4.97%. Calcd for $C_{11}H_{13}O_2Br$: C, 51.38; H, 5.10%.

The second band from the TLC plates gave 88 mg (34%) of **20**: oil; NMR (CCl_4), δ 1.25 (3H, s), 1.35 (3H, s), 3.02—3.35 (1H, br s), 4.07—4.21 (2H, br s), 5.72 (1H, dxd, J=10.2, 3.0 Hz), 6.14 (1H, s), 6.26 (1H, dxd, J=10.2, 1.8 Hz).

Reaction of ***20*** *with Sodium Hydrogencarbonate.* A solution of **20** (129 mg, 0.5 mmol) in 3 cm^3 of methanol and 3 cm^3 of saturated aqueous sodium hydrogencarbonate was stirred for 5 h. The reaction mixture was then extracted with ether, and the combined ether extract was dried over sodium sulfate. After the removal of the solvent, 158 mg (90%) of **22** was obtained as an oil; IR (film), 1710, 1679 cm^{-1}; NMR (CCl_4), δ 1.47 (3H, s), 1.92 (3H, br s), 5.13 (2H, s), 5.73 (1H, dxd, J=12.0, 8.0 Hz), 6.32 (1H, d, J=12.0 Hz), 7.40 (1H, br s), 9.66 (1H, d, J=8.0 Hz); MS, *m/e* (rel intensity), 176 (M^+, 100). Found: C, 74.58; H, 6.81%. Calcd for $C_{11}H_{12}O_2$: C, 74.97; H, 6.86%.

Reaction of ***1*** *with NBS in Methanol.* To a stirred solution of **1** (160 mg, 1 mmol) in 4 cm^3 of methanol, was added 214 mg (1.2 mmol) of NBS. After this mixture had been stirred for 2 h at the ambient temperature, it was extracted with ether. The ether extract was dried over sodium sulfate, the subsequent evaporation of the ether afforded 244 mg (90%) of a mixture of **24** and **25** in a ratio of 9/5, as determined by the study of the NMR spectrum. This mixture was separated by TLC on silica gel, using benzene–dichloromethane (1/1) as the eluent. The first band from the TLC plates gave **24**: IR (CCl_4), 1765 cm^{-1}, NMR (CCl_4), δ 1.22 (3H, s), 1.29 (3H, s), 3.50 (3H, s), 3.84 (1H, m), 4.22 (2H, br s), 6.17 (1H, s), 5.92 (1H, dxd, J=10.8, 2.7 Hz), 6.37 (1H, dxd, J=10.8, 2.7 Hz); MS, *m/e* (rel intensity), 272 (M^+, 1), 270 (M^+, 1), 191 (100), 159 (99). Found: C, 52.14; H, 5.71%. Calcd for $C_{12}H_{15}O_2Br$: C, 53.16; H, 5.58%.

The second band from the TLC plates contained **25** and decomposed material. This portion could not be purified because of its instability: NMR (CCl_4), δ 1.10 (3H, s), 1.19 (3H, s), 2.03—2.23 (2H, m), 3.45 (1H, d, J=10.5 Hz), 3.68 (1H, d, J=10.5 Hz), 5.54 (1H, dxd, J=8.4, 2.7 Hz), 6.18 (1H, dxd, J=8.4, 4.5 Hz).

Reaction of ***2*** *with NBS in THF–H_2O.* To a solution of **2** (174 mg, 1 mmol) in 2.5 cm^3 of THF–H_2O (4/1), was added NBS (214 mg, 1.2 mmol). After the mixture had been stirred for 1 h, it was extracted with ether. The ether extract was dried over sodium sulfate and evaporated under reduced pressure to give 190 mg, (70%) of a solid, which was then recrystallized from CCl_4 to give colorless crystals of **26**: mp 115—117 °C; IR (CCl_4), 3612—3210, 1693 cm^{-1}; NMR (CCl_4), δ 1.14 (3H, s), 1.31 (3H, s), 1.99 (1H, d, J=18.6 Hz), 1.79—1.99 (1H, m), 2.19 (1H, d, J=7.5 Hz), 2.80 (1H, d, J=18.6 Hz), 2.63—3.12 (1H, br s), 3.60 (1H, d, J=9.9 Hz), 3.83 (1H, d, J=9.9 Hz), 5.69 (1H, dxd, J=9.6, 1.5 Hz), 6.12 (1H, dxd, J=9.6, 6.0 Hz); MS, *m/e* (rel intensity), 272 (M^+, 17), 270 (M^+, 18), 149 (100), 105 (98). Found: C, 53.65; H, 5.61%. Calcd for $C_{12}H_{15}O_2Br$: C, 53.16; H, 5.58%.

Reaction of ***2*** *with NBS–Methanol.* To a stirred solution of **2** (174 mg, 1 mmol) in 4 cm^3 of methanol, was added 214 mg (1.2 mmol) of NBS. After this mixture had been stirred for 1 h at the ambient temperature, it was extracted with ether. The ether extract was dried over sodium sulfate and the subsequent evaporation of the ether afforded 240 mg (83%) of **27**: oil; IR (CCl_4), 1688 cm^{-1}; NMR (CCl_4), δ 1.10 (3H, s), 1.36 (3H, s), 1.92 (1H, d, J=18.6 Hz), 2.67 (1H, d, J=18.6 Hz), 2.42 (1H, d, J=8.4 Hz), 1.91—2.14 (1H, m), 3.60 (1H, d, J=10.5 Hz), 3.72 (3H, s), 3.86 (1H, d, J=10.5 Hz), 5.79 (1H, dxd, J=9.4, 1.5 Hz), 6.25 (1H, dxd, J=9.3, 6.6 Hz); MS, *m/e* (rel intensity), 286 (M^+, 4), 284 (M^+, 4), 205 (100), 177 (99). Found: C, 51.02; H, 5.64%. Calcd for $C_{13}H_{17}O_2Br$: C, 54.75; H, 6.01%.

References

1) W. Kitching, *Organomet. Chem. Rev.*, **3**, 61 (1968); D. Sayferth, *J. Organomet. Chem.*, **41**, 155 (1972); **75**, 13 (1974); **98**, 133 (1975).
2) D. Sayferth, *J. Organomet. Chem.*, **143**, 153 (1977).
3) R. C. Larock, *Angew. Chem., Int. Ed. Engl.*, **17**, 27 (1978).
4) M. C. Cabaleiro, A. D. Araya, and M. D. Johnson, *J. Chem. Soc., Perkin Trans. 2*, **1973**, 1207; D. Dodd and M. D. Johnson, *J. Chem. Soc., B*, **1971**, 662.
5) R. D. Bach and R. F. Richter, *Tetrahedron Lett.*, **1973**, 4099; *J. Org. Chem.*, **38**, 3442 (1976).
6) S. J. Christol, J. S. Perry, Jr., and R. S. Beckley, *J. Org. Chem.*, **41**, 1912 (1976).
7) H. C. Brown and J. H. Kawakami, *J. Am. Chem. Soc.*, **95**, 8665 (1973).
8) T. G. Taylor and A. W. Baker, *J. Am. Chem. Soc.*, **85**, 2746 (1963).
9) F. T. Bond, *J. Am. Chem. Soc.*, **90**, 5326 (1968).
10) J. E. Galle and A. Hassner, *J. Am. Chem. Soc.*, **94**, 3930 (1972).
11) F. Freeman, *Chem. Rev.*, **75**, 441 (1975); G. H. Schmid and D. G. Gratt, "Doublebonded Functional Groups," ed by A. S. Patai, Wiley, New York, N. Y. (1977), p. 725.
12) G. H. Schmid and T. T. Tidwell, *J. Org. Chem.*, **43**, 460 (1978).
13) W. Kirms and T. Olbricht, *Chem. Ber.*, **108**, 2616 (1975).
14) J. P-Katalinic, J. Zsindely, and H. Schmid, *Helv. Chim. Acta*, **57**, 223 (1974).
15) V. Bass, R. Gleiter, and P. v. R. Schleyer, *J. Am. Chem. Soc.*, **93**, 3927 (1971); B. Anderson, O. Shallner, and A. de Meijer, *ibid.*, **97**, 3521 (1975).
16) I. C. Ambidge, S. K. Dwight, C. M. Rynard, and T. T. Tidwell, *Can. J. Chem.*, **55**, 3886 (1977).
17) J. Zsindely and H. Schmid, *Helv. Chim. Acta*, **51**, 1510 (1968).
18) M. Nitta, A. Omata, and H. Sugiyama, *Bull. Sci. Eng. Res. Lab. Waseda Univ.*, **94**, 55 (1981).
19) H. C. Brown and P. J. Geoghen, Jr., *J. Am. Chem. Soc.*, **89**, 1552 (1967); *J. Org. Chem.*, **35**, 1844 (1970).
20) Ref. 14; Ref. 22; M. Nitta, H. Sugiyama, and Y. Sekine, *Chem. Lett.*, **1977**, 55.
21) The numerical values presented in parentheses in the structural formulae in this paper are relative downfield shifts of δ's obtained by using $Eu(fod)_3$.
22) G. M-Müller, P. Gilgem, J. Zsindely, and H. Schmid, *Helv. Chim. Acta*, **60**, 1758 (1977).
23) H. C. Brown and P. J. Geoghegen, Jr., *J. Org. Chem.*, **37**, 1937 (1972).
24) N. Takaishi, Y. Fujikura, and Y. Inamoto, *J. Org. Chem.*, **40**, 3767 (1975).
25) The hydroxymercuration-demercuration of **1** afforded a novel 2,4-cyclohexadienone derivative: M. Nitta, A. Omata, and H. Sugiyama, *Chem. Lett.*, **1980**, 1615.
26) J. P-Katalinic, J. Zsindely, and H. Schmid, *Helv. Chim. Acta*, **58**, 2517 (1975).
27) P. G. Gassmann and J. M. Hornback, *J. Am. Chem. Soc.*, **91**, 5817 (1969); M. A. Battiste and J. Mackierman, *Tetrahedron Lett.*, **1972**, 4095.
28) S. P. MacMnus and D. W. Ware, *Tetrahedron Lett.*, **1974**, 4271; M. F. Russe and J. E. Dubios, *J. Org. Chem.*, **39**, 2441 (1974).

 © 1982 The Chemical Society of Japan Bull. Chem. Soc. Jpn., 55, 575—580 (1982)

Computation of Amino Acid Sequences of Polypeptides from Masses of Their Constituent Peptide Fragments and Amino Acid Residues Released in Edman-degradation[1]

Toyoko KITAGISHI, Yeong-Man HONG, Toshifumi TAKAO, Saburo AIMOTO, and Yasutsugu SHIMONISHI*

Institute for Protein Research, Osaka University, Suita, Osaka 565

(Received July 31, 1981)

A computer program ("PROSEQ2") was designed for determining the amino acid sequence of polypeptides from molecular weights and *N*-terminal amino acid residues of two or more sets of peptide mixtures obtained from polypeptides by two or more specific cleavage methods, together with 3-phenyl-2-thiohydantoin derivatives of amino acids released from two or more sets of peptide mixtures by Edman-degradation. Computation of sequences of several polypeptides using this program is described.

Gas chromatography/mass spectrometry is in use for sequencing a peptide mixture obtained from a polypeptide or protein by partial hydrolysis followed by conversion into volatile derivatives. Numerous experimental data thus obtained were handled with computer programs[2,3] capable of deducing the sequence of the original polypeptide or protein.

Recently[4-6] we reported a new method for sequencing a peptide mixture by combination of Edman-degradation and field-desorption mass spectrometry. This method does not involve any extensive chemical processing to convert peptides into volatile derivatives. The principle of this method is to measure mass values of individual "underivatized" peptides in a mixture and their degraded peptide fragments by field-desorption mass spectrometry. *N*-Terminal amino acid residues of individual peptides in a mixture can be determined by calculation of possible mass differences before and after degradation. Amino acid sequences of individual peptides in a mixture can be determined by repeating this operation. If two or more sets of peptide mixtures are to be produced from a polypeptide or protein by two or more specific cleavage methods, the amino acid sequence of the polypeptide or protein can be determined, by use of the computer program "PROSEQ1,"[7] from the molecular weights and *N*-terminal partial amino acid sequences which have been obtained by the above procedure for the peptides present in the resulting peptide mixtures. This method does not necessarily require determination of complete sequences or major portions of sequences for individual peptides.

After attempting sequence determinations on various polypeptides by this new method, we have succeeded in designing a new program which necessarily requires no amino acid sequences of constituent peptides and which can determine the sequence from molecular weights and *N*-terminal amino acid residues of constituent peptides in two or more sets of peptide mixtures and 3-phenyl-2-thiohydantoin derivatives of amino acids (denoted as PTH-amino acids) released in each cycle of Edman-degradation.

In this paper, we describe some applications of the new program (named "PROSEQ2") to determining amino acid sequences for several polypeptides; sequencing of a polypeptide of unknown structure[8] is included.

Methods

The computer program "PROSEQ2" described here is written in FORTRAN, its flow chart being outlined in Fig. 1. The single letter abbreviations for amino acid residues presented by Eck and Dayhoff[9] are adopted as input and output words. The ACOS 700 computer in the Crystallographic Research Center (Institute for Protein Research, Osaka University) was used for calculation.

The analytical data used for the calculation are as follows:

1) The amino acid composition of the sample polypeptide or protein as integer values, as obtained from an amino acid analysis of acid hydrolysate.

2) The *N*- and *C*-terminal amino acid residues of the sample polypeptide or protein, as obtained by well known methods.

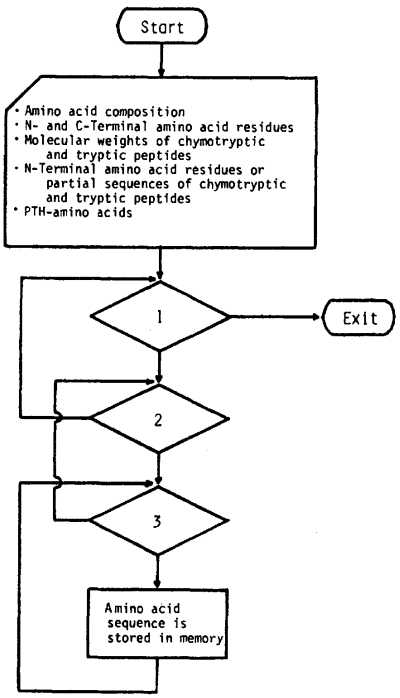

Fig. 1. Flow chart of the computer program "PROSEQ2." The numerals correspond to those given in the explanation of the program in the text.

3) The molecular weights and *N*-terminal amino acid residues of the individual peptides in two or more sets of peptide mixtures prepared from the sample polypeptide or protein by specific cleavage methods, as determined as described in Refs. 4 and 6. Peptide mixtures are degraded by the Edman method[10] with modifications[11] favorable for mass measurements. Mass spectra are obtained with a second-order double focusing mass spectrometer[12] with a mono field-desorption ion source.

4) The kind and compositional ratio, as integer values within some limits between possible maxima and minima, of the PTH–amino acids released from two or more sets of peptide mixtures in each cycle of Edman-degradation and analyzed by high-performance liquid chromatography (HPLC).[13]

In this paper, we use analytical data on peptides obtained from polypeptides by specific cleavage with chymotrypsin and trypsin. Amino acid sequences of polypeptides or proteins are sought by the computer in the following order:

1) Amino acid combinations in chymotryptic peptides are examined in the amino acid composition of the sample polypeptide or protein, and each of the combinations is simultaneously compared with the PTH–amino acids released in each cycle of degradation.

2) Tryptic peptides are aligned in a given order from the *N*-terminus. The tryptic peptide placed at the *N*-terminus has the same *N*-terminal amino acid residue as that of the sample polypeptide or protein. In this case, no amino acid combinations in each tryptic peptide are examined.

3) Chymotryptic peptides are aligned by comparison with the alignment of tryptic peptides from the *N*-terminal position. In this step, the following procedures are carried out simultaneously:

i) Comparison of the molecular weight from the *N*-terminus to the chymotryptic peptide in question with that from the *N*-terminus to the overlapping tryptic peptide.

ii) Collation of the known *N*-terminal amino acid residue of the chymotryptic peptide in question to those of tryptic peptides or the PTH–amino acids released from tryptic peptides.

iii) Collation of the possible amino acid residues in chymotryptic peptides to the PTH–amino acids released from both chymotryptic and tryptic peptides.

iv) Examination of possible similarities of the known *N*-terminal amino acid residues of tryptic peptides with unknown sequences of chymotryptic peptides and also with the PTH–amino acids released from chymotryptic peptides.

In these processes, data on chymotryptic and tryptic peptides are of course interchangeable.

Results and Discussion

In a previous paper,[7] we showed that amino acid sequences of polypeptides or proteins can be deduced from the molecular weights and *N*-terminal partial sequences of their constituent peptides by the computer program "PROSEQ1." By this program, complete sequences or major portions of amino acid sequences of polypeptides or proteins can be determined from sequence

```
INPUT DATA

 AMINO ACID                MOLE WEIGHTS,N-TERMINAL SEQUENCES AND PTH-AMINO ACIDS IN EACH CYCLE
COMPOSITION                 CHYMOTRYPTIC PEPTIDES                                TRYPTIC PEPTIDES

                                          2   3   4                                    2   3

  G   1                396 S*  G  0   0  1,0          174 R  G  0   0
  A   1                431 V   A  0   0   0           652 Y  A 1,0  0
  U   0                477 L   U  0   0   0          1351 A  U  0   0
  S   4                484 T   S 2,0 2,0  0          1356 H* S 1,0  0
  P   0                675 H   P  0   0   0                  P  0   0
  V   1               1106 L   V  0   0   0                  V  0   0
  T   3                        T 1,0  0  1,0                 T  0   0
  L   2                        L  0   0   0                  L 1,0  0
  I   0                        I  0   0   0                  I  0   0
N+D   4                        N  0  1,0  0                  N  0   0
Q+E   3                        D 2,0 1,0  0                  D  0  2,0
  K   1                        Q 1,0 2,0  0                  Q 1,0 2,0
  M   1                        K 1,0  0   0                  K  0   0
  H   1                        E  0   0   0                  E  0   0
  F   2                        M 2,0  0   0                  M  0   0
  R   2                        H  0   0   0                  H  0   0
  Y   2                        F  0   0   0                  F  0   0
  W   1                        R  0   0  1,0                 R  0   0
  C   0                        Y  0  1,0 1,0                 Y  0   0
                               W  0  1,0  0                  W  0   0
TOTAL 29                       C  0   0   0                  C  0   0

 N-TERMINAL AMINO ACID   H
 C-TERMINAL AMINO ACID   T

CANDIDATE SEQUENCES

  1   HSQGTFTSDYSKYLDSRRAQDFVQWLMNT                                              2

  2   HSQGTFTDSYSKYLDSRRAQDFVQWLMNT                                              2

                                                                                 3
```

Fig. 2. Computer out-put sequences of glucagon, sought from the molecular weights, the *N*-terminal amino acid residues and the kind and ratio of PTH–amino acids released by Edman-degradation of the chymotryptic and tryptic peptides, respectively. Peptides with asterisks (*) contain a Lys residue.[4,6] Numerals on the right of sequences show the number of combinations of amino acid residues of chymotryptic peptides and the total number.

```
INPUT DATA

 AMINO ACID                MOLE WEIGHTS,N-TERMINAL SEQUENCES AND PTH-AMINO ACIDS IN EACH CYCLE
 COMPOSITION
                            CHYMOTRYPTIC PEPTIDES                                TRYPTIC PEPTIDES
                                                3   4                                        2   3
   G   1                     396 SK     G   0  1,0                  174 R      G   0    0
   A   1                     431 VQ     A   0    0                  652 Y      A 1,0    0
   U   0                     477 LM     U   0    0                 1351 A      U   0    0
   S   4                     484 TS     S 2,0    0                 1356 H*     S 1,0    0
   P   0                     675 HS     P   0    0                             P   0    0
   V   1                    1106 LD     V   0    0                             V   0    0
   T   3                                T   0  1,0                             T   0    0
   L   2                                L   0    0                             L 1,0    0
   I   0                                I   0    0                             I   0    0
 N+D   4                                N 1,0    0                             N   0    0
 Q+E   3                                D 1,0    0                             D   0  2,0
   K   1                                Q 2,0    0                             Q 1,0  2,0
   M   1                                K   0    0                             K   0    0
   H   1                                E   0    0                             E   0    0
   F   2                                M   0    0                             M   0    0
   R   2                                H   0    0                             H   0    0
   Y   2                                F   0    0                             F   0    0
   W   1                                R   0  1,0                             R   0    0
   C   0                                Y 1,0  1,0                             Y   0    0
 TOTAL 29                               W 1,0    0                             W   0    0
                                        C   0    0                             C   0    0

 N-TERMINAL AMINO ACID   H
 C-TERMINAL AMINO ACID   T

 CANDIDATE SEQUENCES

   1   HSQGTFTSDYSKYLDSRRAQDFVQWLMNT                                                    2

                                                                                        2
```

Fig. 3. Computer out-put sequence of glucagon, sought from the molecular weights, the *N*-terminal sequences of two amino acid residues and the kind and ratio of PTH–amino acids released by Edman-degradation of the chymotryptic and tryptic peptides, respectively.

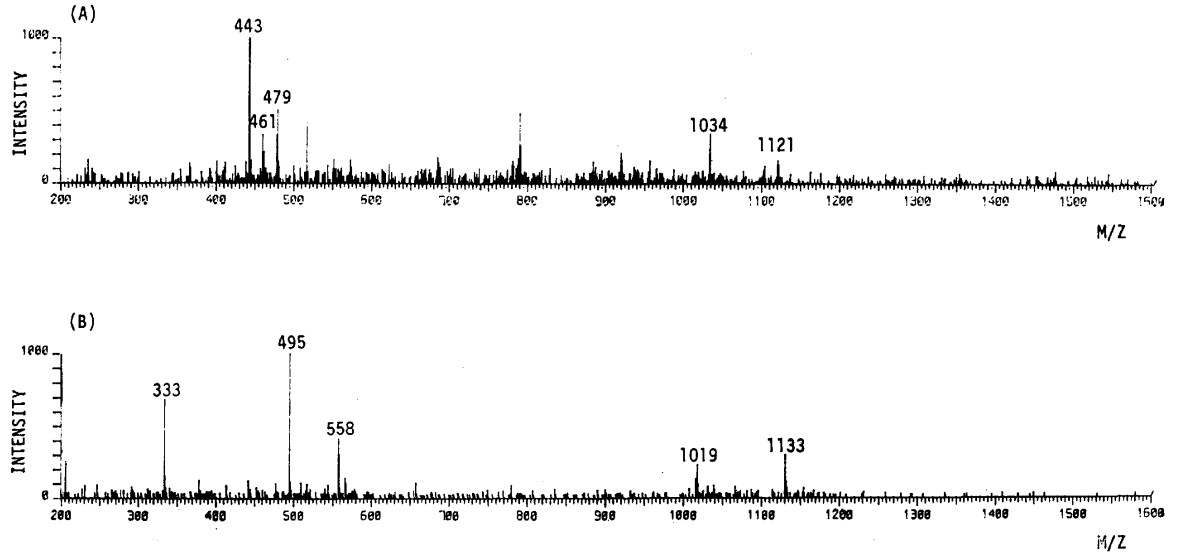

Fig. 4 Field-desorption mass spectra of the chymotryptic (A) and tryptic (B) peptides of human β-endorphin. The spectra were measured with a JMS-DX300 double focusing mass spectrometer equipped with a JMA-2000 mass data analysis system.

information on constituent peptides, but with increasing difficulty with increase in the number of amino acid residues. Therefore, increasing numbers of mass measurements on degraded peptide fragments are necessary to obtain sufficient information on the amino acid sequence of constituent peptides for deducing almost complete amino acid sequences. The present program uses information obtained on PTH–amino acids liberated from peptide mixtures by Edman-degradation in place of that on amino acid sequences of constituent peptides, because using HPLC makes it easy to determine PTH–amino acids liberated from peptide mixtures by successive Edman-degradation.

Figures 2, 3, 5, and 6 show computer output sequences of some polypeptides. The first example (Fig. 2) illustrates the sequence of glucagon, which has been deduced from the molecular weights and *N*-terminal amino acid residues of the chymotryptic and tryptic peptides (Table 1) and the PTH–amino acids released in each cycle of Edman-degradation (Table 2). The output sequences have exchangeable residues (Ser and Asp) at the 8th and 9th positions from the *N*-terminus. This is because PTH–Ser (S) and PTH–Asp (D) were liberated together in the 2nd and 3rd cycles of degradation from the chymotryptic peptides, and the ratio of serine to other amino acids was inaccurate, because

```
INPUT DATA

 AMINO ACID                MOLE WEIGHTS,N-TERMINAL SEQUENCES AND PTH-AMINO ACIDS IN EACH CYCLE
COMPOSITION
                                TRYPTIC PEPTIDES                                CHYMOTRYPTIC PEPTIDES
                                          2   3                                           2   3   4
   G   3                    332 K    G 3,0 3,0                    442 Y    G 2,0 2,0 1,0
   A   2                    494 N*   A 2,0  0                     460 K*   A 2,0 1,0  0
   U   0                    557 N*   U  0   0                     478 V    U  0   0   0
   S   2                   1018 Y*   S  0  1,0                   1033 K*   S  0  1,0  0
   P   1                   1132 S*   P  0   0                   1120 M*   P  0   0  1,0
   V   1                             V  0   0                             V  0   0   0
   T   3                             T 1,0 1,0                            T 2,0 1,0  0
   L   2                             L  0   0                             L  0  1,0  0
   I   2                             I  0  1,0                            I  0   0  1,0
 N+D   2                             N  0   0                             N 2,0  0   0
 Q+E   3                             D  0   0                             D  0   0   0
   K   5                             Q 2,0  0                             Q 1,0  0   0
   M   1                             K 1,0  0                             K 2,0  0  1,0
   H   0                             E 1,0 2,0                            E 1,0 1,0 4,0
   F   2                             M  0   0                             M  0   0   0
   R   0                             H  0   0                             H  0   0   0
   Y   2                             F  0   0                             F  0   0  2,0
   W   0                             R  0   0                             R  0   0   0
   C   0                             Y  0  1,0                            Y  0  1,0  0
                                     W  0   0                             W  0   0   0
TOTAL 31                             C  0   0                             C  0   0   0

 N-TERMINAL AMINO ACID   Y
 C-TERMINAL AMINO ACID   E

CANDIDATE SEQUENCES

   1   YGGFMTSEKSQTPLVTLFKNAIIKNAYKKGE                                                  22

                                                                                        24
```

Fig. 5. Computer out-put sequence of human β-endorphin, sought from the molecular weights, the *N*-terminal amino acid residues and the kind and ratio of PTH-amino acids released by Edman-degradation of the tryptic and chymotryptic peptides, respectively.

```
INPUT DATA

 AMINO ACID                MOLE WEIGHTS,N-TERMINAL SEQUENCES AND PTH-AMINO ACIDS IN EACH CYCLE
COMPOSITION
                                CHYMOTRYPTIC PEPTIDES                                   TRYPTIC PEPTIDES
                                          2   3   4   5   6   7                                   2   3   4   5   6   7
   G   7            252 A    G 1,0 1,0 1,0 1,0 1,0  0                 174 R    G  0   0  1,0 2,0 2,0 1,0
   A   5            385 N    A 2,0 1,0 2,0 1,0  0   0                 626 F*   A 1,0  0  1,0 1,0  0   0
   U   1            439 N    U 1,0 1,0 1,0 1,0 1,0 1,0                 825 A*   U  0   0   0  1,0 1,0 1,0
   S   2            495 Q    S  0  1,0  0   0   0  1,0               1309 A    S 1,0  0   0   0   0   0
   P   1            520 K    P  0  1,0  0   0   0   0                1622 N*   P 1,0  0   0   0   0   0
   V   4            532 N    V 1,0 2,0  0   0   0   0                1817 N    V 1,0 1,0 1,0  0   0   0
   T   3            655 F    T 2,0  0  1,0  0  1,0 1,0                        T 2,0  0   0  1,0 1,0  0
   L   0            924 V*   L  0   0   0   0   0   0                        L  0   0   0   0   0   0
   I   2            934 W*   I 1,0  0   0   0  1,0  0                        I  0   0   0   0  2,0  0
 N+D   7           1309 A    N 2,0  0   0   0   0   0                        N  0   0   0   0   0   0
 Q+E   6                     D  0  1,0  0   0   0  1,0                        D  0  1,0  0   0   0  2,0
   K   3                     Q 1,0 2,0 1,0  0   0   0                        Q  0  1,0 1,0 1,0 1,0 1,0
   M   0                     K 1,0  0  1,0 1,0  0   0                        K  0   0   0  1,0  0   0
   H   1                     E 1,0 1,0 1,0 1,0 1,0 1,0                        E  0  2,0 1,0 1,0 1,0  0
   F   2                     M  0   0   0   0   0   0                        M  0   0   0   0   0   0
   R   2                     H  0   0   0   0   0   0                        H  0   0   0   0   0   0
   Y   6                     F  0   0   0   0   0  1,0                       F  0   0  1,0  0   0   0
   W   3                     R  0   0   0  1,0 1,0  0                       R  0   0   0   0   0   0
   C   0                     Y 2,0 1,0 2,0 2,0  0  1,0                       Y  0  2,0  0  1,0 1,0 1,0
                             W  0  1,0 1,0 1,0 1,0 1,0                       W  0   0  1,0 1,0 1,0 1,0
TOTAL 55                     C  0   0   0   0   0   0                       C  0   0   0   0   0   0

 N-TERMINAL AMINO ACID   A
 C-TERMINAL AMINO ACID   U

CANDIDATE SEQUENCES

   1   ATVAGID(G,S,V,Q,H)RNVDWQYWWNQGKRFAYVKATEGTGYKNPYFAQQYNGSYNIGU                    3242

                                                                                        9276
```

Fig. 6. Computer out-put sequence of the *N*-terminal BrCN fragment of *Streptomyces erythraeus* lysozyme,[14] sought from the molecular weights, the *N*-terminal amino acid residues and the kind and ratio of PTH-amino acids released by Edman-degradation of the chymotryptic and tryptic peptides, respectively.

the recovery of PTH-Ser is generally poor in Edman-degradation. The output sequences suggest that if sequences of two amino acid residues from the *N*-terminus of each peptide are determined as described previously,[4-6] either of the two sequences output is determined. In fact, one sequence was output as illustrated in Fig. 3.

The second example is a sequence determination for human β-endorphin. The mass spectra of the tryptic and chymotryptic peptides are shown in Fig. 4. While the tryptic peptides gave five intense mass peaks of peptides, as expected from the content of basic amino acid residues (4 Lys residues), the chymotryptic peptides gave a number of mass peaks as $[M+H]^+$ and/or $[M+2H]^{2+}$ of expected peptides together with weak mass peaks of peptides, resulting from unspecific cleavage

Table 1. Molecular weights and *N*-terminal amino acid residues of proteolytic fragments of several polypeptides, determined by field-desorption mass spectrometry and Edman-degradation

Glucagon[a]		Human β-endorphin[b]		BrCN *N*-terminal fragment of SE lysozyme[c]	
Chymotryptic	Tryptic	Chymotryptic	Tryptic	Chymotryptic	Tryptic
1106 L	1356 H	1120 M	1132 S	1309 A	1817 N
675 H	1351 A	1033 K	1018 Y	934 W	1622 N
484 T	652 Y	478 V	557 N	924 V	1309 A
477 L	174 R	460 K	494 N	655 F	825 A
431 V		442 Y	332 K	532 N	626 F
396 S				520 K	174 R
				495 Q	
				439 N	
				385 N	
				252 A	

a) Data are cited from Ref. 4. b) Data are based on the mass values in Fig. 4 and PTH-amino acids in Table 3. c) Data are cited from Ref. 8.

Table 2. Recoveries (nmol × 10) of PTH-amino acids released from chymotryptic (1.20 mg) and tryptic (0.66 mg) peptides of glucagon by Edman-degradation

Thr was estimated in addition to Δ-Thr. The 3-phenyl-2-thiohydantoin derivatives of Asn and Gln and Ser and of Ala and Tyr were not satisfactorily separated in some cases. In these cases (*), recoveries were estimated as those of the main component.

	Chymotryptic peptides				Tryptic peptides		
	1	2	3	4	1	2	3
Asp	34	74	44	2	3	4	78
Asn	5	—	41*	1	4		—
Glu		10	19			18	31
Gln		12	30*	2		25	45
Ser	—	—	—		—	—	
Thr	66	12	3	34	6	2	
Gly	8	6	3	18	2	1	5
Tyr	2*	—*	2*	11*	59*	—*	—*
Ala	7*	4*	—*	—*	62*	44*	6
Met	6	60	—		2	10	1
Val	78	5	1	1	2	1	1
Trp		1	1	—	1		
Pro							
Lys	1	1					
Phe	2	1			1		
Ile							
Leu	157	12	3	1	18	58	2
His	64				39		
Arg				26	27		

under the conditions used. The recoveries of the PTH-amino acids liberated from the tryptic and chymotryptic peptides by Edman-degradation are summarized in Table 3. In the method described previously,[4,6] the molecular weights and *N*-terminal amino acid residues of the tryptic and chymotryptic peptides were determined from their mass values and the PTH-amino acids released in the first-cycle of Edman-degradation, as described in Table 1. Figure 5 shows the computer output sequence of human β-endorphin, based on the data described above. The results suggest that the

Table 3. Recoveries (nmol) of PTH-amino acids released from tryptic (0.55 mg) and chymotryptic (0.55 mg) peptides of human β-endorphin by Edman-degradation

See the legend to Table 3 for further details. t means the presence of a trace of material.

	Tryptic peptides			Chymotryptic peptides			
	1	2	3	1	2	3	4
Asp	33	2	1	13	11	2	1
Asn	84	1	t	26	26	1	1
Glu		26	15		12	13	23
Gln		13			t		
Ser	36		2	7	t	3	1
Thr		5	4	13	26	6	
Gly	42	50	24	15	34	45	3
Ala		30		t	30*	10	1
Tyr	55		7	55*	t	12	1
Met	10*	1		33	2*		1
Val	7	t		40	1*	t	
Pro					t	t	6
Phe			1			1	7
Lys	36	3	1	92	35	3	7
Ile			4	t	2	2	4
Leu					1	4	t
His							
Arg							

sequence can be completed by the molecular weights and *N*-terminal amino acid residues of the tryptic and chymotryptic peptides, respectively, and also that the PTH-amino acids released from the second to third cycle of Edman-degradation of the tryptic peptides and from the second to fourth cycle of Edman-degradation of the chymotryptic peptides, although these were rather complicated as shown in Table 3.

Figure 6 shows the amino acid sequence of the *N*-terminal BrCN fragment of *Streptomyces erythraeus* lysozyme,[14] which consists of 55 amino acid residues. The sequence was deduced from the molecular weights, the *N*-terminal amino acid residues of the tryptic and chymotryptic peptides, and the ratios of PTH-amino acids liberated until the 7th step of Edman-degradation. U and W were put in as many data as possible, because

TABLE 4. RECOVERIES (nmol) OF PTH–AMINO ACIDS RELEASED FROM CHYMOTRYPTIC (1.0 mg) AND TRYPTIC (0.7 mg) PEPTIDES OF THE *N*-TERMINAL BrCN FRAGMENT OF *Streptomyces erythraeus* LYSOZYME BY EDMAN-DEGRADATION

See the legend to Table 3 for further details.

	Chymotryptic peptides							Tryptic peptides						
	1	2	3	4	5	6	7	1	2	3	4	5	6	7
Asp	62	30	46	8	4	3	33	24	3	26	4	2	3	20
Asn	277*	113*	11	2	1	1		96	3*			2	2	
Glu	59	16*	75	37	45	9	12			62	11	6	7	1
Gln	—*	11*	65*	31	5	1	1		—*	11*	8*	5	6	5
Ser			—*				1		4*	—*	—*			
Thr		64	13	25	7	7	10	1	80	8	1	12	3	1
Gly	28	51	33	39	43	34	10	6	12	3	25	28	16	7
Tyr		23	—*	25	17*	4	3			22*	—*	6	4	9
Ala	211	102	48*	64	22*	5	1	121	55	—*	32*	17	2	
Met														
Hse														
Val	67	47	75	15	3	2	2	3	58	29	8	3	1	1
Trp	69		—*	1				2			2			
Pro		2	50*	3					40	2				
Lys	113	71	5	29	21	1		1	1			1		
Phe	97	3	1				t	44	2		9	1		
Ile	3	15	2	1	1	39	5	1	4	1		1	20	4
Leu														
His														
Arg	8	8			3	5		26	4					

the former derivative (PTH–Homoser) was not identified and the latter residue (PTH–Trp) was not recovered in good yield under our experimental conditions.[11] The results suggest that the whole sequence was determined except for 4 amino acid residues from the 8th to 11th position from the *N*-terminus and was completed by 4 further cycles of Edman-degradation of the tryptic peptides, as described elsewhere.[8,11] In the calculation reported in this paper, peptides containing a Lys residue[4,6] were used for sequence calculation, and these are shown by asterisks (*) in Figs. 2—5, although the data were not used in the previous paper.[8] This improvement greatly reduced the number of possible combinations of amino acid residues in the peptides with consequent shortening of calculation time.

Thus, the computation by the program described here is very effective for determining amino acid sequences, because all possible candidates of sequences can be searched from a little, simple information. In the current experimental procedure, the recovery of PTH–amino acids from a peptide mixture becomes rather more complicated with increase in the number of peptides in the mixture, because the recovery of PTH–amino acids from smaller or hydrophobic peptides is generally poorer than that from larger or hydrophilic peptides, *etc.* However, the improvement of Edman-degradation increases the usefulness of the present procedure.

References

1) A part of this work was presented at the 18th Symposium on Peptide Chemistry: T. Kitagishi, Y.-M. Hong, and Y. Shimonishi, "Peptide Chemistry 1980," Proceedings of the 18th Symposium on Peptide Chemistry, ed by K. Okawa, Protein Research Foundation, Minoh, Osaka (1981), p. 135.

2) J. A. Kelley, H. Nau, H.-J. Forster, and K. Biemann, *Biomed. Mass Spectrom.*, **2**, 313 (1975).

3) H. Nau, H.-J. Forster, J. A. Kelley, and K. Biemann, *Biomed. Mass Spectrom.*, **2**, 326 (1975).

4) Y. Shimonishi, Y.-M. Hong, T. Matsuo, I. Katakuse, and H. Matsuda, *Chem. Lett.*, **1979**, 1369.

5) T. Matsuo, I. Katakuse, H. Matsuda, Y. Shimonishi, Y.-M. Hong, and Y. Izumi, *Mass Spectroscopy* (*Japan*), **28**, 169 (1980).

6) Y. Shimonishi, Y.-M. Hong, T. Kitagishi, T. Matsuo, H. Matsuda, and I. Katakuse, *Eur. J. Biochem.*, **112**, 251 (1980).

7) T. Kitagishi, Y.-M. Hong, and Y. Shimonishi, *Int. J. Pept. Protein Res.*, **17**, 436 (1981).

8) Y. Shimonishi, Y.-M. Hong, T. Kitagishi, I. Katakuse, T. Matsuo, H. Matsuda, S. Hara, T. Ikenaka, and Y. Izumi, *Chem. Lett.*, **1981**, 499.

9) "Atlas of Protein Sequence and Structure," ed by R. V. Eck and M.O. Dayhoff, National Biomedical Research Foundation Publishers, Silver Spring, Md. (1966): A=Ala, D=Asp, E=Glu, F=Phe, G=Gly, H=His, I=Ile, K=Lys, L=Leu, M=Met, N=Asn, P=Pro, Q=Gln, R=Arg, S=Ser, T=Thr, V=Val, W=Trp, Y=Tyr.

10) P. Edman and A. Henschen, "Protein Sequence Determination," ed by S. B. Needleman, Springer-Verlag, Berlin-Heidelberg- New York (1975), pp. 232—271.

11) Y. Shimonishi, Y.-M. Hong, I. Katakuse, and S. Hara, *Bull. Chem. Soc. Jpn.*, **54**, 3069 (1981).

12) H. Matsuda, *Atomic Masses Fundam. Constants*, **5**, 185 (1976).

13) C. L. Zimmerman, E. Appella, and J. J. Pisano, *Anal. Biochem.*, **77**, 569 (1977).

14) T. Morita, S. Hara, and Y. Matsushima, *J. Biochem.* (*Tokyo*), **83**, 893 (1978).

 © 1982 The Chemical Society of Japan Bull. Chem. Soc. Jpn., 55, 581—586 (1982)

Preparation and Properties of Dealuminated Y Type Zeolite

Akira Yoshida,* Hiromi Nakamoto,** Kazuhito Okanishi,** Tatsuro Tsuru,** and Hiroshi Takahashi**

Mineral Resources Division, National Industrial Research Institute of Kyushu, Shukumachi, Tosu, Saga 841
***Institute of Industrial Science, The University of Tokyo, Roppongi, Minato-ku, Tokyo 106*

(Received May 25, 1981)

The removal of aluminium cations from Y type zeolite, faujasite, was studied by means of three methods of treatment, *i.e.*, acetic acid–sodium acetate buffer treatment, acetate buffer–Na_2H_2EDTA treatment and H_4EDTA treatment. It was confirmed from the results that the reagent for dealumination of faujasite should have two functions, *i.e.* weakly acidic and chelating ability with aluminium cations. When more than 23 aluminium cations were extracted from 53 aluminium atoms in a unit cell, lattice was seriously destroyed. But the analysis of the adsorption isotherms suggested that more than 66% of α-cages remained even in a nearly amorphous sample obtained after dealumination as far as 75%. The differential heat of immersion of the dealuminated Y type zeolite in water showed that the acid strength of the surface increased slightly by dealumination.

Since Kerr[1-3] showed that the tetracoordinate aluminum atoms of faujasite were readily extracted by ethylenediaminetetraacetic acid (H_4EDTA) treatment or by the ion exchange in deep bed method followed by extraction with a sodium hydroxide solution, dealumination of faujasite has been reported by may investigators.[1-12] Beaumont and Barthomeuf[4-6] showed that aluminium atoms could be removed from faujasite with organic solvent such as acetylacetone. They also examined to treat faujasite with diethylenetriaminepeantaacetic acid and 1,2-cyclohexanediamine-*N,N,N',N'*-tetraacetic acid. Miecznikowski *et al.*[7] showed the dealumination of faujasite by the treatment with aqueous tartaric acid solution. Garwood *et al.*[8] reported the partial dealumination of faujasite by chromium salt solution.

The stability of the crystallographic structure of faujasite through dealumination process was mainly related to the silica/alimina molar ratio of starting zeolite. Kerr[2] indicated that the silica/alumina molar ratio should be more than 5.0. Tsutsumi *et al.*[9] attempted dealumination of faujasite whose silica/alumina molar ratio was 4.8 and noted that about 50% of the aluminium atoms was removed by H_4EDTA treatment successfully without collapse of the crystallographic structure. Kerr *et al.*[10] recently reported the technique to remove more than 80% of tetracoordinate aluminium atoms from Y type zeolite retaining 60—70% of the crystallinity. Sherzer[11] produced highly siliceous faujasite with silica/alumina molar ratio over 100 from the starting material whose silica/alumina molar ratio was 5.2.

These reports put focuses on the high crystalline structure retained through the dealumination processes. But, when the starting materials with the silica/alumina molar ratio smaller than 4.8 are dealuminated, the loss of crystallinity is inevitable. This study concerns the amorphous structure of dealuminated faujasite and its properties which were examined by X-ray diffraction analysis, SEM observation, N_2 adsorption, and the measurement of heat of immersion into water.

Experimental

Y type zeolite ($NaY_{4.73}$) used in this work was obtained from Shokubai Kasei Co. Ltd., whose silica/alumina molar ratio

Table 1. Conditions of preparing the samples

Treatment	Sample No.	pH Initial	pH Final	Amount of EDTA g/g zeolite	Reaction time h	V[a] cm³
Acetic acid–sodium acetate	A-1	4.05	4.18	0	20	
	A-2	3.61	3.77	0	20	
	A-3	3.02	3.30	0	20	
	A-4	0.47	1.95	0	20	
Acetic acid–sodium acetate–Na_2H_2EDTA	AE-1	3.61	4.21	1	20	
	AE-2	3.45	4.08	1	20	
	AE-3	3.21	3.64	1	20	
H_4EDTA with Soxhlet extractor	CS-1			0.36	120	20
	CS-2			0.39	240	20
	CS-3			0.47	216	20
	CS-4			0.55	240	20
	CS-5			0.58	264	20
	CS-6			0.66	576	20
	CS-7			0.75	624	7

a) V is the amount of refluxing water poured into the flask at a time.

was 4.73. As the first experiment, $NaY_{4.73}$ (10 g) was mixed only with acetate buffer solution at pH 0.47—4.05 (100 cm^3) in a 300 cm^3 eggplant type flask, and heated at the boiling temperature of the slurry for 20 h. In the second treatment, chelating agent, ten grams of ethylenediamineteraacetic acid disodium salt (Na_2H_2EDTA), was added to the acetate buffer solution to check the role of the chelating agent on the dealumination. The third H_4EDTA treatment was performed with a modified Soxhlet extractor containing 20 g of faujasite and 200 cm^3 of distilled water in the flask of extractor and different amount of H_4EDTA in the extraction room. The conditions of preparing the samples were summarized in Table 1. The amount of refluxing water poured at a time into the flask was controlled by using glass beads between the filter paper thimble and the extraction room to decrease the volume of the extraction room.

The crystallinity of the dealuminated sample was studied by X-ray diffraction analysis. The lattice constant was determined from the interplaner spacing of (533) and (642) with reference to anatase as a standard. The crystallite size was determined from the X-ray line-profile of (533) using silicon as a standard. The appearence of pseudomorphic particles of the sample were observed by MINI SEM of Hitachi-Akashi Co., Ltd. Nitrogen adsorption was measured at −196 °C with Orr Surface-Area Pore-Volume Analyzer 2100D. Heat of immersion was measured in a twin isothermal type calorimeter of Tokyo Rico Co., Ltd. Before measurement, each sample was pretreated at 400 °C under 10^{-5} Torr† for 5 h. The total weight of sample, quartz wool stopper, glass ampule and glass manifold which connected with a vacuum line and a water vapor chamber through glass cocks and joints was measured before and after the pretreatment. Then the different amount of water vapor was injected to the ampule and was adsorbed on the sample. After this adsorption, the amount of water adsorbed was weighed.

Results and Discussion

Dealumination of Faujasite. The properties of the dealuminated Y type zeolite were comparatively studied.

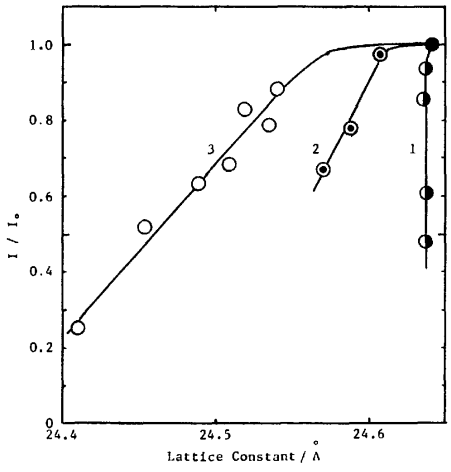

Fig. 1. Correlation between lattice constant and I/I_0.
I: Peak intensity of dealuminated Y type zeolite, I_0: peak intensity of starting material.
1: CH_3COOH–CH_3COONa, 2: CH_3COOH–CH_3COONa–Na_2H_2EDTA, 3: H_4EDTA.

† 1 Torr≈133.32 Pa.

Figure 1 shows the correlation between unit cell constants and the average intensities of (111), (533), and (642) peaks of the dealuminated samples treated with the different three methods. The lattice of faujasite is known to contract through dealumination,[9,12] but the treatment with acetic acid–sodium acetate solution brought about only the collapse of the crystallographic structure without successful dealumination. When Na_2H_2EDTA was added to the acetate buffer solution, a little amount of aluminium was extracted. Na_2H_2-EDTA, as described by Kerr,[2] could not react with sodium zeolite by itself. By the treatment with H_4-EDTA, about 40% of tetracoordinate aluminium of $NaY_{4.73}$ was removed retaining 80% of the crystallinity. These results coincided with the mechanism of dealumination reaction proposed by Kerr.[2] That is, the first step of dealumination reaction is decationization by weak acid, forming basic aluminium hydroxide which is neutralized by Brönsted acid sites, and the second step is the formation of a chelate, NaAlEDTA. The second step of the reaction was not attained by the treatment with acetate buffer solution. The removal of aluminium cations by the chelating agent seems to ensure the partial migration of silicon atoms into the vacant sites by aluminium removal.[12] But this silicon migration did not cause the destruction of the structure of zeolite in H_4EDTA treatment. The limit of dealumination keeping high crystallinity seems to depend on the silica/alumina molar ratio in the starting material.[2,6] The silica/alumina molar ratio of the sample used by Kerr[2] was 5.25, and 37 among 53 aluminium atoms per unit cell were extracted. Barthomeuf *et al.*[6] succeeded to remove 29 aluminium atoms from a unit cell containing 56 aluminium atoms. In our study, the silica/alumina molar ratio of the starting material was 4.73, and 23 among 57 aluminium atoms were extracted with the retention of high crystallinity. The probability of collapse of lattice due to the removal of aluminium atoms seems to increase steeply with the increasing number of the aluminium atoms per unit cell of the starting material. Dealumination and formation of amorphous part from Y type zeolite progressed without noticeable destruction of the shape and the reduction of the size of pseudomorphic particles (Fig. 2). Figure 3 shows the correlation between the ratio of dealumination and the apparent crystallite size determined from the X-ray line-profile of (533). The diameter of pseudomorphic particles of the starting material were between 1000—8000 Å, and their average crystallite size was about 2200 Å. It means that a pseudomorphic particle consists of one or several crystallites. Probably, almost all of the crystallites could be contracted with the dealuminating solution containing H_4EDTA. The process of the formation of amorphous state by dealumination and destruction of the crystal structure of zeolite is schematically described by a model in Fig. 4-a, and is further simplified to the model illustrated in Fig. 4-b. The calculated crystallite sizes from this model are shown in Fig. 3 with dotted line. In this model, $r/r_0=(I/I_0)$,[3] where r and r_0 are the crystallite sizes and I and I_0 are the X-ray diffraction intensities of the dealuminated and original particles,

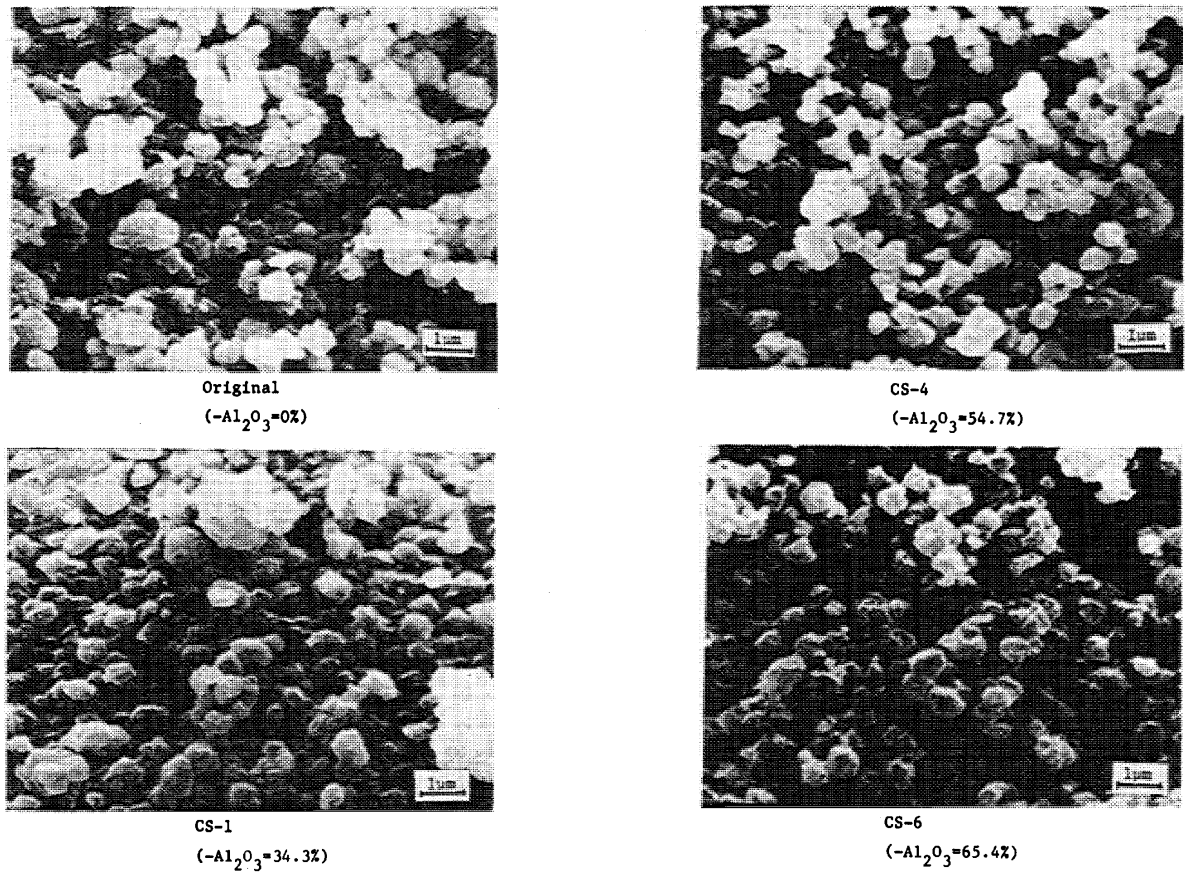

Fig. 2. Electron micrographs of dealuminated Y type zeolite.

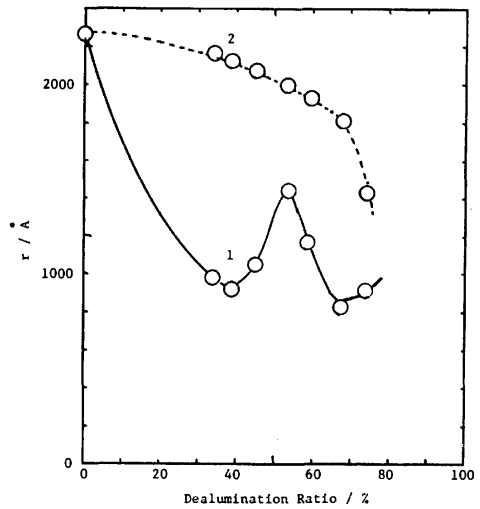

Fig. 3. Changes of apparent crystallite sizes by dealumination.
1: Calculated from line profile of (533), 2: calculated from following equation.
$r/r_0=(I/I_0)^{1/3}$, r,r_0=crystallite sizes of dealuminated and original zeolite, respectively.

respectively. From this calculation, crystallite size of the sample whose dealumination ratio was about 65% should have decreased to 80% of that of the starting material. However, the calculated values did not agree with those observed. Another unexpected phenomenon is the increase of crystallite size after first decrease.

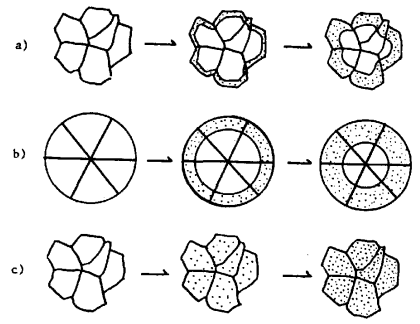

Fig. 4. Models of dealumination and formation of amorphous state.
a): Formation of amorphous state, b): approximation of amorphous state for calculation, c): dealumination.

Since the lattice constant is affected by the silica/alumina molar ratio as described in Fig. 1, the difference of silica/alumina molar ratio in the different crystallites would cause the increase of the half width of X-ray diffraction peak. The first decrease of apparent crystaleite size would be attributed to the heterogeneity of the silica/alumina molar ratio. After the partial dealumination, some part became more siliceous and had extended stability in acid media. Then, the unreacted part of zeolite would be attacked by H_4EDTA. In such a manner, Y type zeolite would be dealuminated nearly homogeneously (Fig. 4-c).

On the assumption that the formation of amorphous state had only negligible effect on the decrease of

Table 2. The molar ratio of faujasite crystal and solid phase of dealuminated Y type zeolite

Sample No.	Dealumination $-Al_2O_3$%	X-Ray analysis $2\theta_{533}$/°	X-Ray analysis $d2\theta_{533}$/°	X-Ray analysis SiO_2/Al_2O_3 (Faujasite)	Chemical analysis SiO_2/Al_2O_3 (Solid phase)
CS-0[a)]	0	23.652	0	4.73	4.73
CS-1	34.3	23.755	0.040	7.3—8.8	7.74
CS-2	38.1	23.775	0.039	8.0—9.8	8.29
CS-3	46.5	23.760	0.033	7.7—8.9	9.74
CS-4	54.7	23.787	0.016	8.9—9.8	11.7
CS-5	57.5	23.807	0.027	9.7—11.3	12.5
CS-6	65.4	23.844	0.054	—	15.6
CS-7	74.2	23.880	0.043	—	21.3

a) CS-0 means the starting zeolite.

crystallite size, the heterogeneity of the silica/alumina molar ratio of the sample was calculated from the increase of half width of (533). The correlation between the silica/alumina molar ratio of faujasite crystal and the unit cell constant was previously reported by Tsutsumi *et al.*[9] On the basis of their results, the silica/alumina molar ratio of the crystalline fraction, and that of the solid phase from the results of chemical analysis, are shown in Table 2. This table shows that in the range of 0 to 38.1% of dealumination, the silica/alumina ratios of faujasite and of the solid phase were similar. The silica/alumina ratio of faujasite in the sample of CS-3 was lower than that of CS-2. In the preparation of CS-1-7, the extent of dealumination was controlled by reaction time and reaction rate. For dealumination to higher extent, the reaction rate must be kept slow to prevent the lattice from destruction, and for this purpose, the more amount of refluxing water was used. In the preparation of CS-3, however, the same amount of refluxing water with and more amount of H_4EDTA than those of CS-2 were used, resulting in the similar reaction time. The rapid dealumination seems to lead to the different silica/alumina molar ratios in faujasite fraction and amorphous fraction. As for CS-6 and CS-7, the lattice constant to be referred to has not been reported. The sample dealuminated at more than 50% of tetracoordinate aluminium have slightly different silica/alumina molar ratios in the faujasite crystal fraction and amorphous fraction. Aluminium atoms in the amorphous state would be extracted easily compared to those in faujasite crystal. The dispersion of silica/alumina molar ratio of faujasite was in the range of 0.9 to 1.8, and the difference of silica/alumina molar ratio between crystalline part and solid phase was in the range of 0 to 2.4.

Changes in Pore Size Distribution. The external forms of particles were not destroyed by acidic H_4EDTA treatment, but their crystallinity decreased to 25%. The change of the pore size distribution due to the treatment was studied next by means of nitrogen adsorption at −196 °C. Figures, 5, 6, and 7 show the pore size distribution curves obtained from the analysis of nitrogen adsorption isotherms in Cranston-Inkley method.[13] For samples CS-1 to CS-4, a large peak of the distribution curves were observed in the range of 12 to 50 Å diameter, and the pores with the larger diameter than 100 Å was negligible. CS-2 has the almost similar distribution curve to those of CS-1, 3, and 4. The peak maxima of these curves are in very narrow range of 14 to 18 Å, and the peak shapes are similar to that of the starting material, CS-0. For CS-5 and CS-6, the pore size distributed to 100—150 Å, and the several peaks lie around 12—120 Å. The pore size seems to distribute over a broader range with the progress of dealumination. But in case of CS-7, the peak shape of the distribution curve is similar to those of CS-1 to CS-4, though the pore size distribution extend to about 100 Å. This would be the result of very slow dealumination, because CS-7 was prepared by the treatment using one third of refluxing water poured at a time than the other samples and the dealumination took 26 d.

The micro pore volume was evaluated by deducing the volume of transitional pores with the diameter of 12—300 Å from the total volume of pores observed as the volume of adsorbed nitrogen at relative pressure of 0.931. At this relative pressure, all pores smaller than 300 Å have been filled by capillary condensation. The wall of pores larger than 300 Å and the external

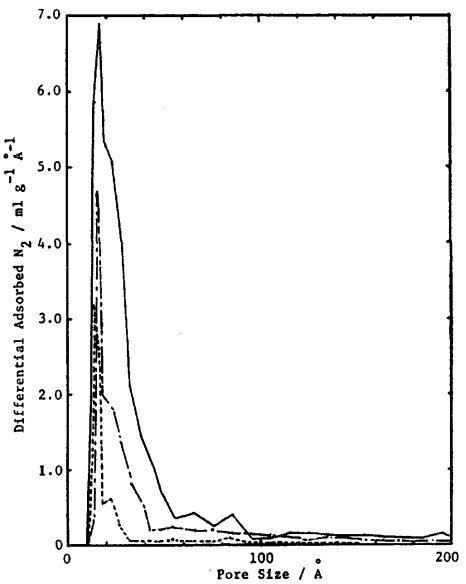

Fig. 5. Pore size distribution of dealuminated Y type zeolite.
---: Starting material, —·—: CS-1($-Al_2O_3$=34.3%), ——: CS-7($-Al_2O_3$=74.2%).

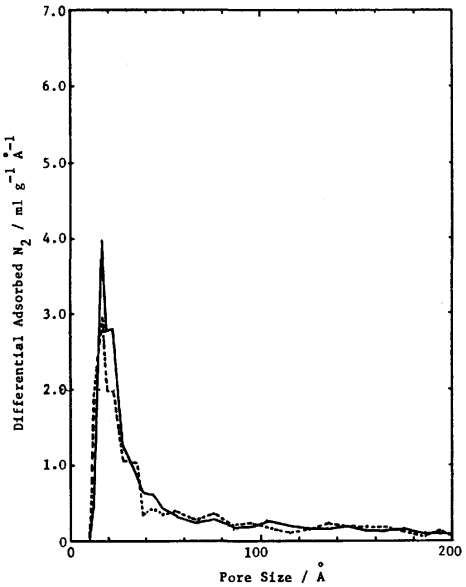

Fig. 6. Pore size distribution of dealuminated Y type zolite.
——: CS-3($-Al_2O_3$=46.5%), ------: CS-4($-Al_2O_3$=54.7%).

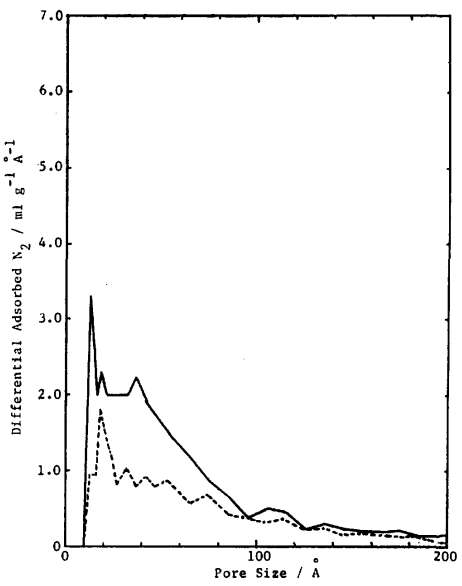

Fig. 7. Pore size distribution of dealuminated Y type zeolite.
------: CS-5($-Al_2O_3$=57.5%), ——: CS-6($-Al_2O_3$=65.4%).

surface were assumed to be negligible. The result are shown in Fig. 8. In these calculations, the specific gravity of nitrogen adsorbed on the solid surface at −196 °C assumed to be that of liquid nitrogen at same temperature. For CS-0, the volume of micro pores is about 0.281 cm³/g. M. M. Dubinin[14] calculated the total void volume of sodium X type zeolite from the known crystal structure to be 0.322 cm³/g. The void volume of faujasite consists of two kinds of cavities, *i.e.* α-cages and β-cages. The ratio of void volume of α-cages to that of β-cages in a unit cell is 6700 Å³/1200 Å³. So, the void volume of α-cages calculated is about 0.271 cm³/g, and this value is slightly lower than the observed micro pore volume of CS-0. Breck *et al.*[15] reported the void volume of α-cages of X type zeolite to be 0.291 cm³/g, which was determined from the adsorption of water. This value is slightly larger than the micro pore volume of CS-0. From these values, it would be considered that the micro pore volume consists mainly of α-cages, or most of α-cages would be evaluated as the micro pores, and the change of micro pore volume would be affected mainly by the decrease of α-cages through dealumination. By dealumination, the volume of α-cages seems to decrease slightly, but even in CS-6 and CS-7, the volume only decreased to 58.1 and 66.2% of the original volume, respectively. The rate of dealumination seems to have an influence on the retention of α-cages. The slow rate of dealumination changes the shapes of α-cages partly, but not the pore size essentially.

Calorimetric Study. To make clear the properties of remaining cationic sites, new structural hydroxyl groups and transitional pores of zeolite after dealumination, immersional heats into water of the dealuminated samples were examined. The results are shown in Fig. 9. The initial immersional heat seems to be related to the acidity at the remaining cationic sites. The

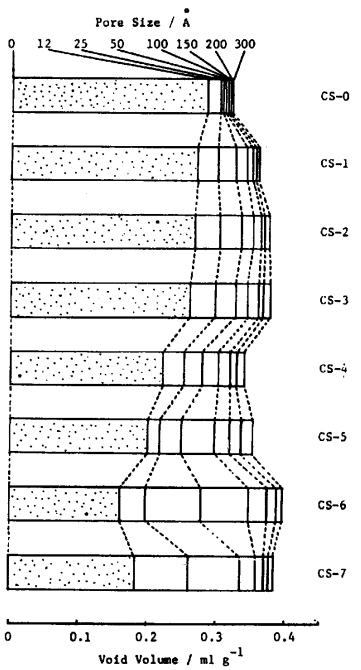

Fig. 8. Void volume of dealuminated Y type zeolite calculated from the amount of N_2 adsorbed using Cranston-Inkley method.

initial heat of immersion on the starting material was in the range of 31.8 to 32.6 kJ/mol, and those on the dealuminated samples were slightly larger, *i.e.* 32.6—33.9 kJ/mol. The amounts of water adsorbed in the range of 31.8 to 33.9 kJ/mol of immersional heat seem to correspond to the amounts of water adsorbed on the cationic sites of the samples, and were 3.7, 3.0, and 1.8 mmol/g for the starting material, CS-1 and CS-5, respectively. The amounts of cationic sites calculated from sodium contents of these samples were 4.0, 3.0, and 1.8 mmol/g, and the amounts of cationic sites

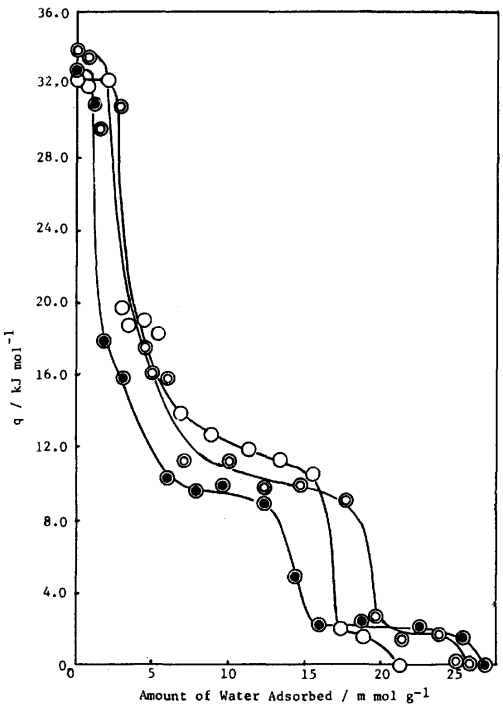

Fig. 9. Differential heat of immersion of dealuminated Y type zeolite.
○: CS-0, ◎: CD-1, ⊙: CS-5.

calculated from aluminium contents were 4.5, 3.2, and 2.2 mmol/g, respectively. After immersion of one water molecule per one sodium ion, the immersional heats of the samples into water decreased sharply to about 11.7 kJ/mol. Each curve of differential heat of immersion has two shoulders at about 10.0—12.5 kJ/mol and at about 1.55—2.51 kJ/mol. The first shoulders seem to be due to the immersion of water molecules in α-cages, partially modified α-cages and β-cages. On the assumption that the volumes of micro pores smaller than 12 Å are nearly equal to the volumes of α-cages and partially modified α-cages of the samples, the amounts of water with different heat of immersion were compared with the pore volumes calculated by Cranston-Inkley method. As for CS-1 and CS-5, it was assumed that the destruction of α-cages accompanied the equivalent collapse of β-cages, and the ratio of the volume of α-cages to that of β-cages in the dealuminated sample was similar to that of the starting material, *i.e.* 6700 Å^3/1200 Å^3, because each silicon or aluminium atom at T site in faujasite belongs to β-cage as well as α-cage. The volume of micro pores smaller than 12 Å in the starting material was 0.281 cm^3/g, and this value corresponds to 0.331 cm^3/g for α-cages and β-cages. The amount of water immersed with the heat larger than 8.37 kJ/mol was about 0.32—0.35 cm^3/g assuming the density of immersed water is the same with that of water at 25 °C. For CS-1, the volume of micro pores smaller than 12 Å was about 0.270 cm^3/g, which leads 0.318 cm^3/g for both cages. The total volume of α-cages, β-cages, and the transitional pores smaller than 25 Å in diameter was about 0.352 cm^3/g which accorded with the amount of water immersed with the heat larger than 8.37 kJ/mol, 0.35—0.39 cm^3/g. For CS-5, the micro pore volume was 0.200 cm^3/g which means 0.235 cm^3/g for both cages. The total volume of pores smaller than 25 Å was 0.254 cm^3/g and the amount of water immersed with the heat larger than 8.37 kJ/mol was about 0.25—0.29 cm^3/g. The electrostatic field of the cationic sites of the starting material seems to affected only the water molecules immersed in both cages, even though in the dealuminated samples the electrostatic field of remaining cationic sites seems to affect the water molecules immersed in the pores smaller than 25 Å. The transitional pores in the starting material would be produced by coagulation of pseudomorphic particles and there would be no cationic site on the wall of transitional pore, but the transitional pores in the dealuminated samples were formed by the partial destruction of α-cages and have some remaining cationic sites and dealuminated sites on the wall. Second shoulder at about 1.55—2.51 kJ/mol seems to correspond to the water molecules immersed in the transitional pores larger than 25 Å. The average immersional heat of water in the large transitional pores seems not to be affected by the dealumination.

References

1) G. T. Kerr, *J. Phys. Chem.*, **71**, 4155 (1967).
2) G. T. Kerr, *J. Phys. Chem.*, **72**, 2594 (1968).
3) G. T. Kerr, *J. Phys. Chem.*, **73**, 2780 (1969).
4) R. Beaumont and D. Barthomeuf, *J. Catal.*, **26**, 218 (1972).
5) R. Beaumont and D. Barthomeuf, *J. Catal.*, **27**, 45 (1973).
6) D. Barthomeuf and R. Beaumont, *J. Catal.*, **30**, 288 (1973).
7) A. Miecznikowski and B. Rzepa, *Rocz. Chem.*, **51**, 1955 (1977).
8) W. E. Garwood, S. J. Luchi, N. Y. Chen, and J. C. Bailar, Jr., *Inorg. Chem.*, **17**, 610 (1978).
9) K. Tsutsumi, H. Kajiwara, and H. Takahashi, *Bull. Chem. Soc. Jpn.*, **47**, 801 (1974).
10) G. T. Kerr, A. W. Chester, and D. H. Olson, *Acta Phys. Chem.*, **24** 169 (1978).
11) J. Sherzer, *J. Catal.*, **54**, 285 (1978).
12) P. Gallezot, R. Beaumont, and D. Barthomeuf, *J. Phys. Chem.*, **78**, 1550 (1978).
13) R. W. Cranston and F. A. Inkley, *Adv. Catal.*, **9**, 143 (1957).
14) M. M. Dubinin, *Izv. Akad. Nauk SSSR, Ser. Khim*, **1964**, 209.
15) D. W. Breck and E. M. Franigen, "Molecular Sieve Zeolite," Society of Chemical Industry, London, (1968), p. 47.

Electron Transfer between Hexacyanoferrate(III) and Thiosulfate. Kinetic Studies in the *trans*-Dihydroxotetraoxoosmate(VIII) Oxidation and the *trans*-Dihydroxotetraoxoosmate(VIII)-catalyzed Hexacyanoferrate(III) Oxidation of Thiosulfate in Aqueous Alkaline Media

Rama Krushna PANDA,* Gautam NEOGI, and Dorai RAMASWAMY†

Department of Chemistry, Berhampur University, Berhampur-760007, India

† *Chemical Laboratories, Central Leather Research Institute, Madras-600020, India*

(Received November 17, 1980)

Kinetics of oxidation of thiosulfate to tetrathionate by *trans*-dihydroxotetraoxoosmate(VIII) (Os(VIII)) and by hexacyanoferrate(III) in the catalytic presence of Os(VIII) have been studied in aqueous alkaline media. The observed pseudo-first-order rate constants for disappearance of Os(VIII) in the Os(VIII)–$S_2O_3^{2-}$ system (k_{obsd}), and those for disappearance of hexacyanoferrate(III) in the Os(VIII)-catalysed $Fe(CN)_6^{3-}$–$S_2O_3^{2-}$ system (k_{cat}) conform, respectively, to Eqs. A and B:

$$k_{obsd}=k_3K_{Os}K_2[S_2O_3^{2-}](1+K_{Os}[OH^-]+K_{Os}K_2[S_2O_3^{2-}])^{-1}, \quad (A)$$

$$k_{cat}=k_6K_{Os}K_2[Os(VIII)][OH^-][S_2O_3^{2-}](1+K_{Os}K_2[S_2O_3^{2-}])^{-1}, \quad (B)$$

where K_{Os} is the stability constant of *trans*-dihydroxotetraoxoosmate(VIII) in aqueous alkaline media, K_2 and k_3 are the formation and decomposition constant of the intermediate complex **1**, and k_6 refers to the rate constant of electron-transfer from **1** to hexacyanoferrate(III). The values of K_{Os} and K_2, as obtained from spectrophotometric titrations and stopped-flow spectrophotometry, respectively, are 19.5 ± 3 dm^3 mol^{-1} and 5.58 ± 0.13; the computed values from kinetic data of K_{Os}, K_2, and k_3 at 30 °C and $\mu=0.32$ mol dm^{-3}, and that of k_6 at 35 °C and $\mu=0.32$ mol dm^{-3} are 22.5 ± 2 dm^3 mol^{-1}, 6.12 ± 0.5, $(3.32\pm0.3)\times10^{-1}$ dm^3 mol^{-1} s^{-1}, and $(3.31\pm0.3)\times10^{-2}$ dm^6 mol^{-2} s^{-1}, respectively. Possible mechanisms for electron-transfer are discussed in terms of an initial equilibrium interaction between Os(VIII) and $S_2O_3^{2-}$ forming an intermediate complex $[OsO_4(OH)(S_2O_3)^{3-}]$ (**1**) followed by (a) a rate-determining decomposition of **1**, with concomitant electron-transfer, in the Os(VIII)–$S_2O_3^{2-}$ system, and (b) a rate-determining outersphere electron-transfer from **1** to hexacyanoferrate(III) in the Os(VIII)-catalyzed $Fe(CN)_6^{3-}$–$S_2O_3^{2-}$ system.

The oxidation of thiosulfate by various metallic oxidants has been shown to proceed either through the intermediacy of metal-thiosulfato complexes[1-5] formed prior to electron-transfer or without a change in the inner co-ordination sphere of the metal.[6-9] We have observed[7] that the oxidation of thiosulfate is zero-order in hexacyanoferrate(III) over a pH range 6.03—12.3, the main reaction being the spontaneous decomposition of thiosulfate. Similar observations were made by Howlett and Wedzicha[6] who reported that the initial 5% reaction of hexacyanoferrate(III) with thiosulfate in the presence of H_2(edta) and acetate was of zero-order in hexacyanoferrate(III). In the presence of 'Osmium Tetraoxide' and an 8—10% aqueous solution of potassium hydroxide, hexacyanoferrate(III) was found to oxidise thiosulfate to sulfate,[10] but the details of the reaction were not presented. In the present study, we are reporting the *trans*-dihydroxotetraoxoosmate(VIII)-catalyzed hexacyanoferrate(III) oxidation of thiosulfate to tetrathionate. Unlike earlier reports on the Os(VIII)-catalyzed electron-transfer reactions, the present kinetics exhibit a first-order dependence in hexacyanoferrate(III).

An understanding of the extent to which Os(VIII) can function as an electron-transfer agent is crucial to the interpretation of kinetics and mechanism of Os(VIII)-catalyzed electron-transfer reactions. Quite a few organic functions have been directly oxidized by Os(VIII); however, no study appears to have been carried out on the direct oxidation of inorganic compounds by Os(VIII). Keeping this in view, the electron-transfer in the Os(VIII)–$S_2O_3^{2-}$ system has been studied as an extension by stopped-flow spectrophotometry.

Experimental

Materials and Methods. All the chemicals used were of Analar grade, and the solutions were prepared using doubly distilled water exclusively. A requisite amount of Os(VIII) solution from the stock (prepared by dissolving 'OsO_4' of Johnson-Matthey in a weakly aqueous alkaline solution, estimated by iodometry[11] and stored in a cool dark place) was taken (as such for the direct oxidation by Os(VIII) or along with hexacyanoferrate(III) solution in the case of catalyzed reactions), made up, thermostated and mixed with the thiosulfate solution at appropriate pH and ionic strength. The ionic strength (μ) of the medium was adjusted by the addition of a required amount of the supporting electrolyte, sodium sulfate. The pH of the medium (±0.01), maintained by the addition of suitable amounts of standard aqueous buffers or carbonate-free hydroxide, as the case may be, was recorded by a Systronics 335 digital pH meter both before and after the reaction; the hydroxide concentrations were calculated from the mean recorded pH after correcting for the ionic strength effect of the medium. The Os(VIII)-catalyzed hexacyanoferrate(III) oxidation reactions were performed by mixing 1 ml aliquots of reactant solutions in a 1 cm-quartz cell by means of semimicro syringes. The course of the reactions was monitored for the decrease in absorbance of hexacyanoferrate(III), continuously as a function of time, at 420 nm (ε_{420} 9.8×10^2 dm^3 mol^{-1} cm^{-1}), in a Pye Unicam SP 1800 spectrophotometer maintained at a desired temperature (±0.1 °C). An extended absorbance scale was used for experiments in which lower concentration of the oxidant was taken.

The electronic spectrum of an aqueous alkaline solution of *trans*-$OsO_4(OH)_2^{2-}$, abbreviated as Os(VIII), showed characteristic bands at 316 nm (ε_{316} 500 $dm^3\ mol^{-1}\ cm^{-1}$) and 247 nm (ε_{247} 690 $dm^3\ mol^{-1}\ cm^{-1}$); earlier workers[11] did not report this observation. In visible region, the solution absorbed strongly around 390 nm, the absorption decreasing with increasing wavelength but without any characteristic maximum in the 390—750 nm region. Tetrathionate, the oxidation product of thiosulfate, absorbed significantly around 247 nm. The kinetic runs for the Os(VIII)-$S_2O_3^{2-}$ system were, therefore, followed by monitoring the disappearance of $OsO_4(OH)_2^{2-}$ at 316 nm in an Aminco stopped-flow spectrophotometer with quartz windows and a 1 cm-light path coupled to a Beckman D. U. monochromator. The nominal mixing time for this spectrophotometer is 0.2 ms. For every entry, at least five replicate runs were performed.

The pseudo-first-order rate constants were computed by least-squares analysis of the expression: $-\ln[(A_t-A_\infty)/(A_o-A_\infty)]=k_{obsd}t$, where A_t, A_o, and A_∞, respectively, represent the absorbance of the reactant at time 't', the initial absorbance and the absorbance at effective infinite time.

For experiments where $[Substrate]_o$—$[Oxidant]_o$, the second-order rate constants (k') were calculated by the usual method; for these experiments the first-order rate constants were calculated from the expression: First-order-rate constant=k' $[Substrate]_o$.

Computations were done by a D. C. M. Data Products minicomputer Microsystem 1121. The self-decomposition of thiosulfate in air was found to be negligible in the conditions employed.

Stoichiometry. The stoichiometric experiments were performed in the presence of 7.8×10^{-7} mol dm^{-3} of Os(VIII) and in the absence of sodium sulfate. The experiments for the stoichiometric runs were carried out at 35 °C under the conditions of $[S_2O_3^{2-}]_o \geq [Fe(CN)_6^{3-}]_o$; for higher concentrations of hexacyanoferrate(III), under the conditions of $[S_2O_3^{2-}]_o \geq [Fe(CN)_6^{3-}]_o$, the runs were carried out at 35 °C and at pH 11.3 till the reaction, with respect to hexacyanoferrate(III), was complete (Table 1). The unconsumed $[S_2O_3^{2-}]_\infty$ was determined iodimetrically. Tests for tetrathionate were done following an earlier procedure.[12] The observed stoichiometric ratio ($\Delta[Fe(CN)_6^{3-}]/\Delta[S_2O_3^{2-}]$) of 0.98±0.02 is in accord with the overall Eq. 1:

$$2Fe(CN)_6^{3-} + 2S_2O_3^{2-} \longrightarrow 2Fe(CN)_6^{4-} + S_4O_6^{2-}. \quad (1)$$

In the oxidation of thiosulfate in aqueous medium at pH 11.3 and 35 °C, 1 mol of Os(VIII) consumed 1.96± 0.03 mol of thiosulfate (Table 1) conforming to the formation of tetrathionate.

$$OsO_4(OH)_2^{2-} + 2S_2O_3^{2-} + 2H_2O \longrightarrow OsO_2(OH)_4^{2-} + S_4O_6^{2-} + 2OH^-. \quad (2)$$

On allowing the final reaction solution to stand for 24 h at room temperature (≈35 °C), it was observed that about 80% of the originally consumed thiosulfate was being reformed. Back-formation of thiosulfate in reaction mixtures of completed thiosulfate oxidation has been reported earlier and explained[1a] to be due to the hydrolysis of tetrathionate. The reformation is, however, very slow and does not complicate the kinetics studied.

Results and Discussion

Electron-transfer in the Os(VIII)-$S_2O_3^{2-}$ System. In weakly alkaline solutions, OsO_4 appears to exist in the form of $OsO_3(OH)_3^-$ which combines with OH^- to yield the reactive form of Os(VIII), *trans*-$OsO_4(OH)_2^{2-}$. This is in accord with the findings of Sauerbrum and Sandell[13] on the dissociation of osmic acid.

$$OsO_3(OH)_3^- + OH^- \overset{K}{\rightleftharpoons} OsO_4(OH)_2^{2-} + H_2O,\ K/[H_2O] = K_{Os}. \quad (3)$$

(K_{Os}=24±4 $dm^3\ mol^{-1}$ at 25 °C and μ=1.0 mol dm^{-3}, ΔH and ΔS associated with this equilibrium are 24±1 kJ mol^{-1} and −146+6 J $K^{-1}\ mol^{-1}$).[11]

Applying Benesi-Hildebrand equation[14] for the determination of equilibrium constant and ε,

$$[Os(VIII)]_o A^{-1} = (K\varepsilon[OH^-])^{-1} + \varepsilon^{-1} \text{ at } [Os(VIII)]_o < [OH^-], \quad (4)$$

where $[Os(VIII)]_o$ is the total analytical concentration

TABLE 1. STOICHIOMETRIC DATA[a] FOR THE OXIDATION OF $S_2O_3^{2-}$ (AQUEOUS MEDIUM, pH 11.3, 35°C)

$Fe(CN)_6^{3-}$–$S_2O_3^{2-}$ system (Os(VIII)[b]-catalyzed)

10^2 $[Fe(CN)_6^{3-}]_o$[c]	10^2 $[S_2O_3^{2-}]_o$	10^2 $[S_2O_3^{2-}]_\infty$[d]
0.01	0.1	—[f]
0.01	0.05	0.039[f,g]
0.1	0.2	0.1[g]
0.2	1.0	0.79[g]
0.4	0.5	0.098[g]
0.5	1.0	0.49[g]
5.0	10.0	4.95[g]
5.0	10.02	8.1[h]
5.0	10.0	9.1[i]
5.01	5.95	4.9[i]

Os(VIII)-$S_2O_3^{2-}$ system

10^3 $[Os(VIII)]_o$[e]	10^3 $[S_2O_3^{2-}]_o$	10^3 $[Os(VIII)]_\infty$[e]	10^3 $[S_2O_3^{2-}]_\infty$[d]
2.0	1.0	1.48	
2.5	1.1	1.94	
3.2	1.2	2.58	
4.1	1.0	3.58	
5.0	1.0	4.49	
0.93	2.1		0.3[g]
0.94	3.0		1.2[g]
0.92	4.0		2.2[g]
0.98	5.2		4.3[g]
5.0	16.7		14.8[h]
10.1	22.0		18.0[i]

a) All concentration units are in mol dm^{-3}. b) In the presence of 7.8×10^{-7} mol dm^{-3} of Os(VIII). c) *Key*: o; initial concentration, ∞; final concentration when the reaction is effectively over. d) Analysis by iodimetry in the presence of zinc sulfate solution just after the reaction is effectively complete. e) Analysis by spectrophotometry at 316 nm. f) At 45 °C. g) Analysis just after the reaction is complete. h) Analysis after keeping the final reaction solution at 35 °C for 24 h. i) Analysis after keeping the final reaction at 60 °C for 5 h (after h).

of Os(VIII) fixed by iodometry, and A and ε respectively refer to the absorbance and molar absorptivity of the complex at 316 nm, the values of K_{Os} and ε_{316} at 30 °C and μ=0.32 mol dm^{-3} have been obtained by a weighted non-linear least-squares programme of the absorbance data at various [Os(VIII)]$_o$ and [OH$^-$] ([Os(VIII)]$_o$ 0.6×10^{-4}—20.4×10^{-4} mol dm^{-3}, [OH$^-$] 1×10^{-3}—40.1×10^{-3} mol dm^{-3}) as 19.5±3 dm^3 mol^{-1} and 500±20 dm^3 mol^{-1} cm^{-1}, respectively; these values should be independent of the concentrations of Os(VIII) and OH$^-$ employed. The K_{Os} value of this work is in good agreement with that obtained earlier.[11]

The Os(VIII)–$S_2O_3^{2-}$ reaction exhibits a first-order dependence on [Os(VIII)] in the range 0.45×10^{-4}—9.06×10^{-4} mol dm^{-3}. At 316 nm, first there is an abrupt increase in the absorbance ($t_{1/2}\approx125$ ms) followed by a subsequent slower step where the absorbance decreases. The first step probably represents a fast formation of an intermediate complex and is followed by a slower decay. The k_{obsd} value (corresponding to the decrease in absorbance) at a constant [$S_2O_3^{2-}$]$_o$ ($=5.0\times10^{-2}$ mol dm^{-3}) registers a marginal increase with the increase in [OH$^-$] from 6.18×10^{-8} mol dm^{-3} to 1.0×10^{-2} mol dm^{-3}, remains almost unchanged till [OH$^-$]$=3.06\times10^{-2}$ mol dm^{-3}, and decreases significantly at much higher [OH$^-$]. The k_{obsd} is found to increase almost linearly with increasing [$S_2O_3^{2-}$] for [$S_2O_3^{2-}$]$_o=1.0\times10^{-4}$—10×10^{-3} mol dm^{-3}; however, beyond [$S_2O_3^{2-}$] of 50×10^{-3} mol dm^{-3}, the k_{obsd} varies only slightly by about 5% for an almost two-fold increase in [$S_2O_3^{2-}$]. The rate expression for the reduction of Os(VIII) should, therefore, include a distinct [$S_2O_3^{2-}$]- dependent term, getting saturated at higher [$S_2O_3^{2-}$].

The k_{obsd} increases with an increase in ionic strength of the medium. It does not appreciably change in the range 25—45 °C. Added acrylonitrile retards the rate, but no polymerisation could be observed.

Rate Law and Mechanism: The preliminary kinetic results suggest that the mechanism of reduction of Os(VIII) by $S_2O_3^{2-}$ involves incorporation of a thiosulfato-ligand into the inner-coordination sphere of Os(VIII) prior to an electron-transfer step.

$$OsO_4(OH)_2^{2-} + S_2O_3^{2-} \overset{K_2}{\rightleftharpoons} [OsO_4(OH)(S_2O_3)^{3-}] + OH^-, \quad (5)$$

$$[OsO_4(OH)(S_2O_3)^{3-}] + H_2O \xrightarrow{k_3} OsO_4(OH)(H_2O)^{2-} + S_2O_3^-, \quad (6)$$

$$OsO_4(OH)(H_2O)^{2-} + S_2O_3^{2-} + H_2O \xrightarrow[\text{fast}]{k_4} OsO_2(OH)_4^{2-} + OH^- + S_2O_3^-, \quad (7)$$

$$2S_2O_3^- \xrightarrow[\text{fast}]{k_5} S_4O_6^{2-}. \quad (8)$$

Since $S_2O_3^{2-}$ is an effective one-electron reducing agent, an Os(VII) species will probably be produced which will further get reduced rapidly to Os(VI) with another $S_2O_3^{2-}$. Os(VII) is known in solution[16] and has been prepared in solid state.[17] Such a one-electron change can take place only with a high activation enthalpy because two very unstable species are formed (Eq. 6) and that the subsequent step, Os(VII)$+e^- \rightarrow$ Os(VI), can proceed without obstacle.

Consequently, the mechanism of the reaction would result in the rate law (Eq. 9), on the basis of Eqs. 3, 5—8, and on applying a steady-state treatment to the intermediate complex [$OsO_4(OH)(S_2O_3)^{3-}$] (**1**)

$$-\frac{d[Os(VIII)]}{dt} = \frac{k_3K_{Os}K_2[Os(VIII)]_T[S_2O_3^{2-}]}{1+K_{Os}[OH^-]+K_{Os}K_2[S_2O_3^{2-}]}, \quad (9)$$

where the total analytical [Os(VIII)]$_T$=[$OsO_3(OH)_3^-$] +[$OsO_4(OH)_2^{2-}$]+[$OsO_4(OH)(S_2O_3)^{3-}$]. If as a first approximation, a reasonable assumption is made that at the low [OH$^-$] employed, K_{Os}[OH$^-$]$\ll$(1+$K_{Os}\times K_2$[$S_2O_3^{2-}$]), Eq. 10 is obtained.

$$-\frac{d[Os(VIII)]}{dt} = \frac{k_3K_{Os}K_2[Os(VIII)]_T[S_2O_3^{2-}]}{1+K_{Os}K_2[S_2O_3^{2-}]}, \quad (10)$$

$$k_{obsd} = k_3K_{Os}K_2[S_2O_3^{2-}](1+K_{Os}K_2[S_2O_3^{2-}])^{-1}, \quad (11)$$

which on rearrangement becomes

$$(k_{obsd})^{-1} = (k_3)^{-1} + (k_3K_{Os}K_2)^{-1}([S_2O_3^{2-}])^{-1}. \quad (12)$$

Eq. 12 predicts that $(k_{obsd})^{-1}$ should be a linear function of $([S_2O_3^{2-}])^{-1}$. From the intercept and slope of this least-squares plot (Fig. 1), using the experimentally determined K_{Os} value, the k_3 and K_2 values have been computed respectively as $(3.32\pm0.3)\times10^{-1}$ dm^3 mol^{-1} s^{-1} and 6.12±0.5 at 30 °C and 0.32 mol dm^{-3} of ionic strength. The computed K_2 is very close to the average value (5.58) of the observed constant pertaining to the first abrupt increase in the absorbance at 316 nm. Also the agreement of the k_{calcd} (Eq. 12) values obtained (employing the estimated values of k_3, K_2, and the experimental value of K_{Os}) with the experimentally determined k_{obsd} is in support of the postulated mechanism.

Eq. 9 can be rearranged to Eq. 13:

$$(k_{obsd})^{-1} = (1+K_2[S_2O_3^{2-}]K_{Os})(k_3K_2[S_2O_3^{2-}]K_{Os})^{-1} + [OH^-](k_3K_2[S_2O_3^{2-}])^{-1}. \quad (13)$$

At [$S_2O_3^{2-}$]$_o=5.0\times10^{-2}$ mol dm^{-3}, employing the value of k_3 computed earlier, K_{Os} has been calculated from the least-squares slope and intercept of the $(k_{obsd})^{-1}$ *vs.* [OH$^-$] plot as 22.5±2 at 30 °C and μ= 0.32 mol dm^{-3}. This value is quite close to that experimentally determined. There is also agreement of the k_{calcd} (Eq. 13) values with the k_{obsd} values (Table 2).

Supporting evidences from kinetics or otherwise,

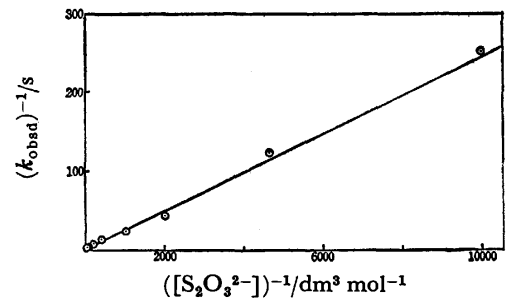

Fig. 1. $1/k_{obsd}$ *vs.* $1/[S_2O_3^{2-}]$ (The Os(VIII)–$S_2O_3^{2-}$ reaction) [Os(VIII)]$=6\times10^{-4}$, [OH$^-$]$=1\times10^{-2}$; Aqueous medium, 30 °C, μ=0.32 (All concentrations are in mol dm^{-3}).

TABLE 2. TYPICAL AVERAGE[a] RATE CONSTANTS FOR THE REACTION BETWEEN Os(VIII) AND $S_2O_3^{2-}$ (Aqueous medium, 30 °C, $\mu=0.32$[b])

10^4 [Os(VIII)]$_o$	10^3 [$S_2O_3^{2-}$]$_o$	10^2 [OH^-]	k_{obsd}/s^{-1} [c]	k_{calcd}/s^{-1}
9.00	52	1.10	0.42[d]	
9.00	50	1.10	0.50[e]	
9.01	51	(6.18×10^{-8})[m]	0.23	0.29[l]
9.04	110	(6.18×10^{-8})[m]	0.24	0.29[l]
9.02	50	(4.28×10^{-6})[m]	0.24	0.29[l]
9.06	51	1.00	0.33	0.282[l]
9.03	50	2.12	0.32	0.274[l]
9.05	51	3.06	0.315	0.27[l]
9.13	50	50.6	0.12	0.12[l]
9.10	50	110	0.07	0.07[l]
9.00	51	1.10	0.32[f]	
9.06	51	1.00	0.33[g]	
9.03	51	1.08	0.33[h]	
3.00	53	1.03	0.32	
3.10	53	1.30	0.33[l]	
3.05	50.5	1.20	0.32[l]	
1.70	49	1.15	0.33	
9.04	51	1.02	0.19[j]	
1.51	5.01	1.03	5.52*	
3.01	5.01	1.02	5.57*	
5.06	5.02	1.00	5.53*	
6.00	5.03	1.00	5.74*	
6.05	5.0	1.05	5.01*[f]	
6.05	5.01	1.06	5.38*[g]	
6.03	5.01	1.01	6.48*[h,k]	
9.03	5.0	1.07	5.71*	
3.02	7.0	1.04	5.50*	
3.02	10.1	1.03	5.46*	
3.02	50.1	1.05	5.61*	

a) Standard deviations range from ±0.02 to 0.1 (at least five experiments for each entry). b) All concentration units in mol dm^{-3}. c) Average first-order rate constants with respect to the disappearance of Os(VIII) at 316 nm. d,e) Respectively at 0.42 and 0.52 mol dm^{-3} of ionic strength. f,g,h) Respectively at 25, 40, and 45 °C. i) For the appearance of $OsO_2(OH)_4^{2-}$ at 500 nm ($\Delta A/\Delta t>0$). j) In the presence of 1×10^{-4} mol dm^{-3} of acrylonitrile. k) Average ΔH^* and ΔS^* respectively 7.1 kJ mol^{-1} and -207 J K^{-1} mol^{-1}. l) Average k_{calcd} from Eq. 13 (representative). m) Calculated from measured pH. * Calculated for the first abrupt increase in absorbance of Os(VIII) at 316 nm.

have been well presented for the formation of intermediate complexes between metal ions and thiosulfate.[1-5] In the Os(VIII)–$S_2O_3^{2-}$ system also, the kinetic evidences and the abrupt increase in absorbance at 316 nm, as soon as Os(VIII) and thiosulfate are mixed, are suggestive of the inner-sphere substitution of a hydroxo-ligand by a thiosulfato-ligand in the *trans*-$OsO_4(OH)_2^{2-}$.

The attack by the sulfur-end rather than by the oxygen-end of thiosulfate is consistent[18,4] with the value of the formation constant of the intermediate complex $[OsO_4(OH)(S_2O_3)^{3-}]$. Spectrophotometric titrations could not be performed because of the rapidity of the change in absorbance of Os(VIII) and also due to the considerable absorption of tetrathionate between 240—290 nm. However, we got indications for the formation of a 1:1 intermediate complex involving Os(VIII) and thiosulfate by the following method. Zero-time absorbance at 316 nm were obtained by extrapolation for different [Os(VIII)]: [$S_2O_3^{2-}$] ratios in isomolar and non-isomolar mixtures. When the increase in the absorbance difference, $+\Delta A$, was plotted against the mole-fraction of Os(VIII), a maximum in ΔA was observed at the mole-fraction of Os(VIII)=0.5.

It is more rational to assume that an electron-transfer from thiosulfate to Os(VIII) has taken place during the substitution. The activated complex could then offer, at the same time, the lowest energy barrier to substitution and also to electron-transfer (Eq. 5), since the orbitals of the central osmium are disturbed (Table 2, foot note for activation parameters pertaining to the first abrupt increase in absorbance at 316 nm); the process starts as a substitution and continues with a one-electron transfer. Since *trans*-dihydroxotetraoxoosmate(VIII) ends up finally as *trans*-dioxotetrahydroxoosmate(VI), an equatorial attack by the outer-sulfur of thiosulfate on osmium is likely,[15b] leading to a fair degree of displacement of the axial hydroxo-ligand.

Os(VIII)-catalyzed $Fe(CN)_6^{3-}$–$S_2O_3^{2-}$ Electron-transfer. Studies on Os(VIII)-catalysed oxidation reactions of various inorganic[11] and organic substrates[19] by hexacyanoferrate(III) are increasingly becoming useful probes in the elucidation of the nature of oscillatory catalysis of Os(VIII). In these studies and in numerous other studies of Os(VIII)-catalyzed oxidations by other oxidants,[20,21] Os(VIII) is involved in an initial equilibrium formation of an intermediate Os(VIII)-substrate complex which breaks down rate-determingly to the products and Os(VI); the Os(VI) formed is oxidised rapidly to Os(VIII) by the main oxidant, resulting in zero-order kinetics with respect to the main oxidant.

In contrast to the earlier observations, the Os(VIII)-catalysed hexacyanoferrate(III) oxidation of thiosulfate is first-order in hexacyanoferrate(III) over the $[Fe(CN)_6^{3-}]_o$ range 0.1×10^{-4}—20.1×10^{-4} mol dm^{-3}. The observation is interesting as it is probably the first report of a main oxidant exhibiting first-order kinetics in the presence of an oscillatory catalyst.

At constant ionic strength and constant $[Na^+]$ ($[Na^+]\gg[K^+]$), the k_{cat} value linearly increases with the increase in [$S_2O_3^{2-}$], [Os(VIII)], or [OH^-] for their respective ranges of concentration: 1.0×10^{-5}—2.46×10^{-3}, 3.9×10^{-7}—97.3×10^{-7}, and 1.0×10^{-5}—50.5×10^{-3} mol dm^{-3} (Fig. 2). Also the good reproducibility of the k_{cat} value obtained by following the first-order disappearance of thiosulfate at 217 nm (in a representative run) with that obtained by monitoring the disappearance of hexacyanoferrate(III), shows that the rate of disappearance of thiosulfate is the same as that of hexacyanoferrate(III). There is a retardation in the rate in the presence of added mannitol, acrylonitrile or hexacyanoferrate(II) in this system (Table 3).

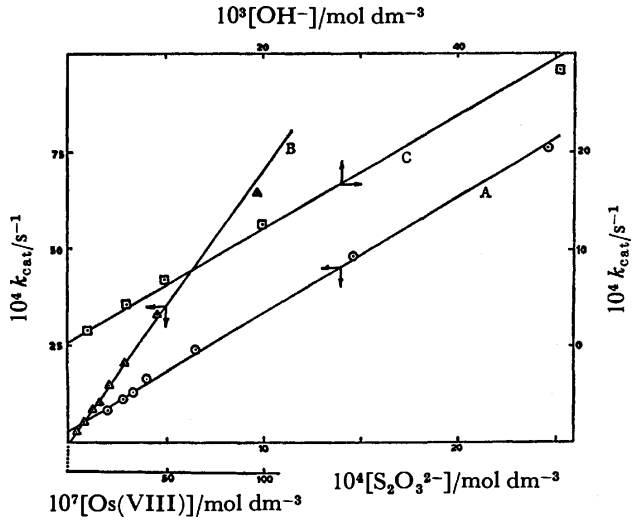

Fig. 2. k_{cat} *vs.* $[S_2O_3^{2-}]$, $[OH^-]$ or [Os(VIII)] (The Os(VIII)-catalyzed $Fe(CN)_6^{3-}$–$S_2O_3^{2-}$ reaction). A: $[OH^-]=1\times10^{-2}$, $[Os(VIII)]=7.8\times10^{-7}$; B: $[S_2O_3^{2-}]=1.2\times10^{-4}$, $[OH^-]=1\times10^{-2}$; C: $[S_2O_3^{2-}]=1.6\times10^{-4}$, $[Os(VIII)]=7.8\times10^{-7}$; $[Fe(CN)_6^{3-}]=1\times10^{-4}$, aqueous medium, 35 °C, $\mu=0.32$ (All concentrations are in mol dm^{-3}).

The k_{cat} value increases linearly with μ. Considerable ion-pairing has been reported in oxidations by alkaline hexacyanoferrate(III), but in the present case as the rate is independent of the $[Fe(CN)_6^{3-}]_o$, any ion-pairing between K^+ or Na^+ and hexacyanoferrate(III) will have no significant effect[22] on the rate. A plot of oxidation rate (k_{cat}) against μ yields a straight line with no zero-rate at zero-electrolyte concentration. This, therefore, appears to be a mere ionic strength effect.[15a] A plot of $\log k_{cat}$ *vs.* $\mu^{1/2}$ is also linear, but no meaningful inference regarding the charge of the reacting ions could be drawn[23a] from the slope of the straight line, as the oxidation process is a multi-step one.

Rate Law and Mechanism: In the absence of Os(VIII), the oxidation of thiosulfate by hexacyanoferrate(III) does not virtually proceed[7] under the conditions employed for the catalysed oxidation, demonstrating that the presence of catalytic amounts of Os(VIII) accelerates the reaction tremendously. The observed kinetic data for the catalyzed system can be presented in terms of a reaction scheme consisting of Eqs. 3, 5, and 14.

$$[OsO_4(OH)(S_2O_3)^{3-}] + Fe(CN)_6^{3-} \xrightarrow[k_6]{OH^-} OsO_4(OH)_2^{2-} + Fe(CN)_6^{4-} + S_2O_3^{-}. \quad (14)$$

Since in the catalysed system, $[S_2O_3^{2-}]\gg[Os(VIII)]\ll[Fe(CN)_6^{3-}]$, the contribution of the catalytic [Os(VIII)] to the direct oxidation of thiosulfate is negligible. Applying steady-state treatment to $[OsO_4(OH)(S_2O_3)^{3-}]$, a rate expression can be derived as in Eq. 15.

$$-\frac{d[Fe(CN)_6^{3-}]}{dt} = \frac{k_6K_{Os}K_2[Os(VIII)][Fe(CN)_6^{3-}][OH^-][S_2O_3^{2-}]}{1+K_{Os}K_2[S_2O_3^{2-}]}, \quad (15)$$

Table 3. Typical average[a] rate constants for Os(VIII)-catalyzed $Fe(CN)_6^{3-}$ oxidation of $S_2O_3^{2-}$

(Aqueous medium, 35 °C, $\mu=0.32$,[b] $[Fe(CN)_6^{3-}]_o=(1.0-1.05)\times10^{-4}$, $[Os(VIII)]=7.8\times10^{-7}$, $[OH^-]=(10.0-10.2)\times10^{-3}$)

10^4 $[S_2O_3^{2-}]_o$	10^4 k_{cat}/s^{-1} [c]	10^4 k_{cat}(calcd)/s^{-1} [d]
1.23	5.00	4.79
1.25	5.17	4.87
1.61	6.70	6.24
2.00	7.78	7.72
2.17	8.84	8.36
2.80	11.15	10.70
3.28	13.20	12.50
4.00	16.40	15.10
6.45	24.00	23.70
14.6	48.0	49.1
24.6	76.0	75.2
2.10	7.53[e]	
0.1	0.4[f]	0.40
1.25	5.20[e]	4.87
2.80	12.20[g]	
2.80	17.74[h]	
2.81	11.26[i]	
2.82	11.25[j]	
2.80	11.22[k]	
2.80	11.10[l]	
3.00	0.07[m]	
2.03	1.36[n]	
2.78	0.35[o]	

a) Standard deviations range from ±0.002 to 0.05. b) All concentration units in mol dm^{-3}. c) Average first-order rate constants with respect to the disappearance of $Fe(CN)_6^{3-}$ at 420 nm. d) Average $k_{cat(calcd)}$ calculated from Eq. 16 (representative). e) Under an atmosphere of nitrogen gas; $[Fe(CN)_6^{3-}]_o=1.0\times10^{-3}$. f) For the disappearance of $S_2O_3^{2-}$ at 217 nm; $[Fe(CN)_6^{3-}]_0=1\times10^{-5}$. g, h) Respectively at 0.42 and 0.52 mol dm^{-3} of ionic strength. i,j,k,l) Respectively at 30, 40, 45, and 60 °C. m,n,o) Respectively in the presence of 1.0×10^{-4} mol dm^{-3} of added mannitol, acrylonitrile or $Fe(CN)_6^{4-}$.

or

$$k_{cat}(1+K_{Os}K_2[S_2O_3^{2-}]) = k_6K_{Os}K_2[Os(VIII)][OH^-][S_2O_3^{2-}]. \quad (16)$$

A plot of k_{cat} $(1+K_{Os}K_2[S_2O_3^{2-}])$ *vs.* $[S_2O_3^{2-}]$ should be a straight-line. At constant [Os(VIII)] and $[OH^-]$, employing the experimental value of K_{Os} and the computed value of K_2, the k_6 value for this system at 35 °C and $\mu=0.32$ mol dm^{-3} can be calculated from the least-squares slope of the above straight-line (neglecting the small value of the intercept) as $(3.31\pm0.3)\times10^{-2}$ dm^6 mol^{-2} s^{-1}. The $k_{cat(calcd)}$ values, calculated with the above values of k_6, K_{Os}, and K_2, agree with those obtained experimentally lending credence to the proposed rate expression.

Inasmuch as the redox potentials[24] for the couples $S_2O_3^{2-}/S_4O_6^{2-}$ and $Fe(CN)_6^{4-}/Fe(CN)_6^{3-}$, are thermodynamically favourable for electron-transfer from thio-

sulfate to $Fe(CN)_6^{3-}$, it is expected that the oxidation of thiosulfate to tetrathionate should proceed by a direct interaction between thiosulfate and hexacyanoferrate(III). In fact, in numerous oxidation studies of thiosulfate by metallic oxidants like complexes of Cu(II),[1] Co(III),[2] Au(III),[3] Cr(VI),[4] and Fe(III),[5] kinetic and other evidences suggest that intermediate metal-thiosulfato complexes (where the metal has lost one formal oxidation state and thiosulfate has gained one) are formed prior to the rate-determining electron-transfer step. Even though hexacyanoferrate(III) oxidations mostly involve outer-sphere electron change, in an analogous system[25] involving hexacyanoferrate(III) and SO_3^{2-}, intermediate complexes of $Fe(CN)_5(CNSO_3)^{5-}$ and $Fe(CN)_5(CNSO_3)^{4-}$ have been evidenced in aqueous alkaline solution and definitely identified. Lancaster and Murray[25] have suggested that many oxidations by transitional-metal complexes which are weak oxidants may proceed *via* intermediate complexes as described in the case of $Fe(CN)_6^{3-}$–SO_3^{2-} system. Legros[26] has also reported that the hydrolysis of $Fe(CN)_5(S_2O_3)^{5-}$ in aqueous medium is accompanied by a high activation energy and positive activation entropy.

In the present system, however, no indication of any intermediate complex could be obtained from repeated and continuous scanning of the reaction solutions (from 250 nm to 650 nm). Also if the experiment is conducted in the presence of $^{14}CN^-$, there is no labelled cyano-ligand in the $Fe(CN)_6^{4-}$ product ensuring the absence of cyano exchange. Any direct interaction between hexacyanoferrate(III) and thiosulfate to form an intermediate complex necessiates a thiosulfato-ligand of very low Lewis-basicity to substitute or attach itself to, a cyano-ligand in a non-labile low-spin d^5-octahedral complex $Fe(CN)_6^{3-}$, and this is inherently not allowed in all probability. A comparison of the divergent pK of CN^- and SO_3^{2-} with that of $S_2O_3^{2-}$ (respectively 9.1, 9.1, and 1.9)[15c] would show that even if any analogous complexes of $[Fe(CN)_5(CNS_2O_3)^{5-}]$ and $[Fe(CN)_5(CNS_2O_3)^{4-}]$ are thought of, they would not be stable enough in aqueous alkaline medium to be experimentally distinguishable.

However, in view of the expected higher redox potential of the couple Os(VIII)/Os(VI), the d^0-configuration of Os(VIII) and the decreased $10Dq$ value of Os(VIII) in the substitution of an octahedral complex, as compared to that in a substitution-inert $Fe(CN)_6^{3-}$, the substitution of a hydroxo-ligand by a thiosulfato-ligand in *trans*-dihydroxotetraoxoosmate (VIII) is possible. The intermediate complex thus formed, between Os(VIII) and $S_2O_3^{2-}$, undergoes hydrolysis (in the direct oxidation reaction by Os(VIII)) with concomitant electron transfer, or is involved in an outer-sphere electron-transfer in the presence of alkaline hexacyanoferrate(III) in a termolecular rate-determining step.

Evidences for the presence of $S_2O_3^-$, thiosulfate(1—), have been well presented.[5] In the present system radical-trapping agents retard the rate; polymerisation, however, is not detected. This may be because $k(S_2O_3^- + S_2O_3^-) \gg k$ (induced polymerisation) so that the induced change is too insignificant to be practically detectable. Moreover, absence of polymerisation does not necessarily mean absence of radical formation; in acidic medium, in the presence of dissolved oxygen, acrylonitrile does not polymerise even if the process is initiated by γ-radiolysis or by thermal decomposition of peroxodisulfate.

A reprisal of the data in Table 3 shows that there is a near-linear-k_{cat} *vs.* $[S_2O_3^{2-}]$-relationship. To verify the validity of Eq. 16, experiments at higher $[S_2O_3^{2-}]_o$ appear necessary; such an investigation is precluded as the $[S_2O_3^{2-}]$-dependence beyond $[S_2O_3^{2-}]_o = 24.6 \times 10^{-4}$ mol dm^{-3} tends to be somewhat different from that observed in the concentration range employed suggesting that another reaction path[27] probably becomes important at higher $[S_2O_3^{2-}]_o$.

The reactions are accompanied by an imperceptible temperature co-efficient in the range 30—60 °C as there is no appreciable change in the rate. This is probably due to the fact that the reaction has been studied at or very near the isokinetic temperature. We cannot offer at this stage any other reasonable explanation for this than that the large negative activation entropy created in the substitution step is probably counterbalanced by the more positive activation enthalpy in the electron-transfer step so that the net $\Delta G^* \approx 0$, thus causing no appreciable rate constant variation.[23b]

Grateful acknowledgements are due to the UGC, New Delhi for the grant of a National Associateship Scheme, and to the Director, CLRI for providing some of the facilities. We thank Prof. P. S. Radhakrishnamurti for helpful discussions. The CSIR, New Delhi for providing a Junior Research Fellowship to G. Neogi, and Mrs. H. Ranganathan, C. K. Ranganathan and D. Rajendra Prasad of CLRI for some technical assistance are acknowledged.

References

1) a) J. J. Beyerley, S. A. Fouda, and G. L. Rampel, *J. Chem. Soc., Dalton Trans.*, **1973**, 889, and references cited therein; b) J. J. Beyerley, S. A. Fouda, and G. L. Rampel, *ibid.*, **1975**, 1329.

2) H. Yoneda, *Bull. Chem. Soc. Jpn.*, **28**, 125 (1955); M. A. Thacker and W. C. E. Higginson, *J. Chem. Soc., Dalton Trans.*, **1975**, 704.

3) G. Nord, L. H. Skibsted, and A. S. Khalonin, *Acta Chem. Scand., Ser. A*, **29**, 505 (1975).

4) I. Baldea and G. Niac, *Inorg. Chem.*, **9**, 110 (1970), and references cited therein.

5) F. M. Page, *Trans. Faraday Soc.*, **56**, 398 (1960); **49**, 1953 (1953).

6) K. E. Howlett and B. L. Wedzicha, *Inorg. Chim. Acta*, **18**, 133 (1976), and references cited therein.

7) R. K. Panda, G. Neogi, and D. Ramaswamy, (Communicated).

8) Y. A. Komkov, N. N. Krot, and A. D. Gel'man, *Radiokhimiya*, **12**, 692 (1970).

9) R. I. Novoselov and Z. A. Muzykantora, *Zh. Neorg. Khim.*, **15**, 3084 (1970).

10) G. S. Deshmukh and M. G. Bapat, *Z. Anal. Chem.*, **156**, 105 (1957).

11) D. Mohan and Y. K. Gupta, *J. Chem. Soc., Dalton*

Trans., **1977**, 1085, and references cited therein.
12) J. H. Karchmer, "The Analytical Chemistry of Sulfur and its Compounds," Wiley Interscience, New York (1970), Chemical Analysis Series, Vol. 29, Part 1, pp. 237—247.
13) R. D. Sauerbrum and E. E. Sandell, *J. Am. Chem. Soc.*, **75**, 4170 (1953).
14) H. A. Benesi and J. H. Hildebrand, *J. Am. Chem. Soc.*, **71**, 2703 (1949).
15) F. Basolo and R. G. Pearson, "Mechanisms of Inorganic Reactions," 2nd ed, John Wiley, New York (1967), (a) p. 35, (b) Chap. 4, (c) p. 140.
16) S. E. Livingstone, "Comprehensive Inorganic Chemistry," ed by J. C. Bailar *et al.*, Pergamon, New York (1973), Vol. 3, pp. 1230—1232.
17) R. Scholder and G. Schatz, *Angew. Chem.*, **2**, 264 (1963).
18) G. P. Haight, P. C. Richardson, and N. H. Coburn, *Inorg. Chem.*, **3**, 1977 (1964).
19) P. S. Radhakrishnamurti and B. Sahu, *Indian J. Chem.*, **17A**, 93 (1979), and references cited therein.
20) G. P. Panigrahi, S. N. Mohapatro, and P. K. Misro, *Indian J. Chem.*, **16A**, 1095 (1978), and references cited therein.
21) P. S. Radhakrishnamurti and B. Sahu, *Indian J. Chem.*, **16A**, 259 (1978), and references cited therein.
22) C. W. Davis, "Ion Association," Butterworths, London, (1962), Chap. 13.
23) J. Lewis and R. G. Wilkins, "Modern-Coordination Chemistry-Principles and Methods," Interscience, New York (1960), (a) D. R. Stranks, Chap. 2, p. 103, (b) F. J. C. Rossotti, Chap. 1, pp. 20—33.
24) W. M. Latimer, "Oxidation Potentials," 2nd ed, Prentice-Hall Inc., Englewood Cliffs, N. J. (1952), p. 75.
25) J. M. Lancaster and R. S. Murray, *J. Chem. Soc.*, *A*, **1971**, 2755, and references cited therein.
26) J. C. R. Legros, *Acad. Sci., Paris*, **242**, 1605 (1956).
27) At higher $[S_2O_3^{2-}]_o$, there is probably a further interaction involving the product $S_4O_6^{2-}$, in addition to the involvement of one more $S_2O_3^{2-}$ molecule; this should, we feel, provide the basis for further fruitful study.

Stability Constants of Some Chromium(II) Complexes

Roderick David CANNON*,† and Mohammad Jan GHOLAMI

Research Laboratory for Nuclear Reactors, Tokyo Institute of Technology, Ō-Okayama, Meguro-ku, Tokyo 152

(Received November 17, 1980)

Equilibria between the binuclear complex $Cr_2(O_2CMe)_4$ and various chelating ligands have been studied spectrophotometrically in acetate buffer media. Combining the results with previous data on the stability of $Cr_2(O_2CMe)_4$, we obtain formation constants for mononuclear chromium(II) complexes with the following ligands: malonate, $\log \beta_2 = 6.0 \pm 0.2$; *N*-methyliminodiacetate, $\log \beta_2 = 12.3 \pm 0.5$; ethylenediamine-*N*,*N*′-diacetate, $\log K_1 = 9.1 \pm 0.2$; at $T = 25$ °C, $I = 1.0$ M (1 M = 1 mol dm^{-3}) ($NaClO_4$).

In a previous paper[1] we showed that the binuclear chromium(II) complex present in aqueous acetate buffer media has the composition $Cr_2(O_2CMe)_4$, the same as in the solid state, and from a combination of solubility and spectrophotometric measurements, we obtained equilibrium constants for the reactions

$$Cr_2(O_2CMe)_4 \overset{K_{DO}}{\rightleftharpoons} 2\,Cr(O_2CMe)_2, \quad (1)$$

$$Cr_2(O_2CMe)_2 \overset{\beta_{A2}^{-1}}{\rightleftharpoons} Cr^{2+} + 2\,MeCO_2^-. \quad (2)$$

The binuclear complex is red-brown in colour, with $\lambda_{max} = 490$ nm, while mononuclear chromium(II) complexes are generally sky-blue, with λ_{max} in the range 600 to 700 nm. The contrast in colours makes it possible to study competitive monomer-dimer equilibria spectrophotometrically, and we have now used this method to obtain stability constants of the mononuclear chromium(II) complexes of malonate, *N*-methyliminodiacetate, and ethylenediamine-*N*,*N*′-diacetate ions.

Experimental

Preparations. Chromium(II) chloride stock solutions were prepared by zinc-reduction of chromium(III), and stored under nitrogen, as described previously.[1] The solutions contained Zn^{2+} ion equal to half the chromium(II) concentration, but this had little effect on the results, as shown by experiments in which an equal additional concentration of Zn^{2+} ion was added (see, Fig. 4).†† Organic acids were Reagent grade, recrystallized twice from water, and standardized by titration with sodium hydroxide. Sodium acetate and sodium perchlorate solutions were prepared by mixing the AnalaR acids with AnalaR sodium hydroxide solution, from freshly opened ampoules.

Measurements. A Beckman DB spectrophotometer was used, with modified temperature-control system.[1] The titration procedure was as previously described.[1]

† On leave from the School of Chemical Sciences, University of East Anglica, Norwich, NR4 7TJ, England; to which correspondence should be addressed.

†† The effect of zinc is expected to be a reduction in the concentration of free ligand by complex formation, thus decreasing the dissociation of the chromium(II) dimer. Since Cr^{2+} and Zn^{2+} stability constants are generally comparable, the greatest perturbation by Zn^{2+} is expected in the system for which dissociation of dimer to monomer is found to be greatest, *i.e.* the malonate system. If the zinc ions are completely complexed as ZnL_2^{2-}, the depletion of free malonate ion is about 10%, giving a reduction of about 0.1 in $\log f$ (see Eq. 15). This is within the experimental error. For the other ligands the effect is expected to be smaller.

Theory

Defining $[Cr_1]$ and $[Cr_2]$ as total concentrations of mononuclear and binuclear species, we may summarise the dimer-monomer equilibria in the solution in the equation

$$Cr_2 \overset{K_D}{\rightleftharpoons} 2\,Cr_1, \quad (3)$$

where K_D is the dimer dissociation constant averaged over all complexes, defined by

$$K_D = [Cr_1]^2/[Cr_2]. \quad (4)$$

In the absence of any ligands other than acetate ion, only one dimer species is important, hence we may write $[Cr_2] = [Cr_2(O_2CMe)_4]$ and $[Cr_1] = [Cr]_T - 2[Cr_2]$, where $[Cr]_T$ denotes the total chromium(II) concentration, giving

$$K_D = ([Cr]_T - 2[Cr_2(O_2CMe)_4])^2/[Cr_2(O_2CMe)_4]. \quad (5)$$

The concentration of $Cr_2(O_2CMe)_4$ may be calculated from the absorbance at 490 nm, using the known extinction coefficient,[1] and assuming that absorption by monomers is negligible. A plot of $[Cr_2(O_2CMe)_4]$ against $([Cr]_T - 2[Cr_2(O_2CMe)_4])^2$ is then expected to be a straight line of slope K_D^{-1}. When an additional ligand L is present which forms mononuclear complexes CrL_n, we have the additional reactions

$$(1/2)[Cr_2(O_2CMe)_4] + nL \overset{\beta_n'}{\rightleftharpoons} CrL_n + 2\,MeCO_2^-, \quad (6)$$

where $n = 1, 2, .. N$, $\beta_n' = (K_{DO})^{1/2}\beta_{A2}^{-1}\beta_n$, and β_n is the overall formation constant:

$$Cr^{2+} + nL \overset{\beta_n}{\rightleftharpoons} CrL_n. \quad (7)$$

(In Eqs. 6 and 7 some ionic charges are omitted). A calculation of the average dimer dissociation constant by the same method as before then yields the value K_D', where

$$K_D' = ([Cr^{2+}] + [CrO_2CMe^+] + [Cr(O_2CMe)_2] + \sum_1^N [CrL_n])^2/[Cr_2(OOCMe)_4]$$
$$= (\beta_{A2}^{-1}[MeCO_2^-]^{-2} + K_{A2}^{-1}[MeCO_2^-]^{-1} + 1 + \sum_1^N \beta_n[L]^n/\beta_{A2}[MeCO_2^-]^2)^2 K_{DO}, \quad (8)$$

where K_{A2} is the second stepwise formation constant of $Cr(O_2CMe)_2$. Equation 8 may be simplified to

$$(K_D')^{1/2} = (K_D)^{1/2} + (K_{DO})^{1/2} \sum_1^N \beta_n[L]^n/\beta_{A2}[MeCO_2^-]^2, \quad (9)$$

where K_D is the dissociation constant observed at the same acetate concentration in the absence of the ligand L. For the purpose of discussion we shall define the function

$$f = [(K_D')^{1/2} - (K_D)^{1/2}][MeCO_2^-]^2, \quad (10)$$

which in turn is related to [L] by

$$f([L]) = (K_{DO})^{1/2}\beta_{A2}^{-1} \sum_{1}^{N} \beta_n[L]^n. \quad (11)$$

The slope of a plot of log f against log ([L]) is equal to $\bar{n}$, the average value of n for complexes formed at a particular value of [L]. Knowing K_{DO} and β_{A2}, the values of β_n may be obtained.

Results

For each ligand, two sets of measurements were obtained. (1) With fixed total chromium(II), acetate, and acetic acid concentrations, the ligand concentration was varied over the range to be used in the later experiments. With increasing added ligand, the momomer and dimer absorbances increased and decreased respectively, and sharp isosbestic points were observed, *i.e.* at λ=600 nm (malonate system, Fig. 1), 620 nm (*N*-methyliminodiacetate system), 395 and 585 nm, (ethylenediamine-*N*,*N*'-diacetate system). This shows that oxidation to chromium(III) is negligible under the conditions of the experiments. (2) With fixed total acetate, acetic acid, and ligand concentrations, the chromium(II) concentration was varied, the first three all being in large excess over chromium(II). At low concentrations, the monomer absorption was dominant, but with increasing concentration the shape of the spectrum steadily changed to that of the dimer (Fig. 2). These experiments were repeated with different acetic acid, acetate and ligand concentrations. Typical plots of $[Cr_2]$ against $[Cr_1]^2$ are shown in Fig. 3.

Malonate (propanedioate) System. The total malonate concentration $[L]_T$ was varied over the range 0—0.09 M and for each malonate concentration, total chromium(II) was varied over the range 2—8 mM. The acetate and acetic acid concentrations were varied over the ranges 0.3—0.6 and 0.3—0.5 M. pK_a values of malonic acid[2] are such that in acetate buffer the first dissociation is complete, and the second partially complete (Eqs. 12—13, $L^{2-}=CH_2(CO_2)_2^{2-}$):

$$H_2L + MeCO_2^- \longrightarrow HL^- + MeCO_2H, \quad (12)$$

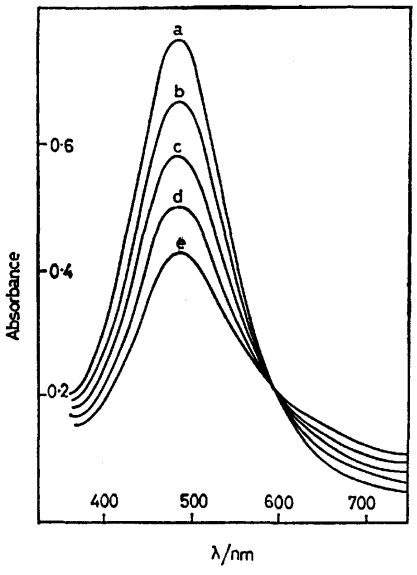

Fig. 1. Spectra of chromium(II) in acetate buffer with various concentrations of added malonic acid (H_2L). $[Cr]_T$=2.75 mM; $[L]_T$=0.0, 2.5, 5.0, 7.4, 9.9 mM (curves a to e respectively); $[MeCO_2H]=[MeCO_2^-]$= 0.2 M; I=1.0 M ($NaClO_4$). Path length 4 cm, T= 25 °C.

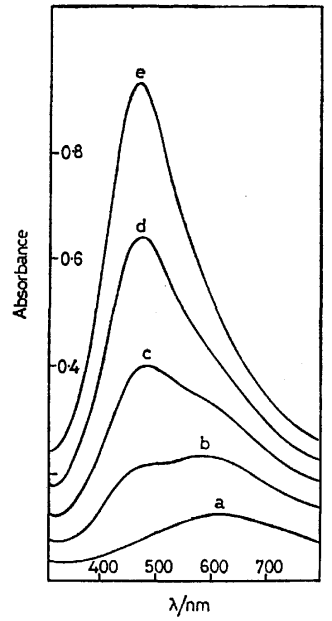

Fig. 2. Spectra of chromium(II) at various concentrations in an acetate-malonate mixture. $[L]_T$=50 mM; $[Cr]_T$=1.9, 3.7, 5.4, 7.0, 8.6 mM (curves a to e respectively); $[MeCO_2H]=[MeCO_2^-]$=0.3 M; I=1.0 M ($NaClO_4$). Path length 4 cm, T=25 °C.

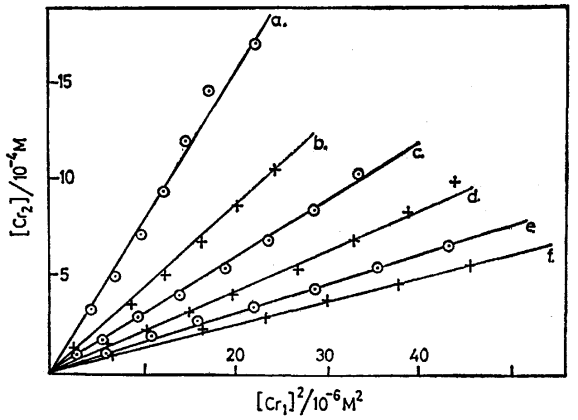

Fig. 3. Variation of chromium(II) dimer concentration with chromium(II) monomer concentration. $[Cr_2]=[Cr_2(O_2CMe)_4]$, $[Cr_1]=[Cr]_T-2[Cr_2]$. H_2L=malonic acid. $[L]_T$=40, 50, 60, 70, 80, 90 mM (curves a to f respectively); $[MeCO_2H]-2[L]_T=[MeCO_2^-]+2[L]_T$=0.3 M; I=1.0 M ($NaClO_4$). T= 25 °C.

$$HL^- + MeCO_2^- \overset{K_{Aa}^{-1}K_{La2}}{\rightleftharpoons} L^{2-} + MeCO_2H. \quad (13)$$

Hence we may write

$$[L^{2-}] = [L]_T/(1+K_{Aa}K_{La2}^{-1}[MeCO_2H]/[MeCO_2^-]), \quad (14)$$

where $[L]_T$ denotes total ligand concentration and K_{Aa} and K_{La2} are acid dissociation constants of $MeCO_2H$ and HL^-. Using $pK_{Aa}=4.58$ (the mean of three literature values at $I=1.0$ M)[2] and $pK_{La2}=5.15$,[3] we have $K_{Aa}K_{La2}^{-1}=3.7$. The plot of $\log f$ against $\log([L^{2-}])$, shown in Fig. 4(a), has the slope 2.0. This is consistent with the equation

$$f([L^{2-}]) = (K_{DO})^{1/2}\beta_{A2}^{-1}\beta_2[L^{2-}]^2, \quad (15)$$

which yields the parameters shown in Table 1.

N-Methyliminodiacetate System. The total ligand concentration was varied over the range $[L]_T=0$ to 0.12 M and total chromium(II) was varied over the range 0.8 to 3.1 mM. Acetate and acetic acid varied from 0.3 to 0.5 M. The acid H_2L has pK_a values 2.2 and 9.3,[4] hance we take $[HL^-]=[L]_T$, where HL^- denotes the ion $MeNH(CH_2CO_2)_2^-$. To show the dependence of f upon $[L^{2-}]$, we have plotted log f against $\log\{[HL^-][MeCO_2^-]/[MeCO_2H]\}$ in Fig. 4(c). The slope of 2.0 is consistent with the formation of CrL_2^{2-} as the predominant species:

$$HL^- + MeCO_2^- \overset{K_{Aa}^{-1}K_{La2}}{\rightleftharpoons} L^{2-} + MeCO_2H, \quad (16)$$

$$Cr^{2+} + 2\,L^{2-} \overset{\beta_2}{\rightleftharpoons} CrL_2^{2-}. \quad (17)$$

Using the equation

$$f([L^{2-}]) = (K_{DO})^{1/2}\beta_{A2}^{-1}\beta_2K_{La2}^2K_{Aa}^{-2} \times [HL^-]^2[MeCO_2^-]^2[MeCO_2H]^{-2}, \quad (18)$$

we obtain the parameters shown in Table 1.

Ethylenediamine-N,N′-diacetate System. With this ligand complexation was less than with the others, and it was necessary to use lower acetate concentrations ($[MeCO_2H]+[MeCO_2^-]=0.4$ M) in order to displace the equilibrium 6 to the right. The total ligand concentration $[L]_T$ was varied over the range 0 to 0.10 M, and total chromium(II) over the range 0.8 to 3.5 mM. The acetic acid-dependence of f was not studied. From the acid dissociation constants, $pK_{La1}=6.7$ and $pK_{La2}=9.9$,[5] we have $[L]_T=[H_2L]$. The plot of $\log f$ against $\log([H_2L])$ has a slope of 1.0 (Fig. 4(b). Hence the equation

$$f([L^{2-}]) = (K_{DO})^{1/2}\beta_{A2}^{-1}K_1K_{La1}K_{La2}K_{Aa}^{-2}[H_2L] \times [MeCO_2^-]^2[MeCO_2H]^{-2}, \quad (19)$$

was used to obtain the parameters shown in Table 1.

Other Ligands. With 5-sulfosalicylate(3-carboxy-4-hydroxybenzenesulfonate) ion, under our conditions ($[L]_T=0.01$ to 0.12 M, $[MeCO_2^-]=0.06$ to 0.3 M, $[MeCO_2H]=0.32$ to 0.62 M), dissociation of the $Cr_2(O_2CMe)_4$ complex was only slightly greater than that observed in the absence of added ligand. Assuming the complex CrL^-, we calculate an upper limit for log K_1 as shown in Table 1. With glycine, no dissociation could be detected. With edta, dissociation of the dimer into monomer was complete.

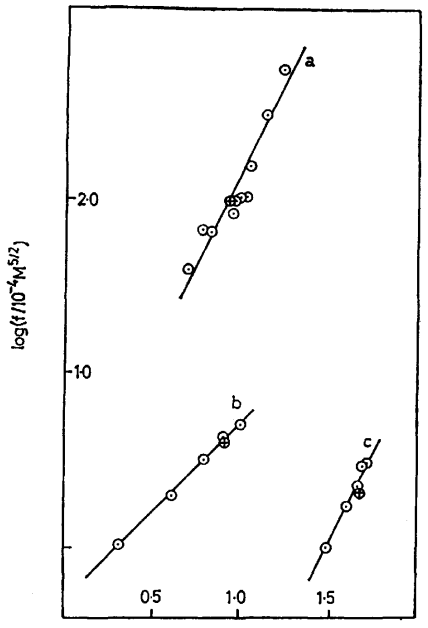

Fig. 4. Plots of log f (see text, Eqs. 10—11) against (a) $\log([L^{2-}]/10^{-3}\,M)$, H_2L=malonic acid; (b) log $([H_2L]/10^{-2}\,M)$, H_2L=ethylenediamine-*N*,*N*′-diacetic acid, $[MeCO_2H]=[MeCO_2^-]$; (c) $\log([HL^-][MeCO_2^-][MeCO_2H]^{-1}/10^{-3}\,M)$, H_2L=*N*-methyliminodiacetic acid. Points ⊙, $[Zn]=(1/2)[Cr]_T$; points ⊕, $[Zn]_T=[Cr]_T$.

Discussion

For the chromium(II)–malonate system, Fukuda

TABLE 1. SUMMARY OF RESULTS

Ligand	Reaction[a]	log Q[b]	log (β_n/M^n)[c]
Malonate	$(1/2)Cr_2A_4+2L^{2-} \rightleftharpoons CrL_2^{2-}+2A^-$	2.23 ± 0.10	$\log\beta_2 = 6.0\pm0.2$
5-Sulfosalicylate	$(1/2)Cr_2A_4+HL^{2-} \rightleftharpoons CrL^-+HA+A^-$	$\leqslant -2.64$	$\log K_1 \leqslant 7.8$
N-Methyliminodiacetate	$(1/2)Cr_2A_4+2HL^- \rightleftharpoons CrL_2^{2-}+2HA$	-0.98 ± 0.03	$\log\beta_2$ 12.3±0.5[d]
Ethylenediamine-*N*,*N*′-diacetate	$(1/2)Cr_2A_4+H_2L \rightleftharpoons CrL+2HA$	-2.30 ± 0.10	$\log K_1 = 9.1\pm0.2$[e]

a) A^-: $MeCO_2^-$, L^{2-} or L^{3-}: the anion specified in column 1. b) Q: equilibrium constant of reaction specified in column 2; units $M^{1/2}$ or $M^{3/2}$. Temperature 25 °C, ionic strength, $I=1.0$ M ($NaClO_4$). Limits of error are root-mean-square deviations of $\log f$ from the lines shown in Fig. 4. c) β_n refers to the reaction $Cr^{2+}+nL \rightleftharpoons CrL_n$, calculated using $\log[(K_{DO}/M)^{1/2}]=-2.17$, $\log(\beta_{A2}/M^{-2})=1.70$ (Ref. 1). Limits of error are rough estimates. d) Calculated using $pK_a=4.6$ for HA (Ref. 2) and $pK_a=9.3$ for HL^- (Ref. 4). e) Calculated using $pK_a=4.6$ for HA (Ref. 2) and $pK_{a2}=6.68$ and 9.85 for H_2L (Ref. 5), neglecting the difference in ionic strength in the latter case.

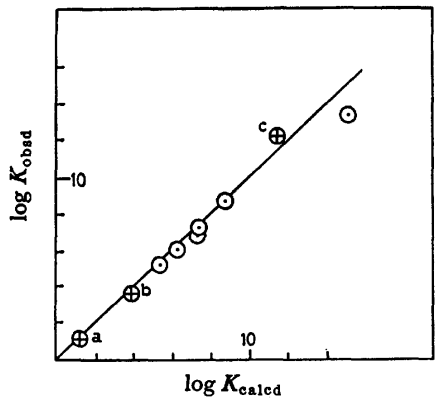

Fig. 5. Comparison of observed stability constants (log K_1) of chromium(II) complexes with those calculated from Eq. 20 of the text. Points ⊙, previous data (Ref. 8). Points ⊕, subsequent data: (a) $MeCO_2^-$ (Ref. 1); (b) malonate (Ref. 6); (c) *N*-methyliminodiacetate (this work). For point (c), log β_2 is plotted, not log K_1. Note that equation 20 yields log K_1= 7.4 (Ref. 8), and log K_2=4.2, using data from the same original sources.

et al.,[6] reported log K_1=3.92, log K_2=3.21. Our value log β_2=6.0 is more consistent with log $K_1 \cong 4$, log K_2=2, bearing in mind the usual difference between first and second stepwise stability constants of chelate complexes.[2] The formation curve reported by Fukuda *et al.*, deviates from the expected S-shape and it seems possible that their value of log K_1 is more reliable than that of log K_2. For the 5-sulfosalicylate system, the limiting value log $K_1 \leqslant 7.8$ is consistent with that of Pecsok and Schaefer (7.1)[7] but not with that of Fukuda *et al.* (9.9).[6]

Cannon[8] previously put forward an empirical expression for stability constants of chromium(II) complexes, based on the Irving-Williams series:

$$\log K_{Cr} = \alpha \log K_{Cu} + \frac{1}{5}(6-\alpha) \log K_{Mn} - \frac{1}{5}(1+4\alpha) \log K_{Zn}. \quad (20)$$

Here K_{Cr}, K_{Cu}, K_{Mn}, and K_{Zn} are stability constants of Cr^{2+}, Cu^{2+}, Mn^{2+}, and Zn^{2+} complexes with the same ligand under the same conditions (they may be step-constants K_n or overall constants β_n), and α=0.55. A comparison of predicted and observed values of log K_{Cr} is shown in Fig. 5, and it can be seen that the new data are in satisfactory agreement with the formula.

The experimental work was carried out at the University of East Anglia. Funds for equipment were provided by the Science Research Council. M. J. G. held an Iranian Government Scholarship for study abroad. R. D. C. held a Foreign Lectureship under the British Council/Mombusho scheme.

References

1) R. D. Cannon and M. J. Gholami, *J. Chem. Soc., Dalton Trans.*, **1976**, 1574.
2) "Stability Constants of Metal-Ion Complexes," ed by L. G. Sillén and A. E. Martell, The Chemical Society Special Publications Nos. 17 and 25, London (1964 and 1971).
3) H. Moriya and T. Sekine, *Bull. Chem. Soc. Jpn.*, **47**, 747 (1974).
4) R. D. Cannon and J. Gardiner, *J. Chem. Soc., Dalton Trans.*, **1972**, 887.
5) N. I. Sevostyanova, L. N. Martynenko, and V. I. Spitsyn, *Zh. Neorg. Khim.*, **15**, 1234 (1970); *Russ. J. Inorg. Chem.*, **15** 633 (1970).
6) Y. Fukuda, E. Kyuno, and R. Tsuchiya, *Bull. Chem. Soc. Jpn.*, **43**, 745 (1970).
7) R. L. Pecsok and W. P. Schaefer, *J. Am. Chem. Soc.*, **83**, 62 (1961).
8) R. D. Cannon, *J. Inorg. Nucl. Chem.*, **38**, 222 (1976).

Polarographic Behavior of 4-Morpholine Carbodithioate and Its Use in the Amperometric Determination of Metal Ions

A. L. J. Rao,* Bikram S. Brar, and B. K. Puri†

Department of Chemistry, Punjabi University, Patiala-147002, India

† *Department of Chemistry, Indian Institute of Technology, Hauz Khas, New Delhi-110016, India*

(Received April 20, 1981)

Polarographic behavior of 4-morpholine carbodithioate has been studied in various base electrolytes. It gives a well defined, diffusion controlled, reversible with one electron change, anodic wave above pH 9 extending over a fairly wide span of potential, +0.2 V to −0.3 V *vs.* SCE. The relation between diffusion current and concentration is linear upto 2.7 mM (1 M=1 mol dm^{-3}) of the reagent. The reagent has been successfully applied for the amperometric determination of Bi^{3+}, Cu^{2+}, Ni^{2+}, Te^{4+}, and Zn^{2+} individually as well as in mixtures like Cu–Zn and Cu–Ni. Conditions have also been developed for the determination of copper, nickel, and zinc in various alloys. The error does not exceed more than ±0.85% in any case. The method is simple, less time consuming and easily adoptable for the micro determination of these metal ions.

4-Morpholine carbodithioates of many metals were prepared and characterized by Brown[1] and Marcotrigiano and coworkers.[2] Zinc complex has been used as a releasing agent in atomic absorption spectrometry of noble metals.[3] Beyer and Ott utilized this compound in the spectrophotometric determination of some metal ions.[4] Recently potassium salt of this reagent has been used in the gravimetric determination of tellurium, copper, bismuth, zinc, cadmium, and mercury.[5–8] Some of the metal ions have also been characterized by thin layer[9] and paper chromatography[10] using this reagent. Extraction behavior of some divalent metals with this reagent have also been studied.[11] In the present paper, the polarographic study of 4-morpholine carbodithioate in various supporting electrolytes has been undertaken with a view to explore the possibility of utilizing it as an analytical reagent for the amperometric determination of various metal ions.

Experimental

Reagents. Sodium 4-morpholine carbodithioate was prepared by the method reported by Marcotrigiano.[2] Stock solution of sodium 4-morpholine carbodithioate was prepared by dissolving a calculated amount in distilled water and standardized against a standard solution of mercury(II) nitrate using diphenyl carbazone as the indicator. The base electrolytes, potassium nitrate, potassium chloride, sodium perchlorate, ammonium tartrate, tetraethylammonium bromide, and buffers like Britton-Robinson, Michaelisborate and ammonia–ammonium chloride were prepared in distilled water from their G. R. samples. Stock solutions of various metal ions were prepared from their G.R. samples and standardized by known methods.[12]

Equipment. Polarograms in all the cases were recorded at 25±0.5 °C with a manual Toshniwal polarograph. An H-type cell with fine porosite sintered glass disk between the two compartments was used. A saturated calomel electrode used as a reference electrode was connected to one compartment of the polarographic cell through potassium chloride-agar bridge. Dropping mercury electrode had the following characteristics, m=2.08 mg/s, t=3.10 s, and H=50 cm in aqueous solution of the base electrolyte with open circuit. In all instances, the solution was deaerated with nitrogen before recording the polarogram. An ECIL digital pH meter with glass electrode was used.

Results and Discussion

Effect of pH on the Polarogram of 4-Morpholine Carbodithioate. Polarograms for 1.25 mM carbodithioate in 0.1 M ammonium tartrate +0.1 M potassium nitrate were recorded at different pH values in the range of 5.75—11.7 using Britton-Robinson buffer. An anodic wave associated with a small prewave at more negative potentials was obtained at all pH values below 9. At pH above 9.0, the prewave was almost disappeared (Fig. 1). Even though the nature of the wave remained unaffected, the values of $E_{1/2}$ shifted towards more negative potentials with

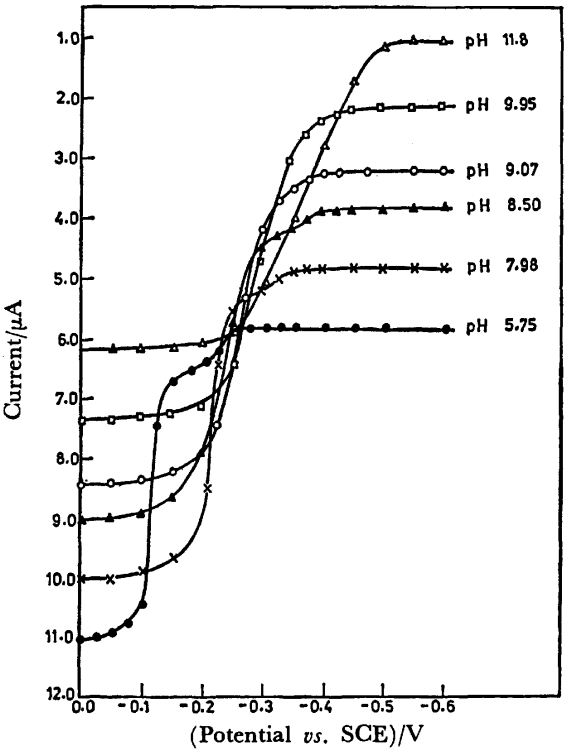

Fig. 1. Effect of pH on the polarograms of 4-morpholine carbodithioate.
4-Morpholine carbodithioate taken=1.25 mM, base electrolyte=0.1 M ammonium tartrate +0.1 M potassium nitrate, m=2.08 mg/s, drop time=3.10 s.

TABLE 1. EFFECT OF pH ON THE HALFWAVE POTENTIAL OF SODIUM 4-MORPHOLINE CARBODITHIOATE

Sodium 4-morpholine carbodithioate = 1.25 mM.
Base electrolyte = 0.1 M ammonium tartrate + 0.1 M potassium nitrate.
m = 2.08 mg/s, t = 3.10 s.

pH	$E_{1/2}$ *vs.* SCE / V	Remarks
5.75	−0.115	Pre-wave appeared
6.18	−0.135	Pre-wave appeared
6.52	−0.150	Pre-wave appeared
7.02	−0.175	Pre-wave appeared
7.51	−0.195	Pre-wave appeared
7.98	−0.215	Pre-wave appeared
8.52	−0.235	Pre-wave appeared
9.07	−0.260	Pre-wave disappeared Well define single wave obtained
9.58	−0.285	Pre-wave disappeared Well define single wave obtained
9.93	−0.300	Pre-wave disappeared Well define single wave obtained
11.26	−0.355	Pre-wave disappeared Well define single wave obtained
11.68	−0.375	Pre-wave disappeared Well define single wave obtained

increase in pH (Fig. 1, Table 1).

Polarograms of 1.25 mM of the reagent solution recorded in different buffers such as Britton-Robinson, Michaelisborate, NH_3–NH_4Cl showed that the nature of the wave was not affected by the constituents of buffers.

Effect of Various Supporting Electrolytes and Solvents. Polarograms of 1.25 mM carbodithioate at pH 9.58 in presence of 0.1 M several supporting electrolytes and solvents were recorded. The nature of the wave remained unchanged and the diffusion current constant was found to increase in the following order:

$(C_2H_5)_4NBr > KNO_3 > KCl > NaClO_4$ and

Acetonitrile > Methanol > Ethanol > DMSO > 2-Propanol.

This may be due to the variation in viscosity of the solution,[13] ($I \propto 1/\text{viscosity}$).

Effect of Mercury Pressure. Polarograms for 1.45 mM of the carbodithioate solution at various heights of the mercury column were recorded. The linear dependence of the limiting current on the square root of the height of the mercury column indicates that the rate of oxidation of 4-morpholine carbodithioate is diffusion controlled.

Effect of 4-Morpholine Carboditioate Concentration. Several polarograms with varying concentration of the reagent were recorded in 0.1 M ammonium tartrate +0.1 M potassium nitrate+ammonia buffer of pH 9.6. The anodic wave extends over a fairly wide span of potential (0.2 V to −0.3 V *vs.* SCE). The plot of diffusion current *vs.* concentration gave a straight line upto 2.7 mM of the reagent. The mean value of diffusion current constant determined with the Ilkovic equation, $I = i_d/cm^{2/3}t^{1/6}$ was found to be 1.64, which indicates the method may be applied

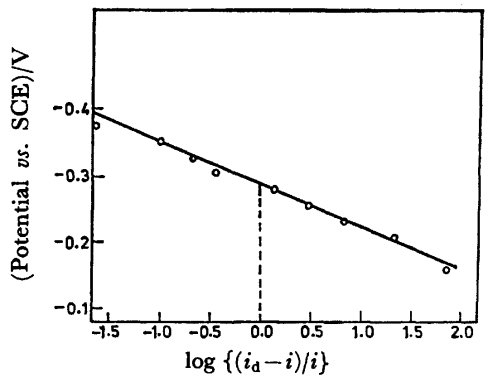

Fig. 2. Plot of $\log\{(i_d-i)/i\}$ *vs.* $E_{d.e.}$ for 2.7 mM sodium 4-morpholine carbodithioate in 0.1 M tartrate buffer (pH 11.7). Rest of the conditions are the same as in Fig. 1.

for the quantitative determination of 4-morpholine carbodithioate.

The electrooxidation of the reagent may not involve the formation of disulfide, RSSR (R=4-morpholine–thiocarbonyl) because the plots of $\log\{(i_d-i)/i\}$ *vs.* E did not yield a straight line with a slope 0.059 V/2, but yield a straight line with a slope of 0.065 V (Fig. 2) for one electron transfer. Also from Lingane equation, 1.5 $n=I$, the value of "n" corresponds to 1 to allow the conclusion that:

$$RSH + Hg \rightleftharpoons RSHg + H^+ + e \quad (1)$$

may represent the electrode reaction. Furthermore, the $E_{1/2}$ values were found to be independent of [RSH] which is characteristics of Eq. 1.

In the amperometric procedures reported for the determination of zinc,[14–15] copper,[16–17] nickel,[18] bismuth,[19] and tellurium,[20–21] the titrations have been carried out at a potential corresponding to the reduction wave of the cation concerned. It may be pointed out that an electroactive organic compound which is capable of forming an insoluble precipitate with these cations may serve as a potential titrant in their estimation. In this connection, the use of 4-morpholine carbodithioate as an analytical reagent for the quantitative estimation of bismuth, copper, nickel, tellurium(IV), and zinc has been investigated. Preliminary observations showed that under regulated conditions of base electrolyte concentration and pH, the reagent reacted with these cations to give characteristic precipitates. These observations paved the way to the estimation of microquantities of these cations by the amperometric titration procedure. The appropriate operative conditions for the quantitative estimation were established by trial experiments and are summarised in Table 2.

The applied potential (−0.2 V for Zn^{2+} and Ni^{2+}, −0.05 V for Bi^{3+}; and Te^{4+}; −0.01 V for Cu^{2+}, *vs.* SCE) was such that the metal ion was not reduced but the reagent was oxidized at the DME. The titration, therefore, involved the measurement of the anodic current of the excess titrant only after complete precipitation. Reverse L shaped curves were obtained by plotting these readings against the volume of the titrant and the end point was located graphically (Fig. 3).

Table 2. Optimum conditions for the amperometric titration of metal ions

Metal	Potential of DME *vs.* SCE V	Supporting electrolytes	pH
Bismuth	−0.05	0.1 M Potassium nitrate 0.1 M Sodium acetate	4.5— 6.5
Copper	−0.01	0.05 M Ammonium tartrate 0.1 M Potassium nitrate	6.2—10.2
Nickel	−0.20	0.05 M Ammonium chloride 0.05 M Ammonium nitrate	7.0— 8.5
Tellurium(IV)	−0.05	0.1 M Sodium acetate acetic acid	5.0— 6.4
Zinc	−0.20	0.1 M Ammonium acetate 0.1 M Potassium nitrate	5.0— 6.4

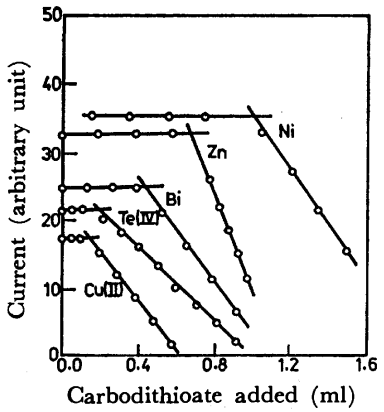

Fig. 3. Typical amperometric titration curves of bismuth, copper, nickel, tellurium(IV), and zinc. Bismuth(M/600): 2.00 ml+0.1 M sodium acetate+acetic acid (pH : 5.8). Applied potential −0.05 V *vs.* SCE. Carbodithioate: 2×10^{-2} M. Copper (1.0×10^{-3} M): 1.50 ml+0.05 M ammonium tartrate +0.1 M potassium nitrate (pH: 8.7). Applied potential: −0.01 V *vs.* SCE. Carbodithioate: 2×10^{-2} M. Nickel (1.0×10^{-3} M): 5.00 ml+0.05 M ammonium chloride+0.05 M ammonium nitrate (pH: 8.0). Applied potential −0.2 V *vs.* SCE. Carbodithioate: 0.01 M. Tellurium(IV) (2.0×10^{-3} M): 0.95 ml+0.1 M sodium acetate+acetic acid (pH: 5.7). Applied potential −0.05 V *vs.* SCE. Carbodithioate: 4×10^{-2} M. Zinc (1.0×10^{-3} M): 3.75 ml+0.1 M ammonium acetate+0.1 M potassium nitrate (pH: 6.4). Applied potential: −0.2 V *vs.* SCE. Carbodithioate: 0.01 M.

Table 3. Amperometric determination of metal ions with 4-morpholine carbodithioate

Conditions same as in Fig. 3.

Cation	Amount taken mg	Amount found mg	Error %
Bismuth	0.348	0.348	0.00
	0.696	0.693	−0.43
	1.393	1.389	−0.28
	1.672	1.675	+0.18
	2.089	2.098	+0.43
Copper	0.095	0.095	0.00
	2.254	0.253	−0.39
	0.635	0.633	−0.31
	0.826	0.829	+0.36
	1.016	1.013	−0.29
Nickel	0.088	0.088	0.00
	0.176	0.175	−0.56
	0.294	0.295	+0.34
	0.352	0.350	−0.56
	0.440	0.438	−0.45
Tellurium(IV)	0.242	0.243	+0.41
	0.497	0.495	−0.40
	0.765	0.769	+0.52
	1.301	1.296	−0.38
	1.607	1.600	−0.43
Zinc	0.098	0.098	0.00
	0.176	0.177	+0.56
	0.359	0.358	−0.28
	0.490	0.492	+0.42
	0.555	0.553	−0.36

In a series of experiments an aliquot of the unknown solution of the cation was taken in the cell containing appropriate base electrolyte. The pH of the medium was adjusted to the desired value (Table 2). The solution was thoroughly deaerated by a slow stream of nitrogen gas. Necessary connections were made and the desired potential was applied to the dropping mercury electrode. A 2 ml microburette was used to deliver the titrant in small increment. In each case, the solution was stirred with nitrogen and the precipitate was allowed to stand for 1—2 min before observing the current reading. The mean deflection of the galvanometer was noted in each case. In all these determinations the solution taken in the burette was kept 20 times stronger than the solution in the cell in order to eliminate dilution effect. The end point was located graphically as the point of intersection of two straight lines (Fig. 3). The results are presented in Table 3, indicate that the microquanties of these cations can be estimated accurately.

Interferences. Metal ions such as Mo(VI), W-(VI), Te(VI), V(V), Th(IV), U(VI), Zr(IV), As-(III), Sb(III), Mg(II), Ca(II), Sr(II), Ba(II), In-(III), upto 10 fold excess; Cr(III), Al(III), and Fe-(III) upto 4-fold excess (they are precipitated as their hydroxide before titration) and Se(IV) in equal quantities can be tolerated in all cases. The interference of Pb(II), Tl(I), and Ag(I) was eliminated with sulfate and chloride ions before the titration. The interference of Cd(II), Ni(II), Hg(II), Co(II), and Zn(II) was eliminated in the determination of Te(IV), and Bi(III) by masking them with cyanide ions[22] (5 ml of 5% solution of sodium cyanide). Te-(IV) only interfered in the determination of bismuth.

In the determination of copper, Cd(II), Ni(II), Co(II), and Bi(III) interfered but the interference of Ni(II) and Co(II) can be eliminated by their successive determinations. Only Zn(II), Cd(II), and Bi(III) interfered in the analysis of nickel. Cd(II), Ni(II), Co(II), Bi(III), and Cu(II) interfered in the determination of zinc. The interference of copper can be eliminated by their successive determination. Obviously these methods are sufficiently selective and may be applied for the determination of these metal ions in complex materials. The method is quite simple rapid and easily adoptable.

It is obvious from the above results (Table 2) that some metals react with this reagent in alkaline medium while other do not. It is thus possible to titrate one metal of a mixture at higher pH and then by changing the pH after the end point to continue the titration of the other metal. This was demonstrated with a mixture of copper–zinc and copper–nickel.

Two methods have been used for the amperometric titrations. The first utilizes the decrease in height of the reduction wave of the uncomplexed copper ion during the course of titration. The second is based on the measurement of the anodic diffusion current of the excess titrating agent after the end point (Fig. 4). A combination of these two methods makes possible the determination of mixture of these metal ions.

Simultaneous Determination of Cu–Zn and Cu–Ni. To an aliquot of the synthetic mixture containing copper+zinc or copper+nickel, added 0.1 M potassium nitrate +0.01% gelatin and aqueous ammonia (pH 9.8) for the first and 0.05 M ammonium acetate +0.05 M potassium nitrate+0.01% gelatin for the second mixture. The total volume was made 20 ml in each case. The residual current of the air free solutions was noted at −0.2 V *vs.* SCE. Under these conditions only copper reacts. The titration was carried out with the reagent solution. In each case, the solution was stirred with nitrogen gas before recording the galvanometer reading. After the copper end point the pH was lowered to ≈6.5 for zinc and 7.2 for nickel by adding 1 M acetic acid at the same potential and determined the mixture end point as the intersection between residual and excess reagent lines. A series of experiments with mixture containing copper+zinc or copper+nickel in different ratios were performed. The results are given in Tables 4 and 5 respectively.

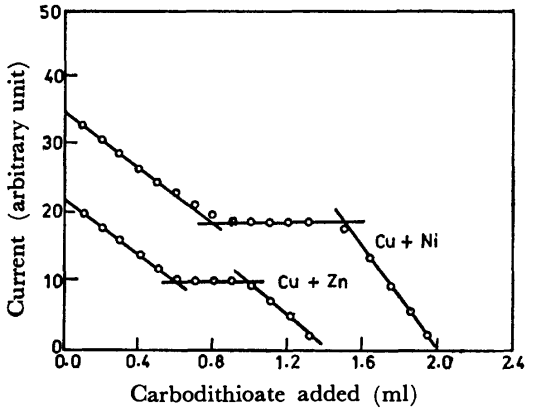

Fig. 4. Typical amperometric titration curves of Cu+Zn and Cu+Ni.
Cu+Zn: Cu(1.0×10^{-3} M): 3.00 ml+Zn(1.0×10^{-3} M): 2.00 ml+0.1 M potassium nitrate +0.01% gelatin+ammonia, pH 9.8 upto copper end point; 0.1 M potassium nitrate +0.01% gelatin+ammonium acetate, pH: 6.4 after copper end point. Applied potential: −0.2 V *vs.* SCE. Carbodithioate: 0.01 M. Cu+Ni: Cu(2.0×10^{-3} M): 4.00 ml+Ni(2.0×10^{-3} M): 3.5 ml+0.05 M ammonium chloride+0.05 M ammonium nitrate, +0.01% gelatin pH 9.5 upto copper, pH 7.2 after copper, end point. Applied potential: −0.2 V *vs.* SCE. Carbodithioate: 2×10^{-2} M.

Analysis of Alloys. 0.1 g of the alloy was taken in a beaker to which were added 10 ml of concentrated hydrochloric acid and a few ml of concentrated nitric acid. This was heated on a hot plate till the mixture dissolved completely and the solution was reduced to about 5 ml. The solution was cooled, added 5 ml of concentrated hydrochloric acid, then diluted and the final volume was made 100 ml exact

Table 4. Simultaneous determination of copper and zinc

Supporting electrolyte=0.1 M potassium nitrate+0.01% gelatin+ammonia, pH 9.8 upto copper end point; 0.1 M potassium nitrate+0.01% gelatin+ammonium acetate; pH 6.4 after copper end point.
Sodium 4-morpholine carbodithioate=0.01 M.
Applied potential=−0.2 V.

Amount taken mg		Amount found mg		Error/%	
Copper	Zinc	Copper	Zinc	Copper	Zinc
0.254	0.098	0.255	0.098	+0.39	0.00
0.222	0.164	0.222	0.165	0.00	+0.64
0.190	0.130	0.191	0.129	+0.52	−0.76
0.159	0.196	0.160	0.197	+0.60	+0.51
0.127	0.262	0.127	0.261	0.00	−0.38
0.095	0.228	0.095	0.227	0.00	−0.43

Table 5. Simultaneous determination of copper and nickel

Supporting electrolyte=0.05 M ammonium chloride+0.05 M ammonium nitrate, ammonia pH 9.5 upto copper end point, pH 7.2 after copper end point.
Sodium 4-morpholine carbodithioate=2×10^{-2} M.
Applied potential=−0.2 V.

Amount taken mg		Amount found mg		Error/%	
Copper	Nickel	Copper	Nickel	Copper	Nickel
0.127	0.734	0.127	0.731	0.000	−0.40
0.317	0.528	0.318	0.530	+0.31	+0.37
0.501	0.411	0.503	0.409	+0.39	−0.48
0.698	0.294	0.695	0.294	−0.43	0.00
0.952	0.117	0.957	0.116	+0.52	−0.85

Table 6. Determination of metals in alloys

Alloy	Composition/% Certified	Found (Average)	Error/%
Mallory No. 3	Cu:99.2 Cr:0.8	Cu:99.0	−0.20
Inconel 600	Ni:74.20, C:0.15, Mn:1.00, Fe:8.10, S:0.50, Cu:0.50 Cr:15.50, Si:0.05	Ni:74.60	+0.54
Brass No. 41.2	Cu:58.20 Zn:39.00, Pb:2.58, Fe:0.09; Sn:0.13	Cu:58.40 Zn:39.20	+0.34 +0.51
Monel wire	Cu:31.10, Ni:66.20 Fe:1.18, Mn:1.08 Mg:0.093, Al:0.93 Si:0.083, C:0.083 S:0.0037	Cu:31.00 Ni:66.60	−0.32 +0.60

in a measuring flask. The results for the determination of copper in Mallory No. 3, Nickel in Inconel-600 and the simultaneous determination of copper+zinc in Brass No. 41.2, copper+nickel in Monel wire are presented in Table 6.

Sincere thanks of the authors are due to CSIR, New Delhi for the award of a Senior Research Fellowship to one of them (BSB).

References

1) D. H. Brown, G. Aravamudan, and D. Venkappayya, *J. Chem. Soc., A*, **17**, 2744 (1971).
2) G. Marcotrigiano, G. C. Pellacani, C. Preti, and G. Tosi, *Bull. Chem. Soc. Jpn.*, **48**, 1018 (1975).
3) D. J. Nicolas and E. A. Jones, *Natl. Inst. Metall. Repub. S. Afr. Rep.* **1825** (1976); *Chem. Abstr.*, **86**, 149963z (1977).
4) W. Beyer and R. D. Ott, *Mikrochim. Inchnoanal. Acta*, 1130 (1965).
5) N. Singh, R. Kumar, and R. C. Agrawal, *Curr. Sci.*, **46**, 851 (1977).
6) N. Singh, R. Kumar, and B. D. Kansal, *J. Indian Chem. Soc.*, **55**, 240 (1978).
7) N. Singh, R. C. Agarwal, V. K. Maheshwari, and R. Kumar, *J. Indian Chem. Soc.*, **55**, 961 (1978).
8) N. Singh, S. K. Kulshreshta, A. K. Agarwal, and T. N. Srivastava, *Curr. Sci.*, **48**, 204 (1979).
9) N. Singh, R. Kumar, and B. D. Kansal, *Chromatographia*, **11**, 408 (1978).
10) R. Kumar and N. Singh, *Curr. Sci.*, **47**, 422 (1978).
11) V. S. Sastri, K. I. Aspila, and C. K. Chakorabarti, *Can. J. Chem.*, **47**, 2320 (1969).
12) A. I. Vogel, "Textbook of Quantitative Inorganic Analysis," Longmans, Green & Co., London (1964).
13) N. A. Lange, "Handbook of Chemistry," McGraw-Hill, New York (1966).
14) G. S. Deshmukh and V. S. S. Rao, *Chem. Ind. (London)*, **42**, 1434 (1968).
15) A. I. Petukhova and V. F. Toropova, *Izv. Vyssh. Uchebn. Zaved., Khim. Khim. Tekhnol.*, **17**, 1253 (1974); *Chem. Abstr.*, **82**, 38228 m (1975).
16) M. Pryszezewska and E. Krzeszowka, *Talonta*, **18**, 638 (1971).
17) F. Freese, H. J. Jasper, and G. Don Boef, *Talanta*, **17**, 945 (1970).
18) V. I. Suprunovich, Zh. B. Kulikovskaya, and S. N. Pirozhok, *Zavod. Lab.*, **45**, 293 (1979).
19) E. F. Denilenko and Yu. I. Usatenko, *Khim. Tekhnol. (Kharkov)*, **18**, 164 (1971).
20) O. A. Songina, V. A. Zakharov, I. M. Bessarabova, P. Rakhimzhanov, and I. I. Safonov, *Zh. Anal. Khim.*, **27**, 1121 (1972).
21) V. V. Voloshina, Yu. I. Usatenko, and A. M. Arishkevich, *Zavod. Lab.*, **36**, 530 (1970).
22) D. D. Perrin, "Masking and Demasking of Chemical Reactions," Wiley-Interscience, New York (1970).

 © 1982 The Chemical Society of Japan Bull. Chem. Soc. Jpn., 55, 603—606 (1982)

Linear Solvation Energy Relationships. 18. Solvent Effects on the Electronic Absorption Spectrum of *p*-Nitrophenoxide Ion

José-Luis M. Abboud,* Robert W. Taft,*,† and Mortimer J. Kamlet*,††

Département de Chimie, Faculte des Sciences, Université Cadi Ayyad, Marrakech, Morocco

† *Department of Chemistry, University of California, Irvine, California 92717, U. S. A.*

†† *Naval Surface Weapons Center, White Oak Laboratory, Silver Spring, Maryland 20910, U. S. A.*

(Received May 6, 1981)

A quantitative analysis of the effects of hydroxylic and aprotic solvents on the electronic absorption spectrum of 4-nitrophenoxide anion is described. By means of linear solvation energy relationships, the contributions of solvent dipolarity, polarizability, and hydrogen bonding are assessed. A significant conclusion is that ion-pairing strongly influences the 4-nitrophenoxide ion in aprotic solvents, but not in hydroxylic solvents. In the latter, specific solvation of both the nitro group and the phenoxide ion center are important.

The last two decades have witnessed a steady effort in the field of study of solvent effects on the UV-visible spectra of polar solutes. An important result of this work has been the development of a number of empirical solvent polarity scales.[1] Recently, the ability of bulk solvents to act as proton donors in hydrogen bonding interactions has also been quantified.[2] Although a number of questions still remain unanswered, we feel that sufficient information is already available to allow the use of these scales in order to gain structural and mechanistic information. Thus the π^* scale of solvent dipolarity/polarizabilities[3] and the α scale of solvent HBD (hydrogen bond donor) acidities[2] have been extensively used[4] to analyze solvent effects on physical properties and chemical reactivity.

Ueji and Kitadani (henceforth abbreviated as U. and K.) have recently described in this journal the influence of solvents on the absorption spectrum of sodium *p*-nitrophenoxide.[5] By adding substantial amounts of 15-crown-5, these authors were able to obtain the spectrum in a wide variety of solvents. The frequencies, $\nu(\mathbf{1})_{max}$, corresponding to the $\pi\rightarrow\pi^*$ electronic transition of 4-nitrophenoxide ion (represented by canonical structures **1a—d**) in a number of solvents are given in Table 1, together with solvent π^* and α values.

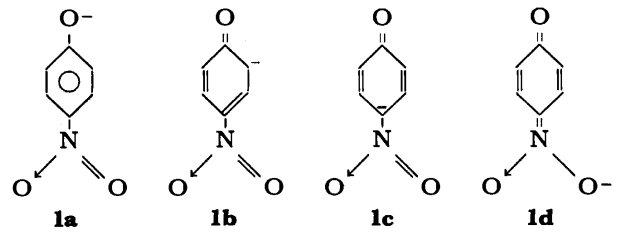

1a **1b** **1c** **1d**

Inspection of the $\nu(\mathbf{1})_{max}$ values shows two different effects: one is a bathochromic shift with increasing solvent dipolarity/polarizability; the other is a hypsochromic shift with increasing HBD acidity of the solvent. U. and K. have pointed out and discussed both effects. While we basically agree with their interpretation of the experimental results, we wish to reexamine them from a somewhat more quantitative standpoint. Our aim is to demonstrate that, when solvent dipolarity, polarizability, and hydrogen bonding effects on $\nu(\mathbf{1})_{max}$ are unravelled by means of the solvatochromic comparison method, the same experimental data can be made to yield additional important information regarding the detailed nature of the electronic transition.

Results and Discussion

When hydrogen bonding effects are excluded, as when solute and solvent are both non-hydrogen bond donors, solvent effects on electronic spectra can take either of two forms. For p$\rightarrow\pi^*$ and $\pi\rightarrow\pi^*$ transitions of uncharged indicators with all solvents considered together, and for other types of electronic transitions when families of solvents with similar polarizability characteristics are treated separately (*e. g.*, only non-chlorinated aliphatic solvents, only polychlorinated aliphatics, or only aromatic solvents) the linear solvation energy relationship (LSER) takes the form,

$$\nu(i)_{max} = \nu(i)_0 + s\pi^*, \quad (1)$$

where s is a measure of the response of $\nu(i)_{max}$ to solvent dipolarity. For the other electronic transitions, when all solvents need to be considered together, the appropriate form of the LSER is,

$$\nu(i)_{max} = \nu(i)_0 + s(\pi^* + d\delta), \quad (2)$$

where δ, a 'polarizability correction term'=0.0 for non-chlorinated aliphatic solvents, 0.5 for polychlorinated aliphatics, and 1.0 for aromatic solvents.

Solvent Dipolarity/Polarizability Effects. Considering first the $\nu(\mathbf{1})_{max}$ values in the six non-protic aliphatic solvents of Table 1 according to Eq. 1, the regression equation with π^* is,

$$\nu(\mathbf{1})_0 = (26.71 - 3.99\pi^*) \times 10^3\ cm^{-1}, \quad (3)$$

r (the correlation coefficient) = 0.980,

sd (the standard deviation) = $0.24 \times 10^3\ cm^{-1}$.

The ν_0 and s values in Eq. 3 provide important mechanistic information. Thus, it is evident from the shift to lower absorption frequencies with increasing π^* that the electronic transition is from a ground state which is relatively more charge-diffuse to an electronic excited state which is relatively more charge-concentrated.

It is profitable to consider Eq. 3 in the context of solvent effects equations for corresponding spectral bands of related indicators as, for example, the [$^+X=C(4)\rightarrow C(1)=NO_2^-$] electronic transitions of the 4-substituted nitrobenzenes, **2—7**, which we reported

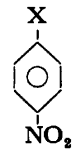

2, X=Me_2N- **5**, X=C_2H_5-
3, X=H_2N- **6**, X=F-
4, X=MeO- **7**, X=H-

earlier.[1d] It was then shown that the $\nu(i)_0$ and s values in the solvatochromic equations for **2**—**7** are linear with the substituent σ^+ values, the correlation equations being,

$$\nu(i)_0 = (6.39\sigma^+ + 39.50) \times 10^3 \text{ cm}^{-1}, \quad (4)$$

and

$$s = 1.021\sigma^+ - 1.685. \quad (5)$$

In order to ascertain whether 4-nitrophenoxide conforms with these relationships, we have back-calculated values of σ^+ for the 4-oxy substituent by substituting the $\nu(\mathbf{1})_0$ and s terms from Eq. 3 into Eqs. 4 and 5, and compared the results with independent estimates of the value of this substituent constant. The $\nu(\mathbf{1})_0$ value of 26.71 in Eq. 4 calls for a σ^+ of −2.00, while the s value of −3.99 in Eq. 5 is consistent with $\sigma^+ = -2.25$. For comparison, Hine[6] has reported that σ^+ for the p-O^- substituent is −2.3, with the comment that σ^+ values for electrically charged substituents are relatively less reliable, being dependent to some extent on solvation and ion pairing.

The at least approximate conformance of 4-nitrophenoxide with Eqs. 4 and 5 indicates that, as with **2**—**7**, the direction of charge migration in the electronic excitation is away from the p-substituent and towards the nitro group. Taken with the finding that there is concentration of charge in the electronic excitation, this leads to the conclusion that electron density in the ground state is delocalized into canonical structures like **1a**—**d** (with **1a** probably being the dominant contributor), whereas in the electronic excited state charge is redistributed and concentrated into canonical structures like **1c** and **1d** (with **1d** being the dominant contributor).

If the data in the non-protic aliphatic, polychloroaliphatic, and aromatic solvents of Table 1 are considered together, the appropriate form of the linear solvation energy relationship is given by Eq. 2. The d value is calculated to be −0.26,[7] and the least squares correlation of $\nu(\mathbf{1})_{max}$ with $(\pi^* - 0.26\delta)$ leads to the regression equation,

$$\nu(\mathbf{1})_{max} = \{26.67 - 3.93(\pi^* - 0.26\delta)\} \times 10^3 \text{ cm}^{-1}, \quad (6)$$
$$n = 11,\ r = 0.988,\ sd = 0.17 \times 10^3 \text{ cm}^{-1}.$$

A plot of $\nu(\mathbf{1})_{max}$ against $(\pi^* - 0.26\delta)$ is shown in Fig. 1.

Since we have shown earlier[1d,7] that the d value in Eq. 2 is effectively zero for the $\pi \rightarrow \pi^*$ transitions of indicators **2**—**7**, it is necessary to inquire why d should have a large negative value for the corresponding transition of indicator **1**. This is particularly important because, in all correlations of electronic spectra which we have hitherto carried out, the general conclusion had been that solvatochromic equations reflected either of two patterns of behavior: (a) If ν_{max} was shifted bathochromically with increasing solvent dipolarity/polarizability, as was usually the case for $\pi \rightarrow \pi^*$ transitions of uncharged indicators, d in Eq. 2 was zero. (b) For all spectra shifted hypsochromically with increasing solvent π^* values, as was usually the case for $n \rightarrow \pi^*$ transitions of uncharged indicators and $\pi \rightarrow \pi^*$ transitions of zwitterionic indicators, d was always finite and negative. 4-Nitrophenoxide is the first example we have investigated of an anionic indicator, and it is of interest that it follows still a third pattern of behavior, *i.e.*, a bathochromic shift with increasing solvent π^* values coupled with a large negative value of d in Eq. 2.

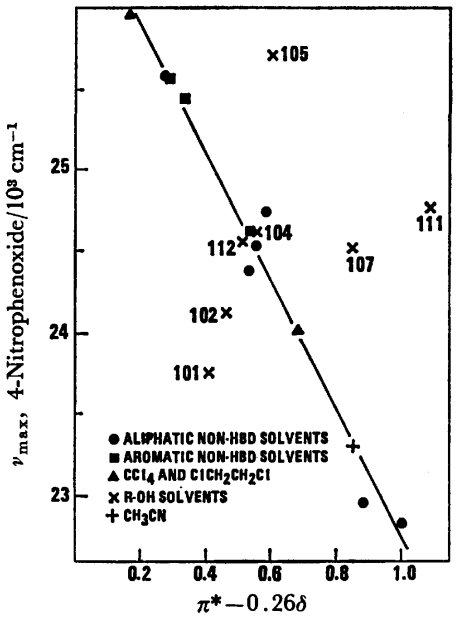

Fig. 1. $\nu(\mathbf{1})_{max}$ plotted against $(\pi^* - 0.26\delta)$.

We had earlier suggested[1d,7] that d is zero when the indicator dipole does not change direction in the electronic excitation (so that solvent molecules which are optimally situated to solvate the indicator ground state are also well oriented to solvate the excited state). Finite negative values of d had been associated with transitions wherein the direction of the indicator dipole changed in the electronic transition and, in conformance with the Franck-Condon principle, solvent molecules which were well situated to solvate the ground state were poorly oriented to solvate the excited state. On this basis the large negative d value for **1** suggests that the dipole changes direction in the electronic excitation and is consistant with canonical structure **1a** being the dominant contributor to the ground state and **1d** the dominant excited state contributor.

Effects of Hydrogen Bonding by Protic Solvents. The correlations become particularly interesting when we consider the HBD (hydrogen bond donor) solvents, $\nu(\mathbf{1})_{max}$ values for which are also plotted in Fig. 1, where it is evident that they do not conform with the correlation with $(\pi^* - 0.26\delta)$. We denote the vertical displacements of the HBD solvent data points from the regression line by $\Delta\Delta\nu(\mathbf{1}-\pi^*)$, and we define this quantity as the additional shift in $\nu(\mathbf{1})_{max}$ caused by hydrogen bonding to **1** by the solvent after the solvent dipolarity/polarizability effects have been accounted for by a correlation with the π^* scale. We

Table 1. Solvent effects on the spectrum of 4-Nitrophenoxide anion (1)

No.[a]	Solvent	π^*	α	$\nu(\mathbf{1})_{max}/10^3$ cm^{-1}	$\Delta\Delta\nu(\mathbf{1}-\pi^*)/10^3$ cm^{-1}
7	Diethyl ether	0.27	0.00	25.58	
9	Dioxane	0.55	0.00	24.54	
13	Tetrahydrofuran	0.58	0.00	24.75	
61	1,2-Dimethoxyethane	0.53	0.00	24.39	
23	*N,N*-Dimethylformamide	0.88	0.00	22.96	
29	Dimethyl sulfoxide	1.00	0.00	22.83	
6	Carbon tetrachloride	0.29	0.00	25.97	
20	1,2-Dichloroethane	0.81	0.00	24.03	
8	Toluene	0.54	0.00	25.57	
14	Benzene	0.59	0.00	25.44	
33	Bromobenzene	0.79	0.00	24.63	
50	Acetonitrile	0.85	0.15	23.31	0.00
101	*t*-Butyl alcohol	0.41	0.67	23.75	−1.31
102	2-Propanol	0.46	0.78	24.13	−0.73
112	1-Propanol	0.51	0.85	24.57	−0.10
104	Ethanol	0.54	0.86	24.63	+0.08
105	Methanol	0.60	0.98	25.71	+1.40
107	Ethylene glycol	0.85	0.92	24.53	+1.01
111	Water	1.09	1.11	24.78	+2.42

a) Solvent numbering is the same in all papers of this series.

calculate this hydrogen bonding effect by,

$$\Delta\Delta\nu(\mathbf{1}-\pi^*) = \nu(\mathbf{1})_{max}^{obsd} - \nu(\mathbf{1})_{Eq.\,3}^{calcd}. \quad (7)$$

Values of $\Delta\Delta\nu(\mathbf{1}-\pi^*)$ for the protic solvents are also assembled in Table 1.

It is seen in the table and the figure that while the net hydrogen bonding effect is essentially *nil* for the very weak HBD solvent acetonitrile (solvent 50), significant displacements from the regression line are observed for the R–OH solvents. For the intermediate strength hydrogen bond donors, *t*-butyl alcohol (101) and 2-propanol (102), the $\Delta\Delta\nu$ terms are negative (shifted bathochromically relative to Eq. 3); for the stronger HBD solvents, methanol (105), ethylene glycol (107), and water (111), $\Delta\Delta\nu$'s are positive (shifted hypsochromically).

While this hints at a complex solvation mechanism, the relationship between $\Delta\Delta\nu(\mathbf{1}-\pi^*)$ and the solvent α values (α being the parameter which measures solvent HBD acidity)[2] is noticeably simple and precise. A plot of $\Delta\Delta\nu(\mathbf{1}-\pi^*)$ against α for the R–OH solvents is shown in Fig. 2. It is seen that linear regression is excellent; the correlation equation is,

$$\Delta\Delta\nu(\mathbf{1}-\pi^*) = (-7.30 + 8.80\alpha) \times 10^3\ \text{cm}^{-1}, \quad (8)$$
$$n = 7,\ r = 0.989,\ sd = 0.20 \times 10^3\ \text{cm}^{-1}.$$

Equations 3 and 8 can be combined to give the total solvatochromic equation for 4-nitrophenoxide spectra in hydroxylic solvents,

$$\nu(\mathbf{1})_{max} = (19.41 - 3.99\pi^* + 8.80\alpha) \times 10^3\ \text{cm}^{-1}. \quad (9)$$

Alternatively the dependence of $\nu(\mathbf{1})_{max}$ on the solvatochromic parameters may be determined by the method of multiple linear regression analysis. For the seven hydroxylic solvents of Table 1, the multiple parameter least squares fit is given by Eq. 10a.

$$\nu(\mathbf{1})_{max} = (19.88 - 3.13\pi^* + 7.67\alpha) \times 10^3\ \text{cm}^{-1}, \quad (10a)$$
$$r = 0.936,\ sd = 0.22 \times 10^3\ \text{cm}^{-1}.$$

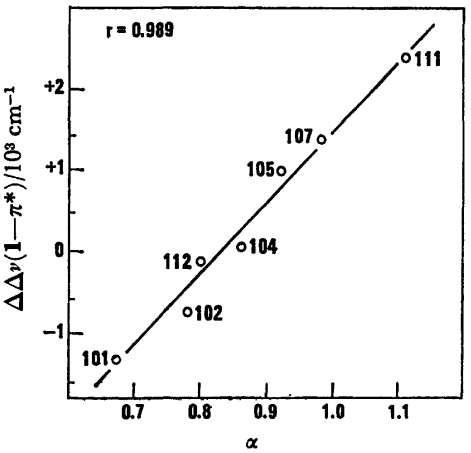

Fig. 2. $\Delta\Delta\nu(\mathbf{1}-\pi^*)$ for hydroxylic solvents plotted against solvent α values.

If, however, the result for ethylene glycol (whose π^* and α values are relatively less certain) is excluded, the correlation equation becomes,

$$\nu(\mathbf{1})_{max} = (19.44 - 3.90\pi^* + 8.66\alpha) \times 10^3\ \text{cm}^{-1}, \quad (10b)$$
$$r = 0.963,\ sd = 0.20 \times 10^3\ \text{cm}^{-1}.$$

The agreement between Eqs. 9 and 10b is surprisingly good if one considers that (a) the *s* values are based on completely different data sets; (b) the π^* values for hydroxylic solvents are somewhat less precise than those for aprotic solvents; and (c) the effects of dipolarity and hydrogen bonding are in different directions and tend to cancel one another, thus narrowing the range of the $\nu(\mathbf{1})_{max}$ values in the hydroxylic solvents compared with the aprotic solvents. The negative sign of the π^* term indicates that increasing solvent dipolarity/polarizability leads to a red shift; the positive sign of the α term indicates that increasing solvent HBD acidity leads to a blue shift. The similar

values of s in Eqs. 3 and 10b imply (perhaps incorrectly or adventitiously, as discussed below) that the dipolarity effects on $\nu(\mathbf{1})_{max}$ are the same in hydroxylic and non-protonic solvents. There are additional considerations, however, which affect the results.

Specific solvation effects are complicated by the expectation of bonding at two sites. For example, hydrogen bonding to the nitro oxygens[8,9] should stabilize canonical structure **1d** and hence the electronic excited state, and thus lead to a bathochromic shift (as has been demonstrated for *N,N*-diethyl-4-nitroaniline).[8] Bonding to the phenoxide oxygen should stabilize structure **1a** and the ground state, and lead to a hypsochromic shift (as mentioned by U. and K.). The phenoxide site being significantly the more basic,[9] the net hypsochromic effect of hydrogen bonding (or other specific solvation)[10] is as expected.

The 7.3×10^3 cm^{-1} difference in the $\nu(\mathbf{1})_0$ values (intercepts) in Eqs. 3 and 10b requires explanation. The $\nu(\mathbf{1})_0$ value represents the regression result in a saturated hydrocarbon environment ($\pi^*=0$, $\alpha=0$ for cyclohexane).

We take the difference in $\nu(\mathbf{1})_0$ as implying that the electronic structures of 4-nitrophenoxide in both ground and electronic excited states are different in aprotic and hydroxylic solvents. From the 7.3 10^3 cm^{-1} higher $\nu(\mathbf{1})_0$ in Eq. 3 relative to Eq. 10b, the difference would appear to derive from significant stabilization of the ground state and/or destabilization of the excited state structure in the aprotic solvents relative to the corresponding 4-nitrophenoxide structures in the hydroxylic solvents. An explanation proposed by U. and K. provides an adequate rationale for such an effect.

These workers have pointed out that in aprotic solvents there is strong ion-pairing between the phenoxide anion and the 15-crown-5-bound sodium cation, whereas in hydroxylic solvents ion-pairing is negligible [indeed, the addition of crown ether produced essentially no effect on $\nu(\mathbf{1})_{max}$ in the hydroxylic solvents]. In the extrapolation of the experimental results of Table 1 back to $\pi^*=0$ and $\alpha=0$, such ion-pairing should significantly stabilize the ground state structure of **1** relative to the excited state in the case of the non-protonic solvents, but not in the hydroxylic solvents. Furthermore, 'tighter' ion-pairing with decreasing solvent dipolarity (as well as the decrease in any specific solvation of the nitro substituent)[10] should increase the magnitude of this effect as the π^* values became smaller in the solvents studied experimentally. It should be recognized, however, that if this rationale is correct, the agreement between Eqs. 9 and 10b may be largely adventitious, or possibly regression equation 10a may be more nearly correct.

Part of the work of J.-L.M.A. was carried out while on leave at Centro Meccanismi di Reazioni Organiche del C.N.R., Istituto di Chimica Organica, Universita di Padova, Italy. Valuable discussions with Professors G. Modena and G. Scorrano, and the financial support from C.N.R. (Rome) are gratefully acknowledged. The work by R.W.T. was supported in part by a grant from the Public Health Service. The work by M.J.K. was done under Naval Surface Weapons Center Foundational Research Task IR-201.

References

1) a) Z scale: E. M. Kosower, *J. Am. Chem. Soc.*, **80**, 3253 (1958); b) $E_T(30)$ scale, K. Dimroth, C. Reichardt, T. Seipmann, and F. Bohlmann, *Ann. Chem. Liebigs*, **661**, 1 (1963); C. Reichardt, *Angew. Chem., Int. Ed. Engl.*, **4**, 29 (1965); c) X_R scale: L. G. S. Brooker, A. C. Craig, D. W. Heseltine, P. W. Jenkins, and L. L. Lincoln, *J. Am. Chem. Soc.*, **87**, 2443 (1965); d) π^* scale: M. J. Kamlet, J.-L. M. Abboud, and R. W. Taft, *J. Am. Chem., Soc.*, **99**, 6027 (1977).

2) R. W. Taft and M. J. Kamlet, *J. Am. Chem. Soc.*, **98**, 2886 (1976); M. J. Kamlet and R. W. Taft, *J. Chem. Soc., Perkin Trans. 2*, **1979**, 349; R. W. Taft and M. J. Kamlet, *ibid.*, **1979**, 1723.

3) The term 'solvent dipolarity' is intended as a more specific description than the frequently misused 'solvent polarity', which has often included as well the effects of hydrogen bonding interactions in varying combinations with the dipole/dipole effects.

4) For a large systematic study, see: M. J. Kamlet, J.-M. L. Abboud, and R. W. Taft, *Prog. Phys. Org. Chem.*, **13**, 485 (1981).

5) S. Ueji and M. Kitadani, *Bull. Chem. Soc. Jpn.*, **50**, 2819 (1979).

6) J. Hine, "Structural Effects on Equilibria in Organic Chemistry," J. Wiley, New York, N. Y. (1975), p. 72.

7) For the method of calculating the d value in Eq. 2, see: R. W. Taft, J.-L. M. Abboud, and M. J. Kamlet, *J. Am. Chem. Soc.*, **103**, 1080 (1981).

8) M. J. Kamlet, E. G. Kayser, J. W. Eastes, and W. H. Gilligan, *J. Am. Chem. Soc.*, **95**, 5210 (1973).

9) M. Fujio, R. T. McIver, and R. W. Taft, submitted to *J. Am. Chem. Soc.*

10) As, for example, by DMSO acting as a non-protonic Lewis acid [*cf.* R. W. Taft, "Kinetics of Ion-Molecule Reactions," ed by T. Ausloos, Plenum Publishing Corp., New York (1979), p. 271].

Dimerization Kinetics of Fluoresceine in Aqueous Solution

Wataru INAOKA, Shoji HARADA, Susumu FUJII, and Tatsuya YASUNAGA*

Department of Chemistry, Faculty of Science, Hiroshima University, Higashisenda-machi, Naka-ku, Hiroshima 730

(Received March 30, 1981)

Synopsis. Kinetic studies of the dimerization reaction of fluorescein (doubly charged anion) in aqueous solution were performed by the ultrasonic absorption method. The data obtained could not be interpreted by the rate equation derived with the usual viscosity effect assumed for the diffusion process. Rather, an experimental equation was found, which adequately fits the data. Here, the viscosity contribution is $k_f=k_f^0/\eta_r$, $k_b=k_b^0$, and $K=K^0/\eta_r$.

The aggregation of many dyes have been investigated both spectrophotometrically and kinetically as a simple model system of molecular aggregation. The kinetics of the aggregation of fluorescein, however, has not been investigated because the aggregate is unstable and the rates of the reaction are too rapid to be studied by conventional techniques.

Ultrasonic absorption of fluorescein in aqueous solution was measured in the frequency range 4.5—95 MHz under the condition of pH 12.0, where the dye exists as the doubly charged anion, 25 °C, ionic strength 5 M.† The absorptions could be explained by a single relaxation.

Since fluorescein is known to form a dimer under the present experimental conditions,[1-5] the relaxation absorption is ascribed to the following equilibrium:

$$2\,M^{2-} \underset{k_b}{\overset{k_f}{\rightleftharpoons}} D^{4-}, \qquad (1)$$

where M^{2-} is the monomer and D^{4-} is the dimer. For this reaction, the relaxation frequency f_r is related to the rate constants by the following equation:

$$(2\pi f_r)^2 = k_b^2 + 8k_fk_bC_0, \qquad (2)$$

where C_0 is the total concentration of the dye. This equation predicts that f_r^2 increases monotonously with C_0, which was not satisfied by the experimental data.

The fact that the viscosity of the solution changes greatly with increase of the dye concentration lead us to consider the viscosity effect on the rate constants. Dimerization reaction involves the diffusion process, whose rate constants are theoretically calculated by the Smoluchowski-Debye-Eigen Equations.[6] Combining with the Stokes-Einstein relation, which represents the viscosity dependence of the diffusion coefficients, the diffusion rate constants are shown to have the viscosity dependence $k=k^0/\eta_r$ where η_r is the relative viscosity, and the superscript 0 represents the value at $\eta_r=1$. Following the usual treatment of the kinetics, k_f and k_b have the same viscosity dependence as that of the diffusion rate constants.[7] Accordingly, Eq. 2 becomes

$$(2\pi f_r)^2 = (k_b^{02} + 8k_f^0k_b^0C_0)/\eta_r^2. \qquad (3)$$

If this is correct, the $(2\pi f_r)^2\eta_r^2$ *vs.* C_0 plot should be linear. As shown in Fig. 1, however, the plot deviates greatly from a straight line. Further, this idea also fails to give a satisfactory explanation for the concentration dependence of the absorption amplitude. Thus we must look further for a satisfactory explanation.

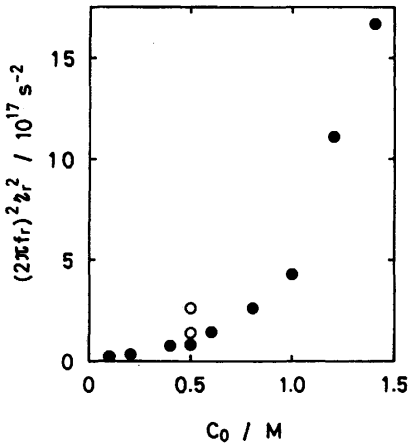

Fig. 1. Plot of $(2\pi f_r)^2\eta_r^2$ *vs.* C_0.
●: Glycerol free, ○: glycerol added.

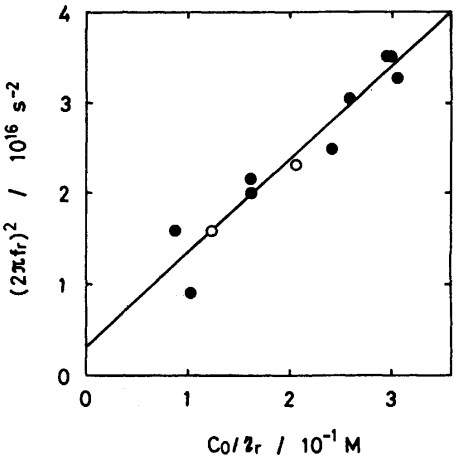

Fig. 2. Plot of $(2\pi f_r)^2$ *vs.* C_0/η_r.
●: Glycerol free, ○: glycerol added.

Petrucci[8] has proposed an empirical formula for the viscosity dependence of the rate constants, *i.e.*, $k_f=k_f^0/\eta_r$ and $k_b=k_b^0$. In this case, Eq. 2 can be rewritten as

$$(2\pi f_r)^2 = k_b^{02} + 8k_f^0k_b^0C_0/\eta_r. \qquad (4)$$

Equation 4 predicts a linear relationship for $(2\pi f_r)^2$ *vs.* C_0/η_r plot, which is well satisfied, as shown in Fig. 2. Further, this type of viscosity dependence of f_r was ascertained by changing the viscosity of the solution with the addition of glycerol, *i.e.*, to the 0.5 M dye solution, 8.3 and 16.6 wt% glycerol were added. The results obtained are also plotted in Fig. 2 with the open circles and the tendency displayed is similar to that for dye alone. From the slope and the intercept of the straight

† In this paper, 1 M=1 mol dm^{-3}.

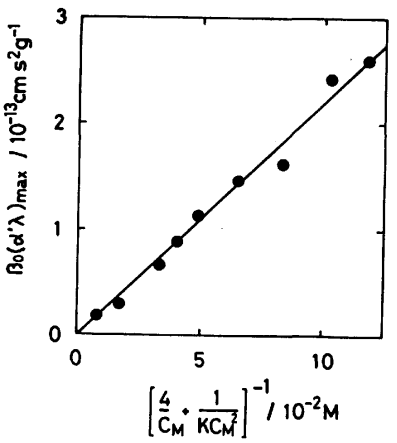

Fig. 3. Plot of $\beta_0(\alpha'\lambda)_{max}$ *vs.* $(4/C_M+1/KC_M^2)^{-1}$ with $C_M=(-1+(1+8KC_0)^{1/2})/4K$.

line, the rate constants were determined to be $k_f^0=2.3\times10^8$ M^{-1} s^{-1} and $k_b^0=5.6\times10^7$ s^{-1}; the equilibrium constant $K^0(=k_f^0/k_b^0)$ was determined to be 4.1 M^{-1}, which is in good agreement with the literature value determined by the spectrophotometric measurements.[1-5] The value of k_f^0 is in the same order of magnitude as that of other dyes,[9,10] which means that the electric charge effect is relatively small in k_f^0, while the value of k_b^0 is the largest of those dyes studied, which is the reason for the small equilibrium constant. The experimental result that the viscosity dependences of k_f and k_b are different from each other, in conflict with the theoretical prediction described before, is interesting.

The result obtained for the rate constants also means that the equilibrium constant changes with the viscosity, *i.e.*, $K=K^0/\eta_r$. This fact was further ascertained by the result of the absorption amplitude. The relaxation absorption $(\alpha'\lambda)_{max}$ of reaction 1 is expressed by

$$(\alpha'\lambda)_{max}=\frac{\pi(\Delta V)^2}{2\beta_0RT}\left(\frac{4}{C_M}+\frac{1}{KC_M^2}\right)^{-1} \quad (5)$$

with

$$C_M=\{-1+(1+8KC_0)^{1/2}\}/4K,$$

where ΔV is the volume change of the reaction and β_0 is the adiabatic compressibility. If we use the viscosity dependent equilibrium constant $K=K^0/\eta_r$, a good linear relationship is obtained, which is well coincident with that predicted by Eq. 5. The value of ΔV was determined from the slope of the straight line in Fig. 3 to be -6.0 cm^3 mol^{-1}.[11]

In conclusion, the viscosity effect on k_f and the fact that the value of k_f is in the same order of magnitude with those of other dyes, show that the association reaction is diffusion controlled. On the other hand, the viscosity independence of k_b implies that the dissociation reaction is limited by some intramolecular process of the dimer.

References

1) Th. Förther and E. König, *Z. Electrochem.*, **61**, 344 (1957).
2) K. K. Rohatgi and G. S. Sighal, *J. Phys. Chem.*, **70**, 1695 (1966).
3) J. Lavorel, *J. Phys. Chem.*, **61**, 1600 (1957).
4) V. L. Levschin and L. V. Krotova, *Opt. Spektrosk.*, **13**, 457 (1962).
5) K. K. Rohatgi and A. K. Mukhopadhyay, *J. Indian Chem. Soc.*, **49**, 1311 (1972).
6) I. Amdur and G. Hammes, "Chemical Kinetics; Principles and Selected Topics," in "Series in Advanced Chemistry," McGraw-Hill, New York (1966), p. 62.
7) P. Warrick, Jr., J. J. Auborn, and E. M. Eyring, *J. Phys. Chem.*, **76**, 1184 (1972).
8) S. Petrucci, *J. Phys. Chem.*, **71**, 1174 (1967).
9) D. H. Turner, R. Yuan, G. W. Flynn, and N. Sutin, *Biophys. Chem.*, **2**, 385 (1974).
10) W. Inaoka, S. Harada, and T. Yasunaga, *Bull. Chem. Soc. Jpn.*, **53**, 2120 (1980).
11) In the ultrasonic absorption measurement, only the absolute value of ΔV can be determined. The sign is assigned considering the pressure dependence of the equilibrium constant of other dyes.[12,13]
12) K. Suzuki and M. Tsuchiya, *Bull. Chem. Soc. Jpn.*, **44**, 967 (1971).
13) D. Pörschke and F. Eggers, *Eur. J. Biochem.*, **26**, 490 (1972).

Infrared Study of the Oxidation of 2-Propanol on TiO_2

Takashi NAKAJIMA, Hisashi MIYATA,* and Yutaka KUBOKAWA*
Department of Applied Chemistry, University of Osaka Prefecture, Mozuumemachi, Sakai, Osaka 591
(Received June 1, 1981)

Synopsis. Oxidation of 2-propanol on TiO_2 was studied by infrared spectroscopy as well as analysis of reaction products. Propene and acetone are formed from isopropoxide species on TiO_2. Only adsorbed acetone is oxidized to carbon dioxide *via* carboxylate species. Propene undergoes no oxidation.

We previously studied surface species formed in oxidation of alcohols on metal oxides such as MgO,[1] NiO,[1] and ZnO[2,3] and concluded that secondary alcohols are dehydrogenated to ketones, which are in turn oxidized to carboxylate species *via* enolate complexes of ketones. However, Walker *et al.*[4] reported that over a UV-irradiated TiO_2 secondary alcohols are oxidized *via* alkenes which have been formed by dehydration. In order to decide to what extent the conclusion obtained with MgO and ZnO is applicable, in the present research similar experiments were extended to the 2-propanol/TiO_2 system for which propene formation is expected to be predominant.

The titanium dioxide used was obtained from Japan Aerosil Co. The details of the apparatus and procedures were as reported previously.[1-3,5] A sample disk was degassed, oxidized at 673 K for several hours, degassed for a short period at the same temperature, and cooled to room temperature. After introduction of 1 cm^3/g of the reactant into an IR cell, an oxygen of 2 kPa was circulated over the TiO_2, the temperature of which was raised in steps. Each of stepwise heat-treatments of the sample was followed by recording infrared spectra at ambient temperature on a JASCO IR-G infrared spectrometer, no reference disk being used.

The infrared spectrum of 2-propanol adsorbed on TiO_2 (1.0 cm^3/g) exhibits a number of bands (Fig. 1a), which does not change significantly on evacuation at 353 K. All the bands except for the one at 3430 cm^{-1} agree with those due to the surface isopropoxide formed on metal oxides,[1,2,6] confirming the formation of the surface isopropoxide species on TiO_2.

The temperature of the disk containing isopropoxide was raised in steps under circulation of oxygen. The bands due to isopropoxide were slightly reduced in intensity at 423 K (Fig. 1b) and disappeared at 523 K (Fig. 1c). The band appearing at 1690 cm^{-1} at 423 K can be attributed to a coordinately adsorbed acetone as will be described later. As regards the new bands appearing at 523 K, the following assignments are possible from comparison of surface carboxylate species on metal oxides.[1-3,7,8] The bands at 1560 and 1360 cm^{-1} are due to the formate species,[7] while those at 1530 and 1440 cm^{-1} are due to the acetate species.[8]

Figure 2 shows the amount of oxygen taken up as well as the amount of reaction products, measured at each step in the stepwise heating in oxygen. At 523 K, formation of water occurs together with uptake of oxygen in an appreciable amount, as expected from the formation of carboxylate species described above.

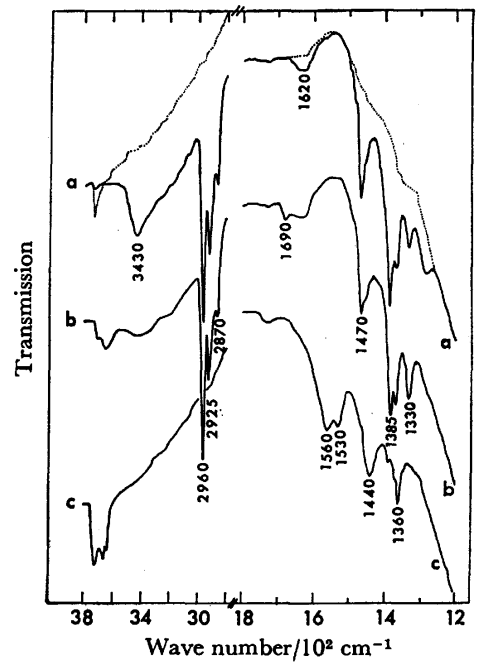

Fig. 1. Interaction of oxygen with 2-propanol adsorbed on TiO_2.
(a): After 1 h adsorption of 2-propanol (1.0 cm^3/g) at 293 K, (b): followed by 1 h at 423 K in oxygen (2.0 kPa), (c): 1 h at 523 K in oxygen.

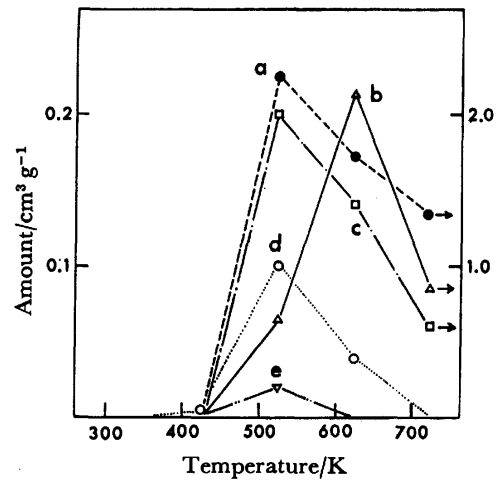

Fig. 2. Reaction of oxygen with 2-propanol adsorbed on TiO_2.
(a): Oxygen uptake or consumed by the reactions, (b): CO_2 formed, (c): H_2O formed, (d): propene formed, (e): acetone formed. Amount of 2-propanol adsorbed at 293 K was 1.1 cm^3/g.

CO_2 is formed above 523 K. In addition, propene and a small amount of acetone are also formed, providing information on intermediates for the oxidation.

In order to obtain information on the pathway of the

oxidation, similar experiments were carried out with propene or acetone adsorbed on TiO_2. When a small amount of propene (500 Pa) was introduced to the TiO_2 at ambient temperature, bands appeared at 2950, 2920, 1635, and 1460 cm^{-1}. Evacuation of the sample at ambient temperature reduced the intensity of the bands, suggesting that propene is weakly adsorbed on TiO_2. On raising the temperature of the sample containing propene in oxygen, few carboxylate bands could be observed. On the other hand, the acetone adsorption was found to be strong. The adsorbed acetone shows bands at 1700, 1620, and 1590 cm^{-1} in the carbonyl stretching region (Fig. 3a). Their corresponding bands were observed at 1690, 1600, and 1570 cm^{-1} with acetone-d_6. The 1700- or 1690-cm^{-1} band of acetone or acetone-d_6 can be assigned to CO-stretching vibrations of coordinately adsorbed species on Lewis acidic sites.[9] The same assignment appears applicable to the bands at 1620 and 1590 cm^{-1}, as proposed by Kiselev and Uvarov.[10] The possibility that these bands arise from mesityl oxide as proposed by Griffiths and Rochester,[9] may be excluded since no mesityl oxide

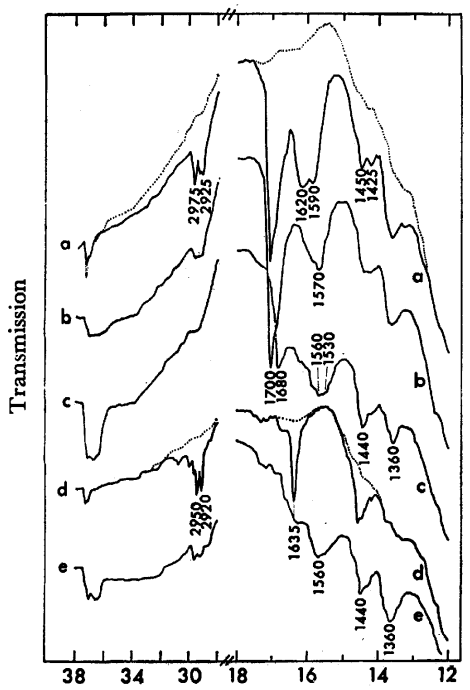

Fig. 3. Interaction of oxygen with acetone or propene on TiO_2.
(a): After 2 h adsorption of acetone (1.0 cm^3/g) at 293 K, (b): followed by 1 h at 353 K in oxygen (1.0 kPa), (c): 1 h at 423 K in oxygen, (d): after introduction of propene (500 Pa) at 293 K, (e): after 1 h reaction at 423 K in a mixture of propene (500 Pa) and oxygen (2.0 kPa). In Figs. 1 and 3, the dotted lines show background spectra.

was detected in the present system. Although at present it is not decided whether or not the band at 1570 cm^{-1} appearing at 353 K is attributable to the enolate species, its formation is supported by the occurrence of hydrogen isotopic exchange between acetone-d_6 and surface OH groups, which proceeds *via* the enolate intermediate.[11] The spectral behavior of adsorbed acetone upon raising the temperature was similar to that of adsorbed 2-propanol in that the carbonyl bands were reduced in intensity, while the carboxylate bands appeared (Fig. 3c).

Contribution of the weakly adsorbed propene to the oxidation was examined by allowing a mixture of propene (500 Pa) and oxygen (2 kPa) to circulate over the TiO_2 at 423 K. The results were compared with those of similar experiments using acetone instead of propene. The amount of carbon dioxide formed in the acetone/oxygen system was found to be more than ten times that in the propene/oxygen system, where carboxylate bands were observed as shown in Fig. 3e.

Figure 2 shows that about 12% of the 2-propanol adsorbed on TiO_2 is converted to propene, in contrast to the negligible formation of propene observed with MgO[1] and ZnO.[2] Such a difference may by expected from acid-base properties of metal oxides. From the results described above, it is concluded that the propene formed on TiO_2 makes no contribution to the formation of oxidation products. It appears that the acetone formed by dehydrogenation is oxidized to carboxylate species, from which CO_2 is formed. About 88% of the 2-propanol adsorbed on TiO_2 was oxidized *via* this reaction pathway. Thus, the same conclusion as that with MgO and ZnO is also applicable to TiO_2.

References

1) H. Miyata, M. Wakamiya, and Y. Kubokawa, *J. Catal.*, **34**, 117 (1974).
2) H. Miyata, K. Hata, T. Nakajima, and Y. Kubokawa, *Bull. Chem. Soc. Jpn.*, **53**, 2401 (1980).
3) H. Miyata, T. Nakajima, and Y. Kubokawa, *J. Catal.*, **69**, 292 (1981).
4) A. Walker, M. Formenti, P. Meriaudeau, and S. J. Teichner, *J. Catal.*, **50**, 237 (1977).
5) H. Miyata, K. Hata, and Y. Kubokawa, *J. Catal.*, **49**, 8 (1977).
6) C. T. Lynch, K. S. Mazdiyashi, J. S. Smith, and W. J. Crawford, *Anal. Chem.*, **36**, 2332 (1964).
7) G. Munuera, F. Gonzalèz, F. Moreno, and J. A. Prieto, *Proc. Int. Congr. Catal. 5th*, 1159 (1973).
8) F. Gonzalez, G. Munuera, and J. A. Prieto, *J. Chem. Soc., Faraday Trans. 1*, **74**, 1517 (1978).
9) D. M. Griffiths and C. H. Rochester, *J. Chem. Soc., Faraday Trans. 1*, **74**, 403 (1978).
10) A. V. Kiselev and A. V. Uvarov, *Surface Sci.*, **6**, 399 (1967).
11) I. R. Shannon, I. J. S. Lake, and C. Kemball, *Trans. Faraday Soc.*, **67**, 2760 (1971).

X-Ray Structure of (1*RS*, 5*RS*, 7*SR*)-1-Acetoxy-7-cyano-5-methylbicyclo-[3.2.0]heptan-2-one, a Photocycloadduct of 2-Acetoxy-3-methyl-2-cyclopenten-1-one and Acrylonitrile

Akio Furusaki,* Katsumi Abe, and Takeshi Matsumoto
Department of Chemistry, Faculty of Science, Hokkaido University, Sapporo 060
(Received July 20, 1981)

Synopsis. The main product of the photocycloaddition between 2-acetoxy-3-methyl-2-cyclopenten-1-one and acrylonitrile has been found to be (1*RS*, 5*RS*, 7*SR*)-1-acetoxy-7-cyano-5-methylbicyclo[3.2.0]heptan-2-one by means of X-ray crystal structure analysis.

Previously, we reported the synthesis of a sesquiterpene through a process involving the (2+2) photocycloaddition between a 2-acetoxy-3-methyl-2-cyclopenten-1-one (**1**) derivative and 1,1-diethoxyethylene.[1] In the course of studies on the synthesis of a related sesquiterpene, it became necessary to investigate the photoaddition of **1** with acrylonitrile (**2**). Few studies seem to have been made on the photoaddition of cycloalkenones with this electron-deficient olefin since the classical work of Corey *et al.*[2] They showed that the reaction of 2-cyclohexen-1-one with **2** was extremely slow, compared with similar reactions with electron-rich olefins, and suggested that the main products were 8-epimeric 8-cyano-*cis*-bicyclo[4.2.0]octan-2-ones. In order to establish the structure of the main product (**3**, 15.7% yield at 56% conversion) of the photocycloaddition between **1** and **2**, we have now undertaken an X-ray crystal structure analysis.

Experimental

Photoaddition. A solution of **1**[3] (1 g, 6.5 mmol) and freshly-distilled **2** (10.33 g, 195 mmol) in a mixture of THF (21 ml) and EtOH (70 ml) was irradiated with a Hanovia 75-W high-pressure mercury lamp under ice-cooling and N_2 atmosphere. A Pyrex filter was used. After 5 h, the mercury lamp was shut off, a white polymeric deposit was removed by filtration, and the filtrate was concentrated *in vacuo*. The residual oil (2.5 g) was chromatographed on silica gel (Kanto, 40 g) using EtOAc–benzene (1 : 9) as the eluent. The first fraction contained the cycloadduct, **3** (98 mg, 7.8%): mp 100.0—101.5 °C; IR (Nujol) 2260 (C≡N), 1752 (ester C=O), 1736 cm^{-1} (cyclopentanone); NMR (CCl_4) δ=1.38 (3H, s), 1.90 (2H, m), 2.11 (3H, s), 2.14 (2H, d, J=6.5 Hz), 2.58 (2H, m), 3.11 (1H, t, J=6.5 Hz). Found: C, 63.39; H, 6.39; N, 6.72%. Calcd for $C_{11}H_{13}NO_3$: C, 63.76; H, 6.32; N, 6.76%. The second fraction was an oily mixture (170 mg) of **3** and an unidentified product, **4** (2 : 1 by NMR). The third fraction was an oil composed of **4** and the other product, **5** (1 : 1 by NMR). From the fourth fraction, 443 mg of **1** was recovered.

X-Ray Measurement. A colorless, single crystal with dimensions of about 0.3×0.3×0.4 mm^3 was used. The crystal data are as follows: $C_{11}H_{13}NO_3$, mol wt 207.2, monoclinic, space group $P2_1$, a=13.852(4), b=6.750(3), c=13.096(4) Å, β=116.69(5)°, Z=4, D_c=1.258 g cm^{-3}. The cell dimensions and diffraction intensities were measured on an automated, four-circle diffractometer with LiF-monochromated Cu $K\alpha$ radiation (λ=1.5418 Å). The θ—2θ scan technique was applied at a θ scan rate of 0.5° min^{-1}; the background was measured for 30—60 s at each end of the scan range. Three standard reflections, measured at intervals of every 62 reflections, showed no significant decrease in intensity during the course of data collection. The intensities were corrected for the Lorentz and polarization factors, but not for the absorption or the extinction effect. In the range of 2θ values up to 140°, 2229 unique structure-factor magnitudes above the $\sigma(F)$ level were selected for the structure determination.

Structure Determination

The structure was solved by the Monte Carlo direct method,[4] using the 30 strongest reflections as the starting set. In order to extend the tentative-phase set derived from random numbers, 12 cycles of the tangent procedure were carried out using 447 $|E|$ values above 1.30. The 21st phase set led to the correct solution; an E-map based on 439 phases revealed the locations of all the 30 non-hydrogen atoms. After all the 26 hydrogen atoms had been located in a difference Fourier map, the structure was refined by the block-diagonal least-squares method with anisotropic temperature factors for the non-hydrogen atoms and isotropic ones for the hydrogen atoms. For this refinement, the following weighting scheme was used:

$$w = 1/\{\sigma(F)^2 \exp(AX^2 + BY^2 + CXY + DX + EY)\},$$

where $X=|F_0|$ and $Y=\sin\theta/\lambda$. The A, B, C, D, and E coefficients are constants which were determined from the $(\Delta F)^2$ values; A=0.001199, B=20.61, C=1.079, D=−0.2608, and E=−30.11. The final R value was 0.044. The final atomic parameters are listed in Table 1.†

The calculations were performed on FACOM 230-75 and HITAC M-200H computers at the Hokkaido University Computing Center, using our own programs. The atomic scattering factors were taken from the International Tables.[5]

Results and Discussion

The two crystallographically-independent molecules, A and B, have almost the same geometries, except that their absolute configurations are opposite. The skeleton of the B molecule is drawn in Fig. 1(a); the structure of **3** has thus been established as shown in Fig. 1(b). The position of the cyano group agrees with that predicted by the frontier-orbital theory.[6] The torsion angles for the bicyclic system are given in Fig. 2. The

† The tables of the anisotropic temperature factors and hydrogen parameters, and the F_o–F_c table are kept at the Chemical Society of Japan (Document No. 8217).

Table 1. The final atomic parameters and estimated standard deviations
The atomic coordinates are multiplied by 10^4.

Atom	x	y	z	B_{eq}[a)]/Å^2	Atom	x	y	z	B_{eq}/Å^2
O(A1)	2814(2)	3225(4)	4074(2)	3.26	O(B1)	3076(2)	475(4)	−556(2)	3.71
O(A2)	2413(2)	693(4)	4921(2)	4.16	O(B2)	1892(2)	2069(6)	−2108(2)	5.07
O(A3)	1038(2)	1101(4)	2301(2)	4.37	O(B3)	943(2)	−114(6)	−716(3)	5.22
N(A)	3179(3)	7762(6)	3238(4)	4.99	N(B)	5118(4)	−735(11)	2023(4)	7.88
C(A1)	1715(2)	3818(4)	3638(2)	2.86	C(B1)	2680(2)	1562(5)	104(2)	3.25
C(A2)	919(2)	2163(5)	2962(3)	3.26	C(B2)	1442(3)	1391(6)	−350(3)	3.81
C(A3)	−19(3)	2228(6)	3258(4)	4.10	C(B3)	1019(4)	3367(9)	−216(4)	5.71
C(A4)	384(3)	3350(6)	4394(3)	4.11	C(B4)	1870(5)	4884(7)	−123(4)	5.95
C(A5)	1279(2)	4739(5)	4439(3)	3.20	C(B5)	2948(3)	3809(6)	360(3)	4.45
C(A6)	866(3)	6540(5)	3610(3)	3.67	C(B6)	3395(5)	3302(9)	1645(4)	6.18
C(A7)	1471(2)	5774(5)	2932(3)	3.30	C(B7)	3294(3)	1054(7)	1394(3)	4.23
C(A8)	3074(3)	1607(5)	4759(3)	3.69	C(B8)	2609(3)	909(7)	−1685(3)	4.10
C(A9)	4254(3)	1165(8)	5262(5)	5.86	C(B9)	3118(4)	−251(11)	−2286(4)	6.27
C(A10)	2104(3)	5314(7)	5629(3)	4.52	C(B10)	3796(5)	4640(10)	33(6)	7.21
C(A11)	2434(3)	6896(5)	3109(3)	3.59	C(B11)	4321(3)	19(9)	1736(3)	5.20

a) $B_{eq}=8\pi^2(u_1^2+u_2^2+u_3^2)/3$, where u_i is the root-mean-square deviation in the ith principal axis of the thermal ellipsoid.

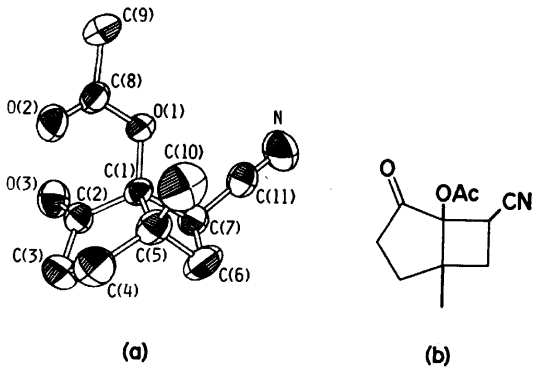

Fig. 1. A perspective view of the **3** molecule, and the corresponding structural formula.

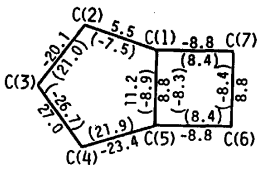

Fig. 2. The torsion angles (ϕ/°) for the bicyclic system. The values for the B molecule are given in parentheses.

cyclopentanone ring takes a half-chair form; the C(4) and C(3) atoms deviate from the C(2)–C(1)–C(5) plane onto the side of the acetyl group and the opposite side, respectively. It should be noted that the acetyl oxygen atom, O(2), approaches closely the ketonic carbon atom, C(2); their distance is 2.661(3) and 2.682(5) Å for the A and B molecules respectively. In this connection, the C(2) atom deviates slightly from the plane through the C(1), C(3), and O(3) atoms onto the side of the O(2) atom; this deviation is 0.018 and 0.011 Å for the A and B molecules respectively. The cyclobutane ring is somewhat puckered; the puckering angle is about 12° for both molecules.

References

1) T. Matsumoto, K. Miyano, S. Kagawa, S. Yü, J. Ogawa, and A. Ichihara, *Tetrahedron Lett.*, **1971**, 3521.
2) E. J. Corey, J. D. Bass, R. LeMahien, and R. B. Mitra, *J. Am. Chem. Soc.*, **86**, 5570 (1964).
3) T. Matsumoto, H. Shirahama, A. Ichihara, S. Kagawa, and S. Matsumoto, *Tetrahedron Lett.*, **1969**, 4103.
4) A. Furusaki, *Acta Crystallogr., Sect. A*, **35**, 220 (1979).
5) "International Tables for X-Ray Crystallography," The Kynoch Press, Birmingham (1974), Vol. IV.
6) K. Fukui, *Acc. Chem. Res.*, **4**, 57 (1971).

Determination of Thermodynamic Properties of Diaspore from Its Solubility Data in NaOH Solutions

Byong-Tae CHANG

Department of Chemistry, Faculty of Science, Korea University, Kodaira, Tokyo 187

(Received February 27, 1981)

Synopsis. Thermodynamic properties of diaspore in the alkaline pH range were determined from its solubility data in NaOH solutions by a method presented earlier by the author. The ionic solubility product, $K_S^\circ = a_{Al}a_H/a_w^2$, of diaspore was found to depend upon temperature between 280 and 325 °C as follows: $\log K_S^\circ = -1367/T - 8.67$.

In the previous paper,[1] the following general equations were derived in order to determine thermodynamic properties of alumina monohydrate from its solubility data in NaOH solutions, they were applied successfully to a dissolution process of boehmite in NaOH solutions:

$$AlOOH(s) + 2H_2O\,(l) = Al(OH)_4^-(l) + H^+(l), \quad (1)$$

$$K_s^\circ = a_{Al}a_H/a_w^2 = K_s\gamma_1^2/a_w^2, \quad (2)$$

$$\left.\begin{aligned} f(I) &= \log(m_{Al}/m_{OH}) + \log(K_w^\circ/a_w) \\ &= \log K_s^\circ + 2\log(\gamma_2/\gamma_1) \end{aligned}\right\}, \quad (3)$$

where $K_S = m_{Al}m_H$, m_i the molality of species i, $\gamma_1^2 = \gamma_{Al}\gamma_H$, $\gamma_2^2 = \gamma_H\gamma_{OH}$, $K_w^\circ = a_Ha_{OH}/a_w$, and a_w the activity of water in a given sodium aluminate and hydroxide. The authors reported solubility data of diaspore in NaOH solutions and discussed its thermodynamic properties by applying an extended Debye-Hückel equation to the solubility data.[2] An essential question arose because the slopes of the straight lines of $\log K_S$ *vs.* $I^{1/2}/(1+1.5I^{1/2})$ or $I^{1/2}/(1+2.0I^{1/2})$ were only about half of the theoretical Debye-Hückel limiting slopes. The purpose of this paper is to revaluate the solubility data according to Eqs. 1—3.

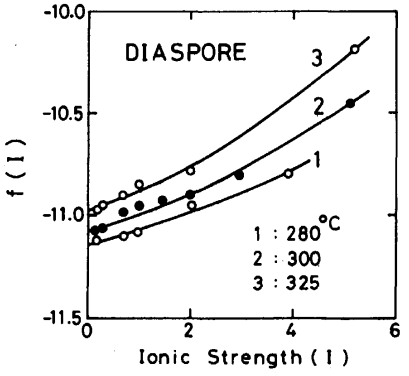

Fig. 1. Relationships between $f(I)$ and ionic strength, I, according to Eq. 3.

Figure 1 gives relationships between $f(I)$ and ionic strength, I, obtained from the solubility data and Eq. 3.[3] Under an assumption of the same ionic size parameters, Eq. 3 can be rewritten as

$$f(I) = \log K_s^\circ + CI + DI^2, \quad (4)$$

where C and D are adjustable parameters. Table 1 gives the values of $\log K_s^\circ$, C, and D determined from the data in Fig. 1 by a method of least squares. Figure 2 shows a temperature dependence of $\log K_s^\circ$ together with that of $\log K_r^\circ$ calculated by following relations:

$$AlOOH(s) + OH^-(l) + H_2O(l) = Al(OH)_4^-(l), \quad (5)$$

$$K_r^\circ = a_{Al}/a_{OH}a_W = K_s^\circ/K_w^\circ. \quad (6)$$

These values are expressed as functions of temperature as follows:

TABLE 1. TEMPERATURE DEPENDENCES OF $\log K_S^\circ$, C, D, AND $\log K_r^\circ$ FOR DIASPORE

No.	Temp/°C	$\log K_S^\circ$	$C\times10^2$	$D\times10^3$	$\log K_r^\circ$
1	280	−11.15	8.56	0.80	−0.13
2	300	−11.06	6.95	8.77	−0.02
3	325	−10.96	6.43	16.46	0.19

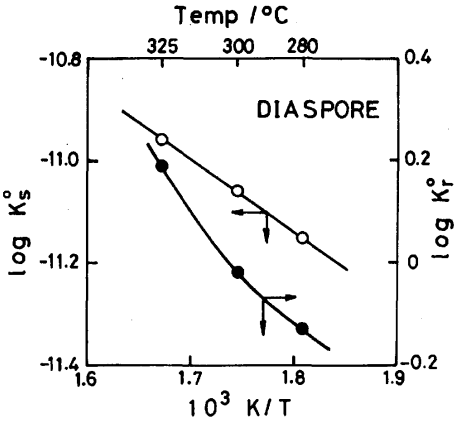

Fig. 2. Temperature dependences of $\log K_s^\circ$ and $\log K_r^\circ$.

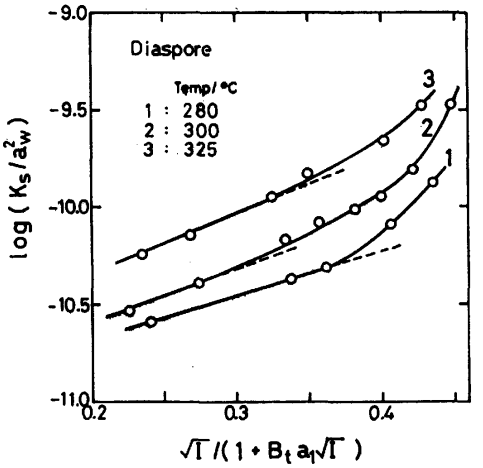

Fig. 3. Plots of $\log(K_s/a_w^2)$ *vs.* $I^{1/2}/(1+B_ta_1I^{1/2})$ at 280, 300, and 325 °C in the case of $a_1 = 4.5$ Å and $a_2 = 5.0$ Å. Values of B_ta_1 are equal to 1.75, 1.79, and 1.87 for curves 1, 2, and 3, respectively.

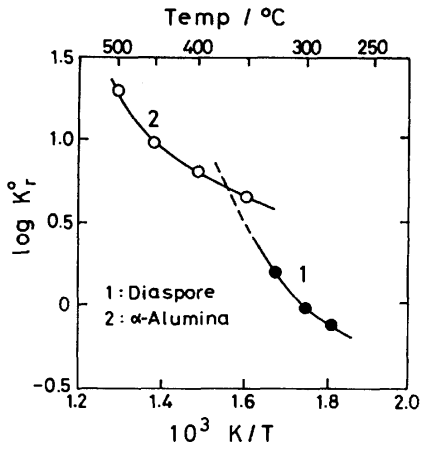

Fig. 4. Temperature dependences of equilibrium constant, K_r°, for diaspore and α-alumina.

$$\log K_s^\circ = -1367/T - 8.67, \quad (7)$$

$$\log K_r^\circ = 2907 - 3.11 \times 10^4/T + 8.27 \times 10^6/T^2, \quad (8)$$

and the heat of Reaction 1 is estimated to be 26.15 kJ.

In the case of different ionic size parameters, the following equations are derived for the dissolution process of alumina monohydrate in NaOH solutions under some assumptions.[1)]

$$\log(K_s/a_w^2) = \log(K_w^\circ/a_w) + \log(m_{Al}/m_{OH}) + 2A_t I^{1/2}/(1 + B_t a_2 I^{1/2}), \quad (9)$$

$$\log(K_s/a_w^2) = \log K_s^\circ + 2A_t I^{1/2}/(1 + B_t a_1 I^{1/2}), + 2c_1 I + 2d_1 I^2, \quad (10)$$

Figure 3 gives plots of log (K_s/a_w^2) *vs.* $I^{1/2}/(1+B_t a_1 I^{1/2})$ at 280, 300, and 325 °C in the case of $a_1=4.5$ Å and $a_2=5.0$ Å. All the curve consist commonly of a straight line in the range of low ionic strength and a positive deviation from it in the range of high ionic strength. Slopes of the straightline are nearly equal to the theoretical Debye-Hückel limiting slopes, $2A_t$. This means that the essential question about the limiting slope described above could be solved by applying more reasonably the extended Debye-Hückel equation. Furthermore, such behaviors of the curves in Fig. 3 are quite consistentwith those of gibbsite[4)] and boehmite.[1)]

Comparison of the temperature dependence of K_s° for diaspore with that of boehmite suggested that the transition temperature between diaspore and boehmite was 170 °C. On the other hand, the transition temperature between diaspore and α-alumina become 368 °C as shown in Fig. 4,[5)] which agrees well with the Al_2O_3-H_2O phase diagram presented by Neuhaus[7)] and Yamaguchi.[8)]

References

1) Thermodynamics of Al_2O_3–Na_2O–H_2O System, Part 4. Part 3: B.-T. Chang, *Bull. Chem. Soc. Jpn.*, **54**, 2579 (1981).

2) B.-T. Chang, L.-H. Pak, and Y.-S. Li, *Bull. Chem. Soc. Jpn.*, **52**, 1321 (1979).

3) The values of m_{Al} and m_{OH} in Ref. 2 were partly corrected in Fig. 1, considering the weight loss of sample in repeated blank tests in pure water, under the same conditions otherwise.

4) B.-T. Chang, *Bull. Chem. Soc. Jpn.*, **54**, 1960 (1981).

5) Values of K_r° for α-alumina were calculated from its solubility data in NaOH solutions[6)] by using $K_r^\circ = a_{Al}/a_{OH}a_w^{3/2}$ and a value of $a_w = 0.97$ at 350 °C.

6) G. Yamaguchi, H. Yanagida, and S. Soejima, *Bull. Chem. Soc. Jpn.*, **35**, 1789 (1962).

7) H. Neuhaus and H. Heide, *Ber. Dtsch. Keram. Ges.*, **42**, 167 (1965).

8) H. Yanagida and G. Yamaguchi, *J. Ceram. Assoc. Jpn.*, **74**, 94 (1966).

The Thermal Decomposition of Crystalline Antimonic(V) Acid

Mitsuo ABE* and Kazufuyu SUDOH

Department of Chemistry, Faculty of Science, Tokyo Institute of Technology, 2-12-1, Ookayama, Meguro-ku, Tokyo 152

(Received December 8, 1980)

Synopsis. The thermal decomposition of crystalline antimonic(V) acid (C-SbA) was studied by means of DTA, DSC, and DTG. The amount of water evolved from the heated C-SbA was determined by the Karl Fischer method. The material heated in the range of 600—1000 °C is Sb_6O_{13}, neither $Sb_3O_6(OH)$ nor $H_2Sb_{12}O_{26}$. The thermal decomposition of C-SbA consists of four dehydration and two reduction steps up to 1000 °C.

The thermal analysis of antimonic(V) acid or hydrous antimony(V) oxide has been studied by various authors.[1-9] The existence of the two forms, valentinite and senarmontite of Sb_2O_3, is unquestionable, and both the Sb_2O_4 dimorphs (α- and β-) have been well characterized by single-crystal X-ray studies. However, much confusion can be found in the literature regarding the higher oxides and their hydrous oxides. Especially, the material heated at 600—800 °C gave an X-ray pattern with a pyrochlore structure (Fd3m) rather than that of Sb_2O_4, which prompted Dihlstöm and Westgren to reassign the Sb_3O_6OH composition.[4] This compound is accepted on the basis of many present texts.

Moreover, the X-ray powder data of material heated at 780 °C is erroneously listed in the ASTM X-ray powder data card file (No. 11-690 in the 1966 edition) as having the composition of Sb_2O_5.[5,7]

Extensive studies of the materials obtained by heating the different antimonic(V) acids (amorphous, glassy, and crystalline) have been carried out by Abe and Ito using X-ray, DTA, TG, IR, and chemical analysis.[5,6] The thermal decomposition of crystalline antimonic(V) acid (C-SbA) up to 1300 °C follows the scheme:

$$(H_3O)_2Sb_2O_5(OH)_2 \xrightarrow{200°C} H_2Sb_2O_5(OH)_2 \xrightarrow{350°C}$$
$$Sb_2O_5 \xrightarrow{550°C} Sb_6O_{13} \xrightarrow{800°C} Sb_2O_4(\alpha\text{- and }\beta\text{-}) \xrightarrow{1200°C}$$
$$Sb_2O_3 \xrightarrow{1250°C} \text{sublimation.}$$

A similar conclusion was recently observed by Stewart *et al.*[7] Kleshchev *et al.* have suggested that the product of the antimonic acid heated at 600—800 °C is $H_2Sb^{III}_5Sb^{V}_7O_{26}$ or $H_2Sb^{III}_{10}Sb^{V}_{16}O_{56}$,[8,9] from structural studies of its pyrochlore phase, and that it is not possible to determine such a hydrogen content by means of gravimetric analysis. Another scheme of the thermal decomposition of crystalline antimonic acid, leading to the stepwise formation of H_3OSbO_3 (148 °C at DTA temp.), Sb_3O_6OH(348 °C), Sb_6O_{13}(620 °C), and Sb_2O_4 (940 °C), has been reported by Novikov *et al.*[10] However, no direct evidence has been obtained for the existence of Sb_3O_6OH or $H_2Sb^{III}_{10}Sb^{V}_{16}O_{56}$.

In the present work, the thermal decomposition of the C-SbA has been reexamined by means of DTA, DTG, and DSC, and the water content has been determined by using the modified Karl Fischer method.[11]

Experimental

The C-SbA was prepared as has been described previously.[5] The C-SbA air dried for over 1 year was humidified on a desiccator over saturated NaCl solution (with a relative humidity of 75% at 20 °C) and was then used in the following experiments.

The inside of the systems of the heating and titration apparatus was free from moisture by passing through dried air at a flow rate of 70 cm^3 min^{-1}. The dried air was obtained by passing through (in the order), silica gel, anhydrated $Mg(ClO_4)_2$, and finally diphosphorus pentoxide. The titration apparatus was set at 20±0.3 °C in order to prevent volumetric error caused by the thermal expansion of the Karl Fischer reagent. The C-SbA of 240 mg was heated in dried air by using a Rigaku Denki Thermoflex 8002 with a thermogravimetric analyser at a heating rate of 10 °C min^{-1} up to the desired temperature, it was then kept for 12 h at that temperature. The water evolved from the heated C-SbA was absorbed into an anhydrous solvent "Mitsubishi ME" (a mixture of methanol and ethylene glycol)supplied by the Mitsubishi Kasei Co.; it was then titrated by using Karl Fischer reagent of SS "Mitsubishi." The strength of the Karl Fischer reagent was standardized with appropriate amounts of deionized water.

For the thermal analysis, about a 40-mg portion of the C-SbA was packed in a platinum crucible. The DTG curve of the C-SbA was determined by differentiating the TG curve obtained with the temperature. The DSC and DTG curves thus obtained were separated into individual peaks by means of non-linear least-squares fit, assuming that each peak of the DSC and DTG curves can be approximated by the following equation:

$$\text{Peak}=A\cdot\exp\{-B\cdot(C-T)^2\}.$$

Where A, B, and C are parameters, and T is the temperature from thermal analysis (°C).

The X-ray diffraction data for the heated C-SbA were determined by using a JEOL X-ray diffractometer, Model JDX-7E, with Ni-filtered Cu $K\alpha$ radiation.

Results and Discussion

The X-ray analysis of the C-SbA heated at 900 °C indicated a mixture of a large amount of α-Sb_2O_4 and a small amount of β-Sb_2O_4, as was observed by Abe.[5] Table 1 showed the weight loss and the evolved water from the C-SbA heated at a different temperature for 12 h. The weight loss of C-SbA was obtained as 20.7% at 600—800 °C and as 22.2% at 900 °C. The evolved water contents, as determined by the modified Karl Fischer method showed an almost constant value of 18.0—18.1%, regardless of the heating temperature in the range of 500—900 °C. The calculated composition of the C-SbA is $Sb_2O_5\cdot3.9H_2O$; this agree well with earlier results.[5]

The observed weight loss of 1.8±0.1%, obtained by heating the material from 750 °C to 900 °C for 30 min,

Table 1. Dependence of the weight loss and the evolved water of the C-SbA at the heating temperature for 12 h

Temp °C	Weight loss %	Water evolution %	Water composition[a] (n)
100	7.5	7.5	
200	13.6	13.6	
300	16.6	16.1	
400	18.3	17.3	
500	20.6	18.0	3.95
600	20.8	18.1	3.97
700	20.7	18.1	3.97
800	20.7	18.0	3.96
900	22.2	18.0	3.96
1000	40.3	18.0	3.96

a) Water composition: $Sb_2O_5 \cdot nH_2O$.

agree well with the theoretical value of 1.70% from Sb_6O_{13} to Sb_2O_4 within the limits of experimental error. If the change from 700 °C to 900 °C corresponds to that of the hydrated material of the antimony oxide, the weight loss should be obtained as 1.8% from $2Sb_3O_6$-OH to Sb_6O_{13}, as 0.97% from $H_2Sb_{12}O_{26}$ to $Sb_{12}O_{25}$, and as 0.45% from $H_2Sb_{26}O_{56}$ to $Sb_{26}O_{55}$. The value of the evolved water from the heated C-SbA is almost constant in the range of 500—900 °C. The evolved water was less than the blank value of 0.1% and/or the same heating conditions of 750—900 °C. Thus, we conclude that the change in the C-SbA heated at 750 to 900 °C is from Sb_6O_{13} to Sb_2O_4. This conclusion agree well with those of Abe[5] and Stewart *et al.*[7]

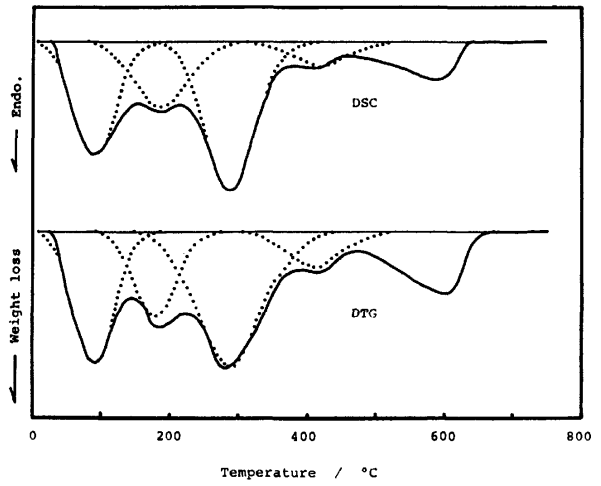

Fig. 1. DSC and DTG curves of C-SbA in H^+ form.
Heating rate: 10 °C min^{-1}, sample size: 100—200 mesh, atmosphere: air.
——: Observed, ····: calculated.

The observed DSC and DTG curves are shown in Fig. 1. The maximum temperatures were observed at about 100, 190, 300, 420, and 600 °C up to 700 °C in five curves. This result is in good agreement with that reported earlier, except for the endothermic peak of 190 °C. Such a small peak as that at 190 °C was detectable because the apparatus of thermal analysis used here is more sensitive than that used earlier. The shape of the last peak at 600 °C was different from the other four peaks and would correspond to the deoxidation of Sb_2O_5. We attempted to separate the first four peaks into four individual peaks by means of a non-linear least-square fit. The sum of the four separated peaks was successfully reproducible on the original DTG curve by means of computer curve-fitting. The weight loss of the C-SbA calculated by means of the total area of the four separated peaks at 90, 180, 290, and 420 °C was 17.9%, almost the same as the water content of the C-SbA in Table 1. Thus, thermal decomposition of the C-SbA in the H^+form follows four dehydration and two deoxidation steps up to 1000 °C:

$$Sb_2O_5 \cdot 4H_2O \xrightarrow{90^\circ C} Sb_2O_5 \cdot 2.9H_2O \xrightarrow{180^\circ C}$$
$$Sb_2O_5 \cdot 2.15H_2O \xrightarrow{290^\circ C} Sb_2O_5 \cdot 0.45H_2O \xrightarrow{420^\circ C}$$
$$Sb_2O_5 \xrightarrow{600^\circ C} Sb_6O_{13} \xrightarrow{940^\circ C} Sb_2O_4.$$

The authors wish to express their thanks to Dr. Takumi Hikida and Dr. Hiroshi Hiratsuka of the Tokyo Institute of Technology for their helpful advices regarding the computer curve fitting.

References

1) J. Szilagyi, *Z. Anal. Chem.*, **57**, 23 (1918).
2) H. Goto, *Nippon Kagaku Zasshi*, **55**, 326 (1934).
3) A. Simon and E. Thaler, *Z. Anorg. Allg. Chem.*, **162**, 253 (1927).
4) K. Dihlström and A. Westgren, *Z. Anorg. Allg. Chem.*, **235**, 153 (1937).
5) M. Abe, *Kogyo Kagaku Zasshi*, **70**, 2226 (1967).
6) M. Abe and T. Ito, *Bull. Chem. Soc. Jpn.*, **41**, 2366 (1968).
7) D. J. Stewart, O. Knop, and C. Ayasse, *Can. J. Chem.*, **50**, 690 (1972).
8) V. Trofimov, A. I. Sheinkman, and G. V. Kleshchev, *Z. Strukt. Khim.*, **14**, 275 (1973).
9) G. V. Kleshchev, V. G. Trofimov, D. G. Kleshchev, and A. I. Sheinkman, *Krystallografiya*, **21**, 832 (1975).
10) B. G. Novikov, F. A. Belinskaya, and E. A. Materova, *Vestn. Leningrad Univ. Fiz. Khim.*, **1969**, 97.
11) K. Yamaya, M. Yoshida, and T. Ozawa, *Nippon Kagaku Kaishi*, **1974**, 2111.

Circular Dichroism Spectra of *cis,cis*-$[Co(OO)(N)_2(py)_2]^+$-Type Complexes

Shuhei FUJINAMI,* Kenshi TSUJI, Ritsuko MUSA, and Muraji SHIBATA

Department of Chemistry, Faculty of Science, Kanazawa University, Kanazawa 920

(Received April 4, 1981)

Synopsis. Four new complexes, *cis,cis*-$[Co(OO)(NH_2C_2H_5)_2(py)_2]^+$($OO=CO_3^{2-}$, ox^{2-}, or mal^{2-}) and *cis,cis*-$[Co(ox)(NH_3)_2(py)_2]^+$, have been prepared and optically resolved. The CD patterns regularly change in the order of carbonato, oxalato, and malonato complexes, the aspect in the change being opposite to that of related *cis,cis*-$[Co(NO_2)_2(OO)(NH_3)_2]^-$-type complexes.

Many complexes of $[Co(N)_4(O)_2]^+$-type have been prepared and optically resolved. The chirality of those complexes is considered to be derived from helical distributions of chelate rings. Recently, *cis,cis*-$[Co(OO)(NO_2)_2(NH_3)_2]^-$ ($OO=CO_3^{2-}$, ox^{2-}, or mal^{2-})[1] and *cis,cis*-$[Co(CO_3)(NH_3)_2(py)_2]^+$ [2] have been prepared and resolved. These complexes are interesting, because the chirality is derived from the arrangement of three kinds of donor atoms. In this paper, the preparations and optical resolutions of *cis,cis*-$[Co(OO)(NH_2C_2H_5)_2(py)_2]^+$ and *cis,cis*-$[Co(ox)(NH_3)_2(py)_2]^+$ complexes are reported. Furthermore, the influence of the chelated OO ligands upon the CD intensity is investigated.

Experimental

Syntheses and Optical Resolutions. a) cis,cis-*Carbonatobis(ethylamine)bis(pyridine)cobalt(III) Chloride Trihydrate*, cis,cis-*[Co(CO$_3$)(NH$_2$C$_2$H$_5$)$_2$(py)$_2$]Cl·3H$_2$O*: Ethylamine (40 cm^3, 0.4 mol) was added to a solution of $[Co(CO_3)_3]^{3-}$ ($Co(NO_3)_2\cdot 6H_2O$, 0.05 mol scale)[3] and the mixture stirred until the solution became blue in color. After filtration, ethanol (150 cm^3) and acetone (100 cm^3) were successively added to the filtrate in an ice-bath. The crude product precipitated was recrystallized from water. The product was *cis*-$K[Co(CO_3)_2(NH_2C_2H_5)_2]\cdot H_2O$. To a solution of the above product (30 g, 0.13 mol, in 30 cm^3 H_2O) pyridine (25 cm^3, 0.31 mol) was added and the resultant solution acidified to pH 5 with $HClO_4$ (60%). After filtration, the filtrate was stirred at room temperature for a day, whereupon some pink crystals deposited. An aqueous solution of the crystals was charged on a column of Dowex 50W-X8 resin in Na^+ form (100—200 mesh, $\phi 7\times 5$ cm^2). By elution with 0.3 mol/dm^3 NaCl, one red band descended. The eluate was concentrated and kept in a refrigerator. The crude product was recrystallized from warm water; yield *ca.* 7 g. Found: C, 39.31; H, 6.52; N, 12.20%. Calcd for $[Co(CO_3)(NH_2C_2H_5)_2(C_5H_5N)_2]Cl\cdot 3H_2O$: C, 39.42; H, 6.57; N, 12.26%.

To a solution of the chloride (4.0 g, 0.017 mol, in 20 cm^3 H_2O) was added $(-)_{546}Ag[Co(ox)_2(en)]$ (3.7 g, 0.017 mol), and the resulting AgCl was filtered off. On concentrating the filtrate, at first, one diastereoisomeric salt of the $(-)_{589}$-carbonato complex deposited, and then another salt of the $(+)_{589}$-one deposited. Since the optical purity of the former salt could not be raised by recrystallization, the latter salt was recrystallized ten times from warm water. The yield was *ca.* 1.0 g.

b) cis,cis-*Bis(ethylamine)oxalatobis(pyridine)cobalt(III) Perchlorate Monohydrate*, cis,cis-*[Co(ox)(NH$_2$C$_2$H$_5$)$_2$(py)$_2$]ClO$_4$·H$_2$O*: $H_2C_2O_4\cdot 2H_2O$ (8 g, 0.089 mol) was added to a solution of *cis,cis*-$[Co(CO_3)(NH_2C_2H_5)_2(py)_2]Cl\cdot H_2O$ (10 g, 0.043 mol) and the mixture was stirred at 35 °C for 2 d. The solution was neutralized with $KHCO_3$. After filtration, the filtrate was charged on a column containing Dowex 50W-X8 resin in Na^+ form (100—200 mesh, $\phi 4\times 30$ cm^2). By elution with 0.1 mol/dm^3 $NaClO_4$, two red bands were discharged from the column (labeled E1 and E2 in the order of elution), and the desired E2 band was collected in a fraction. After concentration and filtration, the filtrate was kept in a refrigerator. The crude product was recrystallized from water. The yield was 4 g. Found: C, 37.73; H, 5.03; N, 10.85%. Calcd for $[Co(C_2O_4)(NH_2C_2H_5)_2(C_5H_5N)_2]ClO_4\cdot H_2O$: C, 37.47; H, 5.12; N, 10.93%.

This complex was partially resolved by column chromatography on SP-Sephadex C-25 ($\phi 2.5\times 95$ cm^2, Na^+ form) using 0.05 mol/dm^3 $K_2[Sb_2(d\text{-tart})_2]$ as an eluent.

c) cis,cis-*Bis(ethylamine)malonatobis(pyridine)cobalt(III) Perchlorate Dihydrate*, cis,cis-*[Co(mal)(NH$_2$C$_2$H$_5$)$_2$(py)$_2$]ClO$_4$·2H$_2$O*: To a solution of *cis*-$K[Co(CO_3)_2(NH_2C_2H_5)_2]\cdot H_2O$(32 g, 0.1 mol, in 120 cm^3 H_2O) potassium malonate (17 g, 0.09 mol) was added, and the mixture acidified to pH 5 with 60% $HClO_4$ in an ice-bath. After filtration, the filtrate was stirred for 1 h, and then adjusted to pH 1 with 60% $HClO_4$. The solution was filtered and the filtrate was chromatographed on a column of Dowex 50W-X8 resin in H^+ form (100—200 mesh, $\phi 7\times 15$ cm^2) using 0.2 mol/dm^3 NaCl as an eluent. A univalent complex species was collected in a fraction. To the fraction was added $KHCO_3$ to adjust pH to 9 and the solution concentrated to *ca.* 50 cm^3. After filtration, pyridine (15 cm^3, 0.19 mol) was added to the filtrate followed by 60% $HClO_4$ to adjust the pH to 5 in the cold. The solution was filtered once and the filtrate stirred at room temperature for 3 d. The solution was charged on a column of Dowex 50W-X8 resin in Na^+ form (100—200 mesh, $\phi 4\times 30$ cm^2). By elution with 0.1 mol/dm^3 NaCl, three bands were discharged. The first eluted band was collected and concentrated to *ca.* 20 cm^3. After filtration, the filtrate was kept in a refrigerator. The product obtained was recrystallized from warm water; yield *ca.* 0.5 g. Found: C, 37.54; H, 5.52; N, 10.44%. Calcd for $[Co(C_3H_2O_4)(NH_2C_2H_5)_2(C_5H_5N)_2]ClO_4\cdot 2H_2O$: C, 37.47; H, 5.56; N, 10.28%.

This complex was partially resolved on a column chromatograph of Dowex 50W-X8 resin in Na^+ form (100—200 mesh, $\phi 4\times 46$ cm^2) using 0.1 mol/dm^3 $K_2[Sb_2(d\text{-tart})_2]$ as eluent.

d) cis,cis-*Diammineoxalatobis(pyridine)cobalt(III) Perchlorate 2.5-Hydrate*, cis,cis-*[Co(ox)(NH$_3$)$_2$(py)$_2$]ClO$_4$·2.5H$_2$O*: This complex was prepared in the same manner as described in *b)* except for the use of *cis,cis*-$[Co(CO_3)(NH_3)_2(py)_2]Cl\cdot H_2O$[2] (10 g, 0.027 mol) instead of *cis,cis*-$[Co(CO_3)(NH_2C_2H_5)_2(py)_2]Cl\cdot H_2O$. The yield was *ca.* 2 g. Found: C, 29.32; H, 4.34; N, 11.48%. Calcd for $[Co(C_2O_4)(NH_3)_2(C_5H_5N)_2]ClO_4\cdot 2.5H_2O$: C, 29.24; H, 4.34; N, 11.58%.

The perchlorate was converted to chloride by column chromatography. The chloride was optically resolved by adding equimolar $(+)_{543}Na[Co(edta)]\cdot 2H_2O$. The less soluble diastereoisomeric salt containing the $(-)_{589}$-oxalato complex was recrystallized from water.

The optical rotation, absorption and CD spectra were measured in the same manner as described in the previous

Table 1. Absorption and CD spectral data

	Absorption $\tilde{\nu}_{max}/10^3$ cm^{-1}		CD $\tilde{\nu}_{ext}/10^3$ cm^{-1}				$\lvert\Delta\varepsilon_1/\Delta\varepsilon_2\rvert$
	(log ε_1)	(log ε_2)	($\Delta\varepsilon_1$)	($\Delta\varepsilon_2$)	($\Delta\varepsilon_3$)	($\Delta\varepsilon_4$)	
$(+)_{589}$[Co(CO_3)-($NH_2C_2H_5$)$_2$(py)$_2$]$^+$	19.2(2.08)	27.2(2.14)	18.1(+0.61)	20.2(−0.77)	27.4(+0.26)		0.79
$(+)_{589}$[Co(ox)-($NH_2C_2H_5$)$_2$(py)$_2$]$^+$	19.2(1.98)	27.0(2.24)	18.0(+0.07)	20.0(−0.16)	28.0(+0.07)		0.44
$(+)_{589}$[Co(mal)-($NH_2C_2H_5$)$_2$(py)$_2$]$^+$	19.1(1.94)	27.0(2.13)	18.0(+0.03)	20.0(−0.13)	27.3(+0.04)		0.23
$(-)_{589}$[Co(CO_3)-(NH_3)$_2$(py)$_2$]$^+$	19.4(2.06)	27.6(2.07)	18.1(−0.76)	20.3(+0.92)	27.8(−0.28)		0.83
$(-)_{589}$[Co(ox)-(NH_3)$_2$(py)$_2$]$^+$	19.7(1.91)	27.6(2.12)	18.5(−0.80)	20.7(+1.52)	27.4(−0.46)		0.53
$(+)_{589}$[Co(H_2O)$_2$-($NH_2C_2H_5$)$_2$(py)$_2$]$^{3+}$	19.1(1.90)	27.0(1.97)	17.4(−0.11)	19.6(+0.24)	25.8(−0.07)	28.4(+0.02)	0.46

paper.[2] Prior to the above measurements, the samples had been converted into chlorides by means of an ion-exchange technique. The absorption and CD spectra of the diaqua complex, after the corresponding carbonato complex was acid-hydrolyzed with 10% $HClO_4$, were measured.

Results and Discussion

The absorption and CD spectral data are summerized in Table 1. The three complexes, $(+)_{589}$[Co(CO_3)-($NH_2C_2H_5$)$_2$(py)$_2$]$^+$, $(+)_{589}$[Co(ox)($NH_2C_2H_5$)$_2$(py)$_2$]$^+$, and $(+)_{589}$[Co(mal)($NH_2C_2H_5$)$_2$(py)$_2$]$^+$, exhibit two CD peaks with opposite sign in the first absorption band region. When the value of the extremum at the lower frequency is designated $\Delta\varepsilon_1$, and that at the higher frequency $\Delta\varepsilon_2$, the ratio, $|\Delta\varepsilon_1/\Delta\varepsilon_2|$, decreases in the order of the carbonato, oxalato, and malonato oomplexes, as is seen in Table 1. The two diammine complexes, $(-)_{589}$[Co(CO_3)(NH_3)$_2$(py)$_2$]$^+$ [2] and $(-)_{589}$[Co(ox)-(NH_3)$_2$(py)$_2$]$^+$, also exhibit two CD peaks, the ratio decreasing in the order of the carbonato and oxalato complexes. Such a decrease is not apparent in [Co(OO)-(en)$_2$]$^+$ or *cis*-[Co(OO)(NH_3)$_2$(en)]$^+$ complexes (OO represents CO_3^{2-}, ox^{2-}, or mal^{2-}),[2] which contain tris or bis bidentate ligands and show a single CD peak in the first absorption band region. These phenomena reveal a difference between the chiral complexes due to the arrangements of three kinds of donor atoms and those due to the helical distribution of bidentate ligands. On the other hand, CD spectra of *cis,cis*-[Co(NO_2)$_2$-(OO)(NH_3)$_2$]$^-$ complexes,[1] which also belong to the same type of chiral complex as the present complexes, exhibit two CD peaks in the first absorption band region. However, the ratio increases in the order of the carbonato, oxalato, and malonato complexes; the values are 0.13, 0.57, and 0.97, respectively (in the case of the malonato complex, an extremely small extremum at the lowest frequency side is neglected). Mason[4] has succeeded in explaining the rotatory strength of *all-cis*-[Co(CN)$_2$(NH_3)$_2$(H_2O)$_2$]$^+$ in terms of a dynamic coupling model in which ligand-polarization induced by other ligands is treated. The different behavior between CD spectra of *cis,cis*-[Co(OO)($NH_2C_2H_5$)$_2$(py)$_2$]$^+$ and those of *cis,cis*-[Co(NO_2)$_2$(OO)(NH_3)$_2$]$^-$ may be explained by the dynamic coupling model rather than a static coupling model,[5] since both complexes approximately belong to the same *cis*-[Co(O)$_2$(N)$_4$]-type complexes. It is considered that a factor such as polarizability or formal charge on the ligands is more intimately associated with the rotatory strength of the present complexes than the ligand field strength. This is supported by the observation that the CD spectrum of $(+)_{589}$[Co($NH_2C_2H_5$)$_2$(py)$_2$(H_2O)$_2$]$^{3+}$ derived from $(-)_{589}$[Co(CO_3)($NH_2C_2H_5$)$_2$(py)$_2$]$^+$ by acid-hydrolysis shows an opposite pattern to that of the $(+)_{589}$-carbonato complex. The ligand field strength of carbonato ligand is nearly equal to that of the aqua ligand. However, the polarizability of the former ligand is very different from that of the latter one.

The absolute configuration of $(-)_{589}$[Co(CO_3)(NH_3)$_2$-(py)$_2$]$^+$ has been assigned *S* on the basis of the CD spectral comparison with related complexes.[2] The CD patterns of three $(+)_{589}$[Co(OO)($NH_2C_2H_5$)$_2$(py)$_2$]$^+$ (OO=CO_3^{2-}, ox^{2-}, mal^{2-}) isomers are opposite to that of $(-)_{589}$[Co(CO_3)(NH_3)$_2$(py)$_2$]$^+$, and the CD spectrum of $(-)_{589}$[Co(ox)(NH_3)$_2$(py)$_2$]$^+$ exhibits the same pattern. Consequently, the three ethylamine complexes are assignable to an *R* configuration, and the ammine complex an *S* configuration. The $(+)_{589}$[Co(NH_2C_2-H_5)$_2$(py)$_2$(H_2O)$_2$]$^{3+}$ species derived from the corresponding $(+)_{589}$-carbonato complex is also assigned to *R*, since the acid-hydrolysis should proceed with retention of the configuration.

References

1) T. Ito and M. Shibata, *Inorg. Chem.*, **16**, 108 (1977).
2) K. Tsuji, S. Fujinami, and M. Shibata., *Bull. Chem. Soc. Jpn.*, **54**, 1531 (1981).
3) M. Shibata, *Proc. Jpn. Acad.*, **50**, 779 (1974).
4) S. F. Mason, *Mol. Phys.*, **37**, 843 (1979).
5) S. F. Mason and R. H. Seal, *Mol. Phys.*, **31**, 755 (1976).

A New Phase of Compound $CaMnO_{2+\delta}$[1)]

Koichiro TAKAHASHI,* Hiroshi YAMAMURA, Kunitaka MURAMATSU, Shin-ichi SHIRASAKI, and Kensuke SUEHIRO**

National Institute for Research in Inorganic Materials, Namiki 1-1, Sakura-mura, Niihari-gun, Ibaraki 305
***Department of Industrial Chemistry, Faculty of Engineering, Tokai University, Tomigaya 2-28, Shibuya-ku, Tokyo 151*

(Received May 8, 1981)

Synopsis. A new phase of $CaMnO_{2+\delta}$ was synthesized by a wet process, followed by calcining. The structure was determined to be orthorhombic, with these lattice constants: $a=5.96$, $b=14.38$, and $c=5.72$ Å. Phase transformations among $CaMnO_{2+\delta}$ compounds were studied in various atmospheres, such as N_2, CO_2, and air.

Compounds of alkaline-earth oxide with transition metals have various crystal structures depending on whether there is an excess or deficiency of oxygen. The $CaMnO_{2+\delta}$ system was chosen in order to study systematically how the crystal structures of manganese oxides change with varied valences of Mn ions.

Mizutani *et al.*[2,3)] reported that $SrMnO_3$ perovskite was transformed to $Sr_2Mn_2O_5$ brownmillerite-type compound, under N_2 atmospheres at 1500 °C. Since both Sr and Ca are alkaline-earth metals, a new phase with the composition of $Ca_2Mn_2O_5$ was expected to be synthesized.

Experimental

The synthesis of the compounds was carried out as follows. The reagents used were: $CaCO_3$ (alkaline metal analysis grade; Kanto Chemical Co., Inc.), Na_2CO_3 (reagent grade; Kanto Chemical Co., Inc.), and $MnCO_3$ (reagent grade; Wako Pure Chemical Industries Ltd.). A mixture of $CaCO_3$ and $MnCO_3$ in a molar ratio of 1:1 was dissolved into an HCl solution. An excess of an aqueous solution of Na_2CO_3 was added to the above solution to coprecipitate both Ca and Mn ions as carbonates in order to prepare a homogeneous materials; washing with distilled water followed to eliminate the Na ions thoroughly. The mixed precipitate was filtered, dried in air, and then calcined in an atmosphere with a volume ratio of $H_2/Ar=1/3$ at 900 °C for 2 h in a platinum crucible. Finally, the compound was heated again in the same atmosphere and at the same temperature for 17 h. The light green product was identified as a cubic (Ca, Mn)O solid solution by X-ray diffractometry. The composition of the solid solution was determined to be $CaMn_{1.01}O_{2.07}$ with 0.05 wt% of Na and 0.089 wt% of H_2O as minor constituents.

Results and Discussion

It is of much interest that a remarkable difference in the oxidation processes of the compound was observed, depending on the heating conditions. When the compound was oxidized in air at 600—610 °C, only one line with a considerable broadness was found in X-ray powder diffractometry, suggesting an amorphous phase[2)] in the range of $\delta=0.74$—0.91. When the solid solution was kept in air above 610 °C, however, $CaMnO_{3-\chi}$ perovskite[4)] was obtained in the stable range of $\chi=0.00$—0.17 in oxygen vacancies. On the other hand, the (Ca,Mn)O in high-temperature oxidation behaves quite differently from that in low-temperature oxidation.

TABLE 1. X-RAY POWDER DIFFRACTION LINES OF $Ca_2Mn_2O_5$

hkl	d_{obsd}/Å	d_{calcd}/Å	I/I_0
?(110)	5.99	(5.51)	14
?(101)	4.84	(4.13)	9
200	3.01	2.98	11
002	2.88	2.86	16
141	2.71	2.71	100
150	2.61	2.59	54
102	2.56	2.58	19
221	2.49	2.48	14
240	2.29	2.29	17
042	2.23	2.24	29
?	2.17	—	12
202	2.07	2.06	18
260	1.88	1.87	15
330	1.84	1.84	24
143	1.63	1.62	11
053	1.58	1.59	14
233 082	1.52	1.52	13
400	1.50	1.49	10
004	1.48	1.43	11
323	1.35	1.35	13

Orthorhombic, $a=5.961$, $b=14.38$, $c=5.72$ Å.

When the (Ca,Mn)O compound was kept at 1000 °C for 2 h in CO_2 ($P_{O_2}=2\times10^{-4}$ atm) and then rapidly quenched to room temperature, a new phase appeared, with the *d*-values shown in Table 1. The phase is very stable, for it was hardly oxidized at all even when kept at 1000 °C for about 1 h in air. The oxidation process was examined using a high-temperature X-ray diffractometer. When the new phase was heated in air at a constant rate of 10 °C/min, the $CaMnO_3$ perovskite peaks appeared at about 1050 °C; this reaction was completed at 1200 °C. The perovskite was reduced to the new phase when held in N_2 gas ($P_{O_2}=5\times10^{-4}$ atm) at 1000 °C for 20 h; it was examined using a rapidly-quenched sample. The transition between the

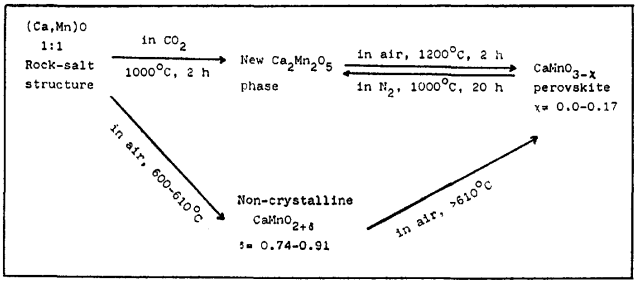

Fig. 1. Reaction diagram for $CaMnO_{2+\delta}$: (Ca, Mn)O solid solution, new $Ca_2Mn_2O_5$ phase and $CaMnO_3$ perovskite.

new phase and $CaMnO_3$ was reversible. These reaction processes are shown in Fig. 1.

Since the X-ray pattern in Table 1 is quite similar to that of orthorhombic $Sr_2Mn_2O_5$ (a brownmillerite-type compound), the new phase was identified as orthorhombic $Ca_2Mn_2O_5$ with the lattice constants of $a=5.96$, $b=14.38$, and $c=5.72$ Å, and with the axis ratios of $b/a=2.42$ and $c/a=0.96$. Using these values, the observed d_{obsd}'s are indexed in Table 1; they are in fair agreement with the calculated d_{calcd}'s except for a few lines. The chemical analysis of the new compound showed the composition of $CaMn_{1.01}O_{2.58}$.

The authors are much indebted to Mr. Hideki Yamamoto of Tokai University, and Dr. Jun-ichi Mohri, Mr. Yuji Sugaya, and Mr. Terumasa Ono of Chiba University for helping with the experiments and for their useful discussions; Mr. Takeshi Nagashima and Mrs. Michiko Kobayashi of NIRIM for their chemical analysis, and Drs. Nobuyasu Mizutani and Masanori Kato of Tokyo Institute of Technology and Mr. Syuzo Tamura and Mr. Eiji Takayama of NIRIM for their helpful suggestions.

References

1) K. Takahashi, H. Yamamura, K. Muramatsu, and S. Shirasaki, Text of the Glass Division Meeting of the Ceramic Society of Japan, April, 1972.

2) N. Mizutani, Ph. D. Thesis, Tokyo Institute of Technology, Tokyo, Japan (1969).

3) N. Mizutani, N. Okuma, A. Kitazawa, and M. Kato, *Kogyo Kagaku Zasshi*, **73**, 1103 (1970).

4) W. O. Wollan and W. C. Koehler, *Phys. Rev.*, **100**, 545 (1955).

Spectrophotometric Determination of Sodium 4-Dodecylbenzenesulfonate with 1-(*N*-Methylpyridinium-4-yl-azo)-4-(4-diethylaminophenylazo)-naphthalene Iodide

Keiro HIGUCHI, Yasuaki SHIMOISHI, Haruo MIYATA,* and Kyoji TÔEI

Department of Chemistry, Faculty of Science, Okayama University, Tsushima-naka 3-1-1, Okayama 700

(Received August 29, 1981)

Synopsis. A new reagent, 1-(*N*-methylpyridinium-4-yl-azo)-4-(4-diethylaminophenylazo)naphthalene iodide, can react with sodium 4-dodecylbenzenesulfonate to show a color change in an aqueous phase in the presence of iodide ion. The calibration graph is straight line up to 1.2×10^{-5} M (1 M= 1 mol dm^{-3}); $\varepsilon=3.25\times10^{4}$ l mol^{-1} cm^{-1} at 580 nm.

The developmental study on the new reagent is invaluable in the determination of micro amounts of anionic surfactant in an aqueous phase.[1] A new reagent, 1-(*N*-methylpyridinium-4-yl-azo)-4-(4-diethylamino-

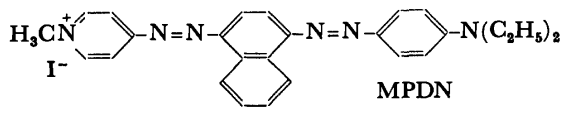

MPDN

phenylazo)naphthalene iodide (MPDN), forms an ion pair with the anionic surfactants such as sodium 4-dodecylbenzenesulfonate (DBS) and dodecyl sulfate (SDS) in the presence of iodide ion. Using this phenomenon, DBS or SDS up to 1.2×10^{-5} M has been determined in an aqueous phase without extraction procedure.

Experimental

Materials. A typical synthetic method of MPDN is as follows. A solution of 1.8 g of 4-aminopyridine in 10 ml of 85% phosphoric acid and 5 ml of concentrated nitric acid were mixed at −8 °C; sodium nitrite (1.4 g) and 25 g of ice were then added successively.[2] The solution was poured into 100 ml of ethanol containing 2.9 g of 1-naphthylamine. After the reaction, the solution was neutralized with sodium carbonate, and the precipitate was filtered off and recrystallized from benzene. The crystals of 4-(4-amino-1-naphthylazo)pyridine (ANP) were reddish violet plates. Found; C, 72.52; H, 4.56; N, 22.18%. Calcd for $C_{15}H_{12}N_4$: C, 72.60; H, 4.87; N, 22.57%.

ANP (1 g) was dissolved in 30 ml of glacial acetic acid, and diazotized with 0.28 g of sodium nitrite by adding in small portions. The solution was poured into 100 ml of ethanol containing 0.6 g of *N,N*-diethylaniline. After the reaction, the solution was neutralized with sodium carbonate, and the precipitate was filtered off and recrystallized from ethanol–water solution. The crystals of 1-(4-pyridylazo)-4-(4-diethylaminophenylazo)naphthalene (PDN) were violet needles. Found: C, 73.70; H, 6.03; N, 20.28%. Calcd for $C_{25}H_{24}N_6$: C, 73.50; H, 5.92; N, 20.58%.

PDN (0.3 g) was quarternized by refluxing with 0.2 g of methyl iodide in 30 ml of *N,N*-dimethylformamide at 50 °C for 8 h. The iodide, 1-(*N*-methylpyridinium-4-yl-azo)-4-(4-diethylaminophenylazo)naphthalene iodide (MPDN), obtained was washed with toluene until the washings were no longer colored and then dried under reduced pressure at 50 °C to a constant weight. A 6.6×10^{-4} M solution of MPDN was prepared by dissolving it in ethanol.

Anionic Surfactants. Anionic surfactants used were sodium 4-dodecylbenzenesulfonate (DBS) and dodecyl sulfate (SDS). They were dried at 50 °C under the reduced pressure to a constant weight.

Procedure. Place a suitable aliquot of the standard DBS or SDS solution, containing less than 1.2×10^{-5} M, into a 25-ml calibrated flask. Add 1 ml of 0.25M sodium iodide and 1.5 ml of 6.6×10^{-4} M MPDN solution. Dilute the solution to the mark with distilled water. Measure the absorbance at 580 nm in 1-cm cell against water as a reference.

Results and Discussion

In addition of iodide ion to the reagent solution at pH between 4 and 10, the blue color of the reagent solution changed into a reddish violet color, and the reddish violet color changed to a blue by the addition of the surfactants. The formation of the ion pair occured instantaneously, and the surfactants could be determined directly in an aqueous phase without extraction. Figure 1 shows the absorption spectra of these solutions; the wavelength of maximum absorption occurs at 620 nm for MPDN, at 520 nm for MPDN containing 10^{-2} M iodide ion, and at 575 nm for MPDN containing 10^{-2} M iodide ion and 1.2×10^{-5} M DBS, respectively. The determination was carried at 580 nm.

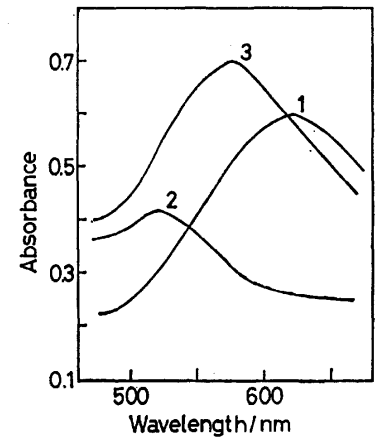

Fig. 1. Absorption spectra.
1: 3.96×10^{-5} M MPDN, 2: 3.96×10^{-5} M MPDN+ 10^{-2} M I^-, 3: 3.96×10^{-5} M MPDN+10^{-2} M I^-+ 1.2×10^{-5} M DBS.

The effect of amounts of sodium iodide on the absorbance at 580 nm was examined. The absorbance difference between the ion pair and the reagent blank was constant within 1 h when iodide ion existed from 5×10^{-3} M to 2×10^{-2} M, and above the concentration,

Table 1. Effect of anions on colouration

Anion	Concentration/M		
	10^{-1}	10^{-2}	10^{-3}
F^-	—	—	—
Cl^-	++*	+	—
Br^-	++*	++	—
I^-	++*	++	+
NO_3^-	++*	+	—
ClO_4^-	—	—	—
CH_3COO^-	—	—	—
SO_4^{2-}	++*	+	—
HPO_4^{2-}	+	—	—

++ Very good, + good, *precipitation.

very fine precipitates appeared on standing. Therefore in the following studies the concentration of iodide ion was kept at 1×10^{-2} M. The effect of other anions on coloration of the reagent solution is shown in Table 1. The most satisfactory results were obtained by use of iodide ion.

The effect of amounts of ethanol was studied. When the amount of ethanol added was 3 ml or more for the total volume of 25-ml, the both absorbances of the reagent blank and the sample solution increased gradually. And a constant absorbance difference was obtained between 1 and 2.5 ml of ethanol to 25 ml of the total solution.

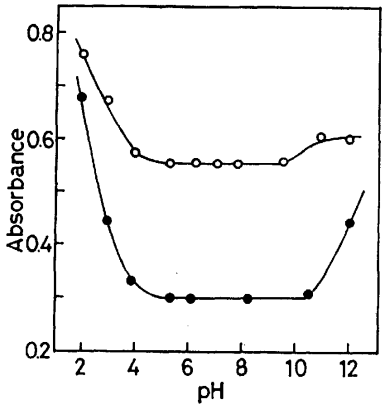

Fig. 2. Effect of pH.
—○—: MPDN-DBS, —●—: MPDN, [MPDN]= 3.96×10^{-5} M, [DBS]=8.0×10^{-6} M, [I^-]=1×10^{-2} M.

Table 2. Tolerance limits for diverse ions

Ion	Tolerance limit/M	Absorbance
None		0.553
Cl^-	10^{-3}	0.558
NO_3^-	10^{-3}	0.550
HCO_3^-	10^{-3}	0.548
SO_4^{2-}	10^{-3}	0.563
HPO_4^{2-}	10^{-3}	0.549
SiO_3^{2-}	10^{-4}	0.553
Na^+	10^{-3}	0.550
K^+	10^{-3}	0.553
NH_4^+	10^{-3}	0.548
Mg^{2+}	10^{-3}	0.558
Ca^{2+}	10^{-3}	0.553
Sodium stearate	10^{-5}	0.556

The effect of pH on the absorbance is shown in Fig. 2. The optimum pH range was between pH 5 and 10. And the pH of the solutions was adjusted with hydrochloric acid or sodium hydroxide solution to avoid the interference from anions intermixed.

The calibration graph obtained by the procedure was linear up to 1.2×10^{-5} M of DBS or SDS. The practical molar absorptivities of DBS and SDS were 3.25×10^4 and 1.45×10^4 l mol^{-1} cm^{-1} at 580 nm, respectively.

The interferences due to various ions were examined, and the results obtained are shown in Table 2. The common cations and anions of 10^{-3} M levels did not interfere with the procedure. Stearate ion above 10^{-5} M caused a positive error, because the precipitate separated out gradually on standing.

References

1) Keiro Higuchi, Yasuaki Shimoishi, Haruo Miyata, and Kyoji Tôei, *Chem. Lett.*, **1981**, 711.
2) R. W. Faessinger and E. V. Brown, *Trans. Ky. Acad. Sci.*, **24**, 106 (1963).

Oxidative Addition of Esters of Formic Acid and β-Lactones to Ni(0)-Complexes Involving Cleavage of the C-O Bond

Takakazu YAMAMOTO,* Junichi ISHIZU, and Akio YAMAMOTO

Research Laboratory of Resources Utilization, Tokyo Institute of Technology, 4259 Nagatsuta, Midori-ku, Yokohama 227

(Received September 12, 1981)

Synopsis. Reactions of esters of formic acid, HCOOR ($R=C_2H_5$, $CH_2C_6H_5$), with Ni(0)-complexes (mixtures of bis(1,5-cyclooctadiene)nickel ($Ni(cod)_2$) and tertiary phosphines (PR'_3)) lead to decarbonylation of HCOOR to afford $(Ni(CO)_n(PR'_3)_{4-n}$ and ROH. Vinyl formate gives a mixture of CH_3CHO, $Ni(CO)_n(PR'_3)_{4-n}$, C_2H_4, and CO_2 on interaction with the Ni(0)-complexes. β-Lactones liberate CO_2 on treatment with the Ni(0)-complexes. Oxidative addition of the reactants to Ni involving cleavage of the C–O bond(s) accounts for the formation of the products.

Oxidative addition of organic compounds to transition metals involving C–O bond cleavage is the subject of recent interest. In the previous papers we reported oxidative addition of aryl carboxylates,[1] vinyl acetate,[1a,2] allyl-O compounds[2] to Ni(0)-complexes. We now report reactions of esters of formic acid, β-lactones, and related compounds with Ni(0)-complexes, where somewhat different types of C–O bond cleavage reactions occur.

Results and Discussion

Table 1 shows products of reactions of formates and β-lactones with mixtures of bis(1,5-cyclooctadiene)-nickel, $Ni(cod)_2$ and tertiary phosphines, PR'_3.

Ethyl and Benzyl Formates. Although the reaction of $HCOOC_2H_5$ with a mixture of $Ni(cod)_2$ and PPh_3 at room temperature causes no C–O bond cleavage of the ester, the reaction at 60 °C causes C–O bond cleavage to afford $Ni(CO)(PPh_3)_3$ and C_2H_5OH. A similar decarbonylation reaction of methyl formate by Mo(0)-complexes to give CH_3OH has been reported.[3]

The following reaction pathway involving the initial cleavage of $HCO-OC_2H_5$ bond best accounts for the reaction products,

$$Ni(cod)_2 + 2L(PPh_3) \underset{}{\overset{-cod}{\rightleftharpoons}} Ni(cod)L_2 \overset{-cod}{\rightleftharpoons} NiL_2$$

$$NiL_2 + HCO-OC_2H_5 \xrightarrow[\text{addition}]{\text{oxidative}} [HCO-NiL_2-OC_2H_5] \quad (1)$$

$$\xrightarrow{\text{decarbonylation}} [H-\overset{\overset{CO}{|}}{Ni}L_2(OC_2H_5)] \quad (2)$$

$$\xrightarrow{-HOC_2H_5} Ni(CO)L_3. \quad (3)$$

We have proposed a similar reaction mechanism involving cleavage of the $RCO-OC_6H_5$ bond of phenyl carboxylates for the reaction of $RCOOC_6H_5$ with Ni(0)-complexes.[1] An alternative mechanism involving initial cleavage of the $H-COOC_2H_5$ bond to give an $H-Ni-COOC_2H_5$ intermediate and ensuing decarbonylation to give $H-Ni-OC_2H_5$ is also conceivable, since the H–C bond in $HCOOC_2H_5$ is considered to have a similar reactivity to that of the C–H bond of –CHO group in aldehydes which are known to oxidatively add to transition metals involving the C–H bond cleavage.[4] This alternative mechanism, however, is less plausible, because alkoxycarbonylnickel(II) complexes, $Ni(X)(COOR)L_n$, are known to liberate CO_2 on their degradation[5] whereas the present reaction releases no CO_2.

When the nucleophilicity of Ni is enhanced by coordination of more basic PEt_3, the oxidative addition of $HCOOC_2H_5$ proceeds under milder conditions (Expt 2). In this case $Ni(CO)_2(PEt_3)_2$[6] is formed

TABLE 1. REACTIONS OF FORMATES AND LACTONES WITH MIXTURES OF $Ni(cod)_2$ AND PHOSPHINE LIGANDS PR_3

Expt	Reactant mol/Ni	PR_3 mol/Ni	Solvent cm^3/cm^3 of reactant	Temp °C	Time h	Product[a] mol%/Ni
1	$HCOOC_2H_5$(38)	PPh_3(2.0)	None	60	40	$Ni(CO)L_3$(60), C_2H_5OH(50), cod-isomers[c]
2	$HCOOC_2H_5$(38)	PEt_3(2.0)	None	25	12	$Ni(CO)_2L_2$[b], C_2H_5OH(50)
3	$HCOOCH_2C_6H_5$(4.0)	PPh_3(3.0)	Eher(4)	65	4	$Ni(CO)L_3$(90), $C_6H_5CH_2OH$(93), C_6H_5CHO(tr), cod-isomers[c]
4	$HCOOCH=CH_2$(1.7)	PPh_3(3.0)	Toluene(4)	26	24	CH_3CHO(15), $Ni(CO)L_3$(51), C_2H_4(2), CO_2(5), 1-butene(tr), butadiene(tr)
5	$HCOOCH=CH_2$(2.0)	PCy_3(2.0)	Toluene(28)	15	28	CH_3CHO(16), $Ni(CO)_3(PCy_3)_2$[b], CO_2(2), C_2H_4(2), 1-butene(4)
6	$\overline{CH_2OCOCH_2}$(120)	PPh_3(2.0)	None	10	12	C_2H_4(45), CO_2[b], polyester, $Ni(CO)_2L_2$[b]
7	$CH_2=\overline{COCOCH_2}$(1.1)	PPh_3(2.1)	Ether(7)	10	9	CO_2(42), polymer
8	$\overline{CH_2CH_2OCOCH_2}$(20)	PPh_3(2.2)	None	65	48	No C–O bond cleavage proceeds

a) L=PR_3. tr=Trace. b) Formation of the compound was confirmed by IR, GLC, and/or NMR, but the amount was not measured. c) Cod isomers: 1,3-cyclooctadiene, 1,4-cyclooctadiene, bicyclooctene-1, and bicyclooctene-2.

instead of the $Ni(CO)L_3$ type complex. The fact that the reaction proceeds more easily by using more basic PEt_3 indicates that the reaction proceeds through nucleophilic attack of the Ni(0) complex at the carbonyl carbon of HCOOR, similarly to the reactions of aryl carboxylates[1] and allyl-O compounds[2] with Ni(0)-complexes.

Employment of $HCOOCH_2C_6H_5$ also leads to a similar type of bond cleavage in the reaction with the mixture of $Ni(cod)_2$ and PPh_3 affording $Ni(CO)(PPh_3)_3$ and $C_6H_5CH_2OH$ (Expt 3).

Vinyl Formate. Vinyl formate undergoes a similar type of bond cleavage to give $Ni(CO)_n(PR'_3)_{4-n}$ and CH_3CHO, a tautomer of vinyl alcohol, in the reaction with the mixture of $Ni(cod)_2$ and PR'_3 ($PR'_3=PPh_3$ and tricyclohexylphosphine (PCy_3)) at room temperature.

$$NiL_2 + HCO\text{-}OCH=CH_2$$
$$\longrightarrow [HCO\text{-}Ni\text{-}OCH=CH_2] \quad (4)$$
$$\longrightarrow [HNi(CO)(OCH=CH_2)] \quad (5)$$
$$\longrightarrow Ni(CO)_nL_{4-n} + CH_2=CHOH \quad (6)$$
$$\downarrow$$
$$CH_3CHO$$

However, in this case the ester undergoes, besides the C–O bond cleavage described above, another type of bond cleavage between HCOO– and $-CH=CH_2$ groups to liberate CO_2 and C_2H_4,

$$NiL_2+HCOO\text{-}CH=CH_2$$
$$\longrightarrow [HCOO\text{-}NiL_2\text{-}CH=CH_2] \quad (7)$$
$$\xrightarrow{-CO_2} [H\text{-}NiL_2\text{-}CH=CH_2] \quad (8)$$
$$\longrightarrow CH_2=CH_2 + NiL_2. \quad (9)$$

This type of bond cleavage has been observed for reactions of Ni(0)-complexes with alkenyl acetates.[2]

β-Lactones. 2-Oxetanone liberates C_2H_4 and CO_2 on interaction with a mixture of $Ni(cod)_2$ and PPh_3, indicating both the O–CH_2 and CO–CH_2 bonds in the lactone are cleaved in the reaction. Oxidative addition of 2-oxetanone involving cleavage of the O–CH_2 or CO–CH_2 bond to form a nickel-containing cyclic compound (*e.g.*, $L_2\overline{Ni\text{-}OCOCH_2CH_2}$) and bond rearrangement in the supposed cyclic intermediate account for the evolution of C_2H_4 and CO_2. A part of 2-oxetanone is converted into polyester, $\{CH_2CH_2COO\}_n$.

A reaction of 4-methylene-2-oxetanone with the $Ni(cod)_2/PPh_3$ mixture also causes cleavage of the C–O bond in the four-membered ring to liberate CO_2, although propadiene which is expected to be formed as the product of the C–O bond cleavage was not obtained. It is known that Ni complexes catalyze polymerization and oligomerization of propadiene,[7] and occurrence of such reactions accounts for the absence of propadiene in the liquid phase. Dihydro-2(3*H*)-furanone having stable 5-membered ring does not undergo the C–O bond cleavage.

Experimental

General Procedures and Materials. Manipulation of complexes and the reactions were carried out under deoxygenated nitrogen or argon or under vacuum. $Ni(cod)_2$ was purchased from Merck Co., Ltd., and recrystallized. Formates and lactones were purified by repeated distillation until their gas chromatogram show no signicant peaks of contaminants. Tertiary phosphine ligands were used as purchased or synthesized by the methods given in the literature.[8] Solvents were dried by usual procedures, distilled, and stored under argon or nitrogen.

Spectral Measurement and Analysis. IR spectra were taken on a Hitachi Model 295 spectrometer using KBr disks under nitrogen. The analysis of gaseous and liquid products was carried out with a Shimadzu GC-3BT or GC-6A gas chromatograph.

Reactions of Formates and Lactones (cf. Table 1). *Expt 1*: Ethyl formate (3 cm^3, 38 mmol) was added to a Schelnk tube containing $Ni(cod)_2$ (0.27 g, 0.98 mmol) and PPh_3 (0.25 g, 2.0 mmol) at −50 °C. The reaction mixture was stirred at 60 °C for 40 h to obtain a brown solution. GLC analysis of the solution showed formation of 0.49 mmol of ethanol. Removing volatile material under vacuum yielded 0.63 g of a light yellow solid whose IR spectrum is almost identical with that of $Ni(CO)(PPh_3)_3$, showing a sharp ν(C=O) band at 1926 cm^{-1}.[9]

Expt 3: Benzyl formate (0.50 cm^3, 4.0 mmol) was added to a Schlenk tube containing $Ni(cod)_2$ (0.25 g, 0.91 mmol), PPh_3 (0.72 g, 2.7 mmol), and diethyl ether (2 cm^3) at room temperature. The mixture was stirred at 65 °C for 4 h to obtain a pale brown homogeneous solution, which was cooled down to −30 °C to yield a yellow solid of $Ni(CO)(PPh_3)_3$ (0.72 g, 90%). GLC analysis of the solution showed formation of 0.84 mmol of benzyl alcohol.

The other reactions listed in Table 1 were carried out analogously. IR spectrum of the viscous polymer obtained in expt. 6 showed absorption bands characteristic of the polyester, $\{CH_2CH_2COO\}_n$ (1750 cm^{-1} (ν(C=O)), 1350 cm^{-1} (ν(C–O)), 1170 cm^{-1}, 1010 cm^{-1}).[10]

References

1) a) J. Ishizu, T. Yamamoto, and A. Yamamoto, *Chem. Lett.*, **1976**, 1091; b) T. Yamamoto, J. Ishizu, T. Kohara, S. Komiya, and A. Yamamoto, *J. Am. Chem. Soc.*, **102**, 3758 (1980).

2) T. Yamamoto, J. Ishizu, and A. Yamamoto, *J. Am. Chem. Soc.*, **103**, 6863(1981)

3) a) T. Tatsumi, H. Tominaga, M. Hidai, and Y. Uchida, *Chem. Lett.*, **1977**, 37; b) T. Tatsumi, H. Tominaga, M. Hidai, and Y. Uchida, *J. Organomet. Chem.*, **215**, 67 (1981).

4) a) J. W. Suggs, *J. Am. Chem. Soc.*, **100**, 640 (1978); b) J. Tsuji and K. Ohno, *Synthesis*, **1**, 157 (1967).

5) H.-F. Klein and H. H. Karsch, *Chem. Ber.*, **10**, 1433 (1973).

6) P. W. Jolly and G. Wilke, "The Organic Chemistry of Nickel," Academic Press, New York (1974), Vol. 1.

7) a) R. J. DePasquale, *J. Organomet. Chem.*, **32**, 381 (1971); b) S. Otsuka, K. Mori, and F. Imaizumi, *J. Am. Chem. Soc.*, **87**, 3017 (1965).

8) a) H. Goetz and S. Domin, *Justus Liebigs Ann. Chem.*, **704**, 1 (1967); b) G. M. Kosolapoff and L. Maier, "Organic Phosphorus Compounds," Wiley, New York (1972), Vol. 1.

9) Y. Inoue, M. Hidai, and Y. Uchida, *Chem. Lett.*, **1972**, 1119.

10) S. Okamura, T. Higashimura, A. Tanaka, R. Kato, and Y. Kikuchi, *Makromol. Chem.*, **54**, 226 (1962).

Reaction of Nitrostyrenes and 1-Nitrohexane with Sodium Polysulfides and Sodium Hydroxide[1)]

Yoshiro OGATA,* Yoshiaki NAKAGAWA, and Morio INAISHI
Department of Applied Chemistry, Faculty of Engineering, Nagoya University, Chikusa-ku, Nagoya 464
(Received March 25, 1981)

Synopsis. The reaction of β-nitrostyrene with NaOH in refluxing EtOH–H_2O (1 : 2) gives benzaldehyde, benzyl alcohol, benzoic acid, phenylacetic acid, β-phenylethyl alcohol, and polymeric materials. On the other hand, the reaction of β-nitrostyrene with Na_2S_4–NaOH in the same solvent gave acetophenone besides the same products obtained with NaOH. Acetophenone was likewise detected in the Na_2S–NaOH and Na_2S_2–NaOH reactions. 4-Nitrostyrene was also allowed to react with Na_2S_4–NaOH in EtOH–H_2O (4 : 1) to give a small amount of 4-aminoacetophenone. The formation of acetophenones suggests the occurrence of the Michael addition of polysulfide ion and supports our mechanism proposed previously for the reaction of *p*-nitrotoluene with Na_2S_4. The reaction of 1-nitrohexane with Na_2S_4–NaOH, in which the Michael addition is not conceivable, gives the same products as the reaction with NaOH.

In our previous report[2)] on the mechanism for the reaction of *p*-nitrotoluene with sodium polysulfides, we assumed the addition of polysulfide ion to a quinonoid isomer of *p*-nitrotoluene as the steps to *p*-(hydroxyamino)thiobenzaldehyde and then to *p*-aminobenzaldehyde (Eq. 1).

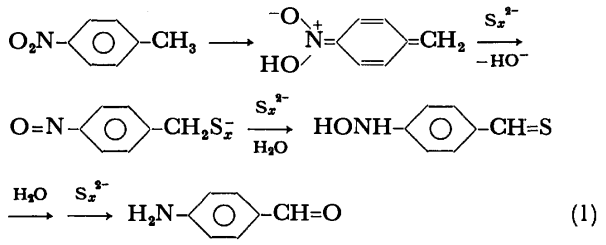

(1)

The similar type of the Michael addition of thiols to olefins bearing electron-withdrawing groups is well known, *e.g.*, a facile addition of thiolate ion to acrylonitrile and acrylate.[3,4)]

In order to confirm the Michael addition step of polysulfide ion in our proposed mechanism (Eq. 1) and to search for other possible substrates which undergo the simultaneous oxidation-reduction, we examined the reaction of Na_2S_x–NaOH (x=4, 2, and 1) with β-nitrostyrene as well as 4-nitrostyrene. The Michael addition of thiols to β-nitrostyrene is known.[5)] For comparison, 1-nitrohexane, the analogous saturated substrate, was examined on the reaction with Na_2S_4–NaOH.

Results and Discussion

β-Nitrostyrene was refluxed with Na_2S_x–NaOH in EtOH–H_2O (1 : 2) for 3 h. The products were acetophenone, benzaldehyde, benzyl alcohol, benzoic acid, phenylacetic acid, β-phenylethyl alcohol, and polymeric materials. The yields of identified products were listed in Table 1. On the other hand, the reaction of β-nitrostyrene with NaOH in the same solvent gave similar products besides acetophenone (Table 1).

Table 1. Products from the reaction of β-nitrostyrene (β-NS) with Na_2S_x–NaOH or NaOH in EtOH–H_2O (2 : 1) by refluxing for 3 h

Product	Yield/%				
	NaOH[a)]	Na_2S[b)]	$Na_2S_{2.1}$[c)]	$Na_2S_{4.3}$[d)]	$Na_2S_{4.8}$[e)]
$PhCOCH_3$	0	1.7	4.5	5.4	8.3
PhCHO	6.4	3.4	4.8	4.4	3.0
$PhCH_2OH$	4.4	0.4	0.6	0.7	0.8
$PhCO_2H$	6.4	0.2	0.2	8.9	15
$PhCH_2CO_2H$	1.3	0.6	0.1	2.0	1.5
$PhCH_2CH_2OH$	0.3	0.2	0.3	0.6	0.6

a) $[\beta\text{-NS}]_0$=0.22 M,† $[NaOH]_0$=0.40. b) $[\beta\text{-NS}]_0$=0.35 M, $[Na_2S\cdot 9H_2O]_0$=0.35 M, $[NaOH]_0$=0.70 M. c) $[\beta\text{-NS}]_0$=0.35 M, $[Na_2S\cdot 9H_2O]_0$=0.35 M, $[S_0]$=0.40 M, $[NaOH]_0$=0.70 M. d) $[\beta\text{-NS}]_0$=0.22 M, $[Na_2S\cdot 9H_2O]_0$=0.09 M, $[S]_0$=0.30 M, $[NaOH]_0$=0.42 M. e) $[\beta\text{-NS}]_0$=0.22 M, $[Na_2S\cdot 9H_2O]_0$=0.22 M, $[S]_0$=0.84 M, $[NaOH]_0$=1.2 M.

$$PhCH{=}CHNO_2 \xrightarrow{Na_2S_x\text{-}NaOH} PhCOCH_3,\ PhCHO,\ PhCH_2OH,\ PhCO_2H,\ PhCH_2CO_2H,\ PhCH_2CH_2OH \quad (2)$$

Hence, a characteristic product in the presence of sulfide and polysulfide ions is only acetophenone. The reactions of β-nitrostyrene with Na_2S–NaOH and Na_2S_2–NaOH gave a rather low yield of acetophenone with the similar products as shown in Table 1. Hence, for the formation of acetophenone the participation of sulfide or polysulfide ion is conceivable.

The mechanism for the formation of acetophenone may be as follows. The α-carbon of β-nitrostyrene is attacked by polysulfide ion to give a Michael adduct (**1**), and then the polysulfide ion in the adduct (**1**) may attack internally the β-carbon with simultaneous elimination of nitrite ion. The resulting cyclic polysulfide **2** will decompose to thioacetophenone which is hydrolyzed to acetophenone (Eq. 3).

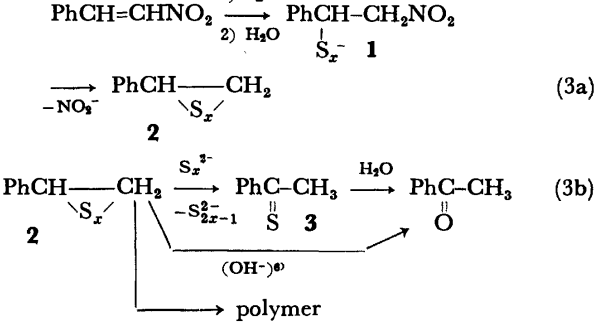

(3a)

(3b)

The step giving **3** from **2** must be the spontaneous intramolecular hydride shift in the case of Na_2S, causing

† 1 M=1 mol dm^{-3}.

the lower yield of acetophenone.

Benzaldehyde may be formed *via* the reverse reaction of the synthesis of β-nitrostyrene,[7] and it can give benzyl alcohol and benzoic acid *via* the Cannizzaro reaction. Benzoic acid may be formed by autoxidation of benzaldehyde. Phenylacetaldehyde which is produced *via* analogous reaction of nitroalkanes with NaOH[8] is autoxidized to give phenylacetic acid.

A decrease of the NaOH concentration resulted in the low yield of acetophenone; *e.g.*, the yield of acetophenone was only 0.4% with 0.15 M NaOH in contrast to 5.4% with 0.42 M NaOH.

The reaction of 4-nitrostyrene with Na_2S_4–NaOH gave a considerable amount of polymeric and monomeric 4-aminostyrenes and a small amount of 4-aminoacetophenone which was detected by NMR in comparison with the authentic specimen. The formation of 4-aminoacetophenone suggests the Michael addition of polysulfide ion to the β-position, and the following path *via* a cyclic sulfide.

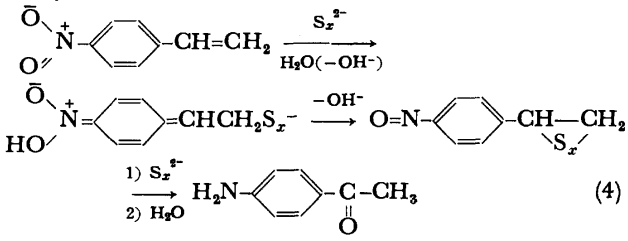

(4)

The formation of acetophenones supports the hypothetical Michael addition of polysulfide ion to the quinonoid form of *p*-nitrotoluene, which has been proposed as a step to the formation of *p*-aminobenzaldehyde from *p*-nitrotoluene (Eq. 1).[2]

On the other hand, the reaction of 1-nitrohexane (a saturated counterpart of nitrostyrenes) with Na_2S_4–NaOH gave hexanal, hexanal oxime, hexanoic acid, *etc.* All the products detected by the GLC peaks were the same as those of the reaction of 1-nitrohexane with NaOH, in which the yields and reaction rates were lower than those with Na_2S_4–NaOH. This fact shows that no oxidation of internal carbon atoms occurs unless a nitro group is conjugated with a C=C bond.

Experimental

Melting points were measured by a Yanagimoto micro melting point apparatus and were not corrected. NMR spectra were recorded on a Hitachi R-24B spectrometer using Me_4Si as an internal standard. The GLC analysis was performed with a Yanagimoto G 180 gas chromatograph with a flame ionization detector. GC-MS analysis was performed with a JEOL JMS-D300 mass spectrometer.

Materials. β-Nitrostyrene was prepared according to the literature;[7] mp 56—58 °C (lit,[7] 57—58 °C); NMR (CCl_4): δ 7.3—8.0 (dd, 2H, -CH=CH-), 7.4 (s, 5H, ArH). 4-Nitrostyrene was prepared by the method of Strassburg *et al.*;[9] NMR (CCl_4): δ 7.8 (d, 2H, ArH), 7.2 (d, 2H, ArH), 6.5 (m, 1H, α-CH), 5.2 (t, 2H, β-CH_2). 1-Nitrohexane was prepared by the method of Kornblum *et al.*;[10] bp 96—98 °C/22 Torr† (lit,[10] 76 °C/10 Torr); NMR (CCl_4); δ 4.3 (t, 2H, 1-CH_2), 1.8 (m, 2H, 2-CH_2), 1.2 (m, 6H, 3,4,5-CH_2), 0.8 (t, 3H, CH_3).

Reaction of β-Nitrostyrene with Na_2S_x–NaOH. A hot aqueous solution (20 ml) of $Na_2S \cdot 9H_2O$ and NaOH (and S) was poured into a 100 ml round-bottomed flask containing a hot ethanolic solution (10 ml) of β-nitrostyrene (1.00 g, 6.7 mmol) (Table 1). The mixture was heated under reflux for 3 h and then cooled in an ice bath. The resulting solution containing the precipitate of polymeric materials and elemental sulfur was filtered off, and the filtrate was steam-distilled. The distillate was extracted with ether, and the extract was dried (Na_2SO_4), and analyzed by GLC using two sorts of columns (2.5 mm × 1 m, packed with PEG 20M and KG-02) at 100—240 °C. Biphenyl was used as an internal standard. The residual solution after distillation was acidified with HCl and, after removal of elemental sulfur precipitated, it was extracted with ether. The extract was esterified by diazomethane and analyzed by GLC (PEG 20M) using benzophenone as an internal standard. Similar work-up was employed for the reaction with NaOH.

Reaction of 4-Nitrostyrene with Na_2S_4–NaOH. The reaction analogous to that of β-nitrostyrene was carried out with a mixture of 4-nitrostyrene (1.00 g, 6.7 mmol), $Na_2S \cdot 9H_2O$ (0.53 g, 2.2 mmol), S (0.28 g, 8.7×10^{-3} g atom), and NaOH (0.53 g, 13 mmol) in EtOH–H_2O (16 ml–4 ml). After refluxing for 3 h the solution was cooled, and the precipitate was removed by filtration. The filtrate was extracted with ether, and the extract was dried over anhydrous sodium sulfate. Then the extract was analyzed by NMR after distilling ether off. 4-Aminoacetophenone was identified by NMR in comparison with its authentic specimen; NMR ($CDCl_3$): δ 7.8 (d, 2H, ArH), 6.6 (d, 2H, ArH), 4.2 (s, 2H, NH_2), 2.5 (s, 3H, CH_3).

Reaction of 1-Nitrohexane with Na_2S_4–NaOH. According to the procedure analogous to that for β-nitrostyrene, 1-nitrohexane (0.21 g, 1.6 mmol), $Na_2S \cdot 9H_2O$ (0.15 g, 0.62 mmol), S (0.06 g, 2×10^{-3} g atom), and NaOH (0.18 g, 4.5 mmol) were refluxed for 9 h in EtOH–H_2O (5 ml–2 ml). The products were extracted with ether from the alkaline solution and also from the acidified solution. Both extracts were analyzed by GLC (PEG 20M) and GC-MS (2.5 mm × 2 m, packed with Silicone OV-1). The similar work-up was applied to the reaction of 1-nitrohexane (0.24 g, 1.8 mmol) with NaOH (0.20 g, 5.0 mmol).

† 1 Torr≈133.322 Pa.

References

1) Contribution No. 290.

2) Y. Ogata, A. Kawasaki, Y. Sawaki, and Y. Nakagawa, *Bull. Chem. Soc. Jpn.*, **52**, 2399 (1979).

3) C. I. Hurd and L. L. Gershheim, *J. Am. Chem. Soc.*, **69**, 2328 (1947).

4) a) E.-A. I. Haiba, *J. Org. Chem.*, **31**, 776 (1966); b) M. S. Kharasch and C. F. Fuchs, *ibid.*, **13**, 97 (1948).

5) D. J. Drain and F. J. Macrae, Brit. Patent, 793965, Apr. 23 (1958); *Chem. Abstr.*, **53**, P2156 g (1959).

6) J. Nakano, M. Suzuki, S. Saheki, and N. Migita, *Mokuzai Gakkaishi*, **13**, 208 (1967).

7) D. E. Worrall, *Org. Synth.*, Coll. Vol. I, 413 (1956).

8) a) R. W. Lockhart, K. W. Ng, P. E. Nott, and A. M. Unrau, *Can. J. Chem.*, **47**, 3107 (1969); b) O. R. Gottlieb, I. S. De Souza, and M. T. Magalkaes, *Tetrahedron*, **18**, 1137 (1962).

9) R. W. Strassburg, R. A. Gregg, and C. Walling, *J. Am. Chem. Soc.*, **69**, 2141 (1947).

10) N. Kornblum, B. Taub, and H. E. Ungnade, *J. Am. Chem. Soc.*, **76**, 3209 (1954).

Synthesis of Unsubstituted Thia Crown Ethers *via* Intramolecular Cyclization

Yohji NAKATSUJI, Yoshitaka WATANABE, and Mitsuo OKAHARA*

Department of Applied Chemistry, Faculty of Engineering, Osaka University, Yamadaoka 2-1, Suita, Osaka 565

(Received May 2, 1981)

Synopsis. A remarkable temperature dependence of the template effect of alkali metal cations was found in the cyclization of thio analogs of penta- or hexaethylene glycols to thia 15-crown-5 or 18-crown-6. The optimum range of the reaction temperature was found to be 80—100 °C.

Thia crown ethers are interesting compounds because they can complex with transition metal cations, unlike normal crown ethers.[1-3] The known synthetic methods, however, are mostly restricted to the condensation reactions between two molecules.[4-6] We previously developed a new synthetic method of preparing crown ethers *via* intramolecular cyclization.[7] Template ions are important in obtaining macrocyclic compounds in good yields. The template effect of alkali metal cations in cyclization of oligoethylene glycols to the corresponding crown ethers was found to be dependent on the reaction temperature.[8] We here applied the intramolecular cyclization method to the synthesis of unsubstituted mono and dithia crown ethers and observed a more remarkable temperature effect on the reaction than occurred in the reaction of oligoethylene glycol.

Monothio oligoethylene glycol (**1**), the precursor of monothia crown ether (**2**), was prepared by the addition of ethylene oxide to 2,2′-thiodiethanol at 80 °C using *N*,*N*-dimethylbenzylamine as a catalyst. The three and four mole ethylene oxide adducts were separated from other adducts by distillation under reduced pressure.

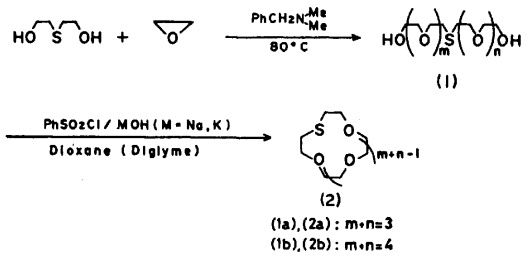

A dioxane solution of **1** and an equimolar amount of benzenesulfonyl chloride was added dropwise to a stirred suspension of powdered sodium hydroxide in dioxane at a fixed temperature for 4 h. The mixture was stirred for another hour to give monothia crown ether (**2**). The yield was best at 100 °C for 15-crown-5 (**2a**) and at 80 °C for 18-crown-6 (**2b**) respectively, as shown in Table 1. It is noteworthy that reaction temperatures over 100 °C drastically lowered the yield. These optimum reaction temperatures (80—100 °C) in the synthesis of thia crown ethers are relatively higher than those of normal crown ethers (60—80 °C[8]). In addition, the temperature dependence of the template effect is remarkable in the reaction of **1**, compared with that of the oligoethylene glycols, so the consideration of the reaction temperature is more important in this case. The stability constant (log K') of **2a** toward Na^+ in methanol at 25 °C was determined to be 2.1 by using a cation-selective electrode, while that toward K^+ was too low to measure. Christensen and coworkers[3] reported that the value for **2b** was 2.57 toward Na^+ and 3.61 toward K^+. This trend in the stability constant may explain why K^+ does not display any template effects in the synthesis of **2a** and yet is suitable as the template ion for **2b**.

3,9,15-Trioxa-6,12-dithiaheptadecane-1,17-diol (**3**), which was obtained from the reaction between bis-(2-mercaptoethyl) ether and 2-(2-chloroethoxy)ethanol, was successfully cyclized to 1,7-dithia-18-crown-6 (**4**) according to the procedure mentioned above. The trend of the template effect of sodium and potassium cations in this case was similar to the case of **2b**.

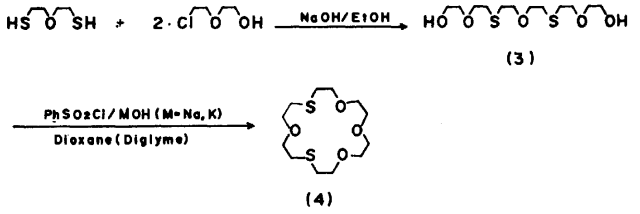

However, the cyclization of 6,9-dioxa-3,12-dithiatetradecane-1,14-diol (**5**) gave very little of the desired crown ether (1,7-dithia-15-crown-5 (**6**)). Instead, a small

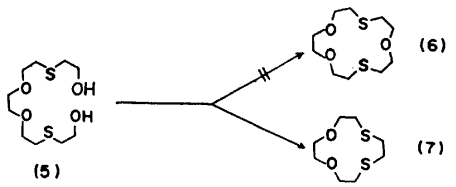

TABLE 1. SYNTHESIS OF THIA CROWN ETHERS

Temperature/°C	Monothia-15-crown-5 (**2a**)		Monothia-18-crown-6 (**2b**)		Dithia-18-crown-6 (**4**)	
	NaOH	KOH	NaOH	KOH	NaOH	KOH
40	24	22	19	43	10	14
60	55	27*	31	53	30	42
80	80	22, 23*	56	62	51	66
100	92	19	52	57	40	51
120	20*	11*	9*	13*	—	8*

Solvent: Dioxane, *diglyme. Yields were determined by GLC.

amount of 1,4-dithia-12-crown-4 (**7**) was isolated by preparative GLC together with the unreacted **5**. The template effect is not effective in this case and **5** may be cyclized to **7** after the removal of ethylene oxide.

Experimental

The ^{1}H NMR spectra were taken at 100 MHz on a JEOL JNM-PS-100 spectrometer using tetramethylsilane as the internal standard. The infrared spectra were obtained on a Hitachi 260-10 spectrometer. The mass spectra were measured with a Hitachi RMU-6E mass spectrometer at an ionization potential of 70 eV.

*Monothia-15-crown-5 (**2a**) (1,4,7,10-tetraoxa-13-thiacyclopentadecane).* A dioxane solution (40 ml) of monothio pentaethylene glycol (**1a**) (3.0 g, 0.012 mol) and benzenesulfonyl chloride (2.12 g, 0.012 mol) was added dropwise to a stirred suspension of sodium hydroxide (1.90 g, 0.048 mol) in dioxane (60 ml) over 4 h at a fixed temperature; then the mixture was stirred for one more hour at that temperature. The insoluble salt was removed by filtration and washed with dichloromethane. The solvent was removed *in vacuo* to give the crude product. The yields were determined by GLC (Shimadzu GC 3BF, FID, 2 m×3 mm packed with 10% Silicone Gum SE-30 on Celite 545, 60—80 mesh, 220 °C) using methyl myristate as the internal standard. Bp 110—114 °C/0.06 Torr† (Kugelrohr apparatus). NMR ($CDCl_3$, δ): 2.66 (t, 4H), 3.55 (s, 12H), and 3.68 ppm (t, 4H). MS (*m/e*): 236 (M^+), 203, 174, 149, 133, 104, 86, 73, 60, and 45. IR (Neat): 2920 (s), 1460 (m), 1355 (m), 1300 (m), 1245 (m), and 1115 cm^{-1} (s). The NMR spectrum of **2a** was coincident with that in the literature.[4]

*Monothia-18-crown-6 (**2b**) (1,4,7,10,13-pentaoxa-16-thiacyclooctadecane).* Monothia-18-crown-6 (**2b**) was prepared according to the procedure mentioned above. The yields were determined by GLC using dihexyl sebacate as the internal standard. The NMR spectrum of **2b** was coincident with that in the literature.[5]

*3,9,15-Trioxa-6,12-dithiaheptadecane-1,17-diol (**3**).* A suspended mixture of bis(2-mercaptoethyl) ether (27.0 g, 0.195 mol) and sodium hydroxide (24.6 g, 0.585 mol) in ethanol (230 ml) was stirred for 1.5 h. Then, 2-(2-chloroethoxy)ethanol (53.44 g, 0.429 mol) was added dropwise to the resultant mixture at 78 °C. The mixture was refluxed for another 1.5 h. The insoluble salt was removed by filtration and washed with ethanol. The solution was neutralized with aq hydrochloric acid and concentrated. The residue was dissolved in a mixed solvent of ethanol and ether and the insoluble salt was removed by filtration again. The solvent was concentrated to give the crude product of **3** (51.3 g, 84%). The crude product was distilled (190—200 °C/0.007 Torr) by using flash distillation apparatus to give **3** in a 48% yield. NMR ($CDCl_3$, δ): 2.75 (t, 8H), 3.00 (s, 2H), and 3.55—3.85 ppm (m, 16H). MS (*m/e*): 314 (M^+), 296, 283, 252, 149, 117, 105, 88, 75, and 45. IR (Neat): 3400 (s), 2920 (s), 1460 (m), 1355 (m), 1200 (m), and 1115 cm^{-1} (s).

*1,7-Dithia-18-crown-6 (**4**) (1,4,7,13-tetraoxa-10,16-dithiacyclooctadecane).* 1,7-Dithia-18-crown-6 was prepared according to the procedure mentioned above. The yields were determined by GLC using ethyl stearate as the internal standard. The NMR spectrum of **4** was coincident with that in the literature.[4]

*6,9-Dioxa-3,12-dithiatetradecane-1,14-diol (**5**).* Purified Yield: 37%. Bp 184—190 °C/0.03 Torr (Kugelrohr apparatus). NMR ($CDCl_3$, δ): 2.75 (t, 8H), 3.30 (s, 2H), and 3.60—3.85 ppm (m, 12H). MS (*m/e*): 252 ($M^+ - H_2O$), 149, 105, 87, 61, and 45. IR (Neat): 3400 (s), 2900 (s), 1640 (m), 1405 (m), 1350 (m), 1100 cm^{-1} (s).

*Cyclization Reaction of **5**.* The cyclization reaction of **5** was carried out according to an analogous procedure. 1,4-Dithia-12-crown-4 (**7**) was detected by GLC, together with unreacted **5**, and isolated by preparative GLC. The analytical data of **7** were as follows: NMR ($CDCl_3$, δ): 2.73 (t, 4H), 2.88 (s, 4H), 3.68 (s, 4H), and 3.78 ppm (t, 4H). MS (*m/e*): 208 (M^+), 149, 120, 104, 86, 73, 61, and 45. IR (Neat): 2870 (s), 1650 (m), 1460 (m), 1350 (m), 1300 (m), and 1130 cm^{-1} (s). The NMR spectrum of this compound was coincident with that in the literature.[4]

† 1 Torr≈133.322 Pa.

References

1) H. K. Frensdorff, *J. Am. Chem. Soc.*, **93**, 600 (1971).
2) R. M. Izatt, R. E. Terry, L. D. Hansen, A. G. Avondet, J. S. Bradshaw, N. K. Dalley, T. E. Jensen, and J. J. Christensen, *Inorg. Chim. Acta*, **30**, 1 (1978).
3) J. D. Lamb, R. M. Izatt, C. S. Swain, and J. J. Christensen, *J. Am. Chem. Soc.*, **102**, 475 (1980).
4) J. S. Bradshaw, J. Y. Hui, B. L. Haymore, J. J. Christensen, and R. M. Izatt, *J. Heterocycl. Chem.*, **10**, 1 (1973).
5) J. S. Bradshaw, J. Y. Hui, Y. Chan, B. L. Haymore, R. M. Izatt, and J. J. Christensen, *J. Heterocycl. Chem.*, **11**, 45 (1974).
6) J. S. Bradshaw, R. A. Reeder, M. D. Thompson, E. D. Flanders, R. L. Carruth, R. M. Izatt, and J. J. Christensen, *J. Org. Chem.*, **41**, 134 (1976).
7) P.-L. Kuo, M. Miki, and M. Okahara, *J. Chem. Soc., Chem. Commun.*, **1978**, 504.
8) N. Kawamura, M. Miki, I. Ikeda, and M. Okahara, *Tetrahedron Lett.*, **1979**, 535.

Regioselective Preparation of 2- and 3-Nitrodibenzofurans by the Direct Nitration of Dibenzofuran

Takashi KEUMI,* Hideyo YAMADA, Hisakazu TAKAHASHI, and Hidehiko KITAJIMA
Department of Fiber and Color Chemistry, Faculty of Engineering, Fukui University, Bunkyo, Fukui 910
(Received May 21, 1981)

Synopsis. Nitration of dibenzofuran with nitric acid in trifluoroacetic acid gave 3-nitrodibenzofuran selectively under very mild conditions. In contrary, the Friedel-Crafts type nitration using alkyl nitrates and aluminium chloride in nitromethane gave 2-nitrodibenzofuran as the main product.

Nitrodibenzofurans are important precursors for many kinds of dibenzofuran derivatives. Nitration of dibenzofuran (**1**) with mixed acids gives 3-nitrodibenzofuran (**2**) as a main product.[1-3] Yamashiro had reported that the nitration of **1** with 12 equiv. of fuming nitric acid in acetic acid gave **2** in a yield of 70%.[3] As for a synthesis of 2-nitrodibenzofuran (**3**), circuitous processes have been taken due to a difficulty of the preparation from the direct nitration of **1** by the usual methods.[4-6] Cullinane had obtained **3** in a total yield of 16% from **1** by the dinitration of **1**, followed by partial reduction and deamination.[4] On the other hand, Gilman had prepared **3** in the total yield of 13% *via* a process of 6 steps starting from **1**.[5]

By choosing the appropriate nitration method, we have succeeded in controlling the main product to **2** or **3** in the direct nitration of **1**. We would like to report the regioselective nitration of **1** to give **2** or **3**.

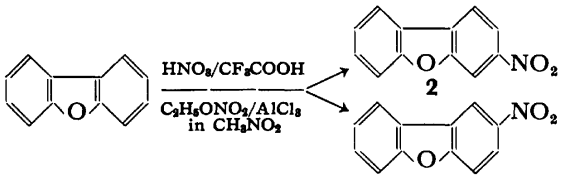

2 **3**

Using trifluoroacetic acid in place of acetic acid in Yamashiro's procedure, the mononitration of **1** was attained in a quantitative yield with 1.2 equiv. of 99% nitric acid under very mild conditions, at 0 °C for 0.5 h. In addition, it was observed that **2** was very predominantly formed in the reaction. The GLC analysis of the crude product showed that a mixture of mononitrodibenzofurans was obtained in a quantitative yield and that the distribution of the 1-, 2-, 3-, and 4-nitroisomers in the mixture was 4 : 6 : 90 : trace. By a recrystallization of the crude product, **2** was isolated in a yield of 80%. In contrast, when the nitration in acetic acid was carried out with 1.2 equiv. of 99% nitric acid at 0 °C for 0.5 h, the yield of mononitrodibenzofurans was only 2% and the distribution of the isomers was 1-, 10 : 2-, 26 : 3-, 62 : 4-, 2.

On the other hand, in the Friedel-Crafts type nitration using alkyl nitrate and Lewis acid, the main product significantly changed from **2** to **3**. It was observed from the GLC analysis that the reaction of **1** with 1-cyano-1-methylethyl nitrate (CMN) in the presence of aluminium chloride in nitromethane gave a mixture of mononitrodibenzofurans in a yield of 92%, in which the distribution of the isomers was 1-, 11 : 2-, 51 : 3-, 36 : 4-, 2. For the preparative method, ethyl nitrate was used in place of CMN. Thus, in the reaction of **1** with 1.2 equiv. of ethyl nitrate and aluminium chloride in nitromethane at 25 °C for 1 h, mononitrodibenzofurans were obtained in a yield of 80%, from which **3** was isolated in a yield of 28% by the column chromatograpy on alumina with benzene. This yield is much higher than the total ones for the derivation from **1** by the indirect methods described in literatures.[4,5]

We can prepare **2** or **3** regioselectively by the direct nitration of **1** with either the nitric acid/trifluoroacetic acid system or with the ethyl nitrate-aluminium chloride/nitromethane system. We believe, therefore, the procedures described here should be much simpler and more convenient for the preparation of **2** and **3** than those reported previously.

Experimental

Materials and Measurements. 1-Nitrodibenzofuran (mp 123 °C, lit,[7] 120—121 °C), 4-nitrodibenzofuran (mp 138 °C, lit,[8] 138—139 °C), and CMN (bp 84 °C/34 mmHg,† lit,[9] 62—65 °C/10 mmHg) were prepared according to the methods described in the literature. Other chemicals were obtained commercially.

The GLC analysis was carried out on a Hitachi GC 163 Model gas chromatograph using a steel column (length 3 m, i.d. 3 mm) packed with 3% Dexil 300 GC on Chromosorb W and a hydrogen flame ionization detector. Isomer distribution of nitrodibenzofurans was calculated from the peak areas obtained using a Takeda TR 2220A Model integrator after calibration against authentic samples.

2-Nitrodibenzofuran (3). To a solution of **1** (5.00 g, 30 mmol) and ethyl nitrate (3.2 g 36 mmol) in nitromethane (30 ml), a solution of aluminium chloride (4.8 g, 36 mmol) in nitromethane (10 ml) was added at 5 °C over 0.1 h and then, the mixture was stirred at 25 °C for 1 h. After an addition of 0.1 mol dm^{-3} hydrochloric acid (30 ml) to the mixture, the solvent and the unreacted **1** were distilled off with steam to yield a crude product of nitrated dibenzofuran; 6.07 g, mp 102—142 °C. The crude product was treated with boiling ethanol (280 ml) and the insoluble by-product, dinitrodibenzofuran was collected; 0.47 g (6.1%), mp 261—269 °C. Evaporation of the filtrate gave a mixture of mononitrodibenzofurans as a light yellow solid, 5.09 g (80%), mp 108—139 °C. After treatment with hot ethanol (first 45 ml, then 35 ml) as above, the resulted ethanol-soluble component (4.12 g, mp 122—134 °C) was chromatographed on alumina with benzene to afford **3**: 1.76 g (28%), mp 152—153 °C (lit,[4] 151 °C), **2**; 1.08 g (17%), mp 162—174 °C, and 1-nitrodibenzofuran; 0.33 g (5%), mp 123 °C (lit,[7] 120—121 °C).

3-Nitrodibenzofuran (2). To a suspension of **1** (4.00 g, 24 mmol) in trifluoroacetic acid (50 ml), a solution of 99% nitric acid (1.82 g, 29 mmol) in trifluoroacetic acid (10 ml) was added dropwise at a rate such as to maintain the temperature

† 1 mmHg≈133.322 Pa.

at 0 °C. The reaction mixture was stirred at 0 °C for 0.5 h and poured into ice–water. The resulted precipitates were filtered and washed thoroughly with alkali and water to give crude nitrodibenzofuran; 5.06 g (100%), mp 168—174 °C. The well refined product was heated with ethanol (50 ml) at 50 °C for 1 h and the insoluble material was recrystallized from acetic acid (29 ml) to give **2** in a almost pure form; 4.07 g (80%), mp 182 °C (lit,[3] 182 °C).

References

1) W. Borsche and W. Bothe, *Ber.*, **41**, 1940 (1908).
2) H. Ryan and N. M. Cullinane, *Sci. Proc. Roy. Dublin Soc.*, **17**, 321 (1924).
3) S. Yamashiro, *Bull. Chem. Soc. Jpn.*, **16**, 61 (1941).
4) N. M. Cullinane, *J. Chem. Soc.*, **1932**, 2365.
5) H. Gilman, G. E. Brown, W. G. Bywater, and W. H. Kirkpatrick, *J. Am. Chem. Soc.*, **56**, 2473 (1934).
6) M. Kuroki, *Nippon Kagaku Zasshi*, **89**, 527 (1968).
7) H. Gilman and J. Swiss, *J. Am. Chem. Soc.*, **66**, 1884 (1944).
8) H. Gilman and R. K. Ingham, *J. Am. Chem. Soc.*, **75**, 4843 (1953).
9) J. P. Freeman and I. G. Shepard, *Org. Synth.*, Coll. Vol. **5**, 839 (1973).

The Direct Synthesis of Methyl 2,4-Di-*O*-benzyl-α-D-xylopyranoside by the Regiospecific Benzylation of Methyl α-D-Xylopyranoside

Naohiko MORISHIMA, Shinkiti KOTO,* Chiharu KUSUHARA, and Shonosuke ZEN

School of Pharmaceutical Sciences, Kitasato University, Shirokane, Minato-ku, Tokyo 108

(Received May 30, 1981)

Synopsis. The regiospecific benzylation of methyl α-D-xylopyranoside with benzyl chloride and sodium hydride produces methyl 2,4-di-*O*-benzyl-α-D-xylopyranoside in a 70% yield, together with the by-products, methyl 2,3- and 3,4-di-*O*-benzyl-α-D-xylopyranosides. The structure of the 2,4-di-*O*-benzyl derivative was confirmed through the alternative synthesis of the 2,3- and 3,4-di-*O*-benzyl derivatives *via* the *O*-isopropylidene and *O*-cyclohexylidene derivatives of methyl α-D-xylopyranoside.

Partially benzylated monosaccharide derivatives are important synthetic intermediates, especially in the synthesis of oligosaccharides.[1] Usually, they are prepared *via* a multi-step sequence of reactions.[2] However, the regiospecific benzylation has often been useful for the ready preparation of the partially benzylated derivative of carbohydrates.[3] This report will present the direct synthesis of methyl 2,4-di-*O*-benzyl-α-D-xylopyranoside (**3**) through the regiospecific benzylation[3] of methyl α-D-xylopyranoside (**1**).

A brief heating of **1** with benzyl chloride containing the stoichiometric amount of sodium hydride, followed by chromatography, furnished crystalline **3** in a 70% yield. Small amounts of two other isomers, 2,3- and 3,4-di-*O*-benzyl derivatives (**2** and **4**), were also isolated through the chromatography. This shows that the reactivity of OH-2 and OH-4 is greater than that of OH-3 under such benzylation reactions.[4] The structure of the main product, **3**, was confirmed through the the alternative synthesis of **2** and **4** from **1**, as will be described below.

The reaction of 2,2-dimethoxypropane with **1** in *N,N*-dimethylformamide containing *p*-toluenesulfonic acid gave the 2,3- and 3,4-*O*-isopropyridene derivatives (**5** and **6**); the former predominated. The structure of the isopropylidene derivatives was confirmed by observing the ^{1}H NMR spectra of their acetates (**7** and **8**). The isopropylidene derivative, **5**, was transformed into **2** *via* allylation, deisopropylidenation, benzylation, and then deallylation, successively. Another isopropylidene compound, **6**, was similarly derived into **4**.

Compounds **2** and **4** were also synthesized *via* the cyclohexylidene derivatives (**9** and **10**) in essentially the same manner as above: 1,1-dimethoxycyclohexane, with *p*-toluenesulfonic acid as the catalyst, in *N,N*-dimethylformamide converted **1** into a mixture of **9** and **10**, which were then derived into **2** and **4** respec-

TABLE 1. PHYSICAL AND ANALYTICAL DATA OF COMPOUNDS[a]

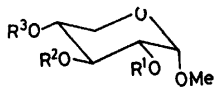

Compound	R^1	R^2	R^3	M$_p$ θ_m/°C	$[\alpha]_D^{20}$/°(*c*)[b]	Mol. form.	Calcd (%) C	Calcd (%) H	Found (%) C	Found (%) H
2	Bn	Bn	H	—	+22(1.6)				69.55	7.01
3	Bn	H	Bn	77—77.5	+63(1.0)	$C_{20}H_{24}O_5$	69.75	7.02	69.75	7.08
4	H	Bn	Bn	89—91	+56(0.4)				69.53	7.08
5	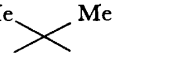		H	—	+139(1.0)				52.71	8.15
6	H			—	+132(1.0)	$C_9H_{16}O_5$	52.93	7.90	52.86	7.85
7	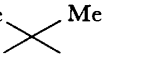		Ac	—	+112(1.0)				53.46	7.52
8	Ac			60—61	+138(0.5)	$C_{11}H_{18}O_6$	53.65	7.37	53.22	7.53
9			H	—	+124(0.6)				59.01	8.44
10	H			65—67	+127(1.3)	$C_{12}H_{20}O_5$	59.00	8.25	58.92	8.40
11	Bn	Bn	All	—	+20(2.0)				71.57	7.31
12	All	Bn	Bn	—	+54(1.6)	$C_{23}H_{28}O_5$	71.85	7.34	71.56	7.30
13	Ac	Me	Ac	—	+109(0.2)	$C_{11}H_{18}O_7$	50.38	6.92	50.37	6.92

a) All=allyl, Bn=benzyl. b) In $CHCl_3$.

tively *via* allylation, decyclohexylidenation, benzylation, and deallylation.

Experimental

The melting points were determined on an MP-1 melting-point apparatus (Yanagimoto); they are uncorrected. The optical rotations were measured in a jacketed 1-dm cell at 20 °C, with a DIP-180 automatic polarimeter (Japan Spectroscopic). The ^{1}H NMR spectra were recorded with a Varian EM-390 spectrometer in $CDCl_3$, using Me_4Si as the internal standard. Column chromatography was carried out on silica gel (Kanto Kagaku); each fraction was examined by TLC on silica gel (Merck, 7731).

Methyl 2,4-Di-O-benzyl-α-D-xylopyranoside (3). A mixture of **1** (Pfanstiehl, 2.0 g, 12 mmol), NaH (Wako, ≈50% disp., 1.2 g, 24 mmol), and benzyl chloride (Tokyo Kasei, 40 ml) was stirred for 1.5 h at 100 °C. After acetic acid (0.1 ml) had then been added, the mixture was evaporated at 95 °C to give an oily residue. This was chromatographed (benzene–butanone, gradient, 100 : 1→3 : 1) to afford three fractions (Fraction A, R_f=0.55; B, 0.30; and C, 0.23 and 0.21; benzene–butanone (10 : 1)). Fraction A (0.05 g, 1%) was crystallized from hexane and identified with methyl 2,3,4-tri-*O*-benzyl-α-D-xylopyranoside.[5] Fraction B (2.88 g, 70%) was crystallized from diisopropyl ether to yield **3** (2.10 g). Fraction C (0.32 g) was rechromatographed to afford **2** (0.15 g, 8%) and then **4** (0.04 g, 1%).

Methyl 2,3- and 3,4-O-Isopropylidene-α-D-xylopyranosides (5 and 6). A solution of **1** (656 mg, 4 mmol), 2,2-dimethoxypropane (Tokyo Kasei, 4.9 ml), and *p*-toluenesulfonic acid monohydrate (Wako, 38 mg) in distilled *N,N*-dimethylformamide (Tokyo Kasei, 13 ml) was heated for 2 h at 70 °C.[6] After a few drops of triethylamine had then been added, the mixture was evaporated and chromatographed (diisopropyl ether–ethylacetate (20 : 1)) to afford **5** (380 mg, 39%) and **6** (123 mg, 13%).

A small portion of **5** was acetylated with acetic anhydride and pyridine to afford the 4-*O*-acetyl derivative (**7**); ^{1}H NMR: δ 1.42 and 1.46 (2s, Me_2C), 2.06 (s, Ac), 3.28 (t, $J_{4,5ax}$=10 Hz, $J_{5ax,5eq}$=10.5 Hz, H-5ax), 3.42 (s, MeO), 3.50 (q, $J_{1,2}$=3 Hz, $J_{2,3}$=10 Hz, H-2), 3.89 (q, $J_{4,5eq}$=5.5 Hz, H-5eq), 4.07 (t, $J_{3,4}$=10 Hz, H-3), 4.99 (d, H-1), and 5.01 (sext, H-4). Compound **6** was similarly converted into the 2-*O*-acetyl derivative (**8**); ^{1}H NMR: δ 1.44 (s, Me_2C), 2.12 (s, Ac), 3.36 (s, MeO), 3.47 (sext, $J_{3,4}$=9 Hz, $J_{4,5eq}$=4.5 Hz, $J_{4,5ax}$=9 Hz, H-4), 3.70 (t, $J_{5ax,5eq}$=9 Hz, H-5ax), 3.87 (q, $J_{2,3}$=10.5 Hz, H-3), 3.94 (q, H-5eq), 4.83 (q, $J_{1,2}$=4 Hz, H-2), and 5.02 (d, H-1).

Methyl 2,3- and 3,4-O-Cyclohexylidene-α-D-xylopyranosides (9 and 10). A solution of **1** (500 mg, 3.05 mmol), 1,1-dimethoxycyclohexane (0.8 ml), and *p*-toluenesulfonic acid monohydrate (5.7 mg) in *N,N*-dimethylformamide (4.0 ml) was heated for 15 h at 140 °C.[7] After triethylamine had then been added, the mixture was evaporated and chromatographed (toluene–butanone, gradient, 100 : 1→3 : 1) to elute **10** (94 mg, 13%) and **9** (467 mg, 63%).

Alternative Synthesis of 2. Compound **5** (180 mg, 0.88 mmol) was stirred in allyl bromide (1.8 ml) containing NaH (≈60% disp., 50 mg) for 1.5 h at 65 °C. The mixture was then filtered and evaporated to give the sirupy 4-*O*-allyl derivative (180 mg). This was treated with a mixture of 0.25 M H_2SO_4, acetone, and 1,4-dioxane (1 : 1 : 1) for 0.5 h at 25 °C. After methanol and $Ba(OH)_2 \cdot 8H_2O$ had been added, the mixture was evaporated to dryness. The residue was stirred in benzyl chloride (3.0 ml) containing KOH (0.8 g) for 5 h at 110 °C, followed by chromatography, to give methyl 4-*O*-allyl-2,3-di-*O*-benzyl-α-D-xylopyranoside (**11**) (150 mg, 44%). Compound **9** was also converted into **11** in a similar way.

Compound **11** (42.5 mg, 0.11 mmol) was heated in dimethyl sulfoxide (0.34 ml) containing potassium *t*-butoxide (Aldrich, 119 mg) for 2.5 h at 110 °C under N_2.[8] The mixture was then diluted with benzene and processed as usual. The organic layer was evaporated, and the residue was heated in a mixture of 2.6 M H_2SO_4† (0.09 ml) and 1,4-dioxane (0.9 ml) for 1 h at 85 °C. After neutralization with $Ba(OH)_2 \cdot 8H_2O$, evaporation and chromatography gave **2** (24.6 mg, 65%).

Alternative Synthesis of 4. Compound **6** was similarly converted into methyl 2-*O*-allyl-3,4-di-*O*-benzyl-α-D-xylopyranoside (**12**), which was, in turn, derived into **4**.

Methyl 2,4-Di-O-acetyl-3-O-methyl-α-D-xylopyranoside (13). Compound **3** (50 mg, 0.15 mmol) was heated in *N,N*-dimethylformamide (0.25 ml) containing methyl iodide (70 μl) and BaO (95 mg) for 1.5 h at 90 °C under stirring.[9] Chromatography gave a homogeneous oil (49.2 mg), which was subsequently hydrogenated over Pd in acetic acid at 340 KPa. The hydrogenolyzate, which was not oxidized with aq $NaIO_4$, was acetylated as usual to give **13** (32.6 mg, 83%); ^{1}H NMR: δ 2.06 (s, Ac), 2.12 (s, Ac), 3.37 (s, MeO), and 3.47 (s, MeO); ^{13}C NMR: δ 20.9, 55.3 (Me-1), 58.5 (C-5), 60.4 (Me-3), 71.1 (C-4), 72.7 (C-2), 77.9 (C-3), 97.1 (C-1), 169.8, and 170.1.

References

1) A. F. Bochkov and G. E. Zaikov, "Chemistry of the *O*-Glycosidic Bond: Formation and Cleavage," English Edition, Pergamon (1979), Chap. 3.

2) J. M. Kuster and I. Dyong, *Justus Liebigs Ann. Chem.*, **1975**, 2179.

3) S. Koto, Y. Takebe, and S. Zen, *Bull. Chem. Soc. Jpn.*, **45**, 291 (1972); S. Koto, S. Inada, T. Yoshida, M. Toyama, and S. Zen, *Can. J. Chem.*, **59**, 255 (1981); S. Koto, N. Morishima, R. Kawahara, K. Ishikawa, and S. Zen, *Bull. Chem. Soc. Jpn.*, in press.

4) A. H. Haines, *Adv. Carbohydr. Chem. Biochem.*, **33**, 11 (1976).

5) S. Tejima, R. K. Ness, R. L. Kaufman, and H. G. Fletcher, Jr., *Carbohydr. Res.*, **7**, 485 (1968).

6) M. E. Evans, F. W. Parrish, and L. Long, Jr., *Carbohydr. Res.*, **3**, 453 (1967).

7) F. H. Bissett, M. E. Evans, and F. W. Parrish, *Carbohydr. Res.*, **5**, 184 (1967).

8) J. Gigg and R. Gigg, *J. Chem. Soc., C*, **1966**, 82.

9) R. Kuhn, H. H. Baer, and Z. Seeliger, *Justus Liebigs Ann. Chem.*, **611**, 236 (1958).

† 1 M=1 mol dm^{-3}.

Synthesis of N^2-Protected L-2,3-Diaminopropanoic Acids

Noriyoshi NOGUCHI, Tsuyoshi KURODA, Minoru HATANAKA, and Toshiyasu ISHIMARU*

The Institute of Scientific and Industrial Research, Osaka University, Suita, Osaka 565

(Received July 11, 1981)

Synopsis. The title compounds have been synthesized from *N*-protected L-aspartic acid *via* Curtius rearrangement.

In the course of synthetic studies of 3-aminonocardicinic acid (the nucleus of nocardicins),[1] we needed N^2-protected L-2,3-diaminopropanoic acid. L-2,3-Diaminopropanoic acid (L-DAPr) is well known as a constituent amino acid of several antibiotics including tuberactinomycins[2] and bleomycins.[3] Although N^2- or N^3-protected L-DAPr and $N^{2,3}$-diprotected L-DAPr have been required for constructing these antibiotics,[4] many of previous methods for the synthesis of these L-DAPr derivatives employ inconvenient procedure.[5,6] We report here a simple synthesis of N^2-protected L-DAPr and $N^{2,3}$-diprotected L-DAPr from *N*-protected L-aspartic acid *via* Curtius rearrangement.

The α-carboxyl groups of *N*-(2,2,2-trichloroethoxycarbonyl)-L-aspartic acid (**1a**) and *N*-benzyloxycarbonyl-L-aspartic acid (**1b**) were protected by the formation of the oxazolidines **2a** and **2b** according to the published method.[7] The oxazolidine **2a** was treated with diphenyl phosphorazidate[8] in benzene to give the acid azide, which was subsequently heated with *p*-methoxybenzyl alcohol in refluxing benzene to produce **3a** in 70% yield. Ring-opening of **3a** with aqueous sodium hydroxide provided the diprotected diamino acid **4a** as an oil, which produced the crystalline dicyclohexylammonium salt. Similarly, the oxazolidine **2b** gave **4b** as crystals. Removal of *p*-methoxybenzyl groups of **4a** and **4b** was carried out with hydrogen chloride in dioxane to give the N^2-protected diamino acids **5a** and **5b** in 73% and 92% yields, respectively. The physical data of the products are shown in Table 1.

Reductive deprotection of **5a** with zinc in formic acid gave L-DAPr, the hydrochloride of which had identical $[\alpha]_D$ value with that reported.[5a] The total synthesis of 3-aminonocardicinic acid using **4** as a starting material will be reported elsewhere.

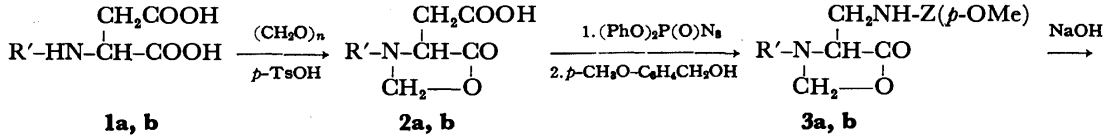

1a, b **2a, b** **3a, b**

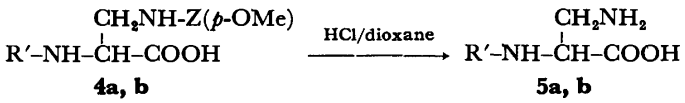

4a, b **5a, b**

a: R′ = Cl_3CCH_2OCO
b: R′ = $C_6H_5CH_2OCO$

Experimental

Melting points (capillary) were uncorrected. Optical rotations were measured with a Perkin-Elmer 241 polarimeter. IR spectra were determined on a JASCO IRA-1 spectrometer. Elemental analyses were performed in the material analysis center of this institute.

(S)-3-(2,2,2-Trichloroethoxycarbonyl)-5-oxo-4-oxazolidineacetic Acid (2a). This compound was prepared in 75% yield by heating **1a** with paraformaldehyde and *p*-toluenesulfonic acid in refluxing benzene according to the procedure described for the preparation of **2a**.[7] The product was crystallized from benzene–hexane; mp 87—88 °C (dec); $[\alpha]_D^{25}$ +177.5° (*c* 1.0, MeOH). Found: C, 30.21; H, 2.49; N, 4.46%. Calcd for $C_8H_8NO_6Cl_3$: C, 29.98; H, 2.51; N, 4.37%.

(S)-4-(p-Methoxybenzyloxycarbonylaminomethyl)-3-(2,2,2-trichloroethoxycarbonyl)-5-oxazolidinone (3a). A solution of **2a**

Table 1. Yields and physical properties of N^2-protected and $N^{2,3}$-diprotected L-2,3-diaminopropanoic acids

Compound	Yield[a] %	Mp θ_m/°C	$[\alpha]_D^{25}$/°	Formula	Found (Calcd) (%) C	H	N
4a·DCHA[b]	50	190—191	+3.7 (*c* 0.9, MeOH)	$C_{27}H_{40}N_3O_7Cl_3$	51.75 (51.89)	6.44 (6.45)	6.52 (6.72)
4b	61	145—147	−13.7 (*c* 0.76, MeOH)	$C_{20}H_{22}N_2O_7$	59.58 (59.69)	5.48 (5.51)	6.90 (6.96)
4b·DCHA[b]		178—180	+4.1 (*c* 0.8, MeOH)	$C_{32}H_{45}N_3O_7$	65.59 (65.84)	7.80 (7.77)	7.21 (7.20)
5a	38	179—180	−15.5 (*c* 0.7, 1 M NaOH)	$C_6H_9N_2O_4Cl_3$	25.68 (25.78)	3.19 (3.25)	9.95 (10.02)
5b	56	213—214 dec[c]	−9.5[c] (*c* 0.4, 1 M NaOH)	$C_{11}H_{14}N_2O_4$	55.20 (55.46)	5.96 (5.92)	11.54 (11.76)

a) Isolated yield on the basis of **1**. b) Dicyclohexylammonium salts. c) Lit,[9] mp 240—241 °C dec, $[\alpha]_D^{22}$ −7.4° (*c* 0.4, 1 M NaOH).

(9.65 g, 0.03 mol) in anhydrous benzene (150 ml) was treated with diphenyl phosphorazidate (9.1 g, 0.033 mol) and triethylamine (3.36 g, 0.033 mol). After the mixture was stirred for 15 h, *p*-methoxybenzyl alcohol (4.14 g, 0.03 mol) was added and the mixture was refluxed for 3 h. The solution was cooled, washed with saturated aqueous $NaHCO_3$, 5% hydrochloric acid and water, dried ($MgSO_4$), and then concentrated *in vacuo*. The residue was chromatographed on silica gel with benzene–ethyl acetate to give **3a** (9.6 g, 70%) as a pale yellow oil; IR (CH_2Cl_2) 1810 and 1735 cm^{-1}.

*(S)-3-Benzyloxycarbonyl-4-(p-methoxybenzyloxycarbonylaminomethyl)-5-oxazolidinone (**3b**).* This compound was prepared from **2b** by the procedure described for **3a** in 80% yield.

N^3-*(p-Methoxybenzyloxycarbonyl)*-N^2-*(2,2,2-trichloroethoxycarbonyl)*-L-*2,3-diaminopropanoic Acid (**4a**).* To a solution of **3a** (9.1 g, 0.02 mol) in aqueous acetone (80 ml), 1 M aqueous NaOH (20 ml) was added dropwise at 0 °C over 1 h. After being stirred for 2 h at 0—5 °C, the solution was concentrated *in vacuo*. The residue was diluted with water (20 ml), washed with ether, acidified with 20% hydrochloric acid, and then extracted with ethyl acetate. The extracts were washed with brine, dried ($MgSO_4$), and concentrated *in vacuo* to give **4a** (8.71 g, 98%) as a pale yellow oil.

The oily product (464 mg) was treated with dicyclohexylamine (227 mg) in ethanol (10 ml) to yield the dicyclohexylammonium salt (595 mg, 91%); mp 190—191 °C.

N^2-*Benzyloxycarbonyl*-N^3-*(p-methoxybenzyloxycarbonyl)*-L-*2,3-diaminopropanoic Acid (**4b**).* This compound was prepared from **3b** according to the procedure described for **4a** in 95% yield. The product was crystallized by trituration in ether; mp 145—147 °C. This compound also produced the crystalline dicyclohexylammonium salt; mp 178—180 °C.

N^2-*(2,2,2-Trichloroethoxycarbonyl)*-L-*2,3-diaminopropanoic Acid (**5a**).* A solution of **4a** (8.7 g, 0.0195 mol) in dioxane (100 ml) was treated with a 4 M HCl–dioxane solution (100 ml). After being stirred for 3 h, the solution was concentrated *in vacuo* and the remaining solid was dissolved in ethanol. The solution was ajusted to pH 7 with triethylamine and left in a refrigerator overnight. The white precipitates were collected by filtration, washed with chilled ethanol, and dried *in vacuo* to give **5a** (4.0 g, 73%); mp 179—180 °C.

N^2-*Benzyloxycarbonyl*-L-*2,3-diaminopropanoic Acid (**5b**).* This compound was prepared from **4b** by the procedure described for **5a** in 92% yield; mp 213—214 °C (dec) [Lit,[9] mp 240—241 °C (dec)].

L-*2,3-Diaminopropanoic Acid Hydrochloride.* The compound **5a** (280 mg) was dissolved in formic acid (10 ml) and cooled in an ice bath. Activated zinc dust (654 mg) was added with vigorous stirring and stirring was continued for 3 h at 0—5 °C. The mixture was filtered and the filtrate was concentrated *in vacuo*. The residue was diluted with water, treated with H_2S, and then filtered. A few drops of 20% hydrochloric acid was added to the filtrate and the solvent was evaporated *in vacuo*. The residue was crystallized from water–ethanol to give 99 mg (71%); mp 233—235 °C (dec); $[\alpha]_D^{25}$ +19.4° (*c* 1, H_2O). [Lit,[5a] mp 236 °C (dec); $[\alpha]_D^{12}$ +19° (*c* 1, H_2O)].

References

1) H. Aoki, H. Sakai, M. Kohsaka, J. Hosoda, Y. Kubochi, and E. Iguchi, *J. Antibiot.*, **29**, 492 (1976); M. Hashimoto, T. Komori, and T. Kamiya, *ibid.*, **29**, 890 (1976).

2) H. Yoshioka, T. Aoki, H. Goko, K. Nakatsu, T. Noda, H. Sakakibara, T. Take, A. Nagata, J. Abe, T. Wakamiya, T. Shiba, and T. Kaneko, *Tetrahedron Lett.*, **1971**, 2043.

3) T. Takita, Y. Muraoka, T. Nakatani, A. Fujii, Y. Umezawa, H. Naganawa, and H. Umezawa, *J. Antibiot.*, **31**, 801 (1978).

4) For example: T. Teshima, S. Nomoto, T. Wakamiya, and T. Shiba, *Bull. Chem. Soc. Jpn.*, **50**, 3372 (1977).

5) a) T. Kitagawa, T. Ozasa, and T. Taniyama, *Yakugaku Zasshi*, **89**, 285 (1969); b) S. Moore, R. P. Patel, E. Atherton, M. Kondo, J. Meienhofer, L-B. R. Bittman, and R. K. Johnson, *J. Med. Chem.*, **19**, 766 (1976).

6) After the completion of this work, an efficient synthesis of N^2-protected L-2,3-diaminopropanoic acids has been reported; M. Waki, Y. Kitajima, and N. Izumiya, *Synthesis*, **1981**, 266.

7) M. Itoh, *Chem. Pharm. Bull. (Tokyo)*, **17**, 1679 (1969).

8) T. Shioiri and S. Yamada, *Chem. Pharm. Bull.*, **22**, 849 (1974); K. Ninomiya, T. Shioiri, and S. Yamada, *ibid.*, **22**, 1398 (1974).

9) F. Brthík and M. Zaoral, *Collect. Czech. Chem. Commun.*, **41**, 2969 (1976).

Preparation of α-Nitro Olefins from α-Halo Ketoximes

Tohru SAKAKIBARA,* Yutaka IKEDA, and Rokuro SUDOH

Department of Chemistry, Faculty of Science, Tokyo Institute of Technology, Ookayama, Meguro-ku, Tokyo 152

(Received July 23, 1981)

Synopsis. α-Nitro olefins were synthesized from α-haloketones through oximation and subsequent oxidation with trifluoroperacetic acid.

α-Nitro olefins are versatile and unique synthetic intermediates, for examples, for the introduction of nucleophiles and electrophiles at the β- and α-carbon atom, respectively, or for annulation reactions.[1,2] Furthermore the nitro group is convertible into such a function as an amino or a carbonyl group.[1]

Although the conversion of α-nitro olefins into the α-chloro ketoximes was reported,[3] the reverse reaction is not developed. This reaction seems to be attractive because α-chloro ketoximes are prepared in good yields by the reaction of olefins with nitrosyl chloride in the presence of hydrochloric acid.[4]

In this paper we described the preparation of α-nitro olefins from α-halo ketones according to Eq. 1, in which the nitro group could be introduced regioselectively.

Although the ketoximes were generally prepared by treatment of the ketones with hydroxylamine acetate or hydroxylamine hydrochloride in the presence of such a weak base as sodium acetate, oximation of 2-chlorocyclohexanone by the conventional methods afforded a complex mixture. However, the desired 2-chlorocyclohexanone oxime was obtained in 64% yield together with 2-chloro-1,1-dimethoxycyclohexane (17.5%) by treatment with hydroxylamine hydrochloride in methanol.[5] Similar treatment of several α-halo ketones provided the corresponding α-halo ketoximes in moderate yields (Table 1). Under the same conditions, however, 2-chloro-2-methylcyclohexanone did not afford the expected oxime, but 2-methyl-2-cyclohexenone oxime (**4**) (39% yield) and 2-methoxy-2-methylcyclohexanone oxime (**5**) (23% yield).

The oximes **2** were oxidized with trifluoroperacetic acid in acetonitrile in the presence of disodium hydrogenphosphate and urea,[6] giving the corresponding α-nitro olefin in moderate yield as shown in Table 1.

Similar oxidation of **5** yielded 2-methyl-1-nitrocyclohexene in 40% yield.

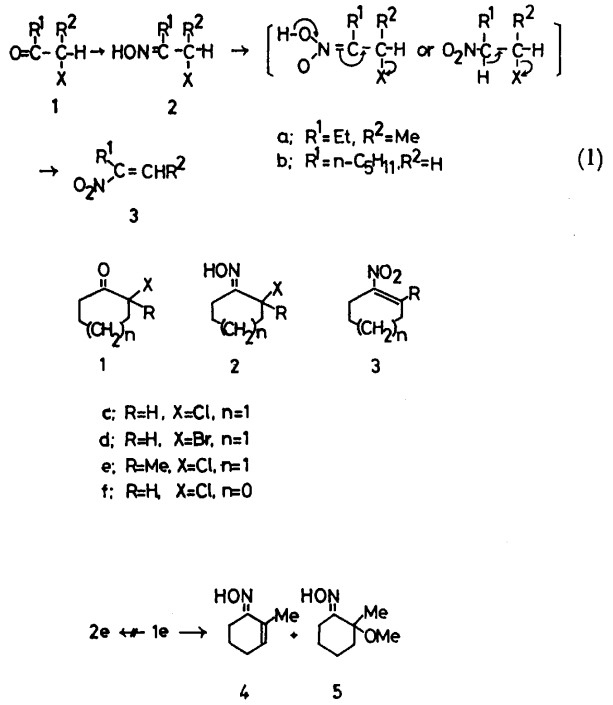

Experimental

IR spectra were recorded with a Hitachi 285 Infrared Spectrophotometer. NMR spectra were determined with a Varian EM 360A NMR Spectrometer. GLC analyses were performed with a Varian 940 instrument equipped with an OV 101 column (*N,N*-diethylaniline as internal standard). Column chromatography was carried out on silica gel (C-300, Wakogel).

2-Chlorocyclohexanone Oxime. Typical Procedure: To a solution of 2-chlorocyclohexanone (1.325 g, 10 mmol) in methanol (6 mL) was added hydroxylamine hydrochloride (765 mg, 11 mmol). The mixture was stirred at room temperature for 2 h and then worked up in the usual way to give a syrup. The syrup was chromatographed on silica gel, eluting with benzene–ethyl acetate (25 : 1, v/v) to afford 944 mg (64%) of the oxime and 312 mg of 2-chloro-1,1-dimethoxycyclohexane (17.5%). Without further purification the oxime was used for oxidation.

1-Nitrocyclohexene. Typical Procedure: An acetonitrile solution (90 mL) of 2-chlorocyclohexanone oxime (590 mg, 4 mmol) was added dropwise a stirred solution of oxidant, prepared by mixing successively acetonitrile (10 mL), trifluoroacetic anhydride (2.0 mL), 90% aqueous hydrogen peroxide

TABLE 1. CONVERSION OF α-HALOKETONES (**1**) INTO α-NITRO OLEFINS (**3**) AND SPECTROSCOPIC DATA OF **3**

α-Halo ketone	Oxime	Yield/%	α-Nitro olefin	Yield/%[a]	IR (NaCl) NO_2 ($\tilde{\nu}$/cm^{-1})	^{1}H NMR ($CDCl_3$) Olefinic proton(s) (δ)
1a	**2a**	61	**3a**	31 (43)	1515, 1335	7.25 (1H, q)
1b	**2b**	63	**3b**	66	1520, 1335	6.36 (1H, d), 5.49 (1H, s[b])
1c	**2c**	64	**3c**	42 (68)	1510, 1335	7.34 (1H, q)
1d	**2d**	58	**3d**	45 (74)	1510, 1335	7.34 (1H, q)
1e	**5**	23	**3e**	40 (62)	1505, 1320	—
1f	**2f**	59	**3f**	38 (61)	1505, 1355	7.00 (1H, m)

a) Isolated yield from **2**; figures in parentheses show the yields based on GLC analyses. b) Broad singlet.

(0.35 mL), disodium hydrogenphosphate (5.2 g), and urea (0.08 g). After the mixture had been stirred for 30 min at ambient temperature, cold water (20 mL) was added gradually. The solution was extracted with diethyl ether (20 mL × 3), and the extracts were successively washed with saturated aqueous solution of sodium hydrogencarbonate and of sodium chloride, dried over $MgSO_4$, and evaporated. The residue was chromatographed on silica gel, eluting with benzene–cyclohexane (1 : 2, v/v) to give 213.4 mg (42%) of 1-nitrocyclohexene, identical with an authentic sample by IR and NMR spectroscopy.

References

1) For general reviews of the chemistry of the nitro group, a) Houben-Weyl, "Methoden der Organischen Chemie," ed by E. Müller, Georg Thieme Verlag, Stuttgart (1971), Band 10/1, pp. 1—462; b) "The Chemistry of Nitro and Nitroso Groups," ed by H. Feuer, Interscience, New York (1964), Part 1 and (1970), Part 2; c) N. Ono and A. Kaji, *Yuki Gosei Kagaku Kyokai Shi*, **38**, 115 (1980).

2) Recently new synthetic methods for preparation of α-nitro olefins have been reported; E. J. Corey and H. Estreicher, *J. Am. Chem. Soc.*, **100**, 6294 (1978); *Tetrahedron Lett.*, **21**, 1113 (1980).

3) A. Dornow, H. D. Jordan, and A. Müller, *Chem. Ber.*, **94**, 67 (1961).

4) Houben-Weyl, "Methoden der Organischen Chemie," ed by E. Müller, Georg Thieme Verlag, Stuttgart (1971), Band 10/4, pp. 92—97.

5) Although 2-chlorocyclohexanone oxime was synthesized from 2-chlorocyclohenanone, general method for preparation of α-halo ketoximes seems not to be reported; A. F. Childs, L. J. Goldsworthy, G. F. Harding, S. G. P. Plant, and G. A. Weeks, *J. Chem. Soc.*, **1948**, 2320.

6) W. D. Emmons and A. S. Pagano, *J. Am. Chem. Soc.*, **77**, 4557 (1955).

Convenient Synthesis of 2,7-Disubstituted 5*H*-1,3,4-Thiadiazolo[3,2-*a*]-pyrimidin-5-ones and Related Compounds

Tadakazu Tsuji* and Keiko Takenaka

Department of Chemistry, Japan Women's University, Mejirodai, Bunkyo-ku, Tokyo 112

(Received July 28, 1981)

Synopsis. 2,7-Disubstituted 5*H*-1,3,4-thiadiazolo[3,-2-*a*]pyrimidin-5-ones were synthesized from the reaction of 3-amino-6-methyl-2-thiouracil with carboxylic acid or from that of thiosemicarbazide with carboxylic acid and β-keto ester in the presence of phosphorus pentaoxide and methanesulfonic acid. The synthesis of related compounds is also described.

Our work on the chemistry of 2,7-disubstituted 5*H*-1,3,4-thiadiazolo[3,2-*a*]pyrimidin-5-ones (**1**)[1] has required a wide and convenient entry to this ring system, which is of their chemical[2,3] and biological[4] interests. Okabe *et al.*[4] have synthesized **1** by the condensation of 5-substituted 2-amino-1,3,4-thiadiazole (**2**) with β-keto ester in the presence of polyphosphoric acid (PPA). However, we failed to obtain the 2-(nitrophenyl or chlorophenyl) derivative of **1** by this method. This paper describes the general and facile methods for the synthesis of **1** and related compounds by the use of 1 : 5 molar ratio of phosphorus pentaoxide (P_2O_5)-methanesulfonic acid (MsOH).[5] The synthetic routes are illustrated in Scheme 1, and the results are summarized in Table 1. PPA was less effective in the present synthesis, since the product yields were generally poor in Method A and B; no desired product was obtained in Method C, D, or E.

The treatment of 3-acylamino-6-methyl-2-thiouracil (**4**) with P_2O_5–MsOH at 70 °C for 10 h, followed by aqueous basic work-up afforded **1** (Method A). Moreover, the reaction of 3-amino-6-methyl-2-thiouracil (**3**) with carboxylic acid (**5**) in the presence of P_2O_5–MsOH gave **1** including the 2-(nitrophenyl and chlorophenyl) derivatives in 37.8—97% yields (Method B).

We then attempted the synthesis of **1** from thiosemicarbazide or its 1-substituted derivatives in the presence of P_2O_5–MsOH. Thus, **1** was obtained from the reaction of acetone thiosemicarbazone (**7**) with β-keto ester (**6**) and **5** (Method C), or from that of 1-acylthiosemicarbazide (**8**) with **6** (Method D), but the yields were unsatisfactory. In connection with these reactions, **2** was prepared by the treatment of thiosemicarbazide with **5** in 40.1—89.9% yields. Based on this result, one pot synthesis of **1** was carried out by

Table 1. Synthesis of 2,7-disubstituted 5*H*-1,3,4-thiadiazolo[3,2-*a*]pyrimidin-5-ones (**1**)

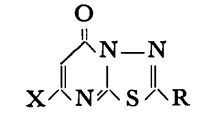

Compound **1** R	X	Methods A[a]	B[b]	C[c]	D[d]	E[e]	Mp θ_m/°C	Formula	Found (Calcd) (%)			Ref.
H	CH_3	65.8			91.1		186—187[f]	$C_6H_5ON_3S$	43.08 (43.10	3.21 3.01	25.24 25.14)	1c, 4
CH_3	CH_3	70.6	57.2	24.8	77.1	72.4	153—154[f]	$C_7H_7ON_3S$	46.50 (46.39	4.01 3.89	23.22 23.19)	4
C_6H_5	CH_3	47.5	97	37.4	37.6	76.5	201—202[g,i]	$C_{12}H_9ON_3S$	59.23 (59.24	3.75 3.73	17.31 17.27)	4
o-$CH_3OC_6H_4$	CH_3		64.3			76.1	246—247[h]	$C_{13}H_{11}O_2N_3S$	57.01 (57.13	4.10 4.06	15.58 15.38)	
p-$CH_3OC_6H_4$	CH_3		78			75.1	245—246[h]	$C_{13}H_{11}O_2N_3S\cdot 1/4H_2O$	56.26 (56.20	3.96 4.17	15.18 15.13)	
o-ClC_6H_4	CH_3		53.5				198[g]	$C_{12}H_8ON_3SCl$	51.75 (51.89	2.70 2.90	14.99 15.13)	
m-ClC_6H_4	CH_3		74.8				192—193[g]	$C_{12}H_8ON_3SCl$	51.58 (51.89	2.70 2.90	15.32 15.13)	
p-ClC_6H_4	CH_3		83.9		29.8		220—221[g]	$C_{12}H_8ON_3SCl\cdot 1/2H_2O$	49.89 (50.26	2.74 3.16	14.94 14.66)	
m-$NO_2C_6H_4$	CH_3		68.4				233—234[g]	$C_{12}H_8O_3N_4S$	49.71 (49.99	2.71 2.80	19.15 19.44)	
p-$NO_2C_6H_4$	CH_3		49.8				303—304[h]	$C_{12}H_8O_3N_4S$	49.78 (49.99	2.76 2.80	19.23 19.44)	
$ClCH_2$	CH_3		37.8				181—183[g]	$C_7H_6ON_3SCl$	39.13 (38.98	2.79 2.80	19.72 19.49)	
CH_3	C_6H_5					72.4	193—194[g]	$C_{12}H_9ON_3S$	59.17 (59.24	3.64 3.73	17.27 17.27)	4

a) From **4**. b) From **3** with **5**. c) From **7** with **5** and ethyl acetoacetate. d) From **8** with ethyl acetoacetate. e) From thiosemicarbazide with **5** and **6** by one-pot reaction. f) Recrystallized from water. g) Recrystallized from methanol. h) Recrystallized from *N*,*N*-dimethylformamide. i) Lit,[4] mp 169—172 °C.

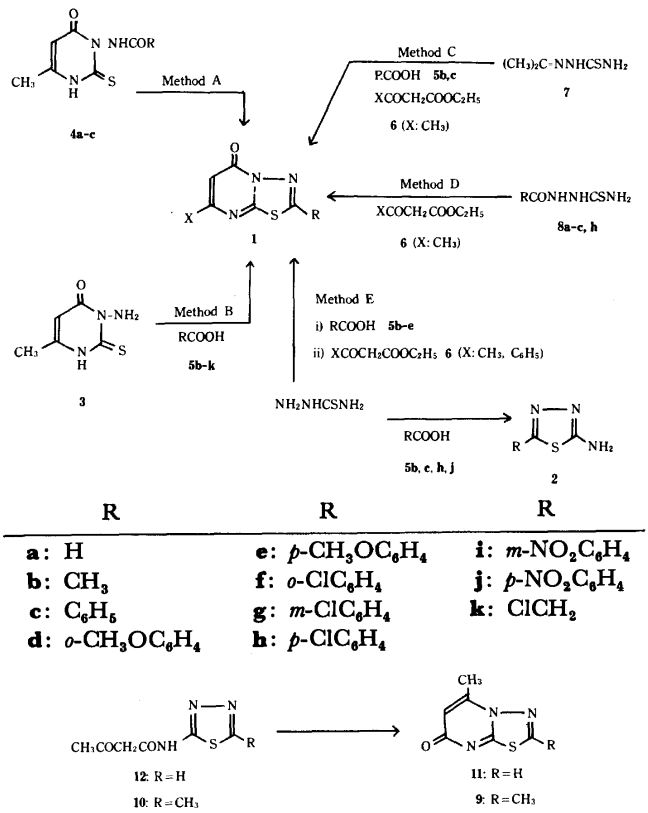

Scheme 1. Synthesis of 2,7-Disubstituted 5*H*-1,3,4-thiadiazolo[3,2-*a*]pyrimidin-5-ones (**1**) and related compounds in the presence of P_2O_5–MsOH.

heating the mixture of thiosemicarbazide and **5** in the presence of P_2O_5–MsOH, followed by the treatment of the above mixture with **6**. The yields were 72.4—76.5% (Method E). This method is inapplicable to the synthesis of **1** which has a 2-(nitrophenyl or chlorophenyl) substituent.

Previously, 2,5-dimethyl-7*H*-1,3,4-thiadiazolo[3,2-*a*]-pyrimidin-7-one (**9**) was prepared by the treatment of 2-acetoacetylamino-5-methyl-1,3,4-thiadiazole (**10**) with PPA in 18% yield.[4] Upon heating **10** with P_2O_5-MsOH, the yield of **9** was raised to 87.4%. Similarly, compound (**11**) was obtained in 61.2% yield.

The P_2O_5–MsOH reagent was at first used for the intramolecular acylation of olefinic acids and the Beckmann rearrangement of ketoxime, since this reagent resembles PPA in reaction rate, product distribution and yield.[5] It is notable that the product yield increased markedly by converting the reagent from PPA to P_2O_5–MsOH in the synthesis of heterocycles.

Experimental

General Procedures for the Preparation of 2,7-Disubstituted 5H-*1,3,4-thiadiazolo*[*3,2-*a]*pyrimidin-5-ones (1). a) From 3 or Its Acyl Derivatives (4)*: Compound **4**[2] (0.01 mol) or a mixture of **3**[1a] (0.01 mol) and **5** (0.01 mol), MsOH (0.05 mol), and P_2O_5 (0.01 mol) was placed in a flask in this order, and heated at 70 °C for 10 h. When nitrobenzoic acids were used for **5**, the reaction was carried out at 100 °C. The reaction mixture was poured into water, and made basic with 10% NaOH to pH 8. The precipitate was extracted with chloroform, and the extract was washed with water. The dried extract was evaporated to dryness in vacuum to obtain **1**.

b) From Acetone Thiosemicarbazone (7): To the mixture of **7** (0.01 mol), ethyl acetoacetate (0.01 mol), and **5** (0.01 mol) was added MsOH (0.05 mol) and P_2O_5 (0.01 mol), and the whole was heated at 100 °C for 10 h. A work-up similar to that in Method A gave **1**.

c) From 1-Acylthiosemicarbazide (8): The mixture of **8** (8 mmol) and ethyl acetoacetate (8 mmol) was heated with P_2O_5 (8 mmol)–MsOH (40 mmol) at 70 °C for 5 h. In the case of **8c** or **8h**, the mixture was heated at 100 °C for 10 h.

d) From Thiosemicarbazide: The mixture of thiosemicarbazide (0.01 mol) and **5** (0.01 mol) was heated at 70 °C for 10 h with P_2O_5 (0.01 mol)–MsOH (0.05 mol). At the end of the reaction time, **6** (0.01 mol) and P_2O_5 (5 mmol) were added to the reaction mixture and the whole was further heated at 70 °C for 10 h. The resulting solution was similarly worked up to give **1**.

Preparation of 5-Substituted 2-Amino-1,3,4-thiadiazole (2). A mixture of thiosemicarbazide (0.01 mol), **5** (0.01 mol), MsOH (0.05 mol), and P_2O_5 (0.01 mol) was heated at 70 °C for 10 h. The reaction mixture was poured into water, and made basic (pH 8) with aqueous ammonia. **2** (R: CH_3,[6,7] C_2H_5,[8] C_6H_5,[6,8] p-$NO_2C_6H_4$,[8] and p-ClC_6H_4[9]) was obtained in 89.9, 64.5, 74.2, 40.4 and 40.1% yields, respectively.

*Preparation of 2,5-Dimethyl-7*H*-1,3,4-thiadiazolo*[*3,2-*a]*pyrimidin-7-one (9).* Upon heating **10** (5 mmol) with P_2O_5 (5 mmol)–MsOH (25 mmol) at 100 °C for 10 h, **9**[4] was obtained in 87.4% yield. In a similar manner, **11**[4] was prepared in 61.2% yield.

References

1) a) T. Tsuji and T. Ueda, *Chem. Pharm. Bull.*, **19**, 2530 (1971); b) T. Tsuji and Y. Kamo, *Chem. Lett.*, **1972**, 641; c) T. Tsuji, *Chem. Pharm. Bull.*, **22**, 471 (1974); d) T. Tsuji and Y. Otsuka, *ibid.*, **26**, 2765 (1978).

2) T. Okabe, E. Taniguchi, and K. Maekawa, *Bull. Chem. Soc. Jpn.*, **47**, 2813 (1974).

3) T. Tsuji and Y. Otsuka, *Heterocycles*, **14**, 197 (1980).

4) T. Okabe, K. Maekawa, and E. Taniguchi, *Agric. Biol. Chem.*, **37**, 1197 (1973).

5) P. E. Eaton, G. R. Carlson, and J. T. Lee, *J. Org. Chem.*, **38**, 4071 (1973). In the original report, 1 : 10 solution by weight of P_2O_5 in MsOH was recommended. However, 1 : 5 molar ratio of reagent was employed in the present work, since the yield did not change and the reagent was readily hydrolyzed by work-up treatment.

6) M. Ohta and T. Higashijima, *Yakugaku Zasshi*, **72**, 376 (1952).

7) S. Ban, *Yakugaku Zasshi*, **74**, 694 (1954).

8) M. Ohta, *Yakugaku Zasshi*, **72**, 1636 (1952).

9) T. J. Kress and S. M. Costantino, *J. Heterocycl. Chem.* **17**, 607 (1980).

The Structure of Alnuserrutriol, a New C_{31} Dammarane-type Triterpenoid from the Male Flowers of *Alnus serrulatoides*

Toshifumi HIRATA, Reiko IDEO, Tadashi AOKI, and Takayuki SUGA*

Department of Chemistry, Faculty of Science, Hiroshima University, Higashisenda-machi, Naka-ku, Hiroshima 730

(Received September 17, 1981)

Synopsis. The structure of a new C_{31} dammarane-type triterpenoid, alnuserrutriol, isolated from the male flowers of *Alnus serrulatoides* CALL. (Betulaceae) has been elucidated to be (3*S*,12*R*, 20*S*)-3,12,20-trihydroxy-24-methylene-dammarane by a combination of chemical and spectroscopic methods.

In our previous studies, we have elucidated the structures of novel C_{31} dammarane-type triterpenoids and glycosides, such as alnuserol,[1] alnuseric acid,[2] alnuselide,[2] and alnuserrudiolone[3] isolated from the male flowers of *Alnus serrulatoides* CALL. (Japanese name: Kawara-hannoki) and monoglycosides of alnustic acid[4] isolated from the female flowers of the plant. In a continuation of these studies, a new C_{31} dammarane-type triterpenoid, named alnuserrutriol (I), has now been isolated from the male flowers of the plant. We here wish to describe evidence leading to the establishment of the structure of this new triterpenoid.

Results and Discussion

The male flowers of *Alnus serrulatoides* CALL. grown naturally on a river side were collected just before the flowering and immersed in acetone. An ether-soluble fraction of the acetone extract exhibited 15 spots on a silica-gel TLC plate with hexane–EtOAc (7: 3 v/v) as a solvent; a small spot (A) was observed between those of alnuserrudiolone (II)[3] and a residue at the origin. The ether-soluble fraction was then subjected to chromatography using silica gel to isolate a constituent corresponding to the spot (A), which gave a new triterpenoid, alnuserrutriol (I).

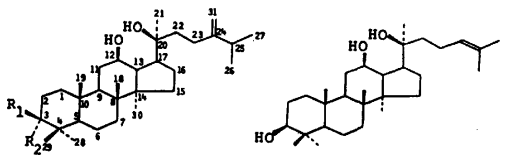

I: R_1=OH, R_2=H
II: R_1, R_2=O

III

The molecular formula $C_{31}H_{54}O_3$ of I was determined by elemental analysis and appearance of a molecular ion peak at *m/z* 474 in the mass spectrum. The IR band at 3350 cm^{-1} and the ^1H NMR signal at δ 3.58 indicated the presence of a hydroxyl group. The existence of a terminal methylene was proved by appearance of the IR bands at 3080, 1635, and 885 cm^{-1} and the ^1H NMR signal at δ 4.78. Comparison of the ^{13}C NMR chemical shifts of I with those of alnuserrudiolone (II)[3] and protopanaxadiol (III)[5] indicated that I possesses a C_{31} dammarane-type skeleton with two secondary hydroxyl groups on C-3 (δ_c 78.9) and C-12 (δ_c 71.1), a tertiary hydroxyl group on C-20 (δ_c 74.1), and a terminal methylene (δ_c 157.0 and 106.5 due to C-24 and C-31, respectively), as shown in Table 1. The configurations of C-3, C-12, and C-20 were suggested to be *S*, *R*, and *S*, respectively, by comparing the ^{13}C NMR chemical shifts with those of (3*S*, 12*R*, 20*S*)-

TABLE 1. ^{13}C CHEMICAL SHIFTS (δ_c) OF I—III IN $CDCl_3$

Carbon No.	I	II	III[a]
1	38.8	39.7	39.0
2	27.4	33.5	27.4
3	78.9	217.8	78.8
4	39.1	47.3	39.0
5	56.0	55.3	56.0
6	18.4	19.7	18.3
7	34.9	33.9	34.8
8	39.8	39.6	39.8
9	50.3	49.4	50.2
10	37.2	36.8	37.1
11	31.5	31.7	31.2
12	71.1	70.5	70.8
13	47.8	47.7	47.7
14	51.7	51.5	51.6
15	31.1	31.0	31.1
16	26.5	26.7	26.6
17	53.8	53.6	53.6
18	16.2[b]	15.9[b]	16.2[b]
19	15.7[b]	15.3[b]	15.7[b]
20	74.1	73.6	74.0
21	27.0	26.7	26.8
22	33.9[c]	34.0	34.8
23	33.5[c]	34.0	22.4
24	157.0	156.5	125.2
25	28.4	28.2	131.4
26	22.0	21.9	25.8
27	22.0	21.9	17.8
28	28.1	26.4	28.1
29	15.5[b]	21.0	15.5[b]
30	17.0	16.8	16.9
31	106.5	106.2	—

a) Referred to the chemical shifts in the Ref. 5. b) and c) The values in any vertical column may be reversed although those given here are preferred.

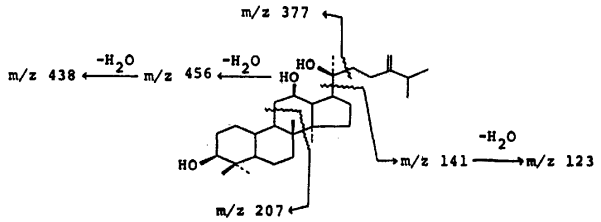

Scheme 1. The MS spectral fragmentation pattern of alnuserrutriol (I).

protopanaxadiol (III)[5] and its related compounds.[5,6] The structure I was thus proposed for alnuserrutriol and possessed all the feature necessary to explain its MS spectrum (Scheme 1). The MS spectral fragmentation pattern was completely supported by the high-resolution MS.

Finally, the proposed structure (I) was confirmed by relating it with a triol which was obtained by the reduction of alnuserrudiolone (II) with $LiAlH_4$. The configuration of C-3 of this triol should be *S*, because it is well known that the $LiAlH_4$ reduction of dammarane-type triterpenoids with the carbonyl group at the 3-position gives exclusively the 3β-hydroxyl derivatives.[7,8] The physical and spectral data of naturally occurring alnuserrutriol (I) were perfectly identical with those of the prepared triol. Thus, the structure of alnuserrutriol (I) has been established to be (3*S*, 12*R*,-20*S*)-3,12,20-trihydroxy-24-methylenedammarane.

Experimental

The ^1H NMR spectra were taken on a varian T-60 spectrometer using TMS as an internal standard. The ^{13}C NMR spectra were obtained on a JEOL JNM FX-60 (15.1 MHz) and a Hitachi R-42 FT NMR (22.6 HMz) spectrometers ($\delta_{TMS}=0$). The EI-MS were obtained on Hitachi RMS-4 and RMU-7L mass spectrometers at 70 eV.

Extraction and Isolation. The male flowers (10.3 kg) of *Alnus serrulatoides* CALL. grown naturally on a river side in the suburbs of Hiroshima city were collected just before the flowering in December. The flowers, after minced mechanically, were immersed in acetone (54 dm^3) at room temp for 2 months. Removal of the solvent from the acetone soln gave a viscous sirup, which was extracted with ether (500 cm^3 × 5) to give a viscous oil (66.0 g). A part (7.0 g) of the viscous oil was subjected to centrifugal chromatography using silica gel (160 g) and a hexane–EtOAc mixture with EtOAc increasing 0 to 100% as a solvent, and then to preparative TLC on a silica-gel plate (Merck; Type 60, GF_{254}, 0.75 mm thick) with hexane–EtOAc (7 : 3 v/v) to give alnuserrutriol (I) (75 mg; R_f 0.05).

Alnuserrutriol (I). Mp 200—202 °C; $[\alpha]_D^{25}$ +89.1° (*c* 0.15, MeOH); IR (Nujol) ν_{max} 3350 (OH), 3080, 1635, and 885 cm^{-1} (C=CH$_2$); ^1H NMR ($CDCl_3$) δ=0.78—1.12 (Me × 8), 3.58 (2H, br, >C<u>H</u>–OH × 2), 4.78 (2H, br, >C=CH$_2$); ^{13}C NMR ($CDCl_3$) (see Table 1); MS *m/z* (rel intensity) 474 (0.5, M$^+$), 456 (11), 438 (23), 377 (12), 341 (37), 207 (43), 189 (26), 141 (69), 123 (71), and 108 (100). High-resolution MS *m/z* 438.3941 ($C_{31}H_{50}O$ (M−2H$_2$O): 438.3859), 377.3010 ($C_{24}H_{41}O_3$: 377.3053), 207.1750 ($C_{14}H_{23}O$: 207.1748), 141.1290 ($C_9H_{17}O$: 141.1279), and 123.1138 (C_9H_{15}: 123.1172).

Found: C, 78.17; H, 11.37%. Calcd for $C_{31}H_{54}O_3$: C, 78.42; H, 11.47%.

Preparation of I from Alnuserrudiolone (II). A soln of alnuserrudiolone (II) (100 mg), which was isolated from *A. serrulatoides*,[3] in dry ether (2 cm^3) was dropped into a suspension of $LiAlH_4$ (10 mg) in dry ether (2 cm^3), followed by stirring for 20 min at 0 °C. The reaction mixture, after acidification, was extracted with ether to give a triol (97 mg): mp 200—203 °C; $[\alpha]_D^{25}$ +87.3° (*c* 0.30, MeOH); IR (Nujol) ν_{max} 3350 (OH), 3080, 1640, and 885 cm^{-1} (>C=CH$_2$); ^1H NMR ($CDCl_3$) δ=3.58 (2H, br, >C<u>H</u>–OH × 2), 4.76 (2H, br, >C=CH$_2$); ^{13}C NMR ($CDCl_3$) δ_c=157.2 (s, C-24), 106.3 (t, C-31), 78.8 (d, C-3), 74.0 (s, C-20), 71.1 (d, C-12), 28.0, 27.1, 21.9, 17.0, 16.0, 15.6, 15.3 (q, Me × 8); MS *m/z* (rel intensity) 474 (0.5, M$^+$), 456 (12), 438 (21), 377 (9), 341 (35), 207 (37), 189 (30), 141 (60), 123 (65), and 108 (100). The physical and spectral data of the triol were identical with those of the naturally occurring alnuserrutriol (I).

The authors thank JEOL Co. Ltd. for obtaining the ^{13}C NMR spectra. The present work was partially supported by a Grant-in-Aid for Scientific Research No. 354189 (1978, to T.A.) from the Ministry of Education, Science and Culture.

References

1) T. Hirata and T. Suga, *J. Chem. Soc., Perkin Trans. 2*, **1978**, 347.

2) T. Suga and T. Hirata, *Bull. Chem. Soc. Jpn.*, **52**, 1153 (1979).

3) T. Hirata, T. Aoki, and T. Suga, *Bull. Chem. Soc. Jpn.*, **54**, 3059 (1981).

4) T. Aoki, S. Ohta, S. Aratani, T. Hirata, and T. Suga, *J. Chem. Soc., Perkin Trans. 1*, in press.

5) J. Asakawa, R. Kasai, K. Yamasaki, and O. Tanaka, *Tetrahedron*, **33**, 1935 (1977).

6) M. Tori, T. Tsuyuki, and T. Takahashi, *Bull. Chem. Soc. Jpn.*, **50**, 3349 (1977).

7) P. Crabbe, G. Ourisson, and T. Takahashi, *Tetrahedron*, **3**, 279 (1958).

8) F. G. Fischer and N. Seiler, *Justus Liebigs Ann. Chem.*, **626**, 185 (1959).

Bis(*p*-methoxyphenyl) Selenoxide as a Mild and Selective Oxidizing Agent

Fumio OGURA,* Hachiro YAMAGUCHI, Tetsuo OTSUBO, and Hiroyuki TANAKA
Department of Applied Chemistry, Faculty of Engineering, Hiroshima University, Sendamachi, Naka-ku, Hiroshima 730

(Received October 2, 1981)

Synopsis. The title compound oxidized thiols to disulfides, sulfides to sulfoxides, hydroquinone or catechol to benzoquinones, and phosphine to phosphine oxide in high yields under very mild conditions. In addition, it functioned as a useful reagent for the syntheses of 1,2,4-thiadiazole derivatives from thioureas or thioamides.

Although the chemistry of organoseleniums is growing rapidly,[1] little attention has been paid to the use of selenoxides as an oxidizing agent for organic syntheses. Selenoxides are usually unfavorable because of their nasty smell, but more reactive due to the greater basicity of the seleninyl oxygen than sulfoxides. For example, dimethyl selenoxide, dibenzyl selenoxide, or diphenyl selenoxide oxidized amines,[2] anilines,[3] catechols,[4] sulfides,[5] phosphines,[6] and thiones[6,7] unlike the sulfur counterparts.

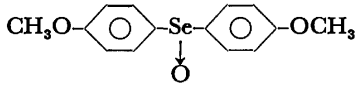

1

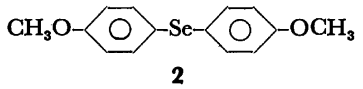

2

Bis(*p*-methoxyphenyl) selenoxide **1** is an odorless, tractable material, and accordingly expected to be of practical use as an oxidizing agent. We now report the reactivity of **1** as shown in Table 1. Like the preceding selenoxides, **1** oxidized sulfides to sulfoxides, hydroquinone or catechol to benzoquinones, and phosphine to phosphine oxide in high yields. In addition, **1** effected the oxidation of thiols to disulfides under very mild conditions, in contrast to the fact that sulfoxides did it under forced conditions.[8] The main by-product was bis(*p*-methoxyphenyl) selenide **2**, which could be used to regenerate **1**. On the other hand, **1** did not react with amines, anilines, phenylhydrazines, alcohols, and simple phenol.

The milder oxidizing properties of **1** relative to the preceding selenoxides were demonstrated by the reactions with thiones. For example, dimethyl selenoxide and dibenzyl selenoxide oxidized thiouracil **3** to uracil **4**[6] and thiourea to urea,[7] respectively. On the other hand, **1** effected milder oxidation to convert thiouracil **3** to 2,2′-dithio-di-4(3*H*)-pyrimidone **5**, and thiourea **6** to 3,5-diamino-1,2,4-thiadiazole **7**. As shown in Table

Table 1. Oxidation of thiols, sulfides, phosphine, hydroquinone, catechol, and thiouracil by **1** at room temperature

Material	Product	Time / min	Solvent	Yield / %	MP θ_m/°C
PhSH	PhSSPh	10	CH_2Cl_2	90	60
$PhCH_2SH$	$(PhCH_2S)_2$	30	CH_2Cl_2	94	69—70
n-$C_{16}H_{33}SH$	$(n$-$C_{16}H_{33}S)_2$	30	CH_2Cl_2	95	54—55
$NH_2CH_2CH_2SH$	$(NH_2CH_2CH_2S)_2$	30	CH_2Cl_2	89	Oil
$HOCH_2CH_2SH$	$(HOCH_2CH_2S)_2$	10	CH_2Cl_2	92	24—24.5
$(PhCH_2)_2S$	$(PhCH_2)_2SO$	40	AcOH	89	130—131
$(n$-$C_{12}H_{25})_2S$	$(n$-$C_{12}H_{25})_2SO$	60	AcOH	87	88—88.5
Ph_3P	Ph_3PO	15	CH_2Cl_2	99	154—155
Hydroquinone	*p*-Benzoquinone	40	MeOH	87	112—113
3,5-Dibutylcatechol	3,5-Dibutyl-*o*-benzoquinone	120	EtOH–Ether (1 : 1)	97	111—112
3	**5**	100	EtOH–$CHCl_3$ (1 : 1)	74	190(dec)

Table 2. Oxidation of thioureas and thioamides by **1**[a]

Material	Product	Solvent	Yield / %	Mp(lit) θ_m/°C
$H_2NC(S)NH_2$	**7**	EtOH	78	168—170 (169—171)[c]
$PhNHC(S)NH_2$	**8**	AcOH	60	179—180 (181)[d]
PhNHC(S)NHPh	**9**	EtOH	84	51—52 (51—52)[e]
$Ph_2NC(S)NH_2$	**10**	EtOH	88	154—155.5 (155)[f]
$CH_3C(S)NH_2$	**11**	EtOH	45[b]	Oil
$PhC(S)NH_2$	**12**	EtOH	86	89.5—90 (90)[g]

a) Reaction time 1 h at room temperature. b) Gas chromatographic analysis. c) F. Kurzer, *J. Chem. Soc.*, **1955**, 1. d) D. S. Hector, *Ber.*, **22**, 1176 (1889). e) Ref. 11. f) T. Charkrabarti and S. Chandra De, *J. Indian Chem. Soc.*, **5**, 661 (1928). g) A. W. Hofmann, *Ber.*, **2**, 645 (1869).

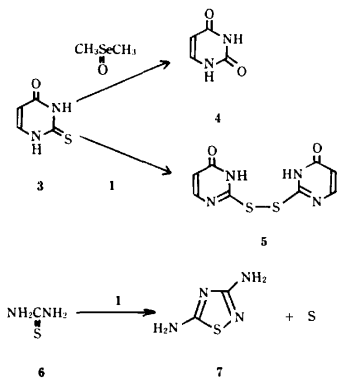

2, some thiadiazole derivatives were prepared not only from thioureas but from thioamides. Phenylthiourea reacted with **1** in a somewhat different way to give 5-imino-4-phenyl-3-phenylamino-4,5-dihydro-1,2,4-thiadiazole **8** as the exclusive product. *N,N'*-Diphenylthiourea can not lead to thiadiazole structure, but was smoothly oxidized by **1** to afford 2,4-diphenyl-3,5-bis(phenylimino)-1,2,4-thiadiazolidine **9**. Hector reported in 1890 that **9** was synthesized by treatment of the same thiourea with hydrogen peroxide,[9] but later the product was claimed to be a different compound **13**.[10] Very recently Kinoshita *et al.* succeeded the formation of **9** by use of benzoyl peroxide as an oxidizing agent.[11] The yield (84%) of **9** by the present method is much higher than that (13%) by Kinoshita's method.

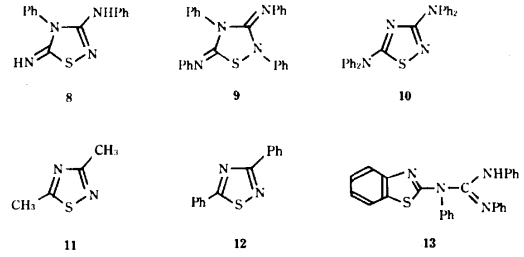

Experimental

Melting points are uncorrected. Solvents are of reagent grade. All products were confirmed by comparison of the melting points and spectroscopic data with those of the authentic samples or the reported data.

Bis(*p*-methoxyphenyl) selenide **2** was readily prepared from a reaction mixture of anisole, selenium dioxide, and water according to the procedure of Boyd *et al.*,[12] and converted to bis(*p*-methoxyphenyl) selenoxide **1** by oxidation with sodium periodate.[13]

General Method of Oxidation by Bis(p-methoxyphenyl) Selenoxide 1. A typical procedure is described in the reaction of thiobenzamide as below. A mixture of thiobenzamide (0.137 g, 1.0 mmol) and **1** (0.339 g, 1.1 mmol) in 6 ml of ethanol was stirred for one hour at room temperature. After the solvent was evaporated, the residue was taken up in chloroform and the insoluble sulfur was removed by filtration. The preparative gel-permeation liquid chromatography (JAI LC-08) of the filtrate using chloroform as eluent gave first bis(*p*-methoxyphenyl) selenide **2** in almost quantitative yield and then 3,5-diphenyl-1,2,4-thiadiazole **12** in 86% yield, colorless needles from methanol.

For isolation and purification in some of the other reactions, column chromatography was employed as well.

References

1) For reviews, see D. L. J. Clive, *Tetrahedron*, **34**, 1049 (1978); H. J. Reich, *Acc. Chem. Res.*, **12**, 22 (1979).

2) M. Poje and K. Balenovic, *Bull. Sci., Cons. Acad. Sci. Arts RSF Yougoslavia Sect. A*, **20**, 1 (1975); *Chem. Abstr.*, **83**, 43558u (1975).

3) V. I. Naddaka, V. P. Gar'Kin, and V. I. Minkin, *Zh. Org. Khim.*, **12**, 2481 (1976); *Chem. Abstr.*, **86**, 89295w (1976).

4) I. Perina, N. Bregant, and K. Balenovic, *Bull. Sci., Cons. Acad. Sci. Arts RSF Yougoslavia Sect. A*, **18**, 3 (1973); *Chem. Abstr.*, **79**, 50966 (1973); J. P. Marino and A. Schwartz, *Tetrahedron Lett.*, **1979**, 3253.

5) D. Barnard and D. T. Woodbridge, *Chem. Ind. (London)*, **1959**, 1603.

6) M. Mikolajczyk and J. Luczak, *J. Org. Chem.*, **43**, 2132 (1978).

7) S. Tamagaki, I. Hatanaka, and S. Kozuka, *Bull. Chem. Soc. Jpn.*, **50**, 3421 (1977).

8) T. J. Wallace, *J. Am. Chem. Soc.*, **86**, 2018 (1964).

9) D. S. Hector, *Ber.*, **23**, 357 (1890).

10) K. S. Suresh and C. N. R. Rao, *J. Indian Chem. Soc.*, **37**, 581 (1960).

11) T. Kinoshita, S. Sato, and C. Tamura, *Bull. Chem. Soc. Jpn.*, **49**, 2236 (1976).

12) G. V. Boyd, M. Doughty, and J. Kenyon, *J. Chem. Soc.*, **1949**, 2196.

13) M. Cinquini, S. Colonna, and R. Giovini, *Chem. Ind. (London)*, **1969**, 1737.

The Conversion of Benzyl Alcohols into Phenylacetic Acid Derivatives by Cobalt Carbonyl Catalyzed Carbonylation

Tsuneo IMAMOTO,* Tetsuo KUSUMOTO, and Masataka YOKOYAMA
Department of Chemistry, Faculty of Science, Chiba University, Yayoi-cho, Chiba 260

(Received October 12, 1981)

Synopsis. Benzyl alcohols were converted into the corresponding one carbon-homologated amides or esters in one pot by cobalt carbonyl catalyzed carbonylation in the presence of ethyl polyphosphate (PPE) and sodium iodide.

Recently, attention is focused on the catalytic carbonylation under mild conditions and many efficient methods including catalytic systems have been developed.[1-6] For example, phase transfer technique has been successfully employed for the carbonylation of benzyl, aryl, and vinyl halides to the homologous acids.[7-10] However, direct carbonylation of alcohols requires drastic conditions (high temperature and high pressure).[11] We report here a facile method for the conversion of benzyl alcohols into one carbon-homologated amides or esters by cobalt carbonyl catalyzed carbonylation under mild conditions.

In the previous papers,[12-14] we noted the synthetic utility of ethyl polyphosphate (PPE).[15,16] The reagent PPE has strong dehydration power as well as the commonly used polyphosphoric acid (PPA), but it is, different from PPA, essentially aprotic and has good solvent power at room temperature. Taking account of these characteristics of PPE, we have examined the title reaction.

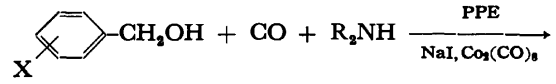

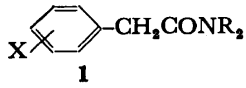

1

Scheme 1.

Our initial work was conducted with the preparation of substituted phenylacetamides (**1**), as is shown in the Scheme 1. This work was undertaken based on the following considerations; a benzyl alcohol is activated by PPE to form a polyphosphoric acid benzyl ester which is subject to nucleophilic attack of iodide ion to generate a benzyl iodide. This intermediate readily undergoes cobalt carbonyl catalyzed carbonylation in the presence of secondary amine to afford an amide (**1**).

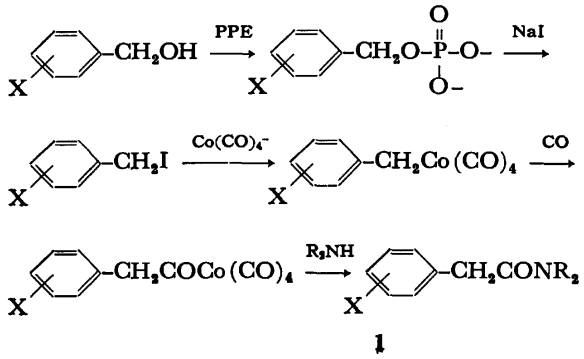

1

After various screenings of the reaction conditions, it was found that the reaction proceeded smoothly at room temperature under carbon monoxide atmosphere by the use of large excess of sterically hindered secondary amine. While, the use of less sterically hindered amine such as diethylamine resulted in poor yields. These results are summarized in Table 1.

Next, we tried the conversion of benzyl alcohol into phenylacetic esters (**2**) in one pot, according to the

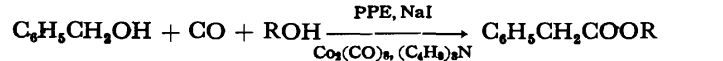

2

Scheme 2.

Scheme 2. In these cases, better results were obtained by initial stirring of a mixture of benzyl alcohol, sodium iodide, and PPE for 2 h, prior to the addition of a mixture of an alcohol, dicobalt octacarbonyl, and tributylamine. The results are shown in Table 2.

From these data, it may be concluded that our method is superior to those[11] reported hitherto, since the procedure is simple and the products are isolated in moderate yields.

Experimental

Spectra. Proton NMR spectra were measured on a JEOL C-60HL spectrometer. The chemical shifts are given in ppm with TMS as an internal standard. Infrared spectra

TABLE 1. CONVERSION OF BENZYL ALCOHOLS TO SUBSTITUTED PHENYLACETAMIDES (**1**)

Benzyl alcohol 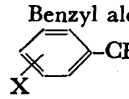	Secondary amine R_2NH	Product	Yield/%[a]
X=H	R=*i*-C_3H_7	**1a**	71
H	Cyclohexyl	**1b**	49
H	C_2H_5	**1c**	20
p-CH_3O	*i*-C_3H_7	**1d**	47
p-Cl	*i*-C_3H_7	**1e**	62
o-Cl	*i*-C_3H_7	**1f**	78
p-Br	*i*-C_3H_7	**1g**	82
p-NO_2	*i*-C_3H_7	**1h**	40

a) Yields after chromatography.

TABLE 2. CONVERSION OF BENZYL ALCOHOL TO PHENYLACETIC ESTERS (**2**)

Alcohol	Product	Yield/%[a]
CH_3OH	$C_6H_5CH_2COOCH_3$	77
C_2H_5OH	$C_6H_5CH_2COOC_2H_5$	47
t-C_4H_9OH	$C_6H_5CH_2COOC_4H_9$-*t*	35
C_6H_5OH	$C_6H_5CH_2COOC_6H_5$	68
—	$C_6H_5CH_2COOCH_2C_6H_5$	37

a) Yields after chromatography.

Table 3. Physical properties and analytical data of substituted phenylacetamides

Compound	Mp θ_m/°C	IR ($\tilde{\nu}_{C=O}$/cm^{-1})	^{1}H-NMR(δ)	Found (Calcd) (%)		
1a	52 Lit,[a] 51	1620	0.65—1.90(m, 12H), 2.95—4.30 (m, 2H), 3.60 (s, 2H), 7.25(s, 5H)			
1b	83—84	1620	0.65—3.75 (s, 22H), 3.60 (s, 2H), 7.25 (s, 5H)	79.85 (80.22)	9.69 (9.76)	4.65 (4.68)
1c	Oil Lit,[a] Bp 120—122 °C/0.3 Torr†	1635	1.00 (t, 3H, J=7.5 Hz), 1.05 (t, 3H, J=7.5 Hz), 3.25 (q, 2H, J=7.5 Hz), 3.30 (q, 2H, J=7.5 Hz), 3.60 (s, 2H), 7.25 (s, 5H)			
1d	63—64	1635	0.65—1.90 (m, 12H), 2.90—4.25 (m, 2H), 3.55 (s, 2H), 3.75 (s, 3H), 6.75 (d, 2H, J=9.0 Hz),7.15 (d, 2H, J=9.0 Hz)	71.99 (72.25)	9.26 (9.30)	5.55 (5.62)
1e	52—53	1640	0.65—1.85 (m, 12H), 2.95—4.30 (m, 2H), 3.55 (s, 2H), 7.25 (s, 4H)	66.01 (66.26)	7.86 (7.94)	5.42 (5.52)
1f	53—54	1640	0.65—1.90 (m, 12H), 2.90—4.35 (m, 2H), 3.65 (s, 2H), 7.25 (m, 4H)	66.03 (66.26)	7.85 (7.94)	5.41 (5.52)
1g	50—51	1630	0.80—1.70 (m, 12H), 3.00—4.25 (m, 2H), 3.65 (s, 2H), 7.15(d,2H, J=8.0 Hz),7.50 (d, 2H, J=8.0 Hz)	56.29 (56.39)	6.72 (6.76)	4.61 (4.70)
1h	77—78	1635	0.75—1.65 (m, 12H), 2.90—4.30 (m, 2H), 3.70 (s, 2H),7.45 (d,2H,J=9.0 Hz),8.15 (d, 2H, J=9 Hz)	63.48 (63.62)	7.55 (7.63)	10.48 (10.60)

a) R. Mukherjee, *J. Chem. Soc., Chem. Commun.*, **1971**, 1113. † 1 Torr ≈ 133.322 Pa.

were recorded on a Hitachi 215 spectrophotometer. Products were identified by NMR and IR spectra together with elemental analyses.

Materials. Ethyl polyphosphate was prepared according to the method described in the Ref. 15. Benzyl alcohols, secondary amines, and tributylamine were distilled or recrystallized before use. Dicobalt octacarbonyl was purchased from Strem Chemicals, Inc. and was used without purification.

*General Procedure for the Preparation of Phenylacetamides (**1a—h**).* A mixture of a benzyl alcohol (2 mmol), sodium iodide (600 mg, 4 mmol), dicobalt octacarbonyl (34 mg, 0.1 mmol), a secondary amine (20 mmol), and PPE (3 ml) was stirred at room temperature under carbon monoxide atmosphere. After 12 h, water was added and the mixture was extracted with chloroform. The combined extracts were dried over sodium sulfate and evaporated. The residual oil was chromatographed on silica gel using benzene–ethyl acetate (6 : 1) as the eluent. The product was further purified by short-path distillation under reduced pressure (Kugelrohr apparatus; *ca.* 190 °C/0.3 Torr). Pure materials thus obtained crystallized on standing at room temperature except *N,N*-diethylphenylacetamide (**1c**). The NMR, IR, and analytical data of the products are listed in Table 3.

*General Procedure for the Preparation of Phenylacetic Esters (**2**).* A mixture of benzyl alcohol (216 mg, 2 mmol), sodium iodide (400 mg, 4 mmol), and PPE (3 ml) was stirred at room temperature for 2 h. To this mixture was added a mixture of an alcohol (8 mmol), dicobalt octacarbonyl (34 mg, 0.1 mmol), and tributylamine (3.7 g, 20 mmol) under carbon monoxide atmosphere. After stirring for 12 h, water was added and the mixture was extracted with chloroform. The combined extracts were dried over sodium sulfate and evaporated. The residual oil was chromatographed on silica gel using benzene as the eluent. The product was further purified by short-path distillation under reduced pressure. The esters thus obtained were identified by comparison of their IR and NMR spectra with those of authentic samples.

References

1) A. Schoenberg, I. Bartoletti, and R. F. Heck, *J. Org. Chem.*, **39**, 3318 (1974).

2) J. J. Brunet, C. Sidot, B. Loubinoux, and P. Caubere, *J. Org. Chem.*, **44**, 2199 (1979).

3) S. Murai and N. Sonoda, *Angew. Chem. Intern. Ed. Engl.*, **18**, 837 (1979).

4) H. Alper and J. K. Currie, *Tetrahedron Lett.*, **1979**, 2665.

5) M. Tanaka, *Bull. Chem. Soc. Jpn.*, **54**, 637 (1981).

6) K. Nagira, K. Kikukawa, F. Wada, and T. Matsuda, *J. Org. Chem.*, **45**, 2365 (1980).

7) H. Alper and H. des Abbayes, *J. Organomet. Chem.*, **134**, C 11 (1977).

8) L. Cassar, M. Foa, and A. Gardano, *J. Organomet. Chem.*, **121**, C 55 (1976).

9) J. J. Brunet, C. Sidot, and P. Caubere, *Tetrahedron Lett.*, **1981**, 1013.

10) L. Cassar and M. Foa, *J. Organomet. Chem.*, **134**, C 15 (1977).

11) H. Bahrmann and B. Cornils, "New Syntheses with Carbon Monoxide," Springer-Verlag, Berlin (1980), pp. 226—242.

12) M. Yokoyama, M. Nakamura, T. Imamoto, and K. Yamaguchi, *J. Chem. Soc., Chem. Commun.*, **1981**, 560.

13) T. Imamoto, H. Yokoyama, and M. Yokoyama, *Tetrahedron Lett.*, **1981**, 1803.

14) T. Imamoto, M. Kodera, and M. Yokoyama, *Synthesis*, in press.

15) W. Pollmann and G. Schramm, *Biochem. Biophys. Acta*, **80**, 1 (1964).

16) L. F. Fieser and M. Fieser, "Reagent for Organic Synthesis," John Wiley and Sons, Inc., New York, N. Y. (1976), Vol. VI, p. 474 and references cited therein.

Mechanochemical Reactions at High Pressures. II. Reaction of Methacrylamide

Yasuhiro Okuri and Yoshiaki Ogo*

Department of Applied Chemistry, Faculty of Engineering, Osaka City University, 3-3-138, Sugimoto, Sumiyoshi-ku, Osaka 558

(Received May 9, 1981)

The mechanochemical behavior of methacrylamide was investigated at room temperature and at static pressures of up to 15 kbar. The determinations of the IR spectrum, the ESR signal, the X-ray diffraction pattern, and the molecular weight by GPC apparatus confirmed that the reaction products were amorphous polymethacrylamide. The reaction of methacrylamide under conditions of high pressure combined with simultaneous shear deformation(HP+SSD) is a free radical polymerization. The concentration of radicals of polymethacrylamide and the relation between the conversion and the shearing degree suggest that an acrylamide crystal is less stable than one of methacrylamide. Methacrylamide was not reached 100% conversion even at about 2π rad shearing.

The first paper[1] of this series described the design and the construction of the apparatus and the reaction of acrylamide. Acrylamide was polymerized under conditions of HP+SSD. We concluded that the polymerization of acrylamide proceeded by the free radical mechanism. The present paper is concerned with methacrylamide. The compound was selected because its similarity to acrylamide suggested that it might undergo an analogous behavior under HP+SSD, and thus allow a comparison of the mechanochemical behavior at high pressure.

Experimental

The experimental procedure is similar to that in the previous paper[1] except for the molecular weight determination. The molecular weight of the product was determined by gel permeation chromatography(GPC) using a Sephadex column constructed in our laboratory.

In this experiment, the reactions proceeded at the constant shearing velocity of 2.51 rad/h(2.4 °/min) at room temperature.

Methacrylamide was a commercial sample which was purified by repeated crystallization from benzene solution and finally vacuum dried at room temperature for 24 h. The purity of this material was confirmed by its melting point, determined as 109—110 °C.

The sample which has been sheared at up to 15 kbar (1 kbar=10^8 Pa) static pressure was extracted from a large amount of methanol for separating into soluble and insoluble fractions. The insoluble fraction (as will be described below) was dried *in vacuo* to constant weight at room temperature, and the conversion was determined. The identifications of the product were carried out by means of the measurements of melting point, IR spectrum, X-ray diffraction patterns and molecular weight distribution.

ESR spectra were recorded at 22 °C on a JEOL JES-ME-3X spectrometer equipped with an X-band microwave unit and 100 kHz field modulation. The concentrations of free radicals were determined by integrations of the spectra and by subsequent comparison with those of 1,3,5-triphenylverdazyl as references.

Results and Discussion

Methacrylamide was polymerized under conditions of HP+SSD, as occurred for acrylamide. The following experimental evidence showed this. The product did not show any definite melting point. The IR spectra of the product were very broad peculiar to a polymer rather than a methacrylamide monomer. The major difference is in the C=C vibration region at 1660—1580 cm^{-1}, where a strong absorption of C=C bonds has disappeared in the product. When X-ray diffraction patterns of methacrylamide monomer were compared with those of the product, the product was found to be in the amorphous state. Therefore, we concluded that the product in this reaction was amorphous polymethacrylamide.

The ESR signal gives a quintet system, and no other signals were detected under our experimental conditions. This signal suggests that the propagating polymer radicals at the side of such methyl groups as $-CH_2-\dot{C}(CONH_2)-CH_3$, which resulted from the rupture of C=C bonds, were generated by this type of reaction. Thus, evidently, the reaction of methacrylamide under conditions of HP+SSD is a free radical polymerization similar to that of acrylamide. Table 1 shows the concentrations of free radicals generated in the sample layer, together with those of polyacrylamide at the same conditions. The concentrations of free radicals increase with the shearing degree. Accordingly, the shearing stresses seem to play a major part in the rupture of C=C bonds. There is no difference in the concentration at each pressure for the same

Table 1. Concentrations of free radicals generated in sample layers

P	Shearing degree		Free radical $\times 10^{-18}$/spin g^{-1}	
kbar	rad	°	Methacrylamide	Acrylamide
5	2.27	130		0.27
5	3.14	180	1.49	
5	4.71	270	3.15	2.56
10	0.52	30	0.076	
10	1.22	70	0.22	
10	2.27	130	0.98	1.27
10	3.14	180	1.39	
10	4.71	270	3.39	4.25
15	1.57	90	0.84	
15	3.14	180	2.93	

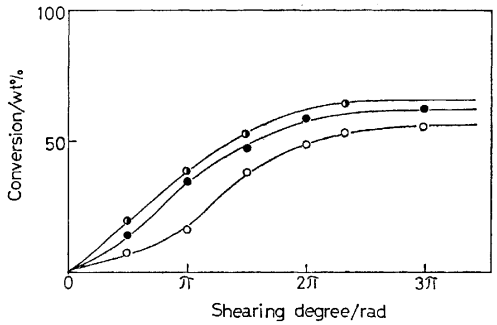

Fig. 1. Relation between conversion and shearing degree at various static pressures.
○: 5 kbar, ●: 10 kbar, ◑: 15 kbar.

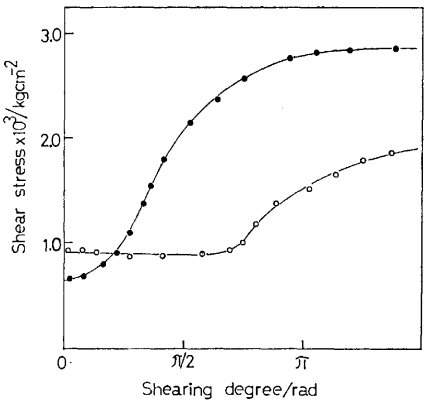

Fig. 2. Shearing curves at 10 kbar.
●: Acrylamide, ○: methacrylamide.

shearing degree (*i.e.* 3.14 rad). The concentration of radicals of polyacrylamide is generally larger than that of polymethacrylamide. It can be seen that the acrylamide crystal is relatively unstable and easily produces radicals due to the mechanical shear force under high pressure. The relation between the conversion and the shearing degree also suggests these conclusions.

Figure 1 shows the dependence of the conversion on the shearing degree at 5, 10, and 15 kbar static pressures, respectively. This relation showed an S-type curve, as do the acrylamide curves. Unlike the relation of acrylamide (refer to Fig. 9 in the previous paper[1]), methacrylamide was not reached 100% conversion even at about 2π rad shearing. Figure 2 shows the relation between the shearing stress and the shearing degree. In Fig. 2, the shearing curve for acrylamide is very similar to its conversion curve. It is therefore concluded that the shearing stress is loaded on the full sample layer and reflects directly on the conversion of polyacrylamide. On the other hand, the value of the shearing stress for methacrylamide is nearly constant up to $\theta=\pi/2$ rad. The shearing force does not affect the whole area of the

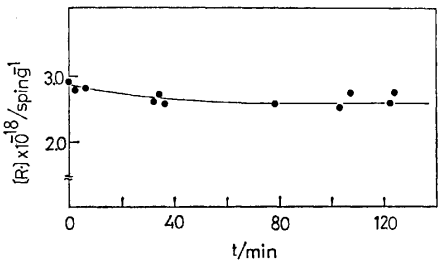

Fig. 3. Time dependence of radical concentrations at room temperature.

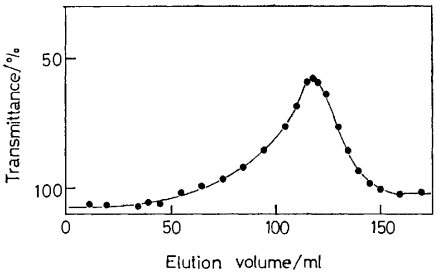

Fig. 4. Molecular weight distribution of the product.

sample, and the only surface destruction which occurs is in the case of methacrylamide. That is presumed from Fig. 3, which shows the time dependence of the polymethacrylamide radical concentrations at room temperature. In this figure, the radical reduction rate was obtained as 13.2%/120 min for polymethacrylamide radicals; this value is larger than that for polyacrylamide radicals, 5.4%/120 min. Polymethacrylamide radicals are thus relatively unstable because most of the radicals are generated in the region of the sample surface.

The relations between the intrinsic viscosity and the molecular weight of polymethacrylamide are unknown. Thus a Sephadex column was prepared in our laboratory to determine the molecular weight and its distribution. The experimental result is shown in Fig. 4. We could determine the average molecular weight of the product from this peak, using a calibration curve for this column. Calibration was undertaken by using polyethylene glycol and dextran as calibrants. The molecular weight determined by this method was about 1000. No variation of the average molecular weight was observed with the change of the reaction conditions. The above value, 1000, was also confirmed by another column (G3000PW, manufactured by Toyo Soda Kogyo Co., Ltd.).

The authors are greatly indebted to Dr. Yozo Miura of Osaka City University for the ESR measurements.

Reference

1) Y. Ogo, N. Nishiguchi, and Y. Okuri, *Bull. Chem. Soc. Jpn.*, **54**, 520 (1981).

Mechanochemical Reactions at High Pressures. III. Reactions of Acrylamide–Methacrylamide and Acrylamide–Propionamide Solid Solutions

Yasuhiro Okuri and Yoshiaki Ogo*

Department of Applied Chemistry, Faculty of Engineering, Osaka City University, 3-3-138, Sugimoto, Sumiyoshi-ku, Osaka 558

(Received May 9, 1981)

The mechanochemical behavior of acrylamide–methacrylamide (AA–MAA) and acrylamide–propionamide (AA–PA) solid solutions was investigated at room temperature and at static pressures of up to 15 kbar. The AA–MAA solid solution was copolymerized under the experimental conditions. On the other hand, the reaction product of AA–PA solid solution was an amorphous homopolymer of polyacrylamide. That is, the mechanochemical reaction of AA–PA solid solution proceeded only in the acrylamide area by a free radical mechanism. The mechanical behavior of both solid solutions was also discussed.

The previous papers[1,2] were concerned with the design and construction of the apparatus and the reactions of acrylamide and methacrylamide. Both compounds were polymerized by a free radical mechanism under conditions of high pressure combined with simultaneous shear deformation(HP+SSD). The present paper deals with acrylamide–methacrylamide(AA–MAA) and acrylamide–propionamide(AA–PA) solid solutions.

The solid-phase reaction of both solid solutions has not been investigated under high pressures. Only polymerization of acrylamide–propionamide with γ-rays has been reported by several investigators.[3–5]

As a general rule, solid solutions have an unstable crystal structure unlike uni-component materials. Crystal instabilities of both solid solutions are expected to appear in some parameters measured in this type of reaction.

In this paper, the mechanochemical behavior and the pressure effect on acrylamide–methacrylamide solid solution and acrylamide–propionamide solid solution are discussed.

Experimental

The principles of the experimental procedure were similar to the preceding papers.[1,2] Acrylamide, methacrylamide, and propionamide were recrystallized from benzene, respectively.

All the solid solutions were prepared by melting the ingredients in the tubes which were closed to the atmosphere, followed by rapid cooling, so that crystalline films were formed on the walls of the tubes.

The molecular weight of the reaction product from AA–MAA solid solution was estimated by gel-permeation chromatographic analysis, using a Sephadex column made in our laboratory and calibrated by using polyethylene glycol and dextran as the standard substances.

The molecular weight of the reaction product from AA–PA solid solution(polyacrylamide, as will be described below) was determined, by means of the following relation,[6] from the viscosity data obtained from the Ubbelohde viscometer at 30 °C.

$$[\eta]_{30}^{H_2O} = 3.73 \times 10^{-4} M_v^{0.66}$$

ESR spectra were recorded at 22 °C on a JEOL JES-ME-3X spectrometer equipped with an X-band microwave unit and 100 kHz field modulation.

Results and Discussion

Reaction of Acrylamide–Methacrylamide Solid Solution. Figure 1 shows the two component phase diagram obtained by a DSC(Differential Scanning Calorimeter) and melting point measurements with the naked eye. This diagram shows that 87 mol% acrylamide–13 mol % methacrylamide mixture melts congruently at 79—80 °C. This congruent transformation is observed for some binary solid solutions. It is thought that this ratio mixture is an optimum experimental sample.

We concluded from the following experimental evidence that AA–MAA solid solution was copolymerized under conditions of HP+SSD. IR spectra of the product were very broad with peak positions at 3200 and 1650 cm^{-1}. The sharp absorption of C=C bonds at 1650 cm^{-1} in IR spectra of the reactant AA–MAA solid solution disappeared during the reaction. The X-ray diffraction patterns of the product showed an

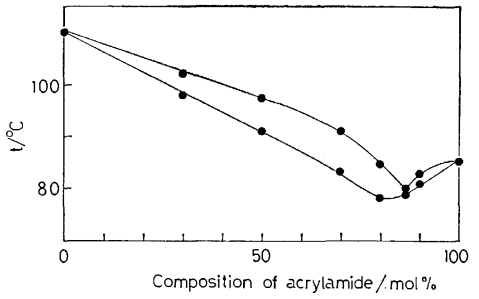

Fig. 1. Binary system phase diagram of acrylamide–methacrylamide.
Upper curve: solidus, lower curve: liquidus.

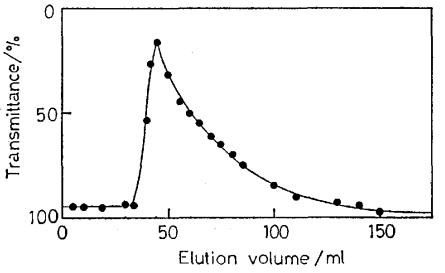

Fig. 2. Molecular weight distribution of the product of AA–MAA solid solution.

amorphous state. The product did not show a definite melting point. In addition, the physical properties of the methanol soluble fraction of the product was the same as the original AA–MAA solid solution. The gel-permeation chromatographic curve showed a single peak as shown in Fig. 2, and its molecular weight was determined as 15000.

Assuming that the ESR data measured immediately after the experiment belong to the growing polymer radical, the molecular weight of the product can be estimated of the order of 10^4 from the following equation if two radicals exist in one polymer chain.

$$(2mNC/n)/m = [R],$$

where m mol of sample, N Avogadro number, C conversion, n the degree of polymerization, and [R] is the radical concentration. The value is similar in magnitude to the chromatographic value.

Table 1. Half widths of X-ray diffraction patterns of various samples

	Acrylamide			
$\frac{2\theta}{^\circ}$	12.0—12.1	19.4	24.1—24.2	28.6—28.7
$\frac{\text{Half width}}{^\circ}$	0.50	0.63	0.62	0.53
	Methacrylamide			
$\frac{2\theta}{^\circ}$	10.8	21.6	23.8	26.4
$\frac{\text{Half width}}{^\circ}$	0.65	0.72	0.75	0.46
	AA–MAA solid solution			
$\frac{2\theta}{^\circ}$	11.8	19.2	23.7	28.2
$\frac{\text{Half width}}{^\circ}$	0.66	0.78	0.75	0.75

Table 1 shows the half widths of the X-ray diffraction patterns of acrylamide,[1] methacrylamide,[2] and AA–MAA solid solution, respectively. The half width of the X-ray diffraction pattern closely relates to the stability of the crystal structure. It seems from Table 1 that the AA–MAA solid solution has a more unstable crystal structure than the others.

The crystal instability or the mechanical weakness of AA–MAA solid solution also appears in Fig. 3, which shows the relation between the conversion and the shearing degree at 5, 10, and 15 kbar (1 kbar= 10^8 Pa) static pressures. The conversion rapidly increased at an earlier shearing stage than those of acrylamide and methacrylamide alone reported in the previous paper.[1,2] The shearing curve at 10 kbar of the congruent solid solution(a) was compared with that of the corresponding (87 mol%AA–13 mol% MAA) mixture(b) as shown in Fig. 4. Although the shearing stress generated in the solid solution was slightly larger than that in the corresponding mixture at an earlier stage of the shearing, the difference gradually increased as the shearing proceeded. The reason for this can be explained by the shear reaction proceeding more actively owing to the instability of the crystal structure of the solid solution. AA–MAA solid solution was not reached 100% conversion even at about 2π rad shearing for the same reason of methacrylamide.[2]

The terminal of this copolymer is an acrylamide radical, because the typical ESR spectrum of the sheared sample is the same as that of acrylamide. No other signals were identified under our experimental conditions. The radical concentrations of the sheared sample at 10 kbar are listed in Table 2 together with the values of the corresponding monomers. Those of AA–MAA solid solution at various shearing degree

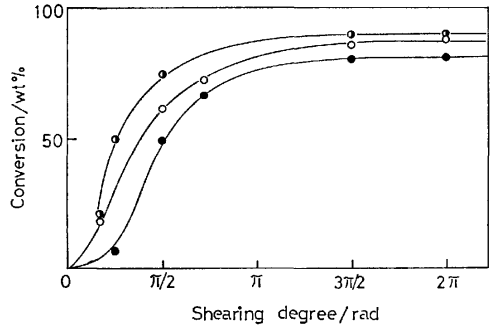

Fig. 3. Relation between conversion and shearing degree at various static pressures for 87AA–13MAA solid solution.
●: 5 kbar, ○: 10 kbar, ◑: 15 kbar.

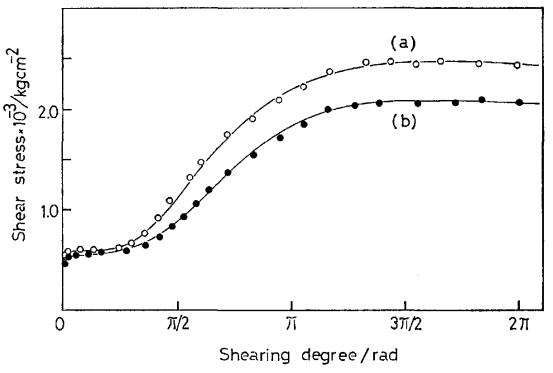

Fig. 4. Shearing curve at 10 kbar for 87AA–13MAA solid solution(a) and 87AA–13MAA mixture(b).

Table 2. Concentrations of free radical generated in sample layer of various samples

P	Shearing degree		Free radical/spin g^{-1}		
kbar	rad	°	Acrylamide[1]	Methacrylamide[2]	AA–MAA solid solution
10	2.27	130	1.29×10^{18}	0.98×10^{18}	9.02×10^{18}
10	3.14	180		1.39×10^{18}	10.7×10^{18}
10	4.71	270	4.25×10^{18}	3.39×10^{18}	12.1×10^{18}

are apparently larger than any other. These facts also suggest the relatively low mechanical stability of the original solid solution.

Reaction of Acrylamide–Propionamide Solid Solution. The crystal structure of propionamide was investigated by Fadner and Morawetz,[3] who described it as monoclinic and the dimensions of the unit cell $a_0=9.74$ Å, $b_0=5.74$ Å, $c_0=9.02$ Å, $\beta=113.5°$. The unit cell of acrylamide is characterized by $a_0=9.69$ Å, $b_0=5.77$ Å, $c_0=8.36$ Å, $\beta=118°$.[7] Therefore acrylamide and propionamide are isomorphous. The mixture of 90 mol% acrylamide–10 mol% propionamide is mainly used as an experimental sample, and 50 mol% acrylamide–50 mol% propionamide and 10 mol% acrylamide–90 mol% propionamide are used for the comparison. Each sample is abbreviated as 90AA–10PA, 50AA–50PA, and 10AA–90PA solid solutions.

A homopolymer was obtained by the reaction of 90AA–10PA solid solution, while the AA–MAA solid solution was copolymerized under the same conditions. The reactive sites of this solid solution are to be polyacrylamide from the following experimental evidence. In the first place, IR spectra of the product were very broad at 1620 cm^{-1}. The sharp absorption of C=C vibration region of 90AA–10PA solid solution has disappeared. Therefore, it is concluded that the C=C bonds of acrylamide were ruptured through this reaction. Secondly, the pattern of the ESR signal of the sheared sample at high pressures was identical with that of polyacrylamide. This fact suggests that the reaction was initiated by the rupture of C=C bonds in acrylamide, in other word, the mechanochemical reaction of this solid solution proceeds only in the acrylamide area by a free radical mechanism, and the propionamide did not participate to the reaction as a reactive monomer.

Figures 5 and 6 show the relations between the conversion and the shearing degree at 5, 10, and 15 kbar static pressures for 90AA–10PA solid solution and for 50AA–50PA solid solution. Figure 6 also shows the range of data because the conversion of this solid solution was fairly low under these experimental conditions. It may be noted that no difference of the conversion with the pressure appear in the latter case. These relations show the S-type curve as well as acrylamide and AA–MAA solid solution. However the values of the conversion of 90AA–10PA and 50AA–50PA solid solutions are respectively smaller and much

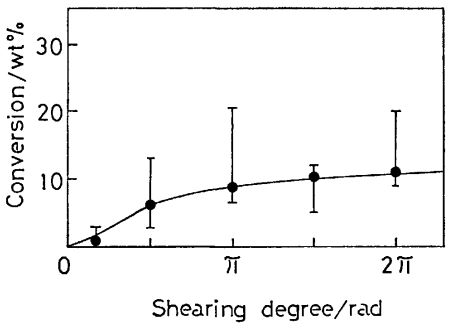

Fig. 6. Relation between conversion and shearing degree for 50AA–50PA solid solution.

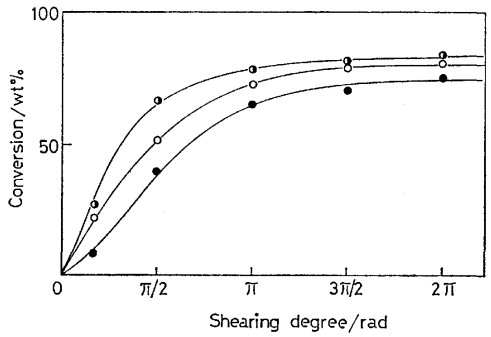

Fig. 5. Relation between conversion and shearing degree at various static pressures for 90AA–10PA solid solution.
●: 5 kbar, ○: 10 kbar, ◐: 15 kbar.

Table 3. Molecular weight of the product polymer of 90AA–10PA

P / kbar	Shearing degree/rad			
	$\pi/2$	π	$3\pi/2$	2π
5	51900	13200	11800	
10	55600	12800	10600	10200
15	26000	12600	8600	

smaller than those of acrylamide[1] and AA–MAA solid solution. These results suggest that propionamide in solid solutions may act as a surprisingly efficient chain transfer agent, that is, a retarder. This assumption is consistent with the experimental results on γ-ray radiation polymerization of AA–PA solid solution reported by Fadner *et al.*[3] It can be seen that propionamide with the active N–H bond reacts with the propagating radicals, and the degradative chain transfer reaction occurs in the reaction system.

Table 3 shows the viscosity-average molecular weight of produced polymer at 5, 10, and 15 kbar at different shearing degrees. The molecular weight of the polymer obtained by HP+SSD was much lower than those of the polymer obtained by the same technique from acrylamide alone.[1] The shorter polymer chain length presents a clear evidence supporting that propionamide may act as a chain transfer agent (a retarder) in solid solutions as just suggested in Figs. 5 and 6. This table also suggests that this polymer degrades, judging from the molecular weight reduction, with the increase in the shearing degree. Consequently, the same conclusion is derived from the above facts as for acrylamide alone.[1]

The Mechanochemical Behaviors of Both Solid Solutions. The shearing stress reflects both on the conversion (polymer production) and on the stability of the crystal structure. In view of many experimental data, at the early stage of the reaction the shearing stress reflects on the stability of the crystal structure, and at the later stage it does on the conversion. The shearing stresses of both solid solutions were nearly equal at the early shearing degree; later the shearing stress of the AA–MAA solid solution was larger than that of the 90AA–10PA solid solution. It can also be concluded from the above experimental result on

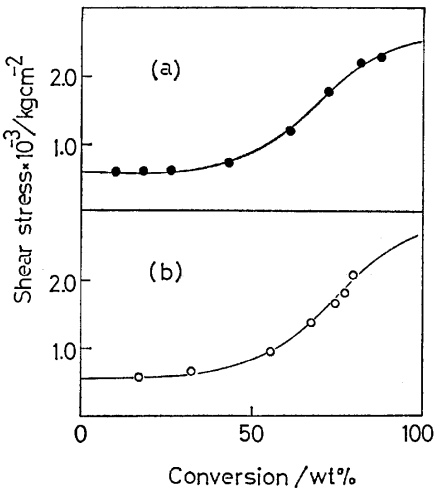

Fig. 7. Relations between shear stress and conversion for AA–MAA(a) and 90AA–10PA(b) solid solutions.

the mechanical behavior that the crystal stability of both solid solutions are similar, and that the conversion of AA–MAA solid solution into copolymer is larger than that of 90AA–10PA solid solution into polymer.

Figure 7 shows the relation between the shearing stress and the conversions of AA–MAA(a) and 90AA–10PA(b) solid solutions.

Some physical properties of two-phase material, k, in which one phase is dispersed randomly in another, can be well-known expressed[8,9] as the corresponding volume fraction, f.

$$k = k_c \frac{1+2f_d\dfrac{1-k_c/k_d}{2k_c/k_d+1}}{1-f_d\dfrac{1-k_c/k_d}{2k_c/k_d+1}} \qquad (1)$$

In this equation the subscripts c and d refer to the continuous phase and to the dispersed phase respectively. This equation is plotted in Fig. 8 for two examples of $k_c/k_d=10$ and $k_d/k_c=10$. As the conversion corresponds to volume fraction of the polymer material in our experiment, measurements should appear between the two curves as a dashed line. The experimental results showed the same relation between the conversion and the shearing stress. It can be concluded, therefore, that the shearing strength of the polymer-monomer composite, τ, may be expressed by the similar equation (2).

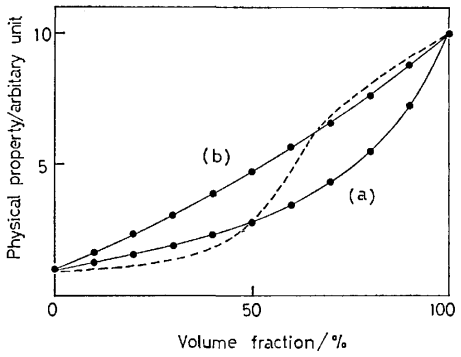

Fig. 8. Plot of Eq. 1.
(a): $k_c/k_d=10$, (b): $k_d/k_c=10$. Dashed line: The curve corresponding to the experimental results. Refer to Fig. 7.

$$\tau = \tau_M \frac{1+2f_d\dfrac{1-\tau_M/\tau_P}{2\tau_M/\tau_P+1}}{1-f_d\dfrac{1-\tau_M/\tau_P}{2\tau_M/\tau_P+1}} \qquad (2)$$

Here the subscripts P and M refer to the polymer and the monomer, respectively, and f_d can be substituted by the conversion into polymer in this case.

The authors wish to thank Dr. Yozo Miura of Osaka City University for the ESR studies.

References

1) Y. Ogo, N. Nishiguchi, and Y. Okuri, *Bull. Chem. Soc. Jpn.*, **54**, 520 (1981).
2) Y. Okuri and Y. Ogo, *Bull. Chem. Soc. Jpn.*, **55**, 645 (1982).
3) T. A. Fadner and H. Morawetz, *J. Polym. Sci.*, **45**, 475 (1960).
4) G. Adler and W. Reams, *J. Polym. Sci., Part A*, **2**, 2617 (1964).
5) B. Baysal, G. Adler, D. Ballantine, and P. Colombo, *J. Polym. Sci.*, **44**, 117 (1960).
6) New Product Bulletin, No. 34, American Cyanamide Co., New York, June 1955.
7) ASTM card, No. 11-920
8) L. H. Van Vlack, "Elements of Materials Science and Engineering," 3rd ed, Addison-Wesley Publishing Company, U.S.A. (1975), p. 351.
9) K. Kanamaru, "Zairyo Bussei Kogaku," Kyoritsu Shuppan, Tokyo (1970), p. 266.

 © 1982 The Chemical Society of Japan Bull. Chem. Soc. Jpn., 55, 651—653 (1982)

ESR Spectra of Anion Radicals of 8,8-Dicyanoheptafulvene and Its 4,5-Benzo Derivative

Yusaku IKEGAMI,* Takashi MURAMATSU,† and Toyonobu ASAO††

Chemical Research Institute of Non-Aqueous Solutions, Tohoku University, Katahira 2-1-1, Sendai 980

†*Research Institute for Science Education, Miyagi University of Education, Aramaki Aoba, Sendai 980*

††*College of General Education, Tohoku University, Kawauchi, Sendai 980*

(Received May 26, 1981)

The hyperfine splitting constants for the 8,8-dicyanoheptafulvene anion radical generated electrolytically at low temperature indicate that the unpaired spin belongs to an a_2 orbital of the group C_{2v}. Its 4,5-benzo derivative gives a stable anion radical by reduction with alkali metals. The odd electron belongs to a b_2 orbital.

8,8-Dicyanoheptafulvene (=2,4,6-cycloheptatrien-1-ylidenepropanedinitrile),[1] which is one of the most stable derivatives of heptafulvene, is not reduced with alkali metals. Electrochemical generation of the anion radical to measure the ESR spectrum at room temperature has also been unsuccessful because of its instability. We have then carried out an electrolytical generation at low temperature. The result will be reported together with results on the anion radical of its 4,5-benzo derivative prepared by reduction with alkali metals.

Results and Discussion

Electrolytic generation of 8,8-dicyanoheptafulvene in degassed butyronitrile was carried out within the cavity of an ESR spectrometer, using a cell modified slightly from Allendoerfer *et al.*[2] and Ohya-Nishiguchi.[3] Tetrabutylammonium perchlorate was used as the supporting electrolyte. The reduction at −100 °C gave the ESR spectrum shown in Fig. 1. A similar spectrum was obtained by an electrolysis in a mixed solvent of acetonitrile and 1,2-dimethoxyethane (DME) (1:9) at −80 °C using tetrapropylammonium perchlorate as the supporting electrolyte. Three splitting constants (Table 1) obtained correspond closely to those of the tropone anion radical (0.858, 0.01, and 0.505 mT).[4]

Similarity of the hyperfine structure to that of the tropone anion radical substantiates that the unpaired spin belongs to an a_2 orbital, in which the spin localizes in the seven-membered ring. Therefore, as has been discussed for the C_{2v} tropone structure,[4] the Hückel MO calculation would show zero spin densities at all atoms in the C=C(CN)$_2$ moiety. The McLachlan spin densities calculated by employing the parameters proposed by Streitwieser are shown in Table 1, demonstrating a good agreement between the experimental and calculated spin densities. Calculations were also carried out by introducing the bond alternation parameter k ($=\beta_s/\beta_d$, the ratio of resonance integral parameters for the C–C and C=C bonds in the seven-membered ring) in order to represent the aromaticity of 8,8-dicyanoheptafulvene. However, the reduction of k-parameter to 0.9 replaced the unpaired spin orbital by the b_2 orbital, with which the observed splitting constants cannot be rationalized. Although such a replacement of the orbitals is avoidable if one adopts other resonance and Coulomb integral parameters for the C=C(CN)$_2$ group, the calculations by the use of some possible parameters show poorer agreements than that seen in Table 1. It is thus concluded that the k-parameter must be close to 1, which means the complete delocalization of π-electrons in the 8,8-dicyanoheptafulvene anion radical, while a considerable bond alternation in the conjugated seven-membered ring has been observed for the neutral species in solid state.[5]

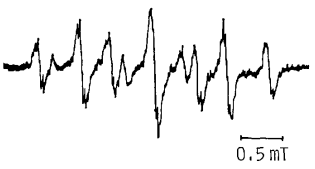

Fig. 1. ESR spectrum of the 8,8-dicyanoheptafulvene anion radical generated by the electrolysis in butyronitrile at −100 °C.

Table 1. Splitting constants (a_i) and spin densities (ρ_i) for the 8,8-dicyanoheptafulvene anion radical

Position	a_i/mT	ρ_i	
		Exptl[a]	Calcd[b]
10, 12			−0.0173
9, 11			−0.0091
8			−0.0098
1			−0.0677
2, 7	0.88	0.37	0.3774
3, 6	0.02	0.01	−0.0111
4, 5	0.50	0.21	0.1989

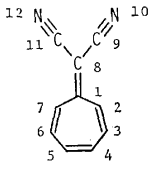

a) With the relation, $a_i = Q^{H}_{CH}\rho_i$, in which $|Q^{H}_{CH}| = 2.37$ mT was adopted. b) Calculated by the McLachlan procedure. Parameters for the calculation: $\alpha_N = \alpha + 0.5\beta$. Resonance integrals for the C-C and C-N bonds are all 1β.

In contrast to the instability of the above, the anion radical of the 4,5-benzo derivative (=7*H*-benzocyclohepten-7-ylidenepropanedinitrile)[6] was produced in a stable form by reduction with an alkali metal at room temperature. The ESR spectra are shown in Fig. 2 for the two solutions prepared by reducing the neutral species with sodium metal in DME and with potas-

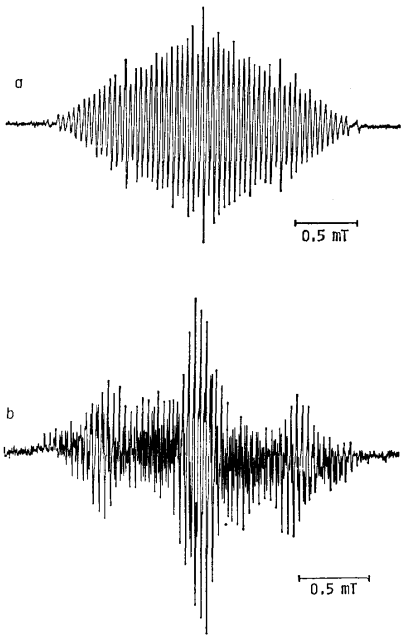

Fig. 2. ESR spectra of the 8,8-dicyano-4,5-benzoheptafulvene anion radical generated by the reduction (a) with Na in DME and (b) with K in THF at room temperature.

TABLE 2. SPLITTING CONSTANTS (a_1) AND SPIN DENSITIES (ρ_1) FOR THE 8,8-DICYANO-4,5-BENZOHEPTAFULVENE ANION RADICAL[a)]

Position	a_1/mT			ρ_1	
	Na-DME	Na-THF	K-THF	Exptl (Na-DME)	Calcd
14, 16	0.087	0.085	0.081		0.0379
13, 15					0.0279
12					−0.0079
1					0.2454
2, 9	0.166	0.168	0.151	0.070	−0.0784
3, 8	0.626	0.630	0.616	0.264	0.2718
10, 11					0.0100
4, 7	0.249	0.251	0.256	0.105	0.0947
5, 6	0.125	0.126	0.108	0.053	0.0372
M+	b)	b)	0.040		

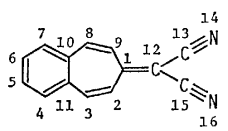

a) See footnotes in Table 1.
b) Not observed.

sium metal in tetrahydrofuran (THF). A much complicated structure in the latter spectrum is caused by an appearance of the splittings due to the potassium ion. Analysis of the hyperfine structures afforded the splitting constants summarized in Table 2 together with those for the Na–THF system. The assignments for the constants were tentatively given according to the type of splitting and by comparing them with the calculated spin densities. As seen from Table 2, the agreement between the calculated and experimental spin densities is satisfactory. An introduction of k-parameter to the seven-membered ring does not lead to the replacement of unpaired spin orbital (b_2 species) by another one, in distinction from the case of 8,8-dicyanoheptafulvene. However, the reduction of the k-value to less than 0.8 makes the agreement between the experimental and calculated spin densities worse. Thus, no information of the bond alternation in the seven-membered ring was obtained.

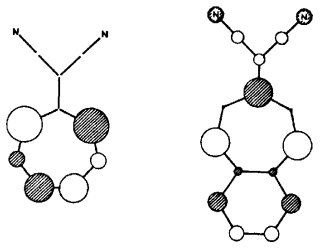

Fig. 3. Illustration of the unpaired-spin distributions for two anion radicals.

The contrast in stability between the above two anion radicals is properly ascribed to the difference in their π-electron systems. The difference can be illustrated with Fig. 3 as an idiomatic expression for the unpaired spin orbitals. In this figure, the radii of the circles are proportional to the absolute value of the LCAO-coefficient in the Hückel MO calculations and blank and shadowed circles refer to relative signs of these coefficients. A noteworthy difference between the unpaired-spin distributions in their dicyanoheptafulvene moieties might be related to the contrast in their stabilities.

Experimental

8,8-Dicyanoheptafulvene, mp 199—200 °C,[1)] and the 4,5-benzo derivative, mp 267 °C,[6)] were prepared by the authentic methods and recrystallized from methanol and a mixture of benzene–cyclohexane, respectively. Solvent butyronitrile (guaranteed reagent) was treated with potassium permanganate and sodium carbonate[7)] and distilled under a nitrogen pressure of 2×10^3 Pa. The middle fraction was degassed and distilled again under a high vacuum to be stored over previously dried molecular sieves 4A in a storage vessel. Other solvents were purified by the procedures reported previously.[8)]

ESR spectra were measured with a Varian E-109E EPR spectrometer. An electrolysis cell for ESR measurements was constructed by modifying slightly from those reported earlier.[2,3)] In this cell, a helical electrode wound with a 0.5 mm diameter silver wire and a straight platinum wire of 0.5 mm diameter are supported in a quartz tube (3.2 mm in inner diameter) connected to a Pyrex tube through a graded seal. The upper Pyrex part, holding two leading wires sealed, has no glass joints and is connected to a branch tube, which can be joined to a vacuum line in order to prepare solutions under vacuum. Spectral simulations were carried out with a JEOL JEC-5 minicomputer.

References

1) T. Nozoe, T. Mukai, K. Osaka, and N. Shishido, *Bull. Chem. Soc. Jpn.*, **34**, 1384 (1961).
2) R. D. Allendoerfer, G. A. Martinchek, and S.

Bruckenstein, *Anal. Chem.*, **47**, 890 (1975).
3) H. Ohya-Nishiguchi, *Bull. Chem. Soc. Jpn.*, **52**, 2064 (1979).
4) Y. Ikegami, H. Watanabe, and S. Seto, *Bull. Chem. Soc. Jpn.*, **45**, 1976 (1972).
5) H. Shimanouchi, T. Ashida, Y. Sasada, M. Kakudo, I. Murata, and Y. Kitahara, *Bull. Chem. Soc. Jpn.*, **39**, 2322 (1966).
6) Y. Sugimura, K. Iino, H. Kawano, N. Sohma, and Y. Kishida, *Chem. Pharm. Bull.*, **20**, 2515 (1972).
7) R. P. Van Duyne and C. N. Reilley, *Anal. Chem.*, **44**, 142 (1972).
8) S. Kubota and Y. Ikegami, *J. Phys. Chem.*, **82**, 2739 (1978).

Electrohydrodynamic Dissipative Structure in Unipolar and Bipolar Injection Cases

Yoshihiro AIKAWA,* Haruhisa SHIMODA,† Kenkichiro KOBAYASHI, Akira TAKAHASHI,††
Shuzaburo TAKEDA,† Toshibumi SAKATA,† and Mitsunori SUKIGARA*

Institute of Industrial Science, The University of Tokyo, Roppongi, Minato-ku, Tokyo 106
†*Department of Electrophotooptics, Tokai University, Hiratsuka, Kanagawa 259-12*
††*Junior College, Tokai University, Miyamae, Shizuoka 420*

(Received June 19, 1981)

An electrohydrodynamic dissipative structure appearing in a suspension system of TiO_2 particles in organic solvents is analyzed from a viewpoint of thermodynamics. This analysis gives rather a general explanation for electrohydrodynamic instability caused by unipolar injection and for that caused by bipolar injection. Dimensionless parameters which are the criteria of the hydrodynamic instability are given as $R=\varepsilon V/\eta\mu$ and $R=\varepsilon^2V^2/nq\mu\eta c^2$ respectively for the former and latter cases. The lattice constant of the hexagonal dissipative structure is derived to be proportional to the thickness of the liquid layer.

It has been known that there exist regular structures which appear only by a constant supply of energy. The Bénard's thermal convection[1-4] and a convection caused by the Felici instability[5] are well known examples. In these cases, energy flux is flowing along a potential gradient across a liquid layer whose surfaces contact respectively with two different systems. The energy flux thus generated causes a periodic structure of convection which usually shows a two-dimensional hexagonal lattice and does not have the translational symmetry of the static liquid layer any more. Such lowering of symmetry means that only some components in the wavenumber spectrum of convective disturbance grows. Both the Bénard and Félici instabilities were considered from the above viewpoint by some authors.[3,6,7] In their treatments the terms of higher order of the small disturbances were neglected and thus linearized equations were solved. In this sense it can be judged by their treatments whether a small fluctuation generated in a fluid system can begin to grow or not, but it is impossible to judge if the growing of the fluctuation can bring the system into a steady convective state.

In the previous paper,[8] we reported a photoelectroexcited convective structure appearing in a suspension of TiO_2 particles in an organic solvent. In the system, TiO_2 particles (1 μm in diameter) had a negative surface charge ($q_d=-48$e, e; unit charge) in the dark. When the system was subjected to a d.c. voltage between a pair of transparent electrodes and to light of the intrinsic absorption region of TiO_2, the sign of the electric charge of the particles is inverted on the anode surface and thus positively charged particles ($q_+=3500$e) showed a photoelectromigration toward the cathode. On the cathode the positively charged particles again acquired a negative charge ($q_-=-660$e) and migrated toward the anode.[9] This process was repeated during illumination. Consequently, TiO_2 particles showed an oscillatory motion between the two electrodes under a stationary illumination, and when the applied voltage exceeded a critical value, a convective flow of insulating fluid with a two-dimensional hexagonal symmetry appeared with a lattice constant proportional to the thickness of the suspension layer.[10] The system looks similar to that of Félici in the sense that the convections in the both cases were generated by amovement of charged particles through a liquid layer, though the charged particles in the Félici instability are ions or electrons and ours were photosensitive TiO_2 particles dispersed in the suspension.

The Félici instability was treated by Schneider and Watson[6] for the case of unipolar injection, while in our case[8-10] there are positively charged TiO_2 particles and negatively charged ones in a suspension system. In the case of Schneider and Watson, the problem was treated as a space charge limited conduction of unipolar carriers. In the present case, however, there is no space charge in the static state with no macroscopic convection. Thus the both cases are physically different from each other. In the present paper we consider which of the two stationary states, *i.e.* the convective state and the non-convective state of the present system, is more favorable and discuss the transition between the two states from the irreversible thermodynamic standpoint, instead of discussing the problem in terms of the growth of small convective fluctuations. The size of a convection cell in the stationary state is estimated with the condition for minimum energy dissipation.[11]

Photoelectrophoresis without Convection. TiO_2 particles may be in two charged states under the stationary illumination, *i.e.* the positively charged state ($q_+=3500$e) and the negatively charged state ($q_-=-660$e).[9] Under an electric field, E, the velocity of TiO_2 particles is given by Stokes' law,

$$v_\pm = \frac{q_\pm E}{6\pi\eta R}, \tag{1}$$

where R and η are the radius of a TiO_2 particle and the viscosity of the surrounding liquid, respectively. Then, the mobility of the particles of each electric charge is given as

$$\mu_\pm = \frac{q_\pm}{6\pi\eta R}. \tag{2}$$

We take the Cartesian coordinates where the z-axis is in the direction vertical to the electrodes (see Fig. 1). We express the number density of total TiO_2 particles, that of the particles carrying positive charge and that carrying negative one by $n(z)$, $n_+(z)$ and $n_-(z)$, respectively. Among the above three quan-

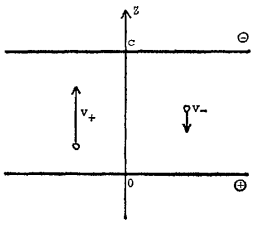

Fig. 1. Co-ordinates of the system for analysis, the anode being at $z=0$ and the cathode at $z=c$.

tities the following relation should hold,

$$n(z) = n_+(z) + n_-(z).$$

By the law of conservation for the particles of each electrical sign under a stationary state, we have

$$\frac{\partial[n_+(z)\cdot v_+(z)]}{\partial z} = \frac{\partial[n_-(z)\cdot v_-(z)]}{\partial z} = 0. \tag{3}$$

The continuity condition at the electrode surfaces ($z=0$ and $z=c$) in a stationary state is given as

$$n_+(0)\cdot v_+(0) + n_-(0)\cdot v_-(0) = n_+(c)\cdot v_+(c) + n_-(c)\cdot v_-(c) = 0. \tag{4}$$

From Eqs. 3 and 4, we have a general condition holding also in the bulk of the liquid layer as

$$n_+(z)\cdot v_+(z) + n_-(z)\cdot v_-(z) = 0. \tag{5}$$

Using Eqs. 1 and 5, we can obtain

$$n_+(z)\cdot q_+(z) + n_-(z)\cdot q_-(z) = 0, \tag{6}$$

that is, there exists no space charge in the bulk of the liquid layer. This suggests that the electric field in the bulk is uniform and can be expressed as V/c, there V is the applied voltage. In consequence, the distribution function of particles, $n_+(z)$ and $n_-(z)$, are also uniform from Eq. 3. Thus the current density in such a stationary state is given as

$$\begin{aligned} i &= n_+\cdot q_+\cdot v_+ + n_-\cdot q_-\cdot v_- \\ &= nq\mu V/c, \end{aligned} \tag{7}$$

where $q\equiv\sqrt{|q_+\cdot q_-|}$ and $v_\pm=\mu_\pm E=\mu_\pm V/c$.

Photoelectrophoresis with Macroscopic Convection Stream Field: As reported before,[8,10] the structure of convection showed a two-dimensional hexagonal lattice. In Fig. 2 intersections of solid lines are the lattice points with the lattice constant, a, and the hexagon given with broken lines is the Wigner-Seitz's unit cell. Vertices, A, B, C, D, E, F of the Wigner-Seitz's unit cell form a dual lattice. If the hexagonal lattice corresponds to the ascending flow, then its dual lattice corresponds to the descending flow of the fluid. The number of lattice points within the dual lattice is twice of that of original hexagonal lattice. Therefore, the ascending flow and the descending flow of the fluid are not symmetrical. This might be the result of the fact that the magnitude of charges carried by a positively charged particle and that by a negatively charged one are not equal. In a unit cell *ABCDEF*, the fluid flows up at the lattice point O, and spreading in the six directions, it falls downward at the boundary of this unit cell, that is, this flow is totally symmetric within this cell.

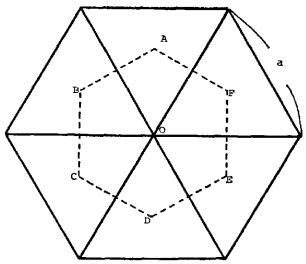

Fig. 2. Two-dimensional hexagonal lattice and the unit cell.
Intersections of real lines are the lattice points. The hexagon shown with dashed line is a Wigner-Seitz's unit cell.

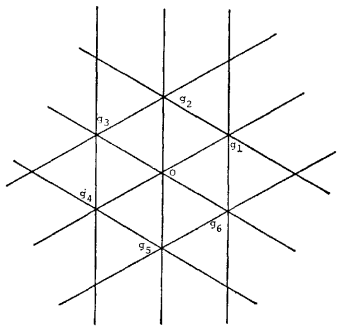

Fig. 3. Reciprocal lattice of convective structure.

We assume that the z-component, $v_z(\boldsymbol{r})$, of the hexagonal stream field, $\boldsymbol{v}(\boldsymbol{r})$, can be expressed as the following form,

$$v_z(x, y, z) = v\cdot f(x, y)\cdot g(z),$$

where v is a constant with the dimension of velocity. Then, $f(x,y)$ must satisfy a periodicity of the two-dimensional hexagonal lattice and $g(z)$ must satisfy a boundary condition at the electrode surfaces. The components of larger wavenumber in $f(x,y)$ will be unfavorable for a stationary state because they will make the larger velocity gradient in the bulk of liquid layer and increase the energy dissipation rate. Thus, taking account of the total symmetry of the flow, we assume that $f(x,y)$ is expressed by Eq. 8, which is constructed with six plane-wave whose wavenumbers are equal to the reciprocal lattice in Fig. 3, $\boldsymbol{g}_i$ ($i=$ 1, 2, 3, 4, 5, 6).

$$f(\boldsymbol{r}_1) = \frac{1}{6}\sum_{i=1}^{6}\exp(i\boldsymbol{g}_i\cdot\boldsymbol{r}_1), \tag{8}$$

where $\boldsymbol{r}_1\equiv(x,y)$ and the factor, 1/6, is a normalization constant making $f(x,y)$ unity at the lattice points. The length of the shortest reciprocal lattice vectors are $g=4\pi/\sqrt{3}a$. Figure 4a illustrates the profile of the function, $f(x,y)$.

With the continuity condition of incompressible fluid flow,

$$\operatorname{div}\boldsymbol{v} = 0, \tag{9}$$

and the relation

$$\left(\boldsymbol{\nabla}_1^2+\frac{4}{3}a^{*2}\right)f = 0, \tag{10}$$

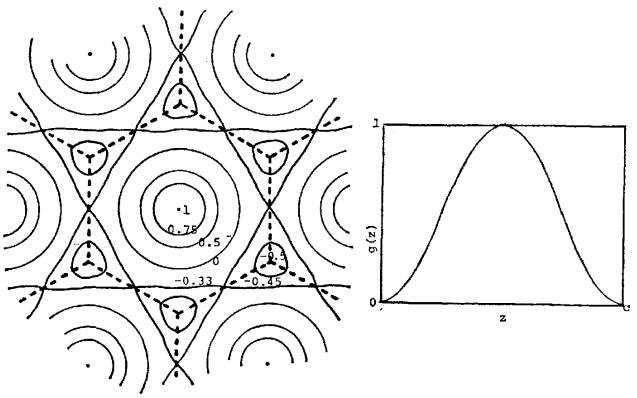

(a) (b)

Fig. 4. Profiles of functions, $f(x,y)$: (a) and $g(z)$: (b).

where $\nabla_1 \equiv \left(\frac{\partial}{\partial x}, \frac{\partial}{\partial y}\right)$ and $a^* \equiv 2\pi/a$, one can obtain the stream field as

$$v_x(x,y,z) = \frac{3}{4}\frac{1}{a^{*2}} v \frac{\partial f(x,y)}{\partial x}\frac{dg(z)}{dz},$$
$$v_y(x,y,z) = \frac{3}{4}\frac{1}{a^{*2}} v \frac{\partial f(x,y)}{\partial y}\frac{dg(z)}{dz}, \qquad (11)$$

and

$$v_z(x,y,z) = v \cdot f(x,y) \cdot g(z).$$

The function, $g(z)$, must be chosen to satisfy the boundary condition, $v_x = v_y = v_z = 0$, at the electrode surfaces ($z=0$, c), so we assume that $g(z)$ has the form as Eq. 12, which satisfies the above conditions with the smallest wave number.

$$g(z) = \frac{1}{2}(1-\cos(c^* z)) \qquad (c^* \equiv 2\pi/c), \qquad (12)$$

where the factor, 1/2, is a normalization constant making $g(z)$ unity at $z=c/2$. The function $g(z)$ is illustrated in Fig. 4b.

Thus, the Eq. 11, together with Eqs. 8 and 12, give the stream field of two-dimensional hexagonal convective domain with the thickness c and the lattice constant a.

Dissipation Function: We assume that TiO_2 particles move on the stream of fluid, then an energy dissipation by the friction between the particles and the fluid will be neglected compared with that within the fluids. The amount of heat generated in a unit volume and a unit time at any point in the fluid is given by the viscous dissipation function,

$$\Phi(x,y,z) = \frac{1}{2}\eta \sum_{i,j}\left(\frac{\partial v_i}{\partial x_j} + \frac{\partial v_j}{\partial x_i}\right)^2. \qquad (13)$$

Substituting Eq. 11 into v_i in Eq. 13, one obtains

$$\Phi(x,y,z) = \eta v^2\left[\left\{4f^2 + \frac{9}{4}\frac{1}{a^{*2}}\left(\left(\frac{\partial^2 f}{\partial x \partial y}\right)^2 - \frac{\partial^2 f}{\partial x^2}\frac{\partial^2 f}{\partial x^2}\right)\right\}\left(\frac{dg}{dz}\right)^2 + \left\{\left(\frac{\partial f}{\partial x}\right)^2 + \left(\frac{\partial f}{\partial y}\right)^2\right\}\left(g + \frac{3}{4}\frac{1}{a^{*2}}\frac{d^2 g}{dz^2}\right)^2\right]. \qquad (14)$$

Substituting Eqs. 8 and 12 into Eq. 14 and integrating it over a unit cell, then dividing the result by the unit cell volume, $(\sqrt{3}/2)a^2 c$, we obtain the mean viscous dissipation function, $\langle\Phi\rangle$,

$$\langle\Phi\rangle = \int_{\text{unit cell}} \Phi(x,y,z) v / \frac{\sqrt{3}}{2} a^2 c$$
$$= \eta\left(\frac{v^2}{c^2}\right)\frac{\pi^2}{16}\left[\frac{a^2}{c^2} + \frac{16}{3}\frac{c^2}{a^2} + 8\right]$$
$$= \eta\frac{v^2}{c^2}\pi^2\left[\frac{1}{3}\gamma^2 + \frac{1}{16}\gamma^{-2} + \frac{1}{2}\right], \qquad (15)$$

where $\gamma = c/a$ is the axial ratio of this stream.

Lattice Constant: The stream field, v_x, v_y, v_z, contains the lattice constant, a, as a parameter, since $f(x,y)$ must satisfy the hexagonal symmetry. Consequently, the parameter, a, also appears in the expression of the mean dissipation function, $\langle\Phi\rangle$. In Fig. 5, the variation of $\langle\Phi\rangle$ corresponding to the virtual variation of the parameter is illustrated. Figure 5 will be interpreted as follows: Under a condition in which the lattice constant is smaller enough than the distance between the two electrodes, *i.e.* the thickness of the suspension layer, c, a large velocity gradient of v_z would occur in the xy-plane, making a large energy dissipation (Fig. 6a). On the other hand, larger enough value of the lattice constant compared with c also increases the dissipation, because the region of fluid transport along the direction perpendicular to the z axis increases and the directions of the flow in the upper and lower parts this region are opposite to each other, so the region where a gradient of v_x and that of v_y along z axis are large becomes wider (Fig. 6c). Consequently a lattice constant of the same order as the thickness of the liquid layer would be most favorable for the smallest dissipation rate of energy (Fig. 6b). We do not have any *a priori* principle to determine the stationary state under a given condition thermodynamically. However, if we assume that the principle of the minimum energy dissipation which

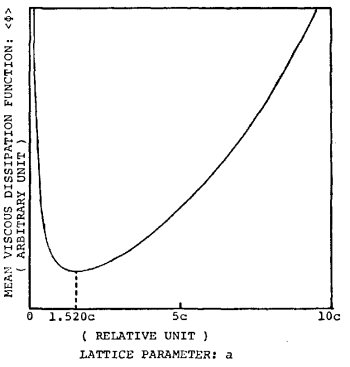

Fig. 5. Variation of $\langle\Phi\rangle$ corresponding to the variation of lattice parameter, a.

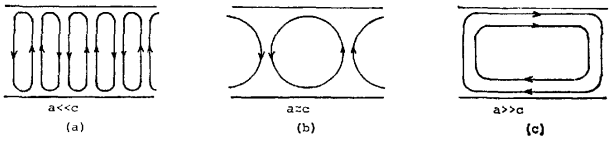

Fig. 6. Illustration of the shapes of cellular convective flows.
(a): Lattice constant, a, is smaller than the electrode spacing, c, (b): a is nearly equal to c, (c): a is larger than c.

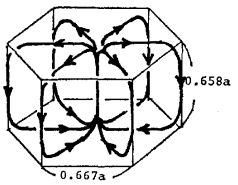

Fig. 7. Most favorable structure of convection.

has been known to be applied close to equilibrium also holds at the stationary state where a dissipative structure has been formed, the most favorable lattice constant can be estimated from Eq. 15 as

$$a = 2 \times 3^{-1/4}c \approx 1.520c. \tag{16}$$

Thus the lattice constant is proportional to the thickness of the liquid layer. The axial ratio of the stream, γ, is given as $\gamma=0.658$ (Fig. 7). The experimental values of γ was 0.86 as reported in the previous paper, which was larger than the theoretical value to some extent. The mean viscous dissipation function at $a=1.520c$ is given as

$$\langle \Phi \rangle = \eta \frac{v^2}{c^2} \frac{\pi^2}{2}\left(1+\frac{1}{\sqrt{3}}\right). \tag{17}$$

Electric Current by Convection: Assuming that TiO_2 particles are moving on the convection stream of the surrounding fluid, their velocity coincides with that of convection of the fluid, $\boldsymbol{v}(\boldsymbol{r})$.

From the continuity equation of the flow in a stationary state, div $\boldsymbol{v}=0$, and that of the TiO_2 particles flow, $\mathrm{div}(n\boldsymbol{v})=0$, we obtain

$$\frac{dn}{dt} = \boldsymbol{v}\cdot\mathrm{grad}\, n = \mathrm{div}(n\boldsymbol{v}) - n\cdot\mathrm{div}\,\boldsymbol{v} = 0. \tag{18}$$

Thus, in a stationary state, there is no change in the particle number density along a stream line. Therefore, there is also no change in the charge density along the stream line. More correctly, since the particles can discharge at the electrodes, there are two regions in a unit cell in each of which v_z is positive or negative, and the charge density along a stream line is kept constant within each region.

The mean number density of TiO_2 particles, n, in the present system was 1.2×10^{11} (cm^{-3}),[9] so if each of them have a positive charge ($q_+=3500e$) and are distributed uniformly in the xy-plane, the charge density on a unit area of a electrode, σ_p, is $3.15\times10^{12}e$ (cm^{-2}). The surface charge induced on an electrode by the application of external voltage, σ_e, is $\varepsilon V/c$, where ε is the dielectric constant of the fluid. In the present case we assume $\varepsilon=3\varepsilon_0$, where ε_0 is the dielectric constant of vaccum. Then, when an external voltage of 100 V is applied between the electrodes, the value of σ_e is $2.25\times10^{10}e$ (cm^{-2}), thus σ_p is about 100 times as large as σ_e. When all the particles have a negative charge ($q_-=-660e$), the absolute value of σ_p is about 20 times as large as σ_e. If the discharge of the TiO_2 particles at the electrodes is a fast process, there exists positive charge in the region of positive v_z, while in the region of negative v_z, there exists negative charge. Thus, spatial separation of the positive charge and the negative charge

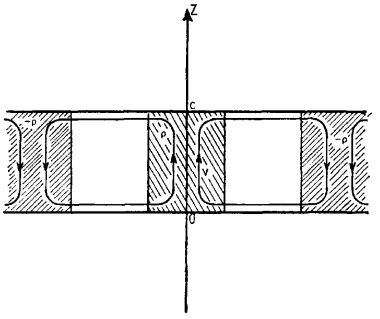

Fig. 8. Model of convective unit cell.

takes place in the periodical convective state, while there is no space charge in the static state without convection. However, the absolute value of the charge density per unit area of the electrode in each region does not exceed σ_e, since, for instance in the region of positive v_z, the increase of the positive charge density reduces the potential gradient near the anode and prevents the discharge of negatively charged particles at the anode, consequently too much increase of the positively charged particles in the region is suppressed. Electric current under this condition is just a space charge limited one. The situation is same in the region of negative v_z.

From the consideration mentioned above, together with Eq. 18, we assume a simple model for such a unit convective cell as shown in Fig. 8. It is assumed that the unit cell can be separated into three regions; the first one is the region in which the positively charged particles are distributed uniformly with the charge density, $+\rho$, and the fluid flows upward. The second region whose cross section area is equal to that of the first one, is that in which the negatively charged particles are distributed uniformely $(-\rho)$ and the fluid falls downward, and the third region between the above two regions is that in which no charge density and no fluid motion exist. The velocity of fluid is v in the first and $-v$ in the second region. From Poisson's equation, we obtain

$$\rho \approx \frac{2\varepsilon V}{c^2}, \tag{19}$$

where V is the applied voltage. The profile of the electric field in the suspension layer along z axis is given as follows:

$$E_1(z) \approx \frac{\rho}{\varepsilon} z \text{ (in the region of positive charge)}, \tag{20}$$

$$E_2(z) \approx \frac{\rho}{\varepsilon}(c-z) \text{ (in the region of negative charge)}. \tag{21}$$

Then we obtain the force by the external field acting on the fluid in the stream tube of a unit cell along a stream line as

$$F \approx \frac{1}{2}S_e\int_0^c \rho E_1(z)dz - \frac{1}{2}S_e\int_0^c (-\rho)E_2(z)dz = 2S_e\varepsilon V^2/c^2, \tag{22a}$$

where S_e is a sum of the cross section area of the first

and the second regions, *i.e.* S_e corresponds to the conducting area in a unit cell. If we assume that S_e is approximately equal to a half of the total cross section area of a unit cell, $S_e=c^2$, we obtain

$$F \approx 2\varepsilon V^2. \tag{22b}$$

Therefore, a work done by the external electric field on the fluid in a unit cell and a unit time is given as

$$W_e = v \cdot F \approx 2v\varepsilon V^2. \tag{23}$$

On the other hand, the energy dissipation within a unit cell and a unit time is written as

$$W_t = 2c^3\langle\Phi\rangle = \pi^2\left(1+\frac{1}{\sqrt{3}}\right)\eta v^2 c, \tag{24}$$

where $2c^3$ is the volume of a unit cell. Since W_e and W_t are equal to each other in the steady state, we obtain the following expression for v by equating Eq. 23 to Eq. 24,

$$v \approx \frac{2}{\pi^2\left(1+\frac{1}{\sqrt{3}}\right)}\frac{\varepsilon V^2}{\eta c} = 0.128\frac{\varepsilon V^2}{\eta c}. \tag{25}$$

One can see in Eq. 25 that v is proportional to the square of the applied voltage. Consequently, the average current density, $\langle i\rangle$, is proportional to V^3:

$$\langle i\rangle \approx \frac{1}{2}\rho v = 0.128\frac{\varepsilon^2 V^3}{\eta c^3}. \tag{26}$$

Transition from the Static State of Fluid to Convective State. When a d.c. voltage is supplied to the TiO_2 particles dispersion system under illumination, migration of the particles transports electric charge between the electrodes in the nonconvective state. The charge transport in this state occurs against the friction between TiO_2 particles and their surrounding insulating fluid, and the current is proportional to the applied voltage as shown in Eq. 7. On the other hand, TiO_2 particles are carried by a flow of fluid in the convective state. In other words, electric charge is transported by a flow of charged fluid between two electrodes. The charge transport in this state occurs against the friction within the fluid. The current in that state is proportional to the cube of the applied voltage as shown in Eq. 26. The two kinds of currents in the both states are illustrated in Fig. 9 as a function of the applied voltage. In the region of lower voltage than V_c, which is the voltage at which two i-V curves in Fig. 9 cross each other, the static state is more favorable than the convective state for electric conduction. On the other hand, in the region of higher voltage than V_c, the state with the convection becomes more favorable. Consequently, a transition between the two states occurs at the critical voltage, V_c. From Eqs. 7 and 26, the critical voltage, V_c is given as

$$V_c \approx 2.8\frac{\sqrt{nq\mu\eta}}{\varepsilon}c. \tag{27}$$

As mentioned in the experimental section of the previous paper,[9,10] $n=1.2\times10^{11}$ cm^{-3}, $q=1520e$, $\mu=1.72\times10^{-5}$ cm^2/V s, $\eta=7.5$ cP, $c=50$—100 μm, $\varepsilon=3\varepsilon_0$. When $c=75$ μm, we estimate $V_c\approx153$ V. The experimental value of the critical voltage[10] was about 200 V which is in good agreement with the theoretical value. A dimensionless parameter indicating the transition between the states is given from Eq. 27 as

$$R_1 = \frac{\varepsilon^2 V^2}{nq\mu\eta c^2}. \tag{28}$$

From the above consideration we may expect that the transition occurs at $R_1\approx8$.

Electrohydrodynamic Instability in the Case of Unipolar Injection. The injection of carriers of one kind and one sign is called as "unipolar injection." In such a case a space charge limited conduction may occur even in the static fluid state if the amount of the injected carriers is large enough (Fig. 10a). Such a case was analyzed by Schneider and Watson[6] and Atten and Moreau,[12] by solving a set of equations which express the turbulance in fluid in the system. However, our method mentioned above is also adequate for such a case and can give a reasonable explanation.

In the space charge limited conductive state without convection, if the charge carriers are of one kind with mobility μ, the current in such a state is given by the Langmuir-Child's law,[13]

$$i = \frac{9}{8}\frac{\varepsilon\mu}{c^3}V^2. \tag{29}$$

Now we consider the current carried by a convective flow in the case of the unipolar injection. We assume tentatively that the carriers are cations. If all the cations which flow up toward the cathode do not discharge as the cathode surface completely, a portion of the cations will remain in the flow toward the anode. When the probability of discharge of cations on the cathode is κ, the charge density in the downward flow is given as $\rho'=(1-\kappa)\rho$, where ρ is the charge

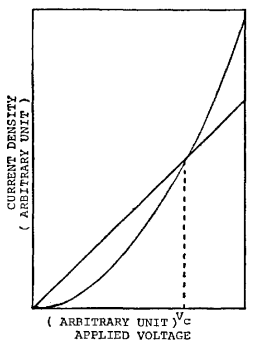

Fig. 9. Current-voltage curves by two state of conduction in bipolar injection.
A transition between two states occurs at the critical voltage, V_c.

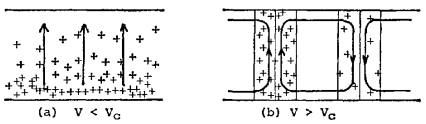

Fig.10. Current-voltage curves by two states of conduction in unipolar injection.
A transition between two states occurs at the critical voltage, V_c.

density in the upward flow, *i.e.* $\rho \approx 2\varepsilon V/c^2$ (see Fig. 10b). And the force acting on the region of upward flow along a stream line in a unit cell, F_1, is given in the same manner as Eq. 22,

$$F_1 \approx \varepsilon V^2.$$

Similarly, the force acting on the region of downward flow along a stream line, F_2, is given as

$$F_2 \approx -(1-\kappa)\varepsilon V^2.$$

Then, the work exerted on a unit cell within a unit time, W_e, is

$$W_e = v(F_1+F_2) \approx \kappa v \varepsilon V^2. \tag{30}$$

Using Eqs. 24 and 30, we obtain the expression for the flow velocity, v, as

$$v \approx \frac{\kappa}{\pi^2\left(1+\frac{1}{\sqrt{3}}\right)}\frac{\varepsilon V^2}{\eta c} = 0.064\kappa\frac{\varepsilon V^2}{\eta c}. \tag{31}$$

Therefore, the average current density, $\langle i \rangle$, is given as

$$\langle i \rangle \approx \frac{1}{4}\kappa\rho v \approx 0.032\kappa^2\frac{\varepsilon^2 V^3}{\eta c^3}. \tag{32}$$

One can see from Eqs. 29 and 32 that the space charge limited current without convection is proportional to the square of the applied voltage but, on the other hand, the current by the convection is proportional to the cube of the voltage. Current densities in the both conduction regimes are illustrated in Fig. 11 which shows that, in the region of the lower voltage, the static state without convection is more favorable for the electric conduction, and in the region of the higher voltage, the convective state is more favorable. The critical voltage, V_c, at which the transition between the two states occurs is given by comparing Eqs. 29 and 32,

$$V_c \approx \frac{27.8}{\kappa^2}\frac{\eta\mu}{\varepsilon}. \tag{33}$$

A dimensionless parameter indicating the transition is given by Eq. 33 as

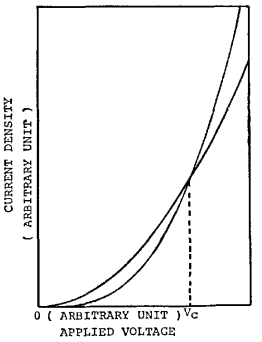

Fig.11. Current voltage curves in the two conduction regimes under unipolar injection.
A transition occurs at the critical voltage, V_c.

$$R_2 = \frac{\varepsilon V}{\eta\mu}. \tag{34}$$

The dimensionless parameter, R_2, coincides with one derived by Schneider and Watson[6] as the criterion of the stability. The transition is expected to occur at $R_2 \approx 27.8/\kappa^2$, while Schneider and Watson calculated the value of R_2 as 99[6] although their boundary condition is somewhat different from the present case.

References

1) H. Bénard, *Rev. Gen. Sci. Pure Appl.*, **11**, 1261 (1900); *Ann. Chim. Phys.*, **23**, 62 (1901).
2) L. Rayleigh, *Philos. Mag.*, **32**, 529 (1916).
3) A. Pellow and R. V. Southwell, *Proc. R. Soc. London, Ser. A*, **176**, 312 (1940).
4) M. J. Block, *Nature*, **178**, 650 (1956).
5) N. Félici, *Revue General de l'Electricite*, **78**, 717 (1969).
6) J. M. Schneider and P. K. Watson, *Phys. Fluids*, **13**, 1948 (1970).
7) S. Chandrasekhar, "Hydrodynamic and Hydromagnetic Stability," Oxford University Press, New York (1961).
8) Y. Toyoshima, A. Takahashi, H. Nozaki, T. Iida, and M. Sukigara, *Photogr. Sci. Eng.*, **21**, 29 (1977).
9) Y. Aikawa, A. Takahashi, H. Shimoda, and M. Sukigara, *Denki Kagaku*, **50**, 167 (1982).
10) Y. Aikawa, A. Takahashi, and M. Sukigara, *J. Colloid Interface Sci.*, in press.
11) Y. Aikawa and M. Sukigara, *Chem. Lett.*, **1981**, 381.
12) P. Atten and R. Moreau, *C. R. Acad. Sci. Paris*, **269A**, 433 (1969); *J. Mecan.*, **11**, 471 (1972).
13) N. F. Mott and R. W. Gurney, "Electronic Processes in Ionic Crystals," Oxford University Press, New York (1940).

Electrolytic Reduction of Carbon Dioxide at Mercury Electrode in Aqueous Solution

Yoshio Hori* and Shin Suzuki

Department of Synthetic Chemistry, Faculty of Engineering, Chiba University, Yayoi-cho, Chiba 260

(Received June 22, 1981)

Cathodic reduction of carbon dioxide at a mercury pool electrode was investigated in aqueous solutions of $NaHCO_3$, NaH_2PO_4–Na_2HPO_4, NaCl, $NaClO_4$, Na_2SO_4, $LiHCO_3$, and $KHCO_3$ as well as their combinations. The reaction product was confirmed to be $HCOO^-$ by a qualitative spot test. $HCOO^-$ was quantitatively analyzed by a permanganate titration. The partial current densities of $HCOO^-$ formation (i_C) and H_2 evolution (i_H) were calculated. In the present paper, relationships between electrode behavior and solution properties, some of which have been qualitatively described in previous papers, are quantitatively clarified as follows. The electrode potential E_C for constant i_C (0.5 mA/cm^2) remains constant irrespective of pH and anions in the pH region of 2.4 to 7.8, whereas the potential E_H for constant i_H (0.5 mA/cm^2) varies linearly with a slope of 125 mV/pH. The present experimental results verify Eyring *et al.*'s presumption that in a relatively high overvoltage region (region 2) the cathodic reduction of CO_2 at Hg proceeds with the charge transfer to CO_2 as the rate determining step. CO_2 reduction and H_2 evolution are concluded to proceed independently at the Hg electrode. The dependence of E_C on electrolyte concentration is interpreted in terms of the diffuse double layer theory. The effect of cation species on E_C also is discussed.

Carbon dioxide has been suggested to be feasible as an energy storage medium by Russell *et al.*[1] and Williams *et al.*[2] Carbon dioxide is electrolytically reduced to methanol or formic acid, which in turn can be fed to a fuel cell or a decomposer to generate hydrogen. This process is superior to the hydrogen energy system, since the transport and storage of these liquid fuels are more convenient and less expensive than hydrogen. In addition to the advantage of energy storage, this process will contribute to fixation of carbon dioxide and prevent the recent increase of atmospheric concentration of carbon dioxide.

The electrolytic reduction of carbon dioxide in aqueous solution has been reported by many authors.[1–11] The principal difficulty of this process appear to be high overvoltage and low current efficiency. Excellent electrocatalysts are consequently requisite for the development of this process. However, the overvoltage and current efficiency depend upon properties of electrolytic solutions as well as electrodes.

Udupa *et al.*[6] studied cathodic reduction of CO_2 at a rotating amalgamated copper electrode in aqueous solutions. They reported that the current efficiency increased in the presence of sodium hydrogencarbonate in the solution as compared with the reaction in the solution containing sodium sulfate alone. Paik *et al.*[5] and Ryu *et al.*[7] studied pH effect on the reaction at Hg. They reported that the current efficiency tends to decrease with increasing acidity of the solution because of the competition with hydrogen evolution. Ito *et al.*[10] studied the reaction at various metal cathodes in several aqueous solutions. According to Ito *et al.*, the current efficiency at In electrode increased in alkali metal carbonate solutions with the sequence of Rb^+, K^+, Na^+, and Li^+, whereas the current efficiency increased with the sequence of PO_4^{2-}, SO_4^{2-}, and CO_3^{2-} in lithium salt solutions.

In these previous papers, effects of pH and species of electrolytes on the electrode reactions of CO_2 reduction and H_2 evolution were only qualitatively reported. In the present paper, they are quantitatively investigated at a mercury electrode which has a smooth and reproducible surface. The results obtained will contribute to the investigation of the electrocatalysis and reaction mechanism.

Experimental

Apparatus and Procedures. The experiments were carried out in a Pyrex H-type cell immersed in a thermostat maintained at 25 °C. The cathode and anode compartments were separated by a sheet of cation exchange membrane (Selemion) donated by Asahi Glass Co., Ltd. The cathode consisted of a pool of purified mercury (4.9 cm^2) which was electrically connected by a Pt wire lead. The anode was a Pt sheet. The potential of the cathode was measured with respect to an Ag/AgCl electrode at room temperature (20±1 °C), which was connected to the cathode by a Pyrex Luggin tube.

The galvanostatic electrolysis measurements were carried out for 15 to 100 min (depending on the current density), by a potentiogalvanostat (Model 2020) manufactured by Toho Giken Co., Ltd. The electrode potential was measured and recorded by a Yokokawa digital voltmeter (Model 2502) and recorder (Model 3066).

The product resulting from the reduction of CO_2 was qualitatively tested by the chromotropic acid test.[12] The solutions in the cell were quantitatively analysed for their $HCOO^-$ content by the permanganate titration technique. pH of the solution was measured before and after electrolysis; the difference between the two pH values was within 0.2.

Materials and Solutions. Commercial reagent grade mercury was washed with 2 M HNO_3,† distilled and again washed with 2 M HNO_3. The mercury thus purified was used as the cathode.

The electrolytes used were aqueous solutions of $NaHCO_3$, Na_2HPO_4–NaH_2PO_4, NaCl, Na_2SO_4, $NaClO_4$, H_3PO_4, and their combinations. The reagents except $NaClO_4$ and H_3PO_4 were triply recrystallized from reagent grade chemicals. The solutions were prepared from distilled water treated with active charcoal and ion exchange resin. The solutions used are tabulated in Table 1.

Commercial nitrogen and CO_2 were purified by passing them through columns of activated copper and wash bottles

† 1 M=1 mol dm^{-3}.

containing aqueous solution of $KHCO_3$. The gases were then introduced to the electrolytic cell and bubbled through the solution under the atmospheric pressure.

Results

Reaction Products and Current Efficiency. The pH-potential diagram was constructed for the system CO_2–water at 25 °C on the basis of the thermochemical data.[13] (Fig. 1) The substances considered in Fig. 1 are CO_2, HCO_3^-, CO_3^{2-}, HCOOH, and $HCOO^-$, the activities of which are taken to be unity.

The product resulting from the electrolytic reduction of CO_2 was confirmed to be formic acid in all the solutions by the chromotropic acid test, which agrees with the previous reports.[1,3,5,7,8] CO_2 stably exists in aqueous media of pH less than 8 (Fig. 1). The equilibrium potential of CO_2 reduction is more cathodic in the lower pH range than that of the competitive reaction of H_2 evolution. Therefore, the reduction of CO_2 would effectively proceed between 7 and 8 of pH.†† Figure 1 shows also $HCOO^-$ to be formed predominantly instead of HCOOH in the solution of pH above 3.7.

The activity of hydrogencarbonate ion $[HCO_3^-]$ is related to the pH value in equilibrium with CO_2 at 1 atm:†††

$$pH = pK_a + \log[HCO_3^-], \quad (1)$$

$$pK_a = 7.82 \ (25\ °C).$$

The pH of phosphoric buffer solution will alter from the value originally prepared with formation of HCO_3^-, according to Eq. 2, if CO_2 is in contact with the solution:

$$HPO_4^{2-} + CO_2 + H_2O = H_2PO_4^- + HCO_3^-. \quad (2)$$

The pH is determined by the following reactions

$$H_2PO_4^- = HPO_4^{2-} + H^+, \quad (3)$$

$$CO_2 + H_2O = HCO_3^- + H^+. \quad (4)$$

The equilibrium concentrations of respective ions are readily calculated in accordance with Eqs. 3 and 4 and corresponding pK_a values; the equilibrium concentrations thus obtained are given in Table 1.

The results of the permanganate titration are to give the values of the current efficiency and the partial current i_C of $HCOO^-$ formation. The experimental current efficiencies are presented as a function of pH in Fig. 2. The trend in Fig. 2 qualitatively agrees with the thermodynamic considerations.

Partial Current of CO_2 Reduction. The limiting current of CO_2 reduction would be approximately 7—10 mA/cm^2,[15] and the present experiments were made under the condition where the partial current density of CO_2 reduction did not exceed 1.5 mA/cm^2.

The electrode potential of cathode remained constant within 2 to 3 mV in every run during the steady state galvanostatic electrolysis of carbon dioxide. The measured potential did not vary by more than 10 mV on different runs in solutions of identical compositions. Each partial current i_C of $HCOO^-$ formation may include an error of up to 2% due to the inaccuracy of the titration technique. The partial current i_H of H_2 evolution was estimated as the difference between the total electrolytic current i and i_C. i, i_C, and i_H are plotted against the electrode potential E (referred to SHE) for the phosphate buffer solution of pH=5.7 (Fig. 3), the composition of which is shown in Table 1. Figure 3 contains also the data obtained in ternary electrolytes consisting of NaCl, $NaClO_4$, or Na_2SO_4 solution mixed with phosphate buffer (NaH_2PO_4–Na_2HPO_4) (pH=5.5). These data for ternary electrolytes were corrected for pH values and zeta potential as described later.

The results for all the solutions showed that the Tafel relationship holds as exemplified in Fig. 3. The values of transfer coefficient α are 0.26—0.28 for CO_2 reduction and 0.41—0.45 for H_2 evolution in the solutions of pH below 6. Thus, the potentials E_C and E_H can be determined at a constant partial current

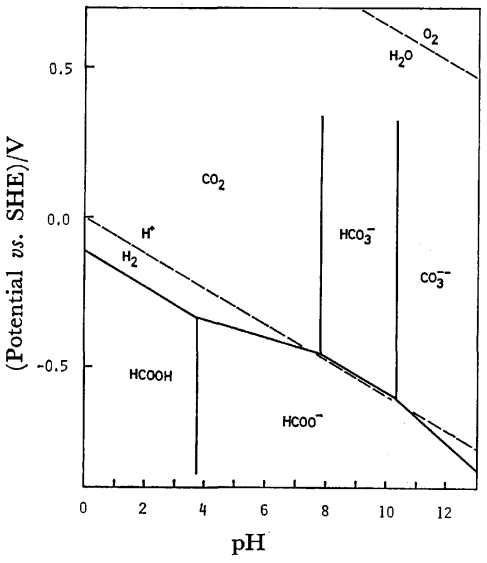

Fig. 1. pH-potential diagram of CO_2 and its related compounds.
pH-potential relations for water are shown in broken lines.

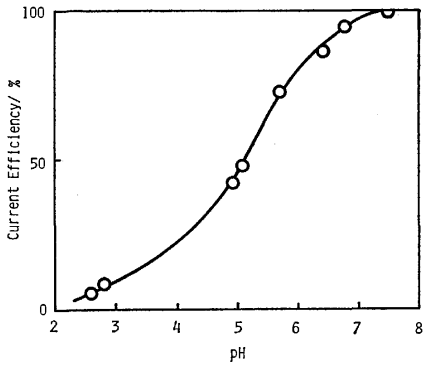

Fig. 2. Current efficiency of CO_2 reduction plotted against pH at constant total current 1 mA cm^{-2}.

†† Iwahara *et al.*[14] recently reported that HCO_3^- was electrolytically reduced on Hg without bubbling CO_2. Their observation contradicts with van Rysselberghe *et al.*'s;[3] the details of this reaction still remain unclarified.

††† 1 atm=1.013×10^5 Pa.

Table 1. Equilibrium composition of aqueous electrolyte solutions

Electrolyte	pH	Total cation concentration/M	Equilibrium composition of electrolyte solution/M							Correction ζ/mV
			H_3PO_4	NaH_2PO_4	Na_2HPO_4	$NaHCO_3$	NaCl	$NaClO_4$	Na_2SO_4	
Phosphate buffer	2.48	0.50	0.16	0.34						15
	2.78	0.50	0.095	0.41						15
	4.86	0.50		0.49	0.0023	0.0011				15
	5.00	0.29		0.28	0.0035	0.0013				1
	5.74	0.26		0.21	0.022	0.010				−1
	6.72	0.29		0.076	0.060	0.076				0
Phosphate-Cl^-	5.48	0.63		0.10	0.0089	0.0084	0.50			21
Phosphate-ClO_4^-	5.47	0.64		0.11	0.012	0.0098		0.50		22
Phosphate-SO_4^{2-}	5.54	0.63		0.11	0.010	0.0091			0.246	21
HCO_3^-	6.57 −7.89	0.056 −1.20				0.056 −1.20				
$HCO_3^-+Cl^-$	6.50 −7.80	1.20				0.050 −1.00	1.15 −0.20			
$HCO_3^-+ClO_4^-$	7.04 −7.86	1.20				0.22 −0.43		0.98 −0.77		
$HCO_3^-+SO_4^{2-}$	6.62 −7.31	1.20				0.10 −0·38			0.55 −0.41	

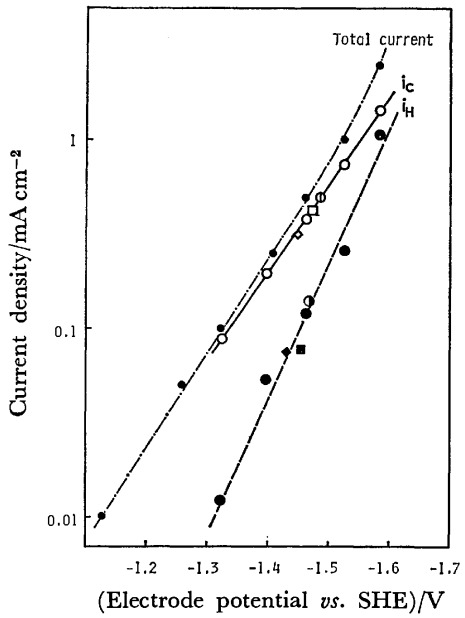

Fig. 3. Current density *vs.* electrode potential (SHE) for cathodic reduction of CO_2 at Hg in aqueous solutions (pH=5.7).
i_C: Partial current of CO_2 reduction, i_H: partial current of H_2 evolution.
Symbols: phosphate buffer; i_C ○, i_H ●, phosphate-Cl^-; i_C ◑, i_H ◑, phosphate-ClO_4^-; i_C ◇, i_H ◆, phosphate-SO_4^{2-}; i_C □, i_H ■.
ζ is corrected with reference to 0.274 M solution of 1-1 electrolyte.

i_C and i_H from the Tafel relationship like Fig. 3.

pH Dependence of Electrode Potentials E_C and E_H. The values of E_C thus obtained at the partial current 0.5 mA/cm² are plotted against pH in Fig. 4. The variation of ζ potential was corrected as mentioned later. E_C values obviously stay constant irrespective

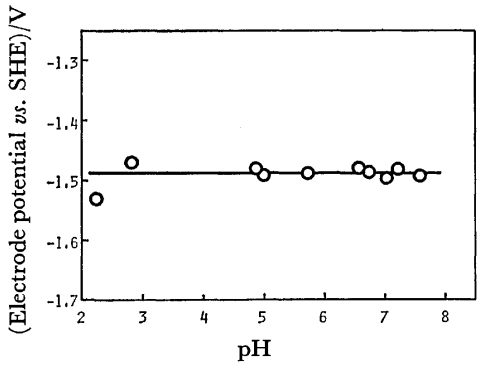

Fig. 4. Electrode potential E_C for CO_2 reduction at i_C=0.5 mA/cm² plotted against pH.

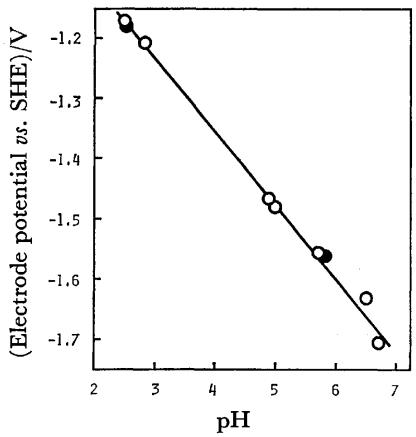

Fig. 5. Electrode potential E_H for H_2 evolution at i_H= 0.5 mA/cm² plotted against pH.
○: E_H observed during CO_2 cathodic reduction,
●: E_H observed under N_2 flow.

of pH. Figure 5 presents the relationship between E_H and pH. The current-potential measurements for hydrogen evolution at Hg under a N_2 flow give the electrode potentials at 0.5 mA/cm², which also are

shown in Fig. 5, falling on the line. The slope is approximately 125 mV/pH. Therefore, the hydrogen evolution reaction, taking place simultaneously with CO_2 reduction, appears to proceed in the same way as in a N_2 flow.

Electrolytes and their Concentrations. The current efficiencies of $HCOO^-$ formation were 100% within the experimental error in the solutions containing $NaHCO_3$ and at pH above 6.6. The potentials E_C at a constant cathodic current density 0.5 mA/cm^2 are shown in Fig. 6 for various concentrations of $NaHCO_3$. E_C varies linearly with $NaHCO_3$ concentration, the slope being approximately 60 mV/decade. However, E_C at 0.5 mA/cm^2 is independent of $NaHCO_3$ concentration, where the total equivalent concentrations of electrolytes are kept constant at 1.2 equiv·dm^{-3} by adding NaCl, $NaClO_4$, or Na_2SO_4. pH in aqueous solution increases from 6.6 to 7.8 with increasing $NaHCO_3$ concentration from 0.05 to 1.2 M while the CO_2 pressure is kept 1 atm. E_C consequently depends upon the total concentration of electrolytes but not upon pH values.

Figure 7 shows the variation of E_C at 0.5 mA/cm^2 of CO_2 reduction with respect to the concentration of electrolytes $LiHCO_3$ and $KHCO_3$. The slopes are about 75 mV/decade and 66 mV/decade for $LiHCO_3$ and $KHCO_3$, respectively. They are close to the value for $NaHCO_3$. E_C for a constant concentration of the electrolyte appears to become remarkably nobler with the sequence of Li^+, Na^+, and K^+.

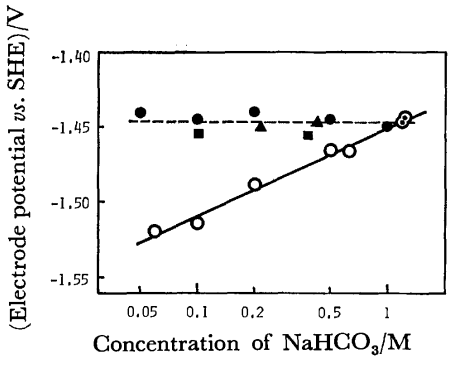

Fig. 6. Electrode potential E_C for CO_2 cathodic reduction in various concentrations of HCO_3^-.
○: Aqueous solution of $NaHCO_3$ alone, ●: mixed electrolyte $NaHCO_3$+NaCl, total equivalent concentration 1.2 mol dm^{-3}, ▲: mixed electrolyte $NaHCO_3$+$NaClO_4$, total equivalent concentration 1.2 mol dm^{-3}, ■: mixed electrolyte $NaHCO_3$+Na_2SO_4, total equivalent concentration 1.2 mol dm^{-3}.

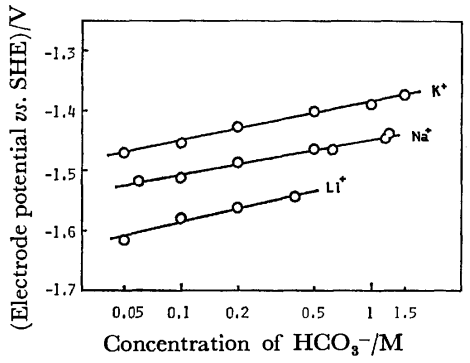

Fig. 7. Electrode potential E_C for CO_2 reduction in various concentrations of $LiHCO_3$, $NaHCO_3$, and $KHCO_3$.

Discussion

Reaction Mechanism and Electrode Potential. Paik *et al.*[5] and Ryu *et al.*[7] studied CO_2 reduction on mercury in neutral aqueous solution. They revealed that the feature of this reaction is the occurrence of two Tafel regions: one at low current densities (region 1) and the other at high current densities (region 2). The present measurements were made in the region 2. They presumed that the following reaction determines the rate of the reaction in region 2:

$$CO_2 + e^- \longrightarrow CO_2^- \text{ (ads)}$$

or

$$CO_2 + H_2O + e^- \longrightarrow HCO_2\cdot\text{(ads)} + OH^-. \quad (5)$$

If one of them is the rate determining step, the electrode potential will be written as follows:

$$E_C = -\frac{RT}{\alpha_C F}\cdot\ln|i| + \zeta + \text{const}, \quad (6)$$

where α_C is the transfer coefficient. This expression suggests that the electrode potential at a constant current will not depend upon pH, if ζ is kept constant. Since E_C obtained experimentally remains constant irrespective of pH (Figs. 4 and 6), the present results confirm Paik *et al.*'s and Ryu *et al.*'s presumptions in the pH region of 2.4 to 7.8.

The point of zero charge (pzc) for the mercury electrode without specific adsorption in aqueous media is about 0.4 to 0.5 V (referred to the normal calomel electrode),[16] and the potential region discussed in this paper is far below pzc. The bulk concentration of Na^+ is much higher than H^+. Na^+ will naturally predominate in the neighborhood of the electrode surface in the present experimental conditions. The surface of the mercury electrode will not significantly be covered with H or H_2, because the discharge of H^+ is considered to be the rate determining step of H_2 evolution. Thus the pH change will not practically affect the ionic distribution near the electrode surface. Accordingly, the CO_2 reduction process will proceed irrespective of pH.

The hydrogen evolution reaction proceeds at mercury in acidic to neutral aqueous media with the discharge of proton as the rate determining process:

$$H^+ + e^- \longrightarrow H. \quad (7)$$

The electrode potential will be expressed as[17]

$$E = -\frac{RT}{\alpha_H F}\cdot\ln|i| + \frac{RT}{\alpha_H F}\cdot\ln[H^+] - \frac{1-\alpha_H}{\alpha_H} + \text{const}$$
$$= -\frac{0.05916}{\alpha_H}\cdot\ln|i| - \frac{0.05916}{\alpha_H}\,\text{pH} - \frac{1-\alpha_H}{\alpha_H} + \text{const (25 °C)}. \quad (8)$$

The values of α_H are between 0.41 and 0.45 as determined from the Tafel plots in the present study. The dependence of E_H on pH with constant current and ζ is thus seen to be *ca.* 137 mV/pH at 25 °C from Eq. 8, which agrees approximately with a value of

125 mV/pH as estimated from the slope in Fig. 5, where CO_2 is simultaneously reduced. The hydrogen evolution process is apparently independent of the competitive CO_2 reduction. Aylmer-Kelly *et al.*[18] studied the intermediate species in the CO_2 cathodic reduction at mercury in aqueous media by means of reflectance spectroscopy. They reported that the coverage of the intermediate CO_2^- on mercury is approximately 0.02. Such a small value of coverage would not affect the hydrogen evolution reaction.

Thus, the two reactions, CO_2 reduction and H_2 evolution, proceed independently at the Hg electrode. The current efficiency of CO_2 reduction varies with pH (Fig. 2) as derived from the pH dependence of H_2 evolution.

Effects of Electrolyte. The zeta potential ζ at the outer Helmholtz plane for mercury and 1-1 electrolyte without specific adsorption varies approximately according to

$$\zeta = \text{const} \pm \frac{RT}{n_1 F} \cdot \ln C, \tag{9}$$

where n_1 and C are the charge number of ion and the bulk concentration of the electrolyte, respectively, and the $\pm$sign holds for $\zeta \gtrless 0$.[16] The above relationship was verified by Delahay for electrode potentials sufficiently positive or negative with respect to the pzc. The pzc for mercury in aqueous media without specific adsorption is about 0.4 to 0.5 V (referred to the normal calomel electrode),[16] and E_C at i_C 0.5 mA/cm^2 is about -1.5 V (referred to SHE) as shown in Fig. 4; Eq. 9 would be applicable to the present experimental situations.

With Eq. 9 inserted into Eq. 6, the electrode potential E_C at constant current is expected to vary with the logarithm of electrolyte concentration with a slope of 0.05916 V/decade at 25 °C. This value is in good agreement with the experimentally observed one as described for $NaHCO_3$ (Fig. 6).

All the electrolysis experiments were not carried out at the same electrolyte concentration; the corrections of ζ were made for different concentrations as mentioned in the previous sections. The correction was made for 1-1 electrolyte according to Eq. 9 with the reference concentration of 0.274 M arbitrarily chosen. The corrections for electrolytes other than 1-1 ones were calculated according to the manner as described in Appendix. Tafel relationship illustrated in Fig. 3 (pH 5.7) contains experimental values for phosphate buffer solutions mixed with NaCl, $NaClO_4$, or Na_2SO_4 after appropriate corrections. The partial current i_H is corrected not only for ζ potential according to Eqs. 9 and 13 but for pH difference, because the electrolyses in phosphate buffer solution mixed with NaCl, $NaClO_4$, or Na_2SO_4 were carried out at pH$\approx$5.5. These data for i_C and i_H fall on the respective lines representing experimental values in phosphate buffer solution without other electrolytes.

Since the electrode potential is far below pzc, anions will hardly affect the structure of the Helmholtz layer of the electrode, if these anions are not specifically adsorbed. The present study confirms this expectation, since any anions employed make no difference in either CO_2 reduction or H_2 evolution (Figs. 3—6).

As pointed out previously, the electrode potential E_C varies to noble values with the sequence Li^+ to Na^+ to K^+. It will qualitatively result from the increasingly specific adsorption of the larger cations, and ζ will become more positive.

The authors would like to thank Mr. Nobuyuki Nakajima for his assistance in part of experiments.

Appendix

The correction of ζ for electrolytes other than 1-1 followed the derivation of Eq. 9 for 1-1 electrolytes given by Delahay.[16] According to the Gouy-Chapman theory of the diffuse double layer, the charge q on the electrode per unit area is deduced as

$$q = \pm\left[\frac{RT\varepsilon}{2\pi} \cdot \Sigma C_i^s \left\{\exp\left(-\frac{n_i F}{RT} \cdot \zeta\right) - 1\right\}\right]^{1/2}, \tag{10}$$

where ε is dielectric constant, and C_i^s and n_i are the bulk concentration of solution and the ionic valence (with sign) of ion i, respectively.

The correction of ζ is exemplified below for an aqueous solution consisting of xM NaH_2PO_4, yM Na_2HPO_4, and zM $NaHCO_3$. The concentrations of each ionic species are tabulated in Table 2. Insertion of these values into Eq. 10 will give

$$\frac{2\pi}{RT} \cdot \frac{q^2}{\varepsilon} = (x+2y+z) \cdot \exp\left(-\frac{F}{RT} \cdot \zeta\right) + (x+z) \cdot \exp\left(\frac{F}{RT} \cdot \zeta\right) + y \cdot \exp\left(\frac{2F}{RT} \cdot \zeta\right) - (2x + 3y + 2z). \tag{11}$$

Then, for $\zeta < -0.1$ V which is applicable to the present case, the terms $\exp\left(\frac{F}{RT} \cdot \zeta\right)$ and $\exp\left(\frac{2F}{RT} \cdot \zeta\right)$ can be dropped. If q is considered to be independent of electrode potential E in the present narrow range of E, the following equation is obtained by differentiation:

$$\frac{F}{RT} \cdot \mathrm{d}\zeta = \frac{\mathrm{d}(x+2y+z)}{x+2y+z} - \frac{\mathrm{d}(2x+3y+2z)}{x+2y+z} \cdot \exp\left(\frac{F}{RT} \cdot \zeta\right). \tag{12}$$

When the variations $\Delta(x+2y+z)$ and $\Delta(2x+3y+2z)$ are small, Eq. 12 is written as

$$\frac{F}{RT} \cdot \Delta\zeta = \frac{\Delta(x+2y+z)}{x+2y+z} - \frac{\Delta(2x+3y+2z)}{x+2y+z} \cdot \exp\left(\frac{F}{RT} \cdot \zeta\right). \tag{13}$$

Table 2. Concentration of each ionic species in an aqueous solution consisting of xM NaH_2PO_4, yM Na_2HPO_4, and zM $NaHCO_3$

Electrolyte	Concentration/M	Na^+	HCO_3^-	$H_2PO_4^-$	HPO_4^{2-}
NaH_2PO_4	x	x		x	
Na_2HPO_4	y	$2y$			y
$NaHCO_3$	z	z	z		
n_i		1	-1	-1	-2
C_i^s		$x+2y+z$	z	x	y

If ions are not specifically adsorbed on the electrode, the value of ζ will be close to the one estimated for NaF solutions.[16] $\Delta\zeta$ is thus calculated as the deviation from the reference solution 0.274 M of 1-1 electrolyte, *i.e.*, $x+2y+z=0.274$ and $2x+3y+2z=0.548$, with ζ -0.11 V. The values of $\Delta\zeta$ are tabulated in the last row of Table 1.

References

1) P. G. Russell, N. Kovac, S. Srinivasan, and M. Steinberg, *J. Electrochem. Soc.*, **124**, 1329 (1977).
2) R. Williams, R. S. Crandall, and A. Bloom, *Appl. Phys. Lett.*, **33**, 381 (1978).
3) T. E. Teeter and P. Van Rysselberghe, *J. Chem. Phys.*, **22**, 759 (1954).
4) J. Jordan and P. T. Smith, *Proc. Chem. Soc.*, **1960**, 246.
5) W. Paik, T. N. Andersen, and H. Eyring, *Electrochim. Acta*, **14**, 1217 (1969).
6) K. S. Udupa, G. S. Subramanian, and H. V. K. Udupa, *Electrochim. Acta*, **16**, 1593 (1971).
7) J. Ryu, T. N. Andersen, and H. Eyring, *J. Phys. Chem.*, **76**, 3278 (1972).
8) U. Kaiser and E. Heits, *Ber. Bunsenges. Phys. Chem.*, **77**, 818 (1973).
9) S. Meshitsuka, M. Ichikawa, and K. Tamaru, *J. Chem. Soc., Chem. Commun.*, **1974**, 158.
10) K. Ito, T. Murata, and S. Ikeda, *Bull. Nagoya Inst. Techn.*, **27**, 209 (1975).
11) K. Hiratsuka, K. Takahashi, H. Sasaki, and S. Toshima, *Chem. Lett.*, **1977**, 1137.
12) F. Feigl, "Spot Test in Organic Analysis," 6th English ed, Elsevier, New York, N.Y. (1960).
13) D. D. Wagman, W. H. Evans, V. B. Parker, I. Halow, S. M. Bailey, and R. H. Schumm, "Selected Values of Chemical Thermodynamic Properties," NBS Technical Note 270 (1968).
14) H. Iwahara, H. Uchida, and M. Kishigami, 48th Meeting of the Electrochemical Society of Japan, Yokohama (1981).
15) Y. Hori and S. Suzuki, *J. Faculty Eng. Chiba Univ.*, **32**, 37 (1981).
16) P. Delahay, "Double Layer and Electrode Kinetics," Interscience Publishers, New York, London, Sydney, Toronto (1965).
17) K. J. Vetter, "Electrochemical Kinetics," Academic Press, New York, San Francisco, London (1967).
18) A. W. B. Aylmer-Kelly, A. Bewick, P. R. Cantrill, and A. M. Tuxford, *Faraday Discuss. Chem. Soc.*, **56**, 96 (1973).

Heterogeneous Photocatalytic Reactions on Semiconductor Materials. III. Effect of pH and Cu^{2+} Ions on the Photo-Fenton Type Reaction

Masamichi Fujihira,* Yoshiharu Satoh, and Tetsuo Osa
Pharmaceutical Institute, Tohoku University, Aobayama, Sendai 980

(Received June 29, 1981)

The effect of pH and Cu^{2+} ions on the heterogeneous photocatalytic oxidation of toluenes by H_2O_2 formed from dissolved O_2 in the presence of illuminated TiO_2 powders, *i.e.* "the photo-Fenton type reaction," was investigated. At low and high pH, a total amount of products increased drastically compared with that of the additive free system (pH 7). In the acidic region (aqueous H_2SO_4), side-chain oxidation prevailed over cresol formation and benzaldehyde was formed quite selectively at pH 1. Oxidation of the side chain in preference to hydroxylation of aromatic ring was also observed in the alkaline region (aqueous NaOH). By adding Cu^{2+} ion to the aqueous H_2SO_4 (pH 1 and 2), the yield of benzaldehyde increased further and cresols, benzyl alcohol, and bibenzyl were formed newly in high yields. At high Cu^{2+} concentrations (pH 2), the cresol formation in preference to the side-chain oxidation was attained. The observation was in good agreement with the Fenton reaction reported in which Cu^{2+} and Fe^{3+} ions are added as oxidants for the intermediate products, such as hydroxycyclohexadienyl and benzyl radicals, formed by HO· attack to toluene. Cu^{2+} ion was more preferable to Fe^{3+} ion as the oxidant, since "short circuiting" by Cu^{2+} due to the reversible redox reaction at semiconductor particles was much lower than that by Fe^{3+}. By adding a large amount of Cl^- ions to the Cu^{2+}–H_2SO_4 aqueous system, no oxidation of toluene resulted.

Previously we described the heterogeneous photocatalytic oxidation of aromatic compounds by the illuminated semiconductor powders under the air atmosphere.[1–3] By this new synthetic method, all the products expected from the Fenton reaction[4] were obtained when the reactions were carried out in the aqueous solutions.[1,2] For example, phenol and biphenyl from benzene and benzaldehyde, cresols, and bibenzyl from toluene were obtained. From the distribution of these products[1] and from the effect of the semiconductor materials on the reaction,[2] it was concluded that the reaction proceeded *via* the same mechanism as the Fenton reaction and consequently the reaction was named "the photo-Fenton type reaction."[1,2] The real oxidant in the aqueous TiO_2 systems was considered to be the hydroxyl radical, HO·, which is formed either from the cathodic reaction product, H_2O_2, (Eqs. 1—3 and 5—7) as in

$$h\nu \longrightarrow e^- + h^+ \quad (1)$$

$$2h^+ + H_2O \longrightarrow 1/2O_2 + 2H^+ \quad (2)$$

$$O_2 + 2H^+ + 2e^- \longrightarrow H_2O_2 \quad (3)$$

Fenton's reagent[5] or from the anodic oxidation of OH^- or H_2O (Eqs. 8 and 22).[6–11] The role of hydroxyl radicals was also suggested in the photodecomposition of hydrocarbons in oxygen-containing aqueous solutions at platinized TiO_2.[12]

On the other hand, the reaction proceeded differently, when TiO_2 powders suspended in the aromatic hydrocarbon themselves were irradiated. For example, irradiation of toluene gave benzaldehyde under the air, and gave bibenzyl under nitrogen very selectively.[3] The observation under the air atmosphere corresponded well to the reported results for vapor-phase oxidation of alkyltoluenes by oxygen in contact with UV irradiated TiO_2 in which alkylbenzaldehydes were yielded selectively.[13] The difference in the distribution of the products caused by the absence of water was interpreted by proposing the other mechanism.[3] In this mechanism, oxidation was initiated by the anodic oxidation of toluene by a photogenerated hole to form a toluene cation radical[14] and inexistence of the reactive oxidant, HO· was assumed. The mechanism explained well not only the absence of the hydroxylated products, but also the reason for failure in oxidation of benzene in the absence of water.[3]

If we compare the results observed in the presence and absence of water, we will readily come to the conclusion that a distinctive feature of "the photo-Fenton type reaction" in the presence of water is its ability to hydroxylation of aromatic rings. Consequently in the present work, we investigated the effect of the solution conditions such as pH and Cu^{2+} ions on "the photo-Fenton type reaction," because these solution conditions are well known in the usual Fenton reaction[4] to affect the distribution of the products, especially the ratio of the yield of hydroxylated product to that of side-chain oxidation product (Scheme 1). We will also describe the effect of these factors on the total yield of product.

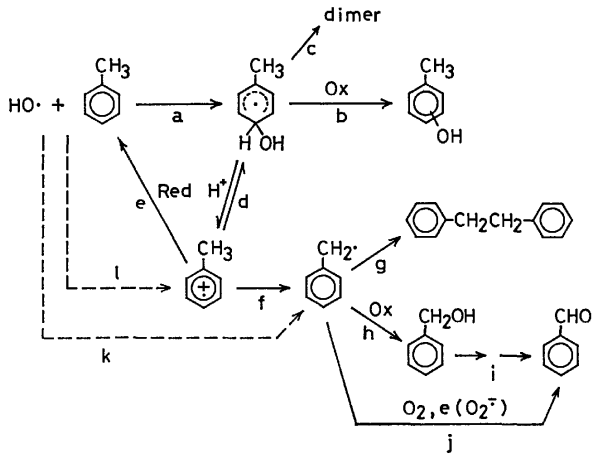

Scheme 1.

Experimental

As a photocatalyst, 99.99% anatase from Rare Metallic Co. was used as received. Each photocatalyst (1 g), in a mixture of aqueous solution of various pH's (100 cm^3) and toluene (5 cm^3), was irradiated for 2 h by a 500 W high pressure mercury arc lamp in a 100 cm^3 Pyrex glass round bottomed flask with a condenser cooled with running water. The solutions were prepared using doubly distilled water and reagent grade chemicals without further purification. To keep the solution saturated with oxygen in the air and to maintain homogeneous mixing of the suspension, the solution was stirred by a magnetic stirrer. After photolysis, the solution was made acidic by HCl addition, then extracted with ether, and finally concentrated under a reduced pressure. A Shimadzu GC-4CM gas chromatograph was used for the analysis of the products. The injection temperature was 250 °C and the column temperature was programmed from 140 °C to 180 °C at the raising rate of 1 °C min^{-1}. Nitrogen was used as the carrier gas at the flow rate of 30 cm^3 min^{-1}. The column used was 2 m × 3ϕ SUS packed with 10% Lanoline on Chromosorb W. Identification of products was based on comparison of the retention times of samples and standards. Acetophenone was used as the internal standard material for quantitative analysis. The amount of a gaseous product, CO_2, was determined by the method in the literature.[12] Total amount of products and the quantum yield were calculated on the basis of the amount of the starting material transformed. Therefore 1 mol of cresols, benzaldehyde, or benzyl alcohol counted as 1 mol of products while 1 mol of bibenzyl counted as 2 mol of product. The number of incident photons (s^{-1}) was estimated by the use of a calibrated Hamamatsu silicon photocell model S 1337-1010 BQ on the assumption that irradiated light through a Toshiba UV filter UV-D35 mainly consisted of photons of 365 nm.

Results and Discussion

Effect of pH. The effect of pH on the distribution of the products and on the total yield of product is shown in Table 1. In these experiments, pH was controlled by adding H_2SO_4 or NaOH and the solutions were irradiated without UV filter except for run Nos. 2 and 3. On calculation of quantum yields, effective light intensity without UV filter was assumed to be about 1.9 times stronger than that with the filter on the basis of the previous results for neutral systems (pH 7).[2] It seems quite reasonable because the quantum yields calculated on the assumption for the experiments at pH 1 with and without the filter are in good agreement with each other (Nos. 1 and 2). By merely adding H_2SO_4, the total amount of products increased with increase in H_2SO_4 concentrations and at pH 1 it becomes about 5 times more than that of additive free system. Although the amount of CO_2 evolved was not determined for every run of the experiment, about 100 μmol of CO_2 was evolved at pH 7 while only a trace amount of CO_2 was detected at pH 1. The suppression of CO_2 formation may explain partly the high yield at low pH.[15] There has been also prediction that the Haber-Weiss reaction can be a potential HO· radical source in the absence of metal impurities at high and low pH.[16] It is also clear from the data in the acidic region (Nos. 1—4) that the yield of side-chain oxidation products prevailed over the yield of cresols and at pH 1 benzaldehyde was formed quite selectively. The total yields increased also with increase in pH in the alkaline region and preferential oxidation of the side chain becomes clearer with increase in pH. But as the side-chain oxidation products, not only benzaldehyde but also bibenzyl was formed and the latter yield is rather higher than the former yield (Nos. 9 and 10) in contrast with the results at pH 1.

The pH dependence of the heterogeneous photocatalytic oxidation of toluene in the acidic region can be interpreted reasonably with reference to the mechanism of the Fenton reaction as previously.[1,2] In the Fenton reaction, H_2O_2 decomposes into hydroxy radical and hydroxide anion by the reductive cleavage with ferrous ion as follows:[4]

$$H_2O_2 + Fe^{2+} \longrightarrow HO^- + HO\cdot + Fe^{3+} \quad (4)$$

In the present system, where the metal ion catalyst for HO· formation such as Fe^{2+} was not added, we considered the following four reactions are responsible for HO· formation as probable paths.[1,2] HO· formed is very reactive and takes part in the hydroxyla-

Table 1. Effect of pH on yields for photo-Fenton type reaction of toluene

Run No.	pH	Product (μmol)[c]								Total[d] μmol	Quantum[d] yield/%
		BzOH	PhCHO	*o*-Cr	*m*-Cr	*p*-Cr	BiBz	Dimer	CO_2		
1	1	3.8	418.2	—	—	—	18.7	—		459.4	1.14
2	1[a]	trace	234.3	—	—	—	—	—	trace	234.3	1.08
3	2[a]	trace	133.7	8.9	3.8	2.7	—	—		149.1	0.69
4	3	trace	84.2	7.5	3.7	1.7	4.7	1.4		106.5	0.26
5	4	—	27.0	31.3	20.2	10.3	11.0	5.4		110.8	0.28
6	7[b]	—	27.3	30.5	19.2	11.2	—	5.0	81.2	88.2	0.22
7	11	—	11.0	19.9	23.8	9.1	18.5	8.0		100.8	0.25
8	12	—	25.1	41.0	39.5	17.5	2.3	trace		127.7	0.32
9	13	trace	46.6	19.9	19.4	6.7	63.8	9.7		220.2	0.55
10	14	trace	58.5	1.5	0.6	0.3	106.0	0.5		272.9	0.68

a) With UV filter. b) Without H_2SO_4 and NaOH. c) BzOH=benzyl alcohol, PhCHO=benzaldehyde, Cr=cresol, BiBz=bibenzyl. d) Calculated by excluding dimer.

$$H_2O_2 + O_2^{\cdot-} \longrightarrow HO\cdot + OH^- + O_2 \quad (5)$$

$$H_2O_2 + h\nu \longrightarrow 2HO\cdot \quad (6)$$

$$H_2O_2 + e^-(TiO_2) \longrightarrow HO\cdot + OH^- \quad (7)$$

$$H_2O(ads) + h^+ \longrightarrow HO\cdot + H^+ \quad (8)$$

tion of aromatic ring and the side-chain oxidation of alkylbenzenes *via* the mechanism as shown in Scheme 1.[17-19] Steps for which there is substantial evidence[18] are indicated by solid arrows, others which are also discussed by dashed arrows. It indicates that most hydroxyl radical attack on aromatics occurs *via* addition, a, to yield hydroxycyclohexadienyl radicals. This is in agreement with conclusions by previous researchers[17-19] and the frequent detection of the hydroxycyclohexadienyl radical by spectroscopic means[20,21] and is strongly supported by the present result described later that phenolic products can be detected in every system in the presence of adequate oxidant, particularly Cu^{2+}, and can be made the major products. This shows that direct side-chain attack, k, cannot be more than a minor reaction path.[22] The rates of hydroxyl radical reactions with aromatics are much faster than would be anticipated for side-chain hydrogen abstraction.[18] In order to account for an apparent high reactivity of aromatic alcohols compared with benzene, Hamilton has proposed either path, l (perhaps concerted with f) or initial formation of a π complex.[23] It is, however, suggested from a correlation of the rate constants with Hammett substituent constant σ[24,25] that sulfate radical anions, $SO_4^{\cdot-}$, form the cation radicals by an electron transfer from the ring to $SO_4^{\cdot-}$ while hydroxyl radicals add to the aromatic ring to form hydroxycyclohexadienyl radicals.

If pH of the solution becomes low, the hydroxycyclohexadienyl radical, will be changed promptly to a radical cation (route d in Scheme 1).[21] The formed cation radical has been known to lose a proton irreversibly to give a benzyl radical (route f) which undergoes dimerization to bibenzyl in the absence of oxidant (route g) or side-chain oxidation to benzyl alcohol (route h) or benzaldehyde (route h and i or route j) in the presence of oxidant. In the systems described above, there is no oxidant added such as Cu^{2+} and Fe^{3+} ions, and therefore only dissolved oxygen acts as the oxidant. Since the yield of benzyl alcohol is much less than that of benzaldehyde (Nos. 1 and 2), benzaldehyde may be formed directly *via* a route j in the presence of dissolved oxygen as in the oxidation in aromatic hydrocarbons.[3] The selective formation of benzaldehyde agrees well with the reaction with Fenton's reagent generated electrochemically in the presence of oxygen.[26] With increase in pH, cresols formation by oxidation of hydroxycyclohexadienyl radical with dissolved oxygen (route b) seems to prevail over the side-chain oxidation described above due to slow down in the water elimination reaction to cation radicals (route d). Above pH 3, another product which may be attributable to a dimer as biphenyl was also detected (route c).

In the alkaline region especially at extremely high pH where only a small amount of cresols was obtained (No. 10), it seems difficult to explain the reaction only by the above described mechanism for the Fenton reaction. For example in such a high pH region, the concentrations of H_2O_2 and $HO\cdot$ are lowered by deprotonation as follows:

$$H_2O_2 \longrightarrow HO_2^- + H^+ \quad (pK_a = 11.62)^{27} \quad (9)$$

$$HO\cdot \longrightarrow O^- + H^+ \quad (pK_a = 11.9^{28,29} \text{ and } 11.8^{30}) \quad (10)$$

Consequently, it is preferable to propose the additional mechanism for the reaction in this pH region. Fortunately, it has been already demonstrated[22,31-34] by pulse radiolysis studies that benzyl radicals can be produced in irradiated aqueous solution by the reaction of O^- with toluene at high pH. Although $HO\cdot$ radicals add to the aromatic ring much more rapidly than they abstract hydrogen from an aliphatic side chain, the situation is reversed when $HO\cdot$ is converted into O^-. At pH>13, the main reaction in irradiated solutions of toluene involves abstraction of H from the methyl group to produce the corresponding benzyl radicals. Consequently, the preferential oxidation of side-chain at high pH (pH>13) in Table 1 can be interpreted by the further reactions of the benzyl radicals formed by this hydrogen abstraction by O^-. In the presence of oxygen, O^- reacts with O_2 very rapidly to form the ozonide ion with the rate constant of $2.6\times10^9\ M^{-1}\ s^{-1}$.[35] However, from careful pulse radiolysis studies, Gall and

$$O^- + O_2 \longrightarrow O_3^- \quad (11)$$

Dorfman[36] concluded that O^- species through thermal dissociation reaction is again the true reactive species in the presence of O_3^-.

$$O_3^- \longrightarrow O_2 + O^- \quad (12)$$

Although the explanation given above is most probable, the alternative mechanism described below was considered at first as a probable mechanism which is similar to the mechanism for the reaction in the absence of water described previously.[3]

$$h\nu \longrightarrow e^- + h^+ \quad (13)$$

$$C_6H_5CH_3 + h^+ \longrightarrow C_6H_5CH_3^{+\cdot} \quad (14)$$

$$C_6H_5CH_3^{+\cdot} \longrightarrow C_6H_5CH_2\cdot + H^+ \quad (15)$$

$$C_6H_5CH_2\cdot \longrightarrow 1/2(C_6H_5CH_2)_2 \quad (16)$$

$$C_6H_5CH_2\cdot + O_2 \longrightarrow C_6H_5CH_2O_2\cdot \quad (17)$$

$$C_6H_5CH_2O_2\cdot + e^- \longrightarrow C_6H_5CHO + OH^- \quad (18)$$

Instead of Eqs. 17 and 18, the alternatives are possible as follows:

$$O_2 + e^- \longrightarrow O_2^{\cdot-} \quad (19)$$

$$C_6H_5CH_2O_2\cdot + O_2^{\cdot-} \longrightarrow C_6H_5CHO + OH^- + O_2 \quad (20)$$

$$C_6H_5CH_2\cdot + O_2^{\cdot-} \longrightarrow C_6H_5CHO + OH^- \quad (21)$$

This seems to be rationalized by the consideration of pH dependent change in energy levels of the band edges of TiO_2[37,38] and the redox potentials of species in solution as shown in Fig. 1. For lack of data, the redox potential of toluene/toluene cation radical measured in acetonitrile[39] is adopted in place of that

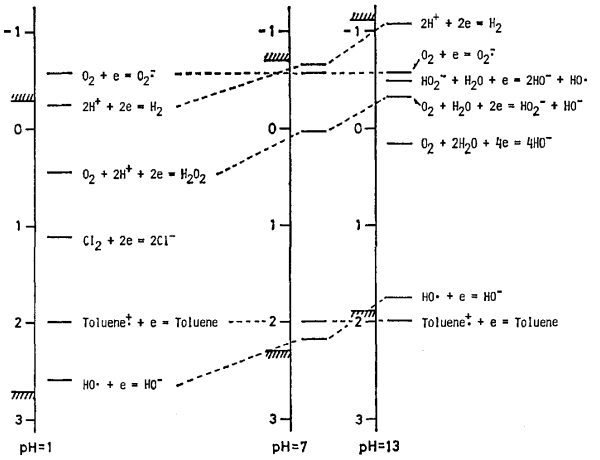

Fig. 1. Changes in position of conduction-band and valence-band edges of TiO_2[37,38] and redox potentials of solution species[39,42,46] in V *vs.* SCE by pH of the aqueous solution.

in water. The potential should be more cathodic than the value shown in Fig. 1 due to the higher solvation energy of cation radical in water than in acetonitrile.[40] Taking this into account, it can be reasonably proposed that toluene is oxidized directly into cation radical even at high pH (Eq. 14) as well as HO^- by positive holes created in the valence band.

$$HO^- + h^+ \longrightarrow HO· \quad (22)$$

Previously the reaction under the air in the absence of water only gave benzaldehyde,[3] but bibenzyl was also formed in the aqueous alkaline solution. The difference may be partly due to the lower solubility of oxygen in water than that in toluene[41] and partly due to the shorter life time of superoxide ion in water[42] than that in hydrocarbon. Furthermore the direct formation of cation radical by positive holes can be considered reasonably as a parallel initiation reaction as well as the reaction initiated *via* addition by HO· at pH<12, since the cation radical formed by $SO_4^{\cdot-}$ gave the similar isomer distributions to those obtained by HO·,[43] but in a strongly alkaline solution, applicability of this parallel mechanism cannot be ascertained since conversion of $SO_4^{\cdot-}$ to HO· should compete with attack on toluene[44] and the HO·–O^- equilibrium becomes significant as described above. If it prevailed, reversible hydration by water to hydroxycyclohexadienyl radicals from the cation radical (route d)[21] would give more phenolic compounds even at high pH. Anyhow, the very low yield of cresols at pH 14 indicates that contribution of the Fenton type reaction by HO· radical is very low, but it is not negligible in contrast with the previous results in the absence of water[3] due to the equilibrium of reaction of Eq. 10.

In addition to the above described pH dependence of CO_2 formation[15] and the yield of Haber-Weiss reaction,[16] the following will partly account for the present observation as to the effect of pH on the total yield of products. In neutral solution, the equilibrium of reaction route d lies to so far to the hydroxycyclohexadienyl radical side and furthermore the rate of reaction route b is limited by the oxidation with dissolved oxygen in the absence of additional oxidants. Consequently if there is another path through which hydroxycyclohexadienyl radicals decay, this accounts for the minimum in the total yield of product in the neutral region. The Hückel theory predicts that the hydrogenated aromatic radical, ArH·, derived from alternant hydrocarbons should have the same half-wave potentials, about −1.1 V *vs.* SCE, since the highest occupied orbital into which a further electron is uptaken is the non-bonding molecular orbital. This fact was ascertained experimentally by Dietz and Peover.[45] Due to its higher electronegativity of HO than H, the reduction potential of hydroxycyclohexadienyl radical can be considered reasonably to be more positive than that of cyclohexadienyl radical of −1.1 V *vs.* SCE. Consequently there is a possibility for hydroxycyclohexadienyl redical to be reduced to yield toluene and HO^- by either electron from conduction band of TiO_2 or superoxide ion. In the alkaline region, the direct formation of benzyl radical by O^- as described above may account for the increase in total yield.

Effect of Cu^{2+} Ions. The effect of Cu^{2+} ion concentrations at pH 1 and pH 2 on "the photo-Fenton type reaction" is summarized in Table 2. On run Nos. 2, 3, and 11—17, pH of the solution was adjusted by adding H_2SO_4, while in run Nos. 18 and 19, HCl was used as acids and in the latter case NaCl was also added. As is evident from the mechanism shown in Scheme 1, the total yield of product will be expected to increase if oxidants are added in the acidic region where the Fenton type reaction mechanism was found to be applicable. This is because the reactions of routes b and h will be accelerated and the backward reaction (route e) will be retarded by the addition of oxidants. As one would expect, the side-chain oxidation products increased by addition of 10 mM Cu^{2+} ions at pH 1 (No. 11). Absence of cresols seems to be reasonable since the reaction between hydroxycyclohexadienyl and cation radicals (route d) lies to the cation radical side at such a very low pH.[4] It is also worthy of note that bibenzyl and benzyl alcohol were formed in additon to benzaldehyde. Cresols formation by further increase in Cu^{2+} ion concentrations (Nos. 12—14) seems to be due to the acceleration of route b which is so high as to be able to compete with the reaction to cation radical (route d). Among the side-chain oxidation products, bibenzyl decreased dramatically with increase in Cu^{2+} ion concentration according to our expectation from Scheme 1. Sudden increase in benzyl alcohol yield by addition of Cu^{2+} ions supports the above interpretation that benzaldehyde was formed directly *via* route j in the presence of only oxygen. The further increase in the formation of benzaldehyde and almost the constant yield of benzyl alcohol with increase in Cu^{2+} ion concentration up to 50 mM indicate that a part of benzaldehyde was formed *via* the intermediate benzyl alcohol in the presence of Cu^{2+} ions (routes h and i). In the presence of high concentration of Cu^{2+} ions (Nos. 13 and 14), cresols formation increased, but the total yield decreased with

Table 2. Effect of Cu^{2+} concentration on yield for photo-Fenton type reaction of toluene[a)]

Run No.	pH	$[Cu^{2+}]$ / mM	Product (μmol)						Total / μmol	Quantum yield/%
			BzOH	PhCHO	*o*-Cr	*m*-Cr	*p*-Cr	BiBz		
2	1	0	trace	234.3	—	—	—	—	234.3	1.08
11	1	10	182.4	315.3	trace	—	—	201.5	901.1	4.17
12	1	50	188.1	646.4	80.7	7.6		70.8	1064.4	4.93
13	1	200	186.8	540.4	130.8	54.7		19.0	950.3	4.40
14	1	500	141.9	206.8	133.0	73.7		8.8	573.0	2.65
3	2	0	trace	133.7	8.9	3.8	2.7	—	149.1	0.69
15	2	50	—	123.9	101.9	44.5	21.1	7.9	307.3	1.42
16	2	200	trace	111.3	208.2	89.7	67.5	—	476.7	2.21
17	2	500	—	24.5	120.9	57.1	50.2	—	252.7	1.17
18	2[b)]	200	—	60.5	165.9	90.0	65.4	—	381.8	1.77
19	2[c)]	200	—	—	—	—	—	—	0	0

a) All experiments were done with UV filter and pH of solutions were controlled by adding H_2SO_4 unless otherwise noted. 1 M=1 mol dm^{-3}. b) 10 mM HCl aqueous solution. c) 3.4 M NaCl in 10 mM HCl aqueous solutinn.

increase in Cu^{2+} concentration. This tendency was also observed in the experiments carried out at pH 2 (Nos. 3, 15—17). At this pH, by adding Cu^{2+} oxidation occurred on the ring in preference to the side chain and furthermore the yield of the side-chain oxidation products rather decreased compared with the result in the absence of Cu^{2+}. In spite of addition of Cu^{2+}, benzaldehyde may be formed mainly *via* route j at this pH as only little benzyl alcohol and bibenzyl are formed. At present the reason for this is not clear. Among the experiments done in H_2SO_4 aqueous solutions, 500 mM of Cu^{2+} ions at pH 2 gave the highest ratio of the yield of hydroxylated products to that of side-chain oxidation products.

In addition to acceleration of routes b and h and retardation of route e, it may be possible that addition of Cu^{2+} ions also increases the total yield by the action of Cu^{+} ions, formed by the oxidation reactions in route b and h, as a catalyst for the Fenton type reaction as follows:

$$H_2O_2 + Cu^{+} \longrightarrow HO\cdot + OH^{-} + Cu^{2+} \quad (23)$$

Here Cu^{+} ion is unstable thermodynamically[46)] because Cu^{+} ion easily disproportionates to Cu^{2+} and Cu metal in H_2SO_4. The decrease in the total yield observed in the high Cu^{2+} concentration, which is not so obvious as in Fe^{2+} addition described previously[1,2)] can be attributed to the "short circuiting" reactions as follows:

$$Cu^{2+} + 2e^{-} \longrightarrow Cu \quad (24)$$

$$Cu + 2h^{+} \longrightarrow Cu^{2+} \quad (25)$$

Sluggishness of Reaction 25, may be the main reason for inefficiency of the "short circuiting" reaction of Cu^{2+} ions.[47)]

If chloride ion is added, cuprous ion will be stable thermodynamically by complex formation[46)] as shown in Eqs. 26—28. The redox couple would also expected to be active as a catalyst for HO· formation.[48)] The result at pH 2 by adding HCl is shown in run No. 18. Almost comparable result to that observed with H_2SO_4 solution was obtained in the aqueous HCl solution, but no product was formed when 3.4 M NaCl was added further (No. 19). The latter result may be explained by the "short circuiting" reaction of the following reversible redox reactions:

$$Cu^{2+} + Cl^{-} + e^{-} \longrightarrow CuCl \quad (26)$$

$$CuCl + h^{+} \longrightarrow Cu^{2+} + Cl^{-} \quad (27)$$

where, in high Cl^{-} concentration, cuprous chloride is in equilibrium with its complexes with chloride anion as follows:[49)]

$$nCuCl + mCl^{-} \rightleftharpoons Cu_nCl_{m+n}^{m-} \quad (28)$$

The preferential hole quenching by the undesirable anodic reaction of chloride anions:[50)]

$$2Cl^{-} + 2h^{+} \longrightarrow Cl_2 \quad (29)$$

also seems to be responsible for no oxidation of toluene.

In conclusion, lowering pH and adding Cu^{2+} ions increased the quantum yield of the heterogeneous photocatalytic oxidation of toluene up to 5% as to total products, which is about 20 times more efficient than that observed in the additive free system. The effect of these solution conditions on the distribution of products was very similar to those observed in the usual Fenton reactions in the acidic media containing H_2O_2, Fe^{2+}, and Cu^{2+}. In the alkaline media, O^{-}, deprotonated form of HO·, abstracts H from side-chain of toluene rather than adds to the aromatic ring and consequently the side-chain oxidation products were formed in preference to the phenolic compounds. In other words, the selective formation of benzaldehyde, bibenzyl, or cresols was possible by controlling pH and/or adding Cu^{2+} ions. By these observations we could confirm further the previous conclusion that the real oxidant in the aqueous TiO_2 system is the hydroxyl radical as in Fenton's reagent. Cu^{2+} ion was not so serious as Fe^{2+} for decreasing the yield due to the "short circuiting" by its redox reaction occurring at the same semiconductor particle, unless the solution contained a large amount of Cl^{-} ions.

References

1) M. Fujihira, Y. Satoh, and T. Osa, *Nature*, **293**, 206

(1981).
2) M. Fujihira, Y. Satoh, and T. Osa, *Chem. Lett.*, **1981**, 1053.
3) M. Fujihira, Y. Satoh, and T. Osa, *J. Electroanal. Chem.*, **126**, 277 (1981).
4) C. Walling, *Acc. Chem. Res.*, **8**, 125 (1975).
5) H. J. H. Fenton, *J. Chem. Soc.*, **65**, 899 (1894).
6) M. D. Archer, *J. Appl. Electrochem.*, **5**, 17 (1975).
7) G. A. Korsunovskii, *Russ. J. Phys. Chem. (Engl. Transl.)*, **52**, 1314 (1978).
8) M. V. Rao, K. Rajeshwar, V. R. P. Verneker, and J. DuBow, *J. Phys. Chem.*, **84**, 1987 (1980).
9) J. M. Kowalski, K. H. Johnson, and H. L. Tuller, *J. Electrochem. Soc.*, **127**, 1969 (1980).
10) S. Sato and J. M. White, *J. Phys. Chem.*, **85**, 336 (1981).
11) C. D. Jaeger and A. J. Bard, *J. Phys. Chem.*, **83**, 3146 (1979).
12) I. Izumi, W. W. Dunn, K. O. Wilbourn, F. F. Fan, and A. J. Bard, *J. Phys. Chem.*, **84**, 3207 (1980); I. Izumi, F. F. Fan, and A. J. Bard, *ibid.*, **85**, 218 (1981).
13) M. N. Mozzanega, J. M. Herrman, and P. Pichat, *Tetrahedron Lett.*, **1977**, 2965.
14) T. Kanno, T. Oguchi, H. Sakuragi, and K. Tokumaru, *Tetrahedron Lett.*, **21**, 467 (1980).
15) B. Kraeutler and A. J. Bard, *J. Am. Chem. Soc.*, **100**, 5985 (1978).
16) J. Weinstein and B. H. J. Bielski, *J. Am. Chem. Soc.*, **101**, 58 (1979).
17) C. R. E. Jefcoate, J. R. L. Smith, and R. O. C. Norman, *J. Chem. Soc., B*, **1969**, 1013.
18) C. Walling and R. A. Johnson, *J. Am. Chem. Soc.*, **97**, 363, (1975).
19) M. K. Eberhardt and M. I. Martinez, *J. Phys. Chem.*, **79**, 1917 (1975).
20) L. M. Dorfman, I. A. Taub, and R. E. Bühler, *J. Chem. Phys.*, **36**, 3051 (1962).
21) K. Sehested, J. Holcman, and E. J. Hart, *J. Phys. Chem.*, **81**, 1363 (1977).
22) K. Sehested, H. Corfitzen, H. C. Christensen, and E. J. Hart, *J. Phys. Chem.*, **79**, 310 (1975).
23) M. E. Snook and G. A. Hamilton, *J. Am. Chem. Soc.*, **96**, 860 (1974).
24) P. Neta, V. Madhaven, H. Zemel, and R. W. Fessenden, *J. Am. Chem. Soc.*, **99**, 163 (1977).
25) P. Neta and L. M. Dorfman, *Adv. Chem. Ser.*, **81**, 222 (1968).
26) T. Matsue, M. Fujihira, and T. Osa, *J. Electrochem. Soc.*, **128**, 2565 (1981).
27) "Handbook of Chemistry and Physics," 54th ed, CRC Press, Cleveland (1973), p. D-130.
28) J. Rabani and M. S. Matheson, *J. Am. Chem. Soc.*, **86**, 3175 (1964).
29) J. Rabani and M. S. Matheson, *J. Phys. Chem.*, **70**, 761 (1966).
30) J. L. Weeks and J. Rabani, *J. Phys. Chem.*, **70**, 2100 (1966).
31) P. Neta, M. Z. Hoffman, and M. Simic, *J. Phys. Chem.*, **76**, 847 (1972).
32) P. Neta and R. H. Schuler, *J. Phys. Chem.*, **77**, 1368 (1973).
33) H. C. Christensen, K. Sehested, and E. J. Hart, *J. Phys. Chem.*, **77**, 983 (1973).
34) M. K. Eberhardt and M. Yoshida, *J. Phys. Chem.*, **77**, 589 (1973).
35) G. E. Adams, J. W. Boag, and B. D. Michael, *Nature*, **205**, 898 (1965).
36) B. L. Gall and L. M. Dorfman, *J. Am. Chem. Soc.*, **91**, 2199 (1969).
37) J. M. Bolts and M. S. Wrighton, *J. Phys. Chem.*, **80**, 2641 (1976).
38) E. C. Dutoit, F. Cardon, and W. P. Gomes, *Ber. Bunsenges. Phys. Chem.*, **80**, 475 (1976).
39) E. S. Pysh and N. C. Yang, *J. Am. Chem. Soc.*, **85**, 2124 (1963).
40) S. Hayano and M. Fujihira, *Bull. Chem. Soc. Jpn.*, **44**, 2051 (1971).
41) R. Battino and H. L. Clever, *Chem. Rev.*, **66**, 395 (1966).
42) D. T. Sawyer and M. J. Gibian, *Tetrahedron*, **35**, 1471 (1979).
43) C. Walling, D. M. Camaioni, and S. S. Kim, *J. Am. Chem. Soc.*, **100**, 4814 (1978).
44) E. Hayon, A. Treinin, and J. Wilf, *J. Am. Chem. Soc.*, **94**, 47 (1972).
45) R. Dietz and M. E. Peover, *Trans. Faraday Soc.*, **62**, 3536 (1966).
46) D. Dobos, "Electrochemical Data," Elsevier, Amsterdam (1975).
47) H. Reiche, W. W. Dunn, and A. J. Bard, *J. Phys. Chem.*, **83**, 2248 (1979).
48) J. F. Skinner, A. Glasel, L. Hsu, and B. L. Funt, *J. Electrochem. Soc.*, **127**, 315 (1980).
49) J. J. Fritz, *J. Phys. Chem.*, **84**, 2241 (1980); **85**, 890 (1981).
50) T. Kobayashi, H. Yoneyama, and H. Tamura, *Chem. Lett.*, **1979**, 457; *J. Electroanal. Chem.*, **122**, 133 (1981).

New Application of PAS for *In Situ* Observation of Semiconductor Electrode Surface

Hideki MASUDA, Akira FUJISHIMA,* and Kenichi HONDA

Department of Synthetic Chemistry, Faculty of Engineering, The University of Tokyo, Hongo, Bunkyo-ku, Tokyo 113

(Received July 15, 1981)

The photoacoustic spectroscopic technique was used to study *in situ* cathodic decomposition of CdS and ZnO semiconductor electrodes and electrochemical deposition of metal ions (Cd^{2+} and Zn^{2+}) on the semiconductor electrodes.

Photoacoustic spectroscopy (PAS) has recently been emphasized as an useful tool for the study of materials.[1-4] In particular, absorption spectra of highly absorbing materials can easily be obtained by the PAS technique. Additionally, thermal conductivity[5] and information regarding to radiationless processes[6,7] can be obtained from photoacoustic effects. Although PAS has extensively been used to study solids, gases, and liquids,[8] application to *in situ* studies of electrode surface is just beginning. In previous publications,[9,10] we reported that change in a few monolayers on electrode surface during anodic oxidation of a gold electrode could easily be detected *in situ* by the PAS technique.

We report here an application of PAS to *in situ* measurement of semiconductor electrode reactions. Specifically, cathodic reactions of n-type semiconductor electrodes (CdS, ZnO) and electrochemical deposition of metal ions (Cd^{2+}, Zn^{2+}) from solution on electrodes are studied.

These reactions were studied by Kolb *et al.*[11,12] by use of differential reflectance spectroscopy, in which mechanically polished surfaces were examined because the surface had to be flat for this technique.

Experimental

The photoacoustic cell, shown in Fig. 1, was constructed of stainless steel and its outside surface was coated with an epoxy resin for the purpose of insulation from the electrolyte.

An electret condenser microphone (SONY Model ECM-150), a pressure transducer, was mounted on the PAS cell. It was favorable for electrochemical study because a high voltage power source was not required. A Pyrex window was situated at the other side of the cell which was directly across the sample electrode, so that the light which was not absorbed by the sample electrode could pass through the window.

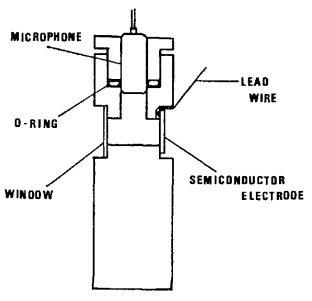

Fig. 1. Photoacoustic cell for semiconductor electrode. The cell width is 20 mm and the height is 60 mm.

Samples measured in this work were a single crystal CdS $(000\bar{1})$ [Teikoku Tsushin (with a donor concentration $N_D = 1.6 \times 10^{16}$ cm^{-3})] and a sintered polycrystalline ZnO which was made with the same procedure as described before.[13] The donor concentration of the polycrystalline ZnO was not known.

Because the amplitude of the photoacoustic signal depends on the thickness of the sample, especially for semiconductors which have lower thermal conductivities than metals, the samples were polished to a thin plate with thickness of less than 0.5 mm.

Ohmic contact was established by evaporating indium on the rear surface of the semiconductor plate, and a lead wire was contacted to the sample with Ag epoxy. Each surface of the samples, CdS and ZnO, was etched with concentrated hydrochloric acid for a few seconds prior to measurement.

The experimental instrumentation was similar to those described previously for the metal electrode-PAS measurement.[9,10] In the present work, a Rhodamin 6G dye laser (Spectra Physics Model 375) which has a wavelength range of approximately 550—660 nm, was used as a high intensity monoenergetic light source in addition to an argon ion laser (Spectra Physics Model 164) and a Xe lamp (Ushio, 1 kW). The light beam from lasers was magnified by a convex lens (f=5 cm) so that the entire surface of the sample electrode except the region of the lead wire contact could be irradiated.

Before a PAS spectrum was taken, the phase angle was adjusted so that the photoacoustic signal due to light absorption at the surface could be optimized. Excitation sources of energy corresponding to the absorption band regions of CdS and ZnO, respectively, were used during the phase adjustment. This procedure was repeated whenever the thickness of samples or modulation frequency was varied.

Results and Discussion

CdS Single Crystal Electrode. Figure 2 shows the photoacoustic signal of the CdS electrode *versus* the wavelength of excitation before and after electrolysis (about 100 mC cm^{-2}) at −2.0 V *vs.* SCE in 1 M KCl (1 M=1 mol dm^{-3}) solution.

In the spectrum of CdS before electrolysis, the photoacoustic signal began to increase when the excitation energy approached the absorption band edge of CdS (2.4 eV or 520 nm). When the energy of radiation is comparable to the band gap energy of the semiconductor electrode, electrons are excited into the conduction band, and when there is no current flow, electrons will recombine with holes in the valence band, and heat will be dissipated.

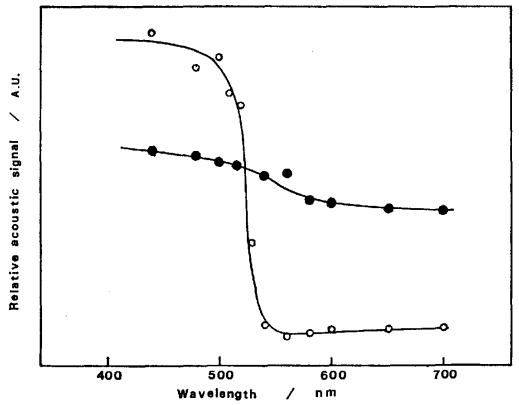

Fig. 2. Photoacoustic spectra of the CdS electrode before (—○—) and after (—●—) electrolysis at −2.0 V *vs.* SCE in 1 M KCl.

When the CdS electrode was electrolyzed at −2.0 V, decomposition of the electrode occurred as follows:

$$CdS + 2e^- \longrightarrow Cd + S^{2-}.$$

The decomposition potential was found to be −1.5 V in the dark. The surface of the CdS was covered with a deposited thin metallic layer of Cd. The photoacoustic signal in the longer wavelength region was due to the intrinsic absorption of the metallic Cd layer. There was a small increase in the photoacoustic signal beginning at an energy corresponding to the absorption band edge of CdS. This extra signal was probably due to the absorption by the CdS underneath the thin metallic Cd layer.

Based on the wavelength response of the photoacoustic signals, we used photons of two different wavelengths, one longer than (610 nm) and the other comparable to (514.5 nm) the absorption band edge of CdS, to prove surface change of the CdS electrode during a reduction and oxidation cycle.

Figure 3 shows the current-potential curve and the relative photoacoustic signal-potential curve of the CdS electrode in 1 M KCl electrolyte solution. The irradiation wavelength was 610 nm. At this wavelength, no photoeffect occurred at the CdS electrode. In the current-potential curve, during the first scan, reduction of oxygen at an onset potential of −0.9 V and hydrogen evolution at an onset potential of −1.4 V were observed, but no cathodic decomposition peak was observed because of the large cathodic current of hydrogen evolution. However, the photoacoustic signal began to increase at −1.5 V. This increase in the photoacoustic signal was due to an increase in the absorption of light at the electrode surface. The increase in the absorption of light reflected the basic change in the absorptivity of the electrode surface and was due to the Cd deposition from lattice at −1.5 V. The photoacoustic signal was not influenced by the oxygen reduction or the hydrogen evolution in the sensitivity region of the present study.

On the anodic scan, a sharp anodic peak appeared at −0.7 V in the current-potential curve, and could be attributed to the dissolution of Cd. At the corresponding potential, the photoacoustic signal decreased and finally returned to its initial value. This behavior suggests that the deposited Cd layer is completely stripped off after an anodic scan.

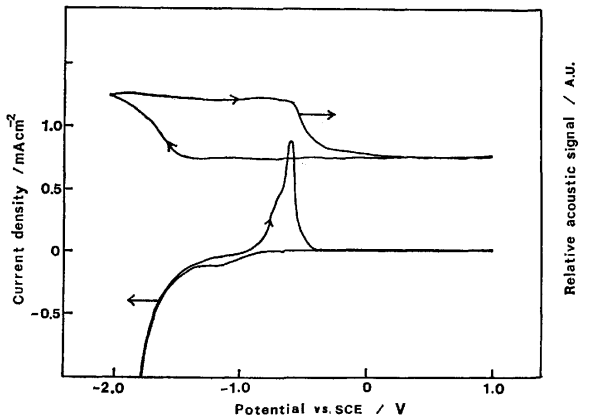

Fig. 3. Photoacoustic signal-potential and current-potential curves of the CdS electrode in 1 M KCl. Potential sweep rate: 40 s/V; λ=610 nm (Rh-6G dye laser irradiation).

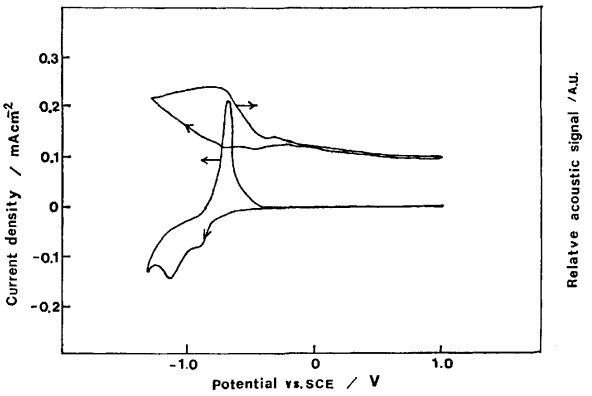

Fig. 4. Photoacoustic signal-potential and current-potential curves of the CdS electrode in the presence of 5×10^{-5} M Cd^{2+} and 1 M KCl.
Potential sweep rate: 40 s/V; λ=610 nm (Rh-6G dye laser irradiation).

Figure 4 shows the current-potential and the photoacoustic signal-potential curves of the CdS electrode in 1 M KCl solution containing 5×10^{-5} M Cd^{2+}. The potential was scanned between 1.0 and −1.4 V, and in this potential range the decomposition of CdS did not take place. A cathodic current at −0.8 V in the current-potential curve was due to the reduction of Cd^{2+} from solution on the CdS surface, thus causing the photoacoustic signal to increase.

Assuming that the deposited layer was uniform, the thickness of the deposited layer was estimated to be about 7 Å from the amount of the charge passed for the electrochemical deposition and the density of Cd (8.7 g cm^{-3}).

We could also detect a change of the CdS electrode surface during the cathodic decompositon by use of the intrinsic absorption wavelength of irradiation (514.5 nm). Figure 5 shows the current-potential and photoacoustic signal-potential curves in 1 M KCl solution using 514.5 nm irradiation. At this wavelength, the anodic photoeffect took place remarkably

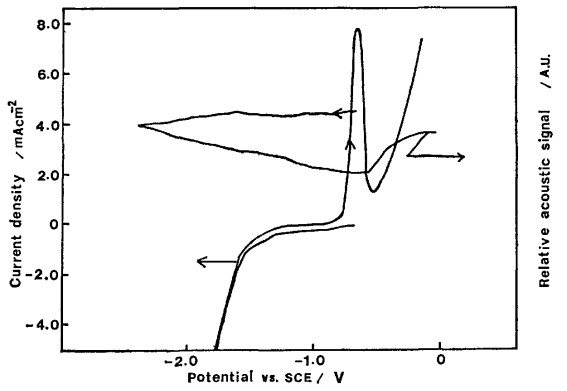

Fig. 5. Photoacoustic signal-potential and current-potential curves of the CdS electrode in 1 M KCl. Potential sweep rate: 50 s/V; λ=514.5 nm (Ar ion laser irradiation).

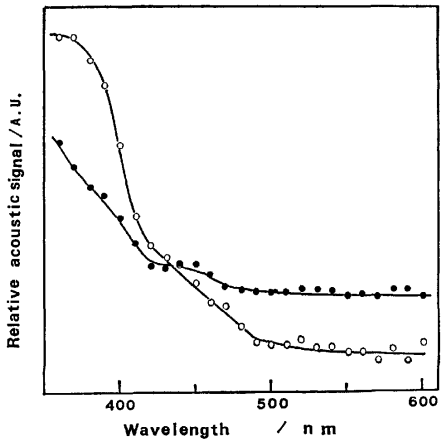

Fig. 6. Photoacoustic spectra of the ZnO electrode before (—O—) and after electrolysis (—●—) at −1.6 V in 1 M KCl.

but the cathodic did negligibly. As was expected, the photoacoustic signal was larger when there was no Cd present on the CdS surface because of the intrinsic absorption of CdS at this wavelength, as shown in Fig. 2. The photoacoustic signal began to decrease at −1.5 V where the CdS decomposition took place. This decrease in signal was due to the Cd deposition. However, the change in the photoacoustic signal was less obvious when the 514.5 nm irradiation was used.

ZnO Polycrystalline Electrode. Photoacoustic spectra of the ZnO electrode before and after electrolysis at −1.6 V (about 100 mC cm^{-2}) in 1 M KCl are shown in Fig. 6. On cathodic polarization, the ZnO electrode decomposed and a deposited Zn layer was formed as follows:

$$ZnO + 2H^+ + 2e^- \longrightarrow Zn + H_2O.$$

After electrolysis the spectra changed, that is, the absorption in the longer wavelength region increased due to deposition of Zn from the ZnO lattice. Because the metallic zinc layer was not uniformly deposited on the surface in the case of polycrystalline ZnO, the absorption of ZnO remained in the spectrum after electrolysis.

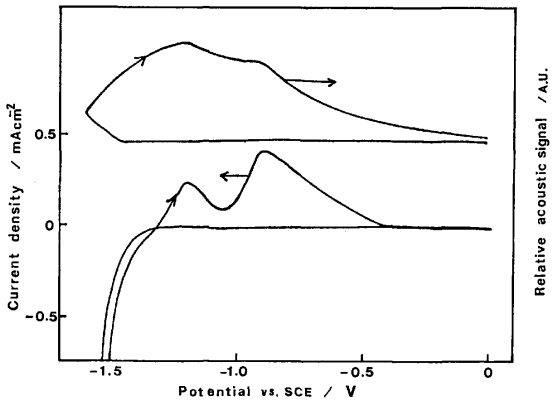

Fig. 7. Photoacoustic signal-potential and current-potential curves of the ZnO electrode in 1 M KCl. Potential sweep rate: 60 s/V; $\lambda \geqq 600$ nm (Xe lamp irradiation with a sharp cut filter).

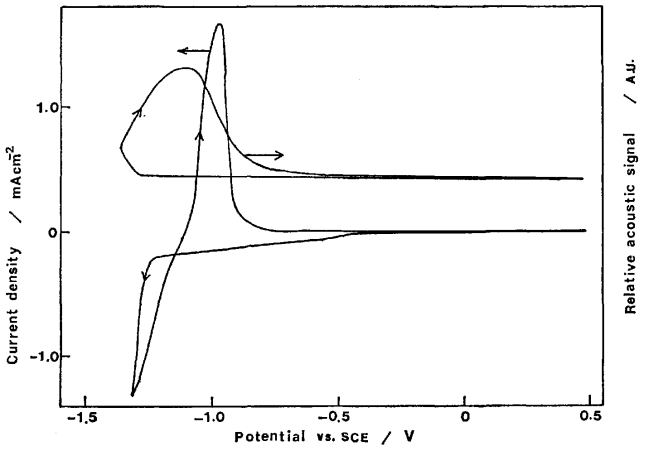

Fig. 8. Photoacoustic signal-potential and current-potential curves of the ZnO electrode in the presence of 10^{-3} M Zn^{2+}, and 1 M KCl.
Potential sweep rate: 30 s/V; $\lambda \geqq 600$ nm (Xe lamp irradiation with a sharp filter).

Figure 7 shows the photoacoustic signal under irradiation at λ>600 nm (Xe lamp irradiation) and current-applied potential curves for ZnO in 1 M KCl electrolyte. The photoacoustic signal began to increase at −1.5 V, which implied decomposition of ZnO. On the anodic scan, two anodic current peaks, both of which seemed to be attributed to dissolution of Zn layer to the solution, were observed in the current-potential curve. The photoacoustic signal decreased stepwise at the corresponding potentials. The photoacoustic signal did not return to the initial value even after the anodic scanning. This behavior implied that the deposited zinc layer could not completely dissolve and remained partially on the polycrystalline ZnO surface.

Figure 8 shows the photoacoustic signal and current-potential curves in 1 M KCl solution containing 10^{-3} M Zn^{2+} ion. A reduction current between −0.5 and −1.25 V was due to the reduction of dissolved oxygen, which did not affect the PAS signal. However, when the large cathodic current flowed from −1.25 V which was attributed to the electrochemical

deposition of Zn^{2+} on the ZnO surface from the solution, the photoacoustic signal began to increase at almost the same potential. On the anodic scan, the anodic current peak was observed at −1.0 V and the photoacoustic signal decreased from −1.1 V. In this case, only one steep peak was observed. Though detailed characters of the two kinds of metallic zinc in the cathodic decomposition (in Fig. 7) are unknown, the results relating to the current-potential and optical measurements of the ZnO in this work are in accord with those by Kolb *et al.*[11,12]

Conclusion

We have demonstrated that photoacoustic spectroscopy is surface sensitive and applicable to *in situ* characterization of the semiconductor electrode surface change during a reduction and oxidation cycle. We could detect deposition of several layers of metal using laser irradiation. This technique is simple and useful for studies of rough or porous surfaces. The problem that the sample has to be thin in our method might be solved by use of other techniques, *e.g.* the piezoelectric photoacoustic detection technique.[14–16] Application of PAS to photoelectrochemical reactions of semiconductor electrodes was described elsewhere.[17]

The authors would like to thank Dr. Boon H. Loo at SRI International for his valuable suggestions.

References

1) A. Rosencwaig, *Opt. Commun.*, **7**, 305 (1973).
2) A. Rosencwaig, *Anal. Chem.*, **47**, 592A (1975).
3) W. R. Harshburger and M. B. Robin, *Acc. Chem. Res.*, **6**, 329 (1973).
4) M. J. Adams, A. A. King, and G. F. Kirkbright, *Analyst*, **101**, 73 (1976).
5) M. J. Adams and G. F. Kirkbright, *Analyst*, **102**, 281 (1977).
6) J. C. Murphy and L. C. Aamodt, *J. Appl. Phys.*, **48**, 3502 (1977).
7) R. G. Peterson and R. C. Powell, *Chem. Phys. Lett.*, **53**, 366 (1978).
8) See for example, Technical Digest, Topical Meeting on Photoacoustic Spectroscopy, Ames., Iowa (1979).
9) A. Fujishima, H. Masuda, and K. Honda, *Chem. Lett.*, **1979**, 1063.
10) H. Masuda, A. Fujishima, and K. Honda, *Bull. Chem. Soc. Jpn.*, **53**, 1542 (1980).
11) D. M. Kolb and H. Gerischer, *Electrochim. Acta*, **18**, 987 (1973).
12) D. M. Kolb, *Ber. Bunsenges. Phys. Chem.*, **77**, 891 (1973).
13) T. Inoue, A. Fujishima, and K. Honda, *J. Electrochem. Soc.*, **127**, 1582 (1980).
14) M. M. Farrow, R. K. Burnham, M. Avzanneau, S. L. Olsen, N. Purdie, and E. M. Eyring, *Appl. Opt.*, **17**, 1093. (1978).
15) W. Jackson and N. M. Amer, *J. Appl. Phys.*, **51**, 3343 (1980).
16) R. E. Malpas and A. J. Bard, *Anal. Chem.*, **52**, 109 (1980).
17) H. Masuda, S. Morishita, A. Fujishima, and K. Honda, *J. Electroanal. Chem.*, **122**, 67 (1981).

^{1}H and ^{19}F Nuclear Magnetic Relaxation Studies of Molecular Motion in Solid Fluoroform

Taro EGUCHI,* Michihiko KISHITA, Hideaki CHIHARA,†
and (the late) Gen SODA

Institute of Chemistry, College of General Education, Osaka University, Toyonaka, Osaka 560
†*Department of Chemistry, Faculty of Science, Osaka University, Toyonaka, Osaka 560*

(Received July 29, 1981)

Spin-lattice relaxation times of proton and fluorine nuclei in solid CHF_3 were measured by the pulsed magnetic resonance technique between 7 and 116 K. In ^{1}H resonance, non-exponential recovery of magnetization was clearly observed. T_1 data as well as magnetization recoveries were interpreted in terms of intramolecular magnetic dipole interactions between like spins and also between unlike spins, which are modulated by the isotropic reorientation of a whole molecule. A calculation of the temperature dependence of T_1 was made by using an activation energy of 17 kJ mol^{-1} and a pre-exponential factor of 1.0×10^{-16} s for the motion, yielding results in agreement with the present experimental results.

Fluoroform (CHF_3) has no phase transition below the melting point, $T_m=118$ K, and has a wide range of liquid phase up to the boiling point, $T_b=191$ K.[1] Nuclear magnetic relaxation studies of fluoroform have been concentrated on its liquid state. Spin-rotational interactions have been found to be the main relaxation mechanism in the ^{19}F resonance in the liquid state[2] as well as in the gas state.[3] The cross relaxation between ^{1}H and ^{19}F connected with the Overhauser effect has also been studied in the liquid state where effects of intermolecular magnetic interactions are predominant over those of intramolecular interactions.[4]

In this paper, we will discuss experimental results of temperature dependence of ^{1}H and ^{19}F spin-lattice relaxation times in order to elucidate the molecular motion in the solid state and to examine the cross relaxation effect between the two kinds of nuclei.

Experimental

A sample of fluoroform was purchased in a cylinder from Seitetsu Kagaku (a product of Dupont), the nominal purity being higher than 99%. The method of purification of the sample and the cryostat used in the measurement of T_1 were the same as in the case of silane reported previously.[5]

The relaxation time measurements were carried out between 7 K and just below the melting point at both 10.00 and 25.54 MHz using pulsed NMR techniques. In the ^{19}F resonance, we measured T_1 by the null-method above 80 K since the magnetization recovery showed exponential behavior over more than one decade within the experimental error.

On the other hand, the magnetization recovery for the ^{1}H resonance showed clear non-exponential behavior as shown in Fig. 1. We therefore used the $\pi/2$(comb)-τ-$\pi/2$ pulse sequences as well as the π-τ-$\pi/2$ pulse method; the two methods gave identical results within the experimental error.

Results and Discussion

The ^{19}F spin-lattice relaxation time T_1 above 80 K is shown in Fig. 2 and that below 80 K is shown in Fig. 3. A minimum in T_1 occurs at 105 K with a value of 10.7 ms at 10.0 MHz. Anomalous T_1 behavior is observed below 50 K where T_1 becomes

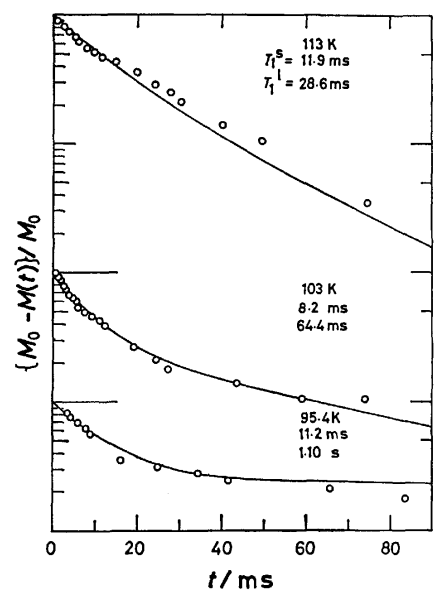

Fig. 1. Reduced magnetization recoveries in ^{1}H resonance.
Solid curves are the results of theoretical fitting.

almost independent of temperature, and on further cooling, the magnetization recovery tends to be more complex with two time constants. The relaxation mechanism in this temperature region is not obvious. The trace of paramagnetic oxygen, which has been detected by a gas chromatographic analysis (less than 0.02%), might be a candidate.[6]

A unique value of ^{1}H spin-lattice relaxation time was not to be determined because of the non-exponential recoveries as shown in Fig. 1. This behavior is due to the cross relaxation effect caused by the dipole coupling between ^{1}H and ^{19}F. In other words, for a quantitative treatment of the ^{1}H resonance data, it is necessary to consider the spin system as one of two unlike spins, ^{1}H (spin S) and ^{19}F (spin I).

In this case, we may describe the equation of motion for the magnetization as follows:[7]

$$\begin{pmatrix} \frac{d\langle I_z\rangle}{dt} \\ \frac{d\langle S_z\rangle}{dt} \end{pmatrix} = -\Gamma \begin{pmatrix} \langle I_z\rangle - I_0 \\ \langle S_z\rangle - S_0 \end{pmatrix}, \quad (1)$$

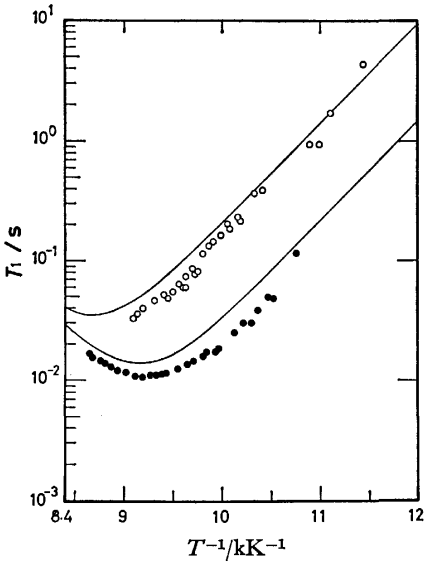

Fig. 2. The temperature dependence of ^{19}F spin-lattice relaxation time above 80 K.
●: At 10.0 MHz, ○: at 25.54 MHz, ——: calculated curves.

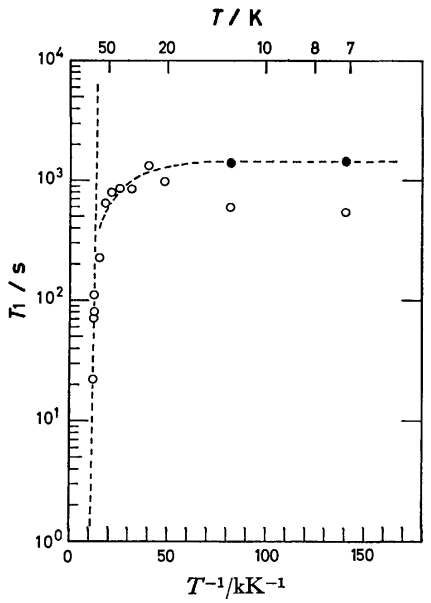

Fig. 3. The temperature dependence of ^{19}F spin-lattice relaxation time below 80 K at 25.54 MHz.

where I_0 and S_0 denote the magnetization at thermal equilibrium, and the relaxation matrix Γ is defined by

$$\Gamma \equiv \begin{pmatrix} \Gamma_{II} & \Gamma_{IS} \\ \Gamma_{SI} & \Gamma_{SS} \end{pmatrix}. \tag{2}$$

For simplicity, with only the intramolecular dipole coupling taken into account, each component of the relaxation matrix may be written as

$$\left.\begin{aligned} &\Gamma_{II} = 2\gamma_{II}^{L} + \gamma_{II}^{U}, \\ &\Gamma_{IS} = \gamma_{IS}^{U}, \\ &\Gamma_{SI} = 3\gamma_{SI}^{U}, \\ \text{and} \\ &\Gamma_{SS} = 3\gamma_{SS}^{U}, \end{aligned}\right\} \tag{3}$$

where the superscripts L and U mean the contribution of a like spin pair and that of an unlike spin pair, respectively. In the case of dipole coupling, theses are given by Abragam as follows:[7]

$$\left.\begin{aligned} \gamma_{II}^{L} &= \frac{9}{8}\gamma_I^4\hbar[J^{(1)}(\omega_I) + J^{(2)}(2\omega_I)] \\ \gamma_{II}^{U} &= \frac{3}{4}\gamma_I^2\gamma_S^2\hbar^2\left[\frac{1}{12}J^{(0)}(\omega_I-\omega_S) + \frac{3}{2}J^{(1)}(\omega_I) + \frac{3}{4}J^{(2)}(\omega_I+\omega_S)\right], \\ \gamma_{IS}^{U} &= \frac{3}{4}\gamma_I^2\gamma_S^2\hbar^2\left[-\frac{1}{12}J^{(0)}(\omega_I-\omega_S) + \frac{3}{4}J^{(2)}(\omega_I+\omega_S)\right], \end{aligned}\right\} \tag{4}$$

and similar equations for γ_{SS}^{U} and γ_{SI}^{U} are obtainable by interchanging the indices I and S, where $J^{(n)}(\omega)$'s are spectral densities.

The observable relaxation rates $\lambda_+ = (T_1^l)^{-1}$ and $\lambda_- = (T_1^s)^{-1}$ are the eigenvalues of the relaxation matrix Γ.

When we use the $\pi/2$(comb)-τ-$\pi/2$ pulse sequences, these eigenvalues determine the magnetization recoveries according to the equations

$$\left.\begin{aligned} &\frac{I_0 - \langle I_z\rangle}{I_0} = a_S\exp(-t/T_1^l) + b_S\exp(-t/T_1^s), \\ \text{and} \\ &\frac{S_0 - \langle S_z\rangle}{S_0} = a_I\exp(-t/T_1^l) + b_I\exp(-t/T_1^s), \end{aligned}\right\} \tag{5}$$

where the coefficients a and b are given by

$$\left.\begin{aligned} &a_S = (\Gamma_{SS}-\lambda_-)/(\lambda_+-\lambda_-) = b_I, \\ \text{and} \\ &b_S = (\Gamma_{SS}-\lambda_+)/(\lambda_+-\lambda_-) = a_I. \end{aligned}\right\} \tag{6}$$

It is worth noting that not only T_1^l and T_1^s but also a and b are temperature-dependent through temperature dependence of correlation time associated with the particular type or types of molecular motion that are responsible for the relaxation. Expressions such as Eqs. 4 and 5 have been used to interprete experimental results on more complicated systems.[8-12] However, the values of a and b were taken as independent of temperature.

In calculating the matrix elements (Eq. 3) for CHF_3, isotropic reorientation of a whole molecule will be assumed to be the dominant relaxation mechanism. The spectral densities are then given by

$$\left.\begin{aligned} &J^{(1)}(\omega) = \frac{4}{15}r_{ij}^{-6}[\tau_c/(1+\omega^2\tau_c^2)], \\ \text{where} \\ &J^{(0)}:J^{(1)}:J^{(2)} = 6:1:4, \end{aligned}\right\} \tag{7}$$

with

$$\tau_c = \tau_0\exp(V/RT), \tag{8}$$

where r_{ij} is the distance between two spins, V is the relevant activation energy, and τ_0 is the pre-exponential factor.

Taking r_{FF}=0.216 and r_{FH}=0.198 nm,[13] we obtain the explicit values of the long and short components, T_1^l and T_1^s, and the coefficients a_S and b_S, which are shown in Fig. 4 as functions of $\omega\tau_c$ in the case of ^{19}F resonance. It is clear that T_1^l has a minimum

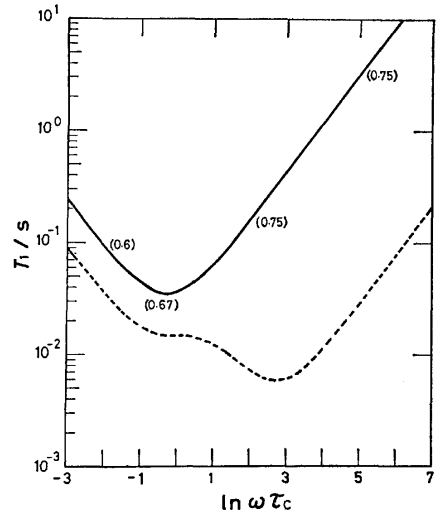

Fig. 4. Theoretical ^{19}F T_1 curves (T_1^l and T_1^s components) *vs.* ln $\omega\tau_c$.
The numbers in the parentheses indicate the coefficient a_S in Eq. 5.

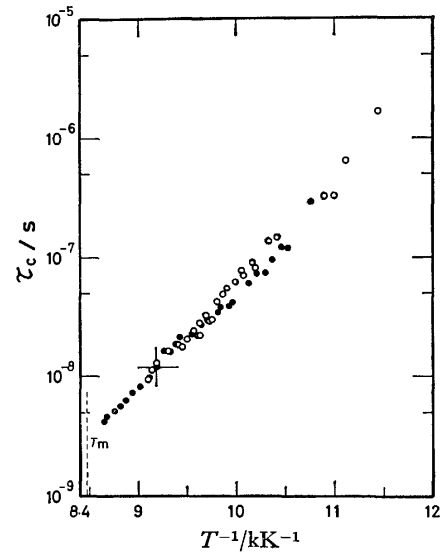

Fig. 5. The temperature dependence of the correlation time associated with isotropic reorientation.
●: From the T_1 data at 10.0 MHz, ○: from the T_1 data at 25.54 MHz.

at $\omega\tau_c=0.75$ ($\ln\omega\tau_c=-0.28$) and a_S assumes a nearly constant value of 0.75 where $\omega\tau_c \gg 0.75$. Judging from the fact that the observed magnetization recovery in ^{19}F resonance can be described by a single exponential function over the time span of experiment, it is reasonable to consider that the observed T_1 is equal to T_1^l. By using the T_1^l curve in Fig. 4 and the observed T_1 values, we can estimate the correlation time τ_c due to isotropic molecular reorientation, the temperature dependence of which is shown in Fig. 5. The straight line in this figure gives us an activation energy $V=17$ kJ mol^{-1} and $\tau_0=1.0\times10^{-16}$ s,[14] as well as the solid curve in Fig. 2.

On the other hand, the magnetization recoveries in ^1H resonance were analyzed by means of Eq. 5 using only one parameter τ_c. A few examples of curve-fitting are drawn in Fig. 1. The two time con-

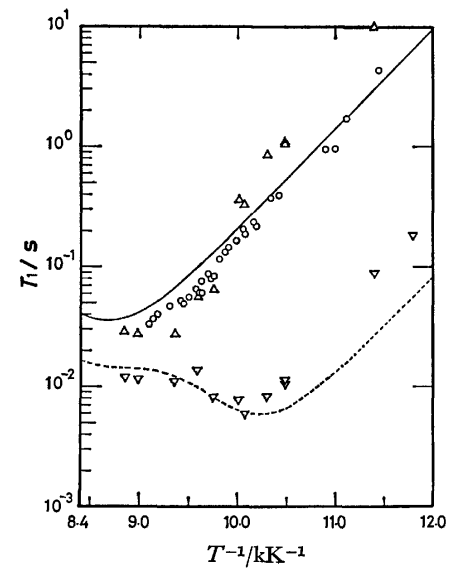

Fig. 6. The temperature dependence of T_1 at 25.54 MHz.
○: ^{19}F resonance, △: T_1^l in ^1H resonance, ▽: T_1^s in ^1H resonance, ——: calculated T_1^l, — —: calculated T_1^s.

stants T_1^l and T_1^s obtained in this manner are plotted against the reciprocal of temperature in Fig. 6, where the T_1^l and T_1^s curves were calculated from the same parameter values as above and are shown by the solid and broken lines, respectively. Here the calculated T_1^s curve has a shoulder around $\omega\tau_c=0.75$ besides a clear minimum at $\omega\tau_c=15$, which arises from the (ω_I—ω_S) terms in Eq. 4.

The calculated minimum value of T_1^l is 13.9 ms at 10.0 MHz and that of T_1^s is 5.8 ms at 25.54 MHz. There are some discrepancies between the calculated and observed T_1 values, which may be caused by the approximation that intermolecular contribution is to be ignored. However, the trend of the temperature dependence of T_1 is described satisfactorily by our simple but more or less rigorous treatment using a single correlation time τ_c.

As is apparent from the foregoing analysis of the experimental results, the data of ^{19}F relaxation can be used to deduce the relaxation behavior of protons in the present case. In other words, when there is a cross-relaxation effect between two nuclear species, one needs to know the relaxation behavior on only one of them which would then permit deductions on the other.

In the absence of structural information on CHF_3 it is difficult to rationalize the magnitude of the activation energy for molecular tumbling (17 kJ mol^{-1}). In the case of the low-temperature phase of CF_4, the activation energy was reported to be 18 kJ mol^{-1}.[15] Because the closest intermolecular approach is probably through F···F contacts, the similarity in the activation energy in these two substances would reflect the similarity in the intermolecular interaction.

The amounts of oxygen in the sample were kindly determined by gas chromatography at Osaka Oxygen Industries, Ltd. This work was supported by a grant

from the Ministry of Education, Science and Culture, to whom the authors express their gratitude.

References

1) R. H. Valentine, G. E. Brodale, and W. F. Giauque, *J. Phys. Chem.*, **66**, 392 (1962).
2) H. S. Gutowsky, I. J. Lawrenson, and K. Shimomura, *Phys. Rev. Lett.*, **6**, 349 (1961).
3) C. S. Johnson, Jr., J. S. Waugh, and J. N. Pinkerton, *J. Chem. Phys.*, **35**, 1128 (1961).
4) J. H. Chaffin III and P. S. Hubbard, *J. Chem. Phys.*, **46**, 1511 (1967).
5) T. Eguchi and H. Chihara, *J. Magn. Reson.*, **26**, 409 (1977).
6) S. Miyajima, N. Nakamura, and H. Chihara, *J. Phys. Soc. Jpn.*, **49**, 1867 (1980).
7) A. Abragam, "The Principles of Nuclear Magnetism," Oxford, New York (1961).
8) J. E. Anderson and W. P. Slichter, *J. Chem. Phys.*, **43**, 433 (1965).
9) D. E. O'Reilly, E. M. Peterson, and Tung Tsang, *Phys. Rev.*, **160**, 333 (1967).
10) S. Albert and H. S. Gutowsky, *J. Chem. Phys.*, **59**, 3585 (1973).
11) C. A. McDowell, P. Raghunathan, and D. S. Williams, *J. Magn. Reson.*, **32**, 57 (1978).
12) S. Albert and J. A. Ripmeester, *J. Chem. Phys.*, **70**, 1352 (1979).
13) S. N. Ghosh, R. Trambarulo, and W. Gordy, *J. Chem. Phys.*, **20**, 605 (1952).
14) The value of τ_0 is much smaller than what may be expected for the libration frequency corresponding to the activation energy.
15) L. Niemelä and M. Niemelä, *Ann. Acad. Sci. Fenn.*, **AVI**, 341 (1970).

Elementary Patterns in Protein-Nucleic Acid Interactions. III.† Crystal Structure of Adenine:Phthalic Acid (3:1) Complex Hexahydrate

Akio TAKENAKA* and Yoshio SASADA

Laboratory of Chemistry for Natural Products, Tokyo Institute of Technology, Nagatsuta, Midori-ku, Yokohama 227

(Received August 5, 1981)

Crystal of adenine:phthalic acid (3:1) complex hexahydrate were obtained from an aqueous solution containing equimolar amounts of adenine and *N,N*-phthaloyl-DL-glutamic acid. The space group is $P\bar{1}$ with unit-cell dimensions of $a=14.232(2)$, $b=16.730(2)$, $c=7.336(1)$ Å, $\alpha=78.97(1)$, $\beta=96.14(1)$, and $\gamma=68.99(1)°$. The structure was solved by the direct method and its parameters were refined by a block-diagonal least-squares technique. The two carboxyl groups of the phthalic acid are dissociated and they are hydrogen-bonded to the amino group and the protonated N(1) of the two adeninium monocations. The geometrical characteristics in adeninium monocations are explained with the electronic structures perturbed by the surroundings. A typical feature of the C–H···N hydrogen bond is observed between the adeninium cations. The third adenine molecule is neutral and disordered. A comparison of the dissociation constants of the related compounds suggests that the protonation of adenine occurs when the hydrogen bonds are formed between the carboxyl group of acidic amino acid residue in protein and the unpaired adenine base in nucleic acid.

We have been engaged in the structural studies on elementary patterns in protein-nucleic acid interactions, using crystals in which nucleotide base and amino acid coexist.[1–6] In case of the systems containing cytosine and carboxyl group, for instance, the α-carboxyl group is dissociated and hydrogen-bonded to the amino group and the protonated N(3) atom in cytosine,[1,2] whereas the γ-carboxyl group of glutamic acids interacts with the amino group of base-paired cytosine.[3] In the present paper, we deal with the system containing adenine and carboxyl group.

Experimental

Single crystals of adenine: phthalic acid (3:1) complex hexahydrate were obtained by slow evaporation of an aqueous solution containing equimolar amounts (0.2 mmol) of adenine and *N,N*-phthaloyl-DL-glutamic acid, both of which were purchased from Tokyo Kasei Kogyo Co. An elementary analysis. Found: C, 40.7; H, 4.5; N, 30.5%. Calcd. for $3C_5H_5N_5\cdot C_8H_6O_4\cdot 6H_2O$: C, 40.6; H, 4.9; N, 30.9%. It means that *N,N*-phthaloyl-DL-glutamic acid is hydrolyzed by heating the solution in presence of adenine. A crystal, $0.2\times0.3\times0.6$ mm³ in size, was used for X-ray data collection on a Rigaku four-circle diffractometer with graphite-monochromated Mo $K\alpha$ radiation ($\lambda=0.71073$ Å). The unit-cell dimensions were calculated with 65 high-angle reflexions. The crystal data are given in Table 1.

Diffraction intensities were measured in the $\omega/2\theta$ scan mode with a scan width of 1.3° (in ω) plus α_1-α_2 divergence and a scan speed of 4° (in 2θ) min^{-1}. Five reference reflexions showed no significant intensity deterioration throughout the data collection. The intensities were corrected for Lorentz and polarization factors but not for absorption effects. Of 7193 independent reflexions in the range $2<2\theta<55°$, 3117 weak reflexions with F_o less than $3\sigma_p(F_o)$ were considered to be unobserved, where $\sigma_p(F_o)$ is evaluated by counting statistics. The standard deviations were estimated by the equation of $\sigma^2(F_o)=\sigma_p^2(F_o)+qF_o^2$, where q (7.77×10^{-5}) was derived from the variations of the monitored reflexions.[7]

TABLE 1. CRYSTAL DATA

Adenine:Phthalic (3:1) complex hexahydrate	
$3C_5H_5N_5:C_8H_6O_4\cdot6H_2O$	*F.W.* 679.6
Space group: $P\bar{1}$	
$a=14.232(2)$ Å	$\alpha=78.97(1)°$
$b=16.730(2)$ Å	$\beta=96.14(1)°$
$c=7.336(1)$ Å	$\gamma=68.99(1)°$
$U=1570.7(4)$ Å³	$Z=2$
$D_x=1.437$ g·cm^{-3}	$D_m=1.43_7$ g·cm^{-3}

Structure Determination

The space group was assumed to be $P\bar{1}$ from normalized structure factor statistics. The phases were derived by using the MULTAN programme[8] with 436 E's ($E>1.9$); two reflexions with the largest E's (>5.0) were omitted in the calculation. Molecular skeletons of phthalic acid and three adenines were found on the E map derived from the phase set with the smallest R_{Karle} value.[9] Subsequent electron density calculations gave the positions of the six water molecules and then revealed that one of the three adenines was disordered in the two modes of orientations and that one of the six waters occupied the two sites. Positional and thermal parameters of the non-hydrogen atoms were refined by block-diagonal least-squares techniques, half occupancies being assumed for the disordered atoms. Hydrogen atoms except for the water and disordered adenine molecules were found on a difference map, which were included in later refinements. The quantity minimized was $\Sigma w(|F_o|-|F_c|)^2$ with $w=1/\sigma^2(F_o)$. The final R was 0.085 for the observed 4076 reflexions; the maximum shift of parameters in the last cycle was 0.2σ for C, N, and O atoms and 0.7σ for H atoms.

Atomic scattering factors used were taken from "International Tables for X-Ray Crystallography."[10] Atomic parameters are listed in Table 2.[11]

† Part II of this series is Ref. 6.

TABLE 2. FRACTIONAL COORDINATES AND ISOTROPIC TEMPERATURE FACTORS

The B values accompanied with $\langle\ \rangle$ are the equivalent isotropic temperature factors calculated from anisotropic thermal parameters using the equation $B=8\pi^2(U_1+U_2+U_3)/3$, where U_1, U_2, and U_3 are principal components of the mean square displacement matrix $\boldsymbol{U}$. Values in $\langle\ \rangle$ are anisotropicity defined by $(\sum(B-8\pi^2U_i)^2/3)^{1/2}$. The e.s.d.'s in ( ) refer to last decimal places.

Atom	x	y	z	B/Å^2	Atom	x	y	z	B/Å^2
N (1A)	0.0199 (2)	0.2197 (2)	0.1283 (5)	3.0⟨9⟩	C (3P)	0.4949 (3)	0.3872 (3)	0.1998 (7)	3.9⟨12⟩
C (2A)	0.1092 (3)	0.2272 (3)	0.1932 (7)	3.4⟨9⟩	C (4P)	0.4598 (3)	0.4414 (3)	0.3196 (7)	3.7⟨7⟩
N (3A)	0.2008 (3)	0.1639 (2)	0.2245 (5)	3.5⟨8⟩	C (5P)	0.3757 (3)	0.5209 (3)	0.2498 (6)	3.2⟨5⟩
C (4A)	0.1978 (3)	0.0884 (3)	0.1839 (6)	3.1⟨5⟩	C (6P)	0.3259 (3)	0.5465 (3)	0.0610 (6)	2.5⟨6⟩
C (5A)	0.1113 (3)	0.0745 (3)	0.1229 (6)	2.7⟨5⟩	C (7P)	0.3123 (3)	0.5189 (3)	−0.2643 (6)	2.8⟨5⟩
C (6A)	0.0147 (3)	0.1440 (3)	0.0914 (6)	3.0⟨7⟩	C (8P)	0.2326 (3)	0.6309 (3)	0.0006 (6)	2.9⟨6⟩
N (6A)	−0.0747 (3)	0.1430 (2)	0.0330 (6)	3.9⟨22⟩	O (71P)	0.3170 (2)	0.4569 (2)	−0.3473 (4)	3.5⟨11⟩
N (7A)	0.1377 (3)	−0.0107 (2)	0.0987 (5)	3.3⟨11⟩	O (72P)	0.2662 (2)	0.5989 (2)	−0.3451 (4)	3.5⟨10⟩
C (8A)	0.2386 (3)	−0.0443 (3)	0.1438 (7)	3.8⟨13⟩	O (81P)	0.1465 (2)	0.6269 (2)	−0.0446 (4)	3.5⟨15⟩
N (9A)	0.2788 (3)	0.0123 (2)	0.1973 (6)	3.8⟨17⟩	O (82P)	0.2441 (2)	0.7015 (2)	0.0071 (5)	4.5⟨26⟩
N (1B)	0.1512 (3)	0.4993 (2)	0.4067 (5)	2.9⟨7⟩	O (1W)	0.4408 (4)	0.1706 (3)	0.0006 (7)	10.6⟨24⟩
C (2B)	0.1457 (3)	0.4244 (3)	0.3687 (6)	3.4⟨7⟩	O (2W)	0.2468 (3)	0.7768 (2)	0.5438 (5)	6.1⟨16⟩
N (3B)	0.0653 (3)	0.4176 (2)	0.2798 (5)	3.3⟨8⟩	O (3W)	0.4284 (3)	0.2809 (2)	0.6613 (6)	6.3⟨16⟩
C (4B)	−0.0160 (3)	0.4969 (3)	0.2272 (6)	2.7⟨5⟩	O (4W)	0.3641 (3)	0.7429 (2)	0.2687 (5)	5.8⟨27⟩
C (5B)	−0.0193 (3)	0.5765 (3)	0.2563 (6)	2.6⟨4⟩	O (5W)	0.3726 (4)	0.2186 (4)	0.3308 (8)	12.2⟨69⟩
C (6B)	0.0702 (3)	0.5784 (3)	0.3546 (6)	2.7⟨3⟩	O (6W)	0.4880 (5)	−0.0459 (6)	0.346 (1)	8.0⟨49⟩
N (6B)	0.0799 (3)	0.6483 (2)	0.3993 (5)	3.4⟨13⟩	O (7W)	0.4796 (6)	−0.0149 (7)	0.176 (2)	11.3⟨77⟩
N (7B)	−0.1164 (3)	0.6415 (2)	0.1834 (5)	3.0⟨4⟩	H (61A)	−0.132 (3)	0.193 (3)	0.013 (6)	2.4 (11)
C (8B)	−0.1677 (3)	0.5990 (3)	0.1108 (6)	3.2⟨7⟩	H (62A)	−0.079 (3)	0.093 (3)	0.007 (6)	2.8 (11)
N (9B)	−0.1112 (3)	0.5111 (2)	0.1340 (5)	3.0⟨7⟩	H (1A)	−0.047 (3)	0.271 (3)	0.104 (6)	2.5 (11)
N (1C)	−0.3346 (3)	0.9882 (4)	0.2741 (7)	7.1⟨37⟩	H (2A)	0.101 (3)	0.291 (3)	0.211 (6)	3.2 (12)
C (2C)	−0.3306 (5)	1.0633 (5)	0.3076 (9)	8.8⟨54⟩	H (9A)	0.352 (4)	−0.004 (3)	0.244 (7)	5.4 (14)
N (3C)	−0.2356 (3)	1.0646 (3)	0.3613 (6)	6.2⟨24⟩	H (8A)	0.281 (4)	−0.111 (3)	0.143 (7)	5.6 (15)
C (4C)	−0.1612 (4)	0.9845 (4)	0.3684 (7)	5.1 (32)	H (61B)	0.143 (3)	0.643 (3)	0.474 (6)	2.3 (11)
C (5C)	−0.1489 (7)	0.8953 (6)	0.333 (1)	3.8⟨14⟩	H (62B)	0.019 (3)	0.714 (3)	0.370 (6)	3.5 (12)
C (6C)	−0.2476 (7)	0.8942 (7)	0.283 (1)	4.9⟨21⟩	H (1B)	0.213 (3)	0.492 (3)	0.490 (6)	1.8 (10)
C (5'C)	−0.2353 (7)	0.9508 (6)	0.309 (1)	3.5⟨11⟩	H (2B)	0.212 (3)	0.369 (3)	0.415 (6)	1.8 (10)
C (6'C)	−0.1847 (7)	0.8662 (6)	0.301 (1)	3.2⟨6⟩	H (9B)	−0.131 (3)	0.467 (3)	0.098 (6)	3.6 (12)
N (6C)	−0.2460 (4)	0.8169 (3)	0.2470 (6)	5.8⟨29⟩	H (8B)	−0.237 (3)	0.625 (2)	0.048 (5)	0.7 (9)
N (7C)	−0.0654 (3)	0.8300 (2)	0.3520 (6)	4.5⟨16⟩	H (2P)	0.476 (3)	0.375 (3)	−0.087 (6)	2.2 (10)
C (8C)	−0.0069 (5)	0.8731 (3)	0.4043 (7)	6.1⟨44⟩	H (3P)	0.560 (3)	0.325 (3)	0.256 (6)	3.6 (12)
N (9C)	−0.0573 (3)	0.9586 (3)	0.4172 (6)	4.7⟨19⟩	H (4P)	0.494 (3)	0.426 (3)	0.466 (6)	2.2 (10)
C (1P)	0.3613 (3)	0.4920 (3)	−0.0592 (6)	2.3⟨3⟩	H (5P)	0.347 (3)	0.562 (3)	0.340 (6)	1.9 (10)
C (2P)	0.4456 (3)	0.4124 (3)	0.0106 (6)	3.2⟨8⟩					

Results and Discussion

Molecular Structure. Both the two carboxyl groups of phthalic acid, I and II, are dissociated and the two adenine molecules, A and B, are monoprotonated at N(1), as confirmed by a difference synthesis. The third adenine, C, is neutral and disordered in the two modes of orientations. Bond distances and angles are shown in Fig. 1.

The two C–O distances in the carboxyl group I differ significantly from each other, while those in the carboxyl group II are almost the same. The longer C(7P)–O(71P) bond suggests that the negative charges are localized mainly on O(71P). The benzene ring of the phthalic acid is planar within 0.002 Å, from which the carboxyl carbon atoms, C(7P) and C(8P), are deviated by −0.050 Å and 0.070 Å, respectively, perhaps owing to repulsions between them. The mean planes of the carboxyl groups make angles of 27.6(2)° for I and 64.6(2)° for II with that of the benzene ring. These values do not seem to be inherent though they resemble those of bivalent phthalic acid salt;[12] the relative orientation of the carboxyl groups varies easily by packing effects of crystal.[13]

It is known that adenine molecule exists in acidic circumstances as mono- or di-cation, whose bond lengths and angles are dependent on protonation.[14,15] The dimensions of the present adeninium cations, A and B, correspond to typical ones of the monocationic species.[14] Figure 2 shows the environments of molecules surrounded by hydrogen bonds. The protonated N(1) and the amino nitrogen N(6) atoms in adeninium B are hydrogen bonded to the carboxylate oxygens, O(71P) and O(72P) of the group I, respectively, while those in A form a similar double-

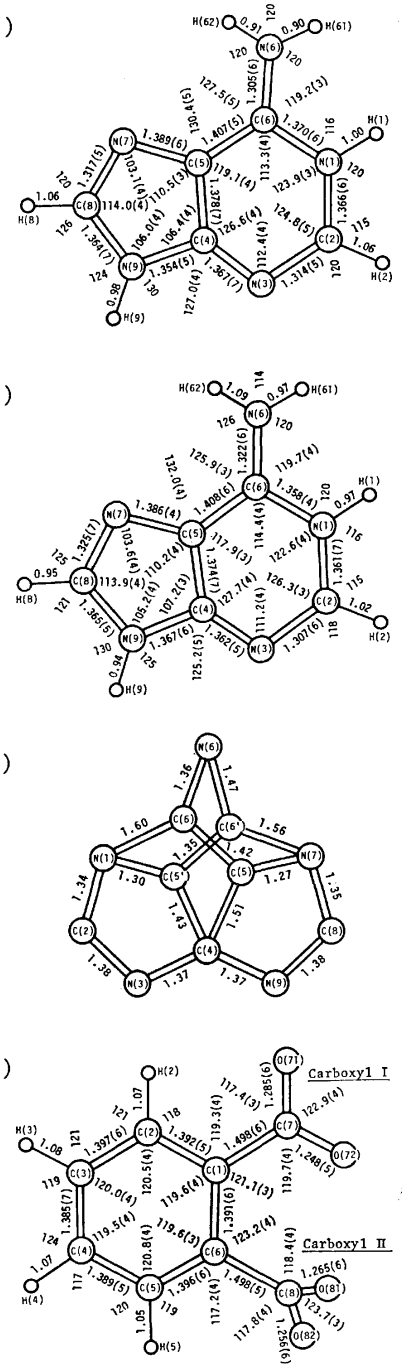

Fig. 1. Bond lengths (l/Å) and angles (ϕ/°) of adenine: phthalic acid (3:1) complex hexahydrate.
(a) Adenine A, (b) adenine B, (c) adenine C, and (d) phthalic acid. E.s.d.'s are 0.05 Å and 4° for H atoms.

hydrogen bond with the carboxyl group II. Here it is noted that the N(1)···O(71P) hydrogen bond (2.594(5) Å) is significantly shorter than the others, and the negative charges are predominant at O(71P), as mentioned above. In such situation, the adeninium B is perturbed, so that the contribution of canonical formula **1** increases, as compared with the adeninium A in which the canonical formula **2** is predominant. The shorter C(6)–N(6) bond of adeninium A, accompanied by the slightly longer C(6)–N(1) bond

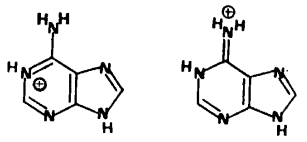

1 **2**

than that of B, is consistent with this anticipation. Table 3 shows the atomic net charges calculated by CNDO approximation[16] for these two adeninium cations. In adeninium A, the positive charges on the amino group increase and those on N(1)–H(1) group decrease, as compared with those in B. These charges, though small, seem to be consistent with the above interpretation.

The adeninium monocations so far analysed show the marked differences in C(6)–N(6) and C(6)–N(1) bond distances, which suggest the change in relative contributions from the two canonical formulae, **1** and **2**. The difference between adenosine hydrochloride[14f] and adenine hydrochloride hemihydrate[14d] can be correlated to the hydrogen bond distances, just as mentioned above. It may be concluded that the adenine cation can be adapted to the various surroundings by changing its electronic structure to some extent.

Crystal Structure. The crystal structure viewed down the c axis is shown in Fig. 3. Hydrogen bond distances and angles are given in Fig. 2 and Table 4.

The adenine C is disordered with a local approximate mirror symmetry; the mirror plane is perpendicular to the adenine plane passing through N(6) and C(4). As seen from Fig. 3, only the C(5) and C(6) atoms give the resolved peaks on the electron density map. The disordered adenine molecules around the inversion centre at 0,0,1/2 may be hydrogen bonded with the scheme shown in Fig. 4. According to this scheme, the water oxygen, O(6W) and O(7W), are also disordered by the hydrogen bonds with the adenine C.

TABLE 3. NET CHARGE DISTRIBUTION

	Adenine A	Sum for the group	Adenine B	Sum for the group
N (1)	−0.112	0.057	−0.109	0.064
H (1)	0.169		0.173	
C (2)	0.241	0.288	0.237	0.280
H (2)	0.047		0.043	
N (3)	−0.165		−0.161	
C (4)	0.243		0.236	
C (5)	−0.045		−0.041	
C (6)	0.335		0.338	
N (7)	−0.164		−0.165	
C (8)	0.190	0.233	0.196	0.240
H (8)	0.043		0.044	
N (9)	−0.105		−0.114	
H (9)	0.168		0.169	
N (6)	−0.203	0.156	−0.200	0.153
H (61)	0.171		0.160	
H (62)	0.181		0.193	

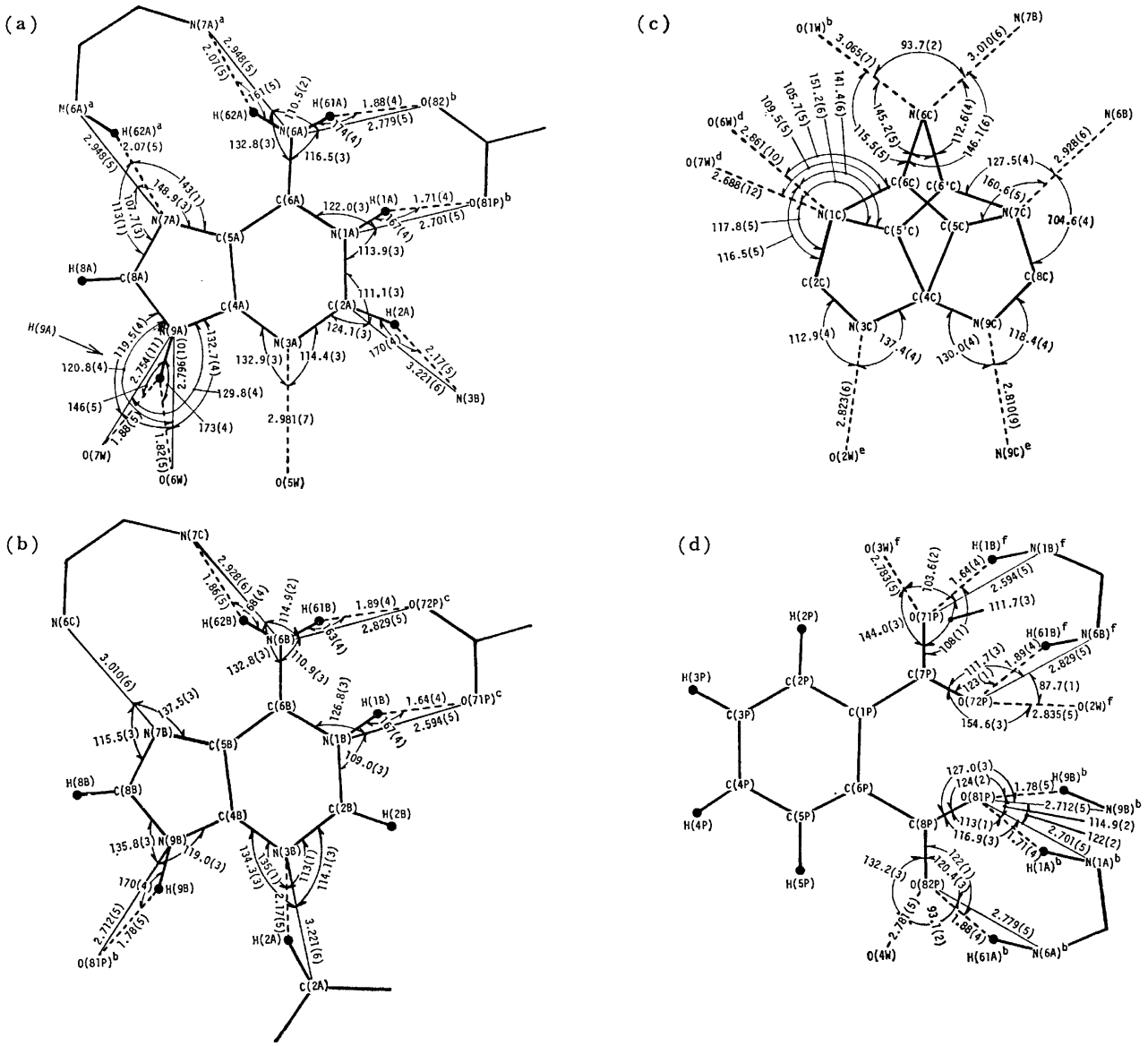

Fig. 2. Hydrogen bond distances (l/Å) and angles (ϕ/°) for (a) adenine A, (b) adenine B, (c) adenine C, and (d) phthalic acid.
The symmetry codes, a—f, are the same as those in Table 4.

The two adeninium A's form a dimer around the inversion centre at 0,0,0 through the N(6)–H···N(7) hydrogen bond. The adeninum B forms a dimer with the adenine C through the N(7B)···H–N(6C) and N(6B)–H···N(7C) [or disordered N(1C)] hydrogen bonds.

Intermolecular stackings are made with different kinds of adenine. The adeninium A and the adenine C at $-x,1-y,-z$ are stacked alternatively along the c axis with the dihedral angle of 2.4(1)° and with the spacings of 3.26 and 3.56 Å. The adeninium B is stacked parallel to that related by the inversions at 0,1/2,0 or 0,1/2,1/2 along the c axis with the spacings of 3.23 and 3.33 Å, respectively. By this way, all kinds of adenines form a layer parallel to the bc plane.

The phthalic acid is linked to the three adeninium cations by the hydrogen bonds between the carboxyl I and the adeninium B [N(6) and the protonated N(1)] and between the carboxyl II and the adeninium A [the same atoms as B] at $-x,1-y,-z$, O(81P) of the latter carboxyl group II being at the same time an acceptor of hydrogen bond from N(9) of adeninium B at $-x,1-y,-z$. The benzene ring of this acid is stacked parallel to that related by the inversion at 1/2,1/2,1/2 with the spacing of 3.45 Å. The water molecules lie between the adenine layers, forming hydrogen bonds with adenine, phthalic acid, and other water molecules.

A short C–H···N contact is observed between the adeninium A and B, as shown in Fig. 2. The C(2)–H(2) bond points to a lone pair lobe of N(3). Since N(3) is significantly negative and the C(2)–H(2) group is positive (Table 3), this contact is favourable to assume the C–H···N hydrogen bond, which has been proposed in hydrogen cyanide,[17] α-1-[(*p*-bromophenyl)-

TABLE 4. HYDROGEN BOND DISTANCES AND ANGLES OF WATER MOLECULES

Some short contacts are also shown. Standard deviations are given in parentheses.

Distances(l/Å)		Angles(ϕ/°)	
O (1W) ··· N (6C) [b]	3.065 (5)	N (6C) [b] ··· O (1W) ··· O (3W) [f]	76.0 (2)
O (1W) ··· O (3W) [f]	2.747 (7)	N (6C) [b] ··· O (1W) ··· O (5W)	103.7 (2)
O (1W) ··· O (5W)	2.853 (8)	N (6C) [b] ··· O (1W) ··· O (7W)	88.6 (3)
O (1W) ··· O (7W)	2.948 (12)	O (3W) [f] ··· O (1W) ··· O (5W)	127.9 (3)
O (1W) ··· O (7W) [j]	3.040 (12)	O (3W) [f] ··· O (1W) ··· O (7W)	141.8 (3)
		O (5W) ··· O (1W) ··· O (7W)	89.4 (3)
O (2W) ··· N (3C) [e]	2.823 (6)	N (3C) [e] ··· O (2W) ··· O (72P) [c]	150.0 (2)
O (2W) ··· O (72P) [c]	2.835 (5)	N (3C) [e] ··· O (2W) ··· O (4W)	111.1 (2)
O (2W) ··· O (4W)	2.768 (5)	O (72P) [c] ··· O (2W) ··· O (4W)	92.6 (2)
O (3W) ··· O (71P) [d]	2.783 (5)	O (71P) [c] ··· O (3W) ··· O (1W) [c]	111.4 (2)
O (3W) ··· O (1W) [c]	2.747 (7)	O (71P) [c] ··· O (3W) ··· O (4W) [g]	105.9 (2)
O (3W) ··· O (4W) [g]	2.810 (5)	O (71P) [c] ··· O (3W) ··· O (5W)	116.5 (2)
O (3W) ··· O (5W)	2.957 (7)	O (1W) [c] ··· O (3W) ··· O (4W) [g]	94.6 (2)
		O (1W) [c] ··· O (3W) ··· O (5W)	113.0 (2)
		O (4W) [g] ··· O (3W) ··· O (5W)	113.2 (2)
O (4W) ··· O (82P)	2.781 (5)	O (82P) ··· O (4W) ··· O (2W)	103.5 (2)
O (4W) ··· O (2W)	2.768 (5)	O (82P) ··· O (4W) ··· O (3W) [g]	134.4 (2)
O (4W) ··· O (3W) [g]	2.810 (5)	O (2W) ··· O (4W) ··· O (3W) [g]	120.3 (2)
O (5W) ··· N (3A)	2.981 (7)	N (3A) ··· O (5W) ··· O (1W)	85.8 (2)
O (5W) ··· O (1W)	2.853 (8)	N (3A) ··· O (5W) ··· O (3W)	131.5 (2)
O (5W) ··· O (3W)	2.957 (7)	O (1W) ··· O (5W) ··· O (3W)	142.6 (3)
O (6W) ··· N (9A)	2.796 (10)	N (9A) ··· O (6W) ··· N (1C) [h]	140.9 (4)
O (6W) ··· N (1C) [h]	2.861 (10)	N (9A) ··· O (6W) ··· O (6W) [i]	108.2 (3)
O (6W) ··· O (6W) [i]	3.026 (17)	N (1C) [h] ··· O (6W) ··· O (6W) [i]	79.9 (3)
O (7W) ··· N (9A)	2.754 (11)	N (9A) ··· O (7W) ··· N (1C) [h]	156.9 (5)
O (7W) ··· N (1C) [h]	2.688 (12)	N (9A) ··· O (7W) ··· O (1W)	96.2 (4)
O (7W) ··· O (1W)	2.948 (12)	N (9A) ··· O (7W) ··· O (7W) [j]	115.9 (5)
O (7W) ··· O (7W) [j]	2.705 (22)	N (1C) [h] ··· O (7W) ··· O (1W)	78.8 (3)
O (7W) ··· O (1W) [j]	3.040 (12)	N (1C) [h] ··· O (7W) ··· O (7W) [j]	82.7 (4)
		O (1W) ··· O (7W) ··· O (7W) [j]	64.9 (3)

Symmetry codes (a) $-x, -y, -z$, (b) $-x, 1-y, -z$, (c) $x, y, 1+z$, (d) $-1+x, 1+y, z$, (e) $-x, 2-y, 1-z$, (f) $x, y, -1+z$, (g) $1-x, 1-y, 1-z$, (h) $1+x, -1+y, z$, (i) $1-x, -y, 1-z$, (j) $1-x, -y, -z$.

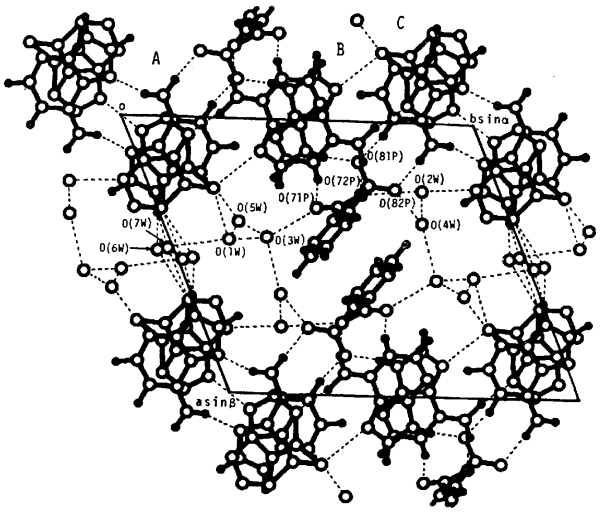

Fig. 3. Crystal structure of adenine:phthalic acid (3:1) complex hexahydrate, projected along the c axis. Adenine, A, B, C, and atomic numbering of water molecules are shown. The broken lines indicate the hydrogen bonds.

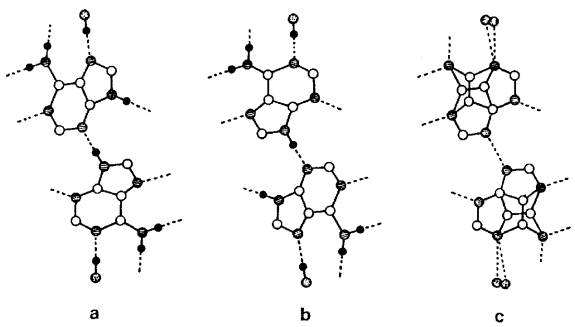

Fig. 4. Hydrogen-bonding scheme of disordered adenine C; (a) and (b) for alternative arrangements. Superposition of (a) and (b) can well explain the electron density map (c).

phenylmethylene]-3-oxo-1,2-diazetidinium inner salt,[18] and (5-methyl-2-pyridinecarbaldehyde 2-pyridylhydrazone)tetracarbonylmolybdenum(0).[19]

Hydrogen Bonding between Adenine and Carboxyl Group. As mentioned above, the two dissociated carboxyl groups of phthalic acid interact respectively with the two protonated adenines by the double hydrogen bond, as shown in Fig. 5. This pattern resembles that found in adenine:*m*-bromobenzoic acid (2:4) complex.[20a] In the latter complex, however, the proton-transfer between the two components is ambiguous due to the disordered structure.[20b]†† The dihedral angle between the base and the carboxyl group is 12.9(2)° for adeninium A and 45.6(2)° for adeninium B; the binding geometry is given in Table 5. Such non-planarity occurs because the phthalic acid is bridged between the two adeninium A and B which are stacked in the different columns, ACAC.. and BB.., respectively. The hydrogen bond scheme with the smaller dihedral angle may be more favourable one.

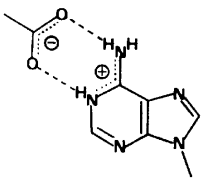

Fig. 5. Interaction pattern between adenine and carboxyl group.

Table 5. Geometrical data to define the interaction between adenine and carboxyl group

The symmetry codes, b and c, are the same as those in Table 4. Hydrogen bond distances and angles are shown in Fig. 2.

i	*j*	*k*	*l*	Torsion angle (ϕ_{ijkl}/°)
C(6P)	C(8P)	O(81P)	N(1A)[b]	175.8
C(6P)	C(8P)	O(82P)	N(6A)[b]	191.9
C(8P)	O(81P)	N(1A)[b]	C(6A)[b]	348.5
C(8P)	O(81P)	N(1A)[b]	C(2A)[b]	174.0
C(8P)	O(82P)	N(6A)[b]	C(6A)[b]	348.2
O(81P)	N(1A)[b]	C(6A)[b]	N(6A)[b]	7.4
O(81P)	N(1A)[b]	C(2A)[b]	N(3A)[b]	172.7
O(82P)	N(6A)[b]	C(6A)[b]	N(1A)[b]	0.2
O(82P)	N(6A)[b]	C(6A)[b]	C(5A)[b]	180.0
C(1P)[c]	C(7P)[c]	O(71P)[c]	N(1B)	143.8
C(1P)[c]	C(7P)[c]	O(72P)[c]	N(6B)	220.7
C(7P)[c]	O(71P)[c]	N(1B)	C(6B)	5.0
C(7P)[c]	O(71P)[c]	N(1B)	C(2B)	199.3
C(7P)[c]	O(72P)[c]	N(6B)	C(6B)	345.1
O(71P)[c]	N(1B)	C(6B)	N(6B)	14.7
O(71P)[c]	N(1B)	C(2B)	N(3B)	166.6
O(72P)[c]	N(6B)	C(6B)	N(1B)	349.9
O(72P)[c]	N(6B)	C(6B)	C(5B)	169.1

†† Lancelot has reported the three types of hydrogen bonds for adenine with butyric acid in chloroform solution from NMR study.[21] Although one of them is similar to the present pattern, the proton transfer is not assumed between the two components.

We have attempted an interpretation in terms of dissociation constant, which was successful for the binding mode in cytosine:glutamic acid system.[2a] Since the pK_a^I value of phthalic acid (2.95) is lower than that of adenine (4.25), the latter molecule is easily protonated by the first dissociation of phthalic acid in solution, but it could scarcely take a proton from the second dissociation because of higher pK_a^{II} (5.41) than that of adenine. In the present crystal, however, even the latter dissociation takes place. It is suggested that when the carboxyl group approaches adenine within a distance sufficient to form hydrogen bonds, their mutual perturbation favours to induce the ionizations.

The pK_a value of acidic side group of proteins is near pK_a of *N*-acetylglutamic acid α-methylamide (4.34),[22] whose value is comparable to that of the second carboxyl group of phthalic acid. On the other hand, adenine bases in nucleic acid would have a pK_a close to that of adenosine-5′-monophosphate (3.74) or its deoxy form (4.4), which is approximate to the adenine's value. Therefore, the pattern of hydrogen bonding, as shown in Fig. 5, would be found in the interaction between the side group of an acidic amino acid residue in protein and an unpaired adenine base in nucleic acid; the proton transfer must occur and their hydrogen bonds would be strengthened by an ionic effect induced.

Figure 3 was drawn by TSD:XTAL[23] for a NOVA 3 computer. The present work was supported in part by a Grant-in-Aid for Scientific Research from the Ministry of Education, Science and Culture, and by the Kawakami Foundation, to which the authors' thanks are due.

References

1) M. Ohki, A. Takenaka, H. Shimanouchi, and Y. Sasada, *Bull. Chem. Soc. Jpn.*, **48**, 848 (1975); C. Tamura, T. Hata, S. Sato, and N. Sakurai, *ibid.*, **44**, 1473 (1971).

2) A. Takenaka, M. Ohki, and Y. Sasada, *Bull. Chem. Soc. Jpn.*, **53**, 2724 (1980); T. Hata, M. Yoshikawa, S. Sato, and C. Tamura, *Acta Crystallogr., Sect. B*, **31**, 312 (1975).

3) M. Ohki, A. Takenaka, H. Shimanouchi, and Y. Sasada, *Bull. Chem. Soc. Jpn.*, **50**, 90 (1977); **49**, 3493 (1976).

4) M. Ohki, A. Takenaka, H. Shimanouchi, and Y. Sasada, *Bull. Chem. Soc. Jpn.*, **50**, 2573 (1977); T. Kaneda and J. Tanaka, *ibid.*, **49**, 1799 (1976).

5) M. Ohki, A. Takenaka, H. Shimanouchi, and Y. Sasada, *Acta Crystallogr., Sect. B*, **33**, 2954, 2956 (1977).

6) M. Takimoto, A. Takenaka, and Y. Sasada, *Bull. Chem. Soc. Jpn.*, **54**, 1635 (1981).

7) L. E. McCandlish and G. H. Staut, *Acta Crystallogr., Sect. A*, **31**, 245 (1975).

8) G. Germain, P. Main, and M. M. Woolfson, *Acta Crystallogr., Sect. A*, **27**, 368 (1971).

9) I. L. Karle and J. Karle, *Acta Crystallogr.*, **21**, 849 (1966).

10) "International Tables for X-Ray Crystallography," Kynoch Press, Birmingham (1974), Vol. IV, p. 71.

11) Lists of structure factors, anisotropic thermal param-

eters, and least-squares plane equations and deviations of atoms from these planes have been deposited as Document No. 8216, at the Office of the Chemical Society of Japan.

12) R. A. Smith, *Acta Crystallogr., Sect. B*, **31**, 1773 (1975).

13) J. W. Bats, A. Kallel, and H. Fuess, *Acta Crystallogr., Sect. B*, **34**, 1705 (1978).

14) a) B. E. Hingerty, J. R. Einstein, and C. H. Wei, *Acta Crystallogr., Sect. B*, **37**, 140 (1981); b) V. Langer, K. Huml, and L. Lessinger, *ibid.*, **34**, 2229 (1978); c) H.-S. Shieh and D. Voet, *ibid.*, **31**, 2192 (1975); d) T. J. Kistenmacher and T. Shigematsu, *ibid.*, **30**, 166 (1974); e) P. L. Johnson, J. K. Frank, and I. C. Paul, *J. Am. Chem. Soc.*, **95**, 5377 (1973); f) K. Shikata, T. Ueki, and T. Mitsui, *Acta Crystallogr., Sect. B*, **29**, 31 (1973).

15) V. Langer and K. Huml, *Acta Crystallogr., Sect. B*, **34**, 1157 (1978).

16) J. A. Pople and D. L. Beveridge, "Approximate Molecular Orbital Theory," McGraw-Hill Book Company, New York (1970).

17) W. J. Dulmage and W. N. Lipscomb, *Acta Crystallogr.*, **4**, 330 (1951).

18) C. J. Fritchie, jun. and J. L. Wells, *J. Chem. Soc., Chem. Commun.*, **1968**, 917.

19) R. St. L. Bruce, M. K. Cooper, H. C. Freeman, and B. G. McGrath, *Inorg. Chem.*, **13**, 1032 (1974).

20) a) C. Tamura, N. Sakurai, and S. Sato, *Bull. Chem. Soc. Jpn.*, **44**, 1473 (1971); b) C. Tamura, private communication.

21) G. Lancelot, *J. Am. Chem. Soc.*, **99**, 7037 (1977).

22) T. Miyazawa, private communication.

23) A. Takenaka and Y. Sasada, *J. Cryst. Soc. Jpn.*, **22**, 214 (1980).

 © 1982 The Chemical Society of Japan Bull. Chem. Soc. Jpn., 55, 687—689 (1982)

The Adsorption of Amino Acids from Water on Activated Carbons

Ikuo Abe,* Katsumi Hayashi, and Mutsuo Kitagawa**

Osaka Municipal Technical Research Institute, Ogimachi, Kita-ku, Osaka 530

***Society for Activated Carbon Research, Ogimachi, Kita-ku, Osaka 530*

(Received August 5, 1981)

Freundlich's adsorption constants of 17 amino acids from aqueous solutions onto an activated carbon have been determined and correlated with various physical constants. A good linear relationship is obtained between the adsorption constants and such physical constants as the molecular refraction and the parachor. The adsorption isotherms of amino acids can be predicted from the molecular refraction or the parachor alone.

The ability to predict the adsorbability for a given adsorbent from a knowledge of the physical properties of the adsorbate is an important objective in adsorbent-adsorbate interaction research. In a previous paper,[1] the partition coefficients of 93 organic compounds between an aqueous solution and activated carbon phases at an infinite dilution have been calculated and correlated with various physical constants. Further, the adsorptive mechanism on activated carbon in an aqueous solution has been discussed.[2] Abe *et al.*[3,4] have presented an adsorption equation for predicting the adsorption isotherms of organic compounds from water on activated carbons and showed that, for aliphatic monofunctional compounds, such physical constants as the molecular refraction or the parachor are useful for the prediction. The present paper aims to examine whether or not the method of prediction is applicable to such multifunctional compounds as amino acids.

Experimental

The adsorbent (Pittsburgh Activated Carbon Co., grade CAL activated carbon) and experimental techniques were the same as those described in a previous paper.[2] All of the adsorbates came from commercial sources (stated minimum assay 99%) and were used without further purification. The substances tested were adsorbed from pure solutions, with no special effort being made to control their pH, since ampholytes in solution tend to maintain pH values near their isoelectric points. A comparison of the pH values of many amino acid solutions before and after adsorption revealed relatively little change in the pH.

Results and Discussion

Figure 1 shows the adsorption isotherms of 17 amino acids onto CAL activated carbon at 25 °C. The adsorption isotherms have been approximated by means of the Freundlich equation:

$$\log X = \log k + \frac{1}{n} \log C, \quad (1)$$

where C is the equilibrium concentration(mg/l), X is the amount of adsorption(mg/g), and k and $1/n$ are constants. The results of regression analysis using Eq. 1 are presented in Table 1.

In order to clarify the adsorptive mechanism of amino acids, the correlation between the adsorption constants and various physical constants has been examined. Table 2 shows the results of the regression analysis for Eq. 2:

$$\log k = a\Phi + b, \quad (2)$$

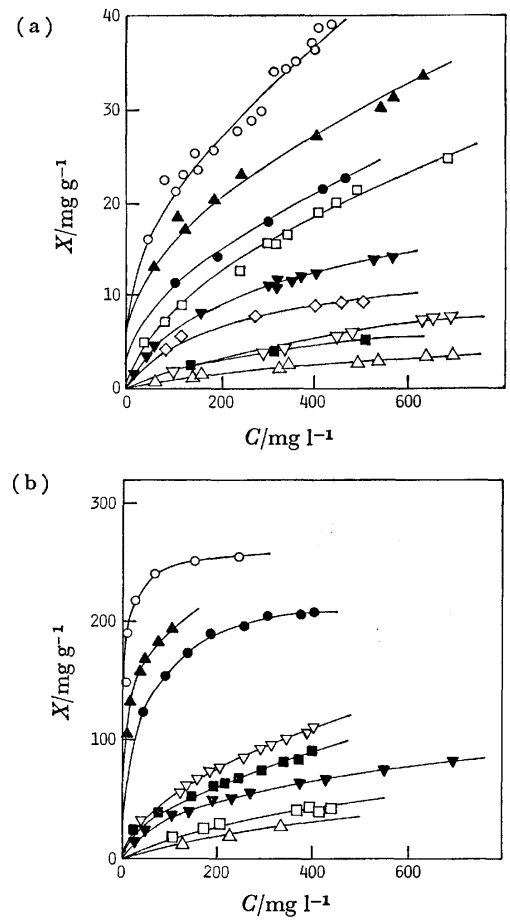

Fig. 1. Adsorption isotherms of 17 amino acids from water onto CAL activated carbon.
(a) ○: L-Glutamic acid, ▲: L-glutamine, ●: L-proline, □: DL-valine, ▼: L-asparagine, ◇: L-threonine, ▽: DL-alanine, ■: L-serine, △: glycine.
(b) ○: L-Tryptophan, ▲: L-tyrosine, ●: L-phenylalanine, ▽: L-methionine, ■: L-histidine, ▼: L-leucine, □: L-isoleucine, △: L-aspartic acid.

where Φ is the physical constant of amino acids and where a and b are constants. In this table, r is the correlation coefficient; s, the standard deviation, and F and t, the values of the statistical test. A high correlation coefficient has been obtained for the molecular-size parameters, such as the molecular refraction, the parachor, or the molecular weight. This result resembles that observed for aliphatic monofunctional compounds.[4] Further, a good linear relationship has been obtained for a very simple value, the carbon-atom number in a molecule. This sug-

gests that the decisive component of the adsorption forces on an activated carbon surface is the hydrophobic interaction. It is well known that compounds with a low solubility are more readily adsorbed than compounds with a high solubility, but the data in Table 2 indicate that solubility is not a dominant factor governing the adsorption of amino acids. Figure 2 shows the relationship between $\log k$ and the molecular refraction.

Table 3 shows the results of regression analysis for Eq. 3:

$$1/n = a\Phi + b. \quad (3)$$

The correlation coefficients for Eq. 3 are lower than those for Eq. 2. Figure 3 shows the relationship between $1/n$ and the molecular refraction.

Table 1. Adsorption parameters of amino acids on CAL activated carbon (25 °C)

Compound No.	Compound	k	$1/n$
1	Glycine	0.0994	0.523
2	DL-Alanine	0.0444	0.774
3	DL-Valine	0.697	0.541
4	L-Leucine	4.84	0.430
5	L-Isoleucine	1.67	0.519
6	L-Serine	0.175	0.534
7	L-Threonine	0.953	0.370
8	L-Tyrosine	62.4	0.247
9	L-Phenylalanine	61.3	0.207
10	L-Tryptophan	129	0.134
11	L-Aspartic acid	0.943	0.553
12	L-Asparagine	0.201	0.693
13	L-Glutamic acid	3.47	0.393
14	L-Glutamine	3.37	0.349
15	L-Histidine	6.44	0.423
16	L-Methionine	5.43	0.499
17	L-Proline	0.524	0.611

In order to examine whether Eqs. 2 and 3 are applicable to the other activated carbons with different adsorptive capacities, the data in two articles have been tested. Cheldelin and Williams[5] measured

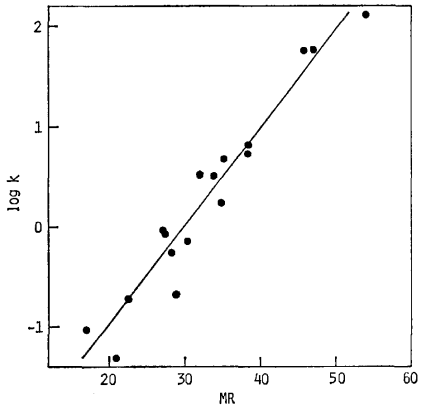

Fig. 2. Relationship between $\log k$ and molecular refraction (MR).

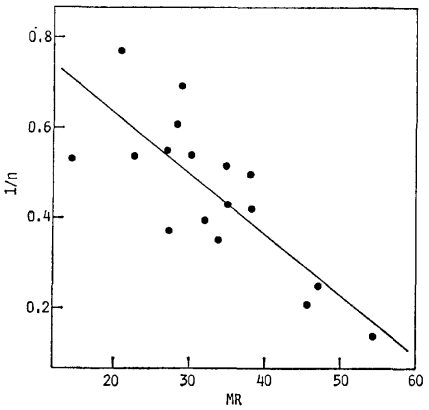

Fig. 3. Relationship between $1/n$ and molecular refraction (MR).

Table 2. Results of regression analysis for the $\log k = a\Phi + b$ equation

Physical constant	Φ	a	b	r	s	F	t
Molecular refraction[a]	MR	0.09802	−2.945	0.9575	0.2953	165.4	12.86***[d]
Parachor[b]	P	0.01341	−3.633	0.9514	0.3154	143.1	11.96***
Molecular weight	MW	0.02905	−3.635	0.9355	0.3620	105.1	10.25***
Carbon number	CN	0.3933	−1.839	0.9308	0.3743	97.31	9.865***
Solubility[c]	$\log C_s$	−0.7891	1.569	−0.6417	0.7855	10.50	−3.240**

a) These physical constants are taken from A. I. Vogel, W. C. Cresswell, G. H. Jeffery, and J. Leicester, *J. Chem. Soc.*, **1952**, 514. b) H. P. Meissner, *Chem. Eng. Progr.*, **45**, 149 (1949). c) The solubilities(C_s), in g/1000 g of water, are taken from "Seikagaku Data Book," ed by Nippon Seikagakukai, Tokyokagakudojin, Tokyo (1979), Vol. 1. d) Significance level: $*<0.05$, $**<0.01$, $***<0.001$.

Table 3. Results of regression analysis for the $1/n = a\Phi + b$ equation

Physical constant	Φ	a	b	r	s	F	t
Molecular refraction	MR	−0.01356	0.9060	−0.7845	0.1072	24.01	−4.900***
Parachor	P	−0.001836	0.9958	−0.7717	0.1099	22.09	−4.700***
Molecular weight	MW	−0.004087	1.011	−0.7797	0.1082	23.26	−4.823***
Carbon number	CN	−0.05698	0.7672	−0.7990	0.1039	26.48	−5.145***
Solubility	$\log C_s$	0.1070	0.2853	0.5157	0.1481	5.435	2.331*

Table 4. Relationship between Freundlich's constants taken from the literature and molecular refraction

Literature	Freundlich's constant	Number of compounds	a	b	r	s	F	t
Ref. 5	log (k/mg)	14	1.385	−4.981	0.9423	0.5461	95.04	9.749***
	log (k/mol)	14	0.03098	−3.596	0.6609	0.3903	9.305	3.050*
	$1/n$	14	−0.01997	1.240	−0.8507	0.1369	31.42	−5.605***
Ref. 6	log (k/mg)	8	0.08790	−2.535	0.9106	0.4501	29.14	5.399**
	log (k/mol)	8	−0.01669	−1.108	−0.4593	0.3644	1.604	−1.266
	$1/n$	8	−0.01924	1.240	−0.8289	0.1465	13.17	−3.630*

Table 5. Results of multiple-regression analysis for the $\log X=\alpha\Phi+\beta+\gamma \log C$ equation

Φ	α	β	γ	r	s	F	$t(\Phi)$	t (log C)
MR	0.07134	−1.983	0.4401	0.9651	0.1505	1004***	44.48***	13.62***
P	0.009583	−2.359	0.4029	0.9556	0.1692	779.0***	39.17***	11.19***
MW	0.01971	−2.147	0.3749	0.9082	0.2404	384.3***	26.17***	7.323***
CN	0.2785	−1.028	0.4081	0.8936	0.2578	293.3***	24.01***	7.337***

the adsorption isotherms of 14 amino acids on Darco G-60, a commercial-grade lignite carbon. Urano et al.[6] measured the adsorption isotherms of 8 amino acids on two activated carbons from coal and petroleum pitch. Table 4 shows the relationship between Freundlich's constants and the molecular refraction. In the original papers, the k values were expressed in mol/g; therefore, the correlation coefficients between log k and the molecular refraction are very low because of the compounds with a high adsorbability, such as tryptophan, phenylalanine, and tyrosine, indicate a maximum adsorption at fairly low concentrations less than 1 mol/l. However, when the k values are expressed in mg/g, the correlation coefficient becomes high. It can be seen from Table 4 that Eqs. 2 and 3 are also applicable to the other activated carbons.

From Eqs. 1 and 2 we obtain the following equation, with a slight change in notation:

$$\log X = \alpha\Phi + \beta + \gamma \log C, \quad (4)$$

where α, β, and γ are constants. The data of 151 plots of 17 amino acids have been given to a NEC PC-8001 computer in order to determine the α, β, and γ values by means of multiple regression analysis. The constants and statistic analysis for several physical constants are given in Table 5. High correlation coefficients have been obtained for the molecular refraction and the parachor. Figure 4 shows a plot of the log X values observed *vs.* the log X values calculated by means of:

$$\log X_{\text{calcd}} = 0.07134\,MR - 1.983 + 0.4401 \log C. \quad (5)$$

We can see from Fig. 4 that the molecular refraction gives a good prediction of the isotherms.

If the α, β, and γ constants for a given activated carbon are determined from the adsorption data of several compounds, the adsorption isotherms of many other amino acids can be predicted from the molecular refraction alone. It should be remembered, however, that the solution pH influences the adsorption of ionized solutes.[7-9] These prediction methods may not be applicable for adsorptions at pH values extremely removed from the isoelectric point.

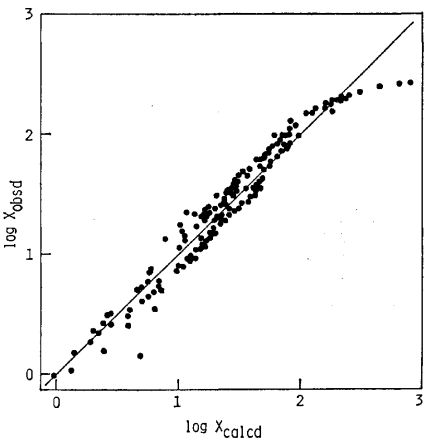

Fig. 4. Relationship between log X observed and log X calculated using Eq. 5.

References

1) I. Abe, K. Hayashi, M. Kitagawa, and T. Urahata, *Bull. Chem. Soc. Jpn.*, **53**, 1199 (1980).
2) I. Abe, K. Hayashi, M. Kitagawa, and T. Urahata, *Bull. Chem. Soc. Jpn.*, **52**, 1899 (1979).
3) I. Abe, K. Hayashi, M. Kitagawa, and T. Urahata, *Nippon Kagaku Kaishi*, **1979**, 830.
4) I. Abe, K. Hayashi, and M. Kitagawa, *Bull. Chem. Soc. Jpn.*, **54**, 2819 (1981).
5) V. H. Cheldelin and R. J. Williams, *J. Am. Chem. Soc.*, **64**, 1513 (1942).
6) K. Urano, Y. Kobayashi, Y. Nishimura, and Y. Yanaga, *Mizushorigijutsu*, **16**, 123 (1975).
7) F. W. Getzen and T. M. Ward, *J. Colloid Interface Sci.*, **31**, 441 (1969).
8) M. R. Rosene and M. Manes, *J. Phys. Chem.*, **81**, 1651 (1977).
9) G. Müller, C. J. Radke, and J. M. Prausnitz, *J. Phys. Chem.*, **84**, 369 (1980).

UV Absorption Studies of the Pyrolysis of Isobutane in Shock Waves

Tohru KOIKE* and Kihei MORINAGA

Department of Chemistry, National Defense Academy, Hashirimizu, Yokosuka 239

(Received March 24, 1981)

The UV absorption measurements at 216 nm were carried out for two shock-heated mixtures, 1.5 and 2.0% i-C_4H_{10} diluted in Ar, in the temperature range of 1300—1800 K, and at an atmospheric pressure of about half. From the initial absorption rise attributed to the CH_3 growth, the rate constant of the initiation reaction, i-C_4H_{10} = CH_3+i-C_3H_7, was evaluated as $k=10^{12.8\pm0.5}\exp[-(60.8\pm4.6)\ \text{kcal}/RT]/\text{s}^{-1}$. A comparison between the k value so derived and the formerly reported values was made. A computer modeling using a 39-reaction mechanism could reproduce the absorption at the early stage of the reaction at temperatures lower than 1550 K, whereas the modeled absorption was smaller than the measured at much high temperatures. The absorption by C_3H_5 (allyl radical) must be taken into account in order to lessen this difference.

Computer modeling has been used often in studying complex reaction mechanisms. We ourselves demonstrated the capability of the method in studies of C_3H_8[1] and n-C_4H_{10}[2] pyrolysis and have proposed reaction mechanisms for them.

In comparison with the n-C_4H_{10} pyrolysis, the i-C_4H_{10} pyrolysis can be interpreted rather simply, as in the case of the C_3H_8 pyrolysis, since it gives only one initiation reaction:

$$i\text{-}C_4H_{10} = CH_3 + i\text{-}C_3H_7. \quad (1)$$

Therefore, if the k_1 value can be determined precisely by means of a time-resolved measurement of the growth or the decay of any species appearing in Reaction (1), only secondary reactions, the k values of most of which are available in the existing literature, need to be examined. Computer modeling shows its usefulness in such a case.

Bradley[3] proposed the basic reaction mechanism of the i-C_4H_{10} pyrolysis from his discernment of alkane pyrolysis at high temperatures. He measured the product distribution of the pyrolysis in the temperature range of 1200—1500 K by means of a single-pulse shock-tube technique and confirmed the validity of the mechanism by computer modeling. At lower temperatures than Bradley's, many studies of the pyrolysis by other experimental techniques have been reported.[4-8] Pratt and Rogers[4] investigated the pyrolysis around 1000 K using a wall-less reactor and proposed a reaction mechanism after surveying almost all of the i-C_4H_{10} pyrolysis studies ever reported. They also compared their own k_1 value with those reported by several other workers.[3,5-8] The k_1 value obtained by Bradley[3] exhibited a distinct fall-off with a smaller activation energy than those reported around 1000 K.

Since Bradley's study is the only one carried out in the high-temperature range, as far as we are aware, and since it gave a k_1 value different from others, another shock-tube study of the pyrolysis, especially devised to check the k_1 value, is required. In this study, we measured the 216 nm absorption in the i-C_4H_{10} pyrolysis behind incident shock waves. From the initial increase in the absorption attributed to the CH_3 growth alone, the k_1 value was evaluated. The k_1 value thus obtained is incorporated into a reaction mechanism of the pyrolysis, and the absorption at 10 μs in lab. time, when C_2H_4 and C_3H_6 are expected to appear much and when these species as well as CH_3 absorb the 216 nm light, is elucidated by computer modeling.

Experimental

The shock tube and the optical system used in this study have been described in detail in a preceding paper.[9] Briefly, the test gases, i-C_4H_{10}/Ar=1.5/98.5 and 2.0/98.0, prepared from 99.8% pure i-C_4H_{10} (Takachiho Co.) and 99.999% pure Ar (Nippon Sanso Co.) at starting pressure of 20.0± 0.5 Torr (1 Torr≈133.322 Pa) were heated up to high temperatures (1300—1800 K) by means of incident shock waves. The reaction profile was observed by means of UV absorption spectroscopy with a D_2-lamp (Hanau, D200F). The light from the lamp was passed through the shock-tube windows and was detected by means of a photomultiplier (Hamamatsu-TV, R208) with a monochromator (Jarrell-Ash, JE25; dispersion=3.3 nm/mm, entrance and exit slit width=1 mm).

Computer modeling was done using the program mentioned previously.[9] The flow model assumed in the modeling was a laminar-boundary-layer growth with a limiting separation. The thermochemical data of each species were taken from several available sources; these sources are shown in the footnote of Table 1.

Results and Discussion

Figure 1 shows a typical oscillogram of the absorption profile at 216 nm obtained in this study. The absorption increases right after the arrival of the shock at the observation window and thereafter maintains a plateau. Since no absorption was observed at the shock front, i-C_4H_{10} does not absorb the 216 nm light. This is in accordance with the former experimental

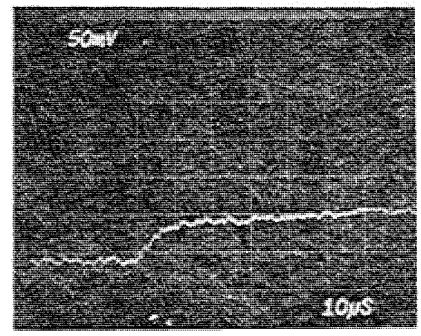

Fig. 1. A representative oscillogram for 1.5% i-C_4H_{10} in Ar mixture, P_1=20 Torr, and T_2=1478 K.

results reported for small alkanes,[10] such as CH_4,[11] C_2H_6,[11,12] C_3H_8,[13] and n-C_4H_{10},[2] having no absorption band in this wavelength region.

The unimolecular decomposition of i-C_3H_7 produced by Reaction (1) also gives CH_3.

$$i\text{-}C_3H_7 = CH_3 + C_2H_4 \qquad (19)$$

The methyl radical so produced reacts mainly with i-C_4H_{10} at early in the reaction as:

$$CH_3 + i\text{-}C_4H_{10} = CH_4 + i\text{-}C_4H_9, \qquad (4)$$

$$CH_3 + i\text{-}C_4H_{10} = CH_4 + t\text{-}C_4H_9. \qquad (5)$$

Methyl recombination is another important step in the CH_3 disappearance:

$$2CH_3 + M = C_2H_6 + M. \qquad (-27)$$

The computer modeling adopted later indicates that the rates of Reactions (4), (5), (19), and (−27) are much smaller than that of Reaction (1) early in the reaction. Thus, the influence of these secondary reactions on the CH_3 profile can be neglected, and the CH_3 growth rate is given by:

$$d[CH_3]/dt = k_1[i\text{-}C_4H_{10}].$$

It has been reported that the absorptivity of i-C_3H_7 at 216 nm is at least 10 times smaller than that of CH_3.[14] Moreover, i-C_3H_7 is very unstable under the present experimental conditions, and the modeled [i-C_3H_7] is about three orders of magnitude smaller than that of CH_3. Thus, the increase in the absorption early in the reaction can be attributed solely to the CH_3 growth. The above equation implies that the evaluation of the initial slope of the absorption provides the k_1 value with an explicit relation of $[CH_3]_t=\log(I_0/I_t)/(a\cdot d)$, where I_0=incident light intensity, I_t=transmitted light intensity at reaction time t (in particle time), a=absorptivity ($cm^2\ mol^{-1}$), and d=optical path length (7.2 cm). The absorptivity of CH_3 was taken from that reported elsewhere.[11,12] Since the absorptivity reported was measured in an effective bandwidth of 1.6 nm, which is almost equal to the present one, it was assumed to be applicable to the present study without any correction.

The k_1 values so evaluated are shown in Fig. 2. The least-squares calculation provides the following Arrhenius expression for k_1 with one standard error (the data points above 1600 K, which deviate from the linear extrapolation of the low-temperature values, were not taken into account in the calculation):

$$k_1 = 10^{12.8\pm0.5} \exp\left[-(60.8\pm4.6)\ \text{kcal}/RT\right]/s^{-1}.$$

Tsang[5] estimated the rate constants of alkane decompositions within the high-pressure limit, k^∞, around 1100 K by means of a single-pulse-shock-tube experiment. Recently, he studied the temperature dependence of the k^∞ value and reached the conclusion that these A factors decrease with an increase in the temperature in the temperature range of 300—1100 K. If such an effect is negligibly small in a narrower temperature range, and if the k_1^∞ value, the k_1 value within the high-pressure limit, is extrapolated to above 1100 K, as is shown in Fig. 2, we can see a distinct deviation of the present k_1 value from the k_1^∞ value with an increase in the temperature, though the present k_1 is almost equal to the k_1^∞ value at temperatures around 1300 K. Besides the k_1^∞ value by Tsang,[5] several k_1^∞ values measured around 1000 K have been reported. One of them is by Golden *et al.*[8] This k_1^∞ value, however, can not be comparable with others, since it is doubtful if the VLPP technique used to obtain it is free from the surface effects, which may lead to a high k_1^∞ value. Another one is by Pratt and Rogers.[4] At 1300 K, their k_1^∞ value extrapolated is about 10 times smaller than the present k_1 value. Even if the decrease of the A_1^∞ factor of the k_1^∞ value is expected as above, we can not explain such a large difference between the two values. Therefore, the k_1^∞ value by Pratt and Rogers[4] seems also to have some error.

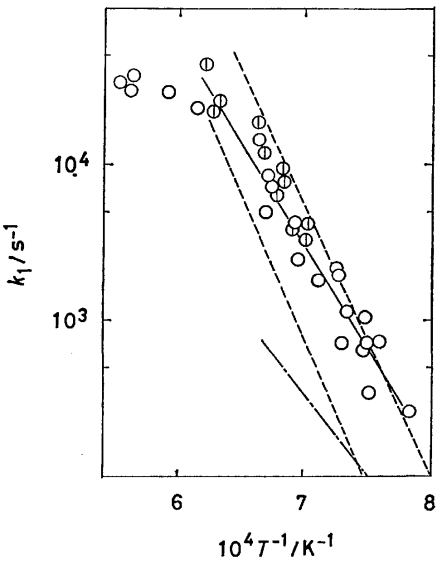

Fig. 2. Arrhenius plots for k_1.
The symbols used are as follows: ○; for 2% i-C_4H_{10} in Ar mixture and ⊕; for 1.5% i-C_4H_{10} in Ar mixture. The solid line shows a least squares fit for the data points below 1600 K. The upper and lower broken lines show the k_1 values in Ref. 5 (Tsang) and in Ref. 4 (Pratt and Rogers), respectively. The chain line shows the k_1 value in Ref. 3 (Bradley).

Although it has been confirmed qualitatively that the present k_1 value above 1300 K is in the fall-off range, it is difficult to find precisely where the present k_1 value is on the fall-off curve, for the present k_1 value was measured at almost equal pressures (P_2=0.45—0.60 atm, 1 atm=101325 Pa) and there is an ambiguity in the k_1^∞ value at high temperatures. Further experiments at different pressures might be necessary to ascertain the exact fall-off behavior of the k_1 value. The k_1 value reported by Bradley,[3] which is considered to be in the fall-off range, will be referred to later.

As the pyrolysis proceeds, many kinds of products appear, and the absorption is an aggregated one by these products. We interpreted the absorption profile with the aid of computer modeling and tried to propose a reaction mechanism of the i-C_4H_{10} pyrolysis. To facilitate the computer modeling, we adopted the absorption at lab. time 10 μs, $A_{10}=\ln(I_0/I_{10})$ for the

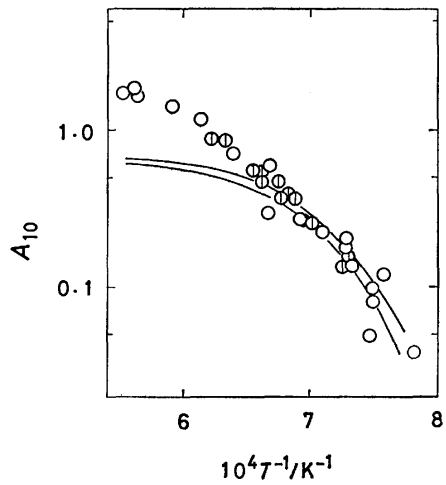

Fig. 3. A comparison between measured and modeled A_{10}.
The symbols are as in Fig. 2. The upper and lower lines show the modeled A_{10} for the 2% and 1.5% mixtures, respectively.

parameter, as in the study of the n-C_4H_{10} pyrolysis reported before. In Fig. 3, the A_{10} values so evaluated are shown *vs.* $10^4/T$. The output of the computer modeling given by the time variation in the concentration of each species is converted to the absorption as: $A=2.303\times a_i[C_i]d$, where $[C_i]$ is the modeled concentration of each species. The A value at the same lab. time is considered to correspond to the above A_{10}. The species which were assumed to absorb the 216 nm light were CH_3,[11,12] C_2H_4,[9] and C_3H_6.[2] The absorptivities of the latter two species, which were measured with the same optical set-up as the present, were mentioned in a previous paper.[9] The absorption by C_2H_2 is expected to be negligible under the present experimental conditions, since a negligible effect of C_2H_2 absorption on the A_{10} value was seen in the modeling of the n-C_4H_{10} pyrolysis previously reported.[2] The absorption by i-C_4H_8 was assumed to be negligible.

Figure 3 shows that a nice agreement between the modeled and measured A_{10} values is established at lower temperatures below 1550 K; at much higher temperatures, however, the modeled A_{10} values are much smaller than the measured ones. The sensitivity test to be discussed later indicates that there might be no way of improving the disagreement only by changing any k values in Table 1. In the modeling of the absorption, there does not seem to be any species which appears in a large amount and which shows a large absorption at higher temperatures.

With an increase in the temperature, the modeled concentration of $C_3H_5(CH_2{=}CH{-}\dot{C}H_2)$ gets much larger than those of other radicals and is comparable to the concentrations of stable products, such as CH_4 and C_2H_4. The strong absorption of C_3H_5 in this wavelength range was observed in the C_3H_6 pyrolysis measured in shock waves[2] and in the 1-C_4H_8 photolysis at room temperature.[16] If we adopt the absorptivity of about 2×10^7 cm^2 mol^{-1} reported in the latter study, the modeled A_{10} values drastically go up to near the measured values. Besides the main route of forming C_3H_5 *via* C_3H_6, the following route *via* i-C_4H_8 may be present in the i-C_4H_{10} pyrolysis:

$$i\text{-}C_4H_8 = CH_3 + (CH_2{=}\dot{C}{-}CH_3).$$

The radicals thus formed is expected to be stabilized to the allyl radical after a few collisions, since it has been reported that,[17] due to the resonance, the heat of formation of the allyl radical is about 20 kcal/mol smaller than that of $(CH_2{=}\dot{C}{-}CH_3)$. Thus, in the modeling of the high-temperature absorption of the i-C_4H_{10} pyrolysis, it is necessary to clarify the route of forming C_3H_5 and to take into account the absorption by the allyl radical.

Table 1 shows the reaction mechanism of the i-C_4H_{10} pyrolysis derived in this study. The reaction mechanism can explain the absorption profile early in the reaction at temperatures lower than 1550 K. Pratt and Rogers' mechanism,[4] which includes explicitly the reactions of C_4H_9 isomers, is the original of the present mechanism. The reactions accompanying the species having more than 5 carbons and the reactions which may have an influence on the overall reaction at a later time were not included. Since the reaction temperature of this experiment is much higher than that of Pratt and Rogers,[4] some of the major products may be expected to decompose further. From this point of view, Reactions (15)—(18), (22)—(26), (28), and (30)—(35) were included as in the study of the reaction mechanism of the n-C_4H_{10} pyrolysis previously reported.[2] Most of the k values of these reactions are identical with those used in the previous study.[2] Among the reactions which were considered to be important under the conditions of Pratt and Rogers' experiment,[4] the k values of unimolecular reactions, (14) and (27), adopted were those determined in an experiment similar to the present one.[13,18]

Since the primary reactions of C_4 species giving the major products have been discussed in detail by Pratt and Rogers,[4] we will give our attention here to the fates of the smaller hydrocarbons produced. The major products in the pyrolysis in the temperature range of 1200—1500 K have been reported to be CH_4, C_2H_6, C_2H_4, C_3H_6, and i-C_4H_8; no appreciable amount of C_3H_8 has been detected.[3] It may be seen from the product distribution reported at that time[3] that $[i\text{-}C_4H_8]$ decreases abruptly with an increase in the temperature and it is less than 5% of the concentration sum of the products at the upper end of the reaction temperature; a similar tendency of the modeled $[i\text{-}C_4H_8]$ above 1500 K will also be seen later. Thus, no consideration will be given here to the fates of i-C_4H_8 and C_3H_8. Among the major products left, CH_4 and C_2H_4 are relatively stable in this temperature range, and their direct decompositions, Reaction (33), $C_2H_4{=}C_2H_2{+}H_2$, and $C_2H_4{=}C_2H_3{+}H$, are considered to be negligible. Only H-atom abstractions, Reactions (34) and (35), are effective in accounting for the disappearance steps of the molecules. Since the reactivities of C_2H_6 and

TABLE 1. REACTION MECHANISM AND RATE CONSTANTS
$k=A\exp(-E/RT)$ (cm, mol, s, and kcal units)

Reaction	log A	E	Footnote
1) i-$C_4H_{10}=CH_3+i$-C_3H_7	12.8	60.8	This work
2) $H+i$-$C_4H_{10}=H_2+i$-C_4H_9	13.7	68.0	a)
3) $H+i$-$C_4H_{10}=H_2+t$-C_4H_9	13.7	68.0	a)
4) CH_3+i-$C_4H_{10}=CH_4+i$-C_4H_9	13.2	16.3	b)
5) CH_3+i-$C_4H_{10}=CH_4+t$-C_4H_9	12.5	12.9	b)
6) i-$C_4H_9=CH_3+C_3H_6$	14.2	32.7	c)
7) i-$C_4H_9=C_2H_4+C_2H_5$	20.2	74.2	a)
8) t-$C_4H_9=H+i$-C_4H_8	14.6	43.1	c)
9) t-$C_4H_9=C_2H_4+C_2H_5$	22.4	92.1	a)
10) CH_3+t-$C_4H_9=CH_4+i$-C_4H_8	$15.0-0.75\log T$	0	d)
11) $H+i$-$C_4H_8=H_2+C_4H_7$	13.7	5.0	a)
12) CH_3+i-$C_4H_8=CH_4+C_4H_7$	14.0	17.6	b)
13) $C_4H_7=C_2H_4+C_2H_3$	14.0	37.0	e)
14) $C_3H_8=CH_3+C_2H_5$	13.6	67.9	f)
15) $CH_3+C_3H_8=CH_4+i$-C_3H_7	12.6	10.3	g)
16) $CH_3+C_3H_8=CH_4+n$-C_3H_7	12.6	10.3	g)
17) $H+C_3H_8=H_2+i$-C_3H_7	13.8	8.0	h)
18) $H+C_3H_8=H_2+n$-C_3H_7	13.8	8.0	h)
19) i-$C_3H_7=C_2H_4+CH_3$	12.0	34.5	c)
20) n-$C_3H_7=C_2H_4+CH_3$	13.8	33.2	c)
21) i-$C_3H_7=H+C_3H_6$	14.3	41.3	c)
22) n-$C_3H_7=H+C_3H_6$	13.8	38.0	c)
23) $C_3H_6+M=CH_3+C_2H_3+M$	18.0	74.0	i)
24) $C_3H_6=C_3H_5+H$	13.0	78.0	j)
25) $H+C_3H_6=H_2+C_3H_5$	10.1	1.5	k)
26) $C_3H_5=C_3H_4+H$	13.6	70.0	k)
27) $C_2H_6+M=2CH_3+M$	$111.3-25.26\log T$	160.0	l)
28) $C_2H_6+H=C_2H_5+H_2$	14.1	9.4	m)
29) $C_2H_5+M=C_2H_4+H+M$	15.3	30.1	l)
30) $CH_3+CH_3=C_2H_5+H$	14.9	26.6	n)
31) $CH_3+CH_3=C_2H_4+H_2$	16.0	32.0	n)
32) $C_2H_5+H=C_2H_4+H_2$	12.3	0	m)
33) $CH_4+M=CH_3+H+M$	17.5	90.6	o)
34) $CH_4+H=CH_3+H_2$	14.9	15.1	p)
35) $C_2H_4+H=C_2H_3+H_2$	15.7	22.9	q)
36) $CH_3+C_2H_5=CH_4+C_2H_4$	11.7	0	r)
37) i-C_3H_7+i-$C_4H_{10}=n$-C_3H_7+i-C_4H_{10}	9.8	9.5	b)
38) t-C_4H_9+i-$C_4H_{10}=i$-C_4H_9+i-C_4H_{10}	9.5	9.5	b)
39) i-$C_4H_9=H+i$-C_4H_8	13.7	36.6	c)

a) Ref. 3. b) Ref. 7. c) S. W. Benson and H. E. O'Neal, "Nat. Stand. Ref. Data Ser.," NBS, No. 21, (1970). d) Ref. 14. e) K. M. Sundaram and G. F. Froment, *Ind. Eng. Chem., Fundam.*, **17**, 174 (1978). f) Ref. 13. g) A. Lifshitz and M. Franklach, *J. Phys. Chem.*, **79**, 686 (1975). h) A. F. Trotman-Dickenson and G. S. Milne, "Nat. Stand. Ref. Data Ser.," NBS, No. 9, (1967). i) A. Burcat, *Fuel*, **54**, 87 (1975). j) K. J. Laidler and B. W. Wojciechowski, *Proc. R. Soc. London, Ser. A*, **259**, 257 (1960). k) A. Amano and M. Uchiyama, *J. Phys. Chem.*, **67**, 1242 (1963). l) Ref. 18. m) P. Camilleri, R. M. Marshall, and J. H. Purnell, *J. Chem. Soc., Faraday Trans. 1*, **70**, 1434 (1974). n) Ref. 11 and K. A. Bhaskaran, P. Frank, and Th. Just, "Proc. 12th Shock Tube Symp.," Hebrew Univ. Press, Jerusalem (1980), in press. o) W. C. Gardiner, Jr., T. Koike, and T. Tanzawa, manuscript in preparation. p) Th. Just and P. Roth, *Ber. Bunsenges. Phys. Chem.*, **79**, 682 (1975). q) Th. Just, P. Roth, and R. Damm, "16th Int. Symp. Combust.," The Combustion Institute, Pittsburgh (1977), p. 961. r) Assumed. The sources of the thermochemical data of species are: i-C_4H_{10}: S. S. Chen, R. C. Wilhoit, and B. J. Zwolinski, *J. Phys. Chem. Ref. Data*, **4**, 859 (1975); C_3H_8 and C_2H_6: S. S. Chen, R. C. Wilhoit, and B. J. Zwolinski, *ibid.*, **2**, 427 (1973); C_3H_6: J. Chao and B. J. Zwolinski, *ibid.*, **4**, 251 (1975); CH_4, C_2H_4, C_2H_2, CH_3, H_2, and H: D. R. Stull and H. Prophet, "JANAF Thermochemical Tables," 2nd ed, NSRDS-NBS, 37 (1971); C_2H_5: Ref. 18; i-C_3H_7, n-C_3H_7, i-C_4H_9, and t-C_4H_9: c) and J. A. Karr, *Chem. Rev.*, **66**, 465 (1966); C_4H_7, C_3H_5, and C_2H_3: R. E. Duff and S. H. Bauer, *J. Chem. Phys.*, **36**, 1754 (1962); i-C_4H_8 and C_3H_4: F. D. Rossini *et al.*, "Selected Values of Properties of Hydrocarbons and Related Compounds," NBS-API Research Project 44, NBS (1947).

C_3H_6 are larger than those of the above two species, the disappearance steps, Reactions (23)—(26) and (27)—(32), are taken into account. At much higher temperatures than the present, the reaction mechanisms of the C_2H_6 and C_3H_6 pyrolysis are not so simple, as has been considered above.[19]

The radicals larger than C_2, such as C_4H_9, C_3H_7, and C_2H_5, are decomposed to produce H or CH_3 with molecules in this temperature range. Therefore, the chain terminations are accomplished by the radical reactions of H and CH_3. The chain termination for the H-atom are $H+H=H_2$ and Reaction (−33); the rate of former reaction is very small compared with those of the other reactions in Table 1, and so it is not included in the reaction mechanism. The disproportionations, Reactions (31) and (36), as well as the recombinations, Reactions (−14), (−27), and (−33), are chain terminations for the CH_3 radical. Reaction (30) can go in either direction and can not be explained simply. Thus, co-radical reactions with CH_3 are not so simple as in the case of the H-atom.

The modeled $[C_3H_6]$ and $[i\text{-}C_4H_8]$ at 1500 K are 1.3×10^{-8} and 1.0×10^{-10} mol cm^{-3} respectively at 10 μs lab. time. At much higher temperatures, for example, at 1700 K, the modeled $[i\text{-}C_4H_8]_{10\mu s}$ is less than 10^{-11}. Thus, because of the smallness of $[i\text{-}C_4H_8]$, it is confirmed that both the influence of the absorption by i-C_4H_8 on the total absorption and the route of forming C_3H_5 *via* i-C_4H_8 are negligible in deriving the present reaction mechanism. On the other hand, it is necessary to examine the C_3H_6 pyrolysis in detail. A recent study of the C_3H_6 pyrolysis in shock waves[19] has predicted that such expressions as Reactions (23)—(26) are not satisfactory in explaining the reaction profile at high temperatures. Also the absorptivity of C_3H_5 at high temperatures is uncertain and must be measured precisely. Since the situation for the C_3H_5 chemistry is as above, we have left the modeling of the absorption profile at high temperatures unfinished.

The results of sensitivity tests at 1500 K and 1700 K are shown in Fig. 4. It may be seen that the sensitivity spectra given by the values of the percent deviations of each reaction are completely different between the two temperatures. At 1500 K, the reactions accompanying the CH_3 radical, the initiation (1), the chain propagations (5) and (30), and the chain terminations, (−14), (−27), and (31), have large influences on the A_{10} value. Since the sensitivities of Reactions (1) and (27) are much larger than those of the other reactions, the k values of these two reactions should be examined carefully. As for Reaction (1), several factors which may give uncertaities in determining the k_1 value have already been discussed in detail, and the error boundary for the expression has been given. The error boundary of the k_1 value may be given as above, but the error boundary seems to be much smaller than that, since the A_{10} value can not be reproduced by computer modeling when a k_1 value different by a factor of 2 from the value in Table 1 is adopted. As for the k_{27} value, we selected the value determined in the C_2H_6 pyrolysis study[18] in which conditions similar

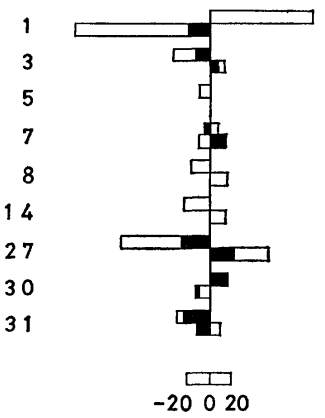

Fig. 4. Sensitivity spectrum for the 2% mixture.
The numbers refer to the reaction number in Table 1. The abscissa is percent deviation defined as: $(A_{10}'/A_{10}-1)\times100$. A_{10} is the standard value modeled using Table 1 mechanism and rate constants. A_{10}' is the perturbed value by multiplying each rate constant by 5, upper bar of each reaction; by 0.2, lower bar. The reactions whose percent deviations are less than 5 are not shown.
The bars used are: □, T_2=1500 K; ■, T_2=1700 K.

to those of the present experiment were adopted, because the k_{27} value is expected to show a pressure dependence. Although we can not find the error boundary of the k_{27} value explicitly,[18] we can elucidate the error boundary to be less by a factor of 2 from the sensitivity spectra shown in the previous report.[18] Likewise, the present A_{10} value can not be reproduced by computer modeling with a changed k_{27} value as above. As for the C_4H_9 decompositions, the value of the percent deviations of Reactions (7) and (8) are given with different signs when each k value is changed with the same factor; *i.e.*, only small variation of the A_{10} value can be seen by changing the k_7 and k_8 values at the same time. On the other hand, very small deviations were observed for Reactions (6), (9), and (39). These results may indicate that it is possible to reproduce the A_{10} value even after making a fall-off correction for each k value of Reactions (6)—(9) and (39) with a similar factor. From the sensitivity spectra at 1700 K, the percent deviations of most reactions can be expected to get smaller with an increase in the temperature, and it is hard to tell which reaction is more sensitive to the A_{10} value. Thus, the A_{10} value at high temperatures can not be reproduced only by changing any of the k values in Table 1.

Since the experimental conditions of the single-pulse shock-tube technique adopted by Bradley[3] is similar to the present (P_5=0.66—0.91 atm), the computer modeling with reaction mechanism shown in Table 1 can be expected to reproduce his experimental results. However, the modeled decay of $[i\text{-}C_4H_{10}]$ is too fast compared with his results. We are led to assume that the gas-cooling effects due to the boundary-layer growth[20] existed in his data also.

References

1) T. Koike and W. C. Cardiner, Jr., *J. Phys. Chem.*, **84**, 2005 (1980).
2) T. Koike and K. Morinaga, *Bull. Chem. Soc. Jpn.*, **54**, 2439 (1981).
3) J. N. Bradley, *Proc. R. Soc. London, Ser. A*, **337**, 199 (1974).
4) G. L. Pratt and D. Rogers, *J. Chem. Soc., Faraday Trans. 1*, **76**, 1694 (1980).
5) W. Tsang, *Int. J. Chem. Kinet.*, **1**, 245 (1969).
6) C. T. Brooks, *Trans. Faraday Soc.*, **62**, 935 (1966).
7) R. S. Konar, R. M. Marshall, and J. H. Purnell, *Trans. Faraday Soc.*, **64**, 405 (1968); *Int. J. Chem. Kinet.*, **5**, 1005 (1973).
8) D. M. Golden, Z. B. Alfassi, and P. C. Beedle, *Int. J. Chem. Kinet.*, **6**, 359 (1974).
9) T. Koike and K. Morinaga, *Bull. Chem. Soc. Jpn.*, **54**, 530 (1981).
10) G. Herzberg, "Molecular Spectra and Molecular Structure," D. Van Nostrand, N. J. (1966), Vol. 3.
11) T. Tsuboi, *Jpn. J. Appl. Phys.*, **17**, 709 (1978).
12) K. Glänzer, M. Quack, and J. Troe, "16th Int Symp. Combust.," The Combustion Institute, Pittsburgh (1977), p. 949.
13) T. Koike and K. Morinaga, manuscript in preparation.
14) D. A. Parkers and C. P. Quinn, *J. Chem. Soc., Faraday Trans. 1*, **72**, 1952 (1976).
15) W. Tsang, *Int. J. Chem. Kinet.*, **10**, 821 (1978).
16) H. E. Van den Bergh and A. B. Callear, *Trans. Faraday Soc.*, **66**, 2681 (1970).
17) S. W. Benson, private communications to W. C. Gardiner, Jr., (1979); M. Rossi, K. D. King, and D. M. Golden, *J. Am. Chem. Soc.*, **101**, 1223 (1979).
18) D. B. Olson, T. Tanzawa, and W. C. Gardiner, Jr., *Int. J. Chem. Kinet.*, **11**, 23 (1979).
19) T. Koike and W. C. Gardiner, Jr., manuscript in preparation.
20) G. B. Skinner, *Int. J. Chem. Kinet.*, **9**, 863 (1977).

Effect of Mixed Surfactant upon Stability and Particle Size of Emulsion

Kimihiko Ogihara,* Minoru Ueno, and Kenjiro Meguro
Department of Applied Chemistry, Faculty of Science, Science University of Tokyo, 1-3 Kagurazaka, Shinjuku-ku, Tokyo 162

(Received June 26, 1981)

An effect of a mixed surfactant of SDS and homogeneous octaethylene glycol dodecyl ether (8ED) upon the stability and particle size of an octane-in-water emulsion was studied. The mixed surfactant solutions were found to exhibit equi-interfacial-tension over a wide concentration region of a mixed 8ED; the SDS concentrations were 6, 8, and 20 mmol dm^{-3}. The emulsion prepared by using mixed surfactant solution in such a concentration region showed a similar mean particle size. When SDS concentration was kept at 8 or 20 mmol dm^{-3}, the emulsions prepared by the mixed surfactant solutions had similar stability, independently of the mixed 8ED concentration. In the presence of 1 mmol dm^{-3} of SDS, the stability of the emulsions increased with the increasing concentration of mixed 8ED. In the case of SDS concentration of 6 mmol dm^{-3}, the emulsion was most stable at 1×10^{-3} mol dm^{-3} of mixed 8ED.

We have so far reported on the surface properties of mixed aqueous solutions containing SDS as an anionic surfactant and a series of polyethylene glycol dodecyl ethers ($C_{12}E_n$: $n=1$—8), having no distribution of poly(oxyethylene) chain lengths, as the nonionic surfactant.[1-3] We have found that an equi-surface-tension exists on the surface tension *vs.* the concentration curve over a wide concentration range of the nonionic surfactant in the presence of 6.3 mmol dm^{-3} of SDS, and also that the mixed micelle exists in the region. The existence of such a plateau region in the surface tension curve will also be expected to appear on the interfacial tension curve for the oil/water system consisting of a similar mixed surfactant solution and octane as the oil. The emulsion prepared by these surfactant solutions and octane will also be anticipated to become more stable over a wide concentration range of a nonionic surfactant.

Additives such as higher alcohols are often utilized as emulsion stabilizers,[4-12] since the emulsion becomes more stable by adding a small amount of a higher alcohol. This effect has so far been explained by formation of some more stable complex between alcohols and emulsifiers[5-7] due to the van der Waals interaction between the hydrocarbons or the ion-dipole interaction between the head groups.[13,14]

In this work, in order to confirm the emulsion stability for the octane-in-water emulsion system in the plateau region of the interfacial tension curve, the interfacial tensions were measured. These tensions are related to the stability of the emulsion produced from the corresponding individual and mixed surfactant solutions; the relation is also justified by the extent of drainage of the emulsion.

Experimental

Materials. The solium dodecyl sulfate (SDS) used here was obtained from Wako Pure Chemical Industries; it was purified by repeated crystallization from either ethanol or a mixture of 2-propanol and water. The purity was confirmed by the absence of any minimum in the surface tension *vs.* concentration curve. The octaethylene glycol dodecyl ether (8ED) supplied by Nikko Chemicals Co. has been confirmed to have a high purity and no distribution of poly(oxyethylene) chain lengths by GLC and TLC. The octane was a GR quality oil which was used without further purification. The water used for all experiments was purified by passing deionized water through a MILLI-Q Reagent-Grade Water System (MILLIPOR Ltd.) until its specific conductivity fell below 0.1 μS cm^{-1}.

Measurements. Interfacial tension was determined at 25 °C by a modified Wilhelmy type surface tensiometer, Shimadzu ST-1. Five ml of surfactant solution and of octane were poured slowly into a weighing bottle, and an octane/surfactant solution interface was formed. Then the bottle was stoppered, and left to stand for 40 min at the measurement temperature. This period was determined from the measurement of the time-dependence of the interfacial tension. After this period the interfacial tension was measured.

Emulsions were prepared as follows: Each mixture consisting of 20 ml of both surfactant solution and octane was emulsified with a Universal Homogenizer (Nihonseiki Kaisha) operated at 6000 min^{-1} for 5 min at room temperature. The emulsion thus prepared was transferred to sedimentation tubes, which had a stop cock, and left standing at 25 °C. The drainage of liquid from the emulsion (degree of separation; *DS*) was determined after 1 h, 2 h, and 24 h. The *DS* value is defined in the present work as follows:

$$DS \text{ value} = \frac{\text{volume of drained phase}}{\text{total volume of emulsion}} \times 100\,(\%)\,.$$

The mean particle size of the emulsions was determined immediately after preparation of each emulsion by a centrifugal particle size analyzer, Shimadzu CP-50.

Results and Discussion

Before discussing the stability of the octane-in-water emulsion system prepared using a surfactant mixture of SDS and 8ED, we must determine whether the properties of the interface of the octane/aqueous solution of each surfactant reflect the stability of the corresponding emulsion. The interfacial tension of 8ED solution against octane is shown in Fig. 1(a). The value decreased from 35 mN m^{-1} to 0.3 mN m^{-1} with the increase of 8ED concentration, and an apparent cmc (critical micelle concentration) was observed at about 1×10^{-3} mol dm^{-3}. Figure 2(a) shows the interfacial tension of SDS solution against octane. The cmc was observed at about 8 mmol dm^{-3}.

Figure 1(b) shows *DS* values of the emulsion which had been prepared with 8ED as an emulsifier. The emulsion began to be stable with increasing concen-

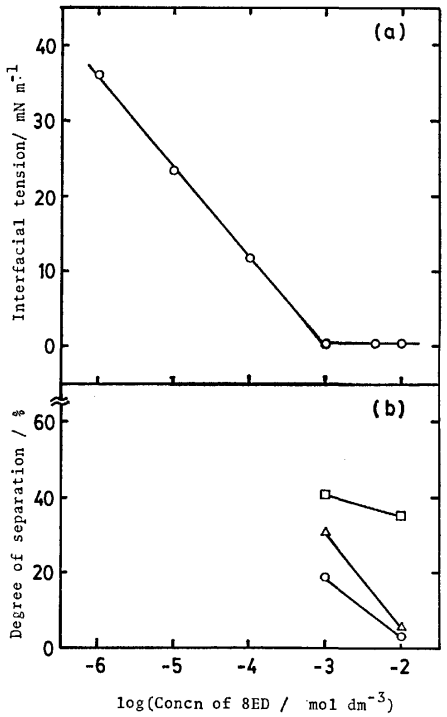

Fig. 1. (a) Interfacial tension of 8ED solution against octane.
(b) Degree of separation of octane emulsion prepared by 8ED, after 1 h (—○—), 2 h (—△—), and 24 h (—□—).

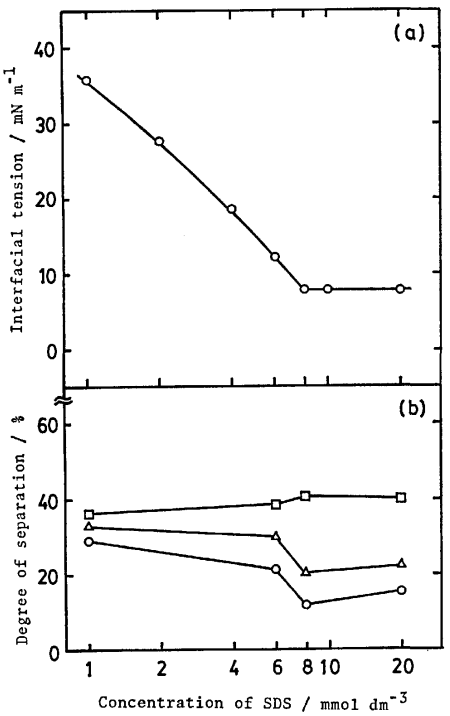

Fig. 2. (a) Interfacial tension of SDS solution against octane. (b) Degree of separation of octane emulsion prepared by SDS, after 1 h (—○—), 2 h (—△—), and 24 h (—□—).

tration above the apparent cmc of 8ED. Figure 2(b) also shows *DS* values of the emulsion prepared with SDS. The *DS* value became smaller as the SDS concentration increased; in the presence of 8 mmol dm^{-3} of SDS the *DS* value was smallest, in the measurement after one hour.

According to our previous data,[1] the surface tension *vs.* concentration curve for the mixed surfactant solution of SDS and homogeneous pentaethylene glycol dodecyl ether (5ED) showed a plateau region (equi-surface-tension region) over a wide concentration range of a mixed 5ED (from 3×10^{-6} to 1×10^{-3} mol dm^{-3}) in the presence of 6.3 mmol dm^{-3} of SDS. The existence of a mixed micelle between SDS and 5ED has been proved by the appearance of this plateau region.[1]

From these findings, such a mixed surfactant will be expected to show an equi-interfacial-tension region even in the interfacial tension curve. The interfacial tension of the mixed surfactant solution of SDS and 8ED against octane is shown in Fig. 3. In the presence of 6, 8, and 20 mmol dm^{-3} of SDS, each interfacial tension curve had an equi-interfacial-tension region.

If the O/W type emulsion of octane is prepared from the mixed surfactant solution which shows the plateau region in the interfacial tension *vs.* concentration curve, a homogeneous emulsion will be formed.

Table 1 indicates the mean particle size of the emulsion prepared from the mixed surfactant solution of SDS and 8ED. In the cases of SDS concentrations of 6, 8, and 20 mmol dm^{-3}, it was found that the mean particle sizes of the emulsions were almost the same for each SDS concentration, independently of the concentration of added 8ED. However, in the

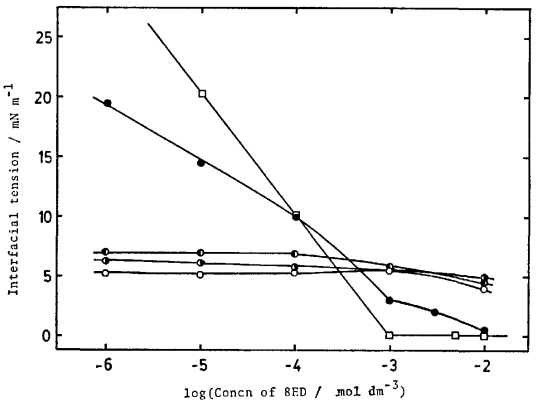

Fig. 3. Interfacial tension of 8ED against octane as a function of SDS additive concentration.
Additive concentration of SDS: 0 (—□—), 1 (—●—), 6 (—○—), 8 (—◑—), and 20 mmol dm^{-3} (—◐—).

Table 1. Mean particle size (μm) of the emulsion

8ED concn / mol dm^{-3}	SDS concn/mmol dm^{-3}			
	1	6	8	20
1×10^{-6}		9.5	8.8	9.9
1×10^{-5}	11.4	9.9	9.5	9.2
1×10^{-4}	10.1	9.5	9.1	9.2
1×10^{-3}	9.7	10.5	9.9	9.5
1×10^{-2}	8.9	10.0	9.2	9.0

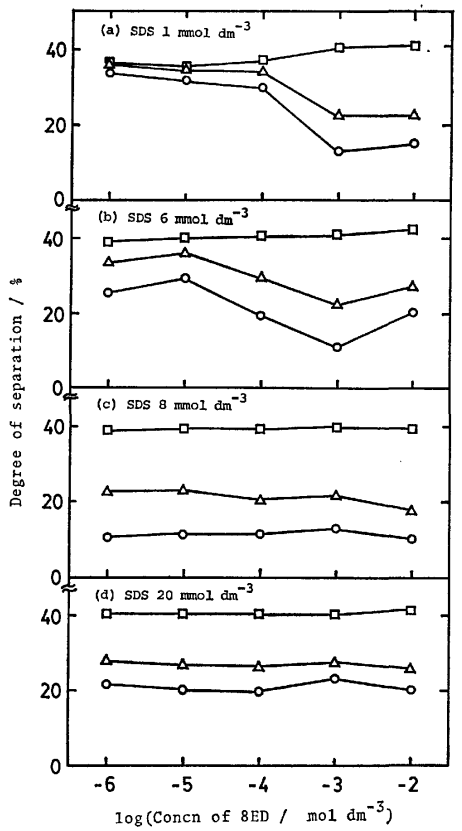

Fig. 4. (a), (b), (c), (d) Degree of separation of octane emulsion prepared by the mixed surfactant of SDS and 8ED, after 1 h (—○—), 2 h (—△—), and 24 h (—□—).

presence of 1 mmol dm^{-3} of SDS, the mean particle size of the emulsion decreased with the increasing concentration of added 8ED.

Figures 4(a), (b), (c), and (d) show the *DS* values of the emulsions prepared by the mixed surfactant solution of SDS and 8ED. At SDS concentration of 1 mmol dm^{-3} (Fig. 4(a)), the *DS* values of the emulsion after one hour began to become smaller at about 1×10^{-3} mol dm^{-3} of added 8ED. On the other hand, in the presence of 6 mmol dm^{-3} of SDS (Fig. 4(b)), in which the mixed surfactant solution gave an equi-interfacial-tension (see Fig. 3.), the *DS* value of the emulsion decreased with the increasing concentration of a mixed 8ED; the emulsion separation was smallest at 1×10^{-3} mol dm^{-3} of 8ED. In the cases of 8 and 20 mmol dm^{-3} (Figs. 4(c) and (d)), the *DS* value of the emulsion was almost constant at the respective SDS concentration, independently of the mixed 8ED concentration. In the presence of 8 mmol dm^{-3} of SDS, the smallest *DS* value in this series of the emulsion was observed after 1 h.

When an oil is emulsified by mixed surfactant solutions which have an equi-interfacial-tension, the emulsion can be expected to have a narrow distribution of emulsion particle sizes, and so the emulsion stability increases; The stability is also explained from the point of view of the properties of the adsorbed film at the oil/water interface. According to our previous data,[15] in the presence of 8 and 20 mmol dm^{-3} of SDS, the properties of the adsorbed layer of the mixed surfactant at octane/water interface are governed primarily by SDS. Thus these emulsions exhibit the same stability independent of the mixed 8ED concentration. However, in the presence of 6 mmol dm^{-3} of SDS, as the properties of the mixed adsorbed layer change from SDS-like properties to 8ED-like ones with increasing concentration of mixed 8ED, the emulsion stability may vary with the concentration of mixed 8ED.

References

1) H. Akasu, M. Ueno, and K. Meguro, *J. Am. Oil Chem. Soc.*, **51**, 519 (1974).
2) K. Meguro, H. Akasu, M. Ueno, and T. Satake, "Colloid and Interface," Academic Press Inc., New York (1976), Vol. 2, p. 421.
3) V. Takasawa, M. Ueno, and K. Meguro, *J. Colloid Interface Sci.*, **78**, 207 (1980).
4) J. H. Schulman and E. K. Rideal, *Proc. R. Soc. London, Ser. B*, **122**, 46 (1937).
5) J. H. Schulman and E. G. Cockbain, *Trans. Faraday Soc.*, **36**, 651 (1940).
6) J. T. Davies and G. R. A. Mayers, *Trans. Faraday Soc.*, **56**, 651 (1960).
7) J. E. Carless and G. Hallworth, *J. Colloid Sci.*, **26**, 75 (1968).
8) H. C. Kung and E. D. Goddard, *J. Phys. Chem.*, **67**, 1965 (1963).
9) H. C. Kung and E. D. Goddard, *J. Phys. Chem.*, **68**, 3465 (1964).
10) R. D. Vold and K. L. Mittal, *J. Colloid Interface Sci.*, **38**, 451 (1972).
11) S. Fukushima, M. Takahashi, and M. Yamaguchi, *J. Colloid Interface Sci.*, **57**, 201 (1976).
12) P. H. Elworthy, A. T. Florence, and H. A. Rogers, *J. Colloid Interface Sci.*, **35**, 34 (1971).
13) J. H. Schulman and E. K. Rideal, *Proc. R. Soc. London, Ser. B*, **122**, 29 (1937).
14) K. Hayase and S. Hayano, *Bull. Chem. Soc. Jpn.*, **50**, 83 (1977).
15) H. Akasu, A. Nishii, M. Ueno, and K. Meguro, *J. Colloid Interface Sci.*, **54**, 278 (1976).

 © 1982 The Chemical Society of Japan Bull. Chem. Soc. Jpn., 55, 699—703 (1982)

Preparation and Physical Properties of EuC_2 and Its Solid Solutions, $R_xEu_{1-x}C_2$ (R=La and Gd)

Tetsuo Sakai, Gin-ya Adachi,* Takeshi Yoshida, Shin-ya Ueno, and Jiro Shiokawa

Department of Applied Chemistry, Faculty of Engineering, Osaka University, Yamadaoka 2-1, Suita, Osaka 565

(Received August 10, 1981)

A cubic-tetragonal phase transformation of EuC_2 was observed at 623 K. The phase transition temperatures of metal dicarbides (MC_2) were discussed in terms of the band structure proposed by previous authors. The compound EuC_2 was a ferromagnet with a zero field curie temperature of 20 K, which was close to the value expected from the Curie temperature *vs.* nearest neighbor Eu–Eu distance relation for the Eu chalcogenides. The solid solutions, $La_xEu_{1-x}C_2$, became ferromagnetic at low temperatures over the whole composition range, while the solid solutions, $Gd_xEu_{1-x}C_2$, have continuously changed the kind of magnetic order from ferromagnetic to antiferromagnetic. All the effective moments obtained for $R_xEu_{1-x}C_2$ were in good agreement with the theoretical values of Eu^{2+} and R^{3+} contained. The electrical resistivities of EuC_2 and its solid solutions had a sharp peak near the Curie temperature. When magnetic field was applied, the peak became broader and shifted to higher temperature.

Metal dicarbides (MC_2), which possess a CaC_2-type tetragonal structure at room temperature, are composed of metal ion (M^{n+}), acetylide ion (C_2^{2-}), and ($n-2$) electrons. Since the ($n-2$) electrons occupy a conduction band,[1] tervalent or quadrivalent metals form metallic dicarbides, while bivalent metals form nonmetallic dicarbides. An isostructural europium dicarbide (EuC_2), whose existence has been established by Gebelt and Eick,[2] is expected to contain bivalent europium ions (Eu^{2+}) and has a variety of interesting physical properties such as observed for Eu chalcogenides.[3] However, in contrast with the tervalent rare-earth dicarbides which have been intensively investigated, the carbide EuC_2 has received the least attention to date. In this paper, we report thermal, magnetic, and electrical properties of EuC_2 and its solid solutions, $R_xEu_{1-x}C_2$ (R=La and Gd).

Experimental

Europium carbide was synthesized by following two techniques. (1) Europium metal of 99% purity (Research Chemicals, Div. of Nucor Corp.) together with spectroscopic grade graphite (Nippon Carbon Corp.) was sealed under a vacuum (10^{-2} Pa) in a silica capsule and heated at 1000 °C for 30 h. (2) Europium oxide of 99.99% (Shin-etsu Chem. Corp.) was mixed with graphite powder in an agate mortar and then pressed into pellets at 10 kbar. The pellets were placed in a molybdenum container and heated at 1800 °C under a flow of argon for 5 h. Solid solutions, $La_xEu_{1-x}C_2$ and $Gd_xEu_{1-x}C_2$, were prepared from mixed lanthanoid oxides and graphite by heating them under the same conditions as the above method (2). The mixed oxides as starting materials were obtained as follows; europium and gadolinium (or lanthanum) trioxides (99.99% purity) were weighed and dissolved in 2 mol dm^{-3} HCl and a saturated solution of oxalic acid was added. The precipitate formed was filtered, oven-dried at 110 °C, and ignited at 900 °C. Strontium dicarbide was synthesized by the reaction of $SrCO_3$ (99.9%, Shin-etsu Chem. Corp.) and graphite at 1600 °C under an argon atmosphere. In all cases, 5 at% excess graphite was used to ensure removal of oxides. The samples obtained here were kept immersed in carbon tetrachloride or in evacuated glass capsules. All manipulations were carried out in an argon dry box in order to prevent hydrolysis.

Powder X-ray diffraction data were obtained with a Rigaku-Denki Rota-flex diffractometer by use of Ni-filtered Cu $K\alpha$ radiation and Si as an internal standard. The atomic ratios (La or Gd:Eu) in the solid solutions were determined with a Rigaku-Denki energy dispersion type X-ray fluorescent spectrograph unit, Ultra trace system. For the purpose of chemical analyses, weighed sample was hydrolyzed in 2 mol dm^{-3} HCl. After the solution was filtered to remove the free graphite, metal content in it was determined by the EDTA titration. Total carbon content was determined by elemental analysis with a Yanagimoto CHN-corder. Bound carbon content was obtained by the difference between the total and free carbon contents. These analyses gave the weight percentages of the free carbon in the range of 1—2% and a metal:bound carbon atomic ratio of 1:2 for all the carbides.

Phase transformation was examined by the method reported previously;[4] differential thermal analysis (DTA) in the range 290—1000 K. Magnetic susceptibility data were obtained with a Curie-chénevea magnetic balance (Shimadzu MB-11) equipped with a low temperature apparatus in the temperature range 4.2—300 K. The samples for magnetic measurements were mixed with apiezon grease L (Apiezon Products Ltd.) to protect them from moist air. Electrical resistivities were measured with strip samples cut from the polycrystalline sintered pellets in the range 1.5—300 K. The measurements were performed on a four-probe d.c. potentiometric technique. Thermoelectric power measurement was carried out in the range 120—300 K. A barshaped sample was held in a place between two copper blocks with Ag paste. Thermal gradient was controlled by small heaters wound on the copper blocks so as to be always less than 5 K.

Results and Discussion

X-Ray Data. Both of the europium carbides obtained by the two different methods possess the CaC_2-type body-centered tetragonal structure though they contain a second phase. This second phase, whose existence has been reported by previous authors,[2] could not be removed by annealing techniques. The lattice constants of the b.c.t. phase are in good agreement with the literature values[2] and those obtained for SrC_2 as shown in Table 1. Since Sr^{2+} in SrC_2 has the almost same ionic radius as Eu^{2+},

this result supports the assumption that all the Eu ions in EuC_2 are bivalent.

Rare-earth dicarbides, LaC_2 and EuC_2, form solid solutions ($La_xEu_{1-x}C_2$) with the b.c.t. structure. The sample of $x=0.08$ contains the same unknown phase as observed for EuC_2, while the sample of the composition range from $x=0.39$ to 0.94 are single phase of b.c.t. The lattice constants of $La_xEu_{1-x}C_2$ are summarized in Table 2.

For the solid solutions, $Gd_xEu_{1-x}C_2$, the compounds with compositions of $x=0.13$, 0.73, and 0.92 are formed with the b.c.t phase, while the compounds of $x=$ 0.40 and 0.62 have a face-centered cubic structure. The occurrence of the f.c.c. phase has been observed by previous authors[5] in the binary systems RC_2–$R'C_2$ (R=rare-earth elements). This phenomenon has been explained successfully in terms of a strain energy in the crystal which was produced by a large difference in the ionic radii of metals.[6,7] The lattice parameters of $Gd_xEu_{1-x}C_2$ are tabulated in Table 3.

The disappearance of the unidentified second phase in the mixed carbides may be in connection with the increase of the conduction electron density.

Phase Transformation. It is well known that the CaC_2-type dicarbides have a transformation from the b.c.t. phase at low temperature to the f.c.c. one at high temperature. The nature of the cubic-tetragonal phase transformation has been studied extensively for metal dicarbides (MC_2) except for EuC_2.[4–14] The data of EuC_2 which we obtained are tabulated in Table 1, compared with those obtained for SrC_2. The f.c.c. modification in EuC_2 occurs at 623 K, which is close to the value observed for SrC_2.

The phase transition temperatures (T_t) of MC_2 vary significantly from 423 K for BaC_2[8] to 2058 K for UC_2.[9] Since the transformation in MC_2 occurs through rotation of the C_2^{2-} group from the c-axis, the T_t values are expected to reflect the M–C_2 bond energy and then depend on two parameters; ionic radius of metal and the number of the conduction electrons. We plotted the T_t values of MC_2 against the ionic radii of metals,[15] $r(M^{n+})$, for coordination number six in Fig. 1. The T_t values are divided into three groups with respect to the number of con-

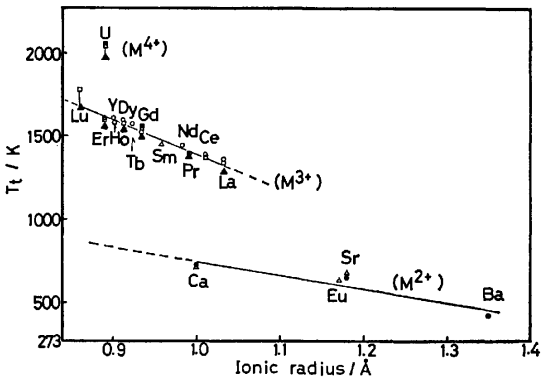

Fig. 1. Ionic radius of M^{n+} *vs.* phase transition temperature (T_t) plots for MC_2.
●: Bredig,[8] ■: Wallace *et al.*,[9] ▲: McColm *et al.*,[7,11] □: Bowman *et al.*,[10] ○: Adachi *et al.*,[13,14] △: this work.

TABLE 1. LATTICE CONSTANTS AND PHASE TRANSITION TEMPERATURES OF EuC_2 AND SrC_2

	Ionic radius of M^{2+} a)	Lattice constants	Transition temperatures
	Å	Å	K
EuC_2	1.17	$a=4.118$	623±3
		$c=6.756$	
SrC_2	1.18	$a=4.103$	675±3
		$c=6.756$	(643) b)

a) Values reported in Ref. 15. b) Values reported in Ref. 8.

TABLE 2. LATTICE CONSTANTS AND MAGNETIC PROPERTIES OF THE SOLID SOLUTIONS, $La_xEu_{1-x}C_2$

x	a/Å	c/Å	T_c/K	θ_p/K	μ_{eff}/μ_B	μ_{cal}/μ_B
0.00a)	4.118	6.756	20	+14	8.04	7.94
0.08a)	4.072	6.696	20	+12	8.15	7.64
0.39	4.022	6.664	19	+15	6.33	6.19
0.47	3.990	6.627	19	+15	5.88	5.76
0.68	3.974	6.613	14	+15	5.02	4.48
0.76	3.944	6.580	11	+2	4.08	3.93
0.94	3.939	6.570	<4	0	2.11	1.90

a) These samples contain the second phase.

TABLE 3. LATTICE CONSTANTS AND MAGNETIC PROPERTIES OF THE SOLID SOLUTIONS, $Gd_xEu_{1-x}C_2$

x	a/Å	c/Å	Phase	$T_{ord.}$/K	θ_p/K	μ_{eff}/μ_B	$\mu_{calord.}/\mu_B$
0.13	4.066	6.551	b. c. t.	20 Fa)	+20	7.94	7.94
0.40	5.835		f. c. c.	12 F	+8	8.05	7.93
0.62	5.813		f. c. c.	<4 AFb)	−13	7.88	7.92
0.73	3.780	6.306	b. c. t.	AF	−28	8.10	7.91
0.92	3.736	6.298	b. c. t.	33 AF	−43	8.06	7.90
1.00	3.722	6.295	b. c. t.	42 AF	−53	7.67	7.90

a) Ferromagnetic. b) Antiferromagnetic.

duction electrons and increase linearly with decreasing the ionic radius of metal, that is, with an increase in the lattice energy. The T_t *vs.* $r(M^{n+})$ plot for $M^{2+}C_2^{2-}$ indicates that EuC_2 is a member of the bivalent metal dicarbide group.

It has been proposed by Atoji[1] that excess electrons occupy the conduction band formed with the d-orbitals (d_{zx} and d_{yz}, z≡c-axis) of metal and the antibonding orbitals of C_2^{2-} and that the increase of conduction electron density causes to increase the C–C bond distance in MC_2. Since the C–C bond distances in MC_2 seem to be independent of the ionic radii of M^{n+},[16,17] their average values are listed in Table 4. Assuming that the C–C bond distances increase with increasing the M–C_2 covalent bond energy, we can expect that the increase in the T_t value has a linear relationship with the C–C bond distance. In order to discuss the T_t values under the same ionic radius of metal, the T_t values at $r(M^{n+})=0.89$ Å, which is identical with the ionic radius of U^{4+}, were estimated from the linear T_t *vs.* $r(M^{n+})$ plots in Fig. 1 and summarized in Table 4. The T_t values of MC_2 are plotted linearly against the C–C bond distances in Fig. 2 in support of the above assumption.

Magnetic Properties. Magnetization (σ) *vs.* temperature (T) curves for EuC_2 are shown at various fields in Fig. 3. Inset is the field dependence of magnetization at various temperatures. These magnetic data exhibit that EuC_2 becomes ferromagnetic at low temperature. Curie temperatures (T_c) at various fields (H) were determined by the method described in Ref. 18; extrapolation of σ^2 *vs.* T plot to $\sigma^2=0$. The zero field Curie temperature, $T_c(H\to 0)=20$ K, was obtained from the $T_c(H)$ *vs.* H plot in Fig. 6. Reciprocal magnetic susceptibility (χ_m^{-1}) *vs.* T plot obeys a Curie-Weiss law, giving an effective moment of

Table 4. Phase transition temperatures estimated at the ionic radius of $r(M^{n+})=0.89$ Å, average values of the C–C bond distances, and the number of conduction electrons, $(n-2)$ for MC_2

	Transition temperature / K	C–C bond distance / Å	$(n-2)$
$M^{2+}C_2$	850	1.191	0
$M^{3+}C_2$	1615	1.286	1
$M^{4+}C_2$	2038	1.340	2

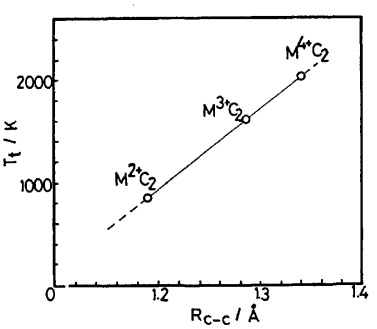

Fig. 2. Estimated phase transition temperature (T_t) *vs.* average C–C bond distance (R_{C-C}) plot for MC_2.

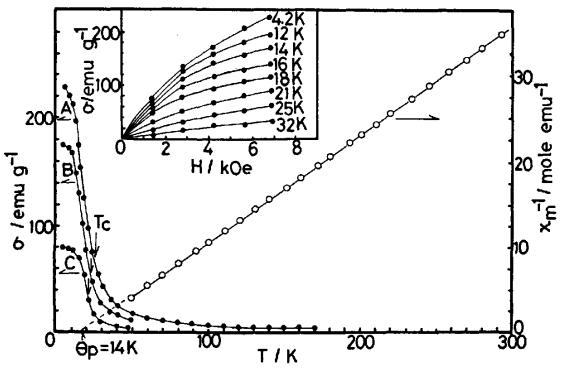

Fig. 3. Temperature dependence of magnetization (σ/emu g^{-1}†, —●—, A: 6.85 kOe††, B: 4.20 kOe, C: 1.40 kOe) and reciprocal magnetic susceptibility (χ_m^{-1}, —○—) for EuC_2.
† emu $g^{-1}=4\pi\times10^{-3}$ MKS kg^{-1}. †† 1 Oe=(1000/4π) A m^{-1}.

8.04 μ_B and a paramagnetic Curie temperature (θ_p) of +14 K. The effective moment is in good agreement with that expected for Eu^{2+}.

The exchange mechanism in EuX (X=O, S, and Se) has been studied by Kasuya.[19] They have proposed that the ferromagnetic interaction is due to the f-f interaction between Eu^{2+} nearest neighbors throughout the 5d-4f exchange interaction. Therefore, the exchange integral between Eu^{2+} nearest neighbours becomes a function of the Eu^{2+}–Eu^{2+} distance. The europium dicarbide has a nearest neighbour Eu^{2+} distance of 4.12 Å, which is very close to that of EuS, 4.21 Å. Since both the values of T_c and θ_p observed for EuC_2 are comparable to those of EuS ($T_c=16$ K, $\theta_p=19$ K), it is reasonable to assume that the exchange mechanism in EuC_2 is the same as that in EuX.

The tervalent rare-earth dicarbides (RC_2), which have one conduction electron per formulae unit, become antiferromagnetic at low temperatures.[20–22] Their magnetic properties have been discussed in terms of the f-f indirect exchange interaction *via* conduction electrons. The replacement of Eu^{2+} with La^{3+} varies two parameters, that is, the concentration of the conduction electron and the magnetic ion, while the replacement of Eu^{2+} with Gd^{3+} varies only the concentration of the conduction electron because the spin configuration of $Gd^{3+}(^8S_{7/2})$ is identical with that of Eu^{2+}. We can expect a continuous change in the exchange mechanism with changing the composition (x) in the solid solutions, $R_xEu_{1-x}C_2$ (R=La and Gd).

The magnetic data of the solid solutions, $R_xEu_{1-x}C_2$ (R=La and Gd), are tabulated in Tables 2 and 3, respectively. All the effective moments obtained from the χ_m^{-1} *vs.* T linear relation are in good agreement with the calculated values on the assumption that all the Eu ions in the compounds are bivalent. The solid solutions, $La_xEu_{1-x}C_2$, become ferromagnetic at low temperatures over the composition range from $x=0.08$ to $x=0.76$. The values of T_c(or θ_p) remain almost constant in the composition range from 0 to 0.47 and decrease rapidly with further dilution. In

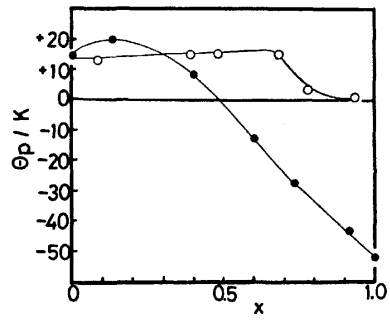

Fig. 4. Paramagnetic Curie temperature (θ_p) as a function of composition (x) for the solid solutions, $La_xEu_{1-x}C_2$ (—○—) and $Gd_xEu_{1-x}C_2$ (—●—).

the solid solutions, $Gd_xEu_{1-x}C_2$, the kind of magnetic order varies from ferromagnetic to antiferromagnetic with increasing the concentration of the Gd^{3+} ion. The composition dependence of θ_p for $R_xEu_{1-x}C_2$ (R=La and Gd) is shown in Fig. 4.

The carbides, $R_xEu_{1-x}C_2$, differ from the Eu chalcogenides such as $R_xEu_{1-x}Se$[23] in the magnetic behavior for small values of x ($x<0.1$). The compounds, $R_xEu_{1-x}Se$, have a drastic increase in θ_p and T_c for very low concentration of dopant (R=La^{3+} or Gd^{3+}) and this behavior was explained theoretically by Kasuya[24,25] in terms of the magnetic impurity model as follows. An excess electron with spin $\vec{s}_i$, which is trapped by a tervalent ion, magnetically polarizes the nearest neighbouring Eu spin, $\vec{S}_n$, by means of a strong exchange interaction between the impurity electron and the 4f electrons (the i-f exchange interaction). The large increase of T_c, ΔT_c, is deduced from the additional i-f exchange interaction, $-2\sum J_{in}\vec{s}_i\cdot\vec{S}_n$, and given by

$$k_B\Delta T_c = 2\sum J_{in}\vec{s}_i\cdot\vec{S}_n. \quad (1)$$

The Eu chalcogenides have a 6s character on the impurity state,[25] while the Eu dicarbides are expected to have a 5d character on the impurity state.[1,26] The almost constant T_c values of the solid solutions, $R_xEu_{1-x}C_2$, for the small values of x seem to be understood in the light of the small special spread of the impurity electron which would suppress the i-f exchange interaction. The magnetic behaviors of $R_xEu_{1-x}C_2$ for higher values of x resemble those of the Eu chalcogenides[23] and would be explained in terms of the change of Ruderman-Kittel function given by[27]

$$F(2k_FR) = [2k_FR\cos(2k_FR) - \sin(2k_FR)](2k_FR)^{-4}, \quad (2)$$

$$k_F = 1/r_0(9\pi z/4)^{1/3}, \quad (3)$$

where R is the distance from the magnetic ion of the reference site, k_F the Fermi wavenumber, r_0 the atomic radius, and z the number of conduction electrons.

Electrical Properties. Electrical resistivities of EuC_2 (ρ) decrease with decreasing temperature down to 160 K, and has a sharp peak at T_p=20 K as shown in Fig. 5. Inset is the ρ *vs.* T curves at various external fields (H). As the H values increase, the peak in ρ decreases, becomes broader, and shifts to higher temperature side. The T_p values exhibit the same

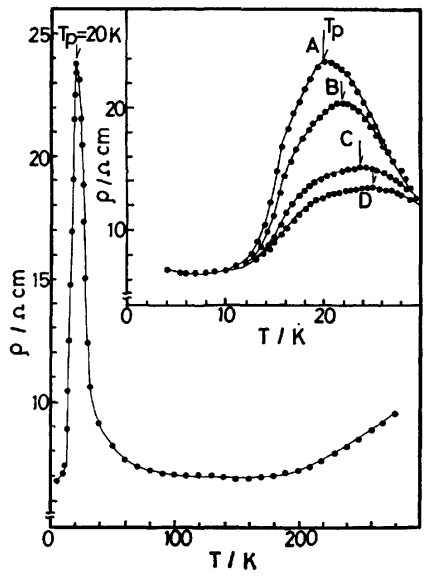

Fig. 5. Electrical resistivity (ρ) *vs.* temperature curve for EuC_2. Inset; the ρ *vs.* T curves at various fields (A: 0 kOe, B: 2.80 kOe, C: 5.60 kOe, D: 6.85 kOe).

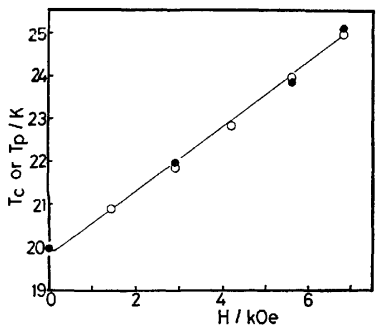

Fig. 6. Magnetic field (H) dependence of the Curie temperature (T_c, —○—) and the temperature at which the resistivity has the peak (T_p, —●—) for EuC_2.

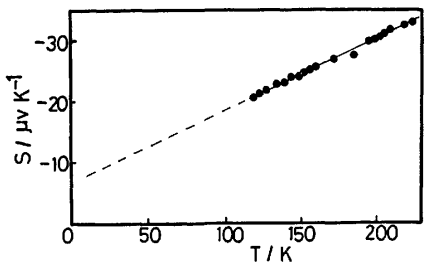

Fig. 7. Temperature dependence of the thermoelectric power (S) for EuC_2.

field dependence as the Curie temperatures (Fig. 6). The temperature dependence of the thermoelectric power (S) in EuC_2 is shown in Fig. 7. The sign of the S values is negative over the whole range of temperatures, indicating electron-type conduction. The creation of the excess electron in EuC_2 may be due to the existence of anion (C_2^{2-}) vacancies in small amount.

The rapid increase in ρ near the Curie temperature was observed previously for the Eu chal-

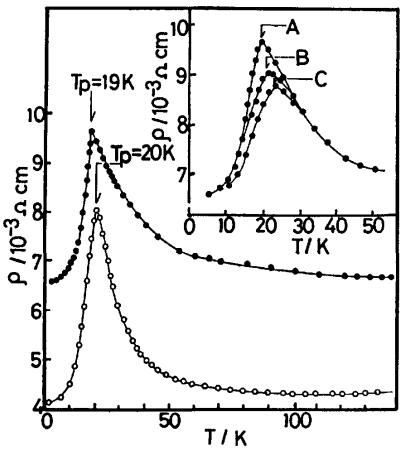

Fig. 8. Electrical resistivity (ρ) *vs.* temperature (T) curves for $La_{0.39}Eu_{0.61}C_2$ (—●—) and $Gd_{0.13}Eu_{0.87}C_2$ (—○—). Inset; the ρ *vs.* T curves at various magnetic fields (A: 0 kOe, B: 3.50 kOe, C: 6.85 kOe) for $La_{0.39}Eu_{0.61}C_2$.

cogenides.[28] Kasuya ascribed this electrical behavior to the exchange interaction between the impurity electron and the 4f electrons.[24,25] The impurity electron aligns the spins of nearest neighbour Eu^{2+} ions throughout the i-f exchange interaction, forming magnetic polarons. Therefore, the mobility of the impurity electron decreases near T_c. Since below T_c all the 4f spins are aligned and the magnetic polarons disappear, the resistivities decrease rapidly. When a magnetic field is applied, an activation energy which is necessary for hopping of the impurity electron is reduced and the peak in ρ decreases.

The electrical resistivity of $La_{0.39}Eu_{0.61}C_2$ or $Gd_{0.13}Eu_{0.87}C_2$, decreases to 1/1000 of that of EuC_2, reflecting the increase of conduction electron density (Fig. 8). A peak in ρ *vs.* T curve is similar to that observed for EuC_2 and would be explained on the basis of the same model as described above.

This work was supported by a Grant-in-Aid for Scientific Research No. 455301 from the Ministry of Education, Science and Culture for one of the authors (G. Adachi).

References

1) M. Atoji, *J. Phys. Soc. Jpn. Suppl.*, B-II **17**, 395 (1962).
2) R. E. Gebelt and H. A. Eick, *Inorg. Chem.*, **3**, 335 (1961).
3) P. Wachter, "Handbook on the Physics and Chemistry of Rare-Earths," ed by K. A. Gschneidner, Jr., and L. R. Eyring, North Holland, New York (1979), Vol. 2, p. 507.
4) G. Adachi, K. Ueno, and J. Shiokawa, *J. Less-Common Met.*, **37**, 313 (1974).
5) G. Adachi, H. Kotani, N. Yoshida, and J. Shiokawa, *J. Less-Common Met.*, **22**, 517 (1970).
6) G. Adachi, T. Nishihata, and J. Shiokawa, *J. Less-Common Met.*, **32**, 301 (1973).
7) I. J. McColm, T. A. Quigley, and N. J. Clark, *J. Inorg. Nucl. Chem.*, **35**, 1931 (1973).
8) M. A. Bredig, *J. Phys. Chem.*, **46**, 801 (1942).
9) T. C. Wallace, N. H. Krikorian, and P. L. Stone, *J. Electrochem. Soc.*, **111**, 1404 (1964).
10) A. L. Bowman, N. H. Krikorian, G. P. Arnold, T. C. Wallace, and N. G. Nereson, U.S.A. Energy Comm. LA-DC-8451 CESTI, **1967**, 7.
11) I. J. McColm, I. Colquhoun, and N. J. Clark, *J. Inorg. Nucl. Chem.*, **34**, 3809 (1972).
12) W. B. Wilson, *J. Am. Ceram. Soc.*, **43**, 77 (1960).
13) G. Adachi, Y. Shibata, K. Ueno, and J. Shiokawa, *J. Inorg. Nucl. Chem.*, **38**, 1023 (1976).
14) G. Adachi, F. Tonomura, Y. Shibata, and J. Shiokawa, *J. Inorg. Nucl. Chem.*, **40**, 489 (1978).
15) R. D. Shannon, *Acta Crystallogr., Sect. A*, **32**, 751 (1976).
16) M. Atoji and R. C. Medrud, *J. Chem. Phys.*, **31**, 332 (1959).
17) M. Atoji, *J. Chem. Phys.*, **35**, 1950 (1961).
18) R. M. Bozorth, "Ferromagnetism," D. Van Nostrand, New York (1951), p. 713.
19) T. Kasuya, *IBM J. Res. Develop.*, **14**, 214 (1970).
20) M. Atoji, *J. Chem. Phys.*, **46**, 1891 (1967); **48**, 3384 (1968); **52**, 6430 (1970); **57**, 2410 (1972).
21) T. Sakai, G. Adachi, and J. Shiokawa, *J. Appl. Phys.*, **50**, 3592 (1979).
22) T. Sakai, G. Adachi, T. Yoshida, and J. Shiokawa, *J. Less-Common Met.*, **81**, 91 (1981).
23) H. Holtzberg, T. R. McGuire, S. Methfessel, and J. C. Suits, *Phys. Rev. Lett.*, **13**, 18 (1964).
24) A. Yanase and T. Kasuya, *J. Appl. Phys.*, **39**, 430 (1968).
25) A. Yanase and T. Kasuya, *J. Phys. Soc. Jpn.*, **25**, 1025 (1968).
26) V. L. Yupko, G. N. Makarenko, and Yu. B. Paderno, "Refractory Carbides," ed by G. V. Samsonov, Consultants Burean, New York (1974), p. 251.
27) B. Coqblin, "The Electronic Structure of Rare-Earth Metals and Alloys: The Magnetic Heavy Rare-Earths," Academic Press, New York (1977).
28) Y. Shapira, S. Foner, and T. B. Reed, *Phys. Rev. B*, **8**, 2299 (1973).

The Analysis of Lanthanoid-induced ^{13}C Shifts for Naphthylamines. Contact Shifts Induced by Gd-chelates and the Spin-delocalization Mechanism

Masatoshi HIRAYAMA,* Kenji AKUTSU, and Kazuko FUKUZAWA

Department of Chemistry, Faculty of Science, Ibaraki University, Bunkyo 2-1-1, Mito 310

(Received August 27, 1981)

The ^{13}C shifts of 1- and 2-naphthylamines induced by $Gd(fod)_3$ and $Gd(dpm)_3$ were shown to consist predominantly of a contact contribution, based on the fact that these shifts excellently correlate with the hyperfine coupling constants obtained from the graphical analysis of ^{13}C shifts induced by other $Ln(fod)_3$, where Ln is La, Pr, Nd, Sm, Eu, Dy, Ho, Er, or Yb. It was found from the INDO MO calculations of the spin densities of ligand moieties that these Gd-induced shifts parallel the spin-density distribution of the naphthylmethyl radical better than that of the naphthylamine cation radical and that these shifts are best interpreted in terms of the superposition of the β-spin of the naphthylmethyl radical and the α-spin of the naphthyl radical. This may suggest that a direct spin transfer occurs through space from Gd^{3+} to the amine molecule, in addition to the normal through-bond delocalization *via* the N-lone pair.

In order to employ lanthanoid-induced shifts(LIS) for the elucidation of molecular structures, particularly of the sterically detailed geometries of molecules, one must separate a purely dipolar contribution from LIS. It has been well recognized that LIS consists of three contributions: contact(cs), pseudo contact(pcs), and complex formation shifts(cfs).[1] The third term can be easily determined from the shifts induced by a La- or Lu-complex on the plausible assumption that the diamagnetic shift due to the adduct formation with a Ln-complex is equal in magnitude along the lanthanoid series. Among several methods proposed for the separation of a pcs term, there is one which can be carried out by a relatively simple procedure using the experimental shifts induced by a Gd-complex.[2] This is based on the theoretical prediction that Gd^{3+} has an isotropic g-tensor[3] and on the expectation that all the other analogous Ln-complexes cause a ligand cs-pattern identical with that due to the Gd-complex. Indeed, this method has successfully been applied to the ^{13}C shifts of several kinds of organic molecules by Ajisaka *et al.*[2] However, no more such studies have been found, probably because of the severe broadening of resonance lines caused by this ion.

The object of this report is to confirm that Gd-induced shifts are only contact in origin in actual complexes and to investigate a spin-delocalization mechanism for such complexes by means of a "relative method." Some of the results have been reported in a preliminary paper.[4] Naphthylamines were chosen because many kinds of carbons assignable to each position are included, their molecular structures are rigid, which are convenient for pcs calculations, and their chemical equilibria are well known.[5]

Experimental

1- and 2-Naphthylamines were of commercial origin (Nakarai Chemicals, Ltd). $CDCl_3$(Merck Sharp & Dohme Canada, Ltd.) was used as a solvent after having been dried over molecular sieves for 24 h. The lanthanoid shift reagents(LSR) were synthesized by the methods in the literatures[6] and were used after having been dried over P_2O_5 in a vacuum desiccator. The LSR employed in the present study are $Ln(fod)_3$,[7] where Ln is La, Pr, Nd, Sm, Eu, Gd, Dy, Ho, Er, or Yb, and $Ln(dpm)_3$,[7] where Ln is La or Gd.

The ratio of LSR(L) to the substrate (S) (ρ) was varied by the addition of well-defined amounts of LSR to a 1 M solution of 1-naphthylamine in $CDCl_3$(0.8 M in 2-naphthylamine). For each LSR, five or six ^{13}C spectra were recorded with ρ values ranging from 0 to 0.2 (0 to 0.03 for $Gd(fod)_3$ and $Gd(dpm)_3$), using TMS as the internal standard at 24 °C, on a Varian CFT-20 spectrometer. The assignments of ^{13}C lines were made by the methods in the literature.[8]

The INDO MO calculations of spin densities were carried out on HITAC 8800/8700 computers at The Computer Center of the University of Tokyo. The program used was Y4CB04[9] of the library programs collected in this center. The LISA2 program prepared by Shapiro *et al.*[10] was used for the nonlinear least-squares analysis of LIS *vs.* ρ plots.

Results and Discussion

The nonlinear least-squares analyses of ^1H-LIS *vs.* ρ plots ($0<\rho<2.5$, the number of data points is 27), carried out for 1-naphthylamine with $Eu(fod)_3$ in $CDCl_3$, indicated that this system is best interpreted in terms of two-step equilibria:

$$L + S \rightleftharpoons LS \quad K_1, \delta_{LS}, \tag{1}$$

$$LS + S \rightleftharpoons LS_2 \quad K_2, \delta_{LS_2}, \tag{2}$$

with no self-association of $Eu(fod)_3$ in solution, $L + L \rightleftharpoons L_2$, where K's, δ_{LS}, and δ_{LS_2} are the equilibrium constants and intrinsic shifts of the 1:1 and 1:2 adducts respectively. The equilibrium constants determined are $K_1=75$—95 and $K_2=1$—5,[11] implying that the second equilibrium is negligible compared with the first. Then, considering the one-step equilibrium, the observed shift, δ_{obsd}, is given by:

$$\delta_{obsd} = \frac{[LS]}{[S_0]}\delta_{LS}, \tag{3}$$

in the fast-exchange limit, where $[S_0]$ is the total concentration of the substrate. When $\rho \ll 1$ and $K_1 \cdot [S_0] \gg 2(1+\rho)$, one has $[LS]/[S_0] \approx \rho$ and Eq. 3 simplifies to:

$$\delta_{obsd} = \rho \cdot \delta_{LS}.^{12} \tag{4}$$

Actually, a good linear relation has been obtained for these ^1H-LIS *vs.* ρ plots in the range of $\rho \ll 1$.

TABLE 1. OBSERVED ^{13}C PARAMAGNETIC SHIFTS OF NAPHTHYLAMINES INDUCED BY $Gd(fod)_3$ AND $Gd(dpm)_3$[a]

	Position	fod			dpm		
		$\delta_{LS}(Gd)$	$\delta_{LS}(La)$	$\delta'_{LS}(Gd)$[b]	$\delta_{LS}(Gd)$	$\delta_{LS}(La)$	$\delta'_{LS}(Gd)$[c]
1-Naphthylamine	1	88±5	−5.4	93±5	40±4	−2.5	43±4
	2	−41±2	8.9	−50±2	−28±3	5.7	−34±3
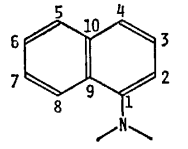	3	30.5	−0.3	30.8	15.8	−0.7	16.5
	4	−22.5	7.8	−30.3	−13.5	4.0	−17.5
	5	−6.0	0.5	−6.5	−6.6	−0.8	−5.8
	6	11.5	1.3	10.2	5.3	0	5.3
	7	−5.0	2.8	−7.8	−4.2	1.1	−5.3
	8	18.0	5.6	12.4	13.4	1.3	12.1
	9	−30.5	3.2	−33.7	−17.0	2.5	−19.5
	10	24.0	0.6	23.4	13.2	0	13.2
2-Naphthylamine	1	−36±4	10.3	−46±4	−19±6	5.6	−25±6
	2	71±10	−5.8	77±10	48±10	−2.7	51±10
	3	−20±2	2.3	−22±2	−7±1	1.8	−9±1
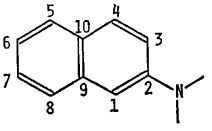	4	16.0	0.9	15.1	9.2	−0.6	9.8
	5	8.8	0.4	8.4	6.6	−0.7	7.3
	6	−8.0	3.8	−11.8	−4.0	0.6	−4.6
	7	9.6	1.3	8.3	4.7	0	4.7
	8	−9.2	1.8	−11.0	−4.0	0.6	−4.6
	9	19.2	−0.8	20.0	10.6	−1.4	12.0
	10	−12.4	4.0	−16.4	−6.6	1.3	−7.9

a) Values in ppm relative to that of the free naphthylamine. Negative signs denote highfield shifts.
b) $\delta_{LS}(Gd(fod)_3)-\delta_{LS}(La(fod)_3)$. c) $\delta_{LS}(Gd(dpm)_3)-\delta_{LS}(La(dpm)_3)$.

Also, in the present ^{13}C experiments, an excellent linear relation between δ_{obsd} and ρ was obtained within the examined range of $\rho(\rho \ll 1)$. Thus, Eq. 4 can be applied to the analyses of the present ^{13}C data. The correlation coefficients(R) in this linear relation with $Gd(fod)_3$ and $Gd(dpm)_3$ were >0.998 for all the carbons except for the C_1 of 1- and the C_2 of 2-naphthylamine, for which the accuracies of measured shifts are poor because of the severe broadening of the resonance lines (>0.9). Thus, in the present system, δ_{LS} can be found from the slope of the δ_{obsd} *vs.* ρ plot. As is generally accepted, the correction of δ_{LS} for a diamagnetic shift can be made by using the $La(fod)_3$- or $La(dpm)_3$-induced δ_{LS} value, the corrected δ_{LS} being denoted as δ'_{LS} in the present paper. The δ'_{LS} values observed for 1- and 2-naphthylamines with $Gd(fod)_3$ and $Gd(dpm)_3$, $\delta'_{LS}(Gd)$, are summarized in Table 1.

In order to examine whether or not $\delta'_{LS}(Gd)$ consists solely of a cs contribution, δ_{LS} values with a series of $Ln(fod)_3$ for 1-naphthylamine were first observed; the δ'_{LS} values were obtained using the $La(fod)_3$-induced δ_{LS} value. For all the carbons with each $Ln(fod)_3$, the R-values in the δ_{obsd} *vs.* ρ plots were >0.999. These were then separated into cs and pcs contributions by the graphical method,[12,13] which has successfully been utilized in recent years: the δ'_{LS} for a given nucleus, i, $\delta'_{LS,i}$ in a lanthanoid adduct can conveniently be expressed as a sum of two terms:

$$\delta'_{LS,i} = A_i \cdot \langle S_z \rangle + G_i \cdot D, \quad (5)$$

where A_i is the hyperfine coupling constant between the nucleus and the unpaired electron, $\langle S_z \rangle$ is the projection of the lanthanoid total electron-spin magnetization in the direction of the external field, G_i is the geometric factor $(3\cos^2\theta-1)r^{-3}$, and D is a constant for a given lanthanoid and temperature. If, for this adduct, the constancy of A_i and G_i can be assumed along the series, the contributions of the two terms can readily be separated. By a rearrangement of Eq. 5, one obtains:

$$\delta'_{LS,i}/\langle S_z \rangle = A_i + G_i \cdot D/\langle S_z \rangle. \quad (6)$$

Using the tabulated values of $\langle S_z \rangle$[14] and of D,[3a] a plot of $\delta'_{LS,i}/\langle S_z \rangle$ against $D/\langle S_z \rangle$ can be constructed; the plot should be linear, with a slope of G_i and an intercept on the ordinate of A_i. However, some scattering of points may be anticipated in view of the fact that the values of D were calculated with an arbitrary set of crystal-field parameters.[3] The present data are plotted in this way in Fig. 1. It may be seen that, apart from some scattering of points, all sets of the data closely obey the linear relationship. The R-values are shown in the footnotes of Fig. 1. The data points from Sm-adducts were excluded, since these deviate considerably from the linear relation because of the great sensitivity of $\delta'_{LS}/\langle S_z \rangle$ to a small experimental error in δ'_{LS} because of the extremely small value of $\langle S_z \rangle$. Thus, it may be said that an effective axial symmetry holds in this system and that G_i and A_i are constant through out the series.

The relative A_i-values determined from Fig. 1 are compared with the relative values of $\delta'_{LS}(Gd)$ in Table 2. These two quantities correspond well with each other ($R=0.985$), considering the A_i-values determined from such plots containing theoretical quantities. Next, the addition of the relative G_i as a pcs pattern to the relative A_i was made tentatively in order to

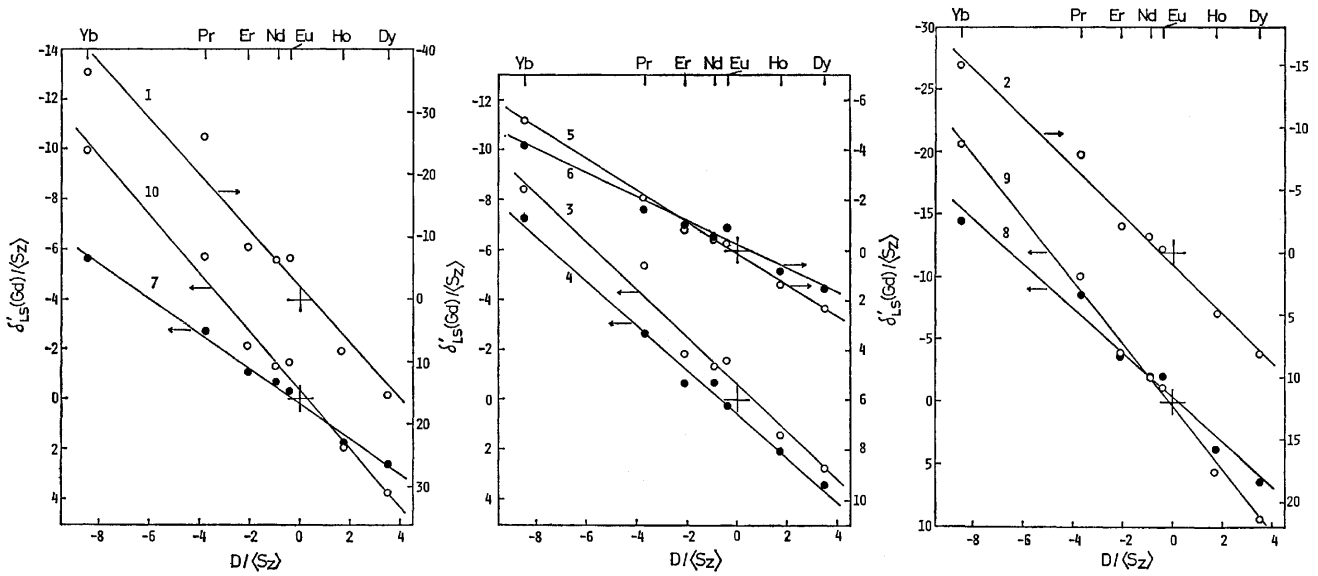

Fig. 1. $\delta'_{LS}(Gd)/\langle S_z\rangle$ *vs.* $D/\langle S_z\rangle$ plots for 1-naphthylamine-Ln(fod)$_3$ system.
Numbers denote positions of carbons. Correlation Coefficients: 0.9714 (C_1), 0.9934 (C_2), 0.9834 (C_3), 0.9945 (C_4), 0.9955 (C_5), 0.9895 (C_6), 0.9947 (C_7), 0.9891 (C_8), 0.9971 (C_9), 0.9908 (C_{10}).

TABLE 2. COMPARISONS OF Gd(fod)$_3$-INDUCED ^{13}C SHIFTS AND HYPERFINE COUPLING CONSTANTS FOR 1-NAPHTHYLAMINE[a]

Position	Relative		
	$\delta'_{LS}(Gd)$[b]	A_1[c]	$\delta_{calcd}(A_1+G_1)$[d]
1	3.08	3.56	3.07
2	−1.65	−1.78	−1.80
3	1.02	1.14	1.02
4	−1.00	−0.95	−0.95
5	−0.21	−0.26	−0.29
6	0.34	0.39	0.33
7	−0.26	−0.31	−0.34
8	0.41	0.68	0.45
9	−1.11	−0.86	−0.96
10	0.77	0.71 (0.985)	0.60 (0.997)

a) The numbers in parentheses are the correlation coefficients of A_1 or $\delta_{calcd}(A_1+G_1)$ to $\delta'_{LS}(Gd)$. b) With Gd(fod)$_3$. c) Relative hyperfine coupling constant estimated graphically from Fig. 1. d) The relative shift values estimated from the least squares fits of the superposition of A_1- and G_1-patterns on $\delta'_{LS}(Gd)$.

TABLE 3. OBSERVED AND CALCULATED RELATIVE GEOMETRIC FACTORS FOR 1-NAPHTHYLAMINE

Position	G_1[a]	GF_{calcd}[b]
1	5.07	5.02
2	2.20	2.47
3	1.08	1.10
4	1.00	0.92
5	0.72	0.69
6	0.54	0.58
7	0.79	0.78
8	2.00	1.87
9	2.84	2.45
10	1.31	1.21 (0.996)

a) Determined graphically from Fig. 1. b) Calculated geometric factors. The geometric parameters used are shown in Ref. 15. The number in parenthesis is the correlation coefficient between G_1 and GF_{calcd}.

interprete $\delta'_{LS}(Gd)$; this resulted in a further, better correlation (R=0.997), as is shown in Table 2. This effectiveness of G_i on the improvement of R may not be completely reliable, considering the effect of the use of theoretical values of D and $\langle S_z\rangle$ on the accuracies of A_i and G_i. However, as long as a relative method is used for the discussion, the possibility of the inclusion of a small amount of a dipolar contribution can not be completely excluded. On the other hand, the G_i-values have fairly well been explained in terms of the geometric factors, calculated using plausible geometric parameters,[15] as is shown in Table 3.

If the observed ^{13}C shifts are purely contact in origin, their intramolecular ratio should correspond to the spin-density distribution of the carbon 2s-orbitals of the ligand (ρ_{2s}). Therefore, the INDO MO calculations of ρ_{2s} were carried out for the cation radicals of naphthylamines, which can be expected to be a real model for the ligand moiety of lanthanoid adducts. The following standard geometries were used with 120° or tetrahedral bond angles: C–H (aromatic), 1.08 Å; C–C (aromatic), 1.40 Å; C–N, 1.37 Å. Considering the pyramidal structure of nitrogen, the angle between the N–C bond and the NH_2 plane (χ) was taken as 50°.[17] The calculated results imply that the highest occupied MO containing an electron spin is of the π-type, as anticipated. In Table 4, the calculated ρ_{2s} values of cation radicals, ρ_{2s}(Naam$^+$), are compared with the $\delta'_{LS}(Gd)$ values observed with Gd(fod)$_3$. The feature of sign alternation is almost identical in both; however, only a poor agreement

Table 4. Comparisons of Gd-induced ^{13}C shifts and spin densities on carbon 2s orbitals[a]

	Position	$\delta'_{LS}(Gd)$[b]	$-\rho_{2s}(Naam^+)$	$-\rho_{2s}(Name)$	$\rho_{2s}(Naph)$	δ_{calcd}[c]
1-Naphthylamine	1	3.1±0.2	0.015	1.262	51.550	2.71
	2	−1.7±0.1	−0.742	−1.377	−2.000	−1.67
	3	1.02	0.576	0.869	4.220	1.13
	4	−1.00	−1.000	−1.000	−1.000	−1.20
	5	−0.21	−0.477	−0.410	0.083	−0.48
	6	0.34	0.295	0.385	0.012	0.46
	7	−0.26	−0.318	−0.418	−0.016	−0.43
	8	0.41	0.008	0.451	0.087	0.47
	9	−1.11	−0.121	−0.689	−0.040	−0.72
	10	0.77	0.538 (0.611)	0.598 (0.937)	0.138	0.62 (0.987)
2-Naphthylamine	1	−3.1±0.3	−8.101	−2.111	−0.822	−2.80
	2	5.1±0.7	0.748	1.840	16.561	4.38
	3	−1.5±0.1	0.896	−1.173	−0.449	−1.55
	4	1.00	−1.000	1.000	1.000	1.40
	5	0.56	1.303	0.728	0.178	0.95
	6	−0.78	−3.950	−0.778	−0.093	−1.01
	7	0.55	3.452	0.667	0.159	0.73
	8	−0.73	−5.450	−0.765	0.037	−0.84
	9	1.32	3.599	1.049	1.318	1.15
	10	−1.09	−1.602 (0.583)	−1.012 (0.925)	−0.224	−1.11 (0.990)

a) Relative values. The numbers in parentheses are the correlation coefficients between $\delta'_{LS}(Gd)$ and ρ_{2s} or δ_{calcd}. b) With $Gd(fod)_3$. The negative signs denote highfield shifts and thus correspond to the negative signs of ρ_{2s}. c) Relative shifts calculated using Eq. 7 from the least-squares fits of the superposition of $\rho_{2s}(Name)$ and $\rho_{2s}(Naph)$ to $\delta'_{LS}(Gd)$.

is obtained.

Horrocks *et al.*[19] and Morishima *et al.*[20] have shown that, for a variety of pyridine-type bases, the $Ni(acac)_2$-induced contact shifts parallel the spin-density distribution in the analogous hydrocarbon radical better than that for the pyridine-like cation radical. Therefore, taking into account this effect for the present system, the spin-density distributions of naphthylmethyl radicals, $\rho_{2s}(Name)$, were calculated. The distance between the ring and the CH_2 group was taken as 1.40 Å. Table 4 implies that, on going from $\rho_{2s}(Naam^+)$ to $\rho_{2s}(Name)$, the agreement with $\delta'_{LS}(Gd)$ becomes considerably better in both 1- and 2-naphthylamines. The difference between these two INDO spin-density distributions may be ascribed mainly to the changes in the σ-π interaction caused by the energy variation in each MO due to the lowering of the nuclear charge of the hetero atom. From this result, one may consider that, in the present system, the interaction between an Ln 4f-orbital and the ligand affects the valence orbital of the ligand fairly much. Thus, the cation radical perturbed in a manner analogous to the effect of lowering the nuclear charge of the hetero atom appears to be a better model for the spin-density distribution of this type of ligand in $Ln(fod)_3$- or $Ln(dpm)_3$-adducts.[21] Comparisons of $\delta'_{LS}(Gd)$ and $\rho_{2s}(Name)$ indicate that a β-spin is delocalized into the ligand π-orbital from Gd^{3+}; this seems to be consistent with the minus sign of $\langle S_z \rangle$ calculated for this ion by Golding *et al.*[14]

Although the feature of sign alternation is completely identical in $\delta'_{LS}(Gd)$ and $\rho_{2s}(Name)$, it is found that an anomalous component of shifts is included in the shifts of carbons bound to the NH_2 group and of its neighbours: considerably large lowfield shifts at C_1 and small highfield shifts at C_2 and C_9 for 1-naphthylamine, and considerably large lowfield shifts at C_2 and small highfield shifts at C_1 and C_3 for 2-naphthylamine. Although an attempt was made to reproduce $\delta'_{LS}(Gd)$ by the superposition of a relative pcs on $\rho_{2s}(Name)$, this was unsuccessful. It is then considered that a second contribution to $\delta'_{LS}(Gd)$ may be required as a cs occurring through another pathway of an electron spin. Taking into account the mixed delocalization, the addition of the spin-density distribution of the lowest vacant MO (ρ_{2s} of the naphthylamine anion radicals) to $\rho_{2s}(Name)$ was tentatively made; however, this was also unsuccessful. From the comparison of $\delta'_{LS}(Gd)$ and $\rho_{2s}(Name)$ in Table 4, one may consider that the distribution of such an anomalous component of shifts is very similar to that expected from a σ-type delocalization of the positive spin placed on C_1 for 1- and on C_2 for 2-naphthylamine into the ring. Naphthyl radicals may thus be expected to have a required spin-density distribution. Then, the relative spin-density distribution of this radical($\rho_{2s}(Naph)$) was added to $\rho_{2s}(Name)$ to obtain the least-squared values in Eq. 7:

$$\delta_{calcd} = X \cdot \rho_{2s}(Name) + Y \cdot \rho_{2s}(Naph), \quad (7)$$

where X and Y are constants. This examination led to a further, better agreement with the $\delta'_{LS}(Gd)$-pattern in both 1- and 2-naphthylamines, as may be

Table 5. Correlation coefficients between δ'_{LS}(Gd) and the relative shifts predicted tentatively

	1-Naphthylamine		2-Naphthylamine	
	fod	dpm	fod	dpm
A_1 only	0.985	0.982	—	—
A_1+G_1	0.997	0.992	—	—
ρ_{2s}(Naam$^+$) only	0.611	0.673	0.583	0.553
ρ_{2s}(Naam$^+$)+ ρ_{2s}(Naph)	0.913	0.898	0.920	0.926
ρ_{2s}(Name) only	0.937	0.970	0.925	0.893
ρ_{2s}(Name)+ ρ_{2s}(Naph)	0.987	0.982	0.990	0.984
ρ_{2s}(Naam$^+$)$+G_1$	0.690	0.711	0.636	0.465
ρ_{2s}(Name)$+G_1$	0.972	0.985	0.940	0.917

seen from Table 4. The correlation coefficients are summarized in Table 5, together with those for the other cases with Gd(fod)$_3$ and Gd(dpm)$_3$. This result may correspond to the delocalization of a significant amount of α-spin into the ligand, in contrast to a β-spin of ρ_{2s}(Name); thus, it may suggest that a through-space transfer of spin occurs from Gd^{3+} to the ligand.

References

1) K. Tori, Y. Yoshimura, M. Kainosho, and K. Ajisaka, *Tetrahedron Lett.*, **1973**, 3127.

2) K. Ajisaka and M. Kainosho, *J. Am. Chem. Soc.*, **97**, 330 (1975).

3) a) B. Bleaney, C. M. Dobson, B. A. Levine, R. B. Martin, R. J. P. Williams, and A. V. Xavier, *J. Chem. Soc., Chem. Commun.*, **1972**, 791; b) B. Bleaney, *J. Magn. Reson.*, **8**, 91 (1972).

4) M. Hirayama, *Chem. Lett.*, **1980**, 1497.

5) The interaction of a series of aromatic amines with LSR has been studied in our laboratory. For the Ln(fod)$_3$–1-naphthylamine system, the equilibrium constants and intrinsic shifts have been estimated, as is described in this text.

6) C. S. Springer, Jr., D. W. Meek, and R. E. Sievers, *Inorg. Chem.*, **6**, 1105 (1967); K. J. Eisentraut and R. E. Sievers, *Inorg. Syn.*, **11**, 94 (1968).

7) fod: 6,6,7,7,8,8,8-heptafluoro-2,2-dimethyl-3,5-octanedionato, dpm: dipyvaloylmethanato.

8) W. Kitching, M. Bullpitt, D. Gartshore, W. Adcock, T. C. Khor, D. Doddrell, and I. D. Rae, *J. Org. Chem.*, **42**, 2411 (1977).

9) This program was prepared based on J. A. Pople, D. L. Beveridge, and P. A. Dobosh, *J. Chem. Phys.*, **47**, 2026 (1967).

10) M. D. Johnston, Jr., B. L. Shapiro, M. J. Shapiro, T. W. Proulx, A. D. Godwin, and H. L. Pearce, *J. Am. Chem. Soc.*, **97**, 542 (1975).

11) Unpublished data. These data have been obtained from the data for H_2 and H_8, which have the largest values of δ_{LS}. Also, for other protons with Eu(fod)$_3$ and several protons with Pr(fod)$_3$-d[27] and Yb(fod)$_3$, the K's have been estimated; however, these show considerable scatter. Nevertheless, in all the cases, K_1 is larger than 50.

12) J. W. M. de Boer, P. J. D. Sakkers, C. W. Hilbers, and E. de Boer, *J. Magn. Reson.*, **25**, 455 (1977).

13) C. N. Reilley, B. W. Good, and R. D. Allendoerfer, *Anal. Chem.*, **48**, 1446 (1976); G. A. Elgavish and J. Reuben, *J. Am. Chem. Soc.*, **99**, 5590 (1977); J. Reuben and G. A. Elgavish, *J. Magn. Reson.*, **39**, 421 (1980); A. D. Sherry, P. P. Yang, and L. O. Morgan, *J. Am. Chem. Soc.*, **102**, 5755 (1980); M. Hirayama and K. Kitami, *J. Chem. Soc., Chem. Commun.*, **1980**, 1030; M. Hirayama and Y. Kawamata, *Chem. Lett.*, **1980**, 1295.

14) R. M. Golding and M. P. Halton, *Aust. J. Chem.*, **25**, 2577 (1972).

15) The following geometric parameters for the aniline–Eu(fod)$_3$ system[16] are also employed for the present system: the distances of Ln–N and N–C are taken as 2.65 and 1.40 Å respectively, and the $\angle$C–N–Ln angle as 150°. When the rotational angle of the Ln–N vector about the N–C bond is taken as 30°, the best agreement is obtained.

16) M. Hirayama, M. Sato, M. Takeuchi, and M. Saito, *Bull. Chem. Soc. Jpn.*, **48**, 2690 (1975).

17) Although ρ_{2s} was calculated with χ values ranging from 20° to 60°, taking into account several works on the conformation of the NH_2 group of aniline,[16,18] this variation had no significant effect on the comparison of ρ_{2s} with δ'_{LS}(Gd). Thus, 50° was adopted.

18) T. Yonezawa, I. Morishima, Y. Akana, and K. Fukuta, *Bull. Chem. Soc., Jpn.*, **43**, 379 (1970).

19) W. DeW. Horrocks, Jr., and D. L. Johnston, *Inorg. Chem.*, **10**, 1835 (1971).

20) I. Morishima, K. Okada, and T. Yonezawa, *J. Am. Chem. Soc.*, **94**, 1425 (1972).

21) The situation is the opposite of that for pyridine-type bases. For a detailed study, the effect of an LSR-ligand interaction must be incorporated into the MO calculation of a model radical, except for the attempt at varying the charge of the hetero atom.

 © 1982 The Chemical Society of Japan Bull. Chem. Soc. Jpn., 55, 709—712 (1982)

Pattern Formation by Rhythmic Crystallization of Methyl Mesitylcarbamate

Kazutoshi Iwamoto, Shun-ichi Mitomo, Jun-ichi Fukide, Tadashi Shigemoto, and Manabu Senō*

Institute of Industrial Science, The University of Tokyo, Minato-ku, Tokyo 106

(Received August 27, 1981)

Rhythmic crystallization behavior of methyl mesitylcarbamate from chloroform solutions under appropriate conditions was found. Effects of temperature, evaporation rate of solvent, and sample weight per area on this behavior are studied in detail, and the qualitative explanation based on the autocatalytic branching process is proposed.

It has been demonstrated that some chemical systems far from equilibrium occasionally show regular changes of the concentrations of intermediate species in space or time during the reactions.[1] The well-known example is the Belousov-Zhabotinskii reaction,[2,3] where malonic acid is oxidized by bromate in the presence of cerium (or iron, manganese) ions. When the reaction is carried out in a well-stirred homogeneous medium, sustained oscillations in concentrations of intermediate chemicals appear spontaneously. On the other hand, when the same reaction is carried out in a thin layer, pattern of developing spiral bands appears.[4]

As a similar example of the periodic spatial structures,[5] the Liesegang rings are well-known since long ago. When crystalline $AgNO_3$ is placed in a thin layer of swollen gelatin gel containing K_2CrO_4, after several days concentric rings of Ag_2CrO_4 crystals are formed around the original $AgNO_3$ crystal. Recently, Feinn *et al.* proposed a model of coupled autocatalytic coagulation and diffusion for explanation of this ring formation.[6,7]

We found occurrence of the rhythmic crystallization on a glass wall of an eggplant type flask, when methyl mesitylcarbamate was crystallized from its chloroform solution in a rotary evaporator equipped with a water-jet pump. A typical example is shown in Fig. 1.

The similar crystallization phenomena of the other substances in the thin films of concentrated solutions or molten substances were sometimes noticed. Miers reported rhythmic crystallization of potassium dichromate from its aqueous solution.[8] The explanation for rhythmic crystallization given by Miers is as follows: the first precipitation ring is formed by inoculation in a labile, supersaturated solution. The precipitates grows so rapidly that the concentration of the solution in an immediate neighborhood decreases within its solubility limit and then the crystallization ceases: in the meantime the next ring of solution becomes labile by vaporization or cooling and induces the next rapid crystallization. Such an explanation seems to meet one aspect of the rhythmic crystallization but more detailed explanation is needed to make clear total mechanism of the rhythmic crystallization. For instances, it should be clarified what switching mechanism is working to produce such periodic patterns.[9] Moreover, it is important to reveal the autocatalytic process involved, if it exists, because an autocatalytic process is always necessary for the appearance of some peculiar behaviors like chemical oscillations or other periodic phenomena according to the recent knowledge on the dissipative structure formation.[10]

In this paper, we wish to report a result of detailed observation of the rhythmic crystallization behavior of methyl mesitylcarbamate following after evaporation of its chloroform solution and to propose a tentative mechanism of the pattern formation involving the autocatalytic process. These investigations serve to systematic understanding of rhythmic crystallization as a typical example of pattern formation in nature.

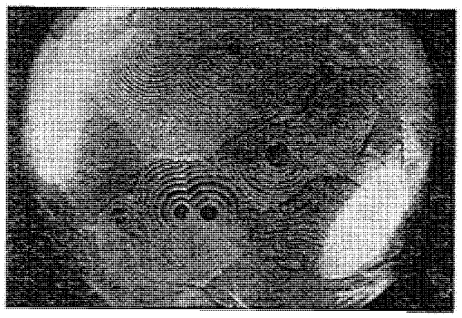

Fig. 1. Typical crystal pattern of methyl mesitylcarbamate from chloroform solution in a 50 cm^3 eggplant type flask.
A rotary evaporator equipped with a water-jet pump was used. Sample weight and bath temperature are about 100 mg and 40 °C, respectively.

Experimental

Materials. Methyl mesitylcarbamate was prepared by the reaction between methanol and mesityl isocyanate, which was produced by thermal rearrangement of mesitonitrile oxide,[11] in xylene at its reflux temperature. Recrystallization of the precipitates from methanol–water solutions yields colorless needle-like crystals. This compound was purified twice by recrystallization. Chloroform was purified with a standard procedure[12] before use.

Procedures. Schematic feature of the apparatus used for observation of crystallization behaviors is shown in Fig. 2. A 0.5 cm^3 portion of a chloroform solution of methyl mesitylcarbamate was put into a watch glass (6 cm in inner diameter and 1 cm in height) settled in a temperature-controlled bath of ethylene glycol. The watch glass was surrounded by a cylindrical polyethylene wall, of which the diameter is fixed to be 7.5 cm and the height is varied from 3 cm to 50 cm in order to control evaporation rate of chloroform. The watch glasses were specially ordered to polish smoothly their inside walls. The temperature of the meas-

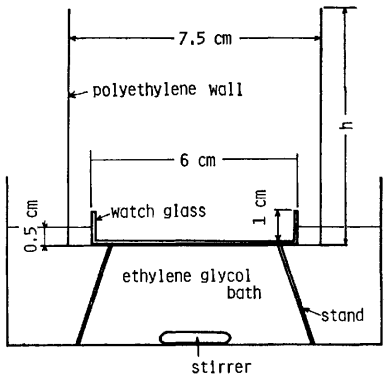

Fig. 2. Schematic feature of measuring apparatus.

uring room was kept constant at about 24±1 °C. Measurements were carried out under the conditions changing the following items: (a) the height of polyethylene wall (the vaporization rate of solvent), (b) the sample weight per area (weight density), and (c) the temperature of bath. All the results were recorded by photographs.

Results

Effect of Wall Height (Vaporization Rate). Each of 0.5 cm^3 chloroform solution containing 60.5 mg (2.14 mg/cm^2) of methyl mesitylcarbamate was put into a watch glass in the temperature-controlled ethylene glycol bath at 39.5 °C, and the rhythmic crystallization behaviors were investigated for various heights of the polyethylene wall. The results are shown in Fig. 3. The evaporation rate of chloroform from the solution decreases with an increase of polyethylene wall height. When the wall height h is 3 cm, the rhythmic crystallization does not appear, and when h is 5 cm, large and small rhythmic patterns appear simultaneously. In the range of h from 6 to 9 cm, we can see clear rhythmic crystallizations and, as h increases higher than 10 cm, the rhythmic patterns become obscure, although the local faint patterns can be observed even at h=50 cm.

Effect of Sample Weight Density. The bath temperature and the wall height are fixed to be 39.5 °C and 7 cm, respectively. Various amounts of methyl mesitylcarbamate were dissolved into 0.5 cm^3 of chloroform and these solutions were put into respective watch glasses. The results are shown in Fig. 4. The rhythmic crystallizations do not appear, when the sample weight density is 0.71 mg/cm^2 or less, but when the weight density is larger than 0.71 mg/cm^2, the rhythmic crystallizations appear in rather wide range of weight density; the clearest pattern is observed at the weight density of 2.14 mg/cm^2.

Effect of Bath Temperature. A 0.5 cm^3 chloroform solution containing 60.5 mg (2.14 mg/cm^2) of methyl mesitylcarbamate was put into a watch glass surrounded by a polyethylene wall of 7 cm in height and the rhythmic crystallization behaviors were investigated at various bath temperatures. The results are shown in Fig. 5. When the bath temperatures are 29.5 and 39.5 °C, the rhythmic crystallizations are clearly observed, but when the bath temperature is 21.0 °C, they disappear completely. When the temperature is 49.5 °C or higher, the rhythmic crystallizations become obscure and only vague periodicity is observed.

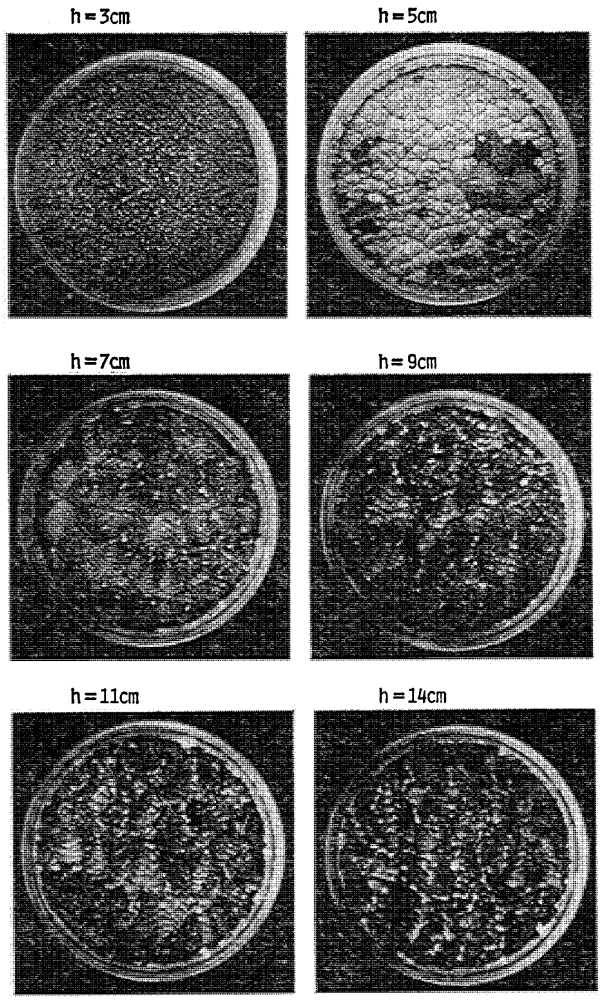

Fig. 3. Effect of polyethylene wall height on the rhythmic crystallization.
Sample weight density and bath temperature are 2.14 mg/cm^2 and 39.5 °C, respectively.

Discussion

The studies of effects of the bath temperature, the sample weight density, and the wall height on the rhythmic pattern formation imply that coupling of the solvent evaporation process with the crystallization process plays an essential role for the phenomena. In order to confirm the steady coupling effect, the following experiment was done: while methyl mesitylcarbamate was rhythmically crystallizing, the atmosphere inside the wall was exchanged by fresh air; by this procedure the evaporation of chloroform increased suddenly. The experimental result is shown in Fig. 6, which shows sudden stop of pattern formation. That is, the increase of evaporation rate of solvent extinguishes the rhythmic crystallization. This result supports our idea.

According to the Mier's explanation,[8] the solvent evaporation leads to formation of a supersaturated solution. As it is labile state, once nucleation occurs

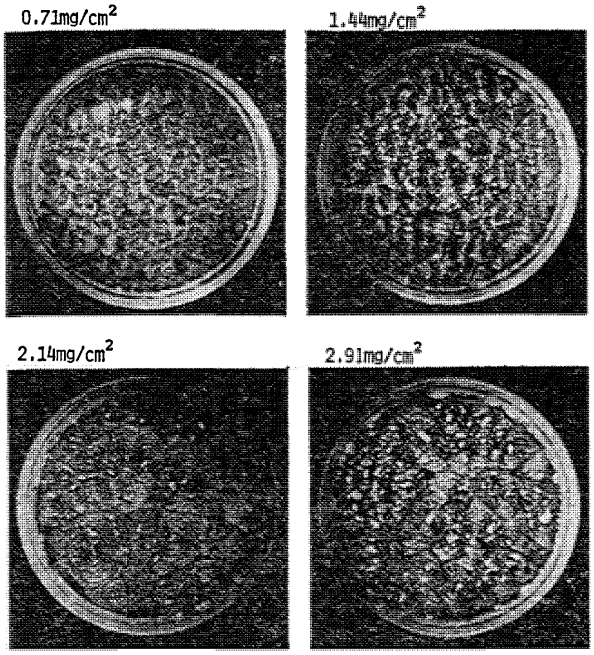

Fig. 4. Effect of sample weight density on the rhythmic crystallization.
Wall height and bath temperature are 7 cm and 39.5 °C, respectively.

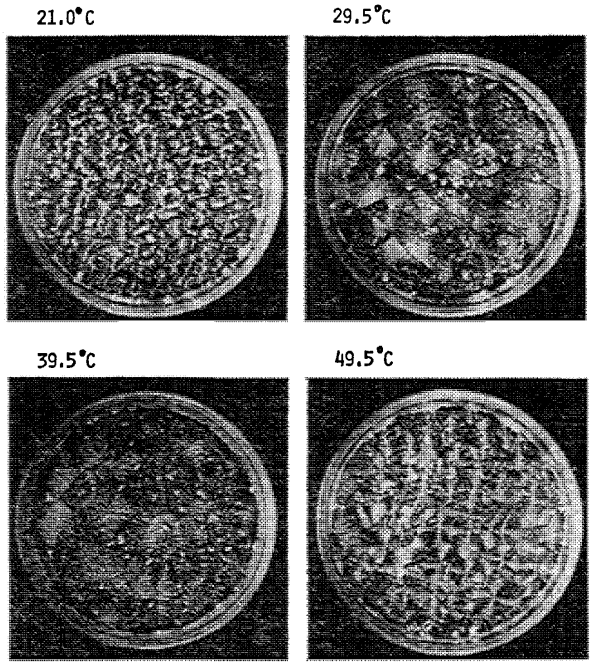

Fig. 5. Effect of temperature on the rhythmic crystallization.
Sample weight density and wall height are 2.14 mg/cm² and 7 cm, respectively.

somewhere, it is followed by a rapid crystal growth. The crystallization process reduces the solute concentration in front of crystals, and slows down until the evaporation process of solvent produces again a new supersaturated state. Repetition of these processes produces the rhythmic crystallization.

Detailed observation of periodic precipitate zones of methyl mesitylcarbamate clarified that two neighboring zones are clearly distinguishable and they are formed alternately. In order to explain completely the precipitate pattern formation, the mechanism of alternating from one zone to another zone should be made clear.

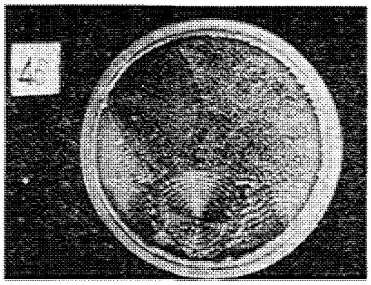

Fig. 6. Effect of sudden change in evaporation rate of chloroform on the rhythmic crystallization.
Sample weight density and wall height are 2.14 mg/cm² and 7 cm, respectively. When the atmosphere inside the wall was exchanged by fresh air, the rhythmic crystallization ceases.

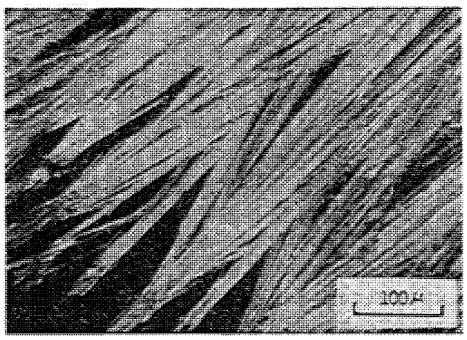

Fig. 7. Feature of crystals near the roots of crystal zone.
Branching and growing of needle-like crystals are clearly observed.

In Fig. 7, the detailed microscopic feature of crystals formed during the rhythmic crystallization is shown. The crossed polaroids were used for the observation with a microscope. The black parts indicate no existence of crystals. The crystals begin to grow from several roots, being followed by repetition of branching to form bundles of needle-like crystals. The branching process is an autocatalytic process, because branching continues to produce new sites for branching. On this account, the number of branches increases nonlinearly as crystallization proceeds. Such an autocatalytic irreversible process may produce a periodic change of crystallization rate, which is recognized as a periodic pattern.

We presume that the number of branches N in every zone is given by

$$\frac{dN}{dx} = f(C, T)N, \tag{1}$$

where $f(C, T)$ represents the number of branches produced per unit length from one branch at the concentration C in the front of crystals and the temperature T, and x is the distance measured from the root of each crystal zone.

The advancing rate of the front at crystal zone

is about a few millimeters per second and it is large compared to the diffusion rate of solute in a liquid phase. Therefore, the front boundary contacts always with a fresh liquid; the concentration of solution at the front of crystals is not practically affected by the crystallization process. This supposition is different from the Mier's view. According to this view, the function $f(C, T)$ is independent of x, and the solution of Eq. 1 is given by

$$N = N_0 e^{fx} \tag{2}$$

at a given temperature, where N_0 is the initial number at $x=0$.

As mentioned already, the crystallization rate is large compared to the diffusion rate and, therefore, we could presume that the total amount w of the substance in a unit volume of crystal zone is constant and expressed by

$$w = \rho N \pi r^2, \tag{3}$$

where N is the number of branches per unit area, r is the radius of each branch, and ρ is the density of crystal. As w is independent of x, the radius r decreases with an increase in N. When N becomes indefinitely large and r becomes indefinitely small, the crystallization rate increases drastically and the solute concentration in the front of the crystal zone reduces remarkably and the diffusion is too slow to compensate this reduction. At this point, the crystallization process ceases. After then, the solution in the vicinity of crystal zone is concentrated by vaporization and the crystallization starts again at some points.

We investigated some specific behaviors of the rhythmic crystallization of methyl mesitylcarbamate and proposed a tentative explanation for it. The explanation is somewhat awkward and a detailed and mathematically elegant treatment is needed. For this purpose, the treatment of Haase *et al.*[9] for the oscillatory zoning in plagioclase feldspar is very suggestive.

We would like to thank Professor D. H. Everett of the University of Bristol for valuable and stimulating discussions.

References

1) G. Nicolis and J. Portnow, *Chem. Rev.*, **73**, 365 (1973).
2) A. M. Zhabotinskii, *Dokl. Akad. Nauk SSSR*, **157**, 392 (1964).
3) R. M. Noyes, R. J. Field, and E. Körös, *J. Am. Chem. Soc.*, **94**, 1394 (1972).
4) A. T. Winfree, *Science*, **175**, 634 (1972).
5) C. L. Stong and R. Sassen, *Sci. Am.*, **220**, 131 (1969).
6) M. Flicker and J. Ross, *J. Chem. Phys.*, **60**, 3458 (1974).
7) D. Feinn, P. Ortoleva, W. Scalf, S. Schmidt, and M. Wolff, *J. Chem. Phys.*, **69**, 27 (1978).
8) H. Miers, *Mineralog. Mag.*, **15**, 39 (1908).
9) C. S. Haase, J. Chadam, D. Feinn, and P. Ortoleva, *Science*, **209**, 272 (1980).
10) G. Nicolis and I. Prigogine, "Self-Organization in Nonequilibrium Systems—From Dissipative Structures to Order through Fluctuations," Wiley, New York (1977).
11) S. Shiraishi, T. Shigemoto, and S. Ogawa, *Bull. Chem. Soc. Jpn.*, **51**, 563 (1978).
12) J. A. Riddick and W. B. Bunger, "Techniques of Chemistry. Vol. II. Organic Solvents," 3rd ed, Wiley, New York (1970).

 © 1982 The Chemical Society of Japan Bull. Chem. Soc. Jpn., 55, 713—716 (1982)

Protolytic Kinetics of Some Pyridine Derivatives in Non-buffered Aqueous Solution

Isao Ando, Kikujiro Ujimoto, and Hirondo Kurihara*

Department of Chemistry, Faculty of Science, Fukuoka University, Nanakuma 11, Nishi-ku, Fukuoka 814-01

(Received August 31, 1981)

The deprotonation rates of the conjugate acids of 2,2′-bipyridine and pyridine, and the protonation rates of 2-aminopyridine and 4-aminopyridine were measured in non-buffered aqueous solution by means of a stopped-flow pH jump method. These pyridine derivatives showed quite slow protolytic behavior, similar to that of 1,10-phenanthroline and cyclopentadienes: the deprotonation rate constants of conjugate acids of 2,2′-bipyridine and pyridine are $(4.8\pm0.7)\times10^{-1}$ and $(6.0\pm2.2)\times10^{-2}$ s^{-1}, respectively. The deprotonation rates of barbituric acid and acetylcyclopentadiene as authentic samples were also measured. Their deprotonation rate constants are in good agreement with the literature values, this demonstrates the validity and the applicability of the stopped-flow pH jump method. This method is superior to the NMR method for the determination of the protontransfer rates of azaaromatic compounds.

It is well known that a proton transfer plays an important role in the reactions in aqueous solution such as complex formation, acid and base catalyses, and enzymatic reaction. In order to clarify the reaction mechanism in aqueous solution, it is necessary to evaluate accurately the contribution of the proton transfer process involved in the reaction. So far the proton transfer reactions of a wide variety of compounds have been kinetically studied by many investigators.[1-13] It was reported that the proton transfer reactions of nitrogen acids and oxygen acids are very fast and their protonation reactions are diffusion-controlled, whereas carbon acids and β-diketones undergo quite slow protolytic reactions.

Previously, we examined the proton transfer reactions of 1,10-phenanthroline, 2-aminopyridine, and 3-aminopyridine by means of a stopped-flow pH jump method, and found that the conjugate acids of these azaaromatic compounds undergo slow deprotonation reactions.[14] So far as we know, these are the first nitrogen acids displaying a slow deprotonation reaction. In order to further investigate the proton transfer reaction of nitrogen acids, in this study the proton transfer rates of 2,2′-bipyridine, pyridine, 2-aminopyridine, and 4-aminopyridine were measured in non-buffered aqueous solution, by means of a stopped-flow pH jump method. The reliability of this method for determining proton transfer rates was also tested by the use of authentic samples with known rate constants.

Experimental

Materials. 2,2′-Bipyridine (bpy), pyridine (py), and 2-aminopyridine (2-ampy) were purchased from Wako Pure Chemical Industries, Ltd., and 4-aminopyridine (4-ampy) and barbituric acid from Nakarai Chemicals, Ltd. Sodium acetylcyclopentadienide (Na-accp) was synthesized from cyclopentadiene according to the method described in the literature[15] and stored under an atmosphere of nitrogen. All other chemicals were of guaranteed grade and used without further purification.

The stock solution of each compound was prepared by dissolving a weighed amount of it in deionized, distilled water. The solution of Na-accp was freshly prepared before each measurement.

pK_a *Measurements.* pK_a values of the conjugate acids of py, 4-ampy, and accp were determined spectrophotometrically by the use of a JASCO Uvidec-2 digital spectrophotometer equipped with a water-jacketed cell holder, as described in the previous paper.[14] The measurements were carried out at 25 °C in the cases of py and 4-ampy and at 30 °C in the case of accp. The ionic strengths of py and 4-ampy solutions were adjusted to 0.20 mol dm^{-3} and that of accp to 0.50 mol dm^{-3} with sodium chloride. The wavelengths employed to determine the concentration ratios of the deprotonated to the protonated species in the sample solutions at various pH values were 256 nm for py, 263 nm for 4-ampy, and 314 nm for accp. The absorbance of accp solution at the time immediately after preparation was used in order to rule out any effects due to decomposition.

Kinetic Measurements. The rates of deprotonation and protonation reactions were measured by the use of a Union RA-1300 stopped-flow spectrophotometer by the following pH jump method. For measuring the deprotonation rate, the pH of a sample solution was adjusted with hydrochloric acid or perchloric acid to values lower than pK_a value of the conjugate acid of the sample. For determining the protonation rate, the pH of the solution was adjusted with sodium hydroxide solution to values higher than the pK_a value. As a perturbing solution, which causes a perturbation of the acid dissociation equilibrium of the sample solution owing to a pH jump up or down by mixing, we used a sodium hydroxide solution or hydrochloric acid at the concentration appropriate for pH jumps smaller than about one pH unit. The ionic strengths of the solutions were adjusted to 0.20 mol dm^{-3} with sodium chloride or sodium perchlorate.

Equal volumes of the sample solution and the perturbing solution were mixed rapidly by a pressure drive device. The changes in absorbances of the mixture were followed at the wavelengths of 300, 256, 302, 263, 257, and 314 nm for bpy, py, 2-ampy, 4-ampy, barbituric acid, and accp, respectively, and were stored in a high speed memory unit and displayed on an X-Y recorder as a function of time. The kinetic measurements using basic solutions were carried out under an atmosphere of purified nitrogen.

Each rate constant for deprotonation and protonation reactions was obtained from fifteen or twenty kinetic runs. The calculation of rate constants was performed by the use of a Hewlett-Packard HP9825A/S desktop computer according to the method reported previously.[14]

The deprotonation rates of barbituric acid and accp were

also measured in non-buffered systems under the same experimental conditions as in the literature.[7,21]

Results and Discussion

Buffers used to keep the pH of a system constant after pH jumping occasionally accelerate the rate of proton transfer in a striking manner. Therefore, the application of the stopped-flow pH jump technique to rate determinations in buffered solutions is rather limited. Recently, we have shown that in non-buffered systems the stopped-flow pH jump method is applicable for the determination of the rate constants for the proton transfer reactions of weak acids.[14] Thus, we utilized the same method for measuring the proton transfer rates of py, bpy, 2-ampy, and 4-ampy in this investigation.

The spectra of the protonated and the deprotonated species of the present azaaromatic compounds were essentially the same as those in the literature.[16-20] Figure 1 shows a typical example of the spectral change of bpy caused by pH jumping, measured by a rapid scanning technique. The comparison between the spectra of the protonated and the deprotonated species revealed that the proton transfer process can be followed spectrophotometrically by the pH jump method.

As in the case of the previous study,[14] the apparent first-order rate constants observed for deprotonation reactions of the present samples, k_{dpo}, were dependent on hydroxide ion concentration, and the apparent second-order rate constants observed for protonation reactions, k_{po}, were dependent on hydrogen ion concentration. This indicates that the proton transfers of the present compounds also proceed in the following reaction scheme:[14]

$$HL^+ \underset{k_p}{\overset{k_{dp}}{\rightleftharpoons}} L + H^+, \quad (1)$$

$$HL^+ + OH^- \underset{k_{H_2O}}{\overset{k_{OH}}{\rightleftharpoons}} L + H_2O, \quad (2)$$

where HL^+ and L are the protonated and the deprotonated species of the sample. The k_{dp} and k_p denote the rate constants for the deprotonation of HL^+ and for the protonation of L, respectively, and k_{OH} and k_{H_2O} those for the protolysis of HL^+ with OH^- and for the hydrolysis of L, respectively.

Since k_{dpo} and k_{po} are defined as

$$-d[HL^+]/dt = k_{dpo}[HL^+] - k_{po}[L][H^+], \quad (3)$$

their values at reaction time zero, $(k_{dpo})_0$ and $(k_{po})_0$, can be expressed as functions of $[H^+]_0$ and $[OH^-]_0$ in the following equation:

$$(k_{dpo})_0 = k_{dp} + k_{OH}[OH^-]_0, \quad (4)$$

$$(k_{po})_0 = k_p + k_{H_2O}([H_2O]/[H^+]_0), \quad (5)$$

where $[H^+]_0$ and $[OH^-]_0$ denote the concentrations of hydrogen and hydroxide ions at reaction time zero in the mixture of the sample and the perturbing solutions. For obtaining k_{dpo}, k_{po}, $[H^+]$ and $[OH^-]$ at any reaction time, the change in pH of the mixed solution caused by the proton transfer of sample was evaluated from the absorbance change of HL^+, presuming that the ionic product of water holds constant at any time of the reaction.

The plot of $(k_{dpo})_0$ against $[OH^-]_0$ and the plot of $(k_{po})_0$ against $[H_2O]/[H^+]_0$ yielded straight lines, as shown in Figs. 2 and 3 for py and 2-ampy, respectively. The values of k_{dp} and k_{OH} (or k_p and k_{H_2O}) were obtained from the intercept and the slope of the linear regression line given in Fig. 2 (or Fig. 3).

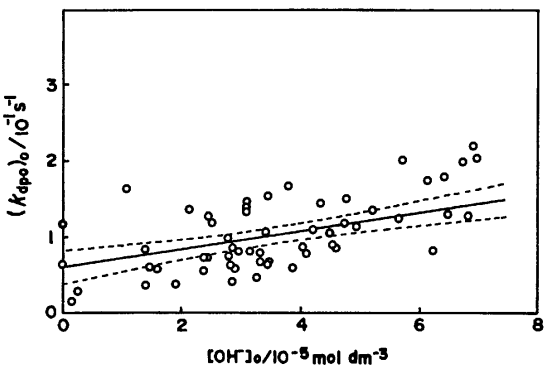

Fig. 2. Plot of $(k_{dpo})_0$ against $[OH^-]_0$ for pyridine.
Solid line: the linear regression line for the plot, broken line: the intervals of the 0.95 confidence for the linear regression.

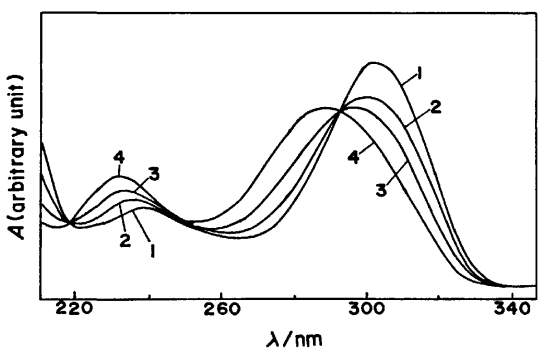

Fig. 1. Rapid scanning spectra of 2,2′-bipridine during the protolytic reaction.
[bpy]$=5.00\times10^{-5}$ mol dm^{-3}; initial pH: 2.00, final pH: 4.49. Curve 1: 0—10 ms, 2: 190—200 ms, 3: 390—400 ms, 4: 790—800 ms.

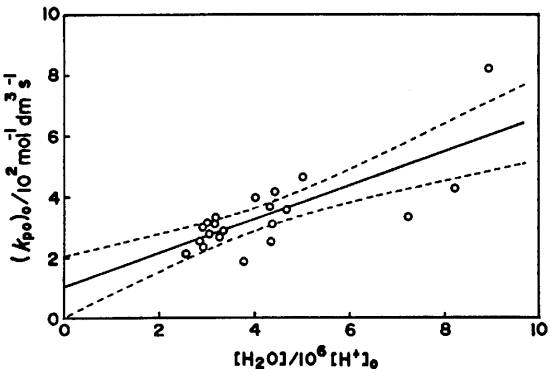

Fig. 3. Plot of $(k_{po})_0$ against $[H_2O]/[H^+]_0$ for 2-aminopyridine.
Solid line: the linear regression line for the plot, broken line: the intervals of the 0.95 confidence for the linear regression.

Table 1. Rate constants and pK_a values[a)]

Sample	pK_a	k_{dp}/s^{-1}	$k_{OH}/mol^{-1}\,dm^3\,s^{-1}$
Barbituric acid	4.00[b)]	5.3±0.9	$(2.9\pm3.3)\times10^4$
accp	8.96±1.05	$(2.9\pm6.7)\times10^{-3}$	$(4.7\pm0.7)\times10^2$
bpy	4.40[c)]	$(4.8\pm0.7)\times10^{-1}$	$(9.3\pm5.7)\times10^4$
phen	5.00[d)]	$(2.5\pm0.8)\times10^{-1}$ [d)]	$(1.2\pm0.7)\times10^4$ [d)]
py	5.31±0.34	$(6.0\pm2.2)\times10^{-2}$	$(1.2\pm0.5)\times10^3$
3-ampy	6.17±0.13[d)]	$(1.8\pm0.6)\times10^{-2}$ [d)]	$(7.4\pm1.6)\times10^2$ [d)]
2-ampy	6.86±0.20[d)]	$(4.2\pm3.6)\times10^{-3}$ [d)]	$(8.7\pm2.8)\times10^2$ [d)]
Sample	pK_a	$k_p/mol^{-1}\,dm^3\,s^{-1}$	$k_{H_2O}/mol^{-1}\,dm^3\,s^{-1}$
2-ampy	6.86±0.20[d)]	$(1.0\pm1.1)\times10^2$	$(5.5\pm2.3)\times10^{-5}$
4-ampy	9.26±0.37	$(0.3\pm17)\times10^5$	$(4.0\pm0.9)\times10^{-4}$

a) Values are shown together with the 0.95 confidence intervals. b) The value was taken from Ref. 21. c) The value was taken from L. G. Sillen and A. E. Martell, The Chem. Soc., Spec. Publ., No. 17 (1964). d) The values were taken from Ref. 14.

Table 1 summarizes pK_a and the rate constants for the azaaromatic compounds obtained in this study and in the previous paper,[14] together with those for barbituric acid and accp employed as authentic samples. The k_{dp} values of the authentic samples in non-buffered systems were in good agreement with the reported values, 10 s^{-1} for barbituric acid[1,21] and 2.5×10^{-3} s^{-1} for accp.[7] The k_{OH} value of accp also agreed well with that observed by Okuyama *et al.*[7] in buffered systems (2.0×10^2 $mol^{-1}\,dm^3\,s^{-1}$). This fact adds a strong support to the validity of the present method for the determination of the rate constants of the proton transfer in non-buffered systems. Thus, the present study has again demonstrated that the rates of the deprotonation reactions of the conjugate acids of the azaaromatic compounds are slow and comparable to those of carbon acids.

The rate constants of the deprotonation, k_{dp} and k_{OH}, for the present azaaromatic compounds decrease with increasing basicity, while those of protonation, k_p and k_{H_2O}, increase with the increasing basicity. The correlations of the logarithms of k_{dp} and k_{OH} with pK_a for the azaaromatic compounds are shown in Fig. 4. Figure 4 also includes the correlations for cyclopentadienes (kinetic data obtained by a stopped-flow method),[7] alkylamines[22-24] and methyl-substituted pyridines[25,26] (by NMR method) for comparison. The log k_{dp} *vs.* pK_a plot for the azaaromatic compounds gives a straight line with a slope of −0.93, while the plot for the cyclopentadienes forms a straight line with a slope of −0.33. The log k_{OH} *vs.* pK_a plots of these two groups also give straight lines, but their slopes are different from each other. These facts imply that the azaaromatic compounds and the cyclopentadienes differ in proton transfer mechanism, though the rate constants for both groups are similar. The slow protolytic reaction of carbon acids including cyclopentadienes has been attributable to the following factors:[4] (i) the electronic and the structural reorganizations on going from the acid to its conjugate base, (ii) the small hydrogen-bonding ability with solvent and (iii) the accompanying reorientation of solvation. Okuyama *et al.*[7] proposed that the nuclear reorganization of carbon is the main factor retarding

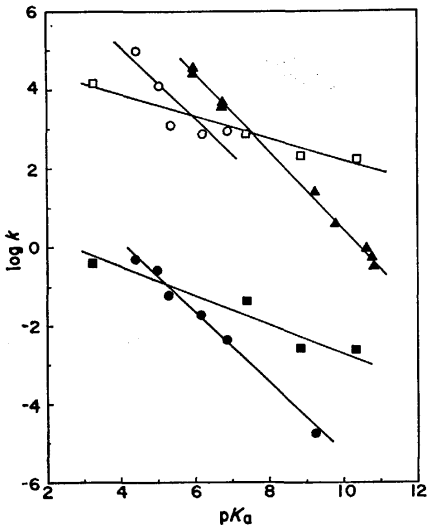

Fig. 4. The correlations between logarithms of the rate constants and pK_a for the azaaromatic compounds in this study (●, ○), the cyclopentadienes (■, □), and the alkylamines and the methyl-substituted pyridines (▲). Solid symbols are the k_{dp} plots and open symbols are the k_{OH} plots.

the proton transfer of cyclopentadienes. On the other hand, we can not explain at present the reason for the slow deprotonation reaction of the azaaromatic compounds.

It is noteworthy that the k_{dp} values determined by the NMR method for the alkylamines and the methyl-substituted pyridines are higher by several orders of magnitude than those for the azaaromatic compounds and the cyclopentadienes. Although the k_{dp} values for the aminopyridines are lower by a factor of 10^7 than those for the methylpyridines, as shown in Fig. 4, it is unlikely that there is such a significant difference in the mechanism of their protolytic reactions. In fact, our preliminary experiment for the deprotonation reaction of 2-methylpyridinium ion showed that the k_{dp} is about 10^{-2} s^{-1}, comparable to the k_{dp} values of the aminopyridines.[27] Accordingly, the fact that the k_{dp} values for the azaaromatic compounds greatly differ from those for the alkylamines

and the methylpyridines may be attributed to the difference in the experimental conditions used for rate-determination. In the present study, the rates were determined in dilute azaaromatic solutions (10^{-5}—10^{-4} mol dm^{-3}) at moderate pH. On the other hand, the rates for the alkylamines and the methylpyridines were determined by means of the NMR method in highly concentrated solutions (more than 0.02 mol dm^{-3}) at higher acidity. It has been reported that in concentrated solution two or more molecules of 1,10-phenanthroline form a stacking compound which can take one proton in acidic solution.[28,29] Though there is no evidence for stacking in the cases of pyridine derivatives, the difference in the concentration of solutes may alter the observed protolytic phenomena. Furthermore, the deprotonation rates determined by NMR method may include the contribution from the proton exchange between R_3N and R_3NH^+ in the crowded state.

Thus, we may conclude that the deprotonation reaction of the conjugate acids of azaaromatic compounds may depend upon the concentration. We believe that the stopped-flow pH jump method is superior to the NMR method for the rate determination, since NMR measurements are usually carried out in highly concentrated solutions in which some intermolecular interactions might affect the rate of the reaction.

The authors are sincerely grateful to Professor S. Kida of Kyushu University for his many useful suggestions and encouragement during this work.

References

1) M. Eigen, W. Kruse, G. Maass, and L. DeMayer, *Prog. Reaction Kinetics*, **2**, 287 (1964).
2) M. Eigen, *Angew. Chem., Int. Ed. Engl.*, **3**, 1 (1964).
3) M. Eigen, *Discuss. Faraday Soc.*, **39**, 7 (1965).
4) F. Hibbert, "Comprehensive Chemical Kinetics," ed by C. H. Bamford and C. H. F. Tipper, Elsevier, Amsterdam (1977), Vol. 8, Chap. 2.
5) A. Hantzsch, *Ber.*, **32**, 575, 3066 (1899).
6) J. C. Reid and M. Calbin, *J. Am. Chem. Soc.*, **72**, 2948 (1950).
7) T. Okuyama, Y. Ikenouchi, and T. Fueno, *J. Am. Chem. Soc.*, **100**, 6162 (1978).
8) W. J. Albery, *Prog. Reaction Kinetics*, **4**, 353 (1967).
9) J. R. Jones, "The Ionization of Carbon Acids," Academic Press, New York (1973).
10) J. R. Jones, *Prog. Phys. Org. Chem.*, **9**, 241 (1972).
11) R. G. Pearson and R. L. Dillon, *J. Am. Chem. Soc.*, **75**, 2439 (1953).
12) J. L. Haslam and E. M. Eyring, *J. Phys. Chem.*, **71**, 4470 (1967).
13) F. Hibbert, *J. Chem. Soc., Perkin Trans. 2*, **1974**, 1862.
14) I. Ando, J. Saito, K. Ujimoto, and H. Kurihara, *Fukuoka Univ. Sci. Reports*, **11**, 47 (1981).
15) K. Hafner, G. Schulz, and K. Wagner, *Justus Liebigs Ann. Chem.*, **687**, 39 (1964).
16) F. H. Westheimer and O. T. Benfey, *J. Am. Chem. Soc.*, **78**, 5309 (1956).
17) R. H. Linnell and A. Kaczmarczyk, *J. Phys. Chem.*, **65**, 1196 (1961).
18) W. A. McBryde, *Can. J. Chem.*, **43**, 3472 (1965).
19) P. Krumholz, *J. Am. Chem. Soc.*, **73**, 3487 (1951).
20) J. M. Essery and K. Schofield, *J. Chem. Soc.*, **1961**, 3939.
21) M. Eigen, G. Ilgenfritz, and W. Kruse, *Chem. Ber.*, **98**, 1623 (1965).
22) E. Grunwald, P. J. Karabatsos, R. A. Kromhout, and E. L. Purlee, *J. Chem. Phys.*, **33**, 556 (1960).
23) E. Grunwald, *J. Phys. Chem.*, **71**, 1846 (1967).
24) M. T. Emerson, E. Grunwald, and R. A. Kromhout, *J. Chem. Phys.*, **33**, 547 (1960).
25) M. Cocivera, *J. Phys. Chem.*, **72**, 2520 (1968).
26) D. Rosenthal and E. Grunwald, *J. Am. Chem. Soc.*, **94**, 5956 (1972).
27) I. Ando *et al.*, unpublished data.
28) P. R. Mitchell, *J. Am. Chem. Soc.*, **102**, 1180 (1980).
29) P. R. Mitchell, *J. Chem. Soc., Dalton Trans.*, **1980**, 1079.

 © 1982 The Chemical Society of Japan Bull. Chem. Soc. Jpn., 55, 717—720 (1982)

Highly Aggregated State of the Dye with the Detergent in the Premicellar Region as Revealed by Resonance Raman Spectra

Masaaki KATSUMATA, Kazuo KASATANI, Masahiro KAWASAKI, and Hiroyasu SATO*

Chemistry Department of Resources, Faculty of Engineering, Mie University, Tsu 514

(Received September 3, 1981)

Resonance Raman spectra of 3,3′-diethylthiacarbocyanine iodide–sodium dodecyl sulfate (SDS) system are characterized by [SDS]-dependent change of band intensities. The change was much larger than that accompanied with the shift of monomer-dimer equilibrium in the aqueous solution. The spectra for [SDS]≪critical micelle concentration (cmc) resemble that of the dye in the solid state, indicating the highly-aggregated state of the dye caused by the interaction with the detergent.

The dye-detergent systems are currently attracting considerable interest from several viewpoints, *e.g.*, highly enhanced energy transfer between the dyes in these systems making these as good model membrane systems of chloroplasts,[1–6] and the study of photophysical processes of the dye in micelles in relation to the improvement of lasing properties of dyes.[7–8]

The presence of peculiar interaction between the dye and detergent carrying the opposite charge has long been known by the color change of the dye which is dependent on the concentration of the detergent (metachromasy).[9] Some investigations have been made on this phenomenon by absorption and fluorescence spectra,[10–12] and also by conductivity measurements.[12] Recently, the fluorescence decay studies provide very efficient means to clarify the nature of the dye-detergent interaction.[2,13–14] All of these investigations indicate the formation of some dye-detergent aggregate *below* the critical micelle concentration (cmc), *i.e.*, in the *premicellar* region.

In this paper, the resonance Raman spectra of 3,3′-diethylthiacarbocyanine iodide (DTC), a cationic dye, was studied in the presence of sodium dodecyl sulfate (SDS), an anionic detergent, to elucidate the nature of change dependent on the concentration of SDS (abbreviated as [SDS]) in the aggregation state of DTC, especially in the premicellar region. The interaction of DTC with SDS was discussed in comparison with its interaction with polyethylene glycol mono-[*p*-(1,1,3,3-tetramethylbutyl)phenyl] ether (PGME), a nonionic detergent, with hexadecyltrimethylammonium bromide (HTAB), a cationic detergent, and with potassium poly(vinyl sulfate) (PVSK), an anionic polyelectrolyte.

Experimental

Laser-grade DTC ("Dotite" reagent from Dojindo), protein-research grade SDS (Nakarai Chemicals), liquid-scintillation grade PGME (Nakarai), G. R. grade HTAB (Nakarai), and PVSK (Wako) were used as received. Water was distilled twice. Spectrograde methanol was used without further purification.

Raman spectra were recorded using a JASCO CT-80D double monochromator and a Hamamatsu R-649/C-1050 photomultiplier-photon counting unit. The excitation lines at 457.9 nm, 465.8 nm, 472.7 nm, 476.5 nm, and 488.0 nm were obtained from a Spectra-Physics model 164 Ar^+ laser. Since some color change was observed for DTC–SDS solutions after mixing, the solutions were kept in the dark until the color change became undetectable (more than 30 min). A flow-cell composed of a 2.5 mm i.d. glass tube was used in the measurements to avoid the degradation of the dye by the continued irradiation. Solid samples were measured as spinning KBr discs.

Absorption and fluorescence spectra were recorded on a Shimadzu UV-200 recording spectrophotometer and on a Hitachi 650-10S fluorescence spectrophotometer, respectively.

The cmc of SDS was determined conductometrically to be 7.4±0.1 mM (at 25±0.1 °C).†

Results

DTC–SDS Solutions. Some of the Raman spectra of DTC–SDS solutions are shown in Fig. 1, together with that of the aqueous solution. The concentration of the dye is 1.0×10^{-5} M. The excitation wavelength is 488.0 nm. The spectra changed with [SDS]. The spectrum at [SDS]≪cmc[15] has a large difference from that of the aqueous solution. The difference decreased with [SDS], and the spectrum above cmc was again similar to that of aqueous solution. While the positions (in cm^{-1}) of Raman bands did not show appreciable shift, their relative inten-

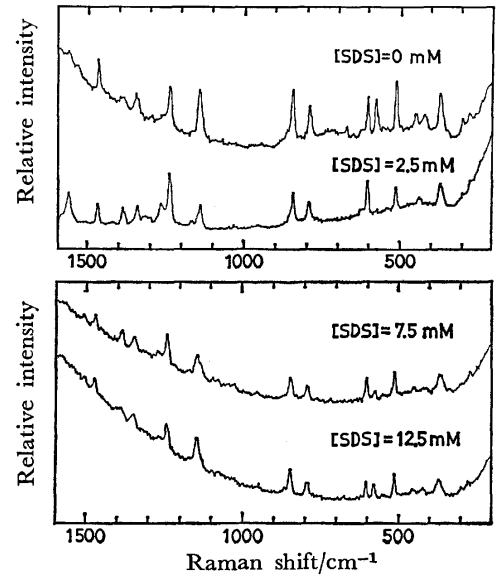

Fig. 1. Raman spectra of aqueous solution of DTC and DTC–SDS, [DTC]=1.0×10^{-5} M, exciting wavelength: 488.0 nm.

† 1 M=1 mol/dm³, 1 mM=1×10^{-3} mol/dm³ in this paper.

sities varied substantially as a function of [SDS], as shown in Fig. 2 for some of the bands. The intensities of each band were corrected for reabsorption in the cell. The intensity of 841 cm^{-1} band was chosen as an internal reference standard.[16] The bands can be classified into three groups by their [SDS]-dependent behavior: (a) the intensity increases for [SDS]$\ll$cmc, (b) the intensity was almost independent of [SDS], and (c) the band disappeared for [SDS]$\ll$cmc. The most peculiar is the band at 569 cm^{-1}, which belonged to the last group.

Aqueous and Methanol Solutions of DTC. The Raman spectra of aqueous solution of DTC were measured in the concentration range 1×10^{-5} M—1×10^{-4} M. The tenfold change in the concentration is accompanied with a large shift in the monomer-dimer equilibrium as shown by the absorption spectra (Fig. 3). The 554 nm and 507 nm peaks can be attributed to monomer and dimer, respectively.[14] However, the intensity change of Raman bands was found to be rather small, as depicted in Fig. 4. The absorption spectra of DTC in methanol show that DTC is present essentially as a monomer, because (1) the shape of the absorption band does not show any appreciable concentration dependence, and (2) it is similar to that of dilute ([DTC]$<2.0\times10^{-5}$ M) aqueous solution, apart from a small red shift. The Raman spectrum of methanol solution of DTC (4.0×10^{-5} M) was quite similar to that of aqueous solution (1.0×10^{-5} M). These results indicate that the shift of monomer-dimer equilibrium in the aqueous solution causes only a small change in the relative intensities of Raman bands.

Solid Spectrum (KBr Disc). The Raman spectrum of DTC in KBr disc is shown in Fig. 5. It is to be noted that relative intensities of the bands in the spectrum of DTC–SDS at [SDS]$\approx$2.5 mM closely resemble those of the solid. The 569 cm^{-1} band disappeared completely in the solid spectrum.

DTC–PGME, –HTAB, and –PVSK. Absorption and Raman spectra of these systems were studied. PGME, a nonionic detergent, has a deaggregation

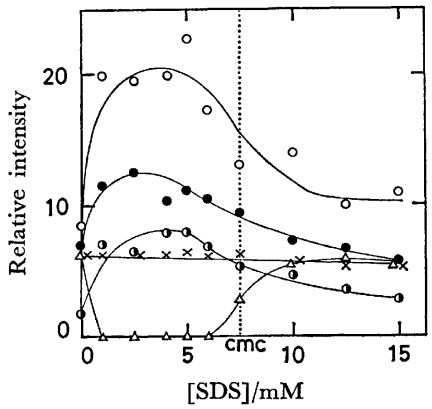

Fig. 2. Dependence of Raman intensities on [SDS]. △ 569 cm^{-1}, ● 601 cm^{-1}, × 791 cm^{-1}, ○ 1238 cm^{-1}, ◑ 1383 cm^{-1} band, [DTC]$=1.0\times10^{-5}$ M, exciting wavelength: 488.0 nm.

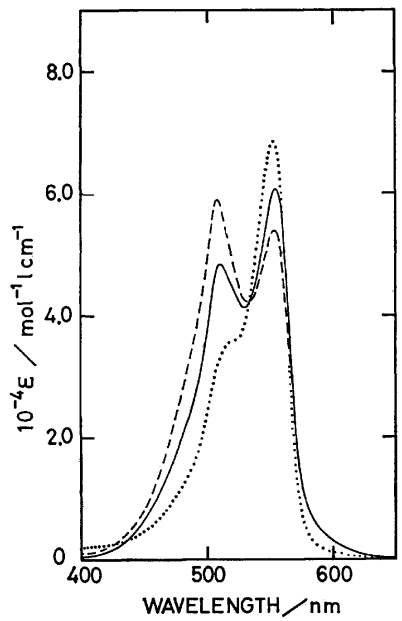

Fig. 3. Absorption spectra of aqueous solution of DTC. [DTC]: - - - 1.0×10^{-4} M, —— 5.0×10^{-5} M, ····· 1.0×10^{-5} M.

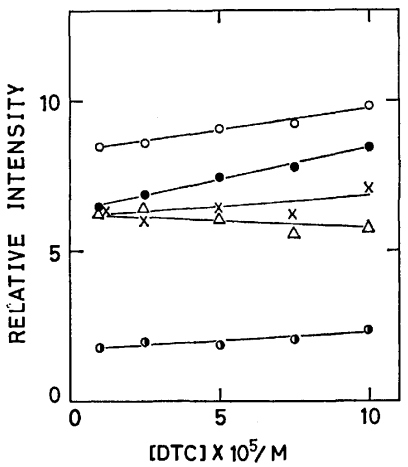

Fig. 4. Dependence of Raman band intensities on [DTC], exciting wavelength: 488.0 nm. The symbols the same as those in Fig. 2.

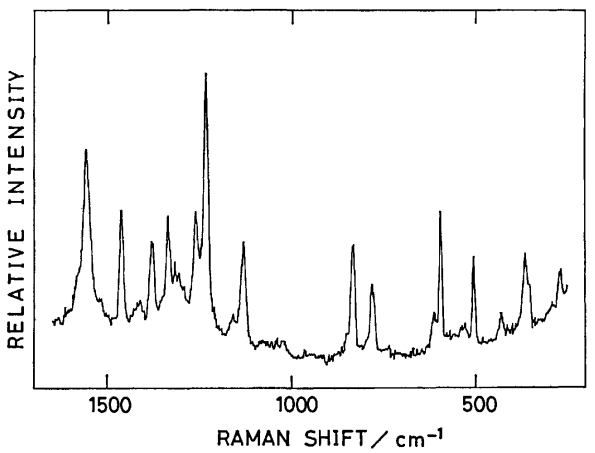

Fig. 5. Raman spectrum of solid DTC (KBr disc), exciting wavelength: 488.0 nm.

effect on DTC as revealed by the decrease of the intensity of dimer band (at 507 nm). However, the corresponding change in the Raman spectra was very little. HTAB, a cationic detergent, did not give any appreciable change in either of absorption and Raman spectra. The positive charge of the HTAB micelle will repel the cationic dye, DTC. PVSK, an anionic polyelectrolyte, (1×10^{-2} g/l—10 g/l)–DTC(1×10^{-4} M) gave the absorption spectra and Raman spectra which are very similar to those of DTC–SDS ([SDS]≈2.5 mM), showing the interaction of $-OSO_3^-$ groups on the polymer chain with DTC.

Effect of Excitation Wavelength. When we measure the resonance Raman spectra of DTC–SDS solutions as a function of [SDS] by exciting at a fixed wavelength, the change in the resonance conditions is inevitable because the absorption spectra changes with [SDS], as shown in Fig. 6. The observed results should be attributed to the joint effect of (1) change in the aggregation state of the dye, and (2) change in the resonance condition. The latter effect can be divided into those due to (2-a) the change in absorption spectra by the shift of monomer-aggregate equilibrium and (2-b) the simple wavelength shift of absorption bands due to environmental effect. The effect (2-a) has the common origin as (1), and what is to be investigated in this study. If the observed results are solely due to (2-b), they are only apparent results, nothing to do with the change in the aggregation state of the dye. In case the observed results are solely due to (2-b), the same results will be obtained by the change in the excitation wavelength. The effect of excitation wavelength on the relative Raman band intensities (the intensity of 841 cm^{-1} being taken as a standard) was studied for aqueous solutions ([DTC]=1.0×10^{-4} M and 1.0×10^{-5} M) and methanol solution ([DTC]=4.0×10^{-5} M). Although the effect of excitation wavelength did exist as shown in Fig. 7 taking [DTC]=1.0×10^{-5} M as an example, there was no direct relationship to the classification of (a), (b), and (c) of [SDS]-dependent intensity change mentioned above. Therefore, the observed [SDS]-dependent change cannot be attributed to the change of resonance condition caused by the shift in the absorption bands (*i.e.* effect 2-b).

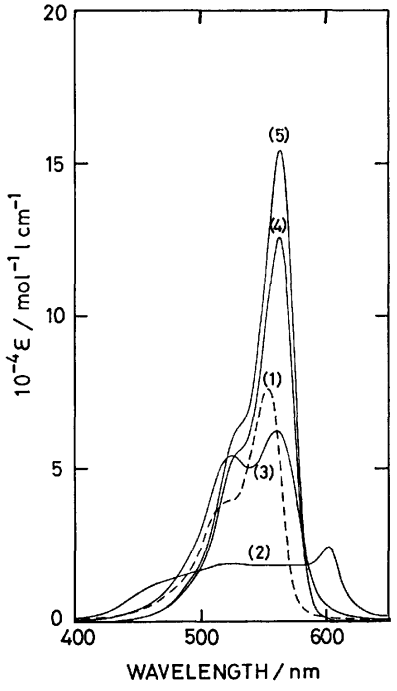

Fig. 6. Absorption spectra of aqueous solution of DTC–SDS.
[DTC]=1.0×10^{-5} M, [SDS]: (1) 0 mM, (2) 2.5 mM, (3) 5 mM, (4) 7.5 mM, (5) 15 mM.

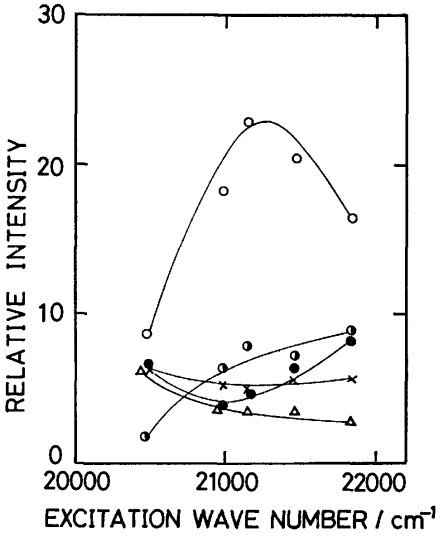

Fig. 7. Dependence of Raman band intensities on excitation wave number, △ 569 cm^{-1}, ● 601 cm^{-1}, × 791 cm^{-1}, ○ 1238 cm^{-1}, ◑ 1383 cm^{-1} band. [DTC]=1.0×10^{-5} M.

Discussion

The dye-detergent interaction was studied with Raman spectra by several authors on several occasions. Verma and Wallach[17] reported the intensities of 1530 cm^{-1} (–C=C– stretching) and 1165 cm^{-1} (=C–C= stretching) of β-carotene were reduced by the addition of SDS. Kim *et al.*[18] found the change of relative intensities of Raman bands at 1420 cm^{-1} and 1155 cm^{-1} of Methyl Orange (MO, an anionic dye) on addition of HTAB below and above cmc. Takenaka and Nakagawa[19] studied the monolayer of MO–HTAB adsorbed at the interface between carbon tetrachloride and aqueous solution. They found a shift of band frequencies of MO in the monolayer from those in bulk aqueous solution toward those of solid MO, indicating that the MO molecules in the monolayer were in an environment similar to a crystal field. Koyama and Matsuo[20] found that 594 cm^{-1} band in the azobenzene–behenic acid system was present in the molten state, but absent in the solid state. They stated that this band can be used as a probe of the aggregation state of the system.

The [SDS]-dependent change of Raman spectra presently studied is not due merely to the change of resonance condition caused by the shift in the absorption bands, and is due to the change of aggrega-

tion state of the dye. For [SDS]≪cmc (*e.g.*, 2.5 mM), the dye is in the aggregation state like in the solid. As the dye is considered to be in a highly aggregated state in the solid, the state of the dye for [SDS]≪ cmc can also be characterized as a highly aggregated state. The comparison with aqueous solution shows that the aggregation state of the dye in SDS solution with [SDS]≪cmc and in solid state is different from that of the dimer in a concentrated aqueous solution. The data in Fig. 2 show that the intensity maxima of bands characteristic to the highly aggregated dye lie around [SDS]=2.5—3.0 mM. When [SDS] approaches cmc, the spectra show the intermediate feature between [SDS]=2.5—3.0 mM and [SDS]>cmc.

The study of absorption and fluorescence spectra, fluorescence intensity and decay behavior as a function of [SDS][14] revealed that there are two regions below cmc. The region [SDS]≪cmc is characterized with a very broad absorption band and the anomolous long-wavelength fluorescence (655 nm). The dye-detergent salt (with nearly 1:1 stoichiometry) as proposed by Mukerjee and Mysels[12] for pinacyanol-SDS seems to be formed. "The highly aggregated dye" must be found in such a dye-detergent aggregate. The resemblance of absorption and Raman spectra to those of DTC–PVSK supports this assumption. For some dye-detergent systems, the dye-detergent aggregate forms a large particle and precipitates from the solution in the low [SDS] region. In the DTC–SDS system presently studied, very minute solid particles seem to be formed in the solution. The formation of such particles can be monitored by the appearance of naturally emitting lines of Ar^+ laser in the observed Raman spectra. These lines are found around [SDS]=1.0 mM. Since the maximum intensities of the bands characteristic to the highly aggregated dye were observed around [SDS]=2.5—3.0 mM, we can safely say that the observed bands are due to dye-detergent aggregate, but not due to solid particles.

For 5.0×10^{-3} M≲[SDS]<cmc, the absorption bands of monomer and dimer dye were observed along with the monomer fluorescence.[14] (Dimers are non-fluorescent.) The energy transfer efficiency between dyes are highly enhanced in this [SDS] region. The presence of dye-rich induced micelles as proposed by Mukerjee and Mysels[12] is plausible in this region. As far as the Raman spectrum is concerned, this region is not characterized by any peculiar feature, but by the intermediate one between [SDS]≪cmc and [SDS]>cmc. In other words, the gradual change of dye-detergent aggregate to micellized monomer dye did not show any peculiarity in the Raman spectra.

For [SDS]>cmc, the absorption spectra draw nearer to the monomer dye. The Raman spectra were similar to those of aqueous and methanol solutions. The deaggregation effect of SDS on the dye did not give any significant change in the Raman spectra.

In summary, resonance Raman spectra proved to be a very useful tool in elucidating the aggregation state of the dye in the dye-detergent systems. The 569 cm^{-1} band works as an useful monitor of the aggregation state of DTC.

The present authors would like to thank Dr. Katsunosuke Machida, Kyoto University, for measurement of solid spectra and for helpful discussions. They are grateful to Miss Yuko Hanyu for her assistance. This study is partly supported by a Grant-in-Aid for Scientific Research No. 447006 from the Ministry of Education, Science and Culture.

References

1) G. S. Singhal, E. Rabinowitch, J. Hevesi, and V. Srinivasan, *Photochem. Photobiol.*, **11**, 531 (1970).
2) E. Lohoczki and J. Hevesi, *Dokl. Akad. Nauk SSSR*, **206**, 1158 (1972).
3) Y. Kusumoto and H. Sato, *Chem. Phys. Lett.*, **68**, 13 (1979).
4) Y. Usui and A. Gotou, *Photochem. Photobiol.*, **29**, 165 (1979).
5) H. Sato, Y. Kusumoto, N. Nakashima, and K. Yoshihara, *Chem. Phys. Lett.*, **71**, 326 (1980).
6) T. Matsuo, Y. Aso, and K. Kano, *Ber. Bunsenges. Phys. Chem.*, **84**, 146 (1980).
7) G. A. Kenney-Wallace, J. H. Flint, and S. C. Wallace, *Chem. Phys. Lett.*, **32**, 71 (1975).
8) H. E. Lessing and A. Von Jena, *Chem. Phys.*, **41**, 395 (1979).
9) The color change was used in the "spectral change method" of determining cmc. *Cf.* M. L. Corrin and W. D. Harkins, *J. Am. Chem. Soc.*, **69**, 683 (1947).
10) N. Mataga and M. Koizumi, *Nippon Kagaku Zasshi*, **75**, 35 (1954).
11) N. Mataga and M. Koizumi, *Bull. Chem. Soc. Jpn.*, **27**, 197 (1954).
12) P. Mukerjee and K. J. Mysels, *J. Am. Chem. Soc.*, **77**, 2937 (1955).
13) J. Knof, F. J. Theiss, and J. Weber, *Z. Naturforsch. Teil A*, **33**, 98 (1978).
14) H. Sato, M. Kawasaki, K. Kasatani, Y. Kusumoto, N. Nakashima, and K. Yoshihara, *Chem. Lett.*, **1980**, 1529.
15) Although cmc shows a small shift towards smaller [SDS] on addition of the dye, the shift is rather small. The shift of 0.5—0.6 mM was reported in the literature (Refs. 3 and 12).
16) The addition of external standard, like MnO_4^- or SO_4^{2-} was tried. It was not successful, however, because the line was too weak, or because the added substance gave some effect on the aggregate formation.
17) S. P. Verma and D. F. H. Wallach, *Biochem. Biophys. Acta.*, **401**, 168 (1975).
18) B. K. Kim, A. Kagayama, Y. Saito, K. Machida, and T. Uno, *Bull. Chem. Soc. Jpn.*, **48**, 1394 (1975).
19) T. Takenaka and T. Nakagawa, *J. Phys. Chem.*, **80**, 475 (1976).
20) Y. Koyama and T. Matsuo, "Laser Raman Bunkogaku To Sono Oyo," ed by T. Shimanouchi, M. Tasumi, and I. Harada, Nankodo, Tokyo (1977), Chap. 11.

 © 1982 The Chemical Society of Japan Bull. Chem. Soc. Jpn., 55, 721—725 (1982)

X-Ray Photoelectron Spectroscopic Study of Highly Conductive Bromine-doped Polyacetylene

Isao IKEMOTO,* Yong CAO, Masamichi YAMADA, Haruo KURODA, Issei HARADA, Hideki SHIRAKAWA,† and Sakuji IKEDA††

Research Center for Spectrochemistry and Department of Chemistry, Faculty of Science, The University of Tokyo, Hongo, Bunkyo-ku, Tokyo 113

†*Institute of Materials Science, University of Tsukuba, Sakura-mura, Ibaraki 305*

††*Research Laboratory of Resources Utilization, Tokyo Institute of Technology, Nagatsuta, Midori-ku, Yokohama 227*

(Received September 10, 1981)

The bromine-doped polyacetylenes were studied by X-ray photoelectron spectroscopy. The IR, Raman, and mass spectra were also measured. We find that below the doping content at which the electrical conductivity shows the maximum, bromine content is higher in the surface region than in the bulk. The C ls peak of X-ray photoelectron spectrum is composed of at least two components with the splitting of about 1.7 eV. The relative intensities of two components change with bromine content. The higher-binding-energy component of C ls peak is attributed to positively charged carbon atoms in the metallic domains where dopant is highly concentrated, and the lower-binding-energy component to carbon atoms in the undoped low-conductive domains. The amount of charge transfer in the metallic domain is estimated to be about 0.3|e| per carbon atom. A possible reaction mechanism of bromine with polyacetylene is discussed.

Recently polyacetylene, $(CH)_x$, has attracted great interests because it exhibits metallic conductivity when treated with various dopants.[1–4] Its electrical conductivity at room temperature varies over twelve orders of magnitude by doping with suitable electron acceptors such as halogens and AsF_5. Although the properties of these doped polyacetylenes have been investigated by many groups, more information concerning their structures and electronic states is needed in order to understand the electrical behaviors of these systems. It is important to determine the chemical state of dopant in the polymer and the nature of interaction between dopants and polymer chains. Previously we reported the results of X-ray photoelectron spectroscopic (XPS) studies of the iodine-doped polyacetylene.[5] The bromine-doped polyacetylene shows an electrical behavior similar to that of the iodine-doped polyacetylene when doping content is low. However, much heavier doping is possible in the case of bromine as compared with iodine.[3] Here we report the results of XPS studies on the bromine-doped polyacetylene.

Experimental

A polyacetylene film was prepared by the method described previously.[6] All samples used in the present experiment were obtained from the same batch of polyacetylene. Polymerization was performed at −78 °C to give *cis*-polyacetylene. A *trans*-polyacetylene film was obtained by heating a *cis*-polyacetylene film at 200 °C for 1 h. Film thickness was approximately 0.1 mm.

Bromine treatment was carried out at room temperature by direct contact of a polyacetylene film with Br_2 vapor. The extent of doping was controlled by measuring the electrical conductivity of a reference film contained in the same vessel by means of the standard four-probe method. The bromine content of a doped sample was determined by elemental analysis.

Prior to XPS studies, a sample film was cut off to several parts to measure Raman, IR, and mass spectra.

X-Ray photoelectron spectra were taken with a McPherson ESCA 36 electron spectrometer employing Mg $K\alpha$ (1253.6 eV) radiation. Special care was taken to prevent samples from exposing to the air prior to XPS measurements. After XPS measurements, sample films were used for elemental analysis and for measurements of Raman and IR spectra. The binding energies of observed photoelectron peaks were calibrated by use of Au $4f_{7/2}$ peak (83.8 eV) of a very thin gold film deposited onto the sample surface.

Raman spectra were taken with a Spex 1401 double monochromator equipped with a Spectra Physics 166-01 Kr ion laser, a JEOL JLG-4A Ar ion laser, and an NEC He-Cd laser. The laser lines between 647.1 nm and 325.0 nm were used to obtain Raman spectrum. The IR spectra were measured by ATR method by use of a HITACHI EPI-G3 double beam grating IR spectrometer.

Mass spectra were obtained on a JMS-D300 mass spectrometer (JEOL) using a direct insertion probe. Polyacetylene samples were directly inserted into the ion source and the mass spectra were measured at room temperature.

Results

The electrical conductivity of bromine-doped *trans*-polyacetylene, $(CHBr_n)_x$ is shown in Fig. 1 as a function of the bromine content, n, which was determined by elemental analysis. The general feature of conductivity change is almost same as those previously reported by other authors,[3] except for small differences as regards the bromine content and the conductivity value at the maximum. It should be noted that a bromine-doped polyacetylene film exhibits conductivity as high as $10^{-2}\,\Omega^{-1}\,cm^{-1}$ even at a high doping level of $n=0.63$. The conductivity abruptly decreased when bromine content was further increased. The variation of conductivity with bromine content was found to be almost same in the case of *cis*-polyacetylene, but the conductivity at the maximum point was a little higher as compared with *trans*-polyacetylene.

As shown in Fig. 2, the Br 3d peak in the XPS spectrum of a bromine-doped polyacetylene film decreased its intensity as we repeated XPS measurements on the same sample, indicating that doped bromine was

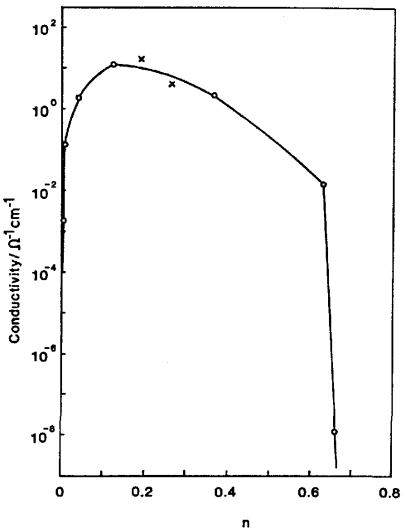

Fig. 1. The electrical conductivity of bromine-doped polyacetylene, $(CHBr_n)_x$, as a function of n determined by elemental analysis.
(○): Trans, (×): cis.

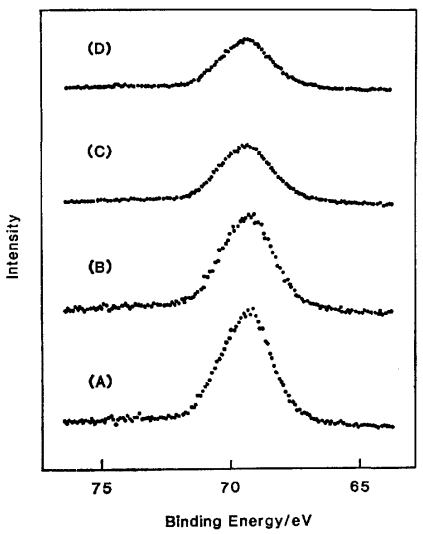

Fig. 2. The time dependent Br 3d spectra of *trans*-$(CHBr_{0.127})_x$.
(A): 5 h, (B): 7 h, (C): 10 h, and (D): 20 h in a vacuum of the spectrometer.

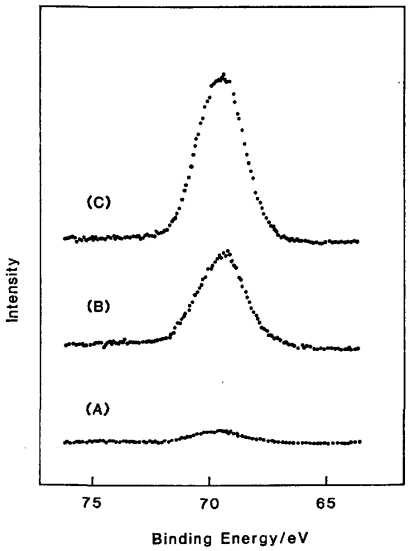

Fig. 3. The Br 3d peaks of *trans*-$(CHBr_n)_x$ obtained by the initial measurement.
(A): n=0.008, (B): n=0.127, (C): n=0.661.

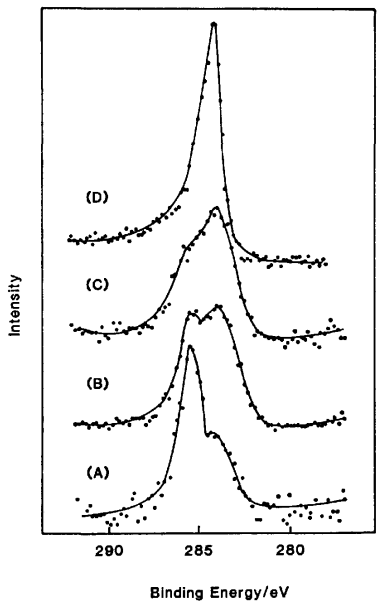

Fig. 4. The C ls peaks of *trans*-$(CHBr_n)_x$ obtained by the initial measurement.
(A): n=0.696, (B): n=0.368, (C): n=0.127, (D): n=0.008.

gradually lost from the film during XPS measurements. We observed a similar phenomenon in the case of iodine-doped polyacetylene.[5] But there is a slight difference between two cases. In the case of bromine-doped polyacetylene, Br 3d peak does not appreciably change its shape accompanying the decrease of its intensity whereas I 3d peak of iodine-doped polyacetylene was found to change its shape.[5]

Figure 3 shows the Br 3d peaks of several films of different bromine content. The spectra shown here are those obtained by the initial measurement on each sample. The binding energy of Br 3d peak did not vary with bromine content. The peak width (FWHM) was about 2.3 eV in the cases of bromine-doped polyacetylene films of $n>0.04$, it being a little larger at lower bromine content. In the cases of bromine-doped *cis*-polyacetylene films, the Br 3d peak width was about 2.6 eV.

In contrast to Br 3d peak, the shape of C ls peak of bromine-doped polyacetylene markedly varies with bromine content as shown in Fig. 4. The observed peak shape suggests that the peak is composed of two components separated by 1.7—2.0 eV, and the intensity of the higher-binding-energy component increases while that of the lower-binding-energy component decreases on increasing bromine content. Figure 5 shows the change of the C ls peak shape of a doped film upon the reduction of bromine content caused by keeping the film in a vacuum. Note that the peak shape varies with bromine content, but the

total intensity remains nearly constant.

We estimated the atomic ratio of bromine to carbon, n_{XPS}, from the ratio of the integrated intensities of Br3d and C1s peaks, with the reference to the relative intensities of the corresponding peaks in the XPS spectrum of tetrabromobenzene. The results are given in Table 1, where the value in the column expressed as "initial" is the Br/C atomic ratio which was determined from the data of the first XPS measurement of the sample concerned, and the value in the column expressed as "final" is the one which was determined from the data of the last measurement of the same sample usually after repetition of XPS measurements for 15—20 h. The XPS atomic ratio n_{XPS} is larger than the atomic ratio n from elemental analysis in the cases of $n \lesssim 0.127$, but they almost agree with each other in the cases of $n > 0.127$. This shows that doped bromine is more concentrated in the surface region than in the bulk at lower bromine content, but is distributed more homogeneously in heavily doped films.

Figure 6 shows the change of n_{XPS} with the time for which the sample has been kept in a vacuum. The

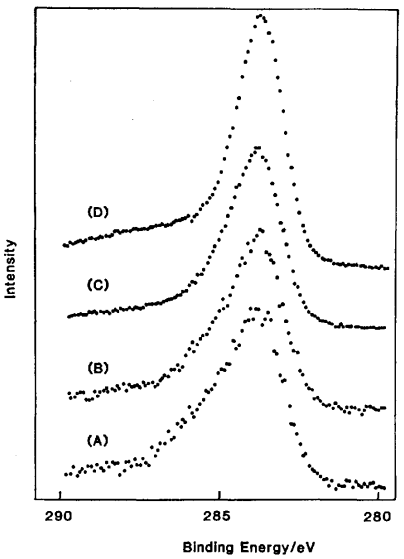

Fig. 5. The change of the C 1s peak shape of *trans*-$(CHBr_{0.042})_x$ upon the reduction of bromine content caused by keeping the sample in a vacuum.
(A): 2 h, (B): 5 h, (C): 11 h, (D): the C 1s peak shape of *trans*-$(CH)_x$.

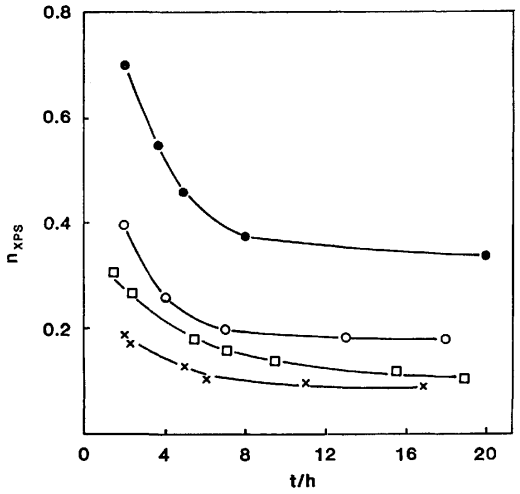

Fig. 6. The change of Br/C ratio n_{XPS}, with the time for which the samples have been kept in a vacuum.
(●): $(CHBr_{0.661})_x$, (○): $(CHBr_{0.368})_x$,
(□): $(CHBr_{0.127})_x$, (×): $(CHBr_{0.042})_x$.

Table 1. XPS results of bromine-doped polyacetylene films

Sample	Electrical conductivity σ / Ω^{-1} cm^{-1}	Br/C Atomic ratio n[a] Initial	n[a] Final	n_{XPS}[b] Initial	n_{XPS}[b] Final	C 1s Binding energy / eV	C 1s FWHM / eV	Br 3d Binding energy / eV	Br 3d FWHM / eV	C1s Peak deconvolution C_1/C[c]	ΔE[d] / eV
trans-$(CHBr_n)_x$	$<10^{-8}$	0.697	0.665	0.76	0.20	285.5 283.8		69.3	2.3	0.74	1.7
	1.2×10^{-8}	0.661	0.647	0.70	0.34				2.3	0.75	1.6
	1.8×10^{-2}	0.633	0.576	0.63	0.19				2.2	0.69	1.7
	3.5×10^{0}	0.368	0.262	0.39	0.18				2.2	0.43	1.7
	1.3×10^{1}	0.127	0.112	0.31	0.12				2.2	0.33	1.8
	3.0×10^{0}	0.042	0.035	0.19	0.09	285.1 283.6		69.3	2.2	0.28	1.5
	1.5×10^{-1}	0.008	0.002	0.03	0.02				2.6		
	2.9×10^{-3}	0.000_4	0.000_3	0.00_9	0.00_2				2.6		
cis-$(CHBr_n)_x$	2.0×10^{1}	0.194	0.188	0.27	0.14	285.7 283.7		69.5	2.6	0.39	2.0
	5.6×10^{0}	0.264	0.246	0.39	0.16	285.6 283.8		69.3	2.6	0.53	1.8
trans-$(CH)_x$						283.8	1.8				

a) Br/C atomic ratio determined by elemental analysis (initial; the value before XPS measurement, final; the value after XPS measurement). b) Br/C atomic ratio determined by XPS measurements at initial and final measurements. c) Relative area ratio of the higher-binding-energy component of C 1s peak to total C 1s peak. d) Splitting of two components of the spectra.

n_{XPS} value rapidly decreases first, but its decrease is leveled off after about 8 h.

Since the C1s peak of a bromine-doped film seems to be composed of two components, we decomposed the observed peak into two component peaks using the C1s peak shape of an undoped polyacetylene film as the standard. The procedures used here are almost the same as those described in our previous paper.[7] Let us denote the carbon atom which is responsible for the higher-binding-energy C1s component, as C_1. We estimated the ratio of C_1 atoms to the total carbon atoms. The C_1/C atomic ratio thus obtained is always close to the Br/C atomic ratio n_{XPS}. Thus we can consider that the atomic ratio of C_1 to Br is always about 1:1.

The Raman spectra of undoped and lightly doped ($n<0.05$) polyacetylene films were previously investigated by several groups.[8-10] It was reported that, according to the observed Raman spectra, doped bromine must be exclusively in the form of Br_3^-. We obtained the same conclusion for lightly doped films. The Raman spectra of heavily doped films were found to be similar to those of lightly doped films showing that doped bromine is primarily in the form of Br_3^- ion, but the possibility of the presence of other bromine species could not be excluded from the observed data. In fact, the band attributable to C–Br stretching vibration was found in the IR spectra of heavily doped films. After XPS measurements, the Raman lines at 158 and 316 cm^{-1}, which are due to the symmetric stretching mode of Br_3^- and its overtone, respectively, appreciably reduced their intensities, indicating the decrease of Br_3^- during the XPS measurements. As we have already mentioned, bromine content decreases when a doped film is kept in a vacuum. It was confirmed by mass spectroscopy that the chemical species which come out from a doped film are mostly HBr in the case of a lightly doped film, and HBr and Br_2 in the case of a heavily doped film. Therefore, we have to consider that the decrease of Br_3^- is accompanied by the formation of C–Br bond. However, it was hard to confirm whether the intensity of C–Br stretching band in IR spectrum increased after XPS measurement or not.

Discussion

According to the conductivity change with bromine content, we can classify the bromine doping of polyacetylene into the following three stages: The stage A ($n\leq0.127$) where conductivity steeply increases with increasing bromine content, the stage B ($0.127<n\leq 0.63$) where conductivity gradually decreases and the stage C ($n>0.63$) where an abrupt decrease of conductivity takes place on further increase of bromine content.

In the case of films of the stage A, the atomic ratio of hydrogen to carbon was found to be 1:1 by elemental analysis. From this fact we can conclude that doped bromine exists primarily as Br_3^- without forming C–Br bond by the substitution of hydrogen of polyacetylene chain with bromine. However, HBr is evolved as a doped film is kept in a vacuum. Possibly this is because Br_3^- can be lost from a film only by performing a reaction with polymer chain to form C–Br bonds with an evolution of HBr.

In the XPS spectrum of a lightly doped film, the C1s peak is asymmetric with a shoulder in the higher-binding-energy side of the main peak. This shoulder is likely to be due to the higher-binding-energy component which clearly appears as a peak in the spectrum of a heavily doped film. One possible interpretation for this higher-binding-energy component could be to attribute it to the carbon atom forming C–Br bond. But this is rather unlikely to be the case since its intensity decreases in parallel to the decrease of bromine content when the film is kept in a vacuum. It should be also noted that the energy separation 1.7 eV from the main peak is too large in comparison with the chemical shift of C1s between C–Br and C–H carbons: the shift is expected to be about 1 eV or less. Thus we consider that the higher-binding-energy C1s component is associated with positively charged carbon atoms which are closely interacting with Br_3^- ions.

Recently Fincher *et al.*[11] proposed, from the investigations of the optical absorption spectra and Raman spectra of doped polyacetylene films, that, in a lightly doped polyacetylene film, the dopant is not uniformly distributed, but forms domains of high dopant concentration, where polyacetylene chain becomes metallic having a uniform C–C bond length, and the remaining regions are in the undoped low-conductive state. This inhomogeneous domain model seems to be consistent with our XPS data. We will attribute the higher-binding-energy C1s component to the carbon atoms in the metallic domain and the other component to the carbon atoms in the low-conductive domain. In the metallic domain, carbon atoms must be positively charged as a result of charge transfer to bromine to form Br_3^-. The positive charge per carbon atom (C_1) of the metallic domain can be estimated from the observed splitting of the two components of C1s peak. Since C1s level is known to be shifted by about 5.6 eV per unit charge,[12] the splitting observed for the doped film of $n=0.127$ corresponds to about $+0.3|e|$. The C_1/Br atomic ratio determined from XPS data provides another independent way to estimate the positive charge per carbon atom since one electron per three bromine atoms should be transferred from polyacetylene chains in the metallic domain, in other words, from C_1 atoms. As shown in Table 2, the values obtained by this way are also about $+0.3|e|$ in agreement with the values from the chemical shift.

It was reported by Salaneck *et al.* that a shoulder appeared on the higher-binding-energy side of C1s peak of polyacetylene upon doping with AsF_5[13] or with iodine.[14] They attributed this shoulder to the plasmon loss associated with charge carriers along polyacetylene chain. However we believe that the shoulder observed in these cases is of the origin similar to the higher-binding-energy C1s component of bromine doped polyacetylene.

Doped bromine must exist mainly in the form of Br_3^- also in the stages B and C, but the substitution

Table 2. Comparison of the charge per C atom estimated from the intensity ratio of higher-binding energy C1s component (C_1) and Br 3d peak and from the splitting of C1s peak of lightly doped polyacetylene

	Estimated from C_1/Br_3 atomic ratio		Estimated from C1s splitting	
	C_1/Br_3^-	Charge per C atom	ΔE/eV	Charge per C atom
trans-$(CHBr_{0.127})_x$	3.2	0.31	1.7	0.30
trans-$(CHBr_{0.042})_x$	4.5	0.22	1.5	0.26
cis-$(CHBr_{0.194})_x$	4.4	0.23	2.0	0.36

or addition reaction of bromine with polyacetylene chain is likely to take place more in these stages. In fact, H/C atomic ratio was found to be 0.95 by elemental analysis in the case of a heavily doped polyacetylene film.

When a film of the stage B is kept in a vacuum, Br3d peak and the higher-binding-energy C1s component decrease their intensities, by evolving HBr from the film. This HBr evolution was markedly enhanced as the film was heated to 150 °C.[15] Probably HBr is formed by the reaction of Br_3^- with polyacetylene chain as in the case of a film of the stage A.

In the stage C, all experimental evidences do suggest that the addition reaction of bromine to C=C double bond significantly takes place in the doping process. The abrupt drop of conductivity in the stage C is likely to be due to the breakdown of π-electron conjugated system of a polyacetylene chain. Thus there must be a considerable amount of carbon atoms having C–Br bond. However even in this case, the higher-binding-energy C1s component which is stronger than the lower-binding-energy one, can not be attributed to the carbon atoms with C–Br bond since its intensity rapidly decreases just by keeping the film in a vacuum at room temperature, by evolving Br_2 and HBr. Seemingly the higher-binding-energy C1s component which appears in the XPS spectra of films of the stage C, is again due to the carbon atoms positively charged by the electron transfer to bromine and in close interaction with Br_3^- ions thus formed, as we have postulated for the stages A and B. Probably the C1s peak due to the carbon atoms with C–Br bond and the one due to the carbon atoms in the undoped regions emerge into the lower-binding-energy C1s component because their energy difference is small, possibly less than 0.5 eV.

Summary and Conclusion

Summarizing all the experimental results obtained in the present study, we postulate the following picture for the bromine doping of polyacetylene. In the first doping stage ($n \leq 0.127$), the doping proceeds inhomogeneously by forming domains in which doped bromine, in the form of Br_3^-, is highly concentrated and polyacetylene chains are in metallic state as the result of charge transfer to bromine by the amount of about 0.3 electron per carbon atom. The conductivity steeply increases on increasing average bromine content because of the increase of the volume fraction of metallic domain.

In the second stage ($0.127 < n \leq 0.63$), the substitution reaction takes place beside the above mentioned doping mechanism, so that the rate of the conductivity-increase with bromine content is leveled down. In the third stage ($n > 0.63$), the addition reaction of bromine to C=C double bond of polyacetylene chain significantly takes place, which results in a marked reduction of the length of π-conjugated system, thus causes an abrupt decrease of conductivity.

The computer used was HITAC-M200H at the Computer Center, the University of Tokyo.

The present work was supported by a Grant-in-Aid for Scientific Research No. 554109 from the Ministry of Education, Science and Culture.

References

1) H. Shirakawa, E. J. Louis, A. G. MacDiarmid, C. K. Chiang, and A. J. Heeger, *J. Chem. Soc., Chem. Commun.*, **1977**, 578.

2) C. K. Chiang, M. A. Drug, S. C. Gau, A. J. Heeger, E. J. Louis, A. G. MacDiarmid, Y. W. Park, and H. Shirakawa, *J. Am. Chem. Soc.*, **100**, 1013 (1978).

3) C. K. Chiang, Y. W. Park, A. J. Heeger, H. Shirakawa, E. J. Louis, and A. G. MacDiarmid, *J. Chem. Phys.*, **69**, 5098 (1978).

4) C. K. Chiang, A. J. Heeger, and A. G. MacDiarmid, *Ber. Bunsenges. Phys. Chem.*, **83**, 407 (1979).

5) I. Ikemoto, M. Sakairi, T. Tsutsumi, H. Kuroda, I. Harada, M. Tasumi, H. Shirakawa, and S. Ikeda, *Chem. Lett.*, **1979**, 1189.

6) T. Ito, H. Shirakawa, and S. Ikeda, *J. Polym. Sci., Polym. Chem. Ed.*, **12**, 11 (1974); **13**, 1943 (1975).

7) I. Ikemoto, M. Yamada, T. Sugano, and H. Kuroda, *Bull. Chem. Soc. Jpn.*, **53**, 1871 (1980).

8) H. Shirakawa, T. Sasaki, and S. Ikeda, *Chem. Lett.*, **1978**, 1113.

9) S. Lefrant, L. S. Lichtmann, H. Temkin, and D. B. Fitchen, *Solid State Commun.*, **29**, 191 (1979).

10) I. Harada, Y. Furukawa, M. Tasumi, H. Shirakawa, and S. Ikeda, *J. Chem. Phys.*, **73**, 4746 (1980); I. Harada, M. Tasumi, H. Shirakawa, and S. Ikeda, *Chem. Lett.*, **1978**, 1411.

11) C. R. Fincher, M. Ozaki, M. Tanaka, D. Peebles, L. Lauchlan, A. J. Heeger, and A. G. MacDiarmid, *Phys. Rev. B*, **20**, 1589 (1979).

12) K. Siegbahn, C. Nordling, G. Johansson, J. Hedman, P. F. Hedén, K. Hamrin, U. Gelius, T. Bergmark, L. O. Werme, R. Manne, and Y. Baer, "ESCA Applied to Free Molecules," North Holland, Amsterdam (1969), p. 114.

13) W. R. Salaneck, H. R. Thomas, C. B. Duke, A Paton, E. W. Plummer, A. J. Heeger, and A. G. MacDiarmid, *J. Chem. Phys.*, **71**, 2044 (1979).

14) W. R. Salaneck, H. R. Thomas, R. W. Bigelow, C. B. Duke, E. W. Plummer, A. J. Heeger, and A. G. MacDiarmid, *J. Chem. Phys.*, **72**, 3674 (1980).

15) W. N. Allen, J. J. Decorpo, F. E. Saalfeld, J. R. Wyatt, and D. C. Weber, *Synth. Metals*, **1**, 371 (1979/1980).

Investigation on the Complex Formation of Some Lanthanoids(III) and Actinoids(III) with Chloride and Bromide

Tetsuo FUKASAWA,† Isamu KAWASUJI,* Toshiaki MITSUGASHIRA, Akiko SATÔ, and Shin SUZUKI

The Research Institute for Iron, Steel and Other Metals, Tohoku University, Katahira 2-chome, Sendai 980

(Received April 17, 1981)

Stability constants (β_1 and β_2) of the chloro and bromo complexes of tervalent Sm, Eu, Gd, Tb, Ac, Am, Cm, Bk, and Cf were determined by a solvent extraction method under the conditions of ionic strength and acidity to be 3.0 and 0.15 M (1 M=1 mol/dm^3), respectively. Stability constants obtained were discussed with respect to the formation mechanism. A much larger contribution from the inner sphere complex formation was observed in chloro complexes than bromo complexes on tripositive actinoids.

Diamond *et al.*[1] reported the difference in the distribution behavior between tripositive actinoids and lanthanoids on the cation exchange resin at high concentrations of HCl. Hulet *et al.*[2] presented the anion exchange method using 10 M LiCl as an eluent to separate tripositive actinoids from lanthanoids, and showed that the distribution ratio(D_v) of actinoids were higher than those of lanthanoids. These phenomena have been explained by the difference in the complex formation between actinoids(III) and lanthanoids(III). Only a few studies have been carried out to determine the stability constants for many actinoids(III) under those conditions.[3] Therefore, the pronounced difference in the complex formation between actinoids(III) and lanthanoids(III) can not be discussed in detail from the available data on stability constants. In this paper, we prepared the adequate tracers of Sm, Ac, Cm, and Bk which are not available in general, determined the stability constants accurately under the same conditions by a solvent extraction method with bis(2-ethylhexyl)hydrogenphosphate, HDEHP, and discussed the phenomena mentioned above.

Experimental

Radioisotopes. ^{152,154}Eu, ^{153}Gd, ^{160}Tb, and ^{252}Cf were obtained from The Radiochemical Centre, Amersham, and ^{241}Am from Oak Ridge National Laboratory. ^{225}Ac was isolated from ^{229}Th which was obtained from ^{233}U.[4] ^{242,243,244}Cm, obtained and purified as reported previously,[5,6] was used in this experiment. ^{145}Sm and the mixture of ^{243}Bk and ^{244}Bk[7] were produced by means of ^{142,143,144}Nd+α and ^{241}Am+α reaction, respectively. For the bombardment, A. V. F. cyclotron at the Cyclotron and Radioisotope Center, Tohoku University, was used. ^{145}Sm was purified by successive extraction with HDEHP. ^{243,244}Bk was separated from irradiated ^{241}Am and fission products by HDEHP extraction of quadrivalent Bk. These tracers were dissolved into 3.0 M $HClO_4$ solutions and stored in Pyrex vessels.

Reagents. The organic extractant HDEHP was purified by the copper-salt precipitation method,[8] and stored as copper salt. LiCl and $LiClO_4$ were prepared from a reagent grade Li_2CO_3. LiBr was obtained in 99.9% purity from MITSUWA Chemical Reagents Co., Ltd. These lithium salts were recrystallized twice before use. All the other chemicals were of the highest grade available.

Apparatus. Gamma-rays of ^{152,154}Eu, ^{153}Gd, ^{160}Tb, ^{241}Am, and ^{243}Cm were counted by means of an auto-well scintillation counter, Packard model 5230. ^{225}Ac, in radioequilibrium with the decay series nuclides, was assayed by the same apparatus. ^{252}Cf was assayed by the prompt fission γ-rays. For the counting, another well type NaI(Tl) ($1.5\phi \times 2''$) counting system was used with a discriminator adjusted to 2.8 MeV with respect to γ-energy. For ^{145}Sm, 61 keV γ-ray was counted by a γ-ray spectrometry system; Tracor Northern TN-11, using an intrinsic Ge(PGT model IGC13) and a Ge(Li) (ORTEC model 8101-1820) detectors. For mixture of ^{243}Bk and ^{244}Bk, the KX-rays of Cm and 218 keV γ-ray were counted by the same γ-ray spectrometry system.

Procedures. Six ml of sample solution was prepared by mixing of appropriate amounts of the stock solution, 3.0 M $LiClO_4$ solution, and 3.0 M LiCl or LiBr solution in a separatory funnel. The sample solution was equilibrated with an equal volume of the HDEHP/octane solution pre-equilibrated by a solution of the same composition as the sample solution. The HDEHP/octane solution was prepared just before the experiment converting the Cu(DEHP)$_2$ to acid form. To determine the relation between distribution ratio and ligand concentration, the acidity was fixed at 0.15 M and the concentration of HDEHP was controlled so that the distribution ratio in the absence of the ligand was to be 1.5—1.8. Extraction equilibrium was reached by shaking for 20 min at about 20 °C. From each phase in equilibrium, a 2 ml portion was taken into a polyethylene test tube and the radioactivity was counted. For the bromide solution, values were corrected for self-absorption of γ-rays by preliminary determined absorption data.

Calculation of the Overall Stability Constants β_1 and β_2. Distribution ratio was calculated by Eq. 1. In the

$$D = \frac{[M]_{org,\ total}}{[M]_{aq,\ total}} \quad (1)$$

presence of complexing anion L^- (L=Cl or Br) in the aqueous phase, complex formation reaction of tripositive cation exists

$$M^{3+} + xL^- \overset{\beta_x}{\rightleftharpoons} ML_x^{3-x},\ (x=1—n), \quad (2)$$

where $\beta_x=[ML_x^{3-x}]/[M^{3+}][L^-]^x$. HDEHP is a cation exchange extractant and the extraction of the complex species can be neglected because of the decrease in the positive charge on the complex species. For example, tervalent lanthanoids and actinoids ions show a distribution ratio a few order of magnitude higher ($>10^3$) than the divalents.[9] Therefore, the distribution ratio can be expressed as follows:

† Present address: Energy Research Laboratory, Hitachi, Ltd., Moriyama-cho, Hitachi 316.

$$D = \frac{[M]_{org,\ total}}{[M^{3+}] + \sum_{x=1}^{n} [ML_x^{3-x}]} = D_0 \frac{1}{1 + \sum_{x=1}^{n} \beta_x [L^-]^x}. \quad (3)$$

And the equation,

$$(D_0/D) - 1 = \beta_1[L^-] + \beta_2[L^-]^2 + \cdots \quad (4)$$

is derived, where D_0 is the distribution ratio in the absence of the ligand. From Eq. 3, the slope of $\log D$ *vs.* $\log [L^-]$ curve is represented as

$$\frac{\partial \log D}{\partial \log [L^-]} = -\sum_{x=1}^{n} x \frac{\beta_x [L^-]^x}{1 + \sum_{x=1}^{n} \beta_x [L^-]^x} = -\sum_{x=1}^{n} x f_x. \quad (5)$$

Where, f_x is a mole fraction of ML_x^{3-x} in the aqueous phase. Equation 4 was used to calculate β_x by the least mean squares fitting of the data points $(D_0/D)-1$ *vs.* $[L^-]$. In order to determine the maximum ligand number, n, a graphic method was applied using the relation of (5).

Results and Discussion

The relation between $\log D$ and $\log [HDEHP]_{org}$ for Bk is shown in Fig. 1. And for Gd, the relation between $\log D$ and $\log [HDEHP]_{org}$ at various ligand concentration is shown in Fig. 2. In these figures, it is shown that D is proportional to the 2.5 power of $[HDEHP]_{org}$ and the relation is not affected by the addition of Cl^- or Br^-. The dependence of $\log D$ on $\log [H^+]_{aq}$ is shown in Fig. 3 for Bk. As shown in Fig. 3, D is inversely proportional to the third power of $[H^+]_{aq}$. The other lanthanoids(III) and actinoids (III) examined in this investigation exhibit the same dependency of D on $[HDEHP]_{org}$ and $[H^+]_{aq}$. HDEHP exists as dimer, $(HA)_2$, in the organic solution. Then the extraction reaction can be written as

$$M^{3+}_{aq} + 2.5(HA)_{2\,org} \rightleftharpoons MA_3(HA)_{2\,org} + 3H^+_{aq}. \quad (6)$$

The relations between $\log D$ and $\log [Cl^-]_{aq}$ or $\log [Br^-]_{aq}$ are shown in Figs. 4 and 5. As shown in these figures, the values of $\partial \log D/\partial \log[L^-]$ at maximum ligand concentration, $[L^-]=2.85$ M, are around -1.5. It is reasonable that f_3, the fraction of the species ML_3, is negligible under the experimental conditions employed in this work. Therefore, we determined the overall stability constants β_1 and β_2 by the least mean squares method based Eq. 4. Some examples of fitting are shown in Figs. 6 and 7. The values of β_1 and β_2 are given in Table 1.

As shown in Table 1, β_1 of the chloro complexes of actinoids(III) are 0.4—0.6 and obviously larger than β_1 of actinoids(III) bromo complexes. And for lanthanoids(III), β_1 of the chloro complexes are also 0.4—0.6 and slightly larger than β_1 of bromo complexes. But for β_2, no significant difference between chloro and bromo complexes was recognized. This means that the second formation constants K_2, calculated as β_2/β_1, of actinoids(III) bromo complexes are obviously larger than those of the others. Moreover, K_2 of the chloro complexes of actinoids(III) and lanthanoids(III) are 0.5—0.7, *i.e.*, almost similar values to $K_1(\beta_1)$. But for Am, Bk, and Cf, K_2 values of the bromo complexes are larger than ≈ 1, as is shown in Table 1.

Tanaka and Yamada[10] proposed that the complex

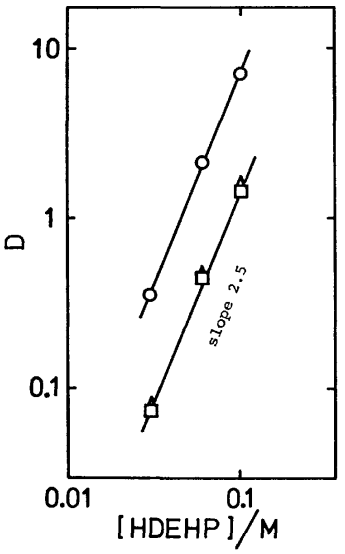

Fig. 2. Dependence of D of Gd on [HDEHP].
○: 3.0 M $(H,Li)ClO_4$, □: 3.0 M $(HClO_4,LiCl)$, △: 3.0 M $(HClO_4,LiBr)$.

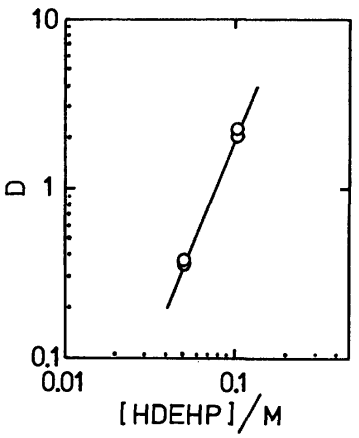

Fig. 1. Dependence of D of Bk on [HDEHP].
$[H^+]=0.15$ M, slope=2.5.

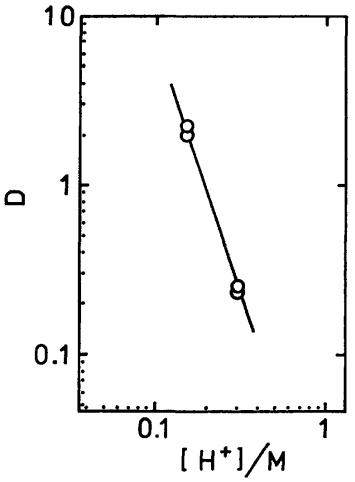

Fig. 3. Dependence of D of Bk on $[H^+]$.
[HDEHP]=0.1 M, slope=−3.0.

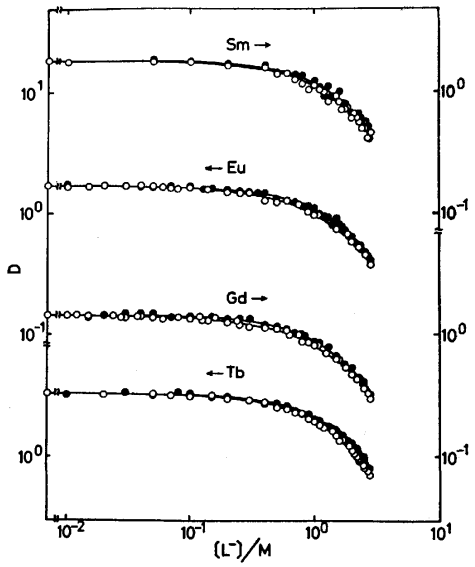

Fig. 4. Dependence of D of some lanthanoids(III) on chloride ion(○) and bromide ion(●).

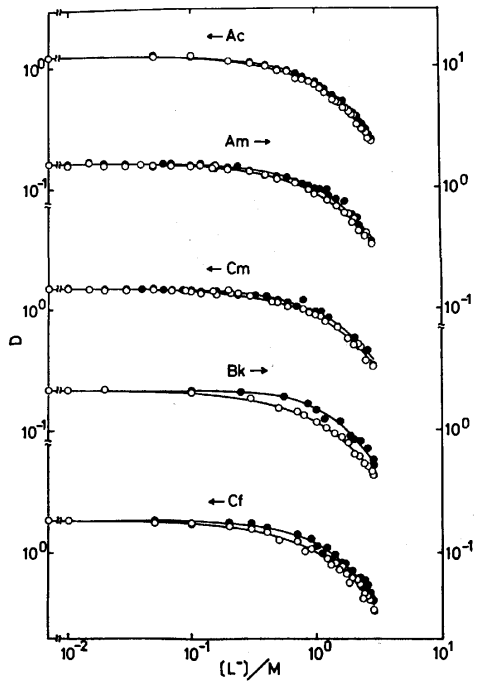

Fig. 5. Dependence of D of some actinoids(III) on chloride ion(○) and bromide ion(●).

formation reaction proceeds along with the Eigen mechanism[11] and the apparent formation constant K is expressed as follows:

$$K = K_{os}(1+K_{is}), \tag{7}$$

where K_{os} is an outer sphere formation constant and K_{is} is a transformation constant of an inner sphere complex. Fuoss[12] proposed an equation which has been applied frequently to the calculation of K_{os};

$$K_{os} = \frac{4\pi Na^3}{3000}\exp[\mu/kT], \tag{8}$$

where $4\pi a^3/3$ is exclusive volume of a cation and μ is the electrostatic energy. This equation gives cal-

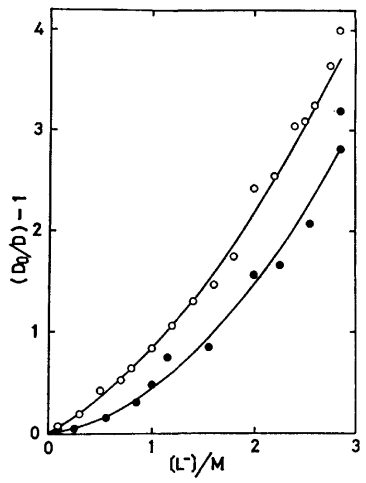

Fig. 6. Dependence of $D_0/D-1$ of Bk on chloride ion(○) and bromide ion(●).

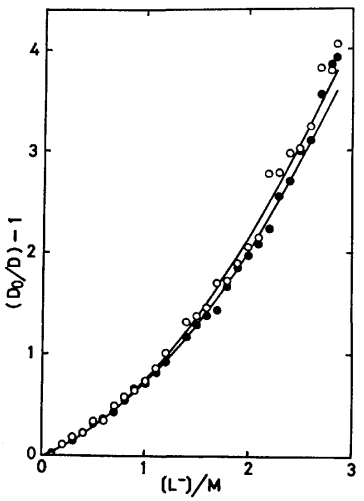

Fig. 7. Dependence of $D_0/D-1$ of Ac on chloride ion(○) and bromide ion(●).

culated formation constants for the bromo complexes of actinoids(III) and lanthanoids(III) of 0.34—0.35 in good agreement with the experimental values of β_1, *i.e.*, K_1. On the other hand for the chloro complexes of actinoids(III), the experimental values of β_1 are obviously higher than the calculated values by Eq. 8, *i.e.*, $K_{os}=0.35-0.36$. According to Eq. 7, this implies that an inner sphere mechanism can not be neglected for the formation of actinoids (III) chloro complexes.

As was mentioned before, in high concentration of LiCl solution actinoids(III) were absorbed by anion exchange resin more strongly than lanthanoids(III), and the distribution ratio(D_v) for actinoids(III) series showed a distinct minimum at Cm, whereas for lanthanoids(III) such trend was not observed.[2] These two facts have been explained by the different complexing ability between two f-series elements and it is widely recognized that actinoids(III) have a much larger ability for complex formation than lanthanoids (III). In order to examine this difference from the data obtained in this work, we calculated the fraction

Table 1. Stability constants of the chloride and bromide complexes of some lanthanoids and actinoids

Anion	Metal	β_1	β_2	K_2	$K_{os\ calcd}$
Cl^-	Sm	0.41±0.04	0.25±0.03	0.60±0.07	0.36
	Eu	0.52±0.02	0.22±0.02	0.41±0.04	0.35
	Gd	0.56±0.02	0.21±0.02	0.38±0.04	0.35
	Tb	0.45±0.02	0.26±0.02	0.58±0.04	0.35
	Ac	0.44±0.02	0.31±0.02	0.72±0.05	0.38
	Am	0.55±0.03	0.22±0.02	0.40±0.05	0.36
	Cm	0.56±0.03	0.20±0.02	0.35±0.05	0.36
	Bk	0.59±0.02	0.25±0.02	0.42±0.03	0.36
	Cf	0.61±0.04	0.25±0.03	0.40±0.04	0.36
Br^-	Sm	0.33±0.04	0.24±0.03	0.71±0.11	0.34
	Eu	0.38±0.02	0.23±0.01	0.59±0.05	0.34
	Gd	0.37±0.02	0.26±0.02	0.69±0.07	0.34
	Tb	0.41±0.03	0.22±0.01	0.53±0.03	0.34
	Ac	0.42±0.02	0.29±0.01	0.71±0.03	0.37
	Am	0.30±0.03	0.28±0.02	0.93±0.11	0.35
	Cm	0.39±0.02	0.22±0.02	0.57±0.05	0.35
	Bk	0.15±0.04	0.29±0.03	1.95±0.46	0.35
	Cf	0.30±0.04	0.30±0.03	0.99±0.13	0.34

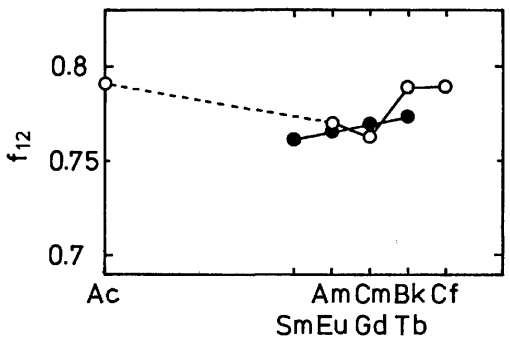

Fig. 8. Variation of f_{12} with atomic number.

of complex species, *i.e.*, $f_{12}=f_1+f_2$, for chloride at $[Cl^-]=2.85$ M, where no anionic complexes are formed. The result is shown in Fig. 8, where f_{12} shows the similar trend as the behavior of D_v for anion exchange and shows a minimum at Cm for actinoids (III), whereas for lanthanoids(III) f_{12} increases continuously with atomic number. However, there is no significant difference in the magnitude of f_{12} between actinoids(III) and lanthanoids(III), thought it has been observed for D_v of anion exchange system. This implies that the large difference in the complex formation between actinoids(III) and lanthanoids(III), which should be observed in the anionic complex formation and gives the experimental basis on the group separation, can not be observed in β_1 and β_2 values experimentally determined in the aqueous system of $\mu=3.0$ and $[Cl^-]\leq 2.85$ M.

The authors wish to thank the members of Cyclotron and Radioisotope Center, Tohoku University, for their handling the cyclotron and monitoring the irradiated sample in the production of Sm and Bk tracers. A part of the expenses for this investigation has been defrayed by a Grant-in-Aid for Scientific Research No. 505002 from the Ministry of Education, Science and Culture.

References

1) R. M. Diamond, K. Street, Jr., and G. T. Seaborg, *J. Am. Chem. Soc.*, **76**, 1461 (1954).
2) E. K. Hulet, R. G. Gutmacher, and M. S. Coops, *J. Inorg. Nucl. Chem.*, **17**, 350 (1961).
3) P. K. Khopkar and J. N. Mathur, *J. Inorg. Nucl. Chem.*, **42**, 109 (1980).
4) S. Suzuki, T. Mitsugashira, Y. Shiokawa, and H. Yamana, 24th Symposium on Radiochemistry, Hirosaki, October 1980, Abstr. No. 2A06.
5) I. Kawasuji, T. Fukasawa, and S. Suzuki, *Radiochem. Radioanal. Lett.*, **40**, 215 (1979).
6) S. Suzuki, A. Satô, M. Hara, T. Mitsugashira, I. Kawasuji, H. Kikuchi, and T. Fukasawa, *Sci. Rep. RITU*, **A28**, 73 (1979).
7) S. Suzuki, A. Satô, T. Mitsugashira, I. Kawasuji, and T. Fukasawa, *CYRIC Annual Report*, **1980**, 119.
8) W. J. McDowell, P. T. Perdue, and G. N. Case, *J. Inorg. Nucl. Chem.*, **38**, 2127 (1976).
9) Y. Marcus and A. S. Kertes, "Ion Exchange and Solvent Extraction of Metal Complexes," Wiley-Interscience, New York (1969), p. 535.
10) S. Yamada and M. Tanaka, *J. Inorg. Nucl. Chem.*, **37**, 587 (1975).
11) M. Eigen and R. Wilkins, *Adv. Chem. Ser.*, **49**, 55 (1965).
12) R. M. Fuoss, *J. Am. Chem. Soc.*, **80**, 5059 (1958).

Reduction of Chromium(VI) by Iron(II) Hydroxide in Alkaline Solution

Toyoaki Aoki* and Makoto Munemori

Environmental Chemistry, College of Engineering, University of Osaka Prefecture, Mozu-umemachi, Sakai 591

(Received May 18, 1981)

Iron(II) hydroxide stoichiometrically reduces CrO_4^{2-} to chromium(III) in alkaline solutions of pH 8 or above. This reduction was finished in less than one minute even at 5 °C. Although chromium(III) dissolves as CrO_2^- above pH 9.5, it did not dissolve in the presence of iron(III) hydroxide which had resulted from the oxidation of iron(II) hydroxide.

This paper reports a fundamental study on the removal of chromium(VI) from wastewaters. In the two-step process[1,2] used at present, chromium(VI) is first reduced to chromium(III) with sulfur dioxide, sodium bisulfite, or iron(II) sulfate below pH 3, and is then precipitated as chromium(III) hydroxide at pH 7.0—8.5 with sodium hydroxide or lime. The first step is always carried out at this low pH because there is a belief that the reduction of chromium(VI) is fast below pH 3 and very slow at pH 4—10.[3]

Recently, we have developed a new process for the chemical treatment of wastewaters which permits simultaneous removal of hazardous metals. In this process, chromium(VI) is reduced by iron(II) at pH 10. A plant for the treatment of laboratory wastewaters was constructed using the new process at the University of Osaka Prefecture and has been in continuous operation since August 1974. Chromium(VI), with a maximum value in influent of 8.2 ppm, is removed to below the detection limit of 0.2 ppm[4] as are the other hazardous metals.

The reduction of chromium(VI) by iron(II) has been studied below pH 7[5,6] and at pH 6.8—7.8,[7] but it has not been studied at pH of 8 or above, at which iron(II) is precipitated as iron(II) hydroxide. In this paper, we report on the heterogeneous reduction of chromium(VI) by iron(II) hydroxide in order to explain the successful treatment of chromium(VI) at the wastewater treatment plant described above.

Experimental

Reagents. All reagents were of analytical-reagent grade. Water was doubly distilled, the second distillation being carried out from alkaline permanganate in an all-Pyrex still. Stock solution of 0.20 mol dm^{-3} chromium(VI) was prepared by dissolving potassium dichromate which had been dried for two hours at 105 °C in redistilled water. Stock solution of 1.00 mol dm^{-3} iron(II) was prepared by dissolving iron(II) sulfate in 0.2 mol dm^{-3} sulfuric acid. When more than 1.0% of the 1.00 mol dm^{-3} iron(II) had been oxidized by oxygen in the air, a stock solution of iron(II) was freshly prepared.

Apparatus. The pHs of the solutions were measured with a Horiba Model F-7DE pH meter. Total iron and total chromium in the solution were determined by atomic absorption spectroscopy using a Nippon Jarrel-Ash Model AA-1W. A Shimadzu Model UV-200 spectrophotometer was used to determine chromium(VI).

Procedure. A solution containing an appropriate amount of 0.2 mol dm^{-3} chromium(VI) solution was adjusted with sodium hydroxide to a pH of 8 or above. Another solution containing an appropriate amount of 1.00 mol dm^{-3} iron(II) solution was similarly adjusted to the same pH. Both solutions were mixed, and stirred at 25 °C. At 0, 2, 5, 10, 20, and 30 min, samples of the resultant mixture were put through glass filters (3G4). Glass filters were used in preference to filter paper, because paper reduced part of the chromium(VI) to chromium(III).

Chromium(VI) in alkaline solution absorbs in the ultraviolet at 370 nm, but chromium(III) does not absorb at this wavelength, so chromium(VI) in the filtrate can be selectively determined in the presence of chromium(III). Total chromium in the filtrate was determined by an atomic absorption method using ammonium perchlorate as a releasing agent to remove interference from other metals and anions.[8]

Futhermore, the reduction of chromium(VI) by iron(II) hydroxide was examined in a nitrogen atmosphere. Commercial nitrogen gas contains traces of oxygen, so this oxygen was removed by passage of the nitrogen gas through an impinger containing an iron(II) hydroxide suspension. With this system, only 1.0% of 500 ppm iron(II) was oxidized after stirring for 30 min at pH 10.

Results and Discussion

Stoichiometry of Reduction Reaction. In order to determine reduction times of chromium(VI) by iron(II) hydroxide at pH 8.0, 10.0, and 11.6, the remaining chromium(VI) in the mixture of a suspension containing iron(II) hydroxide and a solution containing chromium(VI) at the same pH was determined at appropriate time intervals. The sampling and filtering process took two minutes and so the first two minutes of the reaction could not be examined. Within this limitation, Table 1 shows that pHs in this range have no effect on the rate of reduction of chromium(VI) by iron(II) hydroxide in a nitrogen atmosphere. In all of these cases, the reduction of chromium(VI) finished in less than two minutes. In the experimental

Table 1. Effect of pH on reduction of Cr(VI) by iron(II) hydroxide[a]

Time/min	Remaining concentration of Cr(VI)/ppm		
	pH 8.0	pH 10.0	pH 11.6
0	100	100	100
2	24.5	30.2	32.1
5	25.2	30.8	31.8
10	24.1	31.2	31.6
20	24.9	30.4	32.3

a) Initial concentration of iron(II) and chromium(VI) are 224 ppm and 100 ppm, respectively. Experiments were carried out at 25±1 °C in a nitrogen atmosphere.

conditions of Table 1, 30.9 ppm chromium(VI) should have remained in solution if the reduction proceeded at a stoichiometric 3:1 molar ratio of iron(II) to chromium(VI) according to the following equation:

$$3Fe(II) + Cr(VI) \longrightarrow 3Fe(III) + Cr(III). \quad (1)$$

The reduction proceeded stoichiometrically at pH 10.0 and 11.6, but the concentration of chromium(VI) remaining at pH 8.0 was less than the predicted value. It appears that a little of the remaining chromium(VI) was adsorbed at pH 8.0 on iron(III) hydroxide which was the oxidized product of iron(II) hydroxide.[9]

The reduction of chromium(VI) by iron(II) hydroxide was also examined using air instead of nitrogen. In this case, the reduction was also completed in less than two minutes.

To elucidate the stoichiometry of this reduction, the chromium(VI) remaining in the solution after 30 min was determined when various concentrations of iron(II) hydroxide were added to 100 ppm of chromium(VI). Figure 1 shows that the remaining chromium(VI) decreases with increasing iron(II) hydroxide and, in a nitrogen atmosphere, coincides with the curve estimated from the stoichiometry at a 3:1 molar ratio of iron(II) to chromium(VI). On the other hand, experimental data obtained in the presence of air deviated from the stoichiometric curve. In this case, dissolved oxygen competed with the chromium(VI) for the available iron(II) hydroxide.[10] This competition made iron(II) hydroxide unavailable for the reaction with chromium(VI), thereby increasing the concentration of chromium(VI) remaining.

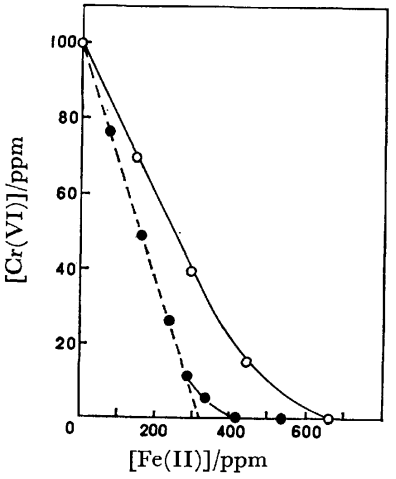

Fig. 1. Relation between remaining concentration of Cr(VI) and concentration of added Fe(II). Experiments were carried out at pH 10.3 (25 °C) in air(○) and in a nitrogen atmosphere(●). Stoichiometric curve is (----).

Chemical Species Taking Part in the Reduction. Chromium(VI) exists in solution as various species as shown in the following equilibria:

$$Cr_2O_7^{2-} + H_2O \rightleftharpoons 2HCrO_4^- \quad pK\ 1.5, \quad (2)$$

$$HCrO_4^- \rightleftharpoons CrO_4^{2-} + H^+ \quad pK\ 6.5. \quad (3)$$

These equilibrium constants were taken from Sillén and Martell.[11]

Chromium(VI) is present as CrO_4^{2-} in alkaline solution of pH 8 or above as in Eq. 3. On the other hand, iron(II) hydrolyzes to produce iron(II) hydroxide above pH 8. From our results and from thermodynamic considerations, it seems that iron(II) hydroxide reduces CrO_4^{2-} by the following reaction:

$$3Fe(OH)_2 + CrO_4^{2-} + 4H_2O \longrightarrow 3Fe(OH)_3 + Cr(OH)_3 + 2OH^-. \quad (4)$$

This reaction indicates that, for every mole of iron(II) hydroxide oxidized, 2/3 mol of hydroxide ion is produced, and in fact, when a suspension of iron(II) hydroxide and a chromium(VI) solution adjusted to same pH were mixed, the pH of the mixture was increased. Therefore, we tried to determine the rate of reduction by following this change of pH. The pH of each mixture became constant immediately after mixing at 5—8 °C. It takes about one minute to mix the solution completely. Thus, the reduction of chromium(VI) by iron(II) hydroxide proceeds in less than one minute in alkaline solutions even at these low temperatures.

Table 2 indicates the increase in pH caused by the reduction at various pHs at 5—8 °C, and the theoretical final pH based on Eq. 4. It is thought that the reduction proceeds stoichiometrically according to Eq. 4 since the theoretical pHs agree very closely with the pHs obtained experimentally.

Removal Mechanism of Chromium(VI). The reaction products are chromium(III) hydroxide and iron (III) hydroxide, according to Eq. 4. However, the precipitate formed from reduction in alkaline solution does not seem to be a simple mixture of these hydroxides.

When a suspension of this precipitate at pH 10 was incubated for 30 min, no chromium(III) was detected in its filtrate, while when a suspension (pH 10) of chromium(III) hydroxide was mixed with a suspension (pH 10) of iron(III) hydroxide, the concentration of dissolved chromium(III) increased with

Table 2. Increase of pH by the reduction of Cr(VI)

Concn of metals/mmol dm^{-3} a)		pH			Temp/°C
Fe(II)	Cr(VI)	Initial	Final(obsd)	Final(theor.)	
3.0	2.0	9.15	11.28	11.28	8.0
3.0	2.0	9.98	11.25	11.30	5.0
5.0	0.5	10.10	11.32	11.32	7.2
5.0	0.5	11.07	11.20	11.33	5.0

a) Volume: 200 cm^3

time, reaching 0.31 ppm at 30 min as shown in Table 3. Chromium(III) hydroxide redissolves in highly alkaline solutions as shown in curve a of Fig. 2. This redissolution is explained by the formation of CrO_2^-. However, the redissolution of chromium(III) was not observed (curve b of Fig. 2) when sodium hydroxide was added to the acidic solution (pH 2) containing chromium(III) and iron(III). This result shows that chromium(III) is coprecipitated with iron(III) hydroxide. From the results above mentioned, when chromium(VI) was reduced by iron(II) hydroxide in alkaline solution, chromium(III) seems to be incorporated in an undissolved form into iron(III) hydroxide. Therefore, the coprecipitation of chromium (III) with iron(III) hydroxide seems to be the incorporation of chromium(III) into iron(III) hydroxide. This can be explained by the similarity of chemical behavior of iron(III) and chromium(III). Both of them have similar polymerization mechanisms[12,13] and hydrolyze even in acidic solutions,[14] and both ions have the same charge and a similar ion radius.

Table 3. Difference between a mixture of $Fe(OH)_3$ and $Cr(OH)_3$[a] and the precipitate from reduction[b]

Time/min	Dissolved Cr(III)/ppm	
	$Fe(OH)_3$+ $Cr(OH)_3$(pH10)	Precipitate(pH10)
10	0.15	0.05
20	0.22	0.05
30	0.31	0.05

a) Initial concentrations of Fe(III) and Cr(III) are 100 ppm and 50 ppm, respectively. b) According to Eq. 4.

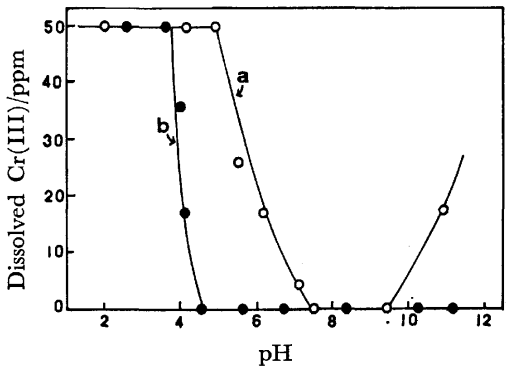

Fig. 2. Precipitation of Cr(III) in the presence of and in the absence of Fe(III).
Initial concentration of Cr(III) and Fe(III) are 50 ppm and 500 ppm, respectively. a; (○) in the absence of Fe(III), b; (●) in the presence of Fe(III).

Conclusion

Iron(II) hydroxide reduces chromium(VI), CrO_4^{2-}, to chromium(III) in less than one minute at pH 8 or above, at 5—8 °C, and at concentrations from 0.5—2.0 mmol dm^{-3}. The chromium(III), concurrently precipitated without adjusting the pH, seems to be incorporated into iron(III) hydroxide which results from the oxidation of iron(II) hydroxide. Thus, iron(II), as iron(II) hydroxide, quickly reduces chromium(VI) even in this heterogeneous system. Therefore, the conventional two-step process mentioned above is not necessary for chromium(VI) removal from wastewaters, since chromium(VI) can be removed, along with other hazardous metals, by iron(II) at pH 8 or above.

The authors thank Mr. Masao Fujita for assistance with experimental measurements.

References

1) "Water Treatment Handbook," John Wiley & Sons, New York (1979), p. 851.
2) H. F. Lund, "Industrial Pollution Control Handbook," McGraw-Hill, New York (1971), Chap. 6.
3) J. W. Patterson, "Wastewater Treatment Technology," Ann Arbor Science, Ann Arbor, Mich. (1975), Chaps. 6 and 7.
4) M. Munemori, T. Aoki, and Y. Inoue, "Toxic and Hazardous Waste Disposal," ed by R. B. Pojasek, Ann Arbor Science, Ann Arbor, Mich. (1980), Chap. 10, p. 97.
5) C. Benson, *J. Phys. Chem.*, **7**, 1 (1903).
6) J. H. Espenson and E. L. King, *J. Am. Chem. Soc.*, **85**, 3328 (1963).
7) E. I. Onstott, W. S. Gregory, and E. F. Thode, *Environ. Sci. Technol.*, **7**, 333 (1973).
8) H. Oguro, *Bunseki Kagaku*, **24**, 361 (1975).
9) T. Aoki and M. Munemori, *Water Res.*, in press.
10) K. Sung and J. J. Morgan, *Environ. Sci. Technol.*, **14**, 561 (1980).
11) L. G. Sillén and A. E. Martell, "Stability Constants of Metal-Ion Complexes," Burlington House, London (1964), p. 89.
12) A. Bell and E. Matijević, *J. Inorg. Nucl. Chem.*, **37**, 907 (1975).
13) W. Stumm and J. J. Morgan, "Aquatic Chemistry," Wiley-Interscience, New York (1970), p. 244.
14) C. F. Baes, Jr., and R. E. Mesmer, "Hydrolysis of Cations," Wiley-Interscience, New York (1976), Chap. 10.

Characterization of Prussian Blue Analogs of the Type $M_3[Fe(CN)_5CO]_2 \cdot xH_2O$

Hidenari INOUE,* Takashi KAWAI, Masaki NAGAO, and Saburo YANAGISAWA

Department of Applied Chemistry, Faculty of Science and Technology, Keio University, 3-14-1, Hiyoshi, Kohoku-ku, Yokohama 223

(Received May 22, 1981)

A series of compounds of the type $M_3[Fe(CN)_5CO]_2 \cdot xH_2O$ (M=Mn, Co, Ni, Cu, and Zn) have been studied by means of the X-ray diffraction powder patterns, magnetic measurements, infrared, electronic, and Mössbauer spectra. Three compounds $M_3[Fe(CN)_5CO]_2 \cdot xH_2O$ (M=Mn, Co, and Ni) crystallize in the face-centered cubic system. Copper compound $Cu_3[Fe(CN)_5CO]_2 \cdot 18.5H_2O$ belongs to the tetragonal system, zinc compound $Zn_3[Fe(CN)_5CO]_2 \cdot 13.5H_2O$ being amorphous. The structure of these compounds is described as a three-dimensional framework of two octahedral coordination units FeC_6 in the low spin state and $MN_{10/3}O_{8/3}$ in the high spin state. The back donation in the $Fe(CN)_5CO^{3-}$ moiety is enhanced by the bridge formation through CN^- and CO ligands, *i.e.* upon the formation of $M_3[Fe(CN)_5CO]_2 \cdot xH_2O$ from the corresponding sodium salt.

A number of Prussian blue analogs have been synthesized by the reaction of hexacyanometalate ions $Me(CN)_6^{n-}$ with the first row transition metal ions. Substituted pentacyanoferrate ions such as $Fe(CN)_5X^{n-}$ (X=NO, CO, NH_3, and H_2O) are also known to react with the first row transition metal ions to yield insoluble polynuclear complexes similar to Prussian blue analogs.[1] Most of these transition metal salts of substituted pentacyanoferrates having a general formula $M[Fe(CN)_5X] \cdot xH_2O$ (M=Mn, Fe, Co, Ni, Cu, and Zn) are shown to crystallize in the face-centered cubic system characteristic of Prussian blue analogs.[2]

In spite of considerable interest in $M[Fe(CN)_5X] \cdot xH_2O$, there have been relatively few systematic studies on the transition metal salts of carbonylpentacyanoferrate(II) ions of the type $M_3[Fe(CN)_5]_2 \cdot xH_2O$. Brown and Brown[3] have investigated transition metal salts of the $Fe(CN)_5CO^{3-}$ ion such as $Co_3[Fe(CN)_5CO]_2 \cdot xH_2O$ to demonstrate the bridge structure of carbonyl ligands. On the basis of Keggin's structure model,[4] Ludi *et al.*[5] have proposed a modified crystal structure model for $Mn_3[Co(CN)_6]_2 \cdot xH_2O$, in which the cubic unit cell contains one and a third formula units. In view of the similarity in composition between $Mn_3[Co(CN)_6]_2 \cdot xH_2O$ and $M_3[Fe(CN)_5CO]_2 \cdot xH_2O$, it is of interest to find whether the crystal structure of transition metal salts of carbonylpentacyanoferrate(II) ions can be understood according to this modified structure model by Ludi *et al.* or not.

In the previous paper we showed that a three-dimensional framework is formed by the bridging of cyanide ligands upon the formation of $Fe[Fe(CN)_5X]$ (X=CO, NH_3, and H_2O) from $Na_3[Fe(CN)_5CO] \cdot H_2O$.[6] Furthermore, we discussed the influence of the bridge formation on the electronic structure of the $Fe(CN)_5X^{3-}$ moiety and the dependence of the electronic structure of the central iron(II) ion on the ligand X. The present work was attempted to characterize Prussian blue analogs of the type $M_3[Fe(CN)_5CO]_2 \cdot xH_2O$ (M=Mn, Co, Ni, Cu, and Zn). This type of compounds provides a good model to study a change in the electronic structure of the $Fe(CN)_5CO^{3-}$ moiety with the systematic change in the counter cation M^{2+} from manganese(II) to zinc(II) ion.

Experimental

Sodium carbonylpentacyanoferrate(II) was prepared by the literature method and purified by recrystallization.[7] A series of compounds of the type $M_3[Fe(CN)_5CO]_2 \cdot xH_2O$ (M=Mn, Co, Ni, Cu, and Zn) were precipitated by the addition of an excess of 0.05 mol dm^{-3} MCl_2 to 0.05 mol dm^{-3} $Na_3[Fe(CN)_5CO]$. The precipitate obtained was allowed to stand for 24 h for aging, collected on a glass filter by suction, washed with distilled water, alcohol, and finally ether, then dried over calcium chloride. The compounds prepared were analyzed chelatometrically: Found: Fe, 12.4; Mn, 18.0%. Calcd for $Mn_3[Fe(CN)_5CO]_2 \cdot 17.5H_2O$: Fe, 12.30; Mn, 18.15%. Found: Fe, 12.9; Co, 19.9%. Calcd for $Co_3[Fe(CN)_5CO]_2 \cdot 15.0H_2O$: Fe, 12.77; Co, 20.21%. Found: Fe, 11.9; Ni, 17.5%. Calcd for $Ni_3[Fe(CN)_5CO]_2 \cdot 18.0H_2O$: Fe, 12.30; Ni, 18.97%. Found: Fe, 12.0; Cu, 20.1%. Calcd for $Cu_3[Fe(CN)_5CO]_2 \cdot 18.5H_2O$: Fe, 11.73; Cu, 20.03%. Found: Fe, 13.0; Zn, 22.1%. Calcd for $Zn_3[Fe(CN)_5CO]_2 \cdot 13.5H_2O$: Fe, 12.88; Zn, 22.61%. X-Ray diffraction powder patterns were taken with a Rigaku-Denki X-ray diffractometer at room temperature. The lattice constants were determined using Fe $K\alpha$ radiation (λ=1.937 Å) and sodium chloride as a standard. Infrared spectra were recorded on a Hitachi Perkin-Elmer Model 225 grating infrared spectrophotometer in the range 200 to 4000 cm^{-1} by the Nujol mull and CsI disk methods. The calibration of wave numbers was made using polystyrene film and water vapor absorption. Diffuse reflection spectra were measured with the Hitachi Perkin-Elmer Model 139 spectrophotometer equipped with the standard integrating attachment using alumina as a standard. Magnetic susceptibilities were measured at room temperature by the Gouy method using $Hg[Co(SCN)_4]$ as a calibrant.[8] Diamagnetic corrections were carried out with Pascal's constants.[9] Mössbauer spectra were measured with a constant-acceleration transducer of the Canberra type. A ^{57}Co source in Pd foil with an original intensity of about 10 mCi which was supplied by Radiochemical Centre, Amersham was used at room temperature. The absorbers with a thickness of about 5 mg of natural iron per cm^2 were kept at 77 or 300 K. The Doppler velocity was calibrated with natural iron foil kept at room temperature.

Results and Discussion

Crystal Structure. A series of compounds of the type $M_3[Fe(CN)_5CO]_2 \cdot xH_2O$ (M=Mn, Co, and Ni)

showed the X-ray diffraction powder patterns very similar to those for Prussian blue analogs belonging to the face-centered cubic system. This indicates that compounds other than copper and zinc compounds are isomorphous with Prussian blue analogs: space group O_h^5–F_{m3m}. According to the modified structure model proposed for $Mn_3[Co(CN)_6]_2 \cdot xH_2O$ by Ludi, *et al.*,[5] the unit cell contains 1 1/3 formula units of $M_3[Fe(CN)_5CO]_2 \cdot xH_2O$. As Fig. 1 shows, 4M coordinated by 3 1/3 nitrogen atoms of cyanide ligands, 2 oxygen atoms of water molecules and 2/3 oxygen atom of carbonyl ligands are distributed at the 4a (0,0,0) positions, while 2 2/3 Fe coordinated by five carbon atoms of cyanide ligands and a carbon atom of the carbonyl ligand occupy the 4b(1/2,1/2,1/2) positions in the face-centered cubic unit cell. The 24e (x,0,0) positions are occupied by 16C, 13 1/3 N, and 10 1/3 O atoms. Eight water molecules coordinate to M to fill the empty nitrogen positions. Additional water molecules are distributed around 8c(1/4,1/4,1/4) positions and have a zeolitic nature. These water molecules could be readily removed on heating and are responsible for the different degree of hydration.

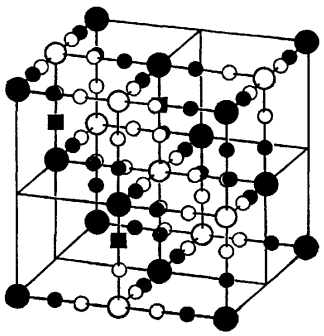

Fig. 1. The structure of $M_3[Fe(CN)_5CO]_2 \cdot xH_2O$.
The number of Fe, C, N, and O does not correspond exactly to the modified structure model and water molecules are not shown for brevity. Symbols: ●, 4M at 4a; ○, 2⅔Fe at 4b; ○, 16C at 24e; ●, 13⅓N at 24e; ■, 2⅔O at 24e.

The crystal structure can be described as a three-dimensional framework of the two octahedral coordination units FeC_6 and $MN_{10/3}O_{8/3}$, where the formula of the latter complex represents an average composition. However, the space group is not O_h^5–F_{m3m} in a strict sense because the symmetry group of the $Fe(CN)_5CO^{3-}$ moiety is not O_h but C_{4v}. In fact, the diffraction powder pattern of the cobalt compound was very diffuse, suggesting that the site symmetry of cobalt ions is lowered due to the C_{4v} symmetry of the $Fe(CN)_5CO^{3-}$ moiety. The preparation of $Fe_3[Fe(CN)_5CO]_2 \cdot xH_2O$ was unsuccessful even in the rigorously purified nitrogen atmosphere since this compound is readily oxidized to give iron(III) carbonylpentacyanoferrate(II) $Fe[Fe(CN)_3CO] \cdot xH_2O$ which is described elsewhere in detail.[6] As reported on $Cu[Fe(CN)_5NO]$,[2] copper compound $Cu_3[Fe(CN)_5CO]_2 \cdot 18.5H_2O$ does not crystallize in the face-centered cubic system but in the tetragonal system. The zinc compound fails to give crystalline precipitate in the present preparative way, *i.e.* it is amorphous. Table 1 lists the lattice constants calculated from the X-ray diffraction powder patterns. The lattice constants obtained fall within the range typical of those commonly found for Prussian blue analogs. Moreover, the lattice constants decrease with the increase of the crystal field stabilization energy of M^{2+} ion in the octahedral weak field, which is quite similar to

Table 1. Lattice constants and magnetic moments

Compound[a]	Lattice constant Å	Magnetic moment μ_{eff}/BM[b]
$Mn_3[Fe(CN)_5CO]_2$	10.38±0.01	5.65
$Co_3[Fe(CN)_5CO]_2$	10.21±0.03	4.77
$Ni_3[Fe(CN)_5CO]_2$	10.13±0.01	2.93
$Cu_3[Fe(CN)_5CO]_2$	a=10.15±0.02 c=10.03±0.02	1.72
$Zn_3[Fe(CN)_5CO]_2$	Amorphous	Diamagnetic

a) Water molecules are not shown for clarity. b) 1 BM $=9.273\times10^{-24}$ A m^2.

Table 2. Infrared absorption frequencies of $M_3[Fe(CN)_5CO]_2 \cdot xH_2O$ and $Na_3[Fe(CN)_5CO] \cdot H_2O$

Compound	Absorption frequencies/cm^{-1}					
	ν_{CN}	ν_{CO}	δ_{Fe-CO}	δ_{Fe-CN}	$\nu_{Fe-C(CO)}$	$\nu_{Fe-C(CN)}$
$Mn_3[Fe(CN)_5CO]_2 \cdot 17.5H_2O$	2113 s	2020 s	625 s	585 s	543 wb	479 m 462 s
$Co_3[Fe(CN)_5CO]_2 \cdot 15.0H_2O$	2122 s	2028 s	624 s	586 s	537 m	500 s 470 sh
$Ni_3[Fe(CN)_5CO]_2 \cdot 18.0H_2O$	2132 s 2095 sh	2017 s	627 s	586 s	546 w	485 sh 466 m
$Cu_3[Fe(CN)_5CO]_2 \cdot 18 \cdot 5H_2O$	2138 s 2097 w	2026 s	626 s	586 s	537 m	492 s 471 m
$Zn_3[Fe(CN)_5CO]_2 \cdot 13.5H_2O$	2132 s	2037 s	626 s	588 s	535 sh	493 s 468 m
$Na_3[Fe(CN)_5CO] \cdot H_2O$	2118 sh 2109 sh 2102 sh 2095 s 2087 s	2033 s 1999 s 1981 s	627 vs 621 s	589 s	537 sh 517 mb	432 sh 427 s

vs=Very strong; s=strong; m=medium; w=weak; sh=shoulder; wb=weak and broad; mb=medium and broad.

the phenomena observed for other Prussian blue analogs.[10]

IR Spectra and Bridge Structure of Cyanide and Carbonyl Ligands. The infrared absorption frequencies observed for $M_3[Fe(CN)_5CO]_2 \cdot xH_2O$ are listed in Table 2 along with those for $Na_3[Fe(CN)_5CO] \cdot H_2O$. In the CN stretching region, very intense absorption bands typical of cyanide complexes were observed in the range 2095 to 2138 cm^{-1}. Since the $Fe(CN)_5CO^{3-}$ moiety belongs to point group C_{4v}, two different species of CN stretching modes $2A_1+E$ are expected to appear in $M_3[Fe(CN)_5CO]_2 \cdot xH_2O$. However, the CN stretching mode was observed as a single intense band with the exception of $M_3[Fe(CN)_5CO]_2 \cdot xH_2O$ (M=Ni and Cu). Taking into account the high site symmetry of the $Fe(CN)_5CO^{3-}$ moiety, the environment of the iron(II) ion is approximated to O_h symmetry even though one of six cyanide ligands is substituted for a carbonyl ligand. On the other hand, four shoulders other than the main strong absorption band were observed for $Na_3[Fe(CN)_5CO] \cdot H_2O$. This splitting of the CN stretching bands must be due to the lowering in the site symmetry of the $Fe(CN)_5CO^{3-}$ moiety. The CN stretching bands of $M_3[Fe(CN)_5CO]_2 \cdot xH_2O$ are observed at higher frequencies than the main strong band (2095 cm^{-1}) of the corresponding sodium carbonylpentacyanoferrate(II). This shift of the CN stretching mode to higher frequencies is considered to be characteristic of the bridge formation of cyanide ligands.[11] Moreover, it is noteworthy that the increasing order in the CN stretching frequencies is very similar to that of the electronegativity of M^{2+} ion or the crystal field stabilization energy in the octahedral weak field.

A strong absorption band assigned to the CO stretching mode appeared at the lower frequencies side of the CN stretching bands. The CO stretching vibration of $M_3[Fe(CN)_5CO]_2 \cdot xH_2O$ was observed as a single broad band whereas the CO stretching modes of $Na_3[Fe(CN)_5CO] \cdot H_2O$ appeared at 1981, 1999, and 2033 cm^{-1} as three strong absorption bands. Of these three bands the absorption bands at 1981 and 1999 cm^{-1} must be caused by hydrogen bonding between the oxygen end of carbonyl ligand and water of crystallization. This is in marked contrast to the fact that the CO stretching band is scarcely affected although the Fe–CO–M bridge is formed in going from $Na_3[Fe(CN)_5CO] \cdot H_2O$ to $M_3[Fe(CN)_5CO]_2 \cdot xH_2O$.

The symmetric and antisymmetric OH stretching modes of water were observed in the range 3340 to 3440 cm^{-1}, while the bending mode appeared in the range 1590 to 1610 cm^{-1}. This observation agrees with that of Prussian blue analogs by Ludi *et al.*;[5] there are two different types of water molecules such as lattice and coordinated water. However, the rocking and wagging vibrations of the coordinated water molecules could not be found probably due to their weakness and/or broadening.

The δ_{Fe-CO} bending and $\nu_{Fe-C(CO)}$ stretching modes appeared in the range 624 to 627 and 535 to 546 cm^{-1}, respectively. It is worth noting that the frequencies of both δ_{Fe-CO} and $\nu_{Fe-C(CO)}$ modes are almost independent of the bridge formation. This is probably because the effect of the bridge formation is compensated by the hydrogen bonding through the oxygen end of the carbonyl ligand. A similar phenomenon was also observed for transition metal salts of substituted pentacyanonitrosylferrates(II).[2] On the other hand, both of the $\nu_{Fe-C(CN)}$ stretching and δ_{Fe-CN} bending modes are simplified in going from $Na_3[Fe(CN)_5CO] \cdot H_2O$ to $M_3[Fe(CN)_5CO]_2 \cdot xH_2O$ because the site symmetry of the $Fe(CN)_5CO^{3-}$ moiety is higher in the latter than the former. The $\nu_{Fe-C(CN)}$ stretching bands observed in the range 462 to 500 cm^{-1} are shifted to higher frequencies upon the formation of $M_3[Fe(CN)_5CO]_2 \cdot xH_2O$ while the δ_{Fe-CN} bending band observed in the range 585 to 588 cm^{-1} is scarcely affected. A shoulder located at the lower frequency side of the $\nu_{Fe-C(CN)}$ stretching band is strong evidence for the bridge structure of cyanide ligand.[12] Indeed, the MN stretching modes were confirmed in nickel and copper compounds. However, no absorption band could be observed in other compounds because the absorption band is very weak in intensity or lies out of the present experimental region.

Electronic Structure and Chemical Environment of M^{2+} Ion. The nature of counter cation, M^{2+} ion, is supposed to affect the electronic structure of the $Fe(CN)_5CO^{3-}$ moiety upon formation of $M_3[Fe(CN)_5CO]_2 \cdot xH_2O$ from $Na_3[Fe(CN)_5CO] \cdot H_2O$. Therefore, it is very important to understand in what ligand field the counter cation is situated or what symmetry the environment of the counter cation has. Magnetic measurements as well as electronic spectra will be a sophisticated mean for this purpose. The effective magnetic moment, μ_{eff}, per M^{2+} ion of $M_3[Fe(CN)_5CO]_2 \cdot xH_2O$ was calculated from the magnetic susceptibilities at room temperature and listed in Table 1. The effective Bohr magnetons calculated agreed with the expectation that Prussian blue analogs of the type $M_3[Fe(CN)_5CO]_2 \cdot xH_2O$ consist of $Fe(CN)_5CO^{3-}$ moieties in the low spin state and M^{2+} ions in the high spin state. As shown in Fig. 2, the absorption bands of electronic spectra in the visible region are very similar in position to those of hexaaqua complexes of M^{2+} ion. This is in good agreement with the magnetochemical conclusion that M^{2+} ion is in the high spin state. Accordingly, the absorption bands are assignable on the basis of the term diagram for M^{2+} ion in the octahedral weak field.[13] Two very weak shoulders occurred in $Mn_3[Fe(CN)_5CO]_2 \cdot 17.5H_2O$ at approximately 17.6 and 23.0×10^3 cm^{-1} which may be assigned to the spin-forbidden transitions, $^6A_{1g} \rightarrow {}^4T_{1g}$ and $^4T_{2g}$ respectively. The absorption band at 16.8×10^3 cm^{-1} for $Co_3[Fe(CN)_5CO]_2 \cdot 15.0H_2O$ is very intense and low in energy as compared with that expected for the corresponding transition $^4T_{1g}(F) \rightarrow {}^4T_{1g}(P)$ in the octahedral weak field, indicating that the environment of Co^{2+} ions is distorted from O_h symmetry. An absorption maximum and a shoulder which appear in $Ni_3[Fe(CN)_5CO]_2 \cdot 18.0H_2O$ at 16.0 and 25.6×10^3 cm^{-1} are assigned to the spin-allowed transitions $^3A_{2g}(F) \rightarrow {}^3T_{1g}(F)$ and $^3T_{1g}(P)$ respectively. The energies of these two transitions are comparable to those of the corresponding hexaaqua complexes. The absorption band of $Cu_3[Fe(CN)_5$-

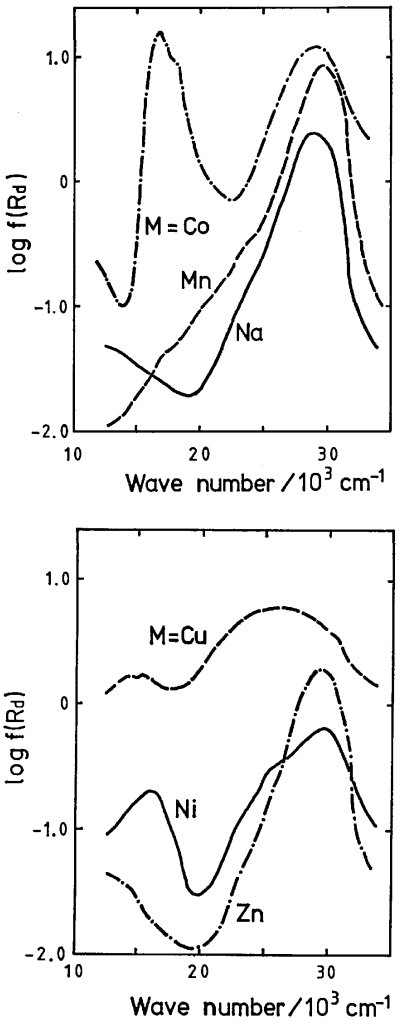

Fig. 2. Electronic spectra of $M_3[Fe(CN)_5CO]_2 \cdot xH_2O$ and $Na_3[Fe(CN)_5CO] \cdot H_2O$.

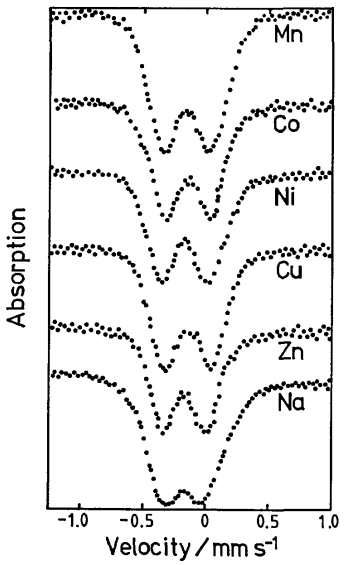

Fig. 3. Mössbauer spectra of $M_3[Fe(CN)_5CO]_2 \cdot xH_2O$ and $Na_3[Fe(CN)_5CO] \cdot H_2O$ at room temperature.

TABLE 3. MÖSSBAUER PARAMETERS OF $M_3[Fe(CN)_5CO]_2 \cdot xH_2O$

Compound[a]	Isomer shift[b] mm s^{-1}		Quadrupole splitting[b] mm s^{-1}	
	78 K	300 K	78 K	300 K
$Mn_3[Fe(CN)_5CO]_2$	−0.085	−0.147	0.338	0.353
$Co_3[Fe(CN)_5CO]_2$	−0.085	−0.154	0.311	0.357
$Ni_3[Fe(CN)_5CO]_2$	−0.087	−0.153	0.362	0.378
$Cu_3[Fe(CN)_5CO]_2$	−0.093	−0.149	0.381	0.371
$Zn_3[Fe(CN)_5CO]_2$	−0.081	−0.148	0.368	0.344
$Na_3[Fe(CN)_5CO]$	−0.058	−0.138	0.287	0.247

a) Water molecules are not given for brevity. b) With uncertainty of 0.008 mm/s.

$CO]_2 \cdot 18.5H_2O$ assignable to the transition $^2E_{2g} \rightarrow {}^2T_{2g}$ is split into two bands (14.1 and 15.2×10^3 cm^{-1}) due to the lowering of the environment of Cu^{2+} ion from O_h symmetry. This splitting of the d-d transition is responsible for the heterogeneous environment around Cu^{2+} ion rather than the Jahn-Teller effect because the Cu^{2+} ion is surrounded by 10/3 N and 8/3 O statistically. A very broad intense band observed at about 26.0×10^3 cm^{-1} is associated with the so-called intervalence electron transfer band. This type of intense absorption band was also observed for $Fe[Fe(CN)_5CO] \cdot xH_2O$.[14]

Influence of Bridge Formation on the Electronic Structure of $Fe(CN)_5CO^{3-}$ Moiety. The bridge formation of the cyanide and carbonyl ligands is expected to influence the electronic structure of the $Fe(CN)_5CO^{3-}$ moiety. The bonding character between iron(II) and carbon atoms would change upon the systematic change in the counter cation. The Mössbauer and electronic spectra afford useful information about these problems. The Mössbauer spectra of $M_3[Fe(CN)_5CO]_2 \cdot xH_2O$ are shown in Fig. 3 where that of $Na_3[Fe(CN)_5CO] \cdot H_2O$ is also presented for comparison. All the compounds of the type $M_3[Fe(CN)_5CO]_2 \cdot xH_2O$ exhibited a relatively small quadrupole splitting doublet which is comparable to that of sodium carbonylpentacyanoferrate(II). The Mössbauer parameters obtained at 77 and 300 K are summarized in Table 3.

As Fig. 2 shows, the intense absorption bands commonly observed for the electronic spectra of $M_3[Fe(CN)_5CO]_2 \cdot xH_2O$ in the range 29.2 to 29.8×10^3 cm^{-1} are assigned to the lowest spin-allowed transition of the $Fe(CN)_5CO^{3-}$ moiety. This assignment is supported by the fact that a relatively strong band is also observed for $Zn_3[Fe(CN)_5CO]_2 \cdot 13.5H_2O$ and $Na_3[Fe(CN)_5CO] \cdot H_2O$ in the near ultraviolet region in which no d-d transition other than that of the $Fe(CN)_5CO^{3-}$ moiety is expected. Since carbonyl and cyanide ligands are located near each other in the spectrochemical series, the iron(II) ion is considered to be situated to a first approximation in the environment of O_h symmetry. Consequently, the intense band in the near ultraviolet region is assigned to the spin-allowed transition $^1A_{1g} \rightarrow {}^1T_{2g}$. This point of view is consistent with the following facts. The solution spectrum of $Na_3[Fe(CN)_5CO]$ resembles closely that of $K_4[Fe(CN)_6]$.[15] The quadrupole splittings of both

$M_3[Fe(CN)_5CO]_2 \cdot xH_2O$ and $Na_3[Fe(CN)_5CO] \cdot H_2O$ are not only small, but also their isomer shifts are comparable to that of potassium hexacyanoferrate-(II).[16] The carbonyl and cyanide ligands are located near each other in the partial isomer shift and partial quadrupole splitting proposed by Bancroft *et al.*[17]

The temperature-variation in the quadrupole splittings may be associated with the thermal vibration of the crystal lattice. Evidently the quadrupole splittings increase upon formation of $M_3[Fe(CN)_5CO]_2 \cdot xH_2O$ from $Na_3[Fe(CN)_5CO] \cdot H_2O$. This indicates that the charge distribution around the iron nucleus in $M_3[Fe(CN)_5CO]_2 \cdot xH_2O$ is more aspherical than that in $Na_3[Fe(CN)_5CO] \cdot H_2O$ because the quadrupole splitting is due to non-zero electric field gradients at the nucleus which are caused by the aspherical charge distribution of ligand and/or crystal lattice. Unfortunately, such systematic tendency as found for the variation in the lattice constants is not always observed for the increasing order of the quadrupole splittings. Therefore, only a single factor of electronegativity of M(II) ions, size of M(II) ions, d_π-orbitals of M(II) ions to form the back donation, etc. does not play a principal role in the electric field gradient at the iron nucleus, but some combination of these factors must contribute to the quadrupole splittings of $M_3[Fe(CN)_5CO]_2 \cdot xH_2O$.

The isomer shifts of $M_3[Fe(CN)_5CO]_2 \cdot xH_2O$ fall within the range characteristic of low-spin iron(II) complexes.[18] The isomer shifts at 300 K are generally smaller than those at 77 K. This temperature shift in the isomer shifts is ascribed to the second-order Doppler effect. The isomer shifts decrease in going from $Na_3[Fe(CN)_5CO] \cdot H_2O$ to $M_3[Fe(CN)_5CO]_2 \cdot xH_2O$. As is well known, the isomer shift of iron compounds is a measure of the total s-electron density at the iron nucleus and the former decreases with the increase in the latter. Thus the decrease of the isomer shifts accompanied by the formation of $M_3[Fe(CN)_5CO]_2 \cdot xH_2O$ is responsible for the increase of the total s-electron density at the iron nucleus, which is caused by the decreased shielding effect of 3d-electrons. This delocalization of iron 3d-electrons is due to the increased back donation, in other words, due to the increased tendency of the cyanide and carbonyl ligands to withdraw electrons from the central iron atom. On the other hand, the spin-allowed transition $^1A_{1g} \rightarrow {}^1T_{1g}$ in $M_3[Fe(CN)_5CO]_2 \cdot xH_2O$ is slightly shifted to higher frequencies compared to the corresponding transition in $Na_3[Fe(CN)_5CO] \cdot H_2O$. As pointed out in Prussian blue analogs of the type $M[Fe(CN)_5NO] \cdot xH_2O$,[2] this blue shift is also correlated with an increase in the back donation. In conclusion, the coordination of M(II) ions to the nitrogen and oxygen ends of carbonyl ligands leads to the increased back donation from the filled iron d_π-orbitals to the empty ligand antibonding π^*-orbitals.

This work was partly supported by a grant from the Kawakami Foundation to which our thanks are due.

References

1) J. B. Ayers and W. H. Waggoner, *J. Inorg. Nucl. Chem.*, **34**, 2045 (1969); A. N. Garg and P. S. Goel, *Inorg. Chem.*, **10**, 1344 (1971); D. B. Brown, *ibid.*, **14**, 2582 (1975).
2) H. Inoue, H. Iwase, and S. Yanagisawa, *Inorg. Chim. Acta*, **7**, 259 (1973); L. A. Gentil, E. J. Baran, and P. J. Aymonino, *ibid.*, **20**, 251 (1976).
3) E. L. Brown and D. B. Brown, *J. Chem. Soc., D*, **1971**, 67.
4) J. F. Keggin and E. D. Miles, *Nature (London)*, **137**, 577 (1936).
5) A. Ludi, H. Güdel, and M. Rüegg, *Inorg. Chem.*, **9**, 2224 (1970).
6) E. Fluck, H. Inoue, M. Nagao, and S. Yanagisawa, *J. Inorg. Nucl. Chem.*, **41**, 287 (1979).
7) A. Vogler and H. Kunkely, *Z. Naturforsch., Teil B*, **30**, 355 (1975).
8) B. N. Figgis and R. S. Nyholm, *J. Chem. Soc.*, **1958**, 4190.
9) P. W. Selwood, "Magnetochemistry," Interscience Publ. Inc., New York (1956), Chap. 5.
10) D. F. Shriver, *Struct. Bonding(Berlin)*, **1**, 32 (1966); A. Ludi and U. Güdel, *ibid.*, **14**, 1 (1973).
11) H. Siebert and M. Weise, *Z. Naturforsch., Teil B*, **30**, 669 (1975).
12) H. Inoue, E. Fluck, and S. Yanagisawa, *Z. Naturforsch., Teil B*, **31**, 167 (1976).
13) B. N. Figgis, "Introduction to Ligand Fields," John Wiley & Sons, New York (1966), Chap. 9.
14) H. E. Toma, *J. Inorg. Nucl. Chem.*, **38**, 431 (1976).
15) H. B. Gray and N. A. Beach, *J. Am. Chem. Soc.*, **85**, 2922 (1968); H. E. Toma, J. M. Malin, E. Giesbrecht, and E. Fluck, *Inorg. Chim. Acta*, **14**, 11 (1975).
16) E. Fluck, W. Kerler, and W. Neuwirth, *Angew. Chem., Int. Ed. Engl.*, **2**, 277 (1963).
17) G. M. Bancroft, M. J. Mays, and B. E. Prater, *J. Chem. Soc., A*, **1970**, 956. G. M. Bancroft and R. H. Platt, *Adv. Inorg. Chem. Radiochem.*, **15**, 59 (1972).
18) P. Gütlich, "Mössbauer Spectroscopy," ed by U. Gonser, Springer-Verlag, Berlin, Heidelberg, N. Y. (1975), p. 53.

Crystallographic Data for New Phases in the $CaSO_3$–H_2O System

Yasuo Arai,* Tamotsu Yasue, Norifumi Nagata, and Hiroaki Shiino
Department of Industrial Chemistry, Faculty of Science and Engineering, Nihon University, Kanda-Surugadai, Chiyoda-ku, Tokyo 101
(Received May 29, 1981)

Among the three modifications of calcium sulfite hemihydrate, two of them, hexagonal β-$CaSO_3 \cdot 1/2H_2O$ with a rhombohedral lattice and γ-$CaSO_3 \cdot 1/2H_2O$ with a simple triangular hexagonal lattice, were found in the authors' recent work.[1] By heating α- and/or γ-hemihydrate at 330—360 °C in a nitrogen atmosphere, the orthorhombic anhydrate α-$CaSO_3$ was formed, with lattice constants of 6.472, 15.93, and 23.44 Å for *a*, *b*, and *c* respectively, while the body-centered tetragonal anhydrate β-$CaSO_3$, with lattice constants of 15.68 and 19.44 Å for *a* and *c* respectively, was formed by heating the β-hemihydrate. The dehydration of three hemihydrates and the hydration of two anhydrates were discussed. The phase relationships in the $CaSO_3$–H_2O system were summarized as follows:

$$\alpha\text{-}CaSO_3 \cdot 1/2H_2O \underset{\text{Hydration (30 °C)}}{\overset{\text{Dehydration (360 °C)}}{\rightleftharpoons}} \alpha\text{-}CaSO_3 + 1/2H_2O;$$

$$\beta\text{-}CaSO_3 \cdot 1/2H_2O \underset{\text{Hydration (30 °C)}}{\overset{\text{Dehydration (340 °C)}}{\rightleftharpoons}} \beta\text{-}CaSO_3 + 1/2H_2O;$$

$$\gamma\text{-}CaSO_3 \cdot 1/2H_2O \xrightarrow{\text{Dehydration (330 °C)}} \alpha\text{-}CaSO_3 + 1/2H_2O;$$

$$\gamma\text{-}CaSO_3 \cdot 1/2H_2O \xrightarrow{\text{Transformation (in water at 20 °C)}}$$

$$\beta\text{-}CaSO_3 \cdot 1/2H_2O \xrightarrow{\text{Transformation (in water at 20 °C)}} \alpha\text{-}CaSO_3 \cdot 1/2H_2O.$$

Calcium sulfite hemihydrate ($CaSO_3 \cdot 1/2H_2O$) is useful as an architectural material since it has a high thermal stability and a low water solubility in comparison with calcium sulfate dihydrate ($CaSO_4 \cdot 2H_2O$). A large amount of the hemihydrate has been produced by the milky-lime process for the desulfurization of flue gas. The hemihydrate has also attracted some attention as an inorganic filler in a plastic composite. The present authors have undertaken several fundamental and applied experiments[1–5] on the hemihydrate for use as industrial material.

In the $CaSO_3$–H_2O system, five compounds have been reported: $CaSO_3 \cdot 4H_2O$;[6] $CaSO_3 \cdot 2H_2O$;[7–10] $CaSO_3 \cdot H_2O$;[11] $CaSO_3 \cdot 1/2H_2O$;[12–16] and $CaSO_3$.[16–18] However, the phase relationships in the $CaSO_3$–H_2O system have not yet been established. The existence of di- and monohydrates has, though, been disproved. The tetrahydrate is known to exist at low temperatures below 4 °C and to be converted into hemihydrate instantly at room temperature. Although several papers on the X-ray diffraction data of the hemi- and anhydrates in the $CaSO_3$–H_2O system have been published,[12–18] they are not consistent with each other.

In recent years, the present authors have found three modifications of the hemihydrate, formed by passing SO_2 through a suspension of $Ca(OH)_2$.[1] The present work was undertaken in order to elucidate the crystallographic data of anhydrate formed by the thermal dehydration of the hemihydrate and to establish the phase relationships in the $CaSO_3$–H_2O system.

Experimental

Preparation of Samples. The chemical composition of the guaranteed reagent used, $Ca(OH)_2$, was 74.9% CaO and 24.1% H_2O. The purity of the SO_2 used was 99.98%, judging from the results of gas chromatography. The three modifications of calcium sulfite hemihydrate were prepared by passing dried and decarboxylated SO_2 through a suspension of 2% $Ca(OH)_2$. After finishing the reaction at pH 6—8, the precipitate was filtered and rinsed with water, methanol, and acetone.

Table 1. Synthesis of calcium sulfite hemihydrate

Conditions	A	B	C
$Ca(OH)_2$ in milky lime/%[a]	2	2	2
Flow speed of SO_2/cm³ min	10	10	100
Temperature/°C	20	80	95

a) 4.1 g $Ca(OH)_2$/200 cm³ H_2O.

Table 1 shows the synthesis conditions of the hemihydrate. The composition of the products under the conditions A, B, and C was 43.1—43.2% CaO, 49.0—49.2% SO_2, 0.5—0.6% SO_3, and 6.86—7.13% H_2O. These values were sufficiently close to the calculated values for $CaSO_3 \cdot 1/2H_2O$ (43.4% CaO, 49.6% SO_2, 7.00% H_2O). The hemihydrates, A—C, were dehydrated at 330—360 °C in a nitrogen atmosphere and then kept them for 1 h to convert in order to the anhydrates. In order to avoid the oxidation and moisture absorption of the products, they were kept in a vacuum desiccator with silica gel.

Measurements. The samples were analyzed by means of the X-ray diffraction method, thermal analysis (micro TG-DTA), infrared spectroscopy, and the scanning-microscope technique. The X-ray diffraction measurement of the samples was made by the use of a Rigaku Denki 2001 diffractometer using Ni-filtered Cu $K\alpha$ radiation (λ=1.5418 Å), with high-purity silicon (d=3.138 Å) as the internal standard. The X-ray diffraction data were obtained as the average values from 15—20 samples of a hemihydrate or an anhydrate. The chemical analyses were made as has been described previously.[3]

Results and Discussion

Identification of the New Phases of Calcium Sulfite Hemihydrate. In the previous paper,[1] three modifications of hemihydrate were reported in detail. The conventional orthorhombic hemihydrate was prepared under the A synthesis conditions in Table 1, the new phase I, with the known phase as part of a mixture, was formed under the B conditions, and the new phase II, including the former two phases, was formed as a mixture under the C conditions. Unfortunately, these new phases could not be distinguished as a single phase. In the previous paper, the above new phases were called Phase I and Phase II as a matter of convenience. In this paper, these three modifications of hemihydrate are named α-$CaSO_3\cdot 1/2H_2O$ (orthorhombic system), β-$CaSO_3\cdot 1/2H_2O$ as Phase I, and γ-$CaSO_3\cdot 1/2H_2O$ as Phase II.

Table 2 lists the crystallographic data for the three modifications. The orthorhombic hemihydrate reported by Waerstad *et al.*[15] will be called α-$CaSO_3\cdot 1/2H_2O$ hereafter.

New Phases of Anhydrous Calcium Sulfite. The dehydrated products of the hemihydrates obtained under the A, B, and C preparing conditions will here-

Table 2. Crystallographic data for three modifications of calcium sulfite hemihydrate

α-$CaSO_3\cdot 1/2H_2O$ (Orthorhombic system)

d_{obsd}/Å	d_{calcd}/Å	h k l	I/I_0
5.556	5.549	0 1 1	70
5.346	5.338	0 2 0	80
4.826	4.830	1 1 1	10
3.806	3.802	1 2 1	83
3.159	3.156	2 2 1	100
3.121	3.121	0 3 1	20
2.966	2.974	1 3 1	33
2.820	2.817	3 1 1	27
2.671	2.670	1 2 2	46
2.626	2.633	2 3 1	62
	2.625	2 1 2	
2.456	2.452	4 0 0	10
2.377	2.394	1 4 1	3
2.345	2.344	2 4 0	6
2.262	2.257	3 3 1	5
2.241	2.243	4 1 1	8
2.206	2.205	2 4 1	25
2.151	2.155	2 3 2	16
2.125	2.122	0 1 3	13
2.112	2.115	3 2 2	3
	2.114	1 0 3	
2.064	2.062	0 4 2	43
2.011	2.018	1 4 2	3
1.959	1.957	4 0 2	30
1.952	1.948	2 1 3	22
1.929	1.928	4 3 1	7
1.849	1.849	5 1 1	47
	1.850	0 3 3	
1.813	1.818	1 3 3	10
1.807	1.800	4 4 0	25
1.780	1.780	3 1 3	7
1.743	1.744	3 4 2	6
1.677	1.677	2 5 2	16
1.620	1.624	0 0 4	20
1.586	1.585	6 0 1	6
1.581	1.584	1 1 4	6
1.520	1.520	6 2 1	5
1.486	1.487	2 6 2	6
1.476	1.477	4 3 3	10
1.425	1.421	5 4 2	14
1.252	1.252	1 2 5	5

$a=9.809$ Å, $b=10.68$ Å, $c=6.496$ Å.

β-$CaSO_3\cdot 1/2H_2O$ (Hexagonal system, rhombohedral lattice)

d_{obsd}/Å	d_{calcd}/Å	h k l*	h k l**	I/I_0
4.270±0.002	4.270	2 2 2	2 0 $\bar{2}$	54
3.408±0.017	3.425	0 2 4	2 2 0	100
3.220±0.008	3.228	1 4 0	2 1 $\bar{3}$	68
3.100±0.011	3.107	2 3 2	3 1 $\bar{2}$	78
3.020±0.012	3.026	0 1 5	2 2 1	34
2.868±0.015	2.853	2 0 5	3 1 1	49
2.847±0.003	2.846	3 3 0	3 0 $\bar{3}$	74
2.740±0.005	2·735	1 4 3	3 2 $\bar{2}$	27
2.182±0.004	2.184	1 0 7	3 2 2	29
1.870±0.003	1.870	2 0 8	4 2 2	41
1.767±0.003	1.770	0 5 7	4 4 $\bar{1}$	31
1.704±0.003	1.701	5 4 4	6 1 $\bar{3}$	18
1.658±0.003	1.657	6 4 2	6 0 $\bar{4}$	21
1.605±0.009	1.614	2 8 0	4 2 $\bar{6}$	17
1.495±0.002	1.495	3 8 1	5 2 $\bar{6}$	12
1.452±0.002	1.451	9 2 1	7 $\bar{2}$ $\bar{4}$	10

$h\,k\,l$*: Hexagonal indices, $h\,k\,l$**: rhombohedral indices $a=17.08$ Å, $c=15.46$ Å, $a_R=11.13$ Å, $\alpha=100.3°$.

γ-$CaSO_3\cdot 1/2H_2O$ (Hexagonal system, simple triangular lattice)

d_{obsd}/Å	d_{calcd}/Å	h k l	I/I_0
5.867±0.038	5.865	1 0 0	6
4.345±0.015	4.346	1 0 2	51
3.474±0.011	3.475	1 0 3	65
3.382±0.007	3.386	1 1 0	100
3.275±0.007	3.276	1 1 1	74
3.004±0.007	3.000	1 1 2	38
2.933±0.009	2.933	2 0 0	22
2.100±0.003	2.097	1 2 2	20
2.024±0.002	2.024	1 0 6	13
1.942±0.002	1.940	2 0 5	55
1.689±0.004	1.693	2 2 0	20
1.685±0.002	1.684	1 2 5	23
1.611±0.003	1.614	1 3 1	18
1.273±0.001	1.274	1 4 1	13

$a=6.773$ Å, $c=12.94$ Å.

Table 3. Compositions of anhydrous calcium sulfite

Sample	Composition (%)				Mole ratio	
	CaO	SO_2	SO_3	Total	SO_2/CaO	SO_3/CaO
A′	46.3	52.6	0.7	99.6	0.994	0.011
B′	46.4	52.7	0.7	99.8	0.994	0.010
C′	46.4	52.8	0.6	99.8	0.996	0.009
Calcd	46.7	53.3	—	100	1.00	—

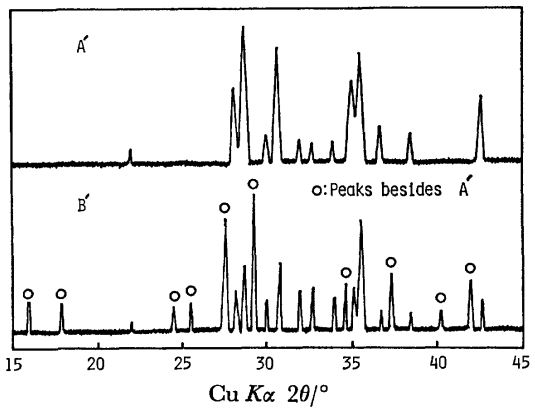

Fig. 1. X-Ray diffraction patterns of anhydrous calcium sulfite.

after be called A′, B′, and C′ respectively. The composition of A′—C′ is shown in Table 3. All of the dehydrated products can be identified as anhydrates. Figure 1 shows the X-ray diffraction patterns for the A′ and B′ anhydrates. The C′ anhydrate gave a pattern identical with that of B′. The X-ray diffraction pattern for A′ agreed generally with that reported by Lutz *et al.*,[18] but it showed many additional diffraction peaks. The X-ray diffraction patterns of B′ and C′ contained peaks identical with those observed on A′, but gave many diffraction peaks which were not observed on A′. Therefore, the existence of two modifications in an anhydrate may be inferred from both the chemical analysis and X-ray diffraction.

Though X-ray diffraction data on anhydrous calcium sulfite have been presented by several investigators,[16–18] their crystallographic information has not yet been published. On the basis of these X-ray diffraction results, obtained with a high accuracy, the crystallographic analysis was carried out by using Hull-Davey's graph[19–20] and a microcomputer. The crystallographic data for two modifications of the anhydrate are shown in Table 4. Thus, it was proved that A′ belonged to an orthorhombic system with a= 6.472 Å, b=15.93 Å, and c=23.44 Å. This phase is named α-$CaSO_3$ in this paper. On the other hand, it was found that B′ and C′ existed as mixtures of α-$CaSO_3$ and another anhydrous phase. In fact, this new phase was found to have a body-centered tetragonal lattice with a=15.68 Å, and c=19.44 Å. This phase is named β-$CaSO_3$. The X-ray diffraction pattern for the mixture of α- and β-anhydrates agreed generally with that reported by Matsuzaki et al.[17]

Table 4. Crystallographic data for two modifications of anhydrous calcium sulfite

α-$CaSO_3$ (Orthorhombic system)					
d_{obsd}/Å	d_{calcd}/Å	h	k	l	I/I_0
4.044±0.013	4.044	1	3	1	9
3.169±0.003	3.171	2	1	0	54
3.117±0.003	3.119	2	0	2	100
2.980±0.006	2.974	1	0	7	17
2.920±0.004	2.923	1	1	7	83
2.803±0.005	2.800	0	5	4	15
2.740±0.004	2.744	2	3	1	13
2.639±0.002	2.639	0	6	1	13
2.560±0.002	2.561	1	4	6	59
2.533±0.002	2.531	1	2	8	80
2.453±0.003	2.456	2	4	2	24
2.345±0.003	2.344	1	6	3	20
2.123±0.002	2.124	1	2	10	47
1.923±0.002	1.925	1	5	9	34
1.887±0.002	1.886	0	8	4	16
1.820±0.002	1.820	1	2	12	15
1.765±0.002	1.765	0	9	1	15
1.665±0.002	1.665	0	5	12	9
1.634±0.002	1.633	0	7	10	8
1.572±0.002	1.571	4	2	2	10
1.472±0.001	1.472	4	4	3	13
1.455±0.001	1.455	0	8	11	8
1.403±0.001	1.403	1	11	2	8
1.344±0.002	1.344	1	1	17	10
1.309±0.001	1.309	0	12	3	7
1.280±0.001	1.281	2	8	12	10

a=6.472 Å, b=15.93 Å, c=23.44 Å.

β-$CaSO_3$ (Tetragonal system, body-centered lattice)					
d_{obsd}/Å	d_{calcd}/Å	h	k	l	I/I_0
5.560±0.021	5.544	2	2	0	20
4.947±0.019	4.959	1	3	0	20
3.642±0.009	3.636	0	4	2	17
3.500±0.007	3.506	2	4	0	20
3.240±0.005	3.240	0	0	6	86
3.054±0.004	3.051	0	4	4	100
2.589±0.003	2.592	3	5	2	31
2.411±0.003	2.408	4	4	4	43
2.243±0.003	2.243	1	4	7	14
2.149±0.002	2.148	1	6	5	37
1.996±0.001	1.997	5	6	1	23
1.962±0.002	1.960	0	8	0	23
1.546±0.002	1.546	4	9	3	17
1.525±0.001	1.525	2	7	9	11
1.492±0.001	1.492	6	8	4	11
1.386±0.001	1.386	8	8	0	11
1.362±0.002	1.362	7	9	2	11

a=15.68 Å, c=19.44 Å.

Phase Relationships in the $CaSO_3$–H_2O System. It was confirmed that three modifications in hemihydrates and two modifications in anhydrates existed. In order to elucidate the mutual relationships of these five phases,

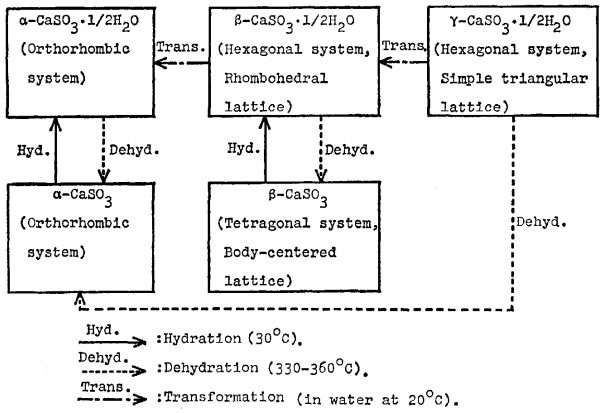

Fig. 2. Phase relationships in the system $CaSO_3$–H_2O.

the phase changes on hydration and dehydration in the $CaSO_3$–H_2O system were traced by means of X-ray diffraction, thermal analysis, and infrared spectroscopy. The phase relationships are summarized in Fig. 2.

The α-$CaSO_3$ anhydrate (orthorhombic system) was formed by the dehydration of both α-$CaSO_3 \cdot 1/2H_2O$ (orthorhombic system) and γ-$CaSO_3 \cdot 1/2H_2O$ (hexagonal system, simple triangular lattice). The β-$CaSO_3$ anhydrate (tetragonal system, body-centered lattice) was formed by the dehydration of β-$CaSO_3 \cdot 1/2H_2O$ (hexagonal system, rhombohedral lattice). When these anhydrates were hydrated in water, α-$CaSO_3$ changed to α-$CaSO_3 \cdot 1/2H_2O$ and β-$CaSO_3$ changed to β-$CaSO_3 \cdot 1/2H_2O$. These results suggest that there were reversible reactions among these phases. In addition, when β- and γ-$CaSO_3 \cdot 1/2H_2O$ were immersed in water, β-$CaSO_3 \cdot 1/2H_2O$ was converted to α-$CaSO_3 \cdot 1/2H_2O$, and γ-$CaSO_3 \cdot 1/2H_2O$ was finally converted to α-$CaSO_3 \cdot 1/2H_2O$ through β-$CaSO_3 \cdot 1/2H_2O$.

The authors wish to thank Mr. Akira Takeshi of Nihon University for his experimental assistance.

References

1) T. Yasue, H. Shiino, and Y. Arai, *Yogyo Kyokai Shi*, **88**, 197 (1980).
2) T. Yasue, K. Miyamoto, and Y. Arai, *Nippon Kagaku Kaishi*, **1978**, 1487.
3) T. Yasue, K. Fukuda, and Y. Arai, *Sekko To Sekkai*, No. 168, 21 (1980).
4) T. Yasue, K. Miyamoto, and Y. Arai, *Sekko To Sekkai*, No. 151, 3 (1977).
5) S. Aoki, E. Sawamura, and Y. Arai, *Sekko To Sekkai*, No. 142, 3 (1976).
6) T. Matsuno and M. Koishi, *Nippon Kagaku Kaishi*, **1979**, 1687.
7) J. S. Muspratt, *Chemist*, **4**, 443 (1843).
8) M. Trontz, *J. Prakt. Chem.*, **122**, 147 (1929).
9) F. A. Miller and C. H. Wilkins, *Anal. Chem.*, **24**, 1243 (1952).
10) F. A. Miller, G. L. Carlson, F. F. Bentley, and W. H. Jones, *Spectrochim. Acta*, **16**, 135 (1960).
11) E. V. Margulis and L. I. Bejsekeeva, *Zh. Prikl. Khim.*, **45**, 178 (1972).
12) K. Murakami, M. Hanada, S. Takahashi, and K. Miyata, *Yogyo Kyokai Shi*, **64**, 43 (1956).
13) K. Setoyama, S. Takahashi, and M. Sekiya, *Sekko To Sekkai*, No. 141, 3 (1976).
14) L. Schröpfer, *Z. Anorg. Allg. Chem.*, **401**, 1 (1973).
15) K. R. Waerstad, R. M. Scheib, and G. H. McClellan, *J. Appl. Crystallogr.*, **7**, 447 (1974).
16) F. W. Matthews and A. O. McIntosh, *Can. J. Res.*, **26B**, 747 (1948).
17) R. Matsuzaki, H. Masumizu, N. Murakami, and Y. Saeki, *Bull. Chem. Soc. Jpn.*, **51**, 121 (1978).
18) H. D. Lutz and S. El-Suradi, *Z. Anorg. Allg. Chem.*, **425**, 134 (1976).
19) A. W. Hull and W. P. Davey, *Phys. Rev.*, **17**, 549 (1921).
20) W. P. Davey, *Gen. Elect. Rev.*, **25**, 565 (1922).

Determination of Trace Amounts of Iron, Nickel, and Tin in Zircaloys by X-Ray Fluorescence Spectrometry after Coprecipitation with Hexamethyleneammonium Hexamethylenedithiocarbamate

Yoshikazu YAMAMOTO,* Michiyuki SUGITA, and Kazumasa UEDA

Department of Industrial Chemistry, Faculty of Technology, Kanazawa University, Kodatsuno, Kanazawa 920

(Received June 8, 1981)

A rapid and precise X-ray fluorescence spectrometry is proposed for the determination of the trace amounts of iron, nickel, and tin in zircaloys. A zircaloy sample was dissolved in a mixture of tetrafluoroboric acid and hydrochloric acid, diluted to a definite volume with water. After the addition of 3 cm³ of 1% (*R*,*R*)-tartaric acid solution as an auxiliary chelating agent and 50 μg of cobalt as an internal standard to an aliquot (less than 200 μg of tin) of the solution, the pH was adjusted to 2 with ammonia solution and 3 cm³ of 1% hexamethyleneammonium hexamethylenedithiocarbamate (HMA–HMDC) was added. The resulting HMA–HMDC complexes were collected on a membrane filter and dried. The contents of iron, nickel, and tin in zircaloys were calculated by the calibration curves with the ratios of *Kα* intensities for each element to that for cobalt. The coefficients of variation (5 results for each metal) were 2.16, 0.63, and 1.52% for 10, 10, and 200 μg of iron, nickel, and tin, respectively. The analytical results of iron, nickel, and tin in zircaloy samples by the proposed method agreed with the certified values.

Various methods for the determination of chromium,[1] iron,[2] nickel,[3] and tin[4] in zircaloys, including atomic absorption spectrometry[5] for the former three elements, have been reported. Polarographic methods[6,7] for tin and spectrographic methods[8,9] for chromiun, iron, and nickel, have suffered from the interference of lead and from relatively high coefficients of variation, respectively. In the determination of tin by a volumetric[10] or coulometric method,[11] meticulous attention must be given to the reduction of tin(IV). X-Ray fluorescence analysis using an "oxide"[12] or "extraction" method[12] needs troublesome treatment and one using a "nondestructive" method[13] can be easily influenced by a matrix effect or by segregation.

The present paper will describe the determination of trace amounts of iron, nickel, and tin in zircaloys by coprecipitation-X-ray fluorescence spectrometry with hexamethyleneammonium hexamethylenedithiocarbamate (shortened to HMA–HMDC), which didn't react with the zirconium matrix but formed stable complexes with these trace elements in a lower pH range. Cobalt was also used as an internal standard in order to improve the accuracy.

Experimental

Apparatus. The X-ray fluorescence measurements were performed using a Rigaku-Denki Model KG-X with a Philips tungsten target tube; lithium fluoride ($2d$=4.028 Å) was used as the analyzing crystal. The detection of the fluorescence X-rays was accomplished using a scintillation counter. The HMA–HMDC complexes of chromium, iron, nickel, tin, and cobalt were collected on membrane filters TM-80 (25 mm in diameter, 0.8 μm pore size). The pH measurements of sample solutions were carried out using a Hitachi-Horiba M-5 pH meter with a glass electrode.

Reagents. Chromium(VI) standard solution: A 1000 μg/cm³ solution was prepared by dissolving potassium dichromate (analytical-reagent grade) with hydrochloric acid (1+5) and by diluting with water.

Iron(III) Standard Solution: A 1000 μg/cm³ solution was prepared by dissolving electrolytic iron with a mixture of nitric acid and hydrochloric acid and by diluting with water.

Nickel(II) Standard Solution: A 1000 μg/cm³ solution was prepared by dissolving nickel metal (99.9%) with hydrochloric acid (1+1) and by diluting with water.

Tin(IV) Standard Solution: A 2500 μg/cm³ solution was prepared by dissolving tin metal (99.999%) with hydrochloric acid and by diluting with water.

Zirconium(IV) Standard Solution: A 4000 μg/cm³ solution was prepared by dissolving zirconium dichloride oxide (analytical-reagent grade) with water.

Cobalt(II) Standard Solution: A 1000 μg/cm³ solution was prepared by dissolving cobalt nitrate (analytical-reagent grade) with nitric acid and by diluting with nitric acid (1+100). The solution was standardized by EDTA titrimetry.

The above standard solutions were diluted as required.

Tetrafluoroboric Acid Solution: Tetrafluoroboric acid solution was prepared by dissolving 50 g of boric acid in 100 cm³ of 47% hydrofluoric acid and was retained in a polyethylene bottle.

HMA–HMDC Solution: A 1% ethanol solution was prepared by dissolving HMA–HMDC which had been synthesized and recrystallized by Busev's method.[14]

All the other chemicals used were of analytical-reagent grade; deionized-distilled water was used throughout the work.

Proposed Procedure. A zircaloy standard sample, 0.2 g, was dissolved in a mixture of 1 cm³ of tetrafluoroboric acid and 14 cm³ of hydrochloric acid (1+1) on a sand bath, and diluted to 100 cm³ with water. After an aliquot (less than 200 μg of tin; corresponding to 10 mg of zircaloys) was pipetted into a 100 cm³-beaker, 3 cm³ of 1% (*R*,*R*)-tartaric acid solution as an auxiliary chelating agent and 50 μg of cobalt as an internal standard were added; the total volume of the solution should be around 50 cm³ with water. The pH of the solution was adjusted to 2 with ammonia solution (1+3). Three cm³ of 1% HMA–HMDC ethanol solution was mixed into the solution. The resulting HMA–HMDC complexes for chromium, iron, nickel, tin, and cobalt were allowed to stand for 20 min at room temperature. After the HMA–HMDC complexes were collected on a membrane filter, the precipitate was washed with 10 cm³ of water three times and dried at room temperature. The precipitate on the filter, covered with a Mylar film, was fixed onto an aluminium holder and fitted with a titanium mask to remove the scattered background

intensity. The X-ray intensity for each element was measured three times for 20 s, operating at 40 kV and 20 mA. The counting was performed for the $K\alpha$ lines of each HMA–HMDC complex for chromium, iron, nickel, tin, and cobalt at the 2θ angles of 69.34°, 57.49°, 48.64°, 14.03°, and 52.81°, respectively. The background correction of each element was made by the blank values measured in a similar manner to that described above. The amounts of the four elements were calculated from their calibration curves, which gave the ratios of the average X-ray intensities for chromium, iron, nickel, and tin to that for cobalt.

Results and Discussion

Effect of the pH on the Formation of HMA–HMDC Complexes. The maximum X-ray intensity of each element was examined for the solutions containing 50 μg each of chromiun, iron, nickel, and cobalt, and 250 μg of tin. The pH range was varied from 1 to 5 with the proposed procedure. The results obtained are shown in Fig. 1. The maximum constant X-ray intensities were shown in the pH range of 1 to 5 for nickel and cobalt, and in that of 1.5 to 5 for chromium and tin. For iron, its maximum constant intensity was found in the pH range of 1.5 to 4. In 1 and 2 molar media of hydrochloric acid, chromium and iron showed an abrupt decrease of their X-ray intensities. The pH range of 1.5 to 4 is available for the formation of HMA–HMDC complexes of these elements; we carried out the experiment at pH 2.

Effect of Adding Amounts of (R,R)-Tartaric Acid Solution. Though HMA–HMDC reacts with tin(IV) to form a complex, the X-ray intensity of its complex shows a poor reproducibility of the results obtained. When (*R,R*)-tartaric acid was added to the solution containing tin, reproducible results were obtained. (*R,R*)-Tartaric acid, therefore, seems to be effective for tin as an auxiliary chelating agent in the formation of the tin–HMA–HMDC complex. To the solutions containing 20 μg each of chromium, iron, and nickel, 200 μg of tin, and 50 μg of cobalt, 1% (*R,R*)-tartaric acid solution was added in the range of 1 to 5 cm^3 and the X-ray intensities of the elements were measured using the proposed procedure. As shown in Fig. 2, the five elements recorded constant X-ray intensities with no marked variations due to tin. Three cm^3 of 1% (*R,R*)-tartaric acid solution, therefore, was used.

Effect of Adding Amounts of HMA–HMDC Solution. The X-ray intensities of the five elements were examined by adding from 1 to 6 cm^3 of 1% HMA–HMDC solution and using the proposed procedure. The results obtained are shown in Fig. 3. The addition of less than 2 cm^3 of HMA–HMDC solution

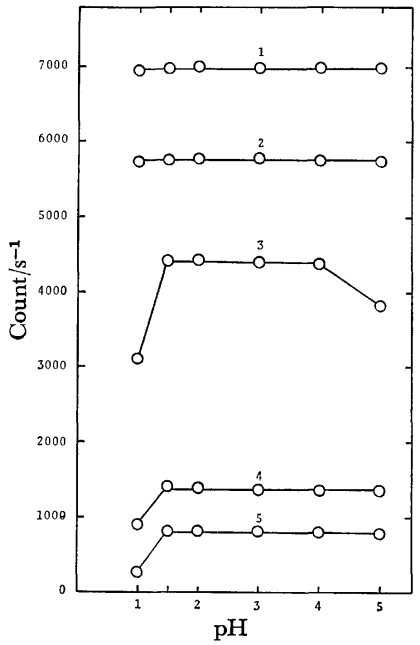

Fig. 1. Effect of the pH on the formation of HMA–HMDC complexes.
1: Ni, 2: Co, 3: Fe, 4: Cr, 5: Sn.

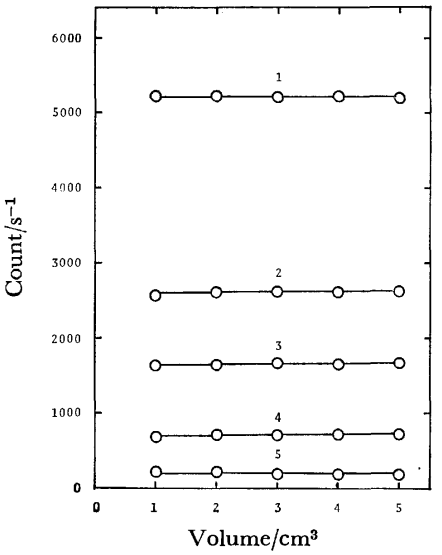

Fig. 2. Effect of adding amounts of 1% (*R,R*)-tartaric acid solution.
1: Co, 2: Ni, 3: Fe, 4: Sn, 5: Cr.

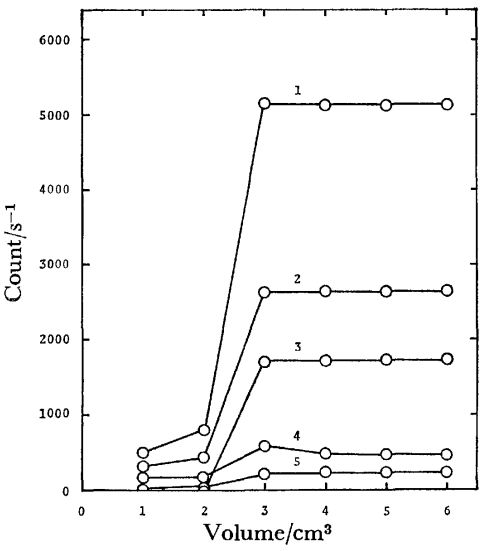

Fig. 3. Effect of adding amounts of 1% HMA–HMDC solution.
1: Co, 2: Ni, 3: Fe, 4: Sn, 5: Cr.

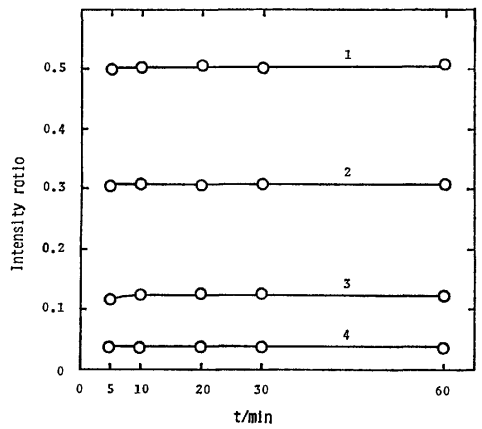

Fig. 4. Effect of aging time of the complexes.
1: I_{Ni}/I_{Co}, 2: I_{Fe}/I_{Co}, 3: I_{Sn}/I_{Co}, 4: I_{Cr}/I_{Co}.

gives extremely low X-ray intensities for each element because a part of the precipitate must pass through membrane filters. The addition of more than 4 cm³ of HMA–HMDC solution makes the filtration of the precipitate more difficult, because of the fine particles of the complexes, and gives lower X-ray intensities of tin. Three cm³ of 1% HMA–HMDC was thus added.

Effect of Aging Time of the Complexes. The aging time required to obtain quantitative complex formation was examined for the same solutions by varying the time over the range from 5 to 60 min. As shown in Fig. 4, the maximum constant ratios of X-ray intensities for chromium, iron, nickel, and tin to that for cobalt were obtained after more than 10 min of aging time. The complexes were thus allowed to stand for 20 min at room temperature.

Calibration Curves. The calibration curves were made for chromium, iron, nickel, and tin as follows. Fifty μg of cobalt as an internal standard and 60 mg of zirconium were added to the solutions containing 5—150 μg of chromium, 5—100 μg each of iron and nickel, and 50—200 μg of tin. By using the proposed procedure, the ratios of X-ray intensities for the elements to be determined to that for cobalt were plotted against the amounts of the elements. The calibration curves were linear in the concentration range of up to 100 μg of iron and nickel, and up to 150 μg of chromium. For tin, a reproducible result could not be obtained in the absence of (*R*,*R*)-tartaric acid, but the calibration curve was linear up to 300 μg in the presence of 3 cm³ of 1% (*R*,*R*)-tartaric acid solution as an auxiliary chelating agent.

The calibration curves of applying zircaloy samples were also made as follows. To the solutions containing 2—15 μg each of chromium and nickel, 5—30 μg of iron and 50—300 μg of tin, also added were 1 cm³ of 5% tetrafluoroboric acid solution, 10 mg of zirconium, 3 cm³ of 1% (*R*,*R*)-tartaric acid solution and 50 μg of cobalt. The procedure mentioned above was then carried out. The calibration curves, which are used for the determination of the amounts less than 300 μg of tin, 15 μg of nickel, and 30 μg of iron in 10 mg aliquots of zircaloy sample, are shown in Fig. 5. For chromium, however, a nonlinear relationship was found with a lowering of sensitivity.

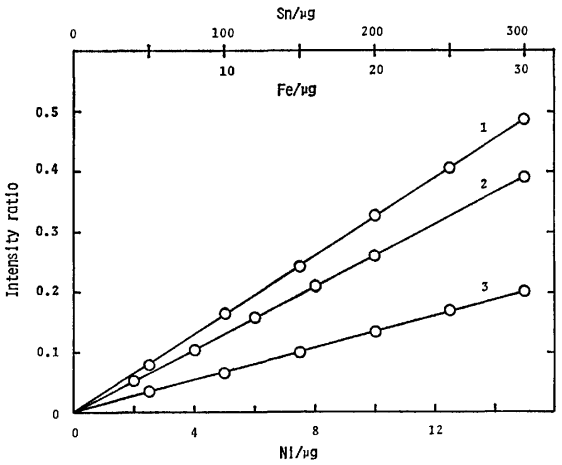

Fig. 5. Calibration curves.
1: I_{Fe}/I_{Co}, 2: I_{Ni}/I_{Co}, 3: I_{Sn}/I_{Co}.

TABLE 1. COMPARISON OF THE PROPOSED METHOD WITH OTHER METHODS

Element	Element added (μg)	Proposed method (μg)	Other method (μg)
Fe	20.0	20.0	20[a]
Ni	20.0	19.8	20[a]
Sn	240.0	243.4	240[b]

a) Determined by atomic absorption spectrometry. b) Determined by extraction spectrophotometry with oxine.

Precision and Detection Limits. The precision of the proposed method was examined for the solution containing 10 μg each of iron and nickel, and 200 μg of tin. The coefficients of variation for iron, nickel, and tin in five determinations were 2.16, 0.63, and 1.52%, respectively.

The detection limits of iron, nickel, and tin were 1.4×10^{-2}, 5.5×10^{-3}, and 3.0×10^{-1} μg, respectively; these amounts correspond to the X-ray intensities that are equal to three times standard deviations of their backgrounds.

Comparison of the Proposed Method with Other Methods. For the solutions containing 20 μg each of iron and nickel or 240 μg of tin, the analytical data obtained by the proposed method were compared with those by atomic absorption spectrometry or spectrophotometry. The results obtained are shown in Table 1. The results by the proposed method agreed with those by other methods.

Effect of Diverse Elements. HMA–HMDC forms complexes with chromium(VI), iron(III), nickel, and tin as well as cobalt, but does not form a complex with zirconium matrix; these complexes can be separated from zirconium by the filtration of them. Negligible interferences of excitation and absorption occurred among the elements studied, because these elements were measured below several hundreds micrograms in total amounts as a thin film.

Simultaneous Determination of the Trace Amounts of Chromium, Iron, Nickel, and Tin in Zircaloys. The analytical results of chromium, iron, nickel, and tin

TABLE 2. ANALYSIS OF ZIRCALOYS

Zircaloys	Element found (%)				Certified values[a] (%)			
	Fe	Ni	Sn	Cr	Fe	Ni	Sn	Cr
Z-9	0.138	0.057	1.45	—	0.148	0.057	1.47	0.097
Z-11	0.200	0.021	1.83	—	0.209	0.021	1.83	0.041
Z-12	0.128	0.095	0.91	—	0.129	0.094	0.92	0.013
Z-13	0.134	0.061	1.48	—	0.136	0.058	1.48	0.098

a) Certified by Japan Atomic Energy Research Institute.

in zircaloy standard samples, JAERI Z-9, Z-11, Z-12, and Z-13, are shown in Table 2, along with their values certified by the Japan Atomic Energy Research Institute. The content of tin is fairly high in zircaloy samples used, compared with the contents of chromium, iron, and nickel, and the intensities of their $K\alpha$ lines are more sensitive than that of tin. Thus 10 mg of sample was sufficient for the determination of their elements, with no addition of standard material. When chromium exists in a trivalent state in the zircaloy samples, the complex formation with HMA–HMDC would not proceed. The oxidations of chromium with hydrogen peroxide, potassium periodate, ammonium persulfate, and potassium permanganate were thus tried, but no effective results were obtained. The analytical results of the other three elements obtained by the proposed method were in agreement with their certified values.

The proposed method is free from the interference by the zircaloy matrix and has advantages in speed (about 2 h), simplicity and precision compared with other chmical methods.

References

1) The Committee on Analytical Chemistry of Nuclear Fuels and Reactor Materials, "Analysis of Zirconium and Its Alloys," JAERI 4050, Japan Atomic Energy Research Institute (1969), pp. 35—39.

2) The Committee on Analytical Chemistry of Nuclear Fuels and Reactor Materials, "Analysis of Zirconium and Its Alloys," JAERI 4050, Japan Atomic Energy Research Institute (1969), pp. 43—47.

3) The Committee on Analytical Chemistry of Nuclear Fuels and Reactor Materials, "Analysis of Zirconium and Its Alloys," JAERI 4050, Japan Atomic Energy Research Institute (1969), pp. 95—99.

4) The Committee on Analytical Chemistry of Nuclear Fuels and Reactor Materials, "Analysis of Zirconium and Its Alloys," JAERI 4050, Japan Atomic Energy Research Institute (1969), pp. 111—119.

5) The Committee on Analytical Chemistry of Nuclear Fuels and Reactor Materials, "Analysis of Zirconium and Its Alloys," JAERI 4050, Japan Atomic Energy Research Institute (1969), pp. 36, 37, 45, and 97.

6) R. T. Clark, *Analyst*, **85**, 245 (1960).

7) T. Mukoyama, T. Yamane, N. Kiba, and M. Tanaka, *Anal. Chim. Acta*, **61**, 83 (1972).

8) N. E. Gordon, Jr., and R. M. Jacobs, *Anal. Chem.*, **25**, 1605 (1953).

9) R. F. Farrell, G. J. Harter, and R. M. Jacobs, *Anal. Chem.*, **31**, 1550 (1959).

10) M. Kawahata, H. Mochizuki, R. Kajiyama, and M. Ishii, *Bunseki Kagaku*, **11**, 963 (1962).

11) T. Yoshimori, I. Matsubara, T. Tanaka, K. Yoshida, K. Tanaka, and T. Tanabe, *Bull. Chem. Soc. Jpn.*, **44**, 731 (1971).

12) R. W. Ashley and R. W. Jones, *Anal. Chem.*, **31**, 1632 (1959).

13) T. Matsumura, N. Kotani, and T. Goto, *Bunseki Kagaku*, **17**, 933 (1968).

14) A. I. Busev, V. M. Byr'ko, A. P. Tereshchenko, N. N. Novikova, V. P. Naidina, and P. B. Terent'ev, *Zh. Anal. Khim.*, **25**, 665 (1970).

Electrochemical Study of Reaction of Hyperoxide with Tris(1,10-phenanthroline)iron(II) in Dimethyl Sulfoxide

Kisaburo Umemoto,* Toyohumi Saeki,* Niro Matsuura,*,† and Katsue Motegi

Department of Pure and Applied Sciences, College of General Education, University of Tokyo, Komaba, Meguro-ku, Tokyo 153

† *Department of Chemistry, School of Medicine, University of Occupational and Environmental Health, Kitakyushu 807*

(Received June 9, 1981)

Reaction of hyperoxide with $Fe(phen)_3^{2+}$ in DMSO was studied by polarography, cyclic voltammetry, and spectroscopy. Voltammetric study of oxygen showed that disproportionation of hyperoxide is promoted by $Fe(phen)_3^{2+}$. Controlled potential coulometry exemplified the stoichiometry of the reaction to be 2:1 for hyperoxide to $Fe(phen)_3^{2+}$ in support of the proposed disproportionation mechanism of hyperoxide. Analysis of reaction products proved that $Fe(phen)_3^{2+}$ decomposes on reaction with hyperoxide in DMSO; the reaction products were iron(III) hydroxide and liberated ligands, neither metal hyperoxide nor oxygen bridged metal complexes being detected.

In aprotic media electrochemical reduction of oxygen occurs in two one-electron steps, the first step being well defined as formation of hyperoxide anion.[1-4] Effects of acids,[1-3] metal ions,[4,5] metal complexes,[6] water,[7] and organic materials[8] on oxygen waves have been studied, general characteristics of reactions of hyperoxide being reviewed by several authors.[9-11]

The discovery of metalloenzyme catalyzing hyperoxide dismutation[12,13] has increased interest in reactions of hyperoxide with transition metal complexes, and some low molecular weight metal complexes containing Mn(III), Cu(II), Fe(II), or Co(II) have been found to catalyze disproportionation of hyperoxide.[6,14-17]

Metal complexes of 1,10-phenanthroline are of interest, since they have heterocyclic nitrogen ligands similar to hystidine imidazole sites thought to be present in the enzyme.[13] However, quite few investigations have been performed on reactions of such complexes with hyperoxide.[14] In a preliminary work,[18] the authors presented that 1,10-phenanthroline complexes of Mn(II), Cu(II), or Fe(II) promote the disproportionation of hyperoxide in DMSO. The present paper is concerned with details of reaction of hyperoxide with $Fe(phen_3)^{2+}$ in DMSO.

Experimental

Materials. Dimethyl sulfoxide (DMSO) of Wako GR grade was shaken with dried activated alumina for one day and distilled twice under a nitrogen of reduced pressure. The portion distilled out at 53—54 °C at *ca.* 3 Torr (1 Torr ≈ 133.322 Pa) was collected. Tetraethylammonium perchlorate (TEAP) was prepared as described elsewhere[19] and $Fe(phen)_3(ClO_4)_2 \cdot H_2O$ by literature method.[20] Potassium hyperoxide obtained from Alfa Division and 1,10-phenanthroline from Wako Pure Chemicals were used as received.

Apparatus and Procedure. The cyclic voltammetry and controlled potential electrolysis were performed on a potentiostat constructed according to a circuit configuration similar to the one cited in literature.[21] Modification was made in the current booster so as to supply max. 700 mA. The platinum electrode used for the cyclic voltammetry was soaked in aqua regia for 30 s and heated in a blue flame. The controlled potential electrolysis was carried out with both a platinum plate and a mercury pool cathode. The counter electrode was a spiral platinum electrode. The two compartments of the cell were separated with a fine sintered glass filter. The current through the cell was recorded on a coulometer by integrating the potential drop across a 10 Ω resistor placed in the electrolysis current path. The coulometer was constructed according to a circuit configuration described elsewhere.[22] Modification was made in the input circuit in such a way that it was replaced with an instrumentational amplifier. Correction for blank current was made in the measurement of electrolysis current. Polarograms were recorded on a Shimadzu RP 50 polarograph. Potentials are all referred to SCE as described previously.[19] All electrochemical measurements were thermostated at 25.0±0.2 °C. The UV and visible absorption spectra were measured on a Hitachi Model 100-60 spectrometer.

The solubility of oxygen in DMSO was determined by gas chromatography. Dry oxygen was bubbled through DMSO in a test tube for 30 min at 25.0 °C and the test tube was then sealed with a serum-type rubber stopper. In order to assure that all the oxygen bubbles had got off the solution, gas chromatographic measurements of oxygen were repeated at 30 min intervals until measured values became constant. The concentration of oxygen saturated in DMSO was determined to be 2.36 mmol dm^{-3} at 25.0 °C. The concentration of oxygen in the aerated DMSO was determined to be 0.42 mmol dm^{-3} at 25.0 °C by comparing the first polarographic reduction wave height of oxygen obtained in the aerated DMSO with that obtained in the oxygen-saturated DMSO.

Results and Discussion

Cyclic voltammograms of oxygen and $Fe(phen)_3^{2+}$ are given in Fig. 1. The cathodic and anodic current peaks of oxygen correspond to the well established reversible one-electron redox process:

$$O_2 + e^- \rightleftharpoons O_2^{\cdot-}. \quad (1)$$

The potential separation between the cathodic and anodic current peaks was 0.079 V, a little greater than 0.059 V, the separation for the reversible process, but sufficiently lower than those reported in literature.[1,9] The usual cyclic polarization method for pretreatment of the platinum electrode in DMSO[17] did not improve the potential separation between the cathodic and anodic current peaks lower than 0.11 V, indicating that the method for pretreatment performed in this work is preferred to the usual method and is recommendable as one of the best methods

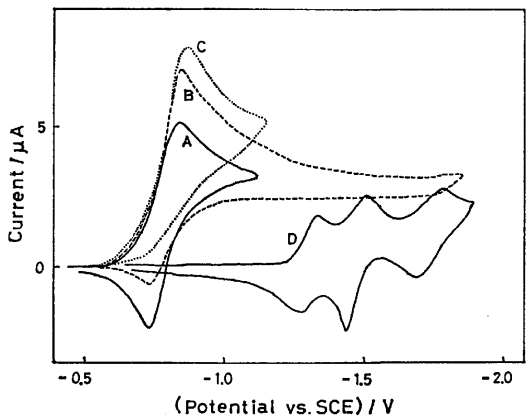

Fig. 1. Cyclic voltammograms of oxygen and Fe(phen)$_3^{2+}$ in DMSO containing 0.1 mol dm^{-3} TEAP. A: 0.42 mmol dm^{-3} O_2, B: 0.42 mmol dm^{-3} O_2+0.50 mmol dm^{-3} Fe(phen)$_3^{2+}$, C: 0.42 mmol dm^{-3} O_2+1.6 mmol dm^{-3} Fe(phen)$_3^{2+}$, D: 0.41 mmol dm^{-3} Fe(phen)$_3^{2+}$. Scan rate: 0.052 V s^{-1}.

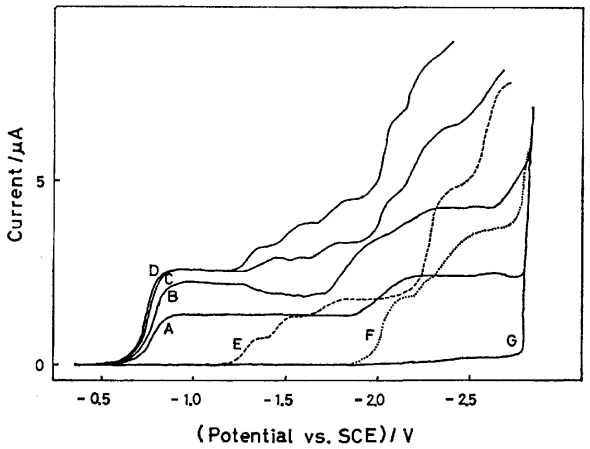

Fig. 2. Polarograms of O_2 and Fe(phen)$_3^{2+}$ in DMSO containing 0.1 mol dm^{-3} TEAP.
A: 0.42 mmol dm^{-3} O_2, B: 0.42 mmol dm^{-3} O_2+0.30 mmol dm^{-3} Fe(phen)$_3^{2+}$, C: 0.42 mmol dm^{-3} O_2+0.80 mmol dm^{-3} Fe(phen)$_3^{2+}$, D: 0.42 mmol dm^{-3} O_2+2.0 mmol dm^{-3} Fe(phen)$_3^{2+}$, E: 1.0 mmol dm^{-3} Fe(phen)$_3^{2+}$, F: electrolyzed solution of 0.41 mmol dm^{-3} Fe(phen)$_3^{2+}$, G: base current.

ever adopted.

Polarograms of oxygen and Fe(phen)$_3^{2+}$ are shown in Fig. 2. The logarithmic analysis of the first wave of oxygen gave a slope of 0.068 V. An ac polarographic current peak was observed at the first wave, showing that the first wave corresponds to the reversible one-electron process as given in Eq. 1.

When Fe(phen)$_3^{2+}$ was added to the solution, the cathodic current peak of the cyclic voltammogram of oxygen increased and the anodic current peak decreased in height as shown in Fig. 1. The first wave of polarogram increased in height with the addition of Fe(phen)$_3^{2+}$ as shown in Fig. 2, approaching asymptotically twice its original height as shown in Fig. 3. The half wave potential slightly shifted to less negative and the slope of the logarithmic analysis was 0.066 V after the first wave attained its maximun

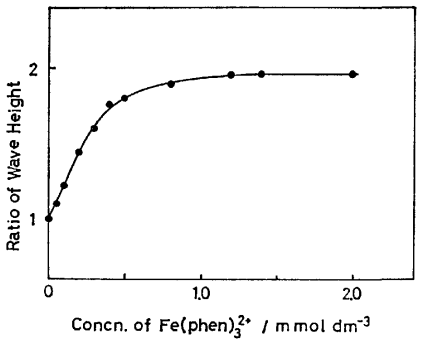

Fig. 3. Effect of Fe(phen)$_3^{2+}$ on the first wave height of the polarogram of O_2 in DMSO containing 0.1 mol dm^{-3} TEAP.
O_2: 0.42 mmol dm^{-3}.

height.

These observations are well explained by the disproportionation mechanism: The regeneration of oxygen is promoted by the reaction of Fe(phen)$_3^{2+}$ on hyperoxide as shown in Eqs. 2—4:

$$Fe(phen)_3^{2+} + O_2^{\cdot-} \longrightarrow Fe(phen)_3^{2+}\cdot O_2^{\cdot-}, \quad (2)$$

$$Fe(phen)_3^{2+}\cdot O_2^{\cdot-} + O_2^{\cdot-} \longrightarrow Fe(phen)_2^{2+}(O_2^{\cdot-})_2 + phen, \quad (3)$$

$$Fe(phen)_2^{2+}(O_2^{\cdot-})_2 \longrightarrow Fe(phen)_2^{2+}O_2^{2-} + O_2. \quad (4)$$

This reaction mechanism is similar to that of the dissociation of Fe(phen)$_3^{2+}$ induced by the attack of nucleophilic anions:[27] The close approach of the metal and hyperoxide due to the formation of an ion pair (Eq. 2) causes the interaction between the π-orbital of hyperoxide and the antibonding d-orbital of the metal with resultant destabilization of the metal ligand bond and subsequent dissociation of the complex, the single bonded ligand in the intermediate being replaced with another hyperoxide (Eq. 3). The liberation of oxygen (Eq. 4) is caused by the formation of stronger Fe–O bonds with the bidentate peroxide ion according to a mechanism similar to that given for the liberation of oxygen in the reaction of hydrogen peroxide with triethylenetetramine-di-hydroxo-iron complex.[28]

The irregular minimum observed in the polarogram B in Fig. 2 appeared at a low concentration of Fe(phen)$_3^{2+}$. This minimum may be due to the adsorption of the reaction product inhibiting part of the electrode process. At higher concentrations of Fe(phen)$_3^{2+}$, the reduction waves of the metal complex and the reaction product are clearly seen to be superimposed on the oxygen wave.

In order to establish the stoichiometry for the reaction, a controlled potential reduction of oxygen was accomplished at −1.0 V *vs.* SCE in a DMSO solution containing 0.2 mmol dm^{-3} Fe(phen)$_3^{2+}$ and 0.1 mol dm^{-3} TEAP under continuous bubbling of dry oxygen. As electrolysis proceeds, the color of the solution changed from red to yellow and simultaneously an yellow substance precipitated on the cathode. The change of the UV and visible absorption spectra of the solution is given in Fig. 4.

The autoxidation of Fe(phen)$_3^{2+}$ within the time frame of the present experiment was completely ruled

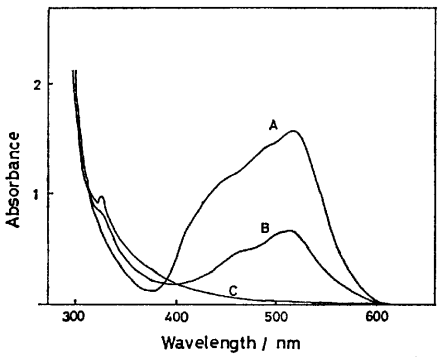

Fig. 4. UV and visible spectra of $Fe(phen)_3^{2+}$ in DMSO containing 0.1 mol dm^{-3} TEAP.
A: 0.20 mmol dm^{-3} $Fe(phen)_3^{2+}$, B: half electrolyzed, C: completely electrolyzed.

out by confirming that the spectrum of a solution with the same composition as that used for the electrolysis showed no substantial change under sunlight as well as in the dark for over 50 h.

By knowing the amount of current used for the electrolysis until the color of the solution turned yellow, 1.93 electrons were found to be required for each $Fe(phen)_3^{2+}$; namely, the stoichiometry of the reaction is 1:2 for $Fe(phen)_3^{2+}:O_2$, in accord with that required for Eqs. 1—4.

The peroxo complex shown in Eq. 4 is not a reaction product with a defined chemical structure but assumed to be a transiently lived reaction intermediate, since no peroxo species could be stable in DMSO.[23] Indeed, the direct mixing of a DMSO solution of KO_2 with one of $Fe(phen)_3^{2+}$ provided a dark violet solution which decayed in a few seconds, yielding an yellow solution and a brown precipitate. Although this transiently lived reaction intermediate has not been identified, it is supposed to be a peroxo complex as shown in Eq. 4. A similar peroxo complex has been found in reaction of Fe^{II}-edta with hyperoxide,[16] where a violet colored reaction intermediate was identified to be a peroxo complex of a formula of Fe^{III}-edta-O_2^{3-}.

Degradation of the peroxo complex may give an oxygen bridged iron complex, since formation of such a complex seems to be favored in aprotic media because it would not require utilization of water or proton donor. Indeed, a stable μ-peroxo-dicobalt(II) complex was obtained in DMSO in reaction of bis(acetylacetonato)Co(II) with hyperoxide.[6] For the autoxidation of iron containing porphyrin, where hyperoxide is considered to play an important role, an oxygen bridged iron dimer was suggested to be formed.[24] In order to check the formation of oxygen bridged iron complex, a μ-oxo complex of iron, $(Fe(phen)_2X)O(ClO_4)_2$, where X is Cl^- or NO_3^-, was prepared by literature method[25] in attempt to use it as a reference.

The cyclic voltammogram of the μ-oxo-diiron(II) complex is shown in Fig. 5. The reversible cathodic and anodic current peaks at -1.3—1.7 V *vs.* SCE are typical for the octahedral 1,10-phenanthroline complex of iron(II) since the lowest vacant molecular

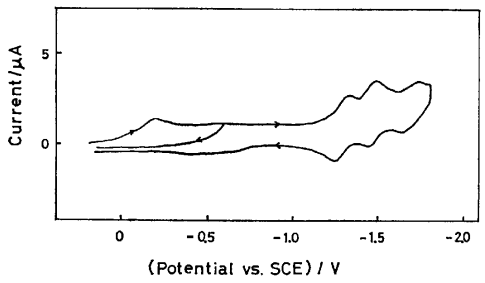

Fig. 5. Cyclic voltammogram of 0.20 mmol dm^{-3} [{$Fe(phen)_2Cl$}O_2]$^{2+}$ in DMSO containing 0.1 mol dm^{-3} TEAP.

orbitals of the complex consist mainly of the π-orbital of the ligand.[26] The yellow colored solutions obtained by the electrolysis and the direct reaction of KO_2 with $Fe(phen)_3^{2+}$ showed no redox current peaks over the potential range shown in Fig. 5. Thus, any oxygen bridged complexes are ruled out as stable reaction products. The presence of hydrogen peroxide also was ruled out since the polarogram of the yellow solution did not give any waves corresponding to hydrogen peroxide.

The qualitative analysis of the yellow solution exemplified chemical properties quite similar to a DMSO solution containing both 1,10-phenanthroline and a saturated amount of iron(III) hydroxide: Addition of Fe^{2+} regenerated the spectrum of $Fe(phen)_3^{2+}$ but addition of 1,10-phenanthroline did not, indicating the presence of liberated 1,10-phenanthroline as well as the absence of free Fe^{2+}: Exposure to mercury gave no color change, showing the absence of free Fe^{3+} since a DMSO solution containing Fe^{3+} and 1,10-phenanthroline generates the spectrum of $Fe(phen)_3^{2+}$ upon reduction with mercury: Addition of hydrogen peroxide evolved oxygen, the spectrum of $Fe(phen)_3^{2+}$ being regenerated.

The yellow substance precipitated on the cathode turned brown when dried. The qualitative analysis of this as well as the brown precipitate obtained by

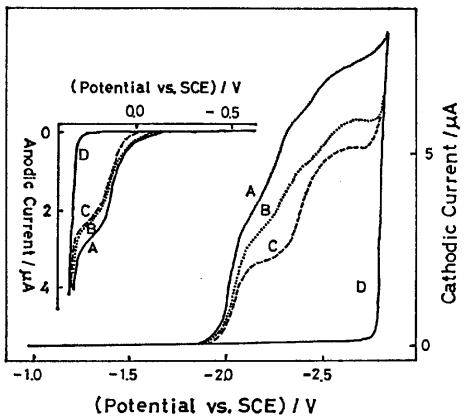

Fig. 6. Polarograms of DMSO solutions containing 0.1 mol dm^{-3} TEAP.
A: Electrolyzed solution of 0.81 mmol dm^{-3} $Fe(phen)_3^{2+}$, B: 1.7 mmol dm^{-3} 1,10-phenanthroline with saturated amount of iron(III) hydroxide, C: 1.9 mmol dm^{-3} 1,10-phenanthroline, D: base current.

direct mixing of KO_2 with $Fe(phen)_3^{2+}$ exhibited chemical properties similar to iron(III) hydroxide: They dissolved in acidic aqueous solution without evolution of gas, ruling out the presence of hyperoxide species in the precipitate; subsequent addition of 1,10-phenanthroline showed no color change, suggesting the absence of free Fe^{2+}; further exposure to mercury generated the spectrum of $Fe(phen)_3^{2+}$ due to the reduction of Fe^{3+}.

The polarographic results shown in Fig. 6 demonstrate that the polarogram of the yellow solution resulting from reaction of 1 mol of $Fe(phen)_3^{2+}$ with O_2^- corresponds quantitatively to that of a solution containing *ca.* 3 mol of 1,10-phenanthroline and a saturated amount of iron(III) hydroxide.

These results indicate that $Fe(phen)_3^{2+}$ decomposes on reaction with hyperoxide. In this sense, $Fe(phen)_3^{2+}$ does not act as a catalyst but acts as a promoter for the disproportionation of hyperoxide, since an alternate reduction and oxidation of Fe^{2+}/Fe^{3+} is not involved in the reaction. The reaction scheme presented in this work is summarized as follows:

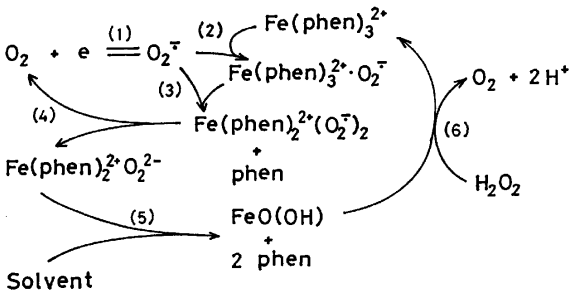

The mechanism of the degradation of peroxo complex (Reaction 5) may consist of the combination of the decomposition of peroxide ion in DMSO yielding hydroxide ion[23] and the fission of bis(phen)-iron(II) complex yielding iron(II) hydroxide with release of ligands.[27] The result that the final product was iron(III) hydroxide may be due to the oxidation of iron(II) hydroxide with DMSO, since the former is a strong reducing reagent and the latter an oxidizing one.

Reaction 6 was found to be too slow to expect to restore the catalytic activity of $Fe(phen)_3^{2+}$ during the electrochemical reaction. However, Reaction 6 would be noticeable as a reaction which demonstrates the restoration of the catalytic activity of $Fe(phen)_3^{2+}$ in DMSO.

References

1) R. L. Maricle and W. G. Hodgson, *Anal. Chem.*, **37**, 1562 (1965).
2) M. E. Peover and B. S. White, *Chem. Commun.*, **10**, 183 (1965); *Electrochim. Acta*, **11**, 1061 (1966).
3) D. T. Sawyer and J. L. Robert, Jr., *J. Electroanal. Chem.*, **12**, 90 (1966).
4) E. L. Johnson, K. H. Pool, and R. E. Hamm, *Anal. Chem.*, **38**, 183 (1966); **39**, 888 (1967).
5) A. Iwase and T. Ito, *Nippon Kagaku Kaishi*, **1972**, 1035.
6) S. Kudo and A. Iwase, *Bull. Chem. Soc. Jpn.*, **52**, 908 (1979).
7) T. Fujinaga, K. Izutsu, and T. Adachi, *Bull. Chem. Soc. Jpn.*, **42**, 140 (1969).
8) D. T. Sawyer, M. J. Gibian, M. M. Morrison, and E. T. Seo, *J. Am. Chem. Soc.*, **100**, 627 (1978); E. J. Nanni, Jr., and D. T. Sawyer, *ibid.*, **102**, 7591 (1980); J. L. Roberts, Jr., and D. T. Sawyer, *ibid.*, **103**, 712 (1981).
9) T. Osa and K. Tezuka, *Denki Kagaku*, **44**, 2 (1976).
10) D. T. Sawyer and E. T. Seo, *Inorg. Chem.*, **16**, 499 (1977).
11) D. T. Sawyer and M. J. Gibian, *Tetrahedron*, **35**, 1481 (1979).
12) J. M. McCord and I. Fridovich, *J. Biol. Chem.*, **244**, 6049 (1969).
13) I. Fridovich, *Acc. Chem. Res.*, **5**, 321 (1972); *Adv. Enzymol.*, **41**, 35 (1974).
14) J. S. Valentine and A. B. Curtis, *J. Am. Chem. Soc.*, **97**, 224 (1975).
15) J. S. Valentine and A. E. Quinn, *Inorg. Chem.*, **15**, 1997 (1976).
16) G. J. McClune, J. A. Fee, G. A. McCluskey, and J. T. Groves, *J. Am. Chem. Soc.*, **99**, 5220 (1977).
17) J. Stein, J. P. Fackler, Jr., G. J. Mclune, J. M. Fee, and L. T. Chan, *Inorg. Chem.*, **18**, 3511 (1979).
18) N. Matsuura, T. Saeki, and K. Umemoto, 7th International Conference on Non-aqueous Solution, Regensburg (1980), Vol. 2, p. 42.
19) N. Matsuura, K. Umemoto, M. Waki, Z. Takeuchi, and M. Omoto, *Bull. Chem. Soc. Jpn.*, **47**, 806 (1974).
20) A. A. Schilt and R. C. Taylor, *J. Inorg. Chem. Nucl Chem.*, **9**, 211 (1959).
21) G. Lauer and R. A. Osteryoung, *Anal. Chem.*, **38**, 1106 (1966).
22) K. Umemoto, *Bull. Chem. Soc. Jpn.*, **54**, 2017 (1981).
23) A. D. Goolsby and D. T. Sawyer, *Anal. Chem.*, **40**, 83 (1966).
24) I. A. Cohen, *J. Am. Chem. Soc.*, **91**, 1980 (1969); N. Sadaswan, H. Eberspaecher, W. Fuchman, and W. Caughey, *Biochem.*, **8**, 534 (1969).
25) J. Lewis, F. E. Mabbs, and A. Richard, *J. Chem. Soc., A*, **1967**, 1014.
26) I. Hanazaki and S. Nagakura, *Bull. Chem. Soc. Jpn.*, **44**, 2312 (1972).
27) D. W. Margerum, *J. Am. Chem. Soc.*, **79**, 2728 (1957); D. W. Margerum and L. P. Morgenthaler, *ibid.*, **84**, 706 (1962); J. Burgess and R. H. Prince, *J. Chem. Soc.*, **1965**, 4697.
28) J. H. Wang, *Acc. Chem. Res.*, **3**, 90 (1970).

An *Ab Initio* MO Calculation for the Bonding Structure of $[Ni(CN)_4]^{2-}$

Mitsuru SANO,* Hiroshi KASHIWAGI,† and Hideo YAMATERA††

Laboratory of Inorganic Chemistry, Faculty of General Education, Nagoya University, Chikusa-ku, Nagoya 464

†*Institute for Molecular Science, Myodaiji, Okazaki 444*

††*Department of Chemistry, Faculty of Science, Nagoya University, Chikusa-ku, Nagoya 464*

(Received June 12, 1981)

An ab initio MO calculation of $[Ni(CN)_4]^{2-}$ has been carried out with a double zeta basis set. The nickel-cyanide interactions are discussed and the electronic change occurring on the coordination of CN^- to Ni^{2+} is shown by using the MO contours and the electron-density difference map. The map shows σ donation from the cyanide orbitals and π back-donation from the metal d_{xy} orbital.

The tetracyanonickelate ion, $[Ni(CN)_4]^{2-}$, is one of the simplest square-planner complexes. Its coordinate bonding is of great interest for inorganic chemists because of its fundamental importance for comparison with the bonding in octahedral complexes. Demuynck *et al.*[1-2] have reported an ab initio molecular orbital (MO) calculation of $[Ni(CN)_4]^{2-}$; however, the bonding structure has not been discussed in detail in terms of the orbital mixing and the electron-density difference on coordination. We have reported the electronic structures of the octahedral complexes, $[M(CN)_6]^{3-}$ (M=Cr, Mn, Fe, and Co) and $[Fe(CN)_6]^{4-}$, by means of both the Hartree-Fock and the discrete-variational-Xα molecular orbital calculations.[3-4] In these reports, the metal-cyanide bonding has been discussed for complexes of different metals and of different oxidation states, and the validity of the orbital mixing rule[3,5,6] has been demonstrated for the coordinate bond.

In the present work, an ab initio MO computation of $[Ni(CN)_4]^{2-}$ has been undertaken to clarify (1) the metal-cyanide bonding structure in $[Ni(CN)_4]^{2-}$ and (2) the electronic change occurring on the coordination of CN^- to Ni^{2+}, on the basis of the MO contours and the electron-density maps.

Computation

The calculation was done in the SCF LCAO MO scheme with a basis set of Gaussian functions ([11s, 7p, 5d][7] for the Ni atom and [9s, 5p][8] for the C and N atoms). The 250 Gaussian functions were reduced to 112 contracted functions. The program JAMOL3 used in the present calculation has been written by Kashiwagi *et al.*,[9] who made the integral calculation more tractable by making use of symmetry properties and an integral approximation scheme based on semi-orthogonalized orbitals.[10-11] The threshold value for the degree of overlap was set at 0.001 in the present calculation. The bond lengths were taken as:[1-2]

Ni-C=1.86 Å and C-N=1.15 Å in D_{4h}.

The x and y axes were taken along the coordinate axes. The calculation of the electron density map was carried out by using the program written by Miyoshi *et al.*[12]

Results and Discussion

The calculated orbital energies and the approximate valence-shell MO's are given in Table 1, together with the corresponding energy values given by Demuynck *et al.*[1] The present results for the orbital energies are 0.02—0.05 a.u. lower than the previous ones. However, the order of MO levels is almost the same as that reported by Demuynck *et al.*,[1] except for two reversals of the orders of adjacent levels. The calculated orbital levels are schematically illustrated in Fig. 1, together with those of the free CN^- ion. Table 2 gives the symmetries of orbitals on the D_{4h} point group. Sigma interactions exist in the orbitals of the a_{1g} and b_{1g} types, π interactions in those of the a_{2u}, b_{2g}, and e_g types, and both interactions in the e_u-type orbitals. The CN^- π orbitals of the a_{2g} and b_{2u} types have no interacting metal orbitals. The important orbitals in forming the metal-cyanide bonds are the 3d, 4s, and 4p orbitals of Ni and the 5σ, 1π, and 2π orbitals of CN^-.

Table 1. Symmetries and energies of valence shell MO's

Symmetry	Energy/a.u.		
	Present results	Literature[1]	
$1a_{2g}$	−0.1449	−0.122	1π
$8e_u$	−0.1457	−0.120	1π
$2e_g$	−0.1495	−0.131	1π
$1b_{2u}$	−0.1589	−0.136	1π
$2b_{2g}$	−0.1746	−0.155	1π
$3a_{2u}$	−0.1821	−0.159	1π
$9a_{1g}$	−0.1923	−0.182	d_{z^2}
$5b_{1g}$	−0.2022	−0.182	5σ
$7e_u$	−0.2136	−0.194	5σ
$8a_{1g}$	−0.2494	−0.231	5σ
$1e_g$	−0.2661	−0.266	d_{zx}, d_{yz}
$4b_{1g}$	−0.3011	−0.262	4σ
$6e_u$	−0.3200	−0.277	4σ
$1b_{2g}$	−0.3371	−0.355	d_{xy}
$7a_{1g}$	−0.4215	−0.378	4σ
$3b_{1g}$	−0.9261	−0.875	3σ
$5e_u$	−0.9268	−0.877	3σ
$6a_{1g}$	−0.9313	−0.879	3σ

The Natures of MO's. We will discuss the natures of MO's and the orbital interactions. Demuynck *et al.*[1-2] reported that the $d_{x^2-y^2}$ and 4p orbitals of the metal are important in the Ni–CN σ bond. However, the mechanism of the orbital interaction has not been reported. Figure 2 shows the important MO wavefunctions which contribute to the Ni–CN bonding; *i.e.* $8a_{1g}$, $9a_{1g}$, and $5b_{1g}$ in the σ system,

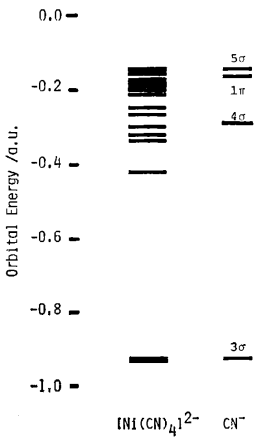

Fig. 1. Schematically illustrated MO energy levels with the levels of free CN^- orbitals.
The MO orderings (from the top to the bottom) are: $1a_{2g}$, $8e_u$, $2e_g$, $1b_{2u}$, $2b_{2g}$, $3a_{2u}$, $9a_{1g}$, $5b_{1g}$, $7e_u$, $8a_{1g}$, $1e_g$, $4b_{1g}$, $6e_u$, $1b_{2g}$, $7a_{1g}$, $3b_{1g}$, $5e_u$, $6a_{1g}$ (See Table 1.).

$1b_{2g}$, $2b_{2g}$, $1e_g$, $2e_g$, and $3a_{2u}$ in the π system, and $7e_u$ and $8e_u$ in the mixed σ and π system. The order of orbital energies in the σ system is $5\sigma<3d\sigma<4s<4p$. In a_{1g} symmetry, two occupied MO's are formed by the combinations of the $5\sigma+3d_{z^2}+4s$ ($8a_{1g}$, Fig. 2a) and $3d_{z^2}-5\sigma-4s$ ($9a_{1g}$, Fig. 2b) types; here the + signs show that the component orbitals have the same sign as that of the main component orbital

Table 2. Symmetry orbitals for D_{4h}

Symmetry	Metal orbital	Cyanide orbital[a]
a_{1g}	s, d_{z^2}	σ
a_{2g}		π
a_{2u}	p_z	π
b_{1g}	$d_{x^2-y^2}$	σ
b_{2g}	d_{xy}	π
b_{2u}		π
e_g	d_{zx}, d_{yz}	π
e_u	p_x, p_y	σ, π

a) Ligand symmetry orbital.

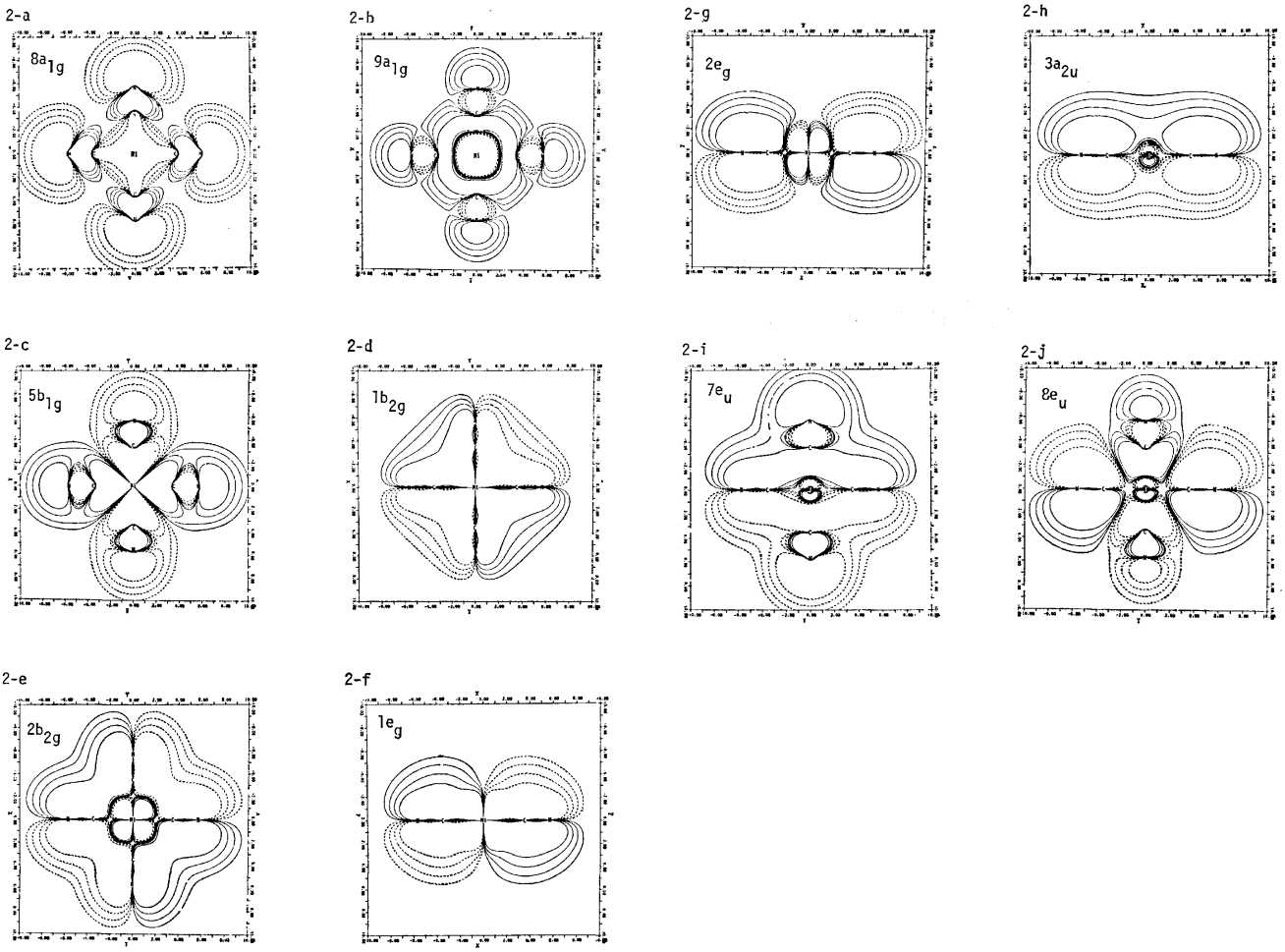

Fig. 2. Selected wavefunction contours for the valence-shell MO's of $[Ni(CN)_4]^{2-}$.
Each set of contours is drawn in a frame of 20 a.u. × 20 a.u. (1 a.u. = 0.529 Å = 52.9 pm). The Ni atom is located at the center of the frame, and four C and four N atoms at the distances of 3.516 a.u. and 5.690 a.u. from the center, respectively, on the xy plane (However, the three figures, f, g, and h, show the wavefunction contours on the xz plane, and two C and two N atoms are located before and behind the Ni atom.). The first solid and dotted contours show ± 0.002, respectively, and neighboring contours differ by a factor of two (For some of the MO's, the signs are reversed.).

(given first) in the region of the Ni–C bonds. If the 4s orbital did not contribute to the two MO's, the linear combinations would be $5\sigma+3d\sigma$ and $3d\sigma-5\sigma$ types; this latter is antibonding and weakens to the Ni–C bonds. This antibonding interaction is relaxed by the mixing of 4s, which thus makes an important contribution to the Ni–CN σ-bond formation. To the b_1 symmetry belongs the occupied $(5\sigma+d_{x^2-y^2})$-type MO ($5b_{1g}$, Fig. 2c), which contributes to the Ni–C bond formation through σ donation.

The order of the energies of π type orbitals is $d\pi<1\pi<4p\pi<2\pi$; $d\pi$ and 1π are originally occupied. The formation of a coordinate bond gives two occupied MO's, $d\pi+1\pi+2\pi$ ($1b_{2g}$, Fig. 2d, and $1e_g$, Fig. 2f) and $1\pi-d\pi-2\pi$ ($2b_{2g}$, Fig. 2e, and $2e_g$, Fig. 2g); the mixing of 2π stabilizes the antibonding $1\pi-d\pi$ MO. In a_{2u}, the $1\pi+4p\pi+2\pi$ combination is formed ($3a_{2u}$, Fig. 2h). The e_u interaction gives the linear combinations $5\sigma+1\pi+4p$ ($7e_u$, Fig. 2i) and $1\pi-5\sigma-4p$ ($8e_u$, Fig. 2j), where the 5σ orbitals of a pair of the CN^- ligands interact with the 1π orbitals of the other pair of the CN^- ligands.

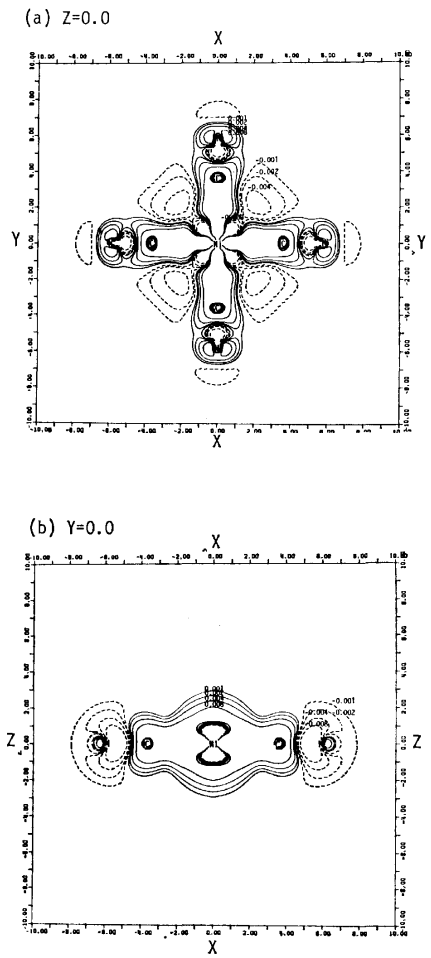

Fig. 3. The electron density difference between $[Ni(CN)_4]^{2-}$ and a cluster of Ni^{2+} (d^8 configuration with unfilled $d_{x^2-y^2}$ orbital) and $(CN^-)_4$: (a) on the xy plane and (b) on the xz plane.
The first solid and dotted contours show ±0.001 e(a.u.)$^{-3}$, respectively, and neighboring contours differ by a factor of two.

As is described above, the interaction of the ligand and the metal occupied orbitals gives rise to two MO's, one with bonding and one with antibonding character; a mixing of the virtual orbitals makes the bonding orbitals more suitable, and the antibonding orbital less unsuitable, to the M–C bonding.

The Electron Density and Population. Figure 3 shows the maps (for the xy and the xz plane) of the electron density difference between $[Ni(CN)_4]^{2-}$ and a system of Ni^{2+} (d^8 configuration with an unfilled $d_{x^2-y^2}$ orbital) and $(CN^-)_4$; the change in the electron density on the formation of the complex is shown in terms of contours. The large positive region between the Ni and C atoms represents a significant σ donation from cyanide to metal. The same feature is also reported by Demuynck *et al.*[2] on the basis of the electron density contours of the localized orbital. The decrease of the electron density in the nickel d_{xy} region results from π back-donation. This π back-donation of d_{xy} increases the nitrogen π_x and π_y populations by the combination of $1\pi-d\pi-2\pi$. This is clearly shown by Fig. 3a. As can be seen from the decrease in the d_{xy} electron density, the extent of π back-donation from d_{xy} is as large as that in $[Fe(CN)_6]^{4-}$ and is larger than that in $[Co(CN)_6]^{3-}$ reported previously.[2,13] There is no indication of the decrease in electron density in the region of d_{zx} (Fig. 3b), suggesting little π back-donation from d_{yz} and d_{zx}. The density increase in the C–Ni–C region and the density decrease in the outer region of CN^- may show the polarization of the coordinated CN^- by the central Ni^{2+} charge and/or the donation of the CN^- electrons to the Ni $3d_{x^2-y^2}$, 4s, and 4p orbitals.

TABLE 3. POPULATION ANALYSIS OF $[Ni(CN)_4]^{2-}$

Orbital	Population (population in free CN^-)			
	Present results		Literature[1]	
Nickel d_{z^2}	1.935		1.96	
$d_{x^2-y^2}$	0.437		0.91	
d_{xy}	1.956		1.95	
d_{yz}	1.956		1.97	
d_{zx}	1.956		1.97	
4s	0.144		0.52	
$4p_x$, $4p_y$	0.235		0.17	
$4p_z$	0.066		0.07	
Atomic charge	+1.533		+0.46	
Carbon 2s	1.660	(1.860)	1.26	(1.62)
$2p\sigma$	1.219	(1.164)	1.14	(1.13)
$2p\pi_y$	0.801	(1.528)	0.84	(0.84)
$2p\pi_z$	0.877		0.91	(0.84)
Atomic charge	−0.549	(−0.546)	−0.14	(−0.43)
Nitrogen 2s	1.647	(1.637)	1.66	(1.69)
$2p\sigma$	1.326	(1.351)	1.53	(1.56)
$2p\pi_y$	1.222	(2.472)	1.18	(1.16)
$2p\pi_z$	1.145		1.10	(1.16)
Atomic charge	−0.335	(−0.454)	−0.47	(−0.57)
Bond overlap population				
Ni-C	0.138			
C-N	1.564	(1.666)		

Although the population analysis is to some extent artificial, especially when based on the double-zeta set,[14] the Mulliken populations are given in Table 3 to allow qualitative considerations. (In the free CN^- ion, for example, the listed Mulliken populations are an overestimate for C and an underestimate for N, probably because the wavefunctions are more diffuse for C than for N. However, a comparison of the Mulliken populations before and after the bond formation will give us at least qualitatively reliable information about the nature of the bond, provided that the populations are calculated with the same basis set.) Table 3 also lists the values reported by Demuynck *et al.*[1] They in general agree with our results, but differ in a couple of respects. The Mulliken populations are known to depend on the basis functions; our $d_{x^2-y^2}$ population may thus be an underestimate, probably because one of the components of the split 2p orbital of carbon was too diffuse. Correspondingly, the calculated charge of the nickel atom is higher and that of the carbon atom is lower than the literature values. A significant donation from the C 2s orbital to the Ni $d_{x^2-y^2}$ and 4s orbitals can be seen in Table 3 and also in Fig. 3. The π back-donation from the Ni d_{xy} orbital to the N $2p\pi$ orbitals, which is not found in Table 3, is clearly shown by Fig. 3a, while the small π back-donation from the Ni d_{zx} (and d_{yz}) orbitals to the CN^- $2p\pi_z$ orbitals and the polarization of the latter are demonstrated both by Fig. 3b and by the present and previous results shown in Table 3. The electron-density difference maps are more useful and probably more reliable than the numerical results of the population analysis in discussing the nature of the bonds.

The work was partly supported by the Joint Studies Program (1979—1980) of the Institute for Molecular Science. The computation has been carried out on a HITAC M-180 computer of the Institute for Molecular Science.

References

1) J. Demuynck, A. Veillard, and G. Vinot, *Chem. Phys. Lett.*, **10**, 522 (1971).
2) J. Demuynck and A. Veillard, *Theoret. Chim. Acta*, **28**, 241 (1973).
3) M. Sano, Y. Hatano, H. Kashiwagi, and H. Yamatera, *Bull. Chem. Soc. Jpn.*, **54**, 1523 (1981).
4) M. Sano, H. Adachi, and H. Yamatera, *Bull. Chem. Soc. Jpn.*, **54**, 2898 (1981).
5) S. Inagaki and K. Fukui, *Chem. Lett.*, **1974**, 509.
6) S. Inagaki, H. Fujimoto, and K. Fukui, *J. Am. Chem. Soc.*, **98**, 4054 (1976).
7) B. Roos, A. Veillard, and G. Vinot, *Theoret. Chim. Acta*, **20**, 1 (1971).
8) T. H. Dunning, Jr., *J. Chem. Phys.*, **53**, 2823 (1970).
9) H. Kashiwagi, T. Takada, E. Miyoshi, S. Obara, and F. Sasaki, "Program JAMOL3," Program Library, Computer Center of Institute for Molecular Science.
10) H. Kashiwagi, *Int. J. Quantum Chem.*, **10**, 135 (1976).
11) H. Kashiwagi and T. Takada, *Int. J. Quantum Chem.*, **12** 449 (1977).
12) E. Miyoshi, M. Sano, C. Watanabe, and H. Kashiwagi, "Program JAPICl," Program Library, Computer Center of Institute for Molecular Science.
13) M. Sano, H. Adachi, H. Kashiwagi, and H. Yamatera, The 29th Symposium on Coordination Chemistry of the Chemical Society of Japan, Hamamatsu, Oct. 1979, Abstr., p. 272.
14) M. Sano, Y. Hatano, and H. Yamatera, *Chem. Lett.*, **1979**, 789.

Determination of Circular Dichroism in Multiple Scattering Systems

Yutaka TANIGUCHI* and Yoichi SHIMURA

Department of Chemistry, Faculty of Science, Osaka University, Toyonaka, Osaka 560

(Received June 12, 1981)

In a thick suspension circular dichroism cannot be directly determined by the Grosjean-Legrand type CD instrument, because Lambert's law does not hold in it. The transfer of light intensity is discussed when polarized light is incident on a plane-parallel scattering medium containing randomly oriented, optically active particles. This problem is analyzed based on a two-beam radiative transfer model. We provide a method to determine the molar CD in a multiple scattering system. The measurements of ellipticity and transmittance with conventional instruments is served for our method by using a plate of opal glass. The molar CD is determined in Nujol mulls of Λ-$[Co(en)_3]Br_3 \cdot H_2O$ and $[Co(NH_3)_6](d\text{-tart})_{1.5} \cdot 5H_2O$. The results are reproducible and reliable.

The measurement of circular dichroism (CD) spectrum is a useful method in the study of molecular structure in solution. The CD spectrum is easily measured by the Grosjean-Legrand method.[1] Because the intensity of incident light decreases in a transparent material exponentially following Lambert's law, the ellipticity of the transmitted light is given by the familiar equations

$$\Theta = (1/4)(k_L - k_R), \tag{1}$$

and

$$\Theta = (1/4)\ln(I_{t,R}/I_{t,L}), \tag{2}$$

where Θ is the ellipticity in radians, k the absorption coefficient, I_t the light intensity transmitted by a sample, and the subscripts L and R denote the left and right circular polarization, respectively. Actually, Θ can be adequately approximated by

$$\Theta = (1/4)(I_{ac}/I_{dc}), \tag{3}$$

where $I_{ac}=I_{t,R}-I_{t,L}$ and $I_{dc}=(I_{t,R}+I_{t,L})/2$. Therefore, Θ is obtained electronically by detecting I_{ac} and I_{dc} as the alternating and direct current signals, respectively, in the photomultiplier of a Grosjean-Legrand type CD instrument.

The CD measurement has recently been extended to suspensions of biological materials.[2,3] The decrease in light intensity transmitted by a dilute suspension also follows Lambert's law. The CD of a suspension, which contains a scattering contribution, is also measured by the conventional Grosjean-Legrand type CD instrument. However, on account of unequal scattering of left and right circularly polarized light by optically active particles, the interpretation of the resulting CD spectra is very complicated. A few investigations based on classical scattering theory were made to analyze the scattering effect on CD spectra,[4] but general approaches to this problem have not been confirmed yet.

In the previous studies suspensions were always assumed to be dilute, where multiple scattering effects were neglected. However, multiple scattering effects are no longer negligible in a somewhat thick suspension. Lambert's law does not hold in it, and hence the Θ measured by the Grosjean-Legrand type CD instrument is not the direct information of CD.

In this paper, we propose a method to determine the molar CD of a thick suspension, a Nujol mull of solid-state complex salt, by the Grosjean-Legrand type CD instrument. The reproducibility of CD data obtained by our method will be shown too.

Principles and Practical Method

Stokes Vector. The light beams suffered multiple scattering have randomly different phases from one another, and hence the scattered beams are incoherent. The polarization state of an incoherent light beam is conveniently expressed by a Stokes vector[5] with four components having the dimensions of light intensity. In this study, the representation based on the left and right circular polarizations[6] will be used instead of the original Stokes vector. It is defined as

$$\boldsymbol{I} = \begin{bmatrix} I_1 \\ I_R \\ I_L \\ I_4 \end{bmatrix} = \begin{bmatrix} \langle E_R E_L^* \rangle \\ \langle E_R E_R^* \rangle \\ \langle E_L E_L^* \rangle \\ \langle E_L E_R^* \rangle \end{bmatrix}, \tag{4}$$

where E is the amplitude of electric field vector, the brackets denote time averages, and the asterisks complex conjugates. In the Grosjean-Legrand type CD instrument, the Stokes vector of the incident beam $\boldsymbol{I}_o$ (total intensity$=I_o$) is

$$\boldsymbol{I}_o = (I_o/2)\begin{bmatrix} \cos(\delta \sin \omega t) \\ 1-\sin(\delta \sin \omega t) \\ 1+\sin(\delta \sin \omega t) \\ \cos(\delta \sin \omega t) \end{bmatrix}, \tag{5}$$

where δ is the maximum phase difference produced in the modulator and ω the modulation frequency.

Equation of Radiative Transfer. The problem of radiative transfer in a scattering medium has been well investigated by Chandrasekhar.[7,8] It is assumed in this paper that a homogeneous scattering medium consisting of randomly oriented particles is bounded by two parallel planes and extends over a region very large compared to its thickness. In such a plane-parallel scattering medium, the radiation field is characterized by the coordinate z on the axis normal to the boundary planes, the polar angle θ with respect to the z-axis, and the azimuthal angle ϕ referred to a suitably chosen x-axis (see Fig. 1). The variation of a light flux travelling through a layer dz in the direction (θ,ϕ) is given by

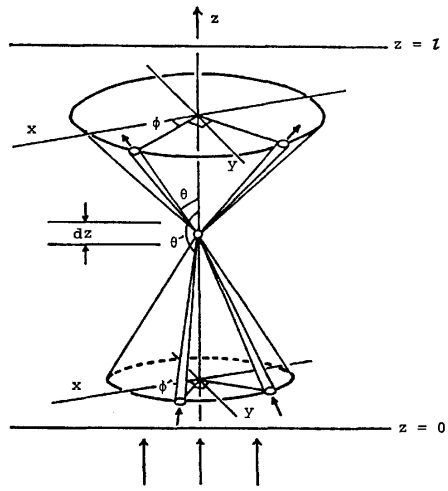

Fig. 1. Coordinate system and the directions of the incident and scattered beams.

$$(\cos\theta/\mathrm{d}z)\mathrm{d}\boldsymbol{I}(z,\theta,\phi) = -(k+s)\boldsymbol{I}(z,\theta,\phi) + (s/4\pi)\int_0^{\pi}\int_0^{2\pi} P(\theta,\phi;\theta',\phi')\boldsymbol{I}(z,\theta',\phi')\sin\theta'\mathrm{d}\theta'\mathrm{d}\phi', \tag{6}$$

where k and s are the absorption and scattering coefficients, respectively, and $P(\theta,\phi;\theta',\phi')$ is the normalized phase matrix defining the angular distribution of the scattered light incident from a direction (θ',ϕ') into the direction (θ,ϕ). The phase matrix is represented by a 4×4 matrix. When scattering particles are optically active, k and s are rewritten by the diagonal matrices, *viz.*,

$$K = \mathrm{diag}(k_1, k_R, k_L, k_4) \text{ and } S = \mathrm{diag}(s_1, s_R, s_L, s_4). \tag{7}$$

For the problem in a plane-parallel scattering medium, the Stokes vector is customarily referred to the directions parallel and perpendicular to the meridian plane,[9] which is defined by the z-axis and the propagation direction of a light beam.

We shall now consider the nature of the radiation scattered from the direction (θ',ϕ') into the direction (θ,ϕ), and that of the radiation from the direction $(\theta',\phi'+\chi)$ into the direction $(\theta,\phi+\chi)$; so the azimuthal angles of both beams are greater for the latter than for the former by an angle χ. The phase matrix depends only on the characteristics of the scattering medium. The phase matrix $P(\theta,\phi+\chi;\theta',\phi'+\chi)$ is identical with the matrix $P(\theta,\phi;\theta',\phi')$ because the scattering medium containing particles with random orientation has, on the whole, an axial symmetry about the z-axis.

When a parallel beam of light is incident into a scattering medium perpendicularly to the boundary plane (parallel to the z-axis), the relation between $\boldsymbol{I}(z,\theta',\phi')$ and $\boldsymbol{I}(z,\theta',\phi'+\chi)$ can be derived as follows. The Stokes vector $\boldsymbol{I}(z,\theta',\phi'+\chi)$ is identical with the new vector which should be yielded in the direction (θ',ϕ') when the reference axes of the original parallel beam are rotated around its propagation axis by the angle χ in the clockwise direction, as viewed in the direction of propagation. The rotation matrix $R(\chi)$ for the Stokes vector $\boldsymbol{I}=(I_1,I_R,I_L,I_4)$ is a diagonal matrix with the elements $(e^{2i\chi}, 1, 1, e^{-2i\chi})$.[6] The components I_R and I_L are invarient for the rotation of the axes. But the other components I_1 and I_4 change with such a rotation. When $\chi=\pi/2$, each of I_1 and I_4 has the value equal in magnitude but opposite in sign to the original value before the rotation.

In the CD measurements, any of the four components of the Stokes vector, (I_1,I_R,I_L,I_4), is not separately detected by our instrument. The CD signals are obtained by measuring the ac and dc components of the total intensity, I_R+I_L, emitted in the forward direction. The total intensities, even in different directions, can be added arithmetically. From the above discussion it is found that the scattering contributions to the total intensity of $\boldsymbol{I}(z,\theta,\phi)$ by the I_1 and I_4 components of $\boldsymbol{I}(z,\theta',\phi')$, and those to the total intensity of $\boldsymbol{I}(z,\theta,\phi+\pi/2)$ by the corresponding components of $\boldsymbol{I}(z,\theta',\phi'+\pi/2)$ are cancelled out each other. The same argument applies to any couple of scatterings having such a directional relation. The azimuthal angles ϕ and ϕ' can be chosen arbitrarily. Therefore, when light beams scattered in the directions with the polar angle θ are all accepted simultaneously, the total intensity is, on the whole, not contributed by the components I_1 and I_4 of the incident beams from the directions with another polar angle θ'. Then the transfer equation of the total intensity is written by a 2-vector with the components I_R and I_L. The matrices P, K, and S are, of course, rewritten by 2×2 matrices.

Two-beam Model. The exact solution of the transfer equation is rarely obtained, because in most cases the phase matrix is seldom known. To a fairly good approximation, a two-beam model, dividing the radiation field into the two streams in the forward and backward directions, has been employed to solve the practical problems of radiative transfer. The scattering particles dealt with in previous papers were always optically inactive. We now extend the two-beam model to an optically active case.

Let $\boldsymbol{I}=(I_R,I_L)^t$ and $\boldsymbol{J}=(J_R,J_L)^t$ represent the streams propagating in the forward and backward directions, respectively (see Fig. 2). The superscript t denotes the transposed matrix. Assuming that the optical activity (circular birefringence and circular dichroism) of a particle is small, we may, as a first approximation, let the elements of the phase matrix be

$$p_{RR} = p_{LL} = 1 \text{ and } p_{RL} = p_{LR} = 0. \tag{8}$$

Within the limits, the transfer equation 6 can be replaced by the two equations of Schuster[10] or Kubelka-

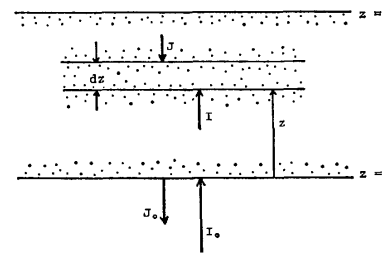

Fig. 2. Directions of the light streams used in the two-beam model.

Munk:[11]

$$dI/dz = -(K+S)I+SJ, \quad (9)$$

$$dJ/dz = (K+S)J-SI, \quad (10)$$

where $K=\mathrm{diag}(k_R,k_L)$ and $S=\mathrm{diag}(s_R,s_L)$. The general solutions of the Eqs. 9 and 10 are

$$I_i = A_i(1-\beta_i)e^{\alpha_i z} + B_i(1+\beta_i)e^{-\alpha_i z};\ i = R, L, \quad (11)$$

$$J_i = A_i(1+\beta_i)e^{\alpha_i z} + B_i(1-\beta_i)e^{-\alpha_i z};\ i = R, L, \quad (12)$$

where A_i and B_i are arbitrary constants to be determined by the boundary conditions, α_i and β_i are constants, given by

$$\alpha_i = [k_i(k_i+2s_i)]^{1/2}, \quad (13)$$

$$\beta_i = [k_i/(k_i+2s_i)]^{1/2}. \quad (14)$$

If

$$I_i = (I_o)_i;\ i = R, L \quad (15)$$

at the illuminated surface ($z=0$), and

$$I_i = (I_t)_i,\ J_i = 0;\ i = R, L \quad (16)$$

at the back surface ($z=l$), we have

$$A_i = -(1-\beta_i)e^{-\alpha_i l}(I_o)_i/[(1+\beta_i)^2e^{\alpha_i l}-(1-\beta_i)^2e^{-\alpha_i l}], \quad (17)$$

$$B_i = (1+\beta_i)e^{\alpha_i l}(I_o)_i/[(1+\beta_i)^2e^{\alpha_i l}-(1-\beta_i)^2e^{-\alpha_i l}]. \quad (18)$$

Therefore, the transmittance of the i component is given by

$$T_I = 4\beta_i(I_o)_i/[(1+\beta_i)^2e^{\alpha_i l}-(1-\beta_i)^2e^{-\alpha_i l}]I_o, \quad (19)$$

when

$$I_o = \Sigma_i(I_o)_i. \quad (20)$$

Determination of Δk. The Eq. 1 between the ellipticity Θ and the circular dichroism $\Delta k=k_L-k_R$ is not valid for a multiple scattering system, because Lambert's law does not hold in it. The Θ measured in such a system only gives the ratio of the ac and dc components of the light intensity transmitted, as indicated in Eq. 3.

The Eq. 3 can be rewritten by the transmittances for the left and right circular polarizations:

$$\Theta = -(1/4)\Delta T/T, \quad (21)$$

where

$$\Delta T = T_L - T_R, \quad (22)$$

and

$$T = (T_R+T_L)/2. \quad (23)$$

From Eqs. 21, 22, and 23 it follows that

$$T_R = T-\Delta T/2 = (1+2\Theta)T, \quad (24)$$

and

$$T_L = T + \Delta T/2 = (1-2\Theta)T. \quad (25)$$

According to Eqs. 13, 14, and 19, k_R and k_L can be calculated from the values of T_R, T_L, s_R, and s_L. The T_R and T_L are evaluated from the Θ and T which are measurable by conventional spectrometers. If the values of s_R and s_L are known, we can determine k_L-k_R, *viz.*, Δk, even in a multiple scattering system.

Estimation of Scattering Coefficients. In the Kubelka-Munk equations, s is the back-scattering coefficient. When scatterers are optically active, the scattering coefficients for left- and right-circularly polarized light are, in general, different from each other. The angular dependence of the difference between scattering of left- and right-circularly polarized light by optically active spheres has been discussed recently.[12,13] It has been indicated that the difference is virtually significant in the forward scattering directions. Therefore, the back-scattering coefficients s_R and s_L may be taken as equal, and hence their values are equal to that for natural light:

$$s_R = s_L = s. \quad (26)$$

In Eq. 19, if k approaches zero, the equation of transmittance becomes the simplified expression

$$\lim_{k\to 0}T = 1/(1+sl). \quad (27)$$

At a wavelength where scattering particles have no absorption, the scattering coefficient s can be calculated by substituting the value of transmittance in Eq. 27.

While the scattering coefficient in an absorption band region cannot be determined directly. The scattering coefficient generally varies with wavelength; it's value normally increases with decreasing wavelength. Kortüm and Oelkrug[14] showed that for the powder samples having no absorption, there exists the empirical relation between s and λ:

$$\log s \propto \log \lambda^{-1}, \quad (28)$$

where λ is wavelength. At any wavelength in an absorption band region, we now estimate the value of the scattering coefficient by extrapolating the linearity between $\log s$ and $\log \lambda^{-1}$ in the wavelength region having no absorption to a desired wavelength (see Fig. 3).

Molar Circular Dichroism. The present paper is concerned with Nujol mulls of complex salts. The Nujol mull is composed of particles of different shapes and sizes. Because the shape and size distributions are different in every mull, neither absorption nor scattering coefficient is identical for every mull, even if it may have the same concentration. Then the values of k and s are not characteristic of a material. Nevertheless, the ratio of Δk to k should be characteristic of a material, even if it is in different mulls. Then we have

$$\Delta k/k = \Delta\varepsilon(\mathrm{cryst})/\varepsilon(\mathrm{cryst}), \quad (29)$$

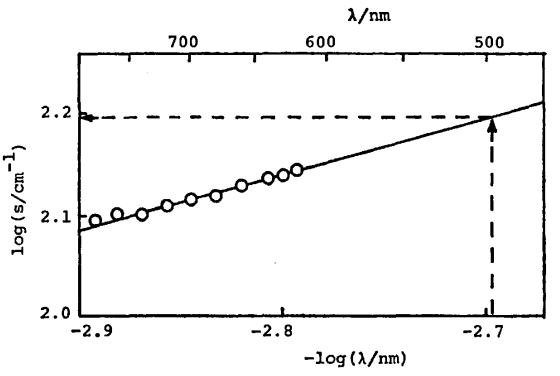

Fig. 3. Extrapolation of the scattering coefficient to a desired wavelength.
This figure is drawn based on the transmittance data in a Nujol mull of Λ-$[Co(en)_3]Br_3\cdot H_2O$.

where $\Delta\varepsilon$(cryst) is the molar circular dichroism and ε(cryst) the molar absorption coefficient in crystalline state.

By using a microspectrophotometer Kondo measured the absorption spectra of nine crystalline hexaamminecobalt(III) complex salts in the d-d transition band region.[15] The spectrum in crystal is not much different from that in aqueous solution, *e.g.*, the molar absorption coefficients of hexaamminecobalt(III) chloride are ε_{max}(cryst)=59.7 and ε_{max}(soln)=57.6 mol^{-1} dm^3 cm^{-1} for the first absorption band. We now assume that the molar absorption coefficient in crystal is equal to that in solution in the d-d transition band region:

$$\varepsilon(\text{cryst}) = \varepsilon(\text{soln}). \tag{30}$$

From Eqs. 29 and 30 the molar CD is given by

$$\Delta\varepsilon(\text{cryst}) = \varepsilon(\text{soln})\Delta k/k. \tag{31}$$

The value of k is, of course, calculated from the values of T and s for natural light.

Experimental

Measurements. In the Kubelka-Munk model the radiation field is divided into two streams in the forward and backward directions. Therefore, the light transmitted in the forward directions ($0 \leqq \theta < \pi/2$) has to be all detected in order to obtain the transmittance based on the Kubelka-Munk model. In a usual measurement parallel light, which passes through the space among suspended particles and hence contains no information from the particles, is more effectively detected by a photomultiplier than scattered light. By setting a plate of opal glass[16] on the unilluminated side of a sample cell, both of the parallel and the scattered light passing through the sample cell are accepted and transformed into diffused light at the plate of opal glass. If the diffused light emerging from the plate of opal glass has the same angular distribution for the incidence of parallel and scattered light, the transmittance is measured by detecting the diffused light on a photomultiplier of a conventional spectrophotometer. The plate of opal glass needs to be much larger than the cross section of light-path in order to prevent missing any of light scattered in the forward directions.

A mull between two parallel plates of quartz may be regarded as a plane-parallel scattering medium. When all of the light scattered into a cone, whose axis is colinear with the z-axis, is accepted simultaneously, the scattering contribution of the Stokes parameters I_1 and I_4 is eliminated from the transfer equation of light intensity. Then the opal glass method is served for the measurement of Θ.

The transmittance was measured with a Shimadzu UV-200 spectrophotometer, and the measurements of Θ were carried out on a JASCO MOE-1 spectropolarimeter at room temperature.

The measurements on Nujol mulls were made by using a quartz cell with demountable window (path length 9.15×10^{-3} cm). The blank values were also obtained by setting the plate of opal glass on the unilluminated side of the blank cell containing the mulling agent Nujol only.

A mull was prepared by adding Nujol (40—50 mg) to a sample complex salt (5—30 mg) in an agate mortar, and good grinding and mixing it.

Materials. The preparation of Λ-$[Co(en)_3]Br_3 \cdot H_2O$ was performed by well-known procedures.[17]

Hexaamminecobalt(III) tartrate was obtained by treating the solution of its chloride salt with an equivalent amount of freshly prepared silver *d*-tartrate. Silver chloride was precipitated and filtered off; the tartrate salt was crystallized from the filtrate. Found: C, 15.00; H, 7.24; N, 17.66%. Calcd for $[Co(NH_3)_6](d\text{-tart})_{1.5}5H_2O$: C, 15.23; H, 7.24; N, 17.76%.

Results and Discussion

In a scattering system, the ellipticity Θ recorded in a usual manner without a plate of opal glass was always smaller than that recorded by the opal glass method. This is because the parallel light, which contributes not to the numerator I_{ac} but to the denominator I_{dc} in Eq. 3, is more effectively detected by the photomultiplier when a plate of opal glass is absent.

When the CD spectrum was measured on mulls in a conventional manner, no reproducibility was found in the intensity and shape of the spectrum. By using a plate of opal glass, the reproducibility of the CD data was obtained. Especially the shape of recorded CD curves was well reproducible on repeated runs. For two complex salts the values of $\Delta\varepsilon$(cryst) at the maximum or the minimum in the first absorption region, which were measured on the samples having various concentrations of the salts, are shown in Table 1. As can be seen from the table, the deviations from the average value of $\Delta\varepsilon$(cryst) are, at most, 5% for Λ-$[Co(en)_3]Br_3 \cdot H_2O$ and 4% for $[Co(NH_3)_6](d\text{-tart})_{1.5} \cdot 5H_2O$. Particles in every mull have different shape and size distributions, so that the values of absorption and scattering coefficients

Table 1. Concentrations and the molar CD in Nujol mulls

Complex	Concentration	$\Delta\varepsilon$(cryst)[a]
Λ-$[Co(en)_3]Br_3 \cdot H_2O$	10.6%	+1.79
	12.3	+1.91
	12.7	+1.86
	14.2	+1.86
	14.6	+1.83
	15.8	+1.84
	15.9	+1.73
	18.3	+1.79
	19.0	+1.81
		av. +1.82
$[Co(NH_3)_6](d\text{-tart})_{1.5} \cdot 5H_2O$	14.6%	−0.61
	24.6	−0.62
	25.0	−0.61
	31.9	−0.65
	33.6	−0.64
	39.2	−0.66
	39.8	−0.65
	40.2	−0.65
		av. −0.64

a) The values are observed at 496 nm for Λ-$[Co(en)_3]Br_3 \cdot H_2O$, and at 478 nm for $[Co(NH_3)_6](d\text{-tart})_{1.5} \cdot 5H_2O$.

are characteristic not of materials but of every mull. Taking this fact into account, the magnitudes of the deviations are not so large; rather good reproducibility can be attained in the CD intensity regardless of the sample concentrations.

The CD spectrum of Λ-$[Co(en)_3]Br_3 \cdot H_2O$ in Nujol, which will be given elsewhere,[18] resembles that in aqueous solution. We have observed $\Delta\varepsilon(\text{cryst}) = +1.83$ at 496 nm, -0.26 at 435 nm, and $+0.24$ at 346 nm in a Nujol mull, and $\Delta\varepsilon(\text{soln}) = +1.89$ at 491 nm, -0.14 at 430 nm and $+0.24$ at 347 nm in an aqueous solution. Since the spectroscopic discrepancy is small, we suppose that the chirality around the central cobalt ion in crystal is not so different from that in solution. Kuroda and Saito have reported the CD data of some cobalt(III) complexes in KBr matrices.[19] For Λ-$[Co(en)_3]Cl_3 \cdot (1/2)NaCl \cdot 3H_2O$ the values of $\Delta\varepsilon = +2.0$ at 505.5 nm, -0.59 at 445.5 nm and $+0.19$ at 352 nm have been obtained. These values are appreciably different from the solid-state CD data obtained for Λ-$[Co(en)_3]Br_3 \cdot H_2O$ in this study. However, this is supposed to be caused by the influence of outer-sphere configuration.[20] Thus the value of $\Delta\varepsilon$(cryst) in our method is regarded as the value of the molar CD in crystal, which seems free from the effects of crystal anisotropies.[21]

On the other hand, the induced CD of $[Co(NH_3)_6]$-$(d\text{-tart})_{1.5} \cdot 5H_2O$ in crystal is more intensive than that in aqueous solution, *i.e.*, the value of $\Delta\varepsilon$(cryst), -0.64, is about 65 times that of $\Delta\varepsilon$(soln), -0.0098, in the first absorption band. It is because the chirality is induced in the achiral complex ion by surrounding tartrate ions more effectively in crystal than in solution.

At present our method is the only approach to determine the molar CD in multiple scattering systems. In the study of solid-state CD, the advantage of our method is that the isotropic solid-state CD, likewise the CD in solution, is obtained by easy experimental procedures, even if a minor error may exist.

References

1) M. Grosjean and M. Legrand, *C. R. Acad. Sci.*, **251**, 2150 (1960).
2) D. W. Urry, T. A. Hinners, and L. Masotti, *Arch. Biochem. Biophys.*, **137**, 214 (1970).
3) M. F. Maestre and C. Reich, *Biochemistry*, **19**, 5214 (1980).
4) D. J. Gordon, *Biochemistry*, **11**, 413 (1972).
5) S. Chandrasekhar, "Radiative Transfer," Dover Publications, New York (1960), p. 25.
6) I. Kuščer and M. Ribarič, *Optica Acta*, **6**, 42 (1959).
7) Chandrasekhar, Ref. 5, Chap. 1.
8) S. Chandrasekhar, "Liquid Crystals," Cambridge University Press, London (1977).
9) Chandrasekhar, Ref. 5, p. 39.
10) A. Schuster, *Astrophys. J.*, **21**, 1 (1905).
11) P. Kubelka, *J. Opt. Soc. Am.*, **38**, 448 (1948).
12) A. Gitter-Amir, K. Rosenheck, and A. S. Schneider, *Biochemistry*, **15**, 3131 and 3138 (1976).
13) C. F. Bohren, *Chem. Phys. Lett.*, **40**, 391 (1976).
14) G. Kortüm and D. Oelkrug, *Z. Naturforsch., Teil A*, **19**, 28 (1964).
15) Y. Kondo, *Sci. Light (Tokyo)*, **10**, 156 (1961).
16) K. Shibata, A. A. Benson, and M. Calvin, *Biochim. Biophys. Acta*, **15**, 461 (1954).
17) A. Werner, *Ber. Dtsch. Chem. Ges.*, **45**, 121 (1912).
18) Y. Taniguchi and Y. Shimura, to be submitted for publication.
19) R. Kuroda and Y. Saito, *Bull. Chem. Soc. Jpn.*, **49**, 433 (1976).
20) L. Dubicki, J. Ferguson, R. J. Geue, and A. M. Sargeson, *Chem. Phys. Lett.*, **74**, 393 (1980).
21) H. P. Jensen, *Acta Chem. Scand., Sect. A*, **30**, 137 (1976).

 © 1982 The Chemical Society of Japan Bull. Chem. Soc. Jpn., 55, 759—763 (1982)

Kinetics of Racemization and Dissociation of Tris(1,10-phenanthroline)-iron(II). Hydrophobic Interaction between the Complex Cation and Alkylammonium Cations

Satoshi TACHIYASHIKI* and Hideo YAMATERA†

Laboratory of Chemistry, Kagawa Nutrition College, Sakado, Saitama 350-02

†*Department of Chemistry, Faculty of Science, Nagoya University, Chikusa-ku, Nagoya 464*

(Received June 16, 1981)

The rates of racemization and dissociation of $[Fe(phen)_3]^{2+}$ were determined in the presence of series of alkali-metal bromides, symmetrical tetraalkylammonium bromides, and alkyltrimethylammonium bromides. The alkali-metal bromides did not affect the racemization rate, but they decreased the dissociation rate. The retarding effect increased with increasing bromide concentrations and decreased in the order of $Li^+ > Na^+ > K^+ > Rb^+ > Cs^+$. The alkylammonium bromides increased the racemization rate up to three fold and decreased the dissociation rate down to half the rate in pure water; alkylammonium ions with longer alkylchains induced greater changes of the rates. The effect of alkylammonium ions on the reaction rates was analyzed in terms of the formation of 1:1 aggregates of the complex cation with the alkylammonium cation caused by hydrophobic interactions. The equilibrium constant for the aggregate formation was greater for the alkylammonium ions with longer alkyl chains. The reaction rate constants of the hydrophobic aggregates remain almost constant with the increase in the alkyl chain length. The rate behaviors of the hydrophobic aggregates are discussed in terms of the reaction mechanisms of racemization and dissociation of $[Fe(phen)_3]^{2+}$.

Tetraalkylammonium ions can be used as model compounds for investigating hydrophobic interactions.[1] Salting-in of a hydrophobic solute by tetraalkylammonium ions has mainly been attributed to hydrophobic interactions between the cations and nonelectrolytes.[2] Tris(1,10-phenanthroline)metal chelates are also considered to be hydrophobic because of the large hydrophobicity of the ligand. Tris(1,10-phenanthroline)nickel(II) is reported to salt-in tris(acetylacetonato)cobalt(III) to water by hydrophobic interactions.[3] A stacking interaction, caused by hydrophobic interaction and a polarization effect, was proposed for the enhancement of the rates of the mixed complex formation of mono(2,2′-bipyridine)-, mono(1,10-phenanthroline)-, and mono(2,2′:6′,2″-terpyridine)-metal complexes with some aromatic nitrogen donors.[4] Thus, it is interesting to study the nature of the interaction between hydrophobic alkylammonium cations and hydrophobic metal complex cations. The rate of aquation of tris(5-nitro-1,10-phenanthroline)iron(II) was reported to be influenced by the addition of alkylammonium cations.[5] The effects were analyzed in terms of salt effects on both the initial and transition states. Jensen *et al.*[6] reported the effect of octadecyltrimethylammonium chloride on the dissociation rate of $[Fe(phen)_3]^{2+}$ (phen=1,10-phenanthroline).

We previously reported the effects of added inorganic salts on the rates of racemization and dissociation of $[Fe(phen)_3]^{2+}$.[7] The racemization rate increased slightly with the increase in the polarizability of the anion, whereas the dissociation rate remarkably increased with the increase in the pK_a value of the conjugate acid of the anion. The racemization of $[Fe(phen)_3]^{2+}$ is known to occur much faster in organic solvents than in aqueous solution.[8] The ability of the solvent to accelerate the racemization rate was correlated with its solvating power to the ligand[9] or with its electron-donating ability.[10] However, the details of the nature of this acceleration effect of the solvents are not clear. Since organic salts can be regarded as compounds intermediate between inorganic salts and organic solvents, the study of the effects of added organic salts such as alkylammonium bromides and sodium alkanesulfonates on the kinetics of racemization and dissociation is expected to give information concerning the nature of the solvent effects. With this expectation, we decided to study the effect of alkali-metal and alkylammonium cations on the rates of racemization and dissociation of $[Fe(phen)_3]^{2+}$. The comparison of the effects of inorganic and organic cations on the reaction rates will lead us to understand the solvent effects and the mechanisms of the dissociation and the intramolecular twist racemization. The present study will also give information about the interactions between the hydrophobic alkylammonium cations and the hydrophobic complex cation. The effect of organic anions on the reaction rates of $[Fe(phen)_3]^{2+}$ will be reported elsewhere.

Experimental

The symmetrical tetraalkylammonium bromides used were reagents of the best grade obtainable from Wako Pure Chemical Industries, Ltd. Ammonium bromide was recrystallized from water, tetramethylammonium bromide from aqueous methanol(1:1), tetraethyl- from ethanol, tetrapropyl- from methanol, tetrabutyl- and tetrapentyl- from acetone. They were dried by heating at 110 °C for 18 h. Alkyltrimethylammonium bromides were guaranteed-grade reagents of Tokyo Kasei Kogyo Co., Ltd. Hexyl-, octyl-, decyl-, dodecyl-trimethylammonium bromides were recrystallized from acetone, while tetradecyl- and hexadecyl-trimethylammonium bromides were recrystallized from 10:1 and 2:1 acetone–ethanol, respectively. They were dried by heating at 90 °C for 24 h. Tetraphenylphosphonium chloride of Dojindo Laboratories, and lithium, sodium, potassium, rubidium, and caesium bromides of Merck(Suprapur) were used without further purification. The concentrations of the solutions of tetraethylammonium bromide, hexyltrimethylammonium bromide, and lithium bromide were determined by argentometry. Those of other salts were deter-

mined by weighing well-dried reagents. The purities of tetrapentylammonium bromide, and octyl-, decyl-, dodecyl-, and tetradecyl-trimethylammonium bromides were more than 99%, as determined by argentometry. Kinetic data were obtained at 32.0 °C using the perchlorate of the complex. The bromide of the metal complex was preferred to the perchlorate for the systems containing dodecyl- and tetradecyl-trimethylammonium ions, since the addition of perchlorate would precipitate alkylammonium perchlorate. In measuring the dissociation rate for the systems containing tetrapentylammonium bromide and alkyltrimethylammonium bromides, hydrochloric acid was added to the solution up to two percent of the alkylammonium bromide concentration; otherwise iron hydroxide might be precipitated in the course of the reaction due to the presence of a trace amount of the alkylamines contained in alkylammonium bromides. Other chemicals and procedures were the same as those described in a previous paper.[7]

Results and Discussion

Alkali-metal Cations. Table 1 and Fig. 1 show the observed first order rate constants of racemization and dissociation of $[Fe(phen)_3]^{2+}$ in the presence of a series of alkali-metal bromides. The racemization rate was not appreciably influenced by the addition of the alkali-metal bromides. The dissociation rate decreased with the increase in the alkali-metal bromide concentration. The order of the cation efficiency in decreasing the rates was $Li^+ > Na^+ > K^+ > Rb^+ > Cs^+$, which is consistent with the previously reported order of $Li^+ > K^+$.[11] As the order is the same as that for the effect of decreasing the activity of water,[12] the effect of cations on the dissociation rates can be at least partly explained in terms of the changes in the activity of water; this change should affect the dissociation rate if the dissociation proceeded through a 7-coordinate transition state with an H_2O ligand.[7]

Alkylammonium Cations. The racemization rate increased and the dissociation rate decreased with the increase in the concentration of tetraalkyl- and alkyltrimethyl-ammonium bromides, as shown in Figs. 2—5. These also show that the extent of the rate change with the alkylammonium ion concentrations becomes greater with increasing length of the alkyl chain for both racemization and dissociation. However, both the racemization and dissociation rates are almost constant above certain concentrations of tetraphenylphosphonium cation and alkyltrimethylammonium cations, as shown in Figs. 2, 3, and 5. The critical concentrations above which the rates were almost constant shifted toward lower concentrations with the increase

Table 1. Racemization rate constants of $[Fe(phen)_3]^{2+}$ in 1.0 mol dm^{-3} alkali-metal bromide solutions at 32.0 °C

Added salt	$k_r/10^{-3}$ s^{-1}
LiBr	1.78, 1.85
NaBr	1.86, 1.88
KBr	1.83, 1.85
RbBr	1.83, 1.85
CsBr	1.86, 1.90

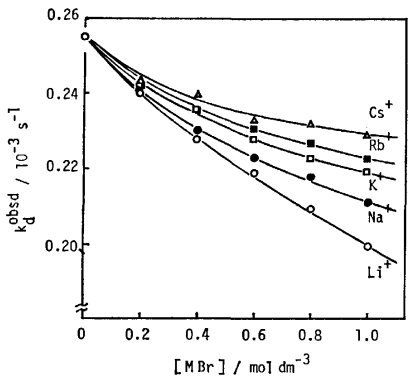

Fig. 1. Dissociation rate constants of $[Fe(phen)_3]^{2+}$ in alkali-metal bromide solutions at 32.0 °C.
○, Li^+; ●, Na^+; □, K^+; ■, Rb^+; △, Cs^+.

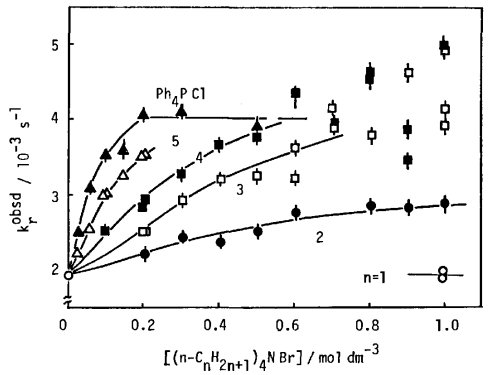

Fig. 2. Racemization rate constants of $[Fe(phen)_3]^{2+}$ in symmetrical tetraalkylammonium bromide and tetraphenylphosphonium chloride solutions at 32.0 °C.
○, $(CH_3)_4NBr$; ●, $(C_2H_5)_4NBr$; □, $(n\text{-}C_3H_7)_4NBr$; ■, $(n\text{-}C_4H_9)_4NBr$; △, $(n\text{-}C_5H_{11})_4NBr$; ▲, $(C_6H_5)_4PCl$.

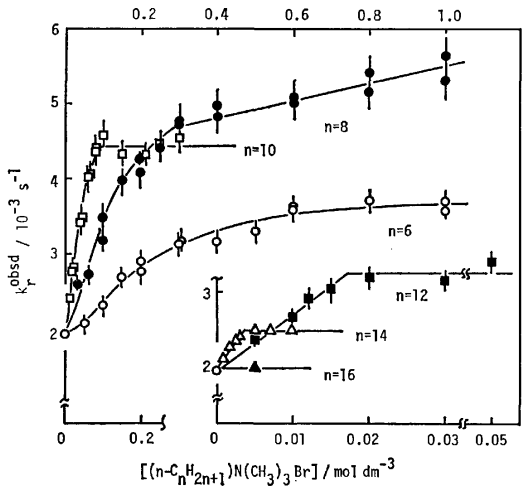

Fig. 3. Racemization rate constants of $[Fe(phen)_3]^{2+}$ in alkyltrimethylammonium bromide solutions at 32.0 °C.
○, $(n\text{-}C_6H_{13})N(CH_3)_3Br$; ●, $(n\text{-}C_8H_{17})N(CH_3)_3Br$; □, $(n\text{-}C_{10}H_{21})N(CH_3)_3Br$; ■, $(n\text{-}C_{12}H_{25})N(CH_3)_3Br$; △, $(n\text{-}C_{14}H_{29})N(CH_3)_3Br$; ▲, $(n\text{-}C_{16}H_{33})N(CH_3)_3Br$.

in the length of the alkyl chain. As is shown in Table 2, the critical concentration is close to the critical micelle concentration (cmc) for each electrolyte. Thus, these phenomena can reasonably be correlated with the micelle formation of the cations above cmc. As the concentration of the monomeric cations remains unchanged above cmc, the kinetic results suggest that the interaction of the complex ion with the monomeric cations is responsible for the observed features of the rate changes. A previously reported phenomenon,[6] that the added octadecyltrimethylammonium chloride had no effect on the rate of dissociation of $[Fe(phen)_3]^{2+}$, can be reasonably accounted for by the very low concentration of the monomeric alkylammonium ion, as indicated by the extremely low cmc value. The slight increase of the rates observed for octyl- and decyl-trimethylammonium ions above cmc would be caused by some interactions of the complex with micelles.

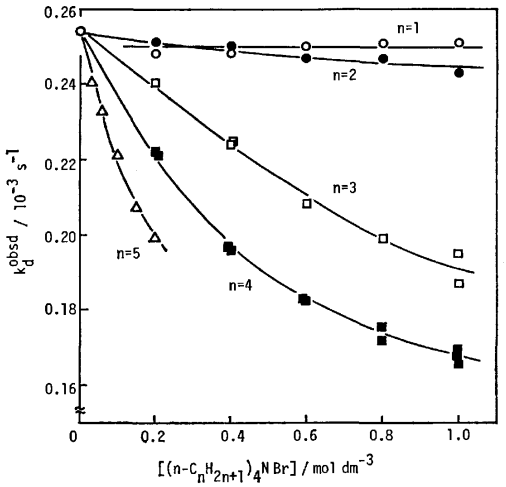

Fig. 4. Dissociation rate constants of $[Fe(phen)_3]^{2+}$ in symmetrical tetraalkylammonium bromide solutions at 32.0 °C.
○, $(CH_3)_4NBr$; ●, $(C_2H_5)_4NBr$; □, $(n\text{-}C_3H_7)_4NBr$; ■, $(n\text{-}C_4H_9)_4NBr$; △, $(n\text{-}C_5H_{11})_4NBr$.

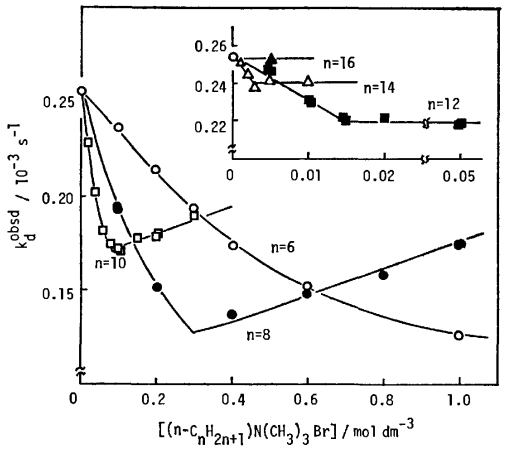

Fig. 5. Dissociation rate constants of $[Fe(phen)_3]^{2+}$ in alkyltrimethylammonium bromide solutions at 32.0 °C.
○, $(n\text{-}C_6H_{13})N(CH_3)_3Br$; ●, $(n\text{-}C_8H_{17})N(CH_3)_3Br$; □, $(n\text{-}C_{10}H_{21})N(CH_3)_3Br$; ■, $(n\text{-}C_{12}H_{25})N(CH_3)_3Br$; △, $(n\text{-}C_{14}H_{29})N(CH_3)_3Br$; ▲, $(n\text{-}C_{16}H_{33})N(CH_3)_3Br$.

As the alkali-metal cations have no effects on the racemization rate, the acceleration of the racemization rate by the monomeric alkylammonium ions can be attributed to the hydrophobic interactions between the complex and the alkylammonium ions. The kinetic results can reasonably be accounted for by assuming the formation of 1:1 hydrophobic aggregates between the alkylammonium ions and complex cations. The following mechanism was considered:

$$[Fe(phen)_3]^{2+} + Br^- \overset{K_1}{\rightleftharpoons} [Fe(phen)_3]^{2+}\cdot Br^-, \quad (1)$$

$$[Fe(phen)_3]^{2+} + R_4N^+ \overset{K_2}{\rightleftharpoons} [Fe(phen)_3]^{2+}\cdot R_4N^+, \quad (2)$$

$$[Fe(phen)_3]^{2+}\cdot Br^- + R_4N^+ \overset{K_3}{\rightleftharpoons} [Fe(phen)_3]^{2+}\cdot Br^-\cdot R_4N^+, \quad (3)$$

$$K_1 = \frac{[Fe(phen)_3{}^{2+}\cdot Br^-]}{[Fe(phen)_3{}^{2+}][Br^-]}\cdot\frac{f_1}{f_2 f_1}, \quad (4)$$

$$K_2 = \frac{[Fe(phen)_3{}^{2+}\cdot R_4N^+]}{[Fe(phen)_3{}^{2+}][R_4N^+]}\cdot\frac{f_3}{f_2 f_1}, \quad (5)$$

$$K_3 = \frac{[Fe(phen)_3{}^{2+}\cdot Br^-\cdot R_4N^+]}{[Fe(phen)_3{}^{2+}\cdot Br^-][R_4N^+]}\cdot\frac{f_2}{f_1 f_1}, \quad (6)$$

$$[Fe(phen)_3]^{2+} \xrightarrow{k_0}, \quad (7)$$

$$[Fe(phen)_3]^{2+}\cdot Br^- \xrightarrow{k_1}, \quad (8)$$

$$[Fe(phen)_3]^{2+}\cdot R_4N^+ \xrightarrow{k_2}, \quad (9)$$

$$[Fe(phen)_3]^{2+}\cdot Br^-\cdot R_4N^+ \xrightarrow{k_3}, \quad (10)$$

where f_z means the activity coefficient of an ion with a charge of $\pm z$, and can be expressed by the Debye-Hückel equation, as discussed previously.[7] The closest distance of approach, a, was assumed to be 8, 9, and 9—11 $\times 10^{-8}$ cm for $z=\pm1$, ±2, and ±3, respectively. The rate constants k_0, k_1, k_2, and k_3 mean the first order rate constants (Eqs. 7—10) for either racemization (r) or dissociation (d) of each chemical species. Additional subscripts, r and d, may be used to specify the type of reaction. The observed

TABLE 2. THE CRITICAL CONCENTRATIONS (C/mol dm^{-3}) ABOVE WHICH THE RATES SHOW CONSTANT VALUES

Salt	Racemization	Dissociation	cmc values[a]
$(C_6H_5)_4PCl$	0.20 ±0.02	—	—
$n\text{-}C_8H_{17}N(CH_3)Br$	0.32 ±0.02	0.29 ±0.01	(≈0.3)
$n\text{-}C_{10}H_{21}N(CH_3)Br$	0.065 ±0.003	0.068 ±0.003	0.068
$n\text{-}C_{12}H_{25}N(CH_3)Br$	0.0173±0.0010	0.0155±0.0005	0.0153
$n\text{-}C_{14}H_{29}N(CH_3)Br$	0.0036±0.0003	0.0030±0.0002	0.00302

a) J. N. Phillips, *Trans. Faraday Soc.*, **51**, 561 (1955).

rate constant is expressed as:

$$k^{obsd} = \frac{k_0 + k_1K_1[Br^-]f_2 + k_2K_2[R_4N^+]f_1f_2/f_3 + k_3K_1K_3[Br^-][R_4N^+]f_1^2}{1 + K_1[Br^-]f_2 + K_2[R_4N^+]f_1f_2/f_3 + K_1K_3[Br^-][R_4N^+]f_1^2}, \quad (11)$$

where $[Br^-]$ and $[R_4N^+]$ can be taken to be equal to the total alkylammonium ion concentration (C_t) at a very low concentration of the complex. At very low alkylammonium ion concentrations, Eq. 11 is transformed to:

$$k^{obsd} = k_0 + (k_1-k_0)K_1[Br^-]f_2 + (k_2-k_0)K_2[R_4N^+]f_1f_2/f_3$$
$$= k_0 + \{(k_1-k_0)K_1 + (k_2-k_0)K_2\}C_t.$$

The gradient (m) of k^{obsd} *vs.* C_t is then;

$$m = (k_1-k_0)K_1 + (k_2-k_0)K_2. \quad (12)$$

For systems containing symmetrical tetraalkylammonium ions, tetraphenylphosphonium ion, hexyl-, octyl-, and decyl-trimethylammonium ions, the kinetic data were analyzed on the basis of Eq. 11. Among the parameter values in Eq. 11, $k_{0r}=k_{1r}=(1.94\pm0.09)\times10^{-3}$ s^{-1}, $k_{0d}=(2.54\pm0.03)\times10^{-4}$ s^{-1}, $k_{1d}=(2.1\pm0.2)\times10^{-4}$ s^{-1}, and $K_1=3$ mol^{-1} dm^3 were previously obtained.[7] Since the simultaneous determination of the values of k_2, K_2, k_3, and K_3 was impossible because of experimental errors in the kinetic data, they were determined in the following way. The formation constant of $[Fe(phen)_3]^{2+}\cdot R_4N^+$ would be small compared with that of $[Fe(phen)_3]^{2+}\cdot Br^-\cdot R_4N^+$. Therefore, we analyzed the kinetic data, considering only the formation of $[Fe(phen)_3]^{2+}\cdot Br^-$ and $[Fe(phen)_3]^{2+}\cdot Br^-\cdot R_4N^+$, to obtain approximate k_3 and K_3 values. Using the approximate k_3 and K_3 values and taking the formation of $[Fe(phen)_3]^{2+}\cdot R_4N^+$ into account, the kinetic data were reanalyzed to obtain approximate k_2 and K_2 values. Then using the values of k_2, K_2, k_3, and K_3 thus obtained as the initial values, the least-squares fitting[13] of the kinetic data to Eq. 11 were carried out to give more reliable values for k_2, K_2, k_3, and K_3. The results of the analysis are listed in Table 3.

For the systems containing dodecyl- and tetradecyltrimethylammonium ions, their small cmc values restricted the measurement of the rates within a narrow range of the ammonium ion concentrations; therefore, Eq. 11 was not applicable in the analysis of the kinetic data. Thus, Eq. 12 was used to analyze the kinetic data for these systems, as well as for the systems containing octyl- and decyl-trimethylammonium ions. As the values of k_0, k_1, and K_1 have been previously obtained, Eq. 12, together with the experimental determination of the value of m, gives us the relation between k_2 and K_2. Then, K_2 can be obtained on the assumption that k_{2d} values for the complex in the hydrophobic aggregates with octyl-, decyl-, dodecyl-, and tetradecyl-trimethylammonium cations are negligibly small, an assumption which seems reasonable if we compare the k_{2d} values for the homologs (see Table 3). Then, the K_2 value thus obtained and the m_r value experimentally determined will be substituted in Eq. 12 to give the value of k_{2r}. The K_2 and k_{2r} values obtained in this manner are listed in Table 3 within parentheses.

The K_2 and K_3 values increased with the increase in the number of carbon atoms of the alkyl chains, as shown in Table 3 and Fig. 6. This implies that the formation of the aggregates is caused by the hydrophobic interaction between the complex and alkylammonium cations, which is presumed to be larger for a longer alkyl chain. The aggregate formation constant (K_2) for the complex and tetraphenylphosphonium ions falls on the line of the K_2 values for tetraalkylammonium ions as shown in Fig. 6; this shows the similarity of the interaction of the complex ion with phenyl groups to that with alkyl groups. Figure 6 also shows that the dependence of the log K_2 value on the total carbon number of the ammonium ion is twice as large for alkyltrimethylammonium ions as for tetraalkylammonium ions. That is, the energies of hydrophobic interaction with complex cations were 0.8 kJ/mol and 0.4 kJ/mol per methylene group for alkyltrimethylammonium cations and tetraalkylammonium cations, respectively.

Table 3. The formation constants of the hydrophobic aggregates and the rate constants of racemization and dissociation of $[Fe(phen)_3]^{2+}$ in the aggregates[a]

Cation	$k_2/10^{-3}$ s^{-1}		K_2/mol^{-1} dm^3		$k_3/10^{-3}$ s^{-1}		K_3/mol^{-1} dm^3	
	Racem.	Diss.	Racem.	Diss.	Racem.	Diss.	Racem.	Diss.
$(C_2H_5)_4N$	7±4	—	0.2±0.2	—	3.6±0.5	—	2.2±1.6	—
$(n\text{-}C_3H_7)_4N$	7±5	0.03 ±0.04	0.2±0.2	0.6±0.2	5.0±0.3	—	2.9±0.8	—
$(n\text{-}C_4H_9)_4N$	5±2	0.04 ±0.02	1.1±0.5	1.4±0.3	4.8±0.2	—	5.7±2.1	—
$(n\text{-}C_5H_{11})_4N$	4±3	0.15 ±0.15	1.9±1.5	1.6±0.7	3.9±0.2	0.187±0.015	45± 20	29± 7
$(C_6H_5)_4P$	5±2	—	4.0±4.0	—	4.2±0.2	—	66± 46	—
$n\text{-}C_6H_{13}N(CH_3)_3$	3±2	0.002±0.015	1.2±0.7	1.5±0.3	4.0±0.1	—	12± 2	—
$n\text{-}C_8H_{17}N(CH_3)_3$	5±2 (8±1)	0.000±0.002	2.5±2.0	2.1±0.3 (2.3±0.2)	5.4±0.2	0.110±0.010	28± 5	15± 3
$n\text{-}C_{10}H_{21}N(CH_3)_3$	8±3 (10±1)	0.003±0.004	5.4±2.9	3.9±2.1 (5.0±0.3)	4.7±0.2	0.162±0.013	171±112	175±120
$n\text{-}C_{12}H_{25}N(CH_3)_3$	(11±2)	—	—	(8.4±1.2)	—	—	—	—
$n\text{-}C_{14}H_{29}N(CH_3)_3$	(9±1)	—	—	(20.9±1.6)	—	—	—	—

a) The values were obtained from the analysis based on Eq. 11, except for a few cases where the results from the analysis based on Eq. 12 are given in parentheses.

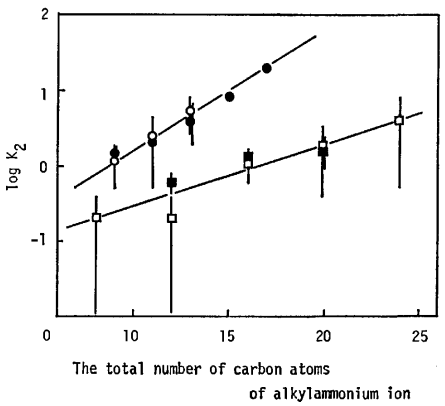

Fig. 6. Plot of $\log K_2$ against the total number of carbon atoms of the alkylammonium ion.
The open marks are the results of the analysis based on Eq. 11 and the closed marks are those based on Eq. 12. ○,●: Alkyltrimethylammonium ion. □,■: Symmetrical tetraalkylammonium ion.

The k_2 and k_3 values both for racemization and for dissociation did not significantly depend on the alkyl chain length, as shown in Table 3. The k_2 values for the racemization rate of the complex were about three times as large as k_0, and for the dissociation rate, the k_2 values were much smaller than k_0 (Table 3). As the alkylammonium ions have no electron-donating ability, the increase in the racemization rates due to the formation of the hydrophobic aggregates may come from a kind of solvating effect of the alkyl groups of the ammonium ions and/or from the modification of the iceberg structure[14] surrounding the complex ion. The exceptionally slow racemization in water, compared with the rates in other solvents, may result from the cage effect of the iceberg structure. The slow dissociation rate of the complex in the aggregate would result from the decrease in the water concentration around the complex cation by the formation of the aggregates and/or from the decrease in the activity of water due to modification of the iceberg structure.

References

1) Wen-Yang Wen, "Water and Aqueous Solutions," ed by R. A. Horne, Wiley Interscience (1972), pp. 613—661.
2) M. J. Blandamer, *Adv. Phys. Org. Chem.*, **14**, 204 (1977).
3) E. Iwamoto, Y. Tanaka, H. Kimura, and Y. Yamamoto, *J. Solution Chem.*, **9**, 841 (1980).
4) D. W. Margerum *et al.*, "Coordination Chemistry," ed by A. E. Martell, American Chemical Society, Washington, D. C. (1978), Vol. II, pp. 140—143.
5) M. J. Blandamer, J. Burgess, and S. H. Morris, *J. Chem. Soc., Dalton Trans.*, **1974**, 1717.
6) A. Jensen, F. Basolo, and H. M. Neumann, *J. Am. Chem. Soc.*, **80**, 2354 (1958).
7) S. Tachiyashiki and H. Yamatera, *Bull. Chem. Soc. Jpn.*, **55**(4), (1982) in press.
8) N. R. Davies and F. P. Dwyer, *Trans. Faraday Soc.*, **50**, 1325 (1954); L. Seiden, F. Basolo, and H. M. Neumann, *J. Am. Chem. Soc.*, **81**, 3809 (1959).
9) F. M. Van Meter and H. M. Neumann, *J. Am. Chem. Soc.*, **98**, 1388 (1976).
10) S. Tachiyashiki and H. Yamatera, *Bull. Chem. Soc. Jpn.*, **54**, 3340 (1981); T. Fujiwara, Y. Okamoto, and Y. Yamamoto, private communication (*Inorg. Nucl. Chem. Lett.*, submitted).
11) J. E. Dickens, F. Basolo, and H. M. Neumann, *J. Am. Chem. Soc.*, **79**, 1286 (1957).
12) O. J. Samoilow, "Die Struktur Wässriger Elektrolytlösungen und die Hydratation von Ionen," B. G. Teubner Verlagsgesellschaft, Leipzig (1961), p. 75.
13) The least-squares fitting was carried out by using the program, "SALS" (Nakagawa and Oyanagi), in the library programs of the Computer Center, The University of Tokyo.
14) H. S. Frank and M. W. Evans, *J. Chem. Phys.*, **13**, 507 (1945).

The Raman Spectra of Cobalt(III) Complexes. III. Differentiation between *cis* and *trans* Isomers of Tetraamminecobalt(III) Complexes

Kan KANAMORI* and Kiyoyasu KAWAI

Department of Chemistry, Faculty of Science, Toyama University Gofuku, Toyama 930

(Received June 19, 1981)

The Raman and the infrared spectra of tetraamminecobalt(III) complexes have been measured to find the vibrational criteria for differentiating between the *cis* and *trans* configurations. Conspicuous differences between the isomers were found in the ν(Co–NH_3) region. Thus, generally the *trans* isomers have two bands at ca. 480 and *ca.* 450 cm^{-1} in the Raman spectra and one band at *ca.* 510 cm^{-1} in the infrared spectra, and the mutual exclusion rule virtually holds. On the other hand, the *cis* isomers have more than three bands in the region of both the Raman and the infrared spectra.

In our previous paper,[1] we identified the Raman criterion for differentiating the geometrical isomers of bis(ethylenediamine)cobalt(III) complexes. Many infrared criteria[2–6] have been also used for these complexes. However little vibrational work has been done to study the stereochemistry of tetraamminecobalt(III) complexes. Faust and Quagliano[7] first applied infrared measurements in the NaCl region to *cis*- and *trans*-tetraamminedinitrocobalt(III) ions and found that the spectrum of the *cis* isomer reveals a slightly more complicated feature than that of the *trans* isomer in the NO_2 stretching region. Conspicuous differences between the geometrical isomers have been found in the skeletal vibration region (200—600 cm^{-1}) in both the infrared[8] and the Raman[9] spectra.

The present study was undertaken to find definite vibrational criteria for differentiating the geometrical isomers of tetraamminecobalt(III) complexes. For this purpose, the Raman and the infrared spectra of a large number of tetraamminecobalt(III) complexes were examined in the ν(Co–NH_3) region (350—550 cm^{-1}). The established criteria were then applied to $[Co(NCS)_2(NH_3)_4]^+$, $[CoCl(NCS)(NH_3)_4]^+$ and $[CoX(NO_2)(NH_3)_4]$-type complexes prepared in the present work (X=Cl^-, H_2O, CN^-).

Experimental

Preparation. *$[Co(NCS)_2(NH_3)_4]Cl$*: One of the isomers has been obtained by Werner.[10] We prepared the isomeric pair by the following method. A solution containing 24 g of cobalt(II) chloride hexahydrate and 76 g of ammonium thiocyanate in 200 cm^3 of 10% aqueous ammonia was oxidized by bubbling air for 6 h at 40 °C, whereupon a red powder separated. The red powder was filtered and washed with a large amount of ethanol. The yield of the crude product was about 13 g. One gram of the crude product was dissolved in 1000 cm^3 of water and the solution was passed through Sephadex cation-exchange resin (SP, C-25; 30 mm×600 mm). By elution with a 0.05 M LiCl solution, two bands, pinkish red one and brick red one, descended in that order. Each eluate was concentrated to a small volume below 40 °C and mixed with ethanol. Each compound thus obtained was recrystallized from water by adding a saturated solution of lithium chloride. Yield 0.3 g for the pinkish red isomer. 0.2 g for the brick red isomer. The infrared spectrum of the brick red isomer is identical with that of the complex obtained by Werner's method.[3] Absorp. max. $10^{-3}\,\sigma/cm^{-1}$ ($\log \varepsilon/mol^{-1}\,dm^3\,cm^{-1}$): 19.5(2.24), 31.75(3.38) for the pinkish red isomer; 20.3 (2.54), 32.3 (3.58) for the brick red isomer. Found: C, 8.66; H, 4.60; N, 30.27% for the former isomer. C, 8.60; H, 4.43; N, 29.72% for the latter isomer. Calcd for $[CoC_2H_{12}N_6S_2]Cl$: C, 8.62; H, 4.34; N, 30.16%.

$[CoCl(NCS)(NH_3)_4]Cl$: The *trans* isomer was obtained according to the method of Poon.[11] The *cis* isomer was obtained by the following method. A solution of 6 g of *trans*-$[CoCl_2(NH_3)_4]SCN$ in 80 cm^3 of water was stirred at 50 °C for half an hour. The resulting reddish violet solution was cooled to room temperature and 80 cm^3 of concd HCl was added. Then a reddish violet precipitate was deposited. The precipitate was added to 400 cm^3 of 6 mol dm^{-3} HCl and the mixture was warmed on a water bath for a few minutes and then filtered. The filtrate was cooled to room temperature and ethanol was added to it. The complex thus precipitated was filtered, washed with methanol and dried in air. The complex was recrystallized from cold water by adding concd HCl. Yield 4 g. Found: C, 4.51; H, 4.96; N, 26.70%. Calcd for $[CoCClH_{12}N_5S]Cl\cdot 0.5H_2O$: C, 4.53; H, 4.76; N, 26.43%.

$[CoCl(NO_2)(NH_3)_4]Cl$: The *trans* isomer was obtained by the method of Werner.[12] Meyer and Rampoldt[13] have shown the scheme for the preparation of the *cis* isomer through a reaction of tetraamminecarbonatocobalt(III) salt with nitrosyl chloride but the detailed procedure has not been described. So, the *cis* isomer was obtained by the following method. A solution of 2.8 g of sodium nitrite in 30 cm^3 of water was added to a solution of 10.8 g of *cis*-$[CoCl(NH_3)_4(H_2O)]Cl_2$ in 400 cm^3 of water and the mixture was stirred at 40 °C for 10 min. The resulting brown solution was evaporated to a small volume below 40 °C under reduced pressure, and a large amount of ethanol was added to it. The precipitate thus obtained was added to 400 cm^3 of 6 mol dm^{-3} HCl and the mixture was stirred for half an hour and then filtered. To the filtrate, 400 cm^3 of methanol was added and the solution was cooled in a refrigerator for 12 h. The desired complex was deposited as brownish red needle-like crystals. Yield 5 g. Found: H, 5.00; N, 28.64%. Calcd for $[CoClH_{12}N_5O_2]Cl$: H, 4.96; N, 28.71%.

$[Co(NO_2)(NH_3)_4(H_2O)](NO_3)_2$: The *trans* isomer was obtained by the method of Jörgensen.[14] The *cis* isomer has been prepared from $[Co(SO_4)(NH_3)_4(H_2O)]NO_2$ by King and Mistry[15] and from $[Co(ONO)(NH_3)_4(H_2O)](NO_3)_2$ by Yalman and Kuwana.[16] However, the isomer was obtained more easily from *cis*-$[CoCl(NO_2)(NH_3)_4]Cl$ by the following method. A solution of 3.4 g of silver nitrate in 20 cm^3 of water was added to a solution of 2.6 g of *cis*-$[CoCl(NO_2)(NH_3)_4]Cl$ in 20 cm^3 of water and the mixture was stirred at 50 °C. The silver chloride deposited was filtered off and 20 cm^3 of concd HNO_3 and then methanol was added to the filtrate. The crude orange powder was recrystallized from hot water by adding concd HNO_3. Yield 1.5 g. Found: H, 4.51; N, 30.99%. Calcd for $[CoH_{14}N_5$-

$O_3](NO_3)_2$: H, 4.48; N, 31.12%.

[Co(CN)(NO$_2$)(NH$_3$)$_4$]Cl: The *trans* isomer was obtained from $[CoCl(CN)(NH_3)_4]Cl$.[17] To a suspension of 1.2 g of $[CoCl(CN)(NH_3)_4]Cl$ in 30 cm^3 of water, 0.35 g of solid sodium nitrite was added and the mixture was stirred at 50 °C for 2 h, then a brownish yellow solution was obtained. Ethanol was added to the solution and the yellow crystals deposited were filtered and recrystallized from hot water by adding ethanol. Yield 0.7 g. Found: C, 4.79; H, 5.59; N, 32.70%. Calcd for $[CoCH_{12}N_6O_2]Cl\cdot H_2O$: C, 4.76; H, 5.59; N, 33.28%.

The *cis* isomer was obtained from *cis*-$[CoCl(NO_2)(NH_3)_4]$-Cl. A solution of 1.7 g of silver nitrate in 30 cm^3 of dimethylsulfoxide (DMSO) was added to a solution of 2.6 g of *cis*-$[CoCl(NO_2)(NH_3)_4]Cl$ in 150 cm^3 of DMSO and the silver chloride deposited was filtered off. Then, 2 g of silver cyanide was added to the filtrate. The suspension was stirred at 60 °C for 5 h; the color of the liquid phase was changed from brownish red to orange yellow. To the suspension, 500 cm^3 of water was added and the insoluble product was filtered off. The filtrate was poured onto Sephadex ion-exchange resin (SP, C-25; 30 mm×700 mm). By elution with a 0.05 M LiCl solution, three bands colored brownish yellow descended. The desired complex was obtained from the second eluate. This eluate was concentrated to a small volume. A brownish yellow precipitate was obtained by the addition of ethanol and recrystallized from warm water. Yield 0.5 g. It was found from absorption measurements that the first eluate contains *trans*-$[Co(CN)(NO_2)(NH_3)_4]^+$ and the third one contains *cis*-$[Co(NO_2)_2(NH_3)_4]^+$. Found: C, 5.00; H, 5.36; N, 33.94%. Calcd for $[CoCH_{12}N_6O_2]Cl\cdot 0.5H_2O$: C, 4.93; H, 5.35; N, 34.51%.

Other Complexes: *trans*-$Na[Co(SO_3)_2(NH_3)_4]$ was prepared by the method of Akamatsu *et al.*[18] All the other complexes are well known and were prepared by standard means.

Measurements. The Raman spectra were recorded on a JASCO R-800 Laser Raman spectrometer with a data processor, using a He–Ne (632.8 nm) or an Ar^+ ion (514.5 nm) laser as an excitation source. The infrared spectra were recorded on a JASCO A-3 spectrometer. The observed frequencies were calibrated by the 533.8 cm^{-1} band of indene for the Raman spectra and the 618.0 cm^{-1} band of polystylene film for the infrared one. The observed frequencies are accurate within ±2 cm^{-1}.

Results and Discussion

If it is assumed that a *trans* isomer of $[Coa_2(NH_3)_4]$-type complexes (a represents a unidentate ligand) possesses a D_{4h} symmetry, the cobalt-ammonia stretching vibrations transform as $(A_{1g}+B_{1g}+E_u)$, the g modes being Raman allowed and the u mode infrared allowed. Therefore mutual exclusion will be expected. Supposing a C_{4v} symmetry for *trans*-$[Coab(NH_3)_4]$-type complexes (a and b represent an unidentate ligand), the cobalt-ammonia stretching vibrations transform as (A_1+B_1+E), all of which are formally Raman active, and A_1+E modes are formally infrared active. However, the A_1 and the E modes are closely correlated with the A_{1g} and the E_u modes of D_{4h} symmetry, respectively. So we expect that the E mode will be hardly detectable in the Raman spectra of $[Coab(NH_3)_4]$-type complexes. In the same way, the infrared intensity of the A_1 mode will be very weak. Thus, the mutual exclusion will virtually hold for this type of complex. If the *cis* isomers of $[Coa_2(NH_3)_4]$-type and $[Coab(NH_3)_4]$-type complexes have a C_{2v} and a C_s symmetry, respectively, the cobalt-ammonia stretching vibrations transform as $(2A_1+B_1+B_2)$ and $(3A'+A'')$, respectively, and all of the modes are active in both the Raman and the infrared spectra.

Figures 1 and 2 show the Raman and the infrared spectra of 350—550 cm^{-1} region, where the cobalt-ammonia stretching vibrations, ν(Co–NH_3), are expected. As shown in Fig. 1, the Raman spectra of the *trans* isomers have a similar spectral feature. Thus, each spectrum shows a very strong band at *ca.* 480 cm^{-1} and a medium or a weak one at *ca.* 450 cm^{-1}, except for that of the dinitro complex in which the two bands are situated at about 10 cm^{-1} higher. The bands at *ca.* 480 and *ca.* 450 cm^{-1} are assigned to the A_{1g} (or A_1) mode and the B_{1g} (or B_1) mode of ν(Co–NH_3), respectively, by polarization measurements. The resemblance in the Raman frequencies of ν(Co–NH_3) among the trans isomers may be interpreted in terms of mechanical couplings among normal modes. The A_{1g} species of D_{4h} symmetry contain ν(Co–NH_3) and ν(Co–a), but the displacement vector of these vibrations are perpendicular to each other. So mechanical coupling between these vibrations will be virtually absent. The B_{1g} species contains only one mode, ν(Co–NH_3). Therefore, the Raman active ν(Co–NH_3) modes of *trans*-tetraamminecobalt(III) complexes are expected to be mechanically free from the other modes. The very weak bands at *ca.* 510 cm^{-1}

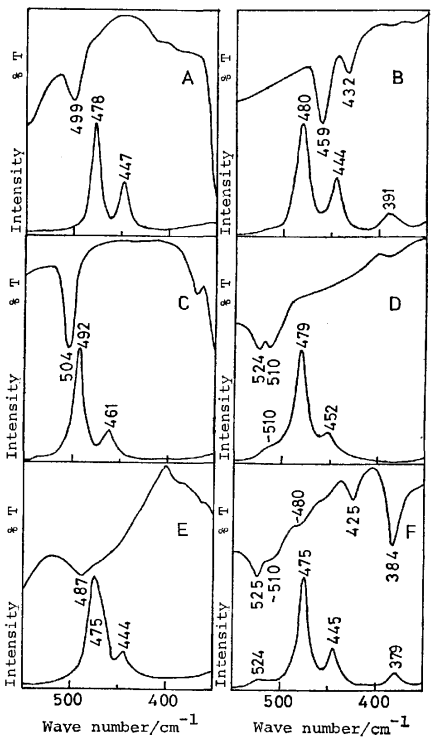

Fig. 1. Raman and infrared spectra of *trans*-$[Coab(NH_3)_4]X$- or *trans*-$M[Coab(NH_3)_4]$-type complexes.
A: a=b=Cl^-; X=Cl^-, B: a=b=CN^-; X=Cl^-, C: a=b=NO_2^-; X=Cl^-, D: a=b=SO_3^{2-}; M=Na^+, E: a=b=Br^-; X=ClO_4^-, F: a=CN^-; b=SO_3^{2-}.

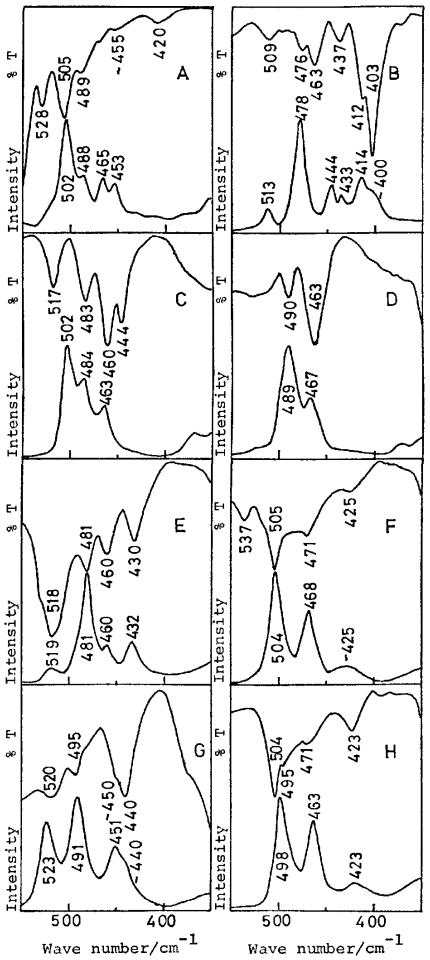

Fig. 2. Raman and infrared spectra of *cis*-[Coab$(NH_3)_4$]X- or *cis*-M[Coab$(NH_3)_4$]-type complexes.
A: a=b=Cl^-; X=Cl^-, B: a=b=CN^-; X=Cl^-, C: a=b=NO_2^-; X=Cl^-, D: a=b=NO_2^-; X=NO_3^-, E: a=b=SO_3^{2-}; M=NH_4^+, F: a=b=F^-; X=Cl^-, G: a=b=H_2O; X=$(NO_3^-)_3$, H: a=Cl^-; b=H_2O; X=$(Cl^-)_2$.

(Fig. 1-D) and at 524 cm^{-1} (Fig. 1-F) are assigned to the degenerate bending of the coordinated sulfito group, $\delta_d(SO_3)$. The bands at 391 cm^{-1} (Fig. 1-B) and at 379 cm^{-1} (Fig. 1-F) are assigned to the ν(Co–CN) by measurements of the deuterated compounds.

The infrared spectra of *trans*-tetraamminecobalt(III) complexes show one band due to the E_u (or E) mode of ν(Co–NH_3) in the region of 490—510 cm^{-1}, except for that of the dicyano complex, in which the ν(Co–NH_3) is observed at 459 cm^{-1} (see Fig. 1). The bands at 524 cm^{-1} (Fig. 1-D) and at 525 cm^{-1} (Fig. 1-F) are assigned to the $\delta_d(SO_3)$ and the bands at 432 cm^{-1} (Fig. 1-B) and at 425 and 384 cm^{-1} (Fig. 1-F) to the ν(Co–CN) or δ(Co–CN). The mutual exclusion with respect to the ν(Co–NH_3) virtually holds in all of the spectra in Fig. 1.

On the other hand, both the Raman and the infrared spectra of the *cis* isomers generally show at least three bands in the region of 400—550 cm^{-1} and many coincidences are found in the frequency between the Raman and the infrared bands (see Fig. 2). Although the Raman spectrum of *cis*-[Co$(NO_2)_2$-$(NH_3)_4$]NO_3 (Fig. 2-D) show two bands similar to that of the *trans* isomer, the Raman bands have counterparts in the infrared spectrum incontrast to that of the *trans* isomer.

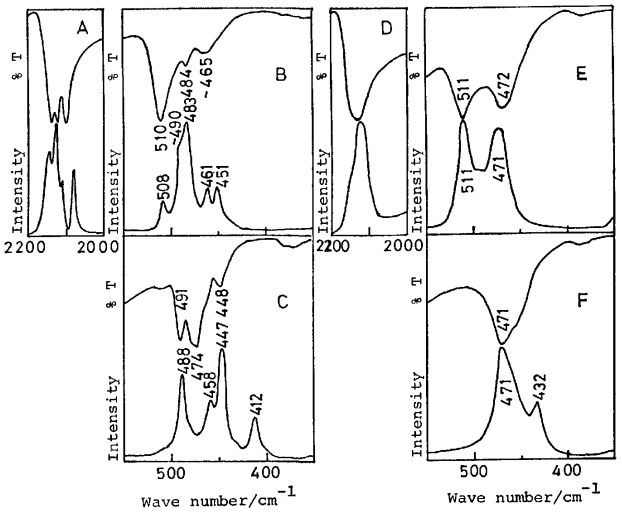

Fig. 3. Raman and infrared spectra of [Co$(NCS)_2$-$(NH_3)_4$]Cl.
A and B: Pinkish red isomer, C: *N*-deuterated pinkish red isomer, D and E: brick red isomer, F: *N*-deuterated brick red isomer.

In conclusion, two criteria will be established for differentiating the geometrical isomers of tetraamminecobalt(III) complexes. The first is based on the number of bands due to ν(Co–NH_3) and their frequencies; *trans* isomer of tetraamminecobalt(III) complexes shows two Raman bands (generally at *ca.* 480 cm^{-1} and at *ca.* 450 cm^{-1}) and one infrared band (generally at 490—510 cm^{-1}), while the *cis* isomer generally shows more than three bands in both the infrared and the Raman spectra. Another is based on mutual exclusion; this mutual exclusion virtually holds in the *trans* isomers and not in the *cis* isomers. It is clear that only a combination of both these two criteria would provide reliable structural diagnosis.

It is obviously of interest to apply these vibrational criteria to tetraamminecobalt(III) complexes of unknown or doubtful configurations. Werner[10] has obtained one of the isomers of [Co$(NCS)_2(NH_3)_4$]$^+$ and the infrared spectrum of this complex has been studied for the C–N and the C–S stretching region by Chamberlain and Bailar.[3] They have regarded this complex as the *trans* isomer. We obtained the other isomer in this work. The Raman and the infrared spectra of the isomeric pair in the region of 350—550 cm^{-1} are shown in Fig. 3, together with the ν(CN) region. The pinkish red isomer (see Experimental section) has three or four bands in the ν(CN) region, while the brick red one shows only one broad band. The splitting of ν(CN) was frequently identified with a *cis* configuration for the related complexes. Also in the region of 400—550 cm^{-1}, the spectra of the pinkish red isomer (Fig. 3-B) are apparently more complicated than those of the brick red one (Fig. 3-E), though more than two bands seem

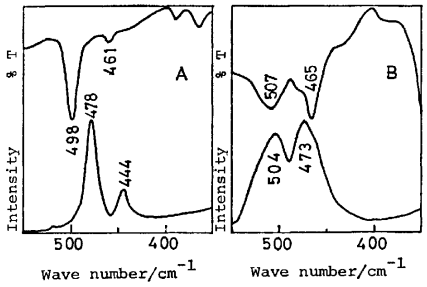

Fig. 4. Raman and infrared spectra of [CoCl(NCS)-$(NH_3)_4$]Cl.
A: The isomer obtained by Poon's method,[11] B: the isomer obtained in this work.

to be overlapped in the spectra of the latter isomer. In these complexes, the bands due to δ(NCS) will appear in the same region as the ν(Co–NH_3). In order to eliminate the bands due to δ(NCS), the spectra of the *N*-deuterated complexes have been measured (Figs. 3-C,F). By the comparison of the spectra of normal complexes with those of the deuterated ones, the bands at *ca.* 490 cm^{-1} and *ca.* 460 cm^{-1} of the pinkish red isomer and a part of the band at *ca.* 470 cm^{-1} of the brick red isomer can be assigned to the δ(NCS). Then the bands at 510 cm^{-1} (very weak in the Raman but very strong in the infrared spectrum), at 483 cm^{-1} (very strong in the Raman but very weak in the infrared spectrum) and at 451 cm^{-1} (which does not appear in the infrared spectrum) are assigned to the ν(Co–NH_3) for the pinkish red isomer. This spectral feature is a characteristic of a *trans* configuration, except for the appearance of the very weak bands. The Raman and the infrared spectra of the brick red isomer show apparently two bands. However, the facts that the intensity of the Raman band at 511 cm^{-1} is very strong and the Raman spectrum has no band at about 450 cm^{-1} suggest that the isomer has not a *trans* configuration but a *cis* configuration. In the *trans* isomer, the appearance of the band at 510 cm^{-1} (E_u mode) in the Raman spectrum and the band at 483 cm^{-1} (A_{1g} mode) in the infrared spectrum, and the complicated feature in the ν(CN) region may be due to the symmetry lowering in the solid state. This assignment of the geometrical configurations is compatible with that on the basis of the relative positions of the absorption maxima in the first d-d absorption band or the "specific band" of thiocyanato groups, and also with the elution order of the column chromatography.

The Raman and the infrared spectra of the isomeric pair of [CoCl(NCS)$(NH_3)_4$]Cl are shown in Fig. 4. On the basis of the observed band positions in the Raman and the infrared spectra and the comparison between the two spectra, the isomer which was obtained by Poon's method[11] is assigned to the *trans* structure and the isomer obtained in this work to the *cis* structure.

The Raman and the infrared spectra of [CoX-$(NO_2)(NH_3)_4$]-type (X=NCS^-, Cl^-, H_2O, CN^-) complexes are shown in Fig. 5. The Raman spectra (Figs. 5-A,C,E, and G) of the complexes, whose geometrical configurations are assumed to be *trans*, show

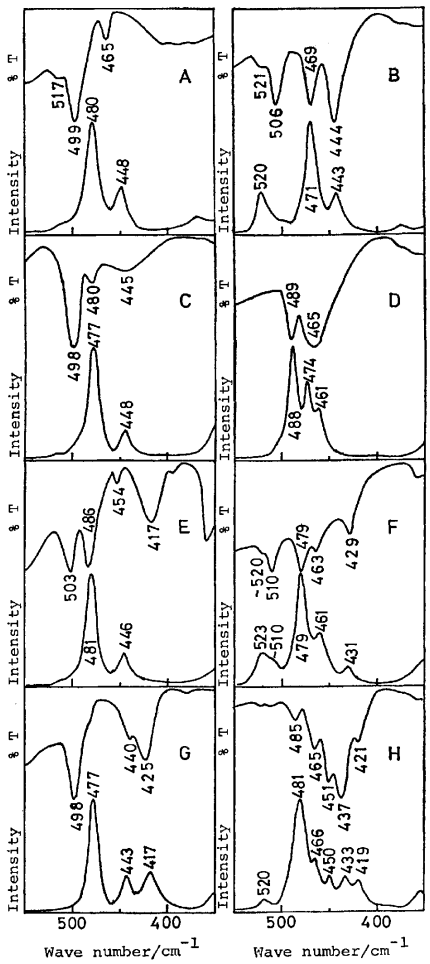

Fig. 5. Raman and infrared spectra of [Coa(NO_2)-$(NH_3)_4$]X-type complexes.
A (*trans*) and B (*cis*): a=NCS^-; X=Cl^-, C(*trans*) and D(*cis*): a=Cl^-; X=Cl^-, E(*trans*) and F(*cis*): a=H_2O; X=$(NO_3^-)_2$, G(*trans*) and H(*cis*): a=CN^-; X=Cl^-.

the characteristic feature of a *trans* configuration. The band at 417 cm^{-1}, which was observed for *trans*-[Co(CN)$(NO_2)(NH_3)_4$]Cl is assigned to the ν(Co–CN). The Raman spectra of the others (Figs. 5-B,D,F, and H) have more than three bands due to ν(Co–NH_3) and most of the bands have counterparts in the infrared spectra, so *cis* configurations are confirmed for these complexes. It is seen from Fig. 5 that the assignments of the geometrical configurations by the infrared spectra alone are not conclusive for these complexes.

The authors wish to express their sincere thanks to Professor Yoichi Shimura, Osaka university, and to Dr. Isao Kanesaka of our university for valuable discussions. Their thanks are also due to Miss Junko Nomura for carrying out a part of the experiments.

References

1) K. Kanamori and K. Kawai, *Bull. Chem. Soc. Jpn.*, **53**, 2520 (1980).
2) P. E. Merritt and S. E. Wiberley, *J. Phys. Chem.*, **59**, 55 (1959).

3) M. M. Chamberlain and J. C. Bailar, Jr., *J. Am. Chem. Soc.*, **81**, 6412 (1959).
4) M. L. Morris and D. H. Busch, *J. Am. Chem. Soc.*, **82**, 1521 (1960).
5) M. E. Baldwin, *J. Chem. Soc.*, **1960**, 4369.
6) M. N. Hughes and W. R. McWhinnie, *J. Inorg. Nucl. Chem.*, **28**, 1659 (1966).
7) J. P. Faust and J. V. Quagliano, *J. Am. Chem. Soc.*, **76**, 5346 (1954).
8) I. Nakagawa and T. Shimanouchi, *Spectrochim. Acta, Part A*, **23**, 2099 (1967).
9) K. Kanamori, T. Morikawa, and K. Kawai, *Bull. Chem. Soc. Jpn.*, **53**, 2787 (1980).
10) A. Werner and H. Müller, *Z. Anorg. Allg. Chem.*, **22**, 91 (1900).
11) C. K. Poon, *J. Chem. Soc., Dalton Trans.*, **1972**, 1701.
12) A. Werner, *Ber.*, **40**, 4120 (1907).
13) J. Meyer and O. Rampoldt, *Z. Anorg. Allg. Chem.*, **214**, 1 (1933).
14) S. M. Jörgensen, *Z. Anorg. Allg. Chem.*, **7**, 289 (1894).
15) H. J. S. King and S. N. Mistry, *J. Chem. Soc.*, **1957**, 2402.
16) R. G. Yalman and T. Kuwana, *J. Phys. Chem.*, **59**, 298 (1955).
17) K. Ohkawa, J. Hidaka, and Y. Shimura, *Bull. Chem. Soc. Jpn.*, **39**, 1715 (1966).
18) K. Akamatsu, J. Hidaka, and Y. Shimura, *Bull. Chem. Soc. Jpn.*, **50**, 533 (1977).

 © 1982 The Chemical Society of Japan Bull. Chem. Soc. Jpn., 55, 769—774 (1982)

Solubility Diagrams of Cobalt(III) Complexes Containing Amino Acid. II.[1] Spontaneous Resolution of Bis(ethylenediamine)glycinatocobalt(III) Salts

Satoshi KAKI,* Kazuaki YAMANARI, and Yoichi SHIMURA

Department of Chemistry, Faculty of Science, Osaka University, Toyonaka, Osaka 560

(Received June 30, 1981)

The binary and ternary solubility phase diagrams of the racemic and optically active complexes $[Co(gly)(en)_2]X_2$ were determined in water ($X_2=SO_4$, S_2O_3, $(NO_3)_2$, $(SCN)_2$, $(CH_3CO_2)_2$, $(ClO_4)_2$, $(CH_3CO_2)ClO_4$, and $[Sb_2(d\text{-tart})_2]$). Spontaneous resolution was found for the double salt of $[Co(gly)(en)_2](CH_3CO_2)ClO_4$ at 5—50 °C and for $[Co(gly)(en)_2]SO_4$ at 39—50 °C; the latter of these has been shown to crystallize as both a racemic compound (below 39 °C) and a conglomerate (above 39 °C).

The solubility diagrams of tetraammine(leucinato)-cobalt(III) sulfate have revealed that the sulfate has a large solubility ratio of DL-complex/L-complex and crystallizes as both a racemic compound (below 30 °C) and a conglomerate (above 30 °C).[1] It is of interest to clarify whether this is characteristic of the counter ion SO_4^{2-} or not. The present paper deals with the binary and ternary solubility diagrams of a variety of salts of the glycinato complex $[Co(gly)(en)_2]X_2$, where X_2 stands for SO_4, S_2O_3, $(CH_3CO_2)_2$, $(ClO_4)_2$, $(CH_3CO_2)ClO_4$, $(NO_3)_2$, $(SCN)_2$, and $[Sb_2(d\text{-tart})_2]$ (tart=tartrate(4—) ion, $C_4H_2O_6^{4-}$).

Experimental

Materials. rac-$[Co(gly)(en)_2]X_2$: Iodide salt obtained by the method of Meisenheimer[2] was converted into acetate salt through an anion exchanger column of Dowex 1-X8 ($CH_3CO_2^-$ form). Found: C, 28.95; H, 7.45; N, 16.79%. Calcd for $[Co(gly)(en)_2](CH_3CO_2)_2\cdot 2.5H_2O=C_{10}H_{31}N_5O_{8.5}Co$: C, 28.85; H, 7.51; N, 16.82%. Sulfate and thiosulfate salts were prepared from an aqueous solution of the acetate salt by adding a calculated amount of $(NH_4)_2SO_4$ or $Na_2S_2O_3$. Found for sulfate salt: C, 17.46; H, 6.44; N, 16.99%. Calcd for $[Co(gly)(en)_2]SO_4\cdot 3.5H_2O=C_6H_{27}N_5O_{9.5}SCo$: C, 17.48; H, 6.60; N, 16.99%. Found for thiosulfate salt: C, 19.52; H, 5.61; N, 18.87%. Calcd for $[Co(gly)(en)_2]S_2O_3\cdot 0.5H_2O=C_6H_{21}N_5O_{5.5}S_2Co$: C, 19.25; H, 5.61; N, 18.71%. For the preparation of perchlorate, nitrate, and thiocyanate salts, a slight excess of $Ba(ClO_4)_2$, $Sr(NO_3)_2$, or $Ba(SCN)_2$ was added to the solution of sulfate salt. The desired crystals were obtained by evaporating the filtrate. Found for perchlorate salt: C, 14.79; H, 4.97; N, 14.31%. Calcd for $[Co(gly)(en)_2](ClO_4)_2\cdot 2H_2O=C_6H_{24}N_5O_{12}Cl_2Co$: C, 14.76; H, 4.96; N, 14.35%. Found for nitrate salt: C, 18.16; H, 5.57; N, 24.98%. Calcd for $[Co(gly)(en)_2](NO_3)_2\cdot H_2O=C_6H_{22}N_7O_9Co$: C, 18.23; H, 5.61; N, 24.81%. Found for thiocyanate salt: C, 25.99; H, 5.46; N, 26.58%. Calcd for $[Co(gly)(en)_2](SCN)_2=C_8H_{20}N_7O_2S_2Co$: C, 26.02; H, 5.46; N, 26.55%. Acetate perchlorate double salt was obtained by mixing equimolar amounts of the perchlorate salt and the acetate salt. Found: C, 23.47; H, 5.67; N, 16.95%. Calcd for $[Co(gly)(en)_2](CH_3CO_2)ClO_4=C_8H_{23}N_5O_8ClCo$: C, 23.34; H, 5.63; N, 17.01%.

Optical Resolution of $[Co(gly)(en)_2]^{2+}$: The resolving agent $Na_2[Sb_2(d\text{-tart})_2]\cdot 5H_2O$ (9.7×10^{-2} mol) was added to the dilute solution of the acetate salt (16.2×10^{-2} mol) in 800 cm^3 of water. The less soluble Λ-diastereomer which deposited was removed by filtration and recrystallized from warm water. Further addition of $Na_2[Sb_2(d\text{-tart})_2]\cdot 5H_2O$ (9.7×10^{-2} mol) to the filtrate gave Λ-diastereomer. Each diastereomer was purified by the fractional crystallization until the CD values became constant. Found for Λ-diastereomer: C, 19.46; H, 3.77; N, 8.11%. Calcd for Λ-$[Co(gly)(en)_2][Sb_2(d\text{-tart})_2]\cdot 4H_2O=C_{14}H_{32}N_5O_{18}Sb_2Co$: C, 19.53; H, 3.75; N, 8.14%. Found for Λ-diastereomer: C, 19.57; H, 3.76; N, 8.20%. Calcd for Λ-$[Co(gly)(en)_2][Sb_2(d\text{-tart})_2]\cdot 4H_2O=C_{14}H_{32}N_5O_{18}Sb_2Co$: C, 19.53; H, 3.75, N, 8.14%. The Λ-diastereomer was added to an aqueous solution containing ion exchange resin Dowex 1-X8($CH_3CO_2^-$ form) and stirred for 2 h at 50 °C. The resin was removed by filtration and the filtrate was evaporated to give the acetate salt. Found: C, 27.84; H, 7.41; N, 16.59%. Calcd for Λ-$[Co(gly)(en)_2](CH_3CO_2)_2\cdot 3H_2O=C_{10}H_{32}N_5O_9Co$: C, 28.24; H, 7.58; N, 16.47%. The other Δ- or Λ-salts were prepared by the same method as was used the corresponding racemic salts. Found for sulfate salt: C, 19.61; H, 6.03; N, 19.11%. Calcd for Λ-$[Co(gly)(en)_2]SO_4\cdot H_2O=C_6H_{22}N_5O_7SCo$: C, 19.62; H, 6.04; N, 19.07%. Found for thiosulfate salt: C, 19.59; H, 5.49; N, 19.19%. Calcd for Λ-$[Co(gly)(en)_2]S_2O_3=C_6H_{20}N_5O_5S_2Co$: C, 19.73; H, 5.52; N, 19.17%. Found for perchlorate salt: C, 15.47; H, 4.84; N, 14.99%. Calcd for Λ-$[Co(gly)(en)_2](ClO_4)_2\cdot H_2O=C_6H_{22}N_5O_{11}Cl_2Co$: C, 15.33; H, 4.72; N, 14.90%. Found for nitrate salt: C, 18.77; H, 5.37; N, 25.75%. Calcd for Λ-$[Co(gly)(en)_2](NO_3)_2\cdot 0.5H_2O=C_6H_{21}N_7O_{8.5}Co$: C, 18.66; H, 5.48; N, 25.39%. Found for thiocyanate salt: C, 26.14; H, 5.45; N, 26.72%. Calcd for Λ-$[Co(gly)(en)_2](SCN)_2=C_8H_{20}N_7O_2S_2Co$: C, 26.02; H, 5.46; N, 26.55%. Found for acetate perchlorate double salt: C, 23.10; H, 5.68; N, 16.92%. Calcd for Λ-$[Co(gly)(en)_2](CH_3CO_2)ClO_4=C_8H_{23}N_5O_8ClCo$: C, 23.34; H, 5.63; N, 17.01%.

Measurements. The solubility of complexes in water was determined in the same way as previously reported.[3] The absorption and CD values which were used for the calculations of concentrations of complexes in solutions are summarized in Table 1. The solid phases were identified from the elemental analysis and the absorption and CD spectra. Optical densities were measured with a JASCO UVIDEC-1 spectrophotometer and CD with a JASCO MOE-1 spectropolarimeter.

Results and Discussion

The binary solubility data are given in Table 2 and Figs. 1 and 3, and the ternary data in Table 3 as well as Figs. 2, 4, and 5. In the triangular isotherms the top part (H_2O corner) is enlarged for the sake of convenience and the tie lines are omitted.

The Sulfate and Thiosulfate Salts. The solubility curves of *rac*-$[Co(gly)(en)_2]SO_4$ and Λ-$[Co(gly)(en)_2]SO_4$ are shown in Fig. 1. The curve of racemate intersects the curve of the active one at *ca.* 21 °C, the solubility of racemic salt being less than that of the active one below this temperature. The solubili-

Table 1. Absorption and CD maximum values used for calculation of solubility of $[Co(gly)(en)_2]X_2$[a]

Absolute configuration	X_2	ε (486 nm) / mol^{-1} dm^3 cm^{-1}	$\Delta\varepsilon$ (508 nm) / mol^{-1} dm^3 cm^{-1}
Λ	SO_4	101.0	−2.61
rac	SO_4	100.7	—
Λ	S_2O_3	102.6	−2.53
rac	S_2O_3	102.7	—
Λ	$(ClO_4)_2$	99.76	−2.65
rac	$(ClO_4)_2$	100.0	—
Λ	$(NO_3)_2$	100.1	+2.55
rac	$(NO_3)_2$	98.83	—
Λ	$(SCN)_2$	100.1	+2.60
rac	$(SCN)_2$	98.83	—
Λ	$(CH_3CO_2)_2$	101.5	−2.57
rac	$(CH_3CO_2)_2$	100.5	—
Λ	$(CH_3CO_2)ClO_4$	98.96	−2.62
rac	$(CH_3CO_2)ClO_4$	98.81	—
Λ	$[Sb_2(d\text{-tart})_2]$	104.5	−2.33
Λ	$[Sb_2(d\text{-tart})_2]$	100.8	+2.30

a) The ε and $\Delta\varepsilon$ values are given in the units of mol^{-1} dm^3 cm^{-1}.

ity curve of racemate shows an inflection at *ca.* 39 °C where the solid phase changes from 3.5-hydrate (below 39 °C) to monohydrate (above 39 °C), whereas the curve of the optically active complex shows no inflection. The slope of the racemic curve above 39 °C is similar to that of the optically active salt. The solubility ratio of racemate/*Λ*-complex is 0.46 at 5 °C, 1.34 at 25 °C, and 2.68 at 40 °C.

Generally spontaneous resolution is expected in the case in which the solubility of racemic salt is more than $2^{1/2}(=1.41)$ times that of the corresponding optically active salt, for a 1:1 electrolyte.[4] Thus, the sulfate salt would be spontaneously resolvable above 39 °C, above which both racemate and *Λ*-complex crystallize as monohydrate salt. To confirm the expectation, the solubility isotherms of the ternary system, H_2O–*Λ*-$[Co(gly)(en)_2]SO_4$–*Λ*-$[Co(gly)(en)_2]SO_4$, were measured at three temperatures: 10, 30, and 45 °C (Fig. 2). The isotherm at 10 or 30 °C shows two invariant points, between which the formation of racemic compound *Λ*-$[Co(gly)(en)_2]\cdot$*Λ*-$[Co(gly)(en)_2](SO_4)_2\cdot 7H_2O$=*rac*-$[Co(gly)(en)_2]SO_4\cdot 3.5H_2O$ is observed. However, this racemic compound disappears in the isotherm at 45 °C, and the two enan-

Table 2. Solubility of the complex salts (grams of anhydrous salt in 100 g of water)

t/°C	No. of complex salt[a]									
	1	2	3	4	5	6	7	8	9	10
5	3.05		6.61				78.2	157	6.32	14.2
10	3.99		6.76						8.15	19.1
15	5.30		6.96	0.157[b]	0.193[b]				10.5	24.2
20	6.90		7.14	0.193	0.228				14.4	32.6
25	9.70		7.26	0.214	0.264				20.5	46.0
30	12.3		7.38	0.236	0.290				29.8	63.7
35	16.1		7.45	0.261		0.326			39.7	
40		20.2	7.55	0.286		0.351			63.2	
45		20.4	7.66	0.314		0.375			83.1	
50		20.5	7.68	0.342		0.417				
55		20.5	7.65	0.370		0.457				

t/°C	No. of complex salt[a]								
	11	12	13	14	15	16	17	18	19
5	13.7	8.79	5.40	8.39[c]	7.14	2.90	3.35	0.0819	0.216
10	14.4	10.0	6.56	10.3[c]	8.51	3.66	4.25	0.0991	0.258
15	16.1	11.0	8.40	13.3[c]	10.7	4.50	5.10	0.121	0.308
20	17.8	12.2	10.6	17.1[c]	13.4	5.65	6.42	0.147	0.360
25	19.6	13.6	13.6	21.6[c]	16.5	7.14	7.93	0.187	0.433
30	21.6	14.9	17.1	28.3[c]	20.9	8.86	10.1	0.209	0.517
35	24.1	16.6	21.6	37.5[c]	25.5	11.0	12.6	0.255	0.607
40	26.4	18.3	27.4	45.5[c]	31.4	14.0	15.8	0.294	0.705
45	28.9	20.0	33.6	57.7[c]	38.6	17.9	20.1	0.354	0.846
50	32.0	22.2	44.3	71.4[c]	50.3[c]	22.3	25.3	0.427	0.991
55								0.512	1.15

a) 1: *rac*-$[\ ]SO_4\cdot 3.5H_2O$, 2: *rac*-$[\ ]SO_4\cdot H_2O$, 3: *Λ*-$[\ ]SO_4\cdot H_2O$, 4: *Λ*-$[\ ]S_2O_3$, 5: *rac*-$[\ ]S_2O_3\cdot 0.5H_2O$, 6: *rac*-$[\ ]S_2O_3$, 7: *rac*-$[\ ](CH_3CO_2)_2\cdot 2.5H_2O$, 8: *Λ*-$[\ ](CH_3CO_2)_2\cdot 3H_2O$, 9: *rac*-$[\ ](ClO_4)_2\cdot 2H_2O$, 10: *Λ*-$[\ ](ClO_4)_2\cdot H_2O$, 11: *rac*-$[\ ](CH_3CO_2)ClO_4$, 12: *Λ*-$[\ ](CH_3CO_2)ClO_4$, 13: *rac*-$[\ ](NO_3)_2\cdot H_2O$, 14: *rac*-$[\ ](NO_3)_2\cdot H_2O$, 15: *Λ*-$[\ ](NO_3)_2\cdot 0.5H_2O$, 16: *rac*-$[\ ](SCN)_2$, 17: *Λ*-$[\ ](SCN)_2$, 18: *Λ*-$[\ ][Sb_2(d\text{-tart})_2]\cdot 4H_2O$, 19: *Λ*-$[\ ][Sb_2(d\text{-tart})_2]\cdot 4H_2O$. b) Measured at 13 °C. c) Metastable solid phase.

TABLE 3. SOLUBILITY IN THE TERNARY SYSTEM, H_2O-Δ-$[Co(gly)(en)_2]X$-Λ-$[Co(gly)(en)_2]X_2$
Solubility is given in mole fraction x of anhydrous salt. Abbreviation for solid phase: Δ-$[Co(gly)(en)_2]X_2 \cdot nH_2O = \Delta$-$X_2 \cdot nH_2O$, Λ-$[Co(gly)(en)_2]X_2 \cdot nH_2O = \Lambda$-$X_2 \cdot nH_2O$, *rac*-$[Co(gly)(en)_2]X_2 \cdot nH_2O$ = *rac*-$X_2 \cdot nH_2O$.

X_2	t/°C	Liquid phase $10^4 x_\Delta$	Liquid phase $10^4 x_\Lambda$	Solid phase
$[Sb_2(d\text{-tart})_2]$	25	0.426	0	Δ-$[Sb_2(d\text{-tart})_2] \cdot 4H_2O$
		0.300	0.468	Δ-$[Sb_2(d\text{-tart})_2] \cdot 4H_2O$
		0.263	0.783	Δ-$[Sb_2(d\text{-tart})_2] \cdot 4H_2O$
		0.249	0.945	Δ-$[Sb_2(d\text{-tart})_2] \cdot 4H_2O$ + Λ-$[Sb_2(d\text{-tart})_2] \cdot 4H_2O$
		0.233	0.958	Λ-$[Sb_2(d\text{-tart})_2] \cdot 4H_2O$
		0	1.01	Λ-$[Sb_2(d\text{-tart})_2] \cdot 4H_2O$
SO_4	10	35.9	0	Δ-$SO_4 \cdot H_2O$
		36.1	1.82	Δ-$SO_4 \cdot H_2O$
		36.8	3.33	Δ-$SO_4 \cdot H_2O$
		37.0	4.21	Δ-$SO_4 \cdot H_2O$ + *rac*-$SO_4 \cdot 3.5H_2O$
		36.5	4.13	*rac*-$SO_4 \cdot 3.5H_2O$
		31.4	4.49	*rac*-$SO_4 \cdot 3.5H_2O$
		27.9	4.90	*rac*-$SO_4 \cdot 3.5H_2O$
		20.8	5.66	*rac*-$SO_4 \cdot 3.5H_2O$
		15.5	7.00	*rac*-$SO_4 \cdot 3.5H_2O$
		13.3	8.09	*rac*-$SO_4 \cdot 3.5H_2O$
		11.2	9.41	*rac*-$SO_4 \cdot 3.5H_2O$
		10.6	10.0	*rac*-$SO_4 \cdot 3.5H_2O$
		10.1	10.1	*rac*-$SO_4 \cdot 3.5H_2O$
SO_4	30	38.1	0	Δ-$SO_4 \cdot H_2O$
		38.6	0.465	Δ-$SO_4 \cdot H_2O$
		39.6	3.38	Δ-$SO_4 \cdot H_2O$
		40.3	5.36	Δ-$SO_4 \cdot H_2O$
		40.4	6.10	Δ-$SO_4 \cdot H_2O$
		41.6	9.60	Δ-$SO_4 \cdot H_2O$
		42.8	13.7	Δ-$SO_4 \cdot H_2O$
		43.6	15.9	Δ-$SO_4 \cdot H_2O$
		44.2	18.7	Δ-$SO_4 \cdot H_2O$
		45.3	23.3	Δ-$SO_4 \cdot H_2O$ + *rac*-$SO_4 \cdot 3.5H_2O$
		42.8	24.3	*rac*-$SO_4 \cdot 3.5H_2O$
		41.1	25.3	*rac*-$SO_4 \cdot 3.5H_2O$
		38.7	26.3	*rac*-$SO_4 \cdot 3.5H_2O$
		35.6	28.5	*rac*-$SO_4 \cdot 3.5H_2O$
		34.0	29.1	*rac*-$SO_4 \cdot 3.5H_2O$
		33.2	29.9	*rac*-$SO_4 \cdot 3.5H_2O$
		31.3	31.3	*rac*-$SO_4 \cdot 3.5H_2O$
SO_4	45	39.1	0	Δ-$SO_4 \cdot H_2O$
		39.4	0.578	Δ-$SO_4 \cdot H_2O$
		39.9	2.51	Δ-$SO_4 \cdot H_2O$
		41.1	5.56	Δ-$SO_4 \cdot H_2O$
		41.7	7.61	Δ-$SO_4 \cdot H_2O$
		42.5	11.6	Δ-$SO_4 \cdot H_2O$
		44.2	16.2	Δ-$SO_4 \cdot H_2O$
		47.2	26.7	Δ-$SO_4 \cdot H_2O$
		50.8	43.1	Δ-$SO_4 \cdot H_2O$
		53.2	53.2	Δ-$SO_4 \cdot H_2O$ + Λ-$SO_4 \cdot H_2O$
$(CH_3CO_2)ClO_4$	20	53.1	0	Δ-$(CH_3CO_2)ClO_4$
		52.0	1.94	Δ-$(CH_3CO_2)ClO_4$
		49.5	5.41	Δ-$(CH_3CO_2)ClO_4$
		49.1	9.75	Δ-$(CH_3CO_2)ClO_4$
		43.6	22.8	Δ-$(CH_3CO_2)ClO_4$

TABLE 3. (Continued)

X_2	t/°C	Liquid phase 10^4x_Δ	Liquid phase 10^4x_Λ	Solid phase
$(CH_3CO_2)ClO_4$	20	40.6	32.0	Δ-$(CH_3CO_2)ClO_4$
		39.3	39.3	Δ-$(CH_3CO_2)ClO_4$ + Λ-$(CH_3CO_2)ClO_4$
S_2O_3	45	1.51	0.193	Δ-S_2O_3
		1.51	0.340	Δ-S_2O_3
		1.51	0.381	Δ-S_2O_3
		1.57	0.451	Δ-S_2O_3
		1.59	0.465	Δ-S_2O_3 + *rac*-S_2O_3
		1.47	0.539	*rac*-S_2O_3
		1.07	0.746	*rac*-S_2O_3
		0.992	0.810	*rac*-S_2O_3
		0.933	0.841	*rac*-S_2O_3
		0.871	0.871	*rac*-S_2O_3
$(NO_3)_2$	45	77.7	77.7	*rac*-$(NO_3)_2\cdot H_2O$
		48.9	126	*rac*-$(NO_3)_2\cdot H_2O$
		38.6	151	*rac*-$(NO_3)_2\cdot H_2O$
		33.7	178	*rac*-$(NO_3)_2\cdot H_2O$
		0	181	*rac*-$(NO_3)_2\cdot H_2O$ + Λ-$(NO_3)_2\cdot 0.5H_2O$
		4.37[a]	182[a]	Λ-$(NO_3)_2\cdot 0.5H_2O$[a]
		8.35[a]	181[a]	Λ-$(NO_3)_2\cdot 0.5H_2O$[a]
		34.2[a]	177[a]	Λ-$(NO_3)_2\cdot 0.5H_2O$[a]
		132[a]	132[a]	*rac*-$(NO_3)_2\cdot H_2O$[a]
		127[a]	137[a]	*rac*-$(NO_3)_2\cdot H_2O$[a]
		123[a]	145[a]	*rac*-$(NO_3)_2\cdot H_2O$[a]

a) Metastable phase.

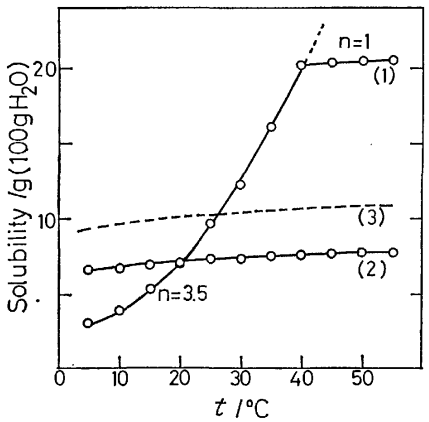

Fig. 1. Solubility curves of *rac*-$[Co(gly)(en)_2]SO_4\cdot nH_2O$(1), Δ-$[Co(gly)(en)_2]SO_4\cdot H_2O$(2), and calculated curve(3): (2)$\times 2^{1/2}$.

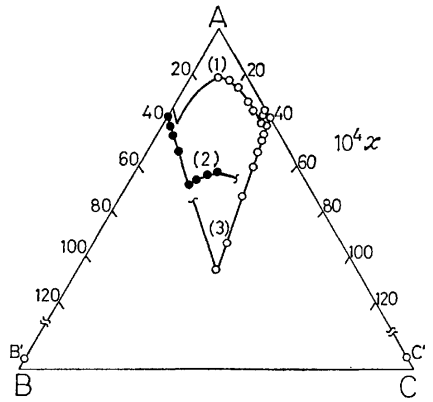

Fig. 2. Solubility isotherms of H_2O(A)–Δ-$[Co(gly)(en)_2]SO_4$(B)–Δ-$[Co(gly)(en)_2]SO_4$(C) at 10 °C(1), 30 °C(2), and 45 °C(3).
The points at 30 °C(●) are plotted at a left side for convenience. The solid phase B′ or C′ is monohydrate of B or C, respectively.

tiomers form a conglomerate.[3] The intersection of the solubility curves at about 21 °C in Fig. 1 has no special meaning with respect to spontaneous resolution. The racemic sulfate $[Co(gly)(en)_2]SO_4$ crystallizes as both a racemic compound (below 39 °C) and a conglomerate (above 39 °C). A similar case has been found for $[Co(leu)(NH_3)_4]SO_4$[1] but the examples such as $K_3[Co(ox)_3]\cdot H_2O$ and $[Rh(rac\text{-cptn})_3](ClO_4)_3\cdot 12H_2O$ reported by Jaeger[5] do not seem to be exact enough in some details (cptn=*trans*-1,2-cyclopentanediamine).

The solubility of racemic thiosulfate salt is larger than that of the corresponding active salt in the range 12—55 °C. The curve has an inflection at *ca.* 35 °C where the solid phase changes from 0.5-hydrate (below 35 °C) to anhydrate (above 35 °C), whereas the solid phase of the optically active salt is anhydrate at 12—55 °C. The curve of racemic salt is lower than $2^{1/2}$ times that of the active salt. The ternary isotherm

at 45 °C confirms the existence of the racemic compound Δ-[Co(gly)(en)$_2$]·Δ-[Co(gly)(en)$_2$](S$_2$O$_3$)$_2$=*rac*-[Co(gly)(en)$_2$]S$_2$O$_3$ (Table 3). It is interesting that the solubility of thiosulfate salt is much lower than that of sulfate salt, whether it is in racemate or active form.

The Acetate Perchlorate Double Salt. The solubility of the optically active perchlorate salt is larger than that of the racemic salt; two enantiomers form a racemic compound. The solubility of the acetate salt is determined at only 5 °C because of its extremely high solubility (Table 2). This salt also crystallizes as a racemic compound.

As described in the Experimental section, the double salt [Co(gly)(en)$_2$](CH$_3$CO$_2$)ClO$_4$ can be prepared from the constituent salt. Figure 3 shows the solubility curves of *rac*- and Δ-[Co(gly)(en)$_2$](CH$_3$CO$_2$)-ClO$_4$. The double salt is not decomposed into the constituent salts in water at 5—50 °C. The solubility of the racemic salt is larger than $2^{1/3}$ times that of the optically active one and both the solid phases are anhydrous at 5—50 °C.[4] Therefore, spontaneous resolution is expected for this double salt at 5—50 °C, though each constituent salt forms a racemic compound. The ternary isotherm at 20 °C is the only invariant point and confirms the formation of a conglomerate (Fig. 4). This case is the first one of spontaneous resolution found for a complex double salt.

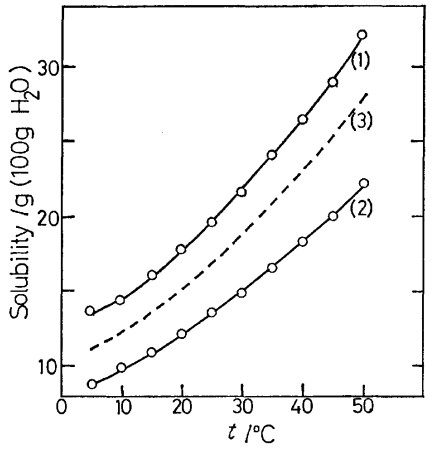

Fig. 3. Solubility curves of *rac*-[Co(gly)(en)$_2$]-(CH$_3$CO$_2$)ClO$_4$(1), Δ-[Co(gly)(en)$_2$](CH$_3$CO$_2$)ClO$_4$ (2), and calculated curve(3): (2)×$2^{1/3}$.

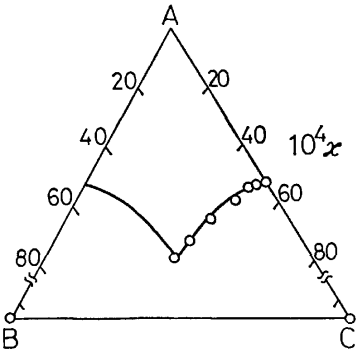

Fig. 4. Solubility isotherm of H$_2$O(A)–Δ-[Co(gly)-(en)$_2$](CH$_3$CO$_2$)ClO$_4$(B)–Δ-[Co(gly)(en)$_2$](CH$_3$CO$_2$)-ClO$_4$(C) at 20 °C.

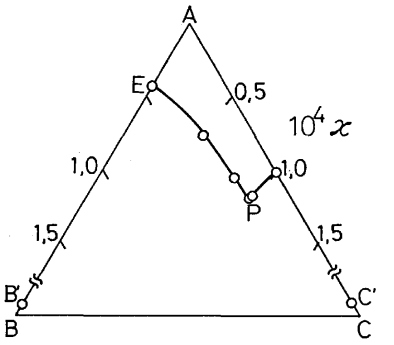

Fig. 5. Solubility isotherm of H$_2$O(A)–Δ-[Co(gly)-(en)$_2$][Sb$_2$(*d*-tart)$_2$](B)–Δ-[Co(gly)(en)$_2$][Sb$_2$(*d*-tart)$_2$] (C).
The solid phase B′ or C′ is 4-hydrate of B or C, respectively.

The Nitrate and Thiocyanate Salts. In the system of nitrate salt, a metastable monohydrate phase is observed for the racemate. This phase is so stable that the solubility could be determined in the range 5—50 °C. The metastable solid phase in contact with the solution was stirred mechanically one day to undergo conversion into the stable solid phase. The solubility of the stable racemate is lower than that of the active one, whereas the solubility of the metastable racemate is larger than $2^{1/3}$ times that of the active complex. However, the ternary isotherm at 45 °C (Table 3) revealed the existence of the racemic compound Δ-[Co(gly)(en)$_2$]·Δ-[Co(gly)(en)$_2$](NO$_3$)$_4$·2H$_2$O=*rac*-[Co(gly)(en)$_2$](NO$_3$)$_2$·H$_2$O.

The solubility of optically active thiocyanate salt is larger than that of the racemate. This salt also forms a racemic compound Δ-[Co(gly)(en)$_2$]·Δ-[Co-(gly)(en)$_2$](SCN)$_4$=*rac*-[Co(gly)(en)$_2$](SCN)$_2$.

The Optical Resolution of [Co(gly)(en)$_2$]$^{2+}$ Complex. This complex have been optically resolved by *d*-BCS[2,6] and Ag$_2$[Sb$_2$(*d*-tart)$_2$][7] as a resolving agent (*d*-BCS=(+)$_{589}$-(1*R*,3*S*,4*S*,7*R*)-3-bromocamphor-9-sulfonate). However, we found that the combination of the acetate salt and the resolving agent Na$_2$[Sb$_2$(*d*-tart)$_2$]·5H$_2$O is more convenient. Figure 5 shows the ternary isotherm of H$_2$O–Δ-[Co(gly)(en)$_2$][Sb$_2$(*d*-tart)$_2$]–Δ-[Co-(gly)(en)$_2$][Sb$_2$(*d*-tart)$_2$] at 25 °C; its only invariant point is P, at the right hand side. When an aqueous solution of an equimolar amount of the two diastereomers is concentrated at this temperature, the less soluble diastereomer Δ-[Co(gly)(en)$_2$][Sb$_2$(*d*-tart)$_2$]·4H$_2$O will crystallize out first and then the solution composition will change along the solubility curve EP. Finally, the solid phase will be composed of the two diastereomers at P. No pseudo racemic compound appears in this system.

References

1) K. Yamanari, S. Naito, and Y. Shimura, *Bull. Chem. Soc. Jpn.*, **54**, 3780 (1981).

2) J. Meisenheimer, L. Angermann, and H, Holsten, *Justus Liebigs Ann. Chem.*, **438**, 217 (1924).
3) Y. Shimura and K. Tsutsui, *Bull. Chem. Soc. Jpn.*, **50**, 145 (1977).
4) K. Yamanari, J. Hidaka, and Y. Shimura, *Bull. Chem. Soc. Jpn.*, **46**, 3724 (1973).
5) F. M. Jaeger, "Optical Activity and High Temperature Measurements," McGraw-Hill, New York (1930).
6) J.-P. Mathieu, *Bull. Soc. Chim. Fr.*, **6**, 873 (1939); I. Lifschitz, *Recl. Trav. Chim. Pays-Bas*, **58**, 785 (1939); *Proc. Acad. Amsterdam*, **42**, 173 (1939).
7) C. T. Liu and B. E. Douglas, *Inorg. Chem.*, **3**, 1356 (1964).

Solubility Isotherms of Systems Containing Optically Active Tris(ethylenediamine)cobalt(III) Ion. III.[1] Quaternary System, (Λ-$[Co(en)_3]^{3+}$, Δ-$[Co(en)_3]^{3+}$, H^+)-(R,R)-$C_4H_4O_6^{2-}$-H_2O, at 25 °C

Akira Fuyuhiro,* Kazuaki Yamanari, and Yoichi Shimura
Department of Chemistry, Faculty of Science, Osaka University, Toyonaka, Osaka 560

(Received July 6, 1981)

A part of quaternary solubility isotherm, (Λ-$[Co(en)_3]^{3+}$, Λ-$[Co(en)_3]^{3+}$, H^+)-(R,R)-$C_4H_4O_6^{2-}$-H_2O, $C_{H^+} \leqq C_{(R,R)\text{-}C_4H_4O_6^{2-}}$, was determined at 25 °C. It was found that three double salts Λ- and Λ-$[Co(en)_3](d\text{-}C_4H_5O_6)\cdot(d\text{-}C_4H_4O_6)\cdot nH_2O$ and Λ-$[Co(en)_3]_{0.48}\cdot\Delta$-$[Co(en)_3]_{0.52}(d\text{-}C_4H_4O_6)_{1.5}\cdot 5H_2O$ exist, three invariant points appearing. The yield for optical resolution of $[Co(en)_3]^{3+}$ found to be constant regardless of $[H^+]$. The existence of complete ternary system containing double salts, Λ-$[Co(en)_3](d\text{-}C_4H_5O_6)(d\text{-}C_4H_4O_6)$-$\Delta$-$[Co(en)_3](d\text{-}C_4H_5O_6)$-$(d\text{-}C_4H_4O_6)$-$H_2O$, was found and the solubilities of Λ- and Λ-$[Co(en)_3](d\text{-}C_4H_5O_6)(d\text{-}C_4H_4O_6)$ were measured at 5—65 °C.

The diastereomer of double salt Λ-$[Co(en)_3]X(d\text{-}H_2tart)$ (X^-=Br^- and I^-; $d\text{-}H_2tart^{2-}$=(R,R)-$C_4H_4O_6^{2-}$) can be used for the optical resolution of $[Co(en)_3]^{3+}$ ion. The particular role of the optically inactive component X^- has been revealed by the solubility phase diagrams of reciprocal salt-pairs, (Λ-$[Co(en)_3]^{3+}$, Δ-$[Co(en)_3]^{3+}$)-(X^-, $d\text{-}H_2tart^{2-}$)-H_2O.[1,2] A similar compound Λ-$H[Co(en)_3](d\text{-}H_2tart)_2\cdot 3H_2O$ was recently reported by Tada *et al.*[3] This diastereomer can be considered to be Λ-$[Co(en)_3](d\text{-}H_3tart)(d\text{-}H_2tart)\cdot 3H_2O$ corresponding to the case of X^-=$d\text{-}H_3tart^-$ in the above formula and have, so to speak, two optically active resolving agents. The system containing this diastereomer will be completely described by a quaternary system (Λ-$[Co(en)_3]^{3+}$, Δ-$[Co(en)_3]^{3+}$, H^+)-$d\text{-}H_2tart^{2-}$-H_2O. When the concentration of H^+ is lower than that of $d\text{-}H_2tart^{2-}$, a part of the system, however, can be formally regarded as the following reciprocal salt-pairs (Λ-$[Co(en)_3]^{3+}$, Δ-$[Co(en)_3]^{3+}$)-($d\text{-}H_3tart^-$, $d\text{-}H_2tart^{2-}$)-H_2O.

In this paper, we report the solubility isotherm of quaternary system (Λ-$[Co(en)_3]^{3+}$, Δ-$[Co(en)_3]^{3+}$, H^+)-$d\text{-}H_2tart^{2-}$-H_2O. This system was covered incompletely by the present experiment because the body of the solubility phase diagram does not form a closed space owing to the lack of solid phases Λ- and Δ-$[Co(en)_3](d\text{-}H_3tart)_3\cdot nH_2O$, and Λ-$[Co(en)_3]_p\cdot\Delta$-$[Co(en)_3]_q(d\text{-}H_3tart)_{3(p+q)}\cdot n'H_2O$. As regards optical resolution, the isotherms of X^-=$d\text{-}H_3tart^-$, however, can be effectively compared with those of X^-=Br^- and I^-.

Experimental

Materials. *$[Co(en)_3](d\text{-}H_2tart)_{1.5}\cdot nH_2O$*: The Λ- and Δ-$[Co(en)_3](d\text{-}H_2tart)_{1.5}\cdot nH_2O$ and the Λ-$[Co(en)_3]_{0.48}\cdot\Delta$-$[Co(en)_3]_{0.52}(d\text{-}H_2tart)_{1.5}\cdot 5H_2O$ diastereomers were the same as reported.[2]

d-*H_4tart*: A guaranteed reagent of Nakarai Chemicals Ltd. was employed.

$[Co(en)_3](d\text{-}H_3tart)(d\text{-}H_2tart)\cdot nH_2O$: The Λ- (or Δ-)$[Co(en)_3](d\text{-}H_3tart)(d\text{-}H_2tart)\cdot nH_2O$ diastereomer was prepared by mixing solutions of Λ- (or Δ-)$[Co(en)_3](d\text{-}H_2tart)_{1.5}\cdot nH_2O$ and $d\text{-}H_4tart$ in a 2:1 mole ratio. Found: C, 28.55; H, 6.62; N, 14.30%. Calcd for Λ-$[Co(en)_3](d\text{-}H_3tart)(d\text{-}H_2tart)\cdot 3H_2O$: C, 28.48; H, 6.66; N, 14.23%. Found: C, 24.84; H, 7.08; N, 12.49%. Calcd for Λ-$[Co(en)_3](d\text{-}H_3tart)(d\text{-}H_2tart)\cdot 7.5H_2O$: C, 25.04; H, 7.20; N, 12.52%.

Measurements. The solubility in water was determined in molality and the calibration of CD was also carried out according to the previous method.[2] The concentration of H^+ was determined by titration with a 0.01 mol dm^{-3} NaOH solution. The solid phases were identified by elemental analysis, absorption and CD spectra. Optical densities were measured with a Hitachi 330 spectrophotometer and CD with a JASCO MOE-1 spectropolarimeter. The absorption maximum value, ε(466 nm)=88.4, was used in this study.

Results and Discussion

Ternary System *Λ-$[Co(en)_3](d\text{-}H_2tart)_{1.5}$-$\Lambda$-$[Co(en)_3](d\text{-}H_3tart)_3$-$H_2O$.* The ternary system, Λ-$[Co(en)_3](d\text{-}H_2tart)_{1.5}$-$d\text{-}H_4tart$-$H_2O$, was partially determined at 25 °C (Fig. 1 and Table 1). The axis (1) expresses the molality of Λ-$[Co(en)_3](d\text{-}H_3tart)_3$, though the salt does not exist as solid. When the concentration of H^+ is lower than that of $d\text{-}H_2tart^{2-}$, the present system can be represented formally as the ternary one, Λ-$[Co(en)_3](d\text{-}H_2tart)_{1.5}$(4)-$\Lambda$-$[Co(en)_3](d\text{-}H_3tart)_3$(1)-$H_2O$, and then can be compared with

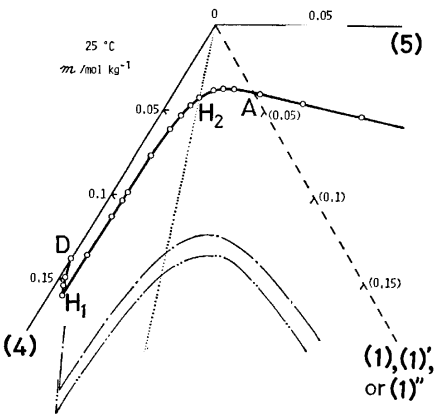

Fig. 1. Solubility isotherm (partial) of the ternary system, Λ-$[Co(en)_3](d\text{-}H_2tart)_{1.5}$(4)-$(d\text{-}H_4tart)_{1.5}$(5)-$H_2O$, at 25 °C.
Solubility is presented in molality m of anhydrous salt.
—·—: The ternary system, Λ-$[Co(en)_3](d\text{-}H_2tart)_{1.5}$(4)-$\Lambda$-$[Co(en)_3]Br_3$(1)'-$H_2O$, —··—: the ternary system, Λ-$[Co(en)_3](d\text{-}H_2tart)_{1.5}$(4)-$\Lambda$-$[Co(en)_3]I_3$(1)"-$H_2O$.

Table 1. Equilibrium of (Λ-$[Co(en)_3]^{3+}$, Δ-$[Co(en)_3]^{3+}$, H^+)-d-H_2tart^{2-}-H_2O system at 25 °C ($[H^+] \leqq [d\text{-}H_2tart^{2-}]$)

In liquid phases, solubility is presented in molality m of the component ions. Abbreviations are as follows: Λ-$[Co(en)_3]^{3+} = \Lambda^{3+}$, Δ-$[Co(en)_3]^{3+} = \Delta^{3+}$, Λ-$[Co(en)_3](d\text{-}H_2tart)_{1.5}\cdot nH_2O (n \gtrsim 7) = \Lambda(tart)_{1.5}$, Δ-$[Co(en)_3](d\text{-}H_2tart)_{1.5}\cdot nH_2O (n \simeq 8) = \Delta(tart)_{1.5}$, Λ-$[Co(en)_3]_{0.48}\cdot\Delta$-$[Co(en)_3]_{0.52}(d\text{-}H_2tart)_{1.5}\cdot 5H_2O = (\Lambda,\Delta)(tart)_{1.5}$, Λ-$[Co(en)_3](d\text{-}H_3tart)(d\text{-}H_2tart)\cdot 3H_2O = \Lambda(Htart)(tart)$, Δ-$[Co(en)_3](d\text{-}H_3tart)(d\text{-}H_2tart)\cdot 8H_2O = \Delta(Htart)(tart)$.

Position of points (Figs. 1—4)	No. of components	Liquid phase[a], $m/10^{-1}$ mol kg^{-1}			Solid phase
		Λ^{3+}	Δ^{3+}	H^+	
D	3	1.49		0.07	$\Lambda(tart)_{1.5}$
↕		1.54		0.12	
H_1					
H_1	3	1.60 (±0.01)		0.202 (±0.002)	$\Lambda(tart)_{1.5}+\Lambda(Htart)(tart)$
H_1	3	1.36		0.204	$\Lambda(Htart)(tart)$
		1.13		0.212	
		1.04		0.217	
		0.985		0.222	
↕		0.769		0.244	
		0.614		0.283	
		0.531		0.320	
		0.471		0.362	
H_2		0.440		0.403	
H_2	2	0.426 (±0.001)		0.426 (±0.001)	$\Lambda(Htart)(tart)$
H_2	3	0.383		0.573	$\Lambda(Htart)(tart)$
↕		0.377		0.693	
A		0.376		0.868	
C	3		3.09	0.108	$\Delta(tart)_{1.5}$
			3.27	0.223	
			3.40	0.349	
			3.42	0.399	
↕			3.53	0.506	
			3.55	0.510	
			3.71	0.671	
F_1			3.81	0.769	
			4.04	0.980	
F_1	3		4.35 (±0.03)	1.31 (±0.03)	$\Delta(tart)_{1.5}+\Delta(Htart)(tart)$
F_1	3		4.29	1.33	$\Delta(Htart)(tart)$
			4.17	1.32	
			3.92	1.33	
			3.24	1.36	
↕			2.91	1.38	
			2.67	1.44	
F_2			2.32	1.52	
			2.15	1.59	
			2.06	1.68	
			1.96	1.75	
F_2	2		1.86 (±0.01)	1.86 (±0.01)	$\Delta(Htart)(tart)$
F_2	3		1.75	2.18	$\Delta(Htart)(tart)$
			1.67	2.58	
			1.67	2.87	
↕			1.70	3.44	
			1.79	4.25	
B			1.89	4.87	
			2.04	5.88	
H_1	4	1.58	0.05	0.205	$\Lambda(tart)_{1.5}+\Lambda(Htart)(tart)$
↕		1.60	0.09	0.217	
P_1		1.63	0.16	0.218	
P_1	4	1.66 (±0.01)	0.21 (±0.01)	0.226 (±0.004)	$\Lambda(tart)_{1.5}+\Lambda(Htart)(tart)$ $+(\Lambda,\Delta)(tart)_{1.5}$

TABLE 1. (Continued)

Position of points (Figs. 1—4)	No. of components	Liquid phase[a], $m/10^{-1}$ mol kg^{-1} Λ^{3+}	Δ^{3+}	H^+	Solid phase
P_1 ↕ P_3	4	1.48	0.23	0.232	Λ(Htart)(tart) +(Λ,Δ)(tart)$_{1.5}$
		1.30	0.25	0.244	
		1.13	0.28	0.262	
		1.03	0.31	0.283	
		0.917	0.343	0.302	
		0.839	0.382	0.323	
		0.787	0.416	0.349	
		0.747	0.435	0.362	
		0.734	0.455	0.371	
		0.698	0.489	0.403	
		0.669	0.509	0.417	
		0.638	0.558	0.452	
		0.554	0.707	0.548	
		0.519	0.811	0.622	
		0.492	0.908	0.706	
		0.48	1.01	0.782	
		0.45	1.18	0.909	
		0.43	1.37	1.07	
		0.42	1.48	1.16	
		0.41	1.79	1.43	
		0.40	2.15	1.73	
P_3	4	0.40 (±0.01)	2.32 (±0.02)	1.90 (±0.02)	Λ(Htart)(tart) +Δ(Htart)(tart) +(Λ,Δ)(tart)$_{1.5}$
G_2 ↕ P_2	4	0.10	3.20	0.128	Δ(tart)$_{1.5}$+(Λ,Δ)(tart)$_{1.5}$
		0.11	3.44	0.368	
		0.11	4.05	0.920	
P_2	4	0.13 (±0.02)	4.48 (±0.02)	1.37 (±0.03)	Δ(tart)$_{1.5}$+Δ(Htart)(tart) +(Λ,Δ)(tart)$_{1.5}$
P_2 ↕ P_3	4	0.17	4.19	1.41	Λ(Htart)(tart) +(Λ,Δ)(tart)$_{1.5}$
		0.18	3.72	1.42	
		0.19	3.64	1.45	
		0.20	3.43	1.45	
		0.20	3.38	1.46	
		0.22	3.28	1.51	
		0.25	2.99	1.55	
		0.30	2.68	1.68	
		0.35	2.48	1.76	
P_3 ↕ I	4	0.39	2.24	1.93	Λ(Htart)(tart) +Δ(Htart)(tart)
		0.37	2.11	1.99	
		0.35	1.99	2.08	
		0.33	1.92	2.24	
I	3	0.33 (±0.01)	1.91 (±0.01)	2.24 (±0.01)	Λ(Htart)(tart) +Δ(Htart)(tart)
I ↕ E	4	0.31	1.85	2.44	Λ(Htart)(tart) +Δ(Htart)(tart)
		0.31	1.78	2.63	
		0.30	1.75	2.75	
		0.30	1.73	2.94	
		0.29	1.72	3.23	
		0.29	1.73	3.46	
		0.30	1.76	3.85	
		0.30	1.76	4.03	
		0.31	1.80	4.41	
		0.32	1.86	4.95	
		0.34	1.94	5.59	
		0.36	2.11	6.69	
		0.39	2.31	8.04	
H_2 ↕ I	3	0.400	0.101	0.501	Λ(Htart)(tart)
		0.390	0.168	0.558	
		0.376	0.248	0.624	
		0.353	0.431	0.784	
		0.335	0.678	1.01	
		0.325	0.941	1.27	
		0.32	1.24	1.57	
		0.32	1.58	1.91	

TABLE 1. (Continued)

Position of points (Figs. 1—4)	No. of components	Liquid phase,[a] $m/10^{-1}$ mol kg^{-1} Λ^{3+}	Λ^{3+}	H^+	Solid phase
F_2 ↕ I	3	0.16	1.88	2.04	Λ(Htart)(tart)

a) Reported data for C, D, G_1, G_2, D→G_1, and G_1→G_2[2] are not shown. Values in parentheses are estimated errors and calculated from twice the standard deviations of measurements repeated 5—8 times.

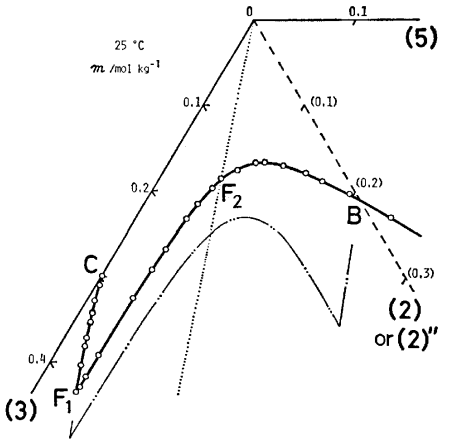

Fig. 2. Solubility isotherm (partial) of the ternary system, Λ-[Co(en)$_3$](d-H$_2$tart)$_{1.5}$(3)–(d-H$_4$tart)$_{1.5}$(5)–H$_2$O, at 25 °C.
Solubility is presented in molality m of anhydrous salt. —·—: the ternary system, Λ-[Co(en)$_3$](d-H$_2$tart)$_{1.5}$ (3)–Λ-[Co(en)$_3$]I$_3$(2)″–H$_2$O.

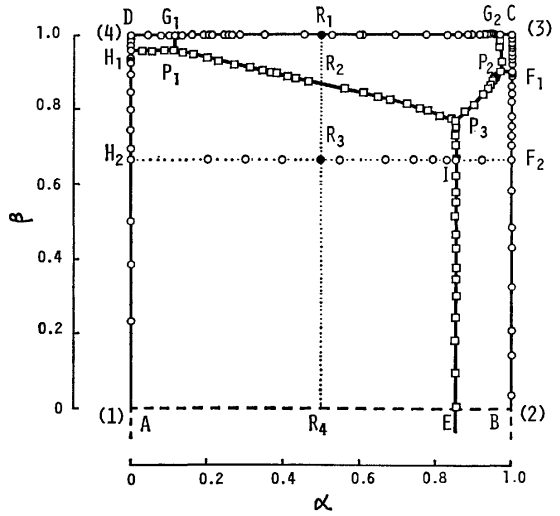

Fig. 3. The clinographic projection of solubility isotherm of the system, (Λ-[Co(en)$_3$]$^{3+}$, Λ-[Co(en)$_3$]$^{3+}$)–(d-H$_3$tart$^-$, d-H$_2$tart^{2-})–H$_2$O, at 25 °C.
α: Mole fraction of Λ-[Co(en)$_3$]$^{3+}$ to all the cations, β: mole fraction of (d-H$_2$tart)$_{1.5}^{3-}$ to {(d-H$_3$tart)$_3^{3-}$+(d-H$_2$tart)$_{1.5}^{3-}$}, (1): Λ-[Co(en)$_3$](d-H$_3$tart)$_3$, (2): Λ-[Co(en)$_3$](d-H$_3$tart)$_3$, (3): Λ-[Co(en)$_3$](d-H$_2$tart)$_{1.5}$, (4): Λ-[Co(en)$_3$](d-H$_2$tart)$_{1.5}$, □: solubility of four-components, ○: solubilities of two- or three-components. Each area has the following solids: $DH_1P_1G_1$: Λ-[Co(en)$_3$](d-H$_2$tart)$_{1.5}$·nH$_2$O, $H_1H_2AR_4EIP_3R_2P_1$: Λ-[Co(en)$_3$](d-H$_3$tart)(d-H$_2$trat)·3H$_2$O, $F_1P_2P_3IEBF_2$: Λ-[Co(en)$_3$](d-H$_3$tart)(d-H$_2$tart)·8H$_2$O, $CG_2P_2F_1$: Λ-[Co(en)$_3$](d-H$_2$tart)$_{1.5}$·nH$_2$O, $G_1P_1R_2P_3P_2G_2R_1$: Λ-[Co(en)$_3$]$_{0.48}$·Λ-[Co(en)$_3$]$_{0.52}$(d-H$_2$tart)$_{1.5}$·5H$_2$O.

the previous systems,[1,2] Λ-[Co(en)$_3$](d-H$_2$tart)$_{1.5}$(4)–Λ-[Co(en$_3$)]X$_3$–H$_2$O, X$^-$=Br$^-$(1)′ and I$^-$(1)″.

Point H$_2$ expresses the binary solubility of double salt Λ-[Co(en)$_3$](d-H$_3$tart)(d-H$_2$tart)·3H$_2$O. The region of the salt occupies a very wide region (H$_1$↔H$_2$↔A↔) and the salt exists in the area where the liquid phase contains little d-H$_2$tart^{2-} (the right area of A). The binary solubility for X$^-$=d-H$_3$tart$^-$ of Λ-[Co(en)$_3$]X(d-H$_2$tart) (m=0.0426 mol kg^{-1}) is much smaller than that for X$^-$=Br$^-$ and I$^-$ (m=0.135 and 0.148 mol kg^{-1}, respectively) at 25 °C. The isotherms of the latter two salts in the ternary systems locate in much lower region than that of the former salt. These facts relate to the appearance of a new ternary system, Λ-[Co(en)$_3$](d-H$_3$tart)(d-H$_2$tart)–Λ-[Co(en)$_3$](d-H$_3$tart)(d-H$_2$tart)–H$_2$O, which is useful for optical resolution.

Ternary System Δ-[*Co(en)*$_3$](d-*H*$_2$*tart*)$_{1.5}$–Δ-[*Co(en)*$_3$](d-*H*$_3$*tart*)$_3$–*H*$_2$*O*. The Λ-ternary system is shown in Fig. 2 and Table 1. Point F$_2$ shows the binary solubility of the new double salt Λ-[Co(en)$_3$](d-H$_3$tart)(d-H$_2$tart), whose region spreads widely as in the case of Λ-system. The corresponding double salt for X$^-$=I$^-$ of Λ-[Co(en)$_3$]X(d-H$_2$tart) has a lower isotherm[1] than that for X$^-$=d-H$_3$tart$^-$, whereas this region for X$^-$=Br$^-$ cannot be measured because of a gelatinous precipitate.[2]

The Solubility Isotherm of Reciprocal Salt-pairs, (Λ-[*Co(en)*$_3$]$^{3+}$, Δ-[*Co(en)*$_3$]$^{3+}$)–(d-*H*$_3$*tart*$^-$, d-*H*$_2$*tart*$^{2-}$)–*H*$_2$*O*. Figure 3 shows the clinographic projection of the system of the reciprocal salt-pairs. The left and right sides correspond to Figs. 1 and 2, respectively, and the upper side is the same ternary system as in the previous systems. However, the lower side shows a imaginary ternary system because neither Λ- nor Λ-[Co(en)$_3$](d-H$_3$tart)$_3$ exists as a solid compound. The boundary curve P$_1$R$_2$P$_3$, where two solids Λ-[Co(en)$_3$](d-H$_3$tart)(d-H$_2$tart)·3H$_2$O and Λ-[Co(en)$_3$]$_{0.48}$·Λ-[Co(en)$_3$]$_{0.52}$(d-H$_2$tart)$_{1.5}$·5H$_2$O coexist, lies at the upper region than the corresponding curves of the Br$^-$ and I$^-$ systems. This fact is advantageous for the optical resolution because the less soluble diastereomer enlarges its region. The double salts Λ- and Λ-[Co(en)$_3$](d-H$_3$tart)(d-H$_2$tart) have a long boundary P$_3$↔I↔E↔. When we utilize the Λ-[Co(en)$_3$](d-H$_3$tart)(d-H$_2$tart) diastereomer for the optical resolution, the point corresponding to maximum yield lies on P$_3$IE. Since the curve is almost parallel to

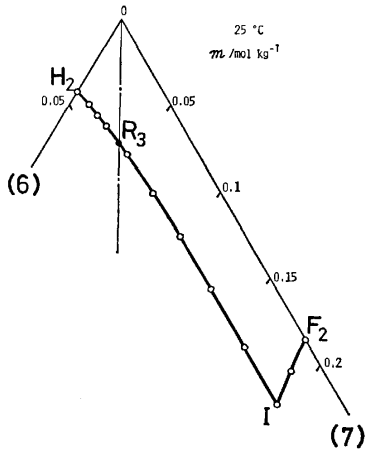

Fig. 4. Solubility isotherm of the ternary system, *Λ*-[Co(en)$_3$](*d*-H$_3$tart)(*d*-H$_2$tart)(6) – *Λ*-[Co(en)$_3$](*d*-H$_3$tart)(*d*-H$_2$tart)(7)–H$_2$O, at 25 °C.
Solubility is presented in molality *m* of anhydrous salt.

the ordinate, the yield is constant at 25 °C (83% for *Λ*-[Co(en)$_3$]$^{3+}$ and 42% for *rac*-[Co(en)$_3$]$^{3+}$) in spite of the large variation of [*d*-H$_3$tart$^-$]/[*d*-H$_2$tart^{2-}] in solution.

Ternary System Λ-[*Co(en)*$_3$](d-*H*$_3$*tart*)(d-*H*$_2$*tart*)–Δ-[*Co(en)*$_3$](d-*H*$_3$*tart*)(d-*H*$_2$*tart*)–*H*$_2$*O*. The ternary system, *Λ*-[Co(en)$_3$]X(*d*-H$_2$tart)–*Λ*-[Co(en)$_3$]X(*d*-H$_2$tart)–H$_2$O, is formed in the present case of X$^-$= *d*-H$_3$tart$^-$ (Fig. 4), though the participation of *Λ*-[Co(en)$_3$]$_{0.48}$·*Λ*-[Co(en)$_3$]$_{0.52}$(*d*-H$_2$tart)$_{1.5}$·5H$_2$O prevents from occurring such kind of ternary system for X$^-$=Br$^-$ or I$^-$. This system corresponds to $\beta=2/3$ in Fig. 3. Though the solubility of *Λ*-[Co(en)$_3$](*d*-H$_3$tart)(*d*-H$_2$tart) slightly decreased with the increase of *Λ*-[Co(en)$_3$](*d*-H$_3$tart)(*d*-H$_2$tart), it is interesting that the *Λ*-double salt shows the reverse relationship.

The solubilities of the double salts are listed in Table 2. The solubility ratio *Λ*/*Λ* becomes maximum (*ca.* 12.2) at the transition temperature (about 47 °C) from 8-hydrate to monohydrate of *Λ*-[Co(en)$_3$](*d*-H$_3$tart)(*d*-H$_2$tart). The ratio is 4.37 at 25 °C, and therefore the yield of optical resolution will be improved by experimenting at 47 °C.

Table 2. Solubility of [Co(en)$_3$]$^{3+}$ salts in water (molality *m*/mol kg^{-1} of anhydrous salt)

T/°C	No. of salt[a]		
	(1)	(2)-α	(2)-β
5	0.0201	0.0411	
10	0.0243	0.0583	
15	0.0295	0.0843	
20	0.0354	0.123	
25	0.0426	0.186	
30	0.0510	0.286	
35	0.0622	0.452	
40	0.0752	0.703	
45	0.0904	1.04	
50	0.110	1.48	1.22
55	0.134	1.95	1.30
60	0.166		1.39
65	0.203		1.50

a) (1): *Λ*-[Co(en)$_3$](*d*-H$_3$tart)(*d*-H$_2$tart)·3H$_2$O, (2): *Λ*-[Co(en)$_3$](*d*-H$_3$tart)(*d*-H$_2$tart)·*n*H$_2$O, $n=8(\alpha)$ and $n=1(\beta)$.

References

1) Part II of this series: A. Fuyuhiro, K. Yamanari, and Y. Shimura, *Bull. Chem. Soc. Jpn.*, **54**, 2317 (1981).
2) A. Fuyuhiro, K. Yamanari, and Y. Shimura, *Bull. Chem. Soc. Jpn.*, **53**, 3577 (1980).
3) T. Tada, Y. Kushi, and H. Yoneda, *Chem. Lett.*, **1977**, 379.

Formation of Mixed-ligand Complexes of Cobalt(II) with Bromide and Substituted Pyridines in 1,2-Dibromoethane

Kiyoshi SAWADA,* Kazue MIURA, and Toshio SUZUKI

Laboratory of Analytical Chemistry, Faculty of Science, Niigata University, Niigata 950-21

(Received July 20, 1981)

The equilibria of a series of complexes of the $CoBr_2(R\text{-}py)_2$ type (where R-py=2-methyl-(2Me-py), 3-methyl-(3Me-py), 4-methyl-(4Me-py), 4-acetyl-(4Ac-py), and 4-cyanopyridine (4CN-py), and pyridine(py)) with TBA·Br (tetrabutylammonium bromide) in 1,2-dibromoethane have been investigated spectrophotometrically. In the presence of an excess of R-py, the dibromocomplex gives rise to the following configurational equilibrium:

$$\underset{\text{(tetrahedral)}}{CoBr_2(R\text{-}py)_2} + 2R\text{-}py \overset{K_c}{\rightleftharpoons} \underset{\text{(octahedral)}}{CoBr_2(R\text{-}py)_4}$$

with log K_C=0.67, 0.11, and 0.53±0.03 for the 4Me-py, 3Me-py, and py complexes respectively. The substitution equilibria of the tetrahedral complexes are written as:

$$CoBr_2(R\text{-}py)_2 + TBA\cdot Br \overset{K_3}{\rightleftharpoons} (TBA)CoBr_3(R\text{-}py) + R\text{-}py,$$

$$(TBA)CoBr_3(R\text{-}py) + TBA\cdot Br \overset{K_4}{\rightleftharpoons} (TBA)_2CoBr_4 + R\text{-}py.$$

The successive formation constants, log K_3, were determined as 2.23, 2.44, and 2.89±0.03 for the 4Me-py, 3Me-py, and py complexes respectively. The constants log K_4 for the 4Me-py, 3Me-py, 2Me-py, py, 4Ac-py and 4CN-py complexes are −1.07, −0.94, 0.09, −0.74, −0.09, and 0.47±0.01 respectively. The values of log K_3 and log K_4 show a linear correlation with the basicity of R-py, pK_b, except for the 2Me-py complex.

In nonaqueous solvents containing an excess of pyridine bases, R-py, the dihalogenocomplex of cobalt(II) is in a configurational equilibrium between tetrahedral $[CoX_2(R\text{-}py)_2]$ and octahedral $[CoX_2(R\text{-}py)_4]$ structures (where X=halogenide ion). Libuś and his co-workers[1,2] have studied the configurational equilibria for a series of complexes of cobalt(II) and other first-row transition metals by means of solubility and spectrophotometric measurements. The thermodynamic data of the equilibria with a series of substituted pyridines have been reported by Nelson *et al.*,[3-5] and the kinetic parameters have been measured by means of nitrogen-14 NMR[6] and T-jump method.[7,8] The addition of the halogenide ion to the dihalogenocomplex solution results in the formation of the tetrahedral trihalogeno $[CoX_3(R\text{-}py)^-]$ and tetrahalogeno $[CoX_4^{2-}]$ complexes.[9] Besides the visible spectra, UV,[10] near-IR,[9,11,12] and far-IR[13-15] spectra of the di- and trihalogenocomplexes in solution and in crystals have been measured.

Nelson *et al.*[5] have interpreted the solution behavior and spectra of the $CoX_2(R\text{-}py)_2$ complexes in terms of Co–N π bonding, which depends mainly on X^- and, to a lesser extent, on R-py and its pK_b. Wayland and Drago[16,17] have explained the effect of the Co–X bond strength on the Co–N bond in terms of the molecular orbital theory, whereas Graddon and Watton[18] and La Mar[19] have attributed the effects to the ligand-ligand repulsion.

The effect of the basicity of pyridine bases on the metal-nitrogen bond strength has been systematically investigated for the zinc complexes, $ZnX_2(R\text{-}py)_2$, by means of the heat of complex formation,[20,21] the far-IR spectra,[20,22-24] and the crystal structure:[24] and the role of the π bonding has been discussed. Almost no such systematic study has been attempted for the cobalt(II) complexes, however.

In a previous paper[9] we have investigated the equilibria of $CoCl_2(R\text{-}py)_2$ with tetrabutylammonium chloride (TBA·Cl) in 1,2-dichloroethane, and reported the linear correlation between the cobalt(II)-pyridine bond strength and pK_b of R-py. In the present paper, the equilibria of $CoBr_2(R\text{-}py)_2$ with TBA·Br in 1,2-dibromoethane are investigated spectrophotometrically, and the results are compared with those for the chlorocomplexes.

Experimental

Reagents. 1,2-Dibromoethane dehydrated by means of the molecular sieve was distilled. Tetrabutylammonium bromide (TBA·Br) was dried at 140 °C, and its purity was determined by argentometry. The substituted pyridines, R-py, and dibromobis(substituted pyridine)cobalt(II) were prepared by a method similar to that described in a previous paper.[9]

Measurements. The $CoBr_2(R\text{-}py)_2$ solution was prepared by dissolving $CoBr_2(R\text{-}py)_2$ crystals in 1,2-dibromoethane containing 10^{-3} mol dm^{-3} of R-py. This solution was titrated with a TBA·Br solution in a stoppered quartz cell (volume: 50 cm^3, light path: 10 mm), and the change in the visible spectra of the solution was measured by a Shimadzu double-beam spectrophotometer UV-200 at 25.0± 0.2 °C.

Results

Configurational Equilibria of Dibromocomplexes. The visible spectra of $CoBr_2(R\text{-}py)_2$ are shown in Fig. 1 (A). By the addition of 10^{-3} mol dm^{-3} of R-py, the formation of a lower pyridine complex such as $CoBr_2(R\text{-}py)$ is surpressed. The fact that the spectra have no peaks of such higher bromocomplexes as the tribromocomplex indicates that they are the spectra of the pure dibromocomplex. The solubilities of the 4Ac-py and 4CN-py complexes are too low for the spectra to be measured.

Upon the addition of a large excess of R-py, the absorbance decreases monotonously, while the ratios of the peak heights do not change. This spectral

change can be interpreted in terms of the formation of an octahedral complex,[1-5,9] which has quite a small molar extinction coefficient compared with that of the tetrahedral complex; *i.e.*, the molar extinction coefficient of the tetrahedral complex of cobalt(II) is about 10^3, as is shown in Fig. 1, whereas that of the octahedral complex is less than 10 in the region of 600—700 nm.[2,25] We thus obtain the following equilibrium:

$$CoBr_2(R\text{-}py)_2 + 2R\text{-}py \overset{K_c}{\rightleftharpoons} CoBr_2(R\text{-}py)_4. \quad (1)$$

As the concentration of R-py, $C_{R\text{-}py}$, is much larger than that of the complex, C_{Co}, and as the absorption of the octahedral complex is negligible, the apparent molar extinction coefficient, $\bar{\varepsilon}$, is written as:

$$\bar{\varepsilon} = \frac{\varepsilon_2}{1+K_cC_{R\text{-}py}{}^2}. \quad (2)$$

We thus obtain Eq. 3 immediately:

$$\log\left(\frac{\varepsilon_2}{\bar{\varepsilon}}-1\right) = \log K_c + 2\log C_{R\text{-}py}. \quad (3)$$

Plot of the log $(\varepsilon_2/\bar{\varepsilon}\text{-}1)$ values of the peaks of the dibromocomplex as a function of log $C_{R\text{-}py}$ gives rise to a straight line with a slope of 2. The equilibrium constants of configurational change, K_c, obtained from the intercept are listed in Table 1.

Formation of Tribromocomplexes. The change in the spectra of the $CoBr_2py_2$ solution (containing 0.05 mol dm^{-3} pyridine) upon the addition of TBA·Br is shown in Fig. 2. These spectra show an isosbestic point at 658 nm. In Fig. 3 the apparent molar extinction coefficient of the pyridine complex at 596 nm is plotted as a function of the mole ratio, $C_{TBA\cdot Br}/C_{Co}$, where $C_{TBA\cdot Br}$ refers to the total concentration of TBA·Br added. These results indicate a reaction of one molecule of bromide with a cobalt(II) complex, *i.e.*, the formation of a tribromocomplex:

$$CoBr_2py_2 + TBA\cdot Br \overset{K_3}{\rightleftharpoons} (TBA)CoBr_3py + py. \quad (4)$$

As will be shown in the next section, the successive formation constant of the tetrabromocomplex, K_4, is much smaller than that of the tribromocomplex, K_3; the formation of the tetrabromocomplex in this region of $C_{TBA\cdot Br}/C_{Co}$ is negligible. Thus, the total concentration of cobalt(II) is given by:

$$C_{Co} = [CoBr_2py_4] + [CoBr_2py_2] + [(TBA)CoBr_3py], \quad (5)$$

where [ ] denotes the equilibrium concentration. As the molar extinction coefficient of the octahedral com-

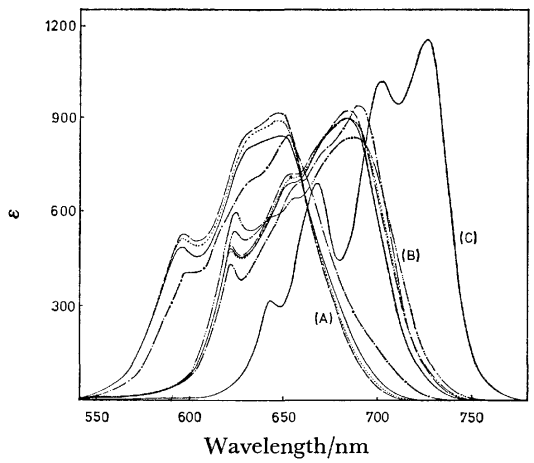

Fig. 1. Absorption spectra of $CoBr_2(R\text{-}py)_2$ (A), (TBA)-$CoBr_3(R\text{-}py)$ (B), and $(TBA)_2CoBr_4$ (C) in dibromoethane.
R-py: ——, 4Me-py; ·····, 3Me-py; —·—, 2Me-py; ——, py; —···—, 4Ac-py; —····—, 4CN-py.

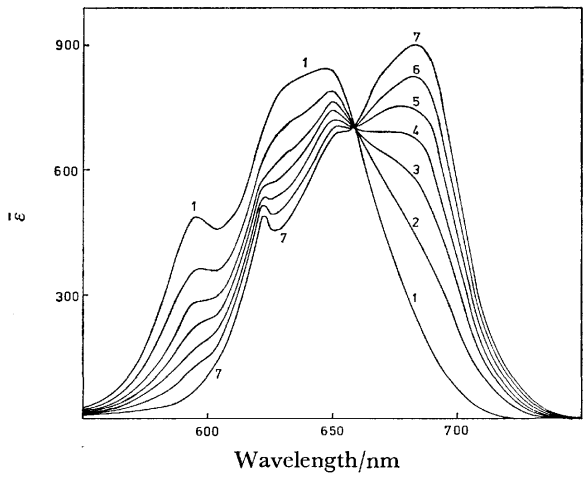

Fig. 2. Absorption spectra of pyridine complex at low TBA·Br concentrations.
$C_{TBA\cdot Br}$: 1, 0; 2, 2.72; 3, 4.50; 4, 6.04; 5, 7.77; 6, 9.89; 7, 25.5×10^{-4} mol dm^{-3}. $C_{Co}=9.84\times10^{-4}$ mol dm^{-3}. $C_{py}=5.00\times10^{-2}$ mol dm^{-3}.

Table 1. Equilibrium constants of configuratioanl change, K_c, and successive formation constants of trichlorocomplexes, K_3, and tetrachlorocomplexes, K_4

R-py	pK_b[a]	log K_c		log K_3		log K_4	
		Chloride[b]	Bromide	Chloride[b]	Bromide	Chloride[b]	Bromide
4Me-py	7.97	0.03±0.03	0.67±0.03	3.48±0.03	2.23±0.03	0.08±0.01	−1.07±0.01
3Me-py	8.32	−0.70	0.11	3.70	2.44	0.27	−0.94
2Me-py	8.04					1.18	0.09
py	8.80	0.27	0.53	4.10	2.89	0.48	−0.74
4Ac-py	10.49					1.06	−0.09
4CN-py	12.12					1.59	0.47

a) D. D. Perrin, "Dissociation Constants of Organic Bases in Aqueous solution, Supplement," Butterworths, London (1972). b) Ref. 9.

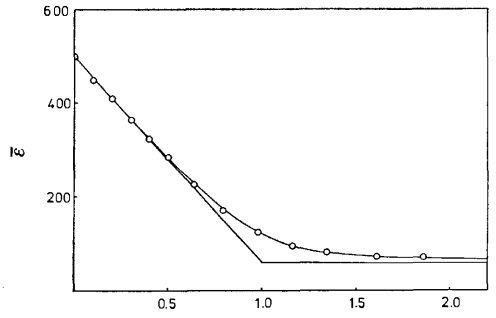

Fig. 3. Plot of apparent molar extinction coefficient at 596 nm as a function of mole ratio, $C_{TBA\cdot Br}/C_{Co}$. $C_{Co}=1.01\times10^{-3}$ mol dm^{-3}. $C_{py}=1.60\times10^{-2}$ mol dm^{-3}. Solid line is the plot of $\bar{\varepsilon}$ calculated by using the values of ε_3, ε_2, and K_3 shown in Fig. 1 and Table 1.

plex is negligibly small at this wavelength, we obtain:

$$\bar{\varepsilon} = \{\varepsilon_2[CoBr_2py_2] + \varepsilon_3[(TBA)CoBr_3py]\}C_{Co}^{-1}, \quad (6)$$

where the molar extinction coefficient of (TBA)-$CoBr_3py$, ε_3, was evaluated by the extrapolation of the plot of $\bar{\varepsilon}$ to $C_{TBA\cdot Br}/C_{Co}=1$. The formation constant of the tribromocomplex:

$$K_3 = \frac{[(TBA)CoBr_3py][py]}{[CoBr_2py_2][TBA\cdot Br]}$$

is calculated by using Eqs. 5 and 6. The spectrum of the tribromocomplex obtained from the ε_3 values at various wavelengths, as evaluated by the extrapolation of the plot of $\bar{\varepsilon}$ to $C_{TBA\cdot Br}/C_{Co}=1$, is shown in Fig. 1. (B).

The value of the apparent molar extinction coefficient calculated by using the ε_2, ε_3, and K_3 values thus obtained is shown in Fig. 3 by a solid line; it is in good agreement with the experimental results. The K_3 of the pyridine complex is listed in Table 1, along with those of the 4Me-py and 3Me-py complexes obtained in the same manner as the pyridine complex.

Formation of Tetrabromocomplexes. 10^{-4} mol of $CoBr_2$ were dissolved in 100 cm^3 of 2×10^{-3}—10^{-1} mol dm^{-3} TBA·Br 1,2-dibromoethane solutions ($C_{R\text{-}py}=0$). The spectra of the solutions (Fig. 1 (C)) show the characteristics of the tetrabromocomplex.[25] The spectra have no peaks of other complexes and do not change upon a change in the concentration of TBA·Br. Concequently, the spectrum of Fig. 1 (C) is that of pure $(TBA)_2CoBr_4$.

The addition of a large excess of bromide to the $CoBr_2(R\text{-}py)_2$ solution causes further spectral change, as is shown in Fig. 4. These spectra show an isosbestic point at 694 nm, and the spectrum at the highest $C_{TBA\cdot Br}$ value shows the characteristics of the tetrabromocomplex. Thus, the reaction in this region of $C_{TBA\cdot Br}$ may be written as:

$$(TBA)CoBr_3(R\text{-}py) + TBA\cdot Br \overset{K_4}{\rightleftharpoons} (TBA)_2CoBr_4 + R\text{-}py. \quad (7)$$

The total concentration of cobalt(II) and the apparent molar extinction coefficient are written as follows:

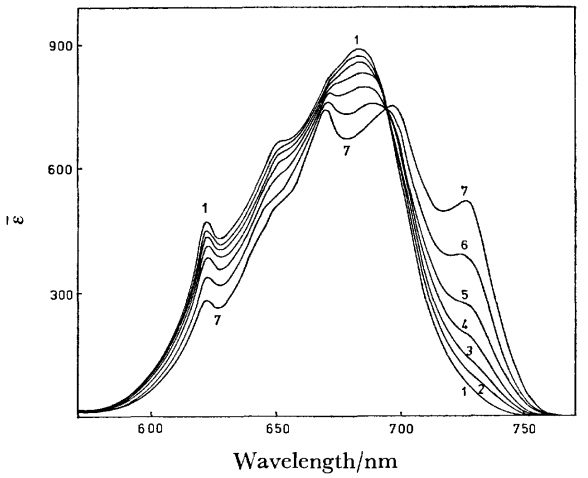

Fig. 4. Absorption spectra of pyridine complex at high TBA·Br concentrations.
$C_{TBA\cdot Br}$: 1, 2.53; 2, 4.51; 3, 6.59; 4, 9.86; 5, 15.5; 6, 25.5; 7, 41.1×10^{-3} mol dm^{-3}. $C_{Co}=1.33\times10^{-3}$ mol dm^{-3}. $C_{py}=0.996\times10^{-2}$ mol dm^{-3}.

$$C_{Co} = [(TBA)CoBr_3(R\text{-}py) + [(TBA)_2CoBr_4], \quad (8)$$

$$\bar{\varepsilon} = \{\varepsilon_3[(TBA)CoBr_3(R\text{-}py)] + \varepsilon_4[(TBA)_2CoBr_4]\}C_{Co}^{-1}, \quad (9)$$

where ε_4 refers to the molar extinction coefficient of $(TBA)_2CoBr_4$. From Eqs. 8 and 9, we obtain the following equation:

$$\frac{[(TBA)_2CoBr_4]}{[(TBA)CoBr_3(R\text{-}py)]} = \frac{\bar{\varepsilon}-\varepsilon_3}{\varepsilon_4-\bar{\varepsilon}}. \quad (10)$$

By using the equilibrium constant of Eq. 7, K_4, and Eq. 10, we obtain:

$$\log\frac{\bar{\varepsilon}-\varepsilon_3}{\varepsilon_4-\bar{\varepsilon}} = \log K_4 + \log\frac{[TBA\cdot Br]}{[R\text{-}py]}. \quad (11)$$

The plot of the left-hand side of Eq. 11 as a function of log [TBA·Br]/[R-py] falls on a straight line with a slope of unity. This indicates the validity of the assumption of the equilibria (7).

In the cases of the 4Ac-py and 4CN-py complexes, the solution of the tribromocomplex, $(TBA)CoBr_3(R\text{-}py)$, was prepared by saturating the 10^{-2} mol dm^{-3} TBA·Br solution with the $CoBr_2(R\text{-}py)_2$ complex. The mole ratio of the TBA·Br and $CoBr_2(R\text{-}py)_2$ of the saturated solution was determined as $C_{TBA\cdot Br}/C_{Co}=1$. Thus, the formation of only the tribromocomplex was ascertained. The spectra of the tribromocomplexes are shown in Fig. 1 (B).

Discussion

As can be seen from Fig. 5, there is no systematic correlation between the K_c and pK_b of R-py. Generally, the configurational change from tetrahedral to octahedral structures is enthalpy-driven, and the enthalpy is largely compensated by the entropy term.[3-5,26] Thus, the effect of the entropy change on the configurational equilibrium is so appreciable that the difference in the basicity of the pyridines may be overwhelmed by the change in the entropy. The K_c of

the 3Me-py complex is considerably smaller than those of the py and 4Me-py complexes. This may indicate steric hindrance in the octahedral complex caused by the substitution at the 3-position of the pyridine.[16-19]

As is revealed in Fig. 5, the plot of log K_3 and log K_4 *vs.* pK_b of R-py shows a linear correlation; *i.e.*, the Co–R-py bond strength decreases upon a decrease in the basicity of R-py. The fact that the constants, K_3 and K_4, of the 3Me-py complexes show normal values indicates that the steric effect of 3Me-py is not important in the tetrahedral complexes. La Mar[19] has suggested the presence of steric hindrance of 3Me-py in the tetrahedral complexes, whereas Wayland and Drago[17] have denied this argument on the basis of the rasults of the molecular model and the contact shift of proton NMR. Our results support the latter conclusion. The K_4 value of the 2Me-py complex is much larger than those of the complexes of the other pyridines having comparable pK_b value. Thus, the steric effect of 2Me-py is significant even in the tetrahedral configuration.

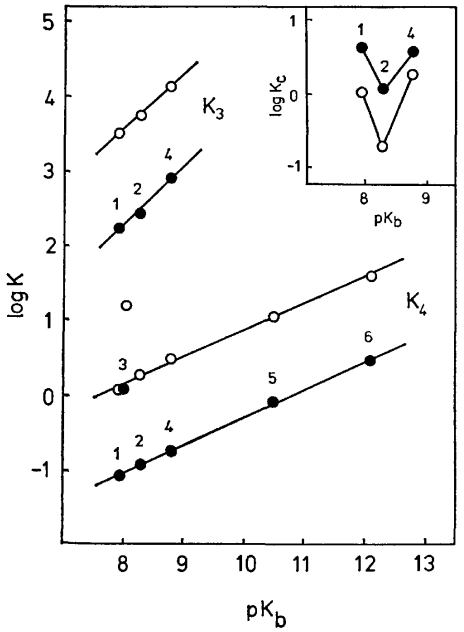

Fig. 5. Plot of log K_c, log K_3, and log K_4 as a function of pK_b of R-py.
R-py: 1, 4Me-py; 2, 3Me-py; 3, 2Me-py; 4, py; 5, 4Ac-py; 6, 4CN-py. Filled circle: bromocomplexes, open circle: chlorocomplexes (Ref. 9).

The ratio of the successive formation constants, K_3/K_4, is much larger than the statistical one, $(K_3/K_4)_{stat}=8/3$. As has been shown in the previous paper,[9] this fact can be interpreted in terms of the steric hindrance increasing in the order of: $CoX_2(R\text{-}py)_2<CoX_3(R\text{-}py)^-<CoX_4^{2-}$.

The formation constants, K_3 and K_4, of the bromocomplexes are smaller than those of the corresponding chlorocomplexes: this trend agrees with the results of other systems.[25] The difference in log K_4 between the chloro- and bromocomplexes (Δ log $K_4=1.16$) is almost the same as that of log K_3 (Δ log $K_3=1.24$). This may indicate that the steric effect of the bromocomplex is of the same magnitude of that of the chlorocomplex. This is consistent with the fact that the magnitude of the steric effects of the octahedral 3Me-py chlorocomplex and the tetrahedral 2Me-py chlorocomplex is almost the same as those of the bromocomplexes respectively.

The effect of the basicity of substituted pyridine on the metal-pyridine bond strength has also been discussed. Wong and Brewer[22] have suggested that, when the substituent on pyridine is more electron-attractive than hydrogen, the metal-nitrogen σ bond is weakened by the decrease in electron density on the nitrogen atom of pyridine, but that the π bond is strengthened by the back-donation of the π electron from metal to nitrogen. Thus, the decrease in metal-pyridine bond strength upon the decrease in σ bonding is partially compensated by the increase in π bonding. Steffen and Palenik[24] have concluded that the linear correlation of the Zn–N bond length in $ZnCl_2(R\text{-}py)_2$ with the pK_b of R-py suggests a minimum contribution of π bonding. As can be seen from Fig. 5 a linear correlation of the Co–N bond strength with pK_b is observed even for the cobalt(II) complex. This can be interpreted in terms of the linear correlation between the π bond and the σ bond, or a minimum contribution of the π bond to the Co–N bond. Wayland and Drago[16] have suggested that the contribution of the π bond is not so significant

Table 2. Frequency of the gravity center and oscillator strength of the absorption band of the tetrahedral halogeno complexes of cobalt(II) in 1,2-dihaloethane, acetic acid, and acetone[a]

		1,2-Dihaloethane		Acetic acid[d]		Acetone[e]
		Chloride[b]	Bromide[c]	Chloride	Bromide	Chloride
CoX_2S_2	$\nu_c/10^3$ cm^{-1}	16.39	15.92	15.93	15.53	15.92
	$f/10^{-3}$	(7.04)	(7.21)	(0.53)[f]	(4.16)[f]	(3.92)
CoX_3S^-	$\nu_c/10^3$ cm^{-1}	15.74	15.13	15.57	14.93	15.39
	$f/10^{-3}$	(6.05)	(6.91)	(4.15)	(4.99)	(4·50)
CoX_4^{2-}	$\nu_c/10^3$ cm^{-1}	15.03	14.38	15.19	14.42	15.11
	$f/10^{-3}$	(5.88)	(6.97)	(6.00)	(8.91)	(5.34)

a) Anionic species form ion-pairs with the tetrabutylammonium ion or the lithium ion. b) Ref. 9. S is pyridine. c) This work. S is pyridine. d) Ref. 25. S is acetic acid. e) Ref. 28. S is acetone. f) Mixture of tetrahedral and octahedral dihalocobalt(II) complexes.

for the ligand with no low-lying empty π orbital such as pyridine.

Much as with the chlorocomplexes, the dibromocomplexes and the tribromocomplexes have virtually the same visible spectra irrespective of the change in the pyridine bases, although those of the 2Me-py complexes are slightly shifted to a higher wavelength (Figs. 1 (A) and (B)). The frequency of the gravity center, ν_c, and the oscillator strength, f, of the absorption band are listed in Table 2, along with the data on chlorocomplexes in 1,2-dichloroethane,[9] bromo- and chlorocomplexes in acetic acid,[25] and chlorocomplexes in acetone.[28]

The plot of ν_c *vs.* the number of the halogenide ion coordinated to cobalt(II) gives rise to a good linear relationship. The ν_c of cobalt(II) coordinated by four pyridine molecules tetrahedrally, $Co(py)_4^{2+}$, is estimated as $\nu_c=17.64\times10^3\,cm^{-1}$. This may indicate that the rule of average environment can be applied to both the ligand-field strength and the electron-repulsion parameter. The trend of change in f with the number of the halogenide ion in the complex depends on the neutral ligand. This may indicate that the structures of the dihalogeno- and trihalogenocomplexes are seriously affected by the structure of the solvent or neutral ligand. On the other hand, as can be seen from Fig. 1, the effect of the basicity of the neutral ligand on the spectra is very small.

We are grateful to the Ministry of Education, Science and Culture for its financial support through Grant No. 374188.

References

1) W. Libuś and I. Uruska, *Inorg. Chem.*, **5**, 256 (1966).
2) W. Libuś, K. Chachulska, and M. Mesik, *Inorg. Chem.*, **19**, 2259 (1980).
3) H. C. A. King, E. Körös, and S. M. Nelson, *J. Chem. Soc.*, **1963**, 5449.
4) S. M. Nelson and T. M. Shepherd, *J. Chem. Soc.*, **1965**, 3284.
5) J. de O. Cabral, H. C. A. King, S. M. Nelson, T. M. Shepherd, and E. Körös, *J. Chem. Soc., A*, **1966**, 1348.
6) G. D. Howald and R. S. Marianelli, *Inorg. Chem.*, **9**, 1738 (1970).
7) R. D. Farina and J. H. Swinehart, *J. Am. Chem. Soc.*, **91**, 568 (1969).
8) R. D. Farina and J. H. Swinehart, *Inorg. Chem.*, **11**, 645 (1972).
9) K. Sawada and T. Suzuki, *J. Inorg. Nucl. Chem.*, **43**, 2301 (1981).
10) Y. Bando and S. Nagakura, *Inorg. Chem.*, **7**, 893 (1968).
11) D. M. L. Goodgame and M. Goodgame, *Inorg. Chem.*, **4**, 139 (1965).
12) A. B. P. Lever and S. M. Nelson, *J. Chem. Soc.*, **1966**, 859.
13) C. Postmus, J. R. Ferraro, A. Quattrochi, K. Shobatake, and K. Nakamoto, *Inorg. Chem.*, **8**, 1851 (1969).
14) R. J. H. Clark and C. S. Williams, *Inorg. Chem.*, **4**, 350 (1965).
15) N. H. Agnew, R. J. Collin, and L. F. Larkworthy, *J. Chem. Soc., Dalton Trans.*, **1974**, 272.
16) B. B. Wayland and R. S. Drago, *J. Am. Chem. Soc.*, **88**, 4697 (1966).
17) R. S. Drago and B. B. Wayland, *Inorg. Chem.*, **7**, 528 (1968).
18) D. P. Graddon and E. C. Watton, *Aust. J. Chem.*, **18**, 507 (1965).
19) G. N. La Mar, *Inorg. Chem.*, **6**, 1939 (1961).
20) P. T. T. Wong and D. G. Brewer, *Can. J. Chem.*, **46**, 131 (1968).
21) L-T. Ang and D. P. Graddon, *J. Inorg. Nucl. Chem.*, **38**, 2279 (1976).
22) P. T. T. Wong and D. G. Brewer, *Can. J. Chem.*, **47**, 4589 (1969).
23) P. T. T. Wong, *Inorg. Chem.*, **14**, 2271 (1975).
24) W. L. Steffen and G. J. Palenik, *Inorg. Chem.*, **16**, 1119 (1977).
25) K. Sawada and M. Tanaka, *J. Inorg. Nucl. Chem.*, **39**, 339 (1977).
26) K. Sawada, T. Nakamura, and M. Tanaka, *J. Inorg. Nucl. Chem.*, **42**, 1471 (1980).
27) U. Carunchio, U. B. Ceipidor, and A. Messina, *Inorg. Chim. Acta*, **6**, 613 (1972).
28) K. Sawada, T. Onoda, and T. Suzuki, *J. Inorg. Nucl. Chem.*, in press.

 © 1982 The Chemical Society of Japan Bull. Chem. Soc. Jpn., 55, 785—791 (1982)

Optically Active Vanadium(IV) and (V) Complexes Containing (*S*)-*N*-[1-(2-Pyridyl)ethyl]iminodiacetate Ion

Kenichi Okazaki and Kazuo Saito*

Department of Chemistry, Faculty of Science, Tohoku University, Aoba, Aramaki, Sendai 980

(Received July 22, 1981)

New optically active vanadium(IV) and (V) and mixed valence(IV,V) complexes containing a quadridentate ligand (*S*)-*N*-[1-(2-pyridyl)ethyl]iminodiacetate (*S*-peida^{2-}) have been prepared: *i.e.* uninuclear distorted octahedral [$V^{IV}O$(*S*-peida)(H_2O)] and Li[$V^{V}(O)_2$(*S*-peida)], a mixed valence binuclear Na[$V_2^{IV,V}O_3$(*S*-peida)$_2$], and an oxo-peroxo complex Na[$V^{V}O(O_2^{(2-)})$(*S*-peida)]. The tertiary amino nitrogen of *S*-peida^{2-} occupies the trans position to the oxo ligand in the first three complexes, but *trans* to the peroxo ligand in the last complex. Three absorption bands of [$V^{IV}O$(*S*-peida)(H_2O)] in the region from 10000 to 30000 cm^{-1} have been assigned to the d-d transitions, $d_{xy}\rightarrow(d_{xz},d_{yz})$, $d_{xy}\rightarrow d_{z^2-y^2}$, and $d_{xy}\rightarrow d_{z^2}$, in the order of increasing frequency. The mixed valence complex gives an intervalence transfer band and two d-d bands in the region from 9000 to 25000 cm^{-1}. It gives a negative and a positive CD peak corresponding to the intervalence transition. The $V^{V}(O)_2$ and the $V^{V}O(O_2)$ complex give a characteristic absorption shoulder at 25000 and a peak at 23500 cm^{-1} with corresponding weak negative CD peaks, respectively. They are assigned to charge transfer bands from oxo and peroxo to V^{V}, respectively. The sign of CD peaks seems to be governed mostly by asymmetric arrangement of the ligating atoms and asymmetric deviation of ligating atoms from regular octahedron.

Oxo complexes of early transition metal ions are attracting increasing interest of coordination chemists. Asymmetric structure of some binuclear optically active $Mo^{V}(d^1)$ complexes was studied in solution and in solid by circular dichroism (CD) spectroscopy and X-ray diffraction.[1] However, much less is known for V^{IV} complexes with the same d^1 configuration. Jones and Larsen[2] first studied CD spectra of optically active oxovanadium(VI) complexes containing (*R*)-lactate, (*S*,*S*)-tartrate, and (*R*)-1,2-diiminopropanebis(acetylacetonate) ions with aims of assigning the absorption peaks. However, they succeeded in the isolation only of the complex with the third ligand. Optical activity was also studied with the complexes containing quadridentate Schiff bases derived from optically active diamines and salicylaldehyde derivatives.[3] Their absorption spectra involve not only d-d transitions (12000—20000 cm^{-1}) but also π-π^* transitions within the azomethine (*ca.* 28000) and the phenyl (*ca.* 36000) chromophore. The relationship between the sign of exciton CD bands of the azomethine chromophore and the configuration of the basal plane was mainly discussed. However, the CD spectra in the d-d region have not been much discussed.

Nishizawa and Saito synthesized new octahedral oxovanadium(IV) complexes with the quadridentate ligands *N*-(2-pyridylmethyl)iminodiacetate (pmida^{2-}) and nitrilotriacetate (nta^{3-}) in crystalline state. X-Ray crystallography of [$V^{IV}O$(pmida)(H_2O)][4] disclosed that only one of the geometrical isomers was exclusively formed with the tertiary amino nitrogen at the apical position. They also prepared a deep blue mixed valence binuclear complex bridged with oxide [$V_2^{IV,V}O_3$(nta)$_2$]$^{3-}$. X-Ray crystallography and ESR spectroscopy in the aqueous solution showed that the two vanadium atoms are equivalent to each other both in crystals and in aqueous solution.[5]

In order to clarify the electronic state and the relationship between the structure and the CD spectrum of the octahedral complexes with $V^{IV}O^{2+}$ and $V^{V}(O)_2^{+}$ core and of the mixed valence complex, we intended to introduce optical activity to those complexes by use of a similar quadridentate ligand (*S*)-*N*-[1-(2-pyridyl)ethyl]iminodiacetate ion (*S*-peida^{2-}).[6] Optically active complexes [$V^{IV}O$(*S*-peida)(H_2O)], [$V_2^{IV,V}O_3$(*S*-peida)$_2$]$^{-}$, [$V^{V}(O)_2$(*S*-peida)]$^{-}$, and [$V^{V}O(O_2^{(2-)})$(*S*-peida)]$^{-}$ have been prepared in crystalline state and their steric and electronic structures discussed.

Experimental

Preparation of Ligand. Sodium (*S*)-*N*-[1-(2-pyridyl)ethyl]iminodiacetate[6] was prepared in aqueous solution by treating (*S*)-1-(2-pyridyl)ethylamine[7] with sodium chloroacetate, and used without separating the crystals for preparing the complexes in aqueous phase.

Preparation of Complexes. [$V^{IV}O$(S-*peida*)(H_2O)]·2H_2O: [$V^{IV}O$(acac)$_2$][8] (Hacac, acetylacetone) (3.2 g, 0.012 mol) was stirred in an aqueous solution of the ligand (prepared from 0.02 mol of (*S*)-1-(2-pyridyl)ethylamine). The pH was maintained at 3 until [VO(acac)$_2$] dissolved completely. The dark blue solution was concentrated under a reduced pressure to about 5 cm^3 and poured onto a column (4 cm×22 cm) of Dowex 50W-X8 (Na^+ form, 100—200 mesh). Elution with dilute $HClO_4$ (pH 4) gave three adsorption bands. The first eluate was dark green and seemed to contain negatively charged complexes. The third band was not eluted and may consist of aqua VO^{2+} complex. The purplish blue eluate (500 cm^3, pH *ca.* 4) of the second band was concentrated to give blue granules of the dihydrate. Yield: 4.0 g (93%). Found: C, 37.27; H, 5.27; N, 8.02%. Calcd for $C_{11}H_{18}N_2O_8V$: C, 36.98; H, 5.08; N, 7.84%.

Na[$V_2^{IV,V}O_3$(S-*peida*)$_2$]·*NaClO*$_4$·H_2O: This complex was prepared by oxidizing [VO(*S*-peida)(H_2O)] with half a mole of nitrite. The [VO(*S*-peida)(H_2O)]·2H_2O (0.21 g, 0.59 mmol) was stirred in methanol (50 cm^3) containing $NaNO_2$ (0.021 g, 0.30 mmol) for 2 h at room temperature. Solid $NaClO_4$ (*ca.* 1 g) was added to the dark blue solution to precipitate dark blue granules, which were filtered off. Addition of diethyl ether to the filtrate gave further crops. Yield: 0.22 g (93%). Found: C, 33.44; H, 3.23; N, 7.00%. Calcd for $C_{22}H_{26}N_4O_{16}ClNa_2V_2$: C, 33.63; H, 3.33; N, 7.13%.

Li[$V^{V}(O)_2$(S-*peida*)]·2CH_3OH·5H_2O: The V^{IV} complex was oxidized with an excess of nitrite. The suspension of

$[V^{IV}O(S\text{-peida})(H_2O)]$ (1 g, 2.8 mmol) in methanol (20 cm^3) containing $LiNO_2$ (0.5 g, 9.4 mmol) was stirred for 3 h at room temperature until the solution turned yellow. The solution was mixed with diethyl ether (25 cm^3) and left in a refrigerator overnight to give yellow crystals. Yield: 1.0 g (89%). Found: C, 39.09; H, 5.14; N, 6.95%. Calcd for $C_{13}H_{21}N_2O_{8.5}LiV$: C, 39.11; H, 5.30; N, 7.02%.

Na[$V^VO(O_2)$(S-peida)]: $[V^{IV}O(S\text{-peida})(H_2O)]$ (0.5 g, 1.4 mmol) was dissolved in 100 cm^3 of water and treated with an excess of hydrogen peroxide (30%, 5 cm^3) at room temperature to give orange solution immediately, which was made pH 6 with aqueous NaOH solution, concentrated to about 10 cm^3, mixed with ethanol (*ca.* 15 cm^3), and left in a refrigerator to give fine orange needles. Yield: 0.3 g (60%). Found: C, 36.85; H, 3.42; N, 7.52%. Calcd for $C_{11}H_{12}N_2O_7NaV$: C, 36.89; H, 3.38; N, 7.82%.

Measurement. The pK_a value of $[VO(S\text{-peida})(H_2O)]$ (Eq. 1) was obtained by titrating the aqueous solution of the complex (30 cm^3, 0.005 mol dm^{-3}) with *ca.* 0.1 mol dm^{-3} NaOH solution at I=0.1 mol dm^{-3} ($NaClO_4$) and 25±0.3 °C in a current of nitrogen. The complex $[V_2^{IV,V}O_3(S\text{-peida})_2]^-$ is in equilibrium with the V^{IV} and V^V complexes in an aqueous solution.[5] The equilibrium constant (see Eq. 2) was determined spectrophotometrically[9] at 740 nm by use of the complex solutions of 2.5—10 mmol dm^{-3} at I=0.1 mol dm^{-3} ($NaClO_4$), pH 4.5, and at 6.3±0.8, 15.0±0.4, and 25.0±0.1 °C.

The absorption and CD spectra were recorded in aqueous solutions and KBr disks with a Hitachi 323 Spectrophotometer, and JASCO Model J-40 A (200—700 nm), J-20 A (700—1000 nm), and J-200 (1000—2000 nm) CD Spectropolarimeters. A Varian A 60 D NMR Spectrometer was used for recording ^{1}H-NMR spectra of the two vanadium(V) complexes in D_2O.

Results and Discussion

Structure. X-Ray crystallography disclosed the structure of $[V^{IV}O(S\text{-peida})(H_2O)]$, $[V_2^{IV,V}O_3(S\text{-peida})_2]^-$, and $[V^V(O)_2(S\text{-peida})]^-$ (Fig. 1); the details are reported elsewhere.[10] The tertiary amine is at the trans position to the oxo ligand in all these complexes, and the methyl group on the asymmetric carbon has an equatorial orientation in the puckered five membered chelate ring.

The $[V^{IV}O(S\text{-peida})(H_2O)]$ and the mixed valence complex have similar CD patterns both in solution and in solid (see CD spectra). ^{1}H-NMR spectrum of the $V^V(O)_2$ complex supports the existence of only one isomer in solution. Its structure estimated by ^{1}H-NMR spectroscopy (*vide infra*) is not in conflict with the X-ray analysis. Hence all these three complexes seem to have the same geometrical isomerism in solution as in crystals.

The ^{1}H-NMR spectrum of the $[V^V(O)_2(S\text{-peida})]^-$ ion in D_2O (Table 1 and Fig. 2) exhibits one doublet, three quartets, and three multiplets from the high field. The doublet and one of the quartets with average chemical shifts 1.73 and 5.23 ppm, respectively, and with a common coupling constant 7 Hz, are assigned to the protons of the methyl group and that on the asymmetric carbon, respectively. The AB patterns centered at 3.46 and 4.18 ppm must arise from methylene protons of the acetates of which the ligating oxygens are at trans and cis to the pyridine nitrogen,

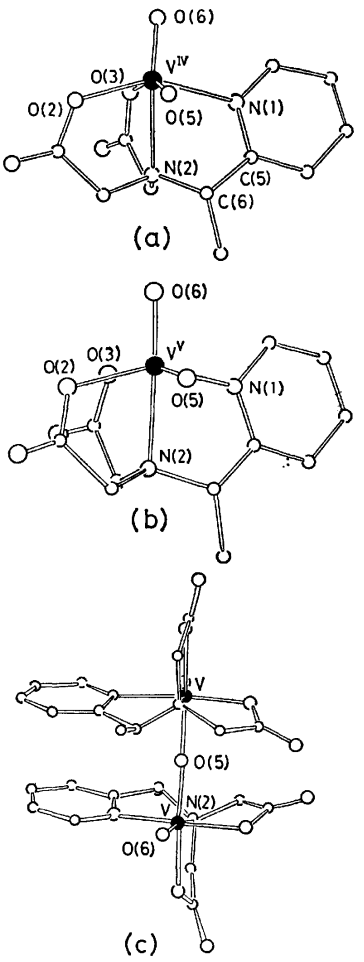

Fig. 1. Structures of the complexes determined by X-ray crystallography.
(a); $[V^{IV}O(S\text{-peida})(H_2O)]$. O(5) is oxygen atom of H_2O. The torsion angle between N(1)–N(2) and C(5)–C(6) is 17.0° (δ). (b); $[V^V(O)_2(S\text{-peida})]^-$. (c); $[V_2^{IV,V}O_3(S\text{-peida})_2]^-$.

respectively. The reasons are follows. The two protons of the cis acetate are subject to a more marked influence of the methyl group on the asymmetric carbon, and have therefore lower chemical shifts than those of the trans acetate; the difference between the anisotropic effects upon the two protons of the cis acetate can also cause a rather large difference of the chemical shifts between them ($\delta_A-\delta_B$ in Table 1). A free pyridine gives three multiplets over 7 ppm which correspond to the 3- and 5-, 4-, and 2- and 6-protons from the high field. Therefore, the multiplets over 7.5 ppm are assigned to the 3- and 5-, 4-, and 6-protons on the pyridine ring from the high field.

The structure of $[V^VO(O)_2(S\text{-peida})]^-$ has not been determined by the X-ray method. Its NMR spectrum shows a similar pattern to $[V^V(O)_2(S\text{-peida})]^-$ in D_2O except that the signal of the 6-proton on pyridine shifts to lower field by *ca.* 0.8 ppm. The similarity suggests that there are two different acetate chelates. The O_2^{2-} ligand may be at the trans site to the tertiary amine, because the signal of the 6-proton has the largest shift and therefore should be nearest to the trans site of the tertiary amine. The

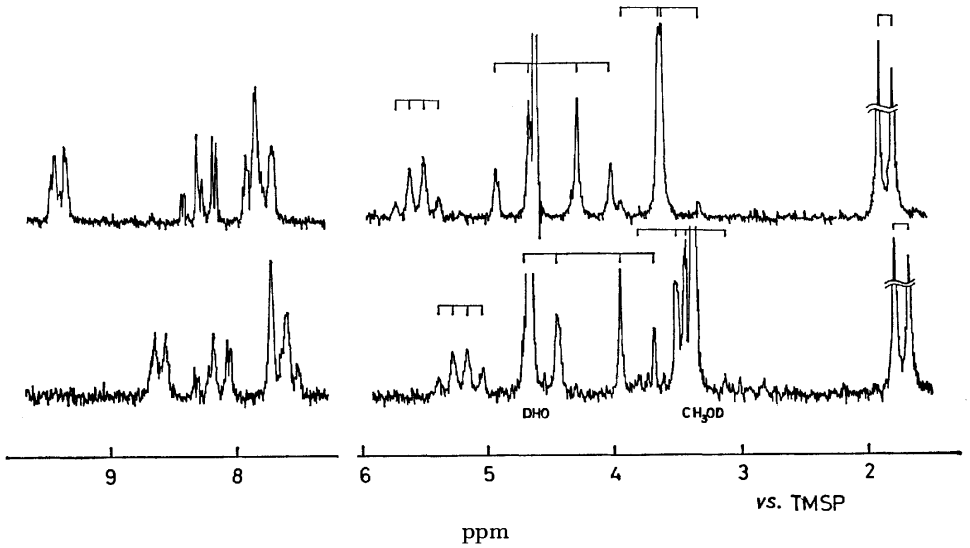

Fig. 2. ^{1}H-NMR spectra of $[V^{V}O(O)_2(S\text{-peida})]^-$ (upper) and $[V^{V}(O)_2(S\text{-peida})]^-$ (lower) in D_2O at *ca.* 30 °C.

Table 1. ^{1}H-NMR Chemical shifts and coupling constants of $[V^{V}(O)_2(S\text{-peida})]^-$ and $[V^{V}O(O_2)(S\text{-peida})]^-$

A. The methylene protons of the two acetate groups.

Complex	$\{(\delta_A+\delta_B)/2\}$	$\delta_A-\delta_B$	J_{AB}/Hz
$V(O)_2^+$	3.46	0.21	18.0
	4.18	0.71	16.0
$VO(O_2)^+$	3.63	0.18	17.5
	4.48	0.59	16.0

B. The methyl and methylidyne protons.

Complex	Proton	δ	J/Hz
$V(O)_2^+$	$-CH_3$	1.73	7.0
	$\geq CH$	5.23	
$VO(O_2)^+$	$-CH_3$	1.86	7.0
	$\geq CH$	5.57	

C. The pyridyl protons.

Complex	Proton	δ
$V(O)_2^+$	3-, 5-	7.6
	4-	8.1
	6-	8.6
$VO(O_2)^+$	3-, 5-	7.8
	4-	8.3
	6-	9.4

NMR spectrum, however, cannot clarify the bonding mode of the peroxo ligand and the geometrical relationship between this ligand and the others. Nevertheless, X-ray structure of the oxo-peroxo complexes[11-13] of early transition metal ions suggests that the present peroxo complex is the isomer in which the peroxide ion is of side-on type and the V=O and the O–O (O_2^{2-}) bonds are across each other (Fig. 3).

Equilibrium. The pK_a of the $V^{IV}O$ complex to give the hydroxo complex is 6.5 at 25 °C and I=1.0 mol dm^{-3} in aqueous solution.

$$[V^{IV}O(S\text{-peida})(H_2O)] \rightleftharpoons [V^{IV}O(OH)(S\text{-peida})]^- + H^+ \quad (1)$$

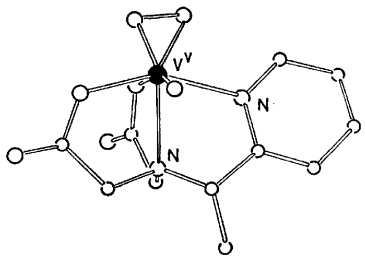

Fig. 3. Estimated structure of $[V^{V}O(O)_2(S\text{-peida})]^-$.

The mixed valence complex of $[V_2^{IV,V}O_3(S\text{-peida})_2]^-$ is in equilibrium with $[V^{IV}O(S\text{-peida})(H_2O)]$ and $[V^{V}(O)_2(S\text{-peida})]^-$ in water as shown in Eq. 2.

$$[V^{IV}O(S\text{-peida})(H_2O)] + [V^{V}(O)_2(S\text{-peida})]^- \rightleftharpoons [V_2^{IV,V}O_3(S\text{-peida})_2]^-(+H_2O) \quad (2)$$

The equilibrium constant, K, is 44±1 mol^{-1} dm^3 at 15 °C, I=0.1 mol dm^{-3} and pH 4.5. The $\Delta H°$ and $\Delta S°$ are −6±3 kJ mol^{-1} and 11±8 J mol^{-1} K^{-1}, respectively, in the temperature region from 5 to 25 °C. The small negative $\Delta H°$ and the small positive $\Delta S°$ suggest that the mixed valence complex is slightly more stable than the mixture of the $V^{IV}O$ and $V^{V}(O)_2$ complexes. Since the number of particles does not change on the reaction, the positive $\Delta S°$ suggests that the formation of mixed valence complex brings about less hydration of the system. The charge distribution in the more bulky $[V_2^{IV,V}O_3(S\text{-peida})_2]^-$ ion should be less concentrated than in the $V^{IV}O$ and $V^{V}(O)_2$ complexes.

Absorption Spectra. *V^{IV} Complex*: Oxo-vanadium(IV) complexes generally give three absorption bands with low intensity (ε=10—200), in the region from 10000 to 30000 cm^{-1} at room temperature. The two lower frequency bands sometimes overlap each other, and the highest frequency band in 21000—30000 cm^{-1} region is not always observed because of the overlap with a band of higher intensity at a higher frequency. Ballhausen and Gray[14] first assigned the three d-d absorption bands of some oxo-

vanadium(IV) complexes to $d_{xy}\rightarrow(d_{xz},d_{yz})$, $d_{xy}\rightarrow d_{x^2-y^2}$, and $d_{xy}\rightarrow d_{z^2}$ transitions in the order of increasing frequency (z axis on the V=O bond, C_{4v} symmetry) with the aid of a molecular orbital energy level scheme. However, Selbin and co-workers[15] found a fine structure with three peaks in the first absorption band (at *ca.* 13000 cm^{-1}) of $[VO(acac)_2]$ (C_{2v} symmetry) at 77 K and assigned the three peaks to those from d_{xy} to d_{xz}, d_{yz}, and $d_{x^2-y^2}$, respectively. They assigned the second band at *ca.* 18000 cm^{-1} to $d_{xy}\rightarrow d_{z^2}$ transitions. Jones and Larsen studied the CD spectra of (*R*)-lactato-, (*S,S*)-tartrato-, and (*R*)-1,2-diiminopropanebis(acetylacetonato)oxovanadium(IV) complexes and discussed the usefulness of CD spectrum for assigning the d-d transitions. However, only the third Schiff base complex was isolated and others were known only in solution. They also failed to observe the important peaks in the low frequency region.

The spectral pattern of the $[V^{IV}O(S\text{-peida})(H_2O)]$ complex gives four peaks at 13200 (ε=27.4), 17700 (16.4), 28200 (357), and 38800 cm^{-1} (4970) and a shoulder at *ca.* 34000 cm^{-1} (642) in aqueous solution of pH *ca.* 4 (Fig. 4). The first three bands are assigned to d-d transitions in the $V^{IV}O$ complex of pseudo C_{4v} symmetry, $d_{xy}\rightarrow(d_{xz},d_{yz})$, $d_{xy}\rightarrow d_{x^2-y^2}$, and $d_{xy}\rightarrow d_{z^2}$. The band in the 13200 cm^{-1} region gives two CD peaks, whilst those at 17700 and 28200 cm^{-1} do one each. Hence the first peak should involve the transition to the degenerated levels, $d_{xy}\rightarrow(d_{xz},d_{yz})$. The other two bands at 17700 and 28200 cm^{-1} are assigned to the $d_{xy}\rightarrow d_{x^2-y^2}$ and $d_{xy}\rightarrow d_{z^2}$, respectively. The band at 28200 cm^{-1} has a larger intensity (ε=357) than the first two bands do. The absorption bands of oxovanadium(IV) complexes of other amino carboxylates without pyridine ring give small ε values (*ca.* 20) at similar wave numbers.[16] Hence the large peak may involve some charge transfer transition related to the pyridine ring. The shoulder at 34000 cm^{-1} gives a CD shoulder (Fig. 4). However, $V^{IV}O$ complexes with amino carboxylates without pyridine ring do not give this absorption shoulder.[16] Hence the transition should be of charge transfer nature involving the pyridine ring. Not only the $V^{IV}O$ complex but also $[V^{V}(O)_2(S\text{-peida})]^-$ and $[V^{V}O(O_2)(S\text{-peida})]^-$ give strong bands near 38800 cm^{-1} (Fig. 4). They are assinged to π-π^* transitions within the pyridine ring, since the π-π^* transitions of pyridine itself exist around 39000 cm^{-1}.

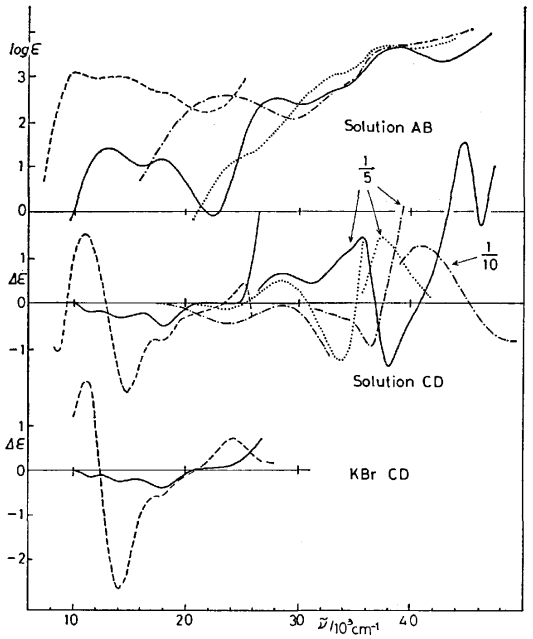

Fig. 4. Absorption and CD spectra of $[V^{IV}O(S\text{-peida})(H_2O)]$ (——), $[V_2^{IV,V}O_3(S\text{-peida})_2]^-$ (— —), $[V^{V}(O)_2(S\text{-peida})]^-$ (……), and $[V^{V}O(O)_2(S\text{-peida})]^-$ (—·—). Upper, absorption in solution; middle, CD in solution; lower, CD spectra in KBr disks.

Mixed Valence Complex: The absorption spectrum was estimated by use of the equilibrium constant, 44 mol^{-1} dm^3. The ε values are calculated per unit molarity of $V_2O_3^{3+}$. To increase the concentration of mixed valence complex in the equilibrium state, a concentrated solution (0.013 mol dm^{-3}) was used in a 0.1 cm cell. Because of the strong absorption in the ultraviolet region under this condition, the discussion is limited in the visible and near infrared region. Three bands are seen in the measurable region: *i.e.* 10200 (ε=1200), 13600 (940), and 17700 cm^{-1} (shoulder, 470), and each overlaps the neighboring band. The frequencies of the second and third bands are similar to those of the first and second bands of $[V^{IV}O(S\text{-peida})(H_2O)]$ and assigned to the d-d transitions, $d_{xy}\rightarrow(d_{xz},d_{yz})$ and $d_{xy}\rightarrow d_{x^2-y^2}$, respectively. The first band should be due to the intervalence transition. The high intensity of the second and third bands may result from partial mixing of the metal d orbitals with the p orbitals of the bridging O atom.

$V^{V}(O)_2$ Complex: The spectrum of $[V^{V}(O)_2(S\text{-peida})]^-$ has two strong bands at *ca.* 33300 (shoulder, ε=1070) and 37700 cm^{-1} (peak, 4640) in aqueous solution of pH 4.5. The former may be the charge transfer band from the pyridine ring to V^{V} and the latter is assigned to the π-π^* transition within the pyridine moiety by the same reason as for the V^{IV} complex. A weak shoulder is seen at *ca.* 25000 cm^{-1} (ε=17.8). The spectrum of $[V^{V}(O)_2(OH_2)_4]^+$ solution prepared by dissolving NH_4VO_3 in *ca.* 4.5 mol dm^{-3} $HClO_4$ has a weak shoulder at 24000 cm^{-1} (ε=7.15).[17] $Na_3[V^{V}(O)_2(edta)]$[18] also gives an absorption shoulder at 25000 cm^{-1} (ε=25.8). Since V^{V} has no d electron, the origin of these shoulders must be a transition involving the oxo or the aqua ligands, most probably a spin-forbidden (singlet to triplet) charge transfer band from oxo to V^{V}. The reasons are as follows: (i) Its low intensity denies the participation of spin allowed charge transfer. (ii) The oxo ligand has π-bonding p orbitals with higher energy than the σ-bonding orbital of oxo and aqua ligands.[14] Hence the charge transfer from the π orbital to the d orbital may possess the lowest energy among the charge transfers from ligand to V^{V}.

$V^{V}O(O)_2$ Complex: The $[V^{V}O(O)_2(S\text{-peida})]^-$ gives two peaks and a shoulder in aqueous solution at 23500 (ε=372), 33300 (shoulder, 500), and 38500 cm^{-1} (3720). Lever and Gray[19] discussed the origin of

electronic spectra of side-on peroxo complexes of some early transition metals and assigned their lowest energy bands to the transition from the highest occupied π antibonding orbital of O_2^{2-} to the metal d orbital. We tend to assign the band at 23500 cm^{-1} to the charge transfer from O_2^{2-} to V^V and those at 33300 and 38500 cm^{-1} to the charge transfer from the pyridine ring to V^V and the π-π^* transition within the pyridine ring, respectively. The possible spin forbidden transition from the oxo ligand to V^V around 25000 cm^{-1} may be hidden by the strong band at 23500 cm^{-1}.

Pattern of CD Spectra. V^{IV} Complex: The CD spectra of $[V^{IV}O(S\text{-peida})(H_2O)]$ and $[V_2^{IV,V}O_3(S\text{-peida})_2]^-$ in KBr disks (Fig. 4) have similar pattern in the region from 10000 to 25000 cm^{-1} to those in aqueous solution. The $V^{IV}O$ complex gives four peaks in the d-d region. The two at 11900 ($\Delta\varepsilon=-0.23$) and 14300 cm^{-1} (-0.33) must correspond to the absorption band at 13200 cm^{-1} [$d_{xy}\rightarrow(d_{xz},d_{yz})$]. This complex has a lower symmetry than C_{4v} and the degenerate levels of d_{xz} and d_{yz} split to give two CD peaks. The peaks at 18100 (-0.53) and 28200 cm^{-1} ($+3.4$) are naturally assigned to the $d_{xy}\rightarrow d_{x^2-y^2}$ (17700 cm^{-1}) and the $d_{xy}\rightarrow d_{z^2}$ band (28200 cm^{-1}), respectively. A positive and a negative peak are seen from lower wave number around 38000 cm^{-1}, corresponding to the π-π^* transition. A large positive peak is also seen at 44800 cm^{-1} (Table 2).

Mixed Valence Complex: The discussion is limited in the infrared and visible region (*vide supra*). This complex gives two CD peaks at 8620 ($\Delta\varepsilon=-1.1$) and 11100 cm^{-1} ($+1.6$) in the intervalence transfer region. The intensities are much larger than those of $V^{IV}O$ complex. It has two peaks at 14700 (-2.0) and 17500 cm^{-1} (-0.84) in the d-d region (13000—20000 cm^{-1}). The patterns in these regions are more or less similar to those of the $V^{IV}O$ complex.

$V^V(O)_2$ and $V^VO(O)_2$ Complexes: The two V^V complexes naturally fail to give CD in the lower wave number region than 19000 cm^{-1}. The $V^V(O)_2$ complex has two negative peaks and one positive peak in the region from 20000 to 34000 cm^{-1} (Table 2). They must correspond to the absorption shoulders at the respective wave numbers. Its large positive peak at 37500 cm^{-1} should correspond to the π-π^* transition of the pyridine moiety. The peroxo complex gives one broad negative peak and one negative shoulder in the 20000 to 34000 cm^{-1} region, corresponding to the broad absorption band at 23500 and a shoulder at 33300 cm^{-1}, respectively. In the π-π^* transition region there are two peaks at 36400 ($\Delta\varepsilon=-4.7$) and 41000 cm^{-1} ($+12.8$).

Source of CD Spectra. It is generally understood that the magnitude of contribution of various sources of asymmetry to the CD of a coordination compound with regular polyhedral structure decreases in the sequence; asymmetric configuration of chelate rings designated by Δ or Λ>asymmetric arrangement of ligating atoms≥vicinal effect including asymmetry on ligating atoms, asymmetry on remote atoms and asymmetric conformation of chelates. The importance of asymmetric deviation of ligating atoms from regular polyhedra has been lately discussed and the magnitude of contribution is sometimes comparable to that of asymmetric configuration of chelate rings.[1,20]

Since both the V^{IV} and the mixed valence complex give similar CD patterns in aqueous solution and in KBr disk, the asymmetric field influencing the CD spectra should not be very different in solution and in the solid state, at least for the transitions in the d-d and intervalence charge transfer region. Hence the relation between structure and CD can be discussed on the basis of X-ray crystal structure.

Table 2. Absorption and CD spectra

	Absorption[a]	CD in solution[b]	CD in KBr[b]
$[V^{IV}O(S\text{-peida})(H_2O)]$	13.2 (27.4)	11.9 (-0.23, -2.4) 14.3 (-0.33, -12)	11.6 (-0.17, -6.2) 14.2 (-0.27, -9.9)
	17.7 (16.4)	18.1 (-0.53, -30)	17.7 (-0.42, -26)
	28.2 (357)	28.2 ($+3.4$, $+9.5$)	
	sh. 34.0 (642)	sh. 34.3 ($+5.6$, $+8.7$)	
	38.8 (4970)	35.8 ($+7.5$, $+1.5$) 38.0 (-7.0, -1.4) 44.8 ($+14$, $+4.4$[c])	
$Na[V_2^{IV,V}O_3(S\text{-peida})_2]$	10.2 (1200)	8.6 (-1.1, -0.92) 11.1 ($+1.6$, $+1.3$)	11.0 ($+2.0$, $+1.7$)
	13.6 (940)	14.7 (-2.0, -2.1)	14.0 (-2.7, -2.9)
	17.7 (470)	17.5 (-0.84, -1.8)	17.5 (-0.55, -1.2)
$Li[V^V(O)_2(S\text{-peida})]$	sh. 25.0 (17.8)	23.7 (-0.081, -4.6)	
	sh. 33.3 (1070)	28.6 ($+0.53$, $+0.50$) 33.9 (-1.25, -1.2)	
	37.7 (4640)	37.5 ($+7.52$, $+1.6$)	
$Na[V^VO(O_2)(S\text{-peida})]$	23.5 (37.2)	24.1 (-0.44, -1.2)	
	sh. 33.3 (500)	sh. 33.3 (-1.39, -2.8)	
	sh. 38.5 (4720)	36.4 (-4.7, -1.0) 41.0 ($+12.8$, $+2.7$)	

a) $\nu/10^3$ cm^{-1} (ε/dm^3 mol^{-1} cm^{-1}). b) $\nu/10^3$ cm^{-1} ($\Delta\varepsilon$/dm^3 mol^{-1} cm^{-1}, $\Delta\varepsilon$ at peak/ε at absorption peak or shoulder ($\times10^3$)). c) $\Delta\varepsilon/\varepsilon$ at 44800 cm^{-1}.

The present *S*-peida complexes have no chilarity coming from the configuration of chelate rings, but the non-equivalent ligating atoms have asymmetric arrangement as shown in Fig. 5. The present V^{IV} complex has configuration (a) of Fig. 5.

There is no established way for expressing the asymmetric deviation, although proposals have been made by some authors.[1,20] The vanadium atom is slightly over the mean basal plane consisting of N(1), O(2), O(3), and O(5) in Fig. 1 (a) by 0.4 Å and the location of ligating atoms deviates largely from a regular octahedron. When one considers an imaginary basal plane which passes the V atom and is perpendicular to the V=O bond, the asymmetric deviation can be expressed by the torsion angles of the basal edges connecting the ligating atoms in cis positions toward the edges of the imaginary plane. These angles are listed in Table 3.

The vicinal effect, the asymmetric arrangement of ligating atoms, and the asymmetric deviation of ligating atoms from regular octahedron can be responsible for the CD. The vicinal effect can come from the asymmetric carbon and the δ-conformation of the five-membered chelate ring containing the asymmetric carbon. Such a vicinal contribution cannot be denied

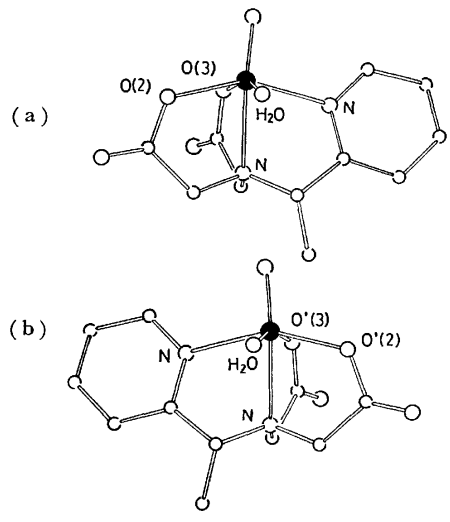

Fig. 5. Optical isomers of $[V^{IV}O(S\text{-peida})(H_2O)]$ due to asymmetric arrangement of ligating atoms.

Table 3. Distorsions around the vanadium[a]

Edge	$V^{IV}O$	$V_2^{IV,V}O_3$		$V^{V}(O)_2$
1) Angles against the perpendicular plane to V–O_6 bond in Fig. 1.				
N_1–O_5	1.92 λ	0.11 δ	0.31 λ	2.77 λ
N_1–O_3	3.97 λ	4.91 δ	6.74 λ	7.10 λ
O_2–O_5	3.51 λ	2.92 λ	2.90 λ	2.93 λ
O_2–O_3	9.87 δ	7.76 δ	10.36 δ	12.92 δ
2) Torsion angles between basal edges.				
(N_1–O_3) *vs.* (O_2–O_5)	10.62 λ	7.88 λ	9.64 λ	10.01 λ
(N_1–O_5) *vs.* (O_2–O_3)	7.84 δ	9.19 δ	10.82 δ	10.59 δ

a) See Ref. 10.

but does not seem predominating because of the following reasons: (i) The 5-membered chelate ring involving asymmetric carbon gives an envelope-like conformation with δ-chilarity and the torsion angle between N(1)–N(2) and C(5)–C(6) (Fig. 1 a) is rather small as compared with other puckered rings of various metal complexes in which significant vicinal contribution is seen in the d-d transition region (*e.g.* (*R*)- or (*S*)-1,2-propanediamine rings in Co^{III} complexes). (ii) The V^{IV} complex of (*S*)-alanine-*N*,*N*-diacetate has a similar skeletal structure to $[V^{IV}O(S\text{-peida})(H_2O)]$, and has a common asymmetrically distorted δ-conformation of the 5-membered chelate ring containing *S*-carbon atom. However, its CD strength is nearly one tenth of that of $[V^{IV}O(S\text{-peida})(H_2O)]$ in the d-d transition region, and the sign is reversed.[16] Hence we tend to consider that the vicinal contribution is not significant. The contribution of asymmetric arrangement and asymmetric deviation can be separated with difficulty, because the ligating atoms are connected by chelate rings. The main origin of CD strength may come from the asymmetric arrangement of the ligating atoms and asymmetric deviation from regular octahedron.

The CD strength of the mixed valence complex is much larger than that of the V^{IV} complex, particularly in the intervalence charge transfer region. This must be related to the large absorption intensity of the former. In the region from 15000 to 23000 cm^{-1}, both patterns are more or less similar, suggesting the function of a common origin. If very small angles less than 1° are ignored (Table 3), both the V^{IV} and the mixed valence complexes are reckoned to have qualitatively similar distorsion. This fact provides support to the above mentioned discussion in the d-d transition region.

The peaks and shoulders of the $V^{IV}O$, $V^{V}(O)_2$, and $V^{V}O(O_2)$ complexes over 30000 cm^{-1} give corresponding CD peaks or shoulders. All the absorption peaks and shoulders are considered to be related to the transitions from the pyridine ring (*i.e.* π-π^* transition or N(pyridine)-V^{IV} charge transfer). However, there does not seem to be simple relationship between the CD sign and the structure of the complexes including the asymmetric distorsion (Table 3). The asymmetry linked to such transitions may be related to the distortion of the N(py)-site from the regular octahedron, or to the orientation of the pyridine ring, both depending on the delicate skeletal structure of the complex. It is difficult to discuss the CD pattern in the UV region more precisely at the present stage.

The authors are grateful to Professor M. Hatano and Dr. T. Murakami of Tohoku University for the use of JASCO Model J-20 A and J-200 CD Spectropolarimeters for the measurement of the spectra in longer wavelength region than 700 nm.

References

1) K. Z. Suzuki, Y. Sasaki, S. Ooi, and K. Saito, *Bull. Chem. Soc. Jpn.*, **53**, 1288 (1980).
2) K. M. Jones and E. Larsen, *Acta Chem. Scand.*, **19**,

1210 (1965).
3) R. L. Farmer and F. L. Urbach, *Inorg. Chem.*, **9**, 2562 (1970); *J. Chem. Soc., D*, **1970**, 1515; *Inorg. Chem.*, **13**, 587 (1974); A. Pasini and M. Gullotti, *J. Coord. Chem.*, **3**, 319 (1974); M. Gullotti, L. Casella, A. Pasini, and R. Ugo, *J. Chem. Soc., Dalton Trans.*, **1977**, 339.
4) S. Ooi, M. Nishizawa, K. Matsumoto, H. Kuroya, and K. Saito, *Bull. Chem. Soc. Jpn.*, **52**, 452 (1979).
5) M. Nishizawa, K. Hirotsu, S. Ooi, and K. Saito, *J. Chem. Soc., Chem. Commun.*, **1979**, 707.
6) T. M. Suzuki, *Ph. D. Thesis, Tohoku Univ.*, (1979).
7) K. Michelsen, *Acta Chem. Scand., Ser. A*, **28**, 428 (1974); E. Bang, *ibid.*, **31**, 495 (1977).
8) *Inorg. Synth.*, Vol. V, 114 (1957).
9) J. F. Ojo, R. S. Taylor, and A. G. Sykes, *J. Chem. Soc., Dalton Trans.*, **1975**, 500.
10) A. Kojima, K. Okazaki, S. Ooi, and K. Saito, submitted to *Inorg. Chem.*
11) NH_4 [$V^{V}O(O_2)(H_2O)$ (pyridine - 2,6 - dicarboxylato)]. R. D. Drew and F. W. B. Einstein, *Inorg. Chem.*, **12**, 829 (1973).
12) $(NH_4)_4[O(V^{V}O(O_2)_2)_2]$, $NH_4[V^{V}O(O_2)_2(NH_3)]$, and $K_3[V^{V}O(O_2)_2(C_2O_4)]$. I. B. Sevensson and R. Stomberg, *Acta Chem. Scand.*, **25**, 898 (1971); R. E. Drew and F. W. B. Einstein, *Inorg. Chem.*, **11**, 1079 (1972); D. Begin, F. W. B. Einstein, and J. Field, *ibid.*, **14**, 1785 (1975).
13) Oxo-peroxo Ti^{IV}, Cr^{VI}, and Mo^{VI} complexes. D. Schwarzenbach, *Inorg. Chem.*, **9**, 2391 (1970); A. J. Edwards, D. R. Slim, J. E. Guerchais, and R. Kergoat, *J. Chem. Soc., Dalton Trans.*, **1980**, 289; R. Stomberg, *Acta Chem. Scand.*, **22**, 1439 (1968); S. E. Jacobson, R. Tang, and F. Mares, *Inorg. Chem.*, **17**, 3055 (1978).
14) C. J. Ballhausen and H. B. Gray, *Inorg. Chem.*, **1**, 111 (1962).
15) J. Selbin, T. R. Ortolano, and F. Smith, *Inorg. Chem.*, **2**, 1315 (1963).
16) K. Okazaki and K. Saito, unpublished.
17) F. A. Cotton and G. Wilkinson, "Advanced Inorganic Chemistry," 4th ed, John Wiley & Sons, New York (1980), p. 712.
18) L. W. Amos and D. T. Sawyer, *Inorg. Chem.*, **11**, 2692 (1972).
19) A. B. P. Lever and H. B. Gray, *Acc. Chem. Res.*, **11**, 348 (1978).
20) For example; M. Ito, F. Marumo, and Y. Saito, *Acta Crystallogr., Sect. B*, **27**, 2187 (1971); R. M. Wing and R. Weiss, *J. Am. Chem. Soc.*, **92**, 1929 (1970); N. C. Payne, *Inorg. Chem.*, **12**, 1151 (1973).

The Phases Formed by the Dehydration of Disodium Zirconium(IV) Bis(orthophosphate) Trihydrate and Their Ion-exchange Behavior

Yasushi INOUE* and Yoshimune YAMADA

Department of Nuclear Engineering, Faculty of Engineering, Tohoku University, Aramaki-aza-Aoba, Sendai 980

(Received August 6, 1981)

The phase transformation of $Na_2Zr(PO_4)_2 \cdot 3H_2O$ which had been obtained from zirconium(IV) bis(hydrogenphosphate) monohydrate(α-zirconium phosphate), prepared by the direct precipitation method, was studied by means of gravimetry, X-ray analysis, and acid-base titration. When the material was heated for 2 d, it was transformed to a monohydrate at 80 °C and then successively to three anhydrous phases, depending on the temperature. The monohydrate was also formed by letting the trihydrate stand over P_2O_5 at room temperature for longer than two weeks. The processes were confirmed to be irreversible by an examination of the rehydration behavior, from which the conditions of the storage of five modifications of disodium zirconium(IV) bis(orthophosphate) were established. It is of special interest that the second anhydrous phase reverted to the first one when it was allowed to stand at room temperature in air or in a desiccator. The rate of the reversion decreased with the temperature of heat-treatment and with a decrease in the relative humidity of the surroundings. The difference between the present results and Clearfield's[1,2] was clarified and attributed mainly to the difference in the crystallinity of the starting α-zirconium phosphate.

During our study of the isotopic exchange rate of Na^+ ions between crystalline disodium zirconium(IV) bis(orthophosphate) trihydrate ($Zr(Na_2PO)_2 \cdot 3H_2O$) and aqueous solutions, it was difficult to obtain reproducible results. This irreproducibility is due to the difference in the crystal structure of the exchanger, which depends subtly on the conditions adopted in the preparation and in the storage of the material. The phases existing under various circumstances should, therefore, be clarified in order to obtain accurate rate data and to give a correct interpretation of the results.

There has been no literature referring to the subject except the studies of Clearfield *et al.*,[1,2] who first elucidated the structure and the dehydration behavior of $Na_2Zr(PO_4)_2 \cdot 3H_2O$, which had been prepared by replacing the H^+ ions in $Zr(HPO_4)_2 \cdot H_2O$ (zirconium(IV) bis(hydrogenphosphate) monohydrate, α-ZP) by Na^+ ions. They made it clear that one monohydrate and three anhydrous phases were irreversibly formed by thermal treatment. Their results will be helpful, but not directly applicable to our purpose, since the exchanger in sodium form prepared from α-ZP synthesized by the method recommended by the present authors will behave differently from that by Clearfield; in fact H^+/Na^+ titration and differential thermal analysis (DTA) studies have clearly shown the difference in crystallinity between these materials.[3]

The present report describes the studies made of the dehydration behavior of sodium-substituted α-ZP and the reversibility of the process by means of gravimetry, X-ray analysis, and pH titration; these studies were enabled us to find the most suitable conditions for the preparation and storage of various phases and to determine the phase changes brought about by immersing them in aqueous solutions.

Experimental

α-Zirconium phosphate was prepared by a procedure recommended previously.[3] Five and a half grams of $ZrOCl_2 \cdot 8H_2O$ were dissolved in distilled water in a polyethylene beaker. The desired amounts of hydrofluoric acid and of phosphoric acid were then vigorously stirred in successively to make the concentrations 0.715 mol dm^{-3} and 9 mol dm^{-3} respectively and to make total volume 130 cm^3. The solution was then kept at 60 °C in a thermostatted water bath for about 100 h. A white, flaky product was separated by filtration, washed with distilled water until the pH of the filtrate became 5, and stored over P_2O_5 for two weeks. The α-ZP thus prepared was then equilibrated with a mixture of 0.1 mol dm^{-3} NaCl and NaOH solutions at pH 12. After filtration, the exchanger was washed with distilled water until the effluent became free of chloride ions; it was then dried in a desiccator over a saturated NaCl solution (relative humidity, 75%) for two weeks. The material thus prepared was confirmed to be $Na_2Zr(PO_4)_2 \cdot 3H_2O$ (hereafter this material will be refereed to as Phase I).

The monohydrate and three anhydrous phases were obtained by the methods established in the present study, as will be described later; the monohydrate phase (Phase II) was obtained by drying Phase I over P_2O_5 for longer than three weeks, while the anhydrous phases (Phases III, IV, and V) were formed by heating Phase I at the desired temperatures (250 °C for Phase III, 700 °C for Phase IV and 820 °C for Phase V) for 2 d. These phases were then stored over P_2O_5.

The other experimental procedures were the same as had been described previously,[3] except for the analysis of sodium ions in the exchanger, which was carried out with a Jarrell-Ash atomic-absorption spectrophotometer, Model AA-782.

Results and Discussion

The material obtained by replacing H^+ by Na^+ in α-ZP in the aqueous solution with a pH of 12 was identified by means of chemical, X-ray, and thermal analyses. The composition was: Found: ZrO_2, 32.63; P_2O_5, 37.23; Na_2O, 16.20; H_2O, 14.57%, which corresponded to the formula of $Na_2Zr(PO_4)_2 \cdot 3H_2O$ (Phase I) and which was in good agreement with the data published by other authors.[2,4,5] The X-ray pattern indicated that this phase had an interlayer distance of 0.983 nm, which agreed well with the Phase D reported by Clearfield *et al.*[1,2] The thermogravi-

metric-analysis (TGA) and DTA curves of Phase I are shown in Fig. 1. The TGA curve reveals that this phase lost water in two steps; that is, it lost two molecules of water up to 100 °C, and then the last molecule of water before 250 °C. In the DTA curve, one large and one small endothermic peak appeared at 110 °C and 150 °C; they apparently corresponded to the release of two molecules of water and one molecule of water respectively, while no exothermic peak appeared.

The static method was then applied to the dehydration studies; Phase I was heated at various temperatures for two days, except as otherwise specified, followed by cooling to room temperature. When Phase I was heated to a constant weight at 80 °C, it lost two molecules of water to form a monohydrate, Phase II, which had an interlayer distance of 0.843 nm. This phase could alternatively be obtained in a pure form by letting Phase I stand over P_2O_5 for longer than two weeks. This can be verified from Fig. 2, which shows the dehydration behavior of Phase I in the P_2O_5 desiccator, and from the agreement of the X-ray pattern of the product with that of the monohydrate mentioned above. This phase will correspond to the Phase E which was prepared by Clearfield *et al.*[2] by heating Phase D at a temperature between 50—100 °C. However they reported that Phase E could not be obtained in pure form by dehydrating Phase D in a desiccator containing P_2O_5.

Over the range of 80—150 °C, an anhydrous phase, Phase III, with an interlayer distance of 0.839 nm, appeared in addition to Phase II. When the mixture was heated above 150 °C, Phase II disappeared, being completely transformed to Phase III, which began transforming to the second anhydrous phase, Phase IV, on further heating (above 300 °C). At 500 °C, Phase III was transformed completely to Phase IV, which had an interlayer distance of 0.763 nm. However, when Phase III was heated for longer than 10 d, it was transformed completely to Phase IV at a far lower temperature (170 °C). Only Phase IV was formed over the range of 500—800 °C. When it was heat-treated at a temperature above 800 °C, the third anhydrous phase, Phase V, which had an X-ray pattern appreciably different from those of the other phases mentioned above, was formed. This phase could not be formed by heating Phase I below 800 °C, no matter how long the heating period was. Figure 3 schematically illustrates the thermal transformation of Phase I.

It must be noted that an interesting phenomenon was observed concerning Phase IV. When being allowed to stand after cooling, Phase IV were transformed to Phase III. To make clear the factors affecting this behavior, the rate of transformation during storage was measured on samples subjected to heat-treatment under different conditions, as is shown in Figs. 4 and 5. The ordinate of these figures shows R, which is defined as $(I_{III}/I_{III+IV}) \times 100$, where I represents the intensity of the diffraction line from the (002) plane which gives the strongest peak in

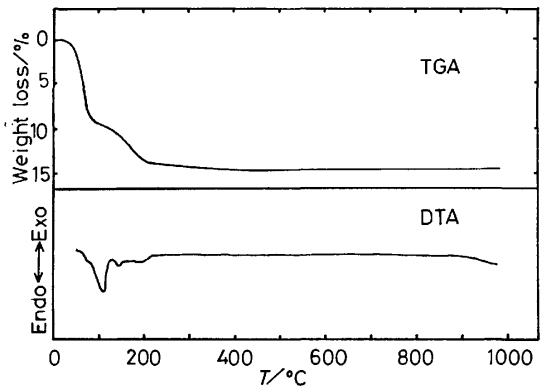

Fig. 1. TGA and DTA curves of Phase I.
Heating rate: 5 °C/min.

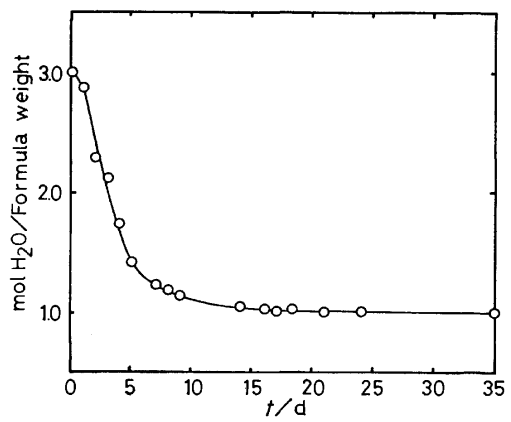

Fig. 2. Water content of Phase I as a function of time of standing over P_2O_5.

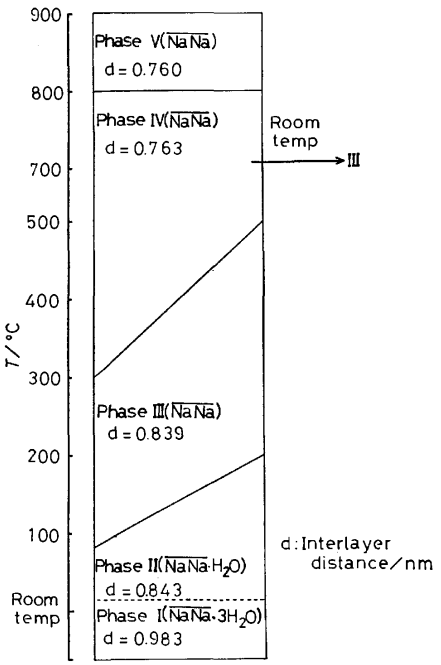

Fig. 3. Phase transformation of disodium substituted ZP.
d: Interlayer distance/nm.

the designated phase. R is considered to be roughly equal to the abundance ratio of Phase III, since the density of the zirconium atom on the plane responsible for the reflection will not be appreciably changed by this phase transformation.

Figure 4 indicates that the rate of transformation was slower with the samples heat-treated at higher temperatures, but was independent of the length of heating. The relative humidity of the atmosphere strongly affected the rate of the transformation, as is shown in Fig. 5. A decrease in the humidity suppressed the transformation. From these facts, we can conclude that Phase IV can be stored in a desiccator over P_2O_5 without suffering from phase transition for at least two weeks. Phases III and IV respectively will correspond to Phases F and G reported by Clearfield *et al.*, but Phase G is more stable than Phase IV; Phase G, obtained by heating Phase F at a temperature higher than 200 °C, did not revert to Phase F at all.[2)]

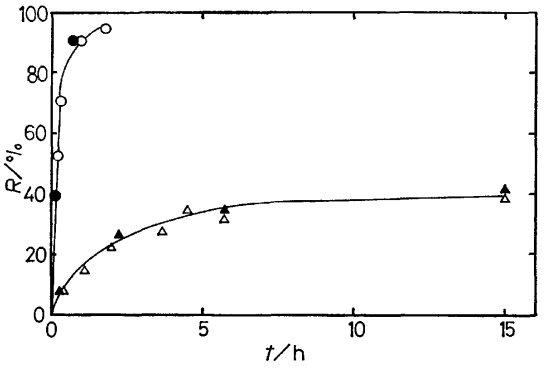

Fig. 4. R as a function of the time of standing-I. Environment; air. Condition for heat-treatment; ○: 600 °C, 2 d, ●: 600 °C, 4 d, △: 700 °C, 2 d, ▲: 700 °C, 4 d.

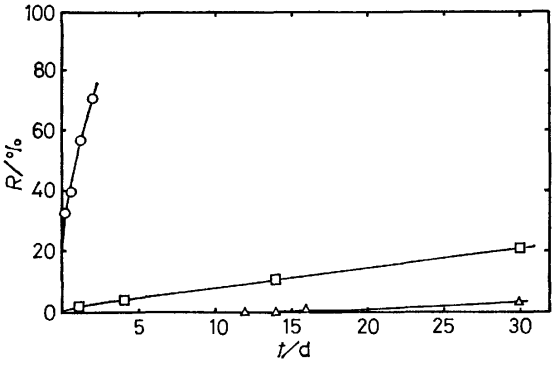

Fig. 5. R as a function of the time of standing-II. Heat-treatment; 700 °C, 2 d. Condition of storage; ○: air, □: silica gel, △: P_2O_5.

In order to examine the reversibility of the dehydration process, the X-ray patterns and the weight recoveries were measured on samples obtained by heat-treatment when they were humidified to a constant weight in a desiccator containing a saturated NaCl solution. Their X-ray patterns were also measured after they had been immersed in 0.1 mol dm^{-3} NaCl, 0.1 mol dm^{-3} NaOH, and H_2O for periods ranging from one day to two weeks. The results are summarized in the 4th through the 8th columns of Table 1. Phase II was gradually rehydrated and partially reverted to Phase I, the degree increasing with the lapse of time. Phase III, though it showed recovered water of 1.48 mole per unit of formula weight during humidifying, did not change its crystal form even when it was immersed in the aqueous solution. As to Phase IV, it completely reverted to Phase III in spite of the fact that it absorbed as much water as the same amount of Phase III. When Phase V was allowed to stand in the aqueous solutions for 10 d, it was transformed to a new phase, the crystal structure of which has not yet been identified.

The titration curves of these phases were constructed in order to ascertain the effect of heat-treatment on their ion-exchange properties, as is shown in Fig. 6. For the convenience of comparison, the abscissas of the figure are represented by percentages converted to hydrogen form. In addition, the samples were separated from the solutions at different stages of exchange, and their X-ray powder patterns were taken while they were wet. The curves for Phases I through IV were similar to each other; they all exhibited two plateaus, each of them corresponding to the replacement of each mole of the Na^+ ion with the H^+ ion. However, a comparison of the X-ray patterns of these four phases at various stages of ex-

TABLE 1. PREPARATION AND STORAGE OF THE VARIOUS PHASES OF DISODIUM ZIRCONIUM BIS(ORTHOPHOSPHATE)

Phase	Formula	Heating temp for preparation / °C	Recovery in weight[a)] %	Recovery in weight[a)] mol H_2O / Formula weight	Phase transition[b)] in aqueous soln 1 d	Phase transition[b)] in aqueous soln One week[c)]	Condition of storage[e)]
I	$Na_2Zr(PO_4)_2 \cdot 3H_2O$	Room temp	—	—	No change	No change	Saturated NaCl soln
II	$Na_2Zr(PO_4)_2 \cdot H_2O$	80	1.50±0.02	1.29	I, 54% II, 46%	I, 72% II, 28%	P_2O_5
III	$Na_2Zr(PO_4)_2$	200—300	8.15±0.02	1.48	No change	No change	P_2O_5
IV	$Na_2Zr(PO_4)_2$	500—800	8.18±0.01	1.49	III, 100%	III, 100%	P_2O_5 *in vacuo*
V	$Na_2Zr(PO_4)_2$	800	4.07±0.05	0.74	No change	New phase, 100% (d=0.840)[d)]	P_2O_5

a) Each phase was allowed to stand for 30 d in a desiccator over a saturated NaCl soln. b) H_2O, 0.1 mol dm^{-3} NaOH, 0.1 mol dm^{-3} NaCl. c) For Phase V, 10 d. d) d: Interlayer distance/nm. e) Kind of desiccant.

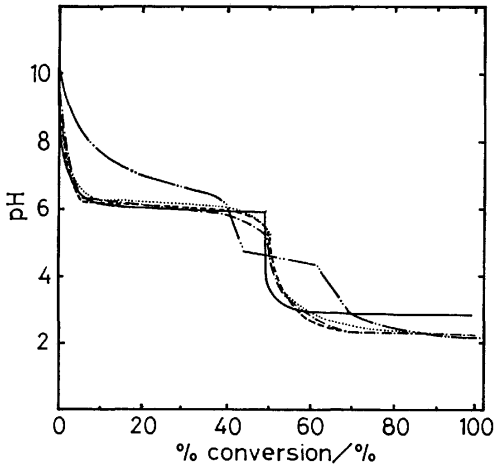

Fig. 6. Na^+/H^+ titration curves for various phases. ——: I, ……: II, ----: III, —·—: IV, —··—: V.

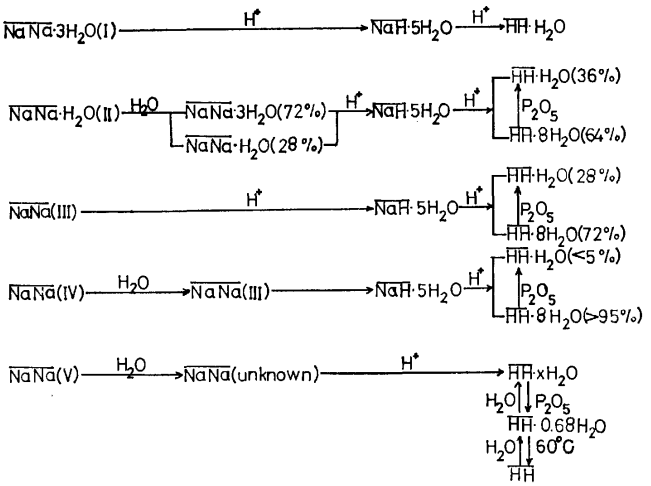

Fig. 7. Phase transformation on replacing Na^+ by H^+. $\overline{NaNa}$: $Zr(NaPO_4)_2$, $\overline{NaH}$: $Zr(NaPO_4)(HPO_4)$, $\overline{HH}$: $Zr(HPO_4)_2$.

change indicated that the replacement of Na^+ ions with H^+ ions proceeded through different paths, as is shown in Fig. 7. At the initial point of titration with acid, the exchangers transformed their crystal structures into low-temperature forms according to the observation mentioned above. In the range of 0—50% H^+ ion-uptake, however, the progressive exchange led to the formation of a monosodium phase of composition, $Zr(HPO_4)(NaPO_4) \cdot 5H_2O$, which was present exclusively at the half-exchange point of the titration, irrespective of the starting materials. Beyond this point, the exchangers in dihydrogen form, which resulted from the replacement of the second Na^+ ions with H^+ ions, consisted of a mixture of $Zr(HPO_4)_2 \cdot H_2O$ and $Zr(HPO_4)_2 \cdot 8H_2O$. The relative amount of the highly hydrated phase ($Zr(HPO_4)_2 \cdot 8H_2O$) differed with the difference in the phase of the starting materials; that is, at the end point of titration, the hydrogen form obtained from Phase II contained 64% $Zr(HPO_4)_2 \cdot 8H_2O$, while the hydrogen form obtained from samples heat-treated at 250 °C (Phase III) and 700 °C (Phase IV) contained 72% and more than 95% of the octahydrate respectively. In contrast, the samples without heat-treatment yielded no highly hydrated phase; *i.e.*, they returned to the original α-ZP. This highly hydrated phase could be converted to $Zr(HPO_4)_2 \cdot H_2O$ by drying over P_2O_5, as had been reported by Clearfield *et al.*[1] The hysteresis (dependence of the curves on the direction of titration) observed in the titration curves of the Phases from II through IV is ascribable to the appearance of $Zr(HPO_4)_2 \cdot 8H_2O$ when these phases are converted to the dihydrogen form. In this connection, it is worthwhile to cite the study of Alberti *et al.*,[6-8] who have described the dependence of the titration curves on the method of synthesizing α-ZP. They made it clear that the degree of crystallinity affected the reversibility of ion exchange and the resolution between two ion-exchange steps in the curves; the reversibility and the resolution became better with an improvement in the degree of crystallinity. Based on this view, it is considered, from the above findings, that the α-ZP prepared by the method recommended by the present authors possesses a very high degree of crystallinity, while a rise in the temperature of the thermal treatment of the sodium-substituted phase reduces the degree of crystallinity of the exchanger.

On the other hand, the Na^+/H^+ titration curve for Phase V exhibited a three-stage ion-exchange, unlike the titrations for the other phases described above. The complete substitution of Na^+ ions for H^+ ions led to the formation of the dihydrogen phase, which has an interlayer distance of 1.047 nm. When this phase was dried in a P_2O_5 desiccator, it was converted to a phase having an interlayer distance of 0.763 nm and the formula of $Zr(HPO_4)_2 \cdot 0.68H_2O$. Furthermore, this phase showed DTA and TGA curves different from those of α-ZP in that the former showed a two-step dehydration up to 150 °C, while the latter showed a one-step dehydration, as is shown in Fig. 1. Therefore, this phase is considered to have a crystal structure different from α-ZP and to be similar to the ι-phase reported by Clearfield *et al.*[9] Figure 8 indicates that the H^+/Na^+ titration curve of this phase was different from that of ι-ZP; the former had three plateaus at pH 2.3, 4.5, and

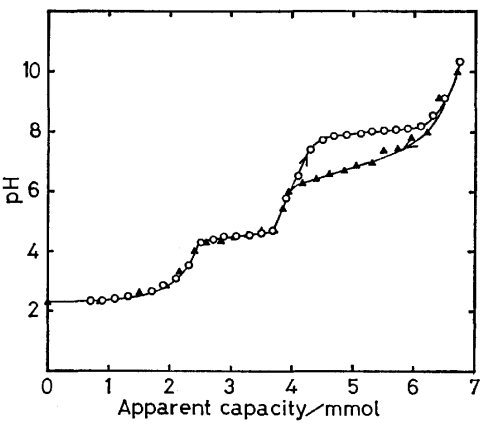

Fig. 8. Titration curves of ZP in H^+ form regenerated from Phase V.
○: Forward titration, 0.1 mol dm^{-3} (NaCl+NaOH),
▲: backward titration, 0.1 mol dm^{-3} (HCl+NaCl).

8.0, whereas the latter exhibited no plateau. Furthermore, the titration curve of $Zr(HPO_4)_2 \cdot 0.68H_2O$ showed hysteresis in the high-pH region. This irreversibility is due to the difference in phases participating in the titration.

There are many other disagreements between the present results and Clearfield's in addition to those explicitly described in this report. They are considered to be attributable mainly to the difference in the crystallinity of the starting α-ZP, as was pointed out in the preceeding paper,[3] although the difference in the details of the experimental conditions may be partly responsible.

In conclusion, the 3rd and the last columns of Table 1 summarize the recommended method for the preparation of, and the conditions for the storage of, five modifications of disodium substituted zirconium phosphate.

References

1) A. Clearfield, W. L. Duax, A. S. Medina, G. D. Smith, and J. R. Thomas, *J. Phys. Chem.*, **73**, 3424 (1969).
2) A. Clearfield and A. S. Medina, *J. Inorg. Nucl. Chem.*, **32**, 2775 (1970).
3) Y. Inoue and Y. Yamada, *Bull. Chem. Soc. Jpn.*, **52**, 3528 (1979).
4) E. Torracca, *J. Inorg. Nucl. Chem.*, **31**, 1189 (1969).
5) A. Clearfield and A. S. Medina, *J. Phys. Chem.*, **75**, 3750 (1971).
6) G. Alberti, U. Costantino, S. Allulli, M. A. Massucci, and M. Pelliccioni, *J. Inorg. Nucl. Chem.*, **35**, 1347 (1973).
7) A. Clearfield and J. A. Stynes, *J. Inorg. Nucl. Chem.*, **26**, 117 (1964).
8) G. Alberti and E. Torracca, *J. Inorg. Nucl. Chem.*, **30**, 317 (1968).
9) A. Clearfield, A. L. Landis, A. S. Medina, and J. M. Troup, *J. Inorg. Nucl. Chem.*, **35**, 1099 (1973).

A Ruthenium(IV)-Ruthenium(III) Dimer, Product of the Reaction of Aqua(ethylenediaminetetraacetato)ruthenium(III) with Chlorate Ions

Masato IKEDA,† Kunio SHIMIZU,* and Gen P. SATÔ

Department of Chemistry, Faculty of Science and Technology, Sophia University, 7-1, Kioi-cho, Chiyoda-ku, Tokyo 102

(Received August 7, 1981)

An oxo-bridged, mixed-valence complex of ruthenium(IV,III), $[(edta)Ru^{IV}ORu^{III}(edta)]^{3-}$, has been obtained from the oxidation of $[Ru^{III}(edta)(H_2O)]^-$ by chlorate ions. The formulation of the complex as a μ-oxo dimer of ruthenium(IV,III) is based on the results of a variety of experiments, including elemental analyses, magnetism, by spectrophotometry, and by electrochemical studies. These studies in acetate buffer solution show that the dimeric ion can be reduced at mercury electrode to $[(edta)Ru^{III}ORu^{III}(edta)]^{4-}$ and then is monomerized to the original $[Ru(edta)(H_2O)]^-$ in a fast reaction.

In the course of the studies of the chemical and electrochemical redox reactions of ruthenium(II)- and (III)-EDTA, it was found that the $[Ru(edta)(H_2O)]^-$ in an acetate buffer solution gave an intense green color on the addition of oxidizing agent such as sodium chlorate or hydrogen peroxide. Examination revealed that the coloration was due to the formation of a mixed-valence μ-oxo ruthenium(IV,III) dimeric complex.

Green or bluish green solutions of ruthenium complexes have become of much interest in recent years. Meyer *et al.*[1,2] have isolated several blue-green complexes of ruthenium, and identified them as μ-oxo dimers of ruthenium(III,III) or (IV,III). As early as 1966, Ezerskaya *et al.*[3,4] obtained a green complex from the reaction between Ru(III)-EDTA and hydrogen peroxide; this seems to be the same as the complex we obtained. They claimed that the complex might be μ-oxo and μ-peroxo double bridged dimer, however, no supporting evidence was presented.

Recently Uehiro *et al.*[5,6] also obtained the green complex from oxidation of Ru(III)-EDTA by Mn(III)-EDTA or platinum electrode, or from irradiation of light.

This paper reports the isolation of mixed-valence ruthenium(IV,III) dimer and the identification and electrochemical properties of the complex.

Experimental

Reagents. Aqua(hydrogenethylenediaminetetraacetato)-ruthenium(III) 4-water, $[Ru(Hedta)(H_2O)]\cdot 4H_2O$, was prepared according to the procedure described previously,[7] and characterized by elemental analysis, alkalimetric titration,[8] and UV-visible, and IR spectra.

Sodium chlorate was recrystallized from water and then dried under a vacuum. The assay was made by alkalimetric titration of the cation-exchanged solution of one-gram samples.

Deionized water distilled in an all-glass apparatus was used throughout the experiment. Nitrogen gas for deoxygenation was purified by passing it through an acid vanadium(II) sulfate solution and then water. The other chemicals were of guaranteed reagent grade and used without further purification.

Apparatus. UV-visible and IR spectra were measured with a Hitachi 624 Digital Spectrophotometer and a Hitachi EPI-G2 IR spectrophotometer.

Polarographic measurement, controlled potential coulometry, and cyclic voltammetry were carried out as described earlier.[9] The flow rate of the dropping mercury electrode (DME) was 1.77 mg s^{-1} under a mercury head of 50 cm. The drop time of the DME was mechanically controlled and the instantaneous currents at 3.50 s after the dislodgement were sampled by means of a dislodger-cutoff device.[10] All the potentials cited here are referred to the saturated calomel electrode (SCE). A Radiometer pH meter 25E was used for pH determination. All the electrochemical measurement was carried out at (25±0.1) °C under a nitrogen atmosphere.

Magnetic properties were measured by the Gouy method. The apparatus was calibrated with $Hg[Co(NCS)_4]$. The observed magnetic susceptibility was corrected for diamagnetism by means of Pascal's constants. The magneton number, magnetic moment $\boldsymbol{m}$ divided by Bohr magneton $\boldsymbol{m}_B$, was calculated by using the following expression:††

$$\boldsymbol{m}/\boldsymbol{m}_B = 798(T/\mathrm{K})^{1/2}(\chi V_m/\mathrm{m^3\ mol^{-1}})^{1/2},$$

where T is the thermodynamic temperature, χ is the corrected magnetic susceptibility, and V_m is the molar volume.

Isolation and Analysis of the Binuclear Complex. One-tenth gram of $[Ru(Hedta)(H_2O)]\cdot 4H_2O$ was dissolved in 50 cm^3 of sodium acetate–acetic acid solution (0.2 mol dm^{-3} each). A 20 cm^3 portion of 0.01 mol dm^{-3} $NaClO_3$ was added dropwise to the mixture. The color of the solution turned from pale yellow to deep green. The green solution was allowed to stand overnight in the dark. After the solution was concentrated to about one-fifth the initial volume by evaporation under a reduced pressure at 30 °C, its pH was adjusted to *ca.* 1 with hydrochloric acid. Ethanol was added to the resulting solution on cooling until fine, green crystals precipitated, which were collected by filtration. The crystals were washed several times with small volumes of ethanol, and then dried *in vacuo* at room temperature (yield 40 mg).

The ruthenium content of the green complex was determined spectrophotometrically according to the ruthenate method.[11] The amount of cation in the product was determined by the cation-exchange method. The elemental analysis of C, H, and N was carried out by means of a Yanagimoto MY2 CHN Corder.

† Present address: Kobayashi Bag Manufactory Co. Ltd., 101 Kitagata, Ikeda, Nagano 395.

†† This expression is based on SI. What is often called inappropriately "molar susceptibility" corresponds to $\chi V_m/4\pi$.

Results and Discussion

D. c. Polarography and Stoichiometry of the Reaction between Aqua-edta-Ru(III) and ClO_3^-. A typical polarogram of the aqua-edta-Ru(III) complex, which shall be abbreviated as Ru(III)L,[†††] is shown in Fig. 1a. The step corresponds to the diffusion-controlled, Nernstian reduction of Ru(III)L to Ru(II)L.[12] When a small amount of sodium chlorate was added to the solution, the pale yellow solution turned green. At the same time, a new step (step A in Fig. 1b) began to appear at a more positive potential, while the original step remained essentially unchanged (step B in Fig. 1b). The limiting current of step A was diffusion-controlled unless a large excess (more than ten times) of chlorate ions was present, and the log-plot analysis indicated that step B was Nernstian (the reciprocal slope was −58 mV). The height of step A gradually increased with respect to time and finally reached a constant value after a few hours. The final step height depended on the amount of the chlorate ions added.

Amperometric and spectrophotometric titrations were carried out: acetate buffer solutions containing known amounts of Ru(III)L and sodium chlorate at various ratios were prepared and left to stand overnight. The polarograms and the UV-visible spectra were then recorded. As shown by the examples in Fig. 2, there was a clear end-point at $n(ClO_3^-)/n(\text{Ru(III)-L}) = 0.083$ or 1/12, where n is the amount of the specified substance. Beyond the end-point, the height of step A of the polarogram remained constant till a large excess of chlorate ions was added; the ratio of the heights of step A and step B was very close to 1:2.

These results are readily explained by assuming that a chlorate ion undergoes a six-electron reduction as in the case of the reaction with vanadium(II) ions,[13] oxidizing six Ru(III)L entities to the Ru(IV) state, and each Ru(IV) species combines with another Ru-

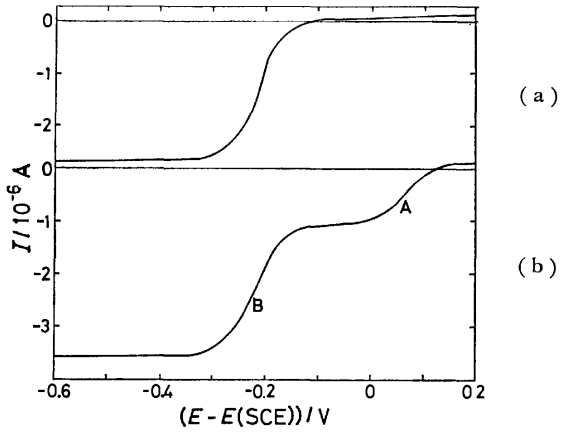

Fig. 1. D. c. polarograms of 1.0 mol m^{-3} [Ru(edta)-(H_2O)]$^-$ in 0.2 mol dm^{-3} sodium acetate-acetic acid buffer (pH=4.7) at 25 °C before (a) and after the addition of 0.1 mol m^{-3} $NaClO_3$ (b).

††† In the pH region under study, this complex actually exists mainly as [Ru(edta)(H_2O)]$^-$ (pK_a=2.65).[7]

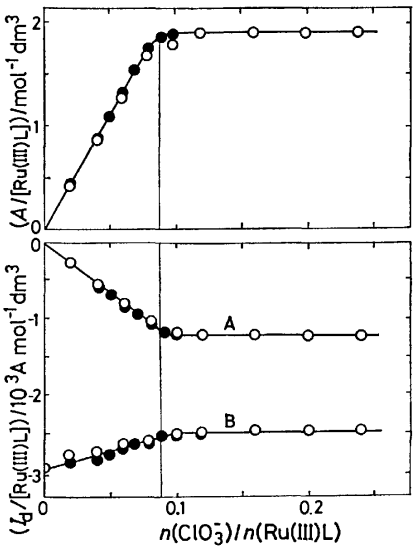

Fig. 2. Titration curves of [Ru(edta)(H_2O)]$^-$ with chlorate ions in 0.2 mol dm^{-3} sodium acetate-acetic acid buffer (pH=4.7) at 25 °C.
Upper: spectrophotometric at 630 nm. Lower: amperometric at −0.1 V (A) and −0.4 V (B). Concentration of [Ru(Hedta)(H_2O)]·$4H_2O$: -⊖-, 1.0 mol m^{-3}; -●-, 2.0 mol m^{-3}

(III)L to form a green mixed-valence dimeric species:

$$12\text{Ru(III)L} + ClO_3^- \longrightarrow 6\text{Ru(IV)-Ru(III)} + Cl^- + \cdots . \quad (1)$$

Here Ru(IV)–Ru(III) represents the green dimeric species; its chemical formula will be discussed later.

If the one-electron, Nernstian step A is the reduction of Ru(IV)–Ru(III), its immediate product should be an Ru(III)–Ru(III) dimer. But the fact that the half-wave potential of step B is the same as that of Ru(III)L indicates that the Ru(III)–Ru(III) dimer is unstable, so that it dissociates rapidly to give two Ru(III)L entities. In fact, a reversible reoxidation peak was observed on the cyclic voltammogram only at a high scan rate. The first-order rate constant of the dissociation reaction was about 1 s^{-1} at pH=4.7 at 25 °C; the details of the kinetics will be reported separately.

The Ru(III)L species thus produced would be reoxidized to Ru(IV)–Ru(III) in the presence of chlorate ions. However, this reaction is too slow to produce an appreciable polarographic catalytic current unless a large excess of chlorate ions is present. Controlled potential coulometry revealed that this reaction did occur. It also corroborated the above stoichiometry.

Coulometry. A green solution containing a known small excess of chlorate ions was electrolyzed with a mercury pool electrode at a potential of the first plateau (−0.1 V) and the polarograms were recorded intermittently by suspending the electrolysis and letting the solution stand for a while. The polarogram remained almost unchanged until a certain quantity of electricity, Q_1, was consumed. The magnitude of the diffusion current of step A, $I_{d,A}$, began to diminish in proportion to the advancement of elec-

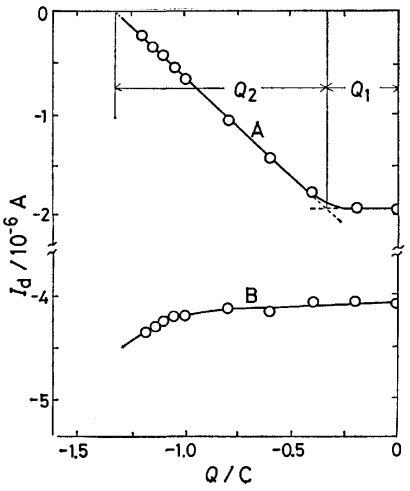

Fig. 3. Coulometric curves of 1.0 mol m^{-3} [Ru(Hedta)(H_2O)]·4H_2O+0.110 mol m^{-3} $NaClO_3$ in 0.2 mol dm^{-3} sodium acetate-acetic acid buffer at 25 °C. Reduction potential=−0.1 V. A, diffusion current at −0.1 V. B, diffusion current at −0.4 V. The current and quantity of electricity for reduction are considered to be negative.

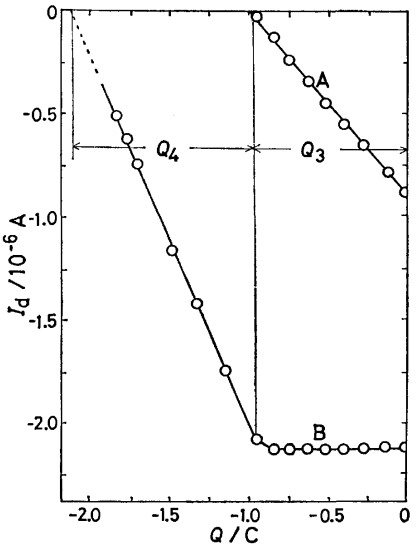

Fig. 4. Coulometric curves of 1.0 mol m^{-3} [Ru(Hedta)(H_2O)]·4H_2O+0.104 mol m^{-3} $NaClO_3$ in 0.2 mol dm^{-3} sodium acetate-acetic acid buffer at 25 °C. Reduction potential=−0.4 V. A, diffusion current at −0.1 V. B, diffusion current at −0.4 V. The current and quantity of electricity for reduction are considered to be negative.

trolysis, whereas the diffusion current of step B, $I_{d,B}$ (total step height less $I_{d,A}$), remained fairly constant (Fig. 3). Another quantity of electricity, Q_2, was consumed before the completion of the electrolysis; the polarogram and UV-visible spectrum of the solution were then the same as those of Ru(III)L. During the first stage of the electrolysis, Ru(III)L produced by the reduction of the mixed valence dimer was reoxidized by the chlorate ions, so that Q_1 was equal to the quantity of electricity that was required for the six-electron reduction of the excess chlorate ions. The roundness of $I_{d,A}$-Q curve reflects the slowness of the reoxidation process. When no more chlorate ions were present, the process was simply the reduction of the mixed-valence dimer, as was indicated by the fact that Q_2 was equal to the quantity of electricity corresponding to the one-electron reduction of half the amount of Ru(III)L originally contained in the solution.

The electrolysis at a potential of the second plateau (−0.4 V) showed that Ru(IV)–Ru(III) reacted with Ru(II)L. In this case, $|I_{d,A}|$ decreased linearly from the beginning until a quantity of electricity, Q_3, was consumed, when step A disappeared (Fig. 4). During this stage, $I_{d,B}$ remained constant and no oxidation step was observed. On further electrolysis, $|I_{d,B}|$ began to decrease and the oxidation step of Ru(II)L began to grow, both in proportion to the advancement of electrolysis. For the completion of the electrolysis another quantity of electricity, Q_4, was consumed. The quantity of electricity Q_3 was equal to that required for the six-electron reduction of all the chlorate ions added to the solution and Q_4 to that required for the one-electron reduction of Ru(III)L which was originally contained in the solution. At this potential the mixed-valence dimer undergoes a three-electron reduction to Ru(II)L, which reacts both with the excess chlorate ions and with the dimer to regenerate Ru(III)L during the first stage:

$$\text{Ru(IV)-Ru(III)} + 3e^- \longrightarrow 2\text{Ru(II)L}, \quad (2)$$

$$6\text{Ru(II)L} + ClO_3^- \longrightarrow 6\text{Ru(III)L} + Cl^-, \quad (3)$$

$$\text{Ru(II)L} + \text{Ru(IV)-Ru(III)} \longrightarrow 3\text{Ru(III)L}. \quad (4)$$

When no more Ru(IV)–Ru(III) and chlorate ions are present, the reduction is simply that of Ru(III)L to Ru(II)L (the second stage).

The coulometric data are summarized in Table 1; the last two columns are the results for the isolated dimer, which will be discussed later. These data reconfirm the above-mentioned stoichiometry of the reaction between Ru(III)L and ClO_3^-.

Characterization of the Green Complex. The isolated green complex is readily soluble in water. The titration curve of the solution with a standard sodium hydroxide solution showed a single pH jump corresponding to the dissociation of carboxylic protons; there was no second pH jump characteristic of the dissociation of the proton of aqua ligand, as observed in the case of Ru(III)L.[12] The amount of the dissociable protons was 1.0 mol per 1 mol of ruthenium. The solution of the complex was passed through a column of an H-form cation-exchange resin, and the eluate was titrated with a standard alkali solution. The results indicated that 1.5 mol of hydrogen ions per 1 mol of ruthenium was present in the eluate, *i.e.* the complex contained 0.5 mol of cations (sodium ions) per 1 mol of ruthenium. These results, together with those of the elemental analysis, are in fair agreement with the values calculated for Na[(Hedta)-RuORu(Hedta)]·10H_2O (molar mass 999.7 g mol^{-1}).

Table 1. Controlled potential coulometry in 0.2 mol dm^{-3} acetate buffer

Sample	Ru(III)L+$NaClO_3$				Green complex	
(E *vs.* SCE)/V	−0.1		−0.4		−0.5	
	$-Q_1$/C	$-Q_2$/C	$-Q_3$/C	$-Q_4$/C	$-Q_3'$/C	$-Q_4'$/C
Obsd	0.33	1.00	0.94	1.15	0.95	1.91
Calcd	0.332[a]	1.02[b]	0.967[c]	1.35[d]	$Q_3'/Q_4'=0.497$	

a) $6F\{n(ClO_3^-)-n(\text{Ru(III)L})/12\}$. b) $Fn(\text{Ru(III)L})/2$. c) $6Fn(ClO_3^-)$. d) $Fn(\text{Ru(III)L})$. F is the Faraday constant and n(X) is the initial amount of substance X.

Table 2. UV-visible spectral data

Compound	λ_{max}/nm (ε/mol^{-1} m^2)			
[(Hedta)RuORu(Hedta)]$^-$ [a]			392 (1790)	630 (38)
[Ru(Hedta)(H_2O)][a]			280 (250)	
[(bpy)$_2$ClRuORuCl(bpy)$_2$]$^{3+}$ [b]	246 (4200)	300 (4600)	470 (1970)	
[(bpy)$_2$ClRuORuCl(bpy)$_2$]$^{2+}$ [b]	244 (6590)	289 (3900)	627 (1790)	
[Ru(bpy)$_2$Cl$_2$]$^+$ [c]	298 (2480)	310 (2240)	380 (565)	

a) In aqueous 0.2 mol dm^{-3} acetate buffer, pH=4.7. b) Ref. 1, in acetonitrile. c) J. N. Braddock and T. J. Meyer, *Inorg. Chem.*, **12**, 723 (1973).

Found: Ru, 20.24; C, 23.94; H, 3.87; N, 5.72; Na, 2.31; rest, 43.98%. Calcd for Ru, 20.22; C, 24.03; H, 4.64; N, 5.60; Na, 2.30; O, 43.21%. The above results show that the overall reaction between Ru(III)L and chlorate ion can be written as follows:

$$12[\text{Ru(edta)}(H_2O)]^- + ClO_3^- \longrightarrow 6[(\text{edta})\text{RuORu(edta)}]^{3-} + Cl^- + 6H^+ + 9H_2O. \quad (5)$$

The IR spectrum (KBr disk) was almost the same as that of Ru(III)L. The absorption bands of coordinated carboxyl groups (1630 cm^{-1}) and of protonated carboxyl groups (1725 cm^{-1}) was observed. According to Hewkin and Griffith,[14] Wing and Callahan,[15] and Filippo *et al.*,[16] for a linear Ru–O–Ru species, a weak, infrared-active asymmetric stretching band should appear in the range of 800 cm^{-1}—900 cm^{-1} (for a non-linear Ru–O–Ru system, at a lower frequency). Attempts to identify this band failed because many small bands covered this region.

The UV-visible spectrum of the green complex was the same as that of the Ru(III)L–ClO_3^- reaction mixture and showed two absorption bands (Table 2). According to Meyer *et al.*[1] an intense, low energy band at about 650 nm is characteristic of the oxo-bridged Ru(III) dimers and this band is considerably blue-shifted for the one-electron oxidized species, *i.e.* the corresponding Ru(IV)–O–Ru(III) dimers.†††† It is most likely that the intense band at 392 nm indicates the presence of the Ru(IV)–O–Ru(III) system in the green complex.

The polarogram of the isolated green complex was the same as that presented in Fig. 1b, except that the height of the second step was a little larger than twice the first step height and varied from sample to sample. The isolated green complex is not very stable and decomposes in the presence of the air and/or light.

The coulometric curves of the reduction at −0.5 V were similar to those in Fig. 4. But in this case the quantity of electricity consumed during the first stage, Q'_3, should be equal to that required for the one-electron reduction of the dimer to Ru(III)L, since no excess chlorate ions were present and reaction(3) was not involved. The quantity of electricity consumed during the second stage, Q'_4, should be that required for the reduction of Ru(III)L to Ru(II)L. Consequently the ratio Q'_3/Q'_4 must be 1/2, as was the case (Table 1).

The molar mass calculated from the coulometric data was 996 g mol^{-1}, while that calculated from the pH titration data was 996.4 g mol^{-1}. These were in good agreement with the calculated value (999.7 g mol^{-1}) for the monosodium decahydrate. However, the thermogravimetric data and coulometric data on other samples, which are not cited in Table 1, indicated that the number of the waters of crystallization might be variable (probably from 8 to 10) according to the condition of crystallization and storage.

The green complex was paramagnetic, and the value of χV_m, corrected for diamagnetism, was 2.34×10^{-8} m^3 mol^{-1} at 23 °C. The magneton number, $m/\underline{m}_B$, was 2.10. This value will be compatible with the existence of one unpaired electron. Dunitz and Orgel[17] have reported that $[Cl_5RuORuCl_5]^{4-}$, a linearly oxo-bridged Ru(IV) dimer, was diamagnetic. In their extensive study of Ru(III)–O–Ru(III) systems Meyer *et al.*[1] explained the magnetic data in terms of the delocalization through the bridging oxide ion and pointed out that the relative stability of [(bpy)$_2$ClRuORuCl(bpy)$_2$]$^{3+}$ is reasonable because the electron lost comes from a π^* level. In the present case too, the observed magneton number can be attributed to the presence of one unpaired electron in the lowest π^* MO delocalized over both ruthenium centers.

Ezerskaya and Solovykin[3,4] reported that a dimer was formed by the oxidation of K[RuCl(Hedta)] with hydrogen peroxide or oxygen. The spectral and polarographic data[4] suggest that their complex was the

†††† "Ru(IV)–O–Ru(III)" is only a formal representaion; the two ruthenium centers are equivalent.[1]

same as or very similar to the present green complex. These authors described the compound as a μ-oxo and μ-peroxo double bridged dimer. But their arguments do not seem to be very convincing. Although no direct evidence is available for the oxo single bridge in the present case, μ-peroxo structure is less plausible than μ-oxo structure in explaining the stoichiometry, electrochemical behavior, and the results of pH titration.

Yoshino *et al.*[5] reported a green substance obtained by oxidizing Ru(III)L either anodically at a platinum electrode, chemically with several oxidizing agents, or photochemically in the presence of oxygen. The substance was later characterized by Uehiro[6] to be the acid form of the present complex: H[(Hedta)RuORu-(Hedta)]·6.5H_2O. His spectral and magnetic data are essentially the same as ours.

Oxidation of Ru(III)L at a Platinum Electrode and with Hydrogen Peroxide. The cyclic voltammogram of Ru(III)L in the acetate buffer with a platinum wire electrode over a range of −0.4 V to +0.5 V showed coupled oxidation and reduction peaks corresponding to Ru(III)L+e^-=Ru(II)L. When the anodic sweep was extended, a shoulder rose on the anodic current at +0.7 V and a new reduction peak at +0.25 V appeared; this reduction peak was attributable to the reduction of the Ru(IV)–O–Ru(III) dimer, since the same peak was observed on the cyclic voltammogram of the green solution prepared by the oxidation of Ru(III)L with chlorate ions. These results confirm the observation of Yoshino *et al.* that the green dimer could be obtained by anodic oxidation of Ru(III)L with platinum electrode. The reduction potential of the dimer at platinum electrode was much more positive than the half-wave potential of the polarographic step A, probably owing to faster decomposition of the Ru(III)–Ru(III) dimer on the platinum surface than on mercury.

The oxidation of Ru(III)L with hydrogen peroxide was reexamined. The UV-visible spectrum and the polarogram of the oxidized solution was the same as those of the solution obtained by the oxidation with chlorate ions. The stoichiometry, however, was complicated. If hydrogen peroxide acted as a two-electron oxidizing agent, $n(H_2O_2)/n(\mathrm{Ru(III)L})$ should be 0.25, whereas the experimental ratio determined from the end-points of the amperometric and spectrophotometric titrations was 0.3. Very likely, partial decomposition of hydrogen peroxide took place owing to the catalytic action of the dimer.[3] No further study was made on this reaction.

Preliminary Study on the Kinetics of the Oxidation of Ru(III)L with Chlorate Ions. The kinetics was examined by measuring the increase of the absorbance at 630 nm and by measuring the growth of the polarographic diffusion current of step A in a weakly acid solution.

If the rate of increase of the concentration of the dimer is proportional to the concentrations of both Ru(III)L and chlorate ions, *i.e.*,

$$dx/dt = k(a-2x)(b-x/6),$$

then

$$[6/(12b-a)] \ln [a(b-x/6)/b(a-2x)] = kt, \quad (6)$$

where x is the concentration of the dimer at time t, and a and b are the initial concentrations of Ru(III)L and chlorate ions, respectively. The value of x was determined either spectrophotometrically or polarographically. In both cases, the experimental plots of the left-hand side of Eq. 6 against time were quite linear up to about 80% of the completion of the reaction. The values of k thus obtained were fairly constant. The average value of the second-order rate constant was 5.3_2 mol^{-1} dm^3 s^{-1} at 25 °C in 0.2 mol dm^{-3} acetate buffer of pH 4.7.

It is rather surprising that this complicated reaction followed a simple second-order rate equation. Uehiro[6] in his study of the oxidation of Ru(III)L with $[Mn(edta)(H_2O)]^-$ observed that the rate equation was compatible with a mechanism that involved the dimerization of Ru(III)L followed by the electron transfer. Since the range of the initial concentration of Ru(III)L was quite limited (1 to 2 mol m^{-3}) in the present study, the above result is not conclusive.

The authors thank Dr. F. S. Howell of the Department of Chemistry of Sophia University for correcting the manuscript. The present work was partially supported by a Grant-in-Aid for Scientific Research No. 547045 from the Ministry of Education, Science and Culture.

References

1) T. R. Weaver, T. J. Meyer, S. A. Adeyemi, G. M. Brown, R. P. Eckberg, W. E. Hatfield, E. C. Johnson, R. W. Murray, and D. Unterecker, *J. Am. Chem. Soc.*, **97**, 3039 (1975).

2) B. A. Moyer and T. J. Meyer, *Inorg. Chem.*, **20**, 436 (1981).

3) N. A. Ezerskaya and T. P. Solovykin, *Zh. Neorg. Khim.*, **11**, 2179 (1966); [*Chem. Abstr.*, **65**, 18145 (1966)].

4) N. A. Ezerskaya and T. P. Solovykin, *Zh. Neorg. Khim.*, **11**, 2569 (1966); [*Chem. Abstr.*, **66**, 34414 (1967)].

5) T. Uehiro, M. Saito, and Y. Yoshino, 26th Meeting of Coordination Chemistry, Sapporo, August 1976, Abstr. No. 4018.

6) T. Uehiro, Ph. D. Thesis, Tokyo University, Tokyo, Japan 1978.

7) K. Shimizu, *Bull. Chem. Soc. Jpn.*, **50**, 2921 (1977).

8) M. Mukaida, H. Okuno, and T. Ishimori, *Nippon Kagaku Zasshi*, **86**, 598 (1965).

9) A. Endo, M. Watanabe, S. Hayashi, K. Shimizu, and G. P. Satô, *Bull. Chem. Soc. Jpn.*, **51**, 800 (1978).

10) K. Shimizu, M. Kobayashi, and G. P. Satô, *Bunseki Kagaku*, **23**, 1537 (1974); K. Shimizu and M. Kobayashi, *Bunseki Kiki*, **12**, 687 (1974).

11) G. A. Stoner, *Anal. Chem.*, **27**, 1186 (1955).

12) K. Shimizu, T. Matsubara, and G. P. Satô, *Bull. Chem. Soc. Jpn.*, **47**, 1651 (1974).

13) G. Gordon and P. H. Tewari, *J. Phys. Chem.*, **70**, 2000 (1966).

14) D. J. Hewkin and W. P. Griffith, *J. Chem. Soc., A*, **1966**, 472.

15) R. M. Wing and K. P. Callahan, *Inorg. Chem.*, **8**, 871 (1969).

16) J. S. Filippo, Jr., R. L. Grayson, and H. J. Sniadoch, *Inorg. Chem.*, **15**, 269 (1976).

17) J. D. Dunitz and L. E. Orgel, *J. Chem. Soc.*, **1953**, 2594.

Cation Exchange Separation of Metal Ions Using HF–H_3BO_3 Media

Takeo Adachi

Analytical Chemistry Laboratory, Japan Atomic Energy Research Institute, Tokai, Ibaraki 319-11

(Received August 14, 1981)

Using hydrofluoric–boric acid media, a new cation exchange method for the mutual separation of metals which form stable fluoride complexes has been developed. The addition of boric acid to a hydrofluoric acid solution reduces the free fluoride ion concentration to about one hundredth because of the formation of fluoroboric acid. This reduction of the free fluoride ion concentration makes it easy to control the formation of metal fluoride complexes, favoring their separation. As the fluoroboric acid has a buffer action relating to the fluoride ion concentration, the distribution coefficients of metal ions are not affected by the increase in the concentrations of metal ions, even at a low concentration of fluoride ions in the solution. By the use of hydrofluoric–boric acid media, such metals as zirconium, titanium, aluminium, and uranium can be separated from each other. The distribution coefficients of eighteen metals were investigated both in hydrofluoric acid and hydrofluoric–boric acid solutions.

Although the ion exchange method in hydrofluoric acid solutions has been widely used for the separation of metals, most of the works have used anion exchange resin in mixed media of hydrofluoric and hydrochloric[1–4] or nitric[5,6] acids. In the absence of hydrochloric or nitric acid, separation can be done to only two groups,[7–9] that is, metals which form stable fluoride complexes and others. The presence of Cl^- or NO_3^- is believed to be effective in differentiating the adsorbabilities of metal fluoride complexes to the anion exchange resin.[6,10] In more than 0.1 M (1 M=1 mol dm^{-3}) of hydrofluoric acid, metals which form stable fluoride complexes, namely hard acid-metals,[11] form highly fluorinated complexes, such as ZrF_6^{2-}, TiF_6^{2-}, and AlF_6^{3-}, and the difference in the adsorbabilities of these complexes either on cation or anion exchange resin is not large enough to separate them from one another.

If the concentration of hydrofluoric acid can be controlled to a certain value far less than 0.1 M, at which such lower fluorinated complexes as ZrF_5^-, TiF_3^+, and AlF^{2+} are formed, the mutual separation of metals based on the difference in the charges of the fluoride complexes may be expected. However, it is not easy to control hydrofluoric acid to a constant concentration of less than 0.1 M in practical operations including the dissolution of the sample in hydrofluoric acid.

By adding boric acid, which is widely used as a masking agent for fluoride ions, the present author has now succeeded in controlling the fluoride ion concentration without reducing the total hydrofluoric acid concentration (C_{HF}). Boric and fluoroboric acids themselves do not form stable complexes with metal ions in acidic solutions, and fluoroboric acid can easily be removed from the solution by evaporation. Hydrofluoric–boric acid media have the practical advantage that the concentration of the free fluoride ion is almost unchanged with the amount of metal ions which consume fluoride ions.

In the present work, cation exchange adsorption data for metal ions in hydrofluoric–boric acid media are investigated in comparison with the data in hydrofluoric acid, and a new mutual-separation method for hard acid-metals is developed using hydrofluoric–boric acid media.

Experimental

Chemicals and Apparatus. Standard solutions of metal ions (0.01 M) were prepared by dissolving the materials described below in 13 M HF with and without the addition of a small amount of nitric acid or hydrochloric acid: V(IV) from $VOSO_4 \cdot 3H_2O$, V(V) from NH_4VO_3, W(VI) from $Na_2WO_4 \cdot 2H_2O$, Mo(VI) from $(NH_4)_6Mo_7O_{24} \cdot 4H_2O$, Nb(V) from Nb_2O_5, and others from metals. After dissolution, the concentration of the residual hydrofluoric acid in each solution was adjusted to about 0.2 M.

A Shimadzu UV-210 spectrophotometer and a Nippon Jarrell-Ash AA-855 atomic absorption spectrophotometer were used for the determination of the metals.

Ion Exchange Resin. A sulfonated, polystyrene-type, strongly acidic cation exchange resin, Diaion SK #1, a product of Mitsubishi Chemical Ind., Ltd. (8% DVB, 75 to 150 μm, H^+-form), was used. After the resin had been washed in a column with sufficient volume of 4 M hydrochloric acid and with distilled water until the effluent was free from chloride, it was dried to a constant weight at 105 °C and stored in a vacuum desiccator.

Determination of Distribution Coefficient. A sample solution containing 2×10^{-4} M of a metal ion and a definite concentration of hydrofluoric acid or hydrofluoric–boric acid was prepared. Fifty ml of the solution was added onto 0.500 g of the dried resin in a 150-ml polyethylene bottle, and the bottle was shaken gently for 24 h at room temperature (the equilibrium was attained within 4 h). After the filtration of the resin, the metal ion concentration in the solution was determined by means of a suitable method (*cf.* Table 1).

The distribution coefficient, K_d, was determined by means of the following equation:

$$K_d = (\text{Amount of metal ion in resin/Amount of metal ion in solution}) \times (\text{ml of solution/g of resin}) \quad (\text{ml/g}).$$

Column Operation. About 4 g of dry-form resin which had been swelled well with distilled water was packed in a polyethylene column (10 mm $\phi \times 120$ mm), and the column was conditioned with about 50 ml of an eluent (with a definite concentration of hydrofluoric acid or hydrofluoric–boric acid the same as in the test solution). After the addition of 10 ml of a test solution containing from 1 to 5 mg of a metal ion, the same eluent was passed through the column. The effluent was collected with a fraction collector, and the concentration of the metal ion in each fraction was determined by the method shown in Table 1.

Results

Distribution Coefficients. The distribution coefficients of 18 elements for cation exchange resin (Diaion SK #1) in hydrofluoric acid and hydrofluoric–0.65 M boric acid media are shown in Tables 2 and 3, along with the stability constants of metal fluoride complexes ($\log K_1$). The metals are arranged in the order of the K_d values in 0.1 M hydrofluoric acid. The K_d values of zirconium, titanium, aluminium, and uranium were investigated more precisely, as is shown in Fig. 1. In both media, the K_d values of metals increased with a decrease in the hydrofluoric acid concentration. The effect of the boric acid concentration on the K_d values is not so great as that of the hydrofluoric acid concentration. For example, when the boric acid concentration was changed from 0.65 M to 0.4 M in 0.2 M HF media, the K_d values of Ti(IV) and Al(III) were decreased to 42 and 420 from 77 and 580 respectively.

Ringbom[12] described how the ion exchange separation of two metals by the column filtration method

Table 1. Methods used for the determination of metal ions

Metal ion	Method
Co(II), Cd(II), Mn(II), Fe(III), Al(III), V(IV), V(V), Cr(III), Ni(II), and Cu(II)	Atomic absorption spectrometry
Sn(IV) and Mo(VI)	Oxine extraction-photometry[a),b)]
U(VI)	Arsenazo III photometry[c)]
W(VI)	Thiocyanate photometry[d)]
Zr(IV) and Hf(IV)	Xylenol Orange photometry[e)]
Ti(IV)	Diantipyrylmethane photometry[f)]
Nb(V)	Sulfochlorophenol S photometry[g)]
Ta(V)	4-(2-Pyridylazo)resorcinol photometry[h)]

a) H. Hashitani *et al.*, *Bunseki Kagaku*, **16**, 478 (1967). b) K. Motojima *et al.*, *Bunseki Kagaku*, **11**, 47 (1962). c) K. Motojima *et al.*, *Bunseki Kagaku*, **18**, 208 (1969). d) E. B. Sandell, "Colorimetric Determination of Traces of Metals," 3rd ed, Interscience, New York (1959), p. 886. e) K. L. Cheng, *Talanta*, **2**, 61 (1959). f) H. Ishii, *Bunseki Kagaku*, **16**, 110 (1967). g) H. Hashitani *et al.*, *Bunseki Kagaku*, **24**, 303 (1975). h) R. Kajiyama *et al.*, *Bunseki Kagaku*, **15**, 153 (1966).

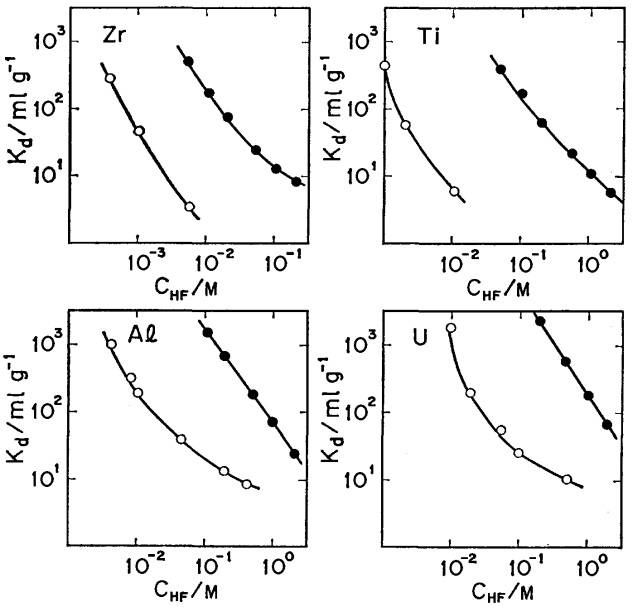

Fig. 1. Distribution coefficients of Zr(IV), Ti(IV), Al(III), and U(VI) in HF (○) and HF–H_3BO_3 (●) media. [H_3BO_3]: 0.65 M.

Table 2. Cation-exchange distribution coefficients of metal ions in HF

Metal ion	HF (M)					$\log K_1$[14)]
	0.1	0.2	0.5	1.0	2.0	
Cd(II)	$>5\times10^3$	$>5\times10^3$	$>5\times10^3$	$>5\times10^3$	2.5×10^3	0.5
Co(II)	$>5\times10^3$	$>5\times10^3$	$>5\times10^3$	$>5\times10^3$	2.0×10^3	—
Mn(II)	$>5\times10^3$	$>5\times10^3$	$>5\times10^3$	$>5\times10^3$	1.9×10^3	0.7
Ni(II)	$>5\times10^3$	$>5\times10^3$	$>5\times10^3$	$>5\times10^3$	1.6×10^3	0.7
Cu(II)	$>5\times10^3$	$>5\times10^3$	$>5\times10^3$	$>5\times10^3$	1.5×10^3	1.0
V(IV)	420	180	80	31	13	3.0
Fe(III)	192	50	10	5	3	5.0
Cr(III)	45	32	25	11	10	4.5
V(V)	30	16	10	3	3	—
U(VI)	20	12	10	8	5	4.5
Al(III)	9	8	7	6	5	6.0
Ti(IV)	3	3	3	3	<3	6.5
Zr(IV)	3	3	3	3	<3	9.1
Hf(IV)	3	3	3	3	<3	—
W(VI)	<3	<3	<3	<3	<3	—
Mo(VI)	<3	<3	<3	<3	<3	—
Sn(IV)	<3	<3	<3	<3	<3	—
Nb(V)	<3	<3	<3	<3	<3	—
Ta(V)	<3	<3	<3	<3	<3	—

TABLE 3. CATION-EXCHANGE DISTRIBUTION COEFFICIENTS OF METAL IONS IN HF–0.65 M H_3BO_3 MEDIA

Metal ion	HF (M)				
	0.1	0.2	0.5	1.0	2.0
Fe(III)	$>5\times10^3$	$>5\times10^3$	4.5×10^3	800	177
Cd(II)	$>5\times10^3$	$>5\times10^3$	2.8×10^3	730	185
Mn(II)	$>5\times10^3$	$>5\times10^3$	2.5×10^3	581	164
Co(II)	$>5\times10^3$	$>5\times10^3$	2.4×10^3	562	154
Ni(II)	$>5\times10^3$	$>5\times10^3$	2.6×10^3	657	118
Cu(II)	$>5\times10^3$	$>5\times10^3$	1.9×10^3	427	97
Cr(III)	$>5\times10^3$	$>5\times10^3$	1.8×10^3	284	145
U(VI)	4.3×10^3	2.1×10^3	580	180	63
V(IV)	2.0×10^3	1.3×10^3	480	190	66
Al(III)	1.6×10^3	580	180	63	20
Ti(IV)	181	77	21	11	7
V(V)	125	90	68	60	58
Mo(VI)	16	10	7	5	3
Sn(IV)	15	7	6	5	3
Zr(IV)	13	10	8	4	<3
Hf(IV)	11	8	6	4	<3
W(VI)	10	6	5	3	<3
Nb(V)	10	8	6	5	<3
Ta(V)	10	6	5	<3	<3

can be achieved when the K_d value of one ion is larger than from 10^2 to $10^{2.5}$ and that of the other is less than from $10^{0.5}$ to 10^1.

According to Ringbom's criterion, the following can be expected for the column-elution behavior of metal ions from the K_d values in Tables 2 and 3: (1) In 2 M hydrofluoric acid, Cd(II), Co(II), Mn(II), Ni(II), and Cu(II) are retained in the column. In addition to these metals, V(IV) and Fe(III) are retained in 0.5 M and 0.1 M HF respectively. The adsorptions of Cr(III), V(V), and U(VI) are not quantitative, not even in 0.1 M. Other metals are not retained in the range from 0.1 to 2 M. (2) In hydrofluoric–boric acid media, the number of elements retained in the column increases. In 2, 0.5, or 0.1 M HF containing 0.65 M H_3BO_3, Cr(III) and Fe(III), U(VI) and Al(III), or Ti(IV) and V(V) are retained respectively, in addition to the metals which are retained in the respective concentration of the hydrofluoric acid medium. Hard acid-metals, such as Zr(IV), Hf(IV), Mo(VI), W(VI), Sn(VI), Nb(V), and Ta(V), are not retained at all in either medium. From the K_d values shown in Tables 2 and 3, the possibility of the mutual separation of Zr(IV), Ti(IV), and Al(III) can be presumed in hydrofluoric–boric acid media

Elution Behavior. In order to ascertain the practical conditions for the separation of metals, the elution behavior of Zr(IV), Ti(IV), Al(III), U(VI), and Fe(III) was investigated in hydrofluoric acid and hydrofluoric–boric acid media using a column filled with 4 g of dry-form resin (10 mmϕ × 120 mm). The elution curves are shown in an integrated form in Fig. 2. The inflection points of the elution curves give the volume of the elution maxima (V_{max}, in ml). The K_d values were calculated from the elution maxima

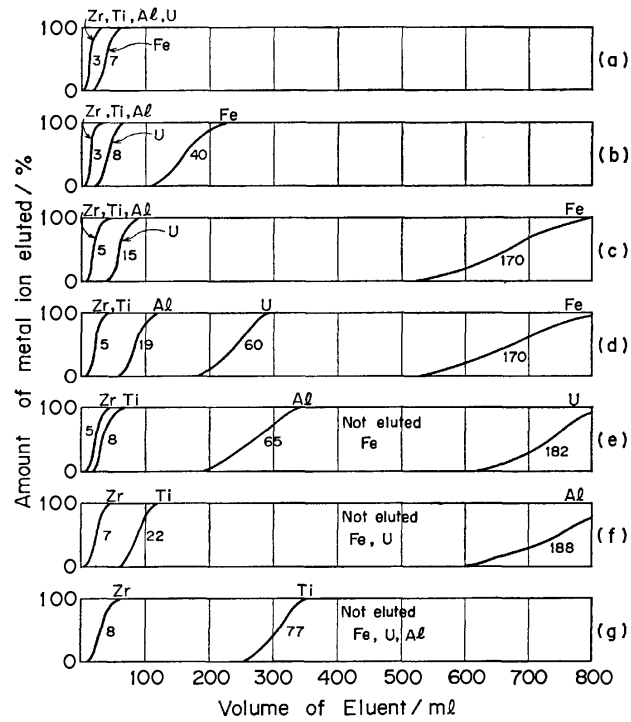

Fig. 2. Column elution behavior of metal ions in HF and HF–H_3BO_3 media.
Diaion SK #1: 4 g, flow rate: 1.2 ml/min. Figures in each column are K_d values obtained. (a): 0.5 M HF, (b): 0.2 M HF, (c): 0.1 M HF, (d): 2 M HF–0.65 M H_3BO_3, (e): 1 M HF–0.65 M H_3BO_3, (f): 0.5 M HF–0.65 M H_3BO_3, (g): 0.2 M HF–0.65 M H_3BO_3.

using the following relation:[13]

$$V_{max} = K_d \times w,$$

where w is the weight of dry resin (g). The calculated K_d values shown in Fig. 2 are in good agreement with the K_d values obtained by the batch method shown in Tables 2 and 3. This fact indicates that the elution was carried out while keeping the ion exchange equilibrium at the flow rate used (1.0 to 1.5 ml/min).

In both hydrofluoric acid and hydrofluoric–boric acid media, metal ions are retained more strongly in the column with a decrease in the concentration of hydrofluoric acid. In hydrofluoric–boric acid media, the metals investigated were retained more tightly than in hydrofluoric acid. For example, as may be seen in Fig. 2 (a), Zr(IV), Ti(IV), Al(III), U(VI), and Fe(III) were eluted when 60 ml of 0.5 M HF was passed through the column, while in 0.5 M HF–0.65 M H_3BO_3 (Fig. 2 (f)) Fe(III) and U(VI) were not eluted even when more than 800 ml of the eluent was passed, and Al(III) was retained in the column until 600 ml.

On the basis of the results shown in Fig. 2, a separation scheme for Zr(IV), Ti(IV), Al(III), U(VI), and Fe(III) was designed. These metals were eluted successively by the following solutions: Zr(IV) by 0.2 M HF–0.65 M H_3BO_3, Ti(IV) by 0.5 M HF–0.65 M H_3BO_3, Al(III) by 2.0 M HF–0.65 M H_3BO_3, U(VI)

Table 4. Effect of amount of metal ion on the distribution coefficient by the batch method

Metal ion	Examined mg	Examined mmol	K_d/ml g^{-1} HF-H_3BO_3	K_d/ml g^{-1} HF
			(0.02—0.65 M)	(10^{-3} M)
Zr(IV)	0.2	2.1×10^{-3}	25	67
	0.5	5.3×10^{-3}	28	97
	2.0	2.1×10^{-2}	30	250
	20.0	2.1×10^{-1}	27	—
			(0.2—0.65 M)	(4×10^{-3} M)
Ti(IV)	1.0	2.1×10^{-2}	77	44
	10.0	2.1×10^{-1}	79	172
	50.0	1.04	75	230
			(1.0—0.65 M)	(0.01 M)
Al(III)	2.0	7.4×10^{-2}	65	106
	20.0	7.4×10^{-1}	63	203
	100	3.7	60	400
			(2.0—0.65 M)	(0.05 M)
U(VI)	1.0	4.2×10^{-3}	63	45
	10.0	4.2×10^{-2}	60	40
	50.0	2.1×10^{-1}	52	40

Dry resin : 4 g, volume of solution : 50 ml.

by 0.1 M HF, and Fe(III) by 0.5 M HF.

Effect of Amounts of Metal Ions on K_d. In the hydrofluoric–boric acid media, the concentration of free fluoride ions is extremely low, as will be discussed in the Discussion section, because the fluoride ions are consumed by the complex formation with boric acid. Therefore, it is considered that the K_d values might be affected by the amount of metal ions as a result of the deficiency of fluoride ions in addition to the loading.

The effect of the amount of metal ions on K_d in the batch method is presented in Table 4. In this experiment, 4 g of the dry resin was used in order to keep the loading less than 0.1, the metal ion solutions were made free from fluoride ions, and the concentration of hydrofluoric acid was chosen so that the K_d values of the metals were between 10 and 100 in solutions containing 1 mg of metal ions.

It is evident that, in hydrofluoric–boric acid solutions, the K_d values are almost unchanged upon variations in the amount of metal ions. On the contrary, in dilute hydrofluoric acid, the K_d values of Zr(IV), Ti(IV), and Al(III) became larger with the increase in the amount of metal ions because of the consumption of free fluoride ions by the metals.

The effect of the amount of zirconium on the column-elution behavior is shown in Fig. 3 as an example. With an increase in the amount of Zr(IV), the elution of Zr(IV) was retarded extensively in 10^{-3} M HF and moderately in 10^{-2} M HF (Figs. 3 (a) and (b)). In 0.1 M HF–0.65 M H_3BO_3, however, the elution of Zr(IV) was hardly affected by an increase in the amount of Zr(IV) up to 250 mg (Fig. 3 (c)). Less than 100 mg of Zr(IV) did not affect the elution of Ti(IV) (Fig. 3 (d)). Although the elution of Ti(IV) is expected to be retarded when

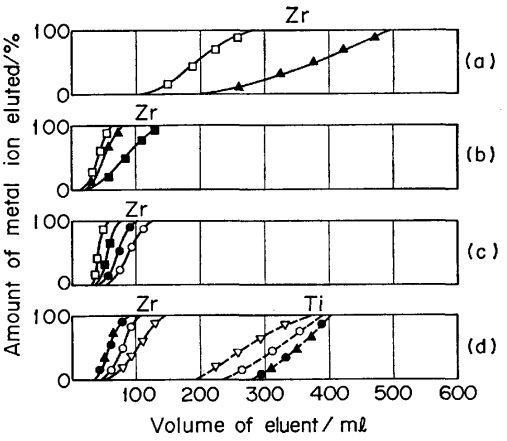

Fig. 3. Effect of amount of Zr(IV) on elution behaviors of Zr(IV) and Ti(IV).
Diaion SK #1: 4 g, flow rate: 1.2 ml/min. (a): 10^{-3} M HF, (b): 10^{-2} M HF, (c): 0.1 M HF–0.65 M H_3BO_3, (d): 0.2 M HF–0.65 M H_3BO_3. Ti: 2 mg, Zr; □: 0.5 mg, ▲: 5 mg, ■: 25 mg, ●: 100 mg, ○: 250 mg, ▽: 500 mg.

the concentration of the fluoride ion is reduced because of the complex formation with a large amount of Zr(IV), the elution of Ti(IV) was slightly accelerated with more than 250 mg of Zr(IV).

Discussion

The experimental results may be summarized as follows:

(1) The K_d values of metals which form stable fluoride complexes are larger in hydrofluoric–boric acid media than in hydrofluoric acid.

(2) The K_d values are scarcely affected by the amount of metal ions in hydrofluoric–boric acid media, whereas they are considerably affected in dilute hydrofluoric acid solutions.

(3) Mutual separations of hard acid-metals using cation exchange resin are possible when hydrofluoric–boric acid solutions are employed as the eluent.

Factors Which Control Cation Exchange Equilibria of Metal Ions in Media Containing Fluoride Ions. The K_d values of metals for the cation exchange resin in a solution involving complexing agent can be expressed by the equation presented by Helfferich.[14] The equation can be rewritten as Eq. 1, considering the adsorption of a metal, M^{n+}, to H^+-form cation exchange resin in a solution containing the fluoride ion as a complexing agent:

$$K_d = \sum_{j=0}^{N} [x_j K^{MF_j}_{(n-j)H}([H^+]_r/[H^+])^{n-j}], \quad (1)$$

$$x_j = [MF_j^{(n-j)+}]/[M^{n+}](1+[F^-]\beta_1+\cdots+[F^-]^N\beta_N)$$

$$= [F^-]^j\beta_j/\sum_{k=0}^{N}([F^-]^k\beta_k), \quad (2)$$

where j is the number of fluoride ions complexed, N is the maximum coordination number of F^- for M^{n+}, β_j is the cumulative stability constant, and r shows the concentration in the resin phase. The $K^{MF_j}_{(n-j)H}$ term is an exchange constant or a selectivity

coefficient which indicates the adsorbability of $MF_j^{(n-j)+}$ to H^+-form resin. As is evident from Eq. 1, the K_d value depends on the fraction, x_j, of a species, $MF_j^{(n-j)+}$, in relating to the total metal species, the selectivity coefficient, $K^{MF_j}_{(n-j)H}$, and the concentration ratio of hydrogen ions in the resin and the solution phase.

Assuming that the ion exchange equilibrium is mainly controlled by one kind of cation species, $MF_j^{(n-j)+}$ $(n-j \geq 1)$, Eq. 1 can be simplified to Eq. 1′:

$$K_d = x_j K^{MF_j}_{(n-j)H}([H^+]_r/[H^+])^{n-j}. \quad (1)'$$

When the amount of metal ion exchanged is negligibly small compared with the capacity of the resin, $[H^+]_r$ is considered to be constant, and, of course, $K^{MF_j}_{(n-j)H}$ is constant. The relation among K_d, x_j, and $[H^+]$ can then be expressed as Eq. 3:

$$\log K_d = \log x_j - (n-j)\log[H^+] + \text{constant}. \quad (3)$$

The charge of the adsorbed species can be obtained from Eq. 3 by changing the hydrogen ion concentration at a constant fluoride ion concentration and, therefore, at a constant x_j.

Ion Exchange Equilibria of Metals in HF. In Fig. 4, the K_d values of various metals in hydrofluoric acid solutions containing 10^{-4} M of free fluoride ions are illustrated as a function of $[H^+]$. From the log K_d—log $[H^+]$ plots of zirconium, titanium, aluminium, uranium, and iron, the linear relations are obtained with slopes of −1.1, −1.7, −1.9, −1.6, and −2.3 respectively. It is considered from these slopes that species of ZrF_3^+, TiF_2^{2+}, AlF^{2+}, UO_2^{2+}, and FeF^{2+} are mainly adsorbed to the resin in the media mentioned above.

In Fig. 5, the K_d values of zirconium and titanium in hydrofluoric acid solutions of pH 1 are illustrated as a function of the concentration of free-fluoride ions, which is calculated using Eq. 4:

$$[F^-] = [HF]/K_{HF}[H^+] = [HF]/10^3 \times 10^{-1} = 10^{-2}\ C_{HF}, \quad (4)$$

where K_{HF} is the stability constant of hydrofluoric acid. The log K_d linearly increases with the decrease

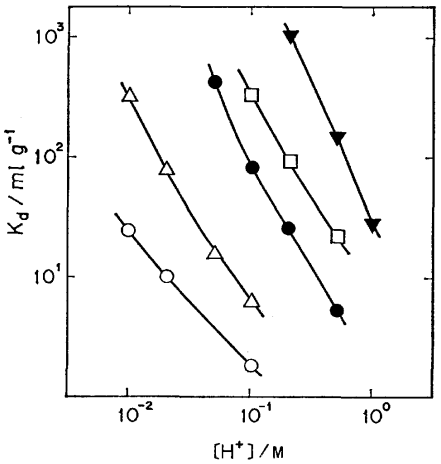

Fig. 4. Relation between K_d and $[H^+]$ in HF at 10^{-4} M $[F^-]$.
○: Zr, △: Ti, ●: Al, □: U, ▼: Fe.

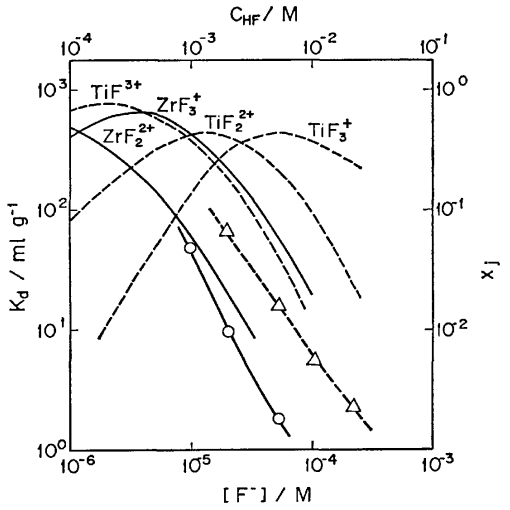

Fig. 5. Relations between changes in K_d in HF at pH 1 and fraction x_j with $[F^-]$.
○: Zr, △: Ti.

in log $[F^-]$. The K_d values of zirconium and titanium increase from 1 to 100 when $[F^-]$ changes from $10^{-4.0}$ to $10^{-5.2}$ M and from $10^{-3.5}$ to $10^{-4.8}$ M respectively. Figure 5 also presents the relations between x_j and $[F^-]$ for zirconium and titanium, calculated using Eq. 2 and the stability constants given in the tables by Sillen and Martell.[15] From these relations, it follows that ZrF_3^+ and TiF_2^{2+} are the main fractions when $[F^-]$ is about $10^{-5.2}$ or $10^{-4.8}$ M respectively. Therefore, it may be considered that ZrF_3^+ and TiF_2^{2+} are the main species which control the adsorption behavior. This estimation agrees with the results obtained from Fig. 4.

Ion Exchange Equilibria of Metals in HF–H_3BO_3 Media. In HF–H_3BO_3 media, $[F^-]$ and $[H^+]$ are calculated according to the chemical equilibria given by the following equations:[15,16]

$$H_3BO_3 + F^- = BF(OH)_3^- \quad (\log \beta_1 = -0.36), \quad (5)$$

$$H_3BO_3 + 2F^- + H^+ = BF_2(OH)_2^- + H_2O \quad (\log \beta_2 = 7.06), \quad (6)$$

$$H_3BO_3 + 3F^- + 2H^+ = BF_3OH^- + 2H_2O \quad (\log \beta_3 = 13.69), \quad (7)$$

$$H_3BO_3 + 4F^- + 3H^+ = BF_4^- + 3H_2O \quad (\log \beta_4 = 19.0), \quad (8)$$

$$H^+ + F^- = HF \quad (\log K_{HF} = 3.0), \quad (9)$$

$$HF + F^- = HF_2^- \quad (\log K_{HF_2^-} = 0.6). \quad (10)$$

The concentrations of hydrogen and fluoride ions in solutions which contain 0, 0.2, 0.4, and 0.65 M H_3BO_3 and various concentrations of hydrofluoric acid (C_{HF}) are summarized in Fig. 6. In the presence of boric acid, $[F^-]$ is extremely low compared with the value in hydrofluoric acid in the absence of boric acid. The reason why K_d in HF–H_3BO_3 media is similar to that in dilute hydrofluoric acid, even at a high concentration of hydrofluoric acid, can be explained by the complex formation of F^- with H_3BO_3 (Eqs. 5 to 8).

For example, the K_d value of titanium in 0.33 M

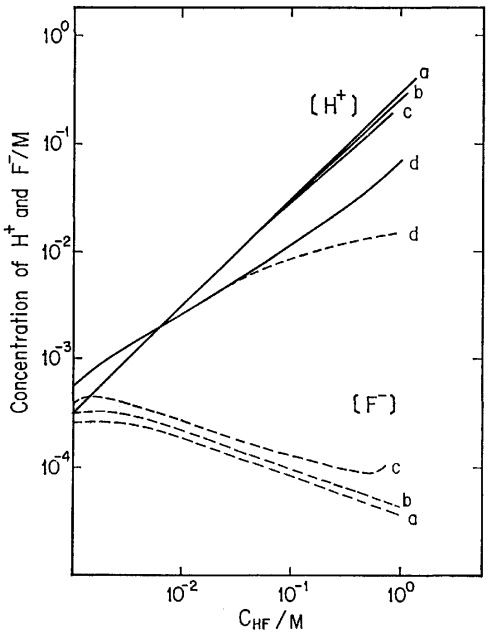

Fig. 6. Calculated concentration of H^+ and F^- in HF-H_3BO_3 media.
[H_3BO_3]; a: 0.65 M, b: 0.4 M, c: 0.2 M, d: 0 M.

HF-0.65 M H_3BO_3 (pH=1) is nearly equal to that in 3.2×10^{-3} M HF, the pH of which is adjusted to 1 (see Figs. 1 and 5). The concentration of the free-fluoride ion in 0.33 M HF-0.65 M H_3BO_3 is considered to be 5.2×10^{-5} M from Fig. 6, while the [F^-] in 3.2×10^{-3} M HF is 3.2×10^{-5} M from Eq. 4.

As is shown in Fig. 6, [F^-] decreases slightly and [H^+] increases proportionally with the increase in C_{HF} in HF-H_3BO_3 media. From Fig. 5 and Eq. 3, the K_d value should increase with the decrease in [F^-] and should decrease with the increase in [H^+]. It can be seen from Fig. 1 that the K_d values of metals in HF-H_3BO_3 media decrease with the increase in C_{HF}. This indicates that K_d in HF-H_3BO_3 media is not governed by the change in [F^-], but by the change in [H^+].

Using the [H^+] value presented in Fig. 6, the K_d values in HF-H_3BO_3 media given in Fig. 1 were replotted against [H^+] instead of C_{HF}: the relations are shown in Fig. 7. The plots of log K_d—log [H^+] are almost straight lines, the slopes of which are similar to those of the lines in Fig. 4. This fact indicates that the adsorbed species in HF-H_3BO_3 media, in which [F^-] is reduced to about 10^{-4} M, are the same as those in a hydrofluoric acid solution, in which [F^-] is about 10^{-4} M.

Fluoride-ion Buffer Action of HF-H_3BO_3. In HF-H_3BO_3 media, BF_4^- and BF_3OH^- are the main species, as is to be expected from the values shown in Eqs. 7 and 8. If a fluoride ion is consumed by a metal ion, fluoride may be supplied from BF_4^- and BF_3OH^- and the concentration of free fluoride ions in the media may thus be kept constant.

This buffer action is effective when the concentration of metal ions is less than one-fifth of the concentration of hydrofluoric acid. For example, the K_d of zirconium in 0.02 M HF-0.65 M H_3BO_3 is not

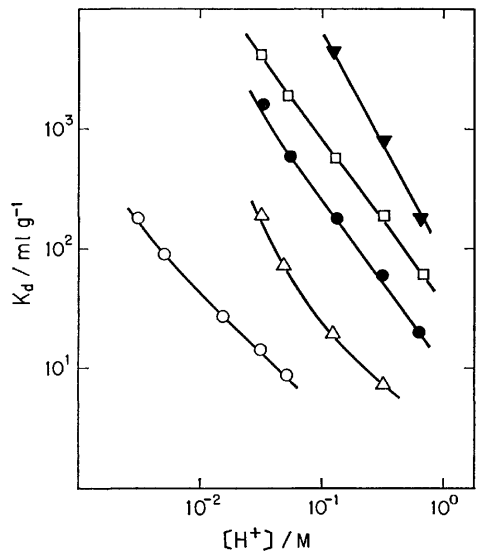

Fig. 7. Relation between K_d and concentration of H^+ in HF-H_3BO_3 media.
[H_3BO_3]: 0.65 M, ○: Zr, △: Ti, ●: Al, □: U, ▼: Fe.

changed up to 4×10^{-3} M of zirconium (20 mg/50 ml), as is shown in Table 4. The F^- buffer action in HF-H_3BO_3 media is remarkable in the column-elution behavior, not only when the amount of an element is changed, but also when the amounts of other co-existing elements are changed, as is shown in Fig. 3.

The F^- buffer action can be expected even in a hydrofluoric acid solution if the concentration is higher than 0.1 M, but the action is not appreciable in the solution with a concentration of less than 0.1 M used in the present work.

Merits of the Use of HF-H_3BO_3 Media in the Cation Exchange Separation of Metals. Using HF-H_3BO_3 media, a successive cation exchange separation of zirconium, titanium, aluminium, and uranium, which has been found difficult in other media, is possible, as is shown in Fig. 2.

From the point of view of practical analysis, the proposed method has the following advantages:

(1) In the analysis of hard acid-metals, anion exchange methods in HF-HCl or -HNO_3 media have been used for separating them from each other. In these methods, metals that form more stable fluoride complexes, M_{ms}, are retained in the column, while metals that form less stable fluoride complexes, M_{ls}, are eluted from the column. Therefore, in the separation of such M_{ls} as aluminium or titanium in a matrix of such M_{ms} as zirconium, an extremely large amount of the resin and an eluent containing hydrofluoric acid are required.[17] In the proposed method using the cation exchange resin, the separation mentioned above can be attained using relatively small amounts of resin and eluent, because M_{ls} are retained in the column and M_{ms} are eluted from the column. The successive elution of impurities retained in the column after eluting matrix elements is also possible. The F^- buffer action of HF-H_3BO_3 media and the reduction of the fluoride-ion concentration with H_3BO_3 are effectively used in the proposed method.

(2) Generally, metals and alloys containing hard acid-metals as the main components are dissolved with the aid of hydrofluoric acid. It is not easy to control the concentration of hydrofluoric acid in the resulting solution to a constant concentration of less than 0.1 M. In HF–H_3BO_3 media, however, it is not so hard to adjust the hydrofluoric acid concentration to the desired value, because separation is carried out at more than 0.1 M HF.

In this connection, the fluoroboric acids in the effluent can easily be evaporated prior to the subsequent determination.

The author wishes to thank Professor Taitiro Fujinaga, Drs. Tooru Kuwamoto, Kakuzo Tada, Hiroshi Hashitani, Sorin Kihara, Osamu Tochiyama and Mr. Hideyo Yoshida for their helpful discussions and useful suggestions.

References

1) K. A. Kraus and G. E. Moore, *J. Am. Chem. Soc.*, **73**, 9, 13, 2900 (1951).
2) J. L. Hague, E. D. Brown, and H. A. Bright, *J. Natl. Bur. Stand.*, **53**, 261 (1954).
3) J. B. Headridge and E. J. Dixon, *Analyst (London)*, **87**, 32 (1962).
4) J. I. Kim, H. Lagally, and H. -J. Born, *Anal. Chim. Acta*, **64**, 29 (1973).
5) E. A. Huff, *Anal. Chem.*, **36**, 1921 (1964).
6) L. Danielsson, *Acta Chem. Scand.*, **19**, 1859 (1965).
7) J. P. Faris, *Anal. Chem.*, **32**, 520 (1960).
8) J. S. Fritz, B. B. Garralda, and S. K. Karraker, *Anal. Chem.*, **33**, 882 (1961).
9) J. Korkish and A. Huber, *Talanta*, **15**, 119 (1968).
10) K. A. Kraus and F. Nelson, "Special Technical Publication," American Society for Testing Materials, Philadelphia (1958), No. 195, p. 27.
11) R. G. Pearson, *J. Chem. Educ.*, **45**, 581, 643 (1968).
12) A. Ringbom, "Complexation in Analytical Chemistry," Wiley-Interscience, New York (1963), p. 229.
13) Ref. 12, p. 220.
14) F. Helfferich, "Ion Exchange," McGraw-Hill, New York (1962), p. 202.
15) L. G. Sillen and A. E. Martell, "Stability Constants of Metal-Ion Complexes," The Chemical Society, London (1964 and 1971), Special Publication Nos. 17 and 25.
16) R. E. Mesmer, K. M. Palen, and C. F. Baes, Jr., *Inorg. Chem.*, **12**, 89 (1973).
17) H. Freund and F. J. Miner, *Anal. Chem.*, **25**, 564 (1953).

Photoreaction of Tris(ethylenediamine)cobalt(III) Ion with Bis(2-hydroxyethyl)dithiocarbamate Ion

Michio NAKASHIMA and Sigeo KIDA*

Department of Chemistry, Faculty of Science, Kyushu University
33, Hakozaki, Higashi-ku, Fukuoka 812

(Received August 20, 1981)

Complete ligand replacement of tris(ethylenediamine)cobalt(III) ($[Co(en)_3]^{3+}$) by bis(2-hydroxyethyl)-dithiocarbamate ion(htc^-) forming $[Co(htc)_3]$ is induced by visible light in aqueous solution. The quantum yield of the reaction depends on the wavelength of the light and on the concentrations of the complex and the ligand. The distinct feature of this photo-induced substitution is that the quantum yield is higher than unity for the solution containing 0.02 mol dm^{-3} $[Co(en)_3]^{3+}$ and 0.13 mol dm^{-3} htc^-. The unusually high quantum yield is explained on the basis of a primary photoredox process followed by a chain reaction involving cobalt(II) species as chain carriers. Cobalt(III) complexes of an N_6 donor set such as $[Co(NH_3)_6]^{3+}$, $[Co(NH_3)_4(pn)]^{3+}$, $[Co(chxn)_3]^{3+}$, and $[Co(dien)_3]^{3+}$ also undergo similar photo-reaction, where pn, chxn, and dien denote 1,2-propanediamine, 1,2-cyclohexanediamine, and diethylenetriamine, respectively.

It is well known that irradiation on cobalt(III) complexes with light in the d-d band region causes ligand substitutions with quantum yields much lower than those of chromium(III) complexes.[1-4] Among cobalt(III) complexes, $[Co(en)_3]^{3+}$ is known to be quite inert for the irradiation of visible light. Recently, however, Matsubara and Kida found that $[Co(en)_3]^{3+}$ reacts with diethyldithiocarbamate ion(dtc^-) in aqueous solution forming solid $[Co(dtc)_3]$ upon irradiation at 550 nm (or even at longer wavelengths).[5] Although they were unsuccessful in determining quantum yield due to the precipitation of the product, they inferred the extremely high quantum yield for this photoreaction. Such a facile replacement of the ligand by the irradiation of light in the d-d band region is unusual for the photochemistry of cobalt(III) complexes. Therefore, the present study was aimed to elucidate the mechanism of this photoreaction by quantitative measurements.

In this study bis(2-hydroxyethyl)dithiocarbamate ion (htc^-) was used instead of diethyldithiocarbamate ion. The use of htc^- enabled quantitative measurements of the reaction, because the product, $[Co(htc)_3]$, is fairly soluble in water. The overall reaction is simply expressed as

$$[Co(en)_3]^{3+} + 3htc^- \xrightarrow{h\nu} [Co(htc)_3] + 3en. \quad (1)$$

Experimental

Materials. $[Co(en)_3]Cl_3 \cdot 3H_2O$,[6] $[Co(NH_3)_6]Cl_3$,[7] $[Co(NH_3)_4(pn)]Cl_3$,[8] $[Co(chxn)_3]Cl_3 \cdot 2H_2O$,[6] $[Co(dien)_2]Cl_3 \cdot 3H_2O$,[9] $[Co(trien)(en)]Br_3$,[10] and $[Cr(en)_3]Cl_3 \cdot 3.5H_2O$[11] were prepared and purified according to the procedures described in the literature. The ligands are abbreviated as: en=ethylenediamine, pn=1,2-propanediamine, chxn=1,2-cycrohexanediamine, dien=diethylenetriamine, trien=triethylenetetraamine. Standard compounds for actinometry, $K[Cr(NH_3)_2(NCS)_4] \cdot H_2O$ and $K_3[Fe(ox)_3] \cdot 3H_2O$ (ox=oxalate ion), were prepared by the procedures described in the literature.[12,13] The crystals were recrystallized in the dark at least three times.

$K(C_2H_4OH)_2NCS_2$: An ethanol solution (100 cm^3) of carbon disulfide (20 g) was slowly added with stirring to a mixture of potassium hydroxide (20 g) and diethanolamine (40 g) in ethanol (300 cm^3). After stirring for 3 h, pale yellow crystals deposited were filtered by suction and dried in air stream. The crude crystals were dissolved in water (70 cm^3), and 300 cm^3 of ethanol was added to this solution. When the solution was cooled in an ice box, colorless crystals were separated out in 4 h. The crystals were recrystallized three times. Since this compound is apt to undergo gradual decomposition at room temperature, it was newly prepared every month and stored in a refrigerator. Found: C, 27.29; H, 4.63; N, 6.53%. Calcd for $C_5H_{10}NO_2S_2K$: C, 27.38; H, 4.60; N, 6.39%.

$[Co(htc)_3]$: An aqueous solution of $[Co(en)_3]Cl_3 \cdot 3H_2O$ (0.6 g in 20 cm^3) was mixed with an aqueous solution of K(htc) (0.5 g in 30 cm^3), and the solution was exposed to room light for three hours. Dark green crystal precipitated was recrystallized from DMF–water (1:1). Found: C, 30.32; H, 5.04; N, 6.84%. Calcd for $C_{15}H_{30}N_3O_6S_6Co$: C, 30.04; H, 5.15; N, 7.01%.

The elementary analyses were carried out at the Kyushu University Elementary Analysis Center.

Apparatus. A tungsten lamp (300 W) was used as a light source. The light beam which passed through a UV filter was monochromatized by an interference filter of transmission maximum at 451 nm (T_{max}=43%, bandwidth at $1/2\,T_{max}$=11 nm). A cell jacket was mounted in a black box which has a window of interference filter. The cell jacket was thermostated at 20±0.1 °C by circulating water with a Taiyo Thermo Unit C-550. Spectroscopic quartz (10 mm) cells were used as reaction vessels. The cells were placed in the jacket at least 30 min before the irradiation so that the solution could reach the temperature of the cell jacket. The wavelength dependence of the photoreaction was studied by irradiating monochromatic lights at 585, 571, 535, 511, 486, and 460 nm with a JASCO Spectroirradiator Model CRM-FA. The irradiator equipped with a 3 kW Xe-lamp gives monochromatic light beams of bandwidth less than 15 nm.

Electronic absorption spectra were measured with a Shimadzu Multipurpose Spectrophotometer Model MPS-5000.

Actinometry. The intensity of 451 nm monochromatic light was measured by the method of Wegner and Adamson (Reineckate actinometry) and by the method of Hatchard and Parker(ferrioxalate actinometry).[12-14] The ratio of the light intensities determined by the different methods was 1.03±0.05, showing the reliability of the measurements. At the actual runs of experiments the intensity of 451 nm light was measured before and after the photoreaction of interest by the ferrioxalate actinometry. For the study of

wavelength dependence of the photoreaction, intensity of the monochromatic lights of 585, 571, 535, 511, 486, and 460 nm were determined by the Reineckate actinometry.

Photoreaction. One milliliter of an aqueous solution of $[Co(en)_3]^{3+}$ and 2 cm^3 of an aqueous solution of htc^- were mixed in a quartz cell under dim light. In order to make the error due to the absorption of $[Co(htc)_3]$ formed as small as possible the irradiation time was adjusted for each 451 nm irradiation so that the internal filtration of the light by the absorption of $[Co(htc)_3]$ formed is less than 5% of the total absorption at the end of the irradiation.

Calculation of Quantum Yield. The amount of $[Co(en)_3]^{3+}$ reacted was determined by measuring the concentration of $[Co(htc)_3]$ formed, because no mixed complexes such as $[Co(htc)(en)_2]^{2+}$ and $[Co(htc)_2(en)]^+$ were detected from the observation of the spectra. The concentration of $[Co(htc)_3]$ formed was determined from the difference of absorbance at 630 nm between the solutions before and after irradiation. Thus, the quantum yield at 451 nm was calculated by the equation,

$$\phi = \frac{C_m}{I(1-\tau)t}, \qquad (2)$$

where, C_m is the concentration of $[Co(htc)_3]$(mol dm^{-3}), and I, τ, and t denote the intensity of light(einstein dm^{-3} s^{-1})-(einstein represents 1 mol of light quanta), transmittance of the initial solution, and irradiation time, respectively. In the cases of irradiation in the range 460—585 nm, quantum yield was calculated by using the equation derived by King *et al.*, in which the internal filtration effect was taken into consideration.[15,16]

Results and Discussion

Absorption spectra of $[Co(en)_3]Cl_3$ and K(htc) are shown in Fig. 1, where quantum yield for the solution containing 0.02 mol dm^{-3} $[Co(en)_3]^{3+}$ and 0.13 mol dm^{-3} htc^- are also plotted in the range 460—585 nm. It is to be noted that very high quantum yields were obtained even at the lower-energy side of the d-d band of $[Co(en)_3]^{3+}$. From this fact it appears that the spin-triplet or -quintet states concern with this photoreaction, although no definite conclusion can be drawn at present.

Cobalt(III) complexes of an N_6-donor set such as $[Co(NH_3)_6]^{3+}$, $[Co(NH_3)_4(pn)]^{3+}$, $[Co(chxn)_3]^{3+}$, and $[Co(dien)_2]^{3+}$ also undergo similar reactions with htc^- upon irradiation of light in the d-d band region forming $[Co(htc)_3]$. The quantum yields were determined for 451 nm irradiation, and are summarized in Table 1. The table shows that the quantum yields determined are unusually high for cobalt(III) complexes. It is to be noted that the quantum yield for $[Cr(en)_3]^{3+}$ is much less than those of the cobalt(III) complexes (see Table 1). This is the reverse relation to the general rule for the photosubstitution of chromium(III) and cobalt(III) complexes.[1-4]

In Fig. 2, quantum yields are plotted against the initial concentration of htc^-, the initial concentration of $[Co(en)_3]^{3+}$ being kept at 0.02 mol dm^{-3}. The quantum yield increases with increasing concentration of htc^-, reaching a plateau at higher concentration of htc^-. In Fig. 3, quantum yields are plotted against the initial concentration of $[Co(en)_3]^{3+}$, the initial concentration of htc^- being kept at 0.13 mol dm^{-3}. As seen in the figure, the quantum yield increases almost linearly with the concentration of $[Co(en)_3]^{3+}$ in this range of concentration. These facts may be interpreted on the assumption that the photoreaction

TABLE 1. QUANTUM YIELDS AND CHAIN REACTION PARAMETERS

Complex	ϕ[a]	$\pm\delta$[b]	ρ[c]
$[Co(NH_3)_6]^{3+}$	2.08	0.12	>10
$[Co(NH_3)_4(pn)]^{3+}$	1.80	0.17	10
$[Co(en)_3]^{3+}$	1.24	0.06	7.8
$[Co(chxn)_3]^{3+}$	1.00	0.05	5.1
$[Co(dien)_2]^{3+}$	0.45	0.02	1.3
$[Co(trien)(en)]^{3+}$	0.04	0.003	1.0
$[Cr(en)_3]^{3+}$	<0.001		1.0

The initial concentrations of the cobalt(III) complexes and htc^- were 0.02 mol dm^{-3} and 0.13 mol dm^{-3}, respectively. a) The quantum yield. b) The maximum error for the quantum yields estimated from repeated (at least three times) experiments. c) The chain reaction parameter, the ratio of the final concentration of $[Co(htc)_3]$ to the initial concentration of $[Co(H_2O)_6]^{2+}$.

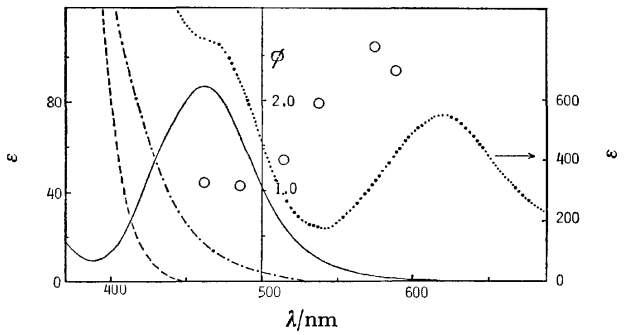

Fig. 1. Absorption spectra and quantum yield.
○: Quantum yield. Absorption spectra; ——: $[Co(en)_3]^{3+}$, — — —: htc^-, —·—: difference spectrum of a solution containing htc^- (0.13 mol dm^{-3}) and $[Co(en)_3]^{3+}$ (0.02 mol dm^{-3}), and a solution containing $[Co(en)_3]^{3+}$ (0.02 mol dm^{-3}) extinction coefficient on left scale, ·····: $[Co(htc)_3]$.

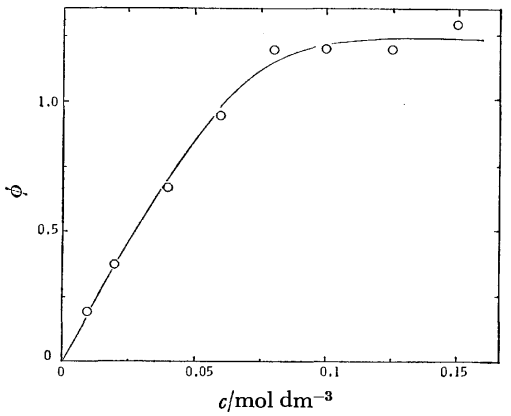

Fig. 2. Quantum yield (at 451 nm) as a function of the initial concentration of htc^-.
Initial concentration of $[Co(en)_3]^{3+}$ was kept at 0.02 mol dm^{-3}.

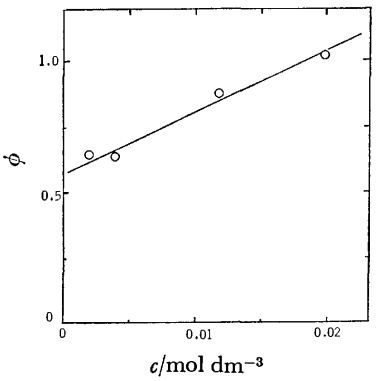

Fig. 3. Quantum yield (at 451 nm, at 15 °C) as a function of the initial concentration of $[Co(en)_3]^{3+}$. The initial concentration of htc$^-$ was kept at 0.13 mol dm^{-3}.

occurs on the ion-pair $[Co(en)_3]^{3+}\cdot$htc$^-$, *i.e.*, the increase of the concentrations of $[Co(en)_3]^{3+}$ and htc$^-$ increases the ratio of concentrations, $[Co(en)_3]^{3+}\cdot$htc$^-$/$[Co(en)_3]^{3+}$.

The formation of ion-pairs is evidenced by the fact that the absorbance of the solution containing $[Co(en)_3]^{3+}$ (0.02 mol dm^{-3}) and htc$^-$ (0.13 mol dm^{-3}) is higher than the sum of the absorbances of the solution of $[Co(en)_3]^{3+}$ (0.02 mol dm^{-3}) and the solution of htc$^-$ (0.13 mol dm^{-3}) in the region <500 nm as shown in Fig. 1. If the above assumption is correct, the quantum yield should be reduced by the addition of the other anions which compete with htc$^-$ in forming ion-pairs with $[Co(en)_3]^{3+}$. In order to elucidate the effect of anions on the quantum yield, the photoreactions were run in the presence of various anions. The results are illustrated in Fig. 4 and summarized in Table 2, together with the formation constants of the ion-pairs. As seen in Table 2, the presence of the anions considerably reduced the quantum yield, and the effect becomes stronger in the order, $NCS^-<I^-<Br^-<Cl^-<C_2O_4^{2-}$, which is the same order as that of the ion-pair formation constants. This fact is in good harmony with the above assumption that the photoreaction initiates at the ion-pair $[Co(en)_3]^{3+}\cdot$htc$^-$.

Since the quantum yields higher than unity can be

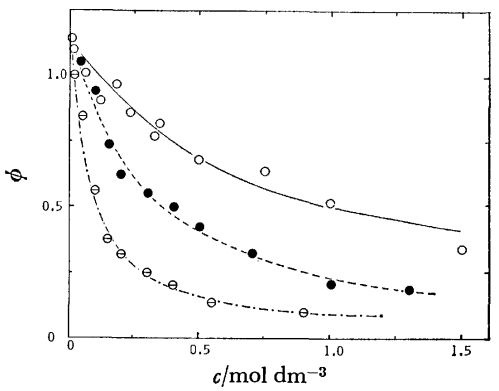

Fig. 4. Effect of anions on the quantum yield (at 451 nm).
○: KCl, ●: KCH_3CO_2, ⊖: $K_2C_2O_4$.

Table 2. The effect of anions on the quantum yield

Anions[a]	Concn/mol dm^{-3}	$\phi\pm\delta$	log K[b]	Ref.
NCS^-	0.33	0.92±0.08	1.34	7
I^-	0.33	0.81±0.08	1.46	7
Br^-	0.33	0.77±0.06	1.68	7
Cl^-	0.33	0.77±0.05	1.72	8
CH_3COO^-	0.30	0.60±0.04	—	
$C_2O_4^{2-}$	0.30	0.25±0.01	3.0	9

a) Potassium salts. b) K is the formation constant of the ion-pair with $[Co(en)_3]^{3+}$.

rationalized only in terms of a chain reaction induced by the photoreaction, we have assumed that the chain-carriers are produced in the reaction as shown below.

$$[Co(en)_3]^{3+}\cdot htc^- \xrightarrow{h\nu} [Co(en)_3{}^*]^{3+}\cdot htc^- \longrightarrow [Co(en)_3]^{2+} + htc\cdot \quad (3)$$

On this assumption, the reaction rate must be affected by the presence of an oxidizing agent, *e.g.*, O_2. In fact, the formation of $[Co(htc)_3]$ was considerably decreased in the reaction under O_2 stream as compared with the case under N_2 stream, (1/30 at the optimum condition so far examined). In the product of a long time irradiation pale yellow solid was detected. It was revealed to be solid sulfur, because it melted at 118 °C and showed no peaks in the IR spectrum.[20] Thus, it is likely that the radical htc· which had been formed in the reaction 3 was removed from the reaction system forming –S–S– bonds finally yielding S_8. Since $[Co(en)_3]^{2+}$ is labile, it readily undergoes the ligand substitution reaction in the solution containing excess of htc$^-$.

$$[Co(en)_3]^{2+} + 3htc^- \longrightarrow [Co(htc)_3]^- + 3en \quad (4)$$

This reaction may be followed by the reaction,

$$[Co(en)_3]^{3+} + [Co(htc)_3]^- \longrightarrow [Co(en)_3]^{2+} + [Co(htc)_3]. \quad (5)$$

Thus, the net reaction of 4 and 5 is

$$[Co(en)_3]^{3+} + 3htc^- \longrightarrow [Co(htc)_3] + 3en, \quad (6)$$

where $[Co(en)_3]^{2+}$ acted as a chain-carrier of the reaction 4 and 5.

In order to examine the validity of the above assumption we have added a small amount of aqueous cobalt(II) chloride to a solution containing $[Co(en)_3]^{3+}$ (0.02 mol dm^{-3}) and htc$^-$ (0.13 mol dm^{-3}) in the dark. The reaction proceeded readily in the dark forming $[Co(htc)_3]^{3+}$. In order to describe the effect of $[Co(H_2O)_6]^{2+}$ on the reaction 6, we defined a parameter ρ= the final amount of $[Co(htc)_3]$/the amount of $[Co(H_2O)_6]^{2+}$ added. In Table 1 quantum yield(ϕ) and ρ for various cobalt(III) complexes of the $[CoN_6]^{3+}$ type are summarized. As seen in the table, ρ is generally larger than unity, except for $[Co(dien)_2]^{3+}$ and $[Co(trien)(en)]^{3+}$, clearly indicating that the chain reaction took place. Table 1 also shows that the increasing order of the quantum yield is exactly in accord with that of ρ. Thus, it is clear that the unusually high quantum yield and the complete replacement of ligands is due to the chain reaction initiated

at the photoredox process 3 and the labile cobalt(II) species $[Co(en)_3]^{2+}$ which undergoes complete ligand replacement in the presence of excess htc^- (reaction 4).

On the basis of the above discussion, we propose the total reaction mechanism as follows:

$$[Co(en)_3]^{3+} + htc^- \longrightarrow [Co(en)_3]^{3+}\cdot htc^- \quad \text{ion-pair formation}$$

$$[Co(en_3]^{3+}\cdot htc^- \xrightarrow{h\nu} [Co(en)_3{}^*]^{3+}\cdot htc^- \longrightarrow [Co(en)_3]^{2+} + htc\cdot \quad \text{photoredox reaction}$$

$$[Co(en)_3]^{2+} + 3htc^- \longrightarrow [Co(htc)_3]^- + 3en$$
$$[Co(htc)_3]^- + [Co(en)_3]^{3+} \longrightarrow [Co(htc)_3] + [Co(en)_3]^{2+} \quad \text{chain reaction}$$

$$[Co(htc)_3]^- \xrightarrow{O_2} [Co(htc)_3]$$
$$[Co(en)_3]^{2+} \xrightarrow{O_2} [Co(en)_3]^{3+}$$
$$htc\cdot \longrightarrow \text{----} \longrightarrow S_8 \quad \text{chain-stopping reactions}$$

The authors wish to acknowledge Prof. M. T. Beck of Kossuth Lajos University, Hungary and Prof. A. W. Adamson of University of Southern California for the discussions and valuable suggestions during their visits to our laboratory.

References

1) P. D. Fleischauer, A. W. Adamson, and G. Sartori, *Prog. Inorg. Chem.*, **17**, 1 (1972).
2) A. W. Adamson, W. L. Waltz, E. Zinato, D. W. Watts, P. D. Fleischauer, and R. D. Lindholm, *Chem. Rev.*, **68**, 541 (1968).
3) V. Balzani and V. Carassiti, "Photochemistry of Coordination Compounds," Academic Press Inc., London (1970).
4) A. W. Adamson and P. D. Fleischauer "Concepts of Inorganic Photochemistry," Willey-Interscience, New York (1975).
5) H. Matsubara and S. Kida, *Proceedings of Annual Meeting of Kyushu-Shikoku Branch of the Chem. Soc. Jpn.*, 1973, p. 18.
6) *Inorg. Synth.*, Vol. II, 221 (1946).
7) W. Biltz, *Z. Anorg. Chem.*, **83**, 178 (1914).
8) M. Kojima, Y. Yoshikawa, and Y. Yamasaki, *Inorg. Nucl. Chem. Lett.*, **9**, 689 (1973).
9) J. E. Pure and G. Schwarzenbach, *Helv. Chim. Acta*, **33**, 985 (1950).
10) F. Basolo, *J. Am. Chem. Soc.*, **70**, 2634 (1948).
11) P. Pfeiffer, P. Koch, G. Lando, and A. Trieschman, *Ber.*, **37**, 4255 (1904).
12) E. E. Wegner and A. W. Adamson, *J. Am. Chem. Soc*, **88**, 394 (1966).
13) C. G. Hatchard and C. A. Parker, *Proc. R. Soc. London, Ser. A*, **235**, 518 (1956).
14) C. A. Parker, *Proc. R. Soc. London, Ser. A*, **220**, 104 (1953).
15) O. Kling, E. Nikolaiski, and H. L. Schlafer, *Ber. Bunsenges. Phys. Chem.*, **67**, 883 (1963).
16) M. Nakashima and S. Kida, *Chem. Lett.*, **1977**, 857. The quantum yields reported in this are one third of the actual values due to miscalculation in the actinometry. Those are corrected in the present report.
17) T. Tanaka and T. Koiso, *Bull. Chem. Soc. Jpn.*, **51**, 1307 (1978).
18) I. L. Jenkins and C. B. Monk, *J. Chem. Soc.*, **1951**, 68.
19) S. Katayama and R. Tanaka, *Bull. Chem. Soc. Jpn.*, **41**, 604 (1968).
20) D. E. Sands, *J. Am. Chem. Soc.*, **87**, 1395 (1965).

 © 1982 The Chemical Society of Japan Bull. Chem. Soc. Jpn., 55, 813—816 (1982)

Temperature-jump Studies of the Complex Formation of Nickel(II) L-Glutamate in Aqueous Solutions

Kiyoshi TAMURA,* Shoji HARADA,† Yoshinori FUNAKI,† and Tatsuya YASUNAGA†

Department of Chemistry, National Defense Academy, Hashirimizu, Yokosuka 239

†*Department of Chemistry, Faculty of Science, Hiroshima University, Higashisenda-machi, Hiroshima 730*

(Received August 27, 1981)

Temperature-jump relaxation studies have been carried out on aqueous nickel(II)–L-glutamic acid solutions. The observed relaxation phenomenon is ascribed to the successive complex formation reactions:

$$Ni^{2+} + L^{2-} \underset{k_{-1}}{\overset{k_1}{\rightleftharpoons}} NiL,$$

$$NiL + L^{2-} \underset{k_{-2}}{\overset{k_2}{\rightleftharpoons}} NiL_2^{2-},$$

$$NiL_2^{2-} + L^{2-} \underset{k_{-3}}{\overset{k_3}{\rightleftharpoons}} NiL_3^{4-},$$

where L^{2-} denotes a glutamate ion. The rate constants are: 2.0×10^4, 1.1×10^4, and 9.2×10^3 M^{-1} s^{-1} (1 M = 1 mol dm^{-3}) for k_1, k_2, and k_3, and 0.048, 0.69, and 27 s^{-1} for k_{-1}, k_{-2}, and k_{-3}, respectively, at 25 °C and I=0.1. The rate-determining step of the complex formation reactions, which follows the initial formation of ion-pairs, is the dissociation of a water molecule from the inner hydration sphere of the nickel; the glutamate ion acts as a bidentate ligand forming a five-membered chelate ring in the complexes.

Recent developments of relaxation kinetics[1,2] have enabled us to study the rapid reactions involved in the metal-ligand interactions. Complex formation reactions of labile metal ions with various ligands have been widely studied,[3,4] and most of them can be interpreted well by a mechanism involving the rate-determining release of the solvent molecule from the inner coordination sphere of the metal ion.[1,3–5] Particular interest has been directed to the metal complexes with amino acid ligands[6–10] not only from the view point of the coordination chemistry but also of their biological importance as model systems of metal-protein interactions. The metal-amino acid complexes are characterized by the formation of five- or six-membered chelate rings, together with especially large complexation constants compared with those of the other non-chelate-forming agents. The above situation inevitably causes a condition where one must study a reaction system containing two or three kinds of complexes and, therefore, be faced with the relaxation treatment of coupled chemical equilibria.

In the present work, we studied nickel(II)–L-glutamic acid interactions by means of a temperature-jump relaxation technique. Glutamic acid is of interest as a potentially terdentate ligand and because it forms mixed ligand complexes with the other chelating agents. However, in spite of the familiar nature and the biological importance of the acid, few kinetic studies[11] have been done on metal-complexes of this ligand. Any information obtained will be helpful in elucidating the metal-glutamic acid interactions.

Experimental

All chemicals used were of a reagent grade. Each solution studied was prepared by mixing aqueous stock solutions of $Ni(NO_3)_2$ and a colorimetric pH indicator, adding sodium hydrogen L-glutamate, and finally diluting. Indicators employed were Phenol Red for pH 7.5—8.5 and Phenolphthalein for pH 9.3—9.8. The ionic strength, I, of the solutions was kept to 0.1 by the addition of KNO_3. The pH of the solution was adjusted with NaOH and/or HNO_3.

The temperature-jump apparatus and the experimental procedure have been described previously.[12,13] All the relaxation experiments were carried out at 25±1 °C.

Results and Treatment of Data

The experimental conditions and the kinetic data observed are summarized in Table 1. All the solutions studied showed a single relaxation phenomenon. The reciprocal relaxation time, τ_{obsd}^{-1}, quoted in Table 1 represents an average of at least four relaxation measurements. The maximum errors are about ±10%. As shown in Table 1, the experiments were carried out in two different pH regions, *i.e.*, around pH 8.0 and 9.8, and the relaxation effect was observed by following the absorbance at the wavelengths 558 (Phenol Red) and 553 nm (Phenolphthalein), respectively. A representative relaxation effect is shown in Fig. 1. Blank solutions of the nickel-indicator and ligand-indicator systems showed no relaxation effect in the same time range. The above fact indicates that the observed relaxation effect is really associated with nickel-ligand interactions.

Under the experimental conditions studied, the formation of nickel(II) glutamate complexes may proceed most generally by the following reaction mechanism:

$$Ni^{2+} + L^{2-} \underset{k_{-1}}{\overset{k_1}{\rightleftharpoons}} NiL \qquad K_1, \qquad (1)$$

$$NiL + L^{2-} \underset{k_{-2}}{\overset{k_2}{\rightleftharpoons}} NiL_2^{2-} \qquad K_2, \qquad (2)$$

$$NiL_2^{2-} + L^{2-} \underset{k_{-3}}{\overset{k_3}{\rightleftharpoons}} NiL_3^{4-} \qquad K_3, \qquad (3)$$

with the rapid protolytic reactions

$$H_2L \rightleftharpoons H^+ + HL^- \qquad K_{a2}, \qquad (4)$$

$$HL^- \rightleftharpoons H^+ + L^{2-} \qquad K_{a3}, \qquad (5)$$

TABLE 1. KINETIC DATA FOR THE NICKEL-GLUTAMIC ACID SYSTEM AT 25 °C AND $I=0.1$

ΣNi (10^{-3} M)	ΣL	pH	τ^{-1}_{obsd} / s^{-1}	τ^{-1}_{calcd} / s^{-1}
HIn=Phenol Red[a]				
2.51	20.2	8.03	42.7	48.6
2.51	40.6	8.03	49.1	51.0
5.01	5.03	8.03	37.4	38.1
5.01	20.3	8.02	65.8	68.7
5.01	40.3	8.04	70.0	69.5
10.0	10.1	8.05	66.2	57.7
10.0	20.4	8.02	113	112
10.0	30.3	7.51	102	106
10.0	30.3	8.02	114	112
10.0	30.3	8.51	114	109
10.0	40.1	8.02	108	111
10.0	60.4	8.03	108	107
20.0	30.1	8.03	207	194
20.0	41.2	8.03	207	205
30.1	40.4	8.02	227	247
HIn=Phenolphthalein[a]				
5.00	10.0	9.32	58.8	64.1
5.00	10.0	9.79	56.0	61.6
5.00	12.5	9.80	78.8	67.1
5.00	15.0	9.76	80.5	70.4
5.01	15.0	9.33	79.3	69.3
10.0	20.0	9.79	94.8	97.8
10.0	25.1	9.78	105	99.3
10.0	30.0	9.81	103	98.7
10.0	35.0	9.82	113	106
10.0	40.0	9.80	112	118
10.0	45.0	9.81	127	136
10.0	50.0	9.83[b]	164	166
20.0	40.0	9.79	176	169

a) ΣIn=2.5×10^{-5} M. b) $I=0.15$.

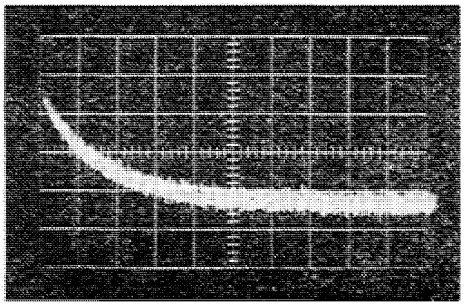

Fig. 1. Relaxation effect in nickel-L-glutamic acid system: ΣNi=0.0100 M, ΣL=0.0204 M, pH=8.02, $I=0.1$ with 2.5×10^{-5} M Phenol Red as an indicator. The abscissa scale is 5 ms per division, and the vertical scale is in arbitrary unit of absorbancy. The relaxation effect corresponds to an increase in absorbance with time.

$$Ni^{2+} + H_2O \rightleftharpoons H^+ + NiOH^+ \qquad K_{OH}, \qquad (6)$$

$$H_2O \rightleftharpoons H^+ + OH^- \qquad K_w, \qquad (7)$$

$$HIn \rightleftharpoons H^+ + In^- \qquad K_{In}, \qquad (8)$$

where the symbols L^{2-} and In^- denote glutamate ion and anionic form of indicator, respectively, and where

TABLE 2. EQUILIBRIUM CONSTANTS FOR THE NICKEL-GLUTAMIC ACID SYSTEM AT 25 °C AND $I=0.1$

Formation constants of nickel(II) glutamate complexes	$K_1=4.17\times10^5$ [a] $K_2=1.59\times10^4$ [a] $K_3=(3.37\pm0.43)\times10^2$ [b]
Dissociation constants of glutamic acid	$pK_{a2}=4.18$[a] $pK_{a3}=9.64$[a]
Nickel(II) hydrolysis constant	$pK_{OH}=10.07$[c]
Ionic product of water	$pK_w=13.79$[d]
Indicator constants	$pK_{In}=7.74$[e] (Phenol Red) $pK_{In}=9.63$[f] (Phenolphthalein)

a) Ref. 14. b) This work. c) Calculated from the value at $I=0$ (Ref. 15) by using the Davies equation for the activity coefficients of the ions (Ref. 16). d) Calculated from the value at $I=0$ (Ref. 17) by using the Davies equation for the activity coefficients of the ions. e) Ref. 18. f) Ref. 19.

K_1, K_2, K_3, K_{a2}, K_{a3}, K_{OH}, K_w, and K_{In} are the equilibrium constants for the corresponding reactions. Since the protolytic reactions (4)—(8) reach equilibrium much faster than the metal complex reactions under consideration here, they can be assumed to be in equilibrium at all times.

All the pertinent equilibrium constants used in this study are given in Table 2. In the earlier equilibrium studies of nickel-glutamate systems,[14,20-22] few investigators[21] reported the presence of the tris-complex NiL_3^{4-}. Therefore, in the preliminary study, we tried to explain the kinetic data in Table 1 by some mechanisms without Eq. 3; *i.e.*, by the complexation reaction (1) or (2), or by coupling the two, or by adopting the disproportionation reaction $Ni^{2+}+NiL_2^{2-}\rightleftharpoons 2\,NiL$. None of them were found to be successful.

By including the three successive complexation equilibria and adopting the usual relaxation treatment, the relaxation times of the system are found to be the solutions of the secular equation:

$$\begin{vmatrix} a_{11}-1/\tau & a_{12} & a_{13} \\ a_{21} & a_{22}-1/\tau & a_{23} \\ a_{31} & a_{32} & a_{33}-1/\tau \end{vmatrix} = 0. \qquad (9)$$

By employing the equilibrium relations $K_n=k_n/k_{-n}$ ($n=1, 2, 3$), the determinant elements a_{ij} are given by

$$\left.\begin{aligned} a_{11} &= k_1\left\{\left(\frac{1-\beta_1}{1+\alpha}\right)[Ni]+(1-\gamma)[L]+\frac{1}{K_1}\right\}, \\ a_{12} &= k_1\left\{\left(\frac{1-\beta_2}{1+\alpha}\right)[Ni]-\frac{1}{K_1}\right\}, \\ a_{13} &= k_1\left(\frac{1-\beta_2}{1+\alpha}\right)[Ni], \\ a_{21} &= k_2\left\{\left(\frac{1-\beta_2}{1+\alpha}\right)[NiL]-[L]\right\}, \\ a_{22} &= k_2\left\{\frac{[NiL]}{1+\alpha}+[L]+\frac{1}{K_2}\right\}, \\ a_{23} &= k_2\left\{\frac{[NiL]}{1+\alpha}-\frac{1}{K_2}\right\}, \end{aligned}\right\} \qquad (10)$$

$$a_{31} = k_3\left(\frac{1-\beta_2}{1+\alpha}\right)[NiL_2],$$
$$a_{32} = k_3\left\{\frac{[NiL_2]}{1+\alpha} - [L]\right\},$$
$$a_{33} = k_3\left\{\frac{[NiL_2]}{1+\alpha} + [L] + \frac{1}{K_3}\right\},$$

with

$$\alpha = \{([HL]+[H_2L]) - ([HL]+2[H_2L])^2/G\}/[L],$$
$$\beta_1 = \gamma\{2([HL]+2[H_2L]) - \gamma([L]+[HL]+[H_2L])\}/G,$$
$$\beta_2 = \gamma([HL]+2[H_2L])/G,$$
$$\gamma = K_{OH}/(K_{OH}+[H]),$$
$$G = [HL] + 4[H_2L] + [H] + [OH] + \gamma[Ni] + [H][In]/(K_{In}+[H]),$$

where the square brackets indicate the molar concentration at equilibrium, and where the charges of the ions are omitted for the sake of simplicity.

Solving Eq. 9, we obtain three relaxation times τ_1, τ_2, and τ_3 ($\tau_1<\tau_2<\tau_3$) as functions of the determinant elements (see Appendix). Since we measured only one relaxation time in each solution studied, we must assign it to one of the three relaxation times predicted by the mechanism. Therefore, we tested the above reaction mechanism for the three cases, in each of which all the experimental data in Table 1 are exclusively associated with only one relaxation time, *i.e.*, (i) τ_1, (ii) τ_2, or (iii) τ_3. The simulation analyses were carried out on computer by iterating the four adjustable parameters K_3, k_1, k_2, and k_3 and by comparing the computed τ^{-1} with the values experimentally observed. The adjustable parameters were optimized by minimizing the root-mean-square percentage deviation between the computed and the observed values of τ^{-1}.

The above simulation analyses revealed that only case (i) gives results consistent with the experiment; case (ii) and (iii) cannot be fitted to the experimental results. As shown in Table 1, the calculated τ_1^{-1} values (denoted by τ_{calcd}^{-1}) agree fairly well with the observed values (r.m.s. % deviation=7.2). The K_3 value determined is shown in Table 2. Considering the differences in ionic strengths, the value garees well with that reported by Gergely and Farkas in their equilibrium studies:[21] K_3=437 at 25 °C and I=0.2. The rate constants determined are shown in Table 3. The contribution of each successive complexation reaction to the relaxation process can be realized from the uncertainty interval of the pertinent rate constant k_n in Table 3.

In the above data treatment, reaction pathways *via* protonated ligands HL^- and H_2L are omitted.

Table 3. Kinetic results for the formation of nickel(II) glutamate complexes at 25 °C and I=0.1

n	k_n/M^{-1} s^{-1}	k_{-n}/s^{-1}
1	$(2.0\pm0.3)\times10^4$	$(4.8\pm0.7)\times10^{-2}$
2	$(1.1\pm0.2)\times10^4$	$(6.9\pm1.4)\times10^{-1}$
3	$(9.2\pm0.5)\times10^3$	$(2.7\pm0.4)\times10$

Reactants of these types lead to additional terms in k_n and k_{-n}. These terms are proportional to either hydrogen-ion concentration or the square of it. Nevertheless, the same set of rate constants gave uniformly good agreement between τ_{obsd} and τ_{calcd} in the pH range 7.5—9.8, without including additional hydrogen-ion dependent terms. We may therefore conclude that, within the experimental error, the major contribution to the relaxation time involves only terms arising from reactions (1)—(3). An additional experiment for the solution containing 0.01 M nickel and 0.01 M glutamic acid, using Methyl Red indicator, at pH 5, where the concentration of glutamate ion L^{2-} is of the order of 10^{-7} M, did not show any relaxation effect.

Discussion

As shown in Table 3, the rate constants k_n are all of the same order of magnitude and show a slightly decreasing tendency of $k_1>k_2>k_3$, which may reflect the electrostatic interactions between the reaction partners. The above result indicates that the successive complex formation reactions (1)—(3) proceed *via* a similar process. The three glutamate ions in the tris-complex NiL_3^{4-} are very likely to be all bidentate, forming five-membered chelate rings, with the γ-carboxylato groups remaining uninvolved in complexation. Therefore, the kinetic result suggests that the glutamate ions in the mono- and bis-complexes NiL and NiL_2^{2-} act as bidentate ligands similar to those in the tris-complex. On the contrary, if the mono- and/or bis-complex contained terdentate ligand, the formation of NiL_2^{2-} or NiL_3^{4-} must involve the cleavage of at least one nickel-ligand bond, and therefore the rate constant k_2 or k_3 would be very different from k_1. This is inconsistent with the present result. The above structural assignment for nickel glutamate complexes is also supported by some equilibrium studies.[21,22]

The k_n values in Table 3 are close to the corresponding rate constants for nickel complexes with univalent α-amino acid ligands such as glycinate,[6] α-alanate,[8] and α-aminobutyrate:[9] $(1.0—2.0)\times10^4$, $(1.5—6.0)\times10^4$, and $(3.0—4.2)\times10^4$ M^{-1} s^{-1} for k_1, k_2, and k_3, respectively, at 20—25 °C and I=0.1—0.15. On the other hand, the k_1 value in Table 3 is significantly smaller than those with bivalent anionic ligands such as oxalate,[23] malonate,[24] and cysteine:[25] $(7.0—15)\times10^4$ M^{-1} s^{-1} at 20—25 °C and I=0.1. According to the widely accepted mechanism of metal-complex formation,[3-5] the rate constants k_n are described in terms of the first-order rate constant k_o for the dissociation of water from the inner hydration sphere of the metal and the association constant K_o of the ion-pair as: $k_n=K_ok_o$. The similarity of the k_n values in Table 3 to those for the univalent anionic ligands indicates that glutamate ion behaves virtually as an univalent anionic ligand for the ion-pair formation. This aspect seems to be reasonable since the negative charge of γ-carboxylato of the ligand resides on a site remote from the chelate-forming groups and the metal ion sees an effective charge

less than −2 owing to the electrostatic shielding of the large ligand.[7] Through the formal estimation of K_o (for 2-1, 1-1, and 0-1 valent ion-pairs) by using Fuoss equation[26] and by setting the minimum approach distance between the reaction partners at 5 Å, the rate constants k_o of ligand substitution were calculated to be 1.0×10^4, 1.4×10^4, and 2.9×10^4 s^{-1} from k_1, k_2, and k_3, respectively, in Table 3. All these values are consistent with the first-order rate constant of the water exchange of nickel ion as determined by an NMR technique:[27] 3×10^4 s^{-1} at 25 °C. The tendency of the increasing water release rate with the higher complexes agrees well with those found in the other nickel-amino acid complexes,[6-9] indicating a significant effect of glutamate ions on the enhancement of the rate of water replacement.

The conclusion is that glutamate ion acts as a bidentate ligand in the nickel complexes and that the formation of the complexes is rate-determined by the release of a coordinated water molecule from the metal rather than by the formation of a chelate-ring closure.

Appendix

Expanding Eq. 9, we obtain the cubic equation

$$\tau^{-3} \quad a\tau^{-2} + b\tau^{-1} - c = 0, \tag{A1}$$

where

$$\begin{aligned} a &= a_{11} + a_{22} + a_{33}, \\ b &= (a_{11}a_{22} - a_{12}a_{21}) + (a_{22}a_{33} - a_{23}a_{32}) \\ &\quad + (a_{33}a_{11} - a_{31}a_{13}), \\ c &= a_{11}(a_{22}a_{33} - a_{23}a_{32}) + a_{12}(a_{23}a_{31} - a_{21}a_{33}) \\ &\quad + a_{13}(a_{32}a_{21} - a_{31}a_{22}). \end{aligned}$$

The secular equation 9 has only real positive eigenvalues of τ^{-1}.[1,5] Thus, by solving Eq. Al, the three relaxation times are given by[28]

$$\begin{aligned} 1/\tau_1 &= a/3 + 2\sqrt{p}\cdot\cos(\theta/3), \\ 1/\tau_2 &= a/3 - 2\sqrt{p}\cdot\cos\{(\theta+\pi)/3\}, \\ 1/\tau_3 &= a/3 - 2\sqrt{p}\cdot\cos\{(\theta-\pi)/3\}, \end{aligned} \tag{A2}$$

with

$$\begin{aligned} \theta &= \cos^{-1}(q/2p^{3/2}) \qquad (0\leqq\theta\leqq\pi), \\ p &= (a^2 - 3b)/9 \qquad (p>0), \\ q &= (2/27)a^3 - ab/3 + c. \end{aligned}$$

As can be realized easily from Eq. A2, we have the inequality relations $\tau_1^{-1} > \tau_2^{-1} > \tau_3^{-1}$ and $\tau_1^{-1} > a/3 > \tau_3^{-1}$.

References

1) M. Eigen and L. De Maeyer, "Technique of Organic Chemistry," 2nd ed, ed by S. L. Friess, E. S. Lewis, and A. Weissberger, Interscience, New York (1963), Vol. 8, Part 2, Chap. 18.

2) "Techniques of Chemistry," 3rd ed, ed by G. G. Hammes, Wiley-Interscience, New York (1974), Vol. 6, Part 2.

3) M. Eigen and R. G. Wilkins, *Adv. Chem. Ser.*, **49**, 55 (1964).

4) D. J. Hewkin and R. H. Prince, *Coord. Chem. Rev.*, **5**, 45 (1970).

5) M. Eigen and L. De Maeyer, Chap. 3 in Ref. 2.

6) G. G. Hammes and J. I. Steinfeld, *J. Am. Chem. Soc.*, **84**, 4639 (1962).

7) J. I. Steinfeld and G. G. Hammes, *J. Phys. Chem.*, **67**, 528 (1963).

8) K. Kustin, R. F. Pasternack, and E. M. Weinstock, *J. Am. Chem. Soc.*, **88**, 4610 (1966).

9) A. Kowalak, K. Kustin, R. F. Pasternack, and S. Petrucci, *J. Am. Chem. Soc.*, **89**, 3126 (1967).

10) J. C. Cassatt and R. G. Wilkins, *J. Am. Chem. Soc.*, **90**, 6045 (1968).

11) S. Harada, K. Higashi, K. Tamura, M. Hiraishi, and T. Yasunaga, *Bull. Chem. Soc. Jpn.*, **51**, 2596 (1978).

12) K. Tamura, *Bull. Chem. Soc. Jpn.*, **46**, 1581, 3626 (1973).

13) K. Tamura, S. Harada, and T. Yasunaga, *Bull. Chem. Soc. Jpn.*, **50**, 2317 (1977).

14) J. H. Ritsma, G. A. Wiegers, and F. Jellinek, *Recl. Trav. Chim. Pays-Bas*, **84**, 1577 (1965).

15) D. D. Perrin, *J. Chem. Soc.*, **1964**, 3644.

16) C. W. Davies, "Ion Association," Butterworths, London (1962), p. 41.

17) T. Ackermann, *Ber. Bunsenges. Phys. Chem.*, **62**, 411 (1958).

18) I. M. Kolthoff, *J. Phys. Chem.*, **34**, 1466 (1930).

19) A. Thiel and G. Coch, *Z. Anorg. Allg. Chem.*, **217**, 353 (1934).

20) "Stability Constants of Metal-Ion Complexes," 2nd ed, ed by L. G. Sillén and A. E. Martell, The Chemical Society, London (1964); *ibid.*, Supplement No. 1 (1971).

21) A. Gergely and E. Farkas, *Magy. Kem. Foly.*, **81**, 471 (1975). These authors reported for the nickel(II) glutamate system: $K_1=10^{5.52}$, $K_2=10^{4.35}$, and $K_3=10^{2.64}$, at 25 °C and $I=0.2$.

22) P. D. Jadhav, D. N. Shelke, and R. A. Bhobe, *J. Inorg. Nucl. Chem.*, **40**, 572 (1978).

23) G. H. Nancollas and N. Sutin, *Inorg. Chem.*, **3**, 360 (1964).

24) F. P. Cavasino, *J. Phys. Chem.*, **69**, 4380 (1965).

25) G. Davies, K. Kustin, and R. F. Pasternack, *Trans. Faraday Soc.*, **64**, 1006 (1968).

26) R. M. Fuoss, *J. Am. Chem. Soc.*, **80**, 5059 (1958).

27) T. J. Swift and G. P. Weinberger, *J. Am. Chem. Soc.*, **90**, 2023 (1968); R. E. Connick and D. Fiat, *J. Chem. Phys.*, **44**, 4103 (1966).

28) T. Uno, "Suchi Keisan," 3rd ed, Asakura, Tokyo (1963), Chap. 4.

 © 1982 The Chemical Society of Japan Bull. Chem. Soc. Jpn., 55, 817—821 (1982)

The Structure of Nickel(II) Bromide in Highly Concentrated Aqueous Solution by X-Ray Diffraction Analysis

Hisanobu WAKITA,* Mitsuyoshi ICHIHASHI, Takeharu MIBUCHI,** and Isao MASUDA

Department of Chemistry, Faculty of Science, Fukuoka University, Nanakuma, Nishi-ku, Fukuoka 814-01

(Received August 31, 1981)

An X-ray diffraction analysis of the aqueous nickel(II) bromide solutions with the concentrations of 2.004, 4.064, and 4.845 mol dm^{-3} demonstrated the presence of the complex $[NiBr(H_2O)_5]^+$. This inner-sphere type complex has interatomic distances of 2.52—2.58 Å for Ni–Br and of 2.04—2.05 Å for Ni–OH_2. With an increase in the concentration the average number of the Ni–Br contacts per one Ni^{2+} ion increased; it was found to be 0.18, 0.47, and 0.68 in the 2.004, 4.064, and 4.845 mol dm^{-3} solutions, respectively.

The X-ray diffraction investigation by Mizuno[1] showed that in crystalline $NiCl_2 \cdot 6H_2O$ the nickel ion has a unitary coordination geometry formulated as *trans*-$[NiCl_2(H_2O)_4]$. Caminiti *et al.*[2] investigated the structure of the aqueous $NiCl_2$ solution by X-ray scattering measurements and showed that the nickel ion existed in the form of the hexaaqua complex $[Ni(H_2O)_6]^{2+}$ even if the concentration was as high as 4 mol dm^{-3}. The neutron diffraction measurement on the aqueous 4.41 mol kg^{-1} $NiCl_2$ solution carried out by Soper *et al.*[3] did not indicate any Ni–Cl interaction, though it confirmed the Ni–OH_2 and Cl–OH_2 interactions. The EXAFS spectra for the aqueous solutions of $NiCl_2$ (0.5 and 4 mol dm^{-3}) and of $NiBr_2$ (0.4 and 4 mol dm^{-3}), obtained by Lagarde *et al.*[4] indicated no contact between Ni^{2+} and halide ions. Sandstrom[5] also demonstrated the EXAFS spectra of the aqueous $NiCl_2$ solutions of 2.78 and 3.74 mol dm^{-3} indicated the presence of only the hexaaqua complex ion with the Ni–OH_2 distance of 2.07 Å.

On the other hand, the ^{17}O-NMR relaxation rate measurements by Hertz *et al.*,[6,7] supported the presence of the Ni–halogen bond in the first coordination sphere in the aqueous $NiCl_2$ and $NiBr_2$ solutions. Libuś *et al.*[8,9] determined the molal-scale stability constant, β_1, of the halogenonickel(II) complex to be 0.10 for X=Cl^- and 0.05 for X=Br^-, in the aqueous 2 mol kg^{-1} NiX_2 solutions; however, they proposed that the Ni–Br interaction occurred with an outer-sphere coordination.

In this paper, in order to determine whether the nickel ion could form a halogeno complex of the inner-sphere type, an X-ray diffraction investigation has been carried out with highly concentrated aqueous $NiBr_2$ solutions.

Experimental and Data Treatment

Sample Solutions. Sample solutions were prepared by dissolving $NiBr_2$, which was obtained by recrystallizing commercially available reagent grade nickel(II) bromide twice from water. The nickel and bromide ion concentrations in the solutions were determined by EDTA titration and the Volhard method, respectively. The density of the solutions was determined pycnometrically. The amount of water in the solutions was calculated from the nickel and bromide ion concentrations and the density. The composition of the sample solutions is shown in Table 1 along with the X-ray linear absorption coefficient of the solutions which were used for the absorption correction of X-ray intensity data.

Table 1. Composition and parameter values of sample solutions

	Solution		
	A	B	C
Ni (mol dm^{-3})	4.845	4.064	2.004
Br (mol dm^{-3})	9.690	8.129	4.008
O (mol dm^{-3})	46.48	47.95	53.02
H (mol dm^{-3})	92.96	95.90	106.0
v/Å^3	342.7	408.6	828.6
ρ/g cm^{-3}	1.896	1.752	1.393
μ/cm^{-1}	76.05	63.97	32.20

v, Stoichiometric volume per one atom of nickel; ρ, density; μ, linear absorption coefficient.

X-Ray Diffraction Measurements. The X-ray diffraction intensity data were recorded on a diffractometer by applying the Bragg-Brentano geometry.[10] A cylindrical quartz-cell with 42 mm in diameter and 21 mm in depth filled with a sample solution was placed in the cell holder. Then the holder was covered with a holder cover which was made of Pyrex-glass and had a double layer Mylar window. The holder was set in a furnace thermostatted by means of circulating water. A Johansson type LiF monochrometer was placed between a receiving slit and a scintillation counter; a pulse height analyzer was used for further effective monochromatization. A Philips Mo X-ray tube (λ=0.7107 Å) was employed. The diffraction intensities were recorded at about 300 points in the angle range 60—0.5°, which corresponds to the s value range 15.3—0.15 Å^{-1}, where $s=4\pi\sin\theta/\lambda$. The time required for accumulating 40000 counts was recorded at every 0.5° to θ=36°, 0.25° to θ=18°, and 0.1° to θ=0.5°. Two sets of divergent and scattering slit combinations, 1°:1° and 1/6°:1/2° were employed. The recording was repeated twice for each sample solution.

Treatment of Diffraction Intensity Data. The diffraction intensities recorded by using each set of the slit combinations were corrected for the background scattering recorded for the cell without solution by using the same slit combination. And the intensities for 1°:1° slit combination were normalized to the intensities measured with the 1/6°:1/2° slit combination by using the data in the overlapping angle regions. Moreover, the intensity data were corrected for the polarization and absorption due to the sample solution. The

** Present address: Idemitsu Kosan Co. Ltd., Sodegaura-machi, Kimitsu-gun, Chiba 292-01.

scaling to the absolute intensities was made by the conventional high angle region method comparing the data in the high angle region ($\theta>45°$) with the sum of the coherent scattering, and by the method proposed by Norman[11] and Krogh-Moe.[12]

The atomic scattering factors for Ni, Br, and O atoms were cited from Cromer and Waber's paper,[13] and for H atom from the International Tables;[14] the incoherent scattering factors for Ni, Br, and O atoms were obtained from Balyuzi[15] and for H atom from Compton and Allison.[16] The incoherent scattering factors were corrected for the Breit-Dirac effect.[17] The values of the anomalous dispersion for these atoms were taken from Cromer's paper.[18] The reduced intensities $i(s)$ due to the combinations of each pair of atoms were evaluated from the scaled intensities $I(s)$ in Eq. 1. In Eq. 1, s represents $4\pi\sin\theta/\lambda$

$$i(s) = I(s) - \sum_i n_i \cdot \{f_i(s)^2 + del(s) \cdot I_i^{inco}(s)\} \quad (1)$$

(λ=0.7107 Å), n_i the number of atoms i, $f_i(s)$ the atomic scattering factor corrected for the anomalous dispersion; $f_i(s)^2=(f_i^\circ(s)+\Delta f_i'(s))^2+(\Delta f_i'')^2$ where $\Delta f_i'$ and $\Delta f_i''$ is the real and imaginary parts of the anomalous dispersion, respectively; $del(s)$ is the fraction of the incoherent radiation $I_i^{inco}(s)$ reaching the counter,[19] and was determined by measuring the resolving power of the monochrometer with the use of a calcite single crystal.[20]

The radial distribution function $D(r)$ was calculated by Eq. 2:

$$D(r) = 4\pi r^2\rho_0 + \frac{2r}{\pi}\int_0^{s_{max}} s \cdot i(s) \cdot M(s) \cdot \sin(r \cdot s) ds, \quad (2)$$

where ρ_0, given in electron units, is the average scattering density of a sample solution, s_{max} (=15.3 Å) the maximum s value during the measurements; the modification function $M(s)$ given by Eq. 2′ was used in this study.

$$M(s) = \{\sum_i n_i \cdot f_i(0)^2 / \sum_i n_i \cdot f_i(s)^2\} \cdot \exp(-0.01 s^2) \quad (2')$$

In the calculated radial distribution curve a small spurious peak appears in the region less than 1 Å where no interatomic interactions besides the O–H interactions in water molecules could be expected to appear. Then the correction for this spurious peak was made with the Fourier inversion method by considering the contribution of the O–H interactions in water molecules.[21] The intensities due to the interatomic interactions were calculated by Eq. 3:

$$i(s)_{calcd} = \sum_i^{i\neq j}\sum_j n_{ij} \cdot f_i(s) \cdot f_j(s) \frac{\sin(r_{ij} \cdot s)}{r_{ij} \cdot s} \exp(-b_{ij} \cdot s^2), \quad (3)$$

where $f_i(s)$ and $f_j(s)$ denote the scattering factors of atom i and j, respectively, and r_{ij} the average distance between atom i and j, b_{ij} the temperature factor ($=\langle\Delta r_{ij}^2\rangle/2$; $\langle\Delta r_{ij}^2\rangle$ is the mean square amplitude of the molecular vibration), and n_{ij} the frequency factor that were refined to minimize the following function U by a least squares method.

$$U = \sum_{s_{min}}^{s_{max}} s^2 \cdot [i(s)_{obsd} - i(s)_{calcd}]^2 \quad (4)$$

In Eq. 4, s_{max} and s_{min} are the upper and lower limits in the selected s regions. Calculations were carried out on a TOSBAC ACOS-600 computer at our University and on a FACOM M-200 computer at Kyushu University; the KURVLR[19] and NLPLSQ[22] programs were used.

Results and Discussion

Both $D(r)$ and $D(r)-4\pi r^2\rho_0$ curves, shown in Figs. 1 and 2, exhibit four distinct peaks at 1.0, 2.1, 2.6, and 3.4 Å. As for the solution C, which is more diluted than the other solutions A and B, the peak at 2.6 Å is rather obscure, though the other three peaks are apparent. The distance of the first peak at 1.0 Å is consistent with that of the O–H bond in water molecules.[23] The second peak at 2.1 Å can be ascribed to the Ni–O interaction in the aqua complexes; a similar peak of the $D(r)$ curves has been reported to appear in the aqueous solutions of 2.491 mol dm^{-3} $Ni(ClO_4)_2$ at 2.04 Å,[22] of 4 mol dm^{-3} $NiCl_2$ at 2.06 Å,[2] and of 1 mol dm^{-3} $Ni(NO_3)_2$ at 2.06 Å.[24]

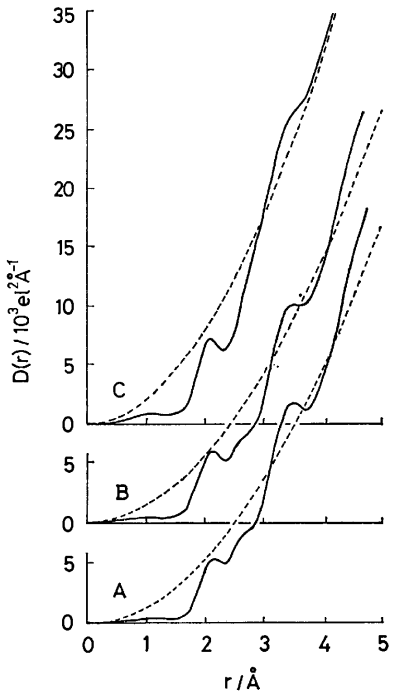

Fig. 1. Radial distribution curves $D(r)$ for the solutions A, B, and C; dashed line shows $4\pi r^2\rho_0$ curve.

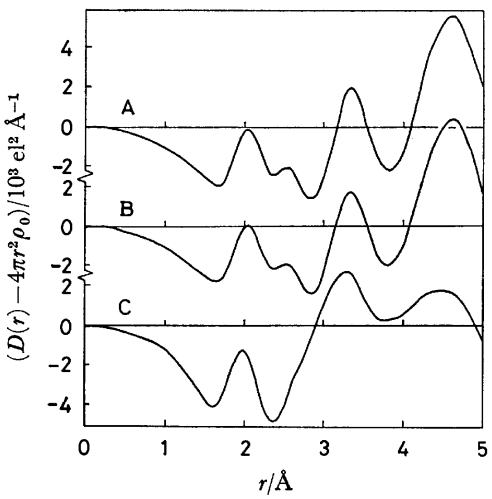

Fig. 2. $D(r)-4\pi r^2\rho_0$ curves for the solutions A, B, and C.

The peak at 2.6 Å may be attributed to the Ni–Br interaction, because the appearance of this peak is reflected by the concentration of $NiBr_2$ and the distance 2.6 Å is very close to the sum of the crystal radii of Ni^{2+} and Br^-, *i.e.* 2.65 Å {=0.83 Å (Ni^{2+})+1.82 Å (Br^-)}.[25] The solution equilibrium investigations indicated the formation of a monobromo complex. However, the formation constants β_1 were very small, ranging from 0.05 to 0.95.[26] By taking the datum β_1=0.05 reported by Libuś *et al.* for the aqueous 2 mol kg^{-1} $NiBr_2$ solution, the monobromo complex presented in our solution C is evaluated to be 16% of the total Ni^{2+} content.

The peak at 3.4 Å can be attributed to the Br–OH_2 interaction, because no comparable peak in this region on the radial distribution curve is observed for the aqueous 2.491 mol dm^{-3} $Ni(ClO_4)_2$ solution, while a clear peak due to the Br–OH_2 interaction is observed at 3.4 Å for the aqueous 2.5 mol kg^{-1} LiBr solution.[27]

On the basis of the above considerations, refinements of the numerical data on the interatomic distances, and frequency and temperature factors of these interactions have been made by the method of Eq. 4. The final data thus obtained are listed in Table 2. And Fig. 3 shows that the $s\cdot i(s)$ curves calculated from these final data are in good agreement with the observed $s\cdot i(s)$ curves in the region above $s>4$. Moreover, subtracting the calculated curve from the radial distribution curve gives a smooth curve indicating a good reliability of the final data, as seen in Figs. 4, 5, and 6.

Table 2. Refined parameters obtained from the reduced intensity curve

Interaction	Parameter	Solution A	Solution B	Solution C
Ni-O	*r*	2.04	2.05	2.04
	b	0.003	0.004	0.004
	n	5.40	5.46	5.73
Ni-Br	*r*	2.52	2.53	2.58
	b	0.007	0.008	0.008
	n	0.68	0.47	0.18

r, Bond distance, Å; *b*, temperature factor, $Å^2$; *n*, frequency factor.

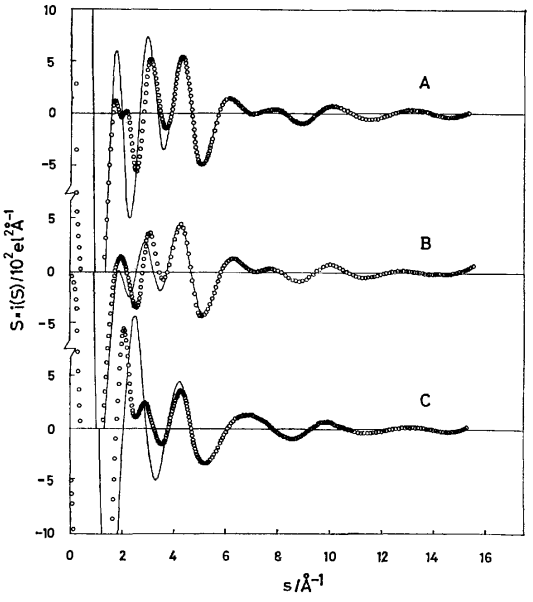

Fig. 3. The reduced intensities $i(s)$ multiplied by s for the solutions A, B, and C.
Observed $s\cdot i(s)$ curve, circles; calculated curve, solid line.

The bond distance of Ni–Br given in Table 2 indicates that the bromo complex is in the inner-sphere type of coordination. Moreover, as seen in the frequency factor, the molar ratio of the bromo complex *vs.* hexaaqua complex increases with an increase in the total $NiBr_2$ concentration. This tendency agrees with the prediction from the stability constant determined by Libuś and Kowalewska.[9] However, they interpreted their formation constant β_1=0.05 for the 2 mol kg^{-1} solution by proposing a monobromo complex with the outer-sphere type of coordination. In fact, on varying the concentration from 0.86 to 4.27 mol kg^{-1}, the ligand field absorption spectra of $NiBr_2$ aqueous solutions changed very little.[28]

For $NiCl_2$ in an aqueous 4 mol dm^{-3} solution, the X-ray investigation was made by Caminiti *et al.*[2] Though they concluded that no chloro complex was formed, a small shoulder is seen around 2.6 Å in their correlation function; this is ascribable to the Ni–Cl

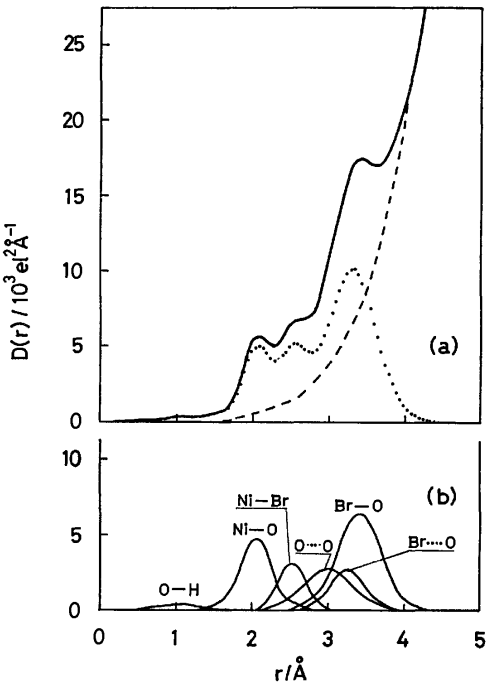

Fig. 4. (a) Radial distribution curve for the solution A. (b) Calculated peak shapes: the O–H interaction is in H_2O; the Ni–O and Ni–Br interactions, and the O···O and Br···O contacts are in $[NiBr(H_2O)_5]^+$; the O···O contact is in hydrogen bonded H_2O molecules; and the Br–O interaction is in $[Br(H_2O)_6]^-$. The O···O peak is composed of two interactions, *i.e.*, the O···O contact in $[NiBr(H_2O)_5]^+$, and the O···O contact in hydrogen bonded H_2O molecules.

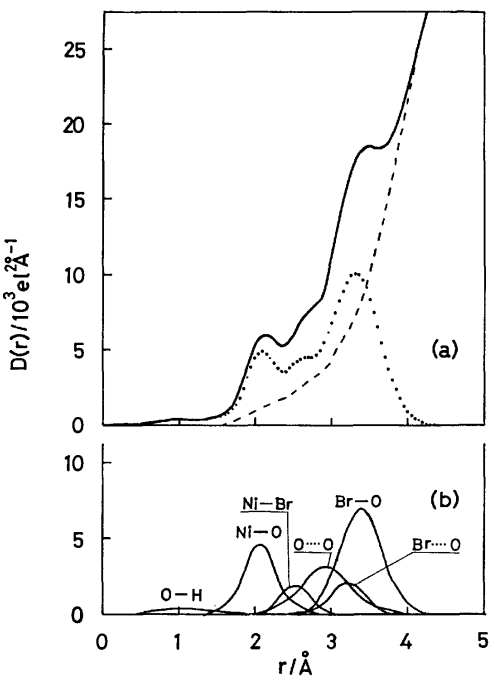

Fig. 5. (a) Radial distribution curve for the solution B. (b) Calculated peak shapes: the O–H interaction is in H_2O; the Ni–O and Ni–Br interactions, and the O···O and Br···O contacts are in $[NiBr(H_2O)_5]^+$; the O···O contact is in hydrogen bonded H_2O molecules; and the Br–O interaction is in $[Br(H_2O)_6]^-$. The O···O peak is composed of two interactions, *i.e.*, the O···O contact in $[NiBr(H_2O)_5]^+$, and the O···O contact in hydrogen bonded H_2O molecules.

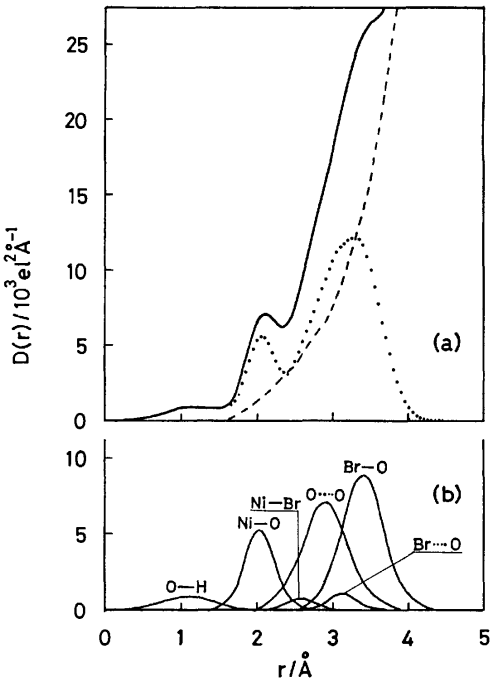

Fig. 6. (a) Radial distribution curve for the solution C. (b) Calculated peak shapes: the O–H interaction is in H_2O; the Ni–O and Ni–Br interactions, and the O···O and Br···O contacts are in $[NiBr(H_2O)_5]^+$; the O···O contact is in hydrogen bonded H_2O molecules; and the Br–O interaction is in $[Br(H_2O)_6]^-$. The O···O peak is composed of two interactions, *i.e.*, the O···O contact in $[NiBr(H_2O)_5]^+$, and the O···O contact in hydrogen bonded H_2O molecules.

interaction. Therefore, in our work the larger X-ray scattering factor of the bromine resulted in the appearance of a pronounced peak of the Ni–Br interaction in the radial distribution curve.

Table 2 shows that the refined data of the bond distance of Ni–Br, 2.52 Å, is smaller than the sum of their ionic radii, 2.65 Å as mentioned above, and is rather approximated by the sum of their covalent bond radii, 2.50 Å {=1.39 Å (Ni^{2+})+1.11 Å (Br^-)}.[29] The bond distance 2.05±0.01 Å of Ni–OH_2 in the bromoaqua complex falls in the same range with those 2.04—2.06 Å of the hexaqua complexes in the aqueous $Ni(ClO_4)_2$[22] and $NiCl_2$[2] solutions. And the temperature factors of the Ni–OH_2 bond in both bromoaqua and hexaaqua complexes are also similar.[22] The Ni–OH_2 distance of the aqua complexes in the solutions seems to be slightly shorter than that of the crystalline $NiCl_2 \cdot 6H_2O$ (2.10 Å).

References

1) J. Mizuno, *J. Phys. Soc. Jpn.*, **16**, 1574 (1961).
2) R. Caminiti, G. Licheri, G. Piccaluga, and G. Pinna, *Faraday Discuss. Chem. Soc.*, **1977**, 62.
3) A. K. Soper, G. W. Neilson, J. E. Enderby, and R. A. Howe, *J. Phys. C*, **10**, 1793 (1977).
4) P. Lagarde, A. Fontaine, D. Raoux, A. Sadoc, and P. Migliardo, *J. Chem. Phys.*, **72**, 3061 (1980).
5) D. R. Sandstrom, *J. Chem. Phys.*, **71**, 2381 (1979).
6) H. Weingärtner and H. G. Hertz, *J. Chem. Soc., Faraday Trans. 1*, **75**, 2700 (1979).
7) H. Weingärtner, C. Müller, and H. G. Hertz, *J. Chem. Soc., Faraday Trans. 1*, **75**, 2712 (1979).
8) Z. Libuś and H. Tialowska, *J. Solution Chem.*, **4**, 1001 (1975).
9) Z. Libuś and G. Kowalewska, *Pol. J. Chem.*, **52**, 709 (1978).
10) H. Ohtaki, M. Maeda, and S. Ito, *Bull. Chem. Soc. Jpn.*, **47**, 2217 (1974).
11) N. Norman, *Acta Crystallogr.*, **10**, 370 (1957).
12) J. Krogh-Moe, *Acta Crystallogr.*, **9**, 951 (1956).
13) D. T. Cromer and J. T. Waber, *Acta Crystallogr.*, **18**, 104 (1965).
14) "International Tables for X-Ray Crystallography," The Kynoch Press, Birmingham (1962), Vol. III, pp. 202—203.
15) H. H. M. Balyuzi, *Acta Crystallogr., Sect. A*, **31**, 600 (1975).
16) A. H. Compton and S. K. Allison, "X-Rays in Theory and Experiment," Van Nostrand, New York (1935).
17) S. Miyake, "X-Sen no Kaisetsu," Asakura Shoten, Tokyo (1969), p. 38.
18) D. T. Cromer, *Acta Crystallogr.*, **18**, 17 (1965).
19) G. Johansson and M. Sandström, *Chemica Scripta*, **4**, 195 (1973).
20) H. Wakita, M. Ichihashi, and I. Masuda, *Fukuoka Univ. Sci. Reports*, **10**, 95 (1980).
21) H. A. Levy, M. D. Danford, and A. H. Narten, "Data Collection and Evaluation with an X-Ray Diffractometer Designed for the Study of Liquid Structure," ORNL-3960 (1966).
22) H. Ohtaki, T. Yamaguchi, and M. Maeda, *Bull.*

Chem. Soc. Jpn., **49**, 701 (1976). The authors are grateful to Prof. H. Ohtaki for the use of this program.
23) A. H. Narten, "X-Ray Diffraction Data on Liquid Water in the Temperature Range 4 °C—200 °C," ORNL-4578 (1970).
24) W. Bol, G. J. A. Gerrits, and C. L. van Panthaleon van Eck, *J. Appl. Crystallogr.*, **3**, 486 (1970).
25) R. D. Shannon, *Acta Crystallogr., Sect. A*, **32**, 751 (1976).
26) L. G. Sillén and A. E. Martell, "Stability Constants," The Chemical Society, London (1964), Spec. Publ. No. 17, pp. 321—322.
27) R. M. Lawrence and R. F. Kruh, *J. Chem. Phys.*, **47**, 4758 (1967).
28) Z. Libus, W. Maciejiewski, and G. Kowaleswka, *Pol. J. Chem.*, **52**, 793 (1978).
29) "Kagaku-binran Kiso-hen II," ed by the Chemical Society of Japan, Maruzen, Tokyo (1966), p. 1266.

Preparation and Physicochemical Properties of New Linear μ-Oxo Bridged Ruthenium(IV) and Osmium(IV) Porphyrin Dimers

Hiroshi Sugimoto,* Teruaki Higashi, Masayasu Mori, Motoi Nagano,†
Zen-ichi Yoshida,† and Hisanobu Ogoshi*,††

Department of Chemistry, Faculty of Science, Osaka City University, Sugimoto, Sumiyoshi-ku, Osaka 558

† *Department of Synthetic Chemistry, Faculty of Engineering, Kyoto University, Yoshida, Sakyo-ku, Kyoto 606*

†† *Department of Material Science, Technological University of Nagaoka, Kamitomioka, Nagaoka 949-54*

(Received September 7, 1981)

μ-Oxo-bis[(hydroxo)(octaethylporphyrinato)ruthenium(IV)] was prepared by the oxidation of (carbonyl)-(octaethylporphyrinato)ruthenium(II) with *t*-butyl hydroperoxide in good yield. Facile replacement of the hydroxyl group with various anions afforded μ-oxo dimer complexes formulated as $[\{Ru^{IV}(oep)X\}_2O]$ (X= Cl, Br, and $OCOCH_3$). The same type of osmium complexes, $[\{Os^{IV}(oep)(OCH_3)\}_2O]$, $\{[Os^{IV}(oep)(OCH_3)\}$-$O\{Os^{IV}(oep)(OH)\}]$, and $[\{Os^{IV}(oep)(OH)\}_2O]$ were obtained from the air oxidation product of (carbonyl)-(methanol)(octaethylporphyrinato)osmium(II) in the presence of 2,3-dimethylindole. These complexes are diamagnetic. The ^1H NMR data are in conformity with the linear oxo-bridged dimer structure which was proved by X-ray crystallography with $[\{Ru^{IV}(oep)(OH)\}_2O]$. The redox potentials were measured by the cyclic voltammetry. These complexes showed three distinct quasi-reversible redox couples assignable to $metal^{II}$/$metal^{III}$, $metal^{III}$/$metal^{IV}$, and porphyrin ligand oxidation, respectively. Significantly lower redox values and anomalous spectral features indicate a strong pπ-dπ interaction between the bridging oxygen atom and the two quadrivalent metal ions.

Higher-valent metalloporphyrins such as quadrivalent iron porphyrins have attracted the attention of chemists in relation to the structure of catalases, horseradish peroxidases, and cytochrome c peroxidases in the redox process.[1] During the course of catalytic cycle of peroxidases, the reaction of the ferric enzyme with hydrogen peroxide and successive reduction with an electron generates the oxidized enzyme which was shown to involve an iron(IV) porphyrin moiety.[2,3] Ruthenium and osmium which have the same number of outer shell (d+s) electrons are considered to form metalloporphyrins analogues to those of iron porphyrins. Complexes of bivalent ruthenium[4] and osmium[5] have been investigated as plausible models for hemoproteins and heme enzymes. For the quadrivalent complex, only one complex of osmium, $[Os^{IV}(oep)(OCH_3)_2]$ has been reported by Buchler *et al.*,[6] and synthesis of ruthenium(IV) porphyrins has never been reported before to our knowledge. Through an investigation of the oxidation of indole derivatives with molecular oxygen catalyzed by various metalloporphyrins, we found that bivalent ruthenium and osmium porphyrins as catalysts were oxidized to quadrivalent complexes.[7,8] Our crystallographic study of the quadrivalent ruthenium complex showed a linear oxo-bridged dimer structure represented as $[\{Ru^{IV}(oep)(OH)\}_2O]$.[9] Moreover spectral data of quadrivalent osmium complexes indicate that they have the same structure. Here we wish to report the first synthesis and physicochemical properties of ruthenium(IV) and osmium(IV) porphyrins.

Experimental

Synthesis of Complexes. *μ-Oxo-bis[(hydroxo)(octaethylporphyrinato)ruthenium(IV)]*, $[\{Ru^{IV}(oep)(OH)\}_2O]$ ***(1)***: To a benzene solution (100 cm^3) of $[Ru^{II}(oep)CO]$ (100 mg)[10] was added 1 cm^3 of 70% aqueous *t*-butyl hydroperoxide. The reaction mixture was stirred at room temperature until the color of the solution turned from orange red to dark brown. After removal of the solvent under reduced pressure, the residual solid was chromatographed on an alumina gel with dichloromethane as an eluent. The purple green fraction was collected and evaporated to dryness. Crystallization of the resulting solid from benzene–petroleum ether afforded slightly hygroscopic dark red crystals (90 mg) in 87% yield. Found: C, 64.59; H, 6.90; N, 8.20%. Calcd for $C_{72}H_{90}N_8O_3Ru_2 \cdot H_2O$: C, 64.68; H, 6.93; N, 8.38%.

μ-Oxo-bis[(chloro)(octaethylporphyrinato)ruthenium(IV)], $[\{Ru^{IV}(oep)Cl\}_2O]$ ***(2)***: The dichloromethane solution (100 cm^3) of **1** was treated with 10% aqueous HCl. The mixture was stirred for 5 h. The solution was dried over anhydrous Na_2SO_4 and condensed to dryness by evaporation. Crystallization of the residual solid from dichloromethane–methanol gave purple crystals (86 mg) in 80% yield. Found: C, 63.51; H, 6.51; N, 8.26%. Calcd for $C_{72}H_{88}N_8Cl_2ORu_2$: C, 63.78; H, 6.54; N, 8.27%.

μ-Oxo-bis[(bromo)(octaethylporphyrinato)ruthenium(IV)], $[\{Ru^{IV}(oep)Br\}_2O]$ ***(3)***: The procedure similar to that descrived for the preparation of **2** by using aqueous HBr instead of HCl gave dark purple crystals of **3**i n 85% yield. Found: C, 59.79; H, 6.26; N, 7.71%. Calcd for $C_{72}H_{88}N_8Br_2ORu_2$: C, 59.85; H, 6.14; N, 7.76%.

μ-Oxo-bis[(aceta)(tooctaethylporphyrinato)ruthenium(IV)], $[\{Ru^{IV}(oep)(OCOCH_3)\}_2O]$ ***(4)***: The mixture of **1** (100 mg) in dichloromethane (100 cm^3) and 10% acetic acid (1 cm^3) was stirred until the color of the solution changed from purple green to green. The dichloromethane solution was washed with water and dried over anhydrous Na_2SO_4. The solution was condensed under reduced pressure to a small volume. Crystallization of the residue from dichloromethane–methanol containing trace amount of acetic acid gave purple red crystals (95 mg) in 90% yield. Found: C, 65.15; H, 7.03; N, 7.70%. Calcd for $C_{76}H_{94}N_8O_5Ru_2$: C, 65.05; H, 6.75; N, 7.99%.

μ-Oxo-bis[(methoxo)(octaethylporphyrinato)osmium(IV)], $[\{Os^{IV}(oep)(OCH_3)\}_2O]$ ***(5)***, μ-Oxo-*[(hydroxo)(octaethylporphyrinato)*-

osmium (IV)] [*(methoxo) (octaethylporphyrinatoosmium (IV)*], [{Os^{IV}(oep)(OH)}O{Os^{IV}(oep)(OCH_3)}], ***(6)***, *and* *μ-Oxo-bis[(hydroxo)(octaethylporphyrinato)osmium(IV)]*, [{Os^{IV}(oep)-(OH)}$_2$O] ***(7)***: To a dichloromethane solution (100 cm^3) of (carbonyl)(methanol)(octaethylporphyrinato) osmium(II) (100 mg)[5,6,11] was added 2,3-dimethylindole (100 mg). The mixture was stirred for about 24 h in air until the color of the solution turned from orange red to brown. After removal of solvent, the residue dissolved in benzene was adsorbed on the silica gel column and first eluted with benzene–acetone (9:1 vol/vol). The dark purple effluent was collected. After removal of solvent the residual solid was recrystallized from benzene to give **5** (30 mg) as dark purple crystals. Found: C, 58.12; H, 6.16; N, 7.46%. Calcd for $C_{74}H_{94}N_8O_3Os_2$: C, 58.32; H, 6.22; N, 7.46%. The dark brown second band was eluted with benzene–acetone (8:2 vol/vol). After removal of solvent the crude crystals obtained were recrystallized from benzene–acetone (1:1 vol/vol) to give 6 (30 mg) as dark purple crystals. Found: C, 58.23; H, 6.16; N, 7.30%. Calcd for $C_{73}H_{92}N_8O_3Os_2$: C, 58.06; H, 6.14; N, 7.42%. Finally the dark brown third band was eluted with benzene–acetone (7:3 vol/vol). After removal of solvent the residual solid was recrystallized from acetone to give **7** (25 mg) as dark purple crystals. Found: C, 56.15; H, 5.91; N, 7.31%. Calcd for $C_{72}H_{90}N_8O_3Os_2\cdot H_2O$: C, 56.45; H, 6.19; N, 7.31%.

Protonated forms of μ-oxo osmium(IV) complexes, *i.e.*, μ-hydroxo complexes were obtained according to the following procedure. To a dichloromethane solution (10 cm^3) of **5** (50 mg) was added 10% aqueous acid HX (1 cm^3, X=Cl and CF_3CO_2). After removal of solvents, the residual solid was recrystallized from benzene to afford purple red crystals.

[{Os^{IV}(oep)Cl}$_2$OH]Cl ***(8)***: Found: C, 55.24; H, 5.81; N, 7.10%. Calcd for $C_{72}H_{89}N_8OCl_3Os_2$: C, 55.49; H, 5.72; N, 7.14%.

[{Os^{IV}(oep)($OCOCF_3$)}$_2$OH]($OCOCF_3$) ***(9)***: Found: C, 51.89; H, 5.09; N, 6.39%. Calcd for $C_{78}H_{88}N_8O_7F_9Os_2$: C, 52.02; H, 4.93; N, 6.22%.

Molecular Weight Measurements. Molecular weights were measured at 31.5 °C in chloroform on a Knour vapor pressure osmometer.

Spectral Measurements. ^{1}H NMR spectra were obtained on a Varian HA-100D and JEOL HM-100 spectrometers. Infrared spectra were measured on Hitachi G-3 and JASCO DS-701G spectrophotometers. Absorption spectra were obtained on a Hitachi model 200-10 spectrophotometer.

Cyclic Voltammetry. Dichloromethane used as a solvent was dried and distilled before use. As a supporting electrolyte, tetrabutylammoium perchlorate (TBAP) was used after being subjected twice to crystallization from benzene. Cyclic voltammograms were obtained on a HA-104 potentiostat (Hokuto Denko) in combination with a HB-107A function generator. A three electrode system was used, consisting of platinum working and counter electrodes and a commercial saturated calomel electrode (SCE). The half-wave potentials were measured as that potential lying midway between the oxidation and reduction peaks for a given couple. Potentials are reported with respect to the saturated calomel electrode.

Results and Discussion

Synthesis. Oxidation of (carbonyl)(octaethylporphyrinato)ruthenium(II) by *t*-butyl hydroperoxide gave the hydroxo derivative **1** of the μ-oxo binuclear ruthenium(IV) porphyrin in a high yield, its axial hydroxyl group being readily replaced with various anions by the treatment with the respective acids. The action of the same oxidant upon (carbonyl)(methanol)(octaethylporphyrinato)osmium(II) gave sexivalent dioxo derivative, [Os^{VI}(oep)O_2] as reported by Buchler *et al.*[6] On the other hand, air oxidation of (carbonyl)-(methanol)(octaethylporphyrinato)osmium(II) in the presence of 2,3-dimethylindole gave three quadrivalent complexes **5**, **6**, and **7**,[8] which could be separated by the chromatography on a silica gel. Thus a sort of peroxide derivative generated *in situ*[7] from 2,3-dimethylindole/air system oxidizes the bivalent complex only to the quadrivalent complex. The bivalent ruthenium complex was also oxidized to the quadrivalent one by this system in good yield.

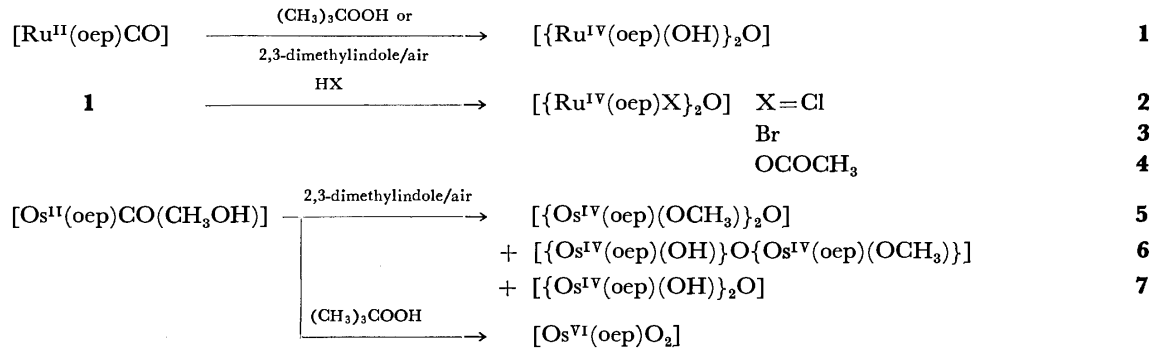

Molecular weight measurements indicate that all of the complexes of Ru(IV) and Os(IV) thus obtained contain two metalloporphyrin moieties.

Molecular weights and infrared, ^{1}H NMR, and absorption spectra are summarized in Table 1.

^{1}H NMR Spectra. All of the binuclear Ru(IV) and Os(IV) complexes obtained in this study are diamagnetic both in solid and solution states,[12] molar susceptibility of **1** in polycrystalline state being $\chi_M = -8.63\times10^{-6}$ cgs emu at 30 °C. ^{1}H NMR spectra of these complexes showed usual diamagnetic spectra.[13] As listed in Table 1, the characteristic features that are common to all of the complexes are the chemical shifts of the meso protons and the coupling pattern of the α-methylene protons of the pheripheral ethyl groups.

The signals for the meso protons of the binuclear ruthenium and osmium complexes appear at higher magnetic field by about 0.5—1.0 ppm than those in monomeric ruthenium(II) and osmium(II) porphy-

Table 1. Molecular weights, IR, absorption maxima and ^{1}H NMR chemical shifts of ruthenium(IV) and osmium(IV) μ-oxo bridged dimers

Compound	Molecular weight Calcd (Found)	IR ν/cm^{-1}	Absorption maxima λ_{max}/nm (log ε) in CH_2Cl_2	^{1}H NMR (δ from TMS in $CDCl_3$) Meso	α-CH_2	β-CH_3	Axial ligand
1	1316 (1270)	3606[a]	377 (5.30) 512 (4.12) 580 (4.32)	9.15	4.18	1.84	−4.20(OH)
2	1355 (1350)		384 (5.40) 500 (4.10) 690 (4.01)	9.29	4.18	1.88	
3	1444 (1450)		387 (5.41) 500 (4.00) 717 (4.08)	9.08	4.06	1.84	
4	1412 (1430)	1659[a] 1255	378 (5.42) 510 (4.03) 667 (4.02)	9.30	4.20	1.87	−3.70($OCOCH_3$)
5	1524 (1520)	2785[b] 1010 525	353 (4.87) 380 sh (4.77) 460 sh (3.97) 500 (3.87) 610 (3.79) 713 (3.56)	9.22 9.42[c]	4.21 4.12	1.82 1.82	−3.54(OCH_3) −4.36(OCH_3)
6	1510 (1500)	2785[b] 1010 3602 863 525 575	351 (4.88) 380 sh (4.72) 470 (3.96) 495 (3.88) 597 (3.77) 695 (3.57)	9.02, 8.98 9.31[c]	4.08 4.04	1.77 1.80	−3.52(OCH_3) −3.5(br OH) −4.48(OCH_3)
7	1496 (1480)	3598[b] 860 575	355 (4.87) 380 sh (4.76) 470 sh (3.96) 490 (3.86) 588 (3.76) 680 (3.56)	9.00	4.06	1.78	−3.4(br OH)
8	1801 (1820)	1715 1170	363 (5.07) 493 sh (3.82) 547 (4.00) 600 (3.87)	9.24	4.10	1.80	
9	1569 (1600)		358 (5.00)[d] 488 (3.87) 553 (4.00) 599 (3.88)				

a) In CCl_4. b) KBr. c) In the presence of 1% CF_3CO_2D. d) In methanol. sh; Shoulder, br; broad.

rins,[10,11] The X-ray crystallography[9] for **1** showed that it is a μ-oxo binulear porphyrinato complex of ruthenium(IV) and that the interplaner distance between the mean planes of the porphyrinato cores is 3.17 Å. The up-field shifts of the meso proton signals are, therefore, explained in terms of the mutual ring current effect in the dimeric complex. It is thus most likely suggested that ruthenium(IV) and osmium(IV) complexes **1**—**7** all have the linear μ-oxo bridged dimer structure.[9] The meso proton signals of mixed ligand complex **6** appear reasonably at 9.02 and 8.98 ppm as two singlets.

Another characteristic ^{1}H NMR feature of the present complexes that suggests the μ-oxo dimer structure is the coupling pattern of the peripheral α-methylene protons. As shown in Fig. 1, all of these complexes showed the ABX_3 coupling pattern which could be analyzed with the aid of the decoupling method. Diastereotopism of the α-methylene protons of ethyl group is due to the different magnetic circumstances above and below the porphyrinato plane. The complicated pattern of the α-methylene signals has been reported for some metalloporphyrins.[14,15] Splitting of the proton signal of α-methylene group in octaethylporphyrin is attributed to out-of-plane central ion or asymmetric axial ligation. The ruthenium atom

in **1** was found to be displaced only 0.03 Å off the plane defined by the four porphyrinato nitrogen atoms.[9] The eight ethyl groups are oriented outside so as to avoid steric constraint between the peripheral ethyl groups of the two porphyrinato cores. Therefore, the hindered rotation of the ethyl group causes the nonequivalence of the α-methylene in the different magnetic atmosphere due to asymmetric ligation.

The proton of the axial ligands OH and $OCOCH_3$ for the ruthenium complexes **1** and **4** resonated at −4.20 and −3.70 ppm respectively as sharp singlets. Methoxyl protons for osmium complexes **5** and **6** appeared at −3.70 and −3.54 ppm, respectively, also as sharp singlets. These anomalous high-field shifts of the proton signal of the axial ligand can be described by a large shielding effect of the ring current in the near proximity of the metal ion. It is noteworthy that the axial hydroxyl protons for the osmium complexes **6** and **7** resonated at about −3.5 ppm as much broader signals compared with those of ruthenium complexes. Such broadening of the signals indicates a more dissociable nature of the proton of the axial hydroxyl group, and suggests lower electron density on the axial oxygen atom in the osmium complex. On the other hand, electronic and ^1H NMR spectra of these binuclear osmium(IV) complexes in the presence of acids show that their bridging oxygen atoms have certain tendency to be protonated while those of similar ruthenium(IV) complexes do not. This suggests higher electron density on the bridging oxygen of the osmium complexes. These problems will be described more fully under a separate section.

IR, VIS, and UV Absorption Spectra. Infrared spectra of **1**, **6**, and **7** showed sharp bands at 3606 (in CCl_4), 3602 (KBr), and 3598 (KBr) cm^{-1}, respectively, assignable to the stretching vibration (ν_{O-H}) of the axial hydroxyl group.[16] Two absorption peaks at 1659 and 1225 cm^{-1} for **4** are due to $\nu_{C=O}$ and ν_{C-O} of the axial acetoxyl group.[16] Three absorption bands at 2785, 1010, and 525 cm^{-1} for **5** and those at similar positions for **6** are due to the axial methoxide ligands.[6]

Data of VIS and UV absorption spectra are given in Table 1. The Soret bands of the binuclear Ru(IV) and Os(IV) complexes are observed at 373—387 and 351—355 nm, respectively, which are considerably in the shorter wave length region than those of the respective bivalent metalloporphyrins,[10] in conformity with the usual empirical rule.

The general features of the absorption spectra of these binuclear complexes at the longer wave length region are considerably different from those of usual porphyrin complexes as shown in Figs. 1 and 2. Since the absorption spectrum of monomeric quadrivalent complex, $[Os^{IV}(oep)(OCH_3)_2]$ has only normal α and β bands at 530 and 497 nm in this region,[6] the band appearing at 550—800 nm of the present osmium(IV) complexes are considered to be the characteristics of the oxo-bridged dimer structure. The same is probably true with the binuclear Ru(IV) complexes, although no mononuclear Ru(IV) porphyrins have been reported to date.

A number of chemically well defined dimeric and oligomeric halogen complexes of ruthenium[17] and osmium[18] are known having a μ-oxo bridging link between halogeno-metal moieties. These complexes exhibit anomalous light absorption mainly in the longer wave length region, which is probably of the similar nature to those of the present complexes. This, as well as other anomalous physical and chemical properties of these series of μ-oxo halogeno complexes have been successfully interpreted using an MO scheme.[17a] Such scheme presupposes a strong electronic coupling between the halogeno-metal moieties and even leads to a sort of a new chemical system. The present complexes seem to be in a more or less similar situation. The above-mentioned absorption peaks appearing at 550—800 nm that characterize such anomalous features of the spectra of these binuclear complexes are sensitive to the kind of the axial ligand. They probably have main contribution from the charge

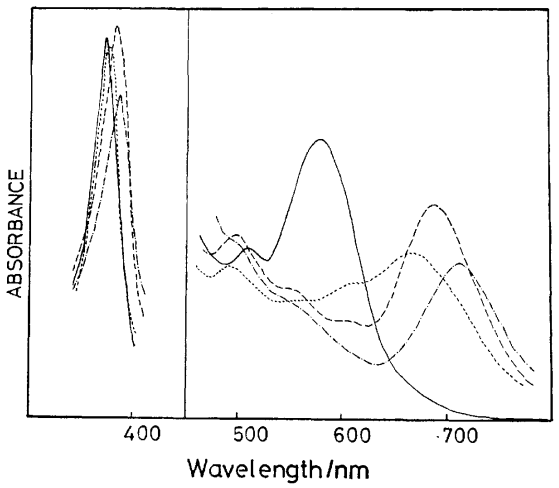

Fig. 1. Absorption spectra of the μ-oxo bridged ruthenium(IV) dimers in CH_2Cl_2.
——: $[\{Ru^{IV}(oep)(OH)\}_2O]$, ·····: $[\{Ru^{IV}(oep)(OCOCH_3)\}_2O]$, — —: $[\{Ru^{IV}(oep)Cl\}_2O]$, and -·-·: $[\{Ru^{IV}(oep)Br\}_2O]$.

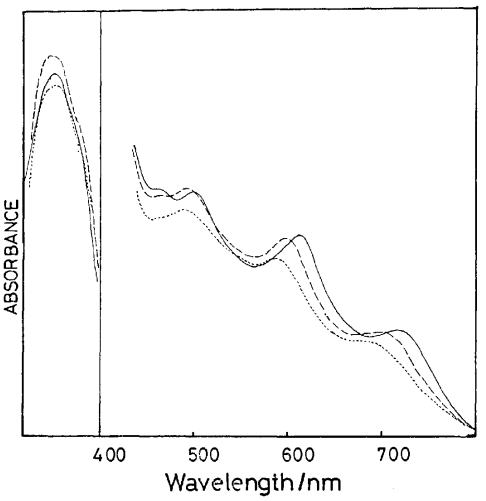

Fig. 2. Absorption spectra of the μ-oxo bridged osmium(IV) dimers in CH_2Cl_2.
——: $[\{Os^{IV}(oep)(OCH_3)\}_2O]$, — —: $[\{Os^{IV}(oep)(OH)\}O\{Os^{IV}(oep)(OCH_3)\}]$, ·····: $[\{Os^{IV}(oep)(OCH_3)\}_2O]$.

transfer of the type $a_{1u},a_{2u}(p\pi)\rightarrow e_g(d_{xz},d_{yz})$. The excitation energy of the transition was in the order OH> $OCOCH_3$>Cl>Br of the axial ligand of the ruthenium complexes, and $(OH)_2>(OH)(OCH_3)>(OCH_3)_2$ of those of osmium complexes. This trend seems to reflect the extent of an interaction between $p\pi$ orbitals of the axial ligand and $d\pi$ orbitals of the metal ions.

Behavior of μ-Oxo Binuclear Complexes toward Acids. As has been described previously, action of acids upon complex **1** replaces the axial hydroxyl group with the respective acid groups to give **2**, **3**, and **4**, leaving μ-oxo group unchanged. Such a change could be followed by observing the change of the absorption spectrum of **1** upon addition, *e.g.*, of aqueous HCl; no more spectral change was observed in the presence of excess amount of acids. Complexes **2**, **3**, and **4** readily regenerate **1**, *e.g.*, by simple column chromatography of them on alumina, due to reverse reaction with trace amount of water on the gel.

The behaviors of the μ-oxo bridged osmium complexes toward acids are considerably different. Treatment of these complexes with acids seems to protonate the bridged oxygen first as evidenced by electronic and ^{1}H NMR spectra. Thus, the absorption spectra of the osmium complexes vary largely with the addition of acids finally to give the same spectra *independent of* the kind of acids. The ^{1}H NMR spectrum of the osmium complex **5** in the presence of 1% CF_3CO_2D is illustrated in Fig. 3. By the addition of trifluoroacetic acid, the meso protons are slightly shifted toward lower magnetic field and the geminal coupling constant of the ABX_3 pattern for α-methylene protons becomes a little smaller. It is noteworthy that the axial methoxide protons are shifted toward higher magnetic field without decrease in the intensity or broadening of the signal. These results indicate that the protonation occurs not on the axial oxygen atom but on the bridged oxygen atom, because if the protonation occured on the oxygen of the axial methoxide, the positive charge on the oxygen would be increased and the methoxyl protons should rather be shifted toward lower magnetic field. However an attempt to isolate the protonated species, $[\{Os^{IV}(oep)(OCH_3)\}_2OH]^+X^-$ only gave the complexes $[\{Os^{IV}(oep)X\}_2OH]^+X^-$ (X=Cl, and CF_3CO_2), respectively, in which methoxyl group were replaced by the chloro and trifluoroacetato groups. Treatment of **8** and **9** with aqueous alkali not only deprives it of the proton from the hydroxyl bridge but also causes hydrolysis resulting

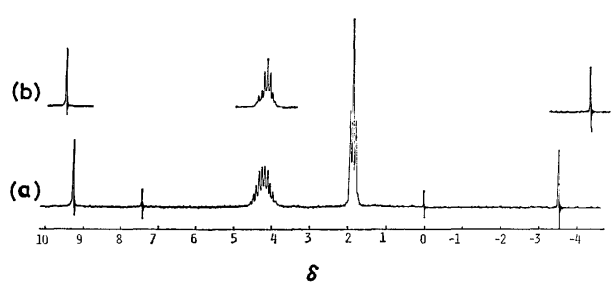

Fig. 3. The ^{1}H NMR spectra of $[\{Os^{IV}(oep)(OCH_3)\}_2O]$ in (a) $CDCl_3$ and (b) $CDCl_3$ containing 1% CF_3CO_2D.

$$[\{Os^{IV}(oep)(OCH_3)\}_2O] \xrightarrow{HX} [\{Os^{IV}(oep)(OCH_3)\}_2OH]^+X^- \xrightarrow{HX} [\{Os^{IV}(oep)X\}_2OH]^+X^-$$

X=Cl **8**

CF_3CO_2 **9**

in the replacement of the axial acid groups by the hydroxyl group. This has so far prevented the authors from obtaining oxo-bridged osmium(IV) complexes having acidic axial ligands comparable to ruthenium complexes **2**, **3**, and **4**.

As shown in Fig. 4, the Soret band for the μ-oxo osmium complexes was shifted to 359 nm and became sharp by the protonation. The charge transfer bands also were largely affected, and absorption at around 700 nm disappeared. The same spectral changes were observed in the presence of other acids such as HCl, HBr, and $HClO_4$. The absorption spectra of complexes **8** and **9** also show similar spectra. This kind of spectrum is, therefore, considered to be characteristic of the species protonated at the bridging oxygen atom represented as $[\{Os^{IV}(oep)(OCH_3)\}_2OH]^+$. The lack of the absorption near 700 nm may be due to the decrease of the interaction between two metalloporphyrins through bridged oxygen caused by the protonation to the oxygen atom. Moreover the same characteristic absorption spectrum could be also observed in the presence of silver perchlorate instead of protons. This means that the silver ion can also react with the bridged oxygen as a Lewis acid, although the adduct of silver perchlorate could not be isolated as analytically pure crystals.

In order to understand the different behavior toward acids between ruthenium(IV) and osmium(IV) complexes in spite of having similar molecular structures, it seems helpful to consider the following canonical structures. The behavior toward acids and ^{1}H NMR data for osmium(IV) complexes indicate considerable contribution of structure (C). Canonical structure (C) points to an easy dissociation of axial hydroxyl protons

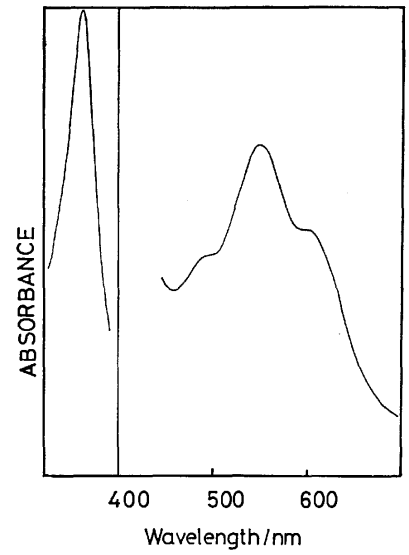

Fig. 4. Absorption spectra of $[\{Os^{IV}(oep)(OCH_3)\}_2O]$ in CH_2Cl_2 containing 1% CF_3CO_2H.

$$HO^- \underset{(A)}{[M{=}\overset{2+}{O}{=}M]} OH^- \leftrightarrow \underset{(B)}{HO\text{-}M\text{-}O\text{-}M\text{-}OH}$$
$$\leftrightarrow H^+ \underset{(C)}{[O{=}M\text{-}\overset{2-}{O}\text{-}M{=}O]} H^+$$

and high affinity of proton toward the bridged oxygen. On the other hand, experimental results for ruthenium(IV) complexes suggest that the more important contribution here is rather structure (A) predicting the easy replacement of axial hydroxyl group and low affinity of proton toward bridged oxygen atom. For a more detailed and quantitative discussion, a theoretical treatment involving the molecular orbital calculations seems to be indispensable.

Electrochemistry. The redox behavior of Ru(IV) and Os(IV) metalloporphyrins seems to form one of the most interesting facets of their chemistry especially from the biological point of view. Unless very accurate data are required, necessary information can be obtained simply from cyclic voltammetry. All of these complexes show three distinct quasi-reversible redox couples (Eo1, Eo2, and Eo3) as shown in Fig. 5, and half-wave potentials estimated therefrom are listed in Table 2. The number of electron concerned in each couple was determined to be about 2 by the controlled coulometry,[19] which means that two metal atoms or porphyrin ligands in a molecule are oxidized and reduced at the same time. In connection with the existing data especially of osmium porphyrins, these three redox couples of both ruthenium and osmium complexes seem to be assignable to metal^{II}/metal^{III}, metal^{III}/metal^{IV}, and to porphyrin ring oxidation, respectively.[20,21] The assignment of Eo3 to the porphyrin ring oxidation is also confirmed by the fact that the redox couple is almost insensitive to the difference of both metal and axial ligand.[20] It is noteworthy that although the redox couple Ru^{II}/Ru^{III} has been confirmed electrochemically for [Ru^{II}(porphyrin)(pyridine)$_2$],[21] the redox couple Ru^{III}/Ru^{IV} has never been observed before, probably because the latter is more positive than that of porphyrin ring oxidation. Appearance of the Ru^{III}/Ru^{IV} in the present complex at a potential lower than that of the ring oxidation, thus, proves the marked stabilization of Ru^{IV} caused by the formation of the linear Ru–O–Ru system in conformity with the successful isolation of Ru(IV) complexes only in the form of oxo-bridged dimers. Here, strong electron-donating ability of the μ-oxo (O^{2-}) ligand probably plays an important role. The Ru^{III}/Ru^{IV} couple of complex **1** having axial hydroxyl groups is somewhat more negative than those of halogeno derivatives **2** and **3**. This means that the electron donation from the axial ligand, which also contributes to the lowering of the Ru^{III}/Ru^{IV} couple is larger in the former.

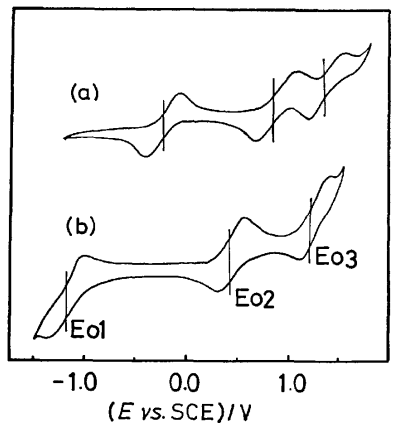

Fig. 5. Cyclic voltammograms of (a) [{Ru^{IV}(oep)Cl}$_2$O], and (b) [{Os^{IV}(oep)(OCH$_3$)}$_2$O] in CH_2Cl_2–TBAP.

Table 2. The half-wave potentials of ruthenium(IV) and osmium(IV) μ-oxo bridged dimer complexes (V *vs.* SCE)

Compound	Eo1	Eo2	Eo3
[{Ru^{IV}(oep)(OH)}$_2$O]	−0.82	+0.68	+1.18
[{Ru^{IV}(oep)Cl}$_2$O]	−0.24	+0.85	+1.32
[{Ru^{IV}(oep)Br}$_2$O]	−0.22	+0.84	+1.30
[{Os^{IV}(oep)(OCH$_3$)}$_2$O]	−1.18	+0.41	+1.20
[{Os^{IV}(oep)(OH)}O-{Os^{IV}(oep)(OCH$_3$)}]	−1.13	+0.40	+1.22
[{Os^{IV}(oep)(OH)}$_2$O]	−1.12	+0.37	+1.23

Formation of the μ-oxo bridges, of course, lowers the redox values of Os^{III}/Os^{IV} and Os^{II}/Os^{III} also. Their redox values for [Os^{II}(oep)(1-methylimidazole)$_2$] were recently reported to be 0.61 and −0.63 V, which are considerably more positive than the values of around 0.4 and −1.1 V for the present osmium dimer complexes. The influence of the protonation to the bridging oxygen on the redox values was also investigated. Figure 6 shows that in the presence of 1% CF_3CO_2H only the redox couple Eo2 was specifically shifted toward positive region by about 0.5 volt. Unfortunately the redox couple Eo1 was completely concealed by the large back ground current due to the presence of trifluoroacetic acid. These results indicate that the protonation on the bridged oxygen considerably decreases the electron donation from the bridged oxygen to the central metals. The redox values for Eo1 and Eo2 of osmium complexes are almost insensitive to the axial ligands, so that the interaction between the metals and the axial ligands acting as electron donors is considered to occur to about the same

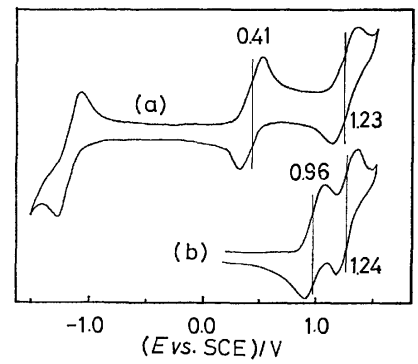

Fig. 6. Cyclic voltammograms of [{Os^{IV}(oep)(OCH$_3$)}$_2$O] in (a) CH_2Cl_2 and (b) CH_2Cl_2 containing of 1% CF_3CO_2H.

extent.

Tervalent iron porphyrins form μ-oxo bridged dimer complexes represented as $[\{Fe^{III}(porphyrin)\}_2O]$.[22] Phillippi and Goff reported[23] that electrochemical oxidation of $[\{Fe^{III}(tetraphenylporphyrin)\}_2O]$ gave both one-electron oxidized ($[Fe^{III}-O-Fe^{IV}]^+$) and two-electron oxidized ($[Fe^{IV}-O-Fe^{IV}]^{2+}$) species at 0.79 and 1.03 V, respectively. This behavior of the iron complex is different from that of ruthenium and osmium complexes, because in ruthenium and osmium binuclear complexes two metal atoms are oxidized at the same time as discussed above. The different redox behavior of the iron complex might be explained in terms of weaker interaction between two metalloporphyrin moieties through bridged oxygen. In fact, X-ray crystallography revealed that the Fe–O–Fe group is not completely linear.[22] Moreover there is still a major question concerning oxidation of the iron complexes, that is, whether electron abstraction occurs formally from the metal (ferryl iron) or from ligand (porphyrin radical).[3c,24]

The present work was partially supported by a Grant-in-Aid for Scientific Research from the Ministry of Education, Science and Culture.

References

1) P. Gerge, *Biochem. J.*, **55**, 220 (1953); A. S. Brill, *Comp. Biochem.*, **14**, 447 (1966); T. Iizuka, M. Kotani, and T. Yonetani, *Biochem. Biophys. Acta*, **167**, 257 (1968); T. H. Moss, A. Ehrenberg, and A. J. Bearden, *Biochemistry*, **8**, 4159 (1969); G. Lang, *Quart. Rev. Biophys.*, **3**, 1 (1970).

2) I. A. Cohen, *Struct. Bonding (Berlin)*, **40**, 1 (1981); H. B. Dunford and J. S. Stillman, *Coord. Chem. Rev.*, **19**, 187 (1976); T. Yonetani, *Adv. Enzymol. Relat. Areas Mol. Biol.*, **33**, 309 (1970); I. Yamasaki, "Molecular Mechanisms of Oxygen Activation," ed by O. Hayaishi, Academic Press, New York (1974), p. 535; T. Yonetani, and A. F. W. Coulson, *Biochemistry*, **14**, 2389 (1975); T. Yonetani, H. Schleyer, and A. Ehrenberg. *J. Biol. Chem.*, **241**, 3240 (1966); H. Yamada, and I. Yamasaki, *Arch. Biochem. Biophys.*, **165**, 728 (1974); P. Jones, and H. B. J. Dunfoed, *J. Theoret. Biol.*, **69**, 457 (1977).

3) a) D. Dolphin, A. Forman, D. C. Borg, J. Fajer, and R. H. Felton, *Proc. Natl. Acad. Sci. U.S.A.*, **68**, 614 (1971); D. Dolphin, Z. Muljiani, K. Rousseau, D. C. Borg, J. Fajer, and R. H. Felton, *Ann. N. Y. Acad. Sci.*, **206**, 177 (1973); c) R. H. Felton, G. S. Owen, D. Dolphin, A. Forman, D. C. Borg, and J. Fajer, *ibid*, **206**, 504 (1973); d) D. Dolphin, R. H. Felton, *Acc. Chem. Res.*, **7**, 26 (1974); e) D. Dolphin, T. Niem, R. H. Felton, and S. Fujita, *J. Am. Chem. Soc.*, **97**, 5288 (1975); f) E. G. Johnson, T. Niem, and D, Dolphin, *Can. J. Chem.*, **56**, 1381 (1978).

4) N. Farrell, D. Dolphin, and B. R. James, *J. Am. Chem. Soc.*, **100**, 324 (1978); H. Ogoshi, H. Sugimoto, and Z. Yoshida, *Bull. Chem. Soc. Jpn.*, **51**, 2369 (1978); D. R. Paulson, A. W. Addison, D. Dolphin, and B. R. James, *J. Biol. Chem.*, **254**, 7002 (1979).

5) J. W. Buchler and P. D. Smith, *Angew. Chem., Int. Ed. Engl.*, **13**, 745 (1974); A. Antipas, J. W. Buchler, M. Gouterman, and P. D. Smith, *J. Am. Chem. Soc.*, **100**, 3015 (1978); J. W. Buchler, W. Kokisch, and P. D. Smith, *Struct. Bonding (Berlin)*, **34**, 79 (1978).

6) J. W. Buchler and P. D. Smith, *Chem. Ber.*, **109**, 1465 (1976).

7) Z. Yoshida, H. Sugimoto, and H. Ogoshi, "Biomimetic Chemistry," ed by D. Dolphin, C. Mckenna, Y. Murakami, and I. Tabushi, American Chemical Society, Washington (1980), Chap. 17.

8) H. Sugimoto and M. Mori, *Chem. Lett.*, **1981**, 297.

9) H. Masuda, T. Taga, K. Osaki, H. Sugimoto, M. Mori, and H. Ogoshi, *J. Am. Chem. Soc.*, **103**, 2199 (1981).

10) G. W. Sovocool, F. R. Hopf, and D. G. Whitten, *J. Am. Chem. Soc.*, **94**, 4350 (1972); T. S. Srivastava, L. Hoffman, and M. Tsutsui, *ibid.*, **94**, 1385 (1972); M. Tsutsui, D. Ostfeld, J. N. Francis, and L. M. Hofman, *J. Coord. Chem.*, **1**, 115 (1971); S. S. Eaton, G. R. Eaton, and R. H. Holm, *J. Organomet. Chem.*, **39**, 179 (1972); J. J. Bonnet, S. S. Eaton, G. R. Eaton, R. H. Holm, and J. A. Ibers, *J. Am. Chem. Soc.*, **95**, 2141 (1973); B. C. Chow and I. A. Cohen, *Bioinorg. Chem.*, **1**, 57 (1971); R. G. Little and J. A. Ibers, *J. Am. Chem. Soc.*, **95**, 8583 (1973).

11) J. W. Buchler and K. Rohbock, *J. Organomet. Chem.*, **65**, 223 (1974).

12) Effective magnetic moments were measured by Evans method in chloroform at 31.5 °C. D. F. Evans, *J. Chem. Soc.*, **1959**, 2003.

13) "The Porphyrins," ed by D. Dolphin, Academic Press, New York (1979), Vol. IV, Chap. 1.

14) H. Scheer, Jr., and J. J. Katz, "Porphyrins and Metalloporphyrins," ed by K. M. Smith, Elsevier, Amsterdam (1975), Chap. 10.

15) R. J. Abraham and K. Smith, *Tetrahedron Lett.*, **1971**, 3335.

16) K. Nakamoto, "Infrared and Raman Spectra of Inorganic and Coordination Compounds," John Wiley and Sons, New York (1977).

17) a) J. D. Dunitz and J. E. Orgel, *J. Chem. Soc.*, **1953**, 2594; b) T. R. Weaver, T. J. Meyer, S. Adeyemi, G. M. Brown, R. P. Eckberg, W. E. Hatfield, E. C. Johnson, R. W. Murray, and D. Untereker, *J. Am. Chem. Soc.*, **97**, 3039 (1975); c) J. E. Earley and T. Fearley, *Inorg. Chem.*, **12**, 323 (1973); d) A. Spencer and G. Wilkinson, *J. Chem. Soc., Dalton Trans.*, **1973**, 1570; e) J. A. Braumann, D. J. Salmon, S. T. Wilson, T. J. Meyer, and W. E. Hatfield, *Inorg. Chem.*, **17**, 3342 (1978); f) J. A. Baumann and T. J. Meyer, *ibid.*, **19**, 345 (1980).

18) K. F. Tebbe and H. G. von Schlering, *Z. Anorg. Allg, Chem.*, **396**, 66 (1973); J. S. Filippo, Jr., R. L. Grayson, and H. J. Sniadoch, *Inorg. Chem.*, **15**, 269 (1976); J. S. Filippo, Jr., P. J. Fagan, and F. J. Disalvo, *ibid.*, **16**, 1016 (1977).

19) Values of n, where n is the number of moles of electrons transferred per mole of complex in an exaustive electrolysis at constant potential, were calculated after measuring the total area under current *vs.* time curves for complete electrolysis. Reactions were judged to be complete when the current had fallen below 1% of its initial value.

20) "The Porphyrins," ed by D. Dolphin, Academic Press, New York (1979), Vol. V, Chap. 1—4.

21) G. M. Brown, F. R. Hopf, J. A. Ferguson, T. G. Meyer, and D. G. Whitten, *J. Am. Chem. Soc.*, **95**, 5939 (1973); G. M. Brown, F. R. Hopf, T. J. Meyer, and D. G. Whitten, *ibid*, **97**, 5385 (1975).

22) E. B. Fleischer and T. S. Srivastava, *J. Am. Chem. Soc.*, **91**, 2403 (1969); A. B. Hoffman, D. M. Collins, V. W. Day, E. B. Fleischer, T. S. Srivastava, and J. L. Hoard, *ibid*, **94**, 3620 (1972).

23) M. A. Phillippi and H. M. Goff, *J. Am. Chem. Soc.*, **101**, 7641 (1979).

24) R. H. Felton, G. S. Owen, D. Dolphin, and J. Fajer, *J. Am. Chem. Soc.*, **93**, 6332 (1971); L. A. Bottomley, and K. M. Kadish, *Inorg. Chem.*, **20**, 1348 (1981).

 © 1982 The Chemical Society of Japan Bull. Chem. Soc. Jpn., 55, 829—832 (1982)

Chemistry of Chiral Vitamin B_6 Analogs. IV. Syntheses of Chiral Pyridoxal and Pyridoxamine Analogs Having a Branched "Ansa Chain" between 2′- and 5′-Positions

Makoto Ando,* Yoji Tachibana, and Hiroyoshi Kuzuhara
The Institute of Physical and Chemical Research, Wako, Saitama 351
(Received June 13, 1981)

Racemic 15-formyl-14-hydroxy-5,5-dimethyl-2,8-dithia[9](2,5)pyridinophane (**4**), an analog of pyridoxal having a branched "ansa chain" between 2′- and 5′-positions, was synthesized from 2,5-bis(chloromethyl)-3-hydroxy-*O*,*O*′-isopropylidene-4-pyridinemethanol. Optical resolution of **4** was achieved *via* the formation of Schiff base with 3-amino-3-deoxy-1,2:5,6-di-*O*-isopropylidene-D-glucofranose, giving the levorotary enantiomer of **4** (**4a**). Racemic 15-aminomethyl-14-hydroxy-5,5-dimethyl-2,8-dithia[9](2,5)pyridinophane (**5**), the same type of pyridoxamine analog as **4**, and its levorotary enantiomer were synthesized from the corresponding **4** and **4a**. Both levorotary and dextrorotary enantiomers of **5** were also obtained by the optical resolution of the racemate *via* the formation of chiral dibenzoyltartaric acid salts of **5**.

In the course of our study on mimics of vitamin B_6-dependent enzymes, we have prepared a new type of chiral analogs of pyridoxal (**1**),[1] pyridoxamine (**2**),[2] and pyridoxine (**3**)[3] which have a straight "ansa chain" between 2′- and 5′-positions. In the presence of a suitable metal ion, **1**[1] and **2**[2] have proved very active in the enzyme-mimics reactions such as racemization or transamination of amino acids. Although such reactions proceed *via* the formation of Schiff base[4] stereospecifically and/or stereoselectively owing to the chirality of the B_6 analogs used, the degree of such steric effects is rather limited in comparison to the corresponding enzymic reactions. This will be because the "ansa chain" to which the B_6 analogs owe their planer chirality is too small and separated too far from the reaction center in the transition state. This prompted us to replace the straight "ansa chain" by a more bulky one. We prepared new B_6 analogs having a branched "ansa chain".

This paper deals with 15-formyl-14-hydroxy-5,5-dimethyl-2,8-dithia[9](2,5)pyridinophane (**4**) and 15-aminomethyl-14-hydroxy-5,5-dimethyl-2,8-dithia[9]-(2,5)pyridinophane (**5**), a new type of pyridoxal and pyridoxamine analogs, and their optical resolution. The levorotary enantiomer of **5** (**5a**) was also obtained by derivation from the corresponding enantiomer of **4** (**4a**).

3,3-Dimethyl-1,5-pentanedithiol (**6**) was prepared by the reaction of 1,5-dibromo-3,3-dimethylpentane (**7**)[5] with thiourea and subsequent alkaline hydrolysis. The ansa compound (**8**) was obtained by slow addition of a benzene solution of an equimolar mixture of **6** and 2,5-bis(chloromethyl)-3-hydroxy-*O*,*O*′-isopropylidene-4-pyridinemethanol (**9**)[1] to a dilute solution of sodium ethoxide in ethanol at 0 °C. Removal of the isopropylidene group in **8** by acidic hydrolysis afforded an analog of pyridoxine (**10**), which was oxidized with manganese(IV) oxide in the presence of *N*,*N*-dimethyl-1,3-propanediamine in pyridine–benzene.[6] The resulting Schiff base was hydrolyzed with acid to give racemic 15-formyl-14-hydroxy-5,5-dimethyl-2,8-dithia[9](2,5)pyridinophane (**4**). The optical resolution of **4** was performed by forming the Schiff base (**11**) by treatment with 3-amino-3-deoxy-1,2:5,6-di-*O*-isopropylidene-D-glucofranose.[1] Levorotary enantiomer of **4** (**4a**) was obtained by recrystallization of one of the less soluble diastereomers of the Schiff base (**11a**) from benzene and subsequent acidic hydrolysis of **11a**. Compounds **4** and **4a** were treated with hydroxylamine in ethanol to give the corresponding (±)-oxime (**12**) and (−)-oxime (**12a**), respectively. Reduction of **12** and **12a** to the corresponding pyridoxamine analogs, **5** and **5a**, were performed with sodium (dihydrotrithio)borate in tetrahydrofuran, following the earlier synthesis of **2**.[2]

We also succeeded in the optical resolution of **5**; that is, when **5** was treated with (−)-(*R*,*R*)-dibenzoyltartaric acid in ethanol, the crude (−)-dibenzoyltartaric acid salt of **5** (neutral equimolar salt) (**13a**) contaminated with its diastereomeric salt was prepared. Owing to the poor solubility of the salt in the usual solvents, fractional crystallization of **13a** proved very difficult. Therefore, such crude **13a** was treated with aqueous sodium hydrogencarbonate to give crude **5a**

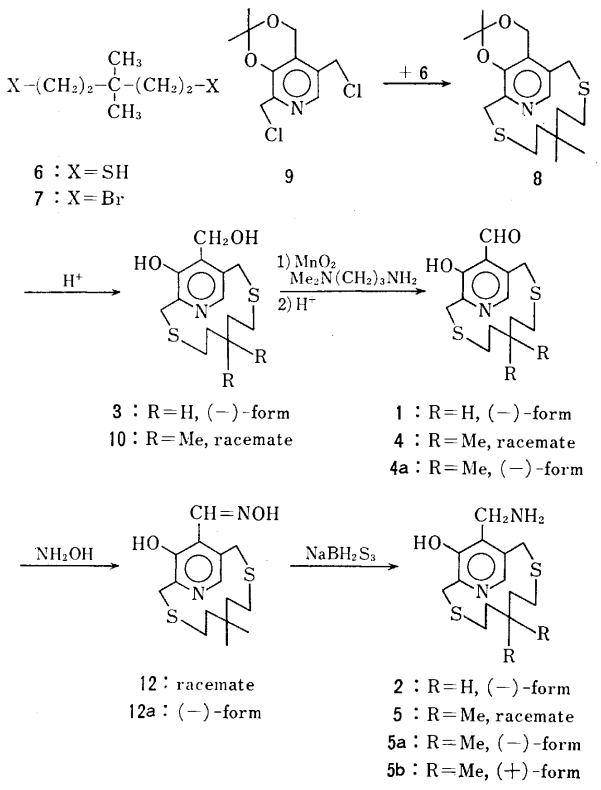

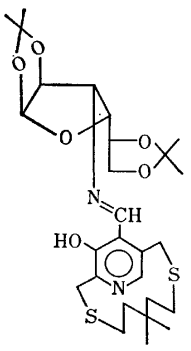

11 : mixture of diastereomer
11a : (−)-form

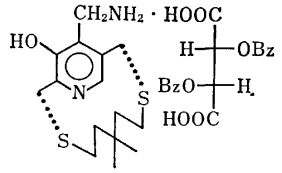

13a

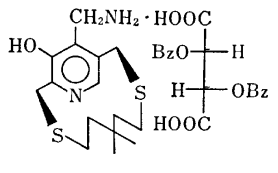

13b

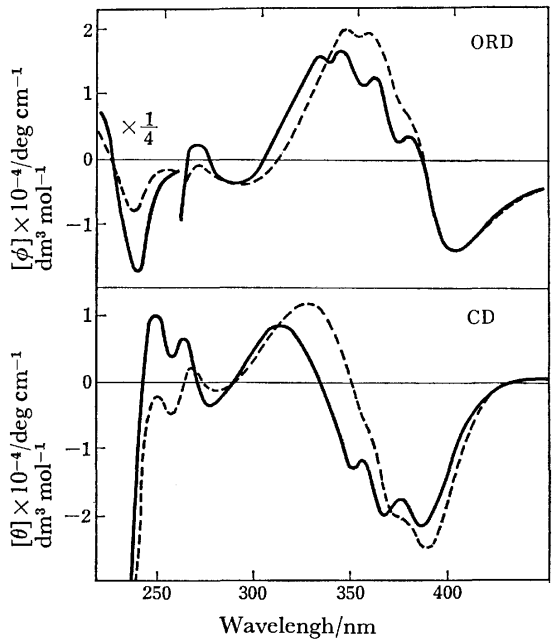

Fig. 1. ORD and CD spectra of **4a** and **1** (1.76×10^{-4} M solution in MeCN at 21 °C.).
4a: ——, **1**: ----.

including a little (+)-enantiomer (**5b**). This was repeatedly treated as described above and gave **5a**. Using (+)-(*S*,*S*)-dibenzoyltartaric acid in the same way resulted in (+)-enantiomer (**5b**). The physical properties, including optical rotation, of **5a** obtained by the resolution of **5** completely agreed with those of **5a** prepared from **12a**.

In order to determine the absolute configuration of **4a**, its ORD and CD spectra were measured. They were very similar to those of **1** (Fig. 1), indicating that **4a** has the same configuration as **1** has. Because **1** had been shown to have *S*-configuration on the basis of the results of X-ray analysis of (−)-pyridoxine analog (**3**) derived from **1**,[3] the absolute configuration of **4a** was determined to be *S*. Therefore, **5a** and **12a** derived from **4a** also had *S*-configuration and the enantiomer **5b** had *R*-configuration.

Studies on the function of these new B_6 analogs with definite configuration are under way. These indicate that in some systems they are very superior to the former analogs, **1** and **2**. The results will be reported in the near furture.

Experimental

All melting and boiling points are uncorrected. Optical rotations were measured with a Perkin-Elmer 241MC polarimater. UV, IR, and ^{1}H NMR spectra were recorded on a Hitachi 124 Spectrophotometer, a Shimadzu IR-27G infrared spectrophotometer, and a JEOL PS-100 spectrometer, respectively. ORD and CD spectra were obtained using a JASCO J20A automatic recording spectropolarimeter. Column chromatography was performed on a Merck silica gel 60 (No. 7734).

*3,3-Dimethyl-1,5-pentanedithiol (**6**).* A stirred mixture of 1,5-dibromo-3,3-dimethylpentane (**7**)[5] (64.8 g), thiourea (61.0 g), and water (45 ml) was refluxed for 20 h. A solution of potassium hydroxide (100 g) in water (200 ml) was added all at once to the resulting solution at room temperature, refluxed for 6 h with stirring, diluted with water, and extracted with ether. The aqueous layer was acidified with hydrochloric acid and extracted with ether. The ethereal extract was dried ($MgSO_4$), concentrated, and distilled, giving 35.8 g (82%) of **6**: bp 100—101 °C/7 mmHg (1 mmHg≈133 Pa); n_D^{23} 1.5141; IR (film) 2550 cm^{-1} (SH). Found: C, 50.84; H, 9.73; S, 39.07%. Calcd for $C_7H_{16}S_2$: C, 51.17; H, 9.81; S, 39.02%.

*14-Hydroxy-15-hydroxymethyl-O,O′-isopropylidene-5,5-dimethyl-2,8-dithia[9](2,5)pyridinophane (**8**).* A solution of **6** (4.6 g) and 2,5-bis(chloromethyl)-3-hydroxy-*O*,*O*′-isopropylidene-4-pyridinemethanol (**9**)[1] (6.9 g) in benzene (500 ml) was added to a stirred solution of sodium ethoxide (prepared from sodium (1.7 g) in ethanol (2.5 l)) over a period of 6 h in an ice bath and kept overnight at 0 °C. The solvents were removed and the residue was extracted with chloroform–water. The organic layer was washed with water, dried ($MgSO_4$), concentrated, and chromatographed. Elution with dichloromethane gave 7.5 g (81%) of **8**: mp 139—140 °C; UV_{max} (MeCN) 297 (ε 6.3×10^3) and 211 nm (ε 15.0×10^3); ^{1}H NMR ($CDCl_3$) δ=7.94; (1H, s), 5.26 (1H, d, J=16 Hz), 4.77 (1H, d, J=16 Hz), 4.15 (1H, d, J=12 Hz), 3.73 (1H, d, J=12 Hz), 3.61 (1H, d, J=13 Hz), 3.50 (1H, d, J=13 Hz), 1.63 (3H, s), 1.59 (3H, s), and 0.70 (6H, s). Found: C, 61.23; H, 7.67; N, 3.92; S, 18.11%. Calcd for $C_{18}H_{27}NO_2S_2$: C, 61.15; H, 7.70; N, 3.96; S, 18.14%.

*14-Hydroxy-15-hydroxymethyl-5,5-dimethyl-2,8-dithia[9](2,5)-pyridinophane (**10**).* A stirred mixture of **8** (7.3 g) in 1 M (1 M=1 mol/dm^3) hydrochloric acid (240 ml) was heated at 80—85 °C for 1 h. Soon **8** was dissolved and the hydrochloride of **10** was deposited. The mixture was made basic with solid sodium hydrogencarbonate and stirred for 1 h at room temperature. Separation of the precipitates gave 5.2 g of **10**. Additional **10** (1.2 g; total 99%) was recovered by concentrating the filtrate to dryness, extracting the residue with pyridine, and removing the pyridine; mp> 280 °C. Found: C, 57.49; H, 7.36; N, 4.30; S, 20.44%. Calcd for $C_{15}H_{23}NO_2S_2$: C, 57.47; H, 7.40; N, 4.47; S,

20.45%.

Hydrochloride: Mp 208—209 °C dec Found: C, 51.50; H, 6.90; Cl, 10.11; N, 3.97; S, 18.38%. Calcd for $C_{15}H_{24}ClNO_2S_2$: C, 51.49; H, 6.91; Cl, 10.13; N, 4.00; S, 18.32%.

(±)-15-Formyl-14-hydroxy-5,5-dimethyl-2,8-dithia[9](2,5)-pyridinophane (4). A stirred mixture of *N,N*-dimethyl-1,3-propanediamine (7.2 ml), manganese(IV) oxide (27.0 g), and a solution of **10** (5.2 g) in pyridine (100 ml) and benzene (70 ml) was refluxed for 4 h while the generated water was azeotropically separated.[6] The insoluble material was filtered off with celite and the filtrate was evaporated to dryness. Dioxane (100 ml) and 1.2 M hydrochloric acid (65 ml) were added to the residue and stirred for 1 h at room temperature. Dilution of the solution with water (*ca.* 1 l) and adjustment of pH to *ca.* 3 with aqueous sodium hydroxide gave precipitates. These were passed through a silica-gel column with dichloromethane, giving 3.6 g (70%) of **4**: mp 147—148 °C; IR (KBr) 1660 cm^{-1} (C=O). Found: C, 57.82; H, 6.73; N, 4.41; S, 20.54%. Calcd for $C_{15}H_{21}NO_2S_2$: C, 57.85; H, 6.80; N, 4.50; S, 20.59%.

(−)-Schiff Base of 4 with 3-Amino-3-deoxy-1,2:5,6-di-O-isopropylidene-D-glucofranose (11a). A solution of **4** (6.24 g) and 3-amino-3-deoxy-1,2:5,6-di-*O*-isopropylidene-D-glucofranose[1] (5.74 g) in benzene (500 ml) was refluxed for 2 h while the generated water was azeotropically separated. Evaporating the solution to *ca.* 100 ml afforded crude **11a**, which was recrystallized twice from benzene, giving 4.17 g (75% based on half of **4**) of **11a**: mp>280 °C; UV_{max} ($CHCl_3$) 353 nm (ε 4.9×10^3); IR (KBr) 1660 cm^{-1} (C=N); $[\alpha]_D^{25}$ −337° (*c* 0.392, $CHCl_3$). Found: C, 58.90; H, 7.30; N, 4.98; S, 11.37%. Calcd for $C_{27}H_{40}N_2O_6S_2$: C, 58.67; H, 7.29; N, 5.07; S, 11.60%.

(−)-15-Formyl-14-hydroxy-5,5-dimethyl-2,8-dithia[9](2,5)-pyridinophane (4a). To a solution of **11a** (3.98 g) in dioxane (400 ml) was immediately added 1 M hydrochloric acid (60 ml). The mixture was stirred for 1 h at room temperature. Treating the solution as described in the preparation of **4** gave 1.80 g (80%) of **4a**: mp 93 °C; $[\alpha]_D^{24}$ −422° (*c* 0.264, $CHCl_3$); UV_{max} (MeCN) 360 (ε 4.0×10^3), 248 (ε 8.2×10^3), and 225 nm (ε 10.8×10^3); IR (KBr) 1660 cm^{-1} (C=O); ^1H NMR ($CDCl_3$) δ=10.53 (1H, s), 8.06 (1H, s), 4.35 (1H, d, J=12 Hz), 4.28 (1H, d, J=14 Hz), 3.77 (1H, d, J=14 Hz), 3.66 (1H, d, J=12 Hz), and 0.70 (6H, s). Found: C, 57.92; H, 6.78; N, 4.42; S, 20.57%. Calcd for $C_{15}H_{21}NO_2S_2$: C, 57.85; H, 6.80; N, 4.50; S, 20.59%.

(−)-14-Hydroxy-15-hydroxyiminomethyl-5,5-dimethyl-2,8-dithia[9](2,5)pyridinophane (12a). To a solution of **4a** (1.22 g) in ethanol (60 ml) was immediately added solid hydroxylamine hydrochloride (0.38 g) and sodium acetate trihydrate (1.0 g). The mixture was stirred overnight at room temperature, concentrated to dryness, and extracted with chloroform–water. After being washed with aqueous sodium hydrogencarbonate and with water, the organic layer was dried ($MgSO_4$), concentrated, and chromatographed. Elution with chloroform afforded 1.01 g (79%) of **12a**: mp 218—219 °C; $[\alpha]_D^{23}$ −363° (*c* 0.204, $CHCl_3$); UV_{max} (MeCN) 330 (ε 4.6×10^3), 260 (ε 9.9×10^3), and 215 nm (ε 18.9×10^3); IR (KBr) 3400 (OH) and 1660 cm^{-1} (CH=N); ^1H NMR (CD_3SOCD_3) δ=12.28 (1H, s), 10.99 (1H, s), 8.73 (1H, s), 8.06 (1H, s), 4.28 (1H, d, J=12 Hz), 4.22 (1H, d, J=12 Hz), 3.77 (1H, d, J=13 Hz), 3.58 (1H, d, J=12 Hz), and 0.65 (6H, s). Found: C, 55.02; H, 6.80; N, 8.51; S, 19.54%. Calcd for $C_{15}H_{22}N_2O_2S_2$: C, 55.19; H, 6.79; N, 8.58; S, 19.64%.

(±)-14-Hydroxy-15-hydroxyiminomethyl-5,5-dimethyl-2,8-dithia[9](2,5)pyridinophane (12). Racemic isomer (**4**) was treated as described in the treatment of **4a**, yielding **12** in 93% yield: mp 205—206 °C. Found: C, 55.05; H, 6.79; N, 8.40; S, 19.58%. Calcd for $C_{15}H_{22}N_2O_2S_2$: C, 55.19; H, 6.79; N, 8.58; S, 19.64%.

(−)-15-Aminomethyl-14-hydroxy-5,5-dimethyl-2,8-dithia[9]-(2,5)pyridinophane (5a). Dry THF (15 ml) was added all at once to a stirred mixture of sulfur (675 mg) and sodium tetrahydroborate (264 mg) under nitrogen atmosphere and stirred for 1 h at room temperature. A solution of **12a** (1.13 g) in dry THF (30 ml) was added to the mixture over a period of 20 min at room temperature with stirring and refluxed for 6 h. After removal of the solvent, the residue was dissolved in hot chloroform–methanol and extracted with dilute hydrochloric acid. The aqueous layer was treated with charcoal, made basic with solid sodium hydrogencarbonate, and extracted with chloroform. The organic layer was dried ($MgSO_4$), concentrated, and chromatographed. Elution with chloroform–methanol (9:1 v/v) gave 617 mg (57%) of **5a**: mp 174—175 °C dec; $[\alpha]_D^{25}$ −262° (*c* 0.409, $CHCl_3$); ORD: λ_{max} 314 ($[\alpha]$ $-1.32°\times10^4$), 285 ($[\alpha]$ $+1.58°\times10^4$), 247 ($[\alpha]$ $-5.0°\times10^2$), and 220 nm ($[\alpha]$ $+4.8°\times10^4$) (*c* 6.4×10^{-5} M, MeCN, 21 °C); CD: λ_{max} 300 ($\Delta\varepsilon$ −22.3), 260 ($\Delta\varepsilon$ +1.65), and 239 nm ($\Delta\varepsilon$ −19.3) (*c* 6.4×10^{-5} M, MeCN, 21 °C); UV_{max} (MeCN) 299 (ε 5.7×10^3) and 214 nm (ε 14×10^3); IR (KBr) 3350, 3200, and 3150 cm^{-1} (NH_2, OH); ^1H NMR (CD_3SOCD_3) δ=7.79 (1H, s), 5.99 (2H, s), 4.18 (2H, s), 4.15 (1H, d, J=11 Hz), 3.78 (1H, d, J=13 Hz), 3.70 (1H, d, J=13 Hz), 3.45 (1H, d, J=11 Hz), and 0.64 (6H, s). Found: C, 57.45; H, 7.79; N, 8.79; S, 20.57%. Calcd for $C_{15}H_{24}N_2OS_2$: C, 57.65; H, 7.74; N, 8.96; S, 20.52%.

(±)-15-Aminomethyl-14-hydroxy-5,5-dimethyl-2,8-dithia[9]-(2,5)pyridinophane (5). The racemate (**12**) was treated as described in the preparation of **5a**, affording **5** in 59% yield: mp 154—155 °C dec. Found: C, 57.37; H, 7.74; N, 8.80; S, 20.43%. Calcd for $C_{15}H_{24}N_2OS_2$: C, 57.65; H, 7.74; N, 8.96; S, 20.52%.

Optical Resolution of 5. (−)-Enantiomer of 5 (5a): A solution of (−)-(*R,R*)-dibenzoyltartaric acid (1.59 g) in ethanol (15 ml) was added to a hot solution of **5** (1.31 g) in ethanol (100 ml), concentrated to *ca.* 30 ml, and cooled in an ice bath. The precipitates were collected and stirred with a mixture of chloroform and saturated sodium hydrogencarbonate solution at room temperature for 1 h. The organic layer was washed with water, dried ($MgSO_4$), and concentrated to dryness, giving crude **5a**. Two more treatments of the crude **5a** with (−)-dibenzoyltartaric acid and sodium hydrogencarbonate, successively yielded 295 mg (45% based on half of **5**) of **5a**: mp 174—175 °C dec; $[\alpha]_D^{21}$ −262° (*c* 0.327, $CHCl_3$).

(−)-Dibenzoyltartarate of 5a (13a): Mp >280 °C; $[\alpha]_D^{23}$ −186° (*c* 0.273, DMF). Found: C, 59.18; H, 5.70; N, 4.14; S, 9.52%. Calcd for $C_{33}H_{38}N_2O_9S_2$: C, 59.09; H, 5.71; N, 4.18; S, 9.56%.

(+)-Enantiomer of 5 (5b): By the use of (+)-(*S,S*)-dibenzoyltartaric acid instead of (−)-optical isomer, **5b** was obtained in 43% yield (based on half of **5**): mp 174—175 °C dec; $[\alpha]_D^{21}$ +262° (*c* 0.330, $CHCl_3$). Found: C, 57.37; H, 7.74; N, 8.78; S, 20.46%. Calcd for $C_{15}H_{24}N_2O_2S_2$: C, 57.65; H, 7.74; N, 8.96; S, 20.52%.

(+)-Dibenzoyltartarate of 5b (13b): Mp >280 °C; $[\alpha]_D^{21}$ +187° (*c* 0.330, DMF). Found: C, 59.19; H, 5.65; N, 4.10; S, 9.55%. Calcd for $C_{33}H_{38}N_2O_9S_2$: C, 59.09; H, 5.71; N, 4.18; S, 9.56%.

The authors wish to express their thanks to Dr. Haruo Homma and his assistants for elementary

analyses and to Dr. Jun Uzawa and Mrs. Tamiko Chijimatsu for measurements of ^{1}H NMR spectra.

References

1) Part I of this series: H. Kuzuhara, M. Iwata, and S. Emoto, *J. Am. Chem. Soc.*, **99**, 4173 (1977).
2) Part II of this series: H. Kuzuhara, T. Komatsu, and S. Emoto, *Tetrahedron Lett.*, **1978**, 3563.
3) Part III of this series: T. Sakurai, H. Kuzuhara, and S. Emoto, *Acta Crystallogr., Sect. B*, **35**, 2984 (1979).
4) E. E. Snell and S. J. Di Mari, "The Enzyme," 3rd ed, ed by P. D. Boyer, Academic press, New York and London (1970), Vol. 2, Chap. 7, p. 335.
5) A. T. Blomquist, E. S. Wheeler, and Y. Chu, *J. Am. Chem. Soc.*, **77**, 6307 (1955).
6) M. Iwata, *Bull. Chem. Soc. Jpn.*, **54**, 2835 (1981).

 © 1982 The Chemical Society of Japan Bull. Chem. Soc. Jpn., 55, 833—837 (1982)

A Kinetic Study on Reduction of 9,9′-Bifluorenylidene by Sodium Isopropoxide

Shoji KAJIGAESHI,* Shizuo FUJISAKI, Yasuhiko NAKASHIGE, and Sadaaki MURAKAMI

Department of Industrial Chemistry, Faculty of Engineering Yamaguchi University, Tokiwadai, Ube 755

(Received February 7, 1981)

The kinetics and mechanism of reduction of 9,9′-bifluorenylidene (**1**) by sodium isopropoxide (**2**) in isopropyl alcohol to yield 9,9′-bifluorenyl (**3**) were investigated spectrophotometrically. The kinetic data suggest that the reduction proceeds autocatalytically, the reduction product **3** acting as the catalyst. It was found that

$$\mathbf{1} \xrightarrow[\mathbf{2}]{k_1} \mathbf{3} \qquad (1) \qquad\qquad \mathbf{1} + \mathbf{3} \xrightarrow[\mathbf{2}]{k_2} \mathbf{3} + \mathbf{3} \qquad (2)$$

Reactions 1 and 2 are of the first order with respect to **1**, but that the former is of the third order with respect to **2**, whereas the latter is of the first. The fourth- and third-order rate constants, k_1 and k_2, for Reactions 1 and 2 were determined to be 3.0×10^{-5} dm^9 mol^{-3} s^{-1} and 1.1×10^{3} dm^6 mol^{-2} s^{-1}, respectively, at 130 °C. Probable mechanisms for Reactions 1 and 2 have been offered on the basis of the reaction order for each molecular species involved.

Obviously, the symmetry of the fulvalene system demands that the central double bond has no dipole moment; however, it would also be expected that it has unusual properties.[1] Indeed, the bond index of that linkage is very low for a double bond and, taking 9,9′-bifluorenylidene (**1**) as an example, the linkage has an unusually high polarizability, which results in various interesting results: *e.g.*, a large molecular refraction[2] and an unusually low reduction potential.[3–5] Among the unusual reactions of fulvalenes, the reduction of the central double bond by sodium alkoxides may be a typical example, since the C=C double bond is, in general, not reducible by such weak reductants.[6] In the previous work[7] it was found that **1** is readily reduced by sodium ethoxide and gives 9,9′-bifluorenyl (**3**). In order to elucidate this mechanism, a kinetic study on reduction of **1** by sodium isopropoxide (**2**) in isopropyl alcohol (Scheme 1) has been made. Sodium isoproxide was chosen as an alkoxide because its oxidation product was acetone, which did not lead to any side reaction, and, in addition, the sequence of the reduction rate of **1** by alkoxide was methoxide<ethoxide<isopropoxide.[8]

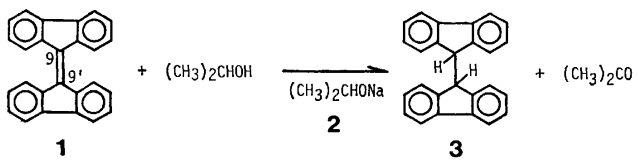

Scheme 1.

Experimental

Reduction of **1** *by Sodium Isopropoxide.* Metallic sodium (0.23 g, 1.0×10^{-2} g-atom) was treated with 5 ml of isopropyl alcohol; the resulting solution was transferred into a glass tube. Then 0.17 g (5.2×10^{-4} mol) of **1** was added. The glass tube was sealed and heated at 130 °C in an oil bath until the orange-red color of the solution disappeared completely. After cooling, the content was poured into water and extracted with benzene–ether (1:1). The solvent was evaporated. Recrystallization of the residue from benzene gave **3**, 0.16 g (93%); mp 245 °C. This compound was identified by direct comparison with an authentic sample. On the other hand, when the chemical components in the distillate from the reduction mixture were analyzed by gas chromatography, acetone was found.

Stock Solutions of **1** *and* **3**. Compounds **1** and **3** were dissolved separately in isopropyl alcohol to a concentration of 2×10^{-3} mol dm^{-3}. These solutions were stored in a dark room and were stable for at least a month. Each solution was diluted with isopropyl alcohol as required for experiments.

Kineitc Measurements. Red compound **1** has an absorption spectrum in the visible region, with its maxium absorbance at 458 nm and with the molar absorptivity of 2.13×10^{4} dm^3 mol^{-1} cm^{-1}, probably attributable to a π-π^* electronic transition, while **3** shows no visible absorption spectrum. The decrease in the absorbance due to the reduction of **1** was a function of the time when measured spectrophotometrically. A required amount of isopropyl alcohol solution of **2** and 2.5 ml of 2×10^{-4} mol dm^{-3} solution of **1** were taken in a 25 ml volumetric flask and diluted with isopropyl alcohol up to the mark. A 5 ml of the aliquot was transferred into a glass tube, 11 mm in external diameter and about 100 mm high, which was used as both a reaction vessel and a spectrophotometric cell.[9] The tube was sealed and then immersed in an oil bath thermostated at 130 °C within an accuracy of 0.2 °C. The oil bath was covered with aluminium foil to prevent any effect of light on the reaction. The absorbance at 458 nm was measured at a given interval (at least 10 min) with a Shimadzu SP-20 spectrophotometer, after taking out the glass tube and wiping off the oil which had stuck on its outside surface. Another glass tube of the same size and quality containing isopropyl alcohol was used as the reference during the spectrophotometry.

Results

The reduction rate of **1** by **2** was measured at 130 °C for various concentrations of **2** (6×10^{-3} to 1.4×10^{-1} mol dm^{-3}) under a constant concentration of **1** (2×10^{-5} mol dm^{-3}). The dimensionless quantity X as a function of the time t was plotted in Fig. 1, where $X=[\mathbf{1}]/[\mathbf{1}]_0$: $[\mathbf{1}]_0$ and $[\mathbf{1}]$ denote the concentrations of **1** at the initial time and at the time of measure-

ment. The reduction for all the cases did not proceed appreciably at the initial stage and only began to proceed after some inductive period; the more the reduction proceeded, the greater the rate became, as seen in Fig. 1. Such behavior of X *vs.* t is frequently observed in the autocatalytic reactions such are as found in the acid-catalyzed hydrolyses of various esters and in various biochemical processes.[10,11]

A kinetic model of conversion from A to B which proceeds by an autocatalytic reaction in addition to the direct conversion would be:

$$\mathrm{A} \xrightarrow{k_1} \mathrm{B}, \tag{1a}$$

$$\mathrm{A} + \mathrm{B} \xrightarrow{k_2} \mathrm{B} + \mathrm{B}. \tag{1b}$$

If the concentrations of the molecular species A at the start and at the measurement time are denoted by A_0 and $A(t)$ and if Reactions 1a and 1b are both of the first order with respect to each substrate, the dimensionless quantity, $X_A(t)=A(t)/A_0$. and the rate, $-\mathrm{d}X_A(t)/\mathrm{d}t$, can be formalized as[10,11]

$$X_A(t) = \frac{k_1+k_2A_0}{k_1e^{(k_1+k_2A_0)t}+k_2A_0}, \tag{2}$$

$$-\frac{\mathrm{d}}{\mathrm{d}t}X_A(t) = \frac{k_1(k_1+k_2A_0)^2e^{(k_1+k_2A_0)t}}{[k_1e^{(k_1+k_2A_0)t}+k_2A_0]^2}. \tag{3}$$

In the above equations, k_1 and k_2 are the first- and second-order rate constants for Reactions 1a and 1b, respectively. The rate reaches its maximum at a particular time, t^*, which satisfies the equation, $\mathrm{d}^2X_A(t)/\mathrm{d}t^2=0$ *i.e.*,

$$k_1e^{(k_1+k_2A_0)t^*} = k_2A_0, \tag{4}$$

when $k_2A_0 \gg k_1$, Approximations 5 to 7 will be derived from the combination of Eqs. 2 to 4.

$$X_A(t^*) \simeq \frac{1}{2}, \tag{5}$$

$$-\frac{\mathrm{d}}{\mathrm{d}t}X_A(t^*) \simeq \frac{1}{4}k_2A_0, \tag{6}$$

$$k_1e^{k_2A_0t^*} \simeq k_2A_0. \tag{7}$$

Approximations 5 to 7 indicate that (i) the dimensionless quantity becomes equal to 1/2 when the conversion rate reaches its maximum, (ii) the k_2A_0 value is four times the slope of the tangential line at $t=t^*$ for the curve of $X_A(t)$ *vs.* t, and (iii) the k_1 value is obtainable with the use of Approximation 7 provided that the values of both t^* and k_2A_0 are known. All the curves of X *vs.* t measured for the reduction of **1** by **2** under the present conditions suggested that $k_2A_0 \gg k_1$, because the reduction rates were at their maximum when $X=1/2$, as seen in Fig. 1.

The apparent first- and second-order rate constants, k_1^{ap} and k_2^{ap}, for each concentration of **2** added were determined from the slope of the tangential line and from the time when $X=1/2$, with the use of Approximations 6 and 7, as indicated by a dashed line and an arrow for Curve 5 in Fig. 1: $k_1^{ap}=2.4\times10^{-10}$ s^{-1} and $k_2^{ap}=2.2\times10$ $dm^3\ mol^{-1}\ s^{-1}$ were obtained for $[\mathbf{2}]=2.0\times10^{-2}$ mol dm^{-3} from Curve 5. The $k_2^{ap}A_0$ values determined were 3.8×10^4 to 2.1×10^7 times larger than the k_1^{ap} values over the concentration range of 1.4×10^{-1} to 6×10^{-3} mol dm^{-3} for **2**.

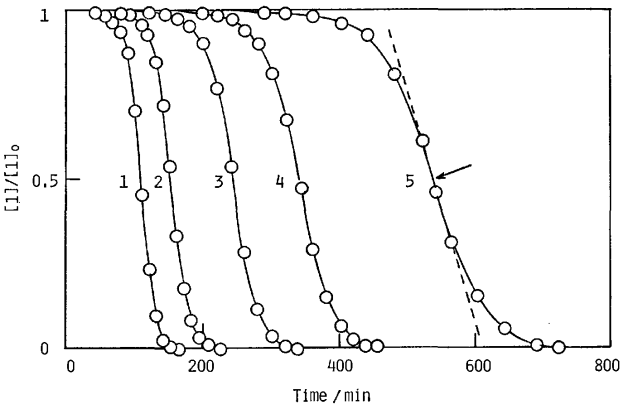

Fig. 1. Reduction of 9,9′-bifluorenylidene (**1**) by sodium isopropoxide (**2**) at 130 °C.
$[\mathbf{1}]_0$: 2.0×10^{-5} mol dm^{-3}. [**2**]: 1—8.0×10^{-2}, 2—6.0×10^{-2}, 3—4.0×10^{-2}, 4—3.0×10^{-2}, and 5—2.0×10^{-2} mol dm^{-3}.

As seen on the curves in Fig. 1, the inductive period in reduction becomes shorter with increase in the concentration of **2** added; in addition, the tangential line at the maximum rate becomes steeper, indicating that both k_1^{ap} and k_2^{ap} are dependent on the concentration of **2**. If Reactions 1a and 1b for the reduction of **1** are of the n- and m-th order with respect to **2**, the apparent first- and second-order rate constants, k_1^{ap} and k_2^{ap}, will be expressed by

$$k_1^{ap} = k_1[\mathbf{2}]^n \quad \text{and} \quad k_2^{ap} = k_2[\mathbf{2}]^m. \tag{8}$$

This is because **2** acts as the catalyst in this reaction and its concentration remains constant during the reaction. Plots of both $\ln k_1^{ap}$ and $\ln k_2^{ap}$ *vs.* $\ln$ [**2**] will give a straight line with each slope of n and m. Each linear plot with a slope of $n=3$ and $m=1$ in Figs. 2 and 3 suggests that Reaction 1a is of the third order and Reaction 1b is of the first order with respect to **2**. The values $k_1=3.0\times10^{-5}$ $dm^9\ mol^{-3}\ s^{-1}$ and $k_2=1.1\times10^3$ $dm^6\ mol^{-2}\ s^{-1}$ are obtained by extrapolating each linear part to $\ln$ [**2**]$=0$.

Summarizing the foregoing discussion, we can say

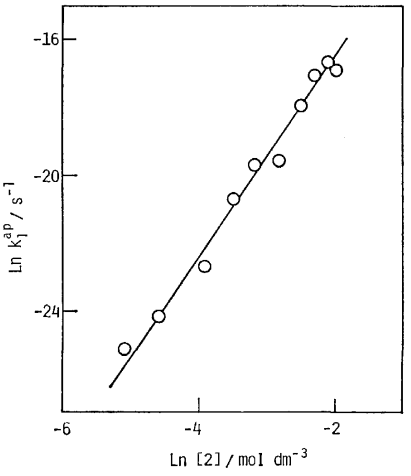

Fig. 2. Dependence of the apparent first-order rate constant, k_1^{ap}, on the concentration of sodium isopropoxide (**2**).

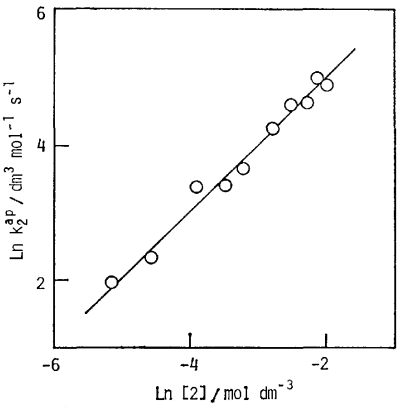

Fig. 3. Dependence of the apparent second-order rate constant, k_2^{ap}, on the concentration of sodium isopropoxide (**2**).

that the reduction of **1** by **2** in isopropyl alcohol to yield **3** proceeds by the following parallel reaction paths:

$$\mathbf{1} \xrightarrow[\mathbf{2}]{k_1} \mathbf{3}, \tag{9a}$$

$$\mathbf{1} + \mathbf{3} \xrightarrow[\mathbf{2}]{k_2} \mathbf{3} + \mathbf{3}, \tag{9b}$$

and its reduction rate is expressed by

$$-\frac{d}{dt}[\mathbf{1}] = k_1[\mathbf{2}]^3[\mathbf{1}] + k_2[\mathbf{2}][\mathbf{1}][\mathbf{3}]. \tag{10}$$

Discussion

It is of interest to note that the reaction rate for Reaction 9a is of the third order with respect to **2**. High-order reactions regarding alkoxide are frequently observed in various reductions by alkoxide, *e.g.*, the second order in reduction of nitrobenzene by sodium methoxide,[12] the first and second orders in benzophenone reduction by aluminium isopropoxide,[13] and the third and forth orders in acetophenone reduction by aluminium isopropoxide.[14] Such a high-order process regarding alkoxide is explaned by the association of alkoxide,[15] and the transition-state complex is formed between the oxidant and the associated alkoxide.[16] According to this interpretation, we offer Scheme 2 as a mechanism of Reaction 9a. The pre-equilibrium 2a between the monomer and trimer of **2** is supposed to exist. The trimer (**4**) reacts with **1** and the hydride ion from **4** is transferred to the C(9) or C(9') atom of **1** to give an intermediate carbanion (**5**) (Step 2b), which will react readily with isopropyl alcohol to yield the final product **3** (Step 2c). Step 2b with a rate constant k_{1b} may be rate-determining: a transition-state complex with a six membered ring,[17,18] as indicated in Formula **6**. Step 2c is in an equilibrium, as will be discussed later, which may shift strongly to the righthand side.

The reduction products of **1** by **2** in isopropyl alcohol were 9,9'-bifluorenyl **3** and acetone. Accordingly, one of these compounds is considered to act as the catalyst in this reaction. The reaction rate was measured in the presence of **3** or acetone. It was found that the reaction was remarkably accelerated in the presence of the former, but no effect was found for the latter. Figure 4 shows plots of X *vs.* t for the various initial concentrations of **3** when 2×10^{-5} mol dm^{-3} of **1** and 2×10^{-2} mol dm^{-3} of **2** were added. On the other hand, the dimensionless quantity $X_A(t)$ for the kinetic model (1) is expressed by Eq. 11, when the intial concentration of B (B_0) is not zero (see Appendix).

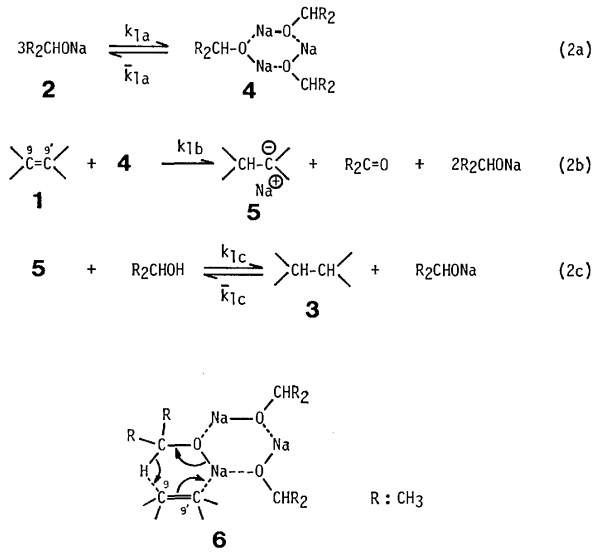

Scheme 2.

$$X_A(t) = \frac{k_1+k_2A_0+k_2B_0}{(k_1+k_2B_0)e^{(k_1+k_2A_0+k_2B_0)t}+k_2A_0} \tag{11}$$

In the case of the reduction of **1** by **2**, k_1 and k_2 in the above equation will be replaced by $k_1[\mathbf{2}]^3$ and $k_2[\mathbf{2}]$, because Reactions 9a and 9b are found to be of the third and first orders with respect to **2**, which acts as the catalyst and keeps its concentration constant during the reaction. The X values for this reaction were calculated for the various initial concentrations of **3** on the basis of Eq. 11, with the use of the k_1 and k_2 values determined above. The experimental plots in Fig. 4 can be explained reasonably by the calculated values; this confirms that the reduction product **3** acts as the catalyst.

A catalytic reaction such as indicated by Scheme 3 is offered as a probable mechanism. Product **3** reacts with **2** to give an intermediate carbanion **5** (Step 3a), which is the reverse reaction of Step 2c. An electron transfer may take place from the carbanion **5** to the compound **1** to give 9-(9-fluorenyl)fluoren-9-yl radical (**8**) and its anion radical (**7**). The protonation of the anion radical **7** to give **8** may be in a rapid equilibrium (Step 3c). One molecule of the radical **8** may attack isopropyl alcohol and an α-hydrogen atom of the alcohol may be transferred to yield a final product **3** and an alcohol radical (**9**) (Step 3d). Another molecule of the radical **8** may react with the alcohol radical **9** produced in Step 3d to yield another molecule of the product **3** and acetone (Step 3e). Step 3b with an rate constant k_{2b} may be rate-determining, because (i) Equilibria 3a and 3c may be established very rapidly and (ii) each radical involved in the process may be very

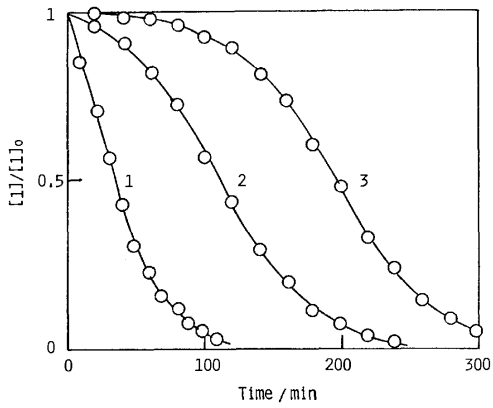

Fig. 4. Reduction of 9,9′-bifluorenylidene (**1**) by sodium isopropoxide (**2**) in the presence of added 9,9′-bifluorenyl (**3**) at 130 °C.
$[\mathbf{1}]_0$: 2.0×10^{-5} mol dm^{-3}. $[\mathbf{2}]$: 2.0×10^{-2} mol dm^{-3}.
$[\mathbf{3}]_0$: 1—1.0×10^{-5}, 2—1.0×10^{-6}, and 3—1.0×10^{-7} mol dm^{-3}.

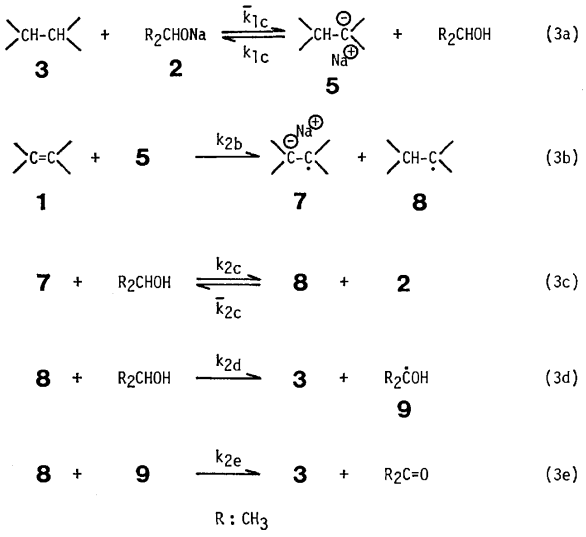

Scheme 3.

reactive.

If the autocatalytic reaction actually proceeds through the foregoing steps, some amount of the pinacol might be formed. This may be explained by that the dimerization of the alcohol radical **9** does not occur in alkaline media.[19,20] The existence of the radicals **7** to **9**, and also the kinetics of various 9,9′-bifluoreylidene derivatives, are now under investigation; we must await these results before giving a valid conclusion for the autocatalytic reaction.

Usually the C=C double bond is not reducible by sodium alkoxide. Regarding Compound **1**, two fluorene moieties are not on a plane, and the central C(9)=C(9′) double bond is twisted sterically.[21,22] Furthermore, despite the symmetry of the molecule, **1** has a considerably larger molar-polarization than expected.[2] This high distortion polarization is also reflected in the particular chemical reactivity of its central double bond; it is capable of adding an organometallic compound[23,24] and amines,[25] of reacting with lithium aluminium hydride,[26] and of undergoing the Michael condensation[27,28]—all reactions typical of high polar substances. Hydrogenation of this double bond by sodium isopropoxide **2** can be interpreted along the same line. However, the direct reduction of **1** by **2**, *i.e.*, Reaction 9a, proceeds very slowly even at 130 °C, as seen in the inductive period in Fig. 1. The most important factor in its reactivity with **2** is that the process involves the autocatalytic reaction 9b; the autocatalytic reaction proceeded 3.8×10^4 to 2.1×10^7 times rapidly as the direct reaction when 2×10^{-5} mol dm^{-3} of **1** and 1.4×10^{-1} to 6×10^{-3} mol dm^{-3} of **2** were reacted.

Appendix

If each process in the kinetic model (1) is of the first order with respect to each molecular species involved, the rate of change in the concentration of A with the time is given by

$$-\frac{d}{dt}A(t) = k_1A(t) + k_2A(t)B(t). \tag{A1}$$

The initial conditions for the above equation are:

$$A(0) = A_0 \quad \text{and} \quad B(0) = B_0. \tag{A2}$$

The total concentration of A and B at any time must satisfy the equation:

$$A(t) + B(t) = A_0 + B_0. \tag{A3}$$

Under the condition A3, Eq. A1 is rewritten as

$$\frac{d}{dt}A(t) + (k_1+k_2A_0+k_2B_0)A(t) - k_2A^2(t) = 0. \tag{A4}$$

The differential equation A4 has the general solution A5:

$$A(t) = \frac{k_1+k_2A_0+k_2B_0}{Ce^{(k_1+k_2A_0+k_2B_0)t}+k_2}, \tag{A5}$$

where

$$C = \frac{K_1+K_2B_0}{A_0}. \tag{A6}$$

From Eqs. A5 and A6, $X_A(t)$ $[=A(t)/A_0]$ is derived as Eq. 9.

References

1) E. D. Bergmann, *Chem. Rev.*, **68**, 41 (1968).
2) E. D. Bergmann, E. Fisher, and J. H. Jaffe, *J. Am. Chem. Soc.*, **75**, 3230 (1953).
3) G. J. Hoijtink, *Recl. Trav. Chim. Pays-Bas*, **74**, 1525 (1955).
4) G. J. Hoijtink, E. de Boer, P. H. van der Meij, and W. P. Weijland, *Recl. Trav. Chim. Pays-Bas*, **74**, 277 (1955).
5) G. J. Hoijtink, J. van Schooten, E. de Boer, and W. Ij. Aalbersberg, *Recl. Trav. Chim. Pays-Bas*, **73**, 355 (1954).
6) Y. Ogata, "Yukikagobutsu No Sanka To Kangen," Nankodo, Tokyo (1963), p. 758.
7) S. Kajigaeshi, S. Fujisaki, I. Aizu, and H. Hara, *Bull. Chem. Soc. Jpn.*, **52**, 3569 (1979).
8) Our unpublished data.
9) T. Yoshino, S. Murakami, H. Takesue, and M. Ishihara, *J. Inorg. Nucl. Chem.*, **42**, 579 (1980).
10) M. Boudart, "Kinetics of Chemical Process," Prentice-Hall, Englewood Cliffs (1968), p. 124.
11) A. A. Frost and R. G. Pearson, "Kinetics and Mechanism," 2nd ed, Wiley, New York (1961), p. 19.
12) Y. Ogata and J. Mibae, *J. Org. Chem.*, **27**, 2048 (1962).

13) W. N. Moulton, R. E. V. Atta, and R. R. Ruch, *J. Org. Chem.*, **26**, 290 (1961).
14) V. J. Shiner, Jr., and D. Whittaker, *J. Am. Chem. Soc.*, **85**, 2337 (1963).
15) V. J. Shiner, Jr., D. Whittaker, and V. P. Fernandez, *J. Am. Chem. Soc.*, **85**, 2318 (1963).
16) Y. Sawaki, "Koza Yukihannokiko 10: Sanka To Kangen Hanno (II)," ed by Y. Ogata, Tokyokagakudojin, Tokyo (1965), p. 286.
17) E. D. Williams, K. A. Krieger, and A. R. Day, *J. Am. Chem. Soc.*, **75**, 2404 (1953).
18) H. Haubenstock and E. B. Davidson, *J. Org. Chem.*, **28**, 2772 (1963).
19) W. E. Bachmann, *J. Am. Chem. Soc.*, **55**, 391 (1933).
20) R. Tanikaga, "Shinjikkenkagakukoza 15: Sanka To Kangen [II]," ed by the Chemical Society of Japan, Maruzen, Tokyo (1977), p. 455.
21) N. A. Bailey and S. E. Hull, *J. Chem. Soc., D*, **1971**, 960.
22) H. L. Ammon and G. L. Wheeler, *J. Am. Chem. Soc.*, **97**, 2326 (1975).
23) R. C. Fuson and H. D. Porter, *J. Am. Chem. Soc.*, **70**, 895 (1948).
24) P. M. G. Bavin, *Can. J. Chem.*, **38**, 882 (1960).
25) L. A. Pink and G. E. Hilbert, *J. Am. Chem. Soc.*, **57**, 2398 (1935).
26) D. Lavie and E. D. Bergmann, *Bull. Soc. Chim. Fr.*, **1951**, 250.
27) K. Suzuki and M. Fujimoto, *Bull. Chem. Soc. Jpn.*, **37**, 1833 (1964).
28) K. Suzuki and S. Kajigaeshi, *Bull. Chem. Soc. Jpn.*, **35**, 408 (1962).

Hydrolysis of Carbohydrates in the Presence of a Reversed Micelle. III. Hydrolysis of Dextrin in Benzene

Kenichiro ARAI* and Yoshitaka OGIWARA
Faculty of Engineering, Gunma University, Kiryu, Gunma 376
(Received May 1, 1981)

The secondary solubilization of dextrin in a dodecylbenzenesulfonic acid (DBSH) reversed micelle in benzene containing a small amount of water was examined; a perfectly clear solution was obtained. The solution showed a CMC of DBSH, estimated by the method of Methylene Blue methachromasis, just like that of sucrose-containing similar reversed-micelle system. The hydrolysis of the dextrin in the system was investigated; the maximum rate enhancement of 285-fold was obtained on the basis of the reaction in DBSH aqueous solution. The CMC and the reaction rate showed changes similar to those in the case of sucrose-containing similar reversed-micelle system with changing the amount of water solubilized, but they showed different changes with changing the concentration of the substrate. These different changes were supposed to result from the differences in the molecular weights of the substrates. These results suggested that the rate enhancement mechanism due to solvent effect and micelle effect which was proposed for the hydrolysis of sucrose in the presence of a DBSH reversed micelle operates in the hydrolysis of the high molecular weight substrate such as dextrin.

Recently, the effective use of carbohydrates as renewable resources has again been recognized to be important. Many modifications of carbohydrates-containing raw and waste materials to, for example, a raw material for preparation of ethanol and livestock feed have been the subject of numerous investigations. In these cases, an effective and economical and if possible, selective depolymerization of the polysaccharides such as cellulose and starch in the raw material is essential.[1]

In previous papers, the hydrolysis of sucrose in the presence of dodecylbenzenesulfonic acid (DBSH) reversed micelles in a dioxane–water mixed solvent[2] and in benzene[3] was investigated. Rate enhancements up to 400-fold were observed on the basis of the reaction in an aqueous solution in the presence of hydrochloric acid. The greater part of the rate enhancement resulted from the formation of the reversed micelle.[3]

In the present paper, we report the hydrolysis of dextrin as a model of polysaccharides, which was carried out to investigate the effect of high molecular weight of the substrate on the reaction in the presence of the reversed micelle.

Experimental

Materials. Commercially available dextrin was purified by pouring a 20% aqueous solution into 5-fold volume of methanol to cause it to precipitate. The number-average molecular weight of the purified dextrin, estimated by the method of end group determination, was 66. Commercially available sodium dodecylbenzenesulfonate was passed through a cation exchange resin column to obtain a free acidic surfactant. Deionized and distilled water was used.

UV Spectrum and Maximum Amount of Solubilized Water. The UV spectra and the maximum amounts of solubilized water in benzene were obtained with the methods previously reported.[2,3]

Measurement of Reaction Rate. DBSH was dissolved in benzene and a dextrin aqueous solution was added with vigorous stirring to get a clear solution. The resulting reaction mixture was maintained at 60 °C in a thermostat, and aliquots were taken out at intervals to determine the amount of reducing sugar according to the method of Somogyi.[4] The logarithm of the ratio of [the amount of reducing sugar at reaction time infinity (r_∞)] to [the difference in the amount of reducing sugar at a reaction time t (r_t) and at infinity (r_∞)] was plotted against the reaction time. A pseudo-first-order rate constant was estimated from the slope of the straight line obtained.

Results and Discussion

In the present experiment, the first problem was whether polysaccharides such as dextrin could be solubilized in benzene in the presence of DBSH or not; polysaccharides could hardly be supposed to be solubilized easily because of their high molecular weights, at least in the same manner as occurs for low molecular weight analogs. In a preliminary experiment, however, addition of dextrin aqueous solution drop by drop to benzene with vigorous stirring was found to give a perfectly clear solution.

Then, we measured the maximum amount of solubilized water containing dextrin. Figure 1 shows the plots of the maximum amount of solubilized water containing dextrin at several concentrations in DBSH

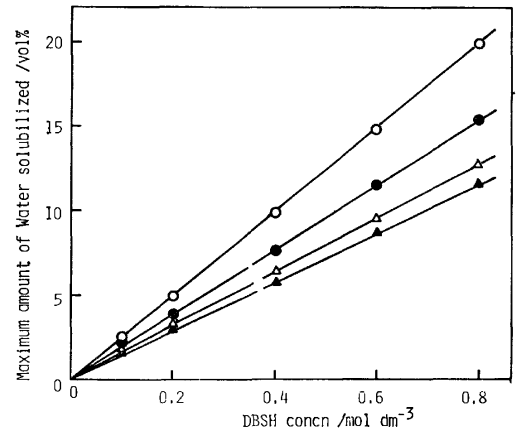

Fig. 1. Plots of maximum amount of solubilized water containing dextrin at several concentrations in DBSH benzene solution against concentration of DBSH, at room temperature.
Concentration of dextrin, %: ○, 0; ●, 2.49; △, 5.79; ▲, 17.7.

benzene solution against concentration of DBSH. The maximum amount of solubilized water was found to increase proportionally with an increasing concentration of DBSH. Figure 2 shows changes in the maximum amount of solubilized water with changing concentration of dextrin in the water. The maximum amounts of solubilized water are found to decrease with an increasing concentration of dextrin, especially in the lower range of the concentration.

The critical micelle concentration (CMC) was estimated with the method of methachromasis of Methylene Blue solubilized in the micelle; we measured the red shift of a peak in the UV spectrum of the added Methylene Blue with changing concentration of DBSH.[2] Figure 3 shows a typical change in the wavelength corresponding to the left-hand side peak in an absorption spectrum of Methylene Blue (shown in the figure), with changing concentration of DBSH. The inflection point of the sigmoidal curve obtained was presumed to be the CMC of DBSH, just as the case of a sucrose-containing reversed-micelle system. Figure 4 shows the plot of the CMC against the amount of water solubilized in the DBSH benzene solution. The CMC is found to increase proportionally with the increasing amount of solubilized water. This result does not conflict with the relationship between the maximum amount of solubilized water and the concentration of DBSH, and agrees with the change in the CMC obtained in the case of a sucrose-containing reversed-micelle system.[2] Figure 5 shows plots of the CMC against concentration of dextrin in water solubilized and the CMC's are found to increase slightly with increasing concentration of dextrin. This tendency is contrary to that observed in the case of the sucrose-containing reversed-micelle system,[3] and is supposed to result from the high molecular weight of dextrin; the higher molecular weight of the substrate is inferred to need more DBSH molecules to form the reversed micelle.

The hydrolysis of dextrin in water solubilized in DBSH benzene solution was investigated. In this case, the concentration of dextrin was expressed as moles of anhydroglucose repeating unit in the total volume, not in water alone. Figure 6 shows typical first-order plots of the amount of reducing sugar in

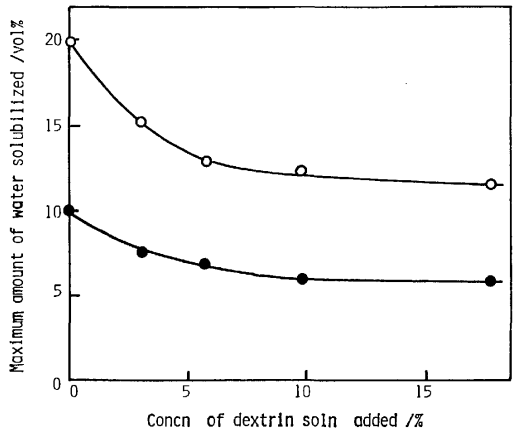

Fig. 2. Changes in maximum amount of solubilized water in DBSH benzene solution, with changing concentrations of dextrin contained in the water, at room temperature.
Concentration of DBSH, mol dm^{-3} as acid: ○, 0.80; ●, 0.40.

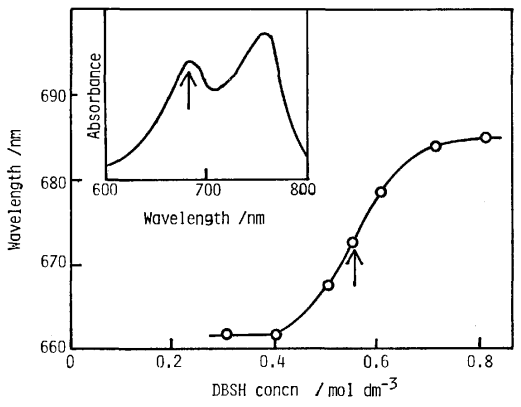

Fig. 3. Typical change in wavelength corresponding to the left-hand side peak in an absorption spectrum of Methylene Blue added to DBSH benzene solution (shown above), with changing concentrations of DBSH. Solubilized water, 5.50 vol%. Concentration of dextrin, 3.68%.

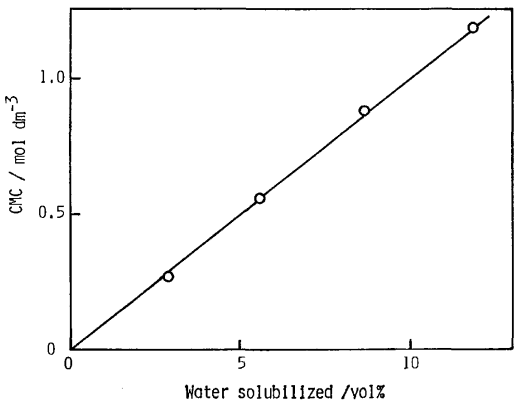

Fig. 4. Plot of CMC estimated with the Methylene Blue methachromasis method against the amount of water solubilized in DBSH benzene solution. Concentration of dextrin, 3.68%.

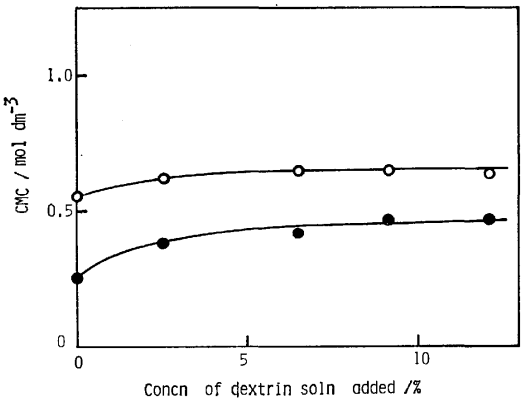

Fig. 5. Plots of CMC against concentration of dextrin in water solubilized in DBSH benzene solution. Water solubilized, vol%: ○, 5.50; ●, 3.50.

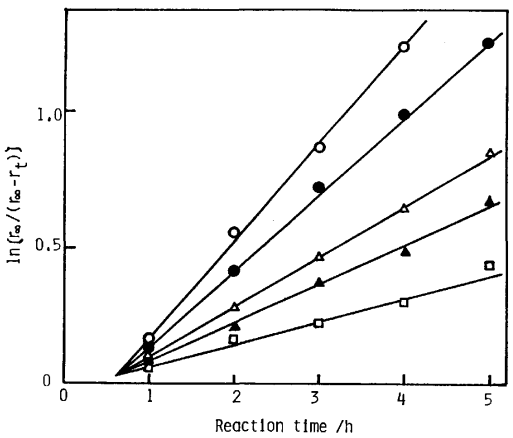

Fig. 6. Typical first-order plots of the changes in the amount of reducing sugar in the reaction mixture at 60 °C.
r_t and r_∞ are the amounts of reducing sugar at a reaction time t and infinity. Concentration of dextrin, 3.29×10^{-3} mol dm^{-3}. Concentration of DBSH, mol dm^{-3}: ○, 0.45; ●, 0.40; △, 0.35; ▲, 0.30; □, 0.25. Solubilized water, 5.50 vol%.

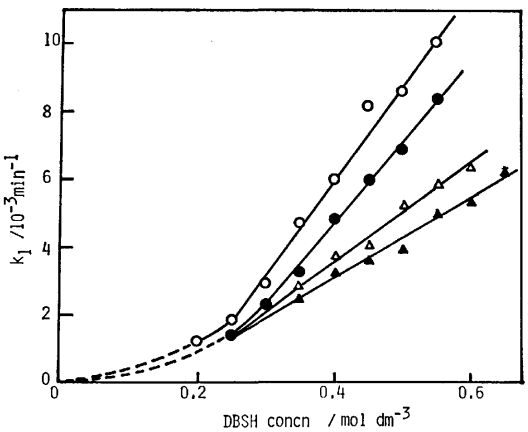

Fig. 7. Plots of pseudo-first-order rate constant, k_1, of dextrin hydrolysis against concentration of DBSH, at 60 °C.
Solubilized water, 4.77 vol%. Concentration of dextrin, 10^{-3} mol dm^{-3}: ○, 1.63; ●, 3.29; △, 4.53; ▲, 6.05.

the reaction mixture; a fairly good straight line is obtained for each plot. A pseudo-first-order rate constant, k_1, was estimated from the slope of the straight line. Figure 7 shows plots of k_1 against concentration of DBSH. The values of k_1 are found to increase proportionally with an increasing concentration of DBSH in the range of the concentration higher than 0.30 mol dm^{-3}. No break point, such as was found in the similar plot in the case of a sucrose-containing reversed-micelle system at CMC of DBSH, was found of the plots in this range, although the CMC of DBSH in this case is in a range of 0.45 to 0.60 mol dm^{-3}. The difference may be related to the solubilizing states of the substrates; the high molecular weight of the substrate may make the solubilizing state of the substrate less stable. The details are now under investigation. The maximum apparent second-order

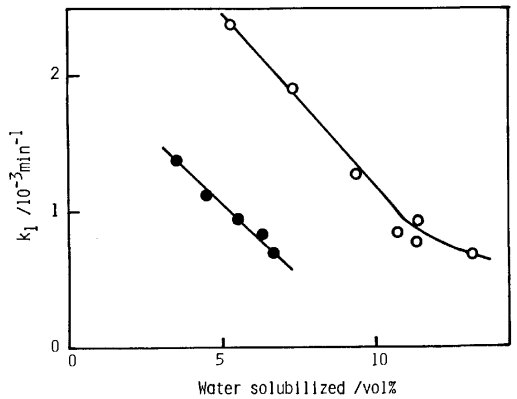

Fig. 8. Plots of k_1 against the amount of solubilized water.
Concentration of dextrin, 13.5×10^{-3} mol dm^{-3}. Concentration of DBSH, mol dm^{-3}: ○, 0.80; ●, 0.40.

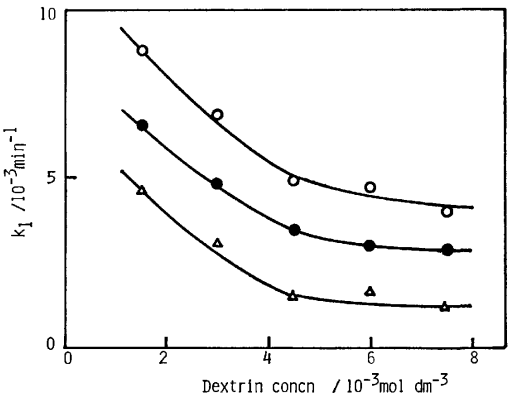

Fig. 9. Plots of k_1 against concentration of dextrin. Solubilized water, 4.77 vol%. Concentration of DBSH, mol dm^{-3}: ○, 0.50; ●, 0.40; △, 0.30.

rate constant estimated from the slope of the straight line in Fig. 7, not considering the amount of solubilized water, is 2.8×10^{-2} dm^3 mol^{-1} min^{-1}, which is about 285-times larger than that of dextrin hydrolysis in aqueous solution in the presence of DBSH normal micelle, under similar conditions.

Figure 8 shows plots of k_1 against the amount of solubilized water. The k_1 is found to decrease considerably with increasing amounts of solubilized water. Figure 9 shows plots of k_1 against concentration of dextrin. The k_1 is found to decrease with an increasing concentration of dextrin, especially in the lower range of concentration. This change in k_1 is contrary in tendency to that observed in a sucrose hydrolysis in the same reversed-micelle system. The difference may result from the difference in molecular weights of the substrates; the higher molecular weight of the substrate is inferred to lead to the less stable reversed micelle.

Conclusion

Even an addition of water containing a higher molecular weight substrate such as dextrin to the DBSH benzene reversed-micelle system gave a perfectly clear solution. The CMC of DBSH estimated

with the method of Methylene Blue methachromasis was observed in the solution, just like in the system containing the low molecular weight analogs. Furthermore in the hydrolysis reaction of the dextrin in this system, large rate enhancement, up to 285-fold, on the basis of the reaction in an aqueous DBSH solution, were observed. Some behaviors different from those in the case of sucrose in the same reversed-micelle system were found in the dependences of CMC and hydrolysis rate on the concentration of substrate and in that of k_1 on the concentration of DBSH. These different behaviors may be due mainly to the high molecular weight of dextrin; the high molecular weight of the substrate influences the stability of the reversed micelle, and consequently the association of the substrate and DBSH molecules and the activity of hydrogen ions. These results suggest that the rate enhancement mechanism due to the solvent effect and micelle effect which was observed in the hydrolysis of sucrose in the same reversed-micelle system operates also on the hydrolysis of the high molecular weight substrate such as dextrin, although the state of association of the substrate with water and DBSH is not apparent at the present time.

References

1) For example: "Bioconversion of Cellulosic Substances into Energy, Chemicals, and Microbial Protein," ed by T. K. Ghose, Swiss Federal Institute of Technology, Zürich (1977); "Proc. Symp. on Bioconversion of Cellulosic Substances into Energy, Chemicals, and Microbial Protein," ed by T. K. Ghose, Indian Institute of Technology, Dehli (1978); Adv. Chem. Ser. No. 181 "Hydrolysis of Cellulose: Mechanisms of Enzymatic and Acid Catalysis," ed by R. D. Brown, Jr., and L. Jurasek, American Chemical Society Washington (1979).

2) K. Arai and Y. Ogiwara, *Bull. Chem. Soc. Jpn.*, **49**, 1059 (1976).

3) K. Arai and Y. Ogiwara, *Bull. Chem. Soc. Jpn.*, **51**, 182 (1978).

4) M. Somogyi, *J. Biol. Chem.*, **195**, 19 (1952).

Photooxygenation Reaction and Chemiluminescence of (Arylmethylenehydrazono)triphenylphosphoranes. Possible Generation of Phospha-1,2-dioxetanes[1]

Nobutaka Suzuki,* Kaniti Sano, Satoshi Wakatsuki, and Yasuji Izawa
Department of Industrial Chemistry, Faculty of Engineering, Mie University, Tsu, Mie 514
(Received May 28, 1981)

Photosensitized oxygenation of (benzylidenehydrazono)-, (diphenylmethylenehydrazono)-, (9-fluorenylidenehydrazono)-, (9-xanthenylidenehydrazono)-, and (10-methyl-9,10-dihydroacridin-9-ylidenehydrazono)triphenylphosphoranes at −78 °C gave the corresponding carbonyl compounds and triphenylphosphine oxide and also gave light emission upon warming-up to room temperature.

In the course of the studies on the 1,2-dioxetanes having a hetero atom in the ring and their chemiluminescence,[1,2] we found that photosensitized oxygenation of (arylmethylenehydrazono)triphenylphosphoranes (**1a—b**) gave the corresponding carbonyl compounds (**5a—b**) and triphenylphosphine oxide (**6**) with chemiluminescent light emission (CL) upon warming-up to room temperature.[1] The reactions above can be extended to the more complex (arylmethylenehydrazono)triphenylphosphoranes (**1c—e**). This phenomenon seems to result from the generation and the decomposition of 1,2,3-dioxaphosphetanes as the intermediates (**4**), which apparently resembles to the 1,2,3-dioxathietanes found on the oxygenation of thioketones.[2] The former reactions were the first examples of chemiluminescent 1,2-dioxetanes containing one hetero atom in the ring. In the present paper, we wish to describe the oxygenation reactions of **1** in details (Fig. 1).

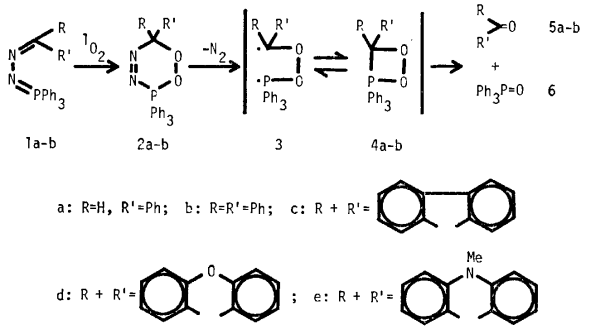

Fig. 1.

Results and Discussion

A solution of **1** (10^{-3}—10^{-2} mol/l) in CH_2Cl_2 with Methylene Blue (10^{-4}—10^{-3} mol/l) was irradiated at −78 °C with a tungsten-halogen lamp through a yellow optical filter (<510 nm cut off) with bubbling O_2. The irradiated solution gave pale-blue light emission upon warming-up to room temperature. The quantum yields of CL (ϕ_{CL}) were *ca.* 10^{-6}—10^{-7} einstein/mol relative to the luminol CL in aqueous solutions.[3] The half life time ($\tau_{1/2}$) of CL were 8.2 s (*ca.* 0 °C) for **1b** and 5.1 s for **1c** at 10^{-4} mol/l for **1**. The CL's were so weak and the $\tau_{1/2}$ were so short that the emission spectra could not be measured, and hence, the emitters were not characterized and the ϕ_{CL} were estimated approximately, provided that the emitter would be the produced ketones or the fluorescer added into the solutions. Lechtken had reported a sensitized photooxidation of acetone azine and the CL of the photooxygenation product, which was assigned to be 3,3,6,6-tetramethyl-3,6-dihydro-1,2,4,5-dioxadiazine (**7**: R=R'=Me) from the NMR spectra of the irradiated solution.[4] Talwar described similar photooxygenation of a several azines which could react through **7** (R=Ph, R'=H; R=Ph, R'=Me; R=R'=Ph).[5]

Recently, Landis and Madoux claimed on Lechtken's report that the supposed peroxide was not a cyclic peroxide **7** but a linear peroxide polymer which was formed by a free-radical oxidation initiated by $^1O_2$.[6]

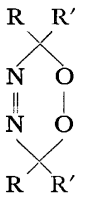

7

A cold photooxygenated solution in CD_2Cl_2 of **1b** was analyzed by ^{13}C-FT NMR at −78 °C: signals centered at δ 103.25 ppm (d, J_{C-P}=197.9 Hz) were assigned as the quart. C in the 6-membered peroxide (**2b**), which disappeared thoroughly upon warming up to room temperature in 5 min. In turn, signals of benzophenone (**5b**) and triphenylphosphine oxide (**6**) took place.

The spent solutions gave only two spots on TLC; the ketones (**5**) and triphenylphosphine oxide (**6**) almost quantitatively (GLC). These data suggest that the 6-membered peroxide (**2**) could be formed as an intermediate with the reaction of $^1O_2$ to **1** and the successive extrusion of N_2 from **2** resulted in the 4-membered peroxide (**4**) which gave the light emission.

Energy liberated on the decomposition of the supposed dioxaphosphetane (**4**) was calculated as *ca.* 66.1 kcal/mol[7] which is not large enough for exciting some of the ketones (**5**) or **6** to the S_1 states (82.3 kcal/mol for **5a**; 68.9 for **5b**; 56.0 for **5c**; 68.8 for **5d**; 65.5 for **5e**; 65.3 kcal/mol for **6**). Therefore, additional energy (maybe the activation energy) is needed for excitation of **5a—b** and **5c** to the singlet state.

Methylene Blue, irradiation, and O_2 were essential for the present photooxygenation. On addition of

KO_2, **1** did not give **5** and/or **6**. Addition of $^1O_2$-quenchers[6] (β-carotene and 1,4-diazabicyclo[2.2.2]-octane (DABCO)) quenched the reaction. A radical scavenger (2,4,6-tri-*t*-butylphenol)[6] did not affect the reaction. These data suggest that the present photooxygenation reactions are non-radical ones initiated by $^1O_2$ and seems to support the Lechtken's mechanism rather than the Landis' one.

Apparently, the "dioxaphosphetane" derivatives, **4**, were the first chemiluminescent dioxetanes having one additional hetero atom instead of the carbon atom.[8]

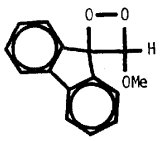

8

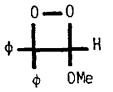

9

Nearly all the dioxetanes studied so far give carbonyl products with lowest excited states of n,π^* configuration.[9] It is conceivable that a dioxetane giving excited carbonyls in which the excitation energy was more delocalized (in a π,π^* state) may be less stable and give relatively more singlet products (greater ϕ_{CL}). A switch from a stepwise mechanism of decomposition (*via* a short-lived diradical-like intermediate as is now generally accepted) to a concerted cleavage may then take place.[9]

Wilson *et al.*[10] compared dioxetanes (**8** and **9**), which produce fluorenone [**5c**: S_1 (π,π^*)] and benzophenone [**5b**: S_1 (n,π^*)] and found significant difference between them: *i.e.*, **8** has much smaller E_a (activation energy) and log A than **9** has. Moreover, **8** gives the singlet excited product, while **9** the triplet one. They suggested that the difference in the electronic configuration of the two ketones (π,π^* instead of n,π^*) allows a change of mechanism of dioxetane cleavage (from a two-step radical mechanism to perhaps a concerted cleavage).[10]

The present results on **1b** and **1c**, however, did not satisfy the expectation of the effect of the electronic configurations of the products on the chemiluminescence efficiency. This might be explained by the fact that **2** may give the radical intermediate (**3**) first, which decomposes directly to the products (**5** and **6**) or indirectly through the dioxaphosphetane (**4**). The direction of the decomposition is in a reverse order to the decomposition of the ordinary 1,2-dioxetanes.

Experimental

Instrumentation. All mp were uncorrected. Following spectrophotometers were used for spectral measurements: IR: JASCO IR-G and A-100; UV: Shimadzu UV-200; NMR JEOL JNM-MH-100 (100 MHz) and FX-100 (99 MHz for ^1H and 25.05 MHz for ^{13}C); MS: JEOL JMS-D-100; Fluorescence: Hitachi MPF-2A. The spectral data are presented as follows: IR in cm^{-1}; UV: in nm (ε given in parentheses); NMR: δ in ppm from int. TMS and J in Hz (accuracy ± 0.5 Hz); MS in m/z; fluorescence: λ_{max} in nm. GLC were carried out by Yanagimoto Yanaco G-80FP and G-180F.

Materials. Ketones (**5a—e**) and $Ph_3P{=}O$ (**6**) were purchased. (Arylmethylenehydrazono)triphenylphosphoranes (**1a—c**) were prepared according to the literatures. **1a**: Yellow-green granules, mp 141—142 °C (lit,[11] 141—142 °C); λ_{max} (KBr) 1435, 1100, 840 cm^{-1}; δ ($CDCl_3$) 7.42 (20H, m), 8.36 (1H, d); m/z 380 (M^+); UV: λ_{max} (CH_2Cl_2) 328 nm (ε 23000); FL: λ_{max} (CH_2Cl_2) 483 nm. **1b**: pale-yellow crystalline powder ($CHCl_3$), mp 167—174 °C (lit,[11] mp 173°); m/z 456 (M^+); UV: λ_{max} (CH_2Cl_2) 231 (ε 20400), 323 nm (9900). **1c**: yellow granules (EtOH), mp 208.5—210 °C (lit,[12] mp 209—210 °C); m/z 454 (M^+); UV: λ_{max} (CH_2Cl_2) 247 (ε 27400), 257 (14200), 294 (6900), 387 nm (10700).

*(9-Xanthenylidenehydrazono)triphenylphosphorane (**1d**)*: A solution of triphenylphosphine (3 g: 1.2×10^{-2} mol) in abs. benzene (50 ml) was cooled in an ice–salt bath under argon streams. Into the solution was added bromine (1 ml: *ca.* 1.0×10^{-2} mol) and then triethylamine (2 g: 2.0×10^{-2} mol). After the resulted solution was stood for a while at room temperature, 9-xanthenone hydrazone[13] (2.1 g: 1.0×10^{-2} mol) in abs. benzene (50 ml) was added and the mixture was stirred overnight at room temperature. After removing triethylamine·HBr with suction and evaporation of benzene gave a redish-brown oil, which resulted in crude crystals of **1d** after crystallization from $CHCl_3$, ether, and pet. ether at 0 °C. Orange-yellow granules, 0.9 g (19.1%). Main parts of the crystals were recrystallized from $CHCl_3$ and pet. ether, purified with Nylon-column chromatography (Woelm Silicagel: *ca.* 30 cm, ϕ 1.9 cm; CH_2Cl_2), and then recrystallized from EtOAc.

Yellow granules, mp 196—199 °C, Found: C, 78.88; H, 4.66%. Calcd for $C_{31}H_{23}N_2PO$: C, 79.14; H, 4.93%. m/z 470 (M^+); ν_{max} (KBr) 1450, 1030, 900 cm^{-1}; δ ($CDCl_3$) 7.26 (m), 10.20 (d); UV: λ_{max} (CH_2Cl_2) 394 (ε 14000), 296 nm (ε 6400).

*(10-Methyl-9,10-dihydroacridin-9-ylidenehydrazono)triphenylphosphorane (**1e**)*: A solution of 9-(*N'*-formylhydrazono)-10-methyl-9,10-dihydroacridine[14] (0.7 g: 2.8×10^{-3} mol) in 15% $HClO_4$ (12 ml) was heated at 100 °C for 2 min and then cooled to room temperature. The resulted perchlorate was collected and recrystallized from EtOH containing a few drop of $HClO_4$ to give dark-tan needles, mp>300 °C. Yield 0.51 g (56.7%). ν_{max} (KBr) 1590, 1465, 760 cm^{-1}; δ (DMSO-d_6) 7.82 (d), 7.40 (m), 3.94 (s). This was used immediately for the following preparation.

To a solution of the perchlorate (565 mg: 1.75×10^{-3} mol) and KOH (1.2 g: 2.1×10^{-2} mol) in EtOH (100 ml) was added HgO (red: 0.4 g: 1.85×10^{-3} mol) and the mixture was stirred overnight at room temperature under argon streams. To the filtrate of the mixture was added a solution of Ph_3P (0.46 g: 1.76×10^{-3} mol) saturated in ether under argon streams and the resulted mixture was stirred overnight at room temperature. After evaporation, the mixture was chromatographed on silica gel (Woelm: 30 cm, ϕ 1.9 cm; CH_2Cl_2). Reddish-brown needles, mp $\approx$189 °C: Yield, 75.4 mg (19.5%). Found; C, 79.66; H, 5.30%. Calcd for $C_{32}H_{26}N_3P$: C, 79.485; H, 5.420%. m/z 277 ($M^+ - 206$); ν_{max} (KBr) 1595, 1360, 1180, 740 cm^{-1}; δ ($CDCl_3$) 8.62 (d), 7.56 (m), 3.80 (s); UV: λ_{max} (CH_2Cl_2) 400 (ε 16000), 382 (12000), 306 (4700), 293 nm (7400).

*Sensitized Photooxygenation of **1a—e**.* A solution of **1** (10^{-3}—10^{-2} mol/l) in CH_2Cl_2 (dried over CaH_2: 5 ml) containing Methylene Blue (10^{-4}—10^{-3} mol/l) was irradiated in a Pyrex cell (ϕ 10 mm) or a quartz cell (ϕ 10 mm) at −78 °C with bubbling O_2 with a 300 W tungsten-halogen lamp (Kondo/Sylvania Projector lamp; ELH 120 V/300 W at 100 V) through a yellow optical filter (Toshiba

Table 1. Photooxygenation of **1** and the CL

1	**5**(%)	**6**(%)	Φ_{CL} (einstein/mol)[a]	τ_{CL} (*ca.* 0 °C)
a:	89	89	3.0×10^{-6}	
b:	75	g.y.[b]	3.1×10^{-6}	8.2 s
c:	91	75	4.5×10^{-6}	5.1 s
d:	100	67	7.5×10^{-7}	
e:	85	86	4.1×10^{-6}	

a) Relative to the CL of luminol (Ref. 3). b) Quantitative yield.

Table 2. Effect of inhibitors on photooxygenation of **1**

Inhibitor(In)	[In]/[**1**]	**1a**	**1b**	**1c**	**1d**
DACCO	25	Q[a]	Q	Q	Q
β-Carotene	5	Q	Q	Q	Q
2,4,6-Tri-*t*-butylphenol	25	N[b]	N	N	N

a) Q: Quenched. b) N: Not effected.

O-52: <510 nm cut off) for 60 min.

Chemiluminescence with/without Fluorescer. The irradiated solutions as above were warmed up to room temperature with/without fluoresceres (9,10-dibromo- and 9,10-diphenylanthracene, or rubrene: 10 mmol/l) in the cell chamber of MPF-2A and the light emitted was recorded. The quantum yields are shown in Table 1.

*^{13}C-NMR of the Irradiated Solution of **1b** in CD_2Cl_2.* CD_2Cl_2 Solution irradiated as above in a Pyrex NMR tube was analysed by ^{13}C-FTNMR at −78 °C. δ (TMS) 103.25 (d, J=197.9) at −78 °C, disappeared when warmed-up to room temperature for 5 min.

Product Analyses. The spent solutions of the irradiated samples were analysed by GLC and TLC: only two spots on TLC were appeared and identified as the ketones and Ph_3PO, which were estimated by GLC as shown in Table 1.

Effect of Inhibitors on CL. Inhibitors were added into the solutions and the effect on the photochemical reactions and the CL was estimated (Table 2).

We thank Drs. T. Kondo and H. Nakamura and Professor T. Goto, Nagoya University, for their taking MS and FT NMR and the Ministry of Education, Science, and Culture of Japan for the financial support (Grant-in-Aid).

References

1) Preliminary commun.: N. Suzuki, S. Wakatsuki, and Y. Izawa, *Tetrahedron Lett.*, **21**, 2313 (1980); A part was presented at the 13th Congress of Heterocyclic Chemistry, Shizuoka, Japan, 1980.

2) N. Suzuki, K. Sano, N. Tani, and Y. Izawa, *Heterocycles*, **16**, 1133 (1981) and references cited therein.

3) J. Lee and H. H. Seliger, *Photochem. Photobiol.*, **4**, 1015 (1965); **15**, 227 (1972).

4) P. Lechtken, *Z. Naturforsch., Teil B*, **31**, 1436 (1976).

5) S. S. Talwar, *Indian J. Chem.*, **16B**, 980 (1978).

6) M. E. Landis and D. C. Madoux, *J. Am. Chem. Soc.*, **101**, 5106 (1979).

7) Heat of decomposition (ΔH) of **4** to a C=O and a P=O compounds was calculated as follows assuming that the ring strain of **4** is not much different from that of the ordinary 1,2-dioxethanes (26 kcal/mol);[15] C–C–O–O→C=O + C=O; C–P–O–O→C=O+P=O: a) 1 C–C ⇝ 1 C–P (ΔHa), b) 1 C–O ⇝ 1 P–O (ΔHb), c) 1 C=O ⇝ 1 P=O (ΔHc), where ΔHa=82.6[16]−65[16]=+17.6; ΔHb=85.5[16]−86[16]=−0.5; ΔHc=179.0[16]−128[16]=+51.0; therefore, $\Delta H'=-(\Delta Ha+\Delta Hb)+\Delta Hc=+33.9$ (kcal/mol); and $\Delta H=\Delta H$ (dioxatane)[15] − $\Delta H'$ = − (*ca.* 100−33.9) = *ca.* −66.1 kcal/mol.

8) For examples of the non-chemiluminescent C–Z–O–O supposed as an intermediate in the literatures, see a) Z=P: W. Adam and J. C. Liu, *J. Am. Chem. Soc.*, **94**, 1206 (1972); C. W. Jefford and G. Barchietto, *Tetrahedron Lett.*, **1977**, 4531; b) Z=S: B. Zwanenburg, A. Wagenaar, and J. Strating, *ibid.*, **1970**, 4683; N. Ishibe, M. Odani, and M. Sunami, *J. Chem. Soc., Chem. Commun.*, **1971**, 118; J. J. Worman, M. Shen, and P. C. Nichols, *Can. J. Chem.*, **50**, 3923 (1972); R. Rajee and V. Ramamurthy, *Tetrahedron Lett.*, **1978**, 5127; S. Tamagaki, R. Akatsuka, M. Nakamura, and S. Kozuka, *ibid.*, **1979**, 3665; J. E. Gano and S. Atik, *ibid.*, **1979**, 4635; S. Tamagaki and K. Hotta, *J. Chem. Soc., Chem. Commun.*, **1980**, 598; N. Ramnath, V. Ramesh, and V. Ramamurthy, *ibid.*, **1981**, 112; c) Z=S or N: W. Ando, S. Kohmoto, and K. Nishizawa, *ibid.*, **1979**, 894; d) Theoretical calculation: L. Carlsen, *J. Chem. Soc., Perkin Trans. 2*, **1980**, 188.

9) J. W. Hastings and T. Wilson, *Photochem. Photobiol.*, **23**, 461 (1976).

10) A. L. Baustark, T. Wilson, M. E. Landis, and P. D. Bartlett, *Tetrahedron Lett.*, **1976**, 2397.

11) W. M. Jones and W. T. Tai, *J. Org. Chem.*, **27**, 1327 (1962).

12) W. Theodore and K. Braunholtz, *J. Chem, Soc.*, **121**, 305 (1922).

13) A. Schönberg and T. Stolpp, *Ber.*, **63B**, 3102 (1930).

14) S. Hümig and H. Herrmann, *Justus Liebigs Ann. Chem.*, **636**, 21 (1960).

15) L. J. Bollyky, *J. Am. Chem. Soc.*, **92**, 3230 (1970); P. Lechtken and G. Höhne, *Angew. Chem., Int. Ed. Engl.*, **12**, 772 (1973).

16) R. F. Hudson, "Structure and Mechanism in Organophosphorus Chemistry," Academic Press, New York, N. Y. (1965), pp. 11 and 68.

 © 1982 The Chemical Society of Japan Bull. Chem. Soc. Jpn., 55, 845—851 (1982)

Preparation and Conformational Properties of Several 1,8-Diarylnaphthalenes

Eiichi Ibuki,* Shigeru Ozasa, Yasuhiro Fujioka, and Hiroshi Mizutani†

Department of Organic Chemistry, Kyoto College of Pharmacy, Misasagi-nakauchi-cho, Yamashina-ku, Kyoto 607

(Received June 5, 1981)

Six new 1,8-diarylnaphthalenes, each having closely held parallel aromatic rings, were synthesized by a Kharash-type Grignard cross-coupling of arylmagnesium iodide and 1,8-diiodonaphthalene in the presence of *N,N'*-bis(1-methyl-3-oxobutylidene)ethylenediaminatonickel(II) as a catalyst. Among them, 1,8-di(1-naphthyl)naphthalene was obtained as *cis* and *trans* rotamers, caused by the restricted rotation at the 1,8-position. Interconversion between the rotamers on heating above their melting points was confirmed by differential scanning calorimetry. The proton magnetic resonance spectral studies of the 1,8-diarylnaphthalenes indicated the presence of a face-to-face arrangement of aromatic rings in the peri-position. Two new 8,8'-diaryl-1,1'-binaphthyls, each having two sets of closely held parallel aromatic rings, were isolated as minor coupling products. *Trans-trans* conformations were proposed for them on the basis of their thermal behavior. Several nickel(II) complexes were found to be effective catalysts for preparative Grignard cross-coupling reaction involving closely crowded geometry.

A number of compounds having closely held parallel aromatic rings, *e.g.* paracyclophanes,[1] janusene,[2] 1,8-diarylnaphthalenes,[3] diarylanthracenes,[4] have been synthesized and studied extensively in view of their specific geometry and their inherent strain due to steric overcrowding. Most of their unusual properties have been ascribed to the existence of such molecules in conformations in which the two benzene rings lie parallel to one another. Recently, Clough and Roberts[5] have found that 1,8-di(*o*-tolyl)naphthalene could be resolved into *cis* and *trans* isomer pair due to a restricted rotation around the tolyl-naphthyl bonds. The two isomers were found to be stable in the crystalline state, but interconversible in solution having a half-life of about one day at room temperature.

The present study was undertaken to synthesize stable rotational isomer pairs of a series of closely related 1,8-diarylnaphthalenes having adjacent parallel π-systems, and to elucidate their structure-physical property correlations. Thus six new 1,8-diarylnaphthalenes (**1**—**6**), having biphenylyl, naphthyl, or terphenylyl groups in the peri-position, were synthesized. Their infrared (IR), ultraviolet (UV), and proton magnetic resonance (^{1}H-NMR) spectra were measured, and the relationship is discussed between the structures and physical properties of the diarylnaphthalenes, especially the characteristics due to the presence of adjacent face-to-face arrangement of two benzene rings. In addition, the characterization and interconversion of the stable *cis* and *trans* rotational isomers of 1,8-di(1-naphthyl)naphthalene (**4**) are also described.

For the synthesis of 1,8-diarylnaphthalenes, the Kharash-type Grignard cross-coupling reaction of the Grignard reagent derived from an appropriate aryl iodide and 1,8-diiodonaphthalene in the presence of nickel(II) complex as a catalyst was employed. Though the similar cross-coupling reaction has already been used for the synthesis of 1,8-di(*o*-tolyl)naphthalene,[5] we introduced the diarylnaphthalenes under modified reaction conditions.

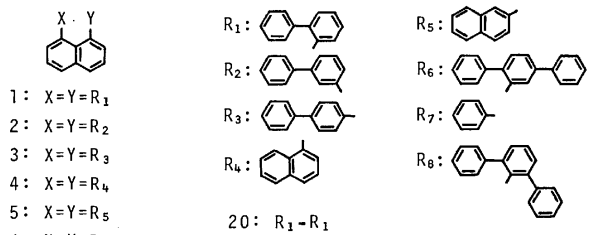

1: X=Y=R_1
2: X=Y=R_2
3: X=Y=R_3
4: X=Y=R_4
5: X=Y=R_5
6: X=Y=R_6
7: X=Y=R_7
8: X=Y=I
9: X=H, Y=R_1
10: X=H, Y=R_2
11: X=H, Y=R_3
12: X=H, Y=R_4
13: X=H, Y=R_5
14: X=H, Y=R_7
15: X=I, Y=R_8

20: R_1-R_1
21: R_2-R_2
22: R_3-R_3
23: R_5-R_5
24: R_6-R_6
25: R_8-R_8

26: R_1I
27: R_2I
28: R_3I
29: R_4I
30: R_5I
31: R_6I
32: R_7I
33: R_8I

16: X=Y=R_1
17: X=Y=R_4
18: X=Y=R_7
19: X=I, Y=R_8

Preliminary experiments using phenylmagnesium iodide and each of two nickel(II) complexes, bis(acetylacetonato)nickel(II) [Ni(acac)$_2$] and *N,N'*-bis(1-methyl-3-oxobutylidene)ethylenediaminatonickel(II) [Ni(acaen)],[6,7] to provide 1,8-diphenylnaphthalene (**7**) indicated that the relative activities of the two complexes were essentially the same (the yields of **7** are 67 and 66%, respectively). Furthermore, alternate preliminary experiments using 1-naphthylmagnesium iodide and each of the following nickel(II) complexes to provide 1,8-di(1-naphthyl)naphthalene showed that all the complexes except potassium tris(L-prolinato)niccolate(II) trihydrate [K[Ni(L-pro)$_3$]·

† Present address: Osaka Kosei-nenkin Hospital, Fukushima, Fukushima-ku, Osaka 553.

$3H_2O$][8] effectively catalyzed the coupling reaction involving considerably crowded geometry: $Ni(acac)_2$, Ni(acaen), bis(4-imino-2-pentanonato)nickel(II) [$Ni(acNH)_2$],[8] bis(η-cyclopentadienyl)nickel(II) [$Ni(C_5H_5)_2$],[8] bis(salicylaldehydato)nickel(II) dihydrate [$Ni(sal)_2 \cdot 2H_2O$],[8] bis(trifluoroacetylacetonato)nickel(II) [$Ni(tfa)_2$],[8] and $K[Ni(L\text{-}pro)_3] \cdot 3H_2O$ (Table 1). On the basis of the foregoing results, Ni(acaen) was used as a catalyst in the preparative experiments.

Among the iodo compounds used, iodobiphenyls[9] (2- (**26**), 3- (**27**), and 4-iodobiphenyl (**28**)) and 2'-iodo-*p*-terphenyl (**31**)[10] were prepared by the methods previously reported. 2'-Iodo-*m*-terphenyl (**33**) was derived by the Ullmann coupling of 1,3-dibromo-2-nitrobenzene and iodobenzene,[11] followed by reduction and then conversion into the iodo compound by the usual method. Although, 1-iodo- (**29**) and 1,8-diiodonaphthalene (**8**)[4] were prepared from corresponding amino compounds, 2-iodonaphthalene (**30**) and iodobenzene (**32**) were commercially available.

The coupling reaction was proceeded by adding a solution of diiodo compound (**8**) and nickel(II) complex (0.1—0.3 mol%) in benzene as a single batch to a refluxing solution of each arylmagnesium iodide (4 fold to 8 fold excess) in an ether–benzene mixture. The reaction products were subjected to column chromatography on alumina. The 1,8-diarylnaphthalenes (**1**—**7**)[12] and by-products thus obtained are given in Table 2.

Table 1. Catalytic activity of various nickel complexes for the cross-coupling of $1\text{-}C_{10}H_7MgI$ with $C_{10}H_6I_2$(1,8-) (**8**)[a]

Catalyst	Conversion of **8**	Products (Yield/%)[b]		
	%	**4**	**17**	**29**
None	91.3	3.2	0	70.2
$Ni(acac)_2$	100	40.8	17.6	1.8
Ni(acaen)	100	42.2	16.2	3.0
$Ni(acNH)_2$	100	43.5	19.2	1.8
$Ni(C_5H_5)_2$	100	38.6	18.0	4.2
$Ni(sal)_2 \cdot 2H_2O$	100	37.4	15.8	2.8
$Ni(tfa)_2$	100	37.4	17.6	3.2
$K[Ni(L\text{-}pro)_3] \cdot 3H_2O$	100	12.3	4.2	4.9

a) Determined by quantitative GLPC, using triphenylamine as an internal standard calibrated against the pure samples. b) Based on the **8** used.

Table 2. Syntheses of 1,8-diarylnaphthalenes by the Grignard cross-coupling of ArMgI with $C_{10}H_6I_2$(1,8-) (**8**)

ArI in ArMgI	Diarylnaphthalene (Yield/%)	Other products
32	**7** (58)	**14**, **18**
26	**1** (27)	**9**, **16**, **20**
27	**2** (41)	**10**, **21**
28	**3** (42)	**11**, **22**
29	**4** (37)	**12**, **17**
30	**5** (31)	**13**, **23**
33	—	**15**, **19**, **25**
31	**6** (11)	**24**

The hitherto-unknown 1,8-diarylnaphthalenes (**1a**, **1b**, **2**, **3**, **4a**, **4b**, **5**, and **6**) thus prepared and 8,8'-diaryl-1,1'-binaphthyl (**16** and **17**) thus isolated as minor products, gave satisfactory analytical results and spectral data (IR, UV, and MS) consistent with the indicated structures. In the coupling reaction, rather low yields of diarylnaphthalenes (**1**—**5**) (27—42%) as compared with that of **7** (58%) may due to enhanced overcrowded conformations of the formers. Furthermore, a very low yield of **6** (11%) and unsuccessful result in the attempted coupling of **8** and Grignard reagent derived from **33**, may also be attributable to the steric crowd during the course of the reactions. The table also shows the formation of 1-arylnaphthalenes (**9**—**14**)[13] and 8,8'-diaryl-1,1'-binaphthyls (**16**—**18**) as common and uncommon by-products, respectively. These by-products formations may reasonably be ascribed to have proceeded *via* the process of Grignard exchange[14] between the Grignard reagent and the iodo compound as follows. In most of the coupling reactions, homo-coupling products (**20**—**25**) of the Grignard reagents were also isolated.

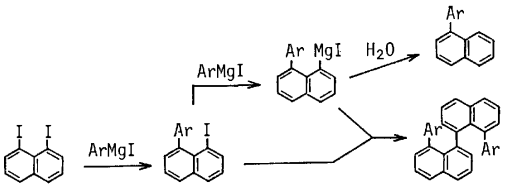

Among the diarylnaphthalenes, **1** was obtained in two forms, **1a** (plates, mp 144.8—145.7 °C) and **1b** (needles, mp 150.3—151.3 °C), from cyclohexane. Repeated crystallizations of **1a** from ethanol yielded **1b**. Both **1a** and **1b** gave slightly different IR spectra, but practically identical ^{1}H-NMR, UV, and mass spectra. The DSC curve for melting of **1a** showed an endothermic peak at 144 °C. After two weeks' annealing period, however, the second run of the melt showed two peaks at 144 °C and 149 °C. While, the DSC curve of **1b** showed a peak originally at 150 °C, after two weeks the second run of the melt showed a new small peak at 144 °C together with the original one at 149 °C. The thermoanalytical analyses suggest the formation of an equilibrium mixture of **1a** and **1b** at or above 150 °C. Though lacking a conclusive proof, it seems very likely that **1a** and **1b** are a rotational isomer pair.

On the other hand, **4** was obtained as more soluble needles **4a** (mp 155.4—156.8 °C) and less soluble plates **4b** (mp 173.3—174.2 °C) in a benzene–ethanol mixture. Both **4a** and **4b** revealed similar UV, slightly different IR, and different ^{1}H-NMR spectra which were found to be compatible with *cis* and *trans* conformations, respectively. The DSC curve of **4a** showed endothermic peaks at 158 °C and 173 °C, having approximately the intensities of 2:1. After cooling, the second run of the melt also showed two peaks at practically the same temperatures but having reverse intensities of 1:5. Further run of the melt did not exhibit any appreciable change compared with

that of the second. However, **4b** displayed at first only one peak at 174 °C. The second run of the melt showed practically the same DSC curve as that of the second run of **4a**, having two peaks at 157 °C and 173 °C with approximate intensities of 1:5. In addition, ^{1}H-NMR spectra ($CDCl_3$) of both melts of each second run of **4a** and **4b** are superimposable, and are compatible to that of a mixture of **4a** and **4b**. On the basis of the foregoing results, it was clarified that **4a** (*cis*) and **4b** (*trans*) were interconversible by heating, and that either of **4a** (*cis*) and **4b** (*trans*) formed same equilibrium mixture of a ratio of approximately 1:4 at or above 176 °C.[15] Both rotamers **4a** and **4b** are quite stable in a solution ($CDCl_3$) at room temperature over two weeks. The stability seems to be remarkable as compared with the half-life of only about one day in solution with respect to interconversion between *cis* and *trans* of 1,8-di(*o*-tolyl)naphthalene at room temperature.[5] Though the *cis* rotamer **4a** would be achiral, the *trans* rotamer **4b** would be a racemic mixture. Identification of the antipodes by resolution was not attempted.

Another crowded diarylnaphthalene, **6** was obtained as colorless needles mp 225.6—227.6 °C, presumably having a *trans* conformation on the basis of its heat stable character.[16] Analogously, both heat stable 8,8′-diaryl-1,1′-binaphthyls, **16** and **17**, may possibly be considered to have *trans-trans* conformations.[16] Although, each of these compounds, **6**, **16**, **17**, and **18**, would be a racemic mixture, their resolutions were not attempted. Each of the other diarylnaphthalenes (**2**, **3**, and **5**) proved to be single substances suggesting a sufficiently low energy barrier to rotation of two aryl rings around the bonds at the peri-position.[4]

The IR spectra of the 1,8-diarylnaphthalenes and related compounds were measured by the KBr-disk method and their characteristic bands in the 680—915 cm^{-1} region were tentatively assigned. These bands are consistent with the kinds of aryl groups and naphthalene ring(s) comprising each of the compounds. All of the compounds show very similar spectra to those of polyphenyls.[9-11] In addition, the characteristic C–C out-of-plane bending vibration bands of substituted naphthalene were observed commonly in the 800—850 cm^{-1} region. However, no significant spectral differences between 1-aryl- and corresponding 1,8-diarylnaphthalenes (presumably due, if any, to the face-to-face arrangement of two benzene or naphthalene rings in the peri-position) were noticed.

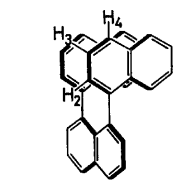

4a

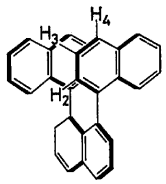

4b

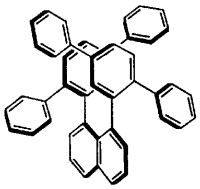
6

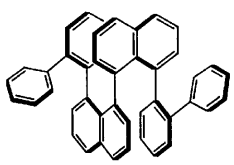
16

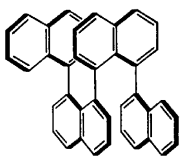
17

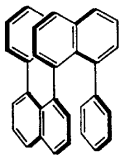
18

The slightly different spectra of **4a** and **4b** in the regions 770—780 cm^{-1} and 820—840 cm^{-1}, assignable to C–H out-of-plane bending on the 1-naphthyl ring and to C–C out-of-plane bending of the naphthalene ring, may be ascribed to their *cis* and *trans* conformation, respectively.

The UV spectra of the 1,8-diarylnaphthalenes and related compounds were measured in cyclohexane solution.

The absorption curves of **4** and **17** were related closely to that of **12**, which corresponds to structural unit of **4** and **17**. Thus, a blue shift and an increase in intensity of the band at 223 nm of **12** with an increase of 1-naphthyl unit were observed.

The spectra of the *cis* rotamer **4a** and the *trans* rotamer **4b** were found to be practically identical. This suggests the lack of significant transannular π-electronic interaction between parallel peri-naphthyl rings of **4a** and **4b**, presumably due to the remote distance of the parallel rings beyond the limit of interaction.[17] Both spectra of 8,8′-diaryl-1,1′-binaphthyls, **18** and **16**, showed similarly a significant red shift (near 316 nm) as compared with that of simpler analog **12**. However, it is difficult to ascertain whether the shifts are due to an increase of aromatic rings[18] or to the transannular π-electronic interaction of parallel aromatic rings. Among the spectra of 1,8-di(biphenylyl)-naphthalenes, that of **3** revealed an increase in intensity of the E-band and a red shift of the longest wavelength absorption band as compared with that of **11**. The spectral differences of **1** with **9**, and of **2** with **10** are essentially similar to that of **7** with **14**.

The foregoing UV spectral results indicated that no significant influence originated from the face-to-face arrangement of the aromatic rings in the peri-positions.

The ^{1}H-NMR spectra of the diarylnaphthalenes and related compounds were measured at 80 MHz in $CDCl_3$ solution.

In the spectrum of the simplest 1,8-diarylnaphthalene **7**, a sharp singlet of phenyl protons appears at higher field by approximately 0.5 ppm compared with that of the monoaryl analog **14**, owing to the anisotropic effect of the faced benzene rings. This high field shift may be comparable to those observed for the faced aromatic protons of [2.2]paracyclophane (δ 6.37)[19] and of janusene (δ 6.60)[2a] as compared with those of *p*-xylene (δ 7.05)[20] and of *o*-xylene (δ 7.10),[2a] respectively. In the spectra of **1**, **2**, and **5**, the aromatic proton signals were also observed at rather high field region as compared with those of corresponding monoaryl analogs **9**, **10**, and **13**, sug-

gesting the presence of a face-to-face arrangement of benzene or 2-naphthyl rings in the peri-position. In the case of **3**, a sharp singlet, which can be assigned to the protons of both phenyl rings, is observed at lower field than that of **7** but similar to that of **14**, indicating that the faced phenyl rings are situated further apart from each other than in **7**.

In the spectrum of isomer **4b**, the chemical shift of naphthyl-C_4 protons (δ 7.03) is nearly comparable to that of the phenyl protons of **7**, whereas the signals of naphthyl-C_2,C_3 protons are shifted appreciably toward higher field presumably owing to the ring current effects caused by the partially parallel naphthyl rings. Analogous but more prominent upfield shifts over 1 ppm have been observed in the spectrum of *anti*-[2.2](1,4)anthracenophane, in which C_2, C_3-protons were located nearly above the opposed anthracene ring.[21] Spectrum of isomer **4a**, however, shows quite different signal pattern of naphthyl-C_2,C_3,C_4-protons (δ 7.00—6.65), but similar signals for other protons in the spectrum of **4b**. Although an assignment of the former pattern is difficult, lack of the characteristic signals of **4b** in the high filed region (δ 6.50—6.14) reflects undoubtedly the absence of protons located nearly above the opposite naphthalene ring.

Thus the foregoing spectral aspects on **4a** and **4b** are obviously compatible with the proposed conformations as *cis* and *trans* rotamers, respectively.

Experimental

Instruments. Low melting points were determined with a Mettler FP-51 or FP-52 apparatus; for those above 300 °C, a Shimadzu DSC-30M differential scanning calorimeter was employed. The calorimeter was also used for thermoanalytical purpose. The UV spectra were measured on a Shimadzu MPS-50L spectrophotometer, IR spectra on a Leitz III-G spectrophotometer, and ^{1}H-NMR spectra on a Varian CFT-20 spectrometer at 80 MHz, using TMS as an internal standard. The molecular weights were determined with a Hitachi RMU-6E mass spectrometer. Quantitative GLPC was performed on a Shimadzu GC-5APTF gas chromatograph using a 1 m×3 mm ϕ glass column 3% Silicone OV-17 on Chromosorb W AW-DMCS.

Materials. 2- (**26**), 3- (**27**), and 4-Iodobiphenyl (**28**),[9] 2′-iodo-*p*-terphenyl (**31**),[10] *N*,*N*′-bis(1-methyl-3-oxobutylidene)ethylenediaminatonickel(II), bis(4-imino-2-pentanonato)nickel(II), bis(salicylaldehydato)nickel(II) dihydrate, bis(trifluoroacetonato)nickel(II), and potassium tris(L-prolinato)niccolate(II) trihydrate[7] were prepared as reported previously. 2′-Iodo-*m*-terphenyl (**33**) was prepared by the Ullmann cross-coupling of 1,3-dibromo-2-nitrobenzene[11] and iodobenzene, followed by reduction and iodo-substitution of the corresponding diazonium compound. Colorless prisms, mp 114.4 °C (Found: C, 60.99; H, 3.87%. Calcd for $C_{18}H_{13}I$: C, 60.69; H, 3.68%). 1-Iodonaphthalene (**29**) was prepared from 1-aminonaphthalene by the usual method. A colorless oil, bp 117—121 °C/2.66×10^2 Pa. 1,8-Diiodonaphthalene (**8**) was prepared by the method used by House *et al.*[4] Tan prisms, mp 110 °C (lit,[4] mp 108.5—110 °C) (Found: C, 31.88; H, 1.63%). 2-Iodonaphthalene (**30**), iodobenzene (**32**), bis(acetylacetonato)nickel(II), and bis(η-cyclopentadienyl)nickel(II) were commercially available.

General Procedure of Grignard Cross-coupling. Magnesium turnings were placed in a four-necked round-bottomed flask equipped with a reflux condenser. To the flask was added *ca.* 20% of an ethereal solution of aryl iodide (c: 0.8—1.0 mol dm^{-3}) under nitrogen atmosphere, and the mixture was stirred and (if necessary) heated to initiate the reaction. The remaining aryl iodide solution was added dropwise just rapidly enough to maintain a gentle reflux (*ca.* 45 min). After additional 0.5 h heating, the resulting solution was diluted with half its volume of benzene. To the refluxing Grignard reagent was added all at once a hot benzene solution of **8** (c: 0.3 mol dm^{-3}) and a catalyst Ni(acaen) (0.13 mol%, based on Grignard reagent), and the reflux then continued to complete the reaction. After cooling, the mixture was hydrolyzed with concentrated ammonium chloride solution. The resulting mixture was extracted with benzene. The organic layer was separated, washed with water, and then dried. The crude mixture, remaining after removal of the solvent, was subjected to chromatography on alumina with a mixture of cyclohexane and benzene as eluent to separate into each product.

Preparation of 1,8-Diphenylnaphthalene (7). The Grignard reagent prepared from the aryl iodide **32** (4.90 g, 24 mmol) was treated with **8** (2.28 g, 6 mmol) in the presence of Ni(acaen) (8.4 mg, 0.03 mmol) and the mixture was refluxed for additional 10 min, as described in the general procedure. The benzene extract of the product was chromatographed on alumina with a cyclohexane–benzene (9:1, v/v) mixture (C–B(9:1)) to separate into the following compounds.

7: Colorless needles from cyclohexane; mp 151.0 °C lit,[3a] mp 149.5—150.5 °C); yield, 0.98 g (58.0%). IR: 698 vs, 706 m (γ_{C-C}, B); 750 s, 758 s, 765 m (γ_{C-H}, M); 775 vs (γ_{C-H}, d); 829 s, 843 m (γ_{C-C}, N); 880 w.[22] UV: $\lambda_{max}(\varepsilon)$ 198 (42400), 215 (39900), 237 (57700), 302 nm (12000) (lit,[3a] $\lambda_{max}(\varepsilon)$ (95% ethanol) 235.5 (54500), 300 nm (11500)). ^{1}H-NMR δ: 6.89 (10H, s, C_6H_5); ν_2 7.36, ν_3 7.49, ν_4 7.90 (6H, $J_{2,3}$=7.0 Hz, $J_{3,4}$=8.5 Hz, $J_{2,4}$=1.4 Hz, $C_{10}H_6$). (Found: C, 94.38; H, 5.92%; mol wt, 280 (M^+)).

1-Phenylnaphthalene (**14**): A colorless oil (lit,[23] bp 147—154 °C/133—160 Pa); 0.18 g (14.8%). IR: 702 s (γ_{C-C}, B); 735 w; 758 s (γ_{C-H}, M); 775 s (γ_{C-H}, α); 800 s (γ_{C-H}, α; γ_{C-C}, N); 840 w (γ_{C-C}, N); 866 w, 909 w. UV: $\lambda_{max}(\varepsilon)$ 227 (65200), 288 nm (10900). ^{1}H-NMR δ: 7.42 (5H, s, C_6H_5), 7.30—8.00 (7H, m, other protons).

8,8′-Diphenyl-1,1′-binaphthyl (**18**): Colorless prisms from cyclohexane; mp 208.9—210.7 °C (lit,[4] mp 210.5—212.0 °C); 0.15 g. IR: 696 vs, 709 m (γ_{C-C}, B); 750 m, 763 s (γ_{C-H}, M); 770 vs (γ_{C-H}, d); 821 s, 831 m (γ_{C-C}, N). UV: $\lambda_{max}(\varepsilon)$ 195 (55200), 220 (52600), 240 (sh) (34800), 318 nm (12700) (lit,[4] $\lambda_{max}(\varepsilon)$ (95% ethanol), 221 (58000), 248 (sh) (29000), 285 (11000), 315 nm (12000)). ^{1}H-NMR δ: 6.05—6.65 (10H, m, C_6H_5), 6.90—7.63 (12H, m, $C_{10}H_6$). (Found: C, 94.82; H, 5.71%; mol wt, 406 (M^+)).

Perylene: Yellow plates from benzene; mp 274.7—275.7 °C (lit,[24] mp 274—275 °C); 0.01 g.

Preparation of 1,8-Di(2-biphenylyl)naphthalene (1). The Grignard reagent prepared from the aryl iodide **26** (48.8 g, 160 mmol) was treated with **8** (7.6 g, 20 mmol) in the presence of Ni(acaen) (0.14 g, 0.5 mmol), and the mixture was refluxed for additional 2 h. The benzene extract of the product, after removal by distillation under reduced pressure of a large part of the biphenyl and naphthalene, was subjected to chromatography on alumina with a C–B (9:1) mixture and separated into the following compounds.

1a: Obtained by concentration and cooling of the mother liquor of **1b**; colorless plates from cyclohexane; mp 144.8—

145.7 °C; 0.31 g (3.4%). IR: 697 sh s, 701 s (γ_{C-C}, B); 720 m, 738 vs, 747 m, 758 s (γ_{C-H}, M, *o*); 772 s (γ_{C-H}, d); 829 s, 847 w (γ_{C-C}, N). Repeated crystallizations of **1a** from cyclohexane or ethanol gave **1b**.

1b: Colorless needles from cyclohexane; mp 150.3—151.3 °C; 2.12 g (23.3%). IR: 701 s, 706 sh s (γ_{C-C}, B); 720 m, 740 vs, 752 s (γ_{C-H}, M, *o*); 775 s (γ_{C-H}, d); 831 s, 846 w (γ_{C-C}, N). UV: $\lambda_{max}(\varepsilon)$ 204 (72500), 218 (sh) (65100), 244 (sh) (42800), 294 nm (10100). ^{1}H-NMR δ: 7.60—7.65 (2H, q, C_4–, C_5–H of $C_{10}H_6$), 6.75—7.30 (22H, m, other protons). Found: C, 94.70; H, 5.32%; mol wt, 432 (M^+). Calcd for $C_{34}H_{24}$: C, 94.40; H, 5.60%; mol wt, 432.

1-(2-Biphenylyl)naphthalene (**9**): Colorless fine needles from ethanol; mp 113.2—114.4 °C; 1.32 g (22.4%). IR: 699 s (γ_{C-C}, B); 738 m, 745 s, 751 s (γ_{C-H}, M, *o*, α); 770 s (γ_{C-H}, *o*, α); 780 vs, 795 m (γ_{C-H}, α); 803 s (γ_{C-H}, α; γ_{C-C}, N); 866 w, 882 w. UV: $\lambda_{max}(\varepsilon)$ 205 (59300), 225 (60200), 290 nm (9600). ^{1}H-NMR δ: 7.00 (5H, s, C_6H_5), 7.18—7.90 (11H, m, *o*-C_6H_4 and $C_{10}H_7$). Found: C, 94.35; H, 5.83%. Calcd for $C_{22}H_{16}$: C, 94.24; H, 5.76%.

trans, trans-8,8′-Di(2-biphenylyl)-1,1′-binaphthyl (**16**): Colorless plates from hexane; mp 270.8—272.1 °C; 0.46 g. IR: 705 s (γ_{C-C}, B); 737 s, 743 vs, 755 s (γ_{C-H}, M, *o*); 762 sh m, 772 vs (γ_{C-H}, d); 820 m, 830 m, 849 w (γ_{C-C}, N); 866 w. UV: $\lambda_{max}(\varepsilon)$ 203 (81400), 224 (77200), 254 (sh) (33300), 316 nm (10400). ^{1}H-NMR δ: 6.25—7.65 (30H, m, all protons). Found: C, 94.30; H, 5.17%; mol wt, 558 (M^+). Calcd for $C_{44}H_{30}$: C, 94.58; H, 5.42%; mol wt, 558.

1,1′:2′,1″:2″,1‴-Quaterphenyl (**20**): Colorless cubes from ethanol; mp 118.7 °C (lit,[9] mp 118—119 °C); 1.86 g.

Preparation of 1,8-Di(3-biphenylyl)naphthalene (2). The Grignard reagent prepared from the aryl iodide **27** (16.8 g, 60 mmol) was treated with **8** (3.8 g, 10 mmol) in the presence of Ni(acaen) (20 mg, 0.07 mmol), and the mixture was refluxed for additional 2.5 h. The benzene extract, after removal by distillation of a large part of the biphenyl and naphthalene, was chromatographed on alumina with C–B(9:1), C–B(4:1), and finally with C–B(1:1).

2: Colorless needles from benzene–ethanol; mp 148.4—150.3 °C; 1.79 g (41.4%). IR: 697 s, 706 s (γ_{C-C}, B); 754 s, 756 s (γ_{C-H}, M); 778 s (γ_{C-H}, *m*, d); 799 m (γ_{C-H}, *m*, d; γ_{C-C}, N); 833 s, 849 w (γ_{C-C}, N); 892 m (γ_{C-H}, *m*). UV: $\lambda_{max}(\varepsilon)$ 204 (70900), 231 (67100), 302 nm (15100). ^{1}H-NMR δ: 7.85—8.01 (2H, q, C_4–, C_5–H of $C_{10}H_6$), 6.90—7.63 (32H, m, other protons). Found: C, 94.11; H, 5.33%; mol wt, 432 (M^+). Calcd for $C_{34}H_{24}$: C, 94.40; H, 5.60%; mol wt, 432.

1-(3-Biphenylyl)naphthalene (**10**): A colorless oil; 1.02 g (36.7%). IR: 690 m, 698 s, 707 s (γ_{C-C}, B); 754 s (γ_{C-H}, M, α); 778 s, 792 s (γ_{C-H}, *m*, α); 799 s (γ_{C-H}, *m*, α; γ_{C-C}, N); 848 w (γ_{C-C}, N); 865 w; 897 m (γ_{C-H}, *m*). UV: $\lambda_{max}(\varepsilon)$ 205 (49600), 225 (59200), 292 nm (sh) (11400). ^{1}H-NMR δ: 7.30—8.08 (16H, m, all protons). Found: C, 94.02; H, 5.78%. Calcd for $C_{22}H_{16}$: C, 94.24; H, 5.76%.

1,1′:3′,1″:3″,1‴-Quaterphenyl (**21**): Colorless leaves from ethanol; mp 87.1 °C (lit,[9] mp 86—87 °C); 1.46 g.

Preparation of 1,8-Di(4-biphenylyl)naphthalene (3). The aryl iodide **28** (16.8 g, 60 mmol), **8** (3.8 g, 10 mmol), and Ni(acaen) (56 mg, 0.2 mmol) were worked up as described in the general procedure, and the mixture was refluxed for additional 3 h. The benzene extract was concentrated to separate a solid (1,1′:4′,1″:4″,1‴-quaterphenyl, **22**, colorless leaves). After filtration of the solid, the mother liquor was distilled to remove a large part of the biphenyl and naphthalene. The resulting residue was chromatographed on alumina with C–B(3:1), C–B(2:1), and finally with C–B(1:2).

3: Colorless needles from benzene–ethanol; mp 202.4—203.8 °C; 1.83 g (42.4%). IR: 699 s, 704 m (γ_{C-C}, B); 733 s, 762 s, 766 s (γ_{C-H}, M); 781 s (γ_{C-H}, d); 829 s, 842 s (γ_{C-H}, *p*; γ_{C-C}, N); 885 w. UV: $\lambda_{max}(\varepsilon)$ 200 (73300), 214 (sh) (59200), 241 (43700), 254 (35000), 304 nm (23300). ^{1}H-NMR δ: 7.11 (8H, d, J=1.5 Hz, *p*-C_6H_4), 7.27 (10H, s, C_6H_5), 7.35—7.73 (4H, m, C_2–, C_3–, C_6–, C_7–H of $C_{10}H_6$), 7.90—8.10 (2H, q, C_4–, C_5–H of $C_{10}H_6$). Found: C, 94.34; H, 5.89%; mol wt, 432 (M^+). Calcd for $C_{34}H_{24}$: C, 94.40; H, 5.60%; mol wt, 432.

1-(4-Biphenylyl)naphthalene (**11**): Colorless needles from benzene–ethanol; mp 149.3—150.7 °C (lit,[25] mp 147—148 °C); 0.59 g (19.2%). IR: 697 s (γ_{C-C}, B); 729 m; 739 w, 751 m, 765 vs (γ_{C-H}, M, α); 781 vs, 792 m (γ_{C-C}, α); 800 s (γ_{C-H}, α; γ_{C-C}, N); 837 m, 848 w (γ_{C-H}, *p*; γ_{C-H}, N); 873 w. UV: $\lambda_{max}(\varepsilon)$ 209 (42200), 228 (45400), 262 (16400), 294 nm (19000). ^{1}H-NMR δ: 7.30—8.10 (16H, m, all protons). (Found: C, 94.41; H, 5.62%).

Preparation of 1,8-Di(1-naphthyl)naphthalene (4). The aryl iodide **29** (20.3 g, 80 mmol), **8** (3.8 g, 10 mmol), and Ni(acaen) (70 mg, 0.25 mmol) were worked up as described for the preparation of **3**. The benzene extract, after removal by distillation under reduced pressure of a large part of the naphthalene, was chromatographed on alumina with C–B(9:1), C–B(4:1), and finally with C–B(1:1). Crystallization of the eluate with C–B(9:1) from benzene–ethanol afforded **4b**. After filtration of **4b**, the mother liquor was concentrated to afford **4a**.

cis-1,8-Di(1-naphthyl)naphthalene (**4a**): Colorless needles from benzene–ethanol; mp 155.4—156.8 °C; 0.46 g (12.2%). IR: 713 w, 724 w, 770 vs, 772 vs, 781 sh s (γ_{C-H}, α); 792 s, 796 s (γ_{C-H}, α, d); 824 w, 837 m (γ_{C-C}, N); 860 w. UV: $\lambda_{max}(\varepsilon)$ 216 (115400), 294 nm (16700). ^{1}H-NMR δ: 6.65—7.00 (6H, m, C_2–, C_3–, C_4–H of $C_{10}H_7$), 7.10—7.64 (12H, m, C_2–, C_3–, C_6–, C_7–H of $C_{10}H_6$; C_5–, C_6–, C_7–, C_8–H of $C_{10}H_7$), 7.94—8.13 (2H, q, C_4–, C_5–H of $C_{10}H_6$). Found: C, 94.90; H, 5.58%; mol wt, 380 (M^+). Calcd for $C_{30}H_{20}$: C, 94.70; H, 5.30%; mol wt, 380.

trans-1,8-Di(1-naphthyl)naphthalene (**4b**): Colorless plates from benzene–ethanol; mp 173.3—174.2 °C; 0.93 g (24.4%). IR: 714 w, 729 w; 773 vs (γ_{C-H}, α); 792 s, 797 s (γ_{C-H}, α, d); 823 m, 837 w (γ_{C-C}, N); 861 w. UV: $\lambda_{max}(\varepsilon)$ 216 (119700), 294 nm (15900). ^{1}H-NMR δ: ν_2 6.27, ν_3 6.43, ν_4 7.03 (6H, $J_{2,3}$=7.0 Hz, $J_{3,4}$=8.5 Hz, $J_{2,4}$=1.4 Hz, $C_{10}H_7$), 7.10—7.64 (12H, m, C_2–, C_3–, C_6–, C_7–H of $C_{10}H_6$; C_5–, C_6–, C_7–, C_8–H of $C_{10}H_7$), 7.94—8.13 (2H, q, C_4–, C_5–H of $C_{10}H_6$). Found: C, 94.76; H, 5.55%; mol wt, 380 (M^+). Calcd for $C_{30}H_{20}$: C, 94.70; H, 5.30%; mol wt, 380.

1,1′-Binaphthyl (**12**): Colorless plates from benzene–ethanol; mp 158.8 °C (lit,[26] mp 147.5 °C); 2.35 g. IR: 740 m, 743 w, 770 vs, 779 vs, 783 vs (γ_{C-H}, α); 805 vs (γ_{C-H}, α; γ_{C-C}, N); 869 w. UV: $\lambda_{max}(\varepsilon)$ 223 (75200), 284 (13400), 295 nm (13300) (lit,[27] $\lambda_{max}(\varepsilon)$ (95% ethanol) 221 (95500), 283 (13200), 294 nm (12900)). ^{1}H-NMR δ: 7.17—8.05 (14H, m, all protons). (Found: C, 94.16; H, 5.73%).

trans,trans-8,8′-Di(1-naphthyl)-1,1′-binaphthyl (**17**): Colorless plates from benzene; mp 287.5—288.0 °C; 0.41 g. IR: 730 m; 770 vs (γ_{C-H}, α); 791 s, 796 m, 802 m (γ_{C-H}, α, d); 826 m, 834 m (γ_{C-C}, N); 865 w. UV: $\lambda_{max}(\varepsilon)$ 212 (146400), 278 (16000), 306 nm (15100). ^{1}H-NMR δ: 6.48—7.69 (26H, m, all protons). Found: C, 95.08; H, 5.30%; mol wt, 506 (M^+). Calcd for $C_{40}H_{26}$: C, 94.82; H, 5.18%; mol wt, 506.

Preparation of 1,8-Di(2-naphthyl)naphthalene (5). The aryl iodide **30** (15.24 g, 60 mmol), **8** (3.8 g, 10 mmol), and

Ni(acaen) (56 mg, 0.2 mmol) were worked up as described for the preparation of **2**. The benzene extract, after removal by distillation under reduced pressure of a large part of the naphthalene, was subjected to crystallization from C–B(9:1). After filtration of a solid (**23**), the solvent of the filtrate was distilled off. The residue was chromatographed on alumina progressively with C–B(9:1), C–B(5:1), C–B(2:1), and finally with C–B(1:1) to give following compounds.

5: Colorless needles from benzene–ethanol; mp 142.4—144.7 °C; 1.16 g (30.5%). IR: 714 w; 738 s, 754 w (γ_{C-H}, β); 766 m, 775 s (γ_{C-H}, β, d); 804 m (γ_{C-H}, d); 814 s, 833 m, 854 m (γ_{C-H}, β; γ_{C-C}, N); 893 m (γ_{C-H}, β). UV: $\lambda_{max}(\varepsilon)$ 220 (sh) (98300), 227 (101200), 282 nm (19500). ^{1}H-NMR δ: 7.90—8.07 (2H, q, C_4–, C_5–H of $C_{10}H_6$), 6.90—7.88 (18H, m, other protons). Found: C, 94.96; H, 5.26%; mol wt, 380 (M^+). Calcd for $C_{30}H_{20}$: C, 94.70; H, 5.30%; mol wt, 380.

1,2′-Binaphthyl (**13**): Colorless needles from ethanol; mp 77.4 °C (lit,[26] mp 78 °C); 0.88 g (34.6%). IR: 737 m, 746 s, 777 s (γ_{C-H}, α, β); 794 m (γ_{C-H}, α); 801 s (γ_{C-H}, α; γ_{C-H}, N); 826 m, 833 m (γ_{C-H}, β; γ_{C-C}, N); 860 m, 866 w; 895 w (γ_{C-H}, β). UV: $\lambda_{max}(\varepsilon)$ 220 (72300), 227 (70300), 283 nm (17000) (lit,[28] $\lambda_{max}(\varepsilon)$ 219 (63100), 226 (61000), 272 (sh) (13500), 282 nm (15900)). ^{1}H-NMR δ: 7.32—7.70 (7H, m, 2-$C_{10}H_7$), 7.72—8.07 (7H, m, 1-$C_{10}H_7$). (Found: C, 94.72; H, 5.59%).

2,2′-Binaphthyl (**23**): Colorless plates from C–B(9:1); mp 186.6 °C (lit,[26] mp 187.0 °C); 0.74 g. IR: 738 s, 749 m (γ_{C-H}, β); 812 vs (γ_{C-C}, β; γ_{C-C}, N); 854 vs (γ_{C-C}, N); 883 s (γ_{C-H}, β). UV: $\lambda_{max}(\varepsilon)$ 205 (sh) (33300), 213 (44100), 248 (sh) (66700), 255 (97500), 272 (sh) (25700), 306 nm (18100) (lit,[27] $\lambda_{max}(\varepsilon)$ 212 (39800), 248 (sh) (63100), 254 (97700), 271 (sh) (27500), 280 (sh) (17000), 305 nm (19500)). ^{1}H-NMR δ: 7.22—8.22 (14H, m, all protons). (Found: C, 94.76; H, 5.57%).

Reaction of **8** *and Magnesium Compound of* **33**. Magnesium turnings (0.83 g, 34 mmol) were placed in a flask as described in the general procedure. To the flask was added a solution of **33** (12.1 g, 34 mmol) in a ether–benzene mixture (80 ml; 3:1, v/v) all at once, and the reaction mixture was refluxed for 5 h. The hot Grignard reagent thus prepared was treated with **8** (3.04 g, 8 mmol) in the presence of Ni(acaen) (22 mg, 0.08 mmol) and the mixture was refluxed for additional 3 h. The benzene extract of the product, after removal of the solvent, was subjected to crystallization from benzene to give 2,2′,6,6′-tetraphenylbiphenyl (**25**). After filtration of **25**, followed by removal of solvent from the filtrate, the residue was chromatographed on alumina with C–B(3:1).

1-Iodo-8-(*m*-terphenyl-2′-yl)naphthalene (**15**): Pale yellow needles from benzene–ethanol; mp 186.5—187.5 °C; 2.04 g. IR: 701 s (γ_{C-C}, B); 739 w; 753 s, 758 s (γ_{C-H}, M); 763 s, 767 s (γ_{C-H}, d); 804 m (γ_{C-H}, *as*); 818 w, 825 w (γ_{C-C}, N); 862 w. Found: C, 69.92; H, 4.20%; mol wt, 482 (M^+). Calcd for $C_{28}H_{19}I$: C, 69.70; H, 3.97%; mol wt, 482.

8-Iodo-8′-(*m*-terphenyl-2′-yl)-1,1′-binaphthyl (**19**): Colorless needles from benzene-ethanol; mp 263.6—266.2 °C; 0.05 g. IR: 699 s (γ_{C-C}, B); 747 m, 758 s (γ_{C-H}, M); 764 s (γ_{C-H}, d); 773 m (γ_{C-H}, d, *as*); 803 w (γ_{C-H}, *as*); 817 m, 827 w, 837 w (γ_{C-C}, N). Found: mol wt, 608 (M^+). Calcd for $C_{38}H_{25}I$: mol wt, 608.

25: Colorless cubes from benzene; mp 390 °C (lit,[29] mp 396 °C); 0.13 g.

*Preparation of 1,8-Di(*p*-terphenyl-2′-yl)naphthalene (***6***).* The Grignard reagent prepared from the aryl iodide **31** (4.98 g, 14 mmol) was treated with **8** (1.24 g, 3.25 mmol) in the presence of Ni(acaen) (9.1 mg, 0.033 mmol) as described for the preceding reaction. The benzene extract of the product, was crystallized to give *p*-terphenyl and 2,2′,5,5′-tetraphenylbiphenyl (**24**). After filtration of the solid, followed by removal of solvent from the filtrate, the residue was chromatographed on alumina with C–B(3:1).

trans-1,8-Di(*p*-terphenyl-2′-yl)naphthalene (**6**): Colorless needles from benzene–ethanol; mp 225.6—227.6 °C; 0.21 g (11.1%). IR: 700 s, 704 s (γ_{C-C}, B); 727 w, 740 m, 744 m, 757 s (γ_{C-H}, M); 779 s (γ_{C-H}, d); 826 w (γ_{C-C}, N); 835 m (γ_{C-C}, N; γ_{C-H}, *as*); 894 m (γ_{C-H}, *as*). UV: $\lambda_{max}(\varepsilon)$ 212 (84400), 225 (sh) (66400), 282 nm (50700). ^{1}H-NMR δ: 7.68—7.82 (2H, q, C_4–, C_5–H of $C_{10}H_6$), 6.63—7.55 (30H, m, other protons). Found: C, 94.74; H, 5.81%; mol wt, 584 (M^+). Calcd for $C_{48}H_{32}$: C, 94.48; H, 5.52%; mol wt, 584.

24: Colorless needles from ethanol; mp 194—195 °C (lit,[10] mp 194—195 °C); 0.11 g.

The authors are indebted to Nippon Shinyaku Co., Ltd. for the measurements of the IR spectra. Thanks are due to Dr. Keiji Hashimoto and Mr. Yasuhiro Fujiwara of this college for their help in MS and ^{1}H-NMR spectral measurements.

References

1) D. J. Cram and H. Steinberg, *J. Am. Chem. Soc.*, **73**, 5691 (1951); C. J. Brown and A. C. Farthing, *Nature*, **164**, 915 (1949).

2) a) S. T. Cristol and D. C. Lewis, *J. Am. Chem. Soc.*, **89**, 1476 (1967); b) W. M. Machintyre and A. H. Tench, *J. Org. Chem.*, **38**, 130 (1973).

3) a) H. O. House, R. W. Magin, and H. W. Thompson, *J. Org. Chem.*, **28**, 2403 (1963); b) R. L. Clough, P. Mison, and J. D. Roberts, *ibid.*, **41**, 2252 (1976).

4) H. O. House, D. G. Koepsell, and W. J. Campbell, *J. Org. Chem.*, **37**, 1003 (1972).

5) R. L. Clough and J. D. Roberts, *J. Am. Chem. Soc.*, **98**, 1018 (1976).

6) P. J. McCarthy, R. J. Hovey, K. Ueno, and A. E. Martell, *J. Am. Chem. Soc.*, **77**, 5820 (1955).

7) The complex Ni(acaen) has been found to be the most effective catalyst for the less crowded cross-coupling of phenylmagnesium bromide and 2-iodobiphenyl to provide *o*-terphenyl: E. Ibuki, S. Ozasa, Y. Fujioka, M. Okada, and K. Terada, *Bull. Chem. Soc. Jpn.*, **53**, 821 (1980).

8) All of these complexes have been found to be the excellent catalysts for the cross-coupling to provide *o*-terphenyl, refer to Ref. 7.

9) E. Ibuki, S. Ozasa, and K. Murai, *Bull. Chem. Soc. Jpn.*, **48**, 1868 (1975).

10) E. Ibuki, S. Ozasa, Y. Fujioka, and H. Kitamura, *Chem. Pharm. Bull.*, **28**, 1468 (1980).

11) S. Ozasa, Y. Fujioka, M. Fujiwara, and E. Ibuki, *Chem. Pharm. Bull.*, **28**, 3210 (1980).

12) Previous attempted Ullmann coupling reactions of **8** and aryl iodide (**26**, **27**, **28**, or **32**) in the presence of copper powder to prepare 1,8-diarylnaphthalenes were unsuccessful.

13) These by-products were identified by mixed-melting-point determination (except **10**), elemental analyses, and comparison of the IR and UV spectra with those of samples prepared alternatively by the analogous Ni(acaen)-catalyzed Kharash-type Grignard cross-coupling of an appropriate Grignard reagent and 1-iodonaphthalene.

14) Clough *et al.* reported that the unfavorable formation of 1-phenylnaphthalene in the attempted coupling of ex-

cess of phenylmagnesium iodide and 1,8-diiodonaphthalene might have proceeded by the Grignard exchange between the both reactants (Ref. 3b).

15) The first scanning of the DSC determination of the melt, which consisted of the equilibrium mixture of **4a** and **4b**, was stopped at 169 °C (just before the second peak). After cooling, the next run of the melt showed only one peak at 174 °C, indicating that the melt used in the present scanning consisted of pure **4b**. The result was compatible with the ^{1}H-NMR spectrum of the melt used. The above experiment provides a novel procedure for obtaining the more stable rotamer in a pure state from an equilibrium mixture of the two rotamers. *Cf.* E. Ibuki, S. Ozasa, Y. Fujioka, and H. Mizutani, *Chem. Pharm. Bull.*, **29**, 2103 (1981).

16) Thermoanalytical data of **6**, **16**, and **17**, measured before and after heat treatment up to *ca.* 50 °C above their melting points, were practically identical, suggesting each of the compounds has the most stable conformation towards heating.

17) Significant differences between λ_{max} and ε_{max} of the spectra of *syn*- and *anti*-[2.2](1,4)anthracenophane, attributable to be caused by the interactions of differently overlapped anthracene rings: A. Iwama, T. Toyoda, M. Yoshida, T. Otsubo, Y. Sakata, and S. Misumi, *Bull. Chem. Soc. Jpn.*, **51**, 2988 (1978).

18) S. C. Dickerman, D. de Souza, and P. Wolf, *J. Org. Chem.*, **30**, 1981 (1965).

19) D. J. Cram, C. K. Dalton, and G. R. Knox, *J. Am. Chem. Soc.*, **85**, 1088 (1963).

20) "Varian N.M.R. Spectra Catalog," Varian Associate, Palo Alto, Calif. (1962), No. 203.

21) See reference cited in Ref. 17.

22) γ_{C-C} and γ_{C-H} refer to vibrations which are primarily out-of-plane C–C and out-of-plane C–H bending motions. M, *o*, *m*, *p*, and *as* in parentheses refer to mono-, ortho-, meta-, para-, and asymmetrically substituted benzene rings. α, β, and d refer to α-, β-, and di-substituted naphthalene rings. B and N refer to benzene ring and naphthalene ring.

23) M. Orchin and L. Reggel, *J. Am. Chem. Soc.*, **69**, 505 (1947).

24) R. Scholl, Ch. Seer, and R. Weitzenböck, *Ber.*, **43**, 2202 (1910).

25) F. Bergmann, J. Szmuszkowicz, and G. Fawaz, *J. Am. Chem. Soc.*, **69**, 1773 (1947).

26) P. G. Copeland, R. E. Dean, and D. McNeil, *J. Chem. Soc.*, **1960**, 1689.

27) H. H. Jaffé and M. Orchin, "Theory and Applications of Ultraviolet Spectroscopy," John Wiley and Sons, Inc., New York (1962), p. 287.

28) R. A. Friedel, M. Orchin, and L. Reggel, *J. Am. Chem. Soc.*, **70**, 199 (1948).

29) E. Ibuki, S. Ozasa, Y. Fujioka, and Y. Yanagihara, *Chem. Pharm. Bull.*, **30** (3), in press.

Nickel(0) Catalyzed [2+2] Cross-addition of Bicyclo[2.2.1]heptene Derivatives with Electron-deficient Olefins[1)]

Hidemasa TAKAYA, Masashi YAMAKAWA,† and Ryoji NOYORI*,†

Chemical Materials Center, Institute for Molecular Science, Myodaiji, Okazaki 444

†*Department of Chemistry, Nagoya University, Chikusa-ku, Nagoya 464*

(Received June 10, 1981)

In the presence of bis(acrylonitrile)nickel(0) or bis(1,5-cyclooctadiene)nickel(0), *exo*-tricyclo[3.2.1.$0^{2,4}$]oct-6-ene cycloadds to acrylonitrile and methyl acrylate to give *anti*- and *syn*-3-cyano-*exo*,*exo*-tetracyclo[4.3.1.$0^{2,5}$.$0^{7,9}$]-decane or the corresponding methoxycarbonyl derivatives. The cycloaddition with dimethyl maleate proceeds with retention of configuration. Benzonorbornadiene also enters into the 2+2 reaction, while *endo*-tricyclo-[3.2.1.$0^{2,4}$]oct-6-ene, bicyclo[2.2.1]heptene, and 5-methylenebicyclo[2.2.1]heptene are unreactive. Origins of the observed selectivities in the catalyzed reaction are discussed.

Under the influence of Ni(0) catalysts, bicyclo-[2.2.1]heptadiene (**1**), a homoconjugated diene[2)] having large strain energy (25.6 kcal/mol[3)]), undergoes a variety of cycloadditions. The diene dimerizes readily to give various regio- and stereoisomers.[4)] Reactions with acetylene and its derivatives afford different types of cycloadducts depending on the nature of the substituents.[4)] Electron-deficient olefins such as methyl acrylate, acrylonitrile, crotononitrile, and dimethyl maleate also react smoothly to yield the formal homo-Diels-Alder adducts of type **2**,[4,5)] while certain strained olefins such as methylenecyclopropane give the endo [2+2] cycloadducts of type **3** as the major product.[6,7)] The endo stereochemistry is considered as originating from the mixed ligand complex, depicted as **4**, in which the diene **1** coordinates to the Ni(0) atom as an endo bidentate ligand. This paper describes a Ni(0) catalyzed reaction of several bicyclo[2.2.1]heptene derivatives that are structurally related to the diene **1**. The principal aim was to determine how, and to what extent, the structural modification of one of the double bonds would affect the reaction course and reactivity with respect to those of the parent diene **1**.

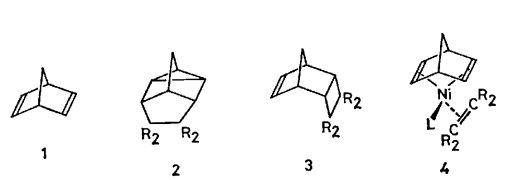

1 2 3 4

Results and Discussion

Nickel(0) Catalyzed [$_{\pi}2+_{\pi}2$] *Cross-addition.* When a solution of the cyclopropanated hydrocarbon **5** in acrylonitrile was kept at 70 °C for 120 h in the presence of a catalytic amount of bis(acrylonitrile)-nickel(0) [Ni(an)$_2$], the [2+2] cycloadducts **6** and **7** were obtained in 55% yield in a ratio of 63:37. Neither other cycloadducts nor dimeric products were obtained. Neither were rearrangement products of the starting hydrocarbon **5** detected. Similarly, the reaction of **5** with methyl acrylate (45 °C, 48 h) in the presence of bis(1,5-cyclooctadiene)nickel(0) [Ni-(cod)$_2$] gave a 78:22 mixture of **8** and **9** in 72% yield. Reaction of **5** with 1,2-disubstituted olefins proceeds more sluggishly. Dimethyl maleate and **5** in toluene

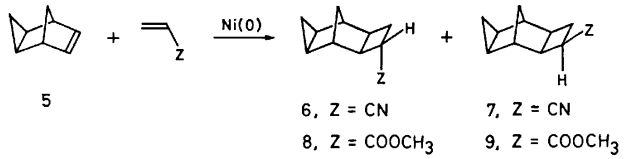

5 6, Z = CN 7, Z = CN 8, Z = $COOCH_3$ 9, Z = $COOCH_3$

10 11 Z = $COOCH_3$

in the presence of Ni(cod)$_2$ (35 °C, 72 h) afforded **10** and **11** (97:3) in 10% yield. Since dimethyl fumarate did not give any adducts under similar conditions, the origin of the production of **11** as a stereo impurity is presently unknown.[8)] The reaction of the benzo derivative **12** and methyl acrylate in the presence of Ni(cod)$_2$ afforded an 87:13 mixture of the stereoisomeric cycloadducts **13** and **14** in 34% yield. On the other hand, the endo cyclopropane isomer of **5** (**15**), bicyclo[2.2.1]heptene (**16**), and 5-methylene-bicyclo[2.2.1]heptene (**17**) gave no or very little cycloadducts with electron-deficient olefins.

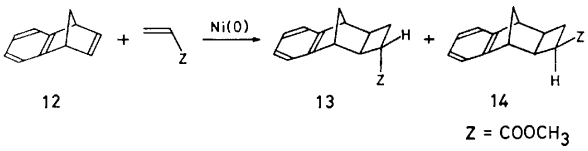

12 13 14 Z = $COOCH_3$

15 16 17

Thus the hydrocarbons **5** and **12** react with olefins in the presence of Ni(0) catalysts under mild reaction conditions to give formal [$_{\pi}2+_{\pi}2$] cycloadducts as the sole products. Characteristic features of these Ni(0)-catalyzed reactions include: (a) The reactions provide new examples of completely selective [2+2] cross-additions promoted by transition metal complexes. (b) The reactions afford only exo adducts, in contrast with the reaction of **1** with methylenecyclopropane

which produced endo adducts as the major products.[6] (c) The cycloaddition proceeds with a high degree of stereospecificity concerning the electron-deficient olefinic substrates. (d) The reactivities of the bicyclo-[2.2.1]heptenes are highly sensitive to the structural change at the site remote from the reacting double bond.

Possible Reaction Paths. Three paths, A, B, and C, may be conceivable "*a priori*" as possible mechanisms which are consistent with the characteristics of the reactions (Scheme 1). The first two, A and

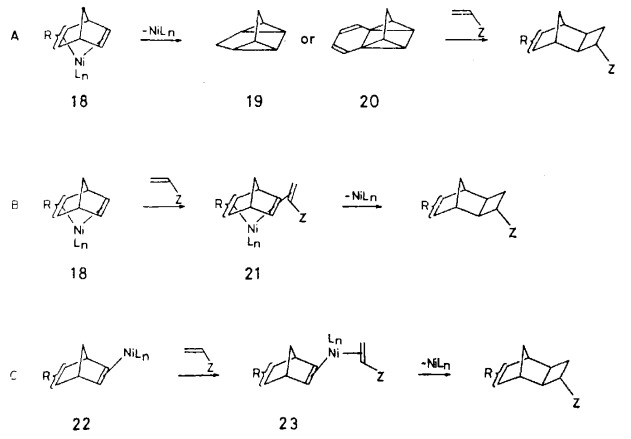

Scheme 1.

B, involve the coordination complex **18** where the strained hydrocarbon is acting as an endo bidentate ligand.[9,10] Thus path A assumes initial metal catalyzed skeletal change of **18** to **19**[11] or **20** and subsequent uncatalyzed, symmetry-allowed [$\sigma 2+\sigma 2+\pi 2$] cycloaddition,[12,13] whereas path B involves the donor-acceptor complex **21** in which the electron-deficient olefin is interacting with the bicycloheptene double bond from the side opposite the coordinated metal atom.[14] Reaction *via* path C goes through the metal complexes **22** and **23** in which the strained olefin binds to the Ni(0) atom as an exo unidentate ligand.

Operation of the path A could be readily dismissed on the basis of the following experiments. Gas chromatographic analysis of the reaction mixture of **5** with methyl acrylate did not indicate the presence of **19**. Moreover, when separately prepared **19**[11] was exposed to the Ni(0) catalyst in methyl acrylate, no traces of cycloadducts **8** and **9** were formed; the compound **19** was recovered unchanged.

Elucidation of the Mode in the Coordination of the Strained Olefins to Nickel(0) Complex. In order to differentiate the remaining two possibilities, B and C, the mode of coordination of the initial strained olefins to the Ni(0) atom was examined by Tolman's method. An olefinic substrate and a Ni(0) complex are known to exist in equilibrium as depicted in Eq. 1.[15]

$$\underset{\mathbf{24}}{\text{Olefin}} + \text{NiL}_3 \rightleftharpoons \underset{\mathbf{25}}{\text{(olefin)NiL}_2} + \text{L} \qquad (1)$$

$$\text{L}=\text{P(O-}o\text{-tolyl)}_3$$

A monoolefin of an appropriate concentration reacts with Ni[P(O-*o*-tolyl)$_3$]$_3$ to give a single 1:1 complex **25**. whose electronic spectrum exhibits an absorption maximum around 350 nm and a shoulder near 400 nm irrespective of the structure of the olefins. Thus two isosbestic points are to be observed when the spectra are taken at various concentration of olefins. The compound **16** presents a typical example (Eq. 2 and Fig. 1). On the other hand, the diene **1** exhibited the complex spectra shown in Fig. 2, where no absorption maxima were observed over the range 300—550 nm. This is ascribed to the fact that **1** acts as both an endo bidentate and an exo unidentate ligand to give a mixture of **27**—**29** (Eq. 3).[15] The

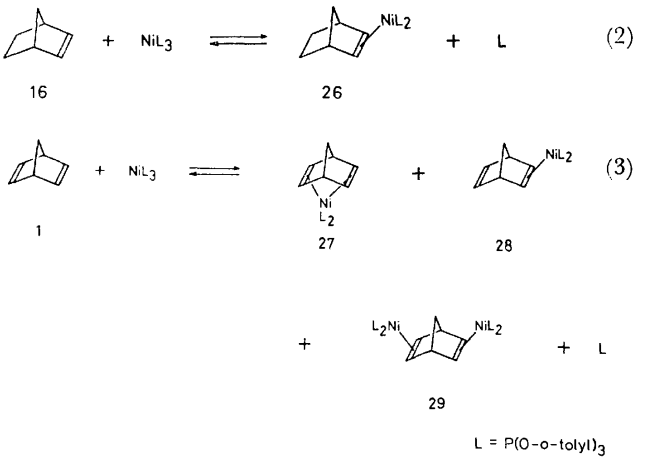

hydrocarbons **5**, **12**, and **15** displayed spectroscopic behavior quite similar to that observed for the monoolefin **16** (Figs. 3, 4, and 5), which indicates that these strained hydrocarbons coordinate to Ni(0) atom as exo unidentate ligands to give complexes **30**—**32**. Although the structure and properties of the complex **24** are different from those of the catalysts employed

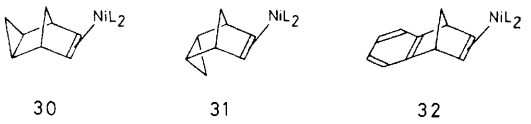

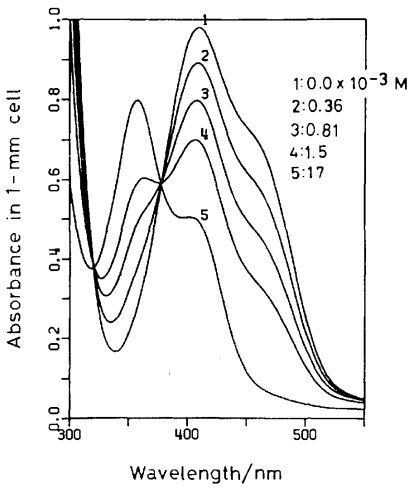

Fig. 1. Electronic spectra of benzene solution containing 1.94×10^{-3} M (1 M = 1 mol dm^{-3}) of Ni[P(O-*o*-tolyl)$_3$]$_3$ and increasing concentration of **16** at 24 °C.

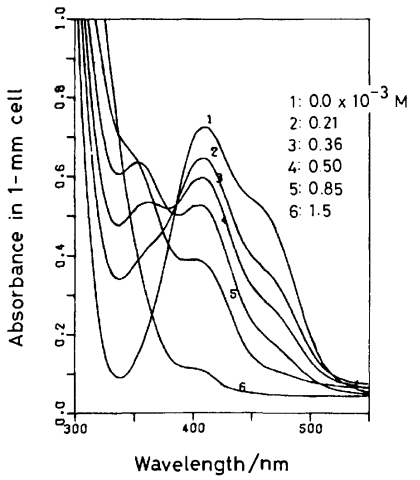

Fig. 2. Electronic spectra of benzene solution containing 1.32×10^{-3} M of Ni[P(O-*o*-tolyl)$_3$]$_3$ and increasing concentration of **1** at 24 °C.

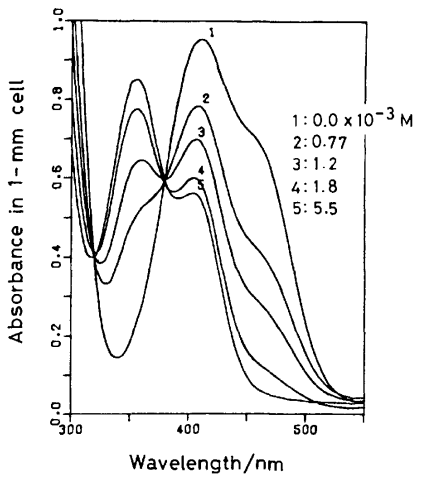

Fig. 3. Electronic spectra of benzene solution containing 1.78×10^{-3} M of Ni[P(O-*o*-toly)$_3$]$_3$ and increasing concentration of **5** at 24 °C.

in the actual catalytic reactions, these results strongly suggest that complexes of a similar type play an important role in the present catalytic reactions. Thus path C is thought to be most probable.

Determination of the Equilibrium Constant of the Complex Formation. Based on the electronic spectra (Figs. 1—5) of the mixtures of the complex **24** and the strained olefins, the equilibrium constants of the complex formation at 24 °C were calculated following Tolman's procedure.[15] The results are summarized in Table 1.

Reactivity of the Strained Olefins. The rate of the reaction of the strained olefins with methyl acrylate catalyzed by Ni(cod)$_2$ was measured at 40 °C. The results are listed in Table 1. The relative reactivities decrease in the order **5**>**12**>**15**. The competition experiments using **5** and **15** at 40 °C showed that the presence of varying amounts of **15** does not affect the reactivity of **5**.

Homoconjugation in the Olefinic Substrates. The existence of homoconjugation in **1**,[2] **5**,[2b] and **12**[2c] has been well-established mainly on the basis of photoelectron and charge-transfer spectra. The influence

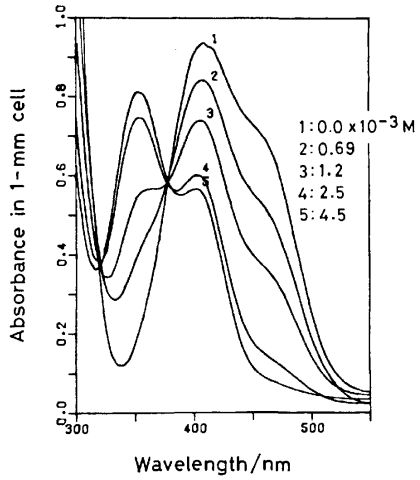

Fig. 4. Electronic spectra of benzene solution containing 1.83×10^{-3} M of Ni[P(O-*o*-toly)$_3$]$_3$ and increasing concentration of **15** at 24 °C.

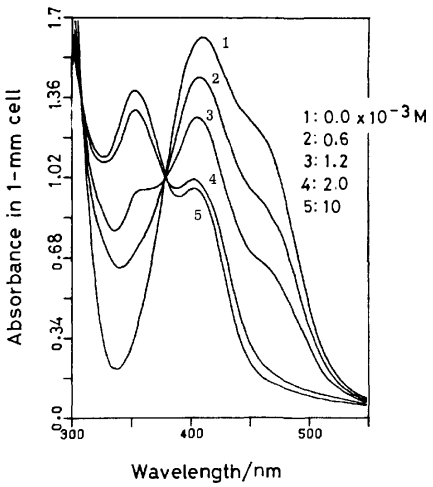

Fig. 5. Electronic spectra of benzene solution containing 1.93×10^{-3} M of Ni[P(O-*o*-tolyl)$_3$]$_3$ and increasing concentration of **12** at 24 °C.

TABLE 1. EQUILIBRIUM CONSTANTS FOR [olefin + NiL_3 ⇌ (olefin)NiL_2 + L] IN BENZENE AT 24 °C

Olefin	K[a]	Relative reactivity
1-Hexene	0.32±0.04	—
16	3.8±0.5	≈0
15	10.3±0.1	≈0
5	30±6	1.6—2.4
12	320±30	1.0
1	—[b]	—

a) $K=[(\text{olefin})NiL_2][L]/[\text{olefin}][NiL_3]$. b) Very large.

of stereoelectronic factors on the degree of these through-space interactions are considerable. In exo derivative **5**, there is substantial homoconjugation which arises from the direct overlap between the π-orbital of the double bond and the Walsh-orbital of the cyclopropane ring. On the other hand, the cyclopropane ring of the endo isomer **15** does not participate

in the cyclic homoconjugation with the double bond.[2b] The extent of the homoconjugative interaction decreases in the order **1**>**12**>**5**≫**15**.

Discussion. It should be emphasized that in these catalytic reactions the benzene ring or cyclopropane rings which are located remote from the reacting carbon–carbon double bond exert definitive influences on the reactivities of the strained hydrocarbons. In certain cases the reactivities of the strained olefinic hydrocarbons can be gauged from the strain energies of these hydrocarbons.[16] There is no appreciable difference in strain energies between these hydrocarbons, because the carbocyclic frameworks are quite similar to each other. Further, as can be seen from the values of equilibrium constants and the results of competitive experiments, there no good correlation seems to exist between the reactivity and the coordination ability of the strained olefins with the Ni(0) atom. For instance, the compound **12** has a large equilibrium constant, but is less reactive than **5**. The exo cyclopropane derivative **5** has an equilibrium constant only three times larger than that of the endo isomer **15**, but only the former compound reacts with methyl acrylate.

The present catalytic reactions can be considered to proceed in a stepwise manner with the initial formation of a transitory five-membered metallacycle **34** as outlined in Scheme 2.[17,18] The observed structure-reactivity relationship leads us to consider that the cyclic homoconjugation between the double bond and cyclopropane or the benzene ring exerts a great influence on lowering the energy of the transition state **33** which gives rise to the metallacyclopentane intermediate **34**. MO considerations are consistent with this assumption; the cyclic homoconjugation in bicyclo[2.2.1]heptene system reduces the bond order of the C=C bond and consequently increases the free valency of C_2 and C_3. This effect facilitates the bonding interaction between C_2 and Ni, and C_3 and C_4, which results in lowering the transition state energy. If the formation of **34** *via* **33** is the rate-determining step, such effects are conceived to determine the reactivity of the strained olefins in the present catalysis.[19]

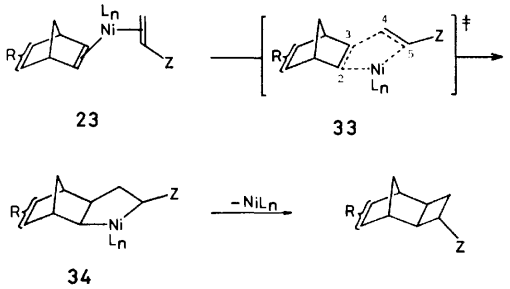

Scheme 2.

Experimental

General. The nuclear magnetic resonance (NMR) spectra were recorded either on a Varian HA-100D (100 MHz) or a JEOL JNM-FX 100 (100 MHz, FT-NMR) spectrometer. Chemical shifts were indicated as parts per million down field from tetramethylsilane as an internal standard. Singlet, doublet, triplet, and multiplet are abbreviated to s, d, t, and m. Infrared (IR) spectra were taken on a JASCO Model DS-402G spectrophotometer in carbon tetrachloride. Analytical gas chromatography (GLC) was done on Hitachi Model 063 instrument equipped with a flame ionization detector using nitrogen as the carrier gas. Preparative gas chromatography was performed on a Varian Model 1700 instrument using helium as the carrier gas. The columns used follow: A, 3 mm×2 m 10% Silicone DCQF-1 on 100—120 mesh Chromosorb W AW; B, 10 mm× 3 m 10% Silicone DCQF-1 on 100—120 mesh Neosorb; C, 3 mm×2 m 10% Silicone DCQF-1 on 100—120 mesh Neopak 1A; D, 1/8 inch×4 m 10% Silicone DCQF-1 on 80—100 mesh Chromosorb W AW; E, 3 mm×2 m 5% poly(ethylene glycol) 20M on 80—100 mesh Chromosorb G NAW. The visible spectra were recorded on a Hitachi Model 323 spectrometer using a 1-mm cell equipped with a serum cap. Low-resolution mass spectra were obtained at 70 eV on Hitachi Model RMU-6C instrument. High resolution mass spectra were taken on a JEOL JMS-D300 spectrometer equipped with JMA-2000 mass data analysis system. Analytical thin layer chromatography (TLC) was done on E. Merck Kieselgel PF_{254} precoated plates (0.25-mm layers). Preparative TLC separation was performed using 20 cm×20 cm glass plates coated with a 1.0-mm thick layer of E. Merck Kieselgel PF_{254}. The positions of spots were visualized by exposure to iodine vapor or a spray of a solution of Cerium(IV) sulfate in 1 mol dm^{-3} H_2SO_4 followed by heating on a hot plate.

Materials. Guaranteed grade 1-hexene and benzene for spectrometry, and reagent grade methyl acrylate, acrylonitrile, acetonitrile, diethyl ether, and hexane for handling air-sensitive metal complexes were distilled under argon over powdered calcium hydride and stored in Schlenk tubes under argon. E. Merck norbornadiene and norbornene were distilled over calcium hydride and stored in the presence of a small amount of hydroquinone. Other reagent grade solvents and reagents were distilled before use.

Ni(an)$_2$-catalyzed Reaction of **5** *and Acrylonitrile.* $Ni(an)_2$ was prepared in a glass ampoule from $Ni(CO)_4$ (34.0 mg, 0.20 mmol) and acrylonitrile (2.5 ml) by the literature procedure[20] and to this was added a solution of **5**[21] (240 mg, 2.26 mmol) in acrylonitrile (1.5 g, 28 mmol). The tube was sealed under argon and the mixture was kept at 70 °C for 120 h. After addition of dichloromethane (20 ml) to the reaction mixture, the nickel complex was decomposed by air. The resulting precipitates were removed by filtration through Celite 545 and the filtrate was evaporated to give a colorless oil. Fractional distillation by Kugelrohr afforded a mixture of *anti*-3-cyano-*exo*,*exo*-tetracyclo[4.3.1.-$0^{2,5}.0^{7,9}$]decane (**6**) and its syn isomer **7** (210 mg, 55% combined yield), bp 90—100 °C (3 mmHg††). No other products were detected by TLC analysis (R_f 3.9, **6**, and **7** unseparable, hexane–ether 10:1). GLC analysis (column A, 150 °C) indicated that **6** (t_R 25.6 min) and **7** (t_R 28.8 min) produced in a ratio of 63:37. Analytical samples of **6** and **7** were obtained by preparative GLC (column B, 180 °C). Spectral and analytical data of the products follow: **6**: IR 2235 cm^{-1} (CN); NMR δ 0.00 (dt, $J_{8a,8s}=J_{8a,7}=J_{8a,9}=7.0$ Hz, H_{8a}), 0.38 (dt, $J_{8s,7}=J_{8s,9}=3.0$ Hz, H_{8s}), 0.59 (dd, H_7, H_9), 0.97 (A part of ABq, $J_{10s,10a}=12.0$ Hz, H_{10s}), 1.12 (B part of ABq, H_{10a}), 1.6—2.0 (m, H_5), 2.13 (broad s, H_6), 2.26 (broad s, H_1), 2.3—2.7 (m, H_2, H_3, $2H_4$). Mass spectrum *m/e* 158 (M^+-1). Found: C, 82.76; H, 8.13; N, 8.58%. Calcd for $C_{11}H_{13}N$: C, 82.97; H, 8.23; N, 8.80%. **7**: IR 2230

†† 1 mmHg≈133.322 Pa.

cm^{-1} (CN); NMR δ −0.03 (dt, $J_{8a,8s}$=8.0 Hz, $J_{8a,7}$=$J_{8a,9}$=6.5 Hz, H_{8a}), 0.44 (dt, $J_{8s,7}$=$J_{8s,9}$=3.0 Hz, H_{8s}), 0.55 (dd, H_7, H_9), 1.09 (A part of ABq, $J_{10s,10a}$=13.0 Hz, H_{10s}), 1.62 (B part of ABq, H_{10a}), 1.6—1.9 (m, H_5), 2.12 (broad s, H_1), 2.2—2.6 (m, H_2, $2H_4$, H_6), 3.0—3.4 (m, H_{3n}). Mass spectrum *m/e* 158 (M^+-1). Found: C, 83.14; H, 8.25; N, 8.61%. Calcd for $C_{11}H_{13}N$: C, 82.97; H, 8.23; N, 8.80%.

Preparation of the Authentic Samples of **6** *and* **7**. *anti*- and *syn*-3-cyano-*exo*-tricyclo[4.2.1.$0^{2,5}$]oct-7-ene (**35**) and (**36**) were prepared by the application of the reported procedure.[12] In a 20-ml reaction ampoule were placed quadricyclane (500 mg, 5.43 mmol), acrylonitrile (3.0 ml), and hydroquinone (3 mg) and the tube was sealed under argon. The mixture was kept at 95 °C for 72 h. Distillation of the reaction mixture *in vacuo* afforded a mixture of **35** and **36** (700 mg, 92%). GLC analysis (column C, 140 °C) indicated that **35** (t_R 14.0 min) and **36** (t_R 12.0 min) were produced in 33:67. Pure samples of the adducts were obtained by GLC purification (column D, 130 °C). Spectral properties of **35** and **36** follow: **35**: NMR ($CDCl_3$) δ 1.40 (d, $J_{9a,9s}$=10.0 Hz, H_{9a}), 1.59 (d, H_{9s}), 2.71 (broad s, H_6), 2.80 (broad s, H_1), 5.99 (m, H_7, H_8), 1.2—2.6 (m, other protons). High resolution mass spectrum. Found: *m/e* 145.087. Calcd for $C_{10}H_{11}N$: *m/e* 145.089. **36**: NMR ($CDCl_3$) δ 1.49 (d, $J_{9s,9a}$=10.0 Hz, H_{9s}), 2.02 (d, H_{9a}), 2.73 (broad s, H_6), 2.98 (broad s, H_1), 3.0—3.4 (m, H_{3n}), 6.01 (broad s, H_7, H_8), 1.5—2.7 (m, other protons). High resolution mass spectrum. Found: *m/e* 145.090. Calcd for $C_{10}H_{11}N$: *m/e* 145.089. Conversion of **35** to **6** was performed by the cyclopropanation by gaseous diazomethane catalyzed by bis[*N*-(1-phenylethyl)salicylideneaminato]copper(II).[22] Purification by GLC (column B, 180 °C) gave pure sample of **6**. Compound **7** was obtained from **36** by the similar procedure. NMR and mass spectra of the authentic samples were superimposable on those of **6** and **7** obtained by metal catalysis.

$Ni(cod)_2$-catalyzed Reaction of **5** *and Methyl Acrylate*. In a 30-ml glass ampoule equipped with a serum cap was placed $Ni(cod)_2$[23] (1.50 g, 5.51 mmol) under argon and to this was added **5** (1.06 g, 10.0 mmol) and methyl acrylate (10.0 ml) with a syringe. The reaction tube was sealed under argon and kept at 45 °C for 72 h. After opening the tube dichloromethane (20 ml) was added to the mixture and air was bubbled gently for 2 h to decompose the nickel complex. The resulting black precipitates were filtered off by passage through a short column packed with Celite 545. The filtrate was concentrated and the residue was analyzed by GLC (column A, 150 °C) indicating that essentially two products *anti*-3-methoxycarbonyl-*exo*,*exo*-tetracyclo[4.3.1.$0^{2,5}$.$0^{7,9}$]decane (**8**) (t_R 15.3 min) and its syn isomer **9** (t_R 14.2 min) were produced in a ratio of 78:22. Distillation by Kugelrohr (1 mm, 150 °C) gave a mixture of **8** and **9** (1.46 g, 72% yield). Analytical samples of **8** and **9** were obtained by preparative GLC separation (column B, 180 °C). The structures of **8** and **9** were determined by the comparison of their spectral data with those of authentic samples prepared as follows. A mixture of **35** and **36** (20 g, 0.138 mol) and KOH (15 g, 0.21 mol) in 80% aqueous ethylene glycol was kept at 140 °C for 12 h. The reaction mixture was acidified by HCl and the resulting carboxylic acid was taken up into ether. Esterification by adding a solution of diazomethane in ether to the acid afforded a mixture of *anti*- and *syn*-3-methoxycarbonyl-*exo*-tricyclo[4.2.1.$0^{2,5}$]oct-7-enes (16.4 g, 67%). The ester (5.6 g, 31.5 mmol) was cyclopropanated by the reported procedure[22] to give a mixture of **8** and **9** (4.0 g, 66%). Separation by preparative GLC (column B, 180 °C) gave pure samples of **8** and **9**. The stereochemistry of the ester groups was determined on the basis of the NMR spectra taken in the presence of $Eu(fod)_3$. Physical properties of **8**: IR 1735 cm^{-1} (C=O); NMR δ −0.06 (dt, $J_{8a,8s}$=$J_{8a,7}$=$J_{8a,9}$=7.0 Hz, H_{8a}), 0.36 (dt, $J_{8s,7}$=$J_{8s,9}$=3.0 Hz, H_{8s}), 0.56 (dd, H_7, H_9), 0.93 (A part of ABq, $J_{10s,10a}$=12.0 Hz, H_{10s}), 1.22 (B part of ABq, H_{10a}), 1.5—1.8 (m, H_5), 2.09 (broad s, H_6), 2.18 (broad s, H_1), 2.2—2.6 (m, H_2, H_3, $2H_4$), 3.61 (s, OCH_3). When the $Eu(fod)_3$-induced shifts were plotted against the relative molar ratios of the shift reagent and the substrate, a linear relationship was observed. The gradients, ppm/mol of $Eu(fod)_3$ per mole of substrate, of these lines were 26.6 (OCH_3), 25.0 (H_3), 20.5 (H_{4n}), 20.0 (H_2), 10.0 (H_5), 7.8 (H_{4x}), 6.1 (H_1), 6.1 (H_{10a}), 3.8 (H_6), 3.3 (H_{10s}). Values for cyclopropane protons could not be determined. Mass spectrum *m/e* 192 (M^+). Found: C, 75.04; H, 8.32%. Calcd for $C_{12}H_{16}O_2$: C, 74.97, H, 8.39%. Physical properties of **9**: IR 1738 cm^{-1} (C=O); NMR δ −0.11 (dt, $J_{8a,8s}$=$J_{8a,7}$=$J_{8a,9}$=7.0 Hz, H_{8a}), 0.31 (dt, $J_{8s,7}$=$J_{8s,9}$=3.0 Hz, H_{8s}), 0.50 (dd, H_7, H_9), 0.78 (A part of ABq, $J_{10s,10a}$=12.0 Hz, H_{10s}), 1.22 (B part of ABq, H_{10a}), 2.07 (broad s, H_6), 1.8—2.6 (m, H_2, $2H_4$, H_5), 3.0—3.4 (m, H_{3n}), 3.60 (s, OCH_3). The gradients of the lines derived from the $Eu(fod)_3$-induced spectra were 19.5 (OCH_3), 20.2 (H_{10a}), 14.6 (H_1), 12.3 (H_{4x}), 9.9 (H_2), 7.8 (H_{4n}), 6.0 (H_{10s}), 5.1 (H_5), 5.0 (H_{3n}), 3.8 (H_6). Values for cyclopropane protons could not be determined. Mass spectrum *m/e* 192 (M^+). Found: C, 75.06; H, 8.33%. Calcd for $C_{12}H_{16}O_2$: C, 74.97; H, 8.39%.

$Ni(cod)_2$-catalyzed Reaction of **5** *and Dimethyl Maleate*. In a 10-ml reaction ampoule was placed $Ni(cod)_2$ (50 mg, 0.18 mmol) under argon and to this was added at −60 °C, a mixture of **5** (110 mg, 1.04 mmol), dimethyl maleate (710 mg, 4.87 mmol), and toluene (1.8 ml). The reaction tube was sealed and dipped in a water-bath kept at 30 °C for 72 h. The colorless oil obtained after the usual work-up was analyzed by GLC (column C, 175 °C) indicating that the adducts *anti*,*anti*-3,4-bis(methoxycarbonyl)-*exo*,*exo*-tetracyclo[4.3.1.$0^{2,5}$.$0^{7,9}$]decane (**10**) (t_R 21.0 min) and its *anti*,*syn*-isomer **11** (t_R 14.0 min) were produced in 10 and 0.3% yields respectively. The GLC analysis also revealed that the recovered diester consisted of dimethyl maleate (30%) and dimethyl fumarate (70%). Pure samples of **10** and **11** (mp 81.0—81.5 °C) were isolated by preparative GLC (column B, 200 °C). Spectral properties of **10**: IR 1740 cm^{-1} (C=O); NMR (benzene as a lock signal): δ −0.02 (dt, $J_{8a,8s}$=$J_{8a,7}$=$J_{8a,9}$=7 Hz, H_{8a}), 0.36 (dt, $J_{8s,7}$=$J_{8s,9}$=3 Hz, H_{8s}), 0.60 (dd, H_7, H_9), 0.93 (A part of ABq, $J_{10s,10a}$=12 Hz, H_{10s}), 0.99 (B part of ABq, H_{10a}), 2.16 (broad s, H_1, H_6), 2.64 (broad s, H_2, H_5), 2.5—2.8 (m, H_3, H_4), 3.57 (s, $2OCH_3$); mass spectrum *m/e* 250 (M^+). Found: C, 67.17; H, 7.35%. Calcd for $C_{14}H_{18}O_4$: C, 67.18; H, 7.23%. Spectral properties of **11**: IR 1734 cm^{-1} (C=O); NMR (benzene as a lock signal): δ −0.07 (dt, $J_{8a,8s}$=$J_{8a,7}$=$J_{8a,9}$=7 Hz, H_{8a}), 0.34 (dt, $J_{8s,7}$=$J_{8s,9}$=3 Hz, H_{8s}), 0.53 (dd, H_7, H_9), 0.70 (A part of ABq, $J_{10s,10a}$=13 Hz, H_{10s}), 1.11 (B part of ABq, H_{10a}), 2.24 (broad s, H_6), 2.32 (broad s, H_1), 2.1—2.6 (m, H_2, H_3, H_5), 2.95 (dd, J=4 Hz, J'=7 Hz, H_4), 3.58 (s, OCH_3), 3.60 (s, OCH_3); mass spectrum *m/e* 250 (M^+). Found: C, 66.93; H, 7.27%. Calcd for $C_{14}H_{18}O_4$: C, 67.18; H, 7.23%. The authentic samples of **10** and **11** were prepared by the cyclopropanation[22] of *anti*,*anti*- and *anti*,*syn*-3,4-bis(methoxycarbonyl)-*exo*-tricyclo[4.2.1.$0^{2,5}$]oct-7-ene,[12] respectively. NMR and IR spectra as well as GLC behavior of **10** and **11** were identical with those of authentic samples.

Attempted $Ni(cod)_2$-catalyzed Reaction of **5** *with Dimethyl Fumarate*. To $Ni(cod)_2$ (46 mg, 0.17 mmol) placed in

a 10-ml reaction ampoule was added a mixture of **5** (117 mg, 1.10 mmol), dimethyl fumarate (287 mg, 1.99 mmol), and toluene (3.0 ml) at −60 °C under argon. The reaction tube was sealed and kept at 30 °C for 72 h with occasional shaking. The reaction mixture was worked up as usual and analyzed by GLC (column C, 175 °C), indicating that no 1:1 adducts were formed.

*Ni(cod)$_2$-catalyzed Reaction of Benzonorbornadiene (**12**) and Methyl Acrylate.* In a 10-ml reaction ampoule equipped with a serum cap was placed Ni(cod)$_2$ (270 mg, 0.99 mmol) and the system was flushed with argon. To this was added a mixture of degassed **12**[24] (250 mg, 1.76 mmol) and methyl acrylate (3.0 ml) with a hypodermic syringe. The reaction tube was sealed and the mixture was kept at 40 °C for 5 d. After opening the tube, the remaining nickel complex was decomposed by introduction of a gentle stream of air. The solid substance was removed by filtration and evaporation of methyl acrylate under reduced pressure gave 460 mg of a colorless oil. Distillation *in vacuo* (160 °C (0.1 mm)) afforded a mixture of *anti*-3-methoxycarbonyl-7,8-benzo-*exo*-tricyclo[4.2.1.0^{2,5}]non-7-ene (**13**) and its syn isomer **14** (130 mg, 32%). GLC analysis (column A, 200 °C) indicated that **13** (t_R 5.4 min) and **14** (t_R 4.9 min) were produced in 80:20 ratio. No distinct coupling between H_1 and H_3, and H_5 and H_6 were observed in NMR spectra of **13** and **14**, which support the exo fusion of cyclobutane rings in these products. The stereochemistries of the ester groups were determined on the basis of the Eu(fod)$_3$-aided NMR spectra. Spectral properties of **13**: IR 1734 cm^{-1} (C=O); NMR δ 1.78 (A part of ABq, $J_{9s,9a}$=10.0 Hz, H_{9s}), 1.6—2.7 (m, H_2, H_3, $2H_4$, H_5), 2.12 (B part of ABq, H_{9a}), 3.13 (broad s, H_6), 3.22 (broad s, H_1), 3.62 (s, OCH_3), 6.8—7.2 (m, aromatic protons). The gradients of the lines derived from the Eu(fod)$_3$-induced spectra were 11.8 (OCH_3), 12.7 (H_3), 11.0 (H_{4n}), 9.7 (H_2), 5.1 (H_{4x}), 3.6 (H_5), 3.0 (H_1), 3.0 (H_{9a}), 1.6 (H_{9s}), 1.5 (H_6). Mass spectrum *m/e* 228 (M^+). Found: C, 79.01; H, 7.02%. Calcd for $C_{15}H_{16}O_2$: C, 78.92; H, 7.06%. Spectral properties of **14**: IR 1737 cm^{-1} (C=O); NMR δ 1.62 (A part of ABq, $J_{9s,9a}$=11.0 Hz, H_{9s}), 1.9—2.6 (m, H_2, $2H_4$, H_5, H_{9a}), 3.0—3.5 (m, H_3), 3.12 (broad s, H_6), 3.32 (broad s, H_1), 3.69 (s, OCH_3), 6.8—7.2 (m, aromatic protons). High resolution mass spectrum. Found: *m/e* 228.1146. Calcd for $C_{15}H_{16}O_2$: *m/e* 228.1150.

*Attempted Ni(cod)$_2$-catalyzed Reaction of **15** and Methyl Acrylate.* Ni(cod)$_2$ (380 mg, 1.38 mmol) was placed in a 20-ml reaction ampoule under argon and the tube was cooled to −70 °C in a Dry Ice–methanol bath. To this was added a solution of **15** (0.56 g, 5.28 mmol) in methyl acrylate (5.0 ml). The sealed reaction tube was kept at 45 °C for 48 h. After decomposition and removal of the resulting precipitates the reaction mixture was analyzed by GLC (column A, 140 °C) indicating that no 1:1 adducts were formed.

*Attempted Ni(cod)$_2$-catalyzed Reaction of **16** with Methyl Acrylate.* In a 10-ml glass ampoule was placed Ni(cod)$_2$ (60 mg, 0.22 mmol) under argon. Then a solution of **16** (100 mg, 1.06 mmol) in methyl acrylate (2.0 ml) was added to this and the tube was sealed. The mixture was kept at 45 °C for 48 h. After opening the tube and addition of dichloromethane (2.0 ml) the catalyst was decomposed by the introduction of a gentle stream of air. Black precipitates were filtered off through a pad of Celite 545 and the filtrate was analyzed by GLC (column A, 140 °C), which revealed that no 1:1 addition compounds were produced.

*Attempted Ni(cod)$_2$-catalyzed Reaction of **17**.* A solution of **17**[25] (56 mg, 0.53 mmol) in methyl acrylate (2.0 ml) was added to Ni(cod)$_2$ (100 mg, 0.37 mmol) placed in a 10-ml reaction ampoule under argon. The yellow solution was kept at room temperature for 20 h and then at 50 °C for 12 h. After the usual work-up, the reaction mixture was analyzed by GLC (column A, 140 °C). No products were detected.

*Comparison of the Reactivities of **5** and **12**.* A competition experiment was done by keeping a mixture of **5** (117 mg, 1.11 mmol), **12** (153 mg, 1.08 mmol), and Ni(cod)$_2$ (100 mg, 0.37 mmol) in methyl acrylate (3.0 ml) at 45 °C under argon. Aliquots of the reaction mixture were taken out with hypodermic syringes after appropriate time intervals and analyzed by GLC (column A, 200 °C). The ratio (**8**+**9**)/(**13**+**14**) varied from 1.6 to 2.4.

*Ni(cod)$_2$-catalyzed Reaction of **5** and Methyl Acrylate with or without Added **15**.* Solutions of Ni(cod)$_2$ (0.37 mmol) and eicosane (0.13 mmol, an internal standard for GLC analysis) in methyl acrylate (2 ml) containing varying amounts of **5** (0.13—0.64 mmol) and **15** (0.56—0 mmol) were kept at 40 °C for 22 h under argon. After the usual work-up, the reaction mixtures were analyzed by GLC (column E, 180 °C). The initial rates of reactions of **5** were calculated based on the above experiments. The results indicated that the presence of varying amounts of **15** caused little change in the reactivity of **5** (only by a factor of 1.0—1.1).

*Spectrophotometric Determination of the Modes and Equilibrium Constants of the Coordination of the Olefins **5**, **12**, and **15** on Nickel Atom.* Special precautions were necessary to get rid of oxygen for handling air-sensitive dilute solutions of the nickel(0) complexes. The olefinic compounds **1**, **5**, **12**, **15**, and **16** were distilled over CaH_2 under argon before use. The complex [P(O-*o*-tolyl)$_3$]$_3$Ni(0) (**24**)[26] was obtained by the procedure described by Tolman. All liquid materials were transferred with gas-tight syringes. The 5 mM (1 M= 1 mol dm^{-3}) benzene solution of **24** (2.0 ml) was freshly prepared just before use and was placed in a 5-ml flask equipped with a Teflon stopcock. To this was added an appropriate amount of the olefinic substrate in benzene. Finally the volume of the solution was adjusted strictly to 5 ml by adding benzene. Thus, 0.8 M solution of **24** in benzene containing variable concentrations (10^{-1} to 10^{-4} M) of strained olefins were prepared. For measurements of visible spectra these solutions were transferred into quartz cells of 1-mm path capped with rubber septa under argon by the use of a gas-tight syringe. The following procedure for determination of the equilibrium constants of the reaction of **5** and **24** is representative for all the other olefins. Visible spectra of a solution of **24** with variable concentration of **5** are shown in Fig. 3. The values of [(olefin)NiL$_2$] where L is P(O-*o*-tolyl)$_3$ were obtained from the loss of absorbance at 450 nm due to the complex **24**, and K was calculated according to the Eq. 4. To minimize the error, which becomes large when the K value is much greater than unity, appropriate amounts of the phosphite ligand were added so that the apparent K values become close to unity. Addition of phosphite ligand, however, causes the formation of NiL$_4$ species as shown in Eq. 5. Thus, the concentration of the each species in Eq. 4 was obtained at first assuming that K is zero, and then the concentration of NiL$_4$ was calculated using the reported formation constant.[15] Finally from the corrected concentration of the each species in

$$K = \frac{[(\text{olefin})\text{NiL}_2][\text{L}]}{[\text{olefin}][\text{NiL}_3]}, \quad (4)$$

$$\text{NiL}_3 + \text{L} \overset{k}{\rightleftharpoons} \text{NiL}_4, \quad (5)$$

Eq. 4, equilibrium constants were obtained (Table 1). Visible

spectra of the solution of **24** and other olefins are shown in Figs. 1, 2, 4, and 5.

We gratefully acknowledge supports of this work by the Kurata Science Foundation, Takeda Science Foundation, and Ito Science Foundation.

References

1) Nickel Catalyzed Reactions Involving Strained Bonds. 18. Part 17: H. Takaya, T. Suzuki, Y. Kumagai, M. Hosoya, H. Kawauchi, and R. Noyori, *J. Org. Chem.*, **46**, 2854 (1981).

2) a) Y. Kobuke, T. Sugimoto, J. Furukawa, and T. Fueno, *J. Am. Chem. Soc.*, **94**, 3633 (1972); b) P. Bischof, E. Heilbronner, H. Prinzbach, and H. D. Martin, *Helv. Chim. Acta*, **54**, 1072 (1971); c) L. N. Domelsmith, P. D. Mollere, K. N. Houk, R. C. Hahn, and R. P. Johnson, *J. Am. Chem. Soc.*, **100**, 2959 (1978).

3) H. K. Hall, Jr., C. D. Smith, and J. H. Baldt, *J. Am. Chem. Soc.*, **95**, 3197 (1973).

4) a) G. N. Schrauzer and P. Glockner, *Chem. Ber.*, **97**, 2451 (1964); b) G. N. Schrauzer and S. Eichler *ibid.*, **95**, 2764 (1962); c) J. Mantzaris and E. Weissberger, *J. Am. Chem. Soc.*, **96**, 1873 (1973).

5) R. Noyori, I. Umeda, H. Kawauchi, and H. Takaya, *J. Am. Chem. Soc.*, **97**, 812 (1975).

6) R. Noyori, T. Ishigami, N. Hayashi, and H. Takaya, *J. Am. Chem. Soc.*, **95**, 1674 (1973).

7) [2+2] type cycloadditions have also been reported for allene and 1,3-butadiene, though yields were very low: A. Greco, A. Carbonaro, and G. Dall'Asta, *J. Org. Chem.*, **35**, 271 (1970); A. Takahashi and T. Inukai, *J. Chem. Soc., D*, **1970**, 1473.

8) During the catalytic reactions dimethyl maleate isomerized to dimethyl fumarate to a considerable extent ($\approx$70%). Dimethyl fumarate, however, does not enter into the catalytic cycloadditions.

9) Coordination of **5** onto Pt(II) as an endo bidentate ligand has been known: H. C. Volger, H. Hogeveen, M. M. P. Gaasbeek, *J. Am. Chem. Soc.*, **91**, 2137 (1969).

10) The benzene ring can participate in the coordination as a dihapto olefinic ligand to form transition metal π complexes: R. E. Rundle and J. H. Goring, *J. Am. Chem. Soc.*, **72**, 5337 (1950); P. W. Turner and E. L. Amma, *ibid.*, **85**, 4046 (1963); R. Victor, R. Ben-Shoshan, and S. Sarel, *J. Org. Chem.*, **37**, 1930 (1972).

11) For the isomerization of **5** to **19** by Rh(I) complexes, see H. C. Volger, H. Hogeveen, and M. M. P. Gaasbeek, *J. Am. Chem. Soc.*, **91**, 218 (1969).

12) I. Tabushi, K. Yamamura, and Z. Yoshida, *J. Am. Chem. Soc.*, **94**, 787 (1972).

13) C. D. Smith, *J. Am. Chem. Soc.*, **88**, 4273 (1966); H. Prinzbach and J. Rivier, *Angew. Chem., Int. Ed. Engl.*, **79**, 1102 (1967); H. Prinzbach, *Pure Appl. Chem.*, **16**, 17 (1968).

14) Such a path is not well-established, but formation of a similar type of complex has been reported for ferrocene and TCNE or tetrafluoroethylene: M. Herberhold, "Metal π-Complex," Elsevier, Amsterdam (1972), p. 309; D. R. Fahey, *Organomet. Chem. Rev.*, **7**, 245 (1972).

15) C. A. Tolman, *J. Am. Chem. Soc.*, **96**, 2780 (1974).

16) It has been pointed out that there exists some relationship between the reactivities of olefinic bonds and their strain energies in metal catalyzed reactions. See Refs. 4b and 6.

17) For the metallacyclopentane formation from transition metal complexes and two moles of olefins, see: A. R. Fraser, P. H. Bird, S. A. Bezman, J. R. Shapley, R. White, and J. A. Osborn, *J. Am. Chem. Soc.*, **95**, 597 (1973); R. H. Grubbs and A. Miyashita, *J. Organomet. Chem.*, **161**, 371 (1978); S. J. McLain, C. D. Wood, and R. R. Schrock, *J. Am. Chem. Soc.*, **101**, 4558 (1979); S. J. McLain, J. Sancho, and R. R. Schrock, *ibid.*, **101**, 5451 (1979). A number of catalytic olefin cyclooligomerization reactions are thought to involve metallacycle intermediates: G. Wilke, *Pure Appl. Chem.*, **50**, 677 (1978).

18) A concerted mechanism has been proposed for metal catalyzed olefin cyclizations, although the mechanistic implication of the concertedness is losing its importance: W. Merk and R. Pettit, *J. Am. Chem. Soc.*, **89**, 4787 (1967); R. Pettit, H. Sugahara, J. Wristers, and W. Merk, *Discuss. Faraday Soc.*, **1969**, 71; F. D. Mango and J. H. Schachtschneider, *J. Am. Chem. Soc.*, **89**, 2484 (1967); G. N. Schrauzer, "Transition Metals in Homogeneous Catalysis," Marcel Dekker, New York, N.Y. (1971), p. 223; W. Slegeir, R. Case, J. S. McKennis, and R. Pettit, *J. Am. Chem. Soc.*, **96**, 287 (1974).

19) Thus, the reactivity of the strained olefins in the present catalytic reactions can be best explained in terms of homoconjugation. The extent of the homoconjugation of **12** is larger than that of **5**,[2b,c] while the former is less reactive than the latter, the reason of this is not clear at present. We need more informations on the energies of the transition states for such quantitative discussion.

20) G. N. Schrauzer, *J. Am. Chem. Soc.*, **81**, 5310 (1959).

21) R. J. Rawson and I. T. Harrison, *J. Org. Chem.*, **35**, 2057 (1970).

22) H. Nozaki, H. Takaya, S. Moriuchi, and R. Noyori, *Tetrahedron*, **24**, 3655 (1968).

23) M. F. Semmelhack, *Org. React.*, **19**, 161 (1972).

24) T. F. Mich, E. J. Nienhous, T. E. Farina, and J. J. Tufariello, *J. Chem. Educ.*, **45**, 272 (1968).

25) J. G. Atkinson, M. H. Fisher, D. Horley, A. T. Morse, R. S. Stuart, and E. Synnes, *Can. J. Chem.*, **43**, 1614 (1965).

26) L. W. Gosser and C. A. Tolman, *J. Inorg. Chem.*, **9**, 2350 (1970).

A Novel Synthesis of 3-Aryl-1,2,4-benzotriazines *via* *N*-Phenylsulfonyl-*N*″-arylbenzamidrazones

Suketaka Ito,* Yumo Tanaka, and Akikazu Kakehi

Department of Industrial Chemistry, Faculty of Engineering, Shinshu University, Wakasato, Nagano 380

(Received June 10, 1981)

3-Aryl-1,2,4-benzotriazines were obtained in good yields by the mercury(II) oxide-oxidation of *N*-phenylsulfonyl-*N*″-arylbenzamidrazones prepared from *N*-(phenylsulfonyl)benzohydrazonoyl chlorides and anilines. From the synthetic viewpoint for benzotriazines, this method may be of high utility on account of the availability of starting materials and higher yields.

The oxidation of 2-substituted (arylsulfonyl)hydrazines leads to the formation of diazonium intermediates with the elimination of arylsulfonyl group as an arenesulfinate anion.[1] An analogous type of reaction is involved in the formation of 2,5-disubstituted tetrazoles from N^2-substituted N^4-(phenylsulfonyl)benzohydrazide hydrazones, in which the cyclization of intermediate formazan, the oxidation product of hydrazide hydrazone, has been postulated to proceed with the elimination of benzenesulfinato moiety.[2]

Such an azo or diazo group formation by the oxidation of (arylsulfonyl)hydrazine derivatives and the subsequent cyclization with the elimination of arenesulfinato moiety may be an attractive method for the synthesis of aza-heterocycles. The present paper deals with the synthesis of 3-aryl-1,2,4-benzotriazines (**1**) by the mercury(II) oxide-oxidation of *N*-phenylsulfonyl-*N*″-arylbenzamidrazones (**2**).

Results and Discussion

N-Phenylsulfonyl-N″-arylbenzamidrazones (2).[3] Amidrazones (**2**)[4] were obtained in good yields by the reaction of *N*-(phenylsulfonyl)benzohydrazonoyl chlorides (**4**)[2a] with anilines (**3**) (Scheme 1, Table 1).

The amidrazones are capable of existing in tautomeric forms, **2**(I)⇄**2**(II), as shown in Scheme 1. Furthermore, the *syn-anti* isomerism can be expected for each tautomer. For each of compounds **2**, plural, wide-spread, definitely unassignable bands due to the NH stretching were noted in the 3400—2950 cm^{-1} region in the IR spectra ($CHCl_3$),[5] and two medium peaks to be assigned to the asymmetric SO_2 stretching vibration at approximately 1380 and 1325 cm^{-1} were also found along with a strong peak due to the symmetric SO_2 stretching vibration near 1160 cm^{-1} (Table 1).

N-Methylbenzanilide phenylsulfonylhydrazone (**5**), prepared as a reference compound from *N*-methylaniline and **4** (X=H), exhibits two broad bands at 3260 and 3030 cm^{-1} (ν_{NH}), a band with a minor side peak (1601 cm^{-1}) at 1590 cm^{-1} ($\nu_{C=N}$), and three peaks at 1377, 1326 (asym. ν_{SO_2}), and 1169 cm^{-1} (sym. ν_{SO_2}, with a shoulder at 1177 cm^{-1}) ($CHCl_3$). Since this type of amidrazone cannot tautomerize, compound **5** would be expected to exhibit one band due to each of the NH, asymmetric SO_2, and symmetric SO_2 stretching vibrations; thus, the origin of the duality of absorption peaks for compound **5** should be related to the *syn-anti* isomerism and/or differences in the type of hydrogen bonding. The IR spectral pattern of each of **2** has a close resemblance to that of **5**; compounds **2**, therefore, may exist in the amide hydrazone form, **2**(I). The characteristics of IR spectra of **2** may reflect also strong hydrogen bonding in these compounds. Several geometrical forms involving intra- or intermolecular hydrogen bonding are conceivable for **2**, and the possibility of hydrazide imide structure, **2**(II), for **2** still remains.

In the ^{1}H-NMR spectra of **2**, broad *N*-H proton signals are concealed by those of aromatic protons appeared at approximately δ 6.5—8.9 ppm.

The amidrazones dissolve both in dilute mineral acids and aqueous alkali solutions. On treatment with

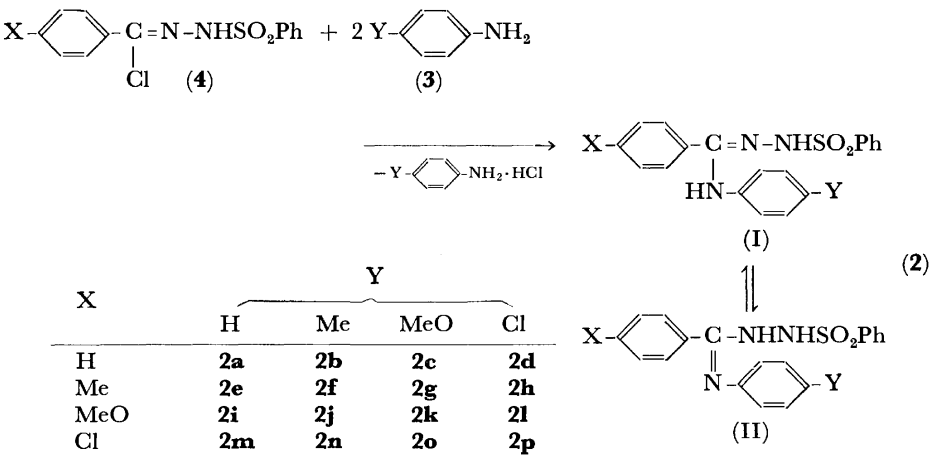

X \ Y	H	Me	MeO	Cl
H	**2a**	**2b**	**2c**	**2d**
Me	**2e**	**2f**	**2g**	**2h**
MeO	**2i**	**2j**	**2k**	**2l**
Cl	**2m**	**2n**	**2o**	**2p**

Scheme 1.

Table 1. Preparation of *N*-phenylsulfonyl-*N''*-arylbenzamidrazones (**2**)

Amidrazone	Yield/%	Mp θ_m/°C	Solvent[a]	IR ($CHCl_3$)[b] $\nu_{C=N}$ cm^{-1}	IR ($CHCl_3$)[b] ν_{SO_2}[c] cm^{-1}		Formula	Found (Calcd)(%) C	H	N
2a	77	153—154	B	1598 s	1380 m 1325 m	1164 s	$C_{19}H_{17}N_3O_2S$	64.68 (64.94	4.85 4.88	11.70 11.96)
2b	82	180—181	B	1600 s	1380 m 1325 m	1165 s	$C_{20}H_{19}N_3O_2S$	65.71 (65.73	5.37 5.24	11.71 11.50)
2c	69	183—184	B-A	1599 s	1382 m 1320 m	1162 s	$C_{20}H_{19}N_3O_3S$	63.00 (62.98	5.02 5.02	11.33 11.02)
2d	86	181—182	B-H	1592 s 1603 d	1378 m 1325 m	1161 s	$C_{19}H_{16}N_3O_2SCl$	59.15 (59.14	4.14 4.14	10.99 10.89)
2e	84	151—153	B-H	1596 s	1378 m 1325 m	1163 s	$C_{20}H_{19}N_3O_2S$	65.45 (65.73	5.27 5.24	11.42 11.50)
2f	86	192—193	B-H	1599 s	1381 m 1320 m	1163 s	$C_{21}H_{21}N_3O_2S$	66.40 (66.47	5.63 5.58	10.97 11.07)
2g	89	169—170	B-H	1598 s	1381 m 1320 m	1163 s	$C_{21}H_{21}N_3O_3S$	63.89 (63.78	5.43 5.35	10.87 10.63)
2h	81	207—208	A	1593 s 1603 sh	1380 m 1325 m	1164 s	$C_{20}H_{18}N_3O_2SCl$	59.71 (60.07	4.50 4.54	10.53 10.51)
2i	80	144—146	B	1596 s 1606 d	1380 m 1320 m	1164 s	$C_{20}H_{19}N_3O_3S$	62.89 (62.98	5.06 5.02	11.34 11.02)
2j	77	153—154	B-H	1606 s 1595 sh	1380 m 1320 m	1164 s	$C_{21}H_{21}N_3O_3S$	63.85 (63.78	5.11 5.33	10.48 10.63)
2k	93	142—144	B-H	1610 s 1600 sh	1381 m 1320 m	1161 s	$C_{21}H_{21}N_3O_4S$	61.19 (61.30	5.13 5.14	9.99 10.21)
2l	77	175—176	A	1609 s 1595 sh	1380 m 1324 m	1166 s	$C_{20}H_{18}N_3O_3SCl$	57.55 (57.76	4.38 4.36	10.25 10.10)
2m	83	190—192	B-E	1599 s	1380 m 1325 m	1165 s	$C_{19}H_{16}N_3O_2SCl$	58.87 (59.14	4.04 4.18	10.95 10.89)
2n	83	181—182	E-H	1598 s	1380 m 1325 m	1161 s	$C_{20}H_{18}N_3O_2SCl$	60.16 (60.07	4.49 4.54	10.58 10.51)
2o	97	178—179	B-H	1599 s	1381 m 1325 m	1162 s	$C_{20}H_{18}N_3O_3SCl$	58.05 (57.76	4.40 4.36	10.16 10.10)
2p	67	198—199	A	1593 s 1600 sh	1376 m 1325 m	1162 s	$C_{19}H_{15}N_3O_2SCl$	54.05 (54.30	3.57 3.60	10.16 10.00)

a) Solvent for recrystallization. A: Acetone, B: benzene, E: diethyl ether, H: hexane. b) Abbreviations are as follows: m, medium; s, strong; sh, shoulder; d, doublet with the counterpart peak. c) The symmetric ν_{SO_2}-peak ($\approx$1165 cm^{-1}) of each compound is accompanied with a shoulder near 1175 cm^{-1}.

hydrogen chloride in an organic solvent, **2a**, for example, gave the corresponding hydrochloride, from which the free amidrazone was recovered by neutralization.

In the amidrazone preparation, in the case of **2a** for example, small amounts of 3,4,5-triphenyl-4*H*-1,2,4-triazole (**6**) and 3,5-diphenyl-4-phenylsulfonylamino-4*H*-1,2,4-triazole (**7**) were formed as by-products. The formation of these by-products can be explained in terms of the intramolecular nucleophilic process with

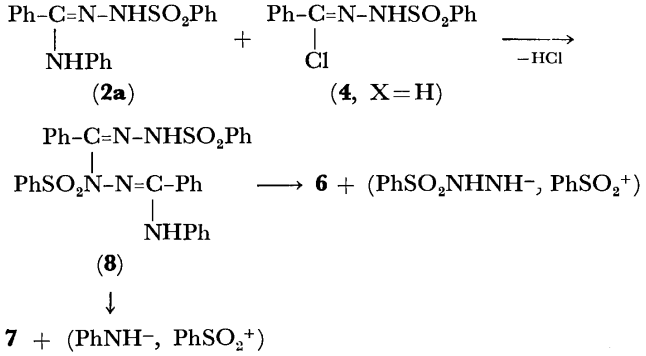

the elimination of anilino or (phenylsulfonyl)hydrazino group *via* *N*-phenylsulfonyl-*N*-[*N*-(phenylsulfonyl)benzohydrazonoyl]-*N''*-phenylbenzamidrazone (**8**) which would be formed from **2a** and **4** (X=H).[6] Amidrazones are a sort of amidines: the formation of 1,2,4-triazoles by the reaction of the hydrazonoyl chloride (**4**, X=H) with amidines has been previously discussed.[7]

Oxidation of Amidrazones (2) with Mercury(II) Oxide. When amidrazone **2a** was stirred with potassium carbonate in dioxane at room temperature for 8 d, 3-phenyl-1,2,4-benzotriazine (**1a**) was obtained in a 33% yield together with benzanilide (**9a**) and small amounts of diphenyl disulfide (**10**) and *S*-phenyl benzenethiosulfonate (**11**). However, on treatment with mercury(II) oxide in the presence of potassium carbonate, the reaction proceeded smoothly to give **1a** in a 55% yield after stirring for 18 h (along with **9a**, **10**, and **11**). The similar treatment of **2b—p** afforded the corresponding 3-aryl-1,2,4-benzotriazines (**1b—p**) in widely changing yields from 11 to 82%, along with benzanilides (**9b—p**), **10**, and **11**. The results are summarized in Tables 2 and 3.

Table 2. Oxidation of amidrazones (**2**) with HgO

Amidrazone	Products[a] (Yield/%)		Mp of **9** θ_m/°C	
	1	**9**	Obsd[b]	(Lit)
2a	**1a** (53)	**9a** (45)	160—162	(161—162)[d]
2b	**1b** (63)	**9b** (36)	157—158	(157—158)[d]
2c	**1c** (61)	**9c** (37)	155—157	(155—156)[d]
2d	**1d** (60)	**9d** (38)	192—193	(191—192)[d]
2e	**1e** (26)	**9e** (72)	146—147	(147)[e]
2f	**1f** (37)	**9f** (62)	163—164	(162—163)[f]
2g	**1g** (50)	**9g** (47)	166—167	(168—169)[d]
2h	**1h** (37)	**9h** (56)	215—216[c]	
2i	**1i** (11)	**9i** (84)	170—171	(171—172)[d]
2j	**1j** (25)	**9j** (73)	151—152	(155—156)[g]
2k	**1k** (22)	**9k** (60)	202—203	(202—203)[d]
2l	**1l** (17)	**9l** (66)	207—209	(207—208)[g]
2m	**1m** (66)	**9m** (32)	200—201	(200—201)[h]
2n	**1n** (82)	**9n** (17)	214—216	(212—213)[e]
2o	**1o** (81)	**9o** (19)	210—211	(208—209)[d]
2p	**1p** (67)	**9p** (32)	211—213	(211—212)[h]

a) Diphenyl disulfide (**10**) and *S*-phenyl benzenethiosulfonate (**11**) were produced in all cases. b) All of the benzanilides were recrystallized from ethanol. c) Mp of a sample prepared from *p*-toluoyl chloride and *p*-chloraniline: 215—216 °C. Found for **9h**: C, 68.38; H, 4.98; N, 5.77%. Calcd for $C_{14}H_{12}NOCl$: C, 68.44; H, 4.92; N, 5.70%. d) S. Ikenoya, M. Masui, H. Ohmori, and H. Sayo, *J. Chem. Soc., Perkin Trans. 2*, **1974**, 571. e) L. A. Tetyueva and P. A. Petyunin, *Zh. Obshch. Khim.*, **28**, 739 (1958); *Chem. Abstr.*, **52**, 17144d (1958). f) D. E. Peason, K. N. Carter, and and C. M. Greer, *J. Am. Chem. Soc.*, **75**, 5905 (1953). g) P. Grammaticakis, *Bull. Soc. Chim. Fr.*, **1964**, 924. h) F. E. R. Gleiter, *Chem. Ber.*, **97**, 472 (1964).

The triazines obtained were identified by their analytical and spectral data, and the confirmation of known compounds was made by direct comparison with authentic specimens prepared according to other synthetic methods.[8] The spectral data of the products are listed in Table 4. In the IR spectra, all the triazines exhibit a similar absorption pattern, exclusive of absorptions due to the substituent at the 7-position (Y) and to that in the 3-aryl group (X). Because of the presence of 3-aryl group, the absorption peaks in the region of aromatic skeletal vibrations cannot be assigned with respect to the benzotriazine skeleton. However, two strong peaks near 1320 and near 1010 cm^{-1} were observed in common with the benzotriazines; these characteristic bands may be assigned to the benzotriazine ring.[9] The maximum absorption in the range of 350—400 nm in the UV spectra should be due to the $n\rightarrow\pi^*$ transition, which also characterizes benzotriazines. The ^{1}H-NMR spectra are consistent with the benzotriazine structures.

Mechanistic Consideration for the Benzotriazine Formation. The oxidation of amidrazone with mercury(II) oxide has been reported to give an imidoylazo compound;[10] thus, by analogy,[11] the primary product in the present reaction can be considered to be an imidoylazo sulfone (**12**), by the intermediacy of which the triazine formation may be reasonably interpreted.

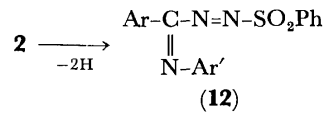

2 $\xrightarrow[-2H]{}$ Ar–C(=N–N–SO_2Ph)–N–Ar′ (**12**)

In the case of reaction without mercury(II) oxide, the same intermediate may be formed by the oxidation with air in the presence of a base. The air oxidation of hydrazine derivatives to azo compounds has been reported for hydrazidines[2a,12] but not for amidrazones.

In view of the fact that the precursor of the disulfide (**10**) and *S*-phenyl benzenethiosulfonate (**11**) is benzenesulfinic acid,[13] the following route involving a diazonium intermediate can be given as the most probable mechanism for the formation of **1** from **12** (Scheme 2).

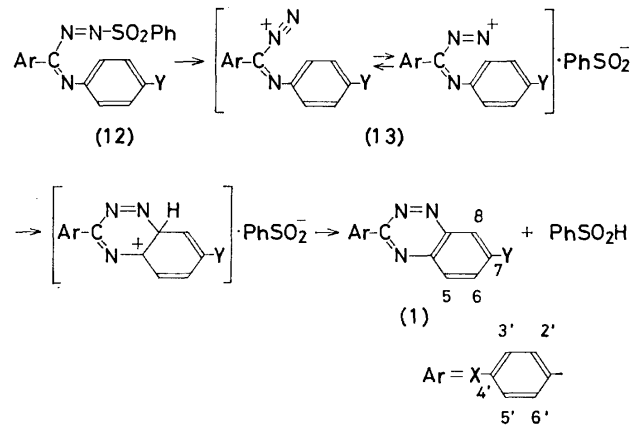

Scheme 2.

The dissociation of azo sulfones to diazonium arenesulfinates is well known,[1,3c,14] and the cyclization process might be an intramolecular diazo-coupling. From the fact that diazonium *p*-toluenesulfinate generated from α-(*p*-tolylsulfonylazo)stilbene does not cyclize to 3-phenylbenzopyridazine,[14a] the imino nitrogen of **13** may play a significant role for the cyclization as an electron-donor. The sequence of reaction shown in Scheme 2 is similar to the mechanism suggested for the acid-catalyzed benzotriazine formation from 1,3,5-triphenylformazan[15] from the viewpoint of electronic structure.

The formation of benzanilides (**9**) can be well interpreted in terms of the hydrolysis of imino-carbonium ion (**14**) which is generated from the diazonium ion (**13**) by releasing molecular nitrogen or directly from **12**.

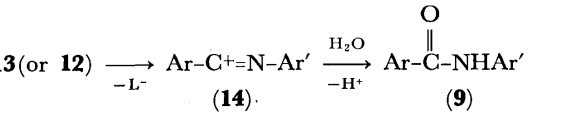

13(or **12**) $\xrightarrow[-L^-]{}$ Ar–C$^+$=N–Ar′ (**14**) $\xrightarrow[-H^+]{H_2O}$ Ar–C(=O)–NHAr′ (**9**)

L = N_2^+(or $PhSO_2N_2$)

The formation of **1** should be competitive with that of **9**. As seen in Table 2, the anilide formation is dominant in such a case that the para-substituent of *C*-phenyl group of **12** is electron-donating (X=Me or MeO), which may be explained in terms of the labilization of the C–N linkage holding phenylazo or diazo group and the increased stability of the imino-

Table 3. Physical and analytical data for 3-aryl-1,2,4-benzotriazines (**1**)

Triazine[a]	Mp θ_m/°C	Solvent[b]	Appearance	Formula	Found (Calcd)(%) C	H	N
1a	124—126[c]	H	Pale yellow needles	$C_{13}H_9N_3$			
1b	127—129	A	Yellow needles	$C_{14}H_{11}N_3$	75.70 (76.00	5.10 5.01	19.17 18.99)
1c	183—184	A-C	Pale yellow needles	$C_{14}H_{11}N_3O$	70.63 (70.87	4.71 4.67	17.82 17.71)
1d	174—175	A	Yellowish orange needles	$C_{13}H_8N_3Cl$	64.43 (64.61	3.31 3.34	17.34 17.39)
1e	119—120	A	Yellowish orange needles	$C_{14}H_{11}N_3$	75.81 (76.00	5.03 5.01	19.10 18.99)
1f	173—174	A	Yellow needles	$C_{15}H_{13}N_3$	76.66 (76.57	5.53 5.57	18.00 17.86)
1g	187—188	A	Pale yellow leaflets	$C_{15}H_{13}N_3O$	71.59 (71.70	5.17 5.21	16.73 16.72)
1h	176—177	A	Pale yellow leaflets	$C_{14}H_{10}N_3Cl$	65.78 (65.76	3.98 3.94	16.67 16.43)
1i	143—144[d]	A	Yellowish orange needles	$C_{14}H_{11}N_3$			
1j	152—154	A	Pale yellow needles	$C_{15}H_{13}N_3O$	71.48 (71.70	5.25 5.21	16.99 16.72)
1k	231—232	A-C	Yellow needles	$C_{15}H_{13}N_3O_2$	67.41 (67.41	4.91 4.90	15.93 15.72)
1l	208—209	A-C	Yellow needles	$C_{14}H_{10}N_3OCl$	61.70 (61.88	3.68 3.71	15.25 15.47)
1m	150—152[e]	A	Yellow needles	$C_{13}H_8N_3Cl$			
1n	183—184	A-C	Yellow needles	$C_{14}H_{10}N_3Cl$	65.70 (65.76	3.91 3.94	16.51 16.43)
1o	259—260	A-C	Pale yellow needles	$C_{14}H_{10}N_3OCl$	61.68 (61.89	3.67 3.71	15.26 15.47)
1p	248—249	A-C	Yellowish orange needles	$C_{13}H_7N_3Cl_2$	56.48 (56.55	4.70 4.75	15.29 15.22)

a) Satisfactory analytical data (±0.3% for C, H, N) were also obtained for known compounds, **1a**, **1i**, and **1m**. b) Solvent for recrystallization. A: acetone, C: chloroform, H: hexane. c) Lit, mp 126—127 °C: R. A. Abramovitch and K. Schofield, *J. Chem. Soc.*, **1955**, 2326. d) Lit, mp 139—140 °C: R. F. Robbins and K. Schofield, *J. Chem. Soc.*, **1957**, 3186. e) Lit, mp 151—152 °C: R. F. Robbins and K. Schofield, *J. Chem. Soc.*, **1957**, 3186.

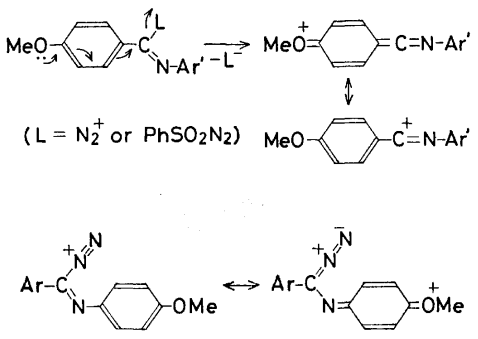

Scheme 3.

carbonium ion (Scheme 3). On the other hand, the para-substitution of *N*-phenyl group with an electron-donor (Y=Me or MeO) seems to be favorable to some extent for the formation of **1**, which may be ascribed to an increase in the stability of diazonium ion (Scheme 3).

It is known that the Bamberger synthesis of 3-aryl-1,2,4-benzotriazines from substituted formazans is widely applicable.[8] In general, however, this method gives two benzotriazines from a mixed formazan in which

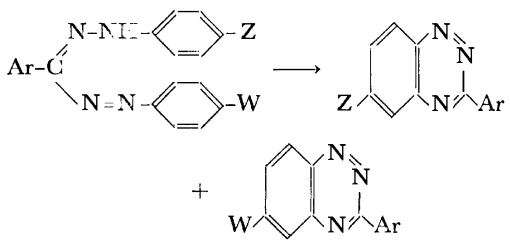

the 1- and the 5-phenyl groups are substituted unsymmetrically,[15] and formazans are not always obtained in high yields depending upon the nature of substituents.[16] On the other hand, the present method gives only one triazine. Furthermore, the starting materials are readily obtainable, and the yield of product is high in general, except the case in which the *C*-phenyl group of **2** is substituted with an electron-donating group. In conclusion, this method possesses a higher synthetic utility for 3-aryl-1,2,4-benzotriazines.

Experimental

The melting points were determined with a Yanagimoto MP-S3 micromelting point apparatus, and are uncorrected.

Table 4. Spectral data of 3-aryl-1,2,4-benzotriazines (**1**)

Triazine	IR (KBr) ν_{ring}/cm^{-1}		UV (EtOH) λ_{max}/nm ($\varepsilon \times 10^{-3}$)		^{1}H-NMR ($CDCl_3$) δ (Coupling constant, J/Hz)
1a	1330	1020	352 (0.91)	261 (12.5)	7.60—8.40 (m; 5,6,7-H, 3',4',5'-H), 8.65—9.10 (m; 8-H, 2',6'-H)
1b	1330	1013	360 (0.91)	261 (11.6)	2.68 (s; 7-Me), 7.55—7.85 (m; 3',4',5'-H), 7.90 (dd, J=9.0, 1.5; 6-H), 8.14 (d, J=9.0; 5-H), 8.41 (brs; 8-H), 8.75—9.05 (m; 2',6'-H)
1c	1320	1015	384 (1.18)	266 (13.5)	4.11 (s; 7-MeO), 7.55—7.90 (m; 6,8-H, 3',4',5'-H), 8.13 (d, J=9.0; 5-H), 8.75—9.05 (m; 2',6'-H)
1d	1315	1010	362 (1.25)	262 (14.7)	7.60—7.90 (m; 3',4',5'-H), 8.00 (dd, J=9.0, 2.0; 6-H), 8.24 (d, J=9.0; 5-H), 8.69 (d, J=2.0; 8-H), 8.80—9.05 (m; 2',6'-H)
1e	1325	1010	358 (1.24)	266 (19.7)	2.53 (s; 4'-Me), 7.57 (d, J=8.5; 3',5'-H), 7.77—8.40 (m; 5,6,7-H), 8.60—8.75 (m; 8-H), 8.85 (d, J=8.5; 2',6'-H)
1f	1320	1010	369 (1.31)	264 (15.3)	2.50 (s; 4'-Me), 2.67 (s; 7-Me), 7.53 (d, J=8.0; 3',5'-H), 7.88 (dd, J=8.5, 2.0; 6-H), 8.33 (d, J=8.5; 5-H), 8.43 (brs; 8-H), 8.80 (d, J=8.0; 2',6'-H)
1g	1320	1015	386 (0.88)	268 (13.1)	2.51 (s; 4'-Me), 4.11 (s; 7-MeO), 7.53 (d, J=8.5; 3',5'-H), 7.72 (dd, J=8.0, 2.0; 6-H), 7.85 (d, J=2.0; 8-H), 8.13 (d, J=8.0; 5-H), 8.78 (d, J=8.5; 2',6'-H)
1h	1315	1010	368 (1.39)	266 (18.0)	2.51 (s; 4'-Me), 7.52 (d, J=8.5; 3',5'-H), 7.97 (dd, J=9.0; 2.0; 6-H), 8.19 (d, J=9.0; 5-H), 8.67 (d, J=2.0; 8-H), 8.78 (d, J=8.5; 2',6'-H)
1i	1325	1020	376 (2.51) 274 (21.3)	302 (18.5)	4.00 (s; 4'-MeO), 7.25 (almost d, J=9.0; 3',5'-H), 7.80—8.27 (m, 5,6,7-H), 8.57—8.80 (m; 8-H), 8.92 (almost d, J=9.0; 2',6'-H)
1j	1325	1015	382 (1.78) 273 (20.3)	301 (12.7)	2.71 (s; 7-Me), 3.99 (s; 4'-MeO), 7.23 (almost d, J=9.0; 3',5'-H), 7.91 (dd, J=9.0, 2.0; 6-H), 8.15 (d, J=9.0; 5-H), 8.45 (brs; 8-H), 8.90 (almost d, J=9.0; 2',6'-H)
1k	1330	1010	396 (1.37) 274 (8.84)	302 (5.37)	a)
1l	1325	1020	386 (3.10) 276 (35.7)	309 (20.6)	a)
1m	1325	1010	350 (1.14) 260 (11.2)	277 (10.8)	7.69 (almost d, J=8.5; 3',5'-H), 7.85—8.30 (m; 5,6,7-H), 8.57—8.75 (m; 8-H), 8.87 (almost d, J=9.0; 2',6'-H)
1n	1310	1005	361 (1.16) 264 (17.4)	277 (14.2)	2.73 (s; 7-Me), 7.70 (almost d, J=8.5; 3',5'-H), 7.97 (dd, J=9.0, 2.0; 6-H), 8.18 (d, J=9.0; 5-H), 8.46 (brs; 8-H), 8.87 (almost d, J=8.5; 2',6'-H)
1o	1320	1015	385 (1.42)	273 (30.6)	4.16 (s; 7-MeO), 7.73 (d, J=9.0; 3',5'-H), 7.90 (d, J=2.0; 8-H), 8.20 (d, J=8.0; 5-H), 8.87 (d, J=8.5; 2',6'-H)[b]
1p	1310	1005	361 (7.06)	265 (21.4)	7.73 (d, J=8.5; 3',5'-H), 8.07 (dd, J=8.0; 2.0; 6-H), 8.23 (d, J=8.0; 5-H), 8.72 (d, J=2.0; 8-H), 8.90 (d, J=8.5; 2',6'-H)

a) Compound **1k** (**1l**) is almost insoluble in $CDCl_3$. b) The signal (dd) of 6-H is partially concealed by those of 8,3',5'-H.

The microanalysis was performed on a Perkin-Elmer 240 elemental analyzer. The UV, IR, and NMR spectra were recorded with a Hitachi 220, a Hitachi 260-10, and a Varian EM-360A spectrometer, respectively. *N*-(Phenylsulfonyl)benzohydrazonoyl chlorides (**4**) were prepared by the method previously reported.[2a]

Preparation of Amidrazones (2). General Procedure: A solution of **3** (21 mmol) in THF (10 ml) was added to a solution of **4** (10 mmol) in THF (30 ml) with stirring at room temperature. After being stirred for 18—20 h, the reaction mixture was poured into cold water. The resulting precipitates were filtered, washed with water, and dried. The crude product was chromatographed on a silica-gel column (100—200 mesh, 2.0 cm × 12 cm) to afford the corresponding amidrazone, which was recrystallized from an appropriate solvent. The results are summarized in Table 1.

N-*Phenylsulfonyl*-N''-*phenylbenzamidrazone (2a). (A Typical Example)*: Compound **2a** (2.71 g) generated from aniline (**3**, Y=H, 1.96 g) and **4** (X=H, 2.95 g) was eluted from a silica-gel column with benzene–ether (50:1, v/v); elution with benzene–ethanol (50:1, v/v; then the proportion of ethanol was increased gradually) gave **6**[7] (100 mg, mp 292—293 °C) and **7**[2b] (150 mg, mp 312—315 °C).

N-*Phenylsulfonyl*-N''-*phenylbenzamidrazone Hydrochloride*. Dry hydrogen chloride was introduced into a solution of

2a (100 mg) in ethanol. Removal of the solvent from the mixture under reduced pressure gave a solid (110 mg), which was crystallized from chloroform–ethanol to afford the hydrochloride as colorless prisms, mp 187—189 °C; IR (KBr): 2960—2650 (ν_{N^+H}), 1625 ($\nu_{C=H}$), 1320, 1155 cm^{-1} (ν_{SO_2}); Found: C, 58.70; H, 4.74; N, 10.65%. Calcd for $C_{19}H_{18}N_3O_2SCl$: C, 58.83; H, 4.68; N, 10.83%. Neutralization with aqueous ammonia or sodium hydrogencarbonate gave the free amidrazone, **2a**.

Oxidation of **2** *with Mercury(II) Oxide. General Procedure*: A mixture of **2** (2 mmol), HgO (yellow, 650 mg, 3 mmol), K_2CO_3 (830 mg, 6 mmol), and $CaSO_4$ (820 mg, 6 mmol) was stirred in dry dioxane (30 ml) for 18—20 h at room temperature. The reaction mixture was filtered to remove insoluble inorganic substances, which were washed with dioxane (20 ml). The filtrate combined with washings was concentrated under reduced pressure to afford a semi-solid residue. By using a hexane–benzene–ether system (4:1:0–1:1:0–0:50:1, v/v) as the eluent, the residue was chromatographed on a silica-gel column (2.0 cm × 10 cm) to give diphenyl disulfide (**10**), *S*-phenyl benzenethiosulfonate (**11**, mp 43—44 °C, lit,[17] mp 45 °C), benzotriazine (**1**), and the corresponding benzanilide (**9**). The results are summarized in Tables 2 and 3. The IR spectra of **10** and **11** were identical with those of authentic samples, respectively.

References

1) W. Koenigs, *Ber.*, **10**, 1532 (1877); "Beilsteins Handbuch der Organischen Chemie," Hw. Bd. XVI, p. 33 (1933); O. Attanasi, L. Caglioti, and F. Gasparrini, *J. Chem. Soc., Chem. Commun.*, **1974**, 138; L. Caglioti, F. Gasparrini, G. Palmiera, and D. Misiti, *Tetrahedron Lett.*, **1976**, 3987.

2) a) S. Ito, Y. Tanaka, and A. Kakehi, *Bull. Chem. Soc. Jpn.*, **49**, 762 (1976); b) S. Ito, Y. Tanaka, A. Kakehi, and M. Kawahata, *ibid.*, **51**, 953 (1978).

3) Concerning *N*-sulfonylamidrazones, the following information is available. N,N-*Disubstituted amide sulfonylhydrazones*: a) Gevaert-Agfa N. V., Neth. Patent, 6509590 (1966); *Chem. Abstr.*, **64**, 18776h (1966); b) J. Jaeken and R. L. Jansseune, U. S. Patent, 3245788 (1966); *ibid.*, **65**, 844d (1966). *Cyclic amide arylsulfonylhydrazones*: c) S. Huenig, *Angew. Chem., Int. Ed. Engl.*, **80**, 343 (1968).

4) Concerning the synthesis of amidrazones, see D. G. Neilson, R. Roger, W. M. Heatlie, and L. R. Newlands, *Chem. Rev.*, **70**, 151 (1970); K. M. Watson and D. G. Neilson, "The Chemistry of Amidines and Imidates," ed by S. Patai, John Wiley & Sons, Inc., New York (1957), Chap. 10.

5) The pressed disks with powdered potassium bromide gave somewhat complex spectra in which absorptions due to the NH and SO_2 stretching vibrations were found at different frequencies.

6) When **2a** was allowed to react with **4** (X=H), a considerable amount of **6** was obtained along with **7**.

7) S. Ito, Y. Tanaka, A. Kakehi, and H. Miyazawa, *Bull. Chem. Soc. Jpn.*, **50**, 2969 (1977).

8) J. P. Horwits, "Heterocyclic Compounds," ed by R. C. Elderfield, John Wiley & Sons, Inc., New York (1961), Vol. 7, Chap. 9; H. Neunhoeffer and P. F. Wiley, "Chemistry of 1,2,3-Triazines and 1,2,4-Triazines, Tetrazines, and Pentazines," ed by A. Weissberger and E. C. Taylor, John Wiley & Sons, Inc., New York (1978), p. 666.

9) Armarego *et al.* have assigned the absorption of 3-phenyl-1,2,4-benzotriazine at 1018 cm^{-1} (strong) to the skeletal stretching vibration: W. L. F. Armarego, G. B. Bartin, and E. Spinner, *Spectrochim. Acta*, **22**, 117 (1966).

10) M. Busch and R. Ruppenthal, *Ber.*, **43**, 3001 (1910).

11) In general, the oxidation of 1,2-disubstituted (or monosubstituted) hydrazine derivatives is well known to give azo compounds.

12) H. von Pechmann, *Ber.*, **27**, 320 (1894); F. D. Chattaway and A. J. Walker, *J. Chem. Soc.*, **127**, 975 (1925).

13) E. Vinkler, F. Klivengi, and J. Szabo, *Acta Chim. Acad. Sci. Hung.*, **15**, 384 (1958); J. L. Kice and K. W. Bowers, *J. Am. Chem. Soc.*, **84**, 605 (1962).

14) a) G. Rosini and R. Ranza, *J. Org. Chem.*, **36**, 1915 (1971); b) G. Rosini and S. Cacchi, *ibid.*, **37**, 1856 (1972); c) L. Caglioti, F. Gasparrini, G. Paollucci, G. Rosini, and P. Masi, *ibid.*, **38**, 920 (1973).

15) D. Jerchel and W. Woticky, *Justus Liebigs Ann. Chem.*, **605**, 191 (1957).

16) A. W. Nineham, *Chem. Rev.*, **55**, 355 (1955).

17) E. Knoevenagel and A. Römer, *Ber.*, **56B**, 215 (1923).

Furan Derivatives. IV. On the Effects of Substituents in the Syntheses of 4,5-Dihydro-3*H*-naphtho[1,8-*bc*]furans

Sakaaki Horaguchi*, Mamoru Hara, and Tsuneo Suzuki†

Department of Chemistry, Faculty of Science, Niigata University, Ikarashi, Niigata 950-21

†*Nippon Dental University, Niigata, 1-8, Hamaura-cho, Niigata 950*

(Received June 13, 1981)

The reaction of (8-oxo-5,6,7,8-tetrahydro-1-naphthyloxy)acetic acids with acetic anhydride and sodium acetate give a mixture of 4,5-dihydro-3*H*-naphtho[1,8-*bc*]furans and lactones. The relative yields of 4,5-dihydro-3*H*-naphtho[1,8-*bc*]furans and lactones varied according to kinds of substituents on the benzene ring of (8-oxo-5,6,7,8-tetrahydro-1-naphthyloxy)acetic acids. Substituents which make the methylene group approach closer to the carbony carbon atom of (8-oxo-5,6,7,8-tetrahydro-1-naphthyloxy)acetic acids by a steric effect seem to favor the production of 4,5-dihydro-3*H*-naphtho[1,8-*bc*]furans. On the other hand, substituents which make the methylene group separate from the carbonyl carbon atom seem to favor the production of lactones. An electron-withdrawing chlorine atom on the benzene ring of (8-oxo-5,6,7,8-tetrahydro-1-naphthyloxy)acetic acids also favors the production of 4,5-dihydro-3*H*-naphtho[1,8-*bc*]furans.

4,5-Dihydro-3*H*-naphtho[1,8-*bc*]furans (**2**) are important intermediates for the syntheses of phenanthro[4,5-*bcd*]furan derivatives.[1] 4,5-Dihydro-3*H*-naphtho[1,8-*bc*]furans (**2**)[2] have been synthesized by heating (8-oxo-5,6,7,8-tetrahydro-1-naphthyloxy)acetic acids (**1**) with acetic anhydride and sodium acetate. However, the yields of 4,5-dihydro-3*H*-naphtho[1,8-*bc*]furans (**2**) were not good because lactones (**3**) were obtained as by-products. Formation of a considerable amount of lactones (**3**) may be due to the long distance between the methylene group adjacent to the carboxyl group and the carbonyl carbon atom of **1**, since the peri-positions in a naphthalene skeleton are too far apart for the formation of the five-membered furan ring.[3] The relative yields of 4,5-dihydro-3*H*-naphtho[1,8-*bc*]furans (**2**) and lactones (**3**) varied according to kinds of substituents (R^1 and R^2). In the present investigation we examined the factors which influenced relative yields of 4,5-dihydro-3*H*-naphtho[1,8-*bc*]furans (**2**) and lactones (**3**); the steric influence of R^1 and R^2 was examined in detail.

Results and Discussion

Some (8-oxo-5,6,7,8-tetrahydro-1-naphthyloxy)acetic acid (**1a—j**) were prepared to investigate the in-

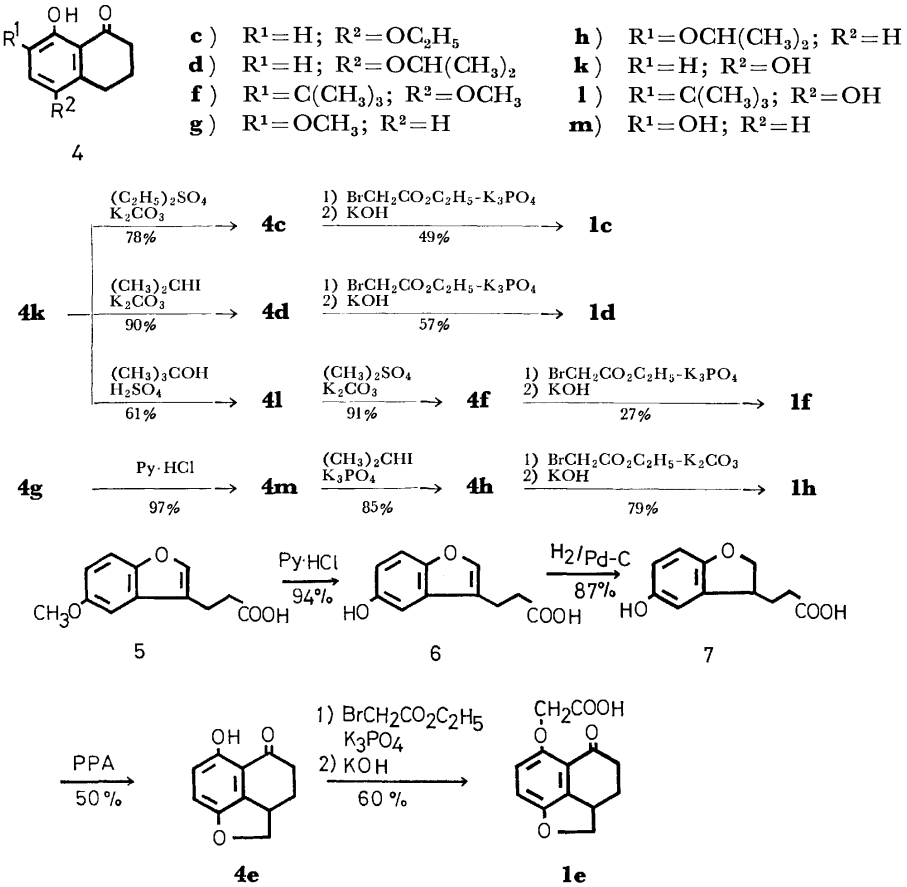

Scheme 1. The synthetic pathways of (8-oxo-5,6,7,8-tetrahydro-1-naphthyloxy)acetic acids (**1c**, **1d**, **1e**, **1f**, and **1h**).

fluence of substituents (R^1 and R^2) in the syntheses of 4,5-dihydro-3*H*-naphtho[1,8-*bc*]furans (**2a—j**) and lactones (**3a—j**). The syntheses of **1a**, **1b**, **1g**, **1i**, and **1j** were carried out according to the methods reported.[2] The synthetic methods of **1c**, **1d**, **1e**, **1f**, and **1h** are summarized in Scheme 1.

When (8-oxo-5,6,7,8-tetrahydro-1-naphthyloxy)acetic acids (**1a—j**) were heated at 150 °C with acetic anhydride and sodium acetate for 1 h, 4,5-dihydro-3*H*-naphtho[1,8-*bc*]furans (**2a—d** and **2f—j**) and lactones (**3a—j**) were obtained. The relative yields and isolated yields of 4,5-dihydro-3*H*-naphtho[1,8-*bc*]furans (**2a—j**) and lactones (**3a—j**) are summarized in Table 1.

Table 1. The reaction of (8-oxo-5,6,7,8-tetrahydro-1-naphthyloxy)acetic acids (**1a—j**) with acetic anhydride and sodium acetate

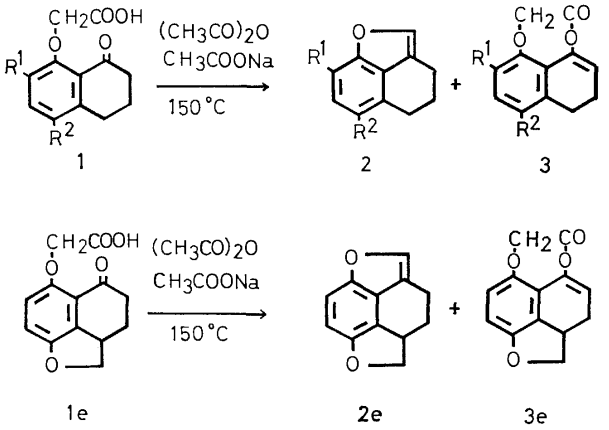

a) R^1=H; R^2=H, **b**) R^1=H; R^2=OCH_3, **c**) R^1=H; R^2=OC_2H_5, **d**) R^1=H; R^2=$OCH(CH_3)_2$, **f**) R^1=$C(CH_3)_3$; R^2=OCH_3, **g**) R^1=OCH_3; R^2=H, **h**) R^1=$OCH(CH_3)_2$; R^2=H, **i**) R^1=OCH_3; R^2=CH_3, **j**) R^1=OCH_3; R^2=Cl.

Starting materials	Product[a]	Relative yields/%	Isolated yields/%
1a	**2a**	48	37
	3a	52	40[b]
1b	**2b**	51	41
	3b	49	40
1c	**2c**	47	37
	3c	53	41
1d	**2d**	49	38
	3d	51	40
1e	**2e**	0	0
	3e	100	48[c]
1f	**2f**	92	77
	3f	8	7
1g	**2g**	65	50
	3g	35	27
1h	**2h**	60	50
	3h	40	33
1i	**2i**	67	60
	3i	33	30[a]
1j	**2j**	87	72
	3j	13	11

a) 4,5-Dihydro-3*H*-naphtho[1,8-*bc*]furans (**2**) are stable under the reaction conditions. b) The lactone was hydrolyzed to the starting material during isolation. c) The yield is low because of the easy hydrolysis of the lactone during isolation.

The results of Table 1 suggest the following conclusions. The reaction of **1a** (R^1=H; R^2=H) with acetic anhydride and sodium acetate gave an almost equal amount of 4,5-dihydro-3*H*-naphtho[1,8-*bc*]furan (**2a**) and a lactone (**3a**) in relative yields of 48 and 52%. Similarly, in the case of **1b—d** (R^1=H; R^2=OCH_3, OC_2H_5, or $OCH(CH_3)_2$), the relative yields of 4,5-dihydro-3*H*-naphtho[1,8-*bc*]furans (**2b—d**) and lactones (**3b—d**) were almost the same in spite of the various kinds of substituents R^2. This suggests that the steric or electronic effect of substituents R^2 have no influence on the relative yields of 4,5-dihydro-3*H*-naphtho[1,8-*bc*]furans (**2a—d**) and lactones (**3a—d**). On the other hand, compound **1e**, in which the electronic effect of a substituent will be similar to that of **1b—d**, gave only a lactone (**3e**) and no 2,2a,3,4-tetrahydronaphtho[1,8-*bc*:4,5-*b'c'*]difuran (**2e**) was obtained. In the case of **1e**, the distance between the methylene group and the carbonyl carbon atom will be longer than that in **1a—d** because the five-membered furan ring of **1e** separates opposite peripositions in the partially saturated naphthalene skeleton.[3] Therefore, the production of **2e** will be difficult because of the strain in the five-membered furan ring. However, the production of **3e** is not so affected by strain owing to formation of the seven-membered lactone ring. The reaction of **1f** (R^1=$C(CH_3)_3$; R^2=OCH_3) with acetic anhydride and sodium acetate gave 4,5-dihydro-3*H*-naphtho[1,8-*bc*]furan (**2f**) and a lactone (**3f**) in the relative yields of 92 and 8% respectively. The large steric effect of the *t*-butyl group in **1f** will make the methylene group approach[4] closer to the carbonyl carbon atom and will favor formation of the five-membered 4,5-dihydro-3*H*-naphtho[1,8-*bc*]-furan (**2f**). The steric repulsion between the *t*-butyl group and the methylene group is observed in the difficult etherification of **4f** with ethyl bromoacetate. The electronic effect of the *t*-butyl group will be negligible.

The reaction of **1g—h** (R^1=OCH_3 or $OCH(CH_3)_2$; R^2=H) with acetic anhydride and sodium acetate gave mainly 4,5-dihydro-3*H*-naphtho[1,8-*bc*]furans (**2g—h**) in the relative yields of 65 and 60% respectively; the yields of lactones (**3g—h**) were 35% and 40% respectively. The steric effect of the methoxyl or isopropoxyl group seems to favor the production of 4,5-dihydro-3*H*-naphtho[1,8-*bc*]furans (**2g—h**), though the substituents are not so bulky as is the *t*-butyl group.

The reaction of **1i** (R^1=OCH_3; R^2=CH_3) with acetic anhydride and sodium acetate gave 4,5-dihydro-3*H*-naphtho[1,8-*bc*]furan (**2i**) and a lactone (**3i**) in the relative yields of 67 and 33% respectively. These yields are similar to those of **2g—h** and **3g—h** and so the effect of the methyl group of **2i** is small. On the other hand, **1j** (R^1=OCH_3; R^2=Cl) with acetic anhydride and sodium acetate gave mostly 4,5-dihydro-3*H*-naphtho[1,8-*bc*]furan (**2j**; 87%) and the yield of a lactone (**3j**) was very low (13%). The electronegative chlorine atom will pull electrons from the benzene ring of **1j** and make the carbonyl carbon

atom more reactive. Therefore, formation of the 4,5-dihydro-3*H*-naphtho[1,8-*bc*]furan (**2j**) will be more favorable than that of the lactone (**3j**).

Experimental

All the melting points are uncorrected. The column chromatography was performed on silica gel (Wakogel C-200). Unless otherwise stated, anhydrous sodium sulfate was employed as the drying agent. The infrared absorption spectra were determined with a Hitachi Model EPI-G grating infrared spectrophotometer. The ultraviolet absorption spectra were determined with a Shimadzu UV-200 spectrophotometer. The nuclear magnetic resonance spectra (^{1}H NMR) were determined at 90 MHz with a JEOL Model JNM-FX 90Q FT NMR spectrometer, using tetrametylsilane as the internal standard.

*A General Procedure for the Reactions of (8-Oxo-5,6,7,8-tetrahydro-1-naphthyloxy)acetic Acids (**1**) with Acetic Anhydride and Sodium Acetate.* A mixture of **1** (1.0 g), acetic anhydride (15 ml), and sodium acetate (4.6 g) was refluxed at 150 °C for 1 h. The mixture was poured into ice–water, stirred for 5 min to decompose excess acetic anhydride, and extracted with ether. The ethereal solution was washed with a 10% potassium carbonate solution and then with water, dried, and evaporated. The resulting oil was chromatographed and eluted with benzene. The first fraction gave 4,5-dihydro-3*H*-naphtho[1,8-*bc*]furans (**2**). The second fraction afforded lactones (**3**).

*6-Ethoxy-4,5-dihydro-3*H*-naphtho[1,8-*bc*]furan (**2c**).* Colorless oil (37% yield); bp 171 °C at 20 Torr (1 Torr≈133.322 Pa). ^{1}H NMR ($CDCl_3$): δ 1.38 (3H, t, J=7 Hz, CH_3), 1.83—2.10 (2H, m, $-CH_2-$), 2.67—2.89 (4H, m, $-CH_2-+-CH_2-$), 4.03 (2H, q, J=7 Hz, $-CH_2-$), 6.78 (1H, d, J=9 Hz, Ar–H), 7.12 (1H, dd, J=1 and 9 Hz, Ar–H), 7.24 (1H, d, J=1 Hz, furan H). UV(EtOH): λ_{max} (ε) 214 (23100), 253 (9200), 291 (2600), 302 nm (2000). Found: C, 77.02; H, 6.83%. Calcd for $C_{13}H_{14}O_2$: C, 77.20; H, 6.98%.

*Lactone (**3c**).* Colorless needles from benzene–hexane (41% yield); mp 87—88 °C. IR (KBr): ν_{max} 1650 (C=C), 1765 cm^{-1} (–COO–). ^{1}H NMR (CD_3COCD_3): δ 1.36 (3H, t, J=7 Hz, CH_3), 2.15—2.41 (2H, m, $-CH_2-$), 2.76 (2H, t, J=8 Hz, $-CH_2-$), 4.03 (2H, q, J=7 Hz, $-CH_2-$), 4.71 (2H, s, $-OCH_2-$), 5.87 (1H, t, J=5 Hz, –OC=CH–), 6.78 (1H, d, J=9 Hz, Ar–H), 6.92 (1H, d, J=9 Hz, Ar–H). Found: C, 68.01; H, 5.49%. Calcd for $C_{14}H_{14}O_4$: C, 68.28; H, 5.73%.

*6-Isopropoxy-4,5-dihydro-3*H*-naphtho[1,8-*bc*]furan (**2d**).* Colorless plates from methanol (38% yield); mp 68—69 °C. ^{1}H NMR ($CDCl_3$): δ 1.31 (6H, d, J=6 Hz, $C(CH_3)_2$), 1.96 (2H, dt, J=7 and 7 Hz, $-CH_2-$), 2.75 (2H, t, J=7 Hz, $-CH_2-$), 2.82 (2H, t, J=7 Hz, $-CH_2-$), 4.37 (1H, m, =CH–), 6.82 (1H, d, J=8 Hz, Ar–H), 7.12 (1H, d, J=8 Hz, Ar–H), 7.24 (1H, s, furan H). UV (EtOH): λ_{max} (ε) 214 (24200), 253 (9400), 292 (2100), 305 nm (1100). Found: C, 77.53; H, 7.29%. Calcd for $C_{14}H_{16}O_2$: C, 77.75; H, 7.46%.

*Lactone (**3d**).* Colorless needles from benzene–hexane (40% yield); mp 90—91 °C. IR (KBr): ν_{max} 1665 (C=C), 1780 cm^{-1} (–COO–). ^{1}H NMR (CD_3COCD_3): δ 1.29 (6H, d, J=6 Hz, $C(CH_3)_2$), 2.17—2.40 (2H, m, $-CH_2-$), 2.57—2.97 (2H, m, $-CH_2-$), 4.49 (1H, m, =CH–), 4.72 (2H, s, $-OCH_2-$), 5.87 (1H, t, J=5 Hz, –OC=CH–), 6.78 (1H, d, J=9 Hz, Ar–H), 6.95 (1H, d, J=9 Hz, Ar–H). Found: C, 68.98; H, 6.09%. Calcd for $C_{15}H_{16}O_4$: C, 69.21; H, 6.20%.

*Lactone (**3e**).* Colorless needles from benzene–hexane (48% yield); mp 104—105 °C. IR (KBr): ν_{max} 1660 (C=C), 1760 cm^{-1} (–COO–). ^{1}H NMR (CD_3COCD_3): δ 2.12—2.86 (4H, m, $-CH_2-+-CH_2-$), 3.46—3.93 (1H, m, =CH–), 4.20 (1H, dd, J=9 and 12 Hz, –OCH=), 4.54—4.95 (3H, m, $-CH_2-+-$OCH=), 5.70 (1H, dd, J=3 and 7 Hz, –OCH=), 6.60 (1H, d, J=8 Hz, Ar–H), 6.72 (1H, dd, J=1 and 8 Hz, Ar–H). Found: C, 67.56; H, 4.41%. Calcd for $C_{13}H_{10}O_4$: C, 67.82; H, 4.38%.

*6-Methoxy-8-t-butyl-4,5-dihydro-3*H*-naphtho[1,8-*bc*]furan (**2f**).* Colorless needles (72% yield); mp 45—46 °C. ^{1}H NMR ($CDCl_3$): δ 1.48 (9H, s, $C(CH_3)_3$), 1.95 (2H, dt, J=6 and 6 Hz, $-CH_2-$), 2.73 (2H, t, J=6 Hz, $-CH_2-$), 2.80 (2H, t, J=6 Hz, $-CH_2-$), 3.85 (3H, s, CH_3), 6.75 (1H, s, Ar–H), 7.26 (1H, s, furan H). UV (EtOH): λ_{max} (ε) 216 (25700), 252 (9800), 292 (3100), 302 nm (2600). Found: C, 78.61; H, 8.21%. Calcd for $C_{16}H_{20}O_2$: C, 78.65; H, 8.25%.

*Lactone (**3f**).* Colorless plates (7% yield); mp 105—106 °C. IR (KBr): ν_{max} 1650 (C=C), 1770 cm^{-1} (–COO–). ^{1}H NMR (CD_3COCD_3): δ 1.37 (9H, s, $C(CH_3)_3$), 2.22—2.38 (2H, m, $-CH_2-$), 2.63—2.79 (2H, m, $-CH_2-$), 3.83 (3H, s, OCH_3), 4.77 (2H, s, $-OCH_2-$), 5.87 (1H, t, J=5 Hz, –OC=CH–), 6.93 (1H, s, Ar–H). Found: C, 70.65; H, 6.83%. Calcd for $C_{17}H_{20}O_4$: C, 70.81; H, 6.99%.

*8-Isopropoxy-4,5-dihydro-3*H*-naphtho[1,8-*bc*]furan (**2h**).* Colorless oil (50% yield); bp 178 °C at 20 Torr. ^{1}H NMR ($CDCl_3$): δ 1.37 (6H, d, J=6 Hz, $C(CH_3)_2$), 1.97 (2H, dt, J=6 and 6 Hz, $-CH_2-$), 2.74 (2H, t, J=6 Hz, $-CH_2-$), 2.81 (2H, t, J=6 Hz, $-CH_2-$), 4.83 (1H, m, =CH–), 6.70 (1H, d, J=8 Hz, Ar–H), 6.84 (1H, d, J=8 Hz, Ar–H), 7.25 (1H, s, furan H). UV (EtOH): λ_{max} (ε) 217 (29200), 249 (10300), 255 (9600), 281 (1600), 291 nm (1100). Found: C, 77.84; H, 7.46%. Calcd for $C_{14}H_{16}O_2$: C, 77.75; H, 7.46%.

*Lactone (**3h**).* Colorless oil (33% yield); bp>200 °C at 2 Torr. IR (neat): ν_{max} 1650 (C=C), 1780 cm^{-1} (–COO–). ^{1}H NMR (CD_3COCD_3): δ 1.27 (6H, d, J=6 Hz, $C(CH_3)_3$), 2.17—2.41 (2H, m, $-CH_2-$), 2.62—2.80 (2H, m, $-CH_2-$), 4.46 (1H, m, =CH–), 4.78 (2H, s, $-OCH_2-$), 5.87 (1H, t, J=5 Hz, –OC=CH–), 6.86 (2H, s, Ar–H). Found: C. 69.04; H, 6.12%. Calcd for $C_{15}H_{16}O_4$: C, 69.21; H, 6.20%.

*8-Methoxy-6-methyl-4,5-dihydro-3*H*-naphtho[1,8-*bc*]furan (**2i**).* Colorless prisms from hexane (60% yield); mp 42—43 °C. ^{1}H NMR (CCl_4): δ 1.82—2.07 (2H, m, $-CH_2-$), 2.22 (3H, s, Ar–CH_3), 2.59—2.76 (4H, m, $-CH_2-+-CH_2-$), 3.95 (3H, s, Ar–OCH_3), 6.41 (1H, s, Ar–H), 7.17 (1H, s, furan H). UV (EtOH): λ_{max} (ε) 217 (3200), 248 (9900), 255 (9400), 284 (2000), 295 nm (1800). Found: C, 77.10; H, 7.06%. Calcd for $C_{13}H_{14}O_2$: C, 77.20; H, 6.98%. The physical properties of **2a**, **2b**, **2g**, **2j**, **3b**, **3g**, and **3j** are described in Ref. 2.

*5-Ethoxy-8-hydroxy-1,2,3,4-tetrahydro-1-naphthalenone (**4c**).* A mixture of **4k** (10 g), diethyl sulfate (11 g), potassium carbonate (17 g), and acetone (100 ml) was refluxed for 6 h. The acetone was distilled off and water was added to the mixture. The mixture was refluxed for 0.5 h to decompose the excess diethyl sulfate and extracted with ether. The ethereal solution was washed with water, dried, and evaporated. The residue was chromatographed and eluted with benzene to give 11.2 g (96%) of **4c**. Recrystallization from methanol gave yellow plates; mp 61.5—62.5 °C. IR (KBr): ν_{max} 1645 cm^{-1} (C=O). ^{1}H NMR ($CDCl_3$): δ 1.38 (3H, t, J=7 Hz, CH_3), 2.05 (2H, dt, J=6 and 6 Hz, $-CH_2-$), 2.65 (2H, t, J=6 Hz, $-CH_2-$), 2.89 (2H, t, J=6 Hz, $-CH_2-$), 3.98 (2H, q, J=7 Hz, $-CH_2-$), 6.72 (1H, d, J=9 Hz, Ar–H), 7.05 (1H, d, J=9 Hz, Ar–H), 11.90 (1H, broad s, Ar–OH). Found: C, 69.75; H, 7.12%. Calcd for $C_{12}H_{14}O_3$:

C, 69.88; H, 6.84%.

*8-Hydroxy-5-isopropoxy-1,2,3,4-tetrahydro-1-naphthalenone (**4d**).* A mixture of **4k** (5.0 g), isopropyl iodide (10 g), potassium carbonate (10 g), and acetone (70 ml) was refluxed.[5] After 1 h, isopropyl iodide (5 g) and potassium carbonate (5 g) were added and the mixture was refluxed for additional 9 h. After removal of the acetone, the residue was extracted with ether. The ethereal solution was washed with water, dried, and evaporated. The resulting oil was chromatographed and eluted with benzene to give 5.6 g (90%) of **4d**. Recrystallization from methanol gave yellow plates; mp 55—56 °C. IR (KBr): ν_{max} 1645 cm^{-1} (C=O). ^1H NMR ($CDCl_3$): δ 1.30 (6H, d, J=7 Hz, $C(CH_3)_2$), 1.97 (2H, dt, J=6 and 6 Hz, $-CH_2-$), 2.64 (2H, t, J=6 Hz, $-CH_2-$), 2.88 (2H, t, J=6 Hz, $-CH_2-$), 4.20—4.47 (1H, m, =CH–), 6.72 (1H, d, J=9 Hz, Ar–H), 7.07 (1H, d, J=9 Hz, Ar–H), 12.00 (1H, s, Ar–OH). Found: C, 70.95; H, 7.30%. Calcd for $C_{13}H_{16}O_3$: C. 70.89; H, 7.32%.

*5,8-Dihydroxy-7-t-butyl-1,2,3,4-tetrahydro-1-naphthalenone (**4l**).* To a *t*-butyl alcohol solution (20 ml) of **4k** (2.0 g) concentrated sulfuric acid (20 g) was gradually added with stirring under cooling with ice–water.[6] The mixture was stirred for 0.5 h, decomposed with ice–water, and extracted with ether. The ethereal solution was washed with water, dried, and evaporated. A high boiling oil was removed by reduced distillation (*ca.* 140 °C at 30 Torr). The residue was chromatographed and eluted with benzene(9)–ether(1) to give 1.6 g (61%) of **4l**. Recrystallization from benzene–hexane gave yellow plates; mp 154—155 °C. IR (KBr): ν_{max} 1615 (C=O), 3360 cm^{-1} (Ar–OH). ^1H NMR ($CDCl_3$): δ 1.38 (9H, s, $C(CH_3)_3$), 1.92—2.20 (2H, m, $-CH_2-$), 2.67 (2H, t, J=7 Hz, $-CH_2-$), 2.83 (2H, t, J=6 Hz, $-CH_2-$), 4.69 (1H, broad s, Ar–OH), 6.02 (1H, s, Ar–H), 12.83 (1H, s, Ar–OH). Found: C, 71.75; H, 7.69%. Calcd for $C_{14}H_{18}O_3$: C, 71.77; H, 7.74%.

*8-Hydroxy-5-methoxy-7-t-butyl-1,2,3,4-tetrahydro-1-naphthalenone (**4f**).* The compound **4f** was prepared from **4l** by a method similar to the synthesis of **4c** from **4k**. Yellow needles from methanol (91% yield); mp 57—58 °C. IR (KBr): ν_{max} 1635 cm^{-1} (C=O). ^1H NMR ($CDCl_3$): δ 1.42 (9H, s, $C(CH_3)_3$), 2.03 (2H, dt, J=6 and 6 Hz, $-CH_2-$), 2.65 (2H, t, J=6 Hz, $-CH_2-$), 2.86 (2H, t, J=6 Hz, $-CH_2-$), 3.79 (3H, s, OCH_3), 7.13 (1H, s, Ar–H), 12.81 (1H, s, Ar–OH). Found: C, 72.70; H, 8.35%. Calcd for $C_{15}H_{20}O_3$: C, 72.55; H, 8.12%.

*(4-Ethoxy-8-oxo-5,6,7,8-tetrahydro-1-naphthyloxy)acetic Acid (**1c**).* A mixture of **4c** (1.0 g), ethyl bromoacetate (4.0 g), potassium phosphate (4.0 g), and dioxane (20 ml) was refluxed for 5 h.[2] After removal of potassium phosphate by filtration the dioxane was evaporated under reduced pressure. The residue was dissolved in ethanol (10 ml) and hydrolyzed with a 20% potassium hydroxide solution (50 ml). The alkaline solution was acidified with 6 M (1 M=1 mol dm^{-3}) hydrochloric acid and the resulting precipitates were extracted with ether. The ethereal solution was washed with water, dried, and evaporated. Trituration of the residue with benzene gave 0.63 g (49%) of **1c**. Recrystallization from methanol gave colorless plates; mp 140—141 °C. IR (KBr): ν_{max} 1655 (C=O), 1765, 1780 cm^{-1} (COOH). ^1H NMR (CD_3COCD_3): δ 1.40 (3H, t, J=7 Hz, CH_3), 1.92—2.20 (2H, m, $-CH_2-$), 2.65 (2H, t, J=6 Hz, $-CH_2-$), 2.92 (2H, t, J=6 Hz, $-CH_2-$), 4.08 (2H, q, J=7 Hz, $-CH_2-$), 4.70 (2H, s, $-CH_2-$), 7.01 (1H, d, J=9 Hz, Ar–H), 7.21 (1H, d, J=9 Hz, Ar–H). Found: C, 63.41; H, 6.19%. Calcd for $C_{14}H_{16}O_5$: C, 63.62; H, 6.10%.

*(4-Isopropoxy-8-oxo-5,6,7,8-tetrahydro-1-naphthyloxy)acetic Acid (**1d**).* The compound **1d** was prepared from **4d** by a method similar to the synthesis of **1c** from **4c**. Colorless plates from methanol (57% yield); mp 130—131 °C. IR (KBr): ν_{max} 1660 (C=O), 1765, 1785 cm^{-1} (COOH). ^1H NMR (CD_3COCD_3): δ 1.32 (6H, d, J=6 Hz, $C(CH_3)_2$), 1.92—2.19 (2H, m, $-CH_2-$), 2.65 (2H, t, J=5 Hz, $-CH_2-$), 2.90 (2H, t, J=6 Hz, $-CH_2-$), 4.58 (1H, m, =CH–), 4.71 (2H, s, $-CH_2-$), 7.00 (1H, d, J=9 Hz, Ar–H), 7.25 (1H, d, J=9 Hz, Ar–H). Found: C, 64.74; H, 6.43%. Calcd for $C_{15}H_{18}O_5$: C, 64.73; H, 6.52%.

*(4-Methoxy-8-oxo-2-t-butyl-5,6,7,8-tetrahydro-1-naphthyloxy)-acetic Acid (**1f**).* The compound **1f** was prepared from **4f** by a method similar to the synthesis of **1c** from **4c**. Colorless plates from ether–hexane (27% yield); mp 139—140 °C. IR (KBr): ν_{max} 1665 (C=O), 1770, 1785 cm^{-1} (COOH). ^1H NMR (CD_3COCD_3): δ 1.43 (9H, s, $C(CH_3)_3$), 1.97—2.17 (2H, m, $-CH_2-$), 2.59 (2H, t, J=7 Hz, $-CH_2-$), 2.84 (2H, t, J=6 Hz, $-CH_2-$), 3.88 (3H, s, OCH_3), 4.41 (2H, s, $-OCH_2-$), 7.20 (1H, s, Ar–H). Found: C, 66.41; H, 7.00%. Calcd for $C_{17}H_{22}O_5$: C, 66.65; H, 7.24%.

*7,8-Dihydroxy-1,2,3,4-tetrahydro-1-naphthalenone (**4m**).* A mixture of **4g** (1.0 g) and pyridinium chloride (10 g) was heated at 200 °C for 1 h.[7] The mixture was poured into ice–water and extracted with ether. The ethereal solution was washed with water, dried, and evaporated to give 0.90 g (97%) of **4m**. Recrystallization from benzene–hexane gave yellow plates; mp 92—93 °C. IR (KBr): ν_{max} 1640 (C=O), 3530 cm^{-1} (Ar–OH). ^1H NMR (CD_3COCD_3): 2.04 (2H, dt, J=6 and 6 Hz, $-CH_2-$), 2.65 (2H, t, J=6 Hz, $-CH_2-$), 2.85 (2H, t, J=6 Hz, $-CH_2-$), 6.62 (1H, d, J=8 Hz, Ar–H), 7.00 (1H, d, J=8 Hz, Ar–H), 7.49 (1H, s, Ar–OH), 12.51 (1H, s, Ar–OH). Found: C, 67.43; H, 5.91%. Calcd for $C_{10}H_{10}O_3$: C, 67.40; H, 5.66%.

*8-Hydroxy-7-isopropoxy-1,2,3,4-tetrahydro-1-naphthalenone (**4h**).* The compound **4h** was prepared from **4m** by a method similar to the synthesis of **4d** from **4k**. Yellow plates from hexane (85% yield); mp 74—75 °C. IR (KBr): ν_{max} 1640 cm^{-1} (C=O). ^1H NMR ($CDCl_3$): δ 1.34 (6H, d, J=6 Hz, $C(CH_3)_2$), 2.06 (2H, dt, J=6 and 6 Hz, $-CH_2-$), 2.65 (2H, t, J=6 Hz, $-CH_2-$), 2.86 (2H, t, J=6 Hz, $-CH_2-$), 4.50 (1H, m, =CH–), 6.59 (1H, d, J=8 Hz, Ar–H), 7.02 (1H, d, J=6 Hz, Ar–H), 12.62 (1H, s, Ar–OH). Found: C. 71.16; H, 7.39%. Calcd for $C_{13}H_{16}O_3$: C, 70.89; H, 7.32%.

*(2-Isopropoxy-8-oxo-5,6,7,8-tetrahydro-1-naphthyloxy)acetic Acid (**1h**).* The compound **1h** was prepared from **4h** by a method similar to the synthesis of **1c** from **4c**. Colorless needles from benzene–hexane (79% yield); mp 89—90 °C. IR (KBr): ν_{max} 1670, 1685 (C=O), 1760, 1775 cm^{-1} (COOH). ^1H NMR (CD_3COCD_3): δ 1.37 (6H, d, J=6 Hz, $C(CH_3)_2$), 1.91—2.18 (2H, m, $-CH_2-$), 2.67 (2H, t, J=6 Hz, $-CH_2-$), 2.94 (2H, t, J=6 Hz, $-CH_2-$), 4.46—4.80 (1H, m, =CHO–), 4.73 (2H, s, $-OCH_2-$), 7.06 (1H, d, J=8 Hz, Ar–H), 7.33 (1H, d, J=8 Hz, Ar–H). Found: C, 64.56; H, 6.68%. Calcd for $C_{15}H_{18}O_5$: C, 64.73; H, 6.52%.

*3-(5-Hydroxybenzofuran-3-yl)propionic Acid (**6**).* A mixture of **5** (15 g) and pyridinium chloride (100 g) was heated for 1 h at 200 °C,[7] poured into ice–water, and extracted with ether. The ethereal solution was washed with 1 M hydrochloric acid and then with water, dried, and evaporated to give 17.4 g (93%) of **6**. Recrystallization from acetone–benzene gave colorless needles; mp 170—171 °C. IR (KBr): ν_{max} 1720 (COOH), 3270 cm^{-1} (Ar–OH). ^1H NMR (CD_3COCD_3): δ 2.59—3.06 (4H, m, $-CH_2-+-CH_2-$), 6.83 (1H, dd, J=2 and 9 Hz, Ar–H), 7.02 (1H, d, J=2 Hz, Ar–H), 7.27 (1H, d, J=2 Hz, Ar–H), 7.27 (1H, d, J=9 Hz, Ar–H), 7.55 (1H, s, furan H). Found: C, 64.19;

H, 4.98%. Calcd for $C_{11}H_{10}O_4$: C, 64.07; H, 4.89%.

*3-(5-Hydroxy-2,3-dihydrobenzofuran-3-yl)propionic Acid (**7**).* An ethanolic solution (50 ml) of **6** (12 g) was hydrogenated for 16 h in the presence of 7% palladium on charcoal (2.4 g) as a catalyst under 7 atm at 65 °C.[8] After removal of the catalyst by filtration the partially produced ester was hydrolyzed with a 30% potassium hydroxide solution. The alkaline solution was acidified with 6 M hydrochloric acid and extracted with ether. The ethereal solution was washed with water, dried, and evaporated to give 10.6 g (87%) of **7**. Recrystallization from acetone–benzene gave colorless needles; mp 117—118 °C. IR (KBr): ν_{max} 1750 (COOH), 3310 cm^{-1} (Ar–OH). ^1H NMR (CD_3COCD_3): δ 1.61—2.16 (2H, m, $-CH_2-$), 2.30—2.49 (2H, m, $-CH_2-$), 3.26—3.57 (1H, m, =CH–), 4.17 (1H, dd, J=6 and 9 Hz, –OCH=), 4.56 (1H, t, J=9 Hz, –OCH=), 6.56—6.76 (3H, m, Ar–H). Found: C, 63.65; H, 5.85%. Calcd for $C_{11}H_{12}O_4$: C, 63.45; H, 5.81%.

*6-Hydroxy-2a,3,4,5-tetrahydro-2H-naphtho[1,8-bc]furan-5-one (**4e**).* A mixture of **7** (20 g) and polyphosphoric acid (300 g) was heated at 80 °C for 5 h under stirring.[8] The mixture was poured into ice–water and extracted with ether. The ethereal solution was washed with a 10% potassium carbonate solution and then with water, dried, and evaporated to give 9.1 g (50%) of **4e**. Recrystallization from benzene–hexane gave yellow needles; mp 123—124 °C. IR (KBr): ν_{max} 1650 (C=O), 3220 cm^{-1} (Ar–OH). ^1H NMR ($CDCl_3$): δ 1.65—2.75 (4H, m, $-CH_2-+-CH_2-$), 3.45—3.85 (1H, m, =CH–), 4.10 (1H, dd, J=9 and 11 Hz, –OCH=), 4.85 (1H, dd, J=8 and 8 Hz, –OCH=), 6.64 (1H, dd, J=1 and 9 Hz, Ar–H), 6.91 (1H, d, J=9 Hz, Ar–H), 9.86 (1H, s, Ar–H). Found: C, 69.62; H, 5.48%. Calcd for $C_{11}H_{10}O_3$: C, 69.46; H, 5.30%.

*(5-Oxo-2a,3,4,5-tetrahydro-2H-naphtho[1,8-bc]furan-6-yloxy)acetic Acid (**1e**).* The compound **1e** was prepared from **4e** by a method similar to the synthesis of **1c** from **4c**. Colorless plates from acetone–benzene (60% yield); mp 155—156 °C. IR (KBr): ν_{max} 1670 (C=O), 1760 (COOH), 3120 cm^{-1} (COOH). ^1H NMR (CD_3COCD_3): δ 1.86—2.52 (2H, m, $-CH_2-$), 2.63—2.78 (2H, m, $-CH_2-$), 3.57—3.99 (1H, m, =CH–), 4.14 (1H, dd, J=8 and 11 Hz, –OCH=), 4.68 (2H, s, $-OCH_2-$), 4.90 (1H, dd, J=8 and 8 Hz, $-CH_2-$), 6.94 (2H, s, Ar–H). Found: C, 62.83; H, 4.69%. Calcd for $C_{13}H_{12}O_5$: C, 62.90; H, 4.87%.

The authors wish to thank Mr. Yoshiaki Takahashi for the elemental analyses.

References

1) T. Horaguchi and T. Shimizu, *Bull. Chem. Soc. Jpn.*, **47**, 485 (1974); T. Horaguchi, *ibid.*, **50**, 3329 (1977).

2) T. Horaguchi, T. Shimizu, and T. Suzuki, *Bull. Chem. Soc. Jpn.*, **48**, 1249 (1975).

3) H. W. W. Ehrlich, *Acta Crystallogr.*, **10**, 699 (1957); A. G. Anderson, Jr., and R. H. Wade, *J. Am. Chem. Soc.*, **74**, 2274 (1952); T. Horaguchi and T. Abe, *Bull. Chem. Soc. Jpn.*, **51**, 2068 (1978).

4) A. Davies and K. Warren, *J. Chem. Soc., B*, **1969**, 873.

5) W. S. Johnson and R. T. Keller, *Org. Synth.*, Coll. Vol. IV, 836 (1963).

6) H. Meyer and K. Hernhauser, *Monatsh. Chem.*, **53** and **54**, 721 (1929); D. Nightingale, R. G. Taylor, and H. W. Smelser, *J. Am. Chem. Soc.*, **63**, 258 (1941).

7) M. S. Newmann and R. L. Childers, *J. Org. Chem.*, **32**, 64 (1967).

8) J. S. H. Davies, D. A. McCrea, W. L. Norris, and G. R. Range, *J. Chem. Soc.*, **1950**, 3206; T. Horaguchi, T. Shimizu, and T. Abe, *Bull. Chem. Soc. Jpn.*, **49**, 737 (1976).

Reactions of Aldonitrones with Phenylphosphonothioic Dichloride and Related Compounds. Formation of 2-Arylbenzothiazoles from α,*N*-Diarylnitrones

Masaaki Yoshifuji, Rihei Nagase, Takayuki Kawashima, and Naoki Inamoto*

Department of Chemistry, Faculty of Science, The University of Tokyo, Hongo, Bunkyo-ku Tokyo 113

(Received June, 19, 1981)

Reactions of α-aryl-*N*-methylnitrones with phenylphosphonothioic dichloride (**1**), diphenylphosphinothioic chloride (**6**), or thiophosphoryl trichloride (**7**) gave *N*-methylbenzamide and *N*-methylthiobenzamide derivatives, and the latter became major in the presence of tertiary amine. α,*N*-Diarylnitrones (**4**) reacted with **1** to give 2-arylbenzothiazoles (**5**) at room temperature in moderate yields. Reaction of **4** with **6** (at room temperature) or **7** (in refluxing THF) gave **5** in a low yield, whereas a similar reaction of **4** with **7** at 0 °C afforded *N*-benzylidene-2-chloroaniline in a high yield. A mechanism for the formation of **5** has been discussed briefly.

During the course of investigations on phosphinothioylidenes (R–P̈=S),[1] we tried reaction of *N*-methyl-α-phenylnitrone with phenylphosphonothioic dichloride (**1**) in the presence of magnesium in an attempt to prepare phosphorus-containing heterocycles such as 1,3,5,2-oxathiazaphospholidine, but the products were *N*-methylbenzamide (**2**) and *N*-methylthiobenzamide (**3**).

$$\underset{\mathbf{1}}{PhP(S)Cl_2} + PhCH{=}N(O)Me \longrightarrow PhCONHMe + PhCSNHMe$$
$$\mathbf{2} \qquad \mathbf{3}$$

Even without magnesium, however, a similar result was obtained. Therefore, reactions of nitrones with **1** and related compounds were investigated and it was found that α,*N*-diarylnitrones gave 6-substituted 2-arylbenzothiazoles.[2] This paper describes these results.

Reactions of N-*Methylaldonitrones.* Reaction of *N*-methyl-α-phenylnitrone with **1** gave **2** (43%) and **3** (41%), together with the nitrone hydrochloride (17%). A similar reaction with diphenylphosphinothioic chloride gave also **2** (61%) and **3** (6%), and that with thiophosphoryl trichloride gave only **3** (60%). However, *N*-methyl-α-phenylnitrone did not react with triphenylphosphine sulfide even at 140 °C.

In order to remove hydrogen chloride evolved during the reaction, a base such as triethylamine and pyridine was added. As shown in Table 1, in the presence of base, formation of **3** was remarkably suppressed.

Similarly, reaction of α-(*p*-methoxyphenyl)-*N*-methylnitrone with **1** gave the corresponding amide (8%) and thioamide (28%), along with the nitrone hydrochloride (17%).

It has been reported that the nitrones rearrange to give the corresponding amide by acid chlorides and anhydrides such as phosphoryl trichloride, phosphorus trichloride, thionyl chloride, benzoyl chloride, benzenesulfonyl chloride, and acetic anhydride.[3] Analogously to these rearrangements,[3e,3f] the formation of thioamide (**3**) is explained as follows:

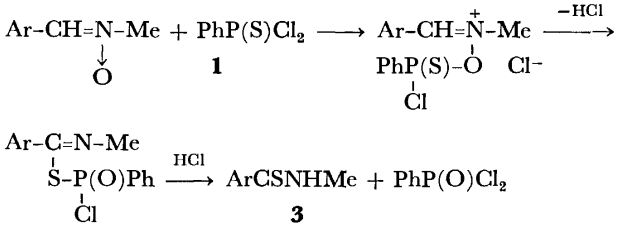

Phenylphosphonic dichloride produced during the reaction can similarly react with the nitrones to give amide (**2**). Therefore, in the presence of a base, hydrogen chloride eliminated during the reaction is trapped by the base, and decomposition of the second intermediate by hydrogen chloride is prevented before work-up. Thus the formation of amide (**2**) is strongly retarded.

Reactions of α,N-*Diarylnitrones.* α,*N*-Diarylnitrones (**4**) reacted with an equimolar amount of **1** in tetrahydrofuran (THF) at room temperature to give 6-substituted 2-arylbenzothiazoles (**5**) unexpectedly, along with the nitrone hydrochloride. The results are summarized in Table 2.

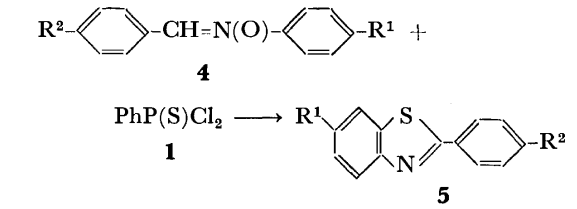

a: $R^1=R^2=H$; **b**: $R^1=H$, $R^2=OMe$; **c**: $R^1=H$, $R^2=Cl$; **d**: $R^1=Me$, $R^2=H$; **e**: $R^1=Me$, $R^2=OMe$; **f**: $R^1=Me$, $R^2=Cl$; **g**: $R^1=H$, $R^2=Me$; **h**: $R^1=H$, $R^2=NMe_2$

The nitrones **4g** and **4h** did not give **5g** and **5h**, respectively. The reason is obscure.

In order to suppress the formation of nitrone hydrochloride, a scavenger of hydrogen chloride such as pyridine and methyloxirane was added. Reaction of **4a** in the presence of pyridine gave thiobenzanilide

Table 1. Effect of base on formation of **2** and **3**

Base	**2** (%)	**3** (%)
None	43	41[a]
Et_3N	9	35[a]
Et_3N	0	60[b]
C_5H_5N	20	41[b]

a) A solution of **1** was added dropwise. b) A solution of nitrone was added dropwise.

Table 2. Yield of 2-arylbenzothiazole (5) from 4

4			
	R^1	R^2	5(%)
4a	H	H	32
4b	H	OMe	54
4c	H	Cl	39
4d	Me	H	33
4e	Me	OMe	34
4f	Me	Cl	39

(36%) instead of **5a**, but that of **4b** in the presence of methyloxirane gave **5b** (57%), indicating no improvement of the yields.

Next, diphenylphosphinothioic chloride (**6**) analogous to **1** was used in order to examine the effect on the yield of **5**. Reaction of **4b** with **6** in the absence or the presence of methyloxirane gave *N*-(4-methoxybenzylidene)-2-chloroaniline (**8**) instead of **5b** in 4 or 18% yield, respectively.

Furthermore, reaction of **4b** with thiophosphoryl trichloride (**7**) also gave **5b** in refluxing THF, but the yield was low (22%). On the other hand, reaction of **4b** with **7** at 0 °C gave **8** in 78% yield, which gave *o*-chloroaniline after hydrolysis. No *p*-chloro derivative was detected.

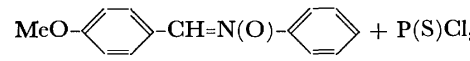

4b **7**

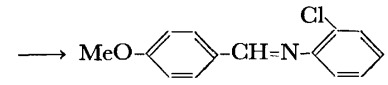

8

It has been reported that α-aryl-*N*-phenylnitrones gave *N*-benzylidene-2-chloroanilines in the reactions with thionyl or carbonyl chloride and gave *N*-benzylidene-2-(chlorooxalyloxy)anilines in the reactions with oxalyl chloride.[4]

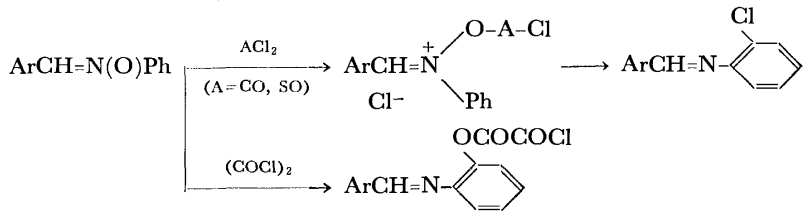

Therefore, the formation of **8** is analogously explained as follows:

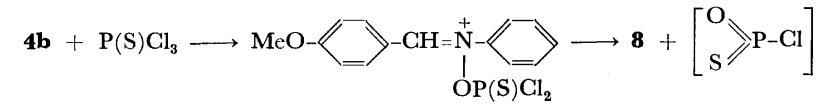

Analogously to reactions of *N*-methylaldonitrones with **1**, it is possible that thiobenzanilide is first formed by reaction of **4** with **1** and then thiobenzanilide may cyclize to **5**. However, thiobenzanilide did not give 2-phenylbenzothiazole with **1** under similar conditions.

Thus, a mechanism for formation of **5** is considered as follows, in connection with the formation of **8**.

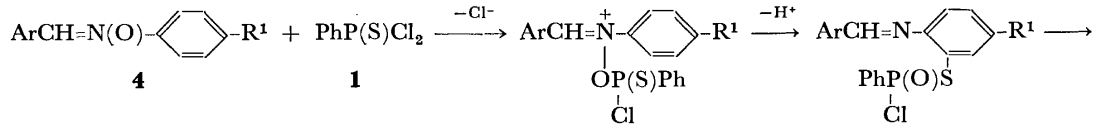

4 **1** **9** **10**

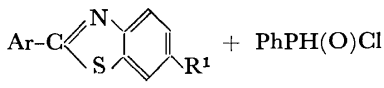

5

An intermediate (**9**) formed by a nucleophilic attack of **4** towards **1** rearranges to second intermediate (**10**) through [3,3] sigmatropic rearrangement containing P=S bond, and then **10** is converted into benzothiazole (**5**).

This new reactions might be used as a preparation method of 2-arylbenzothiazoles under mild conditions.

Experimental

All the melting points are uncorrected. The IR spectra were taken with a Hitachi EPI-G2 spectrophotometer, and the NMR spectra were measured with a Hitachi R-24 or R-20B spectrometer using TMS as an internal standard.

Materials. The following compounds were prepared by reported methods; phenylphosphonothioic dichloride (**1**),[5] diphenylphosphinothioic chloride (**6**),[6] and *N*-methyl-α-phenyl-,[7] *N*-methyl-α-(4-methoxyphenyl)-,[8] α,*N*-diphenyl- (**4a**),[7] α-(4-methoxyphenyl)-*N*-phenyl- (**4b**),[7] α-(4-chlorophenyl)-*N*-phenyl- (**4c**),[9] α-phenyl-*N*-(*p*-tolyl)- (**4d**),[10] α-(4-methoxyphenyl)-*N*-(*p*-tolyl)- (**4e**),[10] α-(*p*-chlorophenyl)-*N*-(*p*-tolyl)- (**4f**),[11] *N*-phenyl-α-(*p*-tolyl)- (**4g**),[3e] and α-(*p*-dimethylaminophenyl)-*N*-phenyl-nitrones (**4h**).[12]

Reaction of N-*Methyl-α-phenylnitrone with* **1**. *Reaction in the Absence of Base*: To a THF solution (25 ml) of the nitrone (1.29 g, 9.6 mmol) was added **1** (2.0 g, 9.5 mmol) with stirring under nitrogen. After the mixture was slightly heated, an exothermic reaction took place and white precipitates were formed. After the reaction mixture was allowed to stand overnight, the precipitates (278 mg) were collected and washed with THF. The filtrate and the washings were evaporated to give a red residue. Since the precipitates contained halogen (by Beilstein test), a mixture of the precipitates and triethylamine in benzene

was stirred overnight at room temperature to give the starting nitrone. Thus, the precipitates were identified with the nitrone hydrochloride (17% yield). The red residue was subjected to dry column chromatography (DCC; SiO_2, CH_2Cl_2) to give recovered **1** (48 mg, 2.3%), **3** (497 mg, 41%), mp 79.5—81 °C (from CCl_4) (lit,[13] mp 79 °C); IR (KBr): 1520, 1340, and 1240 cm^{-1}, and **2** (459 mg, 43%), mp 78—81 °C (from EtOH) (lit,[14] mp 78—80 °C); IR (KBr): 1630, 1540, 1400, and 1300 cm^{-1}. The yields of the amides are based on the nitrone consumed.

Reaction in the Presence of Base: Only typical procedure is described.

To a THF solution (5 ml) of **1** (928 mg, 4.42 mmol) and triethylamine (1.5 ml) was added a THF solution (15 ml) of the nitrone (506 mg, 3.75 mmol) dropwise and the mixture was stirred at room temperature for 1 h. After addition of water, the mixture was extracted with ether, the ethereal extract was dried ($MgSO_4$), and evaporated. The residue was subjected to DCC (SiO_2, CH_2Cl_2) to give **3** (317 mg, 60%) (by IR). The other results were shown in Table 1.

Reaction of N-*Methyl-α-phenylnitrone with Other Phosphorus Chlorides*. Reaction with diphenylphosphinothioyl chloride is described as a typical procedure.

A THF solution (25 ml) of the nitrone (1.30 g, 9.6 mmol) and the phosphinothioyl chloride (2.47 g, 9.8 mmol) was stirred at room temperature overnight. After usual work-up, the recovered chloride (1.70 g, 69%), and **3** (90 mg, 6%), and **2** (786 mg, 61%) were isolated by DCC (SiO_2, CH_2Cl_2).

*Reaction of α-(*p-*Methoxyphenyl)*-N-*methylnitrone with* ***1***. A THF solution (25 ml) of the nitrone (1.41 g, 8.52 mmol) and **1** (1.82 g, 8.64 mmol) was stirred at room temperature overnight. After precipitates (296 mg, 17%) (the nitrone hydrochloride) were removed by filtration, the residue from the filtrate was subjected to DCC (SiO_2, CH_2Cl_2) to give *N*-methyl-*p*-methoxythiobenzamide (365 mg, 28%), mp 118—119 °C (from C_6H_6–hexane (1:1)) (lit,[15] 110—111 °C) and *N*-methyl-*p*-methoxybenzamide (89 mg, 8%), mp 122.5—124 °C (from C_6H_6) (lit,[16] 119.5—120.5 °C).

Reactions of α,N-*Diarylnitrones with* ***1***. Reaction of α-(*p*-methoxyphenyl)-*N*-phenylnitrone (**4b**) is described as a typical procedure.

A mixture of **4b** (2.12 g, 9.33 mmol) and **1** (1.96 g, 9.27 mmol) in THF (25 ml) was stirred at room temperature overnight under nitrogen and precipitates thus obtained were filtered off. The precipitates were the nitrone hydrochloride (340 mg, 14%). The residue (3.27 g) from the filtrate was subjected to DCC (SiO_2, $CHCl_3$) to give **5b** (1.04 g, 54%), mp 123—125 °C (from EtOH) (lit,[17] 121.5—122 °C).

Reactions of other nitrones were carried out similarly. **4a** gave the nitrone hydrochloride (4%) and **5a** (32%), mp 108—113 °C (from EtOH) (lit,[18] 112—114 °C) by DCC (SiO_2, C_6H_6). **4c** gave **5c** (39%), mp 119—120 °C (from EtOH) (lit,[17] 120—121 °C) by DCC (SiO_2, CH_2Cl_2–CCl_4 (1:1)). **4d** gave **5d** (33%), mp 125.5—127 °C (from EtOH) (lit,[19] 125—125.5 °C) by DCC (SiO_2, CH_2Cl_2–CCl_4 (1:2)). **4e** gave **5e** (34%), mp 176—177 °C (from EtOH) (lit,[19] 174 °C) by DCC (SiO_2, CH_2Cl_2). **4f** gave **5f** (39%), mp 160—161 °C (from EtOH) (lit,[20] 160 °C) by DCC (SiO_2, CH_2Cl_2–CCl_4 (1:1)).

Reaction of ***4a*** *with* ***1*** *in the Presence of Pyridine*. To a mixture of **1** (1.14 g, 5.43 mmol) and pyridine (1 ml) in THF (5 ml) was added a solution of **4a** (990 mg, 5.03 mmol) in THF (15 ml) and then the mixture was stirred at room temperature overnight. After addition of water, the reaction mixture was extracted with ether, the ethereal extract was dried with $MgSO_4$, and evaporated. The residue was subjected to DCC (SiO_2, CH_2Cl_2–CCl_4 (1:1)) to give thiobenzanilide (387 mg, 36%), mp 100—101 °C (lit,[13] 97 °C).

Reaction of ***4b*** *with at 0 °C*. A mixture of **4b** (351 mg, 1.5 mmol) and **7** (275 mg, 1.63 mmol) in THF (10 ml) was stirred at 0 °C under nitrogen overnight. After addition of hexane (50 ml), the precipitates thus produced were collected by filtration and washed twice with hexane. The precipitates were suspended in benzene (10 ml) and stirred in the presence of triethylamine (0.3 ml). After precipitates were filtered off, the filtrate was evaporated to give **8** (282 mg, 78%); NMR ($CDCl_3$): δ 3.9 (s, 3H), 6.95—7.6 (m, 6H), 7.86 (d, J=10, 2H), and 8.3 (s, 1H). The NMR spectrum was the same as that of an authentic sample prepared from *p*-methoxybenzaldehyde and *o*-chloroaniline.

References

1) M. Yoshifuji, S. Nakayama, R. Okazaki, and N. Inamoto, *J. Chem. Soc., Perkin Trans. 1*, **1973**, 2065; S. Nakayama, M. Yoshifuji, R. Okazaki, and N. Inamoto, *ibid.*, **1973**, 2069; S. Nakayama, M. Yoshifuji, R. Okazaki, and N. Inamoto, *Bull. Chem. Soc. Jpn.*, **48**, 546, 3733 (1975); **49**, 1173 (1976).

2) Preliminary report: R. Nagase, T. Kawashima, M. Yoshifuji, and N. Inamoto, *Heterocycles*, **8**, 243 (1977).

3) a) J. Hamer and A. Macaluso, *Chem. Rev.*, **1964**, 473; b) A. Padwa, *Angew. Chem., Int. Ed. Engl.*, **15**, 123 (1976); c) B. Umezawa, *Chem. Pharm. Bull. (Tokyo)*, **8**, 698, 967 (1960); d) F. Kröhnke, *Justus Liebigs Ann. Chem.*, **604**, 203 (1957); e) S. Tamagaki, S. Kozuka, and S. Oae, *Tetrahedron*, **26**, 1795 (1970); f) S. Tamagaki and S. Oae, *Bull. Chem. Soc. Jpn.*, **44**, 2851 (1971); g) S. Oae and K. Ogino, *Heterocycles*, **6**, 583 (1977).

4) D. Liotta, A. D. Baker, N. L. Goldman, and R. Engel, *J. Org. Chem.*, **39**, 1975 (1974); D. Liotta, A. D. Baker, S. Goldstein, N. L. Goldman, F. Weinstein-Lanse, D. Felsen-Reingold, and R. Engel, *ibid.*, **39**, 2718 (1974).

5) W. L. Jensen, U. S. Patent, 2662917 (1953); *Chem. Abstr.*, **48**, 13711h (1954); F. Seel, K. Ballreich, and R. Schmutzler, *Chem. Ber.*, **95**, 199 (1962).

6) L. Maier, *J. Inorg. Nucl. Chem.*, **24**, 1073 (1962); *Helv. Chim. Acta*, **47**, 120 (1964).

7) T. Kubota, M. Yamakawa, and Y. Mori, *Bull. Chem. Soc. Jpn.*, **36**, 1552 (1963).

8) O. L. Brady, F. P. Dunn, and R. F. Goldstein, *J. Chem. Soc.*, **1926**, 2386.

9) O. H. Wheeler and P. H. Gore, *J. Am. Chem. Soc.*, **78**, 3363 (1956).

10) E. Bamberger, *Ber.*, **57**, 2082 (1924).

11) V. Bellavita, *Gazz. Chim. Ital.*, **70**, 584 (1940); *Chem. Abstr.*, **35**, 2127[9] (1941).

12) J. S. Splitter and M. Calvin, *J. Org. Chem.*, **20**, 1086 (1955).

13) P. Reynaud, R. C. Moreau, and J.-P. Samama, *Bull. Soc. Chim. Fr.*, **1965**, 3623.

14) E. Schmitz, R. Ohme, and D. Murawski, *Chem. Ber.*, **98**, 2516 (1965).

15) J. Witte and R. Huisgen, *Chem. Ber.*, **91**, 1129 (1958).

16) A. Lassolo, P. D. Waller, A. L. Meyer, and B. V. R. Sastry, *J. Med. Pharm. Chem.*, **2**, 617 (1960); *Chem. Abstr.*, **55**, 27383i (1961).

17) L. W. Wattenberg, M. A. Page, and J. L. Leong, *Cancer Res.*, **28**, 2539 (1968); *Chem. Abstr.*, **71**, 22057s (1969).

18) K. Hideg and H. O. Hankovszky, *Tetrahedron Lett.*, **1965**, 2365.

19) O. Sues, N. Tomanek, and E. Lind, Ger. Patent 1137625 (1962); *Chem. Abstr.*, **59**, P11515f (1963).

20) G. T. Morgan and D. Webster, *J. Chem. Soc.*, **119**, 1070 (1921).

Reactions of α,*N*-Diarylnitrones with *O*-Methyl Diphenylphosphinothioate and Oxidations of *N*-Alkylidene-2-hydroxyanilines with Silver Oxide. Preparation of Benzoxazoles

Masaaki Yoshifuji, Rihei Nagase, and Naoki Inamoto*

Department of Chemistry, Faculty of Science, The University of Tokyo, Hongo, Bunkyo-ku, Tokyo 113

(Received June 19, 1981)

Reactions of α,*N*-diarylnitrones in the presence of *O*-methyl diphenylphosphinothioate at 150 °C gave 2-arylbenzoxazoles (**3**) in fairly good yields. Oxidation of *N*-alkylidene-2-hydroxyanilines with silver oxide afforded 2-alkenyl-, 2-alkyl-, or 2-arylbenzoxazoles (**7** and **3**) in good yields under mild reaction conditions (at room temperature). A plausible mechanism for formation of **3** and **7** has been discussed briefly.

In the previous paper,[1] we reported that reactions of α,*N*-diarylnitrones with phenylphosphonothioic dichloride gave 2-arylbenzothiazoles at room temperature in moderate yields. When *O*-methyl diphenylphosphinothioate (**1**) was used instead of phenylphosphonothioic dichloride, reactions with α,*N*-diarylnitrones (**2**) at 150 °C gave unexpectedly 2-arylbenzoxazoles (**3**).[2] Furthermore, in order to prepare **3** under mild conditions, we investigated oxidations of *N*-alkylidene-2-hydroxyanilines (**4**).[3] This paper describes these detailed results.

Reactions of α,N-*Diarylnitrones (2) with* O-*Methyl Diphenylphosphinothioate (1).* Reactions of **2** with an equimolar amount of **1** did not occur at room temperature, but gave 2-arylbenzoxazoles (**3**) at 150 °C in *o*-dichlorobenzene in fairly good yields. The results are summarized in Table 1.

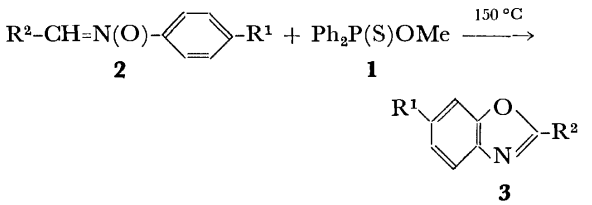

As shown in Table 1, in the case of α,*N*-diphenylnitrone (**2a**), 2-phenylbenzoxazole (**3a**) was not obtained but an intractable mixture was obtained. The reason is obscure.

These reactions in the absence of **1** gave only a trace amount of **3** under similar conditions. For example, in the case of **2g**, the yield of **3g** was only 1%.

Moreover, after the reactions in the presence of **1**, about a half amount of **1** was recovered (see Table 1). The fact suggests that **1** works catalytically. In fact, in the case of **2b**, a similar reaction with a 0.1 molar amount of **1** gave **3b** in 53% yield, and the yield was nearly the same as that with an equimolar amount of **1** (61%).

Table 1. Yields of **3** from **2** and **1**

2	R^1	R^2	Time/d	**3** (%)	Recovery of **1**/%
2a	H	C_6H_5	1	**3a** 0	a)
2b	H	*p*-$MeOC_6H_4$	2	**3b** 61	a)
2c	H	*p*-ClC_6H_4	7	**3c** 50	32
2d	Me	C_6H_5	2	**3d** 69	52
2e	Me	*p*-$MeOC_6H_4$	1	**3e** 56	33
2f	Me	*p*-ClC_6H_4	1	**3f** 47	63
2g	H	*p*-MeC_6H_4	1.75	**3g** 40	53

a) Not determined.

A plausible mechanism for formation of **3** might be as follows:

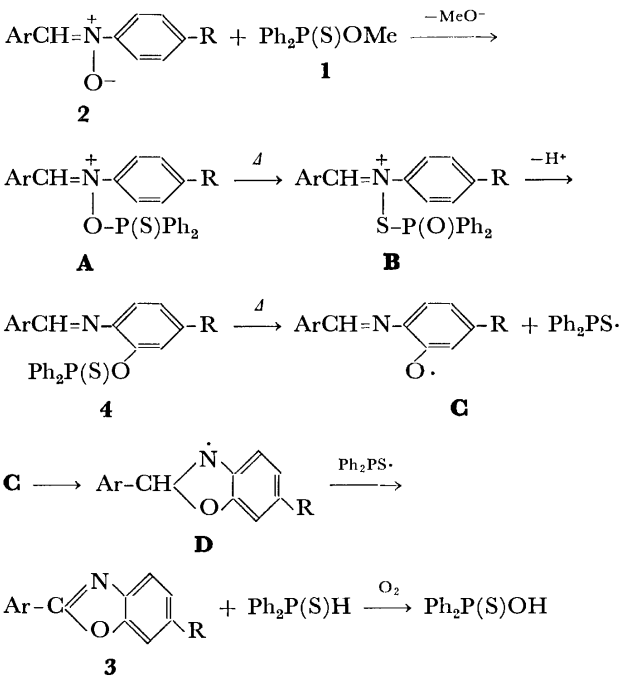

The anionic oxygen atom in the nitrone (**2**) nucleophilically attacks on the phosphorus atom in **1** to afford an intermediate (**A**) which thermally rearranges to a more stable intermediate (**B**) because P=O bond is stronger than P=S bond. Then the intermediate (**B**) is converted into *N*-benzylidene-*o*-(diphenylphosphinothioyloxy)aniline (**4**) by attack of the oxygen atom of the P=O group on the electron-deficient benzene ring. Next, **4** undergoes a homolytic cleavage to produce phenoxyl (**C**) and diphenylphosphinothioyl radicals. The radical (**C**) intramolecularly cyclizes to give a radical (**D**), and diphenylphosphinothioyl radical abstracts hydrogen atom from the radical (**D**) to afford 2-arylbenzoxazole (**3**) and diphenylphosphine sulfide. The latter compound may be oxidized to diphenylphosphinothioic acid under the reaction conditions. Since diphenylphosphinothioic acid can react with **2** to produce **A** analogously to **1**, it is considered that **1** can work catalytically even in a trace amount.

In fact, **2e** gave **3e** in the presence of 0.11 molar

amount of diphenylphosphinothioic acid under similar conditions in 44% yield. On the other hand, **3e** was obtained in a lower yield (23%) in a similar reaction of **2e** with a 0.1 molar amount of **1** under argon atmosphere. A similar reaction of **2e** in the presence of diphenylphosphine sulfide under argon atmosphere afforded **3e** only in 7% yield. These results support the above mechanism.

It was shown in a separate experiment that **4** (Ar= *p*-$MeOC_6H_4$), prepared from diphenylphosphinothioic chloride and *N*-(4-methoxybenzylidene)-2-hydroxyaniline, gave **3b** in 52% yield (based on the Schiff's base) under similar conditions, also supporting the above mechanism.

Oxidations of N-Alkylidene-2-hydroxyanilines (5) with Silver Oxide. If phenoxyl radicals (**C**) can be generated under mild conditions in a high efficiency, it is expected from the above mechanism that 2-substituted benzoxazoles (**3** and **7**) would be produced in high yields under mild conditions.

It has been reported that **5** are oxidized with lead(IV) tetraacetate,[4] lead(IV) tetraphosphate,[5] or nickel peroxide[6] to give **3** or **7** in fairly good yields and the intermediate is phenoxyl radical (**C**),[4] supporting the above mechanism.

In this connection, other oxidizing agents were examined. *N*-(4-Methoxybenzylidene)-2-hydroxyaniline (**5b**) was oxidized with iodine and potassium iodide[7] at room temperature, but the yield of **3b** was only 11%. On the contrary, oxidation of **5b** with silver oxide[8] gave **3b** at room temperature in 92% yield. Therefore, we used silver oxide as oxidizing agent for **5**. It is considered that silver oxide can generate phenoxyl radical from **5**.

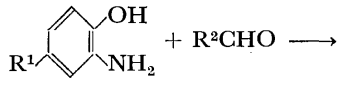

6

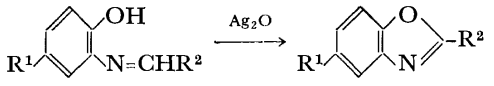

5 **3** or **7**

The Schiff's bases (**5**) are easily prepared from the corresponding aldehydes and *o*-aminophenols (**6**). Since Shiff's bases (**5k**—**m**) could not be purified, these were used in the oxidation reactions without further purification. The results of oxidation reactions of **5** with silver oxide are summarized in Table 2.

2-Alkyl- (**7f** and **7g**) and 2-alkenylbenzoxazoles (**7d**, **7h'**, and **7i**), which have not been prepared by oxidation with lead(IV) tetraacetate, were also obtained by the present method. 2,2'-Bis(benzoxazolyl) (**7j**) was prepared using glyoxal.

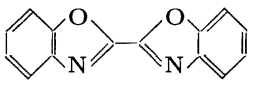

7j

However, in the case of butanal, the product was not 2-propylbenzoxazole, but 2-(1-ethyl-1-pentenyl)-benzoxazole (**7h**) was obtained unexpectedly, showing that an aldol-type condensation occurred at first during the preparation of the corresponding Schiff's base. **7h** was also prepared from the corresponding Schiff's base which was prepared from *o*-aminophenol and 2-ethyl-2-hexenal. 2-(1-Methyl-1-butenyl)benzoxazole (**7i**) was prepared by a similar method.

An aldol-type condensation during the preparation of the Schiff's base is supported by the fact that *N*-butylideneaniline gives *N*-(2-ethyl-2-hexenylidene)aniline through the dimerization followed by elimination of aniline.[9] Thus, we did not further apply this method to aldehydes which can undergo the corresponding reaction easily.

The benzoxazoles are usually prepared by heating *o*-aminophenols with acid anhydrides or acid halides.[10] To the best of our knowledge, yields in the present method were better and the reaction conditions employed were milder than any other methods for preparation of oxazoles. The present method is generally applicable to the 2-substituted benzoxazoles (**3** and **7**).

N-Benzylidene-2-hydroxyethylamine and -*o*-phenylenediamine did not produce the expected 4,5-dihydro-2-phenyl-1,3-oxazole and 2-phenylbenzimidazole, respectively, under similar conditions.

Table 2. Yields of benzoxazoles (**3** and **7**) from Schiff's bases (**5**)

5		R^2	**3** or **7** R^1	Yield/%
5a	**3a**	C_6H_5	H	76
5b	**3b**	*p*-$MeOC_6H_4$	H	92
5c	**3c**	*p*-ClC_6H_4	H	81
5d	**7a**	*p*-$NO_2C_6H_4$	H	80
5e	**7b**	*p*-$MeOC_6H_4$	Me	70
5f	**7c**	*p*-$MeOC_6H_4$	Cl	69
5g	**7d**	PhCH=CH-	H	87
5h	**7e**	α-Furyl	H	45[a]
5i	**7f**	*i*-Pr	H	54[a]
5j	**7g**	*t*-Bu	H	57[a]
5k	**7h**[b]	PrCH=CEt-	H	37[a]
5k'	**7h'**	PrCH=CEt-	H	74[a]
5l	**7i**	EtCH=CMe-	H	41[a]
5m	**7j**	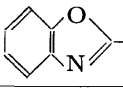	H	25[a]

a) Yield based on *o*-aminophenol used. b) This compound was obtained in the reaction of *o*-aminophenol with butanal followed by silver oxide oxidation (see text).

Experimental

All the melting points are uncorrected. The ^1H NMR spectra were measured with a Hitachi R-24 or R-20B spectrometer using TMS as an internal standard, the IR spectra were taken with a Hitachi EPI-G2 spectrophotometer, and the mass spectra were determined with a Hitachi RMU-6L spectrometer.

Materials. *O*-Methyl diphenylphosphinothioate (**1**) was prepared by reported method.[11] α,*N*-Diarylnitrones (**2a**—**f**) were prepared by the methods described in the previous paper.[1]

Reactions of 2 with 1. A typical procedure is described

on the reaction of **2b**.

Using an Equimolar Amount of ***1***: A solution of **2b** (252 mg, 1.11 mmol) and **1** (288 mg, 1.16 mmol) in *o*-$C_6H_4Cl_2$ (15 ml) was heated at 150 °C for 2 d. After removal of *o*-$C_6H_4Cl_2$ *in vacuo*, the residue was subjected to dry column chromatography (DCC)(SiO_2, CH_2Cl_2) to give **3b** (152 mg) in 61% yield, mp 100—101 °C (from EtOH) (lit,[12] mp 101 °C).

Using a Catalytic Amount of ***1***: A solution of **2b** (458 mg, 2.02 mmol) and **1** (50 mg, 0.2 mmol) in *o*-$C_6H_4Cl_2$ (15 ml) was heated at 150 °C for 24 h. Usual work-up gave **3b** (239 mg, 53%) and unchanged **1** (28 mg, 56%).

These results in reaction of other nitrones (**2**) were summarized in Table 1. Isolation method and mp (lit, mp) of **3** are shown below.

3c: DCC (SiO_2, CH_2Cl_2–CCl_4 (1:1)); mp 151.5—153 °C (from EtOH) (lit,[12] 150 °C). **3d**: DCC (SiO_2, CH_2Cl_2–CCl_4 (1:2)); mp 93—94 °C (from aq EtOH) (lit,[13] 92.5—93.0 °C). **3e**: DCC (SiO_2, CH_2Cl_2); mp 87—90 °C (from EtOH) (lit,[14] 91 °C). **3f**: DCC (SiO_2, CH_2Cl_2–CCl_4 (1:1)); mp 154—155 °C (from EtOH) (lit,[13] 151.5—152.0 °C). **3g**: DCC (SiO_2, CH_2Cl_2–CCl_4 (2:1)); mp 114.5—116.0 °C (from EtOH) (lit,[12] 116—117 °C).

Reaction of ***2e*** *with Diphenylphosphinothioic Acid.* A solution of **2e** (239 mg, 0.99 mmol) and diphenylphosphinothioic acid (27 mg, 0.11 mmol) in *o*-$C_6H_4Cl_2$ (7 ml) was heated at 150 °C for 24 h. After twice DCC (Al_2O_3, CCl_4 and then SiO_2, C_6H_6), **3e** was obtained in 44% yield (105 mg).

Formation of ***3b*** *from* ***4*** *(Ar=*p*-MeOC$_6$H$_4$)*. To a solution of *N*-(4-methoxybenzylidene)-2-hydroxyaniline[15] (1.142 g, 5.03 mmol) in *o*-$C_6H_4Cl_2$ (10 ml) were added triethylamine (0.7 ml, 5.0 mmol) and then diphenylphosphinothioic chloride (1.2 ml, 5.2 mmol) at 0 °C. After stirring at 0 °C for 30 min and then at 20 °C for 3 h, the resulting precipitates (1.65 g) were filtered off and a yellow oil (3.008 g) was obtained as the residue after removal of the solvent from the filtrate *in vacuo*; ^{1}H NMR ($CDCl_3$): δ 3.87 (s, 3H) and 6.5—8.5 (m, 19H); MS (FD): *m/e* 443 (M^+). A solution of the yellow oil (0.271 g) in *o*-$C_6H_4Cl_2$ (10 ml) was heated at 150 °C for 4 d. After removal of the solvent *in vacuo*, the residue was subjected to DCC (Al_2O_3, CCl_4 and then SiO_2, $CHCl_3$) to give **3b** (53.3 mg), yield 52% based on the starting Schiff's base, mp 102—103 °C (from EtOH).

Oxidations of ***5*** *with Silver Oxide.* The following Schiff's bases were prepared by reported methods: **5a**,[15] **5b**,[15] **5c**,[4] **5d**,[6] **5e**,[16] **5f**,[17] and **5g**.[4]

General procedure of oxidation is as follows. A mixture of **5** (1 mmol) and Ag_2O (1.1—1.3 mmol) in CH_2Cl_2 (20—40 ml) was stirred at room temperature for 2—5 h and an insoluble material was filtered off. The filtrate was evaporated and the residue was purified by recrystallization (recryst) or DCC to give pure **7**. The results were shown in Table 2.

Isolation method and mp (lit, mp) of **3** and **7** are shown below.

3a: DCC (SiO_2, CH_2Cl_2); mp 103—105 °C (from EtOH) (lit,[4] 102 °C). **3b**: DCC (SiO_2, CH_2Cl_2); mp 101—102 °C (from aq EtOH) (lit,[12] 101 °C). **3c**: DCC (SiO_2, CH_2Cl_2–CCl_4 (1:1)); mp 151—152 °C (from aq EtOH) (lit,[4] 151—152 °C). **7a**: recryst from xylene; mp 266.5—268.0 °C (lit,[4] 268 °C). **7b**: DCC (SiO_2, CCl_4); mp 109—111 °C (from EtOH) (lit,[18] 98—100 °C). **7c**: DCC (Al_2O_3, CH_2Cl_2–CCl_4 (1:1)); mp 155—156 °C (from EtOH) (lit,[17] 153—154 °C). **7d**: DCC (Al_2O_3, CCl_4); mp 83—85 °C (from aq EtOH) (lit,[4] 83 °C).

Preparation of ***7e*** *from Furfural.* A mixture of *o*-aminophenol (294 mg, 2.7 mmol), furfural (0.2 ml, 2.2 mmol), and anhydrous sodium sulfate (2 g) in benzene (20 ml) was stirred for 20 h at room temperature and filtered. The residual oil (325 mg) (^{1}H NMR ($CDCl_3$): δ 6.45 (q, J=2 Hz, 1H), 6.83—7.3 (m, 6H), 7.52 (d, J=2 Hz, 1H), and 8.4 (s, 1H)) from the filtrate was stirred with Ag_2O (461 mg, 2 mmol) in CH_2Cl_2 (20 ml) overnight and the reaction mixture was subjected to DCC (Al_2O_3, CCl_4) to give **7e** (225 mg, 45%), mp 88—89 °C (from aq EtOH) (lit,[6] 86.0—86.5 °C).

Preparation of ***7f*** *from 2-Methylpropanal.* A mixture of *o*-aminophenol (272 mg, 2.49 mmol), 2-methylpropanal (0.3 ml, 3.31 mmol), and anhydrous sodium sulfate (2 g) in benzene (30 ml) was stirred for 30 min at 0 °C and then for 3 h at room temperature and filtered. The residue (376 mg) from the filtrate was stirred with Ag_2O (769 mg, 3.31 mmol) in CH_2Cl_2 (20 ml) at 0—10 °C overnight and the reaction mixture was subjected to DCC (Al_2O_3, CCl_4) to give oily **7f** (217 mg, 54%) (lit,[19] bp 109—111 °C/10 mmHg, 1 mmHg=133.322 Pa); ^{1}H NMR ($CDCl_3$): δ 1.42 (d, J=7 Hz, 6H), 3.2 (m, 1H), and 7.1—7.85 (m, 4H); MS: *m/e* 161 (M^+, 34%) and 146 (100).

Preparation of ***7g*** *from 2,2-Dimethylpropanal.* A mixture of *o*-aminophenol (253 mg, 2.32 mmol), 2,2-dimethylpropanal (0.3 ml, 2.8 mmol) in benzene (20 ml) was refluxed using Dean-Stark apparatus for 3.5 h, the reaction mixture was concentrated to remove unchange *o*-aminophenol (36 mg), and then evaporated. The residue (360 mg) was stirred with Ag_2O (568 mg, 2.45 mmol) in CH_2Cl_2 (20 ml) at room temperature overnight, and the reaction mixture was subjected to DCC (Al_2O_3, CCl_4) to give oily **7g** (231 mg, 57%) (lit,[20] bp 124 °C/17 mmHg); ^{1}H NMR ($CDCl_3$): δ 1.5 (s, 9H) and 7.15—7.8 (m, 4H); MS: *m/e* 175 (M^+, 32%), 160 (100), and 133 (43).

Preparation of ***7h***. *From Butanal*: A mixture of *o*-aminophenol (259 mg, 2.37 mmol), butanal (0.5 ml, 5.67 mmol), and anhydrous sodium sulfate (2 g) in toluene (15 ml) was stirred at 0 °C for 6 h and filtered. The residue (558 mg) from the filtrate was stirred with Ag_2O (600 mg, 2.58 mmol) in CH_2Cl_2 (20 ml) at 0 °C overnight and the reaction mixture was subjected to DCC (Al_2O_3, CCl_4) to give oily **7h** (191 mg, 37%); ^{1}H NMR ($CDCl_3$): δ 1.0 (t, J=7 Hz, 3H), 1.2 (t, J=7 Hz, 3H), 1.3—1.8 (m, 2H), 2.3 (q, J=7 Hz, 2H), 2.7 (q, J=7 Hz, 2H), 6.71 (t, J=7 Hz, 1H), and 7.1—7.8 (m, 4H); MS: *m/e* 215 (M^+, 41%), 200 (100), 186 (40), 133 (47), and 120 (38).

Found: C, 77.90; H, 8.06; N, 6.75%. Calcd for $C_{14}H_{17}NO$: C, 78.14; H, 7.91; N, 6.51%.

From 2-Ethyl-2-hexenal: A mixture of *o*-aminophenol (275 mg, 2.52 mmol), 2-ethyl-2-hexenal[21] (500 μl), and anhydrous sodium sulfate (2 g) in benzene (50 ml) was refluxed overnight and filtered. The residue from the filtrate (527 mg) was stirred with Ag_2O (570 mg, 2.46 mmol) in CH_2Cl_2 (20 ml) at 0 °C overnight and the reaction mixture was subjected to DCC (Al_2O_3, CCl_4) to give **7h′** (=**7h**) (401 mg, 74%).

Preparation of ***7i*** *from 2-Methyl-2-pentenal.* A mixture of *o*-aminophenol (275 mg, 2.52 mmol) and 2-methyl-2-pentenal (452 mg, 4.61 mmol) in benzene (20 ml) was refluxed for 6 h using Dean-Stark apparatus and evaporated to give a residue (498 mg); ^{1}H NMR ($CDCl_3$): δ 1.1 (t, J=6 Hz, 3H), 2.0 (s, 3H), 2.4 (m, 2H), 6.2 (t, J=7 Hz, 1H), 6.8—7.3 (m, 4H), and 8.2 (s, 3H).

The residue was stirred with Ag_2O (781 mg, 3.37 mmol) in CH_2Cl_2 (20 ml) at room temperature overnight and the reaction mixture was subjected to DCC (Al_2O_3, CCl_4) to give oily **7i** (191 mg, 41%); ^{1}H NMR ($CDCl_3$): δ 1.1 (t,

J=7 Hz, 3H), 2.1 (s, 3H), 2.0—2.5 (m, 2H), 6.8 (t, J= 7 Hz, 1H), 7.3 (m, 3H), and 7.65 (m, 2H).

Found: C, 77.15; H, 7.06; N, 7.57%. Calcd for $C_{12}H_{13}NO$: C, 76.98; H, 7.00; N, 7.48%.

Preparation of ***7j*** *from Glyoxal.* A mixture of *o*-aminophenol (1.50 g, 13.8 mmol), 40% aq glyoxal (1.0 g, 6.9 mmol), and anhydrous sodium sulfate (10 g) in benzene (40 ml) was stirred at room temperature overnight and filtered. The solvent was removed, $CHCl_3$ (50 ml) was added and an insoluble part was filtered off. After removal of $CHCl_3$, the residue (849 mg) was stirred with Ag_2O (1.677 g, 7.23 mmol) in CH_2Cl_2 (50 ml) at room temperature overnight, and the reaction mixture was filtered through Celite. After evaporation of the filtrate, the residue was subjected to DCC (Al_2O_3, $CHCl_3$) to give **7j** (404 mg, 1.71 mmol, 25%), mp 262—263 °C (from EtOH) (lit,[22] 255—257 °C); MS: *m/e* 236 (M^+, 100%).

References

1) M. Yoshifuji, R. Nagase, T. Kawashima, and N. Inamoto, *Bull. Chem. Soc. Jpn.*, **55**, 870 (1982).

2) Preliminary report: R. Nagase, T. Kawashima, M. Yoshifuji, and N. Inamoto, *Heterocycles*, **8**, 243 (1977).

3) Preliminary report: M. Yoshifuji, R. Nagase, T. Kawashima, and N. Inamoto, *Heterocycles*, **10**, 57 (1978).

4) F. F. Stephens and J. D. Bower, *J. Chem. Soc.*, **1949**, 2971; **1950**, 1722.

5) M. S. A. El-Meligy and S. A. Mohamed, *J. Prakt. Chem.*, **316**, 154 (1974).

6) K. Nakagawa, H. Onoue, and J. Sugita, *Chem. Pharm. Bull. (Tokyo)*, **12**, 1135 (1964).

7) L. F. Fieser and M. Fieser, "Reagents for Organic Synthesis," John Wiley & Sons, New York (1974), Vol. 4, p. 260.

8) L. F. Fieser and M. Fieser, "Reagents for Organic Synthesis," John Wiley & Sons, New York (1967), Vol. 1, p. 1011.

9) M. S. Kharasch, I. Richlin, and F. R. Mayo, *J. Am. Chem. Soc.*, **62**, 494 (1940).

10) R. M. Acheson, "An Introduction to the Chemistry of Heterocyclic Compounds," 3rd ed, John Wiley & Sons, New York (1977), p. 353.

11) T. A. Mastryukova, T. A. Melent'eva, and M. I. Kabachnik, *Zh. Obshch. Khim.*, **35**, 1197 (1965); *Chem. Abstr.*, **63**, 11605e (1965).

12) S. Skraup, *Justus Liebigs Ann. Chem.*, **419**, 83 (1919).

13) A. E. Siegrist, *Helv. Chim. Acta*, **50**, 906 (1967).

14) O. Sues, N. Tomanek, and E. Lind, Ger. Patent 1137625 (1962); *Chem. Abstr.*, **59**, P11515b (1963).

15) A. W. Baker and A. T. Shulgin, *J. Am. Chem. Soc.*, **81**, 1523 (1959).

16) V. Bekdrek, J. Klicnar, F. Kristek, and M. Vecera, *Coll. Czech. Chem. Commun.*, **33**, 994 (1968); *Chem. Abstr.*, **68**, 113924b (1968).

17) H. D. Cossey, C. J. Sharpe, and F. F. Stephens, *J. Chem. Soc.*, **1963**, 4322.

18) E. Yu. Belyaev, L. E. Kondrat'eva, and N. A. Shakhov, *Khim. Geterotsikl. Soedin.*, **1972**, 10; *Chem. Abstr.*, **76**, 140615y (1972).

19) N. S. Kozlov and B. I. Kiselev, *Khim. Geterotsikl. Soedin., Akad. Nauk Latv. SSR*, **1966**, 345; *Chem. Abstr.*, **65**, 8889g (1966).

20) L. Oliveros, *Bull. Soc. Chim. Fr.*, **1974**, 2628.

21) S. G. Powell, D. A. Ballard, *J. Am. Chem. Soc.*, **60**, 1914 (1938).

22) S. Hünig, D. Scheutzow, H. Schlaf, and H. Quast, *Justus Liebigs Ann. Chem.*, **765**, 110 (1972).

Photochemical Reaction of Ethyl 3-Oxo-2,4-diphenylbutanoate

Michikazu Yoshioka,* Haruhiko Osawa, and Shinji Fukuzawa
Department of Chemistry, Saitama University, Shimo-okubo, Urawa, Saitama 338
(Received July 6, 1981)

Irradiation of ethyl 3-oxo-2,4-diphenylbutanoate in hexane gave the products formed by recombination of the radicals (Ph–$\dot{C}H_2$ and/or Ph–$\dot{C}H$–CO_2Et) resulting from decarbonylation, together with small amounts of 1,2-diphenylethanol and ethyl α-hydroxyphenylacetate, whereas in benzene no 1,2-diphenylethanol was found. Under oxygen an increased amount of ethyl α-hydroxyphenylacetate and no radical recombination products were observed.

Although the influence of UV-irradiation on the keto-enol equilibrium ratio of β-keto esters has been studied,[1] few reports about the photochemistry of β-keto esters to yield isolatable products have been found.[2,3] Moritur reported[2] that irradiation of the β-keto ester (**1**) gave aldehydes (**2**) resulting from α-cleavage. It is expected that β-keto esters with phenyl group at α-position to both carbonyl groups are easily subject to α-cleavage upon irradiation, and the resulting radicals may couple to yield products. In this paper we wish to report a photolysis of ethyl 3-oxo-2,4-diphenylbutanoate (**3**) which is expected to yield coupling products of radicals resulting from initial α-cleavage of the excited molecule.

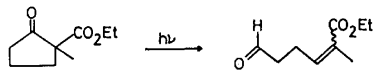

1 2 (E + Z)

Results and Discussion

Irradiation of **3** in hexane with Pyrex filtered light led to the formation of eleven products; bibenzyl (**4**, 13%), ethyl phenylacetate (**5**, 5%), ethyl α-hydroxyphenylacetate (**6**, 5%), 1,2-diphenylethanol (**7**, 2%), ethyl 2,3-diphenylpropionate[4] (**8**, 32%), ethyl *o*-benzylphenylacetate[5] (**9**, 4%), diethyl *meso*-α,α′-diphenylsuccinate[6] (**10**, 7%), diethyl *dl*-α,α′-diphenylsuccinate[6] (**11**, 7%), ethyl *o*-(α-ethoxycarbonylbenzyl)-phenylacetate (**12**, 3%), $PhCH_2C_6H_{13}$ compound (**13**, 4%), and $PhCH(C_6H_{13})CO_2Et$ compound (**14**, 4%). The products **4**, **5**, **6**, and **7** were identified by comparison of their spectroscopic data with those of commercially available authentic samples. The structures of **8**, **9**, **10**, and **11** were established by comparison with the specimens independently synthesized according to published methods.[4–6] The product **12** was confirmed by comparison with an independently synthesized one from *o*-benzoylbenzoic acid by the sequence **15**→**16**→**17**→**18**→**12** (overall yield, 16%).

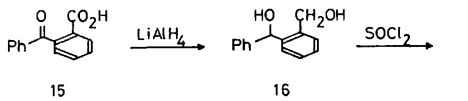

15 16

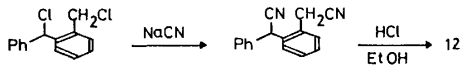

17 18

The products **13** and **14** were characterized by their spectroscopic data (see Experimental), although the structures of the $-C_6H_{13}$ residues of both **13** and **14** were not clear. ^1H NMR spectrum of **13** shows thirteen hydrogen atoms between δ=0.7 and 1.8 ($-C_6H_{13}$), two hydrogen atoms between δ=2.1 and 2.7 ($-CH_2-$ adjacent to the phenyl group) and five hydrogen atoms between δ=7.0 and 7.3 (phenyl), while that of **14** shows a triplet at δ=1.17 and a quartet at δ=4.07 ascribed to the ethoxycarbonyl group.

The formation of **4**—**6** and **8**—**14** may be explained in terms of cleavage of both the C_2–C_3 and the C_3–C_4 bonds of excited **3** to produce a benzyl radical and an α-ethoxycarbonylbenzyl radical. Homogeneous combination of the benzyl radicals and α-ethoxycarbonylbenzyl radicals yields bibenzyl **4** and two diastereomeric diesters **10** and **11**, respectively. Mixed combination of benzyl radical with α-ethoxycarbonylbenzyl radical yields **8**. Attack of the benzyl radical on a phenyl ring of α-ethoxycarbonylbenzyl radical yields **9** through an intermediate **20**. Similarly, coupling of α-ethoxycarbonylbenzyl radicals yields **12** through an intermediate **21**. Reaction of the α-ethoxycarbonylbenzyl radical with the solvent yields either **5** or **14**. Reaction of benzyl radical with the solvent yields **13**. Ethyl α-hydroxyphenylacetate **6** probably arises *via* the reaction of the α-ethoxycarbonylbenzyl radical with oxygen dissolved in the solvent. In fact, irradiation of **3** under oxygen afforded **6** with an increased yield. The formation of 1,2-diphenylethanol **7** may

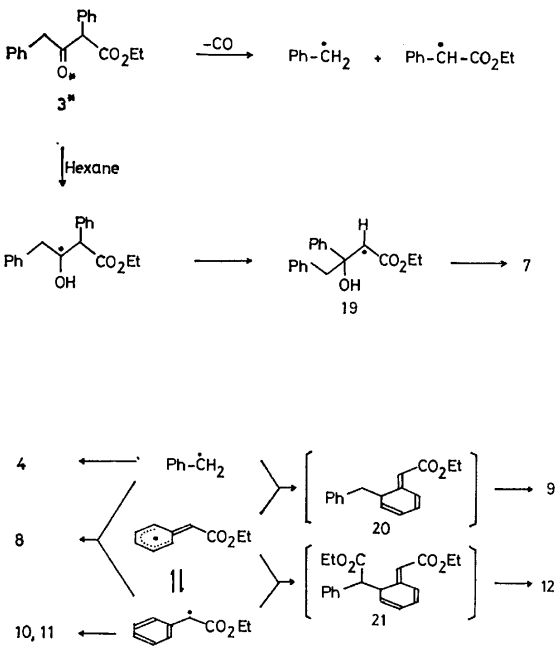

be explained in terms of phenyl migration from C-2 to C-3 of the starting β-keto ester. Since irradiation of **3** in benzene, which is inert toward hydrogen abstraction, affords no **7**, the phenyl migration is considered to follow the hydrogen abstraction by excited **3** from the solvent. Therefore, **7** may arise *via* radical **19**. In conclusion, the present work elucidated that photolysis of a β-keto ester having a phenyl group at the C-2 position proceeded predominantly by an α-cleavage and slightly by hydrogen abstraction from the solvent followed by phenyl migration.

Experimental

^{1}H NMR spectra were recorded on a Varian A-60D apparatus in carbon tetrachloride with tetramethylsilane as the internal standard. IR spectra were recorded on a JASCO IRA-2 spectrometer in carbon tetrachloride. Gas liquid chromatography (GLC) was carried out on a Hitachi K-53 (FID) or a Gasukuro Kogyo KOR-70 (TCD) instrument, using a 2 m×3 mm stainless steel (for K-53) or a 5 m×6 mm aluminium column (for KOR-70), both of which were packed with 10% SE-30 on 60—80 mesh Diasolid L. Irradiations were conducted through a Pyrex filter using an Ushio UM-452 high pressure mercury lamp (450 W). Thin layer chromatography (TLC) was carried out on Merck Silica Gel 60 TLC Plates Art. 5737. Column chromatography was carried out on Merck Silica Gel 60 Art. 7734. Ethyl 3-oxo-2,4-diphenylbutanoate (**3**) was prepared by the published method.[7]

Photolysis. a): A solution of 2.64 g of **3** in 1100 cm^3 of hexane (8.5 mmol/dm^3 solution) was irradiated, and the reaction was monitored by TLC. Irradiation was continued until almost all the starting ester was consumed (*ca.* 8 h). The solvent was removed under reduced pressure, and the residue was analyzed by GLC to reveal the following product distribution: **4** (13%), **5** (5%), **6** (5%), **7** (2%), **8** (32%), **9** (4%), **10** (7%), **11** (7%), **12** (3%), **13** (4%), and **14** (4%). These photo-products were separated from the irradiation mixture by a combination of column chromatography using benzene as eluent and preparative GLC. The products **4**—**12** were identical with authentic samples.

b): A solution of 960 mg of **3** in 400 cm^3 of hexane was irradiated under oxygen for 3 h. The solvent was removed under reduced pressure. Column chromatography of the residue gave only **6** with 37% yield.

c): A solution of 10.1 mg of **3** in 1 cm^3 of benzene was placed in a Pyrex tube and irradiated for 1 h. GLC-analysis indicated that the irradiation mixture contained **4** (18%), **5** (2%), **8** (50%), **9** (4%), **10** (10%), **11** (10%), **12** (3%), and no **7**.

$PhCH_2C_6H_{13}$ Compound ***13***. IR 2950, 2900, 695 cm^{-1}. ^{1}H NMR: δ=0.7—1.8 (m, 13H), 2.1—2.7 (m, 2H) and 7.0—7.3 (m, 5H). Found: C, 88.02; H, 11.22%. Calcd for $C_{13}H_{20}$: C, 88.56; H, 11.44%.

$PhCH(C_6H_{13})CO_2Et$ Compound ***14***. IR: 2950, 2920, 1730, 1160, 1030, 700 cm^{-1}. ^{1}H NMR: δ=1.17 (t, J=7.5 Hz, 3H), 0.6—2.4 (m, 13H), 3.0—3.5 (m, 1H), 4.07 (q, J=7.5 Hz, 2H), and 7.1—7.5 (m, 5H). Found: C, 77.64; H, 9.70%. Calcd for $C_{16}H_{24}O_2$: C, 77.37; H, 9.74%.

Synthesis of ***12***. To a suspension of $LiAlH_4$ (2.0 g) in absolute ether (30 cm^3) under reflux was added slowly a solution of *o*-benzoylbenzoic acid (**15**, 5.0 g) in absolute ether (50 cm^3). After the addition was completed, the mixture was heated under reflux for an additional 2 h. After the remaining $LiAlH_4$ had been destroyed by addition of saturated NH_4Cl solution (40 cm^3), the ether layer was separated. The ethereal solution was washed with water, dried over $MgSO_4$, and evaporated. The residue was submitted to chromatography using hexane-ethyl acetate 1:1 as eluent to give 4.1 g (87%) of diol **16**; bp (bath temp) 190 °C/93 Pa. IR: 3300, 700 cm^{-1}. ^{1}H NMR: δ=3.3—3.8 (broad, 1H), 4.1—4.6 (broad, 1H), 4.45 (AB q, J=14.5 and 12.5 Hz, 2H), 5.95 (s, 1H), and 7.15—7.45 (m, 9H). To a solution of **16** (3.0 g) and pyridine (2.3 g) was added slowly $SOCl_2$ (3.4 g) with stirring under cooling with ice. After the addition was completed, the mixture was stirred for 1 h at room temperature and extracted with ether. The ethereal solution was worked up in the usual way. Column chromatography using benzene as eluent gave 1.75 g (50%) of dichloride **17**; bp (bath temp) 155 °C/53 Pa. IR: 3100, 3050, 1500, 1450, 1265, 695 cm^{-1}. ^{1}H NMR: δ=4.68 (AB q, J=18.5 and 12.0 Hz, 2H), 6.68 (s, 1H) and 7.20—7.70 (m, 9H). Dichloride **17** (382 mg) was added at room temperature to the stirred partially soluble NaCN (210 mg) in dimethyl sulfoxide (2 cm^3). The mixture was stirred at room temperature for 90 min, diluted with water (4.5 cm^3), and extracted with ether. The ethereal solution was worked up. Column chromatography eluted with benzene gave 305 mg (86%) of dicyanide **18**; IR: 2260, 1500, 1460, 700 cm^{-1}. ^{1}H NMR: δ=3.63 (s, 2H), 5.35 (s, 1H), and 7.25—7.90 (m, 9H). Dry hydrogen chloride was bubbled through a solution of **18** (252 mg) in ethanol (5 cm^3). The solution was heated under reflux for 50 h. The reaction mixture was cooled with ice, and the precipitated NH_4Cl was filtered off. The filtrate was concentrated. The residue was extracted with ether, and the ether extract was washed with saturated $NaHCO_3$ and water, dried over $MgSO_4$, and evaporated. The residue was submitted to chromatography using benzene as eluent to yield 153 mg (43%) of diester **12**; IR: 1730, 1150, 1030, 690 cm^{-1}. ^{1}H NMR: δ=1.15 (t, J=7.5 Hz, 3H), 1.19 (t, J=7.5 Hz, 3H), 3.56 (s, 2H), 4.03 (q, J=7.5 Hz, 2H), 4.15 (q, J=7.5 Hz, 2H), 5.32 (s, 1H), and 7.1—7.4 (m, 9H). Found: C, 73.83; H, 6.78%. Calcd for $C_{20}H_{22}O_4$: C, 73.59; H, 6.79%.

References

1) P. Markov, L. Shishkova, and A. Radshev, *Tetrahedron*, **29**, 3203 (1973); D. Veierov, T. Bercovici, E. Fischer, Y. Mazur, and A. Yogev, *J. Am. Chem. Soc.*, **95**, 8173 (1973).
2) J. P. Moritur, G. Bildan, and J. Kossanyi, *Tetrahedron Lett.*, **1975**, 4167.
3) Vo V. Chung, M. Tokuda, A. Suzuki, and M. Itoh, *Bull. Chem. Soc. Jpn.*, **49**, 341 (1976).
4) Ch. Weizmann, E. Bergmann, and M. Sulzbacher, *J. Org. Chem.*, **15**, 918 (1950).
5) N. A. Domnin and R. Ch. Kolinskii, *Zh. Obshch. Khim.*, **30**, 270 (1960).
6) W. G. Kofron, *J. Org. Chem.*, **35**, 2085 (1970).
7) J. Volhard, *Ann.*, **296**, 1 (1897).

Synthetic Approach toward Antibiotic Tunicamycins. II.

Yoshimasa FUKUDA, Hiderou KITASATO, Hiroaki SASAI, and Tetsuo SUAMI*

Department of Applied Chemistry, Faculty of Engineering, Keio University, Hiyoshi, Kohoku-ku, Yokohama 223

(Received July 16, 1981)

Some higher-carbon carbohydrates, dodecose derivatives, have been synthesized by means of the base-catalyzed addition of nitro sugar to sugar aldehyde. The addition reaction of 6,7-dideoxy-1,2:3,4-di-*O*-isopropylidene-7-nitro-α-D-*galacto*-heptopyranose to 2,3:4,5-di-*O*-isopropylidene-D-arabinose yielded three isomeric dodecose derivatives, and their configurations have been studied. The nitro dodecose derivatives were converted into the corresponding hydroxy and acetoxy derivatives.

The higher-carbon carbohydrates, such as the undecose, decose, and octose derivatives, have been found in nucleoside antibiotics, such as tunicamycins,[1,2] anthelmycin[3,4] (hikizimycin), sinefungin,[5] ezomycin,[6] and mildiomycin.[7] The tunicamycins are produced by a strain of *Streptomyces* and exhibit broad-spectrum antitumor activities. They have a unique common structure consisting of uracil, fatty acid, and an undecose derivative named tunicamine, together with *N*-acetyl-D-glucosamine[2] (Scheme 1).

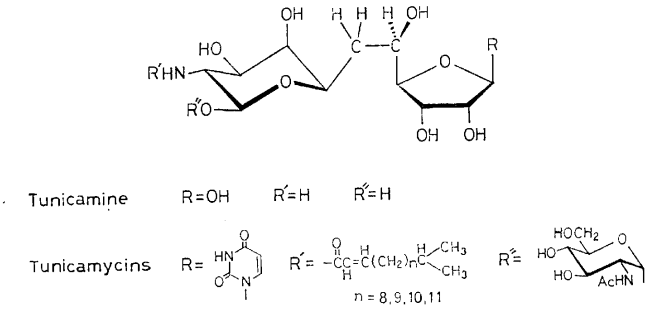

Scheme 1.

The occurrence of the higher-carbon carbohydrates in nature stimulated us to attempt to synthesize higher-carbon carbohydrates. In recent years the development of new methods of chain extension has been described in the literature.[8–14] In a previous paper of this series, we ourselves described the synthesis of 3,5-*O*-benzylidene-6,7-dideoxy-1,2:9,10:11,12-tri-*O*-isopropylidene-7-nitro-α-D-dodecofuranoses by the addition of the 7-nitro-α-D-glucofuranose derivative to 2,3:4,5-di-*O*-isopropylidene-D-arabinose (**5**).[15] Now we wish to report, as a part of a synthetic study toward tunicamycins, the addition reaction of 6,7-dideoxy-1,2:3,4-di-*O*-isopropylidene-7-nitro-α-D-*galacto*-heptopyranose (**3**) to **5**, in which three diastereoisomeric dodecose derivatives have been afforded. The conversion of the nitro group in these derivatives into an oxo or a hydroxyl group has been performed successfully.

This reaction can be used as a general procedure for the conversion of a hindered nitro group of a sugar into an oxo or a hydroxyl group.

Results and Discussion

The oxidation of 1,2:3,4-di-*O*-isopropylidene-α-D-galactopyranose,[16] obtained from D-galactopyranose (**1**), by the method of Pfitzner-Moffatt oxidation[17,18] yielded the aldehyde derivative. A reaction of the intact aldehyde with nitromethane in methanol in the presence of sodium methoxide gave 7-deoxy-1,2:3,4-di-*O*-isopropylidene-7-nitro-DL-*glycero*-D-*galacto*-heptopyranose (**2**). The acetylation of **2** with acetic anhydride in chloroform–pyridine, followed by treatment with sodium borohydride, afforded 6,7-dideoxy-1,2:3,4-di-*O*-isopropylidene-7-nitro-α-D-*galacto*-heptopyranose (**3**) in a 21% yield from **1**. The catalytic hydrogenation of **3** in methanol with Raney nickel and the subsequent acetylation of the reduction product with acetic anhydride in pyridine gave 7-acetamido-6,7-dideoxy-1,2:3,4-di-*O*-isopropylidene-α-D-*galacto*-heptopyranose (**4**) in a 56% yield.

When **3** was reacted with the arabinose derivative, **5**,[19] in the presence of a base catalyst, a mixture of three diastereomers of dodecose derivatives was obtained in a 65—67% yield after chromatography. These three isomeric dodecose derivatives, **6**, **7**, and **8**, were successfully isolated after repeated chromatographic fractionations. Their structures were establish-

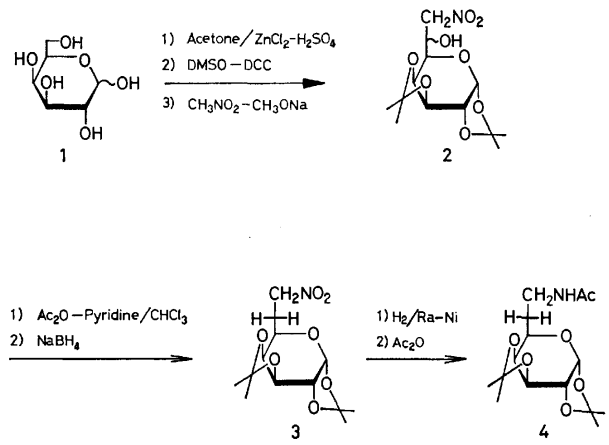

Scheme 2.

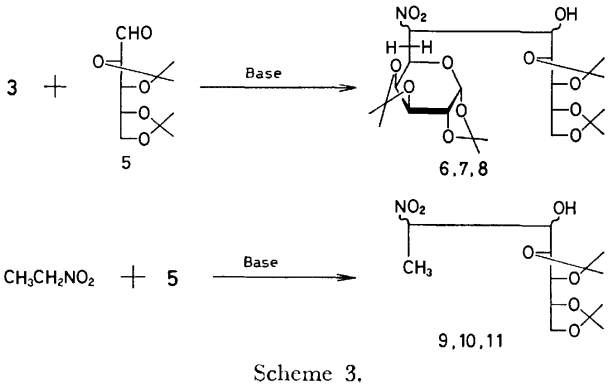

Scheme 3.

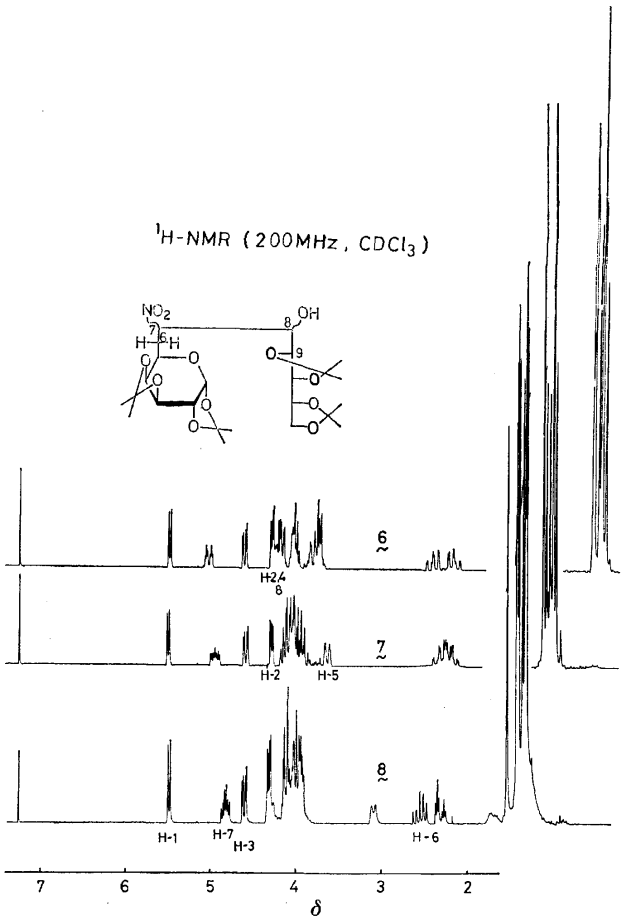

Fig. 1.

ed by means of the ^{1}H NMR, ^{13}C NMR, and IR spectra as 6,7-dideoxy-7-nitro-1,2:3,4:9,10:11,12-tetra-*O*-isopropylidene-α-D-dodecopyranoses.

Concerning the stereochemistry of the two newly introduced chiral centers on the C-7 and C-8 positions of compounds **6**, **7**, and **8**, four diastereomers (**A**)—(**D**) are theoretically possible, as is shown in Scheme 5. Their relative configurations among the C-7, C-8, and C-9 positions of **A**—**D** are *erythro-threo*, *threo-erythro*, *erythro-erythro*, and *threo-threo* respectively. In this reaction, three isomers have been obtained, but the fourth one was scarcely produced at all. As **D**, *threo-threo*, seems to be most unstable; compared to the other three diastereomers, scarcely no **D** is produced. These configurations were determined primarily on the basis of the course of the nucleophilic addition of nitronate anion to the sugar aldehyde, and secondarily on the basis of the course of the protonation of the nitronate anion, according to thermodynamic and kinetic controls.[20,21] Also **C**, *erythro-erythro*, is thermodynamically the most stable among them.

In this reaction, the ratio of the formation of three isomeric dodecose derivatives, **6**, **7**, and **8**, was markedly influenced by the amounts and kinds of catalysts used, as is shown in Table 1, but was little affected by the reaction time. That is, in the presence of a 1.2 equiv. of sodium methoxide as a base catalyst, **8** became the major product. On the other hand, in the presence of triethylamine or a 0.2 equiv.

Table 1. Isomeric ratios of nitrododecoses obtained by condensation of **3** and **5** under various base catalysts

Base	Nitrododecoses 6	7	8
$(CH_3CH_2)_3N$	7—10	: 7—11	: 1
CH_3ONa (0.1 equiv.)	4—7	: 4—8	: 1
CH_3ONa (1.2 equiv.)	0.3—0.6	: 0.3	: 1
CH_3OLi (1.2 equiv.)	0.6—0.8	: 0.7—1	: 1
CH_3OK (1.2 equiv.)	1	: 2	: 1

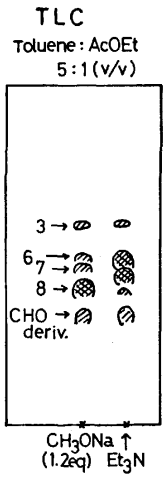

The reaction mixture was developed on TLC (solvent system: toluene-ethyl acetate 3:1 (v/v)) and was charred with 10% sulfuric acid. Then the ratio of dodecose isomers was estimated by by chromatoscan methods (Shimadzu CS-910).

Table 2. ^{13}C-NMR chemical shifts[a] of **6**, **7**, **8**, and **3**

C-No.	6	7	8	3
1	96.4	96.3	96.4	96.2
2	70.6	70.5	70.4	70.4
3	71.2	71.0	70.9	70.9
4	73.1	72.8	72.6	72.5
5	63.9	63.9	64.8	64.1
6	27.0	31.5	30.8	28.0
7	85.6	88.0	86.2	71.8
8	73.7	70.8	69.6	
9	80.3	77.3	77.2	
10	81.6	77.1	77.0	
11	76.1	79.8	79.0	
12	67.9	68.0	67.7	

a) Ppm downfield from internal TMS in $CDCl_3$.

of sodium methoxide, **6** and **7** were formed more readily than **8**.

The epimerization of **7** and **8** in the presence of triethylamine occurred very slowly until the ratio of **7** and **8** reached to *ca.* 7:1, but under the same conditions the epimerization of **6** to another isomer was not observed. These results showed that the configurations of C-8 in **7** and **8** were the same but those of C-7 were different. Compounds **7** and **8** are assigned to be **B** or **C**, while **6** is designated as **A**, since scarcely no **D** is produced because of the instability.

In the ^{13}C NMR spectrum, the chemical shifts of 4 carbon signals, C-9, 10, 11, and 12, of **7** were similar to those of **8**, but they were different from those of **6** as is shown in Table 2. That is, the configurations on the C-8 of **7** and **8** seem to be same.

Then the configurations of the nitro dodecose derivatives were established by the conversion of the nitro groups to amino groups. The catalytic hydrogenation of each one of the nitro dodecose derivatives

in ethyl acetate in the presence of Raney nickel, followed by *N*-acetylation, afforded a corresponding acetamidodideoxy-dodecose, **12** from **6**, **13** from **7**, and **14** from **8**.

The catalytic hydrogenation of the nitro-dodecose isomers, followed by *N*-benzyloxycarbonylation and cyclic *N,O*-carbonylation, gave the corresponding 7,8-*N,O*-carbonyl derivatives; **15** from **6**, **16** from **7**, and **17** from **8**. The structures of **15**, **16**, and **17** were determined by means of ^{1}H NMR and IR spectroscopy as 7-amino-7,8-*N,O*-carbonyl-6,7-dideoxy-1,2:3,4:9,10:11,12-tetra-*O*-isopropylidene-α-D-dodecopyranoses. The ^{1}H NMR spectra showed that the coupling constants of H-7 and H-8 of **15** and **17** were 9 Hz, while that of **16** was 5 Hz. These results suggested that the oxazolidinones of **15** and **17** had *vicinal cis* protons and that the 5 Hz coupling of **16** was due to the *trans* protons.[22,23]

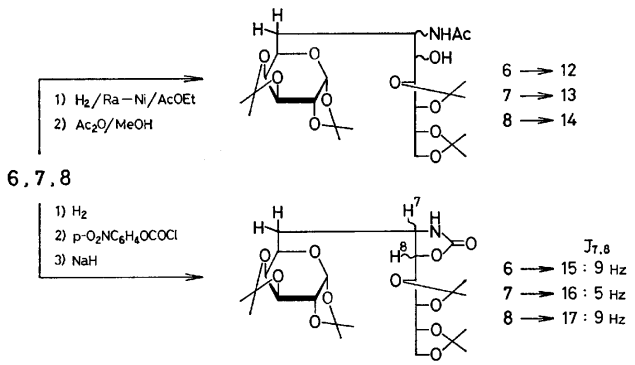

Scheme 4.

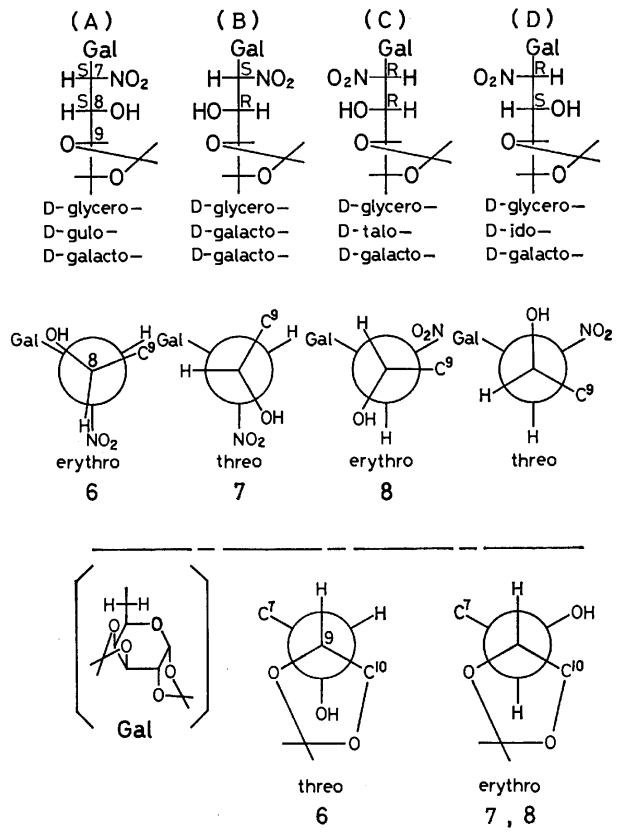

Scheme 5.

Considering the above-mentioned results, the configurations of **6**, **7**, and **8** were tentatively assigned as D-*glycero*-D-*gulo*-D-*galacto*-, **A**, D-*glycero*-D-*galacto*-D-*galacto*-, **B**, and D-*glycero*-D-*talo*-D-*galacto*-dodecose, **C**, respectively (Scheme 5).

The analogous addition reaction between the aldehyde **5** and nitroethane, instead of the D-galactose derivative, **3**, has been carried out as a simple model reaction. The reaction yielded a mixture of all theoretically predictable diastereomers in a 74% yield from **5**. Three of the four diastereomers (**9**, **10**, and **11**) have been isolated by column chromatography. Their structures have been identified as 1,2-dideoxy-4,5:6,7-di-*O*-isopropylidene-2-nitro-D-heptitols by means of ^{1}H NMR and IR spectroscopy. The ratio among the four isomers was not affected by the kind or amount of the catalyst in this model reaction.

The most notable difference between the two above-mentioned addition reactions between **5** and **3** and between **5** and nitroethane was the absence of one of the four diastereomers in the former reaction; this may be due to the existence of the bulky D-galactosyl group.

Then, the conversion of the nitro groups of **6**, **7**, and **8** into hydroxyl groups was attempted under mild conditions where the cleavage of a protective group does not occur. Since the Nef reaction[24,25] and the titanium trichloride method[26,27] are rather drastic, though these reactions have been used widely to convert a nitro group to an oxo group, an oxidative denitration with permanganate[28-31] has been employed in the present experiment.

The oxidation of the intact mixture of the nitro-dodecoses, **6**, **7**, and **8**, with potassium permanganate in water, followed by reduction with sodium borohydride and acetylation with acetic anhydride, afforded a mixture of three 7,8-di-*O*-acetyl derivatives, from which two diastereomers, **18** and **19**, were isolated by column chromatography. The ^{1}H NMR of **18** and **19** showed two acetyl metyl signals each at δ 2.07

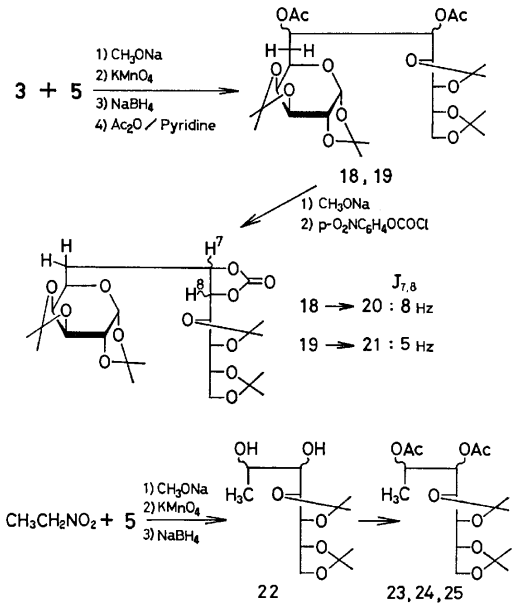

Scheme 6.

and 2.11 for **18**, and at δ 2.04 and 2.16 for **19**.

The deacetylation of **18** and **19** in methanolic sodium methoxide, followed by the cyclic carbonylation of the *vicinal* hydroxyl groups on C-7 and C-8, gave the corresponding 7,8-*O*-carbonyl derivatives, **20** and **21** respectively. In the ^{1}H NMR spectra of **20** and **21**, H-7 was observed as a doublet at δ 4.82 with $J_{7,8}$= 8 Hz on **20** and as a double-doublet at δ 4.49 with $J_{7,8}$=5 Hz on **21**.

The analogous reaction processes were carried out with an addition compound between the aldehyde, **5**, and nitroethane. The reactions gave three of the four theoretically predictable diastereomers after column chromatography. Their structures were established by ^{1}H NMR as 1-deoxy-2,3-di-*O*-acetyl-4,5:6,7-di-*O*-isopropylidene-D-heptitols, **23**, **24**, and **25**.

It has been demonstrated by the present study that a higher-carbon carbohydrate, dodecose, is prepared by the base-catalyzed addition of a nitro sugar to a sugar aldehyde, and that a hindered nitro sugar is converted to the corresponding keto or hydroxy derivative.

Experimental

General Methods. The melting points were taken in capillary tubes in a liquid bath and are uncorrected. The solutions were concentrated under reduced pressure below 50 °C. The IR spectra were measured with a Hitachi 225 spectrophotometer and are expressed in reciprocal centimeters. The ^{1}H NMR spectra were obtained on a Varian EM-390 (90 MHz) and a JEOL FX-200 (200 MHz) spectrometer. The chemical shifts are reported as δ values in parts per million, relative to tetramethylsilane as the internal standard. The TLC was performed on precoated silica gel 60 F-254 plaques (Merck, Darmstadt; Art. 5715, 0.25 mm thickness). The silica-gel column used for chromatography utilized Wako gel C-200 (Wako Pure Chemical Industries, Ltd.).

*7-Deoxy-1,2:3,4-di-O-isopropylidene-7-nitro-*DL*-glycero-*D*-galacto-heptopyranose (**2**) and 6,7-Dideoxy-7-nitro-1,2:3,4-di-O-isopropylidene-α-*D*-galacto-heptopyranose (**3**).* Nitromethane (228 ml) and 1 M† methanolic sodium methoxide (232 ml) were added to a solution of crude 1,2:3,4-di-*O*-isopropylidene-α-D-*galacto*-dialdopyranose-(1,5)[16] in methanol (400 ml), obtained from D-galactose (**1**) (50.0 g), under ice cooling with agitation. After 1 h at the ambient temperature, the solution was neutralized with Amberlite IR-120B(H$^+$) resin, and the resin was filtered off. The filtrate was concentrated to give an oily residue which contained **2** as the main product. A part (1/20) of the residue was purified on a silica-gel column using 7:1 (v/v) toluene–ethyl acetate to give 1.52 g (34%) of a homogeneous oily product of **2**: $[\alpha]_D^{20}$ −51.4° (*c* 0.3, methanol); IR (neat): 3450 (OH), 1550, 1390, 1380 cm^{-1} (NO_2); ^{1}H NMR ($CDCl_3$) δ 5.53 (1H, d, J=5 Hz, H-1), 1.37—1.53 (12H, isopropylidene CH_3). Found: C, 48.60; H, 6.59; N, 4.12%. Calcd for $C_{13}H_{21}NO_8$: C, 48.90; H, 6.63; N, 4.39%.

To a solution of the crude **2** in chloroform (500 ml), was added acetic anhydride (102 ml) and pyridine (68 ml) under ice cooling. After 6 h at the ambient temperature, the solution was washed with water, a saturated sodium hydrogencarbonate solution, and water, and concentrated under reduced pressure at 30 °C. To a solution of the residue in ethanol (600 ml), was added sodium borohydride (24 g) under ice cooling. After 1 h, the solution was neutralized with Amberlite IR-120B(H$^+$) resin, and the resin was filtered off. The filtrate was concentrated, and the residue was purified on a silica-gel column, using 30:1 (v/v) toluene–ethyl acetate, to give 17.0 g (21% yield from **1**) of **3** as a syrup: $[\alpha]_D^{18}$ −35.6° (*c* 3.4, chloroform); IR (neat) 1560, 1380 cm^{-1} (NO_2); ^{1}H NMR ($CDCl_3$) δ 5.35 (1H, d, $J_{1,2}$= 5 Hz, H-1), 1.25—1.75 (12H, isopropylidene CH_3). Found: C, 51.66; H, 6.87; N, 4.54%. Calcd for $C_{13}H_{21}NO_7$: C, 51.48; H, 6.98; N, 4.62%.

*7-Acetamido-6,7-dideoxy-1,2:3,4-di-*O*-isopropylidene-α-*D*-galacto-heptopyranose (**4**).* A solution of **3** (368 mg) in methanol (5 ml) was hydrogenated in the presence of Raney nickel in a hydrogen atmosphere (2.7 kg/cm^2) for 19 h. After the catalyst had then been filtered off, acetic anhydride (0.5 ml) was added to the filtrate. After 3 h, the product was purified on a silica-gel column, using 1:1 (v/v) chloroform–ethyl acetate as the eluent. Fractions corresponding to R_f 0.16 on the TLC in the same solvent were collected and concentrated. The residue was recrystallized from cyclohexane to give 214 mg (56%) of **4**: mp 98—99 °C; $[\alpha]_D^{23}$ −40° (*c* 1.5, methanol); ^{1}H NMR ($CDCl_3$) δ 5.50 (1H, d, $J_{1,2}$=5 Hz, H-1), 4.53 (1H, dd, $J_{2,3}$=2 Hz, $J_{3,4}$=7.5 Hz, H-3), 4.26 (1H, dd, $J_{1,2}$=5 Hz, $J_{2,3}$=2 Hz, H-2), 4.07 (1H, dd, $J_{3,4}$=7.5 Hz, $J_{4,5}$=1.5 Hz, H-4), 3.80 (1H, dt, $J_{4,5}$=1.5 Hz, $J_{5,6}$=6 Hz, H-5), 3.37 (2H, q, J=6 Hz, H-7), 2.93 (3H, s, NHAc), 1.80 (2H, q, J=6 Hz, H-6), 1.50, 1.76, 1.66 (3H×2 and 6H, s×3, isopropylidene CH_3). Found: C, 56.84; H, 7.81; N, 4.36%. Calcd for $C_{15}H_{25}NO_6$: C, 57.13; H, 7.99; N, 4.44%.

*6,7-Dideoxy-7-nitro-1,2:3,4:9,10:11,12-tetra-*O*-isopropylidene-α-*D*-dodecopyranoses (**6**, **7**, and **8**).* *a)*: 1 M Methanolic sodium methoxide (9 ml) was added to a solution of **3** (1.76 g) and **5** (2.01 g) in methanol (17 ml) at the ambient temperature. After 18 h, the solution was neutralized with Amberlite IR-120B(H$^+$) resin under ice cooling, and the resin was filtered off. The filtrate was concentrated, and the residue was chromatographed on a silica-gel column two times. (C-200, 90 g, 10:1 (v/v) toluene–ethyl acetate, wet column), (1:1 (wt/wt) C-200:C-300, 50 g, 6:1 (v/v) toluene–ethyl acetate, dry column). The fractions were combined and concentrated to give 183 mg (6%) of only **6**, 625 mg (20%) of a mixture of **6** and **7**, 443 mg (14%) of **7**, 500 mg (16%) of **7** and **8**, and 329 mg (11%) of only **8** (total yield 2.08 g (67%)); **6**; R_f=0.49 (3:1 (v/v) toluene–ethyl acetate); mp 161—162 °C; $[\alpha]_D^{23}$ −32° (*c* 0.5, methanol); IR ($CHCl_3$ solution) 3540, 3440 (OH), 1550, 1390, 1380 cm^{-1} (NO_2); ^{1}H NMR ($CDCl_3$) δ 5.48 (1H, d, $J_{1,2}$=5 Hz, H-1), 4.29 (1H, dd, $J_{2,3}$=2.5 Hz, H-2), 4.61 (1H, dd, $J_{3,4}$=8 Hz, H-3), 2.40 (1H, m, $J_{5,6}$=2 Hz, $J_{6,6}$=15 Hz, $J_{6,7}$=11.5 Hz, H-6), 2.16 (1H, m, $J_{5,6}$=11 Hz, $J_{6,6}$=15 Hz, $J_{6,7}$=2 Hz, H-6), 5.03 (1H, m, $J_{7,8}$= 3 Hz, H-7). Found: C, 54.27; H, 7.22; N, 2.43%. Calcd for $C_{24}H_{39}NO_{12}$: C, 54.03; H, 7.37; N, 2.63%.

7; R_f=0.45 (3:1 (v/v) toluene–ethyl acetate); mp 121—122 °C; $[\alpha]_D^{23}$ −30° (*c* 0.8, methanol); IR ($CHCl_3$ solution) 3510 (OH), 1555, 1390, 1380 cm^{-1} (NO_2); ^{1}H NMR ($CDCl_3$) δ 5.49 (1H, d, $J_{1,2}$=5 Hz, H-1), 4.28 (1H, dd, $J_{2,3}$=2.5 Hz, H-2), 4.58 (1H, dd, $J_{3,4}$=8 Hz, H-3), 2.24 (2H, m, H-6), 4.95 (1H, m, $J_{7,8}$=7 Hz, H-7). Found: C, 54.22; H, 7.26; N, 2.81%.

8; R_f=0.37 (3:1 (v/v) toluene–ethyl acetate); mp 125—127 °C; $[\alpha]_D^{23}$ −27° (*c* 1.0, methanol); IR ($CHCl_3$ solution) 3410 (OH), 1550, 1390, 1380 cm^{-1} (NO_2); ^{1}H NMR ($CDCl_3$) δ 5.48 (1H, d, $J_{1,2}$=5 Hz, H-1), 4.31 (1H, dd,

† 1 M=1 mol dm^{-3}.

$J_{2,3}$=2.5 Hz, H-2), 4.60 (1H, dd, $J_{3,4}$=8 Hz, H-3), 2.55 (1H, m, $J_{5,6}$=7 Hz, $J_{6,6}$=15 Hz, $J_{6,7}$=7.5 Hz, H-6), 2.30 (1H, m, $J_{5,6}$=4 Hz, $J_{6,6}$=15 Hz, $J_{6,7}$=4 Hz, H-6), 4.82 (1H, m, $J_{7,8}$=7 Hz, H-7). Found: C, 50.85; H, 7.37; N, 4.70%.

b): Triethylamine (0.75 ml) was added to a solution of **3** (426 mg) and **5** (393 mg) in methanol (7 ml) at the ambient temperature. After 4 days, the solution was concentrated at 30 °C under reduced pressure. The residue was chromatographed on a silica-gel column two times, (C-200, 50 g, 10:1 (v/v) toluene–ethyl acetate), (C-200, 20 g, 5:1 (v/v) toluene–ethyl acetate), to give 164 mg (22%) of only **6**, 62 mg (8%) of a mixture of **6** and **7**, 198 mg (26%) of **7**, 49 mg (7%) of **7** and **8**, and 17 mg (2%) of **8** (total yield, 490 mg (65%).

*1,2-Dideoxy-2-nitro-4,5:6,7-di-*O*-isopropylidene-*D*-heptitols (**9**, **10**, and **11**).* Triethylamine (0.67 ml) was added to a solution of **5** (895 mg) and nitroethane (1.68 ml) in methanol (9 ml). After 2 days, the reaction mixture was concentrated to dryness under reduced pressure at 30 °C. The oily residue was purified on a silica-gel column, using 10:1 (v/v) toluene–ethyl acetate (C-200, 33 g, C-300 10 g), to give a mixture of four isomers (800.3 mg, 69% from **5**) as crystals. The chromatography of the mixture was repeated several times to give homogeneous compounds of the three isomers, **9**, **10**, and **11**: **9**; R_f=0.42 (5:1 (v/v) toluene–ethyl acetate); mp 111—113 °C; $[\alpha]_D^{23}$ +8.55° (*c* 1.0, methanol); IR (CCl_4 solution) 3420 (OH), 1560, 1390, 1380 cm^{-1} (NO_2); ^1H NMR ($CDCl_3$) δ 1.78 (3H, d, $J_{1,2}$=6.5 Hz, CH_3), 1.34—1.44 (12H, isopropylidene CH_3). Found: C, 51.36; H, 7.41; N, 4.65%. Calcd for $C_{11}H_{17}NO_7$: C, 51.13; H, 7.59; N, 4.59%.

10; R_f=0.36 (5:1 (v/v) toluene–ethyl acetate); mp 96—98 °C; $[\alpha]_D^{23}$ +31.0° (*c* 1.4, methanol); IR (CCl_4 solution) 3420 (OH), 1560, 1390, 1380 cm^{-1} (NO_2); ^1H NMR ($CDCl_3$) δ 1.64 (3H, d, $J_{1,2}$=6.5 Hz, CH_3), 1.33—1.44 (12H, isopropylidene CH_3). Found: C, 51.36; H, 7.52; N, 4.64%.

11; R_f=0.31 (5:1 (v/v) toluene–ethyl acetate); mp 95—96 °C; $[\alpha]_D^{32}$ +12.7° (*c* 0.9, methanol); IR (CCl_4 solution) 3550 (OH), 1560, 1390, 1380 cm^{-1} (NO_2); ^1H NMR ($CDCl_3$) δ 1.60 (3H, d, $J_{1,2}$=6.5 Hz, CH_3), 1.33—1.44 (12H, isopropylidene CH_3). Found: C, 50.85; H, 7.37; N, 4.70%.

*7-Acetamido-6,7-dideoxy-1,2:3,4:9,10:11,12-tetra-*O*-isopropylidene-α-D-dodecopyranoses (**12**, **13**, and **14**).* One of three compounds, **10**, **11** and **12** (50 mg), was hydrogenated in ethyl acetate (6 ml) with a Raney nickel catalyst in a hydrogen atmosphere (2.7 kg/cm²) for 18 h. The catalyst was then filtered off, and the filtrate was concentrated. The residue was acetylated with acetic anhydride (0.5 ml) in methanol (4 ml) for 4 h. The reaction mixture was then concentrated, and the residue was purified on a silica-gel column, using 1:3 (v/v) toluene–ethyl acetate, to give a 7-acetamido-dodecose derivative: **12**; 68% yield from **6**; R_f=0.12 (1:2 (v/v) toluene–ethyl acetate); mp 178—179 °C; $[\alpha]_D^{28}$ −13.5° (*c* 0.4, methanol); ^1H NMR ($CDCl_3$) δ 5.46 (1H, d, J=5 Hz, H-1), 1.93 (3H, s, NHAc). Found: C, 56.98; H, 7.77; N, 2.52%. Calcd for $C_{26}H_{43}NO_{11}$: C, 57.23; H, 7.94; N, 2.57%.

13; 61% yield from **7**; R_f=0.25 (1:2 (v/v) toluene–ethyl acetate); mp 162—163 °C; $[\alpha]_D^{23}$ −25° (*c* 0.35, methanol); ^1H NMR ($CDCl_3$) δ 5.50 (1H, d, J=5 Hz, H-1), 1.97 (3H, s, NHAc). Found: C, 57.22; H, 7.78; N, 2.56%.

14; 56% yield from **8**; R_f=0.15 (1:2 (v/v) toluene–ethyl acetate); mp 62—63.5 °C (amorphous solid); $[\alpha]_D^{23}$ −30° (*c* 0.7, methanol); ^1H NMR ($CDCl_3$) δ 5.43 (1H, d, J=5 Hz, H-1), 1.97 (3H, s, NHAc). Found: C, 57.31; H, 7.81; N, 2.41%.

*7-Amino-7,8-*N,O*-carbonyl-6,7-dideoxy-1,2:3,4:9,10:11,12-tetra-*O*-isopropylidene-α-D-dodecopyranoses (**15**, **16**, and **17**).* A solution of a 7-nitro-dodecose, **6**, **7**, or **8** (40 mg), in ethyl acetate (5 ml) was hydrogenated analogously to the preparation of **12**, **13**, and **14**, and subsequently reacted with *p*-nitrophenoxycarbonyl chloride (56 mg) in pyridine (2 ml) for 1 d. The reaction mixture, diluted with ethyl acetate (20 ml), was then washed with water, saturated $NaHCO_3$, and water. The ethyl acetate solution was co-evaporated with toluene to give an oily residue, which was subsequently allowed to react with sodium hydride 60% in oil (5 mg) in dioxane (10 ml) to afford a carbamate derivative, **15**, **16**, or **17**, after short silica-gel column chromatography.

15; 59% yield from **7**; R_f=0.35 (1:1 (v/v) toluene–ethyl acetate); mp 48—49.5 °C (amorphous solid); IR ($CHCl_3$ solution) 3400 (NH), 1760 cm^{-1} (C=O); ^1H NMR ($CDCl_3$) δ 5.52 (1H, d, $J_{1,2}$=5 Hz, H-1), 4.59 (1H, dd, $J_{2,3}$=2 Hz, $J_{3,4}$=6 Hz, H-3), 4.53 (1H, dd, $J_{7,8}$=9 Hz, $J_{8,9}$=7.5 Hz H-8), 4.31 (1H, dd, $J_{1,2}$=5 Hz, $J_{2,3}$=2 Hz, H-2). Found: C, 56.55; H, 7.37; N, 2.49%. Calcd for $C_{25}H_{38}NO_{11}$: C, 56.81; H, 7.25; N, 2.65%.

16; 41% yield from **8**; R_f=0.37 (1:1 (v/v) toluene–ethyl acetate); mp 67—69° (amorphous solid); IR ($CHCl_3$ solution) 3460 (NH), 1760 cm^{-1} (C=O); ^1H NMR ($CDCl_3$) δ 5.46 (1H, d, $J_{1,2}$=5 Hz, H-1), 4.57 (1H, dd, $J_{2,3}$=2 Hz, $J_{3,4}$=5.5 Hz, H-3), 4.34 (1H, d, $J_{7,8}$=5 Hz, H-8), 4.28 (1H, dd, $J_{1,2}$=5 Hz, $J_{2,3}$=2 Hz, H-2). Found: C, 57.04; H, 7.39; N, 2.67%.

17; 37% yield from **9**; R_f=0.33 (1:1 (v/v) toluene–ethyl acetate); mp 196—197 °C (crystallized from ethyl acetate–hexane); IR (KBr) 3380 (NH), 1755 cm^{-1} (C=O); ^1H NMR ($CDCl_3$) δ 5.50 (1H, d, $J_{1,2}$=5 Hz, H-1), 4.72 (1H, d, $J_{7,8}$= 9 Hz, H-8), 4.60 (1H, dd, $J_{2,3}$=2 Hz, $J_{3,4}$=7.5 Hz, H-3), 4.32 (1H, dd, $J_{1,2}$=5 Hz, $J_{2,3}$=2 Hz, H-2). Found: C, 56.50; H, 7.28; N, 2.59%.

*7,8-Di-*O*-acetyl-6-deoxy-1,2:3,4:9,10:11,12-tetra-*O*-isopropylidene-α-D-dodecopyranoses (**18** and **19**).* To a solution of **3** (842 mg) and **5** (2.09 g) in methanol (30 ml) was added 1 M methanolic sodium methoxide (3 ml). After 18 h at the ambient temperature, the reaction mixture was poured into ice cold water (250 ml). To the solution was then added a solution of magnesium sulfate (722 mg) in water (18 ml); subsequently, a solution of potassium permanganate (553 mg) in water (430 ml) was stirred, drop by drop, into the mixture under ice cooling. After 1 h at the ambient temperature, acetic acid (1 ml) and chloroform (100 ml) were added to the reaction mixture and the inorganic precipitate was removed by filtration. The chloroform layer was separated, and the aqueous layer was extracted with chloroform (100 ml × 3). The organic layers were combined and concentrated. The residue was dissolved in ethanol (100 ml), and sodium borohydride (150 mg) was added to the solution under ice cooling. After 1 h, the mixture was concentrated under reduced pressure. The residue was dissolved in ethyl acetate (120 ml). The solution was washed with brine and water, and concentrated. The oily residue was purified on a silica-gel column, using 3:1 (v/v) toluene–ethyl acetate (C-200 50 g), and acetylated with pyridine (20 ml) and acetic anhydride (8 ml) for 2 d. The reaction mixture was then concentrated to dryness. The residue was purified on a silica-gel column, using 6:1 (v/v) toluene–ethyl acetate (C-200, 40 g), to give a mixture of isomers of diacetyl-dodecoses (492.4 mg, 30% from **3**). The mixture was chromatographed several times as has been described above to separate **18** and **19** as homogeneous compounds. However, another one, corresponding to R_f 0.51 on TLC using 3:1 (v/v) toluene–ethyl acetate, could not

be isolated.

18; R_f=0.52 (3:1 (v/v) toluene–ethyl acetate); mp 48—50 °C; $[\alpha]_D^{20}$ −24.0° (*c* 2.1, methanol); ^{1}H NMR ($CDCl_3$) δ 5.49 (1H, d, $J_{1,2}$=5 Hz, H-1), 4.27 (1H, dd, $J_{2,3}$=2 Hz, H-2), 4.57 (1H, dd, $J_{2,3}$=8 Hz, H-3), 5.26 (1H, dd, $J_{7,8}$=3.5 Hz, $J_{8,9}$=7 Hz, H-8), 2.11 (3H×2, s×2, Ac). Found: C, 57.30; H, 7.51%. Calcd for $C_{28}H_{44}O_{13}$; C, 57.13; H, 7.53%.

19; R_f=0.46 (3:1 (v/v) toluene–ethyl acetate); mp 98—99 °C; $[\alpha]_D^{20}$ −10.5° (*c* 0.8, methanol); ^{1}H NMR ($CDCl_3$) δ 5.51 (1H, d, $J_{1,2}$=5 Hz, H-1), 4.28 (1H, dd, $J_{2,3}$=2 Hz, H-2), 4.57 (1H, dd, $J_{3,4}$=8 Hz, H-3), 5.25 (1H, dd, $J_{7,8}$=4.5 Hz, $J_{8,9}$=2 Hz, H-8), 2.04, 2.16 (3H×2, s×2, Ac). Found: C, 56.90; H, 7.32%.

*7,8-O-Carbonyl-6-deoxy-1,2:3,4:9,10:11,12-O-isopropylidene-α-D-dodecopyranoses (**20** and **21**).* 1 M methanolic sodium methoxide (1 ml) was added to a solution of an acetyl derivative, **18** or **19** (40 mg), in methanol (5 ml). After 3 h at the ambient temperature the solution was neutralized with Amberlite IR-120B (H^+) resin; the resin was then filtrated off, and the filtrate was concentrated. The residue was reacted with *p*-nitrophenoxycarbonyl chloride (50 mg) in pyridine (3 ml) for 20 h at the ambient temperature. The reaction mixture, diluted with ethyl acetate (20 ml), was washed with water, brine, and water. The solution was then concentrated to give an oily residue, which was purified on a short silica-gel column to give **20** or **21** as a crystal, **20**; 63% from **18**; R_f=0.42 (3:1 (v/v) toluene–ethyl acetate); mp 136—137 °C; IR ($CHCl_3$ solution) 1800 cm^{-1} (C=O); ^{1}H NMR ($CDCl_3$) δ 5.51 (1H, d, $J_{1,2}$=5 Hz, H-1), 4.33 (1H, dd, $J_{2,3}$=2 Hz, H-2), 4.64 (1H, dd, $J_{3,4}$=8 Hz, H-3), 4.94 (1H, m, $J_{7,8}$=8 Hz, H-7), 4.82 (1H, d, $J_{7,8}$=8 Hz, H-8). Found: C, 56.50; H, 7.05%. Calcd for $C_{25}H_{38}O_{12}$: C, 56.60; H, 7.22%.

21; 70% from **19**; R_f=0.44 (3:1 (v/v) toluene–ethyl acetate); mp 159.5—161 °C; IR ($CHCl_3$ solution) 1795 cm^{-1} (C=O); ^{1}H NMR ($CDCl_3$) δ 5.47 (1H, d, $J_{1,2}$=5 Hz, H-1), 4.30 (1H, dd, $J_{2,3}$=2 Hz, H-2), 4.62 (1H, dd, $J_{3,4}$=8 Hz, H-3), 4.88 (1H, m, $J_{7,8}$=5 Hz, H-7), 4.49 (1H, dd, $J_{7,8}$=5 Hz, H-8). Found: C, 56.43; H, 7.03%.

*1-Deoxy-4,5:6,7-di-O-isopropylidene-D-heptitol (**22**) and 2,3-Di-O-acetyl-1-deoxy-4,5:6,7-di-O-isopropylidene-D-heptitols (**23**, **24**, and **25**).* To a solution of **5** (3.30 g) and nitroethane (2.30 ml) in methanol (23 ml), was added 1 M methanolic sodium methoxide (14 ml) under ice cooling. After 3 h at the ambient temperature, the mixture was poured into ice cold water (400 ml) containing sodium hydroxide (6.4 g), and then we added to the solution a solution of magnesium sulfate (3.4 g) in water (70 ml). The mixture was subsequently cooled in an ice–water bath, and potassium permanganate (4.5 g) in water (250 ml) was slowly stirred in. After 2 h, acetic acid (4 ml) and chloroform (100 ml) were added to the mixture, and the inorganic precipitate was removed by filtration. The chloroform layer was separated, and the aqueous layer was extracted with chloroform (250 ml×2). The organic phases were combined and concentrated. To a solution of the residue dissolved in ethanol (150 ml) was added sodium borohydride (1.04 g) under ice cooling. After 2 h, the mixture was evaporated. The residue was dissolved in chloroform (200 ml), and the solution was washed with brine and water, and concentrated. The oily residue was purified on a silica-gel column, using 7:1 (v/v) toluene–ethyl acetate (C-200, 100 g), to give a single isomer, **22**, R_f=0.2 (3:1 (v/v) toluene–ethyl acetate), of a diol derivative (476 mg) and a mixture of two other isomers (827 mg) which could not be separated. (Total yield, 1.3 g, 33.5% from **5**) **22**; recrystallization from cyclohexane–hexane; mp 91—92 °C; $[\alpha]_D^{25}$ +23.5° (*c* 1.0, chloroform); ^{1}H NMR ($CDCl_3$) δ 1.20 (3H, d, $J_{1,2}$=6 Hz, CH_3), 1.40, 1.50 (9H and 3H, s×2, isopropylidene CH_3). Found: C, 56.86; H, 8.30%. Calcd for $C_{13}H_{22}O_6$: C, 56.92; H, 8.09%.

22 (123 mg) was acetylated with acetic anhydride (0.23 ml) and pyridine (0.77 ml) for 18 h. The reaction mixture, diluted with chloroform (30 ml), was then washed with water, a saturated sodium hydrogencarbonate solution, and water, and concentrated to give a syrupy residue. The residue was purified on a silica-gel column, using 7:1 (v/v) toluene–ethyl acetate (C-200, 4 g and C-300, 1 g), to give a homogeneous oily product, **23** (96 mg, 60%); R_f=0.34 (5:1 (v/v) toluene–ethyl acetate); $[\alpha]_D^{20}$ +11.0° (*c* 1.3, methanol); ^{1}H NMR ($CDCl_3$) δ 1.25 (3H, d, $J_{1,2}$=6 Hz, CH_3), 1.35—1.42 (12H, isopropylidene CH_3), 2.04, 2.16 (3H×2, s×2, Ac). Found: C, 56.54; H, 7.77%. Calcd for $C_{17}H_{28}O_8$: C, 56.65; H, 7.83%.

The mixture of the two isomers was acetylated analogously to the method described above to a mixture of the two isomers of **24** and **25** (872 mg, 80.5%). The mixture was chromatographed several times to give two homogeneous products, **24** and **25**; **24**; R_f=0.35 (5:1 (v/v) toluene–ethyl acetate); $[\alpha]_D^{25}$ +29.1° (*c* 0.6, methanol); ^{1}H NMR ($CDCl_3$); δ 1.30 (3H, d, $J_{1,2}$=6.5 Hz, CH_3), 2.00, 2.10 (3H×2, s×2, Ac). Found: C, 56.37; H, 7.64%. Calcd for $C_{17}H_{28}O_8$: C, 56.65; H, 7.83%.

25; R_f=0.31 (5:1 (v/v) toluene–ethyl acetate); $[\alpha]_D^{20}$ +27.5° (*c* 0.2, methanol); ^{1}H NMR ($CDCl_3$); δ 1.30 (3H, d, $J_{1,2}$=6.5 Hz, CH_3), 2.05, 2.10 (3H×2, s×2, Ac). Found: C, 57.06; H, 7.86%.

The authors wish to thank Professor Gakuzo Tamura, Tokyo University, for his helpful suggestions. They also wish to express their appreciation to Shiseido, Ltd., and the Pharmaceutical Development Laboratories, Meiji Seika Kaisha, Ltd., for the NMR spectral data; to Mr. Saburo Nakada for the elemental analyses, and to Mr. Masazumi Kameda for the IR spectral data.

References

1) T. Ito, Y. Kodama, K. Kawamura, K. Suzuki, A. Takatsuki, and G. Tamura, *Agric. Biol. Chem.*, **41**, 2303 (1977).

2) A. Takatsuki, K. Kawamura, M. Okina, Y. Kodama, T. Ito, and G. Tamura, *Agric. Biol. Chem.*, **41**, 2307 (1977).

3) P. L. Hamill and M. M. Hoehn, *J. Antibiot., Ser. A*, **17**, 100 (1964).

4) M. Vuilhorgne, S. Ennifar, B. P. Das, J. W. Pascal, R. Nagarajan, E. W. Hagman, and E. Wenkert, *J. Org. Chem.*, **42**, 3289 (1977).

5) R. Nagarajan, B. Chao, D. E. Dorman, S. M. Nash, L. Occolowitz, and A. Schabei, 17th International Conference on Antimicrobial Agents and Chemotherapy, New York, N. Y., 1977, Abstr. 50.

6) K. Sakata, A. Sakurai, and S. Tamura, *Tetrahedron Lett.*, **1974**, 4327; *Agric. Biol. Chem.*, **39**, 885 (1975); **40**, 1993 (1976).

7) S. Harada, E. Mizuta, and T. Kishi, *J. Am. Chem. Soc.*, **100**, 4895 (1978).

8) H. Paulsen, K. Roden, V. Sinnwell, and W. Koebernick, *Angew. Chem., Int. Ed. Engl.*, **15**, 439 (1976).

9) E. I. Stout, W. M. Doane, and V. C. Trinkus, *Carbohydr. Res.*, **50**, 282 (1976).

10) J. A. Secrist, III, and S. R. Wu, *J. Org. Chem.*, **44**, 1434 (1979).

11) J. A. Secrist, III, and K. D. Barnes, *J. Org. Chem.*, **45**, 4528 (1980).
12) D. Horton and J. Tsai, *Carbohydr. Res.*, **75**, 154 (1979).
13) K. S. Kim and W. A. Szareck, *Can. J. Chem.*, **59**, 878 (1981).
14) S. Hanessian, T. J. Liak, and D. M. Dixit, *Carbohydr. Res.*, **88**, C14 (1981).
15) Y. Fukuda, H. Sasai, and T. Suami, *Bull. Chem. Soc. Jpn.*, **54**, 1830 (1981).
16) D. Horton, M. Nakadate, and J. M. J. Tronchet, *Carbohydr. Res.*, **7**, 56 (1968).
17) K. E. Pfitzner and J. G. Moffatt, *J. Am. Chem. Soc.*, **85**, 3027 (1963).
18) K. E. Pfitzner and J. G. Moffatt, *J. Am. Chem. Soc.*, **87**, 5661 (1965).
19) L. F. Wiggins, *J. Chem. Soc.*, **1946**, 13.
20) H. H. Baer and K. Kovar, *Can. J. Chem.*, **49**, 1940 (1971).
21) J. Kovár, K. Capek and H. H. Baer, *Can. J. Chem.*, **49**, 3960 (1971).
22) P. J. L. Daniels, "Drug Action and Drug Resistance on Bacteria," ed by S. Mitsuhashi, Tokyo Univ. Press, Tokyo (1975), pp. 88—89.
23) J. E. Herweh, T. A. Folglia, and D. Swern, *J. Org. Chem.*, **33**, 4029 (1968).
24) J. U. Nef, *Ann.*, **280**, 263 (1894).
25) W. E. Noland, *Chem. Rev.*, **55**, 137 (1955).
26) J. C. McMurry and J. Melton, *J. Org. Chem.*, **38**, 4367 (1973).
27) J. J. Nieuvenhius and J. H. Jordaan, *Tetrahedron Lett.*, **1977**, 369.
28) H. Shechter and F. T. Williams, Jr., *J. Org. Chem.*, **27**, 3699 (1962).
29) H. H. Baer and M. C. T. Wang, *Can. J. Chem.*, **46**, 2793 (1968).
30) S. W. Gunner, R. D. King, W. G. Overend, and N. R. Williams, *J. Chem. Soc., C*, **1970**, 1954.
31) W. P. Blackstock, C. C. Kuenzle, and C. H. Eugster, *Helv. Chim. Acta*, **57**, 1003 (1974).

Functionalization of *trans*-Decalin. V. A Synthesis of (±)-Nootkatone and (±)-Valencene from 4β,4aβ-Dimethyl-$\Delta^{6,7}$-octalin-1-one Ethylene Acetal

Sigeru Torii,* Tsutomu Inokuchi, and Ko Handa

Department of Industrial Chemistry, School of Engineering, Okayama University, Okayama 700

(Received July 17, 1981)

A synthesis of (±)-nootkatone (**1**) and (±)-valencene (**18**) starting from 4β,4aβ-dimethyl-$\Delta^{6,7}$-octalin-1-one ethylene acetal (**2**) is described. Epoxidation of the double bond of **2** followed by regiospecific reduction of the oxirane ring at the C-6 position gave the corresponding C-7 alcohol **4**. Oxidation of **4** and subsequent methoxycarbonylation at the C-6 position afforded methyl 1,1-ethylenedioxy-4β,4aβ-dimethyl-7-oxodecalin-6-carboxylate (**6**) in good yield. The keto ester **6** was converted to methyl 1,1-ethylenedioxy-4β,4aβ-dimethyldecalin-6α-carboxylate (**10b**) by the reduction with $NaBH_4$ followed by dehydration and subsequent hydrogenation over PtO_2 and epimerization of the 6β-methoxycarbonyl group with MeONa in MeOH. Deacetalization of **10b** followed by reduction and dehydration afforded methyl 4β,4aβ-dimethyl-$\Delta^{1(8a)}$-octalin-6α-carboxylate (**15**). The conversion of **15** into (±)-**18** was carried out directly by the reaction with salt-free methylenetriphenylphosphorane in refluxing tetrahydrofuran (76%) or by hydrolysis of **15** followed by methylation with MeLi, and subsequent Wittig reaction (60%). The allylic oxidation of (±)-**18** with $CrO_3 \cdot (pyridine)_2$ complex gave the desired (±)-**1**, smoothly.

The stereoselective introduction of 4β,4aβ-dimethyl groups of valencene (**18**) is an essential strategy for the nootkatone synthesis.[1] Most of Robinson-type annelation procedures[1f-h,j] for the preparation of (±)-nootkatone (**1**) except for cyclopentenone annulation by Nazarov-type reaction[1k] lack the stereoselectivity on introducing the 4β,4aβ-dimethyl groups in the $\Delta^{1(8a)}$-octalin skeleton. However, an exquisite procedure for the stereoselective synthesis of **1** has been devised by employing a Diels-Alder type reaction.[11] In connection with preparative investigations of eremophilane-type sesquiterpenes,[2] we have also developed the stereo-controlled construction of *trans*-4β,4aβ-dimethyl-$\Delta^{6,7}$-octalin-1-one ethylene acetal (**2**) by Diels-Alder reaction of 4-methyl-3-methoxycarbonyl-2-cyclohexen-1-one with butadiene.[2b] The present work is concerned with the stereoselective synthesis of the flavoring sesquiterpenes **1** and **18**[3] from the adduct **2**.

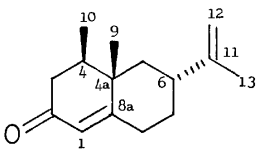

1

The strategy of leading **2** to the targets **1** and **18** involves the introduction of a methoxycarbonyl group at the C-6 carbon of **2**. Epoxidation of **2** with *m*-chloroperbenzoic acid at −60—10 °C gave the corresponding 6α,7α-epoxide **3** in 97% yield. The following reduction of the epoxy ring at the C-6 position of **3** based on the axial ring opening rule[4] with lithium in liquid ammonia afforded the 7α-alcohol **4** in 96% yield. Oxidation of **2** with pyridinium chlorochromate (PCC)[5] gave the ketone **5**, and subsequent methoxycarbonylation at the C-6 position of **5** with sodium hydride in refluxing dimethyl carbonate gave the keto ester **6** in 81% yield (from **4**).[6] The completely enolized form of **6** was characterized by two singlet signals at δ 95.7 and δ 171.5 due to the C-6 and C-7 carbons in homogeneous sixteen peaks in the ^{13}C NMR spectra.[7]

The hydrogenolysis of the ethylene dithioacetal[8] and the lithium metal reduction of methoxymethyl ether in liquid ammonia[9] were explored for the reduction of the β-keto esters. However, we have encountered some difficulties in obtaining the ethylene dithioacetal **11** on treatment of **6** with 1,2-ethanedithiol–boron trifluoride etherate, since the acetal-thioacetal

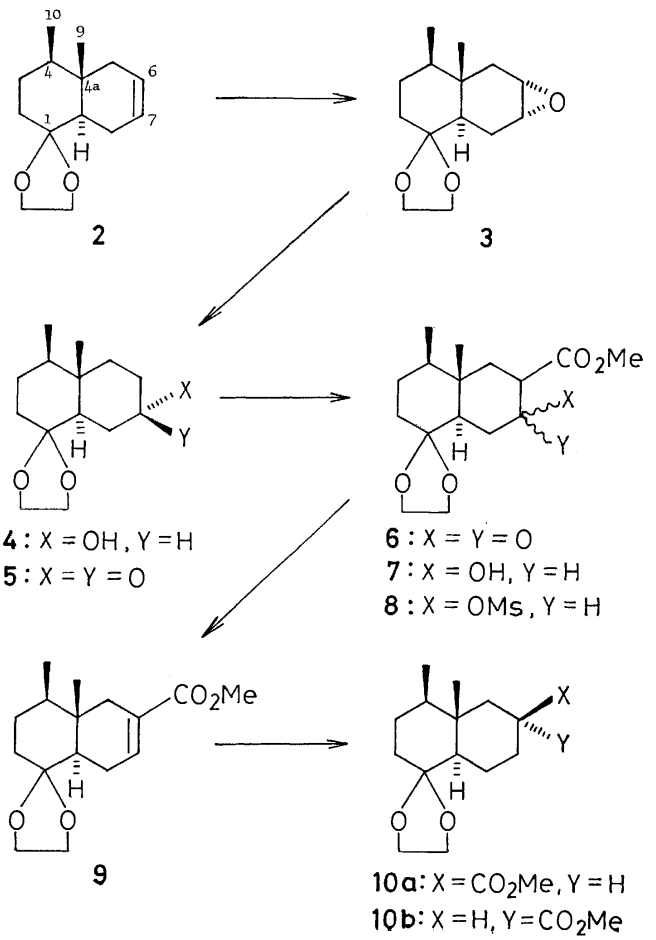

exchange occurred at the C-1 position of **6**, giving **12** exclusively. The lithium metal reduction of **6** was not feasible due to the reduction of the ester moiety to a hydroxymethyl group.

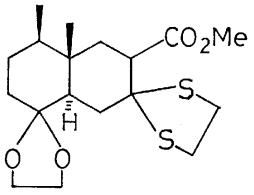

11

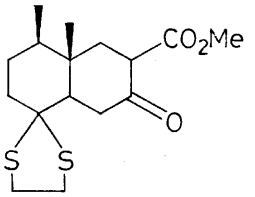

12

Because of the above results, stepwise transformation of **6** to **10** by ways of the dehydration of **7** and subsequent catalytic hydrogenation of **9** seemed to be promising for the present purpose. Reduction of **6** with sodium borohydride gave the epimeric alcohols **7** in 82% yield, and subsequent dehydration of the corresponding mesylates **8** with 1,8-diazabicyclo[5.4.0]-undec-7-ene (DBU) in refluxing benzene afforded α,β-unsaturated ester **9** in 64% yield (from **7**).[10] Catalytic hydrogenation of **9** over platinum oxide gave **10a** bearing the desired 6β-methoxycarbonyl group in 98% yield, as the result of preferential attack of hydrogen to the α side of the $\Delta^{6,7}$-double bond. The ^{13}C NMR spectra of **10a** showed homogeneous peaks, and the assigned configuration was also confirmed by the conversion of **10a** into the thermodynamically favorable 6α-isomer, **10b** on treatment with sodium methoxide at 85—90 °C in methanol (93% yield). The assigned stereochemistry at the C-6 position of **10b** can be rationally interpreted on the basis of downfield shift of ^1H NMR signals due to the angular C-4a methyl protons (δ 0.87) in comparison with that of **10a** (δ 0.72). This is due to the absence of shielding effects of the carbonyl group for a pair of axial and equatorial ester groups.[11]

Hydrolysis of the ethylene acetal of **10b** with perchloric acid and subsequent reduction of **13** with sodium borohydride provided the 1β-alcohol **14** in 95% yield (from **10b**). Dehydration of the hydroxyl group of **14** *via* the corresponding mesylate afforded **15** in 73% yield, the key precursor for the valencene synthesis.

The previous methods reported in the literature for the conversion of an ester into an isopropenyl group comprise the following two methods: one involves hydrolysis of the ester with an aqueous base, and treatment of the produced acid with methyllithium, giving the corresponding methyl ketone, and its subsequent treatment with methylenetriphenylphosphorane, giving the desired product.[1f,k] The other deals with the novel reaction of the ester with an excess of methylenetriphenylphosphorane, giving directly isopropenyl derivatives.[12] The reaction of **15** with an excess of salt-free methylenetriphenylphosphorane in tetrahydrofuran under reflux afforded the desired **18** in 76% yield. Meanwhile, the reaction of the acid **16** prepared by hydrolysis of **15** gave with methyllithium the ketone **17**, and subsequent olefination of **17** by Wittig reaction with methylenetriphenylphosphorane provided **18** (60% yield from **15**). The allylic oxidation of **18** with a slurry of the anhydrous chromium trioxide complex[13] furnished (±)-nootkatone (**1**) in 80% yield.[14]

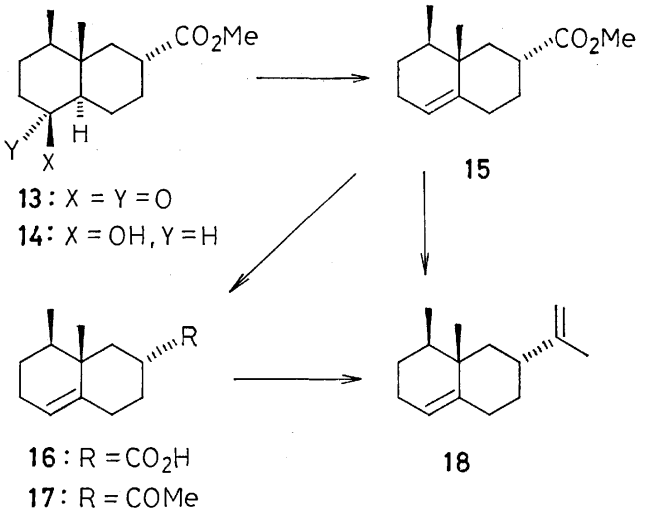

13: X = Y = O
14: X = OH, Y = H
15
16: R = CO_2H
17: R = COMe
18

Experimental

Melting points are uncorrected and boiling points are indicated without correction by the air bath temperature. IR spectra were determined on a JASCO IRA-1 grating spectrometer. ^1H NMR (60 MHz) spectra were obtained on a Hitachi R-24 spectrometer and ^{13}C NMR (25.05 MHz) spectra on a JEOL FX-100 spectrometer. Samples were dissolved in $CDCl_3$ and the chemical shift values (δ) are expressed in parts per million downfield from the internal standard Me_4Si. Elemental analyses were performed in our laboratory.

6α,7α-Epoxy-1,1-ethylenedioxy-4β,4aβ-dimethyl-trans-*decalin (**3**).* To a solution of *m*-CPBA (324 mg, 1.88 mmol) in CH_2Cl_2 (10 ml) was added a solution of **2** (320 mg, 1.44 mmol) in CH_2Cl_2 (10 ml) at −60 °C. After 1 h, the mixture was allowed to be warmed to 10 °C during 5 h, at which temperature it was stirred for 2 h. The mixture was filtered and the filtrate was washed with aqueous 20% KOH and aqueous $NaHCO_3$, dried (Na_2SO_4), and concentrated to give 332 mg (97%) of **3** after chromatography (SiO_2, hexane–AcOEt 5:1): bp 119—121 °C/2 Torr;† IR (neat) 1297, 1277, 1197, 1162, 1150, 1085, 1041 cm^{-1}; ^1H NMR δ 0.75 (s, 3, CH_3), 0.79 (d, J=6 Hz, 3, CH_3), 1.05—2.22 (m, 10, CH_2, CH), 2.80—3.11 (m, 2, CH–O), 3.51—3.96 (m, 4, CH_2O); ^{13}C NMR δ 13.2 (q, C-9), 15.1 (q, C-10), 20.2 (t, C-8), 28.0 (t, C-3), 34.9 (s, C-4a), 35.5 (t, C-2), 39.7 (t, C-5), 42.6 (d, C-4), 42.9 (d, C-8a), 50.3 (d, C-7), 52.7 (d, C-6), 64.0, 65.3 (t, CH_2O), 110.0 (s, C-1). Found: C, 70.65; H, 9.47%. Calcd for $C_{14}H_{22}O_3$: C, 70.56; H, 9.30%.

1,1-Ethylenedioxy-4β,4aβ-dimethyl-trans-*decalin-7α-ol (**4**).* To a blue solution of Li (55 mg, 7.93 mmol) in liquid NH_3 (45 ml) was added a solution of **3** (350 mg, 1.47 mmol) in THF (5 ml) at −70 °C. After being stirred for 3 h at −70 °C and for 1.5 h at −33 °C, the mixture was quenched with NH_4Cl (500 mg), allowed to stand at room temperature until the liquid NH_3 was removed, and worked up in the usual manner to give 340 mg (96%) of **4** after chromatography (SiO_2, hexane–AcOEt 3:1): bp 157—159 °C/0.035 Torr; IR (neat) 3400 (OH) cm^{-1}; ^1H NMR δ 0.80 (m, 3, CH_3), 0.82 (s, 3, CH_3), 1.00—2.10 (m, 12, CH_2, CH), 3.17

† 1 Torr ≈ 133.322 Pa.

(br, 1, OH), 3.54—4.00 (m, 4, CH_2O), 4.11 (complex t, J=2.5, 1 Hz, 1, CH–O); ^{13}C NMR δ 11.5 (q, C-9), 14.8 (q, C-10), 27.1 (t), 28.2 (t), 28.4 (t,) 33.7 (t, C-5), 35.8 (t, C-2), 37.7 (s, C-4a), 42.5 (d, C-4), 44.7 (d, C-8a), 64.0, 65.2 (t, CH_2O), 66.0 (d, C-7), 110.5 (s, C-1). Found: C, 69.87; H, 10.17%. Calcd for $C_{14}H_{24}O_3$: C, 69.96; H, 10.07%.

1,1-Ethylenedioxy-4β,4aβ-dimethyl-trans-*declain-7-one (5).* To a suspension of $Py \cdot CrO_3 \cdot HCl$ (1.06 g, 3.96 mmol) and AcONa (550 mg, 6.70 mmol) in CH_2Cl_2 (15 ml) was added a solution of **4** (320 mg, 1.33 mmol) in CH_2Cl_2 (5 ml). After being stirred for 3 h at 5 °C and for 3 h at room temperature, the mixture was diluted with ether (20 ml) and filtered. The concentrated filtrate was chromatographed (SiO_2, hexane–AcOEt 3:1) to give 294 mg (93%) of **5**: mp 59—61 °C; IR (Nujol) 1705 cm^{-1} (C=O); ^1H NMR δ 0.91 (m, 3, CH_3), 1.04 (s, 3, CH_3), 1.12—2.14 (m, 8, CH_2, CH), 2.15—2.57 (m, 4, CH_2CO), 3.57—4.10 (m, 4, CH_2O); ^{13}C NMR δ 11.7 (q, C-9), 15.3 (q, C-10), 28.3 (t, C-3), 35.6 (t, C-2), 36.4 (t), 37.1 (s, C-4a), 37.7 (t), 39.1 (t, C-5), 42.1 (d, C-4), 50.9 (d, C-8a), 64.1, 65.4 (t, CH_2O), 109.3 (s, C-1), 211.8 (s, C-7). Found: C, 70.63; H, 9.11%. Calcd for $C_{14}H_{22}O_3$: C, 70.56; H, 9.30%.

Methyl 1,1-Ethylenedioxy-4β,4aβ-dimethyl-7-oxo-trans-*decalin-6-carboxylate (6).* A mixture of **5** (340 mg, 1.43 mmol) and NaH (65 mg, 2.71 mmol) in dimethyl carbonate (1.7 ml) was heated under reflux for 3 h and quenched with cold aqueous $NaHCO_3$. The mixture was extracted with benzene–AcOEt (1:1) and the extract was worked up in the usual manner to give 369 mg (87%) of **6** after chromatography (SiO_2, hexane–AcOEt 2:1): mp 99—102 °C; IR (Nujol) 1655 (COO), 1621 cm^{-1} (C=C); ^1H NMR δ 0.78 (s, 3, CH_3), 0.89 (m, 3, CH_3), 1.05—2.00 (m, 6, CH_2, CH), 2.04—2.48 (m, 4, CH_2), 3.72 (s, 3, OCH_3), 3.80—4.12 (m, 4, CH_2O), 12.11 (s, 1, OH); ^{13}C NMR δ 11.8 (q, C-9), 15.3 (q, C-10), 25.4 (t, C-8), 28.1 (t, C-3), 35.5 (t, C-2), 36.4 (s, C-4a), 38.2 (t, C-5), 42.4 (d, C-4), 47.0 (d, C-8a), 51.3 (q, OCH_3), 64.1, 65.5 (t, CH_2O), 95.7 (s, C-6), 109.4 (s, C-1), 171.5 (s, C-7), 173.1 (s, COO). Found: C, 64.93; H, 8.31%. Calcd for $C_{16}H_{24}O_5$: C, 64.84; H, 8.16%.

Methyl 1,1-Ethylenedioxy-7-hydroxy-4β,4aβ-dimethyl-trans-*decalin-6-carboxylate (7).* To a solution of **6** (462 mg, 1.58 mmol) in MeOH (25 ml) was added a solution of $NaBH_4$ (59 mg, 1.56 mmol) in H_2O (1 ml) at 0 °C. The mixture was stirred for 12 h at room temperature, poured into aqueous $NaHCO_3$, and extracted with AcOEt–benzene (1:1). The extract was worked up in the usual manner to give 381 mg (82%) of **7** after chromatography (SiO_2, hexane–AcOEt 1:1): bp 143—145 °C/0.025 Torr; IR (neat) 3500 (OH), 1740 (COO), 1710 cm^{-1} (COO); ^1H NMR δ 0.71, 0.90 (s, 3, CH_3), 0.81 (m, 3, CH_3), 1.05—2.60 (m, 11, CH_2, CH), 2.90 (br, 1, OH), 3.46—4.40 (m, 5, CH_2O, CH–O), 3.66 (s, 3, OCH_3). Found: C, 64.69; H, 8.79%. Calcd for $C_{16}H_{26}O_5$: C, 64.41; H, 8.78%.

Methyl 1,1-Ethylenedioxy-7-methylsulfonyloxy-4β,4aβ-dimethyl-trans-*decalin-6-carboxylate (8).* To a solution of **7** (438 mg, 1.47 mmol) and Et_3N (1.04 g, 2.94 mmol) in ether (10 ml) was added $MeSO_2Cl$ (337 mg, 2.94 mmol) at 0 °C. The mixture was stirred for 2 h at 0 °C and for 1 h at room temperature, poured into cold aqueous $NaHCO_3$, and taken up in AcOEt–benzene (1:1). The extract was worked up in the usual manner to give 480 mg (87%) of **8**: mp 123—126 °C; IR (Nujol) 1718 cm^{-1} (COO); ^1H NMR δ 0.85 (m, 3, CH_3), 0.91 (s, 3, CH_3), 1.00—2.85 (m, 11, CH_2, CH), 2.99 (s, 3, SO_2CH_3), 3.50—4.15 (m, 4, CH_2O), 3.70 (s, 3, OCH_3), 4.50—5.00 (m, 1, CH–O). Found: C, 54.07; H, 7.52%. Calcd for $C_{17}H_{28}SO_7$: C, 54.25; H, 7.50%.

Methyl 1,1-Ethylenedioxy-4β,4aβ-dimethyl-$\Delta^{6,7}$-trans-*octalin-6-carboxylate (9).* A mixture of **8** (460 mg, 1.22 mmol) and DBU (1.36 g, 8.93 mmol) in benzene (20 ml) was heated at reflux for 12 h, poured into aqueous $NaHCO_3$, worked up in the usual manner to give 255 mg (74%) of **9** after chromatography (SiO_2, hexane–AcOEt 5:1): mp 79—81 °C; IR (Nujol) 1718 (COO), 1650 cm^{-1} (C=C); ^1H NMR δ 0.76 (s, 3, CH_3), 0.93 (m, 3, CH_3), 1.10—2.55 (m, 10, CH_2, CH), 3.70 (s, 3, OCH_3), 3.90 (m, 4, CH_2O), 6.95 (m, 1, HC=C); ^{13}C NMR δ 11.8 (q, C-9), 15.2 (q, C-10), 22.4 (t, C-8), 28.3 (t, C-3), 35.5 (t, C-2), 36.1 (s, C-4a), 40.0 (t, C-5), 42.6 (d, C-4), 46.9 (d, C-8a), 51.4 (q, OCH_3), 64.0, 65.5 (t, CH_2O), 109.7 (s, C-1), 128.2 (s, C-6), 138.7 (d, C-7), 167.9 (s, COO). Found: C, 68.50; H, 8.89%. Calcd for $C_{16}H_{24}O_4$: C, 68.55; H, 8.63%.

Methyl 1,1-Ethylenedioxy-4β,4aβ-dimethyl-trans-*decalin-6β-carboxylate (10a).* A mixture of **9** (123 mg, 0.44 mmol) and PtO_2 (40 mg) in AcOEt (7 ml) was treated with excess H_2 for 4 d at room temperature, filtered, and concentrated to give 122 mg (98%) of **10a**: bp 110—111 °C/0.017 Torr; IR (neat) 1730 cm^{-1} (COO); ^1H NMR δ 0.72 (s, 3, CH_3), 0.82 (m, 3, CH_3), 1.00—2.70 (m, 13, CH_2, CH), 3.67 (s, 3, OCH_3), 3.86 (m, 4, CH_2O); ^{13}C NMR δ 12.5 (q, C-9), 14.9 (q, C-10), 16.8 (t, C-8), 26.3 (t, C-7), 28.2 (t, C-3), 35.9 (t, C-2), 37.4 (d, C-4), 38.1 (s, C-4a), 41.2 (t, C-5), 43.0 (d, C-8a), 51.4 (q, OCH_3), 52.7 (d, C-6), 64.3, 65.4 (t, CH_2O), 109.9 (s, C-1), 176.4 (s, COO). Found: C, 70.52; H, 9.46%. Calcd for $C_{16}H_{26}O_4$: C, 70.56; H, 9.30%.

Epimerization of ***10a*** *to* ***10b.*** **10a** (110 mg, 0.39 mmol) was heated in MeOH (6 ml) containing MeONa (540 mg, 10 mmol) at 85—90 °C for 12 h. The mixture was poured into aqueous 5% tartaric acid and extracted with AcOEt–benzene (1:1). The crude product obtained after the usual workup was treated with excess CH_2N_2, giving 102 mg (93%) of **10b**: bp 121—123 °C/0.015 Torr; IR (neat) 1730 cm^{-1} (COO); ^1H NMR δ 0.86 (m, 3, CH_3), 0.87 (s, 3, CH_3), 1.10—2.75 (m, 13, CH_2, CH), 3.64 (s, 3, OCH_3), 4.87 (m, 4, CH_2O); ^{13}C NMR δ 12.7 (q, C-9), 14.8 (q, C-10), 19.0 (t, C-8), 28.4 (t), 28.9 (t), 35.8 (t, C-2), 37.7 (s, C-4a), 38.9 (d, C-4), 42.5 (t, C-5), 42.6 (d, C-8a), 51.4 (q, OCH_3), 51.9 (d, C-6), 64.2, 65.3 (t, CH_2O), 110.0 (s, C-1), 176.7 (s, COO). Found: C, 70.65; H, 9.51%. Calcd for $C_{16}H_{26}O_4$: C, 70.56; H, 9.30%.

Methyl 4β,4aβ-Dimethyl-1-oxo-trans-*decalin-6α-carboxylate (13).* To a solution of **10b** (122 mg, 0.43 mmol) in THF (6 ml) and H_2O (3 ml) was added 70% $HClO_4$ (0.2 ml). The mixture was stirred for 12 h at room temperature and worked up in the usual manner to give 101 mg (98%) of **13**: mp 68—69 °C; IR (Nujol) 1725 (COO), 1705 cm^{-1} (C=O); ^1H NMR δ 0.66 (s, 3, CH_3), 0.90 (d, J=6 Hz, 3, CH_3), 1.10—2.80 (m, 13, CH_2, CH), 3.65 (s, 3, OCH_3); ^{13}C NMR δ 11.7 (q, C-9), 14.5 (q, C-10), 19.8 (t, C-8), 27.8 (t), 31.3 (t), 38.6 (d, C-4), 40.8 (t), 41.2 (t), 41.4 (s, C-4a), 42.5 (d, C-8a), 51.7 (q, OCH_3), 57.2 (d, C-6), 176.3 (s, COO), 212.0 (s, C-1). Found: C, 70.52; H, 9.46%. Calcd for $C_{14}H_{22}O_3$: C, 70.56; H, 9.30%.

Methyl 1β-Hydroxy-4β,4aβ-dimethyl-trans-*decalin-6α-carboxylate (14).* To a solution of **13** (217 mg, 0.91 mmol) in MeOH (10 ml) was added a solution of $NaBH_4$ (35 mg, 0.92 mmol) in H_2O (0.5 ml) at 0 °C. The mixture was stirred for 3 h at room temperature, quenched with aqueous 10% AcOH, and taken up in AcOEt–benzene (1:1). The extract was worked up in the usual manner to give 213 mg (97%) of **14** after chromatography (SiO_2, hexane–AcOEt 3:1): bp 93—94 °C/0.005 Torr; IR (neat) 3480, 3400 (OH), 1730 (COO), 1715 cm^{-1} (COO); ^1H NMR δ 0.81 (m, 3, CH_3), 0.94 (s, 3, CH_3), 1.00—2.85 (m, 13, CH_2, CH), 1.68

(brs, 1, OH), 3.63 (s, 3, OCH_3), 3.67 (m, 1, CH–O); ^{13}C NMR δ 14.3 (q, C-10), 15.1 (q, C-9), 25.2 (t), 25.7 (t), 29.3 (t), 34.1 (t), 36.5 (s, C-4a), 39.2 (d, C-4), 42.7 (t, C-5), 43.1 (d, C-8a), 48.6 (d, C-6), 51.5 (q, OCH_3), 71.9 (d, C-1), 176.9 (s, COO). Found: C, 69.91; H, 10.08%. Calcd for $C_{14}H_{24}O_3$: C, 69.96; H, 10.07%.

Methyl 4β,4aβ-Dimethyl-$\Delta^{1(8a)}$-octalin-6α-carboxylate (15). To a solution of **14** (213 mg, 0.89 mmol) and Et_3N (629 mg, 6.22 mmol) in ether (10 ml) was added $MeSO_2Cl$ (203 mg, 1.77 mmol) at 0 °C. The mixture was stirred for 12 h at room temperature, quenched with aqueous $NaHCO_3$, and worked up in the usual manner. Without purification, the crude product was treated with benzene containing DBU (946 mg, 6.21 mmol) for 12 h under reflux. The usual workup and the subsequent chromatography (SiO_2, hexane–AcOEt 5:1) gave 144 mg (73%) of **15**: bp 74—76 °C/0.025 Torr; IR (neat) 1725 cm^{-1} (COO); ^1H NMR δ 0.85 (m, 3, CH_3), 0.93 (s, 3, CH_3), 1.10—2.60 (m, 12, CH_2, CH), 3.64 (s, 3, OCH_3), 5.35 (m, 1, HC=C); ^{13}C NMR δ 15.5 (q, C-10), 18.0 (q, C-9), 25.8 (t), 27.2 (t), 30.4 (t), 31.7 (t), 37.5 (s, C-4a), 39.7 (d), 40.8 (d), 41.9 (t, C-5), 51.4 (q, OCH_3), 121.0 (d, C-1), 141.6 (s, C-8a), 176.4 (s, COO). Found: C, 75.57; H, 9.97%. Calcd for $C_{14}H_{22}O_2$: C, 75.63; H, 9.97%.

4β,4aβ-Dimethyl-$\Delta^{1(8a)}$-octalin-6α-carboxylic Acid (16). Hydrolysis of **15** (58 mg, 0.26 mmol) in the MeOH (5 ml)–KOH (170 mg, 4.35 mmol)–H_2O (1 ml) system was carried out at room temperature for 24 h, acidified with aqueous 5% HCl, and extracted with AcOEt–benzene (1:1). The usual workup gave 49 mg (91%) of **16**; IR (neat) 3400—2600 (COOH), 1700 cm^{-1} (COO); ^1H NMR δ 0.87 (m, 3, CH_3), 0.93 (s, 3, CH_3), 1.10—2.90 (m, 12, CH_2, CH), 5.35 (m, 1, HC=C), 9.10 (br, 1, OH). Found: C, 75.24; H, 9.87%. Calcd for $C_{13}H_{20}O_2$: C, 74.96; H, 9.68%.

6α-Acetyl-4β,4aβ-dimethyl-$\Delta^{1(8a)}$-octalin (17). To a solution of **16** (54 mg, 0.26 mmol) in ether (5 ml) was added an ethereal solution of 1.05 M MeLi (0.74 ml, 0.78 mmol) at 0 °C. The mixture was stirred for 1 h at 0 °C, quenched with aqueous NH_4Cl, and extracted with AcOEt–benzene (1:1). The extract was worked up in the usual manner to give 43 mg (80%) of **17**: bp 109—112 °C/0.04 Torr (lit,[1h] 100—105 °C/0.02 Torr); IR (neat) 1710 (C=O), 1660 cm^{-1} (C=C); ^1H NMR δ 0.90 (m, 3, CH_3), 0.94 (s, 3, CH_3), 1.00—2.80 (m, 12, CH_2, CH), 2.14 (s, $COCH_3$), 5.32 (m, 1, HC=C).

(±)-Valencene (18) from 15. To a solution of **15** (110 mg, 0.50 mmol) in THF (5 ml) was added a salt-free solution of methylenetriphenylphosphorane prepared from methyltriphenylphosphonium bromide (715 mg, 2.0 mmol) and $NaNH_2$ (200 mg, 5.13 mmol) in THF (4 ml). The mixture was heated for 12 h under reflux and worked up in the usual manner to give 78 mg (76%) of **18**: bp 116—118 °C/14 Torr (lit,[1h] 73—75 °C/0.03 Torr); ^{13}C NMR δ 15.7 (q, C-10), 18.4 (q, C-9), 20.8 (q, C-13), 25.9 (t), 27.2 (t), 32.8 (t), 33.2 (t), 37.9 (s, C-8a), 41.0 (d), 41.1 (d), 45.0 (t, C-5), 108.3 (t, C-12), 120.1 (d, C-1), 143.1 (s, C-8a), 150.6 (s, C-11). IR and ^1H NMR spectra of **18** were identical with those of the reported ones.[3a,15]

Preparation of 18 from 17. To a solution of **17** (62 mg, 0.3 mmol) in benzene (5 ml) was added a benzene solution of 0.5 M methylenetriphenylphosphorane (1.2 ml, 0.6 mmol). The mixture was stirred at room temperature for 5 h, quenched with water, and worked up in the usual manner to give 51 mg (83%) of **18** after chromatography (SiO_2, hexane).

(±)-Nootkatone (1). To a solution of **18** (42 mg, 0.21 mmol) in CH_2Cl_2 (5 ml) was added a slurry of CrO_3·(pyridine)$_2$ complex (553 mg, 3.09 mmol) in CH_2Cl_2 (5 ml). The mixture was stirred for 12 h at room temperature, quenched with aqueous 5% tartaric acid, and worked up in the usual manner to give 36 mg (80%) of **1** after chromatography (SiO_2, hexane–AcOEt 3:1); mp 42—43 °C, crystallized from petroleum ether (boiling range 30—70 °C) at −70 °C (lit,[1f] 44—45 °C); ^{13}C NMR δ 14.9 (q, C-10), 16.8 (q, C-9), 20.8 (q, C-13), 31.7 (t), 33.1 (t), 39.3 (s, C-4a), 40.4 (d), 40.5 (d), 42.1 (t), 43.9 (t), 109.2 (t, C-12), 124.7 (d, C-1), 149.0 (s, C-11), 170.4 (s, C-8a), 199.5 (s, C-2). Except for the optical rotation, the physical data (IR, ^1H and ^{13}C NMR, and TLC analyses) of the product **1** were identical in all respects with those of the authentic sample.[14]

References

1) Isolation: a) H. Erdtman and Y. Hirose, *Acta Chem. Scand.*, **16**, 1311 (1962); b) W. D. MacLeod, Jr., and N. M. Buigues, *J. Food Sci.*, **29**, 565 (1964); c) W. D. MacLeod, Jr., *Tetrahedron Lett.*, **1965**, 4779; d) R. E. Berry, C. J. Wagner, Jr., and M. G. Moshonas, *J. Food Sci.*, **32**, 75 (1967); Synthesis: e) M. Pesaro, G. Bozzato, and P. Schudel, *J. Chem. Soc., Chem. Commun.*, **1968**, 1152; f) J. A. Marshall and R. A. Ruden, *J. Org. Chem.*, **36**, 594 (1971); g) A. Van Der Gen, L. M. Van Der Linde, and J. G. Witteveen, *Recl. Trav. Chim. Pays-Bas*, **90**, 1034 (1971); h) H. M. McGuire, H. C. Odom, and A. R. Pinder, *J. Chem. Soc., Perkin Trans. 1*, **1974**, 1879; i) K. P. Dastur, *J. Am. Chem. Soc.*, **96**, 2605 (1974); j) Y. Takagi, Y. Nakahara, and M. Matsui, *Tetrahedron*, **34**, 517 (1978); k) T. Hiyama, M. Shinoda, and H. Nozaki, *Tetrahedron Lett.*, **1979**, 3529; l) T. Yanami, M. Miyashita, and A. Yoshikoshi, *J. Org. Chem.*, **45**, 607 (1980).

2) a) S. Torii, T. Inokuchi, and K. Kawai, *Bull. Chem. Soc. Jpn.*, **52**, 861 (1979); b) S. Torii, T. Inokuchi, and T. Yamafuji *ibid.*, **52**, 2640 (1979).

3) Isolation: a) G. L. K. Hunter and W. B. Brodgen, *J. Food Sci.*, **30**, 1 (1965); b) J. A. Attaway, A. P. Pieringer, and L. J. Barabas, *Phytochemistry*, **5**, 1273 (1966); c) J. A. Weninger, R. L. Yates, and M. Polinsky, *Proc. Sci. Sect. Toilet Goods Assoc.*, **46**, 44 (1966); *Chem. Abstr.*, **66**, 79794 (1967); d) Ref. 1c; Synthesis: e) R. M. Coates and J. E. Shaw, *J. Org. Chem.*, **35**, 2597 (1970); f) Ref. 1h.

4) A. S. Hallsworth and H. B. Henbest, *J. Chem. Soc.*, **1957**, 4604.

5) E. J. Corey and J. W. Suggs, *Tetrahedron Lett.*, **1975**, 2647.

6) a) R. B. Miller and R. D. Nash, *J. Org. Chem.*, **38**, 4424 (1973); b) D. J. Goldsmith and I. Sakano, *ibid.*, **41**, **2095** (1976).

7) L. F. Johnson and W. C. Jankowski, "Carbon-13 NMR Spectra—A Collection of Assigned, Coded, and Indexed Spectra," John Wiley & Sons, New York, N. Y. (1972), p. 181.

8) a) G. Stork and J. W. Schulenberg, *J. Am. Chem. Soc.*, **84**, 284 (1962); b) T. A. Spencer, T. D. Weaver, R. M. Villarica, R. J. Friary, J. Posler, and M. A. Schwartz, *J. Org. Chem.*, **33**, 712 (1968).

9) R. M. Coates and J. E. Shaw, *J. Org. Chem.*, **35**, 2601 (1970).

10) S. P. Tanis and K. Nakanishi, *J. Am. Chem. Soc.*, **101**, 4398 (1979).

11) a) E. Wenkert, A. Afonso, P. Beak, R. W. J. Carney, P. W. Jeffs, and J. D. McChenesney, *J. Org. Chem.*, **30**, 713 (1965); b) Ref. 3f.

12) A. P. Uijttewaal, F. L. Jonkers, and A. van der Gen, *J. Org. Chem.*, **44**, 3157 (1979).

13) W. G. Dauben, M. Lorber, and D. S. Fullerton, *J. Org. Chem.*, **34**, 3587 (1969).

14) We are grateful to Mr. M. Ishihara, Shiono Koryo Co. Ltd., for a generous gift of natural nootkatone (**1**).

15) H. Hikino, N. Suzuki, and T. Takemoto, *Chem, Pharm, Bull. (Tokyo)*, **16**, 832 (1968).

 © 1982 The Chemical Society of Japan Bull. Chem. Soc. Jpn., 55, 891—898 (1982)

The C(1)–C(10) Bond Cleavage and B Ring Aromatization of Some 6-Hydroxy-5βH-abieta-6,8,11,13-tetraen-18-oic Acid 18,6-Lactones

Takashi MATSUMOTO,* Sachihiko IMAI,* Kenji ONDO, Nobuaki TAKEYAMA, Hideo KATAOKA, Yasuhiro YAMAMOTO, and Kenji FUKUI

Department of Chemistry, Faculty of Science, Hiroshima University, Higashisenda-machi, Naka-ku, Hiroshima 730

(Received July 24, 1981)

Fusion of 6-hydroxy-5βH-abieta-6,8,11,13-tetraen-18-oic acid 18,6-lactone (**2**) with potassium hydrogensulfate at 220 °C afforded bis[3-(2,3-dihydro-7-isopropyl-3,4-dimethyl-2-oxonaphtho[2,3-*b*]furan-3-yl)propyl] ether (**12**) in 37% yield, together with two minor products in 12% yield: 2,3-dihydro-7-isopropyl-3,4-dimethyl-3-propylnaphtho[2,3-*b*]furan-2-one and 3-allyl-2,3-dihydro-7-isopropyl-3,4-dimethylnaphtho[2,3-*b*]furan-2-one. Treatment of **12** with *p*-toluenesulfonic acid at 160 °C gave 2,3-dihydro-7-isopropyl-3,4-dimethyl-3-(3-tosyloxypropyl)naphtho[2,3-*b*]furan-2-one, which was converted into 2,3-dihydro-3-(3-hydroxypropyl)-7-isopropyl-3,4-dimethylnaphtho[2,3-*b*]furan-2-one (**16**). The alcohol **16** was further characterized as its acetate (**17**). After several attempts, the above C(1)–C(10) bond cleavage and B ring aromatization reaction were improved by use of concentrated sulfuric acid in refluxing acetic acid. Under these conditions, **2** gave **17** in 47% yield. Hydrolysis of **17** with hydrochloric acid afforded **16**. Subsequently, 12-hydroxy-, 12-methoxy-, 12-acetoxy-, and 12-nitro-6-hydroxy-5βH-abieta-6,8,11,13-tetraen-18-oic acid 18,6-lactones were each refluxed with concentrated sulfuric acid in acetic acid to give 6-hydroxy-, 6-methoxy-, 6-acetoxy-, and 6-nitro-3-(3-acetoxypropyl)-2,3-dihydro-7-isopropyl-3,4-dimethylnaphtho[2,3-*b*]furan-2-ones, respectively. From the present study, the 12-acetoxy derivative seems to be a suitable intermediate for the synthesis of coleon A.

Coleon A has been isolated from the leaves of *Coleus igniarius* Schweinf. (Labiatae) by Eugster *et al.*[1] On the basis of chemical and spectroscopic studies, they deduced the structure of coleon A to be **1**.[2,3] This is a very unique structure possessing a highly oxygenated 1,10-secoabietane skeleton. During the course of our synthetic studies on natural diterpenes we found[4] that, when 6-hydroxy-5βH-abieta-6,8,11,13-tetraen-18-oic acid 18,6-lactone (**2**) was treated with potassium hydrogensulfate or concentrated sulfuric acid, the C(1)–C(10) bond cleavage and B ring aromatization occurred. This paper[5] describes a novel synthesis of the coleon A skeleton.

Oxidation[7] of methyl abieta-6,8,11,13-tetraen-18-oate (**3**)[6] in chloroform with perbenzoic acid at room temperature afforded a mixture of the B ring oxygenated products, which was immediately treated with *p*-toluenesulfonic acid monohydrate in refluxing toluene to afford **2**. The IR spectrum of **2** showed bands at 1800 and 1692 cm^{-1} corresponding to a γ-lactone and a double bond, and its ^1H NMR spectrum showed signals at δ 2.65 (d, J=2.5 Hz) and 5.96 (d, J=2.5 Hz) due to the C-5 and C-7 protons. The stereochemistry of the C-5 position in **2** was established as follows. Catalytic hydrogenation of **2** in acetic acid over PtO_2, followed by esterification with diazomethane yielded the known methyl 5βH-abieta-8,11,13-trien-18-oate (**4**)[8] (IR: 1725 cm^{-1}), together with 6α-hydroxy-5βH-abieta-8,11,13-trien-18-oic acid 18,6α-lactone (**5**) (IR: 1758 cm^{-1}) and a small amount of its 18,6β-lactone epimer (**6**) (IR: 1760 cm^{-1}); their structures were supported by the following ^1H NMR spectra. The spectrum of **5** showed two singlet signals at δ 1.18 and 1.29 due to the C-10 and C-4 methyls, and signals for the C-5, C-6, and C-7 protons at δ 2.21 (1H, d, J=8.5 Hz), 4.88 (1H, dt, J=8.5 and 4 Hz), and 3.06 (2H, d, J=4 Hz). These spectral data suggested that **5** exists in a steroidal conformation (**5a**) in which the C(6)–O bond is axial to the twist-boat B ring and the A ring is a chair, as has been reported for 6α-hydroxy-5βH-podocarpa-8,11,13-trien-18-oic acid 18,6α-lactone (**7**).[9] While the spectrum of **6** showed the C-4 and C-10 methyl signals at δ 1.41 (6H), and signals for the C-5, C-6, and C-7 protons at δ 1.77 (1H, d, J=11 Hz), 4.38 (1H, dt, J=11 and 5 Hz), and 2.88 (1H, dd, J=15

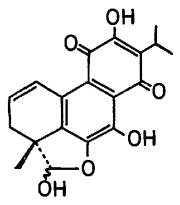

1

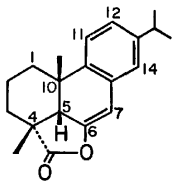

2

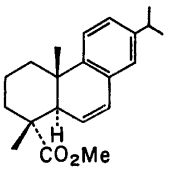

3

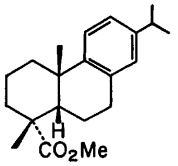

4

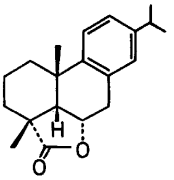

5

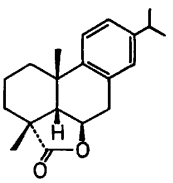

6

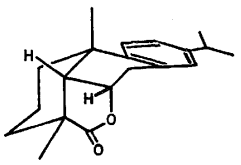

5a

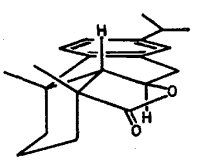

6a

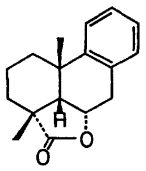

7

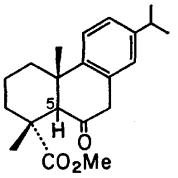

8 5β H
9 5α H

and 11 Hz) and 3.18 (1H, dd, J=15 and 5 Hz). These coupling patterns of the protons in the B ring and the chemical shifts of the C-10 methyl which is deshielded by the aromatic C ring, suggested that **6** exists in the nonsteroidal conformation (**6a**).[10] Methanolysis of **2** with concentrated hydrochloric acid in refluxing methanol afforded an A/B *cis* keto ester, methyl 6-oxo-5β*H*-abieta-8,11,13-trien-18-oate (**8**). On the other hand, the corresponding A/B *trans* keto ester, methyl 6-oxoabieta-8,11,13-trien-18-oate (**9**)[11] which was obtained from the above oxidation mixture of **3** with perbenzoic acid, was never epimerized to **8** with concentrated hydrochloric acid in refluxing methanol.

Fusion of **2** with potassium hydrogensulfate at 220 °C for 12 h afforded three naphthalene derivatives (**10**, **11**, and **12**), which were separated by a careful column chromatography on silica gel. The compound **10** was obtained as a minor product (6%) and showed the presence of a naphthalene chromophore in the UV spectrum,[12] an enol γ-lactone moiety in the IR spectrum (1798 cm^{-1}), and a molecular weight 296 in the mass spectrum. The ^1H NMR spectrum of **10** showed signals due to an isopropyl at δ 1.32 (6H, d, J=7 Hz), two methyls at δ 1.59 and 2.61 (each 3H and s), a propyl at δ 0.7—1.25 (5H, m) and 2.05 (2H, m), and four aromatic protons at δ 7.20 (1H, s), 7.26 (1H, dd, J=8.5 and 2 Hz), 7.50 (1H, d, J=2 Hz), and 7.82 (1H, d, J=8.5 Hz). These spectral data clarified the structure of **10** to be (*R*)-2,3-dihydro-7-isopropyl-3,4-dimethyl-3-propylnaphtho[2,3-*b*]furan-2-one. This structure was further confirmed by the conversion of **10** with dimethyl sulfate in the presence of potassium hydroxide in refluxing acetone to the corresponding methoxy ester (**13**) [IR: 1725 cm^{-1}; ^1H NMR: δ 3.53 (3H, s, $-CO_2CH_3$) and 3.78 (3H, s, $-OCH_3$)].

The compound **11** was also obtained as another minor product (6%), whose IR and ^1H NMR spectra were very similar to those of **10**, except for the presence of an allyl group [IR: 1633, 987, 910 cm^{-1}; ^1H NMR: δ 2.79 (2H, d, J=6.5 Hz) and 4.75—5.60 (3H, m)] instead of the propyl group in **10**. Catalytic hydrogenation of **11** in methanol over Pd–C gave **10**. Thus, the structure of **11** was assigned as (*R*)-3-allyl-2,3-dihydro-7-isopropyl-3,4-dimethylnaphtho-[2,3-*b*]furan-2-one.

The compound **12** was obtained as a major product (37%); its IR and ^1H NMR spectra were also very similar to those of **10**; a molecular weight of 606 was found from the mass spectrum. A triplet signal at δ 3.07 (2H, J=6 Hz) in the ^1H NMR spectrum suggested the structure of **12** to be a dimer possessing an ether linkage at both the ω-positions of propyl groups in two monomers (**10**). The ether dimer **12** was heated at 160 °C with *p*-toluenesulfonic acid in 1,1,2,2-tetrachloroethane to give (*R*)-2,3-dihydro-7-isopropyl-3,4-dimethyl-3-(3-tosyloxypropyl)-naphtho[2,3-*b*]furan-2-one (**14**) (IR: 1795, 1637, 1360, 1172 cm^{-1}), which was converted into the corresponding iodide (**15**) by refluxing with potassium iodide in acetone. Treatment of **15** with potassium *t*-butoxide in dimethyl sulfoxide at room temperature afforded (*R*)-2,3-dihydro-3-(3-hydroxypropyl)-7-isopropyl-3,4-dimethylnaphtho[2,3-*b*]furan-2-one (**16**), together with a small amount of **11**. The alcohol **16** was further characterized as its acetate (**17**) (IR: 1797, 1730, 1640 cm^{-1}). The structures of **14**, **15**, **16**, and **17** were also supported by their ^1H NMR spectra.[12]

Subsequently, we examined the reaction of **2** with concentrated sulfuric acid to find more effective conditions. Treatment of **2** with concentrated sulfuric acid in refluxing toluene for 2 h gave the tosylate **14** in 17% yield. However, when **2** in acetic acid was refluxed for 3 h with concentrated sulfuric acid, the acetate **17** was obtained in 47% yield. Hydrolysis of **17** with hydrochloric acid in refluxing methanol yielded the alcohol **16**, which was converted into the tosylate **14** by treatment with *p*-toluenesulfonyl chloride in pyridine and into a chloride (**18**)

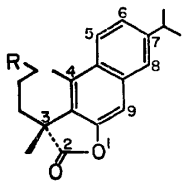

10 R=H
14 R=OTs
15 R=I
16 R=OH
17 R=OAc
18 R=Cl

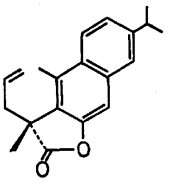

11

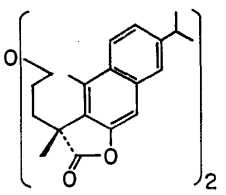

12

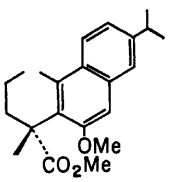

13

by refluxing with triphenylphosphine in carbon tetrachloride.

To obtain further information on the C(1)–C(10) bond cleavage and B ring aromatization leading to a suitable intermediate for the synthesis of coleon A, some C(12)-substituted derivatives of **2** were synthesized. Oxidation of methyl 12-acetoxyabieta-8,11,13-trien-18-oate (**19**)[13,14] with chromium trioxide in aqueous acetic acid afforded methyl 12-acetoxy-7-oxoabieta-8,11,13-trien-18-oate (**20**)[15] which, without purification, was converted into methyl 12-hydroxyabieta-6,8,11,13-tetraen-18-oate (**21**) by reduction with sodium borohydride in methanol, followed by refluxing with *p*-toluenesulfonic acid monohydrate in benzene. The crude hydroxy compound **21** was acetylated with acetic anhydride in pyridine to give methyl 12-acetoxyabieta-6,8,11,13-tetraen-18-oate (**22**), and methylated with methyl iodide in the presence of potassium *t*-butoxide in refluxing *t*-butyl alcohol to give methyl 12-methoxyabieta-6,8,11,13-tetraen-18-oate (**23**). Oxidation of **22** and **23** with perbenzoic acid in chloroform, followed by treatment with *p*-toluenesulfonic acid monohydrate in refluxing toluene, afforded respectively 6,12-dihydroxy-5βH-abieta-6,8,11,13-tetraen-18-oic acid 18,6-lactone (**24**) and 6-hydroxy-12-methoxy-5βH-abieta-6,8,11,13-tetraen-18-oic acid 18,6-lactone (**25**). Acetylation of **24** with acetic anhydride in pyridine yielded 12-acetoxy-6-hydroxy-5βH-abieta-6,8,11,13-tetraen-18-oic acid 18,6-lactone (**26**). The methoxy lactone **25** was also obtained from **24** by methylation with dimethyl sulfate in the presence of anhydrous potassium carbonate in refluxing acetone. Nitration of **2** in acetic anhydride with fuming nitric acid gave 6-hydroxy-12-nitro-5βH-abieta-6,8,11,13-tetraen-18-oic acid 18,6-lactone (**27**), whose ^{1}H NMR spectrum showed two singlet signals at δ 7.08 and 7.69 due to the two aromatic protons, suggesting that the nitration occurred at the C-12 position in **2**. The ^{1}H NMR spectra[12] of **24**, **25**, **26**, and **27** also suggested that the stereochemistry of the C-5 position in these γ-lactones was identical with that of **2**.

Subsequently, the γ-lactones were subjected to the C(1)–C(10) bond cleavage and B ring aromatization. The reaction conditions and yields are summarized in Table 1. The hydroxy γ-lactone **24** in acetic acid was refluxed for 1 h with concentrated sulfuric acid to give (*R*)-3-(3-acetoxypropyl)-2,3-dihydro-6-hydroxy-7-isopropyl-3,4-dimethylnaphtho[2,3-*b*]furan-2-one (**28**) and a small amount of (*R*)-6-acetoxy-3-(3-acetoxypropyl)-2,3-dihydro-7-isopropyl-3,4-dimethylnaphtho-[2,3-*b*]furan-2-one (**29**). Acetylation of **28** with acetic anhydride in pyridine afforded **29**. Similar treatment of **25**, **26**, and **27** also yielded the corresponding 2,3-dihydronaphtho[2,3-*b*]furan-2-one derivatives, **30**, **29**, and **31**, respectively. From the present study, the 12-acetoxy lactone **26** seems to be a useful intermediate for the synthesis of coleon A.

One possible mechanism of the reaction of the 5βH-γ-lactones (**2**, **24**, **25**, **26**, and **27**) with concentrated sulfuric acid in refluxing acetic acid would be the following. These lactones should exist in a non-steroidal conformation (**32**), because no steroidal conformation could be constructed with molecular models. The reaction would be initiated by oxidative elimination of an allylic C-5β hydrogen atom with concentrated sulfuric acid.[16] Then the C(1)–C(10) bond antiperiplaner to the C(5)–H one is cleaved with a back attack of an acetate anion at the C-1 position. This would stabilize the molecule by the B ring aromatization and by the disappearance of any 1,3-diaxial interaction between the C-4 and C-10 methyl groups.

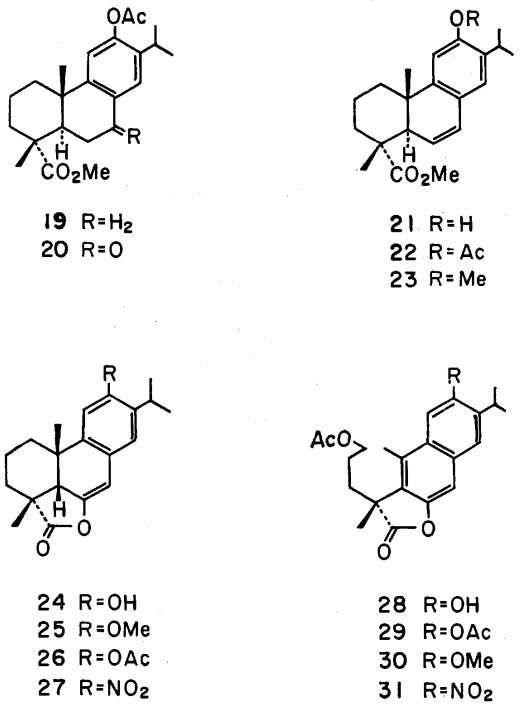

Table 1. The C(1)–C(10) bond cleavage and B ring aromatization of γ-lactones

γ-Lactone	Refluxing time/h	Product	Yield/%
2	3	**17**	47
24	1	**28**+**29**	27
25	1	**30**	32
26	1.5	**29**	42
27	2	**31**	16[a]

a) 64% of **27** was recovered.

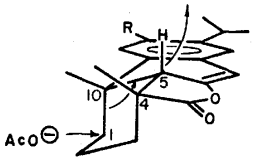

32

Experimental

All melting points are uncorrected. The IR and optical rotations were measured in chloroform, and the ^{1}H NMR spectra in carbon tetrachloride at 90 MHz, with tetramethylsilane as an internal standard, unless otherwise stated. The

chemical shifts are presented in terms of δ values; s: singlet, bs: broad singlet, d: doublet, bd: broad doublet, dd: double doublet, t: triplet, dt: double triplet, m: multiplet. The low-resolution mass spectra were obtained by direct inlet (ion-source temperature 200 °C and ionizing voltage 70 eV). The column chromatography was performed using Merck silica gel (0.063 mm).

6-Hydroxy-5βH-abieta-6,8,11,13-tetraen-18-oic Acid 18,6-Lactone (2). A solution of perbenzoic acid[17] (38.5 mmol) in chloroform (110 ml) was added to a solution of methyl abieta-6,8,11,13-tetraen-18-oate (**3**)[6] (10.8 g, 34.6 mmol) in chloroform (80 ml) at room temperature. After standing at room temperature for 24 h, the solution was diluted with ether (500 ml), and washed successively with aqueous potassium iodide, aqueous sodium thiosulfate, aqueous sodium hydrogencarbonate, and brine. The organic solution was dried over sodium sulfate and evaporated *in vacuo* to give yellowish brown oil (13.2 g).

This oil (13.2 g) was immediately refluxed with *p*-toluenesulfonic acid monohydrate (5.6 g) in toluene (260 ml) for 3 h, cooled, and diluted with ether (250 ml). The solution was washed successively with aqueous sodium hydrogencarbonate and brine, dried over sodium sulfate, and evaporated *in vacuo*. The residual brown oil (10.5 g) was crystallized from hexane to afford **2** (6.4 g) as colorless needles, mp 106—107 °C. The mother liquor of crystallization was evaporated and the residue was chromatographed on silica gel (410 g), using hexane–benzene (1:1) as the eluent, to give some additional **2**, which was crystallized from hexane to give colorless crystals (0.9 g), mp 105—106 °C. The total yield was 70%. Further crystallization gave an analytical sample; mp 106.5—107 °C; $[\alpha]_D$ −116° (*c* 1.54); IR: 1800, 1692 cm^{-1}; ^1H NMR: 1.22 (6H, d, J=7 Hz, $-CH(C\underline{H}_3)_2$), 1.46 and 1.52 (each 3H and s, C_4-CH_3 and $C_{10}-CH_3$), 2.65 (1H, d, J=2.5 Hz, $C_{5\beta}-H$), 2.80 (1H, m, $-C\underline{H}(CH_3)_2$), 5.96 (1H, d, J=2.5 Hz, C_7-H), 6.78 (1H, d, J=2 Hz, $C_{14}-H$), 6.89 (1H, dd, J=8 and 2 Hz, $C_{12}-H$), 7.08 (1H, d, J=8 Hz, $C_{11}-H$); UV: λ_{max}^{EtOH} 271 nm (log ε 4.07), 277 (4.07). Found: C, 80.89; H, 8.19%. Calcd for $C_{20}H_{24}O_2$: C, 81.04; H, 8.16%.

Catalytic Hydrogenation of 2. A mixture of **2** (5.93 g) and PtO_2 (600 mg) in acetic acid (180 ml) was submitted to catalytic hydrogenation with 1 atm hydrogen pressure at room temperature for *ca.* 100 min. After the usual work-up, the crude product was treated with an ethereal diazomethane solution at room temperature for several hours. The solvent was evaporated *in vacuo* and the residue was chromatographed on silica gel (300 g), using hexane–benzene (1:1) at the eluent, to give methyl 5β*H*-abieta-8,11,13-trien-18-oate (**4**)[8] (3.10 g: 49%); $[\alpha]_D$ −79° (*c* 7.35); IR: 1725 cm^{-1}; ^1H NMR: 1.21 (6H, d, J=7 Hz, $-CH(C\underline{H}_3)_2$), 1.31 (6H, s, C_4-CH_3 and $C_{10}-CH_3$), 3.24 (3H, s, $-CO_2CH_3$), 6.76 (1H, bs, $C_{14}-H$), 6.89 (1H, dd, J=8 and 2 Hz, $C_{12}-H$), 7.08 (1H, d, J=8 Hz, $C_{11}-H$); ^1H NMR in $CDCl_3$: 1.22 (6H, d, J=7 Hz, $-CH(C\underline{H}_3)_2$), 1.38 (6H, s, C_4-CH_3 and $C_{10}-CH_3$), 3.42 (3H, s, $-CO_2CH_3$). Found: C, 80.50; H, 9.78%. Calcd for $C_{21}H_{30}O_2$: C, 80.21; H, 9.62%.

Subsequent elution with ether–benzene (1:99) afforded 6β-hydroxy-5β*H*-abieta-8,11,13-trien-18-oic acid 18,6β-lactone (**6**), which was recrystallized from hexane to give colorless crystals (29 mg: 0.5%); mp 133—134 °C; $[\alpha]_D$ −90° (*c* 0.335); IR: 1760 cm^{-1}; ^1H NMR: 1.22 (6H, d, J=7 Hz, $-CH(C\underline{H}_3)_2$), 1.41 (6H, s, C_4-CH_3 and $C_{10}-CH_3$), 1.77 (1H, d, J=11 Hz, $C_{5\beta}-H$), 2.80 (1H, m, $-C\underline{H}(CH_3)_2$), 2.88 (1H, dd, J=15 and 11 Hz, $C_{7\beta}-H$), 3.18 (1H, dd, J=15 and 5 Hz, $C_{7\alpha}-H$), 4.38 (1H, dt, J=11 and 5 Hz, $C_{6\alpha}-H$), 6.87 (1H, bs, $C_{14}-H$), 6.97 (1H, dd, J=8 and 2 Hz, $C_{12}-H$), 7.07 (1H, d, J=8 Hz, $C_{11}-H$). Found: C, 80.76; H, 8.87%. Calcd for $C_{20}H_{26}O_2$: C, 80.49; H, 8.78%.

Further elution with the same solvent afforded 6α-hydroxy-5β*H*-abieta-8,11,13-trien-18-oic acid 18,6α-lactone (**5**), which was recrystallized from hexane to give colorless crystals (1.80 g: 30%); mp 109—109.5 °C; $[\alpha]_D$ −45° (*c* 1.21); IR: 1758 cm^{-1}; ^1H NMR: 1.18 and 1.29 (each 3H and s, $C_{10}-CH_3$ and C_4-CH_3), 1.24 (6H, d, J=7 Hz, $-CH(C\underline{H}_3)_2$), 2.21 (1H, d, J=8.5 Hz, $C_{5\beta}-H$), 2.83 (1H, m, $-C\underline{H}(CH_3)_2$), 3.06 (2H, d, J=4 Hz, C_7-H_2), 4.88 (1H, dt, J=8.5 and 4 Hz, $C_{6\beta}-H$), 6.9—7.1 (3H, m, $C_{11}-H$, $C_{12}-H$, and $C_{14}-H$). Found: C, 80.45; H, 8.88%. Calcd for $C_{20}H_{26}O_2$: C, 80.49; H, 8.78%.

Methanolysis of 2. A mixture of **2** (297 mg) and concentrated hydrochloric acid (0.15 ml) in methanol (15 ml) was refluxed for 1 h, and evaporated *in vacuo*. The residue was dissolved in ether and the ether solution was successively washed with sodium hydrogencarbonate and brine. After drying over sodium sulfate, the solvent was evaporated *in vacuo* and the residue was chromatographed on silica gel (33 g), using benzene as the eluent, to give the starting **2** (15 mg: 5%). Further elution with ether–benzene (1:99) gave methyl 6-oxo-5β*H*-abieta-8,11,13-trien-18-oate (**8**) (265 mg: 81%), which was recrystallized from hexane; mp 126—127 °C; $[\alpha]_D$ +36° (*c* 2.59); IR: 1723, 1700 cm^{-1}; ^1H NMR: 1.09 and 1.18 (each 3H and s, $C_{10}-CH_3$ and C_4-CH_3), 1.23 (6H, d, J=7 Hz, $-CH(C\underline{H}_3)_2$), 2.04 (1H, s, $C_{5\beta}-H$), 2.82 (1H, m, $-C\underline{H}(CH_3)_2$), 2.90 (3H, s, $-CO_2CH_3$), 3.44 (2H, s, C_7-H_2), 6.84 (1H, bs, $C_{14}-H$), 6.99 (1H, dd, J=8 and 2 Hz, $C_{12}-H$), 7.12 (1H, d, J=8 Hz, $C_{11}-H$). Found: C, 76.50; H, 8.56%. Calcd for $C_{21}H_{28}O_3$: C, 76.79; H, 8.59%.

Methyl 6-Oxoabieta-8,11,13-trien-18-oate (9). Chromatographic purification of the crude oxidation product of **3** with perbenzoic acid afforded **9** in *ca.* 30% yield; $[\alpha]_D$ +156° (*c* 1.93); IR: 1720, 1705 cm^{-1}; ^1H NMR: 1.18 (3H, s, $C_{10}-CH_3$), 1.24 (6H, d, J=7 Hz, $-CH(C\underline{H}_3)_2$), 1.44 (3H, s, C_4-CH_3), 2.87 (1H, m, $-C\underline{H}(CH_3)_2$), 3.15 (1H, s, $C_{5\alpha}-H$), 3.52 (2H, s, C_7-H_2), 3.58 (3H, s, $-CO_2CH_3$), 6.90 (1H, bs, $C_{14}-H$), 7.01 (1H, bd, J=8 Hz, $C_{12}-H$), 7.17 (1H, d, J=8 Hz, $C_{11}-H$). Found: C, 76.80; H, 8.38%. Calcd for $C_{21}H_{28}O_3$: C, 76.79; H, 8.59%.

A mixture of **9** (300 mg) and concentrated hydrochloric acid (0.15 ml) in methanol (15 ml) was refluxed for 1 h. The same work-up as described for the methanolysis of **2** gave an oil (270 mg), whose IR and ^1H NMR spectra showed that it was almost the recovered **9** and did not contain the 5β*H*-epimer (**8**).

Fusion of 2 with Potassium Hydrogensulfate. A mixture of **2** (13.31 g) and potassium hydrogensulfate (91.58 g) was heated at 220 °C for 12 h with stirring under a stream of nitrogen. The mixture was cooled, diluted with water, and extracted with ether. The ether extract was washed successively with aqueous sodium hydrogencarbonate and brine, dried over sodium sulfate, and evaporated *in vacuo* The residue was chromatographed on silica gel (800 g), using hexane–benzene (3:2) as the eluent, to give a mixture of naphtho[2,3-*b*]furan-2-one derivatives (3.13 g), whose purification is described later. Subsequent elution with the same solvent recovered the **2** (3.66 g: 27%).

Further elution with ether–benzene (3:97) afforded bis-[3-(2,3-dihydro-7-isopropyl-3,4-dimethyl-2-oxonaphtho[2,3-*b*]furan-3-yl)propyl] ether (**12**) (5.08 g: 37%) as an oil; $[\alpha]_D$ +45° (*c* 1.59); IR: 1780, 1635 cm^{-1}; ^1H NMR: *ca.* 1.1 (4H, m, $2\text{-}CH_2C\underline{H}_2CH_2O-$), 1.31 (12H, d, J=7 Hz, $2\text{-}CH(C\underline{H}_3)_2$), 1.58 (6H, s, $2C_3-CH_3$), *ca.* 2.1 (4H, m, $2\text{-}C\underline{H}_2CH_2CH_2O-$), 2.59 (6H, s, $2C_4-CH_3$), 3.00 (2H, m, 2-

C<u>H</u>$(CH_3)_2$), 3.07 (4H, t, J=6 Hz, 2-$CH_2CH_2C\underline{H}_2O$–), 7.13 (2H, s, $2C_9$–H), 7.26 (2H, dd, J=9 and 2 Hz, $2C_6$–H), 7.47 (2H, d, J=2 Hz, $2C_8$–H), 7.83 (2H, d, J=9 Hz, $2C_5$–H); MS (*m/e*): 606 (M^+); UV: λ_{max}^{EtOH} 235 nm (log ε 5.14), 271sh (4.05), 281.5 (4.08), 292sh (3.93), 312 (3.29), 326.5 (3.36). Found: C, 79.24; H, 7.81%. Calcd for $C_{40}H_{46}O_5$: C, 79.17; H, 7.64%.

The above mixture of naphtho[2,3-*b*]furan-2-one derivatives (3.13 g) was further purified by repeated column chromatography on silica gel.

The less polar fraction gave (*R*)-2,3-dihydro-7-isopropyl-3,4-dimethyl-3-propylnaphtho[2,3-*b*]furan-2-one (**10**) (0.80 g: 6%), which was recrystallized from hexane; mp 130—130.5 °C, $[\alpha]_D$ +81° (*c* 1.52); IR: 1798, 1642, 1595, 1508 cm^{-1}; UV: λ_{max}^{EtOH} 235.5 nm (log ε 4.80), 281.5 (3.76), 293sh (3.63), 312 (3.07), 320sh (2.90), 327 (3.08): ^1H NMR: 0.7—1.25 (5H, m, $-CH_2C\underline{H}_2C\underline{H}_3$), 1.32 (6H, d, J=7 Hz, $-CH(C\underline{H}_3)_2$), 1.59 (3H, s, C_3–CH_3), *ca.* 2.05 (2H, m, $-C\underline{H}_2CH_2CH_3$), 2.61 (3H, s, C_4–CH_3), 7.20 (1H, s, C_9–H), 7.26 (1H, dd, J=8.5 and 2 Hz, C_6–H), 7.50 (1H, d, J=2 Hz, C_8–H), 7.82 (1H, d, J=8.5 Hz, C_5–H; 18% NOE enhancement was observed on irradiation of the signal at δ 2.61); MS (*m/e*): 296 (M^+). Found: C, 81.21; H, 8.18%. Calcd for $C_{20}H_{24}O_2$: C, 81.04; H, 8.16%.

The more polar fraction gave (*R*)-3-allyl-2,3-dihydro-7-isopropyl-3,4-dimethylnaphtho[2,3-*b*]furan-2-one (**11**) (0.83 g: 6%), which was recrystallized from hexane; mp 118—119 °C; $[\alpha]_D$ +130° (*c* 1.25); IR: 1792, 1633, 987, 910 cm^{-1}; ^1H NMR: 1.35 (6H, d, J=6.5 Hz, $-CH(C\underline{H}_3)_2$), 1.64 (3H, s, C_3–CH_3), 2.67 (3H, s, C_4–CH_3), 2.79 (2H, d, J=6.5 Hz, $-C\underline{H}_2CH{=}CH_2$), 3.04 (1H, m, $-C\underline{H}(CH_3)_2$), 4.75—5.60 (3H, m, $-CH_2C\underline{H}{=}C\underline{H}_2$), 7.22 (1H, s, C_9–H), 7.29 (1H, dd, J=9 and 2 Hz, C_6–H), 7.52 (1H, d, J=2 Hz, C_8–H), 7.86 (1H, d, J=9 Hz, C_5–H; 18% NOE enhancement was observed on irradiation of the signal at δ 2.67). Found: C, 81.64; H, 7.61%. Calcd for $C_{20}H_{22}O_2$: C, 81.60; H, 7.53%.

Catalytic Hydrogenation of ***11***. A mixture of **11** (122 mg) and 5% Pd–C (25 mg) in methanol (6.0 ml) was subjected to catalytic hydrogenation at room temperature. After the usual work-up, the crude product was recrystallized from hexane to give a dihydro derivative (95 mg: 77%), mp 129—130 °C, whose IR and ^1H NMR spectra were identical with those of **10**.

*(R)-7-Isopropyl-2-methoxy-3-(1-methoxycarbonyl-1-methylbutyl)-4-methylnaphthalene (**13**).* Dimethyl sulfate (7.5 ml) and 50% aqueous potassium hydroxide (15.5 ml) were added to a stirred solution of **10** (119 mg) in refluxing acetone (15 ml) over a period of 63 min. After addition of acetone (6.0 ml), the mixture was further refluxed for 90 min, diluted with water, neutralized with dilute hydrochloric acid, and then extracted with ether. The ether extract was washed with water, dried over sodium sulfate, and evaporated *in vacuo*. The residue was chromatographed on silica gel (20 g), using benzene as the eluent, to give **13** (68 mg: 50%) as an oil; $[\alpha]_D$ −31° (*c* 1.44); IR: 1725, 1627, 1605 cm^{-1}; ^1H NMR: 0.88 (3H, t, J=6.5 Hz, $-CH_2CH_2C\underline{H}_3$), *ca.* 1.25 (2H, m, $-CH_2C\underline{H}_2CH_3$), 1.30 (6H, d, J=7 Hz, $-CH(C\underline{H}_3)_2$), 1.67 (3H, s, C_3–$\underset{|}{\overset{|}{C}}CH_3$), *ca.* 2.05 (2H, m, C_3–$\underset{|}{\overset{|}{C}}C\underline{H}_2$–), 2.63 (3H, s, C_4–CH_3), 2.98 (1H, m, $-C\underline{H}(CH_3)_2$), 3.53 (3H, s, $-CO_2CH_3$), 3.78 (3H, s, $-OCH_3$), 6.86 (1H, s, C_1–H; 28% NOE enhancement was observed on irradiation of the signal at δ 3.78), 7.14 (1H, dd, J=9 and 2 Hz, C_6–H), 7.37 (1H, d, J=2 Hz, C_8–H), 7.83 (1H, d, J=9 Hz, C_5–H; 22% NOE enhancement was observed on irradiation of the signal at δ 2.63). Found: C, 76.97; H, 8.81%. Calcd for $C_{22}H_{30}O_3$: C, 77.15; H, 8.83%.

*(R)-2,3-Dihydro-7-isopropyl-3,4-dimethyl-3-(3-tosyloxypropyl)-naphtho[2,3-b]furan-2-one (**14**).* A solution of **12** (330 mg) in 1,1,2,2-tetrachloroethane (5.0 ml) was added to *p*-toluenesulfonic acid which was prepared from the monohydrate (270 mg) and 1,1,2,2-tetrachloroethane (5.0 ml) by azeotropic distillation. The mixture was stirred at 160 °C for 12 h under a stream of nitrogen, cooled, and diluted with ether. The ether solution was washed with aqueous sodium hydrogencarbonate and brine, dried over sodium sulfate, and evaporated *in vacuo*. The residue was purified by column chromatography on silica gel (55 g), using benzene as the eluent, to give **14** (232 mg: 45%); $[\alpha]_D$ +69° (*c* 2.13); IR: 1795, 1637, 1360, 1172 cm^{-1}; ^1H NMR: *ca.* 1.2 (2H, m, $-CH_2C\underline{H}_2CH_2OTs$), 1.31 (6H, d, J=7 Hz, $-CH(C\underline{H}_3)_2$), 1.54 (3H, s, C_3–CH_3), *ca.* 2.05 (2H, m, $-C\underline{H}_2CH_2CH_2OTs$), 2.33 (3H, s, $-C_6H_4C\underline{H}_3$), 2.57 (3H, s, C_4–CH_3), 3.01 (1H, m, $-C\underline{H}(CH_3)_2$), 3.77 (2H, t, J=6 Hz, $-CH_2CH_2C\underline{H}_2OTs$), 7.14 (2H, d, J=8 Hz, aromatic protons of *p*-tosyl group), 7.16 (1H, s, C_9–H), 7.28 (1H, dd, J=8.5 and 2 Hz, C_6–H), 7.50 (1H, d, J=2 Hz, C_8–H), 7.58 (2H, d, J=8 Hz, aromatic protons of *p*-tosyl group), 7.84 (1H, d, J=8.5 Hz, C_5–H); UV: λ_{max}^{EtOH} 234 nm (log ε 4.86), 269.5 (3.80), 273.5 (3.81), 281 (3.80), 293sh (3.65), 312.5 (3.07), 318sh (2.92), 326 (3.10). Found: C, 69.66; H, 6.61%. Calcd for $C_{27}H_{30}O_5S$: C, 69.51; H, 6.48%.

Further elution with ether–benzene (3:97) gave the recovered **12** (117 mg: 34%).

*(R)-2,3-Dihydro-3-(3-iodopropyl)-7-isopropyl-3,4-dimethylnaphtho[2,3-b]furan-2-one (**15**).* A mixture of **14** (362 mg), potassium iodide (791 mg), and acetone (13 ml) was refluxed for 5 h in a dark place. After the solvent had been evaporated *in vacuo*, the residue was mixed with water, and extracted with ether. The ether extract was washed with water, dried over sodium sulfate, and evaporated *in vacuo*. The residual oil was chromatographed on silica gel (35 g), using hexane–benzene (2:1) as the eluent, to give **15** (291 mg: 89%) as an oil; $[\alpha]_D$ +19° (*c* 2.91); IR: 1790, 1632 cm^{-1}; ^1H NMR: 1.33 (6H, d, J=7 Hz, $-CH(C\underline{H}_3)_2$), *ca.* 1.4 (2H, m, $-CH_2C\underline{H}_2CH_2I$), 1.64 (3H, s, C_3–CH_3), *ca.* 2.2 (2H, m, $-C\underline{H}_2CH_2CH_2I$), 2.69 (3H, s, C_4–CH_3), 3.03 (2H, t, J=6 Hz, $-CH_2CH_2C\underline{H}_2I$), 3.03 (1H, m, $-C\underline{H}(CH_3)_2$), 7.18 (1H, s, C_9–H), 7.27 (1H, dd, J=8 and 2 Hz, C_6–H), 7.49 (1H, d, J=2 Hz, C_8–H), 7.82 (1H, d, J=8 Hz, C_5–H).

Reaction of ***15*** *with Potassium* t*-Butoxide in Dimethyl Sulfoxide.* A solution of potassium *t*-butoxide (560 mg) in dimethyl sulfoxide (5.0 ml) was added to a stirred solution of **15** (200 mg) in dry benzene (3.0 ml). After being stirred overnight at room temperature under a stream of nitrogen, the mixture was diluted with water, acidified with dilute hydrochloric acid, and extracted with ether. The ether extract was washed with water, dried over sodium sulfate, and evaporated *in vacuo*. The residue was chromatographed on silica gel (20 g), using hexane–benzene (1:2) as the eluent, to give a solid (9 mg: 6%) whose IR and ^1H NMR spectra were identical with those of **11**.

Subsequent elution with ether–benzene (1:3) yielded (*R*)-2,3-dihydro-3-(3-hydroxypropyl)-7-isopropyl-3,4-dimethylnaphtho[2,3-*b*]furan-2-one (**16**) (37 mg: 25%); $[\alpha]_D$ +50° (*c* 0.875); IR: 3620, 3450br, 1795, 1637 cm^{-1}; ^1H NMR: *ca.* 1.1 (2H, m, $-CH_2C\underline{H}_2CH_2OH$), 1.32 (6H, d, J=7 Hz, $-CH(C\underline{H}_3)_2$), 1.59 (3H, s, C_3–CH_3), 1.82 (1H, bs, –OH; disappeared with D_2O), *ca.* 2.1 (2H, m, $-C\underline{H}_2CH_2CH_2OH$), 2.61 (3H, s, C_4–CH_3), 3.02 (1H, m, $-C\underline{H}(CH_3)_2$), 3.33 (2H, t, J=6 Hz, $-CH_2CH_2C\underline{H}_2OH$), 7.21 (1H, s, C_9–H), 7.27 (1H, dd, J=9 and 2 Hz, C_6–H), 7.51 (1H, d, J=2 Hz,

C_8–H), 7.84 (1H, d, J=9 Hz, C_5–H). Found: C, 77.17; H, 7.93%, Calcd for $C_{20}H_{24}O_3$: C, 76.89; H, 7.74%.

*(R)-3-(3-Acetoxypropyl)-2,3-dihydro-7-isopropyl-3,4-dimethylnaphtho[2,3-b]furan-2-one (**17**).* A mixture of **16** (67 mg), acetic anhydride (0.13 ml), and pyridine (0.34 ml) was allowed to stand overnight at room temperature. After the usual work-up, the crude product was purified by column chromatography on silica gel (7.0 g), using benzene as the eluent, to give **17** (70 mg: 92%) as an oil; $[\alpha]_D$ +11° (c 3.75); IR: 1797, 1730, 1640 cm^{-1}; ^1H NMR: *ca.* 1.2 (2H, m, $-CH_2C\underline{H}_2CH_2OAc$), 1.33 (6H, d, J=7 Hz, $-CH(C\underline{H}_3)_2$), 1.62 (3H, s, C_3–CH_3), 1.91 (3H, s, $-OCOCH_3$), *ca.* 2.1 (2H, m, $-C\underline{H}_2CH_2CH_2OAc$), 2.62 (3H, s, C_4–CH_3), 3.01 (1H, m, $-C\underline{H}(CH_3)_2$), 3.83 (2H, t, J=6 Hz, $-CH_2CH_2C\underline{H}_2OAc$), 7.20 (1H, s, C_9–H), 7.26 (1H, dd, J=8 and 2 Hz, C_6–H), 7.49 (1H, d, J=2 Hz, C_8–H), 7.81 (1H, d, J=8 Hz, C_5–H); UV: λ_{max}^{EtOH} 235.5 nm (log ε 4.83), 281.5 (3.78), 293sh (3.62), 313 (2.95), 327 (3.03). Found: C, 74.51; H, 7.46%. Calcd for $C_{22}H_{26}O_4$: C, 74.55; H, 7.39%.

*Reaction of **2** with Concentrated Sulfuric Acid in Toluene.* A stirred mixture of **2** (297 mg), concentrated sulfuric acid (0.33 ml), and toluene (6.0 ml) was refluxed for 2 h. The mixture was cooled, diluted with water, and extracted with ether, The ether extract was washed successively with brine, aqueous sodium hydrogencarbonate, and brine. After drying over sodium sulfate, the solvent was evaporated *in vacuo* and the residue was purified by column chromatography on silica gel (31 g), using benzene as the eluent, to give an oil (78 mg: 17%) whose IR and ^1H NMR spectra were identical with those of **14**.

*Reaction of **2** with Concentrated Sulfuric Acid in Acetic Acid.* A stirred mixture of **2** (148 mg) and concentrated sulfuric acid (0.75 ml) in acetic acid (7.5 ml) was refluxed for 3 h. The reaction mixture was cooled, diluted with water, and extracted with ether. The ether extract was washed successively with water, aqueous sodium hydrogencarbonate, and brine. After drying over sodium sulfate, the solvent was evaporated *in vacuo*. The residue was chromatographed on silica gel (16 g), using benzene as the eluent, to give an oil (83 mg: 47%) whose IR and ^1H NMR spectra were identical with those of **17**.

*Hydrolysis of **17**.* A mixture of **17** (354 mg) and concentrated hydrochloric acid (0.5 ml) in methanol (14 ml) was refluxed for 1 h. After the solvent had been evaporated *in vacuo*, the residue was diluted with water and extracted with ether. The ether extract was washed successively with aqueous sodium hydrogencarbonate and brine, dried over sodium sulfate, and evaporated *in vacuo* to give an oil (306 mg) whose IR and ^1H NMR spectra were identical with those of **16**.

*Reaction of **16** with p-Toluenesulfonyl Chloride.* A mixture of **16** (320 mg) and *p*-toluenesulfonyl chloride (229 mg) in pyridine (1.6 ml) was allowed to stand overnight at room temperature. After the usual work-up, the crude product was chromatographed on silica gel (32 g), using hexane–benzene (1:1) as the eluent, to give (*R*)-3-(3-chloropropyl)-2,3-dihydro-7-isopropyl-3,4-dimethylnaphtho[2,3-*b*]furan-2-one (**18**) (44 mg: 13%), which was recrystallized from hexane; mp 63—65.5 °C; $[\alpha]_D$ +10° (c 0.965); ^1H NMR: *ca.* 1.4 (2H, m, $-CH_2C\underline{H}_2CH_2Cl$), 1.33 (6H, d, J=7 Hz, $-CH(C\underline{H}_3)_2$), 1.63 (3H, s, C_3–CH_3), *ca.* 2.25 (2H, m, $-C\underline{H}_2CH_2CH_2Cl$), 2.64 (3H, s, C_4–CH_3), 3.02 (1H, m, $-C\underline{H}(CH_3)_2$), 3.35 (2H, t, J=6 Hz, $-CH_2CH_2C\underline{H}_2Cl$), 7.20 (1H, s, C_9–H), 7.26 (1H, dd, J=9 and 2 Hz, C_6–H), 7.48 (1H, d, J=2 Hz, C_8–H), 7.82 (1H, d, J=9 Hz, C_5–H); MS (*m/e*): 332 (M^++2), 330 (M^+). Found: C, 72.84; H, 7.30%. Calcd for $C_{20}H_{23}O_2Cl$: C, 72.61; H, 7.01%.

Subsequent elution with benzene afforded a tosylate (228 mg: 49%) whose IR and ^1H NMR spectra were identical with those of **14**.

Further elution with ether–benzene (15:85) recovered some of the **16** (32 mg: 10%).

*(R)-3-(3-Chloropropyl)-2,3-dihydro-7-isopropyl-3,4-dimethylnaphtho[2,3-b]furan-2-one (**18**).* A mixture of **16** (312 mg) and triphenylphosphine (290 mg) in carbon tetrachloride (2.0 ml) was refluxed for 4 h. The solvent was removed *in vacuo* and the residue was purified by column chromatography on silica gel (55 g), using hexane–benzene (1:1) as the eluent, to give a solid (275 mg: 83%) whose IR and ^1H NMR spectra were identical with those of **18**.

*Methyl 12-Acetoxyabieta-6,8,11,13-tetraen-18-oate (**22**).* A solution of chromium trioxide (30 g) in 80% aqueous acetic acid (150 ml) was added dropwise to a stirred solution of methyl 12-acetoxyabieta-8,11,13-trien-18-oate (**19**)[13,14] (37.2 g) in acetic acid (560 ml) at 20—25 °C over a period of 1 h. The mixture was stirred at this temperature for 18 more h, poured into water, and extracted with chloroform. The chloroform extract was washed successively with aqueous sodium hydrogencarbonate and brine, dried over sodium sulfate, and evaporated *in vacuo* to give methyl 12-acetoxy-7-oxoabieta-8,11,13-trien-18-oate (**20**);[15] IR: 1755, 1725, 1678, 1612 cm^{-1}; ^1H NMR: 6.90 (1H, s, C_{11}–H), 7.87 (1H, s, C_{14}–H).

The above crude 7-oxo compound (**20**) (40 g), without purification, was allowed to reduce overnight with sodium borohydride (5.7 g) in methanol (400 ml) at room temperature. After removal of the solvent *in vacuo*, the residue was diluted with water (1.5 l) and acidified with dilute hydrochloric acid. The precipitates were collected, washed with water, and dried at 80—90 °C to yield a mixture of epimeric 7-hydroxy compounds as a solid which, without purification, was used in the next reaction.

This dried solid (36.5 g) in benzene (1.5 l) was refluxed with *p*-toluenesulfonic acid monohydrate (1.8 g) for 2 h. The mixture was concentrated *in vacuo* to a half volume, cooled, and diluted with ether (750 ml). The ether solution was washed successively with aqueous sodium hydrogencarbonate and water, dried over sodium sulfate, and evaporated *in vacuo* to give the crude methyl 12-hydroxyabieta-6,8,11,13-tetraen-18-oate (**21**); IR: 3600, 3330br, 1722 cm^{-1}; ^1H NMR: 2.76 (1H, t, J=2.5 Hz, $C_{5\alpha}$–H), 5.47 and 6.34 (each 1H and dd, J=10 and 2.5 Hz, C_6–H and C_7–H), 6.47 and 6.72 (each 1H and s, C_{11}–H and C_{14}–H).

The crude 12-hydroxy compound (**21**) (32 g) was acetylated with acetic anhydride (32 ml) in pyridine (96 ml) at room temperature for 1 h. After the usual work-up, the crude product was purified by column chromatography on silica gel (350 g), using benzene as the eluent, to give **22** (26.9 g: 73% from **19**) as an oil; $[\alpha]_D$ −19° (c 1.89); IR: 1748, 1715 cm^{-1}; ^1H NMR: 1.08 (3H, s, C_{10}–CH_3), 1.34 (3H, s, C_4–CH_3), 2.22 (3H, s, $-OCOCH_3$), 2.84 (1H, t, J=2.5 Hz, $C_{5\alpha}$–H), 3.60 (3H, s, $-CO_2CH_3$), 5.66 and 6.43 (each 1H and dd, J=10 and 2.5 Hz, C_6–H and C_7–H), 6.68 and 6.89 (each 1H and s, C_{11}–H and C_{14}–H). Found: C, 74.50; H, 8.10%. Calcd for $C_{23}H_{30}O_4$: C, 74.56; H, 8.16%.

*Methyl 12-Methoxyabieta-6,8,11,13-tetraen-18-oate (**23**).* A mixture of the above crude **21** (3.3 g) and potassium *t*-butoxide (1.35 g) in *t*-butyl alcohol (44 ml) was stirred at room temperature for 10 min and methyl iodide (2.82 g) was added dropwise over a 5 min period. The mixture was refluxed for 2 h and evaporated *in vacuo*. The residue was diluted with water, acidified with dilute hydrochloric acid, and extracted with ether. The ether extract was

washed with water, dried over sodium sulfate, and evaporated *in vacuo*. The crude product was chromatographed on silica gel (200 g), using benzene as the eluent, to give **23** (2.4 g: 63% from **19**), which was recrystallized from methanol; mp 73.5—74.5 °C; $[\alpha]_D$ −9.6° (*c* 2.08); IR: 1722 cm^{-1}; ^1H NMR: 1.04 (3H, s, C_{10}–CH_3), 1.15 and 1.18 (each 3H and d, J=7 Hz, $-CH(C\underline{H}_3)_2$), 1.35 (3H, s, C_4–CH_3), 2.79 (1H, t, J=3 Hz, $C_{5\alpha}$–H), 3.21 (1H, m, $-C\underline{H}(CH_3)_2$), 3.60 (3H, s, $-CO_2CH_3$), 3.80 (3H, s, $-OCH_3$), 5.52 and 6.38 (each 1H and dd, J=10 and 3 Hz, C_6–H and C_7–H), 6.57 and 6.78 (each 1H and s, C_{11}–H and C_{14}–H). Found: C, 77.45; H, 9.08%. Calcd for $C_{22}H_{30}O_3$: C, 77.15; H, 8.83%.

*6,12-Dihydroxy-5βH-abieta-6,8,11,13-tetraen-18-oic Acid 18,6-Lactone (**24**).* Oxidation of **22** (45.7 g) in chloroform (340 ml) with a chloroform solution (270 ml) of perbenzoic acid (1.2 mol equivalent) was carried out, followed by refluxing with *p*-toluenesulfonic acid monohydrate (23.4 g) in toluene (1140 ml). This procedure, described for the preparation of **2**, yielded an unstable lactone (**24**) (40.0 g) as a solid. Aliquots of this were recrystallized from benzene; mp 163—165 °C; $[\alpha]_D$ −212° (*c* 0.660); IR: 3600, 3370br, 1794, 1690 cm^{-1}; ^1H NMR: 1.22 (6H, bd, J=7 Hz, $-CH(C\underline{H}_3)_2$), 1.47 (6H, s, C_4–CH_3 and C_{10}–CH_3), 2.62 (1H, d, J=3 Hz, $C_{5\beta}$–H), 3.10 (1H, m, $-C\underline{H}(CH_3)_2$), 5.22 (1H, bs, –OH; disappeared with D_2O), 5.93 (1H, d, J=3 Hz, C_7–H), 6.57 (1H, s, C_{11}–H), 6.71 (1H, s, C_{14}–H); UV: λ_{max}^{EtOH} 286.5 nm (log ε 4.22). Found: C, 77.00; H, 7.68%. Calcd for $C_{20}H_{24}O_3$: C, 76.89; H, 7.74%.

*6-Hydroxy-12-methoxy-5βH-abieta-6,8,11,13-tetraen-18-oic Acid 18,6-Lactone (**25**). a)*: Oxidation of **23** (2.05 g) in chloroform with perbenzoic acid (1.1 mol equivalent), followed by treatment with *p*-toluenesulfonic acid monohydrate (1.14 g) in refluxing toluene, was carried out as described for the preparation of **2**. The crude product was purified by column chromatography on silica gel (70 g), using hexane–benzene (1:1) as the eluent, to afford **25** (1.12 g: 57%) as an oil; $[\alpha]_D$ −101° (*c* 3.40); IR: 1800, 1695 cm^{-1}; ^1H NMR: 1.18 (6H, bd, J=7 Hz, $-CH(C\underline{H}_3)_2$), 1.47 and 1.54 (each 3H and s, C_4–CH_3 and C_{10}–CH_3), 2.65 (1H, d, J=3 Hz, $C_{5\beta}$–H), 3.18 (1H, m, $-C\underline{H}(CH_3)_2$), 3.79 (3H, s, $-OCH_3$), 5.94 (1H, d, J=3 Hz, C_7–H), 6.66 (1H, s, C_{11}–H), 6.74 (1H, s, C_{14}–H). Found: C, 76.97; H, 8.06%. Calcd for $C_{21}H_{26}O_3$: C, 77.27; H, 8.03%.

b): A stirred mixture of the crude **24** (2.44 g), dimethyl sulfate (1.05 ml), anhydrous potassium carbonate (10.8 g), and dry acetone (98 ml) was refluxed for 6 h. After the usual work-up, the crude product was chromatographed on silica gel (350 g), using hexane–benzene (2:3) as the eluent, to give an oil (0.48 g: 19% from **22**) whose IR and ^1H NMR spectra were identical with those of **25**. The compound **25** was so unstable that it converted into a complex mixture during the column chromatography.

*12-Acetoxy-6-hydroxy-5βH-abieta-6,8,11,13-tetraen-18-oic Acid 18,6-Lactone (**26**).* The above crude **24** (20.0 g) was acetylated with acetic anhydride (20 ml) in pyridine (60 ml). After the usual work-up, the product was chromatographed on silica gel (400 g), using benzene as the eluent, to give **26** (15.1 g: 69% from **22**) as an oil; $[\alpha]_D$ −70° (*c* 2.44); IR: 1800, 1758, 1694 cm^{-1}; ^1H NMR: 1.18 (6H, bd, J=7 Hz, $-CH(C\underline{H}_3)_2$), 1.45 and 1.50 (each 3H and s, C_4–CH_3 and C_{10}–CH_3), 2.22 (3H, s, $-OCOCH_3$), 2.67 (1H, d, J=3 Hz, $C_{5\beta}$–H), 2.89 (1H, m, $-C\underline{H}(CH_3)_2$), 5.98 (1H, d, J=3 Hz, C_7–H), 6.76 (1H, s, C_{11}–H), 6.84 (1H, s, C_{14}–H).

*6-Hydroxy-12-nitro-5βH-abieta-6,8,11,13-tetraen-18-oic Acid 18,6-Lactone (**27**).* A mixture of fuming nitric acid (d=1.50: 1.8 ml) and acetic anhydride (3.6 ml) was added dropwise to a stirred solution of **2** (6.0 g) in acetic anhydride (60 ml) at 0—5 °C over a period of 15 min. The mixture was stirred at room temperature for 1 h and then poured into ice–water. The aqueous mixture was stirred for another 30 min and then extracted with ether. The ether extract was washed successively with brine, aqueous sodium hydrogencarbonate, and brine. After being dried over sodium sulfate, the solvent was removed *in vacuo*. The residue was chromatographed on silica gel (350 g), using hexane–benzene (1:1) as the eluent, to give **27** (0.46 g: 7%), which was recrystallized from ethanol; mp 156.5—158 °C; $[\alpha]_D$ −29° (*c* 2.67); IR: 1808, 1690, 1515, 1345 cm^{-1}; ^1H NMR ($CDCl_3$): 1.27 and 1.29 (each 3H and d, J=7 Hz, $-CH(C\underline{H}_3)_2$), 1.55 and 1.62 (each 3H and s, C_4–CH_3 and C_{10}–CH_3), 2.81 (1H, d, J=3 Hz, $C_{5\beta}$–H), 3.48 (1H, m, $-C\underline{H}(CH_3)_2$), 6.15 (1H, d, J=3 Hz, C_7–H), 7.08 (1H, s, C_{14}–H), 7.69 (1H, s, C_{11}–H). Found: C, 70.20; H, 7.08; N, 4.07%. Calcd for $C_{20}H_{23}O_4N$: C, 70.36; H, 6.79; N, 4.10%.

*Reaction of **24** with Concentrated Sulfuric Acid in Acetic Acid.* A mixture of **24** (117 mg), concentrated sulfuric acid (0.61 ml), and acetic acid (5.85 ml) was refluxed for 1 h. After the same work-up as described for the preparation of **17**, the crude product was chromatographed on silica gel (12 g), using ether–benzene (5:95) as the eluent, to give an oil (6 mg: 4%) whose IR and ^1H NMR spectra were identical with those of (*R*)-6-acetoxy-3-(3-acetoxypropyl)-2,3-dihydro-7-isopropyl-3,4-dimethylnaphtho[2,3-*b*]furan-2-one (**29**).

Further elution gave (*R*)-3-(3-acetoxypropyl)-2,3-dihydro-6-hydroxy-7-isopropyl-3,4-dimethylnaphtho[2,3-*b*]furan-2-one (**28**) (32 mg: 23%) as an oil; $[\alpha]_D$ +25° (*c* 2.05); IR: 3600, 3320br, 1793, 1730 cm^{-1}; ^1H NMR: *ca.* 1.2 (2H, m, $-CH_2C\underline{H}_2CH_2OAc$), 1.30 (6H, d, J=7 Hz, $-CH(C\underline{H}_3)_2$), 1.57 (3H, s, C_3–CH_3), *ca.* 2.1 (2H, m, $-C\underline{H}_2CH_2CH_2OAc$), 1.94 (3H, s, $-OCOCH_3$), 2.48 (3H, s, C_4–CH_3), 3.32 (1H, m, $-C\underline{H}(CH_3)_2$), 3.86 (2H, t, J=6.5 Hz, $-CH_2CH_2C\underline{H}_2OAc$), 7.12 (2H, s, C_5–H and C_9–H; 11% NOE enhancement was observed on irradiation of the signal at δ 2.48), 7.43 (1H, s, C_8–H); UV: λ_{max}^{EtOH} 238.5 nm (log ε 4.72), 268.5 (4.00), 279.5 (3.89), 290sh (3.61), 334.5 (3.49), 346.5 (3.57). Found: C, 71.04; H, 7.22%. Calcd for $C_{22}H_{26}O_5$: C, 71.33; H, 7.08%.

The compound **28** (25 mg) was acetylated with acetic anhydride (0.03 ml) in pyridine (0.05 ml) at room temperature for 1 h. After the usual work-up, the crude product was purified by column chromatography on silica gel to give **29** (21 mg); $[\alpha]_D$ +12° (*c* 2.09); IR: 1797, 1753, 1735 cm^{-1}; ^1H NMR: *ca.* 1.2 (2H, m, $-CH_2C\underline{H}_2CH_2OAc$), 1.29 (6H, d, J=7 Hz, $-CH(C\underline{H}_3)_2$), 1.60 (3H, s, C_3–CH_3), 1.91 (3H, s, $-OCOCH_3$), *ca.* 2.1 (2H, m, $-C\underline{H}_2CH_2CH_2OAc$), 2.32 (3H, s, $-OCOCH_3$), 3.05 (1H, m, $-C\underline{H}(CH_3)_2$), 3.83 (2H, t, J=6.5 Hz, $-CH_2CH_2C\underline{H}_2OAc$), 7.20 (1H, s, C_9–H), 7.49 (1H, s, C_5–H), 7.58 (1H, s, C_8–H). Found: C, 70.05; H, 6.98%. Calcd for $C_{24}H_{28}O_6$: C, 69.88; H, 6.84%.

*Reaction of **25** with Concentrated Sulfuric Acid in Acetic Acid.* A mixture of **25** (326 mg), concentrated sulfuric acid (1.48 ml), and acetic acid (16.5 ml) was refluxed for 1 h. After the same work-up as described for the preparation of **17**, the crude product was chromatographed on silica gel (30 g), using ether–benzene (1:99) as the eluent, to give (*R*)-3-(3-acetoxypropyl)-2,3-dihydro-7-isopropyl-6-methoxy-3,4-dimethylnaphtho[2,3-*b*]furan-2-one (**30**) as an oil (123 mg: 32%); $[\alpha]_D$ +25° (*c* 1.93); IR: 1800, 1740 cm^{-1}; ^1H NMR: *ca.* 1.2 (2H, m, $-CH_2C\underline{H}_2CH_2OAc$), 1.29 (6H, d, J=7 Hz, $-CH(C\underline{H}_3)_2$), 1.61 (3H, s, C_3–CH_3), 1.92 (3H, s, $-OCOCH_3$), *ca.* 2.1 (2H, m, $-C\underline{H}_2CH_2CH_2OAc$), 2.59 (3H,

s, C_4–CH_3), 3.38 (1H, m, –C<u>H</u>$(CH_3)_2$), 3.84 (2H, t, J=6.5 Hz, –$CH_2CH_2C\underline{H}_2OAc$), 3.95 (3H, s, –$OCH_3$), 7.07 (1H, s, C_5–H; 20% and 17% NOE enhancements were observed on irradiation of the signal at δ 2.59 and at δ 3.95 respectively), 7.18 (1H, s, C_9–H), 7.49 (1H, s, C_8–H). Found: C, 71.61; H, 7.35%. Calcd for $C_{23}H_{28}O_5$: C, 71.85; H, 7.34%.

Reaction of ***26*** *with Concentrated Sulfuric Acid in Acetic Acid.* A mixture of **26** (1.50 g), concentrated sulfuric acid (6.80 ml), and acetic acid (110 ml) was refluxed for 1.5 h. After the same work-up as described for the preparation of **17**, the crude product was immediately acetylated with acetic anhydride (1.5 ml) in pyridine (4.0 ml) at room temperature for 1 h. The crude acetate, after the usual work-up, was purified by column chromatography on silica gel (75 g), using ether–benzene (5:95) as the eluent, to afford an oil (0.73 g: 42%) whose IR and ^{1}H NMR spectra were identical with those of **29**.

Reaction of ***27*** *with Concentrated Sulfuric Acid in Acetic Acid.* A mixture of **27** (132 mg), concentrated sulfuric acid (0.58 ml), and acetic acid (6.60 ml) was refluxed for 2 h. After the same work-up as described for the preparation of **17**, the crude product was chromatographed on silica gel (12 g), using hexane–benzene (2:3) as the eluent, to give the recovered **27** (85 mg: 64%).

Further elution with ether–benzene (3:97) afforded (*R*)-3-(3-acetoxypropyl)-2,3-dihydro-7-isopropyl-3,4-dimethyl-6-nitronaphtho[2,3-*b*]furan-2-one (**31**) (25 mg: 16%) as an oil; $[\alpha]_D$ +34° (*c* 0.955); IR: 1808, 1740, 1643, 1533, 1355 cm^{-1}; ^{1}H NMR: *ca.* 1.25 (2H, m, –$CH_2C\underline{H}_2CH_2OAc$), 1.37 (6H, d, J=7 Hz, –$CH(C\underline{H}_3)_2$), 1.65 (3H, s, C_3–CH_3), 1.94 (3H, s, –$OCOCH_3$), *ca.* 2.15 (2H, m, –$C\underline{H}_2CH_2CH_2OAc$), 2.71 (3H, s, C_4–CH_3), 3.55 (1H, m, –C<u>H</u>$(CH_3)_2$), 3.87 (2H, t, J=6.5 Hz, –$CH_2CH_2C\underline{H}_2OAc$), 7.32 (1H, s, C_9–H), 7.74 (1H, s, C_8–H), 8.36 (1H, s, C_5–H; 20% NOE enhancement was observed on irradiation of the signal at δ 2.71); UV: λ_{max}^{EtOH} 227 nm (log ε 4.68), 261 (4.36), 278sh (4.18), 361 (3.96), 410sh (3.51), 430sh (3.40). Found: C, 66.03; H, 6.49; N, 3.40%. Calcd for $C_{22}H_{25}O_6N$: C, 66.15; H, 6.31; N, 3.51%.

The authors are grateful to Arakawa Chemical Co. Ltd. for a generous gift of rosin. This work was partially supported by Grant-in-Aid for Scientific Research No. 56540324 from the Ministry of Education, Science and Culture.

References

1) C. H. Eugster, H.-P. Küng, H. Kühnis, and P. Karrer, *Helv. Chim. Acta*, **46**, 530 (1963).
2) D. Karanatsios and C. H. Eugster, *Helv. Chim. Acta*, **48**, 471 (1965).
3) C. H. Eugster, *Ber. Deutsch. Bot. Ges.*, **88**, 141 (1975).
4) T. Matsumoto, S. Imai, K. Ondo, N. Takeyama, and K. Fukui, *Chem. Lett.*, **1980**, 425.
5) A portion of this work was reported in preliminary form: Ref. 4.
6) G. Dupont, R. Dulou, G. Ourisson, and C. Thibault, *Bull. Soc. Chim. Fr.*, **1955**, 708.
7) G. Defaye-Duchateau, *Bull. Soc. Chim. Fr.*, **1964**, 1469.
8) E. Wenkert, A. Afonso, P. Beak, R. W. J. Carney, P. W. Jeffs, and J. D. McChesney, *J. Org. Chem.*, **30**, 713 (1965); E. Wenkert and B. L. Mylari, *ibid.*, **30**, 4387 (1965).
9) S. K. Roy, M. L. Maheshwari, A. C. Rieke, and D. M. S. Wheeler, *J. Org. Chem.*, **37**, 4460 (1972).
10) T. Matsumoto and S. Usui, *Chem. Lett.*, **1978**, 105.
11) R. C. Cambie and R. A. Franich, *Aust. J. Chem.*, **24**, 571 (1971).
12) See Experimental section.
13) R. C. Cambie and R. A. Franich, *Aust. J. Chem.*, **24**, 117 (1971).
14) A. Tahara, M. Shimagaki, M. Itoh, Y. Harigaya, and M. Onda, *Chem. Pharm. Bull.*, **23**, 3189 (1975).
15) A. Tahara, H. Akita, and Y. Ohtsuka, *Chem. Pharm. Bull.*, **22**, 1547 (1974).
16) H. P. Leftin, "Carbonium Ions," ed by G. H. Olah and P. R. Schleyer, J. Wiley & Sons, New York (1968), Vol. I, Chap. 10, p. 389. The evolution of sulfur dioxide during the reaction with **2** was confirmed by the consumption of potassium permanganate.
17) G. Braun, *Org. Synth.*, Coll. Vol. I, 431 (1941).

 © 1982 The Chemical Society of Japan Bull. Chem. Soc. Jpn., 55, 899—903 (1982)

Synthesis and Stereochemistry of Hypusine, a New Amino Acid in Bovine Brain.[1]

Tetsuo SHIBA,* Hitoshi AKIYAMA, Isao UMEDA, Satoshi OKADA, and Tateaki WAKAMIYA

Department of Chemistry, Faculty of Science, Osaka University, Toyonaka, Osaka 560

(Received July 25, 1981)

Hypusine, a new basic amino acid occurring in the homogenate of bovine brain tissue, was synthesized to determine the absolute structure. N^{α}-Benzyloxycarbonyl-L-lysine benzyl ester was coupled with (*S*)- or (*R*)-4-benzyloxycarbonylamino-1-bromo-2-butanol derived from L- or D-malic acid, respectively. The products were deprotected by catalytic hydrogenation. One of the synthetic compounds, *i.e.*, (2*S*,9*R*)-2,11-diamino-9-hydroxy-7-azaundecanoic acid, was completely identical with natural hypusine in all respects.

Hypusine (**1**) had been isolated from bovine brain and its unique structure was determined chemically and spectrometrically to be 2,11-diamino-9-hydroxy-7-azaundecanoic acid.[2] The term of hypusine came from hydroxyputrescine and lysine as composite moieties which joined together by an elimination of ammonia as shown in Fig. 1. Of the two asymmetric carbon atoms in hypusine molecule, the configuration of *C*-2 corresponding to α-carbon atom of lysine had been decided to be of L(*S*) form. This conclusion was given by the fact that periodic acid–permanganate oxidation of hypusine afforded L-lysine.[2] On the other hand, the configuration of *C*-9 in hydroxyputrescine moiety could not be ascertained yet. To clarify the stereochemistry of this carbon atom, we attempted to synthesize two possible isomers, namely (2*S*,9*S*)- and (2*S*,9*R*)-2,11-diamino-9-hydroxy-7-azaundecanoic acid.

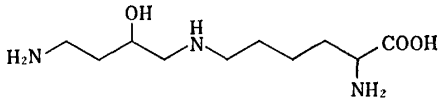

Hypusine (**1**)

Fig. 1. The structure of hypusine.

A principle of the synthesis of this new amino acid is based on the coupling of L-lysine and 4-amino-1-bromo-2-butanol as shown in Scheme 4. Both enantiomers of the latter component can be obtained from L- and D-malic acid, respectively. While L-malic acid was commercially available, D-isomer had to be prepared by optical resolution of the racemic compound with *S*(−)-1-phenylethylamine.

Malic acid (**2**) of either configuration was esterified with diazomethane to give dimethyl ester **3**, which was converted to β-malamic acid (**5**) according to Freudenberg's procedure.[3] Hydrogenation of β-malamic acid (**5**) to 4-amino-1,2-butanediol (**6**) with $LiAlH_4$ failed because of a poor solubility of the acid **5** in ether or THF. However, reduction with diborane could be employed satisfactorily for this purpose. Thus, the suspension of β-malamic acid in THF was heated under reflux with diborane.[4] The product was purified by ion-exchange column chromatography of Dowex 50 W×2 (NH_4^+ form) to isolate the desirable amino alcohol **6**. The amino group of the compound **6** was then protected with benzyloxycarbonyl group to give 4-benzyloxycarbonylamino-1,2-butanediol (**7**).

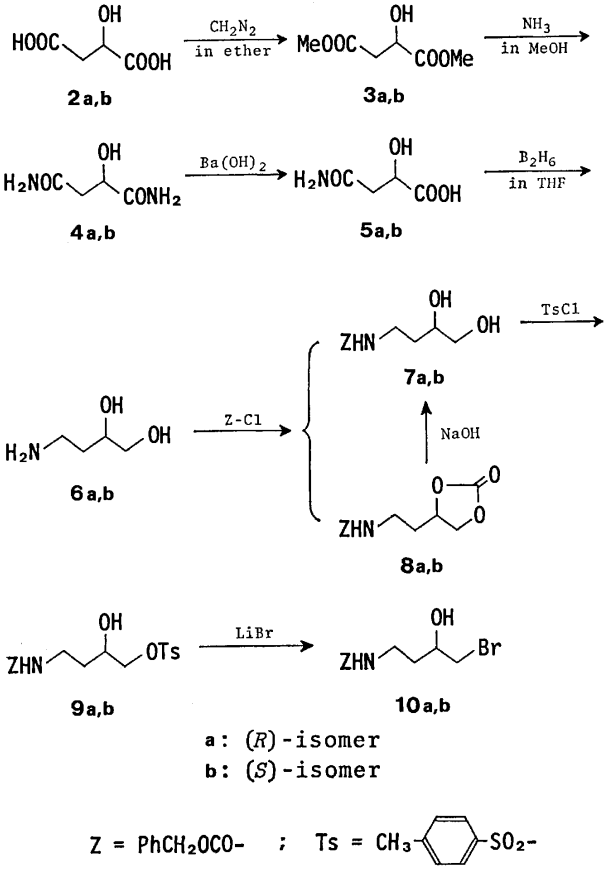

Scheme 1.

Although, a small amount of cyclic carbonate derivative **8** was formed in this reaction as a by-product, the carbonate was quantitatively saponified to **7** giving the total yield of *N*-benzyloxycarbonylation of around 90%. Presumably, benzyloxycarbonylation to primary hydroxyl group occurred in a minor degree and a cyclization through an elimination of benzyl alcohol gave the carbonate **8**.

O-Tosylation of **7** in dichloromethane using pyridine as a base afforded predominantly the primary *O*-tosylate **9** along with formation of the ditosylate as a minor product. *O*-Tosylate **9** was finally converted into 4-benzyloxycarbonylamino-1-bromo-2-butanol (**10**) with LiBr. Thus, we could prepare successfully the carbon unit to construct hydroxyputrescine moiety.

According to this method, two optically active isomers were obtained starting from D- and L-malic acid, respectively.

Parallel to the preparation of optically active **10**, a racemic compound was also synthesized for the preliminary experiment to find out the optimum coupling conditions with lysine residue. The racemic compound **10c** was prepared rather easily from *N*-benzyloxycarbonyl-β-alanine as shown in Scheme 2. Mixed carbonic carboxylic anhydride of *N*-benzyloxycarbonyl-β-alanine (**11**) was allowed to react with diazomethane to give the diazo ketone derivative **12**.[5] The diazo ketone in ether was treated with an equivalent of hydrobromic acid to afford the bromo ketone **13**. Sodium borohydride reduction of **13** gave the racemic bromo alcohol **10c**.

For modification of the lysine moiety to a suitable form for the coupling, L-lysine was first converted to N^{α}-benzyloxycarbonyl-L-lysine (**15**) *via* N^{ε}-benzylidene derivative **14**.[6] Since monoacylated lysine was scarcely soluble in both organic solvents and water, the compound **15** was changed to benzyl ester **16** in the usual way using benzyl alcohol and *p*-toluenesulfonic acid as a catalyst in benzene[7] (Scheme 3).

Coupling reaction of racemic 4-benzyloxycarbonylamino-1-bromo-2-butanol (**10c**) with N^{α}-benzyloxycarbonyl-L-lysine benzyl ester (**16**) was carried out in several organic solvents. The yield of hypusine was estimated by amino acid analysis after hydrogenation of the coupling product without any purification procedure. From the results of this preliminary experiment as shown in Table 1, methanol, ethanol, and *t*-butyl alcohol seemed to be preferable solvents. However, we realized later on that the use of methanol and ethanol caused undesirable ester exchange reaction. This disadvantage could be effectively overcome by employment of *t*-butyl alcohol as a reaction solvent.

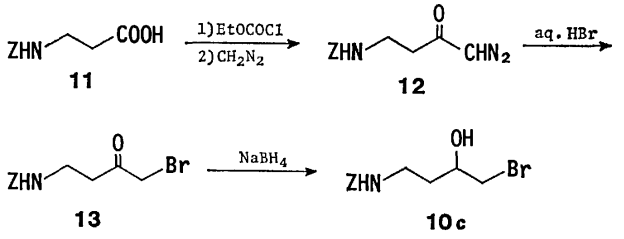

11 12 13 10c

Scheme 2.

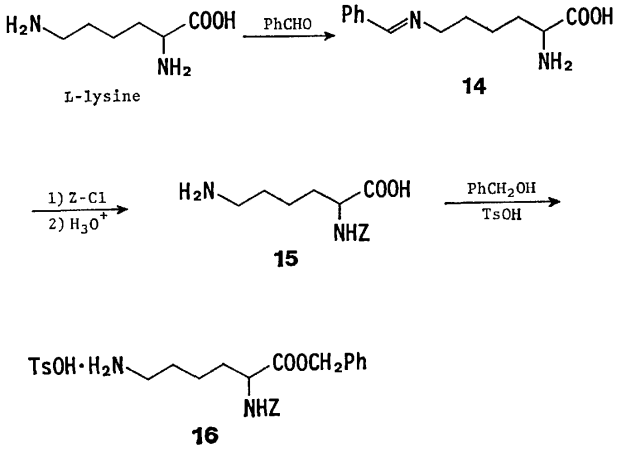

Scheme 3.

Based on the above results, optically active bromo alcohol **10** was condensed with N^{α}-benzyloxycarbonyl-L-lysine benzyl ester *p*-toluenesulfonate (**16**) in *t*-butyl alcohol in the presence of two equivalents of triethylamine.[8] Protecting groups of the coupling product were then removed by catalytic hydrogenation in 50% *t*-butyl alcohol (Scheme 4). Crude hypusine thus obtained was purified by column chromatography of Dowex 50 W×2 (NH_4^+ form) with dilute NH_4OH eluent.

According to the above procedure, both (2*S*,9*S*)- and (2*S*,9*R*)-hypusine were obtained as crystalline dihydrochloride. Several comparisons of synthetic compounds with natural hypusine were achieved physicochemically, chromatographically, and spectrometrically. However, both isomers did not show significant differences in most respects. For example, NMR spectra (Fig. 2) and retention times in amino acid analyses of both synthetic products were virtually identical with those of natural one. Only melting point and

TABLE 1. EXAMINATION OF COUPLING CONDITIONS OF **10c** WITH **16**

Solvent	Base (equiv.)	Temperature	Time d	Yield[a] %
Benzene	TEA[b] (1.0)	reflux	5	0.6
	TEA (2.0)	reflux	5	6.0
	NMM[b] (2.0)	reflux	5	1.0
CH_3CN	TEA (2.0)	reflux	5	6.7
DMF[2]	TEA (2.0)	73 °C	5	11
DMSO[2]	TEA (2.0)	73 °C	5	3.0
Methanol	K_2CO_3 (2.0)	reflux	19 h	11
Ethanol	K_2CO_3 (2.0)	reflux	5	1.0
	TEA (2.0)	reflux	5	20
t-Butyl alcohol	TEA (2.0)	reflux	5	20

a) Yield was obtained by amino acid analysis after hydrogenolysis of the coupling product without any purification. b) Abbreviations: TEA=triethylamine, NMM=*N*-methylmorphorine, DMF=*N*,*N*-dimethylformamide, DMSO=dimethyl sulfoxide.

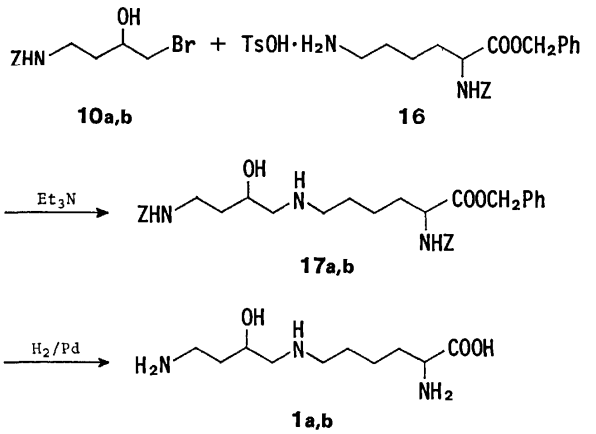

Scheme 4.

specific rotation indicated that the natural compound should be (2*S*,9*R*)-isomer rather than (2*S*,9*S*)-one, though still ambiguously. Fortunately, IR spectra of synthetic compounds showed much difference each other and the spectrum of (2*S*,9*R*)-isomer was completely identical with that of natural hypusine (Fig. 3). Judging from these results thus obtained, we could now determine the absolute structure of hypusine to be (2*S*,9*R*)-2,11-diamino-9-hydroxy-7-azaundecanoic acid.

The total synthesis of hypusine established in this investigation may contribute also to supply an enough amount of the sample of this unique brain amino acid for biological tests.

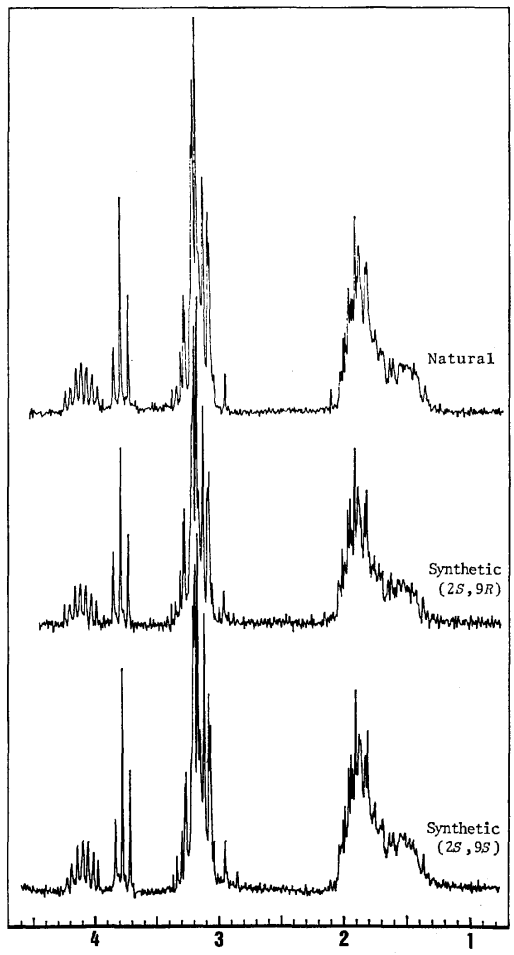

Fig. 2. NMR spectra of natural hypusine and synthetic compounds in D_2O.

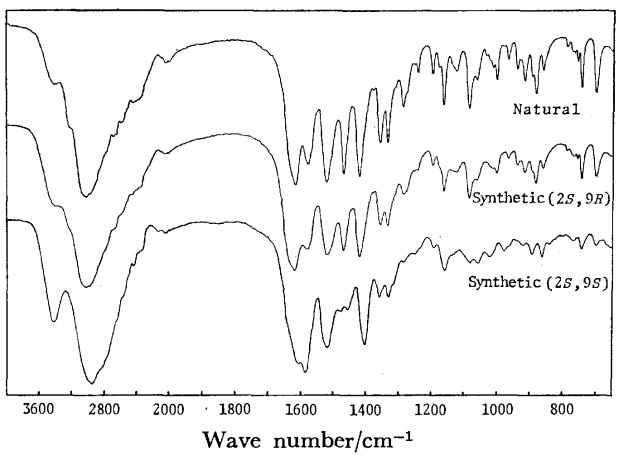

Fig. 3. IR spectra of natural hypusine and synthetic compounds (KBr disk).

Experimental

All melting points are uncorrected. The specific rotations were measured with a Perkin-Elmer 141 polarimeter. NMR spectra were obtained with a Varian XL-100-15 spectrometer and the chemical shifts were given in δ values (ppm) from sodium 2,2-dimethyl-2-silapentane-5-sulfonate (DSS). IR spectra were taken in KBr disk with a Hitachi EPI-G21 spectrophotometer. Amino acid analyses were carried out on a 15 cm column at 55 °C with a Hitachi KLA-3 amino acid analyzer. A buffer solution of 0.7 M (1 M=1 mol dm^{-3}) sodium citrate, pH 5.28, containing 3% NaCl was used for the analysis.

Preparation of D-*Malic Acid by Optical Resolution.* To a solution of DL-malic acid (131 g, 0.98 mol) in 650 ml of water was added *R*(+)-1-phenylethylamine (118 g, 0.98 mol). The mixture was allowed to stand for 2 d and *R*(+)-amine salt of L-malic acid precipitated was filtered off. The filtrate was concentrated *in vacuo* until a small amount of crystals appeared. After allowing to stand overnight, the second precipitate was filtered again. This procedure was repeated three times and the precipitates combined were recrystallized from water.

The filtrate after taking off fourth precipitate and the mother liquor of recrystallization were combined and concentrated *in vacuo*. To the residue was added 310 ml of 4 M NaOH, and then *R*(+)-amine freed was extracted with benzene three times. Aqueous layer was neutralized with 4 M HCl and concentrated *in vacuo*. Solid residue was triturated with acetone several times to extract malic acid and acetone extract was concentrated *in vacuo*. The residue (56 g) was dissolved in 280 ml of water and *S*(−)-1-phenylethylamine (67 g, 0.54 mol) was added. The precipitate of *S*(−)-amine salt of D-malic acid was obtained by the same procedure as mentioned above and crude salt was recrystallized from water. The pure salt (58 g) was dissolved in 120 ml of 4 M NaOH and *S*(−)-amine was extracted with benzene. Aqueous layer was neutralized with 4 M HCl and concentrated *in vacuo*. D-Malic acid was extracted with acetone by the same treatment as mentioned above and recrystallized from anhydrous ether, yield 17 g (13%), mp 97—99 °C,[9] $[\alpha]_D^{14}$ +6.4° (*c* 1.9, acetone).[9] When *S*(−)-1-phenylethylamine was first used for the resolution, actually, optically active D-malic acid in a satisfactorily pure state was not obtained.

*β-Malamic Acid (**5**).* Optically active malic acid dimethyl ester, was converted to β-malamic acid according to Freudenberg's method.[3]

*(R)-4-Amino-1,2-butanediol (**6a**).* Powdered D-β-malamic acid (**5a**) (9.0 g, 0.068 mol) was suspended in 600 ml of anhydrous tetrahydrofuran (THF). To this suspension was introduced diborane, which was generated from boron trifluoride etherate (60 g, 0.42 mol) in diglyme by addition of small portions of sodium borohydride (12.5 g, 0.33 mol) with a gentle stream of nitrogen under cooling in an ice bath. The suspension was then heated under reflux for 3 d and the clear solution obtained was cooled in an ice bath. To the reaction mixture was added water

carefully until no gas generation occurred. The solution was acidified to pH 4 with hydrochloric acid and concentrated *in vacuo*. The residue was dissolved in cold water and insoluble material was filtered off. The filtrate was concentrated *in vacuo* again and the residue was chromatographed on Dowex 50W×2 (200—400 mesh, NH_4^+ form) column, which was first washed with 1 l of water. Elution with 2.8% NH_4OH gave a fraction of positive ninhydrin reaction, which was then concentrated *in vacuo*. (*R*)-4-Amino-1,2-butanediol was obtained as highly hygroscopic oil, yield 4.3 g (61%).

*(S)-4-Amino-1,2-butanediol (**6b**).* L-β-Malamic acid (**5b**) gave (*S*)-amino alcohol **6b** with the same procedure as in the preparation of **6a** in a yield of 56%. A part of (*S*)-amino alcohol was distilled to obtain an analytical sample, bp 172—175 °C/0.10—0.15 mmHg,† $[\alpha]_D^{25}$ −23.0° (*c* 1.87, CH_3OH). Found: C, 41.53; H, 10.40; N, 11.85%. Calcd for $C_4H_{11}NO_2 \cdot 3/5H_2O$: C, 41.43; H, 10.61; N, 12.08%.

*(R)-4-Benzyloxycarbonylamino-1,2-butanediol (**7a**).* To a solution of (*R*)-4-amino-1,2-butanediol (**6a**) (4.20 g, 40.0 mmol) in 20 ml of water and 30 ml of ether were added benzyloxycarbonyl chloride (7.50 g, 44.0 mmol) and 11 ml of 4 M NaOH dropwise with vigorous stirring at 0 °C. After addition of reagents, the reaction mixture was stirred at room temperature overnight and neutralized with 2 M HCl. The product was extracted with ether several times. The extract was dried over magnesium sulfate and concentrated *in vacuo*. Oily residue obtained was purified by silica-gel column chromatography. Elution was carried out with chloroform and methanol (95:5 v/v) to separate (*R*)-4-benzyloxycarbonylamino-1,2-butanediol (**7a**) and its carbonate **8a**. The main product **7a** was recrystallized from chloroform and petroleum ether, yield 7.30 g (76%), mp 67—68 °C, $[\alpha]_D^{22}$ +5.8° (*c* 1.9, $CHCl_3$), and IR 3300 cm^{-1}. Found: C, 60.09; H, 7.15; N, 5.90%. Calcd for $C_{12}H_{17}NO_4$: C, 60.24; H, 7.16; N, 5.85%.

By-product **8a** was recrystallized from ethyl acetate and hexane, yield 1.38 g (13%), mp 36—38 °C, $[\alpha]_D^{22}$ +27.6° (*c* 1.20, AcOEt), and IR 1790 cm^{-1}. Found: C, 59.07; H, 5.73; N, 5.25%. Calcd for $C_{13}H_{15}NO_5$: C, 58.86; H, 5.70; N, 5.28%.

The carbonate **8a** was quantitatively saponified to **7a** in methanol with two equivalents of 2 M NaOH.

*(S)-4-Benzyloxycarbonylamino-1,2-butanediol (**7b**).* The same procedure as in the preparation of **7a** was applied to get (*S*)-isomer (**7b**). Carbonate **8b** was also obtained in 10% yield, mp 37—39 °C, $[\alpha]_D^{25}$ −27.4° (*c* 1.10, AcOEt). Found: C, 58.99; H, 5.72; N, 5.48%. It was quantitatively saponified to **7b** and the total yield of diol **7b** was 80%, mp 66—67 °C, $[\alpha]_D^{25}$ −6.0° (*c* 2.2, $CHCl_3$). Found: C, 59.87; H, 7.13; N, 5.94%.

*(R)-4-Benzyloxycarbonylamino-1-p-tolylsulfonyloxy-2-butanol (**9a**).* (*R*)-4-Benzyloxycarbonylamino-1,2-butanediol (**7a**) (2.00 g, 8.36 mmol) was dissolved in 25 ml of dichloromethane and pyridine (1:1 v/v). To the solution was added *p*-toluenesulfonyl chloride (1.75 g, 9.18 mmol) by portions in 15 min at 5 °C. The reaction mixture was stirred for 21 h at the same temperature. The product was extracted with chloroform several times after an addition of water. The extract was washed with water three times, dried over magnesium sulfate, and concentrated *in vacuo*. Oily residue was chromatographed on silica-gel column. Elution was carried out with benzene–ethyl acetate (9:1 v/v) to separate ditosylate (0.55 g, 12%) and monotosylate **9a** which was recrystallized from ethyl acetate and hexane, yield 2.22 g (68%), mp 68—69 °C, $[\alpha]_D^{22}$ +3.1° (*c* 1.1, AcOEt). Found: C, 57.93; H, 5.97; N, 3.63; S, 8.00%. Calcd for $C_{19}H_{23}NO_6S$: C, 58.00; H, 5.89; N, 3.56; S, 8.15%.

*(S)-4-Benzyloxycarbonylamino-1-p-tolylsulfonyloxy-2-butanol (**9b**).* (*S*)-Monotosylate (**9b**) was prepared similarly to (*R*)-isomer in a yield of 65%, mp 67—69 °C, $[\alpha]_D^{22}$ −3.0° (*c* 1.1, AcOEt). Found: C, 57.69; H, 5.89; N, 3.55; S, 8.14%.

*(R)-4-Benzyloxycarbonylamino-1-bromo-2-butanol (**10a**).* The mixture of (*R*)-monotosylate **9a** (300 mg, 0.76 mmol) and $LiBr \cdot H_2O$ (250 mg, 2.40 mmol) was heated under reflux in 8 ml of acetone for 5 h. Solvent was evaporated *in vacuo* and the residue was dissolved in ethyl acetate. Insoluble material was once filtered off and the filtrate was washed with water several times. Organic layer was dried over magnesium sulfate and concentrated *in vacuo*. Oily residue was chromatographed on silica-gel column using an eluent of benzene–ethyl acetate (4:1 v/v). Bromo alcohol **10a** was obtained in a yield of 95% (220 mg), $[\alpha]_D^{18}$ +15° (*c* 1.6, AcOEt). Found: C, 47.22; H, 5.36; N, 4.62; Br, 26.14%. Calcd for $C_{12}H_{16}NO_3Br$: C, 47.69; H, 5.34; N, 4.64; Br, 26.45%.

*(S)-4-Benzyloxycarbonylamino-1-bromo-2-butanol (**10b**).* (*S*)-Bromo compound **10b** was prepared similarly in a yield of 97%, $[\alpha]_D^{25}$ −15° (*c* 1.7, AcOEt). Found: C, 47.53; H, 5.43; N, 4.56; Br, 26.30%.

*4-Benzyloxycarbonylamino-1-bromo-2-butanone (**13**).* To a solution of *N*-benzyloxycarbonyl-β-alanine (9.4 g, 0.042 mol) in 300 ml of chloroform were added triethylamine (5.8 ml, 0.042 mol) and ethyloxycarbonyl chloride (4.0 ml, 0.042 mol) under cooling in an ice bath. The reaction mixture was stirred for 1 h at 0 °C and then a large amount of anhydrous ether was added to precipitate triethylamine hydrochloride. The precipitate was quickly filtered off and the filtrate was added to an excess of diazomethane in ether which was precooled in an ice bath. The reaction was continued for 1 h at 0 °C. Since a small amount of triethylamine hydrochloride was precipitated again during the reaction, the reaction mixture was once filtered. The filtrate was then warmed at 30 °C to remove unreacted diazomethane and concentrated *in vacuo*. The crude product was purified by silica-gel column chromatography using chloroform as an eluent to give the diazo ketone **12** (5.7 g, 60%).

To a solution of the diazo ketone (1.1 g, 4.5 mmol) in 30 ml of ether was added 0.78 ml of 48% hydrobromic acid (4.5 mmol) dropwise in 1 h under vigorous stirring in an ice bath. After stirring for more 1 h, the reaction mixture was neutralized with aqueous sodium hydrogencarbonate and extracted with ethyl acetate. The extract was dried over magnesium sulfate and concentrated *in vacuo* to obtain 4-benzyloxycarbonylamino-1-bromo-2-butanone (**13**), yield 1.3 g (95%). The crude product was recrystallized from ethanol and petroleum ether, yield 1.0 g (73%), mp 42—43 °C. Found: C, 48.36; H, 4.80; N, 4.84; Br, 26.92%. Calcd for $C_{12}H_{14}NO_3Br$: C, 48.02; H, 4.70; N, 4.67; Br, 26.62%.

*(±)-4-Benzyloxycarbonylamino-1-bromo-2-butanol (**10c**).* 4-Benzyloxycarbonylamino-1-bromo-2-butanone (**13**) (900 mg, 3.0 mmol) was dissolved in methanol and sodium borohydride (38 mg, 1.1 mmol) was added to the solution under cooling in an ice bath. After stirring for 2 h, the reaction mixture was neutralized to pH 7 by an addition of 5% acetic acid and concentrated *in vacuo*. Ethyl acetate was added to the residue and an insoluble material was filtered off. The solution was washed with water, dried over magnesium sulfate, and concentrated *in vacuo*. Oily residue was pu-

† 1 mmHg≈133.322 Pa.

rified by silica-gel column chromatography and racemic 4-benzyloxycarbonylamino-1-bromo-2-butanol (**10c**) was eluted with benzene–ethyl acetate (4:1 v/v) in a quantitative yield (900 mg) as colorless oil. Found: C, 47.55; H, 5.30; N, 4.50; Br, 26.15%. Calcd for $C_{12}H_{16}NO_3Br$: C, 47.69; H, 5.34; N, 4.64; Br, 26.45%.

Coupling Reaction of ***10c*** *and* ***16***. A solution of (±)-4-benzyloxycarbonylamino-1-bromo-2-butanol (**10c**) (30 mg, 0.10 mmol), N^{α}-benzyloxycarbonyl-L-lysine benzyl ester *p*-toluenesulfonate (**16**) (54 mg, 0.10 mmol), and triethylamine (21 mg, 0.20 mmol) in 10 ml of benzene was refluxed for 5 d. The reaction mixture was concentrated *in vacuo*. A solution of the residue in 50% *t*-butyl alcohol, added with 2 M hydrochloric acid, was hydrogenated with Pd catalyst. After the completion of hydrogenation, catalyst was filtered off. The filtrate was concentrated *in vacuo* and the residue was dissolved in water. The solution was applied to an amino acid analysis.

*(2S,9R)-2,11-Diamino-9-hydroxy-7-azaundecanoic Acid (Hypusine) (**1a**) Dihydrochloride*. A solution of (*R*)-4-benzyloxycarbonylamino-1-bromo-2-butanol (**10a**) (0.82 g, 2.7 mmol), N^{α}-benzyloxycarbonyl-L-lysine benzyl ester *p*-toluenesulfonate (1.5 g, 2.8 mmol), and triethylamine (0.76 ml, 5.5 mmol) in *t*-butyl alcohol was refluxed for 5 d. The reaction mixture was concentrated *in vacuo* and the residue was dissolved in 10 ml of 50% *t*-butyl alcohol. It was hydrogenated to remove the protecting groups in the presence of Pd black under a gentle stream of hydrogen. The solution was kept acidic by an addition of 1 M hydrochloric acid through the hydrogenation reaction. After the completion of reduction, catalyst was filtered off and the filtrate was concentrated *in vacuo*. The crude product was purified by column chromatography on Amberlite IRC-50 (CG-Type 1, 1×68 cm, NH_4^+ form) using 0.28% NH_4OH as an eluent. Fractions containing hypusine were collected and concentrated *in vacuo*. The residue was dissolved in water and pH of the solution was adjusted to 5.2 with dilute hydrochloric acid. It was concentrated *in vacuo* to obtain hypusine (**1a**) dihydrochloride, which was recrystallized from 90% methanol, yield 172 mg (21%),[8] mp 234—236 °C (decomp),[10] $[\alpha]_D^{17}$ +6.8° (*c* 0.12, 6 M HCl).[10] Found: C, 38.10; H, 8.24; N, 13.27; Cl, 22.79%. Calcd for $C_{10}H_{25}N_3O_3Cl_2 \cdot 1/2\ H_2O$: C, 38.10; H, 8.31; N, 13.33; Cl, 22.49%.

*(2S,9S)-2,11-Diamino-9-hydroxy-7-azaundecanoic Acid (**1b**) Dihydrochloride*. This was prepared by the same procedure as described above. The hydrochloride was recrystallized from 90% methanol and ethanol in a yield of 21%, mp 238—240 °C (decomp),[10] $[\alpha]_D^{23}$ +16° (*c* 0.10, 6 M HCl).[10] Found: C, 39.14; H, 8.28; N, 13.44; Cl, 23.02%, Calcd for $C_{10}H_{25}N_3O_3Cl_2$: C, 39.22; H, 8.23; N, 13.72; Cl, 23.16%.

The authors wish to express their thanks to Professor Yasuo Kakimoto of Ehime University Medical School and Dr. Teruo Nakajima of Osaka University Medical School for supply of natural hypusine. The present work was partially supported by Grant-in-Aid for Scientific Research No. 921107 from the Ministry of Education, Science and Culture.

References

1) A part of this work was presented at 34th National Meeting of the Chemical Society of Japan, Kanagawa, April 1976, Abstr. No. 4D10.

2) T. Shiba, H. Mizote, T. Kaneko, T. Nakajima, Y. Kakimoto, and I. Sano, *Biochim. Biophys. Acta*, **244**, 523 (1971). In this publication, hypusine was named N^6-(4-amino-2-hydroxybutyl)-2,6-diaminohexanoic acid.

3) K. Freudenberg, *Chem. Ber.*, **47**, 2027 (1914).

4) G. Zweifel, and H. C. Brown, *Org. React.*, **13**, 1 (1963).

5) a) D. S. Tarbell, and J. A. Price, *J. Org. Chem.*, **22**, 245 (1957); b) B. Penke, J. Czombos, L. Baláspiri, J. Petres, and K. Kovács, *Helv. Chim. Acta*, **53**, 1057 (1970).

6) B. Bezas, and L. Zervas, *J. Am. Chem. Soc.*, **83**, 719 (1961).

7) D. Ben-Ishai, and A. Berger, *J. Org. Chem.*, **17**, 1564 (1952).

8) Based on the preliminary experiments, the reaction was stopped before formation of by-products to make easy the isolation of hypusine from the reaction mixture at the sacrifice of the yield. Both starting materials, **10** and **16**, still remained after 5 d reaction indicating that they are relatively stable even under the basic condition mentioned above unless participated to the desired coupling.

9) Authentic L-malic acid showed mp 98—99 °C and $[\alpha]_D^{14}$ −6.3° (*c* 1.9, acetone).

10) Natural hypusine dihydrochloride showed mp 234—238 °C (decomp) and $[\alpha]_D^{16}$ +9.9° (*c* 0.12, 6 M HCl).

Solvent Effects in the Conversion of Phenyldiazomethane into Stilbene and Spirooxetane in the Reaction with Chloranil

Takumi Oshima, Ryoji Nishioka, and Toshikazu Nagai*

Institute of Chemistry, College of General Education, Osaka University, Toyonaka, Osaka 560

(Received July 29, 1981)

A stereochemical study was made of the reaction of phenyldiazomethane(**1**) with chloranil(**2**) at 20 °C in 28 aprotic solvents. The products were *trans*-spirooxetane(**4**) and *cis-trans* mixtures of stilbene(**3**) (*ca.* 2—5 times *cis*-rich). The molar ratios of *cis*-**3** to the sum of the *trans*-**3** and **4** tended to increase, whereas the **4** to *trans*-**3** ratios decrease with the increase in the solvent basicity and polarity. These effects of solvents on the product distributions were interpreted in terms of the effects of the solvent basicity and polarity on the stereoselective formation of the diazonium betaine intermediate and on the conformational isomerism. Moderately successful linear-free-energy(LFE) relationships were established for these product ratios with the aid of the combination of the empirical solvent basicity parameter, D_n, and the Kirkwood function, $f(\varepsilon)$, or E_T values as the solvent polarity parameters.

Our recent studies have shown that the decomposition of phenyldiazomethane (**1**) and its substituted homologs with chloranil(**2**) gives *trans*-spirooxetanes and stilbenes.[1] The stereochemistry of these products was 100% *trans* for spirooxetanes and *cis*-isomer-rich for stilbenes: the *cis*:*trans* ratios of the stilbenes increased with the electron withdrawal of the substituents. The preliminary solvent effects showed that THF brings about higher *cis*:*trans* ratios of stilbenes and lower relative yields of spirooxetanes than 1,2-dichloroethane. We have now extended the work to various aprotic solvents. Thus, the present paper is aimed to make a more penetrating interpretation of the effects of solvents on the stereochemical phenomena and on the product distributions. For this purpose, the use of the linear correlations with solvent basicity and the polarity parameters was examined.

Results and Discussion

As was described in a previous paper,[1] the formation of stilbene (**3**) and *trans*-spirooxetane(**4**) can be well explained by postulating two diazonium betaine intermediates, I and II (Scheme 1). II may be produced by a nucleophilic attack of **1** on I. II is degradated to **3** *via* the elimination of N_2 and **2** (Path a) or to **4** *via* the intramolecular cyclization (Path b). The reaction of **1** with **2** also gave several by-products resulting from the nucleophilic attack of residual water on I.[1]

Our attention in the present study was restricted to the solvent effects in the stereochemical pathway leading to **3** and **4**; thus, the only efforts to determine the distribution of *cis*-, *trans*-**3** and **4** were made by the use of high-performance liquid chromatography. The results in a wide variety of aprotic solvents are tabulated in Table 1.

It is noteworthy that the thermodynamically less stable *cis*-**3** was preferentially formed, *ca.* 2 to 5 times more than *trans*-**3**. The isomer ratios of **3** were high in acyclic ethers, such as diethyl ether and dipropyl ether, but considerably decreased in nitro compounds and nitriles. However, **4** was found to be a stable *trans*-isomer in any solvent, and its relative yields increased in the nonpolar solvents, such as benzene and carbon tetrachloride.

Table 1, Product distributions on the reaction of phenyldiazomethane(**1**) with chloranil(**2**) in various aprotic solvents

	Solvent	Relative yields[a]	
		3(*cis*/*trans*)	**4**
1	Diethyl ether	67.7(5.01)	32.3
2	Dibutyl ether	65.3(4.89)	34.7
3	Dipropyl ether	66.7(4.75)	33.3
4	Carbon tetrachloride	57.7(4.55)	42.3
5	Dimethoxymethane	69.6(4.46)	30.4
6	Tetrahydropyran	78.4(4.32)	21.6
7	Cyclohexanone	86.2(4.03)	13.8
8	Butyl acetate	83.2(3.97)	16.8
9	1,4-Dioxane	70.9(3.94)	29.1
10	1,2-Dimethoxyethane	81.9(3.89)	18.1
11	Tetrahydrofuran	78.9(3.77)[b]	21.1
12	Benzene	60.3(3.70)	39.7
13	Chloroform	59.4(3.65)	40.6
14	Methyl acetate	81.1(3.53)	18.9
15	Isopropyl acetate	79.4(3.45)	20.6
16	Ethyl methyl ketone	87.1(3.40)	12.9
17	1,1-Dichloroethane	63.9(3.39)	36.1
18	1,2-Dichloroethane	61.6(3.34)[b]	38.4
19	Propyl acetate	77.8(3.16)	22.2
20	Nitrobenzene	78.7(3.08)	21.3
21	Butyronitrile	82.3(2.97)	17.7
22	Propionitrile	77.7(2.96)	22.3
23	Acetone	82.9(2.89)	17.1
24	Dichloromethane	59.4(2.88)	40.6
25	Ethyl acetate	81.3(2.71)	18.7
26	Benzonitrile	71.1(2.31)	28.9
27	Acetonitrile	78.2(2.23)	21.8
28	Nitromethane	72.6(1.92)	27.4

a) The total yields of **3** and **4** exceeded 50% in most cases. b) The present values, determined by high-performance liquid chromatographic analyses, are somewhat different from the data obtained by a usual column chromatographic separation method and NMR measurements, probably because of the degradation of **4** into *trans*-**3** and **2** in the previous column-chromatographic treatment.

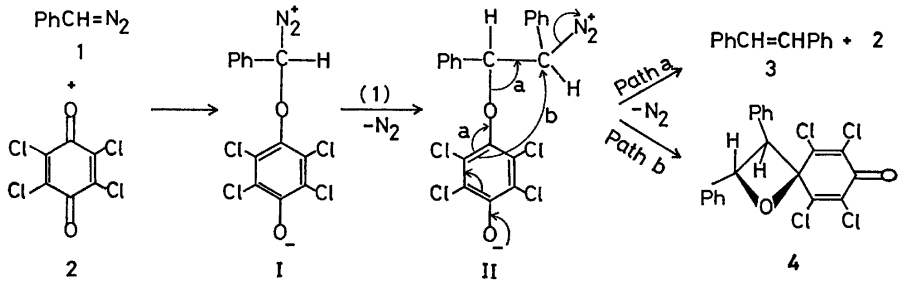

Scheme 1.

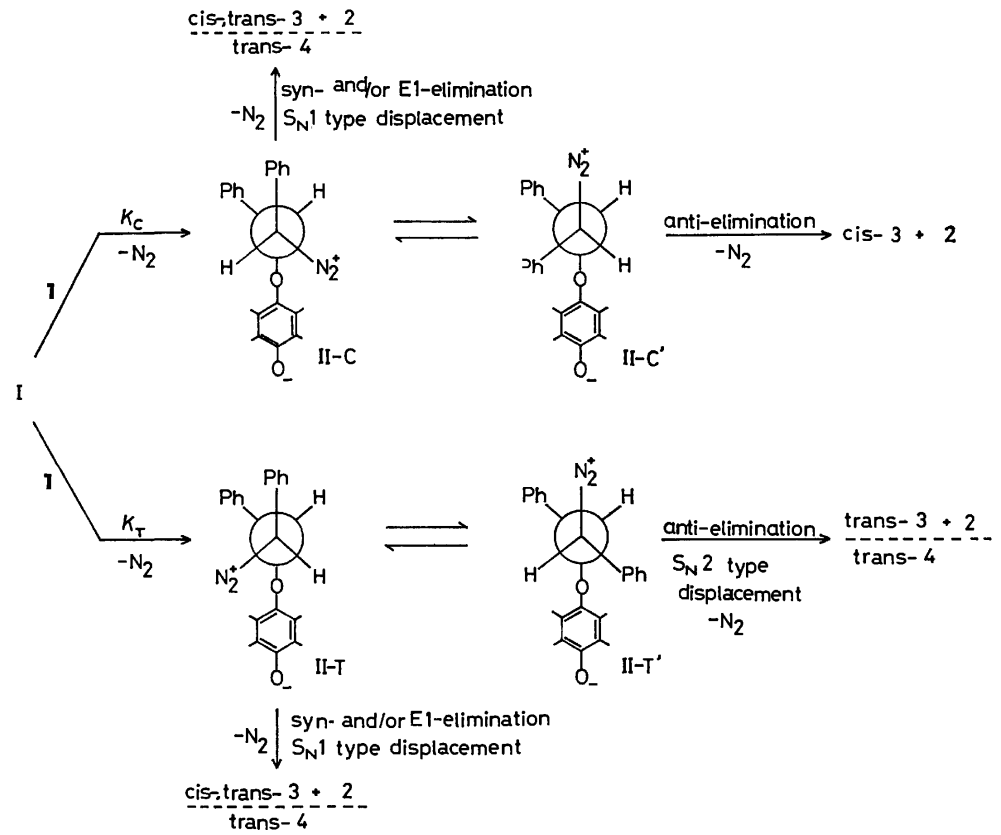

Scheme 2.

Conformational Analysis. As was shown in our previous paper,[1] two conformers, II-C and II-T, may be depicted as the most stable ones for the resulting threo and erythro stereoisomers of II respectively, as may be seen in Scheme 2. From the sterical point of view, II-C is slightly more stable than II-T; *i.e.*, the formation of II-C is a lower-energy process than that of II-T($k_C > k_T$). These conformers, II-C and II-T, can be in equilibrium with each other with the respective conformational isomers, II-C′ and II-T′. On grounds of both the steric and electronic factors, the populations of these threo and erythro rotamers are thought to be in the order of II-C>II-C′, and II-T>II-T′, II-C′ being the most unstable rotamer. The more populous II-C and II-T will afford *cis-trans* mixtures of **3** *via* the syn- and/or *E*1-type elimination, and *trans*-**4** *via* the intramolecular S_N1-type displacement. On the other hand, the less populous II-C′ will prefer to give *cis*-**3** *via* the anti-elimination. II-T′ will prefer to give *trans*-**3** *via* the anti-elimination and *trans*-**4** *via* the intramolecular S_N2-type displacement (Scheme 2).

It should also be noted here that the S_N2-type displacement giving *trans*-**4** is only possible when the bent-ether linkage of these rotamers can be aligned so as to build up a four-membered ring with the central C–C bond, as is represented in the conformational equilibrium of II-T′ (Scheme 3). However, II-C′ will not be transformed into such a crowded structure because of the unfavorable phenyl-phenyl *cis* repulsion. This steric repulsion is the reason why *cis*-**4** was not formed in the present reaction.

Most of the solvents provide a higher yield of *cis*-**3** than the sum of *trans*-**3** and **4**. This apparently means that the reactions from II-C′ and II-T′ proceed more rapidly than those from II-C and II-T.

Solvent Effects on the cis- *to* trans-*Products Ratios.* In the nucleophilic attack of **1**, basic and polar sol-

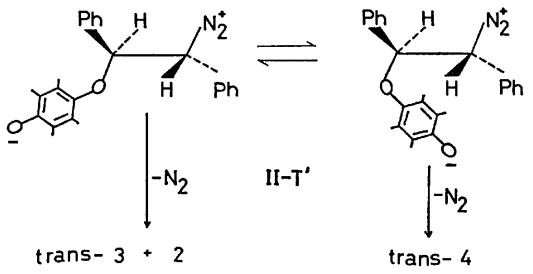

Scheme 3.

vents tend to stabilize the cation center of I, and thereby appear to suppress its reactivity. As a guiding principle of chemical behavior, the reactivity-selectivity principle(RSP)[2] suggests that the less reactive the diazonium betaine, I, the more stereoselective will be the attack of **1**. Assuming that most of the **3** and **4** arise from the II-C′ and II-T′ conformers, as has been mentioned above, the molar ratios of *cis*-**3** to the sum of *trans*-**3** and **4** may be said to be approximately parallel to the rate ratio(k_C/k_T).

Keeping these considerations in mind, we preliminarily attempted to correlate the logarithms of the molar ratios of *cis*-**3** to the sum of *trans*-**3** and **4** with such empirical solvent-basicity parameters as D_π,[3] Kagiya's $\Delta\nu_D$,[4] Gutmann's *DN*,[5] and Kamlet-Taft's β.[6]

When correlated with these conventional parameters, the regression equations are as follows: log *cis*-**3**/(*trans*-**3**+**4**) $= 0.142+0.149D_\pi$($r=0.782$, $n=24$), $=-0.00512+0.0027\Delta\nu_D$($r=0.731$, $n=22$), $=-0.0337+0.0115DN$ ($r=0.808$, $n=14$), and $=-0.142+0.698\beta$ ($r=0.727$, $n=13$), where r and n are the correlation coefficients and the number of data points respectively. However, the correlations with the solvent-polarity parameters, *i.e.*, the Kirkwood function[7] of dielectric constants ε, $f(\varepsilon)=(\varepsilon-1)/(2\varepsilon+1)$ and Dimroth and Reichart's E_T values,[8] provided worse results for $f(\varepsilon)$, ($r=0.156$, $n=23$) and for E_T, ($r=0.102$, $n=20$). Thus, the specific role of the solvent basicity is much more important than its polarity effects. These statistical results are substantially in accordance with the above assumption that the further stereoselective formation of II-C is achieved by the nucleophilic solvation of the cation of I. The better correlation with D_π than with $\Delta\nu_D$ or β is suggestive of a soft acidity of the cation center(N_2^+) of I, because the indicator compounds employed for the determination of D_π and $\Delta\nu_D$ or β are typical soft-acid TCNE and hard-acid methanol or phenol respectively.[9] Though D_π is a slightly less successful parameter than *DN*, the ten more available values for D_π force us to adopt this parameter in the present discussion.

The more basic and the more polar the solvents are, the easier the conformational rotation into II-C′ and II-T′ will be. Thus, II-C′ and II-T′ play a much more significant role in the product distributions, ultimately increasing the net amount of *cis*-**3**. Therefore, we attempted to improve the above unsatisfactory correlation by the use of two parameters, D_π and the polarity parameter, $f(\varepsilon)$ or E_T. Equations 1 and 2

$$\log\frac{cis\text{-}3}{trans\text{-}3+4} = -0.105 + 0.169D_\pi + 0.632f(\varepsilon) \quad (r=0.863,\ s=0.0684,\ n=23) \quad (1)$$

$$\log\frac{cis\text{-}3}{trans\text{-}3+4} = -0.0957 + 0.155D_\pi + 0.00589E_T \quad (r=0.801,\ s=0.0801,\ n=20) \quad (2)$$

were obtained for the D_π-$f(\varepsilon)$ and D_π-E_T systems respectively. The positive coefficients of both D_π and $f(\varepsilon)$ or E_T are in harmony with the hypothesis that the solvent with a more basic and polar nature induces a more stereoselective formation of II-C than II-T and promotes the conformational transformation into II-C′ and II-T′. A plot of log *cis*-**3**/(*trans*-**3**+**4**) (obsd) *versus* log *cis*-**3**/(*trans*-**3**+**4**)(calcd) according to Eq. 1 is shown in Fig. 1. It is noticeable that nonpolar solvents, such as benzene and carbon tetrachloride, afforded exceptionally lower *cis*-**3** values with respect to the *trans*-products; *i.e.*, the logarithmic ratios were below null. These phenomena may be attributed to the more significant participation of the minor syn- and/or *E*1-type elimination and S_N1-type displacement, most probably from II-C. The reason for this may be that the conformational rotation into II-C′ is energetically more costly compared to the corresponding transformation of II-T into II-T′.

*Solvent Effects on the Spirooxetane(**4**) to* trans-*Stilbene (**3**) Ratios.* It is also interesting to examine the solvent effects on the competitive S_N2-type and anti-elimination processes, giving **4** and *trans*-**3**, from II-T′, because the solvent-dependent equilibrium situation between the extended and the crowded structures, as represented in Scheme 3, plays a significant role in these product ratios. The more basic and more polar solvents are liable to separate the opposite charges of II-T′, so that the amount of **4** decreases as a result of the reduced contribution of the crowded structure. On the other hand, in the less basic and

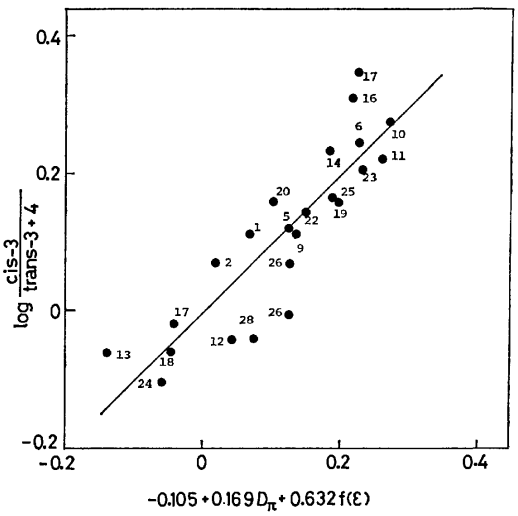

Fig. 1. Plot of $\log\frac{cis\text{-}3}{trans\text{-}3+4}$ (obsd) *versus* $\log\frac{cis\text{-}3}{trans\text{-}3+4}$ (calcd) according to Eq. 1; for point numbers, see Table 1.

less polar solvents the opposed charges should come close together; thus, the growing participation of the crowded structure increases the formation of **4**. A similar type of solvent contribution to product distributions can be expected for the minor S_N1- and/or $E1$-type elimination processes. In consideration of this, we attempted to correlate the logarithms of the molar ratios of **4** to *trans*-**3** with the linear combination of two parameters, D_π and $f(\varepsilon)$ or E_T. Equations 3 and 4 were thus obtained:

$$\log\frac{\mathbf{4}}{\textit{trans}\text{-}\mathbf{3}} = 1.07 - 0.232D_\pi - 2.37f(\varepsilon)$$
$$(r=0.921,\ s=0.0937,\ n=23), \quad (3)$$

$$\log\frac{\mathbf{4}}{\textit{trans}\text{-}\mathbf{3}} = 2.16 - 0.259D_\pi - 0.0514E_T$$
$$(r=0.930,\ s=0.0883,\ n=20). \quad (4)$$

The negative coefficients in both the basicity and the polarity parameters are consistent with the solvation environment expected above.

A comparison of the coefficients in Eqs. 1 and 2 with those in Eqs. 3 and 4 shows that the effects of the solvent basicity are more enhanced in log *cis*-**3**/(*trans*-**3**+**4**) than in log **4**/*trans*-**3**. The reverse is necessarily true for the contribution of the solvent polarity. A plot of log **4**/*trans*-**3**(obsd) *versus* log **4**/*trans*-**3**(calcd) according to Eq. 4 is shown in Fig. 2.

This figure consists of two solvent groups except for 1,4-dioxane. One group on the high side contains aliphatic chlorinated solvents (very low D_π and moderate high E_T) and acyclic ethers and benzene (moderate high D_π and very low E_T). Therefore, the high **4**:*trans*-**3** ratios can be ascribed to the low D_π or E_T values; that is, these solvents can not well stabilize the cation or anion center of II, increasing the population of the crowded structures. On the other hand, the other group on the low side is characterized by such solvent properties as a relatively strong nucleophilicity(high D_π) and/or electrophilicity

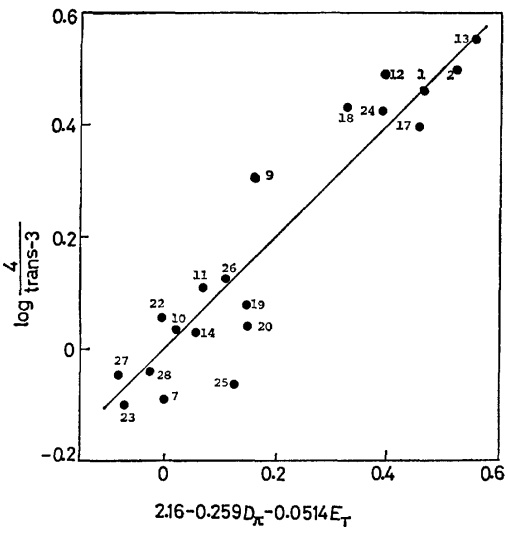

Fig. 2. Plot of $\log\frac{\mathbf{4}}{\textit{trans}\text{-}\mathbf{3}}$ (obsd) *versus* $\log\frac{\mathbf{4}}{\textit{trans}\text{-}\mathbf{3}}$ (calcd) according to Eq. 4; for point numbers, see Table 1.

(high E_T). Thus, the ketones, such as acetone and cyclohexanone, reduce the **4**: *trans*-**3** ratios much more because of both the effective nucleophilic and electrophilic solvations of the respective cation N_2^+ and anion chloranil moieties of II, consequently decreasing the population of the crowded structures. Though the esters have D_π values very close to those of ketones, the **4**:*trans*-**3** ratios appreciably increased on account of the slight decrease in E_T values. Similarly, though the E_T values for nitro compounds and nitriles are higher than those for ketones, the less basic properties (lower D_π) of these solvents induce more formation of **4**.

Experimental

The *cis*:*trans* ratio of **3** and the overall yields of **3** and **4** were determined by means of JASCO tri-rotor high-performance liquid chromatography (HPLC), using naphthalene as the internal standard. The HPLC analysis was carried out at room temperature using a 250 mm×4.6 mm column packed ODS (octadecyl silane on silica gel; methanol–water(4:1 by volume); flow rate, 1—1.5 ml/min. The UV detector was calibrated at 280 nm with standard mixtures of known concentrations of *cis*- and *trans*-**3** and **4**. The average error in the *cis*:*trans* ratio was *ca.* 3% or better. The relative retention times were as follows: naphthalene (1.0), *cis*-**3**(1.8), *trans*-**3**(2.3), and **4**(4.5).

Materials. The phenyldiazomethane(**1**) was prepared according to the procedure described by Closs and Moss[10] and was used without further purification. The chloranil (**2**) was of commercial origin and was recrystallized from benzene. All the solvents used were purified by the usual method.[11]

General Procedure. To a solution or suspension of **2** (0.50 g, 2.03 mmol) in a solvent (30 ml) was added, drop by drop, a solution of **1** (0.50 g, 4.24 mmol) in the same solvent(10 ml) for 10 min at 20 °C. The deep-red color of the mixture rapidly disappeared with a violent evolution of N_2. After 1-h stirring, the solvents (except for benzene) boiling below 100 °C were evaporated, and the pasty residue was redissolved in benzene (40 ml). In the case of the higher-boiling solvents, the reaction solutions were submitted to the following treatment without any work-up. In these reaction solutions, naphthalene(100 mg) was dissolved as an internal standard and two-milliliter aliquots were diluted with benzene until the total volume of solution rose to 25 ml. The sample solutions thus prepared were analyzed by HPLC.

References

1) T. Oshima and T. Nagai, *Bull. Chem. Soc. Jpn.*, **53**, 726 (1980).

2) C. D. Johnson, *Chem. Rev.*, **75**, 755 (1975); B. Giese, *Angew. Chem., Int. Ed. Engl.*, **16**, 125 (1977).

3) T. Oshima, S. Arikata, and T. Nagai, *J. Chem. Res.*, **1981**, (*S*) 204; (*M*) 2518.

4) T. Kagiya, Y. Sumida, and T. Inoue, *Bull. Chem. Soc. Jpn.*, **41**, 767 (1968).

5) V. Gutmann and E. Wychera, *Inorg. Nucl. Chem. Lett.*, **2**, 257 (1966); V. Gutmann and R. Schmid, *Cood. Chem. Rev.*, **12**, 263 (1974); V. Gutmann, *Electrochim. Acta*, **21**, 661 (1976).

6) M. J. Kamlet and R. W. Taft, *J. Am. Chem. Soc.*, **98**, 377 (1976); M. J. Kamlet, J. L. Abboud, M. E. Jones,

and R. W. Taft, *J. Chem. Soc., Perkin Trans. 2*, **1979**, 342.
7) J. G. Kirkwood, *J. Chem. Phys.*, **2**, 351 (1934); K. J. Laidler and H. Eyring, *Ann. New York Acad. Sci.*, **39**, 303 (1940).
8) K. Dimroth, C. Reichardt, T. Siepmann, and R. Bohlmann, *Justus Liebigs Ann. Chem.*, **661**, 1 (1963); C. Reichardt, *Angew. Chem., Int. Ed. Engl.*, **18**, 98 (1979).
9) R. G. Pearson, *J. Am. Chem. Soc.*, **85**, 3533 (1963); R. G. Pearson, *J. Chem. Educ.*, **45**, 581, 643 (1968); T.-L. Ho, "Hard and Soft Acids and Bases Principle in Organic Chemistry," Academic Press, New York (1977), Chap. 2.
10) G. L. Closs and R. A. Moss, *J. Am. Chem. Soc.*, **86**, 4042 (1964).
11) J. A. Riddick and W. B. Bunger, "Techniques of Chemistry, Vol. II, Organic Solvents," 3rd ed, ed by A. Weissberger, John Wiley & Sons, New York (1970).

 © 1982 The Chemical Society of Japan Bull. Chem. Soc. Jpn., 55, 909—913 (1982)

Palladium-catalyzed New Carbon-Phosphorus Bond Formation

Toshikazu Hirao,* Toshio Masunaga, Naoto Yamada,
Yoshiki Ohshiro, and Toshio Agawa
Department of Petroleum Chemistry, Faculty of Engineering, Osaka University,
2-1 Yamada-oka, Suita, Osaka 565
(Received July 30, 1981)

Dialkyl arylphosphonates are prepared by the palladium-catalyzed reaction of aryl bromides with dialkyl phosphite in the presence of triethylamine. The similar treatment of vinyl bromides gives dialkyl vinylphosphonates stereoselectively.

Arbuzov and Michaelis-Becker reactions provide facile procedures for the formation of carbon-phosphorus bonds.[1] These methods, however, are not applicable to the formation of sp^2 hybridized carbon-phosphorus bonds. Only few methods have been reported for the syntheses of arylphosphonates[1,2] and vinylphosphonates.[1,3] For example, the photoinitiated reaction of iodobenzene with trialkyl phosphite[2f,g] or dialkyl phosphite ion[2e] affords dialkyl phenylphosphonate. Direct reaction of aryl[2i] or vinyl halides[3g] with trialkyl phosphite in the presence of nickel halide requires severe reaction conditions, and the stereochemistry of vinylphosphonates has not been clarified. In our preceding reports, we found new and versatile syntheses of dialkyl arylphosphonates[4] and vinylphosphonates[5] using palladium catalyst. The stereoselective synthesis of dialkyl vinylphosphonates has been accomplished by this method. Herein, we wish to report further details of the palladium-catalyzed carbon-phosphorus bond formation.

Results and Discussion

Preparation of Dialkyl Arylphosphonates. Dialkyl arylphosphonates (**1**) were prepared in good yields by the reaction of aryl bromides or iodide with *O,O*-dialkyl phosphonate in the presence of triethylamine and a catalytic amount of tetrakis(triphenylphosphine)-palladium. The results are summarized in Table 1.

$$\underset{\text{X=Br, I}}{\text{ArX}} + \text{HP(O)(OR)}_2 \xrightarrow[\text{Et}_3\text{N}]{\text{catal Pd(PPh}_3)_4} \underset{\mathbf{1}}{\text{ArP(O)(OR)}_2} + \text{Et}_3\text{N}\cdot\text{HX}$$

Use of palladium acetate instead of tetrakis(triphenylphosphine)palladium resulted a moderate yield of **1a**. But palladium chloride was less effective. Triethylamine was superior to tri-*n*-butylamine and pyridine as base. Although bromobenzene readily underwent phosphonation with *O,O*-diethyl phosphonate, chlorobenzene did not react under the same reaction conditions. On treatment of *p*-bromochlorobenzene with *O,O*-diethyl phosphonate, diethyl *p*-chlorophenylphosphonate was obtained in 85% yield as a sole product. *O,O*-Diisopropyl and *O,O*-dibutyl phosphonates were also allowed to react with bromobenzene to give the corresponding phosphonates. Diethyl arylphosphonates, bearing a variety of electron-withdrawing and electron-donating substituents, such as *p*-NO_2, *p*-CN, *p*-MeCO, *o*-COOMe, *p*-MeCONH, *p*-MeO, *p*-Me, *o*-Me, were prepared in high yields. *o*-Bromobenzoic acid was subjected to esterification with diethyl phosphite as well as phosphonation to give diethyl *o*-ethoxycarbonylphenylphosphonate in 24% yield. Attempts to prepare *p*-hydroxy- and *p*-aminophenylphosphonates were unsuccessful. These observations are consistent with the results reported by Heck[6] that aryl bromides with strongly electron-donating substituents do not undergo the palladium-catalyzed vinylic substitution reaction in acceptable yields. The palladium-catalyzed phosphonation of 1-bromonaphthalene and 3-bromopyridine gave the corresponding phosphonates in good yields.

It should be noted that *o*-dibromobenzene reacted with 2 equiv. of *O,O*-diethyl phosphonate to yield *o*-bromophenylphosphonate (34%) and phenylphosphonate (6%), whereas substitution of both bromine atoms of *p*-dibromobenzene was observed. Though the mechanism for the formation of diethyl phenylphosphonate from *o*-dibromobenzene has not been clarified, it is conceivable that diethyl phosphite plays an important role in the present reduction reaction. Previously, we reported a facile reduction of *gem*-dibromo derivatives with diethyl phosphite and triethylamine.[7] In this connection, the dark reactions of *o*-fluoroiodobenzene and *o*-chloroiodobenzene with $(EtO)_2PO^-$ in liquid ammonia were reported to give fluorobenzene and chlorobenzene, respectively, and such a reduction reaction has not been observed for *m*- and *p*-iodohalobenzenes.[8] *o*-Bromobenzyl alcohol was also subjected to reduction of hydroxyl group to produce diethyl *o*-tolylphosphonate in 18% yield.

The formation path of dialkyl arylphosphonates is outlined in Scheme 1. Palladium(0) species undergoes oxidative addition with aryl bromide to give the arylpalladium complex, which may be considered to be a key intermediate. The attack of dialkyl phosphite to the arylpalladium complex leads to dialkyl arylphosphonate. Triethylamine regenerates palladium(0) species with the deposition of $Et_3N\cdot HBr$. Thus obtained palladium(0) species is available to another reaction cycle. In the nickel-catalyzed Arbuzov reaction, arylnickel complexes have also been suggested.[9]

Diethyl sodiophosphonate was able to be employed in the palladium-catalyzed reaction. For prevention of the photoinitiated phosphonation,[2e] the reaction

$$\text{ArBr} + \text{Pd}^0 \longrightarrow \text{ArPd}^{II}\text{Br} \xrightarrow{\text{HP(O)(OR)}_2} \text{ArP(O)(OR)}_2 + \text{HPd}^{II}\text{Br}$$

$$\text{HPd}^{II}\text{Br} + \text{Et}_3\text{N} \longrightarrow \text{Pd}^0 + \text{Et}_3\text{N}\cdot\text{HBr}$$

Scheme 1.

Table 1. Preparation of dialkyl arylphosphonates (**1**)

ArX	$HP(O)(OR)_2$ R	Base	Catalyst	Reaction[a] time/h	Product **1**	Yield/%
PhBr	Et	Et_3N	$Pd(PPh_3)_4$	2.5	$PhP(O)(OEt)_2$ **1a**	92
PhBr	Et	n-Bu_3N	$Pd(PPh_3)_4$	2.5	**1a**	51
PhBr	Et	pyridine	$Pd(PPh_3)_4$	16	**1a**	trace
PhBr	Et	Et_3N	$Pd(OAc)_2$	12	**1a**	58
PhBr	Et	Et_3N	$PdCl_2$	12	**1a**	7
PhBr	i-Pr	Et_3N	$Pd(PPh_3)_4$	2.5	$PhP(O)(OPr\text{-}i)_2$ **1b**	90
PhBr	n-Bu	Et_3N	$Pd(PPh_3)_4$	2.5	$PhP(O)(OBu\text{-}n)_2$ **1c**	94
PhI	Et	Et_3N	$Pd(PPh_3)_4$	2.5	**1a**	96
p-Me-C_6H_4Br	Et	Et_3N	$Pd(PPh_3)_4$	17	p-Me-$C_6H_4P(O)(OEt)_2$ **1d**	94
o-Me-C_6H_4Br	Et	Et_3N	$Pd(PPh_3)_4$	30	o-Me-$C_6H_4P(O)(OEt)_2$ **1e**	91
p-Cl-C_6H_4Br[b]	Et	Et_3N	$Pd(PPh_3)_4$	8	p-Cl-$C_6H_4P(O)(OEt)_2$ **1f**	85
p-MeO-C_6H_4Br	Et	Et_3N	$Pd(PPh_3)_4$	17	p-MeO-$C_6H_4P(O)(OEt)_2$ **1g**	95
p-O_2N-C_6H_4Br[b]	Et	Et_3N	$Pd(PPh_3)_4$	8	p-O_2N-$C_6H_4P(O)(OEt)_2$ **1h**	73
p-MeC(=O)-C_6H_4Br[b]	Et	Et_3N	$Pd(PPh_3)_4$	8	p-MeC(=O)-$C_6H_4P(O)(OEt)_2$ **1i**	90
p-MeC(=O)NH-C_6H_4Br[b]	Et	Et_3N	$Pd(PPh_3)_4$	28	p-MeC(=O)NH-$C_6H_4P(O)(OEt)_2$ **1j**	64
p-NC-C_6H_4Br[b]	Et	Et_3N	$Pd(PPh_3)_4$	2	p-NC-$C_6H_4P(O)(OEt)_2$ **1k**	95
o-MeOC(=O)-C_6H_4Br	Et	Et_3N	$Pd(PPh_3)_4$	35	o-MeOC(=O)-$C_6H_4P(O)(OEt)_2$ **1l**	43
o-HOOC-C_6H_4Br[b]	Et	Et_3N	$Pd(PPh_3)_4$	10	o-EtOC(=O)-$C_6H_4P(O)(OEt)_2$ **1m**[f]	24
p-H_2N-C_6H_4Br[b,c]	Et	Et_3N	$Pd(PPh_3)_4$	35	——	
p-HO-C_6H_4Br[b,c]	Et	Et_3N	$Pd(PPh_3)_4$	24	p-HO-$C_6H_4P(O)(OEt)_2$ **1n**	3
o-$HOCH_2$-C_6H_4Br[b,d]	Et	Et_3N	$Pd(PPh_3)_4$	19	**1e**	18
p-Br-C_6H_4Br[b,e]	Et	Et_3N	$Pd(PPh_3)_4$	8	p-$(EtO)_2P(O)$-$C_6H_4P(O)(OEt)_2$ **1o**	81
o-Br-C_6H_4Br[e]	Et	Et_3N	$Pd(PPh_3)_4$	64	o-Br-$C_6H_4P(O)(OEt)_2$ **1p**	34
					1a	6
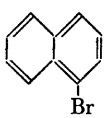	Et	Et_3N	$Pd(PPh_3)_4$	24	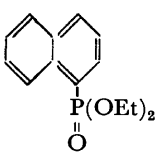 **1q**	96

Table 1. (continued)

ArX	$HP(O)(OR)_2$ R	Base	Catalyst	Reaction[a] time/h	Product **1**	Yield/%
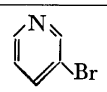	Et	Et_3N	$Pd(PPh_3)_4$	3	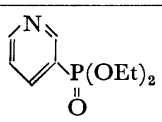 **1r**	77

a) Solvent was not used unless otherwise stated; reactions at 90 °C. b) Toluene was added as a solvent. c) 0.25 equiv of tri-*o*-tolylphosphine was added. d) Reaction temperature, 100 °C. e) 2 equiv. of diethyl phosphite and triethylamine were used. f) Carboxyl group of the product was esterified by ethoxy group of *O,O*-diethyl phosphonate *in situ*.

Table 2. Preparation of dialkyl vinylphosphonates (**2**)

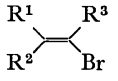	$HP(O)(OR^4)_2$ R^4	Reaction[a] time/h	Product **2**	Yield/%
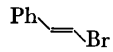	Et	0.2	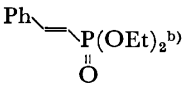 **2a**	93
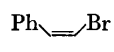	Et	1.5	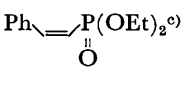 **2b**	91
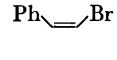	*i*-Pr	12	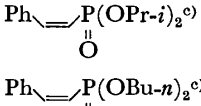 **2c**	81
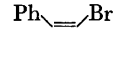	*n*-Bu	1.5	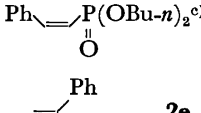 **2d**	92
	Et	30	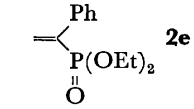 **2e**	66
	Et	9	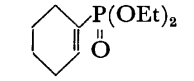 **2f**	69
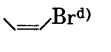 [d]	Et	1.5	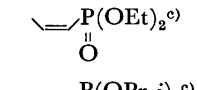 **2g**	98
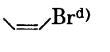 [d]	*i*-Pr	6	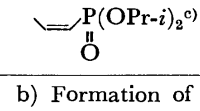 **2h**	92

a) Solvent was not used unless otherwise stated; reactions at 90 °C. b) Formation of no *Z*-isomer was observed in the ^1H NMR spectrum. c) No *E*-isomer was detected in the ^1H NNR spectrum. d) Toluene was added as a solvent. Yields were based on the starting dialkyl phosphite.

was carried out in the dark, but gave diethyl arylphosphonates in moderate yields.

$$ArBr + (EtO)_2PO^-Na^+ \xrightarrow{\text{catal } Pd(PPh_3)_4} ArP(O)(OEt)_2$$

Ar=Ph 54%
=*p*-Me-C_6H_4 36%

Preparation of Dialkyl Alkenylphosphonates. The palladium-catalyzed phosphonation was successfully applied to stereoselective syntheses of dialkyl vinylphosphonates (**2**) from vinyl bromides. The results are summarized in Table 2.

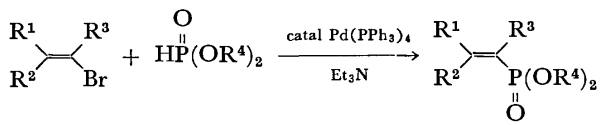

2

Stereoselectivity is illustrated as follows. Treatment of (*E*)- and (*Z*)-β-bromostyrenes with diethyl phosphite in the presence of palladium catalyst gave diethyl (*E*)- and (*Z*)-styrylphosphonates, respectively, without any contamination of the isomer. Phosphonomycin, (−)-(1*R*,2*S*)-1,2-epoxypropylphosphonic acid, is a new antibiotic.[10] Diisopropyl (*Z*)-1-propenylphosphonate, its important synthetic intermediate, was obtained in a high yield by this phosphonation.

1-Monobromodiene was easily prepared by the reaction of *gem*-dibromodiene with *O,O*-diethyl phosphonate and triethylamine according to our method.[8] 1-Bromo-4-phenylbutadiene was converted to diethyl 4-phenylbutadienylphosphonate (**3**) by the palladium-catalyzed phosphonation. One-step synthesis of the dienylphosphonate **3** was attempted by the reaction of 1,1-dibromo-4-phenylbutadiene with *O,O*-diethyl phosphonate in the presence of triethylamine and a

$$PhCH{=}CH{-}CH{=}CBr_2 \xrightarrow[Et_3N]{HP(O)(OEt)_2} PhCH{=}CH{-}CH{=}CHBr$$

$$\xrightarrow[HP(O)(OEt)_2,\ Et_3N]{\text{catal } Pd(PPh_3)_4} PhCH{=}CH{-}CH{=}CHP(O)(OEt)_2$$

78% **3**

catalytic amount of tetrakis(triphenylphosphine)palladium, but only 1-bromo-4-phenylbutadiene was obtained. The substitution with diethyl phosphite was not observed.

Vinylpalladium complexes seem to be involved as key intermediates,[11] and the same mechanism as given for dialkyl arylphosphonates may be operative.

It is well known that the reaction of diene with nucleophiles is catalyzed by palladium complex.[12] But the reaction of dienes with dialkyl phosphite has not been studied. Isoprene was treated with *O,O*-diethyl phosphonate in the presence of a catalytic amount of tetrakis(triphenylphosphine)palladium and 1,2-bis(diphenylphosphino)ethane (DIPHOS) to give diethyl 3-methyl-2-butenylphosphonate (**4**) in 10% yield selectively. Although there are two possible routes of nucleophilic attack of *O,O*-diethyl phosphonate to isoprene, formation of diethyl 1-methyl-2-butenylphosphonate was not observed in the ^1H NMR spectrum.

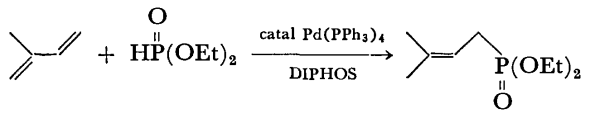

4

The results described here thus show the palladium-catalyzed phosphonation to be a useful method for organophosphorus syntheses, especially in the synthesis of dialkyl aryl- and vinylphosphonates.

Experimental

^1H NMR spectra were obtained on a JEOL JNM-PMX-60 with tetramethylsilane as an internal standard. IR spectra were recorded with a JASCO IRA-1 spectrometer. The mass spectra were taken with a Hitachi RMU-6E spectrometer.

Materials. (*Z*)-*β*-bromostyrene,[13] bromocyclohexene,[13] (*Z*)-1-bromo-1-propene,[14] and 1-bromo-4-phenylbutadiene[8] were prepared by the reported methods. Tetrakis(triphenylphosphine)palladium was easily prepared from palladium chloride.[15] Other reagents and solvents are commercial ones and were purified by distillation under nitrogen atmosphere or recrystallization.

Dialkyl Arylphosphonate (1). General Procedure: To a stirred mixture of *O,O*-dialkyl phosphonate (4.4 mmol), triethylamine (0.61 ml, 4.4 mmol), and tetrakis(triphenylphosphine)palladium (0.23 g, 0.2 mmol), aryl bromide (4.0 mmol) was added under nitrogen atmosphere, and the resultant mixture was stirred at 90 °C for 2—64 h. When aryl bromide is solid, toluene (1 ml) was added as a solvent. After the addition of ether (50 ml), triethylamine hydrobromide was removed by filtration. The residue obtained upon evaporation was purified by Kugelrohr distillation or column chromatography on silica gel to give dialkyl arylphosphonate (Table 1). Dialkyl arylphosphonates (**1a**,[2i] **1b**,[2i] **1c**,[1b] **1d**,[2i] **1e**,[2i] **1f**,[2i] **1g**,[2i] **1h**,[16] **1i**,[2i] **1j**,[2j] **1k**,[17] **1l**,[2i] **1m**,[2i] **1n**,[2i] **1o**,[2i] **1q**,[1b] and **1r**[18]) were identified by comparison of their IR and ^1H NMR spectra with those of authentic samples. **1p**: IR (neat) 1245, 1050—1020, and 965 cm^{-1}; ^1H NMR ($CDCl_3$) δ 1.37 (t, 6H, J=7.0 Hz), 4.20 (dq, 4H, J=7.0 and 7.0 Hz), 7.30—8.30 (m, 4H); MS *m/e* 293 (M^+); Found: C, 40.96; H, 5.05; Br, 27.48; P, 10.32%. Calcd for $C_{10}H_{14}BrO_3P$: C, 40.98; H, 4.81; Br, 27.26; P, 10.57%.

Palladium-catalyzed Reaction of Aryl Bromide with Diethyl Sodiophosphonate. To a stirred mixture of bromobenzene (0.63 g, 4.0 mmol) and tetrakis(triphenylphosphine)palladium (0.23 g, 0.2 mmol) in toluene (3 ml), diethyl sodiophosphonate (4.4 mmol) in toluene (4 ml) was added. The resultant mixture was stirred at 90 °C for 30 h under nitrogen atmosphere. After the addition of ether (20 ml), sodium bromide was removed by filtration. The residue obtained upon evaporation was distilled by Kugelrohr to give diethyl phenylphosphonate (**1a**, 0.46 g, 54%). Diethyl *p*-tolylphosphonate (**1d**) was prepared in 36% yield similarly (reaction time, 24 h).

Dialkyl Vinylphosphonate (2). General Procedure: The vinylphosphonate **2** was prepared in the similar manner as that of **1** (Table 2). In the case of (*Z*)-1-bromo-1-propene as a starting bromide, reactions were carried out by mixing (*Z*)-1-bromo-1-propene (0.58 g, 4.8 mmol), *O,O*-dialkyl phosphonate (4.0 mmol), triethylamine (0.55 ml, 4.0 mmol), and tetrakis(triphenylphosphine)palladium (0.23 g, 0.2 mmol) in toluene (1 ml) at 90 °C. Yields of **2g** and **2h** were based on the starting *O,O*-dialkyl phosphonate. Dialkyl vinylphosphonates (**2a**,[3g] **2e**,[3g] **2f**,[1b] **2g**,[3f] and **2h**[10a]) were identified by comparison of their IR and ^1H NMR spectra with those of authentic samples. **2b**: IR (neat) 1600, 1235, 1050—1020, and 955 cm^{-1}; ^1H NMR ($CDCl_3$) δ 1.12 (t, 6H, J=7.0 Hz), 3.98 (dq, 4H, J=7.0 and 7.0 Hz), 5.78 (dd, 1H, J=14.0 and 14.9 Hz), 6.70—7.90 (m, 5+1H); MS *m/e* 240 (M^+). **2c**: IR (neat) 1605, 1240, and 1030—960 cm^{-1}; ^1H NMR ($CDCl_3$) δ 1.15 (d, 6H, J=6.5 Hz), 1.25 (d, 6H, J=6.5 Hz), 4.25—5.08 (m, 2H), 5.69 (dd, 1H, J=14.0 and 14.5 Hz), 6.53—7.83 (m, 5+1H); MS *m/e* 268 (M^+). **2d**: IR (neat) 1605, 1245, and 1080—950 cm^{-1}; ^1H NMR ($CDCl_3$) δ 0.62—1.75 (m, 14H), 3.19 (dt, 4H, J=6.5 and 6.5 Hz), 5.70 (dd, 1H, J=14.0 and 15.0 Hz), 6.69—7.83 (m, 5+1H); MS *m/e* 296 (M^+).

Diethyl 4-Phenylbutadienylphosphonate (3). The butadienylphosphonate **3** was similarly prepared by the palladium-catalyzed reaction of 1-bromo-4-phenylbutadiene with *O,O*-diethyl phosphonate in the presence of triethylamine. The *E*:*Z* ratio could not be determined.[19]

Diethyl 3-Methyl-2-butenylphosphonate (4). The mixture of isoprene (1.70 g, 25 mmol), *O,O*-diethyl phosphonate (3.45 g, 25 mmol), 1,2-bis(diphenylphosphino)ethane (0.10 g, 0.25 mmol), and tetrakis(triphenylphosphine)palladium (0.29 g, 0.25 mmol) in a sealed tube was heated at 150 °C for 20 h. After evaporation of unreacted isoprene, **4** was isolated in 10% yield by preparative GLC. The structure of **4** was confirmed by the ^1H NMR spectrum.[20]

References

1) a) K. Sasse, "Houben-Weyl, Methoden der Organischen Chemie," 4th ed, ed by E. Müller, Georg Thieme Verlag, Stuttgart (1963), Vol. XII/1, p. 423; b) K. H. Worms and M. Schmidt-Dunker, "Organic Phosphorus Compounds," ed by G. M. Kosolapoff and L. Maier, John Wiley & Sons, New York (1976), Vol. 7, p. 1.

2) a) G. M. Kosolapoff, *Org. React.*, **6**, 273 (1951); b) L. D. Freedman and G. O. Doak, *Chem. Rev.*, **57**, 479 (1957);

c) E. F. Jason and E. K. Fields, *J. Org. Chem.*, **27**, 1402 (1962); d) A. G. Varvoglis, *Tetrahedron Lett.*, **1972**, 31; e) J. F. Bunnett and X. Creary, *J. Org. Chem.*, **39**, 3612 (1974); f) J. B. Plumb, R. Obrycki, and C. E. Griffin, *ibid.*, **31**, 2455 (1966); g) R. Obrycki and C. E. Griffin, *ibid.*, **33**, 632 (1968); h) P. Tavs and F. Korte, *Tetrahedron*, **23**, 4677 (1967); P. Tavs, *Chem. Ber.*, **103**, 2428 (1970).

3) a) G. M. Kosolapoff and I. F. McCullough, *J. Am. Chem. Soc.*, **73**, 855 (1951); b) L. N. Mashljakovskii, B. I. Ionin, I. S. Okhrimenko, and A. A. Petrov, *Zh. Obshch. Khim.*, **37**, 1307 (1967); c) B. I. Ionin and A. A. Petrov, *ibid.*, **33**, 432 (1963); d) G. L. Kenyon and F. H. Westheimer, *J. Am. Chem. Soc.*, **88**, 3557 (1966); e) A. M. Aguiar and D. Daigle, *J. Org. Chem.*, **30**, 2826 (1965); f) A. A. Petrov, B. I. Ionin, and V. M. Ignatyev, *Tetrahedron Lett.*, **1968**, 15; g) P. Tavs and H. Weitkamp, *Tetrahedron*, **26**, 5529 (1970).

4) T. Hirao, T. Masunaga, Y. Ohshiro, and T. Agawa, *Synthesis*, **1981**, 56.

5) T. Hirao, T. Masunaga, Y. Ohshiro, and T. Agawa, *Tetrahedron Lett.*, **21**, 3595 (1980).

6) C. B. Ziegler, Jr., and R. F. Heck, *J. Org. Chem.*, **43**, 2941 (1978).

7) T. Hirao, T. Masunaga, Y. Ohshiro, and T. Agawa, *J. Org. Chem.*, in press.

8) R. R. Bard, J. F. Bunnett, and R. P. Traber, *J. Org. Chem.*, **44**, 4918 (1979).

9) T. M. Balthazor and R. C. Grabiak, *J. Org. Chem.*, **45**, 5425 (1980).

10) a) H. L. Slates and N. L. Wendler, *Chem. Ind. (London)*, **1978**, 430; b) E. J. Glamkowski, G. Gal, R. Purick, A. J. Devidson, and M. Sletzinger, *J. Org. Chem.*, **35**, 3510 (1970).

11) S.-I. Murahashi, M. Yamamura, K. Yanagisawa, N. Mita, and K. Kondo, *J. Org. Chem.*, **44**, 2408 (1979), references therein.

12) W. E. Walker, R. M. Manyik, K. E. Atkins, and M. L. Farmer, *Tetrahedron Lett.*, **1970**, 3817; J. Tsuji, M. Hara, and K. Ohno, *Tetrahedron*, **30**, 2143 (1974).

13) H. Neumann and D. Seebach, *Chem. Ber.*, **111**, 2785 (1978).

14) W. P. Norris, *J. Org. Chem.*, **24**, 1579 (1959).

15) D. R. Coulson, *Inorg. Synth.*, **13**, 121 (1972).

16) A. Sh. Mukhtarov, A. V. Il'yasov, Ya. A. Levin, A. A. Vafina, and S. S. Krokhina, *Zh. Strukt. Khim.*, **17**, 76 (1976).

17) R. A. Naylor and A. Williams, *J. Chem. Soc., Perkin Trans. 2*, **1976**, 1908.

18) D. J. Collins, J. W. Hetherington, and J. M. Swan, *Aust. J. Chem.*, **27**, 1355 (1974).

19) M. Mikolajczyk, S. Grzejszczak, W. Midura, and A. Zatorski, *Synthesis*, **1976**, 396.

20) D. J. Martin, M. Gordon, and C. E. Griffin, *Tetrahedron*, **23**, 1831 (1967).

An X-Ray Crystallographic Study on *cis-trans* Configurational Assignment to "*cis*-" and "*trans*-1,8-Terpins"[1] and a Proposal of New Designation for Discriminating between the Configurational Isomers

Takayuki Suga,* Toshifumi Hirata, and Tadashi Aoki
Department of Chemistry, Faculty of Science, Hiroshima University, Higashisenda-machi, Naka-ku, Hiroshima 730

(Received August 5, 1981)

The crystal structures of "*cis*-terpin" (terpin hydrate) and "*trans*-terpin" were elucidated by X-ray crystallography. This crystal structure elucidation showed that the hydroxyl group at C-1 and the 1-hydroxy-1-methylethyl group at C-4 are in *cis* and *trans* relationships in the "*cis*-" and "*trans*-1,8-terpin" molecules, respectively, similarly to the structures in solutions. A new designation for discriminating between the configurational isomers is proposed on the ground of the IUPAC Rule for Nomenclature.

It has been documented[2-5] that "*cis*-1,8-terpin" and "*trans*-1,8-terpin" are configurational isomers represented by structures (**1**) and (**2**), respectively and that the spatial arrangement of the hydroxyl group at C-1 and the 1-hydroxy-1-methylethyl group at C-4 of **1** was deduced to be *cis* on the basis of the preferential formation of 1,8-cineol (**3**) from **1** on reaction with aqueous sulfuric acid. The stereochemistry of these 1,8-terpins had been deduced by the ease of ring closure to the cineol. However, a controversy as to the stereochemical structure of these terpins was raised on the ground of observation that 1,8-cineol (**3**) had also been produced from "*trans*-1,8-terpin" (**2**) under the same acidic conditions.[6] Reexamination of the *cis-trans* configurational assignment of these terpins by the ^{1}H NMR method[6,7] dispelled the ambiguity, bearing out the earlier assigned structures. All the studies hitherto done have dealt with the configuration of 1,8-terpins in solutions. In order to clarify unambiguously the configurational isomer of "*cis*-" and "*trans*-1,8-terpins," the determination of the molecular structures of the "1,8-terpins" was made by X-ray crystallographic analyses. On the other hand, there have been various designations and no consistency among the nomenclatures[3,8,9] of the "1,8-terpins." A new designation for discriminating between these 1,8-terpins is, therefore, required to standardize their nomenclature.

In this paper, we will deal with the configurational assignment of "*cis*-" and "*trans*-1,8-terpins" in the crystals and propose a new designation for discriminating between the configurational isomers of the "1,8-terpins."

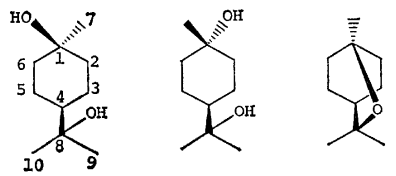

1 **2** **3**

Results and Discussion

*Molecular and Crystal Structures of **1** and **2**.* Crystallographic analyses of "*cis*-1,8-terpin" (**1**) and "*trans*-1,8-terpin" (**2**) were performed by the direct method

Table 1. Final atomic coordinates ($\times 10^4$) and thermal parameters of **1**, with standard deviations in parentheses

(1) The non-hydrogen atoms.

Atom	x	y	z	B_{eq}[a)]/Å^2
C (1)	10261 (3)	1481 (2)	381 (2)	3.0
C (2)	10079 (4)	1492 (2)	−281 (2)	3.9
C (3)	9962 (4)	2250 (2)	−531 (2)	3.5
C (4)	11055 (3)	2735 (2)	−361 (1)	2.8
C (5)	11212 (3)	2736 (2)	308 (1)	3.1
C (6)	11332 (3)	1971 (2)	544 (2)	3.3
C (7)	10439 (5)	713 (2)	612 (2)	4.7
C (8)	10977 (3)	3500 (2)	−631 (2)	3.2
C (9)	9838 (4)	3924 (2)	−447 (2)	4.6
C (10)	11081 (4)	3479 (2)	−1299 (2)	4.4
O (1)	9149 (2)	1773 (1)	626 (1)	3.4
O (2)	11990 (2)	3930 (1)	−410 (1)	3.2
O (3)	9495 (4)	2095 (2)	1779 (1)	5.3

a) $B_{eq}=8\pi^2(U_1+U_2+U_3)/3$, where U_1, U_2, and U_3 are the principal components of U matrix.

(2) The hydrogen atoms.

Atom	x	y	z	B/Å^2
H[C(2)]	1847 (36)	1348 (19)	2138 (16)	4.2
H[C(2)]	3260 (33)	1251 (18)	2030 (14)	3.6
H[C(3)]	2449 (38)	270 (20)	1495 (16)	5.0
H[C(3)]	4212 (33)	2528 (19)	362 (15)	4.0
H[C(4)]	6742 (28)	2487 (15)	516 (12)	1.8
H[C(5)]	9412 (29)	490 (14)	2112 (12)	1.9
H[C(5)]	8000 (38)	470 (21)	2003 (16)	4.3
H[C(6)]	1422 (35)	2012 (18)	1032 (15)	4.3
H[C(6)]	1958 (33)	1772 (17)	410 (14)	2.9
H[C(7)]	9803 (43)	374 (21)	481 (18)	6.7
H[C(7)]	498 (40)	681 (20)	1062 (16)	5.4
H[C(7)]	1138 (34)	450 (18)	466 (14)	3.7
H[C(9)]	5414 (39)	1802 (21)	1450 (16)	5.3
H[C(9)]	6097 (34)	1000 (18)	1443 (14)	3.4
H[C(9)]	6787 (37)	1740 (19)	1400 (15)	4.1
H[C(10)]	4909 (42)	582 (21)	645 (18)	7.0
H[C(10)]	4210 (39)	1261 (20)	573 (17)	4.3
H[C(10)]	4763 (38)	1009 (20)	9 (17)	6.2
H(1)	9210 (46)	1798 (23)	990 (19)	7.0
H(2)	7532 (37)	1226 (20)	512 (15)	4.0
H(3)	9559 (53)	1930 (27)	2189 (22)	10.9
H(4)	9908 (31)	2146 (16)	1782 (13)	2.9

Table 2. Bond lengths and angles of **1**, with standard deviations in parentheses

Bond length(l/Å)		Bond angle(ϕ/°)	
C(1)-C(2)	1.520(5)	C(2)-C(1)-C(6)	109.3(3)
C(1)-C(6)	1.524(5)	C(2)-C(1)-C(7)	111.8(3)
C(1)-C(7)	1.523(5)	C(2)-C(1)-O(1)	105.6(3)
C(1)-O(1)	1.442(4)	C(6)-C(1)-C(7)	111.6(3)
C(2)-C(3)	1.514(5)	C(6)-C(1)-O(1)	109.4(3)
C(3)-C(4)	1.541(5)	C(7)-C(1)-O(1)	108.6(3)
C(4)-C(5)	1.534(5)	C(1)-C(2)-C(3)	113.3(3)
C(4)-C(8)	1.541(5)	C(2)-C(3)-C(4)	112.0(3)
C(5)-C(6)	1.514(5)	C(3)-C(4)-C(5)	109.7(3)
C(8)-C(9)	1.529(6)	C(3)-C(4)-C(8)	112.7(3)
C(8)-C(10)	1.528(5)	C(5)-C(4)-C(8)	113.7(3)
C(8)-O(2)	1.452(4)	C(4)-C(5)-C(6)	111.1(3)
		C(5)-C(6)-C(1)	113.5(3)
		C(4)-C(8)-C(9)	113.8(3)
		C(4)-C(8)-C(10)	111.8(3)
		C(4)-C(8)-O(2)	108.6(3)
		C(9)-C(8)-C(10)	110.3(3)
		C(9)-C(8)-O(2)	104.3(3)
		C(10)-C(8)-O(2)	107.6(3)

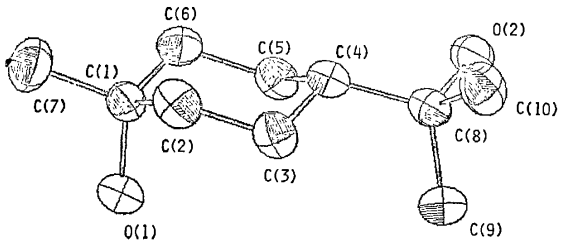

Fig. 1. ORTEP drawing of the molecular structure of "*cis*-1,8-terpin" (**1**).

using MULTAN.[10] Final atomic coordinates, bond lengths, and bond angles are given in Tables 1 and 2 for **1**, and Tables 3 and 4 for **2**. The perspective view (Fig. 1) of the "*cis*-terpin" molecule showed that the hydroxyl group at C-1 is *cis* to the 1-hydroxy-1-methylethyl group at C-4. This corroborates the previously assigned configurational isomer[3-9] of "*cis*-1,8-terpin." Furthermore, it was found that the hydroxyl group at C-1 and the 1-hydroxy-1-methylethyl group at C-4 are axial and equatorial, respectively and also the C-8 hydroxyl group is gauche to the hydrogen atom at C-4. Each hydroxyl group at C-1 and C-8 is linked by intermolecular hydrogen bonding to water of crystallization, as shown in Fig. 2. On the other hand, H(2) is linked to O(1)′ by intermolecular hydrogen bonding. The molecules of the "1,8-terpin" are packed along the a axis and the crystal structure is stabilized by the network of hydrogen bondings (Fig. 2).

On the other hand, the perspective view (Fig. 3) of a molecule of "*trans*-terpin" indicated that the hydroxyl group at C-1 is *trans* to the 1-hydroxy-1-methylethyl group at C-4. Both the hydroxyl group at C-1 and the 1-hydroxyl-1-methylethyl group at C-4 are equatorially oriented, and the C-8 hydroxyl group is gauche to the C-4 hydrogen atom similarly to the

Table 3. Final atomic coordinates ($\times 10^4$) and thermal parameters of **2**, with standard deviations in parentheses

(1) The non-hydrogen atoms.

Atom	x	y	z	B_{eq}[a]/Å^2
C (1)	1200(2)	1324(6)	1428(2)	2.3
C (2)	1807(2)	3108(5)	1425(2)	2.5
C (3)	2548(2)	2400(5)	1137(2)	2.7
C (4)	2931(2)	462(5)	1540(2)	2.0
C (5)	2330(2)	−1357(5)	1509(2)	2.4
C (6)	1593(2)	−637(6)	1804(2)	2.5
C (7)	784(2)	793(7)	689(2)	3.4
C (8)	3718(2)	−236(6)	1313(2)	2.7
C (9)	4318(2)	1568(8)	1429(3)	5.0
C (10)	3614(2)	−1030(8)	553(2)	4.5
O (1)	582(1)	2072(4)	1795(1)	3.2
O (2)	3988(1)	−2027(4)	1758(1)	3.3

a) $B_{eq}=8\pi^2(U_1+U_2+U_3)/3$, where U_1, U_2, and U_3 are the principal components of U matrix.

(2) The hydrogen atoms.

Atom	x	y	z	B/Å^2
H[C(2)]	1558(20)	4295(62)	1127(18)	3.1
H[C(2)]	1974(17)	3590(51)	1944(15)	2.0
H[C(3)]	2898(18)	3673(54)	1167(16)	3.5
H[C(3)]	2420(20)	2119(63)	598(18)	3.2
H[C(4)]	3097(20)	939(61)	2092(18)	1.8
H[C(5)]	2594(20)	−2617(62)	1823(18)	2.6
H[C(5)]	2189(20)	1866(61)	991(18)	3.0
H[C(6)]	1231(20)	−1751(60)	1816(18)	3.7
H[C(6)]	1777(20)	−237(62)	2363(18)	2.4
H[C(7)]	1130(18)	258(56)	373(17)	3.9
H[C(7)]	379(19)	−328(60)	676(17)	4.9
H[C(7)]	536(20)	2272(63)	463(19)	7.1
H[C(9)]	4742(20)	1111(61)	1368(18)	3.9
H[C(9)]	4132(20)	3054(63)	1041(19)	8.8
H[C(9)]	4384(21)	2093(66)	1984(19)	6.8
H[C(10)]	3419(21)	77(64)	213(19)	7.3
H[C(10)]	3244(22)	−2215(69)	440(20)	7.1
H[C(10)]	4109(20)	−1366(61)	419(18)	4.6
H(1)	789(19)	2460(64)	2235(18)	5.5
H(2)	4425(21)	−2300(64)	1737(18)	5.5

case of **1**. As shown in Fig. 4, the "*trans*-1,8-terpin" molecules form an infinite chain along the a axis by intermolecular hydrogen bonding. The chain is coupled with the next chain by other intermolecular hydrogen bonding to form pairs of the chain. These pairs build up the layered structure by the van der Waals force among the hydrophobic groups.

A Proposal of New Designation for Discriminating between "cis-" *and* "trans-*1,8-Terpins.*" 1,8-Terpins have two different substituents, such as the methyl and the hydroxyl groups, at the 1-position. For designating the steric relationship of these terpins, an arbitrary selection of these two substituents as the reference substituent has thrown the nomenclature of the terpins in confusion. The IUPAC Rule for Nomenclature (E. 2.3.4.)[11] has recommended that,

Table 4. Bond lengths and angles of **2**, with standard deviations in parentheses

Bond length(l/Å)		Bond angle(ϕ/°)	
C(1)-C(2)	1.524(5)	C(2)-C(1)-C(6)	109.5(3)
C(1)-C(6)	1.525(5)	C(2)-C(1)-C(7)	112.0(3)
C(1)-C(7)	1.530(5)	C(2)-C(1)-O(1)	108.7(3)
C(1)-O(1)	1.442(4)	C(6)-C(1)-C(7)	112.3(3)
C(2)-C(3)	1.531(4)	C(6)-C(1)-O(1)	109.3(3)
C(3)-C(4)	1.531(5)	C(7)-C(1)-O(1)	104.9(3)
C(4)-C(5)	1.528(4)	C(1)-C(2)-C(3)	113.5(3)
C(4)-C(8)	1.546(4)	C(2)-C(3)-C(4)	111.0(3)
C(5)-C(6)	1.534(4)	C(3)-C(4)-C(5)	109.3(3)
C(8)-C(9)	1.517(5)	C(3)-C(4)-C(8)	113.8(3)
C(8)-C(10)	1.534(5)	C(5)-C(4)-C(8)	113.2(3)
C(8)-O(2)	1.442(4)	C(4)-C(5)-C(6)	111.1(3)
		C(5)-C(6)-C(1)	112.8(3)
		C(4)-C(8)-C(9)	110.6(3)
		C(4)-C(8)-C(10)	112.7(3)
		C(4)-C(8)-O(2)	105.3(3)
		C(9)-C(8)-C(10)	110.9(3)
		C(9)-C(8)-O(2)	109.7(3)
		C(10)-C(8)-O(2)	107.5(3)

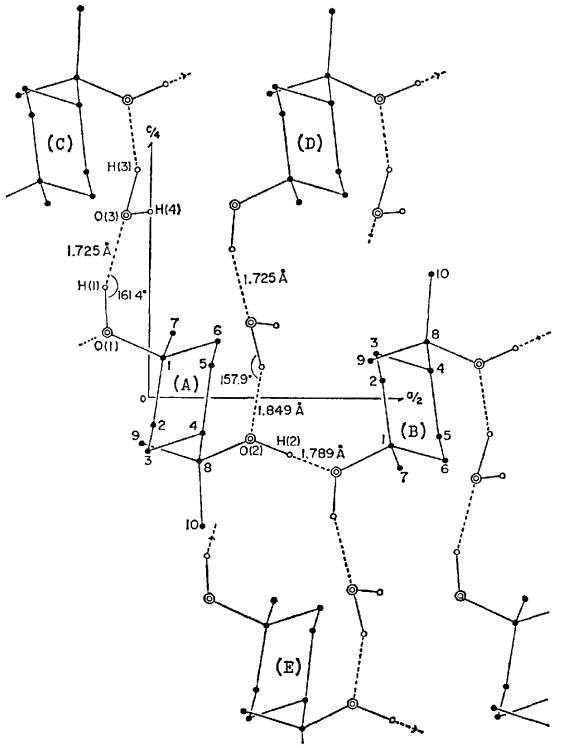

Fig. 2. Projection of **1** viewed along the b axis. The atoms indicated with ●, ◎, and ○ denote carbon, oxygen, and hydrogen atoms, respectively. The transformations of the atomic coordinates are (A) x, y, z; (B) $1/2+x$, $1/2-y$, $-z$; (C) $-1/4+x$, $-1/4+y$, $1/4-z$; (D) $1/4+x$, $1/4+y$, $1/4-z$; (E) $1/4+x$, $3/4-y$, $-1/4+z$.

when two different substituents locate at the same position of a monocycle, a characteristic group or a predominant substituent in the sequence rule is

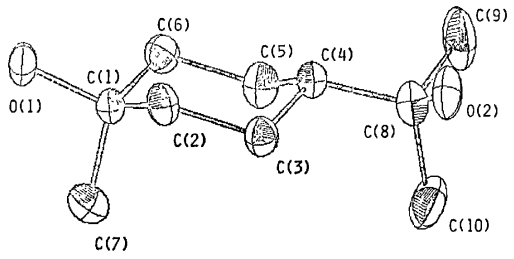

Fig. 3. ORTEP drawing of the molecular structure of "*trans*-1,8-terpin" (**2**).

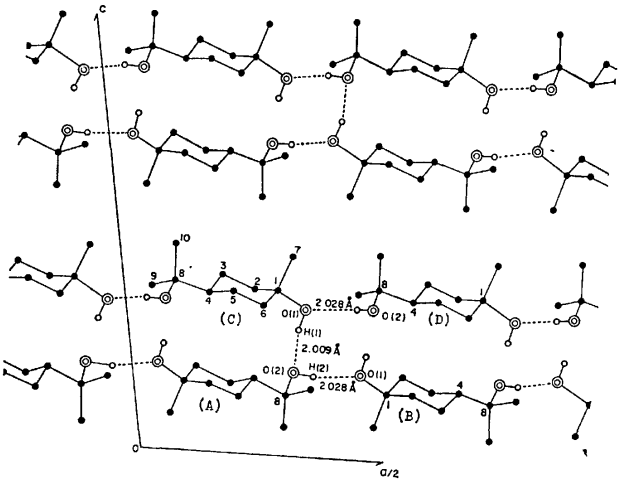

Fig. 4. Projection of **2** viewed along the b axis. The atoms indicated with ●, ◎, and ○ denote carbon, oxygen, and hydrogen atoms, respectively. The transformations of the atomic coordinates are (A) x, y, z; (B) $1/2+x$, $-1/2+y$, z; (C) $1/2-x$, $1/2+y$, $1/2-z$; (D) $1-x$, $1+y$, $1/2-y$.

expressed by adding *r* as the reference substituent and a substituent being in the *cis* or *trans* relationship to this reference substituent is expressed by *c* or *t*, instead of *cis* or *trans*, respectively. According to the IUPAC Rule, therefore, "*cis*-terpin" (**1**) should be represented as *c*-4-(1-hydroxy-1-methylethyl)-1-methyl-*r*-1-cyclohexanol and "*trans*-terpin" (**2**) as *t*-4-(1-hydroxy-1-methylethyl)-1-methyl-*r*-1-cyclohexanol. In the case of using *p*-menthane as a conventional name, **1** and **2** are called *c*-4-*p*-menthane-*r*-1,8-diol and *t*-4-*p*-menthane-*r*-1,8-diol, respectively. However, it is hard to exclude the designation of "terpin" for the reason that this designation has been most widely used for a long time among chemists in the field of terpenoids. For the nomenclature of compounds **1** and **2** by using the appellation of "terpin," we will propose that "*cis*-1,8-terpin" (**1**) is expressed as *c*-1,8-terpin and "*trans*-1,8-terpin" (**2**) as *t*-1,8-terpin, hereafter.

Experimental

Material. "*cis*-1,8-Terpin" (**1**), mp 105—106 °C (lit,[6] 104—105 °C), used for X-ray analysis was obtained by repeated recrystallization of the commercial terpin hydrate (Yoneyama Kogyo Yakuhin Co. Ltd.). "*trans*-1,8-Terpin" (**2**), mp 157—158 °C (lit,[12] 158—159 °C), was prepared from 1,8-cineol (**3**) according to the literature method[12]

and purified by repeated recrystallization. A single crystal of **1** and **2** for X-ray studies was prepared by crystallization from hot water. Spectroscopic data (IR and ^{1}H NMR) of each compound were identical with the data[6,7] reported for the corresponding terpins.

Crystallographic Measurements. The crystallographic analyses were performed on a Syntex R3 diffractometer using graphite-monochromated Mo $K\alpha$ radiation. Cell dimensions were derived by the least-squares method from setting angles of 18 well-centered diffraction peaks for **1** and 15 peaks for **2**. Intensity data were collected by ω-scan ($\theta_{max}=58.0°$), and $I_0>1.96\sigma(I_0)$ were used as observed reflections; 1091 reflections for **1** and 1261 reflections for **2**.

Crystal Data of ***1***. $C_{10}H_{20}O_2\cdot H_2O$, $M=190.28$. Crystal dimensions 0.20 mm×0.25 mm×0.23 mm. Orthorhombic, $a=10.930(2)$, $b=18.425(5)$, $c=22.791(6)$ Å, $U=4589.8$ Å^3, $D_c=1.03$ g cm^{-3}, $Z=16$, $D_m=1.08$ g cm^{-3}, μ(Mo $K\alpha$)=0.8 cm^{-1}. Space group Fdd2.

Crystal Data of ***2***. $C_{10}H_{20}O_2$, $M=172.26$. Crystal dimensions 0.47 mm×0.50 mm×0.30 mm. Monoclinic, $a=17.167(2)$, $b=6.233(2)$, $c=19.325(6)$ Å, $\beta=98.910(2)°$, $U=2043.1$ Å^3, $D_c=1.12$ g cm^{-3}, $Z=8$, $D_m=1.16$ g cm^{-3}, μ(Mo $K\alpha$)=0.8 cm^{-1}. Space group C2/c.

Structure Analyses and Refinements. The phases of 106 reflections with $|E|>1.65$ for **1** and 172 reflections with $|E|>1.80$ for **2** were determined by MULTAN.[10] An E map for the best solution yielded positions for all atoms except hydrogens. These atomic parameters were anisotropically refined, followed by a difference map to find the positions of all hydrogen atoms. Anisotropic refinement for carbon and oxygen atoms and isotropic refinement for hydrogen atom by full-matrix least-squares calculation reduced the R index finally to 0.044 for **1** and 0.049 for **2**.

The complete F_o-F_c data and the tables of anisotropic thermal parameters for **1** and **2** are deposited as Document No. 8208 at the Office of the Editor of the Bulletin of the Chemical Society of Japan.

References

1) The double quotation marks denote the long-standing trivial names used for 1,8-terpins.
2) J. L. Simonsen, "The Terpenes," Cambridge Univ. Press, London (1947), Vol. I, p. 300.
3) C. S. Barnes, *Aust. J. Chem.*, **11**, 134 (1958).
4) R. Lombard and G. Ambrose, *Bull. Soc. Chim. Fr.*, **1961**, 230.
5) A. R. Pinder, "The Chemistry of Terpenes," Chapman & Hall, London (1961), p. 54.
6) B. Singaram, P. M. Abraham, G. M. Saraswathi, and J. Verghese, *Indian J. Chem.*, **14B**, 934 (1976).
7) C. P. Methew and J. Verghese, *Indian J. Chem.*, **17B**, 174 (1979).
8) A. Baeyer, *Ber.*, **26**, 2861 (1893).
9) G. Wagner, *Ber.*, **27**, 1636 (1894).
10) G. Germain, P. Main, and M. M. Woolfson, *Acta Crystallogr., Sect. A*, **27**, 368 (1971).
11) "Rules for the Nomenclature of Organic Chemistry. The IUPAC 1974 Recommendation for Section E (Fundamental Stereochemistry)," by the IUPAC Commission on the Nomenclature of Organic Chemistry (1974).
12) T. Matsuura, H. Komae, and K. Saito, *Bull. Chem. Soc. Jpn.*, **31**, 990 (1958).

Preparation of Homologs of L-2-Amino-5-(*p*-methoxyphenyl)pentanoic Acid

Nobuo Kosui,* Michinori Waki, Tetsuo Kato, and Nobuo Izumiya

Laboratory of Biochemistry, Faculty of Science, Kyushu University 33, Higashi-ku, Fukuoka 812

(Received August 15, 1981)

Lower and higher homologs, L-2-amino-4-(*p*-methoxyphenyl)butanoic acid (L-Amb) and L-2-amino-6-(*p*-methoxyphenyl)hexanoic acid (L-Amh), of L-2-amino-5-(*p*-methoxyphenyl)pentanoic acid were prepared by optical resolution of *N*-acetyl-DL-Amb and of *N*-acetyl-DL-Amh with *Aspergillus* acylase. *N*-Acetyl-DL-Amb or *N*-acetyl-DL-Amh was synthesized from [2-(*p*-methoxyphenyl)ethyl or butyl](acetamido)malonic acid by heating with *p*-xylene.

AM-Toxin I is a host specific phytotoxin, its structure being determined as *cyclo*(-L-Amp[1]-ΔAla[2]-L-Ala[3]-L-Hmb[4]-).[1] Shimohigashi *et al.* synthesized AM-toxin I[2] and its analog, [L-Tyr(Me)[1]]-AM-toxin,[3] and observed that [L-Tyr(Me)[1]]-AM-toxin showed extremely weak necrotic activity toward apple leaves. This finding implies that the methylene length of side chain in L-Amp affects the necrotic activity. Therefore, it is interesting to synthesize L-Amb or L-Amh, which is a lower or higher homolog of L-Amp (Fig. 1), in an attempt to prepare an AM-toxin analog containing an aromatic amino acid residue with a different methylene chain.

Only DL-Amb has been synthesized by Strecker's method,[4] but none of L-Amb, DL- and L-Amh have been prepared so far. This paper deals with the preparation of *N*-acetyl-DL-Amb (Ac-DL-**1a**) and *N*-acetyl-DL-Amh (Ac-DL-**1b**) and their optical resolution by acylase (Fig. 2). The procedure used for resolution is similar to that used for the preparation of L-Amp.[5] In the synthesis of diethyl [2-(*p*-methoxyphenyl)ethyl](acetamido)malonate (**3a**) from arylalkyl bromide (**2a**) and diethyl acetamidomalonate (**5**), we suffered from relatively low yield (27%). In contrast, diethyl [4-(*p*-methoxyphenyl)butyl](acetamido)-malonate (**3b**) in the present study and diethyl [3-(*p*-methoxyphenyl)propyl](acetamido)malonate reported in the previous paper[5] were synthesized in moderate yields of 66% and 64% from the corresponding bromide and the malonate (**5**), respectively. We found that the reaction mixture of the bromide (**2a**) and the malonate (**5**) contained a decarboxylated product (DL-**6**) besides the desired **3a**. The malonic acid derivative (**4a** or **4b**) was obtained in good yield from the diester derivative (**3a** or **3b**) by complete saponification with excess sodium hydroxide. The important intermediate Ac-DL-**1a** or Ac-DL-**1b** was prepared in good yield from **4a** or **4b** by heating in *p*-xylene.

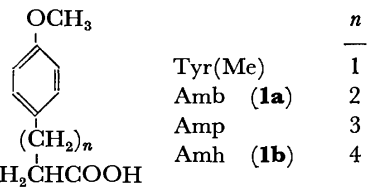

Fig. 1. Structure of homologs of Amp.

Prior to the preparative resolution of Ac-DL-**1a** and Ac-DL-**1b** by *Aspergillus* acylase, the rates of hydrolysis of two substrates were determined using Ac-DL-Tyr(Me) and Ac-DL-Amp as reference substrates, the results being shown in Table 1. It is observed that the rates of hydrolysis are decreased with the increase of the methylene length of side chain in aromatic amino acids. Although Ac-L-**1b** was less susceptible than Ac-L-Tyr(Me), the results indicate that optical resolution of Ac-DL-**1b** is achieved with an increased amount of the acylase. Ac-DL-**1a** or Ac-DL-**1b** was subjected to the action of the acylase, the desired L-amino acid (L-**1a** or L-**1b**) being obtained in a yield of 82% or 81% (Fig. 2). *N*-Acetyl-D-amino acid (Ac-D-**1a** or Ac-D-**1b**) was isolated from the mother liquor, and subsequently D-amino acid (D-**1a** or D-**1b**), which

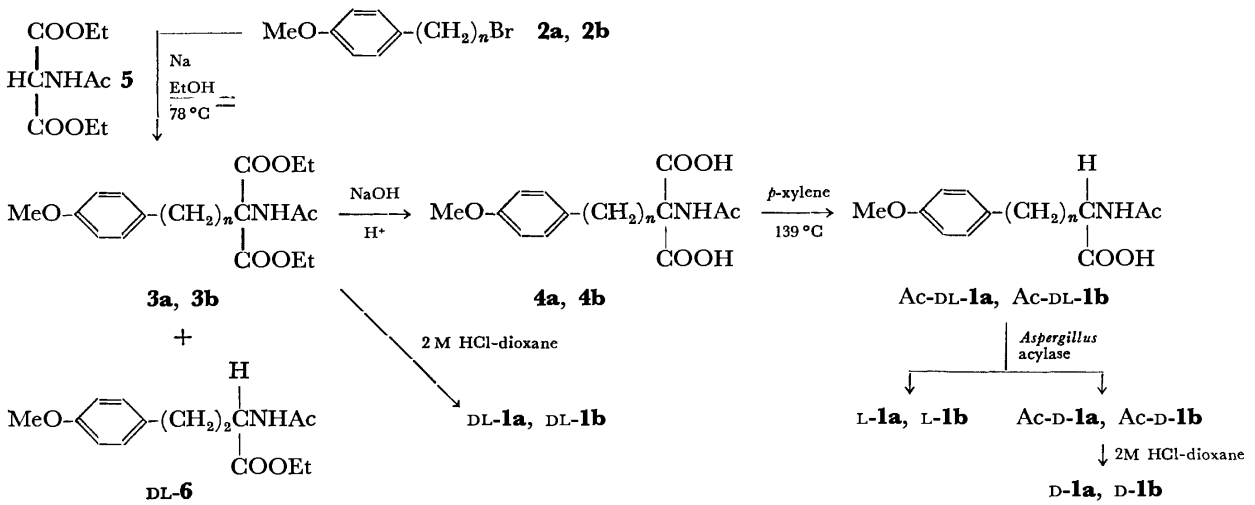

Fig. 2. Synthesis and resolution of *N*-acetyl-DL-amino acids (Ac-DL-**1a**, Ac-DL-**1b**). **a**: $n=2$, **b**: $n=4$.

Table 1. Proteolytic coefficients (C_0) of acetylamino acids by *Aspergillus* acylase

Substrate	C_0[a] at 0.01 M[b]
Ac-DL-Tyr(Me)	28 (100)[c]
Ac-DL-**1a**	24 (86)
Ac-DL-Amp	14 (50)
Ac-DL-**1b**	12 (43)

a) $C_0=K_0/E$ where $K_0=\%$ hydrolysis$\times$min^{-1} of $E=$mg protein $N\times$ml^{-1}; pH 7.3, temp 38 °C. b) Concentration of L-form of substrate. c) The values in the parentheses indicate the relative hydrolytic rate.

is also useful compound for synthesis of AM-toxin analogs, was prepared from Ac-D-**1a** or Ac-D-**1b** by heating in 6 M HCl.

Experimental

All the melting and boiling points are uncorrected. TLC was carried out on silica gel (Merck) with the following solvent systems: R_f^1, benzenea–cetone (1:1); R_f^2, 1-butanol–AcOH–pyridine–H_2O (4:1:1:2). Paper chromatography was carried out on Toyo Roshi No. 52 paper with the following solvent systems: R_f^3, the same solvent as used for R_f^2; R_f^4, 1-butanol–AcOH–pyridine–H_2O (15:3:10:12). The ratio in parenthesis is given in terms of volume. Powder of *Aspergillus* acylase was obtained from Kyowa Hakko Co., Ltd.

*2-(p-Methoxyphenyl)ethyl Bromide (**2a**).* 2-(*p*-Methoxyphenyl)ethanol (**7**) was synthesized following the literature;[6] yield, 76%; bp 121—125 °C/7 mmHg.† Compound **2a** was synthesized from **7** (0.69 mol) and PBr_3 (0.345 mol) by a slight modification of the literature;[7] yield, 77%; bp 122 °C/9 mmHg. In the literature,[7] PBr_5 had been used.

*4-(p-Methoxyphenyl)-1-butanol (**8**).* 4-Oxo-4-(*p*-methoxyphenyl)butanoic acid (**9**) was synthesized from anisole and succinic anhydride by a slight modification of the literature,[8] yield, 89%; mp 142—143 °C. 1-Nitropropane had been used as a solvent in the literature,[8] but anisole was used as a reagent and also as a solvent for the present synthesis of **9**. 4-(*p*-Methoxyphenyl)butanoic acid (**10**) was synthesized from **9** with amalgamated Zn following the literature;[9] yield, 88%; mp 60—61 °C. Compound **8** was synthesized from **10** following the literature.[10] However, the procedure will be described here because the description in the literature was not enough to carry out the experimental work. To a suspension of $LiAlH_4$ (4.75 g, 0.125 mol) in anhydrous ether (180 ml) was added portionwise **10** (19.4 g, 0.1 mol) in ether (450 ml) at 0 °C under stirring within 1 h. The mixture was stirred at 0 °C for another 4 h. Water (300 ml) was added to decompose an excess $LiAlH_4$. To the mixture was added 10% H_2SO_4 (150 ml) and insoluble material was filtered off. The ethereal layer was separated, and the aqueous layer was extracted with ether. The combined ethereal solution was washed with 2 M NaOH, water, and dried (Na_2SO_4). After removal of the solvent, distillation under reduced pressure gave **8**; yield, 13.2 g (73%); bp 135—140 °C/4 mmHg; mp 4 °C. Literature, mp 3—4 °C.[10]

*4-(p-Methoxyphenyl)butyl Bromide (**2b**).* To a solution of **8** (48.3 g, 0.268 mol) in CCl_4 (54 ml) was added dropwise PBr_3 (30.6 g, 0.113 mol) in CCl_4 (27 ml) at 50—55 °C under stirring within 4 h. The mixture was stirred at 40—50 °C for another 2 h and CCl_4 was evaporated. The residue was dissolved in ether, and the solution was washed with water, dried (Na_2SO_4), and evaporated. Then distillation under reduced pressure gave **2b**; yield, 56.3 g (86%); bp 125—130 °C/3 mmHg.

Found: C, 54.13; H, 6.34%. Calcd for $C_{11}H_{15}OBr$: C, 54.34; H, 6.22%.

*Diethyl [2-(p-Methoxyphenyl)ethyl](acetamido)malonate (**3a**).* To a solution of Na (14.4 g, 0.626 mol) in absolute EtOH (840 ml) was added diethyl acetamidomalonate (**5**) (114 g, 0.523 mol) under stirring. A solution of **2a** (113 g, 0.523 mol) in absolute EtOH (260 ml) was added to the previous solution within 1 h. The reaction mixture was stirred under reflux for 8 h, and the precipitate was filtered off and washed with EtOH. The combined filtrates were evaporated *in vacuo* to give an oil which was crystallized by the addition of water and petroleum ether. The product was recrystallized from EtOH–water; yield, 49.4 g (27%); mp 81—84 °C; R_f^1 0.72.

Found: C, 61.39; H, 7.12; N, 3.98%. Calcd for $C_{18}H_{25}O_6N$: C, 61.52; H, 7.17; N, 3.99%.

Ethyl DL-*2-Acetamido-4-(p-methoxyphenyl)butanoate (*DL-*6*).* This was obtained from **2a** (3.9 g, 18 mmol) and **5** (3.9 g, 18 mmol) as described for **3a** except that the reaction mixture was refluxed for 4 d; yield, 1.1 g (22%); mp 94—96 °C; R_f^1 0.66.

Found: C, 63.99; H, 7.49; N, 4.90%. Calcd for $C_{15}H_{21}O_4N$: C, 64.49; H, 7.58; N, 5.01%.

*Diethyl [4-(p-Methoxyphenyl)butyl](acetamido)malonate (**3b**).* This was prepared from **2b** (40.2 g, 0.165 mol) and **5** (35.8 g, 0.165 mol) as described for **3a**. The product was recrystallized from EtOH–water; yield, 41.0 g (66%); mp 37—40 °C; R_f^1 0.83.

Found: C, 63.01; H, 7.72; N, 3.70%. Calcd for $C_{20}H_{29}O_6N$: C, 63.30; H, 7.70; N, 3.69%.

*[2-(p-Methoxyphenyl)ethyl](acetamido)malonic Acid (**4a**).* A solution of **3a** (16.0 g, 46 mmol) and 2 M NaOH (230 ml) in EtOH (500 ml) was allowed to stand at 38 °C for 3 d until none of **3a** and the intermediate 2-acetamido-2-ethoxycarbonyl-4-(*p*-methoxyphenyl)butanoic acid (R_f^2 0.65) were detected in the reaction mixture. The solution was evaporated and acidified with 6 M HCl (138 ml). The liberated oil was extracted with EtOAc and the extract was washed with water, dried (Na_2SO_4), and evaporated. The residue was crystallized by the addition of ether and petroleum ether; yield, 10.5 g (78%); mp 124—126 °C; R_f^2 0.53. Compound **4a** was unstable; on being left to stand at room temperature for 10 d, purified crystals of **4a** gave a small amount of decarboxylated material (Ac-DL-**1a**). The values of elemental analysis of crystalline **4a** deviated from the calculated ones as **4a**.

*[4-(p-Methoxyphenyl)butyl](acetamido)malonic Acid (**4b**).* This was prepared from **3b** (8.1 g, 21.3 mmol) as described for **4a**; yield, 6.1 g (88%); mp 102—103 °C; R_f^2 0.66. Compound **4b** was unstable and its property was similar to **4a**.

DL-*2-Acetamido-4-(p-methoxyphenyl)butanoic Acid (Ac-*DL-*1a).* Compound **4a** (3.0 g, 10.2 mmol) suspended in *p*-xylene (100 ml) was refluxed for 2 h. After being cooled to room temperature, crystals were collected and washed with petroleum ether; yield, 1.96 g (77%); mp 144—145 °C; R_f^2 0.73.

Found: C, 62.03; H, 6.86; N, 5.52%. Calcd for $C_{13}H_{17}O_4N$: C, 62.14; H, 6.82; N, 5.57%.

DL-*2-Acetamido-6-(p-methoxyphenyl)hexanoic Acid (Ac-*DL-*1b).* This was prepared from **4b** (5.87 g, 18.2 mmol) as described for Ac-DL-**1a**; yield, 4.02 g (79%); mp 93—94 °C; R_f^2 0.83.

Found: C, 64.49; H, 7.57; N, 4.96%. Calcd for $C_{15}H_{21}O_4N$: C, 64.49; H, 7.58; N, 5.01%.

† 1 mmHg≈133.322 Pa.

*DL-2-Amino-4-(p-methoxyphenyl)butanoic Acid (DL-**1a**).* A suspension of Ac-DL-**1a** (100 mg, 0.4 mmol) in a mixture of 2 M HCl (20 ml) and dioxane (20 ml) was refluxed on an oil bath at 110 °C for 15 h. The solution was evaporated *in vacuo* several times by the addition of water. The residual solid was recrystallized from 1 M HCl–1 M aqueous Et_3N; yield, 70.3 mg (84%); mp 244—245 °C (dec); R_f^3 0.82, R_f^4 0.76. Literature, mp 245—246 °C.[4]

*DL-2-Amino-6-(p-methoxyphenyl)hexanoic Acid (DL-**1b**).* This was prepared from Ac-DL-**1b** (279 mg, 1 mmol) as described for DL-**1a**; yield, 205 mg (87%); mp 253—254 °C (dec); R_f^3 0.93, R_f^4 0.88.

Found: C, 65.69; H, 8.21; N, 5.82%. Calcd for $C_{13}H_{19}O_3N$: C, 65.80; H, 8.07; N, 5.90%.

Determination of Proteolytic Coefficient (C_0) by Acylase. In a 2-ml flask, an *N*-acetyl-DL-amino acid (0.04 mmol) and 0.2 M NaOH (0.2 ml) were added. Further, 1/7 M Na barbital buffer (1 ml) of pH 7.5, 1/40 M $CoCl_2$ (0.1 ml), and an aqueous enzyme solution (0.2 ml) containing the acylase (0.2 mg) were added. The solution was made up to 2.0 ml with the buffer. The reaction mixture was incubated at 38 °C, aliquots being withdrawn at selected intervals. The rate of appearance of free amino acid was followed by a Hitachi amino acid analyzer KLA-5: column, 0.6 cm × 10 cm; buffer, standard 0.2 M Na citrate at pH 5.28. The hydrolysis of substrates follows zero-order kinetics within experimental error, the results being shown in Table 1.

*Resolution of Ac-DL-**1a**.* L-**1a**: Ac-DL-**1a** (2.51 g, 10 mmol) was dissolved in 0.0125 M aqueous Et_3N (800 ml), the pH being adjusted to 7.5 with AcOH. To the solution were added the acylase (50 mg), 1/80 M $CoCl_2$ (100 ml), and water (100 ml). The solution was left to stand at 38 °C for 5 d, the pH being adjusted occasionally to 7.5. The precipitate formed was collected by filtration (later, the precipitate was subjected to recrystallization). The pH of the combined filtrates was adjusted to 5 with 1 M HCl. A small amount of Norit was added, and the mixture was maintained at 50—60 °C for 10 min. The filtrate was concentrated to a small volume, and its pH was adjusted to 3 with 1 M HCl. The oil separated was extracted with EtOAc and the extract was washed with water (the extract was used for the preparation of Ac-D-**1a**). The aqueous layers were applied to a column of Dowex 50 (H^+ form), and the column was washed with water and eluted with 2 M NH_4OH. The eluate was evaporated, and the residue was combined with the above precipitate. Then, the product was recrystallized from dilute HCl–Et_3N–acetone; yield, 0.86 g (82%); mp 268—271 °C (dec); $[\alpha]_D^{20}$ +42.2 (*c* 0.2, 5 M HCl); R_f^3 0.82, R_f^4 0.76.

Found: C, 62.81; H, 7.44; N, 6.76%. Calcd for $C_{11}H_{15}O_3N$: C, 63.14; H, 7.23; N, 6.69%.

*Ac-D-**1a***: The extract with EtOAc obtained above was dried (Na_2SO_4) and evaporated. The residual solid was recrystallized from EtOH–water; yield, 1.07 g (85%); mp 172—173 °C; $[\alpha]_D^{20}$ −22.5 (*c* 1, EtOH); R_f^2 0.73.

Found: C, 62.05; H, 6.95; N, 5.32%. Calcd for $C_{13}H_{17}O_4N$: C, 62.14; H, 6.82; N, 5.57%.

D-***1a***: This was prepared from Ac-D-**1a** (0.50 g, 2 mmol) as described for DL-**1a**; yield, 0.34 g (81%); mp 268—270 °C (dec); $[\alpha]_D^{20}$ −41.8 (*c* 0.2, 5 M HCl); R_f^3 0.82, R_f^4 0.76.

Found: C, 63.21; H, 7.26; N, 6.42%. Calcd for $C_{11}H_{15}O_3N$: C, 63.14; H, 7.23; N, 6.69%.

*Resolution of Ac-DL-**1b**.* L-***1b***: Ac-DL-**1b** (2.79 g, 10 mmol) was treated with the acylase as mentioned above. Amino acid L-**1b** was obtained from the reaction mixture; yield, 0.96 g (81%); mp 230—233 °C (dec); $[\alpha]_D^{20}$ +31.1 (*c* 0.1, 5 M HCl); R_f^3 0.93, R_f^4 0.88.

Found: C, 65.62; H, 8.12; N, 5.85%. Calcd for $C_{13}H_{19}O_3N$: C, 65.80; H, 8.07; N, 5.90%.

*Ac-D-**1b***: The extract with EtOAc was treated as described for Ac-D-**1a**: yield, 1.15 g (82%); mp 134—135 °C; $[\alpha]_D^{20}$ −13.4 (*c* 1, EtOH); R_f^2 0.83.

Found: C, 64.35; H, 7.65; N, 4.82%. Calcd for $C_{15}H_{21}O_4N$: C, 64.49; H, 7.58; N, 5.01%.

D-***1b***: This was prepared from Ac-D-**1b** (0.56 g, 2 mmol); yield, 0.44 g (93%); mp 234—236 °C (dec); $[\alpha]_D^{20}$ −30.6 (*c* 0.1, 5 M HCl); R_f^3 0.93, R_f^4 0.88.

Found: C, 65.84; H, 8.04; N, 5.77%. Calcd for $C_{13}H_{19}O_3N$: C, 65.80; H, 8.07; N, 5.90%.

We thank Drs. H. Aoyagi, Y. Shimohigashi, S. Lee, and Y. Minematsu for their valuable discussions. We are indebted to Mr. K. Nakajima, Mr. T. Nishi, and Mr. O. Suginoo for their experimental assistances.

References

1) Abbreviation used: Ac, acetyl; Amb, 2-amino-4-(*p*-methoxyphenyl)butanoic acid; Amh, 2-amino-6-(*p*-methoxyphenyl)hexanoic acid; Amp, 2-amino-5-(*p*-methoxyphenyl)-pentanoic acid; ⊿Ala, dehydroalanine; Hmb, 2-hydroxy-3-(methyl)butanoic acid; Tyr(Me), *O*-methyltyrosine.

2) Y. Shimohigashi, S. Lee, H. Aoyagi, T. Kato, and N. Izumiya, *Int. J. Pept. Protein Res.*, **10**, 323 (1977).

3) Y. Shimohigashi, S. Lee, H. Aoyagi, T. Kato, and N. Izumiya, *Int. J. Pept. Protein Res.*, **10**, 197 (1977).

4) W. C. Evans and N. Walker, *J. Chem. Soc.*, **1947**, 1571.

5) Y. Shimohigashi, S. Lee, and N. Izumiya, *Bull. Chem. Soc. Jpn.*, **49**, 3280 (1976).

6) M. V. Grignard, *Chem. Zentralbl.*, **II**, 1751 (1905).

7) J. B. Shoesmith and R. J. Connor, *J. Chem. Soc.*, **1927**, 2234.

8) D. G. Thomas and A. H. Nathan, *J. Am. Chem. Soc.*, **70**, 331 (1948).

9) E. L. Martin, *Org. React.*, **1**, 167 (1947).

10) R. Baird and S. Winstein, *J. Am. Chem. Soc.*, **84**, 788 (1962).

 © 1982 The Chemical Society of Japan Bull. Chem. Soc. Jpn., 55, 921—923 (1982)

Alkaline Hydrolysis of Propella-δ- and ε-lactones

Kiyomi Kakiuchi,* Yoshito Tobe, and Yoshinobu Odaira

Department of Petroleum Chemistry, Faculty of Engineering, Osaka University, Suita, Osaka 565

(Received September 4, 1981)

Second-order rate constants for the alkaline hydrolysis of a series of propella-δ- and ε-lactones at 32.3 °C have been determined. The conclusion to be drawn from the kinetic data is as follows. In the case of propella-δ-lactones, the steric effect of the third ring on the hydrolysis plays an important role, whereas the hydrolysis of propella-ε-lactones is mainly governed by the steric effect attributable to the flexibility of the ε-lactone ring, and, on the contrary, the steric effect of the third ring is of no great consequence.

In a continuation of the studies on the transformation of readily available [*n*.3.2]propellanes into other important polycarbocyclic ring systems,[1] we previously reported on the novel cyclobutyl-cyclopropylcarbinyl rearrangement of propella-δ-lactones (**1**)—(**4**), composed of a cyclobutane ring, a δ-lactone ring, and one of five to eight membered rings as the third ring, to the corresponding dispiro-γ-lactones (**9**)—(**12**) under acidic conditions as well as thermal conditions.[2] In these reactions, the remarkable ring size effect of the third rings on the rearrangement was observed, and it was inferred that the steric effect of the third rings reinforced the puckered geometry of the cyclobutane ring in δ-lactones which was favorable for the rearrangement to the γ-lactones. Of all the propella-δ-lactones, in particular, this was the case for **2** because of the steric requirement of the cyclohexane ring fused to bridgehead positions to adopt the chair conformation. Furthermore, this reasoning could be applicable to the results of the rearrangement of propella-ε-lactones (**5**) and (**6**), being higher homologues of δ-lactones (**1**) and (**2**).[3]

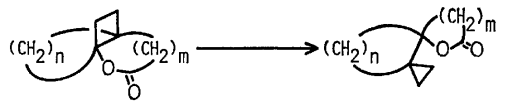

	m	n	
1	2	3	9
2	2	4	10
3	2	5	11
4	2	6	12
5	3	3	—
6	3	4	13

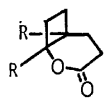

	R
7	H
8	CH_3

On the other hand, it is well-known that the transition state of alkaline hydrolysis of lactones is the formation of the tetrahedral intermediate and that the hydroxide anion attacks perpendicularly to the plane of the carbonyl group.[4] Also, it becomes apparent that the substituent effect which affects the rate of the hydrolysis is primarily due to the steric factor in the transition state.[4c,5]

In this connection, it is very interesting to see if the steric effect of the third ring influences the rate of alkaline hydrolysis of propellalactones. Therefore, we have studied the rate constants for the alkaline hydrolysis of a series of propella-δ- and ε-lactones.

Results and Discussion

The kinetic data for the alkaline hydrolysis of various lactones studied are summarized in Tables 1 and 2.

Firstly, the effect of alicyclic rings or two methyl groups substituted at the 4- and 5-positions of δ-valerolactone on the alkaline hydrolysis was taken up. As shown in Table 1, the rate constants of a series of δ-lactones obviously decreased with going on from δ-valerolactone to tricyclic propella-δ-lactones through bicyclic ones. The striking aspect of the present data is that the rate constant of bicyclic δ-lactone (**7**) compared with that of δ-valerolactone decreased by a factor of about one-twentieth by the fusion of such a small cyclobutane ring. Moreover, the further deceleration was naturally observed in the cases of propella-δ-lactones (**1**)—(**4**), or bicyclic δ-lactone (**8**), being substituted by two methyl groups at the both angular bridgehead positions of **7**. For example, the rate constant of **4** is less than that of **7** by a factor of about twenty-eighth by the additional fusion of a eight membered ring to the bicyclo[4.2.0] ring system. The effect of the third ring on the present alkaline hydrolysis may be regarded as the steric hindrance toward the attack of the hydroxide anion to the carbonyl group which is situated in position β to a bridgehead carbon atom, and, accordingly, it would be expected that the degree of the deceleration of the rate might be consistent with that of enlargement of the third ring size. In fact, however, the rate constants was in the order of **2**>**1**>**3**≈**4**, and that of **2**, having a cyclohexane ring, was twice of that of **1**, having a cyclopentane ring, and was even one and half times larger than that of **8**.

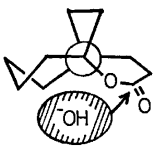

These results are of very significance in connection with those of the rearrangement of **1**—**4** to the corresponding dispiro-γ-lactones (**9**)—(**12**) described in the introduction. The two reactions exhibited very similar feature of the ring size effect of the third ring. As borne out by the inspection of molecular model as well as by the reasoning for the previous rearrangement, this unique feature of **2** in reactivity may be attributed to the puckered geometry of the cyclobutane ring reinforced by the chair conformation of

Table 1. Kinetic data for alkaline hydrolysis of δ-lactone series

Compd	T/°C[a]	k/l mol^{-1} s^{-1}	ΔH^*/kcal mol^{-1}	ΔS^*/eu	k_{rel}[b]
δ-Valerolactone	41.5	24.4±0.3	7.38	−28.9	100
	32.3	17.3±0.0			
	25.0	11.4±0.1			
7	41.5	1.36±0.03	8.79	−30.1	4.8
	32.3	0.854±0.013			
	25.0	0.561±0.006			
8	41.5	0.203±0.002	9.35	−32.1	0.72
	32.3	0.124±0.002			
	25.0	0.0794±0.0005			
1	41.5	0.145±0.002	9.78	−31.4	0.54
	32.3	0.0934±0.0026			
	25.0	0.0544±0.0014			
2	41.5	0.280±0.003	9.33	−31.5	1.0
	32.3	0.179±0.001			
	25.0	0.110±0.002			
3	41.5	0.0309±0.0008	7.69	−40.8	0.14
	32.3	0.0241±0.0008			
4	32.3	0.0290±0.0006			0.17

a) Temperatures are ±0.1 °C. b) Relative rates at 32.3 °C to that of δ-valerolactone=100.

Table 2. Kinetic data for alkaline hydrolysis of ε-lactone series

Compd	T/°C[a]	k/l mol^{-1} s^{-1}	ΔH^*/kcal mol^{-1}	ΔS^*/eu	k_{rel}[b]
ε-Caprolactone	41.5	1.58±0.03	8.33	−31.3	
	32.3	1.04±0.02			
	25.0	0.678±0.009			100
5	41.5	0.458±0.006	8.41	−33.5	
	32.3	0.279±0.010			
	25.0	0.194±0.002			29
6	25.0	0.193±0.002			29

a) Temperatures are ±0.1 °C. b) Relative rates at 25.0 °C to that of ε-caprolactone=100.

the cyclohexane ring. Namely, **2** is packed closely like a compact hemisphere, in other words, **2** has a widespreading room to the direction of endo in comparison with the others, such as **1** and **8**. Therefore, the attack of the hydroxide anion upon the carbonyl carbon atom of **2** may take place more smoothly.

In the case of ε-lactone series, on the other hand, the steric effect of two alicyclic rings fused to ε-caprolactone on the alkaline hydrolysis was much less than in the case of δ-lactone series. Namely, the rate constants of two propella-ε-lactones (**5**) and (**6**), which were the same, were only one-fourth as small as that of ε-caprolactone as shown in Table 2. This marked difference in reactivity between two propellalactone series can be attributed to the difference in flexibility or rigidity between δ- and ε-lactone rings. Inspection of molecular models of two lactone rings clearly indicates that the ε-lactone ring is more flexibile than the δ-lactone one. It may be reasonable that the rate of more flexible ε-lactone for the hydrolysis is much slower than that of more rigid δ-lactone.[6] This consideration implies that the flexibility of the ε-lactone makes it possible to depress the hydrolytic rate by the steric effect of adjacent methylene groups to the carbonyl one in the lactone ring itself. In addition, it is deduced from the kinetic data that the steric effect based on the flexibility of the ε-lactone ring plays more important role than that of the third ring.

In conclusion, from the kinetic study of the alkaline hydrolysis of a series of propella-δ- and ε-lactones, the steric effect of the third ring toward the attack of the hydroxide anion has been elucidated. In particular, in the case of propella-δ-lactones, this effect played as important role as in the case of cyclobutylcyclopropylcarbinyl rearrangement of them. In the case of propella-ε-lactones, on the other hand, the alkaline hydrolysis was dominantly governed by the steric effect attributable to the flexibility of the ε-lactone ring, and, that of the third ring was of no great consequence.

Experimental

δ-Valero- and ε-caprolactones are commercial samples (Wako Pure Chemical Ind. or Tokyo Kasei) and were purified by distillation before use. Bicyclic δ-lactones (**7**) and (**8**) and propellalactones (**1**)—(**6**) were prepared as our previous reports[2b,3] and were purified by silica-gel column chromatography or distillation. Water was prepared by distillation of deionized water under nitrogen atmosphere and was used throughout. Commercially available ethanol (Wako, super special grade) was used without further purification. Hitachi-Horiba pH meter H-7 SD and Horiba combination electrode #6326 were used for pH measure-

ment.

Kinetic Measurement. The rates of the hydrolysis of the lactones were determined by the pH method of Hall *et al.*[4b,d] Water containing 25% ethanol was used as the solvent to form a homogeneous solution.[8] The second-order rate constants were calculated from the pseudo first-order rate constants and were the avarage of at the least three runs of the same lactone concentration. The rate measurements were made at three different temperatures in the range of 25.0—41.5 °C[9] and the activation parameters were evaluated from the slope of the least-square Arrhenius plots.

References

1) a) Y. Sakai, S. Toyotani, Y. Tobe, and Y. Odaira, *Tetrahedron Lett.*, **1979**, 3855; b) Y. Tobe, Y. Hayauchi, Y. Sakai, and Y. Odaira, *J. Org. Chem.*, **45**, 637 (1980); c) Y. Tobe, K. Terashima, Y. Sakai, and Y. Odaira, *J. Am. Chem. Soc.*, **103**, 2307 (1981).

2) a) Y. Tobe, K. Kakiuchi, Y. Kawakami, Y. Sakai, K. Kimura, and Y. Odaira, *Chem. Lett.*, **1978**, 1027; b) K. Kakiuchi, Y. Tobe, and Y. Odaira, *J. Org. Chem.*, **45**, 729 (1980).

3) K. Kakiuchi, T. Tsugaru, Y. Tobe, and Y. Odaira, *J. Org. Chem.*, **46**, 4204 (1981).

4) a) M. L. Bender, *Chem. Rev.*, **60**, 53 (1960); b) H. K. Hall, Jr., M. K. Brandt, and R. M. Mason, *J. Am. Chem. Soc.*, **80**, 6420 (1958); c) J. Grace and M. C. R. Symons, *J. Chem. Soc.*, **1961**, 47; d) H. K. Hall, Jr., *J. Org. Chem.*, **28**, 2027 (1963); e) M. Balakrishnan, G. V. Rao, and N. Venkatasubramanian, *J. Chem. Soc., Perkin Trans. 2*, **1974**, 1093.

5) C. M. Stevens and D. S. Tarbell, *J. Org. Chem.*, **19**, 1996 (1954).

6) This fact may be also explained on the basis of the differences of I-strain between seven and six membered rings as mentioned by Blackburn and Dodds.[7]

7) G. M. Blackburn and H. L. H. Dodds, *J. Chem. Soc., Perkin Trans. 2*, **1974**, 377.

8) In the case of **4**, the satisfactory data were not obtained at 25.0 and 41.5 °C because the solubility was limited at 25.0 °C and ethanol evaporated at 41.5 °C during the long reaction time. Also, the rate constant of **3** at 25 °C did not give reliable data.

9) Since **6** was more reactive and rearranged easily to **13** at 32.3 and 41.5 °C, we could not measure the rate under the above conditions.

The Configurations of Benzylmethyl(*o*- or *p*-tolyl)silylmethylamine and the Stereochemistry of the Reactions of Benzylmethyl-methoxyphenylsilane with Some Organometallic Agents

Daiyo TERUNUMA,* Kazuhisa SENDA, Masato SANAZAWA, and Hiroyuki NOHIRA
Department of Applied Chemistry, Faculty of Engineering, Saitama University, Urawa, Saitama 338
(Received September 9, 1981)

Optically active α-amino organosilanes such as benzylmethyl(*o*- or *p*-tolyl)silylmethylamine were converted into benzylmethylphenyl(*o*- or *p*-tolyl)silane, of which the configurations had been known. From these observations, it was found that (+)- and (−)-benzylmethyl(*o*- or *p*-tolyl)silylmethylamine has *S* and *R* configuration respectively. Furthermore, the stereochemistry of the reaction of benzylmethyl(methoxy)phenylsilane with some organometallic agents was investigated.

Previously, we reported on the successful optical resolutions of the α-amino organosilanes, *i.e.*, benzylmethylphenylsilylmethylamine(**1**), benzylmethyl(*o*-(**2**), *m*-(**3**), and *p*-tolyl(**4**))silylmethylamine, and on the determination of the configuration of **1**.[1] In this paper, we wish to report on the determination of the configurations of **2** and **4**, and on the stereochemistry of the nucleophilic substitutions of benzylmethylmethoxy(phenyl(**23**) and *p*-tolyl(**6**))silane by some organometallic agents.

Results and Discussion

Chemical Conversions of 2 and 4. In order to determine the configuration of **4**, the chemical conversion of **4** into benzylmethylphenyl-*p*-tolylsilane, of which the absolute configuration was known, was undertaken, following the route described in our prior paper[1] (Scheme 1). Thus, (−)-**4**, which was obtained from the less soluble salt of **4** with (+)-tartaric acid by the fractional crystallization, was converted into (+)-benzylmethyl-*p*-tolylsilane(**10**). The treatment of **10** with methanol in the presence of Pd–C at 0 °C, and with a catalytic amount of BPO in CCl_4 at 80 °C gave (−)-benzylmethylmethoxy-*p*-tolylsilane (**11**) and (+)-benzyl(chloro)methyl-*p*-tolylsilane(**12**) respectively. Both reactions of (−)-**11** and (+)-**12** with phenyllithium in ether gave *S*(−)-benzylmethylphenyl-*p*-tolylsilane(**13**). In these chemical conversions, it is already known that the three of them, *i.e.*, the hydrolysis of **8**, the replacement of hydrogen by methoxyl radical, and the reaction of **12** with phenyllithium, proceed with inversion of the configurations, and the others proceed with retention of the configurations.[2]

On the other hand, *R*(−)-benzylmethylphenyl-*o*-tolylsilane(**20**) was obtained from (+)-**2** in the manner similar to that described above.

From these observations, it was noted that (−)-**4** and (+)-**2** had *R* and *S* configurations respectively. These configurations were furthermore confirmed by treating *S*(+)-**12** with *o*-tolyllithium, and *R*(−)-**19** with *p*-tolyllithium to give the product of the same sign of the optical rotation, *i.e.*, *R*(−)-benzylmethyl-*o*-tolyl-*p*-tolylsilane(**21**).

Reaction of the Methoxysilanes with Organometallic Agents. It is generally known that the stereochemistry of nucleophilic substitution at silicon is mainly controlled by the nature of leaving groups on silicon, and the

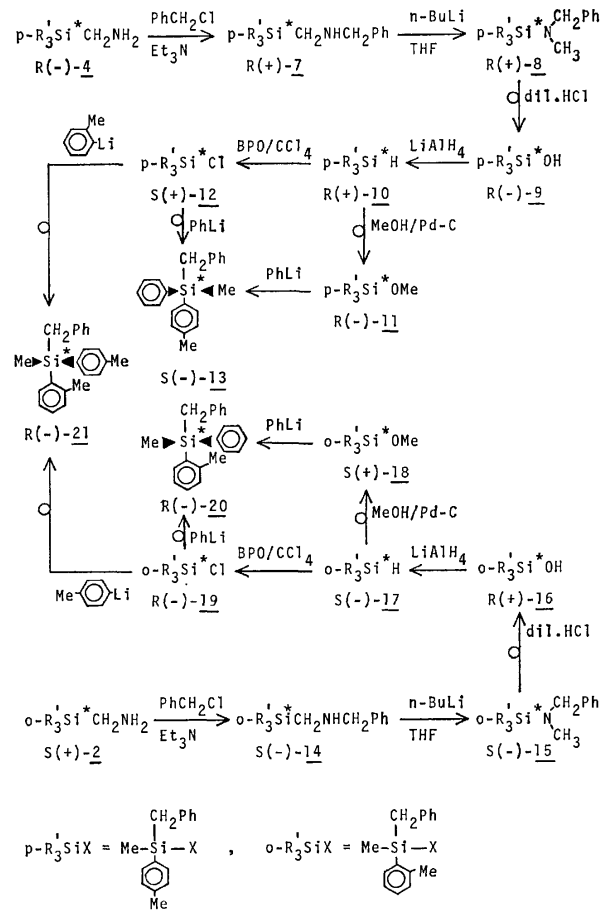

Scheme 1.

electronic character of the nucleophiles.

However, the stereochemistry of the reaction of methoxysilane with organometallic agents seems to be complex. There have been conflicting reports in the literature concerning the stereochemistry of the reaction of methoxysilanes: an inversion reaction of the configuration of benzylphenylmethylmethoxysilane with the aryl Grignard reagents such as mesityl-, and 1-naphthylmagnesium bromide,[3] and a retention reaction of the configuration of methylmethoxy(1-naphthyl)phenylsilane with allyllithium.[4]

On the other hand, we indicated previously that the stereochemical courses of the reaction of *S*(+)-**23** with the organolithium agents such as butyl-, *p*-methoxyphenyl-, and allyllithium, were in agreement with those for methylmethoxy(1-naphthyl)phenylsilane.[1]

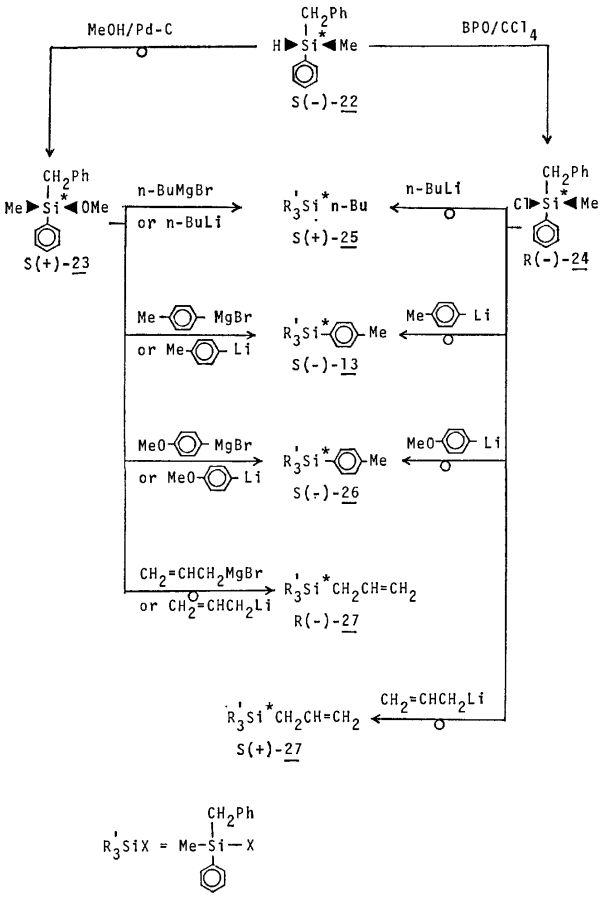

Scheme 2.

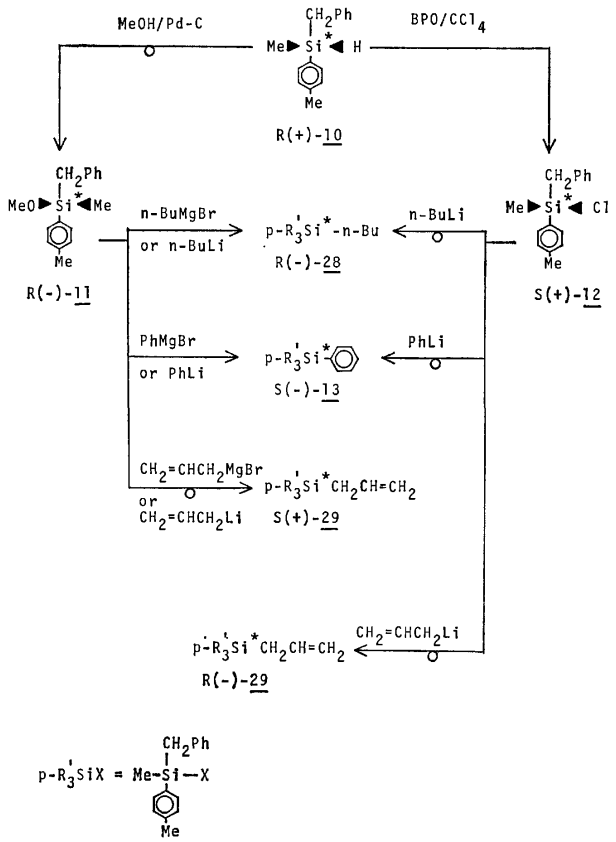

Scheme 3.

Thus, the investigation of the reaction courses of *S*(+)-benzylphenylmethylmethoxysilane(**23**) with the Grignard reagents were carried out (Scheme 2).

The stereochemical courses of the reaction of *S*(+)-**23** with the Grignard reagents were also in accordance with those of organolithium agents, *i.e.*, the reaction of *S*(+)-**23** with the alkyl-, and arylmagnesium bromide proceed with a retention of the configuration, whereas that of *S*(+)-**23** with allylmagnesium bromide proceeds with an inversion of configuration.

Furthermore, the reactions of *R*(−)-**11** and S(+)-**12** with some organometallic agents were investigated (Scheme 3). It was noted that these results were in fair agreement with those of the benzylmethylphenylsilyl system.

Experimental

The boiling points are uncorrected. The IR spectra were determined with a JASCO IR-A2 spectrometer. The NMR spectra were determined at 60 MHz with a Varian A-60D spectrometer in CCl_4, using TMS as an internal standard. The optical rotations were measured with a JASCO DIP-181 polarimeter. All the reactions of the chlorosilanes and methoxysilanes with organometallic agents were carried out under a dry nitrogen atmosphere. Optically active (+)-**2**, (−)-**4**, and (−)-**22** were obtained in manners described in our report.[1)]

(+)-N-Benzylbenzylmethyl-p-tolylsilylmethylamine (7). A solution of (−)-**4** (18.1 g, 0.071 mol) $[\alpha]_D$ −6.6° (c=3, Et_2O), benzyl chloride (9.0 g, 0.071 mol), and Et_3N (21.6 g, 0.213 mol) was stirred for 4 h at 110 °C. Water (30 ml) and hexane (100 ml) were added to the reaction mixture. The organic layer was separated, washed three times with 10% NaOH, and then dried (Na_2SO_4). Subsequent evaporation and distillation gave (+)-**7**. Bp 159—162 °C/0.1 Torr.** Yield 15.0 g (61%). $[\alpha]_D$ 0° (c=2, Et_2O). NMR δ 0.20 (s, 3, Si–CH_3), 1.0 (s, 1, NH), 2.22 (s, 2, $SiCH_2N$), 2.38 (s, 5, $SiCH_2Ph$, C–CH_3), 3.70 (s, 2, N–CH_2Ph), 6.8—7.5 (m, 14, aromatic protons). Found: N, 3.90%. Calcd for $C_{23}H_{27}NSi$: 4.05%.

(+)-N-Benzyl-N-methylbenzylmethyl-p-tolylsilylamine (8). To a solution of (+)-**7** (14.8 g, 0.043 mol) in THF (150 ml), was added *n*-BuLi (5 ml of 10% w/v hexane solution) by means of a syringe under nitrogen atmosphere. After stirring the solution for 10 h at room temperature, water was added to the solution at 0 °C. The organic layer was separated, washed with water, and then dried (K_2CO_3). Subsequent evaporation and distillation gave (+)-**8**. Bp 163—165 °C/0.16 Torr. Yield 14.4 g (97%). $[\alpha]_D$ +3.6° (c=2, Et_2O). NMR δ 0.29 (s, 3, Si–CH_3), 2.38 (s, 6, N–CH_3, C–CH_3), 2.47 (broad s, 2, Si–CH_2Ph), 3.85 (s, 2, N–CH_2Ph), 6.8—7.5 (m, 14, aromatic protons).

(−)-Benzylmethyl-p-tolylsilanol (9). A solution of (+)-**8** (14.3 g, 0.041 mol) $[\alpha]_D$ +3.6° (c=2, Et_2O), in ether (100 ml) was treated with 0.2 M HCl (150 ml)*** in a separating funnel at 0 °C. The organic layer was separated, washed two times with cold water, and then dried (K_2CO_3). Evaporation of the solvent gave (−)-**9**. It was used in the next reaction without further purification. $[\alpha]_D$ −9.7° (c=1, pentane). NMR δ 0.28 (s, 3, Si–CH_3), 2.1 (s, 1, OH), 2.30 (s, 2, $SiCH_2Ph$), 2.35 (s, 3, C–CH_3), 6.8—7.5 (m, 9, aromatic protons).

** 1 Torr ≈ 133.322 Pa.

*** 1 M = 1 mol dm^{-3}.

*(+)-Benzylmethyl-*p*-tolylsilane (**10**).* A solution of (−)-**9** (8.7 g) in dibutyl ether (100 ml) was added to a suspension of $LiAlH_4$ (4.7 g, 0.125 mol) in ether (110 ml). The mixture had been kept at 90 °C for 30 min, and then the ether was removed. The mixture was stirred for additional 3 h at 140—145 °C. The usual workup of the mixture gave (+)-**10**. Bp 106—107 °C/1.0 Torr. Yield 6.0 g (74%). $[\alpha]_D$ +11.1° (c=2, pentane). NMR δ 0.25 (d, J=3.5 Hz, 3, Si–CH_3), 2.33 (s, 5, $SiCH_2$–, CCH_3), 4.45 (q, J=3.5 Hz, 1, Si–H), 6.8—7.5 (m, 9, aromatic protons).

*(−)-Benzylmethylmethoxy-*p*-tolylsilane (**11**).* Methanol (1.6 g, 0.048 mol) was added slowly to the mixture of (+)-**10** (5.8 g, 0.025 mol) $[\alpha]_D$ +11.1° (c=2, pentane), and 5% Pd/C (0.47 g) in pentane at 0 °C. After evolution of hydrogen ceased, the catalyst was removed off by filtration. Subsequent evaporation and distillation gave (−)-**11**. Bp 123 °C/1.0 Torr. Yield 5.8 g (90%). $[\alpha]_D$ −2.6° (c=2, pentane). NMR δ 0.23 (s, 3, Si–CH_3), 2.31 (s, 5, Si–CH_2Ph, C–CH_3), 6.8—7.5 (m, 9, aromatic protons).

*(+)-Benzyl(chloro)methyl-*p*-tolylsilane (**12**).* A solution of (+)-**10** (1.0 g, 4.4 mmol) and BPO (78 mg, 0.23 mmol) in CCl_4 (4 ml) was sealed in a sample tube under nitrogen atmosphere. The tube was then maintained for 11 h at 80 °C. The subsequent evaporation gave (+)-**12**. The chlorosilane (+)-**12** was extreamly moisture-sensitive, and extensive racemization of (+)-**12** was observed in the presence of a trace of H_2O. The product was used without further purification. $[\alpha]_D$ +5.2° (c=1.3, CCl_4). NMR δ 0.55 (s, 3, Si–CH_3), 2.36 (s, 3, C–CH_3), 2.54 (s, 2, $SiCH_2$Ph), 6.8—7.5 (m, 9, aromatic protons).

*Preparation of the Series of the Benzylmethyl-*o*-tolylsilyl Systems, (−)-**14**—(−)-**19**.* In manners similar to that described above, the series of benzylmethyl-*o*-tolylsilyl systems *i.e.*, (−)-**14**, (−)-**15**, (+)-**16**, (−)-**17**, (+)-**18**, and (−)-**19** were obtained from (+)-**2** (22.8 g, 0.089 mol) $[\alpha]_D$ +5.1° (c=2, Et_2O).

*(−)-**14***: Yield 22.8 g (74%). Bp 175—180 °C/0.3 Torr. $[\alpha]_D$ −7.9° (c=2, Et_2O). NMR δ 0.29 (s, 3, Si–CH_3), 0.9 (s, 1, NH), 2.28 (s, 2, $SiCH_2N$), 2.34 (s, 3, C–CH_3), 2.38 (s, 2, $SiCH_2$Ph), 3.68 (s, 2, NCH_2Ph), 6.5—7.5 (m, 14, aromatic protons). Found: N, 4.10%. Calcd for $C_{23}H_{27}NSi$: N, 4.05%.

*(−)-**15***: $[\alpha]_D$ −9.4° (c=2, Et_2O). NMR δ 0.32 (s, 3, Si–CH_3), 2.36 (s, 6, N–CH_3, C–CH_3), 3.90 (s, 2, $SiCH_2$Ph), 6.7—7.5 (m, 14, aromatic protons).

*(+)-**16***: $[\alpha]_D$ +8.2° (c=1.2, pentane). NMR δ 0.33 (s, 3, Si–CH_3), 1.7 (broad s, 1, OH), 2.38 (s, 2, $SiCH_2$Ph), 2.43 (s, 3, C–CH_3), 6.6—7.5 (m, 9, aromatic protons).

*(−)-**17***: Yield 8.5 g (57% from (−)-**14** employed). Bp 114 °C/1.5 Torr. $[\alpha]_D$ −16.8° (c=2.2, pentane). NMR δ 0.29 (d, J=3.5 Hz, 3, Si–CH_3), 2.35 (s, 5, $SiCH_2$–, C–CH_3), 4.55 (q, J=3.5 Hz, 1, SiH), 6.8—7.5 (m, 9, aromatic protons).

*(+)-**18***: Bp 130 °C/1.5 Torr. $[\alpha]_D$ +5.3° (c=2, pentane). NMR δ 0.30 (s, 3, Si–CH_3), 2.39 (s, 5, $SiCH_2$Ph, C–CH_3), 3.40 (s, 3, O–CH_3), 6.8—7.6 (m, 9, aromatic protons).

*(−)-**19***: $[\alpha]_D$ −14.5° (c=1.3, CCl_4). NMR δ 0.65 (s, 3, Si–CH_3), 2.25 (s, 3, C–CH_3), 2.60 (s, 2, $SiCH_2$Ph), 6.8—7.5 (m, 9, aromatic protons).

*(−)-Benzylmethylphenyl-*p*-tolylsilane (**13**).*[1] To a solution of PhLi (*ca.* 12 mmol) in ether (10 ml) was added a solution of (−)-**11** (1.0 g, 3.9 mmol) $[\alpha]_D$ −2.6° (c=2, pentane), in THF (10 ml) at 0 °C by means of a syringe. The mixture was refluxed for 2 h with stirring. The usual workup of the reaction mixture gave (−)-**13** in a 36% (0.43 g) yield. Bp 160 °C/0.2 Torr. $[\alpha]_D$ −1.9° (c=8.7, CH_2Cl_2).

In a manner similar to that described above, the reaction of (−)-**11**, $[\alpha]_D$ −2.6° (c=2, pentane) with PhMgBr gave (−)-**13** in 20% yield. $[\alpha]_D$ −1.7° (c=4.6, CH_2Cl_2). The reaction of (+)-**12**, $[\alpha]_D$ +5.2° (c=1.3, CCl_4) with PhLi gave (−)-**13** in 80% (0.91 g) yield. $[\alpha]_D$ −2.6° (c=8.7, CH_2Cl_2).

*(−)-Benzylmethylphenyl-*o*-tolylsilane (**20**).*[1] In manners similar to that described above, reaction of (+)-**18** with PhLi and PhMgBr, and of (−)-**19** with PhLi was carried out. The reaction of (+)-**18**, $[\alpha]_D$ +5.3° (c=2, pentane) with PhLi gave (−)-**20** in a 52% yield. $[\alpha]_D$ −7.0° (c=2, CH_2Cl_2). The reaction of (+)-**18** $[\alpha]_D$ +5.3° (c=2, pentane) with PhMgBr gave (−)-**20** in a 30% yield. $[\alpha]_D$ −5.2° (c=2, CH_2Cl_2). The reaction of (−)-**19**, prepared from (−)-**17** $[\alpha]_D$ −16.8° (c=2.2, pentane), with PhLi gave (−)-**20** in a 60% yield. $[\alpha]_D$ −12.1° (c=7, CH_2Cl_2).

*(−)-Benzylmethyl-*o*-tolyl-*p*-tolylsilane (**21**).* To a solution of (−)-**19**, prepared from (−)-**17** (1 g, 4.4 mmol) $[\alpha]_D$ −16.8° (c=2, pentane) in Et_2O (10 ml), was added a solution of two fold excess of *p*-tolyllithium by means of a syringe at 0 °C. The mixture was stirred for 1 h at room temperature, and then refluxed for additional 1 h with stirring. The usual workup of the mixture gave (−)-**21** in a 60% (0.84 g) yield. $[\alpha]_D$ −14.5° (c=5.5, CH_2Cl_2). NMR δ 0.41 (s, 3, Si–CH_3), 2.19 (s, 3, *o*-CH_3), 2.32 (s, 3, *p*-CH_3), 2.63 (s, 2, $SiCH_2$Ph), 6.6—7.5 (m, 13, aromatic protons).

In a manner silmilar to that described above, (−)-**21** was obtained from (+)-**10** $[\alpha]_D$ +11.1° (c=2, pentane) in a 51% yield. $[\alpha]_D$ −5.5° (c=3, CH_2Cl_2).

*(+)-Benzylbutylmethylphenylsilane (**25**).*[1] (+)-**23** (1 g, 4.1 mmol) $[\alpha]_D$ +3.5° (c=2, pentane) in Et_2O (10 ml) was added to a large excess amount of *n*-BuMgBr in Et_2O. The mixture was refluxed for 90 h with stirring. The usual workup of the mixture gave (+)-**25** in an 83% (0.92 g) yield. $[\alpha]_D$ +3.5° (c=10, CH_2Cl_2).

*(−)-Benzyl(*p*-methoxyphenyl)methylphenylsilane (**26**).*[1] To a solution of (+)-**23** (1 g, 4.1 mmol) $[\alpha]_D$ +3.5° (c=2, pentane) in Et_2O (10 ml) was added a large excess amount of *p*-methoxyphenylmagnesium bromide in Et_2O. The mixture was refluxed for 80 h with strring. The usual workup of the mixture gave (−)-**26** in a 31% (0.41 g) yield. $[\alpha]_D$ −6.6° (c=4, CH_2Cl_2).

*(−)-Allylbenzylmethylphenylsilane (**27**).*[1] To a solution of (+)-**23** (1 g, 4.1 mmol) $[\alpha]_D$ +3.5° (c=2, pentane) in Et_2O (10 ml), was added a solution of allylmagnesium bromide (*ca.* 6.9 mmol) in Et_2O. The mixture was refluxed for 50 h with stirring. The usual workup of the mixture gave (−)-**27** in a 71% (0.74 g) yield. $[\alpha]_D$ −0.42° (c=12.3, CH_2Cl_2).

*(−)-Benzylbutylmethyl-*p*-tolylsilane (**28**).* To a solution of (−)-**11** (1 g, 3.9 mmol) $[\alpha]_D$ −2.6° (c=2, pentane) in Et_2O (20 ml) was added 4 ml of a 10% w/v solution of *n*-BuLi by means of a syringe at 0 °C. After stirring for 1 h at 0 °C, the mixture was hydrolyzed. The usual workup of the mixture gave (−)-**28**. Yield 59% (0.65 g). $[\alpha]_D$ −3.3° (c=11, CH_2Cl_2). NMR δ 0.19 (s, 3, $SiCH_3$), 0.5—1.5 (m, 9, *n*-Bu), 2.28 (s, 2, $SiCH_2$Ph), 2.34 (s, 3, CCH_3), 6.7—7.4 (m, 9, aromatic protons).

In a manner similar to that described above, the treatment of (−)-**11** with butylmagnesium bromide gave (−)-**28** $[\alpha]_D$ −0.96° (c=14, CH_2Cl_2) in a 73% yield. The reaction of (+)-**12** $[\alpha]_D$ +3.2° (c=1.3, CCl_4), prepared from (+)-**10** (1.0 g, 4.4 mmol) $[\alpha]_D$ +6.8° (c=2, pentane) with *n*-BuLi gave (−)-**28** $[\alpha]_D$ −0.72 (c=10, CH_2Cl_2) in a 56% (0.69 g) yield.

*(+)-, and (−)-Allylbenzylmethyl-*p*-tolylsilane (**29**).* To a solution of allyllithium (*ca.* 8 mmol) in Et_2O (70 ml) was added (−)-**11** (1.0 g, 3.9 mmol) $[\alpha]_D$ −2.6° (c=2, pentane)

in ether (10 ml) with stirring at 0 °C. After the mixture had been stirred for 2 h at 0 °C, the usual workup of the mixture gave (+)-**29** $[\alpha]_D$ +1.6° (c=3, CH_2Cl_2) in a 24% (0.25 g) yield. Bp 140 °C/0.2 Torr. NMR δ 0.20 (s, 3, Si–CH_3), 1.72 (d, J=8 Hz, 2, Si–CH_2–C), 2.29 (s, 2, $SiCH_2Ph$), 2.34 (s, 3, CCH_3), 4.6—5.0 (m, 2, =CH_2), 5.3—6.1 (m, 1, CH=C), 6.7—7.4 (m, 9, aromatic protons).

In a manner similar to that described above, the reaction of (−)-**11** (1.0 g, 3.9 mmol) with Allylmagnesium bromide gave (+)-**29** $[\alpha]_D$ +1.6° (c=6, CH_2Cl_2) in a 76% (0.79 g) yield. The reaction of (+)-**12**, prepared from (+)-**10** (1.0 g, 4.4 mmol) $[\alpha]_D$ +6.8° (c=2, pentane) with allyllithium in Et_2O (70 ml), gave (−)-**29** $[\alpha]_D$ −0.63° (c=4.7, CH_2Cl_2) in a 39% (0.28 g) yield.

The authors wish to thank the Shin-etsu Chemical Industry Co. for the gift of dichlorodimethylsilane.

References

1) D. Terunuma, K. Murakami, M. Kokubo, K. Senda, and H. Nohira, *Bull. Chem. Soc. Jpn.*, **53**, 789 (1980).

2) L. H. Sommer, "Stereochmistry, Mechanism and Silicon," McGraw-Hill, New York (1965).

3) A. Holt and M. J. Smith, *J. Chem. Soc., Perkin Trans. 2*, **1976**, 952.

4) R. Corriu and C. Guerin, *J. Organomet. Chem.*, **195**, 261 (1980).

Coenzyme Models. 30. On the Unusual Spectroscopic Behaviors of Amphiphilic Flavins and 5-Deazaflavins

Seiji SHINKAI,* Akiko HARADA, Osamu MANABE, and Fumio YONEDA†

Department of Industrial Chemistry, Faculty of Engineering, Nagasaki University, Nagasaki 852

†Faculty of Pharmaceutical Sciences, Kumamoto University, Kumamoto 862

(Received September 16, 1981)

At room temperature in aqueous solution, isoalloxazines and 5-deazaisoalloxazines with 10- dodecyl substituent gave a well-resolved, three-banded Sl peak which has been believed to appear only in nonpolar solvents or in enzymic hydrophobic pockets where isoalloxazines and 5-deazaisoalloxazines become free of hydrogen-bonding effects. On the other hand, 3-methyl-10-ethylisoalloxazine and 5-deazaisoalloxazines with 10- ethyl or 10- octyl group did not give such a fine-structured Sl peak. We have found that (i) the fine structure disappears on the addition of organic solvents (ethanol>40 vol% or pyridine>20 vol%), (ii) the fine structure also disappears on the addition of surfactants (CTAB, Brij-35, and SDS) above the critical micelle concentrations, (iii) 10-dodecylisoalloxazine with hydrophilic 3-(thiazolinio)propyl group at 3-position has not the fine structure, and (iv) the fluorescent intensity of 3-methyl-10-dodecyl-5-deazaisoalloxazine is much weaker than that of 3-methyl-10-ethyl-5-deazaisoalloxazine in aqueous solution but these intensities become comparable above 40 vol% ethanol. These findings are consistently rationalized in terms of an aggregation-deaggregation equilibrium of amphiphilic flavin analogues, supporting that the fine structure in aqueous solution is due to the "stacking" association of (5-deaza)isoalloxazine nuclei, like that of dye molecules. The aggregation-deaggregation phenomenon is sensitively reflected by the reactivity: the reaction of 3-methyl-10-ethyl-5-deazaisoalloxazine and cyanide ion gave $k_2=1.27\ M^{-1}\ s^{-1}$ in aqueous solution at 30 °C, whereas aggregated 3-methyl-10-dodecyl-5-deazaisoalloxazine did not react with cyanide ion. These findings have significant implications on the chemistry of flavoproteins, because the absorption spectra of enzyme-bound flavins and 5-deazaflavins have frequently been cited to discuss the flavin reactivities.

The light absorption spectra of a flavin (vitamin B_2) family have characteristic dependence upon the medium polarity and have been used as a useful probe in enzymic and membrane biology. Flavins usually have two characteristic absorption maxima at the ultraviolet region (around 330 nm: peak S2) and the visible region (440 nm: peak S1). The absorption spectra can be classified into three categories on the basis of solvent effects on the S1 peak: a simple gaussian-type peak in aqueous solution (type A), two-to-three shoulders in dipolar solvents (DMF, acetonitrile, tetrahydrofuran, *etc.*) (type B), and a three-banded fine structure in nonpolar solvents (benzene, 3-methylpentane, *etc.*) (type C).[1-5] It is also known that the absorption maximum of S2 shifts to shorter wavelengths in nonpolar solvents.[1,2] Thus, the S2 band is frequently used as an indicator of solvent polarity.

We previously found that the S1 peak of 3-methyl-10-dodecylisoalloxazine (amphiphilic flavin analogue) gives a well-resolved, three-banded fine structure even in aqueous solution at room temperature.[6] Since the fine structure of S1 has been believed to appear only in nonpolar solvents or in enzymic hydrophobic pockets where isoalloxazine becomes free of hydrogen-bonding effects,[1-5,7,8] the novel finding in the nonenzymatic aqueous solution helps understanding the origin of the fine structure in enzymatic systems. Based on the spectral examination, we proposed that the fine structure is attributable to "stacking" association of the isoalloxazine nuclei which is induced by hydrophobic aggregation of 10-dodecyl groups.[6,9]

As an extention of the study, we examined the spectral characteristics of following isoalloxazines (**1**) and 5-deazaisoalloxazines (**2**) (see Table 1 for their 3- and 10- substituents) in aqueous solution. The results support again the importance of the aggregation in the absorption and the fluorescent spectrum.

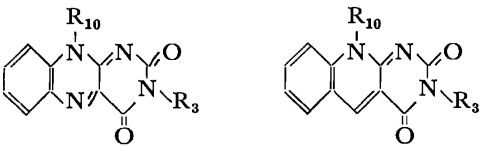

1 **2**

TABLE 1. ABBREVIATIONS OF ISOALLOXAZINES AND 5-DEAZAISOALLOXAZINES

Abbreviation	R_3	R_{10}
1MeEt	CH_3-	CH_3CH_2-
1MeDod	CH_3-	$CH_3(CH_2)_{11}$-
1HDod	H-	$CH_3(CH_2)_{11}$-
1ThDod	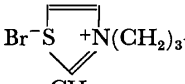	$CH_3(CH_2)_{11}$-
2MeEt	CH_3-	CH_3CH_2-
2MeOct	CH_3-	$CH_3(CH_2)_7$-
2MeDod	CH_3-	$CH_3(CH_2)_{11}$-

Experimental

Preparations of isoalloxazine derivatives (**1**MeEt, **1**MeDod, **1**HDod, and **1**ThDod) were described previously.[9-11] The preparation method of **2**MeEt was also reported.[12] Preparations of **2**MeOct and **2**MeDod will be described soon in a separate paper.

The absorption spectra of isoalloxazines and 5-deazaisoalloxazines were taken at 30±0.1 °C on a Hitachi 200 spectrophotometer equipped with a thermostated cell-holder. The concentration was usually 5.00×10^{-5} M.†† The fluorescent spectra were taken at 30±0.1 °C on a Hitachi 650-10S spectrophotometer equipped with a thermostated cell-holder. The concentration was usually 5.00×10^{-7} M. The excitation wavelengths for isoalloxazines and 5-deazaisoalloxazines were 380 and 330 nm, respectively, and the slit widths of excitation and emission were 3 and

†† 1 M=1 mol dm^{-3}.

15 nm, respectively.

The reaction of cyanide ion and 5-deazaisoalloxazines was monitored spectrophotometrically at 30±0.1 °C by following the disappearance of 5-deazaisoalloxazines at their λ_{max}. The typical conditions were: $[CN^-]=1.00\times10^{-3}$ M and [5-deazaisoalloxazine]$=5.00\times10^{-5}$ M in aqueous 2 vol% DMF solution. The first-order behavior was observed for at least up to three half-lives. The pseudo-first-order rate constants thus obtained were proportional to the cyanide ion concentration. Hence, the reaction is first-order in cyanide ion and 5-deazaisoalloxazine.

Results and Discussion

Absorption Spectra in Various Solvents. The typical absorption maxima of isoalloxazines and 5-deazaisoalloxazines are summarized in Tables 2 and 3, respectively. Table 2 shows that **1**MeEt is subject to typical solvent effects:[1-5] S1 is a gaussian-type peak in aqueous solution (type A), has shoulders in polar solvents (type B), and has a three-banded fine structure in nonpolar solvents (type C). The λ_{max} of S2 shifted to shorter wavelengths with lowering the solvent polarity, as reported by Koziol and others.[1-5] On the other hand, S1 of **1**MeDod and **1**HDod was a well-resolved fine structure even in aqueous solution (*i.e.*, type C: Fig. 1). The shape of the S1 peak was almost unaffected at the concentration range $(0.10—2.40)\times10^{-4}$ M. Although these fine-structured peaks in aqueous solution are similar to that of **1**MeEt in benzene, the blue shift of S2 was not observed for aqueous **1**MeDod and **1**HDod (*e.g.*, 340 and 343 nm, respectively; compare with the blue shift of **1**MeEt, 341 (water)→328(benzene)). The result suggests that the fine structure observed in the aqueous system cannot be rationalized in terms of the simple solvent effect.

Table 2. Absorption maxima(nm) of isoalloxazines in various media (30 °C)[a]

Medium	1MeEt S2	1MeEt S1	1MeDod S2	1MeDod S1	1HDod S2	1HDod S1	1ThDod S2	1ThDod S1
Water	341,	433	340,	427 447 480	343,	423 441 472	345,	437
CTAB(10 mM)	340,	433	338,	440(S)	339,	438(S)	337,	438(S)
SDS(10 mM)			341,	440(S)	343,	440(S)		
Brij-35(10 mM)			340,	445(S)	346,	440(S)		
Ethanol	332,	435(S)	332,	435(S)	332,	435(S)		
Pyridine	327,	438(S)	328,	438(S)	327,	438(S)		
Benzene	328,	418 440 466	329,	420 440 467	327,	417 438 464		

a) (S) indicases that S1 has shoulders. Three values given for S1 indicate each absorption maximum for the fine structure split.

Table 3. Absorption maxima(nm) of 5-deazaisoalloxazines in various media (30 °C)[a]

Medium	2MeEt S2	2MeEt S1	2MeOct S2	2MeOct S1	2MeDod S2	2MeDod S1
Water	323,	392	325,	400	325,	386 403 428
CTAB(10 mM)	322,	393	323,	399	322,	399(S)
SDS(10 mM)	323,	392	323,	397	324,	397(S)
Brij-35(10 mM)	323,	391	323,	398	322,	400(S)
Ethanol	318,	398(S)	320,	398(S)	320,	398(S)
DMF	318,	400(S)			318,	401(S)
CH_3CN	316,	397(S)			316,	398(S)
o-Dichlorobenzene	321(S),	404(S) 426			322(S),	405(S) 427
Benzene	318(S),	405(S) 427			318(S),	405(S) 428

a) (S) indicates that the peak has shoulders. Two-to-three values given for S1 indicate each absorption maximum for the fine structure split.

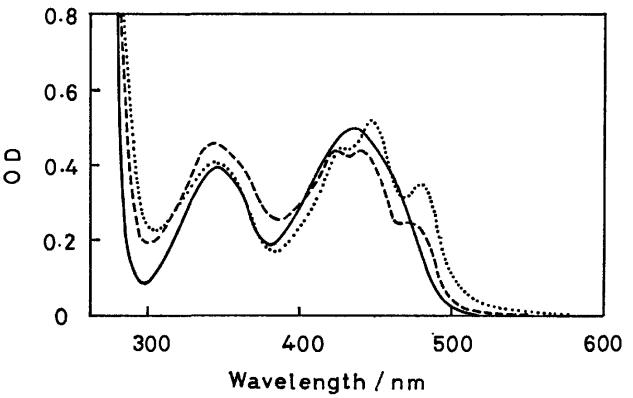

Fig. 1. Absorption spectra of **1**HDod(- - -), **1**MeDod (·····), and **1**ThDod(——) in water. [isoalloxazine]$=5.00\times10^{-5}$ M.

Interestingly, the fine structure of **1**MeDod and **1**HDod has disappeared completely in aqueous solutions containing surfactants above the critical micelle concentrations(cmc), and the spectra were classified as type B (Table 2). Similarly, the fine structure disappeared on the addition of organic solvents (*vide infra*). The fine structure also disappeared by introducing a hydrophilic 3-(thiazolinio)propyl group at 3-position of 10-dodecylisoalloxazine (Fig. 1). These results, together with our previous findings,[6,9] strongly suggest that the fine structure of aqueous **1**MeDod and **1**HDod stems from the association of the isoalloxazine nuclei which is induced by hydrophobic interaction between 10- dodecyl groups. The disappearance of the fine structure in the micellar system is accounted for by the loss of the interaction between the isoalloxazine nuclei in the micellar phase (*i.e.*, dilution effect). The phenomenon is similar to that of the absorption spectrum of dye molecules: "stacking" association of dye molecules induces the split of the absorption bands in aqueous solution, but it disappears in micellar solutions.[13-16] The disappearance of the fine structure by adding organic solvents is accounted for by deaggregation due to the enhanced solubility.

It occurred to us that if the fine structure is induced by the aggregation, the S1 peak of **1**ThDod may split above its cmc. The cmc of cationic C_{12}-surfactants is about 10 mM,[17] so that we measured the spectrum of **1**ThDod at 0.05—30 mM by using 1 cm—0.1 mm width cuvettes. As shown in Fig. 2, the shape of the S1 peak was almost identical below 10 mM while clear shoulders were observed above 20 mM. Probably, the cmc of **1**ThDod is at this concentration. The result supports that the split of the S1 peak is significantly associated with the aggregation phenomenon.

The solvent effect on the absorption spectrum of 5-deazaisoalloxazine has not been examined systematically. Table 3 and Fig. 3 show that in general, the solvent effects on S1 of **2**MeEt are quite similar

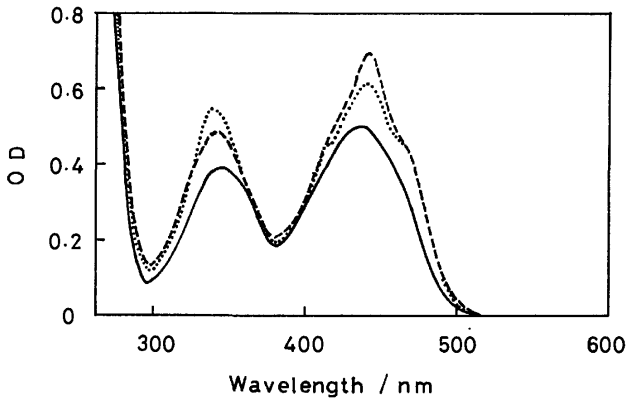

Fig. 2. Absorption spectra of **1**ThDod in water at different concentrations.
——: 10 mM, - - -: 20 mM, ·····: 30 mM. The Y-axis is normalized to 5×10^{-5} M in 1 cm cell.

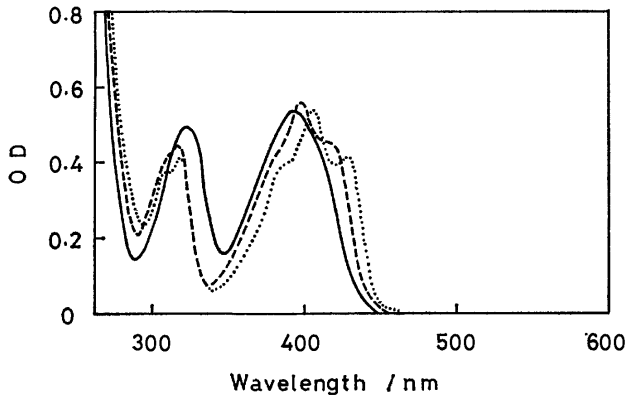

Fig. 3. Absorption spectra of **2**MeEt in water (——), acetonitrile (- - -), and benzene (·····).
[**2**MeEt]$=5.00\times10^{-5}$ M.

to those on **1**MeEt. The following points are noticeable differences: (i) the blue shift of S2 in nonpolar solvents is smaller than that of S2 of isoalloxazines (*e.g.*, 323 nm in water→318 nm in benzene) and (ii) the S2 peak in benzene and *o*-dichlorobenzene(*o*-DCB) has a shoulder at 310 nm (Fig. 3). A similar shoulder on S2 has been observed for tetra-*O*-butyrylriboflavin in carbon tetrachloride.[4] As expected, **2**MeDod (amphiphilic 5-deazaisoalloxazine) gave a three-banded S1 peak. Being different from that of amphiphilic isoalloxazines, the ε_{max} of S2 (12300) is greater than any of S1 (9000, 10400, and 6040). Since the fine structure disappeared in surfactant micellar solutions, the association of 5-deazaisoalloxazine nuclei is responsible for the appearance of the fine structure.

Another amphiphilic 5-deazaisoalloxazine, **2**MeOct in water did not give a three-banded S1 peak but a broad absorption band spreading to 500—600 nm, and the ε_{max} of S1 was smaller than that of S2 (Fig. 4). The longer-wavelength absorption band disappeared in 20 vol% ethanol. One may thus presume that **2**MeOct forms some aggregate in aqueous solution though it is not stable enough to induce a fine structure split. Attempting to stabilize the aggregate, we measured the spectrum of **2**MeOct (5.00×10^{-5} M) in KCl (0.25—2 mM) containing aqueous solutions and at high

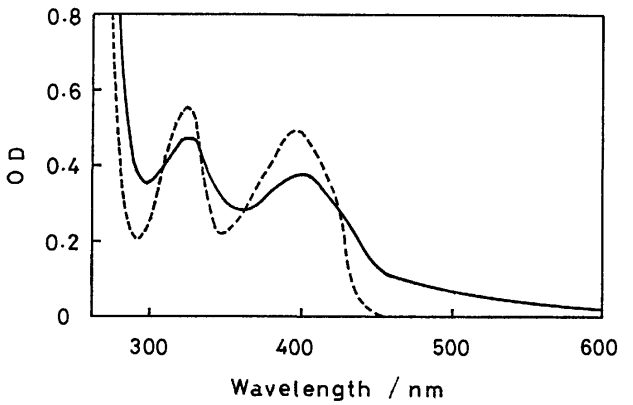

Fig. 4. Absorption spectra of **2**MeOct in water (——) and 20 vol% aqueous ethanol (- - -).
[**2**MeOct]$=5.00\times10^{-5}$ M.

2MeOct concentrations ($\approx2.40\times10^{-4}$ M). However, the spectra were apparently identical under these measurement conditions.

Absorption Spectra in Water–Ethanol and Water–Pyridine Mixed Solvents. Since the fine structure of amphiphilic isoalloxazines and 5-deazaisoalloxazines stems from the association of the nuclei, addition of organic solvents which causes the deaggregation of these amphiphiles would change the shape of the S1 speak. The spectral results are summarized in Tables 4 and 5. Addition of ethanol or pyridine changed the spectral shape of S1 of **2**MeEt from type A to type B (ethanol) or to type C(pyridine). More peculiar spectral changes were observed for **2**MeDod: a new, broad absorption band appeared at 500—600 nm region below 40 vol% ethanol and 20 vol% pyridine, and both the fine structure and the longer-wavelength absorption band disappeared above these solvent compositions (Fig. 5). We previously reported that a similar longer-wavelength absorption band is observed for **1**MeDod in ethanol (<45 vol%) and pyridine (<20 vol%) solutions.[6,9] In particular, the absorption band in aqueous pyridine was so strong (*e.g.*, ε_{550} 4420 in

Table 4. Absorption maxima(nm) of 5-deazaisoalloxazines in ethanol-water mixed solvents (30 °C)[a]

Ethanol (vol%)	**2**MeEt		**2**MeOct		**2**MeDod	
	S2	S1	S2	S1	S2	S1
0	323,	392	325,	400	325,	386 403 428
20	324,	393	325,	395	326,	386 402 428
30					333,	404(S) 428
40	323,	395	324,	397	324,	397(S)
60	322,	396	323,	397	323,	397(S)
80	321,	397(S)	322,	398(S)	322,	398(S)
100	318,	398(S)	320,	398(S)	320,	398(S)

a) (S) indicates that the peak has shoulders. Two-to-three values given for S1 indicate each absorption maximum for the fine structure split.

Table 5. Absorption maxima(nm) of 5-deazaisoalloxazines in pyridine-water mixed solvents (30 °C)[a)]

Pyridine (vol%)	2MeEt		2MeDod	
	S2	S1	S2	S1
0	323,	392	325,	386 403 428
5			328,	388 403 429
7			328,	388 403 429
10	327,	395	329,	404(S) 429
14			330,	405(S) 430
20	326,	396	325,	398
40	323,	397	323,	399
60	322,	399	322,	400
80	321,	400	323,	402
100	319,	402 423	320,	403 423

a) (S) indicates that the peak has shoulders. Two-to-three values given for S1 indicate each absorption maximum for the fine structure split.

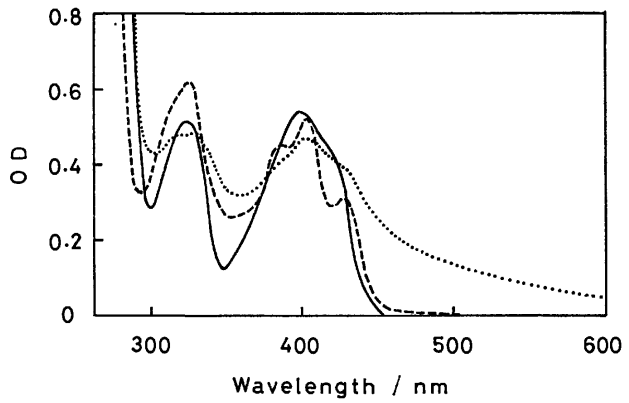

Fig. 5. Absorption spectra of **2**MeDod in water (- - -), 15 vol% pyridine(·····), and 40 vol% pyridine(——).
[**2**MeDod]$=5.00\times10^{-5}$ M.

18 vol% pyridine) that we ascribed the new absorption band to a specific charge transfer interaction between pyridine and isoalloxazine. A similar band was observable in aqueous solutions containing 4-(dimethylamino)pyridine, 3-indoleacetic acid, and *o*-aminobenzoic acid. Since the longer-wavelength absorption band of **2**MeDod in aqueous pyridine was not so strong and was rather comparable with that in aqueous ethanol, this band may not be ascribed to a simple charge transfer interaction. Probably, the electron-acceptability of **2**MeDod may be weaker than that of **1**MeDod.

In Fig. 6, OD_{500} as a measure of the strength of the longer-wavelength absorption band is plotted as a function of solvent compositions. The OD_{500} became largest at 33 vol% ethanol and 13 vol% pyridine and decreased sharply at higher solvent compositions.

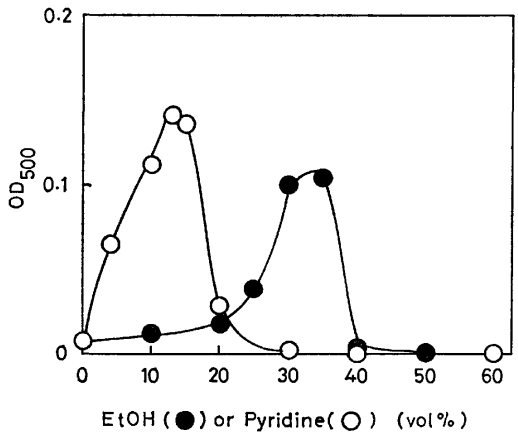

Fig. 6. OD_{500} *vs.* solvent concentration.
[**2**MeDod]$=5.00\times10^{-5}$ M.

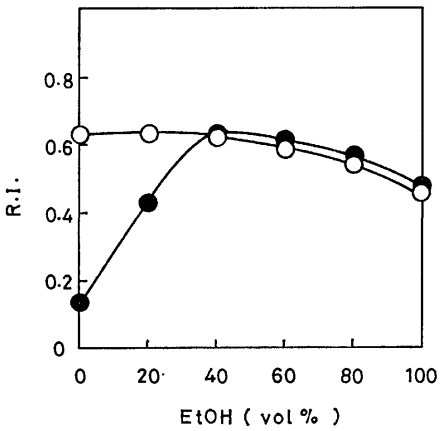

Fig. 7. Relative intensity(R.I.) of emission maxima *vs.* ethanol concentration.
○: **2**MeEt(5.00×10^{-7} M), ●: **2**MeDod(5.00×10^{-7}).

These results indicate that there is a critical transition from the aggregated form to the monomeric form at 40 vol% ethanol or 20 vol% pyridine. In **1**MeDod and **2**MeDod as amphiphiles, (5-deaza)isoalloxazines are hydrophilic head groups. The "stacking" association between the head groups induces the fine structure split of S1. On the other hand, addition of organic solvents, more or less, would disturb the orientation of the aggregation form, and probably, the disturbed orientation would be responsible for the longer-wavelength absorption band. At the transition points, both the fine structure and the longer-wavelength absorption disappear because of the deaggregation to the monomeric forms.

Fluorescent Spectra. Figure 7 shows the influence of added ethanol on the relative intensity (R.I.) of fluorescent maxima (about 460 nm) of **2**MeEt and **2**MeDod in aqueous solution. The R.I. value of **2**MeEt was affected to a smaller extent by added ethanol, slightly decreasing with increasing ethanol concentration. On the other hand, the R.I. of **2**MeDod in water was very small, increasing rapidly with increasing ethanol concentration. The value at 40 vol% was almost equal to that of **2**MeEt. The results indicate that the fluorescent spectra of **2**MeDod

are also explicable on the basis of the aggregation-deaggregation phenomenon: the weak R.I. of **2**MeDod in water is ascribed to concentration quenching due to the association of 5-deazaisoalloxazine nuclei, and solvent-induced deaggregation leads to the increase in R.I. more than expected from the simple solvent effect. The 40 vol% ethanol composition where the abnormality of **2**MeDod disappears is exactly equal to the transition estimated from the absorption spectra.

Nucleophilic Reactivity of Cyanide Ion. It is interesting to assess whether the aggregation-deaggregation equilibrium of **2**MeDod is reflected by its reactivity. To test the possibility, we determined the rate constants for the nucleophilic reaction of cyanide ion toward 5-deazaisoalloxazines[18,19] in water–ethanol mixed solvents.

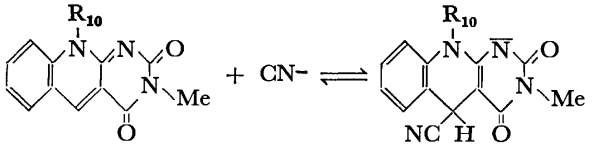

(1)

The reaction was first-order in cyanide ion and 5-deazaisoalloxazine. In Fig. 8, the second-order rate constants (k_2) are plotted as a function of the ethanol concentration. In aqueous solution, the k_2 values for **2**MeEt and **2**MeOct were 1.27 and 0.86 $M^{-1} s^{-1}$, respectively, whereas that for **2**MeDod was not detected at all under the present experimental conditions ($k_2 < 0.001\ M^{-1} s^{-1}$). The k_2 for **2**MeEt increased with increasing ethanol concentration. The reaction rate of **2**MeDod in 20 vol% ethanol was still very slow ($k_2 = 0.003\ M^{-1} s^{-1}$) but suddenly became fast in 30 vol% ethanol ($k_2 = 1.48\ M^{-1} s^{-1}$). **2**MeOct in most cases gave the medium rate constants. The rate constants for three 5-deazaisoalloxazines were almost identical above 40 vol% ethanol. The plots in Fig. 8 are well correlative to those in Figs. 6 and 7, indicating that the reactivity of 5-deazaisoalloxazines is significantly related to the aggregation-deaggregation equilibrium.

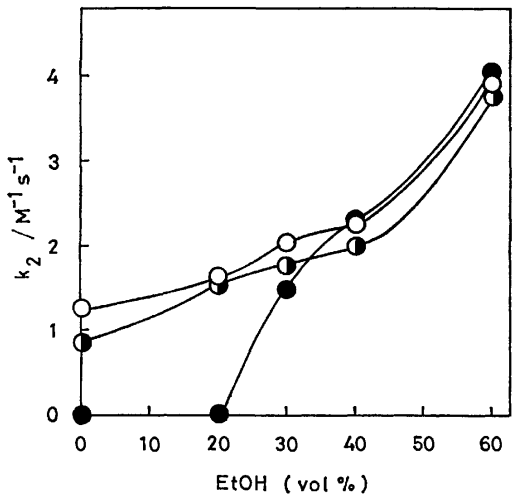

Fig. 8. Second-order rate constants for the reaction of cyanide ion (1.00×10^{-3} M) and 5-deazaisoalloxazines (5.00×10^{-5} M). ○: **2**MeEt, ◑: **2**MeOct, ●: **2**MeDod.

S. S. thanks Ministry of Education of Japan for Grant-in-Aid for Scientific Research (No. 555365).

References

1) J. Koziol, *Photochem. Photobiol.*, **5**, 41 (1966).
2) J. Koziol, *Photochem. Photobiol.*, **9**, 45 (1969).
3) K. Yagi, J. Okuda, A. A. Dmitrovskii, and R. Honda, *J. Vitaminol.* **7**, 276 (1961).
4) A. Kotaki, M. Naoi, J. Okuda, and K. Yagi, *J. Biochem.*, **61**, 404 (1967).
5) A. J. W. G. Visser and F. Muller, *Helv. Chim. Acta*, **62**, 593 (1979).
6) S. Shinkai, A. Harada, Y. Ishikawa, O. Manabe, and F. Yoneda, *Chem. Lett.*, **1981**, 479.
7) K. Yagi and T. Ozawa, *Biochim. Biophys. Acta*, **56**, 413 (1962).
8) V. Massey and H. Ganther, *Biochemistry*, **4**, 1161 (1965).
9) S. Shinkai, A. Harada, Y. Ishikawa, O. Manabe, and F. Yoneda, *J. Chem. Soc., Perkin Trans. 2*, in press.
10) F. Yoneda, Y. Sakuma, M. Ichiba, and K. Shinomura, *J. Am. Chem. Soc.*, **98**, 830 (1976).
11) S. Shinkai, T. Yamashita, Y. Kusano, and O. Manabe, *J. Am. Chem. Soc.*, **104**, 563 (1982).
12) F. Yoneda, Y. Sakuma, S. Mizumoto, and R. Ito, *J. Chem. Soc., Perkin Trans. 1*, **1976**, 1805.
13) J. T. Martin and H. A. Standing, *J. Textil. Institute*, **1949**, 1671.
14) E. Rabinowitch and L. F. Epstein, *J. Am. Chem. Soc.*, **63**, 69 (1941).
15) O. Manabe, K. Nanzyo, S. Matsubara, M. Nagasaki, and H. Hiyama, *Kagaku To Kogyo*, **35**, 12 (1961).
16) H. Sato, M. Kawasaki, K. Kasatani, N. Nakashima, and K. Yoshihara, *Chem. Lett.*, **1980**, 1529.
17) J. H. Fendler and E. J. Fendler, "Catalysis in Micellar and Macromolecular Systems," Academic Press, New York, N. Y. (1975), Chap. 2.
18) R. L. Chan and T. C. Bruice, *J. Am. Chem. Soc.*, **99**, 6721 (1977).
19) M. S. Jorns and L. B. Hersh, *J. Biol. Chem.*, **251**, 4872 (1976).

 © 1982 The Chemical Society of Japan Bull. Chem. Soc. Jpn., 55, 933—937 (1982)

Branched-chain Sugars. XXVIII. Synthesis of 2-*C*-Methyl-L-glyceraldehyde, 2-*C*-Methyl-D-erythrose, and 3-*C*-Methyl-L-erythrose Derivatives[1]

Juji YOSHIMURA,* Kazutoshi HARA, Masanori YAMAURA, Kazutoshi MIKAMI, and Hironobu HASHIMOTO

Laboratory of Chemistry for Natural Products, Faculty of Science, Tokyo Institute of Technology, Nagatsuta, Midori-ku, Yokohama 227

(Received August 19, 1981)

As synthons for the synthesis of bicyclomycin, the title compounds were derived from 1,2:5,6-di-*O*-isopropylidene-3-*C*-methyl-α-D-allofuranose by the descendent method.

Recent advances in the chiral synthesis established the general recognition that monosaccharides are valuable sources of chiral synthons for optically active, non-sugar natural products.[2-4] However, it seems likely that the strategy for the derivation of a desired synthon from a proper monosaccharide is still under development. As a part of the synthetic studies on branched-chain sugars, this paper describes the preparation of 2-*C*-methyl-L-glyceraldehyde, 2-*C*-methyl-D-erythrose, and 3-*C*-methyl-L-erythrose derivatives as synthons for the chiral synthesis of bicyclomycin[5] (**1**) which contains a (1*S*,2*S*)-1,2,3-trihydroxy-2-methylpropyl group attached to a bicyclic 2,5-piperazinedione ring. After a few attemps, the aimed compounds were derived from 1,2-*O*-isopropylidene-3-*O*-benzyl-3-*C*-methyl-α-D-allofuranose,[6] obtained from D-glucose *via* four-step conversions, by the descendent method.

Results and Discussion

In general, two approaches, *i.e.* i) introduction of a methyl-branching into an appropriate tetrose or triose derivative and ii) decrement of carbon number from a higher carbon branched-chain sugar, are considered for the present synthesis.

Firstly, periodate oxidation of 2,5-di-*C*-methyl-L-iditol protected at 1,2,5,6-positions was considered to be the ideal method for the preparation of 2-*C*-methyl-L-glyceraldehyde derivatives, as the preparation of 2,3-*O*-isopropylidene-D-glyceraldehyde from 1,2:5,6-di-*O*-isopropylidene-D-mannitol has been well-known.[7] For the protection of 1,6-positions of 3,4-*O*-isopropylidene-D-mannitol,[8] the usual tritylation with triphenylmethyl chloride in pyridine gave the corresponding di-*O*-trityl derivative (**2**) in 74% yield. However, benzoylation with benzoyl chloride under similar conditions gave a mixture of di- (**4**), tri- (**5**), and tetrabenzoate (**6**) in the ratio of 2:2:1, together with a small amount of monobenzoate and the unchanged starting material. When the benzoylation was conducted in chloroform at 0 °C in the presence of pyridine, the desired **4** was selectively obtained in 80% yield. The structure of **2** and **4** was confirmed by the derivation into the corresponding 2,5-diacetates (**3** and **7**).

Oxidation of **4** with dimethyl sulfoxide (DMSO)–acetic anhydride gave only 5-*O*-acetyl-1,6-di-*O*-benzoyl-3,4-*O*-isopropylidene-D-fructose (**8**) in 90% yield, but did not give the corresponding diketone. The structure of **8** was ascertained by the comparison of its NMR spectrum with that of the corresponding 5-*O*-benzoyl derivative (**9**) obtained by the similar oxidation of **5**. These compounds showed a characteristic larger geminal coupling constant (17.5 Hz) of H-1 and H-1′ protons. Attemped oxidation of **4** with DMSO–phosphorus pentaoxide[9] gave a complex product from which the corresponding monoketone (**10**) was separated. All other oxidations with ruthenium tetraoxide, pyridimium chlorochromate,[10] and potassium permanganate gave unsuccessful results. Moreover, NMR spectra of the reaction products obtained by the reactions of these monoketones with methylmagnesium iodide showed the presence of epimeric *C*-methyl (δ 1.25—1.15) derivatives in the ratios from 1:4 to 1:1. Therefore, this approach was given up.

Secondly, *C*-methylation of known 2,4-*O*-ethylidene-D-erythritol[11] was considered. Partial benzoylation of the substrate with benzoyl chloride gave 1-*O*-benzoyl-2,4-*O*-ethylidene-D-erythritol (**11**) in 80% yield. However, oxidation of **11** with DMSO–trifluoroacetic an-

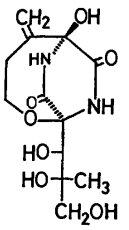

1

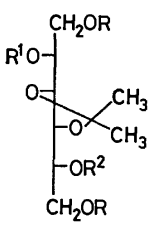

2 R=CPh$_3$, R^1=R^2=H
3 R=CPh$_3$, R^1=R^2=Ac
4 R=Bz, R^1=R^2=H
5 R=R^2=Bz, R^1=H
6 R=R^1=R^2=Bz
7 R=Bz, R^1=R^2=Ac

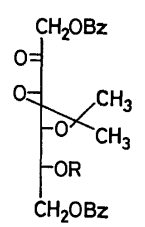

8 R=Ac
9 R=Bz
10 R=H

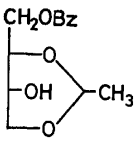

11

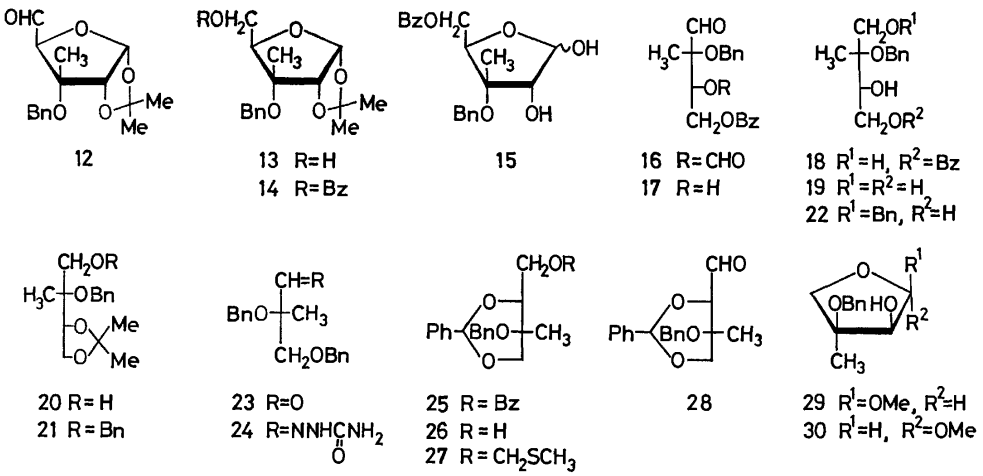

hydride[12] was unsuccessful, probably due to the accompanying β-elimination and also oxidation of the ethylidene group.[13]

From the aforementioned failed results, the descendent method from 1,2-*O*-isopropylidene-3-*O*-benzyl-3-*C*-methyl-α-D-allofuranose,[6] which seems to be the most certain, was thirdly adopted.

Periodate oxidation of the starting α-D-allofuranose gave 3-*O*-benzyl-1,2-*O*-isopropylidene-3-*C*-methyl-α-D-*ribo*-pentodialdofuranose (**12**) quantitatively. Reduction of **12** with sodium borohydride gave the corresponding α-D-ribofuranose (**13**) in 94% yield. The usual benzoylation of **13** gave the corresponding benzoate (**14**) in 95% yield. Partial hydrolysis of **14** with 70% acetic acid gave de-*O*-isopropylidenated product (**15**) in 96% yield. Periodate oxidation of **15** and successive reduction with sodium borohydride gave 4-*O*-benzoyl-2-*O*-benzyl-2-*C*-methyl-D-erythritol (**18**) in 92% yield. The intermediary 4-*O*-benzoyl-2-*O*-benzyl-3-*O*-formyl-D-erythrose (**16**) could not be purified, but characterized by its NMR spectrum, and 4-*O*-benzoyl-2-*O*-benzyl-2-*C*-methyl-D-erythrose (**17**) could be incidentally obtained as crystals from an incomplete reduction products. Treatment of **18** in methanol with a catalytic amount of sodium methoxide gave de-*O*-benzoylated product (**19**) in a good yield.

For the conversion of **19** into branched-chain sugars of L-series, periodate oxidation of **19** was tried. However, the product showed eight kinds of *C*-methyl signals in the NMR spectrum, indicating 2-*O*-benzyl-2-*C*-methyl-L-glyceraldehyde exists in polymeric states. Therefore, **19** was treated with acetone containing sulfuric acid catalyst to give the corresponding 3,4-*O*-isopropylidene derivative (**20**) in 70% yield. Successive benzylation of **20** with sodium hydride and benzyl chloride gave the 1-*O*-benzyl derivative (**21**) in 68% yield, which was partially hydrolyze into the corresponding de-*O*-isopropylidenate product (**22**) in 84% yield. Periodate oxidation of **22** gave the desired 2,3-di-*O*-benzyl-2-*C*-methyl-L-glyceraldehyde (**23**) quantitatively. Because **23** is stable at room temperature only for a few h, it was instantly characterized as the crystalline semicarbazone (**24**).

On the other hand, benzylidenation of **18** with dimethoxytoluene gave the corresponding benzylidene derivative (**25**) which was then converted into the de-*O*-benzoyl derivative (**26**) in a good yield, by treatment with sodium methoxide. Oxidation of **26** with DMSO–dicyclohexylcarbodiimide gave 3-*O*-benzyl-2,4-*O*-benzylidene-3-*C*-methyl-L-erythrose (**28**) and the corresponding methylthiomethyl ether (**27**) in 27 and 25% yield, respectively. The L-erythose derivative **28** was further characterized by the conversion into methyl 3-*O*-benzyl-3-*C*-methyl-α- and β-L-erythrofuranosides (**29** and **30**) by treatment with methanolic hydrogen chloride.

Thus, it was shown that the descendent method of a branched-chain hexose having a proper configuration provides certain pathways to various lower carbon branched-chain sugars of D- and L-series, by the combination of the protection of hydroxyl groups with an aldehyde or a ketone and periodate cleavage of carbon-chain.

Experimental

General Methods. Melting points were determined with a Mel-Temp melting point apparatus and not corrected. Evaporations were conducted under diminished pressure. Optical rotations were measured in a 0.5 dm tube with Carl Zeiss LEP-Al or JASCO DIP-4 polarimeter, using chloroform as a solvent unless otherwise stated. IR spectra were recorded with a Hitachi EPI-G2 grating spectrometer. NMR spectra were recorded with a JEOL JNM PS-100 spectrometer for solutions in chloroform-*d* containing tetramethylsilane as the internal reference. Chemical shifts and coupling constants were recorded in δ and Hz units, respectively, and IR frequencies in cm^{-1}.

3,4-O-Isopropylidene-1,6-di-O-triphenylmethyl-D-mannitol (2) and Its 2,5-Diacetate (3). To a solution of 3,4-*O*-isopropylidene-D-mannitol[8] (10 g, 45 mmol) in pyridine (30 ml) was added triphenylmethyl chloride (27 g, 96.9 mmol) portionwise, and the resulting solution was kept at room temperature for 2 d, poured into ice–water, and extracted with dichloromethane. The extract was washed successively with water, 0.1 M sulfuric acid, saturated aqueous sodium hydrogencarbonate, and water, and then evaporated. The residual syrup was crystallized from ethanol to give **2** as prisms in 74% (23.5 g) yield. Mp 174—175 °C; $[\alpha]_D^{24}$ +10.5° (*c* 1.0, MeOH).

Found: C, 79.25; H, 6.33%. Calcd for $C_{47}H_{46}O_6$: C, 79.86; H, 6.56%.

The usual acetylation of **2** (1.4 g, 2 mmol) in pyridine (2 ml) with acetic anhydride (4 ml) gave **3** as needles in 83% (1.3 g) yield. Mp 154—155 °C (ethanol); $[\alpha]_D^{22}$ −5.5° (*c* 1.0, MeOH); NMR: 7.5—7.1 (m, 30H, 6 Ph), 5.18 (dd, 2H, $J_{2,3}=J_{4,5}=4.5$, H-2 and 5), 3.98 (d, 2H, H-3 and 4), 3.30 (d, 4H, $J_{1,2}=J_{5,6}=4.7$, H-1,1′,6, and 6′), 2.09 (s, 6H, 2Ac), 1.15 (s, 6H, Ip).

Found: C, 76.82; H, 6.32%. Calcd for $C_{51}H_{50}O_5$: C, 77.45; H, 6.37%.

*Benzoylation of 3,4-*O*-Isopropylidene-*D*-mannitol.* To an ice-cooled solution of 3,4-*O*-isopropylidene-D-mannitol (22.2 g, 0.1 mol) in pyridine (100 ml) was added with stirring benzoyl chloride (29.5 g, 0.21 mol) dropwise. The mixture was kept at room temperature overnight, poured into ice-water, and extracted with dichloromethane. The usual processing of the extract and fractionation of the products on a column of silica gel with 50:1 benzene–acetone gave in turn tetra- (**6**), tri- (**5**), and dibenzoate (**4**) in 12% (7.65 g), 24% (12.8 g), and 24% (10.3 g) yield, respectively.

6: mp 120—122 °C; $[\alpha]_D^{24}$ −0.59° (*c* 0.8, MeOH); NMR: 8.0—7.8 and 7.6—7.2 (m, 20H, 4Ph), 5.61 (m, 2H, H-2 and 5), 4.75 (dd, 2H, $J_{1,2}=J_{5,6}=3.2$, $J_{1,1'}=J_{6,6'}=12.2$, H-1 and 6), 4.59 (d, 2H, $J_{2,3}=J_{4,5}=6.0$, H-3 and 4), 4.56 (dd, 2H, $J_{1',2}=J_{5,6'}=6.0$, H-1′ and 6′), 1.49 (s, 6H, Ip).

Found: C, 69.52; H, 5.32%. Calcd for $C_{37}H_{30}O_{10}$: C, 69.58; H, 5.37%.

5: mp 115—118 °C (prisms from EtOH); $[\alpha]_D^{24}$ +5.5° (*c* 0.7, MeOH). NMR and IR patterns were very similar to those of **4**.

Found: C, 67.25; H, 5.42%. Calcd for $C_{30}H_{30}O_9$: C, 67.40; H, 5.66%.

4: mp 96—97 °C; $[\alpha]_D^{20}$ +29.2° (*c* 0.4, MeOH); IR: 3400 (OH), 1720 and 1690 (C=O); NMR; 8.1—7.9 and 7.6—7.2 (m, 10H, 2Ph), 4.63 (bd, 2H, $J_{2,3}=J_{3,4}=11.0$, H-1 and 6), 4.5—4.3 (m, 2H, H-1′ and 6′), 3.97 (bs, 6H, H-2,3,4,5 and OH), 1.40 (s, 6H, Ip).

Found: C, 64.67; H, 6.09%. Calcd for $C_{23}H_{26}O_8$: C, 64.17; H, 6.09%.

The usual acetylation of **4** (200 mg, 0.59 mmol) in pyridine (10 ml) with acetic anhydride (10 ml) gave the corresponding diacetate (**7**) in 83% (198 mg) yield. Mp 75—76 °C (ethanol); $[\alpha]_D^{20}$ +21.1° (*c* 1.0, MeOH); IR: 1760—1720 (C=O); NMR: 8.1—7.9 and 7.6—7.3 (m, 10H, 2Ph), 5.33 (m, 2H, H-2 and 5), 4.68 (dd, 2H, $J_{1,2}=J_{5,6}=3.1$, $J_{gem}=12.0$, H-1 and 6), 4.43 (dd, 2H, $J_{1',2}=J_{5,6'}=6.7$, H-1′ and 6′), 4.24 (d, 2H, $J_{2,3}=J_{4,5}=4.6$, H-3 and 4), 2.07 (s, 6H, 2 OAc), 1.46 (s, 6H, Ip).

Found: C, 62.87; H, 5.84%. Calcd for $C_{27}H_{30}O_{10}$: C, 63.03; H, 5.88%.

When the benzoylation of 3,4-*O*-isopropylidene-D-mannitol (5 g, 22.5 mmol) with benzoyl chloride (6.6 g, 47 mmol) was performed in chloroform (50 ml) at 0 °C in the presence of pyridine (3.3 g, 78 mmol), **4** was selectively obtained in 80% (7.75 g) yield.

*5-*O*-Acetyl-1,6-di-*O*-benzoyl-3,4-*O*-isopropylidene-*D*-fructose (**8**).* A solution of **4** (1.5 g, 3.5 mmol) in dimethyl sulfoxide (DMSO, 35 ml) and acetic anhydride (25 ml) was kept at room temperature overnight, and then evaporated. The residual syrup was extracted with dichloromethane. The usual processing of the extract and purification of the product on a column of silica gel with 50:8 petroleum ether–benzene gave syrupy **8** (1.47 g, 89.7%) which was crystallized from hexane. Mp 54—56 °C; $[\alpha]_D^{22}$ +0.67° (*c* 1.13, acetone); IR: 1760—1720 (C=O); NMR: 8.1—7.9 and 7.6—7.3 (m, 10H, 2 Ph), 5.46 (m, 1H, H-5), 5.28 and 5.08 (ABq, 2H, $J=17.5$, H-1 and 1′), 4.8—4.2 (m, 4H, H-3,4,6, and 6′), 2.08 (s, 3H, OAc), 1.46 (s, 6H, Ip).

Found: C, 63.50; H, 5.72%. Calcd for $C_{25}H_{26}O_9$: C, 63.82; H, 5.72%.

*1,5,6-Tri-*O*-benzoyl-3,4-*O*-isopropylidene-*D*-fructose (**9**).* Compound **5** (4.3 g, 8 mmol) was oxidized with DMSO (75 ml) and acetic anhydride (50 ml) as above. Purification of the product gave syrupy **9** (4.2 g) quantitatively, which was crystallized from ethyl acetate–ligroine. Mp 129—130 °C; $[\alpha]_D^{23}$ +15.5° (*c* 1.4, acetone); IR: 1740—1710 (C=O); NMR: 8.1—7.9 and 7.6—7.2 (m, 15H, 3 Ph), 5.69 (m, 1H, H-5), 5.31 and 5.10 (ABq, 2H, $J=17.5$, H-1 and 1′), 4.73 (dd, 1H, $J_{5,6}=4.0$, $J_{6,6'}=12.5$, H-6), 4.72 (d, 1H, $J_{2,3}=4.2$, H-3), 4.69 (t, 1H, H-4), 4.54 (q, 1H, $J_{5,6'}=6.3$, H-6′), 1.45 (s, 6H, Ip).

Found: C, 67.24; H, 5.32%. Calcd for $C_{30}H_{28}O_9$: C, 67.66; H, 5.30%.

*1,6-Di-*O*-benzoyl-3,4-*O*-isopropylidene-*D*-fructose (**10**).* To an ice-cooled mixture of phosphorus pentaoxide (5 g) and DMSO (50 ml) was added with stirring a solution of **4** (6 g, 14 mmol) in DMSO (40 ml), and the resulting solution was kept at room temperature overnight, poured into excess aqueous sodium hydrogencarbonate, and extracted with dichloromethane. The usual processing of the extract gave a syrup (4.8 g) which showed four spots on TLC, excepting a small amount of the starting material. Separation of the syrup on a column of silica gel with 8:1 benzene–acetone gave **10** as the second polar fraction in 19% (1.15 g) yield. NMR spectrum of the most nonpolar fraction indicated that it is a monobenzoyl derivative. Mp 90—91 °C; NMR: 8.2—8.0 and 7.7—7.3 (m, 10H, 2Ph), 5.31 and 5.21 (ABq, 2H, $J=17.5$, H-1 and 1′), 4.75—4.3 (m, 4H, H-3,4,6, and 6′), 4.14 (m, 1H, H-5), 3.0 (bs, 1H, OH), 1.50 and 1.46 (each s, 6H, Ip).

Found: C, 66.18; H, 5.25%. Calcd for $C_{25}H_{24}O_8$: C, 66.36; H, 5.35%.

*1-*O*-Benzoyl-2,4-*O*-ethylidene-*D*-erythritol (**11**).* The usual benzoylation of 2,4-*O*-ethylidene-D-erythritol[11] (3.16 g, 20 mmol) in pyridine (20 ml) with benzoyl chloride (3.08 g, 22 mmol) at 0 °C gave **11** as crystals in 80% (4.58 g) yield. Mp 103—105 °C; $[\alpha]_D^{26}$ +13.4° (*c* 1.0); NMR: 8.2—8.0 and 7.7—7.3 (m, 5H, Ph), 4.77 (dd, 1H, $J_{1,2}=3.0$, $J_{1,1'}=12.0$, H-1), 4.50 (q, 1H, $J=5.0$, CHMe), 4.44 (dd, $J_{1',2}=2.0$, H-1′), 4.15 (dd, $J_{3,4e}=2.6$, $J_{4e,4a}=10.0$, H-4e), 3.75—3.55 (m, 2H, H-2 and 3), 3.48 (t, 1H, H-4a), 3.02 (s, 1H, OH), 1.36 (d, 3H, CMe).

Found: C, 58.02; H, 6.10%. Calcd for $C_{13}H_{16}O_5$: C, 58.20; H, 6.01%.

*3-*O*-Benzyl-1,2-*O*-isopropylidene-3-*C*-methyl-α-*D*-ribo-pentodialdofuranose (**12**).* A solution of 3-*O*-benzyl-1,2-*O*-isopropylidene-3-*C*-methyl-α-D-allofuranose[6] (10 g, 30.8 mmol) and sodium periodate (7.0 g, 32.7 mmol) in aqueous acetic acid (1:1, 60 ml) was stirred for 30 min at room temperature, diluted with water (60 ml), and then extracted with chloroform. The usual processing of the extract gave **12**, quantitatively. Mp 74—76 °C (ether–petroleum ether); $[\alpha]_D^{23}$ +55.5° (*c* 1.1); IR: 1745 (CHO); NMR: 9.67 (s, 1H, CHO), 7.3 (m, 5H, Ph), 5.85 (d, 1H, $J_{1,2}=4.0$, H-1), 4.64 (s, 3H, H-4 and CH_2Ph), 4.38 (d, 1H, H-2), 1.60 (s, 3H, CMe), 1.40 and 1.29 (each s, 6H, Ip).

Found: C, 65.47; H, 7.01%. Calcd for $C_{16}H_{20}O_5$; C, 65.74; H, 6.90%.

*3-*O*-Benzyl-1,2-*O*-isopropylidene-3-*C*-methyl-α-*D*-ribofuranose (**13**).* To an ice-cooled solution of **12** (8.87 g, 30.3 mmol) in aqueous methanol (1:1, 160 ml) was added sodium borohydride (1.15 g, 30.4 mmol) portionwise, and the mixture

was stirred for 3 h, neutralized with 0.1 M hydrochloric acid, evaporated, and the residue was extracted with chloroform. The usual processing of the extract and crystallization and recrystallization of the product from ether–petroleum ether and ethanol–hexane gave **13** (8.58 g, 94%) as needles. Mp 65—66 °C; $[\alpha]_D^{22}$ +46.3° (*c* 0.99); NMR: 7.3 (m, 5H, Ph), 5.72 (d, 1H, $J_{1,2}$=3.6, H-1), 4.51 (s, 2H, CH_2Ph), 4.22 (d, 1H, H-2), 4.15 (dd, 1H, H-4), 3.74 (dd, 1H, $J_{4,5}$=4.0, $J_{5,5'}$=12.5, H-5), 3.60 (dd, 1H, $J_{4,5'}$=7.0, H-5'), 2.81 (bs, 1H, OH), 1.56 (s, 3H, CMe), 1.31 and 1.14 (each s, 6H, Ip).

Found: C, 65.34; H, 7.47%. Calcd for $C_{16}H_{22}O_5$: C, 65.29; H, 7.53%.

*5-O-Benzoyl-3-O-benzyl-1,2-O-isopropylidene-3-C-methyl-α-D-ribofuranose (**14**).* To an ice-cooled solution of **13** (10g, 34 mmol) in pyridine (100 ml) was added dropwise benzoyl chloride (5.25 g, 37.3 mmol) with stirring, and the mixture was kept for 1 h at room temperature, poured into ice–water, and then extracted with chloroform. The usual processing of the extract and recrystallization of the product from ether–petroleum ether gave **14** as needles (12.7 g, 95%). Mp 84—85 °C; $[\alpha]_D^{22}$ +12.5° (*c* 1.55); IR: 1720 (ester); NMR: 8.1—7.9 and 7.6—7.4 (m, 10H, 2Ph), 5.70 (d, 1H, $J_{1,2}$= 4.0, H-1), 4.55 (s, 2H, CH_2Ph), 4.3—4.5 (m, 3H, H-4, 5, and 5'), 4.23 (d, 1H, H-2), 1.60 (s, 3H, CMe), 1.33 and 1.21 (each s, 6H, Ip).

Found: C, 69.04; H, 6.50%. Calcd for $C_{23}H_{26}O_6$: C, 69.33; H, 6.58%.

*5-O-Benzoyl-3-O-benzyl-3-C-methyl-D-ribofuranose (**15**).* A solution of **14** (5.28 g, 13.3 mmol) in acetic acid (70%, 60 ml) was refluxed for 2 h, diluted with water, and extracted with chloroform. The usual processing of the extract and purification of the product on a column of silica gel with 8:1 benzene–acetone gave pure **15** as a syrup in 96% (4.56 g) yield. $[\alpha]_D^{22}$ +36.3° (*c* 1.67).

Found: C, 66.70; H, 6.35%. Calcd for $C_{20}H_{22}O_6$: C, 67.03; H, 6.19%.

*4-O-Benzoyl-2-O-benzyl-2-C-methyl-D-erythritol (**18**).* To a solution of **15** (1.11 g, 3.1 mmol) in methanol (5 ml) was added a solution of sodium periodate (0.8 g, 3.7 mmol) in water (5 ml), and the resulting suspension was stirred for 30 min at room temperature, neutralized with sodium hydrogencarbonate and then extracted with chloroform. The usual processing of the extract gave 4-*O*-benzoyl-2-*O*-benzyl-3-*O*-formyl-2-*C*-methyl-D-erythrose (**16**, 0.84 g, 83%) as a syrup, but it could not be purified on a column of silica gel. However, the crude product gave reasonable NMR spectrum as follows. NMR: 9.63 (s, 1H, CHO), 8.10 (s, 1H, OCHO), 8.0—7.9 and 7.6—7.2 (m, 10H, 2Ph), 5.74 (dd, 1H, H-3), 4.62 (dd, 1H, $J_{3,4}$=4.0, $J_{4,4'}$=12.0, H-4), 4.60 and 4.52 (ABq, 2H, J=12.5, CH_2Ph), 4.51 (q, 1H, $J_{3,4'}$=7.4, H-4'), 1.49 (s, 3H, CMe).

To an ice-cooled solution of syrupy **16** (0.84 g, 2.56 mmol) in methanol (5 ml) and water (10 ml) was added sodium borohydride (110 mg, 2.9 mmol) with stirring. After stirring at room temperature for 3 h, the reaction mixture was neutralized with 0.1 M hydrochloric acid, and filtered. The filtrate was evaporated, and the residue was extracted with chloroform. The usual processing of the extract and purification of the product on a column of silica gel with 3:1 benzene–acetone gave pure **18** in 92% (0.78 g) yield. $[\alpha]_D^{22}$ +9.1° (*c* 1.03); NMR: 8.1—7.9 and 7.6—7.4 (m, 10H, 2 Ph), 4.66 (dd, 1H, H-4'), 4.57 (s, 2H, CH_2Ph), 4.43 (dd, 1H, $J_{4,4'}$=11.6, H-4), 4.17 (dd, 1H, $J_{3,4'}$=2.6, $J_{3,4}$=7.6, H-3), 3.77 (s, 2H, H-1 and 1'), 1.32 (s, 3H, CMe).

Found: C, 68.62; H, 6.95%. Calcd for $C_{19}H_{22}O_5$: C, 69.07; H, 6.71%.

In one instance, fractionation of the incomplete reduction product on a column of silica gel with 3:1 hexane–ethyl acetate gave 4-*O*-benzoyl-2-*O*-benzyl-2-*C*-methyl-D-erythrose (**17**) as crystals. Mp 97—98 °C (ether–ligroine); $[\alpha]_D^{22}$ +26.8° (*c* 0.98); IR: 3500 (OH), 1740 and 1700 (C–O); NMR: 9.71 (s, 1H, CHO), 8.1—7.9 and 7.6—7.1 (m, 10H, 2 Ph), 4.7—4.4 (m, 4H, H-4,4' and CH_2Ph), 4.24 (dd, 1H, $J_{3,4}$=5.6, $J_{3,4'}$=9.2, H-3), 2.98 (bs, 1H, OH), 1.50 (s, 3H, CMe).

Found: C, 69.47; H, 6.04%. Calcd for $C_{19}H_{20}O_5$: C, 69.50; H, 6.14%.

*2-O-Benzyl-2-C-methyl-D-erythritol (**19**).* A solution of **18** (12 g, 36.3 mmol) in methanol (100 ml) containing a catalytic amount of sodium methoxide was stirred for 3 h at room temperature, neutralized with 0.1 M hydrochloric acid, and then evaporated. The residual syrup was purified on a column of silica gel with 2:1 benzene–acetone to give pure **19** as a syrup (6.1 g, 74%). $[\alpha]_D^{23}$ +8.7° (*c* 1.89); IR: 3600—3100 (OH); NMR: 7.3 (m, 5H, Ph), 4.42 (s, 2H, CH_2Ph), 3.80 (dd, 1H, H-3), 3.78 (dd, 1H, $J_{3,4}$=2.6, H-4), 3.64 (bs, 3H, 3 OH), 3.57 (s, 2H, H-1 and 1'), 3.50 (dd, 1H, $J_{3,4'}$=8.0, $J_{4,4'}$=11.6, H-4'), 1.08 (s, 3H, CMe).

Found: C, 64.00; H, 8.12%. Calcd for $C_{12}H_{18}O_4$: C, 63.70; H, 8.02%.

*2-O-Benzyl-3,4-O-isopropylidene-2-C-methyl-D-erythritol (**20**).* A solution of **19** (5.5 g, 24.3 mmol) in dry acetone (60 ml) containing concd sulfuric acid (1 ml) was stirred for 2 d at room temperature, poured into aqueous sodium hydrogencarbonate, and extracted with ether. The usual processing of the extract and purification of the product on a column of silica gel with 8:1 benzene–acetone gave **20** as crystals in 70% (4.5 g) yield. Mp 42—43 °C (methanol–hexane); $[\alpha]_D^{22}$ +13.2° (*c* 1.02); NMR: 7.3 (m, 5H, Ph), 4.56 and 4.62 (ABq, 2H, J=11.0, CH_2Ph), 4.26 (dd, 1H, $J_{3,4}$=6.0, $J_{4,4'}$=7.6, H-4), 4.1—3.9 (m, 2H, H-3 and 4'), 3.65 (s, 2H, H-1 and 1'), 2.21 (bs, 1H, OH), 1.45 (s, 3H, CMe), 1.24 and 1.35 (each s, 6H, Ip).

Found: C, 67.86; H, 8.44%. Calcd for $C_{15}H_{22}O_4$: C, 67.64; H, 8.33%.

*1,2-Di-O-benzyl-3,4-O-isopropylidene-2-C-methyl-D-erythritol (**21**).* To a solution of **20** (4.5 g, 16.9 mmol) in *N*,*N*-dimethylformamide (20 ml) was added sodium hydride (0.9 g) with stirring portionwise, and the mixture was kept at room temperature for 1 h. Benzyl chloride (3.2 g, 25.3 mmol) was further added dropwise to the above mixture with stirring, and the reaction mixture was stirred for 12 h, poured into water (50 ml), and then extracted with ether. The usual processing of the extract and purification of the product on a column of silica gel with 10:1:20 benzene–ethyl acetate–hexane gave **21** as a syrup in 68% (4.1 g) yield. $[\alpha]_D^{23}$ +2.8° (*c* 2.88); NMR: 7.3 (m, 10H, 2Ph), 4.53 and 4.57 (each s, 4H, $2CH_2Ph$), 4.30 (dd, 1H, $J_{3,4}$= 6.0, $J_{4,4'}$=8.0, H-4), 4.1—3.9 (m, 2H, H-3 and 4'), 3.49 and 3.56 (ABq, 2H, J=10.0, H-1 and 1'), 1.43 (s, 3H, CMe), 1.25 and 1.34 (each s, 6H, Ip).

Found: C, 74.18; H, 7.80%. Calcd for $C_{22}H_{27}O_4$: C, 74.13; H, 7.92%.

*1,2-Di-O-benzyl-2-C-methyl-D-erythritol (**22**).* A solution of **21** (3.65 g, 10.2 mmol) in acetic acid (70%, 30 ml) was stirred at room temperature for 72 h, diluted with water and then extracted with chloroform. The usual processing of the extract and purification of the product on a column of silica gel with 8:1 benzene–acetone gave **22** as a syrup in 84% (2.71 g) yield. $[\alpha]_D^{22}$ −7.5° (*c* 1.72); NMR: 7.3 (m, 10H, 2Ph), 4.52 (s, 4H, $2CH_2Ph$), 3.7—3.9 (m, 3H, H-3,4, and 4'), 3.55 and 3.60 (ABq, 2H, J=11.0, H-1 and 1'), 3.02 and 2.64 (each bs, 2H, 2OH), 1.30 (s, 3H, CMe).

Found: C, 71.60; H, 7.47%. Calcd for $C_{19}H_{24}O_4$: C, 72.12; H, 7.65%.

*2,3-Di-O-benzyl-2-C-methyl-L-glyceraldehyde (**23**).* To a solution of **22** (388 mg, 1.23 mmol) in methanol (5 ml) was added a solution of sodium periodate (299 mg, 1.39 mmol) in water (5 ml), and the mixture was stirred at room temperature for 40 min, neutralized with sodium hydrogencarbonate, and then filtered. Methanol in the filtrate was evaporated and the water layer was extracted with ether. The usual processing of the extract gave **23** as a syrup in 95% (332 mg) yield. IR: 1730 (CHO); NMR: 9.69 (s, 1H, CHO), 7.3 (m, 10H, 2Ph), 4.50 and 4.55 (ABq, 2H, J=10.8, CH_2Ph), 4.51 (s, 2H, CH_2Ph), 3.61 and 3.67 (ABq, 2H, J=9.6, H-3 and 3'), 1.34 (s, 3H, CMe).

*2,3-Di-O-benzyl-2-C-methyl-L-glyceraldehyde Semicarbazone (**24**).* To a solution of **23** (200 mg, 0.7 mmol) in methanol (0.5 ml) was added semicarbazide hydrochloride (78.1 mg, 0.7 mmol), and the mixture was scrached with glass rod to produce crystals (193 mg, 80%) which were recrystallized from benzene. Mp 108—109 °C; $[\alpha]_D^{23}$ +13.2° (*c* 0.68); IR: 1690 (amide); NMR: 10.04 (s, 1H, NH), 7.3 (m, 10H, 2Ph), 7.16 (s, 1H, CH=N), 5.99 (s, 2H, NH_2), 4.50 and 4.39 (each s, 4H, $2CH_2Ph$), 3.54 (s, 2H, H-3), 1.41 (s, 3H, CMe).

Found: C, 66.29; H, 6.22; N, 12.54%. Calcd for $C_{19}H_{23}O_3N_3$: C, 66.84; H, 6.79; N, 12.31%.

*1-O-Benzoyl-3-O-benzyl-2,4-O-benzylidene-3-C-methyl-L-erythritol (**25**).* A solution of **18** (3.1 g, 9.4 mmol), dimethoxytoluene (1.71 g, 11.3 mmol), and catalytic amount of *p*-toluenesulfonic acid (170 mg, 0.89 mmol) in *N,N*-dimethylformamide (5 ml) was stirred at room temperature for 3 h, and then methanol produced was removed for 3 h under diminished pressure. The reaction mixture was neutralized with aqueous sodium hydrogencarbonate, evaporated, and the residual syrup was extracted with ether. The usual processing of the extract gave crystals which were recrystallized from methanol. Yield, 1.8 g (52%); mp 110—111 °C; $[\alpha]_D^{23}$ +58.4° (*c* 1.88); NMR: 8.1—7.9 and 7.6—7.2 (m, 15h, 3Ph), 5.57 (s, 1H, CHPh), 4.73 (dd, 1H, $J_{1,2}$=2.0, $J_{1,1'}$=11.6, H-1), *ca.* 4.52 and 4.57 (ABq, 2H, CH_2Ph), 4.42 (dd, 1H, $J_{1',2}$=8.4, H-1'), 4.41 and 3.87 (ABq, 2H, J=11.0, H-4 and 4'), 4.34 (dd, 1H, H-2), 1.60 (s, 3H, CMe).

Found: C, 74.92; H, 6.35%. Calcd for $C_{26}H_{26}O_5$: C, 74.62; H, 6.26%.

*3-O-Benzyl-2,4-O-benzylidene-3-C-methyl-L-erythritol (**26**).* A solution of **25** (1.3 g, 3.1 mmol) in methanol containing a catalytic amount of sodium methoxide was stirred at room temperature for 2 h, neutralized with 0.1 M hydrochloric acid, evaporated, and the resulting sirup was extracted with chloroform. The usual processing of the extract and purification of the product on a column of silica gel with 1:3 ethyl acetate–hexane gave pure **26** as a syrup in 93% (862 mg) yield. $[\alpha]_D^{23}$ +12.9° (*c* 1.46); NMR: 7.4 (m, 10H, 2Ph), 5.51 (s, 1H, CHPh), 4.44 and 4.56 (ABq, 2H, J=10.4, CH_2Ph), 3.6—4.3 (m, 5H, H-1,1',3,4, and 4'), 2.18 (bs, 1H, OH), 1.53 (s, 3H, CMe).

Found: C, 72.43; H, 7.07%. Calcd for $C_{19}H_{22}O_4$: C, 72.59; H, 7.05%.

*3-O-Benzyl-2,4-O-benzylidene-3-C-methyl-L-erythrose (**28**).* To a solution of **26** (335 mg, 1.12 mmol) in DMSO (3 ml) containing catalytic amount of pyridine and phosphoric acid was added dicyclohexylcarbodiimide (500 mg), and the mixture was stirred at room temperature for 24 h, poured into ice–water, and extracted with ether. The usual processing of the extract and fractionation of the products on a flash column with 1:7 ethyl acetate–hexane gave **28** (91 mg, 27%), together with 3-*O*-benzyl-2,4-*O*-benzylidene-3-*C*-methyl-1-*O*-methylthiomethyl-L-erythritol (**27**: 100 mg, 25%) and the starting material (67 mg, 20%).

28: mp 81—82 °C; $[\alpha]_D^{22}$ +73.7° (*c* 0.93); IR: 1735 (CHO); NMR: 9.78 (s, 1H, CHO), 7.3 (m, 10H, 2Ph), 5.50 (s, 1H, CHPh), 4.88 and 4.64 (ABq, 2H, J=11.4, CH_2Ph), 4.33 (s, 1H, H-2), 3.86 and 4.12 (ABq, 2H, J=10.2, H-4 and 4'), 1.60 (s, 3H, CMe).

Found: C, 73.09; H, 6.41%. Calcd for $C_{19}H_{20}O_4$: C, 73.06; H, 6.45%.

27: syrup; $[\alpha]_D^{23}$ +53.7° (*c* 0.3); NMR: 7.29 (m, 10H, 2Ph), 5.51 (s, 1H, CHPh), 4.67 (s, 2H, OCH_2S), 4.58 and 4.46 (ABq, 2H, J=12, CH_2Ph), 4.07 (t, 1H, $J_{1,2}=J_{1,1'}$=10.0, H-1), 3.84 (dd, 1H, $J_{1',2}$=8.0, H-2), 4.00 and 3.82 (ABq, 2H, J=11.5, H-4 and 4'), 3.65 (dd, 1H, H-1'), 2.11 (s, 3H, SMe), 1.51 (s, 3H, CMe).

Found: C, 67.02; H, 6.95; S, 8.28%. Calcd for $C_{21}H_{26}O_4S$: C, 67.35; H, 7.00; S, 8.56%.

*Methyl 3-O-Benzyl-3-C-methyl-α-L-erythrofuranoside (**29**) and Its β-Anomer (**30**).* A solution of **28** (110 mg, 0.35 mmol) in methanolic hydrogen chloride (1%, 3 ml) was refluxed for 3 h, neutralized with sodium hydrogencarbonate, evaporated, and the residue was extracted with chloroform. The usual processing of the extract and fractionation of the product on a preparative TLC with 1:5 ethyl acetate–hexane gave the corresponding α-(**29**: 4.1 mg, 4.9%, R_f 0.29) and β-glycosides (**30**: 34.7 mg, 41%, R_f 0.39) as syrups.

29: $[\alpha]_D^{23}$ −82.9° (*c* 1.03); NMR: 7.3 (m, 5H, Ph), 4.89 (d, 1H, J=4.8, H-1), 4.63 and 4.52 (ABq, 2H, J=11.0, CH_2Ph), 4.12 and 3.66 (ABq, 2H, J=9.8, H-4 and 4'), 3.84 (dd, 1H, $J_{2,OH}$=10.4, H-2), 3.48 (s, 3H, OMe), 3.00 (d, 1H, OH), 1.48 (s, 3H, CMe).

30: $[\alpha]_D^{23}$ +99.5° (*c* 1.74); NMR: 7.3 (m, 5H, Ph), 4.86 (d, 1H, J=2.4, H-1), 4.52 (s, 2H, CH_2Ph), 4.12 and 3.77 (ABq, 2H, J=10.1, H-4 and 4'), 3.79 (dd, 1H, $J_{2,OH}$=7.8, H-2), 3.42 (s, 3H, OMe), 3.07 (d, 1H, OH), 1.50 (s, 3H, CMe).

Found for **30**: C, 65.32; H, 7.59, and for **31**: C, 65.20; H, 7.69%. Calcd for $C_{13}H_{18}O_4$: C, 65.53; H, 7.61%.

References

1) Part XXVII. N. Hong, M. Funabashi, and J. Yoshimura, *Carbohydr. Res.*, **96**, 21 (1981).

2) B. Fraser-Reid and R. C. Anderson, *Fortschritte. Chem. Org. Naturst.*, **39**, 1 (1978).

3) S. Hanessian, *Acc. Chem. Res.*, **12**, 159 (1979).

4) H. Ohrui, *Yuki Gosei Kagaku*, **39**, 275 (1981).

5) H. Maag, J. F. Blount, D. L. Coffen, T. V. Steppe, and F. Wong, *J. Am. Chem. Soc.*, **100**, 6787 (1978) and papers cited therein.

6) M. Funabashi, S. Yamazaki, and J. Yoshimura, *Carbohydr. Res.*, **44**, 275 (1975).

7) H. O. L. Fischer and E. Baer, *J. Am. Chem. Soc.*, **61**, 761 (1939).

8) T. Horvath and L. Vargha, *Carbohydr. Res.*, **16**, 253 (1971); L. F. Wiggins, *J. Chem. Soc.*, **1946**, 13.

9) K. Onodera, S. Hirano, and N. Kashimura, *J. Am. Chem. Soc.*, **87**, 4651 (1965).

10) J. Corey and J. W. Suggs, *Tetrahedron Lett.*, **1975**, 2647.

11) R. Barker and D. L. MacDonald, *J. Am. Chem. Soc.*, **82**, 2301 (1960).

12) J. Yoshimura, K. Sato, and H. Hashimoto, *Chem. Lett.*, **1977**, 1327.

13) S. J. Angyal and K. James, *J. Chem. Soc., D*, **1970**, 320.

Branched-chain Sugars. XXIX. Synthesis of Moenuronic Acid (4-*C*-Methyl-D-glucuronic Acid)[1]

Ken-ichi SATO, Kazusuke KUBO, Namgi HONG, Hisashi KODAMA, and Juji YOSHIMURA*

Laboratory of Chemistry for Natural Products, Faculty of Science, Tokyo Institute of Technology, Nagatsuta, Midori-ku, Yokohama 227

(Received September 18, 1981)

Moenuronic acid (4-*C*-methyl-D-glucuronic acid), a branched-chain sugar component of moenomycin A, was synthesized by the introduction of an axial *C*-methyl group into methyl 2,3-di-*O*-benzyl-6-*O*-trityl-α-D-*xylo*-hexopyranosid-4-ulose by the reaction with methyllithium, followed by deprotection and platinum-catalyzed oxidation of the *C*-6 position. Stereoselectivities in a few reactions for the introduction of *C*-methyl group were examined.

Moenomycin A[2] is a phosphoglycolipid antibiotic, which inhibits strongly the formation of linear polysaccharide-chain of murein from disaccharide intermediates[3] in the cell-wall biosynthesis. A new brancehd-chain uronic acid called moenuronic acid (**1**; 4-*C*-methyl-D-glucuronic acid) was found as a component.[4] By the ethanolysis of moenomycin A, the moiety was isolated as the corresponding ethyl β-D-glucofurano-sidurono-6,3-lactone(**2**), and the structure was determined by the IR, NMR, CD, and mass spectroscopic data of **2** and its diacetate (**3**).[5] This paper describes the first syn thesis of **3**.

Results and Discussion

The introduction of an axial *C*-methyl group to the *C*-4 position of a D-*xylo*-hexopyranosid-4-ulose and the following oxidation of *C*-6 position of the product are necessary for the synthesis of **1**.

For the former problem, a few pathways from benzyl[6] and methyl 2,3-di-*O*-benzyl-6-*O*-trityl-α-D-*xylo*-hexopyranosid-4-uloses (**4** and **5**) and 4-*C*-methylene derivative (**6**) of **5** were examined. Compound **5** was synthesized by the oxidation of methyl 2,3-di-*O*-benzyl-6-*O*-trityl-α-D-glucopyranoside[7] with dimethyl sulfoxide–trifluoroacetic anhydride in quantitative yield. Compound **6** was obtained in 63% yield by the usual Wittig reaction of **5**.

It is known that the reaction of α-D-*xylo*-hexopyranosid-4-uloses[8] or a α-L-*threo*-pentopyranosid-4-ulose[9] with methyllithium at a low temperature gives axial *C*-methyl derivatives, whereas that with methylmagnesium iodide affords equatorial *C*-methyl derivatives predominantly. Therefore, these reactions of **4** and **5** were examined at first. As shown in Table 1, reaction of **4** with methyllithium at −78 °C in ether gave exclusively the axial attack product (**7**), while that with methylmagnesium iodide in ether at −78 °C gave only the equatorial attack product (**8**). The Grignard reaction in ether–tetrahydrofuran (1:1) under reflux gave **7** and **8** in the ratio of 1 to 1. A similar tendency was also observed in the reaction of **5**, and the corresponding *C*-methyl derivatives (**9** and **10**) were obtained. Configuration of **7**—**10** was determined from the chemical shifts of axially (**7**: δ 15.79 ppm, **9**: δ 14.92 ppm) and equatorially (**8**: δ 22.03 ppm, **10**: δ 22.02 ppm) oriented *C*-methyl carbons in ^{13}C-NMR spectra.[8–10]

On the other hand, diazomethane reaction[11] of **4** and **5** gave one epimer of the corresponding spiro epoxides (**11** and **12**) in 20 and 15% yields, respectively, together with larger amount of ring-expanded products (**13** and **14**). The structures of **13** and **14** were throughly proved by the ^{1}H-NMR spectra (see Experimental). While, epoxidation[12] of **6** with *m*-chloroperbenzoic acid gave a 1:1 mixture of the corresponding spiro epoxides (**12** and **15**) in 80% yield. Reduction of **11**, **12**, and **15** with lithium aluminium hydride gave **7**, **9**, and **10** in fairly good yields, respectively. From these facts, configurations of **11**, **12**,

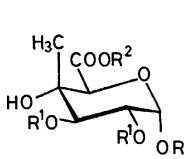

(1) R=R^1=R^2=H
(20) R=Me,R^1=R^2=H
(21) R=Me,R^1=Ac,R^2=Et

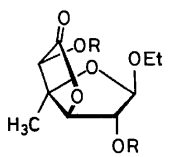

(2) R=H
(3) R=Ac

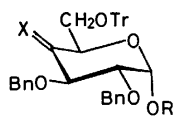

(4) R=Bn, X=O
(5) R=Me, X=O
(6) R=Me, X=CH$_2$

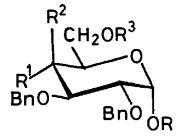

	R	R^1	R^2	R^3
(7)	Bn	OH	Me	Tr
(8)	Bn	Me	OH	Tr
(9)	Me	OH	Me	Tr
(10)	Me	Me	OH	Tr
(16)	Bn	OH	Me	H
(17)	Bn	Me	OH	H
(18)	Me	OH	Me	H

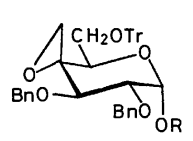

(11) R=Bn
(12) R=Me

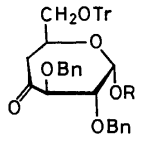

(13) R=Bn
(14) R=Me

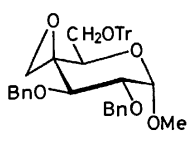

(15)

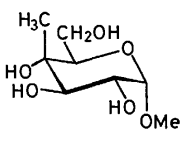

(19)

Bn=benzyl
Tr=trityl

Table 1. Comparison of stereoselectivities in the reactions for the introduction of a 4-*C*-methyl group into **4**—**6**

Substrate	Reagent	Conditions: Solvent	Conditions: Temp/°C	Ratio of products axial : equatorial attack	Yield/%
	CH_3Li	Ether	−78	(**7**) 1 : 0	58
4	CH_3MgI	Ether	−78	0 : 1 (**8**)	84
	CH_3MgI	Ether-THF	Boiling	(**7**) 1 : 1 (**8**)	72
	CH_3Li	Ether	−78	(**9**) 1 : 0	95
5	CH_3MgI	Ether	−78	0 : 1 (**10**)	84
	CH_3MgI	Ether	RT	(**9**) 1 : 2.2 (**10**)	93
4	CH_2N_2	Ethanol	RT	(**11**) 1 : 0	20
5	CH_2N_2	Ethanol	RT	(**12**) 1 : 0	15
6	*m*-$ClC_6H_4CO_3H$	CH_2Cl_2	RT	(**12**) 1 : 1 (**15**)	81

Table 2. Physical constants of 4-*C*-methyl-D-glucuronic acid derivatives

Derivatives	$[\alpha]_D$[a] / °	Chemical shifts (δ) and coupling constants (Hz)[b]: H-1 ($J_{1,2}$)	H-2 ($J_{2,3}$)	H-3	H-5	4-CH_3	OAc	OCH_2 (J_{gem})	CH_3 (J_{CH_2, CH_3})	OMe	$\nu_{C=O}$ / cm^{-1}
2	−47.6	5.14 s	4.41 s	4.60 s	4.16 s	1.67 s	—	3.74 dq, 3.56 dq (9.0)	1.18 t (7.0)	—	1790
3	+55.4	5.12 s	5.42 s	4.62 s	5.17 s	1.63 s	2.24 s 2.13 s	3.86 dq, 3.45 dq (9.0)	1.18 t (7.0)	—	1810 1750
3 (reported)	—	5.14 s	5.42 s	4.60 s	5.19 s	1.63 s	2.25 s 2.13 s	3.70 m	1.19 t	—	1810 1750
20	+87.0	4.77 d (4.0)	3.43 dd (10.5)	3.74 d	4.19 s	1.18 s	—	—	—	3.43 s	1730
21	+112	5.03 d (3.4)	4.77 dd (10.4)	5.41 d	4.37 s	1.30 s	2.12 s 2.07 s	4.30 q	1.35 t (6.8)	3.44 s	1730
22 (reported)	—	5.63 dd (3.5)	3.81 m (10.4)	5.00 d	4.48 s	1.25 s	—	—	—	—	—

a) The rotational values of **2** and **20** were measured in ethanol and methanol, respectively. b) ^{1}H-NMR spectrum of **20** was taken in methanol-*d*. The spectrum of **2** showed signal of hydroxyl protons at δ 2.90 bs.

and **15** were established. Peroxy acid oxidation of methylene derivative such as **6** usually proceeds unselectively,[12] and the selectivities in the reaction of 4-uloses with methyllithium or diazomethane will be discussed in detail in the following papers.

For the oxidation of *C*-6 position, **7**—**9** were partially hydrolyzed with 70% acetic acid to give the corresponding de-*O*-tritylated products (**16**—**18**), respectively. However, attempted oxidation of **16** and **17** with chromium trioxide,[13] potassium permanganate,[14] and oxygen–platinum[15] gave commonly complex results, accompanying with the oxidation of the benzyl groups.[6,16] Therefore, *O*-benzyl groups of **18** were previously removed by hydrogenolysis to give methyl 4-*C*-methyl-α-D-glucopyranoside (**19**) in quantitative yield. Oxidation of **19** in slightly alkaline aqueous solution with oxygen in the presence of platinum–carbon gave the corresponding glucuronic acid (**20**) in 86% yield. Treatment of **20** with 0.1 M ethanolic hydrogen chloride for 16 h under reflux, and then base-catalyzed acetylation of the products gave **3** and methyl 2,3-di-*O*-acetyl-4-*C*-methyl-α-D-glucopyranosiduronic acid ethyl ester (**21**) in 28 and 55% yields, respectively. The formation of **21** implies the incomplete ethanolysis of the glycoside linkage of **20**. A similar ethanolysis of **21** for 3 d gave **2** in quantitative yield. Physical constants of 4-*C*-methyl-D-glucuronic acid derivatives were summarized in Table 2, together with those of 3-*O*-carbamoyl-1-phosphate derivative (**22**) of **1**, obtained by hydrolysis of moenomycin A with trifluoroacetic acid and 2-propanol.[4]

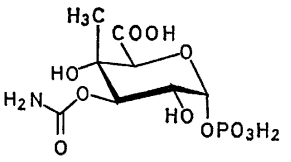

(22)

Although the rotational value and the magnetical non-equivalency of methylene protons in 1-ethoxyl group were not shown in the literature,[5] physical properties of **3** prove that **3** synthesized here is identical with that obtained from Moenomycin A. The non-equivalency of methylene protons will be attributed to the restricted rotation of 1-*O*-CH_2 bond, due to the steric hindrance between 1-ethoxyl and 5-acetoxyl groups oriented into the inside area of *cis*-fused five-membered ring. Data of **2** also support this deduction, though $\Delta\nu$ value of methylene protons is rather smaller. While, the coupling constants ($J_{1,2}$ and $J_{2,3}$) of **20**—**22** indicate their $^4C_1$ (D) conforma-

tions.

Thus, it was conclusively shown that synthesis of methyl glycoside (**20**) of **1** can be accomplished by the pathway of **5**→**9**→**18**→**19**→**20** in 73% overall yield.

Experimental

General Methods. Melting points were determined with a Mel-Temp hot-plate and are uncorrected. The solutions were evaporated under diminished pressure at a bath temperature not exceeding 50 °C. Specific rotations were measured with Carl Zeiss LEP-A1 or JASCO DIP-4 polarimeter, using chloroform as a solvent unless otherwise stated. IR spectra were recorded with Hitachi Model EPL-G2 spectrometer. ^{1}H-NMR spectra were taken with JEOL PS-100 spectrometer in chloroform-*d* unless otherwise stated, using tetramethylsilane as the internal standard. ^{13}C-NMR data were recorded with JEOL FX-100 spectrometer at 25.16 MHz for the solutions in chloroform-*d*, using 8K data points, with proton-noise decoupling. Chemical shifts and coupling constants were recorded in δ (ppm) and Hz units, and IR frequencies in cm^{-1}. Column chromatography was performed on silica gel (Wakogel C-200) and preparative TLC on silica gel (Merck type 60).

*Methyl 2,3-Di-*O*-benzyl-6-*O*-triphenylmethyl-α-*D*-xylo-hexopyranosid-4-ulose (**5**).* A solution of methyl 2,3-di-*O*-benzyl-6-*O*-trityl-α-D-glucopyranoside[7] (3 g, 4.86 mmol) in acetic anhydride (25 ml) and dimethyl sulfoxide (50 ml) was kept overnight at room temperature, poured into ice–water, and then extracted with ether. The usual processing of the extract and purification of the product on a column of silica gel with 15:1 hexane–ethyl acetate gave **5** as a syrup in 72% (2.15 g) yield. $[\alpha]_D^{22}$ +47.1° (*c* 1.2); IR: 1735 (C=O); NMR: 7.55—7.15 (m, 25 H, 5×Ph), 4.82 (d, 1 H, $J_{1,2}$=3.2, H-1), 4.52—4.98 (m, 4 H, 2×CH_2Ph), 4.36 (d, 1 H, $J_{2,3}$=10.0, H-3), 4.20 (dd, 1 H, H-5), 3.78 (dd, 1 H, H-2), 3.56 (dd, 1 H, $J_{6,6'}$=11.0, H-6), 3.53 (s, 3 H, OMe), 3.35 (dd, 1 H, $J_{5,6'}$=7.0, $J_{5,6'}$=10.0, H-6'). Found: C, 78.53; H, 6.31%. Calcd for $C_{40}H_{38}O_6$: C, 78.15; H, 6.23%.

*Methyl 2,3-Di-*O*-benzyl-4-deoxy-4-*C*-methylene-6-*O*-triphenylmethyl-α-*D*-xylo-hexopyranoside (**6**).* To an ice-cooled suspension of methyltriphenylphosphonium bromide (0.6 g, 1.68 mmol) in tetrahydrofuran (THF, 2 ml) was added butyllithium (10%, 8.7 ml, 1.36 mmol) in hexane with stirring, and to the resulting orange-coloured solution, a solution of **5** (1.02 g, 1.6 mmol) in THF (9 ml) was further added. After stirring the mixture for 30 min, the excess reagent was quenched with acetone, diluted with ether (20 ml), and then filtered. The filtrate was evaporated, and the residual syrup was purified on a column of silica gel with benzene to give **6** as a syrup in 63% (640 mg) yield. $[\alpha]_D^{23}$ +40.3° (*c* 0.9); IR: 1660 (C=C); NMR: 7.70—7.10 (m, 25 H, 5×Ph), 5.20—5.40 (bs, 2 H, methylene), 4.60—5.00 (m, 5 H, 2×CH_2Ph and H-1), 4.5—4.2 (m, 2 H, H-3 and 5), 3.53 (s, 3 H, OMe), 3.30—3.50 (m, 3 H, H-6,6', and 2). Found: C, 80.52; H, 6.71%. Calcd for $C_{41}H_{40}O_5$: C, 80.36; H, 6.58%.

Reaction of 4-Uloses with Methyllithium. To a solution of **4** (120 mg, 0.174 mmol) in ether (2 ml) cooled with Dry Ice and acetone was added an excess amount of methyllithium (1.2 M, 1 ml) in ether with stirring, and then the mixture was kept at room temperature for 2 h, poured into saturated ammonium chloride solution. The usual processing of the ether layer and purification of the product on a column of silica gel with 3:1 hexane–ethyl acetate gave pure benzyl 2,3-di-*O*-benzyl-4-*C*-methyl-6-*O*-triphenylmethyl-α-D-glucopyranoside (**7**) as a syrup in 58% (71 mg) yield. $[\alpha]_D^{23}$ +26.8° (*c* 1.1); ^{13}C NMR: CMe, 15.79 ppm; ^{1}H NMR: 7.54—7.12 (m, 30 H, 6×Ph), 5.01—4.40 (m, 6 H, 3×CH_2Ph), 4.80 (d, 1 H, $J_{1,2}$=4.0, H-1), 4.00 (t, $J_{5,6'}$=5.8, H-5), 3.84 (d, 1H, $J_{2,3}$=10.6, H-3), 3.36 (dd, 1H, $J_{5,6}$=5.8, H-6), 3.36 (dd, 1H, H-2), 3.25 (dd, 1H, $J_{6,6'}$=11.6, H-6'), 2.32 (s, 1H, OH), 0.98 (s, 3H, CMe). Found: C, 79.42; H, 6.65%. Calcd for $C_{47}H_{46}O_6$: C, 79.86; H, 6.56%.

A similar reaction of **5** with methyllithium gave methyl 2,3-di-*O*-benzyl-4-*C*-methyl-6-*O*-triphenylmethyl-α-D-glucopyranoside (**9**) in 95% yield. $[\alpha]_D^{23}$ +7.8° (*c* 1.5); ^{13}C NMR: CMe, 14.92 ppm; ^{1}H NMR: 7.60—7.14 (m, 25H, 5×Ph), 5.03—4.52 (m, 4H, 2×CH_2Ph), 4.59 (d, 1H, $J_{1,2}$=3.8, H-1), 3.88 (dd, 1H, $J_{2,3}$=10.0, H-2), 3.87 (t, 1H, $J_{5,6}$=6.0, H-5), 3.51 (d, 1H, H-3), 3.48 (s, 3H, OMe), 3.39 (d, 2H, H-6 and 6'), 2.37 (s, 1H, OH), 1.00 (s, 3H, CMe). Found: C, 78.29; H, 6.78%. Calcd for $C_{41}H_{42}O_6$: C, 78.07; H, 6.71%.

Reaction of 4-Uloses with Methylmagnesium Iodide. To a solution of methylmagnesium iodide, prepared from magnesium turnings (124 mg, 5.17 mmol) and methyl iodide (1 ml, 7 mmol), in ether (5 ml) chilled with Dry Ice and acetone was added dropwise a solution of **4** (187 mg, 2.72 mmol) in ether (2 ml) with stirring, and after 2 h, the reaction mixture was poured into saturated aqueous ammonium chloride solution. The usual processing of the ether layer and purification of the product on a column of silica gel with 3:1 hexane–ethyl acetate gave benzyl 2,3-di-*O*-benzyl-4-*C*-methyl-6-*O*-triphenylmethyl-α-D-galactopyranoside (**8**) as a syrup in 84% (160 mg) yield. $[\alpha]_D^{23}$ +54.9° (*c* 0.8); NMR: 7.64—7.14 (m, 30H, 6×Ph), 5.10—4.25 (m, 6H, 3×CH_2Ph), 4.98 (d, 1H, $J_{1,2}$=3.5, H-1), 3.90 (dd, 1H, $J_{2,3}$=9.5, H-2), 3.79 (t, 1H, $J_{5,6}$=5.0, H-5), 3.59 (d, 1H, H-3), 3.42 (d, 2H, H-6 and 6'), 2.60 (s, 1H, OH), 1.00 (s, 3H, CMe). Found: C, 79.74; H, 6.62%. Calcd for $C_{47}H_{46}O_6$; C, 79.86; H, 6.56%.

The reaction of **4** (16.6 g, 24 mmol) with methylmagnesium iodide in ether–THF (1:1) at refluxing temperature and separation of the products on a flash column of silica gel with 6:1 hexane–ethyl acetate gave **7** and **8** in 35.2% (5.98 g) and 36.3% (6.15 g) yields, respectively.

A similar reaction of **5** (1.02 g, 1.6 mmol) with methylmagnesium iodide in ether at −78 °C and purification of the products on a flash column of silica gel with 6:1 hexane–ethyl acetate gave methyl 2,3-di-*O*-benzyl-4-*C*-methyl-6-*O*-triphenylmethyl-α-D-galactopyranoside (**10**) as a syrup in 84% (850 mg) yield. $[\alpha]_D^{27}$ +18.2° (*c* 1.0); NMR: 7.68—7.16 (m, 25H, 5×Ph), 5.06—4.56 (m, 5H, H-1 and 2×CH_2Ph), 3.90 (dd, 1H, $J_{1,2}$=3.0, H-2), 3.70 (t, 1H, $J_{5,6}$=4.0, H-5), 3.54 (d, 1H, $J_{2,3}$=9.5, H-3), 3.52 (s, 3H, OMe), 3.41 (d, 2H, H-6 and 6'), 0.98 (s, 3H, CMe). Found: C, 77.82; H, 6.83%. Calcd for $C_{41}H_{42}O_6$: C, 78.07; H, 6.71%.

When the reaction of **5** with methylmagnesium iodide in ether is carried out at room temperature, separation of the products on a flash column of silica gel with 6:1 hexane–ethyl acetate gave **9** and **10** in 29 and 64% yields, respectively.

Reaction of 4-Uloses and Diazomethane. To a solution of **4** (138 mg, 2.0 mmol) in ethanol (50 ml) was added dropwise a solution of diazomethane (4.0 mmol) in ether (20 ml) at 0 °C. After keeping the mixture at room temperature for 12 h, the solution was evaporated to give a syrup. Separation of the syrup on a preparative TLC gave a ring-expanded product, benzyl 2,3-di-*O*-benzyl-5-deoxy-7-*O*-triphenylmethyl-α-D-*xylo*-heptaseptanosid-4-ulose (**13**) and corresponding spiro epoxide, benzyl 4,4'-anhydro-2,3-di-*O*-benzyl-4-*C*-hydroxymethyl-6-*O*-triphenylmethyl-α-D-gluco-

pyranoside (**11**) in 60 and 20% yields, respectively.

11: syrup, $[\alpha]_D^{23}$ +56.4° (*c* 2.8); NMR: 7.6—7.1 (m, 30H, 6×Ph), 5.0—4.40 (3×ABq, 6H, J=11.0 and 12.0, 3×CH_2Ph), 4.97 (d, 1H, $J_{1,2}$=3.6, H-1), 4.64 (t, 1H, $J_{5,6}$=4.0, H-5), 4.20 (d, 1H, $J_{2,3}$=10.0, H-3), 3.55 (dd, 1H, H-2), 3.04 (d, 2H, H-6 and 6′), 3.06 and 2.43 (ABq, 2H, J=5.0, epoxy CH_2). Found: C, 80.38; H, 6.33%. Calcd for $C_{47}H_{44}O_6$: C, 80.09; H, 6.29%.

Compound **13** could not be completely purified, but the NMR and IR spectra could be analyzed. IR: 1720 (C=O); NMR: 7.50—7.10 (m, 30H, 6×Ph), 5.03 (d, 1H, $J_{1,2}$=1.8, H-1), 4.95—4.43 (m, 7H, 3×CH_2Ph and H-6), 4.18 (d, 1H, $J_{2,3}$=8.0, H-3), 3.74 (dd, 1H, H-2), 3.35—3.00 (m, 2H, H-7 and 7′) 2.78 and 2.50 (dABq, 2H, $J_{A,B}$=14.0, $J_{5,6}$=11.0, $J_{5',6}$=4.0, H-5 and 5′).

A similar reaction of **5** and diazomethane and the separation of the products on prepative TLC gave a ring-expanded product, methyl 2,3-di-*O*-benzyl-5-deoxy-7-*O*-triphenylmethyl-α-D-*xylo*-heptaseptanosid-4-ulose (**14**), and the corresponding spiro epoxide, methyl 4,4′-anhydro-2,3-di-*O*-benzyl-4-*C*-hydroxymethyl-6-*O*-triphenylmethyl-α-D-glucopyranoside (**12**) 60 and 15% yields, respectively.

12: syrup; $[\alpha]_D^{23}$ +17.8° (*c* 0.8); NMR: 7.56—7.14 (m, 25H, 5×Ph), 4.91—4.59 (m, 4H, 2×CH_2Ph), 4.69 (d, 1H, $J_{1,2}$=3.2, H-1), 4.36 (t, 1H, $J_{5,6}$=4.2, H-5), 4.18 (d, 1H, $J_{2,3}$=10.0, H-3), 3.64 (s, 3H, OMe), 3.58 (dd, 1H, H-2), 3.07 (d, 2H, H-6 and 6′), 3.02 and 2.42 (ABq, 2H, J=5.0, epoxy CH_2). Found: C, 78.01; H, 6.58%. Calcd for $C_{41}H_{40}O_6$: C, 78.32; H, 6.41%.

14: syrup, $[\alpha]_D^{23}$ +19.5° (*c* 0.9); IR: 1720 (C=O); NMR: 7.50—7.15 (m, 25H, 5×Ph), 4.81 (d, 1H, $J_{1,2}$=2.0, H-1), 4.82—4.03 (2×ABq, 4H, 2×CH_2Ph), 4.05—4.35 (m, 2H, $J_{2,3}$=9.0, H-3 and 6), 3.71 (dd, 1H, H-2), 3.42 (s, 3H, OMe), 3.40—2.98 (m, 2H, H-7 and 7′), 2.79 and 2.55 (dABq, 2H, $J_{A,B}$=14,0, $J_{5,6}$=10.0, $J_{5',6}$=2.0, H-5 and 5′). Found: C, 78.30; H, 6.38%. Calcd for $C_{41}H_{40}O_6$: C, 78.32; H, 6.41%.

Reduction of Spiro Epoxides with Lithium Aluminium Hydride. To a solution of **11** (200 mg, 0.28 mmol) in THF (20 ml) was added lithium aluminium hydride (LAH, 50 mg, 1.3 mmol) and then the mixture was refluxed for 2 h. The excess hydride was decomposed with water, and then filterd. The water layer was extracted with chloroform. The combined extract was washed with water, dried, and evaporated to give a syrupy **7** in quantitative yield, which was identical with that obtained by the reaction of **4** and methyllithium at −78 °C.

A similar reduction of **12** (200 mg) in THF (20 ml) as above gave **9** in quantitative yield, which was identical with that obtained by the reaction of **5** and methyllithium at −78 °C.

Reduction of **15** (200 mg) in THF (20 ml) as above gave **10** in quantitative yield, which was identical with that obtained by the reaction of **5** and methylmagnesium iodide at −78 °C.

m-Chloroperoxybenzoic Acid Oxidation of ***6***. A solution of crude **6** (500 mg, 0.82 mmol) and *m*-chloroperoxybenzoic acid (630 mg, 3.65 mmol) in dichloroethane (50 ml) was stirred overnight at room temperature, and then washed successively with aqueous sodium hydroxide (0.1 M), water, saturated sodium chloride, and water, and then dried and evaporated. The residual syrup was separated on a column of silica gel with 5:1 hexane–ethyl acetate to give methyl 4,4′-anhydro-2,3-di-*O*-benzyl-4-*C*-hydroxymethyl-6-*O*-triphenylmethyl-α-D-glucopyranoside (**12**) and -α-D-galactopyranoside (**15**) as syrups each in 21.3% (110 mg) yield. Physical constants of **12** were indentical with the authentic sample that was derived from the reaction of **5** and diazomethane.

15: $[\alpha]_D^{32}$ +4.4° (*c* 0.8): NMR: 7.60—7.10 (m, 25H, 5×Ph), 4.66 (d, 1H, $J_{1,2}$=3.4 H-1), 4.53—4.98 (m, 4H, 2×CH_2Ph), 4.14 (d, 1H, H-3), 4.12 (t, 1H, H-5), 3.73 (dd, 1H, $J_{2,3}$=10.0, H-2), 3.41 (s, 3H, OMe), 3.26 (dd, 1H, $J_{5,6'}$=5.2, H-6′), 2.99 (dd, 1H, $J_{5,6}$=6.2, $J_{6,6'}$=10.0, H-6), 2.89 and 2.74 (ABq, 2H, J=5.0, epoxy CH_2). Found: C, 78.51; H, 6.62%. Calcd for $C_{41}H_{40}O_6$: C, 78.32; H, 6.41%.

*De-O-tritylation of 4-C-Methyl Derivatives (****7****—****9****).* A solution of **7** (1.47 g, 2.05 mmol) in acetic acid (70%, 30 ml) was heated at 100 °C for 5 h, filtered at room temperature, and then evaporated. The resulting syrup was purified on a column of silica gel with 3:1 hexane–ethyl acetate gave pure benzyl 2,3-di-*O*-benzyl-4-*C*-methyl-α-D-glucopyranoside (**16**) as a syrup in 98% (1.1 g) yield. $[\alpha]_D^{23}$ +88.7° (*c* 1.1); NMR: 7.6—6.8 (m, 15H, 3×Ph), 5.02—4.36 (m, 6H, 3×CH_2Ph), 4.81 (dd, 1H, $J_{5,6}$=3.5, H-6), 4.78 (d, 1H, $J_{1,2}$=4.0, H-1), 4.74 (t, 1H, $J_{5,6'}$=3.5, H-5), 4.59 (dd, 1H, $J_{6,6'}$=7.0, H-6′), 3.71 (d, 1H, H-3), 3.38 (dd, 1H, $J_{2,3}$=10.0, H-2), 2.92 (bs, 1H, OH), 1.14 (s, 3H, CMe). Found: C, 72.11; H, 7.07%. Calcd for $C_{28}H_{32}O_6$: C, 72.39; H, 6.94%.

In a similar manner, de-*O*-tritylation of **8** (1.29 g, 1.8 mmol) and purification of the product on a column of silica gel with 3:1 hexane–ethyl acetate gave benzyl 2,3-di-*O*-benzyl-4-*C*-methyl-α-D-galactopyranoside (**17**) as a syrup in 96% (0.96 g) yield. $[\alpha]_D^{23}$ +101° (*c* 1.1), NMR: 7.6—7.1 (m, 15H, 3×Ph), 5.1—4.4 (m, 6H, 3×CH_2Ph), 4.88 (d, 1H, $J_{1,2}$=4.0, H-1), 3.94—3.54 (m, 4H, H-3,5 and 6), 3.42 (dd, 1H, $J_{2,3}$=10.0, H-2), 2.26 (s, 1H, OH), 1.18 (s, 3H, CMe). Found: C, 72.23; H, 7.15%. Calcd for $C_{28}H_{32}O_6$: C, 72.39; H, 6.94%.

In a similar manner, de-*O*-tritylation of **9** (6.3 g, 10 mmol) and purification of the products gave methyl 2,3-di-*O*-benzyl-4-*C*-methyl-α-D-glucopyranoside (**18**) in 90% (3.5 g) yield, together with a small amount of its 6-acetate as syrups.

18: $[\alpha]_D^{23}$ +31.4° (*c* 0.9); NMR: 7.6—7.1 and 5.10—4.52 (m, 14H, 2×CH_2Ph), 4.61 (d, 1H, $J_{1,2}$=4.0, H-1), 4.0—3.5 (m, 5H, H-2,3,4 and 6), 3.40 (s, 3H, OMe), 3.36 (bs, 1H, OH), 1.18 (s, 3H, CMe). Found: C, 67.77; H, 7.10%. Calcd for $C_{22}H_{28}O_6$: C, 68.02; H, 7.27%.

6-Acetate showed the following ^{1}H-NMR deta: 7.6—7.1 and 5.16—4.52 (m, 14H, 2×CH_2Ph), 4.59 (d, 1H, $J_{1,2}$=4.0, H-1), 4.38 (dd, 1H, $J_{5,6}$=2.0, $J_{6,6'}$=12.0, H-6), 4.11 (dd, 1H, $J_{5,6'}$=6.0, H-6′), 3.75 (d, 1H, $J_{2,3}$=9.5, H-3), 3.49 (dd, 1H, H-2), 3.40 (s, 3H, OMe), 2.16 (bs, 1H, OH), 2.05 (s, 3H, Ac), 1.17 (s, 3H, CMe).

*Methyl 4-C-Methyl-α-D-glucopyranoside (****19****).* The usual hydrogenation of **18** (3.9 g, 10 mmol) in ethanol in the presence of palladium-charcoal (10%) gave **19** as a syrup in quantitative (2.08 g) yield. $[\alpha]_D^{23}$ +100° (*c* 0.8, MeOH); NMR (CD_3OD): 4.67 (d, 1H, $J_{1,2}$=4.0, H-1), 3.96—3.10 (m, 5H, H-2,3,5, and 6), 3.43 (s, 3H, OMe), 1.07 (s, 3H, CMe). Found: C, 46.50; H, 7.68%. Calcd for $C_8H_{16}O_6$: C, 46.15; H, 7.75%.

*Methyl 4-C-Methyl-α-D-glucuronic Acid (****20****).* Gaseous oxygen was bubbled into a solution of **19** (1.0 g, 4.8 mmol) in water at 90 °C for 40 h in the presence of platinum-carbon (10%, 0.3 g), and pH of the reaction mixture was maintained about 8.0 with sodium hydrogencarbonate. After **19** has disappeared on TLC, the mixture was filtered, and treated with Amberlite (IR-120) and the filtrate was evaporated to give 20 as a syrup in 86% (917 mg) yield. Physical data of **20** were shown in Table 2. Found: C, 42.97; H, 6.01%. Calcd for $C_8H_{14}O_7$: C, 43.24; H, 6.35%.

Ethyl 2,5-Di-O-acetyl-4-C-methyl-β-D-glucofuranosidurono-6,3-

lactone (3) and Methyl 2,3-Di-O-acetyl-4-C-methyl-α-D-glucopyranosiduronic Acid Ethyl Ester (21). A solution of **20** (500 mg, 2.25 mmol) in ethanolic hydrogen chloride (0.1 M) was refluxed for 16 h, and then evaporated to give a syrup. Acetic anhydride (2 ml) was added to a solution of the syrup in pyridine (2 ml). After keeping overnight at room temperature, the mixture was evaporated together with ethanol to give a syrup. Separation of the syrup on a preparative TLC (benzene–acetone 8:1) gave **21** {mp 99—101 °C (from ether–hexane); Found: C, 50.27; H, 6.61%. Calcd for $C_{14}H_{22}O_9$: C, 50.29; H, 6.63%} and **3** (syrup; Found: C, 51.84; H, 6.26%. Calcd for $C_{13}H_{18}O_8$: C, 51.65; H, 6.00%) in 55% (414 mg) and 28% (190 mg) yields, respectively. Physical constants of **3** and **21** were shown in Table 2.

Ethyl 4-C-Methyl-β-D-glucofuranosidurono-6,3-lactone (2). A similar ethanolysis of **21** (334 mg, 1.0 mmol) as above for 3 d gave syrupy **2** (Found: C, 49.47; H, 6.50%. Calcd for $C_9H_{14}O_6$: C, 49.54; H, 6.47%.) in quantitative (218 mg) yield. Physical data of **2** were shown in Table 2.

The authors thank Mr. Y. Nakamura for measurements of ^{13}C-NMR spectra.

References

1) Part XXVIII. J. Yoshimura, K. Hara, M. Yamaura, K. Mikami, and H. Hashimoto, *Bull. Chem. Soc. Jpn.*, **55**, 933 (1982).

2) W. A. Slusarchyk, *Biotechnol. Bioeng.*, **13**, 399 (1971); V. P. Welzel, F.-J. Witteler, D. Müller, and W. Riemer, *Angew. Chem., Int. Ed. Engl.*, **93**, 130 (1981).

3) Y. van Heijenoort, M. Derrien, and J. van Heijenoort, *F. E. B. S. Letters*, **89**, 141 (1978); P. E. Linett and J. L. Strominger, *Antimicrob. Angents Chemother.*, **4**, 231 (1973).

4) F.-J. Witteler, P. Welzel, H. Duddeck, G. Höfle, W. Riemer, and H. Budzikiewicz, *Tetrahedron Lett.*, **1979**, 3493.

5) N. Langenfeld and P. Welzel, *Tetrahedron Lett.*, **1978**, 1833.

6) M. Matsuzawa, K. Kubo, H. Kodama, M. Funabashi, and J. Yoshimura, *Bull. Chem. Soc. Jpn.*, **54**, 2169 (1981).

7) R. E. Wing, C. L. Collins, and J. N. Bemiller, *J. Chromatogr.*, **32**, 303 (1968).

8) M. Miljkovic, M. Gligorijevic, T. Satoh, and D. Miljkovic, *J. Org. Chem.*, **39**, 1379 (1974); M. Miljkovic, M. Gligorijevic, T. Satoh, D. Glishin, and R. D. Pitcher, *ibid.*, **39**, 3847 (1974).

9) M. Matsuzawa, K. Sato, T. Yasumori, and J. Yoshimura, *Bull. Chem. Soc. Jpn.*, **54**, 3505 (1981).

10) K. Sato, M. Matsuzawa, K. Ajisaka, and J. Yoshimura, *Bull. Chem. Soc. Jpn.*, **53**, 189 (1980).

11) K. Sato and J. Yoshimura, *Carbohydr. Res.*, **73**, 75 (1979); *Bull. Chem. Soc. Jpn.*, **51**, 2116 (1978).

12) J. Yoshimura, K. Sato, and M. Funabashi, *Bull. Chem. Soc. Jpn.*, **52**, 2630 (1979).

13) R. W. Mills, R. D. H. Murray, and R. A. Raphael, *J. Chem. Soc., D*, **1971**, 555; R. Slack and W. A. Waters, *J. Chem. Soc.*, **1948**, 1666; Y. Besace, I. Marszak, and J. Maisse, *Bull. Soc. Chim. Fr.*, **1971**, 2275.

14) W. R. Brasen and C. R. Hauser, *J. Org. Chem.*, **18**, 808 (1953); H. I. E. Zimmermann and J. English, Jr., *J. Am. Chem. Soc.*, **76**, 2285 (1954).

15) H. Weidmann and H. K. Zimmerman, *Ann.*, **684**, 226 (1965); J. Yoshimura, T. Sato, and H. Ando, *Bull. Chem. Soc. Jpn.*, **42**, 2352 (1969).

16) C. L. Stevens and S. H. Czernecki, *Carbohydr. Res.*, **63**, 307 (1978).

© 1982 The Chemical Society of Japan

NOTES

Bull. Chem. Soc. Jpn., 55, 943—944 (1982)

The Crystal Structure of *o*-Phenylenediamine Dihydroiodide

Kozo Kozawa* and Tokiko Uchida

Department of Industrial Chemistry, Faculty of Science and Technology, Science University of Tokyo, Noda, Chiba 278

(Received May 6, 1981)

Synopsis. Crystals of *o*-phenylenediamine dihydroiodide are orthorhombic; $a=7.828(1)$, $b=13.158(1)$, $c=5.043(1)$ Å, $Z=2$, and space group Pmnm. The structure was solved by the heavy-atom method and refined with 1359 diffractometer data points to the final $R=0.052$. It is isostructural with *o*-phenylenediamine dihydrobromide. Protonated amino groups link to iodide ions by hydrogen bonds.

Recently, studies of polyiodides have often been presented in relation to one-dimensional conductors.[1] *o*-Phenylenediamine(OPD)[2] forms many complexes with iodine at various mole ratios and with different crystal systems. In a series of structural studies of OPD–iodine system, we have taken up the crystal structure of OPD dihydroiodide (OPD·2HI). Some OPD–hydrohalides[3] have been studied, but not this one.

Experimental

Colorless a-elongated needle crystals were obtained by mixing an ethanol solution of OPD with an aqueous solution of HI in a nitrogen atmosphere. A crystal with dimensions $0.3\times0.3\times0.25$ mm^3 was sealed in a glass capillary in a nitrogen atmosphere. It was mounted with the a-axis parallel to the ϕ axis of a Rigaku four-circle diffractometer. Intensities and cell parameters were obtained with graphite-monochromatized Mo $K\alpha$ radiation ($\lambda=0.7107$ Å) at room temperature. Intensities of 1620 independent reflections were collected by the 2θ-ω scan method with a scan speed of 4° min^{-1} in 2θ in the range $2\theta\leq75°$, and 1359 intensities ($F_o\geq3\sigma(F)$) were used in the analysis. No absorption correction was applied.

Crystal Data. $C_6H_8N_2\cdot2HI$, $F.W.=364.0$; Orthorhombic, Space group Pmnm, $a=7.828(1)$, $b=13.158(1)$, $c=5.043(1)$ Å, $V=519.4(1)$ Å^3, $D_m=2.27$, $D_x=2.31$ g cm^{-3}, $Z=2$, μ(Mo $K\alpha$)$=59.2$ cm^{-1}, Systematic absences $h0l$ with $h+l=2n+1$.

Structure Determination and Discussion

The structure was solved by the heavy-atom method and refined by full-matrix least-squares with anisotropic thermal parameters for non-hydrogen atoms, and with anomalous dispersion factors for the iodide ion. The hydrogen atoms bonded to carbon atoms were located in the difference synthesis. These hydrogens were introduced and fixed at those positions with temperature factors B of 4.5 Å^2. The discrepancy index, R, was finally reduced to 0.052.

The atomic scattering factors and anomalous dispersion factors were taken from "International Tables for X-Ray Crystallography."[4] The quantity minimized in the refinement was $\Sigma w(|F_o|-k|F_c|)^2$; $w=1.0$ for all the F's. All the computations were performed at the Computer Centre of the University of Tokyo, using the UNICS program system.[5] The final atomic parameters are shown in Table 1. The tables of F_o-F_c data and anisotropic thermal parameters are kept as Document No. 8210 at the Office of the Chemical Society of Japan.

The crystal consists of OPD$^+$ cations and iodide ions, and is essentially isostructural with OPD·2HBr.[3d] Figure 1 shows the molecular arrangement in a cell and the numbering of atoms. OPD molecule is completely planar with an mm symmetry and parallel to the ab plane, except for the amino hydrogens. Partial intercalation of iodide ions permits relatively wide spacing between OPD$^+$ molecular planes, 5.04 Å ($=c$); this suggests the absence of interaction between cations. The distances and angles of OPD skeleton,

Table 1. Atomic coordinates and their standard deviations

Atom	x	y	z
I(1)	$\frac{1}{4}$	0.52924(6)	$\frac{3}{4}$
I(2)	$\frac{1}{4}$	0.25525(6)	$\frac{1}{4}$
N	0.4405(9)	0.6771(5)	$\frac{1}{4}$
C(1)	0.3421(10)	0.7705(6)	$\frac{1}{4}$
C(2)	0.4284(11)	0.8630(6)	$\frac{1}{4}$
C(3)	0.3407(13)	0.9533(6)	$\frac{1}{4}$
H(2)	0.55	0.85	$\frac{1}{4}$
H(3)	0.43	1.02	$\frac{1}{4}$

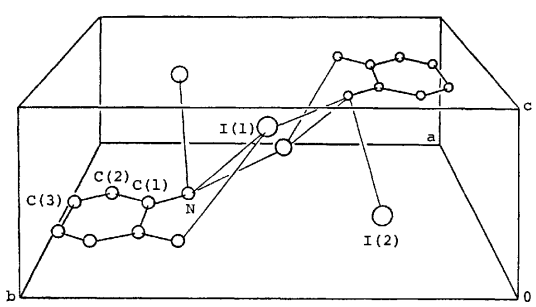

Fig. 1. Perspective view of the non-hydrogen atoms in a cell.

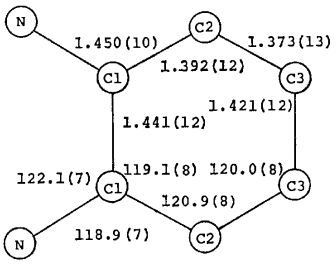

Fig. 2. Bond lengths (Å) and bond angles (°) of OPD^+ skeleton.

shown in Fig. 2, are normal. The C–N length, 1.450 Å, agrees with the C–NH_3^+ bond length, found in the related compounds (1.450—1.501 Å).[3a,3b,3d,6] Domenicano *et al.*[7] proposed that the 'standard' length of the aromatic C–NH_3^+ bond was 1.464 Å, which they calculated as the weighted mean value of 6 ring-substituted anilinium cations. On the other hand, the lengths of reported non-protonated C–NH_2 bond are significantly shorter than those of C–NH_3^+, namely, 1.351—1.391 Å.[3a,6,8] Judging from the C–N bond length, the amino groups in OPD·2HI are protonated. The nitrogen atom is surrounded by 5 iodide ions. Both of the two crystallographically non-equivalent iodide ions, I(1) and I(2), are on the mm symmetry points and surrounded by 4 OPD^+ cations. The I(1) ion has 2 types of I···N distances: 4 equivalent N's to a distance of 3.517 Å and the other 2 equivalent N's at 3.639 Å. The I(2) ion has the only 1 type of 4 I···N distances, 3.608 Å. The reported N···I hydrogen bonding distances are distributed from 3.46 to 4.06 Å.[9]

The authors express their hearty thanks to Professor Yoshio Sasada and Dr. Yuji Ōhashi of Tokyo Institute of Technology for the use of the diffractometer. The authors are also indebted to Mr. Naoya Tanabe and Mr. Hirotaka Hashimoto for their help as undergraduate students.

References

1) L. C. Isset and E. A. Perez-Albuerne, *Solid State Commun.*, **21**, 433 (1977); D. L. Smith and H. R. Luss, *Acta Crystallogr., Sect. B*, **33**, 1744 (1977); C. Lowe-Ma, R. Williams, and S. Samson, *J. Chem. Phys.*, **74**, 966 (1981); R. C. Teitelbaum, S. L. Ruby, and T. J. Marks, *J. Am. Chem. Soc.*, **101**, 7568 (1979); H. R. Luss and D. L. Smith, *Acta Crystallogr., Sect. B*, **36**, 1580 (1980).

2) In this paper, OPD denotes $C_6H_4(NH_2)_2$, and OPD^+ denotes protonated $C_6H_4(NH_3^+)_2$.

3) a) C. Stålhandske, *Acta Chem. Scand.*, **26**, 2962 (1972); *Acta Crystallogr., Sect. B*, **32**, 2806 (1976); b) C. Stålhandske, *ibid.*, **30**, 1586 (1974); c) S. Chandra and M. P. Hemker, *Z. Kristallogr.*, **135**, 320 (1972); d) C. Stålhandske, *Acta Chem. Scand.*, **26**, 3029 (1972); e) T. Uchida, K. Kozawa, and T. Osada, 7th Molecular Crystal Symposium, Nikko, September 1975, Abstr., pp. 177—178.

4) "International Tables for X-Ray Crystallography," Kynoch Press, Birmingham (1974), Vol. IV.

5) UNICS. "Universal Crystallographic Computation Program System," Crystallographic Society of Japan (1967).

6) C. J. Brown, *Proc. R. Soc. London, Ser. A*, **302**, 185 (1968).

7) A. Domenicano, E. F. Serantoni, and L. R. di Sanseverino, *Acta Crystallogr., Sect. B*, **33**, 1664 (1977).

8) M. Chao, E. Schempp, and R. D. Rosenstein, *Acta Crystallogr., Sect. B*, **31**, 2922 (1975); **31**, 2924 (1975).

9) P. H. Davis and J. S. Wood, *Inorg. Chem.*, **9**, 1111 (1970); G. M. Sheldrick and W. S. Sheldrick, *Acta Crystallogr., Sect. B*, **26**, 1334 (1970); J. Verbist, J. P. Putzeys, P. Piret, and M. Van Meerssche, *ibid.*, **27**, 1190 (1971); H. Gillier-Pandraud and S. Jamet-Delcroix, *ibid.*, **27**, 2476 (1971); M. Rossi, L. G. Marzilli, and T. J. Kistenmacher, *ibid.*, **34**, 2030 (1978); W. E. Lee and M. F. Richardson, *Can. J. Chem.*, **54**, 3001 (1976).

Crystal and Molecular Structure of *trans*-2,5-Dimethylpiperazine

Kojun Okamoto,* Kiyotane Sekido, Haruaki Ono,** Teruo Noguchi,**
and Sakutaro Hirokawa

Department of Chemistry, The National Defense Academy, Hashirimizu, Yokosuka 239
***Koa Oil Co., Ltd., Ōtemachi, Chiyoda-ku, Tokyo 100*

(Received October 21, 1981)

Synopsis. The crystal structure of *trans*-2,5-dimethylpiperazine has been determined by means of the X-ray method. The molecule is centrosymmetric, the piperazine ring having a *chair* form. The methyl groups are in the equatorial position. The molecules are linked together by N–H···N hydrogen bonds (N···N=3.305(3) Å) to form infinite ribbons along [011].

As a part of conformation studies of piperazine derivatives, we wish hence to report our structure analysis of *trans*-2,5-dimethylpiperazine(mp 119 °C). The structure thus far determined by means of the X-ray method are *cis*- and *trans*-1,4-dibenzoyl-2,5-dimethylpiperazine(DDP).[1,2]

Experimental and Structure Determination

Colorless prisms elongated along the b axis were obtained by the slow evaporation of a petroleum–benzene solution of the title compound. A prismatic crystal was ground to a cylinder 0.3 mm in diameter and 0.5 mm in length. As the substance was hygroscopic, the sample was sealed in a glass capillary tube 0.3 mm in diameter. The crystal data are as follows: $C_6H_{14}N_2$, F.W.=114.0, space group $P2_1/c$, a=8.582(2), b=5.231(1), c=8.953(2) Å, β=118.09(2)°, V=354.7(3) Å^3, Z=2, D_m=1.06 g cm^{-3} (flotation method), D_c=1.067 g cm^{-3}, μ=0.711 cm^{-1} for Mo $K\alpha$ radiation. The intensity data were obtained for 1097 independent reflections with $|F_o| \geqq 3\sigma(F_o)$ by measuring all the reflections within $2\theta \leqq 60.0°$. Correction for Lorentz-polarization factor was made as usual.

The structure was solved by an interpretation of the three-dimensional Patterson map. Refinement was made with a block-diagonal least-squares program, HBLS V[3]. The calculations were carried out on two computers, the CDC-6600 in the Century Research Center Co., Ltd., and the NEAC-2200/575 in the National Defense Academy. The final R value was 0.059. The atomic parameters are given in Table 1.***

Discussion

The numbering scheme and the thermal ellipsoids are illustrated in Fig. 1, while the bond distances and angles are given in Table 2. The molecule is centrosymmetric, showing that the piperazine ring has

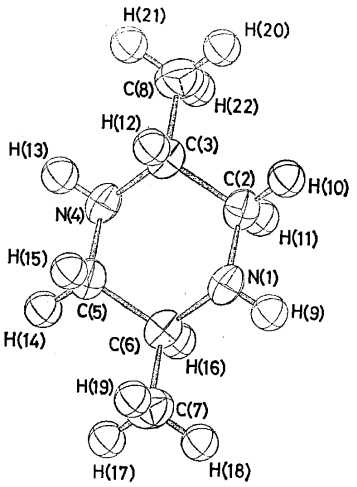

Fig. 1. Thermal vibration ellipsoids[10] for non-hydrogen atoms are drawn at the 50% probability level, viewed along the normal to the C(2), C(3), C(5), C(6) plane. H atoms are shown as spheres with radii of 0.2 Å.

Table 1. Fractional atomic coordinates (×10^4, for H atoms ×10^3) and equivalent or isotropic thermal parameters

The estimated standard deviations given in parentheses refer to the last decimal position.

Atom	x	y	z	$B_{eq}^{a)}$ or B_{iso}/Å^2	Bonding atom
N(1)	71(2)	1315(1)	1405(1)	5.6	
C(2)	−1558(2)	1222(2)	−204(2)	5.6	
C(3)	−1623(2)	−1249(2)	−1129(2)	5.5	
C(7)	3299(3)	1420(2)	2812(2)	6.9	
H(9)	10(2)	272(2)	193(2)	6.4(14)	N(1)
H(10)	−263(2)	127(2)	4(2)	3.4(8)	C(2)
H(11)	−167(2)	274(2)	−96(2)	2.9(7)	C(2)
H(12)	−162(2)	−268(2)	−42(2)	3.5(8)	C(3)
H(17)	437(2)	137(2)	265(2)	4.9(10)	C(7)
H(18)	335(2)	312(2)	339(2)	6.7(12)	C(7)
H(19)	337(2)	−3(2)	352(2)	6.0(12)	C(7)

a) Calculated from the refined anisotropic thermal parameters (deposited) by the method of Willis and Pryor.[11]

***The complete F_o-F_c data are deposited as Document No. 8209 at the Office of the Editor of the Bulletin of the Chemical Society of Japan.

Table 2. Bond distances(l/Å) and bond angles(θ/°)

The estimated standard deviations given in parentheses refer to the least significant figure.

N(1)-C(2)	1.463(3)	C(2)-H(10)	1.04(2)
N(1)-C(6)	1.465(3)	C(2)-H(11)	1.02(2)
C(2)-C(3)	1.521(3)	C(3)-H(12)	0.98(2)
C(6)-C(7)	1.521(3)	C(7)-H(17)	1.00(2)
		C(7)-H(18)	1.02(2)
N(1)-H(9)	0.87(2)	C(7)-H(19)	0.97(2)
N(1)-C(2)-C(3)	109.8(2)	C(3)-C(2)-H(11)	109(1)
C(2)-C(3)-N(4)	107.9(2)	H(10)-C(2)-H(11)	108(2)
C(2)-N(1)-C(6)	110.9(2)	N(4)-C(3)-H(12)	111(1)
C(5)-C(6)-C(7)	111.4(2)	C(2)-C(3)-H(12)	108(1)
N(1)-C(6)-C(7)	110.1(2)	C(8)-C(3)-H(12)	108(1)
		C(6)-C(7)-H(17)	111(1)
C(2)-N(1)-H(9)	110(1)	C(6)-C(7)-H(18)	111(1)
C(6)-N(1)-H(9)	108(1)	C(6)-C(7)-H(19)	110(1)
N(1)-C(2)-H(10)	109(1)	H(17)-C(7)-H(18)	106(2)
C(3)-C(2)-H(10)	109(1)	H(17)-C(7)-H(19)	107(2)
N(1)-C(2)-H(11)	112(1)	H(18)-C(7)-H(19)	112(2)

Table 3. Torsion angles (ϕ/°)

The torsion angle $A(i)$-$A(j)$-$A(k)$-$A(l)$ is viewed down $A(j)$-$A(k)$, with the clockwise rotation of $A(i)$ to $A(l)$ taken to be positive. The e.s.d.'s are 0.5—0.9°.

C(3)-C(2)-N(1)-C(6)	60.8	C(2)-N(1)-C(6)-C(7)	178.5
C(2)-N(1)-C(6)-C(5)	−59.7	C(7)-C(6)-C(5)-N(4)	180.0
N(1)-C(6)-C(5)-N(4)	59.0	C(3)-C(2)-N(1)-H(9)	−179.6
		C(5)-C(6)-N(1)-H(9)	−179.9
		C(7)-C(6)-N(1)-H(9)	−58.8

a *chair* form. The mean N–C bond length, 1.464 Å, is in good agreement with that of *trans*-DDP(1.476 Å),[2] that of *cis*-DDP(1.472 Å),[1] and that of piperazine (1.467 Å).[4] The C–C bond distance is comparable to those found in *N,N'*-dimethylpiperazine(1.521 Å),[5] cyclohexane(1.536 Å),[6] *cis*-DDP(1.535 Å), and *trans*-DDP(1.517 Å). The C(2)–N(1)–C(6) bond angle is comparable to the 109.0° of piperazine or the 112.6° of piperidine.[7] The C(2)–N(1)–H(9) and C(6)–N(1)–H(9) bond angles agree with that of 109° for C–N–H in dimethylamine.[8]

The torsion angles are given in Table 3. The values of the ring torsion angles correspond to the typical chair form. The exocyclic torsion angles show that C(7) is in the equatorial position. This result supports Sudmeier's suggestion.[9] The H(9) atom is in the equatorial position.

The molecular packing with intermolecular distances less than 4.000 Å is shown in Fig. 2. The shortest contact of 3.305 Å is seen between N(1) and the equivalent atom related by a two-fold screw axis. The value of the N–H···N' angle (168°) suggests the presence of a weak hydrogen bond. These hydrogen bonds form infinite ribbons of molecules along the [011] direction. The ribbons of molecules are held together by the van der Waals interactions.

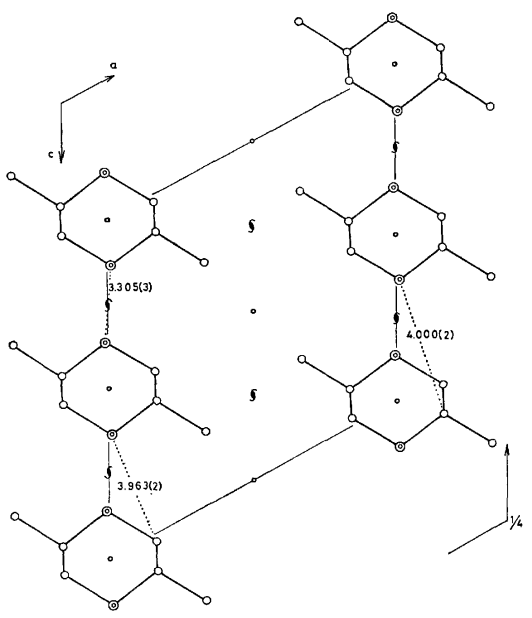

Fig. 2. The molecular packing viewed down the b axis, showing all intermolecular distances less than 4.000 Å.

The authors would like to thank Mr. Kazumasa Maruyama for his kind aid in the computation.

References

1) T. Sakurai, M. Nakamaru, S. Tsuboyama, and K. Tsuboyama, *Acta Crystallogr., Sect. B*, **33**, 3568 (1977).
2) K. Okamoto, K. Sekido, J. Itoh, T. Noguchi, and S. Hirokawa, *Bull. Chem. Soc. Jpn.*, **52**, 1896 (1979).
3) T. Ashida, The Universal Crystallographic Computing System, Osaka, The Computation Center, Osaka University (1973), p. 55.
4) A. Yokozeki and K. Kuchitsu, *Bull. Chem. Soc. Jpn.*, **44**, 2352 (1971).
5) M. Davis and O. Hassel, *Acta Chem. Scand.*, **17**, 1181 (1963).
6) O. Bastiansen, L. Fernholt, H. M. Seip, H. Kambara, and K. Kuchitsu, *J. Mol. Struct.*, **9**, 163 (1973).
7) I. D. Blackburne, R. P. Duke, Richard A. Y. Jones, A. R. Katritzky, and K. A. F. Record, *J. Chem. Soc., Perkin Trans. 2*, **1973**, 332.
8) J. E. Wollrab and V. W. Laurie, *J. Chem. Phys.*, **48**, 5058 (1968).
9) J. L. Sudmeier, *J. Phys. Chem.*, **72**, 2344 (1968).
10) C. K. Johnson, *ORTEP, ORNL-3794*, Oak Ridge National Laboratory, Tennessee (1965).
11) B. T. M. Willis and A. W. Pryor, "Thermal Vibrations in Crystallography," Cambridge Univ. Press, London (1975), pp. 101—102.

Liquid Crystals as Reaction Media. I. Photochemical Dimerization of Acenaphthylene in Cholesteric Liquid Crystal

Tomoko NAKANO* and Hirotaka HIRATA

Niigata College of Pharmacy, 5829 Kamishin'ei-cho, Niigata 950-21

(Received April 13, 1981)

Synopsis. The photodimerization of acenaphthylene in liquid crystalline media exhibiting cholesteric or nematic phase was studied from the view point of the stereoselectivity of the products. In the cholesteric phase *trans*-isomer formation increased remarkably and the ratio of the *trans*-isomer to *cis*-isomer depended significantly upon the acenaphthylene concentration. These results suggest a steric effect of the cholesteric phase structure on stereoselectivity on photodimerization compared with the predominant *cis*-isomer formation in the nematic phase.

The photodimerization of acenaphthylene is known to yield both *trans*- and *cis*-stereoisomer.[1-2] Figure 1 and Table 1 show the results of the photodimerization in cholesteric, nematic liquid crystalline media and in an organic solvent. As reported recently by R. G. Weiss *et al.*[3] the quantum yield of photodimerization considerably increased in cholesteric phase media in comparison with that in nematic phase media or in benzene. The irradiation time required to attain the same degree of conversion was much shortened in the cholesteric phase media than in the nematic media or in benzene (Table 1). *cis*-Isomer formation was dominant in nematic media and in benzene, whereas in cholesteric media the *trans*-isomer formation increased significantly.

In cholesteric or nematic phase systems doped with acenaphthylene, the mesophase appears over a rather narrow concentration range of acenaphthylene, less than about 5%. More acenaphthylene destroys the mesophase structure and generates isotropic phase.

In Fig. 1-(a) it is shown that the dominant *trans*-isomer formation in the cholesteric phase media is restricted to a low concentration range of acenaphthylene. The ratio of *trans*-isomer (**1**) to *cis*-isomer (**2**) is remarkably depended upon the acenaphthylene concentration, increasing with decreasing acenaphthylene. In nematic phase media the ratio of **1** to **2** was rather constant over a wider concentration range, irrespective

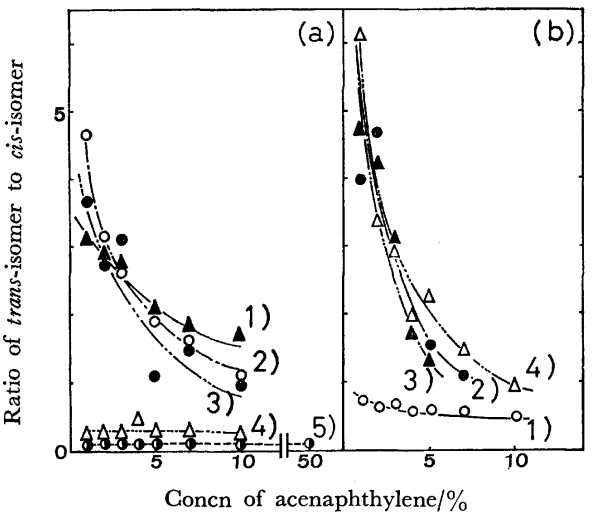

Fig. 1. The ratio of *trans*-isomer (**1**) to *cis*-isomer (**2**) *vs.* acenaphthylene concentration in photodimerization of acenaphthylene.
(a) In cholesteric, nematic liquid crystalline media and organic solvent. 1) In cholesteryl oleyl carbonate [▲], 2) in cholesteryl linolate [○], 3) in cholesteryl oleate [●], 4) In MBBA or EBBA [△], 5) in benzene [◑]. (b) in cholesteryl myristate at various temperatures. 1) at 60 °C (solid phase) [○], 2) at 70 °C (mesomorphic phase) [●], 3) at 75 °C (mesomorphic phase) [▲], 4) at 85 °C (mesomorphic phase) [△].

TABLE 1. THE RESULTS IN PHOTODIMERIZATION OF ACENAPHTHYLENE IN CHOLESTERIC, NEMATIC LIQUID CRYSTALLINE MEDIA AND AN ORGANIC SOLVENT

Acenaphthylene(%) in 1 g solvent media	Not reacted Acenaphthylene (mg)	*trans*-Isomer (**1**) (mg)	*cis*-Isomer (**2**) (mg)	Ratio of (**1**)/(**2**)	Conversion of acenaphthylene %
1% in cholesteryl oleate[a]	0.4	6.4	1.8	3.56	>96[a]
7% in cholesteryl oleate[a]	15.0	25.7	16.2	1.58	79[a]
1% in cholesteryl oleyl carbonate[a]	0.9	5.9	1.9	3.10	>90[a]
7% in cholesteryl oleyl carbonate[a]	30.4	23.0	12.2	1.88	57[a]
1% in cholesteryl linolate[a]	0.15	7.1	1.5	4.73	>98[a]
7% in cholesteryl linolate[a]	20.4	24.0	15.3	1.57	71[a]
1% in EBBA[b]	3.0	1.5	4.9	0.31	70[b]
7% in EBBA[b]	18.3	9.75	29.3	0.33	74[b]
1% in benzene[c]	7.1	0.13	0.91	0.14	29,[c] 15,[d] 40[e]
7% in benzene[c]	50.0	0.91	6.4	0.14	29[c]

a) Irradiation was carried out in a Petri dish at 40 °C for 4 h. b) In a Petri dish at 40 °C for 24 h. c) In a Pyrex tube at room temperature for 6 h. d) For 4 h. e) For 24 h.

of the phase change of the medium.

The effect of a triplet quencher (ferrocene) on the photodimerization in cholesteric phase media was examined. In the presence of 1 w/w% ferrocene, the *trans*-isomer was scarcely detected at acenaphthylene concentrations ranging from 1 to 10 w/w %. The amount of the *cis*-isomer formed was, however, nearly the same as in the absence of ferrocene (*cis*-Isomer was formed to the extent of more than 98%.). These results indicate that the preferable *trans*-isomer formation in the cholesteric phase is to be attributed to the increase of dimerization *via* the triplet state compared to *via* the singlet state.[1] The preferable formation of the *trans*-isomer with high quantum yield in the cholesteric phase implies that photodimerization *via* the triplet state is more enhanced in the cholesteric phase than that *via* the singlet state.

Generally photodimerization *via* the triplet state is more probable in dilute and highly viscous media, such as liquid crystalline media, owing to the difference of the life times of the triplet and singlet states.[3,4] In nematic phase media as highly viscous as cholesteric, dependence of the ratio of **1** to **2** upon the acenaphthylene concentration was scarcely observed, *cis*-isomer formation being dominant and the enhancement of the quantum yield not being observed. Accordingly the preferance for *trans*-isomer formation and the dependence of the ratio of **1** to **2** upon acenaphthylene concentration in the cholesteric phase might scarcely be attributed to the high viscosity of the solvent media, but these results might be characteristic of photodimerization in cholesteric phase media.

The effect of tetralin, which disturbs solvent order but does not interfere electronically with the photodimerization, is shown in Table 2. The ratio of **1** to **2** diminished with increasing tetralin concentration. This effect suggests that the ordered structure of the cholesteric phase definitely affects the *trans*-isomer formation advantageously.

Table 2. The effect of tetralin addition on stereoisomeric product distribution (**1**)/(**2**) in the photodimerization of acenaphthylene in cholesteric phase media

Acenaphthylene (%) in solvent media	Tetralin (%)[a]			
	No addition	5%	10%	20%
1% in cholesteryl myristate (70 °C)	5.40	3.55	2.70	3.02
1% in cholesteryl oleate (40 °C)	3.74	3.01	2.85	2.78

a) Tetralin (%) stands for percentage to the weight of solvent media. The mesophase appears at 5% concentration, whereas it raises the isotropic phase above 10% concentration of tetralin.

In cholesteryl myristate a remarkable change in the ratio of **1** to **2** was recognized between cholesteric phase regions ($T>70$ °C) and the solid phase region (60 °C) (Fig. 1-(b)). The influence of the ordered structure of the cholesteric phase on stereoselectivity is also supported by this result.

Experimental

Materials. Commercially available acenaphthylene was recrystallized several times from methanol. The *trans*-isomer and the *cis*-isomer were isolated from the reaction mixture obtained by irradiation of acenaphthylene in benzene, by silica-gel column chromatography using cyclohexane as eluent. The mp, NMR, and UV spectra of these compounds were identical with those reported by R. Livingston.[1] The mesomorphous reaction media were recrystallized before use.

Photochemical Reaction Procedures. Irradiation was carried out using a 1000 W-high pressure mercury arc lamp (TOSHIBA H 1000 L) filtered through a Toshiba cut-off glass filter UV-34. The sample solutions were irradiated in Pyrex tubes or Petri dishes without de-aeration and the reaction temperature was controlled in a thermostated oil bath with an accuracy of ±2 °C.

LC Measurement. After removal of the reaction media, high performance liquid chromatography(LC) was carried out using a WATERS ASSOCIATES ALC/GPC 204 using a 3.9 mm×30 cm column packed with μ-Bondapack C_{18}. The mobile phase solvent was acetonitrile–water (85:15) at a flow rate of 1.0 ml/min. The detector wavelength was 254 nm. Retention times were 3.86 min for acenaphthylene, 4.90 min for the *cis*-isomer, and 7.24 min for the *trans*-isomer respectively. The ratio of **1** to **2** was determined from the ratio of the peak areas by an external standard method.

DSC Measurements. The transition temperatures for liquid crystals doped with acenaphthylene were measured by differential scanning calorimetry (Rigaku Denki DSC) and polarization microscope observation. It was confirmed that the properties of liquid crystalline reaction media underwent no change under these irradiation conditions.

The authors wish to express their thanks to Dr. Yoshiaki Ohgo and Dr. Yoshihiko Hatano of Niigata College of Pharmacy for their helpful discussions.

References

1) R. Livingston and K. S. Wei, *J. Phys. Chem.*, **71**, 541 (1967).
2) D. O. Cown and R. L. E. Drisko, *J. Am. Chem. Soc.*, **92**, 6281 (1970); **92**, 6286 (1970).
3) J. M. Nerbonne and R. G. Weiss, *J. Am. Chem. Soc.*, **100**, 2571 (1978); **101**, 402 (1979).
4) D. O. Cown and J. C. Kozier, *J. Am. Chem. Soc.*, **97**, 249 (1975).

Infrared Study of 12-Molybdophosphoric Acid Reduced by Organic Compounds

Tian-hsi Tsai, Ken-ichi Maruya,* Mamoru Ai, and Atsumu Ozaki

Research Laboratory of Resources Utilization, Tokyo Institute of Technology, 4259 Nagatsuta, Midori-ku, Yokohama 227

(Received July 24, 1981)

Synopsis. Reaction of 12-molybdophosphoric acid with ethyl methyl ketone, crotonaldehyde, methacrylaldehyde, 1-butene, or 1,3-butadiene is enhanced by the presence of water, and leads to preferential decrease in ν(P–O) at 1060 cm^{-1} with preference over that in ν(Mo–O–Mo) at 880 cm^{-1}, while the reaction with methanol is not dependent on the presence of water and results in rapid disappearance of ν(Mo–O–Mo) and retention of ν(P–O).

The IR spectrum of 12-molybdophosphoric acid (HPA) shows four absorption bands at 1060, 960, 880, and 790 cm^{-1} for the stretching vibrations of the anion structure, which are assigned to ν(P–O), ν(Mo=O), and two ν(Mo–O–Mo), respectively.[1] Tsuneki *et al.*[2] examined H_2 reduction of trisilver 12-molybdophosphate, followed by reoxidation with $^{18}O_2$, by means of IR spectroscopy, and suggested that the oxygen removed by the reduction is not from P–O but from Mo–O–Mo, because the isotope shift associated with the reoxidation by $^{18}O_2$ was observed only for ν(Mo=O) and two ν(Mo–O–Mo)'s. In this paper, we report different behaviors of IR spectral changes in reduction of HPA with various organic compounds.

Experimental

HPA was purchased from Kanto Chemical Co. and used without further purification. Organic compounds were dried on anhydrous $CaSO_4$ or molecular sieve 5A and degassed by distillation *in vacuo*. The film of HPA was prepared as described previously.[3] The film was placed in an IR cell connected with a closed circulating system and evacuated at room temperature for 5 min or at 130 °C for 2 h, after which the vapor of an organic compound with or without water was introduced into the cell. Since the volume of the cell was about 280 cm^3, the amounts of the compound and water were in a large excess over that of HPA (2—5 mg/cm^2).

Results and Discussion

Figure 1 shows IR spectra of HPA treated with ethyl methyl ketone. ν(P–O), $\nu(Mo–O–Mo)_H$ (880 cm^{-1}), and $\nu(Mo–O–Mo)_L$ (790 cm^{-1}) decrease with increase in reaction temperature. The decrease for the HPA preevacuated at lower temperatures is obviously much more eminent, indicating that the reduction of HPA is enhanced by the hydrated water.

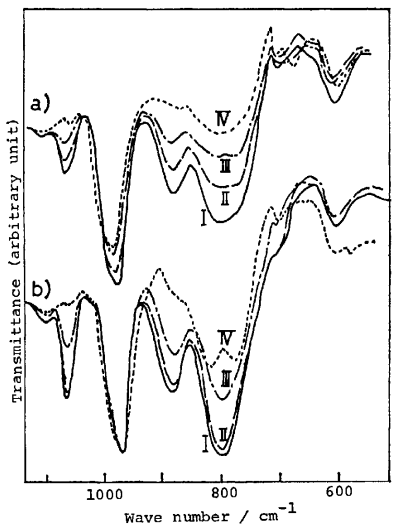

Fig. 1. IR spectra of HPA treated with ethyl methyl ketone (7 mmHg)† for 30 min. a) Preevacuated at 130 °C for 2 h and treated at I: room temp, II: 130 °C, III: 178 °C, and IV: 240 °C. b) Preevacuated at room temp for 5 min and treated at I: room temp, II: 50 °C, III: 90 °C, and IV: 125 °C.

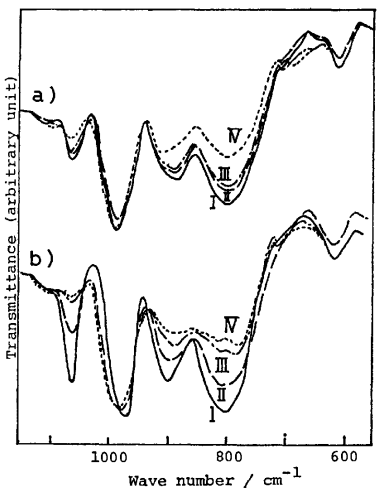

Fig. 2. IR spectra of HPA treated with 1-butene (7 mmHg) for 30 min. a) Preevacuated at 130 °C for 2 h and treated at I: room temp, II: 122 °C, III: 185 °C, and IV: 225 °C. b) Preevacuated at room temp for 5 min, after which water (4 mmHg) was added and treated at I: room temp, II: 124 °C, III: 175 °C, and IV: 220 °C.

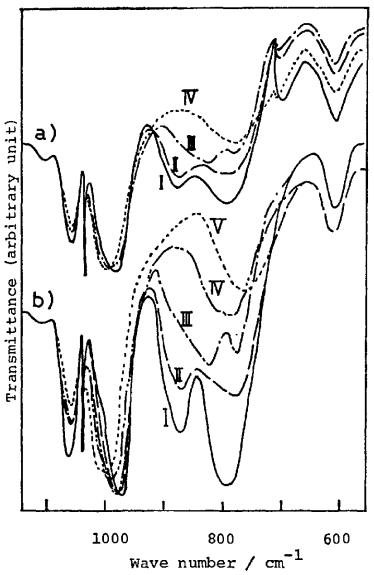

Fig. 3. IR spectra of HPA treated with methanol (4 mmHg) for 30 min. a) Preevacuated at 130 °C for 2 h and treated at I: room temp, II: 125 °C, III: 180 °C, and IV: 225 °C. b) Preevacuated at room temp for 5 min, after which water (4 mmHg) was added, and treated at I: room temp, II: 123 °C, III: 173 °C, IV: 210 °C, and V: 257 °C.

† 1 mmHg≈133.322 Pa.

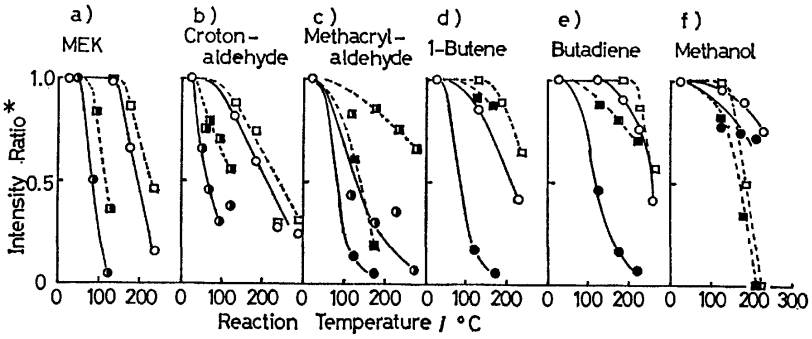

Fig. 4. Changes in peak intensity ratio.
*: $\log(I_0/I)_{\text{react. temp}}/\log(I_0/I)_{\text{room temp}}$ ○ (1060 cm^{-1}) and □ (880 cm^{-1}): evacuated at 130 °C for 2 h. (1060 cm^{-1}) and ◨ (880 cm^{-1}): evacuated at room temp for 5 min. ● (1060 cm^{-1}) and ■ (880 cm^{-1}): evacuated at room temp for 5 min, after which water (4 mmHg) was added.

The decreases in ν(P–O) and $\nu(\text{Mo–O–Mo})_H$ are nearly parallel to each other.

The same dependence on the coexistence of water vapor is found in the reaction with 1-butene, as shown in Fig. 2. The spectra shown in Fig. 2b display quicker decrease of ν(P–O) than that of $\nu(\text{Mo–O–M})_H$. On the other hand, the reaction with methanol results both in almost complete retention of the absorption of ν(P–O) and in disappearance of $\nu(\text{Mo–O–Mo})_H$, as shown in Fig. 3.

The change in both the bands obtained with the above three compounds is plainly plotted together with those obtained with crotonaldehyde, 1,3-butadiene, and methacrylaldehyde in Fig. 4, where it is assumed that either the preevacuation or the reaction conditions have no effect on ν(Mo=O) since the absorption seems to be always superposed as seen in Figs. 1, 2, and 3. Each spectrum is, therefore, normalized on the basis of the intensity of ν(Mo=O), and each change in absorption is represented as the ratio of intensity at a reaction temperature to that at room temperature. With 1-butene and 1,3-butadiene, the intensities of ν(P–O) decrease steeply with increase in reaction temperature, while the lowering of $\nu(\text{Mo–O–Mo})_H$ is very dull, the ratio remaining still more than 0.8 even at 170 °C. With ethyl methyl ketone and crotonaldehyde, too, the decrease in ν(P–O) always precedes that of $\nu(\text{Mo–O–Mo})_H$, although they seem to be nearly parallel. The behavior of the decrease in the two bands with methacrylaldehyde is similar to that with 1-butene in the absence of water and to that with ethyl methyl ketone in its presence. It was reported in our previous paper[3] that absorbed methacrylaldehyde could hardly reduce HPA with or without water at 180 °C, which should be revised. It is, therefore, obvious that the reaction of HPA with all the above five compounds, except methanol, is enhanced by the presence of water and gives rise to the preferential decrease in ν(P–O). The catalytic oxidation of the compounds by HPA is known to depend on the amount of water,[4,5] in conformity with the reduction of HPA. Thus, the lowering of ν(P–O) may be characteristic of reactions in which water participates.

On the other hand, the reaction with methanol results in the striking decrease in $\nu(\text{Mo–O–Mo})_H$ and the almost complete retention of ν(P–O), which seems to be much less affected by water as shown in Figs. 3 and 4f. The catalytic reaction by HPA to produce formaldehyde is not enhanced by water.[5] The decrease in $\nu(\text{Mo–O–Mo})_H$, therefore, may be attributed to the loss of oxygen in Mo–O–Mo.

The results of Fig. 4 show that there would be no appreciable interaction between ν(P–O) and $\nu(\text{Mo–O–Mo})_H$, indicating no fast oxygen exchange between them. In addition, the oxygen mixing between $\nu(\text{Mo–O–Mo})_H$ and $\nu(\text{Mo–O–Mo})_L$ appears to be very slow even at 257 °C, because the latter band remains while the former disappears, as shown in Figs. 2 and 3. In the reduced state, the latter band often splits into two bands at 825 and 780 cm^{-1}, and the splitting was observed both in the disappearance (Figs. 1 and 2) and in the retention (Fig. 3) of ν(P–O), indicating a very complicated behavior. At present, the relation between $\nu(\text{Mo–O–Mo})_L$ and the reduction of HPA is obscure. Katamura *et al.*[6] investigated the mechanism of the H_2 reduction of HPA and the interaction of water with it by means of TPD and IR measurements, suggesting that lower symmetry of the anion structure caused by the reduction may explain the change in IR spectra in the P–O region. It might, however, be suggested from no interaction between the bands that the decrease in ν(P–O) relates to loss of the bridged oxygen showing $\nu(\text{Mo–O–Mo})_L$ but not $\nu(\text{Mo–O–Mo})_H$, if Tsuneki's[2] and Katamura's[6] suggestions would be taken. Another interpretation might be loss of the oxygen in P–O, though there seems to be no change in the band at 610 cm^{-1} which is assigned to δ(O–P–O)[2] as shown in Figs. 1, 2, and 3.

References

1) C. Rocchiccioli-Deltcheff, R. Thouvenot, and R. Frank, *Spectrochim. Acta, Part A*, **32**, 587 (1976).
2) H. Tsuneki, H. Niiyama, and E. Echigoya, *Chem. Lett.*, **1978**, 645 and 1183.
3) T. Tsai, K. Maruya, M. Ai, and A. Ozaki, *Chem. Lett.*, **1981**, 611.
4) M. Misono, K. Sakata, and Y. Yoneda, Preprint of 7th Intern. Congr. Catal., Tokyo, 1980, paper No. B-27.
5) M. Ai, Preprint of 46th Shokubai (Catalyst) Meeting, Sendai, 1980, p. 32; *J. Catal.*, **71**, 88 (1981).
6) K. Katamura, T. Nakamura, K. Sakata, M. Misono, and Y. Yoneda, *Chem. Lett.*, **1981**, 89.

The Effect of Pressure on the Mutual Solubility of a Nonionic Surfactant–Water System

Shoji KANESHINA,* Osamu SHIBATA, and Makoto NAKAMURA

College of General Education, Kyushu University-01, Ropponmatsu, Chuo-ku, Fukuoka 810

(Received July 27, 1981)

Synopsis. The cloud-point temperature (T) of an aqueous hexa(oxyethylene) dodecyl ether solution was determined as a function of the pressure (P) and the composition (x_2). The volume (ΔV) and entropy (ΔS) changes for the separation of the surfactant phase from the water phase were estimated from the T-P-x_2 relation. Both ΔV and ΔS were positive.

An aqueous solution of nonionic surfactants suddenly becomes turbid on being heated to a critical temperature, known as the cloud point, and the solution separates into two phases. This peculiar dissolution phenomenon has been explained especially by an acceptable model based on the thermodynamic properties of a nonionic surfactant–water system,[1,2] since accurate thermodynamic data have been determined for pure nonionics in water. Although the pressure is necessarily an important thermodynamic variable, as well as the temperature and the concentration, defining the state of solution, few studies have been made on the effect of pressure on the solution behavior of nonionic surfactants in water.[3–5] In this paper, the cloud-point temperature of an aqueous hexa(oxyethylene) dodecyl ether solution has been determined as a function of both the pressure and the composition. From the relation of the cloud-point-temperature-pressure-composition, the thermodynamic quantities (volume ΔV and entropy ΔS) accompanied by the separation of the surfactant phase from the water phase were estimated.

Experimental

Homogeneous hexa(oxyethylene) dodecyl ether ($C_{12}E_6$) was obtained from Nikko Chemicals. Its purity was checked by gas chromatography, and it was found to show a single peak. The cloud-point temperature of a 1.0% (w/w) solution was 48.8 °C. The cloud points under a high pressure were determined by a method described previously.[4]

Results and Discussion

The cloud-point temperatures of aqueous $C_{12}E_6$ solutions were determined in the pressure range of 0.1—150 MPa and the composition range of 0.1—10% (w/w). The cloud-point temperatures for all the surfactant solutions increase monotonously with an increase in the pressure up to 150 MPa (Fig. 1). Since the cloud point of a surfactant solution is generally taken to be the temperature where the separation of the liquid-surfactant phase containing dissolved water is caused by the dehydration of ether oxygens of the poly(oxyethylene) group,[1] a pressure of up to 150 MPa seems to favorable for the dissolution of surfactant molecules in water. An increase in the pressure enhances the formation of hydrogen bonds between water and ether oxygens of the poly(oxyethylene) group.[6]

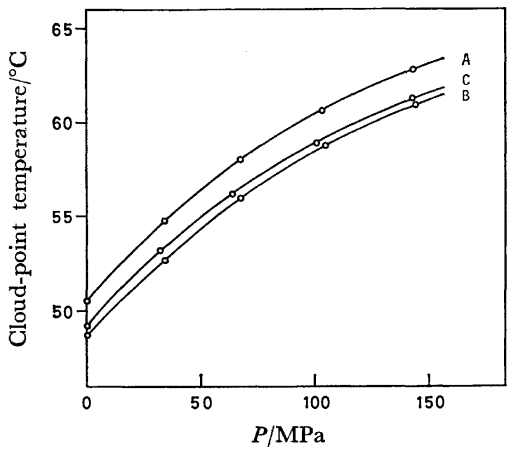

Fig. 1. Cloud-point temperature *vs.* pressure curves for some aqueous hexa(oxyethylene) dodecyl ether solutions. Concentration; A: 0.124, B: 2.06, and C: 5.02 %(w/w).

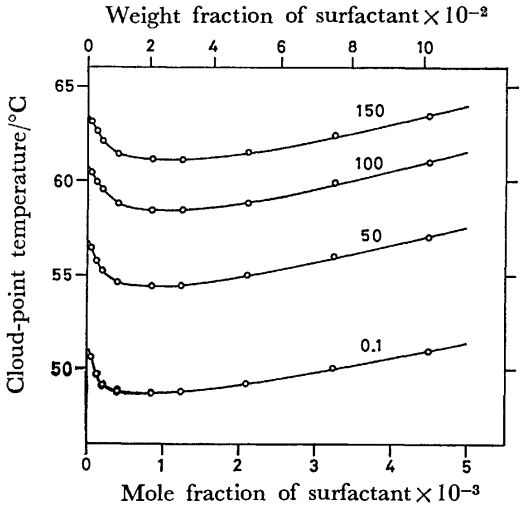

Fig. 2. Cloud-point temperature of aqueous hexa(oxyethylene) dodecyl ether solutions as a function of surfactant concentration at various pressures. Numerical values refer to the pressure in MPa.

In Fig. 2, the cloud points are shown as a function of the concentration of $C_{12}E_6$ at various pressures. Note that each curve in Fig. 2 is a part of the phase diagram representing the liquid-liquid mutual solubility, which has a lower critical solution temperature (LCST). As may be seen from Fig. 2, the LCST can be elevated by increasing the pressure.

At the cloud point, the two phases (an aqueous phase containing a small amount of a singly dispersed surfactant and a liquid surfactant phase containing dissolved water) are in equilibrium.[1,2] In the two-component, two-phase system, the curves of the co-

existence of pairs of phases are described by these equations:[7]

$$\left(\frac{\partial T}{\partial x_2}\right)_P = g_{22}\left(\frac{RT}{y_1\Delta\bar{s}_1+y_2\Delta\bar{s}_2}\right)\left(\frac{x_2-y_2}{x_1x_2}\right), \quad (1)$$

$$\left(\frac{\partial P}{\partial x_2}\right)_T = -g_{22}\left(\frac{RT}{y_1\Delta\bar{v}_1+y_2\Delta\bar{v}_2}\right)\left(\frac{x_2-y_2}{x_1x_2}\right), \quad (2)$$

and:

$$\left(\frac{\partial T}{\partial P}\right)_{x_2} = \frac{y_1\Delta\bar{v}_1+y_2\Delta\bar{v}_2}{y_1\Delta\bar{s}_1+y_2\Delta\bar{s}_2}, \quad (3)$$

where x and y refer to the mole fraction in an aqueous phase and a surfactant phase respectively. $\Delta\bar{s}_1$ and $\Delta\bar{s}_2$ are the partial molal entropy changes in the water and surfactant respectively transferred from the aqueous into the surfactant phase, and $\Delta\bar{v}_1$ and $\Delta\bar{v}_2$ are the partial molal volume changes in the water and surfactant respectively transferred from the aqueous into the surfactant phase. The expression for g_{22} can be written:

$$g_{22} = \left(\frac{\partial \ln a_2}{\partial \ln x_2}\right)_{T,P}. \quad (4)$$

In a dilute solution, the activity is usually proportional to the concentration, and Eq. 4 becomes $g_{22}=1$.

The entropy change on the phase separation of a surfactant solution, ΔS ($\equiv y_1\Delta\bar{s}_1+y_2\Delta\bar{s}_2$), can be estimated by applying Eq. 1 to Fig. 2 (T-x_2 diagram). The volume change on the phase separation of a surfactant solution, ΔV ($\equiv y_1\Delta\bar{v}_1+y_2\Delta\bar{v}_2$), can be estimated by using Eq. 3, the value of ΔS, and the slope of Fig. 1 (T-P diagram).

The values of ΔV and ΔS, which were calculated at the surfactant concentration of $x_2=5.0\times10^{-5}$, are listed in Table 1. Both ΔV and ΔS are positive. These positive changes in volume and entropy are attributable partly to the dehydration of the poly(oxyethylene) chain and partly to the hydrophobic bonding of alkyl chain. The value of ΔV, 2.1 cm^3 is in good agreement with the volume change of 2.2 cm^3, which was determined from the density measurements above and below the cloud point.[8]

The volume change for the transfer of the poly(oxyethylene) chain from the aqueous solution into the pure liquid state amounts to about 2.0 cm^3 per oxyethylene unit.[6] Therefore, the volume change of 12 cm^3 may be expected for the complete dehydration of the hexa(oxyethylene) group. On the other hand, the volume change for the transfer of the hydrocarbon part from the aqueous to the nonpolar environment amounts to 1.2—1.5 cm^3 per methylene group.[9-11] Despite the large volume change to be expected for both the dehydration and the hydrophobic bonding, the volume change calculated thermodynamically or measured directly is appreciably small. Since the liquid-surfactant phase contains a considerable amount of water, the partial dehydration of the poly(oxyethylene) chain and the incomplete transfer of the alkyl chain are considered to be responsible for the small volume change on the separation of the liquid-surfactant phase from the aqueous phase.

Table 1. Thermodynamic parameters on the cloud point of an aqueous hexa(oxyethylene) dodecyl ether solution at the concentration of $x_2=5.0\times10^{-5}$

P / MPa	T / K	ΔS / J K^{-1} mol^{-1}	ΔV / cm^3 mol^{-1}
0.1	323.6	16	2.1
50	329.4	20	1.9
100	333.4	26	1.7
150	336.1	31	1.4

As is shown in Table 1, the value of ΔV decreases with the increase in the pressure, while the value of ΔS increases with the pressure. The large compressibility of the dehydrated system compared with the hydrogen-bonded system is considered to be responsible for the decrease in the ΔV with the pressure. The increased in ΔS with the pressure may be ascribed to the increased numbers of the hydrogen bonds between the poly(oxyethylene) chain and water molecules. In other words, the hydrogen-bonded water, which should be released at the cloud point, is likely to be increased by applying pressure. The hydrophobic bonding may also be responsible for the increase in ΔS with the pressure; the value of ΔS for the hydrophobic bonding (*i.e.*, micelle formation) increases initially with an increase in the pressure and then decreases with the pressure *via* the maximum at about 100 MPa.[11]

References

1) K. Shinoda, *J. Colloid Interface Sci.*, **34**, 278 (1970).
2) K. Shinoda, "Principles of Solution and Solubility," Marcel Dekker, New York (1978), Chap. 9, pp. 157—179.
3) K. Suzuki and M. Tsuchiya, *Bull. Inst. Chem. Res., Kyoto Univ.*, **47**, 270 (1969).
4) S. Kaneshina, O. Shibata, and M. Nakamura, *Bull. Chem. Soc. Jpn.*, **52**, 42 (1979).
5) N. Nishikido, N. Yoshimura, M. Tanaka, and S. Kaneshina, *J. Colloid Interface Sci.*, **78**, 338 (1980).
6) S. Kaneshina, M. Yoshimoto, H. Kobayashi, N. Nishikido, G. Sugihara, and M. Tanaka, *J. Colloid Interface Sci.*, **73**, 124 (1980).
7) J. G. Kirkwood and I. Oppenheim, "Chemical Thermodynamics," McGraw-Hill, New York (1962), Chap. 9, pp. 116—147.
8) S. Kaneshina, I. Ueda, H. Kamaya, and H. Eyring, *Biochim. Biophys. Acta*, **603**, 237 (1980).
9) M. E. Friedman and H. A. Scheraga, *J. Phys. Chem.*, **69**, 3795 (1965).
10) J. M. Corkill, J. F. Goodman, and T. Walker, *Trans. Faraday Soc.*, **63**, 768 (1967).
11) S. Kaneshina, M. Tanaka, T. Tomida, and R. Matuura, *J. Colloid Interface Sci.*, **48**, 450 (1974).

Solvent Effects on the Isomerization of 1-Pentene Catalyzed by Cationic Platinum Complexes

Hiroyoshi KANAI* and Osamu HIRAKO†

Department of Hydrocarbon Chemistry, Faculty of Engineering, Kyoto University, Sakyo-ku, Kyoto 606

(Received September 7, 1981)

Synopsis. The isomerization of 1-pentene with $[PtH(PPh_3)_3]X$ ($X=SO_4H$, ClO_4) occurred only in ethers. The decrease in the concentrations of 1-pentene and the platinum complexes leads to high *cis*-selectivity.

Wells *et al.* deduced that stereoselectivity in the isomerization of 1-alkenes was determined by the degree of molecular congestion at a catalyst site:[1,2] the preferential *cis*-alkene formation occurred when the site of catalytic activity was highly congested.[1-3] A wide range of metal-phosphine complexes catalyze 1-pentene isomerization to 2-pentenes *via* the formation of secondary pentyl intermediates with preferential formation of *cis*-2-pentene.[2-5] The selectivity was explained in terms of the restriction of the normal rotations in the secondary pentyl intermediate by phosphine ligands as low the conformation of molecular volume predominates as possible.[1,2] We observed selective *cis*-isomerization of 1-pentene catalyzed by $NiX(PPh_3)_3$–$SnCl_2$ (X=halogen) systems which was attributed to the bulkiness and *trans*-effect of $SnCl_2X^-$ ligands.[4]

$[PtH(PPh_3)_3]X$ ($X=SO_4H$, ClO_4) isomerized 1-pentene slowly at 50 °C to give 2-pentene having an initial *cis*/*trans* ratio of more than 3 only in ethers (Table 1). No isomerization occurred with $[PtH(PPh_3)_3]SO_4H$ in homogeneous solutions of ethyl methyl ketone, methanol, *N*,*N*-dimethylformamide, acetonitrile, and nitromethane, or in a heterogeneous solution of benzene. However, in homogeneous solutions of benzene and dichloromethane, or in heterogeneous solutions of dioxane, THF, and 1,2-dimethoxyethane (glyme) the isomerization of 1-butene[6] or 1-pentene[7] with $PtH(PPh_3)_2ClO_4$ proceeded readily in preferential formation of the *trans*-isomers. The initial *trans*/*cis* ratio in glyme (Table 1) is in excess of the equilibrium value as is only known in cases of the isomerization of 1-pentene catalyzed by Pt(II)–$SnCl_2$ complex,[8] $RuH_4(PPh_3)_3$, and $RuH_2(N_2)(PPh_3)_3$.[9] $[PtH(PPh_3)_3]ClO_4$ (tris-complex) is lower in reactivity and higher in *cis*-selectivity than $PtH(PPh_3)_2ClO_4$ (bis-complex). Although relative rates are not determined exactly owing to the heterogeneity, isomerization proceeds favorably in glyme among ethers investigated. First-order dependency and constant *cis*/*trans* ratios were observed in ethers listed in Table 1. When excess of PPh_3 was added to the bis-complex, there appeared reaction features characteristic of the tris-complex: the *cis*/*trans* ratios increased gradually from 0.55 to 0.99, 2.00 and 2.70 in accordance with excess PPh_3/bis-complex=0.85, 0.90, 0.95, and 0.97, respectively.

The isomerization catalyzed by the tris-complex occurs *via* a metal-hydride addition-elimination mechanism: (1) Pt–H bond was detected in the IR spectrum after isolation of the catalyst from the reaction mixture of $[PtD(PPh_3)_3]ClO_4$ and 1-pentene in glyme; (2) intermolecular hydrogen transfer between C_2D_4 and C_2H_4 occurred.

The lower the concentrations of 1-pentene and of the platinum complex become, the higher *cis*-selectivity rises (Fig. 1). The increase of 1-pentene results in the dissociation of the tris-complex to give

TABLE 1. ISOMERIZATION OF 1-PENTENE CATALYZED BY PLATINUM COMPLEXES IN ETHERS

Catalyst	Solvent	Temp °C	Time min	Conversion %	*cis*/*trans*	
$[PtH(PPh_3)_3]SO_4H$[a]	Dioxane	50	240	3.5	4.12	Heterogeneous
	THF	50	240	8.3	3.49	Heterogeneous
	Anisole	50	240	0.8	5.84	Heterogeneous
	Glyme	50	240	15.1	4.25	Heterogeneous
$[PtH(PPh_3)_3]ClO_4$[b]	Dioxane	50	240	0.5	4.97	Heterogeneous
	THF	50	240	2.5	6.72	Heterogeneous
	Anisole	50	240	1.4	4.83	Homogeneous
	Glyme[e]	50	240	8.3	4.24	Heterogeneous
$[PtH(PPh_3)_2ClO_4$[d]	Dioxane	r. t.	10	29.5	0.23	Heterogeneous
	THF	r. t.	30	6.0	0.32	Heterogeneous
	Glyme	r. t.	5	4.7	0.13	Heterogeneous
	Glyme[e]	50	240	90.0	0.55	Heterogeneous
	Glyme[f]	50	240	2.4	2.70	Heterogeneous

a) [Pt] 0.1 mmol, [1-pentene] 10 mmol, solvent 20 ml. b) [Pt] 0.05 mmol, [1-pentene] 5 mmol, solvent 10 ml. c) [Pt] 0.025 mmol, [1-pentene] 5 mmol, glyme 10 ml. d) [Pt] 0.05 mmol, [1-pentene] 5 mmol, solvent 10 ml. e) Addition of excess PPh_3/Pt=0.85. f) Addition of excess PPh_3/Ph=0.97.

† Present address: Mitsubishi Motors Corporation, Kyoto Works, Ukyo-ku, Kyoto 615.

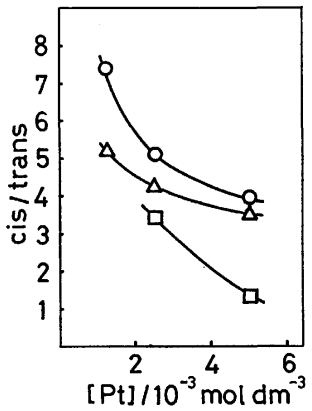

Fig. 1. Plots of *cis*-selectivity *vs.* the concentration of $[PtH(PPh_3)_3]ClO_4$. The ratios of 1-pentene to the Pt complex: 10 (○); 20 (△); 100 (□).

the bis-complex which is high in catalytic activity and low in *cis*-selectivity. Conversions of 1-pentene after 4 h at 10, 20, and 100 of 1-pentene/Pt ratios were 8.6, 10.0, and 11.9%, respectively in 5×10^{-3} mol dm^{-3} of $[PtH(PPh_3)_3]ClO_4$. The opposite tendency in regard to the effect of the concentration of catalysts would be attributed to a gradual increase in the degree of dissociation of the catalyst by losing PPh_3 ligands.[3] The rise in the *cis/trans* ratio with decreasing catalyst concentration in Fig. 1 would be due to the lack of dissociation of the tris-complex in ethers.

The presence of compounds having an ether linkage is essential for catalytic activity of the tris-complex. Diallyl ether and allyl phenyl ether were isomerized by the tris-complex in neat liquid or a non-ether solvent such as ethyl methyl ketone. No isomerization of allylbenzene occurred in neat liquid but it was isomerized to propenylbenzene in glyme.

Experimental

1-Pentene was obtained from Tokyo Kasei Kogyo Co. and distilled prior to use. Tetrahydrofuran, dioxane, and glyme were refluxed over sodium, distilled and stored in a nitrogen atmosphere. Other chemicals were commercial materials and used without further purification.

$[PtH(PPh_3)_3]X$ ($X=SO_4H$, ClO_4)[10] and $PtH(PPh_3)_2ClO_4$[11] were prepared according to the methods given in the literature.

Procedure. A two-necked 100 ml flask was charged in a nitrogen atmosphere with $(2.5—10)\times10^{-4}$ mol of a platinum complex, (10—20) ml of dry, degassed solvent, and a micro stirring bar. The flask was cooled in liquid nitrogen and evacuated, and $(5—10)\times10^{-3}$ mol of 1-pentene was added. The flask was immersed in a bath maintained at 50 °C or r.t. Samples of the solution, *ca.* 0.1 ml, were withdrawn through the side arm at intervals with a syringe and the distillates obtained from thaw-to-thaw distillation were analyzed by a Shimadzu GC gas chromatograph on the 2,4-dimethylsulfolane (30%)/C-22 column operated at ambient temperature.

References

1) D. McMunn, R. B. Moyes, and P. B. Wells, *J. Catal.*, **52**, 472 (1978).
2) D. Bingham, D. E. Webster, and P. B. Wells, *J. Chem. Soc., Dalton Trans.*, **1974**, 1514.
3) D. Bingham, D. E. Webster, and P. B. Wells, *J. Chem. Soc., Dalton Trans.*, **1974**, 1519.
4) H. Kanai, K. Kushi, K. Sakanoue, and N. Kishimoto, *Bull. Chem. Soc. Jpn.*, **53**, 2711 (1980).
5) F. Pennella, *J. Organomet. Chem.*, **78**, C10 (1974).
6) H. C. Clark and H. Kurosawa, *Inorg. Chem.*, **12**, 1566 (1973).
7) O. Hirako, MA Dissertation, Kyoto University 1975.
8) G. C. Bond and M. Hellier, *Chem. Ind. (London)*, **1965**, 35; *J. Catal.*, **7**, 217 (1967).
9) F. Pennella and R. L. Banks, *J. Catal.*, **35**, 73 (1974).
10) F. Cariati, R. Ugo, and F. Bonati, *Inorg. Chem.*, **5**, 1128 (1966).
11) I. V. Gavrilova, M. I. Gel'fman, N. V. Ivannikova, and V. V. Razumovskii, *Zh. Neorg. Khim.*, **16**, 1124 (1971).

Syntheses of Six-membered Cyclopalladated Complexes of 2-Benzoylpyridine

Yoshio FUCHITA, Katsuma HIRAKI,* and Yasunori KAGE

Department of Industrial Chemistry, Faculty of Engineering, Nagasaki University, Bunkyo-machi, Nagasaki 852

(Received July 23, 1981)

Synopsis. 2-Benzoylpyridine reacts with $Pd(OAc)_2$ to give a new six-membered cyclopalladated complex, $[\{Pd(pcph)(OAc)\}_2]\cdot 0.25CH_2Cl_2$ [pcph=2-(2-pyridylcarbonyl)phenyl-C^1,N] (**1**). A chloro-bridged analogue, $[\{Pd(pcph)Cl\}_2]$, prepared by the metathetical reaction of **1** with LiCl, undergoes bridge-splitting reactions with 3,5-lutidine and Tl(acac) to yield the corresponding mononuclear cyclopalladated complexes.

Many studies have been reported on the five-membered cyclopalladated complexes of aryl-substituted nitrogen bases.[1,2] However, as concerns six-membered cyclopalladated complexes having nitrogen donor atoms, only two reports have appeared on *N,N'*-diarylamidines[3] and *N,N*-diethyl-3-phenylthiomethoxy-4-methoxyphenethylamine.[4] Recently, it was found in our laboratory that 2-benzylpyridine readily produces a six-membered cyclopalladated complex by the reaction with palladium(II) acetate.[5] In continuation of our studies about the six-membered cyclopalladated complexes, we wish to report on the cyclopalladation of 2-benzoylpyridine (bzopy) by palladium(II) acetate resulting in the formation of $[\{Pd(pcph)(OAc)\}_2]$ (**1**) [pcph=2-(2-pyridylcarbonyl)phenyl-C^1,N].

Experimental

All the new complexes synthesized in this study were characterized in the same way as described in an earlier paper.[6] Molecular weights were determined in benzene with a Corona Model 114 molecular weight apparatus at 41.7° C.

Preparation of $[\{Pd(pcph)(OAc)\}_2]\cdot 0.25CH_2Cl_2$ (**1**). An acetic acid suspension (20 ml) containing palladium(II) acetate (3.1 mmol) and bzopy (3.7 mmol) was refluxed for 1.5 h, and then filtered, to give a yellow cake and a yellow solution. The yellow cake was successively washed well with water and a small amount of methanol, and recrystallized from dichloromethane/hexane to give 0.56 g of **1** as yellow crystals. An additional amount (0.28 g) of **1** was obtained as yellow precipitates from the yellow solution after extraction of it with dichloromethane, concentration of the extract, and dilution with hexane. Yield 76%; mp 240—243 °C (dec); MW 705.4 (Calcd 716.6).

Preparation of $[\{Pd(pcph)Cl\}_2]$ (**2**). A THF–water (120 ml/10 ml) suspension containing **1** (1.2 mmol) and LiCl (7.5 mmol) was stirred for 12 h. The precipitated yellow solid was filtered, and washed with a methanol/water (20 ml/20 ml) mixture to give **2**. Yield 95%; mp>300 °C.

Reaction of **2** *with 3,5-Lutidine.* A dichloromethane solution (10 ml) containing **2** (0.23 mmol) and 3,5-lutidine (lut) (0.51 mmol) was stirred at room temperature for 5 h. Addition of hexane to the resulting mixture gave $[Pd(pcph)Cl(lut)]\cdot 0.1CH_2Cl_2$ (**3**) as pale yellow crystals. Yield 79%; mp>300 °C.

Reaction of **2** *with Tl(acac).* A dichloromethane suspension (15 ml) of **2** (0.46 mmol) and thallium(I) acetylacetonate (0.95 mmol) was stirred at room temperature for 1 d. After centrifuging the resulting milky suspension, the supernatant solution was passed through a silica-gel column (200 mesh, $20\phi\times 140$ mm) with dichloromethane as an eluent. A pale yellow fraction was collected and concentrated. Addition of hexane gave [Pd(pcph)(acac)] (**4**) as yellow crystals. Yield 39%; mp 229—230 °C (dec).

Results and Discussion

2-Benzoylpyridine reacted with palladium(II) chloride in refluxing ethanol to afford only an addition complex, bis(2-benzoylpyridine)dichloropalladium(II), giving no cyclopalladated complex. However, bzopy reacted readily with palladium(II) acetate in refluxing acetic acid to produce a new six-membered cyclopalladated complex **1** in a high yield. It is noteworthy that bzopy, which contains an electron-attracting carbonyl group, undergoes easily cyclopalladation reaction with palladium(II) acetate, in contrast with the results of the earlier studies concerning the electronic effect on the cyclopalladation reaction of substituted azobenzenes.[7,8] Complex **1** was treated with LiCl to give **2**, which reacted with lut and Tl(acac) to afford the corresponding mononuclear cyclopalladated complexes, **3** and **4**, respectively (Scheme 1). All the new complexes prepared in this study show considerably high thermal stability. The IR spectra of **1**—**4** showed bands at *ca.* 1670 cm^{-1} due to a ν(C=O) vibration in pcph moiety. This band did not shift virtually in comparison with that in free bzopy (1670 cm^{-1}).

The IR spectrum of **1** showed two characteristic bridging acetato bands[9] at 1585 and 1430 cm^{-1}. This

Table 1. Elemental analyses and ^{1}H NMR data of the palladium(II) complexes

Compd	Found (Calcd) (%)			^{1}H NMR (δ)		
	C	H	N	6'-H	Me	Others
1	47.15 (47.35)	3.19 (3.16)	3.66 (3.91)	8.25 d[b]	2.05 s	5.28 s(CH_2Cl_2)
2	44.30 (44.47)	2.58 (2.49)	4.22 (4.32)	—[c]	—[c]	—[c]
3	51.75 (52.17)	3.97 (3.94)	6.27 (6.37)	9.52 dd[b,d]	2.28 s	7.39 s(H^r) 8.29 s(H^α) 5.28 s(CH_2Cl_2)
4	52.38 (52.66)	3.91 (3.90)	3.56 (3.61)	9.08 dd[b,d]	2.01 s 2.06 s	5.04 s(CH)

a) In $CDCl_3$. See the text about the aromatic protons. d=Doublet, dd=double doublet, and s=singlet. b) $^3J_{HH}$=7 Hz. c) Not recorded owing to its poor solubility. d) $^4J_{HH}$=2 Hz.

complex did not show temperature-dependent ^{1}H NMR spectra in the range of 57——50 °C, indicating that the six-membered pcph-palladium ring is virtually planar; if this ring were nonplanar and had a boat conformation, temperature-dependent ^{1}H NMR spectra attributable to an inversion of the ring would be observed as was seen in the palladated 2-(2-picolyl)-phenyl-C^1,N ring.[5] The ^{1}H NMR spectrum of **1** exhibited one sharp singlet due to the μ-acetato-methyl protons at δ 2.05, indicating that **1** has only one (*a*-C^1,*b*-N)(*g*-N,*h*-C^1) typed isomer[10] (Scheme 1).

In the ^{13}C{^{1}H} NMR spectrum of **1** in $CDCl_3$, three aromatic quaternary carbon signals at δ 132.6, 143.2, and 150.5 were ascribed to 2-C, 1-C, and 2'-C, respectively, by comparison with the data of acetophenone (1-C, δ 137.1),[11] a cyclopalladated complex (1-C, δ 143.3),[5] and 2-acetylpyridine (2-C, δ 154.1).[12] These data confirm strongly a cyclopalladated structure of the pcph moiety in **1**. Other eight aromatic tertiary carbon signals appeared as singlets at δ 124.6, 125.4, 126.6, 128.5, 130.4, 134.0, 138.6, and 151.6. Only the last signal (δ 151.6) was assigned to 6'-C (6-C of 2-acetylpyridine, δ 149.5).[12] Two lower field singlets at δ 181.3 and 190.3 were ascribed to μ-acetato-carboxylato carbon [Mo_2(μ-O_2CMe)(Ph)$_3$(PMe_3)$_3$, δ 182.7][13] and carbonyl one, respectively. The μ-acetato-methyl carbon signal also appeared as a singlet at δ 24.5.

Complex **2** was assigned to a chloro-bridged binuclear complex on the basis of the elemental analysis and the characterization of the derivatives from **2** as stated below.

In the ^{1}H NMR spectrum of **3**, eight aromatic protons of the pcph moiety appeared as two sets of well-separated ABCD pattern (Fig. 1). In consideration of the magnetic anisotropy due to the lutidine ring[5,6] and the original chemical shifts of free bzopy,[14] four double doublets at δ 6.69, 7.75, 8.14, and 9.52 were assigned to H^6, H$^{3'}$, H^3, and H$^{6'}$, respectively, and four double triplets at δ 6.98, 7.12, 7.49, and 7.95 were ascribed to H^5, H^4, H$^{5'}$, and H$^{4'}$, respectively. The coupling constants were $^3J_{HH}$=7 Hz and

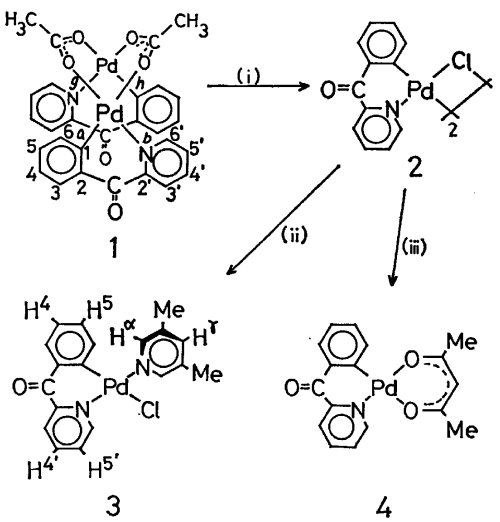

Scheme 1. (i) LiCl. (ii) 3,5-Lutidine. (iii) Tl(acac).

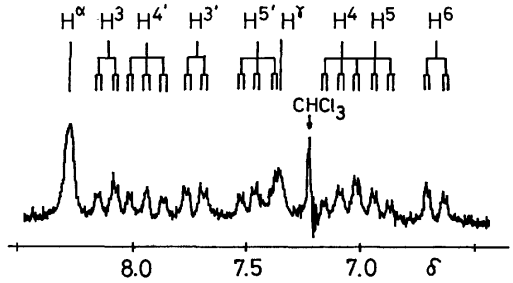

Fig. 1. Low field region of the ^{1}H NMR spectrum of **3**.

$^4J_{HH}$=2 Hz.

The IR spectrum of **4** exhibited two strong bands at 1590 and 1515 cm^{-1}, characteristic of the *O*,*O'*-chelating acetylacetonato ligand. This complex also showed two sets of relatively clear ABCD pattern, which consisted of two doublets at δ 7.72 and 7.78, two double doublets at δ 8.82 and 9.08 (H$^{6'}$) [$^3J_{HH}$=*ca.* 7 Hz, $^4J_{HH}$=*ca.* 2 Hz], two triplets at δ 7.13 and 7.27, and two double triplets at δ 7.51 and 7.98. The mass spectrum exhibited the parent ion peak at *m*/*e* 387, together with the fragment ion peak at *m*/*e* 288 [(P—acac)$^+$].

Styrene reacted with **2** in the presence of tripropylamine in refluxing *m*-xylene for 30 h to give a brownish black oil. After column chromatographic treatment on alumina, this oil was proved to contain both bzopy and *trans*-2-(2-pyridylcarbonyl)stilbene (**5**) in about 68 and 25% yields, respectively. The formation of **5** was confirmed by the ^{1}H NMR spectrum of the oil in CCl_4 [δ 6.82 d ($^3J_{HH}$=16 Hz, 1H, olefinic proton)] and its mass spectrum [*m*/*e* 285 (P$^+$)], supporting the cyclopalladated structure in **2**. However, the separation of these two compounds has not been achieved even after repeated column chromatographic treatments.

References

1) M. I. Bruce, *Angew. Chem., Int. Ed. Engl.*, **16**, 73 (1977).
2) I. Omae, *Chem. Rev.*, **79**, 287 (1979).
3) N. D. Cameron and M. Kilner, *J. Chem. Soc., Chem. Commun.*, **1975**, 687.
4) R. A. Holton and R. V. Nelson, *J. Organomet. Chem.*, **201**, C35 (1980).
5) K. Hiraki, Y. Fuchita, and K. Takechi, *Inorg. Chem.*, **20**, 4316 (1981).
6) Y. Fuchita, K. Hiraki, T. Yamaguchi, and T. Maruta, *J. Chem. Soc., Dalton Trans.*, **1981**, 2405.
7) H. Takahashi and J. Tsuji, *J. Organomet. Chem.*, **10**, 511 (1967).
8) M. I. Bruce, B. L. Goodall, and F. G. A. Stone, *J. Chem. Soc., Dalton Trans.*, **1978**, 687.
9) H. Onoue and I. Moritani, *J. Organomet. Chem.*, **43**, 431 (1972).
10) K. Hiraki, Y. Fuchita, H. Nakaya, and S. Takakura, *Bull. Chem., Soc. Jpn.*, **52**, 2531 (1979).
11) L. F. Johnson and W. C. Jankowski, "Carbon-13 NMR Spectra," John Wiley & Sons, New York (1972).
12) G. Miyajima, Y. Sasaki, and M. Suzuki, *Chem. Pharm. Bull.*, **20**, 429 (1972).
13) R. A. Jones and G. Wilkinson, *J. Chem. Soc., Dalton Trans.*, **1979**, 472.
14) S. Castellano and A. A. Bothner-By, *J. Chem. Phys.*, **41**, 3863 (1964).

The Nafion-H-catalyzed Acylation of Thiophene with Acid Anhydrides

Hisatoshi KONISHI,* Kazuhiro SUETSUGU, Tamon OKANO, and Jitsuo KIJI

Department of Environmental Chemistry and Technology, Faculty of Engineering, Tottori University, Koyama, Tottori 680

(Received May 22, 1981)

Synopsis. The reaction of thiophene with acyclic acid anhydrides in the presence of Nafion-H (fluorocarbon resin sulfonic acid) afforded the corresponding 2-acylthiophenes in moderate yields. Acylation with cyclic acid anhydrides gave only low yields, however. The Nafion-H catalyst could be reused for the acylation with a little loss of activity.

Ion-exchange resins have widely been used as renewable catalysts for organic synthesis. The resin catalysts are insoluble in organic solvents and can be recovered by filtration, with a retention of the catalytic activity. Considerable attention has been focused on the use of fluorocarbon resin (Nafion-H) containing strongly acidic groups, $-CF_2CF_2SO_3H$, in recent years. The catalytic activity and the stability of Nafion-H are superior to those of Amberlyst 15 (polystyrenesulfonic acid).[1] It has previously been shown that Nafion-H is a good catalyst for a variety of reactions, *e.g.*, alkylation,[2] hydration,[3] acylation,[4] and aldol condensation.[5] We have now examined the applicability of the Nafion-H-catalyzed reaction to thiophene chemistry. This paper is concerned with the Nafion-H-catalyzed acylation of thiophene with acid anhydrides and with a comparative study of the catalytic activity of Nafion-H and Amberlyst 15.

Results and Discussion

The results are summarized in Table 1. The reaction of thiophene with aliphatic acid anhydrides (**1a**—**c**) in dichloromethane under refluxing gave the corresponding ketones in sufficient yields. An increase in the chain-length of the acyl group results in a gradual increase in the yield of the ketones. This finding is consistent with the competitive acylation. The acylation rates of propionic anhydride, **1b**, and butyric anhydride, **1c**, relative to acetic anhydride, **1a**, at 38 °C in dichloromethane are as follows: **1a**, 1.00; **1b**, 1.56; **1c**, 1.88. The reactivity of the acid anhydrides increased with an increase in the +I effect of the alkyl group. The electron-releasing groups diminish the reactivity of electrophiles. In these acylations, therefore, the relative reactivity of the acid anhydrides appears to be anomalous. The acylations probably involve the mixed anhydrides intermediate, **A**, as is shown in Scheme 1. The mixed anhydride has been proposed as an intermediate in the acylation.[4]

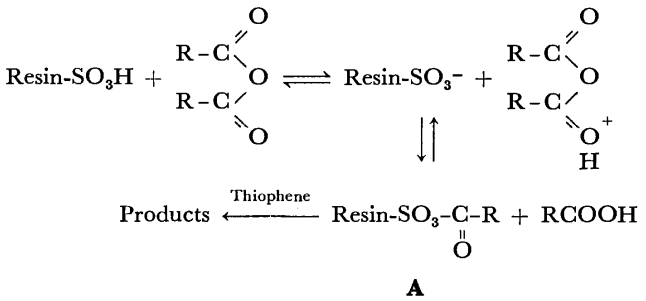

A

Scheme 1.

It has been reported that an equimolar mixture of acetic anhydride and acetic acid was efficient in the Nafion-H-catalyzed acylation of reactive alkylbenzenes, and that acetic anhydride alone was not an effective acylating agent under the reaction conditions.[4] In our reaction conditions, however, the addition of acetic acid decreased the yield of 2-acetylthiophene.

Thiophene reacted with benzoic anhydride in the 1,2-dichloroethane solvent to give 2-benzoylthiophene in a good yield. Acylation with cyclic anhydrides (**2e**—**h**) gave only low yields under similar conditions.

The catalytic activity of Nafion-H was compared with that of Amberlyst 15. Under the same reac-

Table 1. Nafion-H-catalyzed acylation of thiophene with acid anhydrides[a]

Run	Acid anhydride	Reaction conditions	Product	Yield[b] %
1	**1a**	25 °C, CH_2Cl_2	**3a**	70
2	**1a**	Reflux, CH_2Cl_2	**3a**	76
3	**1a**	25 °C, CH_2Cl_2 CH_3COOH[c]	**3a**	31
4	**1b**	Reflux, CH_2Cl_2	**3b**	81
5	**1c**	Reflux, CH_2Cl_2	**3c**	94
6	**1d**	Reflux, CH_2Cl_2	**3d**	20
7	**1d**	Reflux, $(CH_2Cl)_2$	**3d**	89
8	**2e**	Reflux, $(CH_2Cl)_2$	—	0
9	**2f**	Reflux, $(CH_2Cl)_2$	—	0
10	**2g**	Reflux, $(CH_2Cl)_2$	—	0
11	**2h**	Reflux, $(CH_2Cl)_2$	**3h**	6

a) Thiophene (20 mmol), acid anhydride (20 mmol), Nafion-H (0.2 g), and solvent (10 ml), 16 h. b) Determined by GLC analysis. c) Acetic acid (20 mmol) was added to the reaction mixture.

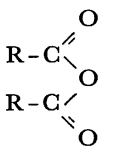

1

R

a: Me
b: Et
c: *n*-Pr
d: Ph

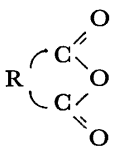

2

-R-

e: 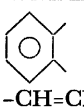
f: -CH=CH-
g: $-(CH_2)_2-$
h: $-(CH_2)_3-$

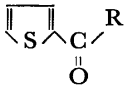

3

R

a: Me
b: Et
c: *n*-Pr
d: Ph
h: $-(CH_2)_3COOH$

Table 2. Repeated use of Nafion-H: acylation of thiophene with acid anhydrides[a)]

Run	Nafion-H (mg)		Acid anhydride	Product	Yield[b)] %
4	Virgin	200	**1b**	**3b**	81
12	Recovered from Run 4	209	**1b**	**3b**	74
13	Recovered from Run 12	225	**1b**	**3b**	52
5	Virgin	200	**1c**	**3c**	94
14	Recovered from Run 5	—[c)]	**1c**	**3c**	78
15	Recovered from Run 14	—[c)]	**1c**	**3c**	70

a) Thiophene (20 mmol), acid anhydride (20 mmol), Nafion-H, and CH_2Cl_2 (10 ml). Reactions were carried out under refluxing for 16 h. b) Determined by GLC analysis. c) Not determined.

tion conditions (Runs 5 and 7), the acylation with **1c** and **1d** catalyzed by Amberlyst 15 gave **3c** and **3d** in 75 and 74% yields respectively. Judging from the yield, the Nafion-H catalyst is superior to the Amberlyst 15 catalyst. We also investigated the stability of Nafion-H under the present reaction conditions. Repeating the reaction of thiophene with propionic anhydride with the recovered catalyst gave the ketone in a somewhat lower yield than that using the original one. (Table 2). The recovered catalyst was black, and its weight increased. The loss of the catalytic activity seems to be ascribable to the adsorption of polymeric materials on the catalyst.

The present procedure offers a convenient method for the preparation of 2-acylthiophenes with an easy work-up. After the removal of the catalyst, the products were obtained by the fractional distillation of the reaction mixture. The yield of **1a** was comparable to that with the standard method.[6)]

Experimental

Catalysts. Nafion-511 resin, as the potassium salt of the fluorocarbon resin sulfonic acid, was obtained from the Mitsui Fluorochemicals Co., Ltd. Nafion-H, the acid form of the resin sulfonic acid, was generated by the treatment of the resin with 15% hydrochloric acid at room temperature for 12 h, followed by washing with deionized water. After the acid-treatment had been repeated four times, the resin was dried under evacuation at 80 °C for 4 h. The dried resin contained 0.80 mequiv. of SO_3H groups per gram of resin. Amberlyst 15 (Rohm & Haas Co.) was dried under a vacuum at 80 °C for 6 h. The ion-exchange capacity of the resin was 2.88 mequiv./g.

Acylation of Thiophene. A mixture of thiophene (20 mmol), acid anhydride (20 mmol), Nafion-H (0.2 g), or Amberlyst 15 (0.06 g), and a solvent (10 ml) was stirred under refluxing for 16 h. The catalyst was then filtered off and washed with dichloromethane. The filtrate was analyzed by gas chromatography. Naphthalene or *p*-di-*t*-butylbenzene was used as the internal standard. The products were identified by means of infrared and ^1H NMR spectroscopies. The recovered catalyst was dried in an air-oven at 105—110 °C for reuse.

Competitive Acylation. A mixture of thiophene (10 mmol), acetic anhydride (10 mmol), propionic anhydride (10 mmol), and Nafion-H (0.1 g) in dichloromethane (5 ml) was stirred at 38 °C for 4 h. The liquid phase was then analyzed by gas chromatography. The relative yield of **3b** to **3a** was 1.56:1. The conversion of propionic anhydride was less than 30% under these conditions.

Competitive acylation with propionic anhydride and butyric anhydride was carried out in a manner similar to that described above. The relative yield of **3c** to **3b** was 1.21:1.

The authors wish to thank the Mitsui Fluorochemicals Co., Ltd., for kindly supplying the Nafion-511 resin.

References

1) J. M. Kapura and B. C. Gates, *Ind. Eng. Chem. Prod. Res. Develop.*, **12**, 62 (1973).
2) G. A. Olah, J. Kapsi, and J. Buhara, *J. Org. Chem.*, **42**, 4187 (1977).
3) G. A. Olah and D. Meider, *Synthesis*, **1978**, 671.
4) G. A. Olah, R. Malhotra, S. C. Narang, and J. A. Olah, *Synthesis*, **1978**, 672.
5) C. U. Pittman, Jr., and Y. F. Liang, *J. Org. Chem.*, **45**, 5048 (1980).
6) A. I. Kosak and H. D. Hartough, *Org. Synth.*, Coll. Vol. III, 14 (1955).

Thermolysis of 6-Hydroxyimino-1,3,5-tri-*t*-butyl-5-methyl-1,3-cyclohexadiene

Renji OKAZAKI,* Masako WATANABE, and Naoki INAMOTO
Department of Chemistry, Faculty of Science, The University of Tokyo, Hongo, Bunkyo-ku, Tokyo 113
(Received May 27, 1981)

Synopsis. Mechanism of the thermolysis of the titile compound has been proposed, which begins with a homolytic cleavage leading to *t*-butyl radical and 2,4-di-*t*-butyl-6-methyl-1-nitrosobenzene. The reaction of the nitrosobenzene with *t*-butyl radical generated from photolysis of 2,2′-dimethyl-2,2′-azopropane is also described.

We have previously reported the photoreaction of cyclohexadienone oxime **1** proceeds *via* α-heterolytic cleavage, a new mode of photoreaction of an oxime.[1] In the present paper, we studied the thermal behavior of **1** and found that **1** underwent a decomposition through a homolytic pathway.

Results and Discussion

Reaction Products. Thermolysis of (*E*)-6-hydroxyimino-1,3,5-tri-*t*-butyl-5-methyl-1,3-cyclohexadiene (**1**) for 30 min at 160—170 °C afforded 2,4-di-*t*-butyl-6-methylaniline (**2**) (39%), 3,5,7-tri-*t*-butyl-2,1-benzisoxazole (**3**) (22%), *N,O*-di-*t*-butyl-*N*-(2,4-di-*t*-butyl-6-methylphenyl)hydroxylamine (**4**) (5%), and *N*-(*t*-butyl)-2,4-di-*t*-butyl-6-methylaniline (**5**) (9%). Identity of the products was established by their spectral and analytical data.

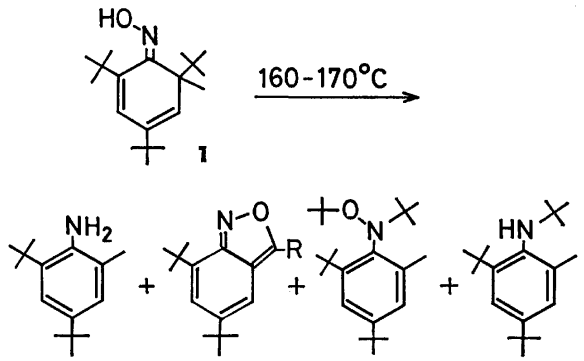

2 **3**: R=*t*-Bu **4** **5**
6: R=H

The structure of **4** was also confirmed by the fact that it was one of the products from the following reaction of 1,5-di-*t*-butyl-3-methyl-2-nitrosobenzene (**7**) with *t*-butyl radical generated from photolysis of 2,2′-dimethyl-2,2′-azopropane. Since the reaction of a nitrosobenzene with radicals is known to give a substituted hydroxylamine[2] or a cyclohexadienone oxime derivative[3,4] depending on the relative bulkiness of the reagents, the formation of the hydroxylamine **4** and the cyclohexadienone oximes **8** is reasonable.

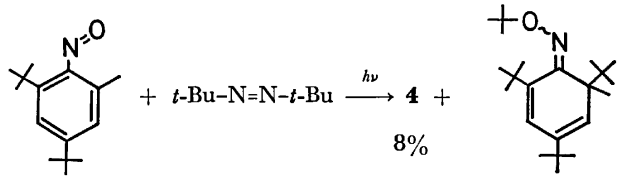

7 **8** 29%

Reaction Mechanism. Formation of **2** and **3** suggests that the nitrosobenzene **7** is formed as an intermediate, because thermal disproportionation of **7** has been reported to afford **2** and 5,7-di-*t*-butyl-2,1-benzisoxazole (**6**).[3]

Since the most reasonable mechanism for the formation of **7** is homolytic cleavage of **1** to give **9**, followed by loss of hydrogen atom, a plausible mechanism for the thermolysis of **1** is considered to be as shown in Scheme 1.[5]

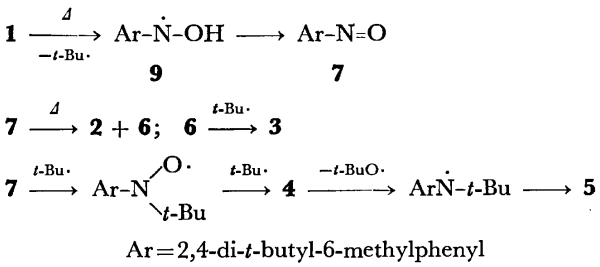

Ar=2,4-di-*t*-butyl-6-methylphenyl

Scheme 1.

Attack of the *t*-butyl radical on **6** affords 3-substituted benzisoxazole **3**, because benzisoxazole is known to undergo a substitution reaction with a radical at the position 3.[3]

Radical attack at the nitroso nitrogen atom of **7** and subsequent reaction of the intermediate nitroxide radical with *t*-butyl radical gave **4**.[2-4] Aniline **5** is probably formed from further thermal reactions of **4** (see Scheme).

It is of interest that the thermolysis proceeds *via* homolysis, contrary to the photolysis which proceeds *via* α-heterolytic cleavage.[1]

Experimental

Thermolysis of Oxime 1. Oxime **1** (400 mg, 1.37 mmol)[6] was kept at 160—170 °C for 30 min in a sealed tube. The reaction mixture was subjected to preparative TLC (silica gel, hexane-dichloromethane (5:1)) to give four fractions. The first fraction afforded 21 mg (5%) of **4** as colorless oil, which was identical with the specimen obtained from the reaction of **7** with *t*-butyl radical (*vide infra*). IR (neat) 1200 cm^{-1} (C–O); NMR (CCl_4) δ 1.06 (9H, s), 1.19 (9H, s), 1.27 (9H, s), 1.52 (9H, s), 2.62 (3H, s), and 6.97 (2H, ABq, J=2.6 Hz, $\Delta\delta$=0.45); MS, *m/e* (rel intensity), 305 ($M^+-C_3H_6$, 2), 291 (3), 235 (7), 219 (16), 204 (66), 188 (8), 57 (78), and 41 (100). The second fraction afforded 80 mg (22%) of **3** as colorless crystals, mp 73—74 °C (CH_3OH). Found: C, 79.56; H, 10.10; N, 4.75%. Calcd for $C_{19}H_{29}NO$: C, 79.39; H, 10.10; N,

4.87%. IR (KBr) 1637, 1560, and 1537 cm^{-1};[3] NMR (CCl_4) δ 1.31 (9H, s), 1.50 (9H, s), 1.59 (9H, s), and 7.13 (2H, ABq, J=1.5 Hz, $\Delta\delta$=0.18); UV_{max} (hexane) 260 (ε 2390), 271.5 (3040), 282.5 (3860), and 317 nm (9520);[3] MS, *m/e* (rel intensity), 287 (M^+, 33), 273 (57), 231 (97), 187 (11), 132 (18), and 57 (100). The third fraction afforded 30 mg (9%) of **5** as pale yellow oily material. IR (neat) 3500 cm^{-1}; NMR (CCl_4) δ 1.21 (9H, s), 1.28 (9H, s), 1.44 (9H, s), 2.32 (3H, s), 3.12 (1H, b), and 6.98 (2H, ABq, J=2.6 Hz, $\Delta\delta$=0.23); UV_{max} (hexane) 248 (ε 5620) and 287 nm (sh, 1590); MS, *m/e* (rel intensity), 275 (M^+, 11), 260 (13), 219 (15), 204 (100), 188 (8), and 57 (28). The fourth fraction afforded 122 mg of yellow oil, which was purified with preparative TLC (silica gel, hexane–dichloromethane (2:3)) to give 107 mg (39%) of **2**, which was identified by comparison with an authentic sample (NMR, MS, and TLC).[7]

Reaction of **7** *with* t-*Butyl Radical.* The nitrosobenzene **7** (235 mg, 1.01 mmol) and 2,2′-dimethyl-2,2′-azopropane (1.49 g, 10.5 mmol) were dissolved in benzene (180 ml), and the solution was irradiated for 1 h at 0—5 °C using a 100 W medium pressure mercury arc filtered through aq. $CuSO_4$ solution to cut off the light below about 340 nm and above 550 nm. Under these conditions, only the azopropane absorbed the light. After the solvent was removed under reduced pressure, the residue was subjected to preparative TLC (silica gel, hexane–dichloromethane (5:1)). The first fraction afforded 206 mg of colorless oily material, which was again subjected to preparative TLC (silica gel, hexane) to give three fractions A, B, and C. Fraction A gave 40 mg of **8** ((*Z*)-form) as white crystals. Fraction B gave 78 mg of colorless oily material, which was subjected to preparative TLC (silica gel, hexane) to afford 39 mg of **8** ((*Z*)-form) and 27 mg (8%) of **4** (by NMR and GLC). Thus the total amount of **8** ((*Z*)-form) was 79 mg (23%). Fraction C afforded 57 mg of colorless oil, which was purified by preparative TLC (silica gel) to give 21 mg (6%) of **8** ((*E*)-form). The configuration of **8** was tentatively assigned by analogy with **1**.[6] **8** ((*Z*)-form): mp 89.0—89.7 °C (CH_3OH). Found: C, 79.75; H, 11.72; N, 3.85%. Calcd for $C_{23}H_{41}NO$: C, 79.48; H, 11.89; N, 4.03%. IR (KBr) 978 and 955 cm^{-1} (NO); NMR (CCl_4) δ 0.78 (9H, s), 1.10 (9H, s), 1.31 (18H, s), 1.55 (3H, s), 5.15 (1H, b, J=2.0 Hz), and 6.08 (1H, d, J=2.0 Hz); UV_{max} (hexane) 264 (sh, ε 2650) and 315 (5630) nm. **8** ((*E*)-form): oil; IR (Nujol) 980 and 960 cm^{-1} (NO); NMR (CCl_4) δ 0.92 (9H, s), 1.09 (9H, s), 1.25 (9H, s), 1.33 (12H, s), 5.37 (1H, d, J=1.5 Hz), and 6.03 (1H, d, J=1.5 Hz); UV_{max} (hexane) 254 (ε 2700) and 308 nm (5420). The second fraction afforded 50 mg (21%) of recovered **7**.

References

1) R. Okazaki, M. Watanabe, and N. Inamoto, *Tetrahedron Lett.*, **1977**, 4515; *Bull. Chem. Soc. Jpn.*, **52**, 175 (1979).

2) *E.g.*, B. A. Gingrass and W. A. Waters, *J. Chem. Soc.*, **1954**, 1920; A. B. Boyd, P. F. Soutern, and W. A. Waters, *ibid.*, **1958**, 2056.

3) T. Hosogai, N. Inamoto, and R. Okazaki, *J. Chem. Soc., C*, **1971**, 3399.

4) *Cf.* S. Terabe and R. Konaka, *J. Chem. Soc., Perkin Trans. 2*, **1973**, 369.

5) The following ionic pathway leading to the nitrosobenzene **7** and the aniline **2** is also possible, but the formation of **3** and **4** (hence **5**) cannot be explained without involvement of *t*-butyl radicals.

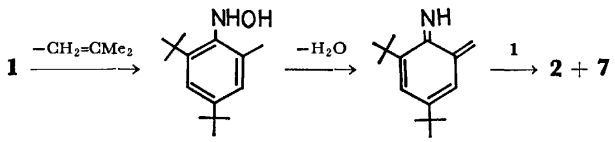

6) Y. Inagaki, R. Okazaki, and N. Inamoto, *Bull. Chem. Soc. Jpn.*, **48**, 621, 3727 (1975).

7) J. Geuze, C. Ruinard, J. Soeterbroek, P. E. Verkade, and B. M. Wepster, *Recl. Trav. Chim. Pays-Bas*, **75**, 301 (1956).

The Enantioface-differentiating Methylation of the *N*-Benzylidene-DL-phenylalanine Methyl Ester in the Presence of Chiral Lithium Amides

Tetsushi YAMASHITA,* Hitoshi MITSUI, Hiroyuki WATANABE, and Nobuo NAKAMURA

Department of Chemistry, Faculty of Science, Osaka City University, Sumiyoshi-ku, Sugimoto-cho, Osaka 558

(Received August 3, 1981)

Synopsis. The asymmetric methylation of the *N*-benzylidene-DL-phenylalanine methyl ester was carried out in the presence of lithium salts of secondary amines derived from (*S*)-proline. The lithium amides of poly(imino-1-isobutylethylene) and its corresponding low-molecular-weight model compound, derived from (*S*)-leucine, were similarly used in order to examine the polymer effects with regard to the stereoselectivity.

Several workers[1-3] have recently used Schiff-base derivatives of α-amino acids in order to prepare the higher amino acids by alkylation routes. Yamada *et al.*[2] have furthermore carried out the diastereoface-differentiating alkylation of Schiff bases derived from chiral ketones and achiral α-amino acid esters in the presence of lithium diisopropylamide, thus obtaining optically active α-amino acids. Duhamel *et al.*[4] have also reported that optically active α-amino acid esters were obtained from the corresponding Schiff bases lithiated with chiral lithium amides, followed by protonation with tartaric acid derivatives.

This paper will describe the enantioface-differentiating methylation of Schiff bases lithiated by the use of chiral lithium salts of secondary amines derived from (*S*)-proline and (*S*)-leucine. The Schiff base (*N*-benzylidene-DL-phenylalanine methyl ester) (**A**) was prepared according to the method of Stork.[1]

The chiral lithium amides used in this experiment are as follows:

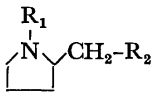

1a R_1=H, R_2=H
1b R_1=Li, R_2=H
2a R_1=H, R_2=N
2c R_1=Li, R_2=N

3a R_1=CH_3, R_2=NHPh
3b R_1=CH_3, R_2=N(Li)Ph
4a R_1=CH_3, R_2=NH

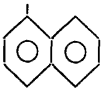

4b R_1=CH_3, R_2=N(Li)

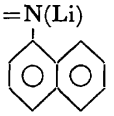

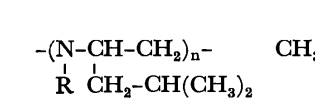

5a R=H **5b** R=Li

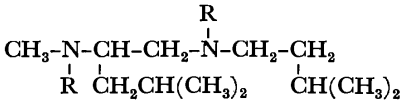

6a R=H **6b** R=Li

The methylation of **A** with methyl iodide in the presence of chiral lithium amides at 0 and −78 °C, followed by hydrolysis and successive acetylation, yielded *N*-acetyl-α-methyl-phenylalanine,[2c] whose optical yields (%) and configurations are shown in Table 1.

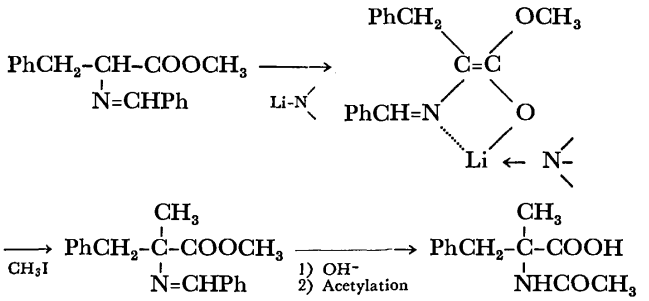

The product for **3b** showed the highest optical yield (31%) at −78 °C. All the amides except **2c** gave the product of the *S*-configuration. In order to examine the polymer effects with respect to the stereoselectivity, polymeric amide (**5b**) and its corresponding low-molecular-weight model compound (**6b**) were similarly used. At −78 °C, the optical yield of the product for **5b** was, albeit low, about six times as high as that for **6b**.

TABLE 1. THE OPTICAL YIELDS AND CONFIGURATIONS OF *N*-ACETYL-α-METHYLPHENYLALANINE OBTAINED WITH CHIRAL AMIDES

Chiral agents	0 °C	−78 °C
1b	1.0(*S*)	1.8(*S*)
2c	1.0(*R*)	2.1(*R*)
3b	6.2(*S*)	31.0(*S*)
4b	1.3(*S*)	1.9(*S*)
5b	6.0(*S*)	13.5(*S*)
6b	1.5(*S*)	2.2(*S*)

Experimental

The Preparation of Chiral Secondary Amines. (*S*)-2-Methylpyrrolidine (**1a**) was prepared by the method of Kostyanovsky.[5] (*S*)-1-(2-Pyrrolidinylmethyl)pyrrolidine (**2a**) (bp 75—80 °C at 4 mmHg,† $[\alpha]_D^{18}$ +9.6° in C_2H_5OH) was obtained by the reduction (sodium in liquid ammonia) of (*S*)-1-[1-tosyl(2-pyrrolidinyl)methyl]pyrrolidine, which had itself been derived from 1-tosyl(2-pyrrolidinyl)methyl iodide (**2b**) and pyrrolidine; **2b** was made by the reaction of (*N,O*-ditosyl) pyrrolidinylmethanol[5] with sodium iodide. (*S*)-1-Methyl-2-(anilinomethyl)pyrrolidine[6] (**3a**) (bp 123—124 °C at 4 mmHg, $[\alpha]_D^{15}$ −59.3° in C_2H_5OH) was obtained by the reduction (lithium aluminium hydride) of *N*(*N*-benzyloxycarbonylprolyl)aniline, which had itself been prepared from *N*-benzyloxycarbonylproline and aniline by the use of 1-ethoxycarbonyl-2-ethoxy-1,2-dihydroquinoline; (*S*)-1-methyl-2-(1-naphthylaminomethyl)pyrrolidine (**4a**) (bp 180—190 °C at 4 mmHg, $[\alpha]_D^{20}$ −5.6° in $CHCl_3$) was obtained

† 1 mmHg≈133.322 Pa.

using *N*-benzyloxycarbonylproline and 1-naphthylamine as starting materials in a manner similar to that described in **3a**. Poly(imino-1-isobutylethylene) (**5a**) and N^1-isopentyl-N^2-methyl-4-methyl-1,2-pentanediamine (**6a**) were derived from (*S*)-leucine according to the procedure reported earlier.[7,8]

The Asymmetric Methylation of ***A*** *with Chiral Lithium Amides.* The methylation with **3b** will be given as an example. To a solution of **3a** (2 mmol) in dry THF (5 ml), we added butyllithium (2 mmol) in hexane at −78 °C under argon. A solution of **A** (2 mmol) in dry THF (1 ml) was then added to the reaction mixture. The color of the solution gradually changed from red-orange to yellow, showing the formation of a lithium ester enolate.[2,3] After 15 min, methyl iodide (2 mmol) was added to the solution at −78 °C, and the mixture was stirred for 1 h. After the subsequent removal of the solvent, ether and water were added to the residue. The organic layer separated out was washed with water, dried, and evaporated to dryness. The methylated Schiff base thus obtained was subjected to hydrolysis without purification. The hydrolysis was carried out in 15 ml of 1 mol dm^{-3} sodium hydroxide solution under reflux for 2 h. The reaction mixture was washed thoroughly with ether and neutralized with 6 mol dm^{-3} hydrochloric acid. On cooling, α-methylphenylalanine precipitated as a white powder; it was then filtered off. Yield, 50%. In order to determine the optical yield and configuration, the amino acid was acetylated with acetic anhydride in pyridine. The rotation of the acetamide was $[\alpha]_D^{15}$ −25° (*c* 2, CH_3OH) (Lit,[2c] optically pure (*R*)-*N*-acetyl-α-methylphenylalanine, $[\alpha]_D^{19}$ +80.3° in CH_3OH). The other lithium amides were similarly used for the methylation of **A**. The amount of polymeric agent (**5b**) was calculated on the basis of that of the monomer used in the polymerization (*e.g.*, 10 mg of **5a** corresponds to 10 mg of (*S*)-2-isobutylaziridine).

The methylation of the *N*-benzylideneglycine ethyl ester (**B**) was also attempted with the chiral amides used for the methylation of **A**. However, all the reagents except (**2c**) yielded a mixture which consisted of mono- and dimethylated **B** and unreacted **B**. The monomethylated **B** obtained with **2c** was hydrolyzed in 1 mol dm^{-3} hydrochloric acid to give (*S*)-alanine in a 13% (10%) optical yield at −78 °C (0 °C).

In this experiment, a JASCO DIP-4 automatic polarimeter was used for the measurement of the optical rotation.

References

1) G. Stork, A. Y. M. Leong, and A. M. Touzin, *J. Org. Chem.*, **41**, 3491 (1976).

2) a) S. Yamada, T. Oguri, and T. Shioiri, *J. Chem. Soc., Chem. Commun.*, **1976**, 136; b) T. Oguri, T. Shioiri, and S. Yamada, *Chem. Pharm. Bull.*, **25**, 2287 (1977); c) S, Terashima, K. Achiwa, and S. Yamada, *ibid.*, **14**, 1138 (1966).

3) J. J. Fitt and H. W. Gschwend, *J. Org. Chem.*, **42**, 2639 (1977).

4) L. Duhamel and J. C. Plaquevent, *Tetrahedron Lett.*, **21**, 2521 (1980).

5) R. G. Kostyanovsky, I. M. Gella, V. I. Markov, and Z. E. Samojlova, *Tetrahedron*, **30**, 39 (1974).

6) T. Mukaiyama, Y. Sakito, and M. Asami, *Chem. Lett.*, **1978**, 1253.

7) S. Tsuboyama, *Bull. Chem. Soc. Jpn.*, **35**, 1004 (1962).

8) T. Yamashita, H. Mitsui, H. Watanabe, and N. Nakamura, *Makromol. Chem.*, **181**, 2563 (1980).

The Influence of Additives on the Decomposition of an Alkaline Manganate(VII) Solution

Eiichi NARITA,* Tatsuhiko HASHIMOTO, Sakae YOSHIDA, and Taijiro OKABE
Department of Applied Chemistry, Faculty of Engineering, Tohoku University, Aramaki, Sendai 980
(Received July 31, 1981)

Synopsis. The decomposition of manganate(VII) in an alkaline solution was significantly enhanced by the addition of hydrous manganese(IV) oxide or metal ions, such as Ni(II) and Co(II). On the other hand, the inhibitive effect of the tellurate(VI) ion on the decomposition was found even in the presence of the additives described above.

The decomposition of manganate(VII) in alkaline solutions, which yields manganate(VI) and oxygen, has been extensively studied and has been shown to be complex. It is well-known that the rate of the decomposition increases with increases in the temperature and alkali concentration.[1,2] In addition, some workers have shown that the decomposition is a function of the surface area of glass[1,3] and the presence of metal oxides, such as MnO_2, SnO_2, and PbO_2.[1,4] Till recently, it has been thought that the decomposition of manganate(VII) in alkaline solutions could be explained by the oxidation of the OH^- ion by manganate(VII) to $OH\cdot$ radicals, which afterwards react to produce oxygen.[1,2,5] However, Vepřek-Šiška and Ettel[6] have recently shown that the kinetic analysis of the earlier workers is invalid because of the presence of traces of Ni(II) and Co(II) ions in the solution, those ions actively assist the decomposition.

Recently some new industrial techniques utilizing a high oxidation potential of manganates have been developed in the field of pollution control. The present authors have also developed the removal of nitrogen oxides from waste gas by using alkaline manganates(VI and VII) solutions.[7] In the course of this development, further information about the decomposition of alkaline manganate(VII) solution was necessary.

This study will deal with the stimulative effect of various kinds of hydrous manganese(IV) oxides (abbreviated as hydrous MnO_2) and of nickel and cobalt ions, and the inhibitive effect by the tellurate(VI) ion on the decomposition of manganate(VII) in an alkaline solution.

Experimental

A 0.5-dm^3 four-necked flask equipped with a reflux condenser, a thermometer, and a stirrer was used as the reaction vessel. Potassium hydroxide was dissolved in distilled water. Then, the concentrated solution of potassium manganate(VII) was added to the alkali solution and the total volume of the reaction solution was immediately adjusted to 200 cm^3 with distilled water. The additives, such as hydrous MnO_2 and metal sulfates, were added, together with distilled water, at the end. At all times the solution was vigorously stirred. The basic conditions were: $KMnO_4$; 0.05 mol dm^{-3}, KOH; 6 mol dm^{-3}, temperature; 80 °C. All the reagents used were commercial, extra pure reagents, and they were used without further purification. The decomposition of manganate(VII) was determined by pipetting 5 cm^3 of the reaction solution from the flask at regular time intervals, filtering out the insoluble matter, and chemically analyzing the manganates(VI and VII) in the filtrate.[8] The analysis of the chemical composition of the insoluble matter was done in the manner previously reported.[9] The amount of the tellurate(VI) ion adsorbed by the hydrous MnO_2 was calculated from the tellurate(VI) ion concentrations in the solution before and after the adsorption was affected. The tellurate(VI) ion was analyzed according to the method of Kishioka *et al.*[10]

Results and Discussion

Stimulative Effect of Hydrous MnO_2 and Ni(II), Co(II) Ions. The decomposition of manganate(VII) in alkaline solutions is well-known to be accelerated by the presence of manganese(IV) oxide, but there remains a lack of understanding of the relationship between this effect and the chemical composition of the manganese(IV) oxide. In this study, several kinds of hydrous MnO_2 (shown in Table 1) were prepared, and their stimulative effects on the decomposition (Eq. 1) were investigated by the addition of 0.05—

$$4MnO_4^- + 4OH^- = 4MnO_4^{2-} + O_2 + H_2O \quad (1)$$

0.06 g (5×10^{-4} mol Mn) of the hydrous MnO_2 to the alkaline manganate(VII) solution. The hydrous MnO_2 substances are amorphous, and their surface areas range from 140 to 160 $m^2\,g^{-1}$. The results given in Fig. 1 show that the stimulative effect of the hydrous MnO_2 increased with an increase in the content of MnO_2. That is, the hydrous MnO_2 with many manganese atoms on its surface became effective in stimulative action. The significant stimulative effect of the hydrous MnO_2 could be similarly explained by the electron-transfer mechanism proposed by Vepřek-Šiška and Ettel,[6] which was previously used to explain the stimulative effect of transition metal ions.

Figure 2 shows the stimulative effect of Ni(II) and Co(II) ions in concentrations of 2.5×10^{-3} mol dm^{-3}

TABLE 1. CHEMICAL COMPOSITION OF THE MANGANESE(IV) OXIDES USED IN THE EXPERIMENTS

MnO_2 sample No.	pH of formation	Composition			
		x in MnO_x	MnO_2 (wt%)	K_2O (wt%)	H_2O (wt%)
1[a]	8.1	2.00	68.4	16.4	15.2
2[a]	4.2	1.94	80.7	8.4	10.9
3[a]	3.2	1.92	83.2	7.7	9.1
4[b]	<1	1.90	86.5	5.2	8.3

a) Disproportionation of 0.6 mol dm^{-3} K_2MnO_4 solution by the addition of 1 mol dm^{-3} H_2SO_4. b) 0.5 mol dm^{-3} H_2SO_4 treatment of Sample No. 1.

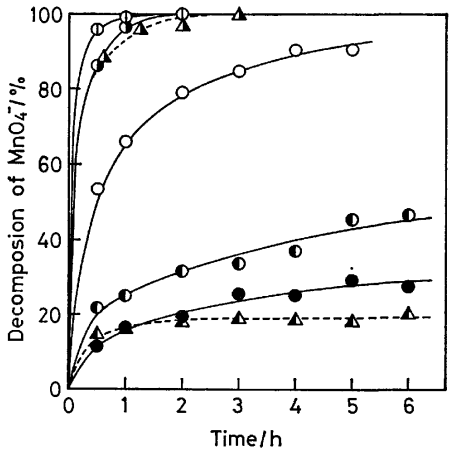

Fig. 1. Effect of several kinds of hydrous manganese (IV) oxides on the decomposition of manganate(VII).

MnO_2 sample No.	TeO_4^{2-} none	TeO_4^{2-} addition
none	●	—
1	◐	◭
2	○	—
3	◑	◭
4	◌	—

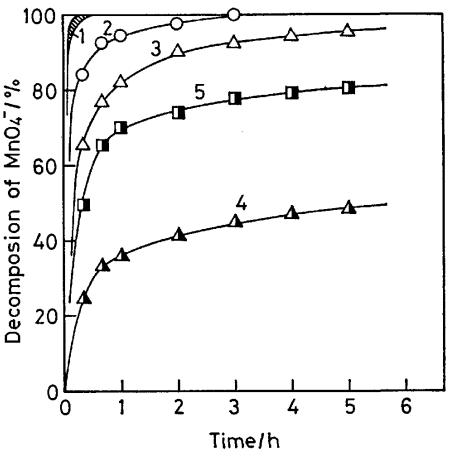

Fig. 2. Effect of metal ions on the decomposition of manganate(VII).
1: Ni^{2+}, Co^{2+}, oxides (Sample Nos. 1 and 3 in Table 1), 2: $Ni(OH)_2$, 3: Ni^{2+} and TeO_4^{2-},
4: Ni^{2+} } MnO_4^- was finally added after sufficient
5: Co^{2+} } mixing of hydroxide suspension containing TeO_4^{2-}.

on the decomposition. It was found that the decomposition was markedly accelarated by the addition of these ions; this agreed well with the result obtained by Vepřek-Šiška and Ettel.[6] Therefore, the resulting precipitates obtained after the decomposition was analyzed here. The results indicate these precipitates were peroxides with a higher oxidation state than trivalent, having potassium and chemically bonded water (*e.g.*, $0.17K_2O \cdot NiO_{1.98} \cdot 2.30H_2O$; $0.04K_2O \cdot CoO_{1.71} \cdot 1.45H_2O$).

Inhibitive Effect of the Tellurate(VI) Ion. According to Issa *et al.*,[11] the inhibitive effect of the tellurate(VI) ion could be explained by the mechanism that the manganese(IV) ion formed by the decomposition of manganate(VII) forms a complex with the tellurate(VI) ion prior to precipitation as MnO_2 and before the stimulation action becomes effective. On the other hand, another mechanism, in which the inhibitive effect is caused by the adsorption of the tellurate(VI) ion on the surface of the metal oxide originating from the impurities in the reagent and on the reaction vessel wall, was also observed in this preliminary experiment.

Figure 1 shows the inhibitive effect of the tellurate(VI) ion on the decomposition in the presence of the hydrous MnO_2 (1 and 3). It was found that the tellurate(VI) ion exhibited a remarkable inhibitive effect on the hydrous MnO_2(1), but not on the hydrous MnO_2(3). The adsorption data of the tellurate(VI) ion on the hydrous MnO_2 obtained under the same conditions as that of the decomposition except that no manganate(VII) ion was present were as follows: hydrous MnO_2(1)—3.85×10^{-4}, (3)—1.96×10^{-4} mol Te(VI) adsorbed/g. The results show that the hydrous MnO_2(1), with a large amount of potassium, adsorbed more of the tellurate(VI) ion than did the hydrous MnO_2(3).[12] This tendency was correlated to the results of the decomposition experiments. These results indicate that the tellurate(VI) ion becomes effectively inhibiting by its adsorption on the surface of the hydrous MnO_2.

Figure 2 shows the similar inhibitive effect of the tellurate(VI) ion on the decomposition in the presence of Ni(II) and Co(II) ions. On changing the addition order of the reagents, namely, by adding the manganate(VII) after a sufficient contact of Ni(II) and Co(II) hydroxides with the tellurate(VI) solution, the inhibitive effect remarkably increased. The inhibitive effect of the tellurate(VI) ion in the presence of the cobalt precipitate was smaller than that in the presence of the nickel precipitate. It was thought to depend upon the small content of potassium in the cobalt precipitate, which caused the less adsorption of the tellurate(VI) ion on it.

References

1) F. R. Duke, *J. Am. Chem. Soc.*, **72**, 3975 (1948).
2) M. C. R. Symons, *J. Chem. Soc.*, **1953**, 3956.
3) M. J. Cotton, *Chem. Ind. (London)*, **1954**, 433.
4) F. R. Duke, *J. Phys. Chem.*, **56**, 882 (1952).
5) R. Landsberg and R. Thiele, *Z. Phys. Chem.*, **221**, 211 (1962).
6) J. Vepřek-Šiška and V. Ettel, *J. Inorg. Nucl. Chem.*, **31**, 729 (1969).
7) A. Obuchi, A. Okuwaki, and T. Okabe, *Nippon Kagaku Kaishi*, **1974**, 1425; T. Okabe, A. Okuwaki, and S. Nakabayashi, U. S. Patents 3929966 (1975); 4001372 (1977), *etc.*
8) E. Narita, J. Goto, T. Imai, and T. Okabe, *Nippon Kagaku Kaishi*, **1980**, 1830.
9) E. Narita and T. Okabe, *Bull. Chem. Soc. Jpn.*, **53**, 525 (1980).
10) A. Kishioka, I. Iwasaki, and Y. Yoshida, *Nippon Kagaku Zasshi*, **85**, 647 (1964).
11) I. M. Issa, S. E. Khalafalla, and R. M. Issa, *J. Am. Chem. Soc.*, **77**, 5503 (1955).
12) E. Narita and T. Okabe, *Bull. Chem. Soc. Jpn.*, **54**, 1251 (1981).

 © 1982 The Chemical Society of Japan Bull. Chem. Soc. Jpn., 55, 965—970 (1982)

Hydrothermally Activated Silica-Alumina. II. Variations in Catalytic Activities for 1-Butene Isomerization and Polymerization, and in the Amount of Acid with Pretreatment Temperature

Shozo FURUYAMA,* Osamu MURASHITA,** Kotomasa ICHISAKA,*** and Tetsuo MORIMOTO

Department of Chemistry, Faculty of Science, Okayama University, Tsushima, Okayama 700

(Received February 27, 1981)

The technique of hydrothermal activation was used to prepare well-mixed and fully hydroxylated silica-alumina catalysts, SA-*n*MHT ($n=13$, 25, or 50 denotes the alumina content (wt%)). Their catalytic activities and *cis*/*trans* selectivities for the 1-butene isomerization (k_i and c/t), the catalytic activities for the 1-butne polymerization (k_p), the amount of acid (A), and the number of the surface hydroxyl group (N_{OH}) were measured as a function of the degassing temperature (T_d) over the 25—700 °C range; the following results were obtained: (1) k_i changed prominently with T_d and reached its maximum around 300 °C. (2) c/t was about 0.9 below 500 °C, but exceeded 1.2 at 700 °C. (3) k_p increased till 300 °C and became constant above that temperature. (4) A was almost independent of T_d above 100 °C. (5) N_{OH} decreased from 11—15 (at 100 °C) to 0.5 group nm^{-2} (at 700 °C). An analysis of these data led to the conclusion that the SA-*n*MHT sample underwent the surface structural changes three times during the thermal dehydroxylation between 25 and 700 °C. The sequence of the structural change was sketched, and the different dependencies upon T_d of k_i, k_p, and A were explained.

Silica–alumina is a strong solid acid and is widely used as a catalyst for various reactions. From the similarities to zeolite in composition, acidic nature, and other aspects, it has been established that the acid center (*i.e.*, the catalytic active site) of silica–alumina originates from the isomorphic replacement of a silicon atom by an aluminium atom in the tetrahedral silicate network.[1-3] To obtain a catalyst with a high acidity and catalytic activity, one must devise a method to complete the isomorphic substitution.

In the previous studies, we developed the technique of hydrothermal activation to prepare a well-mixed and fully hydroxylated silica–alumina catalyst.[4] The relationships between the catalytic activity for the 1-butene isomerization, the amount of acid, and the amount and distribution of the aluminium atom were then investigated on the catalyst.[4]

In the present study, the dependencies upon the degassing temperature of the catalytic activities for the 1-butene isomerization and polymerization, the amount of acid, and the number of the surface hydroxyl group were measured on a hydrothermally activated silica–alumina catalyst. The sequence of the surface structural changes with the dehydroxylation is depicted to explain those dependencies.

Experimental

Materials. Three kinds of silica–alumina SA-*n*M ($n=$ 13, 25, or 50 denotes the alumina content (wt%)) samples were synthesized from purified tetraethyl silicate and aluminium isoproxide as has been described elsewhere.[4] Three kinds of hydrothermally activated silica–alumina SA-*n*MHT samples were prepared by heating the corresponding SA-*n*Ms in hot water in Pyrex ampoules at 110 °C for 14 d.[4] A commercial catalyst, SA-C (FCC high alumina (25 wt%) supplied by the Shokubai Kasei Co., Ltd.) was also used for comparison. The BET (N_2) surface areas of those samples were almost independent of the degassing temperature, T_d, till 700 °C. They were 340, 280, and 310 m^2 g^{-1} for the 13, 25, and 50 MHT samples; 550, 500, and 430 m^2 g^{-1} for the 13, 25, and 50 M samples, and 280 m^2 g^{-1} for the SA-C sample, respectively. Dicinnamylideneacetone was used without further purification. The Hammet (H_0) value of the acid center determined by this indicator is equal to or lower than -3.0; *i.e.* the acid strength of the acid center is equivalent to, or higher than, that of 48 wt% of sulfuric acid.[5]

Apparatus and Procedure. The apparatus and procedures used to measure the catalytic activity for the isomerization and the amount of acid were conventional ones which have been described elsewhere.[4,6,7] To measure the catalytic activity for the polymerization, the catalyst (0.15 g) was placed in an adsorption cell (240 cm^3) and degassed at 25—700 °C for 4 h. Butene gas (16×10^3 Pa$=$120 Torr) was then introduced into the cell maintained at 0 °C, and the drop in pressure of the reacting gas was followed to determine the amount of the butene adsorbed and polymerized. After a certain period, the reacting gas was withdrawn from the adsorption cell into a trap (kept at 77 K). The amount of butene gas which could not be recovered from the catalyst surface was defined as the amount of the butene polymer. The number of the surface hydroxyl group was determined by the successive-ignition loss method.[8]

Results

Isomerization. The apparent rate constant for the conversion of 1-butene to 2-butenes, k_i/min^{-1}(g-catalyst)$^{-1}$, was determined at 0 °C by applying the usual equation for the first-order reaction.[4] The k_i *vs.* T_d curve, plotted in Fig. 1, shows that the maximum activity k_i(max) was obtained around 300 °C in the cases of the 13MHT, 25MHT, and C samples, while it appeared around 320—350 °C in the cases of 50MHT and three kinds of M samples. The appearance of the maximum activity around 300—350 °C accords well with the results obtained by other laboratories.[9-11] The value of k_i(max) of the MHT sample was about 3—4 times as large as that of the corresponding M samples. The position and magnitude of the k_i(max) of the SA-C were almost the same as those of the 25MHT, but its k_i *vs.* T_d curve obviously differed from that of the

** Present address: Scientific Investigation Research Laboratory, Hyogo Prefectural Police, Ikuta-ku, Kobe 650.

*** Present address: Research Laboratory, Sato Special Oil Co. Ltd., Joto-ku, Osaka 536.

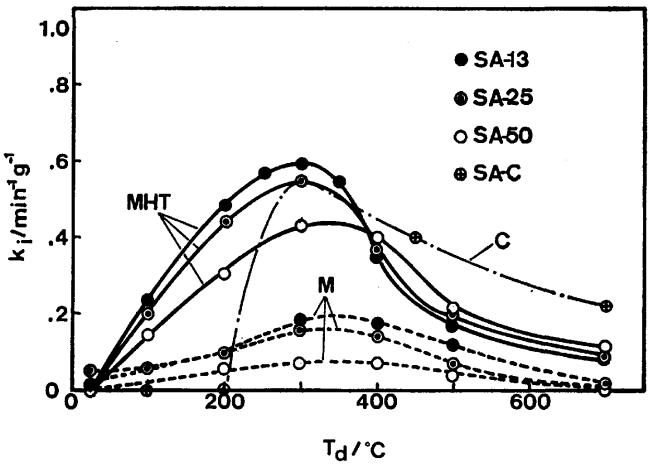

Fig. 1. Variation of apparent rate constant for 1-butene isomerization (k_i) at 0 °C with degassing temperature (T_d).

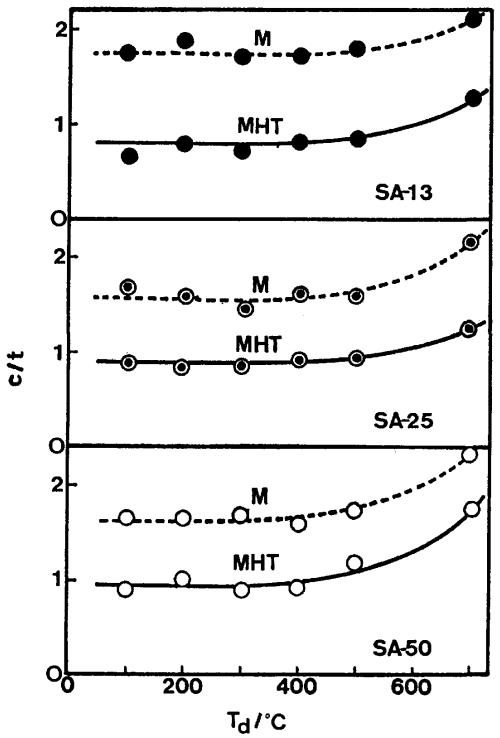

Fig. 2. Variation of c/t ratio for 1-butene isomerization at 0 °C with degassing temperature (T_d).

25MHT.

The value of the selectivity to form *cis*-2-butene against *trans*-2-butene, c/t, was measured at a 10% conversion point; it is plotted against T_d in Fig. 2. The values of the MHT samples fell in a range of 0.8—1.0, while those of the M samples ranged from 1.6 to 1.8 when degassed below 500 °C. The c/t ratio started to increase when degassed at 500 °C and reached about 1.5 and 2.0 at 700 °C in the cases of the MHT and M samples respectively. The increase in the c/t with the increase in T_d above 500 °C was also observed by Gerberich and Hall.[10]

The appearance of the k_i(max) around 300 °C and the increase in the c/t ratio from 500 °C suggest that the

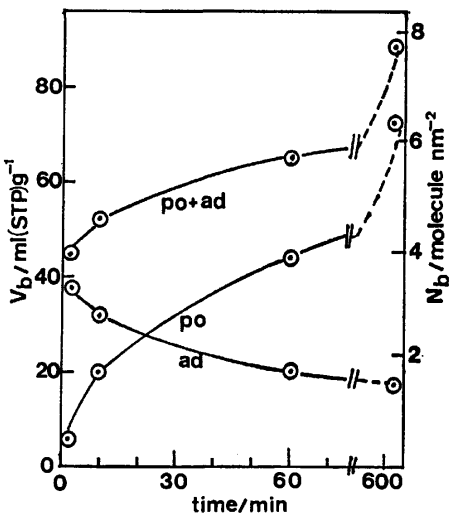

Fig. 3. Variation of amount of butene gas (V_b or N_b) adsorbed (ad) and/or polymerized (po) at 0 °C with contact time. Sample: SA-C degassed at 300 °C.

structure of the catalytic active site of the silica–alumina changed around these temperatures. This will be discussed later.

The dependency upon T_d of the c/t ratio of the SA-C was almost the same as that of the SA-25MHT.

Polymerization. The amounts of butene gas adsorbed and polymerized were measured at 0 °C as a function of the contact period. An example (measured on the SA-C sample degassed at 300 °C) is shown in Fig. 3. It can be seen in Fig. 3 that the adsorption was completed almost instantaneously, while the polymerization proceeded gradually, much slower than the isomeri-

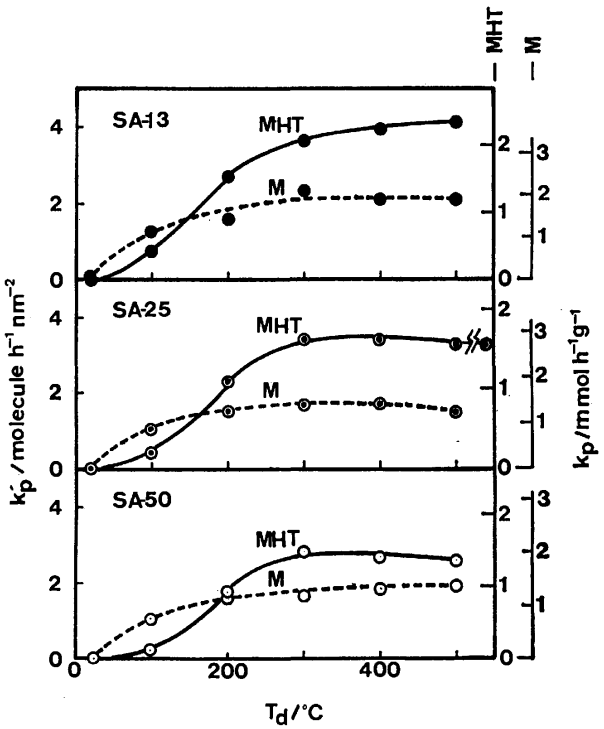

Fig. 4. Variation of amount of butene gas polymerized at 0 °C for 1 h (k_p or k_p') with degassing temperature (T_d).

zation. The amount of gas instantaneously adsorbed was almost 4 molecule nm^{-2}, irrespective of the sample and the degassing temperature. It was concluded that the rapid adsorption was probably a kind of physisorption and had no relation with the isomerization.

The amount of the butene polymer was quite small at first, but reached 4 and 7 molecule nm^{-2} at 1 and 10 h after the reaction started. The amount of butene polymerized in the first 1 h was designated as k_p/mmol h^{-1} g^{-1} or k_p'/molecule h^{-1} nm^{-2}; it is plotted against T_d in Fig. 4. The k_p value increased with the increase in T_d till 300 °C in the cases of the MHT samples and till 200 °C in the cases of M samples, and became almost constant above these temperatures. The k_p value of the MHT sample was smaller than that of the corresponding M samples at lower temperatures, but their values became almost comparable with each other at higher temperatures. These trends clearly differed from the trends observed in the k_i value.

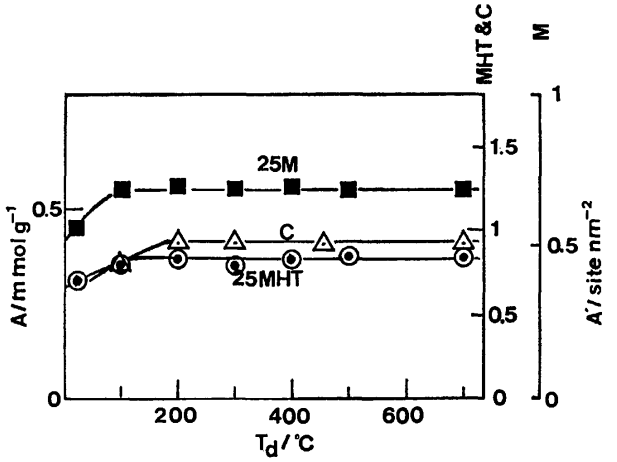

Fig. 5. Variation of acid amount (A or A') with degassing temperature (T_d).

Amount of Acid. The amount of acid, A/mmol^{-1} g^{-1} (or the number of the acid center designated as A'/site nm^{-2}), was measured as a function of T_d, as is shown in Fig. 5. Figure 5 shows that the A value became almost independent of T_d when degassed above 100 °C. Even the value obtained at 25 °C did not differ much from the saturation value. The shape of A *vs.* T_d curve clearly differed not only from the shape of the k_i *vs.* T_d curve, but also from the shape of the k_i *vs.* T_d curve.

The preceding study revealed that the number of the acid center corresponded to the number of the Al atom exposed on the catalyst surface.[4] The value shown in Fig. 5 indicates that almost 0.7—1 molecule nm^{-2} of the Al atom is exposed on the surface of silica-alumina containing 25 wt% of alumina.

Surface Hydroxyl Group. The number of the surface hydroxyl group, N_{OH}, was measured as a function of T_d; it is plotted in Fig. 6. Figure 6 shows that the N_{OH} values of the MHT and C samples were larger than 11 group nm^{-2}, while those of the M samples ranged from 4 to 6 group nm^{-2}, before the heat treatment. It is clear that the surfaces of the MHT and C samples were fully hydroxylated, while those of the M

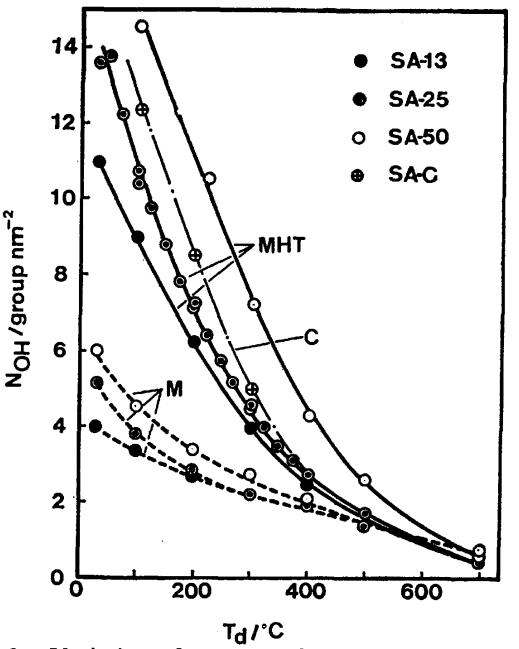

Fig. 6. Variation of number of hydroxyl group (N_{OH}) with degassing temperature (T_d).

samples were only partially hydroxylated. The N_{OH} value decreased with the increase in T_d and became 1/2—1/3, as small as the initial value, when degassed at 300 °C and nearly 1 group nm^{-2} at 600 °C. These values are very suggestive and will later be used to elucidate the sequence of the surface structural change.

Discussion

It was revealed by the present study that the k_i (including c/t ratio), k_i, and A values of the hydrothermally activated silica-alumina are different functions of T_d (and therefore, of N_{OH}), as is shown in Fig. 7. The k_i value varies with T_d very prominently, while the k_p value changes less prominently. The A is almost independent of T_d. These different dependencies upon T_d are very interesting; the causes must be elucidated in the present discussion. A complete set of data for k_i, c/t, k_p, A, and N_{OH} were obtained for the SA-25MHT

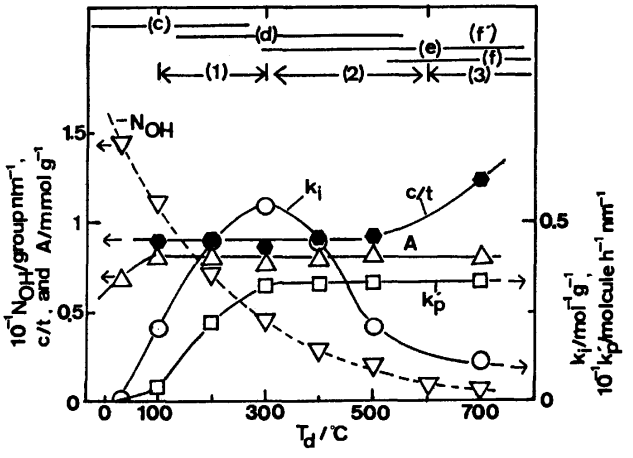

Fig. 7. Dependencies upon T_d of k_i, c/t, k_p', A, and N_{OH} of SA-25MHT sample.

sample. They are used for the explanation. Let us start with the simplest function, A.

The k_i *vs.* T_d curve, when combined with the c/t *vs.* T_d curve, suggests that the surface structure of the SA-25MHT changes three times during the dehydroxylation between 100 and 700 °C. These structural changes are characterized, respectively, by: (1) an increasing k_i value with a constant c/t ratio ≈ 1 between 100 and 300 °C, (2) a decreasing k_i value with a constant c/t ratio ≈ 1 between 300 and 600 °C, and (3) a decreasing k_i value with an increasing c/t ratio >1 above 600 °C. The N_{OH} values of SA-25MHT degassed at 100, 300, 600, and 700 °C are 10.5, 4.5, 1, and 0.5 group nm^{-2} respectively. Therefore, we designate the surface degassed at those temperatures as a highly hydroxylated surface (c), a partially dehydroxylated surface (d), a highly dehydroxylated surface (e), and an extremely dehydroxylated surface (f'), respectively (see Fig. 7).

The accumulated data show that the value of the monolayer capacity of the surface hydroxyl group of various metal oxides falls around 4—8 group nm^{-2}.[12] This implies that the (c) contains the hydronium cation, H_3O^+, as the main acid source. On the other hand, since the A value of the SA-25MHT is 0.8 site nm^{-2}, about 40% of the acid center on the (f') must be of the Lewis-type (*i.e.*, an acid center having no proton, but a vacant orbital). The acid centers on the (d) and (e), therefore, are of the Bronsted-type (*i.e.*, an acid center having either a free proton or an acidic silanol (>SiOH Al<)).

The finding that the A value is almost independent of T_d above 100 °C, simply indicates that the acid strength of all the four structures including the (c) is equivalent to, or higher than, that of 48 wt% sulfuric acid. This conclusion is not surprising, because there must be no free proton, but a hydrated proton, in 48 wt% sulfuric acid.

We will explain the k_p *vs.* T_d curve next. Figure 7 shows that the temperature range of the increasing k_p accords to the temperature range of the surface structural change (c)→(d). This implies that only the (c) is inactive for the polymerization. This can be explained as follows. The butene polymerization may proceed through the cationic polymerization mechanism. Therefore, it is the acid strength which determines the magnitude of the k_p value. Since the acid source of the (c) is the hydronium cation, its acid strength must be much lower than those of (d), (e), and (f') (although they are all equivalent to, or higher than, that of 48 wt% sulfuric acid). This results in the increasing k_p value between 100 and 300 °C. On the other hand, the (d), (e), and (f') possess either a free proton, an acidic silanol, or a vacant orbital; their acid strengths are thus all strong enough to catalyze the polymerization equally. Therefore, the k_p value becomes almost constant above 300 °C. To elucidate how much the acid strength of the (c) differs from those of other structures, anthraquinone ($pK_a = -8.0$) and 4-nitro-toluene ($pK_a = -10.5$) were used.[13] No clear conclusion was obtained, however.

Figure 7 also shows that the k_i values of the (c), (e), and (f') are all much smaller than that of the (d). The reason for the smaller k_i values of the (c) and (f') compared to that of the (d) can easily be explained.

A number of mechanisms have hitherto been proposed for the 1-butene isomerization catalyzed by silica–alumina. Now it is widely accepted that the isomerization proceeds through the intermolecular hydrogen-exchange (IHE) mechanism (*s*-butyl cation intermediate mechanism) on a silica–alumina catalyst.[9-11,14-16] However, a part of the isomerization proceeds through the intramolecular mechanism on the extremely dehydroxylated silica–alumina.[10] According to the IHE mechanism, the transfer of a proton from the acid center to the α-carbon of 1-butene to form the *s*-butyl cation (*i.e.*, proton donation) occurs first. Then a different proton is transferred from the β-carbon of the *s*-butyl cation to the acid center to produce 2-butene (*i.e.*, proton acception). The reason why the c/t ratio becomes nearly unity with the IHE mechanism, but exceeds unity with the intramolecular mechanism, has already been elucidated.[10] From the knowledge about the two mechanisms, we can explain the variations in the k_i and c/t ratio with T_d between 100 and 300 °C, and above 600 °C, as follows.

The acid source of the (c) is the hydronium cation, while that of the (d) is either the free proton or acidic silanol. The acid strength, *i.e.*, the ability of proton donation, of the (d) is much larger than that of the (c). Therefore, the intermolecular hydrogen-exchange reaction proceeds much faster on the (d) than on the (c), resulting in an increase in the k_i value with the constant $c/t \approx 1$ between 100 and 300 °C.

Since the (f') contains a Lewis-type acid center (about 40%), a part of the isomerization proceeds through the intramolecular mechanism. The decrease in the k_i value with the increase in the c/t ratio above 600 °C originates from the slow intramolecular hydrogen shift.

The reason for the decrease in the k_i value with the constant c/t ratio ≈ 1 between 300 and 600 °C is not easily explanable, because both (d) and (e) possess the same number of the Brønsted-type acid centers. To elucidate the reason, we will examine the structural difference between the (d) and (e) in more detail.

Silica glass displays a diffused X-ray diffraction pattern which provides bond parameters close to those obtained from cristobalite.[17] Silica gel and silica–alumina also show a very diffused diffraction peak around $2\theta(\text{Cu } K\alpha) = 22°$, where β-cristobalite shows the most intense peak.[18,19] From these facts, it is widely accepted that the structures of amorphous silica and silica–alumina may be similar to that of β-cristobalite.[3] A crystallographic examination shows that the (100), (110), and (111) planes of β-cristobalite contain about 4, 7, and 4.7 Si atoms per one nm^2 respectively.[20] It is a well-established theory that the plane containing the least number of atoms develops most (Bravais's law[21]). Therefore, it may be reasonable to approximate the surface of SA-25MHT to the (100) plane of β-cristobalite, which is shown in Fig. 8. As can be seen in Fig. 8, the Si (and Al) atom is disposed in an array of "OSiO··· OSiO" linear lines, the spacing of which is about 0.5 nm. Since this spacing is wide enough to prevent interaction between the different lines, we can depict the two-dimensional surface one-dimensionally as in Fig. 9.

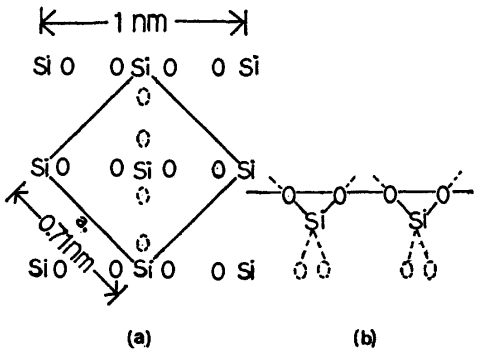

Fig. 8. A schematic representation of surface structure of silica–alumina assumed as the same as surface structure of (100) plane of β-cristobalite. (a): Perpendicular view, (b): horizontal view.

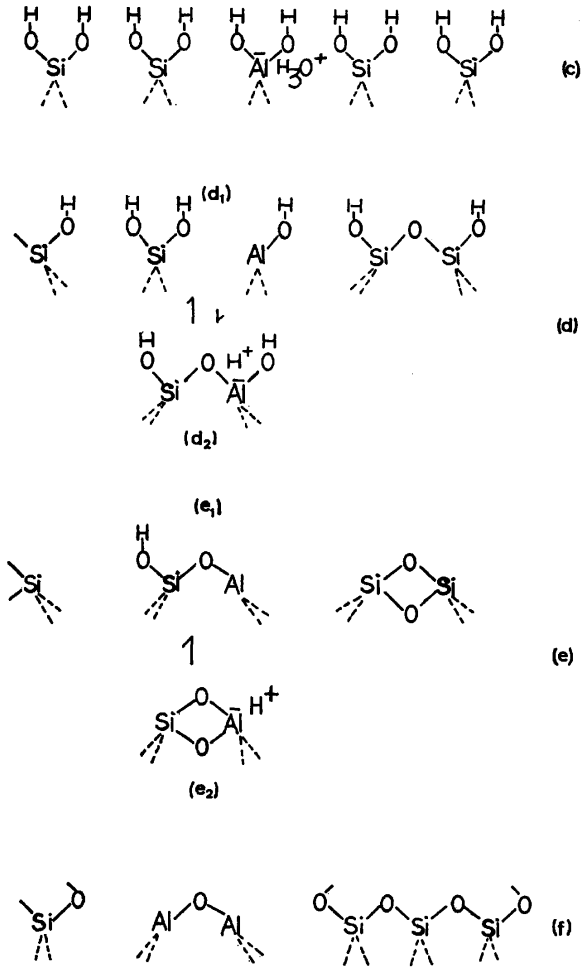

Fig. 9. One-dimensional schematic display of silica–alumina surface at different hydroxylation level. (c): Full hydroxylation (around 100 °C), (d): partial dehydroxylation (around 300 °C), (e): high dehydroxylation (around 600 °C), and (f): complete dehydroxylation (above 600 °C).

Since the acid amount of SA-25MHT is about 0.8 site nm^{-2}, we will set the Al/Si ratio as 1/4 in Fig. 9.

Figure 9 shows that the surfaces of full hydroxylation (c), partially dehydroxylation (d), and high dehydroxylation (e) contain 10.4, 4.8, and 0.8 OH group per one nm^2 respectively. These values coincide with the values of the N_{OH}/group nm^{-2} of 10.5, 4.5, and 1 obtained at 100, 300, and 600 °C. It can thus be concluded that the SA-25MHT takes surface structures like (c), (d), and (e) when degassed at 100, 300, and 600 °C respectively. To eliminate the last proton from the surface, two Al atoms must be paired. To bring about this situation, the surface network must be rearranged greatly. Only a temperature beyond 600 °C can give rise to this rearrangement, resulting in the (f). It must be noticed that the (c), (d), and (e) designations above corespond exactly to the earlier designations, while the (f) does not correspond to the (f'). The (f') consists of 40% of the (f) and 60% of the (e).

When we examine Fig. 9 carefully, we notice that the two M (M=Si or Al) atoms must approach each other to give rise to the structural change (c)→(d). This, in turn, limits the occurrence of the successive dehydroxylation to only the dehydroxylation between the paired M atoms, resulting in the structure of (e) being more strained than that of (d). In general, the surface strain increases with the increase in T_d.[22] This increasing strain may be responsible for the lower k_i value of the structure (e) than that of (d). The following is one possible explanation.

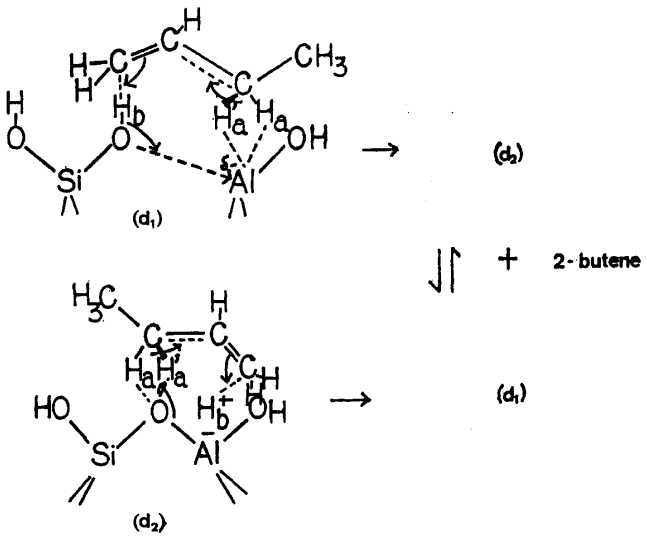

Fig. 10. A schematic representation of intermolecular hydrogen exchange between acid center and butene on the (d_1) and (d_2).

When we compare the structures of (e_1) and (e_2) (the two modifications of the (e)) with each other, we notice that the (e_2) is much more strained and, therefore, thermodynamically much more unstable than the (e_1). Therefore, the mutual transformation between (e_1) and (e_2) is extremely difficult, while the mutual transformation (d_1)⇄(d_2) is easy. As can be seen in Fig. 10, the intermolecular hydrogen exchange can proceed very smoothly (but not necessarily concertedly) on the (d) by using the (d_1)⇄(d_2) transformation. On the other hand, because of the extreme difficulty of the (e_1) ⇄(e_2) transformation, the intermolecular hydrogen exchange does not occur smoothly on the (e). This results in k_i value of the (e) being smaller than that of the (d).

Here we can understand that the k_i value is determined by two factors. One is the acid strength (*i.e.*, the ability of proton donation), and the other is the special configuration (*i.e.*, the ability of proton acception) of the acid center. On the other hand, the k_p is determined by the acid strength alone.

Other Samples. The data for other samples are incomplete. However, the similar dependencies upon T_d of the k_i, c/t, and N_{OH} values show that the surface structures of the 13MHT and 50MHT are both close to that of the 25MHT. The slower appearance (about 20 °C) of the k_i(max) of the 50MHT may arise from its dehydroxylation, slower than that of the 25MHT (see Fig. 6).

Although the curves of c/t, A, and N_{OH} against T_d and the position of k_i(max) are similar to each other, there is a clear difference in the shape of the k_i *vs.* T_d curve between the 25MHT and the C sample (Fig. 1). The surface structures corresponding to the (e) may also be different.

Finally, we should mention the different surface characters between the M and MHT samples. The variations with the T_d of the k_i, k_p, and N_{OH} values of the M sample are not so prominent as those of the corresponding MHT sample. The starting N_{OH} value of the M is much lower than that of the MHT. Moreover, the c/t ratio of the M is much larger than that of the MHT. These facts indicate that the M sample originally contains large fractions of the (e) and (f). The presence of the less active (e) and (f) for the butene isomerization on the 25M sample results in its lower k_i value, with a higher c/t ratio, than those of the 25MHT, although the total acid amount of the 25M is larger than that of the 25MHT (Fig. 5).

Conclusion. The values of k_i, k_p, and A of the hydrothermally activated silica–alumina are different functions of T_d. An analysis of the N_{OH} *vs.* T_d curve shows that the surface structure of the catalyst changes in this fashion: (c)→(d)→(e)→(f) with the increase in T_d. By this, the different dependencies upon T_d of k_i and k_p are consistently explained.

The dependencies upon T_d of k_i, c/t, and k_p of the M sample differ from those of the corresponding MHT sample. This arises from the presence of the (e) and (f) in the original M sample. In other words, the role of the hydrothermal activation exists in the modification of the less active structures, (e) and (f), into the highly active structure (d).

References

1) C. L. Thomas, *Ind. Eng. Chem.*, **41**, 2564 1949); M. W. Tamele, *Discuss. Faraday Soc.*, **8**, 270 (1960).
2) A. Leonard, S. Suzuki, J. J. Fripiat, and C. Dekimpe, *J. Phys. Chem.*, **68**, 2608 (1964); J. J. Fripiat, A. Leonard, and J. B. Uyterhoven, *ibid.*, **69**, 3274 (1965).
3) J. B. Peri, *J. Catal.*, **41**, 227 (1976); *J. Phys. Chem.*, **70**, 3168 (1966); **72**, 2917 (1968).
4) S. Furuyama, O. Murashita, Y. Yukumoto, and T. Morimoto, *Bull. Chem. Soc. Jpn.*, **53**, 3044 (1980).
5) H. A. Benesi, *J. Am. Chem. Soc.*, **78**, 5490 (1956).
6) S. Furuyama, T. Tange, O. Murashita, and Y. Yukumoto, *Rep. Res. Lab. Surface Sci., Okayama Univ.*, **5**, 21 (1980).
7) O. Jǿhnson, *J. Phys. Chem.*, **59**, 827 (1955).
8) T. Morimoto, K. Shiomi, and H. Tanaka, *Bull. Chem. Soc. Jpn.*, **37**, 392 (1964).
9) A. Ozaki and K. Kimura, *J. Catal.*, **3**, 395 (1964).
10) H. R. Gerberich and W. K. Hall, *J. Catal.*, **5**, 99 (1966).
11) J. N. Finch and A. J. Clark, *J. Phys. Chem.*, **73**, 2234 (1969).
12) A. C. Zettlemoyer, F. J. Micale, and K. Klier, "Water," ed by F. Frank, Plenum Press, New York (1975), Vol. 5, p. 280.
13) J. Take, T. Tsuruya, T. Sato, and Y. Yoneda, *Bull. Chem. Soc. Jpn.*, **45**, 3409 (1972).
14) J. W. Hightower and W. K. Hall, *J. Am. Chem. Soc.*, **89**, 778 (1967).
15) D. Ballivet, D. Barthomeuf, and Y. Trambouze, *J. Catal.*, **34**, 423 (1974).
16) M. Misono, N. Tani, and Y. Yoneda, *J. Catal.*, **55**, 314 (1978).
17) S. Tsuchihashi, "Garasu No Kagaku," Kodansha, Tokyo (1972).
18) Many references are available. For instance, H. Mitsushio and K. Matsuoka, *Rep. Res. Lab. Hydrothermal Chem., Kochi Univ.*, **2**, 36 (1978).
19) Unpublished work.
20) "Encyclopedia Chemica," ed by S. Mizushima, Kyoritsu Shuppan, Tokyo (1960).
21) R. Kiriyama, "Kotai Kozo Kagaku," Kyoritsu Shuppan, Tokyo (1978), p. 67.
22) Peri's model is also based on the (100) plane of β-cristobalite and limits the condensation of the hydroxyl group to a narrow region by considering the surface strain. However, his model is made for silica–alumina produced by depositing $AlCl_3$ vapor on a silica-gel surface. Therefore, the surface structure of his catalyst differs considerably from that of the present catalyst.

 © 1982 The Chemical Society of Japan Bull. Chem. Soc. Jpn., 55, 971—974 (1982)

The Crystal Structure of Bis(methyl 3-benzylidenedithiocarbazato)nickel(II)

Tetsuo Uechi* and Takayuki Oniki†

College of General Education, Kyushu University 01, Ropponmatsu, Fukuoka 810
†Pre-dental Course, Kyushu Dental College, Manazuru, Kokurakita-ku, Kitakyushu 803

(Received March 30, 1981)

The title compound crystallizes in the monoclinic space group $P2_1/a$ with two molecules in a unit cell of dimensions; $a=21.479(5)$, $b=4.2092(6)$, $c=14.257(3)$ Å, and $\beta=129.53(2)°$. The structure was refined by block-diagonal least-squares procedures to give a final R value of 0.032 for 1693 reflections with $I>3\sigma(I)$ collected on a four-circle X-ray diffractometer. The complex consists of two methyl 3-benzylidenethiocarbazate groups, each bound to the central Ni atom through the thiol S atom and the hydrazine N atom, to yield a five-membered chelate ring. The NiN_2S_2 moiety is *trans* square-planar, with Ni–S and Ni–N bond distances of 2.1767(9) and 1.927(3) Å respectively. An examination of the bond distances and the planarity of the molecule revealed a delocalization of the π electrons over the chelate ring. The intra-molecular contact of S···H is 2.35(4) Å, which indicates a definite C–H···S interaction or hydrogen bonding.

In the course of our ESR study of $^{63}Cu(II)$ doped in the title compound (abbreviated as $Ni(bdc)_2$), an extra hyperfine structure (hfs) due to azomethine protons was observed.[1,2] The proton hfs was large, though the proton is attached to a carbon atom which is not included in the chelate ring. This proton hfs can be expected to be enhanced through the π electron in a C=N bond, and so the A^H value is sensitive to the geometry around the C=N bond. Therefore, it is interesting to investigate the structure around the C=N bond. The coordination geometry around the nickel atom in $Ni(bdc)_2$ is *trans*, while those in related 1-(2-naphthyl)ethylidene-, 1-(*p*-tolyl)ethylidene-, 1-phenylethylidene-, 1-(*m*-nitrophenyl)ethylidene-, and 1-(*p*-nitrophenyl)ethylidene-dithiocarbazatonickel(II) complexes were found from ESR measurements to be *cis*.[1] This paper will describe the crystal structure of $Ni(bdc)_2$ determined by the single-crystal X-ray-diffraction method.

Experimental

Preparation of Methyl 3-Benzylidenedithiocarbazate. A methanol solution of *S*-methyl dithiocarbazate (10 g), prepared as previously described,[3] was added to a methanol solution of benzaldehyde (11 g). The mixture was heated on a steam bath for 10 min. The deposited crystals were filtered off, washed with methanol, and recrystallized from methanol to give pale yellow crystals of the Schiff base.

Preparation of $Ni(bdc)_2$. A hot methanol solution of the nickel acetate (0.001 mol) was added to a hot methanol solution of the Schiff base (0.002 mol), the solution was heated on the steam bath for 10 min; on cooling, crystals of the $Ni(dbc)_2$ were deposited. Single crystals were obtained by the slow evaporation of the chloroform–methanol solution. Found: C, 44.99, H, 3.71, N, 11.68%. Calcd for $Ni(dbc)_2$: C, 45.29, H, 3.80, N, 11.74%.

X-Ray Diffraction. Preliminary X-ray photographs showed the space group to be $P2_1/a$. The unit cell parameters and intensity data were measured on a Syntex $P\bar{1}$ automated four-circle X-ray diffractometer with monochromated Mo $K\alpha$ radiation ($\lambda=0.71073$ Å). The unit-cell parameters were determined by a least-squares procedure, using 30 reflections within the range of $30<2\theta<43°$. The crystal used for X-ray work was ground to a sphere 0.32 mm in diameter. The density was measured by flotation in an aqueous KI solution. The crystal data are given in Table 1.

Table 1. Crystal data[a]

Molecular formula	$NiS_4N_4C_{18}H_{18}$
Molecular weight	477.31
Space group	$P2_1/a$
$a=21.479(5)$ Å	$Z=2$
$b=4.2092(6)$ Å	$D_m=1.593$ g cm^{-2}
$c=14.257(3)$ Å	$D_x=1.594$ g cm^{-2}
$\beta=129.53(2)°$	$\mu=1.39$ mm^{-1}
$V=994.17(45)$ Å^3	(for Mo $K\alpha$ radiation)

a) Numbers in parentheses here and elsewhere in this paper are the e.s.d.'s in the last significant digits.

The intensity data of 2202 independent reflections within a range of $2\theta<56°$ were collected by the θ-2θ scan technique, with a variable scan rate from 4.0 to 24.0° min^{-1}. Of these, the intensities of 505 reflections were less than $3\sigma(I)$; these reflections were not used in the least-squares refinement. The intensity data were corrected for Lorentz and polarization effects, but not for absorption and extinction.

Structure Determination and Refinement

The Ni atoms must lie on a set of twofold special positions, since there are only two molecules in a unit cell; therefore, the molecule is required to have a center of symmetry. The positions of all the non-hydrogen atoms were deduced from a Patterson synthesis and a subsequent Fourier synthesis. Refinement was carried out by the block-diagonal least-squares method. The function minimized was $\sum\omega(|F_o|-|F_c|)^2$, in which ω was chosen according to Cruickshank's weighting schemes.[4] All the H atoms were located by means of a difference Fourier synthesis. After several further cycles of refinement including all the H atoms, four reflections with $|F_o|-|F_c|>10.0$ were eliminated from the F_o-data set because of the strong imbalances of the background intensities on both sides of each Bragg peak. Refinement was terminated when all the shift/e.s.d. ratios for the non-hydrogen atoms became less than 0.2. The final conventional R index was 0.032 for the 1693 measurable reflections. The final difference Fourier synthesis showed no significant features except for two implausible peaks

Table 2. Fractional atomic coordinates and isotropic thermal parameters[a)]

	x	y	z	B/Å^2
Ni	0	0	0	2.73(0)
S(1)	0.11055(4)	0.26634(21)	0.13102(7)	3.99(3)
S(2)	0.16983(4)	0.54668(18)	0.36153(6)	3.55(3)
N(1)	−0.0179(1)	0.0377(5)	0.1159(2)	2.8(1)
N(2)	0.0340(1)	0.2224(5)	0.2221(2)	2.9(1)
C(1)	0.0948(1)	0.3269(6)	0.2330(2)	2.8(1)
C(2)	0.1352(2)	0.5508(9)	0.4470(3)	4.7(2)
C(3)	−0.0765(2)	−0.0940(7)	0.1058(2)	3.3(1)
C(4)	−0.1023(2)	−0.0779(7)	0.1789(2)	3.2(1)
C(5)	−0.1749(2)	−0.2335(8)	0.1282(3)	4.0(1)
C(6)	−0.2095(2)	−0.2389(9)	0.1827(3)	4.8(2)
C(7)	−0.1717(2)	−0.0724(9)	0.2909(3)	4.7(2)
C(8)	−0.0993(2)	0.0799(10)	0.3442(3)	4.9(2)
C(9)	−0.0645(2)	0.0779(8)	0.2896(3)	4.1(1)
H(2)1	0.174(2)	0.610(8)	0.517(3)	4.9(8)
H(2)2	0.132(2)	0.343(8)	0.457(3)	5.0(7)
H(2)3	0.086(2)	0.641(8)	0.403(3)	4.9(7)
H(3)	−0.109(2)	−0.219(7)	0.035(2)	3.4(6)
H(5)	−0.200(2)	−0.343(7)	0.054(2)	4.2(7)
H(6)	−0.262(2)	−0.352(8)	0.143(3)	4.9(7)
H(7)	−0.203(2)	−0.065(8)	0.320(3)	4.9(8)
H(8)	−0.070(2)	0.170(8)	0.422(3)	5.1(8)
H(9)	−0.018(2)	0.196(7)	0.320(3)	4.2(6)

a) The B's of the non-hydrogen atoms are the equivalent ones of the anisotropic thermal parameters.[15)] The H atoms are labelled in terms of the C atom to which they are attached.

of *ca.* 0.5 eÅ^{-3} in the vicinities of the Ni atom and the center of the chelate ring. The atomic scattering factors for Ni^{2+}, S, N, and C_{cov}, with correction factors for anomalous dispersion for the first two, were taken from International Tables for X-Ray Crystallography.[5)] Those for H atom were adopted from the table of Stewart *et al.*[6)] All the calculations were carried out on a FACOM M-200 computer in the Computer Center of Kyushu University, mainly by the use of the UNICS-II program system.[7)] The drawings were made by the use of the *ORTEP* program.[8)] The final atomic parameters are listed in Table 2, along with their estimated standard deviations. Lists of the structure factors and anisotropic thermal parameters have been deposited with the office of the Chemical Society of Japan as Document No. 8206.

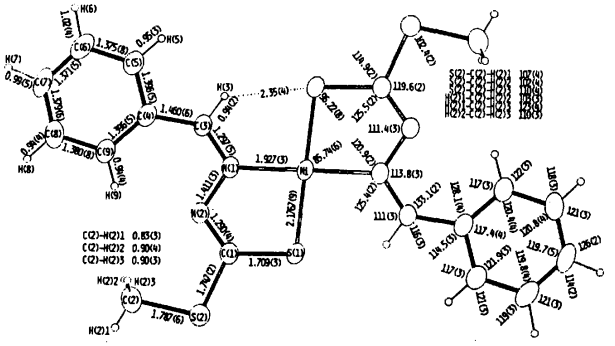

Fig. 1. Bond distances (l/Å) and angles (θ/°) of the molecule. The H atoms are shown as open circles of arbitrary size, and the shapes of the other atoms represent the thermal-motion ellipsoids scaled to enclose 50% probability.

Results and Discussion

The molecular structure is shown in Fig. 1, together with the bond distances(l), bond angles(θ), and atomic nomenclature scheme. The complex consists of two methyl 3-benzylidenedithiocarbazate groups, each bound to the central Ni atom through the thiol S atom and the hydrazine N atom, to yield a five-membered chelate ring. The NiN_2S_2 moiety is *trans* square planar (coordination plane). This coordination geometry is compatible with the results of the ESR measurement of Cu^{2+} doped in $Ni(bdc)_2$.[1,2)]

The Ni–S bond distance of 2.1767(9) Å is in the range of 2.1—2.3 Å found in the four-coordinated Ni(II) complexes, as has been pointed out by Lopez-Castro and Truter.[9)] The Ni–N bond distance of 1.927(3) Å is comparable with the value of 1.896(7) Å found in bis(ethyldithiocarbazate)nickel(II), in which the environment about the Ni atom is similar to that in $Ni(bdc)_2$.[10)] The bond distances of S–C(1.709 Å), C–N(1.290 Å), and N–N(1.411 Å) in the chelate ring are intermediate between the usual values for single and double bonds. The chelate ring is nearly planar, with the maximum deviation of 0.041 Å, as shown in Table 3. The bond distances and the planarity are indicative of an extensive delocalization of π electrons over the chelate ring. Such a large delocalization of π electrons can be expected to give rise to a large proton hfs. The thiomethyl group has the normal S–C(sp^3) bond distance of 1.787(6) Å and is attached to the ring carbon with the C–S–C bond angle of 102.4(2)° and at

TABLE 3. LEAST-SQUARES PLANES AND TORSION ANGLES

(a) Coefficient of least-squares plane equations.

Equations are of the form $lu+mv+nw=d$, where u, v, and w are in Å units referred to the a, b, and c* axes respectively.

	Plane	l	m	n	d/Å
I	Coordination	−0.2870	0.8560	−0.4300	0.0
II	Chelate ring	−0.2722	0.8408	−0.4680	−0.0307
III	Benzene ring	−0.2341	0.8364	−0.4957	−0.3623

(b) Deviations (l/Å) from least-squares planes.

Atoms with an asterisk are not included in the calculation of the plane.

I		II		III	
Ni	0	Ni	0.031	C(3)*	0.064
S(1)	0	S(1)	−0.024	C(4)	0.007
N(1)	0	N(1)	−0.041	C(5)	−0.007
N(2)*	0.120	N(2)	0.025	C(6)	0.002
C(1)*	0.099	C(1)	0.010	C(7)	0.003
C(3)*	−0.092	S(2)*	0.005	C(8)	−0.002
		C(2)*	−0.007	C(9)	−0.003
		C(3)*	−0.138		

(c) Selected torsion angles (θ/°).

S(1)–C(1)–S(2)–C(2)	−178.3(2)	Ni–N(1)–C(3)–C(4)	−175.7(3)
N(1)–N(2)–C(1)–S(2)	−177.1(2)	N(1)–C(3)–C(4)–C(5)	173.5(4)
N(2)–C(1)–S(2)–C(2)	1.0(3)	N(1)–C(3)–C(4)–C(9)	−4.9(7)

the normal S–C(sp^2) distance (1.747(2) Å). These bond distances and angle suggest that the delocalization of π electrons is not extended to this part, although the thiomethylic S–C is almost coplanar with the chelate ring. The coordinated N atom is also bonded to the benzylidene group; the N(1)–C(3) distance (1.297(5) Å) falls within the range of 1.29—1.34 Å established for the coordinated N=C bond;[11] it is longer than the generally accepted value for N(sp^2)–C(sp^2) of 1.24 Å.[12] Judging from the planarity and lengthening of the bonds about N(1), the π electrons seem to be delocalized over C(3). An inspection of the bond angle at C(3) reveals that there is a steric repulsion between the chelate ring and the phenyl group. The benzene ring is planar, with a maximum deviation of 0.007 Å. This ring rotates slightly about the C(3)–C(4) bond; the torsion angles about this bond are 173.5(4) and −4.9(7)°. The intramolecular contact of S(1)···H(3) is 2.35(4) Å, where the C···S distance and the C–H···S angle are 3.053(4) Å and 130.4° respectively. The S···H distance is far shorter than the sum of the van der Waals radii of these atoms (3.05 Å);[13] it indicates a definite C–H···S interaction or hydrogen bonding. The large proton hfs of the ESR spectra of Cu^{2+} doped in Ni(bdc)$_2$ is expected to occur also through this H···S short contact. Such a short contact has also been observed in nickel(II) bis(dipropyldithiocarbamate).[14]

Fig. 2. An edge-on view of the molecule. The H atoms have been omitted for clarity.

An edge-on view of the molecule, as shown in Fig. 2, shows that the molecule is, as a whole, roughly planar. The normal to the coordination plane makes an angle of 31.1° with the b axis; also, the directions of the Ni–N(1) and Ni–S(1) bonds make angles of 85.3 and 59.0° with the b axis respectively. These angles correspond to the angles between the b axis and the g_z, g_x, and g_y directions (30.7, 87.1, and 59.3° respectively) determined from the single-crystal ESR measurement of Cu^{2+} doped in Ni(bdc)$_2$.[1]

The molecular packing projected on the ac plane is

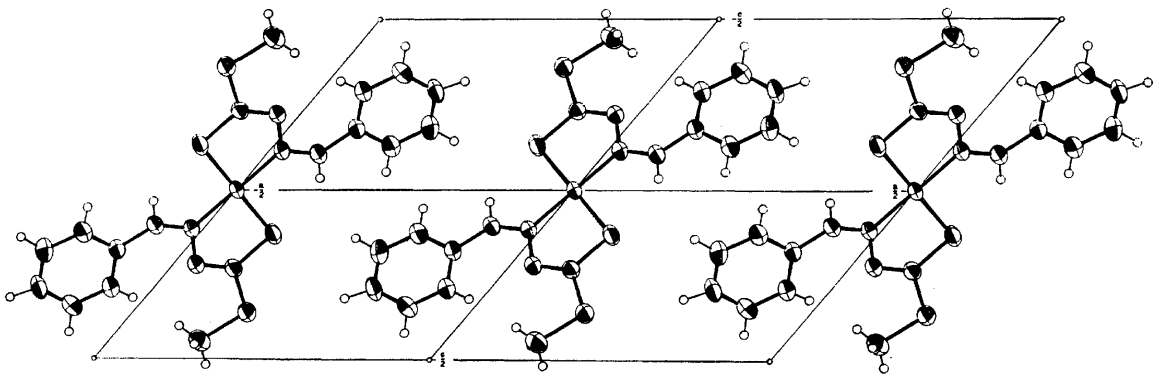

Fig. 3. Projection of the crystal structure on the ac plane.

shown in Fig. 3. There are no unusually close intermolecular contacts; thus, the crystal can be said to be held together primarily by van der Waals forces.

The authors are grateful to Professor Toshio Kawasaki at the Faculty of Pharmaceutical Sciences of Kyushu University for allowing them to use the automated diffractometer, and to Asst. Professor Shigeaki Kawano at the College of General Education of this University for his advice on the computation process.

References

1) T. Oniki, *Bull. Chem. Soc. Jpn.*, **51**, 2551 (1978).
2) T. Oniki, *Bull. Chem. Soc. Jpn.*, **52**, 2584 (1979).
3) G. Bahr and G. Schleitzer, *Z. Anorg. Allg. Chem.*, **280**, 161 (1955).
4) D. W. J. Cruickshank, "Computing Methods in Crystallography," ed by J. S. Rollett, Pergamon Press, Oxford (1965), p. 112.
5) "International Tables for X-Ray Crystallography," Kynoch Press, Birmingham (1974), Vol. IV.
6) R. F. Stewart, E. R. Davidson, and W. T. Simpson, *J. Chem. Phys.*, **42**, 3175 (1965).
7) T. Sakurai, H. Iwasaki, Y. Watanabe, K. Kobayashi, Y. Bando, and Y. Nakamichi, *Rikagaku Kenkyusho Hokoku* (in Japanese), **50**, 75 (1974).
8) C. K. Johnson, ORTEP, Oak Ridge National Laboratory Report ORNL-3794 (1965).
9) A. Lopez-Castro and M. R. Truter, *J. Chem. Soc.*, **1963**, 1309.
10) L. Gastaldi and P. Porta, *Cryst. Struct. Commun.*, **3**, 467 (1973).
11) J. C. J. Bart, I. W. Bassi, M. Calcaterra, and M. Pieroni, *Inorg. Chim. Acta*, **28**, 201 (1978).
12) "International Tables for X-Ray Crystallography," 2nd ed, Kynoch Press, Birmingham (1968), Vol. III.
13) L. Pauling, "The Nature of the Chemical Bond," 3rd ed, Cornell Univ. Press, Ithaca (1960).
14) G. Peyronel and A. Pignedoli, *Acta Crystallogr.*, **23**, 398 (1967).
15) W. C. Hamilton, *Acta Crystallogr.*, **12**, 609 (1959).

 © 1982 The Chemical Society of Japan Bull. Chem. Soc. Jpn., 55, 975—978 (1982)

Polymerization of Silicic Acid Adsorbed on Aluminium Hydroxide

Takushi YOKOYAMA,* Osamu NAKAMURA,** and Toshikazu TARUTANI

Department of Chemistry, Faculty of Science, Kyushu University 33, Hakozaki, Higashi-ku, Fukuoka 812

(Received June 19, 1981)

Factors controlling the absorption of silicic acid on aluminium hydroxide from aqueous solution and the polymerization of adsorbed silicic acid were studied. Measurements included the amount of silicic acid adsorbed on aluminium hydroxide, the amount and size distribution of the polysilicic acid formed, and the differential thermal analysis curve of aluminium hydroxide which had adsorbed silicic acid. The adsorption and the polymerization of silicic acid are affected by pH, the relative amounts of silicic acid and aluminium hydroxide, the reaction time between monosilicic acid and aluminium hydroxide, and the formation of amorphous aluminosilicate. The amount of adsorbed silicic acid and the rate of its polymerization are maximum at pH 9.0—9.5. A part of adsorbed monosilicic acid reacts with aluminium hydroxide to form an aluminosilicate. In an early stage of the polymerization of the adsorbed silicic acid, the polymerization mainly proceeds by the reactions between monosilicic acids and between monosilicic and polysilicic acids; the particle sizes of polysilicic acids gradually increase with time. When the polymer particles grow large enough to touch neighboring polymers, the growth rate of polymer particles becomes faster due to the polymer-polymer reactions.

Siliceous deposits from hot springs generally contain Al_2O_3 and Fe_2O_3; some deposits contain several percent of Al_2O_3.[1-3] Aluminium thus plays an important role in the formation of siliceous deposits. Adsorption characteristics of monosilicic acid on aluminium hydroxide have been studied,[4-6] but only a few reports were published with respect to the polymerization of silicic acid adsorbed on or coprecipitated with aluminium hydroxide.

Hingston and Raupach[7] suggested that a multilayer of silicic acid was formed by polymerization of silicic acid on an aluminium hydroxide surface. Jepson *et al.*[8] reported that, under given conditions, the adsorption of monosilicic acid on gibbsite exceeded the monolayer coverage. Yokoyama and Tarutani[9] reported that, when aluminium hydroxide was placed in a flask and then monosilicic acid solution (150 ppm SiO_2, pH 8) was made to flow continuously through the flask, the monosilicic acid adsorbed on aluminium hydroxide gradually polymerized to form silica particles of larger sizes than 0.1 μm after about 20 d.

In this work, factors controlling the amount of silicic acid adsorbed on aluminium hydroxide and the polymerization of adsorbed silicic acid were studied. The mechanism for the growth of particles of polysilicic acid is proposed.

Experimental

Samples and Reagents. All the reagents used were of analytical reagent grade. A stock solution of monosilicic acid was prepared by dissolving silica gel (Mallinckrodt Chemical Works) in sodium hydroxide solution. A monosilicic acid solution of the desired concentration was prepared by diluting a stock solution before use. Aluminium hydroxide was precipitated by adding sodium hydroxide solution to aluminium chloride solution; the hydroxide was then washed with distilled water. This was prepared immediately before each experiment.

Procedure. The pH of monosilicic acid solution (500 cm^3) of an appropriate concentration was adjusted to a desired pH value with hydrochloric acid or sodium hydroxide solution. A known amount of aluminium hydroxide was then introduced to the solution and the pH of the solution was readjusted. The suspension was stirred vigorously with a magnetic stirrer. The variation of pH of the suspension was maintained within ± 0.1 pH by adding hydrochloric acid or sodium hydroxide solution. Adsorption experiments were carried out in a thermostated bath at 25 °C. After 5 h or at appropriate intervals, an aliquot of suspension was pipetted and filtered through a membrane filter having pore size of 0.1 μm. The concentration of monosilicic acid in the filtrate was determined by colorimetry. The aluminium hydroxide on the membrane filter was dissolved with 1 mol dm^{-3} hydrochloric acid. The resulting solution was filtered and diluted to 100 cm^3 with distilled water (solution A). The amount of monosilicic acid in the solution A was determined by colorimetry and the total silicic acid was determined after decomposing polysilicic acid with alkali. Silica particles larger than 0.1 μm remaining on the filter were determined by colorimetry after the filter had been ashed and the silica was fused with sodium carbonate. Aluminium ion concentration in the solution A was determined by EDTA titration.

The following symbols will be used: Si(M): the amount of monosilicic acid in the solution A; Si($<$0.1): the total amount of silicic acid (particles smaller than 0.1 μm) in the solution A; Si($>$0.1): the amount of silica (particles larger than 0.1 μm) remaining on the filter; Si(T): the sum of Si($<$0.1) and Si($>$0.1); Al(A): the amount of aluminium ion in the solution A; Si/Al(MR): the mole ratio of monosilicic acid to aluminium hydroxide in the initial solution; Si(T)/Al(A): the mole ratio of total silicic acid adsorbed to aluminium hydroxide; Si(M)/Si(T): the mole ratio of monosilicic acid to total silicic acid adsorbed on aluminium hydroxide. Since the difference between Si(M) and Si(T) can be regarded as the amount of polysilicic acid formed on the aluminium hydroxide, this ratio is an indicator of the amount of polysilicic acid formed.

Gel Chromatography. The size distribution of polysilicic acids formed on aluminium hydroxide was measured by gel chromatography. The pH of the solution A was adjusted to 2 and silicic acid was chromatographed on 1 cm × 60 cm column of Sephadex G-75 (Pharmacia Fine Chemicals) according to the procedure of Shimada and Tarutani.[10] After the effluent had been collected with a fraction collector, the amounts of silicic acid in the fractions were measured by colorimetry after decomposition of the polysilicic acid with alkali.

** Present address: Department of Commerce and Industry, Fukuoka Prefectual Office, Hakata-ku, Fukuoka 812.

Differential Thermal Analysis. Aluminium hydroxide which had adsorbed silicic acid was filtered, and then was dried at 25 °C for 10 d. Differential thermal analysis (DTA) was performed using a Rigaku Denki Thermaflex 8002 H/D thermoanalyzer.

Results

Effect of pH. The kinetic data for adsorption of silicic acid on aluminium hydroxide in 300 ppm (SiO_2) monosilicic acid solution of pH 9 showed that a rapid decrease in monosilicic acid concentration occurred in 1 h and then the rate of adsorption of silicic acid became relatively slow. Since, in 300 ppm monosilicic acid solution, monosilicic acid did not polymerize within 5 h, only monosilicic acid was adsorbed by aluminium hydroxide.

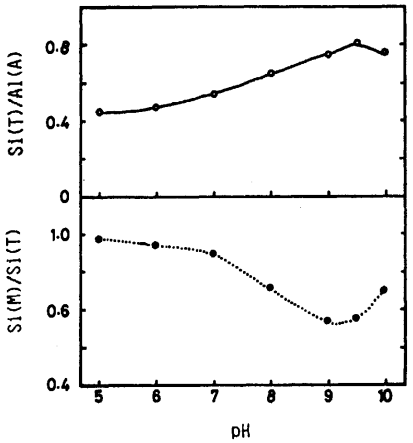

Fig. 1. The effect of pH on Si(T)/Al(A) and Si(M)/Si(T) ratios after 5 h.
Initial monosilicic acid concentration : 300 ppm. Si/Al-(MR)=2.1.

Adsorption of silicic acid by aluminium hydroxide and polymerization of adsorbed silicic acid were examined in the pH range 5—10. The results are shown in Fig. 1. The Si(T)/Al(A) ratio increased with increase in pH range 5.0—9.5, showing a maximum adsorption at pH 9.5. The Si(M)/Si(T) ratio decreased with increasing pH up to 9.0—9.5, increasing with further increase in pH. This indicates that the formation rate of polysilicic acid from silicic acid adsorbed on aluminium hydroxide is most rapid at pH 9.0—9.5. Silicic acid adsorbed on aluminium hydroxide at various pH's was chromatographed on a Sephadex G-75 column. Elution curves obtained are shown in Fig. 2. The dotted line is the elution curve for monosilicic acid, the position V_0 being the elution volume of Blue Dextran 2000, which is not diffusible in the gel phase. Polysilicic acid is eluted between the position V_0 and the elution position of monosilicic acid; the elution volume of monosilicic acid; the elution volume of polymer decreases with increasing particle size. The tailing from the peak for monosilicic acid indicates the presence of polysilicic acid in various sizes. Polymers larger in size than those in the particles separation range available with the gel are eluted together at V_0. As seen from the

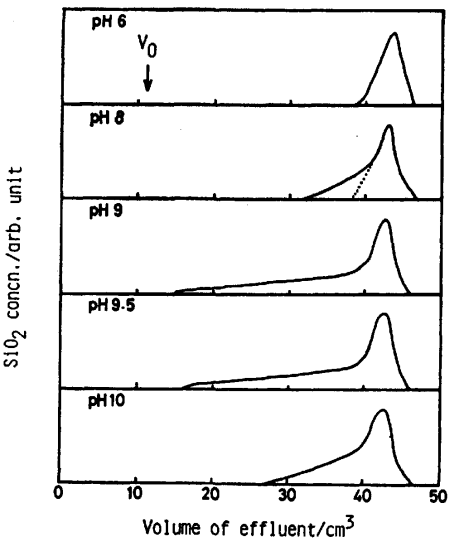

Fig. 2. Gel chromatograms for silicic acid adsorbed on aluminium hydroxide at various pH's after 5 h.
Initial monosilicic acid concentration : 300 ppm. Si/Al-(MR)=2.1. Gel : Sephadex G-75. Column: 1 cm×60 cm.

elution curves shown in Fig. 2, polysilicic acids formed at pH 9.0 and 9.5 have larger particle sizes than those formed at other pH's. This indicates that the rate of growth of polymer particles formed on aluminium hydroxide is most rapid at pH 9.0—9.5.

Effect of Initial Concentration of Monosilicic Acid. The variations of Si(T)/Al(A) and of Si(M)/Si(T) ratios with the initial concentration of monosilicic acid are shown in Fig. 3. The Si(T)/Al(A) ratio increased with increasing initial concentration of monosilicic acid, whereas the Si(M)/Si(T) ratio decreased. The amount of adsorbed silicic acid and the degree of polymerization are strongly affected by the initial monosilicic acid concentration.

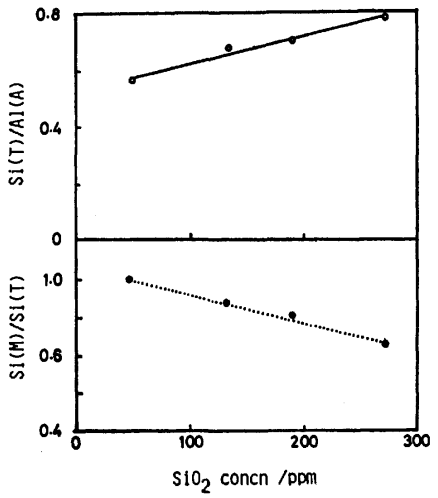

Fig. 3. Variation of Si(T)/Al(A) and Si(M)/Si(T) ratios as a function of initial monosilicic acid concentration.
Si/Al(MR)=0.96. pH : 9. Reaction time : 5 h.

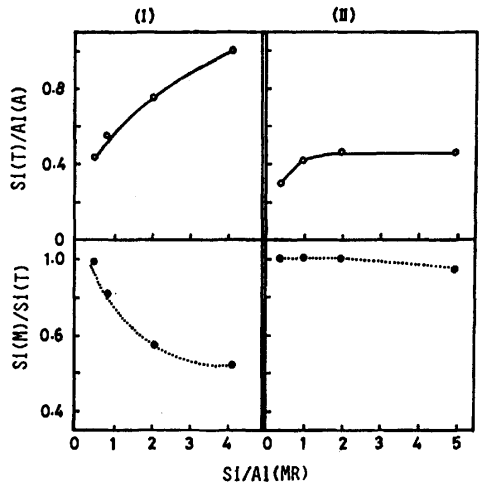

Fig. 4. Variation of Si(T)/Al(A) and Si(M)/Si(T) ratios as a function of Si/Al(MR) ratio.
Initial monosilicic acid concentration : (I) 300 ppm, (II) 100 ppm. pH : 9. Reaction time : 5 h.

Effect of the Relative Amount of Silicic Acid to Aluminium Hydroxide. Figure 4 shows the variations of Si(T)/Al(A) and of Si(M)/Si(T) ratios as a function of Si/Al(MR) ratio. The Si(T)/Al(A) ratio increased with an increase in the Si/Al(MR) ratio in 300 ppm monosilicic acid solution and the Si(M)/Si(T) ratio decreased. In 100 ppm monosilicic acid solution, above the Si/Al(MR) ratio of 2, the Si(T)/Al(A) ratio reached a limiting plateau region. The Si(M)/Si(T) ratio was unity in the Si/Al(MR) range of 0.3—2.0 and was slightly less than unity at the Si/Al(MR) ratio of 5.

Effect of Standing Time. The variations of Si(T)/Al(A), Si(M)/Si(T), and Si(>0.1)/Al(A) ratios with time in 300 ppm monosilicic acid solution are shown in Fig. 5. The Si(T)/Al(A) ratio increased with time, whereas the Si(M)/Si(T) ratio decreased. After 25 h, both ratios became almost constant. On the other hand, silica of particle size above 0.1 μm formed after 35 h; its amount (Si(>0.1)/Al(A)) increased with time.

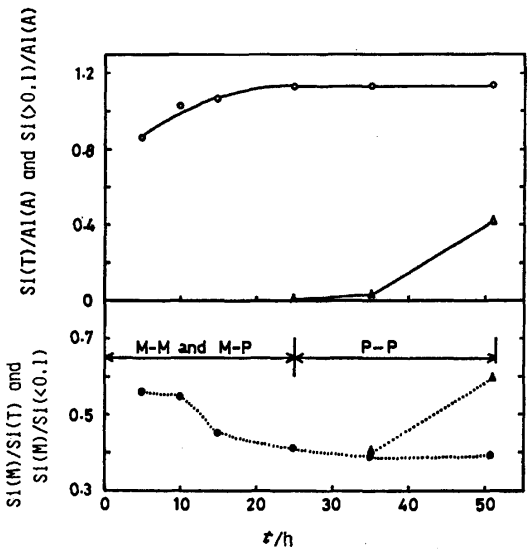

Fig. 5. Polymerization of silicic acid adsorbed on aluminium hydroxide.
Initial monosilicic acid concentration: : 300 ppm. Si/Al(MR)=2.1. pH : 9.3.
—○—: Si(T)/Al(A), —△—: Si(>0.1)/Al(A), —●—: Si(M)/Si(T), —▲—: Si(M)/Si(<0.1).

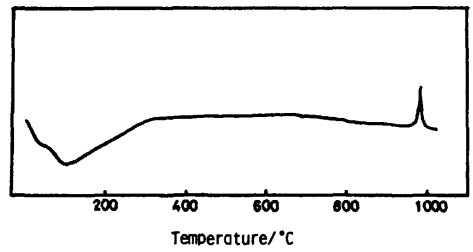

Fig. 6. DTA pattern of sample prepared at pH 8.

Differential Thermal Analysis. Figure 6 shows the DTA curve of aluminium hydroxide which had adsorbed silicic acid, prepared at pH 8. This curve has an endothermic peak at *ca.* 100—300 °C and an exothermic peak at around 1000 °C; it is very similar in basic features to the thermal curve of allophane, that is, amorphous aluminosilicate.[11] Appearance of the exothermic peak at around 1000 °C indicates that aluminosilicate is formed by the reaction of the adsorbed monosilicic acid and aluminium hydroxide. The exothermic peak was observed in all aluminium hydroxide which had adsorbed silicic acid.

Discussion

In 300 ppm (SiO_2) monosilicic acid solution, monosilicic acid did not polymerize within 5 h, whereas the monosilicic acid adsorbed on aluminium hydroxide did polymerize.

The amount of silicic acid adsorbed on aluminium hydroxide, the rate of polymerization of adsorbed silicic acid, and the formation of silica were affected by many factors, such as pH (Figs. 1 and 2), initial monosilicic acid concentration (Fig. 3), Si/Al(MR) ratio (Fig. 4), and standing time (Fig. 5). Amorphous aluminosilicate is formed by the reaction of adsorbed monosilicic acid and aluminium hydroxide (Fig. 6). The process of polymerization of adsorbed silicic acid is discussed on the basis of the data obtained at pH 9.3 (Fig. 5).

According to the preceding report,[12] the polymerization reaction of silicic acid in an aqueous solution is divided into three steps: (1) the reaction between monosilicic acids (M-M reaction), (2) the reaction between monosilicic and polysilicic acids (M-P reaction), and (3) the reaction between polysilicic acids (P-P reaction). Silicic acid adsorbed on aluminium hydroxide may also polymerize through similar reactions. An M-M reaction consists of two reactions, the reaction of the monosilicic acid adsorbed, and the reaction between the adsorbed monosilicic acid and that in the solution. The M-P reaction consists of the reaction between the adsorbed monosilicic acid and the polysilicic acid formed on the surface of solid, and the reaction between monosilicic acid in the solution and the polysilicic acid

formed. The P-P reaction occurs between polysilicic acids formed on the surface of the solid, because polysilicic acid does not exist in the solution.

In Fig. 5, the Si(T)/Al(A) ratio reached nearly a constant value after 25 h. Similarly, the Si(M)/Si(T) ratio showed a constant value after 25 h. However, the Si(>0.1)/Al(A) and Si(M)/Si(<0.1) ratios increased even after 35 h. Since the Si(T)/Al(A) and Si(M)/Al(A) ratios were nearly constant after 25 h, the increase in the Si(M)/Si(<0.1) ratio after 35 h suggests a decrease in the amounts of polymers smaller than 0.1 μm in size (Si(<0.1)) according to P-P reactions.

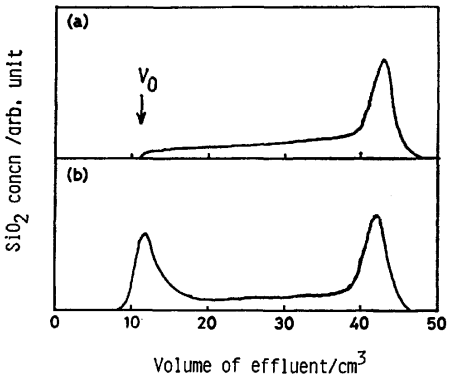

Fig. 7. Gel chromatograms for silicic acid adsorbed on aluminium hydroxide after (a) 20 h and (b) 30 h. Initial monosilicic acid concentration: 300 ppm. Si/Al(MR)=2.1. pH: 9.3. Gel: Sephadex G-75. Column: 1 cm×60 cm.

In order to confirm that a P-P reaction occurred, silicic acid absorbed on aluminium hydroxide after 20 and 30 h was chromatographed on a Sephadex G-75 column. Elution curves for silicic acid are shown in Fig. 7. Figure 7(a) shows no peak at the position V_0, while Fig. 7(b) shows a large peak. Polysilicic acids having larger sizes than the possible separation range of the gel are eluted together at the position V_0. These results suggest that the gradual increase in particle size of polymers occurred for the first 20 h (Fig. 7(a)) and then the further increase between 20 and 30 h occurred by P-P reaction (Fig. 7(b)). If a P-P reaction occurs from the beginning of the polymerization along with M-M and M-P reactions, the elution curve shown in Fig. 7(a) should show a peak at the position V_0, though the peak may be small. As shown in Fig. 5, the Si(T)/Al(A) ratio increased with time until 25 h and the Si(M)/Si(<0.1) (=Si(M)/Si(T)) ratio decreased. From the evidence of gel chromatography, it is concluded that the polymerization of silicic acid mainly proceeds by M-M and M-P reactions in the reaction time up to 25 h.

The process of polymerization of silicic acid adsorbed on aluminium hydroxide can be explained as follows. Monosilicic acid is at first adsorbed on aluminium hydroxide and a part of monosilicic acid adsorbed forms amorphous aluminosilicate (Fig. 6). In an early stage of polymerization of adsorbed silicic acid, the polymerization mainly proceeds by M-M and M-P reactions and the particle sizes of polymers gradually increase with time. When the particles of the polymers grow large enough to touch neighboring polymers, the growth rate of polymers becomes faster due to P-P reaction.

References

1) M. Ichikuni, *J. Soc. Eng. Mineral Springs Jpn.*, **5**, 48 (1968).
2) M. Ichikuni and S. Kobayashi, *Chem. Geol.*, **5**, 131 (1969/1970).
3) M. Ichikuni, *Chem. Geol.*, **6**, 273 (1970).
4) J. A. Mckeague and M. G. Cline, *Can. J. Soil Sci.*, **43**, 83 (1963).
5) F. J. Hingston, R. J. Atkinson, A. M. Ponser, and J. P. Quirk, *Nature*, **215**, 1459 (1967).
6) M. Mcphail, A. L. Page, and F. T. Bingham, *Soil Sci. Soc. Am. Proc.*, **36**, 510 (1972).
7) F. J. Hingston and M. Raupach, *Aust. J. Soil Res.*, **5**, 295 (1967).
8) W. B. Jepson, D. G. Jeffs, and A. P. Ferris, *J. Colloid Interface Sci.*, **55**, 454 (1976).
9) T. Yokoyama and T. Tarutani, *Mem. Fac. Sci., Kyushu Univ. Ser. C*, **13**, 23 (1981).
10) K. Shimada and T. Tarutani, *J. Chromatogr.*, **168**, 401 (1979).
11) J. Ossaka, *Adv. Clay Sci.*, **3**, 225 (1961); **4**, 33 (1962).
12) K. Shimada and T. Tarutani, *Bull. Chem. Soc. Jpn.*, **53**, 3488 (1980).

 © 1982 The Chemical Society of Japan Bull. Chem. Soc. Jpn., 55, 979—984 (1982)

Molecular Structures of [2](2,5)(7,7,8,8-Tetracyanoquinodimethano)[2]-paracyclophane and 14,17-Dimethoxy[2](2,5)(7,7,8,8-tetracyanoquinodimethano)[2]paracyclophane†

Takashi Mizuma,†† Hideaki Matsuura,††† Yasushi Kai, Noritake Yasuoka,†††† and Nobutami Kasai*

Department of Applied Chemistry, Faculty of Engineering, Osaka University, Yamadaoka, Suita, Osaka 565

(Received June 24, 1981)

The molecular structures of two [2.2]paracyclophanes containing a 7,7,8,8-tetracyanoquinodimethan (TCNQ) moiety as an electron acceptor have been determined by means of X-ray diffraction. The electron-donating moieties in these cyclopahnes are benzene (TCNQ-X) and *p*-dimethoxybenzene (TCNQ-X$(OMe)_2$) rings. TCNQ-X crystallizes in a triclinic space group $P\bar{1}$ with two molecules per unit cell; $a=9.772(2)$, $b=18.477(4)$, $c=6.569(1)$ Å, $\alpha=90.38(2)$, $\beta=107.92(2)$, $\gamma=100.32(2)°$. The crystals of TCNQ-X$(OMe)_2$ belong to the orthorhombic system; space group *Fdd2*; $a=25.618(3)$, $b=31.895(5)$, $c=9.808(1)$ Å, $Z=16$. Both structures were solved by the direct method and refined by the block-diagonal least-squares procedure to $R=0.088$ (TCNQ-X) and 0.109 (TCNQ-X$(OMe)_2$) for 3141 and 1695 non-zero rehections. In the two structures determined, the [2.2] paracyclophane skeleton has the usual structure; the benzene ring and six-membered ring of the TCNQ moiety have a boat form, and two $C(CN)_2$ portions in the TCNQ moiety are bent down from the mean plane defined by the C(12), C(13), C(15), and C(16) atoms.

As part of a series of structural studies of layered cyclophanes, the X-ray structure determination of [2,2]paracyclophanes containing a 7,7,8,8-tetracyanoquinodimethan (TCNQ) moiety as an electron acceptor has been carried out. This paper will deal with the molecular structures of **1**, [2](2,5)(7,7,8,8-tetracyanoquinodimethano)[2]paracyclophane (abbreviated as TCNQ-X, hereafter) and **2**, 14,17-dimethoxy[2](2,5)-(7,7,8,8-tetracyanoquinodimethano)[2]paracyclophane (TCNQ-X$(OMe)_2$).

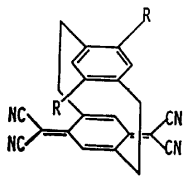

1, R=H
2, R=OCH_3

Experimental

For the X-ray experiment, a Rigaku automated four-circle diffractometer was used.

TCNQ-X. Graphite-monochromatized Mo $K\alpha$ radiation was used. A reddish violet crystal with approximate dimensions of 0.30 mm×0.25 mm×0.17 mm was mounted on a goniometer of the diffractometer. By searching for the locations of strong diffractions, the setting parameters of the crystal with a primitive lattice were first determined. Based on these parameters, a set of 206 diffraction intensities were measured by the θ-2θ scan technique up to $2\theta=14.3°$ as a preliminary work. By statistically treating these data, the point group symmetry of the crystal was determined as $\bar{1}$, and then the space group as $P\bar{1}$. The *SPAGD* program[1] was used. At this stage, the tentative unit-cell was transformed into the reduced cell, the parameters of which were then refined by the least-squares fit.

Crystal Data. $C_{22}H_{14}N_4\cdot C_6H_6$, *F.W.* 412.5, triclinic, space group $P\bar{1}$, $a=9.772(2)$, $b=18.477(4)$, $c=6.569(1)$ Å, $\alpha=90.38(2)$, $\beta=107.92(2)$, $\gamma=100.32(2)°$, $V=1107.8(4)$ Å^3, $D_m=1.240$ (by flotation), $D_c=1.236$ g cm^{-3} for $Z=2$.

The integrated intensities were measured by the θ-2θ scan method at a rate of 4° min^{-1}. The backgrounds were counted for 7.5 s before and after the scan of each peak. A total of 4412 (3141 non-zero) reflections was collected up to $\sin\theta/\lambda=0.62$ Å^{-1}. The usual Lp corrections were made, but absorption corrections were ignored [μ(Mo $K\alpha$)=0.81 cm^{-1}].

TCNQ-X(OMe)$_2$. The space group was determined by means of photographic work. The unit-cell parameters were determined by the least-squares fit of 2θ values of higher-order reflections determined on the Rigaku diffractometer.

Crystal Data. $C_{24}H_{18}N_4O_2$, *F.W.* 394.4, orthorhombic, space group *Fdd2*, $a=25.618(3)$, $b=31.895(5)$, $c=9.808(4)$ Å, $V=8014(3)$ Å^3, $D_m=1.30$, $D_c=1.307$ g cm^{-3} for $Z=16$.

The intensity data were collected on the diffractometer with Zr-filtered Mo $K\alpha$ radiation. The θ-2θ scan technique was employed at a rate of 4° min^{-1}. A bluish violet crystal with approximate dimensions of 0.15 mm×0.18 mm×0.30 mm was used. A total of 2336 reflections was collected up to $2\theta=54°$, of which 1695 $|F|$'s larger than $3\sigma(F)$ were classed as observed. The usual Lp corrections were made, but no absorption correction was applied [μ(Mo $K\alpha$)=0.92 cm^{-1}].

Structure Solution and Refinement

TCNQ-X. The structure was solved by the direct method (*MULTAN* 74)[2] and refined by the block-diagonal least-squares procedure (*HBLS* V).[3] Of the two crystalline benzene molecules centered on (0,0,0) and (1/2,0,1/2), the latter was supposed to be disordered by the feature of peaks on the Fourier map, but the isotropic refinement in which the disorder (two locations with a 3:2 occupancy ratio) was considered was unsuccessful ($R=0.102$). Isotropic refinement was, therefore, again carried out from the beginning, the

† Structural Chemistry of Layered Cyclophanes. VII.

†† Present address: Fuji FACOM Corporation, 23-5 Nishi-Shimbashi 3-chome, Minato-ku, Tokyo 105.

††† Present address: Ehime Works, Sumitomo Chemical Co., Ltd., Niihama, Ehime 792.

†††† Present address: Institute for Protein Research, Osaka University, Yamadaoka, Suita, Osaka 565.

TABLE 1. FRACTIONAL ATOMIC COORDINATES OF TCNQ-X, C_6H_6, WITH ESTIMATED STANDARD DEVIATIONS IN PARENTHESES

(a) C and N atoms with equivalent temperature factors.

Atom	x	y	z	B/Å^2
C(1)	0.7784(4)	0.1871(2)	0.6254(7)	4.52
C(2)	0.8127(5)	0.1746(3)	0.4127(8)	5.94
C(3)	0.7317(4)	0.2174(3)	0.2381(6)	4.39
C(4)	0.5800(4)	0.19937(19)	0.1453(6)	4.22
C(5)	0.4999(4)	0.2535(2)	0.0661(6)	4.11
C(6)	0.5678(5)	0.3260(2)	0.0649(6)	4.26
C(7)	0.7205(5)	0.3398(3)	0.1137(6)	4.91
C(8)	0.8003(5)	0.2865(3)	0.2003(6)	4.82
C(9)	0.4861(6)	0.3879(3)	0.0630(7)	5.83
C(10)	0.5337(5)	0.43102(19)	0.2900(6)	4.46
C(11)	0.5923(4)	0.38191(18)	0.4676(6)	3.61
C(12)	0.7386(4)	0.39009(17)	0.5618(6)	3.49
C(13)	0.8100(4)	0.33154(18)	0.6656(5)	3.23
C(14)	0.7208(4)	0.25729(17)	0.6331(5)	3.25
C(15)	0.5751(4)	0.25388(17)	0.5776(5)	3.25
C(16)	0.5039(4)	0.31536(18)	0.5129(5)	3.29
C(17)	0.9573(4)	0.34794(19)	0.7774(6)	3.64
C(18)	1.0401(5)	0.4211(3)	0.8009(7)	5.22
C(19)	1.0428(4)	0.2977(3)	0.8909(6)	4.42
C(20)	0.3565(4)	0.3075(3)	0.4876(6)	3.93
C(21)	0.2748(4)	0.2395(3)	0.5267(6)	4.89
C(22)	0.2714(5)	0.3641(3)	0.4308(7)	5.43
N(1)	1.1101(5)	0.4785(3)	0.8222(9)	8.90
N(2)	1.1182(4)	0.2609(3)	0.9901(7)	6.60
N(3)	0.2097(4)	0.1858(3)	0.5602(7)	6.89
N(4)	0.1984(5)	0.4069(3)	0.3914(9)	8.46
CB(11)	0.0451(6)	−0.0099(4)	−0.1722(8)	7.3
CB(12)	0.0512(6)	0.0594(3)	−0.0953(9)	6.83
CB(13)	0.0073(7)	0.0703(3)	0.0757(9)	7.28
CB(21)	0.4314(9)	−0.0067(4)	0.2818(12)	11.4
CB(22)	0.3742(7)	0.0257(4)	0.4176(14)	11.4
CB(23)	0.4398(9)	0.0335(4)	0.6328(15)	11.3

(b) H atoms with isotropic temperature factors.

Atom	x	y	z	B/Å^2
H(1A)	0.699(5)	0.151(3)	0.649(7)	6.4(10)
H(1B)	0.865(5)	0.185(2)	0.751(6)	5.6(9)
H(2A)	0.778(5)	0.120(3)	0.374(7)	7.0(11)
H(2B)	0.920(5)	0.188(3)	0.438(7)	7.1(11)
H(4)	0.528(5)	0.148(3)	0.163(7)	6.1(10)
H(5)	0.389(5)	0.240(2)	0.027(6)	5.5(9)
H(7)	0.767(5)	0.391(3)	0.099(6)	5.8(9)
H(8)	0.912(4)	0.301(2)	0.270(6)	5.6(9)
H(9A)	0.369(6)	0.363(3)	0.018(9)	9.5(14)
H(9B)	0.499(5)	0.422(3)	−0.037(7)	6.1(10)
H(10A)	0.619(4)	0.4743(19)	0.299(6)	4.8(8)
H(10B)	0.451(5)	0.453(3)	0.300(7)	6.6(10)
H(12)	0.803(4)	0.4370(18)	0.548(6)	4.4(8)
H(15)	0.512(4)	0.2059(17)	0.571(6)	4.1(8)
HB(11)	0.070(5)	−0.022(3)	−0.298(8)	7.9(12)
HB(12)	0.086(6)	0.103(3)	−0.160(8)	8.7(13)
HB(13)	0.012(7)	0.121(4)	0.143(10)	11.0(16)

TABLE 2. FRACTIONAL ATOMIC COORDINATES OF TCNQ-X(OMe)$_2$, WITH ESTIMATED STANDARD DEVIATIONS IN PARENTHESES

(a) C, N, and O atoms with equivalent temperature factors.

Atom	x	y	z	B_{eq}/Å^2
C(1)	0.0535(4)	0.2173(3)	0.6624(9)	2.4
C(2)	0.1017(5)	0.1961(4)	0.7312(11)	3.2
C(3)	0.1246(4)	0.1608(4)	0.6485(10)	2.8
C(4)	0.1463(4)	0.1687(4)	0.5206(12)	3.0
C(5)	0.1458(4)	0.1374(4)	0.4249(12)	3.4
C(6)	0.1242(4)	0.0977(4)	0.4460(12)	3.0
C(7)	0.1127(4)	0.0874(4)	0.5822(13)	3.6
C(8)	0.1108(4)	0.1198(3)	0.6847(11)	2.8
C(9)	0.1019(5)	0.0720(4)	0.3341(12)	3.8
C(10)	0.0423(4)	0.0736(3)	0.3285(12)	3.2
C(11)	0.0216(4)	0.1147(3)	0.3902(11)	2.4
C(12)	−0.0002(4)	0.1139(3)	0.5169(11)	2.5
C(13)	−0.0027(4)	0.1501(3)	0.6038(9)	1.68
C(14)	0.0277(3)	0.1871(3)	0.5627(10)	1.65
C(15)	0.0381(4)	0.1896(3)	0.4287(10)	2.2
C(16)	0.0319(3)	0.1560(3)	0.3342(10)	2.0
C(17)	−0.0301(4)	0.1478(3)	0.7253(10)	2.4
C(18)	−0.0602(4)	0.1106(4)	0.7571(12)	3.2
C(19)	−0.0362(5)	0.1809(3)	0.8236(13)	3.5
C(20)	0.0391(4)	0.1635(4)	0.1956(12)	3.1
C(21)	0.0497(4)	0.2049(4)	0.1487(11)	3 2
C(22)	0.0367(5)	0.1329(4)	0.0875(12)	3.9
C(23)	0.1778(5)	0.2188(5)	0.3613(16)	5.1
C(24)	0.0794(7)	0.0380(4)	0.7425(16)	6.2
N(1)	−0.0830(5)	0.0820(4)	0.7904(11)	5.4
N(2)	−0.0437(5)	0.2048(3)	0.9065(12)	5.4
N(3)	0.0607(4)	0.2381(4)	0.1097(12)	4.6
N(4)	0.0342(5)	0.1101(4)	0.	5.7
O(1)	0.1623(3)	0.2092(3)	0.4976(9)	4.1
O(2)	0.0935(4)	0.0479(3)	0.6057(10)	4.9

(b) H atoms with isotropic temperature factors.

Atom	x	y	z	B/Å
H(1A)	0.025(4)	0.222(3)	0.720(11)	3.(3)
H(1B)	0.062(4)	0.234(3)	0.609(12)	4.(3)
H(2A)	0.101(5)	0.177(4)	0.794(12)	5.(3)
H(2B)	0.112(5)	0.214(4)	0.788(14)	6.(4)
H(5)	0.146(4)	0.139(4)	0.336(13)	4.(3)
H(8)	0.090(4)	0.109(4)	0.767(13)	5.(3)
H(9A)	0.105(5)	0.043(4)	0.318(13)	5.(3)
H(9B)	0.104(5)	0.087(4)	0.271(14)	7.(4)
H(10A)	0.021(5)	0.081(4)	0.292(14)	7.(4)
H(10B)	0.031(4)	0.054(3)	0.367(12)	4.(3)
H(12)	−0.016(5)	0.084(4)	0.570(13)	6.(3)
H(15)	0.056(4)	0.218(3)	0.391(12)	4.(3)
H(23A)	0.181(5)	0.240(4)	0.357(13)	5.(3)
H(23B)	0.141(5)	0.218(4)	0.299(12)	5.(3)
H(23C)	0.204(5)	0.206(4)	0.371(13)	5.(3)
H(24A)	0.072(4)	0.012(3)	0.738(10)	3.(2)
H(24B)	0.093(5)	0.037(4)	0.849(15)	7.(4)
H(24C)	0.110(5)	0.063(4)	0.806(13)	6.(3)

atoms of the benzene molecules being not included. Six carbon atoms of the benzene molecules were located on the difference Fourier map. The possibility of disorder of the benzene molecule at (1/2,0,1/2) was ignored in the subsequent refinement. All the hydrogen atoms except those belonging to the benzene centered on (1/2,0,1/2) could be located on the difference Fourier map computed during the course of anisotropic refinement; they were included in the subsequent cycles with isotropic temperature factors. The final R was 0.088 for non-zero reflections (R_w=0.124). The weighting schemes used at this stage were $w=\{\sigma^2(F)+0.0204|F_o|+0.0015|F_o|^2\}^{-1}$ for $|F_o|>0$ and $w=0.6236$ for $|F_o|=0$. The final atomic parameters are given in Table 1.**

TCNQ-X(OMe)$_2$. The structure was solved by using the *MULTAN* 74 program.[2] On the E map, 25 atoms of the 30 non-hydrogen atoms could be located. The successive Fourier synthesis revealed the remaining 5 atoms.

The structure was refined, isotropically with the unit weight at the earlier stage and anisotropically at the later stage, by means of the *HBLS* V program.[3] The hydrogen atoms were located on the difference Fourier map and then included in the refinement with isotropic temperature factors. R converged to a rather large value of 0.109 for 1615 observed reflections (R_w=0.113). The weighting schemes used were $w=\{\sigma^2(F)+0.0483|F_o|-0.0002|F_o|^2\}^{-1}$ and $w=0$ for $|F_o|=0$ at the final cycle of the refinement. The final atomic parameters are listed in Table 2.** In the analyses of the two compounds, the atomic scattering factors for C, N, and O were taken from "International Tables for X-Ray Crystallography," Vol. IV,[4] and those for H, from Stewart, Davidson, and Simpson.[5]

Results and Discussion

Molecular Structure. TCNQ-X: A perspective view of the molecule (*ORTEP* II)[6] is shown in Fig. 1, while selected bond distances and bond angles are given in Fig. 2. The most remarkable feature of the structure is that the [2.2]paracyclophane skeleton has the usual structure. The upper benzene ring takes a boat form, as is observed in [2.2]paracyclophane;[7,8] the planes defined by the C(3), C(4), and C(8) atoms and by the C(5), C(6), and C(7) atoms form angles of 12.1(5) and 9.7(5)° respectively with the mean plane made by the C(4), C(5), C(7), and C(8) atoms. The C(3)–C(2) and C(6)–C(9) bonds are further bent down by 12.8(5) and 11.9(5)° from the planes formed by the C(3), C(4), and C(8) atoms and by the C(5), C(6), and C(7) atoms respectively. The TCNQ moiety has a twisted structure. The six-membered ring is in a twisted boat form, the planes formed by the C(13), C(14), and C(15) atoms and by the C(11), C(12), and C(16) atoms are bent up from the mean plane made by the C(12), C(13), C(15), and C(16) atoms by 15.2(4) and 15.7(4)° respectively. On the other hand, both of the two $C(CN)_2$ portions are bent down from the mean plane. The two vectors,

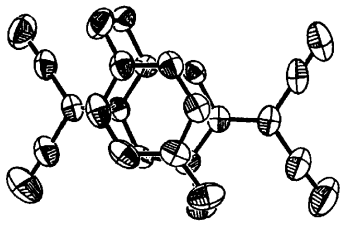

(1) TCNQ-X

Fig. 1. Perspective view of the TCNQ-X molecule.
Non-hydrogen atoms are drawn as thermal ellipsoids at 50% probability level.

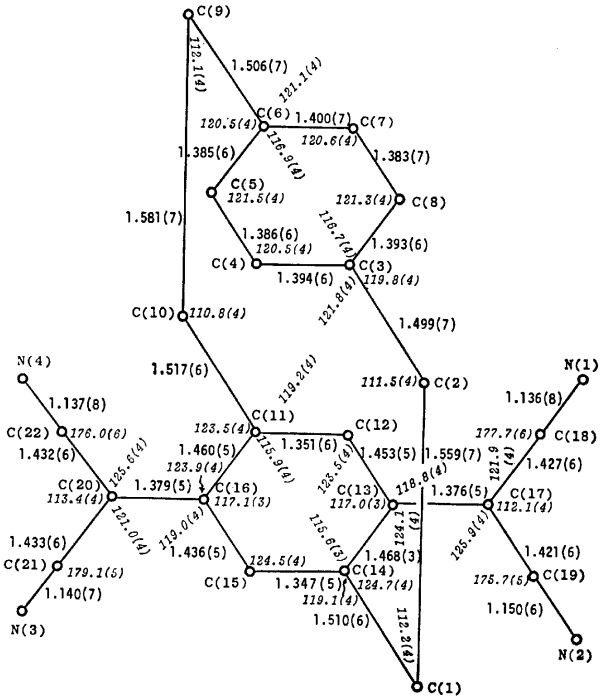

Fig. 2. Bond distances and bond angles in the TCNQ-X molecule (Estimated standard deviations in parentheses).

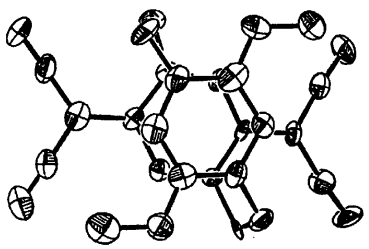

(2) TCNQ-X(OMe)$_2$

Fig. 3. Perspective view of the TCNQ-X(OMe)$_2$ molecule.
Non-hydrogen atoms are drawn as thermal ellipsoids at 50% probability level.

C(13)–C(17) and C(16)–C(20), make angles of 11.9(3) and 12.8(3)° respectively, with the plane defined by the C(12), C(13), C(15), and C(16) atoms. The dihedral angles between two $-C(CN)_2$ planes and the plane made by the C(12), C(13), C(15), and C(16) atoms are 15.0(3) and 15.9(3)°. The C(10)–C(11)–C(16), C(11)–

** Tables of observed and calculated structure factors and anisotropic thermal parameters are kept at the Chemical Society of Japan; Document No. 8207.

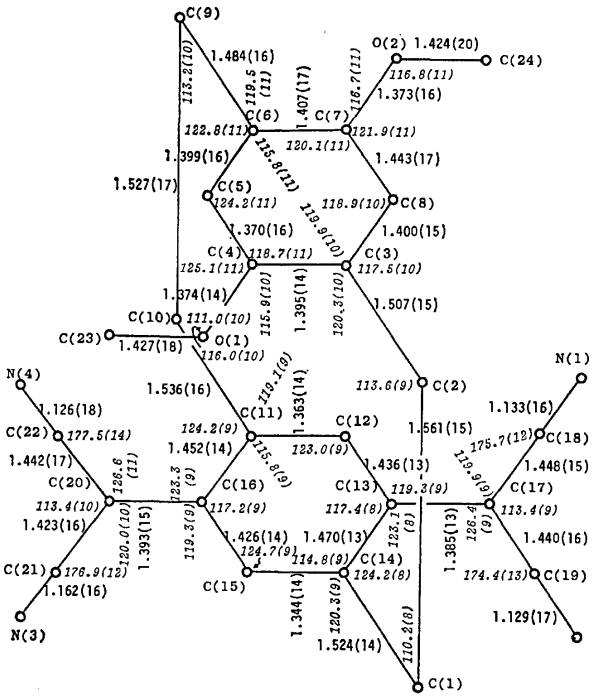

Fig. 4. Bond distances and bond angles in the TCNQ-X-$(OMe)_2$ molecule (Estimated standard deviations in parentheses).

C(16)–C(20), C(16)–C(20)–C(22), C(1)–C(14)–C(13), C(14)–C(13)–C(17), and C(13)–C(17)–C(19) angles ((av. 124.6°) are larger than 120°; they are considered to be due to the repulsions between two pairs of C–C≡N portions and $-(CH_2)_2-$ bridges in the molecule. The C(14)–C(1) and C(11)–C(10) bonds bent up by 7.7(4) and 11.3(4)° from the lower ring. In the $-(CH_2)_2-$ bridges, the torsion angles around the C(1)–C(2) and C(9)–C(10) bonds are −21.0(6) and 5.1(5)° respectively.

TCNQ-X(OMe)$_2$: The molecular structure (*ORTEP* II)[6] is shown in Fig. 3, while the distances and bond angles are given in Fig. 4. The present molecule has a structure similar to that of TCNQ-X except for the OMe portions. As is observed in TCNQ-X, both the upper and lower six-membered rings take boat forms. In the upper ring, the planes formed by the C(3), C(4), and C(8) atoms and by the C(5), C(6), and C(7) atoms are bent down by 8.2(12) and 12.4(12)° respectively from the plane formed by the C(4), C(5), C(7), and C(8) atoms. The OMe groups lie within 0.08 Å on the

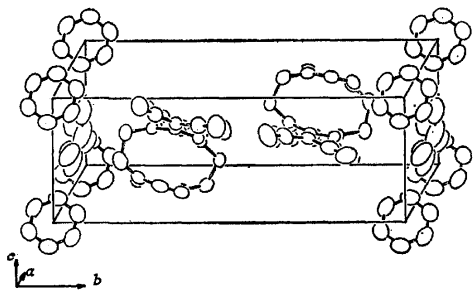

Fig. 5. Perspective view of the crystal structure of TCNQ-X, C_6H_6.

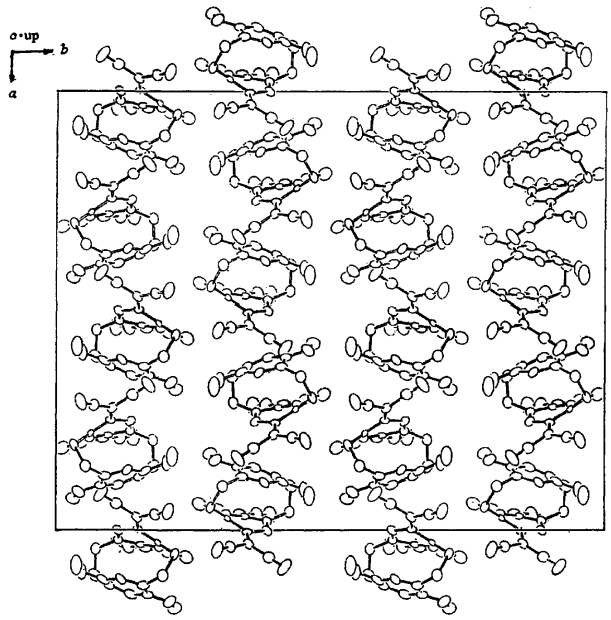

Fig. 6. Crystal structure of TCNQ-X$(OMe)_2$ projected along the c axis.

plane made by the C(4), C(5), C(7), and C(8) atoms. The C(3)–C(2) bond is further bent down by 15.3(12)° from the plane made by the C(3), C(4), and C(8) atoms, and the C(6)–C(9) bond, by 13.0(13)° from the C(5), C(6), and C(7) plane. The TCNQ moiety has a structure similar to that in TCNQ-X. The six-membered ring is also in a boat form; the plane defined by the

Table 3. Short intermolecular atomic contacts less than 3.5 Å
(Estimated standard deviations in parentheses)

TCNQ-X, C_6H_6	
C(20)·····N(2)[a]	3.378(6)
C(21)·····N(2)[a]	3.441(7)
C(22)·····N(2)[a]	3.240(7)
C(6)·····C(15)[b]	3.485(6)
C(6)·····C(16)[b]	3.483(6)
C(7)·····C(13)[b]	3.328(6)
C(7)·····N(1)[c]	3.428(8)
key: a, $-1+x, y, -1+z$; b, $x, y, -1+z$; c, $2-x, 1-y, 1-z$.	
$TCNQ\text{-}X(OMe)_2$	
N(4)·····C(17)[a]	3.379(16)
N(4)·····C(18)[a]	3.394(17)
C(21)·····N(2)[a]	3.371(16)
N(3)·····C(24)[b]	3.43(2)
C(9)·····N(2)[c]	3.305(17)
C(21)·····N(1)[c]	3.397(16)
C(15)·····N(2)[d]	3.378(15)
N(3)·····C(1)[d]	3.293(15)
N(3)·····C(14)[d]	3.320(15)
N(3)·····C(19)[d]	3.386(17)
key: a, $x, y, -1+z$; b, $0.25-x, 0.25+y, -0.75+z$; c, $0.25+x, 0.25-y, -0.75+z$; d, $-x, 0.5-y, -0.5+z$.	

C(13), C(14), and C(15) atoms and the plane defined by the C(11), C(12), and C(16) atoms form angles of 16.9(10) and 16.4(10)° respectively with the mean plane formed by the C(12), C(13), C(15), and C(16) atoms. On the other hand, both of the $C(CN)_2$ portions are bent down from the mean plane, and the C(10)–C(11)–C(16), C(11)–C(16)–C(20), C(16)–C(20)–C(22), C(1)–C(14)–C(13), C(14)–C(13)–C(17), and C(13)–C(17)–C(19) angles (av. 124.6°) are slightly distorted from 120°. The torsion angles around the C(1)–C(2) and C(9)–C(10) bonds in the [2.2] bridges are 23.8(12) and −4.0(12)° respectively.

Crystal Structure. *TCNQ*: Figure 5 shows the crystal structure. The crystalline benzene molecule centered on (1/2,0,1/2) does not give any good shape. Short intermolecular atomic distances less than 3.5 Å are listed in Table 3, the shortest distance being 3.240(7) Å (C(22)(x,y,z)···N(2)($-1+x, y, -1+z$)).

TCNQ-X(OMe)$_2$. The molecular packing in the TCNQ-$X(OMe)_2$ crystal is drawn in Fig. 6. The closest intermolecular atomic contact is 3.293(15) Å (N(3)(x,y,z)···C(1)($-x$, $0.5-y$, $-0.5+z$)), which is listed in Table 3 along with other close contacts.

The calculations were done on an ACOS 700S computer at the Crystallographic Reserach Center, Institute for Protein Research, Osaka University.

The authors wish to express their deep thanks to Professor Soichi Misumi and his co-workers, Institute of Scientific and Industrial Research, Osaka University, for the supply of crystals and for their helpful discussions.

References

1) H. Matsuura, Y. Kai, N. Yasuoka, and N. Kasai, 34th National Meeting of the Chemical Society of Japan, Hiratsuka, April 1976, Abstr. p. 165; Annual Meeting of Crystallographic Society Japan, Nishinomiya, Decemher 1976, Abstr. p. 76.

2) P. Main, M. M. Woolfson, L. Lessinger, G. Germain, and J. P. Declercq, *MULTAN* 74. "A System of Computer Programs for the Automatic Solution of Crystal Structures from X-Ray Diffraction Data," Univ. of York, England and Louvain, Belgium (1974).

3) T. Ashida, "The Universal Crystallographic Computing System-Osaka," The Computation Center, Osaka Univ. (1973), pp. 55—61.

4) "International Tables for X-Ray Crystallography," Kynoch Press, Birmingham (1974), Vol. IV.

5) R. F. Stewart, E. R. Davidson, and W. T. Simpson, *J. Chem. Phys.*, **42**, 3175 (1965).

6) C. K. Johnson, *ORTEP* II, Report ORNL-5138, Oak Ridge National Laboratory, Tennessee (1976).

7) H. Hope, J. Bernstein, and K. N. Trueblood, *Acta Crystallogr., Sect. B*, **28**, 1733 (1972).

8) H. Goto, Y. Kai, N. Yasuoka, and N. Kasai, 10th Symposium on Structural Organic Chemistry, Matsuyama, October 1977, Abstr. p. 219.

9) W. C. Hamilton, *Acta Crystallogr.*, **12**, 609 (1959).

 © 1982 The Chemical Society of Japan Bull. Chem. Soc. Jpn., 55, 985—989 (1982)

Kinetic Study on Conformational Changes of Poly(L-lysine) in Sodium Alkyl Sulfate Solutions. Effects of Surfactant Chain Length and Added NaCl

Kunio TAKEDA,* Akira IBA, and Keishiro SHIRAHAMA†

Department of Applied Chemistry, Faculty of Science, Okayama University of Science, Ridai-cho 1-1, Okayama 700

†*Department of Chemistry, Faculty of Science and Engineering, Saga University, Saga 840*

(Received July 15, 1981)

The conformational changes of poly(L-lysine) (PLL) were observed in alkyl sulfate solutions by a circular dichroic method. PLL forms a β-structure in sodium dodecyl sulfate solution with an apparent first-order rate constant of 3.0×10^{-2} s^{-1} (20 °C). In sodium octyl sulfate (SOS) solution, PLL assumes the α-helix within a certain concentration range of the surfactant, above which the β-structure is favored. The rate of coil to β-structure transition slows down with increase in hydrophobic interaction between surfactants and PLL. The presence of sodium ions decreases the rate of coil to α-helix transition by about two orders of magnitude (2.0×10^{-1} s^{-1} salt free to 3.0×10^{-3} s^{-1} in the presence of 2.0×10^{-2} mol/dm^3 NaCl at 20 °C). These phenomena are explained in terms of a rearrangement process of bound surfactants adjusting for a free energy minimum; a stronger binding force brings about a slower rearrangement rate.

Extensive circular dichroism (CD) studies have been made on the conformational changes of polypeptides in surfactant solutions. Poly(L-lysine) (PLL) has been an interesting material, since it can take on three kinds of conformations depending on experimental conditions.[1-8] For example, the PLL conformation is changed to β-structure in the presence of sodium dodecyl sulfate (SDS) at neutral pH.[1,3,6] However, few kinetic aspects of the conformational changes of PLL in surfactant solutions have been studied. We have applied a CD stopped-flow method to the study of the conformational changes of the PLL in sodium octyl sulfate (SOS) solution.[9] We reported the SOS concentration dependences of both the PLL conformations and the rate constants of the conformational changes; our results are briefly summarized as follows.[9] PLL adopts an α-helix only in a certain concentration range of SOS, taking a disordered structure below the SOS concentration range and β-structure above it. The rate constant of coil to β-structure transition sharply increases with SOS concentration, while that of coil to α-helix transition is almost independent of SOS concentration.

This work examined the above mentioned dependences in the presence of NaCl and also in solutions of an alkyl sulfate with different chain lengths. The main purpose of this paper is to discuss the effects of the chain length of alkyl sulfate and the added NaCl on the conformational changes.

Experimental

The sources of PLL and SOS have been described elsewhere.[9] The SDS is the same sample as before.[10]

The measurements of CD were carried out with a JASCO J-500A spectropolarimeter equipped with a JASCO DP-501 data processor, using a 1.0 mm path length cell with water-circulating jacket. The path length of a cell used in a stopped-flow measurement was also 1.0 mm.[9] Details of the CD and the stopped-flow measurements have been stated previously.[9]

Results

The addition of SDS causes a conformational change of PLL from coil to β-structure, as seen in Fig. 1; this

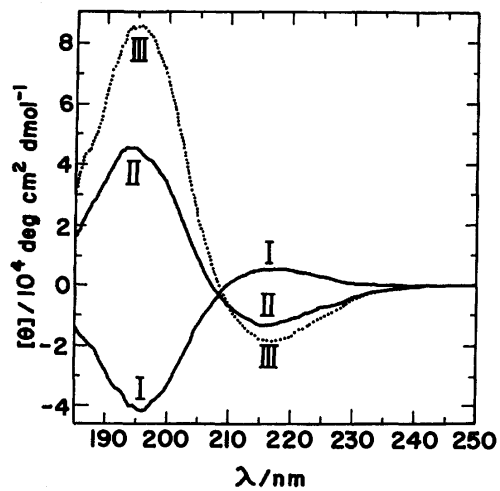

Fig. 1. Typical CD spectra of PLL solutions in the absence (curve I) and the presence (curve II) of 10 mM SDS and the difference CD spectrum between them (curve III) at 20 °C. The concentration of PLL was 2.8×10^{-4} M (residue). The time constant and the scanning speed of the spectropolarimeter were 1.0 s and 20 nm/min, respectively. These spectra are averaged over 8 repetitions and the difference CD spectrum was directly obtained using the data processor.

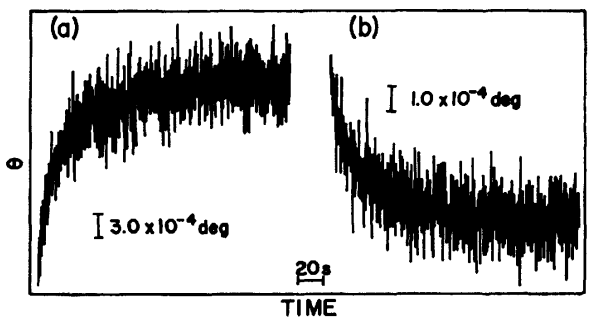

Fig. 2. Typical time courses of ellipticity changes at 195 (a) and 217 nm (b) at 20 °C. The traces (a) and (b) are averages of 8 and 2 repetitions, respectively. The final concentrations of PLL and SDS were 2.8×10^{-4} M (residue) and 10 mM, respectively.

result was previously reported by other investigators.[1,3,6] The CD stopped-flow measurements on the conformational change were made by tracing ellipticities at 195 and 217 nm, where positive and negative peaks appeared in the difference CD spectrum (III in Fig. 1). Typical time courses of the ellipticity changes at both wavelengths are seen in Fig. 2. The direction of the ellipticity change at each wavelength is in accord with the results in Fig. 1, suggesting that the observed process is due to the conformational change from coil to β-structure. The conformational change obeyed first-order kinetics in the ordinary treatment.[9] The rate constant was 3.0×10^{-2} s^{-1} (20 °C), and was independent of the SDS concentration (not shown here).

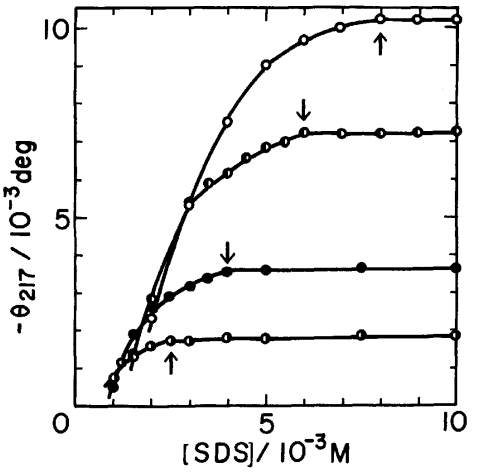

Fig. 3. Effect of PLL concentration on ellipticity, θ_{217} at various SDS concentrations. Residual PLL concentrations are 1.4 (◑), 2.8 (●), 5.6 (◐), and 7.9×10^{-4} M (○). These data were obtained from the measurements under the same experimental conditions as in Fig. 1 except for PLL concentration.

Figure 3 shows the plots of the ellipticities at 217 nm, θ_{217} *vs.* SDS concentration at several PLL concentrations. The conformation of PLL grows with the SDS concentration after a sudden increase in ellipticity. The increase in PLL concentration shifts the range of the SDS concentration where the sudden conformational change of PLL occurs and eventually the conformational change is completed, as seen in Fig. 3.

Figure 4 shows that the CD spectrum of α-helical PLL in the SOS solution is not appreciably affected at a low NaCl concentration; the double negative maximum gradually fades out with increase of NaCl concentration. Since the NaCl added beyond 25 mM (the concentration unit: 1 M=1 mol/dm^3 is used) decreased the ellipticities over the entire wavelength range, the effects of the added salt were examined in the concentration range below 20 mM. The addition of NaCl does not change the characteristic concentration ranges of the surfactants where the conformation of PLL changes, although the critical micelle concentration sharply changes on addition of such an electrolyte. The added NaCl has some effect on the rate constants of the conformational changes in SOS solution and their SOS concentration dependences, as depicted in Figs. 5 and 6. Figure 5 shows the increase of the rate constant with SOS concentration in the presence of NaCl. This exhibits marked contrast with the insensitiveness to SOS concentration in such a concentration range without NaCl.[9] The combination of the 4 figures in Fig. 5 also indicates that the rate constant, k, decreases with increase in the added NaCl concentration at each SOS concentration. As seen in Fig. 6, the presence of NaCl markedly decreases the rate constant of the conformational change at 4.0 mM SOS, which is the lowest concentration where a coil to α-helix transition appears.[9] The rate constant rapidly decreased up to 10 mM NaCl and then gradually leveled off. On the

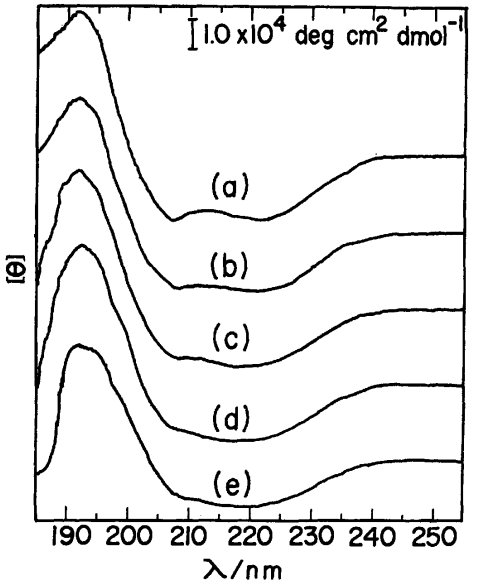

Fig. 4. Changes of CD spectrum of PLL in 5.0 mM SOS solution by addition of NaCl at 20 °C. NaCl concentrations: (a); 0, (b); 5.0, (c); 10.0, (d); 15, and (e); 20 mM.

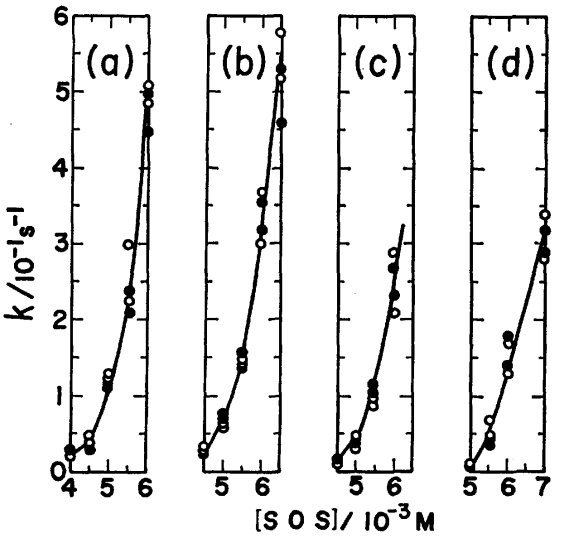

Fig. 5. SOS concentration dependences of rate constant, k, in the presence of NaCl at 20 °C. NaCl concentrations: (a); 5.0, (b); 10.0, (c); 15, and (d); 20 mM. The rate constants were obtained from ellipticity changes at 192 (○) and 221 nm (●) with time. PLL concentration was 2.8×10^{-4} M (residue).

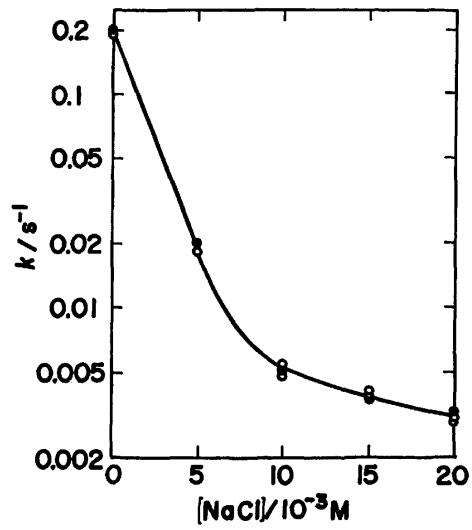

Fig. 6. Effect of NaCl on rate constant of coil to α-helix transition in 4.0 mM SOS solution at 20 °C. The solid and open circles respectively denote the same meanings as in Fig. 5. PLL concentration was 2.8×10^{-4} M (residue).

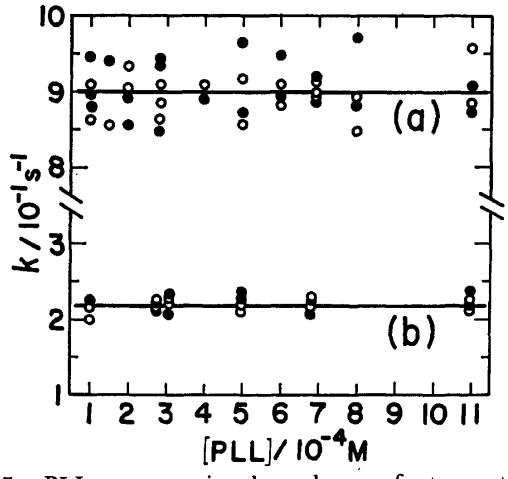

Fig. 7. PLL concentration dependences of rate constants of conformational changes of PLL in 5.0 mM (a) and 8.0 mM (b) SOS solutions at 20 °C. The solid and open circles denote the same meanings as in Fig. 5.

other hand, the presence of NaCl does not affect the rate constant of coil to β-structure transition in SDS solution.

The PLL concentration dependences of two kinds of rate constants, one for the coil to α-helix transition and the other for the coil to β-structure one, were examined in SOS solution, as shown in Fig. 7. The rate constant is almost constant (irrespective of the PLL concentration) in each case. In the same PLL concentration range, the rate constant of coil to β-structure transition induced by SDS is not affected by changing PLL concentration (not shown here).

Discussion

Effect of Chain Length of Alkyl Sulfate on the Conformational Change. As previously reported,[9] PLL adopts an α-helical state in a certain concentration range of SOS. In the PLL residual concentrations between $1.4—7.9\times 10^{-4}$ M, the characteristic SOS concentration range remains almost unchanged. The SOS concentration dependences of residual ellipticities at 192 and 221 nm, $[\theta]_{192}$ and $[\theta]_{221}$ do not differ from those in Fig. 2 of the previous paper.[9] On the contrary, the PLL adopts a β-structure in a solution of SDS whose concentration range is similar to that of SOS. The SDS concentration range where the coil to β-structure transition is observed is clearly dependent on PLL concentration, as seen in Fig. 3; this indicates that about 10 SDS molecules are required for 1 residue of PLL when the conversion to β-structure completes. It is expected that the binding ratio of surfactant to polypeptide determines the conformation of the surfactant-polypeptide complex. The fact that the effect of the PLL concentration on the range of the characteristic surfactant concentration is quite different for these two surfactants may indicate that the β-structured PLL binds a large number of surfactant molecules, while the α-helical PLL does not require so many bound surfactants. It is also expected that the ratio of bound surfactants to free ones is smaller in the case of SOS than in the other because of the difference in binding forces to the polypeptide. Therefore, the SOS concentration range where the coil to α-helix transition is induced is apparently independent of the PLL concentration. This is in line with the results by Satake and Yang[8] that PLL and poly(L-ornithine) (PLO) adopt β-structure and α-helix, respectively, in sodium decyl sulfate solution, and that such a difference is also reflected in the binding isotherm, which is much steeper for the β-structured polypeptide than the α-helical one. Alkyl sulfates may be probably oriented in the same direction on the β-structured polypeptide, while they may be oriented radially on the α-helical one. So, alkyl sulfates would be in contact with each other more efficiently on the β-structure than on the other, leading to a stronger binding. Such a difference in the mode of binding would reflect the difference in the amounts of surfactants bound to PLL.

The conformational change of PLL induced by SDS was followed as the ellipticity changes at 195 and 217 nm with time. The observed process must be the change from random coil to β-structure, on the basis of the comparison of the time courses in Fig. 2 with the changes of CD spectra in Fig. 1. The first-order rate constant of the conformational change of PLL induced by SDS is *ca.* 3.0×10^{-2} s^{-1} (20 °C); it is independent of SDS concentration. This rate constant is slower than that of the SOS-induced coil to β-structure transition ($6—10\times 10^{-1}$ s^{-1}). The clear distinction in the transition rates must be attributed to the differences in the chain length of alkyl sulfates, since binding energies are different for these surfactants. It should be noted that the rate constants of the conformational changes are quite independent of PLL concentrations in SOS solution, as seen in Fig. 7. These facts would suggest that the binding process between the surfactants and the polypeptide is not a rate-determining step in the conformational changes. Alkyl sulfates bound to

polypeptides can be in contact with each other through their alkyl chains, and the conformational changes of the polypeptide must be made together with many surfactant molecules bound on it. In the course of a conformational change of polypeptide, some of the bound surfactants may be forced to move from the initial binding sites to some other sites to achieve a more thermodynamically favorable conformation. Through this process, the bulky hydrophobic groups of surfactants should find maximal contacts between the hydrophobic groups of bound surfactants and the hydrophobic parts of the polypeptide, reconciling with the structure formation to reach minimal free energy. In the initial binding stage before the conformational change, the interaction with SDS is stronger than that with SOS. So, the coil to β-structure transition in SDS solution seems to require a much longer time in the rearrangement process than that in SOS solution.

The rate constant for the coil to β-structure transition sharply depends on SOS concentration, as seen in Fig. 5 of Ref. 9, although it is independent of SDS concentration. The SOS concentration dependence of the rate constant may be due to the transitional concentration range of SOS where the coil to α-helix transition shifts to the coil to β-structure one. Subsequently, it might be expected that the rate of the coil to β-structure transition is independent of surfactant concentration except for a very narrow range of surfactant concentrarion where the cooperative conformational change begins to occur. This indicates that the transitional concentration range of SOS is wider than that of SDS because the cooperativity of conformational change is expected to be greater for SDS than for SOS.

Sarkar and Doty[1] and Li and Spector[3] suggest that the intramolecular β-structure of PLL is formed in SDS solution, but Satake throws some doubt on this.[11] If the intermolecular β-structure is formed, the rate of the coil to β-structure transition should be dependent on PLL concentration. However, the opposite is the case, as stated above, suggesting the probability of the intramolecular structure formation in both α-helix and β-structure. In addition, the coil to β-structure transition obeys first-order kinetics, as in the case of the coil to α-helix one.[9] If the intermolecular β-structure is formed, the kinetics of the coil to β-structure transition will not be of first-order but of mixed order, as previously discussed by Snell and Fasman.[12] All these results would be indicative of the intramolecular β-structure formation in the surfactant solution. Whether the β-structure formation is intramolecular or intermolecular is considered to be essentially responsible for the degree of polymerization of the PLL used.[3,6,13] The intramolecular β-structure seems to be predominant in the present PLL with polymerization degree of 140.[9]

Effect of Added NaCl on the Conformational Change. Addition of NaCl as much as 10 mM seems to cause very slight changes in the α-helical conformation of PLL in SOS solution, as judged from the CD spectra in Fig. 4. The effect of added NaCl is so weak that the α-helical conformation itself does not change to some other conformation, in marked contrast with the effect of added 1-octanol which causes another transition from α-helix to β-structure.[9] The addition of the salt does not alter the surfactant concentration range where the conformation changes, probably because the amount of bound surfactant molecules is not affected by the presence of the salt.

As seen in Figs. 5 and 6, however, the addition of NaCl causes a considerable effect on the rate constant of the coil to α-helix transition in the SOS solution, while that of the coil to β-structure transition in the SDS solution is not affected by the addition of NaCl. As discussed above, the surfactant molecules are considered to be implanted radially on an α-helical polypeptide and the amount of bound surfactants seems to be much smaller on the α-helical polypeptide than on the β-structured one. This indicates that, although the surfactant molecules bound to the polypeptide would be in contact with each other, they are less compact when bound on α-helical polypeptide than on the other one. Sodium ions, as counter ions, must condense around the surfactant-α-helical polypeptide complex and weaken the repulsive force between the surfactants, just as in the case of ordinary micelle formation. Thus, the presence of NaCl can be considered to cause stronger interactions between the surfactants and the α-helical polypeptide. It is expected in such situations that the more strongly bound surfactants have a slower rearrangement process on the α-helical PLL. This phenomenon would markedly appear as the drastic decrease of the rate constant at 4.0 mM SOS, which is the lowest concentration at which the coil to α-helix transition is induced, as seen in Fig. 6. On the contrary, many surfactant molecules can bind onto the β-structured polypeptide with their hydrocarbon chains oriented in the same direction with strong contacts. The interaction between the surfactants is so strong that the added NaCl can hardly change the rate of the rearrangement of surfactant molecules.

In conclusion, the random coiled conformation of PLL changes to β-structure in the presence of SDS. This is because SDS gives a more hydrophobic atmosphere to host polypeptide than SOS which induces the coil to α-helix transition within the limited concentration range. The intramolecular β-structure is considered to be formed in the PLL with the polymerization degree of 140. The rate of coil to β-structure transition has a tendency to become slower with increase in the hydrophobic interactions of surfactants. The rate of the conformational change is affected very little by the added NaCl, probably because of the strong interactions between the surfactant molecules bound to the β-structured polypeptide. On the other hand, the added NaCl appreciably decreases the rate of coil to α-helix. This would be due to the fact that the surfactants bound to the α-helical PLL are less compact, and so the α-helical-surfactant complex is much more influenced by the addition of sodium ions.

This work was partly supported by a Grant-in-Aid for Scientific Research to K. T. from the Ministry of Education, Science and Culture (No. 56540270).

References

1) P. K. Sarkar and P. Doty, *Proc. Natl. Acad. Sci. U. S. A.*, **55**, 981 (1966).
2) M. J. Grourke and J. H. Gibbs, *Biopolymers*, **5**, 586 (1967).
3) L. K. Li and A. Spector, *J. Am. Chem. Soc.*, **91**, 220 (1969).
4) M. M. Feldshtein, A. B. Zezin, and J. J. Gragerova, *Biokhimia (Moscow)*, **37**, 305 (1972).
5) A. B. Zezin, M. M. Feldshtein, V. P. Merzlov, and J. J. Maletina, *Mol. Biol.*, **7**, 174 (1973).
6) I. Satake and J. T. Yang, *Biochem. Biophys. Res. Commun.*, **54**, 930 (1973).
7) I. Satake and J. T. Yang, *Biopolymers*, **14**, 1841 (1975).
8) I. Satake and J. T. Yang, *Biopolymers*, **15**, 2263 (1976).
9) K. Takeda, A. Iba, and K. Shirahama, *Bull. Chem. Soc. Jpn.*, **54**, 1793 (1981).
10) K. Takeda, M. Miura, and T. Takagi, *J. Colloid Interface Sci.*, **82**, 38 (1981).
11) I. Satake, *Hyomen (Surface)*, **15**, 511 (1977) (in Japanese).
12) C. R. Snell and G. D. Fasman, *Biochemistry*, **12**, 1017 (1973).
13) W. L. Mattice and W. H. Harrison, *Biopolymers*, **15**, 559 (1976).

Properties of Magnesium Oxides Prepared from Various Salts and Their Catalytic Activity in 1-Butene Isomerization

Tsuneo MATSUDA,* Jun TANABE, Nobuatsu HAYASHI, Yoh SASAKI, Hiroshi MIURA, and Kazuo SUGIYAMA

Department of Applied Chemistry, Faculty of Engineering, Saitama University, Saitama 338

(Received August 10, 1981)

The basicity, one-electron donor property, and surface area were examined on the magnesium oxide catalysts prepared from six different kinds of magnesium salts. Magnesium oxide prepared from magnesium nitrate, oxalate, and acetate exhibited strong basicity and relatively large surface area and, on the other hand, MgO prepared from magnesium chloride, carbonate and sulfate had relatively weak basicity and small surface area. Number of one-electron donor centers hardly changed in the variety of magnesium oxides, except the one prepared from magnesium chloride. Magnesium oxide prepared from chloride showed both the lowest basicity with less strength than $H_-=15.0$ and surface area in the six kinds of catalysts. In order to examine the influence of remaining anions in MgO a variety of catalysts were prepared by the addition of ammonium chloride, sulfate, and carbonate, respectively in MgO prepared from the nitrate. Ammonium chloride brought the greatest influence on the basicity, one-electron donor property, and surface area. Thus the remaining chloride ion greatly affected such properties as cited above. Sodium nitrite which decomposes at higher temperature than 320 °C was added to the magnesium oxides for the examination of the effect of the sodium cation. The amount of the basicity with a moderate strength ($H_-=15.0$—22.3) increased by the addition of $NaNO_2$. This was ascribed to the formation of the moderate strength of basicity by the interaction of Na_2O, one of the decomposed products of $NaNO_2$ and MgO. Isomerization of 1-butene was carried out on the six kinds of catalysts at 30 °C. The magnesium oxides prepared from nitrate, oxalate, and acetate salts (group A) exhibited isomerization activity and the ones from chloride, sulfate, and carbonate (group B) did not entirely. The isomerization activity could be correlated with the stronger basicity than $H_-=22.3$. Temperature pregrammed desorption curves of acetic acid adsorbed on the catalysts indicated two peaks at around 350 and 420 °C in group A catalysts and only one at 350 °C in group B. The desorbed peak at around 420 °C was assigned to the adsorbed acetic acid on the stronger basic sites than $H_-=22.3$.

It is well known that magnesium oxide is characterized by extremely strong basicity[1-3] and one-electron donor property.[4] Kijenski and Malinowski[5,6] reported that magnesium oxide prepared from magnesium nitrate exhibited such strong basicity as $H_-=33.0$ and that magnesium oxide doped with sodium vapor had further stronger basicity than $H_-=35.0$. Accordingly we examined at first the basicity of magnesium oxide prepared from basic magnesium carbonate, on which sodium vapor was doped as a trace experiment of Kijenski and Malinowski. The results, however, did not entirely show stronger basicity than $H_-=35.0$. Kijenski[7] suggested to us that a trace of remaining carbonate ion in MgO, when it was prepared by from basic magnesium carbonate, would hinder the formation of the stronger basic sites. Consequently, it was considered that the remaining anions, when MgO was prepared from the different magnesium salts, would greatly affect the strength of basicity. On the basis of the consideration basicity, one-electron donor property and surface area of magnesium salts were undertaken to examine in this study. On the six kinds of MgO catalysts isomerization of 1-butene was carried out and their activity was connected with such physico-chemical properties of the catalysts as basicity, one-electron dnor and safaoe area. Temperature progammed desorption (TPD) method of acetic acid adsorbed on the catalysts was also undertaken forthe examination of basicity distribution, as anothermethod from a titration method.

Experimental

Materials. Magnesium oxides were prepared from six different magnesium salts as shown in Table 1. In each of the saturated aqueous solutions of magnesium nitrate, chloride, and sulfate, two times as dilute aqueous ammonia as the concentrated one was gradually added to precipitate magnesium hydroxide. The precipitates were washed well with distilled water; 5 times in the case of nitrate, 11 times in chloride, and 8 times in sulfate, respectively. Thus even by

Table 1. Basicity, number of one-electron donor centers, and specific surface area of MgO prepared from six different magnesium salts

Magnesium salts	Basicity H_-/mmol g^{-1}						Number of one-electron donor centers	Surface area
	9.3—15.0	15.0—17.2	17.2—22.3	22.3—27.0	27.0—33.0	Total	spins g^{-1} × 10^{18}	m^2 g^{-1}
$Mg(NO_3)_2$	0.08	0.01	0.04	0.05	0.03	0.21	1.8	85.7
$MgSO_4$	0.18	0.01	0.01	—	—	0.20	2.1	86.3
$MgCl_2$	0.04	trace	—	—	—	0.04	0.047	19.0
$MgCO_3$-$Mg(OH)_2$	0.02	0.11	—	—	—	0.13	1.8	59.4
MgC_2O_4	0.03	0.12	0.03	0.04	0.03	0.25	1.2	140
$Mg(CH_3COO)_2$	0.04	0.03	0.03	0.03	0.02	0.15	2.1	117

washing with water so well every trace of anion could not be eliminated in every case. Magnesium acetate was dissolved in 6 mol dm^{-3} acetic acid solution, in which the aqueous ammonia of the same concentration as that indicated above was added to precipitate magnesium hydroxide. The precipitate was also washed 5 times with the distilled water All precipitates described above were dried at 120 °C for 12 h and then calcined at 550 °C for 20 h in air. Both magnesium oxalate and basic magnesium carbonate were decomposed to MgO at 550 °C for 20 h in air. Thus prepared samples were analyzed by X-ray diffraction (Rigaku Denki DS type, target Cu $K\alpha$) and could be confirmed to be MgO, and designated as MgO–N (MgO prepared from magnesium nitrate), MgO–Cl (from chloride), MgO–S (from sulfate), MgO–C (from basic carbonate), MgO–O (from oxalate), and MgO–A (from acetate), respectively. Additional compounds of anions and $NaNO_2$ in MgO were prepared as folows; $Mg(OH)_2$ prepared from magnesium nitrate according to the method described above was impregnated in the solutions of ammonium chloride, sulfate, and carbonate, respectively and then evaporated to dryness on the water bath. Thus prepared $Mg(OH)_2$ containing anions was also decomposed at 550 °C for 20 h in air. Sodium nitrite was mixed with MgO and then their mixture was calcined at 400 °C for 2 h under evacuation.

Measurement of Basicity and One-electron Donor Centers. Before the measurements, MgO catalysts were treated at 400 °C for 2 h in a vacuum. The basicity of the catalysts was determined by the titration method with the solution of benzoic acid in benzene (0.05 mol dm^{-3}) in the presence of appropriate Hammett indicatores. The following was applied as basicity indicators;[3,4] phenolphalein ($H_-=9.3$), 2,4-dinitroaniline ($H_-=15.0$), 4-chloro-2-nitroaniline ($H_-=17.2$), aniline ($H_-=27.0$), and triphenylmethane ($H_-=33.0$). By the way the basicity of MgO treated at 500 °C for 2 h in a vacuum showed nearly the same values as the one treated at 400 °C. This agreed with the results of the report of Kijenski that the basicity hardly changed by heat-treatment at the temperature of less than 500 °C.[7] The number of one-electron donor centers was determined by the mesurement of concentration of the anion radical formed by tetracyanoethylene adsorption (in benzene solution) on MgO surface. ESR spectrometer in X-band (Varian E-Line Modulation 100 KHz) was used to record the signal of the resulting radical at room temperature. Spin concentrations were determined by comparison of the area obtained by double integration of the first derivative curves for the sample and for a standard of 2,2-diphenyl-1-picrylhydrazyl benzene solution.

All the reagents used in this study were special grade from Wako Junyaku Co. and used without further purification except benzene and benzoic acid. Benzene and benzoic acid were purified by rectification after reflux in the presence of molecular sieve and recrystallization from water, respectively.

1-Butene Isomerization. 1-Butene isomerization was carried out at 30 °C in a closed system with a volume of 181 cm^3 which was directly connected to a gas chromatograph. The catalysts were evacuated at 500 °C for 2 h before the reaction. Reaction products were analyzed by gas chromatograph equipped with a thermal conductivity detector at 0 °C. The column consisted of 4 m long stainless steel tube (2 mm i.d.) packed with VZ-7. The reaction products released from the system were detected time dependently. The amount of 1-butene fed in the reactor was usually 2.97 mmol and catalysts used was 0.1 g.

TPD of Adsorbed Acetic Acid. TPD of adsorbed acetic acid on MgO consisted of a step-wise heating procedure (5 °C min^{-1}) under flowing N_2 (30 cm^3 min^{-1}). The catalyst (0.2 g) was heated at 550 °C for 2 h under vacuum before adsorption of acetic acid at 35 °C for 30 min. Desorbed compounds were detected by gas chromatograph equipped with the column packed with SiO_2 sand.

Results

Basicity and One-electron Donor Centers of Six Kinds of MgO. The basicity, number of one-electron donor centers and specific surface area of magnesium oxides were summarized in Table 1. The MgO–N, MgO–O, and MgO–A (group A) showed stronger basicity than $H_-=22.3$, but MgO–Cl, MgO–S, and MgO–C (group B) showed a weaker one than that value. However, one could not find stronger basicity than $H_-=35$ in the former catalysts. The MgO–O exhibited both the highest basicity and surface area, and in group B, basicity and surface area of MgO–Cl were the lowest. In the catalysts of group B a trace of anion can be considered to be left. Thus a trace of remaining anions, especially chloride ion, greatly affects basicity and surface area towards the decrease of their values. Number of one-electron donor centers was not almost concerned with the remaining ions except chlorine and was nearly constant.

Additional Effects of Anions and $NaNO_2$. The influences of anions were further examined by the addition of ammonium chloride, sulfate, and carbonate in MgO–N as a standard, since this had a broad distribution of basicity. As shown in Table 2 a large influence

Table 2. Basicity, number of one-electron donor centers, and specific surface area of MgO added with anions

Amount of anion added to 1 g MgO		Basicity H_-/mmol g^{-1}						Number of one-electron donor centers	Surface area
	mmol	9.3—15.0	15.0—17.2	17.2—22.3	22.3—27.0	27.0—33.0	Total	spins $g^{-1}\times 10^{18}$	m^2 g^{-1}
Cl^-	0.12	0.05	0.01	trace	trace	—	0.06	0.6	34.1
	0.28	0.05	trace	—	—	—	0.05	0.6	24.2
	0.58	0.06	trace	—	—	—	0.06	0.3	21.9
SO_2^{4-}	0.11	0.16	0.04	0.14	0.01	0.02	0.37	2.9	107
	0.30	0.18	0.07	0.13	trace	trace	0.38	1.4	110
	0.58	0.20	0.10	0.06	trace	—	0.36	1.7	114
CO_2^{3-}	0.08	0.02	0.07	0.10	0.02	0.01	0.22	1.9	85.9
	0.29	0.10	0.09	0.11	0.01	0.02	0.33	2.1	85.9
	0.58	0.18	0.07	0.09	0.04	trace	0.38	1.9	82.5

Table 3. Basicity of MgO added with $NaNO_2$

Amount of $NaNO_2$ added to 1 g MgO[a)] mmol	Basicity H_-/mmol g^{-1}					
	9.3—15.0	15.0—17.2	17.2—22.3	22.3—27.0	27.0—33.0	Total
0	0.08	0.01	0.04	0.05	0.03	0.21
0.3	0.08	0.02	0.07	0.03	0.01	0.21
0.9	0.08	0.14	0.06	0.03	0.01	0.32
1.8	0.01	0.17	0.06	trace	trace	0.24

a) MgO was prepared frommagnesium nitrate.

Table 4. Basicity of MgO–N, MgO–Cl, MgO–S, and MgO–C added with $NaNO_2$[a)]

Catalysts	Basicity H_-/mmol g^{-1}					
	9.3—15.0	15.0—17.2	17.2—22.3	22.3—27.0	27.0—33.0	Total
MgO–N	0.08	0.14	0.06	0.03	0.01	0.32
MgO–Cl	0.01	0.03	0.01	trace	—	0.05
MgO–S	0.07	0.11	0.02	trace	—	0.20
MgO–C	0.01	0.12	0.02	trace	—	0.15

a) Added amount of $NaNO_2$ is 0.9 mmol/g-MgO.

of chloride ion could also be detected in this case. By addition of only 0.12 mmol as chloride ion per gram of MgO the stronger basic sites than $H_-=17.2$ rapidly diminished. The influences of other ions as sulfate and carbonate were not so remarkable as those of the chloride ion, but stronger basic sites decreased to a large extent in all ions. On the contrary total basicity increased by addition of ammonium salts. Surface area increased by addition of $(NH_4)_2SO_4$ and decreased by NH_4Cl and hardly changed by $(NH_4)_2CO_3$. The extent of the influence of anions on the surface area was in the order; $Cl^- > SO_4^{2-} > CO_3^{2-}$. It could be also confirmed that the number of one-electron donor centers was hardly changed by the addition of anions.

Instead of anions, cation was added to magnesium oxides to examine its influence on physicochemical properties. The results were summarized in Tables 3 and 4. With increase of the added amount of $NaNO_2$ basicity with a moderate strength ($H_-=15.0$—17.2) increased and total basicity attained a maximum of 0.9 mmol/g MgO of $NaNO_2$ (see Table 3). By addition of $NaNO_2$ into the group B catalysts, strong basic sites which did not exist before addition appeared. Total basicity hardly changed except MgO–N. It was confirmed by titration method that $NaNO_2$ did not exhibit any basicity. When $NaNO_2$ was decomposed in air or under vacuum, a fused solid was obtained. The solid was very hard and deliquesced during grinding in air. Therefore, measurement of the basicity of the decomposed solid did not suceed.

1-Butene Isomerization. Isomerization of 1-butene was carried out on the six kinds of MgO catalysts at 30 °C. The group A catalysts alone exhibited isomerization activity and group B did not entirely. Time dependency of 1-butene conversion was shown in Fig. 1. The slope between 2 and 7 or 8 min in a plot of conversion *vs.* reaction time was taken as an initial rate. The good correlation between the rate and the basicity

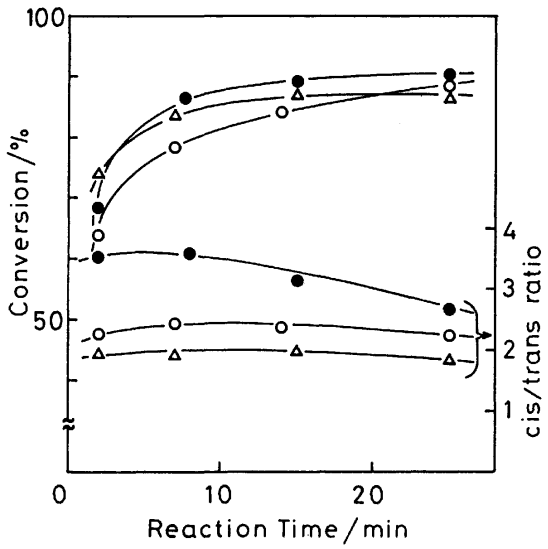

Fig. 1. Conversion-time and *cis/trans* ratio plots of 1-butene isomerization.
○: Reaction over MgO prepared from magnesium nitrate, ●: magnesium oxalate, △: magnesium acetate.

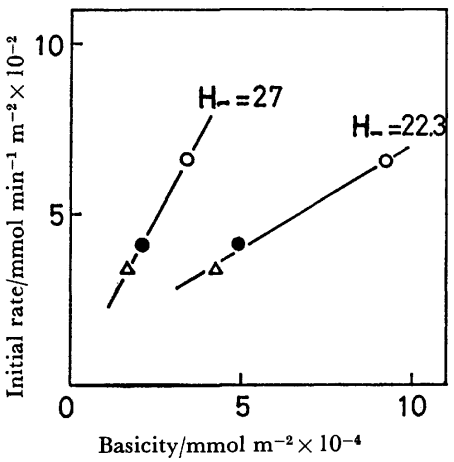

Fig. 2. Relationship between initial rate and basicity with the strength$\geq H_-=22.3$ or 27.
Symbols are the same as those in Fig. 1.

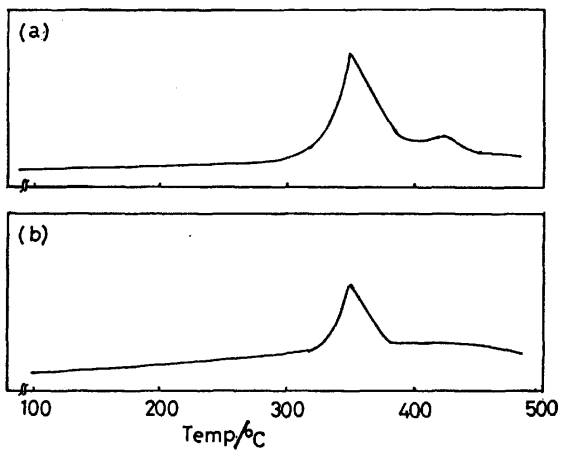

Fig. 3. Typical TPD curves.
(a): MgO–N, (b): MgO–Cl.

stronger than $H_-=22.3$ or 27 per each unit surface area was obtained as shown in Fig. 2.

TPD Measurement. With the aim of examining the basicity distribution by another method except the titration method, and of comparing the results of both methods TPD was carried out. The typical results are shown in Figs. 3(a) and (b). Group A catalysts exhibited two desorbed peaks at near 350 and 420 °C, repectively (Fig. 3(a)). Group B which was inactive for the isomerization exhibited only a peak at 350 °C (Fig. 3(b)). The TPD curve of the catalyst prepared by addition of NH_4Cl in MgO–N was entirely similar to that of Fig. 3(b). It could be demonstrated that the desorbed peak at higher temperature was diminished by the chloride ion left in MgO. By the TPD method a detailed basicity distribution could not be obtained, but a broad one.

Discussion

Basicity nad One-electron Donor Centers of Six Kinds of MgO, Additional Effects of Anions and $NaNO_2$. It is obvious from the results in Tables 1 and 2 that the remaining anions during the preparation of MgO remarkably affect the basicity, one-electron donor centers (only in the case of Cl^-) and surface area. The added ammonium salts decompose evolving gases[8] by heating at 550 °C. In the decomposition of ammonium chloride both NH_3 and HCl are evolved. The strong acid, HCl will interact with MgO to shrink MgO, reducing its basicity and surface area. Chloride ion in HCl probably sinters MgO particles to reduce surface area, as it is known that Cl^- sinters UO_2 particle.[9] The effect of NH_3 would be much smaller than Cl^- in this case. Ammonium sulfate and carbonate decompose as follows:[8]

$$(NH_4)_2CO_3 \longrightarrow 2NH_3 + CO_2 + H_2O,$$

$$(NH_4)_2SO_4 \longrightarrow NH_3 + (NH_4)HSO_4.$$

As the effect of NH_3 seems to be stronger than that of CO_2 or $(NH_4)HSO_4$, more basic sites are produced than acidic sites. The increase of surface area by addition of ammonium sulfate is not due to NH_3, but to sulfate ion, because it was not found in the case of ammonium carbonate.

The basic center is considered mainly to consist of surface O^{2-}.[10,11] Chloride ion added will reduce the electron density of surface O^{2-} by its large electron negativity, leading to the decrease in basicity of MgO. One-electron donor centers consist of anion vacancies in MgO, in which free electron enters.[11,14] Cordischi *et al.*,[15] however, proposed a model of the electron donor surface site consisting of dual site (O^{2-}_{cus}, OH^-), where O^{2-}_{cus}, indicates O^{2-}_{cus} ions in a coordinatively unsaturated site. Thus the accurate structure of one-electron donor centers is still obscure. In either case chloride ions existing in MgO will also attract electron by strong electron affinity, reducing the number of one-electron donor centers. The effect of both sulfate and carbonate ions with weak electron affinity hardly affect the electron donor property. This also agrees with the results in the literature.[15] Both sulfate and carbonate ions do not affect one-electron donor property, as already described, but certainly do the strong basicity, (see Tables 1 and 2) *i.e.*, both affect only the strong basic site to reduce the strength. The strong basic sites ($>H_-=17.2$ or 22.3) will be high in charge density, onto which electrons will easily transfer. Therefore the sites might be affected even by weaker ions such sulfate and carbonate, or one could consider that both ions occlude the strong basic sites. That MgO–S, MgO–C, and MgO added with $(NH_4)_2SO_4$ or $(NH_4)_2CO_3$ had larger surface area than MgO–Cl might be associated with less sintering effect of both ions than Cl^-. Rather larger surface areas of MgO–O and MgO–A might be due to the evolving gases in the decomposition of organic radicals in magnesium salts. Thus, this study provides usuful indications of suitable methods for preparing magnesium oxide having the most favorable catalytic and surface properties.

Sodium nitride decomposes according to the following reaction at more than 320 °C.[16]

$$2NaNO_2 \longrightarrow Na_2O + N_2O_3(=NO+NO_2)$$

and a mechanical mixture or interacted products between them will be formed. By addition of $NaNO_2$ the concentration of the moderate basicity increased, but further addition caused a decrease of the strong basicity, as shown in Table 3. These indicate that Na_2O interacts with the strong basic sites in MgO to reduce the basicity, resulting in the increase of the moderate strength by the increment of Na_2O. Additional details of the interaction of $NaNO_2$ cannot be provided at present, but will be further studied in the future.

1-Butene Isomerization and TPD. As shown in Fig. 2 a good correlation of the initial rate with the stronger basicity than $H_-=22.3$ or 27 indicates that 1-butene isomerization proceeds on such strong basic sites. Therefore the isomerization is inactive on the group B catalysts existing only on weak basic sites. This fact agrees with the results of isomerization of 1-pentene on MgO doped with metalic sodium,[6] requiring stronger basic sites than $H_-=35$. By the reactivity of 1-butene and pentene the isomerization of the former would occur on the weaker basic sites than those in the case of the latter. The reaction mechanism of 1-butene isomerization will be started with proton abstration from the alkene molecule by the stronger

basic site than $H_-=22.3$. Therefore a mechanism similar to that proposed by Pines and Schaap[17] can also hold in this case. As a result an allyl-type carbanion as an intermediate would be formed:

$$CH_2=CH-CH_2-CH_3 + O^{2-} \longrightarrow \underset{\ominus}{CH_2-CH-CH-CH_3} + OH^-,$$

where O^{2-} indicates the basic site. With back donation of one proton from OH^- the intermediate would transform into 2-butene.

$$\underset{\ominus}{CH_2-CH-CH-CH_3} + OH^- \longrightarrow CH_2-CH=CH-CH_3 + O^{2-},$$

It was concluded by Kijenski and Malinowski that the one-electron donor center was independent from the basic site.[6] Cordischi and Indovina reported that there existed a parallelism between basic and one-electron donor properties.[18] In either case the catalytic activity of alkene isomerization and cumene dehydrogenation was unambiguously associated with the one-electron donor center.[6] The center will similarly attract a proton from 1-butene to proceed the reaction, probably in the same way as indicated by Kijenski and Malinowski.[6] As suggested by this study, however, isomerization mainly proceeds on the strong basic sites already described.

The ratio of *cis* to *trans* isomers was rather low in comparison with such a value of 18, as indicated by Tanabe *et al.*[2] This difference might be either due to the concecutive reaction from *cis* to *trans*, as the conversion of 1-butene was so high, or to the thermodynamical stability of *trans* isomer.

TPD curve of the group A catalysts is characterized by two desorption peaks of 350 and 420 °C as shown in Fig. 3(a). The desorption peak at high temperature corresponds to the stronger basicity than $H_-=22.3$ or 27 in comparison with the results of 1-butene isomerization. It should be noted that TPD of adsorbed acetic acid can provide a suitable method to detect the existence of the basicity stronger than $H_-=22.3$. By the way the TPD of adsorbed CO_2 and gaseous HCl did not succeed, because no desorption peak appeared upto 550 °C, but that of magnesium acetate exhibited similar behavior as in Fig. 3(b). Consequently magnesium acetate by adsorption of acetic acid was not formed, which was also confirmed by X-ray analysis. Detailed basicity distribution may be obtained by the TPD method of other acidic compounds adsorbed.

References

1) K. Tanabe, "Solid Acids and Bases," Kodansha Scientific Book, Tokyo (1970).
2) H. Hattori, N. Yoshii, and K. Tanabe, *Proc. 5th Inter. Congr. Catal.* **10**, 233 (1971).
3) J. Take, N. Kikuchi, and Y. Yoneda, *J. Catal.*, **21**, 164 (1971).
4) J. Kijenski and S. Malionwski, *Bull. Acad. Pol. Sci., Ser. Sci. Chim.*, **25**, 329, 427 (1977).
5) J. Kijenski, K. Brzozka, and S. Malinowski, *Bull. Acad. Pol. Sci., Ser. Sci. Chim.*, **26**, 271 (1978).
6) J. Kijenski and S. Malinowski, *J. Chem. Soc., Faraday Trans. 1*, **74**, 250 (1978).
7) J. Kijenski, in private communication.
8) T. Chitani, "Mukikagaku," Sangyo Tosho, Tokyo (1959), pp. 629—632.
9) K. Hashimoto and K. Hamano, "Ceramics No Kiso," Kyoritsu Shuppan, Tokyo (1977), p. 270.
10) O. V. Krylov, Z. A. Markova, I. I. Tretiakov, and E. A. Fokina, *Kinet. Katal.*, **6**, 128 (1965).
11) T. Iizuka, H. Hattori, Y. Ohno, J. Sohma, and K. Tanabe, *J. Catal.*, **22**, 130 (1971).
12) C. Naccache and M. Che, *Proc. 5th Inter. Congr. Catal.*, **101**, 1389 (1972).
13) A. J. Tench, T. Lawson, and I. F. I. Kibblewhite, *J. Chem. Soc., Faraday Trans. 1*, **68**, 1169 (1972).
14) J. Kijenski and S. Malinowski, *Bull. Acad. Pol. Sci., Ser. Sci. Chim.*, **25**, 501 (1977).
15) D. Cordishi, V. Indovina, A. Cimino, *J. Chem. Soc., Faraday Trans. 1*, **70**, 2189 (1974).
16) Y. Shibata, "Mukikagaku II," Iwanami Zensho, Tokyo (1963), p. 42.
17) H. Pines and L. A. Schaap, *Adv. Catal.*, **12**, 117 (1960).
18) D. Cordisgi and V. Indovina, *J. Chem. Soc., Faraday Trans. 1*, **72**, 2341 (1976).

 © 1982 The Chemical Society of Japan Bull. Chem. Soc. Jpn., 55, 995—998 (1982)

Phase Transitions in Tetramethylammonium Hexachloroplatinate(IV), -tellurate(IV), and -stannate(IV) as Studied by ^{35}Cl NQR and Powder X-Ray Diffraction

Yoshihiro FURUKAWA,* Laxman S. PRABHUMIRASHI,† Ryuichi IKEDA, and Daiyu NAKAMURA

Department of Chemistry, Faculty of Science, Nagoya University, Chikusa-ku, Nagoya 464

(Received August 15, 1981)

The ^{35}Cl NQR spectra of $[(CH_3)_4N]_2PtCl_6$, $[(CH_3)_4N]_2TeCl_6$, and $[(CH_3)_4N]_2SnCl_6$ were recorded in a temperature range between 77 and *ca.* 350 K. Below room temperature, the temperature dependence measurements of NQR frequencies for all of these complexes confirmed the presence of structural phase transitions reported very recently. From the experiments of DTA carried out above room temperature, structural phase transitions were located at 385, 351, and 365 K in the same order of the above complexes. The X-ray powder patterns taken in the highest-temperature phase of these complexes (at *ca.* 390 K) were well interpreted as arising from the K_2PtCl_6-type cubic structure with the lattice constant $a_0 = 12.82_8$, 13.05_3, and 12.97_5 Å for the Pt, Te, and Sn complexes, respectively. In this phase of each complex, however, no NQR spectra were observed. The mechanism of the phase transitions detected is discussed in connection with the structure of these complexes.

Recently, tetramethylammonium hexahalometallates(IV), $(tetMA)_2MX_6$, have been extensively studied because of their interesting phase transitions observed at low temperatures.[1-5] In our previous paper,[6] we reported the accurate transition temperatures of $(tetMA)_2PtCl_6$, $(tetMA)_2TeCl_6$, and $(tetMA)_2SnCl_6$ determined from the experiments of differential thermal analysis (DTA) and of proton spin-lattice relaxation time (T_1) carried out below room temperature. However, the nature of these phase transitions is still unclear.

Berg and Søtofte[7] reinvestigated the room-temperature structure of $(tetMA)_2PtCl_6$ by using a single crystal X-ray diffraction method, and found that the structure could be approximately described in the cubic system belonging to the space group Fm3m. In a subsequent paper,[8] Berg and Nielsen also studied the room-temperature structure of $(tetMA)_2TeBr_6$ and found that the complex forms cubic crystals in the space group Fd3c. Based on this new result, they indicated in their paper that the room-temperature structure of $(tetMA)_2PtCl_6$ might be the same because some weak Fm3m-forbidden reflections had been detected in the previous X-ray study. In fact, Mackenzie *et al.*[9] found, very recently, from the neutron powder diffraction study of $[N(CD_3)_4]_2PtCl_6$ that the compound also forms Fd3c crystals. The three hexachlorometallates(IV) described above are known to have the room-temperature crystal structure being isomorphous with each other.[10,11] For these complexes, therefore, a phase transition from the Fd3c structure to the simple Fm3m one may be expected to take place at a higher temperature. The present investigation of ^{35}Cl NQR in these hexachlorometallates(IV) has been undertaken to clarify the nature of the phase transitions already located at lower temperatures, and also to detect another phase transition possibly existing at higher temperature.

† Present address: Chemistry Department, Poona University, Pune 411007, India.

Experimental

The NQR spectra of ^{35}Cl were observed by means of a modified Dean-type super-regenerative spectrometer already described.[12] A chromel-alumel thermocouple was used for the determination of temperature. Observed temperatures were estimated to be accurate within ±1 K. The measurements of DTA were carried out by use of a home-made apparatus.[13] X-Ray powder patterns were taken by means of a Model D-3F diffractometer from Rigaku Denki Co. equipped with a copper anode. A goniometer was calibrated with the standard sample of silicon.

All the sample employed in the present investigation were the same as those prepared in the previous NMR and DTA experiments.[6]

Results and Discussion

Temperature Dependence of ^{35}Cl NQR Frequencies. Figure 1 shows the temperature dependence of ^{35}Cl NQR frequencies in $(tetMA)_2PtCl_6$, $(tetMA)_2TeCl_6$, and $(tetMA)_2SnCl_6$. The resonance frequencies of these complexes determined at various temperatures are listed in Table 1.

At room temperature, a single ^{35}Cl NQR frequency was observed for $(tetMA)_2PtCl_6$ indicating that all the chlorine atoms are crystallographically equivalent in

TABLE 1. ^{35}Cl NQR FREQUENCIES IN $(tetMA)_2PtCl_6$, $(tetMA)_2TeCl_6$, AND $(tetMA)_2SnCl_6$

Compound	T/K	NQR line	ν/MHz
$(tetMA)_2PtCl_6$	286	**a**	26.627±0.002
	170	**a**	26.774±0.002
		b	26.88±0.03
		c	27.00±0.03
	77	**b**	27.00±0.03
		c	27.12±0.03
$(tetMA)_2TeCl_6$	293		16.300±0.003
	77		16.52±0.05
			16.60±0.05
$(tetMA)_2SnCl_6$	292		16.683±0.003
	77		16.70±0.05
			17.51±0.05

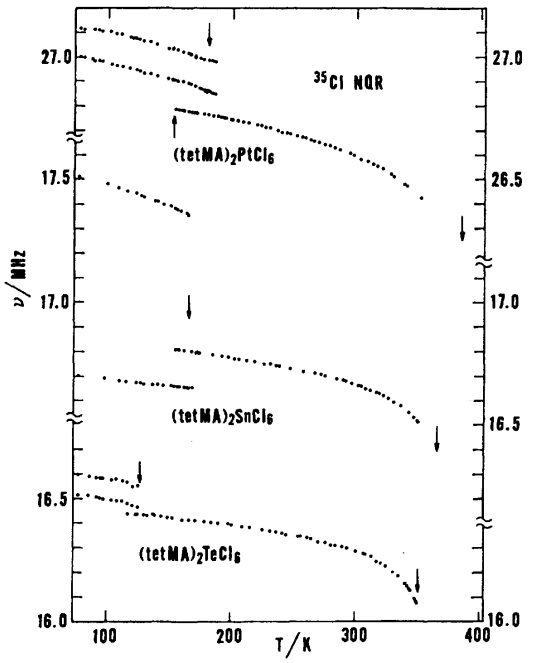

Fig. 1. Temperature dependence of ^{35}Cl NQR frequencies observed for $(tetMA)_2PtCl_6$, $(tetMA)_2TeCl_6$, and $(tetMA)_2SnCl_6$. Arrows indicate T_{tr} determined by the experiments of DTA.[6]

the crystal. With decreasing temperature, it was noticed that the resonance line became suddenly weak at 181 K. On further cooling, two very broad signals appeared at 178 K on the high-frequency side of the weak line labelled as **a**. These experimental facts indicate that $(tetMA)_2PtCl_6$ undergoes a structural phase transition at 181 K in good agreement with the previous DTA experiments.[6] In the temperature range between 181 and 178 K, only the weakened **a** line could be detected. This is presumably because the two new lines appearing at 178 K are too broad to be detected immediately below the transition temperature, T_{tr}. The two broad lines, the lower-frequency one (denoted as **b**) of which was about twice stronger than the higher-frequency one (**c**), could be observed continuously down to 77 K. However, the **a** line gradually weakened with decreasing temperature and disappeared in the noise level at 153 K, which agreed well with the second T_{tr} determined from the measurements of DTA.[6] The fact that three and two NQR lines were observed above and below the lower T_{tr}, respectively, indicates that the phase transition at 153 K is also a structural one. As in the previous paper,[6] we call the three phases determined below room temperature as α, β, and γ in the order of decreasing temperature. The above NQR results indicate that there exist at least three and two nonequivalent chlorine atoms in the β and γ phases, respectively. It is interesting to note that no discontinuity can be seen in the temperature dependence of the **a** line and also of the **b** and **c** lines at $T_{tr}(\alpha\rightarrow\beta)$ and $T_{tr}(\beta\rightarrow\gamma)$, respectively.

When the sample of $(tetMA)_2PtCl_6$ was warmed from 77 K, the **b** and **c** lines followed exactly the same temperature dependence curves obtained on the cooling run. Although both lines became weak above *ca.* 180 K, they could be recorded up to *ca.* 190 K which is higher by *ca.* 10 K than $T_{tr}(\alpha\rightarrow\beta)$. On the other hand, the **a** line did not appear at $T_{tr}(\beta\rightarrow\gamma)$ but it became detectable again at 181 K which agreed well with $T_{tr}(\alpha\rightarrow\beta)$. These experimental facts indicate that, when the sample was heated from 77 K, no phase transition takes place at $T_{tr}(\beta\rightarrow\gamma)$ and both phases α and β may coexist in a narrow range of temperature above 181 K.

It is known from the previous DTA experiments[6] that, on heating $(tetMA)_2PtCl_6$ from a temperature below 107 K, heat anomaly corresponding to the phase transition $\beta\rightarrow\gamma$ disappears, but it reversibly appears unless the sample is once cooled down below 107 K. In the present NQR experiments, the same behavior in the temperature dependence of the NQR frequencies was observed, *i.e.*, the **a** line appeared at 153 K $[T_{tr}(\beta\rightarrow\gamma)]$ on heating the sample which was once cooled down to a temperature not lower than 107 K. This suggests that the phase obtained by cooling the sample to 77 K is different from that existing between 153 and 107 K when the sample was cooled and warmed to and from, respectively, a temperature above 107 K.

Although no heat anomaly could be detected below $T_{tr}(\beta\rightarrow\gamma)$ on both cooling and warming runs, we call the phase obtained by cooling $(tetMA)_2PtCl_6$ to 77 K as δ as was defined in the previous paper.[6] The reason why no heat anomaly corresponding to the phase transitions $\gamma\rightleftarrows\delta$ was observed is considered as that the transition $\gamma\rightarrow\delta$ may take place very gradually as already suggested by Berg,[5] and δ transforms directly into β or α at 181 K. The latter statement means that δ is the stable phase at lower temperatures than 181 K. In the T_1 experiments,[6] two phases γ and δ are clearly distinguishable from one another. However, they are almost indistinguishable in the present NQR experiments. Accordingly, it is thought that the change of the orientation of $tetMA^+$ cations in the crystal or the change of the orientation of methyl groups in a cation may be responsible for the transition $\gamma\rightarrow\delta$. Both changes of the orientations of the cations in the crystal of $(tetMA)_2PtCl_6$ are considered to give only minor influence on the electric field gradient of resonant chlorine nuclei (possibly a change in the NQR linewidth) because $tetMA^+$ is highly symmetric.

With increasing temperature above $T_{tr}(\delta\rightarrow\alpha)$, the frequency of the **a** line decreased quite normally and faded out in the noise level at *ca.* 350 K, indicating the absence of phase transition up to this temperature.

At room temperature, $(tetMA)_2TeCl_6$ yielded a single ^{35}Cl NQR line.[11] With decreasing temperature, the line became gradually weak from *ca.* 150 K and finally disappeared at 117 K. On cooling further, no resonance was observed until two broad signals appeared at 106 K. The two signals became gradually strong with decreasing temperature and could be detected down to 77 K. When $(tetMA)_2TeCl_6$ was heated from 77 K, on the other hand, the doublet lines could be observed up to 128 K, above which temperature a single line was observed at the same frequency as that detected on the cooling run. These experimental facts indicate that $(tetMA)_2TeCl_6$ undergoes a first-order structural phase

transition at 128 K in agreement with the previous DTA and NMR results,[6] and that all chlorine atoms are equivalent in the crystal of the high-temperature phase whereas two nonequivalent chlorine atoms exist in the low-temperature phase crystal.

With increasing the temperature above room temperature, the frequency of the single line of $(tetMA)_2TeCl_6$ decreased unusually before it weakened and disappeared at *ca.* 350 K. This observation suggested the occurrence of another phase transition at a temperature immediately above 350 K.

For $(tetMA)_2SnCl_6$, a structural phase transition showing a thermal hysteresis was located at 168 K from the measurements of the temperature dependence of ^{35}Cl NQR frequencies. The results agree with those of the previous DTA experiments.[6] In the low-temperature phase, two largely separated very broad signals, the lower-frequency one of which was stronger, were observed suggesting that the crystalline lattice of $(tetMA)_2SnCl_6$ undergoes a tetragonal distortion below T_{tr}. With increasing temperature, the frequency of the high-temperature line decreased rather rapidly and the line disappeared at *ca.* 350 K.

DTA above Room Temperature. To locate another high-temperature phase transition expected for the present complexes from the temperature dependence measurements of ^{35}Cl NQR frequencies, we carried out DTA experiments above room temperature. The results were that thermal anomalies indicating the presence of phase transitions were found at 385, 351, and 365 K for the Pt, Te, and Sn complexes, respectively. Hereafter, the highest-temperature phase of these complexes is denoted as α'. It is worthwhile to note here that no ^{35}Cl NQR spectra were observed in the α' phase of these complexes although signals were searched carefully above T_{tr}.

Powder X-Ray Diffraction. The present study has revealed the presence of the high-temperature phase for the three hexachloro complexes. Therefore, we took X-ray powder patterns at various temperatures in order to obtain detailed information on the structure of the complexes in their high-temperature phase as well as on their room-temperature structure.

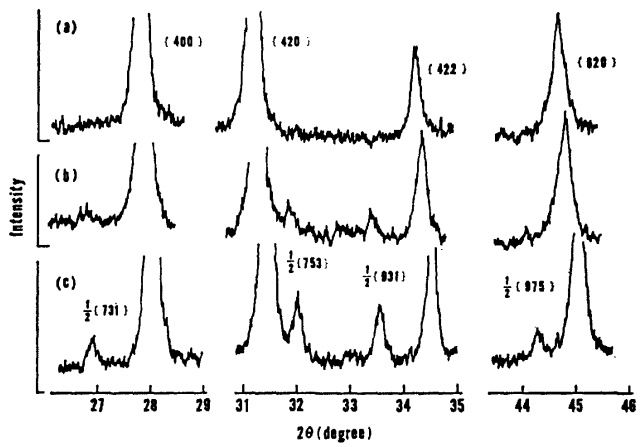

Fig. 2. X-Ray powder patterns of $(tetMA)_2PtCl_6$ taken at (a) *ca.* 400 K, (b) *ca.* 370 K, and (c) *ca.* 300 K. Indices are referred to the Fm3m unit cell.

The diffraction patterns (below $2\theta=60°$) of $(tetMA)_2PtCl_6$ recorded at room temperature could be attributed to the Fm3m cubic lattice with $a_0=12.73_1$ Å, in agreement with the results of Berg and Søtofte.[7] However, there remained four unassignable weak diffraction lines, the *d*-spacing values of which were 3.32_0, 2.79_5, 2.67_1, and 2.04_4 Å (see Fig. 2). These four reflections cannot be indexed by any Fm3m-allowed sets of integers along with $a_0=12.73_1$ Å. If we take a large cubic unit cell consisting of eight Fm3m units, however, the four reflections can be indexed by the following Miller indices, {731}, {753}, {931}, and {975} in the order of the above *d*-spacing values.

Berg and Nielsen reported that $(tetMA)_2TeBr_6$ has approximately the Fm3m structure but exactly it forms cubic crystals belonging to the space group Fd3c with $a_0=26.563$ Å and $Z=32$. The large unit cell is formed by doubling each edge of the Fm3m unit and, therefore, includes eight Fm3m units. Even in this structure, all the bromine atoms are crystallographically equivalent in agreement with the earlier NQR results.[14] Moreover, it is of interest to note that the Fm3m-forbidden reflections observed for $(tetMA)_2PtCl_6$ are allowed for the Fd3c system and are interpreted well. Accordingly, it can be concluded that, at room temperature, $(tetMA)_2PtCl_6$ forms cubic crystals belonging to the space group Fd3c with $a_0=25.46_2$ Å and $Z=32$. Very recently, Mackenzie *et al.* showed that $[N(CD_3)_4]_2PtCl_6$ also forms Fd3c cubic crystals at room temperature.[9] The diffraction patterns of $(tetMA)_2TeCl_6$ and $(tetMA)_2SnCl_6$ could be well described in the Fd3c cubic system with a_0 being 25.86_8 and 25.73_6 Å, respectively.

The diffraction patterns of the complexes studied were recorded at various temperatures above room temperature as shown in Fig. 2 for $(tetMA)_2PtCl_6$. When the temperature was raised, the Fm3m-forbidden reflections became weak and finally disappeared from the patterns taken in the α' phase of the complex. Therefore, the patterns of α'-$(tetMA)_2PtCl_6$ are completely interpreted in terms of the Fm3m lattice with a_0 being 12.82_8 Å at *ca.* 388 K. Similarly, the Fm3m lattice constant a_0 of α'-$(tetMA)_2TeCl_6$ and α'-$(tetMA)_2SnCl_6$ were determined as 13.05_3 Å at *ca.* 394 K and 12.97_5 at *ca.* 389 K, respectively. The lattice constants determined in the present study are estimated to be accurate to 0.010 Å.

This work was supported in part by a Grant-in-Aid for Scientific Research No. 543006 from the Japanese Ministry of Education, Science and Culture. One of the authors (L. S. P.) wishes to express his sincere thanks to the Japanese Ministry of Education, Science and Culture for the award of a research fellowship 1979—1980. He is also grateful to the Poona University authorities for granting him study leave to take up the present research work.

References

1) W. von der Ohe, *J. Chem. Phys.*, **62**, 3933 (1975).
2) W. von der Ohe, *J. Chem. Phys.*, **63**, 2949 (1975).
3) R. W. Berg, F. W. Poulsen, and N. J. Bjerrum, *J.*

Chem. Phys., **67**, 1829 (1977).
4) R. W. Berg, *J. Chem. Phys.*, **69**, 1325 (1978).
5) R. W. Berg, *J. Chem. Phys.*, **71**, 2531 (1979).
6) L. S. Prabumirashi, R. Ikeda, and D. Nakamura, *Ber. Bunsenges. Phys. Chem.*, **85**, 1142 (1981).
7) R. W. Berg and I. Søtofte, *Acta Chem. Scand., Ser.A*, **32**, 241 (1978).
8) R. W. Berg and K. Nielsen, *Acta Chem. Scand., Ser. A*, **33**, 157 (1979).
9) G. A. Mackenzie, R. W. Berg, and G. S. Pawley, *Acta Crystallogr., Sect. B*, **36**, 1001 (1980).
10) R. W. G. Wyckoff, "Crystal Structures," 2nd ed, Interscience Publishers, New York (1966), Vol. 5, p. 158.
11) T. B. Brill, R. C. Gearhart, and W. A. Welsh, *J. Magn. Reson.*, **13**, 27 (1974).
12) D. Nakamura, Y. Kurita, K. Ito, and M. Kubo, *J. Am. Chem. Soc.*, **82**, 5783 (1960).
13) Y. Kume, R. Ikeda, and D. Nakamura, *J. Magn. Reson.*, **33**, 331 (1979).
14) D. Nakamura, K. Ito, and M. Kubo, *J. Am. Chem. Soc.*, **84**, 163 (1962).

Vibrational Spectra and Normal Coordinate Calculations for Trimethylstannane

Yoshika IMAI* and Koyo AIDA

Department of Engineering Science, Faculty of Engineering, Tohoku University, Sendai 980

(Received October 14, 1981)

The infrared and Raman spectra of trimethylstannane and its deuterated analogues were obtained. Assignments for all the fundamentals except internal torsions were made and normal coordinate calculations were carried out to confirm the proposed assignments.

Our previous studies[1,2] have concerned with the reexamination of the vibrational spectra for $(CH_3)_3MH$ (M=Si, Ge). This work extends the studies to trimethylstannane. The vibrational spectra of trimethylstannane have been reported by previous authors,[3,4] but there are some discrepancies in the vibrational assignments. For example, Dillard and May[3] have assigned an infrared band at *ca.* 670 cm^{-1} for $(CH_3)_3SnH$ to the SnH bending vibration, while Kriegsmann and Pischtschan[4] have assigned a band at *ca.* 540 cm^{-1} to this vibration.

Kriegsmann and Pischtschan have calculated the force constants, assuming the methyl groups as a point mass. Our previous studies revealed that for trimethylsilane and trimethylgermane the methyl rocking, the MH bending, and the degenerate MC_3 stretching vibrations are fairly strongly coupled with one another. Since a similar vibrational coupling will be encountered in the case of the present compound, it seems inadequate to make the calculation by assuming that the methyl groups is a point mass.

In this paper we will report the vibrational spectra of trimethylstannane including its three deuterated analogues and the results on normal coordinate calculations without assuming the methyl groups as a point mass.

Experimental

Trimethylstannane and its deuterated analogues were prepared by reacting $(CH_3)_3SnCl$ or $(CD_3)_3SnCl$ with $LiAlH_4$ or $LiAlD_4$ in dibutyl ether. The crude compounds were purified by trap-to-trap fractionations by using a conventional vacuum line. The purity of the compounds was checked by their gas-phase infrared spectra. $(CH_3)_3SnCl$ and $(CD_3)_3SnCl$ were prepared by the reaction of $SnCl_4$ with $(CH_3)_4Sn$ and $(CD_3)_4Sn$, respectively. $(CH_3)_4Sn$ and $(CD_3)_4Sn$ were prepared by reacting $SnCl_4$ with $(CH_3)_2Zn$ and $(CD_3)_2Zn$, respectively, in sealed glass tubes and purified by trap-to-trap fractionations under vacuum. Dimethylzinc and its deuterated analogue were prepared by a method described in the literature.[5]

The infrared spectra were recorded on a Hitachi 345 spectrophotometer (4000—300 cm^{-1}) and on a Hitachi FIS-III spectrophotometer (400—30 cm^{-1}) in the gas phase and in the solid state at liquid nitrogen temperature.

Raman spectra were recorded on a JEOL-JRS-Sl Raman spectrophotometer equipped with a 50 mW NEC GLG 5800 He-Ne laser in the liquid state. Qualitative polarizations were also obtained.

Results and Vibrational Assignments

Since each methyl group of trimethylstannane is staggered with respect to the Sn–H bond,[6] the molecule has a C_{3v} molecular symmetry. Under this symmetry, its normal vibrations distribute as $8A_1+4A_2+12E$, where the A_1 and E modes are infrared and Raman active while the A_2 mode is inactive in both. Symmetry coordinates have been classified, according to the description of the modes, as given in Table 1, where the numbering of the symmetry coordinates is the same as those for the corresponding coordinates for trimethylsilane[1] and trimethylgermane.[2] Infrared spectra of trimethylstannane and its deuterated analogues in the gas phase are shown in Fig. 1. The Raman spectra

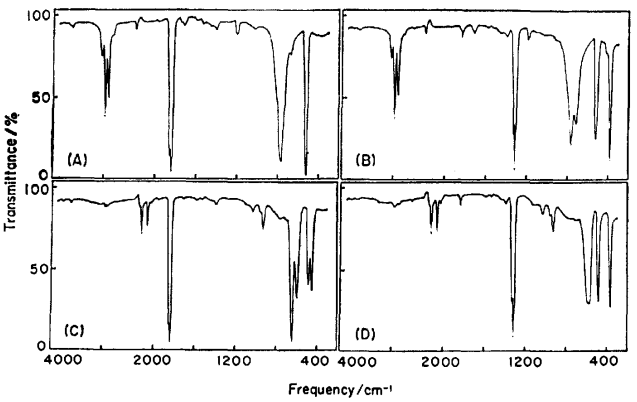

Fig. 1. Infrared spectra of $(CH_3)_3SnH$ (A), $(CH_3)_3SnD$ (B), $(CD_3)_3SnH$ (C), and $(CD_3)_3SnD$ (D) in the gas phase.

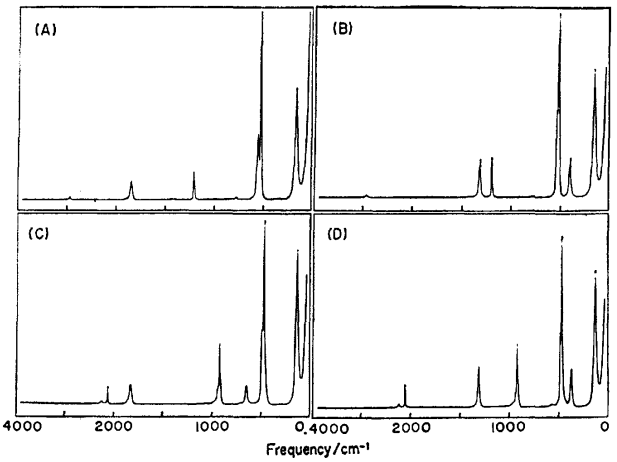

Fig. 2. Raman spectra of $(CH_3)_3SnH$ (A), $(CH_3)_3SnD$ (B), $(CD_3)_3SnH$ (C), and $(CD_3)_3SnD$ (D) in the liquid.

TABLE 1. DESCRIPTION OF THE SYMMETRY COORDINATES FOR TRIMETHYLSTANNANE[a)]

Vibrational mode	Coordinate		
	A_1	A_2	E
Stretching $(CH_3)_a$ or $(CD_3)_a$	S_1	S_9	S_{13}, S_{14}
Stretching $(CH_3)_s$ or $(CD_3)_s$	S_2		S_{15}
Stretching (SnH) or (SnD)	S_3		
Deformation $(CH_3)_a$ or $(CD_3)_a$	S_4	S_{10}	S_{16}, S_{17}
Deformation $(CH_3)_s$ or $(CD_3)_s$	S_5		S_{18}
Rocking (CH_3) or (CD_3)	S_6	S_{11}	S_{19}, S_{20}
Bending (SnH) or (SnD)			S_{21}
Stretching (SnC_3)	S_7		S_{22}
Deformation (SnC_3)	S_8		S_{23}
Torsion		S_{12}	S_{24}

a) Abbreviations used: a, asymmetric; s, symmetric.

TABLE 2. OBSERVED AND CALCULATED FREQUENCIES(cm^{-1}) FOR $(CH_3)_3SnH$

No.	Infrared Gas	Raman Liquid	Calcd	Potential energy distribution
1	2974	2984	2990	$100S_1$
2	2903	2911	2915	$99S_2$
3	1843	1835	1841	$100S_3$
4	1407	1415	1417	$97S_4$
5	1203	1200	1201	$87S_5$ $10S_2$
6	764	761	772	$97S_6$
7	521[a)]	515	518	$100S_7$
8	144	150	149	$82S_8$ $18S_6$
13	2974	2984	2988	$100S_{13}$
14	2974	2984	2993	$100S_{14}$
15	2903	2911	2915	$99S_{15}$
16	1407	1415	1417	$76S_{16}$ $21S_{17}$
17	1407	1415	1417	$76S_{17}$ $21S_{16}$
18	1203	1200	1201	$87S_{18}$ $10S_{15}$
19	764	761	785	$84S_{19}$ $14S_{21}$
20	746[a)]		748	$96S_{20}$
21	547[a)]	544	548	$44S_{21}$ $40S_{22}$ $16S_{19}$
22	514		512	$48S_{22}$ $41S_{21}$ $11S_{19}$
23	144	150	149	$99S_{23}$

a) The frequency is taken from the solid state spectrum.

in the liquid are shown in Fig. 2. Observed fundamental frequencies are listed in Tables 2—4.

The asymmetric and symmetric CH_3 stretches were observed at *ca.* 2980 and *ca.* 2900 cm^{-1}, respectively, for $(CH_3)_3SnH$ and $(CH_3)_3SnD$. For $(CD_3)_3SnH$ and $(CD_3)_3SnD$, these modes were observed at *ca.* 2240 and *ca.* 2120 cm^{-1}.

Polarized Raman bands at *ca.* 1850 cm^{-1} for $(CH_3)_3SnH$ and $(CD_3)_3SnH$ are assigned to the SnH stretching vibration. Upon deuteration of the SnH group, these bands shift to *ca.* 1300 cm^{-1} for $(CH_3)_3SnD$ and $(CD_3)_3SnD$. The corresponding infrared band of each compound in the gas phase has a definite PQR band contour.

Weak infrared bands at *ca.* 1400 cm^{-1} for $(CH_3)_3SnH$ and $(CH_3)_3SnD$ are assigned to the asymmetric methyl deformation. The corresponding Raman bands are

TABLE 3. OBSERVED AND CALCULATED FREQUENCIES (cm^{-1}) FOR $(CH_3)_3SnD$

No.	Infrared Gas	Raman Liquid	Calcd	Potential energy distribution
1	2974	2985	2990	$100S_1$
2	2911	2917	2915	$99S_2$
3	1325	1317	1308	$100S_3$
4	1407	1420	1417	$97S_4$
5	1203	1199	1201	$87S_5$ $10S_2$
6	774	785	772	$97S_6$
7	518[a)]	515	518	$100S_7$
8	144	148	149	$82S_8$ $18S_6$
13	2974	2985	2988	$100S_{13}$
14	2974	2985	2993	$100S_{14}$
15	2911	2917	2915	$99S_{15}$
16	1407	1420	1417	$73S_{16}$ $24S_{17}$
17	1407	1420	1417	$73S_{17}$ $24S_{16}$
18	1203	1199	1201	$87S_{18}$ $10S_{15}$
19	774	785	763	$95S_{19}$
20	728		748	$96S_{20}$
21	392	396	391	$85S_{21}$ $13S_{19}$
22	533	529	532	$97S_{22}$
23	144	148	149	$99S_{23}$

a) See the footnote in Table 2.

TABLE 4. OBSERVED AND CALCULATED FREQUENCIES (cm^{-1}) FOR $(CD_3)_3SnH$

No.	Infrared Gas	Raman Liquid	Calcd	Potential energy distribution
1	2238	2236	2228	$100S_1$
2	2125	2120	2119	$97S_2$
3	1842	1833	1841	$100S_3$
4	1037	1040	1025	$98S_4$
5	933	922	920	$78S_5$ $13S_2$
6	601		590	$94S_6$
7	472[a)]	470	467	$94S_7$
8	124	131	131	$79S_8$ $21S_6$
13	2238	2236	2226	$98S_{13}$
14	2238	2236	2229	$98S_{14}$
15	2125	2120	2119	$97S_{15}$
16	1037	1040	1024	$68S_{16}$ $31S_{17}$
17	1037	1040	1025	$67S_{17}$ $31S_{16}$
18	933	922	920	$78S_{18}$ $13S_{15}$
19	454	450	465	$34S_{19}$ $35S_{21}$ $29S_{22}$
20	601		559	$95S_{20}$
21	651	654	653	$60S_{21}$ $38S_{19}$
22	493	488	487	$50S_{22}$ $31S_{19}$ $14S_{21}$
23	124	131	132	$99S_{23}$

a) See the footnote in Table 2.

broad and very weak. Therefore, their frequencies are fairly indefinite. Upon deuteration of the methyl groups these bands shift to *ca.* 1040 cm^{-1} for $(CD_3)_3SnH$ and $(CD_3)_3SnD$.

For $(CH_3)_3SnH$ and $(CH_3)_3SnD$, weak infrared bands at *ca.* 1200 cm^{-1} are assigned to the symmetric methyl deformation and the correspinding Raman bands are polarized. These bands shift to *ca.* 920 cm^{-1} for $(CD_3)_3$-

Table 5. Observed and calculated frequencies (cm^{-1}) for $(CD_3)_3SnD$

No.	Infrared Gas	Raman Liquid	Calcd	Potential energy distribution
1	2238	2235	2228	$99S_1$
2	2124	2120	2119	$97S_2$
3	1324	1317	1308	$100S_3$
4	1040	1035	1025	$98S_4$
5	932	922	920	$78S_5$ $13S_2$
6	584		590	$94S_6$
7	471[a)]	471	467	$94S_7$
8	124	130	131	$79S_8$ $21S_6$
13	2238	2235	2226	$98S_{13}$
14	2238	2235	2229	$98S_{14}$
15	2124	2120	2119	$97S_{15}$
16	1040	1035	1024	$68S_{16}$ $31S_{17}$
17	1040	1035	1025	$67S_{17}$ $31S_{16}$
18	932	922	920	$78S_{18}$ $13S_{15}$
19	584		588	$83S_{19}$ $14S_{21}$
20	567	570	559	$95S_{20}$
21	375	378	374	$74S_{21}$ $23S_{19}$
22	489	487	482	$89S_{22}$
23	124	130	132	$99S_{23}$

a) See the footnote in Table 2.

SnH and $(CD_3)_3SnD$ upon deuteration of the methyl groups.

Three methyl rocking, two SnC_3 stretching and one SnH or SnD bending vibrations are expected to appear in the region 900—300 cm^{-1}. Raman bands at *ca.* 510 cm^{-1} for $(CH_3)_3SnH$ and $(CH_3)_3SnD$ are strong and polarized. Upon deuteration of the methyl groups these bands shift to *ca.* 480 cm^{-1} for $(CD_3)_3SnH$ and $(CD_3)_3SnD$. Therefore, they are evidently assigned to the A_1 SnC_3 stretching mode. The infrared band due to this mode is weak and could not be observed in the gas phase owing to the obscuration of strong neighbouring bands. However, in the solid state this is clearly observed as a sharp band for each isotopic analogue except for $(CH_3)_3SnH$. For $(CH_3)_3SnH$ three bands were observed at 547, 521, and 512 cm^{-1} in the solid infrared spectrum. The 512 cm^{-1} band is very strong while the 547 cm^{-1} and the 521 cm^{-1} bands are weak and the 521 cm^{-1} band is observed as a shoulder of the 512 cm^{-1} band. Considering its frequency and intensity, we assigned the shoulder to the A_1 SnC_3 stretching mode. Of the 547 cm^{-1} and the 512 cm^{-1} bands, one band should be due to the SnH bending mode and another due to the E SnC_3 stretching mode. Dillard and May have assigned an infrared band at *ca.* 670 cm^{-1} for $(CH_3)_3SnH$ to the SnH bedning mode. We also observed the very weak band at the same position. However, since its intensity was decreased by repeating purification of the compound, it was concluded that this band is due to some other species than trimethylstannane. For $(CH_3)_3SnD$ two bands at *ca.* 530 and *ca.* 390 cm^{-1} were assigned to the E SnC_3 stretching and the SnD bending vibrations, respectively. The 530 cm^{-1} band shifts to *ca.* 490 cm^{-1} for $(CD_3)_3SnH$ and $(CD_3)_3SnD$ upon deuteration of the methyl groups. A strong infrared band at *ca.* 650 cm^{-1} for $(CD_3)_3SnH$ was assigned to the SnH bending, since no corresponding band was observed in the same region for $(CD_3)_3SnD$.

Since the A_1 methyl rocking frequencies are approximately identical with each other for $(CH_3)_3MH$ and $(CH_3)_3MD$ and for $(CD_3)_3MH$ and $(CD_3)_3MD$ (M=Si, Ge),[1,2] we assigned infrared bands at *ca.* 770 cm^{-1} for $(CH_3)_3SnH$ and $(CH_3)_3SnD$, and at *ca.* 480 cm^{-1} for $(CD_3)_3SnH$ and $(CD_3)_3SnD$ to the A_1 methyl rock. For trimethylsilane and trimethylgermane the band due to this mode coincides with that due to one of the E modes. Therefore, it may be considered that the same accidental degeneracy is encountered in trimethylstannane. Assignments of the remaining E modes which appear in the range 900—300 cm^{-1} is impossible without the aid of normal coordinate calculations.

The two skeletal deformation modes should be expected in the region below 300 cm^{-1}. However, only one band is observed in the Raman spectrum for each isotopic compound below 300 cm^{-1}. Since the corresponding infrared band is observed as two closely bands in the solid state and the same modes coincide with each other for $(CH_3)_3SnCF_3$ and $(CD_3)_3SnCF_3$,[7] we assigned bands at *ca.* 150 cm^{-1} for $(CH_3)_3SnH$ and $(CH_3)_3SnD$ and at *ca.* 130 cm^{-1} for $(CD_3)_3SnH$ and $(CD_3)_3SnD$ to the A_1 and E skeletal deformations.

One methyl torsional mode should be expected. However, no band ascribable to this mode was observed in both the infrared and Raman spectra for each isotopic compound.

Normal Coordinate Calculations and Discussion

Normal coordinate calculations were carried out on an ACOS 77/900 computer at the Computer Center,

Table 6. Symmetry force constants for trimethylstannane[a)]

	Constant	σ		Constant	σ
F_1	4.754	0.013	F_{13}	4.750	0.157
F_2	4.723	0.067	F_{14}	4.766	0.157
F_3	1.994	0.009	F_{15}	4.722	0.099
F_4	0.512	0.003	F_{16}	0.511	0.006
F_5	0.471	0.019	F_{17}	0.510	0.006
F_6	0.378	0.019	F_{18}	0.471	0.028
F_7	2.270	0.039	F_{19}	0.381	0.010
F_8	0.453	0.082	F_{20}	0.384	0.006
			F_{21}	0.371	0.013
$F_{2,5}$	−0.385	0.084	F_{22}	2.133	0.057
$F_{5,7}$	−0.152	0.039	F_{23}	0.371	0.028
$F_{6,8}$	−0.158	0.069			
			$F_{15,18}$	−0.388	0.122
			$F_{18,22}$	−0.140	0.056
			$F_{19,21}$	0.088	0.009
			$F_{21,22}$	−0.029	0.023

a) The stretching force constants are given in 10^2 N m^{-1}, the defor mation force constants in 10^{-18} N m rad^{-2}, and the stretching-deformation interaction constants in 10^{-8} N rad^{-1}. The subscript number i in F_i corresponds with that in S_i in Table 1.

Table 7. Comparison of force constants ($10\ N^2\ m^{-1}$)

	f(Sn–C)	f(Sn–H)
$(CH_3)_4Sn$	2.19[10]	
$(CH_3)_3SnH$	2.18[a]	1.99[a]
$(CH_3)_3SnCl$	2.12[4]	
CH_3SnH_3	2.12[11]	2.23[b]
SnH_4		2.27[b]

a) This work. b) The force constant was calculated from the symmetry force constants reported in the earier papers.[11,12]

Tohoku University, by using the interactive least-squares procedure. G-matrix was calculated by use of the structural parameters from the electron-diffraction study[6] and by assuming a tetrahedral angle around carbon atoms; r(Sn–H)=0.1705 nm, r(Sn–C)=0.2147 nm, r(C–H)=0.1086 nm, ∠C–Sn–C=107.5°. The torsional mode of the methyl groups was neglected in the E class.

The least-squares refinement was carried out in the same manner as with the acetonitrile-borane adducts,[8] trimethylsilane,[1] and trimethylgermane.[2] The calculated frequencies have an average error of 0.42% for A_1 vibrations and 0.76% for E vibrations. The sum for the weighted squares of errors $\sum(\lambda_{obsd}-\lambda_{calcd})^2/\lambda_{obsd}$ was 2.0×10^{-3} for A_1 vibrations and 7.7×10^{-3} for E vibrations. The symmetry force constants from the last cycle in the least-squares refinements are given in Table 6, together with their uncertainties.

Potential energy distributions are also given in Tables 1—4. These show that one of the E methyl rocks, the SnH bend, and the SnC_3 stretch in the E class for $(CH_3)_3SnH$ and $(CD_3)_3SnD$ are strongly coupled with each other.

The Sn–C and Sn–H valence force constants derived from the symmetry force constants are compared with those of the related compounds in Table 7. The Sn–C force constants are almost the same in these compounds. However, the Sn–H force constants seem to decrease slightly with increasing the number of methyl groups attached to a tin atom. This trend is quite similar to that found for the Si–H force constants of methylsilanes.[9]

This work was partly supported by a grant from the Asahi Glass Foundation for Industrial Technology to which our thanks are due. One of the authors (Y. I.) wishes to express his thanks to Prof. Fumio Watari, Iwate University, for the computer programs used in calculations.

References

1) Y. Imai and K. Aida, *Bull. Chem. Soc. Jpn.*, **54**, 925 (1981).
2) Y. Imai and K. Aida, *Bull. Chem. Soc. Jpn.*,, **54**, 3323 (1981).
3) C. R. Dillard and L. May, *J. Mol. Spectrosc.*, **14**, 250 (1964).
4) H. Kriegsmann and S. Pischtschan, *Z. Anorg. Allg. Chem.*, **308**, 212 (1961).
5) R. R. Renshaw and C. E. Greenlaw, *J. Am. Chem. Soc.*, **42**, 1472 (1920).
6) B. Beagley, K. McAloon, and J. M. Freemann, *Acta Crystallogr., Sect. B*, **30**, 444 (1974).
7) R. Eujen and H. Bürger, *Spectrochim. Acta, Part A*, **35**, 1135 (1979).
8) F. Watari, *J. Phys. Chem.*, **84**, 448 (1980).
9) L. M. Sverdlov, M. A. Kovner, and E. P. Krainov, "Vibrational Spectra of Polyatomic Molecules," John Wiley and Sons, New York (1974), p. 563.
10) F. Watari, *Spectrochim. Acta, Part A*, **34**, 1239 (1978).
11) H. Kimmel and C. R. Dillard, *Spectrochim. Acta, Part A*, **24**, 909 (1968).
12) I. W. Levin and H. Ziffer, *J. Chem. Phys.*, **43**, 4023 (1965).

Thermodynamic Study of NH_4Br and ND_4Br Crystals under Constant High-pressures†

Kazuo WATANABE,** Masaharu OGUNI, Takasuke MATSUO, Hiroshi SUGA,* and Syûzô SEKI***

Department of Chemistry and Chemical Thermodynamics Laboratory, Faculty of Science, Osaka University, Toyonaka, Osaka 560

(Received October 26, 1981)

Heat capacities and volumes of NH_4Br and ND_4Br crystals were measured in the temperature range from 100 to 260 K at several constant pressures up to 110 MPa with a special attention paid to the behaviors around the point of ND_4Br at 66 MPa and 202 K. The experimental results at an atmospheric pressure were in good agreement with the previously reported ones. The δ-γ and δ-β phase transitions were accompanied with expansion of the volume while the γ-β phase transition with contraction. Detailed phase diagram obtained for ND_4Br disclosed that there was no maximum in any branch of the transition lines. The triple point was represented essentially as the point of intersection of the three straight lines. There was no pressure dependence of the total entropy of transition from the δ to β phase. The entropy values can be explained by the mechanism of the order-disorder change in the orientations of NH_4^+ tetrahedra. The existence of the heat capacity anomaly in the high temperature side of the δ-γ phase transition was discussed as due to the spatial fluctuation of domains of the γ and δ phases. An argument was put forward that the observed δ-γ phase transition was probably superheated. An additional anomalous heat-capacity peak was observed just below the triple point pressure in between the temperatures of the δ-γ and γ-β phase transitions, and explained in terms of the effects of the superheating in the δ-γ phase transition and of the coexistence of the δ and γ phases domains in the crystal.

There have been four phases known to exist in the NH_4Br crystal at the atmospheric pressure.[1] They are named α through δ phases in the order of the high to low temperature in respect of the temperature range of their occurrence. As the pressure increases, the temperature range of the stability of the γ phase becomes small and disappears at the triple point pressure of 160 MPa for NH_4Br and 66 MPa for ND_4Br.[1,2]

These phases are distinguished from one another by the differences in the interrelation of orientations of NH_4^+ ions and in the relative positions of the ions.[3] The α phase has the NaCl structure in which NH_4^+ ions are orientationally disordered. The β phase has the CsCl structure with the NH_4^+ ions in the state of disorder between two different orientations in the octahedral crystal field. The structure of the γ phase is in the tetragonal system; adjacent NH_4^+ ions take a parallel orientation along the c axis and an anti-parallel one within the ab plane, and the Br^- ions accordingly shift themselves slightly along the c-axis with concomitant shortening of the N–H···Br hydrogen bonds. The δ phase has the same cubic structure as the β phase, but with NH_4^+ ions in the parallel ordered state in the orientations.

Two different mechanisms, order-disorder in configurational degrees of freedom and displacement of atoms and ions away from the high symmetry sites, are in general considered as basic atomic processes of phase transitions in ionic crystals. In the transitions among the β, γ, and δ phases there are two competing ordering interactions.[4] A direct octupole-octupole interaction between nearest-neighbor NH_4^+ tetrahedra energetically favors a parallel ordering realized in the δ phase, while an indirect interaction of the tetrahedra through the polarizable Br^- ions stabilizes the anti-parallel ordering accompanied by the displacement of the Br^- ions in the γ phase.

We reported construction of an adiabatic calorimeter working under constant high pressures.[5] In the present paper we report calorimetric and volumetric studies of the phase transitions in NH_4Br and ND_4Br crystals performed with this apparatus with special attention paid to the behavior around the triple point of ND_4Br. In general the behavior of a substance around the triple point involving the gaseous, liquid, crystalline phases is determined only by the difference in the magnitudes of the free energies for these phases. The γ-β and δ-β phase transitions in the present crystals have been well known from various experimental techniques to be of the λ type.[6–9] The behavior around such triple points as associated with phase lines of the λ type was expected to be different from that of the gas-liquid-crystal triple points on account of the continuous interrelation among the crystal structures involved.

Experimental

Materials. Crystalline ammonium bromide NH_4Br (Nakarai Chemical Co. Ltd., special reagent) was purified by sublimation at about 140 °C under vacuum. The powder sample obtained was pressed into pellets of 2 cm in diameter and 0.7 cm in thickness for closer packing in the cell. The mass of the sample used was 37.593 g corresponding to 0.38383 mol.

The sample in the calorimeter cell was pressurized through direct contact with pressure medium, 3-methylpentane, for a uniform hydrostatic pressure. This method is applicable if the sample is insoluble in the liquid. The solubility was checked with a spectroscopic method; NH_4Br was first extracted into water phase from the saturated 3-methylpentane solution, and then the ultraviolet spectra of the aqueous solution was compared with those of the aqueous NH_4Br solutions of known concentration. The amount-of-substance fraction of

† Contribution No. 27 from Chemical Thermodynamics Laboratory.

** Present address: Kanzaki Paper Mtg. Co. Ltd., 1-11, Jōkōji-Motomachi, Amagasaki 660.

*** Present address: Department of Chemistry, School of Science, Kwansei Gakuin University, Nishinomiya 662.

NH_4Br in the pressure medium was estimated to be less than 10 ppm, indicating that the above method of pressurization caused no serious problem in the heat capacity measurements.

Ammonium-d_4 bromide (ND_4Br) sample was prepared by recrystallizing the purified NH_4Br crystals from deuterium oxide (Nakarai Chemical Co. Ltd., 99.8%) solution three times. Deuterium exchange ratio of the powder sample was found by high resolution ^1H-NMR method to be 99.5%. The calorimeter cell contained 35.418 g (0.34734 mol) of the sample in pellet form. All the procedures of the preparation and handling were carried out in the atmosphere of dry nitrogen gas.

The densities of NH_4Br and ND_4Br crystals at room temperature were calculated from data of the mass and volume of the pellet. The volume was obtained by measuring the pellet sizes with a micrometer.

Calorimetric Procedures. The calorimeter cell was loaded with the sample at room temperature and screwed up at liquid nitrogen temperature for tight sealing. Setting-up of the cell in the cryostat and introduction of 3-methylpentane into the high-pressure system were carried out in the same manner as described already.[5]

A series of heat capacity measurement at several constant pressures was performed in the intermittent heating mode with the temperature step of 2—3 K. The volume of the sample at each temperature and pressure was calculated by using the compressibility and expansivity data of 3-methylpentane given in the previous paper.[5]

Results and Discussion

Heat Capacities at an Atmospheric Pressure. Heat capacity values of NH_4Br and ND_4Br crystals at an atmospheric pressure are shown in Figs. 1 and 2, respectively, together with the previously reported data obtained by using an ordinary adiabatic calorimeters.[10-12] They are in good agreement within the inaccuracy of 1% except at temperatures just around the phase transition points. In view of the adverse circumstances in determining the heat capacity values with the present calorimeter, this agreement would be satisfactory. Evidently, unfavorable factors incurred by the high pressure were overcome in the present apparatus. It is now possible to measure high-pressure heat capacities with almost the same accuracy as with the ordinary adiabatic calorimeter under the atmospheric pressure.

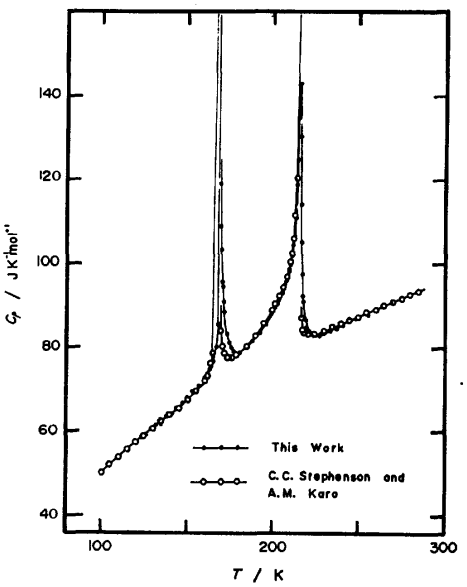

Fig. 2. Molar heat capacity of ND_4Br crystal at an atmospheric pressure.

Table 1. The entropies of the phase transitions in NH_4Br and ND_4Br crystals

Substance	Ref.	$\Delta_\alpha^\gamma S$ / J K^{-1} mol^{-1}	$\Delta_\gamma^\beta S$ / J K^{-1} mol^{-1}	$\Delta_\alpha^\beta S$ / J K^{-1} mol^{-1}
NH_4Br	10	1.1	3.0	4.1
	11	1.1	3.0	4.1
	This work	1.2	2.6	3.8
ND_4Br	12	—	—	5.4
	This work	—	—	5.0

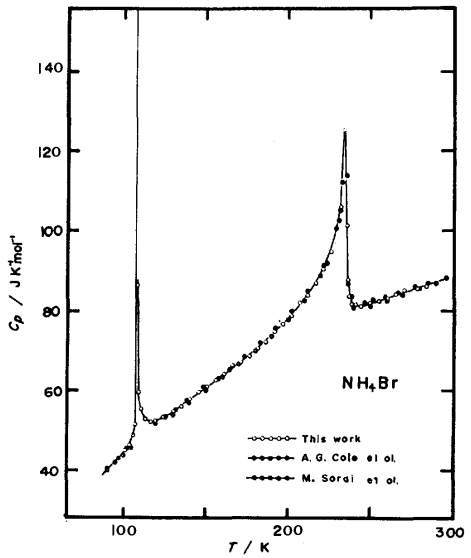

Fig. 1. Molar heat capacity of NH_4Br crystal at an atmospheric pressure.

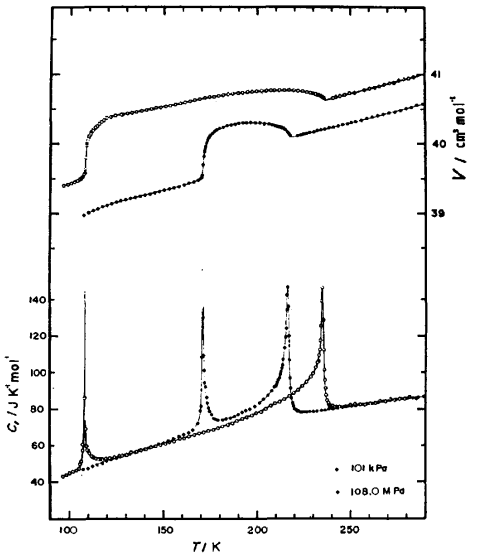

Fig. 3. Molar heat capacity and molar volume of NH_4Br at 0.101 (○) and 108.0 MPa (●).

TABLE 2. MOLAR HEAT CAPACITY AND MOLAR VOLUME OF NH_4Br

T/K	C_p/J K^{-1}mol^{-1}	V/cm^{3}mol^{-1}	T/K	C_p/J K^{-1}mol^{-1}	V/cm^{3}mol^{-1}	T/K	C_p/J K^{-1}mol^{-1}	V/cm^{3}mol^{-1}	T/K	C_p/J K^{-1}mol^{-1}	V/cm^{3}mol^{-1}
P = 101 kPa			217.02	87.04	40.770	232.08	78.70	40.179	181.69	74.03	40.231
			219.46	88.78	40.765	234.10	79.13	40.192	183.79	74.39	40.252
96.81	42.98	39.395	221.83	90.27	40.763	236.10	79.32	40.200	185.88	74.99	40.262
98.78	43.96	39.413	224.15	92.51	40.752	238.27	79.91	40.221	187.97	76.03	40.270
100.71	44.96	39.434	226.37	94.72	40.739	240.67	79.89	40.228	190.04	76.94	40.283
102.49	45.47	39.452	228.51	97.50	40.731	243.16	80.36	40.247	192.09	78.55	40.291
104.13	46.30	39.468				245.64	80.69	40.262	194.14	79.64	40.294
105.29	47.07	39.483	219.89	88.88	40.768	248.14	81.33	40.278	196.34	80.33	40.294
105.93	49.89	39.494	222.40	90.87	40.760	250.37	81.54	40.294	198.75	81.88	40.294
106.44	51.44	39.507	224.91	93.04	40.747	252.82	81.75	40.309	201.18	83.46	40.294
106.84	51.26	39.522	227.41	95.97	40.737	255.85	82.27	40.330	203.60	85.50	40.283
107.17	51.60	39.533	229.78	99.27	40.724	258.86	82.74	40.353	205.85	87.28	40.273
107.52	55.37	39.554	231.15	102.61	40.713	261.83	83.14	40.374			
107.87	60.79	39.577	231.62	103.29	40.710	264.83	83.59	40.398	212.13	97.30	40.231
108.19	86.31	39.634	232.02	105.18	40.705	267.89	84.23	40.416	212.71	98.84	40.223
108.47	219.85	39.793	232.34	105.63	40.703	270.99	84.71	40.439	213.23	101.33	40.221
108.76	67.41	39.970	232.67	107.42	40.697	274.08	84.98	40.450	213.75	103.52	40.213
109.09	59.67	40.023	233.00	108.60	40.695	277.16	85.34	40.479	214.28	107.18	40.208
109.42	58.16	40.056	233.32	111.72	40.692	280.26	85.77	40.502	214.71	111.35	40.200
109.78	57.09	40.080				283.34	86.07	40.523	215.05	115.10	40.192
110.19	57.04	40.103	232.76	106.04	40.697	286.40	86.23	40.554	215.40	122.53	40.184
110.68	55.39	40.129	233.11	109.44	40.697	289.44	86.70	40.572	215.74	131.04	40.171
111.23	54.51	40.150	233.46	112.27	40.690	292.47	87.45	40.596	216.07	148.15	40.155
111.79	53.88	40.174	233.79	117.54	40.690	295.52	87.63	40.617	216.35	162.43	40.150
112.41	53.47	40.197	234.14	125.37	40.679	298.55	87.58	40.643	216.59	148.55	40.132
113.18	52.92	40.221	234.48	138.90	40.761	P = 108.0 MPa			216.83	130.30	40.119
114.16	52.53	40.247	234.79	146.24	40.671				217.15	113.52	40.116
115.35	52.28	40.281	235.10	128.80	40.661	107.56	46.96	38.905	217.47	102.13	40.111
116.64	52.20	40.307	235.40	112.34	40.658	110.56	47.57	39.014	217.82	93.73	40.111
117.93	52.12	40.330	235.72	101.36	40.653	112.60	48.37	39.040	218.19	88.76	40.114
119.52	52.29	40.359	236.03	95.69	40.645	115.03	49.25	39.064	218.58	85.68	40.119
121.58	52.66	40.380	236.35	91.52	40.645	117.53	50.21	39.095	219.01	82.98	40.114
124.23	53.33	40.398	236.67	87.70	40.645	119.98	51.17	39.118	219.54	81.23	40.109
127.06	53.95	40.419	236.99	84.51	40.645	122.44	51.95	39.139	220.07	80.20	40.109
128.14	54.31	40.419	237.32	84.60	40.648	124.95	52.82	39.160	220.60	77.97	40.109
130.58	54.91	40.432	237.64	83.55	40.645	127.44	53.59	39.181	221.13	78.53	40.103
132.98	56.03	40.445	237.98	83.52	40.645	129.95	54.42	39.197	222.46	78.44	40.119
135.51	56.19	40.458	238.43	82.48	40.651	132.54	55.30	39.217			
138.15	57.37	40.471	238.96	81.63	40.653	135.09	56.09	39.233	207.73	89.93	40.262
140.77	57.93	40.484	239.50	81.81	40.648	137.63	57.10	39.249	209.10	91.79	40.257
143.36	58.75	40.499	240.04	81.84	40.648	140.18	57.71	39.267	209.86	92.39	40.241
145.93	59.59	40.510	240.58	80.99	40.656	142.75	58.74	39.280	210.38	93.71	40.239
148.47	60.49	40.520	241.25	81.61	40.661	145.30	59.28	39.296	210.80	94.73	40.236
150.99	61.02	40.536	242.19	81.23	40.671	147.82	60.57	39.316	221.39	95.76	40.231
153.53	62.04	40.549	243.26	80.78	40.679	150.42	61.27	39.332	211.89	96.77	40.231
156.10	62.55	40.562	244.33	81.32	40.687	153.09	62.57	39.350	212.39	98.81	40.223
158.70	63.69	40.580				155.74	63.60	39.368	212.85	100.25	40.226
161.33	64.23	40.598	242.13	80.84	40.671	158.36	64.95	39.379	213.27	102.03	40.221
163.94	65.11	40.614	244.44	81.12	40.687	160.97	66.15	39.405	213.68	104.02	40.215
166.53	66.17	40.627	247.07	81.55	40.703	163.55	67.30	39.426	214.09	107.20	40.210
169.10	66.84	40.643	249.77	82.02	40.721	166.11	68.86	39.447	214.79	113.38	40.202
171.65	67.19	40.656	252.46	81.73	40.739	168.47	71.88	39.470	215.12	119.43	40.192
174.19	67.99	40.664	255.14	82.48	40.755	169.81	78.94	39.499	215.44	124.09	40.184
176.71	68.61	40.679	257.81	82.75	40.773	170.26	81.64	39.517	215.76	134.17	40.171
179.21	69.53	40.690	260.48	83.34	40.794	170.60	108.34	39.546	216.07	142.44	40.155
181.75	70.72	40.700	263.14	83.46	40.810	170.91	284.84	39.692	216.38	146.84	40.142
184.31	71.48	40.710	265.79	84.17	40.833	171.20	130.22	39.814	216.70	135.99	40.132
186.88	72.34	40.724	268.43	84.35	40.851	171.54	109.54	39.874	217.02	119.91	40.122
189.46	73.60	40.724	271.06	85.25	40.867	171.88	100.88	39.916	217.34	106.74	40.111
192.03	74.85	40.734	273.70	85.07	40.886	172.22	94.39	39.957	217.67	96.85	40.111
194.59	75.55	40.742	276.36	85.51	40.905	172.65	92.28	39.999	218.04	91.32	40.116
197.13	76.67	40.747	279.01	85.55	40.929	173.18	86.44	40.043	218.44	86.07	40.114
199.65	77.94	40.755	281.64	86.53	40.945	173.71	83.58	40.072	218.85	83.61	40.119
202.18	78.77	40.760	284.28	85.75	40.963	174.24	80.74	40.098	219.25	82.68	40.116
204.71	80.18	40.755				174.86	78.83	40.116	219.66	81.52	40.109
207.31	81.85	40.765	224.98	78.39	40.132	175.90	77.00	40.142	220.06	80.12	40.109
209.39	83.05	40.765	226.25	78.40	40.142	177.03	74.93	40.171	220.47	79.40	40.103
211.96	83.88	40.768	228.02	78.55	40.155	178.00	74.57	40.189	220.95	79.18	40.106
214.52	85.32	40.768	230.19	78.59	40.163	179.59	74.23	40.208	221.52	78.65	40.109

Agreement between the present and previous data is found also in the entropies of the transition as shown in Table 1.[10-12] The difference (up to 8%) would not be significant because the entropy values depend primarily upon choice of the baseline which one has to assume in the wide temperature range of occurrence of the phase transition.

Heat Capacities under Pressures. Figure 3 shows the results of molar heat capacity and molar volume of NH_4Br at 0.101 and 108.0 MPa. The numerical values are collected in Table 2. Application of the pressure increased the δ-γ phase transition temperature from 108.5 K to 170.9 K and decreased the γ-β one from 234.8 K to 216.4 K. The transition temperatures observed at 108.0 MPa are in good accordance with those on the phase diagram reported before.[13,14] The slope of the transition line, dT_{tr}/dp, is 0.578 K MPa^{-1} for the δ-γ phases and -0.171 K MPa^{-1} for the γ-β phases.

Figure 4 shows the molar heat capacity and molar volume of ND_4Br at 0.101, 50.0, and 111.0 MPa in the temperature range of 130 to 260 K. The numerical values are given in Table 3. The two phase transitions, δ-γ and γ-β, observed at 168.5 and 215.5 K at 0.101 MPa, got close in temperature to each other with the increasing pressure to take place at 194.3 and 206.0 K at 50.0 MPa, and coalesced into one, direct transformation from δ to β phases, around 67 MPa at 201.2 K. The transition temperature was 205.3 K at 111.0 MPa.

The δ-γ phase transition was accompanied with a large expansion in volume, and had a increasingly larger premonitory region on the low temperature side as the pressure was increased. The slope of the transition line, dT_{tr}/dp, was 0.517 K MPa^{-1}. The

TABLE 3. MOLAR HEAT CAPACITY AND MOLAR VOLUME OF ND_4Br

T/K	C_p/J K^{-1}mol^{-1}	V/cm^{3}mol^{-1}
P = 101 kPa		
128.60	60.35	39.351
131.64	61.40	39.400
134.64	61.43	39.426
137.60	61.52	39.440
140.71	64.21	39.460
143.96	65.51	39.469
147.17	66.74	39.498
150.40	67.92	39.506
153.58	69.51	39.503
156.77	70.69	39.521
159.92	72.78	39.549
162.01	73.73	39.567
162.87	74.80	39.572
163.55	75.41	39.578
164.11	75.87	39.584
164.52	76.07	39.584
164.93	76.81	39.584
165.34	77.07	39.587
165.75	77.41	39.584
166.16	78.67	39.584
166.57	79.22	39.584
166.98	80.03	39.587
167.39	80.52	39.601
167.79	85.44	39.598
168.55	261.97	39.739
168.89	192.52	39.898
169.25	119.13	39.995
169.64	108.68	40.047
170.03	103.32	40.099
170.42	95.55	40.131
170.82	94.50	40.145
171.22	90.74	40.171
171.62	88.37	40.191
172.31	85.83	40.217
173.31	83.39	40.249
174.48	81.15	40.286
175.81	79192	40.301
177.48	78.94	40.318
180.46	78.82	40.326
184.40	79.99	40.344
188.32	81.57	40.358
192.20	83.26	40.361
196.04	85.32	40.355
199.80	88.33	40.358
203.18	90.41	40.370
205.75	93.05	40.358
207.99	95.95	40.347
209.27	98.05	40.349
209.80	98.60	40.352
210.22	99.91	40.347
210.64	100.53	40.347
211.06	101.87	40.347
211.48	102.98	40.341
211.90	104.30	40.326
212.32	106.51	40.324
212.73	108.56	40.318
213.15	110.87	40.309
213.56	114.51	40.303
213.97	118.84	40.298
214.38	124.95	40.289
214.78	134.91	40.289
215.18	142.76	40.254
215.58	143.05	40.240
215.99	130.35	40.226
216.39	113.95	40.217
216.80	105.09	40.208
217.22	97.56	40.208
217.65	92.08	40.203
218.07	90.84	40.214
218.49	87.92	40.223
218.91	86.42	40.226
219.34	84.71	40.229
219.87	84.71	40.220
220.51	82.49	40.226
221.46	83.81	40.223
223.68	82.85	40.240
226.91	82.77	40.277
230.06	83.26	40.298
233.49	83.78	40.324
237.24	84.39	40.358
240.96	85.16	40.387
244.66	86.94	40.410
248.34	86.90	40.433
252.00	86.27	40.483
255.65	87.73	40.522
259.29	88.18	40.562
P = 50.0 MPa		
144.70	65.42	39.236
147.73	66.36	39.285
150.74	67.17	39.325
153.89	68.81	39.365
157.39	69.96	39.411
161.02	71.51	39.434
164.61	73.39	39.454
168.16	74.96	39.479
171.16	76.69	39.512
175.16	79.17	39.555
178.61	81.25	39.558
181.68	84.06	39.590
184.07	85.68	39.607
186.09	88.43	39.630
187.43	90.85	39.647
188.09	91.47	39.650
188.76	92.28	39.636
189.42	93.14	39.664
190.08	94.42	39.664
190.74	96.29	39.670
191.29	96.87	39.687
191.72	100.01	39.711
192.16	100.16	39.742
192.59	102.34	39.762
193.45	108.86	39.806
193.88	131.08	39.834
194.26	290.67	39.972
194.62	131.04	40.119
195.02	114.66	40.165
195.45	104.59	40.194
195.88	103.65	40.208
196.42	99.60	40.229
197.07	97.25	40.246
197.72	95.79	40.260
198.37	95.05	40.272
199.18	95.64	40.278
200.15	96.65	40.272
201.12	100.42	40.269
201.82	98.59	40.269
202.25	99.35	40.269
202.68	101.71	40.275
203.10	102.97	40.272
203.53	106.51	40.266
203.95	109.43	40.260
204.37	114.75	40.246
204.79	123.13	40.231
205.20	139.27	40.211
205.59	189.80	40.185
205.97	226.21	40.142
206.35	136.07	40.105
206.77	106.11	40.082
207.30	92.88	40.076
207.94	86.99	40.076
208.59	83.87	40.082
209.24	82.81	40.093
209.89	81.59	40.102
210.87	81.54	40.102
212.82	81.28	40.122
215.72	81.20	40.139
218.94	81.13	40.157
222.15	81.50	40.180
224.91	81.46	40.188
228.08	82.17	40.211
231.56	82.46	40.231
235.33	83.43	40.249
239.09	84.89	40.266
242.83	84.90	40.289
246.54	85.50	40.315
249.01	85.89	40.329
P = 57.0 MPa		
155.58	69.49	39.264
158.47	72.58	39.351
162.05	72.25	39.411
165.59	73.94	39.457
169.09	75.02	39.486
172.56	77.11	39.512
175.99	79.37	39.538
179.39	81.61	39.558
182.75	84.99	39.587
186.07	87.94	39.601
188.25	91.12	39.604
189.23	92.33	39.598
190.21	94.40	39.607
191.02	95.89	39.618
191.68	97.45	39.630
192.33	98.57	39.641
192.99	100.08	39.659
193.64	101.87	39.672
194.29	103.97	39.682
194.94	106.28	39.696
195.59	109.27	39.705
196.23	113.17	39.722
196.74	117.09	39.736
197.12	125.02	39.811
197.49	160.87	39.846
197.84	249.85	39.964
198.19	117.54	40.076
198.57	111.94	40.108
198.95	109.03	40.131
199.34	104.16	40.154
199.73	104.13	40.162
200.11	105.78	40.177
200.50	107.25	40.185
200.88	114.12	40.183
201.26	111.96	40.191
201.65	103.43	40.191
202.03	103.38	40.180
202.42	105.75	40.171
202.80	109.79	40.165
203.18	115.64	40.157
203.56	124.97	40.148
203.93	143.52	40.139
204.28	192.82	40.119
204.62	245.77	40.070
204.97	134.18	40.030
205.34	103.26	40.014
205.73	93.60	40.007
206.25	87.89	40.010
206.90	84.83	40.018
207.55	83.28	40.027
208.21	81.85	40.027
208.86	81.20	40.030
209.85	81.32	40.033
213.00	80.77	40.067
216.14	80.66	40.076
218.41	81.01	40.079
221.64	81.68	40.171
224.85	81.86	40.183
228.04	82.61	40.237
231.22	82.51	40.237
228.34	82.40	40.099
231.47	82.69	40.183
234.58	83.19	40.183
237.98	84.00	40.209
241.68	84.53	40.226
245.36	85.63	40.240
249.04	86.53	40.257
252.68	85.30	40.275
P = 62.0 MPa		
162.70	71.47	39.285
166.30	73.41	39.285
169.85	75.37	39.411
173.37	75.95	39.475
176.86	79.61	39.515
180.31	82.38	39.546
183.72	85.38	39.578
187.10	89.75	39.595
190.44	94.04	39.650
193.73	100.68	39.693
196.02	108.33	39.722
196.99	112.52	39.731
197.63	117.65	39.745
198.26	122.76	39.762
198.76	129.53	39.780
199.13	135.64	93.791
199.50	156.06	39.803
199.86	175.84	39.849
200.21	187.74	39.964
200.57	138.64	40.062
200.93	173.72	40.093
201.29	134.52	40.111
201.67	106.34	40.113
202.06	107.38	40.111
202.44	116.83	40.099
202.81	127.92	40.093
203.18	156.36	40.076
203.53	227.73	40.044
203.87	162.97	40.018
204.24	114.37	40.001
204.75	87.78	39.998
205.41	86.33	39.998
206.06	82.95	40.004
206.72	82.83	40.013
207.37	80.79	40.010
208.69	80.62	39.995
211.30	80.66	40.007
212.15	80.22	39.961
214.92	80.66	40.001
217.83	80.63	40.042
220.90	80.64	40.073
224.11	81.60	40.088
227.31	81.82	40.111
230.49	82.51	40.122
233.66	82.75	40.145
236.82	83.66	40.168
P = 63.5 MPa		
161.35	71.89	39.340
164.96	73.41	39.394
168.54	75.24	39.460
172.07	76.91	39.518
175.57	79.06	39.552
179.03	81.14	39.576
182.46	84.49	39.610
185.84	87.16	39.652
189.19	91.77	39.684
191.48	95.75	39.741
192.86	98.31	39.738
194.17	101.90	39.755
195.47	105.09	39.773
196.76	111.65	39.791
197.72	116.86	39.809
198.35	122.25	39.822
198.85	127.15	39.835
199.23	133.63	39.842
199.60	141.24	39.854
199.96	154.55	39.866
200.32	180.35	39.882
200.66	251.18	40.010
201.00	152.92	40.134
201.37	139.36	40.142
201.74	110.56	40.141
202.12	116.94	40.123
202.86	171.52	40.107
203.21	203.17	40.082
203.56	135.27	40.052
203.94	104.81	40.040
204.33	95.10	40.043
204.85	89.60	40.048
205.50	85.87	40.048
206.16	83.41	40.049
206.98	82.41	40.050
207.96	81.34	40.047
210.09	80.88	40.049
213.35	80.77	40.070
214.58	80.76	40.069
217.82	81.04	40.069
221.05	81.25	40.083
224.26	81.70	40.100
P = 65.0 MPa		
162.38	72.09	39.304
165.98	73.56	39.384
169.54	75.13	39.453
173.08	77.68	39.522
176.57	79.71	39.554
180.02	82.05	39.580
183.43	85.08	39.609
186.81	88.09	39.646
190.15	93.01	39.672
192.47	97.69	39.701
193.81	100.70	39.733
195.11	104.31	39.741
196.40	108.70	39.756
197.68	115.89	39.773
198.50	120.88	39.790
198.88	127.71	39.802
199.26	132.76	39.813
199.63	138.86	39.831
199.99	150.71	39.842
200.35	168.60	39.859
200.70	221.42	39.879
201.03	236.99	40.021
201.39	116.10	40.139
201.76	124.70	40.121
202.13	153.61	40.110
202.48	225.24	40.084
202.82	168.74	40.035
203.19	118.47	40.015
203.57	102.19	40.012
203.96	95.34	40.018
204.35	89.97	40.021
205.03	87.33	40.018
206.01	84.09	40.023
207.00	82.72	40.029
207.98	81.90	40.029
210.10	80.81	40.041
213.36	80.57	40.058
216.61	80.94	40.055
219.85	81.24	40.069
223.06	81.57	40.090
226.26	82.15	40.118
P = 66.0 MPa		
164.76	72.91	39.309
168.33	74.67	39.387
171.86	76.65	39.462
175.36	78.87	39.505
178.99	81.40	39.546
182.60	84.22	39.592
185.98	87.36	39.603
189.33	91.91	39.632
191.98	96.19	39.666
193.65	99.38	39.687
194.95	103.18	39.704
196.24	107.66	39.721
197.53	114.68	39.741
198.48	121.62	39.756
198.98	126.98	39.767
199.36	129.44	39.784
199.73	141.02	39.799
200.09	151.81	39.816

TABLE 3. (Continued)

T / K	C_p / J K^{-1}mol^{-1}	V / cm^{3}mol^{-1}	T / K	C_p / J K^{-1}mol^{-1}	V / cm^{3}mol^{-1}	T / K	C_p / J K^{-1}mol^{-1}	V / cm^{3}mol^{-1}	T / K	C_p / J K^{-1}mol^{-1}	V / cm^{3}mol^{-1}
200.45	170.53	39.831	200.61	174.75	39.916	170.39	74.96	39.264	226.98	82.58	39.958
200.80	230.09	39.856	200.96	229.75	39.833	173.17	76.99	39.282	229.96	82.91	39.978
201.08	709.14	39.954	201.22	687.67	39.868	175.94	78.79	39.313	232.98	83.25	39.967
201.38	122.11	40.009	201.48	246.06	39.911	178.68	79.98	39.336	237.30	84.18	39.986
201.76	114.71	40.012	201.83	96.62	39.940	181.84	82.89	39.400	241.66	84.94	40.065
202.14	124.76	40.003	202.22	90.07	39.951	184.55	84.55	39.431	244.99	85.78	40.099
202.51	112.86	39.997	202.75	86.58	39.954	187.21	86.66	39.457	248.30	86.56	40.128
202.90	102.91	39.995	203.40	84.21	39.966	189.86	89.19	39.474	251.35	86.79	40.134
203.28	96.70	39.889	204.06	82.94	39.969	192.43	93.25	39.509	254.49	86.94	40.168
203.97	92.11	39.889	204.88	82.03	39.974	195.08	96.23	39.529	257.67	87.75	40.185
204.94	87.27	39.986	205.03	81.19	39.972	197.66	103.62	39.609	260.84	88.39	40.240
205.92	84.71	29.983	208.33	80.32	40.012	199.20	109.27	39.584	264.09	88.18	40.272
206.90	83.41	39.980	211.60	80.31	40.023	199.67	112.56	39.590			
208.37	82.29	39.986	214.87	81.22	40.058	200.09	113.21	39.601	191.95	92.12	39.506
210.99	80.98	40.003	218.11	80.86	40.075	200.51	116.70	39.607	193.62	94.21	39.523
214.24	80.76	40.021	215.77	80.76	40.021	200.92	120.07	39.613	194.95	97.00	39.541
216.63	80.72	40.052	219.00	81.23	40.055	201.34	118.28	39.624	196.05	98.80	39.552
219.86	81.10	40.067	222.22	81.47	40.090	201.75	122.66	39.633	197.04	101.55	39.564
223.07	81.36	40.078	225.42	81.67	40.116	202.16	125.71	39.636	197.81	103.36	39.572
			228.62	81.97	40.136	202.58	123.97	39.641	198.24	103.39	39.578
P = 67.0 MPa			231.80	83.12	40.164	202.99	131.93	39.653	198.68	106.44	39.584
159.36	71.18	39.309	234.96	83.37	40.190	203.39	139.07	39.662	199.11	107.49	39.587
162.63	72.10	39.361				203.79	149.90	39.676	199.58	109.39	39.592
166.22	73.82	39.407	P = 111.0 MPa			204.19	161.72	39.693	199.97	110.80	39.598
169.78	75.15	39.451	121.76	58.12	38.861	204.57	192.62	39.708	200.40	112.58	39.607
173.30	77.58	39.497	124.34	58.54	38.913	204.93	271.95	39.731	200.83	115.98	39.616
176.78	79.42	39.517	126.91	59.53	38.962	205.25	485.14	39.762	201.26	117.48	39.624
180.23	80.07	39.552	129.43	60.29	38.944	205.59	127.47	39.803	201.68	121.34	39.630
183.65	85.30	39.589	131.99	61.38	39.014	206.01	95.34	39.808	202.11	123.84	39.636
187.02	88.43	39.612	134.58	61.87	39.046	206.44	88.87	39.805	202.53	128.06	39.639
189.70	92.25	39.620	137.15	62.62	39.072	206.87	86.20	39.817	202.95	132.53	39.650
191.69	95.86	39.643	139.70	63.86	39.086	207.30	84.89	39.817	203.36	141.11	39.662
193.66	99.31	39.672	142.22	64.66	39.109	207.73	82.64	39.826	203.77	150.51	39.679
195.63	104.68	39.695	144.74	65.35	39.123	208.16	84.08	39.828	204.18	165.87	39.693
197.09	111.13	39.721	147.46	66.54	39.146	208.59	82.95	39.834	204.57	194.38	39.708
197.88	116.06	39.733	150.39	67.10	39.155	209.22	82.60	39.841	204.94	291.32	39.722
198.39	119.08	39.741	153.30	67.77	39.161	210.53	78.77	39.846	205.26	467.34	39.762
198.77	124.50	39.759	156.19	69.10	39.169	213.11	81.14	39.849	205.62	120.77	39.808
199.15	127.87	39.764	159.04	70.61	39.184	215.68	81.42	39.866	206.05	92.40	39.811
199.52	132.15	39.781	161.90	71.40	39.195	218.29	81.96	39.889	206.49	87.28	39.817
199.89	141.28	39.793	164.75	72.82	39.215	221.09	81.75	39.903	206.93	86.64	39.823
200.26	153.15	39.805	167.58	74.08	39.214	224.04	82.21	39.935	207.37	84.10	39.826

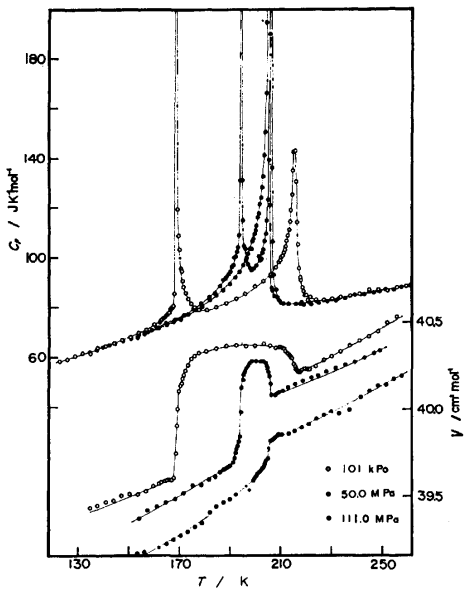

Fig. 4. Molar heat capacity and molar volume of ND_4Br at 0.101 (○), 50.0 (⊕), and 111.0 MPa (●).

γ-β transition, accompanied by the contraction of the volume, got sharper with the increasing pressure. The slope was given as -0.190 K MPa^{-1}. Both slopes of the transition lines changed slightly by deuteration. The deuteration has the same effect on the γ-β transition temperature as Br substitution has in the mixed crystal $NH_4Cl_xBr_{1-x}$.[15] The heat capacities of the β phase above *ca.* 220 K and the δ phase below *ca.* 150 K did not depend on the pressure. This is related to another experimental fact that the volume expansivity is independent of the temperature as required by the thermodynamic relation $(\partial C_P/\partial p)_T = -T(\partial^2 V/\partial T^2)_P$.

Figures 5(a)—(f) shows the temperature dependence of the molar heat capacity and molar volume at the constant pressures (given in the diagram) around the triple point. Those values are tabulated in Table 3. There was another heat capacity anomaly at 57.0 MPa and 62.0 MPa between the temperatures of two phase transitions described above, though the corresponding volume change was too small to be detected. As the pressure increased up to 63.1 MPa to 65.0 MPa, this anomaly overlapped with and merged into the δ-γ phase transition. At 66.0 MPa the heat capacity peak due to the γ-β transition at 202.1 K became quite small, indicating that a very small part of the crystal underwent the transition from the γ to β phases and that most from the δ to β phases. Heat capacity and volume curves at 67.0 MPa were essentially the same as those at 111.0 MPa.

The phase transition temperatures taken as the temperatures of the heat capacity peaks are plotted as a function of pressure as open circles in Fig. 6 where the dashed line stands for the result derived from a dilatometric study by Stevenson.[1] The present result indicates, in contrast to the previous one, that there is no maximum in any one branch of transition lines and the triple point is represented essentially as the point of intersection of the three straight lines. Absence of an exact triplet point in a very close look would be connected with a superheating effect in the δ-γ phase transition and will be discussed later.

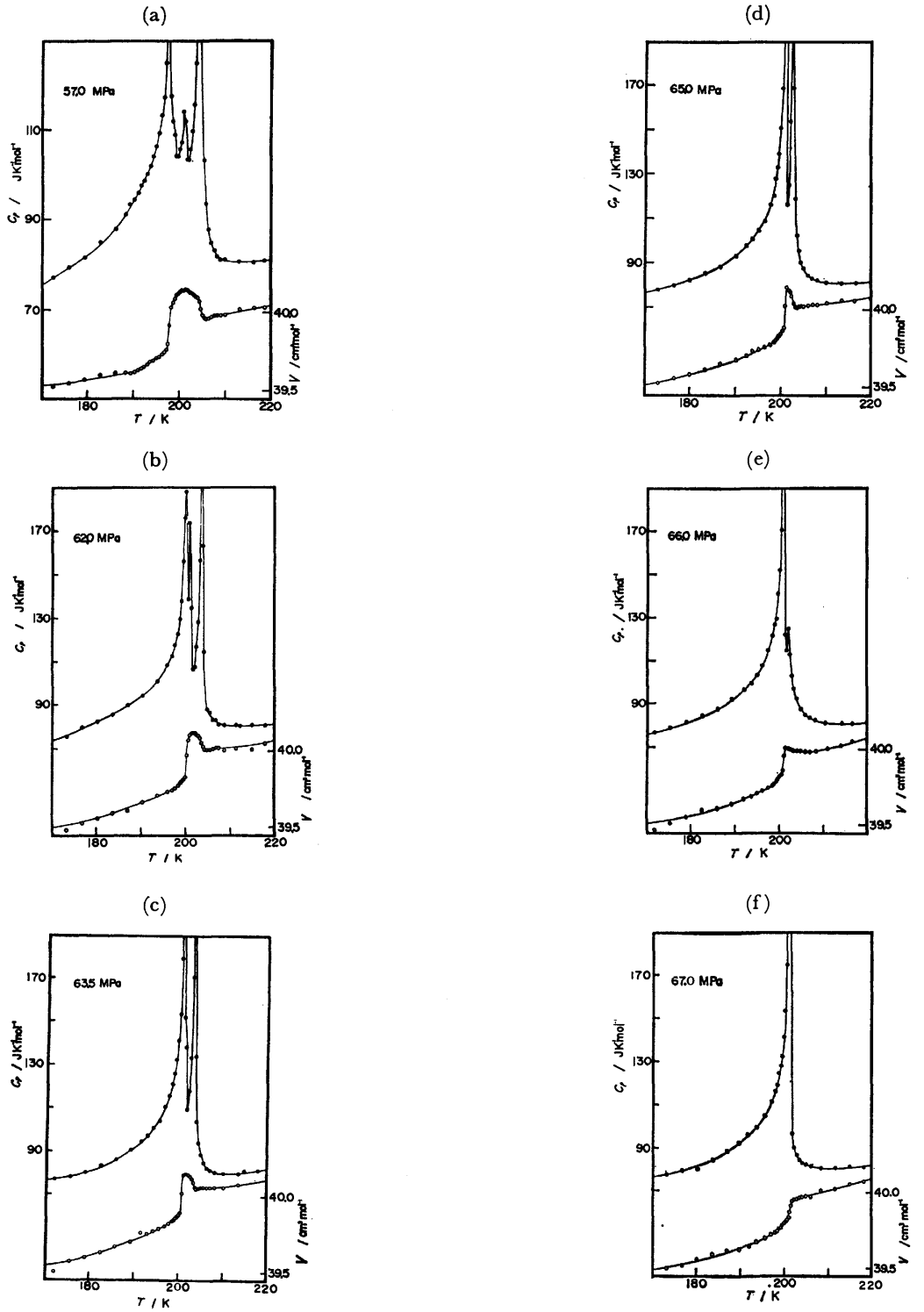

Fig. 5. Temperature dependences of molar heat capacity and molar volume of ND_4Br at the pressures around the triple point.
(a): 57.0 MPa, (b): 62.0 MPa, (c): 63.5 MPa, (d): 65.0 MPa, (e): 66.0 MPa, (f): 67.0 MPa.

Pressure Dependence of the Entropy of the Transition. The excess entropy involved in the successive two transitions for NH_4Br at 0.101 and 108.0 MPa are shown as functions of the temperature in Fig. 7. Here the entropy values were computed by assuming a baseline that joins smoothly the heat capacity curves outside the transition region. The total entropy change associated with the δ-γ-β phase transitions was estimated to be (4.0 ± 0.2) J K^{-1} mol^{-1}.

Figure 8 shows temperature dependence of the entropies of transition in ND_4Br at 0.1, 50.0, and 111.0 MPa and Fig. 9 at six pressures around the triple point. Table 4 lists the total entropy of transition from δ to β phases at all the pressures measured on ND_4Br. There

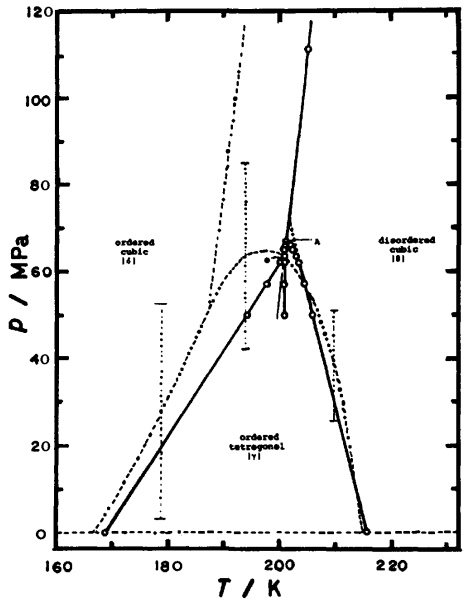

Fig. 6. Phase diagram of ND_4Br crystal as taken from the temperature of heat capacity peak. Previous data by R. Stevenson[1] are represented by dotted lines and error bars.

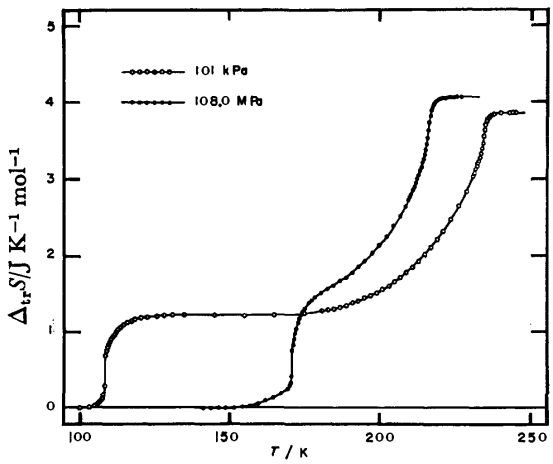

Fig. 7. Temperature dependence of the entropy of δ-γ-β phase transition in NH_4Br.
—○—: 0.101 MPa, —●—: 108.0 MPa.

is no pressure dependence in these values. The values can be explained in terms of the order-disorder mechanism in the orientational degree of freedom of NH_4^+ ions.

Molecular Excitation in the δ Phase. The entropies of transition had a very similar temperature dependence in the δ phase for the five isobaric measurements ranging from 57.0 to 67.0 MPa, as shown in Fig. 15. Correspondingly, the excess heat capacity (ΔC_p) *vs.* temperature curves in the relevant temperature and

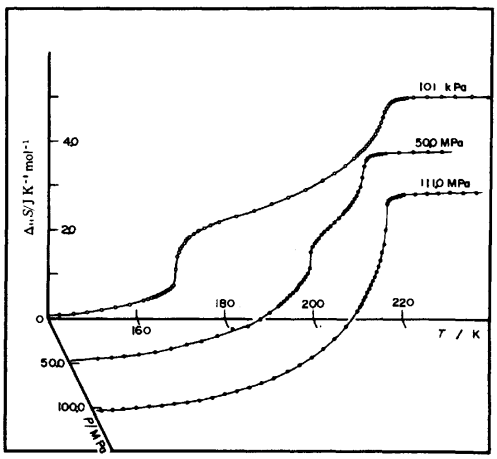

Fig. 8. Temperature dependence of the entropy of δ-γ-β phase transition in ND_4Br.
—○—: 0.101 MPa, —⊕—: 50.0 MPa, —●—: 110.1 MPa.

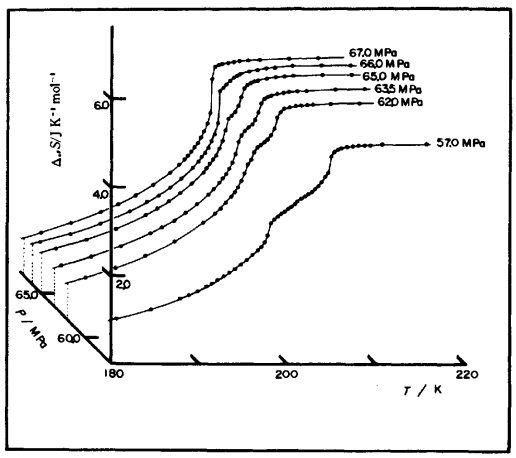

Fig. 9. Temperature dependence of the entropy of δ-γ-β phase transition in ND_4Br at six constant pressures around the triple point.

pressure region were practically independent of pressure as plotted in Fig. 10. It is to be noted here that the crystal transformed from the δ to γ phases below 66.0 MPa and from the δ to β phases at 67.0 MPa. These facts mean that the same process develops in the δ phase irrespective of the phases (γ or β) stable above the transition. This process is considered primarily to be the disordering of the orientation of NH_4^+ tetrahedra in the CsCl lattice, leading to the β phase. The δ-γ phase transition immediately below the triple point pressure therefore takes place between the cubic and tetragonal phases in the stages of low order parameters of the orientational arrangement of NH_4^+ ions.

Table 4. Pressure dependence of the entropy of δ-γ-β phase transition in ND_4Br crystal

$\frac{P}{\text{MPa}}$	0.101	50.0	57.0	62.0	63.5	65.0	66.0	67.0	111.0
$\frac{\Delta_\delta^\beta S}{\text{J K}^{-1}\text{ mol}^{-1}}$	5.00	4.87	4.94	4.86	4.88	4.91	5.00	4.88	4.96

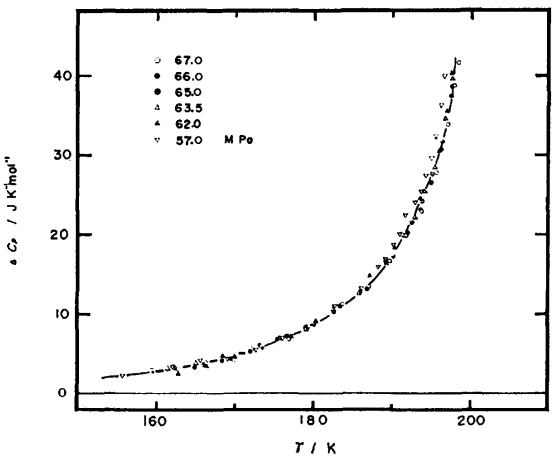

Fig. 10. Pressure and temperature dependences of the excess heat capacity due to the δ-γ or δ-β phase transition in ND_4Br crystal at around the triple point pressure.

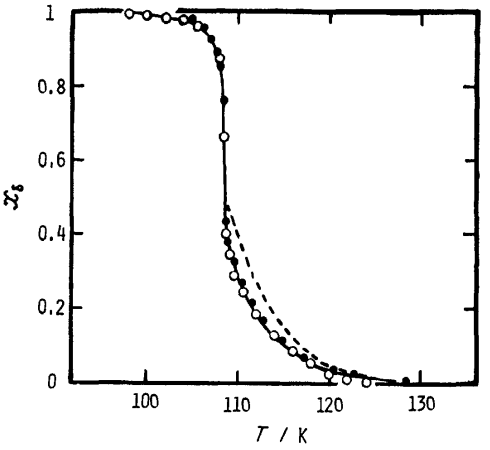

Fig. 11. Mole fraction of δ phase *vs.* temperature relation in the δ-γ phase transition of NH_4Br crystal at an atmospheric pressure.
—○—: Derived from the data of entropy, —●—: from the data of volume, ------: calculated by use of the Eq. 2.

Discussion on the Coexistence of the γ and δ Phases Domains. The δ-γ phase transition is of the first-order in which the entropy and volume undergo discontinuous change at the transition temperature. This is quite reasonable in view of the fact that the transition occurs between the parallel ordered cubic and the anti-parallel ordered tetragonal phases and that it can not proceed continuously as the homogeneous transition from one phase to the other from the viewpoint of crystal symmetry.

The heat capacity curve at 0.101 MPa in Fig. 1, however, shows a large post-transitional effect. The appearance of such an anomaly in a first-order transition as in the present case can be attributed to the coexistence of the domains of the δ and γ phases around the transition point. Actually the temperature dependence of the molar fraction of the δ phase calculated from the changes in entropy and volume associated with the transition can be explained by the spatial fluctuation of the domains as follows.[16-18]

Let x be the molar fraction of the δ phase, N the number of domains whose size is assumed to be the same throughout the crystal and G_δ and G_γ the free energies of the bulk δ and γ phases, respectively. Then the free energy of the crystal is, disregarding their interfacial energies, expressed by

$$G = [(1-x)G_\gamma + xG_\delta] + NkT[x \ln x + (1-x) \ln (1-x)]. \quad (1)$$

Minimization of the free energy at constant N and T gives the molar fraction

$$x = \frac{\exp\{-(G_\delta - G_\gamma)/NkT\}}{\exp\{-(G_\delta - G_\gamma)/NkT\}+1}. \quad (2)$$

Using the experimental values of 1.22 J K^{-1} mol^{-1} for the total entropy of transition and 108.5 K for the transition temperature in NH_4Br at 0.101 MPa, $(G_\delta - G_\gamma)$ can be approximated by the form 1.22 $(T/K - 108.5)$ J mol^{-1}. If one assumes that a single domain contains 6^3 $(=216)$ NH_4^+ ions, the temperature dependence of the molar fraction x could be calculated as drawn with a broken line in Fig. 11.

Comparison of the calculated and the experimental values shows that the heat capacity anomaly described above is reproduced by this model of spatial fluctuation of δ and γ phases domains. The number of domains in the δ phase actually changes depending on the temperature and the pre-history of the sample, and the interfacial energy should be represented in the expression for the sample free energy. This will be discussed in the subsequent paper.

Superheating of the δ-γ Phase Transition. Superheating is possible in principle in the first-order phase transition, though not found frequently in contrast to supercooling. An evidence for the superheating in the δ-γ phase transition could be given by the consideration of the Gibbs free energies for the δ and γ phases. By way of an example the following discussion is established by the use of the calorimetric data at 50 MPa for ND_4Br. The free energies for the δ and γ phases on the basis of that for the β phase would be written down according to the Landau theory of phase transitions of the second kind as follows;

$$G(\eta^2) = G_\beta + \frac{a}{2}(T-T_0)\eta^2 + \frac{b}{4}\eta^4 + \frac{c}{6}\eta^6, \quad (3)$$

and

$$G(\xi^2) = G_\beta + \frac{a'}{2}(T-T_0')\xi^2 + \frac{b'}{4}\xi^4 + \frac{c'}{6}\xi^6, \quad (4)$$

where η and ξ are the order parameters describing the δ-β and the γ-β phase transitions, respectively, and G_β the free energy for the β phase. With coefficients a, b, c, T_0, a', b', c', and T_0' determined appropriately, the problems of which phase is stable at a given T and where the δ-γ phase transition takes place can be solved by the comparison between $G(\eta^2)$ and $G(\xi^2)$.

The coefficients a, b, c, and T_0 were derived by the extrapolation from those at 111.0 and 67.0 MPa at which the δ phase transformed directly into the β phase. The coefficients at the both pressures, 111.0 and 67.0 MPa, were obtained by use of the two equations;

$$\Delta_{tr}S(T) = S_0 - \frac{a}{2}\eta^2, \quad (5)$$

and

$$a(T-T_0) + b\eta^2 + c\eta^4 = 0, \quad (6)$$

where S_0 is the total entropy of the transition. The relation (5) connected with the experimental data of excess heat capacities yielded the temperature dependence of the order parameter, and the least-squares fit of the relation (6) to the T dependence of η^2 determined the coefficients at the respective pressure values. The coefficient values a', b', c', and T_0' were derived, using relations similar to Eqs. 5 and 6 with the order parameter ξ^2, from the experimental data at 50.0 MPa of the excess heat capacities associated with the γ-β phase transition.

Figure 12 shows the temperature dependence of the order parameters η^2 and ξ^2 with the coefficients thus determined. The δ-γ phase transition at 50.0 MPa took place at 194.3 K on heating in the actual experiment. The Gibbs energy against order parameter curves for both the δ and γ phases at the temperature and the pressure 50.0 MPa are shown in Fig. 13. The minimum free energy for the γ phase is definitely lower than that for the δ, contrary to the thermodynamic relation that the minimum values of free energies for the two phases should be equal to each other at the transition point. This means that the temperature of the heat capacity peak observed at 50.0 MPa is higher than the phase transition point as defined by the equality of the Gibbs energies; in other words, the substance in the δ phase at 194.3 K is in a superheated state.

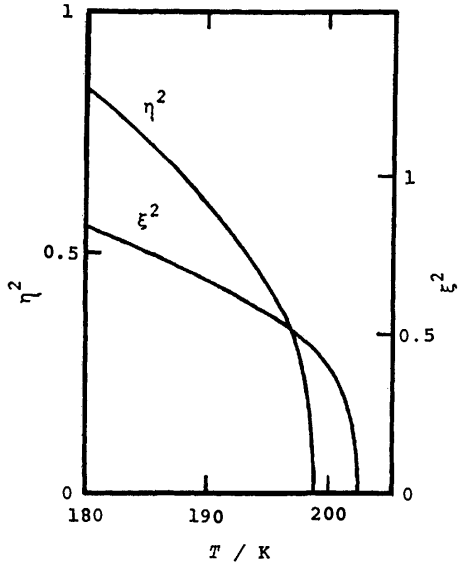

Fig. 12. Temperature dependences of the order parameters for γ and δ phases of ND_4Br at 50 MPa. The order parameter ξ is associated with the γ-β phase transition and η with the δ-β phase transition.

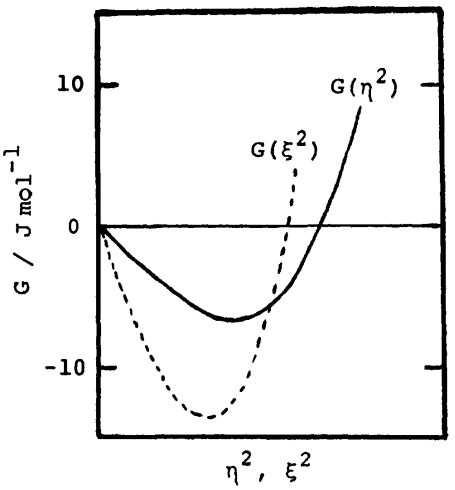

Fig. 13. Gibbs free energy against order parameter curves for the γ and δ phases at 194.3 K and 50 MPa. 194.3 K is the observed δ to γ phase transition point taken as the temperature of heat capacity peak 50.0 MPa.

Interpretation of an Anomalous Heat-capacity Peak. The phase diagram for ND_4Br (Fig. 6) has two peculiarities around the triple point among β, γ, and δ phases; one is the appearance of a new heat-capacity anomaly between the δ-γ and the γ-β phase transitions at pressures just below the triple point pressure, and the other is the apparent presence of two triple-points as shown by A and B. In this section the former phenomenon is discussed as the δ-β phase transition due to the coexistence of the δ and γ domains and of the superheating in the δ to γ phase change, the effects described above.

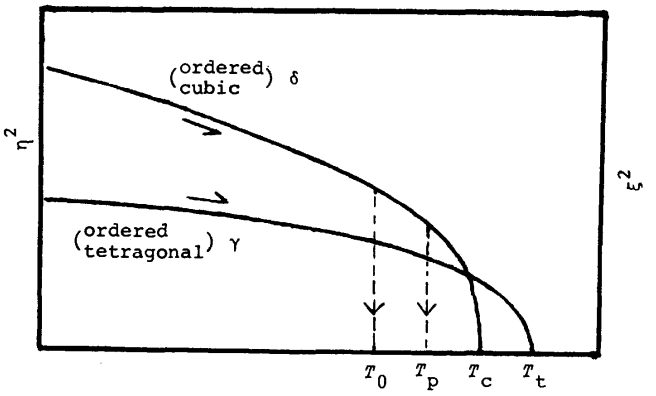

Fig. 14. Schematic temperature dependences of the order parameters for the δ-β and γ-β phase transitions in ND_4Br crystal at a certain constant pressure immediately below the triple point. T_0: the temperature at which $G_\delta = G_\gamma$, T_p: the δ-γ phase transition temperature, T_c: the δ-β phase transition temperature, T_t: the γ-β phase transition temperature.

Figure 14 illustrates diagramatically the path of transformation on heating as curves of order parameter versus temperature, where T_0 is the temperature of equilibrium between the δ and γ phases at which the free energies for the two phases become equal, and T_c and T_t are the temperatures of the δ-β and the γ-β phase changes, respectively. Most of domains of the δ phase transform into the γ phase around T_p with the superheating effect as indicated by an arrows, and subsequently into the β phase at T_t. But some of domains remain in the δ phase until the temperature T_c is reached, at which temperature they transform into the β phase directly. This fluctuational δ-β transition should become important as the pressure approaches

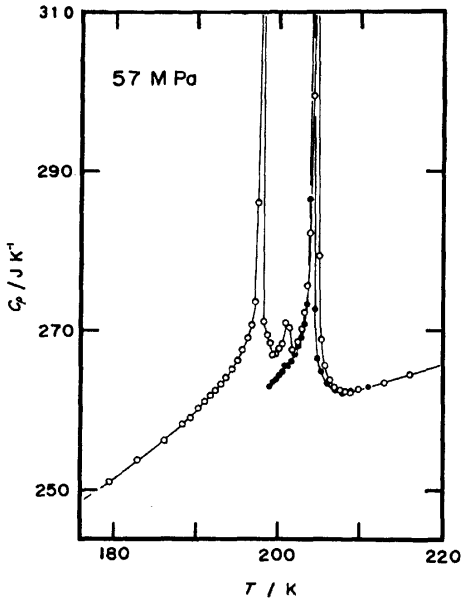

Fig. 15. The effect of thermal hysteresis on the heat capacity curve of ND_4Br crystal at 57.0 MPa. One series of measurement (—○—) was started at 100 K where the crystal was in the δ phase, and the other (—●—) was started at 198 K on the crystal in the γ phase after the treatment of the isothermal pressure increase from 0.101 to 57.0 MPa following the temperature decrease from room temperature to 198 K at 0.101 MPa.

that of the triple point, as the fraction of the substance, namely the number of domains, remaining in the δ phase accordingly increases till T_c.

Figure 15 shows another experimental evidence for the above reasoning with the use of heat capacity curves at 57 MPa as an example, the heat capacity values being the total of contributions from the sample and cell measured in the heating direction. Two sets of data, distinguished by open and solid circles, differed from each other in the prehistories of the sample. The sample in the former case (open circles) was cooled down to liquid nitrogen temperature so as to start the measurement in the δ phase. In the latter, on the other hand, the temperature of the samples was first decreased from 300 K to 198 K at an atmospheric pressure, then the pressure was isothermally increased to 57.0 MPa, and then a set of measurement was started from there in the heating direction. The former sample at 199.5 K, being normally in the γ phase, would consequently still have involved some domains of the δ phase resulting in the anomalous peak at 200.9 K on the subsequent heating while the latter would have been composed of the γ phase and if any the β phase. The results combined with the different thermal-prehistories of the sample therefore indicates the effects of superheating and coexistence as causing the anomalous heat-capacity peak in the decisive way.

It should be pointed out that the extra heat capacity peaks occur practically at the same temperature 200.8—200.9 K even though one would expect the peak temperature to follow the extrapolation of the stable δ-β phase boundary. This cannot be explained by the simplified domain model as discussed above. One would have to incorporate the possibility of distributed internal pressure felt by the less compact γ domains surrounded by the δ or β domains. The situation is, however, not clear at present.

Character of the γ-β Phase Transition around the Triple Point. As already pointed out there appeared two triple points, A and B in Fig. 6, on the phase diagram. The superheating of the δ-γ phase transition explains this unusual behavior of the phase lines (apart from the curvature of the γ-β line) in the close vicinity of the triple point. As we discussed above, the observed δ-γ phase boundary is at higher temperature than the equilibrium phase boundary by several Kelvin. The equilibrium δ-γ phase line which is assumed to be parallel to the observed phase line would then join the point A where the δ-β and γ-β phase boundaries meet thus terminating at a genuine triple point.

The γ-β phase line near the triple point A was found to deviate from a straight line (broken one in Fig. 6). This appears to be an equilibrium properties rather than a hysteretic effect related to the coexistence of the different domains, since the heat capacity measurement performed after approaching the triple point from the lower pressure gave essentially the same γ-β transition temperature. (See Fig. 15) The γ-β phase line is so curved that the β phase region is larger than the linear extrapolation of the γ-β phase line gives. This is explained if one notes that the two ionic interactions stabilizing the γ and δ phases are opposite in nature. The ionic interactions favoring the antiparallel orientation of the NH_4^+ ions within the ab plane stabilizes the γ phase and those favoring the parallel orientation the δ phase. The two interactions have the same strength in the opposite directions at the triple point. They tend to cancel each other resulting in relative stabilization of the disordered β phase, as is experimentally observed. Such fluctuational interaction among different phases does not occur at an ordinary triple point among a solid, liquid, and vapour. It is characteristic of a triple point involving phase transitions of the second kind.[19]

Concluding Remarks

The present results of heat capacity of NH_4Br and ND_4Br crystals evidenced again that the high pressure calorimeter described in the preceding paper has a satisfactory accuracy. The accurate measurements enabled the exact determination of p-T phase diagrams and the detailed examination of phase transitions to be performed under well specified thermodynamic conditions.

The peculiar phenomena observed at high pressures just below a triple point for ND_4Br crystal were reasonably explained in terms of the effects of superheating in the δ-γ phase transition and of coexistence of the δ, γ, and β phases domains (This is quite an instructive point in that the superheating effect causes a new phenomenon in some cases.). The nucleation and growth processes in the δ-γ phase transition is an interesting subject for

further study, as will be described in the subsequent paper. The detailed measurement of the δ-β phase transition line under high pressure (beyond the pressure range of the present apparatus) is desirable for the insight into the competitive interaction between the two different (parallel and anti-parallel) orderings in the disordered β phase.

References

1) R. Stevenson, *J. Chem. Phys.*, **34**, 1757 (1961).
2) C. W. Garland and R. A. Young, *J. Chem. Phys.*, **49**, 5282 (1968).
3) E. L. Wagner and D. F. Horning, *J. Chem. Phys.*, **18**, 305 (1950).
4) Y. Yamada, M. Mori, and Y. Noda, *J. Phys. Soc. Jpn.*, **32**, 1565 (1972).
5) M. Oguni, K. Watanabe, T. Matsuo, H. Suga, and S. Seki, *Bull. Chem. Soc. Jpn.*, **55**, 77 (1982).
6) C. W. Garland and C. F. Yarnell, *J. Chem. Phys.*, **44**, 1112 (1966).
7) R. S. Seymour, *Acta Crystallogr., Sect. A*, **27**, 348 (1971).
8) Y. Yamada, Y. Noda, J. D. Axe, and G. Shirane, *Phys. Rev. B*, **9**, 4429 (1974).
9) C. Rotter and W. Kamitakahara, *Phys. Rev. B*, **14**, 1983 (1976).
10) A. R. Cole, Doctoral Thesis, Massachusetts Institute of Technology, 1950.
11) M. Sorai, H. Suga, and S. Seki, *Bull. Chem. Soc. Jpn.*, **38**, 1125 (1956).
12) C. C. Stephenson and A. M. Karo, *J. Chem. Phys.*, **48**, 104 (1968).
13) W. Mandena and N. J. Trappeniers, *Physica*, **81B**, 285 (1976).
14) C. W. Garland, R. C. Leung, and F. P. Missel, *Phys. Rev. B*, **18**, 4848 (1978).
15) C. W. Garland, R. C. Leung, and C. Zahradnik, *J. Chem. Phys.*, **71**, 3158 (1979).
16) J. Frenkel, "Kinetic Theory of Liquids," Dover, New York (1955), p. 382.
17) A. R. Ubbelohde, "The Molten State of Matter," John Wiley and Sons, New York (1978), p. 86.
18) A. Kosaki, M. Sorai, H. Suga, and S. Seki, *Bull. Chem. Soc. Jpn.*, **50**, 810 (1977).
19) L. D. Landau and E. M. Lifshitz, "Statistical Physics," 3rd ed, Pergamon Press, Oxford (1980), Part 1, p. 497.

 © 1982 The Chemical Society of Japan Bull. Chem. Soc. Jpn., 55, 1014—1021 (1982) [Vol. 55, No. 4

Effect of Nucleophiles on the Rates of Dissociation and Racemization of the Tris(1,10-phenanthroline)iron(II) Ion in Aqueous Solutions

Satoshi TACHIYASHIKI* and Hideo YAMATERA†

Laboratory of Chemistry, Kagawa Nutrition College, Sakado, Saitama 350-02

†*Department of Chemistry, Faculty of Science, Nagoya University, Chikusa-ku, Nagoya 464*

(Received May 13, 1981)

The rates of dissociation and racemization of the tris(1,10-phenanthroline)iron(II) ion were obtained in aqueous solutions containing fourteen kinds of nucleophile. They ranged from 0.7 to 9.3 and from 0.9 to 3.2 times the rates in pure water, respectively. The results were analyzed by considering simultaneous reactions of free and ion-paired complex ions. The rate constants of the dissociation (ligand release) of the complex existing in ion-pairs increased in the following order of the counter-ions: $I^- < Br^- < Cl^- < (H_2O) < NO_2^- < CH_3COO^- < OCN^- < N_3^- < F^- < OH^- \approx CN^-$; here H_2O is regarded as a nucleophile for the free complex ion. This order is similar to that of proton affinities of nucleophiles. The results show that the dissociation is accelerated by σ donation from the nucleophile, suggesting an ion-pair interchange mechanism. The intramolecular racemization rate constant, given by total recemization rate constant minus dissociation rate constant, increased in the following order of nucleophiles: $OH^- \approx CN^- \approx F^- \approx Cl^- < Br^- \approx NO_2^- < (H_2O) < CH_3COO^- < OCN^- < I^- < N_3^- <$ (thiourea) $\approx SCN^- \approx SeCN^- <$ (pyridine). This suggests that the polarizability of nucleophiles has a greater effect than their basicity. The operation of π interaction between the complex ion and the nucleophile in the transition state is also suggested. The ion-association constants obtained from the rate data were in the range of 1 to 8 (I=1.0, 32.0 °C).

Intramolecular twist mechanisms[1] are among the basic reaction mechanisms of the stereochemical rearrangement of metal chelates. The nature of these mechanisms, however, does not seem to be fully understood.[2] Although such mechanisms are suggested in many systems, firm evidence for the mechanism has been presented for only a few cases.[3] The $[Fe(phen)_3]^{2+}$ (phen=1,10-phenanthroline) ion is one of the few inert complexes which racemize by an intramolecular twist mechanism.[4] Thus, studies of the racemization of this complex are expected to give information concerning the characteristics of the twist mechanism.

A variety of different mechanisms have been proposed for substitution reactions of the iron(II) complex. Margerum *et al.*[5] studied the nucleophilic substitution of $[Fe(phen)_3]^{2+}$ with hydroxide, cyanide, and azide. They proposed a mechanism in which nucleophiles enter into the "pocket" between ligands to form an inner-sphere ion-pair with the complex ion and interact with the metal center. An associative mechanism has been proposed for the nucleophilic ligand substitution of $[Fe(bpy)_3]^{2+}$ and $[Fe(phen)_3]^{2+}$.[6] Gillard[7] proposed a mechanism for hydrolysis involving nucleophilic attack at a chelate-ring carbon adjacent to a nitrogen atom. Recently, Lawrance *et al.*[8] proposed a dissociative interchange mechanism based on the values of activation volume obtained from high-pressure experiments. The conjugate base mechanism proposed for the base hydrolysis of cobalt(III) complexes does not seem to be operative in the present case, where the complex has no readily ionizable protons.

In the present study, the kinetics of dissociation and racemization of $[Fe(phen)_3]^{2+}$ were investigated in the presence of nucleophiles to clarify the dissociation mechanism in which nucleophiles are involved and to gain further understanding of the nature of the twist mechanisms.

Experimental

Materials. All the chemicals used were of guaranteed reagent grade except potassium azide, cyanate, and selenocyanate, and were obtained from Wako Pure Chemical Industries, Ltd. unless otherwise noted.

Complex: (+)-$[Fe(phen)_3](ClO_4)_2 \cdot 2H_2O$ was synthesized and resolved according to the method of Dwyer and Gyarfas.[9] $[\alpha]_{589} = 1380°$.

Nucleophiles: Potassium fluoride, chloride, bromide, iodide, thiocyanate, cyanide, acetate, nitrite (Merck), and azide (Alpha), and thiourea were recrystallized from water. Potassium cyanate (Kanto) was recrystallized twice from water below 40 °C to minimize decomposition. Potassium selenocyanate was recrystallized from aqueous alcohol (1:5.5). Pyridine was fractionally distilled using a Widmer distilling column 30 cm long (bp 116.0—116.1 °C). Potassium hydroxide was used without further purification. The concentrations of the solutions of potassium thiocyanate, cyanide, cyanate, and selenocyanate were determined by argentometry. The concentration of the solution of potassium nitrate was determined by iodometry, that of potassium fluoride by the colorimetric method with a zirconium lake of 4-dimethylaminoazobenzene-4'-arsonic acid,[10] and that of potassium acetate by alkalimetry after passing the solution through a column of H-form cation-exchange resin. The solutions of potassium chloride, bromide, iodide, and azide, as well as those of thiourea, were prepared by weighing well-dried reagents.

Other Reagents: Nickel(II) chloride hexahydrate was recrystallized from water. Nickel(II) perchlorate hexahydrate was synthesized from nickel(II) carbonate and perchloric acid. The concentrations of nickel(II) solutions were determined by chelatometry. Other chemicals were used without further purification.

Kinetic Studies. Dissociation Rates: The dissociation rates were obtained at 32 °C from the changes in the absorbance at 510 nm of the solution containing 5×10^{-5} mol dm^{-3} $[Fe(phen)_3](ClO_4)_2$. Nickel(II) chloride (5.19×10^{-4} mol dm^{-3}) was added as the scavenger of the liberated phenanthroline[11] except in the solutions containing KCN and KOH.

A sodium citrate solution of 1.0×10^{-2} mol dm^{-3} was added to the solutions containing potassium cyanate, potassium acetate, and pyridine to prevent the precipitation of any iron hydroxide which might be produced in the course of the reaction. A 1.0×10^{-3} mol dm^{-3} citric acid solution was added to the solutions containing potassium azide and potassium nitrite, and a 2.0×10^{-3} mol dm^{-3} solution of disodium dihydrogen ethylenediaminetetraacetate (Na_2H_2edta) was added to the solutions containing potassium hydroxide for the same reason. The hydroxide ion concentration of the solution was corrected for the Na_2H_2edta added.[5a] The reactions were followed for four half-lives, and were found to be of the first order in the metal-complex concentration in the time range studied. The data were analyzed by the usual method of the first order reactions. The dissociation rates obtained were reproducible within $\pm1\%$. They were independent of the nickel(II) concentration in the range of $(0.02—1.0)\times10^{-2}$ mol dm^{-3}; the rates obtained in Ni(II)-containing KCl solutions agreed with that obtained in acidic solution. The other added reagents had little effect on the dissociation rate, at least at their concentrations up to 1×10^{-2} mol dm^{-3}; the dependence of the rate on the reagent concentration was checked. For the systems containing KSCN and KSeCN, the dissociation rate could not be obtained because of the precipitation of the complex. Without Ni(II) ions, however, no precipitations nor absorbance changes were observed at least for thirty minutes, and the racemization rate could be obtained.

Racemization Rates: A 1.0 ml portion of a 5×10^{-4} mol dm^{-3} solution of the optically active iron-complex perchlorate, cooled with ice water, was added to a thermostated (32.0 °C) solution containing a nucleophile; the resultant solution was adjusted to a volume of 10.0 ml with water at 32.0 °C, and mixed immediately. After being kept for one minute in a thermostat, the solution was transferred into a thermostated (32.0 °C) quartz cell (5 cm path length) and the change in optical rotation of the solution at 546 nm was followed on a recorder using a Union PM-101 automatic polarimeter. Correction was made for the reproducible instrumental error which occurred when the absorbance of the solution decreased in the course of the kinetic measurement. All the reactions were followed for at least four half-lives. The reactions were first order in the concentration of the optically active metal complex in the time range studied.

The racemization rate constant was defined as $k_r=[\ln(\alpha_0/\alpha_t)]/t$, where α_0 and α_t mean the optical rotations at times zero and t, respectively. The reproducibility of the rate data was estimated to be within $\pm5\%$ from the standard deviation of the multiple measurements under the same experimental conditions.

pH Measurements. After each kinetic run, the pH value of the solution was measured by a Radiometer PHM26 pH-meter. In each case, the pH value was at least 2.0 greater than the pK_a value of the nucleophile contained. More than 99% of the nucleophiles thus existed in the free base form, so that the concentrations of the nucleophilic free bases assumed to be equal to those of the nucleophiles added.

Results and Discussion

Rates of Dissociation. Table 1 gives the rate constants for dissociation (k_d) and racemization (k_r) of the complex in aqueous solutions containing various nucleophiles at different concentrations. In the potassium azide system, the final absorbance value of the solution (A_∞) increased with the increase in citric acid and potassium azide concentrations of the solution. This would be caused by the formation of the mixed complex of nickel or iron with citrate and azide ions. However, linear relationships existed between $\log(A_t-A_\infty)$ and the time for four half-lives (A_t represents the absorbance at time t). The rate was not affected by nickel(II) and citric acid concentrations in the range studied. The rate constants thus obtained are considerably greater than those obtained by Margerum *et al.*,[5b] who reported the slowing-down of the apparent dissociation rate after the first 15% decrease in the absorbance. The rate expression proposed by them (Eq. 10) is also different from that proposed here (Eq. 6).

Table 1. The racemization and dissociation rate constants (k_r and k_d) of $[Fe(phen)_3]^{2+}$ in various ionic media at 32.0 °C

Added salt (mol dm^{-3})		$k_r/10^{-3}$ s^{-1}		$k_d/10^{-3}$ s^{-1}		$(k_r-k_d)/10^{-3}$ s^{-1}	
		Obsd	Calcd[a]	Obsd	Calcd[a]	Obsd	Calcd
KCl							
0.00	—	1.94±0.09 (20) [b]	1.94	0.255	0.254[c]	1.69	1.69
0.10	—	1.99	1.90	—	0.254	1.74	1.65
0.20	—	1.80, 1.81	1.88	0.254	0.254	1.55	1.63
0.30	—	1.86	1.86	—	0.254	1.61	1.61
0.40	—	1.72—1.82 (3)	1.83	0.254	0.254	1.51	1.58
0.60	—	1.82, 1.88	1.79	0.255	0.254	1.59	1.55
0.80	—	1.82, 1.85	1.76	0.254	0.254	1.58	1.51
1.00	—	1.70—1.79 (5)	1.74	0.251	0.254	1.49	1.49
KBr	KCl						
0.20	0.80	1.75	1.77	0.244	0.244	1.51	1.53
0.40	0.60	1.76	1.80	0.237	0.237	1.52	1.56
0.60	0.40	1.72, 1.88	1.82	0.231	0.231	1.57	1.59
0.80	0.20	1.80	1.84	0.225	0.225	1.58	1.61
1.00	0.00	1.83—1.86 (3)	1.85	0.221	0.221	1.62	1.65
KI	KCl						
0.20	0.80	2.10	2.13	0.231	0.230	1.87	1.90
0.40	0.60	2.24	2.23	0.213	0.214	2.03	2.02

TABLE 1. (Continued)

Added salt (mol dm^{-3})		$k_r/10^{-3}$ s^{-1}		$k_d/10^{-3}$ s^{-1}		$(k_r-k_d)/10^{-3}$ s^{-1}	
		Obsd	Calcd[a)]	Obsd	Calcd[a)]	Obsd	Calcd
0.60	0.40	2.36	2.27	0.201	0.202	2.16	2.07
0.80	0.20	2.36	2.30	0.193	0.192	2.17	2.11
1.00	0.00	2.22—2.37 (4)	2.31	0.185	0.184	2.10	2.13
0.10	—	—	—	0.233	0.236	—	—
0.20	—	—	—	0.227	0.225	—	—
0.40	—	—	—	0.208	0.210	—	—
0.50	—	—	—	0.206	0.204		
0.60			—	0.200	0.199	—	—
0.80	—	—	—	0.191	0.191	—	—
KI							
0.011	—	1.95	1.93	—	—	—	—
0.099	—	2.03	2.05	—	—	—	—
0.247	—	2.13, 2.17	2.15	—	—	—	—
0.422	—	2.17, 2.23	2.21	—	—	—	—
0.629	—	2.28, 2.28	2.26	—	—	—	—
0.760	—	2.38	2.28	—	—	—	—
0.837	—	2.23, 2.33	2.31	—	—	—	—
KF	KCl						
0.20	0.80	1.96	1.88	0.403	0.397	1.56	1.48
0.40	0.60	1.96	2.04	0.566	0.569	1.39	1.47
0.60	0.40	2.31	2.24	0.765	0.769	1.55	1.47
0.80	0.20	2.41	2.46	0.982	0.996	1.43	1.46
1.00	0.00	2.75	2.72	1.260	1.251	1.49	1.47
0.20	—	—	—	0.589	0.576	—	—
0.40	—	—	—	0.775	0.790	—	—
0.60	—	—	—	0.959	0.970	—	—
0.80	—	—	—	1.127	1.124	—	—
KN_3	KCl						
0.10	0.90	1.85	—	—	—	—	—
0.20	0.80	2.12, 2.15	2.16	0.522	0.526	1.61	1.63
0.30	0.70	2.29	—	—	—	—	—
0.40	0.60	2.47, 2.63	2.51	0.722	0.715	1.83	1.79
0.50	0.50	2.72	—	—	—	—	—
0.60	0.40	2.72, 3.04	2.79	0.855	0.852	2.03	1.93
0.80	0.20	2.91—3.17 (5)	3.03	0.950	0.956	2.07	2.07
1.00	0.00	3.11—3.40 (5)	3.24	1.044[d)]	1.038	2.21	2.20
0.20	—	—	—	0.660	0.662	—	—
0.40	—	—	—	0.825	0.823	—	—
0.60	—	—	—	0.932	0.923	—	—
0.80	—	—	—	0.996	0.992	—	—
KSCN	KCl						
0.10	0.90	2.09	2.01	—	—	—	—
0.20	0.80	2.24	2.20	—	—	—	—
0.30	0.70	2.32	2.34	—	—	—	—
0.40	0.60	2.26, 2.48	2.45	—	—	—	—
0.60	0.40	2.70	2.61	—	—	—	—
0.80	0.20	2.73	2.72	—	—	—	—
1.00	0.00	2.72—2.87 (3)	2.77	—	—	—	—
0.021	—	2.00	2.01	—	—	—	—
0.043	—	2.02	2.07	—	—	—	—
0.070	—	2.03	2.12	—	—	—	—
0.078	—	2.15	2.13	—	—	—	—
0.100	—	2.23	2.16	—	—	—	—
0.162	—	2.40	2.25	—	—	—	—
0.205	—	2.03	2.30	—	—	—	—
0.30	—	2.27	2.39	—	—	—	—
0.40	—	2.53	2.47	—	—	—	—
0.50	—	2.42, 2.55	2.54	—	—	—	—
0.60	—	2.62	2.60	—	—	—	—

TABLE 1. (Continued)

Added salt (mol dm^{-3})		$k_r/10^{-3}$ s^{-1}		$k_d/10^{-3}$ s^{-1}		$(k_r-k_d)/10^{-3}$ s^{-1}	
		Obsd	Calcd[a)]	Obsd	Calcd[a)]	Obsp	Calcd
KOCN	KCl						
0.20	0.80	2.23	2.17	0.408	0.415	1.82	1.75
0.40	0.60	2.29	2.39	0.564	0.561	1.73	1.83
0.60	0.40	2.57	2.57	0.702	0.692	1.87	1.88
0.80	0.20	2.74	2.72	0.814	0.810	1.93	1.91
1.00	0.00	2.85, 2.88	2.85	0.906	0.916	1.96	1.93
KSeCN	KCl						
0.10	0.90	2.18	2.17	—	—	—	—
0.20	0.80	2.41	2.40	—	—	—	—
0.40	0.60	2.51	2.64	—	—	—	—
0.60	0.40	2.83	2.76	—	—	—	—
0.80	0.20	2.76	2.83	—	—	—	—
1.00	0.00	2.83, 3.02	2.89	—	—	—	—
KNO_2	KCl						
0.20	0.80	1.75, 1.88	1.81	0.271	0.270	1.61	1.54
0.40	0.60	1.85, 1.89	1.87	0.290	0.287	1.60	1.58
0.60	0.40	1.91, 1.94	1.92	0.306	0.305	1.63	1.61
0.80	0.20	1.94, 1.95	1.95	0.323	0.322	1.63	1.63
1.00	0.00	1.97, 2.01	1.99	0.340[d)]	0.340	1.67	1.65
KCH_3COO	KCl						
0.20	0.80	1.93	1.87	0.280	0.280	1.55	1.59
0.40	0.60	1.92	1.97	0.308	0.310	1.61	1.66
0.60	0.40	2.10	2.05	0.332	0.340	1.77	1.71
0.80	0.20	2.04	2.12	0.380	0.370	1.66	1.75
1.00	0.00	2.14—2.26 (3)	2.18	0.401	0.400	1.80	1.78
0.40	—	—	—	0.335	0.333	—	—
0.60	—	—	—	0.357	0.359	—	—
KOH	KCl						
0.016	0.98	1.91	1.94	0.488	0.481	1.42	1.47
0.036	0.96	2.16	2.20	0.783	0.761	1.38	1.45
0.056	0.94	2.46	2.46	1.018	1.036	1.44	1.43
0.076	0.92	2.63	2.72	1.284	1.307	1.35	1.41
0.080[e)]	0.90	2.89	2.78	1.343	1.372	1.55	1.42
0.096	0.90	3.02	2.99	1.605	1.573	1.41	1.40
KCN	KCl						
0.020	0.98	2.30	2.21	0.736	0.710	1.56	1.53
0.040	0.96	2.72	2.68	1.110	1.148	1.61	1.57
0.060	0.94	3.08	3.14	1.587	1.570	1.49	1.59
0.080	0.92	3.46, 3.79	3.61	1.981	1.976	1.64	1.63
0.100	0.90	4.05, 4.08	4.07	2.357	2.367	1.71	1.66
Thiourea	KCl						
0.10	1.00	—	—	0.231	—	—	—
0.20	1.00	1.97	2.00	0.225	—	1.75	1.78
0.40	1.00	2.27	2.22	0.217	—	2.05	2.00
0.60	1.00	2.39	2.37	0.209	—	2.18	2.16
0.80	1.00	2.42	2.49	0.203	—	2.22	2.29
0.90	1.00	—	—	0.189	—	—	—
1.00	1.00	2.61	2.58	0.189	—	2.42	2.39
Pyridine	KCl						
0.20	1.00	3.14, 3.32	3.15	0.274	—	2.96	2.87
0.40	1.00	3.98	4.14	0.305	—	3.67	3.84
0.60	1.00	4.66	4.90	0.346	—	4.31	4.56
0.80	1.00	5.50, 6.05	5.50	0.389	—	5.39	5.11
1.00	1.00	5.64—6.15 (3)	5.98	0.433	—	5.52	5.54

a) Calculated with Eq. 6 or 9 using the $K^{1P}_{c(X)}$ and $k^{1P}_{d(X)}$ or $k^{1,1P}_{r(X)}$ values given in Table 2. b) The value in parentheses is the number of observations. c) In KCl solutions, the value of k_d was assumed to be independent of the KCl concentration. d) The value changed only within $\pm 1\%$ in 0—1×10^{-2} mol dm^{-3} citric acid. e) Containing 1.0×10^{-2} mol dm^{-3} Na_2H_2-edta.

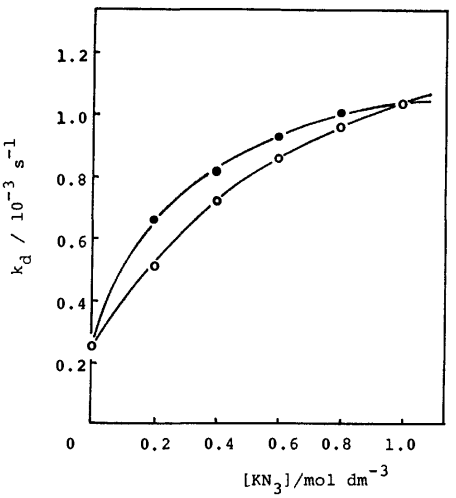

Fig. 1. The dissociation rate constants of $[Fe(phen)_3]^{2+}$ in potassium azide solutions. The solid circles show the rate constants observed in the solutions without ionic-strength adjustment and the open circles are those in the solutions of constant ionic strength (I=1.0, adjusted with KCl).

The effect of nucleophiles on the reaction rate is discussed separately in two groups: anionic and neutral nucleophiles.

Anionic Nucleophiles: An example of the results is shown in Fig. 1. The ion-pair formation mechanism[12] reasonably accounts for the observed dissociation rates. In the systems without added KCl, the proposed mechanism is as follows:

$$[Fe(phen)_3]^{2+} + X^- \overset{K^{IP}_{(X)},\ K^{IP}_{c(X)}}{\rightleftharpoons} [Fe(phen)_3]^{2+}\cdot X^-, \quad (1)$$

$$[Fe(phen)_3]^{2+} \overset{k^0_d}{\longrightarrow} Fe^{2+} + 3\,phen, \quad (2)$$

$$[Fe(phen)_3]^{2+}\cdot X^- \overset{k^{IP}_{d(X)}}{\longrightarrow} Fe^{2+} + 3\,phen + X^-, \quad (3)$$

$$K^{IP}_{(X)} = \frac{[Fe(phen)_3{}^{2+}\cdot X^-]}{[Fe(phen)_3{}^{2+}][X^-]}\frac{f_1}{f_2 f_1} \simeq K^{IP}_{c(X)}\frac{1}{f_2}, \quad (4)$$

where $K^{IP}_{(X)}$ and $K^{IP}_{c(X)}$ represent the thermodynamic and the concentration ion-association constant for reaction (1) and where k^0_d and $k^{IP}_{d(X)}$ are the rate constants for reactions (2) and (3), respectively. The symbol f_z means the activity coefficient of the ion with a charge of $\pm z$; $\log f_z$ can be expressed as:

$$\log f_z = -\frac{z^2 A\sqrt{I}}{1+Ba\sqrt{I}} + bI, \quad (5)$$

where A=0.5181 $mol^{-1/2}\,dm^{3/2}$, B=0.3305$\times 10^8$ cm^{-1} $mol^{-1/2}\,dm^{3/2}$ at 32 °C in water, and the parameters, a and b, are taken to be (7—12)$\times 10^{-8}$ cm and 0.1 z^2, respectively. Then, the observed dissociation rate constant, k_d, is expressed as:

$$k_d = \frac{k^0_d + k^{IP}_{d(X)}K^{IP}_{c(X)}f_2[X^-]}{1+K^{IP}_{(X)}f_2[X^-]}. \quad (6)$$

The $K^{IP}_{(X)}$ and $k^{IP}_{d(X)}$ were obtained by the weighted least-squares fit[13] to Eq. 6 of the kinetic data. The $K^{IP}_{(X)}$ was transformed to the ion-association constant ($K^{IP}_{c(X)}$) at I=1.0 by means of Eqs. 4 and 5.

The following equations were added to Eqs. 1—3 for the systems in which the ionic strength was adjusted to 1.0 with added KCl.

$$[Fe(phen)_3]^{2+} + Cl^- \overset{K^{IP}_{c(Cl)}}{\rightleftharpoons} [Fe(phen)_3]^{2+}\cdot Cl^- \quad (7)$$

$$[Fe(phen)_3]^{2+}\cdot Cl^- \overset{k^{IP}_{d(Cl)}}{\longrightarrow} Fe^{2+} + 3\,phen + Cl^- \quad (8)$$

Then, the observed dissociation rate constant is expressed as:

$$k_d = \frac{k^0_d + k^{IP}_{d(Cl)}K^{IP}_{c(Cl)}[Cl^-] + k^{IP}_{d(X)}K^{IP}_{c(X)}[X^-]}{1+K^{IP}_{c(Cl)}[Cl^-]+K^{IP}_{c(X)}[X^-]}. \quad (9)$$

Since the dissociation rate constants were almost unaffected by the KCl concentration (Table 1), the value of $K^{IP}_{c(Cl)}$ was obtained in the following way.

TABLE 2. THE ION-ASSOCIATION CONSTANTS OF $[Fe(phen)_3]^{2+}$ WITH NUCLEOPHILES ($K^{IP}_{c(X)}$) AND THE DISSOCIATION AND INTRAMOLECULAR RACEMIZATION RATE CONSTANTS ($k^{IP}_{d(X)}$ AND $k^{i.IP}_{d(X)}$) OF THE COMPLEX IN ION-PAIRS AT THE CONSTANT IONIC STRENGTH OF 1.0 (KCl)

Nucleophile	pK_a	$k^{IP}_{d(X)}/10^{-3}\,s^{-1}$	$k^{i.IP}_{r(X)}/10^{-3}\,s^{-1}$	$K^{IP}_{c(X)}$ Dissociation	$K^{IP}_{c(X)}$ Racemization
I	−10	0.165±0.003	2.20±0.09	3.5±0.4	6 ±4
Br	−7	0.210±0.003	1.58±0.11	3.1±1.3	2 ±5
Cl	−4	0.250±0.003	1.37±0.04	2.0±1.0	1.7±0.6
H_2O	−1.7	0.254±0.002	1.74±0.09	—	—
SCN	−0.7	<0.4	3.04±0.17[a]	—	3.4±1.5
Thiourea	0.4	—	2.53±0.18	—	5 ±3
F	3.2	1.78 ±0.03	1.48±0.12	1.9±0.1	1.0±0.9
NO_2	3.4	0.391±0.005	1.64±0.06	1.6±0.2	6 ±11
OCN	3.5	1.14 ±0.06	1.94±0.09	2.9±1.3	17 ±20
SeCN	—	<0.13	2.99±0.10[a]	—	9 ±4
N_3	4.7	1.18 ±0.01	2.4 ±0.3	5.7±0.2	2 ±3
CH_3COO	4.7	0.475±0.011	1.79±0.07	2.0±0.2	6 ±4
Pyridine	5.3	—	6.4 ±0.3	—	5 ±2
CN	9.2	14.2 ±1.6	1.60±0.17	5.0±2.0	5 ±7
OH	15.7	13.6 ±2.0	1.43±0.14	3.2±1.8	0.7±10

a) Rate constants for the total racemization. Other values are for the intramolecular racemization.

Using Eq. 6, an analysis of the kinetic data was made for the systems of various ionic strength containing KI, KN_3, KF, KCH_3COO, and KNO_2 to obtain the values of $k^{IP}_{d(Cl)}$ and $K^{IP}_{e(X)}$. These values were substituted in Eq. 9. The kinetic data for similar systems of the constant ionic strength with added KCl were analyzed with this equation to evaluate $k^{IP}_{d(Cl)}$ and $K^{IP}_{e(X)}$. The latter kinetic data were analyzed again using the resulting $k^{IP}_{d(Cl)}$ and $K^{IP}_{e(X)}$ values to re-evaluate $k^{IP}_{d(X)}$ and $K^{IP}_{e(X)}$. The values thus obtained are in agreement with those derived above from the data for the solutions of variable ionic strength within the experimental error. These $k^{IP}_{d(X)}$ and $K^{IP}_{e(X)}$ values at $I=1.0$ are listed in Table 2.

Margerum[5] reported the rate expression of the type

$$k_d = k_0 + k_1[X] + k_2[X]^2 + k_3[X]^3 \qquad (10)$$

for the azide-, cyanide-, and hydroxide-assisted dissociation of $[Fe(phen)_3]^{2+}$. The square and cubic terms of nucleophile concentration in the rate equation were observed only for hydroxide ions. They were accounted for in terms of the mechanism of the multiple hydroxide attack to the complex, or the multiple hydroxide-association with the complex. However, the rate dependence of the type of Eq. 10 can also be fitted by Eq. 9 for the ion-pair formation mechanism. By substituting C_T(constant) for [Cl]+[X], Eq. 9 is transformed to

$$k_d = \frac{(k^0_d + k^{IP}_{d(Cl)}K^{IP}_{e(Cl)}C_T) + (k^{IP}_{d(X)}K^{IP}_{e(X)} - k^{IP}_{d(Cl)}K^{IP}_{e(Cl)})[X]}{(1+K^{IP}_{e(Cl)}C_T) - (K^{IP}_{e(Cl)} - K^{IP}_{e(X)})[X]}. \qquad (11)$$

On the condition of $\left|\frac{(K^{IP}_{e(Cl)} - K^{IP}_{e(X)})[X]}{(1+K^{IP}_{e(Cl)}C_T)}\right| < 1$, the denominator of Eq. 11 can be expanded to an infinite series and Eq. 11 is then transformed to:

$$\begin{aligned} k_d &= \{(k^0_d + k^{IP}_{d(Cl)}K^{IP}_{e(Cl)}C_T) + (k^{IP}_{d(X)}K^{IP}_{e(X)} - k^{IP}_{d(Cl)}K^{IP}_{e(Cl)})[X]\} \\ &\quad \times \left\{\frac{1}{(1+K^{IP}_{e(Cl)}C_T)} + \frac{(K^{IP}_{e(Cl)} - K^{IP}_{e(X)}}{(1+K_{e(Cl)}C_T)^2}[X] \right. \\ &\quad \left. + \frac{(K^{IP}_{e(Cl)} - K^{IP}_{e(X)})^2}{(1+K^{IP}_{e(Cl)}C_T)^3}[X]^2 + \cdots\right\} \\ &= \frac{(k^0_d + k^{IP}_{d(Cl)}K^{IP}_{e(Cl)}C_T)}{(1+K^{IP}_{e(Cl)}C_T)} + \left\{\frac{(k^0_d + k^{IP}_{d(Cl)}K^{IP}_{e(Cl)}C_T)(K^{IP}_{e(Cl)} - K^{IP}_{e(X)})}{(1+K^{IP}_{e(Cl)}C_T)^2} \right. \\ &\quad \left. + \frac{(k^{IP}_{d(X)}K^{IP}_{e(X)} - k^{IP}_{d(Cl)}K^{IP}_{e(Cl)})}{(1+K^{IP}_{e(Cl)}C_T)}\right\}[X] \\ &\quad + \left\{\frac{(k^0_d + k^{IP}_{d(Cl)}K^{IP}_{e(Cl)}C_T)(K^{IP}_{e(Cl)} - K^{IP}_{e(X)})^2}{(1+K^{IP}_{e(Cl)}C_T)} \right. \\ &\quad \left. + \frac{(K^{IP}_{e(Cl)} - K^{IP}_{e(X)})(k^{IP}_{d(X)}K^{IP}_{e(X)} - k^{IP}_{d(Cl)}K^{IP}_{e(Cl)})}{(1+K^{IP}_{e(Cl)}C_T)}\right\}[X]^2 + \cdots \\ &= k_0 + k_1[X] + k_2[X]^2 + \cdots. \end{aligned} \qquad (12)$$

For KF, KNO_2, KCH_3COO, KCN, and KOH, the observed dissociation rate constants were nicely expressed by Eq. 9 with the parameter values listed in Table 2, although the rate constants could also be expressed by Eq. 10. In fact, the kinetic data for hydroxide-assisted dissociation obtained by Margerum[5a] can also be reproduced by Eq. 9 with a $K^{IP}_{e(X)}$ value of 1.0 ± 0.7, consistent with the value of 3.2 ± 1.8 obtained here. Thus, in our opinion, Eq. 10 may be regarded as an approximation to Eq. 9.

As shown in Table 2, the $k^{IP}_{d(X)}$ values increase in the order:

$$I^- < Br^- < Cl^- < (H_2O) < NO_2^- < CH_3COO^- < OCN^- < N_3^- < F^- < OH^- \approx CN^-,$$

where H_2O means free complex ions not forming ion-pairs. A good correlation is observed between the logarithm of $k^{IP}_{d(X)}$ and the pK_a value of the conjugate acid of the nucleophile, as shown in Fig. 2. Considering that pK_a is a measure of the σ-donating ability of a nucleophile, the dissociation is likely to proceed by an ion-pair interchange mechanism where the nucleophile in an ion-pair would interact directly with the central metal of the complex. The dissociation rate constant of the free complex cation follows the trend observed in Fig. 2, where a water molecule is regarded as a nucleophilic reagent for the free cation. Thus, the free cation would also dissociate by a similar interchange mechanism, *e.g. via* a 7-coordinate transition state with an H_2O ligand, as suggested by Burgess.[14]

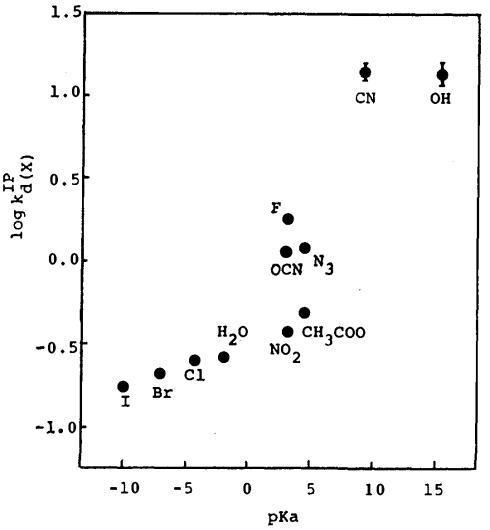

Fig. 2. The plot of the logarithm of $k^{IP}_{d(X)}$ *vs.* the pK_a value of nucleophile.

Alternative mechanisms which may account for the observed dissociation rates are: (i) dissociative mechanism, (ii) associative mechanism, and (iii) Gillard's mechanism. If dissociation of the complex proceeds dissociatively, the rate constant would be independent of the kind of nucleophile. As different rates were observed in the presence of different nucleophiles (Table 2), the dissociative mechanism can be excluded. Maestri *et al.*[15] proposed an associative mechanism for the base hydrolysis of $[Cr(bpy)_3]^{3+}$ to account for the rate expression, $k^{obsd} = [OH^-]/(B + A[OH^-])$, a special case of Eq. 6 with $k^0_d = 0$. The mechanism assumes that, as soon as the heptacoordinate complex is formed by the coordination of a water molecule, it undergoes an acid-base equilibrium, and that the conjugate-base form of the heptacoordinate complex (hydroxide associated species) tends to dissociate; the step of water coordination is considered to be rate-determining. A similar but slightly different mechanism may be considered to account for a rate expression of the type like Eq. 6; the mechanism assumes that a water molecule

associated with the complex is subjected to nucleophilic proton subtraction to form a hydroxide-associated species which undergoes dissociation. In this mechanism, the rate constant for the proton subtraction would be proportional to the probability of the nucleophile approaching the complex (or, in a sense, the ion-association constant) and to the ease of the proton subtraction. As the former does not change very much, the latter may be correlated with the strength of the nucleophile as a base. Although the order in which the nucleophiles increase the dissociation rate of the complex is in general consistent with the trend of increasing basicity of the nucleophiles, the deceleration effect shown by halide ions cannot be explained by this mechanism. Gillard's mechanism supposes the direct nucleophilic attack to a carbon atom of the phenanthroline molecule. The order of nucleophilic reactivity obtained in this study is very different from that obtained from the rate of nucleophilic displacement of the iodide ion from methyl iodide.[16] Thus, Gillard's mechanism is not adequate to interpret the experimental results. Therefore, the ion-pair interchange mechanism proposed in this paper very probably takes place.

Pyridine and Thiourea: In the systems containing pyridine and thiourea, the kinetic data could not be reproduced by Eq. 6 nor by Eq. 9 (see Table 1). The coordination of pyridine molecules to the second coordination sphere of the complex may be important for the system containing pyridine. In the system containing thiourea, a steep decrease in the rate was observed at 0—0.1 and 0.8—0.9 mol dm^{-3} thiourea concentrations. This may reflect the change in water activity or in the solution structure around these thiourea concentrations, if a water molecule is coordinated to the complex ion in the transition state.

Rates of Racemization. The observed racemization rate constants (k_r) are listed in Table 1, along with the dissociation rate constants (k_d) obtained under the same experimental conditions. Since the complex racemizes intramolecularly and dissociatively, the intramolecular racemization rate is given by total racemization rate minus dissociation rate. The total racemization rates increased considerably with added nucleophiles, except in the systems containing KCl and KBr. On the other hand, the intramolecular racemization rates do not appreciably change for the systems containing KF, KCN, and KOH, increase slightly with increasing concentrations of KBr, KNO_2, and KCH_3COO, and increase considerably with the increase in the concentrations of KI, KSCN, KSeCN, KOCN, KN_3, thiourea, and pyridine. The KOH result is in contrast to the intramolecular twist racemization of (ethylenediaminetetraacetato)cobalt(III), for which the racemization was reported to be accelerated by the hydroxide ion.[17] The increase in intramolecular racemization rate of $[Fe(phen)_3]^{2+}$ with increasing nucleophile concentration can resonably be accounted for by considering ion-pair formation, as in the case of dissociation. An analysis similar to that used for the case of dissociation gave the intramolecular racemization rate constants for the ion-paired complex ion ($k_{r(X)}^{I.IP}$) and the ion-association constants ($K_{c(X)}^{I.IP}$); these are listed in Table 2. The variation in the racemization rate constant with different nucleophiles is smaller than that in the dissociation rate constant. The order for $k_{r(X)}^{I.IP}$ is: $OH^- \approx CN^- \approx F^- \approx Cl^- < Br^- < NO_2^- < H_2O < CH_3COO^- < OCN^- < I^- < N_3^- <$ thiourea $\approx SCN^- \approx SeCN^- <$ pyridine. This order of nucleophiles in accelerating the intramolecular racemization rate suggests the importance of the polarizability of nucleophiles rather than their basicity, which was suggested above to be important for nucleophile-assisted dissociation. The order seems to be in rough agreement with that proposed for the reactivity against platinum(II) complexes:[18] $OH^- < H_2O < Cl^-$ < pyridine $< Br^- < NO_2^- < N_3^- \approx SCN^- \approx I^- \approx$ thiourea $< R_3P$. The polarizability of the nucleophile was suggested to be important in determining this order. The absorption spectrum of the complex changed in the presence of KCl, KBr, KI, and KSCN, suggesting a short-range interaction between the complex and the nucleophiles. Red shifts (2—3 nm) of the visible and ultraviolet absorption bands of the complex are observed in the presence of KCl and KBr, while, for KI and KSCN, broadenings of the ultraviolet absorption band (266 nm) toward the longer wave length are observed in addition to the red shift of the visible band. A π interaction between the complex ion (possibly the phen ligand) and a nucleophile would be important for assisting the intramolecular racemization, in contrast to the importance of σ donation of a nucleophile to the central metal of the complex for assisting the dissociation. Thus, it may be said that the central metal of $[Fe(phen)_3]^{2+}$ acts as a hard acid in the dissociation assisted by nucleophilic attack and the ligand phenanthroline acts as a soft acid in the intramolecular racemization assisted by nucleophile. The large accelerating effect of pyridine on the racemization rate may be caused by the solvation-like effect on the complex cation. Remarkable effects of solvents in accelerating the racemization rates were reported for this complex.[19]

The Ion-association Constants. The ion-association constants obtained from the dissociation rates agreed with those obtained from the racemization rates within experimental uncertainties (Table 2). The order of magnitudes of the constants obtained are also in good agreement with the theoretical prediction[20] of $K_{c(X)}^{I.IP} = 1—7$ ($I=1.0$, $a=(3—12)\times10^{-8}$ cm). This can be taken as supporting the ion-pair mechanism for the dissociation and racemization discussed above. The ion-association constant of the complex with an anion increased in the order: $F^- < Cl^- < Br^- < I^-$. The order might seem to be contrary to the theoretical prediction, according to which $K_{c(X)}^{I.IP}$ increases with the increase in the reciprocal of the ionic radius of the nucleophile. However, the reversal of the order can be well understood by considering the hydration of nucleophiles. The hydration number increases with the increase in the reciprocal of the ionic radius. The effective radius of a hydrated ion would increase with the increase in the hydration number. The short-range interactions discussed above may also be a factor affecting the order given above.

References

1) P. Rây and N. K. Dutt, *J. Indian Chem. Soc.*, **20**, 81 (1943); J. C. Bailar, Jr., *J. Inorg. Nucl. Chem.*, **8**, 165 (1958); C. S. Springer, Jr., and R. E. Sievers, *Inorg. Chem.*, **6**, 852 (1967).

2) F. Basolo and R. G. Pearson, "Mechanisms of Inorganic Reactions," 2nd ed, Wiley, New York (1967).

3) F. A. Cotton and G. Wilkinson, "Basic Inorganic Chemistry," Wiley, New York (1967); J. J. Fortman and R. E. Sievers, *Coord. Chem. Rev.*, **6**, 331 (1971); N. Serpone and D. G. Bickley, *Prog. Inorg. Chem.*, **17**, 391 (1972).

4) F. Basolo, J. C. Hays, and H. M. Neumann, *J. Am. Chem. Soc.*, **76**, 3807 (1954).

5) a) D. W. Margerum, *J. Am. Chem. Soc.*, **79**, 2728 (1957); b) D. W. Margerum and L. P. Morgenthaler, *ibid.*, **84**, 706 (1962).

6) R. D. Archer, L. J. Suydam, and D. D. Dollberg, *J. Am. Chem. Soc.*, **93**, 6837 (1971).

7) R. D. Gillard, *Coord. Chem. Rev.*, **16**, 67 (1975).

8) G. A. Lawrence, D. R. Stranks, and S. Suvachittanont *Inorg. Chem.*, **18**, 82 (1979).

9) F. P. Dwyer and E. C. Gyarfas, *J. Proc. Roy. Soc. N. S. Wales*, **83**, 263 (1950).

10) "Shin Jikken Kagaku Koza," ed by The Chemical Society of Japan, Maruzen, Tokyo (1976), Vol. 9 (1), p. 239.

11) L. Seiden, F. Basolo, and H. M. Neumann, *J. Am. Chem. Soc.*, **81**, 3809 (1959).

12) D. J. Farrington, J. G. Jones, and M. V. Twigg, *J. Chem. Soc., Dalton Trans.*, **1979**, 221.

13) The least-squares fitting was carried out by using the program, "SALS" (Nakagawa and Oyanagi), in the library program of the Computer Center, the University of Tokyo.

14) J. Burgess, *J. Chem. Soc., A*, **1967**, 431.

15) M. Maestri, F. Bolletta, N. Serpone, L. Moggi, and U. Balzani, *Inorg. Chem.*, **15**, 2048 (1976).

16) R. G. Pearson, H. Sobel, and J. Songstad, *J. Am. Chem. Soc.*, **90**, 319 (1968).

17) D. W. Cooke, Y. A. Im, and D. H. Bush, *Inorg. Chem.*, **1**, 13 (1962).

18) H. B. Gray, *J. Am. Chem. Soc.*, **84**, 1548 (1962); D. Banerjea, F. Basolo, and R. G. Pearson, *ibid.*, **79**, 4055 (1957).

19) S. Tachiyashiki and H. Yamatera, *Bull. Chem. Soc. Jpn.*, **54**, 3340 (1981).

20) H. Yokoyama and H. Yamatera, *Bull. Chem. Soc. Jpn.*, **48**, 1770 (1975).

The Electronic Structures of Linear Dicyano Complexes

Mitsuru SANO,* Hirohiko ADACHI,† and Hideo YAMATERA††

Laboratory of Inorganic Chemistry, Faculty of General Education, Nagoya University, Nagoya 464
†*Department of Nuclear Engineering, Faculty of Enginneering, Osaka University, Suita 565*
††*Department of Chemistry, Faculty of Science, Nagoya University, Nagoya 464*

(Received June 11, 1981)

Molecular orbital (MO) calculations in the discrete variational Xα (DV-Xα) scheme have been made on linear dicyano complexes, $[Ag(CN)_2]^-$, $[Au(CN)_2]^-$, and $[Hg(CN)_2]$, to clarify their electronic structures. The valence X-ray photoelectron spectra (XPS) for these compounds are also reported. The calculated energy levels are consistent with the XPS results. The relative magnitudes of the bond overlap populations show a good correlation with those of the force constants obtained from infrared data. The calculated MO features show that the mixing of the metal $(n+1)$s orbital is important in stabilizing the linear L–M–L bonds, especially in the partial cancellation of the antibonding character of the σ_g-type highest occupied molecular orbital.

Cyanide complexes have various symmetrical structures belonging to the $D_{\infty h}$, T_d, D_{4h}, and O_h point groups; the simplest of these is a linear two-coordinate complex, NC–M–CN ($D_{\infty h}$), which is formed by heavier ions with d^{10} configuration, such as Ag^+, Au^+, and Hg^{2+}. The study of the linear coordinate bond, L–M–L, is very important for inorganic chemists because it is one of the fundamental structures of coordination compounds. Orgel[1] has attributed the tendency of the d^{10} ions to form linear complexes to the d—s mixing rather than to the special stability of s—p hybrid bonds. Thus, the d_z^2 and s orbitals can be mixed together to give two new orbitals: $(1/\sqrt{2})(d_{z^2}-s)$ and $(1/\sqrt{2})(d_{z^2}+s)$. If the $(1/\sqrt{2})(d_{z^2}-s)$ orbital were occupied and the $(1/\sqrt{2})(d_{z^2}+s)$ orbital left empty, then the ligands in the x-plane would be repelled and a complex ion extending along the z-axis would be stable. However, Orgel's theory does not explain how the metal-ligand bond is formed. Moreover, Mason[2] has carried out absorption and magnetic-circular-dichroism spectral measurements for some linear dicyano complexes and has rejected the argument that metal d orbital predominantly participate in the metal-ligand σ bonding.

We have previously studied the electronic structures of octahedral[3–5] and square-planar[6] cyanide complexes. The studies on the electronic structures of the linear dicyano complexes of Ag^+, Au^+, and Hg^{2+} will complete a series of studies on cyanide complexes. In order to discuss the electronic structures of linear two-coordinate complexes, a systematic investigation of a few representative complexes has been made by means of the molecular orbital (MO) calculations and the measurements of valence X-ray photoelectron spectra (XPS).

Experimental

The complexes studied here are all well-known and were prepared by standard methods. The valence-region X-ray photoelectron spectra were recorded on a JEOL Model JESCA-3A spectrometer. Magnesium $K\alpha_{1,2}$ radiation (1253.6 eV) was used as the X-ray excitation source and the measurements were carried out at a vacuum of 5×10^{-7} Torr (7×10^{-5} Pa) or below.

Computational Method

The computations have been carried out by the discrete-variational Xα (DV-Xα) method, the details of which have been described elsewhere.[7] In the Hartree-Fock-Slater model,[8] the exchange-correlation term is give by

$$V_{xc}(1) = -3\alpha[(3/8\pi)\rho(1)]^{1/3}$$

where $\rho(1)$ is the local charge density and α is the exchange scaling parameter; the value, $\alpha=0.70$, is used for all atoms throughout the present calculations.[9] The DV-Xα self-consistent-charge (SCC) procedure[10] has been performed, where an approximate self-consistent molecular potential is determined from the Mulliken gross orbital populations. The numerical basis functions are obtained with an atom-like potential constructed by spherically averaging the molecular potential around the nucleus for the region inside each atomic sphere.[10] The basis sets include Ag 1s—5p, Au and Hg 1s—6p, and C and N 1s—2p. The molecular geometries for the complexes are assumed as follows:

Ag–C = 2.02 and C–N = 1.13 Å for $[Ag(CN)_2]^-$,

Au–C = 2.12 and C–N = 1.17 Å for $[Au(CN)_2]^-$,

Hg–C = 2.01 and C–N = 1.14 Å for $[Hg(CN)_2]$.

In the present calculations, the complexes are regarded as having the $D_{\infty h}$ symmetry.

Results and Discussion

The MO's of Free CN⁻. The electronic structure of the free cyanide ion is briefly described for convenience of comparison with coordinated cyanide ions. Table 1 shows the orbital energies (with reference to arbitrary zero level) and the Mulliken populations for the free CN^- ion. The contours of the CN^- valence MO's are also shown in Fig. 1. The main features of the CN^- MO's are: (1) the order of the valence MO energies is $3\sigma \ll 4\sigma < 1\pi < 5\sigma$, and (2) the 4σ MO has a higher density on nitrogen, 5σ on carbon, and 1π on nitrogen. The 5σ MO will play the most important role in the coordination of the cyanide ion to a metal ion, and the 4σ, 1π, and 2π MO's also take part in the metal-ligand bond through orbital mixing.

The present result from the DV-Xα calculation and

Table 1. Electronic structure of CN^-

Orbital	Energy/eV	Charge distribution/% C 1s	C 2s	C 2p	N 1s	N 2s	N 2P
2π	11.4			59			41
5σ	3.7		21	41		5	33
1π	2.6			41			59
4σ	0.6		34	8		24	34
3σ	−10.4		22	11		57	10
2σ	−255.8	100					
1σ	−366.6				100		

Carbon orbital	Population	Nitrogen orbital	Population
1s	2.00	1s	2.00
2s	1.54	2s	1.73
$2p\sigma$	1.20	$2p\sigma$	1.54
$2p\pi$	1.63	$2p\pi$	2.37
Atomic charge	−0.37	Atomic charge	−0.63

C–N	Overlap population
2π	−0.598
5σ	−0.194
1π	0.268
4σ	0.002
3σ	0.387

the previous one from an ab initio MO calculation nearly agree in the wavefunction maps,[4] but disagree significantly in the Mulliken populations.[3] The populations are to some extent an artifact and depend on the basis set used in the calculation.[11] The present result showing a higher population on N (in contrast to the previous one showing a higher population on C) is reasonable, considering the electronegativity of N is greater than that of C.

The Natures of MO's. Figure 2 schematically shows the symmetry-allowed interaction between the $(CN^-)_2$ and metal orbitals in a linear cyanide complex. In the formation of the complex, the σ-type metal s (σ_g), $p\sigma$ (σ_u), and $d\sigma$ (σ_g) orbitals interact with the CN^- 4σ and 5σ orbitals, and the π-type metal $d\pi$ (π_g) and $p\pi$ (π_u) orbitals with the CN^- 1π and 2π orbitals. The metal $d\delta$ orbitals do not interact with ligand orbitals because there is no cyanide valence orbital of δ_g symmetry. Table 2 gives the energies and symmetries of the occupied valence MO's together with their atomic components for $[Ag(CN)_2]^-$, $[Au(CN)_2]^-$, and $[Hg(CN)_2]$. Schematical illustrations of the MO energy levels are given in Fig. 3, which also shows the approximate levels of the metal and ligand orbitals for ready comparison. The metal d orbital level is drawn at the same energy as that of the δ_g MO, which consists almost exclusively of the metal $d\delta$ orbital. The level of the CN^- 1π orbital is drawn at the same energy as that of the $6\pi_u$ MO which consists predominantly of the 1π orbital of CN^-; the contributions of the CN^- 2π and the metal $p\pi$ orbitals to this MO are unimportant, as suggested by the orbital populations. Although such layouts of

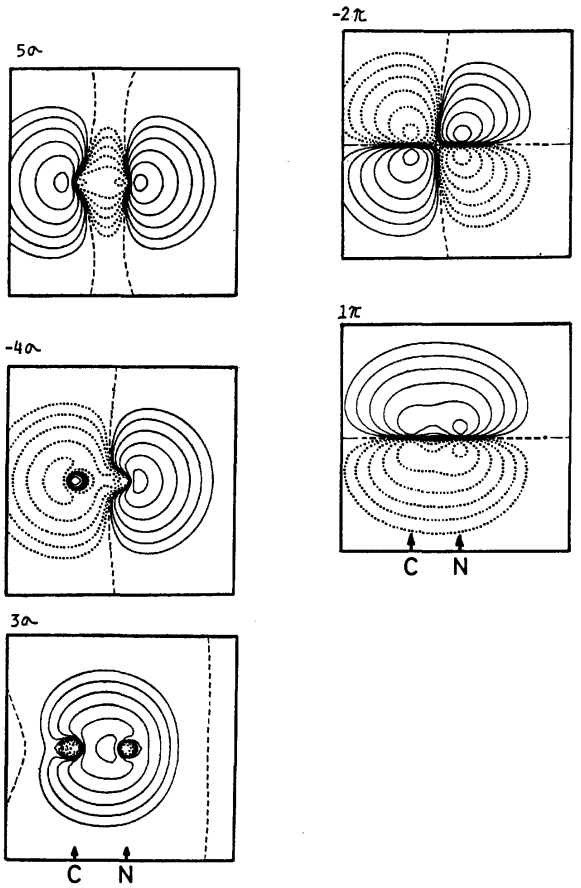

Fig. 1. The wavefunction controus for valence shell MO's of the free CN^- ion. The broken line shows 0.00, and the first solid and dotted contours show ± 0.01, respectively, and neighboring contours differ by a factor of two.

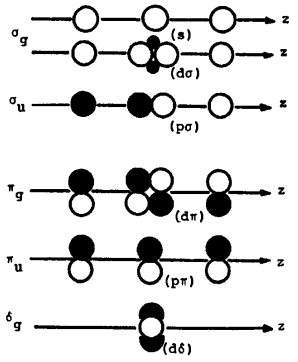

Fig. 2. $D_{\infty h}$ adapted combinations of ligand and metal orbitals.

orbital levels are arbitrary, they show approximate relative positions of the metal and ligand orbital levels in the complexes.

In the case of $[Ag(CN)_2]^-$, selected MO contours are shown in Fig. 4. In the π_g symmetry, the metal $d\pi$ orbital interacts with the 1π and 2π orbitals of CN^-, which lie above the Ag $4d\pi$ orbital. According to the orbital mixing rule,[12] the $2\pi_g$ MO with lower energy

TABLE 2. THE VALENCE SHELL MO's OF $[Ag(CN)_2]^-$, $[Au(CN)_2]^-$, AND $[Hg(CN)_2]$

Symmetry	Energy/eV	Orbital population/%						
		Ag			C		N	
		4d	5s	5p	2s	2p	2s	2p
$11\sigma_g$	−0.77	36.8	28.4		6.7	12.1	2.9	13.1
$3\pi_g$	−0.96	9.1				9.5		61.4
$8\sigma_u$	−1.71			1.3	6.3	21.9	19.2	51.2
$4\pi_u$	−2.52			0.9		48.3		50.7
$10\sigma_g$	−2.70	18.5	1.9		3.2	0.0	28.2	48.2
$2\delta_g$	−3.49	100.0						
$2\pi_g$	−4.00	86.5				12.1		1.3
$7\sigma_u$	−4.63			6.2	42.1	24.1	16.0	11.5
$9\sigma_g$	−6.99	35.7	4.6		27.3	27.6	4.3	0.5
$6\sigma_u$	−16.34			1.5	19.3	15.4	50.2	13.6
$8\sigma_g$	−16.35	0.2	0.7		21.3	13.8	50.4	13.6
		Au			C		N	
		5d	6s	6p	2s	2p	2s	2p
$13\sigma_g$	0.01	46.9	34.4		5.9	7.4	0.4	5.1
$4\pi_g$	−1.34	54.3				10.0		35.7
$10\sigma_u$	−1.74			2.8	9.9	28.7	13.2	45.3
$3\delta_g$	−1.92	100.0						
$6\pi_u$	−2.44			0.9		45.3		53.9
$12\sigma_g$	−2.79	13.8	0.0		0.6	5.6	25.7	54.4
$3\pi_g$	−3.14	41.9				34.0		24.1
$9\sigma_u$	−4.75			5.7	39.5	16.0	20.6	18.1
$11\sigma_g$	−6.47	27.3	6.5		31.2	24.3	8.0	2.7
$10\sigma_g$	−16.07	0.3	0.6		22.0	12.7	52.3	12.0
$8\sigma_u$	−16.07			1.2	20.4	14.2	52.2	12.0
		Hg			C		N	
		5d	6s	6p	2s	2p	2s	2p
$10\sigma_u$	−8.34			1.1	2.31	4.9	24.5	57.1
$13\sigma_g$	−8.38	4.9	14.4		0.9	11.2	20.4	48.1
$4\pi_g$	−8.71	3.7				42.1		54.2
$6\pi_u$	−9.06			1.5		49.5		48.9
$12\sigma_g$	−10.31	27.1	21.8		18.4	5.6	14.2	13.0
$9\sigma_u$	−11.80			8.9	44.3	29.9	11.8	5.0
$3\delta_g$	−13.76	100.0						
$3\pi_g$	−14.14	94.8				4.9		0.4
$11\sigma_g$	−16.31	61.2	2.3		14.3	20.2	2.1	0.0
$10\sigma_g$	−23.08	0.5	0.8		22.3	12.8	49.7	15.9
$8\sigma_u$	−23.09			1.5	19.8	15.0	49.7	14.0

has the dominant contribution from the metal $d\pi$ orbital and consists of the $d\pi+1\pi+2\pi$ combination. (A wavefunction with+sign has positive values in the region between the metal and carbon atoms.) On the other hand, the $3\pi_g$ MO with higher energy is the $1\pi-d\pi-2\pi$ MO (the −sign indicating negative values between M and C), in which the largest component is the 1π orbital. A slight mixing of the 2π orbital with the 1π orbital causes a decrease of the orbital population on nitrogen in the $2\pi_g$ MO and an increase of the same in the $3\pi_g$ MO.

Among σ-type MO's, $6\sigma_u$ and $8\sigma_g$ (not given in Fig. 4) are mainly constructed of the CN^- 3σ orbital. The $7\sigma_u$ and $8\sigma_u$ MO's consist of the $4\sigma+5\sigma+p\sigma$ and $5\sigma-4\sigma-p\sigma$ combinations; the $p\sigma$ orbital of Ag lies far above the 4σ and 5σ orbitals of CN^- and contributes to the MO's only slightly. The calculated orbital populations of these MO's can be explained by assuming an appropriate orbital mixing of the 4σ and 5σ orbitals; thus a mixing of 9: 1 (in the measure of electron-density) gives an estimate of orbital populations (in %) of 49(C2s), 22(C2p), 16(N2s), and 13(N2p) for the $4\sigma+5\sigma$ orbital and 6, 27, 14, and 53 for the $5\sigma-4\sigma$ orbital. These values are very similar to the populations of the $7\sigma_u$ and $8\sigma_u$ orbitals (Table 2). The metal $d\sigma$ ($4d_{z^2}$) and s (5s) orbitals as well as the ligand 4σ and 5σ orbitals belong to the same symmetry, and their energy levels are in the order of $4\sigma<d\sigma<5\sigma<s$. They are mixed together to form the $9\sigma_g$, $10\sigma_g$, and $11\sigma_g$ MO's. The 4σ orbital of CN^- is dominant in the $9\sigma_g$ MO, having

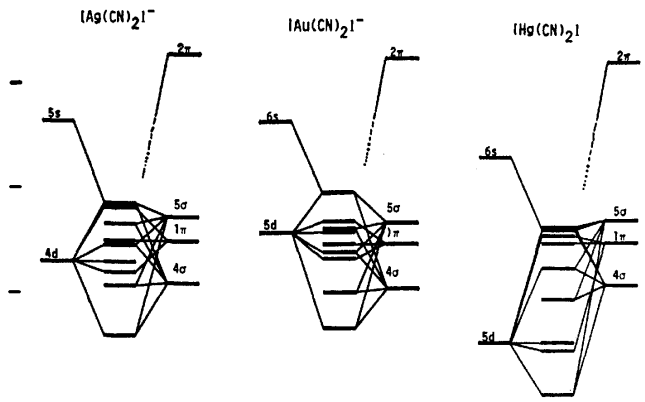

Fig. 3. Schematically illustrated MO energy levels with the levels of metal and cyanide orbitals. The MO level orderings (from the top to the bottom) are: $11\sigma_g$, $3\pi_g$, $8\sigma_u$, $4\pi_u$, $10\sigma_g$, $2\delta_g$, $2\pi_g$, $7\sigma_u$, and $9\sigma_g$ for $[Ag(CN)_2]^-$; $13\sigma_g$, $4\pi_g$, $10\sigma_u$, $3\delta_g$, $6\pi_u$, $12\sigma_g$, $3\pi_g$, $9\sigma_u$, and $11\sigma_g$ for $[Au(CN)_2]^-$; $10\sigma_u$, $13\sigma_g$, $4\pi_g$, $6\pi_u$, $12\sigma_g$, $9\sigma_u$, $3\delta_g$, $3\pi_g$, and $11\sigma_g$ for $[Hg(CN)_2]$.

bonding interactions with the metal orbitals ($4\sigma+5\sigma+d\sigma+s$). Both Table 2 and Fig. 4 show a considerable mixing of the 5σ into the 4σ orbitals (about 4 : 6 in the $9\sigma_g$ MO). They also show that the $10\sigma_g$ MO is nearly nonbonding with regard to the M–C bond and has the highest electron density in the N lone-pair regions; the $10\sigma_g$ wavefunction is expressed as $5\sigma-4\sigma+d\sigma-s$. This minus combination of the 4σ with 5σ orbitals decreases the carbon charge and increases the charge on nitrogen. The HOMO, $11\sigma_g$, is antibonding with respect to the M–C bond and corresponds to a $d\sigma-s$ hybrid orbital with $d\sigma-s-5\sigma(+4\sigma)$ combination (Fig. 5); the antibonding interactions of the $d\sigma$ with the 5σ orbital is relaxed by the mixing of the s orbital of the metal.

In $[Au(CN)_2]^-$, the valence shell MO's are similar to those of the Ag^+ complex. The HOMO is $13\sigma_g$, which corresponds to the $11\sigma_g$ MO of the latter. However, the Au^+ complex gives a slightly different MO level diagram from that for the Ag^+ complex; the relative position of the δ_g MO is higher for the Au^+ complex, indicating that the d level of Au^+ in the complex is higher than that of Ag^+ (Fig. 3). Thus the highest occupied π_g-type orbital, $4\pi_g$, has more the character of the metal $d\pi$ orbital rather than that of the ligand π orbital, while the corresponding orbital of $[Ag(CN)_2]^-$, $3\pi_g$, is characterized as a predominantly ligand orbital.

The atomic d orbital of Hg^{2+} is situated at a lowet energy than those of Ag^+ and Au^+. Thus, in $[Hg(CN)_2]$, the $11\sigma_g$, $3\pi_g$, and $3\delta_g$ MO's are composed predominantly of metal d orbitals, while the HOMO ($10\sigma_u$) is localized mainly on ligands. This feature is very different from those for the Ag^+ and Au^+ complexes. In the σ_g system, the sequence of the orbital energy is $d\sigma<4\sigma<5\sigma<s$. The $11\sigma_g$ MO has the metal $d\sigma$ (d_{z^2}) orbital as the main component, with small contributions of the 4σ, 5σ, and metal s orbitals. This ($d\sigma+4\sigma+5\sigma+s$)-type MO is bonding with respect to the Hg–CN bond. In the $12\sigma_g$ MO, the main component is the 4σ orbital with the combination of $4\sigma-5\sigma-d\sigma+s$, while the 5σ orbital is dominant in the $13\sigma_g$ MO with $5\sigma-4\sigma-d\sigma+s$. The contribution of the metal s orbital in these MO's relaxes the antibonding interaction of the $d\sigma$ with the 4σ or 5σ orbitals, thus strengthening the metal-cyanide bonds.

Main Features of Bonding Structure in NC–M–CN. As can be seen from the MO contours (Fig. 4) and energy-level diagrams (Fig. 3), the σ bond is very strong. This is also suggested by the M–C bond overlap population given in Table 4. The greatest contribution to the stabilization of the complexes is made by the bonding interaction of the metal $d\sigma$ orbital and the ($4\sigma+5\sigma$)-type

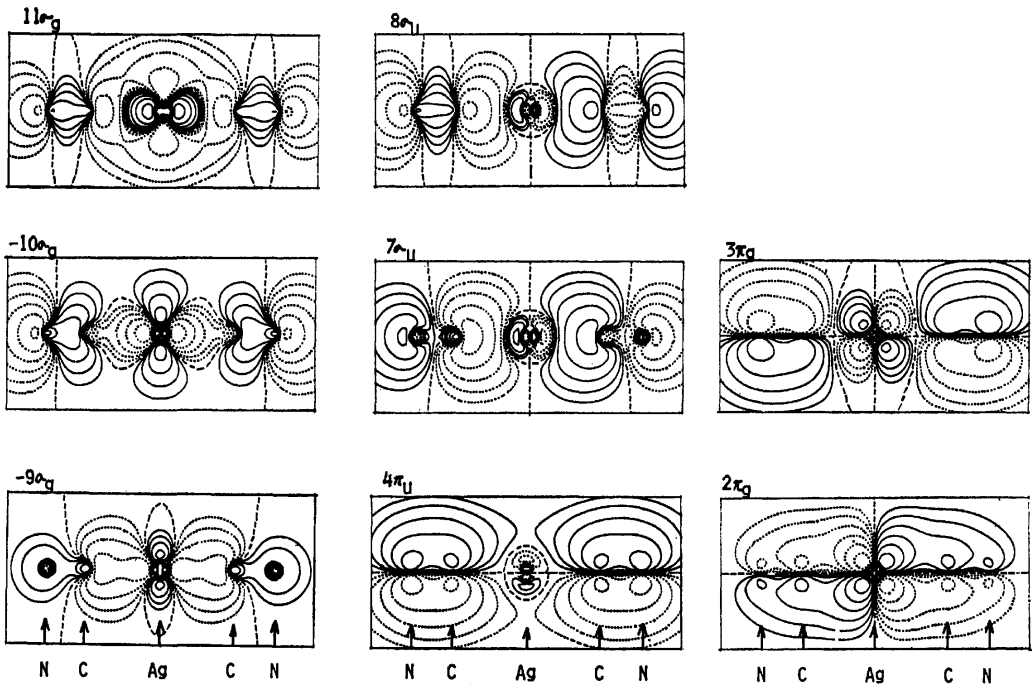

Fig. 4. Selected valence-shell MO contours for $[Ag(CN)_2]^-$.

ligand orbital, resulting in the $9\sigma_g$ (Ag complex) or $11\sigma_g$ (Au and Hg complexes) MO, in which the (dσ+s)-type mixing of the $(n+1)$s with the ndσ orbital also occurs to add a minor contribution to the stabilization of the M–C bond. On the other hand, the (dσ—s)-type metal orbitals interact with the $(5\sigma-4\sigma)$-type ligand orbital to form an antibonding $11\sigma_g$ (Ag complex) or $13\sigma_g$ (Au and Hg complexes) MO, in which the $(n+1)$s orbital is considerably mixed with the ndσ orbital to reduce the antibonding character of the MO. The orbital interactions discussed above are schematically illustrated in Fig. 5.

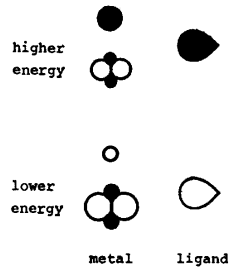

Fig. 5. Orbital interactions of metal dσ and s orbitals and ligand orbitals of σ_g symmetry. (Only one of the ligand orbitals is shown.) The size indicate the magnitudes of orbital components. The positive and negative signs of the orbitals are shown by the white and black area.

The situation mentioned above is in contrast to Orgel's simplified theory,[1] according to which the dσ—s orbital is stabilized while the destabilized dσ+s orbital is empty. However, the bonding structure observed here might be peculiar to the cyanide complexes. In these complexes, the soft cyanide ions strongly interact with the soft noble-metal ion to form bonds of highly covalent character; the cyanide 4σ and 5σ orbitals are mixed with each other to result in the $(4\sigma+5\sigma)$-type orbital, which has an increased electron density at the carbon atoms, and efficiently interact with the metal dσ orbital to form coordinate bonds. Moreover, the small separation of the nd and $(n+1)$s orbital energies (6.7 eV for Ag, 5.7 eV for Au, and 8.8 eV for Hg) results in a large contribution of the metal $(n+1)$s orbital to the valence MO's to relax the antibonding interaction of the dσ and the CN^- σ orbitals, stabilizing a linear complex for Ag^+, Au^+, and Hg^{2+}.

Valence XPS. Figure 6 shows the valence XPS for linear cyanides as well as the calculated energy levels of the MO's with a significant metal d character. The lengths of the lines denote the extents of the metal d contribution, and are roughly proportional to the cross-section of photoionization, because the cross-sections of the d orbitals of heavy atoms are significantly larger than those of cyanide orbitals. For ready comparison, the position of the calculated energy-level of the δ_g orbital with esentially d character is arbitarily adjusted so as to coincide with the largest XPS peak of each spectrum. A reasonably good agreement is observed between the computed d level schemes and the experimental spectra. Thus the main peaks for the silver(I)

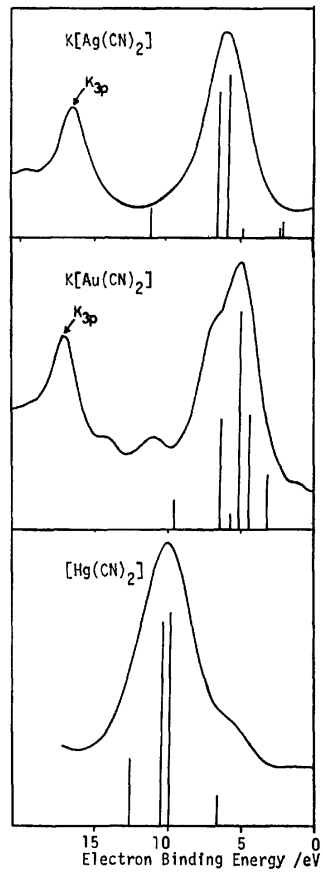

Fig. 6. Valence region of XPS and the orbital energy levels for $K[Ag(CN)_2]$, $K[Au(CN)_2]$, and $[Hg(CN)_2]$. Only the orbitals with large cross-sections are shown.

and gold(I) cyanide complexes appearing near 6.0 and 5.2 eV correspond to the $2\delta_g$ and $3\delta_g$ MO's, respectively. For the mercury(II) cyanide, the main peal at 10 eV is assigned to the $3\delta_g$ and $3\pi_g$ MO's overlapping each other. The complicated structure of the main peak for the Au^+ complex implies a strong interaction between Au and ligands.

Population Analysis. Table 3 gives the results of the Mulliken population analysis for linear dicyano complexes. The deviations of the effective metal charges (+0.42, +0.33, and +1.11) from formal charge for Ag^+, Au^+, and Hg^{2+} are respectively 0.58, 0.67, and 0.89, which show no remarkable difference in the net ligand-to-metal electron donation between uni- and bi-valent metals.

The net negative charge on carbon is largest in the Hg^{2+} complex. This might seem to be in conflict with the conventional argument that the ligand-to-metal electron donation would occur most extensively in the Hg^{2+} complex. However, the consideration of π back-donation will explain the puzzling situation. The variation of carbon charge among these complexes is mainly due to that in the Cpπ population (1.80 for Ag^+, 1.79 for Au^+, and 1.93 for Hg^{2+}). The change in nitrogen charge also results from that in the NPπ population (2.27, 2.27, and 2.07). Since the π back-donation causes a decrease in the carbon population and an increase in nitrogen population, the values of the

Table 3. The Mulliken populations for linear dicyano complexes

		$[Ag(CN)_2]^-$	$[Au(CN)_2]^-$	$[Hg(CN)_2]$
Orbital populations (number of electrons)				
Metal	$d\sigma$	1.82	1.77	1.88
	$d\pi$	3.82	3.86	3.94
	$d\delta$	4.00	4.00	4.00
	s	0.71	0.83	0.79
	p	0.22	0.23	0.29
	Charge	+0.42	+0.33	+1.11
Carbon	2s	1.27	1.29	1.22
	$2p\sigma$	1.15	1.09	1.10
	$2p\pi$	1.80	1.79	1.93
	Charge	−0.22	−0.17	−0.26
Nitrogen	2s	1.71	1.72	1.72
	$2p\sigma$	1.52	1.50	1.51
	$2p\pi$	2.27	2.27	2.07
	Charge	−0.50	−0.49	−0.30
Bond overlap populations				
M–C	σ	0.36	0.40	0.41
	π	0.08	0.07	0.05
C–N	σ	0.38	0.41	0 41
	π	0.88	1.05	1.09

$Cp\pi$ and $Np\pi$ populations show that the π back-donation is smallest in the Hg^{2+} complex. On the other hand, the sum of the Cs and $Cp\sigma$ populations is smallest in the Hg^{2+} complex, indicating that the σ donation is largest in this complex. Both the smallest π back-donation and the largest σ donation is consistent with the highest electronegativity of Hg^{2+}.

The bond overlap populations of M–C and C–N increase in the orders of $Ag^+ < Hg^{2+} < Au^+$ and $Ag^+ < Au^+ < Hg^{2+}$, respectively. The infrared results show the orders of $Ag^+ < Hg^{2+} < Au^+$ and $Ag^+ < Au^+ < Hg^{2+}$ for the force constants of the M–C and C–N bonds,[14] respectively. The good agreement between the orders of the bond overlap populations and of the force constants may suggest that both of them are closely related to the bond strength.

The computations reported in this paper have been carried out on the HITAC M-180 computer of the Institute for Molecular Science.

References

1) L. E. Orgel, *J. Chem. Soc.*, **1958**, 4186.
2) W. R. Mason, *J. Am. Chem. Soc.*, **95**, 3573 (1973).
3) M. Sano, Y. Hatano, and H. Yamatera, *Chem. Phys. Lett.*, **60**, 257 (1979).
4) M. Sano, Y. Hatano, H. Kashiwagi, and H. Yamatera, *Bull. Chem. Soc. Jpn.*, **54**, 1523 (1981).
5) M. Sano, H. Adachi, and H. Yamatera, *Bull. Chem. Soc. Jpn.*, **54**, 2898 (1981).
6) M. Sano, H. Adachi, H. Kashiwagi, and H. Yamatera, The 29th Symposium on Coordination Chemistry of the Chemical Society of Japan, Hamamatsu, Oct. 1979.
7) H. Adachi, S. Shiokawa, M. Tsukada, C. Satoko, and S. Sugano, *J. Phys. Soc. Jpn.*, **47**, 1528 (1979).
8) For a review of the Hartree–Fock–Slater model, see J. C. Slater "Quantum Theory of Molecules and Solids," McGraw-Hill, New York (1974), Vol. 4.
9) E. J. Baerends and P. Ros, *Chem. Phys.*, **2**, 52 (1973).
10) H. Adachi, M. Tsukada, and C. Satoko, *J. Phys. Soc. Jpn.*, **45**, 875 (1978).
11) M. Sano, Y. Hatano, and H. Yanatera, *Chem. Lett.*, **1979**, 789.
12) S. Inagaki, H. Fujimoto, and K. Fukui, *J. Am. Chem. Soc.*, **98**, 4504 (1976).
13) The relative electron densities of the 4σ orbital on the C and N atoms are reversed by a slight mixing (10%) of the 5σ orbital; those of the 5σ orbital are also reversed by a slight orbital mixing.
14) L. H. Jones, *Inorg. Chem.*, **2**, 777 (1963).

Thermal Reactions of Octahedral Nickel(II) Complexes Containing *N,N*- and *N,N'*-Dialkylethylenediamines in a Solid Phase

Yoshinori IHARA,† Eiichi IZUMI, Akira UEHARA, Ryokichi TSUCHIYA,* Shigeo NAKAGAWA,†† and Eishin KYUNO††

Department of Chemistry, Faculty of Science, Kanazawa University, Kanazawa 920
†Laboratory of Chemistry, Faculy of Education, Kanazawa University, Kanazawa 920
††Department of Pharmaceutical Science, School of Pharmacy, Hokuriku University, Kanazawa 920

(Received June 30, 1981)

Thermal reactions of the $[Ni(H_2O)_2(AA)_2]X_2 \cdot nH_2O$ complexes in a solid phase were investigated, where AA is *N,N'*-diethylethylenediamine (*NN'*-deen), *N,N*-dimethylethylenediamine (*NN*-dmen), or *N,N'*-dimethylethylenediamine (*NN'*-dmen), and where X^- is Cl^-, Br^-, I^-, NO_3^- or ClO_4^-. By means of thermal analyses and spectral and magnetic measurements in a series of these complexes before and after heating, the following results were obtained. In the case of the *NN'*-deen complexes, only the perchlorate deaquates to change from octahedral to square-planar, but the other salts, such as the chloride, bromide, iodide, and nitrate, undergo deaquation-anation keeping their octahedral configuration. The deaquation-anation was also observed in the chloride, bromide, and nitrate of the *NN*-dmen complexes, but the iodide deaquated, and so was transformed from octahedral to square-planar. In the *NN'*-dmen complexes, only deaquation-anation was detected, irrespective of the anions (Cl^-, Br^-, I^-, and NO_3^-). The effects of *N*-substituents in the diamines and the anions on the above transformation were discussed.

There are three main types of nickel(II) complexes: the first group consists of blue or green, paramagnetic complexes with an octahedral configuration; the second consists of analogously paramagnetic complexes, but with a tetrahedral configuration, and the third consists of red, orange or yellow, diamagnetic complexes with a square-planar configuration.[1] In 1939, Lifschitz *et al.*[2] pointed out that the $[Ni(stien \text{ or } phenen)_2]X_2 \cdot nH_2O$ complexes (stien: 1,2-diphenyl-1,2-ethanediamine; phenen: 1-phenyl-1,2-ethanediamine; X: Cl^-, $ClCH_2COO^-$, $HCOO^-$, and $1/2SO_4^{2-}$; *n*: 0 to 4) easily undergo mutual transformation (yellow diamagnetic ↔blue paramagnetic species), with a slight variation depending upon the kind of X and the hydration states. Since then, such mutual configurational change or equilibration between any two of the three types has often been found in aqueous and some organic solvents.[3,4] Such changes have also been observed in a solid phase in some limited cases. An example of the change from a square-planar to a tetrahedral configuration was reported in nickel(II) complexes with *N*-methylsalicylideneamine and its derivatives in a solid phase.[5,6] One of the examples of the octahedral-to-square-planar change is seen in $[Ni(H_2O)_2(NN\text{-deen})_2]Br_2 \cdot H_2O$, where *NN*-deen is *N,N*-diethylethylenediamine,[7] while the reverse change, square-planar-to-octahedral, is found in the nickel(II) complex with 2-aminobenzimidazole.[8]

In a series of $[Ni(H_2O)_2(NN\text{-deen})_2]X_2 \cdot nH_2O$-type complexes,[7] the chloride undergoes anation by the counter-chloride ion after the liberation of coordinated water, keeping the octahedral configuration, whereas the bromide loses the coordinated water to form a square-planar structure without anation upon heating in a solid phase, as has been described above. For the iodide and perchlorate, the octahedral complexes were not obtained with two coordinated water molecules; only anhydrous square-planar complexes were formed. In addition to the kind of counter ion, the structure of *N*-alkylethylenediamines is expected to affect the feature of the configurational change of nickel(II) complexes.

The present study aimed to investigate what different changes appear when $Ni(AA)_2X_2 \cdot nH_2O$ are heated. As the diamines, AA, *N,N'*-diethylethylenediamine (*NN'*-deen), *N,N*-dimethylethylenediamine (*NN*-dmen), and *N,N'*-dimethylethylenediamine (*NN'*-dmen) were selected; X^- was Cl^-, Br^-, I^-, NO_3^-, or ClO_4^-.

Experimental

Preparation of Complexes. The *NN'*-deen, *NN*-dmen, and *NN'*-dmen were of a commercial-reagent grade and were used without further purification. The $[Ni(H_2O)_2(NN'\text{-deen})_2]X_2$ (X^-=Cl^-, Br^-, I^-, NO_3^-, and ClO_4^-),[9] $[Ni(H_2O)_2(NN\text{-dmen})_2]Cl_2 \cdot 2H_2O$,[10] $[Ni(H_2O)_2(NN\text{-dmen})_2]X_2$ (X^-=Br^-, I^-, and NO_3^-),[10] and $[Ni(H_2O)_2(NN'\text{-dmen})_2]X_2 \cdot 2H_2O$ (X^-=Cl^-, Br^-, I^-, and NO_3^-)[10] complexes were prepared by a method similar to that of the literature, their chemical formulas being identified by means of elemental analyses and spectral measurements. The perchlorates containing *NN*-dmen and *NN'*-dmen were not obtained in a pure form.

Thermal Analyses. The TG, DTA, and DSC measurements were made with a MOM Derivatograph, Typ-OD-102, and a Rigaku Denki Standard TG-DSC apparatus.

Spectral Measurements. The visible and ultraviolet spectra in a solid state were measured by the diffuse reflectance method with a Hitachi EPU-2A spectrophotometer equipped with a standard Hitachi reflection attachment. The IR spectra were obtained with JASCO-IR-E and -IR-F infrared spectrophotometers.

Magnetic Measurements. The effective magnetic moments were evaluated from the magnetic susceptibilities, as measured by the Gouy method at room temperature.

Results and Discussion

$[Ni(H_2O)_2(NN'\text{-deen})_2]X_2$. DSC Measurements: The TG and DSC curves of $[Ni(H_2O)_2(NN'\text{-deen})_2]X_2$ (X^-=Cl^-, Br^-, I^-, NO_3^-, and ClO_4^-) are given in Fig. 1. From the DSC peak temperatures in Fig. 1, the coordinated water molecules are found to be easily evolved in this order: perchlorate (103 °C)<bromide (96 °C)<iodide (93 °C)<nitrate (74 °C)<chloride (66 °C).

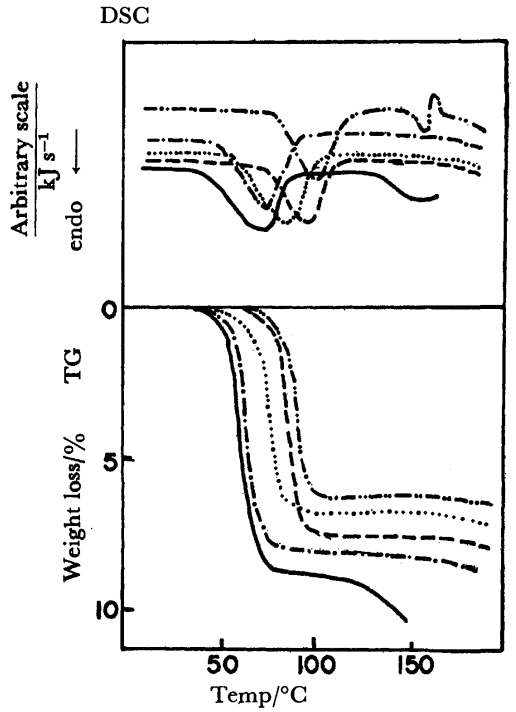

Fig. 1. DSC curves for $[Ni(H_2O)_2(NN'\text{-deen})_2]X_2$, where $X^-=Cl^-$ (——), Br^- (– – –), I^- (------), NO_3^- (-·-·-), and ClO_4^- (-·-·-·-).

A striking difference is, however, seen in the DSC curve for $[Ni(H_2O)_2(NN'\text{-deen})_2](ClO_4)_2$; the successive endo- and exothermic peaks appear at about 160 °C, where no change is observed in the TG curve, which retains a plateau.

Absorption Spectra: The absorption spectra measured by the diffuse-reflectance method for $[Ni(H_2O)_2(NN'\text{-deen})_2]Cl_2$ and $[Ni(H_2O)_2(NN'\text{-deen})_2]Br_2$ before and after heating at 130 °C are shown in Fig. 2.

It can be seen from this figure that both of the aqua complexes give three absorption bands, at 12.5, 17.6, and 27.8×10^3 cm^{-1} at room temperature; these bands can be assigned to the $^3A_{2g}\rightarrow{}^3T_{2g}$, $^3A_{2g}\rightarrow{}^3T_{1g}$ (F), and $^3A_{2g}\rightarrow{}^3T_{1g}$ (P) electron transitions respectively, irrespective of the kind of counter ion, Cl^- or Br^-. The spectra of the anhydrous salts obtained upon heating are almost identical with those of the mother complexes, except for a slight shift of the maximum peaks to the longer-wavelength region (*e.g.*, the third absorption peaks in the chloride and bromide shift to 26.7×10^3 cm^{-1}).

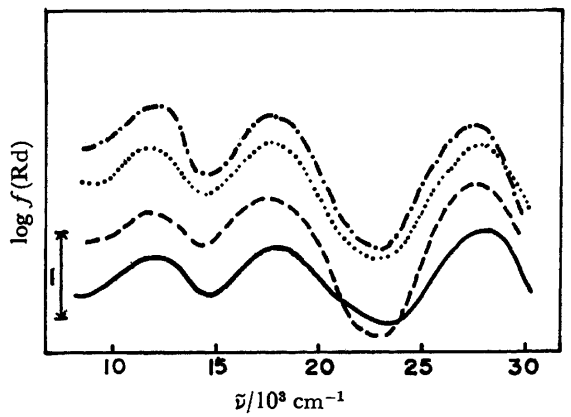

Fig. 2. Absorption spectra for $[Ni(H_2O)_2(NN'\text{-deen})_2]Cl_2$] before (——) and after (– – –) heating, and those for $[Ni(H_2O)_2(NN'\text{-deen})_2]Br_2$ before (------) and after (-·-·-) heating.

Similar patterns were observed in the spectra of the iodide and nitrate (not shown): the third absorption peaks in the iodide and nitrate shift from 28.1 to 26.9×10^3 cm^{-1} and from 28.1 to 27.5×10^3 cm^{-1} respectively. In all these complexes, a color change from violet to blue was observed upon heating, except that the iodide gives a color change from violet to green.

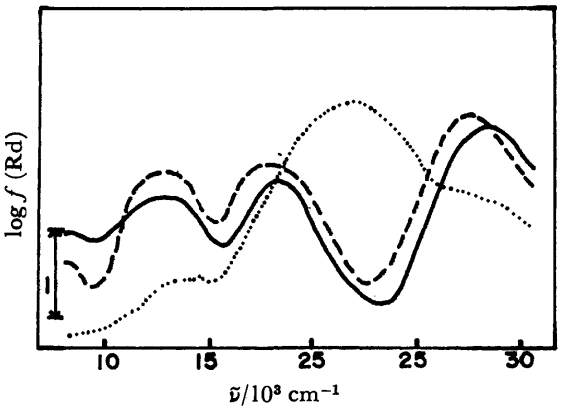

Fig. 3. Absorption spectra for $[Ni(H_2O)_2(NN'\text{-deen})_2](ClO_4)_2$ before (——) and after heating at 130 °C (– – –) and at 160 °C (------).

On the other hand, a color change from violet to orange through gray was observed in the $[Ni(H_2O)_2(NN'\text{-deen})_2](ClO_4)_2$ complex at 160 °C, where a complicated DSC peak appears. The absorption spectra measured at room temperature and those measured at 130 ° and at 165 °C areshown in Fig. 3. As may be seen in the figure, the former two spectra are very similar to each other, indicating three absorption bands characteristic of six-coordinated nickel(II) complexes, although slight shifts are observable in each absorption peak at 130 °C. At 165 °C, however, these three absorption bands disappear, and a strong band at 21.5×10^3 cm^{-1}, characteristic of the square-planar structure and probably assignable to the $^1A_{1g}\rightarrow{}^1A_{2g}$ transition, appears instead.

IR Spectra. The representative infrared absorption spectra before and after heating are given in Fig. 4 for $[Ni(H_2O)_2(NN'\text{-deen})_2](ClO_4)_2$. The figure shows that the considerably weak absorption peak at *ca.* 930 cm^{-1} assignable to the Cl–O stretching vibration grows upon heating at 130 °C as a result of the coordination of ClO_4^- to the metal and is then weakened at 165 °C. This rise and fall of the absorption peak corresponds to the color change of the complex: violet→gray→orange. This suggests that the complex loses the coordinated water to undergo the anation of ClO_4^- at 130 °C, and that ClO_4^- is then liberated from the coordination sphere upon further heating.[11]

Magnetic Susceptibilities. The values of the effec-

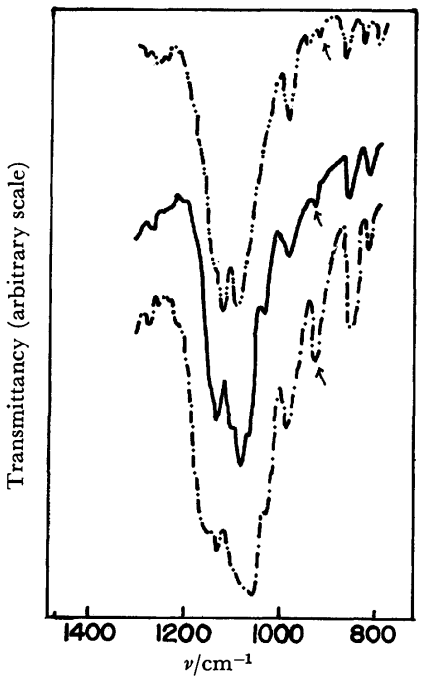

Fig. 4. IR spectra for $[Ni(H_2O)_2(NN'\text{-deen})_2](ClO_4)_2$ at room temperature (——), upon heating at 130 °C (-·-·-) and at 165 °C (-···-···-).

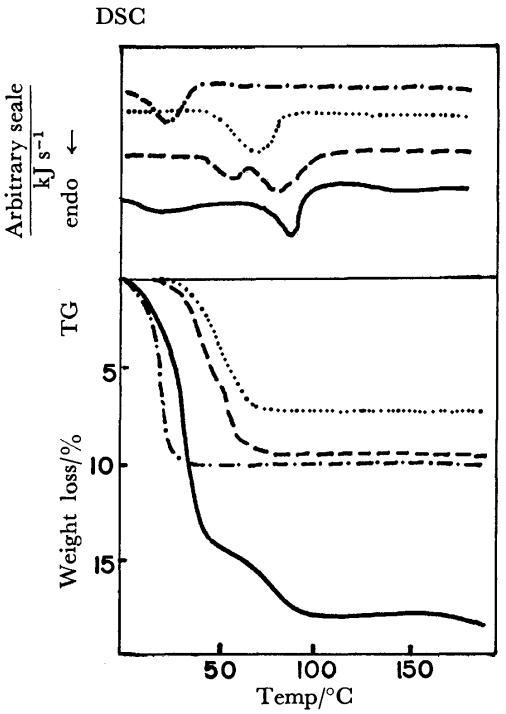

Fig. 5. DSC curves for $[Ni(H_2O)_2(NN\text{-dmen})_2]Cl_2 \cdot 2H_2O$ (——), $[Ni(H_2O)_2(NN\text{-dmen})_2]X_2$, where X= Br^- (----), I^- (·····), and NO_3^- (-·-·-).

tive magnetic moments of the complexes before and after heating are summarized in Table 1. All the $[Ni(H_2O)_2(NN'\text{-deen})_2]X_2$ complexes have paramagnetism corresponding to the two unpaired electrons in octahedral nickel(II) complexes. Upon heating, all except for the perchlorate keep the original paramagnetism. This suggests that the octahedral configuration is still kept as a result of the anation of counter ions in the chloride, bromide, iodide, and nitrate. Only the perchlorate, however, gives a change in the magnetic behavior, paramagnetism→diamagnetism, corresponding to the gray→orange color change. This suggests that ClO_4^- once coordinates to the nickel ion, yielding a six-coordinated complex, and then gets free from the coordination sphere to form a square-planar complex.

$[Ni(H_2O)_2(NN\text{-dmen})_2]X_2 \cdot nH_2O$. DSC Measurements: The TG and DSC curves for $[Ni(H_2O)_2(NN\text{-dmen})_2]Cl_2 \cdot 2H_2O$ and $[Ni(H_2O)_2(NN\text{-dmen})_2]X_2$ (X^-= Br^-, I^-, and NO_3^-) are shown in Fig. 5. The temperature giving DSC peaks becomes lower in this order: chloride (88 °C) >bromide (83 °C) >iodide (70 °C) >nitrate (30 °C).

Absorption Spectra: The absorption spectra of $[Ni(H_2O)_2(NN\text{-dmen})_2]X_2 \cdot nH_2O$ (X^-=Cl^-, Br^-, I^-, and NO_3^-) before and after heating are given in Fig. 6. In the chloride, bromide, and nitrate, the three absorption bands characteristic of the six-coordinated nickel(II) complexes are not quenched, but show a shift to a somewhat longer wavelength region upon heating, the

TABLE 1. EFFECTIVE MAGENTIC MOMENTS OF THE COMPLEXES BEFORE AND AFTER HEATING

Complex	Magnetic moments μ_{eff}/BM	
	Before heating	After heating
$[Ni(H_2O)_2(NN'\text{-deen})_2]Cl_2$	2.96	2.90
$[Ni(H_2O)_2(NN'\text{-deen})_2]Br_2$	3.03	2.95
$[Ni(H_2O)_2(NN'\text{-deen})_2]I_2$	2.96	2.92
$[Ni(H_2O)_2(NN'\text{-deen})_2](NO_3)_2$	2.94	2.94
$[Ni(H_2O)_2(NN'\text{-deen})_2](ClO_4)_2$	2.91	2.94,[a] diamag[b]
$[Ni(H_2O)_2(NN\text{-dmen})_2]Cl_2 \cdot 2H_2O$	3.13	2.90
$[Ni(H_2O)_2(NN\text{-dmen})_2]Br_2$	3.02	2.91
$[Ni(H_2O)_2(NN\text{-dmen})_2]I_2$	3.26	diamag
$[Ni(H_2O)_2(NN\text{-dmen})_2](NO_3)_2$	2.96	3.17
$[Ni(H_2O)_2(NN'\text{-dmen})_2]Cl_2 \cdot 2H_2O$	3.18	3.00
$[Ni(H_2O)_2(NN'\text{-dmen})_2]Br_2 \cdot 2H_2O$	3.08	2.95
$[Ni(H_2O)_2(NN'\text{-dmen})_2]I_2 \cdot 2H_2O$	3.18	2.93
$[Ni(H_2O)_2(NN'\text{-dmen})_2](NO_3)_2 \cdot 2H_2O$	3.16	3.17

a) Upon heating at 130 °C. b) Upon heating at 165 °C.

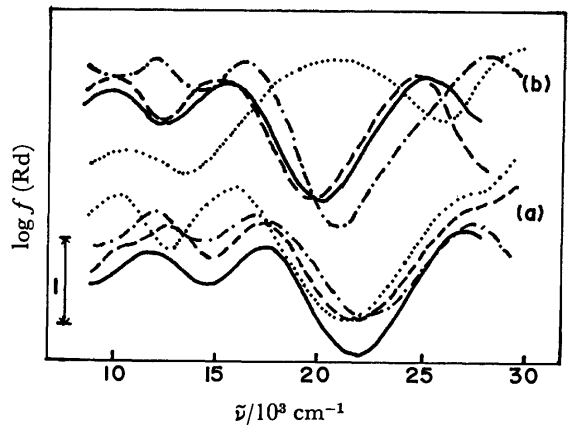

Fig. 6. Absorption spectra for $[Ni(H_2O)_2(NN\text{-dmen})_2]X_2$ before (a) and after (b) heating, where X^-=Cl^- (——), Br^- (——), I^- (·····) and NO_3^- (-·-·-).

color changing from pale blue to greenish blue, to green, and to blue respectively. Only in the iodide does the color change from the original pale blue to orange, and a new strong band due to the formation of a square-planar complex appears after the liberation of the coordinated water.

Magnetic Susceptibilities: As is shown in Table 1, the effective magnetic moments of $[Ni(H_2O)_2(NN\text{-dmen})_2]X_2 \cdot nH_2O$ are all paramagnetic. After heating, the paramagnetism is not lost in the chloride, bromide, and nitrate, indicating that the octahedral configuration is still maintained as a result of the anation of counter ions, whereas only the iodide gives diamagnetism upon heating, suggesting that it undergoes the configurational change to square-planar from octahedral.

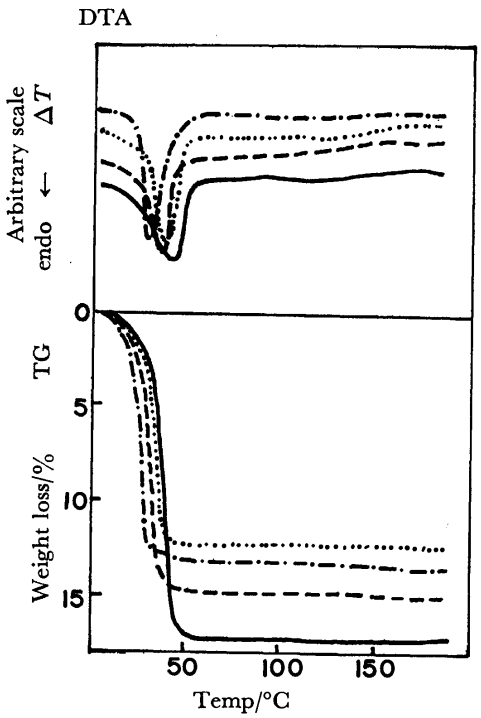

Fig. 7. TG and DTA curves for $[Ni(H_2O)_2(NN'\text{-dmen})_2]X_2 \cdot 2H_2O$, where X^-=Cl^- (——), Br^- (——), I^- (·····), and NO_3^- (-·-·-).

$[Ni(H_2O)_2(NN'\text{-dmen})_2]X_2 \cdot nH_2O$. *DTA Measurements*: The DTA measurements were carried out in this series of compounds because these compounds deaquated even below 50 °C and because our DSC apparatus could not be employed below that temperature. The TG and DTA curves for these compounds are shown in Fig. 7. The temperature giving DTA peaks becomes lower in this order: chloride (52 °C)>iodide (38 °C)>bromide (34 °C)>nitrate (32 °C).

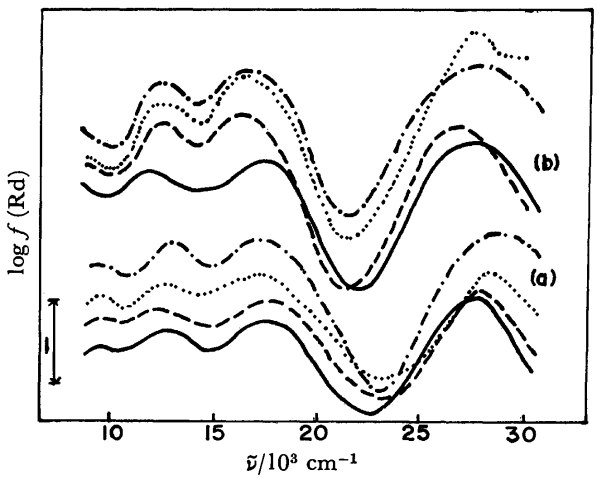

Fig. 8. Absorption spectra for $[Ni(H_2O)_2(NN'\text{-dmen})_2]X_2 \cdot 2H_2O$ before (a) and after (b) heating, where X^-= Cl^- (——), Br^- (----), I^- (·····), and NO_3^- (-·-·-).

Absorption Spectra: The absorption spectra of $[Ni(H_2O)_2(NN'\text{-dmen})_2]X_2 \cdot 2H_2O$ (X=Cl^-, Br^-, I^-, and NO_3^-) before and after heating are given in Fig. 8. In this case, all the complexes are pale blue and give the three absorption bands. After heating, they are still blue, and these absorption bands remain, except for a slight shift to the longer-wavelength region.

Magnetic Susceptibilities: The data in Table 1 show that all the complexes containing *NN'*-dmen, both before and after heating, give paramagnetism, indicating that these complexes undergo the anation of counter ions while keeping their six-coordinated, octahedral configuration.

Effect of N-*Substituents in Ethylenediamine upon Configurational Change*: Table 2 summarizes the configurational changes in $[Ni(H_2O)_2(AA)_2]X_2 \cdot nH_2O$-type complexes.

Table 2. Configurational changes in $[Ni(H_2O)_2(AA)_2]X_2 \cdot nH_2O$-type complexes

AA	X⁻				
	Cl^-	Br^-	I^-	NO_3^-	ClO_4^-
NN'-dmen	A[a]	A	A	A	—
NN'-deen	A	A	A	A	A[b], B[c]
NN-dmen	A	A	B	A	—
NN-deen[d]	A	B[a]	C[a]	C	C

a) A denotes that the complexes undergo deaquation-anation, keeping an octahedral configuration; B, that the complexes deaquate to form square-planar complexes, and C, that square-planar complexes are exclusively obtained. b) At 130 °C. c) At 165 °C. d) Ref. 7.

It shows that the feature of the configurational change is dependent upon the position to which the substituents are attached and upon the kind of substituent, methyl or ethyl. First, in the complexes containing *NN'*-dmen or *NN'*-deen, where two methyl or ethyl groups are combined with different nitrogen atoms, all the complexes undergo anation after liberating coordinated water except for the perchlorate containing *NN'*-deen. On the other hand, in the complexes having *NN*-dmen, where two substituents are combined in the same nitrogen atom, the iodide undergoes the configurational change from octahedral to square-planar after dehydration. In *NN*-deen complexes, on the other hand, the bromide undergoes a similar change to the iodide of the *NN*-dmen complex, while the iodide and perchlorate only give the anhydrous square-planar structure, without any anation. Such differences between the complexes containing *N,N'*- and *N,N*-disubstituted diamines are probably due to the larger steric hindrance of the *N,N*-disubstituent against the anation than that of the *N,N'*-disubstituent. This was because, in the stable form of the *NN'*-dmen and *NN'*-deen complexes, the substituents can all be equatorial, whereas in the *NN*-dmen and *NN*-deen complexes, at least one of the substituents in these diamines is forced to take the axial position.

By inspecting the different behavior in configurational change observed upon heating between octahedral *NN*-dmen and *NN*-deen complexes, the latter has been found more easily to turn or take a square-planar configuration than the former. That is, in the bromide, the *NN*-dmen complex only undergoes anation, while the *NN*-deen complex does not undergo anation, but gives a square-planar configuration, upon heating. In the iodide, where the iodide ion has a larger radius than the bromide ion, the *NN*-dmen complex gives a square-planar configuration after liberating the coordinated water upon heating, but the *NN*-deen complex does not form an octahedral complex with coordinated water, but forms only a square-planar complex. The perchlorate containing *NN*-deen also shows the same behavior as the corresponding iodide. Such differences between *NN*-dmen and *NN*-deen complexes are possibly attributable to the bulkiness of the ethyl group relative to the methyl group. Moreover, the easier formation of square-planar complexes in the iodide than in the bromide is probably also attributable to the larger size of an iodide ion.

References

1) R. S. Nyholm, *Chem. Rev.*, **53**, 263 (1953).
2) I. Lifschitz, J. G. Bos, and K. M. Dijkema, *Z. Anorg. Allg. Chem.*, **242**, 97 (1939).
3) R. H. Holm, *J. Am. Chem. Soc.*, **83**, 4683 (1961).
4) D. R. Eaton, W. D. Philips, and D. J. Caldwell, *J. Am. Chem. Soc.*, **85**, 397 (1963).
5) L. Sacconi, P. Paoletti, and R. Cini, *J. Am. Chem. Soc.*, **80**, 3583 (1958).
6) H. C. Clark and R. J. O'Brien, *Can. J. Chem.*, **39**, 1030 (1961).
7) R. Tsuchiya, S. Joba, A. Uehara, and E. Kyuno, *Bull. Chem. Soc. Jpn.*, **46**, 1454 (1973).
8) Y. Ihara and R. Tsuchiya, *Bull. Chem. Soc. Jpn.*, **53**, 1614 (1980).
9) D. M. L. Goodgame and L. M. Venanzi, *J. Chem. Soc.*, **1963**, 616.
10) D. M. L. Goodgame and L. M. Venanzi, *J. Chem. Soc.*, **1963**, 5909.
11) B. J. Hathaway and A. E. Underhill, *J. Chem. Soc.*, **1961**, 3091.

 © 1982 The Chemical Society of Japan Bull. Chem' Soc. Jpn., 55, 1033—1038 (1982)

The Continuous Determination of Filtered Chemical-oxygen Demand with Potassium Dichromate by Means of Flow-injection Analysis

Takashi KORENAGA

School of Engineering, Okayama University, Tsushima-naka, Okayama 700

(Received August 4, 1981)

A useful method, based on the principle of flow-injection analysis, whose flow system is physically analyzed to operate the apparatus, is proposed for the continuous and rapid determination of chemical-oxygen demand (COD) as a dichromate value in organic-waste-water samples. Potassium dichromate in sulfuric acid (1+2) is pumped as an oxidizing and spectrophotometric reagent stream, and D-glucose is successfully used as a standard substance for COD. A redox reaction between potassium dichromate and organic COD substances is carried out at 100 °C in the poly(tetrafluoroethylene) tubing (0.6 mm i.d. × 50 m) of the system. The peaks, obtained at 445 nm in the recordings, show a good reproducibility over a wide range of COD values. A sampling rate of 10 samples per hour is achieved even when the residence time is 30 min. The precision with this method is 1.3%. Chloride up to 200 mg dm^{-3} does not interfere with the determination even if silver or mercury salts are not added.

Of the water pollution which was recognized in Western countries and in Japan during 1970's, chemical-oxygen demand (COD) due to organic substances was the most common. Hence, in Japan, it was decided that the total loads of COD would be regulated from July, 1981, in Japanese water areas having the characteristics of being semiclosed water bodies around which industries and population have concentrated.[1] In this regulation, it was also decided that only the manual acidic permanganate method (COD_{Mn}),[2] cited as a Japan Industrial Standard (JIS), was to be used officially to measure such organic substances. However, the standard dichromate method (COD_{Cr}),[2,3] based on the reduction of a potassium dichromate solution under specific conditions, is ordinarily used to measure such organic substances as the COD value in Western countries. This method is, though, very time-consuming, poisonous, and dangerous because of its complicated manual procedure (*i.e.*, refluxing for 2 h, the use of mercury sulfate, and the use of a concentrated and hot sulfuric acid solutions).

Previously, the present author proposed an idea for the COD measuring apparatus with potassium permanganate using the flow-injection analysis (FIA),[4] a method which was developed by Růžička and Hansen[5] and reviewed by Betteridge.[6] Since then, this apparatus has been utilized in the field of practical analysis of COD values;[7] the apparatus and its derivatives have, for instance, been used for the continuous determination of the COD values ($COD_{FIA\text{-}Mn}$) of various waste-water samples.[8–11] However, the redox reaction with permanganate was essentially incomplete and was variable for the COD determination. Therefore, the FIA method was fairly troublesome for a continuous operation of the apparatus because of a precipitate formation (*i.e.*, manganese(IV) oxide), Hence, to obtain good continuously operating conditions, potassium dichromate should be used as an oxidizing and spectrophotometric reagent for the COD determination by the FIA method, since the redox reaction with dichromate was much more complete and constant than that with permanganate.

This paper will, therefore, describe a version of a newer FIA method with potassium dichromate for the continuous determination of $COD_{FIA\text{-}Cr}$ values in organic, waste-water samples; an improvement of the previous FIA method with permanganate,[4,7–11] reported in this laboratory, by utilizing potassium dichromate in sulfuric acid (1+2) and by analyzing the flow system of the FIA apparatus, and an evaluation of the present FIA method by comparing it with the manual COD_{Cr} method,[2,3] already optimized as a standard.

Experimental

Reagent. About 3 mol m^{-3} potassium dichromate in a sulfuric acid (1+2) solution was used as an oxidizing and spectrophotometric reagent for a carrier stream. D-Glucose, of an analytical reagent grade, was used as a standard substance for COD.[12,13] Various concentrations of aqueous solutions, the COD_{Cr} values of which had beforehand been measured by the standard manual method,[2,3] were used to determine the operating conditions of the present FIA apparatus with potassium dichromate.

Apparatus and Procedure. A flow diagram of the apparatus for measuring $COD_{FIA\ Cr}$ using potassium dichromate developed here is shown in Fig. 1. The apparatus is simply constructed of commercially available parts for high-performance liquid chromatography and poly(tetrafluoroethylene) (PTFE) tubings to give the highest performance.

The potassium dichromate in a sulfuric acid (1+2) solution (A in Fig. 1), which is filtered with a PTFE membrane filter (B) and degassed with a glass degassor (C), is pumped up to the FIA system with a Kyowaseimitsu Model KHU-52, single-reciprocating micro-pump (D) at a pumping rate of 0.6 cm^3 min^{-1}. The two tubes, (a) and (b), are made of 2-mm inner diameter (i.d.) × 0.5-m length and 0.5-mm i.d. × 0.5-m length PTFE tubings respectively. A small volume (*e.g.*, 20 mm^3) of a properly diluted sample solution is introduced just after a line filter (E) through a sample injector with a septum rubber (F) by means of manual injection using a glass syringe. The sample merged with the carrier solution (A) in a reaction tube (c), made of 0.6-mm i.d. and 50-m length, is heated at 100 °C with a Toyoseisakusyo Model VC-250, thermostatted bath using corn oil (G). The resulting solution is transported to a quartz tubular flow cell (I; 10 mm light path and 8 mm^3 inner volume), placed in a Hitachi Model 200-10 spectrophotometer (H), for the absorbance measurements at 445 nm. The absorbances are continuously recorded with time by using a Hitachi Model 056 multirange recorder (J). A 0.25-mm i.d. and 1-m length PTFE tube is placed just after the flow

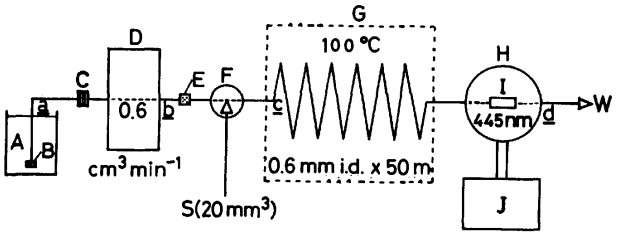

Fig. 1. Block flow diagram of the apparatus for measuring $COD_{FIA\text{-}Cr}$ using potassium dichromate. A: 3×10^{-3} mol dm^{-3} potassium dichromate in sulfuric acid (1+2) solution, B: PTEE membrane filter, C: glass degassor, D: single reciprocating micro-pump, E: line filter, F: sample injector, G: thermostatted bath using corn oil, H: spectrophotometer, I: flow cell, J: multi-range recorder, a: PTFE tubing (2 mm i.d.×0.5 m), b: PTFE tubing (0.5 mm i.d.×0.5 m), c: PTFE tubing as reaction tube (0.6 mm i.d.×50 m), d: PTFE tubing as waste line (0.25 mm i.d.×1 m), S: sample injection (*e.g.*, sample volume: 20 mm³), W: waste.

cell (I) as a waste line (d) in order to prevent bubbling in the reaction tube (c). The calibration curve is made between the peak areas in the recordings and the manual COD_{Cr} values of aqueous glucose solutions.

Results and Discussion

Choice of a Standard. Considering various organic-waste-water samples, many oxidation reactions have to be examined with regard to many organic substances in the sample solutions. However, D-glucose,[12,13] which has been available as the standard substance for COD, was used to determine the optimum operating conditions of the present FIA apparatus using potassium dichromate.

In the previous FIA method with potassium permanganate,[4,7-11] manganese(VII) was reduced by organic substances (*e.g.*, glucose as the standard) to Mn(II), Mn(III), Mn(IV), *etc.* ions in a sulfuric acid solution. For instance, a black precipitate of manganese-(IV) oxide, which had been produced by the redox reaction between permanganate and organic substances, often blocked the PTFE reaction tube of that apparatus. In the present FIA method with dichromate, however, chromium(VI) is quantitatively reduced to Cr(III) by such organic substances, and therefore forms no precipitate in the tube. Hence, the FIA apparatus could be composed of a longer PTFE tubing as the reaction tube, and its continuous operation could easily be achieved for a long time. Moreover, no contamination by organic substances occurred in the tubes of this FIA system because the acidic dichromate solution as a strong oxidant constantly flowed into them.

Design of the Apparatus. With D-glucose as a standard substance for COD, to design the FIA apparatus using potassium dichromate, the effects of such experimental variables as the sulfuric acid concentration, the reaction temperature, the reaction tube (inner diameter and length of PTFE tubing), and the flow rate were examined.

Although a 41.7 mol m^{-3} potassium dichromate in sulfuric acid (1+1) is used as an oxidizing reagent in the standard dichromate method (COD_{Cr}),[2,3] an about 3 mol m^{-3} potassium dichromate in sulfuric acid (1+2) was found suitable as an oxidizing and spectrophotometric reagent for the present FIA method of continuous COD determination because of the high viscosity of sulfuric acid (1+1).

The effect of the temperature on the redox reaction was examined between acidic dichromate and glucose over a long time span (residence time in the reaction tube: almost 30 min). The experiment, controlled with a thermostatted bath using corn oil at 100 °C, was found proper in the case of heating a long-looped PTFE reaction tube. Though the digestion in the COD_{Cr} method[2,3] was carried out for a longer time at a higher temperature (2 h and about 150 °C respectively; see Table 1), glucose was completely digested at 100 °C within 30 min of residence time in this work. However, if large amounts of less oxidizable organic substances than glucose were present in the sample solutions, glucose was not always the best; a more suitable standard substance for COD should be chosen in order to adjust the operating conditions of the FIA apparatus.

The tubing dimensions form one of the most important parameters to minimize the dispersion of the injected sample zone in a reaction tube over a long time span; PTFE tubings of from 0.5 to 1.0 mm i.d. were found usable for the reaction tube of this system. When 0.6-mm i.d. PTFE tubing was, therefore, used as the most promising reaction tube, the effect of the tubing length was examined at 100 °C by using a glucose solution according to the method described in previous papers.[7-10] With an increase in the tubing length, the dispersion of the sample zone also increases in the carrier stream, and so a shorter length is desirable to prevent dispersion. However, the oxidation of organic substances with dichromate is generally slow, so that the redox reaction of the present FIA system at 100 °C requires a longer tubing length. In this work, a suitable length of the 0.6-mm i.d. PTFE tubing was found to be 50 m, since the dispersion severely affected the peak width in the recordings beyond a tube length of 50 m.

The effect of the flow rate of the carrier solution was also examined by using a 0.6-mm i.d. and 50-m length PTFE reaction tube at 100 °C. It was also found that the flow rate should be chosen carefully in order to minimize dispersion over such a long reaction tube. The pumping rate of about 0.6 cm³ min^{-1} was found the most suitable, and the residence time of the injected sample was about 30 min under these operating conditions.

The degassed carrier solution was pumped up into the FIA apparatus, and then the solution was uniformly heated at 100 °C in the looped PTFE reaction tube. To prevent bubbling of the carrier stream solution, 0.25-mm i.d. and 1-m length PTFE tubing had to be connected as a waste line just after the flow cell in order to obtain back pressure.

The present FIA apparatus using dichromate was, therefore, composed as is shown in Fig. 1. Under these operating conditions, the system was satisfactorily operated at a few atm of back pressure, and no bubble

Table 1. Comparison of operating parameters between the FIA and standard methods for COD determination

Parameter	FIA method	Standard method
Sample volume	10—100 mm^3	<50 cm^3
Reaction medium	H_2SO_4 (1+2)	H_2SO_4 (1+1)
Reaction temperature	100 °C	150 °C (reflux)
Reaction time	30 min	2 h
Detection	Spectrophotometry	Titrimetry (indicator: 1,10-phenanthroline, iron(II) sulfate)
Determination range	50—10000 mg dm^{-3}	10—800 mg dm^{-3}
Masking agent for chloride	None	0.4 g $HgSO_4$+0.33 g Ag_2SO_4
Precision	1.3 %	2.6 %
Sampling rate	10 sample h^{-1}	1 sample $(3\ h)^{-1}$
Standard	D-Glucose	None
Reference	This work	2,3

was observed in the recordings. The residence time of the injected sample was almost 30 min, and the oxidation of glucose with dichromate was found not to proceed even when the sample has been stopped in the reaction tube at 100 °C for a further 30 min (the peak area did not change as compared with the case of not stopping the flow).

For reference, the parameters of this method are compared with those of the already optimized COD_{Cr} method,[2,3] as is shown in Table 1.

Analysis of Flow System. To ensure the operating abilities of the FIA apparatus, the present work provides the following considerations for this useful methodology and this valuable technique.

As the analytical results of fluid viscosity in a laminar flow,[14,15] it has been found experimentally that three distinct stable types of flow, that is, laminar flow without rippling, laminar flow with rippling, and turbulent flow, can be observed in a tube. When the value of the Reynolds number (Re) is less than about 2000, the flow is generally laminar. Therefore, it is customary to define the Reynolds number by $Re=D\bar{u}\rho/\mu$, where $D(=2R)$, $\bar{u}$, ρ, μ are the tubing diameter, the fluid average velocity, the fluid density, and the fluid viscosity respectively. Also, the following equation, called the Hagen-Poiseuille law, has been given,[14,15] since the volume rate of the flow (V) is the product of the area (πR^2) and the average velocity ($\bar{u}$):

$$V = (\pi \Delta p R^4)/(8\mu L). \quad (1)$$

Thus, Eq. 2 is well established for the pressure drop (Δp) in the reaction tube:

$$\Delta p = 32\mu L\bar{u}/D^2. \quad (2)$$

In the FIA system proposed here, the flow being, of course, laminar (the Re value is calculated to be about 20), the opearting conditions are found to be best fixed as follows: $L=ca.$ 5000 cm, $D=ca.$ 0.06 cm, $\bar{u}=V/\pi R^2=ca.$ 3 cm s^{-1}, and $\mu=ca.$ 0.0013 Pa.[16] Consequently, the proposed flow system can physically be allowed to operate satisfactorily because the calculated Δp value is as reasonable as (but little smaller than) the observed one ($\Delta p=ca.$ 3 atm; measured by means of a Kyowaseimitsu Model KPG-50N pressure gauge) in this work.

The present paper describes a unique FIA method for the COD determination, one which requires a very long residence time and a high temperature for the carrier stream because this reaction attains equilibrium slowly. However, the injected sample was not dispersed so widely to be measured, since the glutinous flow of sulfuric acid (1+2) as the carrier solution was just a laminar flow (Re: about 20) in the present FIA apparatus for COD. The back pressure, which was obtained by means of a thin PTFE waste line (0.25 mm i.d. × 1 m), would also allow the apparatus to be operated at 100 °C.

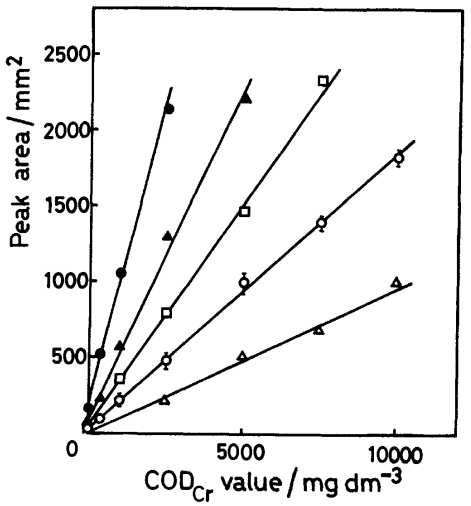

Fig. 2. Calibration curves for glucose.
(△) 10, (○) 20, (□) 30, (▲) 50, and (●) 100 mm^3 of sample solutions are manually injected with a glass syringe.

Calibration Curve and Precision. With the FIA apparatus for COD measurements, peaks at 445 nm in the recordings were obtained with a good reproducibility by using various concentrations of aqueous glucose solutions and by injecting various volumes of the sample solutions. The calibration curves were obtained between the peak areas in the recordings and the COD_{Cr} values of aqueous glucose solutions for several sample volumes (Fig. 2). The curves can be used as the COD_{Cr} value for the range of 50—2500,

100—5000, 150—7500, 200—10000, and 400—10000 mg dm^{-3} when 100, 50, 30, 20, and 10 mm^3 of the aqueous sample solutions are injected respectively. Of course, samples with lower concentrations may be handled whenever a larger volume of the sample can well be introduced into the apparatus. Disappointingly, samples of more than 200 mm^3 were found not to be completely reacted with the carrier solution because of their long sample zones in the reaction tube of this FIA apparatus. The detection limit is, therefore, determined for each sample volume when the increase in the peak area reaches 1.5 times that of the blank peak with distilled water. Accordingly, the detection limits achieved with this method were found to be the COD_{Cr} values of 50, 100, 150, 200, and 400 mg dm^{-3} when 100, 50, 30, 20, and 10 mm^3 of sample solutions were injected respectively. The precision of this method was found to be 1.3% in 16 determinations when 20 mm^3 of a 5000 mg-COD_{Cr} dm^{-3} aqueous glucose solution was injected into the system. A similar precision could also be obtained for other injecting conditions (sample volume and COD concentration) in this work. Moreover, samples with lower concentrations can also be handled, even by using the same sample volume, when a lower concentration of potassium dichromate is used and detected sensitively and stably.

The reproducibility of the total FIA system was also good, and about 10 samples could easily be analyzed in only an hour with the present FIA apparatus. Figure 3 serves as a representative example of this useful method.

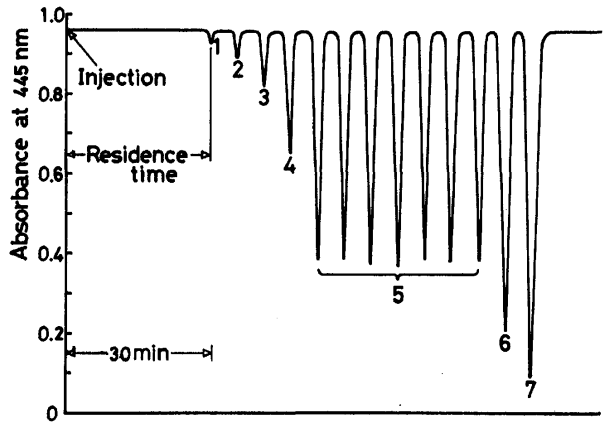

Fig. 3. Typical results of the present FIA for aqueous glucose solutions. 1: 0, 2: 400, 3: 1000, 4: 2500, 5: 5000, 6: 7500, and 7: 10000 mg-COD_{Cr} dm^{-3} of sample solutions of 20-mm^3 volume are manually injected with a glass syringe.

Effect of Chloride. To apply this FIA apparatus to actual organic waste-water samples, the effect of chloride was examined in order to evaluate the interference of co-existing chloride ions in the samples with this COD determination. In this work, it was found that chloride essentially interfered with this method, but its interference could be suppressed by adding suitable amounts of mercury and/or silver salts to the FIA system. However, chloride more than 200 mg dm^{-3} interfered with the determination because of the formation of a silver chloride precipitate, when silver salts (*e.g.*, silver sulfate or nitrate) were added to the carrier reagent solution as a masking agent. As for the results without silver and/or mercury salts, chloride up to 2000 mg dm^{-3} did not interfere with the determination at a COD_{Cr} level of 5000 mg dm^{-3}, whereas more than 200 mg dm^{-3} of chloride interfered with the determination at a COD_{Cr} level of 400 mg dm^{-3} when 20 mm^3 of the sample solution was introduced into the system and the injected sample was properly diluted with the carrier-stream solution by dispersion. Hence, these salts were not used as the masking agent for chloride ions in this work, because the inferference of the co-existing chloride ions was relatively small in comparison with the $COD_{FIA\text{-}Cr}$ values of the organic pollutants, as measured with the present FIA apparatus.

Application to Actual Samples. In order to apply this method to various actual organic-waste-water samples, the following experiments are needed for the pretreatment of the sample solutions. Some of the samples used in this work were highly turbid, so the filtration of the samples was first examined. All the samples were filtered with a 0.45-μm pore-size membrane filter; the filtered samples were then placed in the present FIA apparatus for the continuous determination of the $COD_{FIA\text{-}Cr}$ values.

The samples in glass reservoirs were stored in a refrigerator (about 4 °C) as soon as they were sampled, and then filtered. In this storage, the $COD_{FIA\text{-}Cr}$ values obtained for the filtered samples scarcely changed for at least two weeks.

After the above pretreatment steps, various actual samples such as industrial waste water, civil sewage, human waste, and aqueous waste from the laboratory of a university, could successfully be placed in the proposed FIA apparatus, using potassium dichromate for the determination of organic pollutants as COD values. The results obtained are shown in Table 2. By this continuous determination, about 10 filtered samples could semi-automatically be analyzed in only an hour.

Evaluation of Results. The $COD_{FIA\text{-}Cr}$ values found by this method were evaluated by comparing them with the COD_{Cr} values obtained by the standard dichromate method,[2,3] as is also indicated in Table 2. Both of the methods gave the same results within a permissible error range from −16 to +13%. Of course, samples such as the waste water of the petroleum industry, which contain much less oxidizable susbtances than glucose, probably show lower $COD_{FIA\text{-}Cr}$ values than the COD_{Cr} ones. It was also found that no attention was paid to spectral interferences from organic substances absorbing at 445 nm, since the colored organic substances could generally be changed into colorless ones by an acidic dichromate solution at 100 °C because of their strong oxidizability.

The recovery of $COD_{FIA\text{-}Cr}$ was examined by adding known amounts of glucose to the sample solutions before filtration in order to check the results obtained with this method. As a result, it was found

Table 2. Evaluation of the results obtained with both methods for filtered COD values in actual waste-water samples

Sample		$COD_{FIA\cdot Cr}$ (mg dm^{-3})	COD_{Cr} (mg dm^{-3})	$COD_{FIA\cdot Cr}/COD_{Cr}$
Waste water of chemical industry	1	320	360	0.89
	2	780	820	0.95
	3	1700	1600	1.06
Waste water of textile industry	4	1600	1900	0.84
	5	2300	2200	1.05
Waste water of machinery industry	6	910	1050	0.87
Waste water of food industry	7	550	540	1.02
	8	1700	1800	0.94
	9	3600	4200	0.86
Civil sewage	10	270	280	0.96
	11	450	420	1.07
	12	890	950	0.94
	13	2100	2100	1.00
Human waste	14	600	660	0.91
	15	3400	4000	0.85
	16	5900	5300	1.11
Aqueous waste from laboratory	17	80	95	0.84
	18	700	620	1.13
	19	1000	1020	0.98
	20	2600	2500	1.04
	21	2800	3100	0.90
	22	3400	3700	0.92
	23	3500	4100	0.85
	24	5000	4700	1.06
	25	8600	9300	0.92

that these $COD_{FIA\cdot Cr}$ values could accurately be measured by the present FIA apparatus without loss and gain (the recovery of $COD_{FIA\cdot Cr}$ in the examined range is from 98 to 103%).

Conclusion

The simple apparatus described here succeeded in a continuous determination of the COD in organic-waste-water samples. Although the apparatus is not so good in the determination range for common environmental-water samples, this method will improve COD measurement using dichromate (that is, the FIA method has a much more simple procedure and much less personal error than the standard COD_{Cr} method[2,3]). Furthermore, the present FIA method is more simple, stable, reliable, and less troublesome, though less sensitive, than the previous FIA method using permanganate.[4,7-11] Hence, it possesses the following advantages: (i) the use of potassium dichromate as an oxidant causes a reproducible redox reaction with various organic substances for the $COD_{FIA\cdot Cr}$ values; (ii) no precipitate forms in the PTFE reaction tube of the FIA system; and (iii) an FIA apparatus is simply constructed and easily maintained.

This paper also deals with an analysis of the flow system of the present FIA apparatus. To compose an aqueous system which is operated at 100 °C and has a residence time of almost 30 min, a continuous-flow analysis with air bubbles, which is conventionally available by means of a Technicon Autoanalyzer, will be troublesome. However, this FIA method without air bubbles could succeed in minimizing dispersion by selecting the right tubing dimensions and flow rate of the carrier stream over such a long time span. Although the apparatus presented here may not truly be FIA as a rapid determination method, this application extends FIA to a continuous method of COD analysis based on the acidic dichromate value.

The author is greatly thankful to Professors Kyoji Tôei, Teruo Takahashi, and Tosio Moriwake of Okayama University for their helpful suggestions and encouragement. He also acknowledges the financial support given by the Grant-in-Aid for Scientific Research from the Japanese Ministry of Education, Science and Culture, and by the Nissan Science Foundation.

References

1) Environment Agency, "Quality of the Environment in Japan-1978," Printing Bureau, Ministry of Finance, Tokyo (1979), p. 160.
2) JIS K 0102 (1974).
3) ASTM D 1252 (1978).
4) T. Korenaga, *Bunseki Kagaku*, **29**, 222 (1980).
5) J. Růžička and E. H. Hansen, *Anal. Chim. Acta*, **78**, 145 (1975).
6) D. Betteridge, *Anal. Chem.*, **50**, 832A (1978).
7) T. Korenaga, *Chem. Biomed. Environ. Instrum.*, **10**, 273 (1980).
8) T. Korenaga, *Anal. Lett.*, **13A**, 1001 (1980).
9) T. Korenaga and H. Ikatsu, *Bunseki Kagaku*, **29**, 497

(1980).
10) T. Korenaga and H. Ikatsu, *Analyst*, **106**, 653 (1981).
11) T. Korenaga and H. Ikatsu, *Nippon Kagaku Kaishi*, **1981**, 616.
12) J. E. Shriver and J. C. Young, *J. Water Pollut. Control Fed.*, **44**, 2140 (1972).
13) A. Yamasaki, Y. Tanaka, Y. Kuge, and S. Asada, *Kogai To Taisaku*, **14**, 1133 (1978).
14) S. Kamei, "Kagaku-kikai No Riron To Keisan," Sangyo-tosho, Tokyo (1970), p. 31.
15) R. B. Bird, W. E. Stewart, and E. N. Lightfoot, "Transport Phenomena," Wiley, New York (1960), p. 34.
16) K. Sato, "Bussei-josu Suisanho," Maruzen, Tokyo (1975), p. 261.

 © 1982 The Chemical Society of Japan Bull. Chem. Soc. Jpn., 55, 1039—1045 (1982)

Proton-transfer Reactions of 5-(*m*- and *p*-Nitrophenylazo)salicylic Acids Coupled with Inclusion Reactions with α- and β-Cyclodextrins†

Noboru Yoshida and Masatoshi Fujimoto*

Department of Chemistry, Faculty of Science, Hokkaido University, Sapporo 060

(Received August 7, 1981)

The title azo compounds, 5-(*m*- and *p*-nitrophenylazo)salicylic acids (*m*- and *p*-NPAS), were found kinetically to be included into a cavity of α- or β-cyclodextrin. The rate constants for the inclusion reactions were found to be in the order of magnitude 10^7 and 10^6 mol^{-1} dm^3 s^{-1} for α-cyclodextrin and β-cyclodextrin systems, respectively. The ^1H and ^{13}C NMR data showed that the hydrophobic nitrobenzene ring moiety of *m*- and *p*-NPAS is situated in the α- and the β-cyclodextrin cavity. The proton-transfer reactions of *m*- and *p*-NPAS were accelerated in the presence of α- and β-cyclodextrins. This indicates the possibility that the inclusion force of cyclodextrins contributes to weakening the intramolecular hydrogen bond of *m*- and *p*-NPAS.

Torus-shaped α- and β-cyclodextrins (α- and β-CD), cyclic α-1, 4-linked D-glucose polymers, have 6 and 7 glucose residues per molecule, respectively, and form a number of stereoselective inclusion complexes with azo and triphenylmethane compounds.[1] The driving force for inclusion has been attributed to hydrogen bonding,[2] van der Waals forces,[3,4] hydrophobic interactions,[5] the relaxation of the conformational strain in the cyclodextrin,[6] and the release of non-hydrogen-bonding water molecules with high energy in the cyclodextrin cavity.[4] Recently, a theoretical approach to the aspect of driving force of inclusion by α-cyclodextrin was carried out.[7]

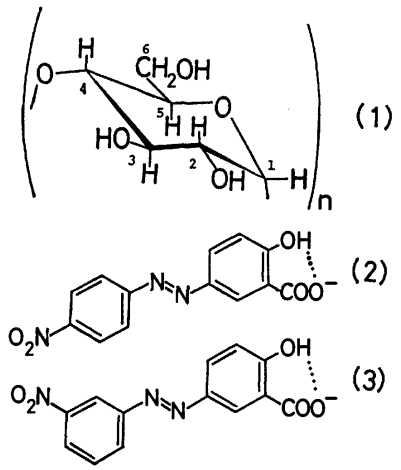

Fig. 1. Structural formulae of α-cyclodextrin ($n=6$; (1)), β-cyclodextrin ($n=7$; (1)); 5-(*p*-nitrophenylazo)salicylate anion (2) and 5-(*m*-nitrophenylazo)salicylate anion (3), HA^-.

5-(*m*- and *p*-Nitrophenylazo)salicylic acids (Fig. 1) were found to form 1 : 1 inclusion compounds with β-CD[8] and α-CD[9] from spectrophotometric and temperature-jump measurements. The ^1H and ^{13}C NMR studies showed that the nitrobenzene ring as hydrophobic portion of *m*- and *p*-NPAS is situated inside the hydrophobic β-CD cavity.[10]

† Presented in part at the 29th Annual Meeting on Coordination Chemistry, Hamamatsu, October 1, 1979, Abstract, p. 300 and 30th Annual Meeting on Coordination Chemistry, Tokyo, October 7, 1980, Abstract, p. 430.

In general the acid dissociation of azo pH indicators is facilitated or retarded by the formation of inclusion compounds with α- and β-CD.[1,8,9,11,13] The enhancement or retardation in acid dissociation has been attributed to Raumalkalität (space alkalinity) in cyclodextrin cavity,[14] topochemische Basizität (topochemical basicity) in cyclodextrin cavity,[15] dipole-ion interaction between dye molecule as nucleophile and cyclodextrin molecule as electrophile,[16] and hydrophobic microenvironment effect of cyclodextrin cavity.[13] On the other hand, it was pointed out qualitatively that the rate constants for the recombination of *m*- and *p*-NPAS with hydroxide ion increase with increasing concentrations of cyclodextrin, irrespective of enhancement or retardation in acid dissociation, namely, the intramolecular hydrogen bond of *m*- and *p*-NPAS is weakened by the formation of inclusion compounds with cyclodextrin molecules.[8,9]

The present paper deals with the detailed quantitative kinetic results on the proton-transfer reactions of *m*- and *p*-NPAS coupled with inclusion reactions with α- and β-cyclodextrins in aqueous solutions.

Experimental

Materials. Water was deionized and distilled. The azo compounds, *m*- and *p*-NPAS, were synthesized by the usual azo coupling method and purified by cellulose column chromatography (Whatman CC 31, 1-butanol : 2 mol dm^{-3} aqueous NH_3 : ethanol=60 : 20 : 20, v/v/v). The monosodium salts of NPAS were acidified with HCl and washed thoroughly with water. The free acids thus obtained were recrystallized from ethanol–water. Found: C, 54.32; H, 3.18; N, 14.41% for *m*-NPAS and C, 54.46; H, 3.23; N, 14.74% for *p*-NPAS. Calcd for $C_{13}H_9N_3O_5$: C, 54.36; H, 3.16; N, 14.63%. Cyclodextrins, α- and β-CD (Tokyo Kasei), were purified by the method of Cramer and Henglein using *p*-cymene, cyclohexane, and fluorobenzene.[17]

A Hitachi-Horiba pH-meter F7-ss was used for the determination of pH values. Acid-dissociation constants were determined spectrophotometrically with a Hitachi recording spectrophotometer Model EPS-3T. The absorption spectra of acid and base forms of *m*- and *p*-NPAS at varying CD concentrations showed isosbestic points at constant pH and ionic strength ($I=0.1$ mol dm^{-3} (KNO_3) at 25 °C). The wavelength of the absorption maximum (λ_{max}) of the absorption spectrum of a solution of NPAS–CD system was dependent on the concentration of CD except for A^{2-} of *m*-NPAS, showing a red shift.[9] Kinetic measurements were carried out with a

Union Giken co-axial-cable temperature-jump apparatus Model RA-105. The reactions were followed on the screen of an oscilloscope Tektronix Type 545 B at a wavelength in the range 350—500 nm.

Deuterium oxide (99.9%) and 40% sodium hydroxide-*d* solution were purchased from E. Merck, Ltd. The NMR spectra of degassed samples (13 mg cm^{-3} *m*-NPAS, 13—180 mg cm^{-3} CD for ^1H NMR and 50 mg cm^{-3} *m*-NPAS, 180 mg cm^{-3} CD for ^{13}C NMR in 0.9 mol dm^{-3} NaOD) were obtained in 5 mm spinning tube at 25±2 °C. The 100 MHz ^1H NMR spectra were taken on a JEOL JNM-FX 100 PFT NMR spectrometer with sodium 2,2-dimethyl-2-silapentane-5-sulfonate as an external reference. The ^{13}C NMR spectra were measured by the PFT NMR spectrometer operating at 25.1 MHz using a deuterium lock. The chemical shifts (measured accuracy approx. ±0.05 ppm) were referred to internal dioxane ($\delta_{TMS} = 67.4 + \delta_{dioxane}$).[18] The assignments of ^{13}C NMR spectra of *m*- and *p*-NPAS were based on proton decoupling, the substituent effects, the additivity rule, and the proton off-resonance irradiation. The theoretical values of chemical shift of *m*- and *p*-NPAS were obtained by the equation δ(substituted benzene)=δ(benzene)+$\sum\Delta\delta$, where $\sum\Delta\delta$ is the sum of the substituent chemical shift.[18] The value of $\Delta\delta$ for azo group of *m*- and *p*-NPAS can be assumed to be approximately equal to that for Ph–N=N– group of azobenzene.[19]

Results and Discussion

Equilibria of the Inclusion Reactions. The formation of 1 : 1 inclusion compounds of *m*- and *p*-NPAS with cyclodextrins in aqueous solutions is confirmed by the presence of isosbestic points in the spectral change. Figure 2 shows the spectral change of *p*-NPAS on addition of α-CD. The equilibria for inclusion reaction in neutral region are expressed as

$$HA^- + \alpha\text{-CD} \underset{K}{\rightleftharpoons} HA\text{-}\alpha CD^-, \quad (1)$$

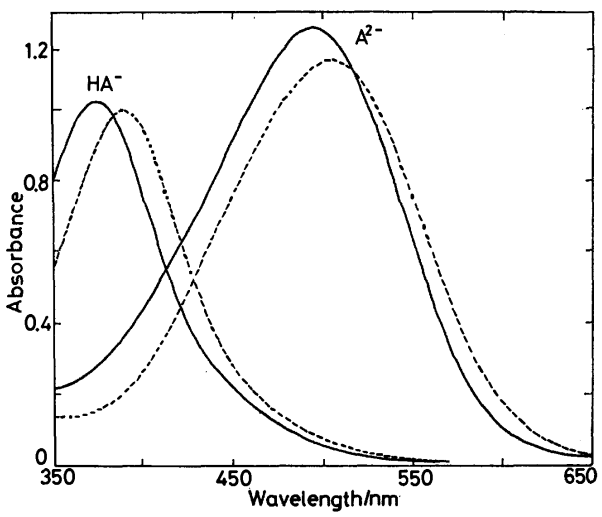

Fig. 2. Absorption spectra of HA^- and A^{2-} forms of *p*-NPAS (full lines) and their inclusion complexes (broken lines).
HA^-: $C_{HA^-}=4.32\times10^{-5}$ mol dm^{-3} and $C_{\alpha\text{-CD}}=(0—6.86)\times10^{-3}$ mol dm^{-3} at pH 7.34. A^{2-}: $C_A=4.32\times10^{-5}$ mol dm^{-3} and $C_{\alpha\text{-CD}}=(0—7.00)\times10^{-3}$ mol dm^{-3} at pH 11.80. At 25 °C and I=0.1 mol dm^{-3} (KNO_3).

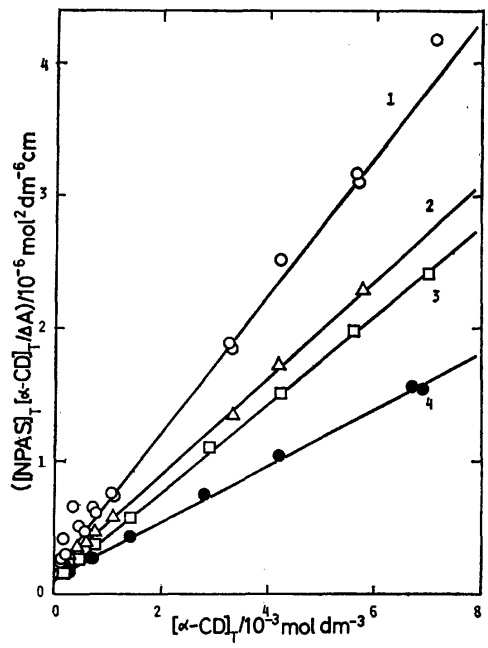

Fig. 3. Plots of $[NPAS]_T[\alpha\text{-CD}]_T/\Delta A$ against $[\alpha\text{-CD}]_T$. (1) A^{2-} of *m*-NPAS at 454 nm, (2) HA^- of *m*-NPAS at 370 nm, (3) A^{2-} of *p*-NPAS at 490 nm, (4) HA^- of *p*-NPAS at 400 nm.

and in alkaline region

$$A^{2-} + \alpha\text{-CD} \underset{K'}{\rightleftharpoons} A\text{-}\alpha CD^{2-} \quad (2)$$

where $K=[HA][\alpha\text{-CD}]/[HA\text{-}\alpha CD]$ and $K'=[A][\alpha\text{-CD}]/[A\text{-}\alpha CD]$, and charges are omitted. A plot of $[NPAS]_T[\alpha\text{-CD}]_T/\Delta A$ against $[\alpha\text{-CD}]_T$ gave a straight line (Fig. 3), where ΔA denotes the change in absorbance of a solution of NPAS-αCD system on addition of α-CD and [ ]$_T$ the total concentration.[8,9,13] The values of the dissociation constants of inclusion compounds, K and K', are determined from the slope and the intercept of Fig. 3.[8,9] The *m*- and *p*-NPAS inclusion complexes with α-CD are 2—7 times more stable compared to those with β-CD (Table 3).

^1H NMR and ^{13}C NMR Spectra of Inclusion Compounds. NMR spectroscopy is an effective technique to study the structure in solution of the inclusion complexes.[20] ^1H NMR spectra were obtained for A^{2-} form of *m*-NPAS (Fig. 4). No ^1H NMR data of HA^- form of *m*-NPAS are available owing to the poor solubility of HA^- form in D_2O. Figure 5 shows ^1H chemical shifts of A^{2-} form of *m*-NPAS on addition of β-CD. By the inclusion into β-CD cavity, most of nitrobenzene ring

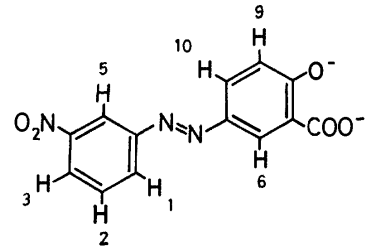

Fig. 4. Structure of the *m*-NPAS bivalent anion (A^{2-}) with the numbering for the protons in nitrobenzene and salicylic acid moieties.

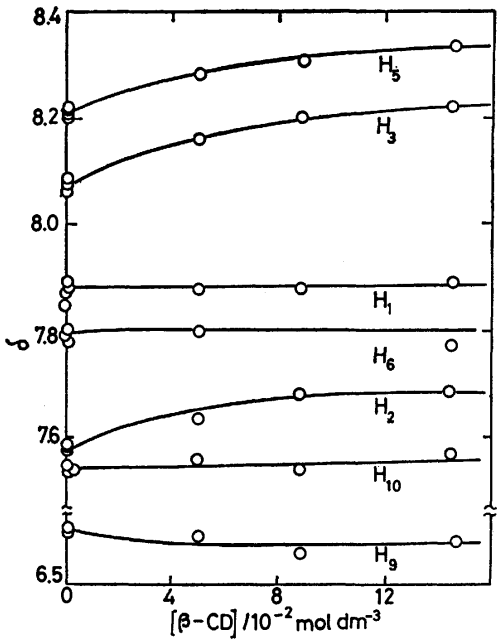

Fig. 5. Chemical shift as a function of β-CD concentration for solutions of the *m*-NPAS–βCD system.

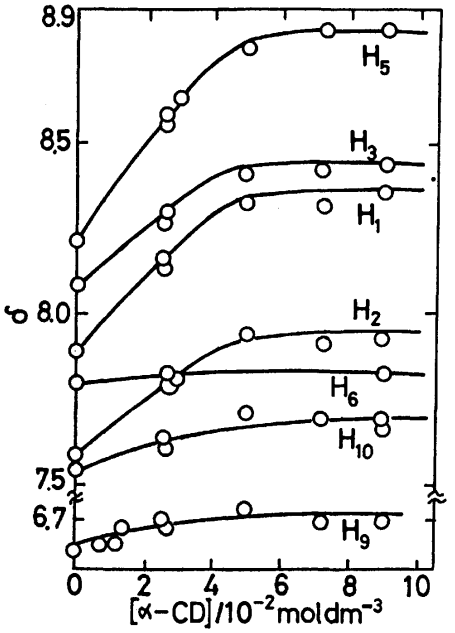

Fig. 6. Chemical shift as a function of α-CD concentration for solutions of the *m*-NPAS–αCD system.

moiety protons showed a downfield shift, while the signals of the hydrophilic moiety protons (H_9, H_{10}, and H_6) changed a little or showed an upfield shift, indicating that the hydrophobic moiety (nitrobenzene ring) of *m*-NPAS is preferentially included into β-CD cavity. Figure 6 shows ^{1}H chemical shifts of A^{2-} form of *m*-NPAS on addition of α-CD.[21] Figure 7 shows ^{13}C spectra of A^{2-} form of *m*-NPAS. The chemical shifts of carbon atoms are shown in Table 1. Nitrobenzene ring moiety carbons show a downfield shift except for C_5, while the hydrophilic moiety carbons an upfield shift. This fact indicates that the nitrobenzene ring moiety of *m*-NPAS preferentially enters the β-CD cavity.[22]

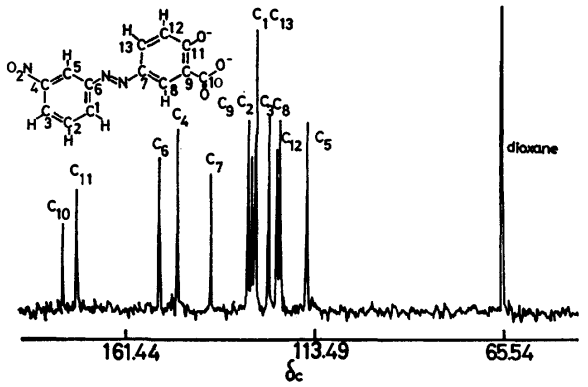

Fig. 7. Carbon-13 NMR spectrum for A^{2-} form of *m*-NPAS in D_2O.

Table 1. Carbon-13 chemical shift (ppm) of *m*-NPAS in the presence and absence of β-cyclodextrin in D_2O

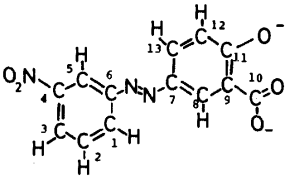

	Without β-CD		With β-CD	$\delta'_{obsd}-\delta_{obsd}$
	δ_{calcd}	δ_{obsd}	δ'_{obsd}	
"Singlet carbon"				
C_{10}	177.96	178.00	177.88	−0.12
C_6	153.4	153.41	153.55	0.14
C_4	148.8	148.84	149.06	0.22
C_7	138.9	140.35	140.52	0.17
C_9	128.6	130.86	130.68	−0.18
C_{11}	171.3	174.33	174.25	−0.08
"Doublet carbon"				
C_5	117.4	115.90	115.80	−0.10
C_1	128.7	128.98	128.98	0.00
C_2	129.6	129.98	130.07	0.09
C_3	125.4	125.70	126.02	0.32
C_8	125.6	123.53	123.32	−0.21
C_{12}	120.6	122.89	122.85	−0.04
C_{13}	127.6	128.98	128.66	−0.32

In the case of smaller molecules such as *m*-nitroaniline as compared with *m*-NPAS, the α-CD ring is found by X-ray analysis to include the nitrophenyl group, while the amino group protrudes outside from the secondary hydroxyl group side of α-CD and is hydrogen-bonded to a primary hydroxyl group of α-CD molecules.[23] As for the inclusion compounds in solution of *p*-nitrophenol with α- and β-CD, the similar preferential inclusion of hydrophobic group (nitro group) was confirmed by ^{1}H and ^{13}C NMR methods.[24]

Acid-dissociation Equilibria in the Presence of Cyclodextrins. The acid-dissociation equilibria coupled with the inclusion equilibria can be expressed as follows,

$$\begin{array}{ccc} HA^- + \alpha\text{-CD} & \overset{K_a}{\rightleftharpoons} & A^{2-} + \alpha\text{-CD} + H^+ \\ \Big\Updownarrow K & & \Big\Updownarrow K' \\ HA\text{-}\alpha CD^- & \overset{K'_a}{\rightleftharpoons} & A\text{-}\alpha CD^{2-} + H^+, \end{array} \qquad (3)$$

where $K_a=[A][H]/[HA]$ and $K_a=[A\text{-}\alpha CD][H]/[HA\text{-}\alpha CD]$ are the acid-dissociation constants of HA^- and $HA\text{-}\alpha CD^-$, and $K=[HA][\alpha\text{-CD}]/[HA\text{-}\alpha CD]$ and $K'=[A][\alpha\text{-CD}]/[A\text{-}\alpha CD]$ the dissociation constants for inclusion compounds of HA^- and A^{2-} with α-CD, respectively. The apparent acid-dissociation constants, $\bar{K}_a$, was determined from the pH-dependence of the absorbance of NPAS solution at each α-CD concentration. At each α-CD concentration the isosbestic point was observed in the pH-dependent spectral change. The absorbance, A, for the system expressed by Scheme 3 is given by

$$A = \varepsilon'_{HA}[HA] + \varepsilon'_{A}[A], \quad (4)$$

where $\varepsilon'_{HA}=\varepsilon_{HA}+\varepsilon_{HA\text{-}\alpha CD}[\alpha\text{-CD}]/K$ and $\varepsilon'_{A}=\varepsilon_{A}+\varepsilon_{A\text{-}\alpha CD}[\alpha\text{-CD}]/K'$. The terms, ε_{HA}, ε_{A}, $\varepsilon_{HA\text{-}\alpha CD}$, and $\varepsilon_{A\text{-}\alpha CD}$, are the molar absorption coefficients for corresponding species. Since the sum of [HA] and [A] is a constant at each α-CD concentration, there must be isosbestic points in the pH-dependent spectral change at the wavelength where $\varepsilon'_{HA}=\varepsilon'_{A}$, even though four absorbing species exist.[25] The apparent acid-dissociation constant, $\bar{K}_a$, at each [α-CD] is expressed as follows,[8,11,12]

$$\bar{K}_a = K_a(1+[\alpha\text{-CD}]/K')/(1+[\alpha\text{-CD}]/K), \quad (5)$$

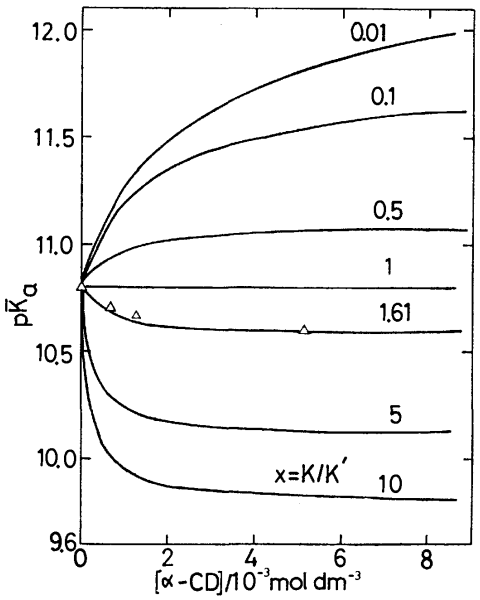

Fig. 8. The dependence of $p\bar{K}_a$ on α-CD concentrations in case of *m*-NPAS–αCD system. $K=4.95\times10^{-4}$ mol dm^{-3} and $\bar{K}_a=1.59\times10^{-11}$ mol dm^{-3}. At $I=0.1$ mol dm^{-3} (KNO_3) and 25 °C. Experimental points are indicated by triangles.

that is, the $\bar{K}_a$ value can be determined by the ratio $x=K/K'$. Figure 8 shows the theoretical curve for the dependence of $p\bar{K}_a$ on α-CD concentrations in case of *m*-NPAS–αCD system. The apparent acid-dissociation constants at each [α-CD] were determined in both *m*-NPAS–αCD and *p*-NPAS–αCD systems (Table 2). The value of $p\bar{K}_a$ decreases with increase in α-CD concentrations, namely, α-CD molecule exerts an enhancement effect on the acid dissociation of *m*- and *p*-NPAS. The quantity $\Delta pK_a=pK'_a-pK_a$ in *p*-NPAS–αCD system is more negative and larger than that in *m*-NPAS–αCD system. The change in $\bar{K}_a$ with increase of α-CD concentrations is larger as compared with the corresponding change for β-CD system.

Kinetics of the Inclusion Reactions. Kinetic study of inclusion reaction of azo compounds with α-CD was investigated for the first time by Cramer *et al.*[26] They indicated that the dissociation constant of inclusion complex (K and K') are almost in the same orders of magnitude, while the rate constants (k_+, k'_+, k_-, and k') varies considerably over the range of 1—8 orders of magnitude. Very recently Ise *et al.* determined the rate constants $\vec{k}$ and $\overleftarrow{k}$ of the inclusion reactions of phenolphthalein to be 1.45×10^5 mol^{-1} dm^3 s^{-1} and 1.30×10^3 s^{-1}, 3.66×10^7 mol^{-1} dm^3 s^{-1} and 1.18×10^3 s^{-1}, and 2.95×10^7 mol^{-1} dm^3 s^{-1} and 1.19×10^3 s^{-1} for α-CD, β-CD, and poly-βCD systems, respectively.[27] Eyring

$$HA^- + CD \underset{\overleftarrow{k}}{\overset{\vec{k}}{\rightleftharpoons}} H_2A\text{–}CD \quad (6)$$

et al. measured the rate constants of inclusion reactions of some inorganic anions with β-CD using ultrasonic relaxation technique.[28]

The kinetic data were obtained under pseudo-first-order conditions using a large excess of α-CD and β-CD. The rate of inclusion reaction was followed at λ_{max} of the inclusion species. The inclusion reaction of α-CD system in neutral region is

$$HA^- + \alpha\text{-CD} \underset{k_-}{\overset{k_+}{\rightleftharpoons}} HA\text{-}\alpha CD^-, \quad (7)$$

and in alkaline region,

$$A^{2-} + \alpha\text{-CD} \underset{k'_-}{\overset{k'_+}{\rightleftharpoons}} A\text{-}\alpha CD^{2-}. \quad (8)$$

The observed relaxation time, τ, for Reactions 7 and 8 can be expressed as

$$\tau^{-1} = k_+[\alpha\text{-CD}] + k_- \quad (9)$$

and

$$\tau^{-1} = k'_+[\alpha\text{-CD}] + k'_-, \quad (10)$$

Table 2. Acid-dissociation constants of *m*- and *p*-NPAS in the presence of α-CD

[α-CD] / mol dm^{-3}	*m*-NPAS $\bar{K}_a(p\bar{K}_a)$		*p*-NPAS $\bar{K}_a(p\bar{K}_a)$	
	Obsd	Calcd	Obsd	Calcd
0	1.59×10^{-11} (10.80)	—	2.06×10^{-11} (10.65)	—
6.47×10^{-4}	1.98×10^{-11} (10.70)	2.14×10^{-11} (10.67)	3.12×10^{-11} (10.51)	3.34×10^{-11} (10.48)
1.29×10^{-3}	2.17×10^{-11} (10.66)	2.29×10^{-11} (10.64)	3.98×10^{-11} (10.40)	3.79×10^{-11} (10.42)
5.18×10^{-3}	2.50×10^{-11} (10.60)	2.48×10^{-11} (10.61)	4.45×10^{-11} (10.35)	4.39×10^{-11} (10.36)
∞	—	2.56×10^{-11} (10.59)	—	4.70×10^{-11} (10.33)

Table 3. Rate and equilibrium constants for the inclusion reactions of *m*- and *p*-NPAS in α-CD and β-CD system

Equilibrium and rate constants	α-CD		β-CD	
	m-NPAS	*p*-NPAS	*m*-NPAS	*p*-NPAS
(1) k_+/mol^{-1} dm^3 s^{-1}	9.3×10^6	6.1×10^7	3.3×10^6	3.2×10^6
(2) k_-/s^{-1}	3.0×10^3	4.1×10^4	4.0×10^3	1.1×10^4
(3) $K=(k_-/k_+)$/mol dm^{-3}	3.2×10^{-4}	6.7×10^{-4}	1.2×10^{-3}	3.4×10^{-3}
(4) K(spectr)/mol dm^{-3}	4.95×10^{-4}	6.80×10^{-4}	9.22×10^{-4}	1.37×10^{-3}
(5) k'_+/mol^{-1} dm^3 s^{-1}	9.0×10^6	2.3×10^7	1.4×10^6	1.5×10^6
(6) k'_-/s^{-1}	2.0×10^3	8.0×10^3	2.2×10^3	4.0×10^3
(7) $K'=(k'_-/k'_+)$/mol dm^{-3}	2.2×10^{-4}	3.5×10^{-4}	1.6×10^{-3}	2.7×10^{-3}
(8) K'(spectr)/mol dm^{-3}	3.07×10^{-4}	2.98×10^{-4}	2.16×10^{-3}	1.12×10^{-3}

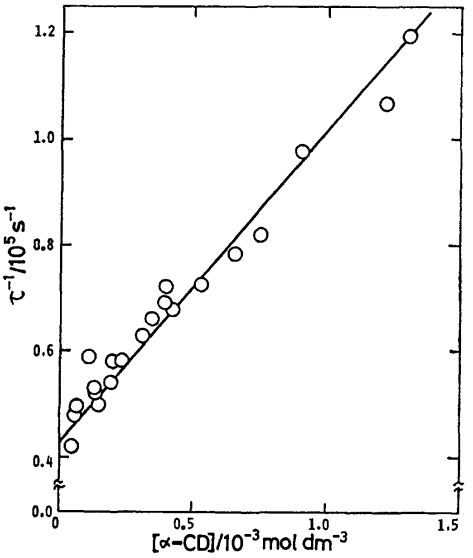

Fig. 9. A plot of Eq. 9 for the inclusion reaction of HA$^-$ form of *p*-NPAS with α-CD.

respectively. The plot of Eq. 9 gave a straight line with a slope k_+ and an intercept k_- (Fig. 9). The values of rate constants, k_+, k_-, k'_+, and k'_- for α-CD and β-CD systems are summarized in Table 3.

In the inclusion processes of *m*- and *p*-NPAS with α-CD, one can expect that the rate constant, k_+ (k'_+), decreases owing to the smaller α-CD cavity.[29] However, the higher stability of inclusion complex with α-CD may be attributed to the increase in k_+ (k'_+).[30] Actually in our investigations, the rate constant k_+ (or k'_+) of α-CD system was considerably larger than that of β-CD system, showing that α-CD exerts the inclusion force more strongly than β-CD does. The value of k_+ in α-CD system was found to depend on the position of the nitro group on *m*- and *p*-NPAS, *i.e.*, the values of k_+ of *m*- and *p*-NPAS was fairly different from each other compared to the case of the β-CD system. Larger steric hindrance of the nitro group in *m*-NPAS contributes to decreasing the rate constants k_+ (or k'_+). This indicates that the inclusion process takes place at the hydrophobic site (nitrobenzene moiety).

The value of k^+ is reported to be almost 2—3 orders of magnitude larger than that of k'_+ when a hydrophilic group such as hydroxyl group is included into α-CD cavity.[26,31] In the present kinetic study, however, the value of k_+ and k'_+ were found to be in the same order of magnitude ($\simeq10^6$ mol^{-1} dm^3 s^{-1} for *m*-NPAS and 10^7 mol^{-1} dm^3 s^{-1} for *p*-NPAS).[32] This fact kinetically supports the inclusion of hydrophobic site of *m*- and *p*-NPAS as a guest molecule into α-CD cavity.

Kinetics of Proton-transfer Reactions Coupled with the Inclusion Reactions. Kinetic data on the proton-transfer reaction coupled with the inclusion reaction with α-CD interpreted in terms of the following scheme,

$$\begin{array}{ccc} HA^- + \alpha\text{-CD} + OH^- & \underset{k_r}{\overset{k_f}{\rightleftharpoons}} & A^{2-} + \alpha\text{-CD} + H_2O \\ k_+ \downarrow\uparrow k_- & & k'_+ \downarrow\uparrow k'_- \\ HA\text{-}\alpha CD^- + OH^- & \underset{k'_r}{\overset{k'_f}{\rightleftharpoons}} & A\text{-}\alpha CD^{2-} + H_2O. \end{array} \quad (11)$$

As mentioned above, it was concluded that the inclusion process takes place at the hydrophobic site (nitrobenzene ring moiety). The apparent rate constants, $\bar{k}_f$ and $\bar{k}_r$, at each α-CD concentration were obtained under pseudo-first-order conditions using a large excess of hydroxide ion. The observed relaxation time, τ, for the proton-transfer reaction can be expressed as

$$\tau^{-1} = \bar{k}_f[\overline{OH}] + \bar{k}'_r, \quad (12)$$

where $[\overline{OH}]$ denotes the equilibrium concentration of hydroxide ion determined from pH-meter readings. The plot of τ^{-1} against $[\overline{OH}]$ gave a straight line at each α-CD concentration. The values of $\bar{k}_f$ and $\bar{k}_r$ at each α-CD concentration are summarized in Table 4. Because of the strong intramolecular hydrogen bond[33] of *m*- and *p*-NPAS, the k_f value (10^7 mol^{-1} dm^3 s^{-1}) is three orders of magnitude smaller as compared with that of diffusion-controlled proton-transfer reactions (10^{10} mol^{-1} dm^3 s^{-1}). Since the interior of α-CD cavity contains a ring of C–H groups, a ring of glycosidic oxygen, and another ring of C–H groups, the interior of α-CD cavity is relatively hydrophobic and apolar as compared with bulk solvent water.[1] Then, the recombination rate constant with OH^- ion, $\bar{k}_f$, should decrease provided the reaction site (–COO$^-$···HO–) of the proton-transfer reaction is included into hydrophobic α-CD cavity,[33] where the dielectric constant is probably small compared with that of the bulk solvent water. As shown in Table 4, $\bar{k}_f$ value increased with increase in α-CD concentrations, which suggests that the reaction site (–COO$^-$···HO–) in the proton-transfer reaction is situated outside the hydrophobic α-CD cavity, and the inclusion force exerts a weakening effect to

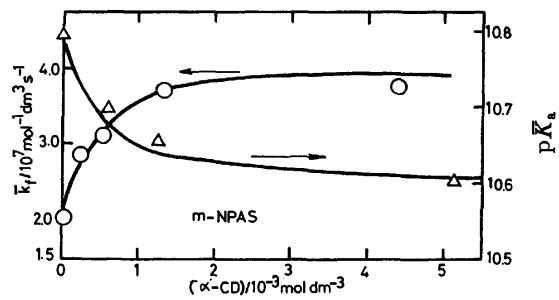

Fig. 10. The dependence of $p\bar{K}_a$ and $\bar{k}_f$ on α-CD concentrations in case of *m*-NPAS–αCD system at I=0.1 mol dm^{-3} (KNO_3) and 25 °C.

the intramolecular hydrogen bond.

The rate constant, $\bar{k}_f$, and $p\bar{K}_a$ of *m*-NPAS thus obtained in the present experiment were plotted against α-CD concentrations in Fig. 10. A definite correlation was observed between the [α-CD]-dependence of $\bar{k}_f$ and $p\bar{K}_a$, that is, with an increase of α-CD concentrations the $p\bar{K}_a$ value decreases and the $\bar{k}_f$ value increases particularly in the α-CD concentration range (0—2)$\times 10^{-3}$ mol dm^{-3}; about 91% of HA^- form of *m*-NPAS is included by α-CD at [α-CD]$=2\times10^{-3}$ mol dm^{-3}. By forming an inclusion compound with *m*-NPAS, α-CD is capable of altering the reactivity of the recombination site in the proton-transfer reaction. Similar observations were made for the proton-transfer reactions of *p*-NPAS in the presence of α-CD and β-CD (Table 4).

Table 4. Rate constants for the proton-transfer reactions of *m*- and *p*-NPAS in the presence of α-CD at 25 °C and I=0.1 mol dm^{-3} (KNO_3)

[α-CD] / mol dm^{-3}	$\bar{k}_f$ / mol^{-1} dm^3 s^{-1}	$\bar{k}_r$ / s^{-1}	K_b^c [a] / mol^{-1} dm^3	$p\left(\frac{\bar{K}_a^c(k)}{\text{mol dm}^{-3}}\right)$ [b]
		m-NPAS		
0	2.0×10^7	3.5×10^4	570	10.97
2.11×10^{-4}	2.9×10^7	3.5×10^4	830	10.81
5.55×10^{-4}	3.1×10^7	3.0×10^4	1000	10.73
1.33×10^{-3}	3.7×10^7	3.1×10^4	1200	10.65
4.44×10^{-3}	3.7×10^7	2.9×10^4	1300	10.62
		p-NPAS		
0	2.1×10^7	1.9×10^4	1100	10.69
5.55×10^{-4}	3.4×10^7	2.2×10^4	1500	10.55
1.33×10^{-3}	3.5×10^7	1.8×10^4	1900	10.45
4.44×10^{-3}	3.9×10^7	1.7×10^4	2300	10.37

a) $K_b^c=k_f/k_r$. b) The values of kinetic $pK_a^c(k)$ were evaluated from the relation, $K_a^c(k)=K_b^c\cdot K_w^c$. K_w^c denotes the apparent ionic product of water.[31]

References

1) M. L. Bender and M. Komiyama, "Cyclodextrin Chemistry," Springer-Verlag (1978); W. Lautsch, W. Broser, W. Biedermann, and H. Gnichtel, *Angew. Chem.*, **66**, 123 (1954); K. Takemoto, "Hōsetsu Kagōbutsu No Kagaku," Tokyo Kagaku Dojin, Tokyo (1969).

2) F. Cramer and W. Kampe, *J. Am. Chem. Soc.*, **87**, 1115 (1965).

3) D. French, *Adv. Carbohydr. Chem.*, **12**, 250 (1957); F. Cramer, *Angew. Chem.*, **73**, 49 (1961).

4) R. L. Vanetten, J. F. Sebastian, G. A. Clowes, and M. L. Bender, *J. Am. Chem. Soc.*, **89**, 3242 (1967).

5) G. Némethyl and H. A. Scheraga, *J. Chem. Phys.*, **36**, 3401 (1962); H. Zahn, *Kolloid Z.*, **197**, 14 (1964).

6) P. C. Manor and W. Saenger, *Nature*, **237**, 392 (1972); *J. Am. Chem. Soc.*, **96**, 3630 (1974); W. Saenger, R. K. Mcmullan, J. Fayos, and D. Mootz, *Acta Crystallogr., Sect. B*, **30**, 2019 (1974).

7) In benzene–*p*-iodoaniline– and Methyl Orange–αCD inclusion complexes. See, I. Tabushi, Y. Kiyosuke, T. Sugimoto, and K. Yamaura, *J. Am. Chem. Soc.*, **100**, 916 (1978). In benzenesulfonic acid–αCD inclusion complexes. See, K. Harata, *Bull. Chem. Soc. Jpn.*, **49**, 2066 (1976).

8) N. Yoshida and M. Fujimoto, *Chem. Lett.*, **1980**, 231.

9) N. Yoshida and M. Fujimoto, *Chem. Lett.*, **1980**, 1377.

10) N. Yoshida and M. Fujimoto, 1980 Winter Hokkaido Meeting of the Japan Society for Analytical Chemistry and the Chemical Society of Japan, Sapporo, February 1, 1980, 2A15, Abstract, p. 39.

11) K. A. Connors and J. M. Lipari, *J. Pharm. Sci.*, **65**, 379 (1976).

12) T. Miyaji, Y. Kurono, K. Uekama, and K. Ikeda, *Chem. Pharm. Bull.*, **24**, 1155 (1976).

13) Y. Matsui and K. Mochida, *Bull. Chem. Soc. Jpn.*, **51**, 673 (1978).

14) F. Cramer, *Angew. Chem.*, **64**, 136, 437 (1952).

15) F. Cramer, *Justus Liebigs Ann. Chem.*, **579**, 17 (1953).

16) W. Broser, *Z. Naturforsch., Teil B*, **8**, 711, 722 (1953).

17) F. Cramer and F. M. Henglein, *Chem. Ber.*, **91**, 308 (1958).

18) J. B. Stothers, "Carbon-13 NMR Spectroscopy," Academic Press (1972); S. Fujiwara, Y. Takeuchi, and H. Ishizuka, "C-13 NMR (Kiso to Ōyō)," Kōdansha, Tokyo (1976).

19) L. F. Johnson and W. C. Jankowski, "Carbon-13 NMR Spectra (A Collection of Assigned, Coded, and Indexed Spectra)," Wiley-Interscience Publication, New York (1972).

20) P. V. Demarco and A. L. Thakkar, *Chem. Commun.*, **1970**, 2; A. L. Thakkar and P. V. Demarco, *J. Pharm. Sci.*, **60**, 652 (1971); J. Sunamoto, H. Okamoto, K. Taira, and Y. Murakami, *Chem. Lett.*, **1975**, 371; M. Otagiri, K. Uekama, K. Ikeda, *Chem. Pharm. Bull.*, **23**, 188 (1975); J. P. Behr and J. M. Lehn, *J. Phys. Colloq. (Paris)*, **1973**, 55; *J. Am. Chem. Soc.*, **98**, 1743 (1976); D. J. Wood, F. E. Hruska, and W. Saenger, *ibid.*, **99**, 1735 (1977); M. Komiyama and H. Hirai, *Chem. Lett.*, **1980**, 1467, 1471.

21) The observed chemical shift (δ_{obsd}) associated with Reaction 2 will be given by

$$\delta_{obsd} = \frac{[A]}{[A]_T}\delta_A + \frac{[A\text{-}\alpha CD]}{[A]_T}\delta_{A\text{-}\alpha CD}$$
$$= \frac{1}{[A]_T}\{[A]_T\delta_A + (\delta_{A\text{-}\alpha CD}-\delta_A)[A\text{-}\alpha CD])\},$$

with

$$[A\text{-}\alpha CD] = [Q-\sqrt{Q^2-4[A]_T[\alpha\text{-}CD]_T)}]/2,$$

and

$$Q = [A]_T + [\alpha\text{-}CD]_T + K',$$

where δ_A, $\delta_{A\text{-}\alpha CD}$, $[\alpha\text{-}CD]_T$, and $[A]_T$ are the chemical shifts of A and A-αCD species and the total concentrations of α-CD and *m*-NPAS anion. The theoretical curves are obtained by plotting δ_{obsd} against $[\alpha\text{-}CD]_T$.

22) Assignments of α-CD and β-CD ^{13}C spectra by Kuge *et al.* were applied to these systems. See, K. Takeo, K. Hirose, and T. Kuge, *Chem. Lett.*, **1973**, 1233. Upon binding to CD of NPAS, CD carbons showed an upfield shift. The order of upfield shifts was $C_4>C_2\gtrsim C_1>C_3\gtrsim C_5\gg C_6$ in *m*-NPAS–βCD system, $C_1\gtrsim C_2>C_3\gtrsim C_4>C_5\gg C_6$ in *p*-NPAS–βCD system, $C_6\gtrsim C_2\gtrsim C_4>C_5>C_1\gg C_3$ in *m*-NPAS–αCD system,

and $C_1 \gtrsim C_2 > C_4 > C_5 > C_3 > C_6$ in *p*-NPAS–αCD system, indicating that the inclusion into CD cavity takes place from the secondary hydroxyl group side.

23) K. Harata, *Bull. Chem. Soc. Jpn.*, **53**, 2782 (1980).

24) R. Bergeron and R. Rowan, *Bioorg. Chem.*, **5**, 425 (1976). R. Bergeron and M. A. Channing, *Bioorg. Chem.*, **5**, 437 (1976). In sodium *p*-nitrophenolate–αCD system, the order of shielding is $C_1 > C_2 > C_3 \approx C_4 > C_5 > C_6$ while with *p*-nitrophenol as a substrate the shielding is $C_1 > C_2 > C_4 \approx C_5 > C_3 > C_6$.

25) A consideration of this problem has been discussed by Drago et al. in another complicated system. See, R. G. Mayer and R. S. Drago, *Inorg. Chem.*, **15**, 2010 (1976).

26) F. Cramer, W. Saenger, and H.-Ch. Spatz, *J. Am. Chem. Soc.*, **89**, 14 (1967).

27) N. Ise, T. Okubo, and M. Kuroda, 23rd Annual Meeting of the Society of High Polymers, Japan, 5A12 (1974).

28) R. P. Rohrbach, L. J. Rodrigues, and E. M. Eyring, *J. Phys. Chem.*, **81**, 944 (1977).

29) 4.5 Å from X-ray crystallographic study. W. J. James, D. French, and R. E. Rundle, *Acta Crystallogr.*, **12**, 385 (1959). The diameter of β-CD cavity is larger than that of α-CD cavity. 7.5 Å from molecular model. See Ref .26.

30) The stability constants of inclusion complexes, K^{-1} and $(K')^{-1}$, are expressed as the ratio of rate constants, k_+/k_- and k_+'/k_-', respectively.

31) N. Yoshida and M. Fujimoto, 1981 Winter Hokkaido Meeting of the Japan Society for Analytical Chemistry and the Chemical Society of Japan, Sapporo, February 2, 1981, 2A03, Abstract, p. 34.

32) The relationship, $k_+' < k_+$, was observed both in α-CD and in β-CD system.

33) N. Yoshida and M. Fujimoto, *Bull. Chem. Soc. Jpn.*, **53**, 101 (1980).

Studies on Characteristics of Electron Capture Responses. VI.[1] A Consideration on the Response Mechanism of the Electron Capture Detector

Masahiro TAKEUCHI

Tokyo Metropolitan Research Laboratory of Public Health, Hyakunincho, Shinjuku-ku, Tokyo 160

(Received August 10, 1981)

In order to improve the understanding of the electron capture detector (ECD), a study on the response mechanism has been carried out by using the pulse sampling technique. The ECD currents in the presence and the absence of electron capturing molecules were measured under various pulse conditions. The responses of the ECD probably arise from the current drop based on the slower electron drift velocity in the presence of electron capturing molecules than that in the absence of them.

The electron capture detector (ECD) has been widely used as the most suitable gas chromatographic detector for trace amounts of halogen-containing compounds on account of its high sensitivity and selectivity. Therefore, the ECD is necessary in laboratories concerned with the analysis of environmental contaminations such as organochloro pesticides and polychlorinated biphenyls. However, the response mechanism of the ECD has not completely establised yet, that is, the details of the events which occur within the ECD are not known so well. Several views have been proposed about the ECD.

Wentworth *et al.*[2] have described the behavior of electrons within a pulse-sampled ECD on the basis of the following assumptions:[3] (1) The current measured is due to electrons which are drawn to the positive electrode during the application of pulses. (2) The relatively immobile ions contribute little to the current. (3) The ECD cell is cleared of electrons during each pulse. (4) Positive ions will be in very large excess of electrons because the electrons diffuse quickly to cell boundaries. (5) The charge associated with negative ions formed by electron capture is quickly lost because of the much faster recombination between positive ions and negative ions than that between positive ions and electrons.

Siegel and McKeown,[4] however, criticised assumptions (3), (4), and (5), and insisted that both electrons and positive ions become characterized by a single (ambipolar) diffusion coefficient. According to this view, the current measured from the ECD should be considered to reflect the motion of electrons and positive ions within one Debye length from the positive electrode surface. Though undeniable for the present, this view has not been commonly accepted.

Grimsrud *et al.*[3] have proposed based on the positive space-charge field created by positive ions, and recalled the Wentworth assumption (3). Their modification has the merit that it does not depart so drastically from the Wentworth view, which has become the conventional one because of being strongly supported in many experiments.[2,5-7]

Under the circumstances described above, the author has measured the ECD currents under various pulse conditions in order to understand the behavior of electrons within the ECD and to reveal its response mechanism.

Experimental

A Shimadzu gas chromatograph Model 5A equipped with a Shimadzu ECD Model EDC-5 was used. The ECD has coaxial geometry and contains a 10 mCi ^{63}Ni or a 300 mCi ^{3}H radioactive source. The radius of the electrode is 2.0 mm, and the distance from the center of the electrode to the surface of the radioactive source is 5.0 mm. The carrier gas used (Nihon Sanso, A grade pure gas) was nitrogen of a purity over 99.9995%. Before being introduced into the gas chromatograph, the gas was passed through a Molecular Sieve 13 X column and an oxygen scrubber (Alltech, Oxy-Trap). For the gas chromatographic column, a 1 m×3 mm i.d. glass column packed with 2% Silicone OV-17 on Chromosorb W (AW-DMCS), 60—80 mesh was used at temperatures up to 200 °C. The other conditions were set up as follows: flow-rate, 60 ml/min; ECD temperature, 220 °C.

Results and Discussion

Effect of Pulse Conditions on ECD Current. As shown in Fig. 1, the ECD current measured increased with increasing the pulse width (t_w), and finally attained a plateau for each different pulse period (t_p).

According to Wentworth *et al.*[1] the current is due to electrons which are drawn to the positive electrode during the application of pulses. The appearance of the plateau indicates that the number of electrons collected by the positive electrode increases with increasing t_w, and all electrons formed between pulses are collected when t_w becomes sufficiently large. This is because slower electrons can drift to the positive electrode with increasing t_w, without recombination with positive ions.

Electron Drift Velocity. The value of $t_w^{1/2}$, which is denoted by an arrow in Fig. 2 and represents the time required for half the electrons drifting to the positive electrode, is the mean time of the electrons drifting to the electrode. Hence, the reciprocal of $t_w^{1/2}$ is proportional to the electron drift velocity, ω:

$$\omega \propto (t_w^{1/2})^{-1}. \quad (1)$$

As shown in Fig. 2, the value of $(t_w^{1/2})^{-1}$ decreases with decreasing the pulse amplitude (V_a), and finally approaches zero at approximately 2 V in any t_p. These results suggest that the positive ion cloud created within the cell reduces the applied field by about 2 V, *i.e.*, about 2 V of the electrical potential is induced by positive ions.

According to Grimsrud *et al.*,[3] the electrical potential, V, expressed in the form of Eq. 2 is induced by positive

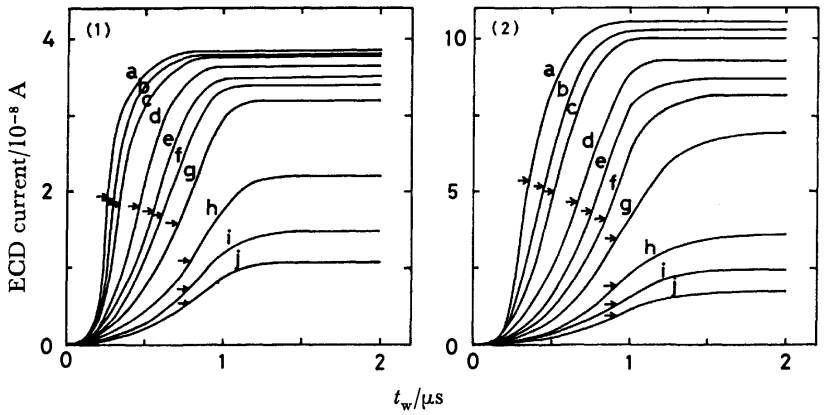

Fig. 1. Effect of t_w on ECD current in various t_p.
t_p/μs: a; 10, b; 100, c; 200, d; 400, e; 600, f; 800, g; 1000, h; 2000, i; 3000, j; 4000. ECD: (1); ^{63}Ni, (2); ^{3}H.

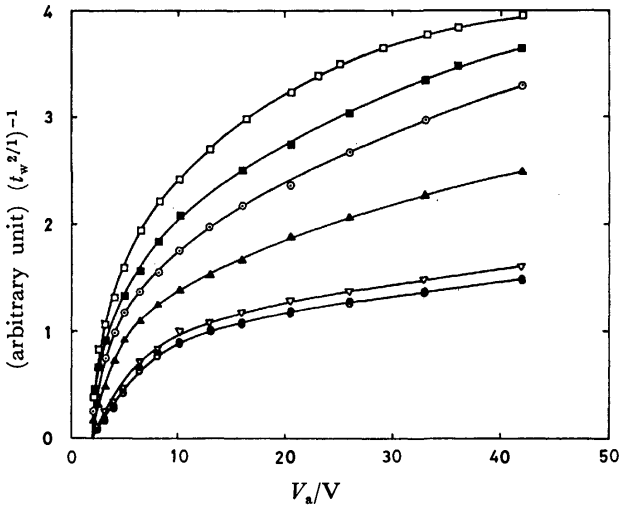

Fig. 2. Effect of V_a on the value of $(t_w^{1/2})^{-1}$ in various t_p.
t_p/μs: □; 10, ■; 100, ⊙; 200, ▲; 400, ▽; 1000, ●; 2000, ○; 4000. ECD; ^{63}Ni.

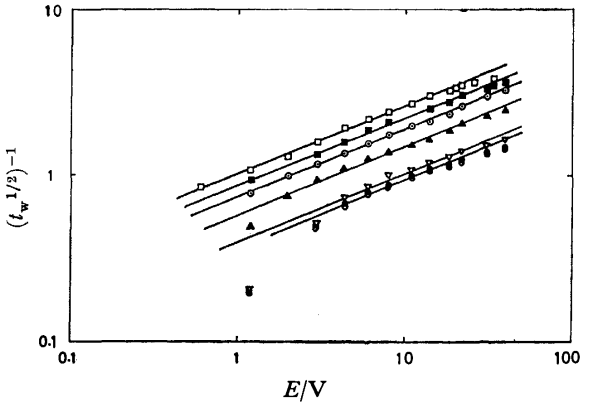

Fig. 3. Plots of ln $(t_w^{1/2})^{-1}$ *versus* E, where $E=V_a-2.0$.
t_p: Same as in Fig. 3.

ions at any point within the cell, if one assumes that the positive ions are uniformly distributed throughout the cell:

$$V=\frac{\rho_o}{4\varepsilon_o}\left\{(b^2-a^2)\frac{\ln(r/b)}{\ln(b/a)}+(b^2-r^2)\right\}. \quad (2)$$

Here ρ_o is the density of the positive ions, ε_o is the permittivity of free space, a is the radious of the electrode, b is the distance from the center of the electrode to the surface of radioactive source, and r is the distance from the center of the electrode to any point within the cell.

The potential calculated from Eq. 2 for the ^{63}Ni ECD used in the present study becomes a maximum value of approximately 10 V at r=2.73 mm. If this value is reasonable, the electrons within the cell will distribute most densely near the middle of the radioactive source and the positive electrode under the field-free, *i.e.*, pulse-free conditions, and then they will drift to the positive electrode against the electrical potential under pulse-sampled conditions. Therefore, the field strength will become lower than that applied to the positive electrode by the maximum value of the induced potential. Consequently, the value of $(t_W^{1/2})^{-1}$ should become zero at approximately 10 V. In practice, however, the value becomes zero at approximately 2 V in any t_P as shown in Fig. 3. This discordance of the theoretical and the observed values suggests the deficiency of Grimsrud's view: The center of the ionization was hitherto considered 1—2 mm for ^{3}H and 6—8 mm for ^{63}Ni, judging from commonly used ECD dimensions.[8,9] Recently, however, Aue *et al.*[9] have reported that the center of ionization is much closer to the radioactive foil than commonly assumed, *i.e.*, at approximately 0.2 mm for ^{3}H and approximately 1 mm for ^{63}Ni in nitrogen at ambient conditions. These experimental facts tend to contradict Grimsrud's view, in which it is assumed that positive ions are uniformly distributed throughout the cell.

The electron drift velocity, ω, in a gas under electric field is expressed in the form of Eq. 3:[10]

$$\omega=\frac{e}{m}\cdot\frac{\lambda}{u}\cdot\frac{E}{p}, \quad (3)$$

where e is the charge, m is the mass, λ is the mean free path, u is the agitation velocity, E is the field strength, and p is the pressure of a gas.

In the ECD used as a gas chromatographic detector, e, m, and p are constant. Hence,

$$\omega \propto \lambda \cdot \frac{E}{u}. \quad (4)$$

On the other hand, electrons which are at thermal equilibrium state under the field-free conditions obtain some kinetic energy proportional to the field strength:

$$\frac{1}{2} \cdot m \cdot u^2 \propto E. \quad (5)$$

Equations 4 and 5 give Eq. 6:

$$\omega \propto \lambda \cdot E^{1/2}. \quad (6)$$

Figure 3 is the ln-ln plots of the curves shown in Fig. 2, where the abscissa is converted into $E=V_a-2.0$. In any t_P, the plot gives a straight line whose slope is approximately 0.5. This result indicates that ω is proportional to $E^{1/2}$.

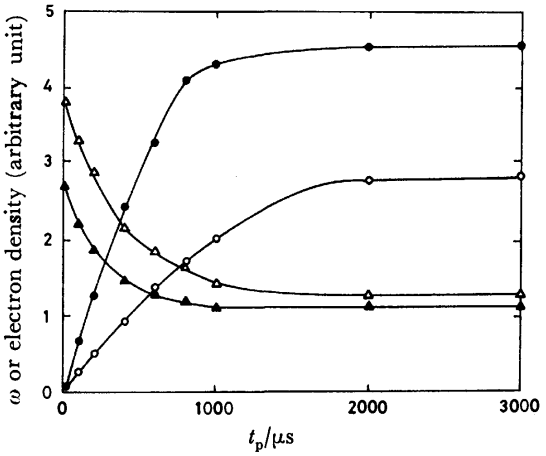

Fig. 4. Variations of ω and electron density with t_p. △: ω (^{63}Ni), ▲: ω (^{3}H), ○: Ion density (^{63}Ni), ●: Ion density (^{3}H). E: 30 V.

Figure 4 shows the variations of ω and the electron density with t_P. The value of ω decreases, and oppositely the electron density increases with increasing t_P for constant E. These results suggest that ω is inversely proportional to the electron density. Since the interaction between electrons and positive ions increases with increasing the electron density, the value of λ should be inversely proportional to the electron density, and consequently ω may be proportional to λ, as in Eq. 5. Therefore, as discussed above, the curves of Fig. 2 are expressed in the form of Eq. 6.

Response Mechanisms. Figure 5 shows the ECD current versus t_w curves in various t_P at 30 °C(a), and 200 °C(b) of column temperatures. In any t_P, the values of $t_w^{1/2}$ increases, *i.e.*, the electron drift velocity decreases, with increasing the column temperature. According to Aue *et al.*,[9] the ECD can simply be considered a non-linear impedance device, whose impedance increases with the introduction of electron capturing molecules. The higher the column temperature is, the more electron capturing molecules which bleed from the column. Consequently, the impedance of the ECD cell increases with the rise of column temperature. The increase of the impedance rusults in the decrease of the electron drift velocity. The curves c, which are the plots for (a−b), correspond to the current drop based on the increase of the impedance. If the drop arises from the increase of the impedance, the curves c should gradually approach zero with increasing t_w. The reason is that even slower electrons can drift to the positive electrode with increasing t_w, and curve b consequently approaches to the corresponding curve a. However, the curves do not practically become zero, but constant in each t_P. These results lead to the probability that the current drop occurs by some other factor rather than the increase of the cell impedance. In the absence of electron capturing molecules, electrons within the ECD attain a thermal equilibrium state through numerous collisions with the carrier gas molecules. In the presence of electron capturing molecules, the thermally equilibrated electrons collide with electron capturing molecules and finally attach to them to form negative ions.[11] Consequently, the value of λ should become smaller than that in the absence of electron capturing molecules. Considered from this view, the curves c correspond to the current drop arising from the decrease of the electron drift velocity, which results from the decrease of λ.

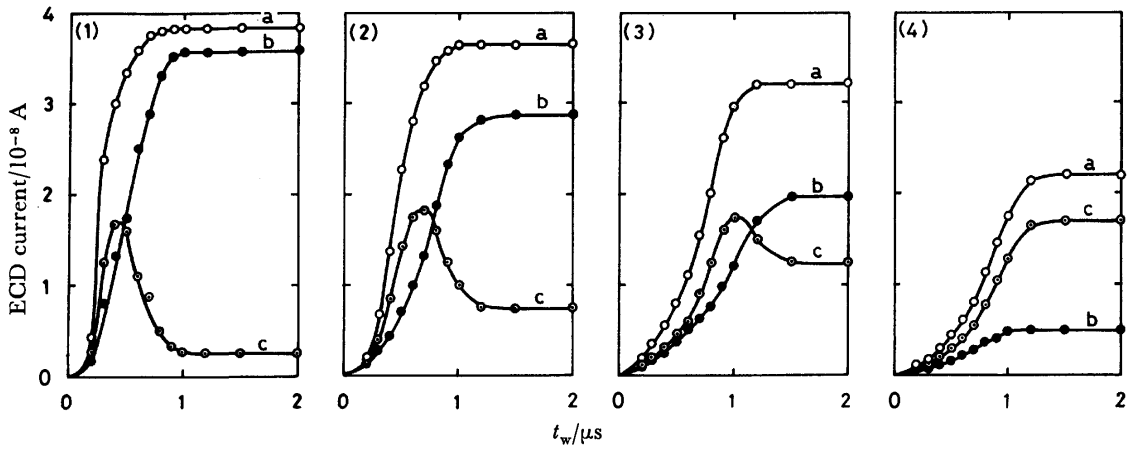

Fig. 5. Effect of t_w on ECD current at column tempertures of 30 °C (a) and 200 °C (b). $t_p/\mu s$: (1); 100, (2); 500, (3); 1000, (4); 2000. V_a: 30 V. ECD: ^{63}Ni. Curves c are the plots of (a−b).

The view described above can explain why the curve c does not become zero, but constant, with increasing t_w. So long as the value of λ is not zero, all electrons within the cell can drift to the electrode by applying a sufficiently large t_w of pulses, *i.e.*, the current drop decreases and finally becomes zero with increasing t_w. However, if the value of λ is zero, the electrons can not drift to the electrode even if sufficiently large t_w of pulses are applied, *i.e.*, the current drop approaches a constant value which is proportional to the number of electrons attached to electron capturing molecules. By applying the above discussion for the region where the current drop remains constant, the proposed view recalls the classical mechanism of electron capture detection by Wentworth *et al.*, *i.e.*, attachment to electron capturing molecules, followed by positive ion-negative ion neutralization.

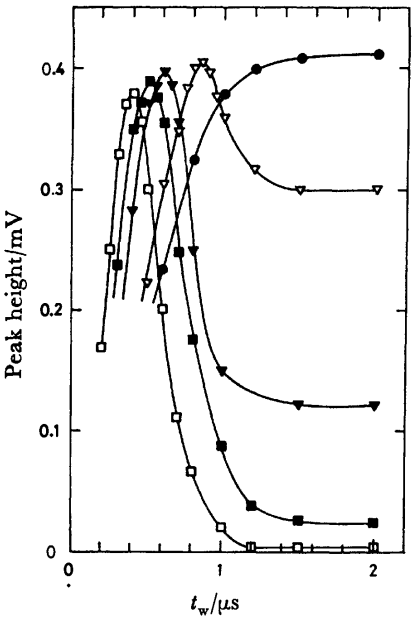

Fig. 6. Effect of t_w on the peak height of γ-BHC.
t_p/μs: □; 10, ■; 100, ▽; 500, ▼; 1000, ●; 2000.
V_a: 30 V. ECD: ^{63}Ni.

Figure 6 shows the variation of the peak height for γ-BHC with t_w. The profile of the peak height, which represents the sensitivity of the ECD, is in accord with the curves c in Fig. 5. Such a profile is not specific for γ-BHC, but general for the other several samples examined, *e.g.*, α-BhC, β-BHC, δ-BHC, *p,p'*-DDE, aldrin, dieldrin, 2,4,5-trichlorobiphenyl, and 2,2',4,4',6,6'-hexachlorobiphenyl.[12] These results lead to the conclusion that the response of the ECD arises from the current drop due to the decrease of the electron drift velocity resulting from the decrease of λ, and the removal of the electrons whose values of λ become zero as the result of attachment to electron capturing molecules.

The author wishes to express his thanks to Emeritus Professor Shun Araki and Professor Shigetaka Suzuki, Tokyo Metropolitan University, for their encouragement and advice.

References

1) Part V: M. Takeuchi, *Bull. Chem. Soc. Jpn.*, **53**, 2466 (1981).
2) W. E. Wentworth, E. Chen, and J. E. Lovelock, *J. Phys. Chem.*, **70**, 445 (1966).
3) E. P. Grimsrud, S. H. Kim, and P. L. Gobby, *Anal. Chem.*, **51**, 223 (1979).
4) M. W. Siegel and M. C. McKeown, *J. Chromatogr.*, **122**, 397 (1976).
5) P. Devaux and G. Guiochon, *J. Gas Chromatogr.*, **5**, 341 (1968).
6) P. G. Simmonds, D. C. Fenimore, B. C. Pettiti, J. E. Lovelock, and A. Zlatkis, *Anal. Chem.*, **39**, 1428 (1967).
7) J. E. Lovelock and A. J. Watson, *J. Chromatogr.*, **158**, 123 (1978).
8) E. D. Pellizzari, *J. Chromatogr.*, **98**, 323 (1974).
9) W. A. Aue and S. Kapila, *J. Chromatogr.*, **188**, 1 (1980).
10) I. Miura, K. Suga, and T. Matano, "Hoshasen-keisoku Gaku," Syokabo, Tokyo (1976), p. 44.
11) "Radioisotope," 3rd ed, ed by Nippon Isotope Kyokai, Maruzen, Tokyo (1975), p. 40.
12) M. Takeuchi, *Nippon Kagaku Kaishi*, **1976**, 1565.

 © 1982 The Chemical Society of Japan Bull. Chem. Soc. Jpn., 55, 1050—1053 (1982) [Vol. 55, No. 4

Multidentate Ligand Kinetics. III. The Ligand-substitution Reaction between the Ethylenediaminetetraacetatocuprate(II) Ion and the Tetraethylenepentaminezinc(II) Ion

Tetsuo KATSUYAMA* and Toshihiko KUMAI

Department of Basic Technology, Faculty of Engineering, Yamagata University, Yonezawa, Yamagata 992

(Received August 24, 1981)

The kinetics and mechanism of the ligand-substitution reaction between the ethylenediaminetraacetatocuprate(II) ion (Cu(II)-edta) and the tetraethylenepentaminezinc(II) ion (Zn(II)-tetren) were studied spectrophotometrically over the pH range from 7.0 to 9.0 at I=0.2 M (1 M= mol dm^{-3}) and 25.0 °C. The substitution reaction was shown to proceed by means of a chain-reaction mechanism where the chainpropagating steps are the reaction of Cu(II)-edta with tetren and the reaction of Zn(II)-tetren with edta. Each chain-propagating step was investigated. The ligand-substitution reaction of Zn(II)-tetren with edta was studied by the use of the chain reaction. The rate law is expressed as

$$-\frac{d[\text{Zn(II)-tetren}]}{dt}=k_L[\text{Zn(tetren)}^{2+}][\text{edta}^{4-}]+k_{HL}[\text{Zn(tetren)}^{2+}][\text{Hedta}^{3-}]+k'_{HL}[\text{Zn(Htetren)}^{3+}][\text{Hedta}^{3-}].$$

The rate constants, k_L,k_{HL}, and k'_{HL} were determined at 25.0 °C and I=0.2 M as: $k_L \approx 3\times10^2$ M^{-1} s^{-1}, $k_{HL}=(4.1\pm0.7)\times10^2$ M^{-1} s^{-1}, and $k'_{HL}=(1.7\pm0.2)\times10^5$ M^{-1} s^{-1}.

Ligand-substitution reactions between two multidentate ligand complexes often proceed by means of a coordination chain-reaction mechanism, in which two free multidentate ligands are the chain-reaction centers and the chain-propagating steps are the reactions of the metal complexes with the free ligands.[1-7]

In a previous paper,[8] the ligand-substitution reactions of the triethylenetetraminecadmium(II) ion and the tetraethylenepentaminecadmium(II) ion with the ethylenediaminetetraacetatocuprate(II) ion (Cu(II)-edta) were reported. The reactions were found to proceed by means of a coordination chain-reaction mechanism. In the present study, the ligand-substitution reaction between the Cu(II)-edta and tetraethylenepentaminezinc(II) ions (Zn(II)-tetren) was undertaken in order to obtain further understanding of the ligand-substitution reaction between two multidentate ligand complexes:

$$\text{Cu(II)-edta} + \text{Zn(II)-tetren} \longrightarrow \text{Cu(II)-tetren} + \text{Zn(II)-edta}. \quad \text{(R1)}$$

The coordination chain reaction of the present system provides a useful method for the study of the ligand substitution of Zn(II)-tetren with edta.

Experimental

Reagents. Reagent-grade zinc(II) and copper perchlorates, and guaranteed reagent-grade sodium perchlorate were recrystallized from their aqueous solutions. GR-grade tetren was purified by distillation under reduced pressure. A standard copper nitrate solution was prepared from copper plate and was subsequently used to standardize the tetren and edta solutions.

Solutions of Cu(II)-edta and Zn(II)-tetren were prepared by the following procedure: a slight excess of the metal perchlorate was added to a solution containing a known quantity of the ligand; the excess metal in the solutions of Cu(II)-edta and Zn(II)-tetren was then precipitated as hydroxide at about pH 9.3 and 9.5 respectively.

Measurements. The reactions were run in the presence of a large excess of Cu(II)-edta and small amounts of edta. The initial Zn(II)-tetren concentration was 1.8×10^{-3} M and the ionic strength was adjusted to 0.2 M with sodium perchlorate. The reaction temperature was controlled at 25.0±0.1 °C. A mannitol–boric acid–sodium borate buffer system was used to control the pH of the solution. The pH values were measured with a Toa Electronics Model HM-15A digital pH-meter. The reaction was followed spectrophotometrically at 575 nm by means of a stopped-flow technique using a Hitachi Model RSP-2 rapidscan spectrophotometer.

Results and Discussion

Rate Equation. The plots of log $(A_\infty-A_t)$ *vs.* t, where A_t and A_∞ denote the absorbances at time t and infinity respectively, were linear over 85% of the reaction. Thus, the reaction was considered to be first-order in Zn(II)-tetren. The conditional first-order rate constant was independent of the concentration of Cu(II)-edta. From these results, it seems that the rate law is given by

$$-\frac{d[\text{Zn(II)-tetren}]}{dt}=k'_o[\text{Zn(II)-tetren}]. \quad (1)$$

In addition, the values of the conditional rate constant, k'_o, at a constant pH are linearly related to the added free edta concentration in the region above the threshold value of b. Thus, the conditional rate constant, k'_o, is given by

$$k'_o = k_o([\text{edta}]_a - b). \quad (2)$$

The values of k_o are plotted against the pH in Fig. 2.

Steady-state Treatment. On the basis of the above results, the ligand-substitution reaction between Cu(II)-edta and Zn(II)-tetren was considered to proceed by means of a chain-reaction mechanism:

$$\text{Cu(II)-edta} + \text{tetren} \underset{k_{-2}}{\overset{k_2}{\rightleftharpoons}} \text{Cu(II)-tetren} + \text{edta}, \quad \text{(R2)}$$

$$\text{Zn(II)-tetren} + \text{edta} \underset{k_{-3}}{\overset{k_3}{\rightleftharpoons}} \text{Zn(II)-edta} + \text{tetren}. \quad \text{(R3)}$$

The conditional equilibrium constants[8] of Reactions R2 and R3 will be useful in the following discussion. The constants were thus calculated from the stability

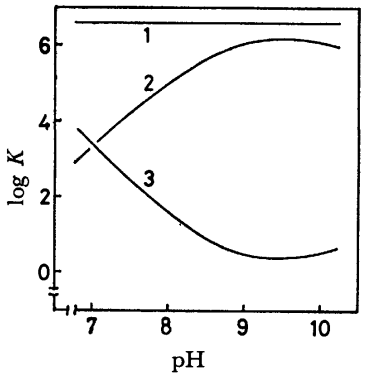

Fig. 1. Dependence of conditional equilibrium constants of reactions R1, R2, and R3 on pH at 25.0 °C and I=0.2 M.
1: R1, 2: R2, 3: R3.

constants of the related complexes and the protonation constants of the related ligands.[9] The calculated values are plotted against the pH in Fig. 1.

According to the proposed mechanism, the following rate law (general equation) is derived from a steady-state treatment reported previously:[8]

$$-\frac{d[\text{Zn(II)-tetren}]}{dt} = \frac{(k_2k_3[\text{Cu(II)-edta}][\text{Zn(II)-tetren}] - k_{-2}k_{-3}[\text{Zn(II)-edta}][\text{Cu(II)-tetren}])[\text{L}]}{k_2[\text{Cu(II)-edta}] + k_{-2}[\text{Cu(II)-tetren}] + k_3[\text{Zn(II)-tetren}] + k_{-3}[\text{Zn(II)-edta}]}, \quad (3)$$

where [L] is the total concentration of free ligands, edta and tetren. Since the R2 equilibrium is highly favored to proceed to the right, the $k_2 \gg k_{-2}$ inequality holds. Therefore, Eq. 3 may be simplified to

$$-\frac{d[\text{Zn(II)-tetren}]}{dt} = \frac{k_2k_3[\text{Cu(II)-edta}][\text{Zn(II)-tetren}][\text{L}]}{k_2[\text{Cu(II)-edta}] + k_3[\text{Zn(II)-tetren}] + k_{-3}[\text{Zn(II)-edta}]}. \quad (4)$$

The conditional rate constant, k_2, was calculated from the rate constants of the reaction of Cu(II)-edta with tetren.[10] The values of k_2 are plotted against the pH in Fig. 2.

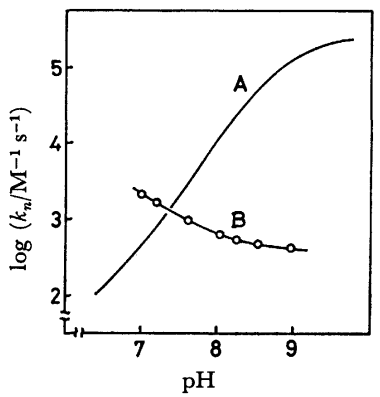

Fig. 2. Dependence of the conditional rate constants of reactions R2 and R3 on pH at 25.0 °C and I=0.2 M ($NaClO_4$).
A: k_2, B: $k_3(=k_0)$. The line A is the curve calculated with the aid of the individual rate constants.[14]

The following approximation seems reasonable from Figs. 1 and 2. In the denominator of Eq. 4, the k_2[Cu(II)-edta] term is predominant, while the other terms may be neglected under the present conditions. Thus, Eq. 4 may be simplified to

$$\frac{d[\text{Zn(II)-tetren}]}{dt} = k_3[\text{Zn(II)-tetren}][\text{L}]. \quad (5)$$

Since Eq. 5 agrees with the rate equation derived experimentally, k_3 corresponds to the k_0 of Eq. 2. The value of k_3 thus determined is plotted against the pH in Fig. 2.

Ligand-substitution Reaction of Zn(II)-tetren with edta. Acid Complex of Zn(II)-tetren: When the successive formation constants of the ammine copper(II) complex, K_n, are compared with those of the ammine zinc(II) complex, K'_n, the constants, K_n and K'_n, differ at n= 1,2,3; however, they are equal at n=4 ($K^{NH_3}_{Cu(NH_3)_4}$= $10^{2.1}$, $K^{NH_3}_{Zn(NH_3)_4}=10^{2.1}$), and the constants over n=4 are extremely small in both complexes.

The successive formation constant, K_1, of the dien (diethylenetriamine : tridentate ligand) copper(II) complex and that of the dien zinc(II) complex differ from one another ($K_{Cudien}=10^{16.0}$, $K_{Zndien}=10^{8.9}$); however, the successive formation constant, K_2, of the copper(II) complex is approximately equal to that of the zinc(II) complex ($K^{dien}_{Cu(dien)_2}=10^{5.3}$, $K^{dien}_{Zn(dien)_2}=10^{5.5}$).

Therefore, in hexadentate polyamine complexes of copper(II) and zinc(II), it may be said that the fifth and sixth nitrogen atoms (which dissociate secondarily and firstly respectively in the dissociation reaction) are weakly bonded to the central metal, and that the intensities of the fifth and sixth Cu–N bonds in the copper(II) complex are approxinately equal to those of the fifth and sixth Zn–N bonds respectively in the zinc(II) complex. Consequently, the protonation constant of the hexadentate polyamine copper(II) complex is expected to be close to that of the zinc(II) complex; in practice, the protonation constant of the penten (tetrakis(2-aminoethyl)ethylenediamine : hexadentate ligand) copper(II) complex is equal to that of the penten zinc(II) complex ($K^H_{CuHpenten}=10^{8.16}$, $K^H_{ZnHpenten}=10^{8.16}$).

If the above considerations can be applied to the pentadentate polyamine complex, it can be assumed that the protonation constant of Cu(II)-tetren ([Cu-(H_2O)tetren]$^{2+}$) is approximatly equal to that of Zn(II)-tetren ([Zn(H_2O)tetren]$^{2+}$). Thus, the protonation constant of Zn(II)-tetren may be estimated as follows: $K^H_{ZnHtetren}=K^H_{CuHtetren}=10^{5.18}$. The protonation constant of Zn(II)-tetren has been reported[11] as $K^H_{ZnHtetren}K^H_{ZnH_2tetren}=10^{9.4}$($K^H_{ZnH_2tetren}$=[Zn($H_2$tetren)$^{4+}$]/[Zn(Htetren)$^{3+}$][H$^+$]). Then, $K^H_{ZnH_2tetren}$ can be calculated to be $10^{4.2}$.

Resolution of the Conditional Rate Constant, k_3: B in Fig. 2 shows the pH dependence of the conditional rate constant for the ligand-substitution reaction of Zn(II)-tetren with edta. The pH dependence of the conditional rate constant was analyzed in the pH range of 7.5—9.0. In this pH range, the dominant species of edta are Hedta^{3-} and edta^{4-}, while the dominant species of acid complex of Zn(II)-tetren is [Zn(Htetren)]$^{3+}$.[12]

Thus, the rate equation for the ligand substitution

of Zn(II)-tetren with edta is given by

$$-\frac{d[\text{Zn(II)-tetren}]}{dt} = k_3[\text{Zn(II)-tetren}][\text{edta}]$$
$$= k_L[\text{Zn(tetren)}^{2+}][\text{edta}^{4-}] + k_{HL}[\text{Zn(tetren)}^{2+}]$$
$$[\text{Hedta}^{3-}] + k'_{HL}[\text{Zn(Htetren)}^{3+}][\text{Hedta}^{3-}], \quad (6)$$

where k_L, k_{HL}, and k'_{HL} are defined as follows:[13]

$$\text{Zn(tetren)}^{2+} + \begin{matrix} \text{edta}^{4-} & \xrightarrow{k_L} & \\ \text{Hedta}^{3-} & \xrightarrow[k_{HL}]{} & \text{Zn(edta)}^{2-}. \\ \text{Zn(Htetren)}^{3+} + \text{Hedta}^{3-} & \xrightarrow{k'_{HL}} & \end{matrix} \quad (7)$$

Hence, the following relationship is derived from Eq. 6:

$$k_3(1+K_1[H^+])(1+K^H_{ZnHtetren}[H^+])$$
$$= k_L + [H^+]K_1k_{HL} + [H^+]^2K_1K^H_{ZnHtetren}k'_{HL}, \quad (8)$$

where K_1 is the formation constant of $Hedta^{3-}$. The rate constant, k_3, was resolved into individual rate constants, k_L, k_{HL}, and k'_{HL}, to fit Eq. 8. The calculation of the resolved rate constants was performed with the aid of an electronic computer. The resolved rate constants are shown in Table 1.

TABLE 1. RATE CONSTANTS FOR THE LIGAND-SUBSTITUTION REACTION OF Zn(II)-tetren WITH edta AT 25.0 °C AND I=0.2 M ($NaClO_4$)

k_L / $M^{-1}s^{-1}$	k_{HL} / $M^{-1}s^{-1}$	k'_{HL} / $M^{-1}s^{-1}$
$\approx 3\times10^2$	$(4.1\pm0.7)\times10^2$	$(1.7\pm0.2)\times10^5$

Mechanism of the Substitution Reaction of Zn(tetren)$^{2+}$ with edta: The reaction scheme can be described as

$$\begin{array}{ccc} \text{ZnL-(edta)}^{2-} & \overset{K_w}{\rightleftharpoons} & \text{ZnL(edta)}^{2-} \\ \Big\uparrow\Big\downarrow K_{os} & & \Big\downarrow k \\ \text{ZnL}^{2+} \overset{K_d}{\rightleftharpoons} \text{ZnL}_d^{2+} & & \text{Zn(edta)}^{2-}, \\ \Big\uparrow\Big\downarrow K'_{os} & & \Big\uparrow k' \\ \text{ZnL-(Hedta)}^{-1} & \overset{K'_w}{\rightleftharpoons} & \text{ZnL(Hedta)}^{-1} \end{array} \quad (9)$$

where K_d is the dissociation constant of ZnL^{2+} to the partially dissociated complex ZnL_d^{2+}, K_{os} is the formation constant of the outer-sphere conplex ZnL-(edta)$^{2-}$, K_w is the equilibrium constant between [ZnL-(edta)]$^{2-}$ and the mixed-ligand intermediate ZnL(edta)$^{2-}$, and L refers to the ligand tetren. Since the structure for the mixed-ligand intermidiate is considered to be the same as that of the nickel system,[14] the structure for the mixed-ligand intermediate (for edta^{4-}) seems to be as follows:

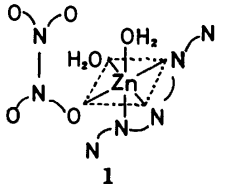

1

where edta^{4-} and tetren are symbolized as 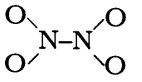 and N–N–N–N–N respectively and where the charges are omitted; the rate-determining step for the formation of [Zn(edta)]$^{4-}$ is considered to be the loss of a water molecule from the intermediate **1**, as in the nickel system.

According to the proposed mechanism, the following equation is obtained:

$$k[\text{ZnL(edta)}^{2-}] + k'[\text{ZnL(Hedta)}^{-1}]$$
$$= K_dK_{os}K_wk[\text{edta}^{4-}][\text{ZnL}^{2+}]$$
$$+ K_dK'_{os}K'_wk'[\text{Hedta}^{3-}][\text{ZnL}^{2+}]$$
$$= k_L[\text{edta}^{4-}][\text{ZnL}^{2+}] + k_{HL}[\text{Hedta}^{3-}][\text{ZnL}^{2+}]. \quad (10)$$

from Eq. 10, the k_L/k_{HL} ratio is given by

$$\frac{k_L}{k_{HL}} = \frac{K_{os}K_wk}{K'_{os}K'_wk'} \quad (11)$$

Since k_L is approximately equal to k_{HL} (Table 1), Eq. 11 becomes

$$\frac{K_{os}K_wk}{K'_{os}K'_wk'} \approx 1. \quad (12)$$

The release of a water molecule from the outer-sphere complex is the rate-determining step in the formation of the inner-sphere complex,[15] and the loss of a water molecule from the mixed-ligand intermediate seems to be the rate-determining step in the formation of [Zn(edta)]$^{2-}$. Therefore, it appears reasonable to assume that $K_w \approx K'_w$ and that $k \approx k'$. Thus, K_{os} is nearly equal to K'_{os}.

In the formation of a metal complex, a charged group removed from the eventual coordination site is relatively unimportant.[16] The negative charge removed from the coordination site in edta thus seems unimportant in the formation of the above mixed-ligand intermediate. Consequently, K_{os} can be expected to be equal to K'_{so}.

Mechanism of the Substitution Reaction of Zn(II)-tetren with Hedta^{3-}: The following reaction mechanism was proposed:

$$\begin{array}{ccccc} \text{ZnL}_d^{2+} & \overset{K_{os}}{\rightleftharpoons} & \text{ZnL-(Hedta)}^{-1} & \overset{K_w}{\rightleftharpoons} & \text{ZnL(Hedta)}^{-1} \\ \Big\uparrow\Big\downarrow K_d & & & & \Big\downarrow k \\ \text{ZnL}^{2+} & & & & \\ \Big\uparrow\Big\downarrow & & & & \text{Zn(edta)}^{2-}. \\ \text{ZnHL}^{3+} & & & & \Big\uparrow k' \\ \Big\uparrow\Big\downarrow K'_d & & & & \\ \text{ZnHL}_d^{3+} & \overset{K'_{os}}{\rightleftharpoons} & \text{ZnHL-(Hedta)} & \overset{K'_w}{\rightleftharpoons} & \text{ZnHL(Hedta)} \end{array} \quad (13)$$

On the basis of the reaction mechanism, the following equation is derived:

$$k[\text{ZnL(Hedta)}^{-1}] + k'[\text{ZnHL(Hedta)}]$$
$$= K_dK_{os}K_wk[\text{Hedta}^{3-}][\text{ZnL}^{2+}]$$
$$+ K'_dK'_{os}K'_wk'[\text{Hedta}^{3-}][\text{ZnHL}^{3+}]$$
$$= k_{HL}[\text{Hedta}^{3-}][\text{ZnL}^{2+}] + k'_{HL}[\text{Hedta}^{3-}][\text{ZnHL}^{3+}]. \quad (14)$$

From Eq. 14, the k_{HL}/k'_{HL} ratio is given by

$$\frac{k_{HL}}{k'_{HL}}=\frac{K_d K_{os} K_w k}{K'_d K'_{os} K'_w k'}. \quad (15)$$

Since it appears reasonable to assume that $K_{os}\approx K'_{os}$, $K_w\approx K'_w$, and that $k\approx k'$, Eq. 15 can be simplified to

$$\frac{k_{HL}}{k'_{HL}}\approx\frac{k_d}{k'_d}. \quad (16)$$

The difference between k_{HL} and k'_{HL} is mostly determined by the difference between K_d and K'_d. Since the k'_{HL}/k_{HL} ratio is about 400 : 1, the partial dissociation rate of the $Zn(Htetren)^{3+}$ complex is 400 times faster than that of the $Zn(tetren)^{2+}$ complex; the proton bonded to the tetren facilitates the partial dissociation.

References

1) D. C. Olson and D. W. Margerum, *J. Am. Chem. Soc.*, **84**, 680 (1962).
2) D. C. Olson and D. W. Margerum, *J. Am. Chem. Soc.*, **85**, 297 (1963).
3) D. W. Margerum and J. D. Carr, *J. Am. Chem. Soc.*, **88**, 1639 (1966).
4) J. D. Carr and D. W. Margerum ,*J. Am. Chem. Soc.*, **88**, 1645 (1966).
5) J. D. Carr, K. Torrance, C. J. Cruz, and C. N. Reilliy, *Anal. Chem.*, **39**, 1258 (1967).
6) E. Mentasti, *J. Chem. Soc., Dalton Trans.*, **1980**, 958 (1980).
7) T. Katsuyama and T. Kumai, *Bull. Chem. Soc. Jpn.*, **48**, 3581 (1975).
8) T. Katsuyama and T. Kumai, *Bull. Chem. Soc. Jpn.*, **51**, 1072 (1978).
9) L. G. Sillén and A. E. Martell, "Stability Constants of Metal-ion Complexes," The Chemical Society, London, (1964).
10) J. D. Carr, R. A. Libby, and D. W. Margerum, *Inorg. Chem.*, **6**, 1083 (1967).
11) P. Paolette and A. Vacca, *J. Chem. Soc.*, **1964**, 5051 (1964).
12) For example, at pH 8.0, the concentrations of $[Zn(Htetren)]^{3+}$ and $[Zn(H_2tetren)]^{4+}$ are 0.2 and 0.00003% respectively of the total concentration of Zn(II)-tetren.
13) In the pH range of 7.5—9.0, $edta^{4-}$ is negligible at a low pH and $[Zn(Htetren)]^{3+}$ is negligible at a high pH; therefore, the reaction of $[Zn(Htetren)]^{3+}$ with $edta^{4-}$ can be omitted in the reaction scheme.
14) D. B. Rorabacher and D. W. Margerum, *Inorg. Chem.*, **3**, 382 (1964).
15) M. Eigen and K. Tamm, *Z. Electrochem*, **66**, 107 (1962).
16) J. C. Cassatt and R. G. Wilkins, *J. Am. Chem. Soc.*, **90**, 6045 (1968).

 © 1982 The Chemical Society of Japan Bull. Chem. Soc. Jpn., 55, 1054—1062 (1982) [Vol. 55, No. 4

Solubility Measurements of Benzene and the Alkylbenzenes in Water by Making Use of Solute Vapor

Isao SANEMASA,* Masatake ARAKI, Toshio DEGUCHI, and Hideo NAGAI
Department of Chemistry, Faculty of Science, Kumamoto University, Kurokami 2-39-1, Kumamoto 860
(Received September 7, 1981)

Aqueous solubilities of benzene and of alkylbenzenes, toluene, ethylbenzene, propyl- and isopropylbenzene, (*o*-, *m*-, and *p*-) xylene, and (1,2,3-, 1,2,4-, and 1,3,5-) trimethylbenzene, have been measured. An apparatus is described which provides a convenient means of obtaining aqueous solutions saturated with solute vapor. The method involves introducing solute vapor, which is in equilibrium with a liquid solute, into water and circulating it in a closed system. This method has three principal advantages: (1) The solubility equilibrium can be attained within 3 min, (2) it can be determined whether the solubility obeys Henry's law, and (3) based on Henry's law, solutions of any desired concentrations of solute at a given temperature of water can be easily prepared.

The solubilities of slightly soluble organic compounds in water have been studied by many reseachers. The solubility measurement generally consists of two steps; the first is a preparation of aqueous solution saturated with solute and the second is a measurement of solute concentration in the solution. The latter step has been markedly improved in sensitivity and selectivity by advances in instruments such as spectrophotometer and gas-liquid chromatography, whereas the former step seems to have remained unchanged for a long time. The former step is still the more important, since it often influences the precission and accuracy of the results. At the present time, it is true to say that the reproducibility of the solubility data mainly depends on this step.

Most of the earlier investigators prepared the saturated solutions by adding an excess quantity of a solute to a water and shaking the mixture mechanically for at least 24 h. The solutions thus prepared were usually allowed to stand for at least another 24 h or centrifuged to ensure removal of any organic droplets entrained in suspension, and then the solute concentrations were determined. Particular attention should be paid to the possible inclusion of a suspended micro-emulsion which may arise when liquid solute has been dispersed by vigorous shaking, and also to the extreme volatility and the strong adsorption on the container walls which are both characteristic of organic solutes in water. Instead of this conventional method, some attempts have recently been made to attain the solubility equilibrium. Sutton and Calder estimated solubilities of alkylbenzenes by equilibrating water with solute vapor in a closed vessel where water and liquid solute were separately placed.[1] Brown and Wasik used an apparatus which made it possible to measure the equilibrium distribution of a hydrocarbon between a gas phase and a liquid phase.[2] Mackay *et al.* estimated Henry's law constants for some liquid and solid hydrocarbons by measuring solute concentrations in aqueous solution while being stripped from solution at a known gas flow rate.[3]

This paper will describe a simple and useful technique that allows a rapid preparation of aqueous solutions of desired solute concentrations at a given temperature of water by making use of solute vapor.

Experimental

Materials. Materials used as solute were analytical reagent grade (Wako Pure Chemical Industries Ltd.) except 1,2,3- and 1,2,4-trimethylbenzene. The stated minimum purities (mass %) were: benzene; 99.5, toluene; 99.0, ethylbenzene, (*o*-, *m*-, and *p*-)xylene, and isopropylbenzene; 98.0, 1,3,5-trimethylbenzene; 97.0, 1,2,4-trimethylbenzene; 95.0, propylbenzene; no description. All these solutes were used without further purification. Redistilled water was used as solvent. Analytical reagent grade chloroform (minimum purity 99.8%) was used for solvent extraction and preparation of standard solution of solute.

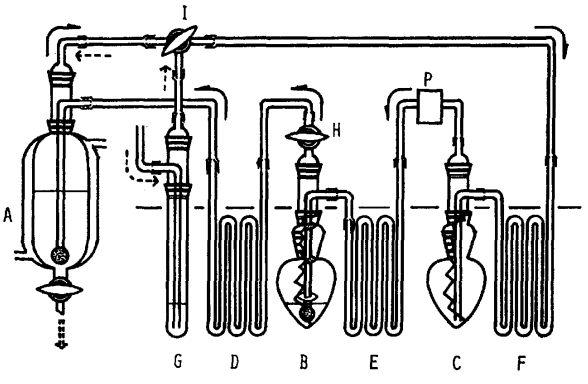

Fig. 1. Solubility apparatus.
The solid and the dotted arrows indicate, respectively, the direction of circulation and the sampling system.

Apparatus and Procedures. The apparatus used is shown in Fig. 1, which is essentially similar to that previously reported,[4] but with some modifications. It is composed of a separatory funnel (300 cm^3), A, two pear-shaped flasks (each 50 cm^3) B, and C, three triplicated-U-shape glass pipes (ϕ 8 mm, each 20 cm^3), D, E, and F, a glass test tube (30 cm^3), G, and a Viton diaphragm pump (Iwaki Type AP-32 Z), P. We will hereafter call A and B by the name "solubility flask" and "solute reservoir," respectively. Gas inlet-type adapters were mounted in A, B, C, and G. Teflon tubes (ϕ 8 mm), a stopcock, H, and a three-way cock, I, were used for connection. The U-shape glass pipes and the flask C serve as traps of water or liquid solute. The test tube, in which was placed some 5 cm^3 of the same liquid solute as the one being measured, was included in the system to facilitate withdrawing sample solution from the solubility flask. In order to prevent liquid solute from being carried over from the solute reservoir by

bubbling air, three sheets of Teflon disks, each of which was bored in the center to fit the glass pipe, were attached to the gas inlet-type adapter inserted in the solute reservoir. Of these three disks, two were made with about 20 pinholes and they were tightly fitted to the lower parts of the ground glass joints and the other was set just above liquid solute phase. The temperature of the solubility flask was held constant by circulating water through a surrounding jacket from a thermostat, and the temperature of the solute reservoir was maintained constant by immersing in another thermostat, in which the other glass wares were also immersed as shown in Fig. 1. These thermostats were controlled within 0.01 °C (in some cases 0.1 °C). The assembled apparatus was placed in a draft chamber, the temperature of which was always kept higher than that of the solute reservoir.

A redistilled water of 100 to 200 cm^3 and a liquid solute of 10 to 20 cm^3 were placed in the solubility flask and in the solute reservoir, respectively. When the conditions of temperature were attained, the pump was started, and the solute vapor, which was generated by bubbling air through the liquid solute *via* a sintered glass ball, was introduced into the water *via* another sintered ball, and circulated as indicated in Fig. 1. The circulation rate, which can be changed by means of a Variac and had been calibrated in advance by a flow meter, was set at 2 dm^3/min in most instances. After the solubility equilibrium was attained, the stopcock (H) was closed and the three-way cock (I) was turned left through 90° so as to connect the system with the test tube (G) as indicated in Fig. 1. Then, by opening a stopcock attached to the bottom of the solubility flask, about 30 cm^3 was first discarded and 10 cm^3 portions were transferred successively into five cylindrical separatory funnels of 50 cm^3 capacity, to which each 10 cm^3 volume of chloroform had previously placed. Each separatory funnel had been calibrated in advance and the volume of aqueous solution poured into it was read off. The mixtures in the separatory funnels were hand shaken and allowed to stand for 30 min, then after dehydrating the chloroform phase with anhydrous sodium sulfate, UV-absorptions were measured using a Hitachi Model 100-50 spectrophotometer against the blank extract as a reference. In the case of benzene, the extracts were further diluted with chloroform. Wavelengths used for the measurements and the molar absorptivities were: benzene; 260.8 nm (126 $dm^3\ mol^{-1}\ cm^{-1}$), toluene; 262.0 (275), ethylbenzene; 261.2 (257), *o*-xylene; 263.0 (324), *m*-xylene; 265.0 (302), *p*-xylene; 268.0 (562), propylbenzene; 261.4 (257), isopropylbenzene; 260.2 (234), 1,2,3-trimethylbenzene; 262.4 (234), 1,2,4-trimethylbenzene; 267.7 (537), 1,3,5-trimethylbenzene; 265.8 (229). Standard solutions were prepared by weighing out suitable quantities of the liquid solutes, followed by dilution with chloroform in volumetric flasks. Calibration curves were made as follows: into separatory funnels aliquots of less than 10 cm^3 of the standard solution were pipetted in succession, diluted with chloroform to 10 cm^3, and then 10 cm^3 portions of redistilled water were added, and the chloroform extracts were measured in the same way as the sample solution. The molar absorptivities described above were thus determined. Values of equilibrium solubilities were the average of at least five determinations.

When the apparatus was used in an open method, the system was modified to remove I, G, P, C, and F from the apparatus. A round-bottom flask of 300 cm^3 capacity was used as the solute reservoir instead of B and the liquid solute of 100 cm^3 was placed in it. Nitrogen gas was allowed to flow continuously through the solute reservoir and to escape through the solubility flask to the atmosphere.

Results

Factors Affecting the Solubility Measurement. When the circulation rate was set at 2 dm^3/min, the solubility equilibrium can be attained after 3 min for each solute. The typical results are shown in Fig. 2. With decreasing the circulation rate, the curve of solubility plotted against time appeared to level off after a somewhat prolonged time, but the solubilities were not affected. In the present method, it is essential to carry out under such experimental conditions that temperature of

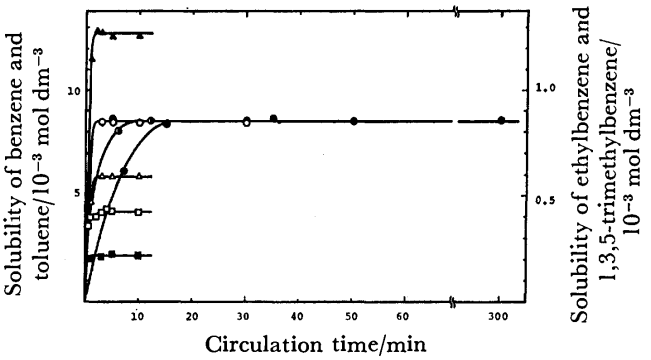

Fig. 2. The effect of circulation rate on the solubilities of benzene, toluene, ethylbenzene, and 1,3,5-trimethylbenzene.
Benzene (○, ◑, ●, ▲), toluene (△), ethylbenzene (□), 1,3,5-trimethylbenzene (■). Circulation rate: 2.0 (○, ▲, △, □, ■), 1.0 (◑), 0.2 dm^3/min (●). Temperature of solubility flask: 35.0 (○, ◑, ●, ▲, □, ■), 25.0 °C (△). Temperature of solute reservoir: 25.0 (△), 21.7 (■), 21.0 (▲), 15.0 (○, ◑, ●), 10.0 °C (□).

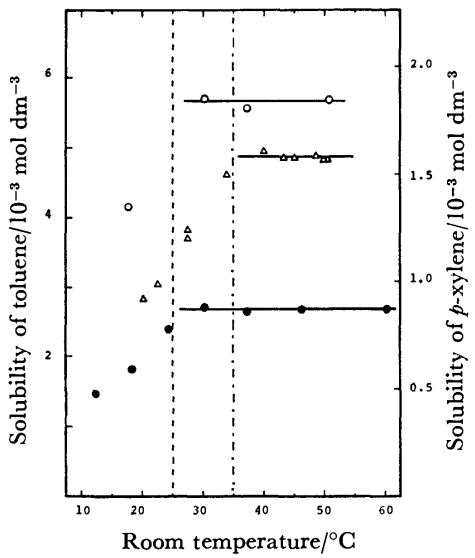

Fig. 3. The effect of room temperature on the solubilities of toluene and *p*-xylene.
Toluene (○, ●), *p*-xylene (△). Temperature of solubility flask: 25.0 (○), 35.0 (△), 45.0 °C (●). Temperature of solute reservoir: 25.0 (○, ●), 35.0 °C (△).

TABLE 1. SOLUBILITIES OF BENZENE AND THE ALKYLBENZENES AS A FUNCTION OF SOLUTE VAPOR PRESSURE

Temperature of liquid solute / °C	Vapor pressure of solute / 10^3 Pa	Solubility / 10^{-3} mol dm^{-3}
Benzene		
Temperature of water 5.00 °C		
5.00	4.682	20.7
Temperature of water 15.00 °C		
0.50	3.672	9.25
2.00	3.985	10.4
5.00	4.682	12.1
6.72	5.126	13.3
10.52	6.241	16.2
15.00	7.818	20.0
Temperature of water 25.00 °C		
0.40	3.652	5.91
5.50	4.808	7.92
5.99	4.934	8.15
10.88	6.357	10.6
15.20	7.895	13.1
19.20	9.595	15.9
25.00	12.61	20.5,20.6,20.7[a]
Temperature of water 35.00 °C		
5.50	4.808	5.63
6.00	4.936	5.44
12.40	6.866	8.00
15.30	7.935	8.92
20.90	10.41	11.5
27.80	14.35	15.9
35.00	19.73	21.5
Temperature of water 45.00 °C		
5.50	4.808	3.85
14.12	7.483	5.80
17.80	8.969	6.87
20.40	10.16	8.08
22.90	11.44	8.92
24.10	12.10	9.25
30.59	16.25	12.5
33.30	18.32	14.1
40.92	25.37	19.1
45.00	30.04	22.2,22.5[a]
Toluene		
Temperature of water 15.00 °C		
−6.18	0.5955	1.55
1.60	0.9925	2.57
9.60	1.619	4.11
15.00	2.210	5.52
Temperature of water 25.00 °C		
2.35	1.041	1.61
11.32	1.790	2.80
17.70	2.568	3.89
25.00	3.793	5.61
Temperature of water 35.00 °C		
8.70	1.535	1.52
17.14	2.490	2.37
17.15	2.491	2.42
19.72	2.868	2.80
29.90	4.864	4.65
35.00	6.239	5.73
Temperature of water 45.00 °C		
18.45	2.676	1.75
31.64	5.301	3.40
40.02	7.894	5.04
45.00	9.883	6.23
Ethylbenzene		
Temperature of water 15.00 °C		
−3.70	0.1923	0.455
2.62	0.3041	0.696
8.30	0.4490	0.988
15.00	0.6934	1.47
Temperature of water 25.00 °C		
1.50	0.2809	0.374
9.50	0.4863	0.626
16.32	0.7532	0.949
25.00	1.268	1.59
Temperature of water 35.00 °C		
8.59	0.4577	0.362
15.47	0.7142	0.549
27.31	1.447	1.10
35.00	2.208	1.62
Temperature of water 45.00 °C		
15.39	0.7106	0.341
29.72	1.656	0.837
37.80	2.558	1.27
45.00	3.682	1.83
o-Xylene		
Temperature of water 15.0 °C		
4.9	0.2384	0.858
7.9	0.2942	1.04
15.0	0.4735	1.50
Temperature of water 25.0 °C		
11.7	0.3810	0.756
19.2	0.6189	1.22
23.7	0.8159	1.49
25.0	0.8820	1.68
Temperature of water 35.0 °C		
14.6	0.4613	0.555
22.9	0.7774	0.919
29.9	1.174	1.39
35.0	1.563	1.84
Temperature of water 45.0 °C		
24.5	0.8561	0.646
30.5	1.215	0.904
38.5	1.889	1.43
45.0	2.649	2.00
m-Xylene		
Temperature of water 15.0 °C		
6.2	0.3361	0.870
9.3	0.4148	1.04
15.0	0.6015	1.46,1.47[a]
Temperature of water 25.0 °C		
6.2	0.3361	0.473
13.4	0.5429	0.783
19.6	0.8012	1.10
22.6	0.9602	1.35
25.0	1.106	1.45
Temperature of water 35.0 °C		
11.2	0.4704	0.417

TABLE 1. (Continued)

Temperature of liquid solute °C	Vapor pressure of solute 10^3 Pa	Solubility 10^{-3} mol dm^{-3}
19.8	0.8111	0.728
27.7	1.293	1.11
35.0	1.938	1.53,1.54[a]
Temperature of water 45.0 °C		
22.6	0.9602	0.550
31.6	1.610	0.885
38.3	2.309	1.264
45.0	3.252	1.69
p-Xylene		
Temperature of water 15.00 °C		
2.62	b)	0.523
5.20	b)	0.701
7.60	b)	0.845
10.36	b)	1.06
15.00	0.6377	1.48,1.48[a]
Temperature of water 25.0 °C		
14.0	0.5985	0.811
15.1	0.6417	0.879
20.0	0.8683	1.16
25.0	1.167	1.44,1.55[a]
Temperature of water 35.0 °C		
13.6	0.5834	0.478
19.4	0.8373	0.682
25.5	1.202	0.990
35.0	2.036	1.55
Temperature of water 45.0 °C		
19.5	0.8424	0.426
28.4	1.418	0.718
34.4	1.972	1.00
45.0	3.403	1.63
Propylbenzene		
Temperature of water 15.0 °C		
6.4	0.1238	0.215
11.3	0.1775	0.290
12.9	0.1990	0.322
15.0	0.2307	0.400
Temperature of water 25.0 °C		
12.1	0.1880	0.179
18.1	0.2854	0.258
21.1	0.3487	0.337
25.0	0.4489	0.421
Temperature of water 35.0 °C		
15.7	0.2422	0.135
24.5	0.4348	0.245
28.8	0.5697	0.308
30.1	0.6170	0.344
35.0	0.8270	0.450
Temperature of water 45.0 °C		
18.4	0.2912	0.113
30.6	0.6361	0.240
36.6	0.9077	0.331
39.7	1.083	0.395
45.0	1.451	0.521
Isopropylbenzene		
Temperature of water 15.00 °C		
6.76	0.1775	0.302
9.45	0.2141	0.327
10.12	0.2242	0.372
15.00	0.3122	0.477
Temperature of water 25.00 °C		
9.03	0.2080	0.212
12.82	0.2697	0.239
18.78	0.4004	0.338
22.40	0.5050	0.414
25.00	0.5946	0.513
Temperature of water 35.00 °C		
17.82	0.3761	0.204
26.80	0.6646	0.368
30.48	0.8311	0.423
31.43	0.8798	0.479
35.00	1.086	0.552
Temperature of water 45.00 °C		
19.20	0.4114	0.146
26.72	0.6614	0.232
33.30	0.9828	0.344
39.62	1.416	0.473
45.00	1.909	0.630
1,2,3-Trimethylbenzene		
Temperature of water 15.00 °C		
6.00	0.06438	0.281
7.76	0.07295	0.314
10.10	0.08594	0.349
15.00	0.1201	0.488
Temperature of water 25.00 °C		
7.58	0.07203	0.165
10.72	0.08973	0.205
16.62	0.1339	0.321
22.82	0.2001	0.414
25.00	0.2297	0.538
Temperature of water 35.00 °C		
5.80	0.06346	0.0792
20.18	0.1689	0.245
23.90	0.2144	0.302
31.13	0.3348	0.469
35.00	0.4213	0.601
Temperature of water 45.00 °C		
12.70	0.09798	0.0932
25.30	0.2341	0.210
33.38	0.3829	0.368
38.08	0.5038	0.474
45.00	0.7438	0.702
1,2,4-Trimethylbenzene		
Temperature of water 15.00 °C		
5.96	0.08054	0.238
12.62	0.1287	0.363
15.00	0.1513	0.463
Temperature of water 25.00 °C		
5.56	0.07825	0.130
11.30	0.1175	0.191
15.73	0.1591	0.256
19.98	0.2108	0.337
25.00	0.2929	0.472
Temperature of water 35.00 °C		
7.12	0.08753	0.0840

TABLE 1. (Continued)

Temperature of liquid solute °C	Vapor pressure of solute 10^3 Pa	Solubility 10^{-3} mol dm^{-3}	Temperature of liquid solute °C	Vapor pressure of solute 10^3 Pa	Solubility 10^{-3} mol dm^{-3}
16.86	0.1715	0.166	5.6	0.1034	0.126
25.26	0.2957	0.305	12.5	0.1658	0.202
29.62	0.3878	0.374	19.7	0.2650	0.295
35.00	0.5360	0.499	25.0	0.3689	0.406
Temperature of water 45.00 °C			Temperature of water 35.0 °C		
13.40	0.1357	0.0795	5.6	0.1034	0.0701
24.50	0.2818	0.171	12.5	0.1658	0.106
32.70	0.4674	0.279	21.7	0.3007	0.221
40.60	0.7419	0.446	28.6	0.4587	0.316
45.00	0.9503	0.569	35.0	0.6675	0.446
1,3,5-Trimethylbenzene			Temperature of water 45.0 °C		
Temperature of water 15.0 °C			7.0	0.1140	0.0507
0.3	0.07081	0.147	20.5	0.2788	0.129
5.6	0.1034	0.211	31.4	0.5416	0.244
9.1	0.1318	0.256	31.8	0.5544	0.257
15.0	0.1957	0.375	38.5	0.8141	0.340
Temperature of water 25.0 °C			45.0	1.163	0.461
0.4	0.07133	0.0865			

a) Determinations were repeated on another days. b) Vapor pressure data are not available.

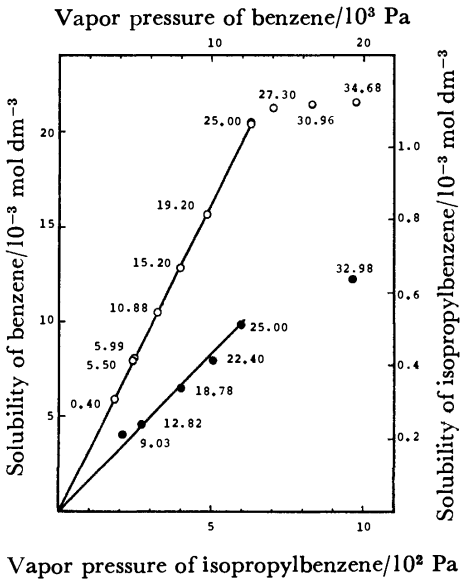

Fig. 4. The effect of temperature of solute reservoir at constant temperature of solubility flask on the solubilities of benzene and isopropylbenzene.
Benzene (○), isopropylbenzene (●). Temperature of solubility flask: 25.00 °C. The figure near each circle indicates the temperature of solute reservoir.

water≥temperature of liquid solute<room temperature. In fact, when the temperature of room was lower than that of the solute reservior, the measured solubilities were lowered correlatively depending on the former temperature. The results are shown in Fig. 3. On the other hand, when the temperature of the solute reservoir was higher than that of the solubility flask, the solute vapor condensed and separated in the solubility flask to form two immiscible phases. Under such conditions, solubilities were found to be considerably higher than those at the same temperature of water and solute. The results are shown in Fig. 4.

Solubility and Vapor Pressure. Solubility runs were made under conditions such that the temperature of the solute reservoir was made to vary while that of the solubility flask was maintained at a constant temperature. The experimental results for all the solutes used here are listed in Table 1. Vapor pressures for pure luquid solutes have been estimated by reference to published tabulations.[5] In this paper, the vapor pressure of liquid solute was taken to be that of pure solute, neglecting the effects of water dissolution in the solute phase and of solute-solvent interaction in the water phase. It can be seen from Table 1 that the concentrations of each solute in aqueous solutions increase linearly with the solute vapor pressure at a constant temperature of water. That is, solubilities obey Henry's law

$$P = K_H X_2, \quad (1)$$

where P is the partial pressure of solute vapor in Pa, X_2 is the mole fraction of the dissolved solute, and K_H is Henry's law constant. Henry's law constants thus determined are given in Table 2. We estimated the solubilities when the temperature of solute was the same as that of water from K_H and P using Eq. 1, since the experimental values under such conditions were somewhat poor in precision. The results are listed in Table 2. To compare the present results with the literature, the reported values, most of which are available only at 25 °C, are summarized in Table 3. In Table 4 are also given some available data of Henry's law constant. Our results are in accord with the literature values except for benzene and propylbenzene. With respect to the latter, the literature value would be overestimated when considered the relationship between the number of methyl group and the solubility.

TABLE 2. HENRY'S LAW CONSTANTS AND THE ESTIMATED SOLUBILITIES OF BENZENE AND THE ALKYLBENZENES

Solute	Temperature of water[a] °C	Henry's law constant 10^7 Pa	γ[b]	Solubility 10^{-3} mol dm^{-3}
Benzene	5.00	1.25[c]		20.7
	15.00	2.15±0.03	0.999	20.2 ±0.3
	25.00	3.38±0.04	0.999	20.7 ±0.1
	35.00	5.03±0.14	0.999	21.8 ±0.6
	45.00	7.34±0.17	0.999	22.8 ±0.5
Toluene	15.00	2.20±0.04	0.999	5.58 ±0.11
	25.00	3.69±0.09	0.999	5.71 ±0.14
	35.00	5.89±0.16	0.999	5.88 ±0.16
	45.00	8.73±0.13	0.999	6.28 ±0.10
Ethylbenzene	15.00	2.55±0.12	0.999	1 51 ±0.08
	25.00	4.43±0.14	0.999	1.59 ±0.05
	35.00	7.44±0.22	0.999	1.65 ±0.05
	45.00	11.2 ±0.3	0.999	1.83 ±0.05
o-Xylene	15.0	1.66±0.11	0.999	1.58 ±0.11
	25.0	2.92±0.11	0.995	1.68 ±0.06
	35.0	4.69±0.04	0.999	1.85 ±0.02
	45.0	7.35±0.06	0.999	2.00 ±0.02
m-Xylene	15.0	2.25±0.06	0.999	1.49 ±0.04
	25.0	4.06±0.15	0.996	1.52 ±0.06
	35.0	6.83±0.41	0.998	1.57 ±0.10
	45.0	10.4 ±0.4	0.999	1.73 ±0.08
p-Xylene	15.00	2.39[c]		1.48
	25.0	4.24±0.17	0.993	1.53 ±0.07
	35.0	7.03±0.33	0.998	1.61 ±0.08
	45.0	11.4 ±0.3	0.999	1.66 ±0.05
Propylbenzene	15.0	3.30±0.12	0.988	0.388±0.015
	25.0	5.90±0.17	0.997	0.423±0.012
	35.0	10.1 ±0.2	0.999	0.455±0.007
	45.0	15.3 ±0.5	0.999	0.528±0.017
Isopropylbenzene	15.00	3.50±0.19	0.985	0.495±0.028
	25.00	6.47±0.52	0.994	0.510±0.045
	35.00	10.6 ±0.4	0.994	0.568±0.022
	45.00	16.6 ±0.6	0.999	0.638±0.024
1,2,3-Trimethylbenzene	15.00	1.34±0.05	0.998	0.498±0.019
	25.00	2.45±0.14	0.989	0.520±0.032
	35.00	3.92±0.25	0.999	0.597±0.041
	45.00	5.88±0.16	0.999	0.702±0.019
1,2,4-Trimethylbenzene	15.00	1.93±0.05	0.998	0.435±0.012
	25.00	3.44±0.05	0.999	0.469±0.007
	35.00	5.79±0.22	0.997	0.514±0.020
	45.00	9.24±0.12	0.999	0.571±0.007
1,3,5-Trimethylbenzene	15.0	2.84±0.11	0.999	0.383±0.015
	25.0	4.93±0.24	0.999	0.415±0.022
	35.0	8.14±0.40	0.998	0.455±0.023
	45.0	13.3±0.8	0.996	0.485±0.032

a) In the course of this study, the thermostats were replaced by new ones, temperature of which could be controlled within 0.01 °C. b) Correlation coefficient of the equation, $X=P/K_H$ (the symbols are described in the text). c) Estimated under the conditions where the temperatures of water and liquid solute were the same.

Solubility in an Open Method. An alterative method may be applicable to attain the solubility equilibrium between the water phase and the saturated solute vapor phase. Thus, solubility runs were undertaken in an open method as described in the experimental section. In the open method, it seems to be natural that the flow rate of nitrogen gas should affect the solubility results to a large extent. The results are shown in Fig. 5. Contrary to our expectation, the nitrogen gas flow rate up to 1.2 dm^3/min had no effect on the solubility and the steady solubility was reached within a relatively short time. The solute vapor generated by bubbling through the liquid solute phase is considered to be sufficient to saturate the nitrogen gas in the wide range of its flow rate. Solubilities of benzene and toluene plotted against vapor pressures are shown in Figs. 6

Table 3. Solubilities of benzene and the alkylbenzenes at 25 °C reported in the literature

Solute	Solubility/10^{-3} mol dm^{-3}
Benzene	22.3,[a,d] 22.9,[b] 23.0,[c] 22.79,[e] 22,[f] 27.8,[g] 22.47,[h] 22.782,[i] 23.3—24.7,[k] 23.8[p]
Toluene	5.8,[a] 6.81,[b] 5.599,[e] 6.22,[h] 5.639,[i] 5.805,[j] 7.16—7.27,[k] 6.01,[n] 5.4[p]
Ethylbenzene	1.58,[a] 1.96,[b] 1.43,[e] 1.67,[h] 1.518,[j] 1.32,[i] 1.55,[m] 1.23,[n] 1.65[p]
o-Xylene	1.92,[a] 1.65,[e] 2.01[h] 1.606,[j] 1.57[n]
m-Xylene	1.63,[a] 1.85,[b] 1.53,[h] 1.375,[j] 1.26,[n] 1.48[o]
p-Xylene	1.88,[a] 1.87,[b] 1.74,[h] 1.469,[j] 1.48,[n] 1.54[o]
Propylbenzene	0.998[p]
Isopropylbenzene	0.61,[a] 0.42,[e] 0.543,[j] 0.402[n]
1,2,3-Trimethylbenzene	0.626[j]
1,2,4-Trimethylbenzene	0.47,[e] 0.491[j]
1,3,5-Trimethylbenzene	0.401[j]

a) L. J. Andrew and R. M. Keefer, *J. Am. Chem. Soc.*, **71**, 3644 (1949). b) R. L. Bohon and W. F. Claussen, *J. Am. Chem. Soc.*, **73**, 1571 (1951). c) H. Hayashi and T. Sasaki, *Bull. Chem. Soc. Jpn.*, **29**, 857 (1956). d) D. S. Arnold *et al.*, *Chem. Eng. Data. Ser.*, **3**, 253 (1958). e) C. McAuliffe, *J. Phys. Chem.*, **70**, 1267 (1966). f) A. A. Taha *et al.*, *J. Chem. Educ.*, **43**, 432 (1966). g) J. D. Worley, *Can. J. Chem.*, **45**, 2465 (1967). h) J. Polak and B. C. Y. Lu, *Can. J. Chem.*, **51**, 4018 (1973). i) Ref. 10. j) Ref. 1. k) F. P. Schwarz, *Anal. Chem.*, **52**, 10 (1980). l) H. Fühner, *Chem. Ber.*, **57**, 510 (1924). m) T. J. Morrison and F. J. Billett, *J. Chem. Soc.*, **1952**, 3819. n) L. C. Price, Ph. D. disertation, University of California, Riverside, Calif. (1973). o) R. B. Hermann, *J. Phys. Chem.*, **76**, 2754 (1972). p) H. B. Klevens, *J. Phys. Colloid. Chem.*, **54**, 283 (1950).

Table 4. Henry's law constants reported in the literature

Solute	Temperature/°C	Henry's law constant/10^7 Pa			
		I[a]	II[b]	III[c]	IV[d]
Benzene	10	1.46			
	15	1.87,1.89			
	20	2.39			
	25	3.06	3.2		3.13
	30	3.82,3.61			
	35			4.702—4.522	
Toluene	25				3.75
Ethylbenzene	25				4.76

a) W. J. Green and H. S. Frank, *J. Solut. Chem.*, **8**, 187 (1979). b) A. A. Taha *et al.*, *J. Chem. Educ.*, **43**, 432 (1966). c) E. E. Tucker and S. D. Christian, *J. Phys. Chem.*, **83**, 427 (1979). d) Ref. 3.

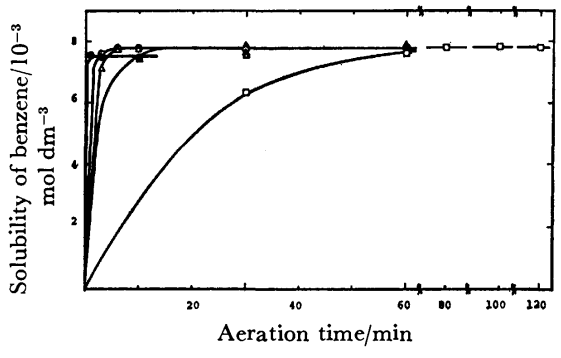

Fig. 5. The effect of nitrogen gas flow rate on the solubility of benzene in the open method.
Temperature of solubility flask; 35.00 °C. Temperature of solute reservoir; 15.00 °C. Flow rate: 3.0 (●), 1.2 (○), 0.5 (△), 0.2 (▲), 0.02 dm³/min (□).

and 7, respectively, where those obtained in the closed method are also given for the sake of comparison. Similarly Henry's law was applied in the open method

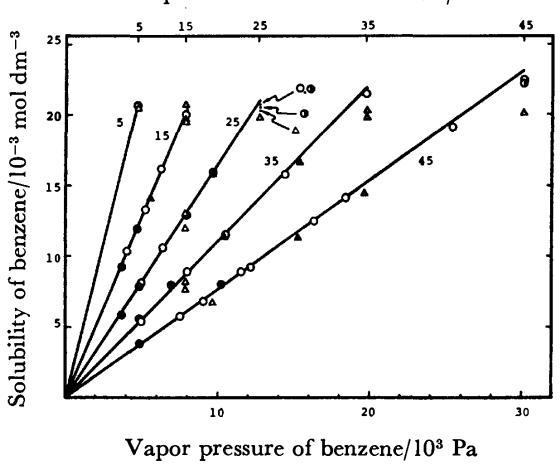

Fig. 6. The solubility of benzene plotted against vapor pressure.
The closed method: circulation rate; 2 dm³/min, time; 5 min, measured on Oct. 26—28 (1980) (●) Dec. 14—16 (1980) (◑) July 25—30 (1981) (○). The open method: nitrogen gas flow rate; 0.2 dm³/min, time; 60 min, measured on May 6—28 (1981) (△) Aug. 3—10 (1981) (▲). The figure near each solid line indicates the temperature of solubility flask in °C.

to these solutes, but the reproducibility was somewhat poor. However, the open method has an advantage that the liquid solute phase is free from contamination with water vapor.

Discussion

The Evaluation of the Present Method. The present method is essentially the same as that previously employed in determining the solubility of metallic mercury in water.[6] In writing this paper, we have searched the literature for the one most similar to the present method and found a paper published by Joris and Taylor.[7] They made use of a similar closed circulatory system

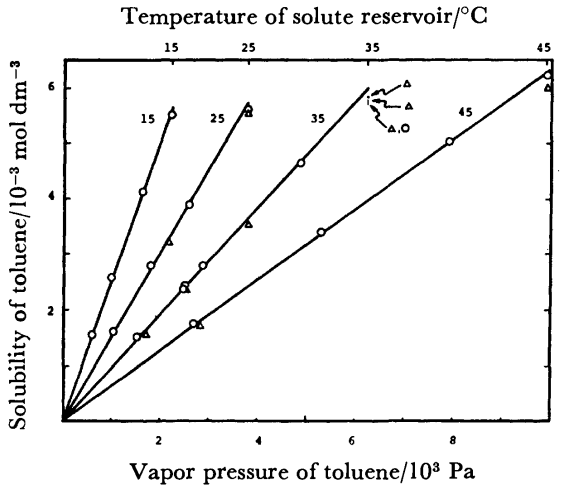

Fig. 7. The solubility of toluene plotted against vapor pressure.
The closed method (○), circulation rate; 2 dm³/min, time; 5 min. The open method (△), nitrogen gas flow rate; 0.2 dm³/min, time; 60 min. The figure near each solid line indicates the temperature of solubility flask in °C.

in determining the solubility of water in organic solvent, which is just the opposite situation to the present study. In their method, temperatures of solvent and solute are nearly equal to each other, while the whole circulatory system is kept at a higher temperature than either.

It is a thermodynamic requirement that the solubility measurement should be done under the same temperature of solvent and solute. From this standpoint, two basic questions arise concerning the validity of the present method; the first is that the temperature of the solute reservoir differs from that of the solubility flask and the second is that the partial pressure of the solute vapor may be affected by the temperature change in a different part of the closed system. The temperature of the solute vapor just before entering the solubility flask certainly differs from that in the solubility flask; the former is higher than that of the solute reservoir owing to the room temperature. However, the solubilities were found to be independent of the room temperature so far as being kept above the temperature of the solute reservoir (Fig. 3). We have assumed that when the solute vapor is bubbled into the water phase through the sintered ball and bubbles come into contact with the water, the temperature of the interface of each bubble can be equated to that of bulk water almost immediately. The temperature change in the bulk water was examined in the preliminary experiment by introducing solute vapor at 2 dm³/min into the solubility flask in which a thermometer was inserted. A slight decrease in the temperature of the bulk water was observed, probably due to the vaporization of water. We have concluded that such temperature change is negligibly small in the solubility measurement.

On the other hand, the second question is more substantial, since the total pressure undoubtedly relates to the temperature of system. In the closed system, however, it seems likely that the different temperature inside the apparatus (solute, solvent, and room) dose not cause the pressure change, but contributes to the flow rate of the gas phase in the corresponding parts of the system. That is, the flow rate of the circulating gas is faster in places of higher temperature. Thus, the total pressure remains constant at atomospheric pressure over the temperature range investigated. This situation may be more easily understood by referring to the open method, where the nitrogen gas carrying the solute vapor is always open to the atmosphere after having been introduced into the water phase. We suppose from the following observation that the total pressure in the closed system is also kept under atmospheric pressure: when the three-way cock was turned prior to sampling so as to connect the system to the test tube as indicated in Fig. 1, only a small change was observed in the liquid solute level inside the glass pipe in the test tube.

Concerning the evaluation of the present method, we have taken account of the serious disagreement of benzene with the literature; some 10% lower than most literature values. After presenting our short communication,[4] we have continued the solubility measurements by the modified apparatus employed here. However, the results always indicated the lower values. The reason is not explicable at present, but it is felt that the present method may give lower saturated solution for such solute exhibiting high vapor pressure as benzene. It can be seen from Figs. 6 and 7 that the solubilities of benzene obtained by the open method are a little lower than those by the closed method, especially at higher temperature of water, and that the agreements between the open and the closed methods are better for toluene than for benzene. It seems likely that an escape of solute vapor from aqueous solution occurs in preference to a dissolution into it in the open system. This escaping tendency may have likewise taken place even under the closed system owing to the extreme volatility of benzene in water. The solubility measured by the present method might be called "steady state solubility," that is, the solubility determined under such condition that the rate of escape of solute vapor from the aqueous phase is equal to the rate of dissolution of solute vapor into it. The balance for benzene may be changed in favor of escape.

Interpretation of the Solubility Results. As suggested by Amidon and Anik,[8] the solution process of liquid hydrocarbon can be divided into two steps; pure liquid to gas and gas to aqueous solution. The present study is concerned with the latter step, that is, the solvation process. The thermodynamic parameters estimated from the temperature dependence of Henry's law constant are tabulated in Table 5, in which are given the solvation enthalpies reported by the two groups. They estimated these values indirectly by subtracting the heat of vaporization to form ideal gas from the energy of solution. Our results are in fair agreement with them. It should be noticed, however, that the present results have been derived on the assumption of ΔH being temperature independent. Thermodynamic features of the solution process of benzene and the alkylbenzenes will be reported and discussed elsewhere.

It can be seen from Table 2 that the number of the methyl groups is predominant in determining the

TABLE 5. THERMODYNAMIC PARAMETERS OF SOLVATION OF SOLUTE VAPOR AT 25 °C DETERMINED FROM TEMPERATURE DEPENDENCE OF HENRY'S LAW CONSTANT[a)]

Solute	ΔG/kJ mol^{-1}	$-\Delta S$/J K^{-1} mol^{-1}	$-\Delta H$/kJ mol^{-1}		
			This work	Literature I[b)]	Literature II[c)]
Benzene	14.4±0.04	157±1	32.3±0.4	31.77±0.06	31.9
Toluene	14.6±0.08	167±1	35.1±0.3	36.26±0.06	36.2
Ethylbenzene	15.1±0.08	177±2	37.8±0.5	40.24±0.06	40.1
o-Xylene	14.0±0.13	173±1	37.7±0.2		
m-Xylene	14.9±0.08	181±2	39.2±0.6		40.0
p-Xylene	15.0±0.08	183±1	39.7±0.2		40.0
Propylbenzene	15.8±0.08	184±2	39.1±0.6	43.9 ±0.1	
Isopropylbenzene	16.0±0.17	186±3	39.6±0.7		41.5
1,2,3-Trimethylbenzene	13.6±0.17	171±3	37.5±0.8		
1,2,4-Trimethylbenzene	14.4±0.04	182±1	39.9±0.2		
1,3,5-Trimethylbenzene	15.4±0.08	183±1	39.2±0.1		

a) Thermodynamic parameters determined in this work were derived based on the assumption of ΔH being temperature independent. b) S. J. Gill, N. F. Nichols, and I. Wadsö, *J. Chem. Thermodyn.*, **8**, 445 (1976). c) R. D. Wauchope and R. Haque, *Can. J. Chem.*, **50**, 133 (1972).

solubility; the solubility decreases to *ca.* 1/3.6 with an increase of one methyl group. Moreover, as pointed out by Sutton and Calder,[1)] the positions of the substituents on the benzene ring are of secondary importance. The expression in terms of Henry's law constant seems to indicate more pronounced differences among the substituted isomers rather than the solubility proper. Henry's law constant might be predictable from the scaled particle theory,[9)] which requires many parameters for a single solute such as molecular diameter, energy parameter, polarizability, and dipole moment. Of these parameters, the last one appears to play an important role in the solubility characteristic of isomers; Henry's law constant decreases with increasing dipole moment of the solute. On the basis of the scaled particle theory, we have tried briefly to correlate Henry's law constants of a series of benzene and the alkylbenzenes with their molecular parameters. The results, however, were not satisfactory.

Applicability of the Present Method. The present method has three principal advantages. Firstly, the solubility equilibria can be attained in quite a short time such as 3 min, and they are easily reproducible. Secondly, it can be easily confirmed whether the solubility obeys Henry's law. Henry's law constant and its temperature dependence should help to clarify the solution process in more detail than the solubility itself. Finally, the apparatus is best suited for preparing aqueous solutions of any desired concentrations of solute, which are equal or below the saturation, at a given temperature of water.

Of these, the last one is the most remarkable feature of the present method and attractive from the practical point of view. For instance, certain specific interaction of a third component such as an electrolyte or another organic compound with organic liquid solutes can be substantiated experimentally by measuring the solubility change in the presence of the third component.

Recent workers have taken it as an advantage that their methods of solubility measurement do not necessarily require the preparation of truly saturated solutions.[2,3,10)] Nevertheless, it is still important and indispensable in some cases to prepare the truly saturated solutions.

References

1) C. Sutton and J. A. Calder, *J. Chem. Eng. Data*, **20**, 320 (1975).
2) R. L. Brown and S. P. Wasik, *J. Res. Natl. Bur. Stand., Sec. A*, **78**, 453 (1974).
3) D. Mackay, W. Y. Shiu, and R. P. Sutherland, *Environ. Sci. Technol.*, **13**, 333 (1979).
4) I. Sanemasa, M. Araki, T. Deguchi, and H. Nagai, *Chem. Lett.*, **1981**, 225.
5) For benzene, vapor pressures were estimated from "International Critical Tables," McGraw-Hill, New York (1928), Vol. III, pp. 208, 221. For the alkylbenzenes, vapor pressures were estimated from "Kagaku Binran, Kiso-Hen II," ed by The Chemical Society of Japan, Maruzene, Tokyo (1975), pp. 710—731.
6) I. Sanemasa, *Bull. Chem. Soc. Jpn.*, **48**, 1795 (1975).
7) G G. Joris and H. S. Taylor, *J. Chem. Phys.*, **16**, 45. (1948).
8) G. L. Amidon and S. T. Anik, *J. Phys. Chem.*, **84**,970 (1980).
9) For example, R. A. Pierotti, *Chem. Rev.*, **76**, 717 (1976).
10) D. Mackay and W. Y. Shiu, *Can. J. Chem. Eng.*, **53**, 239 (1975).

 © 1982 The Chemical Society of Japan Bull. Chem. Soc. Jpn., 55, 1063—1072 (1982)

Structural Study of Optical Resolution. XI. The Crystal Structures of $(+)_{589}$-Tris(biguanide)cobalt(III) Chloride *d*-Tartrate Trihydrate and Racemic Tris(biguanide)cobalt(III) Trichloride

Toshiji TADA, Yoshihiko KUSHI, and Hayami YONEDA*

Department of Chemistry, Faculty of Science, Hiroshima University, Higashi-senda-machi, Naka-ku, Hiroshima 730

(Received September 9, 1981)

The crystal structures of the more-soluble diastereomeric salt, $(+)_{589}$-$[Co(Hbg)_3]Cl(d\text{-tart})\cdot 3H_2O$ (**1**), and the racemic chloride salt, $[Co(Hbg)_3]Cl_3$ (**2**), have been determined by X-ray analysis ($R=0.033$, 2788 reflections for **1** and $R=0.056$, 2785 reflections for **2**), where $Hbg=C_2H_7N_5$, *d*-tart$=C_4H_4O_6^{2-}$. The more-soluble salt **1** is orthorhombic, with the space group $P2_12_12_1$, $Z=4$, $a=15.654(2)$, $b=13.758(2)$, and $c=11.010(1)$ Å. The racemic salt **2** is monoclinic, with the space group C2/c, $Z=8$, $a=19.441(9)$, $b=14.901(7)$, $c=15.911(6)$ Å, and $\beta=127.63(2)°$. In **1**, the complex cations and the Cl^- ions are arranged alternately to form an infinite spiral chain, $\{\Delta\text{-}[Co(Hbg)_3]Cl\}_\infty$. Each *d*-tartrate is hydrogen-bonded to a twofold-screw-axis-related neighbor (-OH··· OOC- 2.792 Å) to form an infinite chain, $(d\text{-tart})_\infty$. In **2** two kinds of similar infinite spiral chains, $\{\Delta\text{-}[Co(Hbg)_3]Cl\}_\infty$ and $\{\Lambda\text{-}[Co(Hbg)_3]Cl\}_\infty$, which are mirror images of each other are found. The structures of these two salts **1** and **2** are compared with those of the less-soluble diastereomeric chloride *d*-tartrate and the optically active chloride in both of which a similar infinite chain has been found, and the mechanism of chiral discrimination *via* the diastereomer formation is discussed.

In a previous paper, we reported the crystal structure of the less-soluble diastereomeric salt, $(-)_{589}$-$[Co(Hbg)_3]Cl(d\text{-tart})\cdot 5H_2O$ **3** (Hbg stands for biguanide, and *d*-tart stands for the *d*-tartrate ion).[1] Two characteristic features were noted to be important in connection with the mechanism of optical resolution *via* the less-soluble diastereomeric salt: 1) The chiral complex and Cl^- ions are arranged alternately to form an infinite spiral chain which is cationic and left-handed as a whole, and 2) two *d*-tart anions exist closely to each other and form a dimeric unit with 4 negative charges, similar in structure to the antimony *d*-tartrate ion. Such a dimeric unit of *d*-tart anions has never been found in the crystal structures determined so far. A similar infinite spiral chain was found in the optically active chloride salt, $(+)_{589}$-$[Co(Hbg)_3]Cl_3\cdot H_2O$.[2] In this case, the spiral chain consists of Δ complexes and is right-handed as a whole. With these findings in mind, we have attempted here to determine the crystal structures of the more-soluble diastereomeric salt, $(+)_{589}$-$[Co(Hbg)_3]Cl(d\text{-tart})\cdot 3H_2O$ **1**, as well as the racemic chloride salt, $[Co(Hbg)_3]Cl_3$ **2**, in order to see whether the infinite spiral chain of the complex ions exists in common and to see how the *d*-tart anions are packed in the more-soluble salt **1**. Through these crystal structure analyses, we have tried to find out a clue to the mechanism of optical resolution of the biguanide complex.

Experimental

Preparation of Compound. Biguanide sulfate was prepared by the method given in the literature.[3] The racemic chloride salt, $[Co(Hbg)_3]Cl_3$ **2**, was prepared by the method of Ray and Dutt.[4] The crystals are brownish yellow parallelepiped. Found: C, 15.60; H, 4.56; N, 45.10%. Calcd for $CoC_6H_{21}N_{15}Cl_3$: C, 15.38; H, 4.52; N, 44.83%. The more-soluble diastereomeric salt, $(+)_{589}$-$[Co(Hbg)_3]Cl(d\text{-tart})\cdot 3H_2O$ **1**, was prepared by the method of Ray and Dutt.[5] After removal of the crystals of the less-soluble diastereomeric salt **3**, the filtrate was allowed to stand at room temperature for several days. Large and thick plate-like crystals of the more-soluble salt were easily separated mechanically from the fine thin plates of the remaining less-soluble salt. The optical purity of the crystals was checked by the CD measurement ($\Delta\varepsilon_{510}=+3.52$ and $\Delta\varepsilon_{452}=-4.76$).[6] Found: C, 19.37; H, 4.96; N, 35.90%. Calcd for $CoC_{10}H_{25}N_{15}O_6Cl\cdot 3H_2O$ ($2H_2O$): C, 20.02 (20.64); H, 5.21 (5.02); N, 35.03 (36.11)%.

Data Collection. The size of crystal used for the X-ray measurement was 0.53 mm × 0.32 mm × 0.15 mm for the more-soluble salt **1** and 0.25 mm × 0.13 mm × 0.08 mm for the racemic salt **2**. For **1**, the systematic absences for *h*00 ($h=2n+1$), 0*k*0 ($k=2n+1$), and 00*l* ($l=2n+1$) indicated the space group $P2_12_12_1$. For **2**, the systematic absences for *hkl* ($h+k=2n+1$) and *h*0*l* ($h=2n+1$ and $l=2n+1$) suggested the following possible space groups: Cc and C2/c. The three-dimensional Patterson map indicated the space group C2/c and the success of the structure determination confirmed the wisdom of this selection. The determination of cell dimensions and the collection of intensity data were carried out on a Rigaku AFC-5 automated four-circle diffractometer with Mo $K\alpha$ radiation ($\lambda=0.71069$ Å) monochromated by a graphite plate. Both unit-cell dimensions were refined by a least-squares method with 23 high angle reflections ($2\theta>26°$). The crystal data are summarized in Table 1. Densities of the

Table 1. Crystallographic data

	a/Å	*b*/Å	*c*/Å	*β*/°	Space group	*Z*	D_m/g cm^{-3}	D_c/g cm^{-3}	*V*/Å^3	(*V*/*Z*)/Å^3
(1)	15.654(2)	13.758(2)	11.010(1)	—	$P2_12_12_1$	4	1.66_3	1.680	2371.2(5)	592.8(1)
(2)	19.441(9)	14.901(7)	15.911(6)	127.63(2)	C2/c	8	1.67_5	1.705	3635(3)	456.3(3)
(3)	24.846(5)	12.970(2)	8.645(2)	—	C222	4	1.51_4	1.516	2785.8(8)	696.5(2)
(4)	18.675(9)	14.086(7)	15.004(7)	—	$C222_1$	8	1.64(2)	1.637	3947(5)	493.4(6)

(1): $(+)_{589}$-$[Co(Hbg)_3]Cl(d\text{-tart})\cdot 3H_2O$. (2): $[Co(Hbg)_3]Cl_3$. (3): $(-)_{589}$-$[Co(Hbg)_3]Cl(d\text{-tart})\cdot 5H_2O$.[1] (4): $(+)_{589}$-$[Co(Hbg)_3]Cl_3\cdot H_2O$ reported by Snow.[2]

TABLE 2. POSITIONAL AND THERMAL PARAMETERS FOR $(+)_{589}$-$[Co(Hbg)_3]Cl(d\text{-tart})\cdot 3H_2O$

Atom	x	y	z	B_{eq}/Å^{2} a)
Co	0.75979(3)	0.60488(3)	0.48673(4)	2.20
Cl	0.99932(7)	0.52598(9)	0.20659(12)	4.42
N(A1)	0.8344(2)	0.5131(2)	0.4089(3)	2.82
N(A2)	0.9003(2)	0.3653(3)	0.3680(4)	3.95
N(A3)	0.7738(2)	0.3687(2)	0.4755(3)	3.37
N(A4)	0.6549(2)	0.3391(2)	0.5902(3)	3.58
N(A5)	0.6923(2)	0.4981(2)	0.5464(3)	2.78
N(B1)	0.8277(2)	0.7079(2)	0.4226(3)	2.63
N(B2)	0.8538(3)	0.8525(3)	0.3179(4)	4.49
N(B3)	0.7256(2)	0.7744(2)	0.2932(3)	3.09
N(B4)	0.6082(2)	0.7043(3)	0.2052(4)	3.39
N(B5)	0.6878(2)	0.6150(2)	0.3447(3)	2.85
N(C1)	0.8315(2)	0.6056(2)	0.6282(3)	2.64
N(C2)	0.9061(2)	0.6837(3)	0.7818(3)	4.02
N(C3)	0.7831(2)	0.7528(2)	0.7089(3)	2.97
N(C4)	0.6505(2)	0.8223(2)	0.6947(4)	3.87
N(C5)	0.6852(2)	0.6933(2)	0.5673(3)	2.48
C(A1)	0.8354(2)	0.4199(3)	0.4163(3)	2.75
C(A2)	0.7046(2)	0.4063(3)	0.5375(3)	2.66
C(B1)	0.8045(2)	0.7744(3)	0.3484(3)	2.78
C(B2)	0.6739(2)	0.6935(3)	0.2834(3)	2.74
C(C1)	0.8409(2)	0.6771(3)	0.7024(3)	2.58
C(C2)	0.7047(2)	0.7542(3)	0.6533(3)	2.54
CT1	0.7490(2)	0.9070(2)	1.0193(3)	3.16
CT2	0.8069(3)	0.9674(3)	0.9368(3)	2.90
CT3	0.8997(3)	0.9562(3)	0.9764(4)	3.39
CT4	0.9589(3)	1.0097(3)	0.8880(5)	4.55
OT1	0.7121(2)	0.8344(2)	0.9740(3)	4.27
OT2	0.7434(2)	0.9334(2)	1.1275(3)	4.63
OT3	0.7973(2)	0.9370(2)	0.8139(3)	3.78
OT4	0.9189(2)	0.8541(2)	0.9802(3)	4.11
OT5	1.0204(2)	0.9662(3)	0.8452(5)	6.47
OT6	0.9421(3)	1.0952(3)	0.8649(5)	7.66
OW1	0.5067(2)	0.7450(3)	0.4974(5)	6.17
OW2	0.9677(5)	0.9341(4)	0.5893(5)	11.00
OW3	0.5431(3)	0.8421(5)	0.0183(6)	11.74
H(NA1)	0.878(2)	0.537(3)	0.359(4)	1.90
H(NA21)	0.882(4)	0.312(5)	0.352(6)	5.91
H(NA22)	0.937(3)	0.359(3)	0.304(4)	2.70
H(NA3)	0.784(3)	0.311(4)	0.472(5)	4.26
H(NA41)	0.661(3)	0.282(3)	0.573(4)	2.15
H(NA42)	0.609(4)	0.362(4)	0.622(5)	4.44
H(NA5)	0.649(3)	0.513(4)	0.585(5)	3.54
H(NB1)	0.880(4)	0.709(4)	0.442(6)	4.62
H(NB21)	0.839(4)	0.885(4)	0.253(5)	4.24
H(NB22)	0.901(3)	0.861(4)	0.356(5)	3.63
H(NB3)	0.713(3)	0.830(3)	0.253(4)	2.14
H(NB41)	0.578(3)	0.650(4)	0.185(5)	3.13
H(NB42)	0.607(4)	0.746(4)	0.163(6)	4.49
H(NB5)	0.658(3)	0.556(3)	0.318(4)	1.92
H(NC1)	0.868(3)	0.553(3)	0.645(4)	1.55
H(NC21)	0.950(4)	0.643(4)	0.769(5)	5.17
H(NC22)	0.906(3)	0.722(3)	0.835(4)	2.30
H(NC3)	0.798(3)	0.806(3)	0.756(4)	1.18
H(NC41)	0.671(4)	0.864(4)	0.738(5)	4.48
H(NC42)	0.599(5)	0.879(6)	0.654(8)	10.52
H(NC5)	0.626(3)	0.693(3)	0.541(5)	2.69
H(CT2)	0.788(3)	1.033(3)	0.948(4)	1.65

Table 2. (Continued)

Atom	x	y	z	B_{eq}/Å^{2} a)
H(CT3)	0.910(3)	0.986(3)	1.057(4)	1.91
H(OT3)	0.792(3)	0.987(3)	0.763(4)	2.54
H(OT4)	0.966(4)	0.838(4)	0.982(5)	4.79
H(OW11)	0.538(4)	0.784(4)	0.451(6)	5.81
H(OW12)	0.497(3)	0.686(4)	0.468(5)	4.13
H(OW21)	0.984(4)	1.007(4)	0.581(7)	6.48
H(OW22)	0.932(4)	0.892(5)	0.668(6)	6.52
H(OW31)	0.616(4)	0.849(5)	0.003(6)	6.37
H(OW32)	0.483(5)	0.769(6)	0.017(10)	11.71

a) $B_{eq}=8\pi^2(U_{11}+U_{22}+U_{33})/3$.

Table 3. Positional and thermal parameters for $[Co(Hbg)_3]Cl_3$

Atom	x	y	z	B_{eq}/Å^{2} a)
Co	0.18928(5)	0.12498(5)	0.25003(6)	1.68
Cl(1)	0.3650(1)	0.3747(1)	0.4800(1)	3.09
Cl(2)	0.4575(1)	0.0066(1)	0.6026(1)	3.30
Cl(3)	0.3950(1)	0.7434(1)	0.6027(1)	3.12
N(A1)	0.2213(3)	0.0615(3)	0.1745(4)	2.44
N(A2)	0.3131(4)	0.0041(4)	0.1408(6)	4.50
N(A3)	0.3557(4)	0.1253(5)	0.2499(7)	5.97
N(A4)	0.4217(4)	0.2469(4)	0.3594(6)	4.25
N(A5)	0.2969(3)	0.1888(4)	0.3259(4)	2.37
N(B1)	0.0817(3)	0.0632(3)	0.1726(4)	2.13
N(B2)	−0.0168(4)	−0.0528(4)	0.1223(5)	3.56
N(B3)	0.1249(3)	−0.0692(3)	0.2699(5)	2.71
N(B4)	0.2532(4)	−0.1104(4)	0.4236(5)	3.51
N(B5)	0.2406(3)	0.0315(3)	0.3545(4)	2.09
N(C1)	0.1358(3)	0.2188(3)	0.1454(4)	2.37
N(C2)	0.0796(5)	0.3615(4)	0.0767(5)	4.43
N(C3)	0.1053(4)	0.3193(4)	0.2303(5)	4.09
N(C4)	0.1121(5)	0.3028(5)	0.3792(6)	5.92
N(C5)	0.1595(3)	0.1875(3)	0.3287(4)	2.31
C(A1)	0.2928(4)	0.0628(4)	0.1871(5)	3.20
C(A2)	0.3566(4)	0.1879(4)	0.3135(5)	2.57
C(B1)	0.0622(4)	−0.0159(4)	0.1856(5)	2.68
C(B2)	0.2089(4)	−0.0453(4)	0.3510(5)	2.57
C(C1)	0.1076(4)	0.2954(4)	0.1489(5)	2.35
C(C2)	0.1259(4)	0.2659(4)	0.3130(5)	2.88
H(NA1)	0.186(4)	0.010(5)	0.135(5)	1.78
H(NA21)	0.368(5)	0.012(6)	0.153(7)	3.56
H(NA22)	0.274(5)	−0.030(5)	0.103(6)	2.76
H(NA3)	0.400(7)	0.119(8)	0.258(8)	5.50
H(NA41)	0.466(5)	0.237(5)	0.366(6)	1.83
H(NA42)	0.426(7)	0.295(7)	0.402(9)	6.36
H(NA5)	0.298(5)	0.236(6)	0.367(7)	3.55
H(NB1)	0.039(5)	0.094(5)	0.127(6)	1.70
H(NB21)	−0.053(5)	−0.024(5)	0.069(6)	2.59
H(NB22)	−0.027(6)	−0.115(6)	0.133(7)	4.01
H(NB3)	0.114(6)	−0.123(7)	0.274(7)	4.30
H(NB41)	0.233(5)	−0.160(6)	0.422(7)	3.27
H(NB42)	0.306(5)	−0.094(6)	0.471(7)	3.15
H(NB5)	0.301(5)	0.048(5)	0.412(6)	2.88
H(NC1)	0.136(4)	0.207(5)	0.091(6)	1.50
H(NC21)	0.063(8)	0.409(8)	0.089(9)	7.17
H(NC22)	0.077(6)	0.367(6)	0.026(7)	4.33
H(NC3)	0.084(5)	0.374(6)	0.227(6)	3.10
H(NC41)	0.132(5)	0.277(5)	0.440(6)	2.46
H(NC42)	0.080(5)	0.360(6)	0.362(6)	3.04
H(NC5)	0.169(5)	0.159(6)	0.380(6)	2.75

a) $B_{eq}=8\pi^2(U_{11}+U_{22}+U_{33})/3$.

crystals were measured by the flotation method in a mixture of chloroform and bromoform. The intensity data were collected in the ω-2θ scan mode up to $2\theta=55°$ with scan rates of 6°/min for **1** and of 16°/min for **2** (50 kV, 170 mA). The ω scan range was $(1.0+0.5 \tan\theta)°$. Of the 2949 and 3322 unique observed reflections, 2788 and 2785 reflections with $|Fo| \geq 3\sigma(F)$ were used for the structure determination in **1** and **2** respectively. Corrections for the absorption effect were neglected (μ(Mo $K\alpha$)=8.96 cm^{-1} for **1** and 14.42 cm^{-1} for **2**).

Determination and Refinement of Crystal Structures

The More-soluble Diastereomeric Salt, $(+)_{589}$-[Co(Hbg)$_3$]Cl(d-tart). 3H$_2$O (1). The structure was determined by the heavy-atom method and refined by the block-diagonal least-squares method. Three kinds of water molecules were found on a difference Fourier map after the other non-hydrogen atoms were located by an application of the Fourier method. The refinement using anisotropic thermal parameters for non-hydrogen atoms reduced the R value (defined as $\sum||F_o|-|F_c||/\sum|F_o|$) to 0.061. At this stage, all the hydrogen atoms were located from a difference Fourier map. The final refinement including the contribution of these H atoms with isotropic temperature factors converged the R value to 0.033. The final difference map showed no peaks higher than 0.4 electron/Å^3. The absolute configuration of $(+)_{589}$-[Co(Hbg)$_3$]$^{3+}$ was assigned as Δ on the basis of the configuration (2R, 3R) of the d-tart anion as an internal reference.[7]

The Racemic Chloride Salt, [Co(Hbg)$_3$]Cl$_3$ (2). The determination and the refinement of the structure were made in a way similar to that used for **1**. The final refinement converged the R value to 0.058. The final difference map showed no peaks higher than 0.4 electron/Å^3.

In the refinement, the quantity minimized was $\sum w(|F_o|-k|F_c|)^2$. The weighting scheme used was $w=(\sigma_{cs}^2+a|F_o|+(b|F_o|)^2)^{-1}$, where σ_{cs} is the standard deviation obtained from the counting statistics for each reflection; the values of a and b were 0.2 and 0.03 respectively. All the atomic scattering factors, with the effect of the anomalous dispersion of Co and Cl atoms were taken from the International Tables for X-Ray Crystallography, Vol. IV.[8]

All the computations were carried out by a HITAC M-180 computer at the Hiroshima University Information Processing Center. The computer programs used were FOUR-MMM, FOUR-2/M,[9] and HBLS-IV with a slight modification.[10] An ORTEP drawing was carried out by a computer system, XTL, in a Syntex R3 automated four-circle diffractometer.[11] The final atomic parameters are listed in Table 2 for the more-soluble salt **1** and in Table 3 for the racemic salt **2**, respectively. The anisotropic thermal parameters and complete lists of the $|F_o|$ and $|F_c|$ values have been preserved by the Chemical Society of Japan (Document No. 8220).

Results and Discussion

The projections of the crystal structure for the more-soluble diastereomeric salt **1**, $(+)_{589}$-[Co(Hbg)$_3$]Cl(d-tart)·3H$_2$O, along the a- and c-axes are shown in Figs. 1 and 2. The projections of the crystal structure for the racemic chloride salt **2**, [Co(Hbg)$_3$]Cl$_3$, to the (110) plane and along the b-axis are shown in Figs. 3 and 4. In Figs. 1 and 3, the part of the components in the unit

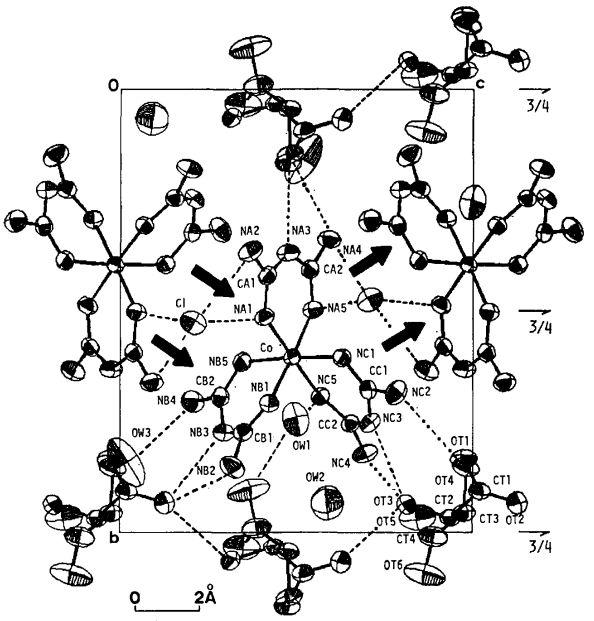

Fig. 1. An ORTEP drawing of the part of the components in the unit cell viewed down the a-axis with the numbering scheme for $(+)_{589}$-[Co(Hbg)$_3$]Cl(d-tart)·3H$_2$O. All atoms are drawn with 50% probability ellipsoids. Possible hydrogen bonds are indicated by broken lines. Hydrogen atoms are omitted for clarity.

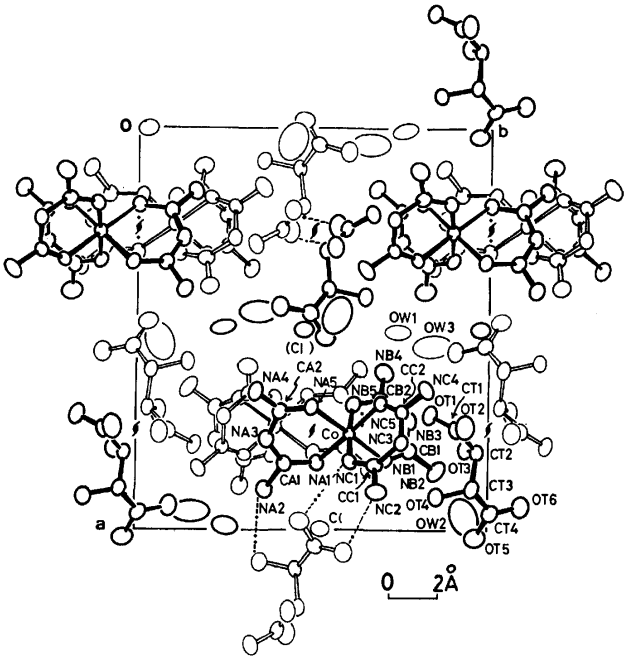

Fig. 2. An ORTEP drawing of the crystal structure viewed down the c-axis for $(+)_{589}$-[Co(Hbg)$_3$]Cl(d-tart)·3H$_2$O.

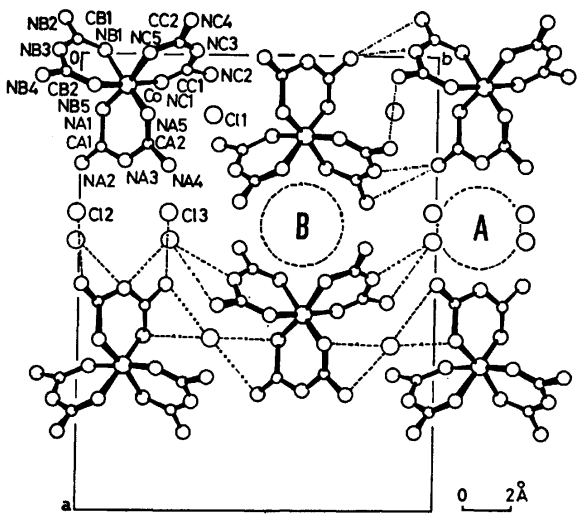

Fig. 3. A drawing of the part of the components in the unit cell projected on the (110) plane with the numbering scheme for $[Co(Hbg)_3]Cl_3$. Possible hydrogen bonds are indicated by broken lines. Hydrogen atoms are omitted for clarity. A and B indicate positions of void A and void B respectively.

cell are omitted in order to show the crystal features more clearly.

Geometry of Complex Cation. The bond distances and angles for the complex cation of both salts **1** and **2** are listed in Tables 4 and 5 respectively. They are in good agreement with those found in the two crystal structures, the less-soluble diastereomeric salt **3**, $(-)_{589}$-$[Co(Hbg)_3]Cl(d\text{-tart})\cdot 5H_2O$,[1] and the optically active chloride salt **4**, $(+)_{589}$-$[Co(Hbg)_3]Cl_3\cdot H_2O$:[2] averaged bond distances all differ by less than 0.012 Å and all averaged bond angles differ by less than 1.9°.

However, there is a small but significant difference in the geometry of complex cations among the four salts, **1**, **2**, **3**, and **4**. While the planarity of a biguanide ligand itself is bearly preserved in all these crystals, the planarity of a chelate ring as a whole (including the Co atom) is lost in some cases. The values of the dihedral angle between the plane of the Hbg ligand and the plane formed by Co and two donor N atoms are summarized in Table 6. The chelate ring A is approximately planar in all these crystals. In these crystals, two Cl^- ions approach the chelate ring A from both sides. Deviation from the planarity is found for the chelate rings B and C in the diastereomeric salts **1** and **3**. In **1** and **3**, both chelate rings B and C are bent inside toward each other. This is clearly reflected by the shorter distances between the central imino-nitrogen atoms of the two chelate rings B and C (Table 6). It is not reasonable to assume the attraction between these two N atoms. The bending of the chelate ring plane being observed only in the crystals containing the *d*-tart anion, such a bending can be attributed to the electrostatic attraction by the *d*-tart anion.

Geometry of d-*Tart.* The bond distances and angles for the *d*-tart anion of the more-soluble salt **1** are listed in Table 4. These values are in accordance with those reported previously.[1,7,12] Five non-hydrogen atoms of each α-hydroxy carboxylate moiety lie approximately on a plane. The dihedral angle between the planes of the two moieties in the more-soluble salt **1** is 62.1°. This value is larger than the corresponding value of 50.8° in the less-soluble salt **3**. Such a relation in the dihedral angle has been found also in the crystal structures of two diastereomeric salt pairs containing the *d*-tartH anion $(C_4H_5O_6^-)$.[13-15]

Crystal Packing. *The More-soluble Salt* ***1***: The intermolecular distances and angles are summarized in Table 7. The complex cation and the Cl^- ion are arranged alternately to form an infinite spiral chain, $\{\Delta\text{-}[Co(Hbg)_3]Cl\}_\infty$, along the twofold screw axis which is parallel to the c-axis through the position $(x=3/4, y=1/2)$ (Figs. 1 and 2). Hydrogen bonds are formed between the N atoms of Hbg A and the Cl^- ion.

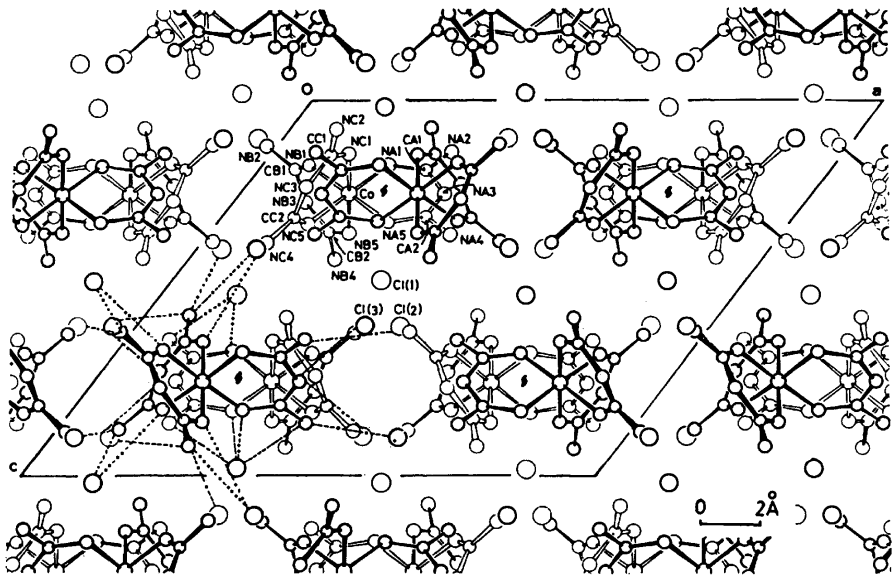

Fig. 4. A drawing of the crystal structure viewed down the b-axis for $[Co(Hbg)_3]Cl_3$. Possible hydrogen bonds are indicated by broken lines.

TABLE 4. BOND DISTANCES AND ANGLES (e.s.d.'s IN PARENTHESES) FOR $(+)_{589}$-$[Co(Hbg)_3]Cl \cdot d$-tart$\cdot 3H_2O$

Bond distances l/Å							
Co–N(A1)	1.921(3)	N(B5)–C(B2)	1.292(5)	C(C2)–N(C3)	1.371(5)	CT2–CT3	1.524(6)
Co–N(A5)	1.925(3)	N(C1)–C(C1)	1.287(5)	C(A1)–N(A2)	1.370(5)	CT3–CT4	1.532(7)
Co–N(B1)	1.907(3)	N(C5)–C(C2)	1.301(5)	C(A2)–N(A4)	1.341(5)	CT1–OT1	1.256(5)
Co–N(B5)	1.933(3)	C(A1)–N(A3)	1.361(5)	C(B1)–N(B2)	1.365(6)	CT1–OT2	1.248(5)
Co–N(C1)	1.919(3)	C(A2)–N(A3)	1.381(5)	C(B2)–N(B4)	1.349(5)	CT4–OT5	1.228(8)
Co–N(C5)	1.904(3)	C(B1)–N(B3)	1.376(5)	C(C1)–N(C2)	1.347(5)	CT4–OT6	1 233(8)
N(A1)–C(A1)	1.285(5)	C(B2)–N(B3)	1.380(5)	C(C2)–N(C4)	1.344(5)	CT2–OT3	1.427(5)
N(A5)–C(A2)	1.281(5)	C(C1)–N(C3)	1.381(5)	CT1–CT2	1.529(5)	CT3–OT4	1.436(6)
N(B1)–C(B1)	1.280(5)						
Bond angles ϕ/°							
N(A1)–Co–N(A5)	89.1(1)	N(C5)–C(C2)–N(C4)	123.2(4)	N(C2)–C(C1)–N(C3)	114 2(3)		
N(B1)–Co–N(B5)	88.4(1)	N(A1)–C(A1)–N(A3)	122.6(4)	N(C4)–C(C2)–N(C3)	115.1(3)		
N(C1)–Co–N(C5)	88.7(1)	N(A5)–C(A2)–N(A3)	121.7(3)	OT1–CT1–OT2	125.3(4)		
Co–N(A1)–C(A1)	129.4(3)	N(B1)–C(B1)–N(B3)	122.4(4)	OT1–CT1–CT2	117.9(4)		
Co–N(A5)–C(A2)	130.0(3)	N(B5)–C(B2)–N(B3)	122.3(4)	OT2–CT1–CT2	116 8(4)		
Co–N(B1)–C(B1)	127.6(3)	N(C1)–C(C1)–N(C3)	122.3(3)	CT1–CT2–OT3	110.1(3)		
Co–N(B5)–C(B2)	125.5(3)	N(C5)–C(C2)–N(C3)	121.7(3)	CT1–CT2–CT3	109 8(3)		
Co–N(C1)–C(C1)	125.9(3)	C(A1)–N(A3)–C(A2)	126.8(3)	OT3–CT2–CT3	110.0(3)		
Co–N(C5)–C(C2)	127.3(3)	C(B1)–N(B3)–C(B2)	124.2(3)	CT2–CT3–OT4	107.9(3)		
N(A1)–C(A1)–N(A2)	122.1(4)	C(C1)–N(C3)–C(C2)	125.0(3)	OT4–CT3–CT4	111.2(4)		
N(A5)–C(A2)–N(A4)	124.0(4)	N(A2)–C(A1)–N(A3)	115.3(3)	CT2–CT3–CT4	110 2(4)		
N(B1)–C(B1)–N(B2)	124.0(4)	N(A4)–C(A2)–N(A3)	114.2(3)	CT3–CT4–OT5	119.0(5)		
N(B5)–C(B2)–N(B4)	123.7(4)	N(B2)–C(B1)–N(B3)	113.6(4)	CT3–CT4–OT6	117.4(5)		
N(C1)–C(C1)–N(C2)	123.4(4)	N(B4)–C(B2)–N(B3)	114.0(3)	OT5–CT4–OT6	123.6(6)		

TABLE 5. BOND DISTANCES AND ANGLES (e.s.d.'s IN PARENTHESES) FOR $[Co(Hbg)_3]Cl_3$

Bond distances l/Å							
Co–N(A1)	1.907(6)	N(A1)–C(A1)	1.279(11)	C(A1)–N(A3)	1.366(14)	C(A1)–N(A2)	1.348(12)
Co–N(A5)	1.912(6)	N(A5)–C(A2)	1.290(10)	C(A2)–N(A3)	1.368(13)	C(A2)–N(A4)	1.334(12)
Co–N(B1)	1.896(6)	N(B1)–C(B1)	1.292(10)	C(B1)–N(B3)	1.386(11)	C(B1)–N(B2)	1.336(12)
Co–N(B5)	1.917(6)	N(B5)–C(B2)	1.285(10)	C(B2)–N(B3)	1.373(11)	C(B2)–N(B4)	1.342(11)
Co–N(C1)	1.922(6)	N(C1)–C(C1)	1.281(10)	C(C1)–N(C3)	1.369(11)	C(C1)–N(C2)	1.351(12)
Co–N(C2)	1.912(6)	N(C5)–C(C2)	1.371(12)	C(C2)–N(C3)	1.371(12)	C(C2)–N(C4)	1.352(13)
Bond angles ϕ/°							
N(A1)–Co–N(A5)	89.6(3)	N(A5)–C(A2)–N(A4)	123.4(8)	N(C5)–C(C2)–N(C3)	122.0(8)		
N(B1)–Co–N(B5)	89.6(3)	N(B1)–C(B1)–N(B2)	124.7(8)	C(A1)–N(A3)–C(A2)	127.4(9)		
N(C1)–Co–N(C5)	89.5(3)	N(B5)–C(B2)–N(B4)	124.5(7)	C(B1)–N(B3)–C(B2)	126.8(7)		
Co–N(A1)–C(A1)	129.5(6)	N(C1)–C(C1)–N(C2)	125.0(8)	C(C1)–N(C3)–C(C2)	126.7(8)		
Co–N(A5)–C(A2)	129.6(6)	N(C5)–C(C2)–N(C4)	122.4(8)	N(A2)–C(A1)–N(A3)	114.4(8)		
Co–N(B1)–C(B1)	130.9(6)	N(A1)–C(A1)–N(A3)	121.7(8)	N(A4)–C(A2)–N(A3)	115.7(8)		
Co–N(B5)–C(B2)	128.9(5)	N(A5)–C(A2)–N(A3)	120.9(8)	N(B2)–C(B1)–N(B3)	114.9(8)		
Co–N(C1)–C(C1)	129.1(6)	N(B1)–C(B1)–N(B3)	120.4(7)	N(B4)–C(B2)–N(B3)	113.1(7)		
Co–N(C5)–C(C2)	129.5(6)	N(B5)–C(B2)–N(B3)	122.4(7)	N(C2)–C(C1)–N(C3)	112.7(7)		
N(A1)–C(A1)–N(A2)	123.9(8)	N(C1)–C(C1)–N(C3)	122.3(7)	N(C4)–C(C2)–N(C3)	115.5(8)		

TABLE 6. DIHEDRAL ANGLES BETWEEN PLANE OF Hbg LIGAND AND PLANE FORMED BY Co AND TWO DONOR N ATOMS, AND DISTANCES BETWEEN CENTRAL IMINO N ATOMS

	Chelate ring ϕ/°			N(X3)···N(Y3) l/Å		
	A	B	C	X=A, Y=B	X=A, Y=C	X=B, Y=C
1	5.6	19.9	19.3	5.98	5.88	4.67
3	3.0	16.4	16.4	5.87	5.87	4.84
4	6.9	6.0	12.8	5.60	5.19	5.89
2	6.3	6.7	6.7	5.51	5.50	5.81

1: More-soluble salt. 2: Racemic salt. 3: Less-soluble salt. 4: Optically active salt.

If we assume a spiral chain which connects the complex and the Cl ions alternately along the hydrogen bonds as shown by broken lines in Fig. 1, the spiral arrangement is left-handed. However, the same spiral arrangement is considered to be right-handed, if we imagine a spiral chain which connects the central Co and Cl ions alternately as shown by arrows in Fig. 1. In this paper we take the latter definition. Such a spiral arrangement has been found in the crystal structures of **3** and **4**, too.[1] It is worth noting that the spiral configuration, $\{\Delta$-$[Co(Hbg)_3]Cl\}_\infty$, in **4** is right-handed, while that, $\{\Lambda$-$[Co(Hbg)_3]Cl\}_\infty$, in **3** is left-handed.

The *d*-tart anions are arranged along the c-axis to

Table 7. Selected intermolecular distances and angles for $(+)_{589}$-$[Co(Hbg)_3]Cl(d\text{-tart})\cdot 3H_2O$

D–H···A	D···A l/Å	H···A l/Å	D–H···A ϕ/°
N(A1)–H(NA1)···Cl	3.415(3)	2.50(4)	156(3)
N(A2)–H(NA22)···Cl	3.233(4)	2.31(5)	153(4)
N(A2)···OT4^{i}	3.291(5)	—	—
N(A3)–H(NA3)···OT1^{ii}	2.803(5)	2 01(6)	170(6)
N(A4)–H(NA41)···OT4^{ii}	3.141(5)	2.47(5)	141(5)
N(A4)^{ii}–H(NA42)···Cl	3.305(4)	2.47(6)	163(5)
N(A5)^{ii}–H(NA5)···Cl	3.495(3)	2.73(6)	154(4)
N(B1)^{iii}–H(NB1)···OW1	3.009(6)	2.19(6)	164(6)
N(B2)–H(NB21)···OT2^{iv}	2.936(6)	2.15(6)	150(5)
N(B2)^{v}–H(NB22)···Cl	3.325(5)	2.83(5)	118(4)
N(B3)–H(NB3)···OT2^{iv}	2.863(5)	2.04(5)	151(4)
N(B3)···OT6^{vi}	3.275(7)	—	—
N(B4)–H(NB41)···OT5^{iii}	2.775(6)	1.87(5)	176(5)
N(B4)–H(NB42)···OW3	2.978(8)	2.30(6)	154(6)
N(C1)–H(NC1)···OT5^{i}	3.023(6)	2.13(4)	161(4)
N(C2)–H(NC21)···OT6^{i}	3.122(7)	2.34(6)	146(5)
N(C2)–H(NC22)···OT4	3.210(5)	2.43(5)	172(5)
N(C2)^{iii}···OW3	3.094(8)	—	—
N(C3)–H(NC3)···OT3	2.794(5)	1.92(4)	158(4)
N(C4)–H(NC41)···OT3	3.082(5)	2.38(6)	147(6)
N(C4)–H(NC42)···Cl^{iii}	3.338(4)	2.54(8)	121(5)
N(C4)···OT1	3.227(5)	—	—
N(C5)–H(NC5)···OW1	2.985(6)	2.06(5)	159(4)
OT3–H(OT3)···OT2^{vi}	2.792(5)	1.93(5)	162(5)
OW1–H(OW11)···OT6^{vi}	2.758(8)	1.94(7)	152(6)
OW1–H(OW12)···OW2^{iii}	2.712(9)	1.83(6)	175(6)
OW2^{vi}–H(OW21)···OW3	3.181(10)	2.23(7)	152(6)
OW2···OT5	2.969(9)	—	—
OW3–H(OW32)···OT4^{iii}	3.327(8)	1.97(11)	167(7)
OW3–H(OW31)···OT1^{iv}	2.693(8)	1.55(7)	167(6)

Roman numerals as superscripts refer to the following equivalent positions relative to the reference molecule at x, y, z:

i ($2-x, -1/2+y, 3/2-z$), ii ($3/2-x, 1-y, -1/2+z$), iii($-1/2+x, 3/2-y, 1-z$), iv($x, y, -1+z$), v ($2-x, -1/2+y, 1/2-z$), vi($3/2-x, 2-y, -1/2+z$)

D, hydrogen donor; A, hydrogen acceptor.

Table 8. Selected intermolecular distances and angles for $[Co(Hbg)_3]Cl_3$

D–H···A	D···A l/Å	H···A l/Å	D–H···A ϕ/°
N(A1)–H(NA1)···Cl(1)^{i}	3.401(6)	2.49(8)	159(7)
N(A2)–H(NA21)···Cl(2)^{ii}	3.218(9)	2.33(10)	152(9)
N(A2)–H(NA22)···Cl(1)^{i}	3.358(9)	2.60(10)	161(9)
N(A3)–H(NA3)···Cl(2)^{iii}	3.487(11)	2.94(13)	129(11)
N(A3)–H(NA3)···Cl(3)^{iv}	3.477(11)	3.17(13)	107(10)
N(A4)–H(NA41)···Cl(3)^{v}	3.233(9)	2.45(9)	162(8)
N(A4)–H(NA42)···Cl(1)	3.333(9)	2.48(14)	149(11)
N(A5)–H(NA5)···Cl(1)	3.387(7)	2.52(11)	151(9)
N(B1)–H(NB1)···Cl(1)^{vi}	3.497(6)	2.73(9)	154(8)
N(B2)–H(NB21)···Cl(1)^{vi}	3.330(9)	2.59(10)	151(9)
N(B2)–H(NB22)···Cl(3)^{vi}	3.233(9)	2.31(11)	157(9)
N(B3)–H(NB3)···Cl(3)^{vii}	3.457(8)	2.74(12)	144(10)
N(B4)–H(NB41)···Cl(3)^{vii}	3.307(8)	2.59(10)	146(9)
N(B4)–H(NB42)···Cl(2)	3.621(8)	2.79(11)	164(9)
N(B5)–H(NB5)···Cl(2)	3.629(7)	2.75(10)	149(8)
N(C1)–H(NC1)···Cl(3)^{i}	3.631(7)	2.81(9)	155(7)
N(C2)–H(NC21)···Cl(2)^{vi}	3.296(9)	2.52(15)	151(13)
N(C2)–H(NC22)···Cl(2)^{ix}	3.290(9)	2.70(12)	133(10)
N(C2)–H(NC22)···Cl(3)^{i}	3.631(7)	3.04(12)	135(9)
N(C3)–H(NC3)···Cl(2)^{vi}	3.463(9)	2.67(10)	146(8)
N(C4)–H(NC41)···Cl(1)^{vii}	3.316(11)	2.58(10)	141(8)
N(C4)–H(NC42)···Cl(2)^{vii}	3.234(11)	2.30(10)	156(8)
N(C5)–H(NC5)···Cl(1)^{vii}	3.482(6)	2.72(10)	151(9)

Roman numerals as superscripts refer to the following equivalent positions relative to the reference molecule at x, y, z:

i ($1/2-x, -1/2+y, 1/2-z$),
ii ($x, -y, -1/2+z$),
iii ($1-x, -y, 1-z$),
iv ($x, 1-y, -1/2+z$),
v ($1-x, 1-y, 1-z$),
vi ($-1/2+x, 1/2-y, -1/2+z$),
vii($1/2-x, 1/2-y, 1-z$),
viii($x, -1+y, z$),
ix ($1/2-x, 1/2+y, 1/2-z$),
x ($1-x, y, 3/2-z$)

D, hydrogen donor; A, hydrogen acceptor.

make an infinite chain, $(d\text{-tart})_\infty$, in which two adjacent anions are related by the twofold screw axis (Figs. 1 and 2). A hydrogen bond is formed between the O atoms of hydroxyl and carboxylato groups of adjacent *d*-tart anions, OT3–H(OT3)···OT2^{vi} 2.792 Å. The pitch of the chain is equal to the length of the c-axis, 11.010 Å. A similar infinite chain related by the twofold screw axis has been found in several crystals containing the *d*-tart anions.[16–20] In these crystals the pitch of the chain shows a wide variation from 6.128 Å in $(NH_4)_2\cdot d\text{-tart}$[18] to 10.989 Å in $[Pt(en)_2]d\text{-tart}$.[20] The pitch in the present case (11.010 Å) is the longest one ever observed. The framework of the crystal structure is built up of two kinds of chains, $\{\Delta\text{-}[Co(Hbg)_3]Cl\}_\infty$ and $(d\text{-tart})_\infty$, along the c-axis. These chains are closely packed with each other (Fig. 2).

As shown in Table 1, the V/Z value, 592.8 Å^3, of **1** is 103.7 Å^3 smaller than that, 696.5 Å^3, of **3**. When the volume (2×20.6 Å^3)[21] corresponding to two water molecules (the difference in the number of water of crystallization between **1** and **3**) is subtracted from the V/Z value of **3**, a large positive value, 62.5 Å^3, still remains. Thus, it can be concluded that the packing density in the more-soluble salt **1** is larger than that in the less-soluble salt **3**. This makes a marked contrast to the cases of two diastereomeric salt pairs containing *d*-tartH, in which the packing density is larger in the less-soluble salt than in the more-soluble salt.[13–15]

The Racemic Chloride Salt **2**: The intermolecular distances and angles are summarized in Table 8. The complex cation of the same chirality and a kind of Cl^- ions (Cl(1)) are arranged alternately along the twofold screw axis to form an infinite spiral chain, $\{[Co(Hbg)_3]Cl\}_\infty$, which is similar to that found in the crystal structures, **1**, **3**, and **4**, (Figs. 3 and 4). Moreover, the spiral chain made up of the *Λ* complex is left-handed and that made up of the *Δ* complex is right-handed. Short contacts between some N atoms of adjacent complexes are 3.21(1)—3.43(1) Å (Fig. 3). The distances between H and N atoms are H(NB22)···N(A4)

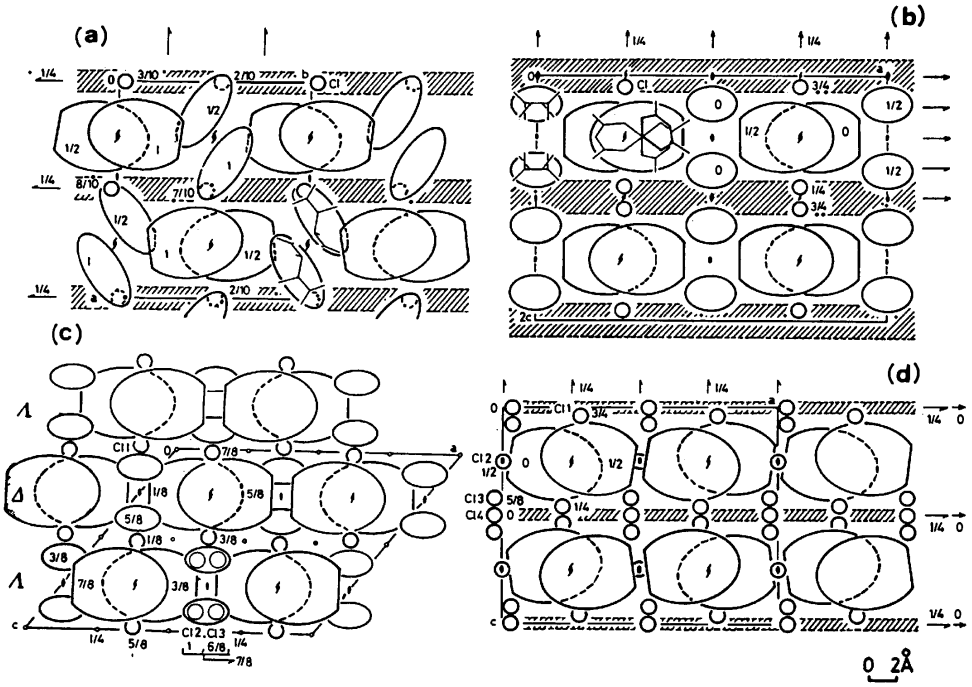

Fig. 5. A schematic drawing of the crystal structures of the four salts, (a) the more-soluble salt $(+)_{589}$-$[Co(Hbg)_3]Cl(d\text{-tart})\cdot 3H_2O$ **1**, (b) the less-soluble salt $(-)_{589}$-$[Co(Hbg)_3]Cl(d\text{-tart})\cdot 5H_2O$ **3**, (c) the racemic salt $[Co(Hbg)_3]Cl_3$ **2**, and (d) the optically active salt $(+)_{589}$-$[Co(Hbg)_3]Cl_3\cdot H_2O$ **4**, along the c-axis for **1** and the b-axis for **2**, **3**, and **4**. Shaded parts indicate positions of water molecules.

2.85(11), H(NB3)···N(A4) 2.63(12), H(NB42)···N(C2) 2.83(11), and H(NC3)···N(A2) 2.65(10) Å. These values are close to the sum, 2.75 Å, of van der Waals radii of H, 1.20 Å, and N, 1.55 Å, atoms.[22] Therefore, the complex cations tend to pack together as closely as their geometry allows in the formation of the spiral chains.

*Comparison of the Packing Modes of the Four Salts, **1**, **2**, **3**, and **4**.* The most characteristic point common to all these four crystal structures is that they contain the infinite spiral chain, $\{[Co(Hbg)_3]Cl\}_\infty$. The four crystal structures projected along the infinite spiral chain are shown schematically in Fig. 5. In these crystals, the spiral chains are packed in parallel with each other.

In the racemic salt **2** and the optically active salt **4**, the spiral chains are arranged almost in contact with each other, and the remaining two Cl^- ions are placed in a void formed by the arrangement of the spiral chains. Here, if we regard the spiral chain as a cylinder, the packing mode in **2** and **4** can be regarded as somewhat irregular, hexagonal and tetragonal packings of parallel cylinders respectively. These two modes, hexagonal and tetragonal, are known as two types of the simplest packings of parallel cylinders. Moreover, the density of the hexagonal packing is larger than that of the tetragonal packing.[23] Indeed, the density of **2** is larger than that of **4** (Table 1).

In the racemic salt **2**, the spiral chains of the same chirality are related along the a-axis by the twofold operation to form a chiral layer on the ab plane as shown in Figs. 4 and 5(c). Also in the less-soluble salt **3** and the optically active salt **4**, the spiral chains are related along the a-axis by the same twofold operation (Figs. 5(b) and 5(d)). Therefore, in these crystals, the voids formed between the adjacent spiral chains on the ab plane can be divided roughly into two groups; one is between two Hbg A (void A) and the other is between Hbg B and C (void B) (see Fig. 3). In **2**, two kinds of Cl^- ions (Cl(2) and Cl(3)) are concentrated in void A to form (4^-)-charged conglomerate. The distances between these Cl^- ions are Cl(2)···Cl(2)^x 3.907(4), Cl(3)···Cl(3)^x 3.908(4), and Cl(2)···Cl(3) 4.106(4) Å. These distances seem to be fairly short, considering the radius of the Cl^- ion of 1.81 Å.[24] In **3**, it has been found that two *d*-tart anions are concentrated in voild A to form a dimeric unit, $(d\text{-tart})_2^{4-}$ (Fig. 5(b)). Therefore, the packing mode in the layer for **2** bears a striking resemblance to that in the layer for **3**. In **4**, three kinds of Cl^- ions (Cl(2), Cl(3), and Cl(4)) are not concentrated in a particular void but scattered in the whole crystal (Fig. 5(d)).

On the other hand, in the more-soluble salt **1**, the spiral chains are related along the b-axis by a unit translation and the relation of the adjacent spiral chains in **1** is different from that in the other three crystals, **2**, **3**, and **4** (Fig. 5(a)). Therefore, in **1**, Hbg A always faces with Hbg B and C in the adjacent spiral chains along the b-axis. The *d*-tart anions are evenly distributed in the void formed by the arrangement of the spiral chains. As a result, the *d*-tart anions themselves form an infinite chain, $(d\text{-tart})_\infty$, through hydrogen bonds (–OH···OOC–). Thus, the packing mode of **1** resembles that of **4** in terms of a dispersive distribution

of the counter anions. Therefore, it might be assumed that the localization of negative charges plays a dominant role in the stabilization of the crystal structure for the less-soluble salt **3** and the racemic salt **2**.

Chiral Discrimination Mode. Since the complex ions, Δ and Λ, in these four crystals are linked together *via* Cl^- ions to form the infinite spiral chains, $\{\Delta\text{-}[Co(Hbg)_3]Cl\}_\infty$ and $\{\Lambda\text{-}[Co(Hbg)_3]Cl\}_\infty$, we can safely conclude that the chiral discrimination by the *d*-tart anion is effected not on the individual complex ion but on these infinite chains in the diastereomer formation. Namely, the crystal-packing mode as a whole is responsible for the chiral discrimination. Here, the question is how the *d*-tart anions collect the spiral chains of the same chirality to form a crystal.

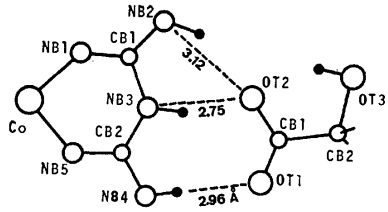

Fig. 6. Disposition of the Hbg ligand and the α-hydroxy carboxylate moiety of the *d*-tart anion for the less-soluble salt **3**. The broken lines indicate hydrogen bonds.

In relation to this point, in the less-soluble salt **3**, a specific close contact between Hbg B (Hbg C is equivalent to Hbg B in crystallography) and *d*-tart has been found along the twofold axis of complex. This specific close contact between the guanidino moiety of Hbg and carboxylato group of *d*-tart is illustrated in Fig. 6. The atoms in Hbg and α-hydroxy carboxylate moiety of *d*-tart lie on nearly the same plane. In the previous paper,[1] it was presumed that this specific close contact (specific interaction) plays a dominant role in collecting left-handed spiral chains. This specific close contact mode is expected to be more stable than any other modes of interaction between the guanidino moiety and the carboxylato group.[25] In other words, it is concluded that this specific close contact mode is most reasonable mode of access for the *d*-tart anion to combine the left-handed spiral chains. It is worth noting that a similar specific interaction has been found between the guanidyl group of arginine and the γ-carboxylato group of glutamate in the crystal structure of L-arginine L-glutamate.[26]

Such a specific close contact mode is not found in the more-soluble salt **1**. A complex cation is surrounded by six *d*-tart anions through hydrogen bonds in different modes of close contact, among which the mode of access to the complex nearly along the threefold axis seems to be important in relation to chiral discrimination as shown in Figs. 2 and 7. One α-hydroxy carboxylate moiety of *d*-tart are hydrogen-bonded to the adjacent *d*-tart anions related by the twofold screw axis to form an infinite chain, $(d\text{-tart})_\infty$, as shown by a broken line A in Fig. 7. On both sides of this infinite chain, are running parallel two infinite spiral chains, $\{\Delta\text{-}[Co(Hbg)_3]Cl\}_\infty$. The other α-hydroxy carboxylate moiety

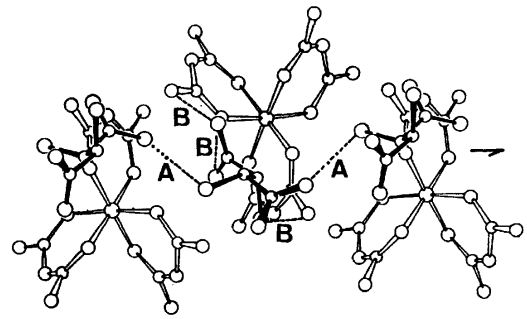

Fig. 7. Disposition of the *d*-tart anions in $(d\text{-tart})^\infty$ and the complex cations in $\{\Delta\text{-}[Co(Hbg)_3]Cl\}_\infty$ for the more-soluble salt **1**. Broken lines A and B indicate OH···O and NH···O hydrogen bonds respectively.

of each *d*-tart is hydrogen-bonded to Hbg A and C of each complex in these two infinite chains, $\{\Delta\text{-}[Co(Hbg)_3]Cl\}_\infty$, as shown by a broken line B in Fig. 7. Through such hydrogen bonds, the right-handed, spiral chains are collected by the infinite chain, $(d\text{-tart})_\infty$. This is supported by the pitch of the two infinite chains (11.010 Å). Namely, in the spiral chain $\{[Co(Hbg)_3]Cl\}_\infty$, the pitch is considerably short when it is compared with pitches of other spiral chains, 12.970, 14.086, and 14.901 Å in **3**, **4**, and **2** respectively (Table 1), and in the chain, $(d\text{-tart})_\infty$, the pitch is long when it is compared with pitches of other chains, $(d\text{-tart})_\infty$, found so far.[16–20]

Therefore, it is clear that the more-soluble salt **1** is quite different from the less-soluble salt **3** in the close contact mode between the complex and *d*-tart ions. Here, the question is why the salt **3** is less-soluble than the salt **1**. Previously, in the crystal structures of two diastereomeric salt pairs containing *d*-tartH, it has been found that the density of the less-soluble salt is larger than that of the more-soluble salt, and the cation and the anion in the less-soluble salt fit with each other more compactly than those in the more-soluble salt (compact fitting model).[13–15] Contrary to the *d*-tartH systems, in the present case the density of the less-soluble salt **3** is smaller than that of the more-soluble salt **1**. In the present diastereomeric salt pair, no significant difference is found in the number of the hydrogen bonds and in the distances between the cation and the anion. Thus, the compact fitting model can not be applied successfully to the present diastereomeric salts. This seems to be due to quite different arrangements of *d*-tart: the infinite chain, $(d\text{-tart})_\infty$, for **1** and the dimeric unit, $(d\text{-tart})_2^{4-}$, for **3**. From the comparison of the crystal structures of the four salts, **1**, **2**, **3**, and **4**, it should be considered that the difference in the arrangement of the *d*-tart anions is important for the solubility difference in the present case. It can be concluded that the localization of the negative charge, which results from the formation of the dimeric unit $(d\text{-tart})_2^{4-}$ containing the specific interaction between Hbg and *d*-tart, plays a dominant role in the stabilization of the crystal structure for the less-soluble diastereomeric salt **3**.

We wish to acknowledge a Grant-in-Aid for Scientific Research from the Ministry of Education, Science and Culture.

References

1) T. Tada, Y. Kushi, and H. Yoneda, *Bull. Chem. Soc. Jpn.*, **54**, 1538 (1981).
2) M. R. Snow, *Acta Crystallogr., Sect. B*, **30**, 1850 (1974).
3) D. Karipides and W. C. Fernelius, *Inorg. Synth.*, Vol. VII, 56 (1963).
4) P. Ray and N. K. Dutt, *J. Indian Chem. Soc.*, **16**, 621 (1939).
5) P. Ray and N. K. Dutt, *J. Indian Chem. Soc.*, **18**, 289 (1941).
6) K. Igi, T. Yasui, J. Hidaka, and Y. Shimura, *Bull. Chem. Soc. Jpn.*, **44**, 426 (1971).
7) J. M. Bijvoet, A. F. Peerdeman, and A. J. van Bommel, *Nature*, **168**, 271 (1951).
8) "International Tables for X-Ray Crystallography," Kynoch Press, Birmingham (1974), Vol. IV, pp. 72—79, 149.
9) Y. Kushi, unpublished work.
10) T. Ashida, "The Universal Crystallographic Computation Program System," ed by T. Sakurai, The Crystallographic Society of Japan (1967).
11) C. K. Johnson, ORTEP, Report ORNL-3794, Oak Ridge National Laboratory, Oak Ridge, Tennessee, U. S. A., 1965.
12) For example, R. Sadanaga, *Acta Crystallogr.*, **3**, 416 (1950); S. Perez, *ibid., Sect. B*, **33**, 1083 (1977); D. H. Templeton, A. Zalkin, H. W. Ruben, and L. K. Templeton, *ibid.*, **35**, 1608 (1979); L. S. Magill, J. D. Korp, and I. Bernal, *Inorg. Chem.*, **20**, 1187 (1981).
13) M. Kuramoto, Y. Kushi, and H. Yoneda, *Bull. Chem. Soc. Jpn.*, **51**, 3251 (1978).
14) M. Kuramoto, *Bull. Chem. Soc. Jpn.*, **52**, 3702 (1979).
15) M. Kuramoto, Y. Kushi, and H. Yoneda, *Bull. Chem. Soc. Jpn.*, **53**, 125 (1980).
16) G. K. Ambady, *Acta Crystallogr., Sect. B*, **24**, 1548 (1968).
17) H. Hinazumi and T. Mitsui, *Acta Crystallogr., Sect. B*, **28**, 3299 (1972).
18) V. S. Yadava and V. M. Padmanabhan, *Acta Crystallogr., Sect. B*, **29**, 493 (1973).
19) S. Perez, *Acta Crystallogr., Sect. B*, **32**, 2064 (1976).
20) W. A. Freeman, *Inorg. Chem.*, **15**, 2235 (1976).
21) K. Harata, *Bull. Chem. Soc. Jpn.*, **49**, 2066 (1976).
22) A. Bondi, *J. Phy. Chem.*, **68**, 441 (1964).
23) M. O'Keeffe and S. Andersson, *Acta Crystallogr., Sect. A*, **33**, 914 (1977).
24) L. Pauling, "The Nature of The Chemical Bond," 3rd ed, Cornell University Press, Ithaca (1960), p. 260.
25) E. Friedem, *J. Chem. Educ.*, **52**, 754 (1975).
26) T. N. Bhat and M. Vijayan, *Acta Crystallogr., Sect. B*, **33**, 1754 (1977).

 © 1982 The Chemical Society of Japan Bull. Chem. Soc. Jpn., 55, 1073—1076 (1982)

Studies of the Separation Mechanism in Ion-exchange Chromatography. III. Elution Order of *cis*-Bis(ethylenediamine)cobalt(III) and *cis*-α-Triethylenetetraminecobalt(III) Complexes on SP-Sephadex C-25 and IEX 510 Resins

Hayami YONEDA,* Shin-Ichi WAKIDA, Hiroshi NAKAZAWA, and Ushio SAKAGUCHI

Department of Chemistry, Faculty of Science, Hiroshima University, Hiroshima 730

(Received September 26, 1981)

Chromatographic separation of *cis*-dianionobis(ethylenediamine)cobalt(III) and *cis*-α-dianionotriethylenetetraminecobalt(III) complexes has been investigated by using SP-Sephadex C-25 and IEX 510 cation-exchange resins. The elution order of the complex cations on both resins are rather similar to each other and the adjusted retention volumes of these complexes correlate very closely with the crystallographic volumes (the unit cell volumes divided by the number of molecules in a unit cell) of $[Co(X)(NH_3)_5]Cl_2$, where $X=CN^-$, Cl^-, NO_2^-, N_3^-, and NCS^-. This has been taken to indicate that the affinity of the complex cation to the functional group of the resins increases as the size of the cation, and hence the character of water-structure breaker of the cation, increases. Thus, the elution order obtained seems to be determined primarily by the difference in the affinities of the complex cations to the resins, rather than by the difference in the association constants for the ion-pairs formed between the complex cation and the eluent anion.

Ion-exchange chromatography has been used widely to separate metal complexes.[1] The mechanism of chromatographic separation of octahedral complexes with different charges or polarities on ion-exchange resins has been explained[2] mainly be electrostatic interactions between the complex ion and the functional group of the resin in the stationary phase and/or by those between the complex ion and the eluent ion in the moving phase. Our recent studies[3,4] were concerned with the inversion of the elution order of differently charged complexes and of geometrically isomeric complexes (*cis*/*trans*). The results pointed clearly to the importance of two processes in chromatographic separation; adsorption on the complex ion to the resin and elution by eluent ions. For example, the separation of the $[Co(N)_6]^{3+}$ type of complexes has been explained[5] by the difference in the strengths of the hydrogen bonding formed between the N–H hydrogen(s) of the complex cation and the eluent anions in the moving phase. Thus, the system can be considered to be a case of elution-governing.

Very few works[6] have, however, been made which discussed the mechanism of the separation of complexes with the same charge and geometric configuration, *e.g.*, the separation of a series of *cis*-$[Co(X)_2(en)_2]^+$ with various substituents X, where en stands for ethylenediamine. For univalent complex cations *cis*-$[Co(X)(Y)(en)_2]^+$ or *cis*-α-$[Co(X)(Y)(trien)]^+$ (trien=triethylenetetramine), if the eluent concentration is not so high, it may be expected that the interaction between the complex cation and the eluent anion is weak and therefore the separation is dominated by the difference in the affinities of the complex cations to the resin; the systems are adsorption-governed. Thus, a detailed mechanism of the adsorption to the resin might be clarified. With this idea in mind, we have measured the retention volumes of substitution-inert complexes, *cis*-$[Co(X)(Y)(en)_2]^+$ and *cis*-α-$[Co(X)_2(trien)]^+$, where X and Y stand for CN^-, NO_2^-, NCS^-, N_3^-, and Cl^-. The resins used were strongly acidic cation-exchangers, SP-Sephadex C-25 and IEX 510, both of which have the sulfonate group as the functional group.

Experimental

Materials. All the complexes used in this work were prepared by the literature methods and identified by UV/VIS absorption spectra, proton magnetic resonance spectra, and chemical analyses. The geometrically isomeric purity was checked by ion-exchange chromatography. All the complexes were confirmed to be stable against hydrolysis and isomerization during the chromatographic experiments.

The resins used were IEX 510 (Toyo soda Manufacturing Co., Ltd., Japan) and SP-Sephadex C-25 (Pharmacia Fine Chemicals, Sweden), which are strongly acidic ($-SO_3^-Na^+$) cation-exchangers based on silica gel and cross-linked dextran, respectively.

Apparatus. All the chromatographic experiments were carried out on a laboratory-built chromatographic apparatus. The sample solution and Blue Dextran 2000, which was used as a marker for the void volume measurement, was injected by a syringe. The detector, Shimadzu UV-140 double beam spectrophotometer, was operated at the first absorption band of each complex. The adjusted retention volume was obtained from the elution curve.

Results and Discussion

Tables 1 and 2 show the adjusted retention volumes of *cis*-$[Co(X)(Y)(en)_2]^+$ and *cis*-α-$[Co(X)_2(trien)]^+$ on IEX 510 and SP-Sephadex C-25, respectively, when eluted by 0.1 M (1 M=1 mol dm^{-3}) aqueous solution of sodium chloride. When IEX 510 was used, the difference in the adjusted retention volumes of these complexes is rather large and the degree of separation is high. With SP-Sephadex C-25, though the degree of separation is not so high as with IEX 510, almost the same elution order was obtained. The elution order of *cis*-$[Co(X)_2(en)_2]^+$ and *cis*-α-$[Co(X)_2(trien)]^+$, expressed in terms of the substituent X, is as follows.

$$CN > Cl > NO_2 > N_3 > NCS$$

It can be seen in Table 1 that the adjusted retention volume of *cis*-$[Co(X)(Y)(en)_2]^+$ with $X \neq Y$ falls midway between the retention volumes of *cis*-$[Co(X)_2(en)_2]^+$ and *cis*-$[Co(Y)_2(en)_2]^+$. This appears to be true also on SP-Sephadex C-25. Further, it will also be apparent

TABLE 1. THE ADJUSTED RETENTION VOLUMES (ml) OF $[Co(X)(Y)(N)_4]^+$ ON IEX 510 WHEN ELUTED BY 0.1 M AQUEOUS SOLUTIONS OF SODIUM CHLORIDE

The column size was 4×300 mm, flow rate 0.30 ml min^{-1}, and void volume 1.38 ml.

(X)(Y)	*cis*-$(en)_2$	*cis*-α-trien
$(CN)_2$	8.07	8.01
$(Cl)_2$	10.78	11.21
$(Cl)(NO_2)$	12.31	
$(NO_2)_2$	12.80	12.60
$(N_3)(NO_2)$	13.41	
$(N_3)_2$	14.98	14.75
(Cl)(NCS)	16.29	
(NO_2)(NCS)	18.17	
$(NCS)_2$	32.00	30.09

TABLE 2. THE ADJUSTED RETENTION VOLUMES (ml) OF $[Co(X)(Y)(N)_4]^+$ ON SP-SEPHADEX C-25 WHEN ELUTED BY 0.1 M AQUEOUS SOLUTION OF SODIUM CHLORIDE

The column size was 6.5×52.5 mm, flow rate 0.69 ml min^{-1}, and void volume 0.72 ml.

(X)(Y)	*cis*-$(en)_2$	*cis*-α-trien
$(CN)_2$	6.93	6.52
$(Cl)_2$	8.20	8.26
$(Cl)(NO_2)$	8.71	
$(NO_2)_2$	8.75	8.44
$(N_3)_2$	8.77	8.79
$(N_3)(NO_2)$	8.81	
(Cl)(NCS)	9.09	
(NO_2)(NCS)	9.16	
$(NCS)_2$	9.70	9.40

TABLE 3. THE ADJUSTED RETENTION VOLUMES (ml) OF *cis*-$[Co(X)_2(en)_2]^+$ ON IEX 510 WHEN ELUTED BY 0.1 M AQUEOUS SOLUTIONS OF VARIOUS SALTS

The conditions are the same as in Table 1.

$(X)_2$	NaCl	$phSO_3Na$	$NaClO_4$	KCl
$(CN)_2$	8.07	8.05	7.94	6.06
$(Cl)_2$	10.78	10.91	10.90	8.83
$(NO_2)_2$	12.80	12.31	12.26	10.22
$(N_3)_2$	14.98	13.13	13.06	10.26
$(NCS)_2$	32.00	30.25	28.54	21.64

from these tables that the *cis*-α-$[Co(X)_2(trien)]^+$ ions show adjusted retention volumes similar in magnitude to those of *cis*-$[Co(X)_2(en)_2]^+$ on both resins (correlation coefficient 0.9995 on IEX 510 and 0.981 on SP-Sephadex C-25). These results imply that two series of complexes are separated on both resins by a similar mechanism and we may discuss collectively the results of two series of complexes on both resins.

We may first confirm that the retention volumes listed in Tables 1 and 2 are obtained under the adsorption-governed conditions. If the system is adsorption-governed, the complex cations will be eluted primarily according to the difference in the affinities of the complex cation and the eluent cation to the resin. Therefore, the adjusted retention volume will be influenced more strongly by the kind of the eluent cation than by the eluent anion which may associate with the complex cation in the moving phase. Thus, the adjusted retention volumes have been measured on IEX 510 by using several eluents. The results for *cis*-bis(ethylenediamine)cobalt(III) complexes are given in Table 3. The adjusted retention volumes obtained by various eluents are highly correlated (correlation coefficients>0.995) and more importantly the change in the adjusted retention volume brought about by changing the eluent cation is much larger than the change caused by changing the eluent anion. Thus, the eluent cation has a dominant effect upon the adjusted retention volumes, which supports the view that the degree of adsorption to the resin is mainly affecting the retention volumes obtained on both resins.

If we look at Table 3 more closely, it can be seen that the adjusted retention volumes decrease, though slightly, as the eluent anion is changed from chloride through benzenesulfonate to perchlorate. This result indicates that the association between the complex cation and the eluent anion in the moving phase does have a contribution, though small, to the retention volumes. That the association between the complex cation and the eluent anion is important in ion-exchange chromatography will be most clearly appreciated by considering the optical resolution of metal complexes. For example, let us consider the case where a racemic complex cation is loaded on a resin and eluted by an aqueous solution containing some optically active anion, *e.g.*, *d*-tartrate or *d*-tartratoantimonate(III). Since in such a case the affinities of the *Λ*- and *Δ*-complex cations are exactly the same, we have to attribute the achievement of optical resolution by such a technique to the difference in the association constants of the *Λ*- and *Δ*-complex cations with the optically active anion.[7] There are many reported examples[8] of chromatographic optical resolution of metal complexes and it is apparent that retention volumes are more or less influenced by the association between the complex cation and the eluent anion in the moving phase. Note here, however, that the degree of optical resolution is always smaller than the degree of separation of different kinds of complexes, which suggests that the effect of elution is smaller than that of adsorption. This is also consistent with the view that our systems are adsorption-governed.

The data of Table 3 also indicate that the degree of ion association increases in the order Cl^-<benzenesulfonate<perchlorate. If we note that this order parallels the order of increasing character of water-structure breaker,[9] it follows that the univalent complexes examined in this work bear the character of water-structure breaker, because a water-structure breaker associates more favorably with water-structure breakers rather than with water-structure makers.[9] This inference gains some support from the works of Oh[10] and Pethybridge and Spiers.[11] Oh showed that for several ethylenediamine complexes of nickel(II), copper(II), and cobalt(III) with an overall charge of +1 or +2 the association of the complex cation with the iodide anion is favored over that with the chloride anion; the iodide ion is a well-known water-structure breaker while the chloride ion is a water-structure

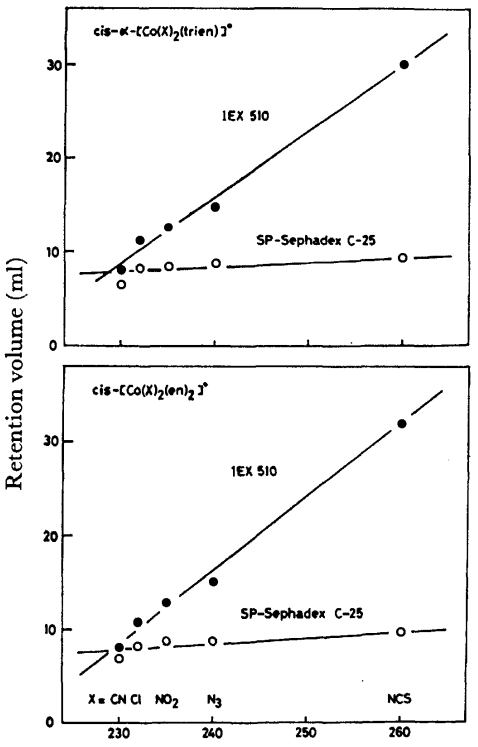

Fig. 1. The correlation between the adjusted retention volumes and the crystallographic volumes of $[Co(X)(NH_3)_5]Cl_2$.

maker.[12] Pethybridge and Spiers showed from conductance measurements that the association constants of $[Co(ox)(en)_2]X$ and *trans*-$[Co(NO_2)_2(en)_2]X$ in water increase in the order $X=Cl^-<Br^-<I^-<ClO_4^-$, where ox stands for the oxalate ion. Though they gave no explanation to these results, their results are most reasonably understood if we consider that univalent and bivalent complex cations bear the character of water-structure breaker.

Since the character of water-structure breaker is expected to get prominent as the volume of the complex cation increases,[9] we have plotted the adjusted retention volumes of *cis*-$[Co(X)_2(en)_2]^+$ and *cis*-α-$[Co(X_2)(trien)]^+$ on both resins against the crystallographic volumes of corresponding anionopentaamminecobalt(III) chlorides, $[Co(X)(NH_3)_5]Cl_2$, all of which are anhydrous and were analysed previously by X-ray diffraction.[13] The abscissa of Fig. 1 is thus the crystallographic volume of $[Co(X)(NH_3)_5]Cl_2$, namely, the unit cell volume divided by the number of molecules in a unit cell. As seen from Fig. 1, the correlation between the two quantities is very good; the correlation coefficients are 0.996 and 0.878 for *cis*-$[Co(X)_2(en)_2]^+$ on IEX 510 and SP-Sephadex C-25, respectively, and 0.995 and 0.754 for *cis*-α-$[Co(X)_2(trien)]^+$ on IEX 510 and SP-Sephadex C-25, respectively. This correlation, in conjunction with the system being adsorption governed, indicates that the complex cation is more tightly bound to the resin function as the crystallographic volume of the cation increases. The correlation in Fig. 1 seems to be quite reasonable in view of the previously reported trend in the association constants of various metal salts. For example, Pethybridge and Spiers[14] reported that the association constants of most 1 : 1 salts in water, including those forming outer-sphere complexes, are primarily determined by the combined size of the two ions; the association constants gets larger as the sum of the crystallographic radii of the two ions increases. It is very interesting to note that the quantity which is correlated with the association constants or the retention volumes is the crystallographic volume of the complex cation, not the hydrodynamic volume of the cation as estimated from, *e.g.*, conductance measurements. In fact, we could find no correlation between the retention volumes and the effective ionic radii of *cis*-$[Co(X)_2(en)_2]^+$, which we have estimated from conductance measurements in water.[15]

Finally, it will be pertinent to point out that the dipole moments of the complex cations do not contribute significantly to the observed retention volumes. This statement follows from the observation that the *trans*-$[Co(X)_2(en)_2]^+$ ions exhibited the same elution order as the corresponding *cis* complexes and the retention volume of *trans*-$[Co(X)(Y)(en)_2]^+$ $(X\neq Y)$ fell midway between the retention volumes of *trans*-$[Co(X)_2(en)_2]^+$ and *trans*-$[Co(Y)_2(en)_2]^+$.[15] Clearly the *trans*-$[Co(X)(Y)(en)_2]^+$ ion can have a dipole moment but the parent complexes can not. Therefore, we conclude that the univalent cations, *cis*-$[Co(X)(Y)(en)_2]^+$ and *cis*-α-$[Co(X)_2(trien)]^+$, assume more and more the character of water-structure breaker and hence get adsorbed to the resins more strongly as the crystallographic volume of the complex cation increases.

The authors thank Mr. S. Yamazaki, Toyo Soda Manufacturing Co., Ltd., for supplying the IEX 510 resin.

References

1) Part II: H. Yoneda, C. E. Oh, and S. Yamazaki, *Bull. Chem. Soc. Jpn.*, **53**, 2403 (1980).

2) See, for a review; L. F. Druding and G. B. Kauffman *Coord. Chem. Rev.*, **3**, 409 (1968).

3) H. Yoneda and S. Yamazaki, *Bull. Chem. Soc. Jpn.*, **52**, 1859 (1979).

4) H. Yoneda, C. E. Oh, and S. Yamazaki, *Bull. Chem. Soc. Jpn.*, **53**, 2403 (1980).

5) See, for example: G. H. Searle, *Aust. J. Chem.*, **30**, 2625 (1977); K. Sakakibara, Y. Yoshikawa, and H. Yamatera, *Bull. Chem. Soc. Jpn.*, **52**, 2725 (1979).

6) See, for example: M. Mori, M. Shibata, and K. Hori, *Bull. Chem. Soc. Jpn.*, **34**, 1809 (1961); M. Mori, M. Shibata, M. Nanasawa, *ibid.*, **29**, 947 (1956); Y. Yoshikawa, M. Kojima, M. Fujita, M. Iida, and H. Yamatera, *Chem. Lett.*, **1974**, 163; K. Kobayashi and M. Shibata, *Bull. Chem. Soc. Jpn.*, **48**, 2561 (1975).

7) H. Nakazawa and H. Yoneda, *J. Chromatogr.*, **160**, 89 (1978); S. Yamazaki and H. Yoneda, *ibid.*, **177**, 227 (1979); H. Yoneda, *J. Liq. Chromatogr.*, **2**, 1157 (1979).

8) See, for a review: Y. Yoshikawa and K. Yamasaki, *Coord. Chem. Rev.*, **28**, 205 (1979).

9) See, *e. g.*: B. G. Cox and A. J. Parker, *J. Am. Chem. Soc.*, **94**, 3674 (1972); C. M. Criss and M. J. Mastroianni, *J. Phys. Chem.*, **75**, 2532 (1971); H. Yoneda, M. Muto, T. Baba, and T. Miura, *Bull. Chem. Soc. Jpn.*, **44**, 689 (1971).

10) C. E. Oh, *J. Sci. Hiroshima Univ., Ser. A*, **44**, 145 (1980).
11) A. D. Pethybridge and D. J. Spiers, *J. Chem. Soc., Faraday Trans. 1*, **72**, 64 (1976).
12) See, *e.g.*: K. Miyoshi, T. Taura, C. Shimada, and H. Yoneda, *Bull. Chem. Soc. Jpn.*, **44**, 783 (1975).
13) Y. Kushi, Ph. D. Thesis, Osaka City University (1968); W. Ozbirn and R. A. Jacobson, *Inorg. Chim. Acta*, **4**, 377 (1970).
14) A. D. Pethybridge and D. J. Spiers, *J. Chem. Soc., Chem. Commun.*, **1974**, 423; A. D. Pethybridge and D. J. Spiers, *J. Chem. Soc., Faraday Trans. 1*, **72**, 64 (1976).
15) S. Wakida, U. Sakaguchi, and H. Yoneda, unpublished.

 © 1982 The Chemical Society of Japan Bull. Chem. Soc. Jpn., 55, 1077—1082 (1982)

Characterization of *trans*(*O*)-*N*,*N*′-Ethylenebis(*S*-methyl-L-cysteinato)-cobalt(III) Perchlorate and the Absolute Configuration of the Complex Determined by X-Ray Analysis

Ken-ichi OKAMOTO,* Takashi ISAGO, Masaaki OHMASA,† and Jinsai HIDAKA

Department of Chemistry, University of Tsukuba, Ibaraki 305

†*Institute of Materials Science, University of Tsukuba, Ibaraki 305*

(Received September 24, 1981)

A cobalt(III) complex with the sexidentate ligand, *N*,*N*′-ethylenebis(*S*-methyl-L-cysteine), was newly synthesized and chromatographically isolated. Of two possible geometrical isomers, trans(O) and trans(N), one isomer was formed selectively. The dark-red crystals are orthorhombic, space group $P2_12_12_1$, $a=9.055(2)$, $b=22.123(7)$, $c=17.111(4)$ Å, and $Z=8$. The structure was solved by the direct method and refined to $R=0.066$ for 2380 non-zero reflections. The complex is trans(O) isomer and the crystal consists of two kinds of complex cations with respect to the absolute configurations of the coordinated asymmetric sulfur atom. One takes an *S*(S),*S*(S) configuration and the other an *R*(S),*S*(S) one. The changes in configuration between the asymmetric sulfur atoms in the crystal and those in aqueous solution are discussed on the basis of NMR (^{13}C and ^1H) spectral studies.

Cobalt(III) complexes with sulfur-containing amino carboxylates have been extensively investigated during the past several years.[1-12] However, the properties of the thioether type sulfur atom which takes *R* or *S* configuration by coordination have been little known yet. Recently, Jackson and Sargeson suggested that a sulfur inversion in the *S*-bonded thioether–cobalt(III) complexes occurs in aqueous solution.[5] The sexidentate ligand in this work, *N*,*N*′-ethylenebis(*S*-methyl-L-cysteine), has two chiral centers, *R*(C) and *R*(C).[13] As seen in Fig. 1, the possible geometrical isomers for the

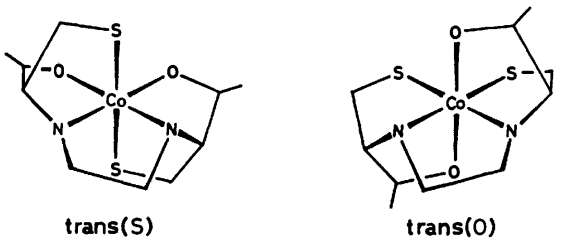

Fig. 1. Two geometrical isomers of [Co(*R*,*R*-ebsmc)]$^+$.

[Co(*R*,*R*-ebsmc)]$^+$ complex are limited to two, *trans*(*O*)-*R*(N),*R*(N) and *trans*(*S*)-*S*(N),*S*(N), where the abbreviation, *R*,*R*-ebsmc, is used for the present sexidentate ligand. For each of the two isomers, three other isomers, *S*(S),*S*(S), *R*(S),*S*(S), and *R*(S),*R*(S), due to the asymmetric sulfur atoms of the coordinated *R*,*R*-ebsmc are possible.

In the present study, the *R*,*R*-H_2ebsmc ligand has been prepared from *S*-methyl-L-cysteine and 1,2-dibromoethane. The [Co(*R*,*R*-ebsmc)]$^+$ complex has been prepared and it has been chromatographically confirmed that only one geometrical isomer is formed. The crystal structure and absolute configuration of the isomer are established by X-ray diffraction studies. The chiral behavior of the sulfur atoms in solution is discussed on the basis of the ^1H and ^{13}C NMR spectra of the isomer, by comparison with the asymmetric sulfur atoms in the crystal. A preliminary report has been presented.[14]

Experimental

Preparation of R,R-H_2*ebsmc.* The *R*,*R*-H_2ebsmc ligand was prepared by a procedure modified from that used in the preparation of ethylenediaminedisuccinic acid.[15] *S*-Methyl-L-cysteine (16.9 g) was dissolved in 30 cm^3 of an aqueous solution containing sodium hydroxide (5.0 g). The solution was poured into a 100 cm^3 round bottom flask fitted with a condenser, and refluxed. To the solution were slowly added 1,2-dibromoethane (11.8 g) and sodium carbonate (6.6 g) over a period of 30 min. The mixture was continuously stirred under reflux for 3 h. The resulting reddish-brown mixture was cooled to room temperature and filtered to remove insoluble materials. When the pH of the filtrate was adjusted to 6 with concentrated hydrochloric acid, white crystals appeared (5.2 g). The crude product obtained was washed well with 80 cm^3 of warm water (*ca.* 60 °C). The product was recrystallized from a dilute aqueous solution of sodium hydroxide by adding concentrated hydrochloric acid. The crystals were collected, washed with water and then with acetone, and dried in a vacuum desiccator over $CaCl_2$. Yield 4.5 g. Found: C, 40.39; H, 6.67; N, 9.36; S, 21.41%. Calcd for $C_{10}H_{20}N_2O_4S_2$: C, 40.52; H, 6.80; N, 9.45; S, 21.63%.

Preparation of trans(O)-[*Co*(R,R-*ebsmc*)]ClO_4. To a suspension of *R*,*R*-H_2ebsmc (0.7 g) in 50 cm^3 of hot water (70 °C) were added $CoCl_2\cdot 6H_2O$ (0.55 g) and lead dioxide (1.5 g). The mixture was stirred at about 70 °C for 20 min, whereupon the solution became orange-red. The reaction mixture was cooled to room temperature and filtered to remove the excess of lead dioxide. The orange-red filtrate was poured onto an ion-exchange column (5 × 15 cm) containing SP-Sephadex C-25 resin (Na^+ form). After sweeping the column with water, the adsorbed band was eluted with 0.2 mol dm^{-3} aqueous solution of $NaClO_4$. Only one orange-red band was eluted and fractionated. It was found, from the absorption and CD spectra of the fractionated eluates, that the eluate contained only *trans*(*O*)-[Co(*R*,*R*-ebsmc)]$^+$. The eluate was concentrated to 20 cm^3 using a rotary evaporator below 30 °C, and then kept in a refrigerator. The dark-red crystals obtained were collected, washed with ethanol and then with ether, and dried in air. Yield 0.06 g. Found: C, 26.49; H, 4.18; N, 6.27%. Calcd for $CoC_{10}H_{18}N_2O_8S_2Cl$: C, 26.53; H, 4.01; N, 6.19%.

The halide (Cl^-, Br^-, or I^-) salt of this complex cation was also obtained by the elution with an aqueous solution of NaCl,

NH_4Br, or NaI instead of that of $NaClO_4$.

Measurements. The electronic absorption spectrum was recorded with a JASCO UVIDEC-1 spectrophotometer,and the CD spectrum with a JASCO J-20 spectropolarimeter. All measurements were carried out in aqueous solution at room temperature.

The ^1H and ^{13}C NMR spectra were recorded in deuterium oxide on a JEOL JNM-FX-100 NMR spectrometer at the probe temperature. For ^1H NMR spectrum, sodium 2,2-dimethyl-2-silapentane-5-sulfonate was used as an internal reference. The ^{13}C chemical shifts were measured relative to external benzene and converted into the chemical shifts from TMS using the relation $\delta_{TMS}=\delta_{benzene}-128.50$ ppm.

The symmetry and approximate cell dimensions of the crystal were determined from Weisenberg and precession photographs. The more accurate cell dimensions were obtained by a least-squares analysis of 2θ measured on a Philips PW 1100 automated four circle diffractometer. The crystal data are summarized in Table 1.

Table 1. Crystal data

Molecular formula	$CoC_{10}H_{18}N_2O_8S_2Cl$
Molecular weight	452.77
Space group	$P2_12_12_1$
Cell constants	$a=9.055(2)$ Å
	$b=22.123(7)$ Å
	$c=17.111(4)$ Å
Density obsd	1.77 g/cm^3
calcd	1.76 g/cm^3
	(for $Z=8$)

A crystal with dimensions of 0.4 mm × 0.2 mm × 0.1 mm was used for data collection. Intensity data were collected on the Philips PW 1100 automated four circle diffractometer with Mo $K\alpha$ radiation monochromatized by graphite. The ω-2θ scan technique was employed and reflections for $2\theta<70°$ were recorded. A total of 2380 independent non-zero reflections were used for the structure determination. The intensities were corrected for the Lorentz and polarization factors, but no absorption correction was applied.

Structure Determination

The structure was solved by the use of MULTAN.[16] Four sets of phases were calculated using the 180 $|E|$'s greater than 1.58. The set of phases with the highest confined figures of merit was used to calculate an E map which yielded the positions of the cobalt, sulfur, oxygen, nitrogen, and chlorine atoms. Fourier and difference-Fourier maps based on these atoms revealed the rest of the structure. The structure was refined by a full-matrix least-squares refinement of the positional and anisotropic thermal parameters (program ORFLS by W. R. Busing, K. O. Martin, and H. A. Levy was used). The final R value ($\sum||F_o|-|F_c||/\sum|F_o|$) was 0.066 for all the non-hydrogen atoms. The atomic scattering factors were taken from "International Tables for X-Ray Crystallography."[17] The calculations were carried out on an ACOS 800II computer at The University of Tsukuba. The final atomic parameters and their standard deviations are given in Table 2. A list of the anisotropic thermal parameters and a table of the observed and calculated structure factors are kept at the Chemical Society of Japan (Document No. 8215).

Table 2. The atomic positional parameters, with their e.s.d.'s in parentheses ($\times 10^4$)

Atom	x	y	z	B_{eq}/Å^2 a)	Atom	x	y	z	B_{eq}/Å^2 a)
Co(1)	7181(2)	884(1)	1761(1)	2.59	N(1)	3991(12)	5469(4)	2462(6)	3.06
Co(2)	7416(2)	3542(1)	3207(1)	2.56	N(2)	4589(10)	5917(5)	3872(5)	3.04
Cl(1)	2347(5)	98(2)	4128(2)	4.51	N(3)	6133(10)	2962(4)	2702(6)	2.88
Cl(2)	2826(5)	2279(2)	983(3)	5.61	N(4)	8589(9)	3553(4)	2244(5)	2.60
S(1)	9188(4)	718(2)	2513(2)	3.97	C(1)	−68(17)	6435(6)	2235(8)	4.74
S(2)	8262(4)	1451(2)	820(2)	3.67	C(2)	1863(17)	5573(6)	1585(8)	4.46
S(3)	5968(4)	3494(2)	4277(2)	4.03	C(3)	3505(16)	5757(5)	1722(7)	4.00
S(4)	1080(4)	9289(2)	1352(2)	3.73	C(4)	3590(15)	6424(6)	1915(7)	3.65
O(1)	3308(9)	6577(3)	2618(4)	3.21	C(5)	105(16)	6057(7)	4528(10)	5.30
O(2)	3874(13)	6793(4)	1390(5)	5.18	C(6)	3052(17)	6249(6)	4956(7)	4.93
O(3)	7561(10)	172(3)	1180(4)	3.30	C(7)	4051(15)	5732(6)	4656(7)	3.75
O(4)	2913(13)	4762(5)	4958(6)	6.79	C(8)	3055(17)	5165(7)	4485(8)	4.95
O(5)	4021(8)	9113(4)	2158(4)	3.13	C(9)	4375(17)	555(6)	2353(8)	4.76
O(6)	3638(8)	4183(4)	2454(5)	3.82	C(10)	4266(14)	505(6)	1449(7)	3.37
O(7)	1201(9)	7958(3)	1470(4)	2.96	C(11)	3364(17)	7900(7)	61(8)	4.89
O(8)	1197(9)	2729(4)	3347(5)	4.20	C(12)	4395(15)	3125(6)	3787(8)	4.24
O(9)	1295(16)	9649(8)	3708(11)	15.38	C(13)	4597(13)	3217(6)	2866(8)	3.56
O(10)	3801(13)	9757(7)	3919(6)	8.60	C(14)	4736(15)	3886(6)	2685(8)	3.33
O(11)	2105(14)	9929(7)	4922(6)	10.10	C(15)	273(17)	9039(7)	411(8)	5.52
O(12)	2251(18)	554(6)	3903(8)	11.19	C(16)	417(14)	4137(6)	2940(8)	3.68
O(13)	3242(35)	2062(8)	342(9)	24.04	C(17)	−108(13)	8538(6)	2443(7)	2.98
O(14)	1343(15)	2310(7)	1012(15)	17.84	C(18)	105(13)	3027(5)	3180(7)	3.14
O(15)	3241(19)	1927(6)	1598(9)	12.89	C(19)	3530(13)	7961(6)	3144(8)	3.29
O(16)	3289(17)	2871(6)	1130(8)	10.86	C(20)	1836(13)	8008(6)	3237(7)	3.33

a) $B_{eq}=8\pi^2(U_1+U_2+U_3)/3$ where U_1, U_2, and U_3 are the principal components of the U matrix.

Results and Discussion

Description of the Structure. Perspective drawings of the complex cations obtained are given in Fig. 2 and their packing mode is illustrated in Fig. 3. The bond lengths and angles with their estimated standard deviations in the complex ions are given in Tables 3 and 4, respectively. There are two crystallographically independent complex cations in an asymmetric unit. In both complex cations, the *R*,*R*-ebsmc ligand is sexidentate and the coordination around cobalt atoms is approximately octahedral. The cobalt atoms are surrounded by two *cis* sulfur, two *cis* nitrogen, and two trans oxygen atoms. Both cations can be designated as trans(O) configuration. The preferred *cis* configiration of the two coordinated sulfur atoms was also recognized in the case of the cobalt(III) complexes with the sulfur-containing amino carboxylates.[10,11] The absolute configuration of the complex cations in the crystal can be confirmed on the basis of the asymmetric carbon atoms, *R*(C),*R*(C), in the coordinated sexidentate ligand. As a result, the absolute configurations of the two nitrogen atoms in each of the two complex cations are determined to be *R*(N),*R*(N), as expected. Each of the two sulfur atoms in these cations becomes chiral by coordination. This means, as seen in Fig. 2, that the two sulfur atoms take the *S*(S),*S*(S) configuration in complex (a), whereas the sulfur atoms are in the *R*(S),*S*(S) one in complex (b). The *S*(S),*S*(S) complex has a pseudo-twofold axis through the Co(1) which bisects the S(1)–S(2) edge of the octahedron, whereas the *R*(S),*S*(S) complex takes a C_1 symmetry (Fig. 2).

The cobalt-ligand bond lengths are all similar to those for the cobalt(III) complexes with the sulfur-containing amino carboxylates.[7-12] The bond angles at the cobalt atoms of both complex cations are slightly distorted from their idealized values, that is, *cis* angles are in the range of 82.6—98.5° and *trans* angles 171.8—177.4° (Table 4). The interatomic distances and bond angles in the two crystallographically independent complex cations corre-

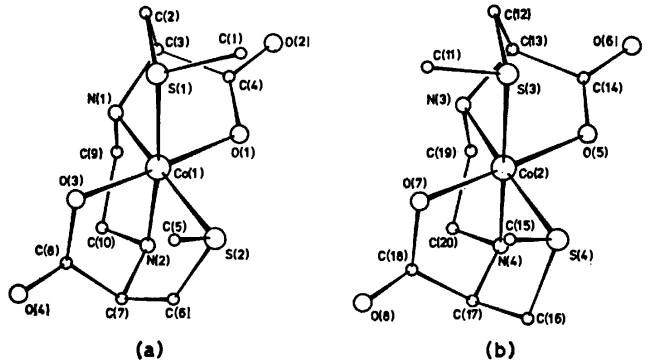

Fig. 2. Structure of *trans*(*O*)-[Co(*R*,*R*-ebsmc)]$^+$ ion; (a) *S*(S),*S*(S) and (b) *R*(S),*S*(S) isomers.

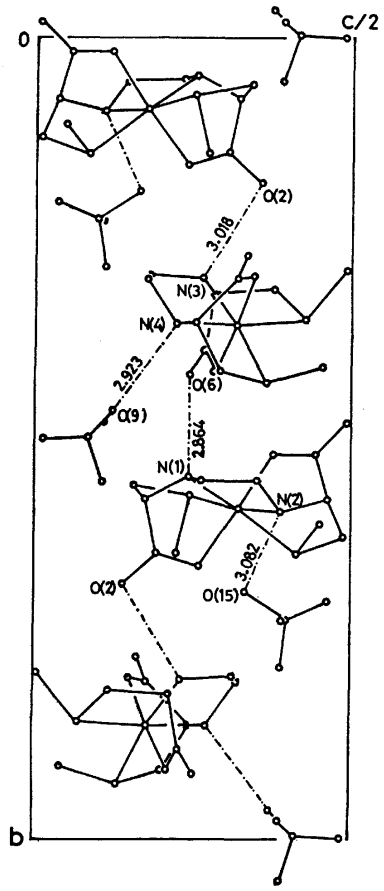

Fig. 3. A projection of the crystal packing viewed along a axis.

Table 3. Intramolecular distances (with e.s.d.'s) for *trans*(*O*)-[Co(*R*,*R*-ebsmc)]ClO_4

	l/Å		*l*/Å
Complex (a)		Complex (b)	
Co(1)–S(1)	2.257(4)	Co(2)–S(3)	2.253(4)
Co(1)–S(2)	2.264(4)	Co(2)–S(4)	2.270(4)
Co(1)–O(1)	1.916(8)	Co(2)–O(5)	1.918(8)
Co(1)–O(3)	1.895(7)	Co(2)–O(7)	1.883(8)
Co(1)–N(1)	1.933(10)	Co(2)–N(3)	1.935(10)
Co(1)–N(2)	1.936(10)	Co(2)–N(4)	1.962(9)
S(1)–C(1)	1.828(13)	S(3)–C(11)	1.838(13)
S(1)–C(2)	1.842(14)	S(3)–C(12)	1.843(14)
S(2)–C(5)	1.816(15)	S(4)–C(15)	1.851(14)
S(2)–C(6)	1.838(14)	S(4)–C(16)	1.849(12)
O(1)–C(4)	1.276(13)	O(5)–C(14)	1.262(14)
O(2)–C(4)	1.240(13)	O(6)–C(14)	1.256(14)
O(3)–C(8)	1.267(14)	O(7)–C(18)	1.334(14)
O(4)–C(8)	1.212(15)	O(8)–C(18)	1.222(13)
N(1)–C(3)	1.483(16)	N(3)–C(13)	1.527(15)
N(1)–C(9)	1.525(17)	N(3)–C(19)	1.479(16)
N(2)–C(7)	1.486(15)	N(4)–C(17)	1.477(14)
N(2)–C(10)	1.486(15)	N(4)–C(20)	1.510(14)
C(2)–C(3)	1.559(20)	C(12)–C(13)	1.600(18)
C(3)–C(4)	1.515(16)	C(13)–C(14)	1.516(17)
C(6)–C(7)	1.547(18)	C(16)–C(17)	1.505(17)
C(7)–C(8)	1.573(18)	C(17)–C(18)	1.554(16)
C(9)–C(10)	1.554(18)	C(19)–C(20)	1.546(16)
ClO_4^- Ion		ClO_4^- Ion	
Cl(1)–O(9)	1.317(12)	Cl(2)–O(13)	1.256(14)
Cl(1)–O(10)	1.401(11)	Cl(2)–O(14)	1.345(14)
Cl(1)–O(11)	1.377(10)	Cl(2)–O(15)	1.361(13)
Cl(1)–O(12)	1.497(13)	Cl(2)–O(16)	1.396(12)

Table 4. Bond angles(with e.s.d.'s) for *trans*(*O*)-[Co(*R*,*R*-ebsmc)]ClO_4

	ϕ/°		ϕ/°
Complex (a)		S(4)-Co(2)-N(4)	86.88(29)
S(1)-Co(1)-S(2)	98.47(15)	O(5)-Co(2)-N(3)	83.33(36)
S(1)-Co(1)-O(1)	90.05(27)	O(5)-Co(2)-N(4)	94.86(35)
S(1)-Co(1)-O(3)	90.99(27)	O(7)-Co(2)-N(3)	94.29(38)
S(2)-Co(1)-O(1)	92.94(25)	O(7)-Co(2)-N(4)	83.98(35)
S(2)-Co(1)-O(3)	90.48(26)	N(3)-Co(2)-N(4)	87.56(40)
S(1)-Co(1)-N(1)	88.44(32)	O(5)-Co(2)-O(7)	177.40(34)
S(2)-Co(1)-N(2)	86.50(29)	S(3)-Co(2)-N(4)	176.51(29)
O(1)-Co(1)-N(1)	82.60(37)	S(4)-Co(2)-N(3)	172.46(31)
O(1)-Co(1)-N(2)	95.05(39)	Co(2)-S(3)-C(11)	110.08(48)
O(3)-Co(1)-N(1)	93.82(38)	Co(2)-S(3)-C(12)	95.84(42)
O(3)-Co(1)-N(2)	83.60(41)	C(11)-S(3)-C(12)	102.66(66)
N(1)-Co(1)-N(2)	87.05(42)	Co(2)-S(4)-C(15)	107.96(55)
O(1)-Co(1)-O(3)	176.25(36)	Co(2)-S(4)-C(16)	95.14(42)
S(1)-Co(1)-N(2)	172.70(34)	C(15)-S(4)-C(16)	103.12(63)
S(2)-Co(1)-N(1)	171.81(33)	Co(2)-O(5)-C(14)	114.32(83)
Co(1)-S(1)-C(1)	110.12(49)	Co(2)-O(7)-C(18)	112.30(72)
Co(1)-S(1)-(C2)	95.13(48)	Co(2)-N(3)-C(13)	102.71(71)
C(1)-S(1)-C(2)	100.27(68)	Co(2)-N(3)-C(19)	108.35(72)
Co(1)-S(2)-C(5)	108.64(54)	C(13)-N(3)-C(19)	111.60(100)
Co(1)-S(2)-C(6)	95.72(41)	Co(2)-N(4)-C(17)	101.44(67)
C(5)-S(2)-C(6)	100.00(70)	Co(2)-N(4)-C(20)	108.07(69)
Co(1)-O(1)-C(4)	110.96(75)	C(17)-N(4)-C(20)	114.60(89)
Co(1)-O(3)-C(8)	113.70(94)	S(3)-C(12)-C(13)	107.65(83)
Co(1)-N(1)-C(3)	102.76(74)	N(3)-C(13)-C(12)	103.78(106)
Co(1)-N(1)-C(9)	109.33(76)	N(3)-C(13)-C(14)	104.34(101)
C(3)-N(1)-C(9)	114.33(103)	C(12)-C(13)-C(14)	109.50(110)
Co(1)-N(2)-C(7)	102.90(72)	O(5)-C(14)-O(6)	124.37(121)
Co(1)-N(2)-C(10)	110.33(72)	O(5)-C(14)-C(13)	114.81(122)
C(7)-N(2)-C(10)	113.17(101)	O(6)-C(14)-C(13)	120.61(123)
S(1)-C(2)-C(3)	107.70(90)	S(4)-C(16)-C(17)	108.00(85)
N(1)-C(3)-C(2)	107.42(110)	N(4)-C(17)-C(16)	108.08(100)
N(1)-C(3)-C(4)	102.53(97)	N(4)-C(17)-C(18)	105.34(91)
C(2)-C(3)-C(4)	109.61(110)	C(16)-C(17)-C(18)	110.06(100)
O(1)-C(4)-O(2)	123.43(119)	O(7)-C(18)-O(8)	123.44(121)
O(1)-C(4)-C(3)	116.92(108)	O(7)-C(18)-C(17)	113.13(99)
O(2)-C(4)-C(3)	119.60(113)	O(8)-C(18)-C(17)	123.41(120)
S(2)-C(6)-C(7)	108.56(79)	N(3)-C(19)-C(20)	107.83(108)
N(2)-C(7)-C(6)	106.71(106)	N(4)-C(20)-C(19)	104.47(99)
N(2)-C(7)-C(8)	103.88(97)	ClO_4^- Ion	
C(6)-C(7)-C(8)	108.45(111)	O(9)-Cl(1)-O(10)	116.32(84)
O(3)-C(8)-O(4)	124.25(157)	O(9)-Cl(1)-O(11)	116.23(106)
O(3)-C(8)-C(7)	114.19(120)	O(9)-Cl(1)-O(12)	103.12(113)
O(4)-C(8)-C(7)	121.56(125)	O(10)-Cl(1)-O(11)	114.24(80)
N(1)-C(9)-C(10)	105.04(113)	O(10)-Cl(1)-O(12)	102.09(85)
N(2)-C(10)-C(9)	106.28(108)	O(11)-Cl(1)-O(12)	101.63(88)
Complex (b)		O(13)-Cl(2)-O(14)	110.53(180)
S(3)-Co(2)-S(4)	96.55(14)	O(13)-Cl(2)-O(15)	111.94(126)
S(3)-Co(2)-O(5)	84.34(25)	O(13)-Cl(2)-O(16)	115.13(120)
S(3)-Co(2)-O(7)	96.68(26)	O(14)-Cl(2)-O(15)	106.04(131)
S(4)-Co(2)-O(5)	92.07(26)	O(14)-Cl(2)-O(16)	104.23(102)
S(4)-Co(2)-O(7)	90.18(26)	O(15)-Cl(2)-O(16)	108.32(96)
S(3)-Co(2)-N(3)	88.96(31)		

spond well with each other. Only the S–Co–S angles are significantly different. The angles S(1)-Co(1)-S(2) and S(3)-Co(2)-S(4) are 98.5° and 96.6°, respectively. The values are significantly larger than the normal ones; these deviations may be attributed to the repulsion between methyl groups on the sulfur atoms.

Several hydrogen bonds are recognized between the two complex ions, and between the complex ions and the perchlorates: *e.g.*, N(1)-O(6), N(3)-O(2), N(2)-O(15), and N(4)-O(9) (Fig. 3). The bond lengths of the Co(1)-O(1) and Co(2)-O(5) are apparently longer than those of the Co(1)-O(3) and Co(2)-O(7), respec-

Table 5. Displacements of atoms from the least-squares plane

Diamine chelate ring			
Plane 1(a);[c] $0.2394X-0.8781Y-0.4144Z+1.4094=0$			
Co(1)*	0.0000	C(9)	−0.3905
N(1)*	0.0000	C(10)	0.3246
N(2)*	0.0000		
Plane 2(b);[c] $0.5636X+0.7475Y+0.3516Z-16.5225=0$			
Co(2)*	0.0000	C(19)	−0.3344
N(3)*	0.0000	C(20)	0.3957
N(4)*	0.0000		
S-Methyl groups			
Plane 3(a); $0.2018X-0.8285Y-0.5224Z+1.8826=0$			
Co(1)*	0.0000	C(1)	−1.3804
S(1)*	0.0000	C(5)	1.3309
S(2)*	0.0000		
Plane 4(b); $0.6105X+0.6852Y+0.3973Z-15.5951=0$			
Co(2)*	0.0000	C(11)	1.7199
S(3)*	0.0000	C(15)	1.4636
S(4)*	0.0000		
S–N chelate ring			
Plane 5(a); $0.1581X-0.8674Y-0.4719Z+2.0899=0$			
Co(1)*	0.0000	C(2)	−0.6010
S(1)*	0.0000	C(3)	−1.0788
N(1)*	0.0000		
Plane 6(a); $0.2832X-0.8326Y-0.4761Z+1.2217=0$			
Co(1)*	0.0000	C(6)	0.6668
S(2)*	0.0000	C(7)	1.1189
N(2)*	0.0000		
Plane 7(b); $0.5598X+0.7477Y+0.3572Z-16.5354=0$			
Co(2)*	0.0000	C(12)	−0.4878
S(3)*	0.0000	C(13)	−1.1001
N(3)*	0.0000		
Plane 8(b); $0.6168X+0.6855Y+0.3868Z-15.5849=0$			
Co(2)*	0.0000	C(16)	0.5965
S(4)*	0.0000	C(17)	1.0801
N(4)*	0.0000		

The *X*, *Y*, and *Z* coordinates in Å are referred to the crystallographic axies. c): (a) and (b) denote the *S*(S),*S*(S) and *R*(S),*S*(S) isomers, respectively.

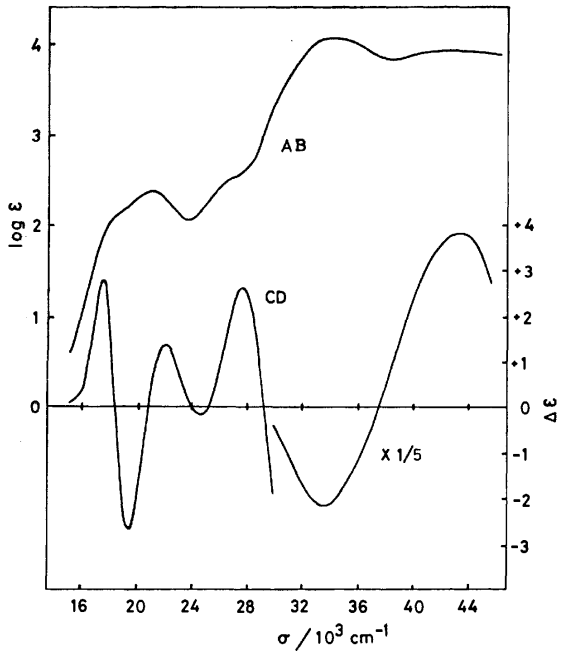

Fig. 4. Absorption and CD spectra of *trans*(*O*)-[Co(*R*,*R*-ebsmc)]$^+$.

Table 6. Absorption and CD spectral data of *trans*(*O*)-[Co(*R*,*R*-ebsmc)]$^+$ ion

Absorption maxima $\sigma/10^3$ cm^{-1} (log ε/mol^{-1} dm^3 cm^{-1})	CD extrema $\sigma/10^3$ cm^{-1} ($\Delta\varepsilon$/mol^{-1} dm^3 cm^{-1})
18.35(2.1 sh[a])	17.33(+2.82)
20.83(2.37)	19.27(−2.68)
	21.93(+1.38)
26.67(2.5 sh)	24.57(−0.17)
	27.47(+2.64)
34.01(4.07)	33.67(−10.8)
42.55(3.92)	43.48(+19.2)
48.78(3.85)	

a) sh: Shoulder.

tively (Table 3). These differences may be reflected by the stronger hydrogen bondings caused by the O(2) and O(6) atoms.

In order to examine the conformations of chelate rings, the displacements of relevant atoms from the chelate ring plane, which is defined by the central cobalt atom and the two coordinated atoms in the chelate ring, were calculated. The results are given in Table 5. The diamine chelate rings in both cations have asymmetric gauche form with λ conformation. This is in line with the case of diamines such as ethylenediamine and its derivatives.[18]

Electronic Absorption and CD Spectra. The electronic absorption and CD spectra of the *trans*(*O*)-[Co(*R*,*R*-ebsmc)]$^+$ are shown in Fig. 4 and their data are summarized in Table 6. The electronic absorption spectrum of the trans(O) complex shows an explicit shoulder on the lower energy side of the major peak in the first absorption band region. The splitting behavior is in line with the results from the semi-empirical calculation on the basis of the ligand field strength order N>S>O.[2,3,6] The sulfur-to-metal charge transfer band of the complex is observed at 34010 cm^{-1}.

The CD spectrum shows (+), (−), and (+) bands, listing from the lower energy side in the first absorption band region. A similar splitting pattern was observed in those of the $(-)_{576}$-[Co(*S*,*S*-edds)]$^-$ [15] and $(-)_{589}$-[Co(*S*,*S*-ebm)]$^+$ [1] which have a similar framework to that of the present trans(O) complex, where *S*,*S*-edds and *S*,*S*-ebm denote the *S*,*S*-ethylenediaminedisuccinate and ethylenebis(*S*-methioninate), respectively.

NMR Spectra. The ^{13}C and ^{1}H NMR spectra of the *trans*(*O*)-[Co(*R*,*R*-ebsmc)]$^+$ complex were measured in D_2O solution. The results are shown in Figs. 5 and 6. Taking the absolute configurations of the coordinated sulfur atoms into consideration, the ^{13}C NMR spectrum of the *S*(S),*S*(S) or *R*(S),*R*(S) isomer having a twofold axis is expected to show a single peak for each of the *S*-methyl, methylene, and methine

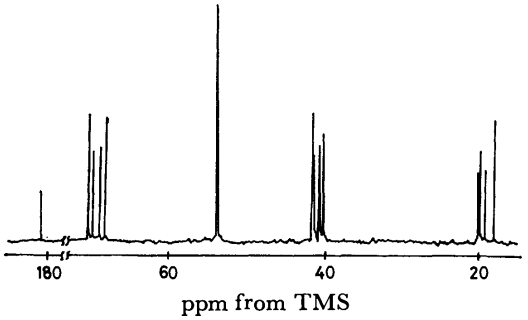

Fig. 5. ^{13}C NMR spectrum of *trans*(*O*)-[Co(*R*,*R*-ebsmc)]$^+$ in D_2O.

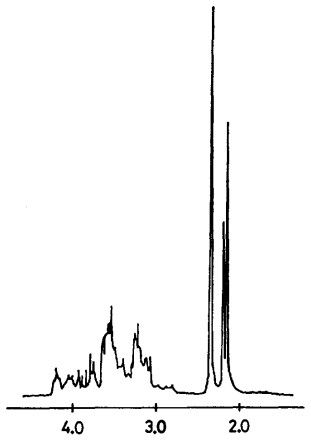

Fig. 6. ^1H NMR spectrum of *trans*(*O*)-[Co(*R*,*R*-ebsmc)]$^+$ in D_2O.

carbons. On the other hand, the *R*(S),*S*(S) isomer is expected to show two peaks for each of them because of a C_1 symmetry of the complex. If the configurations, *S*(S),*S*(S) and *R*(S),*S*(S), in crystal are retained in solution, the ^{13}C NMR spectrum will show the three peaks for each of the *S*-methyl, methylene, and methine carbons. As seen in Fig. 5, the spectrum exhibits the four peaks for each of the *S*-methyl (18.3—20.3 ppm from TMS), methylene (40.3—41.8 ppm), and methine (68.1—70.3 ppm) carbons, respectively. This fact suggests that the sulfur atoms of the *trans*(*O*)-*R*,*R*-ebsmc complex in solution take a different configuration from those in the crystal, that is, the present spectrum indicates a mixture of the *S*(S),*S*(S), *R*(S),*S*(S), and *R*(S),*R*(S) configurations. A similar trend was also observed for the ^1H NMR spectrum.

The ^1H NMR spectrum of *trans*(*O*)-*R*,*R*-ebsmc complex shows three peaks, at 2.19, 2.23, and 2.38 ppm (in the ratio 1.5 : 1.0 : 2.4) from DSS in the *S*-methyl proton region, soon after its dissolution (Fig. 6). It may be considered that the peak at 2.38 ppm is caused by partial overlap of the two peaks due to the two isomers. The peaks did not change significantly in the range from 5 °C to 60 °C. These facts are in agreement with the suggestion from the ^{13}C NMR study and suggest that the rate of the sulfur inversion in the present complex cations is slow on the NMR time scale. The complex chromatographed, however, gave only one adsorbed band and all of its fractionated eluates showed the same CD spectra. The attempt to precipitate fractionally as ClO_4^-, Cl^-, Br^-, and I^- salts from water yielded homogeneous crystals, which exhibited identical CD and NMR spectra. These results suggest that in aqueous solution a sulfur inversion similar to that for the *S*-bonded thioether-cobalt(III) complexes[5] occurs also in the present complex at room temperature, *i.e.*, *S*(S),*S*(S)$\rightleftarrows$*R*(S),*S*(S)$\rightleftarrows$*R*(S),*R*(S).

The authors thank to Prof. Y. Iitaka, The University of Tokyo, for his help in the collection of X-ray data.

References

1) R. J. Magee, W. Mazurec, M. J. O'Conner, and A. T. Phillip, *Aust. J. Chem.*, **27**, 1629 (1974).
2) J. Hidaka, S. Yamada, and Y. Shimura, *Chem. Lett.*, **1974**, 1487.
3) K. Yamanari, J. Hidaka, and Y. Shimura, *Bull. Chem. Soc. Jpn.*, **50**, 2299, 2451, 2643 (1977).
4) D. L. Herting, C. P. Sloan, A. W. Cabral, and J. H. Kreuger, *Inorg. Chem.*, **17**, 1649 (1978).
5) W. G. Jackson and A. M. Sargeson, *Inorg. Chem.*, **17**, 2165 (1978).
6) T. Isago, K. Igi, and J. Hidaka, *Bull. Chem. Soc. Jpn.*, **52**, 407 (1979).
7) H. C. Freeman, C. J. Moore, W. G. Jackson, and A. M. Sargeson, *Inorg. Chem.*, **17**, 3513 (1978).
8) G. J. Gainstord, W. G. Jackson, and A. M. Sargeson, *J. Chem. Soc., Chem. Commun.*, **1979**, 802.
9) P. de Meester and D. J. Hodgson, *J. Chem. Soc., Dalton Trans.*, **1976**, 618.
10) H. M. Helis, P. de Meester, and D. J. Hodgson, *J. Am. Chem. Soc.*, **99**, 3309 (1977).
11) R. J. Geue and M. R. Snow, *Acta Crystallogr., Sect. B*, **33**, 70 (1977).
12) K. Okamoto, K. Wakayama, M. Ohmasa, and J. Hidaka, *Chem. Lett.*, **1981**, 453.
13) *R* and *S* denote the absolute configuration of the asymmetric carbon, nitrogen, and sulfur atoms according to the sequence rule (*R*(C) and *S*(C) for the carbon atom, *R*(N) and *S*(N) for the coordinated nitrogen atom, and *R*(S) and *S*(S) for the coordinated sulfur atom).
14) T. Isago, K. Okamoto, M. Ohmasa, and J. Hidaka, *Chem. Lett.*, **1980**, 319.
15) J. A. Neal and N. J. Rose, *Inorg. Chem.*, **7**, 2405 (1968).
16) G. Germain and M. M. Woolfson, *Acta Crystallogr., Sect. A*, **27**, 368 (1971).
17) "International Tables for X-Ray Crystallography," Kynoch Press, Birmingham (1962), Vol. III.
18) C. J. Hawkins, "Absolute Configuration of Metal Complexes," Interscience Publishers, Inc., New York (1971).

 © 1982 The Chemical Society of Japan Bull. Chem. Soc. Jpn., 55, 1083—1085 (1982)

Stereochemistry of Bis[*N*-(2,6-diisopropylphenyl)salicylideneaminato]-copper(II) and nickel(II) Complexes

Shoichiro YAMADA* and Kuniko YAMANOUCHI

Institute of Chemistry, College of General Education, Osaka University, Toyonaka, Osaka 560

(Received October 3, 1981)

Bis[*N*-(2,6-diisopropylphenyl)salicylideneaminato]copper(II) and nickel(II) complexes have been synthesized. Their configurations in the solid state, in chloroform, and in pyridine have been examined and discussed in comparison with those of the related complexes.

The stereochemistry of copper(II) and nickel(II) complexes with bidentate *N*-arylsalicylideneaminates (I,

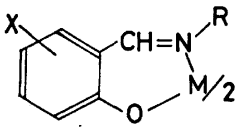

abbreviated as M(X-sal-R)$_2$) has been extensively studied.[1,2] For the most part, the copper(II) complexes of this series are planar, while the nickel(II) complexes are planar or multinuclear.[3] Bis[*N*-(2,6-dialkylphenyl)-salicylideneaminato]copper(II) and nickel(II) complexes, the alkyl being methyl or ethyl, were examined previously, with the view of investigating the effects of the substituents at the 2- and 6-positions of the salicylidene moiety on the structure of the metal complexes.[2-5] According to previous data on crystal structure analyses, the phenyl group is expected to be essentially perpendicular to the salicylideneaminate plane.[1] It also seems to be significant to examine the corresponding complexes with 2,6-diisopropylphenyl, the isopropyl being evidently more bulky than methyl and ethyl. Examination of bis[*N*-(2,6-diisopropylphenyl)-salicylideneaminato]cobalt(II) complexes, abbreviated as Co(X-sal-dpp)$_2$, revealed that the planar structure was neither precluded nor destabilized, but some of the cobalt(II) complexes (X=5-Br and 5-Cl) were forced into the planar structure in the solid state.[5] A similar study has now been extended to the copper(II) and nickel(II) complexes with the same ligands. The present paper describes the accounts of the study.

Experimental

Materials. 2,6-Diisopropylaniline was obtained commercially. Bis[*N*-(2,6-diisopropylphenyl)salicylideneaminato]-copper(II) and nickel(II) and analogous species, which are abbreviated as M(X-sal-dpp)$_2$, were synthesized in the same way as reported previously.[3] They are readily soluble in chloroform, benzene, and acetone, but sparingly soluble in ethanol. The nickel(II) complexes are olive-green, while the copper(II) complexes are brown-olive. Monopyridine adducts of the copper(II) complexes were obtained in dark green crystals by the addition of water or hexane to the pyridine solutions of the parent complexes. Analytical data of these complexes are given in Table 1.

Measurements. Electronic absorption spectra of the complexes in solution and in Nujol were recorded on a Shimadzu MPS-500 spectrophotometer. Magnetic measurements at room temperature were carried out by the Gouy method using CoHg(SCN)$_4$ as a calibrant.

Results and Discussion

Copper(II) Complexes. Bis(*N*-arylsalicylideneaminato)copper(II) complexes (I, R=Ph, Y-C$_6$H$_4$) normally prefer the planar geometry.[1-3] Electronic absorption spectra of Cu(X-sal-dpp)$_2$ (X=H, 5-Br, 5-NO$_2$, and 3-CH$_3$O) in chloroform and in Nujol (Fig. 1) are remarkably similar to each other and bear a close resemblance to the spectra of the copper(II)

Table 1. Analytical data of bis[*N*-(2,6-diisopropylphenyl)salicylideneaminato]-copper(II) and nickel(II) and their monopyridine adducts

Compound	Calcd(%)			Found (%)			μ/BM
	H	C	N	H	C	N	
Cu(H-sal-dpp)$_2$	7.10	73.11	4.49	7.17	73.03	4.55	1.9
Cu(H-sal-dpp)$_2$·py	7.02	73.42	5.97	7.01	73.13	5.94	2.1
Cu(5-Br-sal-dpp)$_2$	5.41	58.35	3.58	5.56	58.22	3.51	1.9
Cu(5-Br-sal-dpp)$_2$·py	5.50	59.97	4.88	5.40	59.83	4.94	2.0
Cu(5-NO$_2$-sal-dpp)$_2$	5.93	63.89	7.84	5.83	64.28	7.77	1.8
Cu(5-NO$_2$-sal-dpp)$_2$·py	5.97	65.09	8.83	6.09	65.40	9.20	2.0
Cu(3-CH$_3$O-sal-dpp)$_2$	7.07	70.20	4.09	6.87	70.41	4.17	1.8
Cu(3-CH$_3$O-sal-dpp)$_2$·py	6.98	70.81	5.51	7.12	70.75	5.56	2.0
Ni(H-sal-dpp)$_2$	7.16	73.68	4.52	7.24	73.54	4.56	dia
Ni(5-Br-sal-dpp)$_2$	5.45	58.72	3.60	5.56	58.84	3.50	dia
Ni(5-Cl-sal-dpp)$_2$	6.15	66.30	4.07	6.10	66.48	4.15	dia
Ni(5-NO$_2$-sal-dpp)$_2$	5.97	64.33	7.90	5.98	64.25	7.91	dia
Ni(3-CH$_3$O-sal-dpp)$_2$	7.12	70.70	4.12	7.36	70.98	4.15	dia

μ: BM at room temperature. dia: Diamagnetic. py: Pyridine.

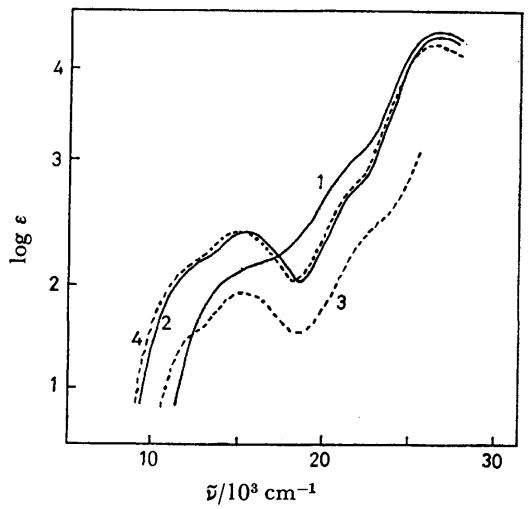

Fig. 1. Electronic absorption spectra of copper(II) complexes: 1, Cu(H-sal-dpp)$_2$ in $CHCl_3$; 2, Cu(H-sal-dpp)$_2$ in pyridine; 3, Cu(H-sal-dpp)$_2$–py in Nujol; 4, Cu(H-sal-2,6-Et_2-C_6H_3)$_2$ in pyridine.

complexes (I, R=Ph, 2,6-Me_2–C_6H_3, and 2,6-Et_2–C_6H_3), which were previously concluded to be planar.[2,3] Some of the representative spectra are shown in Fig. 1. It is thus presumed that the complexes Cu(X-sal-dpp)$_2$ are planar in the solid state and in chloroform.

The spectra of Cu(X-sal-dpp)$_2$ in pyridine have a d-d band maximum at 15.3×10^3 cm^{-1} with a shoulder on the lower frequency side. They are strikingly similar to each other, irrespective of the substituent X, showing that all these copper(II) complexes have essentially the same geometry. The spectra obey Beer's law in pyridine as well as in chloroform and are also remarkably similar to those of the complexes (I, R=Ph, 2,6-Et_2–C_6H_3), as shown in Fig. 1.[3] It is thus presumed that all these copper(II) complexes in pyridine exist exclusively as penta-coordinate monopyridine adducts. The monopyridine addusts can also be isolated in crystals from the pyridine solutions of the parent complexes. Electronic spectra of the monopyridine adducts in Nujol are similar to those of the parent complexes in pyridine (Fig. 1).

Nickel(II) Complexes. The complexes Ni(X-sal-dpp)$_2$ (X=H, 5-Cl, 5-Br, 5-NO_2, and 3-CH_3O) are all diamagnetic and consist of tetra-coordinate planar complexes in the solid state. Their spectra in chloroform and in Nujol are typical of the spin-paired, planar nickel(II) complexes with a d-d band at about $16—17 \times 10^3$ cm^{-1}. Representative spectra are shown in Fig. 2 and the maxima of the d-d bands are set out in Table 2. It is thus found that the steric condition in these complexes does not exclude the planar geometry. In this connection, it is interesting to remark that the complexes Co(X-sal-dpp)$_2$ (X=5-Br and 5-Cl) in the solid state prefer the planar geometry to the tetrahedral one, which is normally adopted by the tetra-coordinate

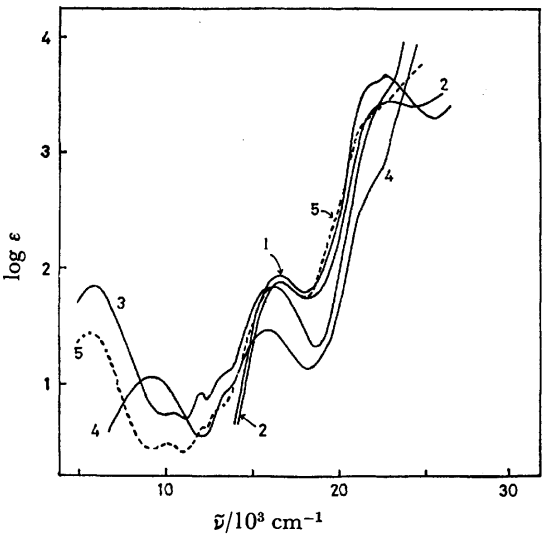

Fig. 2. Electronic absorption spectra nickel(II) complexes: 1, Ni(H-sal-dpp)$_2$ in $CHCl_3$; 2, Ni(H-sal-dpp)$_2$ in pyridine; 3, Ni(5-NO_2-sal-dpp)$_2$ in pyridine; 4, Ni-(3-CH_3O-sal-dpp)$_2$ in pyridine; 5, Ni(5-Cl-sal-dpp)$_2$ in pyridine.

Table 2. Absorption maxima of d-d bands of bis[*N*-(2,6-diisopropylphenyl)-salicylideneaminato]nickel(II), Ni(X-sal-dpp)$_2$

Compound	Medium	$\tilde{\nu}/10^3$ cm^{-1} (log ε)
Ni(H-sal-dpp)$_2$	$CHCl_3$	16.6(1.92)
	Nujol	16.6
	Pyridine	16.5(1.87)
Ni(5-Cl-sal-dpp)$_2$	$CHCl_3$	16.5(2.02)
	Nujol	16.5
	Pyridine	5.5(1.44), 16.5(1.88)
Ni(5-Br-sal-dpp)$_2$	$CHCl_3$	16.4(1.98)
	Nujol	16.5
	Pyridine	5.4(1.56), 16.3(1.84)
Ni(5-NO_2-sal-dpp)$_2$	$CHCl_3$	17.2(2.16)
	Nujol	17.1
	Pyridine	5.8(1.85), 16.1(1.82)
Ni(3-CH_3O-sal-dpp)$_2$	$CHCl_3$	16.1(1.96)
	Nujol	16.1
	Pyridine	9.1(1.06), 15.8(1.47)

cobalt(II) complexes.[5]

The d-d band maxima ($\tilde{\nu}$) of the planar nickel(II) complexes Ni(X-sal-dpp)$_2$ decrease in the following order as to the substituent X: 5-NO_2>H>5-Cl≈5-Br>3-CH_3O (series 1).

The present study indicates that it depends upon X whether or not and to what extent the complexes Ni(X-sal-dpp)$_2$ bind additional pyridine molecules, when dissolved in pyridine. The complex Ni(H-sal-dpp)$_2$ in pyridine exists mostly as the planar species, the penta-coordinate or hexa-coordinate pyridine adducts hardly being detected. The spectrum of the pyridine solution differs very little from that of the chloroform solution (Fig. 2).

On the contrary, Ni(3-CH_3O-sal-dpp)$_2$ in pyridine exists exclusively as hexa-coordinate species. The spectra have d-d bands at 9.4 and 15.9×10^3 cm^{-1} (Table 2), no absorption being observed at about $5—6\times10^3$ cm^{-1} (expected for the penta-coordinated species) or at about $16—17\times10^3$ cm^{-1} (for the tetra-coordinate species).

The complex Ni(5-NO_2-sal-dpp)$_2$ in pyridine exists entirely as penta-coordinate species. The spectrum is strikingly similar to that of the penta-coordinate nickel-(II) complex.[4] Beer's law is found to hold, so that the assumption of equilibria involving various species with different structures is not required.

Table 3. Structures of bis[*N*-(2,6-dialkylphenyl)-salicylideneaminato]nickel(II) complexes Ni(X-sal-R)$_2$ in pyridine[a]

X	R		
	2,6-Me_2-C_6H_3[b]	2,6-Et_2-C_6H_3[b]	2,6-(*i*-Pr)$_2$-C_6H_3
5-NO_2	6	6	5
H	4(65)+5(35)	4(80)+5(20)	4(95)+5(5)
5-Cl	4(20)+5(80)	4(40)+5(60)	4(70)+5(30)
5-Br	4(20)+5(80)	4(50)+5(50)	4(70)+5(30)
3-CH_3O	6	6	6

a) These nickel(II) complexes are tetra-coordinate-planar in non-donor solvents and in the solid state. The numbers in the parentheses are approximate proportions in percentage of the species in the solutions. The numbers of one figure in the table denote the coordination numbers. See also the text. b) The data are taken from Refs. 3 and 4 in the text.

The complexes Ni(5-Br-sal-dpp)$_2$ and Ni(5-Cl-sal-dpp)$_2$ in pyridine exist as equilibrium mixtures of the tetra-coordinate planar and penta-coordinate species. The spectra have a d-d band characteristic of the planar species at about 16.5×10^3 cm^{-1} and another d-d band characteristic of the penta-coordinate species at about 5.5×10^3 cm^{-1}, no absorption being observed at about $9—10\times10^3$ cm^{-1}, where the hexa-coordinate species is expected to absorb. McKenzie and coworkers made some approximate but useful estimates of the relative amounts of the species present in the solutions of the nickel(II) complexes (I, R=2,6-Me_2-C_6H_3 and 2,6-Et_2-C_6H_3) on the basis of the intensities of the various d-d bands in the spectra of these nickel(II) complexes.[4] Similar estimates have been made for the present nickel(II) complexes, following the method of McKenzie. The results of the estimates are shown in Table 3, the relevant data on the related complexes being included for comparison.[3,4] Numbers of one figure in the table represent the coordination numbers at the nickel(II) ion. The number 4 denotes "planar tetra-coordination."

Inspection of Table 3 indicates that the order as to the ability of Ni(X-sal-dpp)$_2$ to bind additional ligands is found to be lower than that of the corresponding dimethylphenyl and diethylphenyl complexes, showing that the steric effect of 2,6-diisopropylphenyl is larger than that of the 2,6-dimethyl- or 2,6-diethylphenyl. For instance, the difference in this respect is apparently noticed in the complexes with X=5-NO_2. Attempts to isolate penta-coordinate pyridine adducts Ni(X-sal-dpp)$_2$·py have not been successful so far, whereas the penta- and hexa-coordinate pyridine adducts of the 2,6-dimethylphenyl and 2,6-diethylphenyl complexes were isolated in crystals.[4]

Inspection of Table 3 also indicates that higher coordination numbers are favored in the following order as to X: 3-CH_3O>5-NO_2>5-Br≈5-Cl>H. The order, which is not in agreement with the series (1), results from the total effects of such factors as bulk steric effects, the electron-withdrawing power of the ring substituent, and the ligand-field strength of the salicyl-ideneaminates. At the moment, however, there seems to be no unambiguous explanation for the order.

Financial support of this work by the Ministry of Education is gratefully acknowledged.

References

1) R. H. Holm and M. J. O'Connor, *Progr. Inorg. Chem.*, **14**, 241 (1971).
2) S. Yamada, *Coord. Chem. Rev.*, **1**, 415 (1966).
3) S. Yamada, E. Ohno, Y. Kuge, A. Takeuchi, K. Yamanouchi, and K. Iwasaki, *Coord. Chem. Rev.*, **3**, 247 (1968); S. Yamada, A. Takeuchi, K. Yamanouchi, and K. Iwasaki, *Bull. Chem. Soc. Jpn.*, **42**, 131 (1969).
4) B. M. Higson, D. A. Lewton, and E. D. McKenzie, *J. Chem. Soc., Dalton Trans.*, **1974**, 1690.
5) S. Yamada and K. Yamanouchi, *Bull. Chem. Soc. Jpn.*, **55**, 418 (9982).

 © 1982 The Chemical Society of Japan Bull. Chem. Soc. Jpn., 55, 1086—1091 (1982) [Vol. 55, No. 4

Binuclear Metal Complexes. XLIV.[1] Crystal Structures and Magnetic Properties of Alkoxo-oxygen Bridged Binuclear Copper(II) Complexes with 2-[2-(Dialkylamino)ethylthio]ethanol

Masahiro MIKURIYA, Hisashi ŌKAWA, and Sigeo KIDA*

Department of Chemistry, Faculty of Science, Kyushu University 33, Hakozaki, Higashi-ku, Fukuoka 812

(Received October 22, 1981)

Six binuclear copper(II) complexes with 2-[2-(dialkylamino)ethylthio]ethanol, $Cu_2\{R_2N(CH_2)_2S(CH_2)_2O\}_2X_2$ (abbreviated as Cu(R-nso)X, where R=CH_3, C_2H_5, n-C_3H_7, n-C_4H_9; X=Cl, Br), were characterized by magnetic susceptibility (80—300 K). The temperature dependence of the magnetic susceptibilities of Cu(C_2H_5-nso)Cl and Cu(n-C_4H_9-nso)Cl can be interpreted by the Bleaney-Bowers equation based on a binuclear structure, while the magnetic data of the other complexes do not obey the Bleaney-Bowers equation. X-Ray structure analyses have revealed that the structures of all the complexes consist of discrete alkoxo-bridged binuclear units, and the coordination geometry of each copper atom is a distorted square pyramid with two oxygen, one sulfur and one chlorine or bromine atoms in the basal plane and a nitrogen atom in the apical position. The major structural difference corresponding to the different magnetic behaviors was attributed to the conformations of the chelate ring Cu–O–C(1)–C(2)–S.

In the preceding paper, we reported the synthesis, structure, spectra and magnetic properties of binuclear copper(II) complexes with 2-[2-(dialkylamino)ethylthio]ethanol, $Cu_2\{R_2N(CH_2)_2S(CH_2)_2O\}_2X_2$ (abbreviated as Cu(R-nso)X, where R=CH_3, C_2H_5, n-C_3H_7, n-C_4H_9; X=Cl, Br).[2] The X-ray structure analysis of Cu(CH_3-nso)Br showed that the crystal consists of discrete binuclear units. However, the temperature dependence of the magnetic susceptibility of Cu(CH_3-nso)Br does not obey the Bleaney-Bowers equation[3] based on a binuclear structure. Similar behaviors were also observed for other Cu(R-nso)X complexes so far prepared except for Cu(n-C_4H_9-nso)Cl. In order to clarify the origin of their unusual magnetic property, it is desirable to compare the detailed structures for a series of this type of complexes in relation to their magnetic behaviors. Hence, in this study, we have undertaken single-crystal X-ray structure analyses for Cu(CH_3-nso)Cl, Cu(C_2H_5-nso)Cl, Cu(n-C_3H_7-nso)Cl, Cu(n-C_4H_9-nso)Cl, Cu(n-C_3H_7-nso)Br and Cu(n-C_4H_9-nso)Br.

Experimental

Crystals of Cu(R-nso)Cl (R=CH_3, C_2H_5, n-C_3H_7, n-C_4H_9) and Cu(R-nso)Br (R=n-C_3H_7, n-C_4H_9) were prepared by the method previously reported.[2] The diffraction data were measured on a Rigaku AFC-5 automated four-circle diffractometer with graphite-monochromated Mo $K\alpha$ radiation (λ=0.71069 Å) at 20±0.5 °C. The unit-cell parameters of each crystal were determined by the least-squares refinement based on 20 high-angle reflections. The crystal data are shown in Table 1. The intensity data were collected by the 2θ-ω scan technique with a scan rate of 8° min^{-1}. For weak reflections the peak scan was repeated up to four times depending on their intensities. Three standard reflections were monitored every 100 reflections, and their intensities showed a good stability. The intensity data were corrected for the Lorentz and the polarization effects, but not for absorption.

The structures were solved by the heavy-atom method. The positions of the copper atoms were obtained from three-dimensional Patterson syntheses. Successive Fourier syntheses revealed all the nonhydrogen atoms. Refinement was

TABLE 1. CRYSTAL DATA AND EXPERIMENTAL DETAILS

Complex	Cu(CH_3-nso)Cl	Cu(C_2H_5-nso)Cl	Cu(n-C_3H_7-nso)Cl	Cu(n-C_4H_9-nso)Cl	Cu(n-C_3H_7-nso)Br	Cu(n-C_4H_9-nso)Br
Crystal system	Triclinic	Triclinic	Monoclinic	Monoclinic	Monoclinic	Monoclinic
Space group	$P\bar{1}$	$P\bar{1}$	$P2_1/a$	$P2_1/a$	$P2_1/a$	$P2_1/a$
a/Å	7.677(1)	8.694(2)	17.829(3)	15.109(2)	17.765(2)	10.284(1)
b/Å	9.131(1)	9.879(2)	10.322(2)	9.915(1)	10.363(1)	19.806(3)
c/Å	7.564(1)	7.591(2)	7.639(1)	11.529(1)	7.831(1)	7.955(1)
α/°	99.68(1)	94.03(2)				
β/°	96.87(1)	114.59(2)	102.73(1)	109.70(1)	102.71(1)	96.76(1)
γ/°	71.79(1)	83.61(2)				
D_m/g cm^{-3}	1.65	1.55	1.46	1.35	1.63	1.55
D_c/g cm^{-3}	1.66	1.55	1.47	1.35	1.64	1.55
Z	1	1	2	2	2	2
μ (Mo $K\alpha$)/cm^{-1}	26.2	22.1	19.2	16.2	44.9	39.3
Crystal size/mm^3	0.27×0.35 ×0.48	0.20×0.20 ×0.25	0.17×0.24 ×0.30	0.17×0.30 ×0.35	0.17×0.25 ×0.33	0.15×0.15 ×0.20
$2\theta_{max}$/°	50	51	50	55	50	52
No. of unique reflections ($F_o>3\sigma(F_o)$)	1677	1957	1831	2946	1920	2330

carried out by the block-diagonal least-squares method. All the hydrogen atoms were located from the subsequent difference Fourier maps. The final R values were $R_1=\sum||F_o|-|F_c||/\sum|F_o|=0.033$, $R_2=[\sum w(|F_o|-|F_c|)^2/\sum w|F_o|^2]^{1/2}=0.048$ for Cu(CH_3-nso)Cl, $R_1=0.049$, $R_2=0.065$ for Cu(C_2H_5-nso)Cl, $R_1=0.043$, $R_2=0.063$ for Cu(n-C_3H_7-nso)Cl, $R_1=0.036$, $R_2=0.054$ for Cu(n-C_4H_9-nso)Cl, $R_1=0.056$, $R_2=0.074$ for Cu(n-C_3H_7-nso)Br and $R_1=0.045$, $R_2=0.070$ for Cu(n-C_4H_9-nso)Br. In the least-squares refinement, the function minimized was $\sum w(|F_o|-k|F_c|)^2$, and the weighting schemes[4] were $w=(2.0+|F_o|+0.018\ |F_o|^2)^{-1}$ for Cu(CH_3-nso)Cl, $(4.0+|F_o|+0.016\ |F_o|^2)^{-1}$ for Cu(C_2H_5-nso)Cl, $(8.0+|F_o|+0.012\ |F_o|^2)^{-1}$ for Cu(n-C_3H_7-nso)Cl, $(6.0+|F_o|+0.010\ |F_o|^2)^{-1}$ for Cu(n-C_4H_9-nso)Cl, $(10.0+|F_o|+0.010\ |F_o|^2)^{-1}$ for Cu(n-C_3H_7-nso)Br and $(10.0+|F_o|+0.009\ |F_o|^2)^{-1}$ for Cu(n-C_4H_9-nso)Br. Final difference Fourier syntheses were featureless.

The atomic scattering factors for Br, Cu, Cl, S, O, N, and C_{val} and the anomalous dispersion corrections, $\Delta f'$ and $\Delta f''$ for Br, Cu, Cl, and S, were taken from the International Tables for X-Ray Crystallography.[5] For the hydrogen atom, the scattering factors were adopted from the Tables of Stewart *et al.*[6] All the calculations were carried out on the FACOM

Table 2. Fractional positional parameters ($\times 10^4$) and thermal parameters of non-hydrogen atoms with their estimated standard deviations in parentheses

Atom	x	y	z	B_{eq}/Å^2
(1) Cu(CH_3-nso)Cl				
Cu	1823.2(4)	−1223.3(4)	129.3(4)	2.4
Cl	3483(1)	−2487(1)	2345(1)	3.9
S	4297(1)	−1435(1)	−1531(1)	2.8
O	519(3)	464(3)	−1206(3)	3.7
N	1324(3)	−3253(3)	−2042(4)	3.1
C(1)	1220(7)	860(7)	−2492(9)	8.2
C(2)	3122(5)	84(4)	−2892(5)	3.5
C(3)	4287(4)	−3219(4)	−3013(5)	3.3
C(4)	2388(5)	−3371(4)	−3570(4)	3.5
C(5)	1930(6)	−4724(4)	−1290(6)	4.7
C(6)	−644(5)	−2875(5)	−2640(6)	5.2
(2) Cu(C_2H_5-nso)Cl				
Cu	342(1)	1468(1)	34(1)	2.7
Cl	660(2)	2730(1)	−2094(2)	4.7
S	2140(1)	2614(1)	2794(2)	3.4
O	896(4)	−56(3)	1717(4)	3.7
N	−1916(5)	2679(4)	754(6)	3.4
C(1)	1590(8)	94(5)	3709(7)	4.7
C(2)	2726(7)	1208(5)	4440(7)	4.8
C(3)	590(6)	3691(5)	3360(7)	3.7
C(4)	−1082(6)	3087(5)	2829(7)	4.1
C(5)	−2709(7)	3893(6)	−394(9)	5.0
C(6)	−3663(9)	3609(8)	−2544(10)	6.9
C(7)	−3101(7)	1634(6)	516(9)	4.8
C(8)	−4548(8)	2082(8)	1135(13)	7.1
(3) Cu(n-C_3H_7-nso)Cl				
Cu	−154.4(3)	1419(1)	−307(1)	3.0
Cl	−260(1)	2766(1)	−2642(2)	4.5
S	−958(1)	2624(1)	1099(2)	3.6
O	−417(2)	−3(3)	1075(5)	3.9
N	883(2)	2401(4)	1987(5)	2.8
C(1)	−625(4)	212(6)	2662(8)	4.4
C(2)	−1128(3)	1369(6)	2630(8)	4.2
C(3)	−253(3)	3673(5)	2467(8)	4.0
C(4)	510(3)	3041(5)	3299(7)	3.7
C(5)	1268(3)	3390(5)	1071(7)	3.5
C(6)	1734(3)	2838(6)	−185(8)	4.1
C(7)	2008(4)	3908(7)	−1257(9)	5.3
C(8)	1418(3)	1407(5)	2894(7)	3.3
C(9)	2087(3)	1886(6)	4348(8)	4.8
C(10)	2587(4)	831(8)	5279(10)	6.0
(4) Cu(n-C_4H_9-nso)Cl				
Cu	−128.7(2)	1513.2(3)	106.2(3)	2.8
Cl	−1334(1)	2782(1)	153(1)	4.2
S	1067(1)	2905(1)	1361(1)	3.6
O	816(1)	119(2)	544(2)	3.7
N	178(2)	2682(2)	−1591(3)	3.3
C(1)	1777(2)	405(3)	1085(4)	3.8
C(2)	1902(3)	1558(3)	1981(4)	4.4
C(3)	1479(2)	3624(3)	183(3)	3.8
C(4)	689(2)	3896(3)	−1000(3)	3.6
C(5)	752(3)	1888(4)	−2157(4)	4.1
C(6)	297(3)	563(4)	−2732(4)	4.7
C(7)	982(4)	−337(5)	−3091(5)	6.7
C(8)	518(6)	−1664(5)	−3648(5)	8.6
C(9)	−742(2)	3075(4)	−2497(3)	4.0
C(10)	−726(3)	4025(4)	−3533(3)	4.7
C(11)	−1704(4)	4433(5)	−4344(4)	6.4
C(12)	−1710(5)	5486(6)	−5290(6)	9.5
(5) Cu(n-C_3H_7-nso)Br				
Br	−315(1)	2811(1)	−2763(1)	4.2
Cu	−160(1)	1408(1)	−302(1)	2.7
S	−969(1)	2594(2)	1046(2)	3.5
O	−420(3)	−26(5)	1052(6)	3.3
N	874(3)	2383(5)	1897(7)	2.8
C(1)	−617(5)	221(8)	2658(9)	3.9
C(2)	−1141(5)	1348(8)	2541(11)	3.9
C(3)	−275(5)	3650(7)	2382(10)	3.8
C(4)	500(4)	3024(7)	3186(9)	3.4
C(5)	1406(4)	1382(7)	2800(9)	3.3
C(6)	2070(5)	1805(9)	4246(11)	4.6
C(7)	2539(6)	720(11)	5176(13)	5.9
C(8)	1272(4)	3353(7)	1046(9)	3.3
C(9)	1735(5)	2784(8)	−196(11)	4.1
C(10)	1995(6)	3838(12)	−1276(13)	5.8
(6) Cu(n-C_4H_9-nso)Br				
Br	2814(1)	332.4(4)	−2180(1)	4.4
Cu	1426(1)	155.4(4)	−11(1)	2.7
S	2609(2)	859(1)	1927(2)	3.6
O	−42(4)	364(2)	1258(5)	3.2
N	2400(4)	−754(2)	1756(6)	2.8
C(1)	205(6)	518(4)	2979(7)	3.5
C(2)	1337(6)	1005(4)	3288(8)	4.0
C(3)	3689(6)	229(3)	3044(9)	4.1
C(4)	3048(6)	−439(3)	3318(8)	3.8
C(5)	3394(6)	−1094(3)	870(8)	3.6
C(6)	2838(7)	−1476(4)	−728(8)	4.3
C(7)	3867(8)	−1718(4)	−1792(9)	4.9
C(8)	4803(10)	−2212(5)	−943(12)	6.8
C(9)	1343(6)	−1210(3)	2157(8)	3.4
C(10)	1757(7)	−1836(4)	3207(10)	4.5
C(11)	593(8)	−2221(4)	3729(10)	4.8
C(12)	966(10)	−2891(4)	4552(11)	6.0

M-200 computer in the Computer Center of Kyushu University by the use of a local version[7] of the UNICS-II[8] and the ORTEP[9] programs. The final positional and thermal parameters with their estimated standard deviations are given in Table 2. The coordinates and isotropic temperature factors of the hydrogen atoms, the anisotropic thermal parameters of the nonhydrogen atoms, and the F_o-F_c tables have been deposited as a Document No. 8213 at the Office of the Editor of Bull. Chem. Soc. Jpn.

Magnetic susceptibilities were measured by the Faraday method in the temperature range from liquid nitrogen temperature to room temperature. The apparatus was calibrated by the use of $[Ni(en)_2]S_2O_3$.[10] All the susceptibilities were corrected for the diamagnetism of the constituting atoms by the use of Pascal's constants.[11]

Description of the Structures and Discussion

The molecular structures of Cu(*n*-C_4H_9-nso)Cl and Cu(*n*-C_4H_9-nso)Br are shown in Figs 1 and 2, respectively. Selected bond lengths and bond angles are listed in Table 3.

The structures of all the complexes studied here are similar to that of Cu(CH_3-nso)Br[2] and consist of alkoxo-bridged binuclear units each of which has a center of symmetry. The coordination around each copper atom is essentially a distorted square pyramid with two alkoxo oxygen, a thioether sulfur and a chlorine or a bromine atoms in the basal plane and an amino nitrogen atom in the apical position. As can be seen in Table 3, the Cu–O and the Cu–O^i bond lengths fall in the range of 1.925—1.957 Å and 1.930—1.945 Å, respectively, and there was no definite relationship between these bond distances and the alkyl substituents, R, or the anions, X. The Cu–X distances (X=Cl or Br) are not much affected by the alkyl substituents and fall in the ranges, 2.229—2.236 Å for Cu(R-nso)Cl and 2.381—2.391 Å for Cu(R-nso)Br. These distances are comparable to the values found in chloro- or bromo[2-(dialkylamino)ethanolato]copper(II) (2.220—2.240 Å for the chloro complexes[12] and 2.333—2.395 Å for the bromo complexes[13]). The Cu–S distances fall in the ranges, 2.330—2.3446 Å for Cu(R-nso)Cl and 2.314—2.316 Å for Cu(R-nso)Br. It is to be noted that the Cu–S distances of Cu(R-nso)Cl are longer than those of Cu(R-nso)Br by 0.02 Å on the average. Since the Cu–S distance of Cu(CH_3-nso)NCS is 2.361(3) Å,[14] the Cu–S bond length decreases in the order Cu(R-nso)NCS>Cu(R-nso)Cl>Cu(R-nso)Br. The observed trend seems to accord with the

Table 3. Selected interatomic distances (l/Å) and bond angles (ϕ/°) of Cu(R-nso)X

Complex	Cu(CH_3-nso)Cl	Cu(C_2H_5-nso)Cl	Cu(*n*-C_3H_7-nso)Cl	Cu(*n*-C_4H_9-nso)Cl	Cu(*n*-C_3H_7-nso)Br	Cu(*n*-C_4H_9-nso)Br
Cu···Cu	2.9955(6)	3.0181(9)	2.999(1)	3.0463(5)	2.992(1)	2.998(1)
Cu–O	1.927(2)	1.931(3)	1.925(4)	1.927(2)	1.940(5)	1.957(4)
Cu–O^i [a]	1.939(2)	1.937(3)	1.945(4)	1.933(2)	1.930(5)	1.933(4)
Cu–S	2.341(1)	2.334(1)	2.330(2)	2.3446(8)	2.315(2)	2.314(2)
Cu–N	2.356(3)	2.421(4)	2.468(3)	2.448(3)	2.443(5)	2.428(5)
Cu–X[b]	2.233(1)	2.229(2)	2.236(2)	2.229(1)	2.381(1)	2.391(1)
O–C(1)	1.316(8)	1.379(5)	1.362(8)	1.403(3)	1.402(10)	1.396(7)
C(1)–C(2)	1.454(6)	1.481(8)	1.490(8)	1.510(5)	1.483(11)	1.509(9)
S–C(2)	1.809(4)	1.819(6)	1.814(6)	1.810(3)	1.814(9)	1.816(7)
S–C(3)	1.817(4)	1.798(6)	1.807(5)	1.820(4)	1.801(8)	1.829(7)
C(3)–C(4)	1.511(5)	1.517(8)	1.516(7)	1.504(4)	1.526(11)	1.507(10)
N–C(4)	1.464(5)	1.482(6)	1.476(7)	1.469(4)	1.483(10)	1.477(8)
Cu–O–Cu^i	101.6(1)	102.6(1)	101.6(2)	104.22(9)	101.3(3)	100.9(2)
O–Cu–O^i	78.4(1)	77.4(1)	78.4(2)	75.78(8)	78.7(2)	79.1(2)
O–Cu–S	84.72(8)	85.00(9)	84.6(1)	84.95(6)	84.9(2)	84.6(1)
S–Cu–X	96.62(3)	95.90(6)	94.78(6)	96.82(3)	94.14(6)	94.63(5)
O^i–Cu–X	98.00(8)	99.2(1)	100.6(1)	98.38(7)	100.5(1)	100.0(1)
O–Cu–N	96.9(1)	99.5(2)	99.1(1)	103.1(1)	99.5(2)	98.5(2)
O^i–Cu–N	100.7(1)	99.8(1)	99.3(1)	107.9(1)	98.7(2)	97.5(2)
S–Cu–N	84.94(8)	84.66(9)	83.9(1)	84.32(6)	84.6(2)	85.0(1)
X–Cu–N	102.87(7)	105.8(1)	103.3(1)	97.40(7)	104.7(1)	106.6(1)
Cu–O–C(1)	123.7(2)	122.4(3)	120.7(3)	122.4(2)	119.1(4)	119.3(3)
Cu^i–O–C(1)	134.7(3)	132.5(3)	130.9(3)	133.0(2)	131.6(4)	131.1(4)
O–C(1)–C(2)	120.2(5)	113.2(5)	113.4(5)	109.2(3)	111.5(6)	110.3(5)
C(1)–C(2)–S	113.8(2)	114.0(3)	113.4(5)	112.3(2)	114.1(6)	113.4(5)
Cu–S–C(2)	97.4(1)	97.0(2)	97.1(2)	95.7(1)	97.2(3)	97.7(2)
Cu–S–C(3)	98.3(1)	99.8(1)	99.6(2)	99.0(1)	99.9(3)	98.9(2)
C(2)–S–C(3)	103.8(2)	104.2(3)	104.4(3)	102.4(2)	104.4(4)	104.9(3)
S–C(3)–C(4)	114.0(2)	114.9(3)	115.4(4)	112.4(3)	115.0(5)	114.7(4)
C(3)–C(4)–N	113.2(3)	113.4(5)	113.9(4)	114.0(2)	114.1(6)	114.3(5)
Cu–N–C(4)	107.6(2)	104.6(3)	106.6(3)	103.2(2)	106.6(4)	106.8(4)

a) Superscript (i) refers to the equivalent position ($-x$, $-y$, $-z$). b) X denotes Cl or Br atom.

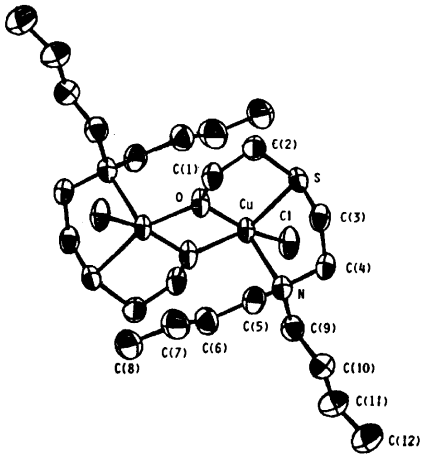

Fig. 1. Molecular Structure of Cu(n-C_4H_9-nso)Cl. Thermal ellipsoids are drawn at 50% probability level.

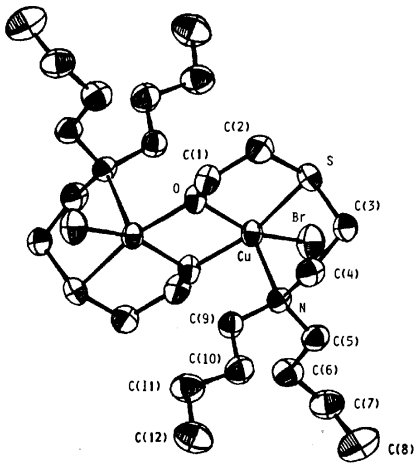

Fig. 2. Molecular Structure of Cu(n-C_4H_9-nso)Br. Thermal ellipsoids are drawn at 50% probability level.

softness of the anion X. It is known that Cu(I)–S bond length is shorter than Cu(II)–S bond length when S is a thioether sulfur.[15] Therefore, our results may be interpreted in the following way: when a donor atom is replaced with softer one, the softness of the copper ion would increase and, consequently, the Cu–S bond would become to be more covalent and shortened. The axial Cu–N bond distances increases in the order Cu(CH_3-nso)X < Cu(C_2H_5-nso)X < Cu(n-C_4H_9-nso)X < Cu(n-C_3H_7-nso)X.

The five-membered chelate ring, Cu–O–C(1)–C(2)–S, assumes two types of conformation. One is the gauche conformation as is usually observed for saturated five-membered chelate rings, *i.e.*, C(1) and C(2) are located below and above the plane defined by Cu, S, and O, respectively. The other is the envelope conformation *i.e.*, both carbon atoms, C(1) and C(2) are placed in the same side of the Cu–S–O plane (Table 4).[16] The chelate ring of Cu(n-C_4H_9-nso)Cl assumes the former conformation and the latter is observed for Cu(CH_3-nso)Cl, Cu(n-C_3H_7-nso)Cl, Cu(CH_3-nso)Br, Cu(n-C_3H_7-nso)Br and Cu(n-C_4H_9-nso)Br. As for Cu(C_2H_5-nso)Cl, the chelate ring is intermediate between the envelope and the gauche conformations. The other chelate ring, Cu–S–C(3)–C(4)–N, is of the gauche conformation for all the Cu(R-nso)X complexes.

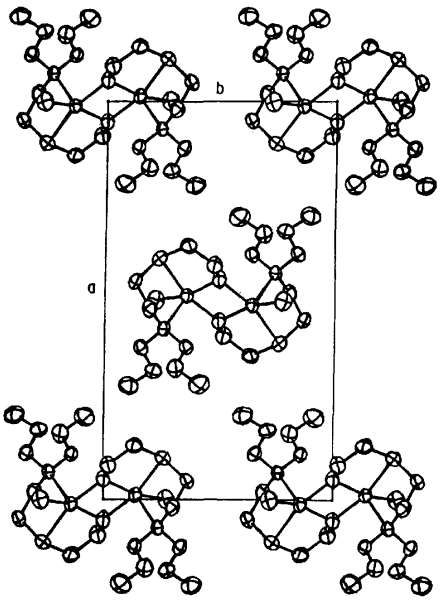

Fig. 3. Projection of the unit cell of Cu(n-C_3H_7-nso)Cl on the ab plane.

The packing diagram is exemplified by the projection of the unit cell of Cu(n-C_3H_7-nso)Cl in Fig. 3. As is evident from the shortest separations between the nonhydrogen atoms of the binuclear units (S···S ($1-x$, $-y$, $-z$ of 3.538(1) Å in Cu(CH_3-nso)Cl, Cl···C(4) (x, y, $z-1$) of 3.534(5) Å in Cu(C_2H_5-nso)Cl, Cl···C(4) (x, y, $z-1$) of 3.669(6) Å in Cu(n-C_3H_7-nso)Cl, Cl···C(4) ($-x$, $1-y$, $-z$) of 3.480(3) Å in Cu(n-C_4H_9-nso)Cl, Br···C(4) (x, y, $z-1$) of 3.772(8) Å in Cu(n-C_3H_7-nso)Br and C(2)···C(12) ($1/2-x$, $1/2+y$, $1-z$) of 3.78(1) Å in Cu(n-C_4H_9-nso)Br), all the crystals consist of discrete binuclear units. Therefore, their magnetic properties were expected to be interpreted by the Bleaney-Bowers equation based on the Heisenberg model on the assumption of a binuclear structure,[3]

$$\chi_A = \frac{Ng^2\beta^2}{3kT}\left[1+\frac{1}{3}\exp(-2J/kT)\right]^{-1} + N\alpha, \qquad (1)$$

where χ_A is susceptibility per copper atom and N, g, J, β, and $N\alpha$ have the usual meanings. However, the temperature dependence of the magnetic susceptibilities of the majority of the Cu(R-nso)X complexes can not be explained by the above equation. This result might be due to the fact that there are polymorphism and by chance the crystal structures of the samples used for magnetic measurements and X-ray analyses are different. In order to check this possibility, magnetic susceptibilities have been measured over the temperature range 80—300 K for crystals taken from the same crop as those used in the X-ray work. Similarly to the previous result, the data for Cu(n-C_4H_9-nso)Cl obey the Bleaney-Bowers equation using $g=2.10$, $-2J=745$ cm^{-1} and $N\alpha=34\times10^{-6}$ cgs emu with very slight deviations from the previous ones ($g=2.10$, $-2J=735$ cm^{-1}, $N\alpha=60\times10^{-6}$ cgs emu)[2] and the experimental χ_A-T curves for the other complexes except for Cu(C_2H_5-nso)Cl

TABLE 4. COEFFICIENTS OF EQUATIONS OF MEAN PLANES[a] AND DEVIATIONS OF ATOMS FROM THE PLANES

(1) Plane through Cu, O, S

Complex	l	m	n	d	Distances from the plane (l/Å)
Cu(CH_3-nso)Cl	0.4426	0.6604	0.5681	−0.0626	C(1) −0.075, C(2) −0.068
Cu(C_2H_5-nso)Cl	0.9256	−0.1988	−0.5834	−0.0285	C(1) −0.353, C(2) 0.018
Cu(n-C_3H_7-nso)Cl	0.6313	0.2206	0.5861	0.0118	C(1) 0.525, C(2) 0.208
Cu(n-C_4H_9-nso)Cl	−0.5641	−0.2410	0.9337	−0.1376	C(1) −0.305, C(2) 0.277
Cu(n-C_3H_7-nso)Br	0.6265	0.2260	0.5898	0.0121	C(1) 0.580, C(2) 0.208
Cu(n-C_4H_9-nso)Br	0.1695	−0.7834	0.5739	0.0023	C(1) 0.590, C(2) 0.173

(2) Plane through Cu, S, N

Complex	l	m	n	d	Distortions from the plane (l/Å)
Cu(CH_3-nso)Cl	0.3418	−0.6122	0.6110	1.2219	C(3) 0.310, C(4) −0.361
Cu(C_2H_5-nso)Cl	−0.3030	−0.7975	0.6569	−1.2298	C(3) −0.158, C(4) 0.493
Cu(n-C_3H_7-nso)Cl	−0.1861	−0.7671	0.6399	−1.2225	C(3) −0.396, C(4) 0.258
Cu(n-C_4H_9-nso)Cl	−0.7212	0.6928	0.2396	1.2089	C(3) −0.280, C(4) 0.441
Cu(n-C_3H_7-nso)Br	−0.1819	−0.7649	0.6429	−1.2166	C(3) −0.389, C(4) 0.262
Cu(n-C_4H_9-nso)Br	0.8403	−0.0295	−0.6365	1.2286	C(3) 0.405, C(4) −0.249

(3) Plane through O, O^i, S, X[b]

Complex	l	m	n	d	Distances from the plane (l/Å)
Cu(CH_3-nso)Cl	0.4311	0.7968	0.4159	−0.0056	O 0.135, O^i −0.124, S −0.097, Cl 0.086, Cu −0.240, N −2.565
Cu(C_2H_5-nso)Cl	0.8795	−0.3733	−0.3909	−0.0093	O 0.206, O^i −0.187, S −0.147, Cl 0.129, Cu −0.281, N −2.668
Cu(n-C_3H_7-nso)Cl	0.7125	0.3748	0.4216	0.0102	O −0.194, O^i 0.174, S 0.142, Cl −0.122, Cu 0.244, N 2.681
Cu(n-C_4H_9-nso)Cl	−0.3830	−0.3224	0.9441	−0.0034	O 0.086, O^i −0.079, S −0.060, Cl 0.053, Cu −0.290, N −2.688
Cu(n-C_3H_7-nso)Br	0.7132	0.3974	0.4063	0.0132	O −0.222, O^i 0.195, S 0.160, Br −0.134, Cu 0.268, N 2.679
Cu(n-C_4H_9-nso)Br	0.3718	−0.8225	0.3838	0.0141	O −0.239, O^i 0.211, S 0.173, Br −0.145, Cu 0.274, N 2.668

a) The equation of the plane is expressed as $lX+mY+nZ=d$, where X, Y, Z are in Å units referred to the crystallographic axes. b) Superscript (i) refers to the equivalent position $(-X, -Y, -Z)$.

largely deviate from the Bleaney-Bowers equation. However, in the case of Cu(C_2H_5-nso)Cl, contrary to the previous result, the present data can almost be fitted to the curve calculated by the Bleaney-Bowers equation with $g=2.10$, $-2J=425\ cm^{-1}$ and $N\alpha=60\times10^{-6}$ cgs emu although the fitness between the calculated and observed curves is slightly poor in the range near room temperature. Thus, we have found that the major structural difference corresponding to these magnetic behaviors lies in the conformation of the five-membered chelate ring. Among the complexes presently studied Cu(n-C_4H_9-nso)Cl and Cu(C_2H_5-nso)-Cl are the only complexes which obey the Bleaney-Bowers equation and are also the only complexes whose chelate ring Cu–O–C(1)–C(2)–S assumes a gauche or an intermediate conformation. As for the other complexes the magnetic behaviors can not be interpreted by any theoretical equations and the Cu–O–C(1)–C(2)–S rings all assume envelope conformations. In the envelope conformation, the strain of the chelate ring may be larger than that for the gauche conformation, although the energy difference between them seems to be little. Therefore, it is likely that an interconversion between the two conformations takes place with change of temperature. Assuming that the envelope conformation changes to a stable gauche conformation with lowering of temperature, this change may cause a slight structural change of the coordination sphere and the geometry

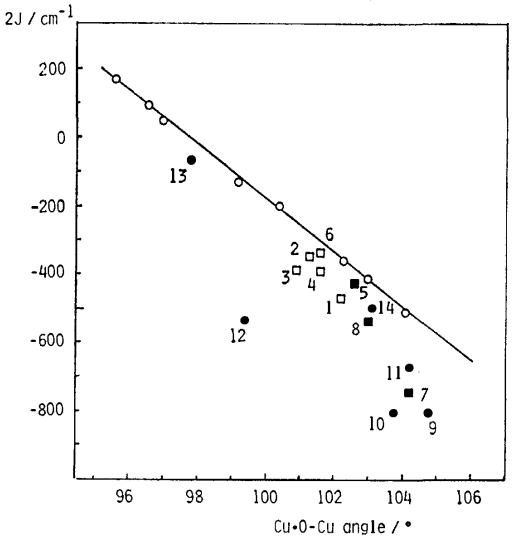

Fig. 4. Plot of the Cu–O–Cu angle *vs.* the $2J$ value.
1; Cu(CH_3-nso)Br, 2; Cu(n-C_3H_7-nso)Br, 3; Cu(n-C_4H_9-nso)Br, 4; Cu(CH_3-nso)Cl, 5; Cu(C_2H_5-nso)Cl, 6; Cu(n-C_3H_7-nso)Cl, 7; Cu(n-C_4H_9-nso)Cl, 8; Cu(CH_3-nso)NCS,[14] 9; α-Cu(C_2H_5-2)Br,[20] 10; α-Cu(n-C_4H_9-2)Br,[20] 11; Cu(n-C_3H_7-2)NCO,[21] 12; Cu(C_2H_5-2-3)$ClO_4\cdot H_2O$,[20] 13; Cu(H-3-2)$I\cdot H_2O$,[22] 14; Cu(bdhe)ClO_4.[23]
The straight line represents the linear relationship observed for the hydroxo-bridged copper(II) complexes.[18]

around the bridging oxygen atom. This may lead to a temperature dependence of the J value, since it is known that a slight change in bond angle may bring about a considerable change in J value.[17,18] In the case of Cu(C_2H_5-nso)Cl, the small deviation from the binuclear model in the magnetic susceptibilities may arise from the intermediate conformation of the chelate ring at room temperature.

In Fig. 4, the exchange parameters, $2J$, for Cu(R-nso)X are plotted against the Cu–O–Cu angles together with the data available in the literature for hydroxo- and alkoxo-bridged binuclear copper(II) complexes. For the complexes which show the unusual magnetic behavior, the values are estimated from Eq. 2[19] by the use of the magnetic moments, μ_{eff}, at room temperature. Hatfield and co-workers found a linear relationship between the spin singlet-triplet separation, $2J$, and the Cu–O–Cu angle for hydroxo-bridged binuclear copper(II) complexes.[18] As shown in Fig. 4, no such clear relationship is found for alkoxo-bridged complexes including Cu(R-nso)X. This may be due to the variation of planarity of the equatorial coordination plane and the effects of axial coordination.

$$-2J = 0.695\,T\ln[3[4.41/\mu_{eff}^2-1)] \quad (2)$$

References

1) Part XLIII: W. Kanda, M. Nakamura, H. Okawa, and S. Kida, *Bull. Chem. Soc. Jpn.*, **55**, 471 (1982).

2) M. Mikuriya, H. Okawa, and S. Kida, *Bull. Chem. Soc. Jpn.*, **53**, 2871 (1980).

3) B. Bleaney and K. D. Bowers, *Proc. R. Soc. London, Ser. A*, **214**, 451 (1952).

4) D. W. J. Cruickshank, "Computing Methods in Crystallography," ed by J. S. Rollet, Pergamon Press, Oxford (1965).

5) "International Tables for X-Ray Crystallography," Kynoch Press, Birmingham (1974), Vol. IV.

6) R. F. Stewart, E. R. Davidson, and W. T. Simpson, *J. Chem. Phys.*, **42**, 3175 (1965).

7) S. Kawano, *Rep. Comp. Cent. Kyushu Univ.*, **13**, 39 (1980).

8) T. Sakurai, H. Iwasaki, Y. Watanabe, K. Kobayashi, Y. Bando, and Y. Nakamichi, *Rep. Inst. Phys. Chem. Res.*, **50**, 75 (1972).

9) C. K. Johnson, Report No. 3794, Oak Ridge National Laboratory, Oak Ridge, Tennessee (1965).

10) N. F. Curtis, *J. Chem. Soc.*, **1961**, 3147.

11) F. E. Mabbs and D. J. Machin, "Magnetism and Transition Metal Complexes," Chapman and Hall, London (1973).

12) W. Haase, *Chem. Ber.*, **106**, 3132 (1973); R. Mergehenn, W. Haase, and R. Allmann, *Acta Crystallogr., Sect. B*, **31**, 1847 (1975); E. D. Estes and D. J. Hodgson, *Inorg. Chem.*, **14**, 334 (1975); N. Matsumoto, I. Ueda, Y. Nishida, and S. Kida, *Bull. Chem. Soc. Jpn.*, **49**, 1308 (1976).

13) A. Pajunen and M. Lehtonen, *Suom. Kemistil. B*, **44**, 200 (1971); W. Haase, *Chem. Ber.*, **106**, 3132 (1973); R. Mergehenn and W. Haase, *Z. Naturforsch., Teil B*, **30**, 155 (1975); R. Mergehenn, L. Merz, and W. Haase, *ibid.*, **30**, 14 (1975); R. Mergehenn, W. Haase, and R. Allmann, *Acta Crystallogr., Sect. B*, **31**, 1847 (1975); R. Mergehenn, L. Merz, W. Haasse, *J. Chem. Soc., Dalton Trans.*, **1980**, 1703.

14) M. Mikuriya, H. Okawa, and S. Kida, *Bull. Chem. Soc. Jpn.*, **54**, 2979 (1981).

15) E. N. Baker and G. E. Norris, *J. Chem. Soc., Dalton Trans.*, **1977**, 877; K. D. Karlin, P. L. Dahlstrom, J. R. Hyde, and J. Zubieta, *J. Chem. Soc., Chem. Commun.*, **1980**, 906; M. M. Olmstead, W. K. Musker, and R. M. Kessler, *Inorg. Chem.*, **20**, 151 (1981).

16) C. J. Hawkins, "Absolute Configuration of Metal Complexes," Wiley-Interscience, New York (1971).

17) E. Sinn, *J. Chem. Soc., Chem. Commun.*, **1975**, 655; R. J. Butcher and E. Sinn, *Inorg. Chem.*, **15**, 1604 (1976).

18) D. J. Hodgson, *Prog. Inorg. Chem.*, **19**, 173 (1975); W. E. Hatfield, "Theory and Applications of Molecular Paramagnetism," ed by E. A. Boudreaux and L. N. Mulay, Wiley-Interscience, New York (1976).

19) M. Kato, Y. Muto, H. B. Jonassen, K. Imai, and A. Harano, *Bull. Chem. Soc. Jpn.*, **41**, 1864 (1968).

20) N. Matsumoto, S. Kida, and I. Ueda, *J. Coord. Chem.*, **9**, 133 (1979).

21) L. Merz and W. Haase, *Acta Crystallogr., Sect. B*, **34**, 2128 (1978).

22) K. Nieminen and M. Nasakkala, *Acta Chem. Scand., Ser. A*, **34**, 375 (1980).

23) L. Banci, A. Bencini, P. Dapporto, A. Dei, and D. Gatteschi, *Inorg. Chem.*, **19**, 3395 (1980).

A Study of the Rapid Anomerization of Poly-*O*-benzyl-β-D-glucopyranosides with Titanium Tetrachloride

Shinkiti Koto,* Naohiko Morishima, Reiko Kawahara, Katsuhiko Ishikawa, and Shonosuke Zen
School of Pharmaceutical Sciences, Kitasato University, Shirokane, Minato-ku, Tokyo 108
(Received March 6, 1981)

Titanium tetrachloride rapidly anomerizes methyl 2,3,4,6-tetra-*O*-benzyl-β-D-glucopyranoside in dichloromethane at 25 °C. Evidence for the proposal that the benzyloxymethyl group on C-5 and the ring oxygen of the glucoside cooperate to prompt the reaction is described. The reagent anomerizes the interglycosidic linkage of several disaccharide derivatives.

The anomerization of per-*O*-acetyl-β-D-glucopyranosides,[1] as well as of per-*O*-benzoyl ones,[2] with titanium tetrachloride (**1**) is useful for preparing the corresponding α-D-glucopyranosides[3] and has been well studied.[4] In spite of this, no report about such a reaction of per-*O*-benzyl-β-D-glucopyranosides has appeared. As has been communicated, however, methyl 2,3,4,6-tetra-*O*-benzyl-β-D-glucopyranoside (**2b**) was anomerized with an extraordinary rapidity into the α-anomer (**2a**) in the presence of **1** in dichloromethane at 25 °C.[5] This paper will present evidence for the mechanism previously proposed[5] in which the benzyloxymethyl group and the ring oxygen of **2b** play an important role in accelerating the reaction. The reagent was applied to the anomerization of the interglycosidic linkage of several disaccharide derivatives.

Results and Discussion

Table 1 shows the dependence of the anomerization reaction of **2b** on the molar ratio of **1** to **2b** and the time course of the reaction. The molar ratio should be greater than 0.5 to keep the efficiency of the reaction high. The equimolar amount of **1** completed the reaction within 10 s.

Table 1. Anomerization of methyl per-*O*-benzyl-β-D-glucopyranoside (**2b**) with titanium tetrachloride in dichloromethane

Mole ratio of $TiCl_4$ to the glucoside	Time/s	Content of the α-anomer/%[a]	Recovery of the glucosides/%[b]
0.2	300	42	96
0.2	3600	76	92
0.5	300	89	93
1.0	4	90	78
1.0	10	96	78
1.0	300	96	77

a) Mol% of α-glucoside to the sum of unchanged β-glucoside and anomerized α-one. b) Sum of yield of α-glucoside and recovery of unchanged β-one.

Interestingly, Table 2 shows that **2b** was anomerized much faster than was methyl 2,3,4,6-tetra-*O*-acetyl-β-D-glucopyranoside (**3b**). The replacement of the acetyl group at C-6 of **3b** with a benzyl one (Compound **4b**) had remarkable accelerating effects on the reaction. However, the replacement of acetyl groups at C-2, -3, and -4 with a benzyl one (Compound **26b**) did not accelerate the reaction appreciably. Compounds **19b**, **21b**, and **25b**, all of them with a benzyloxyl group at C-6, showed fast anomerization rates.

Table 2. Effect of substituents on the anomerization[a]

Compd	R^1	R^2	R^3	R^4	Time/s	Content of the α-anomer/%[b]	Recovery of the glucosides/%[b]
2b	Bn	Bn	Bn	Bn	4	90	78
					300	96	78
3b	Ac	Ac	Ac	Ac	300	3	100
4b	Ac	Ac	Ac	Bn	4	59	88
					300	98	87
12b	Bn	Bn	Bn	Me	4	96	79
13b	Bn	Bn	Bn	—[c]	4	12	67
14b	Bn	Bn	Bn	—[d]	4	7	50
19b	Ac	Bn	Bn	Bn	300	100	67
21b	Bn	Ac	Bn	Bn	300	99	85
25b	Bn	Bn	Ac	Bn	300	100	80
26b	Bn	Bn	Bn	Ac	300	4	70
27b[e]	Bn	Bn	Ac	Ac	300	0	74
28b	Ac	Ac	Ac	Me	4	74	95

a) The mole ratio of $TiCl_4$ to the glucoside was 1.0. b) They are defined in Table 1. c) X=Me. d) X=H. e) A. P. Tulloch and A. Hill, *Can. J. Chem.*, **46**, 2485 (1968).

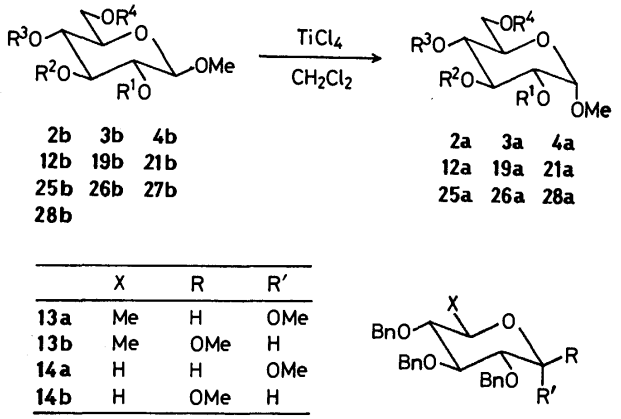

	X	R	R′
13a	Me	H	OMe
13b	Me	OMe	H
14a	H	H	OMe
14b	H	OMe	H

Furthermore, the methoxyl group at C-6 considerably accelerates the reaction; the effect was even greater than that by a benzyloxyl group. This indicates that an ether group at C-6 is essential for the rapid anomerization. The slight retardation shown by **4b** and **28b** at 4 s seems to be due to electron-withdrawing acetoxyl groups, which might depress the affinity of O-5 to **1**

Table 3. Retarding effect of additives on the anomerization[a)]

Additives	Mole ratio to the glucoside, **2b**	Content of the α-anomer/%[b)]	Recovery of the glucosides/%[b)]
5	2.0	34	86
6	1.0	57	84
7	2.0	85	87
8	1.0	7	87
9	1.0	8	86
10	1.0	2	89
11	1.0	21	84

a) The mole ratio of $TiCl_4$ to the glucoside was 1.0; reactions were conducted for 4 s. b) They are defined in Table 1.

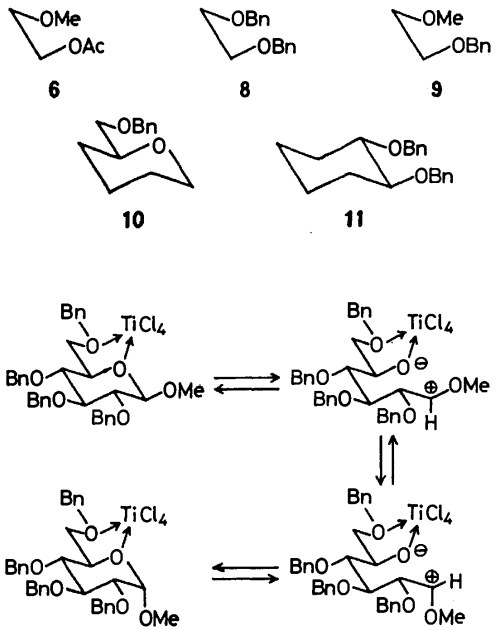

Fig. 1. A mechanism for the rapid anomerization reaction of methyl per-*O*-benzyl-β-D-glucopyranoside.

and/or the ability of C-1 to dissociate the bond between O-5 (Fig. 1).[6)]

These facts caused us to wonder if the benzyloxymethyl group in **2b** or **4b** has a special promoting function, possibly by assisting the interaction between the ring oxygen and **1**.[4a)] Additives which structurally resemble the $C_6H_5CH_2$–O–CH_2–C(5)–O(5)–moiety of **2b** are thought to compete with **2b** in capturing **1**, thus retarding the reaction. Table 3 shows how additives with benzyloxyl and/or acetoxyl group(s) in their structure retard the reaction of **2b**. Additives, such as ethyl acetate(**5**), 2-methoxyethyl acetate(**6**), and benzyl ethyl ether (**7**), did not clearly retard the anomerization of **2b**. This indicates that neither of these additives can be a ligand possessing more affinity to **1** than can **2b** Especially, the fact that **7** did not impede the reaction, while **4b** was anomerized rapidly, suggests that the benzyloxymethyl group of **4b**, and consequently of **2b**, is not fully responsible for the rapidity of the anomerization of **4b** and, hence, of **2b**. However, 1,2-bis(benzyloxy)ethane (**8**) and 1-benzyloxy-2-methoxyethane (**9**), as expected, inhibit the reaction clearly. 2-(Benzyloxymethyl)tetrahydropyran (**10**), whose structure is closely related to the pyranose ring system, hindered the reaction almost completely. This indicates that the $C_6H_5CH_2$–O–CH_2CH_2–O– moiety can effectively compete with **2b** in capturing **1**. It should also be noted that Compound **11**, in which the benzyloxyl groups are linked to the cyclohexane ring, showed a weaker inhibitory effect; this is apparently because benzyloxymethylene groups have lesser flexibility than the benzyloxymethyl one when they complex with **1**. From the things described so far there emerges the conclusion that the difunctional $C_6H_5CH_2$–O–CH_2–C(5)–O(5)– moiety of **2b** is the part which preferentially coordinates with **1**, in competition with other benzyloxyl groups, in the reaction where **1** assists the cleavage of the C(1)–O(5) bond[7,8b)] (Fig. 1). The fact that the 6-*O*-methyl glucoside derivative (**12b**) is rapidly anomerized, while the 6-deoxy one (**13b**) is not, is consistent with the above conclusion (Table 2). In this connection, it is remarkable that methyl 2,3,4-tri-*O*-benzyl-β-D-xylopyranoside (**14b**) was anomerized slower than **2b**, whereas methyl 2,3,4-tri-*O*-acetyl-β-D-xylopyranoside was anomerized faster than **3b**.[8b)]

Table 4. Effect of aglycon on the anomerization

Compd	Aglycon	Time/s	Content of the α-anomer/%[a)]	Recovery of the glucosides/%[b)]
29b	Cyclohexylmethyl	4	100	80
30b	Cyclohexyl	2	100	87
31b	Benzyl	4	100	78
32b	2-Benzyloxyethyl	4	93	54
33b	3-Benzyloxypropyl	4	99	80
34b	6-Benzyloxyhexyl	4	100	76

a) The mole ratio of $TiCl_4$ to the glucoside was 1.0. b) They are defined in Table 1.

As for aglycon, **1** was even more effective for such alkyl groups as cyclohexylmethyl, cyclohexyl, and benzyl (Table 4). In some cases, no trace of β-glucoside was found in the reaction mixture.

The positional effect of the benzyloxyl group in aglycon was then studied in order to ascertain the scope of the reaction.[8a)] Table 4 shows that, when the benzyloxyl group is present at the carbon vicinal to the one which links with the glucosyloxyl residue, the efficiency of the reaction decreases and the recovery of the anomeric glucosides is seriously diminished. In this case, 2,3,4,6-tetra-*O*-benzyl-α-D-glucopyranose was isolated in a fair yield after the chromatography of the reaction mixture. This seems to be produced *via* the hydrolysis of the complex (**15**). Therefore, the reaction is not suitable for anomerizing the interglycosidic linkage of per-*O*-benzylated disaccharides.

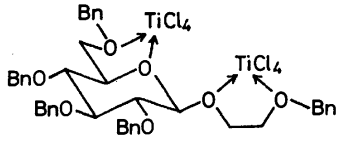

15

Nevertheless, the findings described so far stimulated us to try to anomerize the per-*O*-benzyl derivative of disaccharides.[3a,b] The gentiobiose derivative (**16b**) was rapidly transformed into the isomaltose one (**16a**) with **1** at room temperature. The per-*O*-benzyl derivative (**17b**) of methyl 3-*O*-(β-D-glucopyranosyl)-α-D-xylopyranoside, the aglycon monosaccharide of which has no benzyloxymethyl group, inverted the configuration of its interglycosidic linkage, though the recovery was not so high. To our knowledge, the latter is the first case of the anomerization of the interglycosidic β-linkage of a secondary hydroxyl group of disaccharide.[3a]

	R	R′
16a	H	OGlc[6]
16b	OGlc[6]	H
17a	H	OXyl[3]
17b	OXyl[3]	H
29a	H	OCm
29b	OCm	H
30a	H	OCh
30b	OCh	H
31a	H	OBn
31b	OBn	H
32a	H	$O(CH_2)_2OBn$
32b	$O(CH_2)_2OBn$	H
33a	H	$O(CH_2)_3OBn$
33b	$O(CH_2)_3OBn$	H
34a	H	$O(CH_2)_6OBn$
34b	$O(CH_2)_6OBn$	H

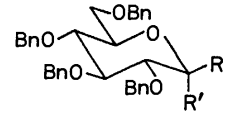

Bn = benzyl
Ch = cyclohexyl
Cm = cyclohexylmethyl

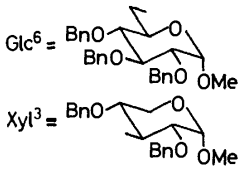

Experimental

The melting points were determined on an MP-1 melting point apparatus (Yanagimoto) and are uncorrected. The optical rotations were measured with a DIP-180 automatic polarimeter (Japan Spectroscopic) in a jacketed 1-dm cell at 20 °C. The ^1H NMR spectra were recorded with a Varian S-60T spectrometer, and the ^{13}C NMR spectra, with a JEOL-PS-100, using TMS as the internal standard. The refractive indexes were determined with an Abbe refractometer, Model 3 (Atago), at 20 °C. Column chromatography was carried out on silica gel (Kanto Kagaku), using an appropriate solvent system of Solvent A (benzene–2-butanone), B (hexane–ethyl acetate), or C (chloroform–methanol); each fraction was examined by means of TLC on silica gel (Merck, 7731). The dichloromethane (Wako) was distilled and stored over a molecular sieve (Linde 3A). The catalyst **1** (Wako) was distilled before use. The ethyl acetate (**5**, Wako), 2-methoxyethyl acetate (**6**, Tokyo Kasei), benzyl ethyl ether (**7**, Wako), and 1,2-bis(benzyloxy)ethane (**8**, Tokyo Kasei) were used without any pre-treatment.

General Procedure for Anomerization. The β-glucoside (0.1 mmol) was dissolved in dichloromethane (1.0 ml) in a stoppered vial, into which **1** was then injected under stirring at room temperature. The reaction was quenched by the addition of a mixture of aq sodium hydrogencarbonate (5%, 1.0 ml) and ice (≈5 g). In the case of the reaction within 4 s, an open vessel was used: dichloromethane was injected into a stoppered vial containing the β-glucoside, and then, just after the removal of the stopper, **1** was shot into the solution under efficient stirring, with care taken to avoid any bubbling. The mixture was extracted with benzene (15 ml), and the organic layer was washed with water (5 ml) and evaporated to give the product mixture, which was then chromatographed.

The additive, when necessary, was injected into the vessel before the addition of **1**.

Preparation of β-Glucosides and Isolation of α-Glucosides Formed by Anomerization. Methyl 2,3,4,6-Tetra-O-benzyl-α-D-glucopyranoside (2a): The treatment of **2b**[9] with **1**, followed by processing and chromatography (Solvent A, 30 : 1), gave **2a** as a syrup, identified with an authentic sample.[10]

Methyl 2,3,4-Tri-O-acetyl-6-O-benzyl-β-D-glucopyranoside (4b): A mixture of methyl β-D-glucopyranoside (1.0 g, 5.2 mmol), sodium hydride (≈50% dispersion, 0.39 g, ≈8.1 mmol), and benzyl chloride (Tokyo Kasei, 30 ml) was stirred for 1.5 h at 100 °C and then evaporated on a boiling water bath to give an oily product mixture. Column chromatography (Solvent C, gradient) and subsequent crystallization from diisopropyl ether containing ethanol gave methyl 6-*O*-benzyl-β-D-glucopyranoside (**18**, 0.28 g, 19%): mp 97—98 °C, $[\alpha]_D$ −36° (*c* 1.0, $CHCl_3$), NMR ($(CD_3)_2CO$) δ=3.51 (s, 3, CH_3O), 4.61 (s, 2, $PhCH_2$), and 7.36 (s, 5, C_6H_5). Found: C, 58.91; H, 7.08%. Calcd for $C_{14}H_{20}O_6$: C, 59.14; H, 7.09%.

The acetylation of **18** with acetic anhydride in pyridine and subsequent crystallization from diisopropyl ether gave **4b**: mp 104—105 °C, $[\alpha]_D$ −1° (*c* 0.7, $CHCl_3$): NMR (CCl_4) δ=1.84 (s, 3, CH_3CO), 1.94 (s, 3, CH_3CO), 1.98 (s, 3, CH_3CO), 3.45 (s, 3, CH_3O), 4.33 (d, 1, *J*=7.8 Hz, H-1), 4.48 (s, 2, $PhCH_2$), and 7.27 (s, 5, C_6H_5). Found: C, 58.24; H, 6.37%. Calcd for $C_{20}H_{26}O_9$: C, 58.53; H, 6.39%.

Methyl 2,3,4-Tri-O-acetyl-6-O-benzyl-α-D-glucopyranoside (4a): The treatment of **4b** with **1**, followed by the aforementioned work-up and chromatographic separation (Solvent B, 6 : 1), gave **4a** as a syrup: $[\alpha]_D$ +131° (*c* 2.0, $CHCl_3$); NMR(CCl_4) δ=1.85 (s, 3, CH_3CO), 1.93 (s, 3, CH_3CO), 2.01 (s, 3, CH_3CO), 3.39 (s, 3, CH_3O), 3.86 (m, 1, H-5), 4.46 (s, 2, $PhCH_2$), 4.72 (dd, 1, *J*=3.5 and 9.0 Hz, H-2), 4.85 (d, 1, *J*=3.5 Hz, H-1), 4.92 (t, 1, *J*=9.0 Hz, H-4), 5.31 (t, 1, *J*=9.0 Hz, H-3), and 7.25 (s, 5, C_6H_5). Found: C, 58.48; H, 6.28%. Calcd for $C_{20}H_{26}O_9$: C, 58.53; H, 6.39%.

Methyl 2-O-Acetyl-3,4,6-tri-O-benzyl-β-D-glucopyranoside (19b): A mixture of 3,4,6-tri-*O*-benzyl-1,2-*O*-(1-ethoxyethylidene)-α-D-glucopyranose[11] (0.88 g), methanol (68 μl), mercury(II) bromide (18 mg), and nitromethane (10 ml) was stirred for 1 h at 100 °C[12] and then evaporated after a few drops of pyridine had been added. The residue was chromatographed (Solvent B, 10 : 1), and the fractions (R_f=0.45, Solvent B, 5 : 1) were collected and crystallized from diisopropyl ether to give **19b** (0.24 g, 28%): mp 51.5—52 °C; $[\alpha]_D$ +4° (*c* 1.0, $CHCl_3$); NMR(CCl_4) δ=1.96 (s, 3, CH_3CO), 3.47 (s, 3, CH_3O), 4.32 (d, 1, *J*=8.0 Hz, H-1), 7.22—7.33 (15, $3C_6H_5$). Found: C, 70.90; H, 6.70%. Calcd for $C_{30}H_{34}O_7$: C, 71.13; H, 6.77%.

Methyl 2-O-Acetyl-3,4,6-tri-O-benzyl-α-D-glucopyranoside (19a): The treatment of **19b** with **1** and subsequent chromatographic separation (Solvent A, 30 : 1) gave **19a** as a syrup: $[\alpha]_D$ +83° (*c* 0.8, $CHCl_3$); NMR(CCl_4) δ=1.90 (s, 3, CH_3CO), 3.30 (s, 3, CH_3O), and 7.13—7.21 (15, $3C_6H_5$). Found: C, 70.70; H, 6.83%. Calcd for $C_{30}H_{34}O_7$: C, 71.13; H, 6.77%.

Methyl 3-O-Acetyl-2,4,6-tri-O-benzyl-β-D-glucopyranoside (21b): A mixture of methyl β-D-glucopyranoside hemihydrate (Tokyo Kasei, 1.02 g, 5 mmol), sodium hydride (≈60% dispersion, 0.80 g, ≈20 mmol), and benzyl chloride (10 ml) was heated under efficient stirring for 3 h at 100 °C. The mixture was processed and chromatographed (Solvent A, gradient) to afford **2b** (0.33 g, 12%, R_f=0.75, Solvent A, 10 : 1) and then methyl 2,4,6-tri-*O*-benzyl-β-D-glucopyranoside (**20**, 0.56 g, 24%, R_f=0.45): $[\alpha]_D$ +19° (*c* 1.0, $CHCl_3$). Found: C,

72.23; H, 7.09%. Calcd for $C_{28}H_{32}O_6$: C, 72.39; H, 6.94%.

The acetylation of **20** with acetic anhydride in pyridine and subsequent crystallization from hexane gave **21b**: mp 109.5—110 °C, $[\alpha]_D$ +18° (*c* 1.0, $CHCl_3$); NMR ($CDCl_3$) δ=1.83 (s, 3, CH_3CO), 3.56 (s, 3, CH_3O), 4.34 (d, 1, J=8.0 Hz, H-1), and 7.22—7.31 (15, $3C_6H_5$). Found: C, 71.29, H, 6.78%. Calcd for $C_{30}H_{34}O_7$: C, 71.13; H, 6.77%.

Methyl 3-O-Acetyl-2,4,6-tri-O-benzyl-α-D-glucopyranoside (21a): The treatment of **21b** with **1** and subsequent chromatographic separation (Solvent A, 30 : 1) gave **21a**, whose ^1H NMR spectrum was identical with that of an authentic sample.[13]

Methyl 4-O-Acetyl-2,3,6-tri-O-benzyl-β-D-glucopyranoside (25b) and Methyl 6-O-Acetyl-2,3,4-tri-O-benzyl-β-D-glucopyranoside (26b): Methyl 2,3-di-*O*-benzyl-β-D-glucopyranoside[14] (**22**, 1.4 g, 3.74 mmol) was heated in benzyl chloride (14 ml) containing sodium hydride (≈50% dispersion, 0.22 g, ≈4.6 mmol) under stirring for 75 min at 75°C. The mixture was then processed and chromatographed (Solvent A, gradient) to afford **2b** (0.28 g, 13%), methyl 2,3,6-tri-*O*-benzyl-β-D-glucopyranoside (**23**, 1.12 g, 60%, R_f=0.40, Solvent A, 10 : 1), and methyl 2,3,4-tri-*O*-benzyl-β-D-glucopyranoside[15] (**24**, 0.34 g, 18%, R_f=0.25).

The acetylation of **23** with acetic anhydride in pyridine furnished **25b**: $[\alpha]_D$ −7° (*c* 2.0, $CHCl_3$); NMR($CDCl_3$) δ=1.73 (s, 3, CH_3CO), 3.51 (s, 3, CH_3O), 4.22 (d, 1, J=7.2 Hz, H-1), and 7.18—7.25 (15, $3C_6H_5$). Found: C, 70.41; H, 6.66%. Calcd for $C_{30}H_{34}O_7$: C, 71.13; H, 6.77%.

The acetylation of **24** gave **26b**: mp 70—70.5 °C (from hexane); $[\alpha]_D$ +19° (*c* 1.0, $CHCl_3$) [lit,[16] mp 61—63 °C; $[\alpha]_D$ +26° ($CHCl_3$)]. Found: C, 70.91; H, 6.68%. Calcd for $C_{30}H_{34}O_7$: C, 71.13; H, 6.77%.

Methyl 4-O-Acetyl-2,3,6-tri-O-benzyl-α-D-glucopyranoside (25a): The treatment of **25b** with **1** and subsequent chromatographic purification (Solvent A, 30 : 1) afforded 25a as a syrup: $[\alpha]_D$ +14° (*c* 2.0, $CHCl_3$); NMR(CCl_4) δ=1.74 (s, 3, CH_3CO), 3.36 (s, 3, CH_3O), and 7.21—7.26 (15, $3C_6H_5$). Found: C, 70.27; H, 6.40%. Calcd for $C_{30}H_{34}O_7$: C, 71.13; H, 6.77%.

Methyl 6-O-Acetyl-2,3,4-tri-O-benzyl-α-D-glucopyranoside (26a): The treatment of **26b** with **1** and subsequent chromatographic separation (Solvent A, 20 : 1) gave **26a** as a syrup: $[\alpha]_D$ +28° (*c* 1.0, $CHCl_3$); NMR CCl_4) δ=1.96 (s, 3, CH_3CO), 3.34 (s, 3, CH_3O), and 7.23—7.27 (15, $3C_6H_5$). Found: C, 70.80; H, 6.79%. Calcd for $C_{30}H_{34}O_7$: C, 71.13; H, 6.77%.

Methyl 2,3,4-Tri-O-benzyl-6-O-methyl-β-D-glucopyranoside (12b): A mixture of **24** (0.41 g), methyl iodide (2.7 ml), and silver oxide (1.0 g) was vigorously stirred for 40 h at room temperature. Chromatography (Solvent A, 30 : 1) and subsequent crystallization from hexane afforded **12b** (0.31 g, 74%): mp 64—65.5 °C; $[\alpha]_D$ +5° (*c* 1.0, $CHCl_3$); NMR(CCl_4) δ=3.31 (s, 3, CH_3O), 3.48 (s, 3, CH_3O), 4.15 (d, 1, J=7.4 Hz, H-1), and 7.15—7.18 (15, $3C_6H_5$). Found: C, 72.69; H, 7.07%. Calcd for $C_{29}H_{34}O_6$: C, 72.78; H, 7.16%.

Methyl 2,3,4-Tri-O-benzyl-6-O-methyl-α-D-glucopyranoside (12a): The treatment of **12b** with **1** and subsequent chromatographic separation (Solvent A, 30 :1) gave **12a** as a syrup: $[\alpha]_D$ +12° (*c* 2.0, $CHCl_3$) [lit,[17] $[\alpha]_D$ +8° (*c* 0.71, $CHCl_3$)]. Found: C, 72.48; H, 7.05%. Calcd for $C_{29}H_{34}O_6$: C, 72.78; H, 7.16%.

Methyl 2,3,4-Tri-O-acetyl-6-O-methyl-β-D-glucopyranoside (28b): The hydrogenolysis of **12b** in acetic acid and methanol in the presence of palladium black at 340 kPa and subsequent acetylation with acetic anhydride and pyridine, followed by crystallization from diisopropyl ether, furnished **28b**: mp 113—113.5 °C; $[\alpha]_D$ −14° (*c* 0.4, $CHCl_3$); NMR ($CDCl_3$) δ=2.03 (s, 3, CH_3CO), 2.06 (s, 6, $2CH_3CO$), 3.40 (s, 3, CH_3O), 3.53 (s, 3, CH_3O), and 4.44 (d, 1, J=8.0 Hz, H-1). Found: C, 50.39; H, 6.75%. Calcd for $C_{14}H_{22}O_9$: C, 50.29; H, 6.63%.

Methyl 2,3,4-Tri-O-acetyl-6-O-methyl-α-D-glucopyranoside (28a): The treatment of **28b** with **1** and subsequent chromatography (Solvent B, 6 : 1) gave **28a**: mp 77.5—78.5 °C; $[\alpha]_D$ +137° (*c* 2.0, $CHCl_3$); +150° (*c* 1.0, MeOH) [lit,[18] mp 73.5—74 °C, $[\alpha]_D$ +145° (*c* 0.99, MeOH)], NMR($CDCl_3$) δ=2.00 (s, 3, CH_3CO), 2.03 (s, 3, CH_3CO), 2.07 (s, 3, CH_3CO), 3.36 (s, 3, CH_3O), and 3.42 (s, 3, CH_3O). Found: C, 50.02; H, 6.71%. Calcd for $C_{14}H_{22}O_9$: C, 50.29; H, 6.63%.

Methyl 2,3,4-Tri-O-benzyl-6-deoxy-β-D-glucopyranoside (13b): Methyl 2,3,4-tri-*O*-acetyl-6-deoxy-β-D-glucopyranoside[19] was benzylated with hot benzyl chloride containing powdered potassium hydroxide to afford **13b**: mp 106.5—107 °C (from hexane); $[\alpha]_D$ +8° (*c* 0.5, $CHCl_3$) [lit,[20] mp 98 °C; $[\alpha]_D$ +6.8° (*c* 0.7, $CHCl_3$)]. Found: C, 74.87; H, 7.14%. Calcd for $C_{28}H_{32}O_5$: C, 74.97; H 7.19%.

Methyl 2,3,4-Tri-O-benzyl-6-deoxy-α-D-glucopyranoside (13a): The treatment of **13b** with **1** and subsequent chromatography (Solvent A, 50 : 1) gave **13a** as a syrup: $[\alpha]_D$ +21° (*c* 0.6, $CHCl_3$) [lit,[20] $[\alpha]_D$ +20.8° (*c* 0.7, $CHCl_3$)]. Found: C, 74.01; H, 6.91%. Calcd for $C_{28}H_{32}O_5$: C, 74.97; H, 7.19%.

Methyl 2,3,4-Tri-O-benzyl-α-D-xylopyranoside (14a): The treatment of **14b**[21] with **1** and subsequent chromatography (Solvent A, 40 : 1), followed by crystallization from hexane, gave **14a**: mp 68—69 °C, $[\alpha]_D$ +16° (*c* 0.7, $CHCl_3$), +50° (*c* 0.7, CH_2Cl_2) [lit,[21] mp 61 °C; $[\alpha]_D$ +50.5° (*c* 5.22, CH_2Cl_2)]. Found: C, 74.41; H, 6.86%. Calcd for $C_{27}H_{30}O_5$: C, 74.63; H, 6.96%.

Cyclohexylmethyl 2,3,4,6-Tetra-O-benzyl-α-D-glucopyranoside (29a): The treatment of **29b**[22] with **1** and subsequent chromatography (Solvent B, 15 : 1) gave **29a** as a syrup, identified with an authentic sample.[22]

Cyclohexyl 2,3,4,6-Tetra-O-benzyl-α-D-glucopyranoside (30a): The treatment of **30b**[10] with **1** and subsequent chromatography (Solvent B, 15 : 1) gave **30a** as a syrup, identified with an authentic sample.[10]

Benzyl 2,3,4,6-Tetra-O-benzyl-α-D-glucopyranoside (31b): The treatment of **31b**[23] with **1** and subsequent chromatography (Solvent B, 15 : 1) furnished **31a**: mp 94.5—95 °C (from hexane); $[\alpha]_D$ +53° (*c* 1.0, $CHCl_3$) [lit,[23] mp 93.5—94.5 °C; $[\alpha]_D^{28}$ +55.8° (*c* 1.63, $CHCl_3$)]. Found: C, 78.02; H, 6.70%. Calcd for $C_{41}H_{42}O_6$. C, 78.07; H, 6.71%.

2-Benzyloxyethyl, 3-Benzyloxypropyl, and 6-Benzyloxyhexyl 2,3,4,6-Tetra-O-benzyl-β-D-glucopyranosides (32b, 33b, and 34b): A mixture of 2,3,4,6-tetra-*O*-acetyl-α-D-glucopyranosyl bromide[24] (1.0 g, 2.4 mmol), 1,2-ethanediol (Wako, 0.27 ml), 4.8 mmol), silver oxide (1.1 g, 4.8 mmol), and benzene (10 ml) was agitated for 20 h at room temperature. The mixture was filtered, evaporated, and then chromatographed (Solvent A, 5 : 1) to afford 2-hydroxyethyl 2,3,4,6-tetra-*O*-acetyl-β-D-glucopyranoside[25] (0.80 g, 84%). This (0.26 g) was treated with hot benzyl chloride (5 ml) containing powdered potassium hydroxide (0.93 g) for 4 h at 100 °C. Usual work-up and chromatography (Solvent A, 30 : 1), followed by crystallization from hexane, gave **32b** (0.36 g, 81%); mp 67.5—68.5 °C; $[\alpha]_D$ +5° (*c* 1.0, $CHCl_3$). Found: C, 76.49; H, 6.88%. Calcd for $C_{43}H_{46}O_7$. C, 76.53; H, 6.87%.

The condensation of the bromide with 1,3-propanediol (Tokyo Kasei) and 1,6-hexanediol (Tokyo Kasei) afforded 3-hydroxypropyl 2,3,4,6-tetra-*O*-acetyl-β-D-glucopyranoside[26] (80%) and 6-hydroxyhexyl 2,3,4,6-tetra-*O*-acetyl-β-D-glucopyranoside[27] (46%) respectively. The yields were substantially improved. The subsequent benzylation of them furnished **33b** and **34b** respectively. **33b**: $[\alpha]_D$ +8° (*c* 2.8, $CHCl_3$). Found: C, 76.33; H, 6.96%. Calcd for $C_{44}H_{48}O_7$: C, 76.71; H, 7.02%. **34b**: $[\alpha]_D$ +4° (*c* 2.6, $CHCl_3$) Found: C, 76.79; H, 7.47%. Calcd for $C_{47}H_{54}O_7$: C, 77.23; H, 7.45%.

2-Benzyloxyethyl, 3-Benzyloxypropyl, and 6-Benzyloxyhexyl 2,3,-4,6-Tetra-O-benzyl-α-D-glucopyranosides (32a, 33a, and 34a): The treatment of **32b**, **33b**, and **34b** with **1**, and subsequent chromatographic separation (Solvent B, 10 : 1) gave **32a**, **33a**, and **34a** respectively. **32a**: $[\alpha]_D$ +37° (*c* 0.3, $CHCl_3$). Found: C, 75.50; H, 6.61%. Calcd for $C_{43}H_{46}O_7$: C, 76.53; H, 6.87%. **33a**: $[\alpha]_D$ +42° (*c* 0.4, $CHCl_3$). Found: C, 75.85; H, 6.97%. Calcd for $C_{44}H_{48}O_7$: C, 76.71; H, 7.02%. **34a**: $[\alpha]_D$ +33° (*c* 1.0, $CHCl_3$). Found: C, 76.25; H, 7.21%. Calcd for $C_{47}H_{54}O_7$: C, 77.23; H, 7.45%.

In the case of the reaction of **32b**, 2,3,4,6-tetra-*O*-benzyl-α-D-glucopyranose (22%), whose IR and NMR spectra were superimposable with those of an authentic specimen,[28] was isolated on chromatography.

Preparation of Additives. 1-Benzyloxy-2-methoxyethane (9): 2-Benzyloxyethanol (Tokyo Kasei) was methylated with methyl iodide in the presence of silver oxide to form **9**: bp 161—163 °C/123 mmHg,† n_D 1.4967 NMR(CCl_4) δ=3.33 (s, 3, CH_3O), 3.55 (s, 4, $(CH_2)_2$), 4.53 (s, 2, $PhCH_2$), and 7.25 (s, 5, C_6H_5). Found: C, 72.22; H, 8.30%. Calcd for $C_{10}H_{14}O_2$: C, 72.26; H, 8.49%.

2-(Benzyloxymethyl)tetrahydropyran (10): The benzylation of 2-(hydroxymethyl)tetrahydropyran[29] with hot benzyl chloride containing powdered potassium hydroxide afforded **10**: bp 169—172 °C/23—25 mmHg; n_D 1.5132; NMR($CDCl_3$) δ=23.2, 26.0, 28.3, 68.5, 73.4, 73.8, 76.8, 127.5, 127.7 (2C), 128.3 (2C), and 138.3. Found: C, 75.46; H, 8.82%. Calcd for $C_{13}H_{18}O_2$: C, 75.69; H, 8.79%.

trans-*1,2-Bis(benzyloxy)cyclohexane (11)*: The benzylation of *trans*-1,2-cyclohexanediol (Aldrich) with hot benzyl chloride and potassium hydroxide furnished **11**: bp 202—204 °C/2.5 mmHg; n_D 1.5470 [lit,[30] bp 182—183 °C/2 mmHg, n_D^{20}1.5468]; NMR(CCl_4) δ=0.93—2.23 (m, 8, $(CH_2)_4$), 3.31 (m, 2, H-1 and H-2), 4.56 (s, 4, $2PhCH_2$), and 7.21 (s, 10, $2C_6H_5$). Found: C, 81.09; H, 8.20% Calcd for $C_{20}H_{24}O_2$: C, 81.04; H, 8.16%.

Anomerization of Disaccharides. Anomerization of Methyl 6-O-(2,3,4,6-Tetra-O-benzyl-β-D-glucopyranosyl)-2,3,4-tri-O-benzyl-α-D-glucopyranoside (16b) into the α-Disaccharide (16a): A solution of **16b**[31] (36.4 mg, 0.037 mmol) in dichloromethane (0.37 ml) was treated with **1** (4.1 μl 0.037 mmol). After 30 s, the reaction was quenched and the mixture was processed as usual. Subsequent chromatographic separation (Solvent A, 30 : 1) gave **16a** (16.6 mg, 46%): mp 105—106 °C; $[\alpha]_D$ +59° (*c* 1.0, $CHCl_3$) [lit,[32] mp 101.5 °C; $[\alpha]_D^{20}$ +59.3° (*c* 1.78, $CHCl_3$)]. Found: C, 75.38; H, 6.71%. Calcd for $C_{62}H_{66}O_{11}$. C, 75.43; H, 6.74%.

The slower-moving, unchanged **16b** (4.9 mg, 14%) was recovered.

Anomerization of Methyl 3-O-(2,3,4,6-Tetra-O-benzyl-β-D-glucopyranosyl)-2,4-di-O-benzyl-α-D-xylopyranoside (17b) into the α-Disaccharide (17a): A solution of **17b**[33] (297 mg, 0.34 mmol) in dichloromethane (3.4 ml) was treated with **1** (38 μl, 0.34 mmol). After 60 s, the reaction was quenched. The mixture was then processed and chromatographed (Solvent B, 4 : 1) to furnish **17a** (40 mg, 14%), which was identified with a sample prepared alternatively:[33] $[\alpha]_D$ +58° (*c* 1.0, $CHCl_3$); NMR($CDCl_3$) δ=96.7 (C_{glc}-1) and 97.7 (C_{xyl}-1). Found: C, 74.04; H, 6.93%. Calcd for $C_{54}H_{58}O_{10}$: C, 74.81; H, 6.94%.

The faster-moving, unchanged **17b** (42 mg, 14%) was recovered.

References

1) E. Pacsu, *Chem. Ber.*, **61**, 1508 (1928).

2) R. E. Reeves and L. W. Mazzeno, Jr., *J. Am. Chem. Soc.*, **76**, 2219 (1954).

3) a) B. Lindberg, *Acta Chem. Scand.*, **3**, 1355 (1949); b) I. Karasawa and R. Onishi, *J. Agr. Chem. Soc. Jpn.*, **35**, 813 (1961); c) J. J. Schneider, *Carbohydr. Res.*, **12**, 369 (1970).

4) R. U. Lemieux, *Adv. Carbohydr. Chem.*, **9**, 1 (1954); b) M. G. Blair and W. Pigman, *Angew. Chem.*, **69**, 422 (1957); c) R. U. Lemieux, "Molecular Rearrangements," ed by P. deMayo, Intersci. Pub., New York (1964), p. 709; d) B. Capon, *Chem. Rev.*, **69**, 407 (1969); e) W. G. Overend, "The Carbohydrates, Chemistry and Biochemistry," 2nd ed, by W. Pigman and D. Horton, Academic Press, New York (1972), Vol. IA, p. 310.

5) N. Morishima, S. Koto, and S. Zen, *Chem. Lett.*, **1979**, 749.

6) In general, the anomeric center of *O*-alkyl sugar derivatives is more reactive than that of *O*-acetyl ones: *e.g.*, T. Ishikawa and H. G. Fletcher, Jr., *J. Org. Chem.*, **34**, 5636 (1969).

7) R. U. Lemieux and W. P. Shyluk, *Can. J. Chem.*, **33**, 120 (1955).

8) a) B. Lindberg, *Acta Chem. Scand.*, **3**, 1153 (1949); b) **4**, 1446 (1950); c) **3**, 1350 (1949).

9) P. W. Austin, F. E. Hardy, J. G. Buchanan, and J. Baddiley, *J. Chem., Soc.*, **1964**, 2128.

10) S. Koto, N. Morhishima, and S. Zen, *Bull. Chem. Soc. Jpn.*, **52**, 784 (1979).

11) M. A. E. Shaban and R. W. Jeanloz, *Carbohydr. Res.*, **52**, 103 (1976).

12) H. B. Boren, G. Ekborg, K. Eklind, P. J. Garegg, A. Pilotti, and C.-G. Swahn, *Acta Chem. Scand.*, **27**, 2639 (1973).

13) S. Koto, Y. Takebe, and S. Zen, *Bull. Chem. Soc. Jpn.*, **45**, 291 (1972).

14) J. C. Dennison and D. I. McGilvray, *J. Chem. Soc.*, **1951**, 1616.

15) S. S. Bhattacharjee and P. A. Gorin, *Can. J. Chem.*, **47**, 1195 (1969).

16) N. Pravdic and D. Keglevic, *Tetrahedron*, **21**, 1897 (1965).

17) A. Liptak, I. Jodal, and P. Nanasi, *Carbohydr. Res.*, **44**, 1 (1975).

18) B. A. Dmitriev, A. A. Kost, and N. K. Kochetkov, *Izv. Akad. Nauk SSSR, Ser. Khim.*, **1969**, 903 (CA-**71**-30665d).

19) J. Compton, *J. Am. Chem. Soc.*, **60**, 395 (1938).

20) B. Bernet and A. Vasella, *Helv. Chim. Acta*, **62**, 1990 (1979).

21) S. Tejima, R. K. Ness, R. L. Kaufman, and H. G. Flectcher, Jr., *Carbohydr. Res.*, **7**, 485 (1968).

22) S. Koto, T. Sato, N. Morishima, and S. Zen, *Bull. Chem. Soc. Jpn.*, **53**, 1761 (1980).

23) M. E. Tate and C. T. Bishop, *Can. J. Chem.*, **41**, 1801 (1963).

24) P. G. Scheuer and F. Smith, *J. Am. Chem. Soc.*, **76**, 3224 (1954).

25) E. Fischer and H. Fischer, *Chem. Ber.*, **43**, 2521 (1910).

26) S. Karjala and K. P. Link, *J. Am. Chem. Soc.*, **62**, 917 (1940).

27) B. R. Bhattacharyya, K. Ramaswamy, and R. K. Crane, *Carbohydr. Res.*, **47**, 167 (1976).

28) S. Koto, N. Morishima, Y. Miyata, and S. Zen, *Bull. Chem. Soc. Jpn.*, **49**, 2639 (1976).

29) *Pat. Belg.* 633, 117 (CA-**61**-P4321f).

30) S. Mamedov and I. L. Nizker, *Zh. Obsch. Khim.*, **33**, 841 (1963).

31) S. Koto, Y. Hamada, and S. Zen, *Chem. Lett.*, **1975**, 587.

32) J.-R. Pougny, J.-C. Jaquinet, M. Nassr, D. Duchet, M.-L. Milet, and P. Sinay, *J. Am. Chem. Soc.*, **99**, 6762 (1977).

33) N. Morishima, S. Koto, C. Kusuhara, and S. Zen, *Chem. Lett.*, **1981**, 427.

† 1 mmHg≈133.322 Pa.

 © 1982 The Chemical Society of Japan Bull. Chem. Soc. Jpn., 55, 1097—1101 (1982)

Phosphatosulfates. Metal-ion Effects on the Acid-catalyzed Hydrolysis of Phenyl Phosphatosulfate in an Acetonitrile-Water Mixed Solvent

Toshio EIKI, Yoshio ASAI, and Waichiro TAGAKI*,†

Department of Chemistry, Faculty of Engineering, Gunma University, Kiryu, Gunma 376

†*Department of Applied Chemistry, Faculty of Engineering, Osaka City University, 3-138, Sugimoto 3-chome, Sumiyoshi-ku, Osaka 558*

(Received March 17, 1981)

The rates of the acid-catalyzed hydrolysis of phenyl phosphatosulfate (PPS) have been found to be highly dependent on the water content in the mixed solvent of acetonitrile–water. A remarkable rate acceleration was observed with a rate maximum near the 1 : 1 ratio of PPS and metal ion, and with a solvent with a low water content. Under such conditions, the site of the cleavage of the P–O–S linkage was observed to be predominantly the S–O bond.

Active sulfates[1] are the key starting intermediates in the sulfur metabolism in biological systems.[2,3] They contain the P–O–S phosphatosulfate linkage, and a number of biological transformations, such as the phosphate- or sulfate-group transfer to various nucleophilic acceptors or the reduction of sulfate groups, are all initiated by the cleavage of the P–O–S linkage. However, the mechanisms of the corresponding enzymatic catalyses have largely been left unclarified. The biomimetic chemistry of the phosphatosulfate linkage has also been relatively unexplored compared to that of the related P–O–P phosphate linkage.

An interesting feature of the chemistry of the P–O–S linkage is the role of metal ions—how they affect the rate and selectivity in the cleavage of the P–O *vs.* S–O bond. Previously we reported that the Mg^{2+} ion enhanced the rate of the acid-catalyzed hydrolysis of PPS, a simple model of active sulfates, in mixed solvents of acetonitrile–water when their water content was low.[4,5] The details will now be described in this paper, along with additional data for some other metal ions (Eq. 1). The substrate PPS was used in the form of diammonium salt.

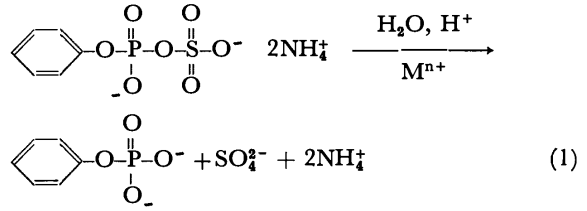

diammonium salt of PPS

(1)

Results and Discussion

Kinetics. The reactions were generally carried out in an acetonitrile–water mixed solvent containing appropriate amounts of PPS ($1.8—2.0\times10^{-3}$ M), a metal ion ($0—4\times10^{-2}$ M) and buffer reagents of $HClO_4$ ($0.3—3.0\times10^{-3}$ M)-*n*-$Bu_4N^+ClO_4^-$ (2×10^{-2} M), at 25 °C (1 M=1 mol dm^{-3}). For some experiments with solvents of a low water content, the water was partially replaced by methanol (see Fig. 2b and Table 3). Under these conditions the hydrolysis of acetonitrile was not detected.

The rates were determined by measuring the formation of phenyl phosphate.[4-6] Most reaction mixtures were homogeneous during the reaction. Occasionally, ammonium sulfate was precipitated out at the end of reaction in the solvents with a low water content (3 M). Nevertheless, good pseudo-first-order rate constants were obtained up to more than 90% completion of the reaction.

Effect of Water Concentration. The rates of acid-catalyzed hydrolysis were found to be highly dependent on the water content of the medium, in both the absence and presence of a metal ion.

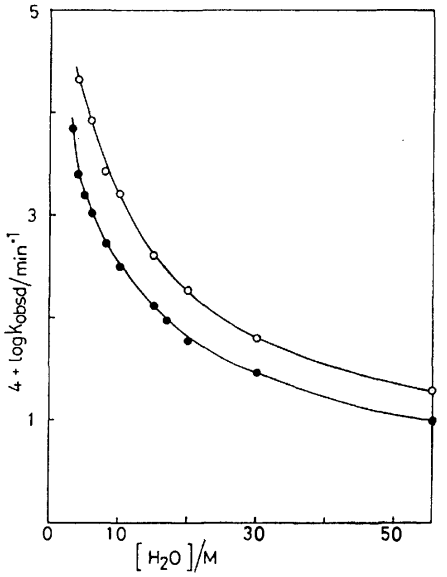

Fig. 1. Effect of water concentration on the rates of hydrolysis of PPS (1.8×10^{-3} M) in the presence of $HClO_4$(●; 2×10^{-3} M, ○ ; 4×10^{-3} M) and $(n\text{-Bu})_4NClO_4$ (2×10^{-2} M) at 25 °C.

In the absence of a metal ion, Fig. 1 shows that the rates in pure water (55.5 M) are enhanced by some 10^3 times in an acetonitrile–water mixed solvent when the water content is reduced to 3 M. A similarly large rate enhancement has also been reported for other acid-catalyzed sulfate hydrolysis in solvents of low polarity (ether or moist dioxane).[7,8] A suggestion has been made that the hydrolysis of aryl hydrogensulfate based on an Al mechanism (Eq. 2) is due to a specific solvation of the zwitter ionic-transition state of sulfur trioxide by ether.[9] Since an Al mechanism to give sulfur trioxide has been suggested for the acid-catalyzed hydrolysis of PPS in pure water,[6,10,11] the specific solvation of sulfur

Table 1. Mg^{2+} ion effect on the rates of hydrolysis of PPS at 25 °C[a)]

$[Mg(ClO_4)_2]\times10^3$/M	k_{obsd}/min^{-1}, $[H_2O]$/M in acetonitrile					
	3	4	4.5	5	6	8
0	2.66×10^{-2}	1.78×10^{-2}	1.30×10^{-2}	1.14×10^{-2}	8.94×10^{-3}	8.28×10^{-3}
0.5	8.88×10^{-2}	—	—	4.57×10^{-2}	1.66×10^{-2}	7.98×10^{-3}
1.0	1.90×10^{-1}	8.82×10^{-2}	7.38×10^{-2}	—	—	—
1.8	2.67×10^{-1}	1.23×10^{-1}	7.74×10^{-2}	5.25×10^{-2}	3.18×10^{-2}	7.80×10^{-3}
2.2	1.44×10^{-1}	8.40×10^{-2}	—	—	—	—
2.5	1.20×10^{-1}	7.20×10^{-2}	3.84×10^{-2}	2.31×10^{-2}	1.38×10^{-2}	5.29×10^{-3}
5.0	2.53×10^{-2}	2.10×10^{-2}	1.27×10^{-2}	8.88×10^{-2}	5.41×10^{-3}	2.96×10^{-3}
10.0	1.06×10^{-2}	9.42×10^{-3}	7.20×10^{-3}	4.09×10^{-3}	4.06×10^{-3}	2.23×10^{-3}
20.0	7.08×10^{-3}	5.10×10^{-3}	3.15×10^{-3}	2.86×10^{-3}	2.44×10^{-3}	1.53×10^{-3}

a) $[PPS]=1.8\times10^{-3}$ M, $[HClO_4]=1.0\times10^{-3}$ M, $[(n\text{-}Bu)_4NClO_4]=2.0\times10^{-2}$ M.

$$ArOSO_2OH \rightleftharpoons Ar\text{-}\overset{+}{\underset{\underset{H}{|}}{O}}\text{-}SO_2\text{-}O^- \rightleftharpoons SO_3 + ArOH \qquad (2)$$
$$\downarrow H_2O$$
$$H_2SO_4$$

trioxide by acetonitrile may also be possible as an explanation in such a medium with a low water content. However, the effect of water seems to be too complex to allow a simple interpretation, as will be described below.

Effects of Metal Ions. The metal-ion effect in water was examined by Benkovic and Hevey.[10] They observed rates faster by 1.26—3.16 times in the hydrolysis of PPS by Mg^{2+}, Ca^{2+}, or Al^{3+} ions at pH 3.1 and 55 °C. They also observed that the rates were 1.2—2.05 times slower in the cases of Mn^{2+}, Co^{2+}, or Zn^{2+} ions. Thus, the effect of these metal ions is not large in pure water. Meanwhile, we have found remarkable metal-ion effects in the medium of acetonitrile–water mixed solvents.[4]

As is shown in Fig. 2a and Table 1, the rate acceleration by the Mg^{2+} ion is not observable when the water content of the medium exceeds 8 M; rather, the addition of the Mg^{2+} ion tends to inhibit the acid catalysis (see the k_{obsd} values in the absence of a metal ion). On the other hand, a large rate acceleration takes place in a medium with a low water content, showing a maximum in each plot of k_{obsd} *vs.* $[Mg(ClO_4)_2]$ where the concentration of the Mg^{2+} ion is very close to the initial concentration of the substrate ($[PPS]=1.8\times10^{-3}$ M). For example, in the solvent of $H_2O=3$ M, the k_{obsd} at

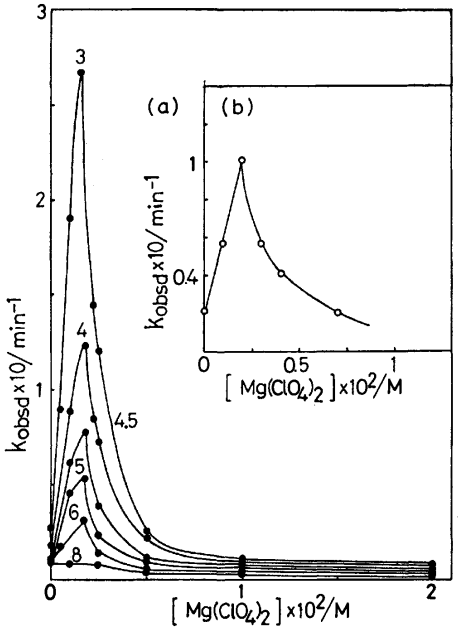

Fig. 2. Mg^{2+} ion effect on the (a) hydrolysis and (b) methanolysis of PPS at 25 °C.
(a): $[PPS]=1.8\times10^{-3}$ M, $[HClO_4]=1.0\times10^{-3}$ M $[n\text{-}Bu_4NClO_4]=0.02$ M. The numbers in the plots are the molar concentrations of water in acetonitrile–water mixed solvent. (b): In acetonitrile containing methanol (1 M), water (3 M), PPS (2.0×10^{-3} M), $HClO_4$ (1×10^{-3} M), and n-Bu_4NClO_4 (0.03 M), 25 °C. The k_{obsd} values are for the formation of phenyl phosphate.

Table 2. Effects of acid and water concentration on the rates of hydrolysis of PPS in the absence (k_o) and the presence of Mg^{2+} ion (k_{max})[a)] in mixed solvents of water–acetonitrile

$[HClO_4]\times10^3$/M	$-\log[HClO_4]$	$k_o(k_{max})$/min^{-1}, $[H_2O]$/M in acetonitrile		
		4.0	5.0	6.0
0.30	3.52	$3.83\times10^{-4}(1.92\times10^{-2})$	$2.63\times10^{-4}(1.06\times10^{-2})$	— (4.06×10^{-3})
0.50	3.30	$2.01\times10^{-4}(4.53\times10^{-2})$	$1.29\times10^{-3}(1.86\times10^{-2})$	$9.54\times10^{-4}(9.96\times10^{-3})$
0.75	3.12	$7.94\times10^{-3}(8.88\times10^{-2})$	$4.83\times10^{-3}(3.92\times10^{-2})$	$3.78\times10^{-3}(2.11\times10^{-2})$
1.00	3.00	$1.78\times10^{-2}(1.23\times10^{-1})$	$1.14\times10^{-2}(5.25\times10^{-2})$	$8.94\times10^{-3}(3.18\times10^{-2})$
1.50	2.82	$7.77\times10^{-2}(2.80\times10^{-1})$	$6.07\times10^{-2}(1.53\times10^{-1})$	$3.37\times10^{-2}(6.78\times10^{-2})$
2.00	2.69	$2.36\times10^{-1}(3.42\times10^{-1})$	$1.54\times10^{-1}(2.13\times10^{-1})$	$1.06\times10^{-1}(9.60\times10^{-2})$
3.00	2.52	$12.3\times10^{-1}(7.80\times10^{-1})$	$4.28\times10^{-1}(3.63\times10^{-1})$	$3.42\times10^{-1}(1.86\times10^{-1})$

a) $[PPS]=1.8\times10^{-3}$ M; $k_o([Mg(ClO_4)_2]=0$ M), k_{max} ($[Mg(ClO_4)_2]=1.8\times10^{-3}$ M) $[(n\text{-}Bu)_4NClO_4^-]=2.0\times10^{-2}$ M, 25 °C.

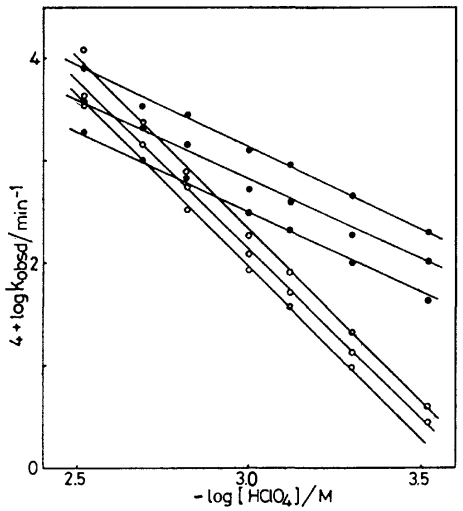

Fig. 3. Effect of acid and water concentration on the rates of hydrolysis of PPS in the absence (○) and presence of Mg^{2+} ion (●) in the mixed solvents of water–acetonitrile. Water concentrations are from the bottom 4,5, and 6 M, respectively (see Table 2).

the maximum ($k_{max}=2.67\times10^{-1}$ min^{-1}) is ten times larger than the k_{obsd} in the absence of the Mg^{2+} ion ($k_0=2.66\times10^{-2}$ min^{-1}). These k_{max} and k_0 values are dependent on both the water and acid concentrations as shown in Fig. 3 and Table 2.

As has previously been reported,[4,10,11] the acid hydrolysis of PPS in water gives a linear pH-log k_{obsd} plot with a slope of −1. In Fig. 3, the corresponding slopes of the plots of $-\log[HClO_4]$ *vs.* $\log k_0$ and $\log k_{max}$ are −3.2 and −1.6 respectively in the ranges of $[HClO_4]=0.3$—3.0×10^{-3} M and $[H_2O]=4$—6 M. Thus, the apparent number of protons involved in the rate-limiting step changes from one in pure water to more than three in the medium with a low water content and in the absence of a metal ion, while the number changes from −3.2 in the absence of the Mg^{2+} ion to −1.6 in its presence. Whatever the cause, these dependencies of k_{max} and k_0 on both the water and acid concentrations lead to the conclusion that the ratio of k_{max}/k_0 (*i.e.*, the metal-ion effect) increases linearly with a decrease in the water concentration (see Table 1) and exponentially with a decrease in the acid concentration (see Fig. 3 and Table 2), at least in the ranges of $[H_2O]=3$—8 M and $[HClO_4]=0.3$—3×10^{-3} M. Conversely, such metal-ion effects become unimportant at higher acid concentrations and in pure water.

The Mg^{2+} ion is most frequently encountered as a cofactor in the reactions of phosphates including active sulfates in biological systems.[2,3,12] The above findings may offer important suggestions regarding the role of the Mg^{2+} ion in such a biological reaction. In order to obtain further knowledge, the effects of some other metal ions have also been examined, as will be described below.

As is shown in Figs. 4 and 5, the effects of Ca^{2+}, Zn^{2+}, Al^{3+}, and Th^{4+} on the rates were found to be similar to those of Mg^{2+} in Fig. 2. For example, the [PPS]/[metal ion]=1 ratio at the k_{max} is the same for both

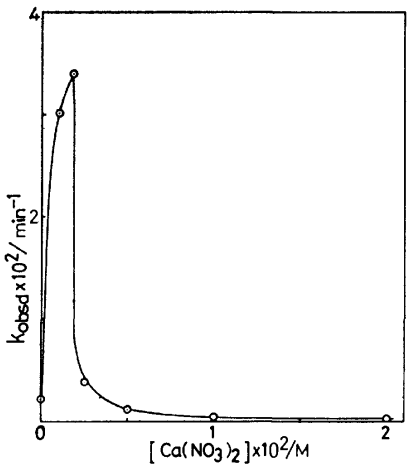

Fig. 4. Effect of Ca^{2+} ion on the rates of hydrolysis of PPS, 25 °C in 4 M water–acetonitrile.
$[PPS]=1.8\times10^{-3}$ M; $[HClO_4]=5.0\times10^{-4}$ M; $[(n\text{-}Bu)_4NClO_4]=0.02$ M.

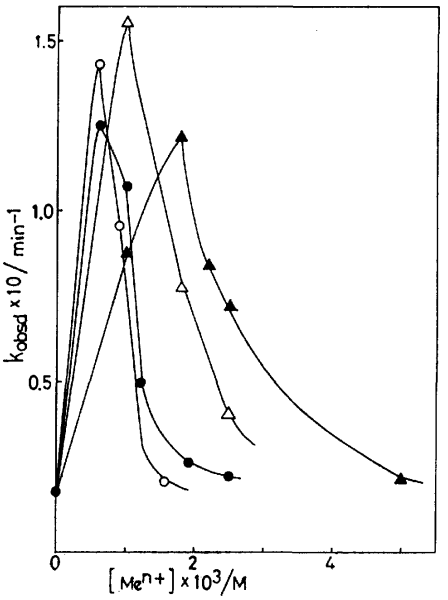

Fig. 5. Effect of metal ions on the rates of hydrolysis of PPS. 25 °C in 4 M water–acetonitrile.
$[PPS]=1.8\times10^{-3}$ M; $[HClO_4]=1.0\times10^{-3}$ M; $[(n\text{-}Bu)_4ClO_4]=0.02$ M; Me^{n+} are Zn^{2+} (△), Al^{3+} (●), Th^{4+} (○), and Mg^{2+} (▲).

Ca^{2+} and Mg^{2+}, and they give comparable k_{max}/k_0 values of 16 and 23 respectively under the same conditions ($[H_2O]=4$ M, $[HClO_4]=5\times10^{-4}$ M). However, the details are different; the metal-ion concentrations which give the rate maximum with $[PPS]=1.8\times10^{-3}$ M are $[Th^{4+}]=0.6\times10^{-3}$ M, $[Al^{3+}]=0.6\times10^{-3}$ M, $[Zn^{2+}]=1.0\times10^{-3}$ M, $[Ca^{2+}]=1.8\times10^{-3}$ M, and $[Mg^{2+}]=1.8\times10^{-3}$ M; all the curves in Figs. 2, 4, and 5 are unusually sharp, but those of Th^{4+} and Al^{3+} are much sharper than for those of Ca^{2+} and Mg^{2+}. Apparently, complicated equilibria are taking place between PPS and a metal ion, which are both highly dependent on both the water and acid concentrations. The fact that [PPS]/[metal ion]=1—3 at the rate maximum suggests

that the 1 : 1, 1 : 2, or 1 : 3 complex of a metal ion and PPS is catalytically active depending on the nature of metal ion, but that a further increase in the metal-ion coordination stabilizes the complex toward the hydrolysis.

Selective S–O Bond Cleavage. It has already been shown by an ^{18}O-tracer study that the S–O bond of PPS was selectively cleaved in the acid-catalyzed hydrolysis in water.[4,10] Similarly, methyl hydrogensulfate was obtained in a reaction in aqueous methanol.[10] However, the metal-ion effect was found to be small in water, as has been mentioned above, and so it was not examined in the latter aqueous methanol.

Table 3. Mg^{2+} ion effect on the rate of hydrolysis of PPS in mixed solvents of methanol (1.0 M)–water (3.0 M)–acetonitrile at 25 °C[a]

$[Mg(ClO_4)_2]$/M	k_{obsd}/min^{-1}
0	2.06×10^{-2}
1.0×10^{-3}	5.69×10^{-2}
2.0×10^{-3}	1.04×10^{-1}
3.0×10^{-3}	5.72×10^{-2}
4.0×10^{-3}	4.15×10^{-2}
7.0×10^{-3}	2.00×10^{-2}

a) $[PPS]=2.0\times10^{-3}$ M; $[HClO_4]=1.0\times10^{-3}$ M; $[(n\text{-Bu})_4NClO_4]=3.0\times10^{-2}$ M.

As is shown in Table 3 and Fig. 2b, a partial substitution of 4 M water by methanol in acetonitrile did not change the essential features of the Mg^{2+}-ion effect; a rate maximum was also observed at [PPS] : [metal ion]=1 : 1. From the reaction mixture at the rate maximum, methyl hydrogensulfate was then detected in a 60% yield by NMR analysis. The alternative formation of methyl phenyl phosphate by the P–O bond cleavage was not detected in spite of the fact that it is stable under the present reaction conditions (Eq. 3a) and should be easily detected by means of the NMR doublet of the CH_3 signal. Thus, the methanolysis of

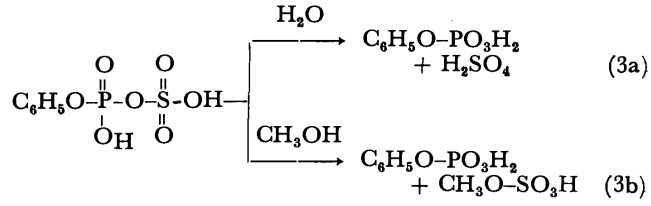

PPS occurs by means of the predominant S–O bond cleavage (Eq. 3b). Here, it should be noted that this S–O cleavage is the subject of Mg^{2+}-ion catalysis.

Mechanism of Metal-ion Catalysis. In the related phosphate hydrolysis, the metal-ion effects have been extensively studied, but the catalysis observed is generally not large.[12] Rate acceleration has been observed only in the hydrolysis of esters which have a neighboring functional group for chelation with a metal ion.[13] In other well-designed models for ATP hydrolysis, neighboring polyamine ligands showed essentially no effect on the metal-ion catalysis.[12] An exception was the observation that the hydrolysis or phosphate group-transfer reaction of ATP was accelerated in the presence of the Mg^{2+} ion when the reactions were conducted in dimethyl sulfoxide with a low water content.[14]

For an efficient catalysis to occur, a metal ion and phosphate (or sulfate) must form a complex. This process would, however, not be favored in water because of the favored hydration of the metal ion and the ester, whereas in an enzymatic reaction the medium at the active site is not necessarily water, but rather would be hydrophobic or dipolar aprotic in favor of metal ion-substrate binding. This idea may be supported by the findings shown above in Figs. 2, 4, and 5. However, even if this is true, the question still remains of how such complexation can activate the selective S–O bond cleavage. One may consider the present metal-ion effect to be electrophilic catalysis, as is illustrated in **1a**.

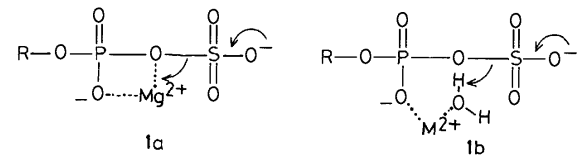

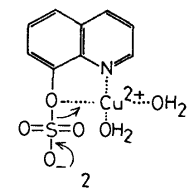

This type of catalysis was proposed in the Cu^{2+}-ion catalyzed hydrolysis of 8-quinolyl sulfate, as is shown in **2**.[13f] However, the present metal-ion effect is highly acid-dependent; under neutral conditions, no such metal-ion-assisted S–O cleavage was detected with divalent metal ions.[15] Therefore, the results may be tentatively accounted for by a mechanism of metal-ion-assisted proton-transfer catalysis, as is illustrated in **1b**, where the leaving group to capture the proton is the phosphoryl group. This type of catalysis is essentially the same as that considered in the hydrolysis of aryl hydrogensulfates, where a neighboring carboxyl or imidazolium group acts as the proton-transfer catalyst to the leaving phenoxyl group.[16,17] In **1b**, the proton transfer seems to be smooth when the metal ion coordinates only to the phosphate group, leaving the sulfate group free. Thus, any further coordination of the metal ion to the sulfate group would stabilize the complex and inhibit the reaction.

Experimental

Materials. The diammonium phenyl phosphatosulfate (PPS) was prepared by the previously reported method.[6] The tetrabutylammonium perchlorate was prepared by the literature method.[18] Deionized water was treated with $KMnO_4$ and distilled twice before use. The metal ions were used in the forms of perchlorate (Mg^{2+}) and nitrate (Zn^{2+}, Ca^{2+}, Al^{2+}, Th^{4+}) of an analytical grade.

Product Analyses. The hydrolysis products were found to be solely phenyl phosphate and inorganic sulfate, regardless of the presence or absence of metal ions. No phenol or other possible organic products were detected. In the reactions shown in Fig. 2b, methyl hydrogensulfate, phenyl phosphate,

and inorganic sulfate were the sole products, and methyl phenyl phosphate was not detected.

Phenyl phosphate was analyzed by UV absorption and paper chromatography.[6] Inorganic sulfate was analyzed colorimetrically by the barium chloranilate method.[19] Methyl hydrogensulfate was analyzed by NMR in the following way: the evaporation of acetonitrile gave $(n\text{-Bu})_4NClO_4$ precipitates, which were then removed by filtration. The filtrate was adjusted to pH 11 with aqueous sodium hydroxide to give insoluble magnesium hydroxide, which was subsequently removed by centrifugation. The supernatant was then neutralized with hydrochloric acid, and the solution was lyophilized. The residue was dissolved in D_2O and analyzed by NMR for phenyl and methyl (3H, δ 3.81, singlet) protons. The yield of methyl hydrogensulfate thus analyzed was 60% for the reaction mixture at the rate maximum shown in Fig. 2b.

Kinetics. The rate of the reaction was followed spectrophotometrically by quenching the reaction mixture with aqueous sodium hydroxide according to the previously reported method, except for the centrifugation of the quenched solutions to remove magnesium hydroxide.[4,11] Good pseudo-first-order rate constants were obtained up to a 90% completion of the reaction in the range of $[HClO_4]=0.3-3.0\times10^{-3}$ M, both in the presence and in the absence of $Mg(ClO_4)_2$ (see Fig. 3), although significant deviation from the first-order kinetics due to autocatalytic rate acceleration was observed below $[HClO_4]=0.3\times10^{-3}$ M. The pseudo-first-order rate constants were computed as usual by using $k_{obsd}=\frac{1}{t}\ln\frac{OD_\infty-OD_0}{OD_\infty-OD_t}$. The rate of reaction shown in Fig. 2b was determined by the same method.

References

1) Adenosine 5′-phosphosulfate (APS) and 3′-phosphoadenosine 5′-phosphosulfate (PAPS).

2) F. Lipmann, *Science*, **128**, 575 (1958).

3) a) H. D. Peck, Jr., *Enzymes*, **10**, 651 (1974); b) A. B. Roy and P. A. Trudinger, "The Biochemistry of Inorganic Compounds of Sulphur," Cambridge Univ. Press, Cambridge, (1970); c) J. A. Schiff and R. C. Hodson, "The Metabolism of Sulfate," *Ann. Rev. Plant Physiol.*, **24**, 381 (1973); d) A. B. Roy, *Enzymes*, **8**, 1 (1971).

4) W. Tagaki, Y. Asai, and T. Eiki, *J. Am. Chem. Soc.*, **95**, 3037 (1973).

5) W. Tagaki and T. Eiki, *Adv. Chem. Ser.*, **191**, 407 (1980).

6) W. Tagaki, T. Eiki, and I. Tanaka, *Bull. Chem. Soc. Jpn.*, **44**, 1139 (1971).

7) S. Burstein and S. Lieberman, *J. Am. Chem. Soc.*, **80**, 5235 (1958).

8) B. D. Batts, *J. Chem. Soc.*, **1966**, 551.

9) A. Williams and K. T. Douglas, *Chem. Rev.*, **75**, 627 (1975).

10) S. J. Benkovic and R. C. Hevey, *J. Am. Chem. Soc.*, **92**, 4971 (1970).

11) T. Eiki, K. Tomuro, S. Aoshima, M. Suda, and W. Tagaki, *Nippon Kagaku Kaishi*, **1980**, 454.

12) B. S. Cooperman, *Biochemistry*, **8**, 5055 (1969).

13) a) R. Hofstetter, Y. Murakami, G. Mont, and A. E. Martell, *J. Am. Chem. Soc.*, **84**, 3041 (1962); b) Y. Murakami, J. Sunamoto, and H. Sadamori, *Chem. Commun.*, **1969**, 983; c) S. J. Benkovic and L. K. Dunikowski, Jr., *J. Am. Chem. Soc.*, **93**, 1526 (1971); d) C. M. Hsu and B. S. Cooperman, *ibid.*, **98**, 5652 (1976); e) R. W. Hay and J. A. G. Edmonds, *Chem. Commun.*, **1967**, 969; f) R. W. Hay, C. R. Clark, and J. A. G. Edmonds, *J. Chem. Soc., Dalton Trans.*, **1974**, 9.

14) N. Nelon and E. Racker, *Biochemistry.*, **12**, 563 (1973).

15) Under neutral or basic conditions, divalent metal ions (Mg^{2+}, Zn^{2+}, Ni^{2+}, Co^{2+}, *etc.*) were found to catalyze nucleophilic reactions on phosphorus to give a P–O cleavage.[5]

16) S. J. Benkovic, *J. Am. Chem. Soc.*, **88**, 5511 (1966).

17) S. J. Benkovic and L. K. Dunikowski, *Biochemistry*, **9**, 1390 (1970).

18) a) H. Sadek and R. M. Fuoss, *J. Am. Chem. Soc.*, **72**, 301 (1950); b) R. L. Buckson and S. G. Smith, *J. Phys. Chem.*, **68**, 1875 (1964).

19) A. Wainer and L. Kock, *Anal. Biol. Chem.*, **3**, 457 (1962).

 © 1982 The Chemical Society of Japan Bull. Chem. Soc. Jpn., 55, 1102—1105 (1982) [Vol. 55, No. 4

Micellar Effects on the Co-catalysis of Magnesium Ion and Imidazole for the Hydrolysis of Phenyl Phosphatosulfate

Toshio EIKI and Waichiro TAGAKI*,†

Department of Chemistry, Faculty of Engineering, Gunma University, Kiryu, Gunma 376
†*Department of Applied Chemistry, Faculty of Engineering, Osaka City University, Sugimoto 3, Sumiyoshi-ku, Osaka 558*

(Received August 3, 1981)

The effects of Mg^{2+} ion and imidazole were examined on the hydrolysis of phenyl and *p*-decylphenyl phosphatosulfate (PPS and DPPS) in the presence of micelle of sodium dodecyl sulfate (SDS). It was observed that Mg^{2+} ion and imidazole increased the rates of hydrolysis cooperatively and the rate enhancement was much larger in the case of DPPS than in the case of PPS. The difference in the reactivities of two esters was discussed in terms of micellar effects.

Active sulfates[1] containing the phosphatosulfate linkage (P–O–S) are the key intermediates in the biological sulfur metabolism.[2] Yet a little has been understood for the mechanism of enzymic catalyses involving P–O–S linkage. In the model reactions, the P–O–S linkage is now known to be susceptible to the hydronium ion catalysis to give a selective S–O bond cleavage.[3,4] Such an acid catalysis can be enhanced by Mg^{2+} ion when the water content of the medium is low.[5,6] However, under the neutral conditions, the effect of Mg^{2+} ion alone is small even in the medium of low water content. Related fact is the requirement of bivalent metal ions as the cofactors in some hydrolytic enzymes of active sulfates which are active under the neutral conditions.[2e] Thus it is interesting to know a mechanism of activation of P–O–S linkage by Mg^{2+} ion under the neutral conditions. In this paper, we describe our observation that Mg^{2+} ion activates the P–O–S linkage toward the attack of imidazole nucleophile and the activation is enhanced under the micellar conditions.

Results and Discussion

Products. The substrates used were phenyl phosphatosulfate (PPS) and *p*-decylphenyl phosphatosulfate (DPPS). Their aminolysis was reported previously.[6,7] In the absence of Mg^{2+} ion and in the neutral or basic media, amines were observed to attack phosphorus to give phosphoramidates and inorganic sufate with a selectivity of 70—85% P–O cleavage. In the presence of Mg^{2+} ion, the selectivity of P–O cleavage increased further up to almost 100%.

In the case of imidazole, the corresponding phosphoramidates were not detected, but presumed to undergo rapid hydrolysis (Eq. 1). This presumption appears to be supported by the formation of methyl phenyl phosphate from PPS when the reaction was conducted in aqueous methanol (Eq. 1), while methyl hydrogensulfate was not detected which would be formed if the alternative cleavage of S–O bond occurred to give imidazole-*N*-sulfonic acid.

Kinetics. *Effect of SDS*: The kinetics of hydrolysis of PPS and DPPS were generally conducted in the micellar solution of SDS (6×10^{-2} M, 1 M=1 mol dm^{-3}), although the latter DPPS and its hydrolysis product diammonium *p*-decylphenyl phosphate (DPP)

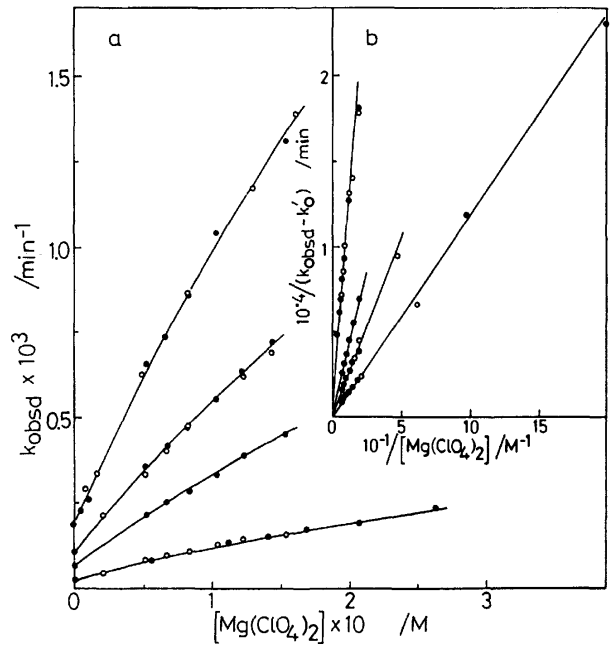

Fig. 1. a) Mg^{2+} ion effects on the imidazole catalyzed hydrolysis of PPS (2×10^{-2} M) in *N*-ethylmorpholine buffer (0.02 M, pH 7.90) at 55.0 °C: ●, in the presence of SDS (6×10^{-2} M); ○, in the presence of NaCl (6×10^{-2} M). Initial total concentrations of imidazole are from the bottom, 0.0, 1.0×10^{-2}, 2.0×10^{-2}, and 4.0×10^{-2} M, respectively. Solid lines are theoretical curves calculated from the values in Table 1 and Eq. 3; b) the reciprocal plots.

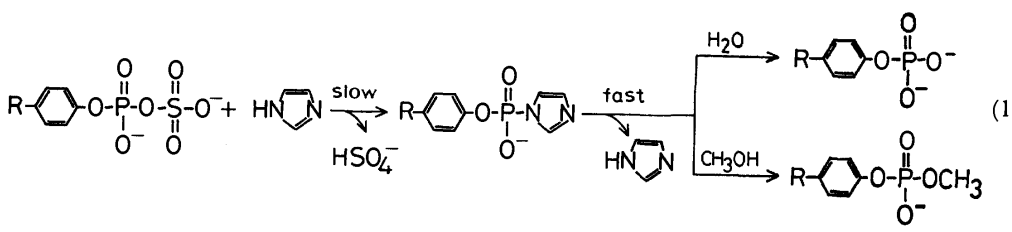

(1)

both form micelles above their CMC.[7] The reason of using SDS was the following. In the absence of SDS, an initially homogeneous reaction mixture of DPPS and Mg^{2+} ion became cloudy as the reaction proceeded due to the formation of an insoluble DPP–Mg^{2+} ion complex which could be solubilized by SDS micelle. The presence of SDS micelle, however, did not cause any detectable effect on the rates (k_{obsd}) of hydrolysis of DPPS.[8] The effect of SDS was also negligible on the hydrolysis of PPS as shown in Fig. 2. Thus in each case of PPS and DPPS, the effect of SDS on the rates was not apparent except for solubilization of the insoluble product. Nevertheless, a higher reactivity of DPPS than PPS appears to be due to a micellar effect as discussed later.

Hydrolysis of PPS: *N*-Ethylmorpholine used as the buffer reagent was confirmed to be unreactive toward the P–O–S linkage.[6,7] The effects of imidazole and Mg^{2+} ion concentration on the rates were then examined as shown in Fig. 1. The figure indicates that there was no difference in the rates between the medium of non-micellar NaCl (0.06 M) and micellar SDS (0.06 M). The figure also indicates that the rates tend to be saturated with increasing Mg^{2+} ion concentration at each fixed concentration of imidazole (0—4×10^{-2} M). On the other hand, the rates were linear with the increase in imidazole concentration at a fixed concentration of Mg^{2+} ion. These observations appear to be accounted for by assuming a reaction scheme involving preequilibrium formation of 1 : 1 complex (M.S) of substrate (S) and Mg^{2+} ion (M), where $[M.S]\ll[M]_T$, according to Eq. 2. From Eq. 2, the pseudo-first-order

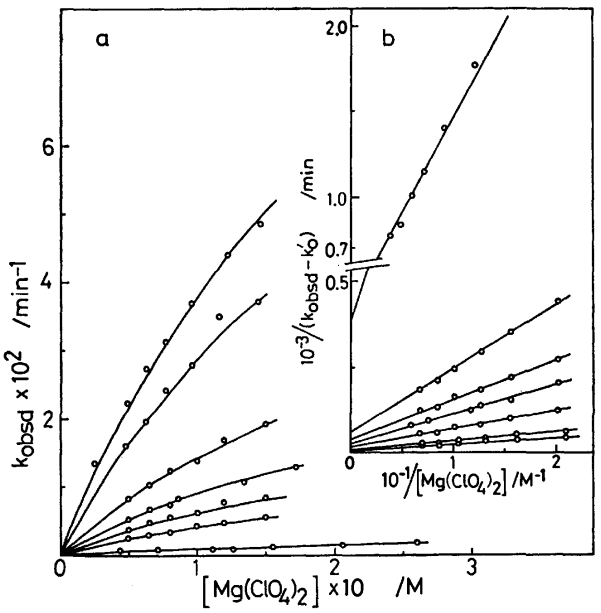

Fig. 2. a) Mg^{2+} ion effects on the imidazole catalyzed hydrolysis of DPPS (2×10^{-2} M) in the presence of SDS (6×10^{-2} M) in *N*-ethylmorpholine buffer (0.2 M, pH 7.90) at 55.0 °C. Initial total concentration of imidazole are from the bottom, 0.0, 2.4×10^{-3}, 4.0×10^{-3}, 6.0×10^{-3}, 1.0×10^{-2}, 2.1×10^{-2}, and 2.8×10^{-2} M, respectively. Solid lines are theoretical curves calculated from the values in Table 1 and Eq. 3; b) the reciprocal plots.

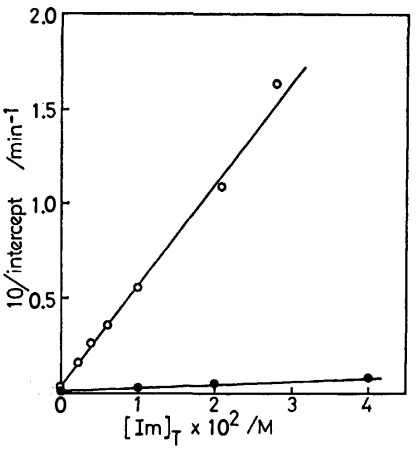

Fig. 3. Plots of 1/intercept *vs.* initial total concentration of imidazole ($[Im]_T$) for DPPS (○) and PPS (●), see text.

rate constant, k_{obsd} is given by Eq. 3, where $[Im]_T$ and $[M]_T$ are the initial stoichiometric concentration of imidazole and Mg^{2+} ion, respectively; k_o, k_o^{Im}, k_m^{Im}, and K_m (association constant) are defined in Eq. 2. Equation 3 gives Eq. 4 (Fig. 1b).

$$M + S \underset{}{\overset{K_m}{\rightleftharpoons}} M.S \xrightarrow{k'_m} \text{products} \qquad (2)$$

$$k'_o$$

$$k'_m = k_m + k_m^{Im}[Im]_T;\ k'_o = k_o + k_o^{Im}[Im]_T$$

$$k_{obsd} = \frac{k'_o + k'_m K_m [M]_T}{1 + K_m[M]_T} \qquad (3)$$

$$\frac{1}{(k_{obsd}-k'_o)} = \frac{1}{(k'_m-k'_o)} + \frac{1}{(k'_m-k'_o)K_m}\cdot\frac{1}{[M]_T} \qquad (4)$$

$$\frac{1}{(\text{intercept})} = (k_m-k_o) + (k_m^{Im}-k_o^{Im})[Im]_T \qquad (5)$$

The intercepts of Eq. 4 (Fig. 1b) should be linearly related to the imidazole concentration (Eq. 5) as verified in Fig. 3. Thus the k_{obsd} values could be analyzed based on these equations to give the kinetic parameters for PPS as listed in Table 1.

Hydrolysis of DPPS: The kinetic procedures and the analysis were essentially the same as in the above hydrolysis of PPS. The results are shown in Figs. 2 and 3, and in Table 1.

Table 1. Rate parameters for the hydrolysis of PPS and DPPS[a]

Constant	PPS	DPPS	k_{DPPS}/k_{PPS}
k_o/min^{-1}	2.57×10^{-5}	2.31×10^{-5}	0.898
k_m/min^{-1}	8.98×10^{-4}	37.6×10^{-4}	4.18
k_o^{Im}/M^{-1} min^{-1}	4.14×10^{-3}	13.3×10^{-3}	3.21
k_m^{Im}/M^{-1} min^{-1}	0.171	5.29	30.9
K_m/M^{-1}	1.19	3.39	

a) pH 7.90, 55 °C, in the presence of 6×10^{-2} M SDS; other conditions, see Figs. 2 and 3.

Comparison of PPS and DPPS Reactivities. The k_o values in Table 1 indicates that the reactivities of two esters toward water are nearly the same at pH 7.9 and

55 °C and in the absence of Mg^{2+} ion and imidazole. These water rates are enhanced by 35 and 163 fold (k_m/k_0 ratio) for PPS and DPPS respectively, when the ester are complexed with Mg^{2+} ion. Similarly the nucleophilic reactivities of imidazole (k_0^{Im}) in the absence of Mg^{2+} ion are enhanced by 41 and 400 fold (k_m^{Im}/k_0^{Im} ratio) for PPS and DPPS respectively by the complexation. Thus these rate enhancements are much larger for DPPS than PPS. Such comparison can also be made by relative rates, k_{DPPS}/k_{PPS} shown in Table 1.

Since DPPS is a surfactant,[7] it is reasonable to assume that DPPS forms a co-micelle with SDS.[9] On the other hand, it is known to be difficult to incorporate such a hydrophilic anion as PPS into an anionic micelle like SDS.[9] Therefore, it can be considered that the reaction of DPPS occurs in the micellar phase, while that of PPS in the bulk water phase. It is known that the binding of a counter ion on an ionic micelle is stronger in general than in the corresponding ion pair formation in the bulk water phase.[9] As expected, the K_m value of DPPS is larger than that of PPS. A plausible structure for the M.S complex (Eq. 3) is a cyclic one as illustrated in **1**, in which the bonding of $P\text{-}O^-\cdots Mg^{2+}$ is presumably stronger than that of $S\text{-}O^-\cdots Mg^{2+}$.

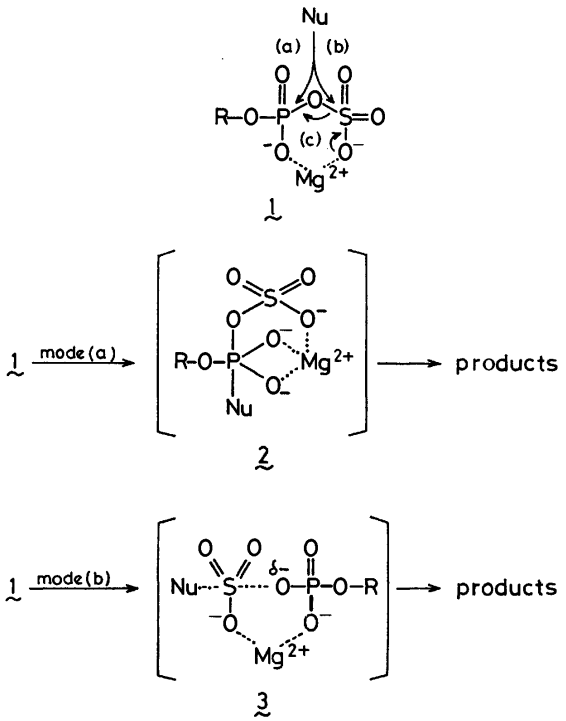

Three modes (a—c) may be conceivable for the cleavage of P–O–S linkage of such a complex **1**. The modes (a) and (b) are the biomolecular nucleophilic attack of imidazole on phosphorus and sulfur, respectively, to give either the P–O or the S–O bond cleavage. The mode (c) is the unimolecular cleavage of the S–O bond. In each case, Mg^{2+} ion is assumed to act as an electrophilic catalyst to polarize the reacting bonds or to neutralize the developing negative charge of the intermediate or the transition state. As mentioned already, what actually observed is the mode (a). Presumably, the formation of pentacovalent intermediate or transition state (**2**) through the mode (a) (Eq. 6) is energetically more favored than to make a S_N2 transition state (**3**) by mode (b) (Eq. 7). The stabilization by charge neutralization by Mg^{2+} ion seems to be more effective in **2** than in **3**, because the developement of negative charge must be more pronounced in **2** than in **3**. Such electrostatic interaction must be stronger in the micellar phase than in the bulk water phase, because of the hydrophobic nature of the micellar phase.[10]

As for the micellar effects on the metal ion catalysis, a positive micellar effect, although small, was reported by Melhado and Gutsche for the catalysis of cationic micellar chelates of 4-alkyl-3,6-diazaoctane-1,8-diamine in the decomposition of acetyl phosphate.[11] Very recently, we also reported a larger micellar effect on the catalytic activity of a lipophilic metal ion chelate in the hydrolysis of carboxylic acid esters in a cationic micelle.[12] In these reactions, the reacting bond undergoing nucleophilic attack is the ester carbonyl group. The present results indicate that a large micellar effect is also possible in the metal ion assisted nucleophilic attack on phosphorus. For enzyme catalysis, the present results suggest that if an enzyme require a bivalent metal ion as the cofactor in the hydrolysis of active sulfates, the medium of the active site is somewhat like a micellar phase and the site of cleavage of the P–O–S linkage is the P–O bond, as suggested by Roy.[2e] The results also suggest the importance of the histidyl residue at the active site of enzymes as the nucleophilic catalyst toward the phosphate substrates.

Experimental

Material. The ammonium salts of DPPS and PPS were prepared by our previous method.[4,7] Inorganic salts, EDTA and SDS were of commercial analytical grade and were used without further purification. Mg^{2+} ion was the perchlorate. All liquid reagents were purified by distillation. Imidazole was recrystallized from benzene. Demineralized water was treated with $KMnO_4$ and distilled twice before use.

Kinetics. A Hitachi-Horiba F-7DE pH meter and a Shimadzu UV-200 spectrophotometer were used for the kinetics. Kinetic procedures were the same as previously described.[7]

Methanolysis. The substrate PPS (144 mg) or DPPS (214 mg) was dissolved in 80% aqueous methanol (25 cm^3) containing imidazole (340 mg) and $Mg(ClO_4)_2$ (1.11 g). This reaction mixture was kept at 55 °C for 24 h and concentrated to dryness. The residue was dissolved in an alkaline solution (pH 11) and centrifuged to remove magnesium hydroxide. The supernatant was concentrated to dryness. The residue dried on P_2O_5 was washed with ether and again dried. The final residue was dissolved in D_2O and analyzed by NMR[6] for methyl phenyl phosphate: $\delta CH_3=3.74$ (3H, doublet). The yield of inorganic sulfate was quantitative as determined by Ba-chloranilate method.[7]

References

1) Active sulfates are adenosine 5′-phosphatosulfate (APS) and 3′-phosphoadenosine 5′-phosphatosulfate (PAPS).

2) a) F. Lipman, *Science*, **128**, 575 (1958); b) H. D. Peck, Jr., *Enzymes*, **10**, 651 (1974); c) A. B. Roy and P. A. Trudinger, "The Biochemistry of Inorganic Compounds of Sulfur," Cambridge Univ. Press, Cambridge (1970); d) J. A. Schiff

and R. C. Hodson, "The Metabolism of Sulfate," *Ann. Rev. Plant Physiol.*, **24**, 381 (1973); e) A. B. Roy, *Enzymes*, **8**, 1 (1971).

3) S. J. Benkovic and R. C. Hevey, *J. Am. Chem. Soc.*, **92**, 4971 (1970).

4) W. Tagaki, T. Eiki, and I. Tanaka, *Bull. Chem. Soc. Jpn.*, **44**, 1138 (1971).

5) W. Tagaki, Y. Asai, and T. Eiki, *J. Am. Chem. Soc.*, **95**, 3037 (1973).

6) W. Tagaki and T. Eiki, *Adv. Chem. Ser.*, **191**, 407 (1980).

7) T. Eiki, K. Tomuro, S. Aoshima, M. Suda, and W. Tagaki, *Nippon Kagaku Kaishi*, **1980**, 454.

8) The SDS concentration was varied in a range of 0—0.1 M under the following conditions: pH 6.86 (0.2 M imidazole/HCl buffer), 55 °C; DPPS=2×10^{-2} M, $Mg(ClO_4)_2$=2.03×10^{-2} M.

9) For example, see J. H. Fendler and E. J. Fendler, "Catalysis in Micellar and Macromolecular Systems," Academic Press, New York (1975).

10) W. Tagaki, D. Fukushima, T. Eiki, and Y. Yano, *J. Org. Chem.*, **44**, 555 (1979).

11) L. L. Melhado and C. D. Gutsche, *J. Am. Chem. Soc.*, **100**, 1850 (1978).

12) T. Eiki, M. Mori, S. Kawada, K. Matsushima, and W. Tagaki, *Chem. Lett.*, **1980**, 1431.

Spirans. XXII.[1] Spiroconjugation in Heteraspirans Studied by UV and ^{13}C NMR Spectra

Stefan SMOLIŃSKI,* Michał BAŁAZY, Hiizu IWAMURA,*,† Tadashi SUGAWARA,† Yuzo KAWADA,† and Michiko IWAMURA††

Stereochemical Laboratory, Institute of Chemistry, Jagellonian University, 30-060 Krakow, Karasia 3, Poland
†*Division of Applied Molecular Science, The Institute for Molecular Science, Myodaiji, Okazaki 444*
††*Department of Chemistry, Faculty of Science, Toho University, 2-2-1 Miyama, Funabashi 274*

(Received May 12, 1981)

UV and ^{13}C NMR spectra of spirocyclic orthocarbonates, a spirobi(benzodithiepin) and a spirobi(naphthopyran) have been measured and compared with those of the "half compounds" to see the spiroconjugation effect. Whereas batho- and hyperchromic shifts are usually brought about by spiroconjugation, hypso- and hypochromic effects have been observed for 2,2′-spirobi[1,3-benzodioxole]. Through-bond interaction similar to the mechanism for the anomeric effect is considered to be operative in attenuating the electron release from the orthocarbonate moiety to the benzene chromophore. The downfield shifts of 20—25 and *ca.* 40 ppm were noted for the spirocarbons of the conformationally flexible and rigid orthocarbonates, respectively, as compared to the corresponding methylene carbons of the half compounds. The largest paramagnetic shift of 66.3 ppm is observed for the orthothiocarbonate and attributed to the presence of the low-lying d-orbitals due to through-space interaction of the four sulfur atoms.

Stimulated by the concept of spiroconjugation put forward by Simmons and Fukunaga,[2] and by Hoffmann *et al.*,[3] a number of theoretical[4] and experimental works[5] have since been carried out to delineate the extent and the mechanism of such conjugative effects. UV absorption and photoelectron spectroscopy have proved to be most instrumental in studying spiroconjugation. In the well-known case of spiro[4.4]nona-1,3,6,8-tetraene (**1**), the effect of spiroconjugation can be shown by comparing the UV spectra of the spiran and its half moiety, cyclopentadiene (**1′**). A large bathochromic shift (35 nm) of the long-wavelength band of the spiran is observed.[5b] The He(I) photoelectron spectra of spirocompounds have revealed that the splitting pattern in the low-energy region provides a measure of splitting of occupied MO's due to spiroconjugation. The spiro-splitting amounts to 1.23, 0.57, and 0.3 eV for **1**, 3,3′-spirobi[3*H*-indene] (**2**) and 9,9′-spirobi[9*H*-fluorene] (**3**), respectively,[6] showing that spiroconjugation is weakened by increasing benzoannelation which enhances the number of mesomeric structures of the "half compound."

In the present work, we would like to report the UV and ^{13}C NMR spectral data for spirocyclic orthocarbonates **4**—**6**, a spirobibenzodithiepin **7**, spirobinaphthopyran **8**, related spiran **9**, and their half compounds **4′**—**9′** to see the effect of spiroconjugation. Because of high electronegativity and consequent contraction of the 2p orbitals of the oxygen atoms, we expect a rather low through-space oxygen lone pair interaction. In such a case other mechanisms can be important. Conformational flexibility and/or rigidity may also affect the conjugation.

Results and Discussion

UV Spectra. Typical absorption spectra are given in Fig. 1. The data for the absorption maxima

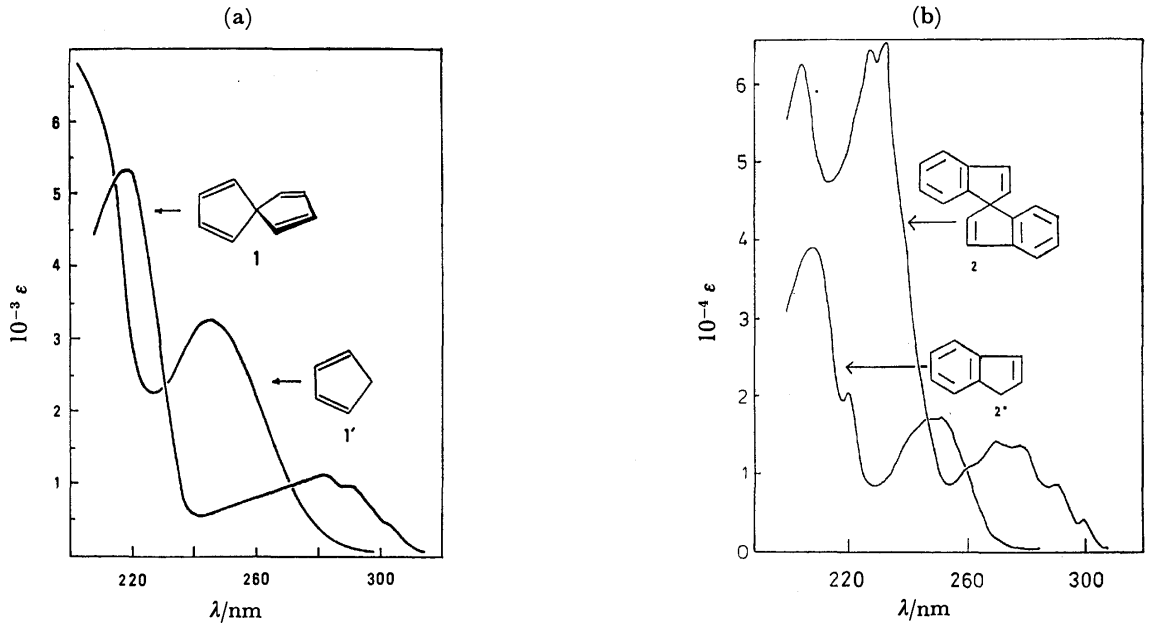

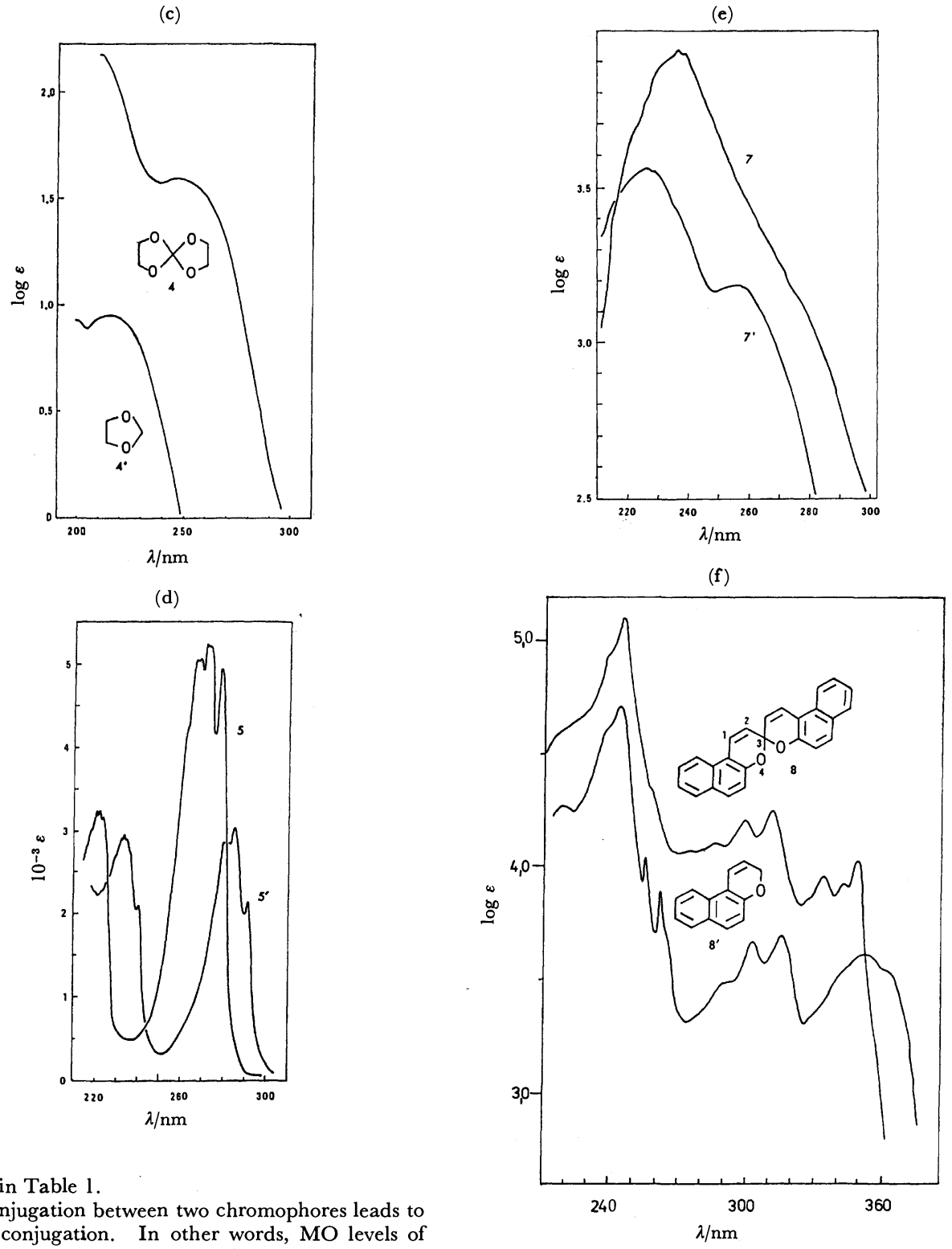

Fig. 1. UV absorption spectra of heteraspirans and their half compounds.

are listed in Table 1.

Spiroconjugation between two chromophores leads to extended conjugation. In other words, MO levels of each chromophore interact to split in energy and to make excitation of electrons more feasible. As a result, bathochromic shift of the UV absorption takes place. This is illustrated by the absorptions of **1** and **2**. There appears to be no exception to this rule for spiroconjugation through carbon $2p\pi$ orbitals. Whereas **4** and **4'** are not the π-system and it is not clearly defined whether the excited state pertinent to the UV absorption should be $n\rightarrow\sigma^*$ or the Rydberg state,[7] they show the spectral pattern similar to those of **1** and **1'** with the exception that the long-wavelength band in **4** has greater intensity than the corresponding band in **4'**. The difference in absorption maxima ($\Delta\lambda=32$ nm$\approx$0.75 eV) approximates the spiro-splitting of 0.55 eV obtained by PE spectroscopy.[8]

2,2'-Spirobi[1,3-benzodioxole] (**5**) provides an excep-

TABLE 1. UV ABSORPTION DATA FOR HETERASPIRANS AND THEIR HALF COMPOUNDS IN HEXANE

Compound	λ_{max}/nm (log ε)
4	247(1.60)[a]
4′	215(0.95)
5	221(3.51), 273(3.72)
5′	233(3.47), 285(3.49)
6	222(1.14), 247(1.24)
6′	213(ī.38), 254(ī.03)
7	229(3.64), 292(2.36)[b,c]
7′	217(3.29), 274(2.45)[c]
8	215(4.58), 244(5.10), 311(4.25), 348(4.03)
8′	219(4.26), 243(4.70), 315(3.70), 350(3.60)
9	218(ī.71), 251(ī.65)

a) 254 (3.57) in ethanol.[6b] b) Shoulder. c) In dioxane.

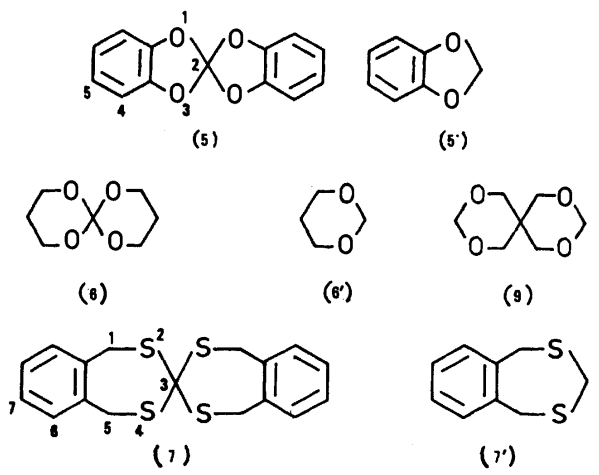

tion. We have encountered for the first time an example in which hypso- and hypochromic effects are observed in the spiroconjugative system relative to the half moiety. The phenomenon is most reasonably explained in terms of inhibition by spiroconjugation of the local charge-transfer absorption from the oxygen lone pair to the benzene ring.

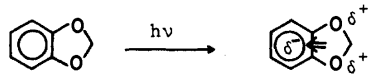

The $^1B_{2u}\leftarrow{}^1A_{1g}$ transition in benzene is forbidden and is observed only because of vibrational interaction. In the case of substituted compounds, the corresponding band is no longer strictly forbidden. When two oxygen atoms are introduced to the ring, the inductive effect affects the ground and excited states about equally and in the same direction. However, the lone pair of electrons on the two oxygen atoms interact with the π-electrons of the benzene ring to give a total of ten electrons on the eight center system. As a consequence of this delocalization, the energy of the highest occupied orbitals rich in the lone pair character is raised and the lowest unoccupied orbitals are affected only to a minor extent. The low-intensity band at 260 nm as well as the 203 nm high-intensity band is shifted to the red. The red shift is greater for the substituent in which the lone pair participation is enhanced by some electron release effect. This is exactly what is observed as we go from anisole (λ_{max}=217 (log ε 3.81) and 269 nm (log ε 3.17) in methanol) to 1,3-benzodioxole (**5′**) (see Table 1). On the other hand, the larger the electronegativity which is directly related to the ionization potential, the more difficult it is to remove an electron. The migration of charge distorts the symmetry responsible for the forbiddenness of the $^1B_{2u}\leftarrow{}^1A_{1g}$ transition of benzene and removes some of the forbiddenness. The absorption intensifies. The greater the migration of charge, the greater the intensification.

With the above generalization of the benzenoid absorption in mind, the observed hypo- and hypsochromic effects for **5** are concluded to be due to the diminution of the ease of electron release from the moiety as compared to . The interpretation is supported by the observed PE spectral data for **5** and **5′**.[9] We note that the HOMO of **5** which is rich in the lone pair orbitals is stabilized relative to that of **5′** by 0.27 eV. There are at least two *a priori* mechanisms possible for the spiroconjugative interaction in orthocarbonates. One is through-space interaction which usually leads to repulsion of the non-bonding orbitals or reduction of ionization potential of the oxygen lone pair,[10] the trend which is not compatible with our observation (see Fig. 2). Second is through-bond interaction in which polar C–O bonds take part.[9] Since a pair of the C–O bonds in one half of the molecule are in the plane perpendicular to the other half in **5**, the skeleton with D_{2d} symmetry is quite adequate for the through-bond interaction. If the lone pair orbitals interact with the high-lying C–O bonding orbital, destabilization of the former would take place. The effect is similar to the through-space lone pair-lone pair interaction. It is the interaction of the lone pair orbitals

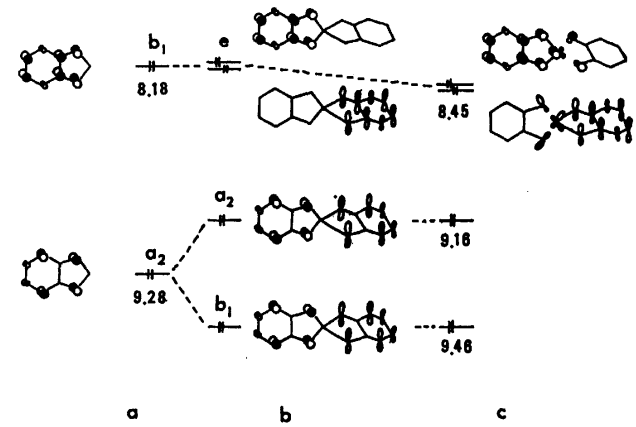

Fig. 2. Schematic correlation diagram for the higher occupied orbitals of **5** and **5′**. Stage (a): b_1 and a_2 orbitals of **5′** with C_{2v} symmetry obtained by mixing of the symmetric and antisymmetric combinations of the lone pair orbitals of 1,3-dioxolane with the HOMO's of benzene. Stage (b): the MO with a_2 symmetry of **5′** (and not the b_1 MO) splits into a_2 and b_1 orbitals as a result of through-space interaction in **5** (D_{2d} symmetry). Stage (c): throug.-bond interaction with the C–O σ^* orbitals of the other half of the 1,3-benzodioxole moiety stabilizes the e orbital (no such effect for a_2 and b_1 orbitals). The numbers are from ionization potential values in the literature.

with the low-lying C–O anti-bonding orbitals which should be responsible for the stabilization of the HOMO of **5** with e symmetry relative to the b_1 orbital of **5'**, and for the observed hypo- and hypsochromic effects in the UV absorptions of **5** and **5'**.

The interaction of the lone pair of electrons with the anti-bonding orbital of the neighboring polar bonds is exactly what is currently adopted for the origin of the anomeric effect in carbohydrate chemistry.[11] The interpretation is also supported by a rather short C_{spiro}–O bond length of 1.38 Å in **5** as compared to the normal value of 1.43 Å.[12]

A pair of 3,3'-spirobi[3*H*-naphtho[2,1-*b*]pyran] (**8**) and 3*H*-naphtho[2,1-*b*]pyran (**8'**) provide an intermediate case where hypsochromic shift is observed only for the long-wavelength band. Through-bond interaction between the carbon 2pπ orbitals and the C–O anti-bonding orbitals would make the C–O single bond weaker and vulnerable to cleavage on heating.[13] As a result, compound **8** shows characteristic thermochromism attributable to reversible formation of **10**.

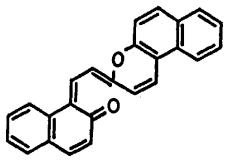

(10)

The spectrum of **7** somewhat resembles that of 1,5,7,11-tetrathiaspiro[5.5]undecane[14] in both bathochromic shift and hyperchromic effect as compared to the half compound. The transition giving rise to the absorption at 274 and 292 nm is considered to arise from an excitation of a non-bonding electron of a sulfur atom to a molecular orbital formed by overlap of d-orbitals on the four sulfur atoms. Let us take the d_{z^2} atomic orbitals, for example, as forming such a molecular orbital. These combine to give a pair of bonding and anti-bonding levels. The former splits further into two levels b_2 and a_1 after spiroconjugative interaction of one ring with another (see Fig. 3). Thus the bathochromic shift can be taken as a measure of the splitting due to spiroconjugation. The splitting amounts to 0.28 eV for **7** and 0.37 eV for the tetrathiaspiroundecane.[14]

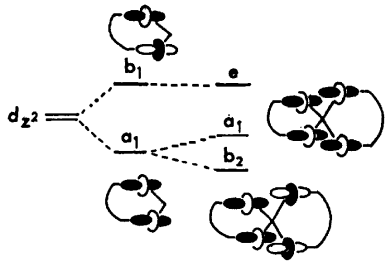

Fig. 3. Splitting of the vacant MO's due to through-space interaction of the d_{z^2} atomic orbitals of four sulfur atoms in orthothiocarbonates. Note that, in contrast to p orbitals where less stable a_2 orbitals are split by spiroconjugation, splitting of more stable a_1 orbitals in the C_{2v} moiety takes place for a combination of d_{z^2} orbitals.

^{13}C NMR Spectra. The proton-noise-decoupled ^{13}C NMR spectra were obtained at 20.1 and/or 25.0 MHz and the data are collected in Table 2. The signal due to the spirocarbons is among the most difficult to measure by the pulsed FT technique owing to their slow spin-lattice relaxation. Spin-lattice relaxation of ^{13}C nuclei in typical organic molecules is practically dominated by dipolar interaction with the near-by proton spins within the molecule. The spirocarbon of **5** which is four bonds apart from the nearest hydrogens thus resisted our effort to detect the signal under the standard pulsed FT measurement conditions of the pulse repetition time as long as 15 s. The difficulty was not overcome by addition of a few mg of a typical relaxation reagent such as $Cr(acac)_2$. The signal was finally obtained by adding a trace of cupper nitrate trihydrate in an acetone solution.[15] In Table 2 are also given differences in chemical shifts on going from the half compounds to the corresponding spiro compounds. The minus sign indicates the upfield shift of the latter signals relative to the former.

Examination of the data in Table 2 shows several trends. First of all, downfield shift of the spirocarbons is most conspicuous. The size of this shifts is 20—40 ppm for orthocarbonates **4**—**6** and ethyl orthocarbonate (**11**), 6—53 ppm for the spirocarbons attached to four carbon atoms, and 66 ppm for orthothiocarbonate **7**. Secondly, the spirocarbon chemical shifts for the orthocarbonates fall in two regions: 20—25 ppm for the conformationally flexible compounds and *ca.* 40 ppm for the rigid tetraoxaspiro[4.4] systems. For a third, upfield shifts up to 5 ppm are observed for the non-spirocarbons attached to oxygens on going from the reference to spiro compounds.

Chemical shifts of ^{13}C nuclei have been shown to be governed by local paramagnetic screening which arises from contributions of higher electronic states to the description of the ground state in the magnetic field. The screening increases as the mean inverse cube of the radius of the 2p orbitals on the carbon atom increases or effective excitation energy of the electron at the carbon decreases.[16] The observed downfield shifts of the central carbons as we go from the acetal (bonded to two oxygens) to the orthocarbonate (bonded to four oxygens) are ascribed to contraction of the radius of the carbon 2p orbitals by bonding to the increased number of the electronegative oxygen atoms. The larger paramagnetic shift in rigid **4** and **5** may be interpreted in terms of two effects; the synergic σ-bond polarization towards oxygen and the steric γ-effect. As described in the discussion of the UV spectra, the lone pair of electrons are donated to the adjacent σ^* orbitals of the C–O bonds. Synergic to this flow of electrons from oxygen to carbon, the C–O bonding orbital, *i.e.*, σ-bonds will tend to polarize more towards oxygen atoms. As a result, contraction of the radius of the spirocarbon 2p orbitals may take place to effect stronger paramagnetic screening of the central spirocarbons. The effect is more pronounced in conformationally rigid **4** and **5** where the lone pair orbitals of the oxygens on one ring and the σ^* orbitals of the C–O bonds on the other ring are

TABLE 2. ^{13}C NMR CHEMICAL SHIFTS (δ VALUES) OF HETERASPIRANS AND RELATED COMPOUNDS

Compound	C-1	C-2	C-3	C-4	C-5	Others
1	150.5	151.0			77.0	
1′	132.8	132.2			41.6	
Δ	17.7	18.8			35.4	
3						90.2[a] 148.8[b] 141.8[c]
3′						36.8 143.2 141.7
Δ						53.3 5.6 0.1
Ph_4C						65.3[d]
Ph_2CH_2						42.0
Δ						23.3
9		94.5		70.5	33.7	
6′		94.5		67.1	27.1	
Δ		0		3.4	6.6	
4		135.3		65.0		
4′		95.3		64.8		
Δ		40.0		0.2		
5		139.6		108.8	123.2	143.5[e]
5′		100.7		108.8	121.8	147.5
Δ		38.9		0	1.4	−4.0
6		114.1		62.1	23.9	
6′		94.5		67.1	27.1	
Δ		19.6		−5.0	−3.2	
11	58.5	14.9				119.9[d]
11′[h]	63.2	15.3				95.1
Δ	−4.7	−0.4				24.8
8			96.0			113.4[f] 149.3[c]
8′			65.3			115.5 130.2
Δ			30.7			−2.1 19.1
7	36.2		104.1			138.9[g]
7′	36.3		37.8			138.6
Δ	−0.1		66.3			0.3

a) C-9. b) C-9a. c) C-4a. d) The central carbon. e) C-3a. f) C-10b. g) C-5a. h) Diethoxymethane.

better aligned. Secondly and perhaps less importantly, there is an additional γ-carbon atom gauche to the spirocarbons introduced as we go from **6′** to **6**. As a result, the stereospecific γ-effect will operate to move the signal due to the spirocarbon somewhat upfield.[17] The same effect may also be operative in the conformationally flexible **11**.

One of the largest downfield shifts ever observed for the spirocarbon is 66.3 ppm in 1,1′,5,5′-tetrahydro-3,3′-spirobi[2,4-benzodithiepin] (**7**). As discussed in the section of its UV absorption, the low-lying d-orbitals are presumably contributing to the low-energy excited states for the 2p electrons of the spirocarbon to be mixed with the ground state.

Dowinfield shift of 53.3 ppm on going from fluorene to **3** may be compared with the shift difference of 23.3 ppm between diphenylmethane and tetraphenylmethane. Here again diminution of effective excitation energy of the carbon 2p electrons is considered to be responsible for the larger paramagnetic screening.

In conclusion, spiroconjugation in heteraspirans is reflected in their characteristic UV and ^{13}C NMR spectra. The spectral changes due to the spiroconjugation in these compounds are often different from those of spirohydrocarbons and are interpreted mainly in terms of the through-bond $n \rightarrow \sigma^*$ interaction.

Experimental

Materials. The previously described procedures were employed to prepare 2,2′-spirobi[1,3-dioxolane](**4**),[18] 2,2′-spirobi[1,3-benzodioxole](**5**),[19] 2,2′-spirobi[1,3-dioxane] (**6**),[20] (**6**),[20] 1,1′,5,5′-tetrahydro-3,3′-spirobi[2,4-benzodithiepin] (**7**),[21] 1,5-dihydro-2,4-benzodithiepin (**7′**),[22] 3,3′-spirobi[3*H*-naphtho[2,1-*b*]pyran] (**8**),[23] 3*H*-naphtho[2,1-*b*]pyran (**8′**),[24] and 5,5′-spirobi[1,3-dioxane] (**9**).[25] Purity of the samples for spectral studies was confirmed by their ^1H NMR spectra and VPC.

Spectra. The UV absorption spectra were taken from hexane solutions, unless otherwise stated, at 25 °C with a UNICAM SP-1800 and a Cary 17 spectrophotometer. Compounds **7** and **7′** were measured in dioxane and their absorption maxima were obtained by resolving the observed curve by using the program BANDF run on a Cyber 72 computer.

^{13}C NMR spectra were recorded on a JEOL FX-100 spectrometer operating at 25 MHz in the pulsed FT mode. A radiofrequency pulse of width 6 μs (45°) was generally employed with the repetition time of *ca.* 10 s. For Fourier transformation, 8 K spectral data points were available for spectral width 4000 Hz. Samples were *ca.* 10% solutions in $CDCl_3$ unless otherwise stated. Only a few mg samples of **7** and **8** were soluble in $CDCl_3$. The chemical shift due to the spirocarbon of **5** was obtained for the solution of 10 mg of **5** and 1 mg of $Cu(NO_3)_2 \cdot 3\,H_2O$ in 0.35 ml of acetone-d_6 with TMS as an internal standard.

We are grateful to Professor Tadashi Suehiro of Gakushuin University for his kindness in furnishing us with a sample of tetraphenylmethane.

References

1) For Part XXI, see: A. Czarny, S. Smoliński, and T. Zyczkowska, *Pol. J. Chem.*, **53**, 2379 (1979).
2) H. E. Simmons and T. Fukunaga, *J. Am. Chem. Soc.*, **89**, 5208 (1967).
3) R. Hoffmann, A. Imamura, and G. D. Zeiss, *J. Am. Chem. Soc.*, **89**, 5215 (1967).
4) M. D. Gordon, T. Fukunaga, and H. E. Simmons, *J. Am. Chem. Soc.*, **98**, 8401 (1976); A. Tajiri and T. Nakajima, *Tetrahedron*, **27**, 6089 (1971).
5) a) R. Boschi, A. S. Dreiding, and E. Heilbronner, *J. Am. Chem. Soc.*, **92**, 123 (1970); b) M. F. Semmelhack, J. F. Foos, and S. Katz, *ibid.*, **95**, 7325 (1973); c) R. Gleiter, D. L. Coffen, H. Bock, W. Schulz, and U. Stein, *Tetrahedron*, **33**, 433 (1977); d) H. Dürr and H. Kober, *Chem. Ber.*, **106**, 1565 (1973).
6) R. K. Hill and D. A. Cullison, *J. Am. Chem. Soc.*, **95**, 1229 (1973); A. Schweig, U. Weidner, R. K. Hill, and D. A. Cullison *ibid.*, **95**, 5426 (1973).
7) M. B. Robin, "Higher Excited States of Polyatomic Molecules," Academic Press, New York, N. Y. (1974), Chap. 3.
8) D. A. Sweigert and D. W. Turner, *J. Am. Chem. Soc.*, **94**, 5599 (1972).
9) R. Gleiter, R. Haider, and H. Quast, *J. Chem. Res. (S)*, 138 (1978).
10) R. Hoffmann, *Acc. Chem. Res.*, **4**, 1 (1971).
11) S. David, O. Eisenstein, W. J. Hehre, L. Salem, and R. Hoffmann, *J. Am. Chem. Soc.*, **95**, 3806 (1973); "Anomeric Effect. Origin and Consequences," ed by W. Szarek and D. Horton, ACS Symp. Ser., American Chemical Society, Washington, D. C. (1979), Vol. 87.
12) H. Meyer and G. Nagorsen, *Angew. Chem., Int. Ed. Engl.*, **18**, 551 (1979).
13) J. H. Day, *Chem. Rev.*, **63**, 65 (1963).
14) D. R. Williams, D. L. Coffen, P. E. Garrett, and R. N. Schwarz, *J. Chem. Soc., B*, 1132 (1968).
15) We thank Prof. Yutaka Kawazoe of Nagoya City University for his suggestion on the usefulness of this reagent.
16) M. Karplus and J. A. Pople, *J. Chem. Phys.*, **38**, 2803 (1963); B. V. Cheney and D. M. Grant, *J. Am. Chem. Soc.*, **89**, 5319 (1967).
17) D. M. Grant and B. V. Cheney, *J. Am. Chem. Soc.*, **89**, 5315 (1967).
18) S. Sakai, Y. Kuroda, and Y. Ishi, *J. Org. Chem.*, **37**, 4198 (1972).
19) H. Gross, A. Rieche, and E. Hoft, *Chem. Ber.*, **94**, 544 (1961).
20) W. E. Willy, G. Binsche, and E. Eliel, *J. Am. Chem. Soc.*, **92**, 5394 (1970).
21) S. Smoliński, J. Nowicka, J. Mokrosz, M. Jaworski, M. Jamrozik, and E. Wiekiera, *Tetrahedron*, **33**, 1219 (1977); S. Smoliński and M. Kubaszek, unpublished work.
22) A. Kotz, *Ber.*, **33**, 730 (1900).
23) R. Dickinson and I. M. Heilbron, *J. Chem. Soc.*, **1927**, 19.
24) I. Iwai and J. Ide, *Chem. Pharm. Bull.*, **10**, 926 (1962); **11**, 1042 (1963); N. Šarčevic, J. Zsindely, and H. Schmid, *Helv. Chim. Acta*, **56**, 1457 (1973).
25) J. Read, *J. Chem. Soc.*, **101**, 2091 (1912).

Photoinduced Intramolecular Substitution. II.[1,2] Absence of *meta*-Favoring Effect in Nucleophilic Photosubstitution of Nitroveratrole Derivatives

Kiyoshi MUTAI,* Kenji YOKOYAMA,† Sei-ichiro KANNO, and Keiji KOBAYASHI

Department of Chemistry, College of General Education, The University of Tokyo, Komaba, Meguro-ku, Tokyo 153

†*The Institute of Physical and Chemical Research, Wako, Saitama 351*

(Received June 2, 1981)

Possible occurrence of the photo-Smiles rearrangement accompanying *meta*-favoring nucleophilic aromatic substitution was examined in a homologous series of 1-(2-methoxy-4-nitrophenoxy)-ω-anilinoalkanes. The structure of reaction products, the reaction kinetics, and absorption spectra of intermediates showed no appreciable alteration of reaction pathway by the introduction of 2-methoxyl group. The photoreaction was exclusively a *para*-directing nucleophilic substitution.

In the previous papers[1,3] we have reported the photo-Smiles rearrangement (intramolecular nucleophilic aromatic substitution) of **1**, along with the reaction mechanism involving a radical ion pair and a *spiro*-type Meisenheimer complex, both ascertained by laser flash photolysis (Scheme 1).

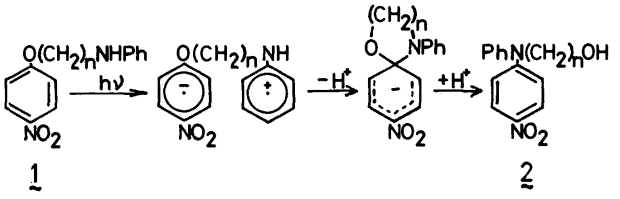

Scheme 1.

The product **2** is also obtained by a catalytic action of strong base such as sodium hydride or sodium ethoxide in DMF. Thus, both the photoinduced and thermal reactions (the Smiles rearrangement) of **1** afford the same product.

On the other hand, intermolecular photoreaction of nitroanisoles and nitroveratrole (3,4-dimethoxynitrobenzene) with nucleophiles shows preference of *meta*- to *para*-substitution.[4,5]

It is worthy of note that the *meta*-orientation observed in the intermolecular photoreactions is not exclusive in contrast with the thermal nucleophilic reactions. Therefore, the coincidence of the product of the photorearrangement with that of the Smiles rearrangement may not be the result of the exclusive photoreaction, but merely due to the lack of an appropriate substituent at the position to undergo the replacement. In other words, the photoreaction of **1** may have several pathways available, the relative importance of which changes according to conditions provided. In this regard, it is interesting to see whether the *meta*-substitution takes place when a methoxyl group is introduced to the *meta* position of the nitro group. Methoxyl is known as a good leaving group in nucleophilic substitution reactions. The present paper is concerned with the photoreaction of the homologs of **3**.

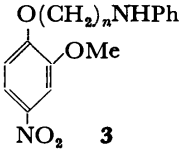

Results and Discussion

Irradiation of **3**. Irradiation of **3** was performed under the same conditions that were applied to **1**.[1] Nitroveratrole type chromophore has UV spectral peaks at *ca.* 300 and 340 nm, and irradiation with any one of 313-, 334-, and 366-nm lines of a high-pressure Hg lamp is plausibly effective for the reaction. However, filter isolation of the longer wavelength lines is accompanied by fairly strong reduction in their intensity, and these lines are also effective for further degradation of photoproducts. For these reasons, only the 313 nm line, isolated through an aqueous solution of $NiSO_4$ (1 cm in path-length), was adopted for the light source.

The photoreaction proceeded with development of yellow color in the solution. The coloration corresponded to the increase in the intensity at *ca.* 410 nm, accompanied by a concomitant decrease in the maxima in the 300—340 nm region in the UV-VIS spectrum. Structures of the products were assigned to **4** on the basis of elemental analysis as well as of the following spectral characteristics: their ^1H NMR spectra showed neither loss of methoxyl group nor remarkable change in the signal patterns of aromatic and polymethylene protons from those of **3**. Appearance of OH group was detected by NMR and IR spectroscopies. Additional evidence was the absorption peak around 410 nm, attributable to *p*-nitroaniline type chromophore.

The $n=2$ and $=3$ homologs dissolved in purified acetonitrile decomposed only to polymeric substances on irradiation, but addition of triethylamine accelerated the photorearrangement to give **4** in high yields. Addition of the amine was unnecessary for the reaction of the $n=4$ homolog. In this case, another nitroaniline derivative (**5**) was obtained as a by-product in a low

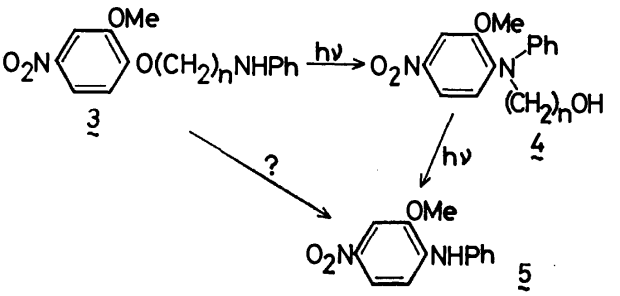

yield. The structure of **5** was confirmed by its ^1H NMR spectrum which showed loss of $(CH_2)_4OH$ group and appearance of a broad singlet at δ 6.75. The UV spectrum (λ_{max} at 401 nm in acetonitrile) and mass spectrum also supported the assignment. Since **5** was also obtained on irradiation of the rearranged product **4**, this compound is probably a secondary photolysis product, though direct formation from **3** cannot completely be eliminated.

Photorearrangement rates were obtained in acetonitrile in the absence and presence of triethylamine by the determination of time dependence of the absorption of **4**, and are summarized in Table 1.

Table 1. Relative initial rate constants (k_{rel}) of the photorearrangement of **3** in acetonitrile

	$\frac{Et_3N}{mol\ dm^{-3}}$	$n=2$	$n=3$	$n=4$
k^0_{rel}	0	*ca.* 0[a)]	*ca.* 0[a)]	4.0
k^{TEA}_{rel}	2.84×10^{-2}	4.4	0.9	1.0[b)]

a) A slight but steady increase in absorbance at 410 nm suggested occurrence of the rearrangement, but accompanying decomposition to unidentified polymeric subustances made it difficult to determine unambiguous values. b) k^{TEA}_{rel} ($n=4$) = 1.0.

From Table 1, it is evident that the reaction is catalyzed by base, especially in the lower homologs ($n=2$ and 3). Furthermore, these homologs scarcely showed reactivity in the absence of base, and only the

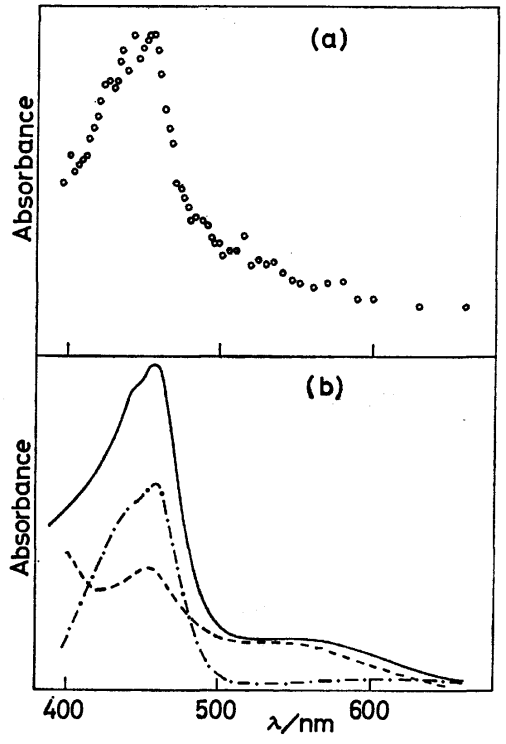

Fig. 1. (a) Transient absorption spectrum of **3** ($n=2$) in CH_3CN (10 ns after excitation). (b) Superposed spectrum (——) of nitroveratrole radical anion (------) and *N*-ethylaniline radical cation (-·-·-).

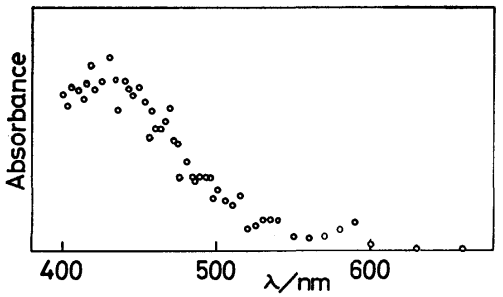

Fig. 2. Transient absorption spectrum of **3** ($n=2$) in CH_3CN–Et_3N (3 μs after excitation).

$n=4$ homolog gave a significant value. These characteristics are similar to those observed in **1**, implying a similar reaction mechanism in the present case.

Intermediates in the Photoreaction. In order to obtain evidence for this mechanism, transient spectra of the solution irradiated with an N_2 laser were observed. The spectra of the $n=2$ homolog observed in the presence of triethylamine at 10 ns and 3 μs after irradiation are reproduced in Figs. 1a and 2, respectively.

The transient species which gave the absorption curve shown in Fig. 1a has a lifetime of *ca.* 75 ns in acetonitrile and 35 ns in the same solvent containing triethylamine, though the spectra in both cases are comparable in shape and peak intensity. The species which gave the spectrum shown in Fig. 2 has a lifetime exceeding 200 μs with no remarkable peak, and its intensity is very low in the absence of triethylamine. These facts seem to suggest that a short-lifetime species formed immediately after the irradiation is converted into a long-lifetime one through a process facilitated by the base.

In all respects these characteristics coincide with the mechanism proposed for the photorearrangement of **1** (Scheme 1). If the same mechanism really works for **3**, the transient species with the shorter lifetime should be a radical ion pair produced by electron transfer from aniline to nitroveratrole moieties, and its spectrum should be a superposition of those of *N*-alkylaniline radical cation and nitroveratrole radical anion.[6] The supposed spectrum is shown in Fig. 1b. Though the peak position is somewhat different, probably due to the difference in the conditions adopted for measurement such as solvent and temperature, other spectral features are almost the same. Therefore, the short-lifetime intermediate is probably the radical ion pair **6**. The long-lived species then should be a *spiro*-type Meisenheimer complex depicted as **7**, but unfortunately any appropriate model anion to be compared has not been known. It may be argued that the spectrum in Fig. 2 is due to the absorption of the triplet state of

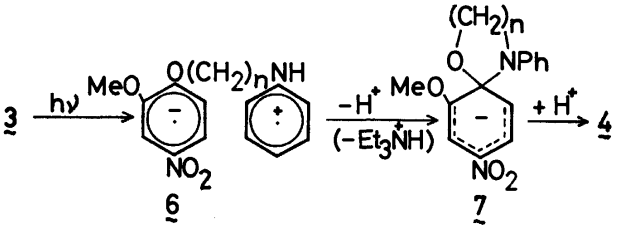

Scheme 2.

nitroveratrole chromophore. This T-T transition, however, was observed at 490 nm with a lifetime of *ca.* 250 ns in acetonitrile, which was reduced to 36 ns in an oxygen saturated solution. Thus the Meinsenheimer complex is a more plausible assignment. A supporting evidence for this is the increase in the intensity due to this species in the presence of triethylamine, since the formation of **7** is greatly facilitated by base (Scheme 2).

In conclusion, it can safely be said that the introduction of a methoxyl group to the *meta*-position of the nitro group has little effect on the reaction pathway of Scheme 1. Consequently the mechanism of the photoreaction of **3** could be written as in Scheme 2.

Experimental

^{1}H NMR spectra were recorded on JEOL-60HL (60 MHz) and MH-100 (100 MHz) spectrometers. The chemical shifts are in ppm with TMS as the internal standard. Electronic spectra were recorded on Hitachi EPS-3T and 100-50 spectrophotometers.

Kinetics of the Photoreaction. The rate constants were determined as described in the previous paper.[1] Acetonitrile (Wako, G. R. grade) used for the solvent was distilled from a mixture with phosphorus pentaoxide.

Transient Spectra Measurement. The absorption spectra of the transient species were determined as described previously.[3]

Materials. 2-Methoxy-4-nitrophenol was prepared by the procedure of Drake *et al.*[7]

1-(2-Methoxy-4-nitrophenoxy)-2-bromoethane: To a mixture of 8.40 g (50 mmol) of 2-methoxy-4-nitrophenol, 11.75 g (62.5 mmol) of dibromoethane, and 50 cm^3 of water, stirred and refluxed, was added 1.95 g (48.8 mmol) of sodium hydroxide in 10 cm^3 of water during 1.5 h, and reflux was further continued for 24 h. After cooling the reaction mixture, the organic layer was extracted with three portions of 20 cm^3 dichloromethane. The solvent was removed from the combined extracts, and a remaining solid mass was charged on a column packed with active alumina. Elution with benzene yielded 5.60 g (40%) of pale yellow crystals of mp 82—83 °C: NMR ($CDCl_3$) δ=3.77 (2H, t, J=6 Hz, CH_2Br), 4.03 (3H, s, OCH_3), 4.53 (2H, t, J=6 Hz, OCH_2), 7.13 (1H, d, J=9 Hz), 7.9 and 8.00 (2H, dd, J=9 and 3 Hz). Found: C, 39.31; H, 3.69; N, 5.21%. Calcd for $C_9H_{10}NO_4Br$: C, 39.15; H, 3.65; N, 5.07%.

1-(2-Methoxy-4-nitrophenoxy)-3-chloropropane: This compound was prepared from 2-methoxy-4-nitrophenol and 1,3-dichloropropane in the same method as was applied for the ethane derivative in 52% yield: mp 79—81 °C; NMR ($CDCl_3$) δ= 2.38 (2H, m, C-CH_2-C), 3.86 (2H, t, J=6 Hz, CH_2Cl), 4.01 (3H, s, OCH_3), 4.35 (2H, t, J=6 Hz, OCH_2), 7.10 (1H, d, J=9 Hz), 7.90 (1H, d, J=3 Hz), and 8.02 (1H, dd, J=9 and 3 Hz). Found: C, 49.02; H, 4.89; N, 5.76%. Calcd for $C_{10}H_{12}NO_4Cl$: C, 48.90; H, 4.92; N, 5.70%.

1-(2-Methoxy-4-nitrophenoxy)-4-bromobutane: This compound was prepared from 2-methoxy-4-nitrophenol and 1,4-dibromobutane in 38% yield: mp 51—52 °C; NMR ($CDCl_3$) δ= 2.01 (4H, m, C-CH_2CH_2-C), 3.71 (2H, t, J=6 Hz, CH_2Br), 4.01 (3H, s, OCH_3), 4.18 (2H, t, J=6 Hz, OCH_2), 7.09 (1H, d, J=9 Hz), 7.9 and 8.02 (2H, dd, J=9 and 3 Hz). Found: C, 43.59; H, 4.67; N, 4.63%. Calcd for $C_{11}H_{14}NO_4Br$: C, 43.44; H, 4.64; N, 4.61%.

Preparation of 1-(2-Methoxy-4-nitrophenoxy)-ω-anilinoalkanes (3): A mixture of the halide (30—50 mmol) and aniline (5 cm^3) was heated at 110 °C for 2 h. After cooling, the reaction mixture was neutralized with 10% aqueous sodium carbonate solution, and unreacted aniline removed by steam distillation. From the remaining liquid was isolated the desired aniline derivative by column chromatography (active alumina, with benzene as an eluent).

1-(2-Methoxy-4-nitrophenoxy)-2-anilinoethane (3, n=2): This compound was obtained in 64% yield as yellow crystals: mp 133—135 °C; UV_{max} (CH_3CN) 297 (ε 8100)and 340 nm (ε 8700); NMR (DMSO-d_6) δ=3.42 (1H, br s, NH), 3.58 (2H, t, J=5 Hz, CH_2N), 3.93 (3H, s, OCH_3), 4.33 (2H, t, J=5 Hz, OCH_2), and 6.7—8.2 (8H, m). Found: C, 62.75; H, 5.52; N, 9.61%. Calcd for $C_{15}H_{16}N_2O_4$: C, 62.49; H, 5.59; N, 9.72%.

1-(2-Methoxy-4-nitrophenoxy)-3-anilinopropane (3, n=3): This compound was obtained in 69% yield as yellow crystals: mp 99—100 °C; UV_{max} (CH_3CN) 298 (ε 8300) and 341 nm (ε 8900); NMR ($CDCl_3$) δ=2.20 (2H, m, C-CH_2-C), 3.43 (2H, t, J=6 Hz, CH_2N), *ca.* 4.0 (1H, br s, NH), 4.00 (3H, s, OCH_3), 4.29 (2H, t, J=6 Hz, OCH_2), 6.6—7.5 (6H, m), 7.87 (1H, d, J=3 Hz), and 8.00 (1H, dd, J=9 and 3 Hz). Found: C, 63.73; H, 6.21; N, 9.28%. Calcd for $C_{16}H_{18}N_2O_4$: C, 63.57; H, 6.00; N, 9.26%.

1-(2-Methoxy-4-nitrophenoxy)-4-anilinobutane (3, n=4): This compound was obtained in 40% yield as yellow crystals: mp 94—95 °C; UV_{max} (CH_3CN) 297 (ε 8600) and 341 nm (ε 9200); NMR ($CDCl_3$) δ=*ca.* 1.9 (4H, m, C-CH_2CH_2-C), 3.28 (2H, t, J=6 Hz, CH_2N), 3.83 (1H, br s, NH), 3.98 (3H, s, OCH_3), 4.20 (2H, t, J=6 Hz, OCH_2), 6.7—7.5 (5H, m), 7.89 (1H, d, J=3 Hz), and 8.03 (1H, dd, J=9 and 3 Hz). Found: C, 64.79; H, 6.67; N, 8.90%. Calcd for $C_{17}H_{20}N_2O_4$: C, 64.54; H, 6.37; N, 8.85%.

N-*(2-Methoxy-4-nitrophenyl)-2-anilinoethanol (4, n=2)*: A solution of 12 mg (0.042 mmol) of **3** (n=2) in 200 cm^3 of acetonitrile containing 1 cm^3 of triethylamine was irradiated with a 100-W high-pressure Hg lamp through an aqueous $NiSO_4$ filter under N_2 for 1.5 h. The process was repeated five times. After removing the solvent and amine from the combined solution, the residue was charged on a slica-gel column, and **4** (n=2) was separated by chromatography using benzene–dichlromethane mixture. The alcohol was obtained in 83% (50 mg) as a viscous dark red liquid: UV_{max} (CH_3CN) 256 (ε 11100) and 411 nm (ε 9000); NMR ($CDCl_3$) δ=2.4 (1H, br s, OH), *ca.* 3.95 (4H, m, NCH_2CH_2O), 3.90 (3H, s, OCH_3), 6.8—7.55 (6H, m), and 7.9—8.15 (2H, m). Found: C, 62.71; H, 5.65; N, 9.57%. Calcd for $C_{15}H_{16}N_2O_4$: C, 62.49; H, 5.59; N, 9.72%.

N-*(2-Methoxy-4-nitrophenyl)-3-anilino-1-propanol (4, n=3)*: This compound was obtained by the same procedure as has been described for the n=2 homolog in 86% isolated yield as a viscous dark red liquid: UV_{max} (CH_3CN) 256 (ε 11100) and 413 nm (ε 9500); NMR ($CDCl_3$) δ=1.86 (2H, m, C-CH_2-C), 2.77 (1H, br s, OH), 3.73 (2H, t, J=6 Hz, CH_2N), 3.80 (3H, s, OCH_3), 3.84 (2H, t, J=6 Hz, OCH_2), 6.7—7.4 (6H, m), and 7.7—7.9 (2H, m). Found: C, 63.81; H, 6.16; N, 9.12%. Calcd for $C_{16}H_{18}N_2O_4$: C, 63.57; H, 6.00; N, 9.26%.

N-*(2-Methoxy-4-nitrophenyl)-4-anilino-1-butanol (4, n=4)*: A solution of 500 mg (1.58 mmol) of **3** (n=4) in 800 cm^3 of acetonitrile was irradiated with a 100-W high-pressure Hg lamp through an aqueous $NiSO_4$ filter under N_2 for 7.5 h. After removing the solvent, the remaining mass was charged on silica gel and eluted with benzene and benzene–dichloromethane mixture. The alcohol (460 mg, 92%) was obtained as a viscous dark red liquid: UV_{max} (CH_3CN) 255 (ε 11200) and 414 nm (ε 9600); NMR ($CDCl_3$) δ=*ca.* 1.65 (5H, m, C-CH_2CH_2-C+OH), 3.5—4.0 (4H, m, CH_2N+OCH_2), 3.79 (3H, s, OCH_3), 6.8—7.4 (6H, m), and 7.7—8.0 (2H, m).

Found: C, 64.66; H, 6.45; N, 8.78%. Calcd for $C_{17}H_{20}N_2O_4$: C, 64.54; H, 6.37; N, 8.85%.

2-Methoxy-4-nitro-N-*phenylaniline* (**5**): This compound was obtained as a first eluate by the chromatograph for the separation of **4** (n=4) described above in 7% yield: yellow crystals, mp 77—78 °C; UV_{max} (95% EtOH) 251 (ε 9900) and 403 nm (ε 17600); NMR ($CDCl_3$) δ=4.01 (3H, s, OCH_3), 6.75 (1H, br s, NH), and 6.9—8.0 (8H, m); MS (70 eV), m/e, 244 (M^+), 229 (M^+-15), 198 (M^+-NO_2), 154, and 148. Found: C, 63.84; H, 4.98; N, 11.63%. Calcd for $C_{13}H_{12}N_2O_3$: C, 63.92; H, 4.95; N, 11.47%.

Photolysis of **4** (n=4) *for the Preparation of* **5**: A solution of 23 mg (0.073 mmol) of the alcohol **4** (n=4) in 240 cm^3 of acetonitrile was irradiated with a 100-W Hg lamp through a Pyrex filter for 6 h. After removing the solvent *in vacuo*, the residue was extracted with three 2-cm^3 portions of chloroform. From the combined extracts, the solvent was distilled off, and the remaining mass was charged on a silica-gel column, eluted with benzene–dichloromethane (1 : 1) mixture. The product **5** was obtained (4.5 mg, 23% yield) as a first eluate, followed by 13 mg of the unreacted starting material.

The authors are grateful to Professor Tadamasa Shida, Kyoto University for providing them with the spectra of the radical ions, and to Professor Saburo Nagakura, Institute for Molecular Science, for his interest and encouragement.

References

1) Part I of this series; K. Mutai and K. Kobayashi, *Bull. Chem. Soc. Jpn.*, **54**, 462 (1981).

2) Preliminary communication; K. Mutai, S. Kanno, and K. Kobayashi, *Tetrahedron Lett.*, **1978**, 1273.

3) K. Yokoyama, R. Nakagaki, J. Nakamura, K. Mutai, and S. Nagakura, *Bull. Chem. Soc. Jpn.*, **53**, 2472 (1980).

4) J. Cornelisse and E. Havinga, *Chem. Rev.*, **75**, 353 (1975).

5) J. Cornelisse, G. P. de Gunst, and E. Havinga, *Adv. Phys. Org. Chem.*, **11**, 225 (1975).

6) The spectra of these radical ions have been provided by T. Shida of Kyoto University.

7) N. L. Drake, H. C. Harris, and C. B. Jaeger, Jr., *J. Am. Chem. Soc.*, **70**, 168 (1948).

The Transition Metal-catalyzed *N*-Alkylation and *N*-Heterocyclization. A Reductive Transformation of Nitroarenes into (Dialkylamino)-arenes and 2,3-Dialkyl-substituted Quinolines Using Aliphatic Aldehydes under Carbon Monoxide

Yoshihisa WATANABE,* Naoki SUZUKI, Yasushi TSUJI, Sang Chul SHIM, and Take-aki MITSUDO
Department of Hydrocarbon Chemistry, Kyoto University, Sakyo-ku, Kyoto 606

(Received June 5, 1981)

The catalytic *N*-alkylation and *N*-heterocyclization of nitroarenes occur at 180 °C under a carbon monoxide pressure of 70 atm and in the presence of aldehyde and such transitionmetal complexes as rhodium and palladium complexes, thus giving 2,3-dialkyl-substituted quinolines and (dialkylamino)arenes in good yields. The product selectivity depends greatly on the catalysts: a binary catalyst, $RhCl(PPh_3)_3$ and $PdCl_2$, is effective for the *N*-heterocyclization, while $[Rh_2Cl_2(cod)_2]$ is effective for the *N*-alkylation.

The reduction of nitroarenes by carbon monoxide using rhodium, palladium, and selenium compounds as catalysts has been of much interest recently.[1] Nitroarenes can be converted into a wide variety of useful *N*-containing compounds, such as aminoarenes,[1a] diarylureas,[1b] aryl isocyanates,[1c] alkyl carbanilates,[1d] and *N*-arylbenzamides.[1e]

On the other hand, during the course of our study of the rhodium-catalyzed *N*-alkylation of amines by means of a carbon monoxide–water system,[2] we found that a rhodium complex is an efficient catalyst for the *N*-heterocyclization, the preparation of quinolines from aminoarenes and aliphatic aldehydes under non-acidic conditions.[3]

Ortho-substituted nitroarenes such as *o*-nitrocinnamaldehyde can also be converted into quinolines by means of an intramolecular cyclization using tetracarbonylferrate(0).[4]

More recently, we also found that nitrobenzene was selectively transformed into substituted quinolines and *N,N*-dialkylanilines by the rhodium- and/or palladium-catalyzed reduction with carbon monoxide in the presence of an aldehyde.[5]

In this paper a detailed study of the reductive transformation of nitroarenes catalyzed by transition-metal complexes to quinolines and aminoarenes will be described.

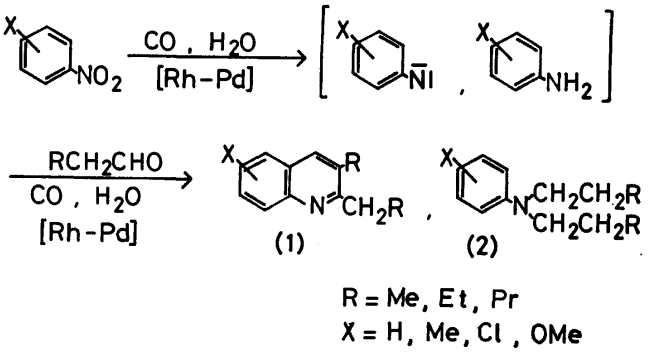

Scheme 1.

Results and Discussion

Effects of Rhodium Complexes as Catalysts. Nitrobenzene combined with butanal in this procedure gave 3-ethyl-2-propylquinoline (**1**) or *N,N*-dibutylaniline (**2**). This combination for the preparation of **1** and **2** was examined in some detail in order to determine the optimum conditions for *N*-heterocyclization and *N*-alkylation.

A variety of rhodium complexes was examined as catalysts; the results are shown in Table 1.

TABLE 1. EFFECTS OF RHODIUM COMPLEXES AS CATALYSTS[a]

Run No.	Rh complexes[b]	Conversion[c] %	Product yield %[c,d] 1	2
1	$RhCl(PPh_3)_3$	51	11	0
2	$RhH(CO)(PPh_3)_3$	50	11	0
3	$RhCl(CO)(PPh_3)_2$	44	10	0
4	$[Rh_2Cl_2(cod)_2]$	37	0	28
5	$[Rh_2Cl_2(nbd)_2]$	43	0	34
6	$[Rh_2Cl_2(nbd)_2]$[e]	64	0	47
7	$Rh_4(CO)_{12}$	65	0	27
8	$[Rh_2Cl_2(CO)_4]$	38	0	23
9	$RhCl_3 \cdot 3H_2O$	55	7	28
10	$RhCl_3Py_3$	47	6	13
11	$Rh_6(CO)_{16}$	100	3	15

a) A mixture of nitrobenzene (40 mmol), butanal (90 mmol), water (2 ml), rhodium complex (0.09 mmol), and ethanol (20 ml) was treated at 180 °C under pressures of carbon monoxide (70 atm) for 4 h. b) [Rh] =0.09 mmol c) Based on the amount of nitrobenzene used. Determined by GLC. d) **1**: 3-Ethyl-2-propylquinoline, **2**: *N,N*-dibutylaniline. e) The reaction time, 8 h.

The products depended greatly on the catalysts. Chlorotris(triphenylphosphine)rhodium(I), (carbonyl)(hydrido)tris(triphenylphosphine)rhodium(I), and (carbonyl)chlorobis (triphenylphosphine)rhodium(I) gave **1** exclusively, while di-μ-chloro-bis[(cyclooctadiene)rhodium(I)], $[Rh_2Cl_2(cod)_2]$, di-μ-chloro-bis[(norbornadiene)rhodium(I)], $[Rh_2Cl_2(nbd)_2]$, dodeca(carbonyl) tetrarhodium(0), and tetra(carbonyl)dichlorodirhodium(I) favored the formation of **2**. Rhodium(III) chloride and hexadeca(carbonyl)hexarhodium(0) gave a mixture of **1** and **2**. The yields of **2** were improved by prolonging the reaction time to 8 h, while the yields of **1** were not. Only trace amounts *N*-butylaniline and aniline were detected as by-products. The reac-

tion by the use of $RhCl(PPh_3)_3$ gave a poor yield and selectivity of **1**. We can suggest two reasons for this. One is that butanal might be reduced to alcohol or suffer condensation to give the unreactive high-molecular-weight species by self-condensation or reaction with nitrobenzene. The other is that nitrobenzene might be reduced and transformed into urea or carbamate.[1] This situation is not yet clear.

Effects of Phosphine and Phosphite Ligands. The product selectivity of the rhodium catalysts appears to be highly affected by the triphenylphosphine coordination. The rhodium complexes with triphenylphosphine as a ligand are favorable for **1**, while $[Rh_2Cl_2(cod)_2]$ is favorable for **2**. Therefore, a combination of several phosphines and phosphite with $[Rh_2Cl_2(cod)_2]$ was tested in the reaction. The results are summarized in Table 2.

When 3 molar equivalents of triphenylphosphine, bis(diphenylphosphino)methane, 1,2-bis(diphenylphosphino)ethane, and 1,3-bis(diphenylphosphino)propane were added to $[Rh_2Cl_2(cod)_2]$, the product selectivity was dramatically changed to **1** from **2**. However, in the case of triphenyl phosphite, trimethyl phosphite, and triethyl phosphite, the product selectivity was not changed. Tributylphosphine combined with $[Rh_2Cl_2(cod)_2]$ showed a unique reactivity. The conversion of nitrobenzene was very high, and *N*-(2-ethylhexylidene)aniline (**3**) was isolated in a 36% yield.

Table 2. Effects of phosphine and phosphite ligands[a]

Run No.	Ligands	Conversion[b] %	Product yield/%[b,c] 1	2
4		37	0	28
12	PPh_3	31	10	0
13	$Ph_2PCH_2PPh_2$	82	10	0
14	$Ph_2P(CH_2)_2PPh_2$	52	12	0
15	$Ph_2P(CH_2)_3PPh_2$	51	12	0
16	$P(OPh)_3$	40	0	24
17	$P(OCH_3)_3$	31	0	20
18	$P(OCH_2CH_3)_3$	35	0	24
19	$P(CH_2CH_2CH_2CH_3)_3$[d]	86	9	0

a) A mixture of nitrobenzene (40 mmol), butanal (90 mmol), water (2 ml), $[Rh_2Cl_2(cod)_2]$ (0.09 mmol), phosphine or phosphite (P/Rh=3), and ethanol (20 ml) was treated at 180 °C under pressures of carbon monoxide (70 atm) for 4 h. b) Based on the amount of nitrobenzene used. Determined by GLC. c) **1**: 3-Ethyl-2-propylquinoline, **2**: *N,N*-dibutylaniline. d) *N*-(2-Ethylhexylidene)aniline (**3**) was isolated in a 36% yield.

Effects of a Binary Catalyst. A binary catalyst, $RhCl(PPh_3)_3$ and palladium(II) chloride, $PdCl_2$, was examined for the preparation of **1**. Several reports have demonstrated that palladium complexes are effective for the reduction of nitrobenzene.[6] Some typical results are listed in Table 3.

The catalytic activity and product selectivity were highly improved by using the binary catalyst. The combination of 0.17 mmol of $RhCl(PPh_3)_3$ and 0.26 mmol of $PdCl_2$ gave an excellent conversion and a fairly good yield of quinolines **1**. The selectivity of **1** amounted to more than 70% (Run 23). $PdCl_2(PhCN)_2$ can also be used for this reaction. On the other hand, the combination of $[Rh_2Cl_2(cod)_2]$ and $PdCl_2$ improved conversion to 100%, but gave a mixture of **1** and **2** with a poorer selectivity.

A palladium species is liable to form an ortho-metallated complex.[7] Therefore, in this study the palladium catalyst may work in activation of the ortho carbon–hydrogen bond.

The Application to a Variety of Nitroarenes and Aldehydes. This produce using butanal can be applied to a variety of nitroarenes for the preparation of 2,3-dialkyl-substituted quinolines and (dialkylamino)arenes. A binary catalyst, $RhCl(PPh_3)_3$ (0.17 mmol) and $PdCl_2$ (0.26 mmol), is effective for the formation of **1** derivatives, while $[Rh_2Cl_2(cod)_2]$ (0.17 mmol) is effective for the formation of **2** derivatives. The results of *o*- and *p*-substituted nitrobenzenes including methyl, methoxyl, and chloro groups are summarized in Tables 4 and 5.

p-Methyl- and *p*-chloronitrobenzene reacted with butanal to give the corresponding 2,3,6-trisubstituted quinolines or *N,N*-dibutylaniline derivatives in fairly good isolated yields. *p*-Nitroanisole, however, gave the products in poor yields, indicating that the methoxyl group located at the para position has an inhibitory

Table 3. The reaction by a binary catalyst[a]

Run No.	Catalyst	Conversion[b] %	Product yield/%[b,c] 1	2
1	$RhCl(PPh_3)_3$(0.09 mmol)	51	11	0
0.09 mmol/4	$[Rh_2Cl_2(cod)_2]$(0.09 mmol)	37	0	28
20	$RhCl(PPh_3)_3$(0.09 mmol), $PdCl_2$ (0.09 mmol)	67	25	0
21	$RhCl(PPh_3)_3$(0.09 mmol), $PdCl_2$ (0.26 mmol)	70	44	0
22	$RhCl(PPh_3)_3$(0.26 mmol), $PdCl_2$ (0.09 mmol)	64	39	0
23	$RhCl(PPh_3)_3$(0.17 mmol), $PdCl_2$ (0.26 mmol)	82	60	0
24	$RhCl(PPh_3)_3$(0.26 mmol), $PdCl_2$ (0.26 mmol)	91	60	0
25	$RhCl(PPh_3)_3$(0.17 mmol), $PdCl_2(PhCN)_2$(0.26mmol)	100	55	0
26	$[Rh_2Cl_2(cod)_2]$(0.17 mmol), $PdCl_2$(0.26 mmol)	100	15	46
27	$PdCl_2$(0.14 mmol)	23	10	0

a) A mixture of nitrobenzene (40 mmol), butanal (90 mmol), water (2 ml), a rhodium and/or palladium complex, and ethanol (20 ml) was treated at 180 °C under pressures of carbon monoxide (70 atm) for 4 h. b) Based on the amount of nitrobenzene used. Determined by GLC. c) **1**: 3-Ethyl-2-propylquinoline, **2**: *N,N*-dibutylaniline

TABLE 4. SYNTHESIS OF QUINOLINE DERIVATIVES FROM *o*- AND *p*-SUBSTITUTED NITROARENES AND ALDEHYDES[a)]

Run No.	Nitroarene	Aldehyde	Product	Yield/%[b)]
23	H	Butanal	3-Ethyl-2-propylquinoline	35
28	*p*-Me	Butanal	3-Ethyl-6-methyl-2-propylquinoline	31
29	*p*-Cl	Butanal	6-Chloro-3-ethyl-2-propylquinoline	44
30	*p*-MeO	Butanal	3-Ethyl-6-methoxy-2-propylquinoline	12
31	*o*-Me	Butanal	3-Ethyl-8-methyl-2-propylquinoline	33
32	*o*-Cl	Butanal	8-Chloro-3-ethyl-2-propylquinoline	29
33	*o*-MeO	Butanal	3-Ethyl-8-methoxy-2-propylquinoline	5
34	H	Propanal	2-Ethyl-3-methylquinoline	53
35	H	Pentanal	2-Butyl-3-propylquinoline	36

a) A mixture of nitroarene (40 mmol), aldehyde (90 mmol), water (2 ml), $RhCl(PPh_3)_3$ (0.17 mmol), $PdCl_2$ (0.26 mmol), and ethanol (20 ml) was treated at 180 °C under pressures of carbon monoxide (70 atm) for 4 h. b) Isolated yield based on the amount of nitroarene used.

TABLE 5. SYNTHESIS OF (DIALKYLAMINO)ARENES FROM *o*- AND *p*-SUBSTITUTED NITROARENES AND ALDEHYDES[a)]

Run No.	Nitroarene	Aldehyde	Product	Yield/%[b)]
36	H	Butanal	*N*,*N*-Dibutylaniline	54
37	*p*-Me	Butanal	*N*,*N*-Dibutyl-4-methylaniline	51
38	*p*-Cl	Butanal	*N*,*N*-Dibutyl-4-chloroaniline	36
39	*p*-MeO	Butanal	*N*,*N*-Dibutyl-4-methoxyaniline	14
			N-(2-Ethylhexylidene)-4-methoxyaniline	22
40	*o*-Me	Butanal	*N*,*N*-Dibutyl-2-methylaniline	34
41	*o*-Cl	Butanal	*N*-Butyl-2-chloroaniline	33
42	*o*-MeO	Butanal	*N*,*N*-Dibutyl-2-methoxyaniline	3
			N-Butyl-2-methoxyaniline	8
43	H	Propanal	*N*,*N*-Dipropylaniline	59
44	H	Pentanal	*N*,*N*-Dipentylaniline	36
45	H	Benzaldehyde	*N*,*N*-Dibenzylaniline	3
46	H	Isobutyraldehyde	*N*,*N*-Diisobutylaniline	10

a) A mixture of nitroarene (40 mmol), aldehyde (90 mmol), water (2 ml), $[Rh_2Cl_2(cod)_2]$ (0.17 mmol), and ethanol (20 ml) was treated at 180 °C under pressures of carbon monoxide (70 atm) for 4 h. b) Isolated yield based on the amount of nitroarene used.

effect on the reaction. With *p*-nitroanisole, the *N*-(2-ethylhexylidene)aniline derivative was also given as a product. *o*-Methylnitrobenzene had a moderate reactivity to give the corresponding products. *o*-Chloronitrobenzene gave the corresponding 2,3,6-trisubstituted quinoline in moderate yields, but it gave *N*-butyl-2-chloroaniline in good yields. The reaction appeared to stop in the step of *N*-monoalkylation, so *N*,*N*-dibutyl-2-chloroaniline was not formed at all. The combination of *o*-nitroanisole with butanal almost failed to give the corresponding products.

This procedure is also applicable to a variety of aldehydes with two α-hydrogens. The combination of nitrobenzene with propanal gave 2-ethyl-3-methylquinoline and *N*,*N*-dipropylaniline in fairly good yields. Pentanal also gave 2-butyl-3-propylquinoline and *N*,*N*-dipentylaniline. In contrast to propanal, butanal, and pentanal, such aldehydes as isobutyraldehyde and benzaldehyde failed to give *N*-heterocyclization products, but did give *N*,*N*-dialkylaniline in poor yields.

Mechanism for the Reactions. The mechanism of the rhodium-catalyzed synthesis of quinolines[3] and (dialkylamino)arenes is not yet clear. An attempt to prepare **2** directly from aniline and butanal was unsuccessful. The rhodium-, even $[Rh_2Cl_2(cod)_2]$, catalyzed reaction between aniline and butanal gives **1** in excellent yields.[3] Thus, the formation pathways are probably different between **1** and **2**. For the formation of **1**, nitrobenzene would be reduced to aniline by the carbon monoxide–water system.[8] The addition of aniline to the aldol condensate, α,β-unsaturated aldehyde, might occur, followed by ring closure with dehydration to form 1,2-dihydroquinoline, which would then be oxidized by nitrobenzene to form **1**. If the aldol condensates, α,β-unsaturated aldehydes, were reduced to saturated aldehyde before the Michael addition, the product **3** would be formed from aniline and the aldehyde. The fact that aldehyde with two α-hydrogens shows a great tendency toward aldol condensation under the conditions used, 200 °C in the presence of a base,[9] suggests that α,β-unsaturated aldehyde is also one of the key intermediates in this reaction, as the case of the Doebner-von-Miller reaction.[10] With the formation of **2**, we believe that the first step involves a catalytic deoxygenation of nitrobenzene to a nitrene, whose subsequent addition to aldehyde would give an oxaziridine and, correspondingly, an isomeric nitrone. A nitrene intermediate has been proposed for the reduction of nitrobenzene with carbon monoxide.[1] Then, the nitrone would be reduced by carbon monoxide to a Schiff base. These steps have been proposed for the synthesis of the Schiff base from nitrobenzene.[11] This Schiff base is

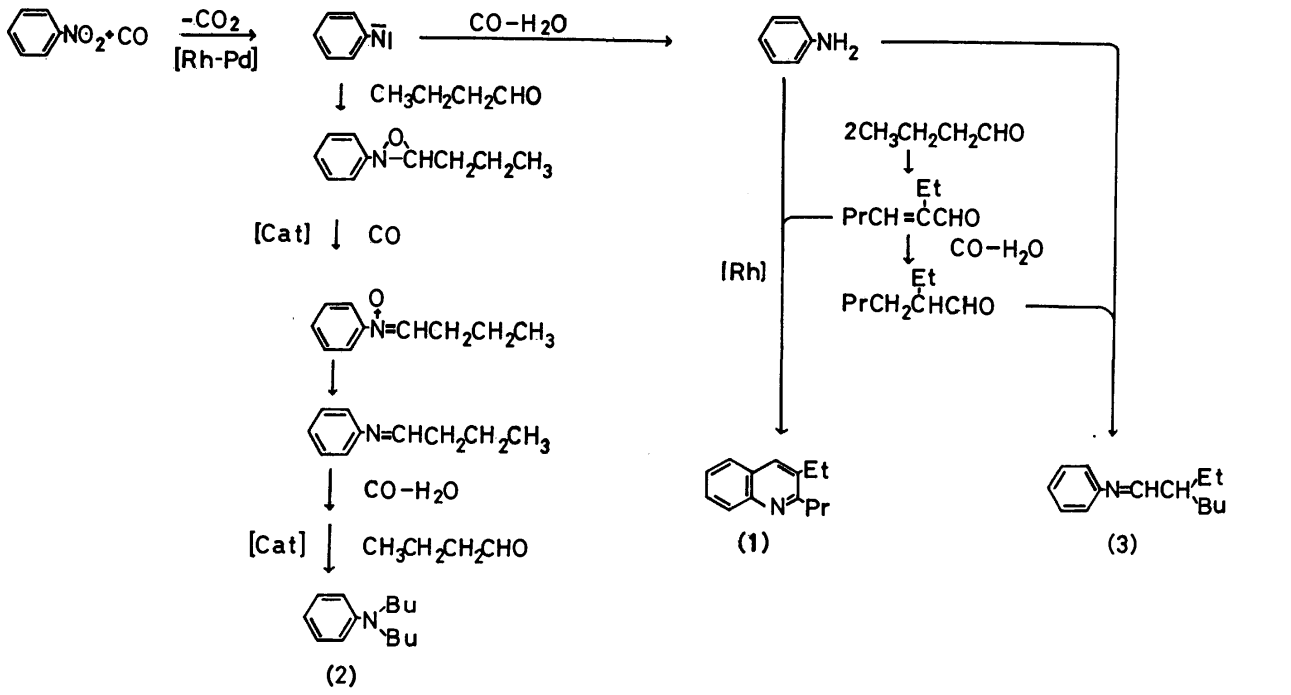

Scheme 2.

easily reduced to the secondary amine, which then reacts with one more aldehyde to form an iminium ion and finally gives **2**.

Experimental

The melting points and boiling points were uncorrected. The melting points were taken on a Yanagimoto capillary melting-point apparatus. The IR spectra were measured on a Hitachi model 215 grating spectrophotometer. The ^{1}H NMR spectra were obtained at 60 MHz with a JEOL JNM-60 or at 220 MHz with a Varian model HR-220 NMR spectrometer. The ^{13}C NMR spectra were determined at 25.05 MHz with a JEOL pulsed Fourier Transform spectrometer, model FX-100. Samples were dissolved in $CDCl_3$, and the chemical-shift values were expressed in δ relative to Me_4Si as the internal standard. Elemental analysis was performed at the Microanalytical Center of Kyoto University. The mass spectra were recorded on a JMS OlSG mass spectrometer.

The aldehydes, nitroarenes, and other compounds employed in this study were commercial products. The aldehydes and nitroarenes were distilled before use. Carbon monoxide was used without further purification. The ethanol was dried by the usual methods.

An autoclave with a capacity of 100 ml, made of stainless= steel and equipped with a magnetic stirrer, was used in the reaction. A typical reaction with butanal and nitrobenzene will be described here to exemplify the general procedure adopted. A mixture of nitrobenzene (4.92 g, 40 mmol), butanal (6.49 g, 90 mmol), water (2 ml), chlorotris(triphenylphosphine)rhodium(I) (0.17 mmol), palladium(II) chloride (0.26 mmol), and anhydrous ethanol (20 ml) was stirred at 180 °C under carbon monoxide (initial pressure, 70 atm).

The autoclave was heated for 20 min to 180 °C and held at this temperature for 4 h. After cooling, the autoclave was discharged and the ethanol was evaporated from the reaction mixture under a vacuum. The GLC analysis of the reaction product was made using bibenzyl as the internal standard with 10% Varsamide on Neopack 60—80 mesh (0.3 cmϕ × 3 m) The reaction products were then subjected to fractional distillation. The identity of the compound was confirmed by IR, ^{1}H NMR, ^{13}C NMR, mass spectra, and elemental analysis.

The analytical data of the quinoline derivatives gave satisfactory results.[3] The (alkylamino)- and (dialkylamino)-arenes and Schiff bases obtained here are described below. Although the products could not be isolated in an analytically pure form, they were identified on the basis of their spectral data.

3-Ethyl-2-propylquinoline (Run 23):[3] Yellow oil, bp 89—91 °C/0.24 Torr.†

N,N-*Dibutylaniline (Run 36)*: Yellow oil, bp 82—84 °C/0.23 Torr. ^{1}H NMR (220 MHz) ($CDCl_3$): δ=0.89 (t, 6H, $2CH_3$), 1.28 (sex, 4H, $2CH_2$), 1.50 (quin, 4H, $2CH_2$), 3.18 (t, 4H, $2CH_2$), 6.57—7.11 (m, 5H, Ar). Found: C, 82.03; H, 11.59; N, 6.87%. Calcd for $C_{14}H_{23}N$: C, 81.89; H, 11.29; N, 6.82%.

N-*(2-Ethylhexylidene)aniline (Run 19)*: Yellow oil, bp 78—82 °C/0.23 Torr. IR (neat) 1650, 1710, 1730 cm^{-1}. ^{1}H NMR (220 MHz) ($CDCl_3$): δ=0.86 (t, 3H, CH_3), 0.91 (t, 3H, CH_3), 1.26—1.39 (m, 4H, $2CH_2$), 1.45—1.61 (m, 4H, $2CH_2$), 2.30 (m, 1H, CH), 6.96—7.28 (m, 5H, Ar), 7.54 (d, 1H, N-CH-). ^{13}C NMR (25.05 MHz) ($CDCl_3$): δ=11.68 (q, CH_3), 14.03 (q, CH_3), 22.84 (t, CH_2), 25.36 (t, CH_2), 29.41 (t, CH_2), 31.82 (t, CH_2), 47.20 (d, CH), 120.53 (ortho), 125.22 (para), 128.86 (meta), 152.41 (arom, C-1), 170.26 (d, CH). Found: C, 80.63; H, 10.15; N, 7.02%. Calcd for $C_{14}H_{15}N$: C, 82.70; H, 10.41; N, 6.89%.

3-Ethyl-6-methyl-2-propylquinoline (Run 23):[3] Yellow oil, bp 110—114 °C/0.35 Torr.

N,N-*Dibutyl-4-methylaniline (Run 37)*: Yellow oil, bp 89—90 °C/0.28 Torr. ^{1}H NMR (220 MHz) ($CDCl_3$): δ=0.94 (t, 6H, $2CH_3$), 1.35 (sex, 4H, $2CH_2$), 1.54 (quin, 4H, $2CH_2$), 2.24 (s, 3H, CH_3), 3.23 (t, 4H, $2CH_2$), 6.56—7.24 (m, 4H, Ar).

† 1 Torr≈133.322 Pa.

6-Chloro-3-ethyl-2-propylquinoline (Run 29):[3] Yellow oil, bp 108—110 °C/0.28 Torr.

N,N-*Dibutyl-4-chloroaniline (Run 38)*: Yellow oil, bp 107—112 °C/0.28 Torr. ^{1}H NMR (220 MHz) ($CDCl_3$): δ=0.92 (t, 6H, $2CH_3$), 1.31 (sex, 4H, $2CH_2$), 1.51 (quin, 4H, $2CH_2$), 3.19 (t, 4H, $2CH_2$), 6.49—7.10 (m, 4H, Ar).

3-Ethyl-6-methoxy-2-propylquinoline (Run 30):[3] Yellow oil, bp 118—120 °C/0.28 Torr.

N,N-*Dibutyl-4-methoxyaniline (Run 39)*: Yellow oil, bp 111—114 °C/0.35 Torr. ^{1}H NMR (220 MHz) ($CDCl_3$): δ= 0.73 (t, 6H, $2CH_3$), 1.14 (sex, 4H, $2CH_2$), 1.34 (quin, 4H, Ar).

N-*(2-Ethylhexylidene)-4-methoxyaniline (Run 39)*: Yellow oil, bp 120—122 °C/0.35 Torr. IR (neat) 1650, 1700, 1730 cm^{-1}. ^{1}H NMR (220 MHz) ($CDCl_3$): δ=0.89 (t, 3H, CH_3), 0.93 (t, 3H, CH_3), 1.27—1.39 (m, 4H, $2CH_2$), 1.48—1.64 (m, 4H, $2CH_2$), 2.32 (m, 1H, CH), 3.73 (s, 3H, $-OCH_3$), 6.84—7.07 (m, 4H, Ar), 7.63 (d, 1H, N=CH–).

3-Ethyl-8-methyl-2-propylquinoline (Run 31):[3] Yellow oil, bp 105—113 °C/0.32 Torr.

N,N-*Dibutyl-2-methylaniline (Run 40)*: Yellow oil, bp 74—78 °C/0.23 Torr. ^{1}H NMR (220 MHz) ($CDCl_3$): δ=0.84 (t, 6H, $2CH_3$), 1.30 (sex, 4H, $2CH_2$), 1.41 (quin, 4H, $2CH_2$), 2.30 (s, 3H, CH_3), 2.92 (t, 4H, $2CH_2$), 6.98—7.26 (m, 4H, Ar).

8-Chloro-3-ethyl-2-propylquinoline (Run 32):[3] Yellow oil, bp 113—118 °C/0.03 Torr.

N-*Butyl-2-chloroaniline (Run 41)*: Yellow oil, bp 76—82 °C/0.50 Torr. IR (neat) 3450 cm^{-1}. ^{1}H NMR (220 MHz) ($CDCl_3$): δ=0.92 (t, 3H, CH_3), 1.41 (sex, 2H, CH_2), 1.60 (quin, 2H, CH_2), 3.09 (t, 2H, CH_2), 4.17 (s, 1H, NH), 6.61—7.27 (m, 4H, Ar).

3-Ethyl-8-methoxy-2-propylquinoline (Run 33):[3] Yellow oil, bp 116—120 °C/0.12 Torr.

2-Ethyl-3-methylquinoline (Run 34):[3] Yellow oil, bp 73—83 °C/0.57 Torr.

N,N-*Dipropylaniline (Run 43)*: Yellow oil, bp 62—66 °C/0.23 Torr. ^{1}H NMR (60 MHz) ($CDCl_3$): δ=0.88 (t, 6H, $2CH_3$), 1.57 (sex, 4H, $2CH_2$), 3.17 (t, 4H, $2CH_2$), 6.48—7.25 (m, 5H, Ar). Found: C, 81.36; H, 10.68; N, 8.00%. Calcd for $C_{12}H_{19}N$: C, 81.30; H, 10.80; N, 7.90%.

2-Butyl-3-propylquinoline (Run 35):[3] Yellow oil, bp 115—118 °C/0.07 Torr.

N,N-*Dipentylaniline (Run 44)*: Yellow oil, bp 110—115 °C/0.32 Torr. ^{13}C NMR (25.05 MHz) ($CDCl_3$): δ=14.1 (q, $2CH_3$), 22.7 (t, $2CH_2$), 26.9 (t, $2CH_2$), 29.4 (t, $2CH_2$), 51.0 (t, $2CH_2$), 111.6 (ortho), 115.1 (para), 129.1 (meta), 148.1 (arom, C-1). Found: C, 82.10; H, 11.80; N, 5.88%. Calcd for $C_{16}H_{27}N$: C, 82.34; H, 11.66; N, 6.00%.

N,N-*Diisobutylaniline (Run 46)*: Yellow oil, bp 72—76 °C/0.40 Torr. ^{1}H NMR (60 MHz) ($CDCl_3$): δ=0.86 (d, 12H, $4CH_3$), 2.07 (m, 2H, 2CH), 3.10 (d, 4H, $2CH_2$), 6.57—7.30 (m, 5H, Ar).

This work was supported by the Grant-in-Aid, Ministry of Education, Science and Culture (No. 56550587).

References

1) See, for example: a) A. F. M. Iqbal, U. S. Patent 3944615; *Chem. Abstr.*, **85**, 20814 (1976); b) H. A. Dieck, R. M. Laine, and R. F. Heck, *J. Org. Chem.*, **40**, 2819 (1975); c) F. J. Weigert, *ibid.*, **38**, 1316 (1973); W. B. Hardy and R. P. Bennett, *Tetrahedron Lett.*, **1967**, 961; T. Yamahara, T. Deguchi, S. Inokuma, and S. Nakamura, Japan Kokai, 75112322; *Chem. Abstr.*, **83**, 205915 (1975); d) U. S. Patent Appl., 459998; *Chem. Abstr.*, **84**, 30723 (1976); H. Yutaka, M. Katsuhara, and M. Aiga, Ger. Offen, 2603574; *Chem. Abstr.*, **85**, 123648 (1976); e) T. Mise, P. Hong, and H. Yamazaki, *Chem. Lett.*, **1980**, 439.

2) Y. Watanabe, M. Yamamoto, T. Mitsudo, and Y. Takegami, *Tetrahedron Lett.*, **1978**, 1289.

3) Y. Watanabe, M. Yamamoto, S. C. Shim, T. Mitsudo, and Y. Takegami, *Chem. Lett.*, **1979**, 1025; Y. Watanabe, S. C. Shim, and T. Mitsudo, *Bull. Chem. Soc. Jpn.*, **54**, 3460 (1981).

4) See, for example: Y. Watanabe, K. Takatsuki, S. C. Shim, T. Mitsudo, and Y. Takegami, *Bull. Chem. Soc. Jpn.*, **51**, 3397 (1978).

5) Y. Watanabe, N. Suzuki, S. C. Shim, M. Yamamoto, T. Mitsudo, and Y. Takegami, *Chem. Lett.*, **1980**, 429.

6) See, for example: T. Yamahara, T. Takano, and S. Nakamura, Japan Kokai, 7552044; *Chem. Abstr.*, **83**, 113938 (1975); P. D. Hammond, W. M. Clarke, and W. I. Denton, U. S. Patent 3832372; *Chem. Abstr.*, **82**, 17729 (1975); P. D. Hammond and N. B. Franco, U. S. Patent 3823174; *Chem. Abstr.*, **82**, 4750 (1975).

7) I. Omae, *Chem. Rev.*, **79**, 287 (1979); A. D. Ryabov and A. K. Yatsimirsky, *Tetrahedron Lett.*, **1980**, 2757; J. M. Thompson and R. F. Heck, *J. Org. Chem.*, **40**, 2667 (1975).

8) A. F. M. Iqbal, *Tetrahedron Lett.*, **1971**, 3385.

9) Y. Watanabe, K. Takatsuki, and Y. Takegami, *Tetrahedron Lett.*, **1978**, 3369.

10) O. Doebner and W. von Miller, *Ber.*, **14**, 2812 (1881); W. H. Mills, J. E. G. Harris, and H. Lambourne, *J. Chem. Soc.*, **119**, 1294 (1921).

11) A. F. M. Iqbal, *J. Org. Chem.*, **37**, 2791 (1972).

 © 1982 The Chemical Society of Japan Bull. Chem. Soc. Jpn., 55, 1121—1126 (1982)

The Replacement of Electronegative Substituents by an Electron-transfer Mechanism. The Factors Governing the Reaction of Carbonyl and Imino Compounds with Organomagnesium Reagents

Masao Ōkubo* and Yumiko Uematsu

Department of Chemistry, Faculty of Science and Engineering, Saga University, Honjō-machi, Saga 840

(Received June 19, 1981)

For the purpose of studying the electron-transfer initiated replacement of *ortho*-methoxy and *ortho*-halogeno substituents of diaryl ketone anils by the aryl group of ArMgBr, eight anils were prepared. The expected *o*-methoxy replacement by the phenyl group of PhMgBr, however, was extremely slow, and no *o*-chloro replacement took place. In contrast, anils of 1-substituted (MeO, Br, Cl) fluorenones gave the replacement products: The distribution of by-products formed *via* radical pathway in the cases of halogeno-anils was clearly different from that in the case of the methoxy-anil. In the reaction with $ArN(MgBr)_2$, 1-halogenofluorenones afforded the normal condensation products, while 1-methoxyfluorenone gave the "condensation-replacement" product. On the basis of the characteristic product-distributions obtained in the two organomagnesium reactions, the mechanism of methoxy replacement was distinguished from that of halogen replacement. Factors governing the two reactions were proposed and discussed: The structures of the substrates favorable to spin-delocalization, the electron-accepting ability of the substrates, the electron-donating ability of the reagents, the leaving ability of substituents, and their leaving manner.

During the past decade, the electron-transfer mechanism in the Grignard addition to carbonyl compounds has been studied extensively, and it was finally established very recently.[1] However, the electron-transfer-initiated replacement of electronegative substituents, such as the methoxy,[2,3] cyano,[2] and halogeno[4] groups of carbonyl and imino compounds, has been reported independently, and a systematic investigation is needed. In this paper, the authors wish to report the results of their study of the replacement of methoxy, bromo, and chloro substituents on the 1-position of 9-fluorenylidene compounds in the reaction with organomagnesium reagents: the reaction of aryliminodimagnesium ($ArN(MgBr)_2$, aryl-IDMg)[5] reagent with fluorenones and that of the Grignard (ArMgBr) reagent with fluorenone anils. The product-distributions found in the reactions with methoxy-substituted substrates are clearly different from those in the reactions with halogeno-substituted ones. On the basis of these results, factors governing the replacement reaction will be discussed.

On the basis of the previous observation[3] that the imino compound, **1**, reacts with PhMgBr (Eq. 1) much more moderately than with carbonyl compounds and that ESR evidence for electron-transfer is obtained in the Grignard reaction with diaryl ketone anils (Eq. 2), a replacement reaction initiated by electron-transfer can be expected to proceed moderately in the Grignard reaction (Eq. 3) with anils of *o*-methoxy- and *o*-chlorobenzophenones, **2**.

In the following, the results of the study to find the best route for preparing anils, **2**, will first be described.

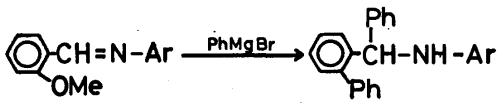

1 (1)

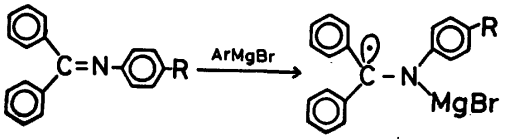

(2)

(3)

2 X = OMe, Cl

The reaction of Eq. 3, however, is too sluggish, and so the study was extended to the reaction of anils with a planar fluorenylidene system (Schemes 4 and 5).

Results and Discussion

Preparation of Anils of o-*Methoxy- and* o-*Chlorobenzophenone.* In order to prepare anils of *ortho*-substituted benzophenones effectively, five possible methods (A—E, Scheme 1) were examined.

Method A is the conventional one, but it cannot be

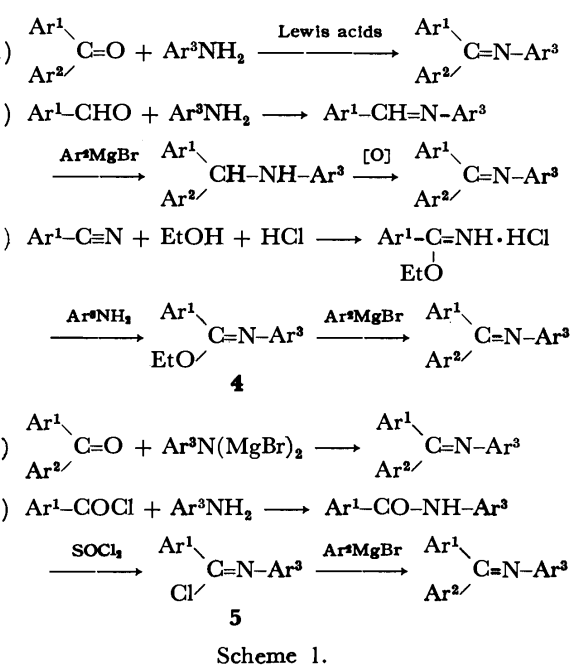

Scheme 1.

used for *o*- and *p*-methoxy-substituted ketones and anilines.[5] Method B proved to be ineffective because the *o*-methoxy group on Ar^1 was replaced by the Ar^2 group of the Grignard reagent (*cf.* Eq. 1).[3]

Method C, which consists of an ethoxy-relacement reaction can be expected to be applicable for synthesizing the anils, since the well-known "*N*-(ethoxymethylene)aniline (**3**) procedure[6] for aldehyde synthesis" involves a quite similar reaction (Eq. 4). After

$$\underset{\mathbf{3}}{EtO\text{-}CH{=}N\text{-}Ph} \xrightarrow{ArMgBr} Ar\text{-}CH{=}N\text{-}Ph \xrightarrow{HCl} ArCHO + PhNH_2 \quad (4)$$

treatment with excess PhMgBr at 55 °C for 5 h, however, *N*-(α-ethoxybenzylidene)-*p*-methylaniline **4** ($Ar^1=C_6H_5$, $Ar^2=p\text{-}MeC_6H_4$) was recovered unchanged: this result will be discussed in the final section.

Method D, using the aryl-IDMg reagent, reported recently, is effective for preparing anils with strongly electron-releasing substituents.[5] However, the reaction of *o*-methoxybenzophenone with phenyl-IDMg gave only a 25% yield of the expected anil, even when excess molar amounts of the reagent were used.[7] The addition of excess metallic magnesium, which acts as a more efficient electron-donor than PhMgBr,[7] caused the methoxy group to be replaced by the Ar^3NH-group, the yield of the replacement product being less than 20%.

Method E proved to be the best one: It was reported earlier,[8] but was not extensively studied. When *N*-(α-chlorobenzylidene)aniline, **5**, obtained almost quantitatively by treating the corresponding benzanilides with $SOCl_2$,[8] was added at 0 °C into a THF solution of equimolar *o*-$MeOC_6H_4MgBr$, a strong exothermic reaction took place. After heating at 55 °C for 2 h and quenching with aqueous NH_4Cl, followed by usual work-up, good yields of the **6**—**13** anils were obtained (Table 1). The *o*-chloro-derivative, **9**, was prepared by the treatment of *N*-(α,*o*-dichlorobenzylidene)aniline, which had been obtained from the corresponding benzanilide, with *p*-MeC_6H_4MgBr. The *p*-chloro-derivative, **12**, was prepared similarly utilizing *o*-MeC_6H_4MgBr.

Twisted Molecular Structure and Sluggish o-*Methoxy Replacement of a Benzophenone Anil in a Grignard Reaction.* Among the anils listed in the table, the *ortho*-unsubstituted anil, **10**, shows unusual physical data. Its wide range of melting temperatures and its split pattern of CH_3-proton signals of NMR (3 : 1.5 : 1.5) indicate that the product is an equimolar mixture of *syn* and *anti* isomers, **10a** and **10b**. Taking the fact and the steric hindrance effect of *ortho*-substituents into account, the data of the other anils are assignable to the sterically preferred configuration, **14** (R=Me, MeO, and Cl).

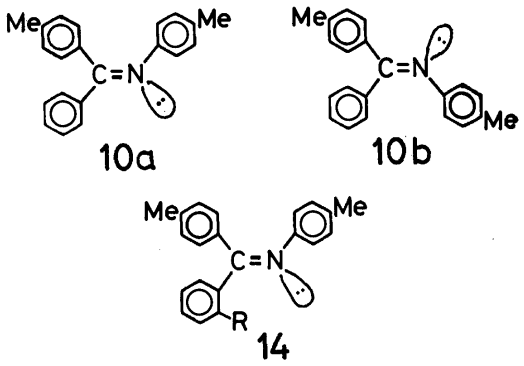

A characteristic purple coloration indicative of radical formation is observed on the treatment of the **8**, **9**, and **10** anils with PhMgBr (*cf.* Eq. 2[3]). The relative concentration of the radicals, as estimated by ESR measurement, is *o*-Cl>H>*o*-MeO.

The expected methoxy replacement of the **8** anil (Scheme 2, Path a) takes place, but the reaction is too sluggish: treatment with five molar equivalents of PhMgBr at 55 °C for 5 h afforded only a 13% yield of the replacement product, which was identified by comparison with an authentic sample prepared by an independent procedure (Path b). The addition of excess metallic magnesium[7] does not improve the yield of the

Table 1. Anils of *ortho*-substituted benzophenones prepared by Method E

No.	Anils[a] $Ar^1(Ar^2)C{=}N\text{-}Ar^3$		Mp θ_m/°C	Yield %	NMR data (δ)
6	C_6H_5, *o*-$MeOC_6H_4$	C_6H_5	78—79	87	6.60—7.92(14H,m) 3.60(3H,s)
7	C_6H_5, *o*-$MeOC_6H_4$	*p*-MeC_6H_4	136—138	73	6.52—7.84(13H,m) 3.62(3H,s) 2.21(3H,s)
8	*p*-MeC_6H_4, *o*-$MeOC_6H_4$	*p*-MeC_6H_4	132—134	79	6.50—7.72(12H,m) 3.56(3H,s) 2.36(3H,s) 2.18(3H,s)
9	*o*-ClC_6H_4, *p*-MeC_6H_4	*p*-MeC_6H_4	136—137	65	6.64—7.68(12H,m) 2.36(3H,s) 2.17(3H,s)
10	*p*-MeC_6H_4, C_6H_5	*p*-MeC_6H_4	57—68	93	6.46—7.86(13H,m) 2.24(3H,s) 2.39(1.5H,s) 2.32(1.5H,s)
11	C_6H_5, *o*-MeC_6H_4	*p*-MeC_6H_4	56—58	95	6.62—7.84(13H,m) 2.18(3H,s) 2.02(3H,s)
12	*p*-ClC_6H_4, *o*-MeC_6H_4	*p*-MeC_6H_4	111—113	61	6.60—7.80(12H,m) 2.20(3H,s) 2.02(3H,s)
13	*p*-MeC_6H_4, *p*-$MeOC_6H_4$	*p*-MeC_6H_4	126—127	81	6.60—7.80(12H,m) 3.80(3H,s) 2.18(3H,s) 2.03(3H,s)

a) Group Ar^2 was introduced as Ar^2MgBr.

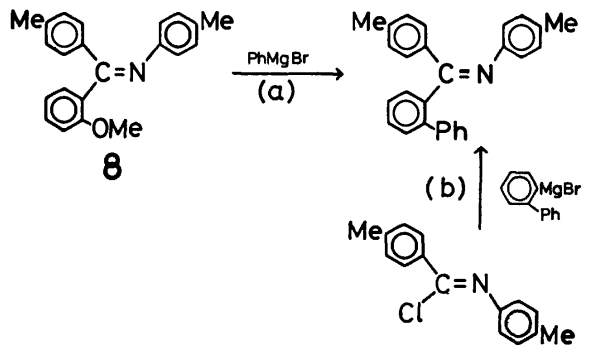

Scheme 2.

replacement product. The *o*-chloro-substituted anil, **9**, was recovered unchanged after being treated under the same reaction conditions.

On the basis of the previous observation that the free spin of the ketyl radicals of hindered benzophenones is delocalized mainly on their unhindered phenyl group,[2] the low replacement reactivity of **8** and **9** is ascribable to restricted spin-delocalization onto their *ortho*-substituted phenyl groups due to their twisting out of the plane of the >C=N- group (*cf.* Scheme 3). This suggestion is verified by the results obtained in the reaction with anils of 1-substituted fluorenones. The ESR spectrum of the radical derived from the non-substituted fluorenone anil show that the free spin is delocalized solely on its fluorenylidene moiety.[3]

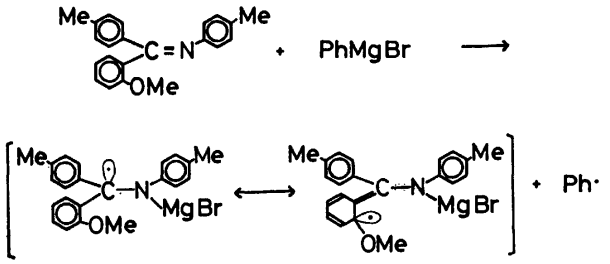

Scheme 3.

Facile Replacement Reaction of 1-Substituted Fluorenones and their Anils with Aryliminodimagnesium and Grignard Reagents. Facile methoxy replacement takes place simultaneously in the condensation of 1-methoxyfluorenone, $\mathbf{15}_{MeO}$, with the *p*-methylphenyl-IDMg reagent, the reaction being carried out in preparing the

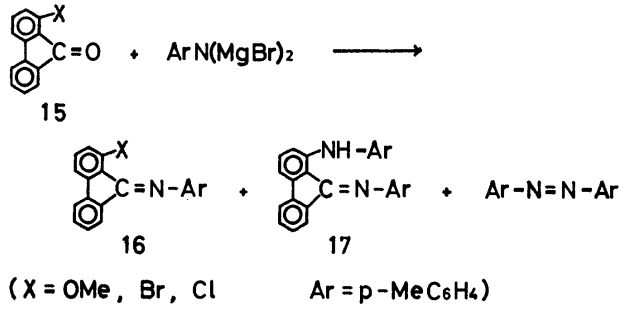

Scheme 4.

Table 2. Products in the reaction (Scheme 4) of 1-substituted fluorenones **15** with *p*-$MeC_6H_4N(MgBr)_2$

Substituent X	Molar ratio	Manner[a] of addition	Yields/%[b] 16	17	Azo	Recovery
MeO	3.0	N	20	38	0	40
MeO	1.5	R	50	11	0	39
Br	3.0	N	44	0	1	52
Cl	3.0	N	56	0	1	40

a) N and R designate "normal" and "reverse" additions respectively. b) Yields obtained after heating the reaction mixture at 55 °C for 2 h.

anil[5] (Scheme 4 and Table 2; *cf.* Scheme 1D): The normal condensation product, $\mathbf{16}_{MeO}$, and condensation-replacement product, **17**, were obtained. In contrast, 1-halogenofluorenones, $\mathbf{15}_{Br}$ and $\mathbf{15}_{Cl}$, afforded only "normal" condensation products, $\mathbf{16}_{Br}$ and $\mathbf{16}_{Cl}$, accompanied by small amounts of the azo compound, the formation of the latter being ascribable to the oxidative coupling of the reagent molecules initiated by electron-transfer due to the higher electron-accepting ability of the halogeno-fluorenones.

Isolated "normal" anils, $\mathbf{16}_{MeO}$, $\mathbf{16}_{Br}$, and $\mathbf{16}_{Cl}$, were submitted to the study of the reaction with *p*-MeC_6H_4MgBr (Scheme 5 and Table 3). The main reaction was the expected replacement affording **18**, the formation of by-products, **19** and **20**, being clearly explainable by the radical pathways given in Scheme 6.

The monomeric reduction product, **19a**, found only in the case of $\mathbf{16}_{MeO}$, originates from the hydrogen-abstraction of the THF molecule (Step 2) by the radical, I, resulting from the initial electron-transfer (Step 1). The dimeric reduction product, **19b**, found in the cases of $\mathbf{16}_{Br}$ and $\mathbf{16}_{Cl}$, originates from the radical, II, produced after the release of the halide anions (Step 3); the structure of the radical II is given tentatively and a detailed mechanism for the formation of **19b** is still equivocal. The dehalogenated anil, **20**, found in the reaction of $\mathbf{16}_{Br}$ and $\mathbf{16}_{Cl}$, originates from the hydrogen-abstraction of the solvent molecule (Step 4) by the radical II. Biaryl, observed in the cases of the halogeno-anils, is formed by the dimerization (Step 7) of the aryl radical generated *via* Step 1: no biaryl was detected in a control experiment carried out without the addition of a substrate. Unexpectedly, in the case of $\mathbf{16}_{MeO}$, a 1-methoxyfluorenone, $\mathbf{15}_{MeO}$, was isolated; its formation is ascribable to the attack of the water molecule upon the I radical because $\mathbf{16}_{MeO}$ itself is not

Table 3. Products in the reaction (Scheme 5) of anils of 1-substituted fluorenones **16** with *p*-MeC_6H_4MgBr

Substituent X	Molar ratio	Yields/%[b] 18	19a	19b	20	15	Ar–Ar	Recovery
MeO	3.0	67	13	0	0	14	0	5
Br	3.0	54	0	20	23	0	14	0
Cl	3.0	30	0	25	23	0	14	22

a) Yields obtained after heating the reaction mixture at 55 °C for 2 h.

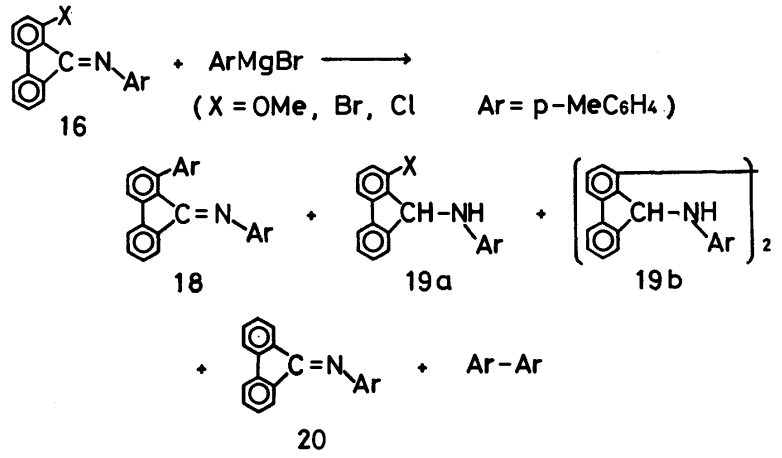

Scheme 5.

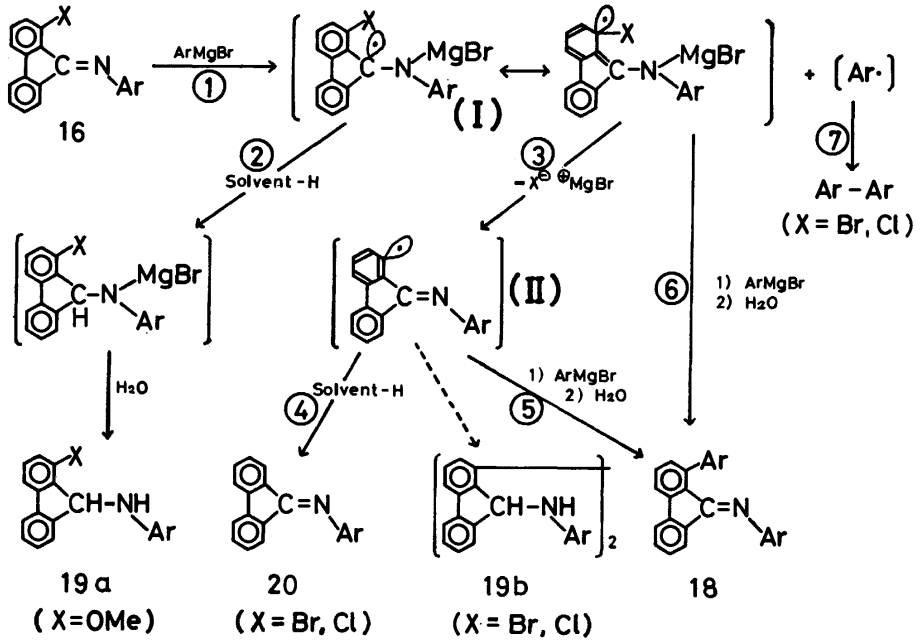

Scheme 6.

hydrolyzed during treatment with aqueous NH_4Cl.

Factors Governing the Replacement Initiated by Electron-transfer. The two clearly different patterns of distribution of the main by-products observed in the Grignard reaction of Scheme 5 should be noted: $\mathbf{16}_{Br}$ and $\mathbf{16}_{Cl}$ give two dehalogenated by-products, **19b** and **20**, while $\mathbf{16}_{MeO}$ affords the methoxy-retaining **19a**. This result is indicative that, according to Scheme 6, the replacement reaction of $\mathbf{16}_{MeO}$ proceeds *via* the methoxy-retaining radical I (Step 6), while the reactions of $\mathbf{16}_{Br}$ and $\mathbf{16}_{Cl}$ proceed *via* the dehalogenated radical II (Step 5). These features are symbolically represented: an S_N1-like mechanism operates for halogen replacement, whereas an S_N2-like one operates for methoxy replacement.

The mechanistic difference is interpretable on the basis of five governing factors: i) The structure of the substrates favorable to spin-delocalization, ii) the electron-accepting (*i.e.*, oxidizing) ability of the substrates, iii) the electron-donating (*i.e.*, reducing) ability of the reagents, iv) the leaving ability of the substituents, and v) their leaving manner. The term "low (or high) reduction potential" can be substituted for "high (or low) electron-accepting ability," and the term "low (or high) oxidation potential" can be substituted for "high (or low) electron-donating ability." The lower electrophilicity of imino compounds in comparison with carbonyl compounds was reported previously;[3] however, the term "electron-accepting ability" should be substituted for "electrophilicity," since the latter term is used for explaining the reactivity in ordinary ionic reactions.

The effect of the first factor, the structure of substrates, is demonstrated by the results given above: the planar fluorenylidene structure is evidently more favorable to replacement than the twisted diarylmethylene structure. The second factor, the electron-accepting ability of the substrates (Cl>Br>MeO),

affects the initial electron-transfer from the reagent.[9] The higher electron-accepting $\mathbf{16}_{Cl}$ and $\mathbf{16}_{Br}$ cause a higher radical concentration which, in comparison with that in the case of the lower electron-accepting $\mathbf{16}_{MeO}$, is responsible for the formation of two dehalogenated products, **19b** and **20**. The formation of biaryl in the Grignard reaction of $\mathbf{16}_{Br}$ and $\mathbf{16}_{Cl}$, like that of azoarene in the IDMg reaction of $\mathbf{15}_{Br}$ and $\mathbf{15}_{Cl}$, is also ascribable to the high electron-accepting ability of the halogeno substrates.

The third factor, the electron-donating ability of the reagents, also affects the intial electron-transfer process. Since the thermographic study of the Grignard reaction[1b] correlates the extent of heat evolution with that of initial electron-transfer, the very slight heat evolution detected in the reaction of $ArN(MgBr)_2$ with benzophenones[5] is indicative that the reagent is moderately electron-donating in comparison with ArMgBr. The absence of the condensation-replacement product, **17**, in the IDMg reaction with highly electron-accepting $\mathbf{15}_{Cl}$ and $\mathbf{15}_{Br}$ is ascribable to the moderate electron-donating ability of the reagent. Even *p*-methoxyphenyl-IDMg, which is more electron-donating than the *p*-methylphenyl reagent, does not afford **17** in the reaction with $\mathbf{15}_{Br}$: an improved yield of the normal anil $\mathbf{16}_{Br}$ (Ar=*p*-$MeOC_6H_4$, 78%), *ca.* a 1% yield of the debrominated anil **20** (Ar=*p*-$MeOC_6H_4$), and a trace amount of the corresponding azoarene were obtained. The effect of the electron-donating ability will be discussed again below in connection with the replacement manner of the methoxy substituent.

The fourth factor, the leaving ability of the substituents (Br>Cl>MeO), is responsible for the considerable recovery of $\mathbf{16}_{Cl}$ in comparison with the absence of any recovery of $\mathbf{16}_{Br}$, even in the reaction with highly electron-donating ArMgBr. This result is compatible with the leaving ability of groups found in ordinary S_N reactions.[10]

The fifth factor, the leaving manner of the substituents, is important for understanding the characteristic behavior of the methoxy substituent in the reactions of Schemes 4 and 5. It should be noted that the group is easily replaced by the use of the "normal addition" procedure, but the replacement is noticeably suppressed by use of the "reverse addition" procedure (Table 2). At the initial stage of the former procedure, an extremely high molar ratio of the moderately electron-donating IDMg reagent to the substrate is realized, the condition being favorable to an S_N2-like replacement of the substituent. In the reaction with the highly electron-donating Grignard reagent, even the least electron-accepting $\mathbf{16}_{MeO}$ affords a sufficiently high concentration of the radical I responsible for the formation of **19a**, which retains the methoxy substituent. The formation of **18** in this case is thus ascribable to its S_N2-like replacement manner.

The behavior of halogeno substituents in the two reactions should be discussed again in terms of their S_N1-like leaving manner. Even by the "normal addition" of the highly electron-accepting halogeno fluorenones, the moderately electron-donating IDMg reagent gives no sufficiently high radical concentration responsible for an S_N1-like halogen release, leading to the formation of **17**. In the reaction with the highly electron-donating Grignard reagent, halogeno-anils give radical concentrations sufficiently high for an S_N1-like halogen release, leading to the formation of **19b** and **20**.

Also explainable in terms of the proposed factors is the apparent contradiction found in the Grignard reactions carried out for preparing benzophenone anils (Scheme 1); Method E owes its success to the high reactivity of chloro-imine **5** whereas Method C fails because of the inertness of ethoxy-imine **4**, despite of their quite similar preferred configurations, **4a**, and **5a**. However, ethoxy-imines, **3** and **21** (Eq. 5), are converted into an aldimine, **22**,[6] and an anil, **23**, respectively, though the latter formation is slower than the former. The sterically preferred configurations and observed reactivities of the three ethoxy-imines suggest that S_N2-like alkoxy replacement requires a "syn-located" lone pair of nitrogen. Regardless of the seemingly unfavorable configuration, **5a**, its high electron-accepting ability and the S_N1-like leaving manner of chlorine supports the success of Method E.

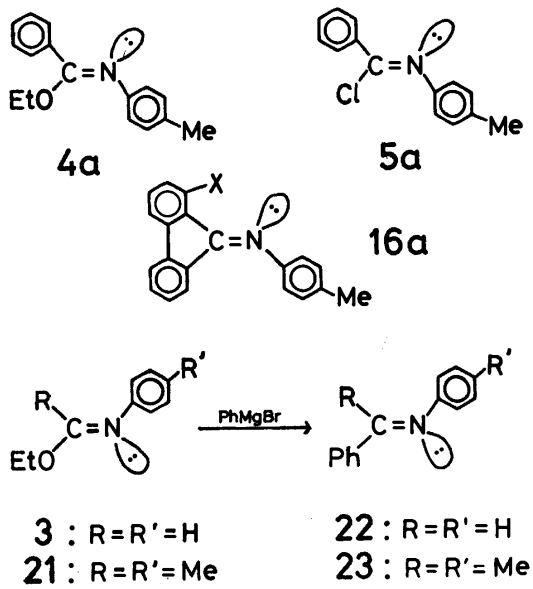

(5)

3 : R=R'=H **22** : R=R'=H
21 : R=R'=Me **23** : R=R'=Me

Taking the additional factor, the configuration of the imines, into account, it is clear that the preferred configuration, **16a**, of the fluorenone anils is responsible not only for the S_N1-like halogen replacement, but also for the S_N2-like methoxy replacement with the Grignard reagent. Properly selected combinations of substrates with reagents, *i.e.*, the combination of highly oxidizing fluorenones with moderately reducing $ArN(MgBr)_2$ as well as that of moderately oxidizing anils with highly reducing ArMgBr, provides useful results for clarifying the factors which depend on each other and which govern the replacement reaction.

Experimental

The melting and boiling points are uncorrected.

Materials. *N*-(α-Ethoxybenzylidene)-*p*-methylaniline, **4**, was obtained by treating a slurry of α-ethoxybenzylideneamine hydrochloride[11] in dry benzene with equimolar *p*-

methylaniline at 60 °C for 5 h:[12] bp 125—128 °C/0.5 mmHg; NMR (CCl_4): δ=6.44—7.38 (9H, m), 4.36 (2H, q), 2.24 (3H, s), 1.40 (3H, t). The similar treatment of α-ethoxybenzylideneamine hydrochloride[11] with *p*-methyl aniline afforded *N*-(α-ethoxyethylidene)-*p*-methylaniline, **21**: bp 63 °C/0.5 mmHg; NMR (CCl_4): δ=6.94 (2H, d), 6.50 (2H, d), 4.14 (2H, q), 2.12 (3H, s), 1.72 (3H, s), 1.26 (3H, t). An authentic sample of *N*-(α-methylbenzylidene)-*p*-methylaniline, **22**, was prepared according to the reported method using $ZnCl_2(p\text{-}MeC_6H_4NH_2)_2$:[13] bp 138—143 °C/0.5 mmHg; NMR (CCl_4): δ=6.60—8.12 (9H, m), 2.45 (3H, s), 2.18 (3H, s).

N-(α-Chlorobenzylidene)-aniline and -*p*-methylaniline, as well as their nuclear-substituted derivatives, **5**, were obtained in good yields by the treatment of the corresponding benzanilides with excess $SOCl_2$.[8] An authentic sample of the *o*-phenylated anil (Scheme 2) was prepared according to Method E using the Grignard reagent derived from 2-bromobiphenyl: mp 106—107 °C; NMR ($CDCl_3$); δ=5.94—7.80 (17H, m), 2.36 (3H, s), 2.16 (3H, s).

1-Methoxyfluorenone, $\mathbf{15}_{Meo}$, was obtained by the methylation of 1-hydroxyfluorenone with Me_2SO_4 and NaOH,[14] the 1-hydroxy derivative being prepared by the diazotation of 1-aminofluorenone, followed by heating at 75—80 °C.[14] 1-Halogenofluorenones, $\mathbf{15}_{Br}$[15] and $\mathbf{15}_{Cl}$.[16] were prepared by the Sandmeyer reaction of 1-aminofluorenone. 1-Aminofluorenone was prepared starting from fluoranthene: oxidation with CrO_3 to 9-oxo-1-fluorenecarboxylic acid[17] and conversion to the amide,[15] followed by a Hofmann reaction using NaOCl.[16] For the purification of 1-substituted fluorenones, **15**, sublimation under reduced pressure was applied more conveniently than column chromatography.[14]

Procedures. All the Grignard reactions of Scheme 5 were carried out using 4.0 mmol of substrates in THF (50 ml) under N_2. The IDMg reactions were done according to the previously reported method[5] using 2.2—2.5 mmol of substrates and THF (40 ml). The Grignard reaction in the presence of metallic Mg was carried out using a reagent solution prepared from bromobenzene and a calculated excess of Mg. The yield of *o*-phenylated product of Scheme 2 was estimated by means of high-pressure liquid chromatography, using the calibration line of an authentic sample: MeOH–H_2O (65 : 35) was used as the eluent.

The ESR measurement was carried out according to the previously reported manner.[18]

Products. For the isolation and purification of the product formed in reactions of Schemes 4 and 5, column chromatography was used.

The melting point and NMR spectrum of **20** were compared with those of an authentic sample.[19] The by-product, **19a** (X=MeO), was identified by converting it into **16** (X=MeO) by dehydrogenation with freshly prepared MnO_2 in refluxing dry benzene.[20] Anils of 1-bromo- and 1-chlorofluorenone, **16**, gave the same by-product, **19b**: its dimeric structure was confirmed by molecular-weight measurement.

The melting points, NMR data, and results of elemental analyses of *N*-fluorenylideneaniline obtained in the reactions of Schemes 4 and 5 are given below: $\mathbf{16}_{Meo}$: mp 143—145 °C; NMR (CCl_4): δ=6.50—7.66 (11H, m), 4.00 (3H, s), 2.40 (3H, s). Found: C, 84.31, H, 5.65, N, 4.69%. Calcd for $C_{21}H_{17}NO$: C, 84.28, H, 5.69, N, 4.68%. $\mathbf{16}_{Br}$: mp 113—115 °C; NMR (CCl_4): δ=6.64—7.88 (11H, m), 2.42 (3H, s). Found: C, 69.01, H, 4.10, N, 3.99%. Calcd for $C_{20}H_{14}BrN$: C, 68.97, H, 4.02, N, 4.02%. $\mathbf{16}_{Cl}$: mp 139—141 °C; NMR (CCl_4): δ=6.58—7.62 (11H, m), 2.42 (3H, s). Found: C, 78.99, H, 4.57, N, 4.65%. Calcd for $C_{20}H_{14}ClN$: C, 79.08, H, 4.61, N, 4.61%. **17**: mp 118—120 °C; NMR (CCl_4): δ=9.92 (1H, s), 6.64—7.64 (15H, m), 2.44 (3H, s), 2.32 (3H, s). Found: C, 86.59, H, 5.82, N, 7.59%. Calcd for $C_{27}H_{22}N_2$: C, 86.63, H, 5.88, N, 7.49%. **18**: mp 171—173 °C; NMR (CCl_4): δ=6.54—7.68 (15H, m), 2.36 (6H, broad s). Found: C, 90.71, H, 5.81, N, 3.48%. Calcd for $C_{27}H_{31}N$: C, 90.25, H, 5.85, N, 3.90%. $\mathbf{16}_{Br}$ (Ar=*p*-$MeOC_6H_4$): mp 144—146 °C; NMR ($CDCl_3$): δ=6.72 (11H, m), 3.88 (3H, s). Found: C, 65.84, H, 3.79, N, 3.87%. Calcd for $C_{20}H_{14}BrNO$: C, 65.93, H, 3.84, N, 3.84%.

References

1) a) M. Ōkubo, *Bull. Chem. Soc. Jpn.*, **48**, 1057, 1327, 2057 (1975); **50**, 2379 (1977); M. Ōkubo, Y. Morigami, and R. Suenaga, *ibid.*, **53**, 3029 (1980); b) T. Holm and I. Crossland, *Acta Chem. Scand.*, **25**, 59 (1971); T. Holm, *ibid.*, *Ser. B*, **28**, 809 (1974); c) E. C. Ashby, Lecture given at the Con, ference of Organometallic Chemistry, Dijon, France, 1979; E. C. Ashby, J. Bowers, and R. Depriest, *Tetrahedron Lett.*, **21**, 3541 (1980).

2) M. Ōkubo, *Bull. Chem. Soc. Jpn.*, **50**, 2379 (1977).

3) M. Ōkubo and S. Ueda, *Bull. Chem. Soc. Jpn.*, **52**, 3346 (1979).

4) T. Holm and I. Crossland, *Acta Chem. Scand.*, **25**, 59 (1971); C. Jongsma and F. Bickelhaupt, *Recl. Trav. Chim. Pays-Bas*, **92**, 1143 (1973).

5) M. Ōkubo and S. Ueda, *Bull. Chem. Soc. Jpn.*, **53**, 281 (1980).

6) L. I. Smith and J. Nichols, *J. Org. Chem.*, **6**, 489 (1941).

7) M. Ōkubo, S. Hayashi, M. Matsunaga, and Y. Uematsu, *Bull. Chem. Soc. Jpn.*, **54**, 2337 (1981).

8) J. V. Braun and W. Pinkernelle, *Chem. Ber.*, **67**, 1218 (1934).

9) M. Ōkubo, *Bull. Chem. Soc. Jpn.*, **48**, 2057 (1975).

10) H. C. Brown and M. Gerstein, *J. Am. Chem. Soc.*, **72**, 2926 (1950); H. C. Brown and A. Stern, *ibid.*, **72**, 5068 (1950).

11) S. M. McElvain and J. W. Nelson, *J. Am. Chem. Soc.*, **64**, 1825 (1942).

12) G. D. Lander, *J. Chem. Soc.*, **1902**, 591.

13) G. Reddelien, *Chem. Ber.*, **43**, 2476 (1910).

14) L. Horner and D. W. Baston, *Justus Liebigs Ann. Chem.*, **1973**, 911.

15) E. H. Huntress, K. Pfister, and K. H. T. Pfister, *J. Am. Chem. Soc.*, **64**, 2845 (1942).

16) N. Kharasch and T. C. Bruice, *J. Am. Chem. Soc.*, **73** 3240 (1951).

17) L. F. Fieser and A. M. Seligman, *J. Am. Chem. Soc.*, **57**, 2174 (1935).

18) K. Maruyama, *Bull. Chem. Soc. Jpn.*, **37**, 1013 (1964).

19) M. Taylor and T. L. Fletcher, *J. Org. Chem.*, **26**, 940 (1961).

20) E. H. Pratt and T. P. McGovern, *J. Org. Chem.*, **29**, 1540 (1964).

 © 1982 The Chemical Society of Japan Bull. Chem. Soc. Jpn., 55, 1127—1132 (1982)

Photocycloadditions of Benzophenone with 6-Methylenetricyclo[3.2.1.$0^{2,7}$]-oct-3-en-8-one and Its Related Compounds. Di-π-methane Photorearrangement of the Primary Photocycloadducts[1]

Makoto NITTA* and Hiroshi SUGIYAMA

Department of Chemistry, School of Science and Engineering, Waseda University, Shinjuku-ku, Tokyo 160

(Received July 3, 1981)

The photocycloadditions of benzophenone with constrained divinylcyclopropanes such as 1,5-dimethyl- and 1,3,5-trimethyl-6-methylenetricyclo[3.2.1.$0^{2,7}$]oct-3-en-8-ones, 5,8-dimethyl-9-methylenetricyclo[3.3.1.$0^{2,8}$]non-3-en-6-one, 5,8-dimethyl-9-methylenetricyclo[3.3.1.$0^{2,8}$]non-3-en-7-one, and their corresponding alcohols were investigated. In no cases, was oxetane formation observed but the formal [2+6] cycloaddition which originates from the cleavage of a cyclopropane ring was observed. In the case of the compounds which have a carbonyl function, benzophenone sensitized di-π-methane or oxadi-π-methane rearrangement of the primary photocycloadducts was observed. The mechanism of the formation of photoproducts is discussed with emphasis on (i) the nature of the intermediates having tricyclo[3.2.1.$0^{2,7}$]oct-3-en-6-yl and tricyclo[3.3.1.$0^{2,8}$]non-3-en-9-yl radicals, (ii) the regioselectivity of the di-π-methane or oxadi-π-methane rearrangement of the primary photocycloadducts.

Rearrangement of free radicals has been observed in reactions with low activation energies.[2] Photocycloaddition of benzophenone with olefins has afforded oxetanes,[3] while with cyclopropylethylenes, oxetanes and tetrahydrooxepins originating from the cleavage of a cyclopropane ring are obtained.[4] An example of this class of cycloaddition reaction involving the constrained divinylcyclopropane moiety was the cycloaddition of benzophenone with barbaralone investigated by Mukai and Kuribayashi.[5] Recently, we have reported that the cycloaddition of benzophenone with 1,5-dimethyl- and 1,3,5-trimethyl-6-methylenetricyclo[3.2.1.$0^{2,7}$]oct-3-en-8-ones (**1a** and **1b**) and 1,5-dimethyl-6-methylenetricyclo[3.2.1.$0^{2,7}$]oct-3-en-8-*endo*-ol (**1c**) afforded formal [2+6] cycloadducts originated from cleavage of the cyclopropane ring.[6] It was recently concluded[7] from product analysis and ESR spectroscopy that of radicals containing the bicyclo[3.2.1]octane skeleton

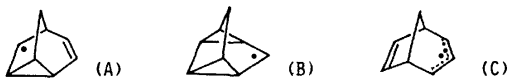

(**A**), (**B**), and (**C**), the allyl radical (**C**) was the most stable. The radical (**A**) or (**B**) rearranges rapidly to radical (**C**). Because of the interest in clarifying the ring size effect and substituent effect[8] of the radical rearrangement and the detailed photochemical behavior of the primary photocycloadduct, we have also investigated the photocycloaddition of benzophenone with the one-carbon ring enlarged compounds such as 5,8-dimethyl-9-methylenetricyclo[3.3.1.$0^{2,8}$]non-3-en-6-*endo*-ol (**2a**), 5,8-dimethyl-9-methylenetricyclo[3.3.1.$0^{2,8}$]-non-3-en-7-ol (**2b**), 5,8-dimethyl-9-methylenetricyclo-[3.3.1.$0^{2,8}$]non-3-en-6-one (**2c**), and 5,8-dimethyl-9-methylenetricyclo[3.3.1.$0^{2,8}$]non-3-en-7-one (**2d**). Through these studies, it was proven that the adduct **3a** is a rearrangement product of a primary photocycloadduct and **4a** has a different regiochemistry from that assigned in an ealier communication.[6] We would like to report the full details of the results.

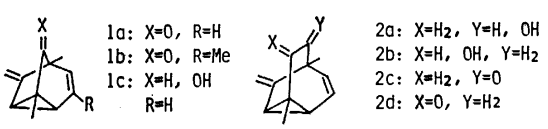

Results and Discussion

Photocycloaddition of Benzophenone with ***1a***, ***1b***, *and* ***1c***. The photocycloaddition of benzophenone with **1a**[9] was performed in anhydrous benzene with RPR-350 nm lamps in a nitrogen atmosphere.[6] The major product was a cycloadduct **3a** (mp 166—167 °C, 47%) and a minor cycloadduct was **4a** (mp 270—271 °C, 15%). The photoreaction of benzophenone with **1b**[9] afforded a similar cycloadducts **3b** and **4b** in 28% and 8% yields respectively. The adduct **3a** exhibited a parent ion peak at 342 in the mass spectrum, and a strong IR absorption

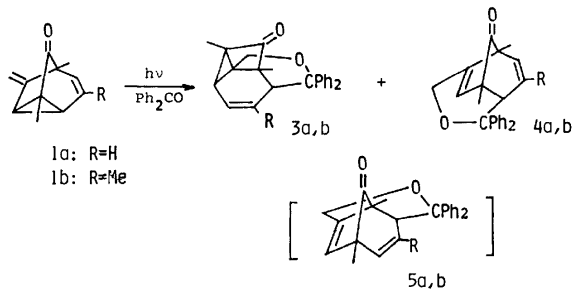

band at 1763 cm^{-1} due to the cyclobutanone ring. The NMR spectrum of **3a** exhibited a proton of the cyclopropane ring at δ 2.10 (d, J=4.0 Hz), and three protons of an allylic moiety at δ 3.50 (d, J=7.8 Hz), δ 5.60 (dxd, J=8.2, 7.8 Hz), and δ 6.02 (dxd, J=8.2, 4.0 Hz), in addition to the protons of two methyl groups at δ 0.92, δ 1.56, two methylene protons at δ 4.34 (d, J=10.0 Hz), δ 4.90 (d, J=10.0 Hz), and ten protons of the phenyl groups. These chemical shifts and the coupling patterns are in good agreement with the proposed structure **3a**. Similarly the structure of **3b** was assessed by the comparison of the spectral data with those of **3a** (see Experimental). The compound **4a** exhibited a parent ion peak at 342, and a strong IR absorption band at 1752 cm^{-1} which is suggestive of a skeleton **4a**. The NMR spectrum of **4a** exhibited a

singlet vinyl proton at δ 4.90 and three protons of an allylic moiety at δ 3.78 (m), δ 5.10 (dxd, J=10.0, 4.0 Hz), δ 5.68 (dxd, J=10.0, 2.0 Hz), in addition to the two methyl signals at δ 0.68, δ 1.57, two methylene protons at δ 4.05 (d, J=13.0 Hz), δ 4.53 (d, J=13.0 Hz), and ten protons of the phenyl groups. These chemical shifts and the coupling patterns suggest the structure **4a**. In our ealier communication, we assigned the structure **5a** for these spectral data, and the structure **4a** was discarded because of the ring strain of the tetrahydrooxepin which contains a *trans* double bond.[10] The following reaction sequences, however, elucidate the correctness of the structure **4a** and **4b**.

The photocycloaddition of benzophenone with **1c**[11] was carried out in a similar manner, and **5c** (mp 74—75 °C) was obtained in 76% yield. The adduct **5c** exhibited a parent ion peak at 344 in the mass spectrum. The NMR spectrum of **5c** exhibited a vinyl proton at δ 6.15 and three protons of allylic moiety at δ 3.17 (m), δ 5.15 (dxd, J=9.5, 3.8 Hz), δ 5.74 (broad d, J=9.5 Hz), in addition to two methyl groups at δ 0.97, δ 1.09, two methylene protons at δ 4.90 (d, J=11.2 Hz), δ 4.38 (d, J=11.2 Hz), a methine proton at δ 3.49 (broad s), hydroxyl proton at δ 1.72 and ten protons of the phenyl groups. Therefore the structure **5c** was deduced as depicted in the scheme. On oxidation with pyridinium chlorochromate[12] in dichloromethane, the adduct **5c** was converted to **5a** (mp 152—153 °C) in 23% yield. The compound **5a** exhibited a parent ion peak at 342

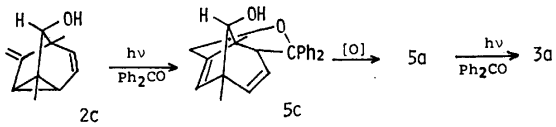

in the mass spectrum, and a strong IR absorption band at 1750 cm^{-1} due to a cyclopentenone moiety. The NMR spectrum exhibited a singlet vinyl proton at δ 6.50, three protons of allylic moiety at δ 3.66 (m), δ 4.98 (dxd, J=9.0, 4.0 Hz), δ 6.00 (dxd, J=9.0, 2.0 Hz), in addition to two methyl signals at δ 1.00, δ 1.17, two methylene protons at δ 4.23 (d, J=10.0 Hz), δ 4.47 (d, J=10.0 Hz), and ten protons of the phenyl groups. Where the vinyl and the allylic moieties are concerned, the coupling patterns of the NMR spectra of **4a**, **b**, and **5a** are very similar to each other. Since the methyl group in **4b** occupies a position corresponding to a proton in an allylic moiety of **4a** (see Experimental), the coupling patterns of **4b** are simplified. However, the relatively high chemical shift of the vinyl proton at δ 4.90 of **4a** or at δ 4.95 of **4b** as compared to δ 6.50 of **5a** or δ 6.15 of **5c** should be ascribed to the anisotropy effect of the phenyl groups, which located very close to the singlet vinyl proton in the case of **4a**, **b**. Therefore the structure of **4a** and **4b** could be reasonably assessed to have a *trans*-tetrahydrooxepin ring.

As reported previously,[6] independent irradiation of **4a**, in the presence or absence of benzophenone, did not cause rearrangement affording **3a**. The benzophenone sensitized photoreaction of **5a**, on the other hand, afforded the di-π-methane rearrangement product **3a** (70% yield), which was identical with an authentic specimen. Therefore **5a** and then **5b** should be the supportive intermediates affording **3a**, **b** in the photocycloaddition of benzophenone with **1a**, **b**.

We proposed a mechanistic scheme for the formation of the photocycloadducts (Scheme 1). The diradical **8** has been considered to be the intermediate[3,4] and it may be produced either because it is more stable than **8'**, or from an initially formed complex of a prefered orientation.[13] Recently kinetic data [E_a 5.9 kcal/mol; log (A/s^{-1}) 12.48] for the cyclopropylcarbinyl→allylcarbinyl radical rearrangement have been obtained from ESR spectroscopy in the temperature range of −120 °C to −140 °C.[14] However, the type (**A**) radical [which has the same skeleton as **8**] has not been detected at −140 °C, and only the rearranged radical species has been detected.[7] These facts may suggest that the rearrangement of the constrained radical species such as **8** may be faster than that of a simple cyclopropylcarbinyl radical itself. Furthermore the combination in **8** affording oxetane should have some degree of F-strain. Therefore the tricyclic radical species **8** rearranges rapidly to the allyl radical species **9** (path 1),

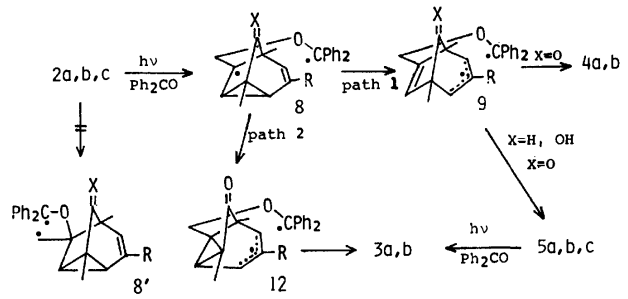

Scheme 1.

and the latter combines to give **4a**, **b**. The cycloadducts **4a**, **b** contains a *trans*-tetrahydrooxepin ring, which seems to be very constained. Therefore the pathway affording **4a**, **b** should be a relatively high-energy process. Another major pathway from **9** to the photocycloadducts should afford **5a**, **5b**, and **5c**, all of which have no *trans*-tetrahydrooxepin ring. However, we have no explanation for the formation of **4a**, **b** in the case of **1a**, **b** as compared to the case of **1c**. It may be impossible for the cycloadduct **5c** to absorb light in the present conditions. Furthermore a benzophenone sensitized di-π-methane rearrangement may be impossible because of its high triplet-state energy. This assumption is reminiscent of the acetone or acetophenone sensitized rearrangement of bicyclo[3.2.1]octadiene.[15] On the other hand, the energy transfer from benzophenone is possible in the case of the corresponding ketones, **5a**, **b** and results in the di-π-methane rearrangement giving **3a**, **b**. The carbonyl group seems to be indespensable for this rearrangement. In an earlier communication, the direct formation of **3a**, **b** from **8** *via* **12** (path 2) was considered.[6] However, the selective formation of **4a**, **b** seems unreasonable because of the high strain energy. In addition, the photochemical behavior of the independently prepared **5a** can contradict the path 2. This explanation is also supported by the experimental results of the similar reaction of the one-carbon ring

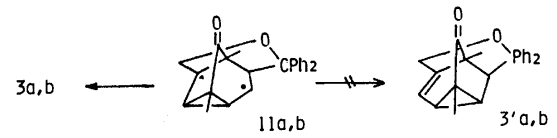

enlarged compounds **2** (*vide infra*). Other di-π-methane rearrangement such as **3'a, b** were not obtained *via* **11**. The examples of the directionality for migration of the vinyl group in the di-π-methane rearrangements are reported.[16] The less substituted or less conjugated double bond can migrate because the high electron density is needed for migration. However, the present selectivity affording **3a, b** might be controlled by the steric factor originated from the $-CH_2-O-CPh_2-$ bridge: In compounds **3'a, b**, an end of $-CH_2-O-CPh_2-$ moiety is attached to a double bond, therefore **3'a, b** are more constained as compared to **3a, b**.

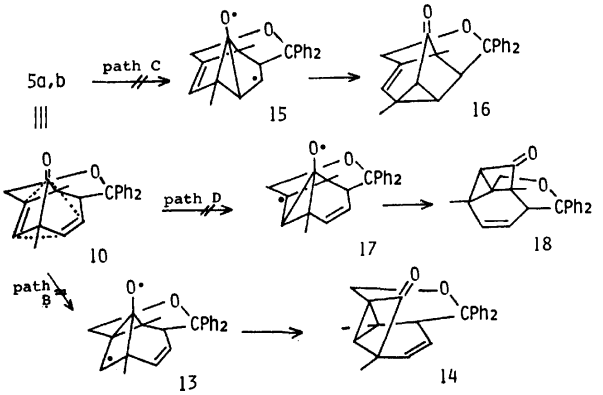

It is noticeable that the oxadi-π-methane rearrangement affording **14, 16,** and **18** were not observed on photoreaction. We think this fact should imply the fully homoconjugated interaction of the carbonyl group with the two basal double bonds, as indicated in the structural formula **10**, and that the full interaction leads to the di-π-methane rearrangement.

Photocycloaddition of One-carbon Ring Enlarged Compounds ***2a—d.*** In order to clarify the ring size effect on the radical rearrangement of **8** or **9** as well as on the photochemical behavior of the primary photocycloadducts such as **5**, photocycloadditions of benzophenone with **2a—d** were also investigated.

The irradiation of a benzene solution of benzophenone and **2a**[17] or **2b**[18] afforded an cycloadduct **6a** or **6b** in 78% or 73% yield, respectively. The chemical shifts and the coupling patterns of the NMR spectra of **6a, b** are very similar to those of **5a, c** (see Experimental). Especially the chemical shifts of the singlet vinyl protons at δ 6.55 of **6a** and at δ 6.17 of **6b** are similar to those of **5a** (δ 6.55) or **5c** (δ 6.50), therefore the structures **6a, b** were deduced. The adduct **6a** or **6b** could arise from the diradical species **20** or **22**, which originate from the rearrangement of the initially formed cyclopropylcarbinyl radical species **19** or **21**, respectively, as in the case of the reaction of benzophenone with **1**.

Irradiation of a benzene solution of **2c**[19] with benzophenone, on the other hand, afforded two photoproducts **6c** and **7c** in 13% and 40% yields, respectively. The mass spectral data and the analytical data of **6c** and **7c** were satisfactory for the 1 to 1 adducts of **2c** and benzophenone. The adduct **6c** exhibited a very similar NMR spectrum to those of **6a** or **6b**, and a strong absorption band at 1715 cm^{-1} in the IR spectrum; therefore the structure was attributed it. The formation of **6c** is explained by the similar reaction sequences to the case of **1** or **2a, b**. The IR spectrum of **7c** exhibited a strong absorption at 1735 cm^{-1} due to the cyclopentanone moiety. The NMR spectrum of **7c** was in full accord with the proposed structure (see Experimental). The double peak at δ 1.34 (J=4.0 Hz) was assigned to a proton on the cyclopropane ring by the help of a decoupling technique. Independent irradiation of a benzene solution of **6c** in the presence of benzophenone afforded **7c** in 80% yield. This fact indicates that **7c** originates from the benzophenone sensitized di-π-methane rearrangement of primary photocycloadduct **6c**.

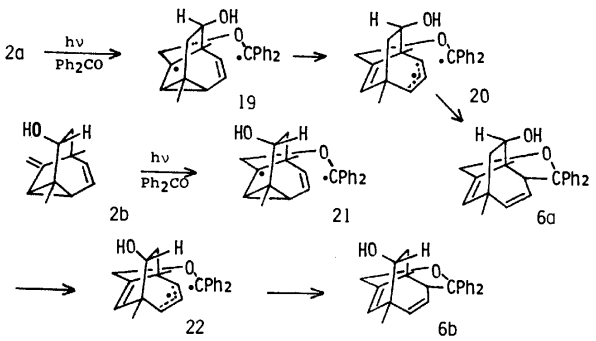

On the other hand, the irradiation of a benzene solution of **2d**[19] and benzophenone in 1/5 molar ratio gave an adduct **7d** (mp 182—183 °C) in 69% yield. The adduct **7d** exhibited a parent ion peak at 356 in the mass spectrum, and a strong absorption band at 1705 cm^{-1} due to a cyclopropyl ketone. The NMR spectrum of **7d** exhibited a cyclopropane proton at δ 2.45 (1H, s) and three protons of an allylic moiety at δ 3.43 (1H, d, J=6.8 Hz), δ 5.50 (1H, dxd, J=8.0, 6.8 Hz) and δ 5.70 (1H, d, J=8.0 Hz), in addition to the protons of two methylene groups, two methyl groups, and two phenyl groups. On LAH reduction, **7a** was converted to the alcohol **23** (mp 158—160 °C)

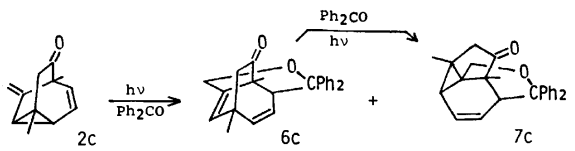

in 65% yield. The stereochemistry of the hydroxyl group of **23** was not determined, however, the NMR spectrum of **23** exhibited a doublet peak at δ 2.06 (J=4.5 Hz), which was assigned to the proton of the cyclopropane ring by the help of a decoupling technique: decoupling of the proton at δ 4.50—4.75 shows change a doublet peak at δ 2.06 to a singlet. This fact and the other spectral data (see Experimental) supported the structures **23** and **7d**, and could eliminate the other possible structure such as **24**, which is expected from the di-π-methane rearrangement on the two basal

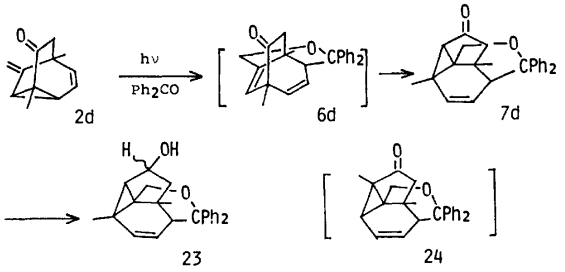

double bonds of the postulated primary photocycloadduct **6d**.

Several remarkable points are noticed here. Tricyclo-[3.2.1.$0^{2,8}$]non-3-en-9-yl radical species, which are derived from the addition of triplet benzophenone to **2a—d**, underwent cyclopropylcarbinyl-allylcarbinyl radical type rearrangement as in the case of type **A** radical or **8**. The rearrangement was independent of the presence of the carbonyl group. The reaction site of the benzophenone sensitized rearrangement of the primary photocycloadducts seemed to be dependent on the position of the carbonyl group in the similar skeleton. The cycloadduct **6c** underwent di-π-methane rearrangement on the two basal double bonds to afford **7c** *via* 1,4-diradical species **25**. This feature is similar to the

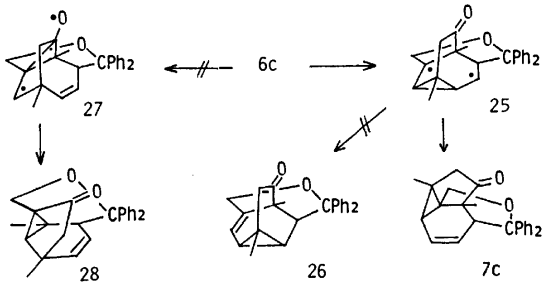

Scheme 2.

rearrangement of **5a** (*vide supra*). The carbonyl group of **6c** can also interact with two basal double bonds in a fully homoconjugated manner as in the case of **5c**. Another isomer **26** should be constrained as mentioned in the case of **3'a**, **b**, therefore the pathway affording **26** should be a higher energy process than that of **7c**. The compound **26** which is a one-carbon ring enlarged derivative of **3'a** seems to be more constrained even than **3'a** judging from a molecular model. The other oxadi-π-methane rearrangement product **28**, which has a very constrained molecular geometry, could not be obtained.

On the other hand, in the postulated primary photocycloadduct **6d**, the carbonyl group and two double bonds build up a special cross homoconjugated system, unlike the case of **5a** or **6c**. The adduct **7d** was considered to be derived from **6d** by the oxadi-π-methane rearrangement *via* **30**. Another oxadi-π-methane rearrangement product **32** was expected to be derived from the interaction of the carbonyl group with another vinyl group *via* **31**, however, it was not obtained. The compound **32** has a similar skeleton to **26** and it is supposed to be constrained, therefore the pathway to **32** should be a high-energy process and **31** possibly goes back to **6d**. Other isomers such as **24** and **34** may be

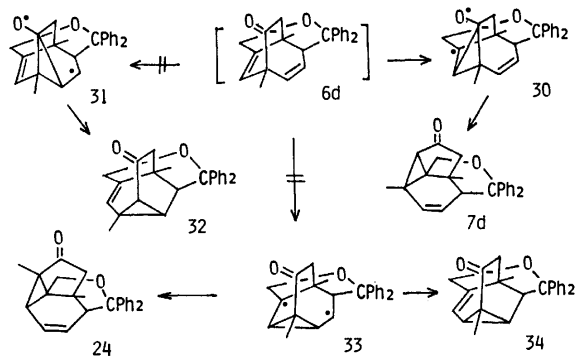

Schelme 3.

derived formally from a di-π-methane rearrangement of the two basal double bonds *via* **33**. Concerning the ring constraint, **34** has a similar skeleton to **26** or **32**, therefore this ring system is suggested to be unfavorable. The compound **24** has a similar skeleton to **7d**, on the other hand, it was not obtained. These observations seem to suggest that excited-state energy is localized on the homoconjugated system of the carbonyl group and a vinyl group.

In conclusion, it was clarified that tricyclo[3.2.1.$0^{2,7}$]-oct-3-en-6-yl or tricyclo[3.3.1.$0^{2,8}$]non-9-yl radical species, which were generated by an initial attack of a triplet benzophenone on **1** or **2**, could not afford oxetanes and rearranged to the less strained bicyclic allyl radical species affording formal [2+6] cycloadducts. The electron-withdrawing carbonyl group which is located to conjugate with the cyclopropane ring in **1** or **2d** could not reflect the electronic property on the radical rearrangement[8] in the present case. The regioselectivity of the subsequent benzophenone sensitized rearrangement of the primary photocycloadducts, however, was much affected by the position of the carbonyl group.

The investigation of photochemical reactions of β,γ-unsaturated carbonyl compounds has been accumulated.[20] Among these investigations, bicyclic ketones such as bicyclo[2.2.2]octenone derivatives undergo acetone sensitized 1,2-acyl migration (oxadi-π-methane rearrangement), 1,3-acyl migration and a bridge elimination.[20,21] The bicyclo[2.2.2]octa-2,5-dien-7-one derivatives are also known to eliminate ketene to afford benzene derivatives. The other noticeable example has been reported by Mukai and Kurabayashi: The triplet photorearrangement of bicyclo[4.2.1]non-2,4,7-trien-9-one, which containes a carbonyl group, a vinyl group and a butadiene moiety in a bicyclic skeleton, afford barbaralone.[23] The presented di-π-methane and oxadi-π-methane rearrangement are good examples reflecting the interactions of the carbonyl group with the two other vinyl groups in the homoconjugated manner. The explanation of the selectivity of the rearrangements is rather qualitative and the ring constraint is proposed as the reason for supressing the possible products such as **14**, **28** or **16**, and **26** and **32**. For profound confirmation of the selectivity for the rearrangement involving the interaction of the carbonyl group with the two other vinyl groups, the study of the compounds containing no $-CH_2-O-CPh_2-$ moiety in **5**, **6c**, and **6d** might be helpfull.

Experimental

IR spectra were measured on a Shimadzu IR-100 spectrometer. NMR spectra were recorded on a JEOL PS-100 high resolution NMR spectrometer. Chemical shifts were determined in carbon tetrachloride or in deuteriochloroform. The abbreviations given in the NMR data are s=singlet, d=doublet, dxd=doublets of doublet, t=triplet, and m=multiplet. VPC analysis was carried out either on Shimadzu GC-6A or on a Varian model-920 gas chromatograph using columns packed with either 5% SE-30 or 5% FFAP on Chromosorb W. The mass spectral studies were conducted using a Hitachi RMU-60 spectrometer. All melting points are uncorrected.

General Procedure of Irradiation. All photoreactions were carried out in a deoxygenated (nitrogen bubbled) benzene solution of a mixture of substrate and benzophenone. Irradiation was made with a RPR-100 photoreactor, which was fitted with RPR-350 nm lamps.

Photoreaction of Benzophenone with **1a**. A benzene (40 cm^3) solution of 3.64 g (20 mmol) of benzophenone and 640 mg (4 mmol) of **1a** was irradiated in a Pyrex cell at room temperature for 7 h. VPC analysis indicated that almost all of **1a** was consumed. Solvent was removed under reduced pressure. The residue was chromatographed on alumina (130 g). Elution with hexane–benzene mixture (19/1) gave a colorless solid. Recrystallization of this solid from chloroform–ethanol mixture gave colorless crystals (647 mg, 47% based on **1a** used), which were characterized as **3a**: mp 166—167 °C; IR (KBr): 3050, 1763, 1630, 1597, 1498, 1447, 1025 cm^{-1}; NMR ($CDCl_3$): δ 0.92 (3H, s), 1.56 (3H, s), 2.10 (1H, d, J=4.0 Hz), 3.50 (1H, d, J=7.8 Hz), 4.34 (1H, d, J=10.0 Hz), 4.90 (1H, d, J=10.0 Hz), 5.60 (1H, dxd, J=8.2, 7.8 Hz), 6.02 (1H, dxd, J=8.2, 4.0 Hz), 7.2—8.2 (1H, m); MS, *m/e* (rel intensity): 342 (M^+, 9), 132 (100). Found: C, 84.04; H, 6.49%. Calcd for $C_{24}H_{22}O_2$: C, 84.17; H, 6.47%. Further elution of the column with hexane–benzene mixture (1/1) gave a colorless solid. Recrystallization of this solid from chloroform–ethanol mixture gave colorless crystals (199 mg, 15% based on **1a** used), which were characeterized as **4a**: mp 270—272 °C; IR (KBr): 1752, 1595, 1025 cm^{-1}; NMR ($CDCl_3$): δ 0.68 (3H, s), 1.57 (3H, s), 3.87 (1H, m), 4.05 (1H, d, J=13.0 Hz), 4.53 (1H, d, J=13.0 Hz), 4.90 (1H, s), 5.10 (1H, dxd, J=10.0, 4.0 Hz), 5.68 (1H, dxd, J=10.0, 2.0 Hz), 7.2—7.8 (1H, m); MS, *m/e* (rel intensity): 342 (M^+, 18), 132 (100). Found: C, 84.53; H, 6.23%. Calcd for $C_{24}H_{22}O_2$: C, 84.17; H, 6.47%.

Photoreaction of Benzophenone with **1b**. A benzene solution (40 cm^3) of 3.64 g (20 mmol) of benzophenone and 696 mg (4 mmol) of **1b** was irradiated in a Pyrex vessel at room temperature for 12 h. VPC analysis indicated that almost all of **1b** was consumed. After solvent removal in vacuo, the resulting residue was chromatographed on alumina (60 g). Elution with hexane–benzene mixture (9/1) gave 430 mg of a colorless solid and 130 mg of the second colorless solid. Recrystallization of the first solid from chloroform–ethanol mixture gave colorless crystals (402 mg, 28% based on **1b** used), which were identified as **3b**: mp 144—145 °C; IR (KBr): 1750, 1598, 1025 cm^{-1}; NMR ($CDCl_3$): δ 0.75 (3H, s), 0.84 (3H, s), 1.54 (3H, s), 2.02 (1H, m), 2.90 (1H, s), 4.12 (1H, d, J=10.0 Hz), 4.64 (1H, d, J=10.0 Hz), 5.57 (1H, m), 7.0—7.7 (1H, m); MS, *m/e* (rel intensity): 356 (M^+, 5), 146 ((100). Found: C 84.02; H, 6.72%. Calcd for $C_{25}H_{24}O_2$: C, 84.24; H. 6.79%. Recrystallization of the second solid from chloroform–ethanol mixture gave colorless crystals (110 mg, 8% based on **1b** used), which were characterized as **4b** by the following physical data: mp 290—291 °C; IR (KBr): 1748, 1600, 1035, 1023 cm^{-1}; NMR ($CDCl_3$): δ 0.50 (3H, s), 0.82 (3H, s), 1.54 (3H, broad s), 3.51 (1H, s), 3.88 (1H, d, J=10.0 Hz), 4.36 (1H, d, J=10.0 Hz), 4.95 (1H, s), 5.43 (1H, broad s), 7.2—7.8 (10H, m); MS, *m/e* (rel intensity): 356 (M^+, 24), 146 (100). Found: C, 83.95; H, 6.45%. Calcd for $C_{25}H_{24}O_2$: C, 84.24; H, 6.79%.

Photoreaction of Benzophenone with **1c**. A benzene solution (10 cm^3) of 182 mg (1 mmol) of benzophenone and 324 mg (2 mmol) of **1c** was irradiated at room temperature for 4 h. After solvent removal *in vacuo*, the residue was chromatographed on alumina (20 g). Elution with benzene–benzene–hexane (1/1) and benzene gave 260 mg (76% based on benzophenone used) of **5c** which was recrystallized from hexane as colorless crystals: mp 74—76 °C; IR (KBr): 3400, 1155, 1125 cm^{-1}; NMR (CCl_4): δ 0.97 (3H, s), 1.09 (3H, s), 1.72 (1H, s), 3.17 (1H, m), 3.49 (1H, broad s), 4.09 (1H, d, J=11.2 Hz), 4.38 (1H, d, J=11.2 Hz), 5.15 (1H, dxd, J=9.5, 3.8 Hz), 5.74 (1H, broad d, J=9.5 Hz), 6.15 (1H, s), 7.1—7.8 (10H, m).

Oxidation of **5c**. To a stirred solution of 204 mg (0.95 mmol) of pyridinium chlorochromate and 164 mg of anhydrous sodium acetate in 5 cm^3 of dichloromethane was added 218 mg (0.63 mmol) of **5c** in a nitrogen stream. Upon completion of the addition, the mixture was stirred at room temperature for 2.5 h. After addition of water, the mixture was extracted with ether (4×20 cm^3). The combined organic portion was dried over sodium sulfate, followed by solvent evaporation. The crude product was purified by TLC on silica gel using benzenes as the eluent to give 50 mg of **5a** (23%) as a colorless crystalline solid, which was recrystallized from ethanol: mp 152—153 °C; IR (KBr): 1750, 1600, 1040, 1007 cm^{-1}; NMR ($CDCl_3$): δ 1.00 (3H, s), 1.17 (3H, s), 3.66 (1H, m), 4.23 (1H, d, J=10.0 Hz), 4.47 (1H, d, J=10.0 Hz), 4.98 (1H, dxd, J=9.0, 4.0 Hz), 6.00 (1H, dxd, J=9.0, 2.0 Hz), 6.50 (1H, s), 7.1—7.6 (10H, m); MS, *m/e* (rel intensity): 342 (M^+, 1), 132 (100). Found: C, 84.01; H, 6.27%. Calcd for $C_{24}H_{22}O_2$: C, 84.17; H, 6.47%.

Irradiation of **4a** *in the Presence or Absence of Benzophenone.* Two Pyrex vessels, which containes **4a** (20 mg, 0.06 mmol) in, (a) benzene (2 cm^3), and (b) benzene (10 cm^3) containing benzophenone (22 mg, 0.12 mmol) were irradiated for 5 h. After removal of the solvent, each of the residues was purified by TLC on silica gel using benzene–dichloromethane (1/1) as the eluent to give **5a**, 90% (a), **5a**, 90% and 17 mg of benzophenone (b).

Benzophenone-sensitized Irradiation of **5a**. A solution containing 22 mg (0.12 mmol) of benzophenone and 20 mg (0.06 mmol) of **5a** in 2 cm^3 of benzene was irradiated in a Pyrex vessel for 3 h. After solvent removal *in vacuo* the resulting residue was separated by TLC on silica gel using benzene–dichloromethane (1/1) as the eluent. The first band isolated from the TLC plates contained 18 mg of benzophenone. The second band from the TLC plates contained 14 mg (70%) of **3a**, which was identical with the authentic specimen.

Photoreaction of Benzophenone with **2a**. A solution of 69 mg (0.38 mmol) of benzophenone and 134 mg (0.76 mmol) of **2a** in 8 cm^3 of benzene was irradiated at room temperature for 2 h. After evaporation of the solvent under reduced pressure, the residue was separated by TLC on alumina using chloroform as the eluent to give 61 mg of **2a** (R_f=0.43, 46%), and 106 mg of **6a** (R_f=0.69, 78% based on benzophenone used). The cycloadduct **6a** gave the following physical data: IR (film): 3450, 1600, 1040 cm^{-1}; NMR (CCl_4): δ 1.06 (3H, s), 1.16 (3H, s), 1.76 (1H, d, J=13.0 Hz), 2.15 (1H, dxd, J=13.0, 8.8 Hz), 3.55 (1H, dxd, J=5.0, 2.0 Hz), 3.84 (1H,

broad d, J=8.8 Hz), 4.10 (1H, d, J=10.0 Hz), 5.62 (1H, d, J=10.0 Hz), 5.70 (1H, dxd, J=11.0, 5.0 Hz), 5.75 (1H, dxd, J=11.0, 2.0 Hz), 6.55 (1H, s), 7.1—8.0 (10H, m). Found: C, 83.37; H, 7.07%. Calcd for $C_{25}H_{26}O_2$: C, 83.76; H, 7.31%.

Photoreactions of Benzophenone with **2b**. A solution of 75 mg (0.41 mmol) of benzophenone and 146 mg (0.83 mmol) of **2b** in 8 cm³ of benzene was irradiated at room temperature for 3 h. After solvent remolval *in vacuo*, the resulting residue was separated by TLC on alumina using hexane–ethyl acetate (3/1) to give 62 mg (R_f=0.40, 42%) of **2b** and 108 mg (R_f=0.23, 73% based on benzophenone used) of **6b**. The cycloadduct **6b** gave the following physical data: IR (film): 3420, 1600, 1045 cm⁻¹; NMR (CCl_4): δ 0.94 (3H, s), 1.22 (3H, s), 1.63 (1H, d, J=15.0 Hz), 2.30 (1H, dxd, J=15.0, 9.0 Hz), 3.06 (1H, dxd, J=4.8, 2.0 Hz), 3.68 (1H, broad d, J=9.0 Hz), 4.05 (1H, d, J=11.0, 4.8 Hz), 4.57 (1H, d, J=10.0 Hz), 4.58 (1H, dxd, J=11.0, 4.8 Hz), 5.52 (1H, dxd, J=11.0, 2.0 Hz), 6.17 (1H, s), 7.7—7.8 (10H, m). Found: C, 84.28; H, 7.12%. Calcd for $C_{25}H_{26}O_2$: C, 83.76; H, 7.31%.

Photoreaction of Benzophenone with **2c**. A solution of 150 mg (0.83 mmol) of benzophenone and 144 mg (0.83 mmol) of **2c** in 9 cm³ of benzene was irradiated at room temperature for 3.5 h. After solvent removal *in vacuo*, the resulting residue was separated by TLC on silica gel using hexane–ethyl acetate (4/1) as the eluent to give 25 mg (R_f=0.85, 17%) of **2c**, 35 mg (R_f=0.45, 13%) of **6c**, and 119 mg (R_f=0.30, 40%) of **7c**. Recrystallization of **6c** gave colorless crystals: mp 205—206 °C: IR (KBr): 1718, 1595, 1045 cm⁻¹; NMR ($CDCl_3$): δ 1.04 (3H, s), 1.26 (3H, s), 2.50 (2H, s), 3.40 (1H, dxd, J=4.0, 2.0 Hz), 4.14 (1H, d, J=10.0 Hz), 4.53 (1H, d, J=10.0 Hz), 4.67 (1H, dxd, J=12.0, 4.0 Hz), 5.75 (1H, dxd, J=12.0, 2.0 Hz), 6.60 (1H, s), 7.00—7.70 (10H, m); MS, *m/e* (rel intensity); 356 (M^+, 1), 132 (100). Found: C, 84.49; H, 6.56%. Calcd for $C_{25}H_{24}O_2$: C, 84.24; H, 6.79%.

The cycloadduct **7c** was crystallized from ethanol to give colorless crystals: mp 139—140 °C; IR (KBr): 1733, 1595, 1040 cm⁻¹; NMR ($CDCl_3$): δ 0.76 (3H, s), 1.40 (3H, s), 1.34 (1H, d, J=4.0 Hz), 2.30 (1H, d, J=18.8 Hz), 2.47 (1H, d, J=18.8 Hz), 3.73 (1H, d, J=6.8 Hz), 3.88 (1H, d, J=11.0 Hz), 4.59 (1H, d, J=11.0 Hz), 5.50 (1H, dxd, J=9.0, 6.8 Hz), 5.72 (1H, dxd, J=9.0, 4.0 Hz), 7.05—7.83 (10H, m); MS, *m/e* (rel intensity): 356 (M^+, 1), 132 (100). Found: C, 84.00; H, 6.90%. Calcd for $C_{25}H_{24}O_2$: C, 84.24; H, 6.79%.

Photoreaction of Benzophenone with **2d**. A solution of 91 mg (0.5 mmol) of benzophenone and 87 mg (0.5 mmol) of **2d** in 5 cm³ of benzene was irradiated at room pemperature for 8 h. After solvent removal *in vacuo*, the resulting residue was separated by TLC on silica gel using ether–hexane (1/1) as the eluent to give 10 mg (R_f=0.90, 10%) of **2d** and 95 mg (R_f=0.50, 69%) of **7d**. Recrystallization of **7d** from ethanol gave colorless crystals: mp 182—183 °C: IR (KBr): 1705, 1595, 1035 cm⁻¹; NMR ($CDCl_3$): δ 0.95 (3H, s), 1.47 (3H, s), 1.86 (1H, d, J=18.8 Hz), 2.34 (1H, d, J=18.8 Hz), 2.45 (1H, s), 3.43 (1H, d, J=6.8 Hz), 4.06 (1H, d, J=11.0 Hz), 4.62 (1H, d, J=11.0 Hz), 5.50 (1H, dxd, J=8.0, 6.8 Hz), 5.79 (1H, d, J=8.0 Hz), 7.05—7.77 (10H, m); MS, *m/e* (rel intensity): 356 (M^+, 1), 132 (100). Found: C, 84.72; H, 6.78%. Calcd for $C_{25}H_{24}O_2$: C, 84.24; H, 6.79%.

Reduction of **7d**. To a suspension containing 19 mg (0.5 mmol) of lithium aluminium hydride in 2 cm³ of anhydrous tetrahydrofuran was added 89 mg (0.25 mmol) of **7d**. After the addition was completed, the reaction mixture was stirred at room temperature for 1 h. The reaction mixture was then treated with water (3 cm³) followed by aqueous ammonium chloride, and extracted with ether (10 cm³×4). The combined organic portion was dried over sodium sulfate. The solvent was removed under reduced pressure and the resulting residue was chromatographed on alumina column using benzene as the eluent to give a colorless crystalline solid, which was recrystallized from carbon tetrachloride to give 58 mg (65%) of **7e**: mp 158—159 °C; IR (KBr): 3450, 1600, 1075, 1010 cm⁻¹; NMR ($CDCl_3$): δ 0.87 (3H, s), 1.35 (3H, s), 1.72 (1H, dxd, J=14.0, 9.6 Hz), 1.96 (1H, dxd, J=14.0, 9.6 Hz), 2.06 (1H, d, J=4.6 Hz), 3.37 (1H, d, J=6.2 Hz), 3.96 (1H, d, J=10.8 Hz), 4.53 (1H, d, J=10.8 Hz), 4.50—4.75 (1H, m), 5.26 (1H, dxd, J=9.0, 6.2 Hz), 5.94 (1H, d, J=9.0 Hz), 7.0—7.75 (1H, m). Found: C, 84.48; H, 7.38%. Calcd for $C_{25}H_{26}O_2$: C, 84.70; H, 7.39%.

References

1) This paper was presented at the 41st National Meeting of Chemical Society of Japan, Tokyo, April 1978, Abstr. II, p. 1038.

2) J. W. Wilt, "Free Radicals," ed by J. K. Kochi, Willey, Interscience, New York (1973), Vol. 1.

3) D. A. Arnold, "Advances in Photochemistry," ed by W. A. Noyes, Jr., G. S. Hammond, and J. N. Pitts, Jr., Interscience, New York (1968), Vol. 6, p. 301.

4) N. Shimizu, M. Ishikawa, K. Ishikura, and S. Nishida, *J. Am. Chem. Soc.*, **96**, 6456 (1974).

5) K. Kurabayashi and T. Mukai, *J. Chem. Soc., Chem. Commun.*, **1972**, 1016.

6) M. Nitta, H. Sugiyama, and Y. Sekine, *Chem. Lett.*, **1977**, 55.

7) R. Sustmann and R. W. Gellert, *Chem. Ber.*, **111**, 388 (1978).

8) M. Nitta, T. Kuroki, and H. Sugiyama, *J. Chem. Soc., Chem. Commun.*, **1980**, 378.

9) J. Zsindely and H. Schmid, *Helv. Chim. Acta*, **51**, 1510 (1968).

10) J. W. Wiseman, H-K. Foon, and C. J. Ahola, *Tetrahedron Lett.*, **1975**, 2647.

11) J. P-Katalinic, J. Zsindely, and H. Schmid, *Helv. Chim. Acta*, **57**, 223 (1974).

12) E. J. Corey and J. W. Suggs, *Tetrahedron Lett.*, **1975**, 2647.

13) R. A. Caldwell, G. W. Sovocool, and R. P. Gajewsky, *J. Am. Chem. Soc.*, **95**, 2549 (1973).

14) B. Maillard, D. Forrest, and K. U. Ingold, *J. Am. Chem. Soc.*, **98**, 7024 (1976).

15) R. Sauer and A. Shurpik, *J. Org. Chem.*, **33**, 799 (1968).

16) S. S. Hixon, P. S. Mariano, and H. E. Zimmerman, *Chem. Rev.*, **73**, 531 (1973); and references cited therein.

17) Prepared stereoselectively by reduction of **2c** with LAH.

18) M. Nitta, O. Inoue, and I. Kasahara, *Bull. Sci. Eng. Res. Lab., Waseda Univ.*, **95**, 27 ,(1981).

19) M. Nitta, A. Omata, and H. Sugiyama, *Bull. Sci. Eng. Res. Lab., Waseda Univ.*, **94**, 55 (1981).

20) K. N. Houk, *Chem. Rev.*, **76**, 1 (1976); and references cited therein.

21) R. S. Givens and F. Oettle, *J. Am. Chem. Soc.*, **93**, 3963 (1971); H. Hart, R. K. Muray, Jr., and G. D. Appleyard, *Tetrahedron Lett.*, **1969**, 4785; D. I. Schuster, F-T. Lee, A. Padwa, and P. G. Gassman, *J. Org. Chem.*, **30**, 2262 (1965).

22) R. S. Givens, W. F. Oettle, R. L. Coffin, and R. G. Carlson, *J. Am. Chem. Soc.*, **93**, 3957 (1971); R. S. Givens and W. F. Oettle, *ibid.*, **93**, 4995 (1971); R. K. Murray, Jr., and H. Hart, *Tetrahedron Lett.*, **1968**, 4995.

23) K. Kurabayashi and T. Mukai, *Tetrahedron Lett.*, **1972**, 1049.

 © 1982 The Chemical Society of Japan Bull. Chem. Soc. Jpn., 55, 1133—1136 (1982)

Photochemical Electrocyclic Reaction Mechanism of Methyleneamine *N*-Oxide to Form Oxaziridine. MINDO/3 CI Study

Osamu KIKUCHI,* Kenji MORIHASHI, and Keizo SUZUKI

Department of Chemistry, The University of Tsukuba, Sakura-mura, Ibaraki 305

(Received July 9, 1981)

The photochemical electrocyclic reaction mechanism of methyleneamine *N*-oxide to form oxaziridine was explored on the basis of the potential energy surfaces obtained by the MINDO/3 CI calculation. The strong interaction between the ground state and the doubly-excited state, which appears in the disrotatory cyclization process of the corresponding hydrocarbon system, was not observed. Instead, a deep potential well, which can be a leakage channel from the excited state to the ground state, was found in the S_1 surface. The predicted reaction path is characteristic of hetero-atom conjugated systems, and an important participation of the oxygen σ lone-pair electrons is expected in this reaction path.

Photochemical isomerization reactions of methyleneamine *N*-oxide, **1**, are quite common;[1-3] they undergo *cis-trans* isomerization reaction and electrocyclic reaction to form oxaziridines, **2**. Although the thermal (ground state) *cis-trans* isomerization reaction of **1**[4] and the photo-isomerization of **2** into amides[5] have been studied theoretically, little attention has been paid to the electron behavior and reaction paths for the photochemical electrocyclic **1**→**2** reaction. From the orbital

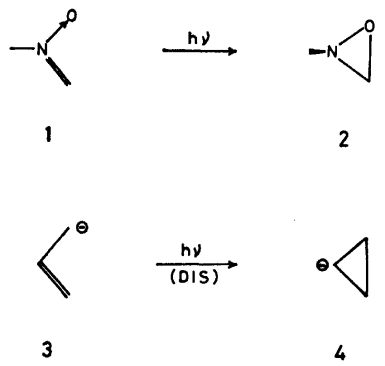

symmetry arguments,[6,7] the allyl anion is expected to cyclize photochemically by disrotatory rotation of the methylene groups. The formal electrocyclic **1**→**2** reaction may be considered to proceed by means of a mechanism similar to that of the **3**→**4** reaction.[2] However, there are two essential differences between the **1**→**2** and **3**→**4** reactions. The first is the mode of rotation of the methylene groups. In the conjugated hydrocarbon system, **3**→**4**, the disrotatory and conrotatory modes give potential curves of very different shapes, while there is no distinction between these two rotation modes in the **1**→**2** reaction, since only one methylene group is involved in methyleneamine *N*-oxide. The second difference is the existence of the lone-pair electrons of the terminal oxygen atom of methyleneamine *N*-oxide. Since the lone-pair electrons distribute on the σ framework where the new σ bond is being formed, the lone-pair electrons should participate in the electrocyclic reaction mechanism of the **1**→**2** reaction, even if the photochemical reaction proceeds from the $\pi\rightarrow\pi^*$ excited state. Because of these essential differences, the mechanism of the **1**→**2** reaction cannot be understood sufficiently well by analogy with the **3**→**4** reaction; therefore it is worthwhile to investigate the reaction process of the **1**→**2** reaction and to compare the reaction mechanism with that of the all-hydrocarbon conjugated system, **3**→**4**. In the present study, the reaction paths of the **1**→**2** reaction will be explored on the basis of the potential energy surfaces obtained by means of the semi-empirical MINDO/3[9] CI calculation.

Method and Results

The structures of the compounds **1** and **2** were optimized by the SCF MINDO/3 (without CI) calculation. They are shown in Fig. 1. The potential energy

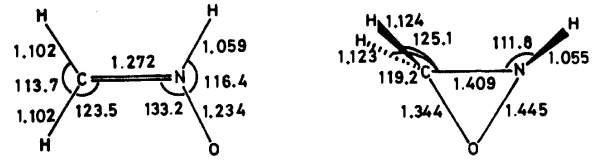

Fig. 1. Molecular structures of methyleneamine *N*-oxide and the oxaziridine optimized by the MINDO/3 method. Bond lengths are in Å and bond angles are in degrees.

surfaces for the **1**→**2** reaction are a function of many geometrical variables. In the present study, the potential energy surfaces were calculated with respect to two independent variables. One of these is the rotation angle, θ, of the methylene group. All the other geometrical variables were allowed to vary simultaneously from their initial to final values. This variation is expressed by the second parameter, d, which varies from 0.0 (initial) to 1.0 (final). In the CI calculation, 40 and 39 configuration functions were selected from the singly- and doubly-excited configurations for the singlet and triplet states respectively. The potential energy surfaces of four lower singlet states are shown in Fig. 2. The symbols W and H correspond to local minimum and maximum points on the potential surfaces respectively. The broken line in Fig. 2-a indicates the concerted path in which all the geometrical variables vary simultaneously. The potential energy curves along this concerted path are shown in Fig. 3. The S_1 and S_2 states of methyleneamine *N*-oxide consist of the $n_o\rightarrow\pi^*$ and $\pi\rightarrow\sigma^*$ excited configurations. The $\pi\rightarrow\pi^*$ configuration is involved in the S_3 and S_5 excited states. The T_1 state is the $\pi\rightarrow\pi^*$ triplet state and the T_3 state is the $n_o\rightarrow\pi^*$ triplet state.

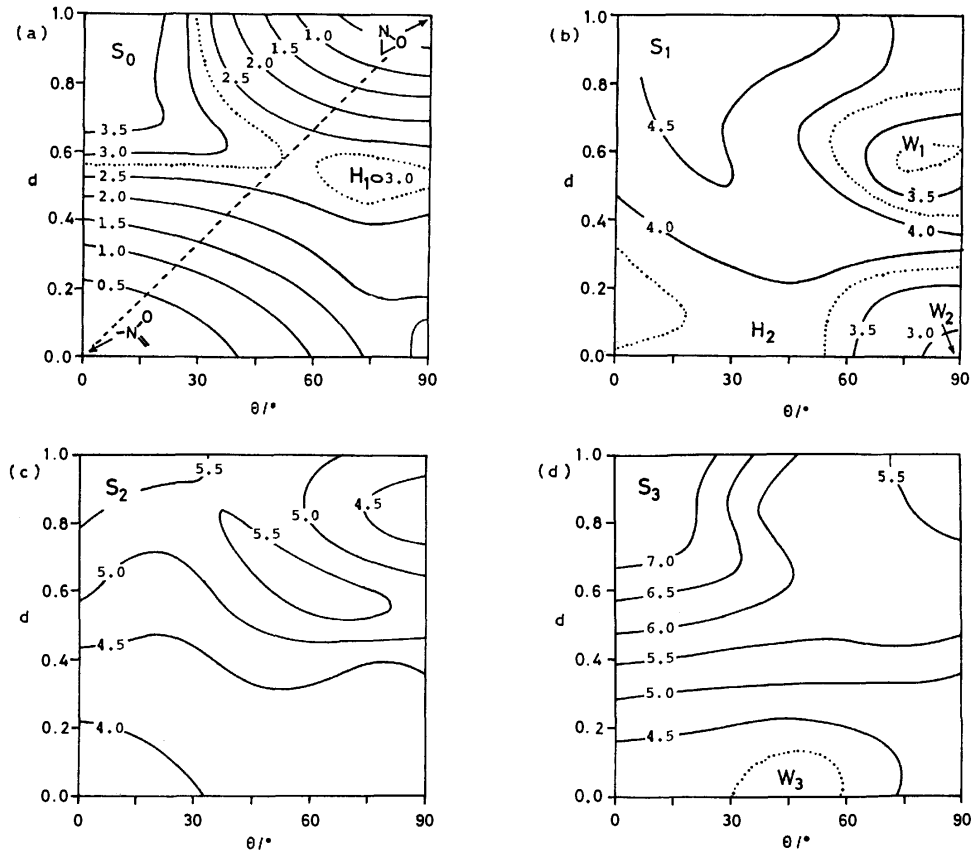

Fig. 2. Two-dimensional potential energy surfaces of (a) S_0, (b) S_1, (c) S_2, and (d) S_3 states of the methyleneamine *N*-oxide–oxaziridine system. The energies (eV) are relative values with respect to the ground state of methylenimine *N*-oxide.

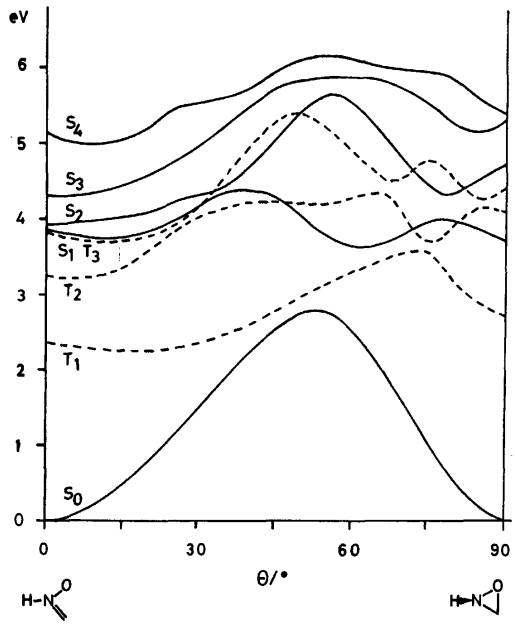

Fig. 3. Potential energy curves for the methyleneamine *N*-oxide–oxaziridine system along the concerted path. All the geometrical variables are varied simultaneously between the optimized structures of methyleneamine *N*-oxide and the oxaziridine.

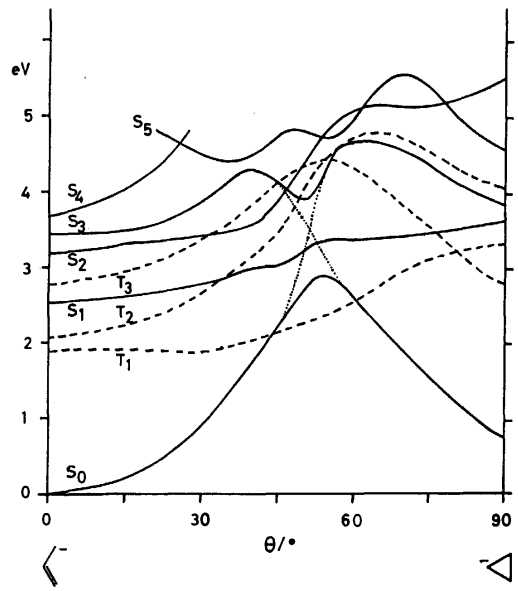

Fig. 4. Potential energy curves along the disrotatory mode of cyclization of the allyl anion into the cyclopropyl anion. All the geometrical variables are varied simultaneously between the two species.

The potential curves for the disrotatory cyclization of the allyl anion along the concerted path are shown in Fig. 4. The S_1 and S_2 states are the $\pi\rightarrow\sigma^*$ singlet states. The S_4 state is the $\pi\rightarrow\pi^*$ singlet state. The $\pi\rightarrow\pi^*$ doubly-excited configuration is involved in the S_5 state. The T_1 state is the $\pi\rightarrow\pi^*$ triplet state. The π_2 and π_3 MO's of the allyl anion cross during the cyclization; avoided crossing at the middle stage of the cyclization involves the ground state and $\pi_2\rightarrow\pi_3$ doubly-excited configurations. The true crossing which involves the $\pi\rightarrow\pi^*$ singly-excited state and its doubly-excited counterpart occurs between the S_4 and S_5 curves at the begining of cyclization. This crossing point lies higher (1 eV) than the S_4 state of the allyl anion; it is expected that the photochemical cyclization of the allyl anion from its $\pi\rightarrow\pi^*$ singlet state is inefficient.

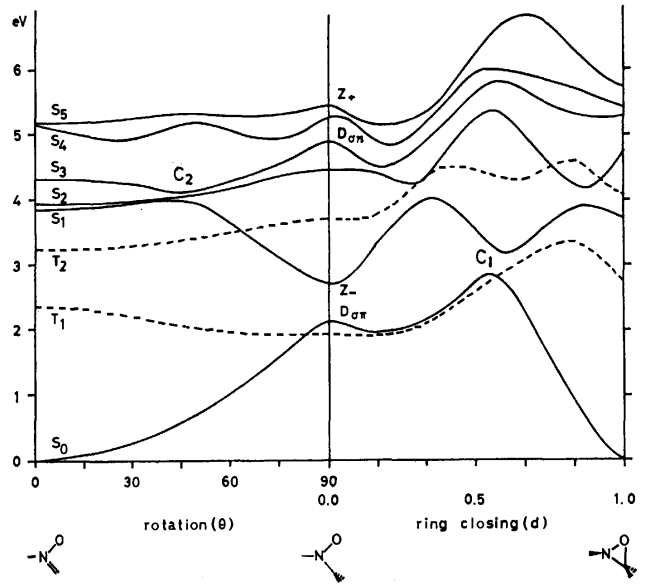

Fig. 5. Potential energy curves for the step-by-step path of the methyleneamine *N*-oxide–oxaziridine system. θ is the rotation angle (degree) of the terminal methylene and d represents the simultaneous change of all the geometrical variables other than θ.

It has been pointed out that the step-by-step path in which the methylene rotation is followed by ring closure may exist in the photochemical electrocyclic reaction of hetero-atom conjugated systems.[8,10] The potential curves along this path are shown in Fig. 5. The vertical

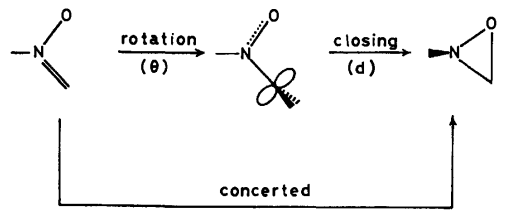

line at the center of Fig. 5 corresponds to the twisted structure of methyleneamine *N*-oxide. The D and Z states of the twisted structure have the following electron configurations. In the twisted structure, the $D_{\sigma\pi}$ diradical state has a symmetry property different from

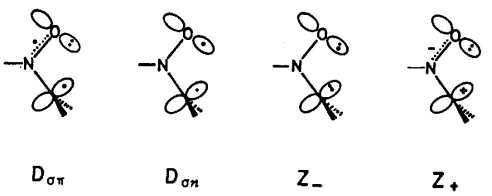

that of the Z–, $D_{\sigma n}$, and Z+ states. The C_1 avoided crossing is caused by pyramidalization of the nitrogen atom during the ring closing.

Discussion

During the photochemical electrocyclic reaction of the allyl anion, the symmetry-allowed crossing occurs between the highest occupied π_2 orbital and the unoccupied π_3 orbital. In this crossing region, strong coupling exists between the ground and the $\pi_2\rightarrow\pi_3$ doubly-excited configurations, and it gives the avoided crossing between the S_0 and S_2 potential energy curves shown in Fig. 4; this is the "C" type of avoided crossing in Salem's classification.[11] In the case of the cyclization of methyleneamine *N*-oxide, the strong coupling between the ground and the doubly-excited configurations does not exist due to the non-symmetric property of the system with respect to the vertical plane; no crossing occurs between π_2 and π_3 orbitals of methyleneamine *N*-oxide. The interaction between the S_0 and S_1 states observed in Fig. 3 is a different kind of avoided crossing. As may be seen from Figs. 2-a and 2-b, the S_0-S_1 interaction observed in Fig. 3 originates from the S_0-S_1 interaction at the W_1 region in the two-dimensional surfaces. Since the θ value at this region is large (80°), this crossing can be understood from the state correlation diagram between the 90°-twisted structure and its cyclization product (Fig. 6). The ground $D_{\sigma\pi}$ state correlates

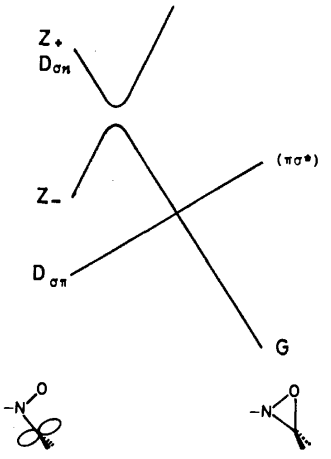

Fig. 6. State correlation diagram between the twisted structure of methyleneamine *N*-oxide and its cyclic structure.

with the $\pi\sigma^*$ excited state of the cyclic product, while the Z+ (or $D_{\sigma n}$) excited state correlates with the ground state of the cyclic product. If the symmetry property with respect to the CN(H)O molecular framework is preserved during the cyclization, the $D_{\sigma\pi}$-Z+ crossing

is allowed symmetrically as shown in the correlation diagram. In reality, however, the N–H hydrogen atom moves out of the plane during the cyclization, and the two states mix. The avoided crossing appeared in Figs. 2-a and 2-b is caused by this geometrical change; this is the "A" type of avoided crossing in Salem's classification.[11]

The clear difference between the potential energy curves of the **1**→**2** and **3**→**4** reactions indicates that the photochemical electrocyclic reaction of **1** proceeds by means of a mechanism different from that of its corresponding all-hydrocarbon system, **3**. The W_1 well in the S_1 surface can be a leakage channel from the excited state to the ground state, and the photochemical formation of the oxaziridine is expected to proceed through the non-adiabatic transition from the W_1 well to the S_0 surface; the reaction mechanism can be expressed by the following scheme.

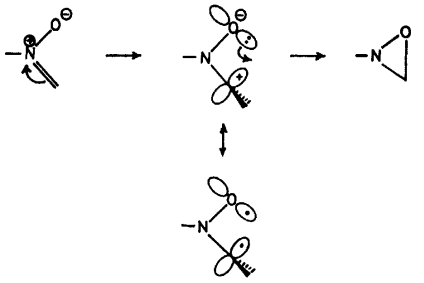

In this mechanism, the oxygen lone-pair electrons on the CNO plane play a key role. The important role of the lone-pair electrons on the terminal hetero atom in the photochemical electrocyclic reaction of hetero-atom conjugated systems has been pointed out in our previous studies on the acrylaldehyde–oxetene system.[8,10]

The calculated potential surfaces (Fig. 2) indicate a strong interaction between the S_3 and S_1 surfaces at the W_3 region. The $\pi\rightarrow\pi^*$ excited state (S_3) of methyleneamine *N*-oxide will have high chance to access the W_1 well and to form the oxaziridine through the $W_3\rightarrow H_2$ transition. On the other hand, the formation of the twisted Z– state (W_2 well in Fig. 2) from the $\pi\rightarrow\pi^*$ excited state results in reproduction of methyleneamine *N*-oxide; this is the *cis-trans* isomerization process. As may be seen from Fig. 2-b, the formation of oxaziridine (the $H_2\rightarrow W_1$ path) competes with the *cis-trans* isomerization (the $H_2\rightarrow W_2$ path). It is expected that the methyleneamine *N*-oxides having a lower W_1 well and a higher W_2 well undergo cyclization to form oxaziridines preferably than the *cis-trans* isomerization. Since the electronic structure at W_1 involves the Z_+ character and that at W_2 is of the Z– type, the electron-donating substituents at the carbon atom increases the formation of the oxaziridine, while the electron-donating substituents at the nitrogen atom decreases it. The oxaziridine formation (%) from the above three compounds[12,13] is parallel to this prediction.

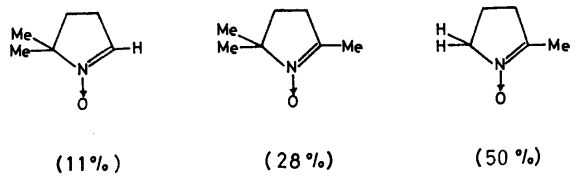

(11%) (28%) (50%)

Since only one methylene group is involved in methyleneamine *N*-oxide, there is no distinction between the conrotatory and disrotatory modes of methylene rotation. However, it may be interesting to illustrate the change in the orbital shape on the oxygen atom, which is induced by the rotation of the terminal methylene group. When the terminal methylene group is rotated, the π_1 orbital fragment on the oxygen atom rotates in the conratatory manner, while other π orbitals remain unchanged.

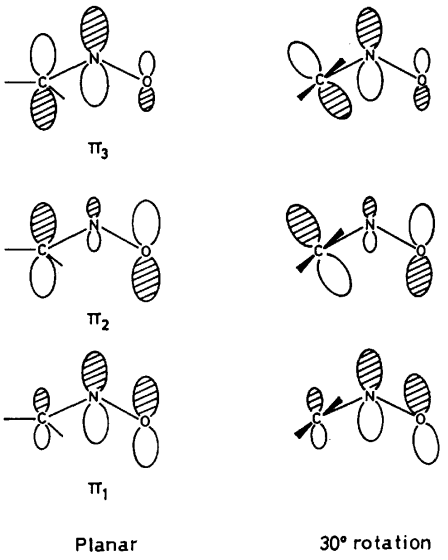

References

1) G. G. Spence, E. C. Taylor, and O. Buchardt, *Chem. Rev.*, **70**, 231 (1970).
2) N. J. Turro, "Modern Molecular Photochemistry," Benjamin/Cummings, Menlo Park, Calif. (1978), p. 510.
3) A. Lablache-Combier, "Photochemistry of Heterocyclic Compounds," ed by O. Buchardt, John Wiley and Sons, New York (1976), p. 207.
4) W. B. Jennings, D. R. Boyd, and L. C. Waring, *J. Chem. Soc., Perkin Trans. 2*, **1976**, 610; W. B. Jennings and S. D. Warley, *Tetrahedron Lett.*, **1977**, 1435.
5) E. Oliveros, M. Riviere, J. P. Malrieu, and Ch. Teichteil, *J. Am. Chem. Soc.*, **101**, 318 (1976).
6) R. B. Woodward and R. Hoffmann, *J. Am. Chem. Soc.*, **87**, 395 (1965).
7) K. Fukui, *Bull. Chem. Soc. Jpn.*, **39**, 498 (1966).
8) O. Kikuchi, H. Kubota, and K. Suzuki, *Bull. Chem. Soc. Jpn.*, **54**, 1126 (1981).
9) R. C. Bingham, M. J. S. Dewar, and D. H. Lo, *J. Am. Chem. Soc.*, **97**, 1285 (1975).
10) O. Kikuchi, *Tetrahedron Lett.*, **22**, 859 (1981).
11) L. Salem, *J. Am. Chem. Soc.*, **96**, 3486 (1974).
12) L. S. Kaminsky and M. Lamchan, *J. Chem. Soc., C*, **1966**, 2295; **1967**, 2128.
13) R. Bonnett, V. M. Clark, and A. Todd, *J. Chem. Soc.*, **1959**, 2102.

A Dimethyl Sulfoxide-mediated Oxidation of Arylalkyl and Alkyl Alcohols to Corresponding Aldehydes and Ketones *via* Tropolonyl Ethers

Hitoshi TAKESHITA,* Hiroaki MAMETSUKA, and Norihide MATSUO†

Research Institute of Industrial Science, 86, Kyushu University, Hakozaki, Higashi-ku, Fukuoka 812

†*Graduate School of Engineering Sciences, 39, Kyushu University, Hakozaki, Higashi-ku, Fukuoka 812*

(Received July 9, 1981)

The arylmethyl and diarylmethyl ethers of tropolones were oxidized to the corresponding carbonyl derivatives by heating in dimethyl sulfoxide. The free alcohols were oxidized at a much slower rate, suggesting that some sort of DMSO-linked intermediates are responsible for the oxidation. Inertness of free alcohols was proven by means of the cross-over experiments, including deuterium-labelling. This oxidation was applicable to alkyl ethers, but not to alkenyl ethers, which are known to cause the Claisen-rearrangement.

Recently, dimethyl sulfoxide (DMSO)-oxidation of alcohols or organic halides has been shown to be useful in organic synthesis.[1] We have found that several tropolonyl ethers, of which the preparations are tabulated in Table 1, are also capable of forming carbonyl compounds in a manner to be described in this paper. The investigations of non-benzenoid aromatic compounds have been hitherto focussed on the peculiarity of their chemical properties, and there seems to have been no attempt to utilize them as a reagent or catalyst.

When a mixture of 2-benzyloxytropone (**1a**)[2] and DMSO in a sealed tube was heated at 180 °C for 2 h, a clean reaction occurred to give tropolone (**2**), dimethyl sulfide, and benzaldehyde (**3a**) in good yields. Although their isolated yields were in the range of 60 to 85%, the NMR spectrometry of **3a** in the reaction mixture proved a nearly quantitative formation. Some other (arylmethoxy)tropones also gave aroyl derivatives, including 2-(diphenylmethoxy)tropone (**1g**) and 2-(1-naphthylmethoxy)tropone (**1h**) to benzophenone (**3g**) and 1-naphthaldehyde (**3h**).

However, the reaction was not applicable to the alkanals, *i.e.*, the yield of hexanal (**4a**) obtained from 2-(hexyloxy)tropone (**5a**) was less than 3% when heated in DMSO. This was at least partly due to the secondary reaction of the aldehyde with regenerated **2**.[3] This was also the case when 2-[4-(methoxycarbonyl)-butoxy]tropone (**5b**) gave ethyl 4-oxobutyrate (**4b**), in a trace amount. Alkanones, inert to tropones under these conditions, were prepared in a moderately good yield; 2-isopropoxytropone (**5c**) gave acetone (**4c**) in a 55% yield.

Table 1. Preparations and characterizations of tropolonyl ethers

	Ethers	Yield/%	Mp θ_m/°C	Found(%)[a] C	Found(%)[a] H	Calcd(%) C	Calcd(%) H (Compositions)	Ref.
	1a: R=CH_2Ph	76	82—83	79.27	5.80	79.22	5.70 ($C_{14}H_{12}O_2$)	
	1b: R=$CH_2C_6H_4Cl(p)$	83	109—110	68.06	4.68	68.16	4.49 ($C_{14}H_{11}O_2Cl$)	
	1c: R=$CH_2C_6H_4Br(p)$	79	105—106	57.67	4.09	57.75	3.81 ($C_{14}H_{11}O_2Br$)	
	1d: R=$CH_2C_6H_4Me(p)$	85	114—115	79.53	6.46	79.62	6.24 ($C_{15}H_{14}O_2$)	
	1e: R=$CH_2C_6H_4Me(o)$	61	89—91	79.63	6.28	79.62	6.24 ($C_{15}H_{14}O_2$)	
	1f: R=$CH_2C_6H_4OMe(p)$	69	124—125	74.53	6.11	74.36	5.83 ($C_{15}H_{14}O_3$))	
	1g: R=$CHPh_2$	33	137—138	288.1152		288.1150	($C_{20}H_{16}O_2$)	
	1h: R=$CH_2C_{10}H_7(1)$	79	121—123	82.21	5.48	82.42	5.38 ($C_{18}H_{14}O_2$)	
	5a: R=$(CH_2)_5Me$	77	Liquid	206.1287		206.1307	($C_{13}H_{18}O_2$)	
	5b: R=$(CH_2)_3COOEt$	45	Liquid	236.1057		236.1049	($C_{13}H_{16}O_4$)	
	5c: R=$CHMe_2$	20	Liquid	164.0830		164.0837	($C_{10}H_{12}O_2$)	
	5d: R=CH_2COPh	50	136—137	74.70	4.96	74.99	5.03 ($C_{15}H_{12}O_3$)	
	7a: R=$CH_2CH=CH_2$	79						6
	7b: R=$CH_2C(Me)=CH_2$	69	Liquid	176.0841		176.0837	($C_{11}H_{12}O_2$)	
	7c: R=$CH_2C(Cl)=CH_2$	17						6
	7d: R=$CH_2CH=CMe_2$	58						11
	10a: R=CH_2Ph	68	Liquid	254.1302		254.1307	($C_{17}H_{18}O_2$)	
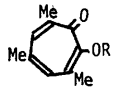	**10d**: R=$CH_2C_6H_4Me(p)$	41	Liquid	268.1454		268.1463	($C_{18}H_{20}O_2$)	
	10e: R=$CH_2C_6H_4Me(o)$	40	Liquid	268.1459		268.1463	($C_{18}H_{20}O_2$)	
	11a: R=$CH_2CH=CH_2$	63						10
	13a: R=$(CH_2)_5Me$	47	Liquid	248.1797		248.1776	($C_{16}H_{24}O_2$)	
	13b: R=$(CH_2)_9Me$	70	Liquid	304.2406		304.2402	($C_{20}H_{32}O_2$)	
	13d: R=CH_2COPh	38	Liquid	282.1254		282.1254	($C_{18}H_{18}O_3$)	

a) Certain tropolonyl ethers were characterized by high-resolution mass-spectra for the samples of more than 99%-purity in respect of high-pressure liquid chromatography (micropolasil-ethyl acetate and hexane).

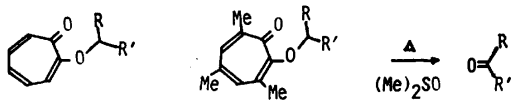

Scheme 1.

TABLE 2. DMSO-OXIDATION OF TROPONYL ETHERS

Starting materials	Conditions T/°C	Conditions t/h	Products: R, R′	Yield/%
1a:	180	2	**3a**: Ph, H	82
10a:	180	1	**3a**: Ph, H	64
1b:	180	2	**3b**: *p*-ClC_6H_4, H	85
1c:	180	2	**3c**: *p*-BrC_6H_4, H	83
1d:	180	3	**3d**: *p*-MeC_6H_4 H	76
10d:	180	1	**3d**: *p*-MeC_6H_4 H	80
1e:	180	2	**3e**: *o*-MeC_6H_4, H	60
10e:	180	1	**3e**: *o*-MeC_6H_4, H	75
1f:	180	2	**3f**: *p*-$MeOC_6H_4$, H	67
1g:	180	4	**3g**: Ph, Ph	77
1h:	180	1	**3h**: 1-$C_{10}H_7$,H	60
5a:	180	17	**4a**: C_5H_{11}, H	+
13a:	180	12	**4a**: C_5H_{11}, H	55
5b:	180	21	**4b**: C_2H_4COOEt, H	+
5c:	180	5	**4c**: Me, Me	70
5d:	180	20	**4d**: PhCO, H	—[a]
13d:	180	20	**4d**: PhCO, H	—[a]
13b:	180	5	**14b**: C_9H_{19}, H	31

a) Me_2S was undetectable.

To determine the responsibility of the troponyl ethers, the reaction was checked by phenyl benzyl ether (**A**); but it was completely recovered unchanged. In addition, a 1 : 1-mixture of **1a** and *p*-chlorobenzyl alcohol (**6b**) gave aromatic aldehydes which consisted of **3a** : **3b** in a ratio of 5 : 1. Furthermore, **1a** and benzyl-2,3,4,5,6-d_5 alcohol (**6a**-d_5), prepared from benzoic-d_5 acid (**B**-d_5),[4] resulted in the overwhelming formation of the deuterium-free aldehyde (**3a**): In the NMR spectrum of the reaction mixture in DMSO-d_6, the intergral ratio for the signals ascribable to aldehydic protons and to 2,6-protons of **3a** was exactly 1 : 2. Even more convincingly, the mass-spectral analysis of the resultant **3a** showed less than 3% of **3a**-d.[5] Thus, within experimental error, hydrolyzed alcohols, if any, are not primarily responsible for the aldehyde formation. Therefore, the present oxidation can be termed a novel DMSO-mediated reaction of tropolonyl ethers.

As in the recently-found radical rearrangement: 2-(arylmethoxy)tropones to 3- and 5-(arylmethyl)-tropolones,[2] the present radical-induced oxidation also revealed a sensitization effect when analyzed kinetically;

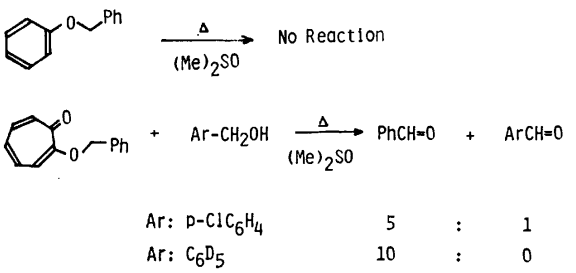

Scheme 2.

throughout the oxidation up to 70% conversion of **1a** in DMSO-d_6, the rate enhancement by addition of the radical sensitizer, benzoyl peroxide (BP, 0.5 mol equiv.), k_{BP}/k_o, was *ca.* 2.7 at 180 °C ($k_o=2.3\times10^{-2}$, $k_{BP}=6.1\times10^{-2}$/min mol). In addition to this, the rate was also increased by addition of 2,4,6-tri-*t*-butylphenol (TB, 0.5 mol equiv.), *i.e.*, $k_{TB}/k_o=1.7$ at 140 °C ($k_{TB}=3.1\times10^{-3}$, $k_o=1.8\times10^{-3}$/min mol). The observed rate increase by introduction of TB, generally regarded as a radical scavenger, may indicate an intermediate formation of some condensate which can be homolyzed to regenerate the benzyl radical. However, these thermodynamic parameters might not be accurate enough to calculate $\Delta S^{\neq}$. But 2-(2-alkenyloxy)tropones, feasible for concerted intramolecular 3,3-sigmatropy, must not yield the oxidation products. Indeed, 2-allyloxytropone (**7a**) and some other analogs (**7b** and **7c**)[6] gave only the Claisen rearrangement products (**8a**—**c**).[7] But 2-(3-methyl-2-butenyloxy)-tropone (**7d**), the Claisen rearrangement product of which should suffer serious steric hindrance, failed to give either oxidation product or Claisen rearrangement product. The identified compounds were regenerated **2** together with isoprene.[8]

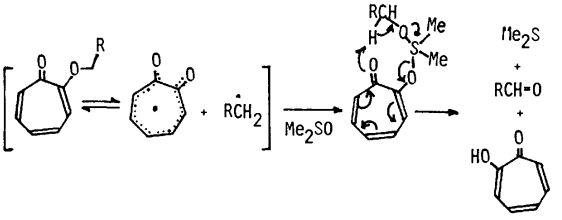

Scheme 3.

As an alternative of **2**, 3,5,7-trimethyltropolone (**9**)[9] can be used; 2-benzyloxy-3,5,7-trimethyltropone (**10a**) gave **3a** in 64% yield after silica-gel chromatographic work up. However, again 2-allyloxy-3,5,7-trimethyltropone (**11a**) gave only a Claisen rearrangement product: 3-allyl-3,5,7-trimethyl-4,6-cycloheptadiene-1,2-dione (**12a**),[10] and no oxidation occurred. On the other hand, the oxidation of 2-alkoxy-3,5,7-trimethyltropones (**13**) proceeded, after an induction period, to give the corresponding aldehydes in good yields; *i.e.*, from 2-hexyloxy-3,5,7-trimethyltropone (**13a**), **4a** was obtained in a 55% yield. This might be a result of blocking of the *o*- and *p*-position with methyl groups to prevent electrophilic attack of the resultant aldehydes. Similar features were observed in several derivatives, as shown in Table 2, and the reaction thus became applicable for the preparation of saturated aldehydes in general.

Related studies are in progress, and will be reported in future.

Experimental

Preparation of Tropolonyl Ethers (General Method). A hexamethylphosphoric triamide (HMPA) solution of tropolones and sodium hydride (1.2 mol equiv.) was treated with alkyl, allyl, or arylmethyl halides until the starting troponoids disappeared. In the cases of alkyl and arylmethyl derivatives, the mixture had to be heated as high as 120 °C,

but allyl and other thermally-sensitive derivatives gave good results when the mixture was kept at room temperature. After dilution with water, the mixture was extracted with ether, dried on $MgSO_4$, and chromatographed on a silica-gel column, if necessary. Yields varied depending on the steric circumstances of the halides, as compiled in Table 1; these are not optimized results.

Reaction of ***1a*** *with DMSO.* A DMSO solution (2 cm³) of **1a** (50 mg) was heated in a sealed tube for 6 h at 180 °C (refluxing *o*-dichlorobenzene bath). After dilution with water, the mixture was extracted with diethyl ether and chromatographed on a silica-gel column to give a colorless oil, **3a**, which was directly identified to be benzaldehyde. The isolated yield was 65%, but the latter fractions of chromatography contained colorless needles, which was identified to be benzoic acid (**B**).

Attempted Reaction of Phenyl Benzyl Ether (A) in DMSO-d_6. A DMSO-d_6 solution (0.5 cm³) of **A** (50 mg) was heated in a sealed tube at 180 °C for 15 h. The NMR spectroscopy revealed that the reaction did not proceeded at all.

The NMR Analysis of the Reaction of ***1a*** *with DMSO-*d_6 *in a Presence of p-Chlorobenzyl Alcohol (****6b****).* A DMSO-d_6 solution (0.5 cm³) of **1a** (25 mg) and **6b** (12 mg) was heated in a sealed tube (in refluxing *o*-dichlorobenzene bath) for 3 h. The mixture was then directly analyzed by an FT-NMR spectrometer: the result was **3a** : **3b**=5 : 1. If we judge only from the NMR spectrum, the reaction was very clean; there are no signals other than those of **1a**, **3a**, **3b**, regenerated **2**, and **6b**.

Reaction of ***1a*** *with DMSO in a Presence of Benzyl-*d_5 *Alcohol (****6a****-*d_5). A DMSO solution (2 cm³) of **1a** (90 mg) and **6a**-d_5 (50 mg)[4] was heated in a sealed tube at 180 °C for 2 h. The product isolated by the usual manner was a colorless oil, **3a**, from which autoxidized benzoic acid (**B**), colorless needles, mp 122—123 °C, were obtained in a pure form, 10 mg (20%). Its mass-spectrum [Found: *m/e*, 122 : 123 : 124 : 125 : 126 : 127=100.0 : 8.1 : 0.7 : 0.2 : 0.6 : 1.3] confirmed that there was only a negligible incorporation of deuterium atoms.[5]

Kinetic Analysis of the Reaction of ***1a*** *in DMSO-*d_6 *in a Presence of BP or TB.* Each DMSO-d_6 solution (0.4 cm³) of **1a** (each 30 mg) with various amounts of BP or TB (0 to 50 mg) was heated in a sealed tube at a constant temperature (140—160 °C), and the rates of formation of **3a** were measured.

Attempted Reaction of 2-(Alkenyloxy)tropones with DMSO. a): A DMSO solution (0.5 cm³) of 2-allyloxy tropone (**7a**, 25 mg) was heated in a sealed tube at 180 °C for 30 min. The product isolated after preparative silica-gel column chromatography was a pale yellow oil, 21 mg (84%), **8a**.[6]

b): A DMSO solution (0.3 cm³) of 2-(2-methyl-2-propenyloxy)tropone (**7b**, 30 mg) was heated in refluxing *o*-dichlorobenzene for 1.5 h. The mixture was then extracted by ether and water, and the organic extract was chromatographed on a silica-gel column to give a colorless oil, which was identified to be the Claisen product (**8b**), 21 mg (70%) [Found: *m/e*, 176.0824 (M^+). Calcd for $C_{11}H_{12}O_2$: 176.0837. δ: 1.33 (3H, d, J=7 Hz), 4.31 (1H, dqt, J=7, 5, 1.5 Hz), 5.13 (1H, dt, J=10, 1.5 Hz), 5.15 (1H, dt, J=17, 1.5 Hz), 5.99 (1H, ddd, J=17, 10, 4 Hz), 6.97 (1H, ddd, J=10, 7, 4 Hz), 7.27 (2H, m), 7.41 (1H, dt, J=10, 1 Hz), and 8.8—9.6 (1H, OH)].

c): A DMSO solution (0.3 cm³) of **7c** (50 mg) was heated in a sealed tube at 180 °C for 1 h. Silica-gel column chromatography of the mixture afforded a colorless oil (**8c**), 48 mg (96%), which was identical with the authentic sample.[6]

d): A DMSO solution (0.3 cm³) of **7d** (50 mg) was heated in a sealed tube at 180 °C for 30 min. Silica-gel column chromatography of the mixture gave only **2**, 31 mg (97%), together with isoprene, which was identified by NMR spectroscopy.

Reaction of 2-(Benzyloxy)-3,5,7-trimethyltropone with DMSO. A DMSO solution (0.3 cm³) of **10a** (50 mg) was heated in a sealed tube in a refluxing decalin bath. Preparative thin-layer chromatography of the mixture yielded benzaldehyde (**3a**), 13 mg (64%).

*Attempted Oxidation of 2-(Allyloxy)-3,5,7-trimethyltropone (****11a****)*[10] *with DMSO.* A DMSO solution of **11a** (50 mg) was heated in a secaled tube at 180 °C for 20 min. After dilution with water, the mixture was extracted with ether to give a colorless oil, 29 mg (58%), whose NMR spectrum was identical with the Claisen rearrangement product (**12a**) described previously:[10] δ: 1.28 (3H, s), 1.91 (3H, d, J=2 Hz), 1.99 (3H, d, J=2 Hz), 2.50 (2H, m), 4.99 (1H, m), 5.12 (1H, m), 5.60 (1H, m), 5.65 (1H, *q*, J=2 Hz), and 6.58 (1H, q, J=2 Hz). No other product was identified.

*Reaction of 2-Alkoxy-3,5,7-trimethyltropones (****13****). a)*: A DMSO solution (2 cm³) of 2-(hexyloxy)-3,5,7-trimethyltropone (**13a**, 50 mg) was heated in a sealed tube at 180 °C for 8 h. The product isolated after silica-gel column chromatography was hexanal (**4a**) [δ: 0.89 (3H, tm, J=7 Hz), 1.2—1.7 (6H, m), 2.38 (2H, td, J=7, 2 Hz) and 9.66 (1H, t, J=2 Hz). δ (C): 14.0, 22.5, 23.3, 31.5, 43.8, and 201.1], 11 mg (55%).

b): A DMSO solution (0.4 cm³) of 2-(decyloxy)-3,5,7-trimethyltropone (**13b**, 50 mg) was similarly heated in a sealed tube at 180 °C for 5 h. Eight mg of decanal (**14b**) was obtained (31%) [δ: 0.87 (3H, tm, J=7 Hz), 1.26 (12H, m), 1.60 (2H, m), 2.38 (2H, td, J=7, 2 Hz), and 9.67 (1H, t, J=2 Hz). δ (C): 14.1, 22.2, 22.8, 29.4 (2C), 29.7 (2C), 32.0, 43.9, and 201.6].

References

1) M. Fieser, "Reagents in Organic Synthesis," Wiley-Interscience Publ., New York (1980), Vol. 8, p. 199. See also previous Vols. 1—7.

2) H. Takeshita, H. Mametsuka, A. Chisaka, and N. Matsuo, *Chem. Lett.*, **1981**, 73.

3) Indeed, by heating of **2** and **4a** in DMSO at 180 °C for 2 h, a decrease of the NMR signals of both compounds occurred by formation of an intractable condensate mixture.

4) The sample of pentadeuteriobenzoic acid kindly provided by Prof. Masashi Tashiro, Research Institute of Industrial Science, Kyushu University, had the following isotope distributions: d_5=70%, d_4=23%, and d_3=7%. However, the deuterium content of 2- and 6-positions is practically 100%. We thank him for the generous gift.

5) Based on the deuterium distributions of the starting **6a—d**, the observed *m/e*: 123 (8.1) must be interpreted as the $(M+1)^+$ peak, but not as the **3a**-d_1.

6) H. Takeshita, I. Kouno, and K. Miyake, *Kyushu Daigaku Seisan Kagaku Kenkyusho Hokoku*, **66**, 1 (1977).

7) In our previous study,[6] Claisen rearrangements on some of these (alkenyloxy)tropones were unsuccessful.

8) Previously, **7d** was converted to the *o*- and *p*-Claisen rearrangement products (33% and 28%) by heating at 150 °C.[11]

9) T. Nozoe, T. Mukai, and K. Takase, *Sci. Reports Tohoku Univ., Ser. I*, **36**, 40 (1952).

10) The Claisen rearrangement product of **11a** (**12a**) is known to cause a further intramolecular Diels-Alder reaction. See R. M. Harrison, J. D. Hobson, and M. M. Al Holly, *J. Chem. Soc., C*, **1971**, 3084.

11) R. M. Harrison and J. D. Hobson, *J. Chem. Soc., Perkin Trans. 1*, **1973**, 1958.

The Cycloisomerization Reaction of [2.2]Metacyclophanes to 1,2,3,3a,4,5-Hexahydropyrenes. Substituent Effects and Directional Selectivity

Takeshi YAMAGISHI, Koichi TORIZUKA, and Takeo SATO*

Department of Chemistry, Tokyo Metropolitan University, Setagaya-ku, Tokyo 158

(Received July 13, 1981)

Substituent effects and directional selectivity in iodine-induced cycloisomerization reaction of [2.2]metacyclophane were tested using several derivatives of the latter. The reaction was found to be highly selective, and electron-donating groups gave a hexahydropyrene preserving a substituted aryl ring. On the other hand, an alkyl group *ortho* to the bridge gave a hexahydropyrene with a hydrogenated substituted ring.

Transannular reactions of mesocyclic compounds constitute an important synthetic strategy for constructing bridged systems.[1] We have found a highly efficient cycloisomerization reaction of [2.2]metacyclophane (**1**) to give 1,2,3,3a,4,5-hexahydropyrene (**2**) by treatment with a catalytic amount of iodine.[2] This remarkable transformation has been shown to be widely applicable for the synthesis, in high yields, of hitherto unaccessible alkyl-substituted hexahydropyrenes,[3] starting from alkyl derivatives of **1**.[2,4]

Instead of iodine, aluminium chloride,[2,5,6] bromine,[2] sulfuric acid[2,5] and silver salts[2] have also been used as the catalyst, but these were less selective and also less efficient than iodine. This paper will describe the substituent effects and directional control of the iodine-induced reaction using substituted [2.2]metacyclophanes, **3a**, **3b**, **6a**, **6b**, **9**, **13a**, **13c**, and **13d**, in which two benzene rings are differently substituted.

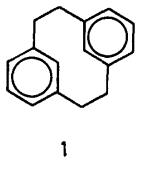

1

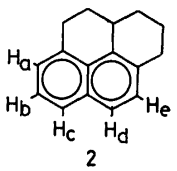

2

Results. [2.2]Metacyclophanes prepared according to the method described before[7] were treated with 0.14 equiv. of iodine in benzene at 60 °C for 15—20 h. The reaction mixture was then analyzed by vapor-phase and column chromatography. The yields shown in Table 1 are for a diastereomeric mixture. The analytical data are shown in Table 2.

TABLE 1. IODINE-INDUCED CYCLOISOMERIZATION REACTION[a]

Compound	Hexahydropyrene(%)	Tetrahydropyrene(%)	Starting material recovery/%
3a	**4a**, 80		20
3b	**4b**, 100		
6a	**7a**, 88	**8a**, 6	6
6b	**7b**, 89	**8b**, 10	1
9	**10**, 98	**12**, 2	
13a	**15**, 100		
13c			100
13d			100

a) The relative yields were determined by gas chromatography after treating the substrate with 0.14 equiv. of iodine in benzene at 60 °C (for **9**, 45 °C) for 15—20 h.

TABLE 2. 1,2,3,3a,4,5-HEXAHYDROPYRENES

Compound	Mp θ_m/°C	Formula	Found (%) C	Found (%) H	Calcd (%) C	Calcd (%) H
4a	97—98	$C_{17}H_{18}$	91.97	8.17	91.84	8.16
4b	116—118	$C_{20}H_{24}$	90.60	9.18	90 85	9.15
7a	101[a]	$C_{19}H_{22}$	91.92	8.23	91.14	8 86
7b	108[a]	$C_{22}H_{28}$	90.45	9.41	90.35	9.65
10	Oil	$C_{20}H_{24}$	90.94	9.17	90.85	9.15
15	140—141	$C_{18}H_{20}$	85.65	8.05	85.67	7.99

a) Half crystalline.

5-Methyl derivative **3a** gave a 80% yield of **4a**, with 20% of the recovered material. That the product was not isomeric **5a** was proved by the appearance of a ^{1}H NMR resonance at δ 2.46 as a singlet. A methyl proton

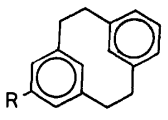

3

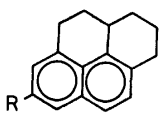

4

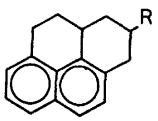

5

a, R=Me
b, R=t-Bu

resonance in **5a** would require a doublet at around δ 1.10, as is observed in the 2,7-dimethyl derivative **14** prepared from **13b**.[2] The substitution pattern in a naphthalene ring was consistent with **4a**, as was proved by the UV and NMR spectra (see below). Similarly, the *t*-butyl derivative **3b** gave a quantitative yield of **4b**.

The directional selectivity was then studied using trialkyl and tetraalkyl derivatives, **6** and **9**. Compound **6a** gave 88% of **7a**. Similarly, **6b** and **9** gave 89 and 98% respectively of **7b** and **10**. In addition, these gave dehydrogenation products, 4,5,9,10-tetrahydropyrenes, **8a** (6%), **8b** (14%), and **12** (2%) as by-products. In any case, no isomeric hexahydropyrene in which a multi-substituted aryl ring was preserved as in **11** was isolated, as was evidenced by a careful examination of the reaction mixture by means of UV and NMR.

Competition between a methyl group and several functional groups were then studied using compounds **13a**, **13c**, and **13d**. Dimethyl derivative **13b** has been shown to give **14** in a quantitative yield.[2] 5-Methoxy-13-methyl derivative **13a** gave **15** exclusively. A methoxy methyl proton resonance at δ 3.90 suggests

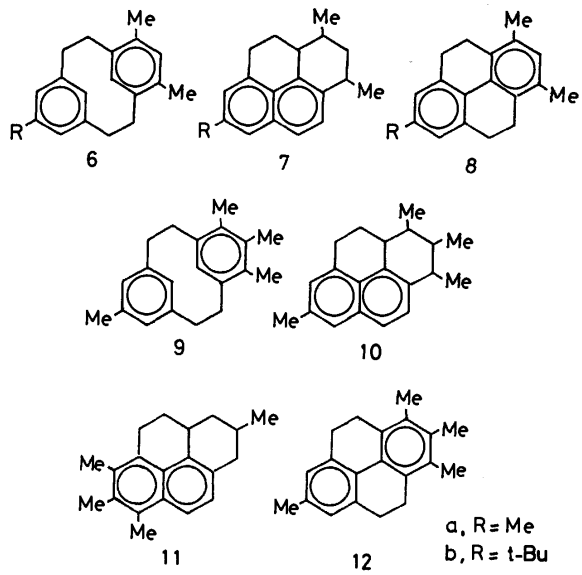

the formation of an aromatic ether **15** but not the isomeric **16**. On the other hand, two bromo and cyano derivatives, **13c** and **13d**, gave no isomerization reaction product and were recovered unchanged under the present reaction conditions.

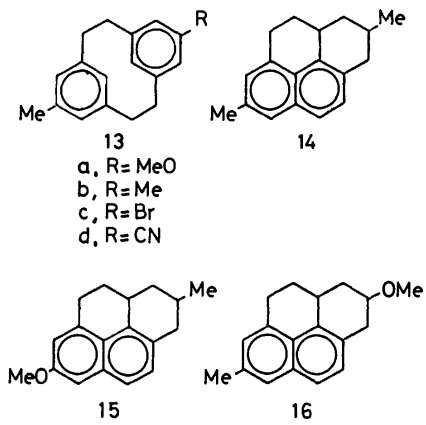

Structural Evidence. When an alkyl-substituted aryl ring becomes hydrogenated, the reaction mixture has been shown to be a diastereomeric mixture.[2] These isomers were separated partially by passing through alumina containing silver nitrate. The mixture could be completely analyzed by means of NMR spectroscopy with the aid of the ASIS and NOE methods and also shift reagents.[2] For example, the tetramethyl derivative **17** has been shown to give three isomeric tetramethylhexahydropyrenes, **18a**, **18b**, and **18c**, each as in a *dl* pair. The possible fourth isomer involving 1,3-diaxial methyl interaction, **18d**, could not be detected.[2]

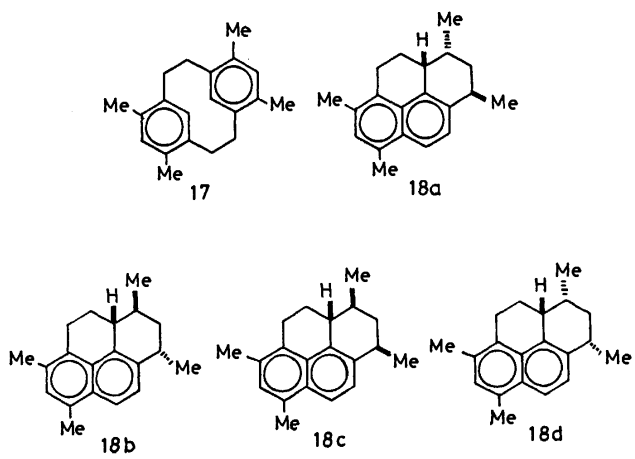

In view of the lack of stereospecificity in this transformation, no attempt was made in the present studies to separate and characterize diastereomers. Structural evidence for the suggested structure is illustrated by the case of **10**, formed from **9**. The assignment of the five aromatic protons in **2**, H_a—H_e, has already been reported.[2] The aryl proton resonances in **10** are in agreement with the suggested substitution pattern. The compound showed a three-proton singlet corresponding to an aromatic methyl resonance at δ 2.38. The methyl groups on saturated carbon showed complex resonances at δ 0.5—1.5, suggesting a diastereomeric mixture.

The substitution pattern in the naphthalene nucleus can conveniently be learned from a UV spectral comparison. Alkyl substitution at an α position causes both bathochromic and hyperchromic shifts of the ^1L_a bands, whereas β substitution results in a red shift and intensity increase in the ^1L_b bands.[8] Figure 1 shows the UV spectra for **10**, **14**, and **18**. The examination of both the ^1L_a and ^1L_b bands suggests that the substitution pattern in the naphthalene ring for **10** is similar to that of **14**.[2] An alternative structure, **11**, would require a further shift of these bands beyond **18**.

Mass-spectral measurements also served as structural

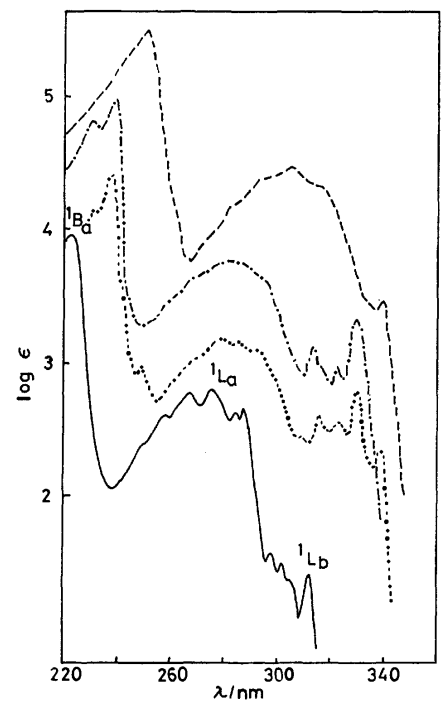

Fig. 1. The UV spectra for —— naphthalene, ------ 1,2,3,7-tetramethyl- (**10**), ····· 2,7-dimethyl- (**14**), and —— 1,3,6,8-tetramethyl-1,2,3,3a,4,5-hexahydropyrenes (**18a**, **18b**, and **18c**) determined in cyclohexane. Absorption, log ε, is for compound **10**.

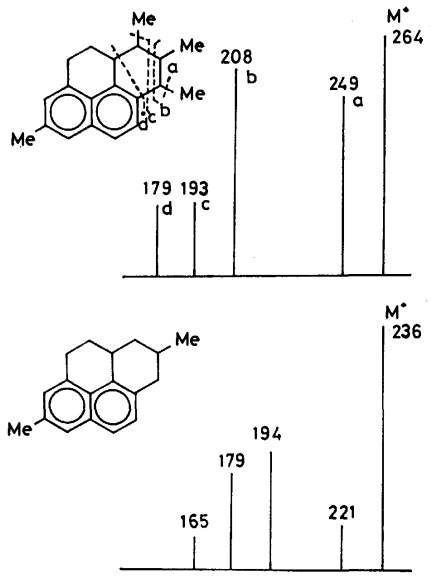

Fig. 2. The mass-spectral fragmentation for 2,7-dimethyl (**14**) and 1,2,3,7-tetramethyl-1,2,3,3a,4,5-hexahydropyrenes (**10**) determined at 70 eV.

proof. Figure 2 shows a comparison of the fragmentation pattern for **10** and **14**. The appearance of assigned peaks for **10** excludes the alternative structure, **11**, which possesses a hydroaromatic partial structure similar to that of **14**.

Compound **7a** gave poor analytical data, probably because of difficulty in purification. Its formation was supported by GC-MS carried out on an OV-1 column, which separated the diastereomeric mixture into two fractions. Both fractions gave essentially the same fragmentation pattern, with *m/e* at 208 ($-C_3H_6$: *cf.* Fig. 2, fragmentation b), 235 ($-CH_3$), and 250 (parent peak). In going into **7a** from **6a**, the NMR signals at δ 2.26, 4.08, and 4.20 in **6a** disapeared and methyl signals appeared at δ 2.40 ($ArCH_3$) and at around 1.3 (aliphatic CH_3).

Conclusion. The results obtained so far can be summarized as follows: 1) The iodine-induced cycloisomerization of substituted [2.2]metacyclophanes proceeds with a high directional selectivity. 2) An electron-donating group at the 5- (or 13-) position directs the transformation toward hexahydropyrene formation, preserving the substituted aryl ring (*cf.* compounds **3a**, **3b**, and **13a**). 3) An electron-withdrawing substituent gives no cycloisomerization reaction products under the present reaction conditions.[9] 4) When an alkyl group is present at the *ortho* position of the bridge (4,6,12,14-positions), the hydrogenation occurs on the alkyl-bearing aromatic ring. 5) An alkyl group ortho to the bridge not only enhance the rate of cycloisomerization, but gives a dehydrogenation product (*cf.* **6**→**8**, **9**→**12**).

With regard to 4) and 5), we have observed[4] that the cycloisomerization reaction of the tetramethyl derivative, **17**, and a hexamethyl derivative[4] are quite rapid compared with that of **1** and also with those of less highly substituted derivatives. The enhanced reactivity for these has been attributed to an additional strain imposed on the bridging methylene group by the vicinal methyl group. The driving force of the cycloisomerization reaction is assumed to be the internal strain of a ten-membered ring, the proximity of two reacting aryl positions, and the π-basicity of the benzene ring(s) for complexation with iodine.[2,4] With **6** and **9**, the additional strain term outweighs the normal substituent effects operating in **3** and directs the reaction toward the formation of **7** and **10**, but not **11** or the isomeric **7**, with a different naphthalene ring disposition.

Experimental

[2.2]Metacyclophane Derivatives. Compounds **3a**,[10] **3b**,[11] **6a**,[10] **6b**,[10] **13a**,[7] **13b**,[2] **13c**,[7] and **13d**[7] were prepared as has been described in the literature.

2,11-Dithia-5,6,7,15-tetramethyl[3.3]metacyclophane. 4,5,6-Trimethyl-α,α'-dichloro-*m*-xylene was treated with thiourea in ethanol and then with a potassium hydroxide solution to give 4,5,6-trimethyl-*m*-xylene-α,α'-dithiol. Benzene solutions (200 cm^3) of the dithiol (5.1 g, 24 mmol) and α,α'-dibromomesitylene (6.7 g, 24 mmol) were dropped, slowly and simultaneously, into a solution of 1.9 g (48 mmol) of sodium hydroxide in benzene (200 cm^3)–ethanol (1000 cm^3) during 24 h under reflux. The solvent was then evaporated, and washed dichloromethane extracts were passed through a silica-gel column. The bis(sulfide) was thus obtained in a 55% yield: mp 123—124 °C: NMR ($CDCl_3$) δ 2,12 (3H, s, Me), 2.16 (9H, s, Me), 3.62 (4H, s, CH_2), 3.68 (4H, s, CH_2), and 6.92 (4H, m, ArH).

Found: C, 72.86; H, 7.27%. Calcd for $C_{20}H_{24}S_2$: C, 73.11; H, 7.36%.

4,5,6,13-Tetramethyl[2.2]metacyclophane (9). The above bis(sulfide) was converted to bis(sulfone), 2,11-dithia-5,6,7,15-tetramethyl[3.3]metacyclophane 2,2,11,11-tetraoxide by oxidation with 30% hydrogen peroxide in benzene–acetic acid at room temperature. The pyrolysis of bis(sulfone) at 550 °C gave **9** (mp 113.5—114.5 °C) after chromatography on silica gel: NMR ($CDCl_3$) δ 2.29 (9H, s, Me), 2.36 (3H, s, Me), 1.9 and 3.2 (8H, m, CH_2), 4.13 (1H, t, C-16H), 4.30 (1H, s, C-8H), and 6.89 (2H, ArH).

Found: C, 90.71; H, 1.13%. Calcd for $C_{20}H_{24}$: C, 90.85; H, 9.15%.

Cycloisomerization of 9 to Give 10. A solution of (820 mg, 3.1 mmol) and iodine (110 mg, 0.43 mmol) in 9.6 cm^3 of benzene was warmed at 45 °C for 14 h. Column chromatography on alumina eluted with hexane gave **10** as an oily diastereomeric mixture in a 98% yield. Further elution gave a 2% yield of tetrahydropyrene **12**:[10] mp 117—121 °C. The cycloisomerization was nearly complete within 20 min at 51 °C, as has been observed in a preliminary experiment carried out in a NMR tube in C_6D_6: NMR ($CDCl_3$) δ 0.5—1.5 (9H, m, Me), 2.38 (3H, m, MeAr), 7.01 (1H, s, a-ArH), 7.33 (1H, s, c-ArH), 7.42 (2H, dd, d,e-ArH) (for the designation of naphthalene proton, see Formula **2**).

References

1) N. J. Leonard and T. Sato, *J. Org. Chem.*, **34**, 1066 (1969); T. Sato, *Yuki Gosei Kagaku Kyokai Shi*, **30**, 109 (1972); N. J. Leonard, *Acc. Chem. Res.*, **12**, 423 (1979).

2) T. Sato, K. Nishiyama, and A. Murai, *J. Chem. Soc., Chem. Commun.*, **1972**, 163; T. Sato and K. Nishiyama, *J. Org. Chem.*, **37**,4254 (1972).

3) "Rodd's Chemistry of Carbon Compounds," 2nd ed, ed by S. Coffey, Elsevier Scientific Publishing Co. (1974), Vol. III, Part F, p. 353; Vol. III, Part H, p. 270.

4) T. Sato and T. Takemura, *J. Chem. Soc., Perkin Trans. 2*, **1976**, 1195.
5) K. Nishiyama, K. Hata, and T. Sato, *Tetrahedron*, **31**, 239 (1975).
6) W. Baker, J. F. W. McOmie, and J. M. Norman, *J. Chem. Soc.*, **1951**, 1114.
7) T. Sato, K. Torizuka, K. Komaki, and H. Atobe, *J. Chem. Soc., Perkin Trans. 2*, **1980**, 561.
8) L. Ruzicka, H. Schinz, and P. H. Muller, *Helv. Chim. Acta*, **27**, 195 (1944).
9) Although 5-nitro[2.2]metacyclophane was also inert toward iodine, it gave, on treatment with aluminium chloride, a dehydrogenation product, 2-nitro-4,5,9,10-tetrahydropyrene; T. Sato and N. Matsumoto, unpublished results.
10) K. Torizuka and T. Sato, *Bull. Chem. Soc. Jpn.*, **53**, 2411 (1980).
11) T. Sato and H. Atobe, unpublished results.

Synthesis of 1,1′-, 2,2′-, 1,2′-, and 2,6′-Biazulenes and Their Derivatives by Ullmann Reaction[1]

Tadayoshi MORITA* and Kahei TAKASE

Department of Chemistry, Faculty of Science, Tohoku University, Aoba Aramaki, Sendai 980

(Received July 20, 1981)

Four kinds of biazulenes, 1,1′- (**1a**), 2,2′- (**2a**), 1,2′- (**3a**), and 2,6′-biazulenes (**4a**), and their derivatives were synthesized by utilizing Ullmann-type coupling of haloazulene derivatives. Ullmann reaction of ethyl 3-iodo- (**5a**) and 2-iodoazulene-1-carboxylates (**6b**) gave diethyl 1,1′-biazulene-3,3′-dicarboxylate (**1b**) and diethyl 2,2′-biazulene-1,1′-dicarboxylate (**2b**), respectively, in excellent yields. The reaction of 2-iodoazulene gave **2a** directly. Diethyl 2-chloroazulene-1,3-dicarboxylate (**7a**) and its 5-alkyl derivatives also reacted to give tetraethyl 2,2′-biazulene-1,1′,3,3′-tetracarboxylate (**2d**) and its 5,5′-dialkyl derivatives, respectively. A mixed Ullmann reaction of **5a** and **6b** afforded a mixture of **1b**, **2b**, and diethyl 1,2′-biazulene-1′,3-dicarboxylate (**3b**). Similarly, a mixed Ullmann reaction of **7a** and diethyl 6-iodoazulene-1,3-dicarboxylate gave a mixture of **2d** and tetraethyl 2,6′-biazulene-1,1′,3,3′-tetracarboxylate (**4b**). The parent hydrocarbons of biazulenes, **1a**, **2a**, **3a**, and **4a**, could be derived from the corresponding ethoxycarbonyl derivatives, **1b**, **2b**, **2d**, **3b**, and **4b**, respectively, by decarboxylation. The planarity of biazulenes and their ester derivatives is also discussed on the basis of the spectral data.

Although benzenoid biaryls, such as biphenyls and binaphthalenes, have been known for a long time and studied extensively from the chemical and physical points of view, no biazulene, one of the non-benzenoid biaryls, had been known until Hagen *et al.*[2] reported the photochemical synthesis of 2,2′- and 3,3′-biguaiazulenes. A number of positional isomers are possible for biazulenes. Recently, 4,4′-,[3] 5,5′-,[4] and 6,6′-biazulenes[5] have been synthesized. The Ullmann-type biaryl coupling of aryl halides using copper at elevated temperature has been utilized for the synthesis of benzenoid biaryls. This reaction was applied on some haloazulene derivatives for synthesis of 1,1′- (**1a**), 2,2′- (**2a**), 1,2′- (**3a**), and 2,6′-biazulenes (**4a**), and their derivatives.

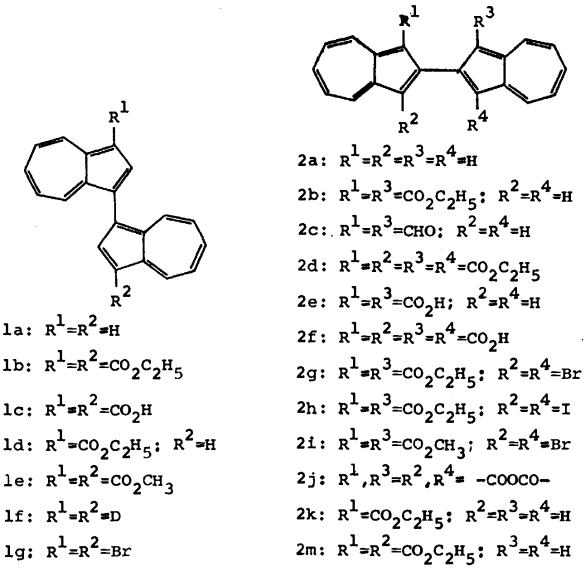

Chart 1.

Results and Discussion

A mixture of haloazulene and activated copper[6] was heated at about 200—220 °C in an evacuated sealed tube and then the products were isolated. The results are listed in Table 1.

1,1′-Biazulene. Ethyl 3-chloro- and 3-bromoazulene-1-carboxylates[7a] did not react at 220 °C, but changed into an unidentified black resinous substance at 250 °C. On the other hand, ethyl 3-iodoazulene-1-carboxylate (**5a**)[7a] easily reacted at 220 °C to give diethyl 1,1′-biazulene-3,3′-dicarboxylate (**1b**), accompanied by a small amount of dehalogenated[8] ethyl azulene-1-carboxylate (**5b**).[9]

The complete hydrolysis of **1b** with alkali, and the subsequent decarboxylation of the resulting dicarboxylic acid (**1c**) upon heating gave the parent hydrocarbon, **1a**, in 55% yield. The mass spectrum of **1a** shows a molecular ion peak at *m/e* 254. A partial hydrolysis of **1b** with alkali, followed by decarboxylation afforded ethyl 1,1′-biazulene-3-carboxylate (**1d**) as a major product. Methylation of **1c** with diazomethane yielded a dimethyl ester (**1e**). Deuteration[10] of **1a** with D_3PO_4 gave 1,1′-biazulene-3,3′-d_2 (**1f**) and bromination of **1a** with NBS gave an expected 3,3′-dibromo derivative (**1g**).

2, 2′-Biazulene. 2-Iodoazulene (**6a**)[7c] and ethyl 2-iodoazulene-1-carboxylate (**6b**)[7b] when heated with activated copper, reacted to give 2,2′-biazulene (**2a**) and diethyl 2,2′-biazulene-1,1′-dicarboxylate (**2b**), accompanied by small amounts of azulene and **5b**, respectively. 2-Iodoazulene-1-carboxaldehyde (**6c**), derived from **6a**, also reacted to give 2,2′-biazulene-1,1′-dicarboxaldehyde (**2c**). 2-Chloroazulene and ethyl 2-chloroazulene-1-carboxylate[7c] did not react at 220—240 °C. However, diethyl 2-chloroazulene-1,3-dicarboxylate (**7a**),[7b,7c] in which two electron-withdrawing ethoxycarbonyl substituents will activate the halogen, easily reacted to give tetraethyl 2,2′-biazulene-1,1′,3,3′-tetracarboxylate (**2d**) in an excellent yield, accompanied by a small amount of dehalogenated diethyl azulene-1,3-dicarboxylate (**7d**).[9] Similarly, 5-methyl (**7b**)[7b] and 5-isopropyl derivatives (**7c**)[7b] also yielded tetraethyl 5,5′-dimethyl- (**8a**) and 5,5′-diisopropyl-2,2′-biazulene-1,1′,3,3′-tetracarboxylate (**8b**), respectively, along with the dehalogenated azulenes (**7e** and **7f**), although some of the starting haloazulenes were recovered unchanged. Besides the direct formation from **6a**, the parant hydrocarbon, **2a**, was derived from **2b** and **2d** by deethoxy-

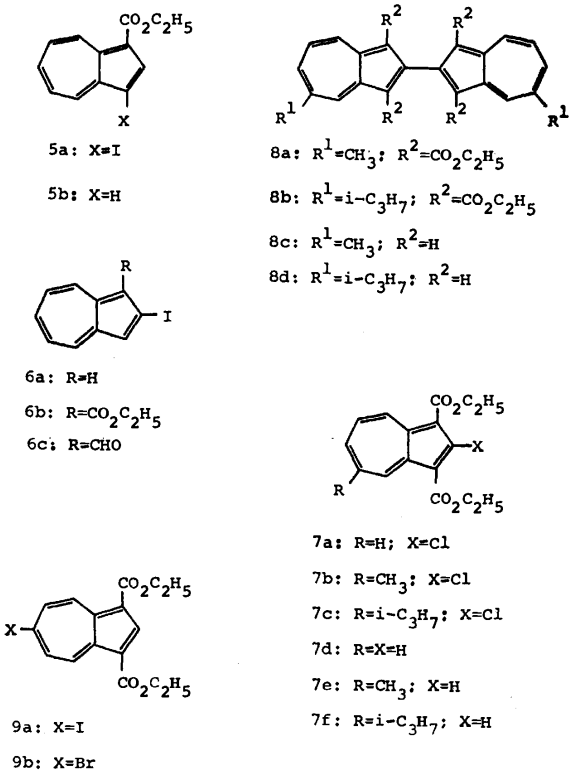

Chart 2.

TABLE 1. THE ULLMANN-TYPE COUPLING OF HALOAZULENES INTO BIAZULENES

Haloazulene	Temp °C	Time h	Products (yield/%) Biazulenes	Others
5a	200	5	**1b** (83)	**5b** (8)
6a	180	6	**2a** (54)	Azulene (trace)
6b	220	6.5	**2b** (82)	**5b** (trace)
6c	220	4.5	**2c** (40)	
7a	220	9	**2d** (83)	**7d** (6)
7b	220	6.5	**8a** (53)	**7e** (7)
7c	235	6	**8b** (11)	**7f** (trace)
5a+**6b**	200	5.5	**1b** (28), **2b** (27), **3b** (22)	**5b** (18)
7a+**9a**	245	6	**2d** (21), **4b** (7)	**7d** (28)

carbonylation. Thus, alkaline hydrolysis of **2b** and **2d** and the subsequent decarboxylation of the resulting di- (**2e**) and tetracarboxylic acids (**2f**) upon heating gave **2a**. Conveniently, **2a** could be obtained directly from **2b** and **2d** by deethoxycarbonylation upon heating with 100% phosphoric acid[7a,7b,11] in excellent yields. Similar treatment of **8a** and **8b** gave 5,5'-dimethyl (**8c**) and 5,5'-diisopropyl-2,2'-biazulenes (**8d**), respectively. The mass spectrum of **2a** shows a molecular ion peak at *m/e* 254.

Vilsmeier reaction of **2a** gave a diformyl derivative which is identical with **2c**. Halogenation of the diester, **2b**, with **NBS** or **NIS** gave diethyl 3,3'-dibromo- (**2g**) or 3,3'-diiodo-2,2'-biazulene-1,1'-dicarboxylates (**2h**). Dimethyl 3,3'-dibromo-2,2'-biazulene-1,1'-dicarboxylate (**2i**) was derived from **2g** by alkaline hydrolysis, followed by methylation. When treated with acetic anhydride, the tetracarboxylic acid, **2f**, yielded a dianhydride (**2j**), whose ethanolysis with sodium ethoxide followed by decarboxylation upon heating afforded a mixture of **2a**, **2b**, ethyl 2,2'-biazulene-1-carboxylate (**2k**), and diethyl 2,2'-biazulene-1,3-dicarboxylate (**2m**).

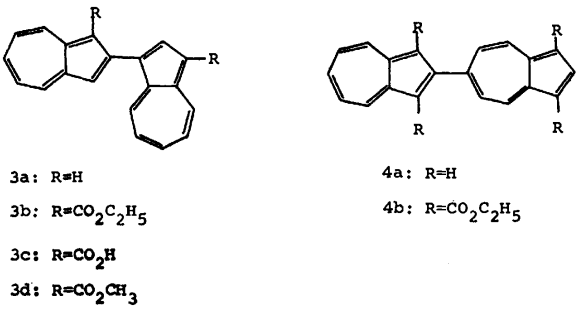

Chart 3.

1,2'-Biazulene. A mixed Ullmann reaction of **5a** and **6b** afforded a mixture of **1b**, **2b**, and diethyl 1,2'-biazulene-1',3-dicarboxylate (**3b**). The parent hydrocarbon, **3a**, was obtained from **3b** upon alkaline hydrolysis followed by decarboxylation of the resulting dicarboxylic acid (**3c**). Its mass spectrum shows a molecular ion peak at *m/e* 254. Dimethyl 1,2'-biazulene-1',3-dicarboxylate (**3d**) was derived from **3c** by methylation.

2,6'-Biazulene. A mixed Ullmann reaction of **7a** and diethyl 6-iodoazulene-1,3-dicarboxylate (**9a**) prepared from 6-bromo compound (**9b**)[12] gave a mixture of **2d** and tetraethyl 2,6'-biazulene-1,1',3,3'-tetracarboxylate (**4b**). The expected 6,6'-biazulene could not be obtained. The parent hydrocarbon, **4a**, was obtained by deethoxycarbonylation of **4b** upon heating with 100% phosphoric acid.

The structures of biazulenes and their derivatives obtained here were confirmed on the basis of the spectral data described below, as well as the above-mentioned chemical evidence.

Infrared Spectra of Biazulenes. The C=O stretching vibrations in the ester derivatives of biazulenes are listed in Table 2. Even for the sterically crowded biazulene derivatives, **2b**, **2d**, **4b**, **8a**, and **8b**, these bands appear in the region comparable to those of the

TABLE 2. CARBONYL STRETCHING VIBRATION OF ETHOXYCARBONYL GROUP OF AZULENE AND BIAZULENES

Compound	ν/cm^{-1} $CHCl_3$[a]	KBr
1b	1684sh 1680	1684
2b	1682sh 1678	1684
2d	1684sh 1678	1684
3b	1684sh 1678	1689 1684
4b		1684
8a	1683sh 1672	1685
8b	1684sh 1673	1684
5b	1683sh 1678	
7d	1686sh 1681	1684

a) sh: Shoulder.

TABLE 3. LONG-WAVE ABSORPTION (BAND A) OF BIAZULENES AND RELATED AZULENES λ/nm (log ε)

Compound	Solvent[a)]	Band A[b)]		
1a	iso	612(2.80)		
1d	cyc	589(2.50)		
1b	iso	575(2.33)		
2a	chl	694(2.43)	635(2.91)	592(3.06)
		554(2.97)		
8c	chl	650(2.61)	608(2.75)	564(2.67)
8d	iso	712(2.50)	640(2.95)	603(3.04)
		565(2.95)		
2k	cyc	644(2.91)	593(3.14)	554(3.10)
2b	iso	640(2.59)	586(2.99)	552(3.01)
2m	chl	627(2.66)[sh]	545(2.95)	510(2.89)[sh]
2d	cyc	597(2.53)	547(2.97)	513(3.02)
8a	iso	610(2.51)	550(2.98)	521(3.03)
8b	iso	600(2.67)	548(3.10)	518(3.12)
3a	iso	614(2.94)	579(2.96)	
3b	iso	564(2.89)	540(2.89)	
4a	chl	595(2.95)		
4b	chl	585(2.56)	530(3.04)	504(3.08)
Azulene	cyc	693(2.24)	663(2.22)	633(2.54)
		604(2.51)	580(2.56)	557(2.40)
		540(2.37)	522(2.23)	
5b	iso	644(2.23)	587(2.60)	545(2.65)
7d	cyc	601(2.21)	551(2.68)	514(2.74)

a) iso: Isooctane; cyc: cyclohexane; chl: chloroform.
b) sh: Shoulder.

conjugated esters in azulene derivatives. This suggests that, in these compounds, the ester groups are favorably in the same plane with the azulene ring and, consequently, the two azulene rings in **2b**, **2d**, **4b**, **8a**, and **8b** are not coplanar.

Electronic Spectra of Biazulenes. Biazulenes show four main electronic absorption bands (A, B, C, and D) in analogy with azulene (shown in Tables 3 and 4). As shown in Figs. 1 and 2, in the spectra of the parent biazulenes, **1a**, **2a**, **3a**, and **4a**, the bands (B, C, and D) in the ultraviolet region show large red shifts with increasing intensities compared with those of azulene, while the visible absorptions (A) exhibit increases in intensities accompanied by loss of the fine structures that appeared in the spectrum of azulene. It is known[13] that the substitution of alkoxycarbonyl groups at C-1 and/or C-3 of azulenes results in blue shift of the band (A) and in red shift of the bands (B and C). The substitution of ethoxycarbonyl groups at C-3 (and C-3′) of 1,1′-biazulene causes blue shifts while decreasing the intensity of band (A), but no apprecible effect on band (B). The substitution of ethoxycarbonyl groups at C-1′, 3 of 1,2′-biazulene results in blue shifts of the bands (A and B).

In the case of 2,2′-biazulene, the substitution of ethoxycarbonyl groups at C-1, 1′ (and C-3, 3′) results in blue shifts of the bands (A and B). Especially the spectra of tetraesters, **2d**, **8a**, and **8b**, are similar to those of diethyl azulene-1,3-dicarboxylates, **7d**, **7e**, and

TABLE 4. THE ULTRAVIOLET ABSORPTION SPECTRA OF BIAZULENES AND RELATED AZULENES λ/nm (log ε)

Compound	Solvent[a)]	Band B		Band C[b)]		Band D[b)]
1a	meth	384(4.19)		308(4.58)	300(4.54)[sh]	263(4.73)
						245(4.51)
1d	meth	375(4.07)		300(4.68)	287(4.72)	260(4.55)
						238(4.53)
1b	meth	382(4.14)		304(4.71)	279(4.82)	239(4.60)
2a	chl	436(4.76)	410(4.45)	328(4.82)	316(4.84)	250(4.30)
			390(4.22)[sh]			
8c	meth	438(4.82)	414(4.63)	332(4.95)	324(4.91)	256(4.38)
8d	meth	434(4.82)	409(4.61)	329(4.99)	317(4.98)	248(4.40)
2k	chl	433(4.45)	411(4.43)	317(4.96)	276(4.14)[e]	246(4.47)
2b	meth	410(4.08)		320(5.00)		245(4.65)[sh]
2m	chl	435(3.80)[sh]	396(4.28)	305(5.13)	270(4.64)[e]	237(4.82)
2d	meth	377(4.18)	348(4.37)	315(5.10)	303(4.85)	238(4.80)
					275(4.66)[e]	
8a	meth	379(4.30)	345(4.41)	317(5.09)	279(4.66)[e]	242(4.78)
8b	meth	380(4.25)	350(4.35)	319(5.02)	282(4.57)[e]	245(4.67)
3a	meth	461(4.27)	441(4.26)	311(4.64)	264(4.54)	232(4.37)
3b	meth	425(4.09)		343(4.40)[sh]	307(4.69)	235(4.55)
				289(4.71)		
4a	chl	448(4.01)[sh]	418(4.55)	338(4.60)	317(5.01)	258(4.27)[sh]
		410(4.55)				
4b	meth	377(4.44)		348(4.54)	317(4.95)	236(4.78)
					273(4.62)[e]	
Azulene	cyc	353(3.14)	341(3.71)	280(4.72)	275(4.74)	238(4.24)
		337(3.63)	326(3.54)	271(4.73)		
		322(3.47)				
5b	cyc	370(3.88)	354(3.78)	299(4.60)	290(4.55)[sh]	234(4.26)
7d	cyc	371(4.14)		302(4.69)	291(4.60)[sh]	234(4.63)
					272(4.53)[e]	

a) meth: Methanol; iso: isooctane; chl: chloroform; cyc: cyclohexane. b) e: A characteritic band in 1,3-bis(ethoxycarbonyl)azulenes and their derivatives; sh: shoulder.

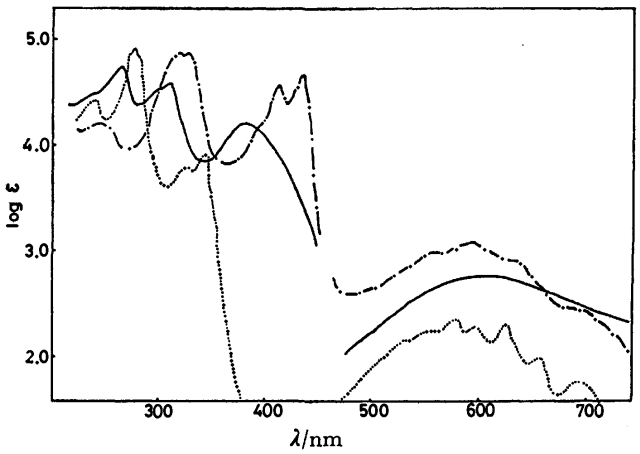

Fig. 1. Electronic Spevtra of **1a** (—— in methanol for UV, isooctane for visible region), **2a** (—·— in chloroform), and azulene (····· in cyclohexane).

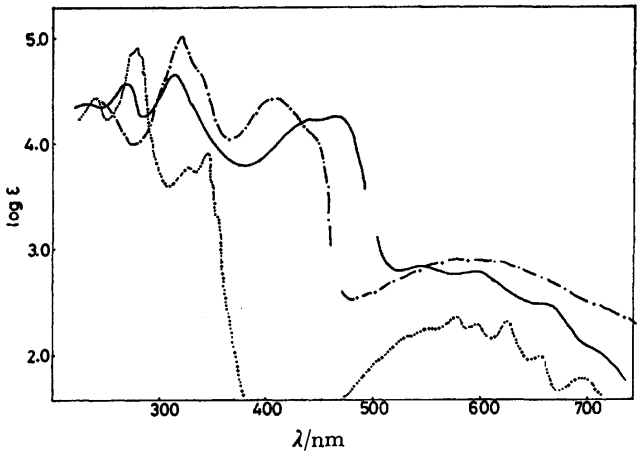

Fig. 2. Electronic Spectra of **3a** (—— in methanol for UV, isooctane for visible region), **4a** (—·— in chloroform), and azulene (····· in cyclohexane).

7f, but the molar absorption coefficients being approximately doubled. This observation suggests that the two azulene rings in **2d**, **8a**, and **8b** are twisted around the 2,2′-bond.

The NMR Spectra of Biazulenes. The NMR spectra data of biazulenes and chemical shift differences ($\Delta\delta$) between biazulenes and the reference compounds are listed in Tables 5 and 6. A study using a Dreiding model of 1,1′-biazulene shows that the steric interactions for H-2···H-8′, H-2′···H-8, and H-8···H-8′ are significant and sugests that the two azulene ring are not coplanar with each other. In fact, in the NMR spectral data of 1,1′-biazulenes, **1a**, **1b**, and **1d**, it is observed that there is no large chemical shift deference ($\Delta\delta$) between the ring protons in **1a** and those in azulene, and between the ethyl protons in esters, **1b** and **1d**, and

Table 5. NMR spectral data of biazulenes (at 60 MHz, in $CDCl_3$, chemical shifts[a,b] in δ from TMS, coupling constants in J/Hz)[g]

Compound	H-1 H-1′	H-2 H-2′	H-3 H-3′	H-4 H-4′	H-5 H-5′	H-6 H-6′	H-7 H-7′	H-8 H-8′	Coupling constants	OCH_2–CH_3 (J=7.0) Others
1a[c]		8.06[d]	7.48[d]	8.30[d]	7.06[t]	7.51[t]	6.96[t]	8.30[d]	$J_{2,3}=3.9$ $J_{4,5}=J_{5,6}=J_{7,8}=9.5$	
1d		8.50[s] 8.01[d]	7.53[d]	9.60[d] 8.32[d]	6.87	—	7.87[m]	8.38[d] 8.24[d]	$J_{4,5}=J_{7,8}=9.5$ $J_{4',5'}=J_{7',8'}=9.5$ $J_{2',3'}=4.0$	4.41[q] 1.43[t]
1b		8.52[s]		9.73[d]	7.10	—	7.95[m]	8.40[d]	$J_{4,5}=J_{7,8}=9.5$	4.46[q] 1.45[t]
2a[d]	7.86[s]		7.86[s]	8.28[d]	7.13[t]	7.50[t]	7.13[t]	8.28[d]	$J_{4,5}=J_{5,6}=9.5$	
8c	7.68[s]		7.68[s]	8.17[br s]		7.37[d]	6.97[t]	8.13[d]	$J_{4,6}<1$ $J_{6,7}=J_{7,8}=10$	2.63[s](CH_3)
8d[e]	7.60[s]		7.60[s]	8.09[d]		7.28[d]	6.93[t]	8.03[dd]	$J_{4,6}=J_{6,8}=1.2$ $J_{6,7}=J_{7,8}=10$	3.05[sept] $C\underline{H}(CH_3)_2$ 1.40[d] $CH(C\underline{H}_3)_2$
2b			7.40[s]	8.39[d]	7.13	—	7.92[m]	9.68[d]	$J_{4,5}=J_{7,8}=9.5$	4.08[q] 0.85[t]
2d				9.83[d]	7.52	—	8.02[m]	9.83[d]	$J_{4,5}=J_{7,8}=9.5$	3.92[q] 0.56[t]
8a				9.81[d]		7.86[d]	7.58[dd]	9.69[dd]	$J_{4,6}=1.5$ $J_{6,7}=9.7$ $J_{6,8}=2.0$ $J_{7,8}=9.5$	3.90[q] 0.53[t] 2.81[s] (CH_3)
8b				9.85[d]		7.88[d]	7.63[dd]	9.68[dd]	$J_{4,6}=1.5$ $J_{6,8}=9.7$ $J_{6,8}=2.0$ $J_{7,8}=9.7$	3.95[q] 0.58[t] 3.16[sept] $C\underline{H}(CH_3)_2$ 1.45[d] $CH(C\underline{H}_3)_2$
3a	7.68[s]	8.25[d]	7.40[d] 7.68[s]	8.16[d] 8.20[d]	6.90	—	7.92[m]	8.96[d] 8.20[d]	$J_{2,3}=3.9$ $J_{4,5}=J_{7,8}=9.5$ $J_{4',5'}=J_{7',8'}=9.5$	
3b		8.56[s]	7.38[s]	9.66[d] 8.33[d]	7.18	—	7.92[m]	8.50[d] 9.51[d]	$J_{4,5}=J_{7,8}=9.5$ $J_{4',5'}=J_{7',8'}=9.5$	4.43[q] 1.43[t](C-3) 4.06[q] 0.82[t](C-1′)
4a[f]	7.81[s] 7.43[d]	7.90[t]	7.81[s] 7.43[d]	8.38[d] 8.48[d]	7.23[t] 7.93[d]	7.60[t]	7.23[t] 7.93[t]	8.38[d] 8.48[d]	$J_{4,5}=J_{5,6}=10$ $J_{1',2'}=3.5$ $J_{4',5'}=10.5$	
4b		8.90[s]		9.83[d] 9.80[d]	7.7 7.73[d]	—	8.1[m] 7.73[d]	9.83[d] 9.80[d]	$J_{4,5}=J_{4',5'}=11$	4.00[t] 0.65[t](C-1,3) 4.45[q] 1.46[t](C-1′,3′)

a) In symmetrical biazulenes (**1a**, **1b**, **2a**, **2b**, and **8a**—**d**), the chemical shifts for two identical protons are listed on upper line. b) In asymmetrical biazulenes, the chemical shifts for protons numbered with prime are listed on lower line. c) 100 MHz. d) 100 MHz, FT-mode. e) In CCl_4. f) 200 MHz. g) s: Singlet; d: doublet; t: triplet; q: quartet; sept: septet; m: multiplet.

Table 6. Chemical shift difference ($\Delta\delta = \delta_{biazulene} - \delta_{azulene}$)[a,b] between biazulenes and reference azulenes

Compound	H-1 H-1′	H-2 H-2′	H-3 H-3′	H-4 H-4′	H-5 H-5′	H-6 H-6′	H-7 H-7′	H-8 H-8′	OCH_2–CH_3		Others
1a		0.11	0.06	−0.01	−0.09	−0.04	−0.19	−0.01			
1b		0.07		0.01				0.09	−0.09	0.02	
2a	0.44		0.44	−0.03	−0.02	−0.05	−0.02	−0.03			
8c	0.35		0.35	−0.29		−0.20	−0.09	−0.15			0.00(CH_3)
8d	0.39		0.39	−0.10		−0.13	−0.03	−0.09			0.06C<u>H</u>(CH_3)$_2$ 0.08CH($C\underline{H}_3$)$_2$
2b			0.09	−0.10				−0.04	−0.40	−0.85	
2d				−0.09				0.09	−0.51	−0.56	
8a				−0.03		−0.06	−0.34	0.01	−0.56	−0.93	0.01(CH_3)
8b				−0.03		−0.02	0.00	−0.05	−0.48	−0.87	0.08C<u>H</u>(CH_3)$_2$ 0.03CH($C\underline{H}_3$)$_2$
3a		0.30	−0.02	−0.15	0.25			0.65			
	0.26		0.26	−0.11				−0.11			
3b		0.11		−0.06				0.01	0.05	0.00	
			0.07	−0.16				−0.21	−0.42	−0.61	
4a	0.39		0.39	0.07	0.08	0.05	0.08	0.07			
	0.01	−0.05	0.01	0.17	0.78		0.78	0.17			
4b				0.09				0.09	−0.43	−0.79	
		0.09		−0.01				0.06	0.02	0.02	

a) In symmetrical biazulenes (**1a**, **1b**, **2a**, **2b**, and **8a**—**d**), the chemical shift differences for two identical protons are listed on upper line. b) In asymmetrical biazulenes (**3a**, **b** and **4a**, **b**), the chemical shift difference for the protons numbered with prime are listed on lower line.

those in **5b**. So, it seems that the two azulene rings in 1,1′-biazulenes, **1a**, **1b**, and **1d**, are not coplanar. In contrast with this, in the NMR spectra of 2,2′-biazulenes, **2a**, **8c**, and **8d**, it is shown that the ring protons (H-1, 1′, 3, and 3′) at the 1 and 3-positions of azulene rings are shifted markedly downfield by 0.35—0.43 ppm and the other ring protons slightly upfield. The downfield shifts of H-1, 1′, 3, and 3′ in 2,2′-biazulenes suggest that these protons are located in the peripheral zone of another azulene ring and consequently, 2,2′-biazulenes, **2a**, **8c**, and **8d**, exist in such a conformation that the two azulene rings are coplanar or nearly coplanar. This result is consistent with the conclusion from the ESR study on 2,2′-biazulene anion radical in which the two azulene rings were found to be coplanar.[14] The NMR spectrum of 2,6′-biazulene, **4a**, also shows downfield shifts of H-1, 3 and H-5′, 7′ by δ 0.39 and 0.78 ppm, respectively, compared with the corresponding protons of azulene. This fact suggests that **4a** also exists in a coplanar conformation.

On the other hand, in the NMR spectra of sterically crowded ester derivatives of 2,2′-biazulenes, **2b**, **2d**, **8a**, and **8b**, the ethyl proton signals of the ethoxycarbonyl groups appear at higher field than of **5b** and **7b**. Such a large upfield shift of ethyl proton signals presumably arises from long-range shielding by another azulene ring. This fact suggests that ethoxyl groups are located above the plane of another azulene ring and consequently, that the two azulene rings in ester derivatives, **2b**, **2d**, **8a**, and **8b**, are twisted to avoid the large steric interactions between the ethoxycarbonyl groups at C-1, 3 and C-1′, 3′.

Experimental

All mp's were uncorrected. Electronic spectra were measured on a Hitachi EPS-3 Spectrometer and IR Spectra on a Shimadzu IR-27 infracord. NMR spectra were obtained by a Varian A-60 D Spectrometer and in some cases on a JNM-100 instrument in Fourier transform mode. Mass spectra were recorded on a Hitachi RMU-6 mass spectrometer at 25 eV.

General Procedure for Ullmann Reaction of Haloazulenes. A mixture of haloazulenes and activated copper[6] was heated in an evacuated, sealed glass tube (see Table 1). After cooling, the reaction mixture was extracted with chloroform. The solvent was evaporated *in vacuo* and the resulting residue was chromatographed.

Reaction of **5a**. A mixture of **5a**[7a] (500 mg) and copper (500 mg) was treated according to the general procedure. A green residue from the extract was chromatographed on a silica-gel column with benzene as an eluent to give two fractions. The first fraction gave 23 mg of **5b**.[9] The second fraction gave 254 mg of **1b** as bluish green needles (from cyclohexane–benzene): mp 211—212 °C; IR (KBr) 1684, 1449, 1414, 1285, 1205, 1044, 781, and 741 cm^{-1}. Found: C, 78.62; H, 5.84%. Calcd for $C_{26}H_{22}O_4$: C, 78.37; H, 5.57%.

Reaction of **6a**. A mixture of **6a**[7c] (300 mg) and copper (600 mg) was treated according to the general procedure. The products were chromatographed on an alumina column with benzene. The first fraction gave a small amount of azulene. The second fraction gave 81 mg of **2a** as green scales (from chloroform): mp 320 °C.

Reaction of **6b**. A mixture of **6b**[7b] (100 mg) and copper (200 mg) was treated in the usual way. The products were chromatographed on an alumina column with benzene to give three fractions. The first fraction gave a small amount of a mixture of **5b** and **6b**. The second fraction gave 50 mg of **2b** as bluish needles (from ethanol); mp 151.5—152 °C. Found: C, 78.63; H, 5.53%. Calcd for $C_{24}H_{18}O_4$: C, 78.37; H, 5.57%. The third fraction eluted with chloroform gave 4 mg of brown needles[15] (from benzene); mp 245—246 °C. [MS, *m/e*: 352 (M^+, 100%); calcd for $C_{24}H_{16}O_3$, 352 (M)].

Reaction of **6c**. A mixture of **6c** (363 mg) and copper

(700 mg) was treated according to the general procedure. The products were chromatographed on an alumina column with chloroform to give 160 mg of **2c** as dark violet scales (from chloroform); mp 284—285 °C (dec); IR (KBr) 1635 cm^{-1}; NMR ($CDCl_3$) δ=7.45 (2H, s, H-3,3'), 7.6—8.1 (6H, m, H-5,5',-6,6' and -7,7'), 8.55 (dm, J=10 Hz, H-4,4'), 9.90 (2H, dm, J=10 Hz, H-8,8'), and 10.37 (s, 2 CHO). Found: C, 85.10; H, 4.34%. Calcd for $C_{22}H_{14}O_2$: C, 85.14; H, 4.55%.

Reaction of 7a. A mixture of **7a**[7c] (100 mg) and copper (200 mg) was treated in the usual way. The products were chromatographed on a silica-gel column with benzene to give three fractions. The first fraction gave 5 mg of **7d**.[9] The second fraction gave 8 mg of **7a**. The third fraction eluted with chloroform gave 73 mg of **2d** as red prisms (from ethanol); mp 181—182 °C. Found: C, 71.01; H, 5.72%. Calcd for $C_{32}H_{30}O_8$: C, 70.83; H, 5.57%.

Reaction of Diethyl 2-Chloro-5-methylazulene-1,3-dicarboxylate (7b). A mixture of **7b**[7b] (1.09 g) and copper (2.18 g) was treated in the usual way. Chromatography of the products on a silica-gel column with benzene gave two fractions. The first fraction gave 140 mg of a mixture of **7b** and diethyl 5-methylazulene-1,3-dicarboxylate (**7e**)[16] (1 : 1 ratio by NMR). The second fraction gave 515 mg of **8a** as red prisms (from benzene–cyclohexane); mp 179—180 °C. Found: C, 71.69; H, 6.25%. Calcd for $C_{34}H_{34}O_8$: C, 71.56; H, 6.01%.

Reaction of Diethyl 2-Chloro-5-isopropylazulene-1,3-dicarboxylate (7c). A mixture of **7c**[7b] (500 mg) and copper (1.0 g) was treated in the manner described above. The chromatography of the products on a silica-gel column with benzene gave two fractions. The first fraction gave a small amount of a mixture of **7c** and diethyl 5-isopropylazulene-1,3-dicarboxylate (**7f**).[17] The second fraction gave 50 mg of **8b** as red prisms (from ethanol); mp 174—175 °C. Found: C, 72.93; H, 6.90%. Calcd for $C_{38}H_{42}O_8$: C, 72.82; H, 6.76%.

Reaction of a mixture of 5a and 6b. A mixture of **5a** (200 mg), **6b** (200 mg), and copper (400 mg) was treated in the usual way. The chromatography of the product on a silica-gel column with benzene gave fractions, a, b, c, and d. The fraction a, b, and d gave **5b** (45 mg), **1b** (68 mg), and **2b** (65 mg), respectively. The yellow fraction c gave 53 mg of **3b** as dark green needles (from cyclohexane); mp 119—120 °C. Found: C, 78.12; H, 5.74%. Calcd for $C_{26}H_{22}O_4$: C, 78.37; H, 5.57%. TNB-complex: brown needles (from ethanol); mp 130—131 °C. Found: C, 63.04; H, 4.42; N, 6.73%. Calcd for $C_{32}H_{25}O_{10}N_3$: C, 62.80; H, 4.12; N, 6.87%.

Reaction of a Mixture of 7a and 9a. A mixture of diethyl 6-bromoazulene-1,3-dicarboxylate (**9b**)[12] (900 mg), potassium iodide (17 g), water (10 cm^3), and acetic acid (80 cm^3) was treated under reflux for 50 h. The reaction mixture was diluted with water and the resulting precipitate was collected by filtration and dried *in vacuo*. Chromatography on a silica-gel column with benzene gave a mixture of diethyl 6-iodoazulene-1,3-dicarboxylate (**9a**) and **9b** (1 : 5 ratio by NMR), which could not be separated by thin layer chromatography. NMR of **9a**: δ=1.45 (t, J=7.0 Hz, 2 $OCH_2C\underline{H}_3$), 4.45 (q, J=7.0 Hz, 2 $OC\underline{H}_2CH_3$), 7.81 (d, J=11.5 Hz, H-5,7), 8.80 (s, H-2), 9.61 (d, J=11.5 Hz, H-4,8). This mixture of 6-haloazulenes (680 mg) was mixed with **7a** (1.0 g) and copper (2.0 g) and the mixture was treated in the manner described above. The chromatography of the crude products on a silica-gel column with benzene gave six bands. The fifth band afforded 61 mg of **4b** as red needles (from ethanol); mp 257—258 °C. Found: C, 70.50; H, 5.31%. Calcd for $C_{32}H_{30}O_4$: C, 70.83; H, 5.51%. From the sixth band 276 mg of **2d** was obtained.

1,1'-Biazulene-3,3'-dicarboxylic Acid (1c). A solution of **1b** (256 mg) dissolved in a solution of potassium hydroxide (100 mg) in ethanol (25 cm^3) containing water (0.5 cm^3) was heated under reflux for 5 h. After cooling the solution was diluted with water (30 cm^3) and acidified with 2 mol dm^{-3} HCl. Greenish crystals separated out were collected by filtration and washed repeated with water, to afforded 224 mg (98%) of **1c** as microcrystals, mp 290—293 °C (dec). IR (KBr): 3000—2570, 1647, 1456, 1287, 1236, 1029, 755, and 732 cm^{-1}. Found: C, 77.02; H, 4.24%. Calcd for $C_{22}H_{14}O_4$: C, 77.18 ; H, 4.12%.

1,1'-Biazulene (1a): Heating of **1c** (280 mg) at 250 °C/15 Torr† in a sublimation apparatus afforded 120 mg of blue crystals which were chromatographed on an alumina column (benzene) to give a single bluish green fraction, yielding 115 mg (55%) of **1a** as bluish green scales (from hexane): mp 104—105 °C; MS, *m/e*, 255 (M^+ +1, 21.4%), 254 (M^+, 100), 253 (M^+ −1, 18.5), 252 (41.4), and 251 (22.8); IR (KBr) 2990 (w), 1567 (s), 1488 (m), 1453 (m), 1406 (w), 1389 (vs), 1304 (m), 1290 (m), 1269 (w), 1212 (m), 1142 (w), 1130 (w), 1043 (w), 967 (w), 961 (w), 943 (m), 900 (m), 877 (w), 855 (w), 827 (m), 787 (vs), 747 (m), 735 (m), and 727 (s) cm^{-1}. Found: C, 94.35; H, 5.83%. Calcd for $C_{20}H_{14}$: C, 94.45; H, 5.55%.

TNB Complex of 1a: Dark blue neeldes (from ethanol): mp 200—201 °C. Found: C, 56.23; H, 3.17; N, 12.06%. Calcd for $C_{32}H_{20}O_{12}N_6$: C, 56.52; H, 2.96; N, 12.13%. IR (KBr) 2990, 1972, 1569, 1488, 1453, 1389, 1304, 1290, 1269, 1212, 1147, 1130, 1043, 967, 961, 943, 936, 900, 877, 855, 827, 787, 747, 735, and ,727 cm^{-1}.

Ethyl 1,1'-Biazulene-3-carboxylate (1d). To a warmed ethanol solution (25 cm^3) of **1b** (76 mg, 0.19 mmol) was added 1 cm^3 of aqueous KOH (11 mg, 0.19 mmol) . The solution was heated under reflux for 15 min and then diluted with water (50 cm^3). The precipitated **1b** (3 mg) was colloected by filtration. The filtrate was acidified with diluted HCl to give a mixture of di- and monocarboxylic acids which was collected by filtration and dried. The mixture, without further purification, was heated at 270—280 °C/10 Torr in a sublimation apparatus to give a mixture of the decarboxylated products, which was chromatographed on an alumina column with benzene. The first elution with benzene afforded 4 mg of **1a**. The second elution with benzene yielded 18 mg of **1d**, blue needles (from ethanol), mp 137—138 °C. Found: C, 84.89; H, 5.72%. Calcd for $C_{23}H_{18}O_2$: C, 84.64; H, 5.56%.

Dimethyl 1,1'-Biazulene-3,3'-dicarboxylate (1e). Treatment of **1c** (51 mg) with ethereal diazomethane gave 39 mg of **1e** as bluish green needles (from benzene–cyclohexane): mp 232—233 °C; UV_{max} (MeOH), nm (log ε), 240 (4.64), 279 (4.83), 304 (4.71), and 405 (4.14), [575 (2.30) in isooctane]; IR (KBr) 1701, 1200, 1029 cm^{-1}. Found: C, 77.76; H, 4.66%. Calcd for $C_{24}H_{18}O_4$: C, 77.82; H, 4.90%.

1,1'-Biazulene-3,3'-d_2 (1f). This compound was prepared by a modification of the method reported.[10] To a solution of **1a** (50 mg) in cyclohexane (5 cm^3) was added 85% D_3PO_4 (3 cm^3) under a nitrogen atmosphere. The solution was shaken until **1a** in the organic layer had transferred completely into the D_3PO_4 phase and then the upper layer was removed by using a small pipette. To the brown phosphoric acid layer obtained was added 3 cm^3 of deuterium oxide. The resulting solution was extracted with cyclohexane. The organic layer was passed through anhydrous sodium sulfate and evaporated under a reduced pressure. The crude product was recrystallized from pentane to give 39 mg of **1f** as bluish green scales: mp 103—104 °C; MS, *m/e*, 256 (M^+,

† 1 Torr≈133.322 Pa.

100%); NMR ($CDCl_3$) δ=6.97 (t, J=9.5 Hz, H-7,7'), 7.05 (t, J=9.5 Hz, H-5,5'), 7.50 (t, J=9.5 Hz, H-6,6'), 8.04 (s, H-2,2'), 8.25 (d, J=9.5 Hz, H-4,4' or H-8,8'), and 8.29 (d, J=9.5 Hz, H-8,8' or H-4,4').

*3,3'-Dibromo-1,1'-biazulene (**1g**).* To a solution of **1a** (50.8 mg) in benzene (2 cm^3) was added NBS (72 mg) with stirring at room temp. After stirring for a day, the reaction mixture was chromatographed on an alumina column with benzene to give 52.8 mg of **1g** as blue needles (from cyclohexane–benzene 9 : 1 mixture): mp 173—175 °C; IR (KBr) 1579, 1381, 862, and 737 cm^{-1}; NMR ($CDCl_3$) δ= 7.20 (t, J=10 Hz, H-5,5' and H-7,7'), 7.78 (t, J=10 Hz, H-6,6'), 7.96 (s, H-2,2'), and 8.20 and 8.35 (d, J=9.5 Hz, H-4,4' and H-8,8'). Found: C, 58.00; H, 3.07%. Calcd for $C_{20}H_{12}Br_2$: C, 58.29; H, 2.94%.

*2,2'-Biazulene-1,1'-dicarboxylic Acid (**2e**).* A solution of **2b** (180 mg) and potassium hydroxide (60 mg) in 0.5 cm^3 of water and 5 cm^3 of ethanol was heated under reflux for 3 h, and diluted water (10 cm^3). After cooling, the solution was acidified by 1 mol dm^{-3} HCl to give 150 mg (97%) of **2e** as red crystals (from ethanol): mp 160—165 °C (dec); IR (KBr) 3030, 1650, 1395, 1239, 950, and 814 cm^{-1}. Found: C, 77.08; H, 4.30%. Calcd for $C_{22}H_{14}O_4$: C, 77.18; H, 4.12%.

Dimethyl 2,2'-Biazulene-1,1'-dicarboxylate was obtained by treatment of **2e** with ethereal diazomethane as blue-violet needles (from methanol): mp 183—184 °C; IR (KBr) 1689 cm^{-1}; NMR ($CDCl_3$) δ=3.63 (s, 2 CO_2CH_3), 7.40 (s, H-3,3'), 7.3—7.9 (m, H-5—7 and H-5'—7'), 8.38 (d, J=9 Hz, H-4,4'), and 9.56 (d, J=9 Hz, H-8,8'). Found: C, 77.73; H, 4.81%. Calcd for $C_{24}H_{18}O_4$: C, 77.82; H, 4.90%.

*2,2'-Biazulene-1,1',3,3'-tetracarboxylic Acid (**2f**).* A solution of **2d** (300 mg) and potassium hydroxide (320 mg) in 0.5 cm^3 of water and 8 cm^3 of ethanol was refluxed for 10 h. The solution was diluted with 20 cm^3 of water and filtreted through a glass-filter to remove an insoluble material. The filtrate was acidified with 2 mol dm^{-3} HCl and then red crystals separated out were collected by filtration and repeatedly washed with water to give 231 mg of **2f** as red crystalline powder, mp 210—215 °C, which is sparingly soluble in organic solvents. IR (KBr) 3030, 1701 sh, 1658, 1449, and 1229 cm^{-1}. Found: C, 67.03; H, 3.41%. Calcd for $C_{24}H_{14}O_8$: C, 66.98; H, 3.28%.

Treatment of **2f** with diazomethane afforded the tetramethyl ether as red prisms (from chloroform): mp—320 °C; NMR ($CDCl_3$) δ=3.45 (s, OCH_3), 7.5—8.0 (m, H-5—7 and H-5'—7'), 9.75 (br d, J=9 Hz, H-4,4' and H-8,8'); IR (KBr) 1695, 1451, 1391, 1193, and 1151 cm^{-1}. Found: C, 68.81; H, 4.54%. Calcd for $C_{28}H_{22}O_8$: C, 69.13; H, 4.56%.

*2,2'-Biazulene (**2a**).* *Decarboxylation of **2e**:* Heating of **2e** (100 mg) at 250 °C/0.5 Torr in a sublimation apparatus afforded green solid which was dissolved in chloroform and the solution was passed through an alumina column. The solvent of the eluent was removed *in vacuo*. The residue was recrystallized from chloroform to give 43 mg of **2a** as green scales with metallic luster: mp>320 °C; IR (KBr) 3030 (w), 1567 (m), 1534 (m), 1451 (m), 1408 (s), 1389 (m), 1359 (m), 1299 (w), 1248 (w), (1096 w), 1012 (w), 989 (w), 971 (w), 899 (w), and 720 (s) cm^{-1}; NMR (DMSO-d_6, at 150 °C) δ= 7.15 (br t, J=9 Hz, H-5,5',7,7'), 7.40 (br t, J=9 Hz, H-6,6'), 7.85 (s, H-1,1', 3,3'), 8.31 (br d, J=9 Hz, H-4,4',8,8'); MS, *m/e*, 255 (M^+ +1, 20.6%), 254 (M^+, 100), and 252 (27.4). Found: C, 94.47; H, 5.41%. Calcd for $C_{20}H_{14}$: C, 94.45; H, 5.55%.

*Decarboxylation of **2f**:* The treatment of **2f** in a manner similar to that described above gave 23 mg of **2a**.

*Deethoxycarbonylation of **2b** with 100% Phosphoric Acid:* A mixture of **2b** (300 mg) and 100% phosphoric acid (3 cm^3) was heated at 95 °C for 1 h. The reaction mixture was diluted with ice–water (10 g). Green crystals were collected by filtration, washed repeatedly with water and dried, yielding 19 mg (99%) of **2a**.

*Deethoxycarbonylation of **2d** with 100% Phosphoric Acid:* A mixture of **2d** (50 mg) and 100% phosphoric acid (3 cm^3) was heated at 95 °C for 2 h. The reaction mixture was treated in a manner to the above, yielding 20 mg (95%) of **2a**.

*5,5'-Dimethyl-2,2'-biazulene (**8c**).* A mixture of **8a** (55 mg) and 100% phosphoric acid (3 cm^3) was treated in a manner similar to the above, yielding 28 mg (99%) of **8c** as green needles (from chloroform): mp 244—245 °C; MS, *m/e*, 282 (M^+, 100%), 265 (14), 141 (M^{2+}, 11); IR (KBr) 2985 (w), 2890 (w), 1572 (m), 1522 (m), 1464 (m), 1418 (m), 1391 (s), 1376 (m), 1302 (w), 1250 (w), 1218 (m), 1157 (w), 1057 (w), 979 (m), 936 (m), 910 (m), 837 (m), 804 (s), 794 (m), 763 (w), and 733 (m) cm^{-1}; NMR (DMSO-d_6) δ=2.58 (s, 2 CH_3), 7.05 (t, J=10 Hz, H-7,7'), 7.47 (d, J=10 Hz, H-6,6'), 7.72 (s, H-1,1',3,3'), 8.18 (d, J=10 Hz, H-8,8'), and 8.27 (br s, H-4,4'). Found: C, 93.13; H, 6.48%. Calcd for $C_{22}H_{18}$: C, 93.57; H, 6.43%.

*5,5'-Diisopropyl-2,2'-biazulene (**8d**).* *Deethoxycarbonylation of **8b** with 100% Phosphoric Acid:* A mixture of **8b** (40 mg) and 100% phosphoric acid (3 cm^3) was treated in a manner similar to the above, afforded 20 mg of **8d** (from pentane): mp 150—151 °C; MS, *m/e*, (M^+ +2, 40%), 339 (M^+ +1, 30), 338 (M^+, 100), 323 (M^+ −15, 40), 308 (M^+ −30, 6), 265 (12), and 169 (M^{2+}, 9); IR (KBr) 2985 (m), 2959 (m), 1572 (m), 1520 (m), 1460 (m), 1445 (m), 1403 (vs), 1381 sh (m), 1333 (w), 1299 (w), 1250 (w), 1220 (w), 1182 (w), 1136 (w), 1101 (w), 1012 (w), 941 (w), 928 (m), 882 (w), 815 (vs), and 770 (m) cm^{-1}. Found: C, 91.86; H, 7.63%. Calcd for $C_{26}H_{26}$: C, 92.26; H, 7.74%.

With Alkaline Hydrolysis: A solution of **8b** (100 mg) and potassium hydroxide (80 mg) in a mixture of water (0.3 cm^3) and ethanol (5 cm^3) was heated under reflux for 3 h. After cooling, the solution was diluted with water (10 cm^3) and acidified with 1 mol dm^{-3} HCl to give 72 mg of a tetracarboxylic acid. Decarboxylation of the acid (60 mg) by heating at 260 °C/0.5 Torr in sublimation apparatus afforded 37 mg of **8d** as green needles, mp 150—151 °C (from pentane).

*2-Iodoazulene-1-carboxaldehyde (**6c**).* To a solution of **6a**[7c] (100 mg) in DMF (0.5 cm^3) was added phosphoryl chloride (0.1 cm^3) at room temp with stirring. After being stirred for another 1 h, the reaction mixture was poured into sat. aq $NaHCO_3$ and extracted with ether. The organic extract was washed with water, dried over Na_2SO_4, and evaporated. The residue was chromatographed on an alumina column with benzene to give 110 mg (99%) of **6c** as red prisms (from ethanol); mp 140—141 °C; IR (KBr) 1639 cm^{-1}; NMR ($CDCl_3$) δ=7.43 (s, H-3), 7.3—8.0 (m, H-5—7), 8.33 (d, J=10 Hz, H-4), 9.70 (d, J=10 Hz, H-8), and 10.12 (s, CHO). Found: C, 47.18; H, 2.70%. Calcd for $C_{11}H_7OI$: C, 46.85; H, 2.52%.

*Formylation of **2a**.* To a suspension of **2a** (20 mg) in DMF (3 cm^3) was added $POCl_3$ at room temp with stirring. The mixture was heated at 60 °C for 1 h and then quenched with water to give green crystals, which were collected by filtration, dried over $CaCl_2$, in a desiccator. The chromatography of the crude products on an alumina column with chloroform gave 24 mg (98%) of **2c**, dark violet scales, mp 284—285 °C (dec).

*Diethyl 3,3'-Dibromo-2,2'-biazulene-1,1'-dicarboxylate (**2g**).* To a solution of **2b** (580 mg) in dry benzene (50 cm^3) was added NBS (636 mg). The mixture was stirred overnight at room temp. The color of the solution turned bluish violet

from reddish violet. The solvent was evaporated and the residue was chromatographed on a silica-gel column with benzene to give 569 mg of **2g** as blue needles (from ethanol): mp 178—179 °C. λ_{max} (MeOH), nm (log ε), 239 (4.37), 315 (4.78), 364 sh, and 380 (3.93) [560 (3.00), 598 (2.97), 656 (2.62) in benzene]; IR (KBr) 1686 cm^{-1}; NMR ($CDCl_3$) δ=0.65 (t, J=7.0 Hz, 2 $OCH_2C\underline{H}_3$), 4.00 (q, J=7.0 Hz, 2 $OC\underline{H}_2CH_3$), 7.35—8.10 (m, H-5—7 and H-5'—7'), 8.58 (d, J=9 Hz, H-4,4'), and 9.73 (br d, J=9 Hz, H-8,8'). Found: C, 56.30; H, 3.72%. Calcd for $C_{26}H_{20}O_4Br_2$: C, 56.16; H, 3.63%.

Diethyl 3,3'-Diiodo-2,2'-biazulene-1,1'-dicarboxylate (2h). To a solution of **2b** (292 mg, 0.73 mmol) in CH_2Cl_2 (3 cm^3) was added *N*-iodosuccinimide (352 mg) with stirring at room temp. After stirring for 1.5 h, the reaction mixture was chromatographed on an alumina column with benzene to give violet crystals (496 mg) of 2 h. Recrystallization from EtOH–CH_2Cl_2 (9 : 1) afforded blue prisms: mp 207—208 °C; IR (KBr) 1675, 1195, and 1031 cm^{-1}; NMR ($CDCl_3$) δ= 0.60 (t, J=7.0 Hz, 2 $OCH_2C\underline{H}_3$), 3.90 (q, J=7.0 Hz, 2 $OC\underline{H}_2CH_3$), 7.36—7.96 (m, H-5—7 and 5'—7'), 8.65 (br d, J=9.5 Hz, H-4,4'), and 9.75 (br d, J=9.5 Hz, H-8,8'). Found: C, 48.26; H, 3.13%. Calcd for $C_{26}H_{20}O_4I_2$: C, 48.04; H, 3.10%.

Dimethyl 3,3'-Dibromo-2,2'-biazulene-1,1'-dicarboxylate (2i). A solution of **2g** (988 mg) and potassium hydroxide (1.5 g) in a mixture of water (5 cm^3) and ethanol (10 cm^3) was heated under reflux for 15 h. The solution was diluted with water and acidified with dilute HCl. The precipitates were collected by filtration, washed with water, dried over $CaCl_2$, and recrystallized from ethanol to give a dicarboxylic acid as black prisms; mp near 300 °C (dec); IR (KBr) 2940 and 1630 cm^{-1}. Found: C, 53.17; H, 2.73%. Calcd for $C_{22}H_{12}O_4Br_2$: C, 52.84; H, 2.24%. This acid was treated with ethereal diazomethane to give **2i** as violet needles (from ethanol): mp 285—286 °C; IR (KBr) 1684 cm^{-1}; NMR ($CDCl_3$) δ= 3.55 (OCH_3). Found: 54.28; H, 3.20%. Calcd for $C_{24}H_{16}O_4Br_2$: C, 54.27; H, 3.04%.

2,2'-Biazulene-1,1' : 3,3'-tetracarboxylic Dianhydride (2j). A mixture of **2f** (1.89 g) in acetic anhydride (15 cm^3) was heated under gentle boiling for 2 h to give 1.6 g of **2j** as red crystals: mp$>$300 °C; IR (KBr) 1706, 1133, 1016, and 762 cm^{-1}. Found: C, 72.81; H, 2.65%. Calcd for $C_{24}H_{10}O_6$: C, 73.10; H, 2.56%.

Ethanolysis of 2j. To an ethanol solution of sodium ethoxide, prepared from 207 mg of sodium, was added 1.3 g of **2j** and the mixture was heated for 1 h. After cooling, the solution was diluted with water (50 cm^3) and acidified with dilute HCl to give precipitates which were collected by filtration, washed with water and dried over $CaCl_2$ in a desiccator. Decarboxylation of the mixture of carboxylic acids by heating at 260—280 °C/10 Torr gave a brown violet substance. Chromatography over a silica-gel column using benzene as an eluent gave four fractions, a, b, c, and d. The fraction a gave 7 mg of **2a**. The fraction b gave 183 mg (15%) of ethyl 2,2'-biazulene-1-carboxylate (**2k**) as blue sacles (from cyclohexane): mp 145—146 °C; IR (KBr) 1682 cm^{-1}; NMR ($CDCl_3$) δ=1.26 (t, J=7.0 Hz, $OCH_2C\underline{H}_3$), 4.41 (q, J=7.0 Hz, $OC\underline{H}_2CH_3$), 6.78—7.83 (9H, m, H-1',3,3', H-5—7, and H-5'—7'). 8.26 (3H, br d, J=9.5 Hz, H-4,4',8'), and 9.28 (br d, J=9.5 Hz, H-8). Found: C, 84.35; H, 5.70%. Calcd for $C_{23}H_{18}O_2$: C, 84.64; H, 5.56%. The fraction c gave 323 mg (22.4%) of diethyl 2,2'-biazulene-1,3-dicarboxylate (**2m**) as blue scales (from ethanol): mp 151—152 °C; IR (KBr) 1677 cm^{-1}; NMR ($CDCl_3$) δ=0.80 (t, J=7.0 Hz, 2 $OCH_2C\underline{H}_3$), 4.08 (q, J=7.0 Hz, 2 $OC\underline{H}_2CH_3$), 7.46 (s, H-1',3'), 7.0—8.0 (m, H-5—7 and H-5'—7'), 8.30 (br d, J=9.5 Hz, H-4',8'), and 9.58 (br d, J=9.5 Hz, H-4,8). Found: C, 78.64; H, 5.79%. Calcd for $C_{26}H_{22}O_4$: C, 78.37; H, 5.57%. The fraction d afforded 528 mg (36.6%) of **2b**.

1,2'-Biazulene-1,3-dicarboxylic Acid (3c). A mixture of **3b** (123 mg) and potassium hydroxide (166 mg) in a mixture of water (0.5 cm^3) and ethanol (3 cm^3) was heated under reflux for 5 h. The solution was diluted with water (10 cm^3) and acidified with 2 mol dm^{-3} HCl. The brown precipitates separated out were collected by filtration, repeatedly washed with water and dried over $CaCl_2$ in a desiccator to give 97 mg of **3c** as brown crystals (from ethanol): mp 240—243 °C (dec); IR (KBr) 2915, 1650, and 1645 cm^{-1}. Found: C, 77.31; H, 4.20%. Calcd for $C_{22}H_{14}O_4$: C, 77.18; H, 4.12%.

Dimethyl 1,2'-Biazulene-1',3-dicarboxylate (3d). Treatment of **3c** with diazomethane gave **3d** as dark brown-blue needles (from ethanol): mp 124—125 °C; IR (KBr) 1686 and 1684 cm^{-1}; UV_{max} (MeOH), nm (log ε), 237 (4.58), 288 (4.71), 306 (4.70), 344 sh (4.45), and 426 (4.14). Found: C, 77.76; H, 4.66%. Calcd for $C_{24}H_{18}O_4$: C, 77.83; H, 4.86%.

1,2'-Biazulene (3a). Heating of **3c** (64 mg) at 215—220 °C/15 Torr afforded 43 mg of crude crystals which were chromatographed on an alumina column with benzene as an eluent to give 34 mg of **3a** as green scales with metallic luster (from pentane): mp 144—145 °C; MS, *m/e*, 255 (M^+ +1, 20.7%), 254 (M^+, 100), 253 (M^+ −1, 65.1), 252 (M^+ −2, 81.7), 226 (12), 148 (33), 127 (M^{2+}, 15), and 126 (37); IR (KBr) 3030 (w), 1590 (w), 1565 (s), 1513 (vs), 1468 (w), 1412 (s), 1391 (vs), 1337 (m), 1297 (m), 1261 (w), 1215 (w), 1193 (w), 1110 (w), 1017 (w), 988 (w), 971 (w), 965 (w), 943 (m), 908 (w), 898 (m), 885 (w), 852 (w), 827 (m), 810 (s), 780 (s), and 722 (s) cm^{-1}. Found: C, 94.29; H, 5.55%. Calcd for $C_{20}H_{14}$: C, 94.45; H, 5.55%.

TNB-complex: Brown scales (ethanol); mp 189—190 °C. Found: C, 67.20; H, 3.51; N, 8.74%. Calcd for $C_{26}H_{17}O_6N_3$: C, 66.81; H, 3.67; N, 8.99%.

2,6'-Biazulene (4a). A mixture of **4b** (13 cm^3) in 5 cm^3 of 100% phosphoric acid was heated at 95 °C for 2 h. The reaction mixture was treated similarly to the cases of **2a** from **2b**, giving 5 mg (90%) of **4a** as green scales (from chloroform): mp 300 °C; MS, *m/e*, 255 (M^+ +1, 21.0%), 254 (M^+, 100), and 252 (35.2); IR (KBr) 3070 (w), 1570 (w), 1445 (w), 1399 (m), 1370 (m), 1227 (w), 1196 (w), 1186 (w), 1110 (w), 1014 (w), 990 (w), 971 (w), 909 (w), 899 (w), 876 (m), 810 (vs), 885 (w), and 727 (m) cm^{-1}. Found: C, 94.70; H, 5.52%. Calcd for $C_{20}H_{14}$: C, 94.45; H, 5.55%.

References

1) This work was presented in part at the 20th National Meeting of the Chemical Society of Japan, Tokyo, April 1967, *cf.* Abstr., p. 437.

2) R. Hagen, E. Heilbronner, and P. A. Staub, *Helv. Chim. Acta*, **51**, 45 (1968).

3) H. Maus, Ph. D. Thesis, University Marburg (1962).

4) M. Hanke and C. Jutz, *Angew. Chem.*, **91**, 227 (1979); *Angew. Chem., Int. Ed. Engl.*, **18**, 214 (1979).

5) M. Hanke and C. Jutz, *Synthesis*, **1980**, 31.

6) E. C. Kleinder and R. Adams, *J. Am. Chem. Soc.*, **55**, 4225 (1933); H. W. Gibson and F. C. Bailey, *J. Org. Chem.*, **34**, 557 (1976).

7) a) T. Morita and K. Takase, *Sci. Repts, Ser. 1. Tohoku University*, **62**, 83 (1980); b) T. Morita, T. Fujita, T. Nakadate, and K. Takase, *ibid.*, **62**, 91 (1980); c) T. Nozoe, S. Seto, and S. Matsumura, *Bull. Chem. Soc. Jpn.*, **35**, 1990 (1962).

8) J. Forrest, *J. Chem. Soc.*, **1960**, 566; **1960**, 581; A. H. Lewin, and T. Cohen, *Tetrahedron Lett.*, **1965**, 4531.

9) T. Nozoe, S. Seto, S. Matsumura, and Y. Murase,

Bull. Chem. Soc. Jpn., **35**, 1179 (1962).
10) A. Bauder and H. H. Guthard, *Helv. Chim. Acta*, **41**, 889 (1958).
11) T. Nozoe, K. Takase, T. Nakazawa, and S. Fukuda, *Tetrahedron*, **27**, 3357 (1971).
12) T. Nozoe, K. Takase, and M. Tada, *Bull. Chem. Soc. Jpn.*, **38**, 247 (1965); R. N. McDonald and J. M. Richmond, *J. Chem. Soc., Chem. Commun.*, **1973**, 605; R. N. McDonald, J. M. Richmnod, J. R. Curtis, H. E. Petty, and T. L. Hoskins, *J. Org. Chem.*, **41**, 1811 (1976).
13) A. G. Anderson, Jr., and J. J. Tazuma, *J. Am. Chem. Soc.*, **75**, 4979 (1953).
14) Y. Ikegami and S. Seto, *Mol. Phys.*, **16**, 101 (1969); *Bull. Chem. Soc. Jpn.*, **43**, 2409 (1970).
15) Details of the structure will be published elsewhere in near future.
16) H. Akino, *Sci. Repts. Hirosaki University*, **11**, 18 (1964); *Chem. Abstr.*, **63**, 1754 (1965).
17) T. Nozoe, S. Seto, S. Matsumura, and T. Asano, *Proc. Jpn. Acad.*, **32**, 339 (1956).

 © 1982 The Chemical Society of Japan Bull. Chem. Soc. Jpn., 55, 1153—1155 (1982)

A New Preparative Method of 2,2-Dimethyl-2*H*-chromenes

Yoshiyuki KAWASE,* Seiji YAMAGUCHI, Hisanori HORITA,
Junko TAKENO, and Hideaki KAMEYAMA
Department of Chemistry, Faculty of Science, Toyama University, Gofuku 3190, Toyama 930
(Received July 24, 1981)

2,2-Dimethyl-2*H*-chromene was prepared from salicylaldehyde and ethyl 3-methyl-2-butenoate (or ethyl α-bromoisobutyrate) in one step. This new method of preparing 2,2-dimethyl-2*H*-chromene was studied and applied to some 2,2-dimethyl-2*H*-chromene derivatives.

Many methods to prepare 2,2-dimethyl-2*H*-chromenes have been reported,[1] but they have involved many reaction steps and low yields. In our preparative study of 2-isopropylbenzofuran, we found a new method to prepare 2,2-dimethyl-2*H*-chromenes. In this paper, we will report this new method.

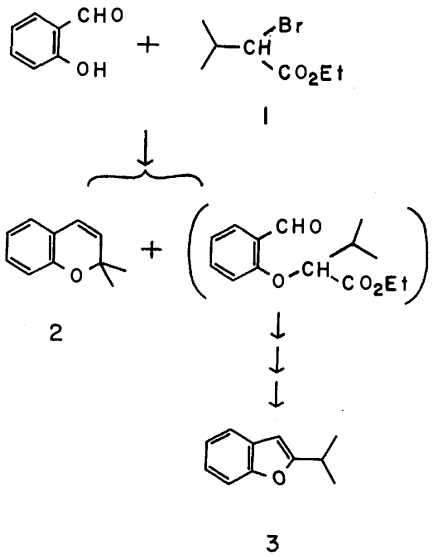

In general, 2-alkylbenzofurans are prepared from salicylaldehyde and ethyl α-bromocarboxylate.[2] In our preparative study of 2-isopropylbenzofuran (**3**) by this method, a solution of salicylaldehyde and ethyl α-bromoisobutyrate (**1**) in DMF was heated at 130 °C in the presence of potassium carbonate, and the products were distilled under reduced pressure. Moreover, the non-volatile part gave the expected 2-isopropylbenzofuran (**3**) after treatment with a 30% aqueous potassium hydroxide solution and sodium acetate-acetic anhydride. The volatile part consisted mainly of 2,2-dimethyl-2*H*-chromene (**2**). It was of great interest that 2,2-dimethyl-2*H*-chromene (**2**) was obtained in a one-step reaction. Next, the reaction of salicylaldehyde and ethyl α-bromoisobutyrate (**1**) was examined under several conditions. The results are given in Table 1. The reactions in DMF or in DMSO gave 2,2-dimethyl-2*H*-chromene (**2**), but those in THF or in pyridine did not. Also, satisfactory yields were obtained after 8 h both in DMF and in DMSO.

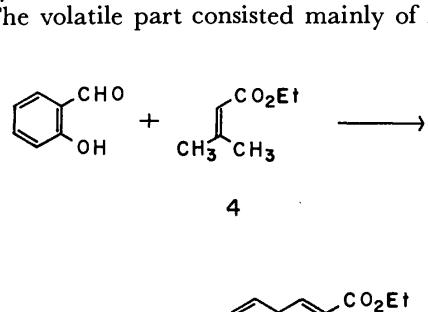

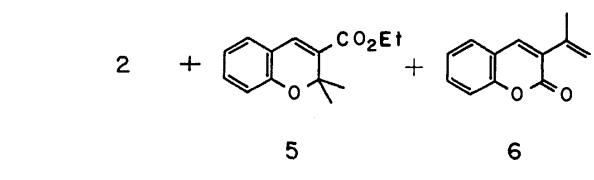

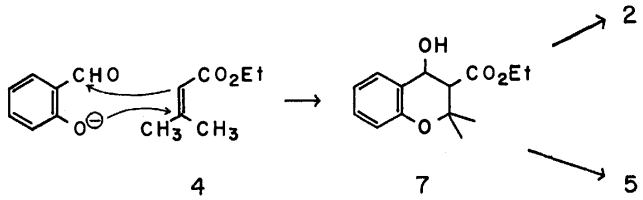

This reaction is thought to proceed as follows. Ethyl α-bromoisobutyrate (**1**) is converted to ethyl 3-methyl-2-butenoate (**4**) by dehydrobromination. Then, the phenolate ion attacks the C=C double bond in ethyl 3-methyl-2-butenoate (**4**), and the resulting carbanion attacks the C=O double bond in salicylaldehyde. These two nucleophilic attacks form ethyl 4-hydroxy-2,2-dimethylchroman-3-carboxylate (**7**) as an intermediate, which then readily loses ethanol and carbon dioxide to give 2,2-dimethyl-2*H*-chromene (**2**).

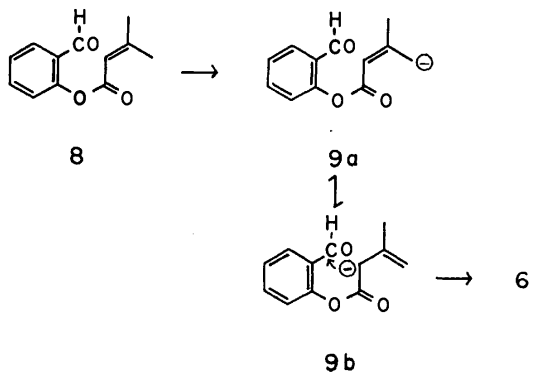

Next, the reaction of salicylaldehyde and ethyl 3-methyl-2-butenoate (**4**) was also examined under similar conditions; the results are given in Table 2. The yield of 2,2-dimethyl-2*H*-chromene (**2**) was the best at 8 h in this reaction. In several cases, 3-isopropenylcoumarin (**6**) was obtained. This new coumarin is thought to be formed as follows: The phenolate ion

TABLE 1. THE REACTIONS OF SALICYLALDEHYDE AND ETHYL α-BROMOISOBUTYRATE (1)

Solvent	Temp/°C	Time/h	Yield of 2/%
DMF	130	5	3
		8	25
		16	29
DMSO	130	8	24
THF	Reflux	8	0
Pyr.	Reflux	8	0

TABLE 2. THE REACTIONS OF SALICYLALDEHYDE AND ETHYL 3-METHYL-2-BUTENOATE (4)

Base	Time/h	Yield/%		
		2	5	6
K_2CO_3	5	17	0	0
	8	35	1	3
	15	32	0	1
NaOEt	8	0	0	7
DBU	8	0	0	2

Solvent: DMF, temp: 130 °C.

attacks the C=O double bond in ethyl 3-methyl-2-butenoate (**4**) to give *o*-formylphenyl 3-methyl-2-butenoate (**8**), which loses the γ proton in 3-methyl-2-butenoate (**8**) to give the mesomery of the γ carbanion (**9a**) and the α carbanion (**9b**). Then, the α carbanion attacks the C=O double bond in the aldehyde to form 3-isopropenylcoumarin (**6**). Ethyl 2,2-dimethyl-2*H*-chromene-3-carboxylate (**5**) was also obtained. This ester is thought to be formed by the dehydration of ethyl 2,2-dimethyl-4-hydroxychroman-3-carboxylate (**7**).

This new method was applied to various salicylaldehydes, and some of them gave the corresponding 2,2-dimethyl-2*H*-chromene derivatives. All the reactions were carried out in DMF at 130 °C, for 8 h or 15 h. The results are given in Table 3. Methoxy-, methyl-, chloro-, bromo-, and phenyl-substituted salicylaldehydes gave the corresponding chromenes in good yields, but the others produced poor yields or nothing at all. This showed that this reaction was useful only for the preparation of 2,2-dimethyl-2*H*-chromenes with electrodonating or less electroaccepting substituents. Also, it was strange that 4-hydroxysalicylaldehyde and 2,4-dihydroxybenzaldehyde gave no corresponding chromene.

TABLE 3. THE REACTIONS OF SUBSTITUTED SALICYLALDEHYDES AND ETHYL 3-METHYL-2-BUTENOATE (4)

Substituted salicylaldehyde	Corresponding chromene	
	Bp θ_b/°C(mmHg)	Yield/%
3-Methoxy-	121—122 (7)	27*
4-Methoxy-	135—146 (8)	25
5-Methoxy-	141—144 (8)	47
6-Methoxy-	118—120 (16)	57
4,5-Dimethoxy-	155—160 (9)	22
4,6-Dimethoxy-	151—157 (9)	31
3-Methyl-	111—113 (24)	44
4-Methyl-	112—113 (21)	42
5-Methyl-	105—108 (21)	35
6-Methyl-	113—117 (14)	42
3-Chloro-	92—94 (9)	3, 5*
4-Chloro-	97—98 (5)	30
5-Chloro-	118—119 (29)	18, 32*
5-Bromo-	143—146 (19)	27
5-Phenyl-	53—55[a]	35
5-Nitro-	.....	0
6-Nitro-	100—105 (18)	2
4-Hydroxy-	.....	0
5-Ethoxy carbonyl-	.....	0
5-Acetyl-6-hydroxy-	.....	0
A[b]	.....	0
B[b]	.....	0
C[b]	.....	0

Solvent: DMF, temp: 130 °C, time: 8 h (*15 h).
a) Mp θ_m/°C (recrystallized from ethanol).
b)

A

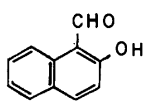

B

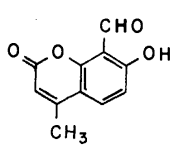

C

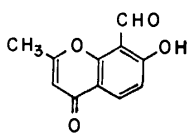

In two cases, the isopropenylcoumarins were also obtained. These two methyl substituted isopropenylcoumarins showed spectra similar to those of 3-isopropenylcoumarin (**6**) (Table 4). Their structures were confirmed by the partial catalytic hydrogenation of 3-isopropenyl-5-methylcoumarin to 3-isopropyl-5-methylcoumarin, which showed a doublet signal (J=7 Hz) at 1.3 ppm in its ^{1}H-NMR spectrum (Table 4).

TABLE 4. THE DATA ON NEW COUMARINS

Substituted coumarin	Mp θ_m/°C	Yield %	IR ν/cm^{-1}	^{1}H-NMR (δ)
3-Isopropenyl-	96.5—97.5	3	1725	2.1(3H,s),5.3(1H,s),5.9(1H,s), 7.0—7.7(4H,m),7.6(1H,s),
3-Isopropenyl-5-methyl-	65—67	6	1725	2.1(3H,s),2.5(3H,s),5.2(1H,s), 5.8(1H,s),6.8—7.2(2H,m), 7.2(1H,dd,J=7+9Hz),7.7(1H,s),
3-Isopropenyl-7-methyl-	65—72	Trace	1710	2.1(3H,s),2.5(3H,s),5.2(1H,s), 5.8(1H,s),7.0—7.2(2H,m), 7.3(1H,d,J=8Hz),7.5(1H,s),
3-Isopropyl-5-methyl-	87—91	—	1720	1.3(6H,d,J=7Hz),2.5(3H,s), 3.0(1H,m,J=7Hz),6.8—7.1(2H,m), 7.1(1H,dd,J=7+8Hz),7.5(1H,s),

Experimental

The boiling points and melting points have not been corrected; the IR spectra were measured on a Hitachi EPI-S2 spectrophotometer, and the ^{1}H-NMR spectra, on a JEOL JNM-MH-60 spectrometer in a carbon tetrachloride solution.

The Reaction of Salicyladehyde and Ethyl α-Bromoisobutyrate (1). A mixture of salicyladehyde (0.1 mol), ethyl 3-bromoisobutyrate (0.1 mol), potassium carbonate (40 g), and the solvent (shown in Table 1) (150 ml) was heated at 130 °C for the time shown in Table 1. After the removal of the solvent and ethyl 3-methyl-2-butenoate (**4**) *in vacuo*, the dark reaction mixture was diluted with water and extracted with ether. The ether solution was washed with 10% hydrochloric acid and a 5% aqueous sodium hydroxide solution, and then dried over anhydrous sodium sulfate. After the removal of the ether, the resulting liquid was distilled. 2,2-Dimethyl-2*H*-chromene (**2**) was thus obtained as a 106—108 °C/29 mmHg† fraction; the yield are summarized in Table 1. The residue was mixed with a 30% aqueous potassium hydroxide solution and refluxed for 3 h with stirring. After cooling, the mixture was treated with water and washed with ether. The aqueous layer was acidified with 10% hydrochloric acid and extracted with ether. The ether solution was washed with water and dried over anhydrous sodium sulfate. After the removal of the ether, the resulting liquid was mixed with a mixture of anhydrous sodium acetate (12 g) and acetic anhydride (18 g). The mixture was then refluxed for 3 h. Still hot, the reaction mixture was poured onto 70 g of ice and extracted with ether. The ether solution was washed with saturated sodium hydrogencarbonate solution and dried over anhydrous sodium sulfate. After the removal of the ether, the resulting liquid was distilled. 2-Isopropylbenzofuran (**3**) was thus obtained as a 111—113 °C/20 mmHg fraction; yield: 7% (8 h).

The Reaction of Salicylaldehyde and Ethyl 3-Methyl-2-butenoate (4). A mixture of salicylaldehyde (0.1 mol), ethyl 3-methyl-2-butenoate (**4**) (0.1 mol), anhydrous potassium carbonate (40 g), and DMF (80 ml) was heated at 130 °C for the time shown in Table 2. After the removal of the solvent and the recovered ethyl 3-methyl-2-butenoate (**4**) *in vacuo*, the dark reaction mixture was diluted with water and extracted with ether. The ether solution was washed with 10% hydrochloric acid and a 5% aqueous sodium hydroxide solution, and then dried over anhydrous sodium sulfate. After the removal of the ether, the resulting liquid was distilled. A fraction of 2,2-dimethyl-2*H*-chromene (**2**), boiling at 106—108 °C/29 mmHg, was then collected. The residue was chromatographed by the use of a silica-gel column with benzene–hexane (1 : 4) to afford ethyl 2,2-dimethyl-2*H*-chromene-3-carboxylate (**5**); bp 185—200 °C/18 mmHg; mp 43—45 °C; IR: 1710 cm^{-1}; ^{1}H-NMR: 1.3 (3H, t, J=7 Hz), 1.6 (6H, s), 4.2 (2H, q, J=7 Hz), 6.5—7.3 (4H, m), 7.2 ppm (1H, s); and 3-isopropenylcoumarin (**6**); mp 96.5—97.5 °C (recrystallized from hexane). The yields are summarized in Table 2, while the spectral data of **6** are sumarized in Table 4.

The General Procedure for the Preparation of Chromenes. A mixture of salicylaldehyde (0.1 mol), ethyl 3-methyl-2-butenoate (**4**) (0.1 mol), anhydrous potassium carbonate (40 g), and DMF (80 ml) was heated at 130 °C for 8 or 15 h. After treatment similar to that described above, the corresponding chromenes were obtained. Their data are summarized in Table 3. Two methyl isopropenylcoumarins were also obtained as white crystals (recrystallized from hexane); their data are summarized in Table 4.

Partial Hydrogenation of 3-Isopropenyl-5-methylcoumarin. 3-Isopropenyl-5-methylcoumarin (151 mg) was dissolved in 50 ml of ethanol, and then mixture was hydrogenated by means of a Raney Ni catalysts (prepared from 1 g of 50% Al–Ni alloy). After 30 m, about 23 ml of hydrogen absorbed. The catalyst was filtered off, and the filtrate was concentrated under reduced pressure and extracted with ether. The ether solution was dried over anhydrous sodium sulfate. After the removal of the ether, 3-isopropyl-5-methylcoumarin (114 mg; 75%) was obtained as white crystals; mp 87—91 °C (recrystallized from hexane).

† 1 mmHg≈133.322 Pa.

References

1) G. P. Ellis, "Chromenes, Chromanones, and Chromones," John Wiley and Sons, New York, N. Y. (1976), p. 43; J. Apsimon, "The Total Synthesis of Natural Products," Wiley-Interscience, New York, N. Y. (1973), Vol. 1, p. 468.

2) T. Abe and R. Shimizu, *Nippon Kagaku Zasshi*, **91**, 753 (1970).

The Total Synthesis of Antibiotic Fortimicin B

Yutaka HONDA and Tetsuo SUAMI*

Department of Applied Chemistry, Faculty of Science and Technology, Keio University, Hiyoshi, Kohoku-ku, Yokohama 223

(Received August 1, 1981)

The total synthesis of antibiotic fortimicin B (**1b**) is described. The sugar component of **1b**: 6-*epi*-purpurosamine B was converted to the sugar chloride: 2,6-bis(2,4-dinitrophenylamino)-2,3,4,6,7-pentadeoxy-β-L-*lyxo*-heptopyranosyl chloride (**5**). The aminocyclitol component of **1b**: fortamine B was also converted to the partially protected aglycone (**9**). The condensation of aglycone **9** with the sugar chloride **5** gave the desired condensation product in 37% yield. The analogous condensation of the DL-form of the aglycone with **5** afforded the same condensation product in 19% yield, it was then converted to **1b** by step-by-step hydrolysis.

Fortimicin A (**1a**), B (**1b**),[1,2] and C,[3,4] SF-1854,[5] SF-2052,[6,7] sporaricin A, B,[8-10] KA-6606 III, and KA-6606 IV[11] are members of a family of structually similar aminocyclitol antibiotics which are found in fermentation broths of various strains of *Actinomycetes*. The general feature of the structures of the antibiotics is a pseudodisaccharide consisting of 6-*epi*-purpurosamine B and a novel aminocyclitol named fortamine. The structural diversity of the antibiotics is due to the configurational difference in the amino group on the 1-position, the existence or the absence of the hydroxyl group on the 2-position, and the variety of aminoacyl groups attached to the methylamino group on the 4-position.

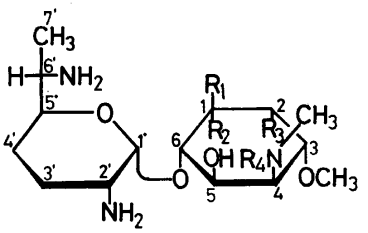

	R_1	R_2	R_3	R_4
Fortimicin A (**1a**):	NH_2	H	OH	$COCH_2NH_2$
B (**1b**):	NH_2	H	OH	H
C:	NH_2	H	OH	$COCH_2NHCONH_2$
SF-1854:	NH_2	H	OH	$COCH_2NHCH{=}O$
SF-2052:	NH_2	H	OH	$COCH_2NHCH{=}NH$
Sporaricin A:	H	NH_2	H	$COCH_2NH_2$
B:	H	NH_2	H	H
KA-6606 III:	H	NH_2	H	$COCH_2NHCONH_2$
KA-6606 IV:	H	NH_2	H	$COCH_2NHCH{=}O$

In preceding papers,[12-14] Suami and his coworkers have reported the synthesis of 6-*epi*-D-purpurosamine B and, in a communication letter,[15] a synthesis of the antibiotic fortimicin B in which natural fortamine B has been used as one of the starting materials. The synthesis of DL-fortamine B from *muco*-inosadiamine-3,6 has been described by a Kyowa Hakko research group.[16] We wish to report here the details of the total synthesis of fortimicin B, together with the synthesis of a DL-fortamine B derivative from 1,4-diazido-1,4-dideoxy-*muco*-inositol.

Fortimicin A, **1a**, the first members of this family to be discovered, exhibits high antimicrobial activities against Gram-positive and Gram-negative bacteria. The structures of **1a** and **1b** have been established by Egan and his coworkers.[17] The important biological activities and unique structures of these antibiotics make then attractive subjects of synthetic studies.

1a differs from **1b** in the existence of a glycyl group on the 1-methylamino group, and the former is converted into the latter by the loss of the glycyl group in an alkaline solution,[17] while it has been described in the literature that **1a** has been reconstructed from **1b** by a selective *N*-acylation.[18] Therefore, we have attempted to synthesize **1b** by condensing a glycosyl halide with a partially protected fortamine B derivative. Scheme 1 represents the reaction sequence leading to the total synthesis of **1b**.

The glycosyl chloride has been prepared by the reaction shown in Scheme 2. The acid hydrolysis of methyl 2,6-di-*N*-acetyl-2,6-diamino-2,3,4,6,7-pentadeoxy-β-L-*lyxo*-heptopyranoside (methyl 2,6-di-*N*-acetyl-6-*epi*-α-purpurosaminide B) (**2**)[13] in hydrochloric acid afforded the dihydrochloride (**3**). On treatment with acetic anhydride in the presence of diethyl ether-boron trifluoride, **3** gave the 1-*O*-acetyl derivative, which was then converted into the bis(*N*-2,4-dinitrophenyl) derivative (**4**) in 52% yield by reaction with 2,4-dinitrofluorobenzene in methanol containing triethylamine. The conversion of **4** into the crystalline glycosyl chloride (**5**) was accomplished in 82% yield by reaction with hydrogen chloride in the presence of acetyl chloride in dry diethyl ether.

The aglycone was synthesized as follows. For the

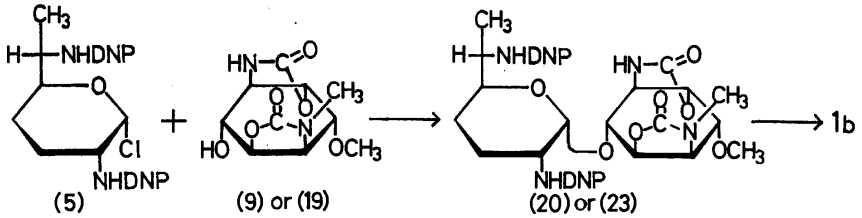

Scheme 1.

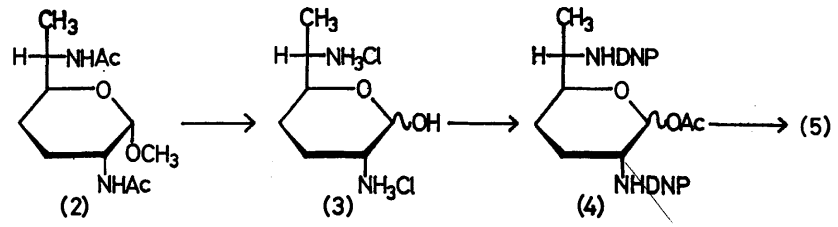

Scheme 2.

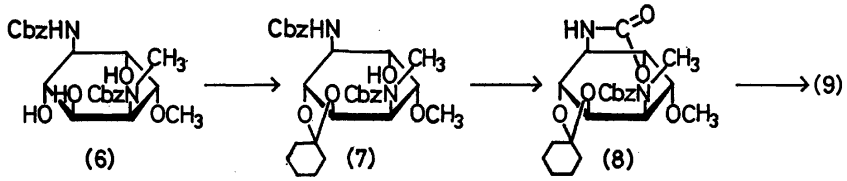

Scheme 3.

conversion of optically active L-1,4-bis(*N*-benzyloxycarbonyl)-4-amino-1,4-dideoxy-6-*O*-methyl-1-methylamino-*chiro*-inositol (**6**)[19] into the partially protected aglycone (**9**), it was necessary to protect selectively the two amino groups on the 1- and 4-positions and the two hydroxyl groups on the 2- and 5-positions with an appropriate protective group, prior to the condensation with the glycosyl chloride **5**. This has been accomplished by the reaction route shown in Scheme 3.

The protection of the two vicinal *trans* hydroxyl groups on the 2- and 3-positions of **6** was achieved by treating **6** with 1,1-dimethoxycyclohexane in *N,N*-dimethylformamide (DMF) in the presence of an acid catalyst. The yield of the 2,3-*O*-cyclohexylidene derivative (**7**) from **6** was 67%. The protection of the 5-hydroxyl group of **7** was accomplished by the reaction of **7** with sodium hydride in DMF, forming a cyclic 4,5-*N,O*-carbamate (**8**) in 91% yield. The transformation of **8** into 1,2:4,5-di-*N,O*-carbonyl-fortamine B (**9**) was performed by the mild hydrolysis of **8** in aqueous acetic acid, followed by cyclic 1,2-*N,O*-carbonylation with sodium hydride in DMF; 83% yield.

The reaction sequence shown in Scheme 4 represents a synthesis of the DL-form of the aglycone. As a starting material, 1,4-diazido-1,4-dideoxy-*muco*-inositol (**10**) was used; it was readily converted to *muco*-inosadiamine-1,4 by catalytic hydrogenation.[20] The stereochemistry of *muco*-inosadiamine-1,4 is similar to that of fortimicin B, except for the 5-hydroxyl group.

The catalytic hydrogenation of **10**, followed by benzyloxycarbonylation with benzyloxycarbonyl chloride in aqueous methanol containing sodium hydrogencarbonate, afforded 1,4-bis(*N*-benzyloxycarbonyl)-*muco*-inosadiamine-1,4 (**11**). The protection of one of the two sets of vicinal *trans* diols of **11** with 1,1-dimethoxycyclohexane in DMF furnished the 2,3-*O*-cyclohexylidene derivative (**12**) in 79% yield.

On treatment with sodium carbonate in aqueous dioxane, **12** was converted into the 4,5-*N,O*-carbamate (**13**) in 82% yield, since the formation of the cyclic carbamate occurs more readily between vicinal *cis*-arranged amino and hydroxyl groups than between those which are *trans*-related.

The *N*-benzylation of **13** in DMF with benzyl bromide and silver oxide afforded a mono-*N*-benzyl derivative (**14**) in 56% yield. The position of the benzyl group, shown in Scheme 4, has been deduced from the ^{1}H NMR spectroscopy and successive reaction products. The methylation of the 1-acylamino and the 6-hydroxyl groups of **14** with methyl iodide and silver oxide in DMF gave the 1-*N*-methyl-6-*O*-methyl derivative (**15**) in 82% yield.

The catalytic hydrogenolysis of **15** in the presence of palladium charcoal, followed by hydrolysis in a barium hydroxide solution, the catalytic hydrogenolysis of *N*-benzyl group in the presence of palladium black, and

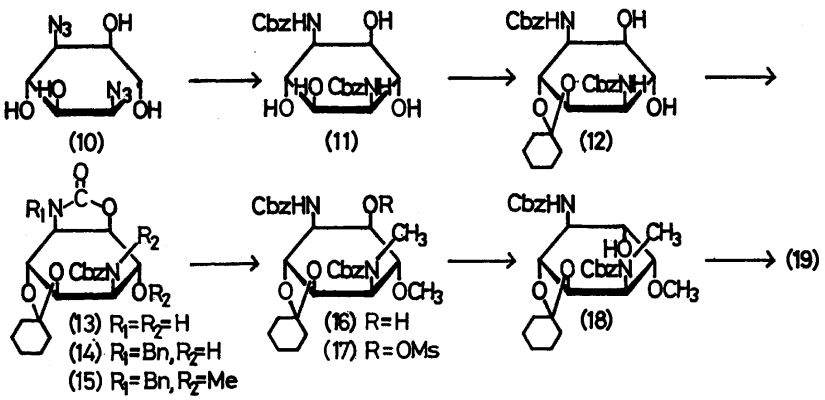

Scheme 4.

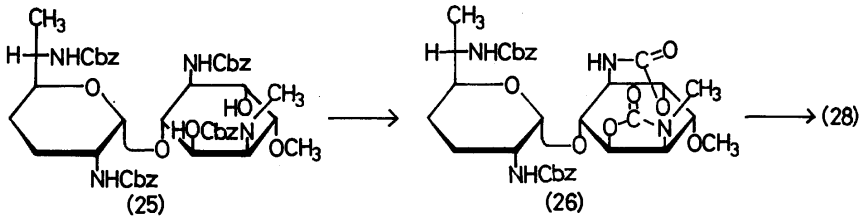

Scheme 5.

N-acylation with benzyloxycarbonyl chloride afforded the 1,4-bis(*N*-benzyloxycarbonyl) derivative (**16**).

The mesylation of the 5-hydroxyl group of **16** with methanesulfonyl chloride in pyridine afforded the 5-*O*-sulfonate derivative (**17**) in 71% yield; this was, in turn, converted to the epimer by reaction with sodium acetate in DMF. The reaction mixture was hydrolyzed in a barium hydroxide solution, followed by *N*-acylation to give 1,4-bis(*N*-benzyloxycarbonyl)-2,3-*O*-cyclohexylidene-DL-fortamine B (**18**).

On treatment with sodium hydride, followed by hydrolysis and again treatment with sodium hydride, **18** was converted into the DL-form of aglycone (**19**) in 72% yield.

The attempted condensation of the optically active aglycone **9** with the glycosyl chloride **5** in dioxane in the presence of silver trifluoromethanesulfonate afforded two condensation products (**20** and **21**) in 37% and 9% yields respectively. The ^{1}H NMR spectrum of the main product **20** revealed a signal at δ 5.53 with a small coupling constant (3.3 Hz) which was due to the anomeric proton of the α-D-glycoside, while the spectrum of **21** showed a signal at δ 5.13 with a large coupling constant (8.1 Hz) which was attributed to the anomeric proton of the β-D-glycoside.

The analogous condensation of the DL-aglycone **19** with the glycosyl chloride **5** gave three component which were subsequently separated by column chromatography to give **22**, **23**, and **24** in 20, 19, and 23% yields respectively. The structural assigments of the condensation products were made by means of ^{1}H NMR spectroscopy. Compound **23** was identical with **20** in all respects, while **22** was identified as its diastereomer containing D-fortamine B. Compound **24** was a mixture of two products possessing β-D-glycosidic linkages. Compounds **20** and **23** were also identical with an authentic sample (**28**) prepared from natural fortimicin B by the reaction sequence shown in Scheme 5.

The removal of the protective groups of **23** by Amberlite IRA-400 (OH^-) resin, followed by hydrolysis in a barium hydroxide solution, afforded **1b** in 98% yield; it was then converted into tetra-*N*-acetylfortimicin B[17] (**25**). Compound **25** was identical with an authentic sample (**29**) prepared from natural fortimicin B by *N*-acetylation.

Experimental

General Procedures. The melting points were determined in capillary-tubes and are uncollected. The solutions were concentrated under reduced pressure below 40 °C. The optical rotations were meassured on a Japan Spectroscopic DIP-SL polarimeter. The infrared spectra were taken on a Hitachi HPL-225 spectrophotometer. ^{1}H NMR spectra were recorded on Varian EM-360A and 390 spectrometers at 60 and 90 MHz respectively. Deutriochloroform was used as a solvent, with tetramethylsilane as the internal standard. The peak position are given in δ values. TLC was preformed on Wakogel B-10 plates (Wako Pure Chemical Co., Ltd.), and silica-gel (Wakogel C-300) was employed for column chromatography.

*2,6-Diamino-2,3,4,6,7-pentadeoxy-*L*-lyxo-heptopyranose Dihydrochloride (6-*epi*-*D*-Purpurosamine B Dihydrochloride) (**3**).* A 1.0 g portion of methyl 2,6-diacetamido-2,3,4,6,7-pentadeoxy-β-L-*lyxo*-heptopyranoside (**2**)[13] was heated in 2 M (1 M=1 mol dm^{-3}) HCl (60 ml) under reflux. After 15 h, the solution was concentrated to give 0.89 g (99%) of crude **2** as a syrupy residue; it was recrystallized from ethanol to give 0.47 g (52%) of **3**; mp 183—184 °C (dec); $[\alpha]_D^{23}$ −15→−9.8° (*c* 1, methanol) $[\alpha]_D^{23}$ −5.4→+23.5° (*c* 1, water). Lit,[19] mp 186—191 °C (dec), $[\alpha]_D^{24}$ +6→+23° (*c* 0.6, water).

Found: C, 36.03; H, 7.50; N, 12.02; Cl, 30.20%. Calcd for $C_7H_{16}N_2O_2 \cdot 2HCl$: C, 36.06; H, 7.78; N, 12.02; Cl, 30.41%.

*1-O-Acetyl-2,6-bis(2,4-dinitrophenylamino)-2,3,4,6,7-pentadeoxy-*L*-lyxo-heptopyranose (**4**).* To a suspention of crude **3** (2.0 g) in acetic anhydride (20 ml), diethyl ether–boron trifluoride (3.3 ml) was added under ice cooling with agitation. After 12 h, the solution was concentrated. To a solution of the residue in 80% aq methanol, 2,4-dinitrofluorobenzene (4.0 g) was added, and a solution of triethylamine (4.8 ml) in methanol (20 ml) was dropped in over 1 h under ice cooling. After 16 h, the solution was diluted with chloroform, it washed with dil HCl and water, dried over Na_2SO_4 and concentrated. The residue was purified by column chromatography using 1 : 15 (v/v) ethanol–toluene. The fractions corresponding to R_f 0.49 on TLC in 1 : 10 (v/v) ethanol–toluene were combined and concentrated to give 2.4 g (52%) of **4**: mp 120—122 °C; ^{1}H NMR ($CDCl_3$) δ 1.48 (2d, 3, J=7.2 Hz, J=6.3 Hz, H-7), 1.97·2.23 (2s, 3, intensity ratio 2 : 1, OAc), 5.65 (d, 2/3, $J_{1,2}$=8.7 Hz), 6.35 (d, 1/3, $J_{1,2}$=3.3 Hz).

Found: C, 47.42; H, 4.30; N, 15.45%. Calcd for $C_{21}H_{22}N_6O_{11}$: C, 47.19; H, 4.15; N, 15.73%.

*2,6-Bis(2,4-dinitrophenylamino)-2,3,4,6,7-pentadeoxy-β-*L*-lyxo-heptopyranosyl Chloride (**5**).* A suspension of **4** (1.0 g) in dry diethyl ether (200 ml) was staturated with dry HCl, and then, to the mixture, acetyl chloride (4 ml) was added. After 18 h, the crystals which was appeared were collected by filtration and washed with diethyl ether to give 0.78 g (82%) of **5**: mp 130—132 °C; $[\alpha]_D^{20}$ +130° (*c* 0.49, acetone); ^{1}H NMR (acetone-d_6) δ 1.45 (d, 3, $J_{6,7}$=6.6 Hz, H-7), 6.72 (d, 1, $J_{1,2}$=3.0 Hz, H-1), 8.69 (d, 1, J=9.0 Hz, NH), 8.80 (d, 1, J=9.9 Hz, NH); IR (KBr) 1610·1580 (Ar), 1510·1325 cm^{-1} (NO_2).

Found: C, 44.38; H, 3.81; N, 16.17; Cl, 7.18%. Calcd for $C_{19}H_{19}N_6ClO_9$: C, 44.67; H 3.75; N, 16.45; Cl, 6.94%.

*1,4-Bis(N-benzyloxycarbonyl)-5,6-O-cyclohexylidenefortamine B (1L,4-Amino-1,4-bis(N-benzyloxycarbonyl)-2,3-O-cyclohexylidene-1,4-dideoxy-6-O-methyl-1-methylamino-*chiro*-inositol) (**7**).* A

mixture of 1,4-bis(*N*-benzyloxycarbonyl)-fortamine B[19] (**6**, 2.0 g) and 1,1-dimethoxycyclohexane (15 ml) in DMF (60 ml) was heated at 70 °C under reduced pressure (30 mmHg)† in the presence of a catalytic amount of *p*-toluenesulfonic acid. After 3 h, triethylamine (1 ml) was added to the solution, and the mixture was concentrated. The residue was purified by column chromatography using 15 : 1 (v/v) benzene–ethanol. Fractions corresponding to R_f 0.52 on TLC in 10 : 1 (v/v) benzene–ethanol were collected and concentrated. The residue was recrystallized from ether–petroleum ether to give 1.46 g (63%) of **7**: mp 94—96 °C; $[\alpha]_D^{24}$ +25.1° (*c* 0.97, methanol) IR (KBr) 1700 (NC=O), 1615 cm^{-1} (NH); ^1H NMR ($CDCl_3$) δ 1.5 (m, 10, C_6H_{10}), 3.07 (s, 3, NCH_3), 3.39 (s, 3, OCH_3), 4.52 (dd, 1, J=3.6 Hz, J=6.1 Hz, H-4), 5.10 (s, 2, CH_2 of benzyl), 5.24 (d, 1, J=7.5 Hz, NH-1), 7.37 (s, 10, $2\times C_6H_5$).

Found: C, 64.73; H, 6.76; N, 4.91%. Calcd for $C_{30}H_{38}N_2O_8$: C, 64.97; H, 6.91; N, 5.05%.

4-N-Benzyloxycarbonyl-1,2-N,O-carbonyl-5,6-O-cyclohexylidene-fortamine B (8). To a stirred solution of **7** (0.50 g) in DMF (10 ml), 50% sodium hydride (0.13 g) was added under ice cooling in a N_2 atmosphere. After 2 h, the solution was neutralized with acetic acid, diluted with water, and extracted with chloroform. The organic layer was concentrated, and the residue was purified by column chromatography, using 15:1 (v/v) benzene–ethanol. Fractions corresponding to R_f 0.67 on TLC in 10 : 1 (v/v) benzene–ethanol were collected and concentrated to give 0.34 g (84%) of crude **8** as an amorphous solid: mp 71 °C. It was recrystallized from chloroform–petroleum ether to give 0.23 g (57%) of **8**: mp 87—90 °C; $[\alpha]_D^{24}$ −9.1° (*c* 0.99, methanol); IR (KBr) 1780 (*trans* cyclic carbamate), 1695 cm^{-1} (NC=O); ^1H NMR ($CDCl_3$) δ 1.62 (m, 10, C_6H_{10}), 3.14 (s, 3, NCH_3), 3.43 (s, 3, OCH_3), 4.75 (m, 1, H-2), 5.17 (s, 2, CH_2 of benzyl), 5.52 (s, 1, NH-1), 7.39 (s, 5, C_6H_5).

Found: C, 62.10; H, 6.91; N, 6.17%. Calcd for $C_{23}H_{30}N_2O_7$: C, 61.87; H, 6.77; N, 6.28%.

1,2:4,5-Di-N,O-carbonylfortamine B (9). To a solution of crude **8** (0.35 g) in methanol (3 ml), 50% aq acetic acid (12 ml) was added, after which the mixture was warmed at 60 °C. After 2 h, the solution was concentrated. To a solution of the residue in DMF (10 ml), 50% sodium hydride (63 mg) was added. After 1 h at 0 °C in a N_2 atmosphere, the solution was neutralized with acetic acid and concentrated. The residue was purified by column chromatography, using 10 : 1 (v/v) benzene–ethanol. Fractions corresponding to R_f 0.42 on TLC in 5 : 1 (v/v) benzene–ethanol were collected and concentrated. The recrystallization of the residue from chloroform gave 168 mg (83%) of **9**: mp 225—228 °C; $[\alpha]_D^{20}$ −84.3° (*c* 1.06, methanol); IR (KBr) 1772 (*trans* cyclic carbamate), 1725 cm^{-1} (*cis* cyclic carbamate); ^1H NMR (CD_3OD) δ 3.01 (s, 3, NCH_3), 3.73 (s, 3, OCH_3), 4.63 (dd, 1, J=6.3 Hz, J=7.9 Hz, H-5).

Found: C, 46.41; H, 5.37; N, 10.59%. Calcd for $C_{10}H_{14}N_2O_6$: C, 46.51; H, 5.46; N, 10.85%.

1,4-Diamino-1,4-bis(N-benzyloxycalbonyl)-1,4-dideoxy-muco-inositol (11). A 1 g portion of 1,4-diazido-1,4-dideoxy-*muco*-inositol[20] (**10**) was hydrogenated in methanol (10 ml) in the presence of Raney nickel under a hydrogen atmosphere (3.4 kg/cm^2). After 14 h, the catalyst was removed by filtration and the filtrate was concentrated. To a solution of the residue in 50% aq methanol containing sodium hydrogencarbonate (1.4 g), a 30% solution of benzyloxycarbonyl chloride in toluene (7.4 ml) was added under ice cooling with agitation. After 12 h, the solution was neutralized with acetic acid and concentrated. The residue was purified by column chromatography using 1 : 5 (v/v) ethanol–toluene. Fractions corresponding to R_f 0.29 on TLC in the same solvent were collected and concentrated to give 1.70 g (88%) of **11**: mp 90—93 °C; IR (KBr) 1695 (NHCOO), 1520 cm^{-1} (NH); ^1H NMR (CD_3OD) δ 5.03 (s, 4, $2\times CH_2$ of benzyl), 7.29 (s, 10, $2\times C_6H_5$).

Found: C, 58.28; H, 5.90; N, 5.88%. Calcd for $C_{22}H_{26}N_2O_8\cdot 1/2\ H_2O$: C, 58.01; H, 5.98; N, 6.15%.

DL-*1,4-Diamino-1,4-bis(N-benzyloxycarbonyl)-2,3-O-cyclohexylidene-1,4-dideoxy*-muco-*inositol (12).* To a solution of **11** (1.0 g) in DMF (20 ml), 1,1-dimethoxycyclohexane (0.7 ml) and a catalytic amount of *p*-toluenesulfonic acid were added at 55—60 °C under reduced pressure (38—40 mmHg). After 2 h, triethylamine (1 ml) was added to the solution and the mixture was concentrated. The residue was purified by column chromatography using 1 : 7 (v/v) ethanol–toluene. Fractions corresponding to R_f 0.47 on TLC 1 : 5 (v/v) ethanol–toluene were collected and concentrated. The residue was recrystallized from ether to give 0.93 g (79%) of **12**: mp 98—100 °C; IR (KBr) 1705 (NHCOO), 1520 cm^{-1} (NH); ^1H NMR ($CDCl_3$) δ 1.5 (m, 10, cyclohexylidene), 5.06 (s, 4, $2\times CH_2$ of benzyl), 5.06 (m, 1, NH), 5.77 (d, 1, J=9 Hz, NH), 7.33 (s, 10, $2\times C_6H_5$).

Found: C, 63.61; H, 6.62; N, 5.19%. Calcd for $C_{28}H_{34}N_2O_8$: C, 63.86; H, 6.51; N, 5.32%.

DL-*1,4-Diamino-1-N-benzyloxycarbonyl-4,5-N,O-carbonyl-2,3-O-cyclohexylidene-1,4-dideoxy*-muco-*inositol (13).* To a solution of **12** (1.0 g) in 60% aq dioxane (30 ml), sodium carbonate (0.2 g) was added. After 17 h at 65 °C the solution was diluted with water (50 ml) and repeatedly extracted with chloroform. The combined layer was concentrated, and the residue was purified by column chromatography, using 2: 3 (v/v) acetone–toluene. Fractions corresponding to R_f 0.26 on TLC in the same solvent were combined and concentrated to give 0.65 g (82%) of **13**: mp 105—107 °C; IR (KBr) 1765 (*cis* cyclic carbamate), 1710 cm^{-1} (NHCOO); ^1H NMR ($CDCl_3$) δ 1.5 (m, 10, cyclohexylidene), 4.72 (t, 1, J=8.7 Hz, H-2), 5.09 (s, 2, CH_2), 5.84 (s, NH-1), 6.79 (s, 1, NH-4), 7.34 (s, 5, C_6H_5).

Found: C, 60.47; H, 6.43; N, 6.50%. Calcd for $C_{21}H_{26}N_2O_7$: C, 60.27; H, 6.26; N, 6.70%.

DL-*1,4-Diamino-4-N-benzyl-1-N-benzyloxycarbonyl-4,5-N,O-carbonyl-2,3-O-cyclohexylidene-1,4-dideoxy*-muco-*inositol (14).* To a stirred solution of **13** (0.10 g) in DMF (4 ml), benzyl bromide (0.06 ml) was added in the presence of silver oxide (0.07 g). After 18 h, the reaction mixture was filtered and the filtrate was diluted with water. The solution was extracted with chloroform and recrystallized from chloroform–ether to give 73 mg (56%) of **14**: mp 166 °C; IR (KBr) 1760 (carbamate); ^1H NMR ($CDCl_3$) δ 1.5 (m, 10, C_6H_{10}), 4.18 (d, 1, J=14.5 Hz, CH_2 of *N*-benzyl), 4.73 (d, 1, J=14.5 Hz, CH_2 of *N*-benzyl), 4.56 (t, 1, J=8.2 Hz, H-5), 5.12 (s, 2, CH_2 of benzyloxycarbonyl), 7.41 (s, 10, $2\times C_6H_5$).

Found: C, 66.31; H, 6.40; N, 5.50%. Calcd for $C_{28}H_{32}N_2O_7$: C, 66.12; H, 6.34; N, 5.51%.

DL-*1,4-Diamino-4-N-benzyl-1-N-benzyloxycarbonyl-4,5-N,O-carbonyl-2,3-O-cyclohexylidene-1,4-dideoxy-1-N-methyl-6-O-methyl*-muco-*inositol (15).* To a stirred solution of **14** (0.56 g) in DMF (10 ml), methyl iodide (0.34 ml) and silver oxide (0.77 g) were added. After 18 h, The mixture was filtered and the filtrate was concentrated. The residue was purified by column chromatography, using 1 : 5 (v/v) acetone–toluene. Fractions corresponding to R_f 0.35 in the same solvent were collected to give 0.49 g (82%) of **15**: mp 107—110 °C; IR (KBr) 1763 (carbamate), 1696 cm^{-1} (NHCOO); ^1H NMR ($CDCl_3$) δ 1.5 (m, 10, C_6H_{10}), 3.30 (s, 3, NCH_3), 3.49 (s, 3,

† 1 mmHg≈133.322 Pa.

OCH_3), 4.15 (d, 1, J=14.5 Hz, CH_2 of *N*-benzyl) 4.49 (t, 1, J=8.8 Hz, H-2), 4.77 (d, 1, J=14.5 Hz, CH_2 of *N*-benzyl), 5.14 (s, 2, CH_2 of benzyloxycarbonyl), 7.37 (s, 10, 2×C_6H_5).

Found: C, 67.36; H, 6.85; N, 5.19%. Calcd for $C_{30}H_{36}N_2O_7$: C, 67.14; H, 6.76; N, 5.22%.

DL-*1,4-Diamino-1,4-bis(*N-*benzyloxycarbonyl)-2,3*-O-*cyclohexylidene-1,4-dideoxy-1*-N-*methyl-6*-O-*methyl*-muco-*inositol* (**16**) Compound **15** (0.32 g) was hydrogenated in ethanol (10 ml) in the presence of 10% Pd on charcoal (30 mg) under a hydrogen atmosphere (3.4 kg/cm²). After 16 h, the catalyst was filtered off and the filtrate was concentrated. The residue was dissolved in dioxane (10 ml) and a 0.04 M $Ba(OH)_2$ solution (10 ml) was added. After 2 h at 100 °C, the solution was neutralized with CO_2 gas, and the resulting precipitate was removed by filtration. The filtrate was concentrated, and the residue was dissolved in aq. methanol (20 ml). To the solution, sodium hydrogencarbonate (0.2 g) and a 30% solution of benzyloxycarbonyl chloride in toluene (1 ml) were under ice cooling. After 4 h, the solution was concentrated, and residue was purified by column chromatography, using 1 : 5 (v/v) acetone–toluene. Fractions corresponding to R_f 0.26 on TLC in the same solvent were collected and concentrated to give 0.28 g (83%) of **16**: mp 77—82 °C; IR (KBr) 1695 (NHCOO), 1520 cm^{-1} (NH); ^1H NMR ($CDCl_3$) δ 1.55 (m, 10, C_6H_{10}), 3.17 (s, 3, NCH_3), 3.32 (s, 3, OCH_3), 3.61 (s, 1, H-3), 4.63 (d, 1, J=5.2 Hz, H-4), 5.08 (s, 2, CH_2 of benzyl), 5.11 (s, 2, CH_2 of benzyl), 5.67 (d, 1, J=7.6 Hz, NH-1), 7.35 (s, 10, 2×C_6H_5).

Found: C, 63.72; H, 6.78; N, 4.85%. Calcd for $C_{30}H_{38}N_2O_8 \cdot 1/2\ H_2O$: C, 63.92; H, 6.97; N, 4.97%.

DL-*1,4-Diamino-1,4-bis(*N-*benzyloxycalbonyl)-2,3*-O-*cyclohexylidene-1,4-dideoxy-1*-N-*methyl-6*-O-*methyl*-chiro-*insoitol* (**18**). To a stirred solution of **16** (0.27 g) in pyridine (10 ml), methanesulfonyl chloride (2.7 ml) was added. After 27 h, the solution was concentrated and the residue was dissolved in chloroform. The solution was washed with water, dried over Na_2SO_4 and concentrated. The residue was purified by column chromatography, using 1 : 7 (v/v) acetone–toluene. Fractions corresponding to R_f 0.36 on TLC in the same solvent were collected and concentrated to give 0.22 g of the 5-*O*-mesyl derivative (**17**) as a residue. The residue (0.69 g) was dissolved in 90% aq DMF (60 ml) containing sodium acetate (4.4 g), after which the solution was heated under reflux. After 22 h, the solution was concentrated and the residue was dissolved in 50% aq dioxane (30 ml) containing barium hydroxide (1.2 g); the solution was then heated under reflux. After 5 h, the solution was neutralized with CO_2 gas and the resulting precipitate was removed by filtration. The filtrate was concentrated, and the residue was dissolved in aq methanol (40 ml). To the solution, sodium hydrogencarbonate (0.36 g) and a 30% solution of benzyloxycarbonyl chloride in toluene (1.85 ml) were added under ice cooling. After 4 h, the solution was concentrated and the residue was purified by column chromatography, using 1 : 5 (v/v) acetone–toluene. Fractions corresponding to R_f 0.40 on TLC in the same solvent were collected and concentrated to give 0.23 g (38%) of **18** as a syrup: ^1H NMR ($CDCl_3$) δ 1.5 (m, 10, C_6H_{10}), 3.08 (s, 3, NCH_3), 3.40 (s, 3, OCH_3), 4.51 (dd, 1, J=3.6 Hz, J=6.1 Hz, H-1), 5.09 (s, 2, CH_2 of benzyl), 5.13 (s, 2, CH_2 of benzyl), 5.20 (d, 1, J=7.5 Hz, NH-4), 7.37 (s, 10, 2×C_6H_5).

DL-*1,4-Diamino-1,2 : 4,5-di*-N,O-*carbonyl-1,4-dideoxy-1*-N-*methyl-6*-O-*methyl*-chiro-*inositol* (**19**). To a solution of **18** (192 mg) in DMF (10 ml), 50% sodium hydride (42 mg) was added under ice cooling. After 3 h, the solution was diluted with water and neutralized with acetic acid. The solution was extracted with chloroform, and the organic layer was concentrated. The residue was hydrolyzed in 50% aq acetic acid (10 ml) at 60 °C for 2 h and then concentrated. To a solution of the residue in DMF (10 ml), 50% sodium hydride (28 mg) was added, after which the mixture was worked up as has been described above. The residual product was purified on a silica-gel column, using 1 : 10 (v/v) methanol–toluene. Fractions corresponding to R_f 0.07 in the same solvent were collected and concentrated. The residue was recrystallized from chloroform to give 64 mg (72%) of **19**: mp 224—228 °C; IR (KBr) 1775 (*trans* cyclic carbamate), 1725 cm^{-1} (*cis* cyclic carbamate); ^1H NMR (CD_3OD) δ 3.02 (s, 3, NCH_3), 3.74 (s, 3, OCH_3), 4.64 (dd, 1, J=6.4 Hz, J=7.7 Hz, H-5).

Found: C, 46.24; H, 5.35; N, 10.57%. Calcd for $C_{10}H_{14}N_2O_6$; C, 46.51; H, 5.46; N, 10.85%.

Condensation of **9** *(*L*-Form) with* **5**. Compound **9** (0.10 g) was dissolved in freshly distilled dioxane (4 ml) at 100 °C. After the solution had cooled to the ambient temperature, **5** (0.58 g) and silver trifluoromethanesulfonate (0.29 g) were added, portion by portion to the solution (under N_2) with agitation in the dark. After 27 h, acetone was added to the reaction mixture, and it was filtered. The filtrate was concentrated, and the residue was purified by column chromatography, using 1 : 3 (v/v) acetone–toluene. Fractions corresponding to R_f 0.26 on TLC in the same solvent were collected and concentrated to give 0.11 g (37%) of **20**: mp 226—228 °C; $[\alpha]_D^{20}$ +43.2° (*c* 1.01, acetone); ^1H NMR (acetone-d_6) δ 1.44 (d, 3, $J_{6',7'}$=6.3 Hz, H-7'), 2.85 (s, 3, NCH_3), 3.61 (s, 3, OCH_3), 4.67 (dd, 1, J=6.0 Hz, J=7.5 Hz, H-5), 5.53 (d, 1, $J_{1',2'}$=3.3 Hz, H-1'), 7.20 (s, 1, NH-1), 7.3 (d, 1, J=9.0 Hz), 7.4 (d, 1, J=9.0 Hz), 8.24 (dd, 2, J=2.4 Hz, J=9.0 Hz), 8.92 (d, 1, J=2.4 Hz), 8.94 (d, 1, J=2.4 Hz) (total 6H, DNP), 8.82 (d, 2, J=8.1 Hz, NH-2',6').

Found: C, 47.50; H, 4.47; N, 14.99%. Calcd for $C_{29}H_{32}N_8O_{15}$: C, 47.54; H, 4.40; N, 15.30%.

Fractions corresponding to R_f 0.23 on TLC were collected to give 25 mg (9%) of the corresponding β-anomer **21**: mp 180—182 °C; $[\alpha]_D^{20}$ −12.5° (*c* 1.00, acetone); ^1H NMR (acetone-d_6) δ 1.47 (d, 3, $J_{6',7'}$=6.3 Hz, H-7'), 2.82 (s, 3, NCH_3), 3.44 (s, OCH_3), 4.48 (dd, 1, J=6.0 Hz, J=7.5 Hz), 5.13 (d, 1, $J_{1',2'}$=8.1 Hz), 6.33 (s, 1, NH-1), 7.33 (d, 1, J=9.3 Hz), 7.49 (d, 1, J=9.3 Hz), 8.29 (dd, 2, J=3.0 Hz, J=9.3 Hz), 8.94 (d, 1, J=3.0 Hz), 8.96 (d, 1, J=3.0 Hz) (total 6H, DNP), 8.64 (d, 1, J=8.4 Hz), 8.9 (d, 1, NH).

Found: C, 47.25; H, 4.45; N, 14.98%. Calcd for $C_{29}H_{32}N_8O_{15}$: C, 47.54; H, 4.40; N, 15.30%.

Condensation of **19** *(*DL*-Form) with* **5**. Compound **19** (49 mg) was dissolved in dioxane (5 ml). To the solution, **5** (288 mg) and silver trifluoromethanesulfonate (145 mg) were added, after which the reaction mixture was worked up as was described in the case of the previous condensation of **9** with **5**. Fractions corresponding to R_f 0.34 on TLC in 1 : 3 (v/v) acetone–toluene were collected and concentrated to give 28 mg (20%) of **22**: mp 306—307 °C; $[\alpha]_D^{20}$ +100.7° (*c* 1.12, acetone); ^1H NMR (DMSO-d_6) δ 1.36 (d, 3, $J_{6',7'}$= 5.1 Hz, H-7'), 2.80 (s, 3, NCH_3), 3.48 (s, OCH_3), 4.60 (dd, 1, J=6.0 Hz, J=7.5 Hz, H-5), 5.20 (d, 1, $J_{1',2'}$=3.0 Hz, H-1'), 8.16 (s, 1, NH-1), 7.23 (d, 2, J=10.8 Hz), 8.23 (m, 2), 8.65 (m, 2) (total 6H, DNP), 8.65 (d, 1, J=9 Hz, NH-2',6').

Found: C, 47.30; H, 4.37; N, 15.10%. Calcd for $C_{29}H_{32}N_8O_{15}$: C, 47.54; H, 4.40; N, 15.30%.

Fractions (R_f 0.26) were collected and concentrated to give 26 mg (19%) of **23**: mp 226—228 °C; $[\alpha]_D^{20}$ +41.9° (*c* 0.48, acetone); ^1H NMR (acetone-d_6) δ 1.44 (d, 3, $J_{6',7'}$= 6.3 Hz, H-7'), 2.87 (s, 3, NCH_3), 3.58 (s, 3, OCH_3), 4.66 (dd, 1, J=6.0 Hz, J=7.5 Hz, H-5), 5.54 (d, 1, J=3.3 Hz), 7.23

(s, 1, NH-1), 7.36 (d, 1, J=9.0 Hz), 7.46 (d, 1, J=9.0 Hz), 8.34 (dd, 2, J=2.4 Hz, J=9.0 Hz), 9.00 (d, 1, J=2.4 Hz), 9.02 (d, 1 J=2.4 Hz) (total 6H, DNP), 8.88 (d, 2, J=8.1 Hz, NH-2',6').

Fractions (R_f 0.23) were collected and concentrated to give 31 mg (23%) of a mixture of β-anomer **24**: ^{1}H NMR (acetone-d_6) δ 1.46 (d, 3, $J_{6',7'}$=6.3 Hz, H-7'), 2.77·2.99 (2s, 3, NCH_3), 3.37·3.40 (2s, 3, OCH_3), 4.91·5.05 (2d, 1, $J_{1',2'}$=8.1 Hz, H-1'), 6.30·6.33 (2s, 1, NH-1), 7.2—7.6 (m, 2), 8.2 (dd, 2, J=3.0 Hz, J=9.0 Hz), 8.86·8.89 (2d, 2, J=3.0 Hz) (total 6H, DNP), 8.56 (d, 1, J=8.1 Hz, NH), 8.8 (d, 1, NH).

*Fortimicin B (**1b**).* To a solution **23** (28 mg) in a mixture of acetone (2 ml) and methanol (6 ml), Amberlite IRA 400 (OH^-) resin (0.23 ml) and water (2 ml) were added. After 15 h at the ambient temperature with agitation, the resin was filtered off and the filtrate was concentrated to give 17 mg of a residue. The residue was dissolved in ethanol (4 ml), and to the solution, a 0.1 M barium hydroxide solution (10 ml) was added. The mixture was then heated at 85 °C overnight and neutralized with CO_2. The precipitate was filtered off, and the filtrate was concentrated. The residue was purified on a column of Amberlite CG-50 (NH_4^+) by the use of 1 M ammonia. Fractions showing ninhydrin-positive and R_f 0.38 on TLC in 1 : 1 : 4 (v/v) chloroform–concd ammonia–isopropyl alcohol were combined and concentrated to give 13 mg (98%) of **1b** as an amorphous residue, $[\alpha]_D^{16}$ +25.3° (c 0.65, water). Lit,[17] $[\alpha]_D^{25}$ +22.2° (c 0.1, water); ^{1}H NMR (D_2O) δ 1.07 (d, 3, $J_{6',7'}$=6.6 Hz, H-7'), 2.40 (s, 3, NCH_3), 3.46 (s, 3, OCH_3), 3.98 (dd, 1, J=4.5 Hz, J=9.2 Hz, H-5), 5.03 (d, 1, $J_{1',2'}$=3.0 Hz).

*Tetra-N-acetylfortimicin B (**25**).* To a solution of **1b** (13 mg) in methanol (4 ml), acetic anhydride (0.5 ml) was added. After 3 h, the solution was concentrated to give 18 mg (96%) of **25** as a monohydrate: mp 161—163 °C; $[\alpha]_D^{20}$ +91.6° (c 0.61, methanol). Lit,[22] $[\alpha]_D$ +92.72° (c 1.0, methanol). ^{1}H NMR (D_2O) δ 1.15 (d, 3, $J_{6',7'}$=6.0 Hz, H-7'), 2.00 (s, 3, NAc), 2.02 (s, 3, NAc), 2.05 (s, 3, NAc), 2.18 (s, 3, NAc), 3.10 (d, 3, J=10.2 Hz, NCH_3), 3.44 (s, 3, OCH_3).

*2',6'-Bis(N-benzyloxycarbonyl)-1,2:4,5-di-N,O-carbonylfortimicin B (**27**).* To a solution of 1,2',4,6'-tetrakis-*N*-(benzyloxycarbonyl)foltimicin B[19] (**26**, 0.50 g) in DMF (6 ml), 50% sodium hydride (70 mg) was added under ice cooling with agitation. After 6 h at the ambient temperature, the pH of the solution was adjusted to 4 by adding acetic acid. The solution was then diluted with cold water, and the precipitates were collected by filtration. Recrystallization of the product from chloroform–ether gave 0.31 g (81%) of **27**: mp 121—128 °C; $[\alpha]_D^{20}$ −1.6° (c, 1.3, methanol); ^{1}H NMR ($CDCl_3$) δ 1.16 (s, 3, $J_{6',7'}$=6.3 Hz, H-7'), 2.83 (s, 3, NCH_3), 3.49 (s, 3, OCH_3), 6.75 (s, 1, NH-1), 7.36 (s, 10, $2\times C_6H_5$).

Found: C, 59.42; H, 6.12; N, 8.16%. Calcd for $C_{33}H_{40}N_4O_{11}$: C, 59.27; H, 6.03; N, 8.38%.

*1,2:4,5-Di-N,O-carbonyl-2',6'-bis(N-2,4-dinitrophenyl)fortimicin B (**28**).* Compound **27** (150 mg) was hydrogenated in methanol (10 ml) in the presence of 10% Pd on charcoal (30 mg) under a hydrogen atmosphere (3.4 kg/cm^2). After 16h, the catalyst was filtered off and the filtrate was concentrated. To a solution of the residue in 67% aq ethanol (25 ml) containing sodium hydrogencarbonate (57 mg), 2,4-dinitrofluorobenzene (104 mg) was added under ice cooling. After 18 h, the solution was diluted with water and repeatedly extracted with chloroform. The combined organic layers were concentrated, and the residue was recrystallized from acetone–chloroform to give 139 mg (85%) of **28**: mp 226—228 °C; $[\alpha]_D^{20}$ +40.7° (c 0.87, acetone); IR (KBr) 1770 (cyclic carbamate), 1624·1594 (nitrophenyl), 1525·1535 cm^{-1} (NO_2); ^{1}H NMR (acetone-d_6) δ 1.45 (d, 3, $J_{6',7'}$=6.3 Hz, H-7'), 2.86 (s, 3, NCH_3), 3.61 (s, 3, OCH_3), 4.66 (dd, 1, J=6.0 Hz, J=7.5 Hz, H-5), 5.53 (d, 1 $J_{1',2'}$=3.3 Hz, H-1'), 7.20 (s, 1, NH-1), 7.32·7.42 (2d, 2, J=9.0 Hz), 8.26 (dd, 2, J=2.4 Hz, J=9.0 Hz), 8.94·8.96 (2d, 2, J=2.4 Hz), 8.83 (d, 2, NH-2' and NH-6').

Found: C, 47.23; H, 4.47; N, 14.91%. Calcd for $C_{29}H_{32}N_8O_{15}$: C, 47.54; H, 4.40; N, 15.30%.

*Tetra-N-acetylfortimicin B (**29**).* To a solution of natural fortimicin B (58.8 mg) in methanol (10 ml), acetic anhydride (4 ml) was added. After 3 h, the solution was concentrated to give 82.2 mg (94%) of **29** as a monohydrate: mp 161—163 °C; $[\alpha]_D^{20}$ +92.5° (c 0.72, methanol); ^{1}H NMR (D_2O) δ 1.17 (d, 1, $J_{6',7'}$=7.2 Hz, H-7'), 2.00 (s, 3, NAc), 2.02 (s, 3, NAc), 2.05 (s, 3, NAc), 2.18 (s, 3, NAc), 3.09 (d, 3, J=10.6 Hz, NCH_3), 3.43 (s, 3, OCH_3).

The authors wish to express their appreciation to Dr. Kunikatsu Shirahata, Kyowa Hakko Kogyo Co., Ltd., for supplying fortimicin A and B; to Mr. Itsuki Sakamoto for his helpful technical assistance, and to Mr. Saburo Nakada for his elemental analysis.

References

1) T. Nara, M. Yamamoto, I. Kawamoto, K. Takayama, R. Okachi, S. Takasawa, T. Sato, and S. Sato, *J. Antibiot.*, **30**, 533 (1977).

2) R. Okachi, S. Takasawa, T. Sato, S. Sato, M. Yamamoto, I. Kawamoto, and T. Nara, *J. Antibiot.* **30**, 541 (1977).

3) M. Sugimoto, S. Ishii, R. Okachi, and T. Nara, *J. Antibiot.*, **32**, 868 (1979).

4) T. Iida, M. Sato, I. Matsubara, Y. Mori, and K. Shirahata, *J. Antibiot.*, **32**, 1273 (1979).

5) S. Inouye, T. Shomura, and K. Ohba, *J. Antibiot.*, **33**, 510 (1980).

6) S. Inouye, K. Ohba, T. Shomura, M. Kojima, T. Tsuruoka, J. Yoshida, N. Kato, M. Ito, S. Amano, S. Omoto, N. Ezaki, and T. Niida, *J. Antibiot.*, **32**, 1354 (1979).

7) T. Shomura, M. Kojima, J. Yoshida, M. Ito, S. Amano, K. Totsugawa, T. Niwa, S. Inouye, T. Ito, and T. Niida, *J. Anitibiot.* **33**, 924 (1980).

8) T. Deushi, A. Iwasaki, K. Kamiya, T. Kunieda, T. Mizuguchi, M. Nakayama, H. Itoh, T. Mori, and T. Oda, *J. Antibiot.*, **32**, 173 (1979).

9) A. Iwasaki, H. Itoh, and T. Mori, *J. Antibiot.*, **32**, 180 (1979).

10) T. Deushi, M. Nakayama, I. Watanabe, and T. Mori, *J. Antibiot.*, **32**, 187 (1979).

11) T. Mori, T. Deushi, A. Iwasaki, T. Kunieda, T. Mizoguchi, K. Kamiya, M. Nakayama, H. Itoh, and T. Oda, Ger. Offen, 2813021, Oct. 5, 1978; Japan Kokai, 79-66603, May 29, 1979.

12) T. Suami, Y. Honda, and T. Kato, *Chem. Lett.*, **1978**, 1125.

13) T. Suami, Y. Honda, T. Kato, M. Masu, and K. Matsuzawa, *Bull. Chem. Soc. Jpn.*, **53**, 1372 (1980).

14) Y. Honda and T. Suami, *Bull. Chem. Soc. Jpn.*, **54**, 2825 (1981).

15) T. Suami and Y. Honda, *Chem. Lett.*, **1980**, 641.

16) H. Sano, K. Shirahata, and Y. Mori, Abstract paper of the Annual Meeting of the Chemical Society of Japan, 3S01, p, 1107 (1980), delivered on April 3, 1980, Osaka, Japan.

17) R. S. Egan, R. S. Stanaszek ,M. Cirovic, S. L. Mueller, J. Tadanier, J. R. Martin, P. Collum, A. W. Goldstein, R. L. Devault, A. C. Sinclair, E. E. Fager, and L. A. Mitscher, *J.*

Antibiot., **30**, 552 (1977).

18) J. Tadanier, J. R. Martin, P. Kurath, A. W. Goldstein, and P. Johnson, *Carbohydr. Res.*, **79**, 91 (1980).

19) H. Sano, T. Sakaguchi, and Y. Mori, *Bull. Chem. Soc. Jpn.*, **52**, 2727 (1979).

20) T. Suami, F. W. Lichtenthaler, and Ogawa, *Bull. Chem. Soc. Jpn.*, **40**, 1488 (1967); a mixture of 2,4,5,6-tetra-*O*-acetyl-1,3-di-*O*-tosyl-*myo*-inositol[21] (3.0 g) and sodium azide (3.0 g) in 90% aq 2-methoxyethanol (54 ml) was heated under reflux. After 45 h, the mixture was filtered and the filtrate was concentrated. The residue was extracted with hot ethyl acetate, and the organic layer was concentrated. The residual product was recrystallized from ethyl acetate to give 0.56 g (53%) of 1,4-diazido-1,4-dideoxy-*muco*-inositol; mp 139—140 °C. Found: C, 31.28; H, 4.38; N, 36.36%. Calcd for $C_6H_{10}N_6O_4$: C, 31.31; H, 4.38; N, 36.51%.

21) S. J. Angyal, P. T. Gilham, and G. J. H. Melrose, *J. Chem. Soc.*, **1965**, 5252.

22) R. L. Giralami and J. M. Stamm, *J. Antibiot.*, **30**, 564 (1977).

 © 1982 The Chemical Society of Japan Bull. Chem. Soc. Jpn., 55, 1163—1167 (1982)

New Building Blocks for Heterocyclic Syntheses. Silylated Methyl Isothiocyanates

Toshikazu HIRAO, Atsushi YAMADA, Ken-ichiro HAYASHI, Yoshiki OHSHIRO,* and Toshio AGAWA

Department of Petroleum Chemistry, Faculty of Engineering, Osaka University, 2-1 Yamada-oka, Suita, Osaka 565

(Received August 3, 1981)

Trimethylsilylmethyl isothiocyanate, bis(trimethylsilyl)methyl isothiocyanate, and tris(trimethylsilyl)methyl isothiocyanate were prepared. The fluoride-catalyzed reaction of trimethylsilylmethyl isothiocyanate with aldehydes or ketones afforded oxazolidine-2-thione derivatives, which involves the isothiocyanato carbanion as an intermediate. Imidazolidine-2-thiones were similarly prepared from imines. The reaction of bis(trimethylsilyl)methyl isothiocyanate with benzaldehyde in the presence of a catalytic amount of *n*-Bu_4NF gave styryl isothiocyanate and 5-phenyl-4-trimethylsilyloxazolidine-2-thione. On the similar treatment of tris(trimethylsilyl)methyl isothiocyanate, 4-benzyl-5-phenyl-4-oxazoline-2-thione, and α-(trimethylsilyl)styryl isothiocyanate were obtained.

The chemistry of functionalized heterocumulene has been recently developed in the field of heterocyclic synthesis.[1] From this point of view, we have previously reported the synthesis of methyl(phenylthio)ketene,[2] methyl(phenylseleno)ketene,[3] α-alkylthio(or arylthio)-vinyl isocyanate,[4] and *N*-[2-(diethoxyphosphoryl)-1-propenylidene]ethylamine,[5] and (2-aryl-2-halovinylidene)arylamine[6] and their cycloaddition reactions.

It is thought to enhance the synthetic utility of isothiocyanates that carbanion center can be generated in the α-position relative to nitrogen. The metalation of activated isothiocyanates was reported by Hoppe,[7] but this method is not applicable to methyl isothiocyanate. We addressed ourselves to this problem by preparing trimethylsilylmethyl isothiocyanate because fluoride ion has been reported to cause bond cleavage between carbon and silicon.[8] In our previous paper, trimethylsilylmethyl isothiocyanate was proved to be an equivalent of isothiocyanatomethanide.[9] Herein, we wish to report further details of the investigation on silylated methyl isothiocyanates as new building blocks for heterocyclic syntheses.

Results and Discussion

Trimethylsilylmethyl Isothiocyanate. Trimethylsilylmethyl isothiocyanate (**1**) was prepared by the addition of sulfur to trimethylsilylmethyl isocyanide in 76% yield. The isothiocyanate **1** is a stable liquid at room temperature, and can be stored under nitrogen atmosphere.

$$Me_3SiCH_2N{\equiv}C + S_x \xrightarrow[\text{reflux}]{\text{PhH}} Me_3SiCH_2N{=}C{=}S$$

1

The cleavage of a carbon-silicon bond by fluoride ion was confirmed by treatment of the isothiocyanate **1** with D_2O in the presence of a catalytic amount of tetrabutylammonium fluoride to give methyl-d_1 isothiocyanate in 76% yield.

The isothiocyanate **1** was subjected to the *n*-Bu_4NF-catalyzed reaction with aldehydes or ketones to produce the oxazolidine-2-thiones **2**. The results are summarized in Table 1. Use of potassium fluoride with triethylbenzylammonium chloride (TEBA·Cl) or 18-crown-6 instead of tetrabutylammonium fluoride also gave the oxazolidine-2-thione **2a** in a good yield.

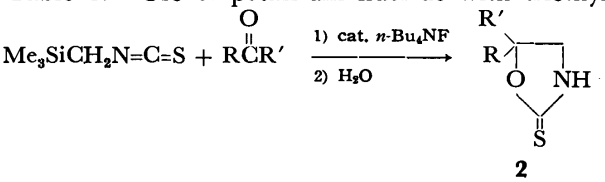

2

A possible reaction path is shown in Scheme 1. The isothiocyanato carbanion **3**, which is generated from the fluoride-catalyzed reaction of **1**, may be involved as a key intermediate. The carbanion **3** reacts with carbonyl compound to give the 1 : 1 adduct, which undergoes intramolecular cyclization resulting in **4**. The following mechanism may be operative to achieve a reaction cycle. The fluoride ion appears to be regenerated by the reaction of trimethylsilyl fluoride with **4**. It is also

Table 1. Preparation of oxazolidine-2-thiones (**2**)

R	R′	F^- (equiv.)	Reaction time/h	Oxazolidine-2-thione, **2** (%)
Ph	H	*n*-Bu_4NF (0.1)	8	**2a** 74
Ph	H	KF (1.0), TEBA·Cl (0.1)	2	**2a** 74
Ph	H	KF (1.0), 18-Crown-6 (0.1)	5	**2a** 65
Et	H	*n*-Bu_4NF (0.1)	5	**2b** 63
i-Pr	H	*n*-Bu_4NF (0.1)	10	**2c** 67
Ph	Ph	*n*-Bu_4NF (0.1)	40	**2d** 25
Ph	Me	*n*-Bu_4NF (0.1)	23	**2e** 35[a]

a) 5-Methyl-3-[methyl(thiocarbamoyl)]-5-phenyloxazolidine-2-thione (**6a**) was obtained in 17% yield.

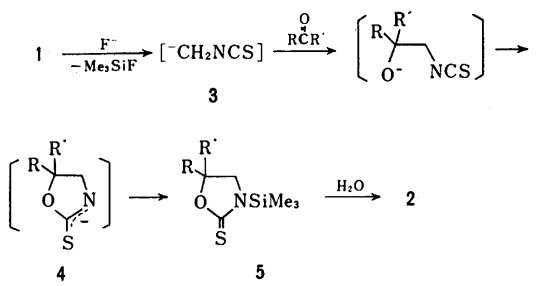

Scheme 1.

conceivable that the attack of **4** to **1** gives the isothiocyanato carbanion **3** and the 3-trimethylsilyloxazolidine-2-thione **5**. It has not been clarified which path is preferred. Thus formed **5** is easily hydrolyzed to **2**.

When the phase-transfer reaction of the isothiocyanate **1** with benzaldehyde was carried out in the presence of potassium fluoride and TEBA·Cl in benzene–water, 3-[methyl(thiocarbamoyl)]-5-phenyloxazolidine-2-thione (**6b**, 30%) was produced together with 5-phenyloxazolidine-2-thione (**2a**, 31%). The formation of the 3-[methyl(thiocarbamoyl)] derivative **6a** (17%) was also observed in the *n*-Bu_4NF-catalyzed reaction of **1** with acetophenone in dry THF, but only a trace amount of the corresponding 3-[methyl(thiocarbamoyl)]oxazolidine-2-thione was given from aldehyde. These 3-[methyl(thiocarbamoyl)] derivatives are considered to be produced by the reaction of **4** with methyl isothiocyanate, which is derived from proton abstraction of **3** from H_2O (phase-transfer reaction) or acetophenone[8a] (Scheme 2). The possibility of desilylation of 3-(*N*-trimethylsilylmethylthiocarbamoyl)oxazolidine-2-thiones, however, could not necessarily be excluded.

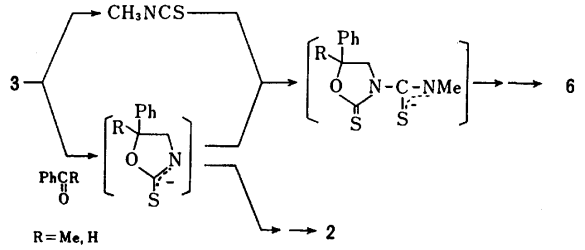

Scheme 2.

Imines were also allowed to react with **1** in the presence of a catalytic amount of *n*-Bu_4NF to produce the imidazolidine-2-thione derivatives **7**.

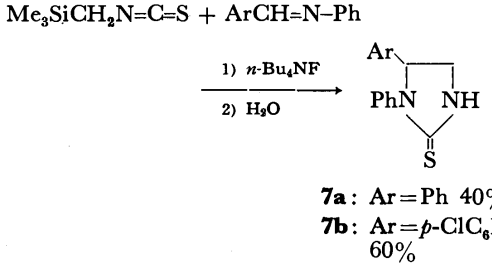

7a: Ar=Ph 40%
7b: Ar=*p*-ClC_6H_4 60%

Bis(trimethylsilyl)methyl Isothiocyanate. Bis(trimethylsilyl)methyl isothiocyanate (**8**) was analogously prepared from the corresponding isocyanide and sulfur in 80% yield. The isothiocyanate **8** was desilylated to methyl-d_2 isothiocyanate by treatment with D_2O and a catalytic amount of *n*-Bu_4NF.

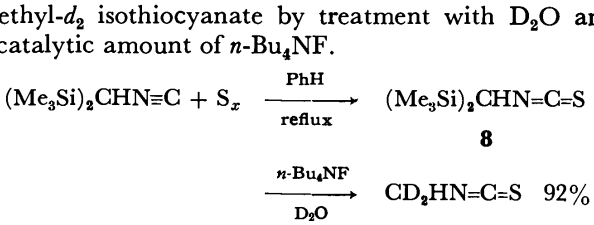

The methodology mentioned above was able to be applied to the reaction of **8** with benzaldehyde, but 5-phenyl-4-trimethylsilyloxazolidine-2-thione (**9**) was produced in only 6% yield. It is of interest that styryl isothiocyanate (**10**) was obtained as a main product in this case.

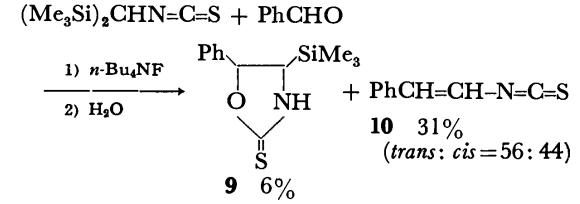

The formation path for styryl isothiocyanate is outlined in Scheme 3. The β-trimethylsilylalkoxide intermediate **12** undergoes elimination of Me_3SiO^- to give styryl isothiocyanate. Both silyl groups of **8** participate in the synthesis of **10**, generation of carbanion by fluoride ion and Peterson-olefination.[14] Ring closure of a rotamer of **12** leads to **9**.

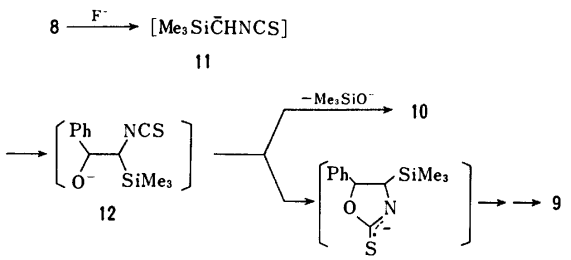

Scheme 3.

Tris(trimethylsilyl)methyl Isothiocyanate. Tris(trimethylsilyl)methyl isothiocyanate (**13**) was prepared by the addition of sulfur to tris(trimethylsilyl)methyl isocyanide in 76% yield. The isothiocyanate **13** was converted to methyl-d_3 isothiocyanate on treatment with D_2O in the presence of a catalytic amount of *n*-Bu_4NF.

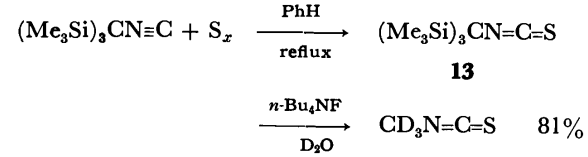

The isothiocyanate **13** reacted with benzaldehyde in the presence of a catalytic amount of *n*-Bu_4NF to afford α-(trimethylsilyl)styryl isothiocyanate (**14**) and 4-benzyl-5-phenyl-4-oxazoline-2-thione (**15**) in 26% and 7% yields, respectively.

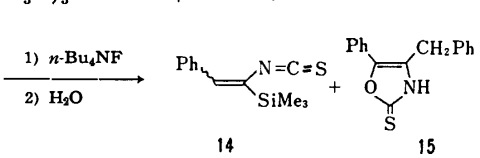

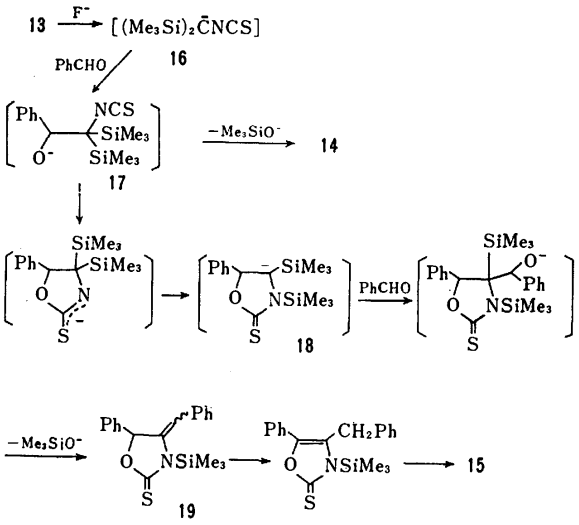

Scheme 4.

The probable reaction path for these products is outlined in Scheme 4. The isothiocyanate **14** was formed by the elimination of Me_3SiO^- from **17**. A rotamer of **17** is subjected to ring closure, followed by transposition of trimethylsilyl group to generate the carbanion **18**. The carbanion **18** reacts with another benzaldehyde to give the benzylideneoxazolidine-2-thione **19**, which may be rearranged and hydrolyzed to **15**.

The fluoride-catalyzed reactions of silylated methyl isothiocyanates provide a facile and mild generation of isothiocyanato carbanions (**3**, **11**, and **16**).

Experimental

Melting points were measured by a Yanagimoto micro melting point apparatus and uncorrected. ^1H NMR spectra were obtained on a JEOL JNN-PMX-60 with tetramethylsilane as an internal standard. IR spectra were recorded with a JASCO IRA-1 spectrometer. The mass spectra were taken with a Hitachi RMU-6E spectrometer.

Materials. Trimethylsilylmethyl isocyanide, bis(trimethylsilyl)methyl isocyanide, and tris(trimethylsilyl)methyl isocyanide were prepared by the reported method.[10] Tetrabutylammonium fluoride was prepared by the literature method[8a] and dried before use. Imines were obtained by the reaction of aldehydes with aniline,[11] and recrystallized prior to use. Carbonyl compounds were purified by distillation or recrystallization.

*Preparation of Trimethylsilylmethyl Isothiocyanate (**1**).* Trimethylsilylmethyl isothiocyanate was prepared by the addition of sulfur to the isocyanide in the same manner as mentioned in the reported method.[12] A mixture of trimethylsilylmethyl isocyanide (12.3 g, 109 mmol) and sulfur (4.2 g, 130 mmol) in benzene (20 ml) was refluxed for 26 h. Hexane (20 ml) was added to the cooled solution. After excess of sulfur was removed by filtration, the solution was distilled *in vacuo* to give **1** (12.0 g, 76%): bp 46 °C/3 mmHg;† IR (neat) 2180 and 2080 cm^{-1}; ^1H NMR ($CDCl_3$) δ 0.18 (s, 9H), 3.00 (s, 2H); MS *m/e* 145 (M^+); Found: C, 41.16; H, 7.98; N, 9.72; S, 22.32%. Calcd for $C_5H_{11}NSSi$: C, 41.33; H, 7.63; N, 9.64; S, 22.07%.

† 1 mmHg≈133.322 Pa.

*Treatment of **1** with D_2O in the Presence of* n-Bu_4NF. To a solution of *n*-Bu_4NF (78 mg, 0.3 mmol) and D_2O (66 mg, 3.3 mmol) in THF (3 ml), the isothiocyanate **1** (0.44 g, 3.0 mmol) in THF (2 ml) was added dropwise at room temperature. The mixture was stirred for 4 h under nitrogen atmosphere. Water (60 ml) was added to the resultant mixture, which was extracted with chloroform (3×30 ml). The combined organic layer was washed with water (10 ml) and dried on anhydrous sodium sulfate. After evaporation, methyl-d_1 isothiocyanate was isolated in 76% yield by preparative GLC (conditions: PS-410 column, 100 °C). IR (neat) 2230 and 2120 cm^{-1}; ^1H NMR ($CDCl_3$) δ 3.27 (t, 2H, J=2.0 Hz); MS *m/e* 74 (M^+).

n-*Bu_4NF-Catalyzed Reaction of **1** with Benzaldehyde.* To a solution of benzaldehyde (0.64 g, 6.0 mmol) and *n*-Bu_4NF (78 mg, 0.3 mmol) in THF (3 ml), the isothiocyanate **1** (0.44 g, 3.0 mmol) in THF (2 ml) was added dropwise at room temperature. The resultant solution was stirred for 8 h under nitrogen atmosphere. Water (60 ml) was added to the resultant mixture, which was extracted with chloroform (3×30 ml). The combined organic layer was washed with water (10 ml) and dried on anhydrous sodium sulfate. After evaporation, the residue was chromatographed on a silica gel column eluting with chloroform to give 0.40 g (74%) of 5-phenyloxazolidine-2-thione (**2a**): mp 130—131 °C; IR (Nujol) 3160 and 1520 cm^{-1}; ^1H NMR ($CDCl_3$) δ 3.68 (dd, 1H, J=8.4 and 10.0 Hz), 4.13 (dd, 1H, J=9.2 and 10.0 Hz), 5.87 (dd, 1H, J=8.4 and 9.2 Hz), 7.35 (s, 5H), 8.20 (br, 1H); MS *m/e* 179 (M^+). Found: C, 60.35; H, 4.89; N, 7.66; S, 17.67%. Calcd for C_9H_9ONS: C, 60.31; H, 5.06; N, 7.81; S, 17.89%.

In a similar manner, 5-ethyloxazolidine-2-thione (**2b**), 5-isopropyloxazolidine-2-thione (**2c**), 5,5-diphenyloxazolidine-2-thione (**2d**), and 5-methyl-5-phenyloxazolidine-2-thione (**2e**) were prepared in 63%, 67%, 25%, and 35% yields, respectively. Reaction time was shown in Table 1. In the preparation of **2e**, 5-methyl-3-[methyl(thiocarbamoyl)]-5-phenyloxazolidine-2-thione (**6a**) was obtained in 17% yield as a by-product.

2b: mp 87—89 °C; IR (Nujol) 3200 and 1520 cm^{-1}; ^1H NMR ($CDCl_3$) δ 1.04 (t, 3H, J=7.0 Hz), 1.87 (dq, 2H, J=6.4 and 7.0 Hz), 3.47 (dd, 1H, J=8.4 and 9.6 Hz), 3.93 (dd, 1H, J=8.8 and 9.6 Hz), 4.97 (ddt, 1H, J=6.4, 8.4, and 8.8 Hz), 8.55 (br, 1H); MS *m/e* 131 (M^+); Found: C, 45.60; H, 6.89; N, 10.70; S, 24.29%. Calcd for C_5H_9ONS: C, 45.78; H, 6.91; N, 10.68; S, 24.44%.

2c: mp 101—101.5 °C; IR (Nujol) 3220 and 1535 cm^{-1}; ^1H NMR ($CDCl_3$) δ 0.97 (d, 3H, J=6.4 Hz), 1.03 (d, 3H, J=6.4 Hz), 2.00 (m, 1H), 3.53 (dd, 1H, J=8.4 and 8.8 Hz), 3.87 (dd, 1H, J=8.8 and 8.8 Hz), 4.76 (ddd, 1H, J=6.4, 8.8, and 8.8 Hz), 8.53 (br, 1H); MS *m/e* 145 (M^+); Found: C, 49.45; H, 7.61; N, 9.68; S, 22.06%. Calcd for $C_6H_{11}ONS$: C, 49.63; H, 7.63; N, 9.65; S, 22.08%.

2d: mp 186—188 °C; IR (Nujol) 3180 and 1530 cm^{-1}; ^1H NMR ($CDCl_3$) δ 4.30 (s, 2H), 7.30 (s, 10H), 8.30 (br, 1H); MS *m/e* 255 (M^+); Found: C, 70.66; H, 5.05; N, 5.47; S, 12.71%. Calcd for $C_{15}H_{13}ONS$: C, 70.56; H, 5.13; N, 5.49; S, 12.56%. **2e**: mp 201—203 °C; IR (Nujol) 3210 and 1510 cm^{-1}; ^1H NMR ($CDCl_3$) δ 1.83 (s, 3H), 3.83 (s, 2H), 7.33 (s, 5H), 8.20 (br, 1H); MS *m/e* 193 (M^+); Found: C, 62.09; H, 5.72; N, 7.29; S, 16.31%. Calcd for $C_{10}H_{11}ONS$: C, 62.15; H, 5.74; N, 7.25; S, 16.59%.

6a: IR (Nujol) 3150 and 1560 cm^{-1}; ^1H NMR (CCl_4) δ 1.85 (s, 3H), 3.15 (d, 3H, J=5.0 Hz), 4.77 (s, 2H), 7.20—7.60 (m, 5H), 11.80 (br, 1H); MS *m/e* 266 (M^+).

*KF-Catalyzed Reaction of **1** with Benzaldehyde in the Presence of TEBA·Cl or 18-Crown-6 in Acetonitrile.* To a mixture of

benzaldehyde (0.64 g, 6.0 mmol), anhydrous KF (0.17 g, 3.0 mmol), and TEBA·Cl (68 mg, 0.3 mmol) or 18-crown-6 (72 mg, 0.3 mmol) in acetonitrile (3 ml), the isothiocyanate **1** (0.44 g, 3.0 mmol) in acetonitrile (2 ml) was added dropwise at room temperature. The resultant mixture was stirred under nitrogen atmosphere for 2 or 5 h, respectively. Work up was carried out in the same procedure as mentioned above. The yields of 5-phenyloxazolidine-2-thione (**2a**) were shown in Table 1.

*KF-Catalyzed Reaction of **1** with Benzaldehyde in the Presence of TEBA·Cl in Benzene–Water.* To 1.5 ml of aqueous solution of TEBA·Cl (68 mg, 0.3 mmol) and KF (1.00 g, 17.2 mmol), benzaldehyde (0.64 g, 6.0 mmol) and the isothiocyanate **1** (0.44 g, 3.0 mmol) in benzene (1 ml) were added at room temperature. The mixture was stirred for 4 h, and then chloroform (10 ml) was added. The organic layer was dried on anhydrous sodium sulfate. After evaporation, the residue was chromatographed on a silica-gel column to give 5-phenyloxazolidine-2-thione (**2a**, 0.17 g, 31%) and 3-[methyl-(thiocarbamoyl)]-5-phenyloxazolidine-2-thione (**6b**, 0.22 g, 30%). **6b**: mp 85—86 °C; IR (Nujol) 3130 and 1545 cm^{-1}; ^1H NMR ($CDCl_3$) δ 3.22 (d, 3H, J=5.0 Hz), 4.62 (dd, 1H, J=8.4 and 11.6 Hz), 5.12 (dd, 1H, J=8.4 and 11.6 Hz), 5.72 (dd, 1H, J=8.4 and 8.4 Hz), 7.40 (br, 5H), 11.80 (br, 1H); MS *m/e* 252 (M^+); Found: C, 52.47; H, 4.79; N, 11.12; S, 25.26%. Calcd for $C_{11}H_{12}ON_2S_2$: C, 52.36; H, 4.79; N, 11.10; S, 25.41%.

*Preparation of 1,5-Diphenylimidazolidine-2-thione (**7a**).* To a solution of *N*-benzylideneaniline (1.09 g, 6.0 mmol) and *n*-Bu_4NF (0.16 g, 0.6 mmol) in THF (3 ml), the isothiocyanate **1** (0.44 g, 3.00 mmol) in THF (2 ml) was added dropwise at room temperature. The resultant solution was stirred for 13 h under nitrogen atmosphere, and worked up in the same procedure as given for **2a**. The imidazolidine-2-thione **7a** was isolated by column chromatography on silica gel eluting with chloroform in 40% yield (0.31 g). **7a**: mp 188—190 °C; IR (KBr) 3200, 1620, 1590, and 1575 cm^{-1}; ^1H NMR ($CDCl_3$) δ 3.63 (dd, 1H, J=7.6 and 9.8 Hz), 4.13 (dd, 1H, J=8.8 and 9.8 Hz), 5.40 (dd, 1H, J=7.6 and 8.8 Hz), 7.00—7.50 (m, 10H); MS *m/e* 254 (M^+); Found: C, 70.56; H, 5.53; N, 11.02; S, 12.38%. Calcd for $C_{15}H_{14}N_2S$: C, 70.83; H, 5.55; N, 11.01; S, 12.61%.

Similarly, 5-(*p*-chlorophenyl)-1-phenylimidazolidine-2-thione (**7b**) was prepared in 60% yield. **7b**: mp 212 °C; IR (KBr) 3200, 1620, 1580, and 1570 cm^{-1}; ^1H NMR ($CDCl_3$) δ 3.55 (dd, 1H, J=7.6 and 10.4 Hz), 4.12 (dd, 1H, J=9.2 and 10.4 Hz), 5.35 (dd, 1H, J=7.6 and 9.2 Hz), 7.05—7.50 (m, 10H); MS *m/e* 288 (M^+); Found: C, 61.96; H, 4.42; Cl, 12.46; N, 9.56; S, 11.13%. Calcd for $C_{15}H_{13}ClN_2S$: C, 62.38; H, 4.54; Cl, 12.28; N, 9.70; S, 11.10%.

*Preparation of Bis(trimethylsilyl)methyl Isothiocyanate (**8**).* The isothiocyanate **8** was prepared in 80% yield by the reaction of bis(trimethylsilyl)methyl isocyanide and sulfur in benzene at 80 °C for 26 h in the same manner as given for **1**. **8**: bp 48—50 °C/0.5 mmHg, mp 45—47 °C; IR (neat) 2140 and 2060 cm^{-1}; ^1H NMR ($CDCl_3$) δ 0.17 (s, 18H), 2.56 (s, 1H); MS *m/e* 217 (M^+); Found: C, 44.35; H, 9.09; N, 6.53; S, 14.37%. Calcd for $C_8H_{19}NSSi_2$: C, 44.18; H, 8.76; N, 6.44; S, 14.74%.

*Treatment of **8** with D_2O in the Presence of* n-*Bu_4NF.* The reaction of **8** (3.0 mmol) with D_2O (6.6 mmol) in the presence of *n*-Bu_4NF (0.3 mmol) was carried out in the same manner as given for **1** to produce methyl-d_2 isothiocyanate in 92% yield. IR (neat) 2220, 2180, and 2100 cm^{-1}; ^1H NMR (CCl_4) δ 3.30 (quintet, 1H, J=2.0 Hz); MS *m/e* 75 (M^+).

*n-Bu_4NF-Catalyzed Reaction of **8** with Benzaldehyde.* In the same manner as described in the preparation of **2a**, *n*-Bu_4NF-catalyzed reaction of **8** with benzaldehyde gave styryl isothiocyanate (**10**)[13] and 5-phenyl-4-trimethylsilyloxazolidine-2-thione (**9**) in 31% and 6% yields, respectively. The *trans-cis* ratio (56 : 44) of **10** was determined by the ^1H NMR spectrum.

9: mp 178 °C (dec); IR (Nujol) 3180 and 1500 cm^{-1}; ^1H NMR ($CDCl_3$) δ −0.18 (s, 9H), 3.89 (d, 1H, J=9.4 Hz), 6.06 (d, 1H, J=9.4 Hz), 7.26—7.47 (m, 5H), 8.20 (br, 1H); MS *m/e* 251 (M^+); Found: C, 57.21; H, 6.88; N, 5.55; S, 13.13%. Calcd for $C_{12}H_{17}ONSSi$: C, 57.33; H, 6.81; N, 5.57; S, 12.75%.

10: IR (neat) 2100, 2040, and 1620 cm^{-1}; ^1H NMR ($CDCl_3$) δ 6.10 (2d, 0.88H, J=8.6 Hz, cis CH=CH), 6.60 (2d, 1.12H, J=12.2 Hz, *trans* CH=CH), 7.20—7.90 (m, 5H); MS *m/e* 161 (M^+).

*Preparation of Tris(trimethylsilyl)methyl Isothiocyanate (**13**).* Tris(trimethylsilyl)methyl isothiocyanate was prepared in 76% yield by the reaction of tris(trimethylsilyl)methyl isocyanide and sulfur in benzene at 80 °C for 29 h in the same manner as given for **1**. The isothiocyanate **13** was purified by column chromatography on silica gel eluting with hexane. **13**: mp>300 °C; IR (KBr) 2140 cm^{-1}; ^1H NMR ($CDCl_3$) δ 0.20 (s, 27H); MS *m/e* 289 (M^+); Found: C, 45.93; H, 9.62; N, 4.60; S, 11.08%. Calcd for $C_{11}H_{27}NSSi_3$: C, 45.61; H, 9.40; N, 4.34; S, 11.07%.

*Treatment of **13** with D_2O in the Presence of* n-*Bu_4NF.* The reaction of **13** (3.0 mmol) with D_2O (9.9 mmol) in the presence of *n*-Bu_4NF (0.3 mmol) was carried out in the same manner as given for **1** to produce methyl-d_3 isothiocyanate in 81% yield. IR (neat) 2260, 2200, and 2120 cm^{-1}; MS *m/e* 76 (M^+).

*n-Bu_4NF-Catalyzed Reaction of **13** with Benzaldehyde.* The *n*-Bu_4NF-catalyzed reaction of **13** with benzaldehyde was carried out at room temperature for 24 h in the same manner as mentioned in the preparation of **2a**. After evaporation of the solvent, the residue was chromatographed on a silica-gel column to give α-(trimethylsilyl)styryl isothiocyanate (**14**) and 4-benzyl-5-phenyl-4-oxazoline-2-thione (**15**) in 26% and 7% yields, respectively, with a small amount of styryl isothiocyanate (6%). **14**: IR (neat) 2040 and 1620 cm^{-1}; ^1H NMR (CCl_4) δ 0.28 (s, 9H), 6.23 (s, 1H), 7.00—7.73 (m, 5H); MS *m/e* 233 (M^+). **15**: mp 182—185 °C; IR (KBr) 1480 cm^{-1}; ^1H NMR ($CDCl_3$) δ 4.06 (s, 2H), 7.00—7.77 (m, 10H); MS *m/e* 267 (M^+).

References

1) J. Goerdeler, *Q. Rep. Sulfur Chem.*, **5**, 169 (1970); E. Van Loock, *Ind. Chim. Belg.*, **39**, 661 (1974); R. Esmail and F. Kurzer, *Synthesis*, **1975**, 301; H. Ulrich, "Cycloaddition Reactions of Heterocumulene," Academic Press, New York (1967).

2) M. Ishida, T. Minami, and T. Agawa, *J. Org. Chem.*, **44**, 2067 (1979).

3) T. Agawa, M. Ishida, and Y. Ohshiro, *Synthesis*, **1980**, 933.

4) K. Takaki, A. Okamura, Y. Ohshiro, and T. Agawa, *J. Org. Chem.*, **43**, 402 (1978).

5) J. Motoyoshiya, A. Teranishi, R. Mikoshiba, I. Yamamoto, H. Gotoh, J. Enda, Y. Ohshiro, and T. Agawa, *J. Org. Chem.*, **45**, 5385 (1980).

6) T. Hirao, K.-i. Hayashi, J. Motoyoshiya, Y. Ohshiro, and T. Agawa, *Chem. Lett.*, **1981**, 1197.

7) D. Hoppe, *Angew. Chem.*, **84**, 956 (1972); D. Hoppe and R. Follmann, *Chem. Ber.*, **109**, 3047 (1976).

8) a) E. Nakamura, T. Morofushi, M. Shimizu, and I. Kuwajima, *J. Am. Chem. Soc.*, **98**, 2346 (1976); b) T. H. Chan,

B. S. Ong, and W. Mychajlowskij, *Tetrahedron Lett.*, **1976**, 3253.
9) T. Hirao, A. Yamada, Y. Ohshiro, and T. Agawa, *Angew. Chem.*, **93**, 95 (1981); *Angew. Chem., Int. Ed. Engl.*, **20**, 126 (1981).
10) R. West and G. A. Gornowicz, *J. Organomet. Chem.*, **25**, 385 (1970).
11) L. A. Bigelow and H. Eatough, *Org. Synth.*, Coll. Vol. I, 80 (1941).
12) J. V. Nef, *Justus Liebigs Ann. Chem.*, **280**, 291 (1894); W. Weith, *Ber.*, **6**, 210 (1873).
13) L. Kniežo, P. Kristian, and S. Velebný, *Collect. Czech. Chem. Commun.*, **43**, 1917 (1978); L. Kniežo and P. Kristian, *Chem. Zvesti*, **28**, 848 (1974).
14) D. J. Peterson, *J. Org. Chem.*, **33**, 780 (1968).

Synthesis of 3β-Hydroxytaxodione and Coleons S and T

Takashi MATSUMOTO,* Hiroyuki KAWASHIMA, and Koji IYO
Department of Chemistry, Faculty of Science, Hiroshima University, Higashisenda-machi, Naka-ku, Hiroshima 730

(Received August 12, 1981)

Hinokiol diacetate was converted into 3β-acetoxyabieta-8,11,13-triene-6β,12-diol *via* 3β,12-diacetoxyabieta-8,11,13-trien-7-one and 3β,12-diacetoxyabieta-6,8,11,13-tetraene. Oxidation of the 6β,12-diol with benzoyl peroxide produced 3β-acetoxy-12-benzoyloxyabieta-8,11,13-triene-6β,11-diol, which was converted into 3β,11,12-triacetoxyabieta-8,11,13-trien-6-one by lithium aluminium hydride reduction, acetylation, and Jones oxidation. Acidic hydrolysis of the triacetoxy ketone, followed by column chromatography on silica gel, afforded 3β-hydroxytaxodione. Oxidation of the 6β,11-diol with *m*-chloroperbenzoic acid afforded 3β-acetoxy-12-benzoyloxy-6β-hydroxyabieta-8,12-diene-11,14-dione. This was further converted into 3β,11,14-triacetoxy-12-benzoyloxyabieta-8,11,13-triene-6,7-dione by a series of reactions: Jones oxidation, reduction with zinc powder and dilute hydrochloric acid, acetylation, and Jones oxidation. Alkaline hydrolysis of the 6,7-dioxo compound afforded coleon T, which was isomerized to coleon S by refluxing with concentrated hydrochloric acid in methanol.

In the previous papers,[1-3] we reported the synthesis of taxodione (**1**), a tumor-inhibitory diterpene quinonemethide isolated from *Taxodium distichum* Rich by Kupchan *et al.*[4] We have now synthesized the analogous quinonemethide compound in order to compare their tumor-inhibiting activity with that of **1**.

Recently, coleon S and coleon T, highly-oxygenated tricyclic diterpenes possessing an abietane skeleton, were isolated from leaf-glands of *Plectranthus caninus* Roth (Labiatae) by Eugster *et al.*[5] On the basis of chemical and spectroscopic studies, they deduced the structures of these coleons, S and T, to be 3β,6,11,12,14-pentahydroxyabieta-5,8,11,13-tetraen-7-one (**2**) and 3β,11,12,-14-tetrahydroxyabieta-8,11,13-triene-6,7-dione (**3**), respectively. As a part of our synthetic studies on the naturally-occurring terpenes, we have attempted the syntheses of these highly-oxygenated tricyclic diterpenes. This paper will describe the syntheses of 3β-hydroxytaxodione (**4**) [3β,11-dihydroxyabieta-7,9(11),13-triene-6,12-dione] and coleons S (**2**) and T (**3**), starting from the optically active hinokiol diacetate (**5**), which has been synthesized[6] from (+)-dehydroabietic acid.

Oxidation of **5** with Jones reagent afforded 3β,12-diacetoxyabieta-8,11,13-trien-7-one (**6**), together with a small amount of 12-acetoxyabieta-8,11,13-triene-3,7-dione (**7**). The diacetoxy ketone **6** was reduced with sodium borohydride in methanol and the resulting mixture of epimeric 7-hydroxy compounds (**8**) was immediately subjected to dehydration with dilute hydrochloric acid in refluxing methanol. Under these conditions, the acetoxyl groups were partially hydrolyzed. Therefore, the crude product was acetylated with acetic anhydride in pyridine and then purified by column chromatography on silica gel to give 3β,12-diacetoxyabieta-6,8,11,13-tetraene (**9**). The 3,7-dioxo compound **7** was also transformed to **9** by a series of reactions: reduction with lithium aluminium hydride in ether, dehydration with dilute hydrochloric acid in refluxing methanol, and acetylation with acetic anhydride in pyridine. The tetraene **9** was subjected to epoxidation at room temperature with *m*-chloroperbenzoic acid in dichloromethane. The resulting epoxide (**10**), without purification, was refluxed with dilute hydrochloric acid in methanol and then acetylated with acetic anhydride in pyridine. Purification of the crude product by column chromatography on silica gel yielded 3β,12-diacetoxyabieta-8,11,13-trien-6-one (**11**) as a major product and 3β,6α,12-triacetoxyabieta-8,11,13-trien-7-one (**12**) as a minor one. The α-configuration of the acetoxyl group at C-6 in **12** was supported by its ^{1}H NMR spectrum, which showed a doublet due to the C-6 proton at δ 5.82 with a coupling constant of 13 Hz, suggesting the presence of a β hydrogen. The minor ketone **12** was easily converted to the major ketone **11** by reduction with lithium aluminium hydride in ether, followed by dehydration with dilute hydrochloric acid in refluxing methanol and acetylation with acetic anhydride. Reduction of **11** with lithium aluminium hydride in refluxing tetrahydrofuran produced abieta-8,11,13-triene-3β,6β,12-triol (**13**), which was partially acetylated at room temperature with acetic anhydride in pyridine to give 3β,12-diacetoxyabieta-8,11,13-trien-6β-ol (**14**) and a small amount of 12-acetoxyabieta-8,11,13-triene-3β,6β-diol (**15**). Similar acetylation of **15** gave **14**. The diacetoxy alcohol **14** was partially hydrolyzed with sodium hydrogencarbonate in refluxing aqueous methanol to yield 3β-acetoxyabieta-

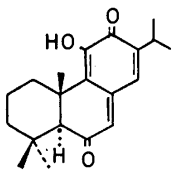

1

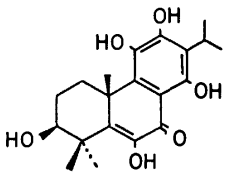

2

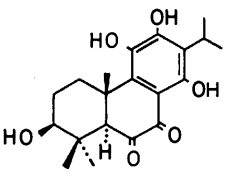

3

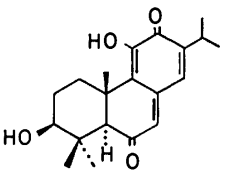

4

8,11,13-triene-6β,12-diol (**16**). Oxidation of **16** with benzoyl peroxide in chloroform at room temperature afforded a phenol (**17**), along with three dienones (**18**, **19**, and **20**) as minor products. The structures of these products (**17**—**20**) were assigned on the basis of the following evidence. The phenol **17** responded positively to the Gibbs test,[7] which suggested the presence of an aromatic proton para to a phenolic hydroxyl group. Oxidation of **17** with *m*-chloroperbenzoic acid in dichloromethane at room temperature afforded a benzoyloxy-*p*-benzoquinone (**21**). The ^{1}H NMR spectrum of **17** showed a singlet signal at δ 6.60 due to the C-14 proton, while for that of **21** no corresponding signal was observed. Thus, the structure of **17** was assigned to be 3β-acetoxy-12-benzoyloxyabieta-8,11,13-triene-6β,11-diol. The ^{1}H NMR spectrum of **18** showed a signal at δ 1.06 due to the equivalent methyls of the isopropyl group. On the other hand, the spectra of **19** and **20** showed two nonequivalent secondary methyl group signals, at δ 0.96 and 1.15 and at δ 0.88 and 1.13, respectively. From these spectral data and those of the IR spectra (see Experimental section), it is obvious that **18** is a para-substituted dienone,[2,8] while **19** and **20** are ortho-substituted dienones.[2,8] Hydrolysis of **18** with potassium carbonate in refluxing aqueous methanol afforded the corresponding trihydroxy ketone (**22**). In the ^{1}H NMR spectrum of **22**, the downfield shift of the signal (δ 1.64) due to the methyl group at C-10 relative to the corresponding signal (δ 1.43) for **18** suggested a 1,3-diaxial-*cis*-relationship between the methyl group and the hydroxyl group at C-8. Thus, the structure of **18** was assigned to be 3β-acetoxy-8β-benzoyloxy-6β-hydroxyabieta-9(11),13-dien-12-one. In order to determine the stereochemistry at C-13 in the ortho-dienones **19** and **20**, the following thermal rearrangements were carried out. A solution of **19** in toluene was refluxed for 4 h to give **17** (6.7%) together with the starting substance (**19**: 93.0%). However, a similar treatment of **20** gave **17** (63.8%) and **18** (26.0%) along with some recovered **20** (10.0%). From the rearrangement of **20** into **18**, the stereochemistry of the benzoyloxyl group in **20** was assigned to be the β-configuration, and therefore, that in **19** to be the α-configuration. Conversion of **17** into 3β-hydroxytaxodione was successfully carried out as follows. In order to change the benzoyloxyl group in **17** into an acetoxyl group which should be easily hydrolyzed under acidic conditions, **17** was reduced with lithium aluminium hydride in ether. The resulting tetrahydroxy compound (**23**), for the protection of the hydroxyl groups at C-3, C-11, and C-12, was partially acetylated with acetic anhydride in pyridine at room temperature to give 3β,11,12-triacetoxyabieta-8,11,13-trien-6β-ol (**24**). The triacetoxy alcohol **24** was oxidized with Jones reagent at 0 °C to afford 3β,11,12-triacetoxyabieta-8,11,13-trien-6-one (**25**), which was easily converted into 3β,11,12-trihydroxyabieta-8,11,13-trien-6-one (**26**) by refluxing with concentrated hydrochloric acid in ethanol under an atmosphere of nitrogen. Column chromatography of **26** on silica gel afforded a quinonemethide compound; its structure was assigned to be that of the desired 3β-hydroxytaxodione by the IR and ^{1}H NMR spectra.

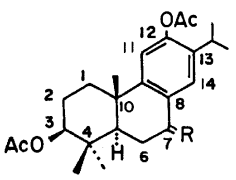

5 R = H_2
6 R = O
8 R = <H, OH

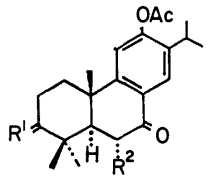

7 R^1=O, R^2=H
12 R^1=α-H, β-OAc; R^2=OAc

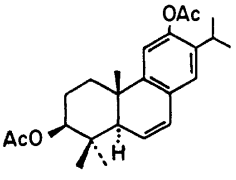

9

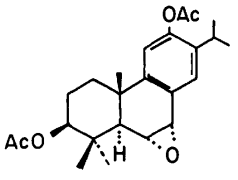

10

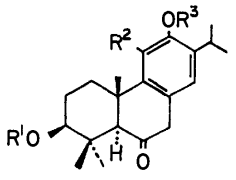

11 R^1=R^3=Ac, R^2=H
25 R^1=R^3=Ac, R^2=OAc
26 R^1=R^3=H, R^2=OH

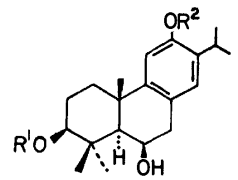

13 R^1=R^2=H
14 R^1=R^2=Ac
15 R^1=H, R^2=Ac
16 R^1=Ac, R^2=H

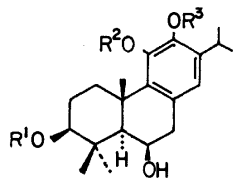

17 R^1=Ac, R^2=H, R^3=Bz
23 R^1=R^2=R^3=H
24 R^1=R^2=R^3=Ac

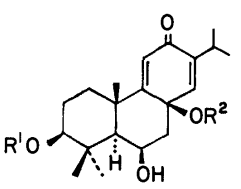

18 R^1=Ac, R^2=Bz
22 R^1=R^2=H

Our next effort was directed toward the syntheses of coleons S and T. Oxidation of **21** with Jones reagent at 0 °C afforded 3β-acetoxy-12-benzoyloxyabieta-8,12-diene-6,11,14-trione (**27**) which, without purification, was used in the next reaction. For the protection of the unstable C ring, the trione **27** was reduced with a mixture of zinc powder and dilute hydrochloric acid in refluxing benzene. The resulting crude phenol (**28**) was acetylated at 85—90 °C with acetic anhydride in pyridine to give 3β,11,14-triacetoxy-12-benzoyloxyabieta-8,11,13-trien-6-one (**29**). Subsequently, oxidation of the C-7 position in **29** was carried out with Jones reagent at room temperature. The crude 6,7-dioxo compound (**30**) was immediately hydrolyzed with aqueous sodium carbonate in refluxing methanol under an atmosphere of nitrogen to give coleon T (**3**), which was further converted into coleon S pentaacetate (**31**) by treatment with acetic anhydride in pyridine. The

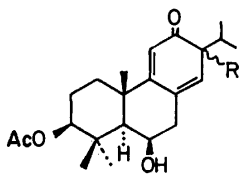

19 R = α-OBz
20 R = β-OBz

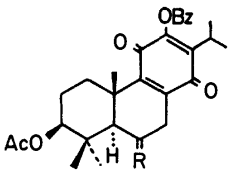

21 R = α-H, β-OH
27 R = O

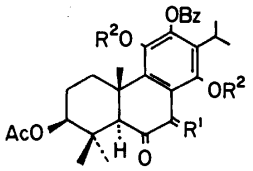

28 R' = H2, R2 = H
29 R' = H2, R2 = Ac
30 R' = O, R2 = Ac

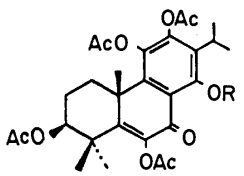

31 R = Ac
32 R = H

synthetic coleon T was finally isomerized with concentrated hydrochloric acid in refluxing methanol to give coleon S (**2**) which was also converted into the pentaacetate (**31**).

Experimental

All melting points are uncorrected. The IR spectra and optical rotations were measured in chloroform, and the ^{1}H NMR spectra in carbon tetrachloride at 60 MHz, with tetramethylsilane as an internal standard, unless otherwise stated. The chemical shifts are presented in terms of δ values; s: singlet, bs: broad singlet, d: doublet, bd: broad doublet, dd: double doublet, bt: broad triplet, m: multiplet. Column chromatography was performed using Merck silica gel (0.063 mm).

Oxidation of Hinokiol Diacetate (5). Jones reagent (2.5 M (1 M = 1 mol dm^{-3}): 13.6 ml) was added dropwise to a stirred solution of hinokiol diacetate[6] (**5**) (4.289 g) in acetone (80 ml) with cooling in an ice-water bath for 15 min. The mixture was stirred at this temperature for 15 min and at room temperature for 6 h. The mixture was then diluted with water and extracted with ether. The ether extract was washed with brine, dried over sodium sulfate, and evaporated *in vacuo*. The residue was chromatographed on silica gel (150 g), using ether–benzene (3 : 97) as the eluent, to give the recovered **5** (1.051 g: 24.5%). Subsequent elution with ether–benzene (5 : 95) afforded 3β,12-diacetoxyabieta-8,11,13-trien-7-one (**6**) (2.284 g: 51.4%), which was recrystallized from methanol; mp 178—179.5 °C; $[\alpha]_D$ +52.5°; IR: 1755, 1725, 1675, 1610 cm^{-1}; ^{1}H NMR 0.95 and 1.03 (each 3H and s, $-\dot{C}(CH_3)_2$), 1.23 (6H, bd, J=7 Hz, $-CH(C\underline{H}_3)_2$), 1.29 (3H, s, $C_{10}-CH_3$), 2.01 and 2.29 (each 3H and s, $2-OCOCH_3$), 2.63 (2H, d, J=8 Hz, $-CH_2CO-$), 2.99 (1H, m, $-C\underline{H}(CH_3)_2$), 4.51 (1H, bt, $W_{1/2}$=16 Hz, C_3-H), 6.90 (1H, s, $C_{11}-H$), 7.90 (1H, s, $C_{14}-H$). Found: C, 71.87; H, 8.25%. Calcd for $C_{24}H_{32}O_5$: C, 71.97; H, 8.05%.

Further elution with ether–benzene (1 : 9) afforded 12-acetoxyabieta-8,11,13-triene-3,7-dione (**7**) (0.213 g: 5.4%) as an oil; $[\alpha]_D$ +12.4°; IR: 1755, 1705, 1675, 1610 cm^{-1}; ^{1}H NMR: 1.12, 1.20, and 1.47 (each 3H and s, $-\dot{C}(CH_3)_2$ and $C_{10}-CH_3$), 1.25 (6H, d, J=6 Hz, $-CH(C\underline{H}_3)_2$), 2.31 (3H, s, $-OCOCH_3$), 6.95 (1H, s, $C_{11}-H$), 7.91 (1H, s, $C_{14}-H$). Found: C, 74.03; H, 8.10%. Calcd for $C_{22}H_{28}O_4$: C, 74.13; H, 7.92%.

3β,12-Diacetoxyabieta-6,8,11,13-tetraene (9). From 6: Sodium borohydride (125 mg) was added at *ca.* 15 °C to a stirred solution of **6** (871 mg) in methanol (35 ml). The mixture was stirred at room temperature for 1.5 h, acidified with dilute hydrochloric acid (10%: 2.0 ml), and refluxed for 1 h. The methanol was evaporated *in vacuo* and the residue was extracted with ether. The ether extract was washed with water, dried over sodium sulfate, and evaporated. The residual oil was acetylated at 78—80 °C with acetic anhydride (2.0 ml) in pyridine (6.0 ml) for 2 h. After the usual work-up, the crude product was chromatographed on silica gel (15 g), using benzene as the eluent, to give **9** (804 mg: 96.2% from **6**) as an oil; $[\alpha]_D$ −7.1°; IR: 1750, 1725 cm^{-1}; ^{1}H NMR: 0.97 (3H, s) and 1.07 (6H, s) ($-\dot{C}(CH_3)_2$ and $C_{10}-CH_3$), 1.18 and 1.21 (each 3H, d, and J=7 Hz, $-CH(C\underline{H}_3)_2$), 2.01 and 2.24 (each 3H and s, $2-OCOCH_3$), 2.93 (1H, m, $-C\underline{H}(CH_3)_2$), 4.50 (1H, m, C_3-H), 5.90 (1H, dd, J=2.5 and 10 Hz, C_6-H), 6.54 (1H, dd, J=2.5 and 10 Hz, C_7-H), 6.68 and 6.95 (each 1H and s, $C_{11}-H$ and $C_{14}-H$). Found: C, 74.79; H, 8.68%. Calcd for $C_{24}H_{32}O_4$: C, 74.97; H, 8.39%.

From 7: A mixture of **7** (361 mg), lithium aluminium hydride (125 mg), and dry ether (10 ml) was stirred at room temperature for 1 h. The mixture was poured into a mixture of ice and dilute hydrochloric acid, and extracted with ether. The ether extract was washed with water, dried over sodium sulfate, and evaporated *in vacuo* to give a crude triol (333 mg); IR: 3605, 3320 cm^{-1}.

A mixture of the crude triol (333 mg) and 10% hydrochloric acid (1.0 ml) in methanol (10 ml) was refluxed for 1 h, and then evaporated *in vacuo*. The residue was extracted with ether. The ether extract was washed with water, dried over sodium sulfate, and evaporated to give an oil (328 mg).

The above oil (328 mg) was immediately acetylated at 81—84 °C with acetic anhydride (2.0 ml) in pyridine (4.0 ml) for 2 h. After the usual work-up, the crude product was purified by column chromatography on silica gel (20 g), using benzene as the eluent, to give an oil (290 mg: 74.4% from **7**), whose IR and ^{1}H NMR spectra were identical with those of **9**.

Epoxidation of 9. A solution of **9** (2.763 g) and *m*-chloroperbenzoic acid (85%: 2.150 g) in dichloromethane (50 ml) was allowed to stand at room temperature for 9 h. The solution was diluted with ether and then washed successively with aqueous potassium iodide, aqueous sodium thiosulfate, aqueous sodium hydrogencarbonate, and water. After being dried over sodium sulfate, the solution was evaporated *in vacuo* to give a crude epoxide (**10**) (2.783 g); IR: 1750, 1723 cm^{-1}; ^{1}H NMR: 1.99 and 2.23 (each 3H and s, $2-OCOCH_3$), 6.68 and 7.37 (each 1H and s, $C_{11}-H$ and $C_{14}-H$). The crude epoxide was immediately subjected to the next reaction.

3β,12-Diacetoxyabieta-8,11,13-trien-6-one (11). From 10: A solution of the crude epoxide (**10**) (2.783 g) and 10% hydrochloric acid (10 ml) in methanol (60 ml) was refluxed for 1 h. The solution was concentrated *in vacuo* and the residue was extracted with ether. The ether extract was washed with water, dried over sodium sulfate, and evaporated. The oily residue was acetylated with acetic anhydride (5.0 ml) in pyridine (7.0 ml) at 80—82 °C for 1.5 h. After the usual work-up, the crude product was chromatographed on silica gel (100 g), using ether–benzene (3 : 97) as the eluent, to give **11** (2.037 g: 70.8% from **9**), which was recrystallized from acetone–hexane; mp 183—187 °C; $[\alpha]_D$ +107°; IR: 1750, 1720 cm^{-1}; ^{1}H NMR ($CDCl_3$): 1.10, 1.20, and 1.37 (each 3H and s, $-\dot{C}(CH_3)_2$ and $C_{10}-CH_3$), 1.19 (6H, d, J=7

Hz, -CH(C$\underline{H}_3$)$_2$), 2.08 and 2.32 (each 3H and s, 2-OCOC$\underline{H}_3$), 2.53 (1H, s, C_5-H), 3.62 (2H, s, -COC$\underline{H}_2$-), 4.45 (1H, m, C_3-H), 6.91 and 7.00 (each 1H and s, C_{11}-H and C_{14}-H). Found: C, 72.08; H, 8.23%. Calcd for $C_{24}H_{32}O_5$: C, 71.97; H, 8.05%.

Further elution with ether–benzene (1:9) afforded 3β,6α,-12-triacetoxyabieta-8,11,13-trien-7-one (**12**) (300 mg: 9.1% from **9**) as an oil; $[\alpha]_D$ +71.5°; IR: 1750, 1735, 1690, 1613 cm^{-1}; ^{1}H NMR: 1.05, 1.08, and 1.45 (each 3H and s, -C(C$\underline{H}_3$)$_2$ and C_{10}-C$\underline{H}_3$), 1.21 (6H, d, J=7 Hz, -CH(C$\underline{H}_3$)$_2$), 2.01, 2.16, and 2.28 (each 3H and s, 3-OCOC$\underline{H}_3$), 2.29 (1H, d, J=13 Hz, C_5-H), 2.97 (1H, m, -C$\underline{H}$(CH$_3$)$_2$), 4.44 (1H, m, C_3-H), 5.82 (1H, d, J=13 Hz, C_6-H), 6.92 (1H, s, C_{11}-H), 7.90 (1H, s, C_{14}-H).

From ***12***: A mixture of **12** (338 mg), lithium aluminium hydride (150 mg), and dry ether (8.0 ml) was refluxed for 1 h. The mixture was poured into a mixture of ice and dilute hydrochloric acid, and extracted with ether. The ether extract was washed with water, dried over sodium sulfate, and evaporated *in vacuo*.

The oily residue (277 mg) was dissolved in methanol (5.0 ml) containing 10% hydrochloric acid (0.5 ml), and then refiuxed for 1 h. The methanol was evaporated *in vacuo* and the residue was extracted with ether. The ether extract was washed with water, dried over sodium sulfate, and evaporated. The oily residue (250 mg) was acetylated at 80—84 °C with acetic anhydride (2.0 ml) in pyridine (3.0 ml) for 1 h. After the usual work-up, the crude product was purified by column chromatography on silica gel (10 g), using ether–benzene (3 : 97) as the eluent, to give an oil (195 mg; 66.1%), whose IR and ^{1}H NMR spectra were identical with those of **11**.

*3β,12-Diacetoxyabieta-8,11,13-trien-6β-ol (**14**).* A solution of **11** (1.401 g) in dry tetrahydrofuran (45 ml) was added to a stirred suspension of lithium aluminium hydride (700 mg) in dry tetrahydrofuran (150 ml) with cooling in an ice–water bath. The mixture was refluxed for 4 h, cooled, poured into a mixture of ice and dilute hydrochloric acid, and extracted with ether. The ether extract was washed with water, dried over sodium sulfate, and evaporated *in vacuo* to give the crude abieta-8,11,13-triene-3β,6β,12-triol (**13**) as a solid which, without purification, was used in the next reaction.

The above crude **13** was acetylated at 18—19 °C for 4 h with acetic anhydride (8.0 ml) in pyridine (15 ml). After the usual work-up, the crude product was chromatographed on silica gel (50 g), using ether–benzene (3 : 97) as the eluent, to give **14** (1.026 g: 72.8% from **11**), which was recrystallized from acetone–hexane; mp 135.5—136.5 °C; $[\alpha]_D$ +45.4°; IR: 3614, 3500, 1750, 1725 cm^{-1}; ^{1}H NMR ($CDCl_3$): 1.04 and 1.32 (each 3H and s, -C(C$\underline{H}_3$)$_2$), 1.20 (6H, d, J=7 Hz, -CH(C$\underline{H}_3$)$_2$), 1.60 (3H, s, C_{10}-C$\underline{H}_3$), 2.09 and 2.32 (each 3H and s, 2-OCOC$\underline{H}_3$), 4.3—4.8 (2H, m, C_3-H and C_6-H), 6.90 and 6.98 (each 1H and s, C_{11}-H and C_{14}-H). Found: C, 71.32; H, 8.74%. Calcd for $C_{24}H_{34}O_5$: C, 71.61; H, 8.51%.

Further elution with ether–benzene (6 : 94) afforded 12-acetoxyabieta-8,11,13-triene-3β,6β-diol (**15**) (133 mg: 10.6% from **11**), which was recrystallized from acetone–hexane; mp 188—189.5 °C; $[\alpha]_D$ +29.7°; IR: 3618, 3444, 1750 cm^{-1}; ^{1}H NMR ($CDCl_3$): 1.15 and 1.25 (each 3H and s, -C(C$\underline{H}_3$)$_2$), 1.20 (6H, d, J=6 Hz, -CH(C$\underline{H}_3$)$_2$), 1.56 (3H, s, C_{10}-C$\underline{H}_3$), 2.32 (3H, s, -OCOC$\underline{H}_3$), 4.70 (1H, m, $W_{1/2}$=8 Hz, C_6-H), 6.89 and 6.98 (each 1H and s, C_{11}-H and C_{14}-H). Found: C, 73.04; H, 9.06%. Calcd for $C_{22}H_{32}O_4$: C, 73.30; H, 8.95%.

The monoacetate **15** (133 mg) was further acetylated with acetic anhydride (1.5 ml) in pyridine (2.0 ml) at 17—19 °C for 4 h. Chromatographic purification of the crude product yielded **14** (110 mg: 74.3%) and the recovered **15** (27 mg: 20.3%).

*3β-Acetoxyabieta-8,11,13-triene-6β,12-diol (**16**).* A stirred mixture of **14** (993 mg), sodium hydrogencarbonate (420 mg), methanol (25 ml), and water (3.0 ml) was refluxed for 15 min. The mixture was concentrated *in vacuo*, diluted with water, and extracted with ether. The ether extract was washed with brine, dried over sodium sulfate, and evaporated *in vacuo*. The residue was recrystallized from benzene to give **16** (601 mg); mp 220—221.5 °C; $[\alpha]_D$ +31.8°; IR: 3610, 3400, 1725 cm^{-1}; ^{1}H NMR ($CDCl_3$): 1.03 and 1.32 (each 3H and s, -C(C$\underline{H}_3$)$_2$), 1.23 (6H, d, J=7 Hz, -CH(C$\underline{H}_3$)$_2$), 1.56 (3H, s, C_{10}-C$\underline{H}_3$), 2.13 (3H, s, -OCOC$\underline{H}_3$), 6.65 and 6.82 (each 1H and s, C_{11}-H and C_{14}-H). Found: C, 73.41; H, 9.16%. Calcd for $C_{22}H_{32}O_4$: C, 73.30; H, 8.95%. The mother liquor of recrystallization was evaporated *in vacuo* and the residue was chromatographed on silica gel (10 g), using ether–benzene (5 : 95) as the eluent, to give an additional **16** (224 mg). The total yield was 92.7%.

*Oxidation of **16** with Benzoyl Peroxide.* A solution of **16** (863 mg) and benzoyl peroxide (2.939 g) in chloroform (10 ml) was allowed to stand at room temperature for 80 h. The chloroform solution was diluted with ether. This ether solution, after addition of acetic acid (9.0 ml) and aqueous potassium iodide (30%: 30 ml), was stirred at room temperature for 3 h. The mixture was washed successively with water, aqueous sodium thiosulfate, aqueous sodium hydrogencarbonate, and water. After being dried over sodium sulfate, the solvent was evaporated *in vacuo* and the residue was purified by repeated column chromatography on silica gel, using ether–benzene (3 : 97) as the eluent, to give four products (**17**—**20**).

a): 3β-Acetoxy-12-benzoyloxyabieta-8,11,13-triene-6β,11,-diol (**17**) (609 mg: 52.9%), which responded positively to the Gibbs test;[7] mp 224—225.5 °C (from methanol); $[\alpha]_D$ +52.2°; IR: 3575, 3430, 1725 cm^{-1}; ^{1}H NMR ($CDCl_3$): 1.05 and 1.31 (each 3H and s, -C(C$\underline{H}_3$)$_2$), 1.18 (6H, d, J=7 Hz, -CH-(C$\underline{H}_3$)$_2$), 1.72 (3H, s, C_{10}-C$\underline{H}_3$), 1.88 (3H, s, -OCOC$\underline{H}_3$), 4.2—4.7 (2H, m, C_3-H and C_6-H), 6.18 (1H, s, -OH), 6.60 (1H, s, C_{14}-H), 7.3—8.4 (5H, m, -C_6H_5). Found: C, 72.81; H, 7.67%. Calcd for $C_{29}H_{36}O_6$: C, 72.47; H, 7.55%.

b): 3β-Acetoxy-8β-benzoyloxy-6β-hydroxyabieta-9(11),13-dien-12-one (**18**) (22 mg: 1.9%); $[\alpha]_D$ −20.1°; IR: 3605, 1725, 1668, 1640 cm^{-1}; ^{1}H NMR ($CDCl_3$): 1.01 and 1.31 (each 3H and s, -C(C$\underline{H}_3$)$_2$), 1.06 (6H, d, J=6.5 Hz, -CH-(C$\underline{H}_3$)$_2$), 1.43 (3H, s, C_{10}-C$\underline{H}_3$), 2.06 (3H, s, -OCOC$\underline{H}_3$), 4.3—4.7 (2H, m, C_3-H and C_6-H), 6.27 and 6.42 (each 1H and s, C_{11}-H and C_{14}-H), 7.3—8.1 (5H, m, -C_6H_5).

c): 3β-Acetoxy-13α-benzoyloxy-6β-hydroxyabieta-8(14),-9(11)-dien-12-one (**19**) (96 mg: 8.4%), which was recrystallized from benzene; mp 184—185 °C; $[\alpha]_D$ +240°; IR: 3500, 1720, 1660, 1603 cm^{-1}; ^{1}H NMR ($CDCl_3$): 0.96 and 1.15 (each 3H, d, and J=7 Hz, -CH(C$\underline{H}_3$)$_2$), 1.02 and 1.31 (each 3H and s, -C(C$\underline{H}_3$)$_2$), 1.57 (3H, s, C_{10}-C$\underline{H}_3$), 2.10 (3H, s, -OCOC$\underline{H}_3$), 4.3—4.7 (2H, m, C_3-H and C_6-H), 5.95 (1H, s, C_{14}-H), 6.15 (1H, s, C_{11}-H), 7.3—8.2 (5H, m, -C_6H_5). Found: C, 72.73; H, 7.66%. Calcd for $C_{29}H_{36}O_6$: C, 72.47; H, 7.55%.

d): 3β-Acetoxy-13β-benzoyloxy-6β-hydroxyabieta-8(14),-9(11)-dien-12-one (**20**) (70 mg: 6.1%), which was recrystallized from ether–hexane; mp 180—180.5 °C; $[\alpha]_D$ −145°; IR: 3525, 1720, 1665, 1605 cm^{-1}; ^{1}H NMR ($CDCl_3$): 0.88 and 1.13 (each 3H, d, and J=7 Hz, -CH(C$\underline{H}_3$)$_2$), 1.07 and 1.33 (each 3H and s, -C(C$\underline{H}_3$)$_2$), 1.59 (3H, s, C_{10}-C$\underline{H}_3$), 2.10 (3H, s, -OCOC$\underline{H}_3$), 4.3—4.7 (2H, m, C_3-H and C_6-H), 5.95 (1H, s, C_{14}-H), 6.13 (1H, s, C_{11}-H), 7.3—8.2 (5H, m, -C_6H_5). Found: C, 72.73; H, 7.78%. Calcd for $C_{29}H_{36}O_6$: C, 72.47; H, 7.55%.

3β-Acetoxy-12-benzoyloxy-6β-hydroxyabieta-8,12-diene-11,14-

dione (21). A solution of **17** (441 mg) and *m*-chloroperbenzoic acid (85%: 280 mg) in dichloromethane (10 ml) was allowed to stand at room temperature for 36 h, and then diluted with ether. The solution was washed successively with aqueous potassium iodide, aqueous sodium thiosulfate, aqueous sodium hydrogencarbonate, and water. After drying over sodium sulfate, the solvent was evaporated *in vacuo* and the crude product was purified by column chromatography on silica gel (40 g), using ether–benzene (1 : 99) as the eluent, to give **21** (338 mg: 74.4%), which was recrystallized from benzene; mp 260.5—261.5 °C; $[\alpha]_D$ +24.2°; IR: 3610, 3535, 1725, 1660, 1607 cm^{-1}; ^1H NMR ($CDCl_3$): 1.01 and 1.31 (each 3H and s, $-\dot{C}(CH_3)_2$), 1.25 (6H, d, J=7 Hz, $-CH(C\underline{H}_3)_2$), 1.68 (3H, s, C_{10}–CH_3), 2.08 (3H, s, $-OCOCH_3$), 4.3—4.8 (2H, m, C_3–H and C_6–H), 7.45—8.30 (5H, m, $-C_6H_5$). Found: C, 70.70; H, 7.04%. Calcd for $C_{29}H_{34}O_7$: C, 70.42; H, 6.93%.

Further elution with ether–benzene (3 : 97) afforded the recovered **17** (52 mg: 11.7%).

3β,6β,8β-Trihydroxyabieta-9(11), 13-dien-12-one (22). A mixture of **18** (18.0 mg), potassium carbonate (54 mg), methanol (2.0 ml), and water (0.5 ml) was refluxed for 75 min. After the methanol had been evaporated *in vacuo*, the residue was extracted with ether. The ether extract was washed with brine, dried over sodium sulafte, and evaporated *in vacuo*. The crude product was chromatographed on silica gel (5.0 g), using ether–benzene (25 : 75) as the eluent, to give **22** (7.0 mg); IR: 3359, 1661, 1630 cm^{-1}; ^1H NMR ($CDCl_3$, 90 MHz): 1.04 and 1.08 (each 3H, d, and J=7 Hz, $-CH(C\underline{H}_3)_2$), 1.11 and 1.27 (each 3H and s, $-\dot{C}(CH_3)_2$), 1.64 (3H, s, C_{10}–CH_3), 2.44 (2H, dd, J=4 and 14 Hz, $-CH(OH)-C\underline{H}_2-$), 4.55 (1H, m, C_6–H), 6.05 and 6.42 (each 1H and s, C_{11}–H and C_{14}–H).

Thermal Rearrangement of Dienones (19 and 20). *a*): A solution of **19** (125 mg) in dry toluene (9.0 ml) was refluxed for 4 h and the crude product, after evaporation of the solvent, was purified by column chromatography on silica gel (10 g), using ether–benzene (3 : 97) as the eluent, to give **17** (8.4 mg: 6.7%). Further elution with ether–benzene (1 : 9) afforded the recovered **19** (116 mg: 93.0%).

b): A solution of **20** (60.0 mg) in dry toluene (5.0 ml) was refluxed for 4 h. The crude product was chromatographed on silica gel (10 g), using ether–benzene (3 : 97) as the eluent, to give **17** (38.3 mg: 63.8%) and **18** (15.6 mg: 26.0%). Further elution with ether–benzene (1 : 9) afforded the recovered **20** (6.0 mg: 10.0%).

3β,11,12-Triacetoxyabieta-8,11,13-trien-6β-ol (24). Lithium aluminium hydride (372 mg) was added to a stirred solution of **17** (1.180 g) in dry ether (30 ml) with cooling in an ice–water bath. The mixture was refluxed for 2 h, poured into a mixture of ice and dilute hydrochloric acid, and extracted with ether. The ether extract was washed with brine, dried over sodium sulfate, and evaporated *in vacuo* to give the crude tetrol (**23**) which, without purification, was used in the next reaction.

The above crude **23** was acetylated at room temperature for 3.5 h with acetic anhydride (3.2 ml) in pyridine (5.0 ml). After the usual work-up, the crude product was chromatographed on silica gel (30 g), using ether–benzene (6 : 94) as the eluent, to give **24** (832 mg: 73.6% from **17**), which was recrystallized from acetone–hexane; mp 186—187.5 °C; $[\alpha]_D$ 38.1°; IR: 3613, 1762, 1724 cm^{-1}; ^1H NMR: 0.96 and 1.25 (each 3H and s, $-\dot{C}(CH_3)_2$), 1.15 and 1.19 (each 3H, d, and J=7 Hz, $-CH(C\underline{H}_3)_2$), 1.53 (3H, s, C_{10}–CH_3), 1.98 (3H, s) and 2.19 (6H, s) (3-$OCOCH_3$), 4.2—4.65 (2H, m, C_3–H and C_6–H), 6.78 (1H, s, C_{14}–H). Found: C, 67.74; H, 7.97%. Calcd for $C_{26}H_{36}O_7$: C, 67.80; H, 7.88%.

3β,11,12-Triacetoxyabieta-8,11,13-trien-6-one (25). A solution of **24** (842 mg) in acetone (4.0 ml) was oxidized at 0—5 °C for 3 min with Jones reagent (2.5 M: 1.2 ml). The mixture was diluted with water and extracted with ether. The ether extract was washed with brine, dried over sodium sulfate, and evaporated *in vacuo*. The residue was chromatographed on silica gel (25 g), using ether–benzene (3 : 97) as the eluent, to give **25** (703 mg: 83.8%), which was recrystallized from acetone–hexane; mp 121—122.5 °C; $[\alpha]_D$ +113°; IR: 1770, 1719 cm^{-1}; ^1H NMR: 1.02 and 1.21 (each 3H and s, $-\dot{C}(CH_3)_2$), 1.16 and 1.20 (each 3H, d, and J=7 Hz, $-CH(C\underline{H}_3)_2$), 1.35 (3H, s, C_{10}–CH_3), 2.00 (3H, s) and 2.24 (6H, s) (3-$OCOCH_3$), 2.73 (1H, s, C_5–H), 3.58 (2H, bs, $-COCH_2-$), 4.40 (1H, m, C_3–H), 6.82 (1H, s, C_{14}–H). Found: C, 68.00; H, 7.55%. Calcd for $C_{26}H_{34}O_7$: C, 68.10; H, 7.47%.

3β-Hydroxytaxodione (4). A solution of **25** (86.0 mg) in ethanol (5.0 ml) was refluxed for 2 h with concentrated hydrochloric acid (1.5 ml) in a stream of nitrogen. The mixture was concentrated *in vacuo*, diluted with water, and extracted with ether. The ether extract was washed with brine, dried over sodium sulfate, and evaporated *in vacuo* to give the crude 3β,11,12-trihydroxyabieta-8,11,13-trien-6-one (**26**).

The crude **26** was subjected to repeated column chromatography on silica gel (10 g and then 8 g), using ether–benzene (8 : 92) as the eluent, to give **4** (46.4 mg: 74.9% from **25**), which was recrystallized from acetone–petroleum benzine; mp 183.5—184.5 °C; $[\alpha]_D$ +69.0°; IR: 3616, 3340, 1674, 1644, 1628, 1616, 1602 cm^{-1}; ^1H NMR ($CDCl_3$): 1.17 (6H, bd, J=7 Hz, $-CH(C\underline{H}_3)_2$), 1.28 (9H, s, $-\dot{C}(CH_3)_2$ and C_{10}–CH_3), 2.60 (1H, s, C_5–H), 6.22 and 6.90 (each 1H and s, C_7–H and C_{14}–H), 7.61 (1H, s, C_{11}–OH). Found: C, 72.57; H, 8.02%. Calcd for $C_{20}H_{26}O_4$: C, 72.70; H, 7.93%.

3β,11,14-Triacetoxy-12-benzoyloxyabieta-8,11,13-trien-6-one (29). A solution of **21** (590 mg) in acetone (30 ml) was oxidized with Jones reagent (2.5 M: 0.8 ml) at 0—5 °C for 2.5 min. The mixture was diluted with water and extracted with ether. The ether extract was washed with water, dried over sodium sulfate, and evaporated to give the crude 3β-acetoxy-12-benzoyloxyabieta-8,12-diene-6,11,14-trione (**27**) (585 mg); IR: 1720, 1660 cm^{-1}.

A stirred solution of the above crude **27** (585 mg) in benzene (12 ml) was refluxed for 20 min with a mixture of zinc powder (1.2 g) and 10% hydrochloric acid (12 ml). After cooling, the mixture was extracted with ether. The extract was washed with brine, dried over sodium sulfate, and evaporated *in vacuo* to give a crude phenol (**28**); IR: 3575, 3425, 1720 cm^{-1}.

The crude phenol **28** was immediately acetylated at 85—90 °C for 2.5 h with acetic anhydride (4.0 ml) and pyridine (4.0 ml). After the usual work-up, the product was purified by column chromatography on silica gel (30 g), using ether–benzene (5 : 95) as the eluent, to give **29** (480 mg: 69.5% from **21**), which was recrystallized from benzene; mp 284—286 °C; $[\alpha]_D$ +126°; IR: 1765, 1740, 1720 cm^{-1}; ^1H NMR ($CDCl_3$): 1.05, 1.27, and 1.37 (each 3H and s, $-\dot{C}(CH_3)_2$ and C_{10}–CH_3), 1.92, 2.04, and 2.38 (each 3H and s, 3-$OCOCH_3$), 2.80 (1H, s, C_5–H), 3.36 (2H, bs, $-COCH_2-$), 4.45 (1H, m, C_3–H), 7.45—8.35 (5H, m, $-C_6H_5$). Found: C, 68.48; H, 6.71%. Calcd for $C_{33}H_{38}O_9$: C, 68.49; H, 6.62%.

3β,11,14-Triacetoxy-12-benzoyloxyabieta-8,11,13-triene-6,7-dione (30). A solution of **29** (195 mg) in acetone (10 ml) was oxidized with Jones reagent (2.5 M: 1.0 ml) at room temperature for 14 h. The mixture was diluted with water and extracted with ether. The ether extract was washed with brine, dried over sodium sulfate, and evaporated *in vacuo* to give a crude **30** (190 mg); ^1H NMR ($CDCl_3$): 1.97, 2.05,

and 2.47 (each 3H and s, 3-OCOCH$_3$), 3.20 (1H, s, C$_5$–H), 7.45—8.35 (5H, m, –C$_6$H$_5$). The crude **30** was immediately subjected to the next reaction.

Coleon T (3). A stirred mixture of the crude **30** (190 mg) in methanol (15 ml) and aqueous sodium carbonate (10%: 3.0 ml) was refluxed for 7 h in a stream of nitrogen. The methanol was evaporated *in vacuo*. The residue was acidified with dilute hydrochloric acid and extracted with ether. The ether extract was washed with brine, dried over sodium sulfate, and evaporated *in vacuo*. The crude product was purified by column chromatography on silica gel (50 g: Mallinckrodt, Silic AR CC-4), using ether–chloroform (1 : 9) as the eluent, to give **3** (71.2 mg: 58.3% from **29**). Crystallization of **3** from acetone–hexane gave an orange powder; mp 134—137 °C decomp; IR (KBr): 3415, 1725, 1613, 1434, 1381, 1296, 1043, 941 cm^{-1}; ^{1}H NMR (acetone-d_6): 1.14, 1.36, and 1.42 (each 3H and s, –C(CH$_3$)$_2$ and C$_{10}$–CH$_3$), 1.33 (6H, d, J=7 Hz, –CH(CH$_3$)$_2$), 3.15 (1H, s, C$_5$–H), 13.54 (1H, s, C$_{14}$–OH).

Acetylation of 3. A solution of **3** (54.0 mg) and acetic anhydride (1.0 ml) in pyridine (2.0 ml) was heated at 70—75 °C for 6 h. After the usual work-up, the crude product was purified by column chromatography on silica gel (10 g), using ether–benzene (7 : 93) as the eluent, to give 3β,6,11,-12-tetraacetoxy-14-hydroxyabieta-5,8,11,13-tetraen-7-one (**32**) (22.9 mg: 29.0%), which was recrystallized from ether–hexane; mp 160.5—162.5 °C; IR (KBr): 3418, 1777, 1728, 1632, 1615 cm^{-1}; ^{1}H NMR (CDCl$_3$, 90 MHz): 1.31 (6H, d, J=7 Hz, –CH(CH$_3$)$_2$), 1.34 and 1.42 (each 3H and s, –C(CH$_3$)$_2$), 1.74 (3H, s, C$_{10}$–CH$_3$), 2.11 (3H, s), 2.30 (6H, s), and 2.35 (3H, s) (4-OCOCH$_3$), 4.83 (1H, m, C$_3$–H), 13.38 (1H, s, C$_{14}$–OH). Found: C, 63.62; H, 6.61%. Calcd for C$_{28}$H$_{34}$O$_{10}$: C, 63.38; H, 6.46%.

Further elution with ether–benzene (15 : 85) afforded 3β,6,-11,12,14-pentaacetoxyabieta-5,8,11,13-tetraen-7-one (colen S pentaacetate) (**31**) (49.6 mg: 58.1%), which was recrystallized from acetone–hexane; mp 215.5—217.5 °C; [α]$_D$ +79.3°; IR (KBr): 1778, 1764, 1722, 1667, 1632, 1602 cm^{-1}; ^{1}H NMR (CDCl$_3$): 1.24 (6H, d, J=7 Hz, –CH(CH$_3$)$_2$), 1.34 and 1.41 (each 3H and s, –C(CH$_3$)$_2$), 1.75 (3H, s, C$_{10}$–CH$_3$), 2.12 (3H, s), 2.35 (9H, s), and 2.41 (3H, s) (5-OCOCH$_3$), 4.83 (1H, m, C$_3$–H). Found: C, 62.96; H, 6.44%. Calcd for C$_{30}$H$_{36}$O$_{11}$: C, 62.92; H, 6.34%. The synthetic **31** was shown to be identical with authentic coleon S pentaacetate by mixed melting point determination and by IR and ^{1}H NMR spectral comparisons.

Coleon S (2). A solution of **3** (51.0 mg) in methanol (6.0 ml) was refluxed for 30 min with concentrated hydrochloric acid (0.5 ml). The mixture was evaporated *in vacuo*, diluted with water, and extracted with ether. The ether extract was washed with brine, dried over sodium sulfate, and evaporated *in vacuo*. The residue was chromatographed on silica gel (10 g: Mallinckrodt, Silic AR CC-4), using ether–chloroform (5 : 95) as the eluent, to give **2** (24.9 mg: 48.8%); IR (KBr): 3383, 1616, 1594, 1561, 1446, 1297, 1259, 1173, 1112, 1061, 1045, 1017, 972, 940, 900, 810, 777 cm^{-1}; ^{1}H NMR (acetone-d_6, 90 MHz): 1.34 (6H, d, J=7 Hz, –CH(CH$_3$)$_2$), 1.40 and 1.55 (each 3H and s, –C(CH$_3$)$_2$), 1.75 (3H, s, C$_{10}$–CH$_3$), 7.55 (1H, s, C$_6$–OH), 13.08 (1H, s, C$_{14}$–OH).

The synthetic **2** was refluxed for 4 h with acetic anhydride in pyridine to give **31**, mp 212.5—214.5 °C (from acetone–hexane), which was shown to be identical with authentic coleon S pentaacetate by mixed melting point determination and by IR and ^{1}H NMR spectral comparisons.

The authors are grateful to the Arakawa Chemical Co. Ltd. for a generous gift of rosin. Thanks are also due to Professor C. H. Eugster for kindly supplying the natural samples. This work was partially supported by a Grant-in-Aid for Scientific Research No. 56540324 from the Ministry of Education, Science and Culture.

References

1) T. Matsumoto, Y. Tachibana, J. Uchida, and K. Fukui, *Bull. Chem. Soc. Jpn.*, **44**, 2766 (1971).

2) T. Matsumoto, Y. Ohsuga, and K. Fukui, *Chem. Lett.*, **1974**, 297; T. Matsumoto, Y. Ohsuga, S. Harada, and K. Fukui, *Bull. Chem. Soc. Jpn.*, **50**, 266 (1977).

3) T. Matsumoto, S. Usui, and T. Morimoto, *Bull. Chem. Soc. Jpn.*, **50**, 1575 (1977).

4) S. M. Kupchan, A. Karim, and C. Marcks, *J. Am. Chem. Soc.*, **90**, 5923 (1968); *J. Org. Chem.*, **34**, 3912 (1969).

5) S. Arihara, P. Rüedi, and C. H. Eugster, *Helv. Chim. Acta*, **60**, 1443 (1977).

6) T. Matsumoto, S. Usui, H. Kawashima, and M. Mitsuki, *Bull. Chem. Soc. Jpn.*, **54**, 581 (1981).

7) F. E. King, T. J. King, and L. C. Manning, *J. Chem. Soc.*, **1957**, 563.

8) D. H. R. Barton, P. D. Magnus, and M. J. Pearson, *J. Chem. Soc., C*, **1971**, 2231.

 © 1982 The Chemical Society of Japan Bull. Chem. Soc. Jpn., 55, 1174—1177 (1982) [Vol. 55, No. 4

The Preparation of Cyclic Dithia and Thiaza Compounds by the Reaction of Potassium Carbonate with Heterocumulenes and Alkylene Dibromides or Carbonate Catalyzed by Organostannyl Compounds

Tatsuo FUJINAMI,* Shinichi SATO, Norimasa UCHIDA, and Shizuyoshi SAKAI

Department of Industrial Chemistry, Faculty of Engineering, Shizuoka University, Hamamatsu 432

(Received August 17, 1981)

Cyclic 1,3-dithia- and 1,3-thiaza-2-ylidene compounds were obtained by the heterogeneous reaction of solid potassium carbonate, a sulfur-containing heterocumulene, such as aryl isothiocyanate, carbon disulfide, or carbonyl sulfide, and alkylene dibromides or ethylene carbonate in the presence of bis(tributylstannyl) compounds. The effect of an organostannyl catalyst on these reactions is discussed.

Alkali carbonates are usually insoluble in aprotic organic solvents and are generally used as weak bases in organic reactions. It was recently reported that potassium and sodium carbonates acted as strong bases for the generation of ylide[1] and carbanions[2] by means of a two-phase procedure catalyzed by a crown ether or quarternary salt. From the viewpoint of the further utilization of alkali carbonates other than a base, the fixation of carbonate ion into organic compounds is attractive, but all attempts to do so have been unsuccessful till lately; Soga[3] has reported that the polycarbonate was obtained by the reaction of potassium carbonate with α,α'-dibromo-*p*-xylene in the presence of a crown ether.

In a previous report,[4] we found that bis(tributylstannyl) compounds were effective two-phase catalysts for the heterogeneous nucleophilic reaction of solid potassium carbonate with alkyl bromides in polar aprotic solvents, affording dialkyl carbonates in good yields (Scheme 1).

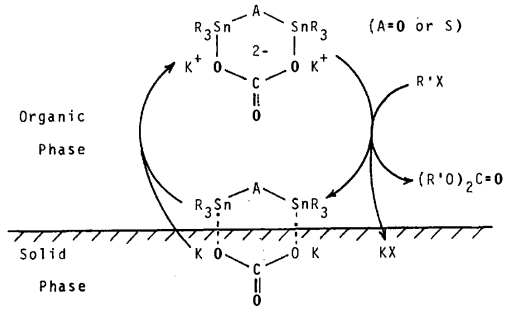

Scheme 1. Preparation of dialkyl carbonates.

Exchange reactions between the CO_2 group in the dimetallocarbamate and heterocumulenes have been observed in organostannyl compounds (Eq. 1).[5]

$$Bu_3SnOSnBu_3 \xrightarrow{+\ O{=}C{=}NR} Bu_3Sn{-}\underset{\displaystyle R}{\overset{\displaystyle |}{N}}{-}\overset{\displaystyle O}{\overset{\displaystyle ||}{C}}{-}O{-}SnBu_3$$

$$\xrightarrow[-CO_2]{+\ R'N{=}C{=}Z} Bu_3Sn{-}\underset{\displaystyle R}{\overset{\displaystyle |}{N}}{-}\overset{\displaystyle NR'}{\overset{\displaystyle ||}{C}}{-}Z{-}SnBu_3 \qquad (1)$$

$Z = O$ or S

It is supposed that, analogously to Eq. 1, the stannate complex proposed for the soluble intermediate in Scheme 1 takes part in the exchange reactions of the CO_2 group in the ate-complex with various heterocumulenes. Also the stannate complexes resulting from the exchange reaction can be expected to give the corresponding heterocyclic compounds by cyclization with bifunctional alkylene compounds. On the basis of this working hypothesis, we wish to report here the use of organostannyl compounds in the activation of potassium carbonate in the preparation of cyclic 1,3-thiaza- and 1,3-dithia-2-ylidene compounds from sulfur-containing heterocumulenes and alkylene dibromides or ethylene carbonate. This procedure is carried out under mild conditions using an insoluble weak base, potassium carbonate, and does not require poisonous or awkward reagents.

Results and Discussion

Reaction of Potassium Carbonate with Aryl Isothiocyanates or Carbon Disulfide and Alkylene Dibromide. Anhydrous potassium carbonate, alkylene dibromide, two equivalents of aryl isothiocyanate, and hexabutyldistannathiane (5 mol%) were stirred for 8 h in refluxing acetonitrile under dry nitrogen to form 1,3-thiaza and 1,3-dithia compounds, **1**—**3**, accompanied by the elimination of carbon dioxide, carbonyl sulfide, and aryl isocyanate (Eq. 2). The carbonyl sulfide was trapped and confirmed by means of its IR spectrum.

$$K_2CO_3 + 2ArNCS + Br(CH_2)_nBr \xrightarrow{\text{Organostannyl catalyst}}$$

$$\underset{\mathbf{1a\text{-}c}}{\text{(1-Ar-2-imino-1,3-thiaza)}} + \underset{\mathbf{2a\text{-}c}}{\text{(1-Ar-2-thioxo-1,3-thiaza)}} + \underset{\mathbf{3a\text{-}c}}{\text{(2-Ar-imino-1,3-dithia)}} \qquad (2)$$

a: Ar=Ph, n=2, b: Ar=p-Tol, n=2, c: Ar=Ph, n=3

From the reaction products, triaryl isocyanurate was isolated; it supported the elimination of aryl isocyanate in the reaction. The cyclic 3-aryl-2-arylimino-1,3-thiaza compound (**1**), 2-thioxo-1,3-thiaza compound (**2**), and 2-arylimino-1,3-dithia compound (**3**) were isolated and identified by their melting points and IR, NMR, and mass spectra. The results are summarized in Table 1.

From the results shown in Table 1, hexaalkyldistannoxane and -distannathiane can be seen to promote Reaction 2 distinctly. The reaction can scarcely

Table 1. Reactions of potassium carbonate, aryl isothiocyanates, and alkylene dibromides[a)]

Ar in ArNCS	n in $Br(CH_2)_nBr$	Catalyst (mol%)[b)]	Reaction time/h	Product yield/% 1	2	3
Ph	2	None	4	5(**1a**)	Trace(**2a**)	Trace(**3a**)
Ph	2	Bu_2SnS(10)	4	26(**1a**)	12(**2a**)	8(**3a**)
Ph	2	$(Bu_3Sn)_2O$(5)	4	51(**1a**)	21(**2a**)	12(**3a**)
Ph	2	$(Bu_3Sn)_2S$(5)	4	48(**1a**)	17(**2a**)	15(**3a**)
Ph	2	$(Me_3Sn)_2S$(5)	4	41(**1a**)	17(**2a**)	13(**3a**)
Ph	2	Bu_3SnCl(10)	4	Trace(**1a**)	Trace(**2a**)	Trace(**3a**)
p-Tol	2	$(Bu_3Sn)_2O$(5)	24	35(**1b**)	18(**2b**)	18(**3b**)
Ph	3	$(Bu_3Sn)_2O$(5)	24	24(**1c**)	19(**2c**)	18(**3c**)

a) Reaction conditions: potassium carbonate (10 mmol), aryl isothiocyanate (20 mmol), alkylene dibromide (10 mmol), acetonitrile (10 ml), at the refluxing temperature. b) Based on the alkylene dibromide used.

proceed without the catalyst. However, dibutylstannathiane existing in a cyclic trimer[6] is less effective, and chlorotributylstannane does not accelerate Reaction 2 at all, although it was an excellent catalyst like the bis(tributylstannyl) compounds in the preparation of dialkyl carbonates. In Reaction 2, hexabutyldistannoxane might be converted to the thiane derivative by a rapid reaction with aryl isothiocyanate.[7]

Bis(tributylstannyl) compounds may act as two-phase catalysts, as is shown in Scheme 1. The bis(tributylstannyl) compounds interact with solid potassium carbonate to form an ate-complex **4**. Since potassium carbonate and 1,2-dibromoethane gave only a low yield (<5%) of ethylene carbonate (**8**) even in the presence of a bis(tributylstannyl) catalyst, under the same conditions, the products, **1**—**3**, cannot be considered to be formed *via* **8**. Therefore, the ate-complex **4** may react with aryl isothiocyanate in the first step to form the ate-complex **5** which further reacts with another molecule of isothiocyanate to form sulfur- and nitrogen-containing ate-complexes, **6A**, **6B**, and **7** (Scheme 2).

Although these ate-complexes have not been established, the mild hydrolysis of the reaction mixture of potassium carbonate with phenyl isothiocyanate in the presence of hexabutyldistannathiane gave *N,N'*-diphenylthiourea which suggests the formation of **7**.

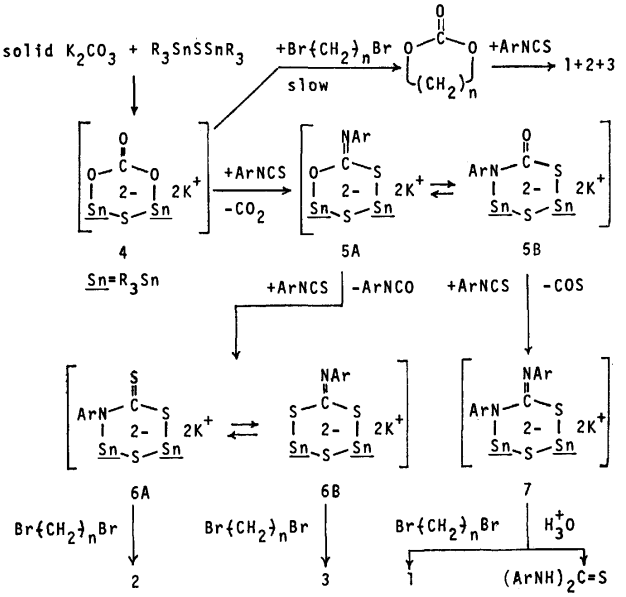

Scheme 2. Preparation of cyclic 1,3-thiaza and 1,3-dithia compounds.

The reaction *via* the ate-complexes **4**—**7** will be the same type of reaction as in the case of a heterocumulene exchange reaction (1) using neutral bis(tributylstannyl) compounds.

The ate-intermediates **6A** and **7** have reactive Sn–N sites and react with alkylene dibromide to afford **1** or **2**. On the other hand, **6B** has no Sn–N site but a less reactive Sn–S site, and the yield of **3**, which may be expected to be a major product from the dithiocarbamate dianion because of the large nucleophilicity of its S⁻ site,[8] is lower than that of **2**.

Hexabutyldistannathiane is inert in many reactions of organostannyl compounds, such as Reaction 1,[5] but in Reaction 2 this compound is highly active. This activity of hexabutyldistannathiane may be ascribed to the formation of ate-complexes.

Contrary to the reaction of aryl isothiocyanate, the reaction of carbon disulfide with potassium carbonate and 1,2-dibromoethane in acetonitrile for 12 h at reflux gave 1,3-dithiolane-2-thione (**9**) in a 90% yield, even in the absence of an organostannyl compound. Potassium trithiocarbonate from carbon disulfide and potassium carbonate is conceived of as the reactive intermediate because of its strong nucleophilicity. Futhermore, the tin atom in organostannyl compounds shows a strong affinity to the sulfur atom serving to stabilize the trithiocarbonate anion by the formation of the ate-complex **10**. This may explain the lowering of the yield of **9** down to 68% by the presence of hexabutyldistannathiane.

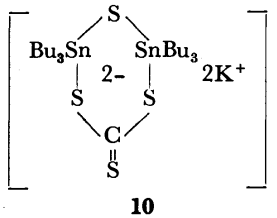

10

Reaction of Potassium Carbonate with Heterocumulenes and Ethylene Carbonate. When ethylene carbonate (**8**) is used instead of dibromoethane in the above reactions, the displacement of the CO_2 group in **8** by other hetero-

TABLE 2. REACTIONS OF ETHYLENE CARBONATE WITH VARIOUS HETEROCUMULENES CATALYZED BY HEXABUTYLDISTANNATHIANE AND/OR POTASSIUM CARBONATE[a)]

Heterocumulene used	Catalyst (mol%)[b)]			Reaction time/h	Solvent	Main product	Yield %
	K_2CO_3	$(Bu_3Sn)_2S$	18-Crown-6				
PhNCS	0	0	0	24	MeCN	—	0
PhNCS	5	0	0	24	MeCN	**3a**	28
PhNCS	5	5	0	24	MeCN	**3a**	50[c)]
PhNCS	5	5	0	24	C_6H_6	—	0
PhNCS	5	5	10	24	C_6H_6	**3a**	49
PhNCS	5	5	10	1	C_6H_6	**3a**	23
PhNCS	5	0	10	1	C_6H_6	**3a**	9
CS_2[d)]	5	0	0	24	MeCN	**9**	0
CS_2[d)]	5	5	0	24	MeCN	**9**	Trace
CS_2[d)]	5	5	10	24	MeCN	**9**	17
COS[d)]	5	0	0	48	MeCN	**11**	40
COS[d)]	5	5	0	48	MeCN	**11**	42

a) Ethylene carbonate (10 mmol), heterocumulene (20 mmol or more), and catalysts were heated in the solvent at reflux. b) Based on ethylene carbonate used. c) Accompanied by the formation of **1a** (11%) and **2a** (34%). d) In an autoclave at 80 °C.

cumulenes can be expected.

These heterocyclic compounds, **1a, 2a,** and **3a**, were obtained in the reaction of **8** with phenyl isothiocyanate in refluxing acetonitrile using 5 mol% of potassium carbonate and hexabutyldistannathiane (Eq. 3). Contrary to Reaction 1, the main product was **3a** (not **1a**).[9)]

$$K_2CO_3 + 2PhNCS + Bu_3SnSSnBu_3 \longrightarrow \mathbf{6A} + \mathbf{6B} + \mathbf{7} \longrightarrow \mathbf{1a} + \mathbf{2a} + \mathbf{3a} \quad (8),\ -K_2CO_3,\ -Bu_3SnSSnBu_3 \qquad (3)$$

Potassium carbonate is reproduced in Reaction 3 so that the carbonate can act as a catalyst. Therefore, the activity of the organostannyl compound as a two-phase catalyst for solid potassium carbonate is less in the catalytic reaction (3) than that in the stoichio reaction (2) of the carbonate.

In a less polar solvent such as benzene, a mixed catalyst system of the distannathiane and 18-Crown-6 was found to be more effective in Reaction 3 as well as in the reaction for the preparation of dialkyl carbonates.[4)]

The analogous reaction of **8** with carbon disulfide or carbonyl sulfide, catalyzed by potassium carbonate in an autoclave at 80 °C, gave **9** and 1,3-dithiolane-2-one (**11**) respectively (Eq. 4).

$$2\ S{=}C{=}Z + \underset{\mathbf{8}}{\text{cyclic carbonate}} \xrightarrow[-CO_2,\ -COS]{K_2CO_3} \underset{\mathbf{9}(Z=S),\ \mathbf{11}(Z=O)}{\text{cyclic trithiocarbonate}} \qquad (4)$$

Z=O or S

The organostannyl catalyst was not effective either in the reaction with carbon disulfide or in that with carbonyl sulfide (Table 2). This can be also explained similarly by the strong Sn–S interaction in the proposed ate-complexes consisting of CS_3^{2-} and COS_2^{2-} as was described about that for **10**.

The attempted analogous reactions using phenyl isocyanate or di-*o*-tolylcarbodiimide, which contains no sulfur atom, gave no corresponding heterocyclic compounds.

Experimental

All the melting points were determined on a micro hot stage and were not corrected. The IR spectra were taken on a JASCO IR A-1 or A-3 spectrometer. The NMR spectra were recorded on a Hitachi R-24 spectrometer. The mass spectra were measured on a Hitachi RMU-7M spectrometer. Commercial potassium carbonate was dried at about 300 °C before use. The other reagents and solvents were dried by the usual methods. All the procedures were carried under a dry nitrogen atmosphere.

Reactions of Potassium Carbonate, Aryl Isothiocyanate, and Alkylene Dibromide. Potassium carbonate (10 mmol), phenyl isothiocyanate (10 mmol), and hexabutyldistannathiane (0.5 mmol) were stirred in refluxing acetonitrile (10 ml) for 8 h. Carbonyl sulfide thus evolved was trapped at −78 °C and identified by means of its IR spectrum (ν_{COS} 2038 cm^{-1}). After the reaction mixture had been filtered to remove the inorganic salts and acetonitrile had been evaporated *in vacuo*, hot diethyl ether was added to precipitate triphenyl isocyanurate: mp 283—287 °C (lit,[10)] 285—286 °C); IR (KBr) 1700 cm^{-1} (C=O). The ether solution was cooled to precipitate 3-phenyl-2-phenylimino-1,3-thiazolidine (**1a**, 48%), contaminated with a small amount of triphenyl isocyanurate, which was removed by recrystallization from diethyl ether. The solvent was evaporated from the ether solution, and then 3-phenyl-1,3-thiazolidine-2-thione (**2a**, 17%) and 2-phenylimino-1,3-dithiolane (**3a**, 15%) were isolated by column chromatography on silica gel (chloroform). **1a**: mp 135—137 °C (lit,[11)] 136—137 °C); IR ($CHCl_3$) 1628 cm^{-1} (C=N); NMR ($CDCl_3$) δ 3.15 (2H, t, J=6.6 Hz, SCH_2), 4.04 (2H, t, J=6.6 Hz, NCH_2), and 6.8—7.6 (10H, m, arom.); MS *m/e* 254 (M^+). **2a**: mp 132—134 °C (lit,[12)] 133—134 °C); IR ($CHCl_3$) 1260 cm^{-1} (C=S); NMR ($CDCl_3$) δ 3.40 (2H, t, J=7.6 Hz, SCH_2), 4.42 (2H, t, J=7.6 Hz, NCH_2), and 7.35 (5H, s, arom.); MS *m/e* 195 (M^+). **3a**: mp 42—44 °C (lit,[13)] 47—48 °C); IR ($CHCl_3$) 1592 cm^{-1} (C=N), NMR ($CDCl_3$) δ 3.36 (4H, s, SCH_2CH_2S) and 6.7—7.4 (5H, m, arom.);

MS *m/e* 195 (M^+).

Similarly, other heterocyclic compounds were obtained. Their yields, melting points, and spectral data were as follows: 3-*p*-Tolyl-2-*p*-tolylimino-1,3-thiazolidine (**1b**): 35%; 107—109 °C (lit,[11] 110 °C); IR ($CHCl_3$) 1629 cm^{-1} (C=N); NMR ($CDCl_3$) δ 2.29 (6H, s, CH_3), 3.16 (2H, t, J=6.6 Hz, SCH_2), 4.02 (2H, t, J=6.6 Hz, NCH_2), and 6.7—7.5 (8H, m, arom.); MS *m/e* 310 (M^+). 3-*p*-Tolyl-1,3-thiazolidine-2-thione (**2b**): 18%, 123—125 °C (lit,[12] 126 °C); IR ($CHCl_3$) 1263 cm^{-1} (C=S); NMR ($CDCl_3$) δ 2.36 (3H, s, CH_3), 3.42 (2H, t, J=7.7 Hz, SCH_2), 4.44 (2H, t, 7.7 Hz, NCH_2), and 7.28 (4H, s, arom.); MS *m/e* 209 (M^+). 2-*p*-Tolylimino-1,3-dithiolane (**3b**): 12%; oil (lit,[13] oil); IR ($CHCl_3$) 1580 cm^{-1} (C=N); NMR ($CDCl_3$) δ 2.32 (3H, s, CH_3), 3.51 (4H, s, SCH_2CH_2S), and 6.8—7.3 (4H, m, arom.); MS *m/e* 209 (M^+). 3-Phenyl-2-(phenylimino)perhydro-1,3-thiazine (**1c**): 24%; 139—141 °C (lit,[10] 139 °C); IR ($CHCl_3$) 1623 cm^{-1} (C=N); NMR ($CDCl_3$) δ 2.24 (2H, m, C-CH_2-C), 3.17 (2H, t, J=6.1 Hz, SCH_2), 3.77 (2H, t, 5.5 Hz, NCH_2), and 6.9—7.5 (10H, m, arom.), MS *m/e* 268 (M^+). 3-Phenylperhydro-1,3-thiazine-2-thione (**2c**): 19%, 105—106 °C; IR ($CHCl_3$) 1232 cm^{-1} (C=S); NMR ($CDCl_3$) δ 2.40 (2H, m, C-CH_2-C), 3.12 (2H, t, J=6.1 Hz, SCH_2), 3.82 (2H, t, J=5.5 Hz, NCH_2), and 7.2—7.5 (5H, m, arom.); MS *m/e* 209 (M^+). 2-Phenylimino-1,3-dithiane (**3c**): 18%; 113—116 °C (lit,[14] 117—118 °C); IR ($CHCl_3$) 1570 cm^{-1} (C=N); NMR ($CDCl_3$) δ 2.17 (2H, m, C-CH_2-C), 3.12 (2H, t, J=6.8 Hz, SCH_2), and 6.7—7.5 (5H, m, arom.); MS *m/e* 209 (M^+).

A reaction mixture from potassium carbonate, phenyl isothiocyanate, and hexabutyldistannathiane (5 mol%), obtained under the conditions described above, was hydrolyzed by the addition of dilute hydrochloric acid after the solvent had been evaporated; the residue was washed with hexane to remove the unreacted phenyl isothiocyanate. A small amount of a water-insoluble precipitate was obtained. By recrystallization from ethanol, *N,N'*-diphenylurea was isolated: mp 149—152 °C (lit,[15] 154 °C); IR (KBr) 1445 cm^{-1}.

Reaction of Ethylene Carbonate (8) with Phenyl Isothiocyanate. Ethylene carbonate (10 mmol), phenyl isothiocyanate (20 mmol), potassium carbonate (0.5 mmol), and hexabutyldistannathiane (0.5 mmol) were stirred in refluxing acetonitrile (10 ml). After the reaction mixture had then been treated as above, **1a** (11%), **2a** (34%), and **3a** (50%) were obtained. By an analogous reaction catalyzed by potassium carbonate (5 mol%), hexabutyldistannathiane (5 mol%), and 18-crown-6 (10 mol%) in refluxing benzene for 24 h, **1a** (16%), **2a** (24%), and **3a** (49%) were obtained.

Reaction of Ethylene Carbonate (8) with Carbon Disulfide or Carbonyl Sulfide. Ethylene carbonate (**8**, 20 mmol), carbon disulfide (40 mmol), potassium carbonate (1 mmol), hexabutyldistannathiane (1 mmol), and 18-crown-6 (2 mmol) were heated in a glass autoclave for 24 h at 80 °C. 1,3-Dithiolane-2-thione (**9**) was then isolated in a 17% yield by means of column chromatography.

By a similar procedure, the reaction of **8** (20 mmol) with carbonyl sulfide (40 mmol), catalyzed by potassium carbonate (1 mmol) and hexabutyldistannathiane (1 mmol) for 48 h at 80 °C, gave 1,3-dithiolane-2-thione (**11**, 42%) and **9** (2%). **11**: mp 31—33 °C (lit, [15] 35 °C); IR ($CHCl_3$) 1716 cm^{-1} (C=O); NMR ($CDCl_3$) δ 3.77 (4H, s, SCH_2CH_2).

References

1) R. M. Boden, *Synthesis*, **1975**, 784.

2) M. Fedorynski, K. Wojiciechowski, Z. Matacz, and M. Makosza, *J. Org. Chem.*, **43**, 4682 (1978).

3) K. Soga, S. Hosoda, and S. Ikeda, *J. Polym. Sci., Polym. Lett. Ed.*, **15**, 611 (1977).

4) T. Fujinami, S. Sato, and S. Sakai, *Chem. Lett.*, **1981**, 749.

5) A. J. Bloodworth, A. G. Davies, and S. C. Vasishtha, *J. Chem. Soc., C*, **1968**, 2640.

6) T. Harada, *Bull. Chem. Soc. Jpn.*, **17**, 283 (1942).

7) A. J. Bloodworth, A. G. Davies, and S. C. Vasishtha, *J. Chem. Soc., C*, **1967**, 1309.

8) We obtained more **3a** (43%) than **2a** (17%) by the reaction of dibromoethane with $PhN(Li)CS_2Li$, which had been prepared *in situ* from aniline, butyllithium, and carbon disulfide; S. Sakai, N. Otani, and T. Fujinami, unpublished.

9) The reason for the formation of **3a** as the main product in Reactions 3 is not yet clear. However, we tentatively consider the reaction scheme to be as follows.

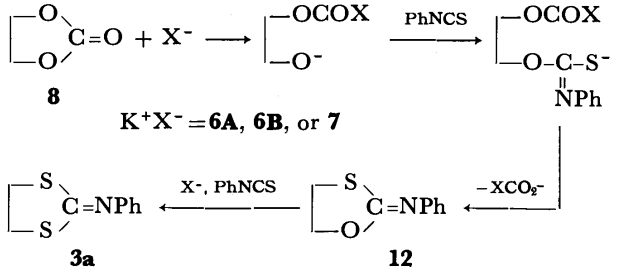

In the first step, the anionic species, X^-(S^- or N^- site in **6A**, **6B**, or **7**) attack the acyl carbon of **8** competitively on the sp^3-carbon. Subsequently, phenyl isothiocyanate adds to the ring-opening product, and a cyclic intermediate is formed by an intramolecular nucleophilic attack of the S^- site. Similar reactions are repeated on **12** to give **3a**.

10) S. L. Shapiro, V. Bandurco, and L. Freedman, *J. Org. Chem.*, **26**, 3710 (1961).

11) F. B. Daines, R. Q. Brewster, J. S. Blain, and W. C. Thompson, *J. Am. Chem. Soc.*, **44**, 2637 (1922).

12) Yu. K. Yur'ev and S. V. Dyatlovitskaya, *Zh. Obshch. Khim.*, **27**, 3148 (1957); *Chem. Abstr.*, **52**, 9077 (1958).

13) T. Nakai and M. Okawara, *Tetrahedron Lett.*, **1967**, 3835.

14) H. Wolfgang, *Arch. Pharm.*, **310**, 409 (1977).

15) H. S. Fry, *J. Am. Chem. Soc.*, **35**, 1539 (1913).

Syntheses of Lividomycin B Analogues, 5-*O*-[3-*O*-(6-Amino-6-deoxy-β-L-idopyranosyl)-β-D-ribofuranosyl]-3′-deoxyparomamine and 5-*O*-[2-*O*-(6-Amino-6-deoxy-β-L-idopyranosyl)-β-D-ribofuranosyl]-3′-deoxyparomamine

Takahiro TORII, Tsutomu TSUCHIYA,* Isamu WATANABE, and Sumio UMEZAWA
Institute of Bioorganic Chemistry, 1614 Ida, Nakahara-ku, Kawasaki 211

(Received August 28, 1981)

The preparation of lividomycin B analogues, the title pseudotetrasaccharides, is described. Condensation of 6-azido-2,3,4-tri-*O*-benzyl-6-deoxy-L-idopyranosyl chloride with 4′,6′-di-*O*-benzoyl-5-*O*-(5-*O*-benzoyl-β-D-ribofuranosyl)-3,2′-bis(*N*-benzyloxycarbonyl)-1-*N*:6-*O*-carbonyl-3′-deoxyparomamine was followed by deblocking and reduction of the azido groups. Structure determinations and the antibacterial activities of the products are described.

Lividomycin B[1] is an amino glycoside antibiotic which belongs to a pseudotetrasaccharide. Since its pseudotrisaccharide[2] portion (**5**; B-A-C portion of lividomycin B) has almost no antibacterial activity, it is suggested that the fourth sugar (D portion) plays an important role in exhibiting the antibacterial activity of lividomycin B. Until now, however, variation of the D portion has rarely been studied. A lividomycin B analogue,[3] which has 2-amino-2-deoxy-α-D-glucopyranose as the fourth sugar, was reported and found to show much less antibacterial activity than lividomycin B having the 2,6-diamino-2,6-dideoxy-β-L-idopyranose. As the continuation of this work, the present study was performed. Since it appeared that the 6-amino group on the β-L-idopyranose portion of lividomycin B would have an important role in its activity, we undertook to synthesize a lividomycin B analogue having 6-amino-6-deoxy-β-L-idopyranose instead of the diamino sugar. This synthesis was carried out by condensation of a protected idopyranosyl halide (**4**) with a pseudotrisaccharide derivative (**8**), leading to the desired glycoside (**14**) and an isomer (**13**).

6-Azido-3-*O*-benzyl-6-deoxy-1,2-*O*-isopropylidene-L-idofuranose[4] (**1**) was prepared from 1,2:5,6-di-*O*-isopropylidene-D-glucofuranose *via* 5,6-anhydro-3-*O*-benzyl-1,2-*O*-isopropylidene-L-idofuranose[5] through 6 steps. Conversion of the furanose (**1**) to the corresponding pyranose was carried out by treating **1** with 95% formic acid and the crude product was treated with α-bromotoluene in the presence of a base to give benzyl 6-azido-2,3,4-tri-*O*-benzyl-6-deoxy-β-L-idopyranoside (**2**). Acidic hydrolysis of **2** gave the free sugar (**3**). Reaction of **3** with thionyl chloride gave the corresponding glycosyl chloride (**4**), which was used without purification.

The pseudotrisaccharide[2] (**5**) obtained from lividomycin B by cleavage[6] of the 2,6-diamino-2,6-dideoxy-L-idopyranose portion was treated with benzyl chloroformate to give 1,3,2′-tris(*N*-benzyloxycarbonyl) derivative (**6**). Treatment of **6** with sodium hydride in *N*,*N*-dimethylformamide, a procedure producing cyclic carbamate developed by Umezawa, Tsuchiya, and Ikeda,[7] gave 3,2′-bis(*N*-benzyloxycarbonyl)-1,6-carbamate (**7**). Structural proof of the five-membered carbamate was obtained from the presence of an absorption peak at 1770 cm^{-1} [8] in its IR spectrum. Treatment of **7** with phenylboronic acid (1 mol equiv. for **6**), followed by benzoylation and removal of the phenylboronate protecting group[9] gave 4′,6′,5″-tri-*O*-benzoyl derivative (**8**) as the main product with the minor 5″-*O*-benzoyl derivative (**9**). The structure of **8** was confirmed by the result of periodate oxidation, and the structure of **9**, by the formation of its 4′,6′:2″,3″-di-*O*-isopropylidene derivative (**10**). This suggests that the intermediary boronate was mainly formed between 2″- and 3″-hydroxyls, and between 4′- and 6′-hydroxyls in a minor extent.

Condensation of the glycosyl chloride (**4**) with the protected pseudotrisaccharide (**8**) was carried out in benzene in the presence of mercury(II) cyanide to give

Table 1. The ^{13}C chemical shifts[a] of lividamine (LA), pseudotrisuccharide (**5**), lividomycin B (LVB), **13** and **14** (all as free bases)

Carbon	LA	5	LVB	13	14
1′	100.8	99.2	99.4	97.4[e]	98.8[l]
2′	49.8	50.1	50.1	49.8	50.0
3′	35.7	35.1	35.4[c]	34.2	34.7
4′	65.4	65.4	65.5	65.1	65.3
5′	74.3	74.3	74.3	74.3	74.3
6′	61.6	61.6	61.6	61.5	61.5
1	51.1	51.1	51.2	51.2[f]	51.1[j]
2	36.3	36.4	35.5[c]	36.0	36.1
3	50.4	51.1	51.2	50.9[f]	51.0
4	88.0	85.4	85.3	86.4	85.5
5	76.7	83.3[b]	82.1[d]	83.1[g]	83.0[k]
6	78.2	78.3	78.5	78.4	78.0
1″		109.6	109.5	108.7	109.5
2″		75.7	74.8	82.9[g]	74.8
3″		70.5	77.1	70.5[h]	77.1
4″		83.8[b]	83.9[d]	81.9[g]	82.1[k]
5″		62.6	62.0	62.4	62.0
1‴			99.8	99.0[e]	99.8[l]
2‴			53.6	70.8[h]	70.5[l]
3‴			71.5	70.1[h]	69.9[l]
4‴			69.4	69.7[h]	69.4[l]
5‴			74.3	74.0	74.3
6‴			41.0	41.5	41.7

a) In ppm downfield from TMS calculated as $\delta^{TMS} = \delta^{dioxane} + 67.4$ ppm. b—l) Figures indicated by the same character may be interconvertible.

2″-*O*- (**11**, 43%) and 3″-*O*-(6-azido-2,3,4-tri-*O*-benzyl-6-deoxy-β-L-idopyranosyl) derivatives (**12**, 19%). Debenzoylation and cleavage[7] of the carbamate groups of the condensation products (**11** and **12**) were carried out with dilute barium hydroxide. Further treatment with sodium metal in liquid ammonia resulted in debenzylation, de(benzyloxycarbonyl)ation and the reduction of the azido into an amino group simultaneously to give the final products (**13** and **14**).

The structures of **13** and **14** were confirmed as follows. The molecular rotations ($[\alpha]_D \times MW/100$) of the final products (**13** : +340; **14** : +310) showed comparative values with that of lividomycin B (+360), but greater than that of **5** (+200), indicating that the contributions of the L-idopyranose moiety of **13** and **14** for their rotations are both positive (*ca.* +120). Since the molecular rotations of α-L- and β-L-idopyranosides are roughly estimated[10] −190 and +100, respectively, it is shown that the L-idopyranoses of **13** and **14** are coupled to the pseudotrisaccharide portion (**5**) with the desired β-L-anomeric configuration. The positions at which the β-L-idopyranose was attached were decided by the ^{13}C-NMR spectra. At first, carbon chemical shifts of lividamine[11] were assigned on the basis of comparison of the data with those of neamine[12] and paromomycin[12] (Table 1); the shifts of pseudotrisaccharide (**5**) were then assigned by comparison of the data with those of lividamine just obtained and paromomycin;[12] finally

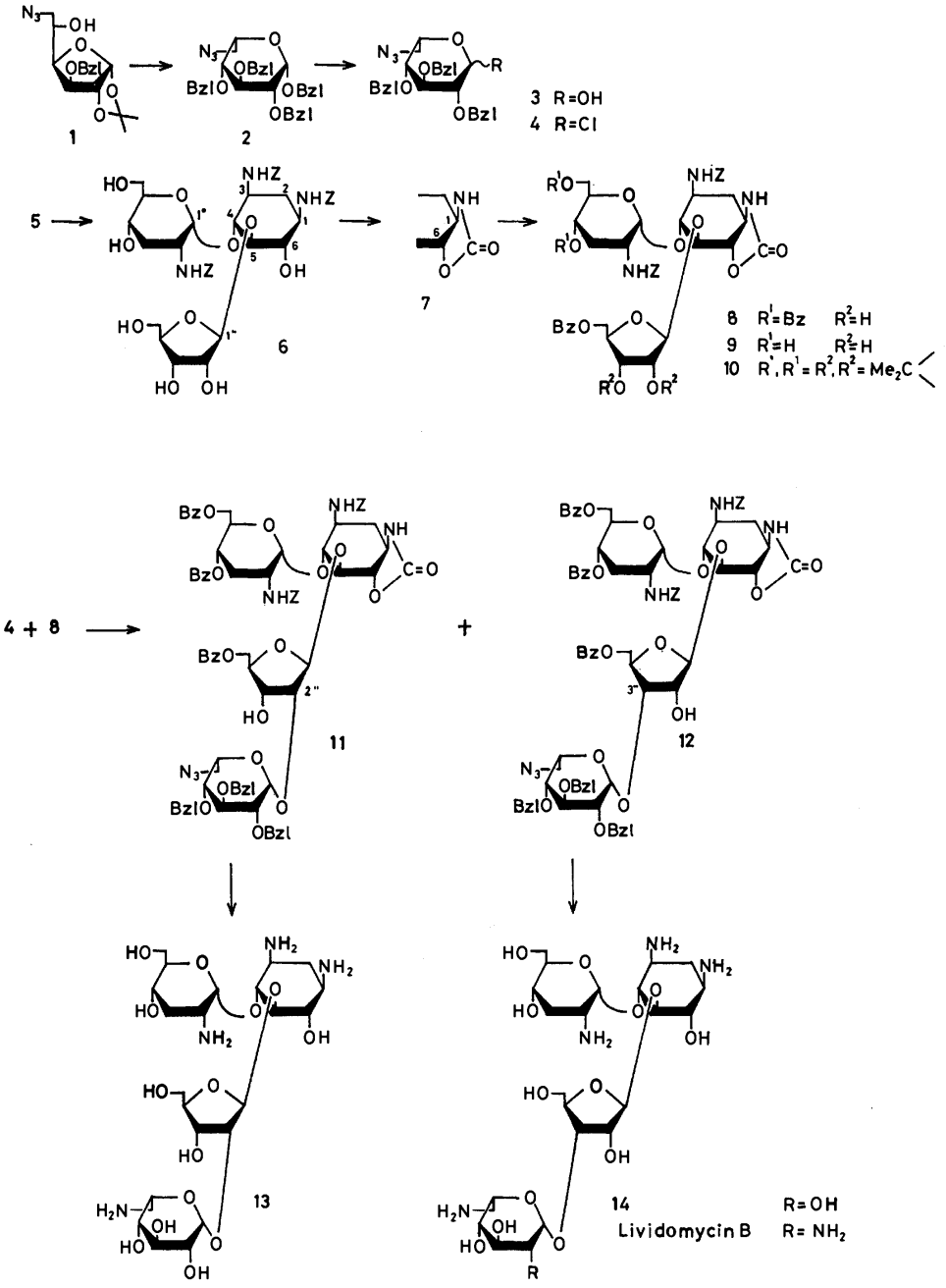

Table 2. Antibacterial spectra of **13**, **14**, and lividomycin B (LVB)

Test organisms[a]	Minimal inhibitory concentration/μg cm^{-3}		
	13	**14**	LVB
Staphylococcus aureus 209P	12.5	6.25	0.78
Bacillus subtilis NRRL B-558	12.5	1.56	1.56
Klebsiella pneumoniae PCI 602	25	6.25	3.12
Salmonella typhi T-63	12.5	6.25	1.56
Escherichia coli K-12	100	25	6.25
Escherichia coli K-12 ML 1629	>100	>100	>100
Escherichia coli K-12 W677	25	3.12	1.56
Pseudomonas aeruginosa A3	100	50	12.5
Mycobacterium smegmatis ATCC 607[b]	6.25	12.5	0.78

a) Agar dilution streak method (nutrient agar, 37 °C, 18 h). b) 48 h.

the shifts of lividomycin B were assigned on the basis of comparison of the data with those of **5** and paromomycin. Shift-assignments of **14** were next made by comparison of the data with that of lividomycin B just obtained. The sole discrepancy in shift-value between **14** and lividomycin B observed was that for C-2‴ at which a hydroxyl group is attached in **14** instead of the amino group in lividomycin B. Downfield shift[13] (6.6 ppm) of C-3″ from the corresponding position of **5** also supported that glycosylation occurred at the 3″-hydroxyl. Compound **14** was, therefore, decided to be 3″-*O*-glycosyl compound. Shift-assignments of **13** were made on the basis of the data of **14**. The chemical shift at 82.9 ppm of **13** can reasonably be assigned to that of C-2″; the shift-difference (7.2 ppm) of the C-2″ between **13** and **5** indicates that **13** is a 2″-*O*-glycosyl isomer.

Antibacterial spectra of **13** and **14** were shown in Table 2 with that of lividomycin B. The results show that **14** has weaker antibacterial activity than that of lividomycin B, and that the position isomer **13** is less active than **14**. This result shows that an important factor with respect to structure-activity relationships in the ring D is the number and location of amino functions, affecting the binding of the antibiotics with bacterial ribosomes. It is noteworthy that the isomer (**13**) does not loss activity against bacteria in spite of the introduction of the D ring at another position of the ribose.

Experimental

^{1}H-NMR spectra were recorded at 90 MHz with a Varian EM-390 spectrometer. ^{13}C-NMR spectra were recorded on a Varian XL-100 spectrometer with Varian 620-L data processing system (25.2 MHz) in deuterium oxide solution containing dioxane as internal reference. Thin-layer chromatography (TLC) was performed on DC-Fertigplatten Kieselgel 60 F_{254} (E. Merck). For column chromatography, silica gel (Wakogel C-200) was used.

*Benzyl 6-Azido-2,3,4-tri-*O*-benzyl-6-deoxy-β-*L*-idopyranoside (**2**).* A solution of **1** (3.00 g) in 95% formic acid (100 ml) was kept at room temperature for 4 h. Evaporation *in vacuo* followed by several coevaporations with toluene gave a residue, which was dissolved in DMF (60 ml). To the solution cooled to 0 °C, α-bromotoluene (5.8 ml. *ca* 3 mol equiv. for **1**), barium oxide (7.26 g) and $Ba(OH)_2 \cdot 8H_2O$ (15 g, powdered) were added and the mixture was stirred overnight at the temperature. Addition of benzene (100 ml) gave precipitates which were removed by centrifugation. Concentration of the solution and the washings (the solid was washed with benzene) combined gave a residue. Column chromatography of the residue with benzene–ethyl acetate (100 : 1) gave a syrup of **2**, 2.90 g (57%), $[\alpha]_D^{24}$ +101° (*c* 1, chloroform).

^{1}H-NMR ($CDCl_3$): δ 3.53 (1H dd, $J_{1,2}$ 2 Hz, $J_{2,3}$ 5 Hz, H-2), and 4.85 (1H d, H-1); IR (KBr): 2100 cm^{-1} (N_3).

Found: C, 72.35; H, 6.31; N, 7.37%. Calcd for $C_{34}H_{35}N_3O_5$: C, 72.19; H, 6.24; N, 7.43%.

*6-Azido-2,3,4-tri-*O*-benzyl-6-deoxy-*L*-idopyranose (**3**).* To a solution of **2** (1.70 g) in acetic acid (93 ml) was added 2 M† sulfuric acid (8.5 ml) and the solution was kept at 80 °C for 3 h. Ice–water (200 g) was introduced and the mixture was extracted with chloroform. The organic solution was washed with sodium hydrogencarbonate solution, water, dried over sodium sulfate and concentrated. The residue was purified by a short column of silica gel with benzene–ethyl acetate (10 : 1) to give a colorless syrup, 1.24 g (86%), $[\alpha]_D^{24}$ +6.5° (*c* 1, chloroform); IR(KBr): 2100 cm^{-1} (N_3).

Found: C, 68.40; H, 6.26; N, 8.88%. Calcd for $C_{27}H_{29}N_3O_5$: C, 68.21; H, 6.11; N, 8.84%.

*6-Azido-2,3,4-tri-*O*-benzyl-6-deoxy-*L*-idopyranosyl Chloride (**4**).* Compound **3** (700 mg) was dissolved in thionyl chloride (7 ml) and the solution was kept at room temperature for 3 h. Evaporation followed by several coevaporations *in vacuo* with dry toluene gave a surup (730 mg).

^{1}H-NMR ($CDCl_3$): δ 5.84 (*ca.* 0.3H d, *J* 3 Hz, α-L-isomer), and 6.16 (*ca.* 0.7 H slightly broadened s, β-L-isomer).

*1,3,2′-Tris(*N*-benzyloxycarbonyl)-3′-deoxy-5-*O*-(β-*D*-ribofuranosyl)paromamine (**6**).* To a cold (−5°C) solution of **5** (4.44 g as the base) in aqueous methanol (1: 1, 50 ml), anhydrous sodium carbonate (4.0 g) and benzyl chloroformate (6.2 g) were added and the solution was kept at 0 °C for 1 h and then at room temperature for 2 h. Concentration followed by addition of water gave a solid, which was thoroughly washed with ether to give a solid, 7.47 g (88%), $[\alpha]_D^{24}$ +27° (*c* 1, methanol).

Found: C, 58.31; H, 6.05; N, 5.13%. Calcd for $C_{41}H_{50}N_3O_{16}$: C, 58.56; H, 5.99; N, 5.00%.

*3,2′-Bis(*N*-benzyloxycarbonyl)-1-*N*:6-*O*-carbonyl-3′-deoxy-5-*O*-(β-*D*-ribofuranosyl)paromamine (**7**).* To a cold (0 °C) solution of **6** (8.0 g) in dry DMF (80 ml), 50% oily sodium hydride (0.6 g as net NaH) was added and the mixture was stirred vigorously for 4 h at the cold. Acetic acid (6.4 ml) was added and the solution was concentrated *in vacuo*. Extraction of the resulting residue with dioxane followed by concentration of the dioxane solution gave a solid, which was chromatographed with chloroform–methanol (8 : 1→ 6 : 1). Starting material (**6**) (1.66 g, 21%) and **7** (4.11 g, 59%) were eluted in this order. **7**: $[\alpha]_D^{24}$ +34° (*c* 1, methanol); R_f 0.24 (TLC with $CHCl_3$–MeOH=6 : 1; **6**: R_f 0.38); IR(KBr): 1770 (cyclic carbamate), and 1710 cm^{-1} (urethane carbonyl).

Found: C, 55.37; H, 6.02; N, 5.43%. Calcd for $C_{34}H_{43}N_3O_{15}$: C, 55.66; H, 5.91; N, 5.73%.

*4′,6′-Di-*O*-benzoyl-5-*O*-(5-*O*-benzoyl-β-*D*-ribofuranosyl)-3,2′-bis(*N*-benzyloxycarbonyl)-1-*N*:6-*O*-carbonyl-3′-deoxyparomamine (**8**).* To a solution of **7** (3.16 g) in dry pyridine (120 ml), phenylboronic acid (527 mg, 1 mol equiv. for **7**) was added and the solution was kept at room temperature for 2 h. To the solution cooled in an ice-bath, benzoyl chloride (7.3 g)

† 1 M=1 mol dm^{-3}.

was added and the solution was kept at room temperature for 2 h. The solution showed a major spot at R_f 0.7 (4′,6′,5″-tri-*O*-benzoyl-2″,3″-boronate derivative), on TLC with chloroform–methanol (10 : 1). After addition of water (2 ml) followed by stirring for 1 h, 1,3-propanediol (1.5 ml) was added and the solution was kept at room temperature overnight. Concentration gave a residue, which was dissolved in chloroform. The solution was washed with 1 M aqueous potassium hydrogensulfate, aqueous sodium hydrogencarbonate, and water, dried over sodium sulfate and concentrated. The residue showed, on TLC with chloroform–methanol (10 : 1), spots of R_f 0.9 (slight, penta-*O*-benzoyl derivative?), 0.43 (slight, another tri-*O*-benzoyl derivative?), 0.38 (major, **8**), 0.22 (minor **9**) and 0.1 (slight, **7**). The residue was chromatographed on a silica-gel column with chloroform–methanol (50: 1→30: 1→15: 1→8: 1→5: 1) as developer to give a solid of **8**, 2.00 g (44%), R_f (0.38 TLC with 10 : 1 chloroform–methanol) and a solid of **9**, 0.84 g (23%), R_f 0.22 (TLC).

8: $[\alpha]_D^{24}$ +48° (*c* 1, chloroform).

Found: C, 63.36; H, 5.35; N, 4.03%. Calcd for $C_{55}H_{55}N_3O_{18}$: C, 63.15; H, 5.26; N, 4.02%.

9: $[\alpha]_D^{24}$ +29° (*c* 1, chloroform).

Found: C, 58.46; H, 5.76; N, 4.77%. Calcd for $C_{41}H_{47}N_3O_{16}$: C, 58.78; H, 5.62; N, 5.02%.

Periodate Oxidation of **8**. To a solution of **8** (10 mg) in ethanol (0.5 ml) was added sodium periodate (5 mg) and the solution was kept at room temperature for 2 h. On checking by TLC with chloroform–methanol (10 : 1), the solution showed a single spot R_f 0.60 (*cf.* **8** : R_f 0.38).

*5-O-(5-O-Benzoyl-2,3-O-isopropylidene-β-*D*-ribofuranosyl)-3,2′-bis(*N*-benzyloxycarobnyl)-1-*N*:6-O-carbonyl-3′-deoxy-4′,6′-O-isopropylideneparomamine* (**10**). A mixture of **9** (50 mg), anhydrous *p*-toluenesulfonic acid (18 mg), and 1,1-dimethoxypropane (1 ml) in DMF (5 ml) was kept at room temperature overnight. Addition of aqueous saturated sodium hydrogencarbonate solution (1 ml) followed by concentration of the mixture gave a residue. Extraction of the residue with chloroform followed by silica gel chromatography of the extracts with benzene–ethyl acetate–triethylamine (1 : 1 : 0.02) gave a solid of **10**, which was reprecipitated from chloroform–hexane, 44 mg (80%), $[\alpha]_D^{25}$ +19° (*c* 1, chloroform): IR(KBr): 1775, and 1725 cm^{-1}; ^{1}H-NMR ($CDCl_3$): δ 1.28, 1.34, 1.42 and 1.46 (each 3H s, Ip).

Found: C, 61.43; H, 5.94; N, 4.61%. Calcd for $C_{47}H_{55}N_3O_{16}$: C, 61.50; H, 6.04; N, 4.58%.

*5-O-[2-O-(6-Azido-2,3,4-tri-O-benzyl-6-deoxy-β-*L*-idopyranosyl)-5-O-benzoyl-β-*D*-ribofuranosyl]-4′,6′-di-O-benzoyl-3,2′-bis(*N*-benzyloxycarbonyl)-1-*N*:6-O-carbonyl-3′-deoxyparomamine* (**11**) *and 5-O-[3-O-(6-azido-2,3,4-tri-O-benzyl-6-deoxy-β-*L*-idopyranosyl)-5-O-benzoyl-β-*D*-ribofuranosyl]-4′,6′-di-O-benzoyl-3,2′-bis(*N*-benzyloxycarbonyl)-1-*N*:6-O-carbonyl-3′-deoxyparomamine* (**12**).

A mixture of **4** (553 mg), **8** (205 mg), mercury (II) cyanide (308 mg, dried at 75 °C under 1 Torr (1 Torr≈133.32 Pa) pressure for 3 h), and Drierite (610 mg, dried at 250 °C for 3 h) in dry benzene (10 ml) was stirred overnight at room temperature. Chloroform (50 ml) was added, filtered, and the organic solution was washed with aqueous saturated sodium hydrogencarbonate and water, dried over sodium sulfate, and concentrated. The residue was chromatographed on a column of silica gel (50 g) with chloroform–methanol (60 : 1) to give a mixture of major products (352 mg). The mixture was separated by preparative TLC (Kieselgel 60 PF_{254}, E. Merck) with chloroform–methanol (30 : 1) to give a solid of **11**, 140 mg (43%, R_f 0.35 on TLC with chloroform–methanol=30 : 1) and **12**, 85 mg (19%, R_f 0.32), with minor products (48 mg, R_f 0.30, a mixture of α-L-isomers?).

11: $[\alpha]_D^{24}$ +51° (*c* 1, chloroform); IR(KBr): 2100 (N_3), 1780, and 1725 cm^{-1}.

Found: C, 65.68; H, 5.48; N, 5.53%. Calcd for $C_{82}H_{82}N_6O_{22}$: C, 65.51; H, 5.46; N, 5.59%.

12: $[\alpha]_D^{24}$ +42° (*c* 1, chloroform); IR (KBr): 2100, 1780, and 1725 cm^{-1}.

Found: C, 65.55; H, 5.44; N, 5.43%.

*5-O-[2-O-(6-Amino-6-deoxy-β-*L*-idopyranosyl)-β-*D*-ribofuranosyl]-3′-deoxyparomamine* (**13**). To a solution of **11** (145 mg) in dioxane (9 ml) was added 0.03 M barium hydroxide solution (2 ml) and the mixture was stirred at 60 °C for 30 min. After introduction of carbon dioxide, the mixture was centrifuged, and the solid was washed thoroughly with dioxane. The solution and the washings combined were concentrated to give a residue. The residue was dissolved in tetrahydrofuran–methanol (1 : 1) and the solution was passed through a column of Sephadex LH-20. The elution was concentrated and the solid was dried thoroughly. A solution of the solid in tetrahydrofuran (3 ml) was adedd to a solution of sodium metal (*ca.* 200 mg) in liquid ammonia (*ca.* 9 ml, −50 °C) and the deep-blue solution was kept at the temperature for 1 h. Addition of water until the solution became colorless, followed by gradual warming to room temperature, and evaporation under diminished pressure, gave a residue. An aqueous solution of the residue was poured onto a column of Dowex 50W×2 (NH_4^+) resin, and the column was washed with water, then eluted with 2 M aqueous ammonia. Ninhydrin-positive fractions were collected and evaporated. The residue was chromatographed on a column of CM-Sephadex C-25 (NH_4^+) with aqueous ammonia (0→0.08 M, gradually changed) to give a solid of **13**, 30 mg (42% as dicarbonate), $[\alpha]_D^{26}$ +47° (*c* 1, water).

^{1}H-NMR (D_2O containing DCl; pD *ca.* 1); δ 1.7—2.7 (4H, H-2,3′), 5.17 (1H d, $J_{1''',2'''} \simeq 1.5$ Hz, H-1‴), 5.43 (1H br s, H-1″), and 5.60 (1H d, $J_{1',2'}$ 3.5 Hz, H-1′).

Found: C, 41.85; H, 6.90; N, 7.69%. Calcd for $C_{23}H_{44}N_4O_{14}\cdot 2H_2CO_3$: C, 41.43; H, 6.68; N, 7.73%.

*5-O-[3-O-(6-Amino-6-deoxy-β-*L*-idopyranosyl)-β-*D*-ribofuranosyl]-3′-deoxyparomamine* (**14**). Compound **12** (145 mg) was treated similarly as described for **13** to give a solid of **14**, 35 mg (50% as dicarbonate), $[\alpha]_D^{26}$ +42° (*c* 0.7, water).

^{1}H-NMR (D_2O containing DCl; pD *ca.* 1): δ 1.7—2.7 (4H, H-2,3′), 5.07 (1H d, $J_{1''',2'''} \simeq 1.5$ Hz, H-1‴), 5.38 (1H br s, H-1″), and 5.62 (1H d, $J_{1',2'}$ 3.5 Hz, H-1′).

Found: C, 41.16; H, 6.96; N, 7.56%. Calcd for $C_{23}H_{44}N_4O_{14}\cdot 2H_2CO_3$: C, 41.43; H, 6.68; N, 7.73%.

The authors wish to express their deep thanks to Prof. Hamao Umezawa of the Institute of Microbial Chemistry for the encouragement.

References

1) T. Oda, T. Mori, H. Ito, and T. Kunieda, *J. Anitibiot.*, **24**, 333 (1971); T. Mori, T. Ichiyanagi, H. Kondo, K. Tokunaga, and T. Oda, *ibid.*, **24**, 339 (1971).

2) T. Yamaguchi, K. Kamiya, T. Mori, and T. Oda, *J. Anitibiot.*, **30**, 332 (1977).

3) I. Watanabe, T. Tsuchiya, S. Umezawa, and H. Umezawa, *Bull. Chem. Soc. Jpn.*, **50**, 2369 (1977).

4) H. Saeki and E. Ohki, *Chem. Pharm. Bull.*, **16**, 2477 (1968).

5) von A. S. Meyer and T. Reichstein, *Helv. Chim. Acta*, **29**, 152 (1946).

6) T. Takamoto and S. Hanessian, *Tetrahedron Lett.*, **46**, 4009 (1974).

7) D. Ikeda, T. Tsuchiya, S. Umezawa, and H. Umezawa,

J. Antibiot., **25**, 741 (1972); *Bull. Chem. Soc. Jpn.*, **47**, 3136 (1974).

8) S. Umezawa, Y. Takagi, and T. Tsuchiya, *Bull. Chem. Soc. Jpn.*, **44**, 1411 (1971).

9) R. J. Ferrier, *J. Chem. Soc., C*, **1961**, 2325; A. M. Yurkevichi, I. I. Kolodkina, L. S. Varshavskaya, V. I. Borodulina-Shvetz, I. P. Rudakova, and N. A. Preobrazhenski, *Tetrahedron*, **25**, 477 (1961); related references are cited therein.

10) N. Baggett, P. J. Stoffyn, and R. W. Jeanloz, *J. Org. Chem.*, **28**, 1041 (1963).

11) T. Oda, T. Mori, and K. Kyōtani, *J. Antibiot.*, **24**, 503 (1971).

12) S. Omoto, S. Inouye, M. Kojima, and T. Niida, *J. Antibiot.*, **26**, 717 (1973).

13) T. Usui, N. Yamaoka, K. Matsuda, K. Tuzimura, H. Sugiyama, and S. Seto, *J. Chem. Soc., Perkin Trans. 1*, **1973**, 2425.

 © 1982 The Chemical Society of Japan Bull. Chem. Soc. Jpn., 55, 1183—1187 (1982)

The Thermal Decomposition of *N,O*-Diacyl-*N*-*t*-butylhydroxylamines. III. Novel Routes to 2-Substituted 1,2-Benzisothiazol-3-(2*H*)-ones[1]

Yuzuru UCHIDA* and Seizi KOZUKA†

Department of Applied Chemistry, Osaka Institute of Technology, Asahi-ku, Osaka 535
†*Department of Applied Chemistry, Faculty of Engineering, Osaka City University, Sumiyoshi-ku, Osaka 558*

(Received September 1, 1981)

The reactions of *N*-alkyl- and *N*-aryl-2-(methylsulfinyl)benzamides and *N*-[2-(methylthio)benzoyl]-*N*-alkylhydroxylamines with thionyl chloride have been found to give 2-substituted 1,2-benzisothiazol-3(2*H*)-ones in nearly quantitative yields. The reactions of *N*-[2-(methylthio)benzoyl]-*N*-arylhydroxylamines with thionyl chloride gave chlorinated anilides as the major products.

2-Substituted 1,2-benzisothiazol-3(2*H*)-ones (**4**) have received much attention in recent years because of their antibacterial and antifungal properties.[2-5] The 2-substituted 1,2-benzisothiazol-3(2*H*)-ones have been synthesized by the reaction of 2-(chlorothio)benzoyl chloride with appropriate amines,[3] cyclization of 2-carbamoylbenzenesulfenyl halides with amines,[4] reaction of bis(2-carbamoylphenyl) disulfides with thionyl chloride,[5] and catalytic cyclization of *N*-substituted 2-(methoxycarbonyl) benzenesulfenamides by strong base.[6]

On the other hand, we have studied the thermal decompositions of *O*-acyl-*N*-[2-(methylthio)benzoyl]-*N*-*t*-butylhydroxylamines (**1**) and found that 2-*t*-butyl-1,2-benzisothiazol-3(2*H*)-one (**4a**) was formed in moderate yield as one of the products.[7] Acylaminosulfonium salt

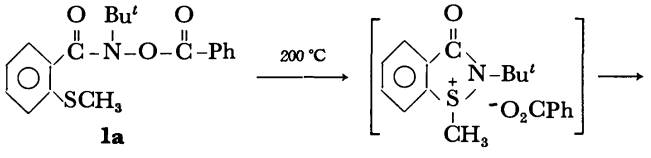

1a **2a**

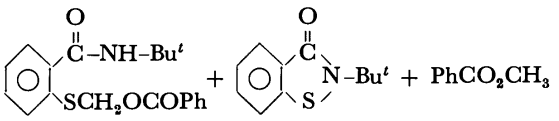

3 **4a**

(**2a**) has been suggested as the intermediate for the thermolysis. In order to prove the intermediacy of **2**, Pummerer reactions of *N*-*t*-butyl-2-(methylsulfinyl)-benzamide (**5a**) with either benzoic anhydride or thionyl chloride were tried; a facile formation of **4a**, by the reaction with thionyl chloride, was found.[7] This reaction would provide a novel and general route to prepare **4**, since a variety of *N*-substituted 2-(methylsulfinyl)benzamides (**5**) can easily be prepared from the corresponding sulfides. Thus, several *N*-alkyl- and *N*-arylbenzamides **5** were prepared and their reactions with thionyl chloride were examined.

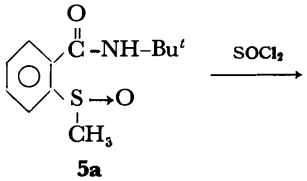

5a

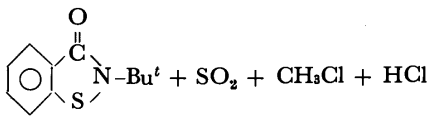

4a

In the thermal decomposition of **1**, the mechanism of the formation of acylaminosulfonium salt (**2**) involves nucleophilic attack of the sulfur atom on the nitrogen atom. A better leaving group would facilitate the formation of **2**. Thus, the reaction of *N*-[2-(methylthio)-benzoyl]-*N*-alkylhydroxylamines (**6**) with thionyl chloride was examined, expecting the formation of the corresponding *N*-chlorosulfinyloxy-2-(methylthio)benzamide (**7**) as the transient product of the reaction. The transient products (**7**) would undergo a subsequent cyclization reaction, since the chlorosulfinate ion would be a better leaving group than the benzoate ion for the nucleophilic attack of the methylthio-sulfur atom on the nitrogen atom.

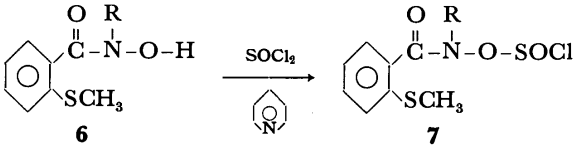

6 **7**

Results and Discussion

Reactions of N-*Alkyl- and* N-*Aryl-(2-methylsulfinyl)-benzamides with Thionyl Chloride.* Several *N*-substituted 2-(methylthio)benzamides (**8a—j**) were prepared from 2-(methylthio)benzoyl chloride (**9**) with appropriate alkyl- and arylamines. The corresponding sulfoxides (**5a—j**) were obtained by periodate oxidation of the sulfides (**8**) in good yields. The reaction of **5**

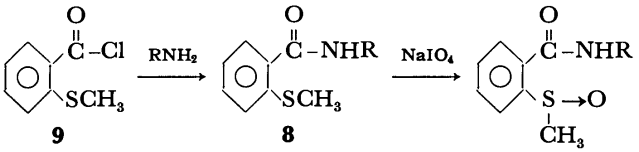

9 **8** **5**

with thionyl chloride was carried out in refluxing dichloromethane or chloroform. Evolution of hydrogen chloride and sulfur dioxide was found during the reaction and the reaction was completed within 30 min. 2-Substituted 1,2-benzisothiazol-3(2*H*)-eones were isolated by chromatographic separation with an alumina column in good yields. The results are given in Table 1. The structures of the products were established by elemental and spectral analyses.

TABLE 1. PREPARATION OF 2-SUBSTITUTED 1,2-BENZISOTHIAZOL-3(2*H*)-ONES (**4**) BY THE REACTIONS OF 2-MeS(O)C_6H_4CONHR (**5**) AND 2-MeSC_6H_4CONROH (**6**) WITH $SOCl_2$

Compd	R	Solvent	Reaction conditions	Product	Yield[a] %
5a	*t*-C_4H_9	CH_2Cl_2	Reflux 10 min	**4a**	92
5b	C_2H_5	CH_2Cl_2	Reflux 10 min	**4b**	96
5c	$(CH_3)_2CH$	CH_2Cl_2	Reflux 10 min	**4c**	97
5d	cyclo-C_6H_{11}	CH_2Cl_2	Reflux 10 min	**4d**	98
5e	$C_6H_5CH_2$	CH_2Cl_2	Reflux 10 min	**4e**	98
5f	C_6H_5	CH_2Cl_2	Reflux 10 min	**4f**	98
5g	*p*-$CH_3C_6H_4$	CH_2Cl_2	Reflux 10 min	**4g**	98
5h	*p*-$CH_3OC_6H_4$	$CHCl_3$	Reflux 30 min	**4h**	84
5i	*p*-$NO_2C_6H_4$	CH_2Cl_2	Reflux 10 min	**4i**	97
5j	1-Naphthyl	CH_2Cl_2	Reflux 30 min	**4j**	98
6a	*t*-C_4H_9	CCl_4	Pyridine, 55 °C, 3 h	**4a**	92
6b	$(CH_3)_2CH$	CCl_4	Pyridine, 55 °C, 3 h	**4c**	81
6c	C_3H_7	CCl_4	Pyridine, 55 °C, 3 h	**4k**	80
6d	C_6H_5	CH_2Cl_2	Pyridine, 30 °C, 3 h	**4f**	Trace[b]
				10a	59[b]
				11	8[b]
				8f	20[b]
6e	*p*-$CH_3C_6H_4$	CH_2Cl_2	Pyridine, 30 °C, 3 h	**5g**	Trace[b]
				10b	66[b]
				8g	8[b]

a) Isolated yields following chromatographic separation. b) The yields were estimated by GLC.

Reactions of N-*Alkyl- or* N-*Aryl*-N-[*2-(methylthio)benzoyl*]*hydroxylamines with Thionyl Chloride.* *N*-[2-(Methylthio)benzoyl]-*N*-*t*-butylhydroxylamine (**6a**) was prepared by alkaline hydrolysis of *N*-[2-(methylthio)-benzoyl]-*O*-benzoyl-*N*-*t*-butylhydroxylamine (**1a**).[7] *N*-Isopropyl (**6b**), *N*-propyl (**6c**), *N*-phenyl (**6d**), and *N*-(4-methylphenyl) derivatives (**6e**) were prepared by the reactions of 2-(methylthio)benzoyl chloride with the corresponding *N*-alkyl- and *N*-arylhydroxylamines.

The reaction of **6a** with thionyl chloride was carried out in carbon tetrachloride at 55 °C in the presence of pyridine. The reaction was monitored by following NMR signals of the *t*-butyl protons. After about 3 h, the spectrum showed the signals of **4a** together with chloromethane (δ, 2.99, s).[7] Although the signal due to **7** was not detected during the reactions, **7** would be the intermediate of the reaction. Similarly, **6b** and **6c** gave **4c** and **4k** by the reactions with thionyl chloride in good yields, respectively. The results are summarized in Table 1. The results show that the reactions of *N*-[2-(methylthio)benzoyl]-*N*-alkylhydroxylamines with thionyl chloride are applicable to syntheses of 2-alkyl-1,2-benzisothiazol-3(2*H*)-ones (**4**). The reaction of **6** with thionyl chloride required somewhat longer heating than that of **5**, but proceeded at much lower temperature than that employed for the thermolysis of **1** (200 °C),[7] as expected from the ability of the leaving groups. Accordingly, the present results also support the mechanism involving the nucleophilic attack of the sulfur atom on the nitrogen which has been suggested as the initial step for the thermolysis of **1**.[7]

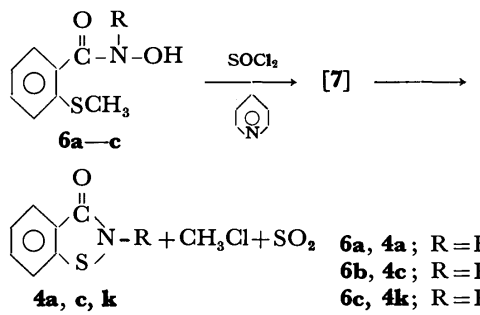

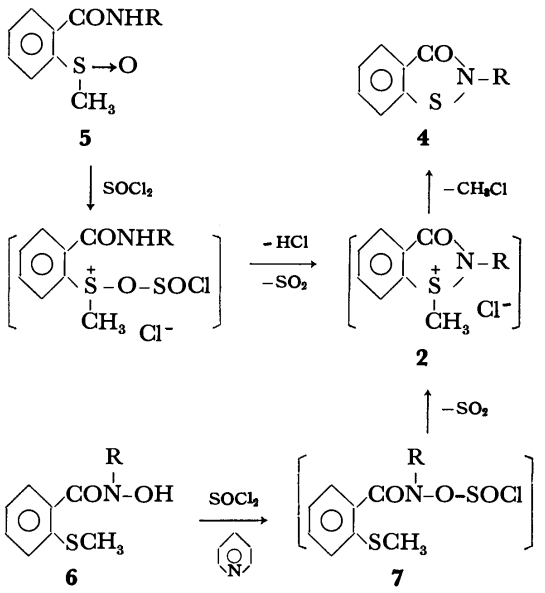

Scheme 1.

Both the reactions examined here appear to be novel and convenient routes to prepare **4**. The probable mechanisms for these reactions are shown in Scheme 1. The acylaminosulfonium salt **2** is involved as the key intermediate of the reactions. The final step of the

reactions would be the nucleophilic attack of the chloride ion on the methyl carbon of the sulfonium ion, since chloromethane was detected as an alternative product.

On the other hand, the reactions of *N*-arylhydroxylamine derivatives (**6d**) and (**6e**) with thionyl chloride gave only trace amounts of **4f** and **4g**, respectively. When the reaction of *N*-[2-(methylthio)benzoyl]-*N*-phenylhydroxylamine (**6d**) with thionyl chloride was carried out in the presence of pyridine, 2'-chloro-2-(methylthio)benzanilide (**10a**), 4'-chloro-2-(methylthio)-benzanilide (**11**), and 2-(methylthio)benzanilide (**8f**) were obtained as the major products. These products were isolated from the reaction products by chromatographic separation and identified by comparison of their physical properties with those of the authentic samples. Similarly, **6e** gave 2'-chloro-4'-methyl-2-(methylthio)-benzanilide (**10b**) and 4'-methyl-2-(methylthio)benzanilide (**8g**). The yields of products were estimated by GLC analysis and the results are summarized in Table 1. A possible mechanism leading to these products involving **7** as the intermediate is shown in Scheme 2.

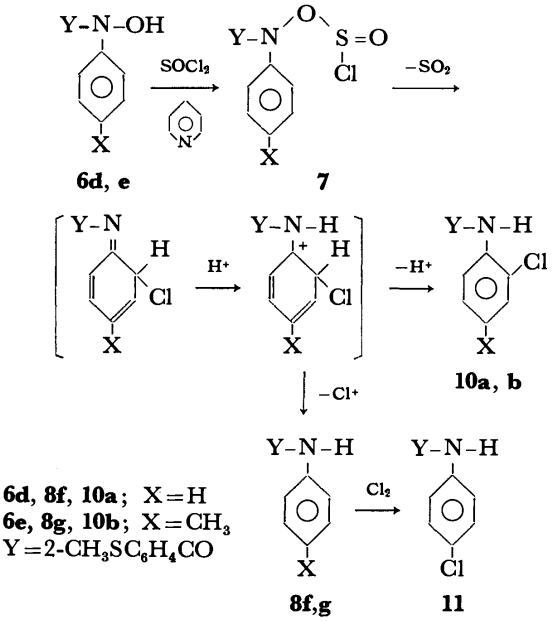

Scheme 2.

Experimental

All the melting points and the boiling points are uncorrected. The IR spectra were recorded on a Shimadzu IR 430 infrared spectrometer. The NMR spectra were recorded on a Varian EM-360 spectrometer using TMS as the internal standard.

Preparation of N-*Alkyl- and* N-*Aryl-2-(methylthio)benzamides (8).* Typical procedures were as follows: (*a*) A solution of 2-(methylthio)benzoyl chloride (9.3 g, 50 mmol) in benzene (50 cm³) was added to a solution of isopropylamine (6.0 g, 102 mmol) in benzene (100 cm³) with stirring. The mixture was heated at 60 °C for 30 min. The reaction mixture was washed with dil HCl, aqueous Na_2CO_3, and water, then the solvent was evaporated. The residue was recrystallized from benzene–ether to give **8c** (7.1 g, 68%); mp 87.5—88.5 °C. IR (KBr): 3400, 3350 (N-H), and 1625 cm^{-1} (C=O). Found: C, 63.10; H, 7.49; N, 6.44%. Calcd for $C_{11}H_{15}NOS$: C, 63.12; H, 7.22; N, 6.69%.

By the same procedure, amides **8a**, **8b**, and **8d—f** were prepared by the reaction of 2-(methylthio)benzoyl chloride with appropriate amines. Amides **8g**, **8h**, and **8j** were prepared by the reaction of 2-(methylthio)benzoyl chloride and an equivalent of amines in the presence of an equivalent of pyridine in benzene. The yields and the physical properties of the amides were as follows: **8a**, 85%; mp 133—134 °C.[7] **8b**, 62%, mp 90.5—91.5 °C. IR (KBr): 3300 (N-H) and 1630 cm^{-1} (C=O). Found: C, 61.73; H, 6.78; N, 7.06%. Calcd for $C_{10}H_{13}NOS$: C, 61.50; H, 6.71; N, 7.17%. **8d**, 79%; mp 138—139 °C. IR (KBr): 3300 (N-H) and 1630 cm^{-1} (C=O). Found: C, 67.30; H, 7.75; N, 5.57%. Calcd for $C_{14}H_{19}NOS$: C, 67.43; H, 7.68; N, 5.62%. **8e**, 98%; mp 131—132 °C. IR (KBr): 3270 (N-H) and 1640 cm^{-1} (C=O). Found: C, 70.10; H, 5.78; N, 5.15%. Calcd for $C_{15}H_{15}NOS$: C, 70.00; H, 5.88; N, 5.44%. **8f**, 98%; mp 148—149 °C. IR (KBr): 3300 (N-H) and 1645 cm^{-1} (C=O). Found: C, 69.04; H, 5.11; N, 5.53%. Calcd for $C_{14}H_{13}NOS$: C, 69.10; H, 5.39; N, 5.76%. **8g**, 93%; mp 145—146 °C. IR (KBr): 3280 (N-H) and 1645 cm^{-1} (C=O). Found: C, 70.15; H, 5.87; N, 5.28%. Calcd for $C_{15}H_{15}NOS$: C, 70.00; H, 5.88; N, 5.44%. **8h**, 91%; mp 137—138 °C. IR (KBr): 3250 (N-H) and 1650 cm^{-1} (C=O). Found: C, 65.99; H, 5.25; N, 5.13%. Calcd for $C_{15}H_{15}NO_2S$: C, 65.91; H, 5.53; N, 5.12%. **8j**, 96%; mp 130.5—131.5 °C. IR (KBr): 3250 (N-H) and 1640 cm^{-1} (C=O). Found: C, 73.62; H, 4.87; N, 4.52%. Calcd for $C_{18}H_{15}NOS$: C, 73.69; H, 5.15; N, 4.77%.

(*b*) A mixture of 2-(methylthio)benzoyl chloride (9.3 g, 50 mmol), *p*-nitroaniline (8.0 g, 58 mmol), and pyridine (20 cm³) was heated under refluxing for 5 h. The reaction mixture was poured into dil HCl (5%, 500 cm³) with stirring. The precipitate was collected by filtration and washed with hot dil HCl, aqueous $NaHCO_3$, and water, then dried. The crude amide (**8i**) was recrystallized from acetone (11.9 g, 83%); mp 165.5—166.5 °C. IR (KBr): 3300 (N-H) and 1655 cm^{-1} (C=O). Found: C, 58.58; H, 3.97; N, 9.86%. Calcd for $C_{14}H_{12}N_2O_3S$: C, 58.32; H, 4.20; N, 9.72%.

Preparation of N-*Alkyl- and* N-*Aryl-2-(methylsulfinyl)benzamides (5).* A typical run was as follows: A solution of sodium periodate (8.6 g, 40 mmol) in water (50 cm³) was added to a solution of **8f** (9.7 g, 37 mmol) in methnoal (300 cm³) with stirring. The mixture was stirred for 2 h at 50 °C. The solvent was evaporated and the residue was washed with water. The residue was crude **5f**, which was recrystallized from methanol-dichloromethane (9.0 g, 94%); mp 194—195 °C. IR (KBr): 3280 (N-H), 1660 (C=O), and 1010 cm^{-1} (S-O). Found: C, 64.86; H, 4.90; N, 5.22%. Calcd for $C_{14}H_{13}NO_2S$: C, 64.84; H, 5.05; N, 5.40%.

Benzamides (**5a—e**) and (**5g—j**) were prepared by the same procedure. The results were as follows: **5a**: 92%; mp 150—151 °C.[7] **5b**, 81%; mp 157—158 °C. IR (KBr): 1640 (C=O) and 1010 cm^{-1} (S-O). Found: C, 56.60; H, 6.08; N, 6.50%. Calcd for $C_{10}H_{13}NO_2S$: C, 56.85; H, 6.20; N, 6.63%. **5c**, 92%; mp 158—159 °C. IR (KBr): 1635 (C=O) and 1010 cm^{-1} (S-O). Found: C, 58.56; H, 6.79; N, 6.12%. Calcd for $C_{11}H_{15}NO_2S$: C, 58.64; H, 6.71; N, 6.22%. **5d**, 83%; mp 138.5—139.5 °C. IR (KBr): 1640 (C=O) and 1010 cm^{-1} (S-O). Found: C, 63.32; H, 7.21; N, 5.07%. Calcd for $C_{14}H_{19}NO_2S$: C, 63.36; H, 7.22; N, 5.28%. **5e**, 82%; mp 142—143 °C. IR (KBr): 1645 (C=O) and 1030 cm^{-1} (S-O). Found: C, 65.85; H, 5.43; N, 5.01%. Calcd for $C_{15}H_{15}NO_2S$: C, 65.91; H, 5.53; N, 5.12%. **5g**, 94%; mp 180.5—181.5 °C. IR (KBr): 1660 (C=O) and 1010 cm^{-1} (S-O). Found: C, 65.79; H, 5.54; N, 5.14%. Calcd

for $C_{15}H_{15}NO_2S$: C, 65.91; H, 5.53; N, 5.12%. **5h**, 99%; mp 176—177 °C. IR (KBr): 1650 (C=O) and 1010 cm^{-1} (S–O). Found: C, 62.34; H, 5.08; N, 4.73%. Calcd for $C_{15}H_{15}NO_3S$: C, 62.26; H, 5.23; N, 4.84%. **5i**, 99%, mp 244—245 °C (dec). IR (KBr); 1670 (C=O) and 1020 cm^{-1} (S–O). Found: C, 55.49; H, 3.99; N, 8.95%. Calcd for $C_{14}H_{12}N_2O_4S$: C, 55.25; H, 3.97; N, 9.21%. **5j**, 96%; mp 213—214 °C (dec). IR (KBr): 1670 (C=O) and 1020 cm^{-1} (S–O). Found: C, 69.83; H, 5.05; N, 4.37%. Calcd for $C_{18}H_{15}NO_2S$: C, 69.88; H, 4.89; N, 4.53%.

Reactions of N-*Alkyl- and* N-*Aryl-2-(methylsulfinyl)benzamides (***5***) with Thionyl Chloride.* A typical run was as follows: Thionyl chloride (1.50 g, 13 mmol) was added to a stirred suspension of **5f** (2.59 g, 10 mmol) in dry dichloromethane (20 cm^3). The reaction mixture was refluxed for 10 min; then the solvent and the excess of thionyl chloride were removed by distillation under reduced pressure. The residue was chromatographed on alumina with dichloromethane as the eluent to give **4f** (2.34 g, 98%), which was recrystallized from carbon tetrachloride–dichloromethane; mp 140.5—141.5 °C (lit,[5a] 140—141 °C). IR (KBr): 1660 cm^{-1} (C=O). By the same procedure, **4a**—**e** and **4g**—**j** were prepared, and the results are given in Table 1. **4a**; mp 57—58 °C. IR (KBr): 1650 cm^{-1} (C=O).[7] **4b**; bp 132 °C/2.5 Torr.†† IR (neat): 1650 cm^{-1} (C=O). NMR (δ, $CDCl_3$): 1.36 (3H, t, J=7 Hz), 3.93 (2H, q, J=7 Hz), and 7.2—8.2 (4H, m). Found: C, 58.64; H, 4.68; N, 7.29%.[8] Calcd for C_9H_9NOS: C, 60.31; H, 5.06; N, 7.82%. **4c**; bp 128 °C/2 Torr. IR (neat): 1650 cm^{-1} (C=O). NMR (δ, $CDCl_3$): 1.33 (6H, d, J=7 Hz), 4.93 (1H, m), and 7.1—8.1 (4H, m). Found: C, 61.12; H, 5.37; N, 6.75%.[8] Calcd for $C_{10}H_{11}NOS$: C, 62.14; H, 5.74; N, 7.25%. **4d**; mp 87—88 °C (lit,[5a] mp 87—88 °C). IR (KBr): 1635 cm^{-1} (C=O). NMR (δ, $CDCl_3$): 1.0—2.3 (10H, broad), 4.6 (1H, broad), and 7.2—8.2 (4H, m). **4e**; mp 87.5—88.5 °C (lit,[5a] mp 88 °C). IR (KBr): 1665 cm^{-1} (C=O). NMR (δ, $CDCl_3$): 5.03 (2H, s) and 7.0—8.2 (9H, m). **4g**; mp 135.5—136.5 °C (lit,[5a] mp 136—137 °C). IR (KBr); 1640 cm^{-1} (C=O). NMR (δ, $CDCl_3$): 2.37 (3H, s) and 7.1—8.2 (8H, m). **4h**; mp 147—148 °C (lit,[6] 147—149 °C). IR (KBr): 1660 cm^{-1} (C=O). NMR (δ, $CDCl_3$): 3.83 (3H, s) and 6.8—8.2 (8H, m). **4i**; mp 238—239 °C. IR (KBr): 1680 cm^{-1} (C=O). Found: C, 57.39; H, 2.68; N, 10.39%. Calcd for $C_{13}H_8N_2O_3S$: C, 57,34; H, 2.96; N, 10.29%. **4j**; mp 154—155 °C. IR (KBr): 1645 cm^{-1} (C=O). Found: C, 73.77; H, 3.75; N, 4.89%. Calcd for $C_{17}H_{11}NOS$: C, 73.62; H, 4.00; N, 5.05%.

Preparation of N-[*2-(Methylthio)benzoyl*]-N-t-*butylhydroxylamine (**6a**).* This compound was prepared by alkaline hydrolysis of *N*-[2-(methylthio)benzoyl]-*O*-benzoyl-*N*-*t*-butylhydroxylamine as described in the previous paper;[7] mp 145—146 °C.

Preparation of N-[*2-(methylthio)benzoyl*]-N-*isopropylhydroxylamine (**6b**).* Aluminium foil (10.5 g) was amalgamated by immersing it in a solution of mercury(II) chloride (3.0 g) in water (200 cm^3). The amalgamated aluminium was washed with water and added to a mixture of ether (500 cm^3) and water (5 cm^3). A solution of 2-nitropropane (18.0 g, 202 mmol) in ether (50 cm^3) was added dropwise into the mixture with stirring under refluxing. After addition of the 2-nitropropane was completed, the reaction mixture was refluxed for 30 min, and then cooled with ice-water. A solution of NaOH (10.0 g) in water (30 cm^3) was added to the mixture with stirring. The ether layer was separated and dried over Na_2SO_4. Into the solution which contained *N*-isopropylhydroxylamine, a solution of 2-(methylthio)benzoyl chloride (9.3 g, 50 mmol) in ether (100 cm^3) was added with stirring. After stirring for 1 h, the reaction mixture was washed with dil HCl and water, and then extracted with aqueous NaOH (5%, 200 cm^3). The extract was acidified with HCl. The crude *N*-[2-(methylthio)benzoyl]-*N*-isopropylhydroxylamine (**6b**) was collected by filtration (6.3 g, 56%), and then recrystallized from dichloromethane–petroleum ether; mp 100.5—101.5 °C. IR (KBr): 3200 (O–H) and 1610 cm^{-1} (C=O). NMR (δ, $CDCl_3$): 1.28 (6H, d, J=7 Hz), 2.47 (3H, s), 3.9 (1H, m), 7.0—7.6 (4H, m), and 8.8 (1H, broad). Found: C, 58.56; H, 6.92; N, 5.69%. Calcd for $C_{11}H_{15}NO_2S$: C, 58.64; H, 6.71; N, 6.22%.

Preparation of N-[*2-(Methylthio)benzoyl*]-N-*propylhydroxylamine (**6c**).* Into an ethereal solution of *N*-propylhydroxylamine which was prepared from 1-nitropropane (18.0 g, 202 mmol) by the procedure described above, pyridine (15.0 g) and a solution of 2-(methylthio)benzoyl chloride (15.0 g, 81 mmol) in ether (100 cm^3) were added with stirring. After the reaction, the mixture was washed with dil HCl and water, and then extracted with aqueous NaOH (5%, 200 cm^3). The extract was acidified with HCl, and the crude *N*-[2-(methylthio)benzoyl]-*N*-propylhydroxylamine (**6c**) was collected by filtration (12.5 g, 69%), and then recrystallized from benzene–petroleum ether; mp 89.5—90.5 °C. IR (KBr): 3100 (O–H) and 1605 cm^{-1} (C=O). NMR (δ, $CDCl_3$) 0.85 (3H, t, J=7 Hz), 1.73 (2H, m, J=7 Hz), 2.50 (3H, s), 3.47 (2H, t, J=7 Hz), 7.0—7.7 (4H, m) and 8.5 (1H, broad s). Found: C, 58.70; H, 6.86; N, 6.04%. Calcd for $C_{11}H_{15}NO_2S$: C, 58.64; H, 6.71; N, 6.22%.

Preparation of N-[*2-(Methylthio)benzoyl*]-N-*arylhydroxylamines (**6d**—**e**).* A solution of 2-(methylthio)benzoyl chloride (5.6 g, 30 mmol) in ether (50 cm^3) was added to a mixture of *N*-phenylhydroxylamine (3.3 g, 30 mmol), pyridine (3.0 g, 38 mmol), and ether (150 cm^3) with stirring. The reaction mixture was refluxed for 30 min, washed with dil HCl, and water, and then extracted with aqueous NaOH (5%, 100 cm^3). The extract was acidified with HCl, and the crude *N*-[2-(methylthio)benzoyl]-*N*-phenylhydroxylamine (**6d**) was collected by filtration (5.6 g, 71%), and then recrystallized from methanol; mp 141.5—142.5 °C. IR (KBr): 3120 (O–H) and 1630 cm^{-1} (C=O). NMR (δ, $CDCl_3$): 2.40 (3H, s), 6.8—7.5 (9H, m), and 9.3 (1H, broad s). Found: C, 64.80; H, 4.83; N, 5.39%. Calcd for $C_{14}H_{13}NO_2S$: C, 64.84; H, 5.05; N, 5.40%.

N-[2-(Methylthio)benzoyl]-*N*-(4-methylphenyl)hydroxylamine (**6e**) was prepared similarly by the reaction of *N*-(4-methylphenyl)hydroxylamine and 2-(methylthio)benzoyl chloride in 80% yield; mp 169—170 °C (decomp). IR (KBr): 3230 (O–H) and 1615 cm^{-1} (C–O). NMR (δ, $CDCl_3$): 2.30 (3H, s), 2.43 (3H, s), 6.8—7.6 (8H, m), and 9.1 (1H, broad). Found: C, 65.86; H, 5.44; N, 4.91%. Calcd for $C_{15}H_{15}NO_2S$: C, 65.91; H, 5.53; N, 5.12%.

Reaction of N-[*2-(Methylthio) benzoyl*]-N-*alkylhydroxylamines (**6a**—**c**) with Thionyl Chloride.* Typical procedure was as follows: Thionyl chloride (1.50 g, 13 mmol) was added to a mixture of **6c** (2.25 g, 10 mmol) and pyridine (1.00 g, 13 mmol) in carbon tetrachloride (100 cm^3). The mixture was stirred for 3 h at 55 °C. The reaction mixture was washed with dil HCl and water, and dried over $CaCl_2$. After evaporation of the solvent, the residue was chromatographed on alumina with dichloromethane as the eluent to give **4k** (1.56 g, 80%), which was distilled under reduced pressure; bp 140 °C/2 Torr (lit,[6] 126—128 °C/0.2 Torr). IR (neat): 1650 cm^{-1} (C=O), NMR (δ, $CDCl_3$): 0.97 (3H, t, J=7 Hz), 1.80 (2H, m), 3.87 (2H, t, J=7 Hz), and 7.2—8.2 (4H, m). By the same procedure, **4a** and **4c** were prepared by the reactions of **6a** and **6b** with thionyl chloride, respectively. The results

†† 1 Torr≈133.322 Pa.

are given in Table 1.

Reactions of N-[*2-(Methylthio)benzoyl*]-N-*arylhydroxylamines (6d and 6e) with Thionyl Chloride.* A solution of thionyl chloride (0.70 g, 6 mmol) in dichloromethane (10 cm^3) was added to a mixture of *N*-[2-(methylthio)benzoyl]-*N*-phenylhydroxylamine (**6d**) (1.176 g, 5 mmol), pyridine (0.80 g, 10 mmol), and dichloromethane (40 cm^3) with stirring. After the reaction for 3 h at room temperature, the reaction mixture was washed with dil HCl, aqueous $NaHCO_3$, and water, then the solvent was removed by distillation under reduced pressure. The residue was subjected to GLC analysis, and the remainder was chromatographed on silica gel to isolate the products. The results are given in Table 1. The reaction of **6e** (1.372 g, 5 mmol) with thionyl chloride (0.70 g) in the presence of pyridine (0.80 g) was carried out in dichloromethane (50 cm^3) by the same procedure. **10a**; mp 93—94 °C. IR (KBr): 3200 (N–H) and 1640 cm^{-1} (C=O). NMR (δ, $CHCl_3$): 2.50 (3H, s), 6.9—8.7 (8H, m), and 8.7 (1H, broad). Found: C, 60.59; H, 4.27; N, 5.00%. Calcd for $C_{14}H_{12}ClNOS$: C, 60.53; H, 4.35; N, 5.04%. **10b**; mp 92.5—93.5 °C. IR (KBr): 3400 (N–H) and 1670 cm^{-1} (C=O). NMR (δ, $CDCl_3$): 2.38 (3H, s), 2.53 (3H, s), 7.0—8.6 (7H, m), and 8.6 (1H, broad). Found: C, 61.54; H, 4.73; N, 4.61%. Calcd for $C_{15}H_{14}ClNOS$: C, 61.74, H, 4.84; N, 4.80%. **11**; mp 137—138 °C. IR (KBr): 3300 (N–H) and 1660 cm^{-1} (C=O). NMR (δ, $CDCl_3$): 2.47 (3H, s), 7.0—7.8 (8H, m), and 8.5 (1H, broad). Found: C, 60.25, H, 4.14; N, 4.97%. Calcd for $C_{14}H_{12}ClNOS$: C, 60.53; H, 4.35; N, 5.04%.

References

1) Preliminary results have been reported. Y. Uchida and S. Kozuka, *J. Chem. Soc., Chem. Commun.*, **1981**, 510.

2) F. Gialdi, R. Ponci, and P. Caccialanza, *Mycopathol. Mycol. Appl.*, **24**, 163 (1964); *Chem. Abstr.*, **63**, 429e (1965).

3) F. Gialdi, R. Ponci, and A. Baruffini, *Farmaco, Ed. Sci.*, **16**, 509 (1961); *Chem. Abstr.*, **60**, 512 (1964); R. Ponci, F. Gialdi, and A. Baruffini, *Farmaco, Ed. Sci.*, **19**, 254 (1964); *Chem. Abstr.*, **61**, 3088e (1964); R. Ponci, T. Vitali, L. Amoretti, and F. Mossini, *Farmaco, Ed. Sci.*, **22**, 935, 999 (1968); *Chem. Abstr.*, **68**, 105078p, 114493x (1968); J. C. Grivas, U. S. Patent, 3761489 (1973); *Chem. Abstr.*, **79**, 137126 (1973).

4) J. S. Morley, Brit. Patent 848130 (1960); *Chem. Abstr.*, **55**, 9430c (1961); R. Ponci, A. Baruffini, M. Croci, and F. Gialdi, *Farmaco, Ed. Sci.*, **18**, 732 (1963); *Chem. Abstr.*, **60**, 2919h (1964); R. Ponci, T. Vitali, F. Mossini, and L. Amoretti, *Farmaco, Ed. Sci.*, **22**, 989 (1967); *Chem. Abstr.*, **69**, 27322t (1968); T. Vitali, L. Amoretti, and F. Mossini, *Farmaco, Ed. Sci.*, **23**, 468 (1968); *Chem. Abstr.*, **69**, 59147f (1968).

5) T. Vitali. L. Amoretti, and V. Plazzi, *Farmaco, Ed. Sci.*, **23**, 1075 (1967); *Chem. Abstr.*, **70**, 37701a (1969); A. Bellotti, E. Coghi, and O. Sgorbati, *Ateneo Parmense, Sez.*, *2*, **7**, 127 (1972); *Chem. Abstr.*, **77**, 48319c (1972).

6) J. C. Grivas, *J. Org. Chem.*, **40**, 2029 (1975).

7) Y. Uchida, Y. Kobayashi, and S. Kozuka, *Bull. Chem. Soc. Jpn.*, **54**, 1781 (1981).

8) The analytical values were lower than the calculated ones, which might be due to evaporation of the liquid samples.

Preferential Crystallization of 2-Amino-2-phenylethanol and Its Application as a Resolving Agent

Kazuhiko SAIGO,* Hisao MIURA, Kozi ISHIZAKI, and Hiroyuki NOHIRA

Department of Applied Chemistry, Faculty of Engineering, Saitama University, Shimo-ohkubo, Urawa 338

(Received September 2, 1981)

(±)-2-Amino-2-phenylethanol (phenylglycinol) prepared from (±)-2-amino-2-phenylacetic acid (DL-phenylglycine) by lithium aluminium hydride reduction was efficiently resolved into a pair of optically active forms by preferential crystallization. The optically active amino alcohol was successfully applied as a basic resolving agent to the resolution of tartaric acid, 2-hydroxy-2-phenylpropionic acid, 2-hydroxy-3-phenylpropionic acid, 2-phenylpropionic acid, and 2-phenyl-2-ureidoacetic acid.

In the fractional crystallization of diastereomers, which is as useful for getting chiral compounds as biological method and asymmetric induction, a natural product or its derivative is widely used as a resolving agent.[1] But, only one of a pair of the enantiomers can be employed as a resolving agent since the other is frequently commercially unavailable. The restriction in utilization of a natural product or its derivative as a resolving agent often becomes to be disadvantageous for fractional crystallization because the desired enantiomer of a chiral compound does not always form the less soluble diastereomer, which is able to be purified by recrystallization, with the resolving agent.[2]

The synthesis of new resolving agents and their optical resolutions by preferential crystallization are tried in our laboratory based on the considerations that preferential crystallization would improve the problem, giving both enantiomers of a resolving agent in preparative quantities and that the desired enantiomer of a chiral compound whould be resolvable as the less soluble diastereomer with either of the enantiomers. The preceding papers presented that 3-*endo*-benzamido-5-norbornene-2-*endo*-carboxylic acid,[3] α-methylbenzylamine,[4] and 1-phenyl-2-(*p*-tolyl)ethylamine[4] were satisfactorily resolved into pairs of enantiomers by preferential crystallization of their achiral amine or carboxylic acid salts. As a part of our further studies along the line concerning the preferential crystallization, the resolution of 2-amino-2-phenylethanol (phenylglycinol) was examined with expectation that it would be useful as a basic resolving agent in the optical resolution of carboxylic acids.

(±)- And (−)-2-amino-2-phenylethanol ((±)-**1** and (−)-**1**) were easily prepared by the lithium aluminium hydride reduction of (±)- and (*R*)-(−)-2-amino-2-phenylacetic acid (DL- and D-phenylglycine), respectively.[5] The optically active **1** has higher melting point and is less soluble in benzene. The physical properties

$C_6H_5CHCH_2OH$
$\quad\quad|$
$\quad\quad NH_2$ **1**

	Mp θ_m/°C	Solubility (g/100 ml C_6H_6 at 20 °C)
(±)-**1**	47—49.5	10.5
(−)-**1**	75—76	1.3

indicate the posibility that crystals of **1** itself are deposited from a supersaturated benzene solution as a conglomerate, which is resolvable by preferential crystallization. Actually, (−)-**1** was obtained from a supersaturated solution of (±)-**1** when (−)-**1** was seeded to the solution and the solution was stood overnight at around 6 °C. Alternate seeding of (+)- and (−)-**1** to the solution supersaturated in a similar magnitude gave (+)- and (−)-**1**, respectively, as shown in Table 1.

TABLE 1. PREFERENTIAL CRYSTALLIZATION OF **1** FROM BENZENE SOLUTION

Run	(±)-**1** (mg)[a]	Seed	Yield mg	$[\alpha]_{435}$/° (*c* 1.00, MeOH)	Optical purity/%[b]
1	—	(−)-**1**	199	−46.8	90
2	375	(+)-**1**	209	+47.3	91
3	254	(−)-**1**	292	−47.7	92
4	232	(+)-**1**	169	+48.2	93

The initial composition of the mother liquor: (±)-**1** (4.00 g) in benzene (100 ml). In all runs, 20—25 mg of seed were added. a) Ammount of (±)-**1** supplied for each run. b) Based on $[\alpha]_{435}^{29.5}$ + and −52.0°(*c* 1.00, MeOH).

The procedure is inapplicable to the optical resolution of (±)-**1** in a preparative scale because only 170—290 mg of optically active **1** is obtainable from 100 ml of benzene solution containing 4.0 g of (±)-**1**. After several examinations on the crystallization conditions such as concentration, cooling temperature, cooling time, and solvent system, it was found that the mixed solvent of benzene and ethanol was more suitable for the preferential crystallization in a preparative scale (see Table 2). Moreover, gentle stirring of the supersaturated solution during crystallization was found to be effective to shorten the cooling time as shown in Table 3. Stirring made the solution uniform and accelerated the crystal growth from seed surface. But, the nucleation of the unseeded antipode crystals of **1** occured when the solution was stirred too vigorously.

Crystals obtained by the preferential crystallization were recrystallized from benzene to yield almost optically pure (+)- and (−)-**1**.

The result that both enantiomers of **1** became obtainable preparatively in high optical purities prompted us to examine the ability of optically active **1** as a basic resolving agent. The resolution of mandelic acid is a unique example, which appears in a patent, for the application of **1** as a resolving agent.[6]

Tartaric acid (**2**), 2-hydroxy-2-phenylpropionic acid (**3**), 2-hydroxy-3-phenylpropionic acid (**4**), 2-phenylpropionic acid (**5**), and 2-phenyl-2-ureidoacetic acid (**6**)

Table 2. Preferential crystallization of **1** from benzene–ethanol mixture on standing

Run	(±)-**1**(mg)[a]	Seed	Cooling time / h	Yield / g	$[\alpha]_{435}$/° (*c* 1.00, MeOH)	Optical purity/%[b]
1	—	(+)-**1**	12	1.71	+47.1	91
2	2.01	(−)-**1**	21	2.47	−45.6	88
3	2.25	(+)-**1**	23	3.32	+47.1	91
4	3.85	(−)-**1**	21	3.24	−47.6	92
5	3.27	(+)-**1**	18	2.61	+48.7	94
6	3.61	(−)-**1**	19	2.94	−43.9	84

The initial composition of the mother liquor: (±)-**1** (38.80 g) and (+)-**1** (0.50 g), which was added to facilitate the preferential crystallization from the first stage, in a mixture of benzene (95 ml) and 99% ethanol (10 ml). In all runs, 0.10 g of seed was added. a) Amount of (±)-**1** supplied for each run. b) Based on $[\alpha]_{435}^{29.5}$ + and −52.0° (*c* 1.00, MeOH).

Table 3. Preferential crystallization of **1** under stirring

Run	(±)-**1**(mg)[a]	Seed	Cooling time / min	Yield / g	$[\alpha]_{435}$/° (*c* 1.00, MeOH)	Optical purity/%[b]
1	—	(+)-**1**	65	2.79	+47.6	92
2	3.00	(−)-**1**	65	3.53	−44.4	85
3	3.50	(+)-**1**	65	3.79	+40.0	77
4	3.60	(−)-**1**	70	2.80	−46.1	89
5	3.30	(+)-**1**	65	2.73	+51.3	99

The initial composition of the mother liquor: (±)-**1** (34.30 g) and (+)-**1** (1.30 g), which was added to facilitate the preferential crystallization from the first stage, in a 9: 1 mixture of benzene and 99% ethanol (84 ml). In all runs, 0.20 g of seed was added. a) Amount of (±)-**1** supplied for each run. b) Based on $[\alpha]_{435}^{29.5}$+ and −52.0° (*c* 1.00, MeOH).

Table 4. Resolution of chiral carboxylic acid by fractional crystallization

Salt (Molar ratio)	Recrystallization: Solvent	Recrystallization: Time	Yield[b] / %	Mp θ_m/°C	$[\alpha]_{435}$/°	N(%) Found (Calcd)
A : (+)-**2**(−)-**1** (1: 2)	MeOH[a]	1	86	193—194	−15.0°[c]	6.54 (6.60)
B : (−)-**2**(+)-**1** (1: 2)	MeOH[a]	2	74	192—193	+16.9°[c]	—
C : (+)-**3**(−)-**1** (1: 1)	EtOAc–C_6H_6 (1: 1)	3	44	117—119	+22.4[d]	4.69 (4.62)
D : (−)-**4**(−)-**1** (1: 1)	EtOAc–2-Propanol (2: 1)	1	71	145—146	−113[d]	4.66 (4.62)
E : (−)-**5**(−)-**1** (1: 1)	EtOAc–EtOH (4: 1)	4	58	149—150	−52.7[d]	4.96 (4.88)
F : (−)-**6**(−)-**1** (1: 1)	75%EtOH	1	76	200—201	−201°[c]	12.8 (12.7)

a) Washing. b) Based on half the amount of (±)-carboxylic acid used. c) (*c* 1.00, H_2O). d) (*c* 1.00, MeOH).

Table 5. Liberation of carboxylic acids from salts (**A**—**F**)

Salt	Product	Method[a]	Total yield[b] / %	M_p θ_m(B_p θ_b) / °C	$[\alpha]_{589}$/°	Optical purity/%
A	(+)-**2**	1	77	163—169	+16.1(*c* 1.02,H_2O)	96
B	(−)-**2**	1	63	165—165.5	−15.9(*c* 1.00,H_2O)	95
C	(+)-**3**	2	41	113—114	+34.7(*c* 1.00,EtOH)	92
D	(−)-**4**	2	67	122—123	−17.5(*c* 1.00,EtOH)	94
E	(−)-**5**	2	55	(108—109/267 Pa)	−88.3(*c* 1.30,C_6H_6)	95
F	(−)-**6**	2	72	188—189	−156(*c* 0.50,EtOH)	94

a) Method 1: The salt was decomposed with ion exchange resin, and the product was eluted with water. Method 2: The salt was decomposed with aqueous HCl, and the product was extracted with ether. b) Based on half the amount of (±)-carboxylic acid used.

were chosen as target compounds for optical resolution. The chiral carboxylic acids successfully resolved in high optical purities by fractional crystallization of the diastereomeric salts with the optically active amine **1**. The results are summarized in Tables 4 and 5.

It is especially noteworthy that tartaric acid, which is valuable and widely used as a resolving agent, can be resolved in a high yield and in a high optical purity.

Experimental

The melting points were determined on a Laboratory Devices Mel-Temp apparatus and are uncorrected. The values of specific roration were obtained on JASCO DIP-181 digital polarimeter.

(±)-2-Amino-2-phenylethanol((±)-**1**) was obtained by the reduction of commercially available (±)-2-amino-2-phenylacetic acid (DL-phenylglycine) with lithium aluminium hydride: mp 47—49.5 °C; bp 106—109 °C/133 Pa (lit,[5] mp 47—49 °C; bp 144—147 °C/1866 Pa). Optically active **1**, (−)- and (+)-**1**, used as seeds were prepared in a similar manner from commercially available (*R*)-(−)-2-amino-2-phenylacetic acid (D-phenylglycine), and (*S*)-(+)-2-amino-2-phenylacetic acid obtained by the reciprocal preferential resolution of the salt of (±)-2-amino-2-phenylacetic acid with (±)-10-camphorsulfonic acid,[7] respectively: mp 75—76 °C; $[\alpha]_{589}^{29.5}$ − and +26.7°, $[\alpha]_{435}^{29.5}$ − and +52.0° (*c* 1.00, MeOH) (lit,[8] mp 78—79 °C, 77—78 °C; $[\alpha]_{589}^{17}$ −25.4°, +23.5° in MeOH).

Preferential Crystallization of (±)-2-Amino-2-phenylethanol ((±)-1). A refluxed solution of (±)-**1** (34.30 g) and (+)-**1** (1.30 g), which was added to facilitate the preferential crystallization from the first stage, in a mixture of benzene and 99% ethanol (9 : 1) (84 ml) was cooled at around 13 °C to give a supersaturated solution. The solution was seeded with (+)-**1** (0.20 g) and stirred gently (about 30 min^{-1}) for 65 min at 4—5 °C. The precipitates appeared were collected by filtration, washed with 1 ml of a mixture of benzene and ethanol (9 : 1), and dried over P_2O_5 and solidified paraffin, giving 2.79 g of (+)-**1** ($[\alpha]_{435}^{38}$ +47.6° (*c* 1.00, MeOH)). The optical purity of the product was 92% based on the specific rotation of (−)-**1** prepared from (−)-2-amino-2-phenylacetic acid by the reduction with lithium aluminium hydride ($[\alpha]_{435}^{29.5}$ −52.0° (*c* 1.00, MeOH)). Successively, (±)-**1** (3.00 g) was added to the filtrate and dissolved at an elevated temperature. The solution was similarly cooled, seeded with (−)-**1** (0.20 g), and stirred gently for 65 min at 4—5 °C. Similar treatment of precipitates appeared gave 3.53 g of (−)-**1** ($[\alpha]_{435}^{35.5}$ −44.4° (*c* 1.00, MeOH); 85% optical purity).

After several stages of the preferential crystallization, the crystals having the same sign of optical rotation were combined and recrystallized. Recrystallization of (+)-**1** (7.24 g; 91% optical purity on the average) from benzene (40 ml) gave 6.32 g (87%) of highly pure (+)-**1** ($[\alpha]_{435}^{29.5}$ +51.6°, $[\alpha]_{589}^{29.5}$ +26.3° (*c* 1.00, MeOH); 99% optical purity). In a similar manner, (−)-**1** (8.22 g; 87% optical purity on the average) was recrystallized from benzene (55 ml), giving 7.15 g (87%) of (−)-**1** ($[\alpha]_{435}^{29.5}$ −50.5°, $[\alpha]_{589}^{29.5}$ −25.9° (*c* 1.00, MeOH); 97% optical purity).

Resolution of (±)-Tartaric Acid (2) with (−)-1. To a solution of (±)-**2** (8.00 g, 53 mmol) in methanol (80 ml) was added a solution of (−)-**1** (14.60 g, 107 mmol) in methanol (20 ml), and the mixture was stood overnight at room temperature. White precipitates appeared were filtered off and dried over P_2O_5 to give crude (+)-**2**·(−)-**1** (1 : 2) salt (10.49 g, 93%): $[\alpha]_{435}^{31.5}$ −19.3° (*c* 1.00, H_2O). The suspension of the salt (10.49 g) in methanol (50 ml) was refluxed for 20 min, and insolubilized crystals and precipitates deposited on cooling at room temperature were collected together by filtration, powdered finely, and dried over P_2O_5 to give 9.70 g (86%) of (+)-**2**·(−)-**1** (1 : 2) salt.

The purified (+)-**2**·(−)-**1** (1 : 2) salt (9.70 g) was dissolved in water (65 ml), and the solution was charged on an ion exchange resin column (Amberlite IR 120B, 77 ml) to decompose the salt. Elution with water (450 ml) gave an aqueous solution of (+)-**2**. After evaporation of the water, white precipitates remained were dried over P_2O_5 to yield (+)-**2** (3.08 g, 77% total yield): mp 163—169 °C; $[\alpha]_{589}^{32}$ +16.1° (*c* 1.02, H_2O); 96% optical purity.

Similarly, (−)-**2** was obtained in 63% total yield by the fractional crystallization of the salt of (±)-**2** with (+)-**1**: mp 165—165.5 °C; $[\alpha]_{589}^{22}$ −15.9° (*c* 1.00, H_2O); 95% optical purity.

The ion exchange resin used for the decomposition of the salt was treated with a large excess of 5 M (1 M=1 mol dm^{-3}) aqueous ammonia solution to recover (−)- or (+)-**1**. The eluate was concentrated under reduced pressure, and slightly yellow oil was treated with 10M NaOH solution and extracted with ether. The ethereal solution was dried with Na_2SO_4 and concentrated under reduced pressure to give (−)- or (+)-**1**. Recovery was over 90% and racemization did not take place.

Resolution of (±)-2-Hydroxy-3-phenylpropionic Acid (4) with (−)-1. A clear solution of (±)-**4** (4.98 g, 30 mmol) and (−)-**1** (4.05 g, 30 mmol) in a mixture of ethyl acetate and 2-propanol (7 : 2) (270 ml) at reflux temperature was cooled with ice bath for 4.5 h to give white precipitates. The precipitates were collected by filtration and dried over P_2O_5, giving crude (−)-**4**·(−)-**1** salt (3.91 g, 87%): $[\alpha]_{435}^{28}$ −74.8° (*c* 1.00, MeOH).

Recrystallization of the salt (3.86 g) from a mixture of ethyl acetate and 2-propanol (2 : 1) (95 ml) gave 3.16 g (71%) of (−)-**4**·(−)-**1** salt: mp 145—146 °C; $[\alpha]_{435}^{25}$ −113° (*c* 1.00, MeOH).

To a solution of purified salt (3.12 g) in water (50 ml) was added 1 M HCl solution (20 ml) to decompose the salt. The liberated acid was extracted with ether (3×40 ml), and the ethereal extracts were combined, dried with Na_2SO_4, and concentrated under reduced pressure to yield (−)-**4** (1.62 g, 67% total yield): mp 122—123 °C; $[\alpha]_{589}^{28}$ −17.5° (*c* 1.00, EtOH); 94% optical purity.

The resolving agent was recovered in 93% yield without racemization by treating the aqueous solution with 1M NaOH solution, followed by extraction with ether.

In a similar fashion, 2-hydroxy-2-phenylpropionic acid (**3**), 2-phenylpropionic acid (**5**), and 2-phenyl-2-ureidoacetic acid (**6**) were resolved in high optical purities (see Tables 4 and 5).

References

1) J. D. Morrison and H. S. Mosher, "Asymmetric Organic Reactions," Prentice-Hall, Inc., New Jersey (1971), Chap. 1-4.

2) S. H. Wilen, A. Collet, and J. Jacques, *Tetrahedron*, **38**, 2725 (1977).

3) K. Saigo, Y. Okuda, S. Wakabayashi, T. Hoshiko, and H. Nohira, *Chem. Lett.*, **1981**, 857.

4) H. Nohira, M. Kai, M. Nohira, J. Nishikawa, T. Hoshiko, and K. Saigo, *Chem. Lett.*, **1981**, 951.

5) M. B. Watson and G. W. Youngson, *J. Chem. Soc.*, **1954**, 2145.

6) R. Nishizawa, A. Mashiba, and Y. Ogawa, Japan Kokai, 53-18529 (1978).

7) H. Nohira, H. Fujii, M. Yajima, and R. Fujimura, unpublished result.

8) L. Apresella and A. Lamanna, *Il Farmaco (Pavia), Ed, Sci.*, **8**, 212 (1953); *Chem. Abstr.*, **48**, 3921 (1954).

 © 1982 The Chemical Society of Japan Bull. Chem. Soc. Jpn., 55, 1191—1194 (1982)

Synthesis of Aubergenone, a Sesquiterpenoid Phytoalexin from Diseased Eggplants[1]

Akio Murai, Atsushi Abiko, Mitsunori Ono, and Tadashi Masamune*

Department of Chemistry, Faculty of Science, Hokkaido University, Sapporo 060

(Received September 11, 1981)

The synthesis of aubergenone, a stress metabolite isolated from diseased eggplants, from α-cyperone, which implies revision of the assigned structure to the metabolite, is described.

In 1975 Stoessl and coworkers[2] reported isolation of the title compound (**1**), aubergenone ("enone sesquiterpene"), as a stress metabolite from diseased eggplants (*Solanum melongena*, Solanaceae) and assigned 11-hydroxy-4β,5α-eudesm-1-en-3-one structure (**2**) on the basis of the extensive spectroscopic studies. However, in 1978 Canadian workers[3] and we[4] independently arrived at the same revised structure, 11-hydroxy-4α,5α-eudesm-1-en-3-one (**1**), by synthesis of 4-epiaubergenone (**2**) and anbergenone (**1**) itself, respectively. The sesquiterpene (**1**) is a sole stress compound with a 5α-eudesmane skeleton among the metabolites of the Family and hence stands unique on biogenetic grounds.[4-6] In the present paper we describe details of the synthesis of aubergenone (**1**) and its 4-epimer (**2**), which is divided into three sections as described in the following.

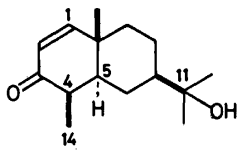

1

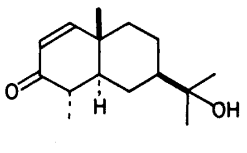

2

Results and Discussion

An Alternative Short-step Transformation of (−)-α-Santonin into (+)-α-Cyperone. A number of synthetic routes of (+)-α-cyperone (**3**) have been reported. Of these routes, most practical ones are those elaborated by Piers,[7] Caine,[8] and coworkers, which start with commercially available (−)-α-santonin (**4**) and (−)-carvone, respectively (overall yields, 20 and 25%). We also started with **4**, which was easily epimerized into epi-α-santonin[7,9] (**5**) in 73% yield. Treatment of **5** with lithium diisopropylamide (LDA, 1.5 equiv.) in tetrahydrofuran (THF) and hexamethylphosphoric triamide (HMPA) at −78 °C followed by addition of methyl iodide afforded 11-methyl-epi-α-santonin (**6**) as a single product, which on hydrogenation in the presence of tris(triphenylphosphine)chlororhodium in degassed dry benzene, formed the 1,2-dihydro derivative (**7**) in 71% yield from **5**. Irradiation of **7** with sunlight by the Ourisson method[10] effected photo-decarboxylation to give 10-epimaalienone,[10] an unstable cyclopropane derivative (**8**), in 68% yield. In accord with the assigned structure, compound **8** exhibited the following spectral data: MS, *m/e* 218 (M^+), 203, 190, and 175; IR, 1665, 1598, 1385, and 1360 cm^{-1}; NMR, δ 0.96, 1.09, 1.23, and 1.77 (each 3H, s). Further treatment of **8** with hydrogen chloride in ethanol gave rise to a known chloride[8] (**9**), mp 86—88 °C, $[\alpha]_D$ +159°, in 82% yield, which was completely identical with the reported data (mp, $[\alpha]_D$, MS, IR, and NMR). The compound (**9**) was converted readily into **3** by a known procedure.[11] This transformation of (−)-α-santonin (**4**) into (+)-α-cyperone (**3**) involved 6 steps and the overall yield amounted to 23.3%.

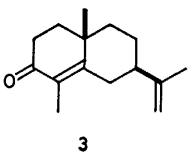

3

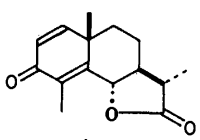

4

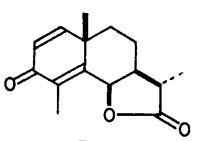

5

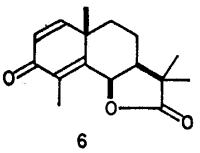

6

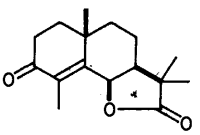

7

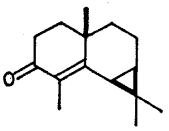

8

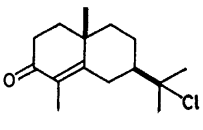

9

Transformation of (+)-α-Cyperone (3) into 4-Epiaubergenone (2). *trans*-Dihydrocarissone[12] (**10**) with the established configuration was first prepared from **3** in two steps (the Birch reduction[13] and oxymercuration-demercuration[14]) in 76% yield. Treatment of **10** with LDA (2.5 equiv.) in THF and then with benzeneselenenyl bromide (2.5 equiv.) in THF at −78 °C afforded its 2α-phenylseleno derivative (**11**) in 75% yield. Oxidation of **11** with sodium periodate (3 equiv.) in 85% aqueous methanol containing sodium hydrogencarbonate (1.5 equiv.) at room temperature[15] led to elimination of benzeneseleninic acid, giving 11-hydroxy-4β,5α-eudesm-1-en-3-one (**2**), mp 105—107 °C, $[\alpha]_D$ −53.5°, in 69% yield, which displayed the following spectra: MS, *m/e* 236 (M^+), 221, 218, 203, 178, and 59; UV_{max}, 228 nm (ε 5700); IR (Nujol), 3500, 1670, and 1655 (sh) cm^{-1}; NMR, δ 1.06 (3H, s, 15-H), 1.13 (3H, d, J=7 Hz, 14-H), 1.22 (6H, s, 12- and 13-H), 2.32 (1H, dq, J=11 and 7 Hz, 4-H), 5.84 and 6.71 (each 1H, ABq, J=10 Hz, 2- and 1-H). While these spectral data were consistent with the formula (**2**), those were different from the reported[2] for aubergenone. Significant difference in the coupling constant $J_{4,5}$ between the synthetic (11 Hz) and natural samples (6 Hz) suggested that the protons at C-4 and C-5 of the latter would probably be oriented *cis* (equatorial-axial).

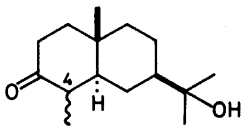

10, 4βH
14, 4αH

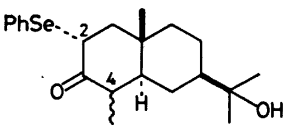

11, 4βH
15, 4αH

Synthesis of Aubergenone (1) from (+)-α-Cyperone (3). The synthesis required *cis*-addition of hydrogen atoms from the rear (α) side to the C-4–C-5 double bond of 4-eudesmene derivatives. Since hydrogenation of carissone, 11-hydroxyeudesm-4-en-3-one, over palladium in acetic acid or in alkaline ethanol gave *trans*-dihydrocarissone (**10**) as a major product, (+)-α-cyperone (**3**) was first transformed into eudesm-4-ene-3β,11-diol[16] (**12**) by a known two-step procedure.[16] Hydrogenation of **12** over platinum in a 40 : 1 mixture of ethyl acetate and acetic acid at room temperature[17] effected the relevant *cis*-hydrogenation to yield 4α,5α-eudesmane-3β,11-diol (**13**) [NMR, δ 3.75 (1H, dt, J=10 and 5.5 Hz, 3-H)], which in turn was oxidized with the Jones reagent, giving 11-hydroxy-4α,5α-eudesman-3-one (**14**) (ORD, a=+2[illegible].0) in 83% yield from **12**. The configurations of C-4 and C-5 of these compounds (**13**) and (**14**) were confirmed by quantitative conversion of **14** into **10** under basic conditions (5% KOH in MeOH, reflux, 6 h). The compound (**14**), when treated with LDA (2.5 equiv.) and then with benzeneselenenyl bromide (2.5 equiv.), afforded the corresponding 2α-phenylseleno derivative (**15**) [NMR, δ 2.61 (1H, qui, J=6 Hz, 4-H) and 4.49 (1H, dd, J=12 and 7 Hz, 2-H)] in 82% yield, which underwent oxidative elimination by treatment with sodium periodate (3 equiv.) in aqueous methanol at room temperature[15] to give α,β-unsaturated ketone, oil, $[\alpha]_D$ −4.0°, in 46% yield. The spectral data (see Experimental) of the ketone were completely identical with those (MS, UV, ORD, IR, ^{1}H and ^{13}C NMR) reported[2] for natural aubergenone. Naturally, aubergenone (**1**) was also converted quantitatively into its 4-epimer (**2**) under the basic conditions. The present result completes the synthesis of aubergenone (**1**) and also establishes the structure.

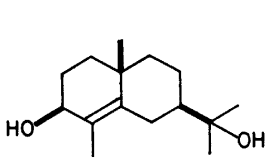

12

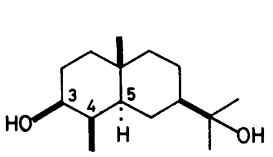

13

Experimental

All the melting points were uncorrected. The homogeneity of each compound was always checked by TLC over silica gel (Wakogel B-5) under various solvent systems, the spots being developed with cerium(IV) sulfate in dilute sulfuric acid and/or iodine. The optical rotations, ORD curves, UV, IR, and NMR (100 MHz) spectra were measured in chloroform, in ethanol, in ethanol, in liquid state, and in chloroform-*d*, respectively, unless otherwise stated.

11-Methyl-epi-α-santonin (6). To a solution of diisopropylamine (0.92 ml, 6 mmol) in dry THF (20 ml) cooled at 0 °C was added dropwise a solution of butyllithium in hexane (3.4 ml, 6 mmol) under nitrogen, and the solution was stirred at 0 °C for 15 min. To the solution cooled at −78 °C was added a solution of epi-α-santonin (**5**) (1 g, 4 mmol) in THF (20 ml) and HMPA (2 ml). The mixture was stirred at −78 °C for 1 h, mixed with a solution of methyl iodide (1 ml, large excess) in THF (2 ml) and HMPA (2 ml), and stirred continuously for 1 h at the same temperature. The reaction mixture was then neutralized with 2 M† hydrochloric acid, concentrated *in vacuo*, diluted with water, and extracted with chloroform. The chloroform solution was washed with water and saturated brine, dried, and evaporated to leave pale yellow oil (4 g), which was purified by chromatography over silica gel. Fractions eluted with benzene–ether (2 : 1) gave **6** (0.83 g), mp 164—165 °C; MS, *m/e* 260 (M$^+$, base), 245, and 217; IR (Nujol), 1762, 1660, and 1625 cm^{-1}; NMR, δ 1.25 [6H, s, 11-$(CH_3)_2$], 1.36 (3H, s, 15-H), 2.04 (3H, s, 14-H), 5.50 (1H, d, J=5 Hz, 6-H), 6.20 and 6.72 (each 1H, d, J=9 Hz, 2- and 1-H). Found: C, 73.52; H, 8.01%. Calcd for $C_{16}H_{20}O_3$: C, 73.85, H, 7.69%.

11-Methyl-1,2-dihydro-epi-α-santonin (7). A solution of **6** (540 mg) in degassed dry benzene (5 ml) was hydrogenated in the presence of tris(triphenylphosphine)chlororhodium (150 mg) for 9 h at room temperature. After the catalyst was removed by filtration through alumina (10 g), the filtrate was evaporated to give crude product (600 mg), which was separated by preparative TLC over silica gel with benzene–ethyl acetate (4 : 1) to give **7** (480 mg), mp 124—125.5 °C (from ether–hexane), $[\alpha]_D$ −113.2°; MS, *m/e* 262 (M$^+$, base), 247, 219; IR (Nujol), 1790, 1695, 1640, and 1400 cm^{-1}; NMR, δ 1.25 [6H, s, 11-$(CH_3)_2$], 1.37 (3H, s, 15-H), 1.72 (3H, s, 14-H), and 5.43 (1H, d, J=5.5 Hz, 6-H). Found: C, 73.44; H, 8.37%. Calcd for $C_{16}H_{22}O_3$: C, 73.28; H, 8.40%.

10-Epimaalienone (8). Compound **7** (135 mg) was exposed under day light (February in Sapporo at about 0 °C) in a Pyrex vessel for 10 d. The reaction mixture was separated by preparative TLC over silica gel with benzene. Fractions (63 mg) with higher R_f value, showing a single spot on TLC, afforded **8**, oil, $[\alpha]_D$ −595°; MS, IR, and NMR, in the text. Found: C, 82.43; H, 10.40%. Calcd for $C_{15}H_{22}O$: C, 82.52; H, 10.16%. The spectral data of **8** were identical with the corresponding reported data.[10] Fractions (32 mg) with lower R_f value, afforded the unchanged starting material (**7**).

11-Chloroeudesm-4-en-3-one (9). A solution of **8** (100 mg) in ethanol saturated with hydrogen chloride (10 ml) was stirred at room temperature for 1 h. The reaction mixture was poured into saturated aqueous sodium hydrogencarbonate and extracted with ether, repeatedly. The ether solution was washed with saturated brine and water, dried, and evaporated to leave crude crystals (111 mg), which were recrystallized from hexane to give **9** (91 mg), mp 86—88 °C, $[\alpha]_D$ +159.4°; MS, *m/e* 254 (M$^+$) and 218; IR (Nujol), 1680, and 1625 cm^{-1}; NMR, δ 1.12 (3H, s, 15-H), 1.59 and 1.61 (each 3H, each s, 12- and 13-H), and 1.73 (3H, s, 14-H). The spectral data of **9** were identical with the corresponding reported data.[8]

trans-*Dihydrocarissone (10).* To liquid ammonia (150 ml) containing lithium (160 mg, 23 mmol) was added dropwise a solution of **3** (500 mg, 2.3 mmol) in ether (25 ml) for 5 min under cooling at −78 °C, and the mixture was stirred at the temperature for 1 h. After addition of ammonium chloride, the mixture was evaporated, mixed with water, and extracted with ether (3 × 50 ml). The ether solution was washed

† 1 M=1 mol dm^{-3}.

with 5% aqueous ammonium chloride and water, dried, and evaporated to leave oily residue (524 mg), which was separated by column chromatography over silica gel (15 g) with hexane. More mobile fractions, showing a single spot on TLC, gave 4β,5α-eudesm-11-en-3-one (340 mg), oil, $[\alpha]_D$ −20.9° (lit,[13] −15.1°); MS, *m/e* 220 (M^+), 205, 177, and 109 (base); IR, 3100, 1720, 1650, 1390, and 890 cm^{-1}; NMR, δ 0.99 (3H, d, J=7.5 Hz, 14-H), 1.10 and 1.74 (each 3H, s, 15- and 13-H), and 4.73 (2H, s, 12-H). Less mobile fractions afforded the unchanged material (**3**) (159 mg).

To a suspended mixture of mercury(II) acetate (611 mg) in THF (2 ml) and water (3 ml) was added the afore-mentioned eudesmene (210 mg, 0.95 mmol) in THF (1 ml), when the mixture became homogeneous and was stirred at 0 °C for 5 min. To the solution was added 3 M aqueous sodium hydroxide (1 ml) and then sodium borohydride (0.5 M) in 3 M aqueous sodium hydroxide (1.6 ml), when mercury precipitated out. After removal of the mercury by filtration over Celite, the filtrate was concentrated, mixed with water (20 ml), saturated with sodium chloride, and extracted with ethyl acetate (4×20 ml). The acetate solution was washed with water, dried, and evaporated to leave crude crystals (280 mg), which on recrystallization from ether–hexane gave **10** (147 mg). The mother liquors obtained on recrystallization was evaporated and purified by chromatography over silica gel (10 g) with benzene–ether (2 : 1) to yield an additional amount (29 mg) of **10**, mp 110—111 °C (from ether–hexane), $[\alpha]_D$ −7.5° (lit,[12] −11.7°), MS, *m/e* 238 (M^+), 223, 220, 205, 180, and 59 (base); ORD (dioxane), $[\phi]^{peak}_{314}$ +2430°, $[\phi]_{278}$ 0°, $[\phi]^{trough}_{272}$ −4180°, a=+66.1; IR ($CHCl_3$), 3480, 1710, and 1390 cm^{-1}; NMR, δ 0.99 (3H, d, J=7 Hz, 14-H), 1.06 (3H, s, 15-H), and 1.20 (6H, s, 12- and 13-H).

*2α-Phenylseleno-11-hydroxy-4β,5α-eudesm-3-one (**11**).* To a solution of LDA in THF, prepared by treatment of diisopropylamine (126 mg, 1.25 mmol) with butyllithium [0.78 M in hexane (0.70 ml)] in THF (5 ml), was added **10** (119 mg, 0.5 mmol) in THF (2 ml) and HMPA (179 mg, 1 mmol) at −78 °C under nitrogen, and the mixture was stirred at the temperature for 1 h. To the mixture was added dropwise benzeneselenenyl bromide (295 mg, 1.25 mmol) in THF (2 ml) at −78 °C, when the mixture became yellow, and was treated with dilute hydrochloric acid and extracted with ether (3× 20 ml). The ether solution was washed with saturated aqueous sodium hydrogencarbonate and saturated brine, dried and evaporated to leave oily residue (300 mg), which was purified by column chromatography over silica gel (10 g) with benzene–ether (1 : 1), giving **11** (141 mg) as needle crystals, mp 154—155 °C (from ethyl acetate–hexane), $[\alpha]_D$ −132.1°; MS, *m/e* 396, 394 (M^+), 392, 378, 376, 374, 218, and 59 (base); IR (Nujol), 3400, 1708, and 1380 cm^{-1}; NMR, δ 1.02 (3H, s, 15-H), 1.06 (3H, d, J=7 Hz, 14-H), 1.19 (6H, s, 12- and 13-H), 2.36 (1H, m, 4-H), and 4.36 (1H, dd, J=13 and 6 Hz, 2-H). Found: C, 63.81; H, 7.71%. Calcd for $C_{21}H_{30}O_2Se$: C, 64.10; H, 7.70%.

*4-Epiaubergenone (**2**)*: A solution of **11** (70 mg, 0.185 mmol) in methanol (5 ml) and water (1 ml) containing sodium hydrogencarbonate (40 mg) and sodium periodate (200 mg, 0.93 mmol) was stirred at room temperature for 3 h, when the solution gradually became heterogeneous. After addition of 10% aqueous sodium thiosulfate, the reaction mixture was concentrated and extracted with ethyl acetate (3×20 ml). The acetate solution was worked up as usual to leave oily residue (57 mg), which was purified by chromatography over silica gel (5 g) with benzene–ether (1 : 1) to yield crude crystals (37 mg). These were recrystallized from ether–hexane to give **2** (30 mg) in pure state, mp 105—107 °C, $[\alpha]_D$ −53.5°; MS, UV, IR, and NMR, in the text; ORD, $[\phi]$ 0°, −50°, −360°, −920°, 0°, +1280°, +510°, +2030°, +510°, and +2850° at 500, 450, 400, 365, 346, 328, 282, 255, 240, and 226 nm. Found: C, 76.43; H, 10.10%. Calcd for $C_{15}H_{24}O_2$: C, 76.22; H, 10.24%.

*4α,5α-Eudesmane-3β,11-diol (**13**).* Eudesm-4-ene-3β,11-diol[16] (**12**) (50 mg) in ethyl acetate (20 ml) and acetic acid (0.5 ml) was hydrogenated over pre-reduced platinum(IV) oxide (20 mg) at room temperature for 2 h, when 4.7 ml of hydrogen (0.9 mol equiv.) had been consumed. After removal of the catalyst, the filtrate was washed with saturated aqueous sodium hydrogencarbonate and saturated brine, dried, and evaporated to leave crystalline substance, which was recrystallized from ethyl acetate–hexane to give **13** (46 mg), mp 166—166.5 °C; $[\alpha]_D$ −2.7°; MS, *m/e* 228 (M^+ −18), 207, 204, 189, and 161 (base); IR ($CHCl_3$), 3360 and 3240 cm^{-1}; NMR, δ 0.86 (3H, d, J=7 Hz, 14-H), 0.89 (3H, s, 15-H), 1.20 (6H, s, 12- and 13-H), and 3.75 (1H, dt, J=10 and 5.5 Hz). Found: C, 74.83; H, 11.71%. Calcd for $C_{15}H_{28}O_2$: C, 74.95; H, 11.74%.

*11-Hydroxy-4α,5α-eudesm-3-one (**14**).* A solution of **13** (111 mg, 0.46 mmol) in acetone (15 ml) was treated with the Jones reagent (*ca.* 0.5 ml, excess) at room temperature for 30 min under stirring. After neutralization by addition of saturated aqueous sodium carbonate, the mixture was filtrated over Celite. The filtrate was concentrated and extracted with ethyl acetate (3×20 ml). The acetate solution was worked up as usual to leave oily residue (110 mg), which was purified by chromatography over silica gel (3 g) with benzene–ether (2 : 1) to give **14** (100 mg), mp 41.5—43 °C (from ether–hexane), $[\alpha]_D$ +2.8°; MS, *m/e* 238 (M^+), 220, 205, 177, and 55 (base); ORD, $[\phi]^{peak}_{314}$ +1100°, $[\phi]_{300}$ 0°, $[\phi]^{trough}_{285}$ −1200°, a=+23; IR, 3500 and 1710 cm^{-1}; NMR, 1.10 (3H, s, 15-H), 1.10 (3H, d, J=7.5 Hz, 14-H), and 1.21 (6H, s, 12- and 13-H). Found: C, 75.27; H, 10.96%. Calcd for $C_{15}H_{26}O_2$: C, 75.58; H, 11.00%.

*2α-Phenylseleno-11-hydroxy-4α,5α-eudesm-3-one (**15**).* To a solution of LDA in THF, prepared by treatment of diisopropylamine (106 mg, 1.05 mmol) with butyllithium [1.7 M in hexane (0.6 ml)] in THF (5 ml), was added dropwise **14** (100 mg, 0.42 mmol) in THF (5 ml) at −78 °C with stirring under nitrogen, and the mixture was stirred at −78 °C for 1 h. To the mixture was added benzeneselenenyl bromide (295 mg, 1.05 mmol) in THF (3 ml) at the temperature, when the mixture became yellow, and was treated with dilute hydrochloric acid and extracted with ether (3×20 ml). The ether solution was worked up as uaual to leave oily residue, which was purified by chromatography over silica gel (10 g) with benzene–ether (2 : 1) to give **15** (130 mg), oil, showing a single spot on TLC, $[\alpha]_D$ −85.5°, MS, *m/e* 396, 394 (M^+), 392, 378, 376, 374, 218, 203, 178, and 59 (base); IR, 3500, 3030, and 1701 cm^{-1}; NMR, δ 1.02 (3H, s, 15-H), 1.14 (3H, d, J= 7.5 Hz, 14-H), 1.18 (6H, s, 12- and 13-H), 2.61 (1H, qui, J= 6 Hz, 4-H), and 4.49 (1H, dd, J=12 and 7 Hz, 2-H). Found: C, 63.83; H, 7.81%. Calcd for $C_{21}H_{30}O_2Se$: C, 64.10; H, 7.70%.

*Aubergenone (**1**).* A solution of **15** (54 mg, 0.14 mmol) in methanol (3 ml) and water (0.5 ml) containing sodium hydrogencarbonate (19 mg) and sodium periodate (94 mg, 0.44 mmol) was stirred at room temperature for 2.5 h, when the solution gradually became heterogeneous. The mixture was treated with 5% aqueous sodium thiosulfate, concentrated, and extracted with ethyl acetate (3×20 ml). The acetate solution was worked up as usual to leave oily residue (48 mg), which was separated by preparative TLC over silica gel with hexane–ethyl acetate (1 : 1). A fraction, showing a single spot, gave **1** (15 mg), oil, $[\alpha]_D$ −4.0°; MS, 236 (M^+), 218, 203, 175, and 59 (base); UV_{max}, 229 nm (ε 5800); ORD,

[ϕ] 0°, 0°, −130°, −520°, −1670°, 0°, +3830°, +4500°, +2800°, and +4500° at 589, 500, 450, 400, 368, 348, 310, 285, 280, and 275 nm; IR, 3400, 1670, 917, 824, and 752 cm^{-1}; ^1H NMR, δ 1.13 (3H, d, J=7.5 Hz, 14-H), 1.16 (3H, s, 15-H), 1.24 (6H, s, 12- and 13-H), 2.44 (1H, dq, J=6 and 8 Hz, 4-H), and 5.87 and 6.78 (each 1H, ABq, J=10 Hz, 2- and 1-H); ^{13}C NMR, δ 13.4, 20.7 (each q), 22.4, 26.0 (each t), 27.1, 27.5 (each q), 36.1 (s), 39.9 (t), 44.3, 45.2, 49.0 (each d), 72.5 (s), 125.8, 160.8 (each d), and 203.8 (s). Found: C, 76.03; H, 10.40%. Calcd for $C_{15}H_{24}O_2$: C, 76.22; H, 10.24%.

Epimerization of ***14*** *to* ***10*** *and* ***1*** *to* ***2***. *a)*: A solution of **14** (20 mg) in methanol (10 ml) containing 5% potassium hydroxide was refluxed for 6 h under nitrogen. The solution was cooled, neutralized with 10% aqueous ammonium chloride, evaporated, and extracted with ethyl acetate (3× 20 ml). The acetate solution was washed with water, dried, and evaporated to leave oil (20 mg), showing a single spot on TLC, which was identified as **10** by comparison of the spectral data (IR and NMR).

b): Compound **1** (10 mg) was treated with 5% potassium hydroxide (10 ml) for 6 h under reflux under nitrogen. The reaction mixture was worked up as mentioned above to give oil (8 mg), showing a single spot on TLC, which was identified as **2** by comparison of the spectral data (IR and NMR).

References

1) Part XXXI of "Studies on the Phytoalexins," and Part XI of "Synthetic Studies of Rishitin and Related Compounds." Part XXX of the former, see, A. Murai, S. Sato, A. Osada, N. Katsui, and T. Masamune, *J. Chem. Soc., Chem. Commun.*, **1982**, 32, and Part X of the latter, see A. Murai, S. Sato, and T. Masamune, *J. Chem. Soc., Chem. Commun.*, in press.

2) A. Stoessl, J. B. Stothers, and E. W. B. Ward, *Can. J. Chem.*, **53**, 3351 (1975).

3) R. B. Kelly, S. J. Alward, K. S. Murty, and J. B. Stothers, *Can. J. Chem.*, **56**, 2508 (1978).

4) A. Murai, A. Abiko, M. Ono, N. Katsui, and T. Masamune, *Chem. Lett.*, **1978**, 1209.

5) A. Stoessl, J. B. Stothers, and E. W. B. Ward, *Can. J. Chem.*, **56**, 645 (1978); J. B. Stothers, *Pure Appl. Chem.*, **53**, 1241 (1981).

6) T. Masamune, A. Murai, and N. Katsui, *Kagaku To Seibutsu*, **16**, 648 (1978).

7) E. Piers and K. F. Cheng, *Can. J. Chem.*, **46**, 377 (1968).

8) D. Caine and J. T. Gupton, III, *J. Org. Chem.*, **39**, 2654 (1974).

9) H. Ishikawa, *Yakugaku Zasshi*, **76**, 504 (1956).

10) A. E. Greene, J-C. Muller, and G. Ourisson, *Tetrahedron Lett.*, **1971**, 4147.

11) A. van der Gen, L. W. van der Linde, J. G. Witteveen, and H. Boelens, *Recl. Trav. Chim. Pays-Bas*, **90**, 1045 (1971).

12) D. C. Humber, A. R. Pinder, and R. A. Williams, *J. Org. Chem.*, **32**, 2335 (1967).

13) *Cf.*, G. L. Chetty, G. S. K. Rao, S. Dev, and D. K. Banerjee, *Tetrahedron*, **22**, 2311 (1966).

14) *Cf.*, A. Asselin, M. Mongrain, and P. Deslongchamps, *Can. J. Chem.*, **46**, 2817 (1968).

15) *Cf.*, H. J. Reich, J. M. Renga, and I. L. Reich, *J. Am. Chem. Soc.*, **97**, 5434 (1975).

16) A. R. Pinder and R. A. Williams, *J. Chem. Soc.*, **1963**, 2773.

17) *Cf.*, C. W. Shoppee, B. D. Agashe, and G. H. R. Summers, *J. Chem. Soc.*, **1957**, 3107.

Synthesis of β- and α-Rotunols. Revision of the Structure of a Stress Metabolite "1-Keto-α-cyperone"[1]

Akio Murai, Mitsunori Ono, Atsushi Abiko, and Tadashi Masamune*
Department of Chemistry, Faculty of Science, Hokkaido University, Sapporo 060
(Received September 11, 1981)

The synthesis of β- and α-rotunols, two sesquiterpene alcohols isolated from nutgrass (*Cyperus rotundus* Linne), is described. This synthetic study also involves revision of the structure of a stress metabolite "1-keto-α-cyperone" isolated from Burley and flue-cured tobaccos (*Nicotiana tabacum* L.).

The title sesquiterpene alcohols, β- and α-rotunols (**1**) and (**2**), were isolated from the crude drug "Ko-bushi," prepared from the dried rhizomes of nutgrass, *Cyperus rotundus* Linne (Cyperaceae) (Japanese name: Hamasuge) by Hikino and co-workers, and the structures were determined in 1969 on the basis of chemical and spectroscopic evidence.[2] In connection with studies on phytoalexins, we preliminarily reported that **1** has been synthesized from α-cyperone (**3**) and has played an important role as a key intermediate for the synthesis of phytuberin, one of the major phytoalexins of the genus *Solanum*.[3] We also found that the structure of a stress compound (**4**), isolated from Burley and flue-cured tobaccos and assigned a formula "1-keto-α-cyperone,"[4] should be represented by structure "2-keto-α-cyperone."[5] In the present paper we describe details of the synthesis of these sesquiterpenes **1**, **2**, and **4**.

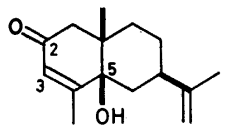

1

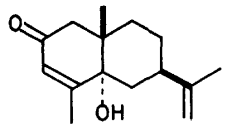

2

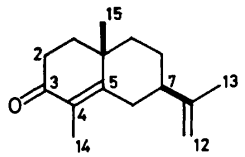

3

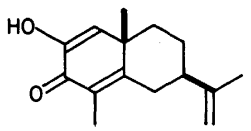

4

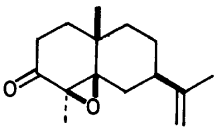

5

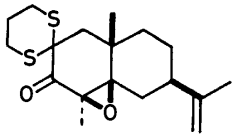

6

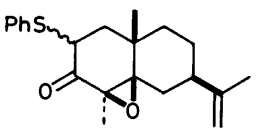

7

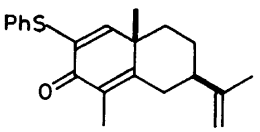

8

Results and Discussion

Revision of the Structure of a Stress Metabolite Named "1-Keto-α-cyperone." The synthesis of β-rotunol (**1**) from α-cyperone (**3**) required oxygenation at C-2 and C-5 as well as removal of the carbonyl group at C-3 of **3**. Thus compound **3** was first transformed into the 4β,5β-epoxy derivative[6] (**5**) in a three-step sequence [(i) reduction ($NaBH_4$ in MeOH), (ii) epoxidation (*t*-BuOOH and $VO(acac)_2$ in benzene), and (iii) oxidation (PCC in dichloromethane)] in 57% overall yield. However, attempted oxygenation reactions at C-2 of **5** under various conditions failed: namely, treatment of **5** with 1,3-propanedithiol di-*p*-toluenesulfonate and base in ethanol[7] gave a complex mixture, no expected dithiane derivative (**6**) being detected. Moreover, the epoxide (**5**), when treated with lithium diisopropylamide (LDA, 1.5 equiv.) in tetrahydrofuran (THF) and then with diphenyl disulfide[8] or benzenesulfenyl chloride, was not converted into the expected 2-phenylthio 3-ketone (**7**) and, instead, produced dienone (**8**) in 62% yield. The structure was assigned easily on the basis of the spectral data (see Experimental). Likewise, treatment of **5** with LDA (1.5 equiv.) in THF at −78 °C followed by addition of molybdenum peroxide $MoO_5 \cdot Py \cdot HMPA$ (MoOPH)[9] (1.5 equiv.) afforded 2-oxo-α-cyperone (**4**) in 75% yield. The structure of **4** was also based on the spectral data: MS, *m/e* 232 (M^+) and 189 (base); NMR, δ 1.28 (3H, s, 15-H), 1.82 (3H, s, 13-H), 1.99 (3H, s, 14-H), 4.84 (2H, s, 12-H), 6.07 (1H, s, 1-H), and 6.53 (1H, s, OH); IR (Nujol), 3400, 3120, 1660(sh), 1635, and 880 cm^{-1}. As expected, compound **8**, when treated with mercury(II) chloride in aqueous acetonitrile[10] under reflux, was converted into **4** in moderate yield (48%).

A plausible pathway for the formation of dienones **8** and **4** is depicted in Scheme 1: unstable 2-phenylthio and 2-oxomolybdenum cyclopropanone derivatives (**10** and **11**) would be formed by initial attack of the C-2 anion to the C-4 oxirane carbon, and subsequent ring cleavage caused by deprotonation at C-1 would produce the dienols (**12** and **13**), which underwent dehydration of the resultant β-hydroxy ketones to yield the dienone derivatives (**8** and **4**). This unexpected result indicated that a hydroxyl group or its equivalent would have to be introduced into C-5 after oxygenation at C-2 of α-cyperone.

Incidentally, the spectral data of the relevant 2-oxo-α-cyperone (**4**) were completely identical with those of a stress compound named "1-keto-α-cyperone," which had been isolated from Burley and flue-cured tobaccos (*Nicotiana tabacum*) by Roberts[4] in 1972 and assigned

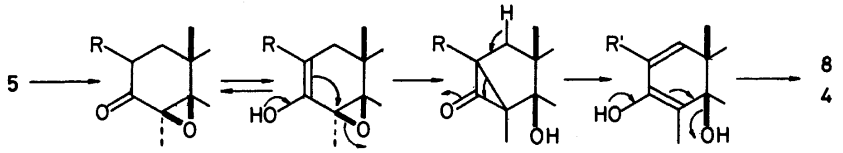

10, R=SPh 12, R'=SPh
11, R=OMoO$_4$L$_2^-$ 13, R'=OH

Scheme 1.

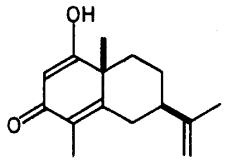

9

formula **9** shown by the name. It follows that this finding implies revision of the assigned structure of the stress metabolite.

Synthesis of β-Rotunol (1). Treatment of α-cyperone (**3**) with LDA (1.5 equiv.) in THF at −78 °C followed by addition of MoOPH effected oxygenation at C-2, giving a *ca.* 2 : 1 inseparable mixture (**14**) of 2β- and 2α-hydroxy-α-cyperones (**14a** and **14b**) in 62% yield, which were converted into the *t*-butyldimethylsilyl ethers (**15a** and **15b**) by treatment with *t*-butyldimethylsilyl chloride and imidazole in *N,N*-dimethylformamide.[11] The β- and α-configurations were assigned to the 2-hydroxyl groups of **14a** and **14b** on the basis of analogy of the contribution ($\Delta\delta$) of the 2-hydroxyl groups to the chemical shift of the 19-methyl protons of Δ^4-3-keto steroids in their NMR spectra:[12] δ_{obsd} 1.34 and 1.22 [total, 3H (2 : 1), each s, 15-H]; δ_{calcd} 1.32 and 1.22 for **14a** and **14b**. This assignment was confirmed by examination of the respective spectra of **14a** and **14b**, which were prepared alternatively as described later: specially, splitting patterns [**14a**, δ 4.21 (1H, dd, J=14 and 6 Hz); **14b**, δ 4.30 (1H, dd, J=12 and 6 Hz)] of the C-2 protons indicated that the A-ring of **14a** and **15a** would take a twist-boat conformation with the relevant functions at C-2 pseudo-equatorial and also with the 3- and 10-carbon atoms at bow-sprit and flag-pole positions, while that of **14b** and **15b** would adopt a half-chair form with the functions at C-2 pseudo-equatorial (Fig. 1). These conformations would probably result from hydrogen bonding between the 2-hydroxyl and 3-oxo groups in **14a** and **14b**, and from large bulkiness of the 2-alkylsilyloxyl group in **15a** and **15b**.

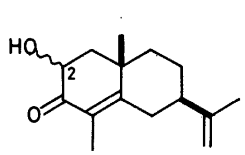

14a, 2α-H
14b, 2β-H

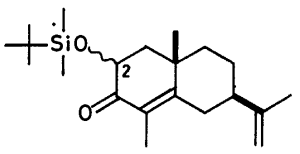

15a, 2α-H
15b, 2β-H

Treatment of the mixture of silyl ethers **15a** and **15b** with lithium tri-*s*-butylborohydride (L-selectride) (1 equiv.) in THF at −78 °C resulted in completely

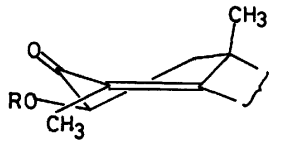

14a, R = H
15a, R = t-BuMe$_2$Si

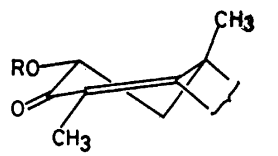

14b, R = H
15b, R = t-BuMe$_2$Si

Fig. 1.

stereoselective reduction of only **15a**, giving 3β-alcohol (**16a**) in 55% yield with 29% yield of the unreacted ketone (**15b**). While reduction of the recovered one (**15b**) with sodium borohydride in methanol afforded a 3 : 1 mixture of 3β- and 3α-alcohols (**16b** and **16c**), treatment with lithium aluminium hydride (LAH) at −78 °C produced 3β-alcohol (**16b**) in 80% yield as a single product. The stereoselective formation of these 3β-alcohols (**16a** and **16b**) with the hydride reagents, specially with L-Selectride, clearly resulted from attack of the reagents to the 3-carbon atom from the less-hindered side. The resultant 3-alcohols were converted into the 3-acetates (**17a**, **17b**, and **17c**), whose NMR spectra [**17a**, δ 3.90 (1H, dt, J=10 and 4.5 Hz, 2-H) and 5.30 (1H, dd, J=4.5 and 2 Hz, 3-H); **17b**, δ 3.90 (1H, m, 2-H, and dd, J=10 and 4.5 Hz, on irradiation at 5.40) and 5.40 (1H, d, J=8 Hz, 3-H); **17c**, 3.90 (1H, dt, J=12 and 4 Hz, 2-H) and 5.28 (1H, d, J= 4 Hz, 3-H)] indicated that **17a** and **17b** would take twist-boat and half-chair conformations, respectively (Fig. 2). The conformation of **17a** was also supported by the long-range coupling (2 Hz) between the hydrogen atoms at C-1 and C-3. Then the 3β-alcohol (**16a**) was oxidized smoothly with activated manganese(IV) oxide[13] in dichloromethane to **15a** in pure state in 93% yield. Moreover, hydrolysis of **15a** and **15b** with acetic acid in aqueous THF[14] gave rise to **14a** and **14b** in pure state quantitatively, respectively.

Introduction of a β-hydroxyl group into C-5 was carried out as follows. Epoxidation of 3β-alcohol **16a** with *t*-butyl hydroperoxide in the presence of bis-(acetylacetonato)oxovanadium(IV) [VO(acac)$_2$][15] in benzene produced 4β,5β-epoxy 3β-alcohol (**18a**), which was converted smoothly into the 3β-mesylate (**19a**) in 84% yield from **16a**: **19a**, δ 3.86 (1H, ddd, J=13, 5,

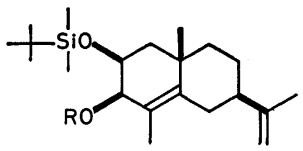

16a, R=H
17a, R=Ac

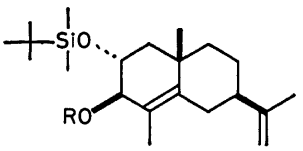

16b, R=H
17b, R=Ac

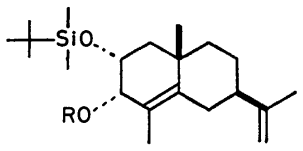

16c, R=H
17c, R=Ac

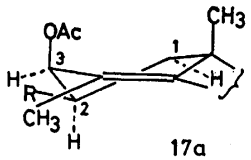

17a

J_{2-3} = 4.5 Hz
$J_{1\alpha-3}$ = 2 Hz

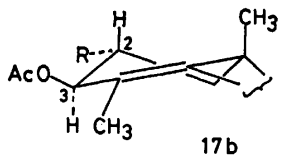

17b

J_{2-3} = 8 Hz

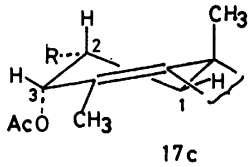

17c

J_{2-3} = 4.5 Hz
$J_{1\beta-3}$ = 2 Hz

Fig. 2.

and 4 Hz, 2-H) and 4.85 (1H, dd, J=4, and 2 Hz, 3-H). These splitting patterns again indicated that compounds **18a** and **19a** would possess a twist-boat form with two β-substituents at C-2 and C-3 pseudo-equatorial and pseudo-axial, respectively. Reductive elimination of the epoxy mesylate (**19a**) with sodium in liquid ammonia and dry THF[16] afforded allyl alcohol (**20a**) in 95% yield, which was hydrolyzed in a 1 : 1 : 2 mixture of acetic acid, water, and THF to give Δ^3-2β,5β-glycol (**21a**) in 90% yield. Likewise, 3β-alcohol **16b**, an isomer of **16a**, was transformed into the corresponding Δ^3-2α,5β-glycol (**21b**) *via* the 4β,5β-epoxy 3β-alcohol (**18b**), the 3β-mesylate (**19b**), and the Δ^3-5β-alcohol (**20b**), in 50% yield from **16b**: **19b**, δ 4.01 (1H, ddd, J=10, 9, and 4 Hz, 2-H) and 4.68 (1H, d, J=9 Hz, 3-H). Oxidation of **21a** and **21b** with activated manganese(IV) oxide in dichloromethane produced the same α,β-unsaturated ketone, mp 117—119 °C, $[\alpha]_D$ +41.4° ($CHCl_3$), in 85 and 90% yields. The ketone was identified as β-rotunol (**1**), mp 118—119 °C, $[\alpha]_D$ +44.8° ($CHCl_3$), by comparison of the spectra of synthetic and natural samples. The overall yield amounted to 29.6% from (+)-α-cyperone (**3**). Since β-rotunol has been transformed into dehydrosolavetivone[2] (**22**) and then into solavetivone[17] (**23**), stress metabolites in diseased potatoes, by Hikino,[2] Anderson and co-workers,[17] respectively, the present synthesis of β-rotunol also constitutes, in a formal sence, the synthesis of the metabolites (**22**) and (**23**).

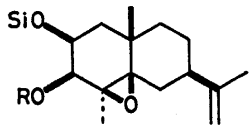

18a, R=H
19a, R=Ms

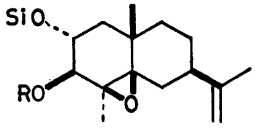

18b, R=H
19b, R=Ms

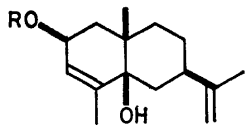

20a, R=t-BuMe$_2$Si
21a, R=H

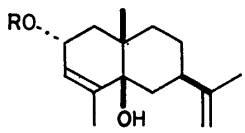

20b, R=t-BuMe$_2$Si
21b, R=H

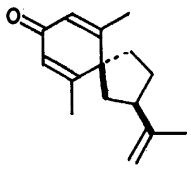

22

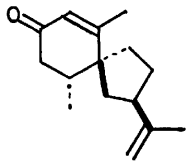

23

Synthesis of α-Rotunol (2). Treatment of α-cyperone (**3**) under the Shapiro conditions[18] effected reductive deoxygenation to give diene (**24**) in 73% yield, which on oxygenation with triplet oxygen in the presence of tungsten(VI) chloride in the dark at −78 °C[19] followed by treatment of the resulting peroxide (**25**) with alumina afforded α,β-unsaturated ketone, mp 102—104 °C, $[\alpha]_D$ +53°, in 88% yield. The ketone was identified as α-rotunol (**2**), mp 87.5—88.5 °C, by comparison of the spectra of synthetic and natural samples.

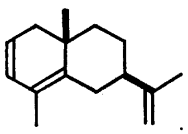

24

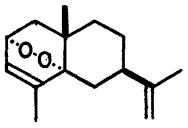

25

Experimental

All the melting points were uncorrected. The homogeneity of each compound was always checked by TLC on silica gel (Wakogel B-5) with various solvent systems, the spots being developed with cerium(IV) sulfate in diluted sulfuric acid

and/or iodine. The optical rotations, UV and NMR (100 MHz) spectra were measured in chloroform, ethanol, and chloroform-*d* respectively, unless otherwise stated.

4β,5β-Epoxyeudesm-11-en-3-one (5). *i)*: To a solution of (+)-α-cyperone (100 mg) in methanol (5 ml) cooled at −50 °C was added sodium borohydride (55 mg) with stirring. After stirring for 1.5 h at −45—−50 °C, the reaction was quenched by addition of acetic acid. The product was extracted with chloroform and the extracts were washed with saturated sodium hydrogencarbonate and saturated brine, dried, and evaporated to give eudesma-4,11-dien-3β-ol (95 mg) as a single product, oil; $[\alpha]_D$ +9.7°, (Ref.[6] +10.9°); NMR, δ 4.05 (1H, br, t, W_H=15 Hz, 3α-H). The spectral data were identical with the reported data.[6]

ii): To a stirred solution of eudesma-4,11-dien-3β-ol (220 mg, 1 mmol) and $VO(acac)_2$ (4 mg, 0.014 mmol) in dry benzene (10 ml) was added dropwise *t*-butyl hydroperoxide (0.186 g, 1.5 mmol) under reflux, and the mixture was stirred under reflux for 10 min. The reaction mixture was poured into aqueous sodium hydrogensulfite. The organic layer was separated and the aqueous solution was extracted with ether. The benzene and ether solution were combined, washed with water, dried, and evaporated to leave an oil (300 mg), which was chromatographed over silica gel (9 g) with benzene–ether (5 : 1) to give 4β,5β-epoxyeudesm-11-en-3β-ol (203 mg), oil; $[\alpha]_D$ +57.6°; IR (neat), 3500, 3100, 1625, and 890 cm^{-1}; NMR, δ 1.08 (3H, s, 15-H), 1.40 (3H, s, 14-H), 1.76 (3H, s, 13-H), 3.80 (1H, br, W_H=7 Hz, 3α-H), and 4.74 (2H, s). The spectral data were identical with the corresponding reported data.[6]

iii): To a mixture of pyridinium chlorochromate (PCC, 323 mg, 1.5 mmol) in dry dichloromethane (5 ml) was added a solution of 4β,5β-epoxyeudesm-11-en-3β-ol (234 mg, 1 mmol) in dichloromethane (3 ml). The whole reaction mixture was stirred at room temperature for 2 h, diluted with dry ether (10 ml) and filtered. The filtrate was evaporated to leave an oil (230 mg), which was separated by chromatography over silica gel with benzene–ether (10 : 1). Fractions (180 mg) with high R_f value, showing a single spot on TLC, afforded **5**, oil; IR (neat), 3080, 1710, 1625, and 890 cm^{-1}; NMR, δ 1.20 (3H, s, 15-H), 1.42 (3H, s, 14-H), 1.76 (3H, s, 13-H), and 4.76 (2H, s). The spectral data were identical with the corresponding reported data.[6]

Attempted Phenylsulfenylation of 5. To a solution of diisopropylamine (0.066 ml, 0.48 mmol) in dry THF (1 ml) cooled at 0 °C was added dropwise a solution of butyllithium in hexane (0.272 ml, 0.48 mmol) under nitrogen, and the solution was stirred at 0 °C for 15 min. To the solution cooled at −78 °C was added a solution of **5** (75 mg, 0.32 mmol) in THF (2 ml). The reaction mixture, after being stirred at −78 °C for 50 min, was mixed with a solution of diphenyl disulfide (105 mg, 0.48 mmol) in dry THF (2 ml) at room temperature and stirred for 1 h at room temperature. The whole mixture was poured into ice–water, and extracted with chloroform. The chloroform solution was washed with water and saturated brine, dried, and evaporated to leave an oil (330 mg), which was separated by preparative TLC over silica gel with benzene–ether (5 : 1). Fractions (39 mg) with higher R_f value, showing a single spot on TLC, afforded the dienone derivative (**8**), gum; $[\alpha]_D$ −98.2°; MS, *m/e* 324; IR (neat), 1640, 1625, and 1065 cm^{-1}; NMR, δ 1.76 (3H, s, 13-H), 1.93 (3H, s, 14-H), 6.12 (1H, s, 1-H), and 7.08—7.56 (5H, br m, C_6H_5). Found: C, 77.70; H, 7.37%. Calcd for $C_{21}H_{24}OS$: C, 77.78; H, 7.41%. Fractions (28.5 mg) with lower R_f value afforded the unchanged starting material (**5**).

Attempted hydroxylation of 5. To a solution of LDA (*ca.* 0.64 mmol), prepared by treatment of diisopropylamine (0.0986 ml, 0.64 mmol) with butyllithium in hexane (0.37 ml, 0.64 mmol) in THF (5 ml) at 0 °C for 15 min, was added a solution of **5** (100 mg, 0.427 mmol) in THF (2 ml) at −78 °C under nitrogen. The reaction mixture, after being stirred at −78 °C for 1 h, was mixed with MoOPH (278 mg, 0.64 mmol) and stirred for 1 h at the same temperature and for 30 min at room temperature. After addition of water to quench the reaction, the mixture was concentrated *in vacuo*, and the residue was diluted with water and extracted with ether, repeatedly. The organic layers were washed with saturated sodium hydrogencarbonate, 2 M† hydrochloric acid, and water, dried, and evaporated to leave an oil (190 mg), which was separated by preparative TLC over silica gel with benzene. Fractions (37 mg) with higher R_f value, showing a single spot on TLC, afforded 2-oxo-α-cyperone (**4**), mp 76—77 °C; $[\alpha]_D$ −166°; UV_{max}, 259.5 nm (ε 18000); MS, IR, and NMR, in the text. Found: C, 77.63; H, 8.59%. Calcd for $C_{15}H_{20}O_2$: C, 77.55; H, 8.68%. Fractions (49 mg) with lower R_f value afforded the unreacted starting material (**5**).

Hydrolysis of 8. A mixture of **8** (100 mg, 0.31 mmol) and mercury(II) chloride (251 mg, 0.93 mmol) in water (2 ml) and acetonitrile (8 ml) was stirred under reflux under nitrogen for 1 h. The resulting precipitates were removed by filtration through Celite and the filtrate was concentrated *in vacuo*, diluted with water, and extracted with chloroform, repeatedly. The chloroform solution was worked up as usual to leave an oil (86 mg), which was separated by preparative TLC with benzene. Fractions (32 mg) with higher R_f value afforded the unchanged starting material (**8**). Fractions (33 mg) with lower R_f value, showing a single spot on TLC, afforded 2-oxo-α-cyperone (**4**), mp 74—76 °C, $[\alpha]_D$ −171.0°, which was identical with the sample (**4**) described above in all respects.

*2-Hydroxy-α-cyperones (**14a** and **14b**).* To a solution of LDA (*ca.* 21 mmol), prepared by treatment of diisopropylamine (3.228 ml, 21 mmol) with butyllithium in hexane (11.58 ml, 21 mmol) in THF (30 ml) at 0 °C for 15 min, was added a solution of **3** (3.0 g, 13.8 mmol) in THF (20 ml) at −78 °C under nitrogen. After being stirred at −78 °C for 1 h, the mixture was mixed rapidly with MoOPH (9.12 g, 21 mmol), and stirred at −78 °C for 1.4 h and at room temperature for 30 min. After addition of water, the mixture was concentrated *in vacuo*, and the residue was diluted with water and extracted with ethyl acetate, repeatedly. The organic solutions were worked up as usual to leave an oil (3.2 g), which was chromatographed over silica gel (100 g) with benzene–ether (10 : 1). More mobile fractions (0.5 g) afforded **4**, and less mobile fractions (2.05 g) gave a 2 : 1 inseparable mixture (**14**) of 2β- and 2α-hydroxy-α-cyperones, (**14a** and **14b**), oil; MS, *m/e* 234 (M^+), 216, 190, 147, and 122; IR (neat), 3550, 3100, 1680 (br), 1615, and 890 cm^{-1}; NMR, δ 4.20 (0.67H, dd, *J*=14 and 6 Hz, 2α-H) and 4.28 (0.33H, dd, *J*=12 and 6 Hz, 2β-H).

*2-(t-Butyldimethylsilyloxy)-α-cyperones (**15a** and **15b**).* A mixture of **14** (250 mg, 1 mmol), imidazole (170 mg, 2.5 mmol), and *t*-butyldimethylsilyl chloride (180 mg, 1.2 mmol) in dry dimethylformamide (0.5 ml) was heated at 35—40 °C for 10 h with stirring under nitrogen. The reaction mixture was poured into ice–water and extracted with ether, repeatedly. The organic solutions were washed with water, dried, and evaporated to leave an oil (396 mg), which was chromatographed over silica gel (10 g) with benzene to give **15** (350 mg) as an 2 : 1 inseparable mixture (**15**) of 2β- and 2α-(*t*-butyldimethylsilyloxy)-α-cyperones (**15a** and **15b**), oil; MS, *m/e* 348 (M^+), 333 (base), and 291; IR (neat), 3080, 1695, 1650, 1620, and 895 cm^{-1}; NMR, δ 4.23 (0.67H, dd, *J*=10

† 1 M=1 mol dm^{-3}.

and 7 Hz, 2α-H), 4.35 (0.33H, dd, J=12 and 7 Hz, 2β-H).

*2α-(t-Butyldimethylsilyloxy)eudesma-4,11-dien-3-one (**15b**) and 2β-(t-butyldimethylsilyloxy)eudesma-4,11-dien-3β-ol (**16a**).* To a stirred solution of **15** (430 mg, 1.24 mmol) in THF (10 ml) was added L-Selectride (1 ml, 1.24 mmol) at −78 °C during 1 h under nitrogen. The solution was stirred at −78 °C for 1 h under nitrogen. After dropwise addition of water (1 ml) to decompose the reagent, the reaction mixture was stirred with 10% aqueous potassium hydroxide and 30% aqueous hydrogen peroxide at room temperature for 30 min and then treated with 5% aqueous sodium thiosulfate (10 ml) under cooling to decompose the hydrogen peroxide, and concentrated *in vacuo*. The residue was diluted with water and extracted with chloroform. The chloroform solution was worked up as usual to leave an oil (452 mg), which was chromatographed over silica gel (13 g) with benzene. Fractions (123 mg) with higher higher R_f value, showing a single spot on TLC, afforded **15b**, oil, $[\alpha]_D$ +50.0°; MS, *m/e* 348 (M^+), 333, and 291 (base); IR (neat), 3100, 1690, 1650, 1618, 1145, and 885 cm^{-1}; NMR, δ 0.09 (3H, s), 0.17 (3H, s), 0.92 [9H, s, $(CH_3)_3C$-], 1.31 (3H, s, 15-H), 1.78 (3H, s, 14-H), 1.80 (3H, s, 12-H), 4.34 (1H, dd, J=12 and 7 Hz, 2β-H), and 4.77 (2H, s). Found: C, 71.97; H, 10.33%. Calcd for $C_{21}H_{36}O_2Si$: C, 72.41; H, 10.34%. Fractions (236 mg) with lower R_f value, showing a single spot, afforded **16a**, mp 72—73 °C; $[\alpha]_D$ −79.4°; MS, *m/e* no M^+, 332, 293, 275, and 117; IR (neat), 3560, 3070, 1645, 1080, and 895 cm^{-1}; NMR, δ 0.09 (6H, s), 0.91 [9H, s, $(CH_3)_3C$-], 1.12 (3H, s, 15-H), 1.76 and 1.82 (each 3H, each s, 13- and 14-H), 3.76—3.86 (total 2H, m), and 4.74 (2H, s). Found: C, 71.99; H, 10.30%. Calcd for $C_{21}H_{38}O_2Si$: C, 72.00; H, 10.34%.

*Reduction of **15b** with Sodium Borohydride.* Compound **15b** (530 mg) was treated with sodium borohydride (200 mg) in methanol (10 ml) at −40—−50 °C for 1 h. After being quenched by addition of acetic acid, the reaction mixture was concentrated and extracted with ether. The ether solution was worked up as mentioned above to leave an oil (540 mg), showing two spots on TLC. The oil was separated into two fractions by column chromatography over silica gel (15 g) with benzene–hexane (1 : 1). Fractions (380 mg) with higher R_f value afforded **16b**, oil, $[\alpha]_D$ −9.4°; MS, *m/e* no M^+, 332 ($M^+ - H_2O$), 293 [$M^+ - C(CH_3)_3$], and 117; IR (neat), 3540 (br), 3090, 1645, 1090, and 885 cm^{-1}; NMR, 0.12 (6H, s), 0.92 [9H, s, $(CH_3)_3C$], 1.15 (3H, s, 15-H), 1.74 and 1.76 (each 3H, each s, 13- and 14-H), 3.72—4.04 (2H, m), and 4.74 (2H, s). Found: C, 71.88; H, 9.98%. Calcd for $C_{21}H_{38}O_2Si$: C, 72.00; H, 10.34%. Fractions (104 mg) with lower R_f value gave **16c**, oil; $[\alpha]_D$ +60.8°; MS, *m/e* no M^+, 332, 293, and 117; IR (neat), 3620, 3550 (br), 3110, 1650, 1080, 895, and 885 cm^{-1}; NMR, δ 0.11 (6H, s), 0.92 [9H, s, $C(CH_3)_3$], 1.10 (3H, s, 15-H). 1.76 and 1.82 (each 3H, each s, 13- and 14-H), 3.76—4.04 (2H, m), and 4.74 (2H, s). Found: C, 71.48; H, 10.71%. Calcd for $C_{21}H_{38}O_2Si$: C, 72.00, H, 10.34%.

*Reduction of **15a** with LAH.* To a stirred solution of **15b** (500 mg) in dry THF (30 ml) was added dropwise a suspension (2 ml) of LAH (100 mg) in dry THF (5 ml) at −78 °C during 5 min. The mixture was stirred at the same temperature for 20 min and, after addition of water (0.5 ml) and 1% aqueous potassium hydroxide (0.5 ml), was filtered. The filtrate was dried and evaporated to leave an oil (519 mg), which was chromatographed over silica gel (15 g) with benzene–hexane (2 : 3). Fractions (145 mg) with higher R_f value, showing a single spot on TLC, afforded the unreacted starting material (**15b**). Fractions (280 mg) with lower R_f value, showing a single spot on TLC, gave **16b** in pure state.

Compounds **16a**, **16b**, and **16c** were converted almost quantiatively into the respective monoacetates (**17a**, **17b**, and **17c**) by treatment with acetic anhydride and pyridine at room temperature, which had the following properties: **17a**, oil; $[\alpha]_D$ −135.8°; MS, *m/e* no M^+, 335, 332, and 117 (base); IR (neat), 3100, 1748, 1657, 1240, 1085, and 885 cm^{-1}; NMR, δ 0.08 (6H, s), 0.86 [9H, s, $C(CH_3)_3$], 1.13 (3H, s, 15-H), 1.68 and 1.76 (each 3H, each s, 13- and 14-H), 2.08 (3H, s, $OCOCH_3$), 3.90 (1H, dt, J=10 and 4.5 Hz, 2α-H), 4.74 (2H, s), and 5.30 (1H, dd, J=4.5 and 2 Hz, 3α-H): **17b**, mp 102—104 °C (from ether); $[\alpha]_D$ −45.6°; MS, *m/e* no M^+, 335, 332, and 117 (base); IR (Nujol), 3100, 1743, 1642, 1240, 1080 and 880 cm^{-1}; NMR, δ 0.04 (6H, s), 0.84 [9H, s, $C(CH_3)_3$], 1.12 (3H, s, 15-H), 1.51 and 1.72 (each 3H, each s, 13- and 14-H), 2.06 (3H, s, $OCOCH_3$), 3.76—4.04 (1H, m, and dd, J=10 and 4.5 Hz on irradiation at 5.40, 2β-H), 4.69 (2H, s), and 5.40 (1H, d, J=8 Hz, 3α-H): **17c**, oil; $[\alpha]_D$ +95.2°; MS, *m/e* no M^+, 335, 332, and 117 (base); IR (neat), 3100, 1743, 1657, 1243, 1110, and 890 cm^{-1}; NMR, δ 0.06 (3H, s), 0.10 (3H, s), 0.88 [9H, s, $C(CH_3)_3$], 1.12 (3H, s, 15-H), 1.63 and 1.74 (each 3H, each s, 13- and 14-H), 2.06 (3H, s, $OCOCH_3$), 3.90 (1H, dt, J=12 and 4 Hz, 2β-H), 4.72 (2H, s), and 5.28 (1H, dd, J=4 and 2 Hz, 3β-H).

*Transformation of **15b** and **16a** into **14a** and **14b**.* Compound **15b** (150 mg) was stirred with acetic acid (1 ml) in water (1 ml) and THF (1.5 ml) at room temperature for 16 h under nitrogen. The mixture was worked up as usual to leave an oily residue (159 mg), showing a single spot on TLC, which was purified by preparative TLC over silica gel with benzene–ether (10 : 1) to yield **14b** in pure state (92 mg), oil; $[\alpha]_D$ +99.1°; MS, *m/e* 234 (M^+), 216, 190 (base), 147, and 122; IR (neat), 3550, 3100, 1676, 1658, 1615, and 890 cm^{-1}; NMR, δ 1.33 (3H, s, 15-H), 1.77 and 1.83 (each 3H, each s, 13- and 14-H), 4.30 (1H, dd, J=12 and 6 Hz, 2β-H), and 4.78 (2H, s). Found: C, 76.91; H, 9.38%. Calcd for $C_{15}H_{22}O_2$: C, 76.92; H, 9.40%.

Compound **16a** (110 mg) was stirred with activated manganese(IV) oxide (500 mg) in dry dichloromethane (10 ml) at room temperature for 24 h. The mixture was worked up as usual to leave an oily residue (120 mg), showing a single spot on TLC, which was purified by preparative TLC over silica gel with benzene to give **15a** (102 mg), oil; $[\alpha]_D$ −162.6°; MS, *m/e* 348 (M^+), 333, and 291; IR (neat), 3100, 1695, 1655, 1620, 1170, and 895 cm^{-1}; NMR, δ 0.10 (3H, s), 0.14 (3H, s), 0.91 (9H, s), 1.77 and 1.80 (each 3H, each s, 13- and 14-H), 1.25 (3H, s, 15-H), 4.22 (1H, dd, J=7 and 10 Hz, 2-H), and 4.79 (2H, s). Found: C, 72.77; H, 10.23%. Calcd for $C_{21}H_{36}O_2Si$: C, 72.41; H, 10.34%.

Compound **15a** (50 mg) was stirred with acetic acid (1 ml) in water (1 ml) and THF (1.5 ml) at room temperature for 16 h under nitrogen. The mixture was worked up as usual to leave an oily residue (61 mg), showing a single spot, which was purified by preparative TLC over silica gel to yield **14a** (43 mg), oil; $[\alpha]_D$ −217.8°; MS, *m/e* 234 (M^+), 216, 190, 147, and 122; IR (neat), 3550, 3105, 1690, 1657 (sh), 1622, and 895 cm^{-1}; NMR, δ 1.23 (3H, s, 15-H), 1.75 and 1.83 (each 3H, each s, 13- and 14-H), 4.21 (1H, dd, J=14 and 6 Hz, 2α-H), 4.76 (2H, s). Found: C, 76.85; H, 9.38%. Calcd for $C_{15}H_{22}O_2$: C, 76.92; H, 9.40%.

*2β-(t-Butyldimethylsilyloxy)-4β,5β-epoxyeudesm-11-en-3β-ol (**18a**) and Its 2α-Epimer (**18b**).* *i)*: To a refluxing green-colored solution of **16a** (1.1 g) in dry benzene (30 ml) containing $VO(acac)_2$ (20 mg) was added rapidly *t*-butyl hydroperoxide (72%, 2 ml), when the solution became red-colored. The solution was further refluxed for 10 min and cooled. The resulting yellow mixture was washed with saturated aqueous sodium thiosulfate, 5% aqueous sodium hydrogencarbonate and water, dried, and evaporated to

leave an oil (1.22 g), showing a single spot on TLC, which was purified by column chromatography over neutral alumina (1 g) with benzene to give **18a** (1.0 g), unstable oil; $[\alpha]_D$ −14.3°; MS, *m/e* 366 (M^+), 351, 291, 217, and 131; IR (neat), 3520, 3060, 1640, 1075, and 900 cm^{-1}; NMR, δ 0.09 (3H, s), 0.11 (3H, s), 0.92 [9H, s, $C(CH_3)_3$], 1.12 (3H, s, 15-H), 1.48 (3H, s, 14-H), 1.76 (3H, s, 13-H), 3.52—3.86 (2H, m, 2α- and 3α-H), and 4.72 (2H, s).

ii): A solution of **16b** (360 mg) in benzene (15 ml) was refluxed with *t*-butyl hydroperoxide (0.6 ml) in the presence of $VO(acac)_2$ (6 mg) for 15 min. The reaction mixture was worked up in the same manner as that of **16a** to leave an oil (405 mg), showing a single spot on TLC, which was purified by column chromatography over neutral alumina (500 mg) with benzene to give **18b** (340 mg), unstable oil; $[\alpha]_D$ −14.2°; MS, *m/e* 366 (M^+), 351, 291, 217, and 131; IR (neat), 3510, 3100, 1651, 1100, 1075, and 895 cm^{-1}; NMR, δ 0.09 (3H, s), 0.11 (3H, s), 0.92 [9H, s, $C(CH_3)_3$], 1.11 (3H, s, 15-H), 1.50 (3H, s, 14-H), 1.75 (3H, s, 13-H), 3.52—3.86 (2H, m), 4.74 (2H, s).

2β-(t-Butyldimethylsilyloxy)-4β,5β-epoxyeudesm-11-ene-3β-ol Mesylate (19a) and Its 2α-Epimer (19b). *i)*: To a solution of **18a** (270 mg) in dry pyridine (1.5 ml) was added methanesulfonyl chloride (0.15 ml). The reaction mixture was stirred at room temperature for 2 h, and then poured into ice–water and extracted with chloroform, repeatedly. The chloroform solution was worked up as usual to leave an oil (320 mg), showing a single spot on TLC, which was purified by chromatography over silica gel (4 g) with benzene to give **19a** (292 mg), solid, $[\alpha]_D$ −28.0°; MS, *m/e* no M^+, 387 [$(M^+ - C(CH_3)_3]$, 349, and 313; IR (neat), 3080, 1640, 1180, 1100, and 875 cm^{-1}; NMR, δ 0.12 (6H, s), 0.90 [9H, s, $C(CH_3)_3$], 1.12 (3H, s, 15-H), 1.50 (3H, s, 14-H), 1.72 (3H, s, 13-H), 3.12 (3H, s, OSO_2CH_3), 3.86 (1H, ddd, J=13, 5, and 4 Hz, 2α-H), 4.72 (2H, s), and 4.85 (1H, dd, J=4 and 2 Hz, 3α-H). Found: C, 59.80; H, 9.39%. Calcd for $C_{22}H_{40}O_5SSi$: C, 59.46; H, 9.01%.

ii): A mixture of **18b** (1.1 g) and methanesulfonyl chloride (0.61 ml) in dry pyridine (6.1 ml) was stirred at room temperature for 3 h. The reaction mixture was worked up in the same manner as that of **18a** to leave crude crystals (1.4 g). showing a single spot on TLC, which were purified by simple column chromatography over silica gel (10 g) with benzene to yield **19b** (1.09 g), mp 105—107 °C (from ether–hexane); $[\alpha]_D$ −38.8°; MS, *m/e* no M^+, 387, 349, and 313; IR (Nujol), 3090, 1655, 1090, 1075, and 895 cm^{-1}; NMR, δ 0.09 (6H, s), 0.89 [9H, s, $C(CH_3)_3$], 1.12 (3H, s, 15-H], 1.49 (3H, s, 14-H), 1.73 (3H, s, 13-H), 4.05 (1H, ddd, J=10, 9, and 4 Hz, 2β-H), 4.68 (1H, d, J=9 Hz, 3α-H), and 4.73 (2H, s). Found: C, 59.91; H, 9.19%. Calcd for $C_{22}H_{40}O_5SSi$: C, 59.46; H, 9.01%.

2β-(t-Butyldimethylsilyloxy)eudesma-3,11-dien-5β-ol (20a) and Its 2α-Epimer (20b). *i)*: To a mixture of **19a** (200 mg) in ammonia (10 ml) and dry THF (4 ml) was added sodium (40 mg, 4-fold excess) at −50 °C (bath temp), when the blue color appeared. The reaction mixture was stirred for 5 min, and then ammonium chloride was added until the blue color disappered. After removal of ammonia and THF, the residue was diluted with cold-water and extracted with chloroform. The chloroform solution was worked up as usual to leave an oil (171 mg), showing a single spot on TLC, which was purified by simple column chromatography over silica gel (2 g) with chloroform to give **20a** (140 mg), oil; $[\alpha]_D$ +9.0°; MS, *m/e* 350 (M^+), 332, 293, and 131; IR (neat), 3450, 3060, 1637, 1060, and 880 cm^{-1}; NMR, δ 0.08 (6H, s), 0.90 [9H, s, $C(CH_3)_3$], 1.02, 1.70, and 1.72 (each 3H, each s, 15-, 13-, and 14-H), 4.30 (1H, br m, 2α-H), 4.65 (2H, s), and 5.44 (1H, br, W_H=6 Hz, 3-H). Found: C, 72.33; H, 10.93%. Calcd for $C_{21}H_{38}O_2Si$: C, 72.00; H, 10.86%.

ii): Compound **19b** (72 mg) was reduced under the same Birch conditions (sodium, 15 mg, THF, 3 ml, and ammonia, 8 ml) as described above to give **20b** (45 mg), oil; $[\alpha]_D$ +71.7°; MS, *m/e* 350 (M^+), 332, 293, and 131; IR (neat), 3500, 3095, 1650, 1055, and 890 cm^{-1}; NMR, δ 0.08 (6H, s), 0.91 [9H, s, $C(CH_3)_3$], 1.05, 1.76, and 1.78 (each 3H, each s, 15-, 13-, and 14-H), 4.18 (1H, br, W_H=12 Hz, 2β-H), 4.76 (2H, s), and 5.56 (1H, br, W_H=12 Hz, 3-H). Found: C, 72.29; H, 11.24%. Calcd for $C_{21}H_{38}O_2Si$: C, 72.00; H, 10.86%.

Eudesma-3,11-diene-2β,5β-diol (21a) and Its 2α-Epimer (21b). *i)*: Compound **20a** (150 mg) was stirred with acetic acid (1 ml) in water (1 ml) and THF (2 ml) at room temperature for 16 h. The mixture was worked up as usual to leave crude crystals (120 mg), showing a single spot on TLC, which were purified by preparative TLC over silica gel with etheyl acetate–hexane (3 : 1) to give **21a** (90 mg), mp 170—171 °C (from ether); $[\alpha]_D$ +48.3°; MS, *m/e* 236 (M^+), 218, and 200; IR (Nujol), 3500, 1635, and 885 cm^{-1}; δ 1.24, 1.70, and 1.76 (each 3H, each s, 15-, 13-, and 14-H), 4.18 (1H, br dd, J=10 and 6 Hz, 2α-H), 4.68 (2H, s), and 5.52 (1H, br s, W_H=5 Hz, 3-H). Found: C, 75.93; H, 10.16%. Calcd for $C_{15}H_{24}O_2$: C, 76.27; H, 10.17%.

ii): Compound **29b** (50 mg) was stirred with acetic acid (0.5 ml) in water (0.5 ml) and THF (1 ml) at room temperature for 19 h. The mixture was worked up as uaual to leave a gum (45 mg), showing a single spot on TLC, which was purified by preparative TLC over silica gel with ethyl acetate–hexane (3 : 1) to give **21b** (27 mg), gum, $[\alpha]_D$ +108.4°; MS, *m/e* 236 (M^+), 218, and 200; IR (neat), 3450 (br), 3110, 1650, and 890 cm^{-1}; NMR, δ 1.07, 1.75, and 1.83 (each 3H, each s, 15-, 13-, and 14-H), 4.30 (1H, br, W_H=16 Hz, 2β-H), 4.76 (2H, s), and 5.72 (1H, br, W_H=7.5 Hz, 3-H). Found: C, 75.81; H, 10.21%. Calcd for $C_{15}H_{24}O_2$: C, 76.27; H, 10.17%.

Conversion of 21a and 21b into (+)-β-Rotunol (1). *i)*: Compound **21a** (1 g) was stirred with activated mangnanese-(IV) oxide (4.8 g) in dry dichloromethane (85 ml) at room temperature for 16 h. The reaction mixture was filtered through a Celite column. The filtrate was evaporated to leave crude crystals (1.1 g), showing a single spot on TLC, which were purified by preparative TLC with ethyl acetate–hexane (1 : 2) to give **1** (844 mg), mp 117—119 °C (needles from ether); $[\alpha]_D$ +41.4°; MS, *m/e* 234 (M^+), 216, 173, and 111; IR (Nujol), 3450, 3090, 1625 (sh), and 890 cm^{-1}; NMR, δ 1.15, 1.75, and 2.00 (each 3H, each s, 15-, 13-, and 14-H), 2.08 and 2.72 (each 1H, ABq, J=17 Hz, 1-H), 4.74 (2H, s), and 5.88 (1H, br s, W_H=4 Hz, 3-H).

ii): Compound **21b** (35 mg) was stirred with activated manganese(IV) oxide (300 mg) in dry dichloromethane (5 ml) at room temperature for 16 h. The reaction mixture was worked up in the same manner as that of **21a** to give **1** (29 mg), mp 116—118 °C (needles from ether), whose spectral data ($[\alpha]_D$, MS, IR, NMR) were identical with those obtained from **21a**. These synthetic samples of β-rotunol (**1**) were completely identical with a sample of the natural compound in the spectral data: natural sample, mp 118—119 °C (needles); $[\alpha]_D$ +44.8° ($CHCl_3$); MS, *m/e* 234, 216, 173, and 111; IR (Nujol), 3450, 3100, 1640, and 890 cm^{-1}; NMR, δ 1.15 (3H, s, 15-H), 1.74 (3H, t, J=1 Hz, 13-H), 1.99 (3H, d, J=1 Hz, 14-H), 2.07 and 2.71 (each 1H, ABq, J=17 Hz, 1-H), 4.75 (2H, q, J=1 Hz, 12-H), and 5.89 (1H, q, J=1 Hz, 3-H).

Eudesma-2,4,11-triene (24). A solution of **3** (248 mg, 1 mmol) in THF (5 ml) containing tosylhydrazine (186 mg, 1 mmol) and concd hydrochloric acid (one drop) was heated under reflux for 7 h. After addition of benzene (10 ml), the mixture was evaporated to remove THF, until the boiling

point became 80 °C, and cooled with an ice-bath. To the benzene solution was added methyllithium [0.7 M in ether (3.2 ml), 2.24 mmol], when nitrogen gas was evolved. The reaction was continued by stirring at room temperature for 30 min and ceased by addition of water. The whole mixture was extracted with hexane (3×20 ml), washed with water, dried, and evaporated to leave oily residue (260 mg), which was purified by column chromatography over silica gel with hexane–ethyl acetate (9 : 1) to give **24** (170 mg), oil; $[\alpha]_D$ +170.2°; MS, *m/e* 202 (M^+), 187, and 131 (base); UV_{max}, 266 nm (log ε 3.79) and 208 (3.78); IR (neat), 3100, 3050, 1650, 1590, 890, and 720 cm^{-1}; NMR, δ 0.93 and 1.71 (each 3H, s, 15- and 13-H), 1.76 (3H, t, J=2, 14-H), 4.72 (2H, s, 12-H), and 5.67 (2H, s, 2- and 3-H). Found: C, 88.89; H, 10.88%. Calcd for $C_{15}H_{22}$: C, 89.04; H, 10.96%.

*Transformation of **24** into α-Rotunol (**2**).* To a solution of **24** (50 mg, 0.216 mmol) in dichloromethane (25 ml) cooled at −78 °C was added rapidly tungsten(VI) chloride (17 mg, 0.043 mmol) under nitrogen. Into the mixture was passed oxygen gas under vigorous stirring in the dark for 2 h. The reaction mixture was then kept at room temperature for 10 min, mixed with water, and extracted with ether (3× 20 ml). The ether solution was washed, dried and evaporated to leave oily crude peroxide (**25**), (64 mg), which without further purification was treated with alumina (Merck, activ basisch, Type E, Activitätsstufe I, 1.6 g) in ether at room temperature for 16 h. The mixture was filtered and the insoluble alumina was washed with ether repeatedly. The combined ether solutions were dried and evaporated to give crude **2** (60 mg), which was purified by preparative TLC over silica gel with hexane–ethyl acetate (3 : 1) to afford **2** (51 mg) in pure state, mp 102—104 °C (from ethyl acetate–hexane); $[\alpha]_D$ +53°; UV_{max} 235 nm (log ε 4.20); IR ($CHCl_3$), 3480, 3100, 1660, 1630 (sh), and 890 cm^{-1}; NMR, δ 1.04 and 1.77 (each 3H, each s, 15- and 13-H), 1.96 (3H, d, J=11 Hz, 14-H), 2.72 (1H, d, J=17 Hz, 1-H), 4.77 (2H, s, 12-H), and 5.81 (1H, s, 3-H).

References

1) Part XXXII of "Studies on the Phytoalexins," and Part XII of "Synthetic Studies of Rishitin and Related Compounds." Part XXXI and Part XI of the respective series; A. Murai, A. Abiko, M. Ono, and T. Masamune, *Bull. Chem. Soc. Jpn.*, **55**, 1191 (1982).

2) H. Hikino, K. Aota, D. Kuwano, and T. Takemoto, *Tetrahedron Lett.*, **1969**, 2921; *Tetrahedron*, **27**, 4831 (1971).

3) A. Murai, M. Ono, A. Abiko, and T. Masamune, *J. Am. Chem. Soc.*, **100**, 7751 (1978).

4) D. L. Roberts, *Phytochemistry*, **11**, 2077 (1972).

5) A. Murai, M. Ono, and T. Masamune, *Chem. Lett.*, **1978**, 1005.

6) H. Hikino, N. Suzuki, and T. Takemoto, *Chem. Pharm. Bull.*, **14**, 1441 (1966).

7) *Cf.*, J. A. Marshall and H. Roebke, *Tetrahedron Lett.*, **1970**, 1555.

8) B. M. Trost, T. N. Saltzmann, and K. Hiroi, *J. Am. Chem. Soc.*, **98**, 4887 (1976).

9) E. Vedejs, *J. Am. Chem. Soc.*, **96**, 5944 (1974); E. Vedejs, D. A. Engler, and J. E. Telschow, *J. Org. Chem.*, **43**, 188 (1978).

10) E. J. Corey and D. Crouse, *J. Org. Chem.*, **33**, 298 (1968).

11) E. J. Corey and A. Venkateswarlu, *J. Am. Chem. Soc.*, **94**, 6190 (1972).

12) K. Tori, *Rep. Shionogi Res. Lab.*, **14**, 136 (1964).

13) *Cf.*, A. J. Fatiadi, *Synthesis*, **1976**, 65.

14) K. K. Ogilivie and D. J. Iwacha, *Tetrahedron Lett.*, **1973**, 317.

15) K. B. Sharpless and R. C. Michaelson, *J. Am. Chem. Soc.*, **95**, 6136 (1973).

16) *Cf.*, A. Yasuda, H. Yamamoto, and H. Nozaki, *Tetrahedron Lett.*, **1976**, 2621.

17) R. C. Anderson, D. M. Gunn, J. Murray-Rust, P. Murray-Rust, and J. S. Roberts, *J. Chem. Soc., Chem. Commun.*, **1977**, 27.

18) W. G. Dauben, M. E. Lorber, N. D. Vietmeyer, R. H. Shapiro, J. H. Duncan, and K. Tomer, *J. Am. Chem. Soc.*, **90**, 4762 (1968).

19) *Cf.*, D. H. R. Barton, R. K. Haynes, P. D. Magnus, and I. D. Menzies, *J. Chem. Soc., Chem. Commun.*, **1974**, 511.

Synthesis of Phytuberin[1]

Akio MURAI, Mitsunori ONO, and Tadashi MASAMUNE*
Department of Chemistry, Faculty of Science, Hokkaido University, Sapporo 060
(Received September 11, 1981)

The first synthesis of phytuberin, which mimics the proposed biogeneses in critical stages, is described. The synthesis also establishes the absolute configuration.

The title compound, phytuberin (**1**), is a potential substance for an effective resistance in diseased potatoes[2] and a representative phytoalexin together with rishitin[3] in the genus *Solanum*. The sesquiterpene was first isolated in 1970 by Varns and Kuć[4] from infected potato tuber tissues (*Solanum tuberosum*), and the structure and relative configuration were determined in 1974 on the basis of the X-ray crystallographic analysis of dihydrophytuberin by Coxon and coworkers.[5] In view of the novel structure characterized by the presence of two hydrofuran rings and the biological importance, **1** is believed to be a subject of intense synthetic investigation. In a preliminary communication[6,7] we reported the synthesis of the compound, which mimics the proposed biogeneses[5,8] (*e.g.*, Scheme 1) in critical stages. The present paper describes details of the transformation of β-rotunol (**2**) into **1**, which, coupled with the synthesis[1] of **2**, completes the synthesis of the title compound.

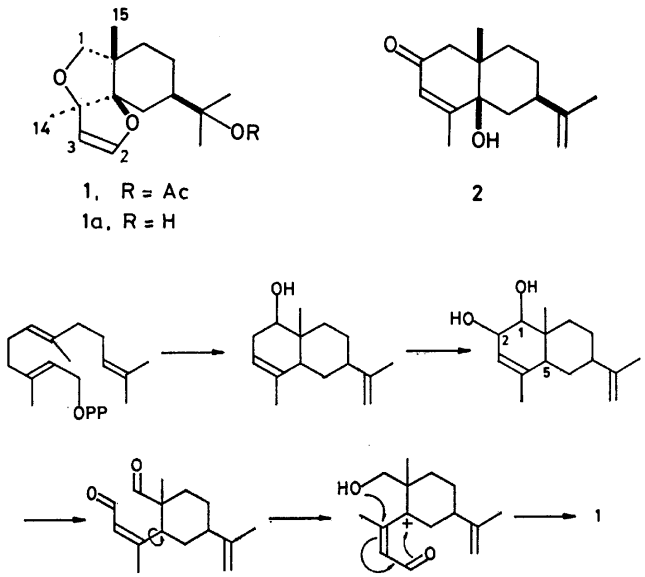

Scheme 1.

Results and Discussion

The proposed biogeneses[5,8] suggested that phytuberin (**1**) would probably be biosynthesized *via* formation of a C-5 and C-1 and/or C-2 oxygenated eudesmane from farnesyl pyrophosphate and subsequent cleavage of the C-1–C-2 bond followed by recyclization. β-Rotunol (**2**) is an eudesmane with oxo- and hydroxyl groups at C-2 and C-5 and hence a starting material suitable for the relevant cleavage and recyclization. Transformation of **2** into **1** was commenced by oxygenation at C-1; namely, **2** was oxidized under the Vedejs conditions[9] to give 1β,5β-diol (**3**) in 57% yield as a single product. Configuration of the hydroxyl group at C-1 was deduced from the formation of acetonide (**4**) by treatment with acetone in the presence of Amberlyst 15 at room temperature for 1 h. Contrary to the expectation, all attempted oxidative cleavage ($NaIO_4$ in aq THF, $Pb(OAc)_4$ in pyridine, or HIO_4 in aq THF) of the α-ketol (**3**) failed, the isopropenyl group being not left intact. Considering the lability of the isopropenyl group under the conditions, **4** was first converted into the corresponding 11,12-epoxide (**5**) by treatment with *m*-chloroperbenzoic acid in a heterogeneous mixture of 5% aqueous sodium hydrogencarbonate and dichloromethane. Reduction of the epoxy group of **5** with hydride reagents was examined under various conditions. The aimed reduction was achieved by treatment of **5** with lithium aluminium hydride (LAH) in a 5 : 2 mixture of 1,2-dimethoxyethane (DME) and tetrahydrofuran (THF) *in an inverse addition manner*, giving tetrahydroxyeudesmane (**6**) in 56% yield from **3**. Smooth oxidative cleavage of the 1,2-diol system was accomplished by treatment of **6** with lead(IV) acetate in dry pyridine at room temperature. The reaction proceeded as expected to afford the relevant formyl γ-lactone (**7**) in a single step in 80% yield. The structure of **7** was assigned clearly on the basis of the spectral data. The mass spectrum displayed parent and fragmentation peaks at *m/e* 266 and 248 (M^+-H_2O). The IR spectrum (2710, 1755, 1720, and 1630 cm^{-1}) revealed the presence of a five-membered lactone and a formyl group. The NMR spectrum exhibited a six-proton singlet at δ 1.19, two three-proton singlets at δ 1.35 and 2.16, and a one-proton singlet at δ 9.36, which were readily assignable to the protons at 12-, 13-, 15-, 14-, and 1-carbon atoms,[10] respectively. Formation of **7** would involve oxidation of an hemiacetal intermediate (**8**) with excess lead(IV) acetate.

The final and most serious problem for the construction of phytuberin skeleton consisted in stereoselective formation of the A and B rings. Owing to difficulty of regioselective reduction of only the hindered formyl group, it was undertaken to reduce simultaneously both the formyl and lactone carbonyl groups. Treatment of the formyl γ-lactone (**7**) with diisobutylaluminium hydride (DIBAH) (3.5 mol equiv.) in DME followed by usual work-up effected reduction of the two relevant carbonyl groups followed by cyclization to two hydrofuran rings, giving alcohol, oil and $[\alpha]_D$ −40.6°, in a single step in 83% yield. The alcohol was converted smoothly into the acetate, oil and $[\alpha]_D$ −38.8°, in 84% yield by treatment with acetic anhydride and triethylamine in the presence of 4-(dimethylamino)pyridine at

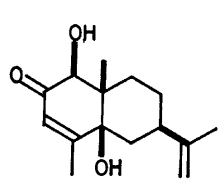

3

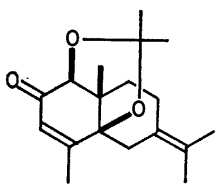

4

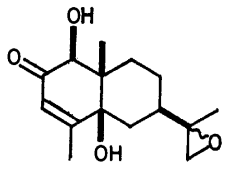

5

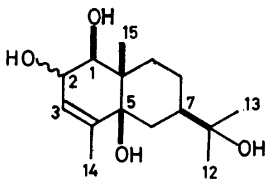

6

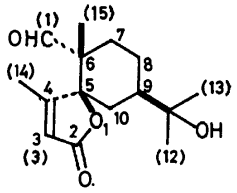

7

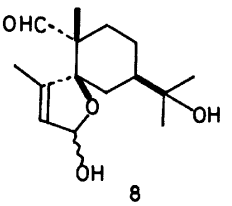

8

room temperature. The alcohol and acetate were identified as phytuberol (**1a**) and phytuberin (**1**), respectively, by direct comparison of the synthetic and natural samples. The result constitutes the first synthesis of phytuberin, and also establishes the undecided absolute configuration of these sesquiterpenes.

Experimental

All the melting points were uncorrected. The homogeneity of each compound was always checked by TLC over silica gel (Wakogel B-5) with various solvent systems, the spots being developed with cerium(IV) sulfate in diluted sulfuric acid and/or iodine. The optical rotations, UV and NMR (100 MHz) spectra were measured in chloroform, ethanol, and chloroform-*d* respectively, unless otherwise stated.

1β-Hydroxy-β-rotunol (3). To a solution of diisopropylamine (0.24 ml, 1.3 mmol) in dry THF (3 ml) cooled at −78 °C was added dropwise butyllithium in hexane (0.94 ml, 1.3 mmol) under nitrogen, and the solution was stirred at 0 °C for 15 min. To the solution cooled at −78 °C was added a solution of β-rotunol (**2**) (138 mg, 0.52 mmol) in dry THF (3 ml). To the reaction mixture, stirred at −78 °C for 1 h, was added rapidly molybdenum peroxide (MoOPH) (738 mg, 1.3 mmol). The whole mixture was stirred continuously for 1 h at −78 °C and then at room temperature for 30 min. After being treated with water, the reaction mixture was concentrated *in vacuo* to leave oily residue, which was extracted with ethyl acetate, repeatedly. The acetate solution was washed with 2 M† hydrochloric acid, saturated sodium hydrogencarbonate, and water, dried, and evaporated to leave an oil (141 mg), which was separated by chromatography over preparative TLC over silica gel with ethyl acetate–hexane (1 : 2). Fractions (70 mg) with higher R_f value, showing a single spot on TLC, afforded **3** with low mp; $[\alpha]_D$ +27.6°; MS, *m/e* 250 (M^+), 232, and 111; IR (neat), 3400 (br), 3100, 1680, 1630, and 890 cm^{-1}; NMR, δ 1.28 (3H, s, 15-H), 1.80 and 2.04 (each 3H, each s, 13- and 14-H), 3.60 (1H, br s, 1α-H), 4.76 (2H, br s), and 5.88 (1H, s, 3-H). Found: C, 71.77; H, 8.45%. Calcd for $C_{15}H_{22}O_3$: C, 72.00; H, 8.80%. Fractions (24 mg) with lower R_f value, showing a single spot on TLC, afforded the unreacted starting material (**2**). Acetate of **3**, oil; MS, *m/e* 292 (M^+), 274, 234, 214; IR (neat), 1745 cm^{-1}; NMR, δ 2.19 (3H, s, $OCOCH_3$), and 4.96 (1H, s). Acetonide (**4**) of **3**, mp 125—129 °C; IR (Nujol), 1696, 1663, 1645, 1405, 1200, 1155, and 1100 cm^{-1}; NMR, δ 0.79 (3H, s, 15-H), 1.30 and 1.41 [each 3H, s, $(CH_3)_2$], 1.94 (9H, s, 12-, 13-, and 14-H), 3.51 (1H, s, 1α-H), and 5.92 (1H, br s, W_H= 5 Hz, 3-H).

1β-Hydroxy-11,12-epoxy-β-rotunol (5). Compounds **3** (55 mg, 0.22 mmol) was stirred with *m*-chloroperbenzoic acid (45.6 mg) in a heterogeneous mixture of dichloromethane (5 ml) and 5% aqueous sodium hydrogencarbonate (5 ml) at −15 °C for 4 h. The reaction mixture was washed with 5% aqueous sodium thiosulfate and water, dried, and evaporated to leave amorphous residue (**5**)(58 mg), showing a single spot on TLC: MS *m/e* 266 (M^+), and 248; IR (neat), 3380, 1680, 1625, 1020, and 910 cm^{-1}; NMR, δ 1.24, 1.32, and 2.00 (each 3H, 15-, 13-, and 14-H), 2.62 (2H, br s, W_H=9 Hz, 12-H), 3.50 (1H, br s, 1α-H), and 5.84 (1H, s, 3-H). This was used for the next reaction without purification because sample of unstability.

Eudesm-3-ene-1β,2ξ,5β,11-tetrol (6). To a stirred solution of **5** (83 mg) in dry DME (5 ml) at −78 °C was added dropwise a suspension (3 ml) of LAH (100 mg) in dry THF (5 ml) during 15 min. The mixture was stirred at room temperature for 2 h, mixed with water (0.5 ml) and 5% aqueous sodium hydroxide (0.5 ml), and was filtered. The filtrate was dried and evaporated to leave amorphous residue (85 mg), which was purified by column chromatography (3 g) over silica gel with ethyl acetate–hexane (4 : 1) to give **6** (77 mg), gum; MS, *m/e* 270 (M^+), 252, and 234; IR (neat), 3580, 3500, and 1620 cm^{-1}; NMR, δ 1.12 (6H, s, 12- and 13-H), 1.20 and 1.22 (total 3H, each s, 14-H), 3.56 (1H, br s, W_H=5 Hz, 1α-H), 4.14 (1H, br, W_H= 10 Hz, 2-H), 5.35 and 5.56 [total 1H (1 : 3), each br, W_H=5 and 9 Hz, 3-H]. Found: C, 66.88; H, 9.55%. Calcd for $C_{15}H_{26}O_4$: C, 66.67; H, 9.63%.

4,6β-Dimethyl-6α-formyl-9β-(2-hydroxy-2-methyl)ethyl-1-oxaspiro-[4.5]dec-3-en-2-one (7). To a stirred solution of **6** (40 mg) in dry pyridine (3 ml) was added lead(IV) acetate (recrystallized freshly from acetic acid, 295 mg) at room temperature. The reaction mixture was stirred for 30 min and, after addition of oxalic acid (950 mg) and water (2 drops) to decompose excess of the reagent, was submitted to filtration. The filtrate was diluted with water and extracted with ethyl acetate, repeatedly. The acetate solution was washed with 2 M hydrochloric acid, saturated sodium hydrogencarbonate, and water, dried, and evaporated to leave an oil (42 mg), showing a single spot on TLC, which was purified by preparative TLC over silica gel with ethyl acetate–hexane (2 : 1) to yield **7** (32 mg), oil; MS, *m/e* 266 (M^+) and 248; IR (neat), 3480, 2710, 1755, 1720, 1630, and 1380 cm^{-1}; NMR,[10] δ 1.19 (6H, s, 12- and 13-H), 1.35 and 2.16 (each 3H, each s, 15- and 14-H), 5.66 (1H, s, 3-H), and 9.36 (1H, s, 1-H). Found: C, 68.00; H, 8.55%. Calcd for $C_{15}H_{22}O_4$: C, 67.67; H, 8.27%.

Phytuberol (1a). To a stirred solution of **7** (17 mg, 0.064 mmol) in dry DME (5 ml) was added DIBAH in hexane (0.13 ml, 0.224 mmol) at −78 °C under nitrogen. The whole reaction mixture was stirred at −78 °C for 30 min,

† 1 M=1 mol dm^{-3}.

at −20 °C for 30 min, and then at 0 °C for 30 min. The reaction was quenched by addition of water (10 drops), and the mixture was diluted with 2 M hydrochloric acid and extracted with ether, repeatedly. The ether solution was washed with saturated sodium hydrogencarbonate and water, dried, and evaporated to leave colorless oil (21 mg), showing a single spot on TLC [ethyl acetate–hexane (1 : 1)], which was purified by preparative TLC over silica gel with ethyl acetate–hexane (1 : 1) to yield **1a** (13 mg), oil; $[\alpha]_D$ −40.6°; MS, *m/e* 252 (M^+) and 234; IR (neat), 3490, 3090, 1625, 1153, 1088, 1040, 1027, and 735 cm^{-1}; NMR, δ 1.00 and 1.55 each 3H, s, 15- and 14-H), 1.20 (6H, s, 12- and 13-H), 3.24 and 3.39 (each 1H, ABq, J=8 Hz, 1-H), 4.66 and 6.42 (each 1H, d, J=2.8 Hz, 3- and 2-H). Natural sample,[5] oil, $[\alpha]_D$ −36.9°; MS, *m/e* 252.1710; IR (neat), 3440, 3080, 1624, 1153, 1088, 1040, 1027, and 735 cm^{-1}; NMR, δ 0.99 and 1.53 (each 3H, s), 1.18 (6H, s), 3.23 and 3.37 (each 1H, ABq, J=8.5 Hz), 4.64 and 6.41 (each 1H, d, J=2.8 Hz).

Phytuberin (1). A mixture of **1a** (12 mg), acetic anhydride (0.5 ml), and 4-(dimethylamino)pyridine (2 mg) in dry triethylamine (2 ml) was stirred at room temperature for 16 h. The mixture was diluted with water and extracted with ether. The ether solution was worked up as usual to leave colorless oil (14 mg), showing a single spot on TLC, which was purified by preparative TLC over silica gel with ethyl acetate–hexane (1 : 4) to yield **1** (9.8 mg), oil; $[\alpha]_D$ −38.8°; MS, *m/e* 294 (M^+), 249, 234, 219, 205, 189, and 107; IR (neat) 3085, 1730, 1625, 1262, 1154, 1080, and 732 cm^{-1}; NMR, δ 1.02, 1.45, 1.48, and 1.57 (each 3H, s, 15-, 12-, 13-, and 14-H), 1.99 (3H, s, $OCOCH_3$), 3.28 and 3.42 (each 1H, ABq, J=8 Hz, 1-H), 4.68 and 6.44 (each 1H, d, J=3 Hz, 3- and 2-H). Natural sample,[5] oil; $[\alpha]_D$ −35.9°; MS, *m/e* 294.1849; 294, 249, 234, 219, 205, 191, 189, 149, and 107; IR (neat), 3080, 1728, 1620, 1260, 1088, and 735 cm^{-1}; NMR, δ 1.02, 1.44, 1.47, and 1.56 (each 3H, s), 1.99 (3H, s), 3.28 and 3.41 (each 1H, ABq, J=8.5 Hz), 4.68 and 6.44 (each 1H, d, J=2.8 Hz).

References

1) Part XXXIII of "Studies on the Phytoalexins," and Part XIII of "Synthetic Studies of Rishitin and Related Compounds." Part XXXII and Part XII of the respective series; A. Murai, M. Ono, A. Abiko, and T. Masamune, *Bull. Chem. Soc. Jpn.*, **55**, 1195 (1982).

2) For recent reviews, see, J. Kuć, "Biochemical Aspects of Plant-Parasite Relationship," ed by J. Fried and D. R. Threlfall, Academic Press, New York, N. Y. (1976), p. 225; T. Masamune, A. Murai, and N. Katsui, *Kagaku To Seibutsu*, **16**, 648 (1978); J. B. Stothers, *Pure Appl. Chem.*, **53**, 1241 (1981).

3) T. Masamune, A. Murai, M. Takasugi, A. Matsunaga, N. Katsui, N. Sato, and K. Tomiyama, *Bull. Chem. Soc. Jpn.*, **50**, 1201 (1977).

4) J. L. Varns, Ph. D. Thesis, Purdue University, Lafayette Indiana, 1970; J. L. Varns, J. Kuć, and E. B. Williams, *Phytopathology*, **61**, 174 (1971).

5) D. L. Hughes and D. T. Coxon, *J. Chem. Soc., Chem. Commun.*, **1974**, 822; D. T. Coxon, K. R. Price, B. Howard, and R. F. Curtis, *J. Chem. Soc., Perkin Trans. 1*, **1977**, 53. *Cf.*, J. Kuć, *Teratology*, **8**, 333 (1973); D. T. Coxon, R. F. Curtis, K. R. Price, and B. Howard, *Tetrahedron Lett.*, **1974**, 2363.

6) A. Murai, M. Ono, A. Abiko, and T. Masamune, *J. Am. Chem. Soc.*, **100**, 7751 (1978).

7) After our publication, three modifications of the synthesis have been reported: D. Caine and T. L. Smith, Jr., *J. Am. Chem. Soc.*, **102**, 7568 (1980); J. A. Findlay, D. N. Desai, G. C.Lonergan, and P. S. White, *Can. J. Chem.*, **58**, 2827 (1980); F. Kido, H. Kitahara, and A. Yoshikoshi, *J. Chem. Soc.,Chem. Commun.*, **1981**, 1236.

8) A. Stoessl, E. W. B. Ward, and J. B. Stothers, *Tetrahedron Lett.*, **1976**, 3271; After completion of our work, almost the same biogenetic pathway as our synthetic route was reported; A. Stoessl, J. B. Stothers, and E. W. B. Ward., *Can. J. Chem.*, **56**, 645 (1978).

9) E. Vedejs, *J. Am. Chem. Soc.*, **96**, 5944 (1974); E. Vedejs, D. A. Engler, and J. E. Telschow, *J. Org. Chem.*, **43**, 188 (1978).

10) The numbering of the carbon atoms (the figures in the parentheses of formula **7**) refer to that of the original eudesmane (**6**).

 © 1982 The Chemical Society of Japan Bull. Chem. Soc. Jpn., 55, 1205—1208 (1982)

Reaction of 1-Lithio-1-arylthio(or alkylthio)methyltrimethylsilane with Acid Derivatives. A Novel Synthesis of Functionalized Vinyl Sulfides

Toshio AGAWA,* Minori ISHIKAWA, Mitsuo KOMATSU, and Yoshiki OHSHIRO

Department of Petroleum Chemistry, Faculty of Engineering, Osaka University, Yamada-oka 2-1, Suita, Osaka 565

(Received September 28, 1981)

Reactions of 1-lithio-1-phenylthiomethyl- (**1a**) and 1-lithio-1-methylthiomethyltrimethylsilane (**1b**) with amides, an ester, acid anhydrides, a urea, and a carbonate are described which provide useful routes to functionalized vinyl sulfides. The reaction of **1** with amides gave β-functionalized vinyl sulfides, 1-dialkylamino-2-phenylthio (or methylthio)ethylenes, in 40—95% yields and the reaction could be extended to the sulfonyl derivatives of **1** to afford 1-dialkylamino-2-phenylsulfonyl(or methylsulfonyl)ethylenes. Although ethyl benzoate and some acid anhydrides were not good substrates for this reaction, tetramethylurea and diethyl carbonate gave α-functionalized vinyl sulfides, 1-amidovinyl- and 1-(ethoxycarbonyl)vinyl sulfides, in moderate yields when treated with **1a** followed by addition of benzaldehyde.

Olefin-forming reaction of α-metallosilanes is known as the Peterson reaction and plays an important role in organic synthesis. For example, 1-lithio-1-arylthio-(or alkylthio)methyltrimethylsilanes **1** react with ketones to give vinyl sulfide derivatives.[1] However, only a few reports mention this type of reactions of the α-metallosilanes **1** with acid derivatives,[2] since they are in general not good substrates for the Peterson olefination.

In our preliminary report we briefly described the reaction of the α-lithiosilanes **1** with several amides which provided a new synthetic method for 2-aminovinyl sulfides.[3] We further investigated the reaction using acid derivatives and found that these reactions can be utilized for preparation of various functionalized vinyl sulfides.

Since vinyl sulfides are very versatile reagents as masked carbonyl compounds,[4] these functionalized vinyl sulfides are expected to have more potential in organic synthesis.[5]

Results and Discussion

Reaction of the α-Lithiosilane 1 with Amides. 1-Lithio-1-phenylthiomethyltrimethylsilane (**1a**) gener-

TABLE 1. YIELDS, BOILING AND MELTING POINTS, AND SPECTRAL DATA OF **3** AND **8**

R	R^1	R^2_2	Yield %	Isomer ratio[a] E : Z	Bp θ_b/°C (mmHg[b]) [M_p θ_m/°C]	IR(ν/cm^{-1}, neat) C=C	^{1}H NMR (δ, $CDCl_3$)	MS(70 eV) m/e (M^+)
3a PhS	H	Me_2	64	100 : 0	90(0.01)	1630	2.80(6H,s),4.56(1H,d,J=13.0Hz),6.55 (1H,d,J=13.0Hz),6.8—7.4(5H,m)	179
3b PhS	*t*-Bu	Me_2	40	20 : 80	65—67(2.0)	1580	1.13(7.2H,s,*Z*-Bu^t),1.19(1.8H,s,*E*-Bu^t), 2.48(1.2H,s,*E*-Me),2.75(4.8H,s,*Z*-Me),5.63(0.2H,s,*E*-CH=),5.99(0.8H,s, *Z*-CH=),7.1—7.4(5H,m)	235
3c PhS	Ph	Me_2	65	96 : 4	112—113(0.03)	1580	2.70(5.76H,s,*E*-Me),2.85(0.24H,s, *Z*-Me),5.00(≈1H,s,*E*-CH=),5.10(≈0H, *Z*-CH=),6.8—7.4(10H,m)	255
3d PhS	Ph	$-(CH_2)_2-$	87	80 : 20	145(0.1)	1580	1.90(3.2H,s,*E*-CH_2),2.11(0.8H, s,*Z*-CH_2),5.73(0.8H,s,*E*-CH=),5.91(0.2H, s,*Z*-CH=),7.0—7.7(10H,m)	253
3e PhS	Ph	$-(CH_2)_5-$	95	100 : 0	130(0.02)	1580	1.2—1.8(6H,m),2.6—3.2(4H,m),5.21 (1H,s,CH=),6.8—7.5(10H,m)	295
3f MeS	Ph	$-(CH_2)_5-$	72[a]	87 : 13	120(2.0)	1580	1.2—1.8(6H,m),2.10(2.6H,s,*E*-Me), 2.27(0.4H,s,*Z*-Me),2.6—3.2(4H,m), 5.03(≈0.9H,s,*E*-CH=),5.12(≈0.1H,s, *Z*-CH=),7.2—7.5(5H,m)	233
8a $PhSO_2$	H	Me_2	60	100 : 0	[131]	1610[c]	2.86(6H,s),4.84(1H,d,J=12.0Hz,CH=), 7.1—8.0(6H,m,CH= and Ph)	211
8b $PhSO_2$	H	$-(CH_2)_5-$	81	100 : 0	150(1.0)[d]	1600	1.2—1.8(6H,m),2.9—3.3(4H,m),4.95 (1H,d,J=13.0Hz,CH=),7.1—8.0(6H, m,CH= and Ph)	251
8c $MeSO_2$	H	Me_2	42	100 : 0	173(1.0)[e]	1600	2.90(9H,s),4.90(1H,d,J=12.0Hz,CH=), 7.17(1H,d,J=12.0Hz,CH=)	149
8d $MeSO_2$	H	$-(CH_2)_5-$	24	100 : 0	150(1.0)[d]	1610	1.4—1.8(6H,m),2.92(3H,s),3.0—3.3 (4H,m),4.98(1H,d,J=12.8Hz,CH=), 7.11(1H,d,J=12.8Hz,CH=)	189

a) Determined by NMR spectroscopy. b) 1 mmHg≈133.322 Pa. c) In Nujol mull. d) Purified by pot distillation. e) Purified by Kugel Rohr.

ated by treating phenylthiomethyltrimethylsilane with butyllithium at 0 °C in THF was reacted with *N,N*-dimethylformamide at the same temperature and was allowed to stand overnight. Usual work-up of the reaction mixture gave 64% of (*E*)-1-dimethylamino-2-phenylthioethylene (**3a**). In this reaction only the (*E*)-isomer was obtained and the structure was determined by spectral data and elemental analysis. Similarly several 2-aminovinyl sulfides were obtained from the α-lithiosilanes **1** and amides **2** in good yields under very mild conditions and the results are summarized in Table 1.

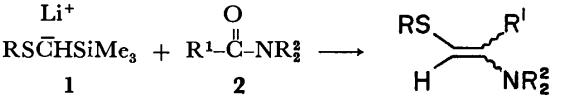

1a: R=Ph
1b: R=Me

In most cases a mixture of (*E*)- and (*Z*)-isomers was obtained and the ratio was determined by NMR spectroscopy. Estimation of the coupling constant between the phenyl carbon and the vinyl proton ($^3J_{CH}$) by ^{13}C-NMR measurement under selective irradiation of the phenyl protons was tried. However, the values for the compounds **3c** (the major isomer only) and **3e** were ≃7 cps which was not decisive for determination of (*E*)- or (*Z*)-form of olefinic compounds. The assignment of (*E*)- and (*Z*)-isomers of the compounds **3c**—**f** was done by comparison of the chemical shifts of the vinyl protons with those of the known compounds **4**,[6] **5**,[7] and **6**.[8] Thus the isomer which

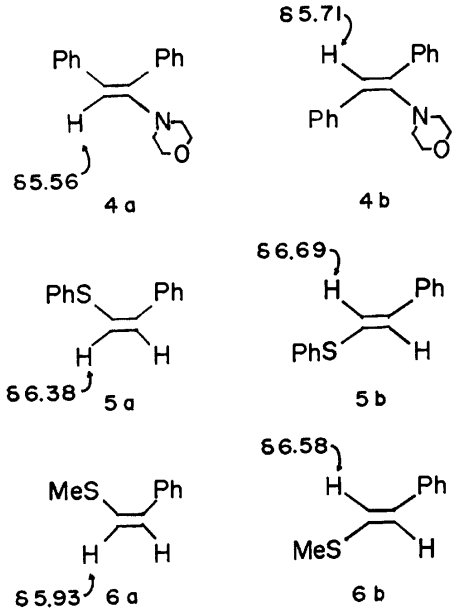

shows the vinyl proton signal in the higher field is determined to be the (*E*)-isomer of **3** (the vinyl proton is *trans* to the phenyl ring) and the other is the (*Z*)-isomer. For the vinyl sulfide **3b**, the methyl group which appears in the lower field is suggested to be that of the (*Z*)-isomer by comparing chemical shifts of the alkylamino groups of **3c** and **3d**. Hence the major product of the reaction was found to be an (*E*)-isomer except for the case of **3b**.

Although the sterically less favorable (*E*)-isomers were predominant, this result is consistent with the observation that **4a**, sterically less favorable, is thermodynamically more stable than **4b**, which is sterically less crowded.[6] This phenomenon was explained by the continuous overlap between the electron pair on the nitrogen atom and the phenyl group in its polar resonance form[9] and the same reason can be applied to the predominance of the (*E*)-isomers in this reaction. The only exception observed for **3b** may be ascribed to the large steric repulsion caused by the bulky *t*-butyl group which suppressed the formation of the (*E*)-isomer.

Extension of the reaction to sulfone derivatives was successful. The reaction of 1-lithio-1-phenylsulfonyl(or methylsulfonyl)methyltrimethylsilane **7** with amides **2** gave 2-aminovinyl sulfones **8** and the results are listed

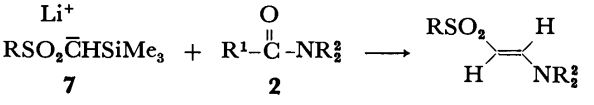

7a: R=Ph
7b: R=Me

in Table 1. Method of lithiation and reaction conditions are different from the preceding reactions (see Experimental). Contrary to the α-phenylthiosilane **1a**, the corresponding phenylsulfonylsilane **7a** gave very poor yields of vinyl sulfones when treated with less reactive amides such as *N,N*-dimethylbenzamide and *N*-benzoylpiperidine. Oxidation of the aminovinyl sulfides to sulfones were also examined, but it was difficult to isolate or to purify the oxidized products. Thus the present reaction is one of the better routes to 2-aminovinyl sulfones.

Reaction with Ester and Acid Anhydride. Reaction of the α-lithiosilane **1a** with ethyl benzoate was carried out in a similar manner to the reaction with amides, and α-phenylthioacetophenone (**9**) was obtained in 60% yield with considerable amount of the starting phenylthiomethylsilane **10**. The anticipated product, 2-ethoxyvinyl sulfide, was not formed at all or the sulfide is quite sensitive to hydrolysis even under basic conditions, since no vinyl proton signals were detected in the NMR spectrum of the reaction mixture immediately after the quenching. Addition of benzaldehyde or

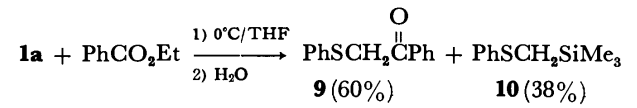

successive addition of lithium diisopropylamide and the aldehyde to the reaction mixture before the quenching was also carried out, but no vinyl sulfide derivatives were detected. Hence, it is not possible that the initial product of the reaction was an acylated phenylthiomethyltrimethylsilane which corresponds to **16** or **18** in Scheme shown later.

Similar reaction of the silane **1a** with benzoic anhydride gave only a small amount of α-phenylthioacetophenone (**9**) and the most part of **1a** was recovered as the starting phenylthiomethylsilane **10**. Some cyclic acid anhydrides such as phthalic anhydride and maleic anhydride were found to be quite unreactive with **1a**.

$$\mathbf{1a} + (PhCO)_2O \xrightarrow[2)\,H_2O]{1)\ rt/THF} \mathbf{9}(18\%) + \mathbf{10}(77\%)$$

Reaction with Urea and Carbonate. The α-lithiosilane **1a** was treated with tetramethylurea at room temperature to give *N,N*-dimethyl-α-phenylthioacetamide (**11**) in 56% yield. As it was likely that the reaction proceeded *via* substitution of the dimethylamino group, benzaldehyde was added to the reaction mixture and was allowed to stand for one day at room temperature. The product was *N,N*-dimethyl-α-phenylthiocinnamamide (**12a**, 41%) and thus one pot synthesis of an 1-amidovinyl sulfide was found. The same treatment of the methylthiomethylsilane **1b** and the urea gave *N,N*-dimethyl-α-methylthiocinnamamide (**12b**, 27%).

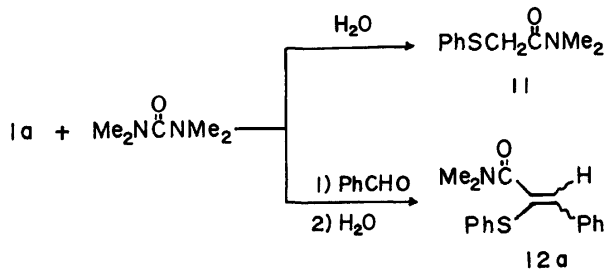

Similarly, the silane **1a** reacted with diethyl carbonate to afford ethyl α-phenylthiocinnamate (**13**) after addition of benzaldehyde. The yield was increased by addition of an equimolar amount of lithium diisopropylamide (LDA) because of its higher basicity than that of lithium ethoxide generated by substitution.

$$\mathbf{1a} + EtO\text{-}\overset{O}{\overset{\|}{C}}\text{-}OEt \longrightarrow$$

$$[PhSCH(SiMe_3)CO_2Et + EtOLi] \xrightarrow{LDA}$$

$$[PhSCLi(SiMe_3)CO_2Et] \xrightarrow[2)\ H_2O]{1)\ PhCHO} EtO\overset{O}{\overset{\|}{C}}(PhS)C{=}CHPh$$

13 (59%)

The paths for the whole reactions are assumed to be as shown in Scheme 1. The two paths from the initially formed intermediate **14** is considered to be controlled by the nature of the substituents Y and Z. When Y is not a hetero-atom substituent, rearrangement of the intermediate **14** to **15** occurs to form an olefinic compound **3** or **17**. Thus the reaction with an amide proceeded *via* the paths (a) and (c). On the other hand, the path (b) seems to be predominant when both Y and Z are hetero atoms such as the urea and the carbonate. Formation of 1-acylvinyl sulfides on addition of benzaldehyde implies the intermediacy of **18** and excludes the formation of **11** by hydrolysis of a 1,1-diaminoethylene corresponding to **3**. The path for the reaction with the ester, however, is not clear at the moment. The result that no olefinic product was obtained by addition of lithium diisopropylamide and benzaldehyde suggests less possibility of the formation of **16** or **18**. But we cannot exclude the formation of α-phenylthioacetophenone (**9**) by hydrolysis of a vinyl ether **3** or a silyl ether **17**.

Experimental

Boiling points were uncorrected. A melting point was determined on a Yanagimoto micro melting point apparatus and was uncorrected. ^1H and ^{13}C NMR spectra were obtained with JEOL JNM PMX-60 and JNM FX-90Q FT spectrometers using TMS as an internal standard. IR spectra were taken on a JASCO IRA-1 spectrophotometer. Mass spectrometry was performed on a Hitachi RMU-6E spectrometer at an ionizing voltage of 70 eV.

All experiments were carried out under a dry nitrogen atmosphere.

Materials. Commercially available butyllithium, ethyl benzoate, tetramethylurea, diethyl carbonate, and *N,N*-dimethylformamide were used. The other amides were prepared by the reaction of the corresponding acid chlorides and the amides and purified by distillation except for *N*-benzoylaziridine. Isopropylamine and THF were dried and distilled by the usual method. Phenylthiomethyltrimethylsilane, methylthiomethyltrimethylsilane, phenylsuflonylmethyltrimethylsilane, and methylsulfonylmethyltrimethylsilane

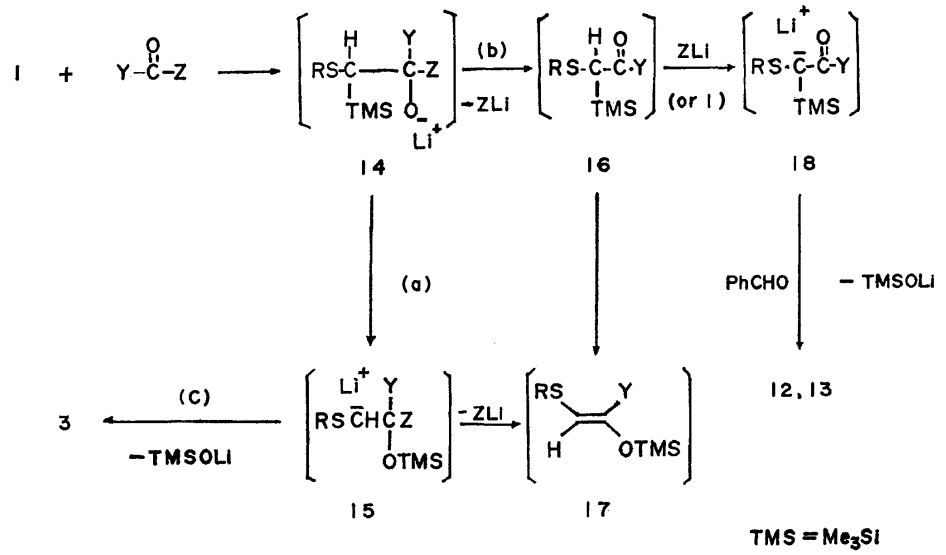

Scheme 1.

were prepared by silylation of methyl phenyl sulfide, dimethyl sulfide, methyl phenyl sulfone, and dimethyl sulfone with triemethylsilyl chloride, respectively, by the known method.[10]

General Procedure for the Reactions of the Silanes **1** *with Acid Derivatives.* To a stirred solution of phenylthio(or methylthio)methyltrimethylsilane (**1**, 5.0 mmol) in THF (5 ml) was added butyllithium (3.8 ml of 15% hexane solution, 6.0 mmol) at 0—5 °C, and the solution was stirred for 2 h at room temperature. An acid derivative (5.0 mmol) in THF (5 ml) was added at 0—5 °C and the stirring was continued for 2 h at the same temperature. The mixture was stood overnight at room temperature, quenched with water after cooling, and extracted (ether). The oragnic layer was dried (Na_2SO_4) and evaporated to give a crude product, which was isolated and purified by distillation and/or chromatography on silica gel. 1-Dialkylamino-2-phenylthio(or methylthio)-ethylenes **3** could be purified only by distillation because of their ready hydrolysis. Hence, some of their elemental analyses were unsatisfactory.

*1-Dimethylamino-2-phenylthioethylene (**3a**)*: Found: C, 66.88; H, 7.43; N, 7.53; S, 18.15%. Calcd for $C_{10}H_{13}NS$: C, 67.02; H, 7.31; N, 7.82; S, 17.86%.

*α-Dimethylamino-β-phenylthiostyrene (**3c**)*: ^{13}C NMR ($CDCl_3$) δ 40.7 (q), 86.8 (d, =CHS–), 158.2 (s, =CPh), and aromatic carbons at δ 123.9, 125.2, 127.6, 127.9, 128.2, 128.8, 136.6 and 141.2. Found: C, 75.17; H, 6.72; N, 5.54; S, 12.38%. Calcd for $C_{16}H_{17}NS$: C, 75.27; H, 6.71; N, 5.49; S, 12.53%.

*β-Phenylthio-α-piperidinostyrene (**3e**)*: ^{13}C NMR ($CDCl_3$) δ 24.5 (t), 25.8 (t), 50.2 (t), 91.2 (d, =CHS–), 158.2 (s, =CPh), and aromatic carbons at δ 124.4, 126.0, 127.8, 128.3, 128.5, 129.3, 137.1, and 140.7. Found: C, 76.81; H, 7.04; N, 4.54; S, 10.90%. Calcd for $C_{19}H_{21}NS$: C, 77.26; H, 7.12; N, 4.74; S, 10.83%.

*α-Phenylthioacetophenone (**9**)*: Bp 120 °C/1.0 mmHg by pot distillation; IR (neat) 1680 cm^{-1} (C=O); ^1H NMR ($CDCl_3$) δ 4.30 (2H, s, CH_2), 7.1—7.5 (8H, m, PhS and a part of PhCO), 7.8—8.0 (2H, m, the rest of PhCO); MS, *m/e* 228 (M^+).

N,N-*Dimethyl-α-phenylthioacetamide (**11**)*: Bp 120 °C/3 mmHg, IR (neat) 1630 cm^{-1} (C=O); ^1H NMR ($CDCl_3$) δ 2.92 (3H, s), 2.98 (3H, s), 3.71 (2H, s), 7.0—7.6 (5H, m).

The Reactions of the Silanes **7** *with Amides.* To a stirred butyllithium (3.8 ml of 15% hexane solution) was added diisopropylamine (0.84 ml, 6.0 mmol) in THF (5 ml) at 0—5 °C. After stirring for 1 h at room temperature, the resulting lithium diisopropylamide (LDA) solution was cooled to −60—−70 °C and phenylsulfonyl(or methylsulfonyl)trimethylsilane (5.0 mmol) was added to the solution. The stirring was continued for 1 h at room temperature followed by addition of an amide (6.0 mmol) in THF (5 ml). Then the mixture was warmed at 50—60 °C for 5 h with stirring. The reaction mixture was quenched with water after cooling, extracted (CH_2Cl_2), dried (Na_2SO_4), and concentrated to give a crude product, which was isolated and purified by crystallization or distillation. Elemental analyses of the products were not satisfactory because of their high sensitivity to hydrolysis.

*1-Dimethylamino-2-phenylsulfonylethylene (**8a**)*: Found: C, 56.69; H, 6.18; N, 6.63; S, 15.10%. Calcd for $C_{10}H_{13}NO_2S$: C, 56.86; H, 6.20; N, 6.63; S, 15.15%.

Formation of the Cinnamamides **12** *and the Cinnamate* **13**. Benzaldehyde (5.0 mmol) in THF (5 ml) was added to a reaction mixture obtained from phenylthiomethyltrimethylsilane (5.0 mmol), butyllithium (6.0 mmol), and tetramethylurea (5.0 mmol) according to the procedure shown above. The mixture was allowed to stand for 1 d at room temperature and was worked up similarly to the previous runs to give 0.58 g (41%) of *N,N*-dimethyl-α-phenylthiocinnamamide (**12a**) as a mixture (57 : 43) of two isomers: bp 130 °C/0.001 mmHg by pot distillation; IR (neat) 1630 cm^{-1} (C=O); ^1H NMR ($CDCl_3$) δ 2.63 (≈1.7H, s), 2.76 (≈1.7H, s), 2.89 (≈1.3H, s), 2.95 (≈1.3H, s), 6.60 (0.57H, s), 6.73 (0.43H, s), 7.1—7.7 (10H, m).

An analytical sample of the major isomer could be isolated by chromatography on silica gel; MS, *m/e* 283 (M^+). Found: C, 71.84; H, 5.01; N, 6.11; S, 11.01%. Calcd for $C_{17}H_{17}NOS$: C, 72.06; H, 4.94; N, 6.05; S, 11.29%.

Similarly 0.30 g (27%) of *N,N*-dimethyl-α-methylthiocinnamamide (**12b**) was obtained from methylthiomethyltrimethylsilane (5.0 mmol), butyllithium (6.0 mmol), the urea (5.0 mmol), and the aldehyde (5.0 mmol) as a mixture (65 : 35) of two isomers: bp 150 °C/5 mmHg; IR (neat) 1620 cm^{-1} (C=O); ^1H NMR ($CDCl_3$) δ 2.24 (1.05H, s), 2.35 (1.95H, s), 2.81 (1.95H, s), 2.98 (≈2H, s), 3.04 (≈1H, s), 3.13 (≈1H, s), 6.48 (0.65H, s), 6.59 (0.35H, s), 7.1—7.6 (5H, m), MS, *m/e* 221 (M^+).

In the case of the reaction starting with phenylthiomethyltrimethylsilane (5.0 mmol), butyllithium (6.0 mmol), and diethyl carbonate (5.0 mmol), THF solution of LDA (5.0 mmol) prepared by the method shown above was added to the reaction mixture at 0 °C. The mixture was stirred for 3 h at the same temperature and overnight at room temperature followed by addition of benzaldehyde (5.0 mmol) in THF (5 ml). The mixture was allowed to stand for 1 d at room temperature and worked up as the previous runs to afford 0.84 g (59%) of ethyl α-phenylthiocinnamate (**13**): bp 150 °C/1 mmHg by pot distillation; IR (neat) 1720 cm^{-1} (C=O); ^1H NMR δ 1.30 (3H, t), 4.07 (2H, q), 7.3—7.9 (10H, m), 8.30 (1H, s, =CH); MS, *m/e* 284 (M^+).

References

1) D. J. Peterson, *J. Org. Chem.*, **33**, 780 (1968); F. A. Carey and A. S. Court, *ibid.*, **37**, 939 (1972); T. Taguchi, H. Okamura, and H. Takei, *Chem. Lett.*, **1975**, 853.

2) D. Seebach, M. Kolb, and B-T. Gröbel, *Chem. Ber.*, **106**, 2277 (1973); R. P. Woodbury and M. W. Rathke, *Tetrahedron Lett.*, **1978**, 709.

3) T. Agawa, M. Ishikawa, M. Komatsu, and Y. Ohshiro, *Chem. Lett.*, **1980**, 335.

4) B-T. Gröbel and D. Seebach, *Synthesis*, **1977**, 357.

5) B. M. Trost, *Chem. Rev.*, **78**, 363 (1978) and references cited therein; K. Iwai, H. Kosugi, and H. Uda, *Chem. Lett.*, **1974**, 1237.

6) M. E. Munk and Y. K. Kim, *J. Org. Chem.*, **30**, 3705 (1965).

7) A. A. Oswald, K. Griesbaum, B. E. Hudson, Jr., and J. M. Bregman, *J. Am. Chem. Soc.*, **86**, 2877 (1964).

8) M. C. Caseiro, R. E. Pratt, and R. J. Holland, *J. Am. Chem. Soc.*, **88**, 5747 (1966).

9) L. W. Haynes, "Enamines," ed by A. G. Cook, Marcel Dekker, New York (1969), Chap. 2, pp. 92—96.

10) D. J. Peterson, *J. Org. Chem.*, **32**, 1717 (1967).

Kinetic Studies on the Amination of Leucoquinizarin

Masashi KIKUCHI, Takamichi YAMAGISHI, and Mitsuhiko HIDA*

Department of Industrial Chemistry, Faculty of Technology, Tokyo Metropolitan University, Fukazawa, Setagaya-ku, Tokyo 158

(Received September 30, 1981)

Leucoquinizarin reacts with amines to give mono- and diaminoanthraquinones. The amination mechanism of leucoquinizarin was investigated on the basis of the kinetics and structures of leuco compounds. The amination reaction of leucoquinizarin was characterized as follows. This amination proceeded in polar solvent but not in nonpolar solvent at all. The reaction rate was not influenced by the addition of a small amount of water (95% ethanol) but enhanced largely in 80% ethanol. This amination reaction has a low activation energy ($\Delta E^*=5.7-9.0$ kcal mol^{-1}) and an extraordinarily small pre-exponential term ($A=10^3-10^5$ l mol^{-1} min^{-1}). Leucoquinizarin was proposed to be aminated by the addition of amine to carbonyl group at its 1,4-position. The oxidation of leuco monoaminohydroxyanthraquinone was also examined.

Leucoquinizarin (**1**) reacts with amines to give mono- and diaminoanthraquinone derivatives, which are among the most important compounds in synthetic dyes. Although many patents[1] and some papers[2] on the amination of **1** have been reported, most of them are nothing but technical reports and no mechanistic investigation has been made. Though some reports concerning the structures of leucoanthraquinones have been published,[3] they have given no convincing data.[4,5] We have recently elucidated the structures of leucoanthraquinones on the basis of ^{13}C-NMR spectra.[6] In this paper we discuss the amination of **1** from the kinetic point of view, and propose that **1** in 1,4-diketo form is the most reactive to amine among the possible tautomeric isomers. The oxidation of leuco monoaminohydroxyanthraquinone was also examined.

Results and Discussion

Kinetics of the Amination of 1 with Butylamine. The reaction of **1** with butylamine in air gave 1-butylamino-4-hydroxyanthraquinone (**2**) and 1,4-bis(butylamino)-anthraquinone (**3**). The reaction under a nitrogen atmosphere gave compounds **2** and **3** in their leuco forms. Since all attempts of quantitative oxidations of these leuco compounds to the anthraquinone derivatives led unsatisfactory results, the amination reaction under a nitrogen atmosphere was followed by taking visible spectra of the amination solution in the presence of citric acid as reducing agent to suppress the oxidations of leuco compounds of **1** and **2**. By using a small amount of butylamine ($C_4H_9NH_2$/**1**=1—5) and by setting the conversion low only leuco compound of **2** was obtained. The reaction was first order on both concentrations of **1** and butylamine and the second order rate constant was independent of these concentrations. The Arrhenius plots showed a good straight line. As shown in Table 1, the reaction proceeded easily in ethanol and DMF, but did not at all in nonpolar solvent such as benzene. These facts show that the polarity of solvent largely enhances the reaction rate and suggest that the reaction intermediate is of ionic character.

If the solvation energy (ΔF_{solv}) of reaction intermediate was approximated by the Born's equation (1), and if the cavity size and the temperature dependency of dielectric constant (D) do not vary with solvent, both values of ΔH^* and ΔS^* will increase with increase in

$$\Delta F_{solv} = C(1-1/D) \quad (1)$$

dielectric constant of the solvent. In accordance with our expectation ΔH^* and ΔS^* have larger values in DMF (D=36.7) than those in ethanol (D=23.2). Since dielectric constant of aqueous ethanol increases in proportion to the amount of water,[7] the reaction rate in aqueous ethanol will increase with increase in water content. But the reaction rate in aqueous ethanol did not increase proportionally to water content and both values of ΔH^* and ΔS^* in 80% ethanol decreased as compared with those in ethanol, though the dielectric constant (D=34) is larger than that of ethanol. Thus the results in aqueous ethanol could not be understood only by the increase in polarity of solvent, but another interaction such as the hydrogen bonding between the reaction intermediate and water should be also assumed.

The amination reaction of **1** was characterized by a low activation energy ($\Delta E^*=5.7$—9.0 kcal mol^{-1}) and extraordinarily small pre-exponential term ($A=10^3$—

Table 1. Solvent effects on the amination of leucoquinizarin

Solvents	$k_{60\,°C}$ / l mol^{-1} min^{-1}	ΔE^* / kcal mol^{-1}	A / l mol^{-1} min^{-1}	ΔH^* / kcal mol^{-1}	ΔS^*[a] / cal deg^{-1} mol^{-1}
DMF	0.989	9.04	7.51×10^5	8.38	−35.21
C_6H_6	No reaction	—	—	—	—
C_2H_5OH[b]	0.523	7.02	1.96×10^4	6.36	−41.07
C_2H_5OH/H_2O[c]	0.532	—	—	—	—
C_2H_5OH/H_2O[d]	1.014	5.72	5.96×10^3	5.05	−43.44

a) This value is shown by correcting a statistic factor 2. b) These values were reinvestigated (see Ref. 6). c) 95% ethanol. d) 80% ethanol.

10^5 l mol^{-1} min^{-1}). In many cases the activation energy and pre-exponential term are reported to be 20—30 kcal mol^{-1} and 10^9—10^{11} l mol^{-1} min^{-1}, respectively, while anomalously small activation energy (ΔE^{*}=10—18 kcal mol^{-1}) and pre-exponential term (A=10^5—10^6 l mol^{-1} min^{-1}) are known in the Menschutkin reaction between pyridine or triethylamine and alkyl iodide[8] and in the semicarbazone formation of acetophenones (ΔE^{*}=4—11 kcal mol^{-1}, A=0.27—10^5 l mol^{-1} min^{-1}).[9] These reactions are known to proceed through ionic intermediates.

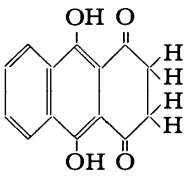

1a

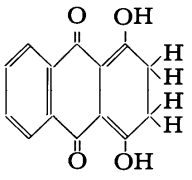

1b

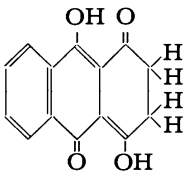

1c

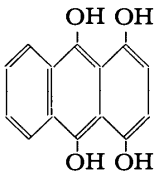

1d

The Structures of 1 and Leuco Compound of 2. The ^{1}H-NMR spectrum of **1** showed methylene protons (4H; singlet, 3.05 ppm), hydroxyl protons (2H; singlet, 13.50 ppm) and aromatic ring protons (4H of A_2B_2 type, 8.42, 7.77 ppm). This result suggests the possibilities of the structures **1a** or **1b**.

With respect to leuco compound of **2**, the five possible structures (**2a**—**e**; R=C_4H_9) can be written as follows.

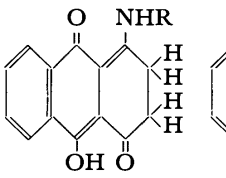

2a

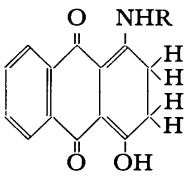

2b

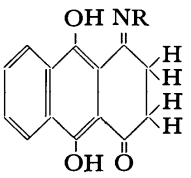

2c

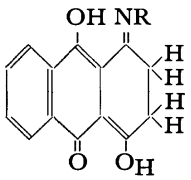

2d

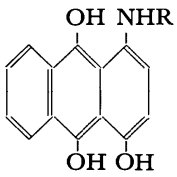

2e

The ^{1}H-NMR spectrum of leuco compound of **2** showed methylene protons (4H; triplet, 2.88 ppm), one hydroxyl proton (1H; singlet, 13.95 ppm), one amino proton (1H; broad, 14.90 ppm) and unsymmetrical ring protons (4H; multiplet, 8.36, 7.62 ppm). This result permits the assignment of leuco compound of **2** to **2a** or **2b**. The presence of the unsymmetrical ring protons seems to demand 4,9-diketo form (**2a**) for leuco compound of **2**.

An examination of ^{13}C-NMR spectra shows that the resonance peaks of carbonyl carbons (C-9, 10) of anthraquinons were characteristically observed at about 180 ppm,[10] but the chemical shifts of carbonyl carbon adjacent to the methylene or methyl carbon are at about 200 ppm.[11] The chemical shift 200.8 ppm of the carbonyl carbon of **1** suggested that **1** may exist in the 1,4-diketo form **1a**. The chemical shifts of the carbonyl carbons of leuco compound of **2** were 199.9 and 172.2 ppm and the latter corresponds to the carbonyl carbon detached from the methylene carbon. These results concluded that the leuco compound of **2** exists predominantly in unsymmetrical 4,9-diketo form **2a** in solution. All ^{1}H-NMR spectra of **1** in $CDCl_3$, DMF-d_7, C_6D_6 and $CDCl_3$–C_2D_5OD (1 : 1) were the same except hydroxyl protons. Also ^{13}C-NMR spectra of **1** in $CDCl_3$, C_6D_6, DMF-d_7 were the same. These spectra showed that **1** retained 1,4-diketo form **1a** predominantly in these solutions. The spectra in C_2D_5OD could not be measured due to low solubility of **1**.

Two possibilities as to the reaction mechanism could be considered as follows.

1. The elementary reaction, which determined the rate of the amination of **1**, has intrinsically a low activation energy and a small pre-exponential term.
2. A very reactive species is one of the tautomers (**1b**—**d**), which exists in a very small amount in the solution.

The compounds of **2a** and 1,4-dimethoxy-9,10-anthracenediol gave no aminated product with butylamine in the same conditions as **1** undergoes amination. This result suggests that **1c** and **1d** are much less reactive than 1,4-diketo form **1a**. Consequently, though the possibility of **1b** to be reactive species cannot be excluded, **1a** could be thought to be the most reactive among tautomeric isomers. The amination of leucoquinizarin seems to proceed by the addition and elimination mechanism as shown in Scheme 1. The addition of amine to carbonyl group of **1a** was led to **2a** *via* an ionic reaction intermediate such as **3**.

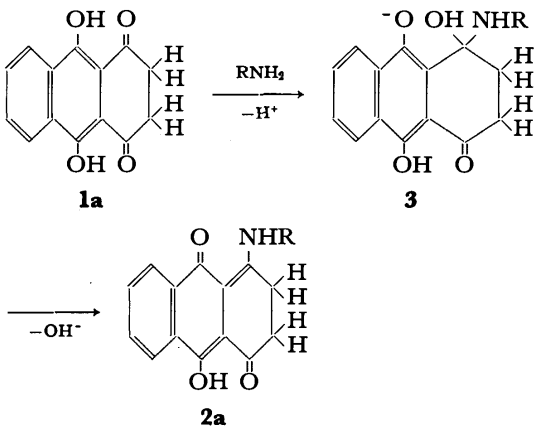

Scheme 1.

Base catalysis by amine can be excluded, because the second order rate constant was independent of amine concentration. The possibility of the reaction intermediate having an ion pair also may be excluded, because the polarity effect of solvent was very large, and then the inner solvation cannot be considered.

Dissociation of 1 in Solution. The possibility of the dissociation of **1** in the reaction media was examined since the dissociation may be promoted by the presence

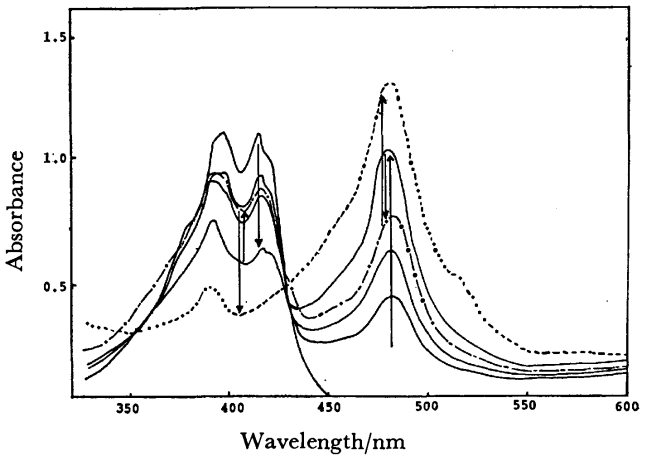

Fig. 1. The visible spectra of leucoquinizarin (**1**) depending on the amount of triethylamine (TEA). [TEA]/mol dm^{-3}: ——; 0—0.358, -·-·-; 0.358—0.574, ------; 0.574—0.717. [**1**]$=8.257\times10^{-5}$ mol dm^{-3}.

of amine. The dissociated **1** may suppress the reactivity of **1** for the nucleophilic attack of amine. Change of the visible spectra of **1** by the presence of triethylamine (inactive for the amination) tells the stepwise dissociation of **1** as shown in Fig. 1. The absorption spectra showed isosbestic points at 353 nm and 429 nm in range of the amine concentration below 0.358 mol dm^{-3}. If a single acid and base equilibrium between **1** and triethylamine can be assumed, the acidity of **1** could be estimated from change of absorbance with the concentration of amine, as shown in Fig. 1, by usual method. But the value of the acid and base equilibrium constant obtained largely depends on wavelength. This means that the single equilibrium cannot be reasonably assumed, but formation of other species, such as radical anion, also should be assumed. Consequently, the amount of dissociated **1** in the amination could not be determined, but it can be considered to be negligible, since the same spectra in the absence and presence of triethylamine were observed in the same conditions as **1** undergoes amination.

The Oxidation of Leuco Compound of **2**. Leuco compounds of aminated product have been oxidized by heating in nitrobenzene,[2a,b] by heating with an excess of amine,[2c] in oleum,[12] or alkaline solution.[1] Currently the heating in nitrobenzene has been reported to be the most plausible method of oxidation of these leuco compounds. As shown in Table 2, the oxidation could not be carried out quantitatively in triethylamine–ethanol solution. The oxidation in nitrobenzene gave **2** in *ca.* 60% at most, accompanied by side reactions such as dealkylation and other reactions. The dealkylated product was confirmed to be 1-amino-4-hydroxyanthraquinone by comparison of its spectra and TLC with those of the authentic sample. The brown product was composed of several compounds and identification of their structures was impossible. It is found that the aminated products are susceptible to dealkylation, while the formation of the brown product is easily formed at lower temperature. Consequently the current method heating in nitrobenzene cannot be approporiate method. The quantitative oxidation method of leuco compounds, which is not accompanied by side reactions, should be investigated.

Table 2. The oxidation of leuco compound of **2**

Solvents	Temp/°C	Time/h	Yield of **2**/%	Conv.
TEA[a]–Ethanol	60	2	72.1	—
Nitrobenzene	160	2	59.6 (4.0)[b]	100
Nitrobenzene	170	2	64.5 (9.2)	100
Nitrobenzene	180	2	61.5 (14.2)	100
Nitrobenzene	Reflux	0.25	62.5 (27.9)	100

a) Triethylamine. b) Parenthesis shows the yield of 1-amino-4-hydroxyanthraquinone.

Experimental

Materials. The leuco compounds and anthraquinone derivatives were prepared and confirmed as reported previously.[6] Leucoquinizarin (**1**): λ_{max} (ethanol) 398 nm (ε; 12700), 415 nm (ε; 12300).[13] Leuco compound of **2**: λ_{max} (ethanol) 432 nm (ε; 17000), 457 nm (ε; 18570).[13] The butylamine was dried by refluxing on sodium metal and distilled under a nitrogen atmosphere. All the solvents were purified by the usual methods, and stored under a nitrogen atmosphere.

Kinetic Measurements. A typical run is as follows. Leucoquinizarin and ethanol were mixed in a flask. After this solution was brought to the reaction temperature, the reaction was initiated by adding butylamine ethanol solution into the leucoquinizarin solution; the concentrations of leucoquinizarin and butylamine were 5 mmol dm^{-3} and 5—25 mmol dm^{-3}, respectively. All above operations were performed under a dry and oxygen-free nitrogen atmosphere. At regular time interval, 0.3 ml portion of reaction solution was withdrawn and diluted to 25 ml with ethanol containing citric acid (0.603 g/250 ml) to suppress the oxidation of leuco compounds. The yield of leuco aminated product **2a** was determined spectrometrically. Visible spectra were measured with Shimazu UV-210 spectrometer.

^{1}H-NMR and ^{13}C-NMR Measurements. ^{1}H-NMR spectrum of leucoquinizarin in $CDCl_3$ was already reported.[6] ^{1}H-NMR spectra in DMF-d_7, C_6D_6, and C_2D_5OD–$CDCl_3$ (1 : 1) were as follows. The parentheses show the chemical shifts (δ, ppm) of α, β protons of aromatic ring, methylene protons and hydroxyl protons, respectively. DMF-d_7: (8.50, 8.00; 3.10; 14.78), C_6D_6: (8.48, 7.36; 2.28; 14.23), C_2D_5OD–$CDCl_3$(1 : 1) : (8.24, 7.64; 2.97; 4.21). The peaks of carbonyl carbons in ^{13}C-NMR were observed at 200.8 ppm ($CDCl_3$),[6] 200.8 ppm (C_6D_6), and 202.6 ppm (DMF-d_7) showing the existence of the carbonyl carbon adjacent to the methylene carbon. In the case of C_2D_5OD solution, the spectrum could not be measured due to low solubility. ^{1}H-NMR spectra were measured using TMS as an internal standard with a Hitachi R-24 spectrometer. ^{13}C-NMR spectra were measured under a nitrogen atmosphere using TMS as an internal standard with a JEOL FX-60 spectrometer.

The Oxidation of Leuco Compound of **2**. A mixture of leuco compound of **2** (20 mg) and nitrobenzene (0.65 ml) was heated in air. The products were separated by column chromatography on silica gel using benzene as eluent and identified to be **2** and 1-amino-4-hydroxyanthraquinone as the dealkylated product by comparison with authentic samples. The yields of products **2** and 1-amino-4-hydroxyanthraquinone were determined spectrometrically.

References

1) M. R. Michael, Brit. Patent 2013701 (Cl C09B1/22) ICI. (1979); *Chem. Abstr.*, **92**, 199751 (1980); J. A. W. George, Brit. Patent 1504137 (Cl D06p1/16) Kodak Ltd. (1978); *Chem. Abstr.*, **89**, 112381u (1978).

2) a) K. Naiki, *Yuki Gosei Kagaku*, **12**, 364 (1954); b) Y. Banshō, *Kogyo Kagaku Zasshi*, **57**, 80 (1954); c) Y. Bansho and K. Kondō, *ibid.*, **57**, 751 (1954); d) M. S. Simon, *J. Am. Chem. Soc.*, **85**, 1974 (1963); M. S. Simon and D. P. Waller, *Tetrahedron Lett.*, **1967**, 1527; e) C. W. Greenhalgh and N. Hughes, *J. Chem. Soc., C*, **1968**, 1284.

3) S. M. Bloom and P. F. Hutton, *Tetrahedron Lett.*, **1963**, 1993.

4) G. S. Egerton, N. E. N. Assaad, and N. D. Uffindell, *J. Soc. Dyers Colour.*, **83**, 45 (1967).

5) C. W. Greenhalgh, *Endeavour*, **35**, 134 (1976).

6) M. Kikuchi, T. Yamagishi, and M. Hida, *Dyes Pigments*, **2**, 143 (1981).

7) E. S. Amis, "Solvent Effects on Reaction Rates and Mechanisms," Academic Press, New York (1966), p. 175.

8) K. J. Laider, "Reaction Kinetics, Vol. II, Reaction in Solution," Pergaman Press, London (1963).

9) R. P. Cross and P. Fugassi, *J. Am. Chem. Soc.*, **71**, 223 (1949).

10) G. Höfle, *Tetrahedron*, **30**, 1963 (1976).

11) M. Kobayashi, Y. Terui, K. Tori, and N. Tsuji, *Tetrahedron Lett.*, **1976**, 619.

12) M. I. Krasnoselśkaya, L. D. Leichenko, N. A. Parfenov, V. I. Kolodyazhnyi, and M. P. Venzelovskii, U. S. S. R. Patent 411077 (Cl C07C, C09b) (1974); *Chem. Abstr.*, **81**, 93052d (1974).

13) These values were determined in ethanol containing citric acid (0.603 g/250 ml) to suppress the oxidation of leuco compounds.

 © 1982 The Chemical Society of Japan Bull. Chem. Soc. Jpn., 55, 1213—1215 (1982)

Upon DNP-aromatic Rule. Effect of Introducing a Methyl Group to the β-Position upon the CD Spectra of DNP Derivatives of Aromatic α-Amino Acids

Masao KAWAI,* Ukon NAGAI, and Atsuko TANAKA

Mitsubishi-Kasei Institute of Life Sciences, Minamiooya, 11, Machida, Tokyo 194

(Received September 30, 1981)

CD spectra of *N*-DNP-*O*-benzoyl derivatives of L-serine, L-threonine, and L-allothreonine and DNP derivatives of L-phenylalanine and (*βR*)- and (*βS*)-*β*-methyl-L-phenylalanines were studied. The effect of methyl substitution at the *β*-position upon their CD spectra was explained by the change in the population of the rotamer g^- ($\chi^1=-60°$) which was shown to be responsible for the characteristic negative Cotton effect at ≈400 nm. The negative sign of the $[\theta]^{max}_{\approx 400}$ values of the DNP derivatives of aromatic L-α-amino acids described by DNP-aromatic rule was proved to be due to the contribution of the rotamer g^-.

The 2,4-dinitrophenyl (DNP) derivatives of L-α-amino acids having aromatic group on the side chain were found to show a negative Cotton effect around 400 nm. Extensive study upon the chiroptical properties of DNP-α-amino acids and related compounds[1-5] lead us to the proposal of DNP-aromatic rule[3] which predicts a negative $[\theta]_{\approx 400}$ for the compounds DNP·NHCHR$_1$R$_2$ with the absolute configuration corresponding to the aromatic L-α-amino acids, where R$_1$ and R$_2$ are an aromatic and a nonaromatic groups, respectively. The R$_1$ group, which carries an aromatic chromophore, must not contain an additional chiral center, since *N*-DNP-*O*-benzoyl-L-threonine (**1a**) was found to exhibit the positive Cotton effect at 410 nm. The corresponding L-serine derivative (**1b**) showed normal CD spectrum expected as an analog of aromatic L-α-amino acid.[3]

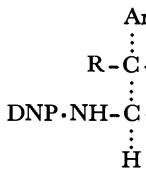

	Ar=OCOPh	Ar=Ph
R=H, R′=CH$_3$	**1a**	**2a**
R=H, R′=H	**1b**	**2b**
R=CH$_3$, R′=H	**1c**	**2c**

For the purpose of investigating the reason why the L-threonine derivative (**1a**), which has one extra methyl group at the *β*-position of the L-serine derivative (**1b**), exhibits an exceptional CD spectrum, *N*-DNP-*O*-benzoyl-L-allothreonine (**1c**) was prepared. The corresponding derivatives (**2a** and **2c**) of DNP-L-phenylalanine (**2b**) were also synthesized. As summarized in Table 1, **1c** exhibited a negative Cotton effect at 405 nm larger than that of **1b**; *i.e.*, the effect of methyl group in **1c** on $[\theta]^{max}_{\approx 400}$ was opposite to that in **1a**. The similar tendency was observed in **2** series, though $[\theta]_{405}$ of **2a** remained negative; *i.e.*, the magnitude of the negative Cotton effects was in the order **2a**<**2b**<**2c**.

Relative orientation of the two chromophores, which is assumed to be the determining factor of the CD spectra, is regulated by the molecular conformation described by the three torsional angles ϕ, χ^1, and χ^2.[6] Restricted rotation around DNP·NH-C$^\alpha$ bond confines the ϕ value to very narrow regions near −160° and near −70°.[7] Assuming that the Cotton effects are due to the exciton coupling between the transition moments of the two chromophores, the rotational strength (RS_1) at the longest wavelength band (400 nm) was calculated using the following equation:[8,9]

$$RS_1 = \frac{2\pi}{ch} \cdot \frac{\lambda_1\lambda_2}{\lambda_1^2-\lambda_2^2} \cdot \left(\frac{(\boldsymbol{\mu}_1\cdot\boldsymbol{\mu}_2)}{R^3} - \frac{3(\boldsymbol{\mu}_1\cdot\boldsymbol{R}_{21})(\boldsymbol{\mu}_2\cdot\boldsymbol{R}_{21})}{R^5}\right) \cdot [\boldsymbol{R}_{21}\cdot(\boldsymbol{\mu}_2\times\boldsymbol{\mu}_1)].$$

The results of the calculation for **2b** with varying χ^1 and χ^2 values were summarized in Fig. 1. As to the side chain conformation, the molecules can be considered to be populated around the three staggered conformations, g^- ($\chi^1=-60°$), g^+ ($\chi^2=+60°$), and t ($\chi^1=180°$), which were expected to exhibit negative, positive, and negligible or slightly negative Cotton effects, respectively. Essentially similar conclusion was obtained by the calculation for **1b**; *i.e.*, in both of **1** and **2** series, the conformer g^- was considered to contribute negative to the observed Cotton effect at ≈400 nm.

Conformational changes induced by the introduction of a methyl group at the *β*-position of **1b** and **2b** were studied by ^{1}H-NMR spectra as summarized in Table 2.[10] As shown in Fig. 2 the *ortho*-proton of the DNP group of **2** was expected to experience an anisotropic shielding effect of the phenyl ring in the conformer g^-, which was considered to be responsible for the negative Cotton

Table 1. CD spectral data recorded in methanol

Compound	Molecular ellipticity($[\theta]\times10^{-2}$) and wavelength(λ/nm) in parentheses[a)]
1a	+34(410),0(360),−19(337),0(290),−135(227),0(213)
1b	−34(408),0(374),+77(340),+20(290),+117(238),0(219)
1c	−80(407),0(361),+73(330),+25(290),+67(270sh),+190(236),+147(220)
2a	−42(405),0(347),+16(320),+13(300),+30(272),0(256),−99(233),0(224)
2b	−91(410),0(363),+74(334),+21(296),+46(270),+23(254),+590(212)
2c	−102(410),−44(350sh),0(316),+70(268),+52(253)

a) sh: Shoulder.

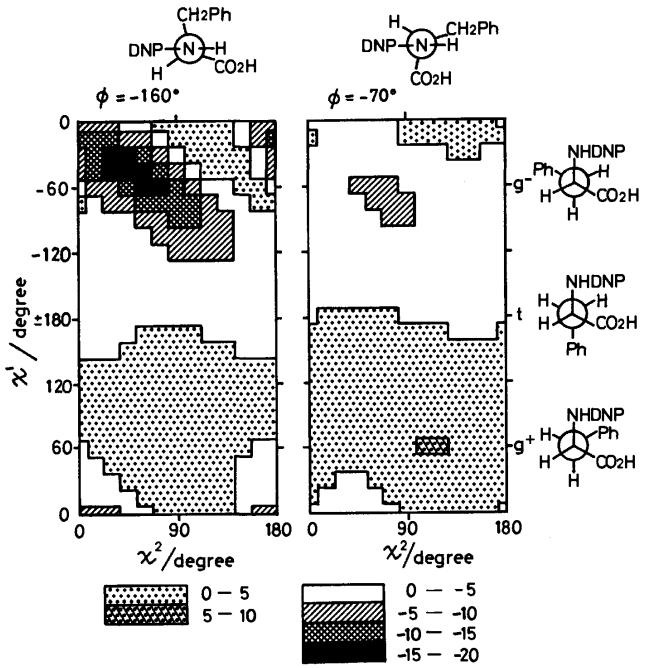

Fig. 1. Calculated rotatory strength (in 10^{-40} c.g.s.) at 400 nm of DNP-L-phenylalanine (**2b**).

TABLE 2. ^{1}H-NMR SPECTRAL DATA

Compound	Chemical shift of aromatic protons[a] (δ)				Coupling constant between $C^\alpha H$ and $C^\beta H$ (J/Hz)
	o	*m*	*m'*	Ph	
1a[b]	7.50	8.40	9.07	7.57,7.70,8.09	2.8
1b[b]	7.45	8.35	8.94	7.52,7.65,7.97	9.2,7.9
1c[b]	7.42	8.30	9.04	7.49,7.65,7.95	2.9
2a[c]	7.12	8.27	9.01	7.37	6.62
2b[c]	7.05	8.24	9.03	7.27	6.63,4.96
2c[c]	6.69	8.06	9.02	7.31	4.47

a) For notations *o*, *m*, *m'*, see Fig. 2. b) Recorded in CD_3COCD_3. c) Recorded in CD_3OD.

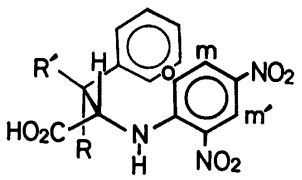

Fig. 2. Conformer g^- of **2a**—**c** in which anisotropic shielding effect of phenyl ring upon the *o*-proton of the DNP group is expected.

effect around 400 nm. The significant difference observed in the chemical shifts of the *ortho*-protons in **2b** and its methyl substituted analogs seem to indicate decrease and increase in the population of the g^- conformer caused by the presence of a methyl group in **2a** and **2c**, respectively, which is consistent with the CD spectral data. In the case of **1b** and its methylated derivatives (**1a** and **1c**), the difference in the chemical shifts of the *ortho*-protons is not prominent, though the same tendency as found in **2** series was observed. The coupling constant between $C^\alpha H$ and $C^\beta H$, however, clearly indicated that the population of g^- conformer is very small for **1a**; *i.e.*, the small coupling constant (2.8 Hz) indicated the two protons to take gauche instead of *trans* positions, to which the g^- conformer corresponds. Thus, the positive $[\theta]_{410}$ value observed for **1a** is explained by significant decrease of the g^- conformer caused by introduction of the methyl group.

In conclusion, the g^- conformer was shown to be responsible for the negative Cotton effect around 400 nm and the effect of methyl substitution at the β-position upon the CD spectra was explained by the change in population of the g^- conformer. Combination of conformational analysis and rotational strength calculation seem to be a useful method for interpreting or predicting chiroptical properties of compounds which show CD spectra due to exciton coupling.

Experimental

Melting points were uncorrected. Compounds **1b** and **2b** were already described in Ref. 3.

N-DNP-O-benzoyl-L-threonine (1a). DNP-L-threonine (713 mg, 2.5 mmol) was benzoylated with Schotten-Baumann method using benzoyl chloride (0.87 cm^3, 7.5 mmol) and NaOH (10 mmol). Crystallization from acetone–benzene afforded **1a** (76 mg) as yellow needles: mp 184—187 °C. Found: C, 52.15; H, 3.85; N, 10.75%. Calcd for $C_{17}H_{15}N_3O_8$: C, 52.45; H, 3.88; N, 10.79%.

N-DNP-O-benzoyl-L-allothreonine (1c). This compound was prepared in the same manner as **1a**, starting from the corresponding L-*allo*threonine derivative: yellow powder; mp 176—177 °C.

As for **2a** and **2c**, the compounds actually synthesized were their enatiomers as described below, starting from the samples supplied by Prof. S. Kuwata of Kōnan University.

(2R,3R)-N-DNP-2-amino-3-phenylbutanoic Acid (Enantiomer of 2a). 2,4-Dinitrophenylation of 38 mg (0.2 mmol) of (2*R*, 3*R*)-2-amino-3-phenylbutanoic acid ($[\alpha]_D^{20}$ +24.2°; *c* 1, H_2O)[11] with the procedure of Sanger[12] afforded the enantiomer of **2a** (45 mg): yellow prisms from ethyl acetate–benzene; mp 169—170 °C. Found: C, 55.59; H, 4.41; N, 12.18%. Calcd for $C_{16}H_{15}N_3O_6$: C, 55.65; H, 4.38; N, 12.17%.

(2R, 3S)-N-DNP-2-amino-3-phenylbutanoic Acid(Enantiomer of 2c). This compound was synthesized from (2*R*, 3*S*)-2-amino-3-phenylbutanoic acid ($[\alpha]_D^{22}$ +6.90°; *c* 1, H_2O)[11] in the same manner as described above. Yellow prisms from ethyl acetate–benzene; mp 159—160 °C. Found: C, 55.58; H, 4.32; N, 12.08%. Calcd for $C_{16}H_{15}N_3O_6$: C, 55.65; H, 4.38, N, 12.17%.

Measurements. CD spectra were recorded on a JASCO spectropolarimeter model J-20 or J-40 at room temperature. PMR spectral data given in Table 2 were measured at 270 MHz on a Bruker WH-270 spectrometer at room temperature.

We wish to thank Prof. Shigeru Kuwata of Kōnan University for his kind gift of the samples of β-methylated phenylalanines. We are also grateful to Dr. Tsutomu Higashijima and Prof. Tatsuo Miyazawa of The University of Tokyo for ^{1}H-NMR measurements and to the members of Analytical Department of System Engineering Laboratory, Mitsubishi-Kasei Industries Ltd., for elemental analyses.

References

1) M. Kawai, U. Nagai, and M. Katsumi, *Tetrahedron*

Lett., **1975**, 2845.

2) M. Kawai and U. Nagai, *Tetrahedron Lett.*, **1977**, 3889.

3) M. Kawai, U. Nagai, M. Katsumi, and A. Tanaka, *Tetrahedron*, **34**, 3435 (1978).

4) U. Nagai, M. Katsumi, T. Yamada, S. Kuwata, and H. Watanabe, *Tetrahedron Lett.*, **1981**, 653.

5) U. Nagai, N. Taki, and M. Kawai, *Chem. Pharm. Bull.*, **29**, 1750 (1981).

6) IUPAC-IUB Comission on Biochemical Nomenclature, *Biochemistry*, **9**, 3471 (1970).

7) M. Kawai and U. Nagai, *Bull. Chem. Soc. Jpn.*, **55**, 1327 (1982).

8) J. A. Schellman, *Acc. Chem. Res.*, **1**, 144 (1968).

9) For the calculation of the rotatory strengths (RS_1), each chromophore was assumed to have the following electric transition moments (wavelength (λ) in nm, dipole strength ($|\mu|^2$) in 10^{-36} c.g.s. and the direction of the moment in degree with respect to the long axis of the chromophore): DNP·NH 400, 8.6, 44;[13,14] $PhCO_2$ 230, 13.3, 6.5;[15] 185, 27.3, 4;[14] Ph 208.5, 7.5, 0; 182.8, 20.9, 0; 182.8, 20.9, 90.[16]

10) ^{1}H-NMR spectra of **1a**—**c** were recorded in acetone-d_6 instead of methanol-d_4. Similar CD spectra were observed in acetone, too, as follows: **1a**, $[\theta]_{403}$ +3100; **1b**, $[\theta]_{407}$ −4200; **1c**, $[\theta]_{402}$ −6900.

11) Y. Kataoka, Y. Seto, M. Yamamoto, T. Yamada, S. Kuwata, and H. Watanabe, *Bull. Chem. Soc. Jpn.*, **49**, 1081 (1976).

12) F. Sanger, *Biochem. J.*, **39**, 507 (1945).

13) M. Kawai, U. Nagai, and T. Kobayashi, *Tetrahedron Lett.*, **1974**, 1881.

14) The direction of the electric transition moment was given by a modified SCF-MO-CI calculaion; Z. Yoshida and T. Kobayashi, *J. Chem. Phys.*, **54**, 4538 (1971).

15) J. Tanaka, *Bull. Chem. Soc. Jpn.*, **36**, 833 (1963).

16) S. Nagakura and K. Kimura, *Nippon Kagaku Zasshi*, **86**, 1 (1965).

A Convenient Method for Preparation of 2-(Methylthio)alkanoic Acids and Their Related Compounds Using the Carbanions of Substituted Malonic Esters

Katsuyuki OGURA,* Hiroshi ITOH, Toshio MORITA, Kunio SANADA, and Hirotada IIDA
Department of Synthetic Chemistry, Faculty of Engineering, Chiba University, Yayoicho 1-33, Chiba 260
(Received October 1, 1981)

Starting from alkyl- or aryl-substituted malonic esters prepared by various methods, 2-(methylthio)alkanoic acids are synthesized by successive treatment with sodium ethoxide and with S-methyl methanethiosulfonate, followed by alkaline hydrolysis which causes concurrent decarboxylation. Production of 2-(phenylthio)alkanoic acids is also achieved in a similar manner.

A 2-(methylthio)alkanoic acid (**1**) and its ester (**2**) are well known to be useful intermediates for making a variety of organic compounds such as a 2-alkenoic acid, an aldehyde, a ketone, and an epoxide.[1-6] For preparation of **1** and **2**, there have been explored many kinds of methods including substitution of 2-haloalkanoic ester with methanethiolate anion,[7] methylation of 2-mercaptoalkanoic ester,[7,8] alkylation of (methylthio)-acetic acid,[4] direct sulfenylation of alkanoic acid or its ester,[3,4,9] Michael addition of a carbanion to methyl α-(methylthio)acrylate,[10] and reaction of (ethoxycarbonyl)(methylthio)methyl cation with 1-alkene or arene.[11] Now we wish to describe a convenient route leading to **1**, which comprises the reaction of *S*-methyl methanethiosulfonate (**5**) with the carbanion (**4**) of an alkyl- or aryl-substituted malonic ester (**3**) and subsequent hydrolysis accompanied by simultaneous decarboxylation. This route provides the following distinct features: (i) Inexpensive and handy sodium ethoxide can be employed as a base; (ii) **1** is selectively produced without formation of 2,2-bis(methylthio)alkanoic acid due to masking the hydrogen at 2-position of **1** with ethoxycarbonyl group; (iii) all the reactions take place smoothly in ethanol at room temperature or in refluxing ethanol; and (iv) many methods are available for production of **3** and **4** to make this route widely applicable (*vide post*).

Results and Discussion

For preparation of alkyl- or aryl-substituted malonic esters (**3**), we employed three methods summarized in Scheme 2. When Y of **3** is an alkyl group or a 2-alkenyl group, the corresponding **3** is synthesized by the so-called malonic ester synthesis [Method A].[12] Ethoxycarbonylation of ethyl arylacetate with diethyl carbonate and sodium ethoxide gives the starting material (**3**) having an aryl group as Y [Method B].[13] The Michael reaction of diethyl malonate with ethyl 2-alkenoate can be utilized to afford **3** (Y=-CHR'CH_2COOEt) [Method C].[14]

Conversion of the thus-obtained **3** into the corresponding **6** was accomplished by successive treatment with sodium ethoxide and with **5** in ethanol. To 0.47 M ethanolic solution (100 ml) of sodium ethoxide, were added **2a** (9.97 g : 33 mmol) and then **5** (5.30 g : 42 mmol),[15] and the resulting mixture was stirred at room temperature for 4 h. The usual workup followed by distillation afforded **6a** in 90% yield. In analogous manners, various derivatives (**6b—g**) of diethyl (methylthio)malonate were obtained. When *S*-phenyl benzenethiosulfonate (**7**)[15] was utilized instead of **5** in the above reactions, the corresponding phenylthio derivatives (**8a**, **8b**, and **8d**) were also produced in high yields. The results are given in Tables 1 and 2.

As shown in Scheme 2, the carbanion (**4**, Y=Ar) is

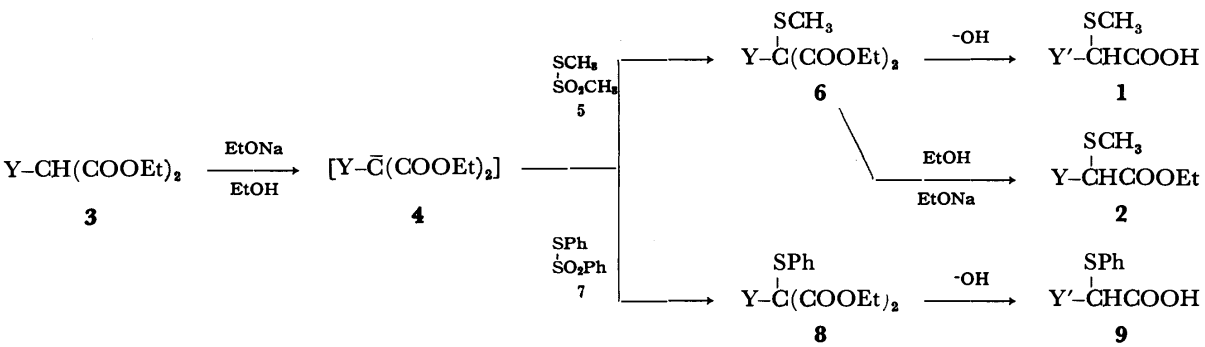

a: Y=*n*-$C_{10}H_{21}$-, b: Y=$PhCH_2$-, c: Y=*n*-$C_5H_{11}CH$=$CHCH_2$-, d: Y=Ph,
e: Y=-CH_2CH_2COOEt [Y'=-CH_2CH_2COOH], f: Y=-CHCH$_2$COOEt [Y'=-CHCH$_2$COOH]
g: Y=-CHCH$_2$COOEt [Y'=-CHCH$_2$COOH]
Ph Ph CH$_3$ CH$_3$

Scheme 1.

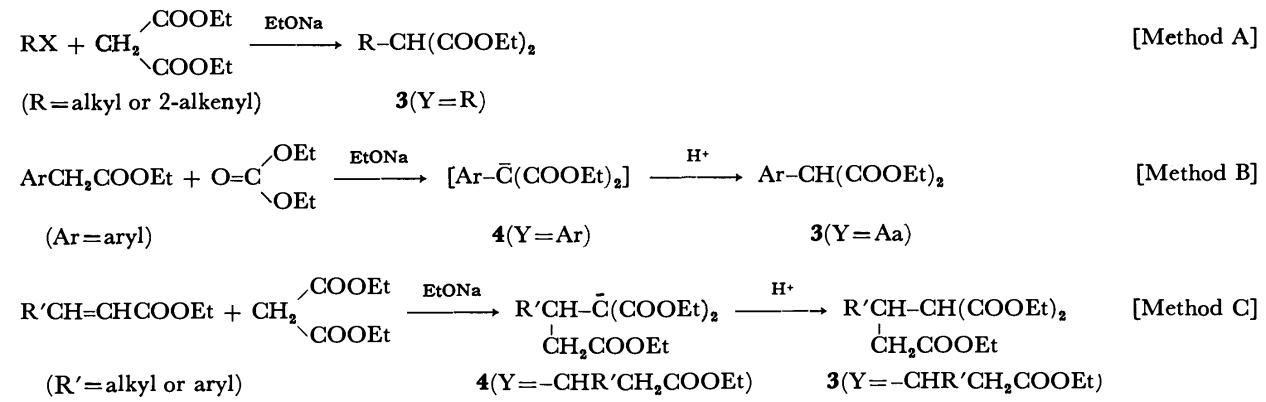

Scheme 2. Preparation of the starting material (**3**)

intermediately formed in Method B. Hence, we examined whether a "one-pot" reaction is feasible for preparation of **6** (Y=Ar) from ethyl arylacetate. Ethyl phenylacetate (16 mmol) and a large excess of diethyl carbonate (15 ml) were added to an ethanolic solution (15 ml) of sodium ethoxide (1.2 equiv.) and the mixture was heated under slow removal of ethanol and diethyl carbonate to afford an insoluble carbanion (**4d**). Then, tetrahydrofuran (50 ml) and **5** (1.3 mol-equiv.) were added to this reaction system and the resulting mixture was stirred at room temperature for 3 h to give **6d** in 92% yield. Analogously, **8d** was given in 90% yield, starting from ethyl phenylacetate and **7**.

Method C of Scheme 2 also suggests that **6** having $-CHR'CH_2COOEt$ as Y can be produced in one flask from ethyl 2-alkenoate by direct treatment of the carbanion **4** (Y=$-CHR'CH_2COOEt$), which is formed in the reaction of ethyl 2-alkenoate with the carbanion of diethyl malonate, with **5**. After a solution containing ethyl 2-alkenoate, diethyl malonate (1—1.2 equiv.), and sodium ethoxide (1—2.2 equiv.) in ethanol was stirred at room temperature or refluxing temperature, **5** (1—2.7 equiv.) was added and the resulting mixture was further stirred at room temperature. The usual workup gave **6f** and **6g** in 67 and 72% yields, respectively. However, preparation of **6e** using this "one-pot" procedure was found to be less effective because the Michael addition of diethyl malonate to ethyl acrylate was always accompanied with formation of diethyl bis[2-(ethoxycarbonyl)ethyl]malonate to lower the yield of the carbanion **4e**. In this case, it is recommended that **3e** is once isolated by distillation and then subjected to the reaction with **5** in the presence of sodium ethoxide in ethanol as mentioned above from a viewpoint of obtaining **6e** in a pure form.

Transformation of **6** into the desired **1** was easily achieved by alkaline hydrolysis. When **6** was treated with excess potassium hydroxide in refluxing ethanol, hydrolysis of the ethoxycarbonyl groups and decarboxylation took place simultaneously to give **1**. However, it should be noted that **6g** afforded ethyl cinnamate and/or cinnamic acid by cleavage of a C–C bond (the retro-Michael reaction) when the hydrolysis was carried out in refluxing ethanol. This was overcome by performing the hydrolysis at room temperature followed by heating at the final stage to form **1g** in 93% yield. 2-(Phenylthio)alkanoic acid (**9**) was also produced in a good yield by alkaline hydrolysis of **8**. These results are also summarized in Tables 1 and 2.

For preparation of **1d**, benzyl cyanide could be employed as a starting material instead of ethyl phenylacetate. Ethoxycarbonylation of benzyl cyanide with diethyl carbonate in the presence of sodium ethoxide gave sodium salt (**10**) of ethyl α-cyanophenylacetate. After the precipitated **10** was again dissolved by addition of tetrahydrofuran to the reaction system, **5** was added and the resulting mixture was stirred at room temperature for 4 h to afford ethyl α-cyano-α-(methylthio)-

Table 1. Yields of **6** and **1**

3 (Y)	**3** → **6**[a]				**6** → **1**[a]		
	EtONa (equiv.)	**5** (equiv.)	Temp (Time/h)	Yield/%	KOH (equiv.)	Temp (Time/h)	Yield/%
3a (n-$C_{10}H_{21}$–)	1.4	1.3	r.t.(4)	90	3.7	reflux(3)	74
3b ($PhCH_2$–)	1.2	1.2	r.t.(4)	70	4.3	reflux(4)	74
3c (n-$C_5H_{11}CH$=$CHCH_2$–[b])	1.5	1.6	r.t.(5)	88	3.9	reflux(6)	87
3d (Ph)	1.2	1.3	r.t.(3)	92[c]	4.1	reflux(3)	79
3e ($-CH_2CH_2COOEt$)	2.1	2.5	r.t.(16)	73	8.9	reflux(3)	82
3f ($-CH(CH_3)CH_2COOEt$)	1.5	1.5	r.t.(4.5)	77	8.2	reflux(4)	71
3g ($-CH(Ph)CH_2COOEt$)	1.6	2.2	r.t.(18)	75	10.0	r.t.(17) → reflux(5)	93

a) In EtOH. b) The (*E*)-isomer was used in this reaction. By an NMR analysis (100 MHz and proton-decoupling), the presence of the corresponding (*Z*)-isomers was not observed in the products **6** and **1**. c) The carbanion (**4**) was obtained by the reaction of ethyl phenylacetate with diethyl carbonate (see Text). This value indicates an overall yield from ethyl phenylacetate.

TABLE 2. YIELDS OF **8** AND **9**

3(Y)	3 ⟶ 8[a]				8 ⟶ 9[a]		
	EtONa (equiv.)	**7** (equiv.)	Temp/°C(Time/h)	Yield/%	KOH (equiv.)	Temp(Time/h)	Yield/%
3a (n-$C_{10}H_{21}$–)	1.0	1.0	r.t.(4) → 50(11)	90	5.2	reflux(2)	77 ·
3b ($PhCH_2$–)	1.1	1.2	r.t.(2) → 50(23)	(83)[b]	4.0	reflux(2)	76[c]
3d (Ph)	1.2	1.3	r.t.(2) → 50(33)	90[d]	5.0	reflux(3)	86

a) In EtOH. b) Contaminated with a small amount of inseparable and unidentified product(s). c) The overall yield from **3**. d) See the footnote (c) of Table 1.

phenylacetate (**11**) in 82% yield. Alkaline hydrolysis of **11** resulted in formation of a complex mixture containing ethyl α-cyanophenylacetate, benzoic acid, and ethyl benzoate. However, transformation of **11** into **1d** was successively accomplished by acidic hydrolysis with 8 M hydrochloric acid to produce the expected **1d** in 76% yield.

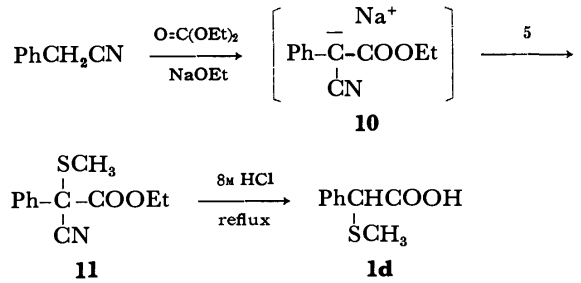

Furthermore, direct conversion of **6** into the ethyl ester (**2**) was examined by retro-ethoxycarbonylation. When a mixture of **6** and sodium ethoxide (about 5 equiv.) was stirred in ethanol, the corresponding **2** was produced (**2a** 93%; **2b** 77%; **2c** 76%; **2d** 80%).

Thus, we have established a convenient method for preparation of 2-(methylthio)alkanoic acids, 2-(phenylthio)alkanoic acids, and their esters. Finally, it should be noted that the present method can be suitably applied to selective synthesis of 3-substituted 2-(methylthio)-pentanedioic acids starting from ethyl 2-alkenoates, which is not achieved by the already-mentioned known methods for making **1** and **2**.

Experimental

Synthesis of ***6a****. Typical Procedure*: To a 0.47 M ethanolic solution (100 ml) of sodium ethoxide, were successively added **3a** (9.967 g, 33 mmol) and **5** (5.297 g, 42 mmol), and the resulting mixture was stirred at room temperature for 4 h. After addition of water (100 ml), the mixture was extracted with diethyl ether (50 ml × 3). The organic layer was dried (Na_2SO_4) and evaporated *in vacuo*. Distillation of the residue gave 10.374 g of **6a** as a colorelss oil: bp 145—148 °C/1 mmHg (1 mmHg≈133.322 Pa); NMR ($CDCl_3$): δ 0.75—1.05 (3H, broad t), 1.15—1.40 (24H, broad), 2.10 (3H, s), and 4.24 (4H, q, J=7 Hz); IR (neat): 1730 cm^{-1}.

Found: C, 62.71; H, 10.06; S, 9.25%. Calcd for $C_{18}H_{34}O_4S$: C, 62.39; H, 9.89; S, 9.25%.

In analogous manners using the conditions given in Tables 1 and 2, the following compounds were synthesized.

6b: A colorless oil which was purified by column chromatography on silica gel using hexane–benzene (1 : 1) as an eluent followed by a short-path distilation (bath temperature: 120 °C/3 mmHg); NMR ($CDCl_3$): δ 1.21 (6H, t, J=7 Hz), 2.15 (3H, s), 3.43 (2H, s), 4.21 (4H, q, J=7 Hz), and 7.21 (s, 5H); IR (neat): 1730 cm^{-1}.

Found: C, 60.90; H, 6.72%. Calcd for $C_{15}H_{20}O_4S$: C, 60.79; H, 6.80%.

6c: A colorless oil; bp 103—103.5 °C/4 mmHg; NMR ($CDCl_3$): δ 0.78—0.91 (3H, broad t), 1.13—1.56 (6H, m), 1.28 (6H, t, J=7 Hz), 1.80—2.24 (2H, m), 2.11 (3H, s), 2.74 (2H, d, J=6 Hz), 4.23 (4H, q, J=7 Hz), 5.40 (1H,dt, J=15.5 and 6 Hz), and 5.52 (1H, dt, J=15.5 and 6 Hz); IR (neat): 1730 cm^{-1}.

Found: C, 60.70; H, 8.84%. Calcd for $C_{16}H_{28}O_4S$: C, 60.71; H, 8.94%.

6e: A colorless oil; bp 108—109 °C/1 mmHg; NMR ($CDCl_3$): δ 1.27 (3H, t, J=7 Hz), 1.30 (6H, t, J=7 Hz), 2.07 (3H, s), 2.30 (4H, s), 4.13 (2H, q, J=7 Hz), and 4.25 (4H, q, J=7 Hz); IR (neat): 1725 cm^{-1}.

Found: C, 51.18; H, 7.21%. Calcd for $C_{13}H_{22}O_6S$: C, 50.96; H, 7.23%.

6f: A colorless oil; bp 114.5—117 °C/0.5 mmHg; NMR ($CDCl_3$): δ 1.14 (3H, d, J=6 Hz), 1.25 (3H, t, J=7 Hz), 1.29 (6H, t, J=7 Hz), 2.14 (3H, s), 2.3—3.2 (3H, m), 4.14 (2H, q, J=7 Hz), and 4.26 (4H, q, J=7 Hz); IR (neat): 1725 cm^{-1}.

Found: C, 52.23; H, 7.48%. Calcd for $C_{14}H_{24}O_6S$: C, 52.48; H, 7.54%.

6g: Colorless crystals; mp 62—63 °C (from hexane); NMR (CCl_4): δ 1.02 (3H, t, J=7 Hz), 1.18 (3H, t, J=7 Hz), 1.25 (3H, t, J=7 Hz), 2.14 (3H, s), 2.80—3.25 (2H, m), 3.85—4.40 (7H, m), and 7.0—7.4 (5H, m); IR (KBr): 1725 cm^{-1}.

Found: C, 59.75; H, 6.82%. Calcd for $C_{19}H_{26}O_6S$: C, 59.66; H, 6.85%.

8a: A colorless oil which was purified by column chromatography on silica gel using benzene as an eluent followed by a short-path distillation (bath temperature: 180 °C/1.5 mmHg); NMR ($CDCl_3$): δ 0.65—1.00 (3H, broad t), 1.0—2.1 (24H, broad), 4.16 (4H, q, J=7 Hz), and 7.22—7.60 (5H, broad s).

Found: C, 67.70; H, 9.09%. Calcd for $C_{23}H_{36}O_4S$: C, 67.61; H, 8.88%.

Synthesis of ***9b*** *from* ***3b*** via ***8b***. To a 0.37 M ethanolic solution (20 ml) of sodium ethoxide, were added **3b** (1.656 g, 6.62 mmol) and **7** (2.010 g, 8.04 mmol), and the resulting mixture was stirred at room temperature for 2 h and at 50 °C for 23 h. After addition of water (20 ml) and extraction with diethyl ether (50 ml × 3), the organic layer was dried (Na_2SO_4), evaporated, and subjected to column chromatography on silica gel to give an oil (1.974 g) which was shown by NMR and TLC analyses to consist mainly of **8b**. However, the impurities could not be separated from **8b** by repeated chromatography.

The oil (0.709 g, about 1.98 mmol) was dissolved in ethanol (10 ml) and, after addition of potassium hydroxide (444 mg, 7.92 mmol), the resulting mixture was refluxed for 2 h. After

water (20 ml) was added, the mixture was acidified to pH 2 with 2 M hydrochloric acid and extracted with diethyl ether (50 ml×3). The extract was dried (Na_2SO_4), evaporated, and separated by column chromatography on silica gel using ethyl acetate as an eluent to give **9b** (465 mg) in 76% overall yield from **3b** as a colorless oil, which was further purified by a short-path distillation (bath temperature: 180 °C/1 mmHg); NMR ($CDCl_3$): δ 3.13 (2H, d, J=7 Hz) 3.85 (1H, t, J=7 Hz), 7.12—7.54 (10H, broad), and 11.06 (1H, s); IR (neat): 3300—2500 and 1715 cm^{-1}.

Found: C, 70.11; H, 5.58%. Calcd for $C_{15}H_{14}O_2S$: C, 69.74; H, 5.46%.

Synthesis of 6d from Ethyl Phenylacetate. Typical Procedure: To a 1.27 M ethanolic solution (15 ml) of sodium ethoxide, were added ethyl phenylacetate (2.630 g, 16 mmol) and diethyl carbonate (15 ml), and the resulting mixture was heated under slow removal of ethanol and diethyl carbonate through the top of the Vigreux column equipped on the reaction flask. After diethyl carbonate (9 ml) was removed, the mixture was cooled to an ambient temperature. Then, tetrahydrofuran (50 ml) and **5** (2.620 g, 20.8 mmol) were added and the resulting mixture was stirred at room temperature for 3 h. After addition of water (30 ml) and extraction with diethyl ether (50 ml×3), the extract was dried (Na_2SO_4), evaporated, and distilled *in vacuo* to give **6d** (4.160 g, 92% yield) as a colorless oil: bp 130—132 °C/1 mmHg; NMR ($CDCl_3$): δ 1.24 (6H, t, J=7 Hz), 1.97 (3H, s), 4.28 (4H, q, J=7 Hz), and 7.2—7.8 (5H, broad); IR (neat): 1725 cm^{-1}.

Found: C, 59.64; H, 6.35%. Calcd for $C_{14}H_{18}O_4S$: C, 59.55; H, 6.43%.

In analogous manners, **8d** and **11** were synthesized.

8d: A colorless oil which was purified by column chromatography on silica gel using benzene as an eluent followed by a shortpath distillation (bath temperature: 180 °C/2 mmHg); NMR ($CDCl_3$): δ 1.50 (6H, t, J=7 Hz), (4H, q, J=7 Hz), and 7.0—7.75 (10H, broad); IR (neat): 1750 and 1730 (sh) cm^{-1}.

Found: C, 66.13; H, 5.88%. Calcd for $C_{19}H_{20}O_4S$: C, 66.26; H, 5.85%.

11; A colorless oil; bp 131 °C/3 mmHg; NMR ($CDCl_3$): δ 1.29 (3H, t, J=7 Hz), 2.25 (3H, s), 4.28 (2H, q, J=7 Hz), and 7.3—7.85 (5H, broad); IR (neat): 2250 and 1750 cm^{-1}.

Found: C, 61.33; H, 5.59; N, 5.98%. Calcd for $C_{12}H_{13}NO_2S$: C, 61.25; H, 5.59; N, 5.95%.

Hydrolysis of 6a. Typical Procedure: To a solution of **6a** (2.007 g, 5.80 mmol) in ethanol (20 ml), was added potassium hydroxide (1.208 g, 21.6 mmol), and the resulting mixture was refluxed for 3 h. Then, water (30 ml) was added and the mixture was acidified below pH 2 with 3 M hydrochloric acid. After extraction with diethyl ether (30 ml ×3), the extract was dried (Na_2SO_4), evaporated, and subjected to column chromatography on silica gel using ethyl acetate as an eluent to give **1a** (1.059 g, 74% yield) as a colorless oil which was further purified by a short-path distillation (bath temperature: 145—148 °C/0.1 mmHg); NMR ($CDCl_3$): δ 0.75—1.10 (3H, broad t), 1.10—1.40 (18H, broad), 2.20 (3H, s), 3.19 (1H, t, J=8 Hz), and 10.77 (1H, s); IR (neat): 3300—2500 and 1715 cm^{-1}.

Found: C, 63.54; H, 10.81%. Calcd for $C_{13}H_{26}O_2S$: C, 63.34; H, 10.64%.

In analogous manners using the conditions given in Tables 1 and 2, the following compounds were obtained.

1b: A colorless oil which was purified by column chromatography on silica gel using ethyl acetate as an eluent followed by a short-path distillation (bath temperature: 150 °C/2 mmHg); NMR ($CDCl_3$): δ 2.19 (3H, s), 2.80—3.60 (3H, m), 7.20 (5H, s), and 8.92 (1H, s); IR (neat): 3300—2400 and 1700 cm^{-1}.

Found: C, 61.15; H, 6.32%. Calcd for $C_{10}H_{12}O_2S$: C, 61.20; H, 6.16%.

1c: A colorless oil which was purified by column chromatography on silica gel using benzene-hexane (2 : 1) as an eluent followed by a short-path distillation (bath temperature: 168—170 °C/0.08 mmHg); NMR ($CDCl_3$): δ 0.75—1.06 (3H, broad t), 1.10—1.55 (6H, m), 1.81—2.17 (2H, m), 2.18 (3H, s), 1.94—2.55 (2H, m), 3.20 (1H, t, J=7.5 Hz), 5.40 (1H, dt, J=15.5 and 6 Hz), 5.52 (1H, dt, J=15.5 and 6 Hz), and 10.4 (1H, broad); IR (neat): 3300—2500 and 1715 cm^{-1}.

Found: C, 60.99; H, 9.24%. Calcd for $C_{11}H_{20}O_2S$: C, 61.06; H, 9.34%.

1d: Colorless crystals which were obtained by column chromatography on silica gel using dichloromethane as an eluent; mp 76—77 °C; NMR ($CDCl_3$): δ 2.09 (3H, s), 4.50 (1H, s), 7.2—7.6 (5H, broad), and 10.98 (1H, s); IR (KBr): 3200—2700 and 1690 cm^{-1}.

Found: C, 59.34; H, 5.49%. Calcd for $C_9H_{10}O_2S$: C, 59.32; H, 5.53%.

1e: Colorless crystals; mp 62.5—63 °C (from benzene); NMR (d_6-DMSO): δ 1.83 (2H, m), 2.04 (3H, s), 2.28 (2H, t, J=8 Hz), 3.18 (1H, t, J=8 Hz), and 12.4 (2H, broad); IR (KBr): 3500—2500 and 1695 cm^{-1}.

Found: C, 40.61; H, 5.56%. Calcd for $C_6H_{10}O_4S$: C, 40.44; H, 5.65%.

1f: Colorless crystals; mp 132—134 °C (from dichloromethane–benzene); NMR (d_6-DMSO): δ 1.04 (3H, d, J= 6 Hz), 2.06 (3H, s), 2.24 (3H, m), 3.16 (1H, diffused d, J=7 Hz), and 12.36 (2H, broad); IR (KBr): 3300—2500 and 1700 cm^{-1}.

Found: C, 43.99; H, 6.30%. Calcd for $C_7H_{12}O_4S$: C, 43.73; H, 6.29%.

1g: Colorless crystals; mp 187—188 °C (from dichloromethane); NMR (d_6-DMSO): δ 2.14 (3H, s), 2.9—3.7 (4H, m), 7.28 (5H, s), and 12.2 (2H, broad); IR (KBr): 3300—2500 and 1700 cm^{-1}.

Found: C, 56.41; H, 5.51%. Calcd for $C_{12}H_{14}O_4S$: C, 56.67; H, 5.54%.

9a: A colorless oil which was purified by column chromatography on silica gel using ethyl acetate as an eluent followed by a short-path distillation (bath temperature: 195 °C/1 mmHg); NMR ($CDCl_3$): δ 0.62—1.03 (3H, broad t), 1.03—1.55 (18H, broad), 3.60 (1H, t, J=7 Hz), 7.15—7.58 (5H, broad), and 10.95 (1H, s); IR (neat): 3400—2400 and 1710 cm^{-1}.

Found: C, 70.15; H, 9.35%. Calcd for $C_{18}H_{28}O_2S$: C, 70.09; H, 9.15%.

9d: Colorless crystals which were obtained by column chromatography on silica gel using ethyl acetate as an eluent and subjected to an elemental analysis; mp 100 °C; NMR ($CDCl_3$): δ 4.88 (1H, s), 7.1—7.55 (10H, broad), and 11.08 (1H, s); IR (KBr): 3200—2400 and 1690 cm^{-1}.

Found: C, 68.58; H, 4.97%. Calcd for $C_{14}H_{12}O_2S$: C, 68.83; H, 4.95%.

Hydrolysis of 11. A mixture of **11** (947 mg, 4.0 mmol) and 8 M hydrochloric acid was refluxed for 12 h. After addition of water (50 ml) and extraction with diethyl ether (100 ml×3), the organic layer was dried (Na_2SO_4), evaporated, and subjected to column chromatography on silica gel using dichloromethane as an eluent to afford colorless crystals (558 mg, 76% yield) which were identified with **1d** by their IR and NMR spectra.

Production of 2a from 6a. Typical Procedure: To a 0.66 M ethanolic solution of sodium ethoxide, was added **6a** (432 mg, 1.25 mmol) and the resulting solution was stirred

at room temperature for 88 h and at 50 °C for 5 h. After addition of water (20 ml) and extraction with diethyl ether (50 ml × 3), the extract was dried (Na_2SO_4), evaporated, and subjected to column chromatography on silica gel using benzene–hexane (1 : 1) as an eluent to give **2a** (317 mg, 93% yield) as a colorless oil which was further purified by a short-path distillation (bath temperature: 145 °C/3 mmHg); NMR ($CDCl_3$): δ 0.70—1.10 (3H, broad t), 1.15—1.45 (21H, broad), 2.15 (3H, s), 3.18 (1H, t, J=7 Hz), and 4.22 (2H, q, J=7 Hz); IR (neat): 1725 cm^{-1}.

Found: C, 65.89; H, 10.77%. Calcd for $C_{15}H_{30}O_2S$: C, 65.64; H, 11.02%.

In analogous manners, **6b**, **6c**, and **6d** were converted to **2b**, **2c**, and **2d**, respectively.

2b: A colorless oil; NMR ($CDCl_3$): δ 1.13 (3H, t, J=7 Hz), 2.10 (3H, s), 2.85—3.50 (3H, m), 4.08 (2H, q, J=7 Hz), and 7.20 (5H, s); IR (neat): 1725 cm^{-1}. These data were in complete accordance with those of an authentic specimen prepared by esterification of **1b** (hydrogen chloride/ethanol).

2c: A colorless oil which was purified by column chromatography on silica gel using benzene–hexane (1 : 2) as an eluent followed by short-path distillation (bath temperature: 118—123 °C/0.03 mmHg); NMR ($CDCl_3$): δ 0.69—1.05 (3H, broad t), 1.10—1.59 (6H, m), 1.28 (3H, t, J=7 Hz), 1.74—2.85 (4H, m), 2.14 (3H, s), 3.19 (1H, dd, J=7 and 9 Hz), 4.19 (2H, q, J=7 Hz), 5.40 (1H, dt, J=15.5 and 6 Hz), and 5.52 (1H, dt, J=15.5 and 6 Hz); IR (neat): 1730 cm^{-1}.

Found: C, 63.88; H, 9.72%. Calcd for $C_{13}H_{24}O_2S$: C, 63.88; H, 9.92%.

2d: A colorless oil; NMR ($CDCl_3$): δ 1.20 (3H, t, J=7 Hz), 2.05 (3H, s), 4.15 (2H, q, J=7 Hz), 4.49 (1H, s), and 7.16—7.55 (5H, broad); IR (neat): 1735 cm^{-1}. These data were completely identical with those of an authentic sample prepared by esterification of **1d** (hydrogen chloride/ethanol).

*Preparation of **6f** from Ethyl Crotonate in One-pot Reaction.*
To a 0.63 M ethanolic solution of sodium ethoxide, were added diethyl malonate (1.695 g, 10.0 mmol) and ethyl crotonate (1.223 g, 10.0 mmol), and the resulting solution was refluxed for 2 h. Then, the mixture was cooled to room temperature and **5** (3.363 g, 27 mmol) was added. The mixture was stirred at room temperature for 39 h and refluxed for 1 h. After addition of water (80 ml) and extraction with dichloromethane (70 ml × 3), the extract was dried (Na_2SO_4) and evaporated to give an oil (4.688 g) which was shown by GLC analysis using *trans*-stilbene as an internal standard to contain 2.25 g (67% yield) of **6f**.

*Preparation of **6g** from Ethyl Cinnamate in One-pot Reaction.*
To a 0.91 M ethanolic solution of sodium ethoxide, were added diethyl malonate (7.986 g, 50 mmol) and ethyl cinnamate (8.924 g, 50 mmol), and the resulting mixture was stirred at room temperature for 25 h. Then, **5** (7.153 g, 56 mmol) was added and the mixture was stirred at room temperature for 21 h. After addition of water (100 ml) and extraction with dichloromethane (100 ml × 3), the extract was dried (Na_2SO_4) and evaporated to give a pale yellow oil containing crystals (21.353 g) which was shown by GLC analysis to contain 13.6 g (72% yield) of **6g**. By recrystallization from hexane, 8.628 g of **6g** was isolated in a pure form.

References

1) For a review, B. M. Trost, *Chem. Rev.*, **78**, 363 (1978).
2) D. Seebach and M. Teschner, *Chem. Ber.*, **109**, 1601 (1976) and the references cited therein.
3) B. M. Trost, T. N. Salzmann, and K. Hiroi, *J. Am. Chem. Soc.*, **98**, 4887 (1976).
4) B. M. Trost and Y. Tamaru, *J. Am. Chem. Soc.*, **99**, 3101 (1977).
5) J. Nogami, M. Kawada, R. Okawara, S. Torii, and H. Tanaka, *Tetrahedron Lett.*, **1979**, 1045.
6) E. Vedejs and G. R. Martinez, *J. Am. Chem. Soc.*, **101**, 6452 (1979).
7) A. Mooradian, C. J. Cavallito, A. J. Bergman, E. J. Lawson, and C. M. Suter, *J. Am. Chem. Soc.*, **71**, 3372 (1949).
8) K. Tanaka, M. Terauchi, and A. Kaji, *Chem. Lett.*, **1981**, 315.
9) D. A. R. Happer, J. W. Mitchell, and G. J. Wright, *Aust. J. Chem.* ,**26**, 121 (1973).
10) R. J. Cregge, J. L. Herrmann, and R. H. Schlessinger, *Tetrahedron Lett.*, **1973**, 2603.
11) Y. Tamura, H. Shindo, J. Uenishi, and H. Ishibashi, *Tetrahedron Lett.*, **21**, 2547 (1980); Y. Tamura, H.-D. Choi, H. Shindo, J. Uenishi, and H. Ishibashi, *ibid.*, **22**, 81 (1981); Y. Tamura, H.-D. Choi, H. Maeda, and H. Ishibashi, *ibid.*, **22**, 1343 (1981).
12) A. C. Cope, H. L. Holmes, and H. O. House, "Organic Reactions," John Wiley & Sons, New York (1957) Vol. 9, p. 107.
13) V. H. Wallingford, A. H. Homeyer, and D. M. Jones, *J. Am. Chem. Soc.*, **63**, 2056 (1941).
14) E. D. Bergmann, D. Ginsburg, and R. Pappo, "Organic Reactions," John Wiley & Sons, New York (1959), Vol. 10, p. 179.
15) Since the reaction of diaryl disulfide with the carbanion of diethyl malonate is reversible,[16] the use of **5** and **7** is recommended in the present reaction.
16) T. Fujisawa, K. Hata, and T. Kojima, *Chem. Lett.*, **1973**, 287.

Mass Spectra of Furanoeremophilane Derivatives[1)]

Hajime NAGANO,† Chiaki KURODA, Yoshihiko MORIYAMA,††
Takahiko TSUYUKI, and Takeyoshi TAKAHASHI*
Department of Chemistry, Faculty of Science, The University of Tokyo, Hongo, Bunkyo-ku, Tokyo 113
(Received September 3, 1981)

Mass spectral fragmentations of furanoeremophilane derivatives bearing oxygen-function on B ring were investigated. It was found that mass spectra measured by direct inlet system gave characteristic *retro*-Diels-Alder fragmentations, while indirect introduction of the samples afforded intense peaks at *m/e* 159 and *m/e* 145 containing the furan moiety. Fragmentation patterns of other poly-functional derivatives were examined by measurements of accurate masses and metastable ions.

In the course of structure determination of sesquiterpenes in plants of the genera *Farfugium*,[2)] *Ligularia*,[3)] and *Syneilesis*,[4)] mass spectra of furanoeremophilane derivatives have been investigated. We now wish to report their characteristic fragmentations which provide useful information for structural studies of furanoeremophilane derivatives.

The *retro*-Diels-Alder fragmentation induced by electron-impact[5)] is one of the most important processes occurring in many sesquiterpenes of a furanoeremophilane type (Fig. 1). However in the case of furanoeremophilane derivatives possessing oxygen-function(s), such as hydroxyl, acyloxyl, and alkoxyl groups, on ring B, the *retro*-Diels-Alder fragmentation was predominant only when the direct introduction of the sample was employed. The spectra of these compounds measured by use of the indirect inlet system showed intense peaks at either *m/e* 159 or *m/e* 159 and 145 and the *retro*-Diels-Alder fragmentation was scarcely observed. The fragmentations leading to the ions at *m/e* 159 and *m/e* 145 are discussed below.

The mass spectra of ligularol (**1**),[6)] epiligularol (**2**),[6)] furanoeremophilan-9α-ol (**3**),[7)] 6β-methoxyfuranoeremophilane (**4**),[8)] 6β-ethoxyfuranoeremophilane (**5**), ligularol acetate (**6**),[6)] and 6β-senecioyloxyfuranoeremophilane (**7**),[2c)] exhibited characteristic peaks at *m/e* 216 (ion **a**), *m/e* 201 (ion **b**), *m/e* 159 (ion **c**), and *m/e* 145 (ion **d**) when the indirect introduction of the sample was employed. The ion **a** must arise by pyrolysis of these compounds prior to ionization at the surface of the heated inlet system. This is supported by comparison of the mass spectrum of 9-dehydrofuranoeremophilane (**8**), a dehydration product of **1**, **2**, and **3**, with those of **1**, **2**, and **3** (Figs. 2 and 3 and Table 1).

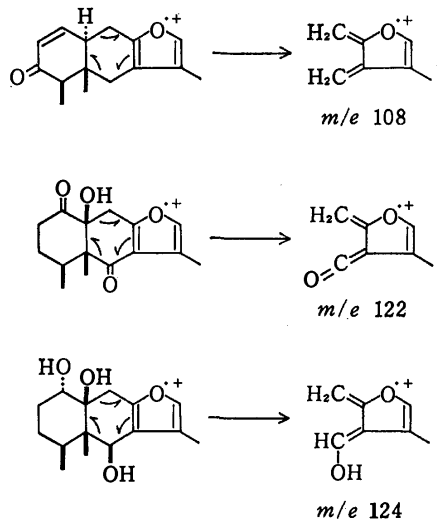

Fig. 1.

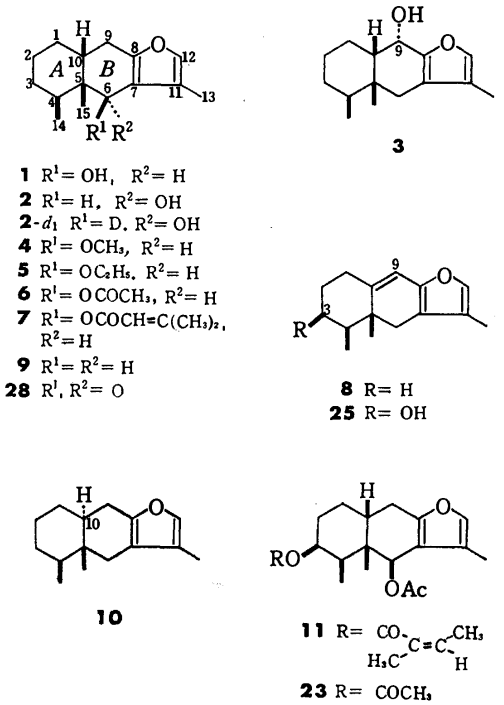

Fig. 2.

Epiligularol (**2**) was treated with *p*-toluenesulfonyl chloride in pyridine under reflux to give 9-dehydrofuranoeremophilane (**8**)[9)] as a major product, formation of which would be explicable by conjugate 1,4-elimination of water followed by [1,5]-hydride shift. The dehydration product (**8**), on hydrogenation over 10% palladium-charcoal, gave an inseparable epimeric mixture, which was revealed to consist of furanoeremophilane (**9**)[10)] and 10-epifuranoeremophilane (**10**)[3a)] in a ratio of 1 : 1 on the basis of comparison of ^{1}H NMR, UV, IR, and mass spectra.

Dehydration of ligularol (**1**) and furanoeremophilan-

† Present address: Department of Chemistry, Faculty of Science, Ochanomizu University, Otsuka, Bunkyo-ku, Tokyo 112.

†† Present address: Institute of Chemistry, Kyoto Prefectural University of Medicine, Taishogun, Kita-ku, Kyoto 603.

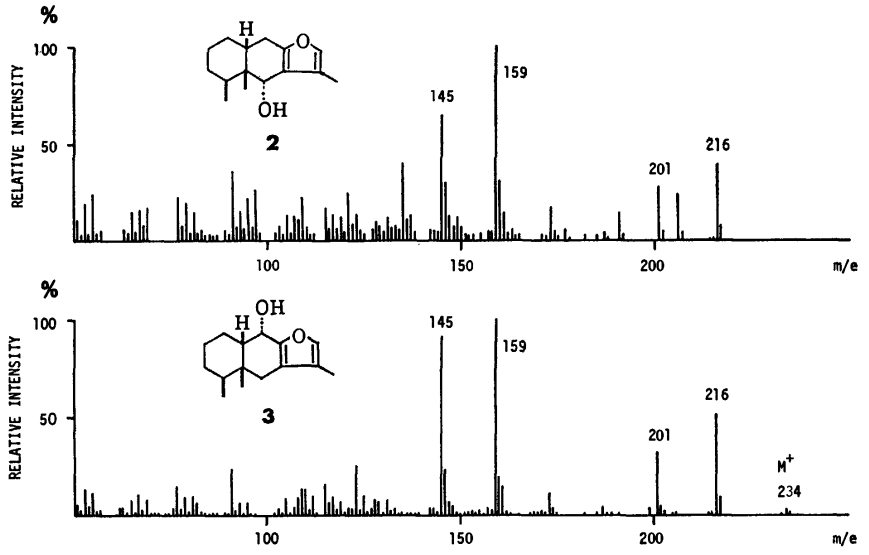

Fig. 3.

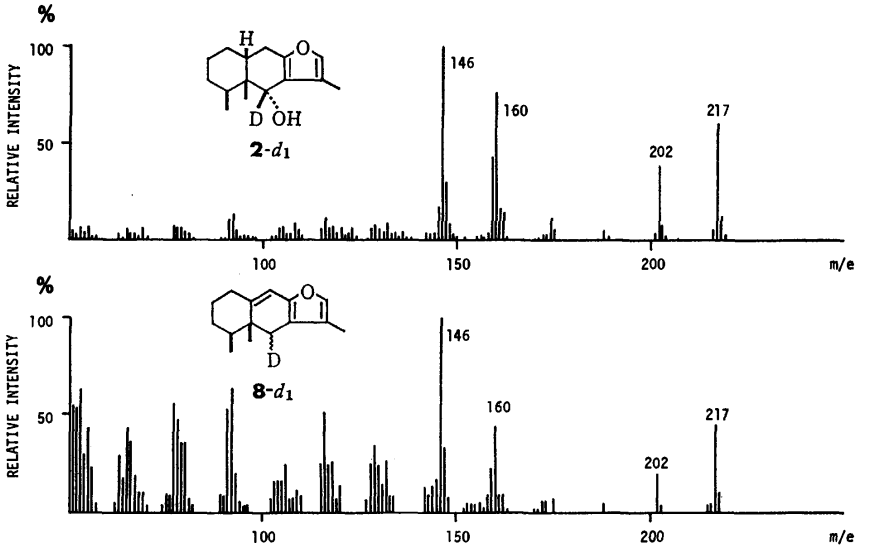

Fig. 4.

9α-ol (**3**) with *p*-toluenesulfonyl chloride in pyridine gave also 9-dehydrofuranoeremophilane (**8**) as a major product. The mass spectrum of **8** measured by direct introduction showed intense peaks at *m/e* 216 (M^+), 201, 159, and 145 and its resemblance to those of **1**, **2**, and **3** is illustrated by the spectra of deuterio compounds, **2**-d_1 and **8**-d_1 (*vide infra*) (Fig. 4 and Table 1).

A plausible mechanism for the fragmentations to afford ion **b**, ion **c**, and ion **d** is depicted in Fig. 5.

The elemental compositions of ion **a** (*m/e* 216.1520; calcd for $C_{15}H_{20}O$: *m/e* 216.1513), ion **b** (*m/e* 201.1297; calcd for $C_{14}H_{17}O$: *m/e* 201.1279), ion **c** (*m/e* 159.0832; calcd for $C_{11}H_{11}O$: *m/e* 159.0810), and ion **d** (*m/e* 145.0652; calcd for $C_{10}H_9O$: *m/e* 145.0655) were determined by the high resolution mass spectrum of epiligularol (**2**). Metastable ions were observed at *m/e* 187.0 (*m/e* 216→*m/e* 201), *m/e* 104.6 (*m/e* 201→*m/e* 145), and *m/e* 117.2 (*m/e* 216→*m/e* 159) in the spectra of epiligularol (**2**), furanoeremophilan-9α-ol (**3**), and ligularol acetate (**6**). These observations indicate that ion **c** arises from ion **a** in one step and ion **d** from ion **a** through ion **b**. The mass spectra of 6β-deuterioepiligularol (**2**-d_1) and its dehydration product (**8**-d_1) showed peaks due to ion **a** at *m/e* 217, ion **b** at *m/e* 202, ion **c** at *m/e* 160 and 159, and ion **d** at *m/e* 146, affording further information for the mechanism of the fragmentations (Table 1). Ion **c** must be derived from ion **a** by the favorable cleavage of $C_{(1)}$–$C_{(2)}$ and $C_{(4)}$–$C_{(5)}$ bonds, both locating β to the Δ^9-double bond. Alternatively, ion **a** loses a methyl radical most probably from the position C-5 to afford ion **b**, the position being allylic to the double bond. The ion **b** may undergo 1,2-hydrogen shift from C-6 to C-5 followed by cleavage of $C_{(1)}$–$C_{(2)}$ and $C_{(4)}$–$C_{(5)}$ bonds to give the fully con-

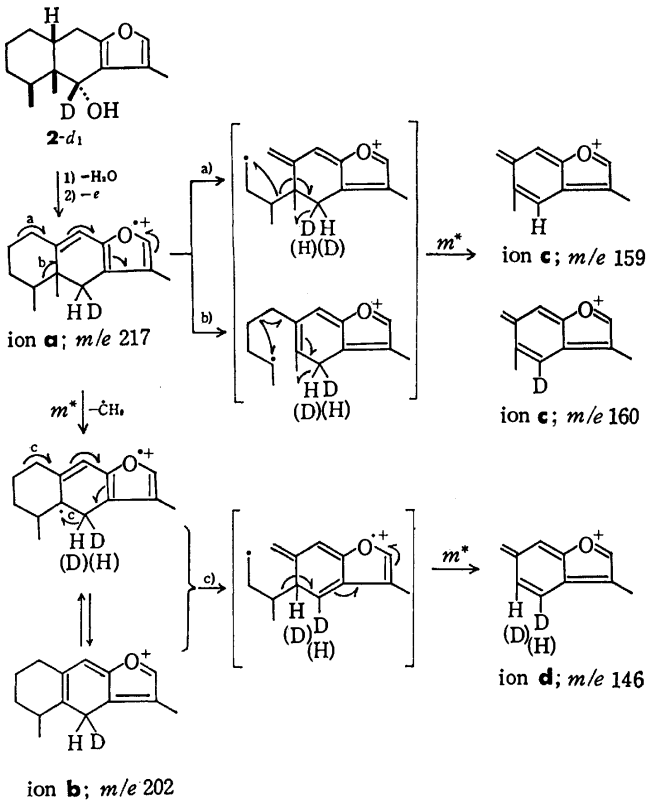

Fig. 5.

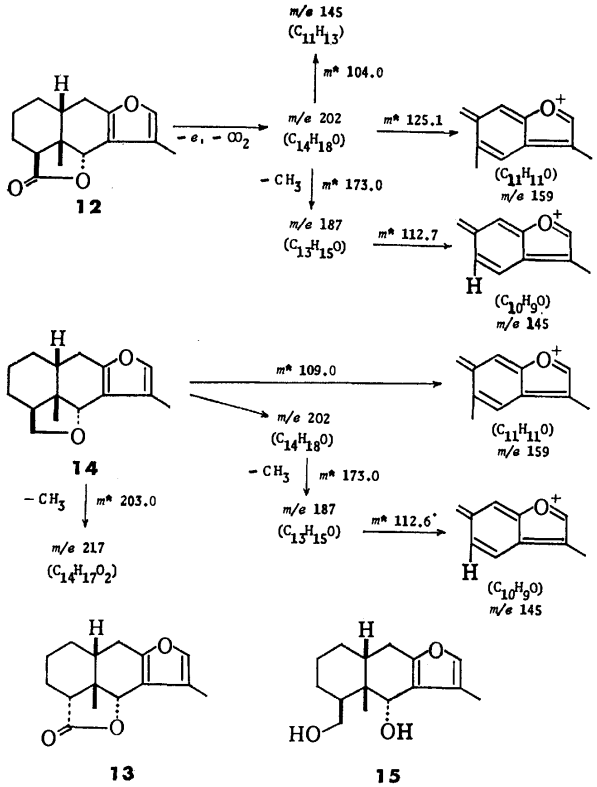

Fig. 6.

jugated ion **d** (Fig. 5).

Now it has been demonstrated that elimination of oxygen-function at C-6 in furanoeremophilane derivatives occurs with ease in mass spectral measurement by the indirect inlet system. A number of natural furanoeremophilanes with different acyloxyl groups at C-3 and C-6 positions have been reported.[11] The electron-impact mass spectral measurement by the indirect inlet method would provide a diagnostic technique for determination of the positions of acyloxyl groups based on the argument developed above.

Mass spectra of 6β-acetoxy-3β-angeloyloxyfuranoeremophilane (**11**)[2b] were then examined by two inlet methods. When mass spectrum of **11** was measured by indirect inlet method, a peak at *m/e* 314 due to elimination of acetic acid by preferential loss of the acetoxyl group at C-6 was observed; a peak at *m/e* 274 due to elimination of angelic acid by loss of the angeloyloxyl group at C-3 was absent. On the other hand, the direct inlet measurement afforded two peaks at *m/e* 314 and *m/e* 274 with an intensity ratio of 9 : 2 (Table 1). This method was successfully applied to determination of the structures of 3β,6β-diacyloxyfuranoeremophilane derivatives obtained from *Syneilesis palmata* (Thunb.) Maxim.[4]

Mass spectra of furanoeremophilan-14,6α-olide (**12**) and its derivatives, **13**, **14**, and **15**,[3b] also exhibited their characteristic ions at *m/e* 159 and *m/e* 145 even when they were measured by the direct inlet method. The fragmentation modes for **12** and **14** are shown in Fig. 6.

Accurate mass measurements for **12** and **14** revealed that the peak at *m/e* 145 splitted into a doublet, a peak at *m/e* 145.0649 (calcd for $C_{10}H_9O$: *m/e* 145.0655) and a peak at *m/e* 145.1001 (calcd for $C_{11}H_{13}$: *m/e* 145.1016). A metastable ion at *m/e* 104.0 for **12** may correspond to the process, $C_{14}H_{18}O^+$ (*m/e* 202)$\rightarrow C_{11}H_{13}^+$ (*m/e* 145). The ion at *m/e* 159 for **12** consists of two species, $C_{11}H_{11}O^+$ (*m/e* 159.0828; calcd: *m/e* 159.0810) and $C_{12}H_{15}^+$ (*m/e* 159.1182; calcd: *m/e* 159.1174). The ion at *m/e* 202 (*m/e* 202.1358; calcd for $C_{14}H_{18}O$: *m/e* 202.1358) for **14** is probably formed from its molecular ion (M^+ at *m/e* 232.1540; calcd: *m/e* 232.1463) by one-step elimination of CH_2O, although the appropriate metastable ion was not observed. In the case of **15**, its dehydration to give **14** dominates over the *retro*-Diels-Alder fragmentation.

Mass spectral fragmentations of the following furanoeremophilane derivatives which have two or three oxygen-functions (Fig. 7) were examined; furanoeremophilane-3β,9β-diol (**16**),[2c] furanopetasine (**17**),[12] furanopetasol (**18**)[12] (Fig. 8), furanoeremophilane-3β,10β-diol (**19**)[2d] (Fig. 8), 3β-angeloyloxy-9β-senecioyloxyfuranoeremophilane (**20**),[2c] furanoeremophilane-6β,10β-diol (**21**)[3c] (Fig. 9), 6β-senecioyloxyfuranoeremophilan-10β-ol (**22**),[2c] 3β,6β-diacetoxyfuranoeremophilane (**23**),[2b] 6β-acetoxy-3β-angeloyloxyfuranoeremophilane (**11**) (*vide supra*), and furanoeremophilane-3β,9β,10β-triol (**24**).[2d] These compounds showed the same fragmentation modes as those of the compounds **1**—**7**; the characteristic fragment ions at *m/e* 159 and *m/e* 145 were observed by the indirect inlet measurement, while the *retro*-Diels-Alder fragmentation was predominant by the direct inlet method (Table 1). Among these compounds, **21**, **22**, and **24** which possess

TABLE 1. PRINCIPAL FRAGMENT PEAKS AND THEIR RELATIVE INTENSITIES

Compound		*m/e* 145 (%)	*m/e* 159 (%)	RDA fragment[b] *m/e* (%)	Other fragments *m/e*(%)
1	i	(48)	(100)		201(11), 216(25, $[M-H_2O]^+$)
	d			124(100)	
2	i	(65)	(100)		201(28), 216(40)
	d			124(100)	
2-d_1	i	(18) (100)[c]	(44) (77)[d]		202(38), 217(61)
	d			124(4.5) 125(100)	
3	i	(92)	(100)		201(32), 216(52), 234(3, M^+)
	d			124(100)	
4	i	(25)	(18)	138(100)	128(89), 248(13, M^+)
5	i	(84)	(100)		201(30), 216(47)
6	i	(100)	(97)		43(100), 60(60), 201(39), 216(53)
	d	(12)	(34)	124(100)	43(35), 216(21), 233(10), 276(2, M^+)
7	i	(29)	(77)		55(23), 83(100), 316(1, M^+)
8	d	(100)	(92)		201(34), 216(54)
8-d_1	d	(100)[c]	(45)[d]		202(20), 217(46)
11	i	(15)	(100)		55(76), 83(83), 199(21), 214(11), 232(18), 314(10)
	d	(10)	(48)	124(100)	43(21), 55(70), 83(82), 274(2), 314(9), 331(6), 374(2, M^+)
12	d	(54)	(41)		246(58, M^+)
13	d	(64)	(56)		95(100), 187(46), 202(46), 246(48, M^+)
14	i	(40)	(52)		187(16), 202(9), 217(5), 232(100, M^+)
15	d	(100)	(87)		232(97, $[M-H_2O]^+$)
16	i	(38)	(100)		199(78), 214(23), 250(1, M^+)
	d	(7)	(15)	124(100)	250(5, M^+)
17	i	(15)	(17)		55(44),83(27), 199(76), 214(100), 314(0.2, $[M-H_2O]^+$) 332(0.2, M^+)
	d	(19)	(18)	124(100)	55(71), 83(33), 109(43),199(61), 214(82), 232(20), 332(2, M^+)
18	i	(68)	(86)		173(98), 199(100), 214(30), 232(74), 250(2, M^+)
	d			124(100)	250(13, M^+)
19	i	(44)	(100)		199(75), 214(28),232(35,$[M-H_2O]^+$)
	d			108(64)	109(100), 250(10,M^+)
20	i	(27)	(94)		55(82), 83(45), 100(78), 314(33,$[M-C_5H_8O_2]^+$)
21	i	(8)	(95)		199(100), 214(67)
	d			124(100)	232(18), 250(2, M^+)
22	i	(8)	(100)		55(75), 100(88), 199(97), 214(64), 232(8)
	d				55(23), 83(100), 232(13), 332(1, M^+)
23	i	(19)	(100)		199(47), 214(18), 274(17, $[M-AcOH]^+$)
24	i	(12)	(100)		230(20, $[M-2H_2O]^+$)
	d			124(100)	
25	i	(44)	(100)		199(79), 214(22), 232(40, M^+)
26	i				199(100), 214(79, M^+)
27	i	(6)	(100)		214(37,M^+)

a) Mass spectra were measured on a Hitachi RMU-6-Tokugata mass spectrometer. Relative intensities are indicated in parentheses and i and d in the second column indicate indirect and direct introduction of samples, respectively. b) RDA fragment represents *retro*-Diels-Alder fragmentation. c) Observed at *m/e* 146. d) Observed at *m/e* 160.

two oxygen-functions at C-10 and either C-6 or C-9 on B ring, showed remarkable intense peak at *m/e* 159 compared with peak at *m/e* 145 by the indirect inlet measurement.

Thermal dehydration of furanoeremophilane-6β,10β-diol (**21**) has been reported to give benzofuran derivatives, farfugins A (**26**) and B (**27**).[2a] The mass spectral investigation showed that farfugin B (**27**) gave a dominant fragmentation due to benzylic cleavage, resulting in the formation of a benzyl (or tropylium) ion at *m/e* 159 (Fig. 9), while the principal peaks in the spectrum of farfugin A (**26**) were a molecular ion at *m/e* 214 and an ion at *m/e* 199 $[M-CH_3]^+$. These results suggest that **21**, **22**, and **24** undergo a facile aromatization into **26** and **27** on the heated surface of the inlet system prior to ionization and give the intense benzyl ion at *m/e* 159, a part of which, however, would be produced through the fragmentation analogous to that shown in Fig. 5. Thus the mass spectral investigation could be applied to the prediction of aptitude for the aromatiza-

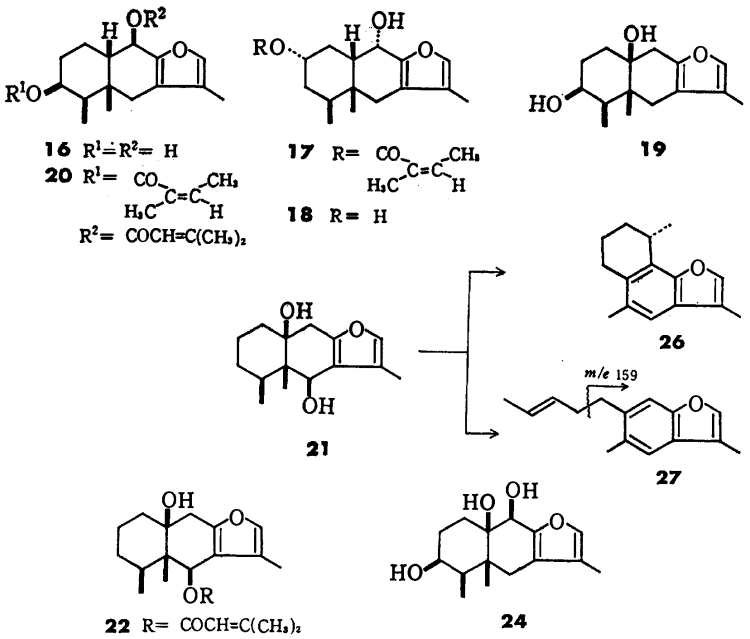

Fig. 7.

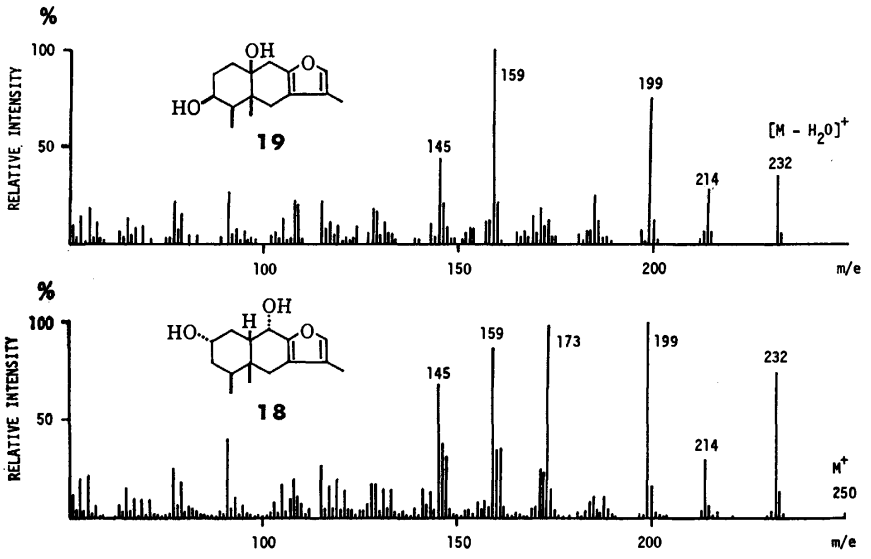

Fig. 8.

tion of furanoeremophilanediol, triol, and their acyl derivatives by elimination of the oxygen-functions to give **27** or its derivatives.[2a,13]

Experimental

Measurement of Mass Spectra. The low-resolution mass spectra were measured on a Hitachi RMU-6-Tokugata mass spectrometer using ionization energy 70 eV with source temperature of 180—230 °C (indirect inlet system) and 120—140 °C (direct inlet system). The high-resolution mass spectra were determined with a CEC 110B type mass spectrometer (indirect inlet system).

Dehydration of Epiligularol (2) with p-Toluenesulfonyl Chloride in Pyridine. *p*-Toluenesulfonyl chloride (100 mg) was added to a solution of **2** (91 mg) in pyridine (8 ml) and the mixture was heated at 120 °C (oil bath temperature) for 2 h under a nitrogen atmosphere. Evaporation of the solvent under reduced pressure gave a residue, which was immediately chromatographed on silical gel (5 g) using light petroleum as an eluent to give an oil (58 mg) containing **8** as the major component. The oil was unstable and therefore further purification was not carried out.

Hydrogenation of 9-Dehydrofuranoeremophilane (8) over Palladium–charcoal. The above product (**8**) prepared from epiligularol (**2**; 67 mg) was hydrogenated over 10% palladium–charcoal (50 mg) in ethanol with stirring for 9.5 h. Filtration of the catalyst and evaporation of the solvent gave a residue (45 mg), which was chromatographed on silica gel using light petroleum as an eluent to afford a mixture of furanoeremophilane (**9**) and 10-epifuranoeremophilane (**10**) in a ratio of 1 : 1. Spectral data of the mixture of **9** and **10** are as

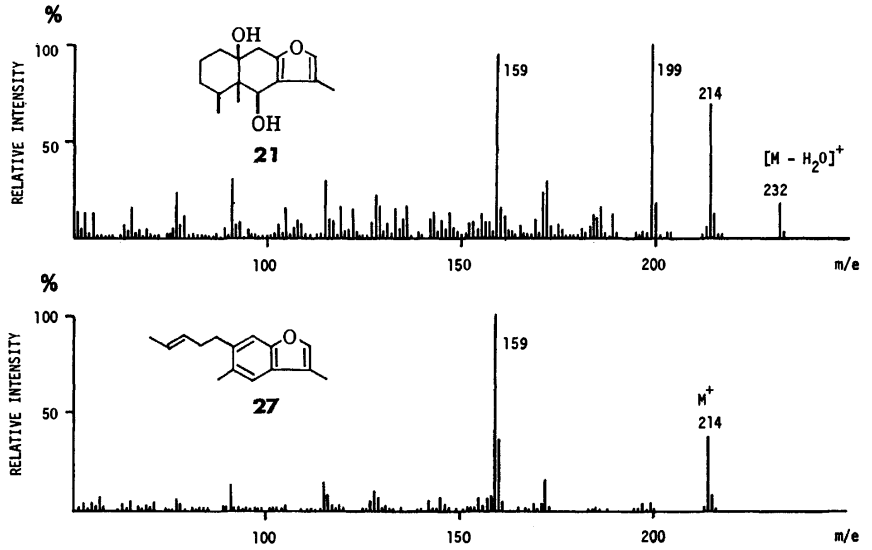

Fig. 9.

follows: UV (EtOH) λ_{max} 220.5 nm (ε 6700); IR (liquid film) 1640, 1560, and 735 cm^{-1}; ^1H NMR (CCl_4) δ 0.69 (s, $C_{(5)}$-CH_3 for **10**), 0.91 (s, $C_{(5)}$-CH_3 for **9**), 1.86 (d, J=*ca.* 1 Hz, $C_{(11)}$-CH_3), and 6.90 (m, $C_{(12)}$-H); ^1H NMR ($CDCl_3$) δ 0.68 (s, $C_{(5)}$-CH_3 for **10**), 0.91 (s, $C_{(5)}$-CH_3 for **9**), 1.89 (d, J=*ca.* 1 Hz, $C_{(11)}$-CH_3), and 7.03 (m, $C_{(12)}$-H); ^1H NMR (C_6D_6) δ 0.61 (s, $C_{(5)}$-CH_3 for **10**), 0.79 (s, $C_{(5)}$-CH_3 for **9**), 1.80 (d, J=*ca.* 1 Hz, $C_{(11)}$-CH_3), and 7.05 (m, $C_{(12)}$-H); the chemical shifts of $C_{(5)}$-CH_3 for furanoeremophilane (**9**) and 10-epifuranoeremophilane (**10**) reported in the literatures[3a,10] are as follows: δ 0.90 ($CDCl_3$) for **9** and δ 0.69 (CCl_4) and 0.61 (C_6D_6) for **10**; MS *m/e* 218 (19%, M^+ ($C_{15}H_{22}O$)) and 108 (100%, *retro*-Diels-Alder fragment).

*6β-Deuterioepiligularol (**2**-d_1).* Ligularone (**28**: 43 mg) in dry ether was stirred with lithium aluminium deuteride (15 mg) for 1 h under a nitrogen atmosphere. The excess of the reagent was decomposed with water, and the reaction product was extracted with ether. The usual work-up gave a crystalline product (34 mg), which was recrystallized from light petroleum to give **2**-d_1. The molecular ion was observed at *m/e* 235.

*6β-Ethoxyfuranoeremophilane (**5**).* A solution of ligularol (**1**; 56 mg) in ethyl iodide (3 ml) was heated under reflux in the presence of silver(I) oxide (113 mg) and *N,N*-dimethylformamide (0.5 ml) for 3 h. After filtration the reaction mixture was evaporated to give an oily residue. The oil was chromatographed on silica gel (3 g) using light petroleum as an eluent to give 6β-ethoxyfuranoeremophilane (**5**; 18 mg).

Extraction of the roots of *Ligularia fischeri* TURCZ. with methanol and ethanol gave 6β-methoxyfuanoeremophilane (**4**) and 6β-ethoxyfuranoeremophilane (**5**), respectively. In the extract of the root of the plant with benzene **4** and **5** were not detected. This indicates that these compounds are artifacts derived from ligularol (**1**) by acid-catalyzed substitution reaction during the extraction procedure. Spectral data of **5**, mp 36—39 °C, are as follows: UV (MeOH) λ_{max} 221 nm (ε 5600); IR (Nujol) 1640 and 1560 cm^{-1}; ^1H NMR ($CDCl_3$) δ 0.77 (d, J=*ca.* 6Hz, $C_{(4)}$-CH_3), 1.03 (s, $C_{(5)}$-CH_3), 1.17 (t, J=7.5 Hz, $-OCH_2\underline{C}H_3$), 2.03 (d, J=*ca.* 1 Hz, $C_{(11)}$-CH_3), 3.67 (q, J=7.5 Hz, $-OC\underline{H}_2CH_3$), 4.22 (br s, $C_{(6)}$-H), and 7.10 (m, $C_{(12)}$-H); Found: C, 77.79; H, 10.59%. Calcd for $C_{17}H_{26}O_2$: C, 77.82; H, 9.99%.

*6ξ-Deuterio-9-dehydrofuranoeremophilane (**8**-d_1).* 6β-Deuterioepiligularol (**2**-d_1) obtained from ligularone (**28**; 50 mg), was treated with *p*-toluenesulfonyl chloride (58 mg) in pyridine (7 ml) under the same conditions as in the case of **2** to afford 6ξ-deuterio-9-dehydrofuranoeremophilane (**8**-d_1).

The authors wish to thank Dr. L. Novotný, Czechoslovak Academy of Science for a gift of furanoeremophilan-9α-ol, furanopetasine, and furanopetasol, and Professor Koji Yamakawa, Science University of Tokyo, for supplying the spectral data of 9-dehydrofuranoeremophilane.

References

1) A part of this work was presented at the 7th Symposium on Mass Spectiometry for Organic Compounds, Kobe, October 21, 1972, Abstr. pp. 36—38.

2) a) H. Nagano, Y. Moriyama, Y. Tanahashi, T. Takahashi, M. Fukuyama, and K. Sato, *Chem. Lett.*, **1972**, 13; H. Nagano, Y. Moriyama, Y. Tanahashi, and T. Takahashi, *Bull. Chem. Soc. Jpn.*, **47**, 1994 (1974); M. Tada, Y. Moriyama, Y. Tanahashi, and T. Takahashi, *Tetrahedron Lett.*, **1972**, 5251; H. Shirasaki, H. Komatsu, H. Nagano, Y. Moriyama, Y. Tanahashi, and T. Takahashi, *Bull. Chem. Soc. Jpn.*, **46**, 2918 (1973); b) H. Nagano and T. Takahashi, *ibid.*, **45**, 1935 (1972); K. Naya, Y. Makiyama, T. Matsuura, N. Ii, H. Nagano, and T. Takahashi, *Chem. Lett.*, **1978**, 301; c) H. Nagano, Y. Tanahashi, Y. Moriyama, and T. Takahashi, *Bull. Chem. Soc. Jpn.*, **46**, 2840 (1973); d) H. Nagano and T. Takahashi, *ibid.*, **51**, 3335 (1978).

3) a) Y. Tanahashi, Y. Ishizaki, T. Takahashi, and K. Tori, *Tetrahedron Lett.*, **1968**, 3739; Y. Ishizaki. Y. Tanahashi, T. Takahashi, and K. Tori, *Tetrahedron*, **26**, 5387 (1970); b) Y. Ishizaki, Y. Tanahashi, T. Takahashi, and K. Tori, *J. Chem. Soc., Chem. Commun.*, **1969**, 551; Y. Moriyama, T. Tsuyuki, T. Takahashi, and K. Koyama, *Phytochemistry*, **13**, 288 (1974); Y. Ishizaki, Y. Tanahashi, T. Tsuyuki, T. Takahashi, and K. Tori, *Bull. Chem. Soc. Jpn.*, **52**, 1182 (1979); c) M. Tada, Y. Moriyama, Y. Tanahashi, T. Takahashi, M. Fukuyama, and K. Sato, *Tetrahedron Lett.*, **1971**, 4007; M. Tada, Y. Moriyama, Y. Tanahashi, and T. Takahashi, *Bull.*

Chem. Soc. Jpn., **47**, 1999 (1974).

4) C. Kuroda, T. Murae, M. Tada, H. Nagano, and T. Takahashi, *Chem. Lett.*, **1978**, 1313.

5) a) Q. N. Porter and J. Baldas, "Mass Spectrometry of Heterocyclic Compounds," Wiley-Interscience, a Division of John Wiley Sons, New York (1971), pp. 128 and 129; b) F. Patil, G. Ourisson, Y. Tanahashi, M. Wada, and T. Takahashi, *Bull. Soc. Chim. Fr.*, **1968**, 1047; c) G. A. Eagle, D. E. A. Rivett, D. H. Williams, and R. G. Wilson, *Tetrahedron*, **25**, 5227 (1969); Y. Nakagawa, 24th National Meeting of the Chemical Society of Japan, Osaka, 1971, Abstr. No. B22240.

6) H. Ishii, T. Tozyo, and H. Minato, *Tetrahedron*, **21**, 2605 (1965).

7) L. Novotný, Z. Samek, J. Harmatha, and F. Šorm, *Collect. Czech. Chem. Commun.*, **34**, 336 (1969).

8) K. Naya, M. Nakagawa, M. Hayashi, K. Tsuji, and M. Naito, *Tetrahedron Lett.*, **1971**, 2961.

9) F. Bohlmann and C. Zdero, *Phytochemistry*, **16**, 135 (1977); K. Yamakawa and T. Satoh, *Chem. Pharm. Bull.*, **26**, 3704 (1978).

10) H. Ishii, T. Tozyo, and H. Minato, *J. Chem. Soc., C*, **1966**, 1545.

11) A. R. Pinder, *Fortschr. Chem. Org. Naturstoffe*, **34**, 81 (1977).

12) L. Novotný, Ch. Tabačíková-Wlotzka, V. Herout, and F. Šorm, *Collect. Czech. Chem. Commun.*, **29**, 1922 (1964).

13) M. Tada, Y. Tanahashi, Y. Moriyama, and T. Takahashi, *Bull. Chem. Soc. Jpn.*, **50**, 463 (1977); M. Tada, Y. Moriyama, Y. Tanahashi, and T. Takahashi, *ibid.*, **48**, 549 (1975).

3β,6β-Bis(acyloxy)furanoeremophilan-14-als and -14-oic Acids from *Syneilesis palmata* (THUNB.) MAXIM.[1]

Chiaki KURODA, Tatsushi MURAE, Masahiro TADA,† Hajime NAGANO,††
Takahiko TSUYUKI, and Takeyoshi TAKAHASHI*

Department of Chemistry, Faculty of Science, The University of Tokyo, Hongo, Bunkyo-ku, Tokyo 113

(Received October 9, 1981)

Structural studies of four new sesquiterpenes, 3β-angeloyloxy-6β-(3-methylbutanoyloxy)- and 3β,6β-bis(angeloyloxy)furanoeremophilan-14-als and 3β-angeloyloxy-6β-(3-methylbutanoyloxy)- and 3β-angeloyloxy-6β-(3-methylpentanoyloxy)furanoeremophilan-14-oic acids, together with 3β,6β-bis(angeloyloxy)furanoeremophilan-14-oic acid from *Syneilesis palmata* (THUNB.) MAXIM. are described.

Investigations on sesquiterpenes in the plants of the genera *Ligularia*,[2] *Eupatorium*,[3] *Farfugium*,[4] and *Cacalia*[5] (Compositae) have been carried out in our laboratory. Furanoeremophilane derivatives have been shown to be main sesquiterpenes for plants of the genera *Ligularia* and *Farfugium*,[6] but benzofuran derivatives[5,7] together with furanoeremophilanes[8] for those of the genus *Cacalia*.[9] In connection with these studies, *Syneilesis palmata* (THUMB.) MAXIM. (Japanese name: Yaburegasa) (Compositae) was now examined. Only a constitutional investigation of *S. palmata* has been reported by Hikichi and Furuya[10] and three alkaloids, syneilesine, acetylsyneilesine, and senecionine have been isolated. While *S. palmata* is classified morphologically into the genus *Syneilesis*, it is also classified taxonomically into the genus *Cacalia* and named *Cacalia Krameri* MAKINO. Therefore, examination on sesquiterpene constituents of this plant is interested from the chemotaxonomical viewpoint.

Chromatographic separation of the ethereal extract of the roots of *S. palmata* afforded two main components **A** and **B**, which were positive to the Ehrlich test.

It was found that the component **A** gave two peaks in high performance liquid chromatographic examination. Since the component **A**, obtained as an oil, crystallized from pentane on standing, separation by fractional crystallization was attempted but was unsuccessful. High performance liquid chromatography (HPLC) was successfully applied to the separation to afford an aldehyde (**1**) and an ether (**2**) in a ratio of 1 : 1. On treatment of the component **A** with sodium borohydride, the ether (**2**) remained unchanged and separated easily from the reaction mixture. The ether (**2**; content: 0.02%), mp 97—98 °C, was found to be a known 3β-angeloyloxy-6α,14-epoxyfuranoeremophilane.[11]

The aldehyde (**1**; content: 0.03%), mp 82—83 °C, was found to be a mixture of two components **1a** and **1b** by appearance of two molecular ions at *m/e* 430.2334 ($C_{25}H_{34}O_6$) and *m/e* 428.2175 ($C_{25}H_{32}O_6$) in the high resolution mass spectrum. HPLC was applied to further separation of **1** into **1a** and **1b** without success, because each retention time was nearly the same due to their structural similarity. Separation by gas-liquid chromatography (GLC) was not available because of thermal unstability of these compounds. Therefore we were obliged to analyze the mixture (**1**) in order to obtain the information for structure determination of **1a** and **1b**.

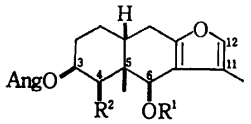

1a $R^1=R_a$; $R^2=CHO$
1b $R^1=R_b$; $R^2=CHO$
3a $R^1=R_a$; $R^2=CH_2OH$
3b $R^1=R_b$; $R^2=CH_2OH$
7a $R^1=R_a$; $R^2=COOH$
7b $R^1=R_b$; $R^2=COOH$
7c $R^1=R_c$; $R^2=COOH$
8a $R^1=R_a$; $R^2=COOCH_3$
8b $R^1=R_b$; $R^2=COOCH_3$
8c $R^1=R_c$; $R^2=COOCH_3$

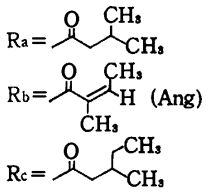

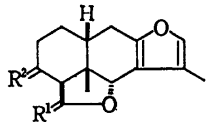

2 $R^1=H_2$; $R^2=\alpha$-H, β-OAng
10 $R^1=O$; $R^2=\alpha$-H, β-OAng
11 $R^1=O$; $R^2=H_2$
13 $R^1=H_2$; $R^2=\alpha$-H, β-OH
14 $R^1=H_2$; $R^2=H_2$
15 $R^1=H_2$; $R^2=O$

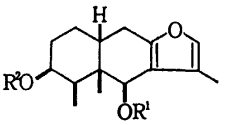

4 $R^1=H$; $R^2=H$
6 $R^1=Ac$; $R^2=Ang$

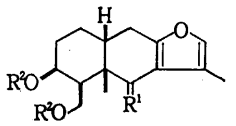

9 $R^1=\alpha$-H, β-OH ; $R^2=H$
12 $R^1=\alpha$-OH, β-H ; $R^2=H$
16 $R^1=\alpha$-H, β-OAc ; $R^2=Ac$

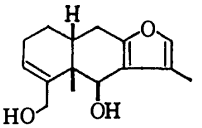

5

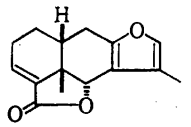

17

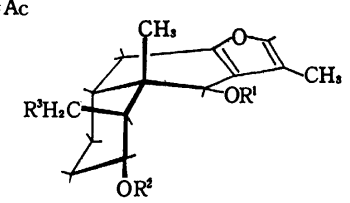

6a $R^1=Ac$; $R^2=Ang$; $R^3=H$
9a $R^1=R^2=H$; $R^3=OH$

† Present address: Laboratory of Bioorganic Chemistry, Tokyo University of Agriculture and Technology, Fuchu, Tokyo 183.

†† Present address: Department of Chemistry, Faculty of Science, Ochanomizu University, Otsuka, Bunkyo-ku, Tokyo 112.

The IR and ^1H NMR spectra of the mixture **1** (**1a** and **1b**) showed the presence of a β-methyl-substituted furan with an α-hydrogen, a tertiary methyl, and an

aldehyde group, together with protons on carbon atoms bearing acyloxyl groups [δ 5.47 (br signal, 1H; $C_{(3)}$–H), 6.28 (m, *ca.* 0.7H; $C_{(6)}$–H of **1a**), and 6.36 (m, *ca.* 0.3H; $C_{(6)}$–H of **1b**)]. Reduction of **1** with sodium borohydride afforded a mixture (**3**) of alcohols, **3a** and **3b**, whose ^{1}H NMR spectrum showed the presence of $-C\underline{H}_2OH$. The mixture of alcohols (**3a** and **3b**) was treated with methanesulfonyl chloride to afford a mixture of mesylates (δ 2.86; $-SO_2CH_3$), which, on reduction with lithium aluminium hydride gave two diols, **4** and **5** in 12% and 57% yields, respectively. The diol (**4**) was identified with a known furanofukinol[12] (furanoeremophilane-3β,6β-diol) by direct comparison with an authentic sample.

In the ^{1}H NMR spectrum of **1**, a doublet signal characteristic of a secondary methyl at C-4 of furanoeremophilanes was not observed, suggesting the formyl group must be attached to the C-4. This was supported by a doublet signal (J=5 Hz) due to the aldehydic proton at δ 9.97. Therefore, **1a** and **1b** were deduced to be 3β,6β-bis(acyloxy)furanoeremophilan-14-als.

The diol (**5**), $C_{15}H_{20}O_3$ (*m/e* 248.1482), was determined to be furanoeremophil-3-ene-6β,14-diol, supporting above conclusion. The presence of a secondary hydroxyl group at C-6 was shown by appearance of a multiplet signal at δ 4.77[13] and a *retro*-Diels Alder fragment ion at *m/e* 124.0518 ($C_7H_8O_2$) as a base peak.[14] The partial structure of 3-en-14-ol for **5** was supported by appearance of a broad signal at δ 5.40 ($C_{(3)}$–H) and an AB quartet signal due to a CH_2OH group attached to a carbon atom carrying no hydrogen atom.

The locations and structures of two acyloxyl groups were determined as follows. The component **A** (a mixture of **1** and **2**) was hydrolyzed with alkali. The carboxylic acids derived from the acyloxyl groups were methylated with diazomethane to give a mixture of methyl esters, which was examined by gas chromatography-mass spectrometry (GC-MS) measurement. Methyl angelate and methyl 3-methylbutanoate were detected in a ratio of *ca.* 3 : 1. From these observations together with the high resolution mass spectral data of **1a** and **1b**, a structure of 3β,6β-bis(angeloyloxy)-furanoeremophilan-14-al was suggested for **1b** and either 3β-angeloyloxy-6β-(3-methylbutanoyloxy)- or 6β-angeloyloxy-3β-(3-methylbutanoyloxy)furanoeremophilan-14-al for **1a**.

It is shown that when mass spectrum of 3β-angeloyloxy-6β-acetoxyfuranoeremophilane (**6**) was measured by direct inlet system, peaks at *m/e* 314 and *m/e* 274 due to fragment ions $(M-AcOH)^+$ and $(M-Angelic\ acid)^+$, respectively, were observed in an intensity ratio of 9 : 2, but when measured by indirect inlet system, only the former peak at *m/e* 314 due to $(M-AcOH)^+$ by elimination of the acetoxyl group on C-6 was observed.[15] These observations mean that an acid moiety at C-6 of 6-acyloxyfuranoeremophilane derivatives is easily eliminated to give the corresponding fragment ion by indirect inlet measurement. Table 1 gives the mass spectral data of **3** measured by the two inlet systems. The mass spectrum measured by indirect inlet system of **3** showed a peak at *m/e* 330 due to elimination of carboxylic acids (3-methylbutanoic acid for **3a** and angelic acid for **3b**) derived from the acyloxyl groups at C-6 with a relative intensity 8.7% but no peak at *m/e* 332 due to elimination of angelic acid, suggesting the presence of the angeloyloxyl group on C-3 for both **3a** and **3b**.

Table 1. Mass spectral data for **3**

m/e	Intensity/% Direct	Indirect	Assignment of ion
432	1.7	—	M^+(**3a**)
430	1.0	—	M^+(**3b**)
348	4.5	—	$(M-R^1+H)^+$
347	1.6	—	$(M-R^1)^+$
332	2.5	—	$(M-AngOH)^+$(derived from **3a**)
330	22[a,b]	8.7[a]	[a]$(M-R^1OH)^+$ (derived form **3a** and **3b**) [b]$(M-AngOH)^+$ (derived from **3b**)
248	6.4	—	$(M-R^1OH-Ang+H)^+$
247	7.5	—	$(M-R^1OH-Ang)^+$
230	37	14	$(M-R^1OH-AngOH)^+$
161	—	24	
159	34	21	
124	22	—	
100	—	24	$(AngOH)^+$
99	29	—	$(AngO)^+$
83	100	36	$(Ang)^+$
55	74	100	$(CH_3CH{=}CCH_3)^+$

In conclusion, **1** is shown to consist of 3β-angeloyloxy-6β-(3-methylbutanoyloxy)furanoeremophilan-14-al (**1a**) and 3β,6β-bis(angeloyloxy)furanoeremophilan-14-al (**1b**) in a ratio of *ca.* 7 : 3.

Component **B** (**7**) was obtained in 0.18% yield as a pale yellow oil and positive to the Ehrlich test. The ^{1}H NMR and mass spectral examination revealed that the component **B** consisted of three carboxylic acids, **7a**, **7b**, and **7c** (deuterium-exchangeable broad singlet at δ 10.05 and molecular ions at *m/e* 446, 444, and 460) and the presence of a β-methyl-substituted furan with an α-hydrogen, a tertiary methyl, and protons [δ 6.28 (*ca.* 0.2H), δ 6.37 (*ca.* 0.7H), and δ 6.48 (*ca.* 0.1H); each assigned to $C_{(6)}$–H, and δ 5.37; $C_{(3)}$–H)] on carbon atoms bearing acyloxyl groups, containing an angeloyloxyl group.

On esterification with diazomethane, **7** gave a mixture (**8**) of **8a** (*m/e* 460.2419, $C_{26}H_{36}O_7$), **8b** (*m/e* 458.2296, $C_{26}H_{34}O_7$), and **8c** (*m/e* 474.2818, $C_{27}H_{38}O_7$). Since HPLC separation of neither the mixture (**8**) nor the mixture (**7**) gave satisfactory results, analysis of the mixture (**8a**, **8b**, and **8c**) was carried out by the same procedures as in the case of **1**.

Reduction of **8** with lithium aluminium hydride afforded a triol (**9**), mp 139—140 °C, which was found to be identical with a triol obtained from **1** by treatment with lithium aluminium hydride. The structure of triol (**9**) was determined to be furanoeremophilane-3β,6β,14-triol by ^{1}H NMR and mass spectral measurements together with the fact that **9** was also derived from **1**. The detail of the structure elucidation of **9** was described below. In the ^{1}H NMR spectrum of **7**, a doublet signal characteristic of a secondary methyl at C-4 is absent. The carboxyl group, therefore, must be

located on C-4 and the acyloxyl groups on C-3β and C-6β for **7**.

Alkaline hydrolysis of **7** gave a mixture of carboxylic acids derived from the acyloxyl moieties. The mixture was methylated with diazomethane and examined by GC-MS measurement. Methyl angelate, methyl 3-methylbutanoate, and methyl 3-methylpentanoate were detected in a ratio of *ca.* 6 : 4 : 1. These observations together with high resolution mass spectral data suggest that 3β,6β-bis(angeloyloxy)furanoeremophilan-14-oic acid could be proposed for **7b**, 3β-angeloyloxy-6β-(3-methylpentanoyloxy)- or 6β-angeloyloxy-3β-(3-methylpentanoyloxy)furanoeremophilan-14-oic acid for **7c**, and 3β-angeloyloxy-6β-(3-methylbutanoyloxy)- or 6β-angeloyloxy-3β-(3-methylbutanoyloxy)furanoeremophilan-14-oic acid for **7a**. The alternatives for **7a** and **7c** were determined by mass spectrum of **8** measured by indirect inlet system (Table 2) and this conclusion was confirmed by the formation of 3β-angeloyloxyfuranoeremophilan-14,6α-olide (**10**) (*vide infra*). Based on arguments developed for **1**, appearance of a fragment peak at *m/e* 358 due to elimination of the acid moieties at C-6 suggests the presence of the angeloyloxyl group on C-3 for **8a**, **8b**, and **8c**. Thus the component **B** (**7**) is shown to consist of 3β-angeloyloxy-6β-(3-methylbutanoyloxy)furanoeremophilan-14-oic acid (**7a**), 3β,6β-bis(angeloyloxy)furanoeremophilan-14-oic acid (**7b**),[11,16] and 3β-angeloyloxy-6β-(3-methylpentanoyloxy)furanoeremophilan-14-oic acid (**7c**) in a ratio of *ca.* 7 : 1 : 2.

TABLE 2. MASS SPECTRAL DATA FOR **8**

m/e	Intensity/% Direct	Indirect	Assignment
474	0.7	—	M^+(**8c**)
460	2.7	—	M^+(**8a**)
458	0.9	—	M^+(**8b**)
376	17	—	$(M-R^1+H)^+$
375	8.7	—	$(M-R^1)^+$
374	0.2	—	$(M-AngOH)^+$ (derived from **8c**)
360	1.5	—	$(M-AngOH)^+$ (derived from **8a**)
358	19[a,b]	1.4[a]	[a] $(M-R^1OH)^+$ (derived from **8a**, **8b**, and **8c**) [b] $(M-AngOH)^+$ (derived from **8b**)
276	25	—	$(M-R^1OH-Ang+H)^+$
275	23	—	$(M-R^1OH-Ang)^+$
258	9.3	2.2	$(M-R^1OH-AngOH)^+$
161	—	8.6	
159	39	15	
124	25	—	
83	100	35	$(Ang)^+$
55	49	100	$(CH_3CH{=}CCH_3)^+$

Bohlmann *et al.*[16] isolated 3β,6β-bis(angeloyloxy)-furanoeremophilan-14-oic acid (**7b**) and related compounds from plants of the genus *Othonna* (Compositae) and these compounds were transformed into the triol (**9**; furanoeremophilane-3β,6β,14-triol) by methylation and reduction with lithium aluminium hydride. The ^{1}H NMR spectrum of our triol (**9**) derived from **8** was kindly measured and compared with that of the specimen (**9**)[11,16] by Professor Bohlmann. However, we were informed that the two compounds are not identical. The physical and ^{1}H NMR spectral data of **9** reported by Bohlmann *et al.*[11,16] were not coincident with those of ours as shown in Experimental. Therefore the structure of triol (**9**) derived from **8** was investigated closely. Treatment of **7** with a mixture of acetic acid and benzene under reflux afforded a lactone (**10**), mp 112—116 °C, IR 1765 cm^{-1}, the purity of which was confirmed by appearance of a single peak on GLC (column: H523, 200 °C, carrier gas: N_2) and a single molecular ion peak at *m/e* 344.1679 ($C_{20}H_{24}O_5$). The mass spectrum of **10** together with ^{1}H NMR spectrum reveals the presence of an angeloyloxyl moiety and the absence of the other two acyloxyl groups, suggesting the angeloyloxyl group remains at C-3β for **10**. The configuration of $C_{(6)}$–H could be established by NOE measurement. It has been reported that the signal due to $C_{(6\beta)}$–H resonated at δ 5.08 shows increase by 28% on irradiation at δ 1.26 assigned to a signal of $C_{(5\beta)}$–Me of furanoeremophilan-14,6α-olide (**11**).[6b] On saturation of a signal due to $C_{(5\beta)}$–Me resonating at δ 1.21, a signal at δ 4.58 due to the $C_{(6)}$–H of **10** resulted in increase by 25%, indicating the structure 3β-angeloyloxyfuranoeremophilan-14,6α-olide for **10**.

Reduction of **10** with lithium aluminium hydride yielded a triol (**12**), mp 170—172 °C [^{1}H NMR ($CDCl_3$) δ 1.21 (s; $C_{(5)}$–Me), 2.06 (d, J=1.5 Hz; $C_{(11)}$–Me], 4.34 [m; $C_{(6)}$–H, and 7.09 (m; $C_{(12)}$–H)], which was *not identical* with the triol (**9**) (*cf.* Experimental). The triol (**12**) is inferred to be furanoeremophilane-3β,6α,14-triol.

On treatment with dilute hydrochloric acid, **9** and **12** gave the same hydroxy ether (**13**), mp 136—138 °C, which was also obtained from the known 3β-angeloyloxy-6α,14-epoxyfuranoeremophilane (**2**)[11] by reduction with lithium aluminium hydride. The presence of a skeletal structure, 6α,14-epoxyfuranoeremophilane (**14**), was confirmed for **2** and **13** by the observed $J_{4,14}$-values (11 and 11.5 Hz, respectively)[6b] and the appearance of the 6β-H signal at δ 4.58 and 4.55 (in $CDCl_3$),[6b] respectively. The $C_{(5\beta)}$–Me of **13** resonates at lower field δ 1.44 (in $CDCl_3$) compared with that (δ 1.16) of **14**[6b] due to deshielding of the 3β(axial)-hydroxyl group. Based on the correlation of **12** with **10** and **13**, the 3β,6α,14-triol structure was shown for the triol (**12**).

From these evidence, the structure of the triol (**9**) derived from **1** and **7**, was unambiguously established to be furanoeremophilane-3β,6β,14-triol. The ^{1}H NMR spectral data[11] of "Bohlmann's triol" are practically identical with those (in $CDCl_3$) of 6α,14-epoxyfuranoeremophilan-3β-ol (**13**) (*cf.* Experimental). This suggests that "the triol" would be **13**, a dehydrated product of the 3β,6β,14-triol (**9**). The epoxy derivative (**13**) can be formed easily from **9** as shown before.

The $C_{(3\alpha)}$–H signal of our triol (**9**) appears as a quintet ($J_{2\beta,3\alpha}$=10, $J_{2\alpha,3\alpha}$=5, and $J_{3\alpha,4\alpha}$=5 Hz; in $CDCl_3$–D_2O) as in the case of 3β-angeloyloxy-6β-acetoxyfuranoeremophilane (**6** and **6a**).[12] This shows that **9** preferentially adopts a non-steroidal-like conformation depicted as in **9a**.

Some compounds (**15**, **16**, and **17**) derived from **13**,

9, and **10**, respectively, are also described.

The fact that benzofuran derivatives are not isolated from *S. palmata* suggests that plants of the genus *Syneilesis* would be chemotaxonomically related to those of the genus *Ligularia* rather than the genus *Cacalia*. Among four new sesquiterpenes (**1a**, **1b**, **7a**, and **7c**), **1a** and **1b** constitute the first examples of natural furanoeremophilanes with a formyl group at C-4.

Experimental

General Procedures. All melting points were measured on a Mel-temp capillary melting point apparatus (Laboratory Devices) and uncorrected. Optical rotations were determined on a JASCO polarimeter DIP-SL. Ultraviolet absorption (UV) spectra and infrared (IR) spectra were measured on a Hitachi EPS-3 and a Hitachi EPI-G2 spectrometer, respectively. Mass (MS) spectra were run on a Hitachi RMU-6 Tokugata mass spectrometer and high resolution mass spectra on a Hitachi RMH-2 or a JEOL JMS-D300 mass spectrometer operating at 70 eV. Gas chromatography-mass spectrometry (GC-MS) was carried out on a Hitachi RM-50 or a Hitachi 063 gas chromatograph connected with a Hitachi RMS-4 mass spectrometer. The relative intensities were expressed in % in parentheses. Proton nuclear magnetic resonance (^{1}H NMR) spectra (60 MHz) were taken using a Hitachi R-20B or a JEOL JNM FX-60 spectrometer. Chemical shifts were expressed in ppm downfield from tetramethylsilane as an internal standard (δ value) and coupling constants in Hz. Gas-liquid chromatography (GLC) was carried out using a Shimadzu GC-4APF or GC-6A equipped with a hydrogen flame ionization detector. Liquid Chromatograph Model ALC/GPC 202/401 (Waters Assoc.) was used for high performance liquid chromatography (HPLC). Thin layer chromatography (TLC) was carried out on Kieselgel 60 PF_{254} or Kieselgel GF_{254} in 0.25 mm- or 0.5 mm-thickness. Wakogel C-200 (Wako) was used for column chromatography.

Plant Material. *Syneilesis palmata* (Thunb.) Maxim. was collected in August 1977 in University Forest at Chichibu, the University of Tokyo.

Extraction and Separation. Extraction of the air-dried roots (7.5 kg) with ether was carried out for 5 d at room temperature. The extract was concentrated to give an oily residue (32 g), which was subjected to separation by silica gel (900 g) column chromatography and eluted (each fraction: 400 ml) with the following solvents: hexane, 100 ml; 5%-ether in hexane, 1000 ml; 10%-, 1500 ml; 20%-, 2500 ml; 25%-, 1000 ml; 50%-, 2000 ml; ether, 1000 ml; and acetone, 500 ml. Fractions 11—14 and fractions 16—18 were subjected to further purification.

Fractions 11—14 (component **A**), containing **1** and **2**, were combined and evaporated to give an oil (4.27 g), which crystallized from pentane. Separation of **1** and **2** was not attained by fractional crystallization, but was successful by HPLC (column; μ-Porasil, solvent: hexane–ether 4 : 1, flow rate: 0.6 ml/min). The mixture afforded **1** (R_t 8.7 min) and **2** (R_t 9.5 min) in a ratio of *ca.* 1 : 1.

Isolation of **2** from the mixture in a large scale was achieved as follows: the mixture (950 mg) in ethanol (100 ml) was treated with sodium borohydride (1.07 g) for 4 h at room temperature and the reaction mixture, after usual work-up, was purified by silica gel column chromatography. Elution with hexane–ether (1 : 1) afforded **2**[11] (387 mg) and **3** (a mixture of **3a** and **3b**; 345 mg).

Fractions 16—18 (component **B**) gave **7** (13.6 g), mp 124—134 °C (decomp.) (from hexane).

*3β-Angeloyloxy-6β-acyloxyfuranoeremophilan-14-als (**1**, a Mixture of **1a** and **1b**).* Mp 82—83 °C (from hexane), one spot on TLC, IR (Nujol) 1725, 1715, 1640, 1565, 1230, and 1160 cm^{-1}; ^{1}H NMR ($CDCl_3$) δ 1.04 (3H, s, $C_{(5)}$–CH_3), 1.83 (3H, d, J=1.5 Hz, $C_{(11)}$–CH_3), 5.47 (1H, br signal, $W_{1/2}$=*ca.* 16 Hz, $C_{(3)}$–H), 6.00 (*ca.* 1.3H, br q, J=7 Hz, $\underline{H}\!>\!C\!=\!C\!<^{CH_3}_{COO-}$), 6.28 (*ca.* 0.7H, m, $C_{(6)}$–H of **1a**), 6.36 (*ca.* 0.3H, m, $C_{(6)}$–H of **1b**), 6.97 (1H, m, $C_{(12)}$–H), and 9.97 (1H, d, J=5 Hz, –CH–CHO); MS *m/e* (%) 430 (M$^+$ of **1a**; 0.9), 428 (M$^+$ of **1b**; 0.5), 346 (8), 345 (1.7), 330 ([**1a** –AngOH]$^+$ [17]; 1.8), 328 ([**1**–R^{1}OH]$^+$ [17] and [**1b**–AngOH]$^+$; 12), 246 (20), 245 (16), 228 (25), 159 (46), 124 (25), 85 (26), 83 (100), 57 (33), and 55 (56); Found for **1a**: *m/e* 430.2334. Calcd for $C_{25}H_{34}O_6$: M 430.2354. Found for **1b**: *m/e* 428.2175. Calcd for $C_{25}H_{32}O_6$: M 428.2197.

*3β-Angeloyloxy-6β-acyloxyfuranoeremophilan-14-oic Acids (**7**, a Mixture of **7a**, **7b**, and **7c**).* An oil (one spot on TLC), IR (liq) 3000, 1730, 1720, 1710, 1645, 1560, 1230, and 1160 cm^{-1}; ^{1}H NMR (CCl_4) δ 1.13 (3H, s, $C_{(5)}$–CH_3), 1.81 (3H, d, J=1.5 Hz, $C_{(11)}$–CH_3), 5.37 (1H, br signal, $W_{1/2}$=*ca.* 15 Hz, $C_{(3)}$–H), 5.59 (*ca.* 1H, br q, J=7 Hz, $\underline{H}\!>\!C\!=\!C\!<^{CH_3}_{COO-}$), 6.28 (*ca.* 0.2H, m, $C_{(6)}$–H of **7c**), 6.37 (*ca.* 0.7H, m, $C_{(6)}$–H of **7a**), 6.48 (*ca.* 0.1H, m, $C_{(6)}$–H of **7b**), 6.97 (1H, q, J=1.5 Hz, $C_{(12)}$–H), and 10.05 (1H, br s, –COOH; disappeared on addition of D_2O); MS *m/e* (%) 460 (M$^+$ of **7c**; 0.05), 446 (M$^+$ of **7a**; 0.17), 444 (M$^+$ of **7b**; 0.07), 362 (0.8), 361 (0.4), 360 ([**7c** –AngOH]$^+$; 0.4), 346 ([**7a**–AngOH]$^+$; 0.2), 344 ([**7** –R^{1}OH]$^+$ and [**7b** –AngOH]$^+$; 2.7), 262 (5.5), 245 (2.3), 244 (3.7), 161 (13), 159 (11), 83 (75), and 55 (100).

*3β-Angeloyloxy-6α,14-epoxyfuranoereomphilane (**2**).* Mp 97—98 °C (from ether), $[\alpha]_D^{22}$ −18° (*c* 1.2, EtOH), IR (Nujol) 1710, 1635, 1560, 1235, and 1155 cm^{-1}; UV (EtOH) 218 nm (ε 28000); ^{1}H NMR ($CDCl_3$) δ 1.40 (3H, s, $C_{(5)}$–CH_3), 2.02 (3H, d, J=1.5 Hz, $C_{(11)}$–CH_3), 3.67 (1H, dd, $J_{4,14\beta}$=11 and $J_{14\alpha,14\beta}$=7.5 Hz, $C_{(14\beta)}$–H), 3.92 (1H, t, $J_{4,14\alpha}$=7.5 and $J_{14\alpha,14\beta}$=7.5 Hz, $C_{(14\alpha)}$–H), 4.58 (1H, m, $C_{(6)}$–H), 5.32 (1H, br s, $W_{1/2}$=*ca.* 7 Hz, $C_{(3)}$–H), 6.07 (1H, q-like, J=7 Hz, $\underline{H}\!>\!C\!=\!C\!<^{CH_3}_{COO-}$), and 7.01 (1H, m, $C_{(12)}$–H); MS *m/e* (%) 330 (M$^+$; 36), 230 (37), 159 (63), 83 (89), and 55 (100). The ^{1}H NMR and mass spectral data are in good agreement with those of **2** reported in lit.[11]

*3β-Angeloyloxy-6β-acyloxyfuranoeremophilan-14-ols (**3**, a Mixture of **3a** and **3b**).* An oil, IR (liq) 3450, 1720, 1710, 1640, 1560, 1230, and 1160 cm^{-1}; ^{1}H NMR (C_6D_6) δ 1.12 (3H, s, $C_{(5)}$–CH_3), 1.90 (3H, d, J=1.5 Hz, $C_{(11)}$–CH_3), 4.36 (1H, br signal, $W_{1/2}$=19 Hz, $C_{(3)}$–H), 4.34 (1H, dd, J=11.5 and J=6 Hz, $C_{(14)}$–H), 4.73 (1H, dd, J=11.5 and J=3 Hz, $C_{(14)}$–H), 5.75 (1H, br q, J=7 Hz, $\underline{H}\!>\!C\!=\!C\!<^{CH_3}_{COO-}$), 6.49 (*ca.* 0.6H, m, $C_{(6)}$–H of **3a**), 6.59 (*ca.* 0.4H, m, $C_{(6)}$–H of **3b**), 6.96 (1H, m, $C_{(12)}$–H); MS are given in Table 1.

*Treatment of **3** with Methanesulfonyl Chloride.* A solution of **3** (135 mg) in pyridine (4 ml) and methanesulfonyl chloride (15 drops) were allowed to stand overnight at room temperature and usual work-up gave a mesylate (crude, 177 mg) as an oil; IR (liq) 1720, 1705, 1635, 1560, 1340, 1230, and 1160 cm^{-1}; ^{1}H NMR (C_6D_6) δ 2.86 (3H, s, $-SO_2CH_3$); MS *m/e* (%) 510 (M$^+$ of a mesylate from **3a**; 0.4), 508 (M$^+$ of a mesylate from **3b**; 0.2), 426 (4.3), 408 (10), 326 (2.7), 325 (3.2), 308 (6.7), 159 (37), 83 (100), and 55 (96).

Reduction of the Mesylates with Lithium Aluminium Hydride.

A mixture of the crude mesylates (177 mg) dissolved in ether (20 ml) and lithium aluminium hydride (200 mg) was stirred at room temperature for 1.5 h and then heated under reflux for 1 h. The reaction mixture was worked up as usual, chromatographed on silica gel, and eluted with ether to give furanoeremophilane-3β,6β-diol (**4**;[12] 9 mg, 12% yield from **3**) and furanoeremophil-3-ene-6β,14-diol (**5**; 44 mg, 57% yield from **3**).

4; Mp 176—179 °C (decomp) (from ether). **5**; An oil, $[\alpha]_D^{27}$ −14° (*c* 0.02, EtOH); IR (liq) 3430, 3250, 1645, and 1565 cm^{-1}; ^{1}H NMR (C_6D_6) δ 1.08 (3H, s, $C_{(5)}$-CH_3), 2.22 (3H, d, J=1.5 Hz, $C_{(11)}$-CH_3), 3.58 (1H, A part of an ABq, J=11 Hz, $C_{(14)}$-H_A), 4.08 (1H, B part of an ABq, J=11 Hz, $C_{(14)}$-H_B), 4.77 (1H, m, $C_{(6)}$-H), 5.40 (1H, br signal, $W_{1/2}$=*ca.* 7.5 Hz, $C_{(3)}$-H), and 7.04 (1H, m, $C_{(12)}$-H); MS *m/e* (%) 248 (M^+; 3.4), 230 (13), 141 (6.1), and 124 (100); Found: *m/e* 248.1482. Calcd for $C_{15}H_{20}O_3$: M 248.1411. Found: *m/e* 124.0518. Calcd for $C_7H_8O_2$: *m/e* 124.0523.

Alkaline Hydrolysis of **1**. A mixture (53 mg) of **1** and **2** was dissolved in methanol (5 ml). Potassium hydroxide (250 mg) in water (1 ml) was added and the reaction mixture was refluxed for 1 h. After addition of water (50 ml), the solution was washed with ether. The aqueous layer was acidified with 2 M** hydrochloric acid to pH 1 and extracted with ether. The ethereal layer was dried (Na_2SO_4) and concentrated carefully. To the concentrated solution, diazomethane in ether was added and the solution was allowed to stand for 1 h. The mixture of methyl esters was analyzed by GC-MS measurement (column: PEG-20M, temperature: heated from 50 °C at a rate of 3 °C/min; carrier gas: He, 0.5 kg/cm^2) and found to be a mixture of methyl angelate (M^+ at *m/e* 114, R_t 15.3 min) and methyl 3-methylbutanoate (M^+ at *m/e* 116, R_t 12.2 min) in a ratio of *ca.* 3 : 1.

Esterification of **7** *with Diazomethane*. 3β-Angeloyloxy-6β-acyloxyfuranoeremophilan-14-oic acids (**7**; 32 mg) was treated with excess diazomethane in ether and the reaction product was purified by silica-gel column chromatography to give methyl 3β-angeloyloxy-6β-acyloxyfuranoeremophilan-14-oates (**8**; 28 mg) as an oil, IR (liq) 1740, 1720, 1640, 1565, 1230, and 1160 cm^{-1}; UV (EtOH) 217 nm (ε 22000); ^{1}H NMR (C_6D_6) δ 1.07 (3H, s, $C_{(5)}$-CH_3), 1.87 (3H, d, J=1.5 Hz, $C_{(11)}$-CH_3), 3.38 (3H, s, -COOCH_3), 5.69 (*ca.* 1H, br q, J=7 Hz, $\underline{H}$>C=C<(COO-, CH_3)), 5.81 (1H, br signal, $W_{1/2}$=13 Hz, $C_{(3)}$-H), 6.50 (*ca.* 0.7H, m, $C_{(6)}$-H of **8a**), 6.60 (*ca.* 0.2H, m, $C_{(6)}$-H of **8c**), 6.63 (*ca*, 0.1H, m, $C_{(6)}$-H of **8b**), and 6.95 (1H, m, $C_{(12)}$-H); MS as given in Table 2; Found for **8a**: *m/e* 460.2419. Calcd for $C_{26}H_{36}O_7$: M 460.2531. Found for **8b**: *m/e* 458.2296. Calcd for $C_{26}H_{34}O_7$: M 458.2442, and Found for **8c**: *m/e* 474.2818. Calcd for $C_{27}H_{38}O_7$: M 474.3021.

Furanoeremophilane-3β,6β,14-triol (**9**). *From* **8**: Methyl 3β-angeloyloxy-6β-acyloxyfuranoeremophilan-14-oates (**8**; 276 mg) in ether (30 ml) was treated with lithium aluminium hydride (530 mg) at reflux temperature for 1.5 h to give **9** (99 mg).

From **1**: A mixture (58 mg) of **1** and **2** was treated with lithium aluminium hydride (100 mg) as above and the reaction mixture was chromatographed on silica gel to yield **9** (16 mg) together with 6α,14-epoxyfuranoeremophilan-3β-ol (**13**).

9; Mp 139—140 °C (from ether; derived from **8**), 137—138 °C (from ether; derived from **1**), mp of the admixture 137—140 °C; lit,[14] 148 °C; lit,[11] 122 °C; $[\alpha]_D^{25}$ −12° (*c* 1.45, EtOH; derived from **8**), $[\alpha]_D^{26}$ −11° (*c* 0.63, EtOH; derived from **1**); lit,[14] $[\alpha]_D^{24}$ −36.9° (*c* 1.48, $CHCl_3$); IR (Nujol) 3250, 1635, and 1560 cm^{-1}; UV (EtOH) 218 nm (ε 8600); ^{1}H NMR [$(CD_3)_2CO$] δ 0.97 (3H, s, $C_{(5)}$-CH_3), 2.03 (3H, d, J=1.5 Hz, $C_{(11)}$-CH_3), 4.46 (1H, m, $C_{(6)}$-H), and 7.02 (1H, br s, $W_{1/2}$=4 Hz, $C_{(12)}$-H); ^{1}H NMR ($CDCl_3$-D_2O, determined by Prof. Bohlmann) δ 1.04 (3H, s, $C_{(5)}$-CH_3), 2.08 (3H, d, J=1.1 Hz, $C_{(11)}$-CH_3), 2.20 (1H, d-like, J=17.5 Hz, $C_{(9\alpha)}$-H), 2.81 (1H, m, $C_{(9\beta)}$-H), 3.89 (1H, dd, J=10.5 and J=3 Hz, $C_{(14)}$-H), 4.14 (1H, t, J=10.5 Hz, $C_{(14)}$-H), 4.45 (1H, quintet, $J_{2\beta,3\alpha}$=10, $J_{2\alpha,3\alpha}$=5, and $J_{3\alpha,4\alpha}$=5 Hz, $C_{(3\alpha)}$-H), 4.89 (1H, br s, $W_{1/2}$=*ca.* 5.5 Hz, $C_{(6)}$-H), and 7.05 (1H, br s, $W_{1/2}$=*ca.* 4 Hz, $C_{(12)}$-H); lit,[14] [$(CD_3)_2CO$] δ 1.48 (3H, s, $C_{(5)}$-CH_3), 2.06 (3H, d, J=1 Hz, $C_{(11)}$-CH_3), 3.95 (2H, d, J=9 Hz, $C_{(14)}$-H_2), 4.29 (1H, ddd, J=2.5, J=2, and J=2 Hz, $C_{(3)}$-H), 4.59 (1H, t, J=1 Hz, $C_{(6)}$-H), and 7.04 (1H, br s, $C_{(12)}$-H); lit,[11] ^{1}H NMR (solvent not registered, probably $CDCl_3$) δ 1.45 (3H, s, $C_{(5)}$-CH_3), 2.03 (3H, d, J=1 Hz, $C_{(11)}$-H), 3.92 (2H, m, $C_{(14)}$-H_2), 4.25 (1H, dd, J=5 and J=2 Hz, $C_{(3)}$-H), 4.57 (1H, t, J=1 Hz, $C_{(6)}$-H), and 7.01 (1H, br s, $C_{(12)}$-H); MS *m/e* (%) 266 (M^+; 4.7), 248 (2.3), 230 (2.5), and 124 (100); Found: C, 67.78; H, 8.63%. Calcd for $C_{15}H_{22}O_4$: C, 67.64; H, 8.33%.

Alkaline Hydrolysis of **7**. A mixture of **7** (158 mg) in methanol (15 ml) and potassium hydroxide (700 mg) in water (3 ml) was heated under reflux for 1.5 h and the reaction product was treated and analyzed by the same procedures as in the case of the alkaline hydrolysis of **1** (*vide supra*) and was found to be a mixture of methyl 3-methylbutanoate (M^+ at *m/e* 116, R_t 12.2 min), methyl angelate (M^+ at *m/e* 114, R_t 15.3 min), and methyl 3-methylpentanoate (M^+ at *m/e* 130, R_t 15.6 min) in a ratio of *ca.* 4 : 6 : 1.

3β-Angeloyloxyfuranoeremophilan-14,6α-olide (**10**). A mixture (207 mg) of **7** in benzene (30 ml) and acetic acid (30 ml) was refluxed under a nitrogen atmosphere for 5 h. After addition of water, the reaction product was extracted with ether and the ethereal layer was washed with sodium hydrogencarbonate solution. The usual work-up gave 111 mg of **10**, mp 112—116 °C (from hexane-ether); $[\alpha]_D^{23}$ +18° (*c* 1.63, EtOH); IR (Nujol) 1765, 1720, 1645, 1635, 1565, 1235, and 1145 cm^{-1}; UV (EtOH) 216 (ε 16000); ^{1}H NMR (C_6D_6) δ 1.21 (3H, s, $C_{(5)}$-CH_3), 1.80 (3H, q, J=*ca.* 2 Hz, CH_3>C=C<(COO-, $\underline{CH_3}$)), 1.93 (3H, d, J=1.5 Hz, $C_{(11)}$-CH_3), 2.01 (3H, dq, J=7 and J=*ca.* 2 Hz, $\underline{CH_3}$>C=C<(COO-, CH_3)), 4.58 (1H, m, $C_{(6)}$-H), 5.43 (1H, br s, $W_{1/2}$=7 Hz, $C_{(3)}$-H), 5.71 (1H, br q, J=7 Hz, $\underline{CH_3}$>C=C<(COO-, CH_3)), and 6.88 (1H, m, $C_{(12)}$-H); MS *m/e* (%) 344 (M^+; 26), 262 (63), 245 (25), 244 (39), 83 (96), and 55 (100); Found: *m/e* 344.1679. Calcd for $C_{20}H_{24}O_5$: M 344.1622.

Furanoeremophilane-3β,6α,14-triol (**12**). 3β-Angeloyloxyfuranoeremophilan-14,6α-olide (**10**; 70 mg) in ether (10 ml) was treated with lithium aluminium hydride (200 mg) at reflux temperature for 1.5 h to give **12** (50 mg), mp 170—172 °C (from acetone); $[\alpha]_D^{17}$ ±0° (*c* 2.37, EtOH); IR (Nujol) 3300, 1645, and 1565 cm^{-1}; ^{1}H NMR ($CDCl_3$) δ 1.21 (3H, s, $C_{(5)}$-CH_3), 2.06 (3H, d, J=1.5 Hz, $C_{(11)}$-CH_3), 4.00 and 4.08 (2H, m, $C_{(14)}$-H_2), 4.34 (1H, m, $C_{(6)}$-H), 4.95 (1H, br signal, $W_{1/2}$=*ca.* 18 Hz, $C_{(3)}$-H), and 7.09 (1H, br s, $W_{1/2}$=*ca.* 3.5 Hz, $C_{(12)}$-H); ^{1}H NMR [$(CD_3)_2CO$] δ 1.18 (3H, s, $C_{(5)}$-CH_3), 2.00 (3H, d, J=1.5 Hz, $C_{(11)}$-CH_3), 3.90 (2H, br signal, $W_{1/2}$=*ca.* 12 Hz, $C_{(14)}$-H_2), 4.26 (1H, m, $C_{(6)}$-H), 4.70 (1H, br signal, $W_{1/2}$=*ca.* 12 Hz, $C_{(3)}$-H), and 7.10 (1H, br s, $W_{1/2}$=*ca.* 4 Hz, $C_{(12)}$-H); MS *m/e* (%) 266 (M^+; 1.7), 248 (2.5), 230 (1.1), 160 (3.4), 159 (2.9), and 124 (100).

6α,14-Epoxyfuranoeremophilan-3β-ol (**13**). *From* **9**: Furanoeremophilane-3β,6β,14-triol (**9**; 30 mg) in methanol

** 1 M=1 mol dm^{-3}.

(a few drop) was stirred with 0.05 M hydrochloric acid (18 ml) at room temperature for 10 min under a nitrogen atmosphere. Extraction with ether and washing with sodium hydrogencarbonate solution afforded **13** (27 mg).

From 12: Furanoeremophilane-3β,6α,14-triol (**12**; 16 mg) in acetone (a few drop) was treated with 0.2 M hydrochloric acid (5 ml) under the same conditions as above to give **13** (9 mg).

From 2: A mixture of 3β-angeloyloxy-6α,14-epoxyfuranoeremophilane (**2**; 72 mg) in ether (10 ml) and lithium aluminium hydride (100 mg) was heated under reflux for 1 h to give **13** (63 mg).

13; Mp 136—138 °C (from ether); $[\alpha]_D^{25}$ −30° (*c* 0.49, EtOH; derived from **9**), $[\alpha]_D^{22}$ −27° (*c* 1.1, EtOH; derived from **12**), $[\alpha]_D^{23}$ −27° (*c* 0.88, EtOH; derived from **2**); IR (Nujol) 3470, 1635, and 1565 cm^{-1}; UV (EtOH) 210 nm (end absorption, ε 8800); ^1H NMR (C_6D_6) δ 1.40 (3H, s, $C_{(5)}$-CH_3), 2.14 (3H, d, J=1.5 Hz, $C_{(11)}$-CH_3), 3.56 (1H, br s, $W_{1/2}$=6 Hz, $C_{(3)}$-H), 3.70 (1H, t, $J_{4,14\alpha}$=7 and $J_{14\alpha,14\beta}$=7 Hz, $C_{(14\alpha)}$-H), 3.87 (1H, dd, $J_{4,14\beta}$=11.5 and $J_{14\alpha,14\beta}$=7 Hz, $C_{(14\beta)}$-H), 4.54 (1H, m, $C_{(6)}$-H), and 6.99 (1H, m, $C_{(12)}$-H); ^1H NMR ($CDCl_3$) δ 1.44 (3H, s, $C_{(5)}$-CH_3), 2.01 (3H, d, J=1.5 Hz, $C_{(11)}$-CH_3), 3.84 and 4.00 (2H, m, $C_{(14)}$-H_2), 4.26 (1H, br s, $W_{1/2}$=6 Hz, $C_{(3)}$-H), 4.55 (1H, m, $C_{(6)}$-H), and 7.02 (1H, br s, $C_{(12)}$-H); MS *m/e* (%) 248 (M^+; 100), 161 (23), 160 (30), 159 (38), and 108 (31); Found: C, 72.40; H, 8.40%. Calcd for $C_{15}H_{20}O_3$: C, 72.55; H, 8.12%.

6α,14-Epoxyfuranoeremophilan-3-one (15). Chromium trioxide (700 mg) was dissolved in a solution of pyridine (1 ml) and dichloromethane (20 ml) and stirred at room temperature for 15 min. 6α,14-Epoxyfuranoeremophilan-3β-ol (**13**; 246 mg) was added to the solution and the whole was stirred for 5 h. The reaction mixture was filtered, and the precipitate was washed with ether. The filtrate and washing were combined and washed with 5% sodium hydroxide solution, 1 M hydrochloric acid, 10% sodium hydrogencarbonate solution, and brine, in turn. The usual work-up gave **15** (103 mg), mp 172—175 °C (from ether); $[\alpha]_D^{24}$ −31° (*c* 1.29, $CHCl_3$); IR (Nujol) 1710, 1630, and 1560 cm^{-1}; ^1H NMR (C_6D_6) δ 0.78 (3H, s, $C_{(5)}$-CH_3), 2.06 (3H, d, J=1.5 Hz, $C_{(11)}$-CH_3), 3.85 (1H, t, $J_{4,14\alpha}$=8 and $J_{14\alpha,14\beta}$=8 Hz, $C_{(14\alpha)}$-H), 4.15 (1H, dd, $J_{4,14\beta}$=11 and $J_{14\alpha,14\beta}$=8 Hz, $C_{(14\beta)}$-H), 4.43 (1H, m, $C_{(6)}$-H), and 6.94 (1H, m, $C_{(12)}$-H); MS *m/e* (%) 246 (M^+; 100), 231 (16), 160 (51), 159 (37), and 145 (43); Found: *m/e* 246.1264. Calcd for $C_{15}H_{18}O_3$: M 246.1255.

3β,6β,14-Triacetoxyfuranoeremophilane (16). Treatment of furanoeremophilane-3β,6β,14-triol (**9**; 28 mg) in pyridine (4 ml) with acetic anhydride (1 ml) at room temperature gave a crude acetate, which was purified by silica-gel column chromatography. Elution with petroleum ether–ether (1 : 1) afforded **16** (33 mg) as an oil, $[\alpha]_D^{30}$ −35° (*c* 1.2, EtOH); IR liq) 1740, 1640, 1560, and 1240 cm^{-1}; UV (EtOH) 217 nm (ε 7700); ^1H NMR (C_6D_6) δ 1.09 (3H, s, $C_{(5)}$-CH_3), 1.68, 1.69, and 1.79 (each 3H, s, -OCOCH_3), 1.88 (3H, d, J=1.5 Hz, $C_{(11)}$-CH_3), 4.33 (2H, m, $C_{(14)}$-H_2), 5.43 (1H, br signal, $W_{1/2}$=*ca.* 16 Hz, $C_{(3)}$-H), 6.49 (1H, m, $C_{(6)}$-H), and 6.94 (1H, m, $C_{(12)}$-H); ^1H NMR [$(CD_3)_2CO$] δ 1.17 (3H, s, $C_{(5)}$-CH_3), 1.87 (3H, d, J=1.5 Hz, $C_{(11)}$-CH_3), 1.99, 2.02, and 2.12 (each 3H, s, -OCOCH_3), 4.29 (2H, d, J=5 Hz, $C_{(14)}$-H_2), 5.28 (1H, dt, J=8 and J=5 Hz, $C_{(3)}$-H), 6.28 (1H, m, $C_{(6)}$-H), and 7.18 (1H, m, $C_{(12)}$-H); MS *m/e* (%) 392 (M^+; 1.8), 350 (7.1), 332 (10), 290 (6.4), 272 (5.8), 230 (15), 212 (20), 166 (10), 159 (30), and 124 (100).

Furanoeremophil-3-en-14,6α-olide (17). Aqueous methanol (80%, 50 ml) and then sodium carbonate (900 mg) in water (10 ml) were added to a solution of 3β-angeloyloxyfuranoeremophilan-14,6α-olide (**10**; 70 mg) in methanol (3 ml), and the mixture was stirred at room temperature for 45 min under nitrogen. The usual work-up afforded **17** (34 mg), mp 103—107 °C (from ether); $[\alpha]_D^{18}$ −68° (*c* 0.96, EtOH); IR (Nujol) 1740, 1670, 1640, and 1560 cm^{-1}; UV (EtOH) 218 nm (ε 28000); ^1H NMR ($CDCl_3$) δ 1.43 (3H, s, $C_{(5)}$-CH_3), 2.05 (3H, d, J=1.5 Hz, $C_{(11)}$-CH_3), 5.25 (1H, m, $C_{(6)}$-H), 6.28 (1H, t-like, J=3 Hz, $C_{(3)}$-H), and 7.03 (1H, m, $C_{(12)}$-H); MS *m/e* (%) 244 (M^+; 59), 187 (48), 185 (27), and 121 (100).

The authors wish to thank Mr. Masaya Sakata and Mr. Noboru Saito, University Forest at Chichibu, the University of Tokyo, for collecting *Syneilesis palmata* (THUNB.) MAXIM. The authors are also grateful to Professor F. Bohlmann, Technical University Berlin, for the discussions and the measurements of the ^1H NMR spectrum (270 MHz) of furanoeremophilane-3β,6β,14-triol.

References

1) Preliminary account of this report: C. Kuroda, T. Murae, M. Tada, H. Nagano, and T. Takahashi, *Chem. Lett.*, **1978**, 1313.

2) H. Hirota, Y. Tanahashi, and T. Takahashi, *Bull. Chem. Soc. Jpn.*, **53**, 785 (1980) and references cited therein.

3) T. Takahashi, T. Ichimura, and T. Murae, *Chem. Pharm. Bull.*, **27**, 2539 (1979) and references cited therein.

4) H. Nagano and T. Takahashi, *Bull. Chem. Soc. Jpn.*, **51**, 3335 (1978) and reference cited therein.

5) M. Terabe, M. Tada, and T. Takahashi, *Bull. Chem. Soc. Jpn.*, **51**, 661 (1978).

6) *E.g.* a) Y. Moriyama, T. Sato, H. Nagano, Y. Tanahashi and T. Takahashi, *Bull. Chem. Soc. Jpn.*, **48**, 112 (1975); b) Y. Ishizaki, Y. Tanahashi, T. Tsuyuki, T. Takahashi, and K. Tori, *ibid.*, **52**, 1182 (1979).

7) *E.g.* J. Correa and J. Romo, *Tetrahedron*, **22**, 658 (1966).

8) L. Rodoriguez-Hahn, A. Guzmán, and J. Romo, *Tetrahedron*, **24**, 477 (1968).

9) A. R. Pinder, *Fortschr. Chem. Org. Naturst.*, **34**, 81 (1977).

10) M. Hikichi and T. Furuya, *Tetrahedron Lett.*, **1974**, 3657; *Chem. Pharm. Bull.*, **24**, 3178 (1976).

11) F. Bohlmann and N. Rao, *Tetrahedron Lett.*, **1973**, 613.

12) K. Naya, Y. Makiyama, T. Matsuura, N. Ii, H. Nagano, and T. Takahashi, *Chem. Lett.*, **1978**, 301 and references cited therein.

13) Y. Moriyama, T. Sato, H. Nagano, Y. Tanahashi, and T. Takahashi, *Chem. Lett.*, **1972**, 637.

14) M. Tada, Y. Moriyama, Y. Tanahashi, and T. Takahashi, *Bull. Chem. Soc. Jpn.*, **47**, 1999 (1974).

15) H. Nagano, Doctoral Thesis, the University of Tokyo (1974), p. 138.

16) F. Bohlmann, C. Zdero, and M. Granz, *Chem. Ber.*, **107**, 3928 (1974).

17) "Ang" represents an angeloyl group, $\begin{matrix}CH_3\\H\end{matrix}\!\!>\!C\!=\!C\!<\!\begin{matrix}CO-\\CH_3\end{matrix}$ and R^1 refers to acyl moieties as a part of the acyloxyl group at C-6.

Synthesis of 3-Aminonocardicinic Acid, the Basic Nucleus of Nocardicins

Minoru HATANAKA,* Noriyoshi NOGUCHI, and Toshiyasu ISHIMARU
The Institute of Scientific and Industrial Research, Osaka University, Suita, Osaka 565
(Received October 27, 1981)

A short and high-yielding synthesis of optically active 3-aminonocardicinic acid (3-ANA) is described. The fourth component condensation reaction of N^2-protected L-2,3-diaminopropanoic acid with *p*-benzyloxybenzaldehyde and butyl isocyanide gave directly the amide derivatives of 3-ANA, as a diastereomeric mixture, which was, after conversion of the amide group into the benzhydryl ester, led in good yield to a single disatereomer with natural chirality *via* epimerization. Deprotection of the 3-ANA derivative gave 3-ANA.

Attension has been given to the synthesis of nocardicins, *e.g.*, **1**, which are unusual monocyclic β-lactam antibiotics isolated from Nocardia species.[1,2] In this paper, we wish to report a short and high-yielding synthesis of optically active 3-aminonocardicinic acid (3-ANA, **2**) which is the key intermediate for the synthesis of nocardicins. It is based on the Ugi reaction using isoncyanides as azetidinone forming reagents.[3] In this reaction, the use of L-2,3-diaminopropanoic acid as a chiral starting material would permit direct formation of the 3-ANA derivatives with the natural chirality at the position 3. On the contrary, one of the most successful approaches to the synthesis of 3-ANA has used D-*p*-hydroxyphenylglycine as a chiral strating material, following asymmetric induction to the position 3 *via* ketene-imine cycloaddition for the azetidinone construction.[2a] The noteworthy feature of our route will be shown by quantitative transformation *via* epimerization of the resulting diastereomeric mixture into a single diastereomer with the natural chirality.

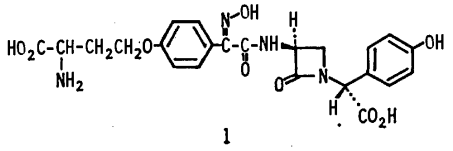

1

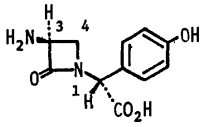

2

Results and Discussion

The starting materials, N^2-protected L-2,3-diaminopropanoic acids (**3a**—**c**), were prepared according to our previous report[4] or the published method.[5] The amino acids **3a**—**c** were allowed to react with *p*-benzyloxybenzaldehyde and butyl isocyanide in methanol at room temperature. In each case, the product was a diasteromeric mixture, in a ratio of approximately 1 to 1, which could be separated by column chromatography on silica gel. The results are summarized in Table 1. The azetidinones **4a** and **5a** were chosen as precursors of 3-ANA because these compounds were obtained in the best yield and the 2,2,2-trichloroethoxycarbonyl *N*-protecting group possessed the advantage of permitting stepwise deprotection of the resulting protected 3-ANA derivative.

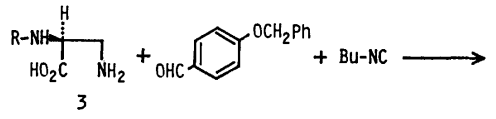

3

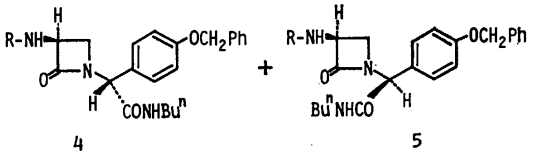

4 5

a, R = CCl_3CH_2OCO
b, R = $C_6H_5CH_2OCO$
c, R = Bu^tOCO

TABLE 1. YIELDS AND PHYSICAL PROAERTIES OF THE UGI REACTION PRODUCTS

Substrate	Products 4 Mp θ_m/°C	4 $[\alpha]_D^{b)}$/°	5 Mp θ_m/°C	5 $[\alpha]_D^{b)}$/°	Yield[a)] %
3a	182—184	−119.0 (*c* 1.0)	100—101	+35.2 (*c* 1.0)	68
3b	151—152	−120.5 (*c* 0.99)	175—176	+33.5 (0.94)	31.3
3c	161—162	−104.8 (*c* 1.02)	Oil	—	59

a) Isolated total yield on the basis of **3**. b) In methanol.

Selective cleavage of the exocyclic amide bond was achieved *via* the imidoyl chloride. The azetidinone **4a** was treated with phosphorus pentachloride in dichloromethane in the presence of pyridine, and successively with methanol. The acidic work-up of the reaction mixture gave a 4 : 1 mixture of the methyl esters **6** and **7** in 66% yield together with recovery (16.3%) of a 2 : 1 mixture of **4a** and **5a**, indicating that epimerization at the exocyclic C–H took place to a considerable extent under the reaction conditions. Similarly, the 1 : 1 mixture of **4a** and **5a** gave a 5 : 3 mixture of **6** and **7** in 68% yield.

Hydrolysis of the methyl ester **6** with aqueous sodium hydroxide or lithium iodide–pyridine was also accom-

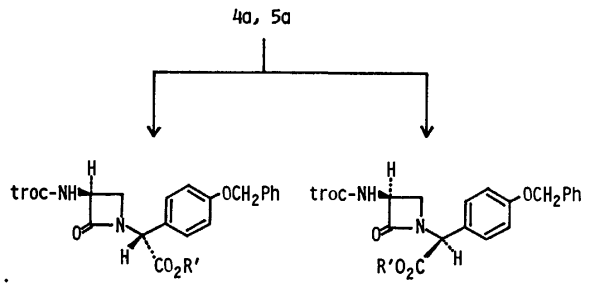

6, R'=CH_3
8, R'=H
10, R'=CH_2Ph
12, R'=$CHPh_2$

7, R'=CH_3
9, R'=H
11, R'=CH_2Ph
13, R'=$CHPh_2$

troc = CCl_3CH_2OCO

panied by epimerization to result in a mixture of the acids **8** and **9**. Thus, the epimerization was extremely facile as reported previously.[2b] Therefore, the methyl esters **6** and **7**, in the form of the 5 : 3 mixture, were converted into the benzyl esters **10** and **11** (62% yield as a 4 : 3 mixture) or the benzhydryl esters **12** and **13** (91% yield as a 4 : 3 mixture) by saponification, followed by treatment with benzyl chloride or diphenyldiazomethane. Treatment of **11** with triethylamine in aqueous methanol resulted in an equilibrium mixture of the diastereomers **10** and **11** to provide more **10**. The benzhydryl ester was found to be more convenient in terms of its easy crystallization. The crude product, in the form of the 4 : 3 mixture of **12** and **13**, was directly crystallized from aqueous methanol containing triethylamine to give a single isomer **12** in 85% overall yield from the methyl esters **6** and **7**.

Table 2. ^{1}H-NMR chemical shifts of 4-protons[a]

Compound	4β-Protons	4α-Protons
4a	3.27	3.93
5a	3.57	3.31
4b	3.25	3.84
5b	3.55	3.40
4c	3.27	3.82
5c	3.53	3.09
6	3.11	3.96
7	3.59	3.45
10	3.09	3.92
11	3.56	3.42
12	3.08	3.92

a) In ppm downfield from internal TMS in $CDCl_3$.

Stereochemistry of the diastereomers was assigned on the basis of the ^{1}H-NMR spectral data. It has been reported that in the NMR spectra of nocardicin series the 4β-protons always appeared in higher field than the 4α-protons.[2a] In agreement with this fact, the 4β-protons of **4a**—**c**, **6**, **10**, and **12** with the natural chirality appeared in higher field by 0.66—0.85 ppm than their 4α-protons, while in the cases of **5a**—**c**, **7**, **11**, and **13** the 4α-protons resonanced in slightly higher field than the 4β-protons (Table 2).

Removal of the 2,2,2-trichloroethoxycarbonyl group

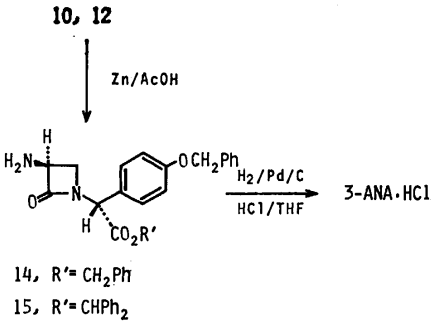

14, R'=CH_2Ph
15, R'=$CHPh_2$

of **10** was carried out with zinc in aqueous acetic acid to yield quantitatively the free amine **14**, the ^{1}H-NMR spectrum of which corresponded well with that of the dibenzyl derivative of 3-ANA previously reported.[2b] Catalytic deprotection of **14** with 10% palladium on carbon as catalyst in the presence of hydrogen chloride produced 3-ANA hydrochloride. Similarly, the benzhydryl ester **12** gave 3-ANA hydrochloride in quantitative yield. Total yield from **3a** was 38%.

Experimental

Melting points (capillary) were uncorrected. IR spectra were recorded on a JASCO IRA-1 spectrometer. NMR spectra were determined with tetramethylsilane as an internal standard on a Hitachi R-600 or a JEOL FX-100 spectrometer, chemical shifts being given in ppm unit. Optical rotations were measured with a Perkin-Elmer 241 polarimeter. Elemental analyses were performed in the material analysis center of this institute. Columns of chromatography were packed with Wakogel C-200.

(3S)-1-(α-Butylcarbamoyl-p-benzyloxybenzyl)-3-(2,2,2-trichloroethoxycarbonylamino)-2-azetidinone (4a, 5a). A mixture of **3a** (2.80 g, 0.01 mol), *p*-benzyloxybenzaldehyde (2.55 g, 0.012 mol) and butyl isocyanide (1.25 g, 0.015 mol) in methanol (80 ml) was stirred at room temperature for 3 d. The methanol was removed *in vacuo*, and the residue was crystallized from ethyl acetate–diisopropyl ether to give **4a** (1.15 g). The filtrate was evaporated *in vacuo*, and the residue was chromatography on silica gel with benzene–ethyl acetate to give **4a** (0.86 g, 36% total yield) and **5a** (1.77 g, 32% yield). The individual properties of **4a** and **5a** follow. **4a**: mp 182—184 °C; $[\alpha]_D$ −119.0° (*c* 1.0, MeOH); IR (Nujol) 1765, 1740, and 1663 cm^{-1}; NMR ($CDCl_3$) δ 0.90 (3H, t, *J*=6, CH_3), 1.41 (4H, m, $(CH_2)_2$), 3.27 (3H, m, NCH_2 and H4β), 3.93 (1H, t, *J*=5, H4α), 4.70 (2H, s, CH_2CCl_3), 4.83 (1H, m, H3), 5.07 (2H, s, OCH_2Ar), 5.23 (1H, s, methine), 5.48 (1H, m, NH), 5.97 (1H, m, NH), and 6.68—7.53 (9H, m, Ar). Found: C, 46.06; H, 4.55; N, 8.85; Cl, 22.95%. Calcd for $C_{25}H_{28}N_3O_5Cl_3$: C, 46.32; H, 4.75; N, 9.00; Cl, 22.78%.

5a: mp 100—101 °C; $[\alpha]_D$ +35.2° (*c* 1.0, MeOH); IR (nujol) 1743, 1733, and 1658 cm^{-1}; NMR ($CDCl_3$) δ 0.93 (3H, t, *J*=6, CH_3), 1.47 (4H, m, $(CH_2)_2$), 3.31 (3H, m, NCH_2 and H4α), 3.57 (1H, dd, *J*=2.7 and 6.6, H4β), 4.46 (1H, m, H3), 4.74 (2H, ABq, *J*=12, CH_2Cl_3), 5.06 (2H, s, OCH_2Ar), 5.44 (1H, s, methine), 5.68 (1H, broad d, *J*=7.5, NH), and 6.92—7.36 (10H, m, Ar and NH).

(3S)-3-(Benzyloxycarbonylamino)-1-(α-butylcarbamoyl-p-benzyloxybenzyl)-2-azetidinone (4b, 5b). By the use of the procedure described above, this compound was obtained in 31.3% yield from **3b** as a solid, in the form of a diastereomeric mixture of **4b** and **5b** in the ratio 10 : 9 (determined by NMR spectra). Repeated column chromatography of the mixture

gave pure **4b** and **5b**, the individual properties of which were as follows. **4b**: mp 151—152 °C; $[\alpha]_D$ −120.5° (*c* 0.99, MeOH); IR ($CHCl_3$) 3420, 3350, 1760, 1728, and 1680 cm^{-1}; NMR ($CDCl_3$) δ 0.89 (3H, t, J=6, CH_3), 1.40 (4H, m, $(CH_2)_2$), 3.25 (3H, m, NCH_2 and H4β), 3.84 (1H, t, J=5.4, 4Hα), 4.80 (1H, m, H3), 5.06 (4H, s, OCH_2Ar), 5.18 (1H, s, methine), 5.37 (1H, m, NH), 6.30 (1H, m, NH), and 6.95—7.50 (14H, m, Ar). Found: C, 69.61; H, 6.41; N, 8.12%. Calcd for $C_{30}H_{33}N_3O_5$: C, 69.88; H, 6.45; N, 8.15%. **5b**: mp 175—176 °C; $[\alpha]_D$ +33.5 °C (*c* 0.94, MeOH); IR ($CHCl_3$) 3440, 3360, 1763, 1720, and 1665 cm^{-1}; NMR ($CDCl_3$) δ 0.93 (3H, t, J=6, CH_3), 1.50 (4H, m, $(CH_2)_2$), 3.40 (3H, m, NCH_2 and H4α), 3.55 (1H, dd, J=2.4 and 6.6, H4β), 4.35 (1H, m, H3), 5.05 (2H, s, OCH_2Ar), 5.13 (2H, s, OCH_2Ar), 5.44 (1H, s, methine), 5.55 (1H, m, NH), and 6.86—7.50 (14H, m, Ar). Found: C, 69.64; H, 6.36; N, 8.11%. Calcd for $C_{30}H_{33}N_3O_5$: C, 69.88; H, 6.45; N, 8.15%.

*(3S)-3-(t-Butoxycarbonylamino)-1-(α-butylcarbamoyl-*p*-benzyloxybenzyl)-2-azetidinone (**4c**, **5c**).* By the use of the procedure described above, this compound was prepared from **3c**. The yield of *ca.* a 1 : 1 diastereomeric mixture of **4c** and **5c** was 59%. The individual properties of **4c** and **5c** follow. **4c**: mp 161—162 °C; $[\alpha]_D$ −104.8° (*c* 1.02, MeOH); IR (nujol) 3300, 1765, 1700, and 1665 cm^{-1}; NMR ($CDCl_3$) δ 0.90 (3H, t, J=6, CH_3), 1.41 (9H, s, Bu^t), 1.50 (4H, m, $(CH_2)_2$), 3.27 (3H, m, NCH_2 and H4β), 3.82 (1H, t, J=5.4, H4α), 4.72 (1H, m, H3), 5.06 (2H, s, OCH_2Ar), 5.14 (1H, s, methine), and 6.88—7.50 (9H, m, Ar). Found: C, 67.10; H, 7.34; N, 8.64%. Calcd for $C_{27}H_{35}N_3O_5$: C, 67.34; H, 7.33; N, 8.73%. **5c**: oil; IR (neat) 3320, 1755, 1690, and 1655 cm^{-1}; NMR ($CDCl_3$) δ 0.93 (3H, t, J=6, CH_3), 1.45 (9H, s, Bu^t), 1.20—1.65 (4H, m, $(CH_2)_2$), 3.09 (1H, t, J=5.5, H4α), 3.30 (2H, m, NCH_2), 3.53 (1H, dd, J=2.7 and 5.5, H4β), 4.20 (1H, m, H3), 5.03 (2H, s, OCH_2Ar), 5.44 (1H, s, methine), and 6.86—7.50 (9H, m, Ar).

*(3S)-1-(α-Methoxycarbonyl-*p*-benzyloxybenzyl)-3-(2,2,2-trichloroethoxycarbonylamino)-2-azetidinone (**6**, **7**).* Phosphorus pentachloride (313 mg, 1.5 mmol) was added at −20 °C to a suspension of **4a** (557 mg, 1 mmol) and pyridine (237 mg, 3 mmol) in dichloromethane (6 ml). The mixture was stirred at 0 °C for 5 h, and then cooled to −60 °C. After addition of anhydrous methanol (0.6 ml), the mixture was brought gradually to 0 °C, then stirred at 0 °C for 1.5 h, and poured into ice–water (5 ml). The mixture was vigorously stirred at 0 °C for 1 h. The aqueous layer was extracted with dichloromethane. The combined extracts were dried ($MgSO_4$) and evaporated *in vacuo*. The residue was chromatographed on silica gel with benzene–ethyl acetate to give **6** (273 mg, 53%), **7** (68 mg, 13.2%), and a 2 : 1 mixture of **4a** and **5a** (91 mg, 16.3% recovery). The physical properties of **6** follow. Mp 139—140 °C; $[\alpha]_D$ −141.3° (*c* 0.98, MeOH); IR (Nujol) 3240, 1760, and 1735 cm^{-1}; NMR ($CDCl_3$) δ 3.11 (1H, dd, J=2.4 and 5.6, H4β), 3.75 (3H, s, OCH_3), 3.96 (1H, t, J=5.6, H4α), 4.69 (2H, s, CH_2Cl_3), 4.90 (1H, m, H3), 5.07 (2H, s, CH_2Ar), 5.51 (1H, m, NH), 5.57 (1H, s, methine), and 6.94—7.48 (9H, m, Ar). Found: C, 51.27; H, 4.01; N, 5.39, Cl, 20.88%. Calcd for $C_{22}H_{21}N_2O_6Cl_3$: C, 51.23; H, 4.10; N, 5.43; Cl, 20.62%. The physical properties of **7** follow. Oil; $[\alpha]_D$ +65.0° (*c* 3.31, MeOH); IR (neat) 3300 and 1740 cm^{-1}; NMR ($CDCl_3$) δ 3.45 (1H, t, J=5.6, H4α), 3.59 (1H, dd, J=2.4 and 5.6, H4β), 3.76 (3H, s, OCH_3), 4.73 (2H, s, CH_2Cl_3), 4.80 (1H, m, H3), 5.07 (2H, s, OCH_2Ar), 5.55 (1H, s, methine), 5.85 (1H, m, NH), and 6.88—7.50 (9H, m, Ar).

A similar experiment was repeated with the 1 : 1 mixture of **4a** and **5a** on the 0.01 mol scale, yielding a 5 : 3 mixture of **6** and **7** (3.51 g, 68%).

*Benzyl O-Benzyl-N-(2,2,2-trichloroethoxycarbonyl)-3-aminonocardicinate (**10**).* To a solution of the 5:3 mixture of **6** and **7** (346 mg, 0.67 mmol) in 80% aqueous acetone (10 ml), 1 M† aqueous KOH was added dropwise at 0 °C over 1 h. After being stirred at 0 °C for 2 h, the solution was evaporated to dryness *in vacuo*. The residue was suspended in DMF (5 ml), and treated with benzyl chloride (102 mg) and a few drops of *N,N,N′,N′*-tetramethylethylenediamine . The mixture was stirred overnight at room temperature, poured into ice–water (20 ml), and then extracted with ethyl acetate. The extracts were washed with brine, dried ($MgSO_4$), and evaporated *in vacuo*. The residue was separated by preparative TLC in benzene–ethyl acetate to give **10** (135 mg, 34%) as needles and **11** (111 mg, 28%) as an oil. The physical properties of **10** follow. Mp 128—129 °C; $[\alpha]_D$ −104.4° (*c* 0.94, MeOH); IR ($CHCl_3$) 1760 and 1740 cm^{-1}; NMR ($CDCl_3$ δ 3.09 (1H, dd, J=2.4 and 5.6, H4β), 3.92 (1H, t, J=5.6, H4α) 4.68 (2H, s, CH_2Cl_3), 4.87 (1H, m, H3), 5.06 (2H, s, OCH_2Ar), 5.18 (2H, s, OCH_2Ar), 5.47 (1H, m, NH), 5.61 (1H, s, methine), 6.94 (2H, d, J=9, Ar), 7.17 (2H, d, J=9, Ar), 7.30 and 7.39 (10H, each s, Ar). Found: C, 57.88; H, 4.29; N, 4.72%. Calcd for $C_{28}H_{25}N_2O_6Cl_3$: C, 56.82; H, 4.26; N, 4.73%. The physical properties of **11** follow. Oil; $[\alpha]_D$ +42.24° (*c* 0.76, MeOH); IR ($CHCl_3$) 1755 and 1740 cm^{-1}; NMR ($CDCl_3$) δ 3.42 (1H, t, J=5.6, H4α), 3.56 (1H, dd, J=2.4 and 5.6, H4β), 4.70 (2H, s, CH_2CCl_3), 4.83 (1H, m, H3), 5.05 (2H, s, OCH_2Ar), 5.19 (2H, s, OCH_2Ar), 5.59 (1H, s, methine), 5.80 (1H, broad d, J=8, NH), 6.93 (2H, d, J=8.8, Ar), 7.13 (2H, d, J=8.8, Ar), 7.29 and 7.38 (10H, each s, Ar).

The oily isomer **11** (95 mg) was dissolved in aqueous methanol. After addition of a few drops of triethylamine, the solution was allowed to stand at room temperature for 3 days, while the epimerization of **11** was effected to result in a new diastereomeric mixture of **10** and **11** in a ratio of 4 : 3. The solution was seeded with crystals of **10**, and left for an additional day to yield pure **10** (51 mg).

*Benzhydryl O-Benzhyl-N-(2,2,2-trichloroethoxycarbonyl)-3-aminonocardicinate (**12**).* To a solution of the 5 : 3 diastereomeric mixture of **6** and **7** (516 mg, 1 mmol) in 80% aqueous acetone (10 ml), 0.5 M aqueous NaOH (2.2 ml) was added dropwise at 0 °C over 1 h. The solution was stirred at 0 °C for 2 h, and concentrated to 5 ml *in vacuo*. The remaining solution was acidified with hydrochloric acid, and extracted with ethyl acetate. The ethyl acetate solution was dried ($MgSO_4$), and then treated with a small excess of diphenyldiazomethane until the red colour no longer disappeared. The solution was evaporated *in vacuo*, and the residue was purified through a short column of silica gel to yield *ca.* a 4 : 3 mixture of **12** and **13** (610 mg, 91%) as a pale-yellow oil.

The mixture (610 mg) was dissolved in hot aqueous methanol (4 ml) containing one drop of triethylamine. The solution was seeded with crystals of **12** and allowed to stand at room temperature for 3 h. The crystals were colloected by filtration to yield pure **12** (480 mg). Repeated procedure on the filtrate gave an additional crop of **12** (88 mg, 85% total yield).

The physical properties of **12** follow. Mp 135—136 °C; $[\alpha]_D$ −123.2° (*c* 0.44, MeOH); IR (Nujol) 1760 and 1735 cm^{-1}; NMR ($CDCl_3$) δ 3.08 (1H, dd, J=2.4 and 5.6, H4β), 3.92 (1H, t, J=5.6, H4α), 4.68 (2H, s, CH_2CCl_3), 4.86 (1H, m, H_3), 5.07 (2H, s, OCH_2Ar), 5.41 (1H, broad d, J=8, NH), 5.69 (1H, s, methine), 6.91 (2H, d, J=9, Ar), 7.11 (2H, d, J=9, Ar), and 7.00—7.46 (16H, m, $CHPh_2$ and Ar). Found: C, 60.90; H, 4.13; N, 4.29; Cl, 15.56%. Calcd for $C_{34}H_{29}$-

† 1 M=1 mol dm^{-3}.

$N_2O_6Cl_3$: C, 61.14; H, 4.38; N, 4.19; Cl, 15.92%.

Benzyl O-Benzyl-3-aminonocardicinate (14). The compound **10** (150 mg, 0.25 mmol) was dissolved in a mixture of 1 M aqueous KH_2PO_4 (0.25 ml), 90% aqueous acetic acid (2 ml) and THF (3 ml). Zinc powder (165 mg) was added and the mixture was vigorously stirred for 1 h and then filtered. The filtrate was concentrated *in vacuo* below 30 °C. The residue was diluted with water (10 ml), neutralized with $NaHCO_3$, and extracted with ethyl acetate. The extracts were washed with brine, dried ($MgSO_4$), and then evaporated *in vacuo*. The residue was purified by passing through a short column of silica gel with benzene–ethyl acetate to yield **14** (101 mg, 96%) as a colourless oil. The physical properties of **14** were as follows and corresponded well with those previously reported.[2b] $[\alpha]_D$ −128.2° (*c* 0.71, MeOH) [lit,[2b] $[\alpha]_D$ −138° (TFE)]; NMR ($CDCl_3$) δ 2.81 (1H, dd, J=2.2 and 5.4, H4β), 3.86 (1H, t, J=5.4, H4α), 4.22 (1H, dd, J=2.2 and 5.4, H3), 5.06 (2H, s, OCH_2Ar), 5.17 (2H, s, OCH_2Ar), 5.58 (1H, s, methine), 6.93 (2H, d, J=8.8, Ar), 7.16 (2H, d, J=8.8, Ar), 7.29 and 7.39 (10H, each s, Ar).

Benzhydryl O-Benzyl-3-aminonocardicinate (15). By the use of the procedure described above, this compound was obtained from **12** in quantitative yield as an oil, $[\alpha]_D$ −129° (*c* 0.61, THF); NMR ($CDCl_3$) δ 1.67 (2H, broad s, NH_2), 2.80 (1H, dd, J=2 and 5, H4β), 3.85 (1H, t, J=5, H4α), 4.20 (1H, m, H3), 5.07 (2H, s, OCH_2Ar), 5.70 (1H, s, methine), and 6.80—7.60 (20H, m, $CHPh_2$ and Ar).

3-Aminonocardicinic Acid (3-ANA, 2). *From 15*: A mixture of **15** (98 mg, 0.2 mmol) and 10% palladium on carbon (50 mg) as catalyst in anhydrous THF–ethanol (*ca.* 1 : 1, 6 ml) containing hydrogen chloride (0.2 mmol) was placed under a hydrogen atmosphere at atmospheric pressure, and stirred for 6 h at room temperature. The catalyst was removed by filtration and the filtrate was concentrated *in vacuo*. The residue was triturated in ether to give 3-ANA hydrochloride (54 mg, quantitative yield) as a white solid, $[\alpha]_D$ −207° (*c* 0.3, H_2O); NMR (D_2O) δ 3.29 (1H, dd, J=2.2 and 6.5, H4β), 3.93 (1H, t, J=6.5, H4α), 5.57 (1H, s, methine), 6.96 (2H, d, J=8.5, Ar), and 7.30 (2H, d, J=8.5, Ar).

From 14: By the use of the procedure described above the compound **14** (167 mg, 0.4 mmol) was deprotected to give 3-ANA hydrochloride (106 mg), which was identical with that obtained from **15** (NMR, TLC, $[\alpha]_D$ value).

References

1) Isolation and structure: a) H. Aoki, H. Sakai, M. Kohsaka, T. Konomi, J. Hosoda, Y. Kubochi, and E. Iguchi, *J. Antibiot.*, **29**, 492 (1976); b) M. Hashimoto, T. Komori, and T. Kamiya, *ibid.*, **29**, 890 (1976); *J. Am. Chem. Soc.*, **98**, 3023 (1976).

2) Synthesis: a) T. Kamiya, T. Oku, O. Nakaguchi, H. Takeno, and M. Hashimoto, *Tetrahedron Lett.*, **1978**, 5119; T. Kamiya, M. Hashimoto, O. Nakaguchi, and T. Oku, *Tetrahedron*, **35**, 323 (1979); b) G. A. Koppel, L. McShane, F. Jose, and R. D. G. Cooper, *J. Am. Chem. Soc.*, **100**, 3933 (1978); c) H. H. Wasserman and D. L. Hlasta, *ibid.*, **100**, 6780 (1978); d) K. Chiba, M. Mori, and Y. Ban, *J. Chem. Soc., Chem. Commun.*, **1980**, 770; e) P. G. Mattingly and M. J. Miller, *J. Org. Chem.*, **46**, 1557 (1981).

3) I. Ugi and C. Steinbrückner, *Chem. Ber.*, **94**, 2802 (1961); I. Ugi and E. Wishhöfen, *ibid.*, **95**, 136 (1962); I. Ugi, *Angew. Chem.*, **74**, 9 (1962).

4) N. Noguchi, T. Kuroda, M. Hatanaka, and T. Ishimaru *Bull. Chem. Soc. Jpn.*, **55**, 633 (1982).

5) T. Teshima, S. Nomoto, T. Wakamiya, and T. Shiba, *Bull. Chem. Soc. Jpn.*, **50**, 3372 (1977).

The Enrichment of Tritium in Hydrogen or Deuterium by Thermal Diffusion

Osamu TAKAYASU,* Ikuro MAKINO, Susumu YAMAGAMI, and Toyosaburo TAKEUCHI*
Faculty of Science, Toyama University, Gofuku, Toyama 930
(Received October 3, 1980)

Tritium in H_2 or D_2, 1.7×10^{-2} Ci mol^{-1}, was enriched by means of thermal diffusion at the bottom of a 100-cm glass column with a gas reservoir on top. Four columns with different diameters (8, 20, 30, and 41 mmϕ) were used. The temperature of the wire stretched along the axis of the column was changed over a range from 200 °C to 450 °C. The maximum equilibrium separation factors in hydrogen and in deuterium were 17 and 4.5 respectively. The optimum diameters were estimated by a modification of Waldmann's equation, which can be used for the separation using the flat-type system.

The enrichment of the tritium present in the stable hydrogen isotopes is important in connection with the nuclear-fusion reaction of tritium with deuterium and with the treatment of tritium wastes. This report is concerned with the enrichment of low concentrations of tritium present in hydrogen or deuterium by means of thermal diffusion using a 100-cm glass column with a gas reservoir on top. A short column is desirable because of its ease of handling in a laboratory. The correlation between the column length and the separation factor has been reported elsewhere.[1] In this study, the diameter of the column and the temperature of the wire were changed over wide ranges, and the separation factor was obtained in each case. The possibility of an extended application of Waldmann's equation,[2,3] which can be used for a flat-type system, was examined in the hot-wire type columns, and the optimum diameter was predicted.

Experimental

The main part of the apparatus is shown in Fig. 1, where A is the separation column, constructed of Pyrex glass.

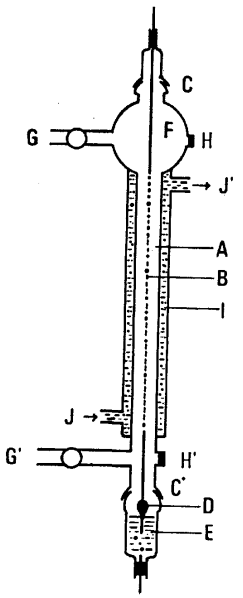

Fig. 1. Thermal diffusion column.
A: Separation column, B: nichrome wire, C and C': greaseless spherical joints, D: weight; E: mercury, F: gas reservoir, G and G': tube, H and H': sampling orifices, I: water jacket, J and J': running water.

Columns of four different diameters, 8, 20, 30, and 41 mmϕ, were used. The nichrome wire, B, stretched in the column was 0.5 mmϕ in diameter and 100 cm in length. The wire could be set along the center of the column by moving the spherical joints, C and C'. In order to stretch the wire, a small lead weight, D, was hung at the end of the wire, and it was immeresed in a mercury reservoir, E, which was connected at the end of the column. The temperature of the wire was changed over the range from 200 °C to 450 °C by means of a direct current. Each temperature was measured by means of the thermal expansion of the wire. Prior to use, the wire was heated in 100 kPa of hydrogen at 500 °C for 5 h; then the evacuation was carried out at a pressure of 10^{-3} Pa for 5 h in order to remove any active oxygen on the surface of the wire. The outside of the column was always kept at 20 °C by the use of running water. The volume of the gas reservoir, F, was 500 cm^3.

Before the study, the effect of the gas reservoir connected to the column was ascertained using the Kr–N_2 system, which had previously been tested in the same type of apparatus by Tanaka *et al.*[4] Their apparatus was devised to circulate readily the gas in the gas reservoir by the aid of a circulation tube, and they concluded that the connection of the gas reservoir with the column is quite effective for the separation. Our results were very similar to those of Tanaka *et al.*

The operating pressure of the gas was 107 kPa. The amount of sampling in each case was 30 mm^3. The concentration of tritium was measured by means of a radio-gas chromatograph.

The carrier-free tritium was diluted with hydrogen or deuterium to a volume of 1.7×10^{-2} Ci mol^{-1}. Prior to use, the gas mixture was put into contact with nickel plates at 100 °C for about 50 h in order to change completely the tritium (T_2) to tritiated hydrogen (HT) or tritiated deuterium (DT), since the following catalytic reaction on nichrome wire took place during the enrichment experiment:

$$T_2 + H_2 = 2HT, \quad T_2 + D_2 = 2DT. \qquad (1)$$

Results

The tritium at the bottom of the column was rapidly concentrated soon after the temperature of the wire had been elevated; the concentrations at both ends of the column became constant within 100 min. The results on H_2–HT in various columns of different diameters are shown in Figs. 2 and 3. The results on D_2–DT are shown in Figs. 4 and 5. The change in the concentration at the bottom occured faster than that at the top, as a result of the large difference in volume between the two ends. The radioactivities of the gas

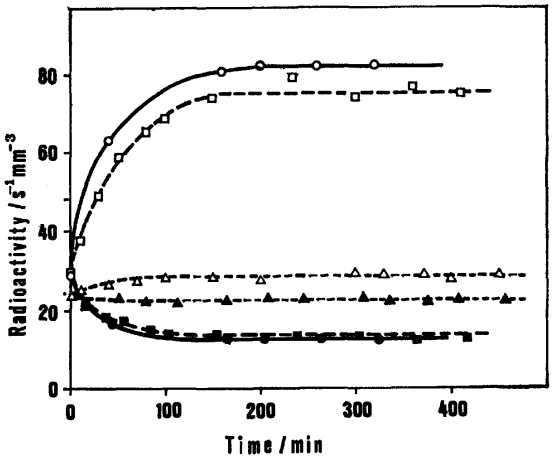

Fig. 2. Enrichment of tritium in the mixture of H_2–HT. Each specimen was taken out of the bottom (white symbols) or of the top (black symbols). The diameters of the column and the wire temperatures were: (○, ●) 20 mmϕ and 300 °C; (□, ■) 20 mmϕ and 200 °C; (△, ▲) 8 mmϕ and 450 °C.

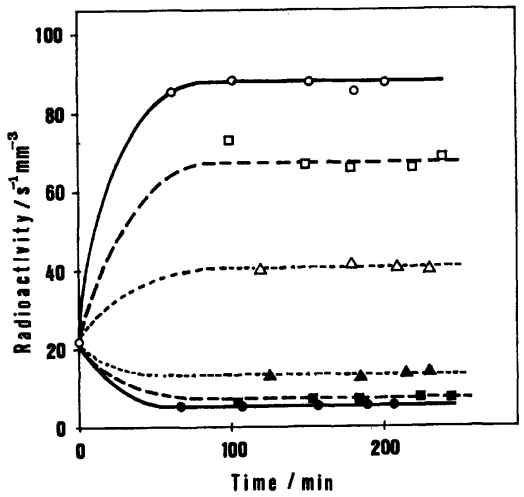

Fig. 3. Enrichment of tritium in the mixture of H_2–HT. Each specimen was taken out of the bottom (white symbols) or of the top (black symbols). The diameters of the column and the wire temperatures were: (○, ●) 30 mmϕ and 450 °C; (□, ■) 30 mmϕ and 300 °C; (△, ▲) 41 mmϕ and 300 °C.

at both ends in the equilibrium state are listed in Table 1, where c and c' are the radioactivities of the bottom and the top respectively. Since the concentration of tritium was extremely low, the equilibrium separation factor, q_e, can be written as:

$$q_e = c/c'. \tag{2}$$

The correlations between the equilibrium-separation factor and the temperature of the wire are shown in Figs. 6 and 7, together with the theoretical values, which will be explained later. In the case of H_2–HT, the separation factors of 8 mmϕ and 20 mmϕ increased initially with the elevation of the wire temperature, and then gradually decreased. However, no decrease was found on the columns of 30 mmϕ and 41 mmϕ up to

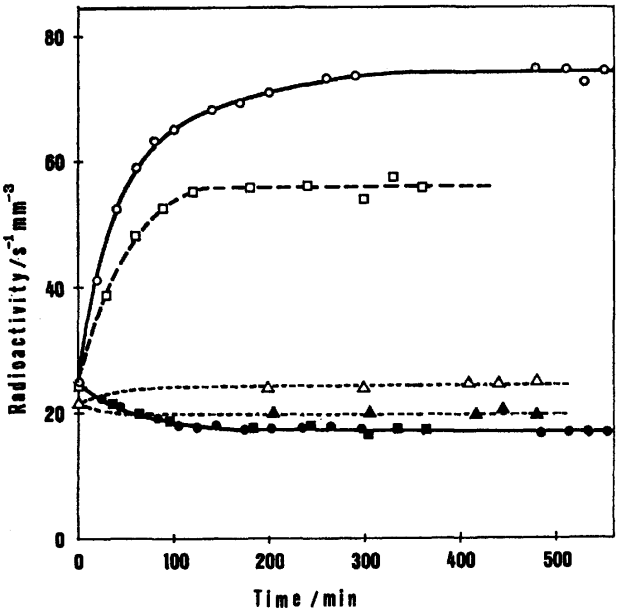

Fig. 4. Enrichment of tritium in the mixture of D_2–DT. Each specimen was taken out of the bottom (white symbols) or of the top (black symbols). The diameters of the column and the wire temperatures were: (○, ●) 20 mmϕ and 450 °C; (□, ■) 20 mmϕ and 200 °C; (△, ▲) 8 mmϕ and 200 °C.

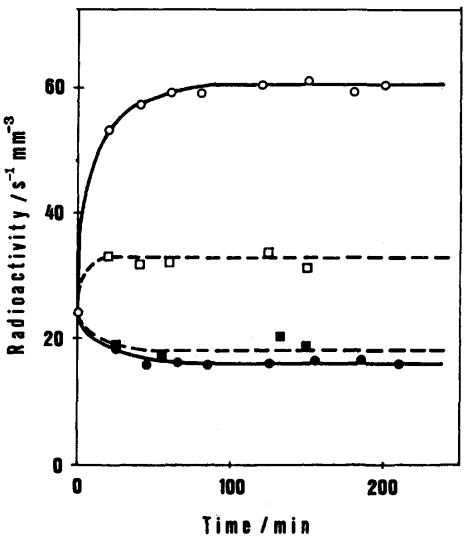

Fig. 5. Enrichment of tritium in the mixture of D_2–DT. Each specimen was taken out of the bottom (white symbols) or of the top (black symbols). The diameters of the column and the wire temperatures were: (○, ●) 30 mmϕ and 450 °C; (□, ■) 30 mmϕ and 200 °C.

450 °C. In the case of D_2–DT, all the separation factors were smaller than those of H_2–HT. It is noticeable that the separation factor of 20 mmϕ in this case became larger than that of 30 mmϕ at all temperature regions investigated.

Discussion

The optimum diameter for the enrichment in a wire-type column may be obtained simply by making

TABLE 1. RADIOACTIVITIES OF TRITIUM AT THE BOTTOM AND THE TOP OF THE COLUMN IN THE EQUILIBRIUM STATE

Mixtures	Column diameter (mmϕ)		Radioactivities/s^{-1} mm^{-3} Temperature of the wire/°C					
			200	250	300	350	400	450
H_2–HT	8(bottom)	c	30.34	32.98	31.74	40.02	33.74	29.02
	(top)	c'	25.09	23.18	22.16	27.51	23.97	21.77
	20(bottom)	c	75.26	84.07	88.68	85.33	87.56	87.46
	(top)	c'	13.62	12.72	12.04	9.44	9.45	9.76
	30(bottom)	c	47.92	—	56.24	59.92	85.62	88.16
	(top)	c'	7.13	—	5.74	5.17	5.93	5.21
	41(bottom)	c	31.55	—	39.72	—	53.55	59.43
	(top)	c'	14.80	—	13.05	—	10.04	8.95
D_2–DT	8(bottom)	c	24.87	—	24.47	28.44	—	28.68
	(top)	c'	20.16	—	19.57	23.13	—	23.08
	20(bottom)	c	56.52	62.10	66.87	—	70.92	70.51
	(top)	c'	17.72	16.03	16.01	—	15.46	15.56
	30(bottom)	c	32.13	39.67	47.29	—	55.05	60.09
	(top)	c'	18.26	19.65	20.63	—	17.77	16.33

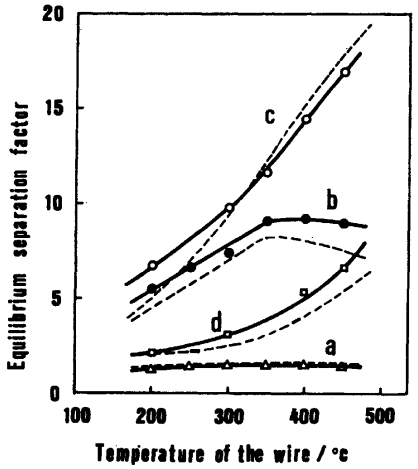

Fig. 6. The temperature dependence of experimental q_e (——) and theoretical q_e (------) in H_2–HT.
(a): 8, (b): 20, (c): 30, (d): 41 mmϕ.

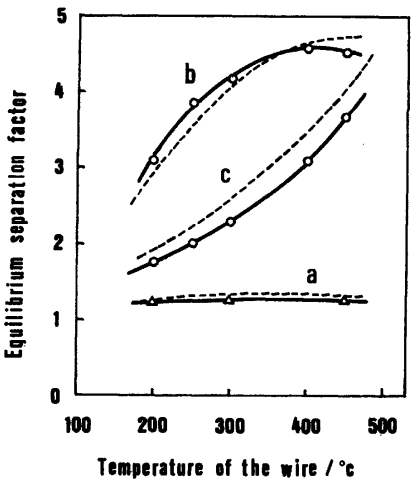

Fig. 7. The temperature dependence of experimental q_e (——) and theoretical q_e (------) in D_2–DT.
(a): 8, (b): 20, (c): 30 mmϕ.

small modifications of Waldmann's method, developed for flat-type systems. Waldmann's equation is written as Eq. 3[4] when the concentration of one component is very low:

$$\ln \Lambda'/\Lambda = -h/H^*, \tag{3}$$

where Λ and Λ' are the concentrations at both ends of the flat-type system and where h is the effective length of the system. H^* is given as follows:

$$H^* = \frac{T_0}{\Delta T} \frac{1+\alpha\left(\frac{d}{d^*}\right)^6}{\beta\left(\frac{d}{d^*}\right)^3} d, \tag{4}$$

where d is the distance between two walls, where T_0 is the average temperature of two walls: $(T_1+T_2)/2$ and

$$\Delta T = T_1 - T_2, \tag{5}$$

where α is the constant which depends on the intermolecular potential of the gas, and where β is the constant which depends not only on the intermolecular potential, but also on the ordinary diffusion coefficient and the thermal-diffusion coefficient. The optimum distance between the two walls, d^*, is given by:

$$d^* = \sqrt[3]{610 \frac{R}{\mu g P} \frac{T_0^2}{\Delta T} D\eta}, \tag{6}$$

where R is the gas constant, g is the gravitational acceleration, P is the pressure of the gas, D is the ordinary diffusion coefficient, η is the viscosity of the gas, and

$$\mu = M_1X_1 + M_2(1-X_1), \tag{7}$$

where M_1 and M_2 are the molecular weights of the two components of the mixture and X_1 is the mole fraction of M_1.

When these equations are applied to wire-type columns, α and β must be modified, and the distance between the two walls, d, is replaced by the radius of the column. The optimum radius of the wire-type column can be simply calculated from d^* by multiplying it by the constant corresponding to α. The constants, α and β, for the column used are evaluated by fitting

the calculated q_e value to the experimental q_e value. The calculated results are shown by dotted lines in Figs. 6 and 7. In the case of H_2–HT, α and β were given as 1.8 and 0.14 respectively, while in the case of D_2–DT, α and β were given as 1.8 and 7.0×10^{-2} respectively. In this calculation, the concentration of tritium was rewritten in terms of radioactivity:

$$\ln c/c' = -h/H^*, \quad (8)$$

and the theoretical separation factor, q_e, was obtained from Eqs. 2 and 8 as follows:

$$q_e = \exp(h/H^*). \quad (9)$$

The viscosity of hydrogen at T_0 was available from the literature.[5] The viscosity of deuterium at T_0 was obtained by postulating that the isotope effect is 1.39[6] at all the temperatures used. The diffusion coefficient of H_2-HT was available from the literature,[7,8] but that of D_2–DT was not. The diffusion coefficient of D_2–DT used was the average of D_2-HT[7] and D_2–T_2.[7] In these cases, the coefficient of each system at T_0 was obtained from the linear relation between $\log D$ and $\log T$. Figs. 6 and 7 show two cases where each calculated q_e value comes closest to the experimental q_e value. Accordingly, it can be said that α and β are independent of the wire temperature. Figures 6 and 7 can be rewritten as Figs. 8 and 9, where the dependence of q_e on d/d^* at various temperatures is shown. These figures indicate that q_e is greatly affected by d/d^* and that the maximum q_e is given at 0.80 on the d/d^* abscissa in both cases, irrespective of the temperature of the wire.

The following results were obtained from this study:

1. The separation factors of tritium in H_2–HT and D_2–DT (1.7×10^{-2} Ci mol^{-1}) systems for thermal-diffusion columns 100 cm in length could be obtained by changing the diameter of the column and the wire temperature.
2. It was found that a modified application of Waldmann's equation to the hot-wire-type column was possible by introducing two parameters. These parameters were independent of the wire temperature.
3. The optimum radius of the column for the enrichment was given as 80% of the optimum distance of a flat-type apparatus.

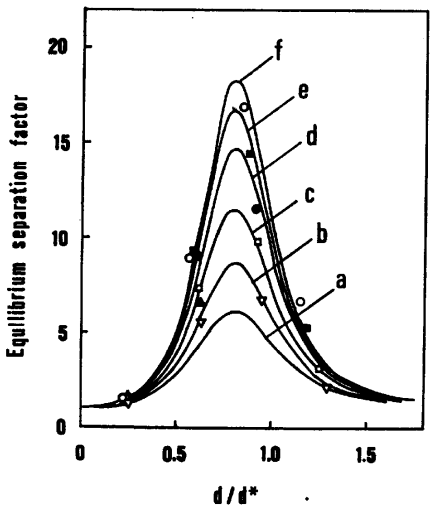

Fig. 8. Dependence of theoretical q_e and experimental q_e on d/d^* in H_2–HT.
The wire temperatures were in the case of theoretical q_e: (a) 200; (b) 250; (c) 300; (d) 350; (e) 400; (f) 450 °C; in the case of experimental q_e: (▽) 200; (▲) 250; (□) 300; (●) 350; (■) 400; (○) 450 °C.

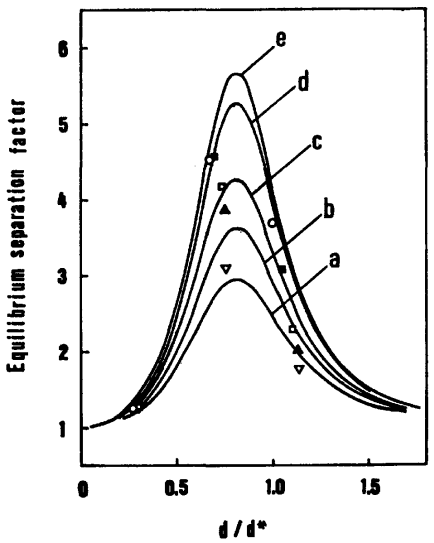

Fig. 9. Dependence of theoretical q_e and experimental q_e on d/d^* in D_2–DT.
The wire temperatures were in the case of theoretical q_e: (a) 200; (b) 250; (c); 300; (d) 400; (e) 450 °C; in the case of experimental q_e: (▽) 200; (▲) 250; (□) 300; (■) 400; (○) 450 °C;.

The authors wish to acknowledge the helpful suggestions and criticisms offered by Professor Emeritus Kozo Hirota (Osaka Univ.) in the course of many fruitful discussions.

References

1) R. C. Jones and W. H. Furry, *Rev. Mod. Phys.*, **18**, 151 (1946).
2) L. Waldmann, *Z. Phys.*, **114**, 53 (1939).
3) K. Hirota, *Nippon Kagaku Kaishi*, **63**, 292 (1942).
4) Y. Tanaka, M. Aoki, Y. Ogino, Y. Okuzaki, K. Nakamura, and K. Hirota, *Nippon Kagaku Kaishi*, **1975**, 1630.
5) Landolt-Boernstein Zahlenwerte und Funktionen, 6 Aufl., Bd. II/5a, Springer-Verlag, Berlin (1969), s. 20.
6) N. E. Menabde, *Atomnaya Energiya*, **17**, 307 (1964); **19**, 453 (1966); **25**, 42 (1968); Landolt-Boernstein Zahlenwerte und Funktionen, 6 Aufl., Bd. II/5a, Springer-Verlag, Berlin (1969), s. 23.
7) I. Amdur and J. W. Beatty, Jr., *J. Chem. Phys.*, **42**, 3361 (1965).
8) "Bussei-Jyosu," ed by the Society of Chemical Engineers Japan, Maruzen, Tokyo (1967), Vol. 5, p. 199.

Electronic Structure of Transition Metal Complexes. III. A Comparative Study of Bondings in Metal Porphyrins

Eiko KAI and Kichisuke NISHIMOTO*

Department of Chemistry, Faculty of Science, Osaka City University, Sumiyoshi-ku, Osaka 558

(Received March 18, 1981)

In order to elucidate π-type interaction between the metal and the ligand, the electronic structure of various metal porphyrins, [M(Por)], where M=Mn, Fe, Co, Ni, and Cu, has been investigated by the CNDO/2 method. The present calculation shows that the nature of σ-type interaction in M–N bond of porphyrin complex is similar to that of the corresponding ammine complex. The calculated ionization potentials reproduce the experimental data. The electron population of macrocycle π-electron systems in metal porphyrins is about 18 which accords with Hückel's $4n+2$ rule.

In the previous paper,[1] we discussed the mutual influence in ammine complexes of the first transition metals, in which a ligand, NH_3, coordinates to the metal with the lone pair of atom N and has no π-type MO's available. Our next interest is to consider the π-type interaction between the metal and the ligand. Probably, porphyrin is the most interesting ligand for such a purpose. Therefore, in this paper, the electronic structure of various planar metal porphyrins is investigated by the MO theory.

As well known, metal porphyrins are important in the fields of chemistry and biology. For this reason, many experimental and theoretical works have been done.[2] Several *ab initio* and semiempirical MO calculations of metal porphyrins have been carried out in order to elucidate their physicochemical properties.[3] However, most of them have been concerned with heme(Fe-porphyrin) and there are quite a few theoretical works on metal porphyrins in which central metal ions are varied widely. A systematic study of metal porphyrins has been done only with the EHMO method by Zener and Gouterman.[4]

In order to elucidate the nature of metal-ligand bond, particularly, π-type interaction, we have carried out the CNDO/2 calculations of various metal porphyrins systematically using our new bonding parameters.[5] The reason why we use the CNDO/2 method is as follows: The surprising progress in the computer as well as the development of new methods has resulted in the application of the *ab initio* MO method to medium sized molecules. It is, however, not easy to do such calculations on very large molecules, for example, metal porphyrins. In this respect, the semiempirical MO method is still useful for comparative theoretical study of similar and very large molecules.

Calculations

In this paper, metal porphyrins, [M(Por)], where M=Mn, Fe, Co, Ni, and Cu, are considered (see Fig. 1). As the bivalent ions and the porphyrin dianion are taken into consideration, the complex is neutral. Standard values have beenused for CNDO/2 parameters associated with atoms C, N, and H,[6] while a new parameter set which we proposed in the previous paper[5] has been used for those associated with the metals.

Fleischer[7] and Fleischer *et al.*[7] determined molecular dimensions of various metal porphyrins by X-ray analysis. For the sake of simplicity, we assumed the D_{4h} symmetry for the porphyrin molecular framework.[8] The interatomic distances associated with M–N bonds are fixed at 2.0 Å from Mn to Cu. Furthermore, metal porphyrins are supposed to be of planar structure, because they are assumed to be in the low spin state.[9] As we make a comparative study of a series of metal porphyrins, the above-mentioned simplification on the molecular geometry is acceptable.

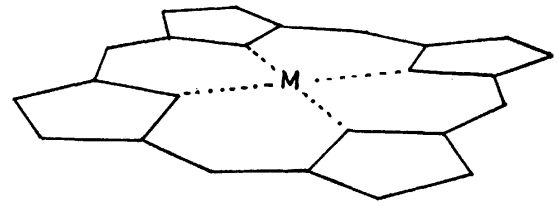

Fig. 1. Planar metal porphyrins, M(Por), where M= Mn, Fe, Co, Ni, and Cu.

Results and Discussion

Binding Energy and Stability. The calculated binding energies of metal porphyrins are shown in Fig. 2. This figure shows that the order of the binding energies is as follows:

$$Mn > Fe > Co > Ni \gtrsim Cu,$$

and that the shape of the binding energy curve is very

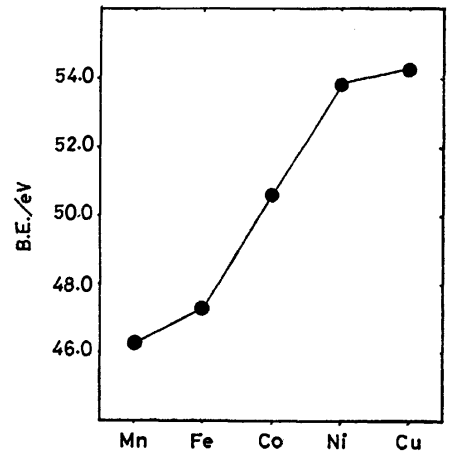

Fig. 2. Calculated binding energies (B.E.) of M(Por)'s.

similar to that of hexaammine or hexaaqua complex.[1] Unfortunately, no experimental data of the binding energies of metal porphyrins are available. However, when calculated binding energies of metal porphyrins are plotted against log (K/mol^{-3} dm^9) (K is stability constant) of the corresponding ethylenediamine complexes determined experimentally,[10] a linear relation is obtained (Fig. 3). Thus, the strength of metal-ligand bonds in metal porphyrins is parallel to that of the corresponding ethylenediamine complexes. This suggests that the strength of metal-ligand bond is determined mainly by the σ-type interaction and that the π-type interaction contributes little to it.

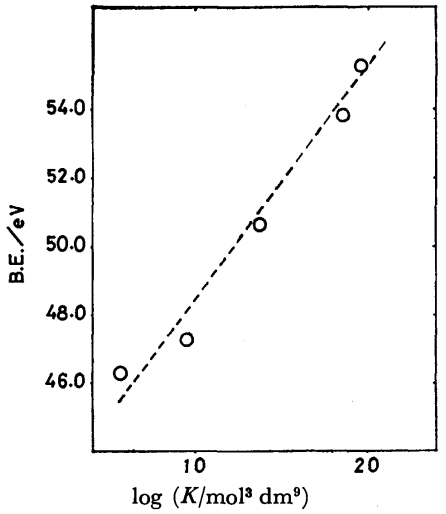

Fig. 3. Binding energy (B.E.) of M(Por) *vs.* log (K/mol^{-3} dm^9), where K is a stability constant of the corresponding ethylenediamine complex.

Bond Order and Bond Strength. As seen from Fig. 2, the calculated binding energy of Cu-porphyrin is nearly equal to that of Ni-porphyrin. This peculiar tendency has been found also with hexaammine and hexaaqua complexes.[1] In order to elucidate this problem, the strength of M–N bond is analyzed from calculated bond orders.

Bond strength is proportional to atomic bond order.[11] However, atomic bond order should not be regarded as a simple sum of bond orders associated with each orbital pair. Therefore, the relative bond strength of M–N bond is considered by comparison of bond orders associated with each orbital pair. The calculated bond orders are shown in Fig. 4. This figure shows that the change of the bond orders associated with 4s-2pσ, 4pσ-2pσ, 3dσ-2s, 3dσ-2pσ, and 3dπ-2pπ is remarkable.

The pattern of the bond-order changes in metal porphyrins is almost the same as those of hexaammine and hexaaqua complexes, as far as σ-type interaction is concerned. The bond orders associated with 3dσ-2s and 3dσ-2pσ decrease abruptly at Cu-porphyrin, as in hexaammine and hexaaqua complexes. This is due to the fact that one of the 3d electrons should enter into the antibonding orbital in the Cu complex. Thus, the decrease in the bond energy contributed from the 3dσ-2s and 3dσ-2pσ pairs cancels out the increase in

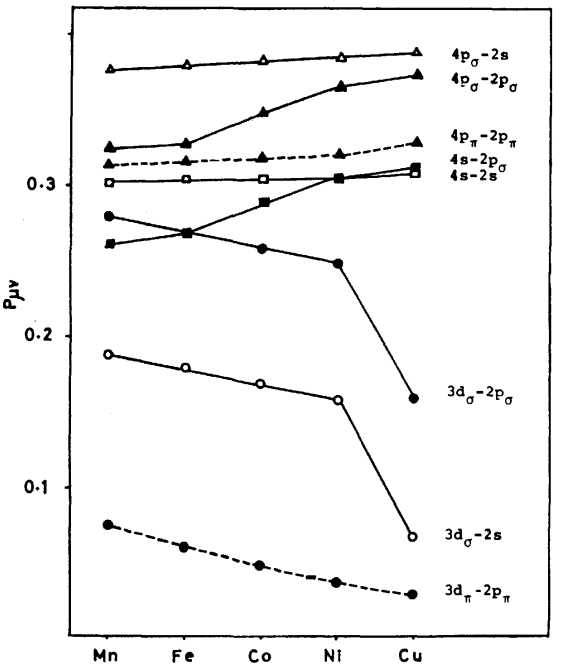

Fig. 4. Calculated bond orders associated with M–N bond in M(Por).

that contributed from the 4s-2pσ and 4pσ-2pσ pairs. Consequently, the shape of binding energy curve shown in Fig. 2 is obtained.

As we expected, the interaction of 3dπ-2pπ is small, because all the complexes are assumed to be in the low spin state in this work. The bond order associated with 3dπ-2pπ decreases according to the increase in atomic number. The reason for this is as follows: Although the ionic radii of the central metal ions decrease according to the increase in atomic number, we fixed the M–N bond distance at 2.0 Å. Therefore, the overlap integral between the metal and ligand will be caused to decrease due to the orbital contraction of the central metal ions.

It can be concluded that the nature of σ-type interaction in the M–N bonds of the porphyrin complexes is similar to that of the corresponding ammine complexes.

Orbital Energy and Ionization Potential. As we assumed these complexes to be in the low spin states, Fe- and Ni-porphyrins are in singlet states, while the others are in doublet states. Figure 5 shows orbital energies of the metal porphyrins. From this figure, some interesting results are derived.

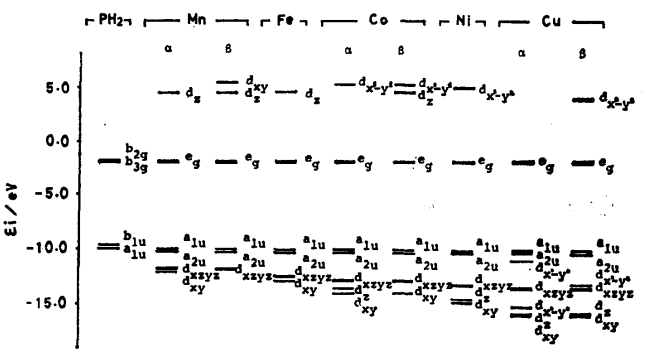

Fig. 5. MO energies (ε_i) of PH_2 and M(Por).

TABLE 1. SPIN DENSITIES OF M(Por)

	Mn	Co	Cu
$3d_{z^2}$	0.0	0.970	0.0
$3d_{x^2-y^2}$	0.0	0.0	0.891
$3d_{xy}$	0.986	0.0	0.0
$3d_{yz}$	0.0	0.0	0.0
$3d_{zx}$	0.0	0.0	0.0

First of all, the change in central metal ions affects MO's which are contributed mainly by the metal itself but barely affects them which are contributed by porphyrin. Although UHF calculations have been done with respect to Mn-, Co-, and Cu-porphyrins which have the open shell structure, the orbital energies of porphyrin parts associated with α- and β-spins resemble each other. In SOMO which has 3d character, the α-spin orbital is different from the β-spin orbital (*e.g.*, d_{xy}-orbital in Mn-porphyrin). This is similar to the result obtained by *ab initio* MO calculations.[12] These results may be due to the following fact that, since most of the MO's are localized on either the ligand or the central metal ion, those belonging to the latter are characterized by the metal itself. The results of calculated spin density given in Table 1 confirm this expectation. It should be noted that in Mn-porphyrin the unpaired spin has π-character, whereas it has σ-character in Co- and Cu-porphyrins. The calculated results accord with the experimental data.[2]

Secondly, although HOMO is b_{1u} (a_{2u} in D_{4h} symmetry) and NHOMO (next HOMO) is a_{1u} in PH_2 (free porphyrin), HOMO is a_{1u} and NHOMO is a_{2u}

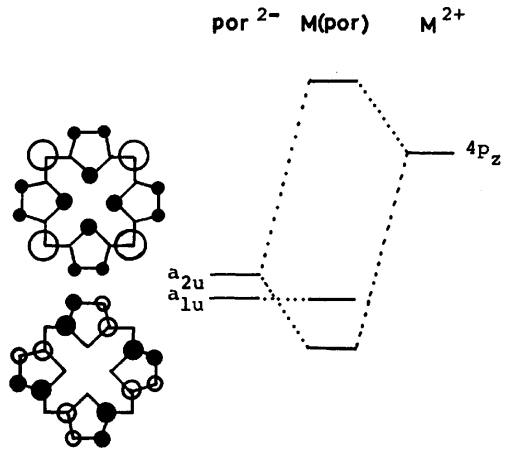

Fig. 6. MO interaction between HOMO and NHOMO of Por^{2-} and 4p-AO of the metal ion.

TABLE 2. IONIZATION POTENTIALS, I_p, OF PH_2 AND M(Por)

		I_p/eV			
		PH_2	Fe	Co	Ni
This calcd	a_{1u}	8.82	8.88	8.88	8.88
	a_{2u}	8.57	9.03	9.07	9.10
Ab initio[a]	a_{1u}	8.78		6.82	
	a_{2u}	8.42		7.12	
Obsd[b]	a_{1u}	6.72	6.50		6.44
	a_{2u}	6.39	6.80		6.62

a) Ref. 12. b) Ref. 13.

in all metal porphyrins. The a_{2u} goes down due to $4p\pi$-$2p\pi$ interaction. Figure 6 shows the orbital interaction diagram. This figure indicates that the $4p\pi$-orbital of the metal ion interacts with the a_{2u} of Por^{2-} (porphyrin dianion) but not with the a_{1u} because of its nonbonding character. Therefore, the a_{1u} energy of PH_2 is almost the same as that of metal porphyrin. Table 2 gives calculated ionization potentials which are obtained by using Koopmans' theorem together with experimental data.[13] As shown from this table, the calculated results reproduce the experimental data, that is, the order of the a_{1u} and a_{2u} is reversed when PH_2 coordinates to the metal. Thus, the present results also suggest that the bonding parameter, $\beta_\mu^0(4p)$, is reasonable. Furthermore, the experiment using ESCA shows that the MO energy of PH_2 is almost the same as that of metal porphyrin. The present calculation also explains this fact. Accordingly, it is suggested that Por^{2-} becomes neutral by coordinating to a bivalent metal. This is different from the results calculated by the *ab initio* MO method which are shown in Table 2 for comparison.

Electronic Spectra. The lowest electronic transitions are contributed mainly by the HOMO and LUMO of the complex. In the present study, we obtained the result that the HOMO and LUMO of the complex are localized entirely in the porphyrin part and that their character is very similar among complexes. Therefore, the variation in transition energy is proportional to that in the orbital energy difference between the HOMO and LUMO.

Figure 5 shows that both HOMO and LUMO are almost unchanged by the replacement of metal ions, so that the difference between them is nearly constant. This fact consists with the results obtained through measurement of electronic spectra in which absorption maxima of metal porphyrins are almost the same.[14]

Electronic Population and Net Charge. Let us consider charge densities. Figure 7 shows the calculated

TABLE 3. ELECTRON POPULATION ON THE METAL ION OF M(Por)

	This calcd					EHMO[a]	*Ab initio*[b]
	Mn	Fe	Co	Ni	Cu	Co	Co
Net charge	+0.317	+0.305	+0.260	+0.223	+0.258	+0.342	+1.78
4s	0.457	0.473	0.523	0.563	0.576	0.442	0.11
4p	0.940	0.966	1.003	1.040	1.084	0.599	0.13
3d	5.285	6.258	7.214	8.174	9.083	7.637	6.98

a) Ref. 4. b) Ref. 12.

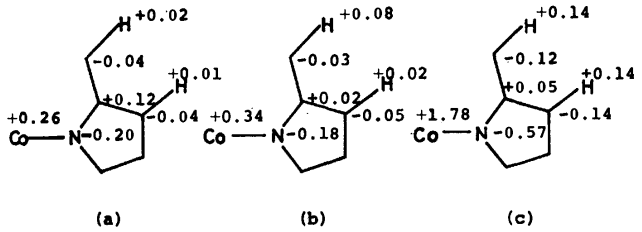

Fig. 7. Calculated net charges of Co-porphyrin.
(a): This calcd, (b): EHMO method, Ref. 4, (c): *ab initio* MO method Ref. 12.

net charge of Co-porphyrin. For comparion, the results obtained by the EHMO and *ab initio* MO methods are also shown. Although the values of calculated net charges depend greatly on the method used, the aspects of polarization resemble each other. The calculated net charge based on the CNDO/2 or EHMO method shows that the central metal ion is almost neutral. This result is different from that calculated by the *ab initio* MO method. For comparison, the calculated charge densities of the central metal ion are shown in Table 3. From this table, it is seen that both the CNDO/2 and EHMO methods calculate the large electron population in the 4s- and 4p-AO's. This is the reason why the central metal ion is neutralized by the coordination. In the EHMO method, the value of q(3d) is also large. Our results coincide with recent X-ray data in which the valence electron distribution is analyzed in detail[15] and also with the results of ionization potential obtained from the photoelectron spectra mentioned above.

In free porphyrin, its macrocycle is highly conjugated and a number of resonance forms can be written. There are nominally 22 π-electrons, but only 18 of them are included in any one delocalization pathway.[2] In metal porphyrin, the very large stability of the porphyrin part may be due to the high aromaticity of the macrocycle part, which is expected to have 18 π-electrons (Hückel's $4n+2$ rule). In order to confirm this, the calculated π-electron density of the macrocycle part is given in Table 4, together with the result calculated by the P-P-P method.[8] This table shows that the number of π-electrons in macrocycle is nearly equal to 18 as expected.

Table 4. Charge densities of macrocycle part of M(Por) and Por^{2-}

	This calcd					P-P-P[a]
	Por^{2-}	Mn	Fe	Co	Ni	Cu	M(Por)
Q	17.49	17.58	17.57	17.57	17.56	17.54	17.75

a) Ref. 8.

The authors would like to express their gratitude to the Computer Center of Institute for Molecular Science for the use of the HITAC M-200H computer and to the Data Processing Center of Kyoto University for the use of the FACOM M-200 computer.

References

1) E. Kai, T. Misawa, and K. Nishimoto, *Bull. Chem. Soc. Jpn.*, **53**, 2481 (1980).
2) "Porphyrins and Metalloporphyrins," ed by K. M. Smith, Elsevier, New York (1975).
3) For example, "Horizons of Quantum Chemistry," ed by K. Fukui and B. Pullman, Reidel, London (1980); D. A. Case, B. H. Huynh, and M. Karplus, *J. Am. Chem. Soc.*, **101**, 4433 (1979); Z. S. Herman and G. H. Loew, *ibid.*, **102**, 1815 (1980).
4) H. Zerner and M. Gouterman, *Theor. Chim. Acta*, **4**, 44 (1966).
5) E. Kai and K. Nishimoto, *Int. J. Quantum Chem.*, **XVIII**, 403 (1980).
6) J. A. Pople and D. L. Beveridge, "Approximate Molecular Orbital Theory," McGraw-Hill, New York (1970).
7) E. B. Fliescher, *J. Am. Chem. Soc.*, **85**, 146 (1963); E. B. Fliescher, C. K. Millerand, and L. E. Webb, *ibid.*, **86**, 2342 (1964).
8) K. Tomono and K. Nishimoto, *Bull. Chem. Soc. Jpn.*, **49**, 1179 (1976).
9) C. A. Read, T. Mashiko, W. R. Scheidt, K. Spartalian, and G. Lang, *J. Am. Chem. Soc.*, **102**, 2302 (1980).
10) D. P. Mellar and L. Maley, *Nature*, **159**, 370 (1947); **161**, 436 (1948).
11) K. Nishimoto and L. S. Forster, *Theor. Chim. Acta*, **3**, 407 (1975).
12) H. Kashiwagi, T. Takada, S. Obara, E. Miyoshi, and K. Ohno, *Int. J. Quantum Chem.*, **XV**, 13 (1978).
13) S. C. Khandelwal, *Chem. Phys. Lett.*, **34**, 355 (1975).
14) J. W. Buchler, G. Eikelmann, L. Puppe, K. Rohbock, H. H. Schneehage, and D. Weck, *Ann. Chem.*, **745**, 135 (1971).
15) M. Iwata and Y. Saito, *Acta Crystallogr., Sect. B*, **29**, 822 (1973).

Molecular Mechanical Calculation on Cyclodextrin Inclusion Complexes. I. The Structures of α-Cyclodextrin Complexes Estimated by van der Waals Interaction Energy Calculation

Yoshihisa MATSUI

Department of Agricultural Chemistry, Shimane University, Nishikawazu, Matsue 690

(Received April 23, 1981)

The geometries of inclusion complexes of α-cyclodextrin (α-CD) with krypton, methanol, 1-propanol, and *p*-nitrophenol were estimated on the basis of the calculation of energies (E_{vdw}) due to the van der Waals interactions between the CD and the guest molecules. The E_{vdw} values were computed by the use of Hill's potential equation. A spatial relationship at which the E_{vdw} value became minimal was in good agreement with that observed by X-ray crystallography for such a guest molecule as 1-propanol or *p*-nitrophenol, which is large in size and less polar. On the other hand, a significantly large deviation was found between the observed and the calculated geometries of the inclusion complex in such polar and/or small guest molecules as methanol and krypton.

Cyclodextrin (CD) is a truncated cone-shaped oligosaccharide composed of six (α-CD), seven (β-CD), or more D-glucose residues attached by α-(1,4) linkages. The CD catalyzes a variety of organic reactions in a stereospecific manner *via* the preceding inclusion of guest molecules within its intramolecular cavity.[1,2] For a comprehensive understanding of the stereospecificity in the binding and catalytic processes of CD, it is essential to define the spatial relationships (geometries) within the inclusion complexes. In this regard, the three-dimensional structures of CD and its inclusion complexes have been investigated by means of X-ray crystallography,[2,3] and NMR[4,5] and CD[6,7] spectrometries. However, these methods are too toilsome to be readily applied to any host-guest molecular system. Instead, Corey-Pauling-Koltum (CPK) molecular models have been widely used to predict the geometries of CD inclusion complexes.[1] The CPK models are constructed on the basis of van der Waals radii of atoms and are a convenient tool for the examination of intermolecular spatial relationships in molecular adducts. However, no one can estimate, with the aid of the models, which of the possible geometric isomers of CD–guest inclusion complexes is actually dominant in the complexation process, owing mainly to the lack of information on interaction energies. In order to estimate the geometry of a CD–guest complex more definitively, it is required to evaluate energy differences between the possible geometric isomers. Molecular mechanical calculation (semiempirical force-field calculation)[8,9] is a method available at hand for this purpose. This method involves the calculation of bond stretching, bond angle strain, torsional, and van der Waals interaction energies. Recently, Tabushi *et al.*[10] have successfully applied this method to α-CD systems to elucidate some aspects of the driving force of inclusion.

The present study deals with a structural analysis of some α-CD–guest inclusion complexes on the basis of the calculation of the van der Waals interaction energy (E_{vdw}) alone, as a first step with the intention of relating the structures, stabilities, and reactivities of CD inclusion complexes to energies estimated by molecular mechanical calculation. The van der Waals interaction, together with hydrophobic interaction, is regarded as a dominant binding force contributing to the association of CD with a guest molecule.[10–14] Since the magnitude of the van der Waals interaction is highly dependent on the interatomic distance, the geometry of a CD–guest complex may be largely governed by this interaction. The disregard of other interactions may inevitably result in some discrepancy between observed and calculated geometries. Even so, it is worthwhile to make clear the scope or limitation of this simplified method. For this purpose, the calculation was carried out on several guest molecules, such as krypton, methanol, 1-propanol, and *p*-nitrophenol, which differ in size and in polarity from one another. The molecular structures of α-CD complexes with these guest molecules have already been determined by the X-ray method.[15–18] The E_{vdw} values were computed for each molecular system at a variety of geometric relationships, and the position at which the E_{vdw} value becomes minimum was searched for by the use of the steepest descent method for nonlinear optimization programming.

Method for Calculation

The energy, E_{vdw}, was calculated by the use of Hill's potential equation (Eq. 1),[19] which was first utilized by Tabushi *et al.*[10] for the calculation of CD inclusion.

$$E_{vdw}=a\sum_i\sum_j \varepsilon_{ij}\,(r_{ij}/d_{ij})^6 + b\sum_i\sum_j \varepsilon_{ij}\,\exp(d_{ij}/cr_{ij}) \quad (1)$$

In this equation, the subscripts, i and j, denote interacting atoms belonging to α-CD and a guest molecule respectively, d_{ij}, the interatomic distance, r_{ij} and ε_{ij},

TABLE 1. VAN DER WAALS PARAMETERS FOR THE HILL EQUATION

Atom	r/nm	ε/kJ mol^{-1}
H	0.120[a,b,c]	0.176[a,b]
C(sp^2)	0.185[d]	0.084[d]
C(sp^3)	0.170[b,c]	0.448[b]
N	0.155[c]	0.397[e]
O	0.152[c]	0.485[f]
Kr	0.207[a]	1.368[a]

a) Ref. 19. b) N. L. Allinger, M. A. Miller, F. A. Van Catledge, and J. A. Hirsch, *J. Am. Chem. Soc.*, **89**, 4345 (1967). c) A. Bondi, *J. Phys. Chem.*,**68**, 441 (1964). d) N. L. Allinger, J. A. Hirsch, M. A. Miller, and I. J. Tyminski, *J. Am. Chem. Soc.*, **91**, 337 (1969). e) Ref. 8. f) N. L. Allinger, M. A. DaRooge, and R. B. Hermann, *J. Org. Chem.*, **26**, 3626 (1961).

the sum of van der Waals radii (r) and a geometrical mean of energetic parameters (ε) respectively with regard to the interacting atoms of i and j, and a, b, and c, constants equal to -2.25, 8.28×10^5, and -0.0736[19] respectively. The values of r and ε used in the present study are summarized in Table 1. All of the atoms were taken into account in the calculation except hydrogen atoms attached to oxygen atoms of α-CD. Thus, 36 carbon atoms, 30 oxygen atoms, and 42 hydrogen atoms of α-CD were chosen. The structure of a α-CD–guest complex in which E_{vdw} becomes minimum was determined by the steepest descent method with a FACOM M-140F computer at Shimane University.

The Coordinates of Atoms Composing of α-CD. The atomic coordinates of α-CD used in the calculations were determined on the basis of the following three assumptions. (1) Each glucopyranose skeleton of α-CD has the same structure as the "Gl" glucopyranose residue of a α-CD–potassium acetate complex.[20] (2) The α-CD macrocycle retains a regular hexagonal structure with the C_6 element of symmetry, irrespective of the guest molecule. In this connection, the Cartesian coordinates were fixed so that the Z-axis refers to the six-fold axis of rotation, the XY plane to a plane defined by the six O(4) atoms of α-CD, and X-axis to a diagonal through G3O (4) and G6O (4) atoms. (3) The angle of each glucopyranose residue to the Z-axis is determined so as to minimize the conformational energy (E_{conf}) of α-CD. The value of E_{conf} was calculated by the use of semiempirical force-field parameters for the van der Waals and angle bending energies. Since it was assumed that the structure of each glucopyranose residue is unchanged, the conformational energies due to the interactions between atoms belonging to the same residue were excluded from this calculation. The E_{conf} value was minimal at $\phi=12.30°$, where ϕ denotes an angle of a plane defined by C(1), C(3), and C(5) atoms of a glucopyranose residue to the Z-axis. Table 2 shows a part of the atomic coordinates of α-CD obtained, together with a few parameters which represent the aspects of the conformation of the α-CD macrocycle. The ϕ value calculated is slightly larger than that observed.[20] The bond angle (θ) of a glucosidic linkage and the distance (r_d) between a pair of diagonal O(4) atoms for the calculated structure are virtually equal to those for the observed one.

Geometry of an Organic Guest Molecule. The geometry of an organic guest molecule was determined by calculation using bond lengths taken from the literature[21] and with bond angles which were taken as 109.5° for aliphatic carbon and alcoholic oxygen atoms and 120.0° for aromatic carbon atoms. It was also assumed that a straight-chain alkyl group always retains a zigzag *trans* planar conformation.

Table 2. A part of α-CD atomic coordinates used for the calculation of the van der Waals interaction energy[a]

Atom	x/nm	y/nm	z/nm
GlC(1)	0.1759	0.5014	−0.0352
GlC(2)	0.0949	0.5567	0.0819
GlC(3)	−0.0303	0.4702	0.1054
GlC(4)	−0.1126	0.4663	−0.0228
GlC(5)	−0.0250	0.4159	−0.1399
GlC(6)	−0.0983	0.4255	−0.2710
GlO(2)	0.1791	0.5601	0.1990
GlO(3)	−0.1108	0.5274	0.2093
GlO(4)	−0.2145	0.3716	0.0000
GlO(5)	0.0919	0.5001	−0.1505
GlO(6)	−0.0196	0.3752	−0.3787
GlH(1)	0.2638	0.5637	−0.0534
GlH(2)	0.0634	0.6584	0.0581
GlH(3)	−0.0007	0.3688	0.1333
GlH(4)	−0.1545	0.5645	−0.0453
GlH(5)	0.0055	0.3129	−0.1217
GlH(6) A	−0.1229	0.5301	−0.2902
GlH(6) B	−0.1901	0.3671	−0.2643

a) Parameters representing the conformation of the α-CD macrocycle: $\phi=12.30°$ (obsd, $8.7\pm0.5°$), $\theta=119.26°$ (obsd, $119.1\pm0.2°$), and $r_d=0.8581$ nm (obsd, 0.849 ± 0.011 nm).

Results

The atomic coordinates obtained by the E_{vdw} calculation are compared with those observed in Table 3 to 6. Only the z-coordinates of atoms are given in the tables in order to simplify the representation. The observed atomic coordinates were re-calculated from the X-ray crystallographic data.[15–18] In this calculation, the Cartesian coordinates were transformed so that the observed least-squares plane of six O(4) atoms of α-CD accords with the XY plane and the y-coordinates of a pair of diagonal O(4) atoms become equal to zero.

The X-ray study[15] revealed that, in a α-CD–Kr adduct obtained under Kr pressure of 304 kPa, the Kr is statistically disordered over three positions. Each Kr atom is approximately located on the Z-axis. The

Table 3. The z-values of Kr in a α-CD–Kr complex[a]

	z/nm		
	Site A	Site B	Site C
Obsd	−0.168	−0.016	−0.073
Calcd	−0.158	−0.076	—

a) Parameters representing the conformation of the α-CD macrocycle observed: $\phi=11.4\pm4.2°$, $\theta=118.2\pm0.5°$, and $r_d=0.845\pm0.008$ nm.

Table 4. The z-values of the constituent oxygen and carbon atoms of methanol in a α-CD–methanol complex[a]

Atom	z/nm		
	Obsd		Calcd
	Site A	Site B	
O	−0.2832	−0.0723	−0.1572
C	−0.2541	0.0577	−0.0150

a) Parameters representing the conformation of the α-CD macrocycle observed: $\phi=12.1\pm4.4°$, $\theta=119.0\pm0.4°$, and $r_d=0.845\pm0.021$ nm.

Table 5. The z-values of the constituent oxygen and carbon atoms of 1-propanol in a α-CD-1-propanol complex[a)]

Atom	z/nm		
	Obsd		Calcd
	Site A	Site B	
O	−0.243	−0.249	−0.252
C(1)	−0.168	−0.168	−0.174
C(2)	−0.019	−0.019	−0.025
C(3)	0.075	0.061	0.059

a) Parameters representing the conformation of the α-CD macrocycle observed: $\phi=11.3\pm4.1°$, $\theta=119.9\pm0.6°$, and $r_d=0.846\pm0.006$ nm.

Table 6. The z-values of the constituent atoms of p-nitrophenol in a α-CD–p-nitrophenol complex[a)]

No.[b)]	Atom	z/nm	
		Obsd	Calcd
1	C	0.2696	0.2714
2	C	0.2042	0.2029
3	C	0.0665	0.0635
4	C	0.0001	−0.0073
5	C	0.0658	0.0612
6	C	0.2002	0.2006
7	O	0.4028	0.4074
8	O	−0.2023	−0.2143
9	O	−0.2051	−0.2163
10	N	−0.1453	−0.1543
11	H	0.2671	0.2580
12	H	0.0291	0.0102
13	H	0.0109	0.0062
14	H	0.2401	0.2539
15	H	0.4449	0.4552

a) Parameters representing the conformation of the α-CD macrocycle observed: $\phi=9.7\pm2.3°$, $\theta=118.5\pm0.4°$, and $r_d=0.846\pm0.027$ nm. b) The number of each atom is refered to Fig. 2.

E_{vdw} calculation for this adduct showed two energy minima at $z=-0.158$ and -0.076 nm. The former is close to the z observed for Kr at site A, whereas the latter deviates considerably from those observed. Fairly large deviations were also found between geometries observed and calculated for a α-CD–methanol complex. The methanol molecule observed is two-fold disordered in sites A and B with equal probability. However, both are located far from the position calculated. In contrast to these cases, the geometries calculated are in good agreement with those observed in the cases of α-CD complexes with 1-propanol and p-nitrophenol. The X-ray study[17] showed that the hydroxyl and methyl groups of 1-propanol are two-fold disordered in the α-CD cavity, with site A occupied 80%, site B 20%. The average and standard deviations between the atomic coordinates observed and calculated for 4 atoms of oxygen and carbon of 1-propanol are as follows (standard deviations are in parentheses): x, 0.005 (0.022) and 0.012 (0.048) nm, y,

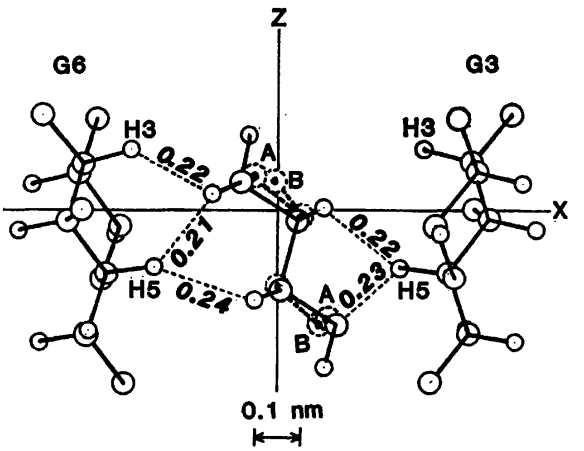

Fig. 1. Geometries calculated (solid lines) and observed (bold dashed lines) for 1-propanol in its α-CD adduct. Letters A and B represent the disordered sites observed for 1-propanol. Interatomic distances are shown in bold italics on fine dashed lines (nm).

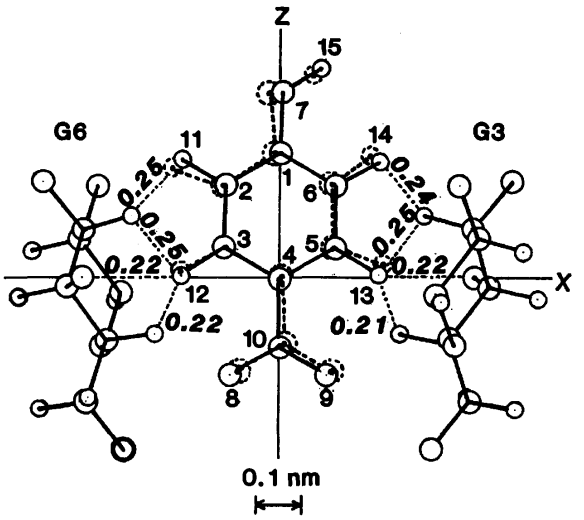

Fig. 2. Geometries calculated (solid lines) and observed (bold dashed lines) for p-nitrophenol in its α-CD adduct. The figures given in roman on the atoms of p-nitrophenol refer to those shown in Table 6. Interatomic distances are shown in bold italics on fine dashed lines (nm).

0.001 (0.032) and −0.004 (0.052) nm, and z, 0.010 (0.005) and 0.005 (0.002) nm for site A and B respectively. On the whole, the coordinates observed for site A are in better agreement than those for site B with the calculated coordinates. Corresponding values for the 15 atoms of p-nitrophenol are −0.004 (0.014) nm for x, 0.028 (0.036) nm for y, and 0.003 (0.010) nm for z. Such deviations, as are shown above, are acceptably small, when taking into account the fact that the atomic coordinates of α-CD and the guest molecules used for the calculation are not exactly the same as those observed. The geometric relationships are illustrated for the adducts of 1-propanol and p-nitrophenol in Figs. 1 and 2 respectively. The calculation of atomic distances between the constituent atoms

of the α-CD complexes revealed that the hydrogen and oxygen atoms of 1-propanol or the hydrogen atoms of *p*-nitrophenol are in van der Waals contact with some of H(3), H(5), and/or O(4) atoms of α-CD as are shown in the figures.

Discussion

Geometric relationships obtained by the E_{vdw} calculation were in good agreement with those observed by the X-ray method in the cases of α-CD complexes with 1-propanol and *p*-nitrophenol. These guest molecules are large enough in size to give significantly large stabilization energies due to the van der Waals interaction ($-E_{vdw}$=57.36 and 52.26 kJ mol^{-1} for 1-propanol and *p*-nitrophenol adducts respectively). On the other hand, deviations between observed and calculated geometries are appreciably large for the krypton and methanol adducts. These molecules are small in size so that the stabilization energies due to the van der Waals interaction are small ($-E_{vdw}$=26.15 or 26.12 kJ mol^{-1} for the krypton adduct and 29.16 kJ mol^{-1} for the methanol adduct). Thus interactions other than the van der Waals one, such as hydrogen bonding and dipole-dipole and hydrophobic interactions, may considerably influence the geometries of these adducts.

The present method of calculation sometimes provides a criterion to judge which of the possible geometric isomers of a α-CD–guest inclusion complex is actually dominant in the complexation process. Harata[18] showed that *p*-nitrophenol is included in such a specific manner that the nitro group is located within the α-CD cavity, whereas the phenolic hydroxyl group protrudes from the O(2), O(3) side. However, it is geometrically possible that *p*-nitrophenol is situated upside down in the cavity. The stabilization energy due to the van der Waals interaction was calculated to be 52.26 kJ mol^{-1} for the former and 41.17 kJ mol^{-1} for the latter. Thus, it is possible to predict the specific orientation of the guest molecule in the α-CD cavity on the basis of the E_{vdw} calculation alone.

A number of problems still remain to be solved. First, it was assumed in the present study that the conformation of α-CD is unchanged during the complexation process. Actually, it has been found that the macrocyclic conformation of α-CD is affected by the inclusion of a guest molecule. The primary hydroxyl groups of α-CD shows both *gauche-gauche* and *gauche-trans* conformations, although only the latter was taken into account in the present study. On the other hand, the E_{vdw} values obtained may serve to elucidate the role of the van der Waals interaction in the stabilization of any α-CD–guest inclusion complexes. In addition, the method can easily be extended so as to include β- and γ-CD systems. These problems will be dealt with in subsequent work.

References

1) D. W. Griffiths and M. L. Bender, *Adv. Catal.*, **23**, 209 (1973).
2) W. Saenger, *Angew. Chem., Int. Ed. Engl.*, **19**, 344 (1980).
3) W. Saenger, "Environmental Effects on Molecular Structure and Properties," ed by B. Pullman, D. Reidel Publishing, Dordrecht-Holland (1976), p. 265.
4) D. J. Wood, F. E. Hruska, and W. Saenger, *J. Am. Chem. Soc.*, **99**, 1735 (1977).
5) R. J. Bergeron, M. A. Channing, and K. A. McGovern, *J. Am. Chem. Soc.*, **100**, 2878 (1978).
6) R. J. Bergeron and P. McPhie, *Bioorg. Chem.*, **6**, 465 (1977).
7) K. Harata, *Bull. Chem. Soc. Jpn.*, **52**, 1807 (1979).
8) E. L. Elliel, N. L. Allinger, S. J. Angyal, and G. A. Morrison, "Conformational Analysis," John Wiley and Sons, New York, N. Y. (1965), p. 449.
9) N. L. Allinger, *Adv. Phys. Org. Chem.*, **13**, 1 (1974).
10) I. Tabushi, Y. Kiyosuke, T. Sugimoto, and K. Yamamura, *J. Am. Chem. Soc.*, **100**, 916 (1978).
11) K. Harata, *Bull. Chem. Soc. Jpn.*, **49**, 2066 (1976).
12) K. Harata, H. Uedaira, and J. Tanaka, *Bull. Chem. Soc. Jpn.*, **51**, 1627 (1978).
13) R. J. Bergeron, M. A. Channing, G. J. Gibeily, and D. M. Pillor, *J. Am. Chem. Soc.*, **99**, 5146 (1977).
14) Y. Matsui and K. Mochida, *Bull. Chem. Soc. Jpn.*, **52**, 2808 (1979).
15) W. Saenger and M. Nortemeyer, *Chem. Ber.*, **109**, 503 (1976).
16) B. Hingerty and W. Saenger, *J. Am. Chem. Soc.*, **98**, 3357 (1976).
17) W. Saenger, R. K. McMullan, J. Fayos, and D. Mootz, *Acta Crystallogr., Sect. B*, **30**, 2019 (1974).
18) K. Harata, *Bull. Chem. Soc. Jpn.*, **50**, 1416 (1977).
19) T. L. Hill, *J. Chem. Phys.*, **16**, 399 (1948).
20) A. Hybl, R. E. Rundle, and D. E. Williams, *J. Am. Chem. Soc.*, **87**, 2779 (1965). X-Ray crystallographic studies so far reported showed that each glucopyranose skeleton of α-CD is rigid enough to give virtually similar structure, irrespective of the guest molecule. An advantage of the choice of the α-CD–potassium acetate complex system is that not only the atomic coordinates of the carbon and oxygen atoms but also those of hydrogen atoms attached to the carbon atoms are discussed in the article. The atomic coordinates of the hydrogen atoms attached to the oxygen atoms are not given. However, these atoms are so mobile that the contribution of the atoms to the van der Waals interactions may be regarded as negligible.
21) A. J. Gordon and R. A. Ford, "The Chemist's Companion; A Handbook of Practical Data, Techniques, and References," John Wiley and Sons, New York, N. Y. (1972), p. 107.

Formation of Electronically Excited Fragments (H, CH, NH) by the Electron Impact of Pyrrole and Pyrrolidine

Ikuo Tokue,* Masami Ikarashi, and Yoshio Ito

Department of Chemistry, Faculty of Science, Niigata University, Ikarashi, Niigata 950-21

(Received July 9, 1981)

In the wavelength region of 200—600 nm, photoemissions from electronically excited fragments (H, CH, NH, CN, and C_2) were observed when pyrrole and pyrrolidine were excited by electron impact (0—70 eV). Hydrogen atoms and CH and NH radicals from pyrrole and pyrrolidine are produced *via* a single collision excitation. The appearance potentials for these fragments from pyrrole are 19.4±0.8 eV for the hydrogen Balmer β (H_β), 19.7 ±0.8 eV for the CH($A^2\Delta$-$X^2\Pi$) band, and 20.0±1.0 eV for the NH($A^3\Pi$-$X^3\Sigma$) band. Those from pyrrolidine are 18.7±0.8 eV for H_β, 23.0±0.8 eV for the CH(A-X) band, and 21.8±1.0 eV for the NH(A-X) band. Dissociation processes forming these electronically excited fragments are discussed.

Fragmentation of several cyclic molecules has been studied by electron impact mass spectroscopy.[1,2] Information thus obtained has been restricted to relatively large ionic fragments. Formation of neutral species could be, only indirectly, detected by mass spectroscopy. When atoms and diatomic molecules are produced in their excited states they are easily detected by photoemission spectroscopy. Photoemissions from neutral excited fragments produced by electron impact of aromatic molecules have been investigated extensively.[3—5] However, a few papers[6,7] concerned with large heterocycles have reported emissions from fragments produced by electron impact; very little is known about the formation of neutral fragments from excited parent species.

Appearance potentials of neutral fragments in their excited states produced by electron impact[7] of pyridine and pyrazine are higher than first ionization potentials of parent molecules. In these cases, the formation of ionic fragments can compete with fragmentation to neutral excited species, or ionic fragments seem to be by-products in the formation of neutral fragments. Therefore, we expect that information obtained by mass spectroscopy is also useful for studying the fragmentation mechanism of large heterocycles by electron impact as well as by photoemission spectroscopy.

In the present paper, emission spectra of fragments produced by electron impact of pyrrole and pyrrolidine are identified and appearance potentials for the H_β, CH($A^2\Delta$-$X^2\Pi$), and NH($A^3\Pi$-$X^3\Sigma$) bands are determined. Possible dissociation processes forming H(n=4), CH($A^2\Delta$), and NH($A^3\Pi$) from pyrrole and pyrrolidine are discussed in consideration of thermochemical data.

Experimental

The apparatus and experimental details have been described in the previous paper.[7] The apparatus consists of an electron source, a collision chamber, and an optical detection system. Sample pressures during emission measurements, as measured by an ionization gauge, were 5—40 mPa. Negative potentials from the threshold to 70 eV were applied to a tungsten filament and the maximum beam current measured at Faraday cage was about 0.8 mA for 70 eV. Electron-beam currents of 10 μA at thresholds and 40—50 μA at higher energies were used for the measurement of excitation functions.

In preliminary measurements, the photoemission in the region of 200—600 nm modulated at 225 Hz by a mechanical chopper was detected by a combination of a 30 cm Czerny-Turner monochromator and an HTV R374 photomultiplier connected to a lock-in amplifier. For the measurement of excitation function, an HTV R585 photomultiplier cooled at about −20 °C and an HTV C1230 photon-counter were used with spectral resolution of 0.6 nm ((FWHM).

Pyrrole and pyrrolidine (Nakarai Chemicals, guaranteed grade) were degassed by several freeze-pump-thaw cycles just before use.

Results

Emission Spectra. Figure 1 shows emission spectra produced by electron impact on pyrrole and pyrrolidine in the region of 260—510 nm. The observed spectra were assigned to the hydrogen Balmer series (n= 4—13→2), the NH($A^3\Pi$-$X^3\Sigma$) band around 336 nm, the CN($B^2\Sigma$-$X^2\Sigma$) band around 385 nm, the CH($A^2\Delta$-$X^2\Pi$) band around 431 nm, and the C_2($A^3\Pi$-$X^3\Pi$) band around 470 nm. The NH($c^1\Pi$-$a^1\Delta$) band from neither pyrrole nor pyrrolidine was detected.

The photoemission intensities of the H_β, CH(A-X), and NH(A-X) bands from pyrrole and pyrrolidine were found to be proportional to the electron-beam current up to 0.5 mA and to the sample pressure up to 40 mPa in the collision chamber. The excitation functions for

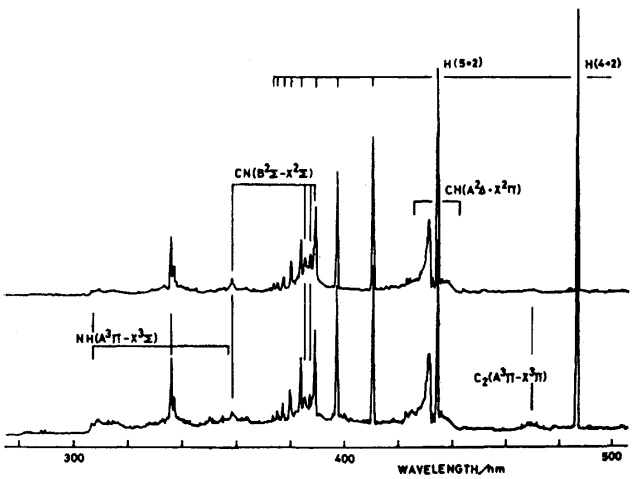

Fig. 1. Emission spectra by electron impact (70 eV, 0.5 mA).
Top view: pyrrolidine at 11 mPa, bottom view: pyrrole at 12 mPa.

these fragment species were observed at sample pressures of 5—11 mPa and the appearance potentials were found to be independent of the sample pressure. Therefore, the excited fragments, H atoms and CH and NH radicals, from pyrrole and pyrrolidine, seem to be formed from fragmentation *via* a single collision excitation by electrons. The two-step collision with another electron seems to be negligible.

Appearance Potentials for Fragment Species. The energy for the impinging electron was calibrated on the basis of both the peak of the excitation function for the (1,0) band of the $N_2(C^3\Pi\text{-}B^3\Pi)$ emission reported by Finn *et al.*[8] and the appearance potential for the (0,0) band of the $N_2^+(B^2\Sigma\text{-}X^2\Sigma)$ emission reported by Borst and Zipf.[9] Nitrogen was mixed with the sample vapor and their emission intensities were measured simultaneously. Slight discrepancies were observed in the steepness of the excitation function for the (1,0) band of the N_2(C-B) emission in the threshold region, probably because of the energy spread of about 2 eV in the present experiment.[7]

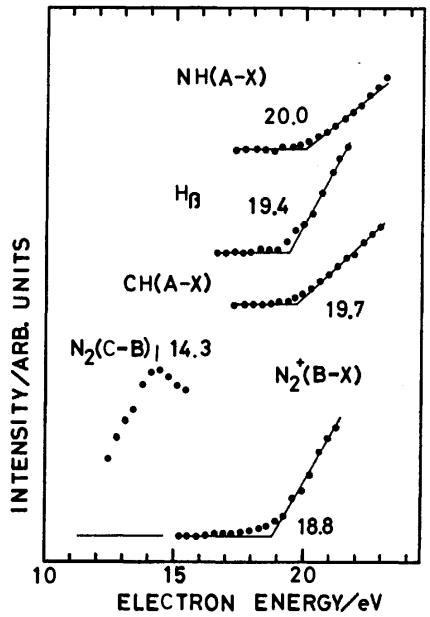

Fig. 2. The excitation functions for the H_β, the CH(A-X) and the NH(A-X) emissions from pyrrole, and those for the N_2(C-B) and N_2^+(B-X) emissions from nitrogen molecule. Typical data are presented and the standard deviation is as large as the diameter of the circles.

The excitation function for the NH(A-X) band could not be measured simultaneously from the gaseous mixture of the sample and nitrogen because the head of the (0,0) band of the N_2(C-B) emission, 337.1 nm,[10] is accidentally overlapped with the head of the (0,0) band of the NH(A-X) emission, 336.0 nm.[11] Therefore, the excitation function for the NH(A-X) band was measured with those for the H_β and CH(A-X) bands from the pure sample vapor, and the appearance potential for NH(A) was calibrated indirectly from those for H(n=4) and CH(A).

Figure 2 shows the excitation functions for the H_β, CH(A-X), and NH(A-X) emissions from pyrrole near their thresholds, together with those for the (1,0) band of the N_2(C-B) emission and the (0,0) band of the N_2^+(A-X) emission measured simultaneously. Figure 3 shows the excitation functions for the same fragments from pyrrolidine. The appearance potentials thus obtained for H(n=4), CH(A), and NH(A) from pyrrole are listed in the third column of Table 1, and those from pyrrolidine are also listed in the third column of Table 2. Dissociation processes which are expected to play an important role in the formation of H(n=4), CH(A), and NH(A) from pyrrole and pyrrolidine are shown in the first column of each table. The threshold energies

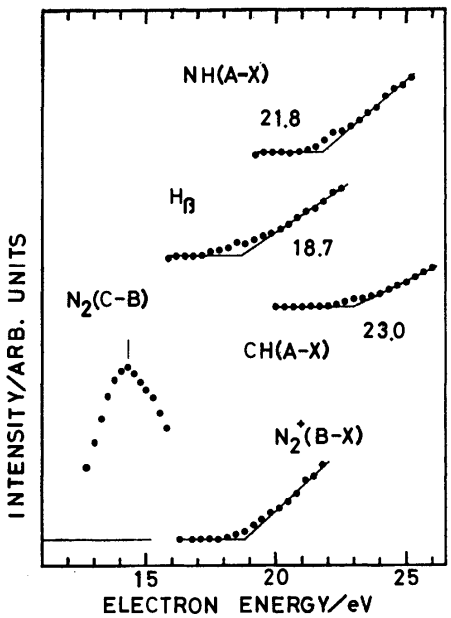

Fig. 3. Same as Fig. 2 from pyrrolidine.

Table 1. Dissociation processes for the formation of H(n=4), CH($A^2\Delta$), and NH($A^3\Pi$) from pyrrole

	Dissociation processes	Threshold eV Calcd	Threshold eV Obsd
(1)	$C_4H_5N \longrightarrow C_4H_4N(\tilde{X})+H(n=4)$	17.3±0.3[a]	19.4±0.8
(2)	$\longrightarrow C_2H_3(\tilde{X})+HCN(\tilde{X})+CH(A^2\Delta)$	12.2[a]	
(3)	$\longrightarrow C_3H_2^+(\tilde{X})+NH_2(\tilde{X})+CH(A^2\Delta)$	18.7±0.5[b]	19.7±0.8
(4)	$\longrightarrow 2C_2H_4(\tilde{X})+NH(A^3\Pi)$	10.8[a]	
(5)	$\longrightarrow C_3H_2^+(\tilde{X})+CH_2(\tilde{X})+NH(A^3\Pi)$	19.5±0.5[b]	20.0±1.0

a) See Text. b) Calculated from the appearance potential for $C_3H_2^+$ ion, 15.8±0.5 eV, and the electronic energy of CH(A) or NH(A).[12]

Table 2. Dissociation processes for the formation of H(n=4), CH($A^2\Delta$), and NH($A^3\Pi$) from pyrrolidine

	Dissociation processes	Threshold / eV Calcd[a]	Threshold / eV Obsd
(1)	$C_4H_9N \longrightarrow C_4H_8N(\tilde{X})+H(n=4)$	17.1±0.2[b]	18.7±0.8
(2)	$\longrightarrow CH_3CH_2NH(\tilde{X})+CH_2(\tilde{X})+CH(A^2\Delta)$	14.8	
(3)	$\longrightarrow C_3H_5^+(\tilde{X})+NH(\tilde{X})+H_2(X)+CH(A^2\Delta)$	22.5±0.5	23.0±0.8
(4)	$\longrightarrow C_3H_3^+(\tilde{X})+NH_3(\tilde{X})+H_2(X)+CH(A^2\Delta)$	23.7±0.5	
(5)	$\longrightarrow C_2H_3(\tilde{X})+C_2H_5(\tilde{X})+NH(A^3\Pi)$	11.2	
(6)	$\longrightarrow C_2H_3^+(\tilde{X})+C_2H_5(\tilde{X})+NH(A^3\Pi)$	20.0±0.5	21.8±1.0
(7)	$\longrightarrow C_2H_2^+(\tilde{X})+C_2H_6(\tilde{X})+NH(A^3\Pi)$	21.6±1.0	

a) See Text. b) Calculated from bond dissociation energy of the C–H or N–H bond estimated according to the method by Allen.[13]

Table 3. Heats of formation used for the calculation of the thresholds

Species	ΔH°_{f0} / kJ mol^{-1}	Ref.
Pyrrole	108.28	13
Pyrrolidine	−3.6	14 and estimated
H_2	0	15
CH	590.8±0.4	15
CH_2	386±4	15
C_2H_3	278	13 and estimated
C_2H_4	61.0±0.3	15
C_2H_5	107.5	13
C_2H_6	−84.68	13
NH	339±10	15
NH_3	−47.7	13
CH_3CH_2NH	174	13 and estimated
$C_2H_2^+$	1328	2, 16
$C_2H_3^+$	1125	17
CH_2=$CHCH_2^+$	964	2, 17
$C_3H_3^+$ (cyclopropenyl)	1075	2, 17
CH≡C–CH_2^+	1175	2, 17

of the dissociation processes leading to the formation of the excited fragments, listed in the second column of Tables 1 and 2, are calculated by using the electronic energies of the excited species and the thermochemical data. The heats of formation used for the calculation of the thresholds are summarized in Table 3.

Discussion

Formation of H(n=4). The onset for the H_β from pyrrole is found at 19.4±0.8 eV. By comparison of the observed threshold energy with the bond dissociation energy of the C–H bond estimated from benzene,[18] 4.86 eV, or the N–H bond,[13] 4.24 eV (estimated), and with the excitation energy of H(n=4), 12.74 eV, the dissociation process for the formation of H(n=4) from pyrrole is considered to be mainly process (1) in Table 1. The onset for the H_β from pyrrolidine is found at 18.7±0.8 eV. A similar consideration on the threshold energy for pyrrolidine leads to process (1) in Table 2. The excess energy of 1.6—2.1 eV for the difference between the observed and calculated threshold in these processes (Tables 1 and 2) is probably dissipated as the kinetic energy of the leaving hydrogen atom. These dissociation processes for the formation of excited H atoms are similar to those with benzene[5,7] and pyridine and pyrazine.[7]

Formation of CH(A) and NH(A). The onsets for the CH(A-X) and NH(A-X) emissions from pyrrole are found at 19.7±0.8 and 20.0±1.0 eV, respectively, and those from pyrrolidine are also found at 23.0±0.8 and 21.8±1.0 eV, respectively. These appearance potentials observed for CH(A) and NH(A) are much higher than the first ionization potentials for pyrrole, 8.97 eV,[19] and for pyrrolidine, 9.0 eV;[2] accordingly, it appears that ionic fragments are possible to be by-products in the formation of CH(A) and NH(A). Dissociation processes leading to the formation of CH(A) and NH(A) from pyrrole and pyrrolidine are still uncertain because available heats of formation of ionic products are insufficient. Nevertheless, if one assumes that the threshold energy consists of the thermochemical values and electron excitation energies of CH(A) and NH(A), main dissociation processes leading to the formation of CH(A) and NH(A) from pyrrolidine seems to include an ionic by-product. Namely, in Table 2, processes (3) and (4) and processes (6) and (7) seem to play an important role in the formation of CH(A) and NH(A) from pyrrolidine, respectively.

Dissociation processes (3) and (5) in Table 1 are expected to play an important role in the formation of CH(A) and NH(A) from pyrrole, respectively. The threshold energies for these processes from pyrrole were calculated from the appearance potential for $C_3H_2^+$ ion from pyrrole reported by Hissel[1] because the heat of formation of $C_3H_2^+$ ion is not known. Furthermore, Gallegos and Kiser[2] have pointed out that the appearance potentials reported by Hissel[1] from tetrahydrofuran and pyrrolidine are in every case lower than the appearance potentials reported by Gallegos and Kiser[2] with the exception of the parent-molecule ions in both molecules. According to these facts, the threshold values for processes (3) and (5) in Table 1 seem to be the lower limits. The threshold energies for dissociation processes from pyrrole including other relatively abundant ions reported by Hissel,[1] $C_3H_3^+$, $C_3H_4^+$, and $C_2H_2N^+$, are higher than the observed values.

Another possibility for the formation of CH(A) and NH(A) from pyrrole and pyrrolidine is that by-products

are formed in their electronically excited states, because the thresholds calculated for the dissociation processes including only neutral by-products in their ground state are much lower the observed thresholds. This possibility will be examined by the photon-photon coincidence technique.[20]

In summary, the appearance potential for H_β from pyrrolidine is slight lower than that from pyrrole, but $H(n=4)$ atoms from both molecules are probably formed *via* a similar mechanism following neither cleavage of skeletal bonds nor new bond formation. The dissociation processes for the formation of CH(A) and NH(A) from pyrrole and pyrrolidine seem to include a fragment ion as a by-product.

References

1) J. Hissel, *Bull. Soc. R. Sci. Liege*, **21**, 457 (1952).
2) E. J. Gallegos and R. W. Kiser, *J. Phys. Chem.*, **66**, 136 (1962).
3) D. A. Vroom and F. J. de Heer, *J. Chem. Phys.*, **50**, 573 (1969).
4) T. Ogawa, M. Tsuji, M. Toyoda, and N. Ishibashi, *Bull. Chem. Soc. Jpn.*, **46**, 2637 (1973).
5) C. I. M. Beenakker and F. J. de Heer, *Chem. Phys. Lett.*, **29**, 89 (1974).
6) T. Ogawa, M. Toyoda, and N. Ishibashi, *Engineering Sci. Repts. Kyushu Univ.*, **2**, 17 (1980).
7) I. Tokue and M. Ikarashi, *Bull. Chem. Soc. Jpn.*, **54**, 1852 (1981).
8) T. G. Finn, J. F. M. Aarts, and J. P. Doering, *J. Chem. Phys.*, **56**, 5632 (1972).
9) W. L. Borst and E. C. Zipf, *Phys. Rev. A*, **1**, 834 (1970).
10) R. W. B. Pearse and A. G. Gaydon, "The Identification of Molecular Spectra," Chapman and Hall, London (1965).
11) L. Wallace, *Astrophys. J. Suppl. Ser.*, **7**, 165 (1962).
12) G. Herzberg, "Spectra of Diatomic Molecules," 2nd ed, Van Nostrand, Princeton (1950).
13) J. D. Cox and G. Pilcher, "Thermochemistry of Organic and Organometallic Compounds," Academic Press, New York (1970).
14) S. W. Benson, "Thermochemical Kinetics," 2nd ed, John Wiley and Sons, New York (1976).
15) D. R. Stull and H. Prophet, "JANAF Thermochemical Tables," 2nd ed, Natl. Stand. Ref. Data Ser., Natl. Bur. Stand., **37**, 1141 (1971).
16) D. D. Wagman, W. H. Evans, V. B. Parker, I. Halow, S. M. Bailey, and R. H. Schumm, "Selected Values of Chemical Thermodynamic Properties," National Bureau of Standards Tech. Note 270-3, U. S. Govt. Printing Office, Washington D. C. (1968).
17) H. M. Rosenstock, K. Draxl, B. W. Steiner, and J. T. Herron, *J. Phys. Chem. Ref. Data*, **6**, Suppl. No. 1 (1977).
18) H. S. Rogers, D. M. Golden, and S. W. Benson, *J. Am. Chem. Soc.*, **89**, 4578 (1967).
19) I. Omura, H. Baba, and K. Higashi, *J. Phys. Soc. Jpn.*, **10**, 317 (1955).
20) N. Böse, *J. Phys. B*, **11**, L309 (1978).

Crystal Structure and Photochemistry of Isopolymolybdates. I. The Crystal Structures of Hexakis(propylammonium)heptamolybdate(VI) Trihydrate and Hexakis(isopropylammonium)heptamolybdate(VI) Trihydrate

Yuji OHASHI,* Kazunori YANAGI, Yoshio SASADA, and Toshihiro YAMASE†

Laboratory of Chemistry for Natural Products, Tokyo Institute of Technology, Nagatsuta, Midori-ku, Yokohama 227

†*Research Laboratory of Resource Utilization, Tokyo Institute of Technology, Nagatsuta, Midori-ku, Yokohama 227*

(Received July 15, 1981)

The crystal structures of $(NH_3CH_2CH_2CH_3)_6[Mo_7O_{24}]\cdot 3H_2O$ and $(NH_3CH(CH_3)_2)_6[Mo_7O_{24}]\cdot 3H_2O$ have been determined by X-ray analysis. The crystal of the propylammonium salt is triclinic; the space group is $P\bar{1}$; $Z=2$, with $a=14.118(2)$, $b=15.977(2)$, $c=11.368(1)$ Å, $\alpha=90.23(1)$, $\beta=93.00(1)$, $\gamma=111.79(1)°$. That of the isopropylammonium salt is monoclinic; the space group is P2/n; $Z=4$, with $a=23.904(6)$, $b=10.504(1)$, $c=20.652(9)$ Å, and $\beta=115.40(2)°$. The structures were deduced by the direct method and refined by the block-diagonal least-squares technique. The final R values were 0.035 for 8084 observed reflections of the former and 0.060 for 9934 of the latter. The heptamolybdate anion of the two crystals has an approximate 2mm symmetry and its structure is similar to that observed in the crystals of the ammonium, potassium and sodium salts. The propyl- and isopropylammonium cations form some hydrogen bonds to the bridging oxygens of the heptamolybdates. Such hydrogen bonds play an important role in the UV-induced photochromism of these crystals.

Recently it has been reported that various alkylammonium polymolybdates show photochemical and photochromic properties in aqueous solution and in the solid state.[1] On exposure to UV light, they turn blue from colorless in deaerated solutions, whereas they change from colorless to red in the solid state. The photoreduced blue compound of isopropylammonium polymolybdate, $(NH_3CH(CH_3)_2)_4[Mo_{13}O_{40}]_{0.33}[H_4Mo_{12}O_{40}]_{0.67}$, was crystallized and its structure has been reported.[2] The crystal structure of the isopropylammonium salt, $(NH_3CH(CH_3)_2)_6[H_2Mo_8O_{28}]\ 2H_2O$, (IPAM2) has been analyzed by X-rays.[3] It has been proposed from the structure and the ESR measurement of the crystal that the photoreduction from Mo(VI) to Mo(V) in a MoO_6 octahedral site proceeds on irradiation with UV light, accompanying a transfer of a hydrogen-bonding proton from the isopropylammonium nitrogen to a bridging oxygen atom of the octamolybdate.[4]

In order to ascertain the mechanism, crystal structures of the propylammonium and isopropylammonium salts of the polymolybdate with somewhat different compositions have been analyzed. Hereafter the former crystal is abbreviated to PAM and the latter to IPAM.

Experimental and Structure Determination

The preparation of the two crystals was reported in the previous paper,[1] in which their chemical formulae were erroneously given owing to the low accuracy of the elemental analysis.

PAM, $(NH_3CH_2CH_2CH_3)_6[Mo_7O_{24}]\cdot 3H_2O$. Preliminary unit cell dimensions and the space group were obtained from oscillation and Weissenberg photographs. Accurate cell dimensions were determined by a least-squares technique from 19 reflections measured on a Rigaku automated four-circle diffractometer. Crystal adata re summarized in Table 1. Intensity data up to $2\theta\leqq 55°$ were collected on the diffractometer with Mo $K\alpha$ radiation ($\lambda=0.71069$ Å) monochromated by graphite. An ω-2θ scan was employed with a scan rate of 4° (2θ) min^{-1}. A total of 8084 independent reflections, ($|F_o|\geqq 3\sigma(|F_o|)$), were used for the structure determination.

Table 1. Crystal data

	PAM	IPAM
Chemical formula	$(C_3H_{10}N)_6[Mo_7O_{24}]\cdot 3H_2O$	$(C_3H_{10}N)_6[Mo_7O_{24}]\cdot 3H_2O$
F.W.	1470.3	1470.3
Crystal system	triclinic	monoclinic
Space group	$P\bar{1}$	P2/n
a/Å	14.118(2)	23.904(6)
b/Å	15.977(2)	10.504(1)
c/Å	11.368(1)	20.652(9)
α/°	90.23(1)	
β/°	93.00(1)	115.40(2)
γ/°	111.79(1)	
V/Å^3	2377.1(7)	4684(3)
Z	2	4
D_c/g cm^{-3}	2.054	2.085
μ(Mo $K\alpha$)/cm^{-1}	18.28	18.56

Although the crystal turned red on X-ray exposure, the intensities of the monitor reflections did not change significantly during the data collection. The intensities were corrected for Lorentz and polarization factors but absorption correction was not applied.

The positions of the seven Mo atoms were obtained by the direct method using program MULTAN 78.[5] The C, N, and O atoms and three water molecules appeared on the successive Fourier maps. The structure was refined by the block-diagonal least-squares method with the anisotropic temperature factors. After several cycles of refinement, six atoms of the three propylammonium ions and a water molecule, respectively, were found to be distributed over two positions. The occupancy factors of the disordered atoms were fixed at a value which was estimated from their isotropic temperature factors. All the H atoms bonded to the N atoms and to the O atoms of the ordered water molecules were located on a difference map. Some of the H atoms of the ordered propyl groups obtained from a difference map and the positions of the remaining ones were calculated geometrically. In the final refinement, the disordered atoms and the H atoms except the propyl H atoms were included with the isotropic temperature factors. The final R value became 0.035 for 8084 reflections.

TABLE 2. FINAL ATOMIC PARAMETERS OF PAM, MULTIPLIED BY 10^5 FOR Mo ATOMS, 10^4 FOR C, N, O ATOMS AND 10^3 FOR THE DISORDERED ATOMS WITH *

Atom	x	y	z	B or B_{eq}/Å^2	Atom	x	y	z	B or B_{eq}/Å^2
Mo(1)	26485(3)	9179(2)	44423(3)	2.3	N(2)	3142(4)	4068(3)	−1720(4)	3.6
Mo(2)	22464(3)	2745(3)	16807(3)	2.4	N(3)	4623(4)	1725(3)	−2429(4)	3.9
Mo(3)	49615(3)	33497(2)	35450(3)	2.3	N(4)	6127(5)	4634(3)	6357(4)	4.8
Mo(4)	45757(3)	26910(3)	7684(3)	2.6	N(5)	5177(3)	933(3)	2750(5)	3.9
Mo(5)	31452(3)	29676(3)	53102(3)	2.5	N(6)	−354(3)	992(3)	967(5)	4.4
Mo(6)	23451(3)	15954(3)	−4732(3)	2.8	O(W2)	5484(5)	4824(3)	−1438(4)	7.3
Mo(7)	25140(3)	24267(2)	23739(3)	2.2	O(W3)	4299(5)	66(4)	−925(6)	8.4
O(1)	1556(2)	−1(2)	4699(3)	2.8	C(11)	148(4)	2276(4)	6352(5)	3.9
O(2)	1208(3)	−617(2)	2067(3)	3.2	C(12)	−107(5)	2438(5)	5116(6)	5.3
O(3)	5745(3)	4389(2)	3116(3)	3.1	C(13)	−257(7)	3326(6)	5009(10)	8.8
O(4)	5370(3)	3766(3)	439(3)	3.9	C(31)	5716(5)	2179(5)	−2610(6)	4.5
O(5)	3566(3)	862(2)	5451(3)	2.9	C(32)	6236(6)	1544(5)	−2654(8)	6.5
O(6)	2914(3)	−191(2)	850(3)	3.1	C(33)	7370(6)	1994(7)	−2939(10)	8.8
O(7)	5645(2)	3078(2)	4670(3)	2.7	C(51)	5819(5)	960(5)	3857(7)	5.1
O(8)	5049(3)	1980(3)	93(3)	3.5	C(52)	6956(6)	1325(6)	3617(8)	6.9
O(9)	3900(3)	2929(2)	6524(3)	3.0	C(53)	7338(6)	2237(7)	3213(10)	8.8
O(10)	2728(3)	964(3)	−1406(3)	3.6	C(21)	2388(5)	4231(5)	−993(6)	5.3
O(11)	2432(3)	3547(2)	5814(3)	3.1	C(61)	−808(8)	1657(6)	1071(9)	7.9
O(12)	1465(3)	1902(3)	−1286(3)	3.7	O(W1)	−291(4)	446(4)	3283(5)	5.2(1)[a]
O(13)	2158(2)	1752(2)	5272(3)	2.4	C(22)	2126(9)	5015(8)	−1380(10)	7.3(2)[a]
O(14)	1458(2)	622(2)	417(3)	2.4	C(23)	1678(11)	5021(10)	−2406(13)	8.9(3)[a]
O(15)	4166(2)	3879(2)	4484(3)	2.3	C(62)	−592(9)	2231(8)	60(11)	7.7(3)[a]
O(16)	3521(3)	2706(2)	−450(3)	3.0	C(63)	−986(12)	3027(10)	273(14)	13.6(4)
O(17)	2134(2)	2991(2)	3440(3)	2.7	C(41)	7314(10)	4803(8)	6195(11)	6.3(3)[a]
O(18)	1801(3)	2444(2)	1089(3)	3.0	C(42)	7705(17)	4793(15)	7603(19)	12.5(6)[a]
O(19)	3122(2)	457(2)	3114(3)	2.1	C(43)	8795(13)	4982(11)	7324(15)	14.8(5)
O(20)	5144(2)	2586(2)	2325(3)	2.1	O(W1*)	−122(3)	14(2)	298(3)	6.0(8)[a]
O(21)	1846(2)	1215(2)	2820(3)	2.0	C(22*)	141(4)	440(3)	−153(4)	9.1(10)[a]
O(22)	3813(2)	3284(2)	2046(3)	2.1	C(23*)	133(4)	512(3)	−100(4)	8.7(10)[a]
O(23)	3542(2)	2260(2)	3901(2)	1.8	C(41*)	698(2)	478(2)	701(2)	6.3(6)[a]
O(24)	3175(2)	1643(2)	1193(2)	1.9	C(42*)	783(3)	444(2)	658(3)	8.5(8)[a]
N(1)	394(3)	1459(3)	6454(4)	3.5	C(62*)	−137(4)	198(3)	42(4)	6.8(10)[a]

a) The occupancy factors of O(W1), C(22), C(23), C(62), C(41), C(42), O(W1*), C(22*), C(23*), C(41*), C(42*), and C(62*) are 0.80, 0.80, 0.75, 0.80, 0.65, 0.65, 0.20, 0.20, 0.25, 0.35, 0.35, and 0.20, respectively.

The weighting scheme was $w=(0.00069F_o^2-0.11048|F_o|+5.42077)^{-1}$ for $3.90\leqq|F_o|\leqq156.14$ and $w=0.2$ for $|F_o|<3.90$ and $|F_o|>156.14$. The atomic scattering factors were taken from the International Tables for X-Ray Crystallography.[6] Positional and isotropic or equivalent isotropic temperature factors are given in Table 2.

IPAM, $(NH_3CH(CH_3)_2)_6[Mo_7O_{24}]\cdot 3H_2O$. Experimental details were nearly the same as those in PAM. Refinement of the unit cell dimensions was based on 18 reflections. Crystal data are listed in Table 1. A total of 9936 independent reflections were used for the structure determination.

The positions of the seven Mo atoms were obtained by using program MULTAN 78.[5] The C, N, and O atoms and three water molecules appeared on the successive Fourier maps. The structure was refined by the block-diagonal least-squares method. After several cycles of refinement with anisotropic temperature factors, an isopropylammonium cation (N(6), C(61), C(62), and C(63)), and a water molecule (O(W3)) were found to occupy two disordered positions. The occupancy factors for the two equivalent atoms were assumed to be 0.6 and 0.4, which were estimated from the isotropic temperature factors of the atoms and were not refined in the least-squares calculation. Out of 60 H atoms, 18 were located on the difference map. The H atoms were included in the final refinement with the isotropic temperature factors. Two strong reflections, 010 and 200, were excluded because they seemed to suffer from secondary extinction. The final R value became 0.060 for 9934 reflections. The weighting scheme used in the final stages was $w=[\sigma^2(F_o)+(0.015F_o)^2]^{-1}$. Positional and equivalent isotropic temperature factors are given in Table 3.** The FACOM-HITAC system M-160 and M-170 computers were used in the calculation.

Results

The Structure of Heptamolybdate. The geometries of the heptamolybdate anions in both crystals are quite similar. Seven MoO_6 octahedra are condensed by edge sharing into a structure that has an approximate

** Lists of the positional and isotropic temperature factors of the H atom, lists of the anistropic temperature factors of the Mo, C, N, and O atoms, tables of the bond angles and tables of the observed and calculated structure factors for both crystal structures are kept in the office of the Chemical Society of Japan (Document No. 8214).

Table 3. Final atomic parameters of IPAM, multiplied by 10^5 for Mo atoms and 10^4 for C, N, O atoms

Atom	x	y	z	B or B_{eq}/Å^2	Atom	x	y	z	B or B_{eq}/Å^2
Mo(1)	2614(3)	67851(6)	15724(3)	2.4	C(11)	−1714(4)	8145(9)	1617(5)	4.4
Mo(2)	−9147(3)	47911(7)	10288(3)	2.9	C(12)	−1956(5)	8802(14)	891(5)	7.3
Mo(3)	3174(3)	67699(6)	36462(3)	2.4	C(13)	−1977(5)	8725(15)	2082(7)	8.6
Mo(4)	−8702(3)	48120(6)	30659(3)	2.9	N(2)	1609(3)	6721(6)	1064(3)	3.1
Mo(5)	14141(3)	66003(6)	31304(3)	2.5	C(21)	1559(4)	8141(8)	885(4)	4.0
Mo(6)	−9734(3)	24895(7)	20165(5)	4.2	C(22)	1864(4)	8402(9)	383(4)	4.9
Mo(7)	3420(3)	42658(5)	26335(3)	2.1	C(23)	1877(5)	8824(9)	1588(5)	5.2
O(1)	293(2)	6551(6)	776(3)	3.7	N(3)	458(4)	3318(9)	729(4)	6.8
O(2)	−823(3)	4651(6)	250(3)	4.3	C(31)	1039(7)	2848(16)	935(7)	10.1
O(3)	368(3)	6493(5)	4490(3)	3.8	C(32)	1117(6)	1915(12)	440(6)	7.5
O(4)	−753(3)	4708(5)	3940(3)	4.1	C(33)	1493(10)	2995(36)	1734(10)	27.9
O(5)	248(3)	8406(5)	1669(3)	3.7	N(4)	479(4)	3541(7)	4796(4)	5.6
O(6)	−1688(2)	5089(6)	764(3)	4.4	C(41)	602(9)	2215(13)	4861(7)	11.2
O(7)	301(3)	8385(5)	3557(3)	3.8	C(42)	1021(6)	1889(12)	5682(6)	8.3
O(8)	−1644(2)	5088(6)	2602(3)	4.4	C(43)	233(11)	1405(15)	4369(10)	16.2
O(9)	1539(2)	8191(5)	3175(3)	3.9	N(5)	679(3)	234(6)	2849(4)	4.0
O(10)	−1771(3)	2496(7)	1623(5)	7.7	C(51)	1331(12)	1145(23)	3403(13)	21.6
O(11)	2148(2)	5932(5)	3476(3)	3.7	C(52)	1797(7)	1791(15)	3444(10)	13.0
O(12)	−763(3)	900(5)	2114(4)	6.3	C(53)	1735(12)	510(25)	4136(11)	21.4
O(13)	1153(2)	6415(5)	2127(3)	2.8	N(6)	−2133(6)	3772(13)	3722(7)	5.5
O(14)	−863(2)	2939(5)	1187(3)	3.8	C(61)	−1731(7)	2570(16)	3990(10)	6.1
O(15)	1196(2)	6413(5)	3916(2)	2.8	C(62)	−1914(9)	1825(22)	3340(11)	7.6
O(16)	−830(2)	2961(5)	2953(3)	3.9	C(63)	−1886(10)	1963(21)	4583(9)	7.8
O(17)	1147(2)	4323(5)	3011(3)	3.1	N(6′)	1861(15)	6648(18)	5489(11)	8.5
O(18)	166(2)	2659(4)	2544(3)	3.9	C(61′)	1644(14)	8006(28)	5569(11)	6.6
O(19)	−613(2)	6525(4)	1294(2)	2.5	C(62′)	1802(14)	8777(25)	5231(12)	6.2
O(20)	−569(2)	6528(4)	3079(2)	2.6	C(63′)	1741(12)	8412(27)	6382(15)	6.2
O(21)	145(2)	4688(4)	1679(2)	2.6	O(W1)	2492(5)	3778(9)	4445(5)	10.9
O(22)	182(2)	4682(4)	3417(2)	2.4	O(W2)	−145(5)	897(10)	943(6)	11.0
O(23)	419(2)	6410(4)	2661(2)	2.0	O(W3)	1688(5)	4652(12)	4980(6)	6.0
O(24)	−700(2)	4498(4)	2127(3)	2.6	O(W3′)	−2793(9)	5478(23)	1419(10)	8.0
N(1)	−1037(3)	8284(6)	1972(3)	3.0					

Table 4. Bond distances (l/Å) of $[Mo_7O_{24}]^{6-}$ in PAM and IPAM

Bond	Distance		Type	Bond	Distance		Type
	PAM	IPAM			PAM	IPAM	
Mo(1)–O(1)	1.729(3)	1.696(6)	a	Mo(4)–O(20)	1.938(3)	1.937(5)	b
Mo(1)–O(5)	1.713(4)	1.717(6)	a	Mo(4)–O(22)	2.253(3)	2.303(5)	c
Mo(1)–O(13)	1.973(3)	1.977(5)	b	Mo(4)–O(24)	2.144(3)	2.169(5)	c
Mo(1)–O(19)	1.931(3)	1.935(5)	b	Mo(5)–O(9)	1.714(4)	1.693(6)	a
Mo(1)–O(21)	2.258(3)	2.243(5)	c	Mo(5)–O(11)	1.717(4)	1.733(6)	a
Mo(1)–O(23)	2.156(3)	2.151(5)	c	Mo(5)–O(13)	1.923(3)	1.900(5)	b
Mo(2)–O(2)	1.702(4)	1.719(6)	a	Mo(5)–O(15)	1.917(3)	1.914(5)	b
Mo(2)–O(6)	1.715(4)	1.717(6)	a	Mo(5)–O(17)	2.506(3)	2.461(6)	d
Mo(2)–O(14)	1.978(3)	1.968(6)	b	Mo(5)–O(23)	2.171(3)	2.158(5)	c
Mo(2)–O(19)	1.946(3)	1.949(5)	b	Mo(6)–O(10)	1.700(4)	1.723(10)	a
Mo(2)–O(21)	2.224(3)	2.306(5)	c	Mo(6)–O(12)	1.723(4)	1.731(9)	a
Mo(2)–O(24)	2.183(3)	2.123(5)	c	Mo(6)–O(14)	1.926(3)	1.901(6)	b
Mo(3)–O(3)	1.708(4)	1.720(6)	a	Mo(6)–O(16)	1.927(4)	1.881(7)	b
Mo(3)–O(7)	1.715(4)	1.705(6)	a	Mo(6)–O(18)	2.546(4)	2.469(7)	d
Mo(3)–O(15)	1.984(3)	1.965(5)	b	Mo(6)–O(24)	2.160(3)	2.192(5)	c
Mo(3)–O(20)	1.932(3)	1.949(5)	b	Mo(7)–O(17)	1.729(3)	1.739(6)	a
Mo(3)–O(22)	2.264(3)	2.238(5)	c	Mo(7)–O(18)	1.736(4)	1.730(7)	a
Mo(3)–O(23)	2.171(3)	2.183(5)	c	Mo(7)–O(21)	1.897(3)	1.873(5)	b
Mo(4)–O(4)	1.722(4)	1.708(6)	a	Mo(7)–O(22)	1.895(3)	1.868(5)	b
Mo(4)–O(8)	1.713(4)	1.704(7)	a	Mo(7)–O(23)	2.285(3)	2.259(5)	c
Mo(4)–O(16)	1.986(4)	1.965(6)	b	Mo(7)–O(24)	2.285(3)	2.264(5)	c

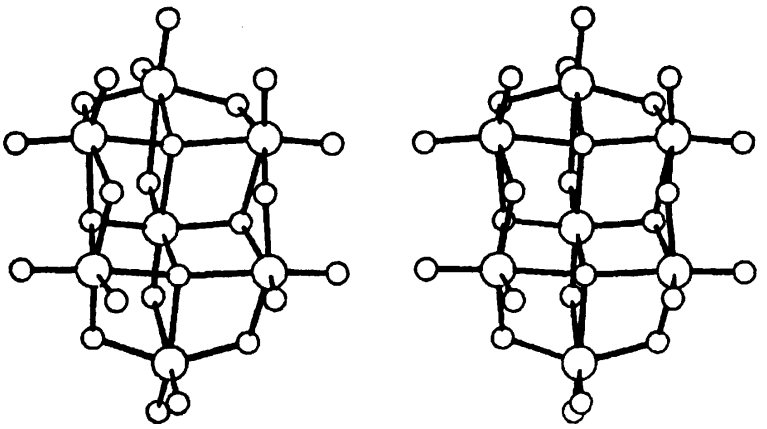

Fig. 1. Stereoscopic drawing of the heptamolybdate anion in PAM.

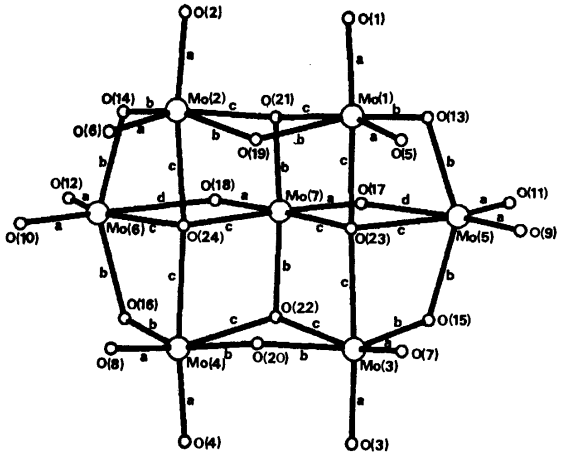

Fig. 2. The numbering of the atoms and the bond types in the heptamolybdate anion.

point symmetry 2mm(C_{2v}). Figure 1 shows the stereoscopic drawing of the heptamolybdate ion in PAM. Such a structure of $[Mo_7O_{24}]^{6-}$ is also found in the crystal of the ammonium,[7] potassium,[7] and sodium[8] salts.

Bond distances of the heptamolybdate ions in PAM and IPAM are listed in Table 4. The corresponding values are in fair agreement, although some distances and angles relevant to O(16), O(21), O(22), and O(24) are significantly different between the two crystals. The discrepancy is probably due to the different hydrogen bonding scheme.

The Mo–O bonds can be classified into four types by their bond distances; *a*(1.69—1.73 Å), *b*(1.90—1.97 Å), *c*(2.16—2.30 Å), and *d*(2.46—2.55 Å). Figure 2 shows the numbering of the atoms and the types of the bonds. The seven MoO_6 octahedra are divided into two classes; five octahedra of Mo(1), Mo(2), Mo(3), Mo(4), and Mo(7) have three types of Mo–O bonds, whereas two octahedra of Mo(5) and Mo(6) have four types of the bonds. The electronic state of Mo(5) and Mo(6) may be different from that of the other Mo atoms. The seven MoO_6 octahedra in the ammonium salt are also divided into two classes.

The Structure of Propylammonium and Isopropylammonium Cations. Bond distances of the propyl- and isopropylammonium ions are listed in Table 5. The rather large deviations from the normal values may be brought

Table 5. Bond distances (*l*/Å) of propyl- and isopropylammonium ions

Propylammonium ion		Isopropylammonium ion	
N(1)–C(11)	1.47(1)	N(1)–C(11)	1.47(1)
C(11)–C(12)	1.48(1)	C(11)–C(12)	1.52(2)
C(12)–C(13)	1.51(1)	C(11)–C(13)	1.49(2)
N(2)–C(21)	1.48(1)	N(2)–C(21)	1.53(1)
C(21)–C(22)	1.49(1)	C(21)–C(22)	1.53(1)
C(22)–C(23)	1.30(2)	C(21)–C(23)	1.50(1)
N(3)–C(31)	1.47(1)	N(3)–C(31)	1.36(2)
C(31)–C(32)	1.46(1)	C(31)–C(32)	1.48(2)
C(32)–C(33)	1.55(2)	C(31)–C(33)	1.55(4)
N(4)–C(41)	1.62(2)	N(4)–C(41)	1.42(2)
C(41)–C(42)	1.67(3)	C(41)–C(42)	1.59(3)
C(42)–C(43)	1.51(3)	C(41)–C(43)	1.33(3)
N(5)–C(51)	1.50(1)	N(5)–C(51)	1.77(3)
C(51)–C(52)	1.53(1)	C(51)–C(52)	1.27(4)
C(52)–C(53)	1.44(2)	C(51)–C(53)	1.55(4)
N(6)–C(61)	1.44(1)	N(6)–C(61)	1.54(3)
C(61)–C(62)	1.45(2)	C(61)–C(62)	1.45(3)
C(62)–C(63)	1.59(2)	C(61)–C(63)	1.56(3)
C(21)–C(22*)	1.59(4)	N(6′)–C(61′)	1.55(5)
C(22*)–C(23*)	1.33(4)	C(61′)–C(62′)	1.23(5)
N(4)–C(41*)	1.33(4)	C(61′)–C(63′)	1.65(5)
C(41*)–C(42*)	1.60(4)		
C(42*)–C(43*)	1.52(4)		
C(61)–C(62*)	1.30(4)		
C(62*)–C(63)	1.56(4)		

Table 6. Torsion angles (ϕ/°) of the central N–C–C–C bonds of the propylammonium cations

N(1)–C(11)–C(12)–C(13)	174.4
N(2)–C(21)–C(22)–C(23)	63.8
N(3)–C(31)–C(32)–C(33)	175.6
N(4)–C(41)–C(42)–C(43)	178.3
N(5)–C(51)–C(52)–C(53)	62.0
N(6)–C(61)–C(62)–C(63)	173.3
N(2)–C(21)–C(22*)–C(23*)	135.7
N(4)–C(41*)–C(42*)–C(43)	163.4
N(6)–C(61)–C(62*)–C(63)	126.7

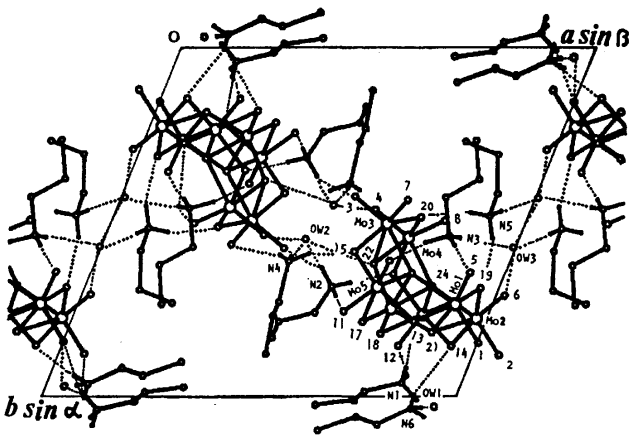

Fig. 3. Crystal structure of PAM viewed along the c axis. The hydrogen bonds are drawn with dotted lines. The hydrogen atoms of the propyl group and the minor portions of the disordered atoms are omitted for clarity.

about by the disordered structures of these ions. Table 6 shows the torsion angles of the central C–C bond in the propylammonium ions. The conformation of the ions may be easily changed in the crystal.

Crystal Structure and Hydrogen Bonding Scheme. The crystal structure of PAM viewed along the c axis is shown in Fig. 3. The hydrophobic groups of the propylammonium ions are brought together around the $(1/2,0,z)$ region. All the N–H groups of the propylammonium ions and O–H groups of the water molecules make hydrogen bonds with the heptamolybdate anion or the water molecules. The hydrogen bonds construct a three-dimensional network. The distances of X···O, X–H, and H···O and the angles of X–H···O are listed in Table 7, where X means the N or O atoms. The N(1)–H(N13) and N(2)–H(N32) groups make trifurcate hydrogen bonds with O(1), O(2), and O(W1), and O(8), O(10), and O(W3), respectively. However, the distances of H..O and the angles of N–H···O indicate that N(1)–H(N13)..O(2), N(1)–H(N13)···O(W1), N(3)–H(N32)···O(8), and N(3)–H(N32)···O(10) may

TABLE 7. HYDROGEN BOND DISTANCES (l/Å) AND ANGLES (ϕ/°) IN PAM

X means N or O atoms and unit number indicates the equivalent position as follows:

(i) (x,y,z) (ii) $(-x,-y,-z)$ (iii) $(1-x,-y,-z)$
(iv) $(1-x,1-y,-z)$ (v) $(x,y,1+z)$ (vi) $(-x,-y,1-z)$
(vii) $(1-x,1-y,1-z)$ (viii) $(x,y,-1+z)$.

X–H···O	Unit	X···O	X–H	H···O	X–H···O
N(1)–H(N11)···O(13)	i	2.776(6)	0.75(5)	2.04(5)	172(5)
N(1)–N(N12)···O(12)	v	2.859(7)	0.78(6)	2.14(6)	152(6)
N(1)–H(N13)···O(1)	vi	3.092(6)	0.92(8)	2.22(8)	158(7)
N(1)–H(N13)···O(2)	vi	2.812(6)	0.92(8)	2.51(8)	100(6)
N(1)–H(N13)···O(W1)	vi	3.010(8)	0.92(8)	2.52(8)	114(6)
N(2)–H(N21)···O(16)	i	2.814(6)	0.83(6)	1.99(6)	176(6)
N(2)–H(N22)···O(11)	viii	2.937(6)	0.81(7)	2.14(7)	169(7)
N(2)–H(N23)···O(3)	iv	2.912(6)	0.82(8)	2.29(8)	133(7)
N(2)–H(N23)···O(W2)	i	3.068(9)	0.82(8)	2.41(8)	138(7)
N(3)–H(N31)···O(5)	viii	2.829(6)	0.71(8)	2.12(8)	177(8)
N(3)–H(N32)···O(8)	i	2.894(7)	0.71(7)	2.43(7)	124(6)
N(3)–H(N32)···O(10)	i	2.812(7)	0.71(7)	2.53(7)	106(6)
N(3)–H(N32)···O(W3)	i	3.062(9)	0.71(7)	2.40(7)	157(7)
N(3)–H(N33)···O(9)	viii	2.740(7)	0.96(7)	1.88(7)	147(6)
N(4)–H(N41)···O(7)	i	2.982(7)	0.57(5)	2.44(5)	162(6)
N(4)–H(N42)···O(W2)	v	2.763(10)	0.70(7)	2.07(7)	171(7)
N(4)–H(N43)···O(15)	vii	2.727(7)	0.90(6)	1.85(6)	163(5)
N(5)–H(N51)···O(20)	i	2.704(6)	0.77(5)	1.95(5)	163(5)
N(5)–H(N52)···O(W3)	iii	2.900(9)	0.67(5)	2.23(5)	176(6)
N(5)–H(N53)···O(19)	i	2.767(6)	0.84(5)	1.97(5)	158(5)
N(6)–H(N61)···O(14)	ii	2.878(6)	0.73(6)	2.15(6)	174(7)
N(6)–H(N62)···O(14)	i	2.927(6)	0.55(7)	2.44(7)	151(8)
N(6)–H(N62)···O(18)	i	3.061(7)	0.55(7)	2.65(7)	135(8)
N(6)–H(N63)···O(W1)	i	2.785(8)	1.15(8)	1.64(8)	176(7)
N(6)–H(N63)···O(W1*)	i	2.771(5)	1.15(8)	1.82(8)	137(6)
O(W2)–H(W21)···O(4)	i	2.702(8)	0.87(7)	1.88(7)	158(7)
O(W2)–H(W22)···O(22)	iv	2.909(8)	0.80(8)	2.22(7)	144(7)
O(W3)–H(W31)···O(6)	i	2.809(8)	0.83(9)	1.98(9)	177(8)
O(W3)–H(W32)···O(W3)	iii	2.874(13)	1.07(6)	2.62(6)	93(3)
O(W1)···O(1)	vi	2.908(7)			
O(W1*)···O(1)	vi	2.697(3)			

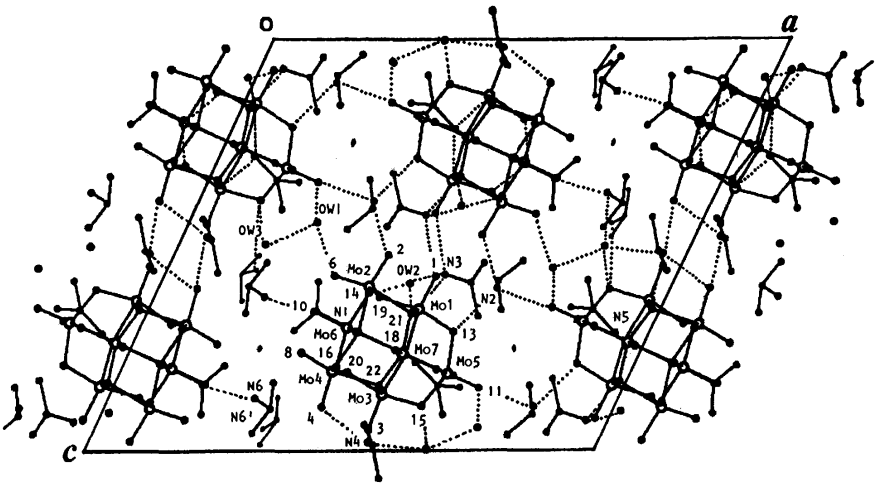

Fig. 4. Crystal structure of IPAM viewed along the b axis. The hydrogen bonds are drawn with dotted lines. The hydrogen atoms of the isopropylammonium cation and the minor portions of the disordered water molecule, O(W3'), are omitted for clarity.

Table 8. Hydrogen bond distances (l/Å) in IPAM

The unit number indicates the equivalent position as fllows:

(i) (x,y,z) (ii) $(1/2-x,y,1/2-z)$
(iii) $(-1/2-x,y,1/2-z)$ (iv) $(x,1+y,z)$
(v) $(-x,1-y,-z)$ (vi) $(1/2+x,1-y,1/2+z)$
(vii) $(x,-1+y,z)$ (viii) $(-x,1-y,1-z)$.

Hydrogen bond	Unit	l/Å
N(1)···O(19)	i	2.76(1)
N(1)···O(12)	iv	2.81(1)
N(1)···O(20)	i	2.77(1)
N(2)···O(2)	v	2.93(1)
N(2)···O(11)	ii	2.83(1)
N(2)···O(13)	i	2.86(1)
N(3)···O(1)	v	2.85(1)
N(3)···O(21)	i	2.78(1)
N(3)···O(W2)	i	3.05(2)
N(4)···O(4)	i	2.97(1)
N(4)···O(4)	viii	3.03(1)
N(4)···O(3)	viii	2.97(1)
N(4)···O(22)	i	2.88(1)
N(4)···O(W3)	i	2.99(2)
N(5)···O(5)	vii	2.92(1)
N(5)···O(7)	vii	2.80(1)
N(5)···O(9)	vii	2.85(1)
N(5)···O(18)	i	2.78(1)
N(6)···O(10)	iii	2.75(2)
N(6)···O(W3)	viii	2.93(2)
N(6')···O(15)	i	2.95(4)
N(6')···O(W3')	vi	2.83(4)
O(W1)···O(6)	vi	2.85(1)
O(W1)···O(11)	i	2.90(1)
O(W1)···O(W3)	i	2.75(2)
O(W2)···O(5)	vii	2.96(1)
O(W2)···O(14)	i	2.92(1)
O(W3)···O(15)	i	2.72(1)
O(W3')···O(8)	i	2.82(3)
O(W3')···O(8)	iii	2.90(3)

not be those of hydrogen bonds, although the N···O distances of these bonds are rather shorter than those of N(1)–H(N13)···O(1) and N(3)–H(N32)···O(W3).

The crystal structure of IPAM viewed along the b axis is shown in Fig. 4. The isopropylammonium cations occupy the space between the heptamolybdate anions. Interatomic distances of the possible hydrogen bonds are listed in Table 8.

Discussion

It has been proposed from the X-ray analysis[3] and ESR measurement[4] of the IPAM2 crystal that the photoreduction of Mo(VI) to Mo(V) proceeds *via* UV-induced charge transfer in the terminal Mo=O bond of a MoO_6 site, followed by a transfer of a hydrogen-bonding proton from an isopropylammonium nitrogen to a bridging oxygen of the MoO_6 site as follows.

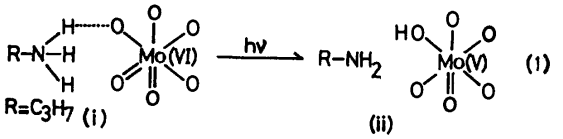

Figure 5 shows the geometry in the environment of the photoreducible MoO_6 site found in the IPAM2 crystal.

In the heptamolybdate anion of the present PAM and IPAM crystals, the photoreducible Mo atom is considered to be Mo(5) or Mo(6), because each of them has a long Mo–O bond, as is observed in the photoreducible site of the IPAM2 crystal. Figure 6(a) and (b) show the geometries of the hydrogen bonding scheme at the Mo(5) and Mo(6), respectively, in the PAM crystal. There are five hydrogen bonds between the N–H groups of the propylammonium cations and the bridging oxygen atoms of the Mo(5) and Mo(6) sites. One of the hydrogen bonds may be responsible for the proton transfer from the cation to the anion. In the crystal of IPAM, only the Mo(5) site has such a hydrogen bonding scheme, which is shown in Fig. 7. One of the two hydrogen bonds may bring about the

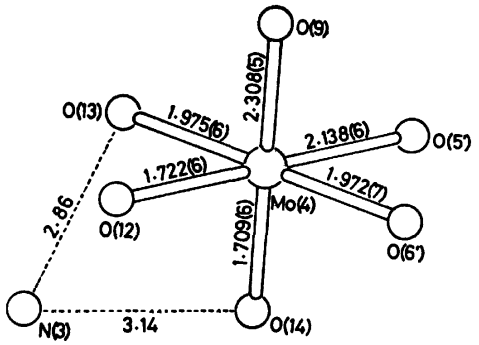

Fig. 5. Bond distances (l/Å) and interatomic distances (l/Å) between the non-bonded atoms in the environment of the photoreducible MoO_6 site in IPAM2. These values are taken from the reference 3. Positions of H atoms are omitted for clarity.

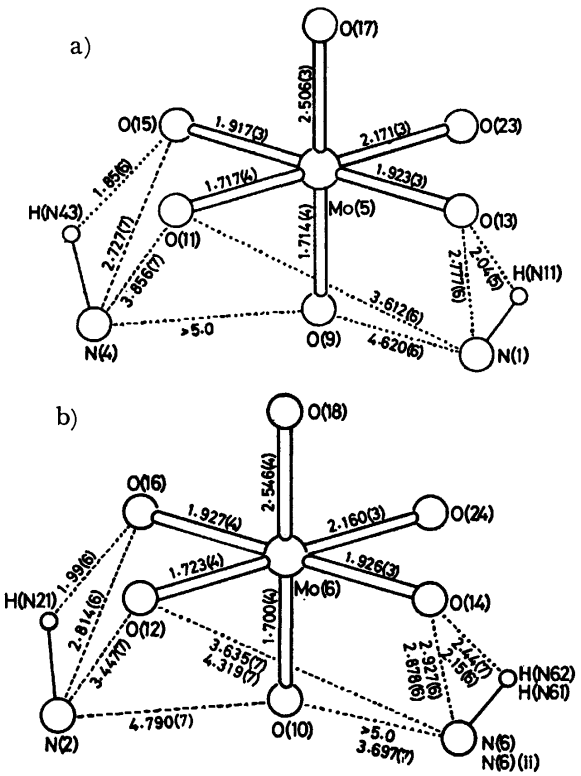

Fig. 6. Bond distances (l/Å) and interatomic distances (l/Å), (less than 5 Å), between non-bonded atoms in the environment of the (a) Mo(5) and (b) Mo(6) sites in PAM. In the Mo(6) site, O(14) makes two hydrogen bonds with N(6)–H(N62) and N(6)–H(N61) in the unit of (ii), $(-x, -y, -z)$. The upper and lower values correspond to the former and latter hydrogen bonds, respectively.

proton transfer.

It should be noted that the crystal of the ammonium heptamolybdate does not exhibit photoreduction on irradiation with UV light,[1] although it has a similar hydrogen bonding scheme.[7] This indicates that some additional factors should be taken into account for the photoreduction. If the positively charged terminal oxygen atom forms a charge transfer complex with the negatively charged alkylamine nitrogen atom in the complex (ii), the Mo(V) species formed by the UV

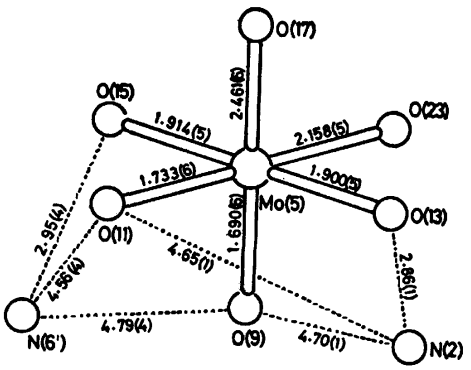

Fig. 7. Bond distances (l/Å) and interatomic distances (l/Å), (less than 5 Å), between the non-bonded atoms in the environment of the Mo(5) site in IPAM. Positions of H atoms are omitted for clarity.

irradiation would be stabilized. Since the propyl- and isopropylammonium cations have considerably loose contacts with the neighboring molecules in the crystal, such a charge transfer complex would be easily formed in the solid state. When the crystal is allowed to stand in the dark after irradiation, the charge transfer complex returns to the initial hydrogen bonding complex (i) and its color is bleached.[1] On the other hand, the ammonium cation has more than four hydrogen bonds with the neighboring heptamolybdates and water molecules. Moreover, it is closely packed in the crystal. The formation of the charge transfer complex may be inhibited and the coloration cannot be observed even if the crystal is exposed to UV light.

It is concluded that the photochromism of alkylammonium isopolymolybdates is brought about by the following reaction process (2) instead of (1) in the

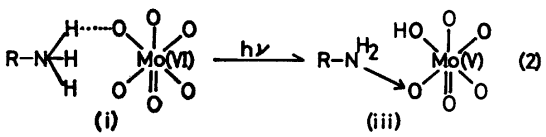

crystal. The mechanism of the change in color when the photoreduced crystal is dissolved in water has been discussed elsewhere.[9]

References

1) T. Yamase and T. Ikawa, *Bull. Chem. Soc. Jpn.*, **50**, 746 (1977).
2) T. Yamase, T. Ikawa, Y. Ohashi, and Y. Sasada, *J. Chem. Soc., Chem. Commun.*, **1979**, 697.
3) M. Isobe, F. Marumo, T. Yamase, and T. Ikawa, *Acta Crystallogr., Sect. B*, **34**, 2728 (1978).
4) T. Yamase, *J. Chem. Soc., Dalton Trans.*, **1978**, 283.
5) P. Main, "MULTAN 78, A System of Computer Programms for the Automatic Solution of Crystal Structures from X-Ray Diffraction Data," University of York, York (1978).
6) "International Tables for X-Ray Crystallography," Vol. IV, The Kynoch Press, Birmingham (1974), p. 72.
7) H. T. Evans, B. M. Gatehouse, and P. Leverett, *J. Chem. Soc., Dalton Trans.*, **1975**, 505.
8) K. Sjöbom and B. Hedman, *Acta Chem. Scand.*, **27**, 3673 (1973).
9) T. Yamase, R. Sasaki, and T. Ikawa, *J. Chem. Soc., Dalton Trans.*, **1981**, 628.

 © 1982 The Chemical Society of Japan Bull. Chem. Soc. Jpn., 55, 1261—1266 (1982)

The Effect of Diluents on the Mechanochemical Change in the Solid State of Amobarbital

Akiko IKEKAWA* and Sohachiro HAYAKAWA†

Faculty of Pharmaceutical Sciences, Showa University, Hatanodai, Shinagawa-ku, Tokyo 142
†*Department of Applied Physics, Faculty of Science, Tokyo Institute of Technology, Oh-okayama, Meguro-ku, Tokyo 152*
(Received July 30, 1981)

The effect of ball-milling with dextran 2000, microcrystalline cellulose, or methylcellulose (MC) on the solid state of amobarbital was investigated. There are three kinds of polymorphs for amobarbital; Crystals I, II, and III. Crystal I is obtained by heating Crystal II recrystallized from a 25 v/v % aqueous ethanol solution at 150 °C. The part of Crystal I decreased remarkably at the first stage of ball-milling, while the amorphous part increased gradually. The heat of fusion decreased remarkably; this was considered to be due to the increase in the amorphous part. The peak of fusion in the DTA thermogram was broadened, and the temperature at which amobarbital began to fuse was lowered. This phenomenon was considered to be due to the increase in the lattice imperfection. The solubility in the KH_2PO_4–Na_2HPO_4 buffer solution with a pH of 6.0 increased; the increase in the amorphous part was considered to contribute to this increase. This phenomenon was the most remarkable in the case of the mixture with MC. The interaction of amobarbital with MC was suggested by the heat of fusion and the DTA thermograms. It was also suggested that the interaction of amobarbital with the diluent was one of the most important reasons for the increase in the solubility upon ball-milling.

It was reported previously that the solubility of amobarbital in the KH_2PO_4–Na_2HPO_4 buffer solution with a pH of 6.0 increased upon ball-milling with such diluents as methylcellulose,[1] though the solubility also increased slightly upon ball-milling in the absence of any diluents at all.[2] In a previous paper, the effect of ball-milling in the absence of diluents on the solid state of amobarbital was investigated.[2] In this paper, the effect of ball-milling with diluents on the solid state of amobarbital was investigated in order to clarify the mechanism of solubilization.

Experimental

The amobarbital (5-ethyl-5-isopentylbarbituric acid), dextran 2000, microcrystalline cellulose (MCC), and methylcellulose (MC) used were described in a previous paper.[1]

A 10-g portion of amobarbital, a mixture of 2 g of amobarbital and 3 g of MC, a mixture of 1 g of amobarbital and 9 g of MCC, a mixture of 3 g of amobarbital and 7 g of MCC, and a mixture of 3 g of amobarbital and 7 g of dextran were ball-milled in the way reported in the previous paper.[1] The following measurements were carried out in the way reported in the previous papers;[1,2] X-ray diffraction diagrams, DTA and DSC thermograms, and the particle-size distribution of amobarbital in the mixture with dextran or MC (dextran and MC are soluble in distilled water). The dissolution of amobarbital from the mixture into a KH_2PO_4–Na_2HPO_4 buffer solution (pH; 6.0, ionic strength; 0.08) at 30 °C was measured by shaking the suspension as has been reported in a previous paper. The concentration of amobarbital in the filtrate of the suspension was obtained from the absorbance at 238 nm.[1]

Results and Discussion

X-Ray Diffraction. Three kinds of polymorphs of amobarbital were obtained in a previous paper. Crystal I was obtained by heating Crystal II (at 150 °C), which had been recrystallized from a 25 v/v % aqueous ethanol solution. Crystal III was obtained by freeze-drying an aqueous solution of amobarbital. The X-ray diffraction intensities at 9.0° and 24.7° of 2θ for Crystal I were higher than those for Crystal III, where 2θ is the angle between the incident X-ray and the scattering X-ray. The intensity at 12.6° of 2θ was lower than the intensity at 16.0° of 2θ, and no line was observed at 14.9° of 2θ in the diagram of Crystal I, while the intensity at 12.6° of 2θ was a little higher than the intensity at 16.0° of 2θ and a line was observed at 14.9° of 2θ in the diagram of Crystal III.[2]

Figure 1 shows the X-ray diffraction patterns of a mixture of amobarbital and MC. No diffraction line was observed in the diagram of MC. The diffraction intensities for amobarbital at 9.0°, 16.0°, and 24.7° of 2θ decreased, while the intensities at 12.6° and 14.9° of 2θ increased, upon ball-milling with diluents; these increases were considered to be due to the transformation of Crystal I into Crystal III. The percentage of Crystal

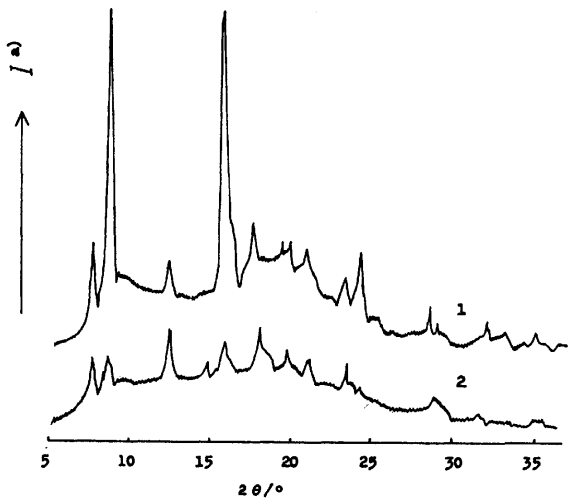

Fig. 1. Variation in the X-ray diffraction pattern of amobarbital with ball-milling in the presence of MC.
1: The physical mixture of MC containing 40 w/w % of amobarbital, 2: the powders obtained by ball-milling "1" for 101 h.
a) *I* is the diffraction intensity.

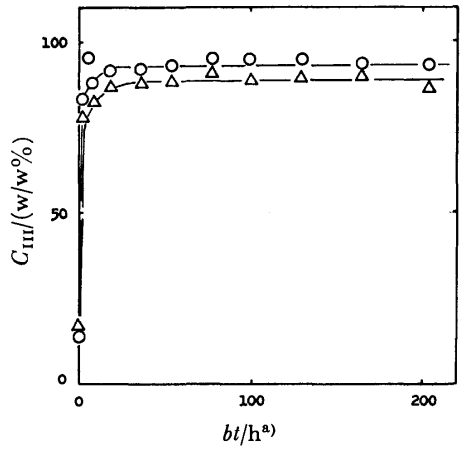

Fig. 2. Increase in C_{III} upon ball-milling with diluents.
The content of amobarbital; 30 w/w%, diluent: △; dextran, ○; MCC.
a) bt is the ball-milling time.

III in the crystal part, C_{III}, was obtained from the ratio of the diffraction intensity at 12.7° of 2θ to the intensity at 16.0° of 2θ. As is shown in Fig. 2, C_{III} increased remarkably at the first stage of ball-milling, while C_{III} was nearly constant after ball-milling with MC for 10 min.

Ruland reported that the crystallinity, x_{cr}, could be obtained by means of Eq. 1, where λ is the wave length of the X-ray, $I_{cr}(s)$ is the intensity of the diffraction line at s, $I(s)$ is the total intensity of the scattering X-ray at s and K is a constant:[3)]

$$x_{cr} = KF_{cr}/\int_{s_o}^{s_p} s^2 I(s)\mathrm{d}s, \qquad (1)$$

$$F_{cr} = \int_{s_o}^{s_p} s^2 I_{cr}(s)\mathrm{d}s, \qquad s = 2\sin\theta/\lambda.$$

The value of $\int_{s_o}^{s_p} s^2\, I(s)\ \mathrm{d}s$ was assumed to be constant in the case of ball-milling with diluents, though the value could not be obtained experimentally. F_{cr} was obtained for the range between 5° and 30° of 2θ, and x_{cr} was obtained from the ratio of F_{cr} for the ball-milled

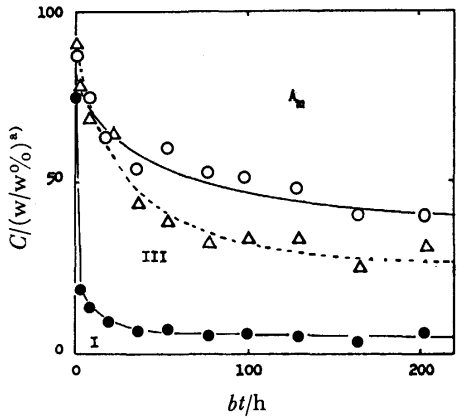

Fig. 3. Effect of ball-milling with dextran on the solid state of amobarbital.
●: The content of crystal I, ○: x_{cr}, △: $x_{cr\ heat}$, I: crystal I, III: crystal III, A_m: amorphous part.
a) C is the composition.

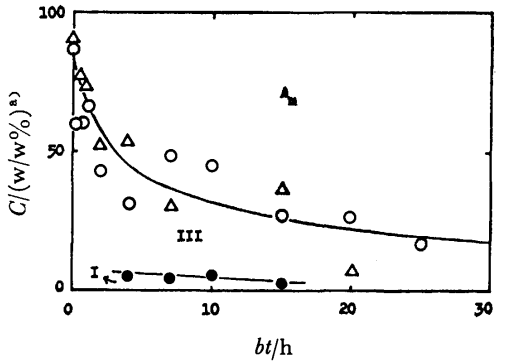

Fig. 4. Effect of ball-milling with MCC on the solid state of amobarbital.
The content of amobarbital: 10 w/w%. ●: the content of crystal I, ○: x_{cr}, △: $x_{cr\ heat}$, I: crystal I, III: crystal III, A_m: amorphous part.
a) C is the composition.

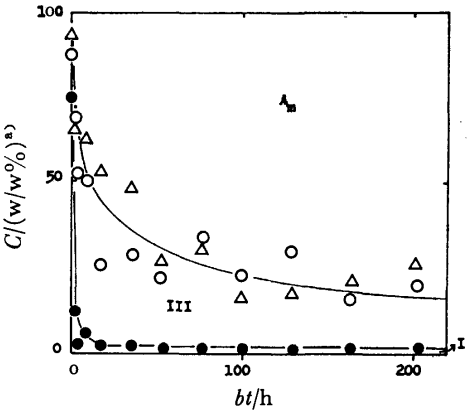

Fig. 5. Influence of ball-milling with MCC on the solid state of amobarbital.
The content of amobarbital: 30 w/w%, ●: the content of crystal I, ○: x_{cr}, △: $x_{cr\ heat}$, I: crystal I, III: crystal III, A_m: amorphous part.
a) C is the composition.

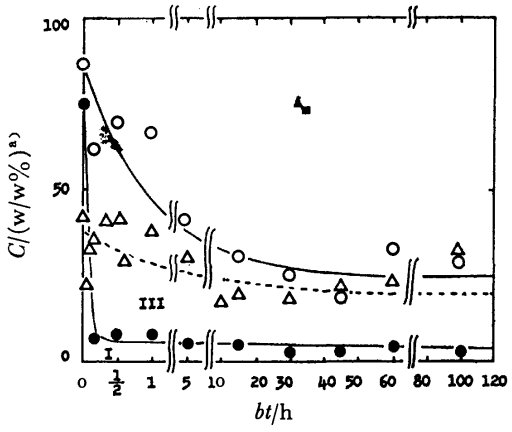

Fig. 6. Effect of ball-milling with MC on the solid state of amobarbital.
●: The content of crystal I, ○: x_{cr}, △: $x_{cr\ heat}$, I: crystal I, III: crystal III, A_m: amorphous part.
a) C is the composition.

Table 1. Influence of ball-milling with diluents on the width of the X-ray-diffraction lines of amobarbital

Diluent	—[a]	—[a]	Dextran	Dextran	MCC[b]	MCC[b]	MC	MC
bt[c]/h	0	60	0	2—203[d]	0	100—200[d]	0	0.17—61[d]
2θ/°				$\Delta H_{1/2}$/°[e]				
7.8	0.38	0.40	0.34	0.43	0.32	0.44	0.34	0.42
8.9	0.42	0.38	0.40	0.43	0.34	0.50	0.38	0.45
12.7	0.38	0.40	0.36	0.45	0.36	0.49	0.38	0.45
16.1	0.44	0.43	0.42	0.47	0.34	0.48	0.42	0.47
23.6	0.36	0.40	0.32	0.48			0.28	0.44

a) The content of amobarbital is 100%. b) The content of amobarbital is 30 w/w%. c) bt is the ball-milling time. d) The mean values for the data between the times are tabulated. e) $\Delta H_{1/2}$ is the separation of 2θ where the diffraction intensity is half the maximum intensity at the line.

mixture to the value for the physical mixture of amobarbital ball-milled for 60 h in the absence of any diluents, a mixture whose crystallinity was assumed to be 0.82.[2] The results are shown in Figs. 3, 4, 5, and 6. Some of the values of C_{III} could not be obtained for the mixture with MCC containing 10 w/w% of amobarbital, as diffraction lines were observed in the diagram of MCC at the first stage of ball-milling. However, in all cases, Crystal I decreased remarkably at the first stage of ball-milling, while the amorphous part increased gradually upon ball-milling.

Table 1 suggests that the line-width of amobarbital increases upon ball-milling with diluents; this is probably a result of the increase in the lattice imperfection.

Heat of Fusion. The heat of fusion of amobarbital, ΔH_{obsd}, decreased remarkably upon ball-milling with diluents, as is shown in Fig. 7. In a previous paper, Eq. 2 was applied to the relation between ΔH_{obsd} and x_{cr}:[2]

$$\Delta H_{obsd} = 29.3\, x_{cr} + 5.0\,(1-x_{cr}). \quad (2)$$

The crystallinity which is obtained by Eq. 2 using the data of ΔH_{obsd} is defined as $x_{cr\ heat}$ in this paper. The data of $x_{cr\ heat}$ are shown in Figs, 3, 4, 5, and 6 by the triangles. In the case of the mixture with MC, $x_{cr\ heat}$ was much smaller than x_{cr} even for the physical mixture. This phenomenon is considered to be due to the interaction between amobarbital and MC. However $x_{cr\ heat}$ and x_{cr} were nearly identical for the other mixtures.

Melting Point. As is shown in Fig. 8, the peak of fusion of amobarbital was broadened and caused to branch into two peaks by ball-milling with diluents. In Fig. 8, T_1 is the temperature at which amobarbital begins to fuse, T_2 and T_3 are the melting points for the two peaks, T_3* is the temperature at the beginning of the shoulder, and T_4 is the temperature at which the fusion comes to an end. Table 2 shows the numerical values of these temperatures. T_1 was lowered by ball-milling with diluents. In each case, T_1 was lower when x_{cr} was smaller, as is shown in Fig. 9. These results suggest that the lowering of T_1 by ball-milling is due to the increase in the amorphous part. The relations between T_1 and x_{cr} were influenced by the kind of diluent. The lowering of T_1 was more remarkable for the mixture with MC than for the other mixtures, and T_1 was lowered even by physically mixing amobarbital

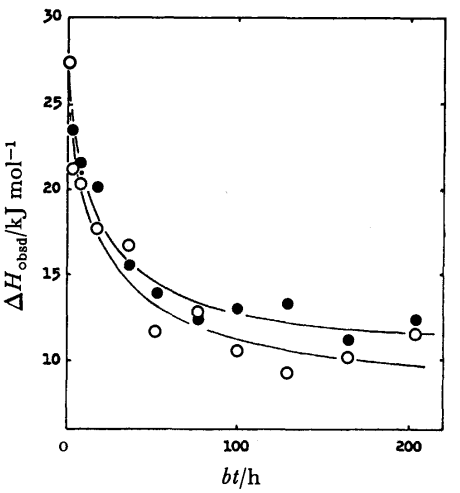

Fig. 7. Decrease in the heat of fusion of amobarbital by ball-milling with diluents.
The content of amobarbital: 30 w/w%, diluent: ●; dextran, ○; MCC.

with MC. In the case of the mixtures with dextran or MCC, T_4 was not influenced and T_3 was lowered slightly by ball-milling, but T_3 and T_4 were lowered by ball-milling the mixture with MC. A signal was observed in the DTA thermograms of the mixture with dextran or MCC when the sample was heated from room temperature to 200 °C, left alone at room temperature, and then heated again immediately after cooling, and the signal was nearly identical with the signal by heating for the first time. However, in the case of the mixture with MC, no signal was observed upon the same preparation, while only a small signal was observed when the sample was set aside for more than a day at room temperature after heating to 200 °C. This phenomenon was more remarkable for the mixture ball-milled for a long time. It can be considered, on the basis of the above facts, that interaction occurs between amobarbital and the diluents and that the interaction with MC is more remarkable than the interaction with the other diluents. It has also been reported that MC prevented the amorphous noboviocin from crystallization in the aqueous suspension.[4]

Particle Size. Variation in the particle size of amobarbital with ball-milling in the presence of dextran

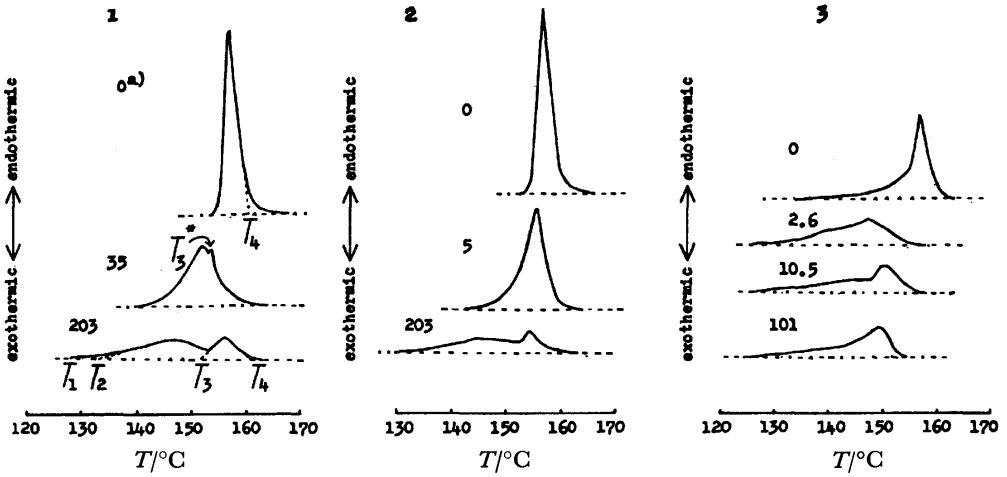

Fig. 8. Influence of ball-milling with diluents on DTA thermograms of amobarbital.
The content of amobarbital in the mixture with MCC is 30 w/w%. Diluent: 1; dextran, 2; MCC, 3; MC. a) The figure on each of the curves is the ball-milling time/h.

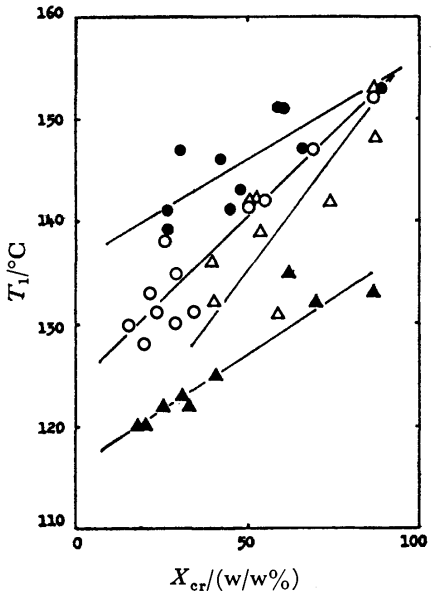

Fig. 9. Relation between T_1 and x_{cr}.
Ball-milling condition.

	Diluent	C_a[a] (w/w %)
△	Dextran	30
●	MCC	10
○	MCC	30
▲	MC	40

a) C_a is the content of amobarbital in the mixture.

TABLE 2. BROADENING OF THE PEAK OF FUSION OF AMOBARBITAL IN THE DTA THERMOGRAM UPON BALL-MILLING WITH DILUENTS

Diluent	C_a[a] (w/w%)	bt h	T_1 °C	T_2 °C	T_3 °C	T_3* °C	T_4 °C
—	100	0	153		155		159
		60	149		154		159
Dextran	30	0	153		153		159
		2	148		153		158
		35	142	146	154		158
		203	132	139	154		158
MCC	10	0	153		155		159
		1	147		154		159
		10	141		146		158
		15	141	145		154	159
MCC	30	0	152		154		159
		2	147		152		158
		5	142		151		158
		8	142	151		155	158
		36	135	143		153	158
		203	128	133	153		158
MC	40	0	133		156		159
		0.17	135		147		160
		2.6	123		134		154
		10	126	130	143		154
		30	122	128	141		154
		101	120	124	140		152

a) C_a is the content of amobarbital in the mixture.

or MC was also investigated. In Figs. 10 and 11, D_{50} is the median diameter by weight base, and $W_{0.3}$ is the weight percentage of the particles smaller than 0.3 μm in diamter. In Fig. 10, D_{50} decreased remarkably in the first stage of ball-milling. $W_{0.3}$ increased gradually, and it stayed nearly constant after ball-milling for more than 2 h for the mixture with MC. For the mixture with dextran, D_{50} was at a minimum at a ball-milling time between 17 and 100 h. A similar phenomenon has also been reported for many kinds of inorganic powders.[5] As is shown in Figs, 2, 10, and 11, the change in C_{III} with the ball-milling time was parallel to the decrease in D_{50} at the first stage of ball-milling. It is considered that the transformation of Crystal I into Crystal III is remarkable when the particles are broken at nearly the center. In Figs. 3, 6, 10, and 11, the increase in the amorphous part with ball-milling is parallel to the increase in $W_{0.3}$ at a ball-milling time within 50 h. It is suggested that the amorphous part increases markedly when the particles are broken at the edge. It is also probable that the agglomeration rate is larger than the rate of decrease in the particle size when the amorphous

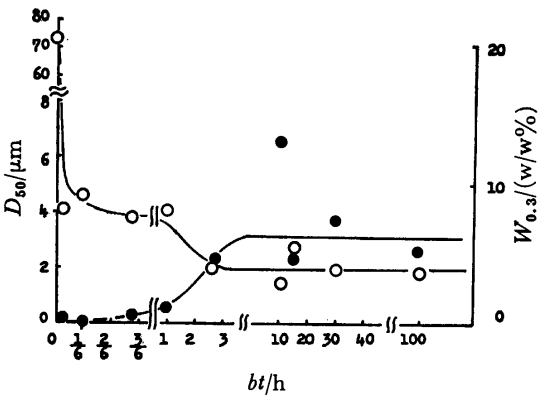

Fig. 10. Variation in the particle size of amobarbital by ball-milling with MC.
○: D_{50}, ●: $W_{0.3}$.

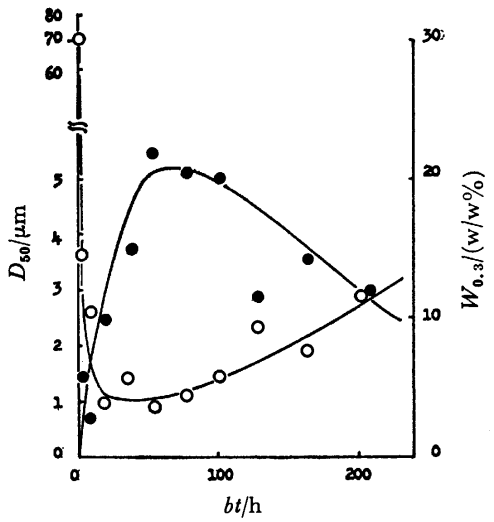

Fig. 11. Variation in the particle size of amobarbital by ball-milling with dextran.
○: D_{50}, ●: $W_{0.3}$.

part increases slightly after ball-milling for more than 100 h in the case of a mixture with dextran.

Solubility. In the case of the mixture with MC, the concentration of amobarbital in the filtrate of the suspension of the KH_2PO_4–Na_2HPO_4 buffer solution increased gradually with shaking, and then it stayed nearly constant after shaking for more than 2 h. However the concentration was at a maximum at the shaking time of 5 min for the other mixtures. In Figs. 12, 13, and 14, $c_{5\,min}$, $c_{2\,h}$, and c_e are the concentrations for the suspension shaken for 5 min, for 2 h, and set aside at 30 °C for a week after shaking for 2 h, respectively. The values of $c_{2\,h}$ or $c_{5\,min}$ for amobarbital in the ball-milled mixture were larger than the values for amobarbital ball-milled in the absence of the diluent. In Fig. 12, the $c_{5\,min}$ value for the mixture with dextran was at a maximum at a ball-milling time around 30—70 h; this was probably attributable to the fact that the surface energy of the amobarbital particles was at a maximum at this stage. In Figs. 10 and 11, D_{50} for the mixture with MC was larger than that for the mixture with dextran, but c_{2n} and c_e for the mixture with MC were larger than $c_{5\,min}$ for the mixture with dextran. To judge from this fact, it does not seem that the surface energy is the main reason for the increase in the solubility of amobarbital.

The amorphous part in the amobarbital particles in the ball-milled mixtures was larger than the part for amobarbital ball-milled in the absence of diluents. In Figs, 3, 4, 6, 12, 13, and 14, the increase in $c_{5\,min}$ upon ball-milling with dextran or MCC at the first stage and the increase in c_e for the mixture with MC were parallel to the increase in the amorphous part. These facts suggest that the increase in the solubility of amobarbital upon ball-milling is due to the increase in the amorphous part. The solubility of amobarbital in the ball-milled mixture is expected to be 6—8.5 times as high as that of the original amobarbital, from the thermodynamical consideration using the data of ΔH_{obsd} and T_2, if the solid state of amobarbital in the ball-milled mixture is equilibrated with amobarbital in the solution.[2)]

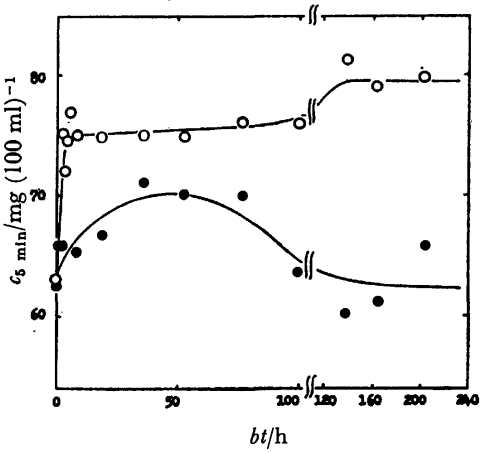

Fig. 12. Effect of ball-milling with the diluent on dissolution of amobarbital in the KH_2PO_4–Na_2HPO_4 buffer solution.
The content of amobarbital: 30 w/w%, diluent: ●; dextran, ○; MCC.

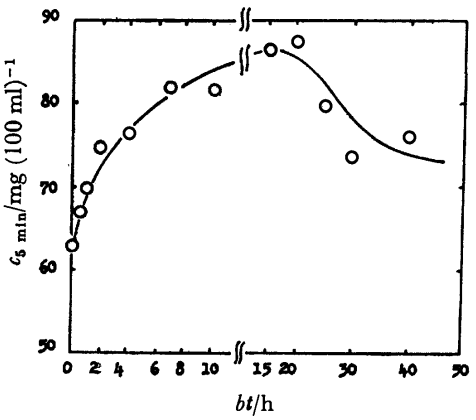

Fig. 13. Effect of ball-milling with MCC on dissolution of amobarbital in the KH_2PO_4–Na_2HPO_4 buffer solution.
The content of amobarbital: 10 w/w%.

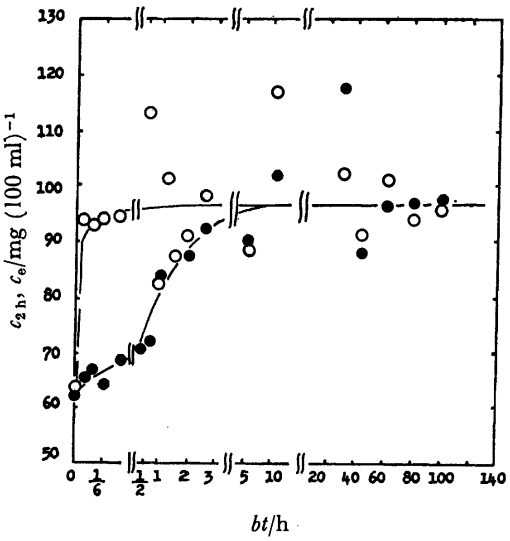

Fig. 14. Effect of ball-milling with MC on dissolution of amobarbital in the KH_2PO_4–Na_2HPO_4 buffer solution.
○: c_{2h}, ●: c_e.

In Figs, 3, 4, 5, and 6, the percentage of the amorphous part in amobarbital for the mixture with MC is nearly equal to the percentage for the mixture with MCC, though the percentage for the mixture with dextran is a little smaller than the percentage for the other mixtures. However, the c_{2h} for the mixture with MC was larger than the $c_{5\,min}$ for the other mixtures. For the mixture with MC, c_e was nearly identical with c_{2h}, but for the other mixtures c_e was smaller than $c_{5\,min}$ and nearly identical with the solubility of the original amobarbital. This fact suggests that the interaction of amobarbital with the diluent caused by ball-milling is one of the important reasons for the increase in the solubility. More details will be reported in another paper concerning this problem.

References

1) N. Kaneniwa, A. Ikekawa, and M. Sumi, *Chem. Pharm. Bull.* (*Tokyo*), **26**, 2734, 2744 (1978).
2) A. Ikekawa and S. Hayakawa, *Bull. Chem. Soc. Jpn.*, **54**, 2587 (1981).
3) W. Ruland, *Acta Crystallogr.*, **14**, 1180 (1961).
4) J. D. Mullins and T. J. Macek, *J. Am. Pharm. Assoc.* (*Sci. Ed.*), **49**, 245 (1960).
5) R. Schrader, *DECHEMA-Monogr.*, **41**, 287 (1962).

 © 1982 The Chemical Society of Japan Bull. Chem. Soc. Jpn., 55, 1267—1271 (1982)

Effects of Mechanical and Electrical Anharmonicities on Local Mode Spectrum

Keietsu TAMAGAKE,* Shi-aki HYODO,† and (the late) Tsunetake FUJIYAMA††

Faculty of Pharmaceutical Sciences, Okayama University, Tsushima, Okayama 700

†*Department of Chemistry, Faculty of Science, Tokyo Metropolitan University, Setagaya-ku, Tokyo 158*

††*Institute for Molecular Science, Myodaiji, Okazaki 444*

(Received August 3, 1981)

The first and second order dipole moment parameters along the CH bond in benzene, chloroform, and cyclohexane were obtained by deducing the local mode intensities on the basis of the one-dimensional Morse oscillator model. The validity of the one-dimensional model is discussed according to a newly introduced formula which helps us to understand the nature of local mode absorptions. The relative intensities of the first overtones to the other bands were found to be crucially important in determining M_2/M_1 together with its sign, because the contributions of the mechanical and electrical anharmonicities to M_1/M_2 are often cancelled out each other accidentally. The M_2/M_1 values for benzene, cyclohexane, and chloroform were 2.3, 1.45, and -0.93 Å^{-1} respectively. These values for benzene and cyclohexane were excellently reproduced by the *ab initio* calculations for benzene and methane respectively.

The local mode idea has been recognized as a convenient representation for highly excited vibrational states, where anharmonic characters can never be neglected, since it was introduced by Henry and Siebrand[1] and later developed by Albrecht *et al.*[2] Surprisingly simple features in high overtone spectra of many hydrocarbons were successfully explained by a virtually isolated diatomic model which represents each local CH bond. However, these facts do not immediately mean that highly excited vibrational states are always so simple. What an absorption spectrum tells us directly is change in dipole moments rather than motions of atoms. There could exist many other vibrational motions which are not responsible for an absorption spectrum line. A question is why intensities tend to concentrate into some particular transitions among many other candidates, or in other words, what restrictions on the Hamiltonian and the dipole moment operator are required for the formation of a so-called local mode spectrum. Understanding of this point is important to clarify the usefulness and the limitations of the one-dimensional oscillator model, which is used to determine dipole moment parameters from the intensities observed for both fundamental and very high overtones.

In this paper we will express the absorption spectrum in a general way using more physically meaningful basis states rather than eigenstates. Such a formulation would be convenient when the eigenstates of the Hamiltonian are severely mixed states of many physically meaningful basis states. Then we apply the formulation to deducing one-dimensional dipole moment functions of benzene, cyclohexane, and chloroform. The experimental parameters thus obtained will be compares with the theoretical values and with the results obtained by Burberry and Albrecht.[3] More rigorous treatment was necessary to analyze the 1st and 2nd overtones of 1,1-dichloroethylene because of the mixings between the combinations and pure overtones which have non-zero intrinsic intensities. The result will appear in a separate paper.

Theoretical Background for Intensity Analysis

An absorption intensity at a frequency ν is generally expressed by:

$$B(\nu) = C\nu|\langle 0|M|E\rangle|^2 \tag{1}$$

where $|E\rangle$ is an eigenstate of the Hamiltonian with an eigenvalue $E=h\nu$, $|0\rangle$ is the ground state, M is the dipole moment function, and C is a constant. Inserting an identity operator,

$$I = \sum_v |v_1,v_2,\cdots\rangle\langle v_1,v_2,\cdots|, \tag{2}$$

into Eq. 1, we obtain the relation

$$B(\nu) = C\nu|\sum_v \langle 0|M|v_1,v_2,\cdots\rangle\langle v_1,v_2,\cdots|E\rangle|^2, \tag{3}$$

where $|v_1,v_2,\cdots\rangle$'s are basis states which are not necessarily eigenstates as far as Eq. 2 is satisfied. Here we express the density of a basis state $|v_1,v_2,\cdots\rangle$as a function of E as

$$\rho(E) = \langle v_1,v_2,\cdots|E\rangle^2. \tag{4}$$

Equation 4 represents the probability function of finding a state $|v_1,v_2,\cdots\rangle$ at E or the contribution of $|v_1,v_2,\cdots\rangle$ to the eigenstate $|E\rangle$. If $|v_1,v_2,\cdots\rangle$ is an eigenstate, $\rho(E)$ is a delta function which has a non-zero value only when E is the eigenvalue of the Hamiltonian. In this case Eq. 3 becomes

$$B(\nu) = C\nu\sum\langle 0|M|v_1,v_2,\cdots\rangle^2\delta(\nu-E_v). \tag{5}$$

This is a conventional expression which uses a continuous function. If $|v_1,v_2,\cdots\rangle$ is not an eigenstate but a more physically meaningful state such as local mode state or a normal mode state, on the other hand, $\rho_v(E)$ can not be so simple anymore; there appears splitting or braodening because of the mixings. Even in such a case, Eq. 3 can be reduced approximately to

$$B(\nu) = C\nu\sum_v\langle 0|M|v_1,v_2,\cdots\rangle^2\rho_v(E), \tag{6}$$

unless both of the mixing partners have non-zero intrinsic intensities at the same time. Here, the intrinsic intensity associated with a basis state, $|v_1,v_2,\cdots\rangle$, is defined by

$$I'(v_1,v_2,\cdots) = C\nu\langle 0|M|v_1,v_2,\cdots\rangle^2. \tag{7}$$

Therefore, Eq. 6 becomes

$$B(\nu) = \sum_{v} I'(v_1,v_2,\cdots)\rho_v(E). \quad (8)$$

Equation 8 or 6 means that an absorption band which is associated with one of the basis states, $|v_1,v_2,\cdots>$, must have the same structure or lineshape as $\rho_v(E)$ and that the integrated intensity over the whole band is directly related to the square of the matrix element represented by the same states used for the assignment. Any complicated interactions with other states which do not have intrinsic intensities will not affect the integrated intensity at all and the center of gravity of the band will remain unchanged, to the first order approximation, at the position which would be expected for the unperturbed state.

The above description is the theoretical basis for the intensity analysis of the present work. Equation 8 can be conveniently applied to a band which is broadened by the interactions with almost continuous background states of highly excited vibrational modes as well as external lattice mode, because such background states do not usually have their own intrinsic intensities.

Experimental

The absorption spectra of liquid benzene, cyclohexane and chloroform were observed for the C–H stretching fundamental and its overtones. A Fourier transform spectrometer (NICOLET 7199) was used for the observation of 1,2,3←0 bands, while UV-visible spectrophotometers (CARY 17 and Shimadzu D-40R) were used for the observation of 4,5,6←0 bands. 6←0 bands were also measured by the use of a dual-beam thermal lensing spectrometer which was designed and constructed in our laboratory. The optical path lengths of the cells used were 25 μm, 58 μm, and 10 mm depending upon the intensity of each absorption band. The fundamental bands of benzene and cyclohexane were so strong that the 1 : 10 diluted solutions in carbon tetrachloride were used with a 25 μm cell instead of the pure liquid.

The observed spectra were integrated over the whole of the bands corresponding to the C–H stretching modes. The integrated intensity Γ is defined by the relation:

$$\Gamma = \frac{1}{cl}\int_{\text{band}} \ln\left(\frac{I_0}{I}\right) \mathrm{d}\ln\nu \quad (\text{cm}^2/\text{mol}), \quad (9)$$

where c is the concentration of the sample in mol/cm^3, l is the thickness of sample in cm, and I_0 and I are the intensities of the incident and transmitted light, respectively. The observed integrated intensity was corrected for the dielectric effect. The corrected integrated intensity, Γ^c, can be expressed in terms of a transition matrix element as,

$$\Gamma^c = \frac{8\pi^3 N}{3hc}|<0|M|v>|^2$$

$$= 2.508 \times 10^5 M_{0v}^2 \quad (\text{cm}^2/\text{mol}), \quad (10)$$

where $M_{0v} \equiv <0|M|v>$ is a transition moment and M is a dipole moment operator. If we experess M in Debye units, Γ^c can be expressed in the units of cm^2/mol.

Results and Discussion

Observed Spectra. The spectral patterns observed in the present work are essentially the same as those of the previous work.[3,4]

The fundamental band of benzene consists of three peaks. The v=2←0 bands are more complicated. Such complex structures were explained by Fermi resonances between the pure C–H stretching mode and overtones and/or combinations of other lower frequency modes which are probably skeletal stretching modes.[5] These overtones and combination tones do not seem to have their own intensities, because all three peaks in the C–H fundamental region of benzene disappear in deuterated benzene.[5] Then we assumed that the total integrated intensities over each v←0 band were responsible for the C–H stretching mode.

The structure of the fundamental and the overtones of cyclohexane was primarily doublet, although it contained other weak peaks or shoulders. The doublet of the fundamental vibrations can be assigned to the in-phase and out-of-phase stretching modes of the two nearly identical C–H bonds which share a common carbon atom. On the other hand, the doublet structure of the high overtones should be considered as a reflection of the difference between the axial and equatorial C–H bonds, since local mode characters are dominant in highly excited states. However, independent analyses for each bond are still very difficult. Thus, we integrated the intensity over the doublets for the determination of the effectively averaged dipole moment parameters.

In Table 1 the integrated intensities, corrected for the

Table 1. Observed $\Gamma^c_{0,v}$ values in (cm^2 mol^{-1})

v	Benzene	Cyclohexane	1,1-Dichloroethylene	Chloroform
1	2448	22000	328	422
2	30.8	41.5	18.8	16.4
3	3.66	11.73	0.822	0.973
4	0.237	0.770	0.0332	0.357
5	0.0189	0.0730	2.19×10^{-3}	5.97×10^{-3}
6	3.75×10^{-3}	5.93×10^{-3}	—	—

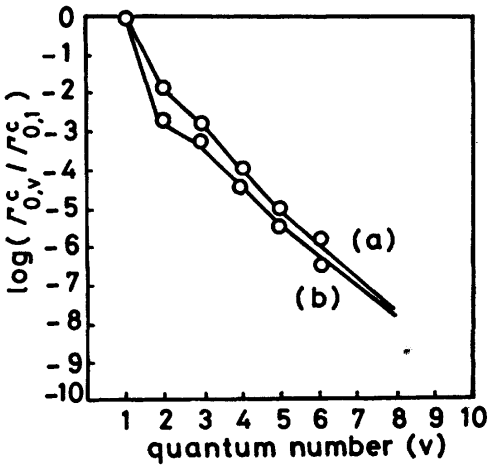

Fig. 1. The logarithmic relative intensities, $\Gamma^c_{0,v}/\Gamma^c_{0,1}$, for liquid benzene (a) and liquid cyclohexane (b) plotted against a vibrational quantum number, v. Open circles represent the observed values, while the solid line connect these values calculated from the best-fit parameter, M_2/M_1=2.30 Å^{-1} for benzene and M_2/M_1=1.45 Å^{-1} for cyclohexane.

local field effect, $\Gamma^c_{0,v}$, are summarized. In Fig. 1(a) the logarithmic relative intensities, $\Gamma^c_{0,v}/\Gamma^c_{0,1}$, observed for benzene are plotted against the vibrational quantum number, v. It can be seen from the figure that the intensity of the $v=2\leftarrow0$ band is about half of that expected from the interpolation of other $\Gamma^c_{0,v}$ values. A similar plotting for cyclohexane is shown in Fig. 1(b). The decrease in the intensity of the $v=2\leftarrow0$ band is more pronounced in cyclohexane than in benzene. In the experimental results reported by Albrecht[3] and Yamamoto,[4] the same tendencies are clearly observed. Unfortunately they did not pay any attention to this point, but rather emphasized the monotonous decrease in $\ln(\Gamma^c_{0,v}/\Gamma^c_{0,1})$ with the increase of v. We will focus our attention on this singular behaviour of the $v=2\leftarrow0$ band intensity because it is far beyond the experimental error.

Calculation of Intensity and Dipole Moment Function. We assume a one-dimensional Morse oscillator for the local mode oscillator. The Morse parameters, D_e and α, were determined from these spectral parameters: $\omega_e=3173\ \mathrm{cm}^{-1}$ and $\omega_e\chi_e=60.7\ \mathrm{cm}^{-1}$ for benzene, and $\omega_e=3020\ \mathrm{cm}^{-1}$ and $\omega_e\chi_e=65.94\ \mathrm{cm}^{-1}$ for cyclohexane, which were obtained from the observed frequencies of the local mode spectra. Using these Morse potentials, we have numerically calculated the wavefunctions and the dipole matrix elements.[6] The dipole moment function, $M(R)$, is expanded as a power series of a displacement coordinate, $R-R_e$, as

$$M(R) = M_0 + M_1(R-R_e) + M_2(R-R_e)^2, \qquad (11)$$

and the effects of M_1 and M_2 on the absorption intensities are to be studied. After determining the M_2/M_1 value so as to reproduce the relative intensities of the overtones, the absolute values of M_1 and M_2 were determined by scaling to the absolute intensity of the fundamental band. In order to clarify the origin of the anomalous intensity behaviour observed for the $v=2\leftarrow0$ band, the magnitude of M_2/M_1 and the signs of M_1 and M_2 were investigated in relation with the calculated intensity values. In Fig. 2 we demonstrate the dependency of the calculated $\Gamma^c_{0,v}/\Gamma^c_{0,1}$ value of benzene on the magnitude of M_2/M_1. The general qualitative feature which can be observed from Fig. 2 does not change much with the slight change in the Morse potential parameters. It can be seen from Fig. 2 that the relative intensity of the $v=2\leftarrow0$ band is quite sensitive to the M_2/M_1 value: the relative intensity of the $v=2\leftarrow0$ is diminished for a small positive M_2/M_1 value, while it is enhanced for a negative M_2/M_1 value. It is also clarified that the relative intensity of the $v=2\leftarrow0$ band is also enhanced if M_2/M_1 takes a large positive value; this situation is illustrated in Fig. 3. So far as we know, this is the first time for anyone to recognize the fact that the overtone intensity is so sensitive to a slight change in M_2/M_1. This anomalous behaviour of the $v=2\leftarrow0$ band intensity is considered to arise from the accidental cancellation of the mechanical and electrical anharmonicities. The magnitudes of the matrix elements are, for benzene,

$$\langle 0|(R-R_e)|2\rangle = -0.0077064\ \text{Å},$$
$$\langle 0|(R-R_e)^2|2\rangle = 0.0079453\ \text{Å}^2.$$

So the mechanical and electrical anharmonicities can completely cancel out each other if $M_2/M_1=0.970\ \text{Å}^{-1}$ (see Eq. 11). Of course, this accidental cancellation can occur even for the v values other than 2. The M_2/M_1 value which brings about the abnormality of the $v=2\leftarrow0$ band intensity, however, is not likely to bring about this accidental cancellation for other v values.

The observed intensities of benzene were reproduced best for $M_2/M_1=2.3\ \text{Å}^{-1}$ (see Fig. 1(a)), while those of cyclohexane were reproduced best for $M_2/M_1=1.45$

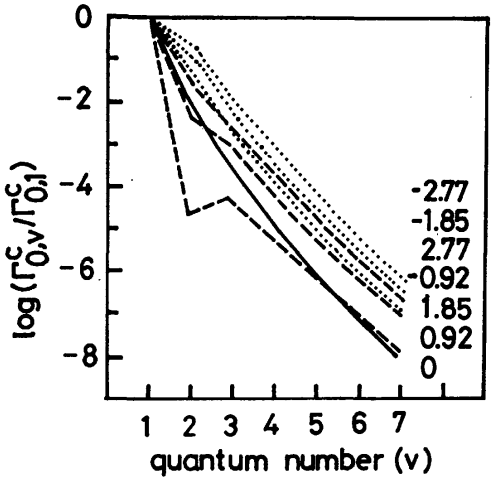

Fig. 2. The dependence of the logarithmic relative intensity, $\Gamma^c_{0,v}/\Gamma^c_{0,1}$ of liquid benzene on the parameter, M_2/M_1. The numbers at the ends of the curves indicate the M_2/M_1 value.

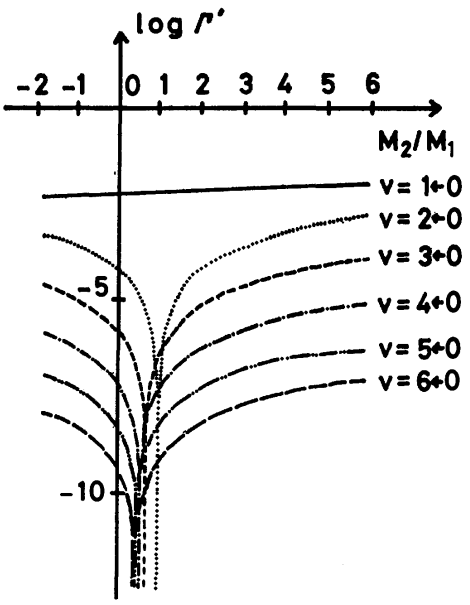

Fig. 3. The dependence of the absolute intensities of the overtones on the M_2/M_1 value in Å^{-1}. At $(M_2/M_1)\simeq1$, the effects of the mechanical and electrical anharmonicities cancell out with each other. The absolute intensity, Γ', is defined by this relation,
$\Gamma'=|\langle 0|(R-R_e)+(M_2/M_1)(R-R_e)^2|v\rangle|^2$
$=\frac{3hc}{8\pi^3N}\cdot\frac{\Gamma^c_{0,v}}{M_1^2}$.

TABLE 2. MATRIX ELEMENTS $\langle v|(R-R_e)^m|0\rangle$ FOR BENZENE

v	$(R-R_e)$	$(R-R_e)^2$	$(R-R_e)^3$	$(R-R_e)^4$
0	0.016115	6.30049×10^{-3}	3.62064×10^{-4}	1.24637×10^{-4}
1	0.077329	4.19587×10^{-3}	1.60029×10^{-3}	1.82516×10^{-4}
2	-7.70646×10^{-3}	7.94528×10^{-3}	8.03216×10^{-4}	3.71245×10^{-4}
3	1.26623×10^{-3}	-1.97764×10^{-3}	8.84528×10^{-4}	1.2578×10^{-4}
4	-2.72909×10^{-4}	5.20610×10^{-4}	-4.08416×10^{-4}	9.45319×10^{-5}
5	7.08451×10^{-5}	-1.53061×10^{-4}	1.56648×10^{-4}	-7.57525×10^{-5}
6	-2.11962×10^{-5}	4.99765×10^{-5}	-6.02466×10^{-5}	4.04809×10^{-5}
7	7.13530×10^{-6}	-1.79200×10^{-5}	2.42181×10^{-5}	-1.98537×10^{-5}

TABLE 3. THE COEFFICIENTS, M_1 AND M_2, OF THE DIPOLE MOMENT FUNCTION, AND THE CORRESPONDING (R_m-R_e) VALUES

	M_1/D Å^{-1}	M_2/D Å^{-2}	(R_m-R_e)/Å
C_6H_6	−0.48(−0.55)	−1.10(−1.40)	−0.22(−0.20)
C_6H_{12}	−0.91(−0.85)*	−1.32(−1.30)*	−0.35(−0.33)*
CH_2CCl_2	−0.36 (—)	−0.90 (—)	−0.20 (—)
$CHCl_3$	0 (−0.08)	−1.25(−1.0)	0 (−0.04)
CH_2CH_2	— (−0.64)	— (−1.24)	— (−0.26)

( ): Obtained from *ab initio* calculations. ( )*: Obtained from the *ab inito* calculation for methane.

Å^{-1} (see Fig. 1(b)). The disagreement between the observed and calculated intensities for the $v=5\leftarrow0$ and $v=6\leftarrow0$ bands may be due to the neglect of these terms higher than M_2 (see Eq. 11). We did not try to add the higher order terms to get better agreement, although it is not particularly difficult, because the one-dimensional oscillator model is not accurate enough. The final results are summarized in Table 3. In addition to the absolute value, the sign of M_2/M_1 was determined to be positive. However, the signs of M_1 and M_2 could be determined separately only after the *ab initio* calculations which will be described in the next section.

A chloroform molecule has only one C–H bond. Therefore, the one-dimensional oscillator model is considered to be most appropriately applied to this molecule. Actrually, the situation was not so simple, because the intensity of the ν_1 fundamental (the C–H stretching vibration) is abnormally weak and is extremely sensitive to the molecular environment. A detailed study on this problem will be described in a separate paper.[11] We only report here the final result, that M_1 is almost zero.

For 1,1-dichloroethylene, we adopted the two-dimensional oscillator model and obtained the M_{12} value, which is the coefficient of the cross-term, $(R_1-R_e)(R_2-R_e)$, in addition to M_1 and M_2. Although the details of this analysis will also appear in a separate paper,[12] we include the final results in Table 3. Here again $M_1M_2>0$.

Ab Initio *Calculation of Dipole Moment Function.* A dipole moment function has been determined only for a very few diatomic molecules like HCl and HF. Therefore, we cannot ascertain the validity of the dipole moment functions obtained here on the basis of the local mode representation. So we tried to compare the present results with the predictions of the *ab initio* calculation for benzene, chloroform, ethylene, and methane. Methane was chosen as a model system for cyclohexane, and ethylene was added for the convenience of understanding those molecules having double bonds. The program used for the present calculation was IMSPACK GAUSSIAN 70.[7] As a basis set, the 4-31G[8] was chosen for methan and ethylene, while the 6-31G*[9,10] was chosen for the calculations of benzene and chloroform. The calculated results are summarized in Table 3, in the brackets.

Dipole Moment Functions. From the comparison of the experimentally determined M_1 and M_2 values of Table 3, we can understand the following facts. First, M_1 and M_2 take the same sign for all the molecules except chloroform. This corresponds to the fact that the dipole moment function takes a extremum at a distance smaller than R_e. We designated this distance as R_m, and calculated the deviation from the equilibrium distance, R_e-R_m; these results are summarized in the last column of Table 3. It can be seen from the table that chloroform is quite different from other molecules in the sense that R_m is very close to R_e.

The M_1 values are different for different molecules, while the M_2 values are rather constant for all the molecules studied: that is, $-1.3<M_2<-0.9$. It is of same interest to emphasize that even the M_2 value for chloroform was obtained in this range of magnitude.

The *ab initio* calculation reproduces the observed M_1 and M_2 values very well. So far, very few experimental M_2 values have been compared with the M_2 values calculated by the *ab initio* calculation, because the corresponding experimental values have been so poor. The present study shows that the agreement between the calculated and observed M_2 values are excellent for various hydrocarbons. The characteristic features of the dipole moment function of chloroform are also well reproduced by the *ab initio* calculation: M_2 is not very different from those of the other molecules, although M_1 is exceptionally small in magnitude. It may be giving too many compliments to the *ab initio* calculation to say that the slight deviations of the calculated dipole moment functions from the observed ones may be

Table 4. The dipole moment function for liquid benzene obtained by Burberry and Albrecht.[a)]

	Semiempirical		Theoretical	
	Morse potential	Quartic potential	CNDO	*Ab initio*
M_1/D Å^{-1}	−0.81	−0.59	−1.0	−1.78
M_2/D Å^{-2}	0.20	−1.16	−0.99	−1.48

a) See Ref. 3.

ascribed to the over-simplification of the oscillator model, *i.e.* the one-dimensional local mode model.

Burberry and Albrecht[3)] determined the dipole moment function of benzene by the use of an oscillator model which is analogous to ours; their results are given in Table 4. It is puzzling to see from the table that the signs of M_1 and M_2 are different, although they use a Morse potential in their calculation. We do not see any clear reasons for this. We only emphasize the fact that Burberry and Albrecht do not seem to have paid special attention to the anomalous intensity decrease of the $v=2\leftarrow0$ bands, although the anomaly can clearly be seen in their intensity data. Strange to say, their calculation has led to a dipole moment function which is very close to our present result; they used the quartic potential function in the place of the Morse potential. We are not sure at present why the quartic potential is preferrable to the Morse potential for the treatment of an oscillator whose anharmonic character is very strong. Perhaps the dipole moment function is sensitive to the anomalous intensity behaviour of the $v=2\leftarrow0$ band.

Mechanical and Electrical Anharmonicities. Next, we consider the contributions of mechanical and electrical anharmonicities on overtone spectra.

If a potential is completely harmonic, the dipole term related with M_2 simply allows the $v=2\leftarrow0$ transition. If a potential is of a Morse type, on the other hand, all the highly excited vibrational bands can be expected to have considerable intensities even if $M_2=0$. For example, about 10% of the observed intensity for the $v=6\leftarrow0$ band in liquid benzene can be ascertained to be originating from the Morse potential only ($M_2=0$). In other words, M_2 contributes only to the appearence of a $v=2\leftarrow0$ band under a harmonic potential, while it can have large contributions to the appearence of the high overtones other than $v=2\leftarrow0$ under the influence of a harmonic potential. Thus, we can conclude that the mechanical and electrical anharmonicities cooperatively contribute to the appearance of the high overtones. In some cases, the contribution of mechanical and electrical anharmonicities cancel out each other, as we have seen in the $v=2\leftarrow0$ band. This phenomenon is most distinct in the $v=2\leftarrow0$ band, simply because M_2 contributes directly to the $v=2\leftarrow0$ transition. Thus, we can recognize that the present system was only a lucky case for the determination of M_2/M_1 in the sense that we could use the anomalous intensity decrease of the $v=2\leftarrow0$ band. If the intensity of the $v=2\leftarrow0$ band were normal, in comparison with the other high overtones, or if it were enhanced instead of diminished, we could not determine even the sign of M_2/M_1.

Incidentally, the present theoretical treatment is quite general, provided that the dipole matrix elements related with the other modes are negligible and that the cross terms in a dipole moment function which represent the couplings between each mode in question and the other modes can be neglected. The coupling originating from the nature of the Hamiltonian does not spoile the generality of the present theory. The effects of the cross term in a dipole moment function can properly be treated by introducing a coupled oscillator model; the results of this treatment will appear in a separate paper.

Conclusion

The absolute intensities of the high overtones were observed for liquid benzene, cyclohexane, and chloroform. From these intensity values, the dipole moment functions were obtained up to quadratic terms, based upon the one-dimensional oscillator model. The corresponding parameters for benzene, methane, chloroform, and ethylene were estimated by the *ab initio* calculations. The agreement between the experimental and theoretical dipole moment functions, in turn, confirmed the validity of the one-dimensional oscillator model and the reliability of the *ab initio* calculation simultaneously.

The anomalous intensity behaviour of the $v=2\leftarrow0$ band was ascertained to be arising from the accidental interaction between the mechanical and electrical anharmonicities. This effect was conveniently used for the determination of the M_2/M_1 value.

We are indebted to Dr. Shigeki Kato of Institute for Molecular Science for his invaluable assistance with the *ab initio* calculations.

References

1) B. R. Henry and W. Siebrand, *J. Chem. Phys.*, **49**, 5369 (1968).
2) M. E. Long, R. L. Swofford, and A. C. Albrecht, *Science*, **191**, 183 (1976).
3) M. S. Burberry and A. C. Albrecht, *J. Chem. Phys.*, **70**, 147 (1979).
4) N. Yamamoto, N. Matsuo, and H. Tsubomura, *Chem. Phys. Lett.*, **71**, 463 (1980).
5) G. Herzberg, "Molecular Spectra and Molecular Structure. II," D. Van Nostrand Co., Inc., New York (1949). p. 365.
6) K. Tamagake and D. W. Setser, *J. Chem. Phys.*, **67**, 4370 (1977).
7) K. Morokuma, S. Kato, K. Kitaura, I. Ohmine, S. Sakai, and S. Obara, IMS Computer Center Library Program, No. 0372 (1980).
8) R. Ditchfield, W. J. Hehre, and J. A. Pople, *J. Chem. Phys.*, **54**, 4297 (1971).
9) P. C. Hariharan and J. A. Pople, *Theoret. Chim. Acta.*, **28**, 213 (1973).
10) The number of the inner-shell orbitals of a chlorine atom was four.
11) S. Hyodo, K. Tamagake, and T. Fujiyama, *Bull. Chem. Soc. Jpn.*, **55**, 1272 (1982).
12) K. Tamagaki, S. Hyodo, and T. Fujiyama, *Bull. Chem. Soc. Jpn.*, **55**, 1277 (1982).

 © 1982 The Chemical Society of Japan Bull. Chem. Soc. Jpn., 55, 1272—1276 (1982) [Vol. 55, No. 4

High-overtone Spectra and Dipole Moment Functions for the C-H Stretching Vibration of Chloroform

Shi-aki Hyodo,† Keietsu Tamagake,*,†† and (the late) Tsunetake Fujiyama

Institute for Molecular Science, Myodaiji, Okazaki 444

†*Department of Chemistry, Faculty of Science, Tokyo Metropolitan University, Setagaya-ku, Tokyo 158*

††*Faculty of Pharmaceutical Sciences, Okayama University, Tsushima, Okayama 700*

(Received August 10, 1981)

The absorption spectra of liquid chloroform were observed for the C–H stretching fundamental vibration and its overtones up to $v=\leftarrow 50$. The spectral parameters were analyzed on the basis of the one-dimensional local mode representation, which led to the determination of the mechanical and electrical anharmonicities. The solvent effects on the absorption intensities are discussed from the viewpoint of the solvent effect on the dipole moment function. The finally obtained dipole moment function was compared with that obtained by the *ab initio* calculation.

The absolute intensity of the C–H stretching fundamental band of chloroform in the gas phase has been known to be anomalously weak in comparison with the absolute intensity of its pure overtone, *i.e.*, the $v=2\leftarrow 0$ band. The reason of this anomaly has been vaguely attributed to same electric anharmonicity related with this vibrational mode.[1] Since the intensities of overtones are influenced by both mechanical and electrical anharmonicities, however, we cannot obtain any definite conclusions about this problem without analyzing these two kinds of anharmonicities simultaneously.

Previously we have reported the intensity analysis of the C–H stretching overtones for a few molecules.[2] In the report, we emphasized the usefulness of the one-dimensional local mode model for the analysis of intensity data. At the same time, the choice of the Morse-type potential function was found to give a satisfactory approximation for the elucidation of the mechanical anharmonicity, if we are able to define the absorption bands in terms of the local mode representation. This result indicates, at the same time, that we are now able to obtain accurate knowledge about the electrical anharmonicity for a system in which a local mode can be well defined.

A chloroform molecule has only one C–H bond. Therefore, it is the most appropriate molecule to which to apply our one-dimensional oscillator model. The intensity of the $v=1\leftarrow 0$ band of chloroform is sensitive to the change of molecular environment. Such spectral changes of the $v=1\leftarrow 0$ band have been interpreted in terms of the hydrogen bonding in the liquid or solution phase.[3] Suzuki *et al.* have reported that the concentration dependence of the intensities and the line width of the C–H stretching vibration of chloroform in carbon tetrachloride solutions can be well explained by considering the coexistence of two different types of chloroform molecules; one is a molecule which interacts with other molecules and the other is a non-interacting molecule.[4] The role of the carbon tetrachloride molecule is to break the interaction between chloroform molecules.

The present work has examined the absorption spectra of the C–H stretching vibration of chloroform observed for the fundamental and overtone bands. The observed spectral parameters will be analyzed on the basis of the one-dimensional local mode model to obtain the dipole moment function. Based upon these results, the remarkable solvent effect observed for the intensity of the fundamental band will be discussed in relation to the solvent effect on the dipole moment function.

Experimental

All the chemicals used in this work were commercially available reagents. Chloroform was purified by column chromatography on alumina to remove ethanol.

The absorption spectra were measured for the C–H stretching vibrations of liquid chloroform with the use of a Fourier transform infrared spectrometer (NICOLET 7199) at room temperature. For the measurement of the $v=1\leftarrow 0$ band, a water-cooled Glober source and a mercury cadmium telluride detector were used. The used beam-splitter was a Ge on KBr substrate. An NaCl window cell having a thickness of 0.0025 cm was used for the $v=1\leftarrow 0$ band intensity measurement. For the measurements of the $v=2\leftarrow 0$, $v=3\leftarrow 0$, and $v=4\leftarrow 0$ bands, a water-cooled tungsten-halogen lamp, a quartz beam-splitter, and an InAs detector were used. An NaCl window cell having a thickness of 0.0107 cm was used for the $v=2\leftarrow 0$ band, while a quartz cell having a thickness of 1 cm was used for the $v=3\leftarrow 0$ and $v=4\leftarrow 0$ bands.

The concentration dependences of the absorption spectra were observed in the carbon tetrachloride solutions at the concentrations of 80, 60, 40, and 20 mol %.

For the measurement of the $v=5\leftarrow 0$ band, a UV-visible spectrometer (CARY 17) and a quartz cell having an optical path length of 10 cm were used.

All the absorption spectra were measured with a resolution of about 1 cm^{-1}.

Results and Discussion

Analysis of Intensity Data. The absolute intensity $\Gamma_{n',n''}$ related with the $v=n''\leftarrow n'$ transition can be expressed in terms of the experimentally observable quantities as

$$\Gamma_{n',n''} = \frac{f_d}{nl}\int_{band} \ln\left(\frac{I_0}{I}\right) d\ln \nu \qquad (1)$$

where n is the concentration of sample, l is the sample thickness, I_0 and I are the intensities of the incident and transmitted light, respectively, and ν is the frequency of light. f_d is the correction factor for the dielectric-field effect. Since the absolute intensities of the observed

Table 1. The band parameters observed for the C–H stretching vibration in the liquid and CCl_4 solutions phases

Molar concentration of $CHCl_3$ (%)		100	80	60	40	20	Gas[a]
ν_1	ν_0/cm^{-1}	3019.5	3019.5	3019.5	3019.5	3019.5	3032.9
	Γ/cm^2 mol^{-1}	245	216	190	172	134	5.247
$2\nu_1$	ν_0/cm^{-1}	5912	5910	5908	5907	5906	5941.4
	Γ/cm^2 mol^{-1}	16	17	16	17	18	17.32
$3\nu_1$	ν_0/cm^{-1}	8674	8672	8672	8670	8669	—
	Γ/cm^2 mol^{-1}	0.61	0.63	0.61	0.59	0.55	—
$4\nu_1$	ν_0/cm^{-1}	11315	11315	11315	11315	11315	—
	Γ/cm^2 mol^{-1}	0.0251	0.0268	0.0266	0.0268	0.0306	—
$5\nu_1$	ν_0/cm^{-1}	13850	—	—	—	—	—
	Γ/cm^2 mol^{-1}	2.46×10^{-3}	—	—	—	—	—

a) After Rossi *et al.* (see Ref. 1).

bands are weak, the Polo-Wilson's scheme[5] can safely be applied to the dielectric-field correction.[6] Thus, the correction factor f_d can be expressed as

$$f_d = \frac{9n_D}{(n_D^2+2)^2}, \tag{2}$$

where n_D is the refractive index of the solution. The used n_D data were found in the International Critical Tables.[7]

Concentration Dependence of Absolute Intensity. The cencentration dependence of band parameters (the peak frequency and the intensity) observed for the carbon tetrachloride solutions are summarized in Table 1. The intensities of the $v=1\leftarrow0$ and $v=2\leftarrow0$ bands observed for the gas phase by Rossi *et al.*[1] are also included in the last column of Table 1.

The absolute intensity of the $v=1\leftarrow0$ band in 20 mol% of carbon tetrachloride solution is about half of that in the pure liquid chloroform. No remarkable solvent effects on the intensities were observed for the overtone bands; this result in sharp contrast with that for the fundamental band. It has been shown in our previous report that the intensities of overtone bands are determined by both the electrical and the mechanical anharmonicities.[2] Let us consider the mechanical anharmonicity first.

Mechanical Anharmonicity and Absorption Frequency. The mechanical anharmonicity is directly related with the potential term of the Hamiltonian. Therefore, it can be determined by the frequency measurement of the absorption maximum for the fundamental and overtone bands. It has been established that the frequencies of the absorption maxima of the overtone bands are well approximated by the Birge-Sponer equation, if we can assign the overtone spectra on the basis of the local mode representation,[8–10] that is

$$\frac{E_v-E_0}{v} = A + Bv, \tag{3}$$

where A and B are constants and E_v and E_0 are the eigenvalues of the vibrational states $|v>$ and $|0>$ respectively. Equation 4 shows that the anharmonic character of the vibrational eigenvalues can be well explained by considering the v and v^2 dependences. We assume a one-dimensional Morse oscillator for the local mode oscillator. The Morse parameters, D_e and α, were determined from these spectral parameters: $\omega_e=3130\,\text{cm}^{-1}$ and $\omega_e\chi_e=60.0\,\text{cm}^{-1}$, which were obtained from the observed frequencies of the local mode spectra. Thus we could quantify the mechanical anharmonicity and, therefore, the wavefunction $|v>$.

Electrical Anharmonicity and Intensity. Next we consider the electrical anharmonicity. Using the Morse potential, we have numerically calculated the wavefunctions and the dipole matrix elements.[11] The dipole moment function, $M(R)$, is expanded as a power series of a displacement coordinate, $R-R_e$, as

$$M(R) = M_0 + M_1(R-R_e) + M_2(R-R_e)^2 \tag{4}$$

and the effects of M_1 and M_2 on the absorption intensities are to be studied. We have already described, in our

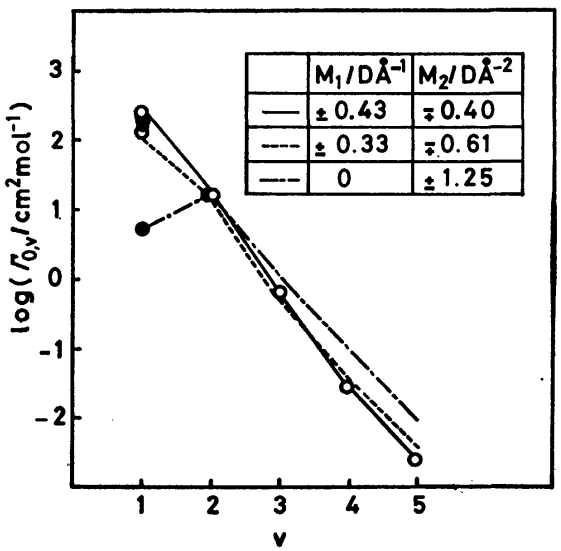

Fig. 1. The logarithmic absolute intensity plotted against the vibrational quantum number.
○: Observed values for the liquid phase, ●: observed values for the gas phase, ——: best fit curve for the pure liquid data, ——: best fit curve for the 20 mol% solution data, –·–·–: best fit curve for the gas phase data. The Taylor expansion of the dipole moment function is truncated at the quadratic term, $M=M_0M_1(R-R_e)+M_2(R-R_e)^2$.

previous report,[2] the way of determining the M_1 and M_2 values on the basis of the one-dimensional local mode model. Here again, we adopt this one-dimensional oscillator model and determine the M_1 and M_2 values for chloroform. As we did not see any remarkable solvent effects on the intensities for the $v=2\leftarrow0$, $v=3\leftarrow0$, and $v=4\leftarrow0$ bands, we may regard the absolute intensity value observed at the concentration of 20 mol% as the absolute intensity value in the gas phase. In facts the intensity values for the $v=2\leftarrow0$ band were observed to be almost identical in the gas and solution phases.

Figure 1 shows the logarithms of the observed absolute intensities plotted against the vibrational quantum number of the upper state, v. The open circles correspond to the absolute intensities in solutions, while the closed circles correspond to the absolute intensities in the gas phase reported by Rossi *et al.*[1] The open circles arranged on the vertical line at $v=1$ correspond to the $\Gamma_{0,1}$ values associated with the pure liquid and the solutions of 80, 60, 40, and 20 mol%. The concentration dependence of the $\Gamma_{0,2}$, $\Gamma_{0,3}$, or $\Gamma_{0,4}$ values were too small to be identified in this logarithmic scale.

Using the intensity data for pure liquid chloroform,

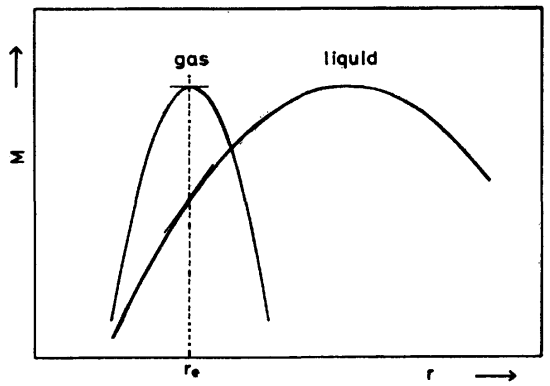

Fig. 2. The schematic drawing of the dipole moment functions for the gas and liquid phases.

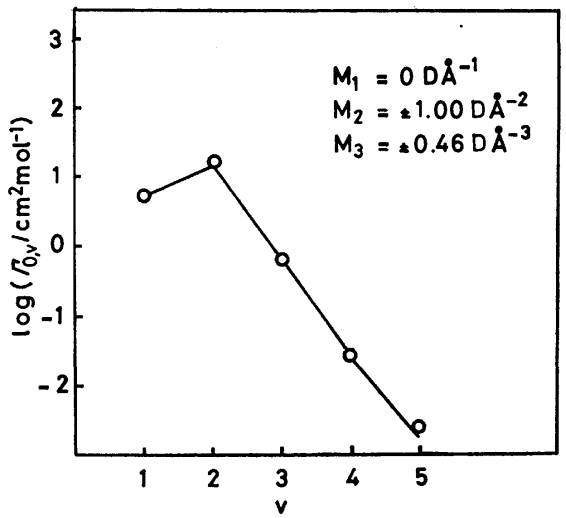

Fig. 3. The best fit curve for the gas phase intensity data. The Taylor expansion of the dipole moment function is truncated at the cubic term, $M=M_0+M_1(R-R_e)+M_2(R-R_e)^2+M_3(R-R_e)^3$.

the best fit parameters were obtained to be: $M_1=\pm0.43$ D Å^{-1} and $M_2=\mp0.40$ D Å^{-2}. In Fig. 3 the best fit values for this case are shown by the solid line. The dotted line, on the other hand, shows the intensity values calculated for the parameter values of $M_1=\pm0.33$ D Å^{-1} and $M_2=\mp0.61$ D Å^{-2}, which are the best fit parameter values for the intensity observed in the 20 mol% solution. The dot-and-dash line indicates the theoretical values calculated from the M_1 and M_2 values which were determined from the gas phase intensities of the $v=1\leftarrow0$ and $v=2\leftarrow0$ bands, namely, $M_1=0$ D Å^{-1} and $M_2=\mp1.25$ D Å^{-2}. Similarly, the best fit parameters, M_1 and M_2, were determined for various concentrations: these results are summerized in Table 2.

Table 2. The M_1 and M_2 values of chloroform in the liquid, carbon tetrachloride solution, and gas phases

Mole fraction of $CHCl_3$		M_1/D Å^{-1}	M_2/D Å^{-2}	M_3/D Å^{-3}
1.0 (Pure liquid)		±0.43	∓0.40	—
0.8		±0.41	∓0.49	—
0.6		±0.39	∓0.58	—
0.4		±0.37	∓0.58	—
0.2		±0.33	∓0.61	—
Gas	a)	0	∓1.25	—
	b)	0	∓1.00	∓0.46
Ab initio		-0.08	-1.00	—

a) The Taylor expansion of the dipole moment function was truncated at the quadratic term. The observed intensities for the $v=1\leftarrow0$ and $v=2\leftarrow0$ bands were used. b) The Taylor expansion of the dipole moment function was truncated at the cubic term. The observed intensities for the $v=1\leftarrow0$, $v=2\leftarrow0$, $v=3\leftarrow0$, $v=4\leftarrow0$, and $v=5\leftarrow0$ were used for the fitting.

Miyazaki and Yamamoto have calculated the M_1 and M_2 values for the C–H stretching vibration of methylchloride, methylenechloride, and chloroform by the CNDO method.[12] The $\Gamma_{1,0}/\Gamma_{2,0}$ ratio of chloroform obtained from their calculation agrees well with the observed one, although the absolute intensities are smaller than the observed ones by about an order of magnitude. Their results agrees with the present experimental results in the sense that the M_1 value of chloroform is smaller than those of the other molecules. However, the M_2 values were calculated to be four times as small as our present results, presumably because the absolute intensity values which were calculated by the CNDO method were too small. The potential energy calculated from the CNDO method for the C–H stretching vibration does not seem appropriate, because the energy increase with the displacement from the equilibrium distance is much larger than those generally found. Therefore, we will perform the *ab initio* closed shell SCF calculation and compare the results with the experimental ones.

Ab Initio *Calculation of Dipole Moment Function.*

A dipole moment function has been determined experi-

mentally only for a very few diatomic molecules like HCl and HF. Therefore, we cannot ascertain the reliability of the dipole moment function obtained on the basis of the local mode representation. So we tried to compare the present result with the prediction of the *ab initio* closed shell SCF calculation. The programme used for the present calculation was IMSPACK GAUSSIAN 70.[13] As a basis set, the 6-31G*[14] was chosen for this calculation. The number of the inner-shell orbitals for a chlorine atom was set to be four. The 3d orbital for a chlorine atom was taken into account to improve the accuracy in the calculation of force constants or dipole matrix elements. The geometry optimization was carried out by the energy gradient technique.[15] The dipole moment derivatives were obtained by numerizal differentiations of calculated dipole moments in the Cartesian Coordinate system. The final results for M_1 and M_2 are given at the bottom of Table 2. It can be understood that the calculated M_1 and M_2 values agree well with those observed in the gas phase. It is noticeable that the M_2 values was calculated to be almost zero, which is in good agreement with the experimental result. As for the sign of these parameters, we may safely conclude that M_2 should be negative from this *ab initio* calculation. The sign of M_1, on the other hand, cannot be determined from this calculation, because the magnitude was calculated to be almost zero.

Dipole Moment Function and Solvent Effect. Let us consider now the concentration dependence of the dipole moment function observed in the carbon tetrachloride solutions. It can be seen from Table 2 that M_2 increases its magnitude and M_1 decreases its magnitude with the increase in concentration. Of course we cannot give too much quantitative meaning to the M_1 and M_2 values obtained for the liquid or solution phases, because it has been established that there exist two types of chloroform molecules in the liquid and solution phases. One is a molecule which interacts with other molecules and the other is a non-interacting molecule.[4] Therefore, the true M_1 value of the interacting molecule, for example, in pure liquid chloroform may be much larger than ± 0.43 D Å^{-1}. Thus, the M_1 and M_2 values in the liquid phase should be regarded as effective values. However, the general tendency of the concentration dependence of M_1 and M_2 is important. We remember that M_1 and M_2 values approach those of the gas phase in the infinite dilution limit.

The parameter values of $M_1 \simeq 0$ means that the dipole moment function M takes an extremum at the equilibrium distance of the C–H bond or at the distance where the C–H internuclear potential function takes a minimum value. On the other hand, the increase of M_1 with the increasing concentration corresponds to the fact that the distance at which the dipole moment function takes an extremum deviates from that of the potential minimum. This deviation may be due to the intermolecular interaction of the hydrogen bonding type between chloroform molecules. We discussed the details of this interaction in our previous reports,[4,16] where the effect of the charge transfer complex formation has been emphasized. If this charge transfer model can be applied to the present case, the sign of M_1 should be positive in the liquid and solution phases.[16] This conclusion is consistent with the fact that M_1 and M_2 should have opposite signs (see Fig. 1); the latter conclusion is drawn from the present intensity analysis.

The decrease in the absolute value $|M_2|$ with the increasing chloroform concentration corresponds to the decrease in the curvature of the dipole moment function. Taking these situations into account together with the signs of M_1 and M_2, we can draw the dipole moment functions in the gas and liquid phases schematically in Fig. 2. We cannot give any further meanings to the behavior of M_2 with the concentration change at this stage. But we can conclude that the apparent anomalous intensity behavior of the fundamental band is not due to the electrical anharmonicity M_2, but to the harmonic term M_1. The fundamental band looks quite sensitive to the change of the molecular environment, simply because the dipole moment function takes a extremum at the equilibrium distance of the C–H bond, which brings about the anomalously weak intrinsic intensity for the fundamental band. The $\Gamma_{0,1}$-value change from 5.2 cm^2/mol to 245 cm^2/mol on passing from the gas to the pure liquid phases is only a small change from the viewpoint of the hydrogen bonding. As we have proposed in our report,[16] the strength of the hydrogen bonding should be evaluated by the $(\sqrt{\Gamma_b}-\sqrt{\Gamma_f})$ value instead of the Γ_b/Γ_f value, where Γ_b and Γ_f correspond to the absorption intensities of the hydrogen-bonded and free molecules, respectively. The $(\sqrt{\Gamma_b}-\sqrt{\Gamma_f})$ value of the present case is $\sqrt{245}-\sqrt{5.2} \simeq 10$, which is equivalent to an excess enthalpy of only 200 cal/mol.

The reflection of the dipole moment function on the intensities will be understood in more detail if we watch the numerically calculated matrix elements. The absolute intensity $\Gamma_{0,v}$ corresponding to the transition from the ground state $|0>$ to a vibrationally excited state $|v>$ is proportional to the square of the dipole matrix element $|<0|M|v>|$. Therefore,

$$\begin{aligned}\Gamma_{0,v} &\propto |<0|M|v>|^2 \\ &= M_1^2<0|R-R_e|v>^2 \\ &\quad + 2M_1M_2<0|R-R_e|v><0|(R-R_e)^2|v> \\ &\quad + M_2^2<0|(R-R_e)^2|v>. \end{aligned} \tag{5}$$

The numerical values for the three terms of Eq. 5 are summarized in Table 3. It can be seen from the table that the intensity of the $v=1\leftarrow 0$ band is governed by rather complicated factors. In the gas phase, the intensity is determined completely by the third term. As the concentration and, therefore, the intermolecular interaction increase, the intensity comes to be governed by the first term. The concentration dependence of the $v=1\leftarrow 0$ band is obviously governed by the magnitude of M_1. In the case of the $v=2\leftarrow 0$ band, on the other hand, the three terms can equally contribute to the intensity. It is noticeable that the second term is almost independent of the concentration. The third term decreases, while the first term increases, with the increase of the chloroform concentration. The increase and decrease of the first and third terms compensate each other, which keeps the $v=2\leftarrow 0$ band intensity almost independent of the chloroform

Table 3. The numerical values for the dipole matrix elements of chloroform

$\Gamma_{0,v}/(8\pi^3N/3hc) = M_1^2\langle 0|\Delta r|v\rangle^2 + 2M_1M_2\langle 0|\Delta r|v\rangle\langle 0|\Delta r^2|v\rangle + M_2^2\langle 0|\Delta r^2|v\rangle^2$

Mole fraction of $CHCl_3$	$v=1$			$v=2$		
	1st term	2nd term	3rd term	1st term	2nd term	3rd term
1.0 (Pure liquid)	1.1065×10^{-3}	-1.1397×10^{-4}	2.9346×10^{-6}	1.1434×10^{-5}	2.1452×10^{-5}	1.0062×10^{-5}
0.8	1.0060×10^{-3}	-1.3312×10^{-4}	4.4037×10^{-6}	1.0395×10^{-5}	2.5057×10^{-5}	1.5100×10^{-5}
0.6	0.9102×10^{-3}	-1.4988×10^{-4}	6.1699×10^{-6}	0.9406×10^{-5}	2.8212×10^{-5}	2.1156×10^{-5}
0.4	0.8193×10^{-3}	-1.4219×10^{-4}	6.1699×10^{-6}	0.8466×10^{-5}	2.6766×10^{-5}	2.1156×10^{-5}
0.2	0.6517×10^{-3}	-1.3338×10^{-4}	6.8247×10^{-6}	0.6734×10^{-5}	2.5107×10^{-5}	2.3401×10^{-5}
Gas	0.0	0.0	2.8658×10^{-5}	0.0	0.0	9.8266×10^{-5}

concentration.

Higher Order Terms in Dipole Moment Function. In Fig. 1, it is seen that the dash-and-dot line deviates from the observed values at the higher vibrational quantum numbers. If we choose the parameter values which can explain the intensities of the $v=3\leftarrow0$, $v=4\leftarrow0$, and $v=5\leftarrow0$, we cannot explain the intensity of the $v=1\leftarrow0$ band. This is probably arising from the fact that the effects of the higher order term of the dipole moment function on the intensities are relatively accentuated at the higher v values, because M_1 is extremely small in chloroform. Conversely speaking, it may be possible to determine the higher term in the dipole moment function for this particular case, although the one-dimensional oscillator model may be too over-simplified to do so in general.[2] We only add here the results of the intensity analysis by taking into account the cubic term M_3 in the dipole moment function. In Fig. 3, the best fit values are shown by the solid line, while the observed values are given by the open circles. The best fit parameter values were: $M_1=0$ D Å^{-1}, $M_2=1.00$ D Å^{-2}, and $M_3=0.46$ D Å^{-3}. The sign of M_2 is probably negative, while that of M_3 can be negative because M_2 and M_3 should have the same signs.

Conclusion

The dipole moment functions of chloroform were determined from the observed intensities. The solvent effects on the absorption intensity were discussed as related to the concentration dependence of the dipole moment function. The anomalous intensity behavior of the fundamental band was clarified to arise from the accidental coincidence of the positions at which the potential function and the dipole moment function take extrema, which brings about the anomalously weak intrinsic intensity of the fundamental band. The reliability of the finally determined electrical anharmonicity parameters was confirmed by the *ab initio* calculation.

Incidentally, the one-dimensional local mode representation was shown to be useful for an intensity data analysis in the sense that a mechanical anharmonicity can be fairly easily determined for a complicated polyatomic molecule like chloroform. This, in turn, makes it possible to elucidate an electrical anharmonicity or a higher order term of a dipole moment function.

We are indebted to Dr. Shigeki Kato of Institute for Molecular Science for his assistance with the *ab initio* calculation.

References

1) C. C. Robinson, S. A. Tare, and H. W. Thompson, *Proc. R. Soc. London, Ser. A*, **269**, 492 (1962); I. Rossi, Ngnyen-van-Than, and C. Haeusler, *Can. J. Chem.*, **47**, 3319 (1969). The absolute intensity in their report is expressed in the units of A/cm^{-2} atm^{-1}. For convenience, we converted their value into the units of Γ/cm^2 mol^{-1} by the use of the conventional relation, $\Gamma=22415A/\nu_0$.

2) K. Tamagake, S. Hyodo, and T. Fujiyama, *Bull. Chem. Soc. Jpn.*, **55**, 1267 (1982).

3) There are many papers concerning this topic. The earliest one is: W. Klemper, M. W. Crown, A. H. Maki, and G. C. Pimentel, *J. Am. Chem. Soc.*, **76**, 5846 (1954).

4) T. Suzuki, Y. K. Tsutsui, and T. Fujiyama, *Bull. Chem. Soc. Jpn.*, **53**, 1931 (1980).

5) S. R. Polo and M. K. Wilson, *J. Chem. Phys.*, **23**, 2376 (1955).

6) T. Fujiyama and B. L. Crawford, Jr., *J. Phys. Chem.*, **73**, 4040 (1969).

7) "International Critical Tables of Numerical Data; Physics, Chemistry and Technology," National Research Council, McGraw-Hill, New York (1929).

8) R. L. Swofford, M. E. Long, and A. C. Albrecht, *J. Chem. Phys.*, **65**, 179 (1976).

9) N. Yamamoto, N. Matsuo, and H. Tsubomura, *Chem. Phys. Lett.*, **71**, 463 (1980).

10) Y. Mizugai and M. Katayama, *Chem. Phys. Lett.*, **73**, 240 (1980).

11) K. Tamagake and D. W. Setser, *J. Chem. Phys.*, **67**, 4370 (1977).

12) T. Miyazaki and H. Yamamoto, *Bull. Chem. Soc. Jpn.*, **45**, 1669 (1972).

13) K. Morokuma, S. Kato, K. Kitaura, I. Ohmine, S. Sakai, and S. Obara, IMS Computer Center Library Program, No. 0372 (1980).

14) P. C. Hariharan and J. A. Pople, *Teor. Chim. Acta*, **28**, 213 (1973).

15) P. Pulay, "Applications of Electronic Structure Theory," ed by H. F. Schaefer, Plenum, New York (1977), Vol. III, Chap. 4.

16) M. Okazaki, I. Hara, Y. K. Tsutsui, and T. Fujiyama, *Bull. Chem. Soc. Jpn.*, **54**, 2399 (1981).

 © 1982 The Chemical Society of Japan Bull. Chem. Soc. Jpn., 55, 1277—1283 (1982)

Symmetrized Local Mode Analysis of CH_2 Stretching Mode in 1,1-Dichloroethylene

Keietsu TAMAGAKE,* Shi-aki HYODO,† and (the late) Tsunetake FUJIYAMA††

Faculty of Pharmaceutical Sciences, Okayama University, Tsushima, Okayama 700

††*Department of Chemistry, Faculty of Science, Tokyo Metropolitan University, Setagaya-ku, Tokyo 158*

††*Institute for Molecular Science, Myodaiji, Okazaki 444*

(Received September 10, 1981)

A symmetrized local mode (SLM) model based on the two dimensional Morse oscillator was developed and applied to the analysis of the spectrum of the CH stretching modes in 1,1-dichloroethylene in the range of 3000—17000 cm^{-1}. More than twelve absorption peaks were assigned in terms of the mixed SLM states. The calculated frequencies with finally determined parameters: $\omega_e=3191.6$ cm^{-1}, $\omega_e\chi_e=57.63$ cm^{-1}, and $f_{12}=2170$ cm^{-1} agreed well with the observed ones. The kinetic coupling was found to be more responsible for the mixings between SLM states than the potential coupling. The observed intensity data were analyzed by the use of the obtained mixing coefficients and the two dimensional dipole moment function parameters: M_1, M_2, M_{12}, and θ. The finally determined dipole moment function parameters were: $M_1=-0.290$ D $Å^{-1}$, $M_2=-0.875$ D $Å^{-2}$, $M_{12}=0.386$ D $Å^{-2}$, and $\theta=38.4°$. Careful examination of the influence of M_{12} upon the integrated intensities clarified the validity of the one dimensional intensity analysis of our preceding work. An SLM representation was confirmed to be useful for the systematic analysis of the CH stretching spectrum through the fundamental and the high v local mode bands which include highly structured low v summation bands. An SLM representation was also found to be convenient for making a simple correlation between local mode and normal mode pictures.

Many reports on local mode (LM) spectra[1] have been published in recent years since the idea was introduced by Henry and Siebrand[2] and later developed by Albrecht.[3] Our preceding articles[4,5] on the determinations of the dipole moment functions of CH bonds in benzene, cyclohexane, and chloroform were based upon the one-dimensional LM model. A simple LM picture is not adequate, however, for an explanation of the complicated spectral structures in the fundamental band and low v overtone bands. These structured bands are usually analyzed by the conventional method[6,7] developed in a normal mode (NM) picture, although the NM picture is not so convenient either, because of the large Darling-Dennison resonance[8] in the summation band regions. In relation to the above statment, there still exist some problems which have been not solved thoroughly. One is how to express the states which are assigned in the NM picture in terms of the LM picture, or how to clarify the correlation between LM and NM quantitatively. The other is to examine the magnitude of the interactions between equivalent LM states quantitatively. The latter would be necessary to test the validity of the one-dimensional LM approximation when it is applied to various particular subjects, such as the deduction of dipole moment parameters.

In this paper, we introduce symmetrized local mode states (SLM) for the analysis of the spectrum of the CH stretching modes in 1,1-dichloroethylene. An SLM representation would be one of the most convenient pictures because some of the large interactions between equivalent LM states are automatically included in the diagonal elements in zero-th order and because it could be easily correlated to the states in a NM picture which were intrincically symmetrized at the stage of the construction of the coordinates. Two dimensional analysis of the CH_2 stretching modes in an SLM picture would also enable us to determine two-dimensional dipole moment parameters.

The vibrational spectra of 1,1-dichloroethylene and its deuterated compounds were measured by Winter *et al.*[9] and by Enomoto *et al.*[10] Yamaoka and Machida[11] have analyzed these spectra, including the overtones and the combinations, and have determined some anharmonic potential parameters. It would be interesting to compare their parameters for the CH_2 group with ours, which are determined by a completely different method.

Experimental

The absorption spectra of 1,1-dichloroethylene in the liquid phase were measured with a Fourier transform spectrometer (NICOLET 7199) in the frequency region of 2800—10000 cm^{-1} and with a UV-visible spectrometer (CARY 17) in the visible region. The sample was purchased from Tokyo Chemical Industry Co., Ltd. and used without further purification.

The observed frequencies at the absorption maxima, ν_{obsd}, and the integrated intensities, Γ_{obsd}, are listed in the first and the second columns of Table 1, respectively. The definition of Γ and the correction for the dielectric field are the same as those described in our preceding paper.[4]

Results and Discussion

NM Approach and LM Approach. In Fig. 1, two different approaches to reach the eigenstates are schematically summarized. In the NM approch, the coordinates of the oscillators are first delocalized by symmetrization and diagonarization of a GF matrix[12] prior to the quantizations and the quantum mechanical mixings caused by the anharmonic characters of the potential. On the other hand, the quantizations precede the symmetrizations and mixings in the LM approach. The differences between these two approaches may be analogized with those of the MO and VB theories for electronic structures, since orbitals are symmetrized and delocalized in MO before adding electrons whereas electronic structures in VB are constructed by making

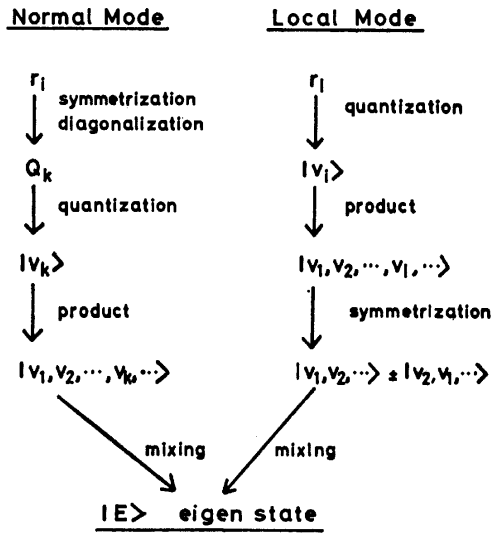

Fig. 1. Two different approaches to the eigen states.

proper pairs of the electrons which already belong to individual localized atomic orbitals.

The most different step in both approaches is the quantum mechanical mixings which may correspond to configuration interactions (CI) in the electronic theory. Therefore, the question of which method is more suitable must be answered from several points of view. One is to see which representation would cause smaller mixing or which can give closer states to the true eigenstates when the mixing process is discarded. The mixings in the NM representation are caused only by anharmonic terms in the potential, whereas any cross terms in kinetic and potential parts can cause mixings in the LM representation even in a completely harmonic system. So the NM approch would be better for fundamentals and also for low v overtones and combinations of skeletal vibrations where anharmonic characters are usually not so significant. However, hydrogen stretching motions in CH, OH, or NH are very anharmonic because of their large amplitude and high frequency. If there is a large anharmonic coupling term in the potential, and if there are more than two equivalent or nearly equivalent anharmonic oscillators, the anharmonic coupling term causes a mixing of the NM states, even if these two anharmonic oscillators are completely independent of each other in the internal coordinate system, that is,

$$v = \frac{1}{2}kq_1^2 + hq_1^3 + \frac{1}{2}kq_2^2 + hq_2^3$$
$$= \frac{1}{2}kQ_s^2 + \frac{1}{2}kQ_a^2 + \frac{h}{\sqrt{2}}Q_s^3 + \frac{3h}{\sqrt{2}}Q_sQ_a^2, \quad (1)$$

where

$$Q_s = \frac{1}{\sqrt{2}}(q_1+q_2) \text{ and } Q_a = \frac{1}{\sqrt{2}}(q_1-q_2). \quad (2)$$

Such induced anharmonic coupling causes very strong perturbations in the overtone region of CH_2 or CH_3 stretching modes, which are known by the name of Darling-Dennison resonances. The LM approach in such an anharmonic system, however, may not cause such strong mixing since all the effects of the anharmonic character can be considered at the stage of a one-dimensional oscillator problem. Although the harmonic coupling is large in this representation, the symmetrization procedure can greatly reduce the final mixings, as will be seen in the following section.

The second point of view on the choice of the LM or NM representation is to see which representation makes it easier to obtain the interaction terms related with the mixing. The third is to see which can give more physically meaningful descriptions for the finally obtained eigenstates. The answers from these points of view are obvious. Perturbation terms in the NM representation cannot be so simple because a normal coordinate itself is an already complicated linear combination of internal coordinates. By the same reason, an eigenstate expressed by a linear combination of NM states is difficult to visualize. On the other hand, an LM or SLM representation would make it much easier to obtain the perturbation terms as well as to understand the meaning of each eigenstate because of the simplicity of the basis modes. It must be emphasized that this advantage of LM or SLM is extremely important for wider application of the assigned spectra rather than for prediction of the absorption frequencies.

Hamiltonian of Coupled Morse Oscillator. The Hamiltonian of two equivalent interacting Morse oscillators may be written as

$$H = H_1 + H_2 + H_{12}, \quad (3)$$

where

$$H_i = \frac{1}{2m}p_i^2 + D_e(1-\exp(-\alpha q_i))^2, \quad (4)$$

$$H_{12} = g_{12}p_1p_2 + f_{12}q_1q_2. \quad (5)$$

H_i is the one-dimensional Hamiltonian for the i-th oscillator and H_{12} is the perturbation which couples the two oscillators. The first and second terms in Eq. 5 correspond to the kinetic and potential coupling, respectively. The higher order anharmonic coupling terms in the potential were neglected in Eq. 5. The eigenvalue of the H_i is expressed by

$$E_{v_i} = \omega_e\left(v_i+\frac{1}{2}\right) - \omega_e\chi_e\left(v_i+\frac{1}{2}\right)^2, \quad (6)$$

where

$$\omega_e = \left(\frac{\alpha}{\pi c}\right)\sqrt{\frac{D_e}{2m}}, \quad (7a)$$

$$\omega_e\chi_e = hc\omega_e^2/4D_e. \quad (7b)$$

Then the matrix elements of the two dimensional Hamiltonian, H, can be written as

$$\langle v_1,v_2|H|v_1,v_2\rangle = E_{v_1} + E_{v_2} + g_{12}\langle v_1|p|v_1\rangle\langle v_2|p|v_2\rangle + f_{12}\langle v_1|q|v_1\rangle\langle v_2|q|v_2\rangle, \quad (8)$$

$$\langle v_1,v_2|H|v_1',v_2'\rangle = g_{12}\langle v_1|p|v_1'\rangle\langle v_2|p|v_2'\rangle + f_{12}\langle v_1|q|v_1'\rangle\langle v_2|q|v_2'\rangle, \quad (9)$$

where $|v\rangle$ is an eigenstate of a one-dimensional Hamiltonian H_i, and

$$|v_1,v_2\rangle = |v_1\rangle|v_2\rangle. \quad (10)$$

Harmonic approximation for the matrix elements of H_{12} may be convenient for a preliminary analysis or for qualitative understanding of the mixing effects,

although the exact matrix elements based on the Morse oscillator wavefunctions are not so difficult to obtain. Some values used for 1,1-dichloroethylene are tabulated in the Appendix. The off-diagonal elements other than $v_1'=v_1\pm1$ and $v_2'=v_2\pm1$ are all zero in harmonic approximation or small even in exact solution.

Introducing the symmetrized local mode (SLM) states as

$$(u_1,v_2)^{\pm}=\begin{cases}\frac{1}{\sqrt{2}}(|v_1,v_2\rangle\pm|v_2,v_1\rangle) & \text{for } v_1>v_2\\ |v_1,v_2\rangle & \text{for } v_1=v_2 \text{ and } (+) \text{ state}\end{cases}, \quad (11)$$

the Hamiltonian matrix is reduced to

$$\langle v_1,v_2,\pm|H|v_1',v_2',\pm\rangle=\langle v_1,v_2|H|v_1',v_2'\rangle \pm\langle v_1,v_2|H|v_2',v_1'\rangle \quad \text{for } v_1>v_2 \text{ and } v_1'>v_2', \quad (12)$$

$$\langle v,v,+|H|v,v,+\rangle=\langle v,v|H|v,v\rangle, \quad (13)$$

$$\langle v,v,+|H|v_1,v_2,+\rangle=\sqrt{2}\langle v,v|H|v_1,v_2\rangle. \quad (14)$$

Since the states which have the same value of v_1+v_2 form a nearly degenerate group, and since the off-diagonal elements are very small compared to the energy difference between the different groups, the mixing of the states may essentially occur between these states belonging to the same group.

The degenerate pair states in LM, (v_1,v_2) and (v_2,v_1), split into doublets, $(v_1,v_2)^+$ and $(v_1,v_2)^-$, in SLM. The magnitude of the splitting, however, is large only when $v_2=v_1-1$, as easily seen in harmonic approximation. For other states, splitting is mainly caused by small differences of mixings between (+) and (−) states through higher order perturbations, although the anharmonic character of the off-diagonal matrix elements may be also responsible to some extent. The splitting of $(v,0)^{\pm}$ decreases rapidly with the increase of v and the states behave as a pure local mode state. Figure 2 shows a schematical energy diagram which correlates NM states to LM states from the above considerations.

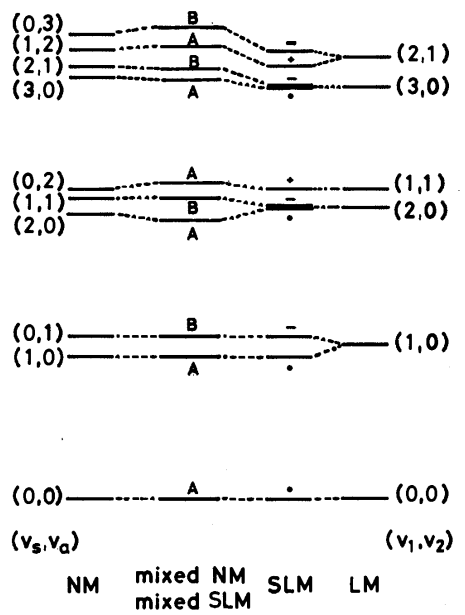

Fig. 2. Schematical energy diagram wich correlates NM states to LM states. The structure in NM was drawn using the tentative values for the parameters, $(\omega_e\chi_e)_s$ and $(\omega_e\chi_e)_a$, the effects of $\chi_{s,a}$ were taken in mixed NM. A and B denote the symmetric stretching and antisymmetric stretching states for the C_2 operation around the molecular axis. (+) and (−) states were defined by Eq. 11.

Frequency Analysis and Potential Parameters. Prior to the two dimensional analysis of the spectrum, ω_e and $\omega_e\chi_e$ were estimated to be 3194 cm^{-1} and 58 cm^{-1} respectively by the use of the Birge-Sponner relation[13] for the overtone series, assuming a one dimensional oscillator model. There were two more parameters, f_{12} and g_{12}, necessary for the two dimensional calculation. It was, however, very difficult to determine these two parameters independently because $\langle v_1,v_2|H|v_1+1,v_2-1\rangle$, which is most responsible for mixing, always contains f_{12} and g_{12} in the same combined form in harmonic approximation, although such constraint is to be destroyed in $\langle v_1,v_2|H|v_1+1,v_2+1\rangle$ which connects different groups and also in the anharmonic calculation. Therefore, we used the calculated value of $(1/m_C)\cos(\angle HCH)=-0.04167$ amu^{-1} for g_{12} using the assumed angle of $\angle HCH=120°$. g_{12} was fixed at this value throughout the present analysis.

A preliminary calculation was done neglecting f_{12} under a harmonic approximation for the off-diagonal

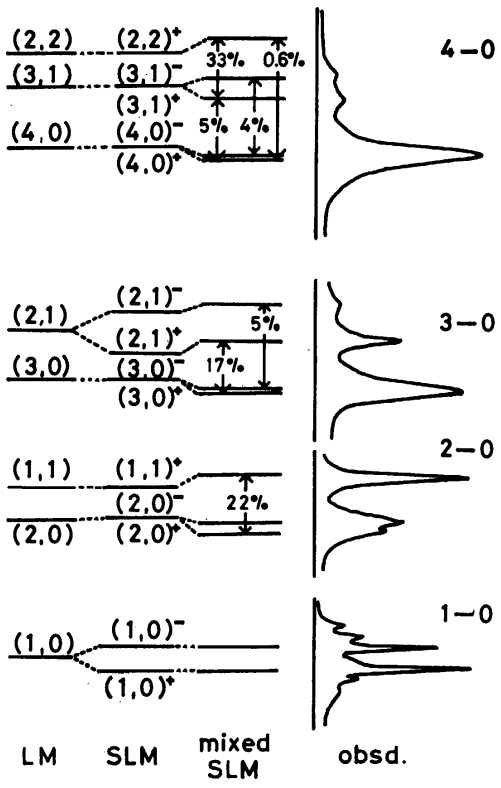

Fig. 3. Observed spectrum and their assignment. The energy diagram was shown by the diagonal elements in each representation in order to show how to approach to the eigen values. The numbers in % show the degree of the mixing between the two states which are connected by the arrows.

TABLE 1. OBSERVED PEAK FREQUENCIES (ν-obsd), OBSERVED INTENSITIES (Γ-obsd), THEIR ASSIGNMENTS, CALCULATED PEAK FREQUENCIES (ν-calcd), AND CALCULATED EIGENSTATES AS A LINEAR COMBINATIONS OF SLM

ν-obsd / cm^{-1}	Γ-obsd / cm^2 mol^{-1}	Assign.[a]	ν-calcd / cm^{-1}	Eigenstates (mixed SLM)		
3035	197	$(1,0)^+$	3032	$(1,0)^+$		
3130	131	$(1,0)^-$	3124	$(1,0)^-$		
5990	3.26	$(2,0)^+$	5993	$0.882(2,0)^+$	$+0.471(1,1)^+$	
6025	4.3	$(2,0)^-$	6042	$(2,0)^-$		
6210	5.2	$(1,1)^+$	6205	$0.882(1,1)^+$	$-0.471(2,0)^+$	
8860	0.54	$(3,0)^+$	8849	$0.912(3,0)^+$	$+0.410(2,1)^+$	
		$(3,0)^-$	8869	$0.974(3,0)^-$	$+0.228(2,1)^-$	
9070	0.21	$(2,1)^+$	9076	$0.912(2,1)^+$	$-0.410(3,0)^+$	
9230	0.03	$(2,1)^-$	9226	$0.974(2,1)^-$	$-0.228(3,0)^-$	
11601	0.051	$(4,0)^+$	11599	$0.970(4,0)^+$	$+0.227(3,1)^+$	$+0.080(2,2)^+$
		$(4,0)^-$	11601	$0.977(4,0)^-$	$+0.212(3,1)^-$	
11880	0.003	$(3,1)^+$	11897	$0.784(3,1)^+$	$+0.576(2,2)^+$	$-0.231(4,0)^+$
11990	0.003	$(3,1)^-$	11994	$0.977(3,1)^-$	$-0.212(4,0)^-$	
—	0	$(2,2)^+$	12191	$0.814(2,2)^+$	$-0.577(3,1)^+$	$+0.068(4,0)^+$
14204	0.006	$(5,0)^+$	14219	$0.982(5,0)^+$	$+0.184(4,1)^+$	$+0.052(3,2)^+$
		$(5,0)^-$	14220	$0.983(5,0)^-$	$+0.181(4,1)^-$	$+0.027(3,2)^-$
14705	0.002	$(4,1)^+$	14649	$0.821(4,1)^+$	$+0.542(3,2)^+$	$-0.182(5,0)^+$
—	0	$(4,1)^-$	14694	$0.946(4,1)^-$	$+0.270(3,2)^-$	$-0.182(5,0)^-$
16722	0.0008	$(6,0)^\pm$	16720			

a) Most dominant SLM state.

matrix elements. The results were good enough to assign all the peaks in the observed spectra. The three peaks at 5990 cm^{-1}, 6025 cm^{-1}, and 6210 cm^{-1} in the first overtone region were assigned to the $(2,0)^+$, $(2,0)^-$, and $(1,1)^+$ dominant states. These bands were assigned to $2\nu_1$, $\nu_1+\nu_9$, and $2\nu_9$, respectively, in the NM representation by Yamaoka and Machida.[11] The 8860 cm^{-1} peak was assigned to the unresolved $(3,0)^+$ and $(3,0)^-$ pairs corresponding to $3\nu_1$ and $2\nu_1+\nu_9$ respectively, whereas $(2,1)^+$ and $(2,1)^-$ were assigned to the 9070 cm^{-1} peak ($\nu_1+2\nu_9$, in the NM representation) and 9230 cm^{-1} peak ($3\nu_9$, in the NM representation), respectively, which show larger splitting. Other peaks were also assigned as shown in the third column of Table 1 and in Fig. 3.

Next, f_{12} and more refined ω_e and $\omega_e\chi_e$ values were determined by the least squares methods still within the harmonic approximation. The final parameters in Table 2 were obtained using the exact matrix elements based on the Morse potential which are listed in the Appendix. The calculated frequencies were in good agreement with the observed ones, as shown in the fourth column of Table 1. The last column of Table 1 shows the calculated eigenstates as a linear combination of SLM.

TABLE 2. SPECTROSCOPIC PARAMETERS

ω_e/cm^{-1}	3191.6
$\omega_e\chi_e$/cm^{-1}	57.63
f_{12}/cm^{-1} Å^{-1}	2170 (0.043 mdyne Å^{-1})
g_{12}[a]/amu^{-1}	−0.04167
D_e/cm^{-1}	44190
α/Å^{-1}	1.755

a) Calculated assuming $\angle$HCH=120°.

The changes of the spectral structures with the change of the basis representations are schematically shown in Fig. 3 together with the observed spectra. The degeneracy of the fundamental bands, (1,0) and (0,1) in LM, was easily resolved into $(1,0)^+$ and $(1,0)^-$ in the SLM representation as well as in the other $(v,v-1)$, $(v-1,v)$ pair states. However, (2,0) and (0,2) in LM were still practically degenerate in pure SLM. The splitting of these levels were caused by a second order perturbation which mixed $(2,0)^+$ and $(1,1)^+$ by 22%. The other pair states which did not show splitting in SLM were also split by mixing to a greater or lesser degree, although the splitting of $(v,0)$ states became smaller with the increase of v, as stated in the previous paragraph.

Intensity Analysis and Dipole Moment Function. The change of the dipole moment with the displacement of q_1 and q_2 could be expressed by

$$\boldsymbol{D}(q_1,q_2) = \boldsymbol{D}_1(q_1) + \boldsymbol{D}_2(q_2) + \boldsymbol{D}_{12}(q_1,q_2), \tag{15}$$

where $\boldsymbol{D}_1$ or $\boldsymbol{D}_2$ is the change induced by the change of q_1 or q_2, respectively, while the other coordinate q_2 or q_1 remains unchanged. $\boldsymbol{D}_{12}$ expresses the interacting effect which appears when q_1 and q_2 change simultaneously. Instead of Eq. 15, $\boldsymbol{D}(q_1,q_2)$ may be written in another form as

$$\boldsymbol{D}(q_1,q_2) = D_{//}(q_1,q_2)\,\boldsymbol{i} + D_{\perp}(q_1,q_2)\,\boldsymbol{j}, \tag{16}$$

where $\boldsymbol{i}$ and $\boldsymbol{j}$ are the unit vectors parallel and perpendicular to the molecular axis respectively, as shown in Fig. 4. Here, we assume that directions of $\boldsymbol{D}_1$ and $\boldsymbol{D}_2$ do not change because of the magnitude of q_1 and q_2. Let θ be the angle of $\boldsymbol{D}_1$ measured from the direction of $\boldsymbol{i}$ and let M be the scalar part of $\boldsymbol{D}_1$. Then we obtain this relations:

$$D_{//} = (M(q_1) + M(q_2))\cos\theta + M_{12}q_1q_2, \tag{17}$$

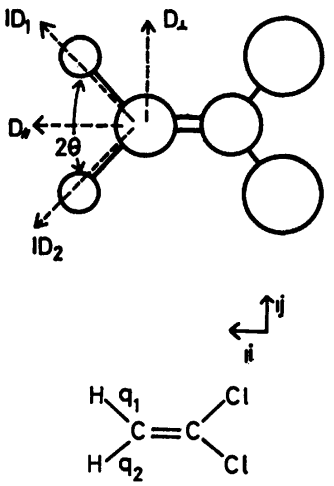

Fig. 4. The change of the dipole moment of CH_2CCl_2 and its relation to the molecular framework.

$$D_\perp = (M(q_1) - M(q_2))\sin\theta. \quad (18)$$

Here, we make a further approximation by neglecting the higher order terms in $\boldsymbol{D}_{12}(q_1,q_2)$ such as $M_{122+}(q_1q_2^2+q_1^2q_2)\,\boldsymbol{i}$ and $M_{122-}(q_1q_2^2-q_1^2q_2)\boldsymbol{j}$. $M(q)$ is a dipole moment function in one dimensional approximation as treated in our preceding paper[4] and we can expand it in a power series of q:

$$M(q)=M_1q+M_2q^2+\cdots. \quad (19)$$

The higher order terms in Eq. 19 were again neglected. θ is an unknown parameter because $\boldsymbol{D}_1$ will not necessarily be parallel to the direction of the displacement of q_1. So we have four parameters to be determined from the intensity analyses of the observed spectra.

The symmetry considerations show that a transition from the ground state to any (+)-state or to any (−)-state must be induced by $D_{//}$ or $D_\perp$, respectively. The transition moments in the SLM representation are given by

$$\langle v,0,+|\boldsymbol{D}|0\rangle = \sqrt{2}\cos\theta\langle v|M|0\rangle\,\boldsymbol{i} + \sqrt{2}\,M_{12}\langle v|q|0\rangle\langle 0|q|0\rangle\,\boldsymbol{i}, \quad (20)$$

$$\langle v,0,-|\boldsymbol{D}|0\rangle = \sqrt{2}\sin\theta\langle v|M|0\rangle\,\boldsymbol{j}, \quad (21)$$

$$\langle v_1,v_2,+|\boldsymbol{D}|0\rangle = \begin{cases} \sqrt{2}\,M_{12}\langle v_1|q|0\rangle\langle v_2|q|0\rangle\,\boldsymbol{i} & \\ \qquad\qquad \text{for } v_1\neq v_2>0 & \\ M_{12}\langle v|q|0\rangle^2\,\boldsymbol{i} \quad \text{for } v_1=v_2>0. & \end{cases}$$

The second term of Eq. 20 is smaller than the first term because an anharmonic character is necessary for $\langle 0|q|0\rangle\neq 0$. Thus, we may say that M is responsible for the appearence of the fundamental and pure overtone bands whereas M_{12} is responsible for the appearence of pure combinations with (+)-symmetry. Pure combination bands with (−)-symmetry are inactive in this approximation, although they may appear in higher order approximation through the terms such as M_{122-}.

The transition moment corresponding to a mixed state, $|n\rangle=\sum C_{nv}|v\rangle$, is written as

$$\langle n|D|0\rangle = \sum C_{nv}\langle v|D|0\rangle \quad (24)$$

where $|v\rangle$ is a representative of a pure SLM state $|v_1,v_2\rangle$ and C_{nv} is a linear combination coefficient as listed in Table 1.

Deduction of the Dipole Moment Parameters. The appearence of the combination bands would be totally attributed to the degree of mixing with allowed pure overtones in the absence of M_{12}. The 6210 cm^{-1} peak assigned to the $(1,1)^+$ dominant state, however, was stronger than the 5990 cm^{-1} assigned to the $(2,0)^+$ dominant state, although the calculation showed only 22% of mixing between the two SLM's. This fact indicated considerable contribution of M_{12} to the spectrum.

Analyzing the observed intensities of the five peaks in the fundamental and the first overtones using Eqs. 20—24 and the matrix elements of the Appendix, we obtain:

$$|\langle 1|M|0\rangle| = 2.56\times10^{-2}\ \text{D},$$
$$|\langle 2|M|0\rangle| = 4.76\times10^{-2}\ \text{D},$$
$$|M_{12}| = 0.386\ \text{D Å}^{-1},$$
$$\theta = 38.4°\pm0.2°.$$

Here, the sign of M_{12} depends on M. It must be chosen so that it can be constructive with M in the $(1,1)^+$ dominant band but destructive in the $(2,0)^+$ dominant band.[14] From these values, the contribution of M_{12} to the total integrated intensity over the second overtone region was estimated to be less than a few per cent, and much less for the higher overtones. Thus we could use the one-dimensional approximation for the other $|\langle v|\boldsymbol{D}|0\rangle|$'s with $v>2$. In the determination of M_1 and M_2 in M, the procedure described in our preceding papers[4,5] was employed. The intensity values were converted to those of the one-dimensional model by subtracting small contributions from M_{12}. These corrected values showed a slight dip in the 2←0 transition (see Fig. 5) as seen in benzene and cyclohexane.[4] Therefore, the relation, $M_1M_2>0$, could be obtained.[4] It would be reasonable to choose $M_1<0$ and $M_2<0$, according to the *ab initio* calculation for ethylene and also

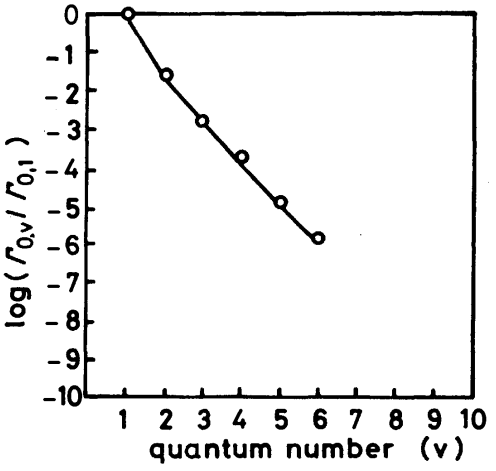

Fig. 5. The logarithmic relative intensity, $\Gamma_{0,v}/\Gamma_{0,1}$, for liquid 1,1-dichloroethylene plotted against a vibrational quantum number, v. Open circles represent the observed values, while the solid line connects these values calculated from the best-fit parameter, $M_2/M_1=3.03$ Å^{-1}.

TABLE 3. DIPOLE MOMENT PARAMETERS

	This work	Ethylene (*Ab initio*)
M_1/D Å^{-1}	−0.29	−0.64
M_2/D Å^{-2}	−0.88	−1.23
M_{12}/D Å^{-2}	0.39	0.57
θ/°	38.4	52.3

considering the results of benzene and cyclohexane. This choice of the sign for M enforced $M_{12}>0$. The finally obtained parameters are listed in Table 3.

Comments on the Final Results. There are two causes which mix the states in the SLM representation, namely, kinetic coupling and potential coupling. We ignored the anharmonic coupling in the potentials. The excellent agreement between the calculated and observed frequencies seems to confirm this approximation. The contributions from these two types of coupling were evaluated numerically to see which is more effective in the 1,1-dichloroethylene system. One off-diagonal elements, shown as

$$\begin{aligned}\langle 2,0,+|0|1,1,+\rangle &= \sqrt{2}(q_{12}\langle 2|p|1\rangle\langle 0|p|1\rangle \\ &\quad + f_{12}\langle 2|x|1\rangle\langle 0|x|1\rangle) \\ &= -111.5\ \mathrm{cm^{-1}} + 26\ \mathrm{cm^{-1}}\end{aligned}$$

indicated that f_{12} was less effective in the mixing. This might be one of the reasons why the preliminary calculation with $f_{12}=0$ led to the frequencies which are satisfactory enough to allow assignment of the observed spectrum.

The f_{12} value determined in this work was positive, unlike that of Yamaoka and Machida.[11] Our value is close to f_{12} of ethylene, 0.0185 mdyne/Å, including its sign, which was obtained by the same authors.[15] D_e and the Morse parameter, α, were deduced from ω_e and $\omega_e\chi_e$ and are listed in Table 2. The α-value of 1.75 Å^{-1} was 10% larger than Machida's value.

Our approach has the advantage of giving more physically meaningful assignments for the spectrum as well as some simplicity of the analysis. The assignments in the NM representation, such as $2\nu_1$ or $\nu_1+2\nu_9$, may not have much physical meaning except for the symmetry because of the strong mixing due to the Darling-Dennison reasonance in the CH overtone regions. Although the mixing can never be neglected in SLM, the meaning of the mixing is still clear. We found the $(v,0)^{\pm}$ dominant states tended to be more isolated and tended to degenerate rapidly for $v>3$. This corresponds to the formation of pure local modes in spectra. The other states, however, did not show these tendencies even in the highest states examined. So we may say that the LM representation is surely preferable in the cases of the optically allowed high v states. But we should remember that there are many other excited states which neither LM nor NM can describe in a simple form, although they are almost forbidden in absorption spectra.

The intensities calculated from the parameters in Table 3 are listed in the fourth column of Table 4. The numbers in the parentheses are the intrinsic intensities of the pure SLM bands in the absence of mixing. The contributions of M and M_{12} to each transition moment are separately listed in the sixth and seventh columns respectively. The last column shows the percent contribution of M_{12} to the total integrated band intensities, f_{M12}. It can be seen that f_{M12} is not very large. It is only 13.6% even in the largest case, for the 2←0 band. The second largest is 3.4% for the 3←0 band. If the effects of M_{12} in other molecules are the same order in magnitude, the one-dimensional analysis in the preceding paper[4] would be

TABLE 4. CALCULATED INTENSITIES AND THE CONTRIBUTION OF M_{12}

ν_0 / cm^{-1}	Assign.	Γ-obsd / cm^2 mol^{-1}	Γ-calcd / cm^2 mol^{-1}	Γ-intrinsic / cm^2 mol^{-1}	$\langle n\|M\|0\rangle$ / 10^{-3} D	$\langle n\|M_{12}q_1q_2\|0\rangle$ / 10^{-3} D	$f_{M_{12}}$ / %
3035	$(1, 0)^+$	197	198	(198)	−28.7	0.61	0.03
3130	$(1, 0)^-$	131	129	(129)	−22.7	0	
5990	$(2, 0)^+$	3.26	3.25	(7.2)	−4.62	1.65	13.6
6025	$(2, 0)^-$	4.3	4.39	(4.39)	−4.18	0	
6210	$(1, 1)^+$	5.2	5.28	(1.33)	2.50	2.03	
8860	$(3, 0)^+$	0.54	0.38	(0.57)	1.36	−0.135	3.4
	$(3, 0)^-$		0.33	(0.34)	1.14	0	
9070	$(2, 1)^+$	0.27	0.20	(0.025)	0.69	0.33	
9230	$(2, 1)^-$	0.03	0.016	(0)	0.25	0	
11601	$(4, 0)^+$	0.051	0.036	(0.038)	−0.39	0.01	0.7
	$(4, 0)^-$		0.024	(0.024)	−0.31	0	
11880	$(3, 1)^+$	0.003	0.004	(0.0006)	0.097	0.040	
11990	$(3, 1)^-$	0.003	0.004	(0)	0.075	0	
—	$(2, 2)^+$	0	0.0003	(0.0001)	−0.027	−0.010	
14204	$(5, 0)^{\pm}$	0.006	0.0036	(0.0036)	0.12	−0.002	0.0
			0.0025	(0.0025)	0.10	0	
14705	$(4, 1)^+$	0.0002	0.0002	(0.0000)	−0.022	−0.009	
16722	$(6, 0)^{\pm}$	0.0008	0.0006	(0.0006)			0.0

Intensities and matrix elements are connected by the following relation:

$$\Gamma = \frac{8\pi^3 N}{3hc}|\langle 0|M|v\rangle|^2 = 2.508\times 10^5|\langle 0|M|v\rangle|^2 \quad \text{(see Ref. 4).}$$

practically assured.

M_{12}, however, shows a great deal of perturbations on the intensity distributions in the overtones. This is due to interferring interactions with M which happened to contribute to the same transition moment through mixing of the states. From columns 6 and 7, we see that M alone and M_{12} alone explained only 31% and 20% of the total intensity of the $(1,1)^+$ dominant transition. The remaining 49% must be attributed to the constructive property[14] of M and M_{12} in the transition moment. In contrast to this transition, $(2,0)^+$ dominant states were 40% smaller in intensity than what M alone could induce. This was attributed to the destructive[14] contribution of M_{12}.

The obtained dipole moment parameters were compared with the *ab initio* values of ethylene, since we failed to find the corresponding experimental parameters in the literature. The *ab initio* calculation was the one described in the preceding paper.[4] The sign of M_{12} was found to be positive, as shown in Table 3. However, θ was smaller than expected. The direction of the change of the dipole moment induced by a displacement of one CH bond deviates more than 20° from the direction of the displacement, whereas the *ab initio* value of θ in ethylene was very close to what we expected from the direction of the displacement. We believe the experimental error in θ is not so large, since it is strongly correlated to the ratio of the intensities of $(1,0)^-$ and $(1,0)^+$ bands. Polarization of the electrons in chlorine atoms induced by the stretching of CH bonds might be responsible for such small values of θ.

Appendix

MATRIX ELEMENTS FOR MORSE OSCILLATOR WITH THE PARAMETERS IN TABLE 2

$\langle v|q|v'\rangle/10^{-2}$ Å

	0	1	2	3	4	5	6
0	1.57						
1	7.71	4.80					
2	−0.748	11.00	8.18				
3	0.120	−1.32	13.60	11.7			
4	−0.025	0.25	−1.91	15.90	15.47		
5	0.0064	−0.059	0.40	−2.52	17.96	19.40	
6	−0.0019	0.016	−0.105	0.59	−3.14	19.87	23.53

$\langle v|q^2|v'\rangle/10^{-4}$ Å^{-2}

	0	1	2	3	4	5	6
0	62.41						
1	40.64	205.2					
2	79.15	118.5	377.2				
3	−19.19	132.8	224.6	582.2			
4	4.90	−38.2	181.0	357.0	825		
5	−1.414	11.19	−60.1	224.0	517	1109	
6	0.453	−3.53	19.5	−84.23	260	699	1428

$\langle v|p|v'\rangle/i$(cm^{-1} amu)$^{1/2}$

	0	1	2	3	4	5
0	0.668					
1	−37.457	1.925				
2	6.274	−51.665	3.082			
3	1.294	10.748	−61.629	4.190		
4	0.314	−2.600	15.005	−69.211	5.099	
5	−0.082	0.714	−4.124	19.127	−75.139	5.958
6	0.028	−0.212	1.257	−5.842	23.077	−79.778

i: The unit pure imaginary number.

In the final stage of preparing this paper, we received a preprint of a new work on local mode spectra of dihalomentanes from B. R. Henry. We should point out an accidental similarity in the way of approach between their work and this work.

References

1) Y. Mizugai and M. Katayama, *Chem. Phys. Lett.*, **73**, 240 (1980); N. Yamamoto, N. Matsuo, and H. Tsubomura, *Chem. Phys. Lett.*, **71**, 463 (1980).

2) B. R. Henry and W. Siebrand, *J. Chem. Phys.*, **49**, 5369 (1968).

3) R. L. Swofford, M. E. Long, and A. C. Albrecht, *J. Chem. Phys.*, **65**, 179 (1976); M. E. Long, R. L. Swofford, and A. C. Albrecht, *Science*, **191**, 183 (1976).

4) K. Tamagake, S. Hyodo, and T. Fujiyama, *Bull. Chem. Soc. Jpn.*, **55**, 1267 (1982).

5) S. Hyodo, K. Tamagake, and T. Fujiyama, *Bull. Chem. Soc. Jpn.*, **55**, 1272 (1982).

6) M. Goldsmith, G. Amat, and A. H. Nielsen, *J. Chem. Phys.*, **24**, 1178 (1956).

7) H. H. Nielsen, "Handbuch der Physik," ed by S. Flugge, Springer-Verlag, Berlin (1959), Vol. 37.

8) B. T. Darling and D. M. Dennison, *Phys. Rev.*, **57**, 128 (1940).

9) F. Winter and D. O. Hummel, *Spectrochim. Acta, Part A*, **23**, 1839 (1967).

10) S. Enomoto and S. Ichinohe, *Nippon Kagaku Zasshi*, **79**, 1343 (1958).

11) Y. Yamaoka and K. Machida, *J. Mol. Spectrosc.*, **83**, 21 (1980).

12) E. B. Wilson, T. C. Decius, and P. C. Cross, "Molecular Vibrations," McGraw-Hill, New York (1955).

13) R. T. Birge and H. Sponner, *Phys. Rev.*, **28**, 259 (1926).

14) The absorption intensity, I, is expressed in terms of M and M_{12} as,

$$I \propto (\langle M\rangle + \langle M_{12}\rangle)^2$$
$$= \langle M\rangle^2 + \langle M_{12}\rangle^2 + 2\langle M\rangle\langle M_{12}\rangle.$$

The effect of M_{12} is said to be "constructive" or "destructive" with M according to whether the sign of the $\langle M\rangle\langle M_{12}\rangle$ term is "positive" or "negative," respectively.

15) K. Machida and Y. Tanaka. *J. Chem. Phys.*, **61**, 5040 (1974).

Salting-out Phenomenon and Clathrate Hydrate Formation in Aqueous Solution of Polar Nonelectrolyte

Tadashi KATO,* Masako YUDASAKA, and (the late) Tsunetake FUJIYAMA

Institute for Molecular Science, Myodaiji, Okazaki 444

(Received August 14, 1981)

The Salting-out Phenomenon has been carefully observed by adding ammonium chloride into aqueous solutions of *t*-butyl alcohol, acetone, dioxane, and 2-butoxyethanol. The experimental results have been well explained by considering the formation of a clathrate hydrate-like local structure in the aqueous solution of each nonelectrolyte. In addition, the role of the chloride ion has been found to be the promotion of the aggregation of the clathrate hydrate-like local structures. The line-width measurement of ^{35}Cl-NMR spectra has been shown to be an extremely powerful method for studying the state of mixing of ions in solutions.

The mutual solubility of a nonelectrolyte and water is decreased by the addition of inorganic salts. The interpretation of this salting-out phenomenon from a molecular viewpoint originated in the work of Debye *et al.*[1] They presented an equation which relates the solubility of a nonelectrolyte with the salt concentration in terms of the dielectric constant of the solution. Later on, some modifications of Debye's theory have been reported.[2-4] These theories are based on the idea that the solubilities of nonelectrolytes diminish by adding salts into aqueous solutions because the ions draw water molecules around themselves and, therefore, rob the water molecules from the nonelectrolytes. The scaled particle theory has been proposed from a completely different point of view.[5] This theory does not imply any model for the structure of the solvent and calculates thermodynamic quantities through the estimation of a free energy which is necessary first to make cavities in solvents and, then, to introduce nonelectrolyte molecules into the cavities. There are currently many attempts to explain salting-out phenomena by the use of this theory.[6,7]

In general, the solubilities of polar nonelectrolytes in water are much larger than those of nonpolar molecules; sometimes the two components are miscible in all proportions. Therefore, the salt concentration required to cause a phase-separation is higher than that in the case of nonpolar molecules. However, the application of the foregoing theories has been limited to the very low concentration range of salt or nonelectrolyte. Solubility curves such as those shown in Fig. 1 cannot be explained by these theories even qualitatively.

In our previous reports, the existence of clathrate hydrate-like local structures has been suggested in aqueous solutions of polar nonelectrolytes such as *t*-butyl alcohol (TBA) and acetone.[8-10] Although these nonelectrolytes are miscible with water in all proportions, the addition of salt causes phase-separation.

In the present work, we consider the salting-out phenomena based on the results of the above studies and emphasize the role of a clathrate hydrate-like local structure formed in the aqueous solutions of a nonelectrolyte. It will be shown that the line-width measurement of the ^{35}Cl-NMR spectrum is a useful method for the clarification of these problems. Ammonium chloride was chosen as a salt because it has been known that ammonium chloride changes the structure of water very little.[11]

Experimental

Materials. Dioxane, *t*-butyl alcohol, 2-butoxyethanol, and ammonium chloride were commercially available in a guaranteed grade; they were used without further purification. Water was distilled and passed through an exchange resin.

Determination of Solubility Curve. Weighed ammounts of water, nonelectrolyte, and ammonium chloride were sealed in glass tubes. The phase-separation temperature, T_p, of each ternary solution was determined in a water bath by the observation of the temperature at which the solution became turbid. The accuracy of T_p was ± 0.5 °C. The solubility curves at various temperatures were determined by the observation of T_p at various concentrations.

NMR Measurement. The ^{35}Cl-NMR spectra were recorded on a Varian FT80A spectrometer at 7.794 MHz. For a spectral width of 4000 Hz and an aquisition time of 0.4 s. 8000 data points are available in the time domain spectra. The alpha delay was kept at 1000 s, while the Fourier number was kept at 16384. No weighting function was applied; this avoided artificial broadening of the line-widths. The accuracy of the half-line-width was ± 1.5 Hz.

Results and Discussion

Solubility Curve. The solubility curves of ternary solutions of water, ammonium chloride, and various nonelectrolytes (TBA, acetone, dioxane, and 2-butoxyethanol) at 40 °C are shown in Fig. 1. We define two kinds of concentrations, X_2' and X_3,

$$X_2' = \frac{n_2}{n_1+n_2}$$

and

$$X_3 = \frac{n_3}{n_1+n_2+n_3},$$

where n_1, n_2, and n_3 are the number of moles of a water, nonelectrolyte, and ammonium chloride, respectively. In Fig. 1, X_2' is plotted as abscissa, while X_3 as ordinate. We define here a new quantity, $X_3^{\min}$ as the minimum value of the mole fraction of ammonium chloride which is necessary to make the ternary solution separate into two liquid phases. The figure shows that $X_3^{\min}$ decreases rapidly as X_2' increases in the low concentration range. For each system, there exists a concentration range where ammonium chloride is precipitated before phase-separation occurs. This concentration range is defined as $0 \leq X_2' \leq X_2^{\mathrm{p}}$.[12] For example, X_2^{p} is about 0.03 for the TBA system. Figure 2 shows the

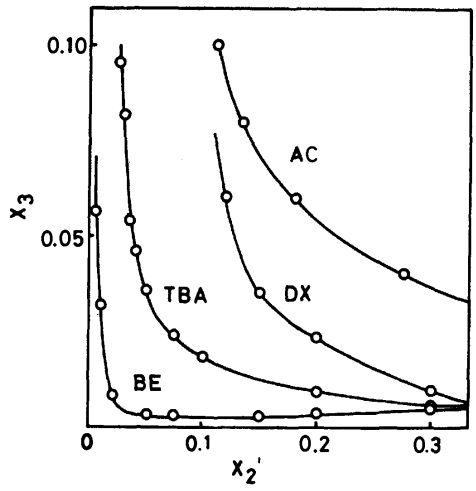

Fig. 1. Solubility curve for ternary solutions of water, ammonium chloride, and various nonelectrolytes (acetone(AC), dioxane(DX), *t*-butyl alcohol(TBA), and 2-butoxyethanol(BE)) at 40 °C.

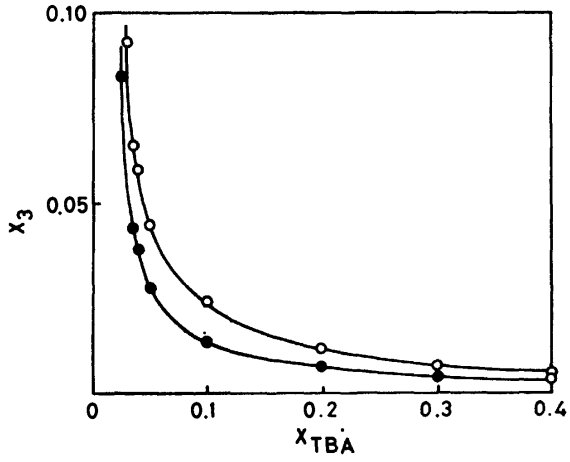

Fig. 2. Solubility curve for TBA–water–ammonium chloride solution at 30 °C (○) and 50 °C (●).

solubility curves for the TBA system at 30 °C and 50 °C. The figure shows that X_3^{min} decreases as the temperature increases, but that X_2^s is only slightly dependent on temperature. These results may depend on the mixing state of the binary solution of water and the nonelectrolyte. We will thus compare the solubility curves with the mean-square concentration fluctuations for the binary solution, which sensitively reflect the mixing state.

Concentration Fluctuations for Binary Solution and Solubility Curve. Figure 3 shows the mean-square concentration fluctuation, $N<(\Delta X)^2>$, for the aqueous solutions of TBA,[8] dioxane,[8] and 2-butoxyethanol[13] at 40 °C where N is the mean number of total molecules included in the field within which the concentration fluctuations are considered. It is seen from the figure that the $N<(\Delta X)^2>$ value is nearly equal to that for an ideal solution in the low concentration range and begins to increases abruptly at a certain mole fraction, X_2^s. For example, X_2^s is about 0.04 for the TBA system. Figures 1

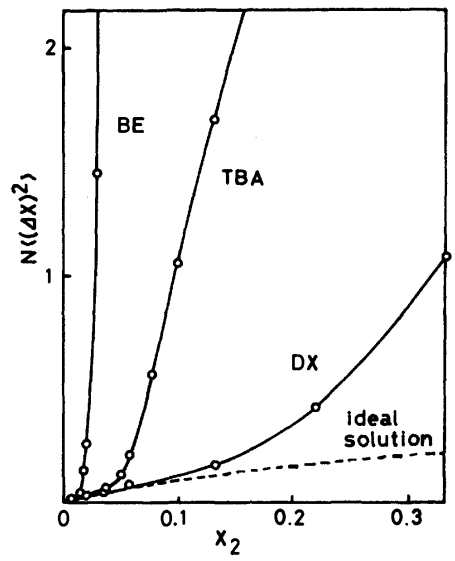

Fig. 3. Concentration dependence of mean-square concentration fluctuation for aqueous solutions of dioxane (DX), *t*-butyl alcohol(TBA), and 2-butoxyethanol(BE) at 40 °C.

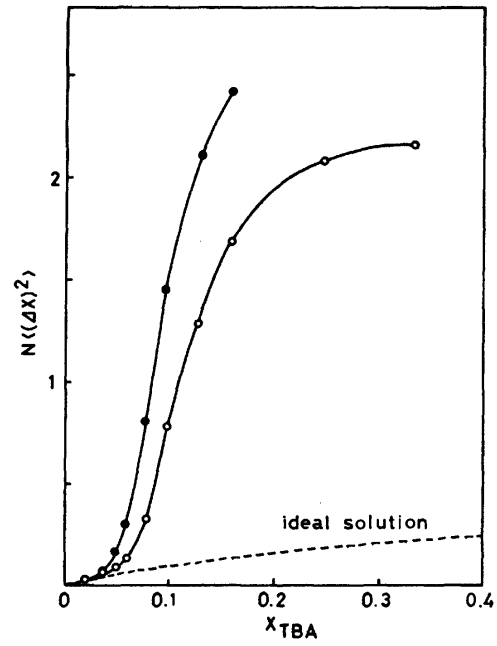

Fig. 4. Concentration dependence of mean-square concentration fluctuation for TBA–water solution at 24 °C (○) and 50 °C (●).

and 3 show that X_2^s is nearly eaual to X_2^p. Figure 4 shows the temperature dependence of the $N<(\Delta X)^2>$ values for the TBA–water system. $N<(\Delta X)^2>$ increases in magnitude with the elevation of temperature in the concentration range of $X_{TBA}>X_{TBA}^s$. Similar results have been obtained for other systems. These results suggest that the solution is rapidly approaching the phase-separation with the increase of the temperature. In fact, 2-butoxyethanol(BE)–water system has a lower critical temperature. The phase diagram (T-X_2 curve) for this system is shown in Fig. 5.[14] Figures 3 and 5 show

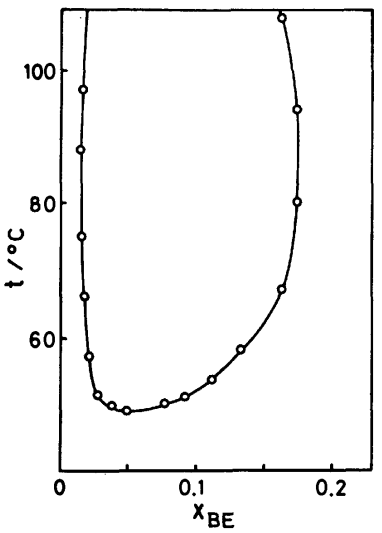

Fig. 5. Phase diagram for 2-butoxyethanol–water solution.

that the phase diagram is strongly correlated with the concentration dependence of the $N\langle(\Delta X\rangle)^2$ value. The phase-separation temperature decreases with the increase of $N\langle(\Delta X)^2\rangle$ in the concentration range of $X_{BE}<X_{BE}^s$ and the phase-separation does not occur in the concentration range of $X_{BE}<X_{BE}^s$. Similar results have been obtained for other systems, such as, the 2,6-lutidine–water system.[13] The relation between the X_3-X_2' curve (Fig. 1) and the concentration dependence of the $N\langle(\Delta X)^2\rangle$ value is similar to that between the T-X_2 curve and the concentration dependence of the $N\langle(\Delta X)^2\rangle$ value. X_2^{min} rapidly decreases with the rapid increase of the $N\langle(\Delta X)^2\rangle$ value and salting-out does not occur in the concentration range of $X_2<X_2^s$. It can be concluded that an addition of salt causes phenomenologically the same change of the mixing state of the binary aqueous solutions as that caused by an elevation of temperature.

The temperature dependence of the mixing state for the TBA–water system has been discussed based on the quantitative analysis of the concentration fluctuations.[8,10] The conclusion is as follows. In the concentration range of $0<X_{TBA}<X_{TBA}^s$, water molecules form a polyhedron which encages a TBA molecule in water. In the concentration range of $X_{TBA}>X_{TBA}^s$, the polyhedra gather together in TBA. As the temperature increases, the polyhedra continue gather in this concentration range. This suggest that microscopic phase-separation occurs in the solution. One is a TBA-rich phase and the other is a water-rich phase. In the water-rich phase, almost all the molecules take part in the formation of polyhedra.

The salting-out phenomenon is considered to be governed by a mechanism similar to that described above. Namely, on adding ammonium chloride into an aqueous solution of TBA, the polyhedra formed in the TBA–water solution gather together; this results in the separation of the water-rich layer.

Surroundings of Ion in Aqueous Solution of Nonelectrolyte. We now consider the state of mixing of ammonium chloride in the aqueous solution of a nonelectrolyte based on the results of the measurement of the ^{35}Cl-NMR spectra. The half-line-width of ^{35}Cl-NMR spectra, $\Delta\nu$, is proportional to the product of the square of the electric field gradient at the nucleus, q^2, and the correlation time of the fluctuation of the electric field gradient at the nucleus, τ_c.[15] The magnitude of q^2 depends on the local asymmetry of the local structure around the chloride ion. If τ_c is assumed to be proportional to viscosity η, we can discuss the concentration or temperature dependence of the asymmetry of the local structure around the chloride ion from the concentration or temperature dependence of the quantity, $\Delta\nu^\circ\equiv\Delta\nu/(\eta/\eta_0)$, where η_0 is the viscosity of the solution whose $\Delta\nu$ value is chosen as reference.[16] As an absolute value of $\Delta\nu^\circ$ will not be discussed in the present report, the η_0 value will be fixed to 10^{-3} Pa s.

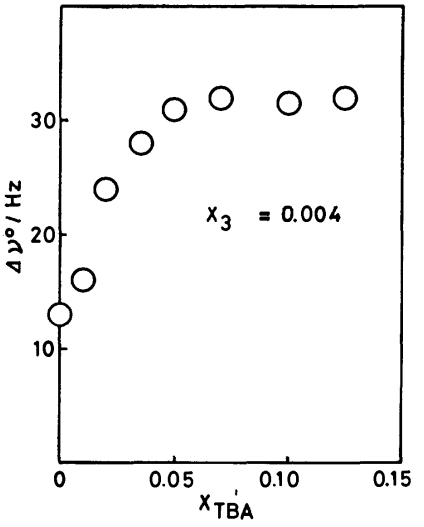

Fig. 6. Dependence of the $\Delta\nu^\circ$ value (see tle text) for TBA–water–ammonium chloride solution on the mole fraction of TBA at 32 °C (mole fraction of ammonium chloride is 0.004).

Figure 6 shows the relation between $\Delta\nu^\circ$ and X'_{TBA} for $X_3=0.004$ at 32 °C. It is seen from the figure that $\Delta\nu^\circ$ increases in magnitude as X'_{TBA} increases in the concentration range of $0<X'_{TBA}<0.05$. In the aqueous solution of ammonium chloride ($X'_{TBA}=0$), the $\Delta\nu^\circ$ value was observed to be only about 13 Hz for the wide salt concentration range from dilute to $X_3=0.11$. As the molar ratio of (ammonium ion) : (chloride ion) : (water) at $X_3=0.11$ is about 1 : 1 : 9, there are only two layers of water molecules between ammonium and chloride ions. This result indicates that $\Delta\nu^\circ$ increases only when the symmetry of the local structure around a chloride ion is broken down. The increase of $\Delta\nu^\circ$ observed in the TBA–water–ammonium chloride solution may reflect the break-down of the local symmetry around the chloride ion. Some chloride ions probably take part in the formation of the polyhedra in the solution. The concentration dependence of $\Delta\nu^\circ$ confirms the validity of the above picture. As ammonium chloride is only slightly soluble in TBA by itself, the number of chloride ions which take part in the formation

of the polyhedra is expected to be proportional to the number ratio, R, of water molecules which form polyhedra to all the water molecules. According to the results obtained from the analysis of concentration fluctuations, R can be calculated from the relations:[8]

$$R = lX_{TBA}/(1-X_{TBA}) \text{ for } 0<X_{TBA}<X^{s}_{TBA},$$

$$R = 1 \quad \text{for } X_{TBA}>X^{s}_{TBA},$$

where $l(\simeq 20)$ is the number of water molecules which encage a TBA molecule. Figure 7 shows the concentration dependence of R calculated for $l=20$. It can be seen from Figs. 6 and 7 that $\Delta\nu^{\circ}$ is nearly proportional to R.

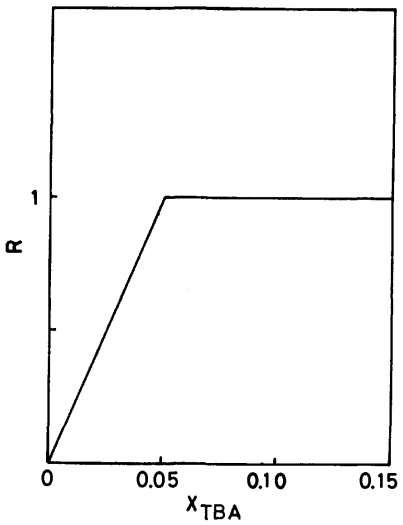

Fig. 7. Dependence of the number ratio of water molecules which form polyhedra to all the water molecules for TBA–water solution on the mole fraction of TBA.

For an ammonium ion, we have no experimental information about its state of mixing in this solution. However, it is only natural to consider that an ammonium ion is also taking part in the formation of a polyhedra, because an ammonium ion has similar size and property to those of a water molecule. Therefore, the water molecule which forms a polyhedra can be replaced by an ammonium ion much more easily than by a chloride ion.

Role of Ammonium Chloride in Phase-separation. Next, we focus our attention on the dependence of the $\Delta\nu^{\circ}$ value on salt-concentration. The acetone (AC) system was chosen for this experiment because the salt-concentration can be widely changed in a one-phase region. In Fig. 8, the $\Delta\nu^{\circ}$ values observed for $X'_{AC}=0.3$ at 32 °C are plotted against the salt-concentration, X_3. It can be seen from the figure that $\Delta\nu^{\circ}$ decreases its magnitude with the increase of the ammonium chloride concentration. Note that the phase-separation occurs at $X_3>0.004$. These results cannot be explained if we consider that all the chloride ions are engaged in the formation of polyhedra, because the local symmetry around a chloride ion should attain higher symmetry with the increase of salt-concentration. Therefore, it may be reasonable to consider that, at high salt-concentration, some chloride ions can exist in this solution,

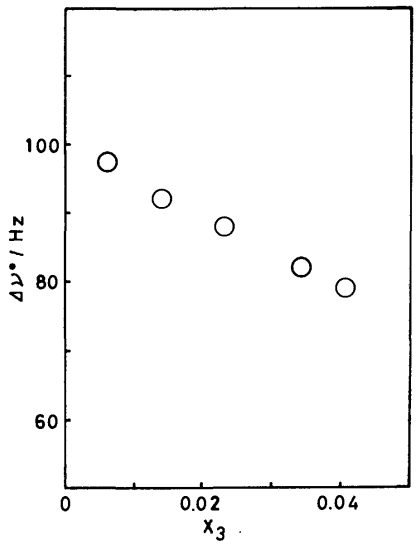

Fig. 8. Dependence of the $\Delta\nu^{\circ}$ value for acetone–water ammonium chloride solution on the mole fraction of ammonium chloride at 32 °C (mole fraction of acetone is 0.3).

surrounded by polyhedra. In other words, some chloride ions can attract polyhedra around themselves, which results in the formation of a high local symmetry around the chloride ion. As the aggregation of polyhedra is one of the necessary conditions for phase-separation, it can be said that chloride ions promote the phase-separation by attracting polyhedra around themselves.[17]

From the above discussion, the picture for the salting-out phenomenon can be drawn as follows. When ammonium chloride is added to the aqueous solution of nonelectrolyte in the concentration range of $X_2>X^{s}_{2}$, not only water molecules but also ammonium and chloride ions form polyhedra and each of them encages a nonelectrolyte molecule. As the concentration of ammonium chloride increases, the polyhedra begin to gather around a chloride ion. When the concentration of ammonium chloride is raised to X_3^{min}, the aggregate of the polyhedra grows into a macroscopic phase and the phase-separation occurs. This situation is schematically visualized in Fig. 9.

Lastly, we consider the temperature dependence of the mixing state at a constant salt-concentration. The temperature dependence of the $\Delta\nu^{\circ}$ value observed for $X'_{AC}=0.3$ and $X_3=0.04$ is shown in Fig. 10. Note that phase-separation occurs at 33 °C at this concentration. It can be seen from the figure that the $\Delta\nu^{\circ}$ value decreases with the elevation of temperature. This experimental result corresponds to the fact that, as the temperature approaches the phase-separation temperature, polyhedra begin to gather together around a chloride ion, which in turn results in the formation of a symmetric local field around a chloride ion.

Concluding Discussion. We have shown the existence of the clathrate hydrate-like local structure plays an important role in the salting-out phenomena in the aqueous solutions of polar nonelectrolytes such as TBA and acetone. Even if the solution does not contain

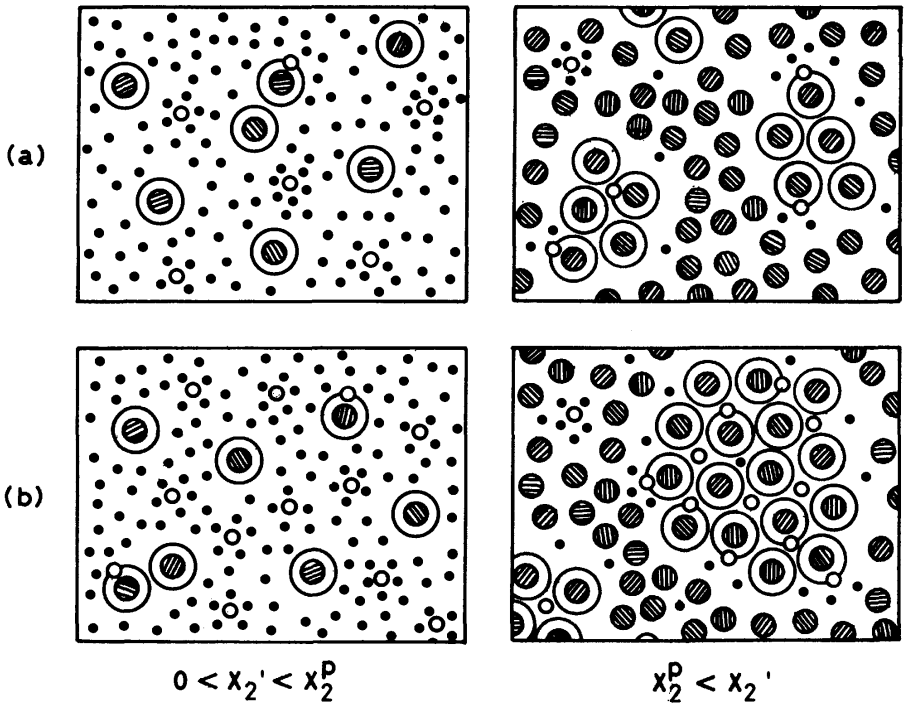

Fig. 9. Mixing state of ternary solution of water–ammonium chloride–nonelectrolyte (schematic) in the low (a) and high (b) concentration range of ammonium chloride. (•) and (●) represent a water and a TBA molecule, respectively. (◍) Represents the clathrate hydrate-like local structure. (○) Represents an ammonium or chloride ion.

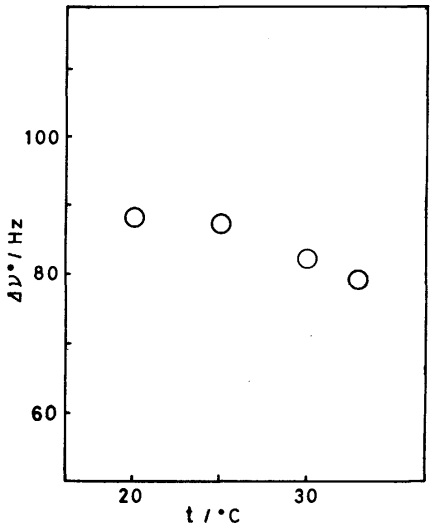

Fig. 10. Temperature dependence of the $\Delta\nu^\circ$ value for acetone–water–ammonium chloride solution (mole fractions of acetone and ammonium chloride are 0.3 and 0.04, respectively).

salts, the chlathrate hydrate-like local structure grows with the increase of the temperature. That is, the number of polyhedra which gather increases as the temperature increases. This property of the solution is considered to originate in the difference between the affinity of the polyhedron (strictly speaking, the water molecules which form a polyhedron) for nonelectrolyte and the affinity of the polyhedron for the polyhedron. The salt performs the task of promoting the gathering of the polyhedra. The present result shows that the ions take part in the formation of polyhedra; this may arise from the fact that the affinity of the ion for nonelectrolyte is weaker than that of the ion for water. The facts that the salting-out does not occur in the concentration range of $X_2 < X_2^s$ can be explained from this point of view. Roughly speaking, the polyhedra rarely contact with nonelectrolyte molecules in this concentration range because most of the nonelectrolyte molecules are encaged by water molecules. So, the phase-separation does not occur.

The above picture is rather different from the classical picture that ions rob the water molecules from the nonelectrolyte. Of course, we are not going to deny this classical picture wholly. In fact, the result that X_2^p is slightly smaller than X_2^s may arise from the fact that the number of water molecules which can form polyhedra is decreased by some ions which rob water molecules from the polyhedra. However, the rapid decrease of X_3^{min} with the increase of X_2', and the existence of the concentration range where salting-out does not occur cannot be explained by the classical picture.

The strong correlation between the solubility curve for the ternary solution and the concentration dependence of the concentration fluctuation for the binary solution indicates that the phase behavior is determined principally by the mixing state of the binary solution at least in the concentration range near X_2^s. So, the validity of our picture is considered to be dependent

on the validity of the picture for the mixing state of the binary solution.

The authors wish to express their sincere thanks to Dr. Tadashi Sugawara for his helpful advice on the measurement of NMR spectra.

References

1) P. Debye and J. McAulay, *Phys. Z.*, **26**, 22 (1925).
2) P. Debye, *Z. Phys. Chem.*, **130**, 56 (1927).
3) F. A. Long and W. F. McDevit, *Chem. Rev.*, **51**, 119 (1952).
4) G. Wada and T. Ito, *Nippon Kagaku Zasshi*, **78**, 1500 (1957).
5) S. K. Shoor and K. E. Gubbins, *J. Phys. Chem.*, **74**, 1776 (1970).
6) R. Aveyard and R. Hselden, *J. Chem. Soc., Faraday Trans. 1*, **71**, 312 (1975); M. Fromon and C. Treiner, *ibid.*, **75**, 1837 (1979).
7) R. A. Pierotti, *Chem. Rev.*, **76**, 718 (1976).
8) K. Iwasaki and T. Fujiyama, *J. Phys. Chem.*, **81**, 1908 (1977), **83**, 463 (1979).
9) T. Kato, M. Yudasaka, and T. Fujiyama, *Bull. Chem. Soc. Jpn.*, **54**, 1632 (1981).
10) N. Ito, T. Kato, and T. Fujiyama, *Bull. Chem. Soc. Jpn.*, **54**, 2573 (1981).
11) According to the classification proposed by Desnoyer, an ammonium ion is a weak structure breaker and an chloride ion is a weak structure breaker. See "Mizu No Kōzō To Bussei," ed by M. Nakagaki, Nankōdō, Tokyo (1974), p. 111; J. E. Desnoyers and G. Perron, *J. Solution Chem.*, **1**, 199 (1972).
12) In the concentration range of $X_2 > X_{\frac{1}{2}}^{P}$, the concentration at which ammonium chloride is precipitated is higher than X_3^{min}.
13) N. Ito, unpublished data.
14) H. L. Cox and L. H. Crether, *J. Am. Chem. Soc.*, **48**, 451 (1926).
15) S. Fujiwara, N. Nakagawa, and H. Shimizu, "Kōbunkainō Kakujikikyōmei, Kagaku E No Ōyō," Maruzen, Tokyo (1962).
16) M. Yudasaka, T. Sugawara, H. Iwamura, and T. Fujiyama, *Bull. Chem. Soc. Jpn.*, **53**, 1933 (1981).
17) Similar pictures can be drawn for other systems. As $X_{\frac{1}{2}}^{P}$ is nearly equal to $X_{\frac{1}{2}}^{S}$, the difference in $X_{\frac{1}{2}}^{P}$ values is considered to come from the difference in the size of the hydrophobic group of the molecule. See Ref. 9.

An Ion-impact Study of Singlet-Triplet Transitions in Ethylene and Alkyl-substituted Ethylenes

Yukinori SATO,* Kazuki SATAKE, and Hokotomo INOUYE
Research Institute for Scientific Measurements, Tohoku University, Sanjyo-machi, Sendai 980
(Received August 21, 1981)

The $T \leftarrow N$ ($\pi \rightarrow \pi^*$) transitions in ethylene, all of its methyl derivatives, and 1-butene were observed by means of He^+-impact energy-loss spectroscopy. With a resolution of better than 0.1 eV, a vibrational structure was just resolved in the $T \leftarrow N$ excitation spectrum of ethylene. The $T \leftarrow N$ transition energy was measured for the alkylethylenes with a lower resolution. The results are in good agreement with the electron-impact data, indicating that the vibro-rotational excitation due to the impulsive momentum transfer is negligible in the present method. The $T \leftarrow N$ excitation cross-sections were found to decrease by half upon the unit substitution of alkyls. The relative invariance of the $T \leftarrow N$ transition energy and the decrease in the $T \leftarrow N$ cross-sections upon alkyl substitution may be attributable to the decrease in the intra- and intermolecular Coulomb and exchange interactions between π- and π^*- orbitals.

The alkylation red shift has been of some interest in studies of the electronic spectra of ethylene and alkyl-substituted ethylenes.[1-3] After earlier studies using optical spectroscopy,[4,5] electron-impact methods have been applied to observe the bathochromic shift in the spin-forbidden $T \leftarrow N$ ($\pi \rightarrow \pi^*$) transition for a series of fundamental mono-olefinic hydrocarbons.[6-8] It has been revealed that the shift is much smaller in the $T \leftarrow N$ transition than in the optically allowed $V,R \leftarrow N$ transitions.

Measurements of energy loss by ion impact have also proved to be useful for observing spin-exchange transitions.[9-11] In the ion-impact method, a singlet-triplet transition of a target molecule is induced by electron exchange between the projectile ion and the target molecule. Therefore, the proton impact on a singlet spin-state molecule results in excitations only to singlet states, whereas the He^+ impact, for example, can induce both singlet-singlet and singlet-triplet transitions in the molecule. Under a suitable collision energy, the lowest energy singlet-triplet transition of a molecule may be observed as the most intense peak in the ion-impact spectrum. Moore and his co-workers have performed several ion-impact experiments in order to investigate the effect of substitution on the $T,V,R \leftarrow N$ transition energies in substituted ethylenes[9] and in methyl-substituted butadienes[10] and the effect of ring size on the $T,V,R \leftarrow N$ transition energies in cycloalkenes.[11]

In the present study, the He^+-impact method was used for observing the $T \leftarrow N$ transition in ethylene and alkylethylenes. Semiempirical calculations of the transition energies were also performed in order to analyze the experimental results. The purposes of the present study were; (1) to achieve a better energy resolution in the ion-impact spectroscopy; (2) to accumulate systematic data by means of ion impact to see if the ion-impact and electron-impact methods are consistent in determining the $T \leftarrow N$ transition energy; (3) to obtain some insight into the cause of the alkylation red shift, and (4) to investigate the effect of alkylation on the cross-section of $T \leftarrow N$ excitation induced by the ion-molecule interaction.

Experimental

The apparatus consists of an ion source, a mass analyzer, an energy monochromator for the incident-ion beam, a collision cell, an energy analyzer for the scattered ions, and a detector. The projectile He^+ ions are produced in a low-voltage plasma source.[12] The ions extracted from the source are focused into a beam, mass-analyzed by means of a Wien filter (COLUTRON Model 300), and directed into the ion spectrometer which is schematically shown in Fig. 1.

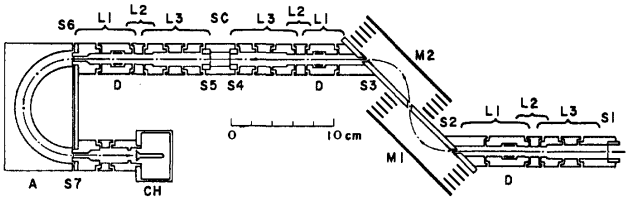

Fig. 1. Schematic of the ion spectrometer.
S1—S7: Apertures, L1: fixed ratio lens, L2: field lens, L3: variable ratio lens, D: beam steering deflectors, M1 and M2: parallel plate deflectors for an energy monochromator, SC: scattering cell, A: hemispherical energy analyzer, CH: channel electron multiplier.

The mass-analyzed beam is decelerated to an energy of 15—30 eV and focused into the electrostatic energy monochromator. The monochromator consists of two parallel-plate deflectors with an incident angle of $\pi/4$. The two deflectors are symmetrical in geometry and are directly connected so that they have a common inner plate. A coupling hole ($5 \times 10\ mm^2$) is bored at the center of the inner plate for the ion beam to pass from the first deflecting stage to the second deflecting stage. The entrance and the exit apertures (0.5 mm in diam.) are 116 mm apart and are held on the inner plate equidistantly from the coupling hole.

The ion beam transmitted through the monochromator is accelerated to an energy in the range of 2—3 keV through an acceleration-lens system and then enters into the collision cell. The target gas is introduced into the collision cell at a sufficiently low pressure to assure the single collision condition. The entrance and the exit apertures of the cell are 0.6 mm in diameter. The scattered ions are decelerated and focused onto the entrance aperture of the energy analyzer. The acceleration and deceleration of the ions are performed by means of a series of electrostatic cylinder lenses. The lenses

consist of a variable ratio lens (L1) and a fixed ratio lens (L3). An einzel lens (L2) is inserted as a field lens between the L1 and L3 lenses. The lenses are designed by using the optical properties of the two-element cylinder lens calculated by Read *et al.*[13]

A hemispherical electrostatic deflector is used for the energy analyzer. The hemispheres are made of aluminum alloy. The mean radius of the outer and the inner hemispheres is 47.5 mm. The entrance and the exit apertures are 0.3 mm in diameter. The entrance aperture of the analyzer is 132 mm from the exit of the collision cell. The geometrical acceptance angle of the analyzer for scattered ions is 6.8×10^{-3} rad in a scattering plane, which is a measure of the present angular resolution. The voltage difference between the outer and inner hemispheres is held constant so as to pass ions at a constant transmission energy in the range of 15—30 eV.

After passing the analyzer, the ions are again accelerated and detected by a channel electron multiplier (MULLARD B318-AL).

The whole system is housed in connected metal vessels and pumped by means of oil-diffusion pumps. The ultimate pressure is 3×10^{-5} Pa, and the working background pressure is 5×10^{-4} Pa when the target gas and the ion-source gas are introduced.

An energy-loss spectrum is obtained by tracing the intensity of ions transmitted through the analyzer as a function of the deceleration potential between the collision cell and the analyzer. A voltage ramp applied to the deceleration lens is generated by a D/A converter, which is controlled by a personal-computer (SHARP MZ80-K). Output pulses from the detector are amplified, discriminated, and accumulated in the computer.

For a small-angle scattering at a high collision energy, the laboratory energy lost by the projectile is approximately given by:

$$\Delta E = (M_p/M_t)E\theta^2 + Q,$$

where M_p and M_t are the masses of the projectile and the target respectively; E is the laboratory collision energy; θ, the laboratory scattering angle, and Q, the change in the internal (vibrational, rotational, and electronic) energy. The term proportional to the collision energy, E, is the elastic loss due to the momentum transfer from the projectile to the target. The elastic loss can be minimized by observing the glancing collision at the forward scattering angle ($\theta=0$). The internal energy defect, Q, is also dependent on the scattering angle, because the vibro-rotational excitation, in addition to the vertical electronic excitation, is induced by the impulsive momentum transfer from the projectile to the target.[14,15] The degree of the impulsive vibro-rotational excitation is dependent on the impact parameter and can also be minimized in the forward scattering. In the present study, observations are made only for the forward scattering. Under the present angular resolution, the energy loss is expected to correspond to the vertical electronic transition energy, and the vibrational excitation is expected to follow the Franck-Condon principle. This is verified by the results to be presented in the following section. An overall energy resolution of better than 0.1 eV FWHM is achieved. This enables us to observe the vibrational structures in the electronic excitation spectrum of ethylene.

Results and Discussion

T←N *Spectrum of Ethylene.* The spectrum of ethylene in the energy-loss region from 3 to 6 eV is shown in Fig. 2. The spectrum was obtained with a resolution of 95 meV FWHM by the impact of 2.3 keV He^+. A broad feature modulated by small structures appears with its maximum intensity at around 4.25 eV. The shape and position of the gross feature are in good agreement with those obtained by Moore.[9] The whole band has been assigned to the transition of ethylene from the ground state, N, to the lowest lying triplet state, T ($\pi \rightarrow \pi^*$). The small structures superimposed on the envelope are reproducible under the present resolution and show a spacing of 0.13 eV. The structures have an essential similarity, both in spacing and intensity distributions, with the high-resolution electron-impact spectrum obtained by Wilden and Comer,[16] though the present resolution is lower than theirs. The structures have been assigned to the vibrational progressions in the C–C stretching mode (ν_2). The spacing of 0.13 eV (1050 cm^{-1}) is the vibrational energy spacing of the ν_2 mode in the triplet state.

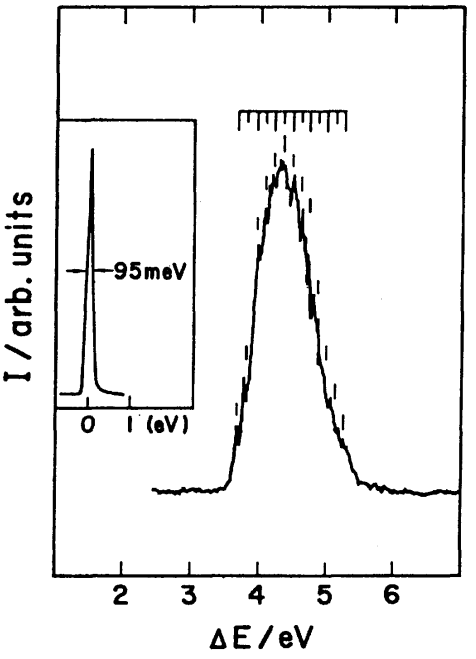

Fig. 2. Energy loss spectrum of ethylene by 2.3 keV He^+ impact. The inset shows the elastic peak.

The similarity of the vibrational structures obtained from the ion-impact and electron-impact methods is evidence that the momentum transfer from the projectile to the target is not significant in the present observation; it can be thought, then, that the electronic excitation occurs in the Franck-Condon manner. The $T \leftarrow N$ excitation requires exchange interaction between the collision pair. It should be noticed that the exchange interaction, whose range is much shorter than the range of direct Coulomb interaction, is still effective in these glancing collisions.

Alkylation Shift in T←N *Transition.* The energy-loss spectra obtained by means of 2.5 keV He^+ impact are shown in Fig. 3 for ethylene, its six methyl derivatives, and an ethyl derivative. Because of a considerable decrease in the $T \leftarrow N$ excitation intensity in alkylethylenes, a lower resolution of about 0.35 eV FWHM was employed to accumulate these spectra. Common

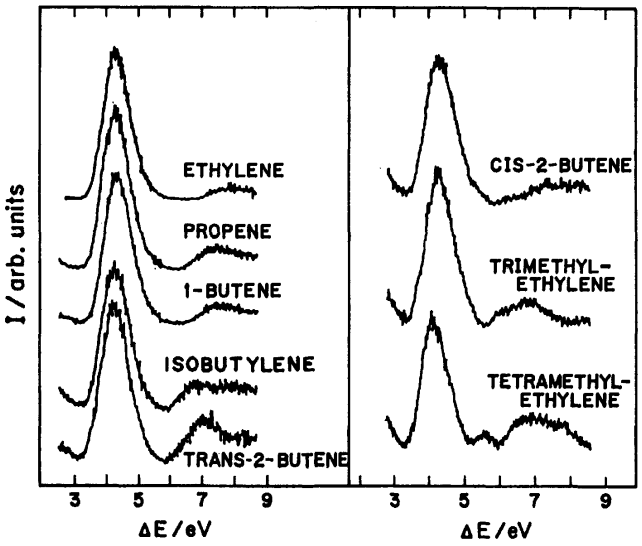

Fig. 3. Energy loss spectra of ethylene and alkyl-substituted ethylenes by 2.5 keV He^+ impact.

spectral features are seen for all of the alkylethylenes studied. The most intense $T \leftarrow N$ band at about 4.2 eV is followed by weaker $V,R \leftarrow N$ bands at higher-energy losses. The relative intensities of the $T \leftarrow N$ band and the $V,R \leftarrow N$ bands are dependent on the impact energy. The shape and position of the $T \leftarrow N$ band are relatively invariant with respect to the alkyl substitution, while the $V,R \leftarrow N$ bands rise at lower energies as the number of substitution increases from zero to four. The separation of the $R \leftarrow N$ bands from the $V \leftarrow N$ band is not possible at this level of resolution, but the growth of the low-energy tail of the 7 eV peak with an increase in substitution may be attributable to the rapid red shift of the $2R \leftarrow N$ band.[7,8] A small peak at 5.5 eV is distinguishable in the tetramethylethylene; it has been assigned to the $2R \leftarrow N$ ($\pi \rightarrow 3s$) transition.[7,8] The position of the maximum intensity of the $T \leftarrow N$ band is listed in Table 1. Data obtained by the use of a variety of methods are included for comparison. The consistency of the present data with the electron-impact data indicates again that glancing collision without any significant momentum transfer is observed on these target molecules under the present scattering angular resolution. The present measurement gives an overall red shift of 0.20 eV for the $T \leftarrow N$ transition in going from ethylene to tetramethylethylene. The degree of shift in the $T \leftarrow N$ transition is much smaller than the corresponding 1.75 eV shift[8] in the $2R \leftarrow N$ transition.

Mulliken has indicated that the alkylation decrease in the ionization potential and the red shift in the $R \leftarrow N$ transition are largely attributable to a change in the effective nuclear charge of carbons due to charge transfer within the sigma system, while the red shift in the $V \leftarrow N$ transition may be entirely explained by the hyperconjugation in the pi system. The relative invariance of the $T \leftarrow N$ transition energy upon the alkylation has been predicted from VESCF-CI calculations by

Table 1. $T \leftarrow N$ transition energy in alkyl-substituted ethylenes

Molecule	Vertical transition energy/eV						
	Present work[a]	Other					
		Ion-impact[b]	Electron-impact			Optical	
Ethylene	4.25	4.3	4.32,[c] 4.205,[g]	4.30,[d] 4.290,[g]	4.2[e] 4.330[g]	4.6[f]	
1-Butene	4.25	4.3					
Propene	4.25		4.28,[c]	4.23,[d]	4.35[e]	4.20[h]	
Isobutene	4.20		4.22,[c]	4.21[d]		4.09,[h]	4.2[i]
cis-2-Butene	4.20	4.2	4.21,[c]	4.21,[d]	4.3[e]		4.2[i]
trans-2-Butene	4.20	4.2	4.24,[c]	4.22,[d]	4.4[e]	4.07,[h]	4.2[i]
Trimethylethylene	4.15		4.16,[c]	4.16[d]		3.70[h]	
Tetramethylethylene	4.05		4.10,[c]	4.05[d]		3.65[h]	

a) The error of the peak position is estimated to be +0.05 eV. b) From Ref. 9. c) From Ref. 7. d) From Ref. 8. e) From Ref. 6. f) From Ref. 4. g) From Ref. 16. h) From Ref. 5. i) From Ref. 25.

Table 2. Calculated results for π- and π^*-orbital energies and coulomb and exchange energies between π- and π^*-orbitals, and $T \leftarrow N$ and $V \leftarrow N$ transition energies

Units are in eV.

Molecule	$-\varepsilon_\pi$	$\varepsilon_{\pi^*}-\varepsilon_\pi$	$J_{\pi\pi^*}$	$2K_{\pi\pi^*}$	$E(V \leftarrow N)$[a]	$E(T \leftarrow N)$[a]
Ethylene	11.158	11.377	7.740	4.934	7.581	3.637
Propene	10.429	10.647	7.054	4.188	7.324	3.385
Isobutylene	9.954	10.313	6.845	3.963	7.001	3.467
trans-2-Butene	10.066	10.064	6.613	3.741	6.797	3.235
cis-2-Butene	9.526	9.598	6.567	3.442	5.899	2.832
Tetramethylethylene	9.234	9.255	6.260	3.309	6.304	2.994

a) The transition energies are the CI results within single-excitation configurations.

Allinger *et al.*[17] and by Watson *et al.*[18] In order to see more specifically how this invariance arises, semiempirical calculations of the vertical $T\leftarrow N$ and $V\leftarrow N$ transition energies were performed by using a CNDO/S program made by Tajiri *et al.*[19] In the SCF level of the calculation, the $\pi\rightarrow\pi^*$ transition energy is given by;

$$E(T\leftarrow N) = (\varepsilon_{\pi^*}-\varepsilon_{\pi}) - J_{\pi\pi^*} \quad (1)$$

for the $T\leftarrow N$ transition and by;

$$E(V\leftarrow N) = (\varepsilon_{\pi^*}-\varepsilon_{\pi}) - J_{\pi\pi^*} + 2K_{\pi\pi^*} \quad (2)$$

for the $V\leftarrow N$ transition, where ε_{π} and ε_{π^*} are the SCF orbital energies and where $J_{\pi\pi^*}$ and $K_{\pi\pi^*}$ are, respectively, the Coulomb and the exchange energies between π- and π^*-orbitals. The calculated values for the quantities appearing in Eqs. (1) and (2) are listed in Table 2. The transition energies, $E(V\leftarrow N)$ and $E(T\leftarrow N)$, in the table are the results of partial configuration mixing within single-excitation configurations. The calculated results of $E(T\leftarrow N)$ are lower than the corresponding experimental data by more than 0.5 eV. This would be improved by taking the configuration mixing including double excitations at the expense of the worse agreement for the $V\leftarrow N$ transition energy.[20,21] Our attention will be confined to the gross results appearing in the SCF level. The differences $(\varepsilon_{\pi^*}-\varepsilon_{\pi})$ in the orbital energy, the Coulomb energy, and the exchange energy decrease altogether upon the methyl substitution. A remarkable point is that the degrees of change in $(\varepsilon_{\pi^*}-\varepsilon_{\pi})$, $J_{\pi\pi^*}$ and $2K_{\pi\pi^*}$ are all comparable in their magnitudes. Thus, the changes in $(\varepsilon_{\pi^*}-\varepsilon_{\pi})$ and $J_{\pi\pi^*}$ cancel each other to result in a small net change in the $T\leftarrow N$ transition energy upon the substitution. The changes in $J_{\pi\pi^*}$ and $K_{\pi\pi^*}$ may be taken to reflect, to some extent, the degree of hyperconjugation. The decrease in $(\varepsilon_{\pi^*}-\varepsilon_{\pi})$ arises mostly from the change in ε_{π}, which is largely attributable to the charge-transfer effect in the sigma system according to Mulliken. Thus, the relative invariance of the $T\leftarrow N$ transition energy arises from the cancellation of the hyperconjugation effect in $J_{\pi\pi^*}$ with the charge-transfer effect in $(\varepsilon_{\pi^*}-\varepsilon_{\pi})$, while the hyperconjugation effect in $K_{\pi\pi^*}$ remains, resulting in the red shift in the $V\leftarrow N$ transition to an extent similar to the decrease in $2K_{\pi\pi^*}$.

Alkylation Effect in T←N *Excitation Cross-section.* It was found that the scattering intensity of the $T\leftarrow N$ excitation was considerably influenced by the alkyl substitution. The relative $T\leftarrow N$ cross-section decreases by almost half when the number of substitution increases by one. The $T\leftarrow N$ cross-section of 1-butene is nearly equal to that of propene. Three dimethylethylenes (*trans*- and *cis*-2-butene, and 2-methylpropene) have nearly identical $T\leftarrow N$ cross-sections. These facts indicate that the number of substitution is more important for the hypochromic effect than is either the size of a substituent or the site of substitution. It was also observed that the $V,R\leftarrow N$ cross-sections were less sensitive to the degree of substitution than were the $T\leftarrow N$ cross-sections. Quite the same hypochromic effect has been observed in the ion-impact study of methyl-substituted butadienes.[10]

Mechanisms of excitation in heavy-particle collisions may be divided into two types.[22,23] In low-energy collisions, an electronic excitation requires a close encounter of a collision pair. A quasi-molecular description and the potential crossing mechanism will be adequate for these collisions. In this mechanism, the threshold law of impact parameter holds and an excitation occurs for scattering angles larger than a threshold value. For high-energy collisions, on the other hand, excitations are possible in a distant encounter by means of the direct Coulomb or the exchange mechanism. Because of the delocalized character of the mechanism, one expects an excitation with no definite impact-parameter threshold. This is the case in the present experiment. The effective range of the ion-molecule interaction leading to the $T\leftarrow N$ excitation may be longer than the spatial extent of the surrounding alkyl groups. Otherwise, the momentum transfer between projectile and target would be considerable and would violate the vertical excitation. The spatial shielding effect does not seem to be important for the present hypochromic effect. We suggest that the hypochromic effect occurs through a change in the π- and π^*-wavefunctions upon the alkyl substitution, and that this in turn causes a decrease in the ion-molecule interaction. The exchange interaction for singlet-triplet transition[24] includes an integral such as;

$$\langle\pi^*(1)\chi(2)|r_{12}^{-1}|\pi(2)\chi(1)\rangle, \quad (3)$$

where χ is the electronic wavefunction of the projectile He^+ ion and where r_{12} is the distance between the electrons to be exchanged. Since we have seen the decrease upon the substitution in the intramolecular Coulomb and exchange integrals between π- and π^*-orbitals, a decrease can also be expected in the ion-molecule exchange integral given by Eq. 3. The same reasoning leads to a decrease upon the substitution in the ion-molecule Coulomb interaction responsible for the $V,R\leftarrow N$ excitation. However, the alkylation decrease in the energy defect of the $V,R\leftarrow N$ excitation favors for an increase in the cross-section and makes the hypochromic effect less obvious than in the $T\leftarrow N$ excitation.

The authors wish to express their thanks to Dr. Noriyuki Shimakura for his help in the CNDO/S calculations. The present work was partially suported by a Grant-in-Aid for Scientific Research No. 454117 from the Ministry of Education, Science and Culture. The present work was also partially suported by the Nishina Memorial Foundation.

References

1) R. S. Mulliken, *Rev. Mod. Phys.*, **14**, 265 (1942).
2) A. J. Merer and R. S. Mulliken, *Chem. Rev.*, **69**, 639 (1969).
3) M. B. Robin, "Higher Excited State of Polyatomic Molecules," Academic Press, New York (1975), Vol. 2, Chap. IV. A, pp. 2—68.
4) D. F. Evance, *J. Chem. Soc.*, **1960**, 1735.
5) M. Itoh and R. S. Mulliken, *J. Phys. Chem.*, **73**, 4332 (1969).
6) D. F. Dance and I. C. Walker, *Proc. R. Soc. London, Ser. A*, **334**, 259 (1973).
7) W. M. Flicker, O. A. Mosher, and A. Kupperman,

Chem. Phys. Lett., **36**, 56 (1975).
8) K. E. Johnson, D. B. Johnston, and S. Lipsky, *J. Chem. Phys.*, **70**, 3844 (1979).
9) J. H. Moore, Jr., *J. Phys. Chem.*, **76**, 1130 (1972).
10) J. H. Moore, Y. Sato, and S. W. Staley, *J. Chem. Phys.*, **69**, 1092 (1978).
11) I. Sauers, L. A. Grezzo, S. W. Staley, and J. H. Moore, *J. Am. Chem. Soc.*, **98**, 4218 (1976).
12) M. Menzinger and L. Wahlin, *Rev. Sci. Instrum.*, **40**, 102 (1969).
13) F. H. Read, A. Adams, and J. R. Soto-Monitiel, *J. Phys. E*, **4**, 625 (1971).
14) H. Inouye, K. Niurao, and Y. Sato, *J. Chem. Phys.*, **64**, 1250 (1976).
15) Y. Sato, K. Niurao, H. Takagi, and H. Inouye, *J. Chem. Phys.*, **65**, 3952 (1976).
16) D. G. Wilden and J. Comer, *J. Phys. B*, **12**, L371 (1979).
17) N. L. Allinger, J. C. Tai, and T. W. Stuart, *Theor. Chim. Acta*, **8**, 101 (1967).
18) F. H. Watson, Jr., A. T. Armstrong, and S. P. McGlynn, *Theor. Chim. Acta*, **16**, 75 (1970).
19) A. Tajiri, N. Ohmichi, and T. Nakajima, *Bull. Chem. Soc. Jpn.*, **44**, 2347 (1971).
20) T. H. Dunning, W. J. Hunt, and W. A. Goddard, *Chem. Phys. Lett.*, **4**, 147 (1969).
21) R. J. Buenker, S. D. Peyerimjhoff, and W. E. Kammer, *J. Chem. Phys.*, **55**, 814 (1971).
22) N. Andersen, T. Andersen, K. Bahr, C. L. Cocke, E. H. Pedersen, and J. O. Olsen, *J. Phys. B*, **12**, 2529 (1979).
23) N. Andersen, "Electronic and Atomic Collisions," ed by N. Oda and K. Takayanagi, North-Holland, Amsterdam (1980), Proceedings of XIth ICPEAC, Kyoto, 1979, Invited Papers and Progress Reports, pp. 301—312.
24) D. R. Bates and D. S. F. Crothers, *Proc. Phys. Soc.*, **90** 73 (1967).
25) F. H. Watson, Jr., and S. P. McGlynn, *Theor. Chim. Acta*, **21**, 309 (1979).

The Aggregation of a Merocyanine Dye in Solution and Film

Fumio Mizutani,* Sei-ichiro Iijima, and Keishiro Tsuda
Research Institute for Polymers and Textiles, Yatabe-Higashi, Tsukuba, Ibaraki 305

(Received August 27, 1981)

Two low-energy bands, one near 595 nm and the other near 630 nm, were observed in the visible absorption spectra of a merocyanine dye (3-carboxymethyl-5-[2-(3-octadecyl-2-benzothiazolinylidene)ethylidene]-2-thioxo-4-thiazolidinone) dissolved in methanol–water mixtures containing KOH and Triton X-100. From the dye-concentration dependence on the spectra, the band near 595 nm was assigned to the tetramer, and the one near 630 nm, (probably) to the hexamer of the carboxylate form of the dye. The same bands were observed in the dye films when they were soaked in aqueous solutions of pH$\geq$5.5. The relative intensities of the two bands were strongly affected by the ionic strength of the aqueous solution.

Merocyanine dyes have come to attract particular interest as materials for photoelectric[1–8] or photoelectrochemical[8–12] devices because of their high quantum efficiencies. We have reported previously[11] that a thin film of 3-carboxymethyl-5-[2-(3-octadecyl-2-benzothiazolinylidene)ethylidene]-2-thioxo-4-thiazolidinone (MD) showed two low-energy absorption bands near 595 and 625 nm. This spectral change seems of interest because it is induced by a simple treatment, *i.e.*, by soaking the MD film in an aqueous solution of an adequate pH and ionic strength, and also because it is accompanied by a drastic enhancement of the cathodic photocurrent at the MD-coated electrode.[11] Sugi *et al.* have also reported[6,7] that Langmuir multilayers containing MD or its analogue exhibited an enhanced photoconductivity in the lateral direction, associated with the appearance of a low-energy band near 595 nm. Although these low-energy bands have been taken as aggregates of MD,[6,7,11] only a limited number of experiments have so far been carried out, and little is known about the nature of the bands.

We have found that methanolic aqueous solutions of MD containing KOH show low-energy bands depending on the concentration of methanol as well as on that of MD. In this paper, the visible absorption spectra of MD in the solution system are investigated in order to characterize the low-energy bands. The spectral change in the MD film is also discussed with the aid of the results obtained for the solution system.

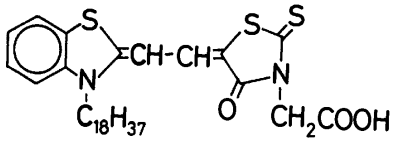

Experimental

The MD was obtained from the Japanese Research Institute for Photosensitizing Dyes and used without further purification, since preliminary tests showed that the purification of MD by means of column chromatography on silica gel (eluent; chloroform containing 10% v/v methanol) brought about no discernible change in the results. The other reagents used were of an analytical GR grade and were also used without further purification.

Methanolic aqueous solutions, each containing 0.01 M† KOH, were employed as solvents of MD, and 0.005% v/v of Triton X-100 was added to each solution in order to prevent the precipitation of MD. The visible absorption spectra of the MD solutions were recorded 2 h after the preparation of each solution using a Cary 17 DX spectrophotometer. An absorption cell with the optical path of 10 cm was mostly employed because the measurements had to be carried out on very dilute MD solutions.

MD films were prepared by means of the vacuum evaporation of the dye onto Pyrex-glass plates (size; 0.9 × 4.5 cm^2) below 5×10^{-4} Pa using a tungsten boat heated up to *ca.* 220 °C. Film with an absorption of 0.25±0.01 at 516 nm was used for the experiments. For IR spectral measurements, CaF_2 single crystal plates were employed as bases of the MD films in place of the glass plates. The permeability of the MD film to an aqueous solution was checked by soaking the film on a water-soluble substrate in the solution. In the present study, a KBr tablet coated with epoxy resin on only one side was used as the substrate; MD was evaporated onto the uncoated side. A phosphate buffer solution (KH_2PO_4 plus K_2HPO_4, pH 7.0; ionic strength, 0.01) was prepared, and the ionic strength of the solution used for the experiments was adjusted by diluting the buffer solution with water or by adding KCl to it. The MD film on glass was placed in an absorption cell (size; $1.0\times1.0\times4.5$ cm^3), and the visible absarption spectra were recorded using a Shimadzu UV-220 spectrophotometer before and after adding an aqueous solution to the cell. The IR spectrum of the MD film soaked in an aqueous solution and then dried was measured using a JEOL JIR 40 IR spectrophotometer.

The chemical stability of MD during the course of the experiment was always checked by means of silica-gel thin layer chromatography.[3] No degradation products were observed on the silica-gel plate after soaking the film.

All the spectral measurements were carried out at 25±1 °C.

Results and Discussion

Aggregation of MD in Solutions. Methanolic solutions of MD gave a single peak at 524 nm, along with a discernible shoulder at 495 nm, on their visible absorption spectra, and they followed Beer's law, at least in the concentration range from 0.1 μM to 14.0 μM (which corresponds to the saturated solution of MD). Since conformity to Beer's law was found at such a low concentration, the absorption of the methanolic solution can be assigned to the monomer of MD. The shape of the monomer-absorption spectrum of MD is typical of the monomers of polymethine dyes.[13,14] The peak absorption is induced by the 0←0 transition, and the shoulder on the high-energy side is a result of the

† Throughout this paper, 1 M = 1 mol dm^{-3}.

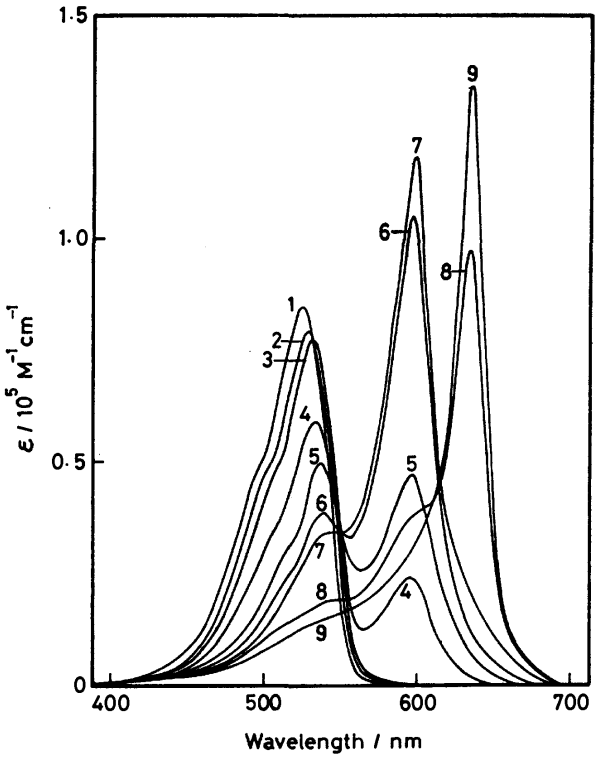

Fig. 1. Absorption spectra of 0.75 μM MD in methanolic aqueous solutions containing 0.01 M KOH and 0.005% v/v Triton X-100. The methanol concentrations in the solvents are given in M: (1) 22.5; (2) 20.0; (3) 17.5; (4) 15.0; (5) 13.5; (6) 12.5; (7) 11.0; (8) 9.0; (9) 7.5.

"forbidden" transition of high energy due to molecular vibration.[13,14] The addition of an alkaline aqueous solution to the methanolic solution of MD strongly affected the shape of the absorption spectrum. Figure 1 shows the visible absorption spectra of 0.75 μM MD in mixed solution of methanol and water, each containing 0.01 M KOH and 0.005% v/v Triton X-100. The features of the spectra can be roughly classified into three groups, depending on the methanol concentration of the solution. The MD solutions containing 17.5 M or above methanol give an absorption similar in shape to that obtained in the methanolic solution (Lines 1—3). On the other hand, a new band starts to appear near 595 nm in addition to the above absorption, and the intensity of the new band increases with a decrease in the concentration of methanol, in the concentration range of methanol from 15.0 M to 11.0 M (Lines 4—7). Further decreasing methanol concentration below 11.0 M brings about the appearance of another low-energy band near 630 nm associated with a significant intensity lowering of the band near 595 nm (Lines 8 and 9).

The similarity of Lines 1—3 to the absorption of the methanolic solution of MD indicates that MD is in the monomeric form in the mixed solvents containing 17.5 M or more methanol. The MD in these solvents followed Beer's law over a relatively wide concentration range; *i.e.*, the solution containining 20.0 M methanol follows the low from 0.1 μM to 2.0 μM of MD. As can be seen from Lines 1—3, the monomer band of MD exhibits a small shift to the low-energy side and a

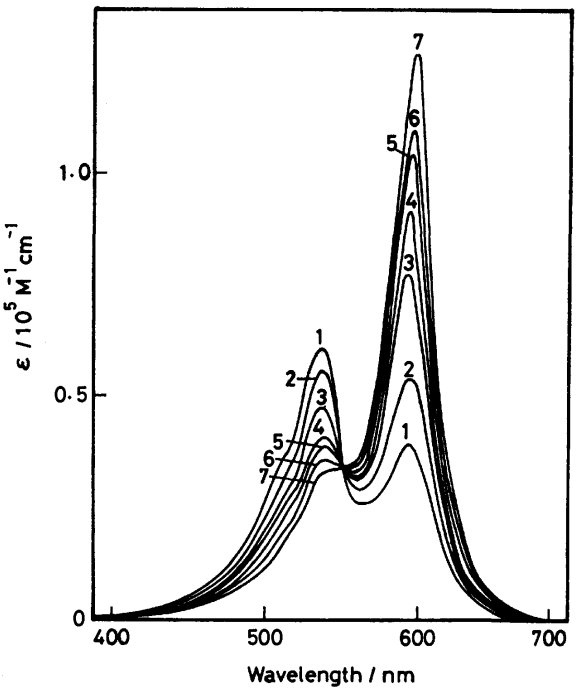

Fig. 2a. Absorption spectra of MD of various concentrations in 12.5 M methanol–water containing 0.01 M KOH and 0.005% v/v Triton X-100. MD concentrations are given in μM: (1) 0.2; (2) 0.3; (3) 0.4; (4) 0.6; (5) 0.75; (6) 1.2 (7) 1.4.

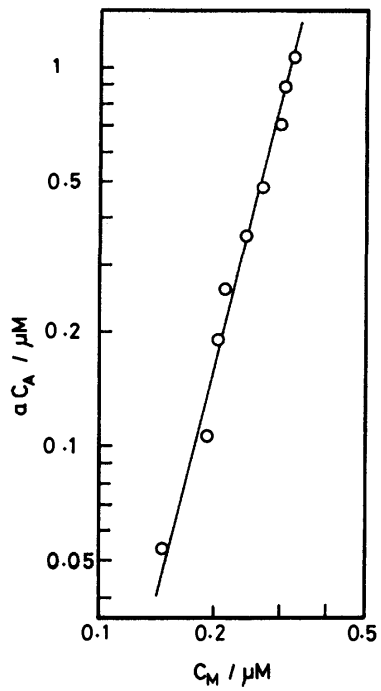

Fig. 2b. Determination of the aggregation number a, for the equilibrium $aC_M \rightleftharpoons C_A$. C_M and C_A are the concentrations of monomer and aggregate, respectively, and they derived from Fig. 2a.

lowering of the molar absorptivity, ε_M, with a decrease in the concentration of methanol in the mixed solvent; this could be explained by the increase in the dielectric

constant of the solvent, since the monomer band obtained in methanol and in other organic solvents (such as benzene, tetrahydrofuran, acetone, *N*,*N*-dimethylformamide, and diethyl sulfoxide) showed a slight shift to the low-energy side with the increase in the dielectric constant of the solvent, and since the ε_M of the band decreased when the dielectric constant of the solvent was above *ca.* 30.

Deviations from Beer's law become noticeable when low-energy bands appear in addition to the monomer band. Figure 2a shows the dependence of the absorption spectra on the MD concentration in the solvent containing 12.5 M methanol. An isosbestic point is observed near 550 nm; this indicates that the monomer band and the band near 595 nm are expressed by a single equilibrium. Since the decreased intensity of the monomer absorption near 535 nm and the accompanied enhancement of the low-energy band near 595 nm are observed with a growing MD concentration, the curves in Fig. 2a can be analyzed in termes of an equilibrium between the monomeric and aggregate forms of MD:

$$aC_M \rightleftharpoons C_A, \quad K = C_A/(C_M)^a, \qquad (1)$$

where C_M and C_A are the concentrations of the monomer and the aggregate respectively, a is the number of monomer units in the aggregate, and K is the association constant. Hence, the a-value is determined by plotting log aC_A and log C_M. The peak intensity of the monomer band and that of the aggregate band were evaluated according to the procedure of West and Pearce.[14] The molar absorptivity of the monomer at the peak, ε_M, was taken as 7.40×10^4 M^{-1} cm^{-1} in the solvent by extrapolating the ε_M *vs.* methanol concentration curve measured in the methanol-concentration region where only the monomer band is given. By subtracting the C_M thus determined from the total dye concentration, C_T, aC_M $(=C_T-C_M)$ was evaluated. As is shown in Fig. 2b, the plots follows a straight line, and the a-value is determined as *ca.* 4. Accordingly, the spectral change is explained by a monomer⇌tetramer equilibrium, and the low-energy band near 595 nm can be assigned to the tetrameric form of MD. The molar absorptivity of the tetramer at the peak, ε_4, was obtained as 6.27×10^5 M^{-1} cm^{-1}.

Similarly, the dependence of the band near 630 nm on the MD concentration was examined in the solvent containing 7.5 M methanol (Fig. 3a). In this case, however, the absorption change cannot be described by a simple equilibrium, because two bands, the monomer and the tetramer bands, appear in addition to the band near 630 nm. Since the relative intensities of the monomer and tetramer absorptions decreased and the absorption of the band near 630 nm increased with a growing MD concentration, the band near 630 nm may well be assigned to a higher-order aggregate. The following equilibrium is, therefore, proposed in addition to the monomer⇌tetramer equilibrium:

$$C_4 + bC_M \rightleftharpoons C_{(4+b)}, \quad K' = C_{(4+b)}/C_4\cdot(C_M)^b, \qquad (2)$$

where $C_{(4+b)}$ is the concentration of the aggregate which shows the band near 630 nm; $(4+b)$, the number of monomer units of the aggregate; C_4, the concentration of the tetramer; and K', the association constant. If the total dye concentration is given by C_T, the following relations are obtained:

$$\log[(4+b)C_{(4+b)}/C_4] = b\log C_M + \log[(4+b)K'], \qquad (3)$$

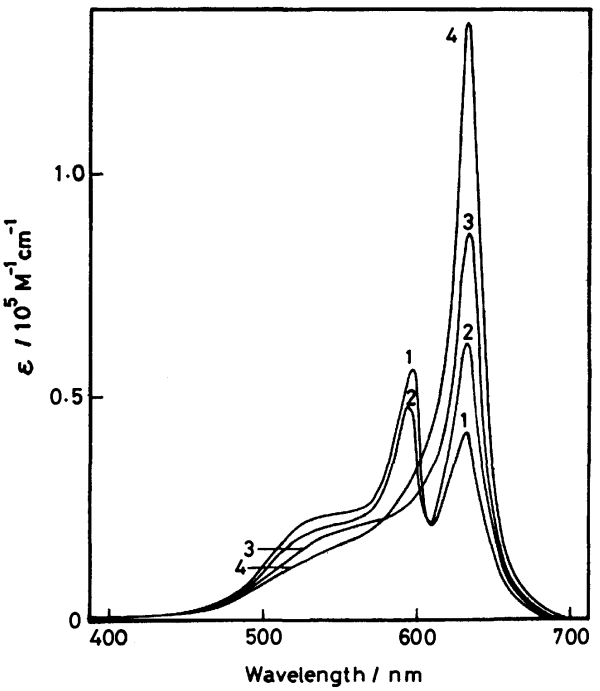

Fig. 3a. Absorption spectra of MD of various concentrations in 7.5 M methanol–water containing 0.01 M KOH and 0.005% v/v Triton X-100. MD concentrations are given in μM: (1) 0.1; (2) 0.2; (3) 0.5; (4) 0.75.

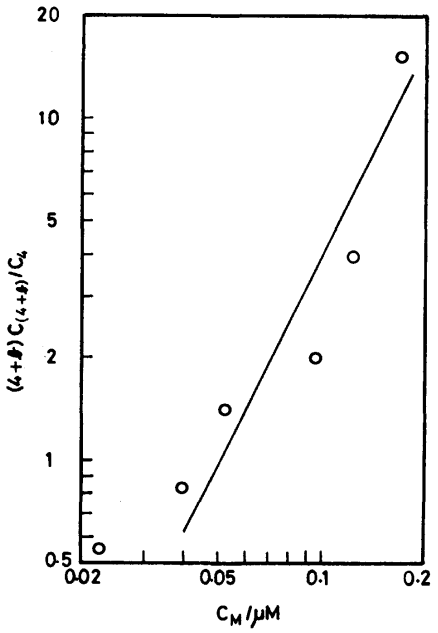

Fig. 3b. Determination of the b-value, for the equilibrium $C_4 + bC_M \rightleftharpoons C_{(4+b)}$. C_M, C_4, and $C_{(4+b)}$ are the concentrations of monomer, tetramer, and aggregate which shows the band near 630 nm, respectively, and they are derived from Fig. 3a. See Eqs. 2—4 and text for details.

$$(4+b)C_{(4+b)} = C_T - C_M - 4C_4. \quad (4)$$

By evaluating the peak intensities of the monomer and tetramer bands according to the procedure of West and Pearce[14] and by applying the value of ε_M and ε_4 obtained for the mixed solvent containing 12.5 M methanol, C_M and C_4 were determined, and the values according to Eq. 3 were plotted. The results are shown in Fig. 3b. Although the data scatter somewhat, the b-value can be roughly estimated as 2. The low-energy band near 630 nm is, therefore, (probably) assigned to the hexamer of MD.

In the methanol-water mixtures containing KOH, MD is considered to be in the anionic form because of the dissociation of the carboxymethyl group of MD. For the formation of the above-mentioned tetramer and hexamer, the anionic form is concluded to be essential, since such aggregates were not formed when MD was dissolved in any methanol-water mixtures containing HCl, in which MD is considered to be in the neutral molecule form. As MD anions are polymerized by overcoming the electrostatic repulsive force between the anions, the addition of cations may play an important role in the screening effect.[13-16] Our preliminary results indicate that the addition of KCl to the alkaline solution used in the present study enhanced the formation of both kinds of aggregates, especially of the hexamer. On the contrary, the increase in the concentration of Triton X-100 enhanced the intensity of the monomer band because of the dissociation of the aggregates, as has previously been reported in the case of a cyanine dye solution.[13]

Aggregation of MD in Films. The vacuum-deposited MD film exhibits, similarly to the cast film of MD,[11] two visible absorption peaks at 516 nm and at 546 nm. The peak at 516 nm has been assigned to the dimeric (or oligomeric) form, and the one at 546 nm, to the monomeric form, of MD molecules since a dicrease in the absorbance at 516 nm was observed in the cast film of MD which contained arachidic acid as a diluent.[11] MD is insoluble in water as well as in aqueous solutions which are free from surfactants in the pH range from 0 to 13. Therefore, no coloration of aqueous solutions was observed when MD film was soaked in them. A slight alteration has been observed in the spectrum of the film soaked in a 0.5 M HNO_3 aqueous solution,[11] while the monomer and the dimer (or oligomer) bands remain practically unchanged. Similar results were obtained for the film soaked in any aqueous solution with a pH below 5.5. When the film was soaked in aqueous solutions of pH 5.5 or above, on the other hand, the spectrum was changed to form two low-energy bands, at 595 nm and at 625 nm. Figure 4 shows the spectral change in the MD film in the aqueous solution of pH 7.0 and an ionic strength of 0.10. The observed absorption bands for the MD film at 595 nm and at 625 nm are very similar, with regard to the peak position and the band shape, to those near 595 nm and near 630 nm for the methanolic aqueous solutions of MD described in the preceding section. Therefore, it can be concluded that the observed low-energy band at 595 nm and at 625 nm for the film are also to be assigned to the tetramer and (probably) the hexamer of the MD anion respectively.

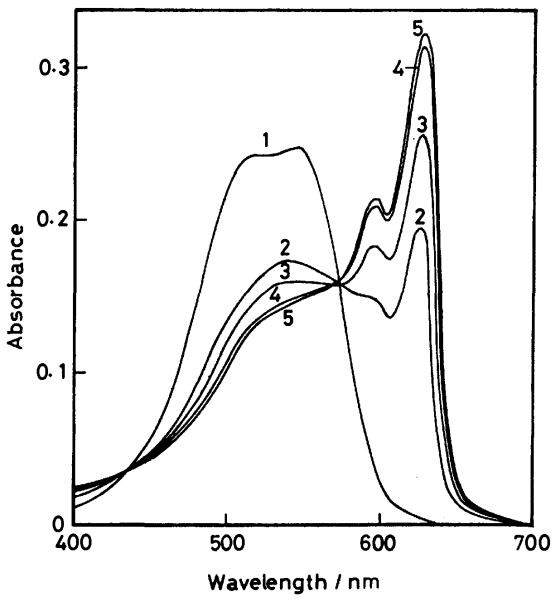

Fig. 4. Absorption spectra of the MD film (1) before and after sorking in an aqueous solution of pH 7.0 and ionic strength 0.10 for (2) 5 min, (3) 30 min, (4) 2 h, and (5) 24 h.

When the MD film on a KBr tablet was soaked in an aqueous solution of pH 7.0 with an ionic strength of 0.10, the tablet immediately began to dissolve (within a few seconds). The finding indicates that the solution can permeate rapidly into the film. Accordingly, the dissociation of the carboxymethyl group of MD in the bulk of the film is expected to proceed immediately after soaking the film in the aqueous solution. The formation of the MD anion in the bulk of the film was ascertained by IR measurements. The deposited film shows a C=O stretching absorption band for -COOH at 1740 cm^{-1}. The intensity of the absorption band becomes almost negligible after the film is dipped in the solution, probably because of the formation of the carboxylate form. The spectral change in the MD film is, on the contrary, very slow, as is shown in Fig. 4; the film needs *ca.* 2 h to give an almost stationary spectrum after being soaked in the aqueous solution. Therefore, slow processes for the aggregation, such as the re-arrangement, of MD anions proceed after the fast permeation of the aqueous solution into the film.

As has been described in the preceding section, the addition of KCl to the solution (which corresponds to the increment in the ionic strength of the solution) significantly affects the relative intensities of the two low-energy bands. In the case of the MD film/solution system, the change in the ionic strangth of the aqueous solutions also showed a marked effect on the relative intensities of the two bands. The results are given in Fig. 5, where the values of absorbance at 595 nm and at 625 nm are recorded after the MD film has been soaked for 2 h in each solution. As is shown in Fig. 5, the lowering of the ionic strength below 0.08 brings about a decrease in the absorbance at 625 nm and a simultaneous increase in that at 595 nm; further, only

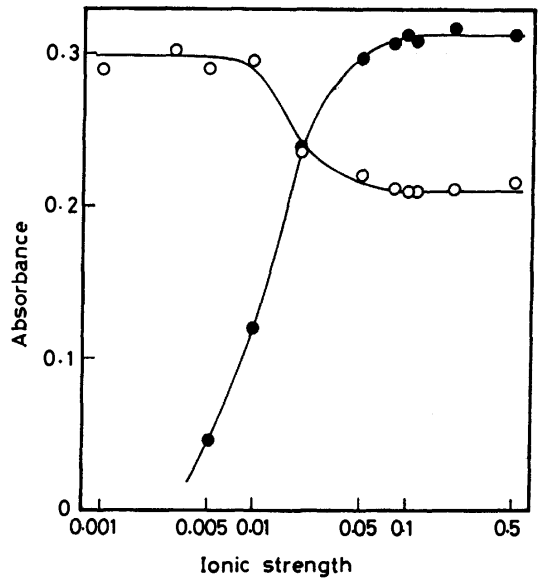

Fig. 5. Role of ionic strength of aqueous solutions on the absorptions of (○) the peak at 595 nm and (●) that at 625 nm.

the band at 595 nm is observed below the ionic strength of 0.003. Similar results were given by Sugi *et al.*[7] and also by Nakahara *et al.*;[17] they found[7,17] that the MD containing monolayer which was spread on an aqueous subphase of 0.4 mM $CdCl_2$ (pH *ca.* 6.5 and ionic strength *ca.* 0.001) exhibited only a low-energy absorption near 595 nm. The results given in Fig. 5 clearly indicate that very concentrated cations surrounding MD anions lead to a highly-ordered aggregation.

The dye film with aggregate(s) which shows a low-energy band is of practical importance as a photosensitizer[7,11,18–22] because of its high quantum efficiency, broad spectral response, and high stability. The change in the electrochemical behavior of the MD-coated electrode due to the formation of the aggregates will be described in detail in the following paper.

The authors are grateful to Drs. Masahiko Yoshiura, Keiji Iriyama, Michio Sugi, and Yukio Shimura for their informative suggestions. The authors are also grateful to Dr. Shigeo Yasui for synthesizing the MD.

References

1) D. L. Morel, A. K. Ghosh, T. Feng, E. L. Stogryn, P. E. Purwin, and A. Fishman, *Appl. Phys. Lett.*, **32**, 495 (1978).
2) A. K. Ghosh and T. Feng, *J. Appl. Phys.*, **49**, 5982 (1978).
3) K. Iriyama, M. Shiraki, K. Tsuda, A. Okada, M. Sugi, S. Iizima, K. Kudo, S. Shiokawa, T. Moriizumi, and Y. Yasuda, *Jpn. J. Appl. Phys.*, **19**, *Supplement* **19-2**, 173 (1980).
4) K. Kudo and T. Moriizumi, *Jpn. J. Appl. Phys.*, **19**, 1683 (1980).
5) G. A. Chamberlain, P. J. Cooney, and S. Dennison, *Nature*, **289**, 45 (1981).
6) M. Sugi and S. Iizima, *Thin Solid Films*, **68**, 199 (1980).
7) M. Sugi, T. Fukui, S. Iizima, and K. Iriyama, *Mol. Cryst. Liq. Cryst.*, **62**, 165 (1980).
8) G. A. Chamberlain and R. E. Malpas, *Faraday Discuss. Chem. Soc.*, **70**, 299 (1980).
9) H.Meier, W.Albrecht, U.Tschirwitz, E.Zimmerhackel, and N. Geheeb, *Ber. Bunsenges. Phys. Chem.*, **81**, 592 (1977).
10) F. Mizutani, M. Yoshiura, and K. Iriyama, *J. Chem. Soc., Chem. Commun.*, **1980**, 393.
11) K. Iriyama, F. Mizutani, and M. Yoshiura, *Chem. Lett.*, **1980**, 1399.
12) Y. Morishita, M. Isono, Y. Itoh, and S. Nozakura, *Chem. Lett.*, **1981**, 1149.
13) A. H. Hertz, *Photogr. Sci. Eng.*, **18**, 323 (1974).
14) W. West and S. Pearce, *J. Phys. Chem.*, **69**, 1894 (1965).
15) P. Mukerjee and A. Ghosh, *J. Phys. Chem.*, **67**, 193 (1963).
16) R. Robinson, A. Loffler, and G. Schwartz, *J. Chem. Soc., Faraday Trans. 1*, **69**, 56 (1973).
17) H. Nakahara and D. Möbius, to be published.
18) W. J. Dulmage, W. A. Light, S. J. Marino, C. D. Salzberg, D. L. Smith, and W. J. Staudenmayer, *J. Appl. Phys.*, **49**, 5543 (1978).
19) P. M. Borsenberger, A. Chodry, D. C. Hoestery, and W. Mey, *J. Appl. Phys.*, **49**, 5555 (1978).
20) H. Hada, Y. Yonezawa, and H. Inaba, *Chem. Lett.*, **1980**, 467.
21) H. Hada, Y. Yonezawa, and H. Inaba, *Ber. Bunsenges. Phys. Chem.*, **85**, 425 (1981).
22) M. Matsumura, S. Matsudaira, H. Tsubomura, M. Tanaka, and H. Yanagida, *Ind. Eng. Chem., Prod. Res. Dev.*, **19**, 415 (1980).

 © 1982 The Chemical Society of Japan Bull. Chem. Soc. Jpn., 55, 1300—1305 (1982) [Vol. 55, No. 4

Interaction between Ethidium Bromide and Various Polyelectrolytes and DNA with Emphasis on Spectral Characteristics and Binding Curves of the Bound Dye[1)]

Kiwamu YAMAOKA,* Takumi MATSUDA, Daisuke SHIBA, and Mineo TAKATSUKI
Faculty of Science, Hiroshima University, Higashisenda-machi, Naka-ku, Hiroshima 730
(Received September 19, 1981)

Visible and ultraviolet absorption spectra of ethidium bromide (EB) were measured by the optical titration method in the presence of each of three synthetic polyelectrolytes—sodium salts of poly(*p*-styrenesulfonate) (NaPSS), polyphosphate (NaPP), and polyacrylate (NaPA)—and native and heat-denatured DNA at 25 °C. By use of the principal component analysis (PCA) method, the number of EB species present in each EB–polymer system was determined to be two, *i.e.*, free and bound EB, in the range of the polymer residue-to-EB ratio between zero and about one. The spectrum and the fraction of EB species bound to each polymer were determined by the extended PCA method. The bound-EB spectra are bathochromic and hypochromic relative to the spectrum of free EB, but they show no metachromasy band. The apparent binding constants K_a for EB bound to polymers are in the order of NaPSS>denatured DNA>NaPP>NaPA≒native DNA.

In order to understand the general mechanism of metachromasy which results from the binding between dyes of particular classes and polyelectrolytes with highly charged sites, the pure spectrum of a given dye species bound to a particular polymer site, *i.e.*, the bound-dye spectrum, should be studied. This spectrum reflects the mode of interaction between the dye and the polymer site. Its extraction with a high resolution from observed absorption spectra of a dye–polymer system is, however, not an easy task because of the overlapping of the spectra of an unknown number of free and bound dye species and also because of the complicated reaction schemes with which the binding proceeds. It has been shown that the principal component analysis (PCA) method can be utilized to unravel the bound-dye spectrum.[2–8)] The bound-dye spectra of Crystal Violet (CV) and Trypaflavine (TF) show the characteristics of metachromasy, *i.e.*, the appearance of more than one absorption band, hypsochromism, and hypochromism.[3–6)] In the absence of polymers, CV and TF show a broad absorption band in the visible wavelength region, which consists of more than one electronic transition.[9,10)] A recent work on simpler acridine dyes, *N*-methylacridinium, and 9-aminoacridinium chlorides, has revealed that these bound-dye spectra exhibit only bathochromism and hypochromism.[5,7,8,11)]

Ethidium bromide (EB) has two amino groups at 3-, and 8-positions, but it belongs to a class of dyes different from 3,6-diaminoacridines such as Proflavine and TF. The interaction of EB with various biomolecules and biopolymers, particularly nucleic acids, has been studied by a number of physicochemical methods,[12–32)] but, precise information on the optical property of EB is still needed. In the present work, therefore, attempts were made to extract the bound-EB spectra by the PCA method. For this purpose, the spectroscopic interaction of EB with three polyelectrolytes with different functional groups and native and heat-denatured DNA was investigated in the low region of polymer residue-to-EB mixing ratio (P/D), where the binding scheme is rather simple. The empirical formula previously utilized for binding reactions was also improved upon to fit the thermodynamic concepts.

Experimental

Materials. Ethidium bromide (EB), 3,8-diamino-5-ethyl-6-phenylphenanthridinium bromide, was purchased from Sigma Chemical Co. (St. Louis, Mo., USA). It was purified by the method of column chromatography. The three synthetic polyanions used in this work are sodium salts of poly(*p*-styrenesulfonate) (NaPSS, the degree of polymerization $DP=1360$),[3)] polyphosphate (NaPP, $DP=154$),[3,4)] and polyacrylate (NaPA, $DP=7700$).[3)] Calf thymus DNA was obtained from Worthington Biochemical Corp. (Freehold, N. J., USA).

Preparation and Measurement of Sample Solutions. Throughout optical titration measurements, the concentrations of EB were kept constant at about 7×10^{-5} and 1.5×10^{-5} mol dm^{-3} in the visible and ultraviolet regions, respectively. The concentrations were determined by using the molar absorption coefficient, ε, of 5850 mol^{-1} dm^3 cm^{-1} at 480 nm.[18,19,27)] No ionic additives, such as neutral salt and buffer reagent, were added to EB–polyanion solutions to avoid undesired side effects, while EB–DNA solutions contained 1×10^{-3} mol dm^{-3} NaCl to prevent denaturation. The hyperchromicity of DNA was about 34%.[33)] The concentration of native DNA (nDNA) solution was 9.35×10^{-4} mol dm^{-3}; this was determined by using the ε value of 6400 at 260 nm. Heat-denatured DNA (dDNA) was prepared by the heating-shock cooling method.[33)] Optical titrations were carried out by adding a stock polymer solution, prepared as before,[3,4)] to an EB solution in an absorption cell successively in about 20—60 μl portions with a graduated or a Gilson microburet. The mixture was stirred for a few minutes and its absorption spectrum was recorded at 25 °C.[3)] Volume corrections were made whenever necessary.[3,4)] The P/D ratio was defined as the concentration of polymer in monomer unit per concentration of EB present in a mixture.[33)] Path lengths of quartz cells were 2 cm in the visible and 1 cm in the ultraviolet region.

Data Analysis by the Principal Component Analysis. The principal component analysis (PCA) method has been described in detail[2–5)] and also in outline.[6)] By this method, the number of light-absorbing species, *i.e.*, *components*, can be determined. These components are responsible for serial changes in the absorption spectra of a given dye successively titrated with a given polymer in solution. When the number was two, the apparent equibrium constant, K, and the pure absorption spectrum, ε^b_λ, of the dye bound to the polymer

could be evaluated by the extended PCA method with the following equilibrium scheme:[3-8]

$$K = \frac{[DP^*]}{[D][P]^{\alpha}}, \quad (1)$$

where DP* is the dye–polymer complex or the bound dye in the low P/D region, D is the unbound or free dye, P is the polymer residue which is not occupied by the dye, the brackets indicate the equilibrium concentration of each species, and α is a single adjustable parameter. The fraction of the bound dye in a dye–polymer solution, f_b ($=[DP^*]/[D]_0$), may be calculated at any given P/D, $[D]_0$ being the initial concentration of the dye.[1-3,5]

Equation 1 is an empirical one which was introduced to explain observed optical titration curves for various dye–polymer combinations.[3-9] The problem associated with this formula is that the dimension of K is given by $[dm^3/mol]^{\alpha}$ rather than $[dm^3/mol]$. This irregularity is now resolved by dividing both side of Eq. 1 by $[D]_0^{1-\alpha}$, which is a constant, because optical titrations are carried out at the constant initial dye concentration. Equation 1 is rewritten as

$$K_a \equiv \frac{K}{[D]_0^{1-\alpha}} = \frac{[DP^*]}{[D][P]}\left(\frac{[P]}{[D]_0}\right)^{1-\alpha}. \quad (2)$$

According to Tanford,[34] the apparent association constant, k, for the ligand–polymer site may be expressed as

$$k = \frac{(DP^*)}{(D)(P)} = \frac{[DP^*]}{[D][P]}\left(\frac{\gamma_{DP}}{\gamma_D\gamma_P}\right)e^{-\phi(\tilde{\nu})} \quad (3)$$

where the parentheses stand for the activity, γ's for the activity coefficients, and $\phi(\tilde{\nu})$ is a general function for electrostatic interaction. It is interesting to note that Eq. 2 may be transformed into Eq. 3 by formally equating the appropriate factors:

$$\left(\frac{D}{P}\right)^{\alpha-1}\exp[(1-\alpha)\ln(1-\tilde{\nu})] = \left(\frac{\gamma_{DP}}{\gamma_D\gamma_P}\right)\exp[-\phi(\tilde{\nu})], \quad (4)$$

since $f_b = \tilde{\nu} \times (P/D)$ and since $[D]_0/P \equiv D/P$. Not entering into theoretical implications of this relationship in the present work, we shall discuss the experimental results by using values of K_a in Eq. 2.

Results and Discussion

Three EB–Polyanion Systems. A series of observed visible spectra of EB–NaPSS solutions are shown in Fig. 1 as an example. These spectra reveal two isosbestic points, at 513 and 395 nm, in the low P/D range. By dropwise addition of NaPSS, the peak of EB at 480 nm decreases and concurrently shifts toward the long wavelength. This spectral behavior is also observed for EB–NaPP (isosbestic points 527 and 395 nm) and EB–NaPA (516 and 392 nm) solutions. A similar result has been reported for the EB–NaPP system.[18] Optical titrations of EB are shown in Fig. 2, where values of ε_{480} of EB–polyanion solutions are plotted against P/D. Values of ε_{480} decrease less for NaPA and NaPP than for NaPSS. In any case, they do not decrease linearly but are curved, the curvature being convex at the initial P/D (<0.5). This sigmoidal trend in titration curves has already been pointed out.[3-5]

The presence of isosbestic points in each EB–polyanion system indicates that this may be a binary system, but the possibility that it contains three or more independent components cannot be excluded. (If the molar absorption coefficients of these components have an identical value at some wavelength, this would be an isosbestic point.) By applying the PCA method to each EB–polyanion system, the exact number of components was determined. The results are shown in Fig. 3, where ratios of the eigenvalue of the ith component to the largest eigenvalue of the *first component*, Λ_i/Λ_1, are plotted on a logarithmic scale. A large gap is seen between the second and third components in each case; the ratio of $\Lambda_1 : \Lambda_3$ is larger than $10^5 : 1$. These results confirm that each EB–polyanion system contains two absorbing species. Thus, it is reasonable to conclude that observed spectral changes are an interplay of two EB species, *i.e.*, free EB and EB–polyanion complex (bound EB),

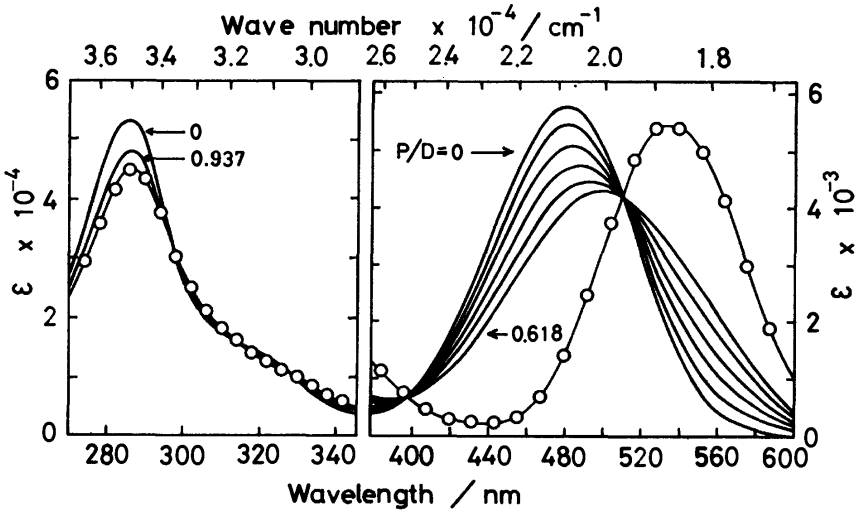

Fig. 1. Visible and ultraviolet spectra of EB titrated with salt-free NaPSS solution. The ordinates are the apparent molar absorption coefficients, ε, expressed in $mol^{-1}\,dm^3\,cm^{-1}$. Values of P/D are 0 (EB alone), 0.125, 0.243, 0.368, 0.493, and 0.618 in this order for the right, while they are 0 and 0.937 for the left. The concentration of EB $= 7.47 \times 10^{-5}$ mol dm^{-3}. Open circles represent the molar absorption coefficients, ε_λ^b, or the bound-EB spectra.

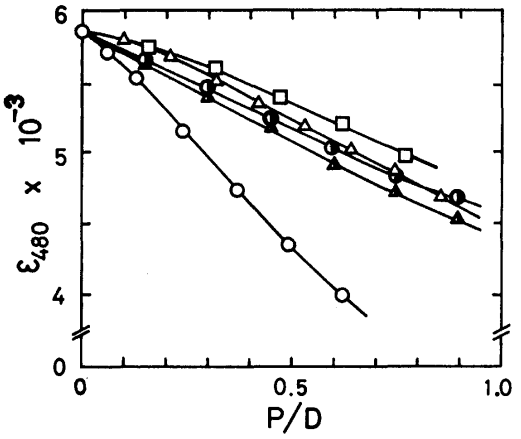

Fig. 2. Optical titration of EB with five different polymer solutions. The ordinate is the value of ε at 480 nm where the free EB shows the absorption peak. The abscissa is the mixing ratio. (○) NaPSS, (△) NaPP, (□) NaPA, (◑) native DNA, and (◭) heat-denatured DNA.

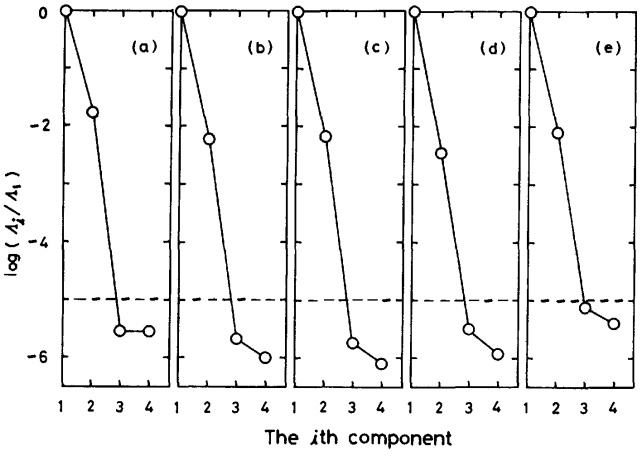

Fig. 3. Variations in the eigenvalue A_i with the ith light-absorbing component for five different EB–polymer systems. (a) NaPSS, (b) NaPP, (c) NaPA, (d) native DNA, and (e) heat-denatured DNA. The ordinate is the ratio of the eigenvalue of the ith component to that of the first. Dashed lines represent the upper limit to any significant components and are set under due considerations of experimental conditions.[2]

TABLE 1. THE APPARENT EQUILIBRIUM CONSTANTS, K_a AND K', AND THE EMPIRICAL PARAMETER α FOR EB–POLYMER SYSTEMS IN THE LOW P/D RANGE

Systems	α	$K_a \times 10^{-4}$ / dm^3 mol^{-1}	$K' \times 10^{-4}$ a) / dm^3 mol^{-1}
EB–NaPSS	1.4	9.9	6.6
EB–NaPP	1.7	1.4	1.0
EB–NaPA	1.4	1.2	1.0
EB–nDNA	1.1	1.2	1.1
EB–dDNA	1.1	1.6	1.5

a) $K' = K_a\left(\frac{[P]}{[D]_0}\right)^{\alpha-1}$. Values of K' were calculated at $P/D=1$.

in the low P/D range.

The Extended PCA Procedure and Bound-EB Spectra. On the basis of the above conclusion, Eq. 2 was used for evaluating the apparent equilibrium constant K_a and the empirical parameter α. The results are summarized in Table 1. Values of α are larger than unity for three EB–polyanion systems, corresponding to the convex curvature observed for titration curves in Fig. 2.[3-7] Values of the commonly-postulated apparent equilibrium constant, $K'=[DP^*]/[D]\cdot[P]=K_a([P]/[D]_0)^{\alpha-1}$, were computed at a convenient P/D value, *i.e.*, $P/D=1$.[3,4,6-8] They are given in Table 1, so that they may be compared with values reported for other dye–polymer systems.

With the optimized elements of the **t** matrix [Eq. 5 in Ref. 3], the spectrum of bound EB in the EB–NaPSS complex was calculated in the visible region (circles in Fig. 1). The spectral change of EB in the ultraviolet region is small, when a polyanion solution is added, and the strong absorption of free EB dominates the 340—235 nm region; hence, application of the extended PCA procedure is restricted. The ultraviolet spectrum of bound-EB, ε_λ^b, was therefore calculated with the fraction of bound EB, f_b, as

$$\varepsilon_\lambda^b = \varepsilon_\lambda^f + \frac{\varepsilon_\lambda - \varepsilon_\lambda^f}{f_b}, \qquad (5)$$

where ε_λ^f and ε_λ are the molar absorption coefficients at λ of EB and EB–polymer solutions, respectively. The ultraviolet spectrum of EB bound to NaPSS is shown in Fig. 1. It is hypochromic relative to the spectrum of free EB.

The bound-EB spectra of three EB–polyanion complexes are summarily shown in Fig. 4, and their spectral characteristics are given in Table 2. These visible spectra are bathochromic and hypochromic to different degrees. The bathochromic shift is about 37 nm (NaPA)—55 nm (NaPSS). The hypochromism of bound-EB spectra was expressed with the absorption maxima, $1-(\varepsilon_{max}^b/\varepsilon_{max}^f)$, and also with the oscillator strengths, $1-(F^b/F^f)$. When EB is bound to a charged polymer site, neither band-broadening, new peak, nor shoulder seems to appear in the bound-EB spectrum above 400 nm; the number of transition moments probably remains unchanged, as judged both from values of the half-intensity band width ($\Delta\tilde{\nu}_{1/2}$) and from values of the oscillator strength F. Since the 480 nm band of free EB is due to a single electronic transition,[17,35,36] the same probably holds for the visible band of bound EB. It may be concluded from the data in Table 2 that EB bound to various polyanions exhibits neither the metachromatic blue shift nor the metachromasy band. This conclusion is based on the fact that the bound-EB spectra were obtained in the low P/D range, where possible dye-stacking would be maximum, and lead to the most pronounced metachromatic behavior, if any. Hence, possessing two amino groups, EB differs markedly from many 3,6-diaminoacridine dyes[3,4,18,37,38] but resembles the unsubstituted acridinium or 9-aminoacridinium chloride.[7]

Spectral Characteristics of EB–DNA Complexes. In order to obtain the spectrum of EB bound to DNA,

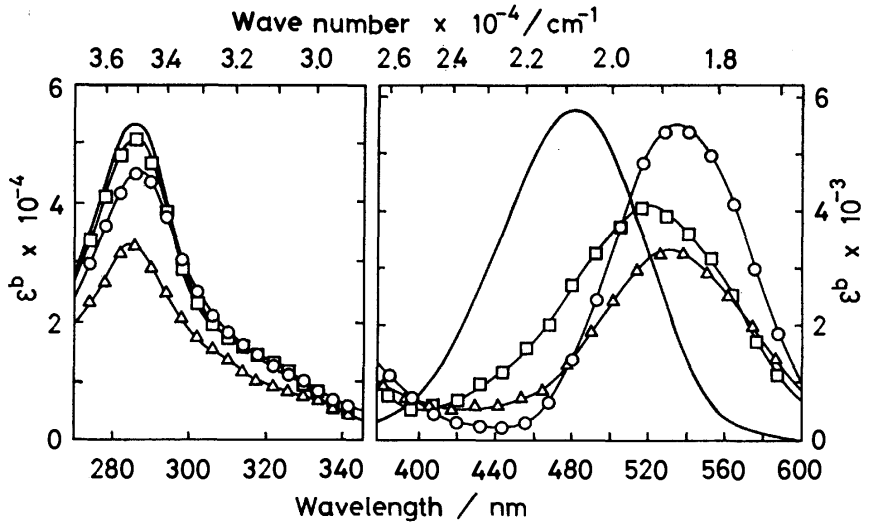

Fig. 4. Visible and ultraviolet spectra of EB bound to three different polyanions. (○) NaPSS, (△) NaPP, and (□) NaPA. The ultraviolet spectra were calculated at $P/D=0.937$ for NaPSS, 0.727 for NaPP, and 1.045 for NaPA. The concentration of EB is 7.47×10^{-5} mol dm^{-3}. Spectra of free EB are shown with solid lines for comparison.

Table 2. Characteristics of bound-EB spectra in the visible wavelength region

Systems	λ^b_{max} [a] / nm	ε^b_{max} [b] / mol^{-1} dm^3 cm^{-1}	H[c]	$\Delta\tilde{\nu}_{1/2}$ [d]	F[e]	H'[f]
EB[g]	480	5850	0	3920	0.107	0
EB–NaPSS	536	5550	5.1	2820	0.0751	29.5
EB–NaPP	532	3350	42.7	3410	0.0552	48.3
EB–NaPA	518	4160	28.9	3930	0.0785	26.4
EB–nDNA	524	4190	28.4	2950	0.0613	42.5
EB–dDNA	524	4090	30.1	3030	0.0595	44.2

a) Absorption peak of bound-EB spectrum. b) Molar absorption coefficient of bound EB at λ^b_{max} c) Hypochromicity in % defined as $[1-(\varepsilon^b_{max}/5850)]\times100$. d) Half-intensity band width, where $\varepsilon=\varepsilon^b_{max}/2$. e) Oscillator strength defined as $(4.315\times10^{-9})\int_{1/\lambda_1}^{1/\lambda_2}\varepsilon^b(\tilde{\nu})\cdot d\tilde{\nu}$, where λ_1 is set at 660 nm and λ_2 is the wavelength at which ε^b_λ is minimum. f) Hypochromicity in % defined as $[1-(F_{\text{bound EB}}/F_{\text{free EB}})]\times100$. g) Free EB as the reference.

the series of optical titration spectra were measured for EB–nDNA (isosbestic points 518 and 392 nm) and EB–dDNA (517 and 391 nm) systems. The results of optical titrations are similar to those in Fig. 1 and to those previously reported;[12,18,27] therefore, no detail will be reproduced here. Values of ε_{480} of EB decrease almost monotonously by addition of either native or denatured DNA solution, *i.e.*, the least convex curvature was observed (Fig. 2). The PCA result reveals that the number of EB components responsible for the visible spectra (the DNA moiety does not absorb in this wavelength region) is most probably two in the EB–nDNA and –dDNA systems, as indicated by the relative magnitudes of the eigenvalues in Fig. 3 (d and e). Hence, one free and one bound EB species are present in the low P/D range, regardless of the conformations of DNA.

By the extended PCA procedure, both K_a and α were evaluated (Table 1). Values of α are close to unity, indicating that the frequently-postulated binding scheme K' is nearly applicable to the EB–DNA system. Indeed, the value of K' calculated at $P/D=1$ (and that of K_a) is in good agreement with equilibrium constants previously reported for various EB–nDNA systems.[19,27] Figure 5 shows that the bound-EB spectrum in the native DNA complex (circles) is practically identical with that in the denatured DNA complex (triangles). These spectra are similar to a bound-EB spectrum which was obtained by equilibrium dialysis under different conditions.[19] The bound-EB spectra for DNA are very similar to those for three synthetic polyanions as regards their spectral characteristics, such as the red-shift and the absence of any new metachromasy band (Table 2). This close similarity suggests that the binding site of DNA may be related neither to the overall DNA conformation nor to the presence or absence of base-pairs. The polymer conformations or the functional groups thereof seem to be only of secondary importance for the bound-EB spectra. Thus, the most likely binding site is the charged moiety of the polymer, which is the common factor in the low P/D range.

Because of the reasons stated in the preceding section, the PCA procedure could not be applied to the ultraviolet spectra of EB–nDNA and –dDNA systems. By subtracting the contribution of the moiety of native and denatured DNA, the bound-EB spectra in the ultraviolet region were calculated with values of K_a and α according to Eq. 5 and are shown in Fig. 5. They are again very close to each other and to a reported spectrum.[16]

Fraction of Bound EB and Binding Curves. Values of the fraction of bound EB, f_b, or free EB, $1-f_b$, were calculated with K_a and α in Table 1 or with the elements of the **t** matrix. They are plotted against P/D on a

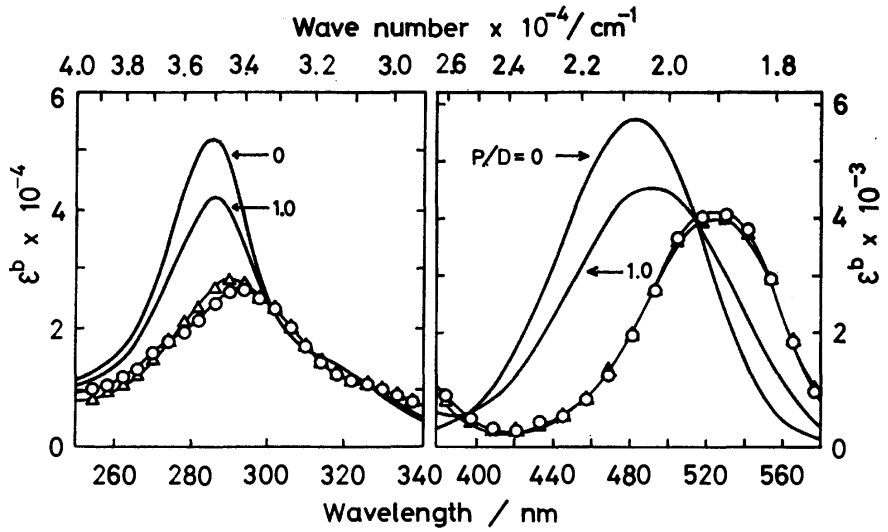

Fig. 5. Visible and ultraviolet absorption spectra of EB titrated with the 1×10^{-3} mol dm^{-3} NaCl-containing DNA solutions and the bound-EB spectra. Observed spectra are at $P/D=0$ and 1.0 for EB–nDNA solutions only. (○) EB bound to native DNA and (△) bound to heat-denatured DNA. The concentration of EB is 7.12×10^{-5} mol dm^{-3} in 1×10^{-3} mol dm^{-3} NaCl.

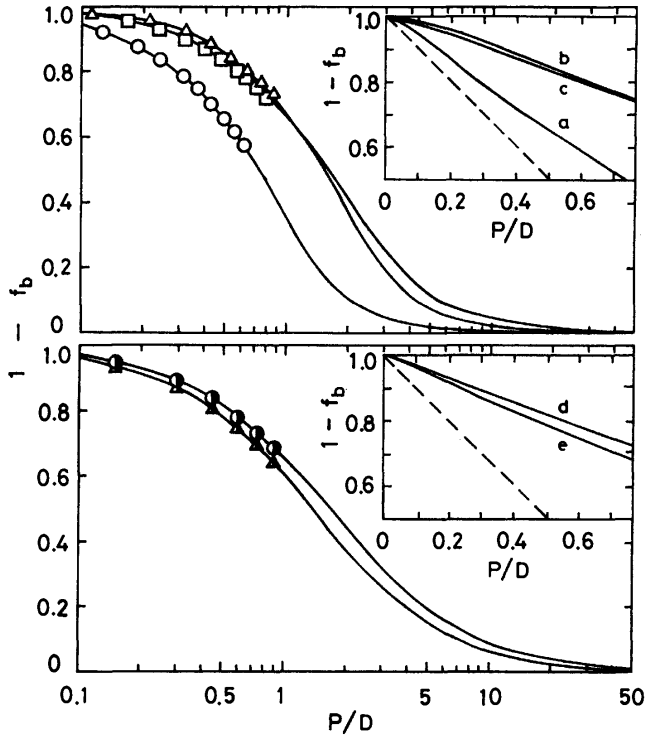

Fig. 6. Fractions of bound-EB in EB–polymer solutions and binding curves as a function of P/D. The ordinates are the fraction of free EB in EB–polymer solution, $1-f_b$. (○) NaPSS, (△) NaPP, (□) NaPA, (◑) nDNA, and (▲) dDNA. Binding curves, calculated with values of K_a and α, are shown by solid lines. In inserts, values of $(1-f_b)$ are plotted against P/D on a decadic scale. Dashed lines should be referred to the text. Each point was calculated with the aid of Eq. 4 in Ref. 4.

semi-logarithmic scale in Fig. 6. The fraction of free EB decreases gradually with the increase in P/D. Almost all EB molecules are estimated to be bound to NaPSS at $P/D>20$ but to NaPA, nDNA, and dDNA only at $P/D>50$, provided that the binding proceeds according to Eq. 1 or 2. The binding affinity of various polymers toward EB expressed by f_b at $P/D=1$ is in the order of NaPSS>dDNA (1 mM NaCl)>nDNA (1 mM NaCl)> NaPP≒NaPA. NaPSS has been noted for its high binding affinity toward various acridine dyes,[3,7] for which the strong ability for counterion condensation may be responsible.[39] Sigmoidal changes of binding curves are well reproduced for EB–polyanion systems ($\alpha>1$), as are indicated in the inserts of Fig. 6, where P/D values are plotted on a decadic scale. The binding curves decrease almost linearly for EB–DNA system ($\alpha=1.1$). In any case, it is worth mentioning that, except for NaPSS, no more than 50% of EB are bound to polymer sites when EB and the polymer residue are present in solution at equimolar amounts ($P/D=1$). Dashed lines in the inserts represent the relation $(1-f_b)=1-(D^b/P)(P/D)$, where $D^b/P=1$, *i.e.*, the number of bound EB per polymer residue in solution is unity. Hence, even in the P/D region where the amount of EB is in large excess ($P/D<1$), polymer sites are only partially occupied by EB (Fig. 6).

Closing Remarks. The common spectral features of five EB–polymer complexes are in that the absorption maximum of each bound-EB spectrum in the visible region shows both bathochromism and hypochromism but none of new "metachromasy" band, band-broadening, or hypsochromism. These features are in accord with those observed for *N*-methylacridinium and 9-aminoacridinium chlorides, but in contrast with the more complex acridine dyes. A possible explanation rests on the fact that the visible absorption band of metachromatic 3,6-disubstituted acridine dyes consists of two mutually perpendicular but overlapping transition moments,[10] while the visible band of EB[35,36] or

simple acridine cations[7,40] consists of a single electronic transition moment. Theoretical interpretations of these spectral characteristics would undoubtedly promote the understanding of metachromasy. For this purpose, accumulations of bound-dye spectra are highly desired for diverse combinations between metachromatic dyes of various chemical structures and polyelectrolytes with different conformations and functional groups.

References

1) This is Part X of *Metachromasy*. For the preceding paper of this series, see K. Yamaoka, T. Matsuda, and T. Murakami, *Bull. Chem. Soc. Jpn.*, **54**, 3859 (1981).

2) M. Takatsuki and K. Yamaoka, *J. Sci. Hiroshima Univ., Ser. A*, **40**, 387 (1976).

3) K. Yamaoka and M. Takatsuki, *Bull. Chem. Soc. Jpn.*, **51**, 3182 (1978).

4) M. Takatsuki and K. Yamaoka, *Bull. Chem. Soc. Jpn.*, **52**, 1003 (1979).

5) M. Takatsuki, *Bull. Chem. Soc. Jpn.*, **53**, 1922 (1980).

6) K. Yamaoka and T. Matsuda, *Biophys. Chem.*, **12**, 235 (1980).

7) K. Yamaoka, M. Takatsuki, and K. Nakata, *Bull. Chem. Soc. Jpn.*, **53**, 3165 (1980).

8) K. Yamaoka and M. Takatsuki, *Bull. Chem. Soc. Jpn.*, **54**, 293 (1981).

9) Y. Matsuoka and K. Yamaoka, *Bull. Chem. Soc. Jpn.*, **52**, 2244 (1979).

10) Y. Matsuoka and K. Yamaoka, *Bull. Chem. Soc. Jpn.*, **52**, 3163 (1979); **53**, 2146 (1980).

11) K. Yamaoka and M. Masujima, *Biopolymers*, **17**, 2485 (1978).

12) M. J. Waring, *J. Mol. Biol.*, **13**, 269 (1965).

13) J.-B. Lepecq and C. Paoletti, *J. Mol. Biol.*, **27**, 87 (1967).

14) W. Bauer and J. Vinograd, *J. Mol. Biol.*, **33**, 141 (1968).

15) W. Bauer and J. Vinograd, *J. Mol. Biol.*, **47**, 419 (1970).

16) D. G. Dalgleish, A. R. Peacocke, G. Fey, and C. Harvey, *Biopolymers*, **10**, 1853 (1971).

17) C. Houssier, B. Hardy, and E. Fredericq, *Biopolymers*, **13**, 1141 (1974).

18) G. Löber, J. Koudelka, and E. Smekal, *Biophys. Chem.*, **2**, 158 (1974).

19) J. L. Bresloff and D. M. Crothers, *J. Mol. Biol.*, **95**, 103 (1975).

20) T. R. Krugh and C. G. Reinhardt, *J. Mol. Biol.*, **97**, 133 (1975).

21) J. Paoletti, B. B. Magee, and P. T. Magee, *Biochemistry*, **16**, 351 (1977).

22) D. J. Patel and L. L. Canuel, *Biopolymers*, **16**, 857 (1977).

23) C. C. Tsai, S. C. Jain, and H. M. Sobell, *J. Mol. Biol.*, **114**, 301 (1977).

24) S. C. Jain, C. C. Tsai, and H. M. Sobell, *J. Mol. Biol.*, **114**, 317 (1977).

25) H. M. Sobell, C. C. Tsai, S. C. Jain, and S. G. Gilbert, *J. Mol. Biol.*, **114**, 333 (1977).

26) R. V. Kastrup, M. A. Young, and T. R. Krugh, *Biochemistry*, **17**, 4855 (1978).

27) J. Pauluhn and H. W. Zimmermann, *Ber. Bunsenges. Phys. Chem.*, **82**, 1265 (1978).

28) C. G. Reinhardt and T. R. Krugh, *Biochemistry*, **17**, 4845 (1978).

29) M. Hogan, N. Dattagupta, and D. M. Crothers, *Biochemistry*, **18**, 280 (1979).

30) J. Pauluhn and H. W. Zimmermann, *Ber. Bunsenges. Phys. Chem.*, **83**, 76 (1979).

31) A. W. Braithwaite and B. C. Baguley, *Biochemistry*, **19**, 1101 (1980).

32) H.-W. Wu, N. Dattagupta, M. Hogan, and D. M. Crothers, *Biochemistry*, **19**, 626 (1980).

33) K. Yamaoka and R. A. Resnik, *J. Phys. Chem.*, **70**, 4051 (1966).

34) C. Tanford, "Physical Chemistry of Macromolecules," John Wiley and Sons, New York (1961), p. 535.

35) I. Zimmermann and H. W. Zimmermann, *Ber. Bunsenges. Phys. Chem.*, **80**, 991 (1976).

36) A. Waleh, B. Hudson, and G. Loew, *Biopolymers*, **15**, 1637 (1976).

37) V. Vitagliano, L. Costantino, and A. Zagari, *J. Phys. Chem.*, **77**, 204 (1973).

38) M. Dourlent and C. Hélène, *Eur. J. Biochem.*, **23**, 86 (1971).

39) G. S. Manning, *Acc. Chem. Res.*, **12**, 443 (1979).

40) V. Zanker and A. Wittwer, *Z. Phys. Chem. (Frankfurt am Main)*, **24**, 183 (1960).

Mechanism of Copper Transport through a Diaphragm-type Liquid Membrane

Takeshi KATAOKA, Tadaaki NISHIKI,* and Koretsune UEYAMA

Department of Chemical Engineering, College of Engineering, University of Osaka Prefecture, Mozu-Umemachi, Sakai, Osaka 591

(Received March 13, 1981)

The permeation mechanism of copper with a liquid membrane process was studied by measuring the permeation rate of copper, which was allowed to permeate through a diaphragm-type liquid membrane with LIX64N as a mobile carrier at various concentrations of carrier and acid. The permeation rate is explained approximately by the diffusional process in the membrane for a chelating complex between copper and carrier and by the succeeding stripping reaction at the interface between the membrane and stripping phase.

A novel technique which can separate and concentrate dissolved solutes and ions in aqueous solution with liquid membranes has attracted special interest recently.[1,2] Especially, the liquid membrane process containing a mobile carrier can be expected to give high selectivity and concentrating effect, so researches have been actively advanced to apply the process to hydrometallurgy and waste water treatment.

The liquid-liquid extraction of copper with LIX reagents has been one of important commercial solvent extractions for practical applications in hydrometallurgical processes. Therefore, a number of studies on equilibria and kinetics of extraction reactions have been reported. However, concentration and separation of copper with liquid membrane containing LIX reagents as a mobile carrier has not sufficiently been studied,[3-6] and the mechanism of permeation through such a membrane has not been elucidated.

The purpose of the present investigation is to clarify the permeation mechanism of copper ion with a liquid membrane. The permeation rate of copper ion through a diaphragm-type liquid membrane was measured by adopting LIX64N as a mobile carrier. The effect of the concentration of carrier and acid on the permeation rate was examined, and the permeation mechanism was discussed.

Theoretical

Model for Permeation of Copper. The permeation mechanism of copper ion through a liquid membrane containing LIX64N as a mobile carrier is shown schematically in Fig. 1. Copper ion M^{2+} in the left cell diffuses to the interface $x=0$, where it undergoes chelating complex formation with the carrier RH. The complex R_2M formed diffuses across the membrane toward the interface $x=L$, reacts with hydrogen ion H^+ and liberates copper ion in the right cell. The regenerated carrier RH diffuses back to the left side of membrane and reacts again with M^{2+} in the left cell. As a result of repetition of such a mechanism, copper ions are permeated and concentrated from the left into the right cell.

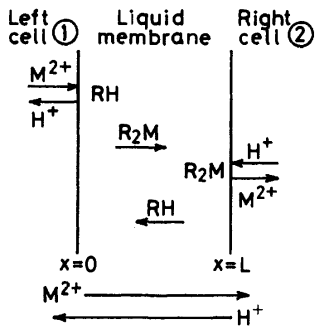

Fig. 1. Permeation mechanism.

Permeation Rate. If the permeation rate is controlled both by the diffusion process in the membrane and by the stripping process at the interface between the membrane and the right cell, the quasi-steady state may be assumed, and the fluxes J in the membrane and J in the right cell are respectively given by

$$J_M = \bar{k}_M\{(\bar{C}_T/2)-\bar{C}_{ML}\}, \quad (1)$$

$$J_{RH} = -\bar{k}_{RH}\bar{C}_{RHL}, \quad (2)$$

$$J_{M2} = k_{M2}(C_{ML}-C_{M2}), \quad (3)$$

where k is the mass-transfer coefficient and $\bar{C}_T$ the total concentration of mobile carrier. The bar superscript and the subscripts L and 2 denote the membrane phase, the interface $x=L$, and the right cell, respectively.

The following interfacial reaction model[7] may be applied to the stripping reaction at $x=L$:

$$(\overline{R_2M})_i + (H^+)_i \underset{k_{-r1}}{\overset{k_{r1}}{\rightleftharpoons}} (RM^+)_{ad} + (\overline{RH})_i \quad K_1, \quad (4)$$

$$(RM^+)_{ad} + (H^+)_i \rightleftharpoons (M^{2+})_i + (RH)_{ad} \quad K_2, \quad (5)$$

$$(RH)_{ad} \rightleftharpoons (\overline{RH})_i \quad K_3, \quad (6)$$

where K is the equilibrium constant, the subscript "ad" denotes the interfacially adsorbed species, and "i" denotes the species adjacent to the interface, either on the membrane side or on the right cell side. If the reaction shown in Eq. 4 is a rate-controlling step, the stripping reaction rate is expressed as

$$r = k_{r1}[\overline{R_2M}]_i[H^+]_i - \frac{k_{-r1}[M^{2+}]_i[RH]_{ad}[\overline{RH}]_i}{K_2[H^+]_i}$$

$$= k_{r1}\bar{C}_{ML}C_{HL} - \frac{\alpha C_{ML}\bar{C}_{RHL}}{C_{HL}}, \quad (7)$$

where $\alpha=\bar{k}_{-r1}[RH]_{ad}/K_2$.

From Eqs. 1, 2, 3, and 7, the concentration $\bar{C}_{ML}$ of the complex at the interface $x=L$ is given by

$$\bar{C}_{ML} = (1/4\alpha\beta\gamma)[2\alpha\beta\gamma\bar{C}_T + k_{r1}C_{HL}^2 + \bar{k}_M C_{HL} + 2\alpha\beta C_{M2} - \{k_{r1}C_{HL}^2(4\alpha\beta\gamma\bar{C}_T + k_{r1}C_{HL}^2 + 2(\bar{k}_M C_{HL} + 2\alpha\beta C_{M2})) + (\bar{k}_M C_{HL} + 2\alpha\beta C_{M2})^2\}^{1/2}], \quad (8)$$

where $\beta=\bar{k}_M/\bar{k}_{RH}$ and $\gamma=\bar{k}_M/k_{M2}$.

Consequently, with $\bar{C}_{ML}$ obtained from Eq. 8, the concentration C_{M1} of copper in the left cell can be calculated successively as a function of time by using Eq. 1 and the following equation:

$$-V(dC_{M1}/dt) = SJ_M, \quad (9)$$

where V and S represent the volume of cell and the area of diaphragm, respectively.

In the initial contact time, the second term on the right-hand side of Eq. 7 may be neglected and the copper concentration with time is expressed as

$$\frac{C_{M1}}{C_{M1,0}} = 1 - \frac{1}{2}\left(\frac{S}{V}\right)\left\{\frac{k_{r1}C_{HL}}{1+(k_{r1}/\bar{k}_M)C_{HL}}\right\}\left(\frac{\bar{C}_T}{C_{M1,0}}\right)t, \quad (10)$$

where $C_{M1,0}$ is the initial concentration of copper in the left cell.

The mass-transfer coefficient k_{M2} was evaluated from the following equation:

$$\frac{kd}{D} = 0.158\left(\frac{\mu}{\rho D}\right)^{1/3}\left(\frac{\omega d^2\rho}{\mu}\right)^{0.63}, \quad (11)$$

where D is the diffusivity, d the diameter of impeller, ρ the density, μ the viscosity, and ω the rotational speed of impeller. This equation is correlated with the mass-transfer coefficients obtained from the following experiment. Namely, benzoic acid was cast in a circular depression corresponding to the membrane in the same apparatus as used in this study. Rates of dissolution of benzoic acid from the flat surface into several liquids were measured for various speeds.

Experimental

Apparatus. The permeation apparatus used is illustrated in Fig. 2. The membrane was clampled between two glass half-cells with inner diameter of 8 cm. A Teflon millipore membrane filter, which has a thickness of 125 μm, a porosity of about 68%, and a pore size of 10 μm, was used as a diaphragm throughout this study. The volume of each cell is 370 cm^3 and the contact area between the membrane and aqueous solution is 33.2 cm^2. The turbine impellers of 4 cm diameter with six flat-blades filtted at the center of cell length were driven in the same direction at a constant speed of 82 min^{-1} with variable-speed motors in both cells. The apparatus was placed in an air bath which was maintained at 25 °C. In addition, all metal surfaces were coated with Teflon.

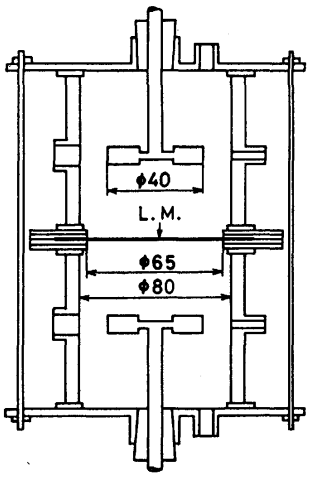

Fig. 2. Permeability cell.

Method. The pores in the membrane were filled up by immersing the membrane filter in the membrane solution. The membrane solution was prepared by dissolving LIX64N as a mobile carrier in kerosene. The concentration of active ingredient of LIX64N in kerosene was determined by measurement of the ultimate copper loading of LIX64N. The aqueous solutions were prepared by saturating degassed deionized water with kerosene.

The aqueous copper sulfate solution containing acetic acid–sodium acetate buffer was carefully poured into the left cell and the aqueous hydrochloric acid or sulfuric acid solution into the right cell so that the liquid levels in both cells might become equal. The time when the aqueous solution had come into contact with whole surface of membrane was taken as the beginning of experiment. After each cell was filled with the solution, both cells were stirred immediately.

Samples were taken from the left cell at regular time intervals by replacing them with fresh solution. The amount of sample was about 5 cm^3 and the number of samples was 5 or 6 in each run. The copper concentration was determined by titration with a standardized EDTA solution.

Results and Discussion

Effects of pH and Initial Concentration of Copper. The effect of pH on the partition equilibrium of copper between LIX64N in kerosene and aqueous solution was investigated by the batchwise method. The result obtained shows that the percent extraction of copper becomes constant around 100% above pH=3.

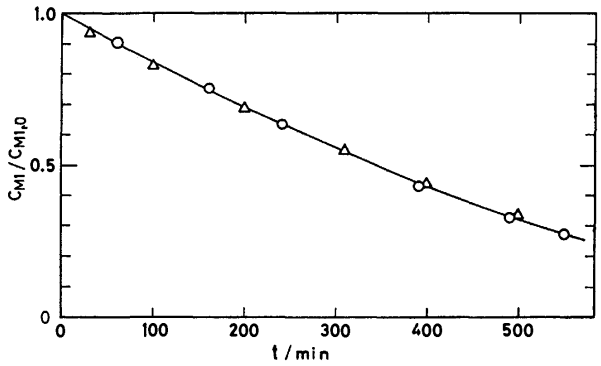

Fig. 3. Effect of pH on permeation rate of copper.
System: 0.01 mol dm^{-3} $CuSO_4$–L.M. ($\bar{C}_T$=0.490 mol dm^{-3})–2 mol dm^{-3} HCl. △: pH=3.5, ○: pH=4.5.

To examine the effect of pH on the permeation rate of copper, the copper concentration in the left cell with time was followed with time by keeping the pH in the left cell at 3.5 and 4.5. These results are shown in Fig. 3. No appreciable difference in permeation rate is detected for the above two pH values. Therefore, all the runs described below were performed for pH=4.5.

Figure 4 shows a result where differences in concentration, *i.e.*, the decreased amounts of copper in the left cell, were plotted against time for the initial copper concentrations of 0.01, 0.02, and 0.05 mol dm^{-3}. There

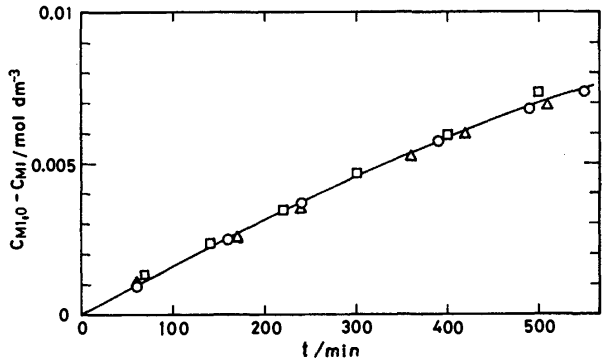

Fig. 4. Effect of initial coper concentration on permeation rate of copper.
System: $CuSO_4$(pH=4.5)-L.M. ($\bar{C}_T$=0.490 mol dm^{-3}) -2 mol dm^{-3} HCl. ○: $C_{M1,0}$=0.01, △: $C_{M1,0}$=0.02, □: $C_{M1,0}$=0.05 mol dm^{-3}.

is no change in concentration difference with the variation of initial concentration and the effect of the initial copper concentration on the permeation rate may be neglected.

From the above results, the foregoing assumption that the permeation rate is controlled both by the diffusion process in the membrane and by the stripping process seems to be reasonable.

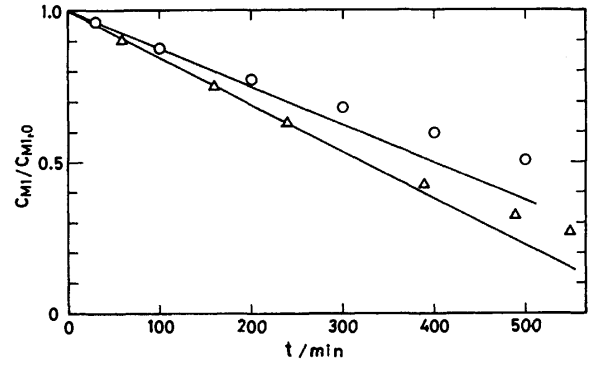

Fig. 5. Copper concentration in left cell *vs.* time (determination of k_{r1}).
System: 0.01 mol dm^{-3} $CuSO_4$(pH=4.5)-L.M.($\bar{C}_T$= 0.490 mol dm^{-3})-2 mol dm^{-3} acid. ○: H_2SO_4, △: HCl.

Determination of Reaction Rate Constant k_{r1}. Figure 5 shows results of runs in which time-dependent concentrations of copper in the left cell were measured by using 2 mol dm^{-3} hydrochloric acid or sulfuric acid as an acid in the right cell at the carrier concentration of 0.49 mol dm^{-3}. The solid lines are the slopes for each straight region near contact time zero. The values of k_{r1} obtained from each slope and Eq. 10 are 2.5 for HCl and 0.95 cm^4 mol^{-1} min^{-1} for H_2SO_4. The value of $\bar{k}_M$ in the membrane adopted in this calculation was evaluated by the same method as in the case of the concentration of chloride ion[8] and by using the diffusivity estimated from the Wilke-Chang equation. The estimated value of $\bar{k}_M$ is shown in Table 1. In the figure, the experimental values tend to deviate upward

TABLE 1. ESTIMATED VALUES OF MASS-TRANSFER COEFFICIENTS

$\bar{C}_T$ / mol dm^{-3}	$\bar{k}_M$ / cm min^{-1}	$\bar{k}_{RH}$ / cm min^{-1}
0.490	8.3×10^{-4}	1.3×10^{-3}
0.193	2.1×10^{-3}	3.2×10^{-3}
0.100	2.7×10^{-3}	4.2×10^{-3}

Acid	C_{HL} / mol dm^{-3}	k_{M2} / cm min^{-1}
HCl	2.0	4.6×10^{-2}
	1.0	4.8×10^{-2}
H_2SO_4	4.0	2.9×10^{-2}
	2.0	3.8×10^{-2}

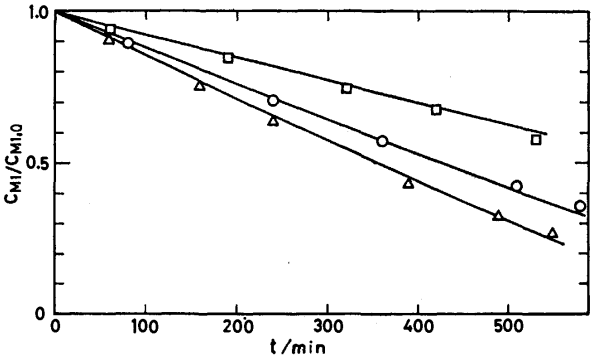

Fig. 6. Copper concentration in left cell *vs.* time (effect of carrier concentration).
System: 0.01 mol dm^{-3} $CuSO_4$ (pH=4.5)-L. M.-2 mol dm^{-3} HCl. α=0.16 cm min^{-1}. □: $\bar{C}_T$=0.100, ○: $\bar{C}_T$=0.193, △: $\bar{C}_T$=0.490 mol dm^{-3}.

from each straight line. This is caused by neglecting the second term on the right hand side of Eq. 7.

Effect of Carrier Concentration. Figure 6 shows the effect of the carrier concentration on the permeation rate at 2 mol dm^{-3} of hydrochloric acid. The solid lines are the concentrations as a function of time for each carrier concentration which were calculated from Eqs. 1, 8, and 9 by using the above value of k_{r1} and those of $\bar{k}_M$ and $\bar{k}_{RH}$ in Table 1. In this case, the mass-transfer coefficient k_{M2} in the right cell was obtained from Eq. 11 by using the diffusivity of copper ion estimated from the Nernst-Einstein equation, and is shown in Table 1. In addition, the value of α, which is constant because the value of $[RH]_{ad}$ becomes the saturated value at the high concentrations of LIX64N used, was determined by the trial and error method. The calculated values agree with the experimental results over the wide range of contact time for each carrier concentration.

The effect of carrier concentration on the permeation rate at 2 mol dm^{-3} of sulfuric acid is shown in Fig. 7. The solid line represents the calculated values for α= 0.20 cm min^{-1} obtained in the same way as in the case of hydrochloric acid by using the k_{r1} obtained above and the mass-transfer coefficients presented in Table 1. The calculated values agree with the observed over the whole range of contact time for all the carrier concentrations. The value of α for H_2SO_4 is a little different

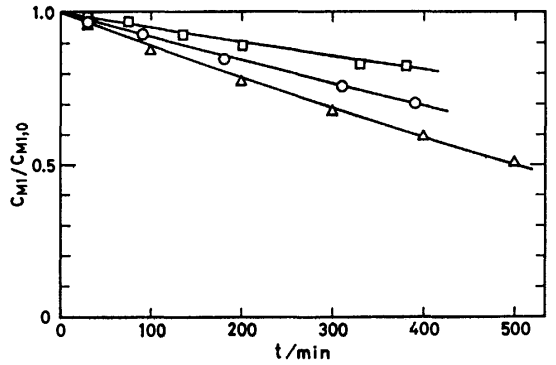

Fig. 7. Copper concentration in left cell *vs.* time (effect of carrier concentration).
System: 0.01 mol dm^{-3} $CuSO_4$ (pH=4.5)–L.M.–2 mol dm^{-3} H_2SO_4. α=0.20 cm min^{-1}. □: $\bar{C}_T$=0.100, ○: $\bar{C}_T$=0.193, △: $\bar{C}_T$=0.490 mol dm^{-3}.

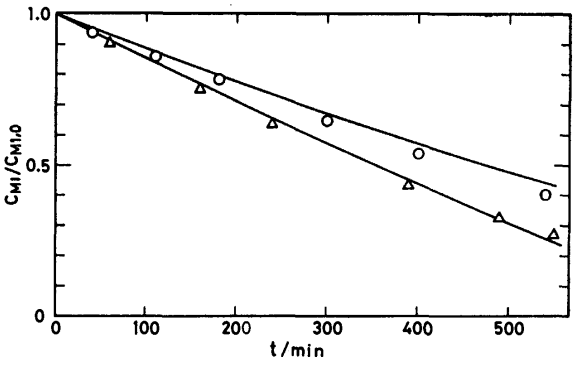

Fig. 8. Copper concentration in left cell *vs.* time (effect of hydrochloric acid concentration).
System: 0.01 mol dm^{-3} $CuSO_4$ (pH=4.5)–L. M. ($\bar{C}_T$= 0.490 mol dm^{-3})–HCl. α=0.16 cm min^{-1}. ○: HCl concn=1.0, △: HCl concn=2.0 mol dm^{-3}.

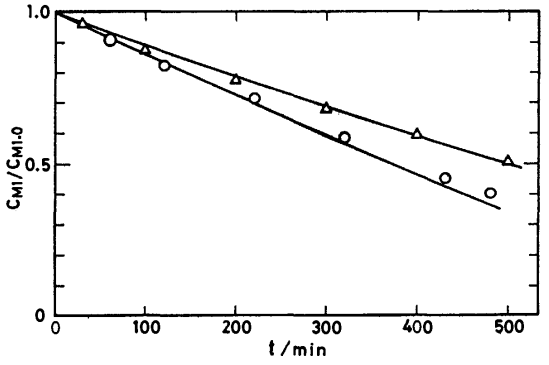

Fig. 9. Copper concentration in left cell *vs.* time (effect of sulfuric acid concentration).
System: 0.01 mol dm^{-3} $CuSO_4$ (pH=4.5)–L. M. ($\bar{C}_T$= 0.490 mol dm^{-3})–H_2SO_4. α=0.20 cm min^{-1}. △: H_2SO_4 concn=2.0, ○: H_2SO_4 concn=4.0 mol dm^{-3}.

from α=0.16 cm min^{-1} for HCl. This may be caused by a difference in k_{-r1} value between the two acids.

Effect of Acid Concentration. To clarify the effect of acid concentration in the right cell on the permeation rate, the copper concentration with time was measured by varying the concentration of hydrochloric acid at a constant carrier concentration of 0.49 mol dm^{-3}. These results are shown in Fig. 8. The solid lines are the calculated values obtained by using the same values of k_{r1} and α as in the case of the variation of carrier concentration. The calculated values agree approximately with the experimental ones, althought there are slight deviations between the calculated and experimental values in the region of long contact time.

Figure 9 shows results of the time-dependent concentration for sulfuric acid of 2 and 4 mol dm^{-3}. The agreement between the calculation and experiment is approximately good to the same extent as in the case of hydrochloric acid.

Conclusion

To clarify the permeation mechanism of copper ion with a liquid membrane, the time-dependent concentration of copper was measured for a diaphragm-type liquid membrane impregnated with LIX64N as a mobile carrier.

The permeation rate of copper ion is affected by the concentration of carrier and of the acid in the stripping phase. It has become apparent that the mechanism for the present permeation can be expressed by the diffusional process in the membrane for a chelating complex between copper and carrier and by the succeeding reaction at the interface between the membrane and stripping phase.

This work was supported by Grant-in-Aid for Scientific Research of the Ministry of Education, Science and Culture, Japan, Grant No. 355406. The authors wish to acknowledge the support leading to the publication of this article.

References

1) N. N. Li and A. L. Shrier, "Recent Developments in Separation Science," ed by N. N. Li, CRC Press, Cleveland (1972), Vol. 1, p. 163.
2) J. W. Frankenfeld and N. N. Li, "Recent Developments in Separation Science," ed by N. N. Li, CRC Press, Cleveland (1977), Vol. 3, p. 285.
3) R. W. Baker, M. E. Tuttle, D. J. Kelly, and H. K. Lonsdale, *J. Membr. Sci.*, **2**, 213 (1977).
4) A. Kopp, R. Marr, and F. Moser, presented at CHISA '78 Conference, 12.6 (1978).
5) K. H. Lee, D. F. Evans, and E. L. Cussler, *AIChE J.*, **24**, 860 (1978).
6) W. Volkel, W. Halwachs, and K. Schügerl, *J. Membr. Sci.*, **6**, 19 (1980).
7) I. Komasawa, T. Otake, and T. Muraoka, *J. Chem. Eng. Jpn*, **13**, 204 (1980).
8) T. Kataoka, T. Nishiki, Y. Tamura, and K. Ueyama, *J. Chem. Eng. Jpn.*, **13**, 35 (1980).

Photodimerization of Indeno[2,1-*a*]indene

Sang Chul SHIM* and Jeong Seok CHAE

Department of Chemistry, The Korea Advanced Institute of Science and Technology, P. O. Box 150 Chongyangni, Seoul, Korea

(Received October 16, 1980)

Indeno[2,1-*a*]indene, a *trans*-stilbene analogue with fixed planar configuration, yielded a head-to-head and a head-to-tail C_4-cyclodimer on direct irradiation with 300 nm UV light. The fluorescence quenching and sensitization studies indicated the reaction to proceed through excited singlet state, very likely through the singlet excimer intermediate.

Twisting around the C=C bond is normally an important decay mode of electronically excited singlet as well as triplet states of olefins as shown in stilbenes. However, fluorescence is the major decay route for stilbenes where the C=C bond is incorporated into a small ring such as cyclopropene, cyclobutene, or cyclopentene so that the twisting around the C=C bond is forbidden because of the ring strain.[1-3]

The photochemistry of stilbene has been extensively studied but relatively little is known about the photochemistry of the stilbene chromophore in small ring systems. Irradiation of 1,2-diphenylcyclobutene with 335 nm light in the crystal or in hexane solution yields $2\pi+2\pi$ C_4-cyclodimer, 1,2,5,6-tetraphenyltricyclo[4,2,-0,$0^{2,5}$]octane, through a finite-lived metastable singlet excimer along with the ring splitted photoproducts, diphenylacetylene and ethylene[1] while 1,2,3-triphenylcyclopropene yields no photoproduct with quantum yield greater than 10^{-2} on direct irradiation with 313 nm light but gives $2\pi+2\pi$ C_4-cyclodimer and a noncyclic hydrogen transfer dimer on triplet sensitization with benzophenone.[3] Thus, the photochemistry of stilbene chromophore in small ring systems is dependent on the size of the ring. The structure of indeno[2,1-*a*]indene, a *trans*-stilbene analogue, is restricted to a planar configuration and the compound cannot undergo *cis*⇌*trans* photoisomerization. Saltiel and coworkers utilized the fluorescence quantum yield of unity of the compound for backing up the singlet mechanism for the direct *cis*⇌*trans* photoisomerization of stilbene.[2,4] However, nothing is known about the photochemistry of indeno-[2,1-*a*]indene and photodimerization of the compound is studied in this report.

Experimental

Materials. *Indeno[2,1-a]indene*: Indeno[2,1-*a*]indene was synthesized by the method reported from benzyl chloride[5-7] and recrystallized from ethyl acetate and acetone. Mp 203—205 °C; NMR: δ 3.63 (s, 4H), 7.35 (m, 8H); IR: 3035, 2905, 1608, 1461, 1397, 1203, 775, 714 cm^{-1}; UV: 314 (ε_{max} 32500), 236 nm (ε_{max} 16500).

Spectra: UV spectra were recorded on a Cary 17 spectrophotometer. Infrared spectra were measured on a Perkin-Elmer Model 267 spectrophotometer in KBr pellet. Nuclear magnetic resonance spectra were measured on a Varian T-60A spectrometer against tetramethylsilane standard in chloroform-*d*. Mass spectra were determined with Hewlett Packard 5985 A GC/MS system. Fluorescence spectra were recorded on a Aminco Bowman spectrofluorometer with Aminco XY-recorder. Elemental analysis were carried out on a Coleman C, H, N analyzer.

Determination of Fluorescence Quantum Yields. Fluorescence quantum yield (Φ_F^s) of dilute solutions were calculated by Eq. 1.

$$\Phi_F^s = \Phi_F^r \times \frac{\int I_F^s(\tilde{\nu})d\tilde{\nu}}{\int I_F^r(\tilde{\nu})d\tilde{\nu}} \times \frac{O \cdot D_\lambda^r}{O \cdot D_\lambda^s} \times \frac{n_r^2}{n_s^2}, \quad (1)$$

where Φ_F^r is the fluorescence quantum yield of the reference compound. $I_F(\nu)$ and n are the corrected fluorescence intensity and refractive index respectively ($\tilde{\nu}$ in cm^{-1}). The reference compound, 2,5-diphenyloxazole (DPO) from Aldrich Chemical Co. was dissolved in benzene. Absolute quantum yield of the reference DPO in benzene is known to be 0.58. All sample compounds were dissolved in ether. The corrected fluorescence spectra were recorded on a Perkin-Elmer spectrofluorometer Model MPF-3.

Fluorescence-lifetime Measurements. The fluorescence lifetimes were measured at room temperature with an SLM-Model 480 phase-modulation spectrofluorometer utilizing continuous light that had been sinusoidally modulated.

Irradiation of the Sample and Separation of Dimers. Purified benzene solution of indeno[2,1-*a*]indene (100 mg/100 ml) was degassed by bubbling nitrogen through the solution for 30 min and irradiated in a Rayonet reactor (The Southern New England Ultraviolet Company) equipped with 300 nm fluorescence lamps for 10 h. The solvent was evaporated off and compound A was isolated by extraction of the residue with ethanol and recrystallized from methanol–water mixture. Compound B was isolated from the remaining residue by recrystallization from ethanol.

Found: Compound A; C, 94.00; H, 5.59%, compound B; C, 94.13; H, 5.98%. Calcd for $C_{32}H_{24}$: C, 94.09; H, 5.91%.

Quantum Yield Measurements. A solution of 3 ml of indeno[2,1-*a*]indene (2.3×10^{-3} M†) in several purified solvents[6] was put into a Pyrex ampoule and degassed by three freeze-pump-thaw cycles with cooling in liquid nitrogen and then sealed. Thus prepared samples were irradiated in a "merry-go-round" unit with 450 W Hanovia mercury arc lamp (Type 679 A 36). A Corning glass filter #7-54 and a solution filter of 2.5×10^{-3} M potassium chromate in 1% sodium carbonate aqueous solution were used to get a monochromatic light of 313 nm. The light intensity was measured by tris(oxalato)ferrate(III) actinometry and the amounts of photoproducts were analyzed by UV spectrophotometer at 314 nm.

Results and Discussion

Product Analysis. A benzene solution of indeno-

† 1 M=1 mol dm^{-3}.

[2,1-*a*]indene (4.9 mM) was irradiated for 10 h in a Rayonet reactor equipped with 300 nm fluorescent lamps. Separation of products by extraction and recrystallization gave products A and B in 2: 1 ratio. The photochemical conversion was almost complete. Both compounds were pure as shown by their Mp; compound A 183—184 °C, compound B decomposes at 290 °C before melting. The structures of compounds A and B were determined by their IR, ^{1}H NMR, mass, UV spectral data and elemental analyses.

Mass spectra of both compounds A and B show molecular ion peak at *m/e* 408 which is twice the molecular weight of indeno[2,1-*a*]indene. The base peak appears at *m/e* 204 which is exactly the molecular weight of starting material in both compounds. This indicates that compounds A and B easily undergo splitting into starting materials on electron impact suggesting compounds A and B to be C_4-cyclodimers. The elemental analyses of compounds A and B gave exactly the same data which are consistent with the dimeric structure.

The central double bond stretching of starting material at 1608 cm^{-1} are not apparent in the infrared spectra of compounds A and B and λ_{max} at 314 nm disappeared. These observations further substantiate the structure of compounds A and B to be $2\pi+2\pi$ type C_4-cyclodimers.

The ^{1}H NMR spectrum of compounds A in chloroform-*d* shows two doublets at 2.8 (d, 4H, J=17 Hz) and 3.2 (d, 4H, J=17 Hz) and two mutiplets at 6.9 (m, 8H) and 7.2 (m, 8H) ppm (δ). That of compound B also shows two doublets at 3.1 (d, 4H, J=17 Hz) and 3.7 (d, 4H, J=17 Hz) and a multiplet at 6.9 (m, 16H). The data are in agreement with the C_4-cyclodimers of indeno[2,1-*a*]indene, compound A being a head-to-tail (HT) cyclodimer and compound B being a head-to-head (HH) cyclodimer.

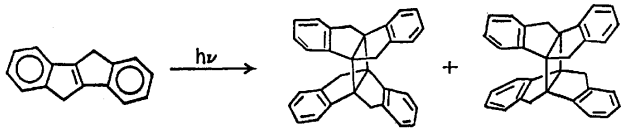

Indeno[2,1-*a*]indene Head-to-Head Head-to-Tail

Fig. 1

In HT dimer, H_b, the outer proton of methylene bridge is deshielded by the ring current of upper benzene ring, but H_a, the inner proton of methylene group, is shielded by the same ring current. Thus H_b resonance corresponds to 3.2 ppm peaks and that of H_a corresponds to 2.7 ppm peaks. The same ring currents cause the ring protons H_c and H_d to be shielded and the protons H_e and H_f to be deshielded as two multiplets appear in the NMR spectrum of compound A.

In HH dimer, H_a is deshielded in contrast to that of HT dimer and 3.7 ppm peaks correspond to H_a resonance. All ring protons, H_c, H_d, H_e, and H_f of HH dimer are shielded by the ring current of upper benzene ring and only one multiplet appears in the NMR spectrum of compound B.

Fluorescence Studies. Indeno[2,1-*a*]indene is strongly fluorescent and the fluorescence quantum yield is reported to be unity. However, the fluorescence quantum yield of the compound in ether was determined to be 0.85 when 2,5-diphenyloxazole which has same UV absorption characteristics as indeno[2,1-*a*]indene was used as a reference compound. This implicates that there is some radiationless decay routes other than fluorescence from the excited singlet state of indeno-[2,1-*a*]indene in contrast to the results reported earlier.[2)]

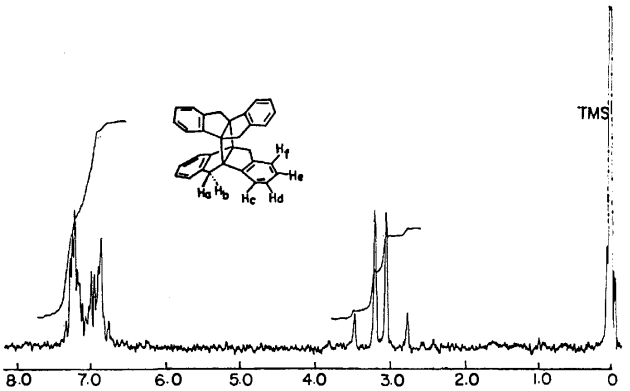

Fig. 2. ^{1}H NMR spectrum of H-T dimer of indeno[2,1-*a*]indene.

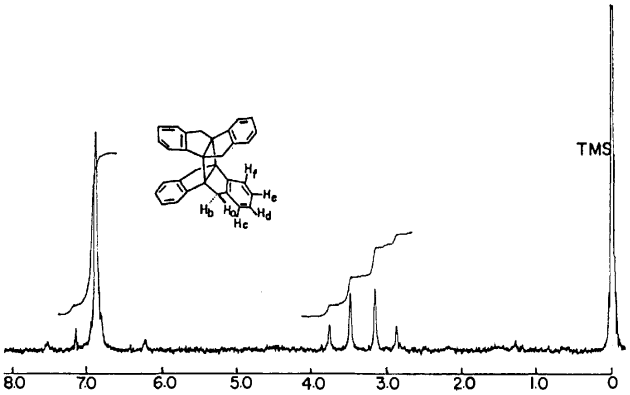

Fig. 3. ^{1}H NMR spectrum of H-H dimer of indeno[2,1-*a*]indene.

The fluorescence quenching of indeno[2,1-*a*]indene by electron deficient olefins, fumaronitrile and dimethyl fumarate, is very efficient while electron rich olefin, 2,3-dimethyl-2-butene (TME) does not quench fluorescence of indeno[2,1-*a*]indene.

The lifetime calculated from the slope of Stern-Volmer plot for fluorescence quenching by fumaronitrile and dimethyl fumarate is about 3.3 ns if $k_q = k_{diff} = 2.25 \times 10^{10}$ M^{-1} s^{-1} is assumed. This value is in agreement with the value of 1.99 ns measured directly from the fluorescence.

Reaction Mechanism. If the cyclodimerization occurs *via* a singlet excimer, the following mechanistic scheme can be proposed for the reaction

$$I \longrightarrow I^*, \quad (2)$$

$$I^* \xrightarrow{k_f} I + h\nu_f', \quad (3)$$

$$I^* \xrightarrow{k_d} I, \quad (4)$$

Table 1. Solvent effects and external heavy atom effects on the photocyclodimerization of indeno[2,1-*a*]indene

Solvent	Hexane	Acetonitrile	Benzene	Methyl iodide	Ethyl bromide
Viscosity	0.294 cP†	0.345 cP	0.564 cP	0.500 cP	0.402 cP
Quantum yield	1.80×10^{-2}	1.35×10^{-2}	0.75×10^{-2}	Undetectable	0.62×10^{-2}

† 1 P=0.1 Pa s.

$$I^* + I \underset{k_{-e}}{\overset{k_e}{\rightleftharpoons}} \text{Excimer}, \quad (5)$$

$$\text{Excimer} \xrightarrow{k_{dim}} \text{Dimers}, \quad (6)$$

$$\text{Excimer} \xrightarrow{k_{ed}} 2\,I, \quad (7)$$

where I is indeno[2,1-*a*]indene.

By steady state approximation,

$$\Phi_{dim}^{-1} = \frac{(k_f+k_d)(k_{-e}+k_{dim}+k_{ed})}{k_{dim}\,k_e}[I]^{-1} + \frac{k_{dim}+k_{ed}}{k_{dim}}. \quad (8)$$

The linear relationship between Φ_{dim}^{-1} and $[I]^{-1}$ is expected if the mechanism is valid.

When Φ^{-1} is plotted against $[I]^{-1}$ for the [I] of 5×10^{-3}—2×10^{-2} M in benzene solution at 21 °C, a good linear relationship (correlation coefficient: 0.999) is obtained as shown in Fig. 4.

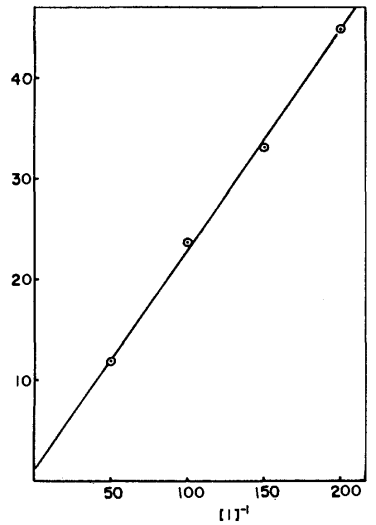

Fig. 4. Plot of the reciprocal of the quantum yield for photodimerization *vs.* the reciprocal of the indeno[2,1-*a*]indene concentration in benzene solution at 21 °C.

The intercept, $(k_{dim}+k_{ed})/k_{dim}$, is 1.20 and the slope which is given by $(k_f+k_d)(k_{-e}+k_{dim}+k_{ed})/k_{dim}k_e$ is 0.22. From these results and $\tau=1/(k_f+k_d)=1.99$ ns in dilute solution,

$$k_e\times\frac{k_{dim}}{k_{-e}+k_{dim}+k_{ed}} = k_e\,\frac{1}{\dfrac{k_{-e}}{k_{dim}}+\dfrac{(k_{dim}+k_{ed})}{k_{dim}}}$$

$$= 2.3\times10^9\ M^{-1}\,s^{-1}.$$

Thus the minimum value for k_e which is the rate constant for singlet excimer formation is $2.76\times10^9\ M^{-1}\,s^{-1}$ and the maximum value for that will be diffusion controlled rate constant of $2.25\times10^{10}\ M^{-1}\,s^{-1}$, the value obtained by the simplified Debye expression, $k_{diff}=8RT/3000\eta$, taking the viscosity of hexane as 0.294 cP at 25 °C.[8]

The ratio of A/B monitored by NMR is about two and is independent on indeno[2,1-*a*]indene concentration indicating that the two dimers are formed through a common intermediate.

From these results, it is suggested that two dimers, HH and HT, are formed through a singlet excimer. The direct evidence for this mechanism will be obtained through the investigation of the temperature effect[9,10] on the

$$k_e\times\frac{k_{dim}}{k_{-e}+k_{dim}+k_{ed}},$$

and this work is in progress.

The quantum yield of cyclodimerization in various solvents are shown in Table 1. The higher quantum yields are obtained in less viscous solvents indicating that the photocyclodimerization is dependent on the diffusion and association of solute molecules. External heavy atom effect as shown in methyl iodide decreases cyclodimerization quantum yield drastically indicating unequivocally that the excited singlet state is the reactive state for cyclodimerization. This mechanism was strongly substantiated by the triplet sensitization studies. No dimerization was observed when the benzene solution of indeno[2,1-*a*]indene was irradiated for 20 h with 366 nm UV light in the presence of benzophenone as a triplet sensitizer (E_T=68.3 kcal/mol). In acetonitrile solvent, the intersystem crossing from singlet to triplet state is perhaps enhanced as in the case of pyrimidine bases[11] and this enhanced intersystem crossing along with the slower diffusion of singlet excited molecules decreases the photocyclodimerization yield.

We thank Mr. Minjoong Yoon of Texas Tech University for fluorescence quantum yield and lifetime measurements. This work is supported by the Korea Science and Engineering Foundation.

References

1) C. D. DeBoer and R. H. Schlessinger, *J. Am. Chem. Soc.*, **90**, 803 (1968).
2) J. Saltiel, O. C. Zafirion, E. D. Megarity, and A. A. Lamola, *J. Am. Chem. Soc.*, **90**, 4759 (1968).
3) C. D. DeBoer and R. Breslow, *Tetrahedron Lett.*, **1967**, 1033.
4) J. Saltiel, Al. Marinari, D. W. L. Chang, and J. C. Mitchener, *J. Am. Chem. Soc.*, **101**, 2982 (1979).
5) K. Brand and K. O. Müller, *Ber.*, **55B**, 601 (1922).
6) Chen. C. Chuen and S. W. Fenton, *J. Org. Chem.*, **23**, 1538 (1958).
7) C. T. Blood and R. P. Linstead, *J. Chem. Soc.*, **1952**, 2255.
8) D. O. Cowan and R. L. Drisko, "Elements of Organic Photochemistry," Plenum Press, New York (1976), p. 67.
9) O. L. Chapman and R. D. Lura, *J. Am. Chem. Soc.*, **92**, 6352 (1970).
10) O. L. Chapman and R. D. Lura, *J. Am. Chem. Soc.*, **93**, 2804 (1971).
11) A. A. Lamola and J. P. Mittal, *Science*, **154**, 1560 (1966).

©1982 The Chemical Society of Japan

Spectral Changes in X-Ray *K* Emission Lines of Potassium in Various Compounds

Seiji YASUDA* and Hitoo KAKIYAMA

The Government Industrial Research Institute, Kyushu, Shuku-machi, Tosu, Saga 841

(Received May 16, 1981)

Synopsis. The chemical shifts and profile changes in the $K\alpha_{1,2}$, $K\beta_{1,3}$ and their satellite lines of potassium from 21 chemical compounds were measured with a two-crystal X-ray spectrometer. The data obtained are discussed qualitatively and related to the nature of the surrounding groups.

The valences or coordination numbers of elements in unknown samples or the ionic character of chemical bonds can be readily distinguished by the spectral changes in X-ray emission lines.[1] Such studies have received considerable attention from analytical chemists. However, so far as the elements such as potassium and calcium are concerned, only a few measurements have been directed to the theoretical interpretation of the $K\beta_{1,3}$ and its satellite lines.[2-4]

In the previous paper,[5] we have shown that the surrounding atoms or anions give appreciable line shifts and profile changes in the $K\alpha$ and $K\beta$ emission lines of calcium. The present note deals with potassium in an analogous way by measuring the chemical shifts and profile changes in the potassium $K\alpha_{1,2}$, $K\alpha_{3,4}$, $K\beta_{1,3}$, $K\beta''$, and $K\beta_5$ lines from 21 chemical compounds. The purpose for our previous and present studies is to examine whether a change of the nature of the surrounding groups leads to line shifts or profile changes in X-ray K emission lines of elements with constant formal charges in most compounds.

Experimental

The potassium X-ray emission spectrum was measured automatically by a step-scanning method at regular intervals of 0.005° 2θ using a Rigaku two-crystal X-ray spectrometer with Ge(111) crystals ($2d$=6.5327 Å). The primary radiation used for exciting the spectrum was provided by a chromium X-ray tube operated at 50 kV, 30 mA. The detector was a flow proportional counter. The 2θ position of the potassium $K\alpha_1$ was determined by averaging the goniometer settings at which the same intensity was measured on either side of the peak at the half-maximum intensity. The $K\alpha_2$, $K\alpha_4$, and $K\beta_{1,3}$ positions were also determined in the same way at approximately 70% intensity, whereas the $K\beta''$ and $K\beta_5$ positions were estimated from their apparent maxima. The chemical shift was calculated as an energy difference between the respective lines from the compound under study and KF. The experimental errors in such procedures were estimated to be±0.02 eV in the $K\alpha_1$, $K\alpha_2$, and $K\beta_{1,3}$ shifts and ±0.06 eV in the other lines. No corrections were made on the spectrum measured.

All potassium compounds used were of the highest commercial grade available and were confirmed by X-ray diffraction.

Results and Discussion

Potassium Kα *Spectrum.* The potassium $K\alpha$ emission spectrum consists of the $K\alpha_{1,2}$ doublet and its high energy satellites, namely the $K\alpha_{3,4}$ group. For all compounds, the $K\alpha_1$ full width at half-maximum intensity and the peak separation in the doublet seemed nearly constant at about 1.90 and 2.68 eV, respectively. In addition, the observed chemical shifts of both the $K\alpha_1$ and $K\alpha_2$ lines did not exceed the limits of the experimental errors at ±0.02 eV. The potassium $K\alpha_{3,4}$ group of satellites was observed on the high energy tails of the parent $K\alpha_{1,2}$ doublet. In every case, three components $K\alpha'$, $K\alpha_3$, and $K\alpha_4$ could be resolved, about 11, 18, and 22 eV apart from the $K\alpha_1$, respectively. However, there were no significant changes in the energy positions, profiles and relative intensities of the resolved satellite components in all compounds. These results indicate that the $K\alpha_{1,2}$ and its high energy satellite lines of potassium in different compounds are little affected by the changes of surrounding groups or of the crystal structures of compounds.

Potassium Kβ *Spectrum.* The potassium $K\beta$ spectrum from KF is shown in Fig. 1. According to the relative positions in similar spectra which have appeared in the literature,[2,6] the main peak was assigned to $K\beta_{1,3}$ and its high energy satellites were assigned to $K\beta''''$, $K\beta'''$, $K\beta_5$, and $K\beta''$ beginning from the high energy side in every case. The weak emission structures on the

Table 1. Characteristic data of the spectral changes in the potassium $K\beta$ lines

Compound	Chemical shift/eV			$\Delta E_{K\beta_1-K\beta_{1'}}$
	$K\beta_{1,3}$	$K\beta''$	$K\beta_5$	eV
$K_2S_2O_8$	+0.10	0.0	−0.4	9.6
K_2SO_4	+0.05	0.0	−0.2	9.9
$KHSO_4$	+0.03	0.0	−0.2	9.9
KF	—	—	—	10.1
KH_2PO_4	+0.05	0.0	+0.1	10.2
$K_4P_2O_7$	+0.03	−0.2	+0.1	10.2
KNO_3	+0.03	−0.3	+0.6	10.7
K_2SO_3	+0.03	−0.2	+1.1	11.2
$KBrO_3$	+0.10	−0.2	+1.2	11.2
$KHCO_3$	+0.03	−0.3	+1.2	11.3
KNO_2	+0.03	−0.3	+1.2	11.3
$KClO_3$	+0.08	−0.3	+1.4	11.4
$KMnO_4$	+0.13	−0.3	+1.5	11.5
$KClO_4$	+0.10	−0.2	+1.5	11.5
$K_3C_6H_5O_7\cdot H_2O$	+0.05	−0.3	+1.7	11.8
$KOOCC_6H_4COOH$	+0.10	−0.3	+1.8	11.8
KCl	+0.05	−0.3	+1.8	11.9
K_2CO_3	+0.03	−0.3	+1.8	11.9
CH_3COOK	+0.05	−0.1	+2.1	12.2
KBr	+0.05	−0.4	+2.8	12.9
KI	+0.03	−0.4	+3.5	13.6

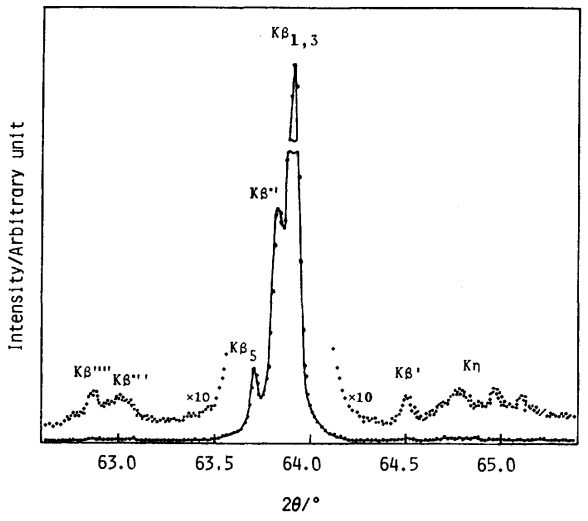

Fig. 1. Potassium $K\beta$ spectrum from KF.

low energy side of the $K\beta_{1,3}$ were assigned to $K\beta'$ and $K\eta$. The observed spectrum of each compound was characterized by the chemical shifts of the $K\beta_{1,3}$, $K\beta''$, and $K\beta_5$ relative to the respective lines in KF and the energy difference (ΔE) between $K\beta_5$ and $K\beta_{1,3}$. The measured data of these four parameters are listed in Table 1, according to the increase of the last parameter.

The potassium $K\beta_{1,3}$ line had an almost constant full width at half-maximum intensity of 1.67 eV for all compounds, but a slight difference in the energy positions was detectable. The experimentally observed shifts of the $K\beta_{1,3}$ lay in the range +0.03 to +0.13 eV, although they rarely exceeded +0.05 eV. However, a simple correlation in relating the observed $K\beta_{1,3}$ shifts to the nature of surrounding atoms or anions could not be found. The potassium $K\beta''$ bands was found to occur at about 4 eV higher energies than those of the $K\beta_{1,3}$. This band of most compounds was shifted slightly to lower energies by 0.1—0.4 eV relative to that of KF. The $K\beta''$ is generally regarded as a satellite, but the origins of this band and the observed shifts are at present unclear.

At 10—14 eV above $K\beta_{1,3}$, the potassium $K\beta_5$ band appeared as a well-defined peak in the spectra from potassium halides, carbonate and nitrate, while the other compounds gave the broad asymmetric $K\beta_5$ band with some structure and an ambiguous maximum. The chemical shifts of this band were as much as several electron Volts in the range −0.4 to +3.5 eV; these shifts are remarkably larger than those of the $K\beta_{1,3}$ and result in an increase in the energy difference ΔE with increasing the $K\beta_5$ shifts toward higher energies; these are shown in the last two columns of Table 1. A similar trend has been found by the photographic determinations of the potassium $K\beta_{1,3}$ and $K\beta_5$ energies from potassium carbonate, sulfate, and halides.[6] Since the $K\beta_5$ bands of potassium sulfates and phosphates shifted slightly to lower energies by 0.2—0.4 eV and to higher energies by 0.1 eV, respectively, the energy difference ΔE in these compounds was rather close to the value 10.1 eV for the reference material, KF. The remaining compounds showed the $K\beta_5$ shifts in the range +0.7 to +3.5 eV, which are almost comparable to those of calcium compounds.[5] On the other hand, the energy differences ΔE by 11—12 eV in most compounds were about 0.5 times as large as those in calcium compounds. In a series of potassium halides, the $K\beta_5$ maximum was found to shift toward higher energies with a decrease in the electronegativity of surrounding atoms with a consequent decrease in the charge of the potassium atom. This finding was the only possible regularity obtained in the present study on the spectral changes in the potassium X-ray K emission lines.

Every measured spectrum revealed very broad high energy structures $K\beta''''$ and $K\beta'''$ at about 53 and 44 eV above $K\beta_{1,3}$ and the low energy structures $K\beta'$ at about 31 eV below $K\beta_{1,3}$ and $K\eta$ with several maxima mostly occurring at about 42, 52, and 60 eV below $K\beta_{1,3}$. However, their profile changes and line shifts could not be investigated in detail because of the extremely faint intensities.

References

1) A. Meisel, "Rontgenspektren und Chemische Bindung," Akademische Verlagsgesellschaft Geest and Portig K.-G., Leipzig (1977), Chaps. 5 and 6.
2) J. Valasek, *Phys. Rev.*, **53**, 274 (1938).
3) J. Utriainen and M. Linkoaho, *J. Phys. Chem. Solids*, **32**, 2493 (1970).
4) P. E. Best, *J. Chem. Phys.*, **54**, 1512 (1971).
5) S. Yasuda and H. Kakiyama, *X-Ray Spectrom.*, **10**, 85 (1981).
6) S. Kiyono, *Sci. Rep. Tohoku Univ.* [1], **39**, 129 (1956).

The Raman Spectra of Cobalt(III) Complexes. IV. Differentiation between *cis* and *trans* Isomers of Bis(trimethylenediamine)cobalt(III) Complexes

Kan KANAMORI,* Hiroko ICHINOSE, and Kiyoyasu KAWAI

Department of Chemistry, Faculty of Science, Toyama University, Gofuku, Toyama 930

(Received June 19, 1981)

Synopsis. The Raman and the infrared spectra of bis(trimethylenediamine)cobalt(III) complexes have been studied to establish a definite distinction between the *cis* and *trans* isomers. A differentiation between the isomers can be made on the bases of the number of the Raman bands in the region of 480—550 cm^{-1} and of the mutual exclusion in the region of 400—500 cm^{-1}.

In the previous paper,[1] the Raman criterion has been established for differentiating *cis* and *trans* isomers of bis(ethylenediamine)cobalt(III) complexes. Many infrared studies[2-6] have been done on the stereochemistry of bis(ethylenediamine)cobalt(III) complexes, but few vibrational studies of bis(trimethylenediamine)cobalt(III) complexes have been reported. Kawaguchi and Kawaguchi[7-9] have applied Baldwin's criteria[5] and Hughes and McWhinnie's criteria[6] for bis(ethylenediamine)cobalt(III) complexes to isomeric pairs of bis(trimethylenediamine)cobalt(III) complexes. They have noted that the former criteria have not been useful for $[Co(NCS)_2(tn)_2]Cl$ and $[Co(N_3)_2(tn)_2]NO_3$, and the latter were not useful for $[Co(CN)(SO_3)(tn)_2]$.

In the present work, we tried to establish vibrational criteria for differentiating *cis* and *trans* isomers of bis(trimethylenediamine)cobalt(III) complexes on the basis of the Raman and the infrared spectra. The established criteria were then applied to the isomeric pair of $[Co(NH_3)_2(tn)_2]Cl_3$ obtained in the present work.

Experimental

Preparation. *Isomeric Pair of* $[Co(NH_3)_2(tn)_2]Cl_3$: This complex has been obtained by Ogino[10] through the reaction of $[Co(NH_3)_5(H_2O)]^{3+}$ with trimethylenediamine, but he did not refer to its geometrical configuration. We have prepared the isomeric pair by two methods.

Method I. Powdered *trans*-$[CoCl_2(tn)_2]Cl$ (5 g) was dissolved in 100 cm^3 of liquid ammonia. The ammonia was then allowed to evaporated spontaneously, leaving behind an orange powder. This powder was washed with a large amount of ethanol and dissolved in a minimum amount of warm water, then the solution was cooled in a refrigerator. The reddish orange precipitate (isomer I) was filtered and dried. The other isomer was obtained by adding a large amount of ethanol to the filtrate as an orange powder (isomer II). Yields: isomer I: 1.5 g; isomer II: 0.3 g.

Method II. Powdered *trans*-$[CoCl_2(tn_2)]Cl$ (5 g) was dissolved in 200 cm^3 of methanol which was saturated with ammonia. The solution was warmed on a water bath for 5 min. The orange powder which deposited was filtered and washed with ethanol. The same compounds as those obtained by method I were isolated by a fractional crystallization, but the ratio of the yields was reversed. Yields: isomer I: 0.7 g; isomer II: 2.5 g. Found: C, 19.16; H, 8.15; N, 22.45% for isomer I. C, 19.18; H, 8.07; N, 22.46% for isomer II. Calcd for $[CoC_6H_{26}N_6]Cl_3 \cdot 1.5H_2O$: C, 19.24; H, 7.81; N, 22.45%.

Isomeric Pair of $[Co(NO_2)_2(tn)_2]Cl$: This isomeric pair was first obtained by Kawaguchi and Kawaguchi.[7,8] Later, Celap *et al.*[11] have prepared it by different methods; they have shown that the property of the *cis* isomer is different from that obtained by Kawaguchi and Kawaguchi.[8] We have prepared the isomeric pair from the reaction mixture obtained by Kawaguchi's method[7] for the *trans* isomer by using an ion-exchange column chromatography (SP-Sephadex, C-25; ϕ 30 mm × 500 mm; eluent-0.04 mol/dm^3 KCl solution). The electronic spectrum of each isomer obtained by this method is identical with that of respective isomer observed by Celap *et al.*[11]

Other Complexes. All the other complexes were obtained by the method of Kawaguchi and Kawaguchi.[7-9]

Measurements. The Raman spectra were recorded on a JASCO R-800 Laser Raman spectrometer, using a He–Ne (632.8 nm) or an Ar^+ ion (514.5 nm) laser as an excitation source. The infrared spectra were recorded on a JASCO A-3 spectrometer. The observed frequencies were calibrated by the 533.8 cm^{-1} band of indene for the Raman spectra and the 618.0 cm^{-1} band of polystylene film for the infrared spectra. The observed frequencies are accurate within ± 2 cm^{-1}.

Results and Discussion

The most consistent variation between the vibrational spectra of *cis* and *trans* isomers has been found in the region of 400—550 cm^{-1}. The Raman and the infrared spectra in this region for the *cis* and *trans* isomeric pair of bis(trimethylenediamine)cobalt(III) complexes are shown in Fig. 1 and those of other *trans* isomers are in Fig. 2. The very strong Raman bands at *ca.* 450 cm^{-1} can be confidently assigned to the Co–N(tn) stretching mode, ν(Co–N(tn)), by comparison with the Raman

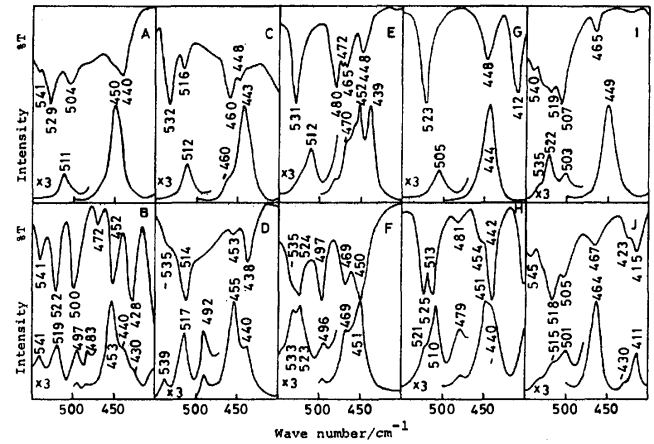

Fig. 1. The Raman and the infrared spectra of the isomeric pair of $[Coab(tn)_2]X$-type complexes. A(*trans*) and B(*cis*); a=b=CN^-, X=Cl^-. C(*trans*) and D(*cis*); a=b=NO_2^-, X=Cl^-. E(*trans*); a=b=NCS^-, X=Br^-. F(*cis*); a=b=NCS^-, X=Cl^-. G(*trans*) and H(*cis*); a=b=N_3^-, X=NO_3^-. I(*trans*) and J(*cis*); a=CN^-, b=SO_3^{2-}.

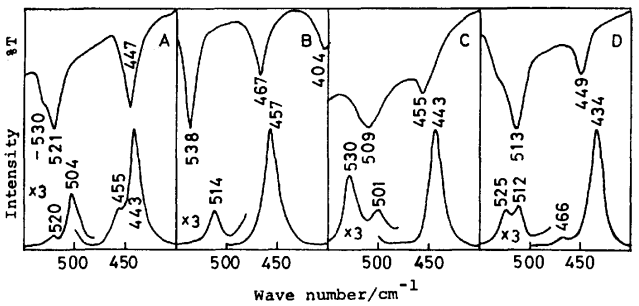

Fig. 2. The Raman and the infrared spectra of *trans*-[Coab(tn)$_2$]X-type or M[Coab(tn)$_2$]-type complexes. A; a=b=Cl$^-$, X=Cl$^-$. B; a=b=NO$_3^-$, X=NO$_3^-$, C; a=b=SO$_3^{2-}$, M=Na$^+$. D; a=Cl$^-$, b=SO$_3^{2-}$.

spectra of bis(ethylenediamine)cobalt(III) complexes.[1] Therefore, the infrared bands in the vicinity of 450 cm^{-1} may be assigned to the ν(Co–N(tn)), though Kawaguchi and Kawaguchi[8,9] have regarded the infrared bands in the region of 500—550 cm^{-1} as the ν(Co–N(tn)). The bands in the region of 480—550 cm^{-1} are assignable to the deformation vibration of the chelate ring, δ(CCN), by considering the assignment for ethylenediamine complexes based on the normal coordinate analysis.[12]

It can be seen from Figs. 1 and 2 that the *trans* isomers generally show one band due to δ(CCN) in the 480—550 cm^{-1} region of the Raman spectra and also in the infrared region. Further, the mutual exclusion between the Raman and the infrared spectra occurs, as expected from the approximate symmetry (D_{2h}) of the *trans* isomers. All the *cis* isomers have at least two bands in the 480—550 cm^{-1} region of the Raman spectra and most bands have their counterparts in the infrared spectra. Thus a complex which has one band in the Raman spectra and/or in the infrared spectra of 480—550 cm^{-1} region can be unambiguously assigned to the *trans* isomer. In the sulfito-containing complexes, the band due to the degenerate bending of the sulfito group, δ_d(SO$_3$), obscured the band due to the δ(CCN), so this region is not helpful for structural diagnosis. Forbidden vibrations under the assumption of a D_{2h} symmetry appear as a very weak band in the infrared spectrum of the *trans*-dinitro complex and in the Raman spectrum of the *trans*-dichloro complex, but the mutual exclusion approximately holds between the strongest band of the Raman spectrum in the 480—550 cm^{-1} region and that of the infrared one in the same region, in contrast to the *cis* isomers. The bands in the region of 460—480 cm^{-1} for the bis(isothiocyanato)complexes can be assigned to the δ(NCS).

The mutual exclusion generally holds also in the region of the ν(Co–N(tn)) of the *trans* isomers (see Figs. 1 and 2). This criterion can be used even for the sulfito-containing complexes. But in the *trans*-dinitro and the *trans*-diazido complexes, the mutual exclusion does not hold. This may be interpreted as a symmetry lowering in the solid state or as an accidental degeneracy.

In conclusion, three criteria for differentiating the geometrical isomers of bis(trimethylenediamine)cobalt-(III) complexes are established: the first is based on the

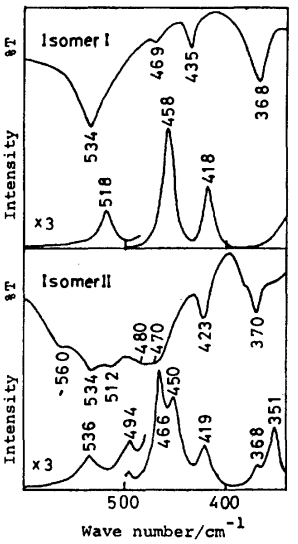

Fig. 3. The Raman and the infrared spectra of the isomeric pair of [Co(NH$_3$)$_2$(tn)$_2$]Cl$_3$.

number of bands in the region of 480—550 cm^{-1}, the second on the mutual exclusion in the same region, and the last on the mutual exclusion in the ν(Co–N(tn)) region. But each criterion has some exceptions, so only a combination of the three criteria would provide reliable diagnosis.

These criteria were applied to the isomeric pair of [Co(NH$_3$)$_2$(tn)$_2$]Cl$_3$. The Raman and the infrared spectra of the isomers are shown in Fig. 3. It is clear that isomer I has a *trans* configuration and isomer II has a *cis* configuration.

We wish to express our sincere thanks to Professor Yoichi Shimura of Osaka University, and to Dr. Isao Kanesaka for valuable discussions. We also thank Miss Naomi Shimizu for carrying out a part of the experiment

References

1) K. Kanamori and K. Kawai, *Bull. Chem. Soc. Jpn.*, **53**, 2520 (1980).
2) M. M. Chamberlain and J. C. Bailar, Jr., *J. Am. Chem. Soc.*, **81**, 6412 (1959).
3) P. E. Merritt and S. E. Wiberley, *J. Phys. Chem.*, **59**, 55 (1959).
4) M. L. Morris and D. H. Busch, *J. Am. Chem. Soc.*, **82**, 1521 (1960).
5) M. E. Baldwin, *J. Chem. Soc.*, **1960**, 4369.
6) M. N. Hughes and W. R. McWhinnie, *J. Inorg. Nucl. Chem.*, **28**, 1659 (1966).
7) H. Kawaguchi, T. Yano, and S. Kawaguchi, *Bull. Chem. Soc. Jpn.*, **42**, 136 (1969).
8) H. Kawaguchi and S. Kawaguchi, *Bull. Chem. Soc. Jpn.*, **43**, 2103 (1970).
9) H. Kawaguchi and S. Kawaguchi, *Bull. Chem. Soc. Jpn.*, **46**, 3453 (1973).
10) H. Ogino, *Bull. Chem. Soc. Jpn.*, **50**, 2459 (1977).
11) M. B. Celap, M. J. Malinar, and P. N. Radivojsa, *Inorg. Chem.*, **14**, 2965 (1975).
12) Y. Omura, I. Nakagawa, and T. Shimanouchi, *Spectrochim. Acta, Part A*, **27**, 2227 (1971).

The Viscosities of Aqueous Solutions Containing Metal Complexes. IV. Nitrilotriacetato Complexes

Kiyoshi MIZUTANI and Motoo YASUDA*

College of General Education, Nagoya University, Chikusa-ku, Nagoya 464

(Received July 17, 1981)

Synopsis. Viscosity *B*-coefficients of bivalent metal complexes formed with nitrilotriacetic acid (H_3nta) were determined with Cannon-Fenske capillary viscometers at 25±0.01 °C. The *B*-coefficients obtained are smaller for metal chelates having larger stability constants, and larger for metal chelates having smaller stability constants.

The viscosities of aqueous electrolyte solutions have been measured by many authors, but few data are available for the metal complexes. In the previous papers of this series, the viscosity *B*-coefficients were reported for metal complexes formed with several amino polycarboxylic acid.[1-3] The results showed valuable information concerning the metal complexes. For example, it was shown that for a particular ligand a bivalent metal ion with a greater affinity for the ligand generally formed a chelate with a smaller *B*-value. In order to extend these conclusions further, a viscosity study was made of aqueous solutions of bivalent metal chelates formed with nitrilotriacetic acid.

Experimental

Viscosity measurements were made using Cannon-Fenske capillary viscometers with efflux times of *ca.*240—320 s for distilled water. The time of flow was measured with a stopwatch graduated to 0.1 s. All measurements were made at 25±0.01 °C. Solutions of metal chelates were made up using metal nitrate (or chloride) and K_3nta stock solutions.

For each of the 1 : 1 chelates studied, the variation in the relative viscosity η_{rel} with the solute concentration c was expressed by the Jones-Dole equation:[4]

$$\eta_{rel} = \frac{\eta}{\eta_0} = 1 + A\sqrt{c} + Bc, \qquad (1)$$

where η and η_0 are viscosities of solution and water. respectively. A is a constant depending on the ion-ion interaction between the solute ions, and B is a constant depending on the size of the ion and on the interaction between the ion and the surrounding solvent molecules. A and B are called the Jones-Dole viscosity A- and B-coefficients. These constants were fully discussed by Gurney,[5] who showed the *B*-coefficient of the electrolyte was composed additively of contributions from each of the solute species present in the solution. So *B*-values of the complex ions were obtained by subtracting a relatively smaller correction for the coexisting species.

Results and Discussion

In each case the *A*-coefficient was found to be zero within experimental error. The same was also found, for example, in ethylenediaminetetraacetato chelates[6] $[M(edta)]^{2-}$ and *trans*-1,2-cyclohexanediaminetetraacetato chelates[2] $[M(cydta)]^{2-}$. The *B*-coefficients of the nitrilotriacetato chelates obtained here at 25 °C are listed in Table 1, together with stability constants reported by Schwarzenbach *et al.*[7] For metal ions studied, the stability constants of nitrilotriacetato chelates are sufficiently large, and so even for magnesium chelate, which is the least stable, the estimated error due to dissociation of the complex is less than 0.01 in *B*-value.

TABLE 1. *B*-VALUES, STABILITY CONSTANTS k, AND AVERAGE RADII r OF NITRILOTRIACETATO COMPLEXES

Metal	B / dm³ mol⁻¹	log k[7]	r / Å
Cu^{2+}	0.52	12.96	4.4
Ni^{2+}	0.63	11.54	4.6
Co^{2+}	0.61	10.4	4.6
Zn^{2+}	0.62	10.66	4.6
Pb^{2+}	0.50	11.39	4.3
Mg^{2+}	0.71	7.0	4.8
Ca^{2+}	0.74	8.2	4.9

Larger *B*-values seem to indicate more free carboxylato groups of the ligand, which will make the chelates less stable. As seen from Table 1, the more stable the chelate is, in general, the smaller is its *B*-value. This was already seen in the case of amino polycarboxylato chelates studied previously.[2,3,6] It is interesting to compare the *B*-values of amino polycarboxylato chelates for a particular metal ion. The order of the *B*-value for each bivalent metal is as follows:

$$[M(nta)]^- < [M(ida)_2]^{2-} < [M(mida)_2]^{2-} \approx [M(edta)]^{2-} < [M(cydta)]^{2-},$$

where H_2ida is iminodiacetic acid and H_2mida is *N*-methyliminodiacetic acid. This order meets our expectations. However, there seems to be no special relation between the *B*-values of nta-chelate and those of $(ida)_2$-chelate, although a linear relationship[2] was found between *B*-values of edta- and cydta-chelates. This might be due to the fact that $[M(nta)]^-$ and $[M(ida)_2]^{2-}$ chelates do not have such similar structures, whereas $[M(edta)]^{2-}$ and $[M(cydta)]^{2-}$ do. The difference between *B*-values of $[M(nta)]^-$ and $[M(ida)_2]^{2-}$ chelates decreases as follows:

$$Pb > Cu > Zu > Ni \approx Co.$$

In this connection it is interesting to note that the ratio of the 1st and 2nd stability constants of iminodiacetato chelates, that is k_1/k_2, decreases in the order:[8]

$$Cu > Pb \gg Zn > Ni > Co.$$

This means that lead and copper form relatively unstable 1 : 2 chelates compared with the corresponding 1 : 1 chelate and so that $[Pb(ida)_2]^{2-}$ and $[Cu(ida)_2]^{2-}$ chelates may have relatively large *B*-values.

Since the *A*-value of each chelate was within experimental error of zero, we may calculate the volume of the hydrated chelate v_h from Eq. 2, because its radius is large compared with that of the solvent molecules:[2]

$$v_h = \frac{4000\,B}{6.02}\ (\text{Å}). \qquad (2)$$

Thus the average radius of the chelate r can be obtained from its B-coefficient, and is also listed in Table 1. This varies from 4.3 Å for the lead chelate to 4.9 Å for the calcium chelate. The variation may be in part due to the difference in effective ionic radii of metal ions, but cannot be wholly explained by this difference. For example, though the effective ionic radii of octahedral Mg^{2+} and Ca^{2+} are 0.86 and 1.14 Å, respectively,[9] both average radii of the chelates calculated are about the same. As we discussed previously,[2] the larger average radius may be ascribed to the larger extent of free carboxylato groups of nitrilotriacetic acid ligand which do not attach to the metal ion.

References

1) M. Yasuda, *Bull. Chem. Soc. Jpn.*, **41**, 139 (1968).
2) M. Yasuda, *Bull. Chem. Soc. Jpn.*, **42**, 2547 (1969).
3) K. Mizutani and M. Yasuda, *Bull. Chem. Soc. Jpn.*, **46**, 157 (1973).
4) G. Jones and M. Dole, *J. Am. Chem. Soc.*, **51**, 2950 (1929).
5) R. W. Gurney, "Ionic Processes in Solution," McGraw-Hill Book Company, New York (1953).
6) R. G. Charles, *J. Am. Chem. Soc.*, **78**, 3946 (1956).
7) G. Schwarzenbach, E. Kampitsch, and R. Steiner, *Helv. Chim. Acta*, **28**, 828 (1945); G. Schwarzenbach and R. Gut, *ibid.*, **39**, 1589 (1956).
8) S. Chaberek and A. E. Martell, *J. Am. Chem. Soc.*, **74**, 5052 (1952); M. Kodama and S. Takahashi, *Bull. Chem. Soc. Jpn.*, **44**, 697 (1971).
9) R. D. Shannon and C. T. Prewitt, *Acta Crystallogr., Sect. B*, **25**, 925 (1969).

Synthesis and Circular Dichroism Spectra of *mer*(*N*)-*cis*(NH_3)-[Co(OO)(NH_3)$_2$-(py)(H_2O)]$^+$ and *mer*(*N*)-[Co(OO)(en)(py)(H_2O)]$^+$ Complexes

Shuhei FUJINAMI,* Kenshi TSUJI, Kumiko MINEGISHI, and Muraji SHIBATA

Department of Chemistry, Faculty of Science, Kanazawa University, Kanazawa 920

(Received August 13, 1981)

Synopsis. The *mer*(*N*)-*cis*(NH_3)-[Co(OO)(NH_3)$_2$-(py)(H_2O)]$^+$ and *mer*(*N*)-[Co(OO)(en)(py)(H_2O)]$^+$ complexes (OO=ox^{2-} or mal^{2-}) have been prepared and optically resolved. The CD spectra are different. The difference seems to be due to the additional optical activity derived from the helical arrangement of two bidentate ligands in the latter ethylenediamin complexes.

Recently, the complexes of *cis,cis,cis*-[Co(a)$_2$(b)$_2$-(c)$_2$],[1,2] *cis,cis*-[Co(a)$_2$(b)$_2$(CC)],[2] *fac*(*D*)-[Co(a)(b)-(c)(DDD)],[3] and *fac*(*a*)-[Co(a)$_3$(b)(CD)] types,[4] which derive their dissymmetry mainly from the distribution of donor atoms, have been prepared in our laboratory. In this note, novel complexes, *mer*(*N*)-*cis*(NH_3)-[Co-(OO)(NH_3)$_2$(py)(H_2O)]$^+$, and related complexes, *mer*(*N*)-[Co(OO)(en)(py)(H_2O)]$^+$ (OO=ox^{2-} ormal^{2-}), are reported. The CD spectra of these complexes are of interest in investigating the optical activity of *mer*-[Co(N)$_3$(O)$_3$] chromophore.

Experimental

Preparation and Optical Resolution. *a)* mer(N)-cis(NH_3)-*Diammineaquaoxalatopyridinecobalt(III) Perchlorate*, mer(N)-cis-(NH_3)-[*Co(ox)*(NH_3)$_2$(*py*)(H_2O)]ClO_4: To a solution of *cis*-K[Co(CO_3)(ox)(NH_3)$_2$]·H_2O[5] (20 g, 0.067 mol, in 200 cm^3 H_2O) was added pyridine (17 cm^3, 0.21 mol), and the solution was adjusted to pH 5.5 with 60% $HClO_4$ in an ice-bath. After filtration, the filtrate was stirred at room temperature for 0.5 h. The crude product which deposited was recrystallized from warm water. The yield was *ca.* 5 g. Found: C, 22.26; H, 3.47; N, 10.84%. Calcd for [Co(C_2O_4)(NH_3)$_2$(C_5H_5N)-(H_2O)]ClO_4: C, 22.26; H, 3.48; N, 11.13%.

The perchlorate was converted into chloride by using a column of Dowex 50W-X8 in Na^+ form. To a solution of the chloride (6 g, 0.02 mol, in 90 cm^3 H_2O) was added $(+)_{546}$-K[Co(edta)]·2H_2O (4 g, 0.01 mol) with mechanical stirring, and the whole was kept in an ice-bath. The less-soluble diastereoisomeric salt containing the $(-)_{589}$-oxalato complex was recrystallized five times from water. The final yield was *ca.* 1.5 g. Found: C, 31.17; H, 4.31; N, 10.16%. Calcd for [Co(C_2O_4)(NH_3)$_2$(C_5H_5N)(H_2O)][Co($C_{10}H_{12}N_2O_8$)]·2H_2O: C, 30.87; H, 4.43; N, 10.59%.

b) mer(N)-*Aquaethylenediamineoxalatopyridinecobalt(III) Chloride*, mer(N)-[*Co(ox)(en)(py)*(H_2O)]*Cl*: Pyridine (24 cm^3, 0.3 mol) was added to a solution of K[Co(CO_3)(ox)(en)]·H_2O[5] (32.5 g, 0.1 mol, in 100 cm^3 H_2O), and pH of the solution was adjusted to 5.5 with 60% $HClO_4$. After filtration, the filtrate was stirred at room temperature for a day. The solution, once filtered, was chromatographed on a column of Dowex 50W-X8 in Na^+ form (5 cm×30 cm) using a 0.15 mol/dm^3 NaCl solution. The red-violet band which descended was collected. After concentrating the effluent to *ca.* 30 cm^3, followed by filtering, the filtrate was kept in a refrigerator. The crude product thus obtained was recrystallized from warm water. The yield was 5.5 g. Found: C, 31.83; H, 4.45; N, 12.36%. Calcd for [Co(C_2O_4)($C_2H_8N_2$)-(C_5H_5N)(H_2O)]Cl: C, 31.97; H, 4.39; 12.46%.

Optical resolution was performed by using $(+)_{546}$Na[Co-(edta)]·2H_2O in a way similar to that in *a)*. The less-soluble diastereoisomeric salt of the $(-)_{589}$-oxalato complex was recrystallized from water. Found: C, 33.95; H, 4.42; N, 10.48%. Calcd for [Co(C_2O_4)($C_2H_8N_2$)(C_5H_5N)(H_2O)][Co-($C_{10}H_{12}N_2O_8$)]·H_2O: C, 34.09; H, 4.33; N, 10.46%.

c) mer(N)-cis(NH_3)-*Diammineaquamalonatopyridinecobalt-(III) Chloride Monohydrate*, mer(N)-cis(NH_3)-[*Co(mal)*(NH_3)$_2$-*(py)*(H_2O)]*Cl*·H_2O: A solution containing a *cis*-[Co(CO_3)-(mal)(NH_3)$_2$]$^-$ complex, which had been prepared according to the literature method[5] (*cis*-K[Co(CO_3)$_2$(NH_3)$_2$]·H_2O, 27 g, 0.1 mol scale), was treated in the same manner as *b)*. By elution with 0.15 mol/dm^3 NaCl, red-violet and pink bands successively descended. The aimed red-violet band was collected, and the effluent was concentrated to *ca.* 20 cm^3. After filtration, the filtrate was kept in a refrigerator. The product thus obtained was recrystallized from warm water. The yield was *ca.* 0.2 g, Found: C, 27.62; H, 5.01; N, 12.35%. Calcd for [Co($C_3H_2O_4$)(NH_3)$_2$(C_5H_5N)(H_2O)]Cl·H_2O: C, 27.79; H, 4.92; N, 12.15%.

This complex was partially resolved by means of chromatography on a column of Dowex 50W-X8 in Na^+ form (100—200 mesh, 2 cm×30 cm), using 0.1 mol/dm^3 K_2[Sb_2(*d*-tart)$_2$] as the eluent. The earlier eluted species was the $(+)^{CD}_{500}$-isomer.

d) mer(N)-*Aquaethylenediaminemalonatopyridinecobalt(III) Chloride Trihydrate*, mer(N)-[*Co(mal)(en)(py)*(H_2O)]*Cl*·3H_2O: This complex was prepared by the same way as described in *c)* except for the use of a [Co(CO_3)(mal)(en)]$^-$ complex,[5] which had been prepared from K[Co(CO_3)$_2$(en)]·H_2O (30 g, 0.1 mol scale). The yield was *ca.* 0.3 g. Found: C, 29.47; H, 5.75; N, 10.77%. Calcd for [Co($C_3H_2O_4$)($C_2H_8N_2$)(C_5H_5N)-(H_2O)]Cl·3H_2O: C, 29.45; H, 5.64; N, 10.31%.

This complex was partially resolved in a way similar to that in *c)*, except for the use of a long column (2 cm×60 cm). The earlier eluted species was the $(+)_{589}$-isomer.

Measurement. The absorption spectra were measured with a Hitachi 323 spectrophotometer. The CD spectra were recorded on a JASCO J-40CS automatic recording spectropolarimeter. Samples were converted into the chloride by an ion-exchange technique, and the $\Delta\varepsilon$ values were evaluated from the absorption spectral data. For the measurements of the optical rotation, a JASCO DIP-SL automatic polarimeter was used.

Results and Discussion

For the [Co(OO)(NH_3)$_2$(py)(H_2O)]$^+$ complexes four geometrical isomers are possible: (a) *mer*(*N*)-*cis*-(*NH_3*), (b) *mer*(*N*)-*trans*(*NH_3*), (c) *fac*(*N*)-*cis*(*py*, *H_2O*), and (d) *fac*(*N*)-*trans*(*py*, *H_2O*). On the other hand, for the [Co(OO)(en)(py)(H_2O)]$^+$ complexes, three geometrical isomers are possible: (e) *mer*(*N*), (f) *fac*(*N*)-*cis*(*py*, *H_2O*), and (g) *fac*(*N*)-*trans*(*py*, *H_2O*). Among these isomers, (a), (c), (e), and (f) are resolvable into enantiomeric pairs. All complexes prepared in the present work could be resolved as described in the Experimental section.

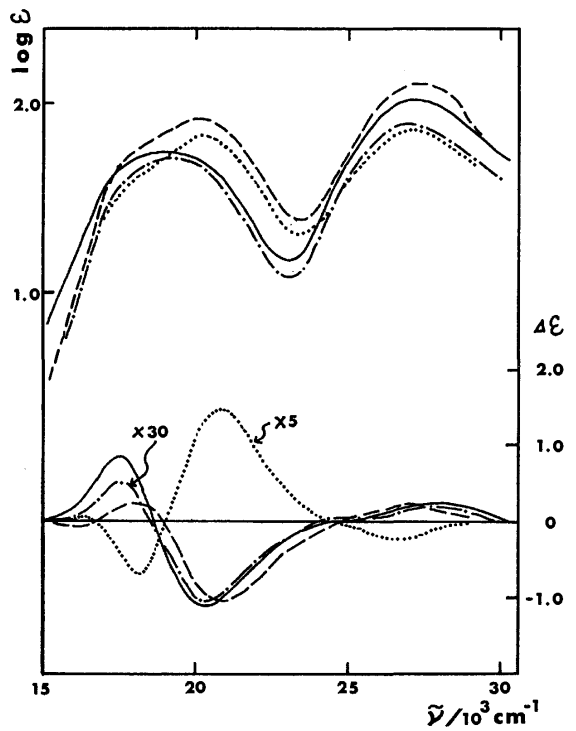

Fig. 1. Absorption and CD Spectra.
——: *mer*(*N*)-*cis*(*NH*$_3$)-(−)$_{589}$[Co(ox)(NH$_3$)$_2$(py)(H$_2$O)]$^+$, ——: *mer*(*N*)-(−)$_{589}$[Co(ox)(en)(py)(H$_2$O)]$^+$, —·—·: *mer*(*N*)-*cis*(*NH*$_3$)-(−)$^{CD}_{500}$[Co(mal)(NH$_3$)$_2$(py)(H$_2$O)]$^+$, ·····: *mer*(*N*)-(+)$_{589}$[Co(mal)(en)(py)(H$_2$O)]$^+$

As shown in Fig. 1, the first absorption bands of the [Co(OO)(NH$_3$)$_2$(py)(H$_2$O)]$^+$ complexes are broad, and those of the [Co(OO)(en)(py)(H$_2$O)]$^+$ complexes exhibit obvious shoulders, suggesting that these complexes have *mer*-[Co(N)$_3$(O)$_3$] chromophores. On this basis, the present [Co(ox)(NH$_3$)$_2$(py)(H$_2$O)]$^+$ and [Co(mal)(NH$_3$)$_2$(py)(H$_2$O)]$^+$ complexes can be assignable to *mer(N)-cis(NH$_3$)* isomers, and the [Co(ox)(en)(py)(H$_2$O)]$^+$ and [Co(mal)(en)(py)(H$_2$O)]$^+$ complexes to *mer(N)* isomers.

The CD spectra of the diammine complexes exhibit two Cotton peaks with opposite signs in the first absorption band region. The peaks at the higher-frequency side are dominant: 17300 cm^{-1} ($\Delta\varepsilon$=0.90) and 20300 cm^{-1} ($\Delta\varepsilon$=−1.07) for the (−)$_{589}$[Co(ox)(NH$_3$)$_2$(py)(H$_2$O)]$^+$ complex, and 17600 cm^{-1} ($\Delta\varepsilon$=0.017) and 20400 cm^{-1} ($\Delta\varepsilon$=−0.035) for the (−)$^{CD}_{500}$[Co(mal)(NH$_3$)$_2$(py)(H$_2$O)]$^+$ complex. On the other hand, the CD spectra of the ethylenediamine complexes exhibit three peaks with alternating signs, the peaks at the lowest frequency being extremely weak compared with the dominant peaks at the highest frequency: 16100 cm^{-1} ($\Delta\varepsilon$=−0.03), 18000 cm^{-1} ($\Delta\varepsilon$=0.26), and 20800 cm^{-1} ($\Delta\varepsilon$=−1.05) for the (−)$_{589}$[Co(ox)(en)(py)(H$_2$O)]$^+$ complex, and 16200 cm^{-1} ($\Delta\varepsilon$=0.016), 18200 cm^{-1} ($\Delta\varepsilon$=−0.09), and 20800 cm^{-1} ($\Delta\varepsilon$=0.28) for the (+)$_{589}$[Co(mal)(en)(py)(H$_2$O)]$^+$ complex.

The CD spectral shapes are little affected by the change of a five-membered oxalato chelate to a six-membered malonato chelate, while a large difference in CD spectral shapes is observed between the diammine and the corresponding ethylenediamine complexes. It is considered that the optical activity of [Co(OO)(NH$_3$)$_2$(py)(H$_2$O)]$^+$ is mainly derived from an arrangement of four kinds of ligating atoms, two O donors in OO and aqua, and two N donors in ammine and pyridine. On the other hand, that of [Co(OO)(en)(py)(H$_2$O)]$^+$ is mainly derived from two sources, one of which is an arrangement of four kinds of donor atoms, and the other is a helical distribution of two chelate rings. Therefore, the CD spectral difference between the diammine and ethylenediamine complexes, which is clearly observable at the lower frequency side, may be attributed to the additional optical activity derived from the helical distribution of the chelates.

Dividing the optical activity between the two sources is justified by the CD spectral comparison between the *all-cis*-[Co(C)$_2$(N)$_2$(O)$_2$] complexes, which have a rhombic crystal field like the present complexes.[1] A CD spectrum of *all-cis*-[Co(CN)$_2$(H$_2$O)$_2$(NH$_3$)$_2$]$^+$ resembles that of *cis,cis*-[Co(CN)$_2$(H$_2$O)$_2$(en)]$^+$. On the other hand, a spectrum of *cis,cis*-[Co(CN)$_2$(ox)(NH$_3$)$_2$]$^-$ is different from that of *cis*-[Co(CN)$_2$(ox)(en)]$^-$; the former exhibits two extrema in the first absorption band region, and the latter, three extrema. From these comparisons, the chiral environments are considered not to be derived by the ethylenediamine chelate itsel but to be derived by forming a ring pair with the oxalate chelate.

References

1) T. Ito and M. Shibata, *Inorg. Chem.*, **16**, 108 (1977).
2) K. Tsuji, S. Fujinami, and M. Shibata, *Bull. Chem. Soc. Jpn.*, **54**, 1531 (1981).
3) S. Shimba, S. Fujinami, and M. Shibata, *Chem. Lett.*, **1979**, 783.
4) S. Fujinami and M. Shibata, *Chem. Lett.*, **1981**, 495.
5) S. Muramoto, K. Kawase, and M. Shibata, *Bull. Chem. Soc. Jpn.*, **51**, 3505 (1978).

Studies of 8-Quinolinethiol as Chelating Agents. III.[1] Distribution Behavior of 8-Quinolinethiol between Chloroform and Aqueous Solutions

Eiichi SEKIDO,* Tadashi KOBAYASHI, and Yoshitaka MASUDA
Department of Chemistry, Faculty of Science, Kobe University, Rokkodai, Nada-ku, Kobe 657
(Received September 4, 1981)

Synopsis. The distribution behavior of 8-quinolinethiol between chloroform and aqueous solutions was examined and compared with that of 8-quinolinol. The distribution coefficient was $K_{D_R}=2140$ and macroscopic acid dissociation constants were $pK_{a_1}=2.05$ and $pK_{a_1}=8.39$.

8-Quinolinethiol is a useful organic reagent for the chloroform extraction and photometric determination of heavy metals.[2,3] Equilibrium constants for the extraction of the reagent itself are necessary to study the stoichiometric extraction of metals with 8-quinolinethiol. It is also interesting to compare the extraction behavior of 8-quinolinethiol with that of 8-quinolinol because it is assumed that 8-quinolinethiol exists predominantly as the zwitter ionic form in aqueous solutions,[4] but that almost all 8-quinolinol exists as the neutral form.

Experimental

Reagents. 8-Quinolinethiol was prepared by the method of Kealey and Freiser[5] and its sodium salt by the method of Nakamura and Sekido.[6] The sodium salt was purified by recrystallization three times from ethanol and dried *in vacuo*. 8-Quinolinol was also recrystallized three times from ethanol. The chloroform solution of 8-quinolinethiol was prepared as following. Into a 200 ml separatory funnel containing 10 ml of pH 4—5 buffer solution was added the required amount of sodium salt of 8-quinolinethiol under nitrogen gas, and then the resulting solution was shaken for 3 min with the aliquot of chloroform taken so as to obtain the required concentration of the reagent, 2×10^{-5} M (1 M=1 mol dm^{-3}).

Apparatus. Extraction was made with a Taiyo M-100N type incubator. UV and visible absorption spectra were taken with a Hitachi 124 type double beam spectrophotometer. A Hitachi-Horiba pH meter M-5 with a glass-calomel electrode pair was used.

Procedures. Into a 50 ml cylindrical tube containing 10 ml of 2×10^{-5} M 8-quinolinethiol chloroform solution was added 10 ml of the aqueous solution, which was adjusted to the desired pH by a buffer solution and to 0.1 ionic strength by the addition of sodium perchlorate. After shaking at 25 °C until the equilibrium was attained, two phases were separated with a centrifuge for 2 min, then 5 ml of the aqueous phase was pipetted out and its pH was measured. Concentrations of the reagent in the chloroform phase and/or the aqueous phase were spectrophotometrically obtained and distribution ratios were calculated.

Results and Discussion

8-Quinolinethiol exists as both the neutral form, HR, and the zwitter ionic form, H^+R^-, in a solution. Therefore, acid dissociation phenomena of 8-quinolinethiol are represented by the following explanatory Scheme 1. The relationships between the various equilibrium constants in Scheme 1 and macroscopic acid dissociation constants, called K_{a_1} and K_{a_2}, are as follows:

$$K_{a_1} = K_{a_A} + K_{a_B}, \tag{1}$$

$$\frac{1}{K_{a_2}} = \frac{1}{K_{a_C}} + \frac{1}{K_{a_D}}, \tag{2}$$

$$K_t = \frac{[\text{Zwitter ion}]}{[\text{Neutral}]} = \frac{[H^+R^-]}{[HR]} = \frac{K_{a_A}}{K_{a_B}} = \frac{K_{a_D}}{K_{a_C}}. \tag{3}$$

As it is expected that the species existing in the organic phase is only HR, the distribution ratio of the reagent, D_R, is represented by Eq. 4:

$$D_R = \frac{[HR]_o}{[H_2R^+]+[HR]+[H^+R^-]+[R^-]}, \tag{4}$$

where the subscript o represents the concentration in the organic phase. The simplifications of Eq. 4 on the lower pH (<2) and the higher pH (>8) media and the appropriate substitutions give Eqs. 5 and 6 respectively:

$$D_R = \frac{[HR]_o}{[H_2R^+]+[HR]+[H^+R^-]} = \frac{K_{a_1}K_{D_R}}{(1+K_t)\{[H^+]+K_{a_1}\}}, \tag{5}$$

$$D_R = \frac{[HR]_o}{[HR]+[H^+R^-]+[R^-]} = \frac{[H^+]K_{D_R}}{(1+K_t)\{[H^+]+K_{a_2}\}}, \tag{6}$$

where K_{D_R} is the distribution coefficient of the reagent, defined as $K_{D_R}=[HR]_o/[HR]$. Moreover, on the condition of $[H^+]\gg K_{a_1}$, and $[H^+]\ll K_{a_2}$ Eqs. 5 and 6 are simplified and expressed in logarithmic forms as Eqs. 7 and 8, respectively.

$$\log D_R = \log\frac{K_{D_R}}{1+K_t} - pK_{a_1} + pH \tag{7}$$

$$\log D_R = \log\frac{K_{D_R}}{1+K_t} + pK_{a_2} - pH \tag{8}$$

The plots of $\log D_R$ for 8-quinolinethiol as a function of pH are shown in Fig. 1 with those for 8-quinolinol. A horizontal portion of maximum $\log D_R$ for 8-quinolinethiol, $\log D_{R_{max}}=2.65$, appears in the range of pH 4 to 7, which indicates that the reagent exists completely as HR and H^+R^-. As K_{D_R} is related with $D_{R_{max}}$ by Eq. 9, $K_{D_R}=2140$ is obtained by substituting the values $D_{R_{max}}=10^{2.65}=447$ and $K_t=3.8$[3] in Eq. 9. A linear

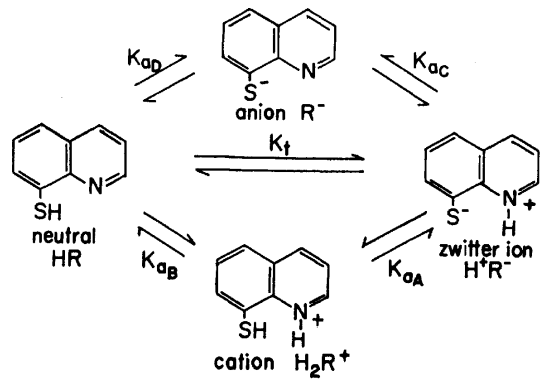

Scheme 1.

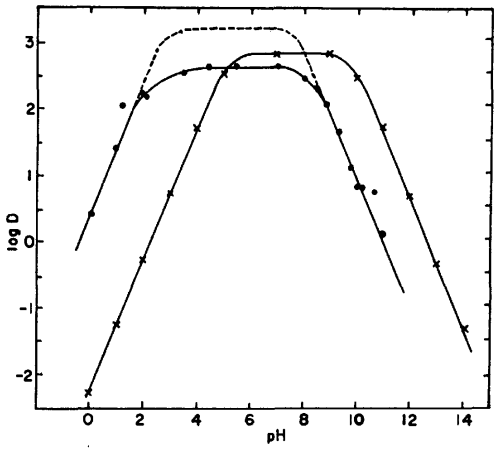

Fig. 1. Effects of pH on distribution of 8-quinolinethiol and 8-quinolinol between chloroform and aqueous solutio.
—•—: 8-Quinolinethiol, —×—: 8-quinolinol, ——: i all 8-quinolinethiol were the neutral form.

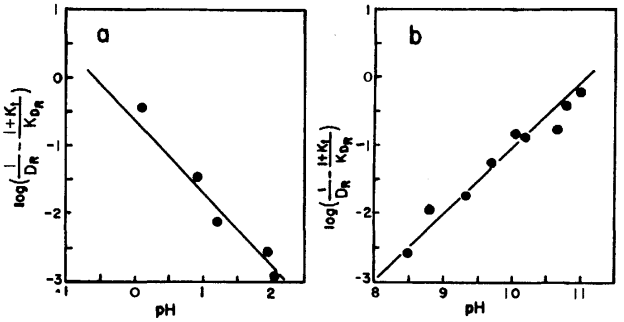

Fig. 2. Plots of log $\{(1/D_R)-(1+K_t)/K_{DR}\}$ *vs.* pH.
(a) In acidic region and (b) in alkaline region.

$$K_{DR} = D_{Rmax}(1+K_t) \quad (9)$$

portion with the slope of +1 in the range of pH −0.5 to 1.5 and that with the slope of −1 in the range of pH 8.5 to 11 are found as expected from Eqs. 7 and 8, respectively, and $pK_{a_1}=2.05$ and $pK_{a_2}=8.39$ were obtained from the pH values at log $D_R=0$. As was expected from the values of $pK_{a_1}=5.13$ and $pK_{a_2}=9.89$ for 8-quinolinol,[6] 8-quinolinethiol is extracted into chloroform in the lower pH range than that which 8-quinolinol is extracted. Although $K_{D_R}(2140)$ for 8-quinolinethiol is much larger than $K_{D_R}(772)$ for 8-quinolinol, the horizontal portion of the maximum distribution ratio for 8-quinolinethiol is lower than that for 8-quinolinol, because about 78% of 8-quinolinethiol

Table 1. Equilibrium consstants for 8-quinolinethiol

	Present work	Previous work
K_t		3.8[a]
pK_{a_1}	2.05	2.0[b]
pK_{a_B}	2.15	2.10
pK_{a_A}	2.73	2.68
pK_{a_2}	8.39	8.36[c]
pK_{a_C}	8.29	8.26[c]
pK_{a_D}	7.72	7.68[c]

a) Ref. 3. b)Ref. 7. c) Ref. 8.

in aqueous solution exists as the zwitter ionic form, while almost all 8-quinolinol exists as the neutral form.[4] If all of 8-quinolinethiol exists as the neutral form, the horizontal portion of the log D-pH curves will be higher than that for 8-quinolinol, as shown on the broken line in Fig. 1. Equations 10 and 11 are derived from Eqs. 5 and 6, respectively.

$$\log\left(\frac{1}{D_R}-\frac{1+K_t}{K_{DR}}\right) = -\mathrm{pH} - \log K_{D_R} + pK_{a_B} \quad (10)$$

$$\log\left(\frac{1}{D_R}-\frac{1+K_t}{K_{DR}}\right) = \mathrm{pH} - \log K_{D_R} - pK_{a_D} \quad (11)$$

The plots of log $\{(1/D_R)-(1+K_t)/K_{D_R}\}$ *vs.* pH are shown in Figs. 2a and 2b. Two straight lines with slopes of −1 and 1 are given and $pK_{a_B}=2.73$ and $pK_{a_D}=7.72$ are obtained from the values of log K_{D_R} and of the pH on log $\{(1/D_R)-(1+K_t)/K_{D_R}\}=0$. Thus, the values of pK_{a_A}, pK_{a_C}, pK_{a_1}, and pK_{a_2} are calculated by using Eqs. 1, 2, and 3, and these values are tabulated in Table 1 with values obtained by potentiometric and photometric methods. As shown in Table 1, these values are in fair accord with those reported previously.[7,8] Such agreement confirms that 8-quinolinethiol exists predominantly as the zwitter ionic form in aqueous solutions.

References

1) Part II: Y. Mido and E. Sekido, *Bull. Chem. Soc. Jpn.*, **44**, 2130 (1971).
2) V. I. Kuznetsov, Yu. A. Bankovsky, and A. F. Iyevinsh, *Zh. Anal. Khim.*, **13**, 267 (1958).
3) Yu. A. Bankovsky, L. M. Chera, and A. F. Iyevinsh, *Zh. Anal. Khim.*, **18**, 668 (1963).
4) S. F. Mason, *J. Chem. Soc.*, **1957**, 5010.
5) D. Kealey and H. Freiser, *Talanta*, **13**, 1381 (1966).
6) A. Albert and A. Hampton, *J. Chem. Soc.*, **1954**, 505.
7) E. Sekido, Q. Fernando, and H. Freiser, *Anal. Chem.*, **36**, 1768 (1964).
8) N. Nakamura and E. Sekido, *Talanta*, **17**, 515 (1970).

Cycloadditions of Constrained Dicyclopropylethylenes and Divinylcyclopropanes with Tetracyanoethylene

Makoto NITTA* and Toshio KUROKI

Department of Chemistry, School of Science and Engineering, Waseda University, Shinjuku-ku, Tokyo 160

(Received May 14, 1981)

Synopsis. 2,4-Dimethyl-7-methylenetetracyclo[3.3.0.0^{2,8}0^{4,6}]octan-3-one and its corresponding alcohol were reacted with TCNE to give $\pi 2+\pi 2$ cycloadducts at the exomethylene group. On the other hand, 1,5-dimethyl-6-methylenetricyclo[3.2.1.0^{2,7}]oct-3-en-8-one did not react with TCNE, whereas its corresponding alcohol and 1,5-dimethyl-6,8-dimethylenetricyclo[3.2.1.0^{2,7}]oct-3-ene afforded $\pi 2+\pi 2$ cycloadducts. The reactivities were correlated with the ^{13}C-NMR data of the exomethylene groups, the electron densities of which are affected by the carbonyl group.

The electronic state and chemical reactivity of cyclopropane have attracted the continuous attention of organic chemists. Previously it has been reported that the photocycloaddition of benzophenone to 2,4-dimethyl-7,-methylenetetracyclo[3.3.0.0.^{2,8}0^{4,6}]octan-3-one (**1a**)[1] or its corresponding alcohol **1b**[1] afforded an oxetane, **3a** or **3b** and an adduct, **3c**.[2] The product composition of these reactions was understood by means of the electron-withdrawing property of the carbonyl group. A similar reaction of 1,5-dimethyl-6-methylenetricyclo[3.2.1.0^{2,7}]oct-3-en-8-one (**2a**)[3] or its corresponding alcohol **2b**[4] was also investigated to afford **4a** or **4b**, as is summarized in Scheme 1.[5] A $\pi 2+\pi 2$ cycloaddtion of cyclopropylethylenes with tetracyanoethylene (TCNE) is generally accepted to proceed *via* a zwitterionic intermediate.[6] In this article, the cycloaddition of **1a** and **1b** and of **2a** and **2b**, to TCNE was investigated, and it was clarified that the reactivity of the exomethylene group toward TCNE was affected by the presence of the carbonyl group.

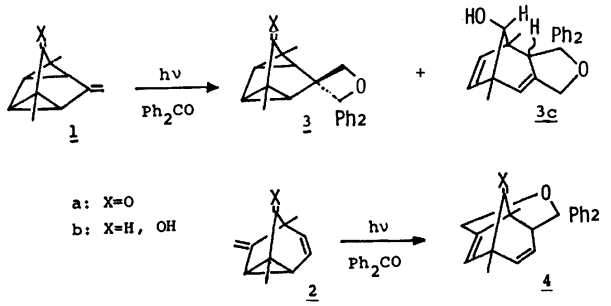

Scheme 1.

The reaction of **1a** and TCNE in acetonitrile at a refluxing temperature for 6 h provided, after recrystallization, an adduct **5a** in a 24% yield. The similar reaction of **1b** in refluxing dichloromethane for 1 h afforded an adduct **5b** in a 37% yield. The reaction of **1b** was faster than that of **1a** and proceeded at a lower temperature. The assignment of these structures, **5a** and **5b** was deduced from the spectral data (see Experimental). The hydroxyl proton in an NMR spectrum of **5b** could not be assigned distinctly. The stereochemistry of oxetane rings of **3a** and **3b** has been confirmed, as is depicted in Scheme 1.[2] This orientation of the benzophenone moiety must be favored by a steric hindrance. On the basis of a comparison with this observation, the stereochemistry of the cyclobutane rings of **5a** and **5b** depicted in Scheme 2 was proposed.

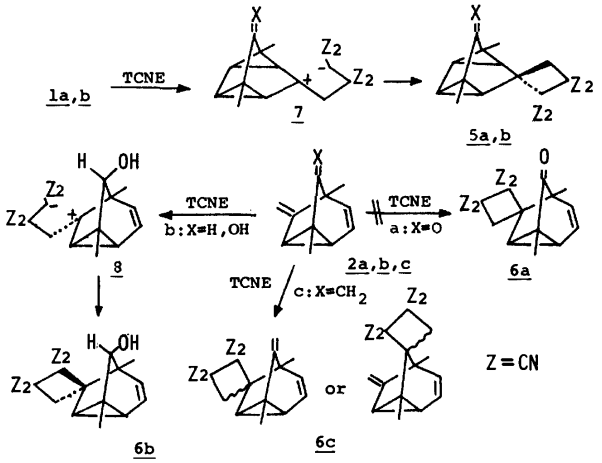

Scheme 2.

On the other hand, the reaction of the tricyclic ketone **2a** and TCNE in refluxing dichloromethane or acetonitrile did not afford any cycloadduct. The similar reaction of **2b** and TCNE in refluxing acetonitrile for 5 h, however, afforded an adduct **6b** in a 31% yield. The NMR spectrum of **6b** exhibited the proton signals of a vinylcyclopropane moiety and a resonable geminal coupling constant (J=14.0 Hz) for the hydrogens of the cyclobutane ring.[7] Therefore, the structure **6b** was deduced to be as is depicted in Scheme 2. Although the evidence for the stereochemistry of the cyclobutane ring of **6b** is not presented, the exo orientation of the TCNE moiety must be favorable because of the steric hindrance.[8]

The zwitterionic species, such as **7** and **8**, would be the intermediate in the present cycloaddition reactions.[6] The following intramolecular combination in **7** and **8** from the less sterically hindered site afford the cycloadducts, **5a**, **5b**, and **6b**. The rearrangement of the intermediate **7** or **8** could not be observed. This feature is not like the case of radical reactions.[2,3,9] The corresponding radical species in the photocycloaddition of **1b** or **2a** and **2b** with benzophenone has been observed to rearrange (Scheme 1). The inertness of **2a** toward TCNE is noticeable. The inclusion of an electron-withdrawing substituent, such as CN or CO_2Me, in a

Table 1. ^{13}C-NMR chemical shifts of exomethylene group in $CDCl_3$

$\overset{A}{>}C=\overset{B}{C}H_2$	**1a**	**1b**	**2a**	**2b**
A	149.6	152.9	148.3	154.2
B	110.9	107.7	112.4	104.5
$\Delta\delta_{AB}$	38.7	45.2	35.9	49.7
$\Delta\Delta\delta_{AB}$	6.5		1.38	

cyclopropane ring has been demonstrated to preclude its reaction with TCNE.[10] The rate of the reaction of **1b** with TCNE was faster than that of **1a**. Therefore, the inertness of **2a** toward TCNE under the present conditions may be attributed to the presence of an electron-withdrawing carbonyl group.

The ^{13}C-NMR spectra of **1a**, **1b**, **2a**, and **2b** were recorded, the data for the carbons of the exomethylene groups are summarized in Table 1. Regarding the $\Delta\delta_{AB}$ value in the **1a**—**1b** and **2a**—**2b** pairs, **1b** and **2b** exhibit larger values than the corresponding ketones, **1a** and **2a** respectively. This fact seems to indicate that the polarization of the exomethylene group of **1b** or **2b** is greater than that of **1a** or **2a** respectively.[11] The $\Delta\Delta\delta_{AB}$ value between **1a** and **1b** is 6.5, while the

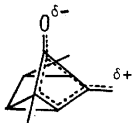

9

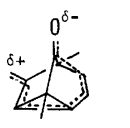

10

value between **2a** and **2b** indicates the larger value of 13.8. This fact may suggest that the difference in the polarization of the exomethylene group between **2a** and **2b** is very large as compared to that between **1a** and **1b**. The reduction of the polarization may be ascribed to the carbonyl group, which withdraws the electron of the exomethylene group of **1a** or **2a** through the cyclopropane ring, as is depicted in the structural formulae, **9** and **10**. This effect also seems to be reflected by the values of δ_A and δ_B of **1a**, **1b**, **2a**, and **2b**. Therefore, the exomethylene group of **2a** is probably electron-deficient as compared to that of **2b**, so **2a** would be inert to the present reaction. Support for the deactivation by the carbonyl group in **2a** may be given by the following observation. The reaction of TCNE with 1,5-dimethyl-6,8-dimethylenetricyclo[3.2.1.0^{2,7}]oct-3-ene (**2c**), which has a π-electron system similar to that of **2a**, was achieved to afford an adduct **6c** in a 30% yield. The structure of **6c** was deduced from the spectral data to have a cyclobutane ring. There are still two possible structures concerning the reaction site for the **6c** adduct.

Experimental

*Reaction of **1a** with TCNE.* A solution of **1a** (160 mg, 1 mmol) and TCNE (192 mg, 1.5 mmol) in 2 cm^3 of acetonitrile was refluxed for 6 h. The reaction mixture was then treated with 100 mg of Norit, and the filtrate was concentrated to give 56 mg (24%) of **5a**: mp 199—200 °C (from benzene): IR (KBr) 2955, 2250, 1710 cm^{-1}; NMR (DMSO-d_6) δ 1.12 (6H, s), 2.24 (2H, d, J=5.0 Hz), 2.72 (2H, d, J=5.0 Hz), 3.37 (2H, s); MS *m/e* 288 (M$^+$). Found: C, 70.56; H, 3.91; N, 19.80%. Calcd for $C_{17}H_{12}ON_4$: C, 70.82; H, 4.20; N, 19.44%.

*Reaction of **1b** with TCNE.* A solution of **1b** (324 mg, 2 mmol) and TCNE (379 mg, 2.4 mmol) in 2 cm^3 of dichloromethane was refluxed for 1 h. The subsequent evaporation of the solvent afforded a brown solid. This solid was dissolved in 5 cm^3 of acetone, followed by the addition of Norit. The Norit was removed by filtration, and then the acetone was evaporated. The residue was recrystallized from benzene to afford 199 mg (37%) of **5b**: mp 150—151 °C; IR (KBr) 3550, 2250 cm^{-1}; NMR (DMSO-d_6) δ 1.15 (6H, s), 1.70 (2H, d, J=5.0 Hz), 1.98 (2H, d, J=5.0 Hz), 3.30 (2H, s), 3.50 (1H, s); MS *m/e* 290 (M$^+$). Found: C, 70.16; H, 4.56; N, 19.35%. Calcd for $C_{17}H_{14}ON_4$: C, 70.33; H, 4.86; N, 19.30%.

*Reaction of **2a** with TCNE.* A solution of **2a** (160 mg, 1 mmol) and TCNE (128 mg, 1 mmol) in dichloromethane (3 cm^3) was refluxed for 31 h. After the removal of the solvent *in vacuo*, the residue was chromatographed on florisil, using benzene as the eluent, to give 144 mg (90%) of the starting material **2a**. A similar reaction in refluxing acetonitrile for 10 h afforded no adduct except **2a** in a 77% yield.

*Reaction of **2b** with TCNE.* A solution of **2b** (162 mg, 1 mmol) and TCNE (154 mg, 1.2 mmol) in 5 cm^3 of acetonitrile was refluxed for 5 h. After the removal of the solvent, the residue was chromatographed on florisil. The elution with benzene–dichloromethene (1/1) afforded 94 mg (31%) of **6b**, which was recrystallized from ethanol: mp 186—187 °C; IR (KBr) 3550, 2250 cm^{-1}; NMR (DMSO-d_6) δ 1.26 (3H, s), 1.41 (3H, s), 1.88 (2H, m), 3.13 (1H, d, J=14.0 Hz), 3.29 (1H, d, J=7.0 Hz), 3.31 (1H, d, J=14.0 Hz), 4.56 (1H, d, J=7.0 Hz), 5.17 (1H, d, J=8.0 Hz), 6.38 (1H, m); MS *m/e* 290 (M$^+$). Found: C, 70.47; H, 4.68; N, 19.00%. Calcd for $C_{17}H_{14}ON_4$: C, 70.33; H, 4.86; N, 19.30%.

*Reaction of **2c** with TCNE.* A solution of **2c**[12] (158 mg, 1 mmol) and TCNE (128 mg, 1 mmol) in acetonitrile (5 cm^3) was refluxed for 7 h. After the removal of the solvent *in vacuo*, the residue was chromatographed on florisil, using benzene as the eluent to give a crystalline solid. This solid was recrystallized from ethanol to give 110 mg (38%) of **6c**: mp 178—179 °C; IR (KBr) 2275, 1650 cm^{-1}; NMR (acetone-d_6) δ 1.16 (3H, s), 1.42 (3H, s), 2.32 (2H, m), 2.66 (1H, d, J=11.0 Hz), 2.75 (1H, d, J=11.0 Hz), 4.78 (1H, s), 4.85 (1H, s), 5.75 (1H, dxd, J=7.0, 2.0 Hz), 6.30 (1H, m); MS *m/e* 286 (M$^+$). Found: C, 75.15; H, 4.71; N, 19.29%. Calcd for $C_{18}H_{14}N_4$: C, 75.50; H, 4.93; N, 19.57%.

*^{13}C-NMR Spectra of **1a,b**, and **2a,b** in $CDCl_3$.* **1a**: 212.3, 149.6, 110.9, 44.8, 44.0, 38.9, 17.2 ppm. **1b**: 152.9, 107.7, 80.6, 42.7, 41.6, 37.8, 20.3 ppm. **2a**: 212.6, 148.3, 132.8, 125.5, 112.4, 52.0, 37.8, 36.9, 30.4, 12.2, 11.7 ppm. **2b**: 154.2, 131.6, 131.1, 104.5, 81.7, 51.4, 37.1, 36.6, 33.1, 20.9, 19.4 ppm.

References

1) M. Nitta, O. Inoue, and M. Tada, *Chem. Lett.*, **1977**, 59.
2) M. Nitta, T. Kuroki, and H. Sugiyama, *J. Chem. Soc., Chem. Commun.*, **1980**, 378.
3) J. Zindely and H. Schmid, *Helv. Chim. Acta*, **51**, 1510 (1968).
4) J. P-Katalinic, J. Zindely, and H. Schmid, *Helv. Chim. Acta*, **57**, 223 (1974).
5) M. Nitta, H. Sugiyama, and Y. Sekine, *Chem. Lett.*, **1977**, 55.
6) S. Nishida, I. Moritani, and T. Teraji, *J. Org. Chem.*, **38**, 1878 (1973); F. Effenberger and W. Podszen, *Angew. Chem. Int. Ed. Engl.*, **8**, 976 (1969); F. Effenberger and O. Gerlach, *Chem. Ber.*, **107**, 278 (1974).
7) R. Huisgen and J. P. Ortega, *Tetrahedron Lett.*, **1978**, 3975.
8) M. Nitta, Y. Yajima, and A. Omata, unpublished results.
9) R. Sustmann and R. W. Gellert, *Chem. Ber.*, **111**, 388 (1978).
10) M. Langbeheim and S. Sarel, *Tetrahedron Lett.*, **1978**, 1219.
11) R. W. Hoffmann, H. R. Kurtz, and J. Becherer, *Chem. Ber.*, **111**, 1275 (1978).
12) P. Gilgen, J. Zsindely, and H. Schmid, *Helv. Chim. Acta*, **56**, 681 (1973).

A New Efficient and Stereoselective Synthesis of Ubiquinone-10

Yoshiji FUJITA,* Michihiro ISHIGURO, Takashi ONISHI, and Takashi NISHIDA
Central Research Laboratories, Kuraray Co. Ltd., Sakazu, Kurashiki, Okayama 710
(Received May 25, 1981)

Synopsis. Coupling reaction of 6-cupro-2,3-dimethoxy-5-methylhydroquinone bis(2-methoxyethoxymethyl) ether with (2*E*)-1-(phenylsulfonyl)-2-methyl-4-chloro-2-butene afforded the sulfone-functionalized prenylhydro quinone (**6**) in 82% yield. Stereoselective synthesis of ubiquinone-10 was achieved by the condensation of **6** and solanesyl bromide (yield 92%), reductive elimination of the sulfone group by sodium–ethyl alcohol in THF (yield 80%), and followed by air oxidation of the hydroquinone.

Recently much attention has been paid to ubiquinone-10 (**1**) owing to its remarkable physiological and clinical activity.[1] Various synthetic routes to **1** have been developed and these involve alkylation of the appropriate quinone or hydroquinone precursor.[2,3] However, the alkylating agent, decaprenyl bromide is obtained as a *Z*/*E* (=3/7) mixture *via* multi-step procedures from solanesol.[4] Thus, its use presents an intrinsic disadvantage for obtaining all-*E* ubiquinone-10. Terao and coworkers have demonstrated an efficient route to **1** using a sulfone-functionalized prenylhydroquinone **6**.[5] However, a simpler procedure for the synthesis of **6** starting with 2,3-dimethoxy-5-methylhydroquinone (**2**) still remains. Previously we have developed a new effective and simple method[6] for the introduction of the sulfone-functionalized isoprene skeleton into aromatic moieties using (2*E*)-1-(phenylsulfonyl)-2-methyl-4-chloro-2-butene (**5**) as a building block which is easily obtainable by the reaction of isoprene and benzenesulfonyl chloride in the presence of copper(I) chloride-triethylamine hydrochloride catalyst.[7] Here we extend the investigation to a stereoselective synthesis of **1** applicable to large scale production.

Alkylation of **3**[8] with 2-methoxyethoxymethyl [MEM] chloride[9] according to the previously reported procedure[8] afforded **4** in 91% yield, and the coupling reaction of **4** with **5** in the presence of copper(I) bromide afforded **6** in 82% yield.[6]

Condensation of **6** and solanesyl bromide in the presence of potassium *t*-butoxide, gave **7** in 92% yield. The next problem is to find the method of selective and economical reduction of the sulfone group. The well established method for this purpose is use of lithium-ethylamine system,[10] but it requires low reaction temperature (*ca.* −70 °C) and the product usually contains *ca.* 10—15% of $\Delta^{3,4}$-isomer. Then the modified Bouveault-Blanc reduction recently reported by Tsuchihashi *et al.*[11] was very attractive as an alternative. *The reaction could be carried out at room temperature by treating* **7** *with sodium (8 equiv.)–ethyl alcohol (12 equiv.) in THF.* The product **8** obtained in 80% yield was found to contain a trace of $\Delta^{3,4}$-isomer, although its amount could not be quantitatively determined because the retention time in high pressure chromatography (HPLC) is same as that of **8**. The mixture was treated with 48% hydrobromic acid catalyst in isopropyl alcohol at 50 °C to remove the protecting group. Neutralization of the reaction mixture with potassium hydroxide in methyl alcohol, followed by air oxidation at room temperature yielded a mixture consisting of 93% of **1** and 7% of $\Delta^{3,4}$-isomer (HPLC). Pure (all *E*)-ubiquinone-10 (mp 50 °C) was obtained by recrystallization of the mixture from ethyl alcohol.

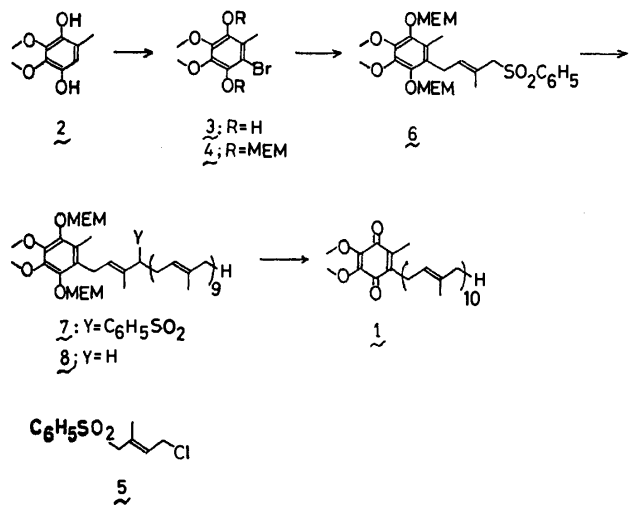

Experimental

Boiling points and melting points are uncorrected. IR spectra were determined on a Digilab FTS-20 C/D spectorometer. NMR spectra were taken with a Varian EM 390 (with hexamethyldisiloxane as an internal standard) and mass spectra with Finnigan 9500 or JEOL JMS-D 300 instruments. HPLC analyses were made with a Waters Associate.

6-(4-Phenylsulfonyl-3-methyl-2-butenyl)-2,3-dimethoxy-5-methylhydroquinone Bis(2-methoxyethoxymethyl) Ether (6). This compound was synthesized in 82% yield according to the procedure reported previously[6] by the reaction of **5** (0.5 mol) and copper derivertive of **4** prepared by treating the Grignard reagent of **4** with copper (I) bromide (0.5 mol). NMR δ (in $CDCl_3$) 1.87 (s, 3H, CH_3), 1.97 (s, 3H, CH_3), *ca.* 3.03—4.00 (m, 24H, $6\times CH_2+4\times CH_3O$), 5.00, 5.07 (s, 4H, $2\times CH_2$), *ca.* 4.90—5.20 (m, 1H, -CH) and *ca.* 7.23—7.80 (m, 5H, arom).

6-(4-Phenylsulfonyl-3,7,11,15,19,23,27,31,35,39-decamethyltetraconta-2,6,10,14,18,22,26,30,34-decaenyl)-2,3-dimethoxy-5-methylhydroquinone Bis(2-methoxyethoxymethyl) Ether (7). Into a solution of **6** (20.5 g; 36 mmol) and solanesyl bromide (purity 95%; 17.5 g; 24 mmol) in THF–DMF (9 : 1; 150 ml) was added potassium *t*-butoxide (22.5 g; 29 mmol) at −20 °C under nitrogen atmosphere. Stirring was continued for 1 h at −20 °C, and further for 1 h at 20 °C. The reaction mixture was poured into saturated ammonium chloride solution and extracted with diisopropyl ether. Evaporation of the solvent and purification of the residue with silica-gel column chromatography (dioxane–hexane=3 : 7) afforded **7** (26.0 g) in 92% yield. IR (neat) 1660, 1450, 1300, 1250, 975, and 875 cm^{-1}. NMR δ (in $CDCl_3$) 1.53, 1.63 (s, 30H, $10\times CH_3$), 1.75 (s, 3H,

CH_3), *ca.* 1.95 (s, 35H, $16\times CH_2+CH_3$), *ca.* 2.68 (m, 2H, CH_2), *ca.* 3.00—4.00 (m, 23H, $4\times CH_3O+5\times CH_2+CH$), 4.97, 5.05 (s, 4H, $2\times CH_2$), 5.07 (broad s, 10H, $10\times CH$) and 7.20—7.80 (m, 5H, arom). Found: C, 73.95; H, 9.34%. Calcd for $C_{73}H_{112}O_{10}S$: C, 74.19; H, 9.55%.

Ubiquinone-10 (1). Into a solution of **7** (118 g; 0.1 mol) in ethyl alcohol (70 ml) and dry THF (350 ml) was added a small pieces of sodium (18.4 g; 0.8 atom) at 10—15 °C under nitrogen stream. After stirring was continued for 12 h, additional 100 ml of ethyl alcohol was dropped to consume the excess sodium, the reaction mixture was poured into saturated ammonium chloride solution and extracted with diisopropyl ether, washed with water, and dried over magnesium sulfate. Evaporation of the solvent, and purification with silica gel column chromatography (dioxane: hexane= 15 : 85) afforded **8** (83.6 g) in 80.4% yield. IR (neat) 2950, 1670, 1390, 1110 and 980 cm^{-1}. NMR δ (in $CDCl_3$) 1.57, 1.61, 1.69 (s, 33H, $11\times CH_3$), 1.97, 2.10 (s, 39H, $18\times CH_2+CH_3$), 3.32 (s, 6H, $2\times CH_3O$), 3.98 (s, 6H, $2\times CH_3O$), *ca.* 3.30—3.95 (m, 10H, $5\times CH_2$), *ca.* 5.05 (broad s, 10H, $10\times CH$) and 5.17 (s, 4H, $2\times CH_2$). Found: C, 77.02; H, 10.18%. Calcd for $C_{67}H_{108}O_8$: C, 77.26; H, 10.45%.

The NMR spectra agreed very closely with that of authentic sample obtained by reacting the Grignard reagent of **4** and (all *E*)decaprenyl bromide except for the signal of δ *ca.* 2.50 (m) which was supposed to originate from $\Delta^{3,4}$-isomer. Quantitative analyses by HPLC resulted in failure because the retention time was same as that of **8**. Deprotection of **8** was carried out with 48% hydrobromic acid (5 ml) in isopropyl alcohol (1500 ml) at 50 °C for 3 h under nitrogen atmosphere. After neutralization with 10% KOH–MeOH, air was bubbled into the reaction system at 25 °C for 3 h. After evaporation of the solvent, the mixture was poured into water, extracted with hexane, and dried over magnesium sulfate. Reaction product was purified with silica gel column chromatography (diisopropyl ether: hexane= 2 : 8) to obtain **1** (67.9 g) quantitaively. HPLC analyses [Lichrosorb SI 60-5; butyl acetate: hexane=6 : 94] showed that the product consisted of 93% of **1** (5.8 min) and 7% of $\Delta^{3,4}$-isomer (5.5 min). Pure all *E*-**1** (58.4 g; yield 77%) was obtained by recrystallization of the mixture from ethyl alcohol (2.5 l) at 5 °C. Mp 50 °C [lit,[5a] mp 48—49 °C].

References

1) G. P. Littaru, L. H. Ho, and K. Folkers, *Int. J. Vitanm. Natr. Res.*, **42**, 291, 413 (1972); A. B. Combs, D. Acosta, and K. Folkers, *IRCS. Med. Sci. Biochem.*, **4**, 403 (1976).

2) S. Inoue, R. Yamaguchi, K. Saito, and K. Sato, *Bull. Chem. Soc. Jpn.*, **47**, 3098 (1974); L. S. Hegedus, B. R. Evans, D. E. Korte, E. L. Waterman, and K. Sjöberg, *J. Am. Chem. Soc.*, **98**, 3901 (1978); C. D. Snyder and H. Rapoport, *ibid*, **86**, 8046 (1974); Y. Naruta and K. Maruyama, *Chem. Lett.*, **1979**, 885; I. Tabushi, Y. Kuroda, K. Fujita, and H. Kawakubo, *Tetrahedron Lett.*, **1978**, 2083.

3) C. H. Shunk, R. E. Erickson, E. L. Wong, and K. Folkers, *J. Am. Chem. Soc.*, **81**, 5000 (1959).

4) R. Rüegg, U. Gloor, N. R. Ryser, O. Wiss, and O. Isler, *Helv. Chim. Acta*, **42**, 2626 (1959).

5) S. Terao, K. Kato, M. Shiraishi, and H. Morimoto, *J. Org. Chem.*, **44**, 868 (1979); S. Terao, M. Shiraishi, and K. Kato, *Synthesis*, **1979**, 467.

6) Y. Fujita, M. Ishiguro, T. Onishi, and T. Nishida, *Synthesis*, **1981**, 469.

7) W. E. Truce, C. T. Goralski, L. W. Christensen, and R. H. Bavery, *J. Org. Chem.*, **35**, 4217 (1970).

8) K. Sato, S. Inoue, and R. Yamaguchi, *J. Org. Chem.*, **37**, 1889 (1972).

9) E. J. Corey, J-L. Gras, and P. Ulrich, *Tetrahedron Lett.*, **1976**, 809.

10) E. M. Kaiser, *Synthesis*, **1972**, 391.

11) K. Ogura, T. Noguchi, S. Mita, and G. Tsuchihashi, 7th Congress of Organo Sulfur and Phosphorus Compound, Kyoto, 1979, Abstr. p. 76.

Upon DNP-aromatic Rule. Effect of Chromophore Exchange on the CD Spectra of *N*-DNP-arylalkylamines

Masao KAWAI* and Ukon NAGAI

Mitsubishi-Kasei Institute of Life Sciences, Minamiooya 11, Machida, Tokyo 194

(Received September 30, 1981)

Synopsis. CD spectra of the analogs of aromatic DNP-α-amino acids and the related *N*-DNP-arylalkylamines, in which the positions of the two chromophoric groups were exchanged with each other, were studied. The analogs, in which the DNP-amino group is separated from the asymmetric carbon, did not show any marked Cotton effect near 400 nm, indicating the importance of direct attachment of the DNP-NH group to the chiral carbon atom for showing the characteristic CD spectra of *N*-DNP-aromatic α-amino acids.

Chiroptical properties of 2,4-dinitrophenyl (DNP) derivatives of aromatic α-amino acids and related compounds were studied extensively[1-6] and DNP-aromatic rule was proposed.[3] According to the rule the sign of $[\theta]_{\approx 400}$ is negative for the compounds of the formula **1**, where Ar and R are an aromatic and a nonaromatic groups, respectively. The symbol X represents a methylene chain, in which a hetero atom or such a group as ester, amide, *etc.* can be included.

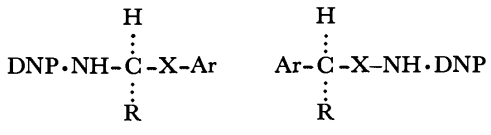

1 **2**

(for Ar, R, and X see Table 1)

As an attempt to investigate the basis of the rule, DNP-amino compounds **2**, which are the chromophore exchanged analogs of **1**, were prepared and their CD spectra were compared. Assuming that the Cotton effects are due to the exciton coupling between the two chromophores,[7] essentially same spectra are expected for the compounds having the same relative orientation of the electric transition moments. Thus, if the transition moments of both chromophores have similar orientation relative to the attaching bond and exchange of the chromophoric groups doesn't cause significant change of molecular conformation, similar CD spectra can be expected for each pairs of **1** and **2**.

CD spectra of **1a—g** and **2a—g** measured in methanol are summarized in Table 1. All of the type **1** compounds exhibited distinctly negative Cotton effect around 400 nm reflecting the absolute configuration of the chiral center as stated by DNP-aromatic rule. In all the pairs examined, however, the molecular ellipticities of **2** at 400 nm were much weaker than those of **1**, and apparently no simple relation was found between the sign of the Cotton effect and the absolute configuration. Since the assumption of similar molecular conformation of **1** and **2** seems reasonable, the unexpected low $[\theta]_{\approx 400}$ values of **2** are attributed to the increased freedom of rotation around the DNPNH–C bond in **2** compared to that in **1**, which results in different average relative orientation of the transition moment. Direct attachment of DNP–NH to the asymmetric carbon restricts rotation around that bond as confirmed by the conformational energy calculation of DNP-L-alanine using ECEPP program;[8] *i.e.*, only the values −60°——85° and

Table 1. CD spectral data of **1** and **2** recorded in methanol

	Ar	R	X	Molecular ellipticity($[\theta] \times 10^{-2}$) and wavelength(λ/nm) in parentheses[a]
1a	Ph	CO_2H	CH_2	−91(410),0(363),+74(334),+21(296),+46(270),+23(254)
2a	Ph	CH_3	CH_2	−19(415sh),−47(355),0(290)
1b	$PhCO_2$	CH_3	CH_2	−61(400),0(347),+23(325),+9(300),+170(238)
2b	$PhCO_2$	CH_3	CH_2	−4(420sh),−78(343),0(287),+22(268),0(253),−6(247),0(243)
1c	PhCONH	CH_3	CH_2	−97(409),−70(370sh),0(300),+45(372),+166(238)
2c	PhCONH	CH_3	CH_2	+10(415),0(390),−91(345),0(275),−115(243)
1d	PhCONH	CO_2H	$(CH_2)_3$	−59(405),0(341),+11(324),+3(308),+75(264)
2d	PhCONH	CO_2H	$(CH_2)_3$	+8(415),0(380),−16(345),0(280)
1e	PhCONH	CO_2H	$(CH_2)_4$	−42(408),0(352),+22(332),0(300),+28(265),0(244)
2e	PhCONH	CO_2H	$(CH_2)_4$	+11(420),0(380),−8(340),0(300),−8(275)
1f	p-$NO_2C_6H_4NHCO$	CH_3	$CONHCH_2$	−112(395),0(355),+82(337),0(313),−13(300),0(287),+6(280),0(270)
2f	p-$NO_2C_6H_4NHCO$	CH_3	$NHCOCH_2$	−43(400),−40(386),−42(375),0(348),+37(325),0(302),−25(275)
1g	p-$NO_2C_6H_4NHCO$	CO_2H	$(CH_2)_2$	−108(402),0(371),+202(432),0(319),−20(306),0(292),+13(275),0(260)
2g	p-$NO_2C_6H_4NHCO$	$NHCO_2$-$C(CH_3)_3$	$(CH_2)_3$	−4(420sh),−40(345),0(313),+2(295)

a) sh: Shoulder. The underlined values are those of $[\theta]^{max}$ near 400 nm.

$-145°$——$-165°$ are allowed for ϕ.[9] Thus, much smaller ellipticities of **2** compared to those of **1** were deduced to be due to the loss of restricted rotation of DNP–NH group caused by the presence of intervening achiral chain X between the DNP–NH group and the chiral center.

It is noteworthy that introduction of just one methylene between the DNP–NH and asymmetric carbon of (*S*)-DNP-NHCH(CH_3)Ph ($[\theta]_{406}+16200$) affords **2a** possessing very low $[\theta]_{400}$ value. Insertion of a methylene chain [$(CH_2)_n$, $n=1$—5] between the asymmetric carbon and the phenyl group of L-DNP-NHCH(CO_2H)-Ph doesn't cause marked change of the CD spectra.[1,3]

Experimental

Melting points were uncorrected. Compounds **1a**—**e** and **1g** were described in Ref. 3. The DNP derivatives **1a**, **1f**, **2a**, and **2g** were prepared in enantiomeric form. 2,4-Dinitrophenylations were performed with the procedure of Sanger[10] unless otherwise stated. All the PMR spectra (Hitachi R-24 spectrometer; $CDCl_3$, acetone-d_6, or DMSO-d_6) of the compounds synthesized were consistent with the assigned structures.

(2R)-N-DNP-2-phenylpropylamine (Enantiomer of 2a). Dinitrophenylation of 404 mg (1 mmol) of (2*R*)-2-phenylpropylamine L-malate ($[\alpha]_D^{22}$ +21.1°, *c* 4.1, H_2O)[11] afforded enantiomer of **1a** (195 mg): orange crystals from benzene; mp 89—90 °C. Found: C, 59.30; H, 4.94; N, 13.83%. Calcd for $C_{15}H_{15}N_3O_4$: C, 59.79; H, 5.02; N, 13.95%.

(2R)-N-DNP-O-benzoyl-1-amino-2-propanol (2b). Dinitrophenylation of 112 mg (1 mmol) of (2*R*)-1-amino-2-propanol ($[\alpha]_D^{22}$ −32.8°, *c* 2, CH_3OH)[12] afforded *N*-DNP derivative (80 mg, mp 94—96 °C) as yellow needles from benzene–hexane. This compound was benzoylated with benzoyl chloride–pyridine to give **2b** (73 mg) as yellow powder from benzene: mp 131—132 °C. Found: C, 55.10; H, 4.35; N, 12.10%. Calcd for $C_{16}H_{15}N_3O_6\cdot(1/4)H_2O$: C, 54.94; H, 4.47; N, 12.01%.

(2R)-N¹-DNP-N²-benzoyl-1,2-propanediamine (2c). To a stirred mixture of 0.75 g (2 mmol) of (2*R*)-1,2-propanediamine L-tartrate ($[\alpha]_D^{23}$ +21.2°, *c* 1.63, H_2O) and $NaHCO_3$ (0.6 g, 7 mmol) in H_2O were added 1-fluoro-2,4-dinitrobenzene (0.37 g, 2 mmol) in acetone and then benzoyl chloride (0.47 ml, 4 mmol) and $NaHCO_3$ (1 g, 12 mmol). The main product **2c** was isolated using preparative TLC (SiO_2, developed 7 times with $CHCl_3$) as yellow powder (47 mg), which had slightly higher R_f value than that of the isomer **1c**.[3]

N^δ-DNP-N^α-benzoyl-L-ornithine (2d). N^δ-DNP-N^α-*t*-butoxycarbonyl-L-ornithine (mp 65—72 °C; 100 mg, 0.25 mmol), prepared from N^α-*t*-butoxycarbonyl-L-ornithine, was treated with trifluoroacetic acid and was benzoylated with benzoyl chloride (0.06 cm^3, 0.5 mmol) and NaOH to afford **2d** (78 mg) as yellow powder from methanol–H_2O: mp 181—183 °C. Found: C, 53.36; H, 4.67; N, 13.41%. Calcd for $C_{18}H_{18}N_4O_7\cdot(1/4)H_2O$: C, 53.14; H, 4.58; N, 13.77%.

N^ϵ-DNP-N^α-benzoyl-L-lysine (2e). N^α-Benzoyl-L-lysine (125 mg, 0.5 mmol) was dinitrophenylated to give **2e** (210 mg) as yellow crystals from ethyl acetate–hexane: mp 110—113 °C. Found: C, 54.23; H, 4.89; N, 13.35%. Calcd for $C_{19}H_{20}N_4O_7\cdot(1/4)H_2O$: C, 54.22; H, 4.91; N, 13.31%.

DNP-L-alanylglycine p-Nitroanilide (Enantiomer of 1f). DNP-L-alanine *N*-hydroxysuccinimide ester (mp 148—152 °C; 260 mg, 0.73 mmol) and trifluoroacetate of glycine *p*-nitroanilide, prepared from *t*-butoxycarbonylglycine *p*-nitroanilide (mp 180—181 °C; 200 mg, 0.67 mmol), were allowed to react in DMF to give enantiomer of **1f** (180 mg) as yellow fine needles from acetone: mp 292—295 °C. Found: C, 47.47; H, 3.96; N, 19.27%. Calcd for $C_{17}H_{16}N_6O_8$: C, 47.22; H, 3.73, N, 19.44%.

DNP-glycyl-L-alanine p-Nitroanilide (2f). Coupling reaction of *t*-butoxycarbonylglycine (117 mg, 0.67 mmol) and L-alanine *p*-nitroanilide trifluoroacetate, prepared from *t*-butoxycarbonyl-L-alanine *p*-nitroanilide (mp 130—135 °C; 103 mg, 0.33 mmol), using dicyclohexylcarbodiimide (83 mg, 0.4 mmol) in DMF afforded *t*-butoxycarbonylglycyl-L-alanine *p*-nitroanilide (90 mg) as an oil. This compound was treated with trifluoroacetic acid and dinitrophenylated to give **2f** (90 mg) as yellow crystals from ethyl acetate: mp 224—227 °C (decomp). Found: C, 47.03; H, 3.69; N, 19.23%. Calcd for $C_{17}H_{16}N_6O_8$: C, 47.22; H, 3.73; N, 19.44%.

N^δ-DNP-N^α-t-butoxycarbonyl-L-ornithin p-Nitroanilide (Enantiomer of 2g). N^δ-DNP-N^α-*t*-butoxycarbonyl-L-ornithine (120 mg, 0.3 mmol), *p*-nitroaniline (137 mg, 1 mmol), and dicyclohexylcarbodiimide (103 mg, 0.5 mmol) in THF afforded enantiomer of **2g**, which was purified by preparative TLC (SiO_2, developed 3 times with $CHCl_3$): yellow powder (7 mg); mp 190—200 °C (decomp).

We are grateful to the members of System Engineering Laboratory, Mitsubishi-Kasei Industries Ltd., for elemental analyses and computing facilities.

References

1) M. Kawai, U. Nagai, and M. Katsumi, *Tetrahedron Lett.*, **1975**, 2845.
2) M. Kawai and U. Nagai, *Tetrahedron Lett.*, **1977**, 3889.
3) M. Kawai, U. Nagai, M. Katsumi, and A. Tanaka, *Tetrahedron*, **34**, 3435 (1978).
4) U. Nagai, M. Kawai, T. Yamada, S. Kuwata, and H. Watanabe, *Tetrahedron Lett.*, **1981**, 653.
5) U. Nagai, N. Taki, and M. Kawai, *Chem. Pharm. Bull.*, **29**, 1750 (1981).
6) M. Kawai, U. Nagai, and A. Tanaka, *Bull. Chem. Soc. Jpn.*, **55**, 1213 (1982).
7) J. A. Schellman, *Acc. Chem. Res.*, **1**, 144 (1968).
8) F. A. Momany, R. F. McGuire, A. W. Burgess, and H. A. Scheraga, *J. Phys. Chem.*, **79**, 2361 (1975).
9) IUPAC-IUB Comission on Biochemical Nomenclature, *Biochemistry*, **9**, 3471 (1970).
10) F. Sanger, *Biochem. J.*, **39**, 507 (1945).
11) W. R. Brode and W. S. Raasch, *J. Am. Chem. Soc.*, **64**, 1449 (1942).
12) R. L. Clark, W. H. Jones, W. J. Raich, and K. Folkers, *J. Am. Chem. Soc.*, **76**, 3995 (1954).

Reduction of α,β-Unsaturated Carbonyl Compounds to the Saturated Alcohols Using Hydridocarbonyliron Complexes

Masakazu YAMASHITA,* Kanako MIYOSHI, Yasuhiro OKADA, and Rikisaku SUEMITSU
Department of Applied Chemistry, Faculty of Engineering, Doshisha University, Kamikyo-ku, Kyoto 602
(Received October 2, 1981)

Synopsis. Tetracarbonylhydridoferrate was found to be effective for the selective reduction of α,β-unsaturated carbonyl compounds to the corresponding saturated alcohols. The reactions proceeded stereospecifically and (−)- and (+)-neodihydrocarveol were obtained exclusively from (+)- and (−)-carvone respectively. The reaction mechanism is briefly discussed.

Hydridocarbonyliron complex $[HFe_m(CO)_n^-]$ have been reported to be useful hydrogenating reagents for α,β-unsaturated carbonyl compounds,[1,2] conjugated dienes,[3] and the C=N double bond of *N*-benzylideneaniline,[4] giving saturated carbonyl compounds, monoenes, and *N*-benzylaniline, respectively. But the reduction of a carbonyl group to an alcohol has never been reported.

In the course of our research on the selective reduction of several essential oils with α-enone moiety using tetracarbonylhydridoferrate $[HFe(CO)_4^-]$ (**1**), we found unexpectedly that **1** in tetrahydrofuran was effective for the selective reduction of carbonyl groups to the corresponding alcohols. In this paper, we wish to report about these reactions.

Experimental

Infrared spectra were recorded on a Hitachi 260-10 Infrared Spectrophotometer, NMR spectra were measured on a Hitachi R-600 FT-NMR Spectrophotometer, and mass spectra were measured on a RM-50 Hitachi GC-MS. Gas chromatography was carried out on a Yanagimoto G-180 Model equipped with a glass column packed with polyethyleneglycol 20 M† (10%) on Chromosorb (0.3 cmϕ × 1.5 m) and a Yanagimoto G-8 Model equipped with a stainless column packed with Silicone Gum SE-30 (10%) on Chromosorb (0.3 cmϕ × 2 m). Optical rotations were measured on a Union High Sensibility Specific Rotary Meter PM-71.

Materials. Tetrahydrofuran (THF) was distilled over lithium aluminum hydride under argon just before use. Pentacarbonyliron and deuterium oxide (Merck) were used without further purification. The following organic compounds, (+)- and (−)- carvone, α- and β-ionone, diethyl ketone, benzylideneacetone and triethylenediamine, were commercial products of the highest available purity. Piperitenone was supplied from Ogawa and Co., Ltd. All reduction experiments were carried out under argon atmosphere.

Preparation of 1 in THF. To the THF solution (40 ml) of triethylenediamine (3.7 g, 33 mmol), deionized water (0.59 ml, 33 mmol) or D_2O (0.66 ml, 33 mmol) was injected by syringe and the mixture was stirred for 30 min at 60 °C under argon atmosphere. Then, pentacarbonyliron (1.5 ml, 11 mmol) was injected and the reaction mixture was stirred for further 1 h at the same reaction conditions. The solution was used for the next reaction *in situ*.[5]

Representative Reduction of α-Ionone Using 1. To the solution of **1** (22 mmol) in THF, α-ionone (1.13 ml, 5.5 mmol) was injected, and the mixture was stirred at 60 °C under argon atmosphere till the reaction was completed perfectly. After the air oxidation of the solution at room temperature for 1 d, iron oxide was centrifuged. And THF was removed with a rotary evaporator. The residue was purified by column or thin layer chromatography (silica gel, hexane: ethyl acetate= 4 : 1). The product was identified as 4-(2,6,6-trimethyl-2-cyclohexenyl)-2-butanol by means of IR, NMR, MS, and GLC. Yield >98% (GLC).

4-(2,6,6,-Trimethyl-2-cyclohexenyl)-2-butanol. IR (cm^{-1}): 3300, 2900, 1440, 1110; MS (*m/e*); 196 (M^+); NMR ($CDCl_3$) (δ): 0.88 (6H, d, $C(CH_3)_2$), 1.24 (3H, s, $=C-CH_3$). 1.44 (3H, s, $O-C-CH_3$), 0.98—2.2 (8H, m), 3.6—4.0 (1H, m), 5.25—5.6 (1H, m).

4-(2,6,6,-Trimethyl-1-cyclohexenyl)-2-butanol. IR (cm^{-1}): 3350, 2900, 1460, 1120; MS (*m/e*): 196 (M^+); NMR ($CDCl_3$) (δ): 0.97 (6H, s, $C(CH_3)_2$), 1.13 (2H, s, $=CH_2-$), 1.23 (2H, s, $-CH_2-$), 1.59 (3H, s, $O-C-CH_3$), 1.1—2.0 (6H, m), 3.4—3.92 (1H, m).

(−)-Neodihydrocarveol. IR (cm^{-1}): 3400, 880; MS (*m/e*): 154 (M^+); NMR ($CDCl_3$) (δ): 0.95 (3H, d, $-CH_3$), 1.05—1.65 (8H, m), 1.72 (3H, s, $=C-CH_3$), 3.2—3.7 (1H, m), 3.58 (1H, s), 4.76 (2H, s).

Results and Discussion

For example, **1** in THF generated *in situ* reacted with (+)-carvone at 60 °C for 9 d under argon atmosphere to give (−)-neodihydrocarveol in almost quantitative yield. This shows that **1** in THF is an efficient reductant of α,β-unsaturated carbonyl compounds to the corresponding saturated alcohols (Eq. 1), although **1** in

$$R^1-\underset{\underset{O}{\|}}{C}-CH=CH-R^2 \xrightarrow[THF]{HFe(CO)_4^- (1)} R^1-\underset{\underset{OH}{|}}{\overset{\overset{H}{|}}{C}}-CH_2-CH_2-R^2 \quad (1)$$

ethanol gives only (−)-dihydrocarvone from (+)-carvone. Other results are summarized in Table 1. As shown in Table 1, the compounds with α-enone moiety were reduced to the corresponding saturated alcohols in high yields. Piperitenone which has two carbon–carbon double bonds of α-enone moiety was also reduced to the corresponding menthol using 6 equiva-

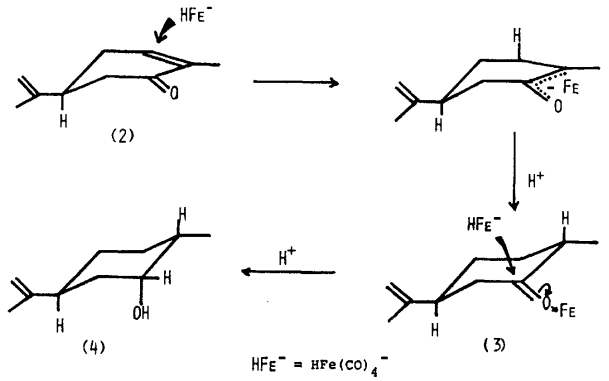

Scheme 1.

† 1 M = 1 mol dm^{-3}.

Table 1. The reduction of α,β-unsaturated carbonyl compounds using tetracarbonylhydridoferrate in THF

Run	Substrate	Reaction time/d	Product	Yield/%[a]
1	(+)-Carvone[b]	9	(−)-Neodihydrocarveol[c]	>98
2	(−)-Carvone[d]	9	(+)-Neodihydrocarveol[e]	>98
3	Piperitenone	26	(±)Menthol	>98
4	α-Ionone	20	4-(2,6,6-Trimethyl-2-cyclohexenyl)-2-butanol	>98
5	β-Ionone	13	4-(2,6,6-Trimethyl-1-cyclohexenyl)-2-butanol	>98
6	Benzylideneacetone	3	4-Phenyl-2-butanol	>98
7	Diethylketone	—	No reaction	—

a) Yields were determined by GLC. b) $[\alpha]_D^{20}$ +49.8° (*c* 9.66, EtOH). c) $[\alpha]_D^{20}$ −13.5° (*c* 1.01, Et OH). d) $[\alpha]_D^{20}$ −60.1° (*c* 9.65, EtOH). e) $[\alpha]_D^{20}$ +21.4° (*c* 1.03, EtOH).

lents of **1**.

As to the stereochemistry, it was found that (+)- and (−)-carvone reacted with **1** to give exclusively (−)- and (+)-neodihydrocarveol respectively, but the corresponding diastereomers such as isodihydrocarveol, dihydrocarveol, and neoisodihydrocarveol were not produced, showing that these reactions proceeded stereospecifically.

The reaction mechanism was assumed as follows (Scheme 1). First, **1** attacked the carbon-carbon double bond of α,β-unsaturated carbonyl moiety of (+)-carvone (**2**) from the sterically less hindered side to form dihydrocarvone (**3**),[6] which was detected in the reaction mixture by means of GLC. Subsequently, **3** is reduced selectively to give (−)-neodihydrocarveol (**4**). However, although it is still uncertain, it seems that **3** exists as a complex with carbonyliron and that the carbonyl group is to some extent activated, because saturated ketones such as diethyl ketone did not react with **1** in THF.

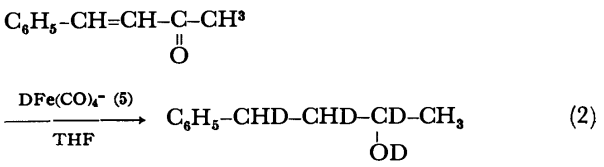

(2)

Besides, the introduction of deuterium was tried using deuterium oxide (D_2O) instead of water (H_2O) for the preparation of tetracarbonyldeuterioferrate (**5**). The reaction of **5** with benzylideneacetone in THF at 60 °C for 3 d gave the corresponding deuterated alcohol, which was identified by means of IR, NMR, and MS. The similar introduction of deuterium was also noticed in the case of the reaction with (+)- and (−)-carvone.

The authors are grateful to Mr. Y. Enomoto of Ogawa and Co., Ltd. for providing of piperitenone.

References

1) R. Noyori, I. Umeda, and T. Ishigami, *J. Org. Chem.*, **37**, 1542 (1972).

2) J. P. Collman, R. G. Finke, P. L. Matlock, R. Wahren, and J. I. Brauman, *J. Am. Chem. Soc.*, **98**, 4685 (1976).

3) Y. Takegami, Y. Watanabe, I. Kanaya, T. Mitsudo, T. Okajima, Y. Morishita, and H. Masada, *Bull. Chem. Soc. Jpn.*, **41**, 2990 (1968).

4) Y. Watanabe, M. Yamashita, T. Mitsudo, M. Tanaka, and Y. Takegami, *Tetrahedron Lett.*, **1974**, 1879.

5) (**1**) in diethyl ether has been prepared by the similar method; see Ref. 1.

6) M. Yamashita, K. Miyoshi, Y. Okada, and R. Suemitsu, 24th Symposium of the Chemistry of Terpenes, Essential Oils, and Aromatics, Kōriyama, September 1980, Abstr. p. 185.

Carbon-Carbon Bond Formation by the Use of Chloroiodomethane as a C_1 Unit. IV.[1] The Mannich Reaction of Ketones by Means of Dihalomethane and Secondary Amine[2]

Sotaro MIYANO,* Akira MORI, Hiroshi HOKARI, Katsuaki OHTA, and Harukichi HASHIMOTO

Department of Applied Chemistry, Faculty of Engineering, Tohoku University, Aramaki-Aoba, Sendai 980

(Received October 2, 1981)

Synopsis. Treatment of ketones with dihalomethane (CH_2Br_2, CH_2ClI, and CH_2I_2) in the presence of secondary amine, preferably pyrrolidine, gave the corresponding Mannich base in varing yields depending on the substrate and/or combination of the reagents.

In previous papers[3] we have reported that chloroiodomethane reacts in the sense of I–CH_2Cl, in either homolytic or heterolytic fashion, enabling the introduction of chloromethyl moiety into various substrates. In a study to extend the scope and utility of the transformation by the use of CH_2ClI as a C_1 unit, we have for some time been trying to chloromethylate active methylene compounds with the aid of various base catalysts.

Although such attempts have not yet been realized,[4] it has been found that α-methylene protons of ketones (**1**) can be replaced with (dialkylamino)methyl moiety by a combination of dihalomethane (**2**) and secondary amine (**3**) (Eq. 1). The important features of the amino ketone products, the Mannich base, have been well documented for a long time,[5] and here we wish to report the results of the aminomethylation reaction.

$$\underset{\mathbf{1}}{R^1\text{–}\overset{\overset{O}{\|}}{C}\text{–}CHR^2R^3} + \underset{\mathbf{2}}{CH_2XY} \xrightarrow[(-HX,\ -HY)]{2R_2NH\ \mathbf{3}} \xrightarrow{NaOH/H_2O} \underset{\mathbf{4}}{R^1\text{–}\overset{\overset{O}{\|}}{C}\text{–}\underset{\underset{CH_2NR_2}{|}}{CR^2R^3}} \quad (1)$$

(X, Y = Cl, I; Br, Br; I, I)

The reaction was simply carried out by adding amine (**3**) to a stirred solution of the substrate ketone (**1**) and CH_2XY (**2**) in THF, followed by stirring the mixture under the conditions indicated in Table 1. Typical results obtained are as follows: 1) Among secondary amines examined, *i.e.* pyrrolidine, Et_2NH, and *i*-Pr_2NH, the first gave the best results while the last was almost ineffective. Attempted reactions of propiophenone with **2** in the presence of tertiary amine such as Et_3N or 1,4-diazabicyclo[2.2.2]octane resulted in the quaternization of the amine by the halide leaving the ketone almost intact. 2) The choice of the dihalide (**2**) should depend on the substrate **1**. For reactive ketones such as cyclohexanone and acetophenone, CH_2ClI gave better results than CH_2I_2; the latter yielded larger amounts of intractable tarry materials with the expense of **4**. On the other hand, CH_2I_2 was preferred for the less reactive ketones such as propiophenone and diethyl ketone. Dibromomethane showed intermediate character, and could be applicable to both types of ketones. 3) Heptanal was also aminomethylated in a low yield, while esters (ethyl butyrate, methyl phenylacetate, *etc.*) were recovered unchanged.

Table 1. Aminomethylation of ketones with CH_2XY/R_2NH[a]

Substrate (**1**)	CH_2XY (**2**) X,Y	R_2NH[b] (**3**)	Time / h^{-1}	Mannich base (**4**)	Yield / %[c]
Ph–CO–Et	I, I	A	4	**4a**	60 (73)
	Br,Br	A	3		54 (61)
	Cl,I	A	5		32 (40)
	Cl,I	B	5	**4a′**	29 (37)
	I, I	C	5.5	**4a″**	(1.6)
Ph–CO–Me	Br,Br	A	3	**4b**	27 (60)
	Cl,I	A	3		(54)
	I,I	A	3		(0)[d]
Ph–CO–*i*-Pr	Cl,I	A	3	**4c**	(trace)
Ph–CO–CH_2Ph	Cl,I	A	3	**4d**	64
Et–CO–Et	I, I	A	3	**4e**	62 (71)
	Br,Br	A	3		53 (61)
	Cl,I	A	3		44 (53)
	Cl,I	B	4	**4e′**	11 (30)
i-Pr–CO–Me	Br,Br	A	3	**4f**	67 (84)[e]
	Cl,I	A	2		64 (80)
t-Bu–CO–Me	Br,Br	A	5	**4g**	(0)[d]
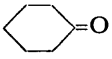	Cl,I	A	5[f]	**4h**	21 (66)
	Br,Br	A	3		15 (53)
	Cl,I	B	5	**4h′**	8.8 (34)
n-Hex–CHO	Cl,I	A	3[f]	**4i**	(48)
	Br,Br	A	3[f]		8.3 (45)

a) **1**, *ca.* 80 mmol; **1** : **2** : **3** ≈ 1 : 1.2 : 2.4 (molar ratio); THF 100 ml; under reflux. b) A, pyrrolidine (*c*-$(CH_2)_4$NH); B, Et_2NH; C, *i*-Pr_2NH. c) Isolated yields. Figures in parentheses refer to the crude products (see Experimental). d) Resulted tarry material with complete consumption of the substrate. e) Only *i*-Pr–CO-CH_2- 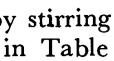 was detected. f) Room temp.

As is encountered in literatures,[6] attempts to isolate pure sample by distillation sometimes suffered from poor yields of **4**, probably due to thermal instability of the Mannich base. Although the conventional Mannich reaction with formaldehyde–R_2NH in the presence of acid catalyst,[5] or recent version by means of preformed methyleneiminium reagents,[7] has widely been utilized for the synthesis of amino ketones, the transformation described here may have some synthetic utility because of its operational simplicity and reasonable yields for certain ketone substrates.

The aminomethylation depicted in Eq. 1 seems to proceed *via* initial formation of methyleneiminium species **5** which is formed according to Eq. 2; upon

mixing pyrrolidine with CH_2ClI in DMSO-d_6, a new ^1H NMR absorption signal appeared at δ 8.8 (broad), which may be assigned to methylene protons of the iminium species,[8] and the strength of which was reduced gradually on addition of propiophenone. The Mannich reaction of ketones by means of preformed methyleneiminium species such as $Me_2\overset{+}{N}=CH_2,\bar{X}$ has well been precedented in the last decade.[10]

$$R_2NH + CH_2XY \xrightarrow[-HY]{R_2NH} R_2N\text{-}CH_2X \longleftrightarrow \underset{\mathbf{5}}{R_2\overset{+}{N}=CH_2,\bar{X}} \quad (2)$$

Experimental

Materials and measurements were the same as those described in a previous paper.[1]

The aminomethylation reactions were conducted in essentially the same manner under nitrogen, and the reaction of diethyl ketone is illustrative. To a water-chilled, stirred solution of diethyl ketone (7.13 g, 82.8 mmol) and CH_2Br_2 (16.5 g, 94.9 mmol) in 90 ml of THF was added dropwise 13.7 g (193 mmol) of pyrrolidine in 10 ml THF; the mixture was heated under reflux for 3 h. The cooled reaction mixture was diluted with 100 ml of 2 M HCl.† Non-basic components were extracted with portions of cyclohexane. The aqueous phase was made alkaline with 10% NaOH, and basic products were extracted with ether (100 ml×3), washed successively with 1 M Na_2CO_3, brine, and water, and then dried over $MgSO_4$. Evaporation *in vacuo* of the solvents, unchanged pyrrolidine, and di(1-pyrrolidinyl)methane, which was formed by the reaction of pyrrolidine and CH_2Br_2, left 8.60 g of the crude Mannich base (61% yield). Trap-to-trap distillation of the residue gave a middle cut boiling at 65—70 °C/6 mmHg†† (**4e**, 7.45 g, 53% yield); IR (neat) 2780 and 1710 cm^{-1}; ^1H NMR (CCl_4, hexamethyldisiloxane) δ 0.7—1.2 (6H, 2× $-CH_3$), 1.4—2.0 (4H, $-CH_2-(C\underline{H}_2)_2-CH_2-$, m), and 2.0—2.8 (9H, m). Found (Calcd for $C_{10}H_{19}NO$): C, 71.06 (70.96); H, 11.45 (11.32); N, 8.58 (8.27)%.

4a: Bp ≈123 °C/3 mmHg; IR (neat) 2780 and 1680 cm^{-1}; MS *m/e* (%) 146 (M−*c*-$(CH_2)_4NH$, 31.1), 118 (10.1), 105 (28.8), and 77 (7.1).

4a': Bp 105—108 °C/2.2 mmHg; IR (neat) 2800 and 1680 cm^{-1}; MS *m/e* (%) 146 (M−Et_2NH, 12.0), 118 (7.8), 105 (38.9), and 77 (24.9).

4b: Bp 100—110 °C/1—1.5 mmHg; IR (neat) 2800 and 1690 cm^{-1}. Found (Calcd for $C_{13}H_{17}NO$): C, 76.78 (76.81); H, 8.42 (8.42); N, 6.86 (6.89)%.

4c: IR (neat) 2800 and 1680 cm^{-1}.

4d: Mp 98—99 °C; IR (KBr) 2780 and 1685 cm^{-1}. Found (Calcd for $C_{19}H_{21}NO$): C, 82.10 (81.68); H, 7.67 (7.58); N, 4.76 (5.01)%.

4e': Bp 42 °C/4 mmHg; IR (neat) 2800 and 1710 cm^{-1}. Found (Calcd for $C_{10}H_{21}NO$): C, 69.95 (70.12); H, 12.25 (12.36); N, 8.37 (8.18)%.

4f: Bp 69—70 °C/5—6 mmHg; IR (neat) 2780 and 1710 cm^{-1}. Found (Calcd for $C_{10}H_{19}NO$): C, 71.35 (70.96); H, 11.25 (11.31); N, 8.66 (8.28)%.

4h: Bp 61—64 °C/3—5 mmHg; IR (neat) 2780 and 1710 cm^{-1}; MS *m/e* (%) 181 (M^+, 1.4), 111 (11.7), 84 (58.4), 82 (7.0), and 67 (13.0).

4h': Bp 62 °C/2.5 mmHg; IR (neat) 2800 and 1710 cm^{-1}; MS *m/e* (%) 111 (11.7), 84 (7.0), and 67 (13.0).

4i: Bp 35—40 °C/1.5 mmHg; IR (neat) 2800 and 1725 cm^{-1}.

† 1 M=1 mol dm^{-3}.

†† 1 mmHg≈133.322 Pa.

References

1) Part III of this series describes the Mannich reaction of enol silyl ethers by a combination of CH_2ClI and *N,N,N',N'*-tetramethylmethanediamine: S. Miyano, H. Hokari, and H. Hashimoto, *Bull. Chem. Soc. Jpn.*, **55**, 534 (1982).

2) Part of this work was presented at the 42nd Autumn Annual Meeting of the Chemical Society of Japan, Sendai, 1980, Abstr. No. 1L13.

3) S. Miyano and H. Hashimoto, *Bull. Chem. Soc. Jpn.*, **46**, 892 (1973); S. Miyano, Y. Izumi, K. Fujii, Y. Ohno, and H. Hashimoto, *Bull. Chem. Soc. Jpn.*, **52**, 1197 (1979); S. Miyano, H. Hokari, Y. Umeda, and H. Hashimoto, *Bull. Chem. Soc. Jpn.*, **53**, 770 (1980).

4) For example, KOH-catalyzed reaction under phase-transfer catalysis conditions of RH with CH_2ClI resulted in the formation of $R\text{-}\dot{C}H_2\text{-}R$, where R-=PhĊHCN or Ph-CO-ĊHCH$_3$.

5) M. Tramontini, *Synthesis*, **1973**, 703; H, O. House, "Modern Synthetic Reactions," 2nd ed, W. A. Benjamin, Inc., California (1972), pp. 654—660; F. F. Blicke, *Org. React.*, **1**, 303 (1942).

6) For example, see footnote 13) in J. Hooz and J. N. Bridson, *J. Am. Chem. Soc.*, **95**, 602 (1973).

7) T. A. Bryson, G. H. Bonitz, C. J. Reichel, and R. E. Dardis, *J. Org. Chem.*, **45**, 524 (1980); N. Holy, R. Fowler, E. Burnett, and R. Lorenz, *Tetrahedron*, **35**, 613 (1979), and references cited therein.

8) ^1H NMR of methylene protons of $Me_2\overset{+}{N}=CH_2,\bar{I}$ appears at δ 8.2 in DMSO-d_6.[1,9] See also, "Iminium Salts in Organic Chemistry," ed by H. Böhme and H. G. Viehe, Wiley-Interscience, New York (1976), Part I, pp. 23—105.

9) J. Schreiber, H. Maag, N. Hashimoto, and A. Eschenmoser, *Angew. Chem.*, **83**, 355 (1971).

10) For example, Y. Jasor, M. Gaudry, M. J. Luche, and A. Marquet, *Tetrahedron*, **33**, 295 (1977).

Weathering of H_3BO_3-ZnO Bond for Forming Glass Fiber Reinforced Composite

Yoshikazu UTSUMI,* Tadaki MURAKAMI, and Isao ISHII
Mitsubishi Electric Corporation, 80 Nakano, Minami-shimizu, Amagasaki, Hyogo 661
(Received August 14, 1981)

Synopsis. H_3BO_3–ZnO bond stored in humidity above 75% causes the bending strength of a fiber reinforced composite to decrease. The lowering behavior corresponds to formation of $2ZnO \cdot 3B_2O_3 \cdot 7H_2O$ and to a decrease of H_3BO_3. The weathering of the bond is attributed to the decreasing of H_3BO_3, which becomes liquid during hot pressing.

A powder mixture of H_3BO_3 and ZnO can be used as a bond for forming a glass fiber reinforced composite with hot pressing and subsequent heat treatment.[1] Hot pressing at 170 °C makes the powder mixture melt and makes it penetrate into the spaces of the reinforcing elements. Heat treatment advances the reaction in the bond and makes the composite durable. However, long term storage of the mixture sometimes decreases its bonding power. The decreasing behavior resembles the weathering of portland cement.

This study deals with the cause of weathering in this H_3BO_3–ZnO bond.

Experimental

The bond was prepared with a powder mixture in 3 : 1 mole ratio of H_3BO_3 and ZnO. It was stored in various humidity atmospheres at 30 °C for 7 d. Humidities were kept constant with water vapor of saturated aqueous solutions of salts, which were KNO_3, KCl, NaCl, and $Mg(NO_3)_2 \cdot 6H_2O$ for 92, 84, 75, and 52%, and with drying silica gel for 0%. A composite was prepared from the stored powder and glass fiber mats with the composition of 40 wt% and 60 wt%. To form a composite, the powder layer and the glass layer were laminated one after the other and were pressed under 100 kg cm^{-2} at 170 °C. The pressure was sometimes taken away to eliminate excess water produced by dehydration of H_3BO_3. The composites were used for testing the bending strength. On the other hand, the crystal phases and their behavior in the stored bond were examined by X-ray diffraction and differential thermal analysis.

Results and Discussion

In forming a composite, the bonds which were stored in low humidity penetrated fully into the spaces of glass fiber mats, whereas those which were stored in high humidity penetrated only partly into the spaces. The test pieces for the bending strength were taken from a part of a composite into which the bond had penetrated. Figure 1 shows the relationship between bending strength of composites and storing humidity of bond. As shown in Fig. 1, there was no significant difference between the bending strength of a composite which was formed by the bond stored in 0% humidity and the bending strength of one which was formed by the bond immediately after mixing. Moreover, the bending strength was independent of storing humidity up to 75%. However, the storage of the bond in humidity above

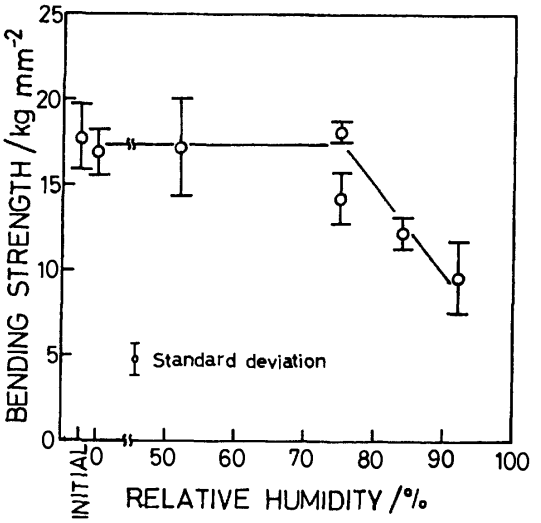

Fig. 1. Bending strength of composite formed with bond stored in various humidity.

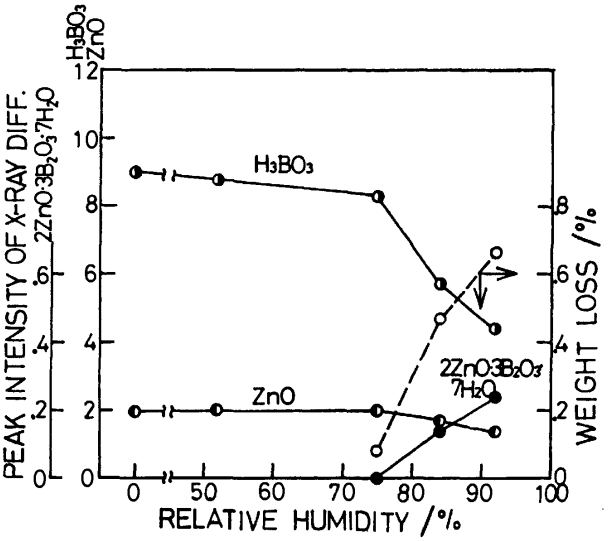

Fig. 2. Peak intensity of X-ray diffraction of crystal phases in bond stored in various humidity.

75% caused the bending strength to decrease.

The X-ray diffraction pattern of the bond immediately after mixing showed peaks of H_3BO_3 and ZnO crystals. However, the patterns showed that the bond stored in humid atmosphere contained not only H_3BO_3 and ZnO but also $2ZnO \cdot 3B_2O_3 \cdot 7H_2O$ crystal.[2,3]

The variation in each one of the diffraction peaks of H_3BO_3, ZnO, and $2ZnO \cdot 3B_2O_3 \cdot 7H_2O$ crystals is plotted as a function of storing humidity in Fig. 2. In humidity above 75%, H_3BO_3 was decreased in the bond and a new crystal of $2ZnO \cdot 3B_2O_3 \cdot 7H_2O$ was produced instead of H_3BO_3. The starting humidity of the decrease

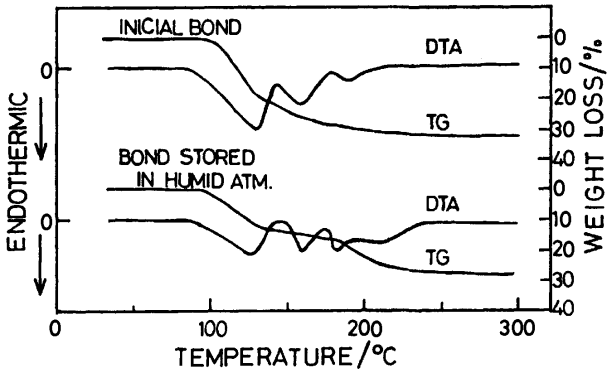

Fig. 3. DTA and TG of initial bond and of bond stored in 84% humidity.

or the production agrees with that of bending strength. Figure 2 also shows weight loss from the initial bond. The crystal $2ZnO \cdot 3B_2O_3 \cdot 7H_2O$ contains less water than the composition of initial bond, that is, $2ZnO \cdot 6H_3BO_3 = 2ZnO \cdot 3B_2O_3 \cdot 9H_2O$. The weight loss in Fig. 2 seems mainly to be water loss caused by production of the new crystal and partly to be H_3BO_3 loss due to its sublimation in humid atmosphere.[4]

Differential themal analysis of the bond is shown in Fig. 3. A broad peak appears from about 170 °C to 240 °C, omitting the three peaks of H_3BO_3 dehydration; this peak corresponds to dehydration of $2ZnO \cdot 3B_2O_3 \cdot 7H_2O$ crystal. The crystal became amorphous as a result of its dehydration. It seems to behave as a filler in a composite, because its dehydration temperature is rather higher than the hot pressing temperature. However, its production may somewhat obstruct the flow of the bonding liquid under hot pressing by bridging between ZnO particles. On the other hand, the decrease of H_3BO_3 causes the bonding liquid to decrease under hot pressing. H_3BO_3 considerably decreased as humidity increased above 75%, as shown in Fig. 2. Therefore the decreasing behavior of bending strength is attributed to H_3BO_3 decreasing in the bond due to the production of $2ZnO \cdot 3B_2O_3 \cdot 7H_2O$ crystals.

It is concluded that the decrease of H_3BO_3 in humid air gives rise to the weathering of the bond in the system $H_3BO_3 \cdot ZnO$.

References

1) Y. Utsumi, T. Murakami, and I. Ishii, *J. Am. Ceram. Soc.*, **64**, C-164 (1981).

2) H. A. Lehmann, K. Sperschneider, and G. Kessler, *Z. Anorg. Allg. Chem.*, **354**, 37 (1967).

3) J. M. Gallagher pointed out that pattern of $2ZnO \cdot 3B_2O_3 \cdot 7H_2O$ crystal in diffraction file 9-88, which is based on C. B. Tennant's data, published by JCPDS agrees with the pattern of H. A. Lehmann's paper,[2] although it is not in agreement with the diffraction file 21-1471 based on Lehmann's paper.

4) F. C. Kracek, G. W. Morey, and H. E. Merwin, *Am. J. Sci., 5th Ser. A*, **35**, 143 (1938).

 © 1982 The Chemical Society of Japan Bull. Chem. Soc. Jpn., 55, 1335—1339 (1982)

Conformational Change of Delta-chymotrypsin Caused by Sodium Dodecyl Sulfate as Studied by Stopped-flow Circular Dichroic Method

Kunio TAKEDA

Department of Applied-Chemistry, Faculty of Science, Okayama University of Science, 1-1 Ridai-cho, Okayama 700

(Received April 8, 1981)

The conformational change of delta-chymotrypsin was studied in a sodium dodecyl sulfate (SDS) solution containing 3.33 mmol/dm^3 NaH_2PO_4 and 3.56 mmol/dm^3 Na_2HPO_4 (pH 7.0, μ=0.014) by means of the circular dichroism (CD) and absorbance stopped-flow methods. The protein adopts a conformation with a higher helix content than the native state upon the addition of SDS. The rate of the conformational change strongly depends on the SDS concentration. The corresponding rate constant sharply increases in the range of 5—12 mmol/dm^3 SDS, indicating that the higher the helix content, the faster the coil to α-helix transition. The nature of the conformational change was examined by parallel measurements of the CD, the difference spectra, and the binding isotherm. As a result, it was concluded that, at a certain SDS concentration above 5 mmol/dm^3, the native conformation of the protein is directly transformed to another conformation without passing through any intermediate one which may be caused when the SDS concentration is below the one mentioned above.

Sodium dodecyl sulfate (SDS) is now widely used in the purification and characterization of proteins.[1] The interactions of surfactants with proteins *per se* are interesting enough, and so have been extensively investigated.[2,3] However, the kinetic aspects of the interactions have been little studied, although many kinetic studies have been done on the conformational changes of proteins induced by other agents.[4] As is well known, several proteins clearly adopt conformations with high helix contents than their native states upon the addition of anionic surfactants such as SDS.[5,6] This is in marked contrast with the denaturation processes induced by the other denaturants. In this work, delta-chymotrypsin has been used as an example of a protein which can be converted in part to the α-helical conformation. As is also well known, the conformation of protein in an aqueous solution can be more clearly detected by the circular dichroism (CD) measurements. Although a few CD stopped-flow studies of conformational changes of proteins have recently been carried out, most of them have been done in the visible and near-ultraviolet regions.[7–11] Since the ellipticity in the far-ultraviolet region reflects the change of the protein backbone structure, such kinetic studies should be done in this region as well. The present author wishes to report on the SDS-induced conformational change of the protein followed by means of the far-ultraviolet CD and the near-ultraviolet absorbance stopped-flow methods. The main purpose of this paper is to discuss the characteristic process of the conformational change of the protein in the presence of the surfactant.

Experimental

Crystalline delta-chymotrypsin from beef pancreas (MW: 25400) was obtained from Miles Laboratories. The SDS and the phosphate buffer used have been described in a previous paper.[12]

The CD measurements were carried out with a JASCO J-500A spectropolarimeter equipped with a JASCO DP-501 data processor. The details of CD and CD stopped-flow measurements have been stated elsewhere.[13] The absorbance stopped-flow measurements were made with a rapid mixer of a stopped-flow apparatus, RA-401 of Union Giken Co., combined with a single-beam spectrophotometer, Unispec A of the same company, the time constant of which was modified to be less than 1.0×10^{-3} s. The static measurements of the ultraviolet absorbance were made with a Hitachi double-beam spectrophotometer, Model 200-10.

The binding isotherm of SDS to the protein was obtained by the use of gel chromatography, as has been reported before.[12]

Throughout the experiments, the protein concentration was constant, 1.0×10^{-5} M (as a concentration unit, 1 M= 1 mol/dm^3 was used), and its solution was used within 6 hours after preparation. The spectra of the CD and the absorbance of the protein were measured within 5 min after mixing the solutions of the protein with those of SDS.

Results and Discussion

The SDS-induced conformational change of delta-chymotrypsin was studied primarily by observing the changes in the CD spectra in the far-ultraviolet region in order to make clear the changes of the backbone structure of the protein polypeptide. Figure 1 shows the typical CD spectra of the protein in the absence (I) and in the presence (II) of 20 mM SDS and the difference CD spectrum(III) between them. The difference CD spectrum clearly indicates an increase in the α-helix content upon the addition of SDS, as in the case of alpha-chymotrypsin.[6] The SDS concentration dependence of the residue ellipticity at 206 nm, $[\theta]_{206}$, is shown in Fig. 2. The value of $[\theta]_{206}$ sharply increases at first and then attains a plateau at about 12 mM SDS, indicating that the helix content of the protein increases in such a concentration range of SDS.

Figure 3 shows the effect of added SDS on the absorbance spectra of delta-chymotrypsin. It is well known that the denaturation blue shift observed here is attributable to the exposure of chromophores, such as tryptophan and tyrosine, to an aqueous environment (the protein contains 9 tryptophan residues and 3 tyrosine ones). The difference spectrum of absorbance shows a blue shift and has a positive peak around 255 nm and a major negative peak at 295 nm. The SDS-induced difference absorption coefficient at 295 nm, $\Delta\varepsilon_{295}$, is plotted against SDS in Fig. 2. The

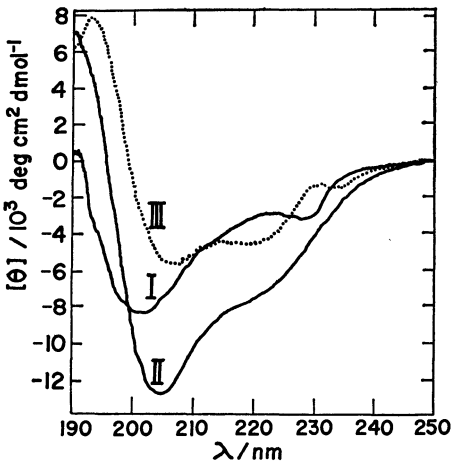

Fig. 1. Typical CD spectra of delta-chymotrypsin in the absence (curve I) and the presence (curve II) of 20 mM SDS and the difference CD spectrum between them (curve III) at 25 °C.
The difference spectrum was directly obtained by the use of the data processor. The concentration of the protein was 1.0×10^{-5} M. The thickness of cell used was 1.0 mm. These spectra are averaged over 8 repetitions.

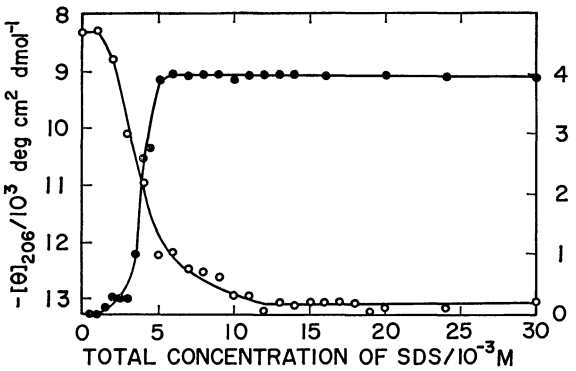

Fig. 2. The effects of total SDS concentration on the residue ellipticity at 206 nm, $[\theta]_{206}$ (○) and the difference absorption coefficient at 295 nm, $\Delta\varepsilon_{295}$ (●) at 25 °C.
The both values were obtained on the basis of the results at 1.0×10^{-5} M delta-chymotrypsin.

value of $\Delta\varepsilon_{295}$ increases just like that of $[\theta]_{206}$, but flattens out at a lower SDS concentration, 5 mM. Their importance will be referred to later in discussion of a reaction process and a transition state of the conformational change.

It is characteristic of the conformational change of a protein in a surfactant solution that large amounts of surfactant molecules bind to the protein. The binding isotherm of SDS to delta-chymotrypsin, as obtained by the gel chromatography, is shown in Fig. 4. The amounts of SDS bound to the protein (the protein concentration $=1.0\times10^{-5}$ M) are also plotted against the total SDS concentration (solid curve) in order to compare them with the total SDS concentration dependences of $[\theta]_{206}$ and $\Delta\varepsilon_{295}$. The amounts of SDS bound to the protein increase discontinuously at 1—2 and 4—5 mM of total SDS, and finally reach

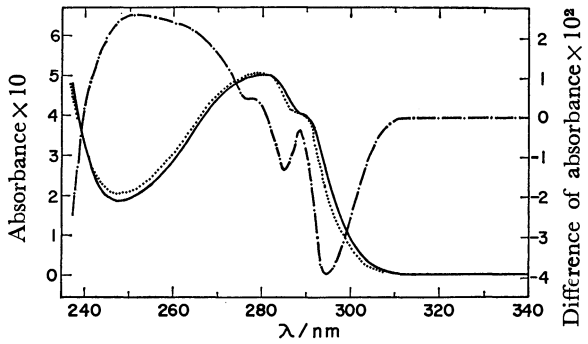

Fig. 3. Typical absorbance spectra of delta-chymotrypsin in the absence (solid curve) and the presence (dotted-curve) of 20 mM SDS and the difference spectrum of them (dot-dashed curve) at 25 °C.
The concentration of the protein was 1.0×10^{-5} M.

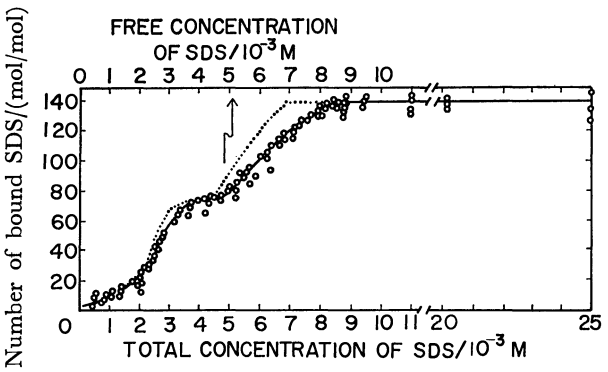

Fig. 4. Binding curve of SDS to delta-chymotrypsin *vs.* total concentration of SDS at 25 °C.
The dotted line indicates the binding isotherm plotted against free concentration of SDS. The total concentration of SDS was determined by the addition of the molar concentration of bound SDS per 1.0×10^{-5} M protein to its free concentration on the basis of the plot of number of bound SDS (mol/mol) *vs.* its free concentration.

a maximum, 140 mol of SDS per mole of the protein, in the vicinity of 8.5 mM SDS. This trend is the same as in the case of the system of SDS and bovine serum albumin.[12] We can approximately divide the binding curve into two stages, that is, the first binding stage of 70 mol of SDS per mole of the protein below 5 mM SDS and the second binding stage of a further 70 mol of SDS. In comparing the stepwise binding curve in Fig. 4 with the SDS concentration dependences of $[\theta]_{206}$ and $\Delta\varepsilon_{295}$, the exposure of chromophores to an aqueous environment completes in the first binding stage and the helix content also predominantly increases in this stage. The second binding of 70 mol of SDS can occur without a large-scale conformational change of the polypeptide chain.[14]

The CD stopped-flow measurements were carried out at 192 and 206 nm, where the positive and the negative maxima appeared in the difference spectrum of CD. The representative time courses of the conformational change are presented in Fig. 5. As is to be expected from the CD spectra in Fig. 1, the

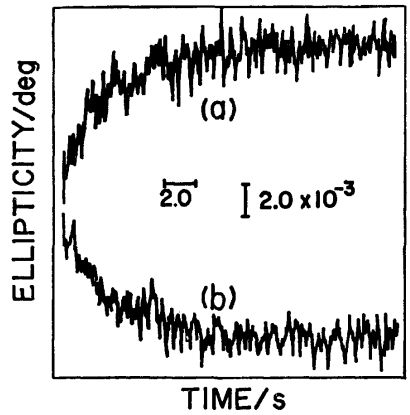

Fig. 5. Representative time courses of ellipticity changes at 192 (a) and 206 nm (b) at 25 °C.
The traces (a) and (b) are the averages of 32 and 2 repetitions, respectively. The final concentrations of SDS and delta-chymotrypsin were 20 mM and 1.0×10^{-5} M, respectively.

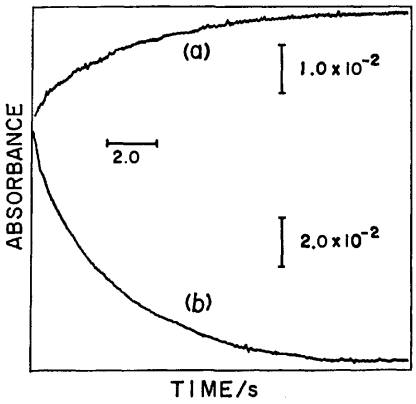

Fig. 6. Representative time courses of absorbance changes at 255 (a) and 295 nm (b) at 25 °C.
The experimental conditions were identical with those in Fig. 5.

ellipticity at 192 nm changed from the negative ellipticity to the positive one, while the negative ellipticity at 206 nm increased with time. The observed process, therefore, seems to correspond to an increase in the helix content. The absorbance stopped-flow measurements were made at 255 and 295 nm. The representative time courses are shown in Fig. 6. The directions of absorbance changes with time are in accordance with those expected from the difference spectrum of absorbance, as in the case of the CD stopped-flow measurements.

By the analysis of the curves shown in Figs. 5 and 6, the first-order rate constant, k, of the SDS-induced conformational change of the protein was obtained. The analysis was made by the ordinary treatment.[13] The magnitude of k is of the same order as those of the thermal denaturations of alpha-chymotrypsin[15] and lysozyme[16] and the denaturation of lysozyme by guanidine,[17] although the conformational changes caused by these agents are essentially different from that caused by SDS by which the helix content increases. The SDS concentration dependence of k is

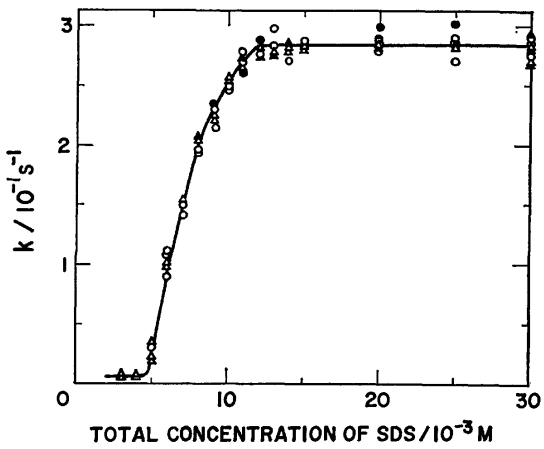

Fig. 7. Plot of rate constant, k *vs.* total concentration of SDS at 25 °C.
The values of k were obtained from time courses of ellipticity changes at 195 (●) and 206 nm (○), and those of absorbance changes at 255 (▲) and 295 nm (△).

presented in Fig. 7. It is noticeable that the same values of k are obtained, irrespective of the method of detection, and that the behavior of chromophores is useful in following the conformational changes of the protein. The rate constant, k, begins to increase around 5 mM, reaching a constant value around 12 mM SDS. The sharp increase of the rate constant in the range of 5—12 mM SDS indicates that the higher the helix content, the faster the rate of coil to α-helix transition. The rate constant, k, is independent of the SDS concentration in the range below 5 mM,[18] where the values of $[\theta]_{206}$ and $\Delta\varepsilon_{295}$ change as is shown in Fig. 2. Thus, the discussion given below will be limited to the conformational change in the range of SDS concentrations above 5 mM.

It is expected that the binding ratio of surfactants to protein determines the conformation of the surfactant-protein complex. In reference to the results of the interactions of bovine serum albumin with some ionic surfactants,[3,19–24] there may be some limited particular binding ratios (surfactants/protein) in the present system. Therefore, the following process may be easily assumed for the complex formation and the accompanying conformational change:

$$P_0 \xrightarrow{a_1 S} \cdots \rightarrow P_x S_l \xrightarrow{a_2 S} P_y S_m \rightarrow \cdots \xrightarrow{a_i S} P_z S_n \qquad (1)$$

where P_0 is the native protein, S is the surfactant molecule, a_i is a particular number, and $\cdots P_xS_l$ and $P_yS_m \cdots P_zS_n$ denote the complexes (the helix content increases in the order $\cdots$ x, y, $\cdots$ z; the binding number of surfactants, $70 \leqq l < m < \cdots < n$). The reaction model (1) indicates that the longest time is required for the transition from P_0 to P_zS_n with the highest helix content. However, the transition rate becomes faster as the final helix content increases as seen in Fig. 7. On the other hand, with reference to many results of micellization kinetics,[25] the binding rate of

SDS to a protein seems to be rapid compared to the time range of the conformational change, since it should be of approximately the same order as the time of the association of surfactant molecules in a micelle formation. This suggests that the protein cannot adopt various different conformations as reaction intermediates in the presence of a certain quantity of SDS, because they would rapidly bind to the protein, causing the transition only to a particular conformation of the protein. The features of the conformational change may be drawn schematically as follows,

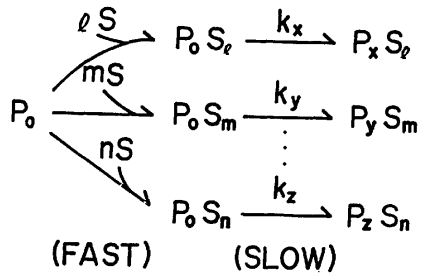

(2)

where k_x, k_y, and k_z denote rate constants of the corresponding processes ($\cdots k_x < k_y < \cdots < k_z$). This reaction model means that the binding of the surfactants completes before the conformational change of the native protein is completed. The conformation of the protein polypeptide must change together with many of the surfactant molecules bound to it. Through the particular conformational change of the protein polypeptide, the bound surfactants must be rearranged; that is, they may be forced to move from the initial binding sites to more favorable ones. Through this process, the bulky hydrophobic groups of the surfactant should come into maximum contact with the hydrophobic parts of the polypeptide, reconciling with the structure formation to reach a minimal free energy. Reaction 2 seems to be more suitable as an explanation of the present kinetic results, although Reaction 1 may be favorable for an understanding of the growth of the complex. Reaction 2 is also reminiscent of conformational changes of poly(L-lysine) in an octyl sulfate solution: the polypeptide, which adopts a disordered structure in the absence of the surfactant, takes an α-helix and a β-structure at low and high concentrations of the surfactant respectively, but the disordered structure of the polypeptide directly turns to the β-structure.[13] The author considers that, at a certain SDS concentration above 5 mM, the native conformation of the protein is directly transformed into another conformation without passing through any intermediate conformation such as may be caused when the SDS concentration is below the one mentioned above.

The temperature dependence of k was examined at 20 mM SDS in order to evaluate the activation parameters of the corresponding conformational change. Table 1 shows the temperature dependence of k and the activation parameters, ΔH^* and ΔS^*, of the process evaluated in a usual manner.[26] In the case of the conformational change induced by the surfactant, the entropic contributions must be due not only to the folding and unfolding of the polypeptide chain, but also to the rearrangement of the surfactant molecules bound to the polypeptide and the solvent-ordering process around the hydrophobic groups of the surfactant molecule exposed to an aqueous environment. The latter two contributions must be negative. If the new ordered structure is merely added to the original structure of the native protein, the value of ΔS must be negative, while that of ΔS^* may also be negative. However, the observed value of ΔS^* is positive and large. It is interesting to compare the present results with the activation parameters of the conformational change of lysozyme caused by other agents.[16,17] The values of ΔH^* and ΔS^* are similar to those of the unfolding process of the lysozyme. It may be noted here that the value of ΔS^* in the present study is similar to that of the conformational change in which the ordered structure decreases. As has been mentioned above, the helix content increases through the conformational change caused by SDS, while the degree of exposure of chromophores becomes greater in the denatured conformation than in the native one. Subsequently, the polypeptide chains must have been partially refolded in the transition process; that is, part of the polypeptide chains must have been unfolded, followed by a continuous refolding together with the bound surfactants in the transition process. As a result of the conformational change of the protein, more chromophores are exposed to the aqueous environment in the denatured state than in the native one. Therefore, the degree of unfolding becomes significant in the transition state relative to the native state, and the value of ΔS^* may reflect such a large-scale conformational change of the complex.

Table 1. KINETIC PARAMETERS OF CONFORMATIONAL CHANGE OF DELTA-CHYMOTRYPSIN BY SDS

Temperature/°C	15	20	25	30	35
$k/10^{-1}\,s^{-1}$ a)	0.40	0.85	2.9	7.0	15
ΔH^*/kJ mol^{-1}			140		
ΔS^*/J K^{-1} mol^{-1}			160		

a) These values were calculated from the results at 1.0×10^{-5} M protein and 20 mM SDS.

Further studies comparing the kinetic parameters of the same conformational change of proteins similar to the protein used here are in progress and will be reported in due course.

This work was partly supported by a Grant-in-Aid for Scientific Research No. 374149 from the Ministry of Education, Science and Culture of Japan.

References

1) T. V. Waehneldt, *Biosystems*, **6**, 176 (1975).
2) C. Tanford, *Adv. Protein Chem.*, **23**, 213 (1968).
3) J. Steinhardt and J. A. Reynolds, "Multiple Equilibria in Protein," Academic Press, New York (1969), pp. 239—302.
4) R. L. Baldwin and T. E. Creighton, "Protein Folding (Proc. Conf. Ger. Biochem. Soc., 28th, 1979)," ed by R.

Jaenicke, Elsevier, Amsterdam (1980), pp. 217—260.
5) B. Jirgensons, *J. Biol. Chem.*, **242**, 912 (1967).
6) A. H. Hunt and B. Jirgensons, *Biochemistry*, **12**, 4435 (1973).
7) P. M. Bayley and M. Anson, *Biopolymers*, **13**, 401 (1974).
8) K. Nitta, T. Segawa, K. Kuwajima, and S. Sugai, *Biopolymers*, **16**, 703 (1977).
9) I. Tabushi, K. Yamamura, and Y. Nishiya, *Tetrahedron Lett.*, **49**, 4921 (1978).
10) J. Luchins and S. Beychok, *Science*, **199**, 427 (1978).
11) Y. Sano and H. Inoue, *Chem. Lett.*, **1979**, 1087.
12) K. Takeda, M. Miura, and T. Takagi, *J. Colloid Interface Sci.*, **82**, 38 (1981).
13) K. Takeda, A. Iba, and K. Shirahama, *Bull. Chem. Soc. Jpn.*, **54**, 1793 (1981).
14) Although the binding is visually saturated around 8.5 mM SDS in Fig. 4, it may be expected that the amounts of bound SDS will continue to increase up to the total SDS concentration at which $[\theta]_{206}$ reaches a constant value.
15) F. M. Pohl, *Eur. J. Biochem.*, **4**, 373 (1968).
16) S. Segawa, Y. Husimi, and A. Wada, *Biopolymers*, **12**, 2521 (1973).
17) C. Tanford, R. H. Pain, and N. S. Otchin, *J. Mol. Biol.*, **15**, 489 (1966).
18) The enzymic activity of the delta-chymotrypsin completely disappears below 5 mM SDS (K. Takeda and Y. Mikane, unpublished data). The mechanism of the conformational change in the low concentration range of SDS will be discussed in the future.
19) M. J. Pallansch and D. R. Briggs, *J. Am. Chem. Soc.*, **76**, 1396 (1954).
20) K. Aoki and J. F. Foster, *J. Am. Chem. Soc.*, **79**, 3385 (1957).
21) K. Aoki, *J. Am. Chem. Soc.*, **80**, 4904 (1958).
22) R. V. Decker and J. F. Foster, *Biochemistry*, **5**, 1242 (1966).
23) R. V. Decker and J. F. Foster, *J. Biol. Chem.*, **242**, 1526 (1967).
24) J. Oakes, *J. Chem. Soc., Faraday Trans. 1*, **70**, 2200 (1974).
25) N. Muller, "Solution Chemistry of Surfactants," ed by K. L. Mittal, Plenum Press, New York (1979), Vol. 1, pp. 267—295.
26) S. Glasstone, K. J. Laidler, and H. Eyring, "The Theory of Rate Processes," McGraw-Hill, New York (1941).

A Temperature-dependent Desorption Process of Molecular Ions in Field Desorption Mass Spectrometry

Hiroaki SHIRAISHI,* Akira OTSUKI, and Keiichiro FUWA

Department of Chemistry and Physics, National Institute for Environmental Studies, Yatabe, Ibaraki 305

(Received April 17, 1981)

A temperature dependent desorption process of molecular ions operating in field desorption mass spectrometry (FDMS) was examined by means of measurements of desorption rates using cholesterol, stearic acid, and poly(oxyethylene) nonylphenyl ether. The desorption of ions formed under high electric field followed the first order kinetics. The desorption rate constants were measured at several emitter currents, and apparent activation energies for the desorption of molecular ions were calculated. A mass transfer process operating in FDMS is discussed.

Field desorption mass spectrometry (FDMS) has been successfully applied for various qualitative and quantitative analyses of organic compounds in many kinds of samples during the last several years.[1] In this technique, an activated emitter of 10 μm diameter tungsten wire covered with carbon microneedles is commonly employed in order to attain the high electric field essential to the ionization. The desorption of ions from the emitter is often assisted with heating by passing current through the emitter. Thus, the emitter temperature can strongly influence the FD mass spectra which are obtained.

Several types of emitter current programmers have been developed to control the emitter temperature.[2-4] Further detailed study for the temperature dependence of FD mass spectra is needed by use of these programmers in order to understand the picture of the FD process. A simple model for sample supply to activation sites of a tip emitter by field-enhanced surface diffusion from large reservoirs of adsorbed molecules on the shank of the tip has been proposed by Beckey *et al.*[5] in order to explain the results from angular distribution studies, and was supported by Cocke *et al.*[6] But, Holland *et al.* reported that the electric field has little effect on mass transfer from the activated emitter and proposed a model for the FD process which was later argued against by Beckey and Röllgen.[8] The uncertainty in the picture of the processes operaing in conventional FDMS may arise from the use of an activated emitter with many activated points under different field strengths and different temperatures.

This paper describes the temperature dependence of the field desorption process of molecular ions and the effect of high electric field on mass transfer operating in conventional FDMS.

Experimental

Mass spectrometry was performed on a JEOL JMS O1-SG double focusing mass spectrometer with a combined field desorption/field ionization/ electron impact ion source, connected to JMS-2000 mass data analysis system (Japan Electric and Optics Laboratory). The FD emitter used was 10 μm tungsten wire with carbon needles grown at high temperature.[9] An anode potential of 10 kV and cathode potential of −3 kV were applied. Emitter current was controlled by use of a modified emitter current programmer. The emitter was loaded with samples from a stock solution (1 μg/μl) using a dipping technique. Sample loading by dipping resulted in more reproducible determination of the desorption rate constants than that by microsyringe technique. Initial focusing was done on acetone introduced *via* the batch inlet, and finally using an FD ion of a sample at room temperature. A profile of FD ion current was measured by single ion monitoring. Ion current was integrated for every 0.2 s and stored in a computer. The mass chromatogram of poly(oxyethylene) nonylphenyl ether was measured by repetitive magnet scanning at an interval of 10 s. After measurement of each sample, the emitter current was increased to 60 mA in order to clean the emitter.

The emitter current-emitter temperature relationship was obtained in the following manner. An emitter was introduced into an electrically heated air bath, and its resistance was measured by means of an LCR meter (Yokokawa, Hewlett-Packard; model 4216A). Then the same emitter was introduced in an ion source and heated by passing direct current through it; the applied potential was measured by means of a voltmeter. Resistance was calculated according to the equation $R=V/I$.

All chemicals supplied by Wako Pure Chemical Industries, Ldt. were used without further purification.

Results and Discussion

Generation of many types of ions, such as molecular ion(M^+), protonated and cationated molecular ion ($(M+H)^+$, $(M+\text{cation})^+$), cluster ion ($(nM+H)^+$, multiple charged ion (M^{n+}, $(M+nH)^{n+}$), and fragment ion, make it difficult to investigate the mechanism of ion formation and desorption in FDMS. In order to simplify the mechanism of ion formation and desorption, typical samples, which give only molecular ions in their FD mass spectra, were used in the present study.

When the emitter current was kept constant during the measurement, the intensity of molecular ions was observed to decrease exponentially with time, as shown in Fig. 1. If the desorption process of ions formed under high electric field follows the following equation at a constant temperature:

$$C_t = C_0 e^{-kt},$$

C_t: Amount of neutral material to be ionized (or ions) remaining on the emitter at time t.

C_0: Initial amount of neutral material to be ionized (or ions) remaining on the emitter at time, 0.

k: First order rate constant (desorption rate constant).

a plot $\log[C_t]$ against time should give a linear relation.

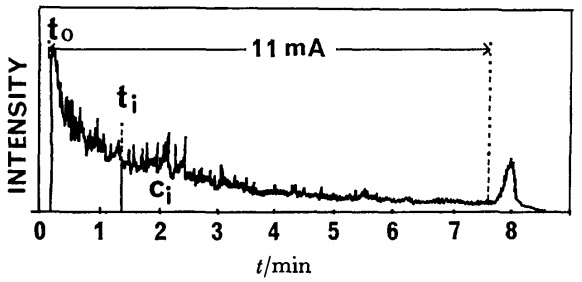

Fig. 1. Ion current profile for molecular ion of cholesterol (m/z 386) at 11 mA followed by linear increase in emitter current.

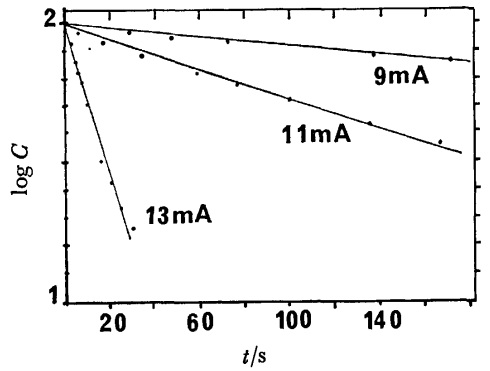

Fig. 2. log[C_t]-time plot for molecular ion of cholesterol (m/z 386) at 9, 11, and 13 mA.

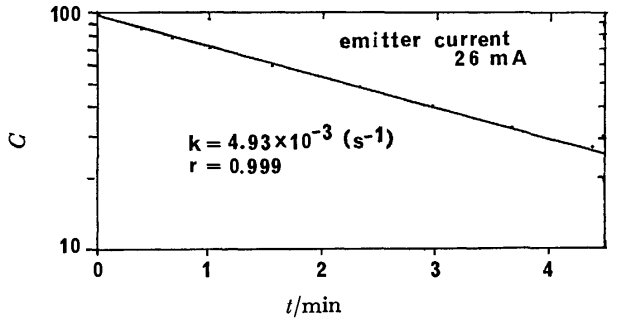

Fig. 3. log[C_t]-time plot for lithium ion attached molecular ion of lithium iodide (Li_2I^+, m/z 141) at 26 mA.

Figures 2 and 3 show log[C_t]-time plots for molecular ions of cholesterol at three different emitter currents and lithium-ion-attached molecular ion of lithium iodide (m/z 141) at 26 mA in emitter current, respectively. These results indicate that the desorption process of ions from the activated emitter at high electric field follows the first order kinetics. Table 1 shows first order rate constants for desorption of poly(oxyethylene) nonylphenyl ether containing different degrees of polymerization of ethylene oxide, calculated from each slope in the log[C_t]-time plots. Rate constants of lower molecular weight components have larger values than those of higher molecular weight components, and rate constants of each component are larger at higher emitter current than at lower emitter current. These results are consistent with the fact that fractional desorption occurs during increase in emitter current when a mixture is analyzed, permiting the analysis of a mixture under controlled conditions of emitter current.[4]

Table 1. First order rate constants k for desorption of molecular ions of poly(oxyethylene) nonylphenyl ether

m/z	8 mA	10 mA	11 mA
396	6.11×10^{-3}	1.73×10^{-2}	5.37×10^{-2}
440	3.69×10^{-3}	8.11×10^{-3}	1.88×16^{-2}
484	2.66×10^{-3}	5.79×10^{-3}	1.00×10^{-2}

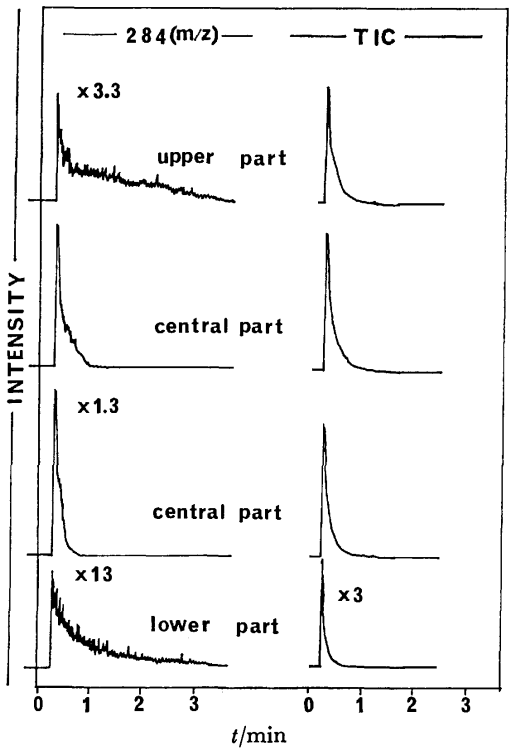

Fig. 4. Influnce of *axial* focus on ion current profile for molecular ion of stearic acid (m/z 284) at 10 mA. TIC (total ion current).

It was concluded from these results that desorption of ions formed under high electric field can be expressed as a first order reaction. Therefore, it is suggested that not only qualitative but also quantitative discussion about the fractional desorption should be done by use of desorption rate constants for each compound. However, it should be mentioned that these values given in Table 1 are relative because of uncertainty of the temperature gradient along the emitter wire and also along the carbon needles under the conditions used. Fugure 4 presents the evidence which suggests that a temperature gradient may be present in an activated emitter with 5 mm separation between the two supporting poles even if the emitter current is kept constant. In a Mattauch-Herzog type mass spectrometer, accelerated ions are focused by radial and axial foucs lens on the ion detector, but all widths of ion beam band desorbed from the 5 mm long emitter cannot be simultaneously focussed on the ion detector. Thus, one part of the ion beam band, usually the central part, is focussed on the ion detector by adjusting the axial foucs lens.

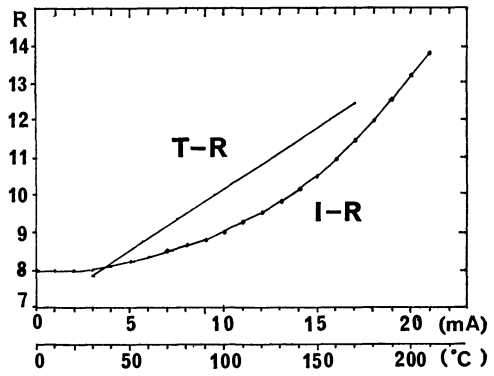

Fig. 5. Relations between emitter temperature and emitter resistance, and between emitter current and emitter resistance.

In Fig. 4, the molecular ion beam band of stearic acid was roughly divided into four parts: upper quarter, two central quarters, and lower quarter. Although similar profiles of the total ion current in each quarter were observed in every measurement, desorption profiles of the molecular ions from the two central parts of the emitter were different from the other two and the initial ion intensities were also much higher than those in the other two. These data would mean that there exists a temperature gradient on the activated emitter, and that the upper and lower parts near the two supporting poles were at a lower temperature than in the two central parts.

Since the average emitter temperature is one of the most important factors in the desorption process of ionization under high electric field, we tried to estimate the emitter temperature inside the ion source by a different way from that used in earlier papers on the estimation of emitter temperature.[10,11] Figure 5 shows a typical example of relations between emitter temperature and emitter resistance, and between emitter current and emitter resistance of 10 μm tungsten wire 5 mm long with carbon needles 20—30 μm in length. In this emitter, when the emitter current was adjusted to 9 mA, the emitter temperature was estimated to be about 65 °C with 9 Ω. The resistivity of tungsten varies as a function of temperature following the equation

$$R = R_0(1+\alpha\Delta T),$$

where $\alpha=0.0047\ K^{-1}$ is the temperature coefficient of resistivity. For the activated emitter, the tungsten wire is partially converted to tungsten carbide whose temperature coefficient of resistivity is $0.0049\ K^{-1}$.[12] The calculated coefficients of the activated emitters were in the range of about 0.0047 to 0.0050. The result indicated that each emitter has slightly different relations depending upon the length and number of carbon microneedles. Thus, the relations given in Fig. 5 may be used as a relative measure of the emitter temperature for the other emitters.

Using these relations, the apparent activation energy for desorption of ions formed under high electric field was obtained. Figure 6 shows an example of the Arrhenius plots (log k *vs.* $1/T$) for cholesterol and stearic acid. Apparent activation energies for the desorption of molecular ions of cholesterol and stearic acid at high electric field were calculated from the slopes to be 30 and 55 kcal/mol, respectively. The apparent activation energy obtained in the present study is not equivalent to that in field desorption, but may mean that required for an overall process of field desorption including migration of sample molecules to activation sites of carbon microneedles. Theoretically, the activation energy required for FD of ions under high electric field should be smaller than that for desorption of neutral molecules under no electric field.[13] These calculated values were apparently lower than the ionization potentials of both compounds, suggesting the importance of the electric field.

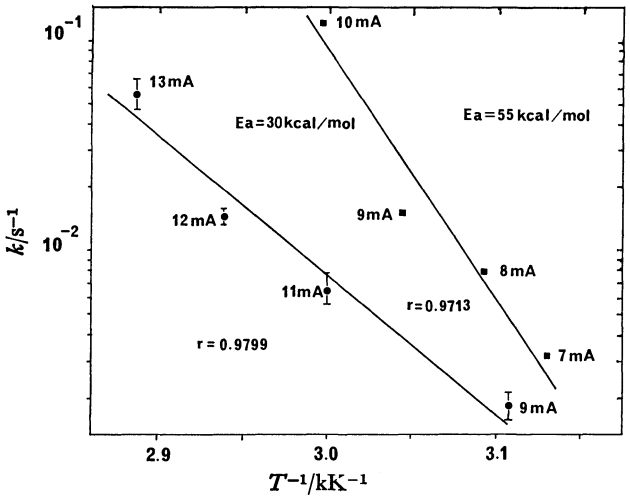

Fig. 6. $\log k - 1/T$ plot for desorption of molecular ions of cholesterol (●) and stearic acid (■).

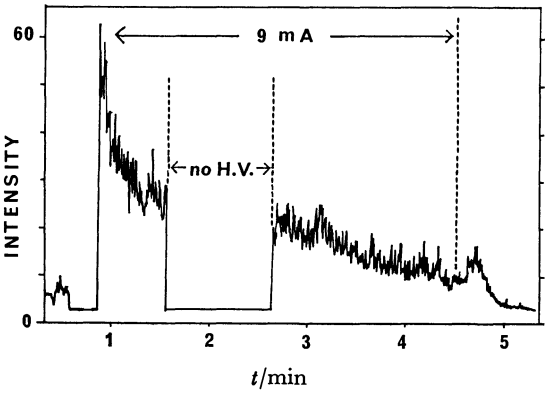

Fig. 7. Mass chromatogram of molecular ion of stearic acid measured at 9 mA followed by linear increase. High electric field was turned off for 1.5 to 2.7 min in the time course of measurement.

The fact that the desorption process follows the first order kinetics gives us the opportunity to investigate the role of high electric field for the desorption process. Figure 7 shows the mass chromatogram of molecular ions of stearic acid measured at 9 mA, followed by a linear increase. When the high electric field was turned off for 1.5 to 2.7 min in the time course of measurement, the molecular ion intensity was observed to become zero. Figure 8 shows the

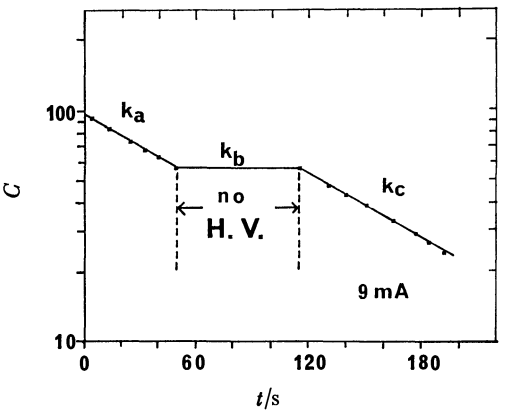

Fig. 8. log[C_t]-time plot for molecular ion of stearic acid, assuming that desorption of stearic acid did not occur under low electric field.

log [C_t]-time plot, assuming that desorption of stearic acid from the emitter under low electric field did not occur. As shown in Fig. 8, the desorption rate constant in the first stage was equal to that in the third stage when the high electric potentials were again applied. This result means that desorption of stearic acid under low electric field did not occur at 9 mA.

The same kind of experiment was carried out using cholesterol at 8 mA. It was found that the desorption rate of cholesterol under low electric field was nearly equal to that under high electric field. This result suggests that the desorption rate of cholesterol was little affected by the electric field. Similar field-independent desorption was reported by Holland *et al.*[7] and was explained on the basis of field ionization processes by Beckey and Röllgen, assuming the sample molecules to be evaporated before ionization takes place.[8] This means that the calculated apparent activation energy for desorption of cholesterol (30 kcal/mol) is mainly due to the heat of desorption of neutral molecules of cholesterol. Although there is no report on the heat of adsorption of stearic acid on the activated carbon surface, the fact that stearic acid was not desorbed at 9 mA under low field suggests that stearic acid having a carboxy group may be more strongly adsorbed on an emitter surface than cholesterol having a hydroxy group.

In conclusion, the present study indicated that desorption of ions formed under high electric field follows the first order kinetics, and that the desorption rate is temperature dependent.

References

1) H. D. Beckey, "Principle of Field Ionization and Field Desorption Mass Spectrometry," Pergamon Press, Oxford (1977).
2) H. R. Schulten and H. D. Beckey, *Cancer Treat. Rep.*, **60**, 501 (1976).
3) J. W. Maine, B. Soltmann, J. F. Holland, N. D. Young, J. N. Gerber, and C. C. Sweeley, *Anal. Chem.*, **48**, 427 (1976).
4) H. Shiraishi, A. Otsuki, and K. Fuwa, *Bull. Chem. Soc. Jpn.*, **52**, 2903 (1979).
5) H. D. Beckey, J. Dahmen, and H. Knöppel, *Z. Naturforsch., Teil A*, **21**, 141 (1966).
6) D. L. Cocke, G. Abent, and J. H. Block, *Int. J. Mass Spectrom. Ion Phys.*, **24**, 271 (1977).
7) J. F. Holland, B. Soltmann, and C. C. Sweeley, *Biomed. Mass Spectrom.* **3**, 340 (1976).
8) H. D. Beckey and F. W. Röllgen, *Org. Mass Spectrom.*, **14**, 188 (1979).
9) H. D. Beckey, E. Hilt, and H.-R. Schulten, *J. Phys. E: Sci. Instr.*, **6**, 1043 (1973).
10) H. U. Winkler and B. Linden, *Org. Mass Spectrom.*, **11**, 327 (1976).
11) D. Kümmler and H.-R. Schulten, *Org. Mass Spectrom.*, **10**, 813 (1975).
12) S. N. L'vov, M. I. Lesnaya, I. M. Vinitskii, and V. Ya Naumenko, *High Temp. (Engl. Transl.)*, **10**, 1196 (1972).
13) R. Gomer, *J. Chem. Phys.*, **31**, 341 (1959).

Solvation Effect on the Complex Formation between *o*-Quinones and Metal Chlorides in Nonaqueous Media

Kazuaki KATAOKA, Tatsuya TAKAGI, and Yoshio SASAKI*

Faculty of Pharmaceutical Sciences, Osaka University, Yamadaoka 1-6, Suita, Osaka 565

(Received April 22, 1981)

The complex formation of *o*-quinones with metal chlorides was studied by means of spectrophotometry in CH_3NO_2 and CH_3CN, where the metal chloride behaved as a nonelectrolyte. The results obtained in both solutions showed that the complex formation was obviously affected by the solvation of CH_3CN to the metal chloride. The participation of CH_3CN in the *o*-quinone–$ZnCl_2$ complex was assumed as a result of comparing the $\Delta\nu_{max}$ values, and the results obtained by NMR and spectrophotometry proved the coordination of two molecules of CH_3CN to the complex. The values of K_c in CH_3NO_2 increased in the order of $BiCl_3 < ZnCl_2$, whereas those in CH_3CN were in the reverse order; this fact was ascribed to the number of the solvent molecules liberated in the complex formation. The conventional elimination of the solvation effect from the observed K_c was proposed in order to obtain a parameter of solvation-free K_c.

o-Quinones have been reported to form intensively colored complexes with various kinds of metal halides.[1,2] An extensive study of these complexes was first carried out by Crowley and Haendler.[2] However, there have been few reports on the equilibrium of the complex formation of *o*-quinones with metal halides in solution. The complex between *o*-quinones and some metal chlorides has already been examined in CH_3NO_2 by spectroscopy,[3] where the metal chloride behaved as a nonelectrolyte and a correlation was observed between the stability constants, K_c, and the complex shifts, $\Delta\nu_{max}$ ($=\nu_{max}$ of the free ligand $-$ ν_{max} of its complex) or $\Delta\delta_{ML}$ ($=\delta_{ML}-\delta_L$), of the 1:1 complex. On the other hand, when CH_3CN is used as a solvent, the order of the increment of K_c's is not consistent with that in CH_3NO_2, particularly in the case of the *o*-quinone–$ZnCl_2$ complex. The coordination of CH_3CN is reasonable, since the donor strength of CH_3CN is larger than that of CH_3NO_2 (the donor numbers of CH_3CN and CH_3NO_2 are 14.1 and 2.7 respectively[4]). The purpose of this paper is to investigate the solvation for the *o*-quinone–$ZnCl_2$ complex in detail. In this work, cryptotanshinone and related compounds are used as the ligands, since some *o*-quinones having ether-type oxygen atoms form more stable complexes with metal chloride than does 1,2-naphthoquinone or 9,10-phenanthraquinone.[5]

Experimental

Materials. The cryptotanshinone(1,2,6,7,8,9-hexahydro-1,6,6-trimethylphenanthro[1,2-*b*]furan-10,11-dione) was isolated from the Chinese drug "Tan-shen" by the method of Takiura.[6] The 4,5-dimethoxy-1,2-benzoquinone and 4,5-diethoxy-1,2-benzoquinone were synthesized by the methods of Wanzlich and Jahnke.[7] Commercially available metal chlorides were purified by sublimation or distillation under reduced pressure. The CH_3CN was fractionally distilled from P_2O_5. The CH_3NO_2 and CH_2ClCH_2Cl were purified by distillation after drying on $CaCl_2$. The remaining water in the rectified solvents was checked by the measurement of the degree of the dissociation of the cryptotanshinone–$FeCl_3$ complex, which is liable to be decomposed by water;[5] the data were reproducible.

Procedures. In order to determine K_c, sample solutions containing a fixed overall concentration of the ligand and varying amounts of the metal chloride were prepared; stoppered cells were placed in a dry box under an N_2 atmosphere. The visible absorption spectra were measured on a Shimadzu UV-200 spectrophotometer at 25 or 34 °C. Changes in the absorbance by the complex formation were significant between 460 and 500 nm, and measurements of the absorbance were made at several wavelengths in this range. The K_c values of 1:1 complex formation were obtained by the curve-fitting method;[3] the root mean-square deviations of the absorbance were always within 0.003. The proton NMR spectra were measured in a Hitachi R-22 spectrometer (90 MHz) at 34 °C. The chemical shifts were determined by a frequency counter within an error of ± 0.1 Hz, relative to the internal reference, TMS. The molar conductances ($\Lambda/\Omega^{-1}\,mol^{-1}\,cm^2$) of millimolar solutions of the metal chlorides, measured at room temperature on a Kyoto Denshi CM-07 conductivity meter, were as follows; $ZnCl_2=1.7$ and $BlCl_3=2.4$ in CH_3NO_2, and $ZnCl_2=2.2$ and $BiCl_3=1.2$ in CH_3CN. The values of the molar conductances of complexes prepared by adding an excess amount of cryptotanshinone to the above solutions were essentially invariable.

Results and Discussion

Stability Constant and Complex Shift. The K_c and $\Delta\nu_{max}$ values on the complex formation between cryptotanshinone and $BiCl_3$ or $ZnCl_2$ in CH_3NO_2 and CH_3CN are listed in Table 1. The values of K_c in CH_3CN are smaller than those in CH_3NO_2; this is reasonable considering the donor strength of the two solvents. However, the order of K_c in CH_3CN differs from that in CH_3NO_2. A detailed discussion of this disagreement will be given below.

On the other hand, the values of $\Delta\nu_{max}$ are almost invariable with the solvent, but those of K_c are much

Table 1. The $\log K_c$ and $\Delta\nu_{max}$ values of the complex formation between cryptotanshinone and metal chlorides in two solvents at 25 °C

Solvent	MX_n	$\log(K_c/mol^{-1}\,dm^3)$	$\Delta\nu_{max}/10^3\,cm^{-1}$
CH_3NO_2	$ZnCl_2$	3.27 ± 0.03	3.68
	$BiCl_3$	2.63 ± 0.03	2.73
CH_3CN	$ZnCl_2$	0.83 ± 0.06	3.35
	$BiCl_3$	1.39 ± 0.03	3.00

ν_{max} of cryptotanshinone/$10^4\,cm^{-1}=2.273$ in CH_3NO_2, 2.304 in CH_3CN.

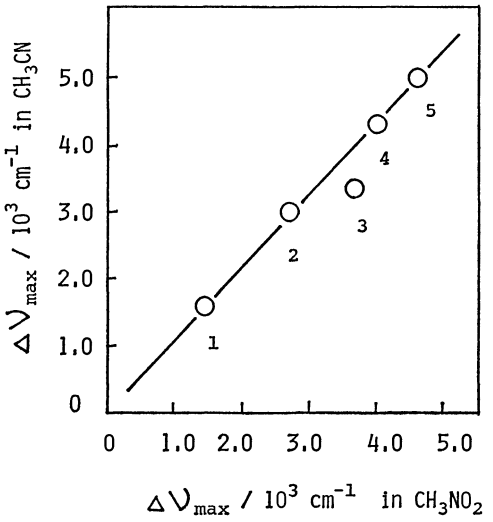

Fig. 1. Plot of $\Delta\nu_{max}$ of cryptotanshinone–MX_n complexes; CH_3CN *vs.* CH_3NO_2.
MX_n: 1; $HgCl_2$, 2; $BiCl_3$, 3; $ZnCl_2$, 4; $InCl_3$, 5; $SnCl_4$.

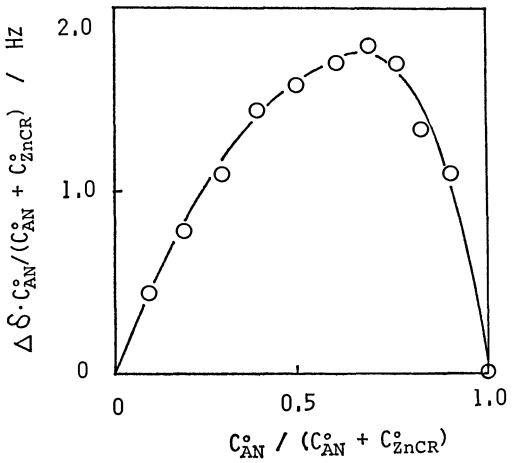

Fig. 2. Continuous variation method of cryptotanshinone–$ZnCl_2$+CH_3CN in 1,2-dichloroethane by NMR.
C°_{AN}: concn of CH_3CN, C°_{ZnCR}: concn of cryptotanshinone–$ZnCl_2$, $C^\circ_{AN}+C^\circ_{ZnCR}=0.13$ mol dm^{-3}, $\Delta\delta=\delta_{obsd}-\delta_{CH_3CN}$.

affected by the solvent. This fact suggests that $\Delta\nu_{max}$ does not depend on the donor strength of the solvent. A slope of *ca.* 1.0 was also given by plotting the values of $\Delta\nu_{max}$ in CH_3CN against those in CH_3NO_2, as shown in Fig. 1, where the plots of the $\Delta\nu_{max}$ values of other metal chlorides have been added. The value of the slope is consistent with the ratio of CH_3CN *vs.* CH_3NO_2 in the dielectric constant.

Participation of Solvent. The $\Delta\nu_{max}$ values of the cryptotanshinone–metal chloride complexes obtained in CH_3CN were of the same order as those obtained in CH_3NO_2. However, the plot of the $\Delta\nu_{max}$ values of the cryptotanshinone–$ZnCl_2$ complex deviated from the linear relation, as is shown in Fig. 1. This deviation should first be examined. Taking into account the complex formation of CH_3CN with $ZnCl_2$[8] or the reports[9,10] on the solvent participation in the complex, this deviation is probably to be ascribed to the coordination of the solvent molecules to the cryptotanshinone–$ZnCl_2$ complex in CH_3CN. The report on the Ni(II) complex[10] is cited as an example of the studies of the solvent participation, where the solvated species were estimated by the shift of the d-d transition band of the Ni(II) complex. In this work, however, the formation of the solvated species can not be confirmed by the method discribed above. Accordingly, the coordination of CH_3CN to the cryptotanshinone–$ZnCl_2$ complex was examined. In this work, CH_2ClCH_2Cl was used as a suitable solvent, since the cryptotanshinone–$ZnCl_2$ complex is sufficiently soluble in this solvent; in addition, the donor strength of CH_2ClCH_2Cl is very weak (*e.g.*, the donor number is 0[4]).

The chemical shifts of aromatic protons of the cryptotanshinone–$ZnCl_2$ complex, prepared by dissolving equimolar amounts of cryptotanshinone and $ZnCl_2$ in CH_2ClCH_2Cl, are concentration-independent in the range from 0.1 to 0.01 mol dm^{-3} of the complex. This suggests that cryptotanshinone and $ZnCl_2$ were almost transformed into the complex. It can therefore, be expected that the values of K_c of the cryptotanshinone–$ZnCl_2$ complex in CH_2ClCH_2Cl are very large. In order to obtain the number of CH_3CN coordinated, the continuous-variation method was performed by the NMR method. As is shown in Fig. 2, the results suggest that two molecules of CH_3CN take part in this equilibrium. In spite of the small displacement of the observed shift, the data were well reproduced. In addition, the molar conductance indicates that $ZnCl_2$ and the cryptotanshinone–$ZnCl_2$ complex in CH_3CN behave as nonelectrolytes. Accordingly, the above results lead to the following two equilibria, the addition type (Eq. 1) and the replacement type (Eq. 2):

$$CR\text{-}ZnCl_2 + 2CH_3CN \rightleftharpoons CR\text{-}ZnCl_2\text{-}2CH_3CN, \quad (1)$$

$$CR\text{-}ZnCl_2 + 2CH_3CN \rightleftharpoons CR + ZnCl_2\text{-}2CH_3CN, \quad (2)$$

where CR denotes cryptotanshinone. The possibility of Eq. 1 is a matter of concern in the present work, though the possibility of Eq. 2 will be estimated by considering the value of K_c of the cryptotanshinone–$ZnCl_2$ complex in CH_3CN.

The formation of solvated species was further examined by means of spectrophotometry. The change in the spectra of cryptotanshinone with $ZnCl_2$ in CH_2ClCH_2Cl having isosbestic points is shown in Fig. 3. When the concentration of CH_3CN increases gradually while the concentrations of cryptotanshinone and $ZnCl_2$ are held constant (*cf.* Fig. 3 IV), the absorption curves deviate from the isosbestic point, as is shown in Fig. 3 C. This fact suggests that the species containing cryptotanshinone, other than free cryptotanshinone and the cryptotanshinone–$ZnCl_2$ complex, are formed by the addition of CH_3CN. This result supports the priority of Eq. 1. In the case of the complex formation in CH_3CN, therefore, the cryptotanshinone–$ZnCl_2$ complex is almost completely transformed into the solvated species cryptotanshinone–$ZnCl_2$–$2CH_3CN$. On the other hand, the cryptotanshinone–$ZnCl_2$ complex is inert to CH_3NO_2.

It is well known that the partial charge on the metal

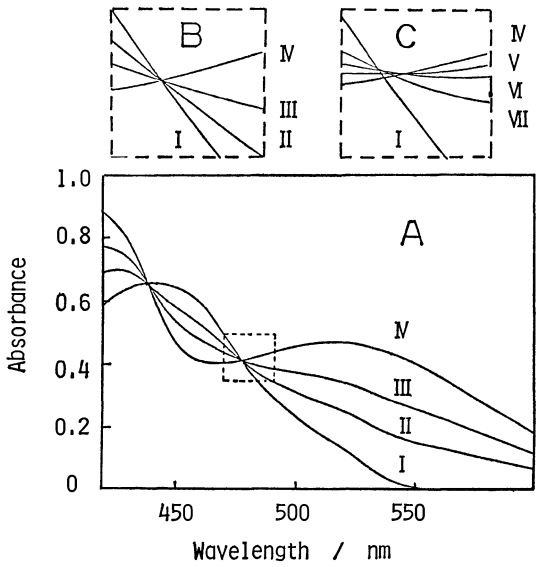

Fig. 3. Spectral change of cryptotanshinone with $ZnCl_2$ in 1,2-dichloroethane and the effect of CH_3CN. Concn of cryptotanshinone/mol dm^{-3}; 0.001 constant, concn of $ZnCl_2$/mol dm^{-3}: I; 0, II; 0.0003, III; 0.0006, IV—VII; 0.0009, concn of CH_3CN/mol dm^{-3}: I—IV; 0, V; 0.09, VI; 0.14, VII; 0.28. B and C are in the wavelength region surrounded by the dotted line in A.

atom of metal chloride is one of the factors controlling the complex formation.[3] The partial charges in the Zn of $ZnCl_2$ and $ZnCl_2$–$2CH_3CN$, as calculated by the method of Sanderson,[11] were 0.36 and 0.32 respectively. The decrease in the partial charge on the addition of CH_3CN (0.36→0.32) is consistent with the deviation of the plot of $\Delta\nu_{max}$ in the cryptotanshinone–$ZnCl_2$ complex (*cf.* Fig. 1). This fact also supports the presence of the solvated cryptotanshinone–$ZnCl_2$ complex in CH_3CN.

Number of Solvent Molecules Liberated in Complex Formation. In general, the complex formation in donor solvents is a replacement reaction, as is expressed by Eq. 3:

$$MS_m + L \overset{K_{obsd}}{\rightleftharpoons} MS_{m-n}L + nS, \quad (3)$$

where M, L, and S are the metal, the ligand, and the solvent, respectively. When $m=n$, K_{obsd} (the K_c of the complex formation is expressed by Eq. 3; *i.e.*, the K_c given in Table 1 corresponds to K_{obsd}) can be approximately expressed by Eq. 4, where K_{ML} and K_{MS} are the K_c's of the complex formation between M and L and between M and S in the inert solvents:

$$\log K_{obsd} = \log K_{ML} - \log K_{MS}. \quad (4)$$

In the complex formation of a given ligand with a series of metals, if $\log K_{MS} \ll \log K_{ML}$, or if the n's are constant in this series, K_{obsd} will be proportional to K_{ML}. That is, the increasing order of K_{obsd} agrees with that of K_{ML}. On the other hand, if the relative values of K_{MS} can not be ignored, and if the n's are variable between metals, the order of K_{obsd} probably disagrees with that of K_{ML}. In this work, the values of K_c in CH_3NO_2 increased in the order of $BiCl_3 < ZnCl_2$, whereas those in CH_3CN were in the reverse order. This disagreement in the order seems to be responsible for the difference of n. Accordingly, the values of n in the complex formation of cryptotanshinone with $ZnCl_2$ and $BiCl_3$ were examined.

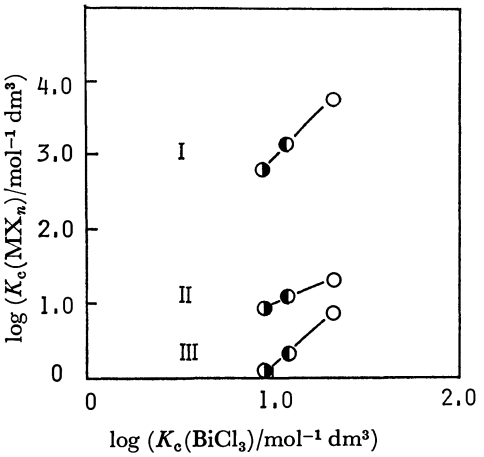

Fig. 4. Plots of $\log K_c$ of the complex formation of *o*-quinones with MX_n against that with $BiCl_3$ in CH_3CN.
MX_n: I; $InCl_3$, II; $BiCl_3$, III; $ZnCl_2$. *o*-Quinones: ○; cryptotanshinone, ◐; 4,5-diethoxy-1,2-benzoquinone, ◑; 4,5-dimethoxy-1,2-benzoquinone.

Formerly, a procedure for the determination of the number of solvent molecules liberated in the complex formation, utilizing the solubility equation and the solubility parameter,[13] was proposed by Tanaka.[12] In his work, $\log K_c$ is expressed in terms of the solubility parameter (δ) and the molar volume (V) as follows:

$$\log K_c = 0.43(V_M + V_L - V_{ML})\delta_S^2/RT + 0.86(V_M\delta_M + V_L\delta_L - V_{ML}\delta_{ML})\delta_S/RT + \text{constant}. \quad (5)$$

Equation 5 is modified to Eq. 6, providing $V_M+V_L-V_{ML}=nV_S$ and $\delta_{ML}=(V_M\delta_M+V_L\delta_L)/V_{ML}$:

$$\log K_c = 0.43\, nV_S\delta_S^2/RT + \text{constant}, \quad (6)$$

where n is the number of solvent molecules liberated in the complex formation. As two solvents were used in this work, n is given by solving two simultaneous equations for CH_3CN and CH_3NO_2; the values of δ_s are 11.9 and 12.6, while those of V_s are 52.9 and 54.0, respectively.[13] For $ZnCl_2$ and $BiCl_3$, the n values were 3.1 and 1.6 respectively. The calculated values of n are not integral: however, it is important that the value of n for $ZnCl_2$ is about twice that for $BiCl_3$.

In the case of the complex formation in CH_3NO_2, K_{MS} is negligible because of the weak donor strength of CH_3NO_2. It can be considered that there is no effect of the number of the liberated solvent molecule against the order of K_{obsd}. However, the donor strength of CH_3CN is strong, so K_{MS} could not be neglected. Therefore, it is estimated that the disagreement of the order of K_c among two solvents results from the difference in the number of the solvent molecule liberated in the complex formation.

Elimination of Solvation Effect. As was described in the previous section, it is evident that the order

Table 2. The $\log K_c$ and $\Delta\log K_c$ values of the complex formation between *o*-quinones and metal chlorides in CH_3CN at 34 °C

	$\log (K_c/\text{mol}^{-1}\,\text{dm}^3)$		$\Delta\log K_c$
	(a)	(b)	
$InCl_3$	3.15±0.04	2.81±0.04	0.34
$ZnCl_2$	0.34±0.04	0.08±0.04	0.26
$BiCl_3$	1.18±0.04	0.95±0.04	0.13

(a); 4,5-Diethoxy-1,2-benzoquinone, (b); 4,5-dimethoxy-1,2-benzoquinone, $\Delta\log K_c = \log K_c$ of (a) $-\log K_c$ of (b).

of K_c is very much affected by solvation, so information about solvation-free K_c is necessary in order to examine the acidity of metal chloride. However, the solubility of metal chloride inevitably requires donor solvents. As for the procedure for eliminating the term of solvation from an enthalpy of complex formation in donor solvents, ESP (Elimination of Solvation Procedure) has been proposed by Drago *et al.*[14] In ESP, the solvation term is cancelled by using a replacement reaction: A basic solvent is used to compare the donor strength of a series of bases, whereas an acidic solvent is used to compare the acceptor strength of a series of acids. In this work, a basic solvent is employed in order to compare the acceptor strength of a series of metal chlorides. ESP is not applicable as an intact whole, but the essentials of ESP are extended in this work. That is, the information of solvation-free K_c should be obtained from a comparison with $\Delta\log K_c$, given by subtracting the log K_c of ML′ from that of ML, where L and L′ are ligands with the same coordination geometry. On the other hand, to promote the quantitative accuracy, the slope a defined in Eq. 7 must be evaluated:

$$\log K_c \text{ of ML} = a \log K_c \text{ of M'L} + b. \quad (7)$$

The slope a indicates the relative value of the acidity of M to M′; it is given by the plots of log K_c of the complex formation of M and M′ with a series of ligands.

At first, the evaluation of a was attempted in CH_3CN. When M′ is $BiCl_3$, the a values of $InCl_3$, $ZnCl_2$, and $BiCl_3$ are 2.4, 2.0, and 1.0, respectively, as is shown in Fig. 4. This order of a was consistent with both the order of K_c in CH_3NO_2 and that of $\Delta\nu_{max}$ in the two solvents. For the sake of convenience, the values of $\Delta\log K_c$ can subsequently be compared with each other. The values of $\Delta\log K_c$ increased in the order of $BiCl_3 < ZnCl_2 < InCl_3$, as is shown in Table 2; this fact also supports the above results. Therefore, either $\Delta\log K_c$ or a is valid as a parameter of K_c without solvation.

References

1) K. H. Meyer, *Ber.*, **41**, 2568 (1908); J. Knox and H. R. Innes, *J. Chem. Soc.*, **105**, 1451 (1914); S. Patai, "The Chemistry of the Quinonoid Compounds," John Wiley and Sons, New York (1974).

2) P. J. Crowley and H. M. Haendler, *Inorg. Chem.*, **1**, 904 (1962).

3) K. Kataoka, S. Kimura, F. Shirakawa, and Y. Sasaki, *Bull. Chem. Soc. Jpn.*, **54**, 2237 (1981).

4) V. Gutmann and E. Wychera, *Inorg. Nucl. Chem. Lett.*, **2**, 257 (1966); V. Gutmann, *Coord. Chem. Rev.*, **18**, 225 (1976).

5) K. Takiura, K. Kataoka, and Y. Sasaki, *Chem. Pharm. Bull. (Tokyo)*, **25**, 2477 (1977).

6) K. Takiura, *Yakugaku Zasshi*, **61**, 475 (1941).

7) H. W. Wanzlich and V. Jahnke, *Chem. Ber.*, **101**, 3744 (1968).

8) J. C. Evans and G. Y. S. Lo, *Spectrochim. Acta*, **21**, 1033 (1965).

9) C. Floriani, R. Henzi, and F. Calderazzo, *J. Chem. Soc., Dalton Trans.*, **1972**, 2640.

10) Y. Fukuda, R. Morishita, and K. Sone, *Bull. Chem. Soc. Jpn*, **49**, 1017 (1976).

11) R. T. Sanderson, "Inorganic Chemistry," Reinhold Publishing Corp., New York (1967), p. 69.

12) M. Tanaka, *Z. Phys. Chem. N. F.*, **96**, 239 (1975).

13) J. H. Hildebrand, J. M. Pransnitz, and P. L. Scott, "Regular and Related Solutions," Van Nostrand Reinhold Co., New York (1970); A. F. M. Barton, *Chem. Rev.*, **75**, 731 (1975).

14) R. S. Drago, M. S. Nozari, and G. C. Vogel, *J. Am. Chem. Soc.*, **94**, 90 (1972); M. S. Nozari, C. D. Jensen, and R. S. Drago, *ibid.*, **95**, 3162 (1973).

Pressure Effect on Reaction Rate of Cycloaddition of Tetracyanoethylene with α-Methylstyrene in Some Aprotic Solvents

Hideaki Tsuzuki, Yasuhiro Uosaki, Masaru Nakahara,
Muneo Sasaki,* and Jiro Osugi

Department of Chemistry, Faculty of Science, Kyoto University, Kitashirakawa, Sakyo-ku, Kyoto 606

(Received May 22, 1981)

The high-pressure kinetic study of the title reaction was carried out at 25 °C up to 1500 bar in carbon tetrachloride, chloroform, 1,2-dichloroethane, and acetonitrile, taking into account the role of the EDA complex formation. The dipole moment at the transition state is as large as 8.5±0.5 debye by Kirkwood's electrostatic model. The solvent effect is also ascribable to the polarity change upon activation. The intrinsic volume of activation is −27±3 cm³/mol for the cycloadding process and −3.3±3 cm³/mol for the reverse reaction.

Styrene was believed to give only the electron-donor-acceptor(EDA) complex with tetracyanoethylene (TCNE) in nonaqueous solvents at the ambient pressure and temperature.[1] Thereafter it was found[2] that a species other than the EDA complex was accumulated sufficiently at pressure as high as several kilobars and that its reversible decomposition after pressure withdrawal could be retarded at temperature as low as 0 °C. This species was identified as the 1,4-cycloadduct from the ^{13}C NMR and other spectra.[2] Careful examination confirmed that not only styrene but some of its derivatives gave the 1,4-cycloadduct with TCNE even at 1 bar, coexisting with the EDA complexes.[2-5] α-Methylstyrene(MS) reacts with TCNE more rapidly than styrene in some alkyl halides as solvent at room temperature to give the 1,4-cycloadduct.[3,4]

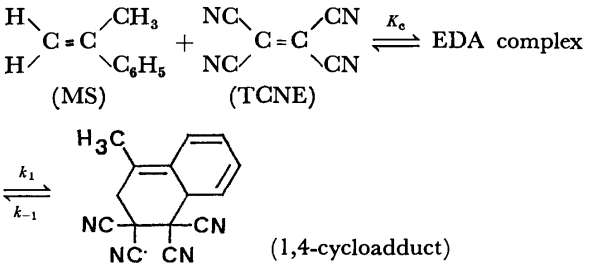

Scheme 1.

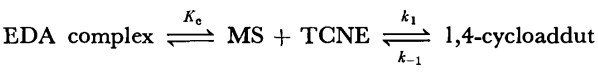

Scheme 2.

Whether the EDA complex is an intermediate of the reaction (Scheme 1) or it is formed only in a dead-end equilibrium (Scheme 2) is of interest. However, it is impossible to distinguish the two schemes only by a simple kinetic study. We reported previously[5] that the second-order rate constant for the forward process being denoted by k_f, the reaction constant of its Hammett plot for the para-substituted styrenes was as negative as −5.5±0.2. Moreover, a linear correlation was induced between $\log k_f$ and $\log K_c$; k_f increased with increasing equilibrium constant K_c for the EDA complex formation. The latter fact will support Scheme 1; otherwise the overall free energy of activation would not be correlated necessarily with the free energy change of the EDA complex formation. A similar scheme is presented for the reaction of TCNE with 9,10-dimethylanthracene,[6] in which the overall enthalpy of activation is negative. We have pointed out already the importance of the role of the EDA complex in the reaction between TCNE and enol ethers.[7]

Moreover the present reaction attracts much attention in a sense that unlike most [4+2] reactions the reaction rate depends significantly on solvent polarity.[3,4] This paper deals with the pressure and solvent effects on the reaction rate for the purpose of elucidating the transition state character. While a volume of activation, as a result of pressure effect on a reaction rate, is known to provide an important knowledge to understand a reaction mechanism,[8,9] the kinetic study on the thermal reaction faster than *ca.* half an hour has been hardly done at high pressure by a usual convenient method because it takes long time to attain the thermal equilibrium at a desired pressure after initiating the reaction. We could overcome the problem by developing a high pressure stopped-flow method.[10]

Experimental

Materials. All reagents were commercially obtained (Nakarai Chemicals Co. Ltd.). Tetracyanoethylene (TCNE) was sublimed three times *in vacuo* at 50—55 °C in the presence of active carbon, mp 200—201 °C. α-Methylstyrene (MS) was washed twice with slightly alkaline water and stored for 24 h over KOH. After being refluxed with CaH_2, it was distilled twice under a reduced pressure. Chloroform was treated with molecular sieves 5A, and then distilled twice just before use, bp 61—62 °C. Acetonitrile was refluxed with $NaHCO_3$ and P_2O_5, then distilled, bp 81—82 °C. Spectrograde 1,2-dichloroethane and carbon tetrachloride were used without further purification.

Kinetic Measurement. The rate of the cycloaddition was spectrophotometrically determined by following the absorbance of the 1,4-cycloadduct. At 1 bar (1 bar=0.1 MPa) was used a Shimadzu UV-200S spectrophotometer equipped with a rapid mixing apparatus(Union Giken MX 703). At high pressure the kinetic measurement was done by using a high-pressure stopped-flow apparatus up to 1500 bar,[10] the absorbance change being traced in the whole course of the reaction. The weighed-in concentration of MS was less than 0.2 mol/dm³ and that of TCNE was less than 1 mmol/dm³. In all cases the former was *ca.* 100 fold over the latter. Temperature was maintained at 25±0.2 °C by circulating the thermostated fluid around the high-pressure vessels.

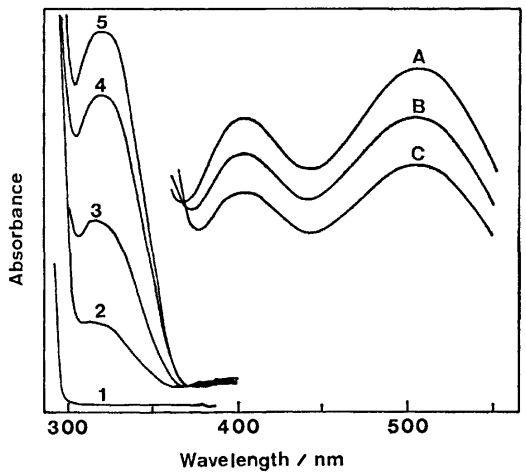

Fig. 1. Electronic spectra of the EDA complex (A—C, $[MS]_0=0.2$ mol/dm³, $[TCNE]_0=5$ mmol/dm³), and the 1,4-cycloadduct (2—5, $[MS]_0=0.1$ mol/dm³, $[TCNE]_0=1$ mmol/dm³) in chloroform at 1 bar at the following time/s after mixing.
A: 5, B: 90, C: 120, 1: TCNE, 2: 10, 3: 60, 4: 180, 5: 480.

Results and Discussion

The reaction mixture of TCNE and MS exhibited the increasing absorbance at 325 nm of the 1,4-cycloadduct with time, while the absorbances at 400 and 510 nm of the EDA complex decreased (Fig. 1); an isosbestic point appeared at 371 nm. When MS existed in large excess over TCNE, the rate of appearance of the adduct obeyed a first-order rate equation. Under the conditions that the EDA complex is always in equilibrium with TCNE and MS during the whole course of the reaction, we can represent the observed pseudo first-order rate constant k_{obsd} by Eq. 1 in terms of the rate and equilibrium constants as defined in Scheme 1:

$$k_{obsd} = \frac{k_1 K_c [D]_0}{1+K_c[D]_0} + k_{-1}, \quad (1)$$

where $[D]_0$ is the initial concentration of MS in molarity at a desired pressure. The correction of the weighed-in concentration for compression was made on the basis of the density data of Newitt *et al.*[11] for carbon tetrachloride, chloroform, and 1,2-dichloroethane, and of Srinivasan *et al.* for acetonitrile.[12] In chloroform and 1,2-dichloroethane where K_c was known even at high pressure,[13] the plot of k_{obsd} *vs.* $K_c[D]_0/(1+K_c[D]_0)$ was straight line to give k_1 and k_{-1} from the slope and the intercept, respectively (Fig. 2). In acetonitrile K_c being expected to be small enough, $1 \gg K_c[D]_0$, we obtain Eq. 2.

$$k_{obsd} = k_1 K_c [D]_0 + k_{-1}. \quad (2)$$

Hence, by the k_{obsd} *vs.* $[D]_0$ plot, $k_1 K_c$ and k_{-1} can be readily determined. In carbon tetrachloride in which K_c was unknown at high pressure, we first estimated k_{-1} at the region of $K_c[D]_0 \ll 1$, then obtained k_1 by

$$\frac{1}{k_{obsd}-k_{-1}} = \frac{1}{k_1 K_c [D]_0} + \frac{1}{k_1}. \quad (3)$$

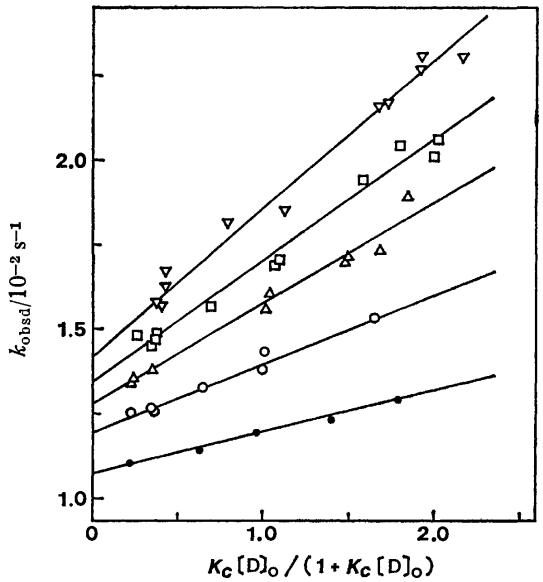

Fig. 2. Variation of k_{obsd} with $[D]_0$ according to Eq. 1 in chloroform at 25 °C.
●: 1 bar, ○: 250 bar, △: 500 bar, □: 750 bar, ▽: 1000 bar.

Table 1 shows the k_1 and k_{-1} values with K_c.

The volumes of activation ΔV_1^* for the step from the EDA complex to the 1,4-cycloadduct and ΔV_{-1}^* for the reverse one are calculated by the relation;

$$\Delta V^* = -RT\left(\frac{\partial \ln k}{\partial p}\right)_T, \quad (4)$$

where R, p, T, k, and ΔV^* are the gas constant, pressure, temperature, the rate constant(k_1 or k_{-1}) and the volume of activation(ΔV_1^* or ΔV_{-1}^*). The reaction volume ΔV_1 as calculated by $\Delta V_1^* - \Delta V_{-1}^*$ coincides with that by the equilibrium study.[13] In acetonitrile, K_c and k_1 are not reliable enough for the reaction volume associated with the EDA complex formation, ΔV_c, and ΔV_1^* to be recorded. If the volume of activation reflected only the structural change upon activation, the present value of ΔV_{-1}^* should be positive. It is worthy to note that ΔV_{-1}^* is negative in any solvent, since the volume decreases even for a bond-breaking process. As a consequence, in this case we are enforced to consider the electrostatic solvation in the transition state.

The solvent effect in which the electrostatic interaction plays an important role is sometimes successfully explained with Kirkwood's model,[14] which leads to Eq. 5 for the rate constants. Since the change of μ^2/r^3 terms with pressure is negligible up to a few kilobars compared to that of q, the volume of activation is represented by Eq. 6.

$$\ln k_1 = \ln k_{0(1)} + \frac{N}{RT}\left(\frac{\mu_*^2}{r_*^3} - \frac{\mu_{EDA}^2}{r_{EDA}^3}\right)q \quad (5a)$$

$$\ln k_{-1} = \ln k_{0(-1)} + \frac{N}{RT}\left(\frac{\mu_*^2}{r_*^3} - \frac{\mu_P^2}{r_P^3}\right)q \quad (5b)$$

$$\Delta V_1^* = \Delta V_{0(1)}^* - N\left(\frac{\mu^{*2}}{r^{*3}} - \frac{\mu_{EDA}^2}{r_{EDA}^3}\right)\left(\frac{\partial q}{\partial p}\right)_T \quad (6a)$$

$$\Delta V_{-1}^* = \Delta V_{0(-1)}^* - N\left(\frac{\mu_*^2}{r_*^3} - \frac{\mu_P^2}{r_P^3}\right)\left(\frac{\partial q}{\partial p}\right)_T \quad (6b)$$

Table 1. Rate and equilibrium constants at 25 °C

Solvent	Pressure / bar	K_c / dm³ mol⁻¹	k_1 / 10^{-2} s⁻¹	k_{-1} / 10^{-3} s⁻¹	$k_c k_1$ / 10^{-2} dm³ mol⁻¹ s⁻¹
CCl_4	1	1.39	0.130	0.861	0.180
	200		0.172	1.03	0.245
	400		0.198	1.15	0.296
	600		0.252	1.24	0.408
	800		0.329	1.34	0.583
$CHCl_3$	1	0.422	2.80	6.50	1.18
	200	0.430	6.70	6.88	2.88
	400	0.435	8.32	7.30	3.17
	500	0.438	9.86	7.57	4.32
	600	0.441	10.8	8.00	4.76
	1000	0.452	14.6	8.86	6.60
	1500	0.466	21.4	9.88	9.97
$ClCH_2CH_2Cl$	1	0.094	12.5	10.7	1.19
	250	0.098	22.3	11.9	2.19
	500	0.100	30.0	12.8	3.00
	750	0.103	35.3	13.5	3.64
	1000	0.109	44.5	14.2	4.85
CH_3CN	1			37.5	0.7
	200			41.2	1.1
	400			43.4	2.0
	600			47.0	1.1
	800			49.7	1.4

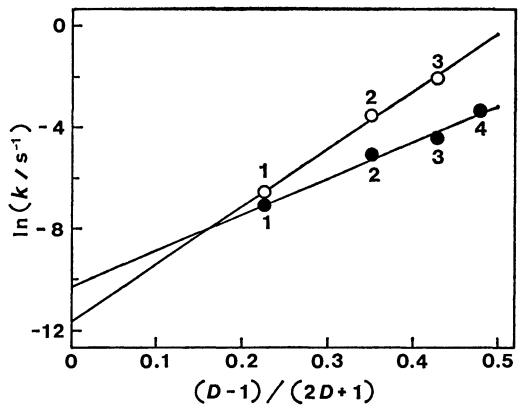

Fig. 3. Variation of k_1 (○) and k_{-1} (●) with the solvent dielectric constant parameter (Eq. 5).
1: Carbon tetrachloride, 2: chloroform, 3: 1,2-dichloroethane, 4: acetonitrile.

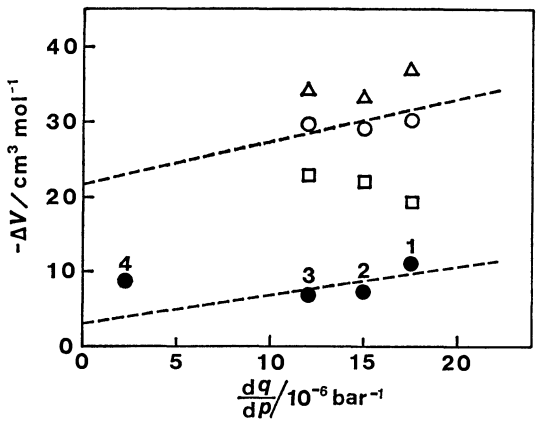

Fig. 4. Variation of the activation and the reaction volumes with solvent dielectric constant parameter (Eq. 6).
The number is the same as in Fig. 3. ○: ΔV_1^*, ●: ΔV_{-1}^*, □: ΔV_1, △: $\Delta V_c + \Delta V_1^*$.

$$q = \frac{D-1}{2D+1} \tag{7}$$

Here N is Avogadro's number, and r_*, r_{EDA}, and r_P are the radii of the transition state, the EDA complex and the 1,4-cycloadduct, respectively, and μ's denote the dipole moments. D is the dielectric constant of the solvent, and subscript 0 refers to the state free from the electrostatic interaction with the solvent. $\Delta V_{0(1)}^*$ and $\Delta V_{0(-1)}^*$ are the so-called intrinsic volumes of activation, and the second terms in Eq. 6 represent the volume contraction due to the solvation. The numerical values of q and $(\partial q/\partial p)_T$ are utilizable from the literatures.[12,15] The estimation of the radii was made on the assumption of the spherical model as follows:

$$r_{EDA}^3 = \frac{3}{4\pi N}\{\Delta V_c + V(\mathrm{TCNE}) + V(\mathrm{MS})\}, \tag{8a}$$

$$r_*^3 = \frac{3}{4\pi N}\{\Delta V_1^* + \Delta V_c + V(\mathrm{TCNE}) + V(\mathrm{MS})\}, \tag{8b}$$

$$r_P^3 = \frac{3}{4\pi N}\{\Delta V_1 + \Delta V_c + V(\mathrm{TCNE}) + V(\mathrm{MS})\}, \tag{8c}$$

and these approximated to be $r_{EDA}=4.6$, $r_* \approx r_P = 4.4$ Å.[4,16]

The plot of $\ln k$ *vs.* q exhibits a good straight line

Table 2. Reaction and activation volumes at 25 °C

Solvent	ΔV_0 / cm³ mol⁻¹	ΔV_1 / cm³ mol⁻¹	ΔV_1^* / cm³ mol⁻¹	ΔV_{-1}^* / cm³ mol⁻¹
CCl_4		-19 ± 2	-30 ± 1	-11 ± 1
$CHCl_3$	-4.0 ± 0.6[a]	-22 ± 2 -20 ± 1[a]	-29 ± 1	-7 ± 1
$ClCH_2CH_2Cl$	-6.9 ± 0.6[a]	-23 ± 2.4 -21 ± 1[a]	-30 ± 1.2	-7 ± 1.2
CH_3CN				-9 ± 1.2

a) Ref. 13.

for k_1 and k_{-1} as seen in Fig. 3; the slopes and r's provide the magnitudes of μ_* and μ_P to be 8.5 ± 0.5 and 6 ± 1 debye, respectively. Equation 6 is a severer test of this electrostatic model than Eq. 5. If not only the solvent effect on a reaction rate is expressed by Eq. 5 but also the volume of activation lies on a line of Eq. 6, the application of Kirkwood's theory is more justified, and the obtained value of μ_* becomes more reliable. That idea does not apply satisfactorily to the present results, as seen in Fig. 4. However, the relationship of Eq. 6 is useful to estimate the intrinsic volume terms. The slopes of the broken lines of Fig. 4 correspond to those of Fig. 3. The intercepts fall on -22 ± 3 and -3 ± 3 cm³/mol for the cycloaddition and the reverse reaction, respectively. The volume changes for most EDA complex formations, arising mainly from the intrinsic contribution are around -5 cm³/mol,[13,17] hence the intrinsic volume change from the reactants to the transition state results in about -27 cm³/mol; this is larger than the values for many reactions of Diels-Alder type,[8,9] -35—-40 cm³/mol. The fact that $\Delta V_{0(-1)}^*$, which should not be negative, is practically zero, suggests that the geometric structure at the transition state is not far from that of the cycloadduct. The apparent negative values for ΔV_{-1}^* must then be an indication of their difference in electronic character as reflected in the difference in their dipole moments.

The [2+2] cycloaddition of TCNE with a vinyl ether where the concerted mechanism is symmetrically forbidden by the Woodward-Hoffmann rule,[18] proceeds *via* a zwitterionic intermediate, and the dipole moment in the transition state is as large as 10—14 D.[19] Therefore, the volume contraction due to the electrostriction must be substantial in the transition state.[20,21] On the other hand, in many Diels-Alder reactions the dipole moment does not vary so much upon activation that the reaction rate cannot be affected by solvent and that the electrostriction hardly contributes to the volume of activation.

The present results that μ_* is large enough for the solvent polarity to affect the reaction rate remarkably and that ΔV_1^* is less negative than in usual Diels-Alder reactions strongly suggest that the 1,4-cycloaddition reaction undergoes a transition state of much higher polarity than do most [4+2] reactions.

References

1) T. Arimoto and J. Osugi, *Rev. Phys. Chem. Jpn.*, **44**, 25 (1974), and the references cited therein.

2) M. Nakahara, Y. Uosaki, M. Sasaki, and J. Osugi, *Rev. Phys. Chem. Jpn.*, **47**, 119 (1977); *Bull. Chem. Soc. Jpn.*, **53**, 3395 (1980).

3) Y. Uosaki, M. Nakahara, M. Sasaki, and J. Osugi, *Chem. Lett.*, **1979**, 727; Y. Uosaki, M. Nakahara, and J. Osugi, *Bull. Chem. Soc. Jpn.*, **54**, 2569 (1981).

4) Y. Uosaki, M. Nakahara, and J. Osugi, *Bull. Chem. Soc. Jpn.*, **55**, 41 (1982).

5) Y. Uosaki, M. Nakahara, and J. Osugi, *Bull. Chem. Soc. Jpn.*, **54**, 3681 (1981).

6) V. D. Kiselev and J. G. Miller, *J. Am. Chem. Soc.*, **96**, 4036 (1975).

7) M. Sasaki, H. Tsuzuki, and J. Osugi, *J. Chem. Soc., Perkin Trans. 2*, **1980**, 1596.

8) C. A. Eckert, *Ann. Rev. Phys. Chem.*, **23**, 239 (1972).

9) T. Asano and W. J. le Noble, *Chem. Rev.*, **78**, 407 (1978).

10) M. Sasaki, F. Amita, and J. Osugi, *Rev. Sci. Instrum.*, **50**, 1104 (1979).

11) D. M. Newitt and K. E. Weale, *J. Chem. Soc.*, **1951**, 3092.

12) K. R. Srinivasan and R. L. Kay, *J. Solution Chem.*, **6**, 357 (1977).

13) Y. Uosaki, M. Nakahara, M. Sasaki, and J. Osugi, *Bull. Chem. Soc. Jpn.*, **54**, 2893 (1981).

14) J. G. Kirkwood, *J. Chem. Phys.*, **2**, 351 (1934).

15) J. F. Skinner, E. L. Cussler, and R. M. Fuoss, *J. Phys. Chem.*, **72**, 5057 (1968); H. Hartmann, A. Newmann, and A. P. Schmidt, *Ber. Bunsenges. Phys. Chem.*, **72**, 875 (1968).

16) The averaged partial molar volumes in solvents used in this work are V(TCNE)$=107.3\pm1.0$ and V(MS)$=131.7\pm1.1$ cm³/mol. The values of r's do not change within ±0.1 Å in spite of the changing volume terms in Eq. 8 from solvent to solvent.

17) T. Nakayama, *Rev. Phys. Chem. Jpn.*, **49**, 25 (1979).

18) R. B. Woodward and R. Hoffmann, *Angew. Chem.*, **81**, 797 (1969).

19) G. Steiner and R. Huisgen, *J. Am. Chem. Soc.*, **95**, 5056 (1973); *Tetrahedron Lett.*, **39**, 3769 (1973); R. Huisgen, R. Schug, and G. Steiner, *Bull. Soc. Chim. Fr.*, **1976**, 1813.

20) K. Fleischman and H. Kelm, *Tetrahedron Lett.*, **39**, 3773 (1973); J. V. Jouanne and H. Kelm, *High Temp.-High Pressures*, **9**, 515 (1977).

21) M. Sasaki, H. Tsuzuki, and M. Okamoto, *J. Org. Chem.*, **44**, 652 (1979).

The Penetration of Lysine into the Monolayers of Lecithin from the Underlying Aqueous Solutions

Masayuki NAKAGAKI and Emiko OKAMURA*
Faculty of Pharmaceutical Sciences, Kyoto University, Yoshida-Shimoadachicho, Sakyo-ku, Kyoto 606
(Received May 27, 1981)

The surface pressure of the monolayers of dimyristoyl phosphatidylcholine (DMPC) on the lysine solutions was measured. The monolayer was more expanded on the solution than on pure water. The amount of lysine penetrating into the DMPC monolayer was calculated by means of a successive approximation. It was found that the amount of lysine penetrating increased with the increase in the concentration of the solution and with the decrease in the area per molecule of a DMPC monolayer, but it decreased with the further decrease in the area per molecule of DMPC. The average area per molecule of the monolayer consisting of lysine and DMPC was linearly related to the mole fraction of lysine. This linear relation indicates that partial molecular areas of both DMPC and lysine are independent of the amount of lysine in the monolayer. It is concluded that lysine and DMPC do not interact in the monolayer, although the monolayer of lysine and DMPC is formed as a result of the interaction between DMPC and lysine in a subsolution.

It has been widely believed, according to the fluid mosaic model of Singer and Nicolson,[1] that the biomembranes consist essentially of bimolecular lipid layers in which some proteins are dissolved. Much attention has been paid to the studies of the penetration of proteins into phospholipid monolayers, since lipid molecules in monolayers are oriented just as in the bimolecular layers. In these studies, the increase in either the area per molecule at a constant surface pressure or the surface pressure at a constant area per molecule has been measured for a phospholipid monolayer spread on an aqueous solution,[2,3] and the formation of mixed monolayers of phospholipid and protein has been discussed.[4] The monolayer method has thus been proved to be useful for investigating the lipid-protein interaction at the liquid-air interface.

In this work, the change in the surface pressure, caused by the penetration of L-lysine into the monolayer of lecithin, was measured. L-Lysine is an essential amino acid which is indispensable to growth and which plays various other important roles, for example, in the regulation of emzyme reactions[5] and in inactivating viruses,[6] and lecithin is the most typical component of biomembranes. As the lecithin, L-α-dimyristoyl phosphatidylcholine(DMPC) was used in this work; the amount of lysine penetrating into the monolayer of DMPC was calculated using the data obtained. The features of the interaction between lysine and DMPC were discussed.

Experimental

Materials. L-Lysine(free base) from Nakarai Chemicals, Ltd, was dissolved in redistilled water. DMPC from the Sigma Company was dissolved in distilled chloroform and the solution preserved in a refrigerator for several days before use.

Surface-tension Measurement. The surface tension of the lysine solution, γ_{lys}, was measured by the capillary-height method, while the surface pressure of lysine, F_{lys}, was obtained by means of Eq. 1:

$$F_{lys} = \gamma_0 - \gamma_{lys}, \quad (1)$$

where γ_0 is the surface tension of pure water. The temperature of the solution was kept at 25±0.5 °C.

Surface-pressure Measurement. The surface pressure of the DMPC monolayer was measured by Wilhelmy's plate method. Since the surface tension of a subsolution is not always equal to that of pure water, the surface pressure, F, was calculated by means of Eq. 2:[7]

$$F = \gamma_0 - \gamma = F' + F_{lys}, \quad (2)$$

where γ is the surface tension of a lysine solution covered with a lipid monolayer, while F' is the practical surface pressure defined by:

$$F' = \gamma_{lys} - \gamma, \quad (3)$$

and is measured directly by Wilhelmy's plate method as the decrease in the surface tension of a lysine solution upon the spreading of a lecithin monolayer. That is:

$$F' = (T_{lys} - T')/l, \quad (4)$$

where l is the length around the horizontal cross section of the plate. The values of T_{lys} and T' were measured as follows. A lysine solution of 57 cm³ was poured into a trough (5.0 cm×20.0 cm×0.4 cm) coated with Teflon: the temperature of the solution was kept at 25±0.5 °C by circulating thermostatted air. After the surface of lysine solution had been swept by a barrier covered with a Teflon sheet, a ground glass plate was suspended vertically on the liquid surface and the force acting on the plate, T_{lys}, was measured by means of a torsion balance, Shimadzu T-NR. The value of T_{lys} was measured several times until the equilibrium value was obtained. Then a lipid monolayer was spread from an AGLA micrometer syringe(accuracy ±0.0002 cm³) and left for 5 min. Then, the force acting on the plate, T', was measured by compressing the monolayer with a barrier. The equilibrium value of T' was obtained within 10 min.

The trough was used after any contaminants had been wiped off with ethanol and it had been rinsed well with redistilled water. The Teflon sheet and the ground glass plate were used after they had been immersed in heavy chromic acid and in fuming nitric acid respectively for more than one night and then rinsed well with redistilled water.

Results

Surface Tension of the Lysine Solution. Figure 1 shows the surface tension of a lysine solution. It is seen that the surface tension decreases slightly with the increase in the concentration of lysine, C_2. There-

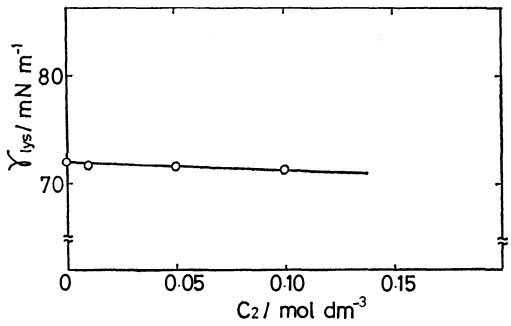

Fig. 1. The relation of surface tension, γ_{lys}, and the concentration of lysine, C_2.
Temp 25±0.5 °C.

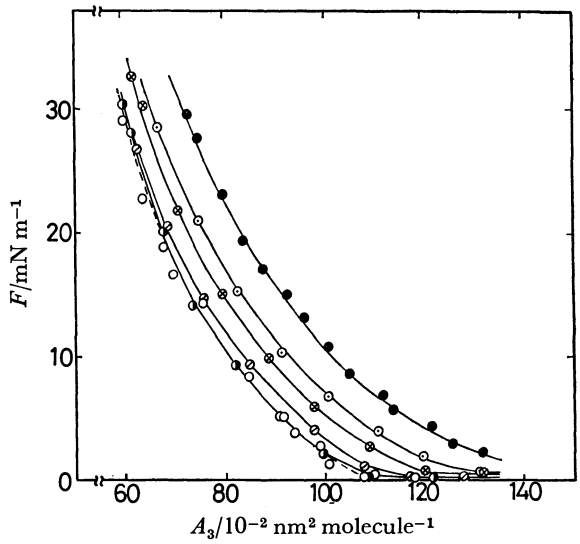

Fig. 2. F-A_3 curves of the DMPC monolayers on the lysine solutions.
C_2/mol dm^{-3}: ○ 0, ◑ 0.01, ⊘ 0.02, ⊗ 0.05, ⊙ 0.07, ● 0.10.

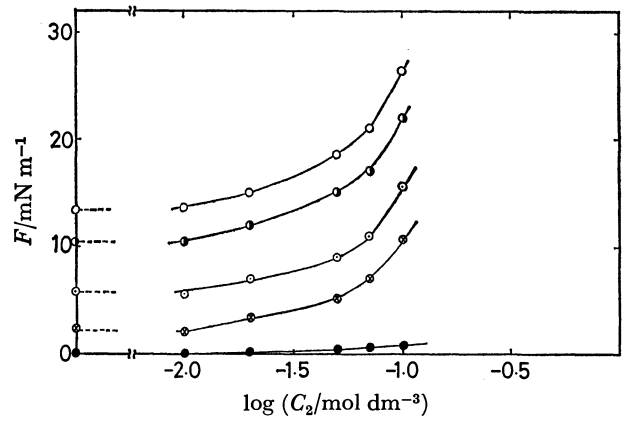

Fig. 3. The relation of the surface pressure, F, and the concentration of lysine, log C_2, at various areas per molecule of DMPC, A_3.
A_3/10^{-2} nm^2 molecule^{-1}: ● No insoluble monolayer, ⊗ 100, ⊙ 90, ◑ 80, ○ 75.

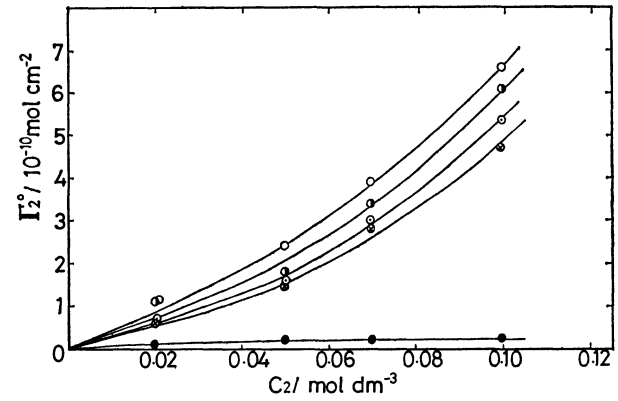

Fig. 4. The amount of lysine adsorbed onto DMPC monolayer, Γ_2°, *vs.* C_2.
Calculated from Eq. 5. A_3/10^{-2} nm^2 molecule^{-1}: ● No insoluble monolayer, ⊗ 100, ⊙ 90, ◑ 80, ○ 75.

fore, lysine is not adsorbed appreciably onto the liquid-air interface.

Surface Pressure-area Curves of the DMPC Monolayers. Figure 2 shows the relation between the surface pressure of the DMPC monolayer on an L-lysine solution, F, and the area per molecule of DMPC, A_3. When the concentration of lysine, C_2, is lower than 0.01 mol dm^{-3}, the F-A_3 curve of the DMPC monolayer on a lysine solution nearly coincides with that on pure water. This is because the amount of lysine penetrating into or adsorbed onto the monolayer is not so large as to change the surface pressure. When C_2 is higher than 0.01 mol dm^{-3}, the F-A_3 curve of the higher C_2 shifts to the right with an increase in C_2. This is attributable to the fact that the monolayer is expanded by the adsorption or penetration of lysine from the subsolution.

The Amount of Lysine Adsorbed. The relation between the surface pressure, F, and the concentration of lysine, C_2, at a constant area per molecule of lecithin, A_3, is shown in Fig. 3, from which the amount adsorbed may be calculated by use of Gibbs' adsorption equation:

$$\Gamma_2^\circ = \frac{1}{RT}\left(\frac{\partial F}{\partial \ln C_2}\right)_{A_3}, \tag{5}$$

where R is the gas constant, T is the absolute temperature, and Γ_2° is the amount of lysine adsorbed onto the portion of the interface where lecithin does not exist. The value of Γ_2° thus obtained is shown in Fig. 4 as a function of the concentration of lysine, C_2. It seems that lysine is not adsorbed appreciably onto the interface without a lecithin monolayer, but the amount of lysine adsorbed increases with the increase in C_2 when a lecithin monolayer exists at the interface.

In Eq. 5, the existence of an insoluble component, DMPC, at the interface is disregarded. Actually, however, both adsorbed lysine and the DMPC monolayer coexist at the interface, and the part of the interface already occupied by DMPC is not available for the adsorption of lysine. Gibbs' adsorption equation 5 is, therefore, modified by taking the partial molecular area of DMPC, $\overline{A}_3$, into account. The designed modification of Gibbs' adsorption equation is given by:

$$\Gamma_2 = (1-\overline{A}_3/A_3)\Gamma_2^\circ, \tag{6}$$

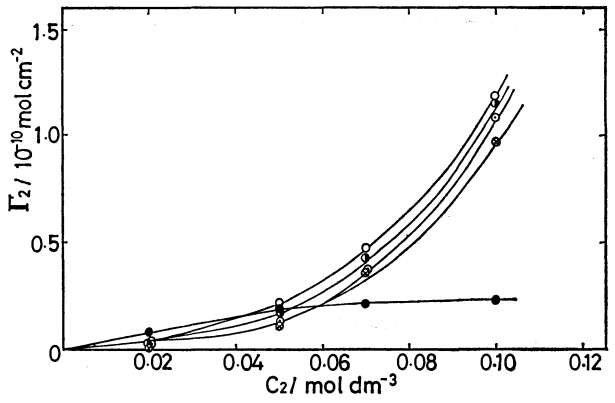

Fig. 5. The amount of lysine adsorbed onto DMPC monolayer, Γ_2, *vs.* C_2.
Calculated from Eq. 7. $A_3/10^{-2}$ nm^2 molecule^{-1}: ● No insoluble monolayer, ⊗ 100, ⊙ 90, ◑ 80, ○ 75.

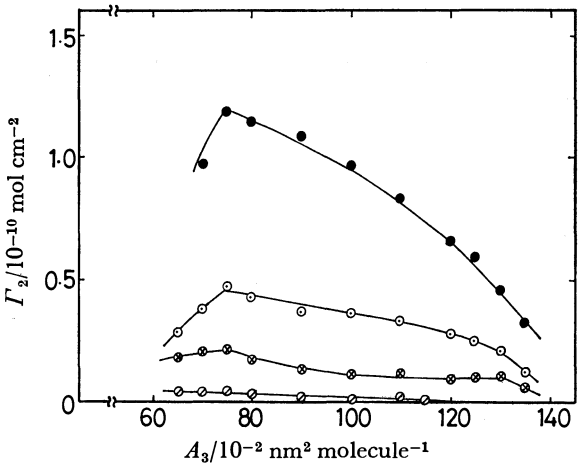

Fig. 6. The relation of the amount of lysine adsorbed, Γ_2, and the area per molecule of DMPC, A_3.
C_2/mol dm^{-3}: ∅ 0.02, ⊗ 0.05, ⊙ 0.07, ● 0.10.

where Γ_2 is the amount of lysine adsorbed onto the unit area of the interface in the presence of DMPC. According to Pethica,[8] $\overline{A}_3$ is approximated by the molecular area of DMPC on pure water, $A_3°$; Eq. 6 is, therefore, rewritten as follows:

$$\Gamma_2 = (1 - A_3°/A_3)\Gamma_2°. \tag{7}$$

Hereafter, this will be called the first approximation. This equation has been used to calculate the amount of solute molecules adsorbed onto the monolayer on subsolutions.[9,10]

The relation between the amount of lysine adsorbed, Γ_2, as calculated from Eq. 7, and the concentration of lysine, C_2, is shown in Fig. 5. The amount of lysine adsorbed decreased in the presence of an insoluble component at the interface, but it is still larger than the value in the case of no insoluble component, at least in the high-C_2 region. This would indicate that there exists a strong affinity between lysine and lecithin.

If the concentration of lysine, C_2, is kept constant, the amount of lysine adsorbed, Γ_2, changes with the area per molecule of DMPC, A_3, as is shown in Fig. 6. The amount adsorbed is higher at a higher concentration of lysine, and the curve has a maximum at high values of C_2. This would indicate the following points. As has already been shown in Fig. 1, lysine is not adsorbed appreciably onto a clean interface. The value of Γ_2 is, therefore, small when A_3 is large. Lysine is, however, adsorbed more onto a lecithin monolayer than onto a clean interface, and the amount adsorbed increases with the density of lecithin, that is, with the decrease in A_3. However, lysine is excluded from the monolayer, and the amount adsorbed decreases with the further decrease in the area per molecule of lecithin.

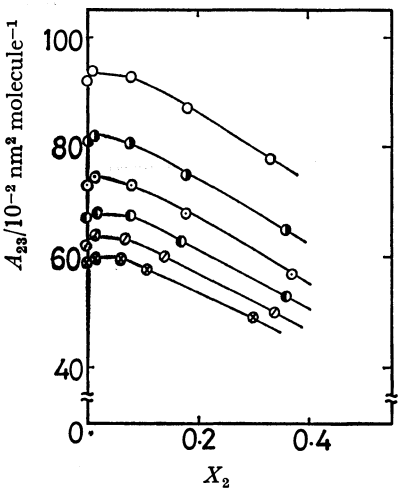

Fig. 7. The relation of the average area per molecule, A_{23}, of a lysine-DMPC mixed monolayer, and the mole fraction of lysine, X_2.
F/mN m^{-1}: ○ 5, ◑ 10, ⊙ 15, ◐ 20, ∅ 25, ⊗ 30.

Discussion

The Mixed Monolayers Formed by the Penetration of Lysine. It may be stated that a mixed monolayer of lysine and DMPC is formed as a result of the penetration of lysine into a DMPC monolayer when a lysine solution is used as a subphase. The mole fraction of lysine in this mixed monolayer, X_2, is given by:

$$X_2 = \frac{\Gamma_2}{\Gamma_2 + \Gamma_3}. \tag{8}$$

Here, Γ_3 is the moles of DMPC per unit of area defined by:

$$\Gamma_3 = \frac{1}{A_3 \cdot N_A}, \tag{9}$$

where N_A is the Avogadro number. The average area per molecule of a lysine–DMPC mixed monolayer, A_{23}, is defined by:

$$A_{23} = \frac{1}{(\Gamma_2 + \Gamma_3)N_A}. \tag{10}$$

The relation between the average area per molecule and the mole fraction of lysine at a constant surface pressure is shown in Fig. 7. It may be seen from this figure that the partial molecular areas of both DMPC and lysine are dependent on X_2, but they

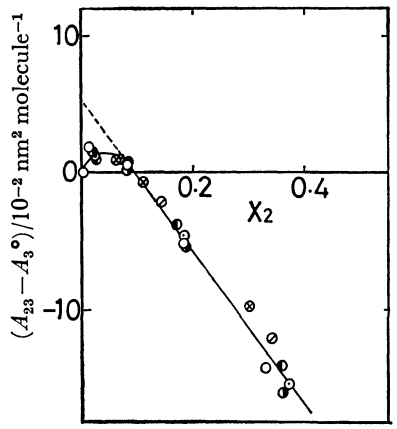

Fig. 8. $(A_{23}-A_3°)$ *vs.* X_2.
F/mN m^{-1}: ○ 5, ◑ 10, ⊙ 15, ◐ 20, ⊘ 25, ⊗ 30.

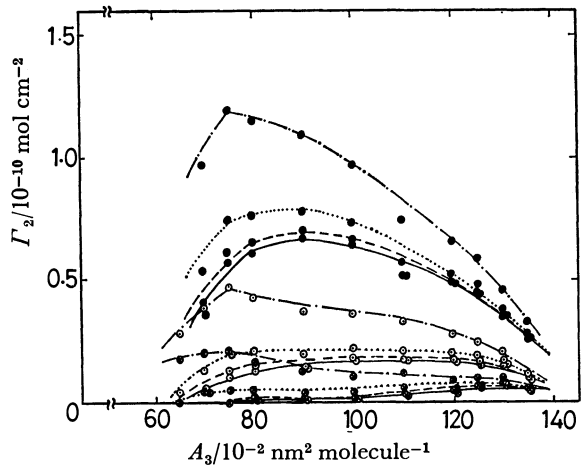

Fig. 9. The amount of lysine adsorbed onto DMPC monolayer, Γ_2, *vs.* A_3.
—·—·: By the 1st approximation, ·····: by the 2nd approximation, ----: by the 3rd approximation, ——: by the 4th approximation.
C_2/mol dm^{-3}: ⊗ 0.05, ⊙ 0.07, ● 0.10.

are practically independent of X_2 and are nearly constant in the region where X_2 is larger than 0.07. By extrapolating the linear portion of X_2, it is found that the partial molecular area of DMPC on a lysine solution, $\overline{A}_3$, is not equal to that on pure water, $A_3°$, at each surface pressure. This indicates that the approximation, $\overline{A}_3=A_3°$, used in Eq. 7 was not appropriate.

Since all the curves on Fig. 7 had the same shape, $(A_{23}-A_3°)$ was plotted against X_2 in Fig. 8. It was found that all the plots come on one curve and that $(A_{23}-A_3°)$ is linearly related to X_2 when X_2 is larger than 0.07. This linear portion is written by:

$$A_{23}-A_3° = 5.1—55.0X_2, \quad (11)$$

and when X_2 is equal to zero, Eq. 11 is rewritten as follows:

$$\overline{A}_3 = A_3° + 5.1. \quad (12)$$

The amount adsorbed, Γ_2, was, therefore, recalculated by Eqs. 6 and 12; this will be called the second approximation. The successive approximation was repeated until the value of Γ_2 converged to a defined value.

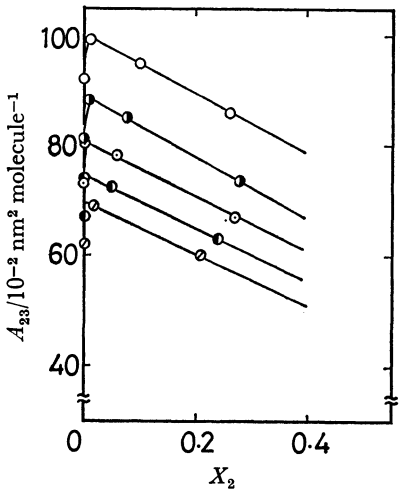

Fig.10. The relation of the average area per molecule, A_{23}, and the mole fraction of lysine, X_2, by the 4th approximation.
F/mN m^{-1}: ○ 5, ◑ 10, ⊙ 15, ◐ 20, ⊘ 25.

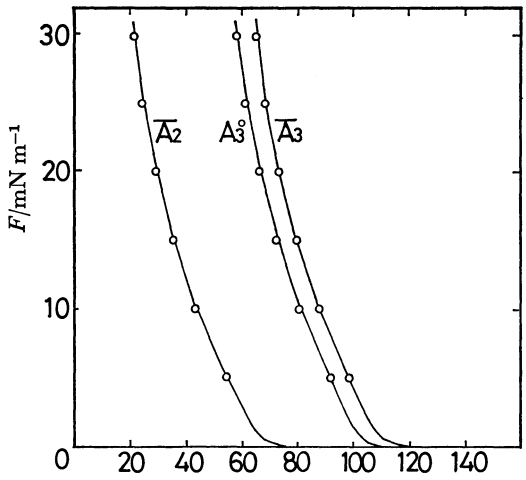

Fig.11. The relation of the surface pressure, F, and the partial molecular areas of lysine, $\overline{A}_2$, and DMPC, $\overline{A}_3$.
The F-A_3 curve of DMPC on pure water was designated as $A_3°$.

The approximation was repeated in this way, by using $\overline{A}_3-A_3°=6.5$ for the third and 7.0 for the fourth approximation. The values of Γ_2 thus obtained are plotted against A_3 in Fig. 9. Although the value of Γ_2 decreased with higher approximations, the general features did not change; *i.e.*, (1) Γ_2 increases with the increase in C_2 and (2) Γ_2 increases with the decrease in A_3 at a constant C_2, but decreases at a small value of A_3.

The Interaction between Lysine and DMPC. The relation between the average area per molecule, A_{23}, and the mole fraction of lysine, X_2, obtained by the fourth approximation is shown in Fig. 10. By com-

paring it with Fig. 7, we may conclude that A_{23} is linearly related to X_2, in the higher approximations at each surface pressure and that the relation may be expressed by the following empirical equation:

$$A_{23} = A_3^\circ + 7.0 - 44.0X_2. \quad (13)$$

This yields the following equations for the partial molecular areas of lysine and DMPC, $\overline{A}_2$ and $\overline{A}_3$, respectively:

$$\overline{A}_2 = A_3^\circ - 37.0, \qquad \overline{A}_3 = A_3^\circ + 7.0. \quad (13a)$$

The dependence of these quantities on the surface pressure is shown in Fig. 11.

The linear relation between A_{23} and X_2 shown in Fig. 10 thus shows that the partial molecular areas of both DMPC and lysine are independent of the extent of mixing as long as X_2 is smaller than about 0.3. This means that lysine and DMPC do not interact in the monolayer, although a mixed monolayer is formed by the interaction between lysine and DMPC. It can, therefore, be concluded, with regard to the intermolecular interaction between two components of a mixed monolayer formed by the penetration of one component, that the lateral interaction in the monolayer is quite different from the longitudinal interaction effective for the formation of a mixed monolayer, as is naturally to be expected from the high degree of orientation of molecules in the monolayer.

References

1) S. J. Singer and G. L. Nicolson, *Science*, **175**, 720 (1972).
2) D. Papahadjopolous, M. Cowden, and H. Kimelberg, *Biochim. Biophys. Acta*, **330**, 8 (1973).
3) D. Papahadjopolous, M. Moscarello, E. H. Eylar, and T. Isac, *Biochim. Biophys. Acta*, **401**, 317 (1975).
4) M. Nakagaki and H. Ichihashi, *Yakugaku Zasshi*, **99**, 999 (1979).
5) O. Tosaka, H. Hirakawa, K. Takinami, and Y. Hirose, *Agric. Biol. Chem.*, **42**, 1501 (1978).
6) A. Murata, K. Tanaka, K. Nakatsumi, S. Genno, F. Kato, R. Saruno, and M. Kondo, *Nippon Nôgei Kagaku Kaishi*, **52**, 385 (1978).
7) M. Nakagaki and T. Handa, *Bull. Chem. Soc. Jpn.*, **49**, 880 (1976).
8) B. A. Pethica, *Trans. Faraday Soc.*, **51**, 1402 (1955).
9) M. Nakagaki and T. Handa, *Bull. Chem. Soc. Jpn.*, **49**, 2934 (1976).
10) M. A. McGregor and G. T. Barnes, *J. Colloid Interface Sci.*, **54**, 439 (1976).

Relation between Exchange Interaction and Crystal Structure of Verdazyl Radicals. As Studied by Means of McConnell's Spin Density Hamiltonian*

Nagao AZUMA†

Department of Chemistry, Faculty of Science, Kyoto University, Sakyo-ku, Kyoto 606

(Received July 15, 1981)

The exchange interactions in four kinds of verdazyl crystals, 2,4,6-triphenylverdazyl (TPV), 2,4,6-triphenyl-3-methylverdazyl (MeTPV), 2,4,6-tri-*p*-tolylverdazyl (TTV), and 2,6-di-*p*-tolyl-4-phenylverdazyl (DTPV), have been studied by means of McConnell's spin density Hamiltonian. The calculated exchange parameters, J, have been compared with the experimental values derived from the magnetic susceptibilities. The observed order of J's, $J/k=-5.4$ (TPV), -9.1 (MeTPV), -11.1 (DTPV), and 0——0.3 K (TTV), can be qualitatively explained by the following equation:

$$J \propto \sum_{ij} (-1/r_{ij})\rho_i^l \rho_j^{l+1},$$

where ρ_i^l and ρ_j^{l+1} are π-spin densities on atoms i and j of the l-th and $(l+1)$-th molecules in the *crystallographic column* and r_{ij} is the interatomic distance between atoms i and j. The magnetic susceptibility data of MeTPV and TTV between 1.6 and 300 K are presented and interpreted with the Heisenberg linear chain model. The susceptibility of DTPV is re-interpreted in the same framework as above.

The magnetic susceptibilities of some organic free-radical solids show a characteristic temperature dependence[1] which can be well explained based on the Heisenberg-type magnetic linear chain model.[2] The spin Hamiltonian for the exchange interaction in the magnetic linear chain can be given by a familiar form:

$$H = -2J \sum_l \boldsymbol{S}_l \boldsymbol{S}_{l+1}, \quad (1)$$

where $\boldsymbol{S}_l$ and $\boldsymbol{S}_{l+1}$ are the spin operators for the l-th and $(l+1)$-th magnetic electrons, and J is the exchange interaction parameter which depends on the crystal structure. However, the relation between J and the crystal structure has not been understood well.

The verdazyls first synthesized by Kuhn and Trischmann[3] are a series of stable organic radicals containing four nitrogen atoms per molecule with unpaired electrons over the entire molecules. The magnetic susceptibility of 2,4,6-triphenylverdazyl (TPV) between 77 and 300 K[4] has indicated existence of the substantial exchange interaction between the unpaired electrons. We have studied the magnetic susceptibilities of TPV, 2,4,6-triphenyl-3-methylverdazyl (MeTPV), 2,4,6-tri-*p*-tolylverdazyl (TTV), and 2,6-di-*p*-tolyl-4-phenylverdazyl (DTPV) (*cf.* Fig. 1) in order to understand the relationship between J and the crystal structure. J's determined from the magnetic susceptibilities are very different depending on the radicals in spite of the similarity in their spin distributions. X-Ray studies have shown that the crystal structures of these radicals are different from one another. Therefore, these four verdazyls form a suitable set for such a study.

In order to understand the observed J from the crystal structure, we have calculated the exchange parameter using McConnell's spin density

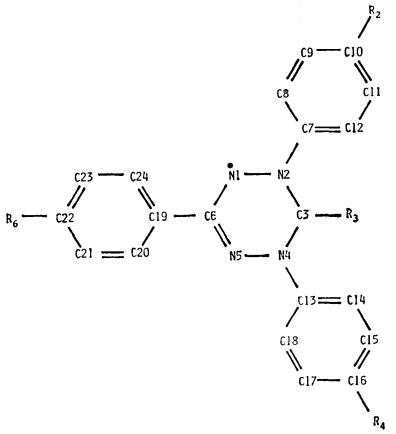

Fig. 1. Chemical structures and numbering system of verdazyls.

Radical	R_2	R_3	R_4	R_6
TPV	H	H	H	H
MeTPV	H	CH_3	H	H
TTV	CH_3	H	CH_3	CH_3
DTPV	CH_3	H	H	CH_3

Hamiltonian:[5]

$$H^{AB} = -\boldsymbol{S}^A \boldsymbol{S}^B \sum_{ij} J_{ij}^{AB} \rho_i^A \rho_j^B, \quad (2)$$

where $\boldsymbol{S}^A$ and $\boldsymbol{S}^B$ are the spin operators for Molecules A and B, and where ρ_i^A and ρ_j^B are the π-spin densities on Atoms i of Molecule A and j of B, respectively. In evaluating the two-center exchange integral J_{ij}^{AB}, four trial functions of the distance, r_{ij}^{AB}, between Atoms i and j were used. The observed order of J's was qualitatively explained when J_{ij}^{AB} was assumed as a function of $1/r_{ij}^{AB}$.

Experimental

Following the process of Kuhn and Trischmann,[6] the samples were prepared by the ring formation of the corresponding formazans with formaldehyde or acetaldehyde, followed by reduction with alkaline solutions of these aldehydes. The radicals were purified a few times through

* Part XIV of "The Magnetic Properties of Verdazyl Free Radicals."

† Present address: Laboratory of Chemistry, Faculty of General Education, Ehime University, Bunkyo-cho Matsuyama 790.

TABLE 1. SPIN DENSITY DISTRIBUTION IN TPV

Atom[a)]	π-Spin density
N1, N5	0.1944
N2, N4	0.2040
C6	−0.0461
C7, C13	−0.0345
C8, C12, C14, C18	0.0473
C9, C11, C15, C17	−0.0179
C10, C16	0.0505
C19	0.0032
C20, C24	−0.0179
C21, C23	0.0067
C22	−0.0131

a) The numbering system refers to Fig. 1.

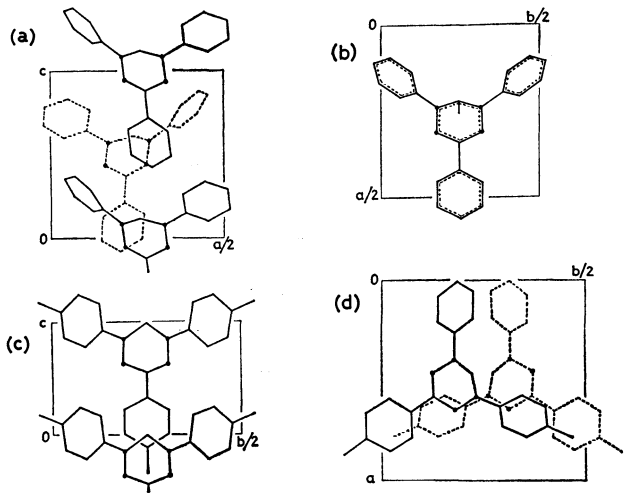

Fig. 2. Molecular packings of TPV(a),[13] MeTPV (b),[9] TTV(c),[10] and DTPV(d)[11] viewed along the b, c, a, and c axes, respectively.
Solid circle stands for the nitrogen atom. The molecule drawn with broken line is lower than one with solid line respective to the axis perpendicular to the projected plane.

recrystallization from a mixture of acetone and methanol. The results of the elementary analyses were in agreement with the calculated values within experimental errors.

The magnetic susceptibilities from 1.6 to 300 K were measured on the powdered samples of MeTPV and TTV by means of a magnetic torsion balance with an accuracy of 3%.[7] The temperature was measured with a carbon resister and an AuCo–Cu thermocouple calibrated by measurements of the susceptibility of manganese Tutton salt and of the vapour pressure of liquid helium.

The experiments of ESR and ENDOR in solution have been described elsewhere.[8] The analyses of the crystal structures of MeTPV, TTV, and DTPV by X-ray diffraction have been reported previously.[9–11]

Summary of Previous Results

Spin Density Distribution. The present radicals in dilute solution have exhibited nine-line ESR spectra due to four nearly equivalent nitrogen nuclei.[8] The nitrogen hyperfine coupling constants have ranged from 0.56 to 0.58 mT. The proton hyperfine coupling

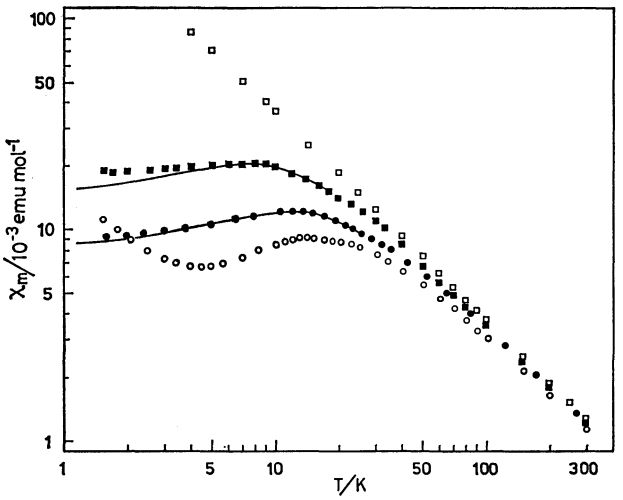

Fig. 3. Molar paramagnetic susceptibilities of crystalline verdazyls.
The solid square stands for the observed susceptibility of TPV, the solid circle of MeTPV, the open square of TTV, and the open circle of DTPV. The solid lines are theoretical susceptibilities calculated with the Heisenberg linear chain model.

constants of TPV, MeTPV, and TTV have been measured by means of the ENDOR technique.[8] The changes in the proton coupling constants caused by methyl substitutions are less than 5%. The spin densities in TPV calculated by Fischer[12] are given in Table 1. As these values explain the hyperfine coupling constants, we use these values for the calculation of the exchange parameters.

Crystal Structure. The molecular overlappings of four verdazyls are compared with one another in Fig. 2. TPV and DTPV molecules are arranged in zigzag chains along the respective c axes, and MeTPV and TTV ones form Venetian blinds along the respective c axes. No alternation is observed in the intermolecular distances in these chains and blinds (columns). The angular orientation of $p_z\pi$-orbitals in TTV crystal is much more unfavourable for overlapping than that in the MeTPV crystal. The order of the mean values of the interatomic distances between the π-frameworks of the neighbouring molecules in the columns is as follows: DTPV<MeTPV<TTV<TPV (see Table 3).

Magnetic Susceptibility

The susceptibility data were corrected for the diamagnetic contribution using Pascal's constants.[14] The molar paramagnetic susceptibility, χ_m, of MeTPV follows the Curie-Weiss law with the negative Weiss constant of $\theta = -10.3$ K in the high temperature region. In the low temperature region, however, it deviates from the Curie-Weiss law and exhibits a broad maximum, χ_{max}, at T_m (=11.7 K). When the temperature, T, is lowered below T_m, χ_m decreases towards a non-zero value at 0 K. This finite value, $\chi_{T=0}$, was estimated by extrapolation. The susceptibility of TTV complies with the Curie-Weiss law

Table 2. Results from susceptibility measurements

	TPV	MeTPV	TTV	DTPV
θ/K	−8.0	−10.3	−0.3	−14.6
T_m/K	6.9	11.7		14.2
T_n/K	1.7			
$\chi_{max}/10^{-3}$ emu mol^{-1} a)	20.3	12.1		9.15
$\chi_{T=0}/10^{-3}$ emu mol^{-1} a)	17.0	8.5		2.5
(J/k)/K	−5.4	−9.1	0—−0.3	−11.1

a) The value of the molar susceptibility in m^3 mol^{-1} (SI) can be obtained by multiplying the value in emu mol^{-1} (cgs) by $4\pi\times10^{-6}$.

with a small negative Weiss constant of −0.3 K over the whole temperature region examined. The spin concentrations of MeTPV and TTV, as determined from the susceptibilities in the Curie-Weiss region, were 100% within the experimental accuracy.

The susceptibilities of TPV[15] and DTPV[16] have been reported previously. However, the susceptibility of DTPV, which has been explained tentatively by the Ising model, is re-interpreted in the framework of the Heisenberg model in this paper. The susceptibility of DTPV displays a round maximum and a broad minimum at 4 K. An approximated $\chi_{T=0}$ is estimated by the extrapolation of the curve between the maximum and minimum. The susceptibilities of the verdazyls and the results obtained from the susceptibilities are shown in Fig. 3 and Table 2, respectively, together with the data of TPV. In Table 2, T_n for TPV shows the temperature at which χ_m-T curve exhibits a discontinuity in its slope.

Discussion

Susceptibility. The susceptibilities of the verdazyls are discussed here in order to obtain the experimental parameters for the exchange interactions. The columnar structure with a uniform intermolecular distance suggests a linear chain spin system, that is, the Heisenberg linear chain model with an isotropic exchange interaction or the Ising linear chain model with an extremely anisotropic one. In our case, therefore, the former is more adequate than the latter in view of the practically isotropic g-values of the verdazyls, $g=2.003$.[17] Edelstein[18] employed the Ising linear chain model to interpret the susceptibilities of organic radicals of BDPA and PAC at an earlier date. Recently, however, those susceptibilities were interpreted quantitatively in terms of the Heisenberg-type interaction.[1a,b]

According to the study of Bonner and Fisher,[2] the susceptibility of the Heisenberg linear chain with an antiferromagnetic exchange coupling exhibits a round maximum of height

$$\chi_{max}T_m = 0.142 \tag{3}$$

at

$$kT_m/|J| = 1.282, \tag{4}$$

where k is the Boltzmann constant. J parameters of TTV[15] and MeTPV have been estimated from Eq. 4 (see Table 2). The observed $\chi_{max}T_m$ values of TPV and MeTPV are 0.140 and 0.142, respectively. The ratios of $\chi_{max}/\chi_{T=0}$ estimated for TPV and MeTPV are, respectively, 1.19 and 1.42, while theory predicts 1.45.[2] These values indicate that the MeTPV crystal is a typical Heisenberg linear chain spin system. On the other hand, the TPV crystal is not an ideal one, which is indicated also by the discontinuity in the slope of the χ_m-T curve. However, the dominant exchange interaction is the Heisenberg-type one.

J value for TTV has been estimated by a familiar relation of $\theta=2\zeta JS(S+1)/3k$ given by the molecular field theory,[19] where the nearest-neighbour parameter, ζ, is 2 and $S=1/2$.

DTPV Spin System: The susceptibility of DTPV exhibited a maximum and a broad minimum, and $J/k=-17$ K was obtained by means of the Ising linear chain model.[16] However, application of the Ising model to such susceptibility may underestimate the contribution from magnetic chains with odd spins. Therefore, we re-interpreted the susceptibility of DTPV based on diamagnetic dilution.

When a magnetic linear chain with an infinite length is diluted by diamagnetic impurities, the resultant diluted system is composed of paramagnetic chains of various finite lengths; such finite chains will be called segments. When the interaction between the segments is disregarded, the susceptibility of the diluted system is given by

$$\chi_m = \sum_{n=1}^{\infty} P_{n,c}\chi_n, \tag{5}$$

where $P_{n,c}$ is a probability making the segment with n spins at c spin-concentration, and χ_n is the susceptibility of the n-spin segment. For random diamagnetic dilution of the linear chain, $P_{n,c}$ is approximately given by

$$P_{n,c} = nc^n(1-c)^2. \tag{6}$$

Because there is no analytical representation of χ_n, the susceptibility of DTPV is treated graphically in Fig. 4. The solid circles are the experimental values based on $J/k=-11.1$ K which is estimated from Eq. 4. The open circles were obtained by adjusting the experimental value at T_m to the theoretical value of the Heisenberg linear chain at the same temperature. The adjusting factor is 1.09; this corresponds to the spin concentration of 0.92, which is very close to 0.94 determined from the susceptibility measurement. The adjusted susceptibility is close to the mean of the theoretical values for 10- and 11-spin segments. This mean susceptibility is very similar to that of the Heisenberg linear chain except for the region below $kT/|J|=0.3$. On the other hand, $n=12$ is obtained from the equation derived by $\partial P_{n,c}/\partial n=0$ with $c=0.92$. These results suggest strongly that the DTPV spin system is characterized by the Heisenberg linear chain with $J/k=-11$ K.

Relationship between J and Crystal Structure. Comparing Eq. 2 with Eq. 1, the quantity in the summation in Eq. 2 is identified as $2J$ in Eq. 1, which is the exchange integral between the l-th and $(l+1)$-th radicals. In order to obtain a tractable form of J_{ij}^{AB}, we have calculated the summation for pairs of the

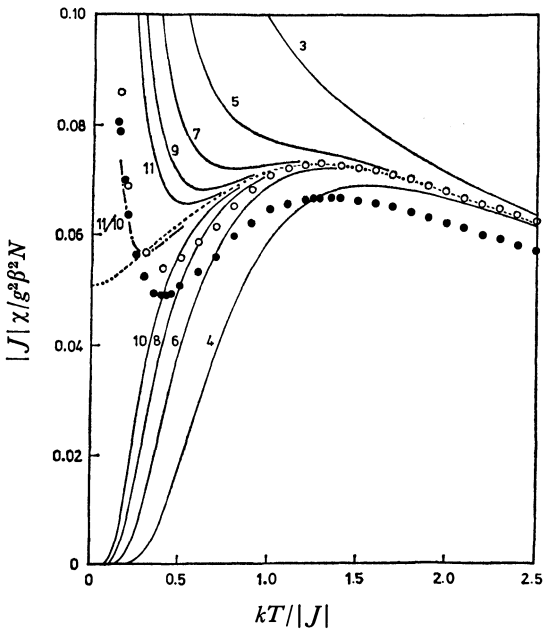

Fig. 4. Paramagnetic susceptibility of DTPV.
The solid circles are the experimental values. The open circles are the values corrected for the diamagnetic impurities. The broken line is the susceptibility of the Heisenberg linear chain.[2] The solid lines with n figures are the theoretical susceptibilities from rings of n Heisenberg-spins and dashed line is the mean of those of 10 and 11 spins.[2]

neighbouring molecules in the crystal. By analogy with the hydrogen molecule, the antiparallel spin-arrangement may be favourable with negative J_{ij}^{AB}. The negative J_{ij}^{AB} was assumed previously in this series[15] and also by Duffy *et al.*[20] in order to estimate J in DPPH-benzene crystal. Four trial functions with negative sign are adopted for J_{ij}^{AB}.

$$\text{Type A} \quad J_{ij}^{AB} = -C \exp[-Dr_{ij}^{AB}], \tag{6}$$

where C and D are positive constants. This equation can be derived from the result of the numerical calculation made by Dulčić and Herak[21] who have treated two carbon atoms in a radical pair by using the explicit form for the exchange integral given by Löwdin.[22]

On the other hand, it has been considered that the overlap between the orbitals occupied by the unpaired electrons serves as the path of the exchange interaction and the overlap has been used as a measure of the magnitude of the exchange interaction.[23] Then, this measure is adopted as the second trial function:

$$\text{Type B} \quad J_{ij}^{AB} \propto -S_{ij}^{AB}, \tag{7}$$

where S_{ij}^{AB} is the overlap integral between $p_z\pi$-orbitals of atoms i and j. The overlap integral can be easily computed with the recurrence formulae.[24]

In order to obtain the third trial function, the Hamiltonian for hydrogen molecule written by using the familiar symbols is referred:

$$H = -(h^2\nabla_1^2/8\pi^2m + e^2/r_{a1}) - (h^2\nabla_2^2/8\pi^2m + e^2/r_{b2}) + (-e^2/r_{a2} - e^2/r_{b1} + e^2/r_{12} + e^2/R).$$

The quantity in the last parentheses is known as the interaction operator, H'; $(H' - e^2/R)$ is the operator for the Heisenberg exchange interaction. The energy given by $(H' - e^2/R)$ approaches $-e^2/R$ when R becomes large. Then, the intermolecular exchange interaction may be approximated by

$$\text{Type C} \quad J_{ij}^{AB} \propto -1/r_{ij}^{AB}. \tag{8}$$

Several investigators have noted the linear correlation between the singlet-triplet energy separation and the zero-field splitting parameter for a number of aromatic hydrocarbons and biradicals.[25] This correlation suggests that the exchange energy follows r^{-3} where r is the mean distance between the unpaired electrons, so we adopted the following trial function.

$$\text{Type D} \quad J_{ij}^{AB} \propto -1/(r_{ij}^{AB})^3. \tag{9}$$

The exchange integral depends on both the distance and the angle between the $p_z\pi$-orbitals. However, the angular dependence is neglected in Types A, C, and D. A possible angular correction can be made by multiplying the trial functions by $\cos\theta_i^A \cos\theta_j^B$ where θ_i^A and θ_j^B are the angles between the respective axes of the $p_z\pi$-orbitals and the interatomic vector distance r_{ij}^{AB}.[20] However, we adopted the following correction factor, p,

$$p = \begin{cases} 1 & \text{when } r_{ij}^{AB} \leq 6\,\text{Å} \\ 0 & \text{when } r_{ij}^{AB} > 6\,\text{Å}. \end{cases} \tag{10}$$

Such a correction gives almost the same effect as that obtained by the cosine squared factors in our case.

The results of the calculation are shown in Table 3. Type A predicts J less than 1% of the observed one. This result arises from the short-range character of Eq. 6 which gives $J_{ij}^{AB}/k = -3.9$ and -0.01 K for $r_{ij}^{AB} = 3.4$ and 4.6 Å, respectively. Type B as well as Type A reverse the observed order of J's strikingly. Contrary to the case of Types A and B, Types C (and D) explain the order of the observed J's when the summation in Eq. 2 is performed over the pair of the neighbouring molecules in the column along the c axis of each crystal. This result shows that the magnetic chains in the present crystals are along the respective c axes and correspond to the *crystallographic columns*. The ratios of the interchain coupling to the intrachain one calculated by using Type C are 0.2, 0.04, 0.1, and 0.04 for TPV, MeTPV, TTV, and DTPV, respectively. This is consistent with the following fact based on the susceptibility: TPV crystal is not a typical Heisenberg linear chain spin system, while MeTPV and DTPV crystals are typical ones. Since the molecular packing along the column is generally different from those perpendicular to the column in the crystals of organic radicals, the ratios of the exchange coupling between the chains to the intrachain one may be hence more adequately estimated by using Type C than Types A and B.

Concluding Remarks

The susceptibilities of TPV, MeTPV, and DTPV can be explained in the framework of the Heisenberg linear chain model. The exchange parameters estimated from the susceptibilities are $J/k = -5.4$, -9.1, -11.1, and 0——0.3 K for TPV, MeTPV, DTPV,

Table 3. Results of summation in McConnell's spin density Hamiltonian

Direction in the crystal	Type of J_{ij}^{AB}	Sum in Eq. 2[a]			
		TPV	MeTPV	TTV	DTPV
Along a axis	A	0.0012	0.00071	0.00019	0.00028
	B	−0.032	0.20	0.48	−0.013
	C	−1.0	0.22	0.18	−0.35
	D	−0.79	0.25	0.26	−0.33
	$\langle r \rangle$[b]	10.27	10.38	9.77	11.45
Along b axis	A	0.00037	0.00000	−0.0029	−0.0029
	B	0.41	0.00	−1.9	−0.14
	C	0.24	0.00	−0.33	0.38
	D	0.24	0.00	−0.54	0.38
	$\langle r \rangle$	8.85	12.61	11.40	9.43
Along c axis	A	−0.046	−0.00026	−0.00043	−0.071
	B	−1.1	−0.64	0.13	−11
	C	−5.8	−5.8	−2.7	−11
	D	−5.1	−4.2	−2.1	−11
	$\langle r \rangle$	7.86	7.76	7.82	7.15
Obsd (J/k)/K		−5.4	−9.1	0—−0.3	−11.1

a) The constants in Eq. 6 (Type A) were obtained from the exchange integrals (in [K]) in Ref. 21. Those in Eqs. 7—9 were adjusted to give −11 K for the DTPV pair along the c axis. b) $\langle r \rangle$ is the mean value of the relevant interatomic distances [l/Å].

and TTV, respectively. These differences arise from the differences in the crystal structures. The McConnell's spin density Hamiltonian with $-1/r_{ij}^{AB}$ in place of J_{ij}^{AB} may be useful in finding the direction of the dominant exchange interaction and in estimating the order of the exchange coupling between the magnetic chains in crystals of aromatic radicals.

The author is much obliged to Professors Hiroaki Ohya-Nishiguchi and Yasuo Deguchi for continuous encouragement throughout this work and also indebted to Professors Noboru Hirota and Kazuo Mukai for illuminating discussions. Encouraging advices have been given by Professor Kazuhiko Ishizu, to which the author's thanks are due. Thanks are also due to the co-authors in this series for hearty cooperation. The calculations were performed at the Computer Centers of Kyoto and Ehime Universities.

References

1) a) J. Yamauchi, *Bull. Chem. Soc. Jpn.*, **44**, 2301 (1971); b) W. Duffy, Jr., and D. L. Strandburg, *J. Chem. Phys.*, **46**, 456 (1967); c) O. Takizawa, J. Yamauchi, H. Ohya-Nishiguchi, and Y. Deguchi, *Bull. Chem. Soc. Jpn.*, **44**, 3188 (1971); Yu. S. Karimov, *Zh. Eksp. Teor. Fiz. Pis'ma Red.*, **8**, 239 (1968); *Zh. Eksp. Teor. Fiz.*, **57**, 1962 (1969).

2) J. C. Bonner and M. E. Fisher, *Phys. Rev. A*, **135**, 640 (1964).

3) R. Kuhn and H. Trischmann, *Angew. Chem.*, **75**, 294 (1963).

4) R. Kuhn, F. A. Neugebauer, and H. Trischmann, *Monatsh. Chem.*, **97**, 525 (1966).

5) H. M. McConnell, *J. Chem. Phys.*, **39**, 1910 (1963).

6) R. Kuhn and H. Trischmann, *Monatsh. Chem.*, **95**, 457 (1964).

7) M. Mekata, *J. Phys. Soc. Jpn.*, **17**, 796 (1962).

8) K. Mukai, T. Yamamoto, M. Kohno, N. Azuma, and K. Ishizu, *Bull. Chem. Soc. Jpn.*, **47**, 1797 (1974).

9) N. Azuma, Y. Deguchi, F. Marumo, and Y. Saito, *Bull. Chem. Soc. Jpn.*, **48**, 825 (1975).

10) N. Azuma, Y. Deguchi, F. Marumo, and Y. Saito, *Bull. Chem. Soc. Jpn.*, **48**, 819 (1975).

11) N. Azuma, *Bull. Chem. Soc. Jpn.*, **53**, 2671 (1980).

12) P. H. H. Fischer, *Tetrahedron*, **23**, 1939 (1967).

13) D. E. Williams, *Acta Crystallogr., Sect. B*, **29**, 96 (1973).

14) P. W. Selwood, "Magnetochemistry," 2nd ed, Interscience Publisher, New York (1956).

15) N. Azuma, J. Yamauchi, K. Mukai, H. Ohya-Nishiguchi, and Y. Deguchi, *Bull. Chem. Soc. Jpn.*, **46**, 2728 (1973).

16) K. Mukai, N. Azuma, and K. Ishizu, *Bull. Chem. Soc. Jpn.*, **43**, 3618 (1970).

17) Unpublished data; *e.g.*, g_{xx}, g_{yy}, and g_{zz} of TTV are 2.0023, 2.0042, and 2.0038, respectively.

18) A. S. Edelstein, *J. Chem. Phys.*, **40**, 488 (1964).

19) See *e.g.*, T. Oguchi, "Statistical Theory of Magnetism," Syokabo, Tokyo (1970).

20) W. Duffy, Jr., D. L. Strandburg, and J. F. Deck, *J. Chem. Phys.*, **68**, 2097 (1978).

21) A. Dulčić and J. N. Herak, *Mol. Phys.*, **26**, 605 (1973).

22) P. O. Löwdin, *Rev. Mod. Phys.*, **34**, 80 (1962).

23) See *e.g.*, O. Takizawa, *Bull. Chem. Soc. Jpn.*, **49**, 583 (1976).

24) O. Kikuchi, "A Series of Monographs Modern Trends in Chemistry," Kohdansha, Tokyo (1971), Vol. 6, p. 137.

25) J. S. Brinen and M. K. Orloff, *Chem. Phys. Lett.*, **1**, 276 (1967); P. W. Kopf and R. W. Kreilick, *J. Am. Chem. Soc.*, **91**, 6569 (1969).

ESR Investigation of Alkali Metal Complexes of Galvinoxyl-labeled Benzo-15-crown-5 in Frozen Solution

Kazuo Mukai,* Nobuhito Ida, and Kazuhiko Ishizu
Department of Chemistry, Faculty of Science, Ehime University, Matsuyama 790
(Received July 18, 1981)

A stable galvinoxyl derivative (**1**) of benzo-15-crown-5 was prepared and the complex formation between the spin labeled crown ether **1** and the alkali metal and ammonium salts was studied by the ESR technique. Existence of the (2:1) complex of **1** with potassium, rubidium, and ammonium salts was confirmed by the observation of the triplet ESR spectra in ethanol rigid matrix at 77 K. Essentially the same ***g***- and ***D***-tensor values are observed for all the (2:1) complexes, indicating similar conformation of the ligand molecule **1**. The zero-field splitting parameters (*D* and *E*) are calculated on the basis of the spin distribution of **1** and the assumed molecular structures for the (2:1) complex. By comparing the observed *D* and *E* parameters with the calculated ones, the structure of the (2:1) complex in ethanol rigid matrix is discussed. On the other hand, the sodium complexes of **1** show a slightly asymmetric single line, suggesting the (1:1) complex formation between **1** and the sodium salts. No anions (SCN^-, Br^-, and I^-) have any appreciable effect on the ESR spectra of both the (2:1) and (1:1) complexes.

It is well known that the cyclic polyethers synthesized by Pedersen form stable complexes with alkali and alkaline earth metal ions, both in solution and in the solid state.[1-3] The stoichiometry of the crystalline complexes depends on the relative size of the "hole" in the cyclic polyether and of the cation. For instance, benzo-15-crown-5 with a hole 1.7—2.2 Å in diameter usually forms a (1:1) complex with sodium (1.90 Å in diameter), and (2:1) complexes with the ions larger than the hole. Recently, we have prepared a galvinoxyl derivative (**1**) of benzo-15-crown-5 (*i.e.*, galvinoxyl-benzo-15-crown-5 (**1**)) (see Fig. 1) and studied the complex formation of the spin-labeled crown ether (**1**) with NaSCN or KSCN salt by using the ESR technique.[4] A triplet ESR spectrum has been observed for the KSCN complex of **1** in ethanol rigid matrix at 77 K, indicating the formation of a sandwiched dimer. On the other hand, the result of ESR measurement of the NaSCN complex suggested a (1:1) complex formation between **1** and NaSCN.

In the present paper, in order to obtain further information on such complex formations, we have measured ESR spectra of the complexes of **1** with eight kinds of salts in ethanol rigid matrix. Typical triplet ESR spectra have been observed for the K^+, Rb^+, and NH^+_4 complexes of **1**, clearly showing the (2:1) complex formation between **1** and the salts. The zero-field splitting (ZFS) parameters (*D* and *E*) were calculated for the assumed molecular structures by using McLachlan's spin densities of **1** which is a monoradical half of the sandwiched dimer. On the basis of these data, the structure of the (2:1) complex has been discussed. Solvent effect on the structure of the (2:1) complex has also been studied. On the other hand, the sodium complexes of **1** showed a slightly asymmetric single line, suggesting the (1:1) complex formation between **1** and the sodium salts. Three anions, SCN^-, Br^-, and I^-, used in this study have been found to have little effect on the spectral characteristics of either the (2:1) or the (1:1) complex.

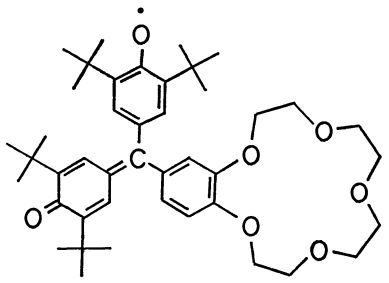

1

Fig. 1. Molecular structure of galvinoxyl-benzo-15-crown-5 (**1**).

Experimental

The phenol precursor of **1** was synthesized by condensation of 2,6-di-*t*-butylphenol (2.06 g) with 4′-formylbenzo-15-crown-5 (2.96 g) in KOH (0.66 g)–ethanol (30 cm^3) solution under a nitrogen atmosphere at 30 °C, as described in a previous paper.[4] An orange crystal of the phenol precursor showed a melting point 209—211 °C (softens at 176 °C): Found: C, 74.13; 8.74%. Calcd for $C_{43}H_{60}O_7$: C, 74.97: H, 8.78%. UV and visible (C_2H_5OH) 276 (ε 18500) and 434 nm (ε 30200); NMR (CCl_4) δ=1.23 (18H, s, *t*Bu, ring A), 1.43 (18H, s, *t*Bu, ring B), 3.5—4.2 (16H, m, $-CH_2-$), 5.37 (1H, s, OH, ring A), 6.70—6.82 (3H, m, ring C), 7.00 (2H, s, aromatic H, ring A), and 7.08 (2H, s, aromatic H, ring B).

Compound **1** was prepared by oxidation of the above phenol precursor with alkaline potassium hexacyanoferrate-(III) in diethyl ether solvent under a nitrogen atmosphere, with the temperature kept between 0—5 °C. Compound **1** was isolated as a stable dark brown crystal from the etherial solution: UV and visible (C_2H_5OH) 280 (ε 17000), 388 (ε 18400), and 455 nm (ε 49500).

The magnetic susceptibility of **1** was measured in the temperature range 55—300 K. The data have been corrected for the diamagnetic contribution of $\chi_{dia}=-0.437\times10^{-3}$ emu/mol calculated by Pascal's method. The susceptibility follows the Curie-Weiss law, with a paramagnetic Curie constant of 0.369±0.010 K·emu/mol and a Weiss constant of −2±3 K. The radical concentration of **1** calculated from the above Curie constant is 98%. All the ESR spectra were measured in a sealed, degassed system.

Table 1. *D*- and *g*-tensor values of the complexes of **1** with several salts in ethanol at 77 K

Salt	Complex	$\frac{\lvert D\rvert}{G}$ [a]	$\frac{\lvert E\rvert}{G}$ [a]	g_{zz} [b]	g_{yy}	g_{xx}	g_{av} [c]
KSCN	(2 : 1)	76.2	8.9	2.0032	2.0052	2.0072	2.0052
KBr	(2 : 1)	76.4	8.8	2.0030	2.0049	2.0069	2.0049
KI	(2 : 1)	75.9	8.7	2.0029	2.0049	2.0073	2.0051
RbI	(2 : 1)	76.4	8.8	2.0028	2.0048	2.0067	2.0048
NH_4SCN	(2 : 1)	76.2	8.6	2.0029	2.0050	2.0066	2.0048
NaSCN	(1 : 1)	a slightly asymmetric single line ($\Delta H_{msl}\simeq 6.6$ G)					
NaBr	(1 : 1)						
Na_2SO_4	(1 : 1)						

a) The experimental errors in the values of $|D|$ and $|E|$ are ± 0.3 G. 1 G $=10^{-4}$ T. b) The experimental errors in the values of g_{xx}, g_{yy}, g_{zz}, and g_{av} are ± 0.0002. c) $g_{av}=1/3(g_{xx}+g_{yy}+g_{zz})$.

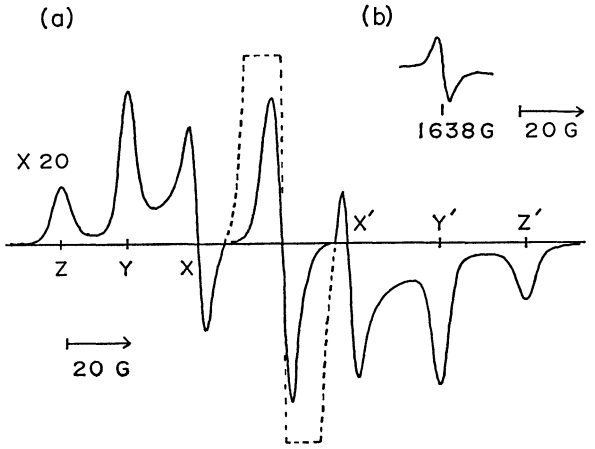

Fig. 2. ESR spectrum of the KI complex of **1** in ethanol at 77 K; (a) $\Delta m_s=\pm 1$ transition and (b) $\Delta m_s=\pm 2$ transition.

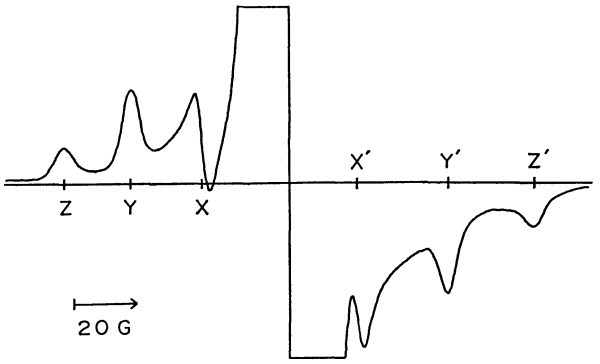

Fig. 3. ESR spectrum of the RbI complex of **1** in ethanol at 77 K.

Results and Discussion

Ethanol Rigid Matrix ESR Spectra of the Alkali Metal Complexes of ***1***. An ethanol solution of **1** (3.0×10^{-3} mol dm^{-3}) containing equimolar KI salt clearly shows three pairs of absorption lines with the same order of intensity at 77 K, as shown in Fig. 2(a). A slightly asymmetric central line with a width of about 6.0 G (1 G $=10^{-4}$ T) at $g\simeq 2.005$ shows a shape essentially the same as that of the metal-free **1** ($\Delta H_{msl}=$ 6.5 G and $g\simeq 2.005$), and the relative intensity of this central line changes depending on the ratio of the potassium salt to **1**. Therefore, this line is attributable to the metal-free **1** and/or the (1:1) complex between **1** and KI. The three pairs of absorption lines apparently represent zero-field splittings arising from the intermolecular spin-spin dipolar interaction of two electrons in a triplet state. In fact, the forbidden transition ($\Delta m_s=\pm 2$) was observed at about 1638 G, as shown in Fig. 2(b). These results clearly indicate the (2:1) complex formation between **1** and KI.

The spin Hamiltonian for the triplet radical pair may be expressed by

$$H=\beta \boldsymbol{H}\cdot\hat{\boldsymbol{g}}\cdot\boldsymbol{S}+\boldsymbol{S}\cdot\hat{\boldsymbol{D}}\cdot\boldsymbol{S} \quad (1)$$

$$=\beta \boldsymbol{H}\cdot\hat{\boldsymbol{g}}\cdot\boldsymbol{S}-XS_x^2-YS_y^2-ZS_z^2, \quad (2)$$

where $\hat{\boldsymbol{g}}$ is $\boldsymbol{g}$ tensor, $\hat{\boldsymbol{D}}$ is the fine structure tensor with principal values of $-X$, $-Y$, and $-Z$, and the other symbols have the usual meanings. The separations (ZZ', YY', and XX') between the three pairs of absorption lines in the spectrum of the KI complex are 151.8 $\pm$0.6, 102.0$\pm$0.6, and 49.8$\pm$0.6 G, respectively, so the ZFS parameters, $|D|$ and $|E|$, were evaluated as 75.9$\pm$0.3 and 8.7$\pm$0.3 G, respectively, by the method of Wasserman *et al.*[5] Assuming that the principal axes of the *D*- and *g*-tensors are coaxial, *g*-tensor values have been estimated from the positions of three pairs of turning points (ZZ', YY', and XX').[5,6] They are $g_{zz}=2.0029\pm 0.0002$ (Z, Z'), $g_{yy}=2.0049\pm 0.0002$ (Y, Y'), and $g_{xx}=2.0073\pm 0.0002$ (X, X').

First, the effect of the negative ions on the structure of the KI complex of **1** was examined. The ESR spectra of both the KBr and KSCN complexes of **1** in ethanol at 77 K are similar to that of the KI complex of **1**, and the observed *D*- and *g*-tensor values of these (2:1) complexes are summarized in Table 1. Live and Chan[7] have measured the proton NMR spectra of some crown ethers and their alkali metal complexes in organic solvents, and studied the solution structure of the "crown" cyclic polyether rings in detail. They observed the variation in chemical shifts of ether protons with anions (I^-, SCN^-, and ClO^-_4), and concluded that the difference in the shifts is due to the ion-pair formation. However, as it is clear from the results shown in Table 1, the variation in ZFS parameters with anions is almost negligible in the present (2:1) complexes. The result

indicates that the ion pairing is unimportant in determining the structure of the (2:1) complex.

Second, the effects of the positive ions on the complex formation and on the molecular structure of the complex were studied. The ESR spectrum of the RbI complex of **1** in ethanol rigid-matrix at 77 K shows a shape essentially the same as that of the KI complex (see Fig. 3), except for the difference in the central signal intensity, indicating the (2:1) complex formation. The ZFS parameters (D and E) and g-tensor values have been estimated from the positions of the three pairs of turning points (ZZ', YY', and XX'), as performed for the KI complex of **1**. These values are $|D|=76.4\pm0.3$ G, $|E|=8.8\pm0.3$ G, $g_{zz}=2.0028\pm0.0002$, $g_{yy}=2.0048\pm0.0002$, and $g_{xx}=2.0067\pm0.0002$. The ethanol rigid-matrix ESR spectrum of the NH_4SCN complex of **1** is also quite similar to that of the KI complex of **1**, giving the ZFS parameters of $|D|=76.2\pm0.3$ G and $|E|=8.6\pm0.3$ G. The ZFS constants are the same for all the (2:1) complexes of **1** examined in the present work. We can then conclude that the same molecular conformation persists in all the (2:1) complexes studied. On the other hand, the solution of **1** (3.0×10^{-3} mol dm^{-3}) containing the equimolar NaSCN salt shows a slightly asymmetric single line with a width of 6.6 G located at $g\simeq2.005$ at 77 K, unequivocally suggesting (1:1) complex formation between **1** and NaSCN. Further, by changing the anion of Na salt from SCN^- to Br^- and SO_4^{2-} in the ethanol solution, no detectable changes were observed in the ESR spectra (see Table 1).

*The Structure of the (2:1) Complexes of **1** with K, Rb, and NH_4 Salts.* The crystal structure of a (2:1) complex of benzo-15-crown-5 with potassium iodide has been investigated by Mallinson and Truter.[8] The crystal system of the complex is tetragonal with a space group of P4/n and with lattice constants of $a=b=17.84$, $c=9.75$ Å, and $z=4$. The complex cation has crystallographic symmetry $\bar{1}$, the potassium being 'sandwiched' between the two centro-symmetrically related ligand molecules. In each of these, the five ether-oxygen atoms are approximately coplanar, the cation lying 1.67 Å away from this plane, so that the ten oxygen neighbors form a pentagonal antiprism. The benzo-group is nearly coplanar with the oxygens, the greatest deviation being 0.11 Å. If the KI complex of **1** takes a conformation (hereafter referred to as the "*trans*" conformation) similar to that of the benzo-15-crown-5 complex, the interatomic distance between the central triphenylmethyl carbon atoms in the pair of **1** will become about 13 Å. A zero-field splitting of $|D|=75.9$ G has been observed for the KI complex of **1**, as described above. Consequently, the calculated average interelectronic distance, using a model of two-point dipoles ($|D|=(3/2)g\beta r^{-3}$), is about 7.2 Å. From comparison of these distances, the "*trans*" conformation is not acceptable for the KI complex of **1**. Therefore, in order to clarify the structure of the (2:1) complex of **1** with KI in ethanol rigid matrix, the calculations of the D-tensor values were performed for the assumed structure of the complex, using McLachlan's spin densities of **1** which is considered to be a monoradical half of the (2:1) complex.[9,10]

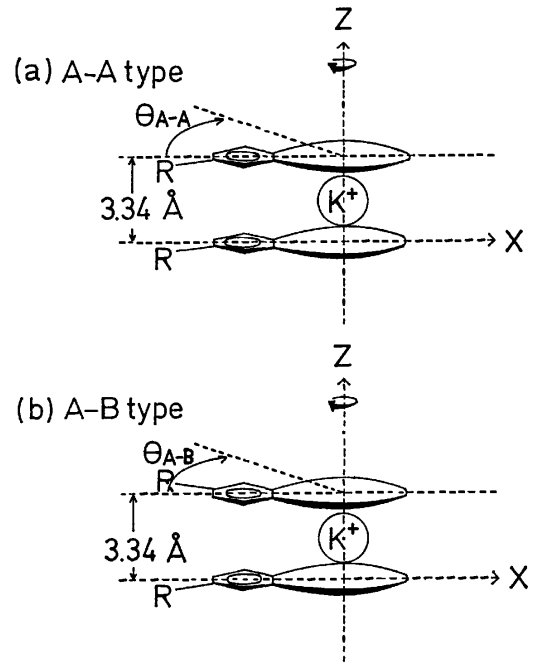

Fig. 4. Molecular structures and the coordinate systems chosen for "*cis*" conformation of the K complex of **1**.
(a) A–A type, (b) A–B type.

For the KI complex of **1**, we can expect two possible structures, (i) and (ii), in which each monoradical half is considered to have a planar structure, as a whole molecule. These two structures, (i) and (ii), are shown in Fig. 4 and named as "A–A type" and "A–B type" structures, respectively. Thus, as a most plausible case, the D-tensor values were calculated, assuming that the interplanar spacing between the two monoradical halves is 3.34 Å and varying the rotation angles θ_{A-A} and θ_{A-B}. The coordinate systems (x, y, and z) chosen for both the structures are shown in Fig. 4, where $\theta=0°$ corresponds to a planar "*cis*" conformation and $\theta=180°$ is a planar "*trans*" conformer in each structure.

The orbital containing the unpaired electron of phenylgalvinoxyl radical has, at least in the Hückel approximation, a node in the central phenyl ring; in fact, the results of McLachlan MO calculation of phenylgalvinoxyl[11] showed the exsistence of a very small unpaired electron density (1.0—1.5%) in the phenyl ring, and, further, an ENDOR study found a small hyperfine splitting ($a^H=0.207$ G) for the phenyl-ring protons.[11] In such a case, the unpaired electron distribution of **1** must be similar to that of phenylgalvinoxyl. In fact, the values of the hyperfine splittings ($a_m^H=1.31\pm0.02$ G) of the *meta* ring protons and the isotropic g_{iso} value ($=2.0044\pm0.0001$) of **1** show an excellent agreement with the corresponding values ($a_m^H=1.32\pm0.02$ G, $g_{iso}=2.0044\pm0.0001$) of phenylgalvinoxyl.

The D-tensor components of the dipolar splittings

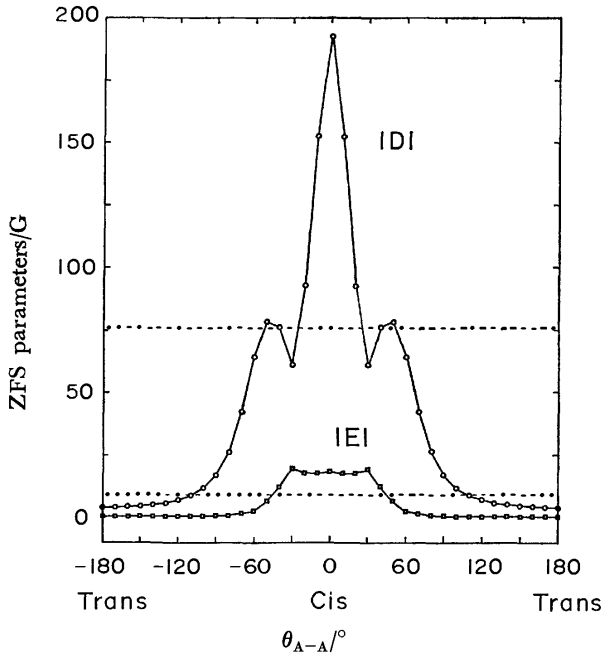

Fig. 5. The variation of the ZFS parameters $|D|$ and $|E|$ as a function of the rotation angle θ_{A-A}. Broken lines represent the observed $|D|$ (75.9 G) and $|E|$ (8.7 G) values for the KI complex of **1**.

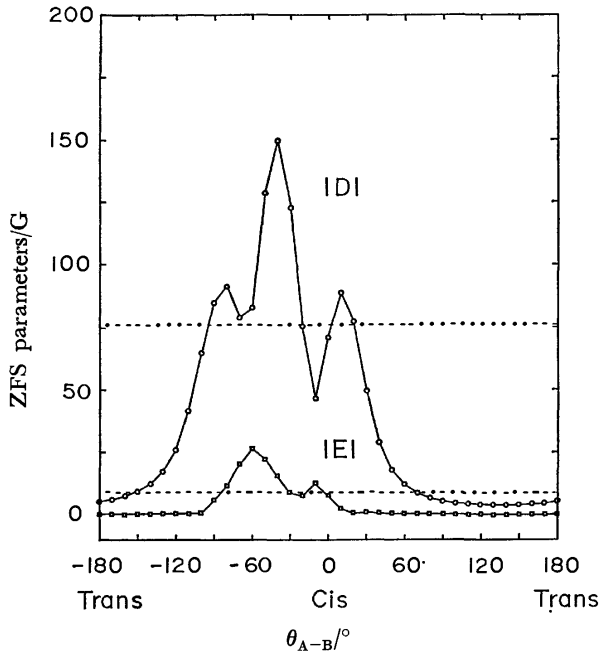

Fig. 6. The variation of the ZFS parameters $|D|$ and $|E|$ as a function of the rotation angle θ_{A-B}. Broken lines represent the observed $|D|$ (75.9 G) and $|E|$ (8.7 G) values for the KI complex of **1**.

can be calculated with the aid of the following equations:

$$D_{mm} = (1/2)g^2\beta^2 \sum_{i,j} \rho_i\rho_j(r_{ij}^2 - 3m_{ij}^2)/r_{ij}^5, \quad (3)$$

$(m = x, y, z)$

$$D_{mn} = (1/2)g^2\beta^2 \sum_{i,j} \rho_i\rho_j(-3m_{ij}n_{ij})/r_{ij}^5, \quad (4)$$

$(m, n = x, y, z;$ but $m \neq n)$

where r_{ij} is the distance between the i and j atoms, and ρ_i and ρ_j are the McLachlan π-spin densities[11] on the i-th atom in one phenylgalvinoxyl group and the j-th atom in the other phenylgalvinoxyl group, respectively, in a (2:1) complex. Here we have used the following bond lengths for the galvinoxyl group: the C–O bond length is 1.27 Å and the C–C bond length is 1.40 Å on the average, as obtained by an X-ray analysis of the galvinoxyl radical.[12] Atomic coordinates of benzo-15-crown-5 are taken from its KI complex reported by Mallinson and Truter.[8] Then, the resulting tensor was diagonalized, giving the principal values (X, Y, and Z) and thus, the zero-field splitting parameters, D and E.

Figures 5 and 6 show just how the ZFS parameters D and E vary as a function of θ_{A-A} and θ_{A-B}, respectively. In the case of A–A structure, the D parameter varies with θ_{A-A} from 192.3 G for $\theta_{A-A}=0°$ to 3.9 G for $\theta_{A-A}=180°$ and the E parameter from 19.3 G for $\theta_{A-A}=30°$ to 0.1 G for $\theta_{A-A}=180°$, but the dependence on the changes in θ_{A-A} is not simple. Similarly, in the case of A–B structure, the D and E parameters vary with θ_{A-B} from 149.3 G ($\theta_{A-B}=-40°$) to 3.9 G ($\theta_{A-B}=140°$) and from 26.2 G ($\theta_{A-B}=-60°$) to 0.1 G ($\theta_{A-B}=170°$), respectively. By comparing the observed D and E parameters ($|D|=75.9$ G, $|E|=8.7$ G) with the calculated ones, agreements were found for two cases of about $\theta_{A-A}=\pm45°$ ($|D|=77.5$ G, $|E|=9.1$ G) in A–A structure, and in A–B structure, for two cases of about $\theta_{A-B}=0°$ ($|D|=71.3$ G, $|E|=7.6$ G) and $\theta_{A-B}=-20°$ ($|D|=75.9$ G, $|E|=7.5$ G).

Unfortunately, it is not possible to decide whether the KI complex takes an "A–A" or "A–B" structure because both the D and E values experimentally obtained can be well explained by those calculated for the above structures. Although the calculation presented here is of a very approximate nature for the (2:1) complex of **1**, the result has shown that the "*trans*" conformation observed for the KI complex of benzo-15-crown-5 by the X-ray analysis is improbable for the present KI complex of **1** in ethanol rigid matrix. This is consistent with our previous expectation. The results of the calculation of the ZFS parameters suggest that the complex has a structure near to "*cis*" conformation rather than "*trans*" one, showing the overlap between two galvinoxyl groups in the complex. It is probable that the van der Waals interaction between two galvinoxyl groups induces such a conformation.

As described in a previous section, **1** makes the (2:1) complex with Rb and NH_4 salts as well. If the Rb and NH_4 complexes of **1** also have a "sandwiched" structure with an alkali metal ion between the two benzo-15-crown-5 rings, we can expect the increase in the interplanar spacing between the two crown ether rings, as the ion diameter increases from K^+ (2.66 Å) to Rb^+ (2.96 Å) or NH^+_4 (2.84 Å). This will induce the decrease in the ZFS parameter $|D|$. However, the $|D|$ and $|E|$ values observed for the K, Rb, and NH_4 complexes remain constant, within the limit of experimental error (see Table 1). As

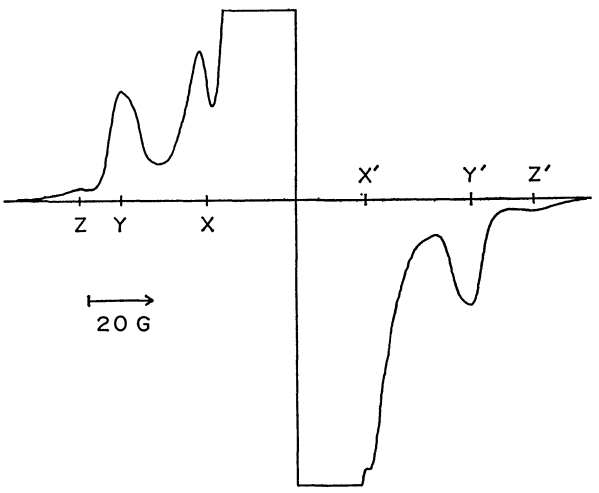

Fig. 7. ESR spectrum of the KSCN complex of **1** in 1,2-dichloroethane at 77 K.

Table 2. *D*- and *g*-tensor values of the KSCN complex of **1** in several solvents at 77 K

Solvent	$\frac{\lvert D\rvert}{G}$	$\frac{\lvert E\rvert}{G}$	g_{zz}	g_{yy}	g_{xx}	g_{av}
Ethanol	76.2	8.9	2.0032	2.0052	2.0072	2.0052
2-Propanol	76.1	8.8	2.0029	2.0048	2.0069	2.0049
1-Butanol	76.9	8.8	2.0032	2.0052	2.0073	2.0052
1,2-Dichloroethane	73.5	13.3	2.0029	2.0050	2.0072	2.0050

the results of the calculation of the ZFS parameters indicate, the KI complex of **1** is thought to have a structure close to "*cis*" conformation, in which the galvinoxyl skeletons stack over one another. In such a case, because of the overlapping of the bulky tertiary butyl group, the real interplanar spacing between the two crown ether rings will become larger than that (3.34 Å) reported for the KI complex of benzo-15-crown-5.[8] Therefore, the cavity which exists between the two polyether rings can accommodate the K^+, Rb^+, and NH^+_4 ions without varying the intermolecular distance between the two galvinoxyl group. Thus, we can understand the experimental fact that the ZFS constants are the same for all the (2:1) complexes of **1**.

Solvent Effect on the Structure of the Potassium Complex of 1. In addition to the above van der Waals interaction, the asymmetric environment due to frozen solvent molecules may contribute to the change in molecular structure found for the K complex of **1** in the low-temperature rigid matrix. Therefore, solvent effect on the structure of the (2:1) complex of **1** with KSCN has been studied. The solubilities of **1** and KSCN place some restriction on the choice of solvents. For this reason, ethanol, 2-propanol, 1-butanol, and 1,2-dichloroethane solvents could only be used in the present study. In the KSCN complex of **1**, identical triplet spectra were obtained in frozen ethanol, 2-propanol, and 1-butanol solutions, while a different triplet spectrum was obtained in frozen 1,2-dichloroethane solution, as shown in Fig. 7. The observed $|D|$ and $|E|$ values are summarized in Table 2. The result indicates that the change in conformation for the (2:1) complex is almost negligible for the above alcoholic solvents. On the other hand, the $|D|$ (73.5 G) and $|E|$ (13.3 G) values in 1,2-dichloroethane are 2.7 G smaller and 4.4 G larger than the corresponding ones in ethanol, respectively. These results may be explained by assuming that the rotation angle θ_{A-A} or θ_{A-B} varies several degrees in 1,2-dichloroethane solvent, as it can be seen from the results shown in Figs. 5 and 6. It has been reported that solvent molecules may play an important role in fixing the conformation of the triplet molecules in frozen solution.[13–15] However, the present experimental results suggest that such a role of solvent molecules is not notable in the (2:1) complex of **1**.

We wish to thank Miss Yoshiko Kumamoto for her kind help in the synthesis of **1**.

References

1) C. J. Pedersen, *J. Am. Chem. Soc.*, **89**, 7017 (1967).
2) C. J. Pedersen, *J. Am. Chem. Soc.*, **92**, 386 (1970).
3) J. J. Christensen, D. J. Eatough, and R. M. Izatt, *Chem. Rev.*, **74**, 351 (1974), and references cited therein.
4) K. Mukai, N. Iida, Y. Kumamoto, H. Kohama, and K. Ishizu, *Chem. Lett.*, **1980**, 613.
5) E. Wasserman, L. C. Snyder, and W. A. Yager, *J. Chem. Phys.* **41**, 1763 (1964).
6) K. Mukai, T. Mishina, and K. Ishizu, *J. Chem. Phys.*, **66**, 1680 (1977).
7) D. Live and S. I. Chan, *J. Am. Chem. Soc.*, **98**, 3769 (1976).
8) P. R. Mallinson and M. R. Truter, *J. Chem. Soc., Perkin Trans. 2*, **1972**, 1818.
9) N. Azuma, H. Ohya-Nishiguchi, J. Yamauchi, K. Mukai, and Y. Deguchi, *Bull. Chem. Soc. Jpn.*, **47**, 2369 (1974).
10) K. Mukai and A. Sogabe, *J. Chem. Phys.*, **72**, 598 (1980).
11) K. Mukai, T. Kamata, T. Tamaki, and K. Ishizu, *Bull. Chem. Soc. Jpn.*, **49**, 3376 (1976).
12) D. E. Williams, *Mol. Phys.*, **16**, 145 (1969).
13) A. Calder, A. R. Forrester, P. G. James, and G. R. Luckhurst, *J. Am. Chem. Soc.*, **91**, 3724 (1969).
14) T. Ito and J. Higuchi, *Chem. Lett.*, 1519 (1974).
15) B. J. Scheve and P. J. Wagner, *Chem. Phys. Lett.*, **25**, 324 (1974).

The Structure of the Cyclodextrin Complex. XII. Crystal Structure of α-Cyclodextrin-1-Phenylethanol (1 : 1) Tetrahydrate

Kazuaki HARATA

Research Institute for Polymers and Textiles, 1-1-4, Yatabe-Higashi, Tsukuba, Ibaraki 305

(Received August 1, 1981)

The crystal structure of the α-cyclodextrin–1-phenylethanol (1:1) tetrahydrate, $C_{36}H_{60}O_{30}\cdot C_8H_{10}O\cdot 4H_2O$, was determined by the X-ray method. The crystal is monoclinic, the space group being $P2_1$ with $Z=2$; the cell dimensions are $a=8.176(1)$, $b=23.930(2)$, $c=13.853(1)$ Å, and $\beta=106.69(1)°$. The structure was solved by means of the Patterson map and the trial-and-error method combined with the rigid-body least-squares technique. Refinement was carried out by the block-diagonal least-squares method to the final R-value of 0.040 for 3565 reflections. α-Cyclodextrin molecules are stacked along the a axis in the head-to-tail fashion to form a channel-type structure, and are tilted by 17.0° against the channel axis. Owing to the lateral shift of α-cyclodextrin ring parallel to the molecular plane, neighboring α-cyclodextrin molecules along the channel are linked by only one weak hydrogen bond. The 1-phenylethanol molecule is sandwiched between stacked α-cyclodextrin molecules. S-(−) and R-(+) isomers of 1-phenylethanol are each located at the same position with the statistical disorder of the hydroxyl group with the occupancy of 0.5. Columns formed by the stack of α-cyclodextrin are closely packed, being linked with one another by many hydrogen bonds. Water molecules are located in two kinds of intermolecular spaces between α-cyclodextrin columns.

Cyclodextrins form diastereoisomers with optically active guests since they consist of optically active glucose residues. On this basis, complexation of cyclodextrins has been applied as a method for resolution of racemic molecules.[1] We have investivated the host-guest stereospecificity in the complex formation of cyclodextrins with benzene derivatives by the X-ray method.[2] In this paper, we deal with the α-cyclodextrin complex with racemic 1-phenylethanol to investigate the interaction with optically active molecules.

Experimental

α-Cyclodextrin was dissolved in a hot aqueous solution saturated with 1-phenylethanol to prepare a 5% solution, and then the solution was allowed to stand at 40 °C. Colorless plate-like crystals were obtained. Measurements of lattice parameters and reflection intensities were carried out on a Nicolet P3/F diffractometer with graphite-monochromated Cu $K\alpha$ radiation. By the θ-2θ scan mode, 3565 independent reflections with $|F_o|\geqq 3\sigma(F)$ were obtained up to 115° in 2θ. No corrections were made for absorption and extinction effects.

Crystal Data: $C_{36}H_{60}O_{30}\cdot C_8H_{10}O\cdot 4H_2O$; F.W.=1239.1; monoclinic; space group $P2_1$; $Z=2$; $a=8.176(1)$, $b=23.930(2)$, $c=13.853(1)$ Å, $\beta=106.69(1)°$; $V=2596.2$ Å^3; $D_x=1.585$ and $D_m=1.577$ g cm^{-3}.

Determination and Refinement of the Structure

The orientation of α-cyclodextrin in a unit cell was deduced by inspection of a Patterson map. The position of the molecule was determined by the trial-and-error method. The positional and orientational parameters of each glucose residue were corrected by the rigid-body least-squares method. 1-Phenylethanol and water molecules were found on Fourier and difference-Fourier maps. Both S-(−) and R-(+) isomers of 1-phenylethanol are found with the statistical disorder of the hydroxyl group. The occupancy was estimated from an electron-density map but not refined. Hydrogen atoms were found on a difference-Fourier map. Refinement of the structure was carried out by the block-diagonal least-squares method. The quantity minimized was $\Sigma w(|F_o|-|F_o|)^2$ with $w=1.0$ for all the reflections. The final R-value was 0.040. The atomic scattering factors were taken from the "International Tables for X-Ray Crystallography."[3] Final atomic coordinates are given in Table 1. Tables of anisotropic temperature factors of non-

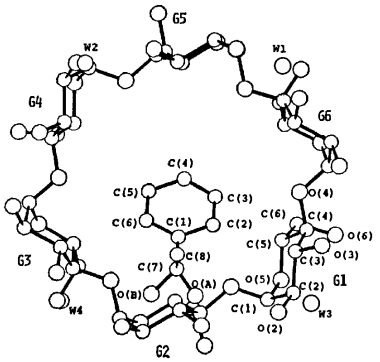

Fig. 1. A numbering scheme of the α-cyclodextrine–1-phenylethanol (1:1) tetrahydrate.
O(A) and O(B) denote disordered hydroxyl groups, corresponding to S-(−) and R-(+) isomers, respectively. Water molecules are denoted by W1, W2, W3, and W4.

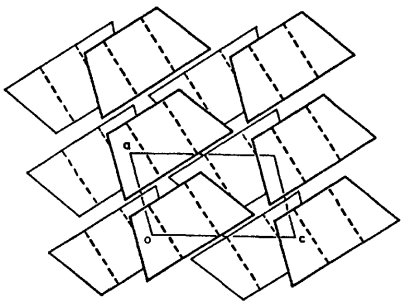

Fig. 2. A packing feature of α-cyclodextrin molecules viewed down along the b axis.

TABLE 1. FRACTIONAL COORDINATES ($\times 10^4$) AND B_{eq}[a] (B/Å^2) OF NON-HYDROGEN ATOMS[b]

	x	y	z	B_{eq}		x	y	z	B_{eq}
C(1,G1)	-809(7)	1144(2)	-315(4)	2.61	O(3,G4)	805(5)	4588(2)	4557(3)	3.82
C(2,G1)	-1855(7)	762(2)	150(4)	2.66	O(4,G4)	1998(4)	4291(2)	2852(2)	2.31
C(3,G1)	-1062(7)	743(2)	1284(4)	2.63	O(5,G4)	5816(4)	4078(2)	4991(3)	2.61
C(4,G1)	800(6)	581(2)	1543(4)	2.26	O(6,G4)	5911(8)	4898(3)	3378(5)	4.52
C(5,G1)	1785(7)	942(2)	979(4)	2.58	C(1,G5)	5097(7)	1659(2)	6254(4)	2.46
C(6,G1)	3564(7)	726(3)	1088(5)	4.15	C(2,G5)	4091(8)	2006(2)	6812(4)	3.43
O(2,G1)	-3551(5)	977(2)	-79(3)	3.24	C(3,G5)	3520(7)	2553(2)	6248(4)	3.30
O(3,G1)	-2002(5)	346(2)	1693(3)	3.49	C(4,G5)	5070(7)	2869(2)	6096(4)	2.51
O(4,G1)	1486(4)	694(2)	2603(3)	2.36	C(5,G5)	6110(6)	2483(2)	5612(4)	2.67
O(5,G1)	901(4)	946(2)	-87(3)	2.59	C(6,G5)	7770(7)	2735(3)	5550(5)	3.30
O(6,G1)	3533(6)	150(2)	759(3)	5.25	O(2,G5)	2678(6)	1681(2)	6864(3)	4.86
C(1,G2)	-1687(7)	3342(2)	-764(4)	2.49	O(3,G5)	2724(6)	2909(2)	6814(4)	5.21
C(2,G2)	-3264(7)	2998(2)	-810(4)	2.49	O(4,G5)	4390(4)	3316(1)	5405(3)	2.31
C(3,G2)	-2760(7)	2448(2)	-225(4)	2.72	O(5,G5)	6531(5)	1971(2)	6176(3)	2.52
C(4,G2)	-1437(7)	2144(2)	-616(4)	2.32	O(6,G5)	8921(6)	2850(2)	6518(3)	3.92
C(5,G2)	75(6)	2523(2)	-607(4)	2.48	C(1,G6)	2402(7)	267(2)	3237(4)	2.56
C(6,G2)	1317(7)	2262(2)	-1111(4)	2.88	C(2,G6)	1724(7)	235(2)	4155(4)	2.83
O(2,G2)	-4404(5)	3309(2)	-407(3)	3.32	C(3,G6)	2025(7)	790(2)	4705(4)	2.65
O(3,G2)	-4257(5)	2122(2)	-375(3)	3.54	C(4,G6)	3882(7)	958(2)	4964(7)	2.47
O(4,G2)	-827(5)	1689(2)	78(3)	2.46	C(5,G6)	4567(7)	933(2)	4043(4)	2.50
O(5,G2)	-539(5)	3033(2)	-1157(3)	2.71	C(6,G6)	6464(7)	1016(2)	4293(4)	3.24
O(6,G2)	466(5)	2064(2)	-2112(3)	3.03	O(2,G6)	-57(5)	108(2)	3801(3)	3.73
C(1,G3)	1623(7)	4723(2)	2127(4)	2.50	O(3,G6)	1490(5)	726(2)	5597(3)	4.08
C(2,G3)	-299(7)	4794(2)	1756(4)	2.85	O(4,G6)	4007(4)	1534(1)	5295(3)	2.26
C(3,G3)	-1109(7)	4242(2)	1337(4)	2.75	O(5,G6)	4172(5)	393(2)	3560(3)	2.58
C(4,G3)	-362(7)	4052(2)	498(4)	2.54	O(6,G6)	7361(5)	708(2)	5158(3)	3.75
C(5,G3)	1597(7)	4052(2)	827(4)	2.53	C(1,PE)	-3629(8)	2492(3)	2297(4)	4.00
C(6,G3)	2318(8)	3971(3)	-66(5)	3.70	C(2,PE)	-2796(10)	1981(3)	2505(5)	5.21
O(2,G3)	-916(5)	4965(2)	2587(3)	3.14	C(3,PE)	-1141(11)	1952(4)	3031(6)	6.92
O(3,G3)	-2915(5)	4295(2)	940(3)	3.81	C(4,PE)	-203(9)	2420(6)	3364(5)	7.81
O(4,G3)	-939(5)	3485(2)	258(3)	2.58	C(5,PE)	-1000(13)	2948(5)	3149(7)	8.28
O(5,G3)	2236(5)	4578(2)	1294(3)	2.62	C(6,PE)	-2705(11)	2974(3)	2604(6)	5.90
O(6,G3)	1390(6)	4280(2)	-935(3)	4.04	C(7,PE)	-5505(9)	2506(5)	1712(5)	6.87
C(1,G4)	4975(7)	3870(2)	5679(4)	2.54	C(8,PE)	-6628(9)	2505(4)	2432(5)	5.81
C(2,G4)	3436(7)	4237(2)	5646(4)	2.59	O(A,PE)	-6080(11)	2225(5)	998(7)	5.86
C(3,G4)	2193(7)	4222(2)	4587(4)	2.55	O(B,PE)	-6016(11)	2881(5)	1027(7)	5.37
C(4,G4)	3123(7)	4404(2)	3832(4)	2.45	O(W1)	-762(6)	985(2)	7150(3)	4.24
C(5,G4)	4776(7)	4078(2)	3945(4)	2.68	O(W2)	-600(6)	3928(2)	7115(3)	4.16
C(6,G4)	5868(8)	4318(3)	3331(5)	4.01	O(W3)	4409(12)	489(7)	-1628(10)	22.98
O(2,G4)	2623(5)	4060(2)	6372(3)	3.08	O(W4)	4845(8)	4221(2)	-1740(4)	5.92

a) $B_{eq}=8\pi^2(u_1^2+u_2^2+u_3^2)/3$, where u_i is the root-mean-square deviation in the i-th principal axis of the thermal ellipsoid. b) Occupancy of each of O(A,PE) and O(B,PE) is 0.5.

hydrogen atoms, atomic parameters of hydrogen atoms, observed and calculated structure factors, bond distances, angles, and conformation angles in α-cyclodextrin are kept at The Chemical Society of Japan (Document No. 8218). The calculations were performed on a FACOM M-200 computer at the RIPS Center, Tsukuba.

Description and Discussion of the Structure

Outline of the Structure. Structure and numbering scheme of the complex are shown in Fig. 1. A packing feature of α-cyclodextrin in the crystal is illustrated in Fig. 2. α-Cyclodextrin molecules are stacked with a head-to-tail mode along the a axis. The molecules are laterally shifted to each other parallel to the molecular plane. Both *S*-(−) and *R*-(+) isomers of the guest 1-phenylethanol molecule are sandwiched at the same position with a statistical disorder of the hydroxyl group by the two adjacent α-cyclodextrin molecules along the channel.

Conformation of α-Cyclodextrin. Average bond distances and angles over six glucose residues are shown in Fig. 3. Geometrical data of α-cyclodextrin ring are given in Tables 2 and 3. Average bond distances and angles are in good agreement with those of the α-cyclodextrin–benzaldehyde complex[2] having a similar crystal structure. All primary hydroxyl groups are in a *gauche-gauche* conformation; average conformation angles of O(5)–C(5)–C(6)–O(6) and C(4)–C(5)–C(6)–O(6) are −71.7° and 50.0°, respectively. Distances between adjacent glycosidic oxygen atoms (O(4)) are in the range from 4.17 to 4.31 Å with the average value of 4.23 Å. Torsion-angle indexes of glucose residues lie in rather a narrow region (124.5—137.5), indicating that the conformation of each pyranose ring is nearly identical.

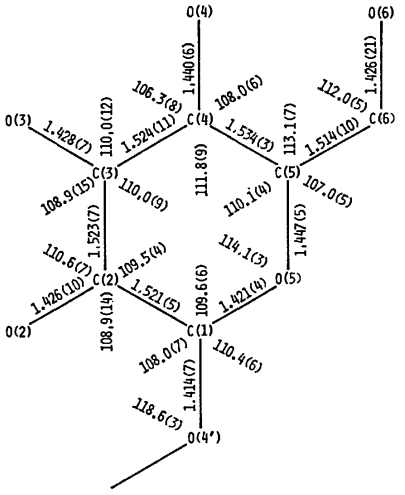

Fig. 3. Average bond distances and angles over six glucose residues in α-cyclodextrin.
Standard deviations in parentheses were estimated according to the equation: $\sigma=[\sum_{i=1}^{6}(x_i-\bar{x})^2/5]^{1/2}$ where x_i referes to bond distance or angle in i-th glucose residue and $\bar{x}$ is the average value.

Diagonal distances measured between glycosidic oxygen atoms and the good planarity of these atoms (Table 3) show that the α-cyclodextrin ring is a nearly regular hexagon although the G1···G4 distance is slightly larger than the G2···G5 distance. Distances between O(2) and O(3) of adjacent glucose residues

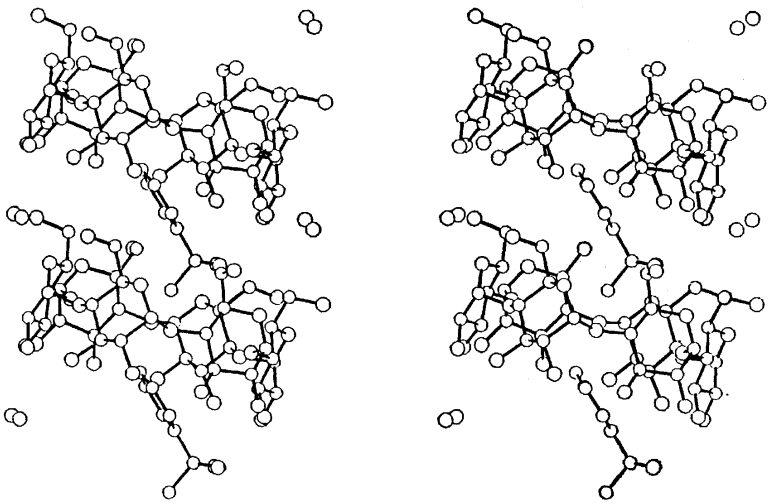

Fig. 4. A stereo-drawing of stacking feature of α-cyclodextrin.

Table 2. Selected geometrical data for α-cyclodextrin ring

I. O(4)···O(4) distances

Distance (l/Å)		Distance (l/Å)	
O(4,G1)···O(4,G2)	4.21	O(4,G5)···O(4,G6)	4.27
O(4,G1)···O(4,G6)	4.22	O(4,G1)···O(4,G4)	8.62
O(4,G2)···O(4,G3)	4.31	O(4,G2)···O(4,G5)	8.35
O(4,G3)···O(4,G4)	4.18	O(4,G3)···O(4,G6)	8.40
O(4,G4)···O(4,G5)	4.22		

II. Torsion-angle index[a] and tilt angle[b]

Residue	Torsion-angle index(ϕ/°)	Tilt-angle(ϕ/°)
G1	131.2	14.6
G2	124.5	8.1
G3	137.5	11.5
G4	132.5	8.7
G5	130.4	4.1
G6	132.9	10.1

a) The torsion-angle index is defined as: $|\phi(C(1)-C(2))|+|\phi(C(2)-C(3))|+|\phi(C(5)-O(5))|+|\phi(O(5)-C(1))|-|\phi(C(3)-C(4))|-|\phi(C(4)-C(5))|$. b) The tilt-angle is defined as the angle made by the plane through six O(4) atoms and the plane through C(1), C(4), O(4), and O(4′) of each glucose residue.

vary in the range from 2.81 to 3.04 Å. These hydroxyl groups form a round circle with six intramolecular O(2)···O(3) hydrogen bonds. Significant conformational differences in the macrocyclic ring, compared with the benzaldehyde complex,[2] are observed in the tilt-angles of glucose residues against the least-squares planes through six O(4) atoms, in spite of the similarity in the molecular packing. The tilt-angles of the 1-phenylethanol complex (4.1—14.6°) are smaller than those values of the benzaldehyde complex (10.9—19.9°). This may be interpreted in terms of differences in the molecular packing and intermolecular hydrogen bonds. As will be discussed later, the more tilted orientation of glucose residue in the benzaldehyde complex is held by intermolecular hydrogen bonds along the channel. In the 1-phenylethanol complex, however, the small tilt of glucose residue may be preferable to form hydrogen bonds with neighboring α-cyclodextrin molecules arranged in sheets parallel to the molecular plane.

Table 3. Least-squares planes and deviations of atoms from the plane

The plane equation is of the $AX+BY+CZ=D$ from, where X, Y, and Z are the coordinates in Å units along the a, b, and c* axes, respectively.

I. The plane through six O(4) atoms			
$0.956X-0.016Y-0.292Z=-0.887$			
O(4,G1)	0.023	O(4,G4)	0.097
O(4,G2)	0.117	O(4,G5)	0.044
O(4,G3)	−0.177	O(4,G6)	−0.104
II. The benzene plane			
$-0.517X-0.041Y+0.855Z=4.354$			
C(1,PE)	0.014	C(6,PE)	−0.011
C(2,PE)	−0.009	C(7,PE)	0.022
C(3,PE)	−0.001	C(8,PE)	1.462
C(4,PE)	0.004	O(A,PE)	−0.664
C(B,PE)	0.001	O(B,PE)	−0.716

α-Cyclodextrin–Guest Interaction. Bond distances and angles in 1-phenylethanol and intermolecular distances between 1-phenylethanol and α-cyclodextrin are shown in Fig. 5. The planarity of the phenyl group is quite good (Table 3). The hydroxyl group of 1-phenylethanol is statistically disordered with the same occupancy; O(A) and O(B) belong to *S*-(−) and *R*-(+) isomers, respectively. The C(7)-O(A) and C(7)-O(B) bonds are significantly short, and the C(1)-C(7)-O(A) and C(1)-C(7)-O(B) angles are somewhat large. This may be interpreted in terms of the thermal displacement and/or slight disorder of 1-phenylethyl moiety as discussed by Kim and Rosenstein.[4] The relatively large temperature factor indicates that the position of the 1-phenylethyl moiety of the two isomers is slightly shifted to each other in the asymmetric environment although such small disorder is not resolved on the electron-density map.

1-Phenylethanol is sandwiched between adjacent α-

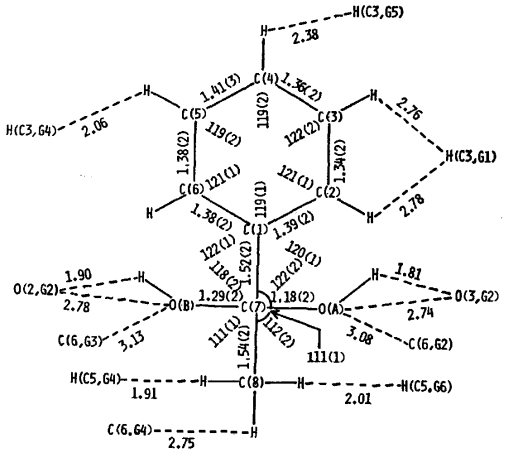

Fig. 5. Bond distances and angles in 1-phenylethanol and selected intermolecular distances between 1-phenylethanol and α-cyclodextrin.

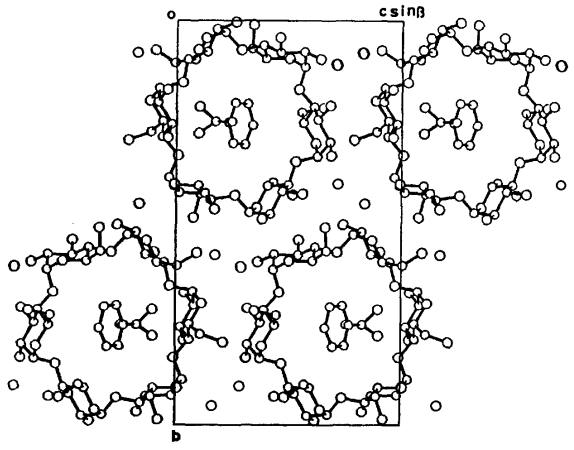

Fig. 6. Crystal structure viewed down along the a axis.

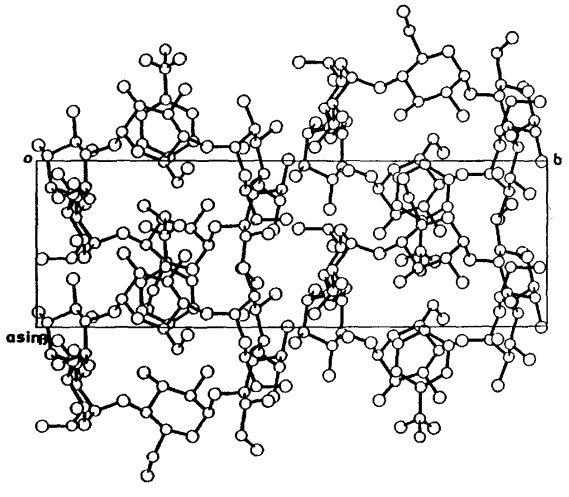

Fig. 7. Crystal structure viewed down along the c axis.

cyclodextrin molecules stacked along the channel (Fig. 4). The phenyl group is in contact with the secondary hydroxyl side of α-cyclodextrin, while the ethanol moiety is located at the O(6) side of the next α-cyclodextrin. The phenyl plane makes an angle of 42.0° with the plane through the six O(4) atoms. O(A) and O(B) hydroxyl groups form O(A)–H···O(3,G2) and O(B)–H···O(2, G2) hydrogen bonds, respectively. The C(7)–C(8) bond is inserted into the next α-cyclodextrin from the primary hydroxyl side. This type of the host-guest interaction has not yet been found. In the α-cyclodextrin complexes with other benzene derivatives,[2] the benzene ring is included at the O(2), O(3) side nearly parallel to the α-cyclodextrin axis. In the 1-phenylethanol complex, however, such inclusion geometry may be unfavorable since the hydrogen bonds involving O(A) and O(B) should be broken to include the phenyl group parallel to the α-cyclodextrin axis, and moreover, such parallel inclusion may cause steric hindrance between the C(8) methyl group of 1-phenylethanol and C(6) methylene groups of the next α-cyclodextrin. Somewhat short contacts involving hydrogen atoms are found between α-cyclodextrin and 1-phenylethanol; H(C3,G4)···H(C5,PE) (2.06 Å), H(C5,G4)···H(C8, PE) (1.91 Å), H(C5,G6)···H(C8,PE) (2.01 Å), and C(6,G4)···H(C8,PE) (2.75 Å). This suggests that the guest 1-phenylethanol molecule is bound in the channel by hydrogen bonds and the van der Waals force.

Molecular Packing and Hydrogen Bonds. Projections of crystal structure are shown in Figs. 6 and 7. α-Cyclodextrin molecules are stacked along the a axis forming an endless column. Since the α-cyclodextrin ring is tilted by 17.0° against the plane perpendicular to the channel axis, the rings are laterally shifted to each other parallel to the molecular plane. Except for a weak O(3,G5)–H···O(6,G5) hydrogen bond, no intermolecular hydrogen bonds along the column are formed. Most of the intermolecular hydrogen bonds are found between neighboring α-cyclodextrin molecules arranged parallel to the molecular plane. In other channel-type structures,[2] the stacked α-cyclodextrin molecules are linked by many hydrogen bonds along the column. In those complexes, the inclination and lateral shift of the α-cyclodextrin ring are so small that the hydrogen bonds cannot be broken; in the benzaldehyde complex, the glucose residues are remarkably tilted to compensate the effect of the molecular shift on the hydrogen bond formation. Moreover, α-cyclodextrin molecules belonging to different columns are linked with one another by hydrogen-bond bridges involving water molecules rather than by direct hydrogen bonds. In contrast to those complexes, α-cyclodextrin columns in the 1-phenylethanol complex are linked mainly by direct hydrogen bonds, and as the result, they are more closely packed in the crystal as indicated by the comparison of cell volumes; 2645.1 Å^3 in the benzaldehyde complex and 2596.3 Å^3 in the 1-phenylethanol complex. Between columns, adjacent glucose residues are faced to each other as shown in Fig. 6. The G1 and G3 residues are linked by the O(3,G3)–H···O(6,G1) and O(6, G3)–H···O(3,G1) hydrogen bonds. Two hydrogen bonds, the O(6,G2)–H···O(6,G5) and O(2,G5)–H··· O(6,G2), are also found between the G2 and G5 residues, but only the O(2,G6)–H···O(3,G4) hydrogen bond is formed between the G4 and G6 residues.

Table 4. Hydrogen-bond distances (l/Å) and angles (ϕ/°)

O	H	O	CODE	DISTANCE O-H	DISTANCE H···O	DISTANCE O···O	ANGLE O-H···O
O(2,G1)	-H(O2,G1)	O(W3)	(b)	0.96	1.64	2.583	171
O(3,G1)	-H(O3,G1)	O(2,G6)		0.87	2.09	2.952	171
O(2,G2)	-H(O2,G2)	O(W4)	(b)	1.19	1.65	2.811	163
O(3,G2)	-H(O3,G2)	O(2,G1)		0.99	1.82	2.806	180
O(6,G2)	-H(O6,G2)	O(6,G5)	(e)	0.94	1.79	2.713	166
O(2,G3)	-H(O2,G3)	O(W1)	(h)	0.82	2.00	2.773	157
O(3,G3)	-H(O3,G3)	O(2,G2)		0.98	2.12	3.037	157
O(3,G3)	-H(O3,G3)	O(6,G1)	(f)	0.98	2.13	3.049	156
O(6,G3)	-H(O6,G3)	O(3,G1)	(f)	1.10	1.86	2.858	150
O(2,G4)	-H(O2,G4)	O(3,G5)		0.88	2.02	2.817	151
O(3,G4)	-H(O3,G4)	O(2,G3)		1.13	1.72	2.835	172
O(6,G4)	-H(O6,G4)	O(2,G3)	(a)	0.84	2.58	3.097	121
O(2,G5)	-H(O2,G5)	O(6,G2)	(c)	0.89	1.87	2.756	170
O(3,G5)	-H(O3,G5)	O(6,G5)	(b)	1.19	2.05	3.021	136
O(6,G5)	-H(O6,G5)	O(W2)	(a)	1.02	1.70	2.703	166
O(2,G6)	-H(O2,G6)	O(3,G4)	(j)	1.00	1.85	2.809	159
O(3,G6)	-H(O3,G6)	O(2,G5)		0.81	2.08	2.875	169
O(A,PE)	-H(OA,PE)	O(2,G2)		1.07	1.81	2.743	144
O(B,PE)	-H(OB,PE)	O(2,G2)		1.04	1.90	2.870	154
O(W1)	-H(1,W1)	O(6,G2)	(c)	0.78	2.09	2.850	168
O(W1)	-H(2,W1)	O(6,G6)	(b)	1.09	1.79	2.824	156
O(W2)	-H(1,W2)	O(6,G3)	(c)	1.20	1.68	2.851	165
O(W2)	-H(2,W2)	O(2,G4)		0.97	2.63	3.108	111
O(W3)	-H(1,W3)	O(6,G4)	(i)	0.91	1.86	2.753	164
O(W4)	-H(1,W4)	O(6,G1)	(g)	0.69	2.34	2.740	119
O(W4)	-H(2,W4)	O(2,G4)	(d)	0.86	1.92	2.750	162

None	x,	y,	z
a	$1+x$,	y,	z
b	$-1+x$,	y,	z
c	x,	y,	$1+z$
d	x,	y,	$-1+z$
e	$-1+x$,	y,	$-1+z$
f	$-x$,	$1/2+y$,	$-z$
g	$1-x$,	$1/2+y$,	$-z$
h	$-x$,	$1/2+y$,	$1-z$
i	$1-x$,	$-1/2+y$,	$-z$
j	$-x$,	$-1/2+y$,	$1-z$

In the crystal, the hydrogen-bond network is built up of branched chains and circles of hydrogen bonds as shown in Fig. 8. Six intramolecular hydrogen bonds are observed between adjacent glucose residues. Except for the O(2,G4)–H···O(3,G5) hydrogen bond, the O(3) hydroxyl groups act as a hydrogen donor (Table 4). The G4 residue donates hydrogen atoms to the G3 and G5 resiues, while the G5 residue accepts two hydrogen atoms from the G4 and G6 residues. O(2,G4), O(3,G5), O(6,G5), and O(W2) from a four membered hydrogen-bond circle. O(2,G2), O(3,G3), O(6,G1), and O(W4) also form a cyclic hydrogen bond, although O(3,G3) donates a hydrogen atom to O(2,G2) and O(6,G1), forming weak bifurcated hydrogen bonds.[5] Water molecules are located in two kinds of intermolecular spaces as shown in Fig. 6; W1 and W3 are located in one space, while

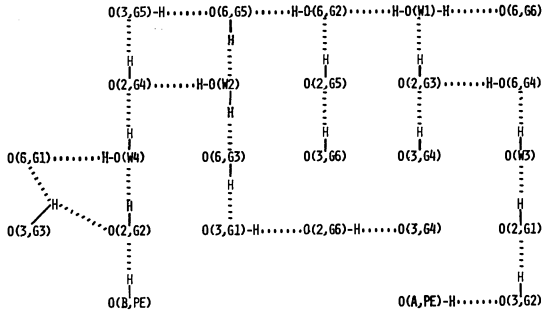

Fig. 8. A schematic representation of hydrogen-bond network.

W2 and W4 are in the other space. W2 and W4 are linked by the O(W2)–H···O(2,G4)···H–O(W4) hydrogen-bond bridge. W1 forms three hydrogen bonds with O(2,W3), O(6,G2), and O(6,G6), linking three columns surrounding it. W4 forms similar tripod-like hydrogen bonds with each of O(6,G1), O(2,G2), and O(2,G4) in different columns. W3 links two columns with the O(2,G1)–H···O(W3)–H···O(6,G4) hydrogen-bond bridge. Unlike these three water molecules, W2 links α-cyclodextrin rings along the column axis with the O(6,G5)–H···O(W2)–H···O(2,G4) hydrogen-bond bridge, and is also hydrogen-bonded to O(6,G3) of the neighboring column.

References

1) F. Cramer and W. Dietsche, *Chem. Ber.*, **92**, 378 (1959); H. P. Benshop and G. R. Van der Berg, *J. Chem. Soc., Chem. Commun.*, **1970**, 1431; M. Mikolajczyk, J. Drabowicz, and F. Cramer, *ibid.*, **1971**, 317; *J. Am. Chem. Soc.*, **100**, 2510 (1978).

2) K. Harata, K. Uekama, M. Otagiri, F. Hirayama, and H. Ogino, *Bull. Chem. Soc. Jpn.*, **54**, 1954 (1981), and references therein.

3) "International Tables for X-Ray Crystallography," Kynoch Press, Birmingham (1974), Vol. IV, pp. 72—75.

4) S. H. Kim and R. D. Rosenstein, *Acta Crystallogr.*, **22**, 648 (1967).

5) G. A. Jeffrey and S. Takagi, *Acc. Chem. Res.*, **11**, 264 (1978).

The Crystal and Molecular Structure of Strontium Bis(thiocyanate)-Hexaethylene Glycol (1/1)

Iwao YAMAGUCHI,† Kunio MIKI, Noritake YASUOKA,†† and Nobutami KASAI*

Department of Applied Chemistry, Faculty of Engineering, Osaka University, Yamadaoka, Suita, Osaka 565

(Received August 8, 1981)

The molecular structure of strontium bis(thiocyanate)–hexaethylene glycol(1/1) has been determined from single crystal X-ray diffraction data(3121 observed reflections): triclinic, space group $P\bar{1}$, $a=12.086(4)$, $b=8.732(2)$, $c=10.628(2)$ Å, $\alpha=80.88(2)$, $\beta=101.99(3)$, $\gamma=100.55(2)°$, $D_m=1.48$, $D_c=1.48$ g cm^{-3} for $Z=2$. The central Sr ion is coordinated by seven O atoms from the hexaethylene glycol moiety and two N atoms from the SCN groups; the Sr–O distances range from 2.603(5) to 2.750(5), while the Sr–N distances are 2.628(8) and 2.634(8) Å. The hexaethylne glycol moiety assumes a $GT_2\bar{G}T_2GT_2\bar{G}T_2GTG_2$ conformation.

In connection with the studies of the metal-ion complexation of non-cyclic poly(oxyethylene) derivatives by Yanagida, Okahara, and their co-workers,[1] X-ray diffraction studies have been made of strontium bis(thiocyanate)–heptaethylene glycol(1/1) and –hexaethylene glycol(1/1) (EO7–$Sr(SCN)_2$ and EO6–$Sr(SCN)_2$) in order to examine the chelating behavior of heptaethylene glycol(EO7) and hexaethylene glycol (EO6) to the strontium. An account of the structure of the former, EO7–$Sr(SCN)_2$, has been reported.[2] This paper will deal with the structure of the latter, EO6–$Sr(SCN)_2$.

Experimental

Colorless, transparent, and prismatic crystals were recrystallized from acetone-hexane. A crystal with approximate dimensions of 0.5 mm × 0.2 mm × 0.1 mm was used for the X-ray experiments. The unit-cell parameters and diffraction intensities were measured on a Rigaku automated, four-circle diffractometer. Zr-filtered Mo $K\alpha$ radiation was used.

Crystal Data. $(C_{12}H_{26}O_7)\cdot Sr(SCN)_2$, *F.W.* 478.02, triclinic, space group $P\bar{1}$, $a=12.086(4)$, $b=8.732(2)$, $c=10.628(2)$ Å, $\alpha=80.88(2)$, $\beta=101.99(3)$, $\gamma=100.55(2)°$, $V=1070(1)$ Å^3, $D_m=1.48$, $D_c=1.48$ g cm^{-3} for $Z=2$, μ(Mo $K\alpha$)$=28.6$ cm^{-1}. The intensity data were measured by the θ-2θ scan technique at a 2θ rate of 2° min^{-1}. The scan width was $\Delta(2\theta)=(2.4+0.7\tan\theta)°$. Backgrounds were measured for 7.5 s at both ends of a scan. A total of 3957 reflections ($2\theta<50°$) were measured, of which 3121 ($|F_o|>3\sigma(F_o)$) were non-zero reflections. Usual Lorentz and polarization corrections were applied, but no absorption correction was made [max(μR)$=0.8$].

Structure Solution and Refinement

The structure was solved by the heavy-atom method. The positions of the Sr and S atoms were determined from the Patterson function. The subsequent Fourier map revealed the remaining non-hydrogen atoms.

The structure was refined anisotropically by the block-diagonal least-squares procedure (*HBLS*-V).[3] The difference Fourier map calculated at the stage with $R=0.085$ revealed the positions of 26 H atoms, those atoms were included in the subsequent cycles and refined isotropically. The final R was 0.061 for non-zero reflections ($R_w=0.069$). The weighting schemes used in the final cycle were $w=\{\sigma_{cs}(F_o)+a|F_o|+b|F_o|^2\}^{-1}$, where $a=0.0223$ and $b=0.0008$, for $|F_o|>0$ and $w=0.0508$ for $|F_o|=0$. The final atomic parameters are summarized in Table 1.†††

The atomic scattering factors used were taken from the International Tables for X-Ray Crystallography, Vol. IV.[4] Computations were done on an ACOS Series 77 NEAC System 900 computer at Osaka University.

Results and Discussion

The molecular structure as drawn by the *ORTEP* program[5] is shown in Fig. 1. The interatomic dis-

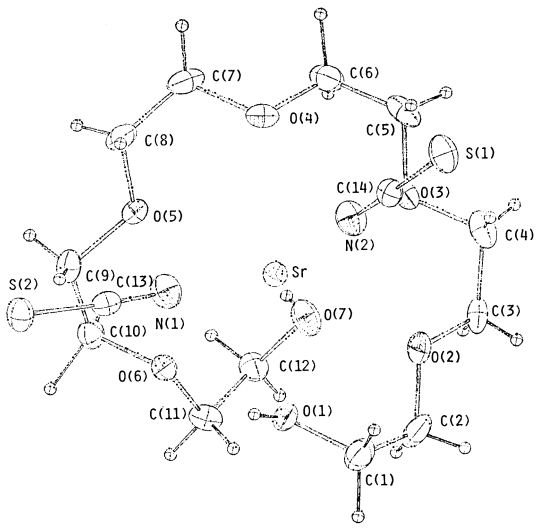

Fig. 1. A prespective view[5] of EO6–$Sr(SCN)_2$ molecule with the numbering scheme of non-hydrogen atoms.
Non-hydrogen atoms are expressed as thermal ellipsoids at 50% probability level and hydrogen atoms as spheres with the radius of 0.1 Å.

† Present address: Nissho-Iwai Corporation, 3-30 Imabashi, Higashi-ku, Osaka 540.

†† Present address: Institute for Protein Research, Osaka University, Yamadaoka, Suita, Osaka 565.

††† Lists of the observed and calculated structure factors and anisotropic thermal parameters are kept at the Chemical Society of Japan (Document No. 8219).

TABLE 1. FRACTIONAL ATOMIC COORDINATES, WITH ESTIMATED STANDARD DEVIATIONS IN PARENTHESES

(a) Non-hydrogen atoms with equivalent temperature factors.

Atom	x	y	z	B_{eq}[6]/Å^2
Sr	0.25433(7)	0.24284(9)	0.18693(7)	3.36
S(1)	0.1495(3)	−0.3421(3)	0.4327(3)	5.58
S(2)	0.3557(3)	−0.0048(3)	−0.1954(3)	5.19
O(1)	0.4722(5)	0.2261(7)	0.2461(5)	4.3
O(2)	0.3633(5)	0.2392(7)	0.4371(5)	5.2
O(3)	0.1319(5)	0.2512(6)	0.3690(5)	4.3
O(4)	0.0245(5)	0.1966(7)	0.1201(6)	4.8
O(5)	0.1490(5)	0.3573(7)	−0.0558(5)	4.2
O(6)	0.3667(5)	0.4812(6)	0.0341(5)	3.6
O(7)	0.2810(6)	0.5304(7)	0.2402(6)	5.5
N(1)	0.3059(7)	0.0802(9)	0.0251(8)	5.5
N(2)	0.2087(7)	−0.0477(8)	0.2978(8)	5.5
C(1)	0.5292(8)	0.2002(12)	0.3753(9)	5.7
C(2)	0.4816(8)	0.2798(13)	0.4562(9)	6.3
C(3)	0.3042(9)	0.2992(10)	0.5176(8)	4.8
C(4)	0.1859(9)	0.2146(10)	0.5026(9)	5.5
C(5)	0.0172(8)	0.1715(12)	0.3424(10)	6.0
C(6)	−0.0389(8)	0.2299(12)	0.2092(10)	5.9
C(7)	−0.0310(8)	0.2340(11)	−0.0119(10)	5.7
C(8)	0.0535(8)	0.2412(11)	−0.0966(9)	5.4
C(9)	0.2244(8)	0.4105(10)	−0.1454(8)	4.7
C(10)	0.3092(8)	0.5407(10)	−0.0934(8)	4.5
C(11)	0.4228(7)	0.6062(10)	0.1103(9)	4.7
C(12)	0.3388(8)	0.6626(10)	0.1688(8)	4.6
C(13)	0.3300(7)	0.0432(9)	−0.0646(8)	3.8
C(14)	0.1851(7)	−0.1676(9)	0.3543(8)	3.8

(b) Hydrogen atoms with isotropic temperature factors.

Atom	x	y	z	B/Å^2
H(1)	0.477(8)	0.163(11)	0.198(9)	5(3)
H(2)	0.616(9)	0.248(12)	0.390(10)	6(3)
H(3)	0.507(8)	0.094(11)	0.394(9)	6(3)
H(4)	0.508(9)	0.261(13)	0.539(11)	7(3)
H(5)	0.497(12)	0.403(17)	0.427(14)	12(5)
H(6)	0.313(6)	0.410(9)	0.496(7)	2.2(17)
H(7)	0.341(10)	0.290(13)	0.588(11)	8(4)
H(8)	0.183(7)	0.102(10)	0.514(9)	4(3)
H(9)	0.142(9)	0.262(12)	0.544(10)	6(3)
H(10)	−0.014(7)	0.188(9)	0.403(8)	3.2(19)
H(11)	0.024(9)	0.053(12)	0.356(10)	7(3)
H(12)	−0.031(13)	0.343(17)	0.212(14)	13(5)
H(13)	−0.125(9)	0.157(12)	0.181(10)	7(3)
H(14)	−0.053(7)	0.338(10)	−0.016(8)	4(2)
H(15)	−0.105(10)	0.161(13)	−0.033(11)	8(4)
H(16)	0.030(9)	0.288(13)	−0.172(11)	7(3)
H(17)	0.079(8)	0.126(11)	−0.093(9)	5(3)
H(18)	0.176(8)	0.438(11)	−0.217(9)	5(3)
H(19)	0.258(9)	0.302(12)	−0.153(10)	6(3)
H(20)	0.262(8)	0.617(11)	−0.087(9)	6(3)
H(21)	0.389(11)	0.569(15)	−0.142(12)	9(4)
H(22)	0.468(10)	0.695(13)	0.064(11)	8(4)
H(23)	0.478(8)	0.546(11)	0.165(9)	5(3)
H(24)	0.286(9)	0.708(12)	0.092(10)	7(3)
H(25)	0.371(8)	0.736(11)	0.216(9)	5(3)
H(26)	0.244(9)	0.564(12)	0.202(10)	6(3)

TABLE 2. SELECTED INTERATOMIC DISTANCES AND ANGLES IN EO6-$Sr(SCN)_2$, WITH ESTIMATED STANDARD DEVIATIONS IN PARENTHESES

Interatomic distances (l/Å)			
Sr-O(1)	2.603(6)	Sr-N(1)	2.628(8)
Sr-O(2)	2.709(6)	Sr-N(2)	2.634(8)
Sr-O(3)	2.686(5)	N(1)-C(13)	1.160(11)
Sr-O(4)	2.691(6)	N(2)-C(14)	1.141(11)
Sr-O(5)	2.750(5)	S(1)-C(14)	1.645(8)
Sr-O(6)	2.762(5)	S(2)-C(13)	1.618(9)
Sr-O(7)	2.609(6)		
C(1)-O(1)	1.406(12)	C(11)-O(6)	1.445(10)
C(2)-O(2)	1.389(12)	C(12)-O(7)	1.429(11)
C(3)-O(2)	1.431(12)		
C(4)-O(3)	1.446(12)		
C(5)-O(3)	1.426(12)	C(1)-C(2)	1.447(15)
C(6)-O(4)	1.428(12)	C(3)-C(4)	1.474(14)
C(7)-O(4)	1.438(11)	C(5)-C(6)	1.491(14)
C(8)-O(5)	1.431(11)	C(7)-C(8)	1.483(14)
C(9)-O(5)	1.421(10)	C(9)-C(10)	1.478(12)
C(10)-O(6)	1.451(10)	C(11)-C(12)	1.485(13)
Interatomic angles (ϕ/°)			
O(1)-Sr-O(2)	60.2(2)	O(1)-Sr-N(1)	71.0(3)
O(1)-Sr-O(3)	121.6(2)	O(1)-Sr-N(2)	89.9(3)
O(1)-Sr-O(4)	168.1(2)	O(2)-Sr-N(1)	122.5(3)
O(1)-Sr-O(5)	123.0(2)	O(2)-Sr-N(2)	73.7(3)
O(1)-Sr-O(6)	71.9(2)	O(3)-Sr-N(1)	147.9(3)
O(1)-Sr-O(7)	94.0(2)	O(3)-Sr-N(2)	73.2(2)
O(2)-Sr-O(3)	61.4(2)	O(4)-Sr-N(1)	100.1(3)
O(2)-Sr-O(4)	122.3(2)	O(4)-Sr-N(2)	80.3(3)
O(2)-Sr-O(5)	159.4(2)	O(5)-Sr-N(1)	74.2(3)
O(2)-Sr-O(6)	109.6(2)	O(5)-Sr-N(2)	124.7(3)
O(2)-Sr-O(7)	73.8(2)	O(6)-Sr-N(1)	79.7(3)
O(3)-Sr-O(4)	62.0(2)	O(6)-Sr-N(2)	154.7(2)
O(3)-Sr-O(5)	111.9(2)	O(7)-Sr-N(1)	140.8(3)
O(3)-Sr-O(6)	131.2(2)	O(7)-Sr-N(2)	139.8(3)
O(3)-Sr-O(7)	70.9(2)		
O(4)-Sr-O(5)	59.5(2)	N(1)-Sr-N(2)	77.9(3)
O(4)-Sr-O(6)	115.2(2)		
O(4)-Sr-O(7)	97.8(2)		
O(5)-Sr-O(6)	58.5(2)		
O(5)-Sr-O(7)	85.6(2)		
O(6)-Sr-O(7)	61.1(2)		
O(1)-C(1)-C(2)	109.5(9)	C(2)-O(2)-C(3)	117.3(8)
O(2)-C(2)-C(1)	110.6(9)	C(4)-O(3)-C(5)	112.1(7)
O(2)-C(3)-C(4)	108.1(8)	C(6)-O(4)-C(7)	111.3(7)
O(3)-C(4)-C(3)	107.3(8)	C(8)-O(5)-C(9)	115.3(7)
O(3)-C(5)-C(6)	109.6(8)	C(10)-O(6)-C(11)	112.1(6)
O(4)-C(6)-C(5)	107.7(8)		
O(4)-C(7)-C(8)	107.9(8)		
O(5)-C(8)-C(7)	107.4(8)	N(1)-C(13)-S(2)	176.2(8)
O(5)-C(9)-C(10)	107.4(8)	N(2)-C(14)-S(1)	178.8(8)
O(6)-C(10)-C(9)	107.8(7)		
O(6)-C(11)-C(12)	110.4(7)		
O(7)-C(12)-C(11)	108.0(7)		

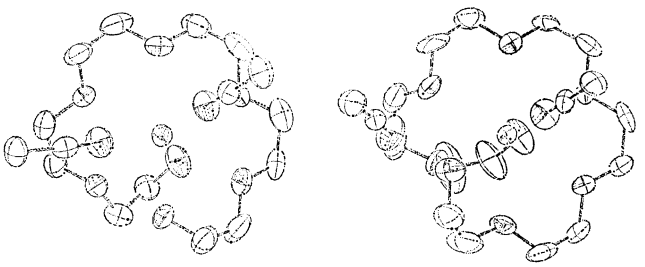

Fig. 2. Molecular structure of EO6-$Sr(SCN)_2$ (a) compared with that of EO7-$Sr(SCN)_2$[2] (b).
A similar conformation is observed at the central portions of the EO6 and EO7 chanis (See also Fig. 3).

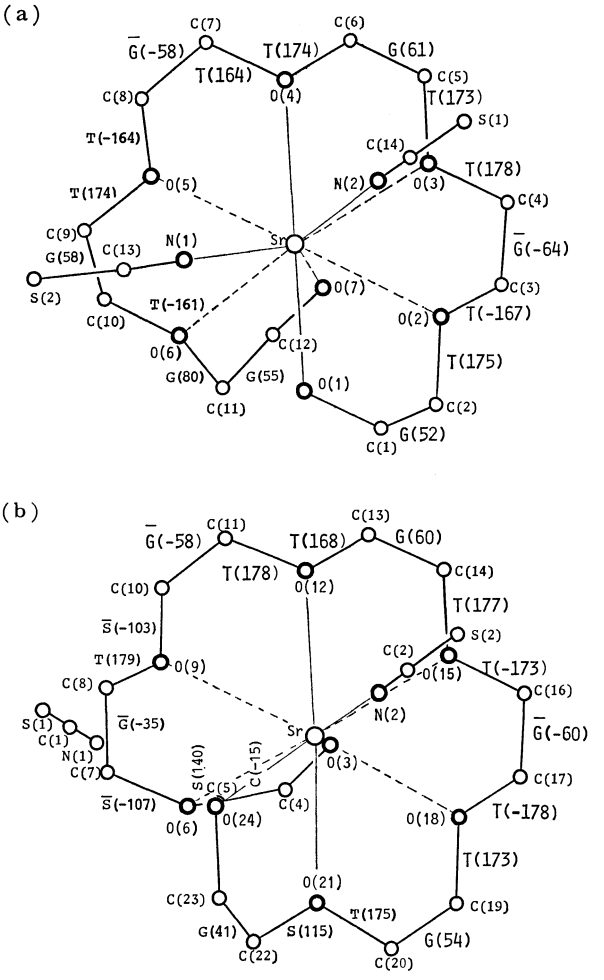

Fig. 3. Conformations and torsion angles(ϕ/°) in oligoethylene glycol part.
(a) EO6-$Sr(SCN)_2$, (b) EO7-$Sr(SCN)_2$.[2] Thick circles represent atoms coordinated to the Sr. Solid and broken lines respectively show the coordination bonds between the Sr and atoms above and below the planes defined by the (a) O(1), O(2), O(3), O(4), and O(5), (b) O(9), O(12), O(18), O(21), and O(24) atoms.

tances and angles are given in Table 2.

Coordination Geometry. Seven O atoms from the EO6 chain and two N atoms from two SCN anions are coordinated to the Sr ion. In EO7–$Sr(SCN)_2$, the eighth O atom takes part in the coordination instead of the N atom of the second SCN anion. The two Sr–N distances in the present complex are equal, within the limits of experimental error: 2.628(8) and 2.634(8) Å. The seven Sr–O distances are classed into three groups. Both of the terminal O atoms, O(1) and O(7), of the EO6 are rather close to the Sr atom; the Sr–O distances being 2.603(6) and 2.609(7) Å. The Sr–O(2), Sr–O(3), and Sr–O(4) distances are the second longest [2.709(6), 2.686(5) and 2.691(6) Å], while the Sr–O(5) and Sr–O(6) are the longest distances [2.750(5) and 2.762(5) Å].

Conformations of the EO6 Chain. The structure of and torsion angles in the EO6 chain are compared in Figs. 2 and 3 respectively with those found in the EO7 chain in EO7–$Sr(SCN)_2$.[2] The EO6 chain assumes a $\mathbf{GT_2\bar{G}T_2GT_2\bar{G}}T_2GTG_2$ conformation About 2/3 of the EO6 chain has a conformation similar to that of the central part of the EO7 chain in EO7–$Sr(SCN)_2$($\mathbf{GT_2\bar{G}T_2GT_2\bar{G}}$). This fact, and the similarity between the corresponding Sr–O distances in the EO6 [2.709(6), 2.686(5) and 2.691(6) Å] and EO7 chains [2.71(2), 2.69(2) and 2.72(2) Å], suggest that some part of the EO6 chain (from O(1) to O(5)) and the corresponding part of the EO7 chain (from O(21) to O(9)) have "rigid structure."

Crystal Structure. The crystal structure is drawn in Fig. 4. Close intermolecular distances (less than 3.5 Å) are listed in Table 3; the closest contact is S(2)(x, y, z)···O(1)($1-x$, $-y$, $-z$)=3.258(6) Å.

The authors wish to express their deep thanks to Dr. Shozo Yanagida and Professor Mitsuo Okahara of Osaka University for the supply of crystals and for their helpful discussions. The authors' thanks are also due to Miss Nobuko Kanehisa for the *ORTEP* drawings. A part of the cost of the present study was defrayed by a Grant-in-Aid (No. 535038) from the Ministry of Education, Science and Culture.

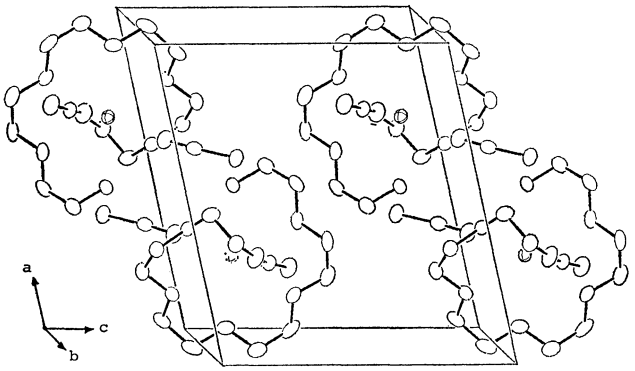

Fig. 4. Crystal structure of EO6–$Sr(SCN)_2$.[5]

Table 3. Short intermolecular atomic contacts(l/Å) (less than 3.5 Å), with estimated standard deviations in parentheses

O(7)···S(1)[a]	3.267(7)	key: a, x, $1+y$, z;
S(2)···O(1)[b]	3.258(6)	b, $1-x$, $-y$, $-z$;
S(2)···C(1)[b]	3.393(11)	c, $1-x$, $1-y$, $-z$.
O(6)···C(11)[c]	3.479(10)	
O(6)···O(6)[c]	3.394(10)	

References

1) S. Yanagida, K. Takahashi, and M. Okahara, *Bull. Chem. Soc. Jpn.*, **51**, 3111 (1978).
2) H. Ohmoto, Y. Kai, N. Yasuoka, N. Kasai, S. Yanagida, and M. Okahara, *Bull. Chem. Soc. Jpn.*, **52**, 1209 (1979).
3) T. Ashida, "The Universal Crystallographic Computing System-Osaka," The Computation Center, Osaka Univ. (1973), pp. 55—60.
4) "International Tables for X-Ray Crystallography," Kynoch Press, Birmingham, (1974), Vol. IV, pp. 71—73.
5) C. K. Johnson, *ORTEP* II, Report ORNL-5138, Oak Ridge National Laboratory, Tennessee (1976).
6) W. C. Hamilton, *Acta Crystallogr.*, **12**, 609 (1959).

The Binding of Sodium Dodecyl Sulfate to Lysozyme in Aqueous Solutions. II. The Effect of Added NaCl

Kohsuke FUKUSHIMA,* Yoshio MURATA, Gohsuke SUGIHARA, and Mitsuru TANAKA

Department of Chemistry, Faculty of Science, Fukuoka University, Fukuoka 814-01

(Received August 12, 1981)

The isotherms for the binding of sodium dodecyl sulfate (SDS) to lysozyme have been investigated as a function of the concentration of added NaCl at pH 5.8 and 25 °C by a potentiometric method utilizing a surfactant-selective electrode. The equilibrium surfactant concentration at which the binding begins to occur increases with increasing NaCl concentration. The equilibrium surfactant concentration giving the same binding number above 10, on the contrary, decreases with increasing NaCl concentration. Thermodynamic analysis shows that there takes place not only the exchange between chloride ion (Cl^- ion) and dodecyl sulfate ion (DS^- ion) but also the binding of DS^- ion to the positively charged site unoccupied by Cl^- ion. The addition of NaCl does not change the equilibrium SDS concentration at which the binding number begins to exceed 10. This equilibrium concentration is regarded as a characteristic one at which the affinity between lysozyme and SDS can be evaluated. The value of standard free energy change upon DS^- ion binding and the number of Na^+ ions bound to a DS^- ion which forms a cluster on lysozyme were estimated from a thermodynamic equation based on the phase separation model.

In the previous paper, we discussed the binding mode of SDS to lysozyme and the accompanying structural change of lysozyme.[1] It was suggested from the previous experiments that the driving force of the initial binding (the binding number, $\bar{\nu}<10$) was mainly electrostatic, and that of the subsequent binding ($\bar{\nu}\geq 10$) was hydrophobic. If the binding force is different in the two regions, *i.e.*, regions of $\bar{\nu}<10$ and $\bar{\nu}\geq 10$, the addition of NaCl must give different effects on the binding in the respective regions. The effect of NaCl on the binding isotherm, therefore, is expected to give more detailed information about the binding mechanism of SDS to lysozyme.

A surfactant-selective electrode was used for potentiometry.[2-4] In this work, a poly(vinyl chloride) gel membrane was used as the ion exchange membrane instead of the nitrobenzene membrane, to prevent the solubilization of nitrobenzene.

Experimental

The solutions of hen egg-white lysozyme and other chemicals were prepared in the same way as in the previous paper.[1] The binding isotherms were made by means of potentiometry, as described previously,[1] except that the poly(vinyl chloride) gel membrane was used instead of the nitrobenzene liquid membrane. The carrier used in the surfactant-selective electrode was prepared by mixing equivalent amounts of SDS and dimethyldioctadecylammonium chloride (Kaō Soap Co. Ltd.,) in water. The details of the preparation of poly(vinyl chloride) gel membrane have been mentioned in the paper by Shirahama *et al.*[2] In the present case, a voltage follower amplifier was connected to the digital multimeter (Takeda Riken TR 6885) in order to raise the input impedance.

All measurements were carried out at pH 5.8 and 25 °C. NaCl concentrations were 10, 20, 30, 50, and 100×10^{-3} mol dm^{-3}. Every calibration curve of the electromotive force (emf) of SDS in NaCl solutions showed a good linearity over the concentration range from 3×10^{-5} mol dm^{-3} to the concentration near its critical micelle concentration(CMC) and gave a slope which was very close to a Nernstian response (55.2 ± 0.6 mV per decade of change in SDS at 25 °C).

In order to examine the accuracy of each emf value for the sample solution, emf's for several SDS solutions of known concentration were also measured after measurements of the three sample solutions.

Results and Discussion

As is shown in Fig. 1, the equilibrium concentration of SDS in the initial binding region ($\bar{\nu}<10$) increases with increasing concentration of NaCl. On the contrary, the equilibrium concentration of SDS in the region of subsequent binding ($\bar{\nu}\geq 10$) decreases with increasing concentration of NaCl. One should pay attention to the fact that all isotherms intersect each other at the equilibrium concentration of SDS at which $\bar{\nu}=10$.

The flat region in Fig. 1, where $\bar{\nu}$ could be kept at 10, becomes narrower with increasing NaCl concentration. The free energy difference of DS^- ion

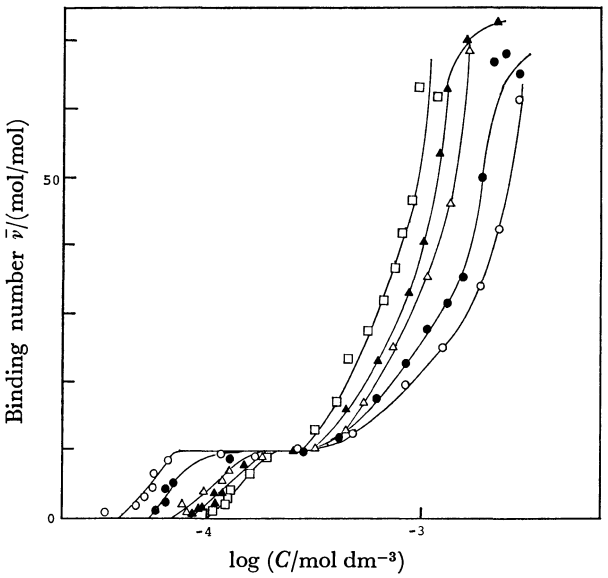

Fig. 1. Binding isotherms of lysozyme–SDS system at 25 °C and pH 5.8.
$\bar{\nu}$: Binding number, C: equilibrium SDS concentration, NaCl concentration: ○ 10, ● 20, △ 30, ▲ 50, □ 100 mmol dm^{-3}.

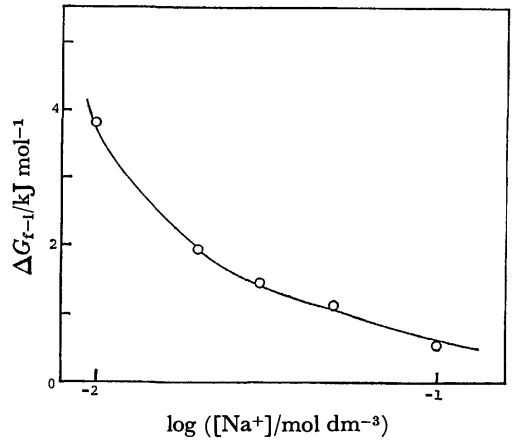

Fig. 2. ΔG_{f-1} *vs.* log [Na$^+$] plot evaluated from Eq. 1.

between the states of the initial and final points at this region can be obtained from the respective equilibrium SDS concentration as follows:

$$\Delta G_{f-1} = RT \ln \frac{a_f}{a_i} \simeq RT \ln \frac{C_f}{C_i}, \quad (1)$$

where a_i and a_f are the activities of DS$^-$ ions in solution at the initial and final points of the region, respectively, and C_i and C_f are the respective equilibrium SDS concentrations. The results obtained from Eq. 1 are shown in Fig. 2. ΔG_{f-1} is considered to be the free energy accumulation for the subsequent binding. ΔG_{f-1} decreases with increasing NaCl concentration and seems to approach zero. When ΔG_{f-1} becomes zero, the binding isotherm will show an inflection at the binding number of 10.

The plots of log $C_{\bar{\nu}}$ *vs.* log [Na$^+$] are given in Fig. 3. $C_{\bar{\nu}}$ and [Na$^+$], here, represent the equilibrium SDS concentration where $\bar{\nu}$ ions of DS$^-$ are bound to lysozyme and the total Na$^+$ ion concentration originating in NaCl and SDS, respectively. The plot of log $C_{0.5}$ *vs.* log [Na$^+$] gives a straight line with the positive slope of 0.5.

In the initiation of the binding of SDS to lysozyme, the Cl$^-$ ion must be taken into account along with the dodecyl sulfate ion (DS$^-$ ion), because both DS$^-$ and Cl$^-$ ions may be bound to the positively charged sites on lysozyme.[5] The initiation of SDS binding to the lysozyme–Cl$^-$ complex can be treated as the exchange reaction between Cl$^-$ and DS$^-$ ions, since lysozyme has been dissolved in respective NaCl solutions before the addition of SDS. The reaction scheme for the first step of initial binding of DS$^-$ ion to lysozyme is written as

$$\mathrm{P{\cdot}Cl}_m^- + \mathrm{DS}^- \overset{K}{\rightleftharpoons} \mathrm{P{\cdot}Cl}_{m-n}^-{\cdot}\mathrm{DS}^- + n\mathrm{Cl}^-, \quad (2)$$

$$K = \frac{[\mathrm{P{\cdot}Cl}_{m-n}^-{\cdot}\mathrm{DS}^-][\mathrm{Cl}^-]^n}{[\mathrm{P{\cdot}Cl}_m^-][\mathrm{DS}^-]}, \quad (3)$$

where P represents lysozyme and n is the number of Cl$^-$ ions excluded by the first binding of one DS$^-$ ion. Now, a special case, where $\bar{\nu}$ is 0.5 in average, is considered. The meaning is that 50% of the lysozyme molecule is bound by one DS$^-$ ion and the rest is not. This situation is realized if the concentration of SDS is reasonably low. Under this condition,

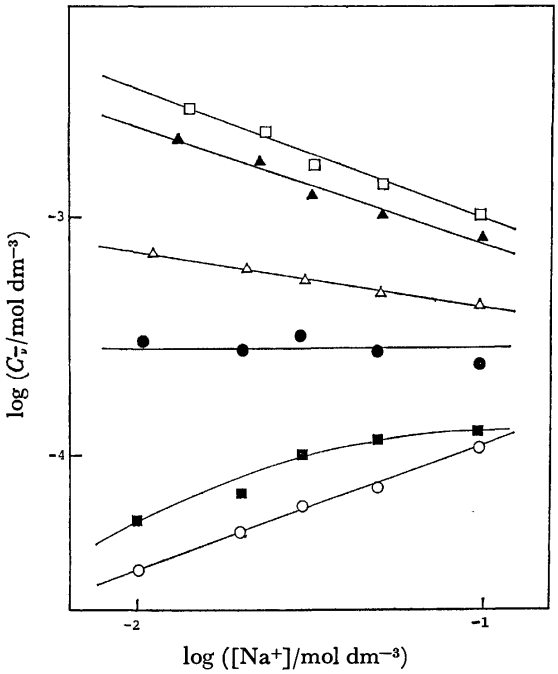

Fig. 3. Log $C_{\bar{\nu}}$ *vs.* log [Na$^+$] plots.
$C_{\bar{\nu}}$: Equilibrium SDS concentration at binding number $\bar{\nu}$, $\bar{\nu}$: ○ 0.5, ■ 5, ● 10, △ 17, ▲ 40, □ 60.

[P·Cl$_{m-n}^-$·DS$^-$] equals [P·Cl$_m^-$]. Then, Eq. 3 at the binding number of 0.5 can be rewritten as

$$\log [\mathrm{DS}^-] = n \log [\mathrm{Cl}^-] - \log K. \quad (4)$$

In Eq. 4, [Cl$^-$] can be replaced by [Na$^+$], because the concentration of NaCl is sufficiently large compared with those of SDS and lysozyme at a binding number of 0.5. Hence n is almost equal to the slope (0.5) of the plot of log $C_{0.5}$ *vs.* log [Na$^+$] in Fig. 3. As mentioned above, the slope n means the number of Cl$^-$ ions which are excluded by a DS$^-$ ion. The fact that n is not equal to unity but to 0.5, therefore, implies that the exchange between Cl$^-$ and DS$^-$ ions and the binding of DS$^-$ ions to the positively charged sites take place at the same time. This leads to the decrease in the number of positively charged sites and hence to the precipitation of lysozyme.[1]

For $\bar{\nu}$=5, the plot of log C_5 *vs.* log [Na$^+$] gives a convex curve, as is shown in Fig. 3. In this case, the assumption used in deriving Eq. 4 from Eq. 3 cannot be used, since lysozyme–Cl$^-$–DS$^-$ complexes with different numbers of Cl$^-$ and DS$^-$ ions distribute around the mean binding number ($\bar{\nu}$=5). It is difficult, therefore, to estimate the value of n from a log C_5 *vs.* log [Na$^+$] plot. The evaluation of n could not be made for other lysozyme–Cl$^-$–DS$^-$ complexes having different binding numbers either, without estimating the concentrations of the complexes from other experiments.

As is shown in the plot of log C_{10} *vs.* log [Na$^+$] in Fig. 3, C_{10}, the equilibrium SDS concentration at which $\bar{\nu}$ begins to exceed 10, is independent of the concentration of NaCl added. This equilibrium SDS concentration corresponds to the intersection point of the isotherms in Fig. 1. At this point, the Cl$^-$ ions on the positively charged sites are completely

replaced by DS^- ions. The lysozyme molecule has ionizable amino acid residues, *i.e.*, 6 Lys's, 11 Arg's, and 1 His, as basic residues and 7 Asp's and 2 Glu's as acidic residues. At the pH studied (pH 5.8), Lys and Arg are positively charged, since their pK values on lysozyme are within the ranges of 10.3—10.6 and 12.7—13.3[5] respectively. This means that a lysozyme molecule has 17 positive charges at this pH. On the other hand, the negatively charged residues are 7 Asp's and one Glu[7], since their pK values are within the ranges of 3.0—4.7 and 2.7—4.7[5] respectively. Therefore, the net charge of lysozyme is $+9(+17-8=+9)$ at pH 5.8. Accordingly, a lysozyme–DS^- complex is almost electrically neutral at C_{10}. The further binding of ions to the electrically neutral lysozyme–DS^- complex will be restricted to the ions having a hydrophobic part like DS^-. From these points of view, such an equilibrium concentration as C_{10} may be looked upon as a characteristic concentration of the lysozyme–DS^- system. The other system of charged protein-ionic surfactant also might have the same characteristic concentration as that of the lysozyme–SDS system.

Plots of log C_{17}, C_{40}, and C_{60} *vs.* log [Na^+] give straight lines with negative slopes, as is shown in Fig. 3. These trends seem to reflect the effect of added NaCl on micelle formation of an ionic surfactant on the surface of lysozyme. In the previous paper,[1] the site number of the first layer at pH 5.8 was estimated from the analysis by the use of BET equation to be about 17, which corresponds to the number of positively charged residues of lysozyme,[5] and it was suggested that the hydrophobic interaction between DS^-'s was expected for the subsequent binding over the first layer. Such behavior may be considered thermodynamically the same as that of the micelle formation. The standard free energy change of the micelle formation from the phase separation model is expressed as

$$\Delta G^\circ/RT = \ln X_{CMC} + \beta \ln X_{Na^+}, \quad (5)$$

where X_{CMC} and X_{Na^+} are the mole fractions of the surfactant and Na^+ ion in the intermicellar solution at CMC, respectively, and β is the binding number of Na^+ ions per surfactant molecule in micelle.[6] If the binding of SDS is assumed to proceed like a micelle formation above the first layer of SDS on the complex, the intercept and slope of the straight line in the plot of ln $X_{\bar{\nu}}$ *vs.* ln X_{Na^+} will give $\Delta G^\circ_{\bar{\nu}}$ and β, where $\Delta G^\circ_{\bar{\nu}}$ is the difference between the standard Gibbs free energy of a mole of monomeric hydrated DS^- ion with β counterion and that of a mole of DS^- ion with β counterion bound to the complex, and $X_{\bar{\nu}}$ is the mole fraction of DS^- ion in solution at the binding number $\bar{\nu}$. Equation 5 can be applied to the plots log $C_{\bar{\nu}}$ *vs.* log [Na^+] above $\bar{\nu}=17$ in Fig. 3, if the common logarithmic concentration in mol dm^{-3} is converted into the natural logarithmic mole fraction. The linearity of the plots is maintained even in the plots of the mole fraction unit. The results obtained by applying Eq. 5 to the plots in Fig. 3 are listed in Table 1.

TABLE 1. THERMODYNAMIC PARAMETERS

$\bar{\nu}$	β	ΔG°/kJ mol^{-1}
17	0.25	−33
40	0.50	−35
60	0.55	−36

The β increases with increasing binding number and seems to approach the value for the micelle of SDS. The negative charged density on the surface of the complex will increase with increasing DS^- ion binding above the binding number 10, which will cause the binding of Na^+ to the complex and hence the increment in β. The negative charge density on the surface of the complex is smaller than that of SDS micelle, because the surface area of the former is larger than that of the latter. Therefore, β of the complex must be smaller than β of the micelle.

$\Delta G^\circ_{\bar{\nu}}$'s are comparable to ΔG° (−37 kJ/mol at 25 °C estimated roughly by putting $\beta=0.7$) of SDS micelle formation. The difference between $\Delta G^\circ_{\bar{\nu}}$ and ΔG° can be attributed to the fact that the hydrocarbon part of the DS^- ion on the complex is in a less hydrophobic environment than in micelle. This suggests that lysozyme is somewhat loosely covered by DS^- ions. The results obtained here support the concept that the driving force of initial binding ($\bar{\nu}<10$) is electrostatic, and that of subsequent binding ($\bar{\nu}\geq 10$) is hydrophobic in nature.

The authors are grateful to Professor Keishiro Shirahama, Saga University, for his helpful discussion, and to Mr. Hiroshi Ninomiya, Fukuoka University, for his preparation of the voltage follower amplifier.

References

1) K. Fukushima, Y. Murata, N. Nishikido, G. Sugihara, and M. Tanaka, *Bull. Chem. Soc. Jpn.*, **54**, 3122 (1981).
2) K. Shirahama, H. Yasuda, and S. Sugimoto, *Bull. Chem. Soc. Jpn.*, **54**, 375 (1981).
3) I. Satake, T. Gondo, and H. Kimizuka, *Bull. Chem. Soc. Jpn.*, **52**, 361 (1979).
4) K. M. Kale, E. L. Cussler, and D. F. Evans, *J. Phys. Chem.*, **84**, 598 (1980).
5) T. Imoto, L. N. Johnson, A. T. C. North, D. C. Phillips, and J. A. Rupley, "Enzyme," 3rd ed, ed by P. D. Boyer, Academic Press, New York (1972), Vol. 7, p. 740.
6) M. Tanaka, "Ōyo Colloid Kagaku," ed by R. Matuura and T. Kondo, Hirokawa Publishing Co., Tokyo (1969), p. 205.

 © 1982 The Chemical Society of Japan Bull. Chem. Soc. Jpn., 55, 1379—1386 (1982)

Internal Heavy Atom Effect on the T_1 States of Halogen-substituted Benzonitriles

Yoshinori Asahi and Noboru Hirota*,†

Department of Chemistry, Faculty of Science, Kyoto University, Kyoto 606

(Received August 22, 1981)

The magnetic and decay properties of the ortho-, meta-, and para-substituted benzonitriles have been investigated and the nuclear charge and the position dependences of the internal heavy atom effects are examined in detail. From the single crystal EPR studies spin densities at the halogen atoms (ρ_H) are found to be in the order $\rho_H(\text{para}) > \rho_H(\text{ortho}) > \rho_H(\text{meta})$, but $\rho_H(\text{meta})$ is found to be much larger than that expected from the spin distribution in benzonitrile. The changes in the ZFS on going from the chloro-substituted molecules to the bromo-substituted molecules correlate with ρ_H and are explained in terms of the second order effect of the spin orbit mixing with $^3\sigma\pi^*$ ($^3\pi\sigma^*$) and $^3n\pi^*$ states. In the para-substituted molecules the relative increases of the T_y sublevel decay rates (k_y) are much greater than those of the T_z sublevel decay rates (k_z). The dependence of the average decay rate, $1/2(k_y+k_z)$ on the atomic spin orbit coupling constant (ζ), is considerably larger than expected from the ζ^2 dependence. These results were discussed in connection with the closeness of the $^3\sigma\pi^*$ ($^3\pi\sigma^*$) states in bromine containing molecules. A correlation between the decay rate and ρ_H is observed and the factors affecting the position dependence are examined.

When a halogen atom is substituted into an aromatic molecule, drastic changes in the properties of a triplet state molecule are observed.[1] The magnitude of this so-called internal heavy atom effect depends on the nuclear charge of the substituent, the type of molecule and the position of substitution. The nuclear charge dependence has been investigated rather intensively and in the systems so far studied the magnitude of the effect appears to be roughly proportional to the squares of the atomic spin orbit coupling constant ζ of the substituent.[1-5] Although this dependence has been rationalized qualitatively on the basis of the spin orbit matrix elements between the T_1 state and the perturbing singlet states, further examination of this dependence, especially in connection with the decay rates of the spin sublevels, may be useful in clarifying the relative importance of the different decay mechanisms.

The magnitude of the internal heavy atom effect is also dependent on the type of molecule. For example, the effects of the bromine substitution on the zero field splitting (ZFS) and the decay rates of the substituted benzenes[6,7] are far greater than those of naphthalene.[8,9] As for the position dependence Miller *et al.*[4] found in naphthalene and phenanthrene that there is a correlation between the magnitude of the heavy atom effect on the decay rate and the spin density on the carbon to which the heavy atom is attached. However, the data on the position dependence are scarce and further investigation seems to be worthwhile.

In the present work we have studied the T_1 states of the halogen-substituted benzonitriles by means of zero field optically detected magnetic resonance (ZFODMR) and EPR in order to examine the above mentioned dependences further. The main motives of the present study are the following.

(1) Benzonitrile may be considered as a typical example of the substituted benzenes having quinoid structures in the T_1 states. Our previous EPR investigation[10] has shown that the spin densities on the para, ortho, and meta positions are 0.33, 0.12, and 0.007, respectively. Because of the large differences in the spin densities it was thought that the halogen-substituted benzonitriles might be suited to investigate the position dependence of the internal heavy atom effect in detail.

(2) Previous ODMR studies on the bromine containing substituted benzenes have indicated that $^3\sigma\pi^*$ ($^3\pi\sigma^*$) and $^3n\pi^*$ states are likely to be rather close to the T_1 states.[6,7] This may lead to a nuclear charge dependence which is very different from those found for the other aromatics previously.

(3) The previous works on the nuclear charge dependence were made using the total decay rate constants. However, since different perturbing states are involved in the decay processes of the different sublevels nuclear charge dependence may depend on the sublevel significantly.

Here we first discuss the spin densities on the halogen atoms from the analysis of the hyperfine structures and the zero field splittings. We then examine the factors which affect the nuclear charge and position dependences of the decay rates in detail and discuss the observed dependences in connection with the spin distributions and the energy separations between the T_1 states and the main perturbing states.

Experimental

Guest molecules investigated here are 4-, 3-, and 2-fluorobenzonitrile (FBN), 4-, 3-, and 2-chlorobenzonitrile (ClBN), and 4-, 3-, and 2-bromobenzonitrile (BrBN). Hereafter we use the abbreviations given in parentheses. 3FBN and 2FBN were purified by distillation under reduced pressure and the others were purified by recrystallization from ethanol followed by sublimation under vaccum. The host crystals used here are *p*-xylene (PX), *o*-xylene (OX), *m*-xylene (MX) which were purified by distillation under reduced pressure and 1,4-dibromobenzene (DBB) and 1,4-dichlorobenzene (DCB) which were purified by recrystallization from ethanol and extensive zone refining. The molecular structure, the axis system and the numbering of the carbon atoms of para-substituted benzonitriles are

† Also at Department of Chemistry, State University of New York at Stomy Brook, New York, 11794, U.S.A.

Table 1. Observed and calculated hyperfine coupling constants of 2- and 3-fluorobenzonitriles

2FBN					3FBN				
Spin density ($2P_x$)		Hfcc A_x/mT			Spin density ($2P_x$)		Hfcc A_x/mT		
	Calcd		Calcd[a]	Obsd		Calcd		Calcd[a]	Obsd
C1	0.3049				C1	0.3021			
C2	0.1233				C2	0.0815	H2	0.196	
C3	−0.0235	H3	0.056		C3	0.0074			
C4	0.3192	H4	0.766	0.77	C4	0.3402	H4	0.816	0.83
C5	0.0040	H5	0.009		C5	−0.0125	H5	0.030	
C6	0.0888	H6	0.213	0.54	C6	0.1162	H6	0.279	0.44
C7	−0.0387				C7	−0.0389			
N	0.2046			0.69	N	0.2001			0.70
F	0.0167	F	3.064	2.60	F	0.0031	F	0.385	2.00

a) Hfcc of H was calculated using the values of Q and A_x^d for triplet benzene,[14] and hfcc of F was calculated by the analytical evaluation of dipolar integral.[12]

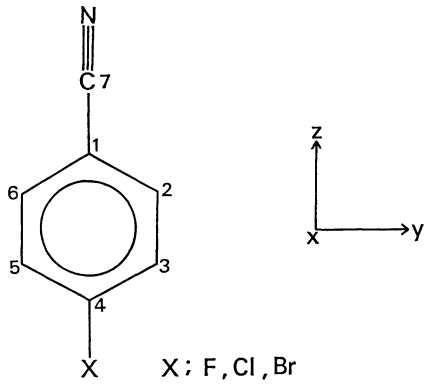

Fig. 1. Molecular structure, axis system, and numbering of the carbon atoms of the para-substituted benzonitriles.

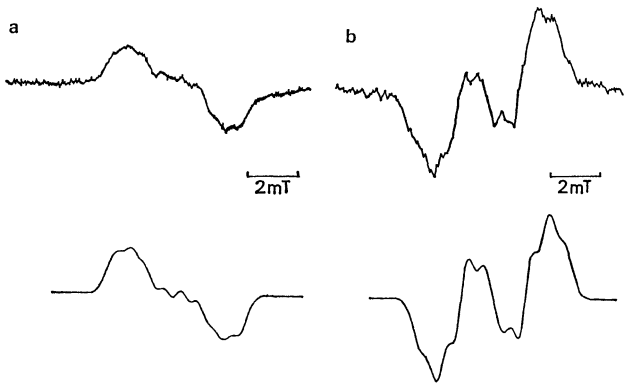

Fig. 2. Observed and simulated hyperfine structures when the applied field is perpendicular to the molecular plane.
(a): 3-Florobenzonitrile in DBB, (b): 2-fluorobenzonitrile in DBB. The upper spectra are experimental and the lower are simulated.

shown in Fig. 1.

The crystals were melt grown using the Bridgman method. When the host crystal was OX or MX, the solution containing a small amount of guest molecule was degassed by freeze-pump-thaw method and sealed in a 4 mm quartz tube. The sample mounted in the helical slow wave structure was cooled slowly to the liquid nitrogen temperature and was inserted rapidly into the helium cryostat. In other cases the crystals cut to the appropriate sizes were mounted in the helical slow wave structure in the ZFODMR experiments or on the acryl resin sample holder in the EPR experiments. The experimental setups and the procedure are essentially the same as those reported previously.[11,12]

Results and Disscussion

Hyperfine Splittings and Spin Distributions in the Halogen-substituted Benzonitriles. The spin densities in the T_1 state benzonitrile at the para, ortho, and meta positions were estimated to be 0.33, 0.12, and 0.007, respectively.[10] Halogen substitution, especially fluorine substitution, does not perturb the spin distribution of the parent molecule in the aromatic molecules such as naphthalene.[13] Fluorine or bromine substitution to benzonitrile at the para position also does not change the spin distribution much, although considerable spin delocalization of the unpaired electron into the halogen atom takes place.[12] The spin densities at the carbon 4 and the fluorine atom in 4FBN are 0.32 and 0.046, respectively.[12]

In Fig. 2 EPR spectra of 2FBN and 3FBN in DBB host taken with the applied field **B** perpendicular to the molecular plane are shown together with the simulated spectra. The fluorine splittings (A_x) estimated from the simulation are 2.6 mT for 2FBN and 2.0 mT for 3FBN. In the previous work on 4FBN[12] it was shown that a good agreement between the observed and calculated splittings was obtained using the molecular geometry of benzonitrile obtained from the bond orders calculated by the PPP UHF method for the T_1 state of benzonitrile. We have made similar calculations for 2FBN and 3FBN assuming the same geometries. The calculated A_x agrees reasonably well with the observed one in 2FBN, but the experimental value is far greater than the calculated one in 3FBN as shown in Table 1. This result seems to indicate that the structure of the T_1 state 3FBN is substantially different from that of benzonitrile. The normally used assumption[13] that the fluorine substitution does not perturb the spin distribution of

Table 2. Zero field splittings of halogen containing benzonitriles

System		ν_{00}/cm^{-1}	$\lvert D\rvert/cm^{-1}$	$\lvert E\rvert/cm^{-1}$
4BrBN	in PX	25766	0.168[a]	0.0129[a]
	in DBB	26202	0.156	0.0176
	in DCB	26235	0.157	0.0186
3BrBN	in MX	26535	0.160	0.0119
	MX doped	26095	0.148	0.0112
2BrBN	in OX	26295	0.183	0.0161
	OX doped	26286	0.153	0.0096
4ClBN	in PX	25799	0.135	0.0050
	in DBB		0.132	0.0045
	in DCB	26239	0.133	0.0058
	PX poped	25673	0.132	0.0042
3ClBN	MX doped	26041	0.134	0.0145
2ClBN	neat	26378	0.139	0.0133

a) Taken from Ref. 6.

the parent molecule appears to be no longer correct in the case of 3FBN. Nevertheless, the spin densities on the fluorine $2P_x$ orbitals are in the order $\rho(4FBN)>\rho(2FBN)>\rho(3FBN)$ following the order of the spin densities on the carbon atoms of the corresponding positions of benzonitrile.

In view of the fact that the delocalization of the unpaired electron into the bromine $4P_x$ orbital is greater than that into the fluorine $2P_x$ orbital, deviation from the benzonitrile structure may even be more serious in 3BrBN than in 3FBN.

Zero Field Splittings and the Contribution of Spin Orbit Coupling. It is known that the ZFS of the para-bromo-substituted benzenes are greately affected by the second order effect of the spin orbit coupling.[6,7] We determined the magnitudes of the ZFS of the ortho-, meta-, and para-substituted benzonitriles from the microwave frequencies for the zero field ODMR transitions. From the previous EPR study[6] the relative ordering of the sublevels of 4BrBN are known to be $T_z>T_y>T_x$: Here, the z axis is parallel to the C–Br direction, the x axis is perpendicular to the molecular plane, and the y axis is perpendicular to the other two. For the ortho- and meta-substituted molecules the relative ordering of the zero field sublevels as well as the directions of the in-plane principal axes of the fine structure tensor are not known. In these cases we designate the sublevels $T_{z'}$, $T_{y'}$, and $T_{x'}$ from the top.

The ZFS of the halogen-substituted benzonitriles studied here are listed in Table 2. The ZFS of the bromo- and chloro-substituted molecules are substantially affected by the choice of the host crystal. However, if we compare the $|D|$ of the bromo-substituted molecules with those of the chloro-substituted molecules in the same host or in the X traps, the $|D|$ of the bromo-substituted molecules are always larger. This seems to indicate that the contribution of the second order effect of the spin orbit coupling is significant in both 2BrBN and 3BrBN.

The depression of the sublevel energy caused by the spin orbit mixing with the perturbing state p is given by[15,16]

$$\Delta E^1 = \sum_{p\neq T_1}\sum_{v}\frac{|\langle\Psi^0_{pv}|H_{so}|\Psi^0_{T_1o}\rangle|^2}{E^0_{T_1O}-E^0_{pv}}, \quad (1)$$

where $\Psi^0_{T_1^0}$ is the wave function of the sublevel i of the zeroth vibrational unperturbed T_1 state and Ψ^0_{pv} are of the zeroth order perturbing states. v stands for the vibrational states of the perturbing state. It was suggested that the spin orbit mixing with the $^3\sigma\pi^*$ ($^3\pi\sigma^*$) and $^3n\pi^*$ states primarily affects the sublevel energies of the bromine containing substituted benzenes. In 4BrBN the T_z and T_x sublevels are lowered by the spin orbit mixing with the $^3\sigma\pi^*$ ($^3\pi\sigma^*$) state, while the T_y and T_x sublevels are lowered by the mixing with the $^3n\pi^*$ state. The spin orbit interaction is given by[1]

$$H_{so} = \Sigma\xi(l_xs_x+l_ys_y+l_zs_z), \quad (2)$$

where the summation is taken over the electrons. Then the electronic matrix elements which govern the depressions of the sublevel energires due to these mixings are given by

$$\left.\begin{aligned} a &= \frac{|\langle\sigma|\xi l_y|\pi\rangle|^2}{4[E(^3\pi\pi^*)-E(^3\sigma\pi^*)]}\begin{pmatrix}\text{for the mixing with}\\ \text{the } ^3\sigma\pi^* \text{ state}\end{pmatrix}\\ b &= \frac{|\langle n|\xi l_z|\pi\rangle|^2}{4[E(^3\pi\pi^*)-E(^3n\pi^*)]}\begin{pmatrix}\text{for the mixing with}\\ \text{the } ^3n\pi^* \text{ state}\end{pmatrix}\end{aligned}\right\}. \quad (3)$$

If we only consider the one center integrals at the bromine atoms a and b are given by the following expressions.

$$\left.\begin{aligned} a &= \frac{(C^{\sigma}_{Br}C^{\pi}_{Br})^2|\langle p^{Br}_z|\xi l^{Br}_y|p^{Br}_x\rangle|^2}{4[E(^3\pi\pi^*)-E(^3\sigma\pi^*)]}\\ b &= \frac{(C^{n}_{Br}C^{\pi}_{Br})^2|\langle p^{Br}_y|\xi l^{Br}_z|p^{Br}_x\rangle|^2}{4[E(^3\pi\pi^*)-E(^3n\pi^*)]}\end{aligned}\right\} \quad (4)$$

Here, C^{σ}_{Br}, C^{n}_{Br}, and C^{π}_{Br} are the coefficients of the bromine atomic orbitals in the σ, n and π molecular orbitals, respectively. ξ is defined by the relation

$$\xi = \frac{1}{4\pi\varepsilon_0}\frac{e^2}{2m^2c^2}\frac{r^3}{Z}, \quad (5)$$

where Z and r are the atomic number of the bromine and the distance of electron from the bromine nucleus, respectively. In the cases of 2BrBN and 3BrBN the z' and y' directions are not parallel or perpendicular to the C–Br direction, and both the z' and y' sublevels are lowered by the mixings with the $^3\sigma\pi^*$ and $^3n\pi^*$ states. When we take θ as the angle between the y' axis and the C–Br direction, $T_{z'}$, $T_{y'}$ and $T_{x'}$ sublevels are depressed by $a\cos^2\theta+b\sin^2\theta$, $a\sin^2\theta+b\cos^2\theta$ and $a+b$, respectively. Thus it is convenient to take $\delta=\Delta E_{z'x'}+\Delta E_{y'x'}$ as a measure of the effect of the spin orbit coupling on ZFS. Here ΔE_{ij} are the changes of the energy difference between i and j sublevels on going from the chloro-substituted molecule to the bromo-substituted molecule. δ is equal to $|a+b|$, namely the sum of the contributions due to the mixings with both $^3\sigma\pi^*$ ($^3\pi\sigma^*$) and $^3n\pi^*$ states. These values amount to 0.066 cm^{-1} for the para-substituted benzonitrile in PX, 0.028 cm^{-1} for the ortho- and meta-substituted benzonitriles in the X trap. If we assume that the energy denominators are similar for the para-, ortho-, and meta-substituted molecules, δ are proportional to the spin densities

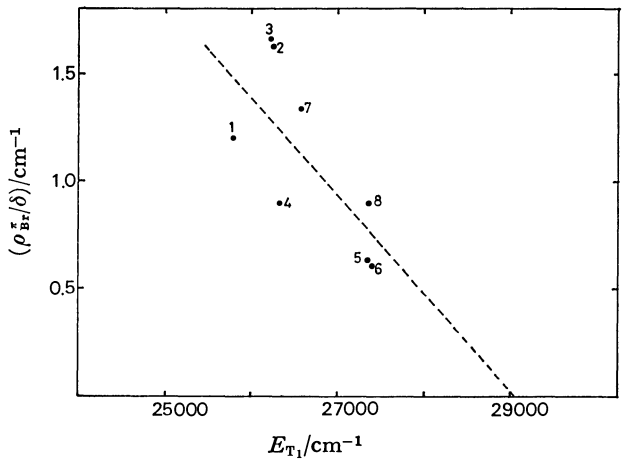

Fig. 3. Plot of ρ^{π}_{Br}/δ *vs.* E_{T_1}; (1) 4-bromobenzonitrile in PX, (2) 4-bromobenzonitrile in DCB, (3) 4-bromobenzonitrile in DBB, (4) 2-bromobenzonitrile X trap, (5) 1,4-dibromobenzene in PX,[7,21] (6) 1-bromo-4-chlorobenzene in PX,[7,21] (7) 4-bromoaniline in PX,[6,22], (8) 4-bromoanisole in PX.[6,22]

on the bromine atom ρ^{π}_{Br}. The observed values of δ are in the order of $\delta(\text{para}) > \delta(\text{ortho}) \simeq \delta(\text{meta})$ in qualitative agreement with that expected from the spin densities on the bromine $4P_x$ orbitals.

Possible Locations of the Perturbing States. From Eqs. 1—5 we obtain

$$\frac{(C^{\pi}_{Br})^2}{\delta} \propto \frac{1}{\zeta^2}\left\{\frac{(C^{\sigma}_{Br})^2}{E(^3\sigma\pi^*)-E(^3\pi\pi^*)}+\frac{(C^{n}_{Br})^2}{E(^3n\pi^*)-E(^3\pi\pi^*)}\right\}^{-1}. \quad (6)$$

If C^{σ}_{Br} and C^{n}_{Br} do not change much from one molecule to the other, $(C^{\pi}_{Br})^2/\delta$ approaches zero as the perturbing triplet states become close to the T_1 state. In Fig. 3 we plot ρ^{π}_{Br}/δ against the triplet state energy for these systems assuming that $(C^{\pi}_{Br})^2$ is proportional to ρ^{π}_{Br}. ρ^{π}_{Br} were estimated from the bromine hyperfine splittings when the bromine hyperfine splittings were observed. In others they were estimated from the fluorine hyperfine splittings by using the ratio of the fluorine splitting in 4FBN and the bromine splitting in 4BrBN. Though the points are scattered there seems to be a correlation between ρ^{π}_{Br}/δ and the triplet state energy (E_{T_1}) as indicated by the broken line in Fig. 3. The broken line intersects the horizontal axis at $\cong$29000 cm^{-1}. This seems to indicate that there are perturbing states around 29000 cm^{-1}. From the fact that both T_z and T_y sublevels are depressed by the bromine substitution for the para-substituted molecules both $^3\sigma\pi^*$ ($^3\pi\sigma^*$) and $^3n\pi^*$ states are likely to be in the vicinity of 29000 cm^{-1}.

Phosphorescence Spectra and the Main Radiative Mechanisms. The phosphorescence spectra of the representative systems are shown in Fig. 4. The phosphorescence spectra of 4- and 3BrBN, and 4- and 3ClBN in the corresponding xylenes and DCB are well resolved. On the other hand, the resolution of the phosphorescence spectra of 2BrBN and 2ClBN in OX are somewhat poorer, but they still give structures. In the X trap systems which contain small amount of the corresponding xylenes the phosphorescence spectra are broad with some structures. Nevertheless the frequencies of some of the main vibrations observed in the spectrum are similar to those of well resolved one in xylene. Therefore, it is considered that poorly resolved spectra are genuinely due to BrBN and ClBN.

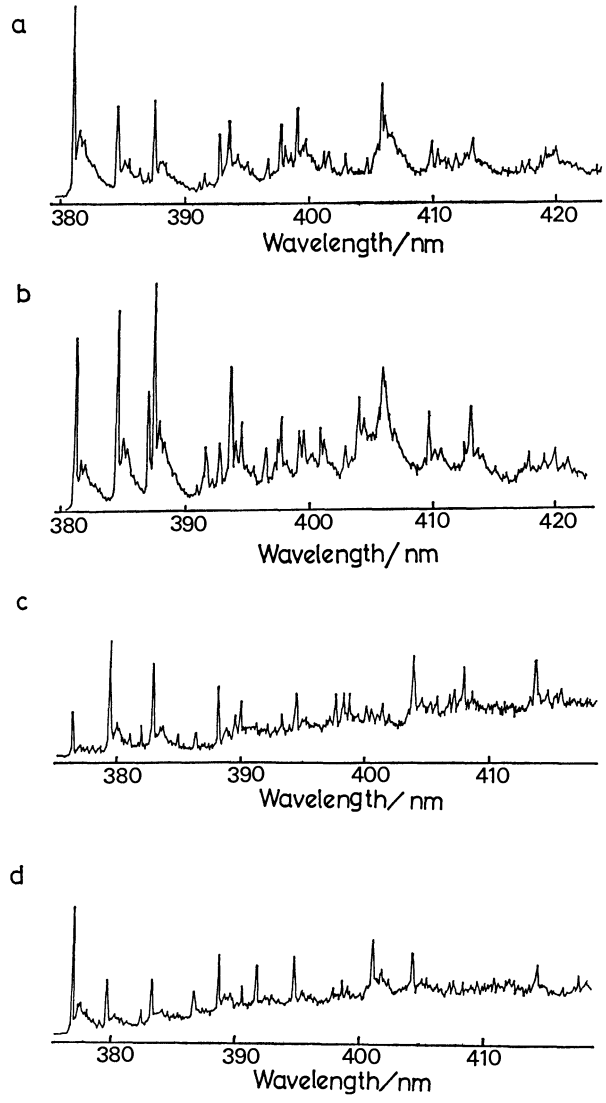

Fig. 4. Phosphorescence spectra of (a) 4-chlorobenzonitrile in DCB, (b) 4-bromobenzonitrile in DCB, (c) 3-chlorobenzonitrile in MX, (d) 3-bromobenzonitrile in MX.

The vibrational analyses of the phosphorescence spectra of 4BrBN and 4ClBN in DCB are given in Table 3. We have made assignments in reference to the infrared and Raman data.[17] In the 4ClBN spectrum the 0-0 band is the strongest. The vibrations of the a_1, b_1, and b_2 symmetries have moderate to weak intensities. On the other hand, in the spectrum of 4BrBN vibrations of the b_1 symmetry are the strongest. The possible mechanisms of the radiative transitions are summarized in Table 4. Since the perturbing states are close to the T_1 state vibronic coupling within the triplet manifold is considered to be dominant. The sublevel spectra of 4BrBN show that the enhanced intensity of the b_1 vibration of

TABLE 3. VIBRATIONAL ANALYSIS OF THE PHOSPHORESCENCE SPECTRUM OF 4-CHLOROBENZONITRILE AND 4-BROMOBENZONITRILE IN DCB AT 4.2 K

ν/cm^{-1}	$\Delta\nu$/cm^{-1}	Relative intensity	Assignment	ν/cm^{-1}	$\Delta\nu$/cm^{-1}	Relative intensity	Assignment
4-Chlorobenzonitrile				26007	228	s	b_1
26229		s	(0, 0)	25835	400	m	
25997	242	m	b_1	25806	429	s	b_1
25889	350	w	a_1	25532	703	m	b_1
25836	403	w		25459	776	m	a_1
25801	438	m	b_1	25407	828	s	b_1
25559	681	w		25379	856	w	
25536	703	w		25350	885	m	
25457	782	m	a_1	25228	1006	m	a_1
25408	831	m	b_1	25178	1057	w	a_1
25212	1027	w	a_1	25146	1089	m	b_2
25150	1089	m	a_1	25056	1179	w	a_1
25120	1119	w	b_2	25033	1202	w	
25064	1175	m	a_1	24951	1284	w	b_2
25049	1190	w	a_1	24931	1304	w	
24929	1310	w	b_2	24825	1410	w	b_2
24820	1419	w	b_2	24760	1475	m	a_1
24644	1596	m		24736	1499	w	
24625	1614	w		24642	1593	m	
4-Bromobenzonitrile				24633	1602	w	
26235		s	(0, 0)				

Relative intensity; s>m>w.

TABLE 4. MAIN PERTURBING STATES FOR THE $^3A_1 \rightarrow {}^1A_1$ RADIATIVE TRANSITION ALLOWED BY GROUP THEORY

Vibronic band	T_1 sublevel	Spin-orbit	Vibronic-spin-orbit
0, 0	z	$^3A_2(\pi\pi^*) \leftrightsquigarrow {}^1A_2(n\pi^*)$	
a_1	y	$^3B_1(\pi\pi^*) \leftrightsquigarrow {}^1B_1(\sigma\pi^*)$	
	x		
b_1	z		$^3A_2(\pi\pi^*) \leftrightarrow {}^3B_2(\sigma\pi^*) \leftrightsquigarrow {}^1B_2(\pi\pi^*)$
	y		$^3B_1(\pi\pi^*) \leftrightarrow {}^3A_1(\sigma\pi^*) \leftrightsquigarrow {}^1A_1(\pi\pi^*)$
	x		$^3B_2(\pi\pi^*) \leftrightarrow {}^3A_2(\sigma\pi^*) \leftrightsquigarrow {}^1A_2(n\pi^*)$
b_2	z		$^3A_2(\pi\pi^*) \leftrightarrow {}^3B_1(\pi\pi^*) \leftrightsquigarrow {}^1B_1(\sigma\pi^*)$
	y		$^3B_1(\pi\pi^*) \leftrightarrow {}^3A_2(\pi\pi^*) \leftrightsquigarrow {}^1A_2(n\pi^*)$
	x		$^3B_2(\pi\pi^*) \leftrightarrow {}^3A_1(\pi\pi^*) \leftrightsquigarrow {}^1A_1(\pi\pi^*)$
a_2	z		$^3A_2(\pi\pi^*) \leftrightarrow {}^3A_1(n\pi^*) \leftrightsquigarrow {}^1A_1(\pi\pi^*)$
	y		$^3B_1(\pi\pi^*) \leftrightarrow {}^3B_2(n\pi^*) \leftrightsquigarrow {}^1B_2(\pi\pi^*)$
	x		$^3B_2(\pi\pi^*) \leftrightarrow {}^3B_1(n\pi^*) \leftrightsquigarrow {}^1B_1(\sigma\pi^*)$

State symbols give the total symmetries.

4BrBN is mainly due to the T_y sublevel emission. Then the importance of the spin orbit vibronic mechanism involving $^3\pi\pi^* \leftrightarrow {}^3\sigma\pi^*$ ($^3\pi\sigma^*$) vibronic coupling increases on going from 4ClBN to 4BrBN (Fig. 5).

In the case of the meta-substituted benzonitrile the 0-0 band is stronger in the bromo-substituted molecule than in the chloro-substituted molecule. This indicates that the relative importance of the mechanism involving the $^1\sigma\pi^*$ ($^1\pi\sigma^*$) state increases on going from the chloro-substituted molecule to the bromo-substituted molecule.

In spite of the poor molecular symmetry of 3BrBN the T_y' and T_x' sublevel spectra are very different (Fig. 6). If we assume that only one center integral at the bromine atom is important in determining the radiative decay, this observation implies that the directions of the z′ and y′ axes are either nearly parallel or perpendicular to the C–Br direction. This result is in agreement with the conclusion obtained from the analysis of hfs and ZFS that the halogen substitution at the meta position perturbs the spin distribution of the present molecule greately.

Nuclear Charge and Position Dependence of the Decay Rates. We measured the total and relative radiative decay rate constants of the sublevels by the technique of microwave induced delayed phosphorescence (MIDP). The decay properties of the halogen-substituted benzonitriles are summarized in Table 5. The decay rate constants obtained in methylcyclohexane glass at 77k are also shown in Table 5. In order to study the position dependence of the decay rates we use $k_{av}=1/2(k_{y'}+k_{z'})$, because many molecules

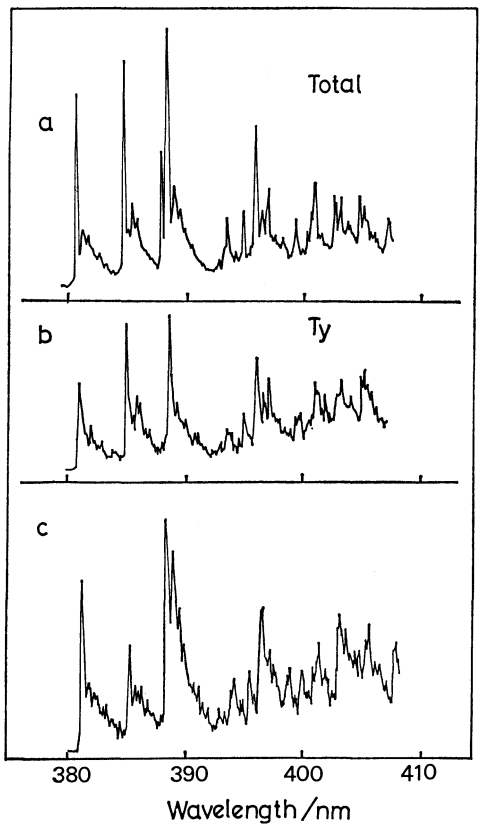

Fig. 5. MIDP and time resolved spectra of 4-bromobenzonitrile in DCB.
(a) Total phosphorescence spectrum. (b) MIDP spectrum obtained by the application of microwave at 4.1 GHz. (c) Time resolved spectrum obtained at 10 ms after excitation.

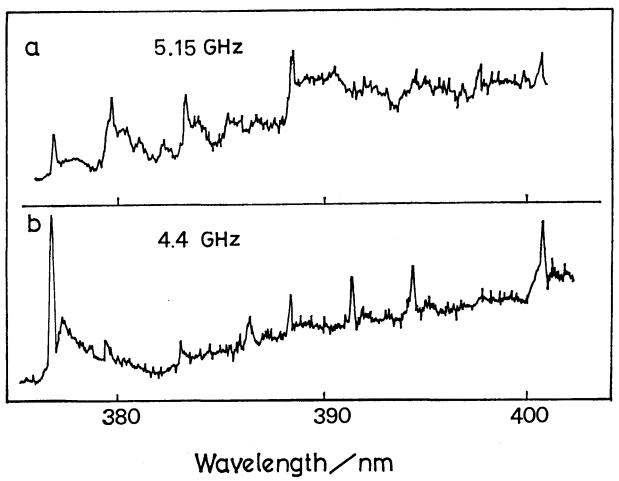

Fig. 6. MIDP spectra of 3-bromobenzonitrile in MX, (a) obtained by the application of microwave at 5.15 GHz, (b) obtained by the application of microwave at 4.4 GHz.

do not have C_{2v} symmetry and it is not possible to discuss the heavy atom effect on k_z' and k_y' seperately. Important results concerning the nuclear charge and position dependence may be summarized in the following.

(1) In the cases of the para-substituted benzonitrile the nuclear charge dependence is very dependent on the sublevel. $k_y(\mathrm{Br})/k_y(\mathrm{Cl})$ are 88 and 52 in PX and DCB host, respectively. These values are much larger than $\zeta^2_{Br}/\zeta^2_{Cl}$. On the other hand, $k_z(\mathrm{Br})/k_z(\mathrm{Cl})$ are only 22 and 11 in PX and DCB, respectively. $k_x(\mathrm{Br})/k_x(\mathrm{Cl})$ is also relatively small.

(2) $k_{av}(\mathrm{Br})/k_{av}(\mathrm{Cl})$ are 58, 35, and 35 for the para-substituted benzonitrile in PX, in DCB and in methylcyclohexane, 30 and 33 for the meta-substituted one in MX and in methylcyclohexane, and 38 and 34 for the ortho-substituted one in OX and in methylcyclohexane. These values are also substantially larger than those found for other systems (for 1- and 2-halonaphthalene in EPA glass these values are 20.9 and 21.4, respectively), though they depend on the host. The nuclear charge dependences are shown schematically in Fig. 7.

Table 5. Dynamic properties of halogen containing benzonitriles

Molecule		k[a) / s^{-1}]	$k^r(00)$[b)]	k_{av}[c) / s^{-1}]	k_{av}[d) / s^{-1}]
4BrBN (in PX)[f)]	z	110	10		
	y	580	25	345	352
	z	3.9	1		
(in DCB)	z	85			
	y	540		313	
	x	4.9			
3BrBN (in MX)	z′	190			
	y′	89	30	140	145
	x′	6.5	1		
(MX doped)	z′	92	13		
	y′	110	39	101	
	x′	5.1	1		
2BrBN (in OX)	z′				
	y′			184[e)]	165
	x′				
(OX doped)	z′	130	13		
	y′	75	11	103	
	x′	3.7	1		
4ClBN (in PX)[f)]	z	5.0	13.5		
	y	7.0	25	6.0	10.0
	x	0.28	1		
(in DCB)	z	7.6			
	y	10.4		9.0	
	x	0.52			
(PX doped)	z	3.2			
	y	19.6		11.0	
	x	0.30			
3ClBN (in MX)	z′				
	y′			4.5[e)]	4.4
	x′				
2ClBN (in OX)	z′				
	y′			4.9[e)]	4.8
	x′				
4FBN					0.85
3FBN					0.65
2FBN					0.73

a) Total decay rates. b) Relative radiative decay rates obtained at the 0-0 band. c) $k_{av}=1/2(k_y+k_z)$ or $1/2(k_{y'}+k_{z'})$ except where indicated. d) $k_{av}=1/2(k_{x'}+k_{y'}+k_{z'})$ in methylcyclohexane at 77 K. e) $k_{av}=1/2(k_{x'}+k_{y'}+k_{z'})$. f) Taken from Ref. 6.

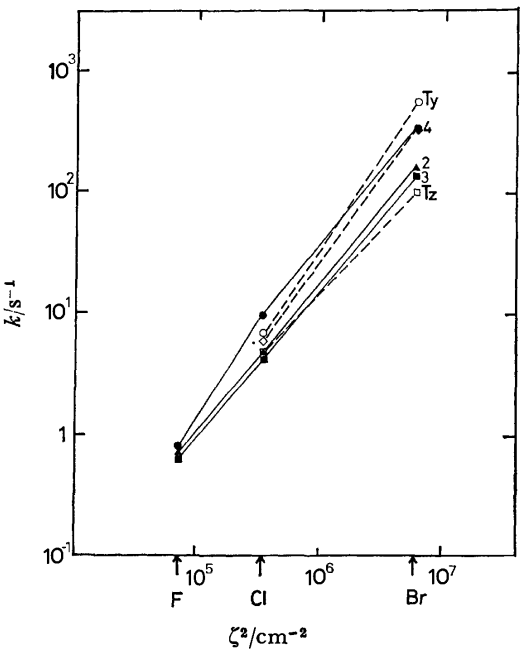

Fig. 7. Nuclear charge and position dependences of the decay rates.
●: k_{av} of the para-substituted molecules, ▲: the ortho-substituted ones, ■: the meta-substituted ones in methylcyclohexane. ◇: k_{av}, ○: T_y sublevel decay rate, □: T_z sublevel decay rate of the para-substituted ones in *p*-xylene.

(3) k_{av} are in the following order, $k_{av}(\text{para}) > k_{av}(\text{ortho}) > k_{av}(\text{meta})$. Although the decay rate constants depend on the host considerably, k_{av}(para) are 2—3 times larger than k_{av}(ortho) and k_{av}(meta).

We discuss these results based on the factors which govern the radiative and nonradiative decay rates. The transition moment $\boldsymbol{M}(T_1 \rightarrow S_0)$ between the T_1 state and the ground state is given by[18]

$$\boldsymbol{M}(T_1 \rightarrow S_0) = \sum_k \frac{1}{E^0(T_1) - E^0(S_k)} \left\{ \langle S_k | H(1) | T_1 \rangle + \sum_n \frac{\langle S_k | H(2) | S_n \rangle \langle S_n | H(1) | T_1 \rangle}{E^0(T_1) - E^0(S_n)} + \sum_{n \neq 1} \frac{\langle S_k | H(1) | T_n \rangle \langle T_n | H(2) T_1 \rangle}{E^0(T_1) - E^0(T_n)} \right\} \langle S_k | \Sigma \boldsymbol{er}_l | S_0 \rangle, \quad (7)$$

where $H(1) = H_{so}^{(e)}$, $H(2) = \sum_k (\partial H_0 / \partial Q_k) Q_k$, and Q_k are the normal vibrational coordinates of the given electronic state. The first term inside the parentheses gives the transition at the electronic origin induced by the direct spin orbit coupling, while the second and the third terms embody the vibronic spin orbit mechanisms. In the present systems $^3\sigma\pi^*$ ($^3\pi\sigma^*$) and $^3n\pi^*$ states are close to the T_1 state and the vibronic interactions involving these states are considered to be dominant. The important singlet states which couple with the $T_1(\pi\pi^*)$ state are $^1\sigma\pi^*$ and $^1n\pi^*$ states. The matrix elements such as $\langle ^1\sigma\pi^* | H_{so} | ^3\pi\pi^* \rangle$ and $\langle ^1n\pi^* | H_{so} | ^3\pi\pi^* \rangle$ are reduced to $C_h^{\sigma} C_h^{\pi} \langle P_z^h | \xi | l_y^h | P_x^h \rangle$ and $C_h^{n} C_h^{\pi} \langle P_y^h | \xi | l_z^h | P_x^h \rangle$, when only one center integrals at the halogen atoms are taken into consideration. Here, C_h^{π}, C_h^{σ}, and C_h^{n} are the AO coefficients of the halogen atomic orbitals which constitute the π, σ and n orbitals. Similar expressions are obtained for the spin orbit couplings between the $^1\pi\pi^*$ state and $^3\sigma\pi^*$ and $^3n\pi^*$ states.

In the case of nonradiative decay we use the expression for nonradiative transition obtained by Metz *et al.*;[19] the pure spin Born-Oppenheimer functions are used as a zeroth order basis set,[20] the dominant perturbation is assumed to be the spin orbit coupling operator, and the electronic transition moment is expanded about the equilibrium nuclear configuration of the ground state, *viz.*,

$$\begin{aligned} \langle T_1 | H_{so} | S_0 \rangle &= \langle T_1^0 | H_{so} | S_0^0 \rangle \\ &+ \sum_{j,k} \{ (E_{S_0}^0 - E_{S_j}^0)^{-1} [\langle T_1^0 | H_{so} | S_j^0 \rangle \langle S_j^0 | H_{vlb} | S_0^0 \rangle]_0 Q_k \} \\ &+ \sum_{m,k} \{ (E_{T_1}^0 - E_{T_m}^0)^{-1} [\langle T_1^0 | H_{vlb} | T_m^0 \rangle \langle T_m^0 | H_{so} | S_0^0 \rangle]_0 Q_k \}. \end{aligned} \quad (8)$$

Here the superscript zeros denote the zeroth order wave functions and energies, the subscript zeros denote the reference configuration, H_{vlb} is the vibronic coupling operator and Q_k are the normal coordinates describing the displacements from the reference configuration. We neglect spin vibronic term.

The first term in Eq. 8 is vanishingly small for planar conformation because of $\pi\pi^*$ character of the T_1 state. The spin orbit matrix elements in the second and third terms in Eq. 8 depend on the coefficients of the halogen atomic orbitals as in the case of the radiative decay. The dependence of the spin orbit matrix elements on the coefficients of the halogen atomic orbitals and the relevant energy denominators for the radiative and nonradiative transitions are given in Table 6.

In the present approach the decay rate constants depend on the energy denominator, AO coefficient of the halogen atomic orbital, the matrix element for the vibronic interaction, the transition moments for $S_0 \rightarrow S_k$ transitions involved in the main decay mechanisms, and the spin orbit coupling constant ζ. If the factors other than ζ do not change on going from the chloro-substituted molecule to the bromo-substituted molecule, the decay rate constants would be approximately proportional to ζ^2. Since the extent of the spin delocalization into the halogen atom increases on going from fluorine to iodine, the increase in the decay rate may be somewhat larger than expected from ζ^2. When we take account of this increase, the ratio of the spin orbit coupling matrix elements for bromine and chlorine is 24.4. The values observed for naphthalene and phenanthrene are indeed close to this value.[14] In these systems the above condition may be satisfied.

Since different sublevels couple with different perturbing states, the heavy atom enhancement is in principle sublevel dependent. In 4BrBn the enhancement was found to be much larger for the T_y sublevel decay than for the T_z sublevel decay. The T_y sublevel decay is mostly due to the mechanisms involving the vibronic interaction between the T_1 state and the $^3\sigma\pi^*$ ($^3\pi\sigma^*$) state. The larger value of k_y(Br)/k_y(Cl) seems to imply that the energy denominator for the $^3\sigma\pi^*$ ($^3\pi\sigma^*$) state substantially decreases on going from 4ClBN to 4BrBN. On the other hand

Table 6. The radiative and nonradiative decay mechanisms, relevent spin orbit matrix elements and energy denominators

	Decay mechanism	Spin-orbit matrix element[b]	Energy denominator
Radiative decay			
spin-orbit	$^3\pi\pi^* \longleftrightarrow {}^1\sigma\pi^*$	$C_h^x C_h^z \langle P_x^h \vert \xi 1_{y'}^h \vert P_{z'}^h \rangle$	$\Delta E(^1\sigma\pi^* - {}^3\pi\pi^*)$
	$^3\pi\pi^* \longleftrightarrow {}^1n\pi^*$ [a]	$C_h^z C_h^n \langle P_z^h \vert \xi 1_{x'}^h \vert P_{y'}^h \rangle$	$\Delta E(^1n\pi^* - {}^3\pi\pi^*)$
vibronic-spin-orbit	$^3\pi\pi^* \longleftrightarrow {}^3\sigma\pi^* \longleftrightarrow {}^1\pi\pi^*$	$C_h^z C_h^x \langle P_{z'}^h \vert \xi 1_{y'}^h \vert P_x^h \rangle$	$\Delta E(^1\pi\pi^* - {}^3\pi\pi^*) \times \Delta E(^3\sigma\pi^* - {}^3\pi\pi^*)$
	$^3\pi\pi^* \longleftrightarrow {}^3n\pi^* \longleftrightarrow {}^1\pi\pi^*$	$C_h^n C_h^x \langle P_{z'}^h \vert \xi 1_{y'}^h \vert P_x^h \rangle$	$\Delta E(^1\pi\pi^* - {}^3\pi\pi^*) \times \Delta E(^3\sigma\pi^* - {}^3\pi\pi^*)$
	$^3\pi\pi^* \longleftrightarrow {}^3\pi\pi^* \longleftrightarrow {}^1\sigma\pi^*$	$C_h^z C_h^z \langle P_x^h \vert \xi 1_{y'}^h \vert P_{z'}^h \rangle$	$\Delta E(^1\sigma\pi^* - {}^3\pi\pi^*) \times \Delta E(^3\pi\pi^* - {}^3\pi\pi^*)$
	$^3\pi\pi^* \longleftrightarrow {}^3\pi\pi^* \longleftrightarrow {}^1n\pi^*$	$C_h^z C_h^n \langle P_x^h \vert \xi 1_{z'}^h \vert P_{y'}^h \rangle$	$\Delta E(^1n\pi^* - {}^3\pi\pi^*) \times \Delta E(^3\pi\pi^* - {}^3\pi\pi^*)$
Nonradiative decay			
	$^3\pi\pi^* \longleftrightarrow {}^3\sigma\pi^* \longleftrightarrow G$	$C_h^{z*} C_h^z \langle P_x^h \vert \xi 1_{y'}^h \vert P_{z'}^h \rangle$	$\Delta E(^3\sigma\pi^* - {}^3\pi\pi^*)$
	$^3\pi\pi^* \longleftrightarrow {}^3n\pi^* \longleftrightarrow G$	$C_h^{z*} C_h^n \langle P_x^h \vert \xi 1_{z'}^h \vert P_{y'}^h \rangle$	$\Delta E(^3n\pi^* - {}^3\pi\pi^*)$
	$^3\pi\pi^* \longleftrightarrow {}^1\sigma\pi^* \longleftrightarrow G$	$C_h^z C_h^z \langle P_x^h \vert \xi 1_{y'}^h \vert P_{z'}^h \rangle$	$\Delta E(^1\sigma\pi^* - G)$
	$^3\pi\pi^* \longleftrightarrow {}^1n\pi^* \longleftrightarrow G$	$C_h^z C_h^n \langle P_x^h \vert \xi 1_{z'}^h \vert P_{y'}^h \rangle$	$\Delta E(^1n\pi^* - G)$

a) Only for meta and orhto substituted molecules. b) The x axis is perpendicular to the molecular plane, the z′ axis is parallel to the C–Br direction, and the y′ axis is perpendicular to the other two.

the energy denominator for the $^3n\pi^*$ state may not change much.

The increase of the T_y sublevel decay rate because of the reduction in the energy denominator seems to be manifested in the large change of the T_y sublevel decay rate on going from 1-bromonaphthalene[9] through 4BrBN to 1-bromo-4-chlorobenzene.[7] The decay rate constants are 159 s^{-1}, 580 s^{-1}, and 1540 s^{-1}, respectively following the order of the T_1 state energy. The $^3\sigma\pi^*$ ($^3\pi\sigma^*$) state should be very close to the T_1 state of 1-bromo-4-chlorobenzene as also indicated by the analysis of ZFS.[7]

When the increase of the $T_{y'}$ sublevel decay rate is much larger than that expected from ζ^2, $k_{av}(Br)/k_{av}(Cl)$ also becomes larger than that expected from ζ^2. $k_{av}(Br)/k_{av}(Cl)$ of the ortho- and meta-substituted benzonitrile are also considerably larger than expected from ζ^2 as in the case of para-substituted benzonitrile. This is expected when the decay mechanism involving the $^3\sigma\pi^*$ ($^3\pi\sigma^*$) state is dominant as in the case of 4BrBN.

The present analysis shows that the relationship between the decay rate and the spin density is not so straightforward, because the decay rate is determined by a number of factors. When the T_1 state is approximated by the single excitation from the HOMO (π) to the LUMO (π^*), the spin density on the halogen atom is given by $|C_h^H|^2 + |C_h^L|^2$. Here C_h^H and C_h^L denote the AO coefficients of halogen in the HOMO and the LUMO, respectively. The radiative decay rate depends on $|C_h^H|^2$. If the π^* orbital relevant to the spin orbit matrix elements governing the nonradiative decay is the LUMO, the nonradiative decay rate depends on $|C_h^L|^2$ and $|C_h^H|^2$. Therefore, a qualitative correlation between the spin density on the halogen atom and the decay rate may be obtained as observed in phenanthrene, if other factors such as energy denominators remain the same. In the present systems, $k_{av}(\text{para}) \simeq 2k_{av}$ (ortho) also correlates well with $\rho_{Br}(\text{para} \simeq 3\rho_{Br}$ (ortho). In spite of the complexities of the factors governing the decay rates, the correlation between the decay rate and the spin density may not be uncommon.

References

1) S. P. McGlynn, T. Azumi, and M. Kinoshita, "Molecular Spectroscopy of Triplet State," Prentice Hall, Englewood Cliffs, N. J. (1969), Chap. 7.
2) D. S. McClure, *J. Chem. Phys.*, **17**, 905 (1949).
3) S. P. McGlynn, R. Sunseri, and N. Christodouleas, *J. Chem. Phys.*, **37**, 1818 (1962).
4) J. C. Miller, J. S. Meek, and S. J. Strikler, *J. Am. Chem. Soc.*, **99**, 8175 (1977).
5) F. Masetti, U. Mazzucato, and G. Galuazzo, *J. Lumin.*, **4**, 8 (1971).
6) S. Niizuma, L. Kwan, and N. Hirota, *Mol. Phys.*, **35**, 1029 (1978).
7) H. Shinohara and N. Hirota, *J. Chem. Phys.*, **72**, 4445 (1980).
8) G. Kothandraman, H. J. Yue, and D. W. Pratt, *J. Chem. Phys.*, **61**, 2102 (1974).
9) H. Saigusa and T. Azumi, *J. Chem. Phys.*, **71**, 1408 (1979).
10) N. Hirota, T. C. Wong, E. T. Harrigan, and K. Nishimoto, *Mol. Phys.*, **29**, 903 (1975).
11) T. H. Cheng and N. Hirota, *Mol. Phys.*, **27**, 281 (1974).
12) Y. Asahi and N. Hirota, *Mol. Phys.*, **41**, 1211 (1980).
13) J. Mispelter, J.-Ph, Grivet, and J. M. Lhoste, *Mol. Phys.*, **21**, 999 (1971).
14) A. M. P. Goncalves and C. A. Hutchison, Jr., *J. Chem. Phys.*, **54**, 2962 (1971).
15) C. R. Jones, A. H. Maki, and D. R. Kearns, *J. Chem. Phys.*, **59**, 873 (1973).
16) H. Hayashi and S. Nagakura, *Mol. Phys.*, **24**, 801 (1972).
17) J. H. S. Green and D. J. Harrison, *Spectrochim. Acta*, **32**, 1279 (1976).
18) E. C. Lim, "Excited States," ed by E. C. Lim, Academic, New York (1977), Vol. 3, Chap. 5.
19) F. Metz, S. Friedrich, and G. Hohlneiher, *Chem. Phys. Lett.*, **16**, 353 (1972).
20) B. R. Henry and W. Siebrand, *J. Chem. Phys.*, **54**, 1072 (1971).
21) In the cases of 1-bromo-4-chlorobenzene and 1,4-dibromobenzene, the spin densities on the bromine were assumed to be proportional the spin densities on carbon 4 (0.33).
22) Y. Asahi and N. Hirota, *Mol. Phys.*, in press.

Calculation of the Pair Correlation Functions for Fluids Composed of Diatomic Polar Molecules Based on the Interaction Site Model

Masaharu Ohba and Kiyoshi Arakawa*

Research Institute of Applied Electricity, Hokkaido University, Sapporo 060

(Received October 2, 1981)

A reference hypernetted chain (RHNC) like approximation of the interaction site model is proposed, which is the extension of Lado's RHNC equation of simple fluids to the case of molecular fluids. By using the proposed RHNC like integral equation, pair correlation functions, structure factors and some thermodynamic quantities for fluids composed of diatomic polar molecules are calculated, where the molecules consist of two fused hard-spheres with each center located at a distance l, and at each center charges $+q$ and $-q$ are sited. Calculated pair correlation functions are successful in showing well-marked characteristics of the fluid, such as cusps, not observed for simple fluids like argon. The isothermal compressibility at a constant reduced density and dipole moment has a weak l-dependence in sharp contrast to the total internal energy showing a strong l-dependence.

The statistical mechanical theory of fluids based on the interaction site model (ISM)[1-4] has turned out to be successful in studying the equilibrium properties of those composed of polyatomic molecules. It was also applied to fluids composed of molecules with electrostatic potentials. The theory of polar fluids based on the ISM was proposed first by Chandler and others.[5,6] We applied the ISM to ionic solutions.[7] These theories concern with general properties of dielectric constant, pair correlation functions and others for polar and ionic fluids. Recently, Morriss and Perram have obtained a formal solutions of the mean spherical approximation of RISM-1 (see below) for polyatomic polar fluids,[8] but numerical results have not been given yet.

As the method of obtaining site-site pair correlation functions, three modifications of reference interaction site model integral equations (RISM-1, RISM-2, and RISM-3) coupled with a certain approximation, such as the Percuss-Yevick (PY) like approximation, the hypernetted chain (HNC) like approximation and mean spherical approximation, are proposed.[1,4,9,10] These integral equations were solved for molecular fluids with short-ranged intermolecular forces,[11-13] and the RISM-1 equation gives the most accurate site-site pair correlation functions in comparison with computer simulation results or experimental results.[4] Since the differences between the results of the PY like approximation and the HNC like approximation are similar to those of simple fluids,[4] it is expected that the PY like and HNC like approximations are appropriated to fluids with short-ranged forces and with long-ranged forces, respectively.

For simple fluids composed of molecules with a short-ranged force and a long-ranged tail, the reference hypernetted chain (RHNC) approximation gives a fairly good result.[14-16] In the theory, the system without long-ranged tails is treated as a reference system whose properties are obtained from the PY approximation or computer simulations, and the correction due to the long-ranged tail is calculated by the HNC approximation. So, by considering the properties of the PY like and HNC like approximations, a similar treatment will also be appropriated to the case of polyatomic molecular fluids.

In this paper, we propose an RHNC like approximation of RISM-1 and solve it for diatomic polar fluids. In Theory section, the definition of a model is made and the RHNC like approximation is proposed.

Theory

Model. We assume that the molecule has n interaction sites and a charge q_α is sited on the α-th site of the molecule. The total potential energy for the molecular fluid is assumed to be the sum over all pairs of the intermolecular potentials. The pair interaction between the i-th molecule and the j-th molecule $U(i,j)$ is given by

$$U(i,j) = \sum_{\alpha=1}^{n} \sum_{\gamma=1}^{n} u_{\alpha\gamma}(|\boldsymbol{r}_i^\alpha - \boldsymbol{r}_j^\gamma|), \tag{1}$$

where $u_{\alpha\gamma}(|\boldsymbol{r}_i^\alpha - \boldsymbol{r}_j^\gamma|)$ is an interaction potential between the pair of the site α of the i-th molecule and the site γ of the j-th molecule, and $\boldsymbol{r}_i^\alpha$ the position of the site α of the i-th molecule. An illustration of the molecule is shown in Fig. 1. The site-site interaction

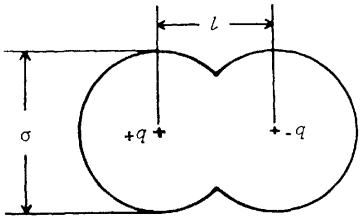

Fig. 1. The shape of the diatomic polar molecule considered in this paper.

can be divided into two parts,

$$u_{\alpha\gamma}(r) = u_{\alpha\gamma}^{(0)}(r) + u_{\alpha\gamma}^{(1)}(r). \tag{2}$$

Here, $u_{\alpha\gamma}^{(0)}(r)$ is a short ranged part of the site-site interaction, which is treated as a reference potential, and $u_{\alpha\gamma}^{(1)}(r)$ a long-ranged Coulomb tail, that is,

$$u_{\alpha\gamma}^{(1)}(r) = \frac{q_\alpha q_\gamma}{4\pi\varepsilon_0 r}, \tag{3}$$

where ε_0 is the dielectric constant of vacuum.

RHNC like Approximation. In the following formulation, we attempt to extend Lado's formalism of simple fluids[14,15] to polyatomic molecular fluids. We start with the Ornstein-Zernike type equation[1,4] as follows,

$$\boldsymbol{h}(\boldsymbol{r}) = \boldsymbol{\omega} * \boldsymbol{c} * \boldsymbol{\omega}(\boldsymbol{r}) + \rho \boldsymbol{\omega} * \boldsymbol{c} * \boldsymbol{h}(\boldsymbol{r}), \tag{4}$$

where the * denotes a convolution, ρ the number density of molecules and $\boldsymbol{h}(r)$, $\boldsymbol{\omega}(r)$, and $\boldsymbol{c}(r)$ are matrices with elements $h_{\alpha\gamma}(r)$, $\omega_{\alpha\gamma}(r)$, and $c_{\alpha\gamma}(r)$, respectively. The site-site total correlation function $h_{\alpha\gamma}(r)$ and the intramolecular pair correlation function $\omega_{\alpha\gamma}(r)$ are defined as reported,[7] and the site-site direct correlation function $c_{\alpha\gamma}(r)$ is defined in Eq. 4. The Fourier transform of Eq. 4 is

$$\tilde{\boldsymbol{h}} = \tilde{\boldsymbol{\omega}}\tilde{\boldsymbol{c}}\tilde{\boldsymbol{\omega}} + \rho\tilde{\boldsymbol{\omega}}\tilde{\boldsymbol{c}}\tilde{\boldsymbol{h}}, \tag{5}$$

where $\tilde{\boldsymbol{A}}$ denotes a matrix with the element $\tilde{A}_{\alpha\gamma}(k)$ and $\tilde{A}_{\alpha\gamma}(k)$ the Fourier transform of $A_{\alpha\gamma}(r)$,

$$\tilde{A}_{\alpha\gamma}(k) = \int \mathrm{d}\boldsymbol{r} A_{\alpha\gamma}(r)\mathrm{e}^{-i\boldsymbol{k}\cdot\boldsymbol{r}}.$$

The function, $\tilde{\omega}_{\alpha\gamma}(k)$, for rigid molecules is expressed as

$$\tilde{\omega}_{\alpha\gamma}(k) = \delta_{\alpha\gamma} + (1-\delta_{\alpha\gamma})\frac{\sin kl_{\alpha\gamma}}{kl_{\alpha\gamma}}, \tag{6}$$

where $\delta_{\alpha\gamma}$ is the Kronecker delta and $l_{\alpha\gamma}=|\boldsymbol{r}_i^\alpha-\boldsymbol{r}_i^\gamma|$ the distance between the α-th site and γ-th site of the same molecule.

The Ornstein-Zernike type equation for a reference system is

$$\tilde{\boldsymbol{h}}^{(0)} = \tilde{\boldsymbol{\omega}}\tilde{\boldsymbol{c}}^{(0)}\tilde{\boldsymbol{\omega}} + \rho\tilde{\boldsymbol{\omega}}\tilde{\boldsymbol{c}}^{(0)}\tilde{\boldsymbol{h}}^{(0)}, \tag{7}$$

where superscript (0) denotes the reference system quantity. From Eqs. 5 and 7, we obtain

$$\delta\tilde{\boldsymbol{h}} = (\tilde{\boldsymbol{\omega}}+\rho\tilde{\boldsymbol{h}}^{(0)})\{\boldsymbol{1}-\rho\delta\tilde{\boldsymbol{c}}(\tilde{\boldsymbol{\omega}}+\rho\tilde{\boldsymbol{h}}^{(0)})\}^{-1}\delta\tilde{\boldsymbol{c}}(\tilde{\boldsymbol{\omega}}+\rho\tilde{\boldsymbol{h}}^{(0)}), \tag{8}$$

where $\boldsymbol{A}^{-1}$ denotes the matrix inverse of matrix $\boldsymbol{A}$, $\boldsymbol{1}$ the unit matrix. $\delta\tilde{\boldsymbol{h}}$ and $\delta\tilde{\boldsymbol{c}}$ are the matrices with elements $\delta\tilde{h}_{\alpha\gamma}(k)$ and $\delta\tilde{c}_{\alpha\gamma}(k)$, the Fourier transforms of $\delta h_{\alpha\gamma}(r)$ and $\delta c_{\alpha\gamma}(r)$, respectively, which are defined as follows,

$$\delta h_{\alpha\gamma}(r) = h_{\alpha\gamma}(r) - h_{\alpha\gamma}^{(0)}(r) \tag{9}$$

and

$$\delta c_{\alpha\gamma}(r) = c_{\alpha\gamma}(r) - c_{\alpha\gamma}^{(0)}(r). \tag{10}$$

$\delta h_{\alpha\gamma}(r)$ and $\delta c_{\alpha\gamma}(r)$ are the perturbation corrections to $h_{\alpha\gamma}(r)$ and $c_{\alpha\gamma}(r)$, respectively, due to the perturbation potential $u_{\alpha\gamma}^{(1)}(r)$.

A closure relation between $\delta h_{\alpha\gamma}(r)$ and $\delta c_{\alpha\gamma}(r)$ is derived as follows. We consider the following relation as

$$c_{\alpha\gamma}(r) = h_{\alpha\gamma}(r) - \ln g_{\alpha\gamma}(r)\mathrm{e}^{\beta u_{\alpha\gamma}(r)} + B_{\alpha\gamma}(r), \tag{11}$$

where $g_{\alpha\gamma}(r)=h_{\alpha\gamma}(r)+1$ is the site-site radial distribution function, $\beta=(k_\mathrm{B}T)^{-1}$, k_B the Boltzmann constant and T the absolute temperature. $B_{\alpha\gamma}(r)$ defined in Eq. 11 is the residual term. If we put $B_{\alpha\gamma}(r)=0$, we obtain the HNC like approximation for RISM-1.[4,17] Different from the case of simple fluids, $B_{\alpha\gamma}(r)$ cannot be expressed as a sum of allowed cluster diagrams.[17] Subtraction of the similar equation for the reference system yields

$$\delta c_{\alpha\gamma}(r) = \delta h_{\alpha\gamma}(r) - \ln\frac{g_{\alpha\gamma}(r)}{g_{\alpha\gamma}^{(0)}(r)}\mathrm{e}^{\beta u_{\alpha\gamma}^{(1)}(r)} + \delta B_{\alpha\gamma}(r), \tag{12}$$

where

$$\delta B_{\alpha\gamma}(r) = B_{\alpha\gamma}(r) - B_{\alpha\gamma}^{(0)}(r).$$

Here, we assume that $\delta B_{\alpha\gamma}(r)=0$. Then we have a new approximation as follows

$$\delta c_{\alpha\gamma}(r) = \delta h_{\alpha\gamma}(r) - \ln\frac{g_{\alpha\gamma}(r)}{g_{\alpha\gamma}^{(0)}(r)}\mathrm{e}^{\beta u_{\alpha\gamma}^{(1)}(r)}, \tag{13}$$

which we call an RHNC like approximation for RISM-1. Combining Eq. 8 with Eq. 13, we can solve the integral equation when the reference system quantities are given. The RHNC like integral equation for RISM-1, that is, Eqs. 8 and 13, is the extension of Lado's RHNC integral equation for simple fluids[14,15] to the case of polyatomic molecular fluids.

Computational Procedures

A system calculated is a fluid composed of diatomic polar molecules which is shown in Fig. 1. A fluid composed of fused hard-spheres with the same diameter σ is considered as a reference system, so the reference potential is given as

$$u_{\alpha\gamma}^{(0)}(r) = \begin{cases} \infty, & r<\sigma \\ 0, & r>\sigma. \end{cases} \tag{14}$$

Because of the symmetry, we have $g_{++}(r)=g_{--}(r)$, $g_{+-}(r)=g_{-+}(r)$ and $g_{++}^{(0)}(r)=g_{--}^{(0)}(r)=g_{+-}^{(0)}(r)=g_{-+}^{(0)}(r)\equiv g^{(0)}(r)$ for the systems considered here.

The functions $\delta h_{\alpha\gamma}(r)$ and $\delta c_{\alpha\gamma}(r)$ have a discontinuity at $r=\sigma$. Thus, we define a new function $H_{\alpha\gamma}(r)$ as follows,

$$H_{\alpha\gamma}(r) = \delta h_{\alpha\gamma}(r) - \delta c_{\alpha\gamma}(r). \tag{15}$$

$H_{\alpha\gamma}(r)$ is a continuous function of r. By the use of this, Eqs. 8 and 13 can be written as

$$\tilde{\boldsymbol{H}} = (\tilde{\boldsymbol{\omega}}+\rho\tilde{\boldsymbol{h}}^{(0)})\{\boldsymbol{1}-\rho\delta\tilde{\boldsymbol{c}}(\tilde{\boldsymbol{\omega}}+\rho\tilde{\boldsymbol{h}}^{(0)})\}^{-1}\delta\tilde{\boldsymbol{c}}(\tilde{\boldsymbol{\omega}}+\rho\tilde{\boldsymbol{h}}^{(0)}) - \delta\tilde{\boldsymbol{c}} \tag{16}$$

and

$$\delta c_{\alpha\gamma}(r) = g_{\alpha\gamma}^{(0)}(r)\{\exp[H_{\alpha\gamma}(r)-\beta u_{\alpha\gamma}^{(1)}(r)]-1\} - H_{\alpha\gamma}(r). \tag{17}$$

From Eqs. 13 and 15, we obtain

$$H_{\alpha\gamma}(r) = \beta u_{\alpha\gamma}^{(1)}(r) + \ln\frac{g_{\alpha\gamma}(r)}{g_{\alpha\gamma}^{(0)}(r)}. \tag{18}$$

For polar fluids, $h_{\alpha\gamma}(r)$ decays as r^{-6} at large r.[5,6] Thus, the following asymptotic forms of $H_{\alpha\gamma}(r)$ and $\delta c_{\alpha\gamma}(r)$ at large separations are derived from Eqs. 15 and 18,

$$H_{\alpha\gamma}(r) \sim \beta u_{\alpha\gamma}^{(1)}(r), \text{ and } \delta c_{\alpha\gamma}(r) \sim -\beta u_{\alpha\gamma}^{(1)}(r).$$

Since $u_{\alpha\gamma}^{(1)}(r)$ is the long-ranged Coulomb potential, serious truncation errors can arise when these functions are numerically integrated over a finite range. Thus, we define a new short-ranged function $H_{\alpha\gamma}^{s}(r)$ and $\delta c_{\alpha\gamma}^{s}(r)$ as follows,

$$H_{\alpha\gamma}^{s}(r) = H_{\alpha\gamma}(r) - H_{\alpha\gamma}^{L}(r) \tag{19}$$

and

$$\delta c_{\alpha\gamma}^{s}(r) = \delta c_{\alpha\gamma}(r) + H_{\alpha\gamma}^{L}(r), \tag{20}$$

where

$$H_{\alpha\gamma}^{L}(r) = \frac{\beta q_\alpha q_\gamma}{4\pi\varepsilon_0 r}(1-\mathrm{e}^{-ar}) \tag{21}$$

and a is a disposable parameter chosen so as to make the function $\Psi_{\alpha\gamma}^{s}(r)$, defined below, negligibly small at the termination of the finite range of r. By the use of new functions $H_{\alpha\gamma}^{s}(r)$ and $\delta c_{\alpha\gamma}^{s}(r)$, Eqs. 16 and

17 can be written as

$$\tilde{\boldsymbol{H}}^{S} = (\tilde{\boldsymbol{\omega}}+\rho\tilde{\boldsymbol{h}}^{(0)})\{\boldsymbol{1}-\rho(\delta\tilde{\boldsymbol{c}}^{S}-\tilde{\boldsymbol{H}}^{L})(\tilde{\boldsymbol{\omega}}+\rho\tilde{\boldsymbol{h}}^{(0)})\}^{-1} \times (\delta\tilde{\boldsymbol{c}}^{S}-\tilde{\boldsymbol{H}}^{L})(\tilde{\boldsymbol{\omega}}+\rho\tilde{\boldsymbol{h}}^{(0)}) - \delta\tilde{\boldsymbol{c}}^{S} \quad (22)$$

and

$$\delta c^{S}_{\alpha\gamma}(r) = g^{(0)}_{\alpha\gamma}\{\exp[H^{S}_{\alpha\gamma}(r)-\Psi^{S}_{\alpha\gamma}(r)]-1\}-H^{S}_{\alpha\gamma}(r), \quad (23)$$

where

$$\Psi^{S}_{\alpha\gamma}(r) = \frac{\beta q_\alpha q_\gamma}{4\pi\varepsilon_0 r}e^{-ar}$$

and

$$\tilde{H}^{L}_{\alpha\gamma}(k) = \frac{\beta q_\alpha q_\gamma a^2}{\varepsilon_0 k^2(k^2+a^2)}.$$

Equations 22 and 23 involve only short-ranged functions that can be numerically handled in the usual way. An iteration procedure is carried out for solving Eqs. 22 and 23 numerically. The iteration was started with the initial guess $H^{a}_{\alpha\gamma}(r)=0$, and has been continued until the self consistency of

$$\left|\frac{H^{S}_{\alpha\gamma}(r)_{out}-H^{S}_{\alpha\gamma}(r)_{in}}{H^{S}_{\alpha\gamma}(r)_{in}}\right| < 10^{-7} \quad (24)$$

is satisfied. The site-site radial distribution function is finally obtained as

$$g_{\alpha\gamma}(r) = g^{(0)}_{\alpha\gamma}(r)\exp\{H^{S}_{\alpha\gamma}(r)-\Psi^{S}_{\alpha\gamma}(r)\}. \quad (25)$$

The solution of Lowden's RISM computer program[18] is used as a reference system site-site radial distribution function $g^{(0)}_{\alpha\gamma}(r)$.

Results and Discussion

A system considered is characterized by three parameters, that is, the reduced density $\rho^*=\rho d^3$, the reduced dipole moment $\mu^*=(\mu^2/4\pi\varepsilon_0 k_B T d^3)^{1/2}$ and the reduced bond length $L^*=l/\sigma$. Here, $\mu=ql$ is the magnitude of the dipole moment of the molecules and d, the diameter of the hard sphere whose volume is the same as the molecule considered here, is defined by the following relations as

$$d^3 = \sigma^3\left(1+\frac{3L^*}{2}-\frac{L^{*3}}{2}\right). \quad (26)$$

Iteration procedures described above diverge when L^* is 0.2 or less.

Distribution Functions. Figures 2—5 show the site-site radial distribution functions calculated according to the procedures described in the preceding section. All of $g_{\alpha\gamma}(r)$ shown in these figures have cusps at $r/\sigma=1+L^*$. These cusps are characteristic of fluids composed of diatomic molecules with a hard core repulsion. For the system with continuous potentials, these cusps are rounded off.[4] It is noted that all the curves of $g_{++}(r)$ and $g_{+-}(r)$ in Figs. 2—5 are nearly symmetrical with respect to the curve of $g^{(0)}(r)$, and have oscillatory structure around the curve of $g^{(0)}(r)$. These behaviors are explained as follows: Let the center of the + atom of one molecule fix the origin. Then, if the + atom of the other molecule exist at $r\simeq\sigma$, the − atom of its molecule necessarily exist at $r\simeq\sigma+l$. Thus, because of the decrease of the value of $g_{++}(r)$ at $r\simeq\sigma$ due to the electrostatic repulsion in comparison with the value of $g^{(0)}(r)$, the value of $g_{+-}(r)$ decrease at $r\simeq\sigma+l$. Similar effects will cause the behaviors described above.

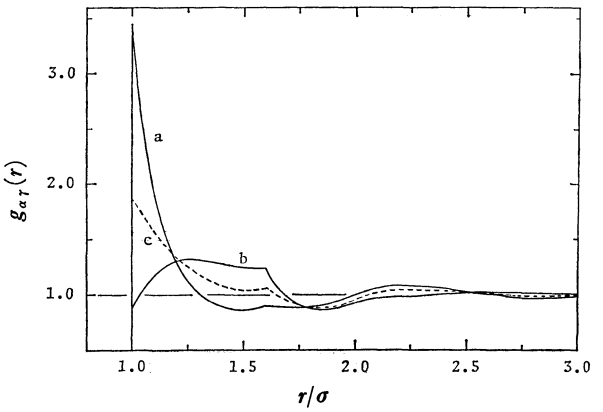

Fig. 2. The site-site radial distribution functions, $g_{\alpha\gamma}(r)$, for diatomic polar fluid at $\rho^*=0.8$, $\mu^{*2}=3.0$ and $L^*=0.6$. a; $g_{+-}(r)=g_{-+}(r)$, b; $g_{++}(r)=g_{--}(r)$, c; $g^{(0)}(r)$.

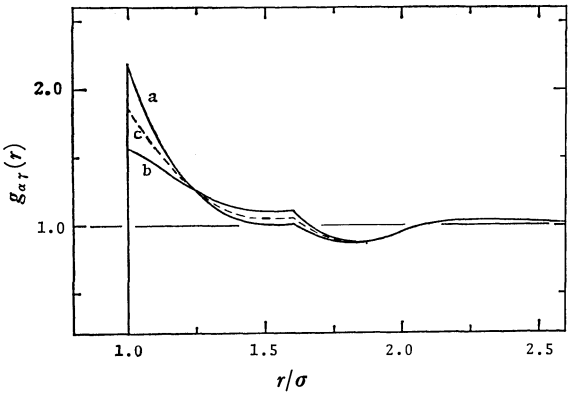

Fig. 3. Same as Fig. 2, except $\mu^{*2}=0.5$.

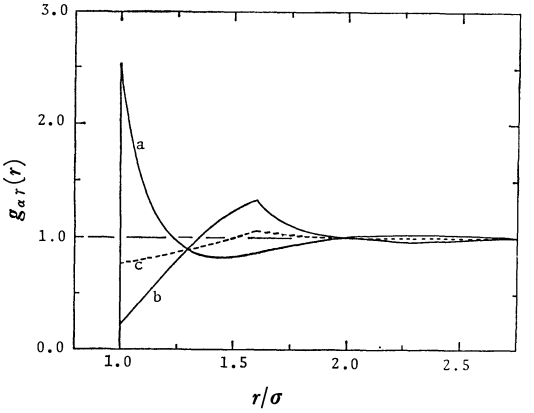

Fig. 4. Same as Fig. 2, except $\rho^*=0.2$.

A large deviation of $g_{\alpha\gamma}(r)$ from $g^{(0)}(r)$ are shown at $\rho^*=0.8$, $\mu^{*2}=3.0$ and $L^*=0.6$ (Fig. 2). The deviation at $\rho^*=0.8$, $\mu^{*2}=0.5$ and $L^*=0.6$ (Fig. 3) are smaller than that shown in Fig. 2 and $g_{\alpha\gamma}(r)$ almost agree with $g^{(0)}(r)$ at $r>2\sigma$. It is shown in Fig. 4 that $g^{(0)}(r)$ at $\rho^*=0.2$, $\mu^{*2}=3.0$ and $L^*=0.6$ is nearly equal to one, on the other hand the deviations of $g_{\alpha\gamma}(r)$ from $g^{(0)}(r)$ are similar to those shown in Fig. 2. Figure 5 shows $g_{\alpha\gamma}(r)$ at $\rho^*=0.6$, $\mu^{*2}=1.0$ and $L^*=0.3$. The shapes of curves are considerably dif-

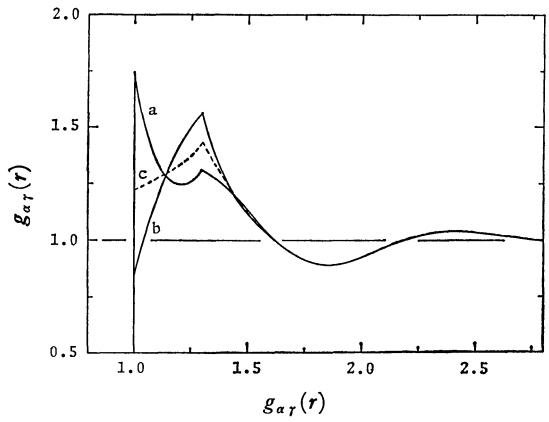

Fig. 5. The site-site radial distribution functions, $g_{\alpha\gamma}(r)$, for diatomic polar fluid at $\rho^*=0.6$, $\mu^{*2}=1.0$ and $L^*=0.3$. a; $g_{+-}(r)=g_{-+}(r)$, b; $g_{++}(r)=g_{--}(r)$, c; $g^{(0)}(r)$.

ferent from those at $L^*=0.6$. This difference is due to the difference of the shape of $g^{(0)}(r)$. On the other hand, the deviation of $g_{\alpha\gamma}(r)$ from $g^{(0)}(r)$ is similar to that at $L^*=0.6$.

Structure Factors. The structure factor is expressed in terms of site-site correlation functions as follows,[11]

$$S(k) = (\sum_{\alpha} b_\alpha)^{-2} \sum_{\alpha}\sum_{\gamma} b_\alpha b_\gamma \{\tilde{\omega}_{\alpha\gamma}(k) + \rho\tilde{h}_{\alpha\gamma}(k)\}$$

$$= \frac{(b_+^2+b_-^2)\{1+\tilde{h}_{++}(k)\}+2b_+b_-\{\tilde{\omega}_{+-}(k)+\tilde{h}_{+-}(k)\}}{(b_++b_-)^2}, \quad (27)$$

where we use the relations $h_{++}(r)=h_{--}(r)$ and $h_{+-}(r)=h_{-+}(r)$ in the second equality and b_α denote the coherent scattering amplitude for an atoms of type α. Figures 6 and 7 show the structure factors calculated under the assumptions of $b_+=b_-$ and $b_+=10b_-$, respectively. The structure factor at $b_+=b_-$ is nearly equal to that of reference system except at small k. This result arises from the fact that the deviation of $g_{++}(r)$ from $g^{(0)}(r)$ cancells that of $g_{+-}(r)$. Because of the decrease of these cancellations, $S(k)$ at $b_+=10b_-$ fairly deviate from $S^{(0)}(k)$. The values of $S(k)$ increase in small range of $k\sigma$ in comparison with $S^{(0)}(k)$. The behavior of the structure factors at small k seems to be due to the contribution of averaged attractive potentials.[4,19]

Thermodynamic Quantities. The total internal energy U and the isothermal compressibility κ_T are expressed in terms of the site-site pair correlation functions as follows,

$$\frac{U}{Nk_BT} = \frac{\rho}{2k_BT}\sum_{\alpha}\sum_{\gamma}\int d\boldsymbol{r} u_{\alpha\gamma}(r) g_{\alpha\gamma}(r), \quad (28)$$

and

$$\rho k_BT\kappa_T = S(0) = 1 + \rho\tilde{h}_{\alpha\gamma}(0), \quad (29)$$

where N is the number of molecules. Figures 8 and 9 show the internal energy and the isothermal compressibility at $L^*=0.6$, respectively. The L^* dependence of the internal energy and the isothermal compressibility are also shown in Figs. 10 and 11, respectively. In Fig. 10, the values at $L^*=0$ are those

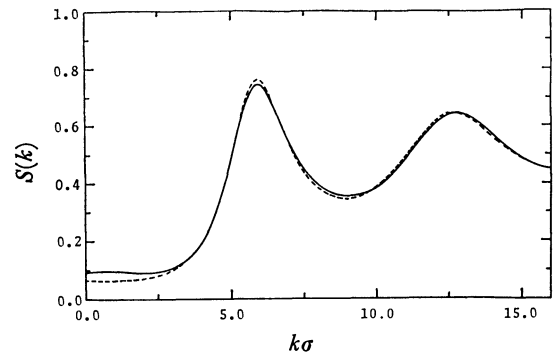

Fig. 6. The structure factor, $S(k)$, for diatomic polar fluids at $\rho^*=0.8$, $\mu^{*2}=3.0$, $L^*=0.6$ and $b_+=b_-$.
——: The structure factor for diatomic polar fluid,
----: the structure factor for the reference system.

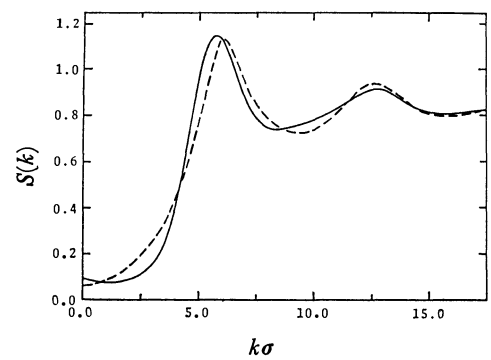

Fig. 7. Same as Fig. 6, except $b_+=10b_-$.

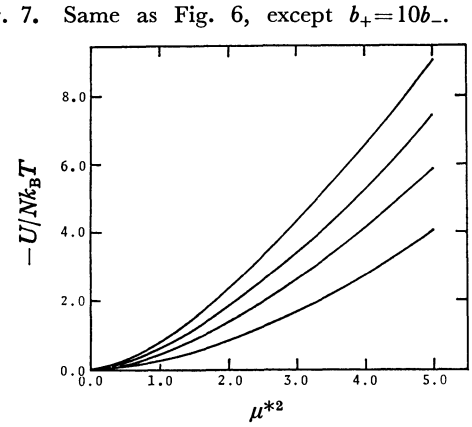

Fig. 8. The internal energy for diatomic polar fluids at $L^*=0.6$.
From top to bottom, the curves are for $\rho^*=0.8$, 0.6, 0.4, and 0.2, respectively.

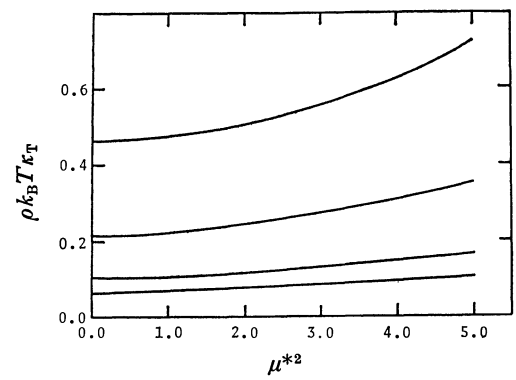

Fig. 9. The isothermal compressibility for diatomic polar fluids at $L^*=0.6$. From top to bottom, the curves are for $\rho^*=0.2$, 0.4, 0.6, and 0.8, respectively.

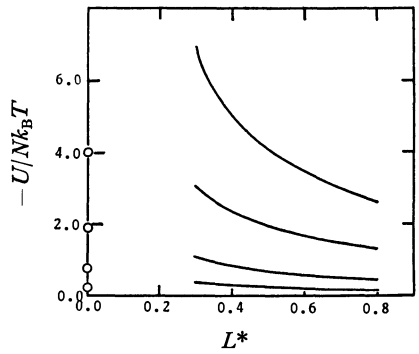

Fig. 10. The L^* dependence of the internal energy for diatomic polar fluids. From top to bottom, the curves and circles are for $(\rho^*, \mu^{*2})=(0.6, 3.0)$, (0.2, 3.0), (0.6, 1.0), and (0.2, 1.0), respectively.
○: LHNC results for dipolar hard sphere fluids,
—: this work.

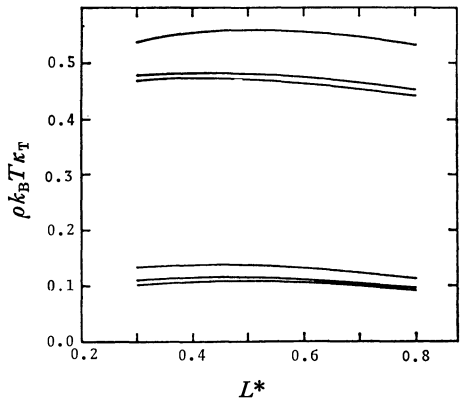

Fig. 11. The L^* dependence of the isothermal compressibility for diatomic polar fluids. From top to bottom, the curves are for $(\rho^*, \mu^{*2})=(0.2, 3.0)$, (0.2, 1.0), (0.2, 0.0), (0.6, 3.0), (0.6, 1.0), and (0.6, 0.0), respectively.

of fluids composed of dipolar hard spheres at the same reduced density and dipole moment calculated by the LHNC integral equations.[20] All the values of Patey *et al.* are nearly equal to those at $L^*=0.5$. It is shown in Figs. 10 and 11 that the values of $\rho k_B T\kappa_T$ are nearly constant with respect to the values of L^*, in sharp contrast to the case of the internal energy which has a large L^* dependence.

In this paper, we have proposed the RHNC like integral equations of RISM-1 type for polyatomic molecular fluids, and applied the equation to diatomic polar fluids. This calculation made from the first principles gives some new informations with respect to the structure and properties of diatomic polar fluids.

References

1) D. Chandler and H. C. Andersen, *J. Chem. Phys.*, **57**, 1930 (1972).
2) B. M. Ladanyi and D. Chandler, *J. Chem. Phys.*, **62**, 4308 (1975).
3) D. Chandler and L. R. Pratt, *J. Chem. Phys.*, **65**, 2925 (1976).
4) K. Kojima and K. Arakawa, *Bull. Chem. Soc. Jpn.*, **51**, 1977 (1978); **53**, 1795 (1980).
5) D. Chandler, *J. Chem. Phys.*, **67**, 1113 (1977).
6) J. S. Høye and G. Stell, *J. Chem. Phys.*, **65**, 18 (1976).
7) M. Ohba and K. Arakawa, *J. Phys. Soc. Jpn.*, **50**, 743 (1981).
8) G. P. Morriss and J. W. Perram, *Mol. Phys.*, **43**, 669 (1981).
9) D. Chandler, *J. Chem. Phys.*, **59**, 2742 (1973).
10) D. Chandler, *Mol. Phys.*, **31**, 1213 (1976).
11) L. J. Lowden and D. Chandler, *J. Chem. Phys.*, **59**, 6587 (1973); **61**, 5228 (1974).
12) E. Johnson and R. P. Hazoume, *J. Chem. Phys.*, **70**, 1599 (1979).
13) C. S. Hsu and D. Chandler, *Mol. Phys.*, **36**, 215 (1978).
14) F. Lado, *Phys. Rev. A*, **8**, 2548 (1973).
15) F. Lado, *Mol. Phys.*, **31**, 1117 (1976).
16) J. P. Hansen and J. J. Weis, *Mol. Phys.*, **33**, 1379 (1977).
17) R. P. Hazoume, *Mol. Phys.*, **39**, 1445 (1980).
18) L. J. Lowden, RISM, RISMGR, RISMSK: program number QCPE306; Quantum Chemistry Program Exchange, Indiana University, Bloomington, Indiana 47401, U.S.A.
19) J. D. Weeks, D. Chandler, and H. C. Andersen, *J. Chem. Phys.*, **54**, 5237 (1971); **56**, 3812 (1972).
20) G. N. Patey, D. Levesque, and J. J. Weis, *Mol. Phys.*, **38**, 219 (1979).

A Hypervirial Theorem Aspect of Koopmans' Theorem

Makoto ISIHARA

Department of General Education, Shotoku-Gakuen Women's Junior College, Gifu 500

(Received October 9, 1981)

Koopmans' theorem is interpreted as a hypervirial theorem requirement; the implication of Koopmans' theorem is thereby clarified. A hypervirial theorem standpoint gives a physically sound ground to a leading correction of Koopmans' relation. Attention is paid to the orbital ambiguity associated with the correction, a possible utilization of the ambiguity being suggested.

Koopmans' theorem[1] is one of the most important characteristics of the standard Hartree-Fock(HF) method,[2] giving a definite physical meaning to occupied canonical HF orbitals. However, what is implied in the theorem does not seem to be fully recognized; a well-known approximate evaluation of the vertical ionization energy

$$I_i = -\varepsilon_i^c \quad (\varepsilon_i^c\text{: } i\text{th canonical HF orbital energy}) \tag{1}$$

is rather misleadingly referred to as Koopmans' theorem.[3,4] In this paper Koopmans' theorem is examined from the viewpoint of the hypervirial theorem(HVT),[5] which leads us not only to transparent understanding of a nature of Koopmans' theorem but also to a physically sound ground for a leading correction to Koopmans' relation.

Preliminaries

Let us start with writing the Hamiltonian for a system of electrons in a fixed nuclear framework as

$$H = \sum_{\xi\eta} h_{\xi\eta} a_\xi^\dagger a_\eta + \frac{1}{2}\sum_{\xi\eta\theta\tau} v_{\eta\tau}^{\xi\theta} a_\xi^\dagger a_\theta^\dagger a_\tau a_\eta, \tag{2}$$

where $a_\xi^\dagger$ and a_ξ are, respectively, the creation and annihilation operators for the one-particle quantum state ξ. Taking a relevant hermitian one-particle operator

$$X = \sum_{\xi\eta} x_{\xi\eta} a_\xi^\dagger a_\eta,$$

which is to be determined later, going through an eigenvalue problem

$$\sum_\eta (h_{\xi\eta} + x_{\xi\eta}) u_{\eta j} = u_{\xi j}\varepsilon_j, \tag{3}$$

we rewrite Eq. 2 in the molecular orbital representation as

$$H = K + V^{(1)} + V^{(2)} \tag{4}$$

with

$$K = \sum_j \varepsilon_j a_j^\dagger a_j, \tag{5}$$

$$V^{(1)} = -\sum_{jk} x_{jk} a_j^\dagger a_k, \tag{6}$$

and

$$V^{(2)} = \frac{1}{2}\sum_{jklm} v_{km}^{jl} a_j^\dagger a_l^\dagger a_m a_k. \tag{7}$$

Postulating that an eigenstate $|\psi\rangle$ of H is attainable from the corresponding unperturbed eigenstate $|\phi\rangle$ of K through a unitary transformation:

$$|\psi\rangle = \exp(S)|\phi\rangle, \tag{8}$$

where S is an antihermitian operator independent of state indices, we expand S perturbation-theoretically as

$$S = S_1^{(1)} + S_1^{(2)} + \text{second and higher orders}$$

with

$$S_1^{(1)} = \sum_{jk} s_{jk} a_j^\dagger a_k \tag{9}$$

and

$$S_1^{(2)} = \frac{1}{2}\sum_{jklm} s_{km}^{jl} a_j^\dagger a_l^\dagger a_m a_k. \tag{10}$$

Then the first order one-particle HVT[5] affirms that

$$\sum_j (y_{jp}\langle a_j^\dagger a_q\rangle - y_{qj}\langle a_p^\dagger a_j\rangle + \sum_{kl}(y_{pi}^{jk}\langle a_j^\dagger a_k^\dagger a_l a_q\rangle - y_{ji}^{qk}\langle a_p^\dagger a_k^\dagger a_l a_j\rangle)) = 0 \quad (\text{any } p, q) \tag{11}$$

with

$$y_{jk} = -x_{jk} + (\varepsilon_j - \varepsilon_k)s_{jk} \tag{12}$$

and

$$y_{km}^{jl} = v_{km}^{jl} + (\varepsilon_j + \varepsilon_l - \varepsilon_m - \varepsilon_k)s_{km}^{jl}, \tag{13}$$

the simple bracket $\langle\cdots\rangle$ in Eq. 11 standing for the expectation value in $|\phi\rangle$. We confine ourselves to single-configurational $|\phi\rangle$'s in the following.

Koopmans' Theorem

First the case without S is considered. Denoting the N-electron Fermi sea state of K by $|F\rangle$:

$$|F\rangle = a_N^\dagger \cdots a_2^\dagger a_1^\dagger |\text{vacuum}\rangle, \tag{14}$$

and sets of the occupied and unoccupied orbitals by F and $\bar{F}$ respectively, we can write the one-particle HVT for the ground state $|F\rangle$ as

$$\langle F|[H, a_p^\dagger a_q]|F\rangle = 0 \qquad (\text{any } p, q) \tag{15}$$

and that for the ionized state $a_i|F\rangle$ $(i\epsilon F)$ as

$$\langle F|a_i^\dagger [H, a_p^\dagger a_q] a_i|F\rangle = 0 \quad (\text{any } p, q). \tag{16}$$

By making use of Eqs. 11, 12, and 13 with all s_{jk}'s and s_{km}^{jl}'s vanishing, Eqs. 15 and 16 are easily converted into

$$(-x_{qp} + \bar{v}_{qp})(\mathrm{f}(q) - \mathrm{f}(p)) = 0 \tag{17}$$

and

$$(-x_{qp} + \bar{v}_{qp} - v(i)_{qp})(\mathrm{f}(q) - \mathrm{f}(p) - \delta_{iq} + \delta_{ip}) = 0 \tag{18}$$

respectively, where we introduce the occupation indicator

$$\mathrm{f}(j) = \begin{cases} 1 & (j\epsilon F) \\ 0 & (j\epsilon \bar{F}) \end{cases} \tag{19}$$

and the abbreviations

$$t(l)_{jk} = t_{kl}^{jl} - t_{lk}^{jl}$$

and

$$\tilde{t}_{jk} = \sum_{l\epsilon F} t(l)_{jk}.$$

While Eq. 17 gives the HF condition[5]

$$x_{jk} = \bar{v}_{jk} \quad (j\epsilon F,\ k\epsilon\bar{F},\ \text{and } \textit{vice versa}), \tag{20}$$

Eq. 18 results in

$$\begin{cases} x_{ij} = \bar{v}_{ij} \text{ and } x_{ji} = \bar{v}_{ji} & (j\epsilon F') \quad (21) \\ v(i)_{jk} = 0 & (j\epsilon F',\ k\epsilon\bar{F},\ \text{and } \textit{vice versa}) \quad (22) \end{cases}$$

with Eq. 20 assumed, the prime on F indicating the exclusion of i: $F'=F-\{i\}$. Since we cannot satisfy Eq. 22 in general, Eqs. 15 and 16 are intrinsically prevented from holding simultaneously.

Now for the ionized state, contented with the HVT in a restricted region

$$\langle F|a_i^\dagger[H, a_p^\dagger a_q]a_i|F\rangle = 0 \quad (p, q\epsilon F, \text{ and } p, q\epsilon\bar{F}') \tag{23}$$

with $\bar{F}'=\bar{F}+\{i\}$, we are free from Eq. 21; the two HVT's, Eqs. 15 and 23 are compatible with each other and lead together to

$$x_{jk} = \bar{v}_{jk} \quad (j\epsilon F, k\epsilon\bar{F} \text{ and } \textit{vice versa};\ j, k\epsilon F,\ j \text{ or } k=i). \tag{24}$$

Thus we see a HVT aspect of Koopmans' theorem: When the molecular orbitals are determined so as to satisfy Eq. 24, a single-configurational approximation of the vertical ionization energy

$$\begin{aligned} I_i &= \langle F|a_i^\dagger H a_i|F\rangle - \langle F|H|F\rangle \\ &= -h_{ii} - \bar{v}_{ii} \end{aligned} \tag{25}$$

is at its best.

Conversely, we can formally make Eq. 16 compatible with the ground state HVT in a restricted region. This coalition is, however, unnatural and disadvantageous, as long as the matrix elements $\{h_{\xi\eta}\}$ and $\{v_{\gamma\tau}^{\xi\theta}\}$ are set to be appropriate to the more stable ground state.

A sufficient way to satisfy Eq. 24 is obviously to put

$$x_{jk} = \bar{v}_{jk} \quad (\text{any } j, k) \tag{26}$$

or in the initial representation

$$x_{\xi\eta} = \sum_{\theta\tau} (v_{\eta\tau}^{\xi\theta} - v_{\tau\eta}^{\xi\theta})\rho_{\tau\theta} \tag{27}$$

with

$$\rho_{\tau\theta} = \sum_{j\epsilon F} u_{\tau j}u_{\theta j}^*. \tag{28}$$

The eigenvalue problem obtained by substituting Eq. 27 into Eq. 3 can be solved with Eq. 28 self-consistently, giving the canonical HF orbitals. If canonical HF orbitals are used, we can rewrite Eq. 25 as Eq. 1. This step is, however, just only rewriting of no physical content.[6] It seems to be desired to call Eq. 1 itself not Koopmans' theorem but relation.

It should be emphasized that Eq. 24 leaves many of x_{jk}'s for $j,k\epsilon F$ and all x_{jk}'s for $j,k\epsilon\bar{F}$ undetermined. This ambiguity is to be utilized purposively. We can require Eq. 23 consistently for all $i\epsilon F$ besides Eq. 15, if necessary, the resultant condition being

$$x_{jk} = \bar{v}_{jk} \quad (j\epsilon F, k\epsilon\bar{F} \text{ and } \textit{vice versa};\ j, k\epsilon F, j\neq k). \tag{29}$$

We have Eq. 26 again as a sufficient choice of X. It is worth while to note that x_{jj}'s remain still undetermined even for $j\epsilon F$ in Eq. 29. Since all x_{jk}'s for $j,k\epsilon\bar{F}$ are not conditioned in Eq. 24, Koopmans' theorem is valid in the hole potential method.[5,7] The electron-hole potential choice of X is generally inconsistent with Eq. 24.[5,8]

A Leading Correction to Koopmans' Relation

Next let us consider to fulfil the one-particle HVT's for the ground and ionized states,

$$\langle F|\exp(-S)[H, a_p^\dagger a_q]\exp(S)|F\rangle = 0 \quad (\text{any } p, q) \tag{30}$$

and

$$\langle F|a_i^\dagger \exp(-S)[H, a_p^\dagger a_q]\exp(S)a_i|F\rangle = 0 \quad (\text{any } p, q), \tag{31}$$

simultaneously to first order by using simple S. Putting $|\phi\rangle=|F\rangle$ and $|\phi\rangle=a_i|F\rangle$ in Eq. 11 respectively, we immediately obtain

$$(y_{qp}+\tilde{y}_{qp})(\mathrm{f}(q)-\mathrm{f}(p)) = 0 \tag{32}$$

and

$$(y_{qp}+\tilde{y}_{qp}-y(i)_{qp})(\mathrm{f}(q)-\mathrm{f}(p)-\delta_{iq}+\delta_{ip}) = 0. \tag{33}$$

The former gives

$$-y_{jk} = \tilde{y}_{jk} \quad (j\epsilon F, k\epsilon\bar{F}, \text{ and } \textit{vice versa}), \tag{34}$$

letting the latter result in

$$\begin{cases} -y_{ij} = \tilde{y}_{ij} \text{ and } -y_{ji}=\tilde{y}_{ji} & (j\epsilon F') \quad (35) \\ y(i)_{jk} = 0 & (j\epsilon F', k\epsilon\bar{F}, \text{ and } \textit{vice versa}). \quad (36) \end{cases}$$

Forming a striking contrast to Eqs. 22 and 36 merely asserts that

$$s(i)_{jk} = v(i)_{jk}/(\varepsilon_k-\varepsilon_j) \quad (j\epsilon F', k\epsilon\bar{F}, \text{ and } \textit{vice versa}). \tag{37}$$

The other s_{km}^{ii}'s are allowed to be zero. We have alternatives with regard to fulfilment of Eq. 34.

If we make all s_{jk}'s vanishing, Eq. 34 becomes

$$x_{jk} = \bar{v}_{jk} - v(i)_{jk} \quad (j\epsilon F, k\epsilon\bar{F}, \text{ and } \textit{vice versa}) \tag{38}$$

by virtue of Eq. 37. From Eq. 35 we have

$$x_{ij} = \bar{v}_{ij} \text{ and } x_{ji} = \bar{v}_{ji} \quad (j\epsilon F'). \tag{39}$$

Because $v(i)_{ij}$ and $v(i)_{ji}$ vanish identically for any j, Eqs. 38 and 39 can be achieved by the standard HF calculation for the ionized configuration. There is no first order correction to the ionized state; we have

$$S_1^{(2)}|F\rangle = \sum_{j\epsilon\bar{F},\ k\epsilon F'} v(i)_{jk}/(\varepsilon_k-\varepsilon_j)a_j^\dagger a_k|F\rangle. \tag{40}$$

The resultant approximation of the vertical ionization energy is, to second order, given by

$$I_i = -h_{ii} - \bar{v}_{ii} + \sum_{j\epsilon\bar{F},\ k\epsilon F'} |v(i)_{jk}|^2/(\varepsilon_j-\varepsilon_k). \tag{41}$$

Note that x_{jk}'s for $j,k\epsilon F'$ and $j,k\epsilon\bar{F}$ are not conditioned in Eqs. 38 and 39; Eq. 41 remains ambiguous.

Another way, usually fitting real situations better than the preceding, consists in adhering to the ground state HF condition, Eq. 20. In consequence it follows from Eq. 34 that

$$s_{jk} = v(i)_{jk}/(\varepsilon_j-\varepsilon_k) \quad (j\epsilon F, k\epsilon\bar{F}, \textit{vice versa}) \tag{42}$$

after substitution of Eq. 37. The other s_{jk}'s can be set to vanish; we have Eq. 39 as before from Eq. 35. This time the first order state correction does not appear in the ground state, but does in the ionized:

$$(S_1^{(1)}+S_1^{(2)})a_i|F\rangle = \sum_{j\epsilon\bar{F},\ k\epsilon F'} v(i)_{jk}/(\varepsilon_j-\varepsilon_k)a_j^\dagger a_k a_i|F\rangle. \tag{43}$$

Accordingly, in place of Eq. 41, we have

$$I_i = -h_{ii} - \bar{v}_{ii} - \sum_{j\epsilon\bar{F},\, k\epsilon F'} |v(i)_{jk}|^2/(\varepsilon_j - \varepsilon_k). \quad (44)$$

Again it should be noted that the ambiguity in x_{jk}'s for $j,k\epsilon F'$ and $j,k\epsilon\bar{F}$ leaves Eq. 44 undetermined. Although how to utilize this ambiguity is not very evident, it seems much more plausible to use the orbitals satisfying

$$x_{jk} = \bar{v}_{jk} - v(i)_{jk} \qquad (j,k\epsilon F' \text{ and } j,k\epsilon\bar{F}) \quad (45)$$

rather than to hold on the canonical HF orbitals for the ground state configuration; the second order term in Eq. 44 exclusively comes from the correction concerning the ionized state.

In order to have Eqs. 20, 39, and 45 hold, it is sufficient to take X as

$$x_{jk} = \bar{v}_{jk} - \mathrm{f}(j)v(i)_{jk}\mathrm{f}(k) - (1-\mathrm{f}(j))v(i)_{jk}(1-\mathrm{f}(k)). \quad (46)$$

Denoting the one-particle quantum state by the round bra and ket, we employ the projection operators[7]

$$\mathrm{P} = \sum_j |j)\mathrm{f}(j)(j| \quad (47)$$

and

$$\bar{\mathrm{P}} = \sum_j |j)(1-\mathrm{f}(j))(j|, \quad (48)$$

which are invariant under unitary transformations within each of the orbital subsets F and $\bar{F}$. With the abbreviations

$$\rho_{\xi\eta} = (\xi|\mathrm{P}|\eta) = \sum_{j\epsilon F} u_{\xi j}u^*_{\eta j} \quad (49)$$

and

$$\bar{\rho}_{\xi\eta} = (\xi|\bar{\mathrm{P}}|\eta) = \sum_{j\epsilon\bar{F}} u_{\xi j}u^*_{\eta j} \quad (50)$$

we can rewrite Eq. 46 in the initial representation as

$$x_{\xi\eta} = \sum_{\theta\tau} ((v^{\xi\theta}_{\eta\tau} - v^{\xi\theta}_{\tau\eta})\rho_{\tau\theta} - \rho_{\xi\theta}v(i)_{\theta\tau}\rho_{\tau\eta} - \bar{\rho}_{\xi\theta}v(i)_{\theta\tau}\bar{\rho}_{\tau\eta}). \quad (51)$$

However, to solve Eq. 3 with Eqs. 49, 50, and 51 seems unreasonably inefficient. A stepwise method is practical: First perform the standard HF calculation for the ground state configuration to obtain the canonical HF orbitals $\{\underline{j}\}$ and their energies $\{\varepsilon_{\underline{j}}\}$. Selecting a relevant occupied orbital $\underline{i}$, next work out the two separate eigenvalue problems

$$\sum_{\underline{k}\epsilon F'} (\delta_{\underline{k}\underline{l}}\varepsilon_{\underline{k}} - v(\underline{i})_{\underline{k}\underline{l}})c_{\underline{l}\underline{j}} = c_{\underline{k}\underline{j}}\varepsilon_j \qquad (\underline{k}\epsilon F') \quad (52)$$

and

$$\sum_{\underline{l}\epsilon\bar{F}} (\delta_{\underline{k}\underline{l}}\varepsilon_{\underline{k}} - v(\underline{i})_{\underline{k}\underline{l}})c_{\underline{l}\underline{j}} = c_{\underline{k}\underline{j}}\varepsilon_j \qquad (\underline{k}\epsilon\bar{F}), \quad (53)$$

which give rise to the new orbitals $\{j\}$ with their energies $\{\varepsilon_j\}$, the orbital i being identical with $\underline{i}$. No iterative procedure for self-consistency is involved in solving Eqs. 52 and 53.

The simultaneous fulfilment of the one-particle HVT's for the ground and ionized states leads us to taking it into account the effect of the charge distribution rearrangement through ionization.[9]

References

1) T. Koopmans, *Physica*, **1**, 104 (1933).
2) For example, a) A. C. Hurley, "Introduction to the Electron Theory of Small Molecules," Academic Press, London (1976), Chap. 7, § 7.2; b) S. Huzinaga, "Bunshikidoho," Iwanami Shoten, Tokyo (1980), Chap. 5.
3) M. D. Newton, *J. Chem. Phys.*, **48**, 2825 (1968).
4) R. K. Nesbet, *Adv. Chem. Phys.*, **9**, 321 (1965).
5) M. Isihara, *Bull. Chem. Soc. Jpn.*, **54**, 3312 (1981).
6) Reference 4, p. 327; Reference 2b, p. 111.
7) S. Huzinaga and C. Arnau, *Phys. Rev. A*, **1**, 1285 (1970); *J. Chem. Phys.*, **54**, 1948 (1971).
8) K. Morokuma and S. Iwata, *Chem. Phys. Lett.*, **16**, 192 (1972); S. Iwata and K. Morokuma, *Theor. Chim. Acta*, **33**, 285 (1974).
9) G. Born, H. A. Kurtz, and Y. Öhrn, *J. Chem. Phys.*, **68**, 74 (1978).

 © 1982 The Chemical Society of Japan Bull. Chem. Soc. Jpn., 55, 1395—1400 (1982)

The Quenching of Excited Zinc(^3P_J) Atoms by Alkane Hydrocarbons

Shunzo YAMAMOTO* and Norio NISHIMURA

Department of Chemistry, Faculty of Science, Okayama University, Tsushima, Okayama 700

(Received October 16, 1981)

The intensities of the 307.6 nm resonance line of zinc were measured at different pressures of alkane hydrocarbons, and the quenching-rate constants were determined on the basis of the Stern-Volmer plots. A remarkable dependence of the quenching cross-section on the C–H bond strength was observed, and the relative decrease in the quenching cross-section with an increase in the C–H bond strength was interpreted in terms of the semiempirical bond-energy-bond-order(BEBO) method.

Recently, Breckenridge and Renlund have measured the quenching cross-sections of Cd(^3P_J) by the use of several alkane hydrocarbons.[1] They have then compared their values with those for the quenching of Hg($^3P_0$) and Hg($^3P_1$). They summarized the important aspects of their results as follows: (1) The Cd(^3P_J) quenching-rate constants are remarkably small for alkane hydrocarbons. (2) There is a slight increase in the quenching cross-section in the order of primary, secondary, and tertiary C–H bonds. (This is in contrast to the fact that there is a remarkable dependence of the quenching cross-section on the C–H bond strength in the case of Hg($^3P_{0,1}$)). (3) The direct abstraction of a hydrogen atom to form CdH appears to be a major quenching pathway for all the alkanes studied, with the possible exception of methane. (4) The quenching of Cd(^3P_J) by alkane hydrocarbons differs substantially from the quenching of Hg($^3P_1$). (They suggested that the difference in the quenching behavior between Cd(^3P_J) and Hg($^3P_1$) can be understood if the mechanistic pathway for Hg($^3P_1$) is merely energetically inaccessible to the low-energy Cd(^3P_J) atom.

Since the excitation energy of Zn(^3P_J) lies between those of Cd(^3P_J) and Hg($^3P_1$), we expected that the study of the quenching of Zn(^3P_J) would give further detailed information about the mechanism. The present paper will deal with the quenching of Zn(^3P_J) by several alkane hydrocarbons.

Experimental

The apparatus was the same as that previously described,[2] except for the use of a zinc-resonance lamp made of Pyrex. This lamp emits only resonance line, at 307.6 nm, which gives rise to Zn($^3P_1$) atoms. The reaction cell and the zinc lamp were kept in a furnace at 305±2 °C for most of the measurements. The light intensity from the cell was measured by means of a Hitachi spectrophotometer, Model 139. The pressures of the gases were measured by means of a Bourdon pressure gauge (W & T model 62-075, Nagano Keiki Co.). The low pressures of the quenching gases were measured using calibrated expansion volumes.

The zinc metal used was high-purity zinc (99.9999%) manufactured by Osaka Asahi Metal Co. The ethane, propane, ethylene, and propylene (Gasukuro Kogyo Co., Ltd.), and cyclopropane (Santetsu Kagaku Kogyo Co., Ltd.) were freeze-pumped several times. The isobutane and neopentane (Tokyo Kasei Kogyo Co., Ltd., E. P. grade) and other alkanes (Tokyo Kasei Co., Ltd., G. R. grade) were freeze-pumped several times and repeatedly subjected to trap-to-trap distillation. Pure-grade argon (Daido Sanso Co., 99.999%) was used without further purification.

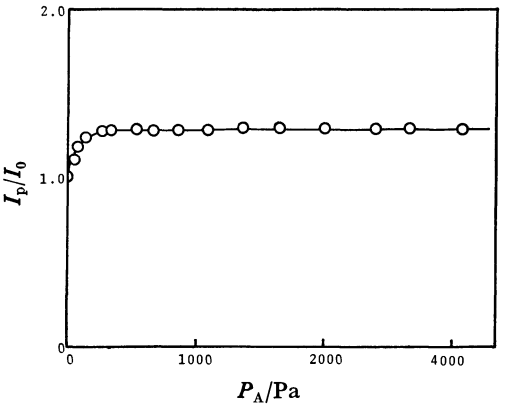

Fig. 1. Intensity of resonance line at 307.6 nm as a function of argon pressure.

Results

Pressure Dependence of the Emission Intensity at 307.6 nm. When a cell containing zinc vapor was illuminated by the exciting lamp, a resonance line was observed at 307.6 nm. Upon the addition of argon, the intensity of the line increased with the increase in the pressure, as is shown in Fig. 1. This was attributed to the increase in the light intensity absorbed by zinc atoms as a result of the pressure broadening of the absorption line.[2] In order to minimize such pressure dependence of the absorption of the resonance line, quenchers were diluted with a large amount of argon(total pressures 1000—3000 Pa).

Quenching of the 307.6 nm Resonance Line. In a previous paper,[2] the following reaction scheme was proposed:

$Zn(^1S_0) + h\nu(307.6\,nm) \longrightarrow Zn(^3P_1)$	I_a
$Zn(^3P_1) \longrightarrow Zn(^1S_0) + h\nu(307.6\,nm)$	k_0
$Zn(^3P_1) + M \rightleftharpoons Zn(^3P_0) + M$	k_1, k_{-1}
$Zn(^3P_1) + M \rightleftharpoons Zn(^3P_2) + M$	k_2, k_{-2}
$Zn(^3P_0) + Q \longrightarrow$ quenching	k_3
$Zn(^3P_1) + Q \longrightarrow$ quenching	k_4
$Zn(^3P_2) + Q \longrightarrow$ quenching	k_5.

Here, M denotes Ar and/or quenchers. As before, the ratio of the emission intensities in the absence and in the presence of quenchers can be given as:

$$\frac{I^{\circ}_{307.6}}{I_{307.6}} = 1 + \frac{1}{k_0}\left(\frac{k_1}{k_{-1}}k_3 + k_4 + \frac{k_2}{k_{-2}}k_5\right)[Q]. \quad (1)$$

Some typical Stern-Volmer plots for the quenching of the resonance line by several alkanes are shown

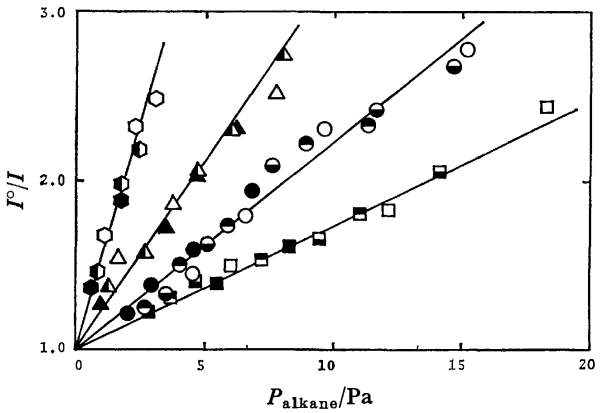

Fig. 2. Stern-Volmer plots for quenching of resonance line at 307.6 nm by alkanes diluted with argon 1) ethane: Total pressures are 2800 (◓), 2100 (□), 1700 (◒), and 1300 Pa (■). 2) Propane: 2800 (○), 2100 (◒), 1700 (◓), and 1300 Pa (●). 3) Butane: 2800 (△), 2100 (◭), and 1700 Pa (▲). 4) Cyclopentane: 2800 (⬡), 2100 (◐), and 1700 Pa (⬢).

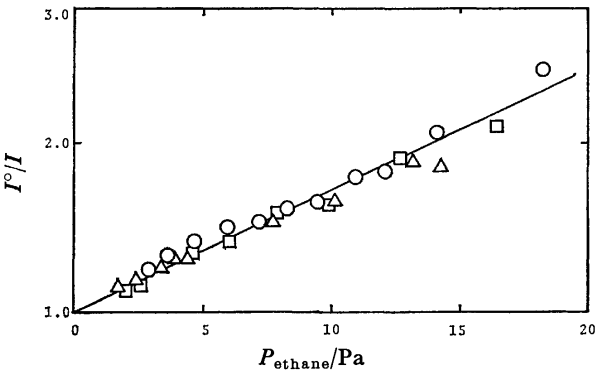

Fig. 3. Stern-Volmer plots for quenching of resonance line at 307.6 nm by ethane at various temperatures. 1) 290 °C (△), 2) 300 °C (○), 3) 320 °C (□).

in Fig. 2, where I° and I are the intensities of the resonance line in the absence and in the presence of quenchers respectively. Similar plots were obtained for other alkanes and alkenes. These Stern-Volmer plots are accounted for by Eq. 1.

As the f-value of the zinc 307.6 nm line is about one-tenth that of the cadmium 326.1 nm line,[3] the absorption of the 307.6 nm line by the zinc vapor (0.36 Pa at 305 °C) seems to be too small to cause any significant radiation trapping. If the lengthening of the effective radiation lifetime of $Zn(^3P_1)$ caused by radiation imprisonment is not negligible, the effective lifetime must be dependent on both the zinc pressure and the total pressure. In Fig. 3, the values of I°/I obtained for propane at various temperatures and at various total pressures are plotted as functions of the partial pressure of propane. The points lie on a straight line, and no dependence of the zinc pressure (from 0.25 Pa at 290 °C to 0.77 Pa at 320 °C) or the total pressure (1300—2700 Pa) can be seen. This suggests that the effective lifetime of the $Zn(^3P_1)$ is not lengthened by the radiation imprisonment under the present conditions. Therefore, k_0 can be taken as the reciprocal of the natural lifetime of $Zn(^3P_1)$ ($\tau_0=2.0\times10^{-5}$ s).[4]

Table 1. Quenching of $Zn(^3P_J)$ by alkanes and alkenes

Gas	$10^{11}k_q$ / cm^3 molecule^{-1} s^{-1}	$10^{16}\sigma_q$ / cm^2
H_2	106.6±7.2	42.7±2.8
D_2	64.1±4.5	35.5±2.5
CH_4	0.50±0.01	0.50±0.03
C_2H_6	2.88±0.06	3.74±0.06
C_3H_8	4.74±0.09	6.94±0.13
c-C_3H_6	12.8±0.2	18.4±0.4
n-C_4H_{10}	9.14±0.21	14.5±0.9
i-C_4H_{10}	5.02±0.12	8.70±0.20
n-C_5H_{12}	11.9±0.2	21.8±0.4
i-C_5H_{12}	8.53±0.12	14.3±0.21
neo-C_5H_{12}	4.45±0.10	7.41±0.22
c-C_5H_{10}	22.5±0.4	41.1±0.7
c-C_6H_{12}	34.5±0.6	60.0±1.0
C_2H_4	121.7±2.4	153.9±3.1
C_3H_6	89.7±1.2	129.7±1.9

From the slope of the Stern-Volmer plots, the composite rate constants for the quenching, $(k_1/k_{-1})k_3+k_4+(k_2/k_{-2})k_5$, were estimated. Since the three triplet states are in equilibrium, $k_1/k_{-1}=(1/3)\exp(2300/RT)$ and $k_2/k_{-2}=(5/3)\exp(-4730/RT)$, and at 305 °C k_1/k_{-1} and k_2/k_{-2} are 0.54 and 0.62 respectively. The quenching rate constants, $k_q(=0.54k_3+k_4+0.62k_5)$, and the corresponding quenching cross-sections for equilibrated $Zn(^3P_{0,1,2})$ calculated by means of:

$$\sigma_q = k_q\left[\frac{8RT}{\pi}\cdot\frac{M_{Zn}+M_Q}{M_{Zn}\cdot M_Q}\right]^{-1/2}, \quad (2)$$

are listed in Table 1.

As may be seen in Table 1, because the quenching cross-sections for alkanes determined here are considerably smaller than those for hydrogen and alkenes, it is important to discuss the possible effects on these measurements of very small amounts of impurities in the gases. Any hydrogen initially present in these gases would have been removed by many careful freeze-pump cycles performed. The alkanes used were at least 99.5% pure, except for neopentane (96% pure). Most of the impurities are thought to be other alkanes, and these alkane impurities at this level would not be sufficient to cause any considerable error in the measurements. For example, a 0.5% cyclopentane impurity causes about a 1% error in the cross-section for butane. On the other hand, alkenes have large cross-sections, and if the propane used contain 0.1% propylene, it would cause about a 1.8% error. This error is, however, within the limits of experimental error. Therefore, it is thought that, for alkanes except for neopentane, the errors attributable to possible impurity contents are negligibly small. As neopentane has a little larger amount of impurities, we regard the k_q value obtained for neopentane as the upper limit.

TABLE 2. COMARISON OF QUENCHING CROSS-SECTIONS AND CORRELATION OF THOSE CROSS-SECTIONS WITH C–H BOND STRENGTHS OF ALKANE HYDROCARBONS

Gas	Quenching cross-section $10^{16}\sigma_q$/cm^2			C–H bond strength[a] kJ mol^{-1}	
	$Zn(^3P_J)$	$Cd(^3P_J)$[b]	$Hg(^3P_1)$[c]	Weakest	Average
CH_4	0.50	0.0041	0.3	435	435
C_2H_6	3.74	0.016	0.5	410	410
C_3H_8	6.94	0.0082	7.2	395	406
c-C_3H_6	18.4	—	5.0	423	423
n-C_4H_{10}	14.5	—	18	396	404
i-C_4H_{10}	8.73	0.011	22	381	407
n-C_5H_{12}	21.8	—	42	396	403
i-C_5H_{12}	14.3	—	53	381	405
neo-C_5H_{12}	7.44	—	6.6	416	416
c-C_5H_{10}	41.1	—	60	398	398
c-C_6H_{12}	60.0	0.19	63	393	393

a) W. H. Breckenridge and O. K. Malmin, *J. Chem. Phys.*, **74**, 3307 (1981); J. G. Calvert and J. N. Pitts, "Photochemistry," Wiley, New York (1966). b) Ref. 1. c) Includes quenching to $Hg(^3P_0)$. Ref. 5.

Discussion

The reaction and quenching of $Hg(^3P_{0,1})$ by alkane hydrocarbons have been very thoroughly studied,[5-9] and several mechanistic schemes have been proposed to explain the large body of data. In the case of $Hg(^3P_{0,1})$, a remarkable dependence of the quenching rate on the C–H bond strength was observed. On the other hand, there is virtually no dependence in the case of $Cd(^3P_J)$, and the cross-sections for methane, propane, and isobutane can be fit by assuming an additive cross-section of 0.0010×10^{-16} cm^2 for each C–H bond, irrespective of the type of bond.[1]

Table 2 compares the quenching cross-sections of $Zn(^3P_J)$, $Cd(^3P_J)$, and $Hg(^3P_1)$ by alkanes; the C–H bond strength is also shown. It may be noted that the quenching cross-section of $Zn(^3P_J)$ depends greatly on the C–H bond strength, and that the dependence is very similar to that of $Hg(^3P_1)$. Since the quenching cross-sections of such alkanes as methane, ethane, and neopentane, which contain neither secondary nor tertiary C–H bonds, are considerably smaller than those of alkanes which do contain secondary and/or tertiary C–H bonds, it is plausible that, in the latter case, the weaker secondary and tertiary C–H bonds are predominantly ruptured in the primary quenching act. An inspection of Table 2, however, shows that the quenching cross-section of $Zn(^3P_J)$ by alkanes is more closely correlated with the average C–H bond strength than with the weakest C–H bond strength. The correlation between the average quenching cross-section per C–H bond and the average C–H bond strength for $Zn(^3P_J)$, $Cd(^3P_J)$, and $Hg(^3P_1)$ is shown in Fig. 4. In general, the cross-sections increase with a decrease in the C–H bond strength for $Zn(^3P_J)$ and $Hg(^3P_1)$, but those for $Cd(^3P_J)$ are almost constant. This figure also shows that the cross-sections increase more regularly for $Zn(^3P_J)$ than for $Hg(^3P_1)$. In the latter case, the plots are somewhat scattered. The

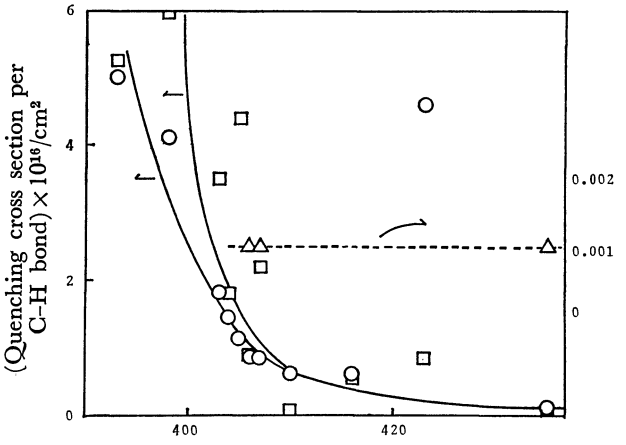

Fig. 4. The quenching cross section per C–H bond plotted against average C–H bond strength. $Zn(^3P_J)$ (○), $Cd(^3P_J)$ (△), and $Hg(^3P_1)$ (□).

good correlation shown indicates that the excited zinc do not attack only the weakest C–H bond, but all kinds of C–H bonds, with efficiencies which depend on the bond strength.

The quenching cross-section, σ_q, of a certain molecule is defined as the sum of the quenching cross-section, σ_i, for each individual quenching site (C–H bond):

$$\sigma_q = \Sigma\,\sigma_i. \quad (3)$$

Conversely, from the obtained quenching cross-section, σ_q, an effective cross-section, σ_i, for each C–H bond can be calculated. The effective cross-section per C–H bond in methane and that per primary C–H bond are obtained by:

$$\sigma_i(CH_3\text{–}H) = \sigma_q(CH_4)/4$$

$$\sigma_i(\text{primary}) = \sigma_q(C_2H_6 \text{ or } \textit{neo}\text{-}C_5H_{12})/(\text{number of C–H bonds}).$$

The effective cross-sections per secondary or tertiary

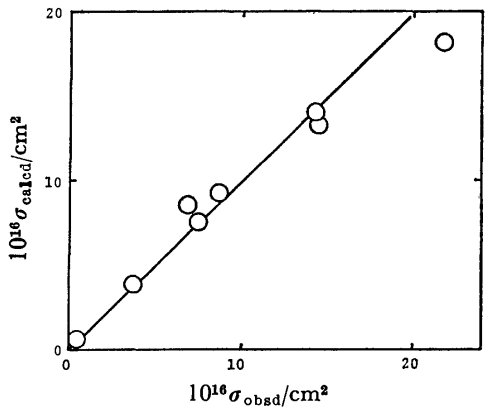

Fig. 5. Relationship between σ_{calcd} and σ_{obsd}.

C–H bond are estimated by means of:

$$\sigma_1(\text{secondary}) = \frac{\sigma_q(C_3H_8,\ n\text{-}C_4H_{10},\ \text{or}\ n\text{-}C_5H_{12}) - 6\sigma_1(\text{primary})}{\text{number of secondary C–H bonds}},$$

$$\sigma_1(\text{tertiary}) = \sigma_q(i\text{-}C_4H_{10}) - 9\sigma_1(\text{primary}) = \sigma_q(i\text{-}C_5H_{12}) - 9\sigma_1(\text{primary}) - 2\sigma_1(\text{secondary}).$$

The values of σ_1 thus obtained are given in Table 3. The average values of σ_1 for primary, secondary, and tertiary C–H bonds are 0.62, 2.4, and 3.6 respectively, corresponding to a ratio of 1:3.9:5.8. These values are different from those of 1:65:350 for $Hg(^3P_1)$ quenching.[10] In Fig. 5, the cross-sections, σ_{calcd}, calculated by summing the cross-sections, σ_1, for primary, secondary, and tertiary C–H bonds shown in Table 3 are plotted against the observed cross-section, σ_{obsd}. This figure shows that the quenching cross-sections for alkanes can be reproduced fairly well by summing the σ_1-values.

As is shown in Tables 2 and 3, the cross-sections for cyclopentane and cyclohexane are quite high. These high cross-sections for cycloalkanes were also observed in the cases of $Cd(^3P_J)$ and $Hg(^3P_1)$.[5] The higher cross-sections for cyclopentane and cyclohexane could be due to less steric repulsion in the cycloalkane C–H bond attack by excited atoms.

Table 4 shows the estimated enthalpies of reaction for the abstraction of a hydrogen atom by $Zn(^3P_J)$, $Cd(^3P_J)$, and $Hg(^3P_1)$ atoms from various types of C–H bonds in the alkane hydrocarbons. In the $Cd(^3P_J)$- and $Zn(^3P_J)$-photosensitized decomposition of alkanes, the major primary step is thought to be the C–H bond cleavage, which becomes energetically feasible only if the process is a true hydrogen transfer:

$$RH + Cd^*(Zn^*) \longrightarrow R + CdH(ZnH).$$

The formation of CdH in the course of the reaction can be readily detected spectroscopically.[11,12] In the case of the $Hg(^3P_1)$-photosensitized decomposition, however, the direct cleavage of C–H bonds without the intermediate formation of HgH is also energetically possible; the enthalpy of reaction for this process is shown in Table 4. It seems interesting that the dependence of the quenching cross-section on the C–H bond strength decreases in this order: $Hg(^3P_1) > Zn(^3P_J) > Cd(^3P_J)$. This order is consistent with the order of the decrease in the enthalpy of reaction for the abstraction of a hydrogen atom.

Table 3. Effective cross-section, σ_1, for each C–H bond

		$10^{16}\sigma_1$ / cm^2
CH_3–H		0.13
Primary		0.62
		0.62
	Average	0.62
Secondary		1.6
		2.7
		3.0
	Average	2.4
Tertiary		3.2
		3.9
	Average	3.6

Table 4. Enthalpy of reaction for the abstraction of a hydrogen atom by excited metal atoms

	ΔH / kJ mol^{-1}			
	$Zn(^3P_1)$	$Cd(^3P_1)$	$Hg(^3P_1)$	$Hg(^3P_1)$[a]
CH_3–H	−38	0	−77	−37
Primary				
C_2H_5–H	−63	−25	−102	−62
$(CH_3)CH_2$–H	−57	−19	−96	−56
Secondary				
$(CH_3)_2CH$–H	−78	−40	−117	−77
Tertiary				
$(CH_3)_3C$–H	−92	−54	−131	−91

In the case of $Hg(^3P_1)$, several workers[5–8] have proposed mechanism in which the initial step is the formation of a weak complex between $Hg(^3P_1)$ and the alkane quencher. The resulting complex can decompose (if there is sufficient energy) by surmounting a potential barrier, the height of which is dependent on the type of C–H bond. Such a general model was originally proposed by Yang,[6] and the rate of passage over the barrier has been estimated by the use of Kassel,[6] RRKM,[7] and BEBO[8] treatments. All of these theories would predict large variations with the C–H bond strength in quenching cross-sections for lower-energy $Cd(^3P_J)$ and $Zn(^3P_J)$. As has been mentioned above, however, the variation for $Zn(^3P_J)$ is considerably smaller than that for $Hg(^3P_1)$, and there is virtually no dependence on the C–H bond strength in the quenching of $Cd(^3P_J)$ by alkanes. Therefore, it is obvious that previous models based on $Hg(^3P_1)$ quenching data are not directly applicable for $Zn(^3P_J)$ and $Cd(^3P_J)$.

Recently, Breckenridge and Renlund have pointed out that the mechanistic pathways which have been proposed for $Hg(^3P_{0,1})$ quenching are not energetically accesible for $Cd(^3P_J)$ quenching and have proposed

a possible mechanism which is consistent with several observations in the Hg($^3P_1$)–alkanes system and explains the small variation of Cd(^3P_J) quenching cross-sections among the alkane hydrocarbons studied.

In this paper, it is shown that the Zn(^3P_J)-photosensitized decomposition of alkanes can be considered as a simple hydrogen-atom transfer reaction; consequently, it is possible to calculated the relative potential energies of activation of these reactions by a modified BEBO method.[13]

In the BEBO method, the potential energy of activation for hydrogen-atom abstraction by a radical as a function of the bond order, n, of the bond being broken is given by:

$$V = E_b(1-n^p) - E_f(1-n)^q + V_{tr}, \quad (4)$$

where E_b and E_f are the single-bond energies of the bond being broken and formed, V_{tr} is the triplet repulsion term, and p and q are the bond-energy indices defined by the expression:

$$p \text{ or } q = \frac{0.26 \ln (D_e/\varepsilon_x)}{r_x - r_e}, \quad (5)$$

in which ε_x and r_x are the potential depth and the equilibrium internuclear distance of the analogous diatomic noble gas cluster, while D_e and r_e are the bound dissociation energy and the equilibrium internuclear distance of the bond in question. Strausz *et al.*[8] calculated the potential energies of activation for the mercury-photosensitized decomposition of alkanes by assuming the following model:

$$RH + Hg^* \longrightarrow R\cdots H\cdots Hg \longrightarrow R + HHg,$$

and by neglecting the repulsive triplet term, V_{tr}. They described since the model assumed is somewhat oversimplified, only the relative values are significant.

In the case of Zn(^3P_J), we could not obtain information about the bond-energy index (q). Therefore, we estimated only the relative potential energy of activation for the following process:

$$RH + Zn^* \longrightarrow R\cdots H\cdots Zn \longrightarrow R + HZn.$$

If it can be assumed that the bond order, n, for the transition state and the bond-energy index, q, are constant, irrespective of the type of C–H bond being broken, the activation energy referred to that for CH_3–H is expressed by the following equation:

$$\Delta V = E_b(1-n^p) - E_b^{CH_4}(1-n^{p_0}), \quad (6)$$

where $E_b^{CH_4}$ and p_0 are the bond energy of CH_3–H and the p-value for the CH_4–Zn* system. If $p=p_0$, as was assumed for the alkane–Hg* system by Strausz *et al.*, the above equation becomes:

$$\Delta V = (E_b - E_b^{CH_4})(1-n^p). \quad (7)$$

The cross-section, σ_1 is expressed by the following equation:

$$\sigma_1 \propto k_1 = A \exp(-V/RT). \quad (8)$$

Therefore, $\sigma_1/\sigma_1^{CH_4}$ can be expressed as follows:

$$\ln \sigma_1/\sigma_1^{CH_4} = -\Delta V/RT. \quad (9)$$

From Eqs. 7 and 9, the following equation is obtained:

$$\ln \sigma_1/\sigma_1^{CH_4} = -\frac{(1-n^p)}{RT}(E_b - E_b^{CH_4}). \quad (10)$$

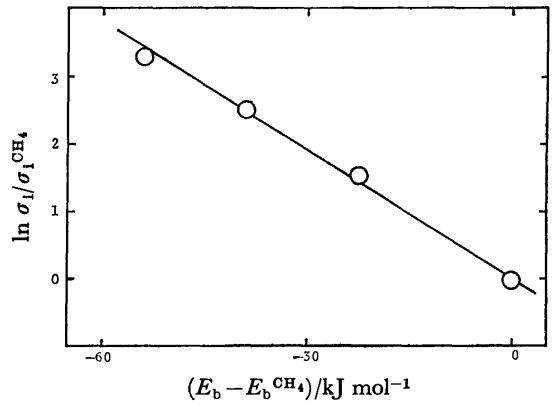

Fig. 6. Relationship between $\ln \sigma_1/\sigma_1^{CH_4}$ and $E_b - E_b^{CH_4}$.

In Fig. 6, $\ln \sigma_1/\sigma_1^{CH_4}$ is plotted as a function of $E_b - E_b^{CH_4}$. From the slope of the straight line in Fig. 6, the value of $(1-n^p)/RT$ can be estimated to be 0.063 mol/kJ. If we used the same p-value as that used for the alkane–Hg($^3P_1$) system, a bond order, n, of about 0.7 is obtained. This value is almost the same as that obtained for the alkane–Hg($^3P_1$) system and so may be thought to be valid.

By the BEBO method, the relative values of the cross-section of the Zn(^3P_J) quenching by alkanes can be explained. As was mentioned above, however, it is difficult to explain the difference in the variations with the C–H bond strength in quenching cross-sections between those obtained for Zn(^3P_J) and for Hg($^3P_1$) by means of the BEBO method.

Strausz *et al.* calculated the potential energy of activation for the Hg($^3P_1$)-photosensitized decomposition of alkanes and described the BEBO calculation predicts the observed trends. By using the values of the potential energy of activation obtained by them, and by assuming that the relative quenching cross-sections of the various types of C–H bonds are governed only by the difference in the activation energy, the relative quenching cross-sections for primary, secondary, and tertiary C–H bonds can be calculated. These calculated values of 1:8:43 are considerably smaller than the observed values. The temperature at which the Hg($^3P_1$)-photosensitized reaction was carried out was lower than that for the Zn(^3P_J)-photosensitized reaction; therefore, the selectivity appears to be somewhat emphasized for the former. However, it seems to be impossible to explain the large variation with the C–H bond strength in the quenching cross-section for higher-energy Hg($^3P_1$) in terms of the same mechanism as that used for Zn(^3P_J).

In the case of Hg($^3P_1$), the quenching by alkanes appears to result in a direct cleavage of the C–H bonds without the intermediate formation of HgH, as was pointed out by Breckenridge and Renlund.[1] The cleavage with the formation of hydride, as in the Zn(^3P_J)-photosensitized decomposition, involves a transition state in which the Zn–H bond is partly formed. The formation of the Zn–H bond somewhat lowers the potential energy and seems to make the Zn(^3P_J) quenching less sensitive to the C–H bond strength.

References

1) W. H. Breckenridge and A. M. Renlund, *J. Phys. Chem.*, **83**, 303 (1979).
2) S. Yamamoto, T. Takei, N. Nishimura, and S. Hasegawa, *Chem. Lett.*, **1976**, 1413; *Bull. Chem. Soc. Jpn.*, **53**, 860 (1980).
3) A. C. G. Mitchell and M. W. Zemansky, "Resonance Radiation and Excited Atoms," Cambridge University Press, Cambridge (1961).
4) F. W. Byron, M. N. McDermott, R. Novick, B. W. Perry, and E. Saloman, *Phys. Rev. A*, **134**, 47 (1964).
5) R. J. Cvetanovic, *Prog. React. Kinet.*, **2**, 39 (1964).
6) K. Yang, *J. Am. Chem. Soc.*, **89**, 5344 (1967).
7) A. Vikis and H. Moser, *J. Chem. Phys.*, **53**, 2333 (1970).
8) H. Guning, J. Campbell, H. Sandhu, and O. P. Strausz, *J. Am. Chem. Soc.*, **95**, 746 (1973).
9) H. Horiguchi and S. Tsuchiya, *Bull. Chem. Soc. Jpn.*, **50**, 1661 (1977), and the references cited therein.
10) R. A. Holroyd and G. W. Klein, *J. Am. Chem. Soc.*, **67**, 2273 (1963).
11) P. J. Young, G. Greig, and O. P. Strausz, *J. Am. Chem. Soc.*, **92**, 413 (1970).
12) W. H. Breckenridge and A. B. Callear, *Trans. Faraday Soc.*, **67**, 2009 (1971).
13) H. S. Johnston and C. Parr, *J. Am. Chem. Soc.*, **85**, 2544 (1963).

Effect of Polar Group on the Polypeptide–Lipid Interaction at the Air-Water Interface

Akira SHIBATA,* Shinsuke YAMASHITA, and Takuya YAMASHITA
Faculty of Pharmaceutical Sciences, Tokushima University, Shomachi, Tokushima 770
(Received October 19, 1981)

The effect of polar group on the interaction of synthetic polypeptides with lipids at the air-water interface was investigated. Methyl stearate interacts with benzyloxycarbonyl derivative of basic poly(α-amino acid) or benzyl ester of acidic poly(α-amino acid) on distilled water and KF, KSCN, and urea subsolutions. No interaction between polypeptide and stearamide on various subsolutions was observed except for the mixed system of stearamide with benzyl ester of acidic poly(α-amino acid) in α-helical conformation. The components in mixed monolayers exhibit characteristic miscibilities depending upon the flexibility of polymer side chain, the conformation of polymer and the steric factor of head group in lipid molecules. All of the mixed polypeptide–lipid monolayers spread on the subsolution containing SCN^- as a breaker of water structure become miscible. The dipole-dipole interaction between stearamide and benzyl ester of acidic poly(α-amino acid) in α-helical conformation is weakened by the action of urea.

The hydrophobic bonding is important in stabilizing macromolecular structures such as proteins and biological membranes.[1] Water is considered to affect the stability of macromolecular structure and the interaction of macromolecule with lipid at the interface.[2] In relation to the structure of water at the interfacial region, we have reported the effects of salts and urea on the interaction of polypeptide with fatty acid in monolayers.[3,4] The effects of anions on increasing the surface pressure were in the order $SCN^->Br^->Cl^->F^-$ in line with that of these anions as breakers of water structure.[5] KSCN, urea, and KF are known as breakers and a maker of water structure, respectively.

We have found that the interaction of polypeptide-(benzyloxycarbonyl derivatives of basic poly(α-amino acid), benzyl esters of acidic poly(α-amino acid), and poly(L-leucine)) and lipid(fatty acid, fatty alcohol and cholesterol) at the air-water interface is mainly of hydrophobic nature.[6] The interaction was found to take place between side chain of polypeptide and lipid. The interaction of polypeptide with myristic acid was stronger than that between polypeptide and myristyl alcohol. This suggests that weak interactions may exist between the polar group of lipid and polypeptide side chain. These polymer side chains consist of polar group and methylene groups. The polar groups in polymer side chain, as well as polar group in stearamide and methyl stearate, are ROCONHR′ for benzyloxycarbonyl derivative of basic poly(α-amino acid) and RCOOR′ for benzyl ester of acidic poly(α-amino acid).

In this study, by the use of methyl stearate and stearamide, the effect of the polar groups on the interaction of polypeptide with lipid was investigated in relation to the structure of water at the interfacial region.

Experimental

Poly(N^ε-benzyloxycarbonyl-L-lysine)(PLL(Z)), poly(γ-benzyl L-glutamate) (PBLG), and poly(γ-benzyl DL-glutamate) (PBDLG) were prepared by the polymerization of the *N*-carboxy anhydrides of respective amino acids. The molecular weights determined from the viscometry at 25 °C were 3.8×10^5, 3.0×10^5, and 6.4×10^4, respectively. Infrared spectra indicate that PLL(Z) and PBLG are in the α-helical conformation in the solid state. The helical content of PBDLG was 13% regular α-helix and 60% perturbed α-helix. No β-conformation was found for PBDLG. The regular α-helix and perturbed α-helix have been designated by Tsuboi *et al.*[7] The perturbed α-helix portion in a polypeptide molecule contains an antipode residue, the sequence length being relatively short. Lipids used were methyl stearate and stearamide. These materials were chromatographically pure.

The spreading solvents (*N*,*N*-dimethylformamide (DMF), dichloromethane (DCM)) were distilled under nitrogen atmosphere. The spreading solvents were DCM for mixed PBLG– and PBDLG–lipid systems, a 9:1(v/v) mixture of DCM and DMF for mixed PLL(Z)–lipid systems. The solutions of polypeptide and lipid were prepared separately, and mixed in the desired ratio immediately before spreading.

Salt and urea solutions were treated with activated charcoal in order to remove surface active contaminants. A 10 to 1 compression of the surface of the salt or urea subsolutions, after standing 10 min, produced less than 0.1 dyn/cm film pressure.

The initial spreading-area was 50 Å²/residue or molecule. The trough (65 cm × 15 cm × 1 cm) and compressing barriers were made of Teflon. The surface pressure was measured by Whilhelmy method at 20 °C. The film was compressed at a rate of 0.5 mm/min (1 Å²/residue or molecule).

Results

Figure 1 shows the surface pressure-area(π-A) curves for PLL(Z), PBLG, and PBDLG. Plateau which is characteristic of a number of synthetic polypeptide in α-helical conformation in the monolayer state are seen in the curves. The plateau is associated with the collapse or the transition of monolayer from a two-dimensional oriented state to a three-dimensional disoriented state.[6,8,9]

Figures 2 and 3 show the π-A curves of mixed PLL-(Z)–methyl stearate and mixed PLL(Z)–stearamide monolayers. The π-A curves of methyl stearate and stearamide are also shown in Figs. 2 and 3. These lipids form condensed films with the cross sectional area of about 20 Å² on distilled water. The areas are in agreement with those reported by other workers.[10,11] The transition pressure for mixed PLL(Z)–methyl stearate monolayer increases with methyl stea-

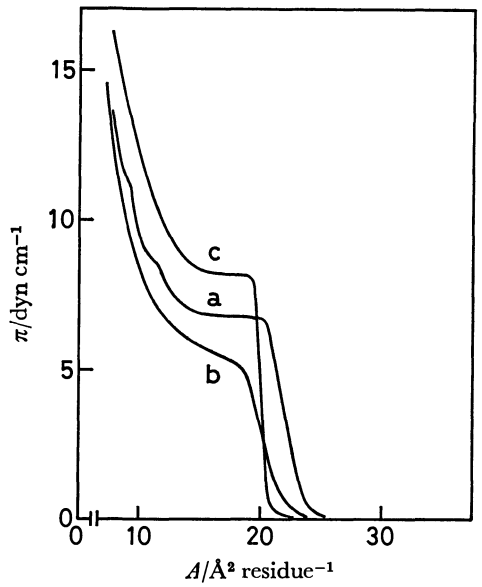

Fig. 1. Surface pressure-area curves of polypeptide monolayers on distilled water.
1 dyn=10^{-5} N, 1 Å=0.1 nm. a: PLL(Z), b: PBLG, c: PBDLG.

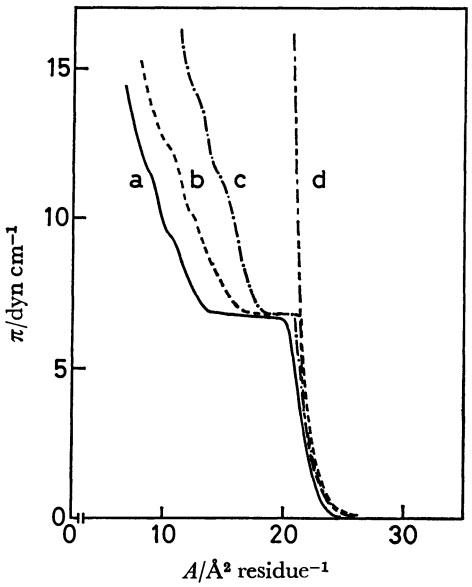

Fig. 3. Surface pressure-area curves of mixed PLL(Z)–stearamide monolayers on distilled water.
a; PLL(Z), b; 4:1(residue mol:mol), c; 1:1(residue mol:mol), d; stearamide.

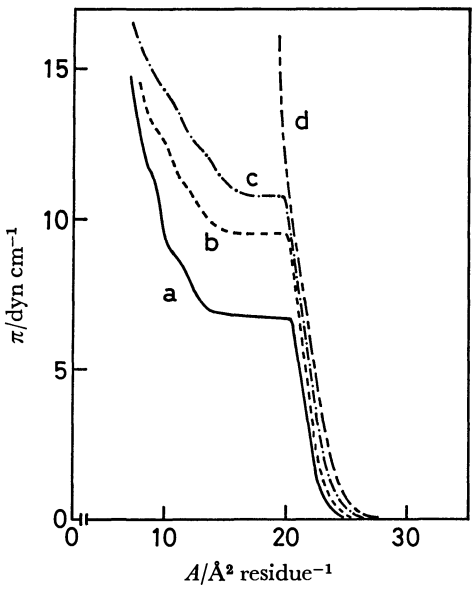

Fig. 2. Surface pressure-area curves of mixed PLL(Z)–methyl stearate monolayers on distilled water.
a; PLL(Z), b; 9:1(residue mol:mol), c; 1:1(residue mol:mol), d; methyl stearate.

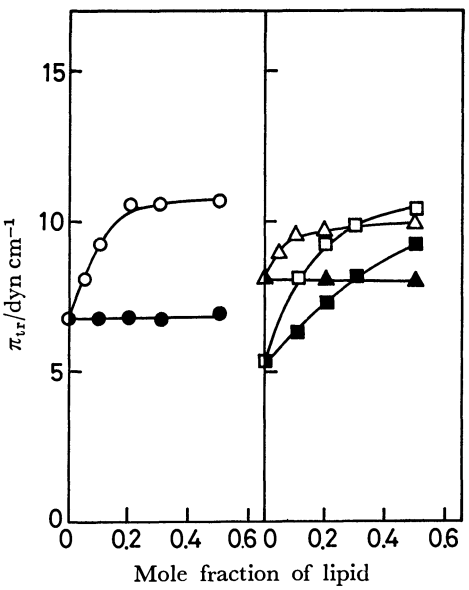

Fig. 4. Transition pressures of single and mixed monolayers as a function of lipid mole fraction.
○: PLL(Z)–methyl stearate, ●: PLL(Z)–stearamide, □: PBLG–methyl stearate, ■: PBLG–stearamide, △: PBDLG–methyl stearate, ▲: PBDLG–stearamide.

rate mole fraction, while for mixed PLL(Z)–stearamide monolayer is independent of stearamide mol fraction.

Figure 4 shows the relationship between the transition pressure and the composition of lipid in mixed monolayers for PLL(Z)–lipid, PBLG–lipid, and PBDLG–lipid systems on distilled water. For mixed polypeptide–methyl stearate systems, up to methyl stearate mol fraction of about 0.2, the transition pressures caused by the polymer components increase steeply, the increase becoming gradual beyond this mole fraction. On the other hand, no significant change in transition pressure is observed for mixed monolayer of stearamide and either PLL(Z) or PBDLG. The transition pressures for mixed PBLG–stearamide system increase with stearamide mol fraction different from those for mixed systems of stearamide and either PLL(Z) or PBDLG.

As a example of mixed monolayers on salt subsolutions, Fig. 5 shows the π-A curves for mixed PLL(Z)–methyl stearate (1:1 residue mol: mol) spread on distilled water, 6 M urea, 3 M KSCN and 3 M KF subsolutions (1 M=1 mol dm^{-3}). The transition pressures caused by PLL(Z) are much higher on the subsolution containing KSCN or urea than on distilled water. In the presence of KF, on the other hand,

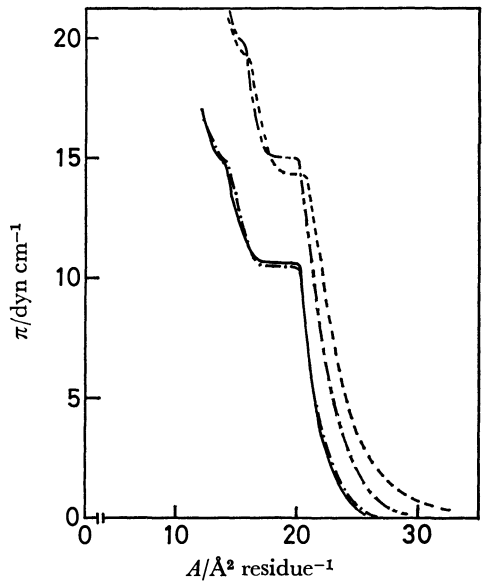

Fig. 5. Surface pressure-area curves of mixed PLL(Z)–methyl stearate (1:1(residue mol : mol)) monolayers on different subsolutions.
——: Distilled water, ——— 3 M KSCN, —·—: 3 M KF, ----: 6 M urea.

the film transition pressure becomes slightly lower. The film expansion is observed in the presence of KSCN or urea. The effect of KF on expansion is quite small. Similar tendencies were observed for the other mixed monolayers on salt and urea subsolutions.

Discussion

Interaction on Distilled Water. The application of the two-dimensional phase rule provides an important tool for detecting miscibility in two-component monolayers.[12] If a polypeptide and a lipid are miscible in the monolayer and the new three-dimensional phase begins to appear at the transition point, the transition pressure should vary with composition. If, on the other hand, the monolayer components are immiscible, the transition pressure is independent of composition. As can be seen in Fig. 4, the mixed systems of methyl stearate with PLL(Z), PBLG, or PBDLG are miscible. Stearamide is immiscible with PLL(Z) or PBDLG except PBLG. Both monolayers of methyl stearate and stearamide are the condensed type. Because of the similarity of cross sectional area between polypeptide and lipid monolayers, the deviation from the additivity rule was difficult to detect.

To obtain a further information concerning polypeptide–lipid interaction, the work of collapse of mixed monolayers was estimated. The work of collapse, W, is given by[6]

$$W = \pi_{tr} \cdot \Delta A,$$

where π_{tr} is the transition pressure, and ΔA is the difference between initial and final areas of collapse. Figure 6 shows the work of collapse as a function of lipid mole fraction. It can be seen that with the exception of mixed PLL(Z)–stearamide and PBDLG–stearamide systems, the maximum work of collapse

Table 1. Miscibility between polypeptide and lipid

Mixed System	Miscibility			
	Water	KF	KSCN	Urea
Methyl stearate-PLL(Z)	+	+	+	+
Methyl stearate-PBLG	+	+	+	+
Methyl stearate-PBDLG	+	+	+	+
Stearamide-PLL(Z)	−	−	+	−
Stearamide-PBLG	+	+	+	−
Stearamide-PBDLG	−	−	+	−

+: Miscible, −: immiscible.

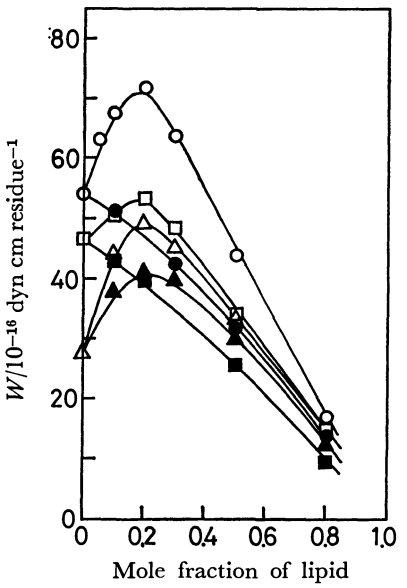

Fig. 6. Work of collapse for mixed monolayers as a function of lipid mole fraction.
○: PLL(Z)–methyl stearate, ●: PLL(Z)–stearamide, △: PBLG–methyl stearate, ▲: PBLG–stearamide, □: PBDLG–methyl stearate, ■: PBDLG–stearamide.

is found at about 0.2 lipid mol fraction. At this fraction, the surface adhesive forces might be reinforced as a result of the formation of the 4:1 complex (residue:molecule) of polypeptide and lipid as reported previously for mixed polypeptide–fatty acid and polypeptide–fatty alcohol systems.[6] In the lipid rich region, the adhesive force of polypeptide decrease steeply, the film collapsing more easily in the case of polypeptide alone. There is a remarkable difference in W values between mixed PLL(Z)–stearamide and mixed PBLG–stearamide systems (Fig. 6). This would be due to the difference between the polar groups, RCOOR', in PBLG side chain and ROCONHR' in PLL(Z) side chain.

Effect of Salts. The effect of polar group on interaction could be discussed in more detail by the use of subsolutions containing either KSCN or urea as a breaker and KF as a maker of water structure.

The polypeptide and mixed monolayers of polypeptide with methyl stearate or stearamide on salt subsolutions expand with salt concentration. The order of film expansion is KSCN>KF>distilled water, and independent of the difference in miscibility between polypeptide and either methyl stearate or ste-

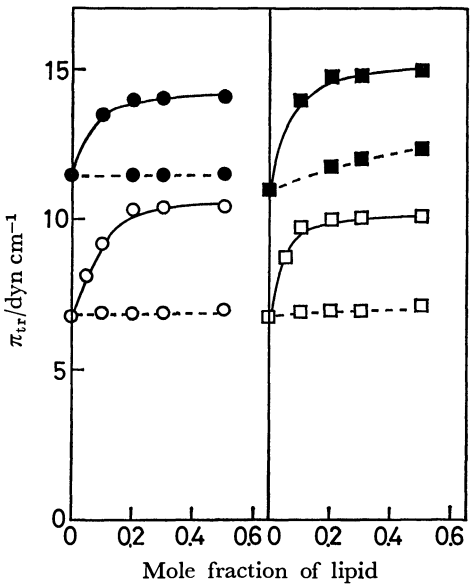

Fig. 7. Transition pressures of single and mixed monolayers as a function of lipid mole fraction on different subsolutions.
——: PLL(Z)–methyl stearate, ----: PLL(Z)–stearamide, ○: distilled water, ●: 6 M urea, ■: 3 M KSCN, □: 3 M KF.

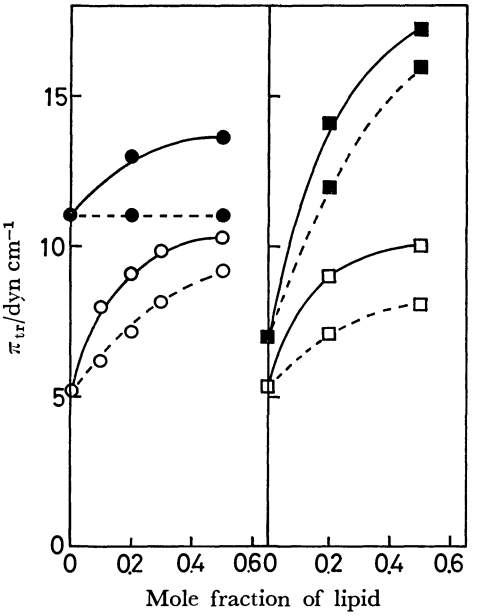

Fig. 8. Transition pressures of single and mixed monolayers as a function of lipid mole fraction on different subsolutions.
——: PBLG–methyl stearate, ----: PBLG–stearamide, ○: distilled water, ●: 6 M urea, ■: 3 M KSCN, □: 3 M KF.

aramide. This order was essentially the same as obtained for mixed polypeptide–fatty acid systems.[6] Salts may be transferred into the interface relative to the monolayer free surface. Ralston and Healy[13] reported that salts are transferred into fatty alcohol monolayer in terms of interfacial water structure and this process continued until the surface and bulk concentration become equal.

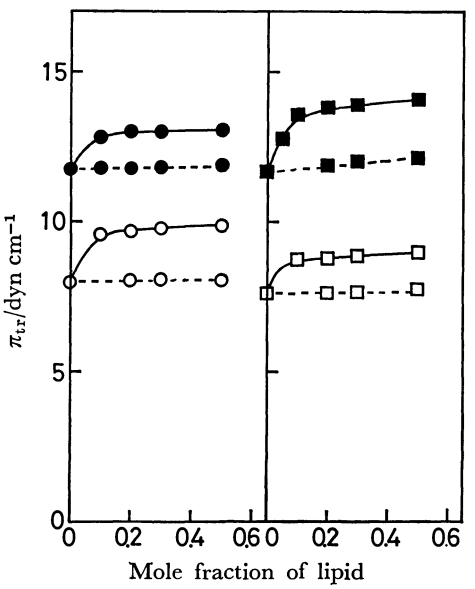

Fig. 9. Transition pressures of single and mixed monolayers as a function of lipid mole fraction on different subsolutions.
——: PBDLG–methyl stearate, ----: PBDLG–stearamide, ○: distilled water, ●: 6 M urea, ■: 3 M KSCN, □: 3 M KF.

The general tendencies relating to the miscibility of polypeptide with lipid on various subsolutions was summarized in Table 1. The miscibilities between polypeptide and stearamide are extremely poor compared with polypeptide–methyl stearate systems.

Figures 7, 8, and 9 show the relationship between the transition pressure and the composition of lipid in mixed PLL(Z)–lipid, PBLG–lipid, and PBDLG–lipid monolayers spread on distilled water, 6 M urea, 3 M KSCN and 3 M KF subsolutions, respectively. The transition pressures for single and mixed monolayers spread on KSCN subsolution are higher than those on distilled water, and is independent of miscibility between polypeptide and lipid. For mixed polypeptide–methyl stearate monolayers on KSCN or urea subsolution, up to 0.2 methyl stearate mole fraction, the transition pressure caused by the polymer component increases steeply, the increase becoming almost constant beyond this mol fraction. The hydrated structure around the hydrocarbon moieties of the side chains of polypeptide is disrupted by SCN^- ion preferentially accumulated on the surface. As a result of the disruption, the affinity of the hydrocarbon moieties to water may increase.

The transition pressures for both miscible and immiscible mixed systems on KF subsolution becomes slightly low compared with that on distilled water (Figs. 7, 8, and 9). In the presence of F^- ion as a maker of water structure, the adhesive force of polypeptide to water become weak with the formation of hydrated structure around the mixed films.

The molecular structure of urea is similar to the polar group in stearamide molecule and PLL(Z) side chain, and urea acts as a breaker of water structure.[14] The expansion of single and mixed films may be ascribed to the penetration of polypeptide monolayer

by urea in the subsolution (Fig. 5).[15] As shown in Figs. 7 and 8, the transition pressures of mixed PLL-(Z)-lipid and PBLG–lipid monolayers on urea subsolution are higher than those on distilled water. The hydrated structure around hydrophobic moieties of polypeptide side chain would be disrupted by the action of urea.

It is noteworthy that stearamide becomes practically immiscible with PBLG on urea subsolution (Table 1 and Fig. 8). In the presence of urea, the dipole-dipole interaction between $RCONH_2$ in stearamide molecule and RCOOR′ in PBLG side chain may be weakened by urea because of the similarity of polar group in stearamide and urea molecule.

Effect of Polypeptide Conformation. The perturbed helix portion of PBDLG is unfolded at the interface owing to relatively weak stability of the helix.[6,7] As shown in Fig. 1, the difference in shape of the π-A curves between PBLG and PBDLG is accounted for as arising essentially from the conformation of these polymer at the interface.[6,16] The change in transition pressure for mixed PBLG–lipid monolayer is larger than that of mixed PBDLG–lipid monolayer (Fig. 4). The PBLG monolayer is more compressible than the PBDLG monolayer.[4] The flexible side chains of PBLG might undergo a rearrangement more easily into position favorable to the interaction with alkyl chain of methyl stearate or stearamide The strength of van der Waals forces of lipid molecules in condensed monolayers and the flexibility of polypeptide side chain seem to affect the degree of interaction as in the case of mixed systems of polypeptide and either fatty acid or fatty alcohol.[4]

The effect of stearamide on interaction in mixed monolayers is much more pronounced than that of methyl stearate. PBLG interacts characteristically with stearamide. However, PBDLG interacts with considerable difficulty (Fig. 4). The conformation of a polymer may also be important for the interaction at the interface.

The transition pressures of mixed PBDLG–methyl stearate monolayer spread on KF subsolution are smaller than those on distilled water. For mixed PBLG–methyl stearate system, on the other hand, there is little difference between KF and KF free subsolutions. The formation of hydrated structure around PBDLG molecule unfolded considerably at the interface may be caused by F^- ion as a maker of water structure.

The transition pressures of mixed monolayers of lipid and either PBLG or PBDLG spread on KSCN subsolution become higher than those on distilled water (Figs. 8 and 9). In the presence of KSCN, the increment of transition pressure for mixed PBLG–lipid systems is larger than that of mixed PBDLG–lipid systems. The geometry of the α-helix in the monolayer state is such that the side chains of adjacent helices can interpenetrate to form good hydrophobic contacts.[16] PBLG might become more hydrophobic than PBDLG unfolded considerably at the interface since the polypeptide main chain is appreciably shielded from the interaction with water molecules. Therefore, the interaction of the amide group in the main chain with SCN^- ion would accompany the difficulty. SCN^- ion is considered to act primarily as a breaker of water structure around the hydrophobic moieties in mixed PBLG–lipid film.

Irrespective of the composition of subsolution, methyl stearate is miscible with PBLG or PBDLG. On the other hand, mixed PBLG–stearamide and PBDLG–stearamide monolayers are miscible and immiscible on distilled water, respectively (Table 1 and Figs. 8 and 9). As such the case of mixed PBLG–cholesterol system,[6] PBLG interacts characteristically with stearamide on distilled water. In the presence of urea, however, both mixed monolayers become immiscible through the interaction between the polar group, $RCONH_2$, in stearamide and urea molecule.

PBDLG is miscible for methyl stearate though immiscible for stearamide on distilled water and urea subsolution. The head group, $RCOOCH_3$, of methyl stearate in monolayer state exists under the surface. The methyl group under the surface shields the ester group from attack by polar group of polypeptide side chains,[17] and in addition, is able to interact with hydrophobic moieties of polypeptide side chains. On the other hand, stearamide monolayer on distilled water or urea subsolution may be stabilized by the intermolecular hydrogen bonding between C=O and NH_2 groups in stearamide molecules or by the interaction with urea. Therefore, it seems that the miscibility between PBDLG and stearamide becomes less.

References

1) W. B. Dandliker and V. A. de Saussure, "The Chemistry of Biosurface," ed by M. L. Hair, Marcel Dekker, New York (1971), Vol. 1, p. 1.

2) W. Drost-Hansen, "Chemistry of the Cell Interface," ed by H. D. Brown, Academic Press, New York (1971), Part B, p. 1.

3) A. Shibata, S. Yamashita, and T. Yamashita, *Nippon Kagaku Kaishi*, **1978**, 917.

4) A. Shibata, S. Yamashita, and T. Yamashita, *Bull. Chem. Soc. Jpn.*, **51**, 2757 (1978).

5) T. Yamashita, A. Shibata, and S. Yamashita, *Chem. Lett.*, **1978**, 11.

6) T. Yamashita, A. Shibata, and S. Yamashita, *Bull. Chem. Soc. Jpn.*, **51**, 2751 (1978).

7) M. Tsuboi, Y. Mitsui, A. Wada, T. Miyazawa, and N. Nagashima, *Biopolymers*, **1**, 297 (1963).

8) B. R. Malcolm, *Proc. R. Soc. London, Ser. A*, **305**, 363 (1968).

9) B. R. Malcolm, *Prog. Surface Membrane Sci.*, **7**, 183 (1973).

10) N. K. Adam, *Proc. R. Soc. London, Ser. A*, **101**. 452 (1922).

11) W. D. Harkins and E. Boyd, *J. Phys. Chem.*, **45**, 20 (1941).

12) G. L. Gaines, Jr., "Insoluble Monolayers at Liquid-Gas Interfaces," Interscience, New York (1966), p. 281.

13) J. Ralston and T. W. Healy, *J. Colloid Interface Sci.*, **42**, 629 (1973).

14) S. Subramanian, D. Balasubramanian, and J. C. Ahluwalia, *J. Phys. Chem.*, **73**, 266 (1969).

15) D. F. Sears, *J. Colloid Interface Sci.*, **29**, 288 (1969).

16) B. R. Malcolm, *Adv. Chem. Ser.*, **145**, 338 (1975).

17) A. W. Adamson, "Physical Chemistry of Surfaces," Interscience, New York (1960), p. 103.

The Existence of an Unstable Limit Cycle in the Oregonator Model for the Belousov-Zhabotinskii Reaction

Shinji SAKANOUE* and Mitsuo ENDO

Department of Chemistry, Faculty of General Education, The Tokyo University of Agriculture and Technology, Saiwai-cho, Fuchu, Tokyo 183

(Received October 20, 1981)

With an Oregonator model for the mechanism of the Belousov-Zhabotinskii reaction (an oscillatory chemical system), the coexistence of a stable and an unstable limit cycle was confirmed from the results of computer simulations and the real unstable limit cycle was shown. The relation of the amplitude of the unstable limit cycles to the parameters f and p in Tyson's equation[4] was found.

The Belousov-Zhabotinskii reaction (B-Z reaction) is a well known example of an oscillatory chemical reaction. Field, Körös, and Noyes[1] presented the mechanism for this reaction in the homogeneous system and proposed a simple reaction model for sustained oscillation, which is called an Oregonator. Subsequently, Noyes *et al.*[2] Murray *et al.*[3] and Tyson[4] examined precisely the oscillation conditions based on the model. Tyson predicted the existence of a pair of stable and unstable limit cycles for a parameter p close to a critical one, p_c, in his analysis. However, he did not show any real unstable limit cycles. In this study the conditions for an unstable steady state are given over a wide range of the parameters f, p, and q in Tyson's equation; the coexistence of stable and unstable limit cycles, which is called "hard self-excitation", is confirmed for a parameter p not only close to p_c, but also far from it. The relation of the amplitudes of the unstable limit cycles to the parameters f and p is also clarified from the results of computer simulations.

The mechanism of the B-Z reaction to be expressed with the Oregonator is as follows:[2]

$$\mathrm{A} + \mathrm{Y} \xrightarrow{k_1} \mathrm{X} + \mathrm{P}, \tag{1-1}$$

$$\mathrm{X} + \mathrm{Y} \xrightarrow{k_2} 2\mathrm{P}, \tag{1-2}$$

$$\mathrm{B} + \mathrm{X} \xrightarrow{k_3} 2\mathrm{X} + \mathrm{Z}, \tag{1-3}$$

$$2\mathrm{X} \xrightarrow{k_4} \mathrm{B} + \mathrm{P}, \tag{1-4}$$

$$\mathrm{Z} \xrightarrow{k_5} f\mathrm{Y}. \tag{1-5}$$

The symbols correspond to the chemical species in the B-Z reaction system as follows;

$\mathrm{X} = \mathrm{HBrO_2}$, $\mathrm{Y} = \mathrm{Br^-}$, $\mathrm{Z} = 2\mathrm{Ce^{4+}}$, $\mathrm{A} = \mathrm{B} = \mathrm{BrO_3^-}$, $\mathrm{P} = \mathrm{HOBr}$.

The parameter f is a stoichiometric factor and is twice the number of $\mathrm{Br^-}$ ions generated per $\mathrm{Ce^{4+}}$ to be reduced. During the following calculations, it is assumed that the concentrations of A and B remain constant, effectively treating the system as open.

The kinetic behavior of the reaction (1) was represented by Tyson[4] with the following dimensionless equations:

$$\varepsilon\frac{dx}{d\tau} = x + y - qx^2 - xy, \tag{2-1}$$

$$\frac{dy}{d\tau} = -y + fz - xy, \tag{2-2}$$

$$p\frac{dz}{d\tau} = x - z, \tag{2-3}$$

Here x, y, and z *etc.* are the variables including X, Y, Z, A, B, and k_i, *etc.* which represent the concentrations of species and the rate constants, *etc.* as follows:

$$\begin{aligned} x &= k_2(k_1A)^{-1}X, \\ y &= k_2(k_3B)^{-1}Y, \\ z &= k_2k_5(k_1k_3AB)^{-1}Z, \\ p &= k_1k_5^{-1}A, \\ q &= 2k_1k_4(k_2k_3B)^{-1}A, \\ \varepsilon &= k_1A(k_3B)^{-1}, \\ \tau &= k_1At. \end{aligned}$$

The constant solution ("steady state") of Eq. 2 without the origin ($x=y=z=0$) is

$$\left.\begin{aligned} x_0 = z_0 &= \{1-f-q+\sqrt{(1-f-q)^2+4q(f+1)}\}(2q)^{-1} \\ y_0 &= fx_0(1+x_0)^{-1} \end{aligned}\right\}. \tag{3}$$

In order to examine the trajectory in the neighborhood of the steady state, Eq. 2 is expressed in terms of deviations from the steady state, which are $\bar{x}=x-x_0$, $\bar{y}=y-y_0$, $\bar{z}=z-z_0$, as follows:

$$\varepsilon\frac{d\bar{x}}{d\tau} = -\alpha\bar{x} - \beta\bar{y} - q\bar{x}^2 - \bar{x}\bar{y}, \tag{4-1}$$

$$\frac{d\bar{y}}{d\tau} = -\gamma\bar{x} - \delta\bar{y} + f\bar{z} - \bar{x}\bar{y}, \tag{4-2}$$

$$p\frac{d\bar{z}}{d\tau} = \bar{x} - \bar{z}, \tag{4-3}$$

where

$$\left.\begin{aligned} \alpha &= -1 + y_0 + 2qx_0 = qx_0 + y_0x_0^{-1} > 0 \\ \beta &= x_0 - 1 > 0, \qquad \text{for } q<1 \\ \gamma &= y_0 > 0 \\ \delta &= x_0 + 1 > 0. \end{aligned}\right\}. \tag{4-4}$$

When $\varepsilon\to 0$ as in the real B-Z reaction,[1] the following condition is maintained, from Eq. 4-1:

$$q\bar{x}^2 + (\alpha+\bar{y})\bar{x} + \beta\bar{y} = 0.$$

Thus

$$X(\bar{y}) = \bar{x} = \{-(\alpha+\bar{y}) \pm \sqrt{(\alpha+\bar{y})^2 - 4q\beta\bar{y}}\}(2q)^{-1}. \tag{5}$$

Here, only the positive sign of $\pm$ in Eq. 5 is taken, because, if the negative sign is taken, $x<0$, this would a negative concentration, which is physically unacceptable.

From Eqs. 5, 4-2, and 4-3, the following two

ordinary differential equations can be obtained:

$$\left.\begin{aligned}\frac{d\bar{y}}{d\tau} &= -\delta\bar{y} + f\bar{z} - (\gamma+\bar{y})X(\bar{y}) = Y(\bar{y},\bar{z}) \\ \frac{d\bar{z}}{d\tau} &= \frac{1}{p}X(\bar{y}) - \frac{1}{p}\bar{z} = Z(\bar{y},\bar{z})\end{aligned}\right\}. \quad (6)$$

Since $\bar{y} \ll y_0$, $\bar{z} \ll z_0$, Eq. 6 can be linearized as follows:

$$\left.\begin{aligned}\frac{d\bar{y}}{d\tau} &= Y_{\bar{y}}\bar{y} + Y_{\bar{z}}\bar{z} \\ \frac{d\bar{z}}{d\tau} &= Z_{\bar{y}}\bar{y} + Z_{\bar{z}}\bar{z},\end{aligned}\right\}, \quad (7)$$

where

$$Y_{\bar{y}} = \left(\frac{\partial Y(\bar{y},\bar{z})}{\partial\bar{y}}\right)_{\substack{\bar{y}=0\\ \bar{z}=0}} = \frac{\beta\gamma-\alpha\delta}{\alpha}, \quad (8\text{-}1)$$

$$Y_{\bar{z}} = \left(\frac{\partial Y(\bar{y},\bar{z})}{\partial\bar{z}}\right)_{\substack{\bar{y}=0\\ \bar{z}=0}} = f, \quad (8\text{-}2)$$

$$Z_{\bar{y}} = \left(\frac{\partial Z(\bar{y},\bar{z})}{\partial\bar{y}}\right)_{\substack{\bar{y}=0\\ \bar{z}=0}} = -\frac{\beta}{p\alpha}, \quad (8\text{-}3)$$

$$Z_{\bar{z}} = \left(\frac{\partial Z(\bar{y},\bar{z})}{\partial\bar{z}}\right)_{\substack{\bar{y}=0\\ \bar{z}=0}} = -\frac{1}{p}. \quad (8\text{-}4)$$

The behaviors of $\bar{y}$ and $\bar{z}$ in the neighborhood of the steady state are determined by the eigenvalues, λ, of the matrix

$$A = \begin{pmatrix} Y_{\bar{y}} & Y_{\bar{z}} \\ Z_{\bar{y}} & Z_{\bar{z}} \end{pmatrix}$$

which satisfies the following secular equation

$$\lambda^2 - Tr\lambda + \mathrm{Det} = 0,$$

where

$$Tr = Y_{\bar{y}} + Z_{\bar{z}} = \frac{\beta\gamma-\alpha\delta}{\alpha} - \frac{1}{p},$$

$$\mathrm{Det} = Y_{\bar{y}}Z_{\bar{z}} - Y_{\bar{z}}Z_{\bar{y}} = \frac{\alpha\delta-\beta\gamma+f\beta}{p\alpha}.$$

Stability of Steady State

The boundary condition that determines the stability of a steady state for the periodic solutions is given by $Tr=0$, that is

$$Tr = \frac{\beta\gamma-\alpha\delta}{\alpha} - \frac{1}{p} = 0. \quad (9\text{-}1)$$

As is obvious from Eqs. 3 and 4-4, each of α, β, γ, and δ can be a function of q and f. Equation 9-1, then, can be generally represented as follows:

$$F(f,p,q) = 0. \quad (9\text{-}2)$$

Here, $F(f,p,q)=(\beta\gamma-\alpha\delta)/\alpha-1/p$. Thus, for a certain fixed set of two values from three parameters the remaining parameter which satisfies Eq. 9-2 gives a critical value. For p fixed, Eq. 9 gives a critical value of f as a function of q, which is shown in Fig. 1. For a value of q less than 0.0809, the critical f takes two values, f_{c_1} and f_{c_2}, where $f_{c_1}<f_{c_2}$. If $f_{c_1}<f<f_{c_2}$, $Tr>0$ and the steady state is unstable. On the other hand, if $f<f_{c_1}$ or $f>f_{c_2}$, $Tr<0$ and the steady state is stable. For example, when $p=\infty$ and $q=0$, $f_{c_1}=0.5$, and $f_{c_2}=1+\sqrt{2}=2.414$. The region of f in which a steady state is unstable becomes narrower with increasing values of q, as shown in Fig. 1.

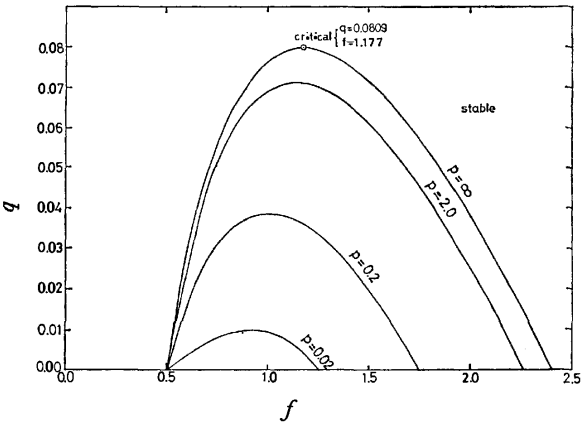

Fig. 1. Stability of the steady state as a function of parameters q and f for the various values of p. The steady state is unstable for the values of f and q inside a curve for p fixed.

For q fixed, a critical p, p_c, is given as a function of f by Eq. 9 as follows:

$$p_c = \frac{\alpha}{\beta\gamma-\alpha\delta} \quad (10)$$

If $p<p_c$, $Tr<0$ and then the steady state is stable; if $p>p_c$, $Tr>0$ and then the steady state is unstable.

The boundary condition for whether a trajectory around a steady state is a periodic spiral or not, that is, whether a steady state is a focus or node, is given by $Tr^2=4\mathrm{Det}$. The critical parameter p, $p_\pm$, is represented by

$$p_\pm = \{(p_c^{-1}+2\xi) \pm 2\sqrt{\xi p_c^{-1}+\xi^2}\}p_c^2, \quad (11)$$

where

$$\xi = \mathrm{Det}\cdot p = \frac{\alpha\delta-\beta\gamma+f\beta}{\alpha}.$$

Since $p_\pm$ is a function of q and f only, its value can be determined for a certain set of q and f values. If $p_-<p<p_+$, $Tr^2<4\mathrm{Det}$ and a steady state is a focus; on the other hand, if $p<p_-$ or $p>p_+$, $Tr^2>4\mathrm{Det}$ and it is a node.

Tyson[4] calculated p_c and $p_\pm$ by using an approximation which is calculated for a very low value of q. Here, without the approximation, p_c and $p_\pm$ were calculated directly from Eqs. 3, 4-4, 10, and 11 for q fixed. A result for $q=0.006$ is shown in Fig. 2, which represents a f-p parameter phase space. It differs from the approximate result obtained by Tyson in the regions near the values of 0.5 and 1.0 of f.

If f and p have the values in the unstable focus region (uf) in Fig. 2, a steady state is unstable, the behavior of the trajectory surrounding it is periodic, and the existence of a stable limit cycle can be predicted: that is the situation called "soft self-excitation". The real limit cycle was obtained by Tyson[4] with a numerical integration of Eq. 2 for $dx/d\tau=0$ or $\varepsilon=0$.

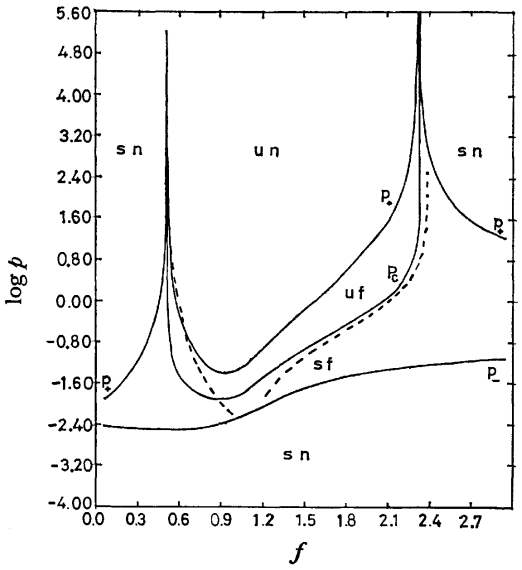

Fig. 2. Stability of the steady state and periodicity of the trajectory as a function of the parameter p and f for $q=0.006$.
------: Tyson's approximate expression of p_c for $q=0.006$, sn: stable node, sf: stable focus, un: unstable node, uf: unstable focus.

Coexistence of Stable and Unstable Limit Cycles[5)]

There should be no stable limit cycle in the case where f and p have the values in the stable focus (sf) region in Fig. 2, unless an unstable limit cycle surrounds a stable focus (Poincarè-Bendixon's theorem). In regard to the Oregonator, it was confirmed with computer simulations that a stable limit cycle coexists with an unstable limit cycle which surrounds a stable focus in the case of $p_c>p>p_d$, where p_d is a critical parameter for the existence of an unstable limit cycle. That is, the situation called "hard self-excitation" can appear not only for the condition of $p\simeq p_c$, but also for every p value in the range of $p_c>p>p_d$, even when $p_c\gg p_d$. For an example, in the case of $q=0.006$ and $p=\infty$, $f_{c_1}=0.519$, and $f_{c_2}=2.354$ (Fig. 1), $p_+=1.584\times10^5$, $p_-=5.141\times10^{-2}$, $p_c=90.24$ (Fig. 2), and $p_d=0.849$ (Fig. 5). These values come from the results of numerical calculated solutions of Eq. 2 under $\varepsilon\to0$ for various values of p. The hard self-excitation under this condition is shown in Fig. 3. In the situation, there could be two kinds of trajectories, A and B in Fig. 3, starting from the two different initial values near to each other, one of which asymptotically reaches a stable steady state, and the other a stable limit cycle. In the former case the oscillation is damped, while in the latter it is sustained. These two kinds of temporal changes on the variable y are shown in Fig. 4. In this case, the bifurcation can occur with a small change of a value of p for a certain initial value. In this situation, a final behavior of a system is decided due to the result of a fluctuation in the initial values of y and z, or in a parameter p. However, the hard self-excitation phenomenaon has not yet been found experimentally in

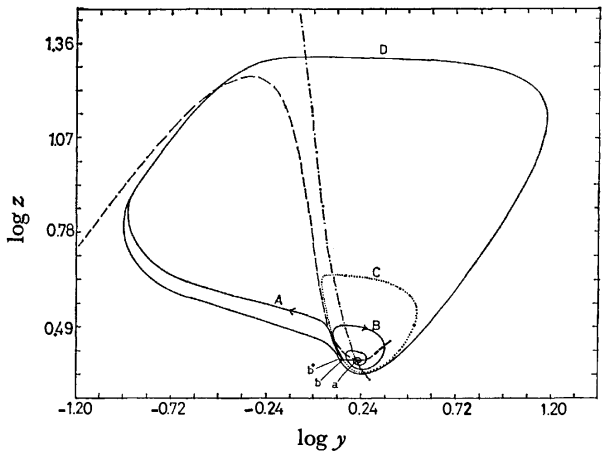

Fig. 3. Phase plane plot of log z *vs.* log y obtained numerical integration of Eq. 2 under $\varepsilon\to0$ for $q=0.006$, $f=2.350$, and $p=2.0$.
A: Trajectory to reach a stable limit cycle (initial values; $y=1.411$, $z=2.444$), B: trajectory to reach a steady state (initial values; $y=1.412$, $z=2.444$), C: unstable limit cycle, D: stable limit cycle, a: steady state, ab: *AMP*, ----: solution of Eq. 2 for $dx/d\tau=0$ and $dy/d\tau=0$, —·—·: solution of Eq. 2 for $dx/d\tau=0$ and $dz/d\tau=0$.

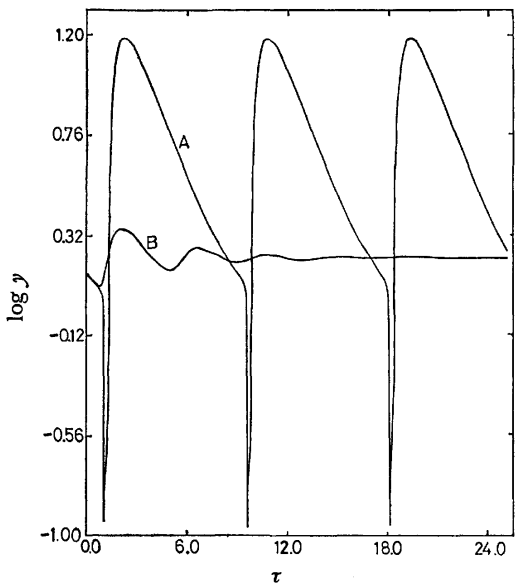

Fig. 4. Temporal behaviors of log y for $q=0.006$, $f=2.350$ and $p=2.0$.
A: Sustained oscillation (initial values; $y=1.411$, $z=2.444$), B: damped oscillation (initial values; $y=1.412$, $z=2.444$).

a real B-Z reaction. The chemical equation, Eq. 1-5 in the Oregonator corresponds to the real reaction:

$$2Ce^{4+} + \frac{1}{2}BrCH(COOH)_2 + H_2O \longrightarrow$$

$$2Ce^{3+} + \frac{1}{2}HCOOH + CO_2 + \frac{1}{2}Br^- + \frac{5}{2}H^+.$$

Therefore, the value of k_5 includes not only the rate constant of this reaction, but also the concentration of $BrCH(COOH)_2$, (BrMA). Since $p=k_1k_5^{-1}A$, an

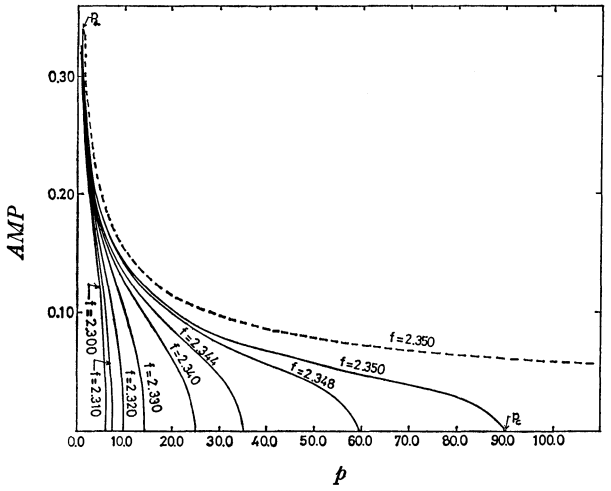

Fig. 5. Plot of *AMP* *vs.* p for $q=0.006$.
——: Amplitude of unstable limit cycle, $\overline{ab}$ in Fig. 3, ----: amplitude of stable limit cycle, $\overline{ab}'$ in Fig. 3.

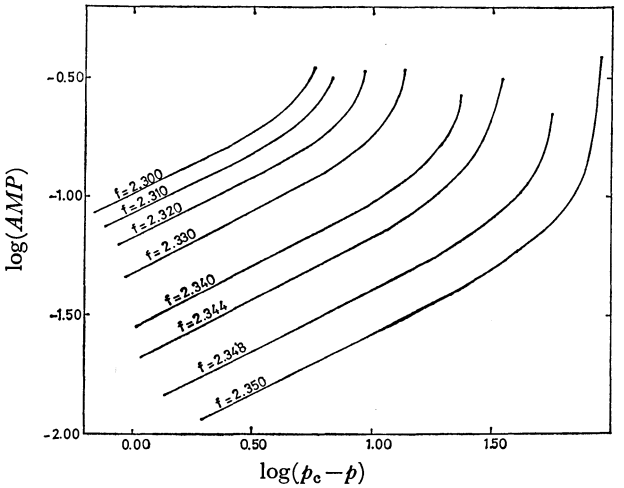

Fig. 6. Plot of $\log(AMP)$ *vs.* $\log(p_c-p)$.

increase of temperature, which increases the value of the rate constant, or of the concentration of BrMA should result in a decrease of p. If p could reach a value in the range of $p_d<p<p_c$ through as adjustment of these conditions, it may be possible to realize a hard self-excitation in the real B-Z reaction.

Relation of Amplitudes of Unstable Limit Cycles with p

In Fig. 3, a steady state ($y=y_0$, $z=z_0$) is represented by the symbol "a", and the point which a line $z=z_0$ intersects an unstable limit cycle is denoted by the symbol "b"; then it is convenient to define the distance, $\overline{ab}$, between the points "a" and "b" as the amplitude of an unstable limit cycle, *AMP*. These amplitudes for various values of f and p were obtained from computer simulations. Figure 5 shows the plots of *AMP* against p for various f values and Fig. 6 shows the plots of $\log(AMP)$ against $\log(p_c-p)$. These are linear with a slope of 1/2 in the range of low values of (p_c-p), but $\log(AMP)$ increases rapidly with $\log(p_c-p)$ in its high value range. This relation and the behavior of periodic trajectories in the hard self-excitation can be treated quantitatively with Landau's theory, in which a transition from a steady flow to a turbulent one in a stream could be elucidated. The quantitative treatment of this problem will be dealt with later.

The authors should like to thank Dr. Chiaki Murase for his suggestion that Landau's theory could be applied to this problem.

References

1) R. J. Field, E. Körös, and R. M. Noyes, *J. Am. Chem. Soc.*, **94**, 8649 (1972).
2) R. J. Field and R. M. Noyes, *J. Chem. Phys.*, **60**, 1877 (1974).
3) S. P. Hastings and J. D. Murray, *SIAM J. Appl. Math.*, **28**, 678 (1975).
4) J. J. Tyson, *J. Chem. Phys.*, **66**, 905 (1977).
5) S. Sakanoue and M. Endo, 42nd National Meeting of the Chemical Society of Japan, Sendai, September 1980, Abstr. p. 138.

Identification and Quantification of Poly(oxyethylene) Alkyl Ether Nonionic Surfactants in River Water at Trace Levels by Field Desorption Mass Spectrometry

Hiroaki SHIRAISHI,* Akira OTSUKI, and Keiichiro FUWA

Department of Chemistry and Physics, National Institute for Environmental Studies, Yatabe, Ibaraki 305

(Received January 8, 1981)

Field desorption mass spectrometry (FDMS) was applied to the identification and quantification of poly(oxyethylene) alkyl ethers in natural waters at trace levels. The FD mass spectrum of poly(oxyethylene) (POE) derivatives, which produce $(M+H)^+$, $(M+\text{cation})^+$, and cluster ions of the type $(M_1+M_2+H)^+$, was mainly affected by emitter current, amount of sample loading, and the presence of metal salts. POE alkyl ethers were extracted from water by means of XAD-4 resin adsorption or solvent extraction under nitrogen bubbling, and determined by FDMS using tetradeuterioocta(oxyethylene) dodecyl ether as an internal standard. Sample sizes from 10^{-6} to 10^{-8} g are suitable for the quantification of POE alkyl ethers. The mole ratio of POE methyl-substituted undecyl ethers to POE dodecyl ethers was estimated by comparison with the FD mass spectra of the HPLC fractions of the extract.

Although gas chromatograph-mass spectrometry (GCMS) has successfully been applied for identification and quantification of organic pollutants in natural waters, relatively high molecular weight pollutants, which could not be determined by GCMS, remain to be analyzed. Therefore, field desorption mass spectrometry (FDMS), which is one of the most useful tools for identifying and quantifying relatively high molecular weight and thermally labile organic compounds, is being applied to the analysis of environmental samples.[1]

Use of poly(oxyethylene) (POE) derivatives nonionic surfactants in place of anionic surfactants is increasing because of their high biodegradability and low toxity in aquatic environment. Though some colorimetric determinations of POE derivatives were reported,[2,3] they have rarely been applied to the analysis of environmental samples. The reasons may be limitations of the colorimetric methods, such as the lack of selectivity and the dependence of color development upon the degree of polymerization of ethylene oxide (EO). Jones and Nickless reported that the macroreticular resin Amberlite XAD-4 was a useful adsorbent for the separation of POE derivatives from water,[4] but they could not determine individual components in environmental samples by means of UV, IR, and NMR analysis even after a long clean-up procedure.[5]

In the preceding paper, we developed a method for concentration and quantification of poly(oxyethylene) alkylphenyl ethers in water by high pressure liquid chromatograph (HPLC) with UV detector; FDMS was applied to confirm the presence of these compounds in the HPLC fractions.[6] POE alkyl ethers, however, could not be determined by this method, because they have no UV absorption. This paper describes how POE alkyl ethers in water can easily be determined by FDMS using a stable isotope labeled internal standard, and shows that the ratio of POE alkyl ethers having normal alkyl groups to those having branched alkyl groups can be estimated by HPLC-FDMS.

Experimental

Apparatus. Mass spectrometry was performed on a JEOL JMS-O1SG double focusing mass spectrometer with a combined field desorption/field ionization/electron impact ion source, connected to a JMS-2000 mass data analysis system (Japan Electric and Optics Laboratory). The FD emitter used was a 10 μm tungsten wire with carbon needles grown at high temperature.[7] An anode potential of 10 kV and a cathode potential of −3 kV were applied. Emitter current was increased linearly by use of an emitter current programmer.[8] The sample was loaded on the emitter by the microsyringe technique.[9] FD mass spectra were obtained by integration of each individual FD mass spectrum, which was measured by repetitive magnet scanning at an interval of 10 s.

HPLC was performed on a Waters ALC/GPC-204 liquid chromatograph equiped with two 6000 A pumps, a model 660 solvent programmer, a U6K injector, a model 400 UV detector operating at 254 nm, and a model R-400 RI detector.

Materials. Methanol (Mallincklodt) was nanograde and pure water was prepared by passing distilled water through a Milli-Q system(Millipore). POE dodecyl ethers and monodisperse POE dodecyl ethers (degree of polymerization; $m=1$ to 8), supplied by Daiichi Seiyaku Co., Ltd. and Tokyo Kasei Co., Ltd. respectively, were used.

Poly(oxyethylene) hexadecyl ethers were prepared from hexadecyl bromide and sodium salt of polyethylene glycol 400.

Nona- and deca(oxyethylene) dodecyl ether were prepared from dodecyl bromide and sodium salt of nona- and decaethylene glycol,[10] respectively.

Octa(oxyethylene)-$\alpha,\alpha,\beta,\beta$-$d_4$ dodecyl ether was prepared from the sodium salt of ethylene-d_4 glycol (E. Merck, G. F. R.) and 1-chloro-3,6,9,12,15,18,21-heptaoxatritriacontane, which was synthesized from thionyl chloride and hepta(oxyethylene) dodecyl ether.

These POE derivatives were purified by column chromatography (silica gel/ethyl acetate:acetone:water=55:35:10) before use. Other chemicals of the highest grades from Wako Pure Chemical Ind., Ltd. were used without further purification.

HPLC Separation of POE Alkyl Ethers. UV Detection: To the 200 μL solution of POE alkyl ethers (1 mg/mL ethyl acetate), freshly distilled 2 mg 3,5-dinitrobenzoyl chloride and a small piece of magnesium turnings were added, and the mixture was heated at 80 °C for 15 min. After cooling, 1 μL of the reaction mixture was injected. The mobile phase was methanol–water at the flow rate 2 mL/min and stationary phase was Radialpak C_{18} (Waters). The percentage of methanol in water was increased from 50% to

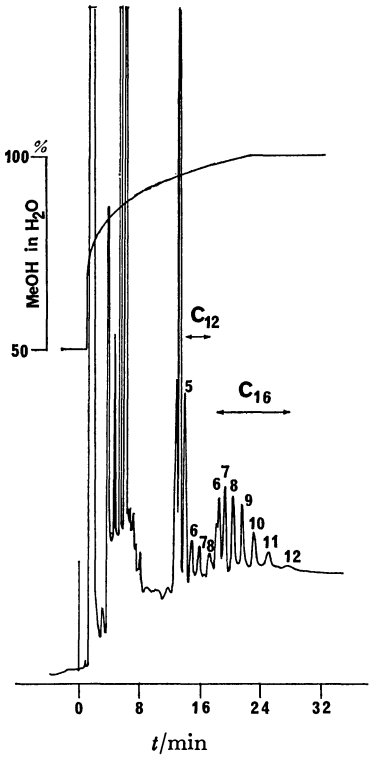

Fig. 1. Typical liquid chromatogram of the separation of POE dodecyl and hexadecyl ethers. Flow rate of 2 mL/min.

100% on the mode 2 in the Waters programmer, as shown in Fig. 1. The programming time was 20 min.

Refractive Index Detection: The Mobile phase was methanol–water (80:20) at the flow rate 1 mL/min and the stationary phase was μ-Bondapak C_{18} (Waters). A sample was dissolved in methanol–water (80:20) and injected. Fractions were collected as needed. All experiments were done at ambient temperature.

Extraction from Water. XAD-4 Adsorption:[5] The resin (5 g) was mixed with acetone and the slurry was packed into the column (55 cm long × 1.1 cm I.D.). A 50 mL volume of acetone–hexane (1:1), 50 mL acetone, 100 mL ethanol, and another 50 mL acetone were passed through the column in order to wash the resin. Before use, the resin was washed with 1 L distilled water and then the water sample was passed through the column at 20 mL/min. POE derivatives were eluted by 70 mL acetone and concentrated by a rotary evaporator.

Solvent Extraction:[11] One hundred grams of sodium chloride were added to a 1 L water sample in a concentration apparatus by gas bubbling. After the sodium chloride was dissolved, 100 mL ethyl acetate was added to the sample and nitrogen saturated with ethyl acetate was bubbled through a glass filter from the bottom of the apparatus for 10 min. The upper layer was separated, and the same extraction procedure was repeated twice. The extracts were combined and concentrated by the rotary evaporator.

Results and Discussion

Concentration from Water and Separation by HPLC. Sensitive determination of POE alkyl ethers by HPLC would be possible, if they can be transformed into derivatives which have UV absorption. Thus, 3,5-dinitrobenzoyl chloride was used as a UV labeling agent. Figure 1 shows a typical liquid chromatogram of the separation of POE dodecyl ethers and POE hexadecyl ethers by gradient elution. Each peak was assigned in comparison with the retention time of standard monodisperse POE dodecyl and hexadecyl ethers. Though separation was performed according to both the carbon atom number in each alkyl group and the number of EO units, POE dodecyl ethers with less than five EO units had the same retention time and those with more than nine EO units were overlapped with POE hexadecyl ethers.

XAD-4 resin adsorption[5] and solvent extraction under nitrogen bubbling,[11] reported as excellent methods for concentration of POE derivatives, were reexamined. It was found that nearly quantitative recovery was achieved at 100 μg/L levels by both methods.

FDMS of POE Derivatives. The FD mass spectrum of POE derivatives was mainly affected by the emitter current, amount of sample on emitter, and the presence of metal salts. Table 1 a) shows characteristics of typical FD mass spectrum of poly(oxyethylene) dodecyl ethers. In contrast to the case of POE alkylphenyl ethers, protonated molecular ions $(M+H)^+$ were found in every 44 mass units corresponding to an EO unit. It was observed that lower molecular weight components of the mixture were desorbed at lower emitter currents. This temperature dependence of the spectrum was identical to that of POE alkylphenyl ethers.[8] Table 1 b) shows the effect of the amount of sample loading. When a large amount (*ca.* 10 μg) was loaded on the emitter, intense cluster ions, corresponding to two molecules plus one proton $(M_1+M_2+H)^+$, were observed. Intensities of these cluster ions were also dependent on the emitter current. At higher emitter currents (*ca.* 15 mA), these cluster ions were not observed. Table 1 c) shows the effect of the presence of metal salts. When an FD mass spectrum of POE alkyl ethers was measured after several measurements of salts of sodium, another series of ions due to attachment of sodium ions to molecules was observed. The same FD mass spectrum was obtained by pretreatment of emitter or sample by salts of sodium. FD mass spectrum of POE dodecyl ethers, which was concentrated from 10% sodium chloride solution by the solvent extraction method, shows sodium-ion-attached molecular ions $(M+Na)^+$, potassium-ion-attached molecular ions $(M+K)^+$ with weaker intensity, and no $(M+H)^+$ ion (Table 1 d).

The fact that ammonium, lithium, potassium rubidium, caesium, and silver could be involved in the ionization by cation attachment (Fig. 2) suggested that ionization of POE alkylphenyl ethers by cation attachment can occur, though they formed molecular ions under usual conditions. This was confirmed by the experiment using these salts. Especially in the case of the sample extracted from natural water by solvent extraction, $(M+Na)^+$ ions were major ion species.[12] Since many kinds of cations can be involved in ionization, special care has to be taken to prevent erroneous identification. For example, $(M+H)^+$ ions of POE hexadecyl ethers and (M+

TABLE 1.

a) Typical FD mass spectrum of POE dodecyl ether; 1 μg was loaded on new emitter.

m/z	319	363	407	451	495	539	583	627	671	715	759	769	803	813
Rel. int.	28	59	63	77	90	100	96	92	68	60	40	13	26	15
Assignment[a)]	H3	H4	H5	H6	H7	H8	H9	H10	H11	H12	H13	C9	H14	C10

b) FD mass spectrum of POE dodecyl ether; 10 μg was loaded on emitter.

m/z	275	319	363	407	451	495	539	561	583	593	605
Rel. int.	31	71	100	86	70	61	64	14	43	19	13
Assignment[a)]	H2	H3	H4	H5	H6	H7	H8	N8	H9	C5	N9
m/z	627	637	649	671	681	693	715	725	759	769	813
Rel. int.	40	32	13	34	45	14	20	51	13	46	46
Assignment[a)]	H10	C6	N10	H11	C7	N11	H12	C8	H13	C9	C10

c) FD mass spectrum of POE dodecyl ether measured after several measurements of sodium salts.

m/z	319	363	407	451	473	495	517	539	561	583
Rel. int.	19	30	41	59	10	73	23	97	49	100
Assignment[a)]	H3	H4	H5	H6	N6	H7	N7	H8	N8	H9
m/z	605	627	649	671	693	715	737	759	781	813
Rel. int.	54	70	59	67	42	49	35	32	22	22
Assignment[a)]	N9	H10	N10	H11	N11	H12	N12	H13	N13	H14

d) FD mass spectrum of POE dodecyl ether, which was extracted from the 10% sodium chloride solution.

m/z	429	477	517	561	577	605	621	649	665	693	709	737	781	825
Rel. int.	19	61	81	100	13	85	13	66	12	48	10	30	14	11
Assingment[a)]	N5	N6	N7	N8	K8	N9	K9	N10	K10	N11	K11	N12	K12	N13

a) Hm, Nm, Km, and Cm mean types of ions: *i.e.* $(M+H)^+$, $(M+Na)^+$, $(M+K)^+$, and $(M_1+M_2+H)^+$, respectively (m indicates total number of EO units in the ions).

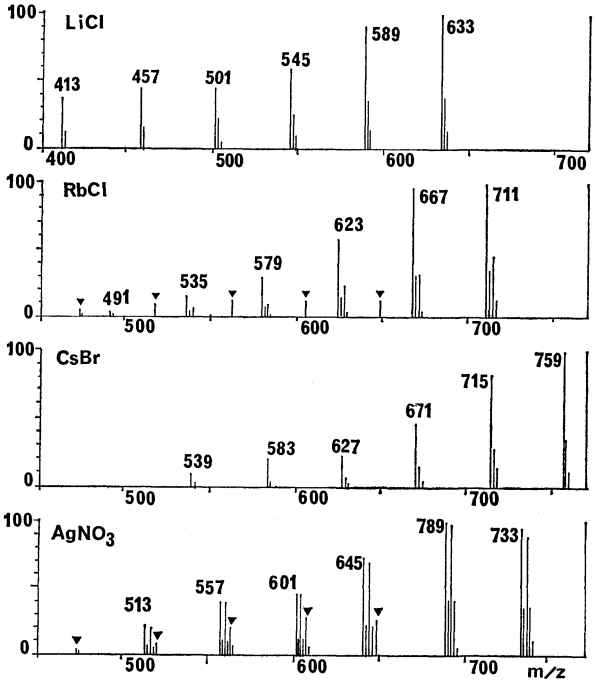

Fig. 2. FD mass spectra of equimolar mixture of monodisperse POE dodecyl ether (degree of polymerization of 5 to 10) which were measured in the presence of LiCl, RbCl, CsBr, and $AgNO_3$. ▼ indicates $(M+Na)^+$ ions of POE dodecyl ether.

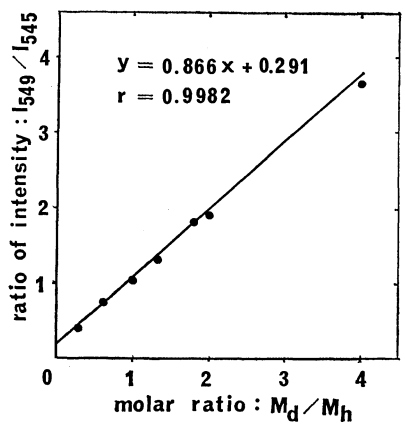

Fig. 3. Calibration curve for determination of octa(oxyethylene) dodecyl ether.

$Na)^+$ ions of POE nonylphenyl ethers gave the same *m/z* values. However, the two spectra could be easily differentiated by the addition of another cation source, *e.g.*, when lithium chloride was added to samples, one can observe $(M+H)^+$ ions and $(M+Na)^+$ ions to shift by 6 *m/z* to higher and 16 *m/z* to lower *m/z* values, respectively.

Use of a stable-isotope-labeled internal standard is essential in quantitative FDMS, because of fluctuations of ion current. In this study, tetradeuterioocta(oxyethylene) dodecyl ether was systhesized and used as

Table 2. Relative intensity of quasi-molecular ions $(M+Li)^+$ in the FD mass spectrum of an equimolar mixture of monodisperse poly-(oxyethylene) dodecyl ether (m=5—10)

m	5	6	7	8	9	10
Rel. int.	59.1	76.9	83.0	100.0	120.6	97.1
SD	11	8.3	4.6	—	5.8	10
CV %	19	11	5.6	—	4.8	10

an internal standard. The calibration curve for octa-(oxyethylene) dodecyl ether was constructed by use of intensities of $(M+Li)^+$ ions (m/z 545 and 549) and a good linear relationship between the amount of sample and added internal standard was obtained (Fig. 3). The reproducibility of the relative intensity of m/z 545 to m/z 549 in each FD mass spectrum was within ±3% at 10^{-7} g levels. Optimum sample size for determination was from $3—5\times10^{-6}$ g to 10^{-8} g.

The integrated FD mass spectrum was used for determination of each component which had a different degree of polymerization of EO. The relative sensitivities of each component to octa(oxyethylene) dodecyl ether were determined by using intensities of $(M+Li)^+$ ions in the integrated FD mass spectrum of an equimolar mixture of monodisperse POE dodecyl ether, which was measured in the presence of lithium nitrate. Table 2 summarizes the realtive intensities of $(M+Li)^+$ ions, its standard deviations (SD), and variation coefficient (CV). m/z 545 (degree of polymerization; m=8) was chosen as a base peak in order to determine the relative sensitivities to this ion. Since the relative sensitivity may reflect the ionization efficiency of each compound by lithium ion attachment, the fact that the sensitivity increases with increase in the number of EO units suggests that the EO unit plays an important role in ionization.

Application. Figure 4 shows FD mass spectrum of mixture extracted from urban stream water by XAD-4 resin adsorption. Since lithium chloride was loaded on the emitter together with the extract, $(M+Li)^+$ ions of POE compounds should be observed. The peak at m/z 549 is due to the added internal standard. Seven series of the ion peaks with differences of 44 mass units were found. The series of the peaks at m/z 1) 415, 459, 503, 547, 591; 2) 443, 487, 531, 575, 619, 663, 707; 3) 413, 457, 501, 545, 589, 633, 677, 721; 4) 427, 471, 515, 559, 603, 647, 691, 735, 779; 5) 441, 485, 529, 573, 617, 661, 705, 749; 6) 469, 513, 557, 601, 645, 689, 733, and 7) 447, 491, 535, 579, 623, 667, 711, 755 may be due to POE 1) nonyl, 2) undecyl, 3) dodecyl, 4) tridecyl, 5) tetradecyl, 6) hexadecyl, and 7) nonylphenyl ethers, respectively. Another series of peaks with difference of 58 mass units at m/z 489, 547, 605, 663, 721, and 779 may be due to $(M+Li)^+$ ions of polypropylene glycol. These identifications were confirmed from the shift of each peak in the FD mass spectrum of the same sample, which was measured in the presence of sodium citrate.

Further confirmation was tried by HPLC fractionation followed by FDMS. Figure 5 shows the liquid

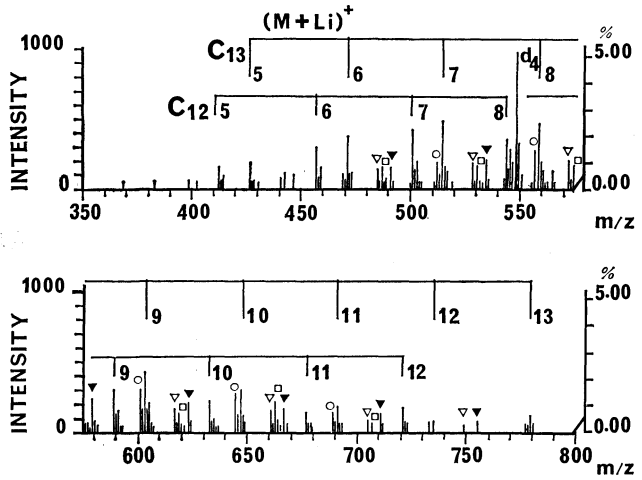

Fig. 4. FD mass spectrum of the extracted organic compounds from 1L polluted stream water. Tetradeuterioocta(oxyethylene) dodecyl ether (16.8 μg) was added as an internal standard. □, ▽, ○, and ▼ indicate $(M+Li)^+$ ions of POE undecyl, tetradecyl, hexadecyl, and nonylphenyl ethers, respectively.

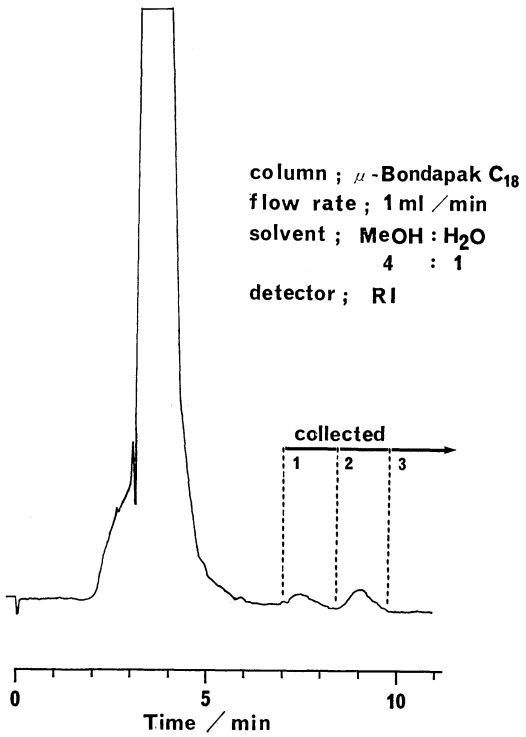

Fig. 5. Liquid chromatogram of the organic compounds extracted from polluted urban stream water.

chromatogram of the extract containing tetradeuterioocta(oxyethylene) dodecyl ether as the internal standard. After the large peak of unidentified compounds was eluted, fractions containing POE alkyl ethers were collected. Although POE alkyl ethers could hardly be detected by the RI detector, the presence of POE alkyl ethers was confirmed by FDMS. Figures 6 and 7 show the FD mass spectra of the fraction 1 and 3, respectively. From the analysis of the FD mass spectra, we could determine that fraction 1 contained POE nonylphenyl, dodecyl, and small amount of un-

TABLE 3. CONCENTRATION (μg/L) OF POE-ALKYL AND ALKYLPHENYL ETHERS IN THE POLLUTED STREAM WATER

n	*m*									Total
	5	6	7	8	9	10	11	12	13	
8				1.3						1.3
9		1.7	2.7	3.1	3.6	2.9	2.1			16.1
10						4.0				4.0
11		2.1	3.1	2.9	2.6	2.4	4.5	1.5		19.2
12	3.4	5.5	7.8	6.2	4.6	4.6	2.9	3.9		39.9
13	4.2	7.2	9.2	7.3	6.6	6.4	4.0	1.8	2.8	49.5
14	2.0	2.9	3.9	3.7	2.7	3.1	2.0			20.4
16	2.7	4.0	5.8	5.7	4.6	3.1	1.7			27.5
Nonyl	2.5	3.1	4.3	4.3	3.3	3.6	2.7	1.9		25.5
Total	14.8	26.5	36.8	34.4	28.0	30.1	19.9	9.1	2.8	202.4

n and *m* indicate carbon numbers of alkyl group and numbers of EO units, respectively. Nonyl indicates POE nonylphenyl ether.

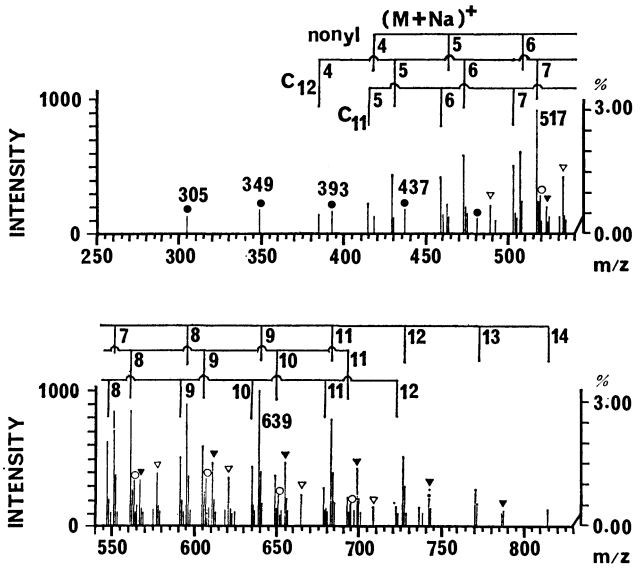

Fig. 6. FD mass spectrum of the fraction 1. ○, ▽, ▼, and ● indicate $(M+K)^+$ ions of POE undecyl, dodecyl, nonylphenyl ethers, and $(M+Na)^+$ ions of polyethylene glycol, respectively.

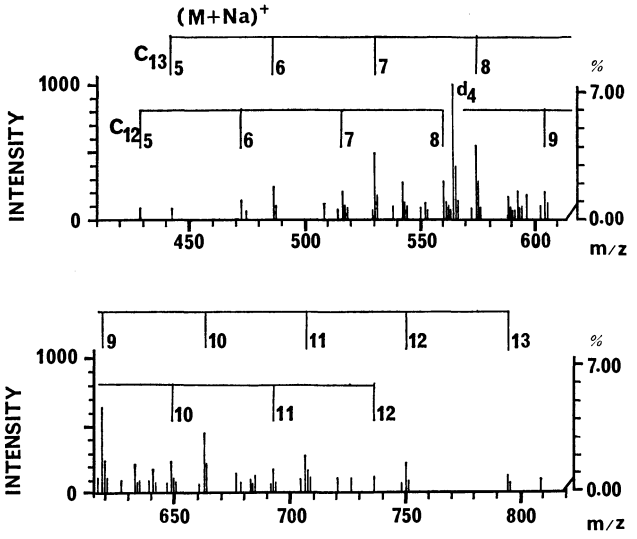

Fig. 7. FD mass spectrum of the fraction 3.

decyl ethers, and that fractions 2 and 3 contained POE dodecyl, tridecyl ethers, and the spiked internal standard. The result means that POE dodecyl ethers were contained in every fraction. In the reversed phase separation, the compounds having alkyl groups are generally eluted according to the number of carbon atoms in each alkyl group, that is, retention time increases with increase in the number of carbon atoms in each alkyl group, but compounds having branched alkyl groups have shorter retention time than those having normal alkyl groups of the same carbon number. This suggests the presence of POE compounds having branched alkyl groups in the extract. Indeed, the spiked internal standard was not found in fraction 1. Since the internal standard has a dodecyl group, the isomers of POE dodecyl ethers found in the fraction 1 may be POE methyl-substituted undecyl ethers, which are usually used as detergents. From the comparison between the relative intensity of *m/z* 545 to *m/z* 549 in fraction 3 and that in the extract (Fig. 4), the mole ratio of POE methyl-substituted undecyl ethers to POE dodecyl ethers was estimated to be 0.2.

The concentration of POE alkyl and alkylphenyl ethers were calculated on the assumption that sensitivities do not depend upon the number of carbon atom in alkyl group, and the total concentration of POE derivatives was determined to be 202 μg/L (Table 3).

The present study has demonstrated that POE alkyl ethers in water at trace levels can be easily determined by FDMS. Cation attachment ionization in FDMS makes selective and sensitive determination of POE derivatives possible. Distinction between normal and branched alkyl group in POE alkyl ethers may become possible by HPLC–FDMS.

References

1) H. D. Beckey, "Principles of Field Ionization and Field Desorption Mass Spectrometry," Pergamon Press, London (1977).

2) L. Favetto, B. Stancher, and F. Tunis, *Analyst*, **105**, 833 (1980).
3) E. G. Brown and T. J. Hayes, *Analyst*, **80**, 755 (1955).
4) A. Otsuki and H. Shiraishi, *Anal. Chem.*, **51**, 2329 (1979).
5) P. Jones and G. Nickless, *J. Chromatogr.*, **156**, 87 (1978).
6) P. Jones and G. Nickless, *J. Chromatogr.*, **156**, 99 (1978).
7) H. D. Beckey, E. Hilt, and H. -R. Schulten, *J. Phys. E: Sci. Instr.*, **6**, 1043 (1973).
8) H. Shiraishi, A. Otsuki, and K. Fuwa, *Bull. Chem. Soc. Jpn.*, **52**, 2903 (1979).
9) H. D. Beckey, A. Heindlichs, and H. U. Winkler, *Int. J. Mass Spectrom. Ion Phys.*, **3**, 9 (1970).
10) R. Fordyce, E. L. Lovell, and H. Hibbert, *J. Am. Chem. Soc.*, **61**, 1905 (1939).
11) R. Wickbolt, *Tenside Detergents*, **9**, 173 (1972).
12) A. Yasuhara, H. Shiraishi, M. Tsuji, and T. Okuno, *Environ. Sci. Technol.*, **15**, 570 (1981).

A Polarographic Study of Bis(benzoylacetonato)nickel(II) in Dimethyl Sulfoxide

Setsuko KUDO,† Akio IWASE,* Iwao MOGI, and Nobuyuki TANAKA††

Department of Chemistry, Faculty of Science, Yamagata University, Koshirakawa-machi, Yamagata 990

††Department of Chemistry, Faculty of Science, Tohoku University, Aoba, Aramaki, Sendai 980

(Received April 10, 1981)

The chemical equilibria of bis(benzoylacetonato)nickel(II) in dimethyl sulfoxide solutions were investigated, mainly by means of d.c. polarography. In 0.05—0.1 mol dm^{-3} $NaClO_4$, TMAP, and TBAP solutions, the following chemical equilibria were found: $Ni(bi\text{-}bzac)_2 \rightleftharpoons Ni(bi\text{-}bzac)(uni\text{-}bzac) \rightleftharpoons Ni(bi\text{-}bzac)^+ \rightleftharpoons Ni(uni\text{-}bzac)^+$ where bi- and uni- are the abbreviations of bidentate and unidentate respectively. The species of $Ni(bi\text{-}bzac)_2$ and $Ni(bi\text{-}bzac)(uni\text{-}bzac)$ comprised 35% and 57% respectively of the total complex of 1 mmol dm^{-3} in a TMAP or TBAP solution, while they accounted for 15% and 77% respectively in a $NaClO_4$ solution. Such a difference in the equilibrium distribution was explained on the basis of the interaction between π electrons of the ligand and cations of the supporting electrolytes. The tris-complex was formed by the addition of excess benzoylacetonate to the complex solution.

In a previous paper,[1] the d.c. polarographic reduction of bis(acetylacetonato)nickel(II) and bis(hexafluoroacetylacetonato)nickel(II) was studied in dimethyl sulfoxide as a solvent. The study led to the conclusion that the dissolved state of bis(β-diketonato)-nickel(II) complexes is dependent on the nature of their ligands; therefore, a systematic study of the complexes with various ligands was required.

In the present paper, a d.c. polarographic study of bis(benzoylacetonato)nickel(II) will provide useful information about the chemical equilibria of the complex in the same solvent. To judge from the conductance and the cryoscopic data, the complex existed predominantly in the monomeric $Ni(bzac)_2 \cdot 2DMSO$ form. However, three or four kinds of species were polarographically observed in the presence of such supporting electrolytes as alkali-metal perchlorates and tetraalkylammonium perchlorates. The coexisting sodium ion significantly influenced the chemical equilibria of bis(benzoylacetonato)nickel(II). The dissolved state of bis(β-diketonato)nickel(II) complexes in nonaqueous solvents thus far reported, except in a few papers,[1,4,26] was confined to that in noncoordinating solvents.[3,18–20] Choplin-Gast and Hugel[20] determined the equilibrium constant of $Ni_3(bzac)_6 \rightleftharpoons 3Ni(bzac)_2$ in dichloromethane by the spectroscopic method: $\log K = -4.7$ at 25 °C.

Experimental

Reagents. The dimethyl sulfoxide (DMSO), nickel(II) perchlorate hexahydrate, tetramethylammonium perchlorate (TMAP), and tetrabutylammonium perchlorate (TBAP) were the same as described in the previous paper.[1] The TBAP was recrystallized from ethanol when necessary. The sodium perchlorate and potassium perchlorate were dried *in vacuo* at 60 to 70 °C for a minimum of 24 h prior to use. The rubidium perchlorate and caesium perchlorate of a 99.9% purity were used.

Bis(benzoylacetonato)nickel(II) monohydrate was prepared by the following procedure. Into 20 cm^3 of an aqueous solution of 2 mmol of nickel(II) acetate ($Ni(CH_3COO)_2 \cdot (H_2O)_4$), a solution of 4 mmol of benzoylacetone (Hbzac) in *ca.* 20 cm^3 of ethanol was added, followed by the addition of *ca.* 10 cm^3 of an aqueous solution containing 7 mmol of sodium acetate ($CH_3COONa \cdot (H_2O)_3$). The mixed solution was then kept for *ca.* 30 min at 50 °C. The product thus precipitated was recrystallized twice from methanol and then dried *in vacuo* at room temperature. Found: C, 59.87; H, 5.05%. Calcd for $C_{20}H_{20}O_5Ni$: C, 60.19; H, 5.05%.

Tetrabutylammonium benzoylacetonate ($Bu_4N(bzac)$) was prepared according to Buchta and Evans.[2] The salt was stored in the dark under nitrogen. Found: C, 76.73; H, 11.19; N, 3.52%. Calcd for $C_{26}H_{45}O_2N$: C, 77.36; H, 11.23; N, 3.47%.

Reagent-grade chemicals were used unless otherwise stated.

Apparatus. The current-potential curves were obtained with a Yanagimoto Voltammetric Analyzer P-1000 and a Watanabe X-Y Recorder WX-4404. The electrolysis cell and other apparatus have been reported previously.[1] Two dropping-mercury electrodes were used. The A electrode had an m value of 0.89_0 mg s^{-1} and a drop time, t_d, of 6.60 s in a deaerated 0.05 mol dm^{-3} TBAP–DMSO solution at -1.0 V *vs.* SCE at a height of the mercury reservoir, h, of 50 cm. The B electrode had an m value of 1.06_2 mg s^{-1} and a t_d value of 6.18 s in a deaerated 0.05 mol dm^{-3} TMAP–DMSO solution at -1.0 V and $h=47$ cm.

In the following sections, the word "current" denotes the mean current.

Procedures. Nickel(II) perchlorate was made to react with tetrabutylammonium benzoylacetonate in deaerated solutions containing 0.05 mol dm^{-3} of the supporting electrolyte at room temperature in the dark overnight (Fig. 3). The reaction of the complex with tetrabutylammonium benzoylacetonate was also carried out under the same conditions (Fig. 2). Unless otherwise stated, the polarographic measurements were made at 25.0±0.2 °C. All the test solutions were deaerated for 30 min with nitrogen gas in a thermostat before measurements.

Results and Discussion

Conductance, Molecular Weight, etc. The molar conductivity of 2 mmol dm^{-3} of bis(benzoylacetonato)-nickel(II) was 0.4 Ω^{-1} cm^2 mol^{-1} at 25 °C. According to the conductance results of DePalma and Arnett,[10] the molar conductivity at an infinite dilution (Λ_0) and the dissociation constant of tetrabutylammonium dibenzoylmethanate were 30.8±1.6 Ω^{-1} cm^2 mol^{-1} and (62±24)×10^{-4} mol dm^{-3} respectively in dimethyl sul-

† Present address: Chemical Laboratories, Yamagata Building Service Co., Ltd., Iizuka-machi, Yamagata 990.

Table 1. Polarographic data for the reduction of $Ni(bzac)_2$, Hbzac, and $Bu_4N(bzac)$ in DMSO

Compound	Supporting electrolyte	($E_{1/2}$ *vs.* SCE)/V	Slope/mV	$\bar{i}_j/(\bar{i}_t)_B$[a]
$Ni(bzac)_2$	0.05 mol dm^{-3} $NaClO_4$	−1.12		0.08
		−1.30		
		−1.63	115	0.77
	0.05 mol dm^{-3} TMAP	−1.21	45	0.03
		−1.38		0.05
		−1.63	110	0.57
		−2.16	63	0.35
	0.05 mol dm^{-3} TBAP	−1.24		0.08
		−1.36		
		ca. −1.7 (Max.)		0.57
		−2.24	86	0.35
		−2.68		
Hbzac	0.05 mol dm^{-3} TBAP	−1.54	70	
		−2.44	63	
		−2.70		
$Bu_4N(bzac)$	0.05 mol dm^{-3} TBAP	−2.65		

a) The $\bar{i}_j/(\bar{i}_t)_B$ ratios for $Ni(bzac)_2$ were obtained at the concentration of 1 mmol dm^{-3} under the controlled drop time of 2.0 s, where the $(\bar{i}_t)_B$ represents the $\bar{i}_t$ in a TMAP or TBAP solution. The meanings of $\bar{i}_j$ and $\bar{i}_t$ are shown in Fig. 1.

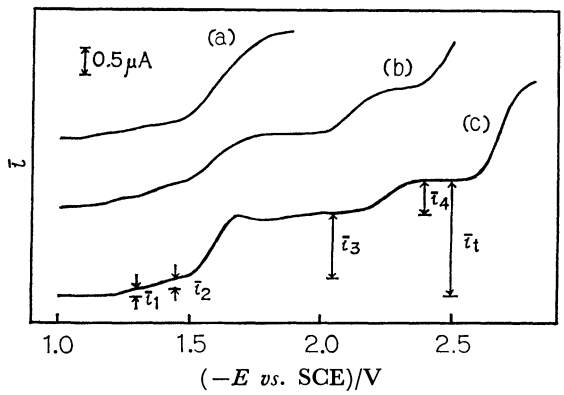

Fig. 1. Polarograms of 1 mmol dm^{-3} $Ni(bzac)_2$ in DMSO solutions. Supporting electrolyte: (a) $NaClO_4$, (b) TMAP, (c) TBAP. Each in 0.05 mol dm^{-3}. With the DME (A).

foxide at 25 °C. The investigators of the conductance of quaternary ammonium halides in dimethyl sulfoxide have reported that these salts are almost entirely dissociated[15,16] and that the Λ_0 values are 32—43 Ω^{-1} cm^2 mol^{-1} at 25 °C.[15] In our preliminary experiments, the Λ_0 value of bis(hexafluoroacetylacetonato)nickel(II) was 38 Ω^{-1} cm^2 mol^{-1} at 25 °C: This complex was considerably dossociated into the 1:1 electrolyte, but the Λ *vs.* $C^{1/2}$ plot did not follow quantitatively the Onsager relation,[17] where Λ and C denote the molar conductivity and the concentration respectively. It therefore seems likely that the degree of dissociation of 2 mmol dm^{-3} of bis(benzoylacetonato)nickel(II) is less than 2%. The cryoscopic data of the complex agreed with the molecular weight of $Ni(bzac)_2 \cdot 2DMSO$. Thus, the complex probably exists in the predominant form of the monomeric bis-complex in the absence of electrolytes. The spectroscopic data indicate that the complex has a hexacoordinate octahedral structure.[3,4]

Polarographic Behavior. Some typical polarograms of the complex are shown in Fig. 1. The polarographic data of the complex, benzoylacetone, and tetrabutylammonium benzoylacetonate are summarized in Table 1. The complex gave three waves in the presence of sodium perchlorate as the supporting electrolyte. On the other hand, it gave four waves in a solution of tetramethylammonium perchlorate and five waves in one of tetrabutylammonium perchlorate. These polarograms were not appreciably affected by the change in the concentration of each supporting electrolyte in the range of 0.05—0.1 mol dm^{-3}.

The fifth wave at the most negative potential in a TBAP solution corresponds to the reduction of benzoylacetonate, judging from a comparison of the two half-wave potentials (Table 1).

For the complex of 1 mmol dm^{-3}, the total limiting current in a $NaClO_4$ solution was 85% of that at −2.30 V in a TMAP solution and of that at −2.45 V in a TBAP solution, under a controlled drop time. The latter currents were approximately equal to that of 1 mmol dm^{-3} of nickel(II) perchlorate. The diffusion coefficient for the solvated nickel(II) ion obtained from the Ilkovič equation was $2.3_3 \times 10^{-6}$ cm^2 s^{-1} in all the supporting-electrolyte solutions of 0.05 mol dm^{-3}. It is known that the coordinated water of nickel(II) perchlorate hexahydrate is replaced by dimethyl sulfoxide in this solvent.[5] The controlled-potential coulometry at −2.30 V in a TMAP solution gave the number of electrons participating in the electrode processes, n, of 2. All the waves, except for the wave at the most negative potential in a TBAP solution, are considered to be due to the reduction of nickel(II).

The first limiting current ($\bar{i}_1$) at the least negative potential was diffusion-controlled: it was proportional to $h^{1/2}$. The i_2/i_3 ratio was dependent on the drop time, indicating that the second wave included a kinetic current; however, all the $\bar{i}_j/\bar{i}_t$ ratios were constant at $t_d \leqslant 2.0$ s, where $j=1$—4. These results were con-

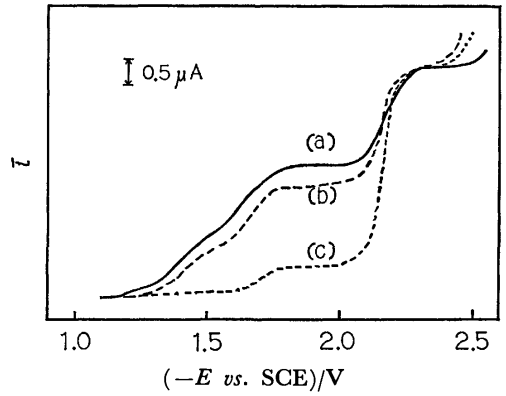

Fig. 2. Effect of addition of free ligand to 2 mmol dm^{-3} $Ni(bzac)_2$ in 0.05 mol dm^{-3} TMAP–DMSO solutions. Concn (mmol dm^{-3}) of $Bu_4N(bzac)$ added: (a) 0, (b) 0.5, (c) 3.0. With the DME (A).

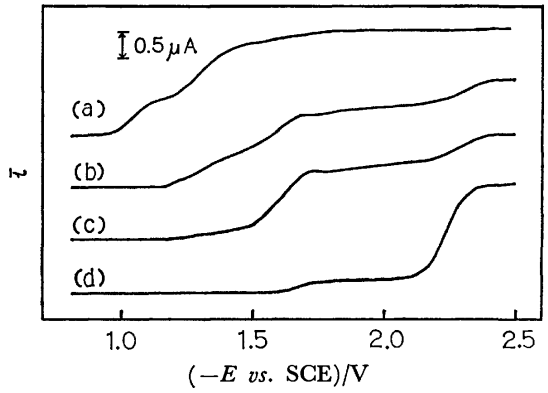

Fig. 3. Polarograms of bzac-complexes of nickel(II) in DMSO solutions containing the ligand in different concentrations. 1 mmol dm^{-3} $Ni(ClO_4)_2$, 0.05 mol dm^{-3} TBAP. Concn (mmol dm^{-3}) of Bu_4N-(bzac): (a) 0.7, (b) 1.5, (c) 2.0, (d) 5.0. t_d=2.0 s. With the DME (A).

firmed in all the supporting-electrolyte solutions. The i_t was proportional to the concentration of the complex in solutions containing TMAP or TBAP. None of the i_f/i_t ratios were affected by the addition of 0.14 mol dm^{-3} of water.

The effect of the addition of free benzoylacetonate to the complex is shown in Fig. 2. The two waves at less negative potentials disappeared successively as the concentration of benzoylacetonate increased, and the low wave at *ca.* −1.7 V and the high wave at −2.16 V finally remained. Evidently, the chemical equilibria exist between the species giving each reduction wave in Fig. 2, judging from the above findings. The limiting current at the least negative potential in Figs. 2(a) and (c) was diffusion-controlled, while that in Fig. 2(b) was partially kinetic-controlled. The constant diffusion-controlled i_t values for the three curves suggest that the diffusion coefficients of all the species are almost equal; the i_f/i_t ratio obtained under the controlled drop time of $t_d \leqslant 2.0$ s in a TMAP or TBAP solution in Fig. 1 represents the molar fraction for each species.

No wave in the least negative potential in Fig. 1 is due to the reduction of the free nickel ion, because it is reduced at *ca.* −1.0 V.[5,6] Figure 3 shows the polarograms measured after the reaction of 1 mmol dm^{-3} of nickel(II) perchlorate with tetrabutylammonium benzoylacetonate in various concentrations. In Fig. 3 (a), the two waves at less negative potentials correspond to the reduction of the main species, which are the nickel ion and the mono-complex. The first two waves in Figs. 1 (a)—(c) appear, judging from a comparison of the half-wave potentials of Curves (a) and (c) in Fig. 3, to be due to the mono-complex reduction. This was confirmed by the plot of (i_1+i_2) *vs.* bzac/Ni mole-ratio, where each (i_1+i_2) value was the diffusion-current obtained under the controlled drop time of 1.0 s. Provided that the first and the second waves, the third wave, and the fourth wave of Curve (c) in Fig. 3 come from the reduction of $Ni(bzac)^+$, $Ni(bzac)_2$, and $Ni(bzac)_3^-$ respectively, the total concentration of the ligand bonded to the nickel ion comes to be higher than that actually contained in the solution; thus, this assumption can not be accepted. Further, the i_3/i_4 ratio was constant in Figs. 3(a)—(c). It is, therefore, reasonable to consider that the complex behaves as a mixture of $Ni(bzac)^+$ and $Ni(bzac)_2$ in the supporting-electrolyte solution. Octahedral complexes involving unsymmetrical β-diketonates and unidentate ligands of the $M(AB)_2X_2$ type possess five possible geometrical isomers, three with the two X ligands *cis* to one another, and two with the two X ligands *trans* to each other.[7] In view of the known structure of $Ni(acac)_2 \cdot 2H_2O$,[3] the latter isomers may be present for $Ni(bzac)_2 \cdot 2DMSO$. Even if these isomers exist in the solution, however, they are not responsible for the third and the fourth waves in Fig. 1, because bis(dibenzoylmethanato)nickel(II) involving symmetrical β-diketonates also gave four polarographic waves due to the reduction of nickel(II). Consequently, the possible assignments for the four waves in a TMAP or TBAP solution are as follows:

$$\begin{array}{ccc} Ni(uni\text{-}bzac)^+ & \rightleftharpoons & Ni(bi\text{-}bzac)^+ \rightleftharpoons \\ \downarrow 2e & & \downarrow 2e \\ \text{1st wave} & & \text{2nd wave} \end{array}$$

$$\begin{array}{ccc} Ni(bi\text{-}bzac)(uni\text{-}bzac) & \rightleftharpoons & Ni(bi\text{-}bzac)_2 \\ \downarrow 2e & & \downarrow 2e \\ \text{3rd wave} & & \text{4th wave} \end{array}$$

where uni- and bi- are the abbreviations of unidentate and bidentate respectively. The second wave includes the kinetic current due to the preceding reaction, $Ni(bi\text{-}bzac)(uni\text{-}bzac) \rightleftharpoons Ni(bi\text{-}bzac)^+$. As will be shown below in Fig. 5, the temperature effect on the i_f and i_t values is consistent with the above conclusion. In a $NaClO_4$ solution, the existence of $Ni(bi\text{-}bzac)_2$ of 15% is presumed for the total complex of 1 mmol dm^{-3} from a comparison of the i_t in this solution with that in a TMAP or TBAP solution, though the wave of its species can not observed because of the overlap with that of the sodium ion. In accord with the general expectations, the kinetic nature of the second wave suggests that the rate of the dissociation of Ni(bi-

bzac)(uni-bzac) is faster than that of Ni(bi-bzac)$_2$.

The three waves at less negative potentials were little observed in the solution containing 0.5 mmol dm^{-3} Ni(bzac)$_2$, 25 mmol dm^{-3} Bu_4N(bzac), and 0.05 mol dm^{-3} TBAP. Further, the i_1/i_2 ratio decreased by the addition of benzoylacetonate to the complex under the controlled drop time of $t_d \leqslant 2.0$ s. These findings and Fig. 3 suggest that there are several paths for the reaction of nickel ions with benzoylacetonate, as is shown in the following scheme:

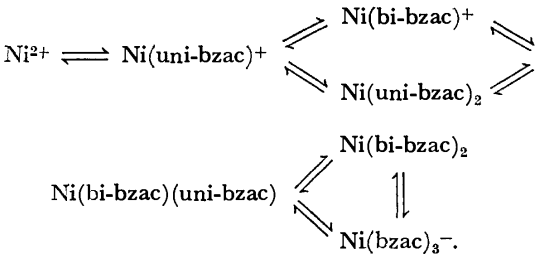

With an increase in the concentration of tetrabutylammonium benzoylacetonate added to a solution of nickel ions, the above equilibria shifted to the right. In the curves of (b) and (c) in Fig. 2, and in the curve of (d) in Fig. 3, the formation of the tris-complex is apparent as a consequence of the mass-action law; however, it is unknown polarographically whether or not Ni(bzac)$_3^-$ is electroactive at the fourth wave. The several species would likely be formed for Ni(bzac)$_3^-$ in the bulk of the solution. Though the quantitative treatment of the equilibrium distribution in Fig. 3 is a very interesting subject, it is really complicated. At the present stage, the accurate evaluation of the free-ligand concentration is also difficult in the presence of a large excess of electrolytes. Generally, β-diketones themselves have been used as the ligands for the determination of the formation constants of their metal complexes.[21-23] This method can not be applied in the present work, because the species of Ni(bi-bzac)(uni-bzac) and Ni(bi-bzac)$_2$ are reduced at more negative potentials than the first wave of benzoylacetone, which is considered to come from the hydrogen reduction of the enol form[2,24] (see Table 1). This is the reason for the use of tetrabutylammonium benzoylacetonate. The formation constants of the nickel(II) complex with benzoylacetonate anion have been determined only in 75 vol% dioxane–25 vol% water at 15, 25, and 40 °C: $\log K_1=9.13$ and $\log K_2=7.76$ at 25 °C.[25] In this paper, the only change in the equilibrium distribution is shown in the complex concentration range of 0.5—5 mmol dm^{-3} in the presence of 0.05 mol dm^{-3} TMAP (Fig. 4). A higher dissociation of Ni(bi-bzac)$_2$ to Ni(bi-bzac)(uni-bzac) attendant upon a decrease in the total complex concentration was found, but the molar fractions for Ni(uni-bzac)$^+$ and Ni(bi-bzac)$^+$ were constant within the range of experimental error. The total molar fraction of Ni(uni-bzac)$^+$ and Ni(bi-bzac)$^+$, 0.08, in the solutions containing the electrolyte is higher than would be expected on the basis of the conductance, indicating the electrolyte effect on the dissociation of the bis-complex to the mono-complex.

In the concentration of the supporting electrolyte

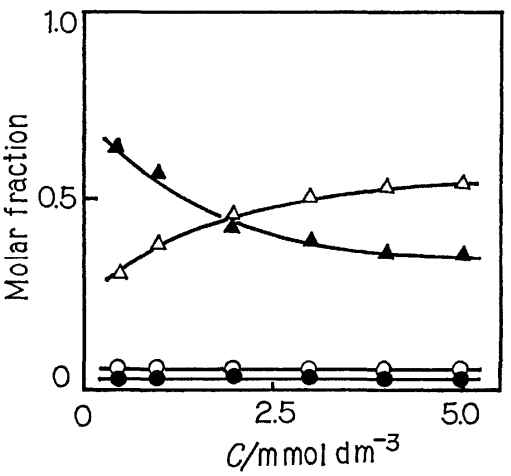

Fig. 4. Equilibrium distribution of four nickel(II) species present in 0.05 mol dm^{-3} TMAP–DMSO solutions containing Ni(bzac)$_2$ in different concentrations. (●) Ni(uni-bzac)$^+$, (○) Ni(bi-bzac)$^+$, (▲) Ni(bi-bzac)(uni-bzac), (△) Ni(bi-bzac)$_2$.

Table 2. Effect of sodium-ion concentration on the $\bar{i}_j/(\bar{i}_t)_B$ ratios

$NaClO_4$ (mol dm^{-3})[a]	$(\bar{i}_1+\bar{i}_2)/(\bar{i}_t)_B$[b]	$\bar{i}_3/(\bar{i}_t)_B$[b]
0.010	0.08	0.65
0.025	0.08	0.74
0.050	0.08	0.77

a) The total concentration of the supporting electrolyte was adjusted to 0.050 mol dm^{-3} with TBAP. b) See Table 1.

of 0.05 mol dm^{-3}, the species of Ni(bi-bzac)(uni-bzac) comprised 57% of the total complex of 1 mmol dm^{-3} in a TMAP or TBAP solution, while its species formed 77% in a $NaClO_4$ solution (Table 1). It should be noted that the concentration of Ni(bi-bzac)(uni-bzac) is high in a $NaClO_4$ solution. The complex gave three waves in each supporting-electrolyte solution—in 0.05 mol dm^{-3} portions of $KClO_4$, $RbClO_4$, and $CsClO_4$, where each i_t was roughly equal to $(i_1+i_2+i_3)$ at −2.00 V in a TBAP solution. In these solutions, the distribution of the species is similar to that in a TMAP or TBAP solution: the waves for Ni(bi-bzac)$_2$ could not be observed because of overlap with those of potassium, rubidium, and caesium ions. The $\bar{i}_3/(\bar{i}_t)_B$ ratio, *i.e.*, the molar fraction of Ni(bi-bzac)(uni-bzac), increased with an increase in the concentration of sodium perchlorate, as is shown in Table 2, where $(\bar{i}_t)_B$ denotes the $\bar{i}_t$ in a TMAP or TBAP solution. Apparently, the sodium ion is related to the dissociation of Ni(bi-bzac)$_2$ to Ni(bi-bzac)(uni-bzac). Probably the cations in the solutions cause the decrease in the π delocalization in the ligand, thereby labilizing the complex; the sodium ion is considered to be the most effective among the cations used here. This cationic effect will be reported on in detail in the polarographic studies of the nickel(II) complexes with 2-thenoyltrifluoroacetonate, 2-furoyltrifluoroacetonate, and benzoyltrifluoroacetonate anions in the following paper. The sodium ion may con-

tribute to the chelation with free benzoylacetonate anion as well as with several β-diketonate anions:[8-12]

$$\mathrm{Ni(bi\text{-}bzac)_2} \rightleftharpoons \mathrm{Ni(bi\text{-}bzac)(uni\text{-}bzac)} \rightleftharpoons \mathrm{Ni(bi\text{-}bzac)^+ + bzac^-}$$

$$\downarrow\uparrow \qquad \downarrow\uparrow \mathrm{Na^+}$$

$$\mathrm{Ni(uni\text{-}bzac)^+} \qquad \mathrm{Na(bzac)}$$

However, as can be seen in Table 1, the $(i_1+i_2)/(i_t)_B$ ratio, *i.e.*, the molar fraction of the mono-complex, in a $NaClO_4$ solution is equal to that in a TMAP or TBAP solution; thus, it seems unlikely that the chelation of the sodium ion by benzoylacetonate anion plays an appreciable role in the equilibrium distribution of Ni(II)-complexes.

Murray *et al.*[27] found that the reduction potentials of a number of metal acetylacetonates in acetonitrile are shifted to less negative potentials by the addition of lithium perchlorate to tetraethylammonium perchlorate as the supporting electrolyte. Their detailed studies of $Fe(acac)_3$ led to the conclusion that this effect is caused by a coordinative relaxation reaction of the $Fe(acac)_3^-$ reduction product, where an acetylacetonate ligand is transferred to the lithium ion. The interaction between reduction products and the lithium ion has been studied for complexes of the $[ML_n]^\circ$ type in such nonaqueous solvents as acetonitrile[28] and *N*,*N*-dimethylformamide.[29,30] According to the results of Gritzner *et al.*,[31] the reduction product, $Mn(acac)_3^-$, of $Mn(acac)_3$ forms ion-pairs with lithium, sodium, and potassium ions in various solvents. There was no difference between the half-wave potential of the third wave in a $NaClO_4$ solution and that in a TMAP solution in the present work (Table 1). In the case of a completely irreversible electron transfer, however, special experimental approaches will be required to discuss the above interaction.[27]

The temperature effect on the i_1 and i_t of the complex was examined in a TMAP solution (Fig. 5). The species of $Ni(bi\text{-}bzac)_2$ and $Ni(bi\text{-}bzac)(uni\text{-}bzac)$ were readily dissociated in the bulk of the solution with an increase in the temperature, and there was a marked tendency for the latter. Little dissociation of $Ni(bi\text{-}bzac)^+$ to $Ni(uni\text{-}bzac)^+$ was observed, judging from the temperature coefficient of *ca.* 1.6% K^{-1} for i_1.

A study was not made as to whether or not $Ni(bi\text{-}bzac)_2$ is somewhat dissociated to $Ni(bi\text{-}bzac)(uni\text{-}bzac)$ in the absence of the electrolyte. No useful information from the electronic spectra can be expected concerning such a study. However, the observation of such species involving a unidentate ligand as $Ni(bi\text{-}bzac)(uni\text{-}bzac)$ and $Ni(uni\text{-}bzac)^+$ in the present work is of interest in connection with the intermediates in the various reaction mechanisms of metal complexes in solution. The high basicity of dimethyl sulfoxide[13,14] might contribute to the stabilization of those species. Further, the properties of the central metal seem to be very important for the stabilization, but the solution to this problem will require a systematic study of β-diketonate complexes with various metals.

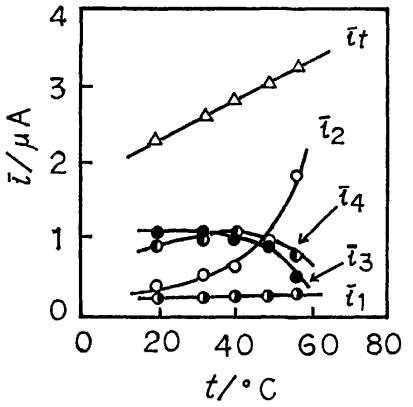

Fig. 5. Effect of temperature on the limiting currents of 1 mmol dm^{-3} $Ni(bzac)_2$ in 0.05 mol dm^{-3} TMAP–DMSO solution. With the DME (B).

References

1) S. Kudo, A. Iwase, and N. Tanaka, *Bull. Chem. Soc. Jpn.*, **54**, 207 (1981).
2) R. C. Buchta and D. H. Evans, *Anal. Chem.*, **40**, 2181 (1968).
3) J. P. Fackler, Jr., "Progress in Inorganic Chemistry," ed by F. A. Cotton, Interscience Publishers, John Wiley & Sons (1966), Vol. 7, p. 407.
4) F. A. Cotton and J. P. Fackler, Jr., *J. Am. Chem. Soc.*, **83**, 2818 (1961).
5) I. M. Kolthoff and I. B. Reddy, *J. Electrochem. Soc.*, **108**, 980 (1961).
6) G. J. Janz and R. P. T. Tomkins, "Nonaqueous Electrolytes Handbook," Academic Press, New York (1973), Vol. 2, p. 495.
7) R. C. Mehrotra, R. Bohra, and D. P. Gaur, "Metal β-Diketonates and Allied Derivatives," Academic Press, New York (1978), p. 94.
8) L. G. Van Uitert, W. C. Fernelius, and B. E. Douglas, *J. Am. Chem. Soc.*, **75**, 455 (1953).
9) M. Raban, E. A. Noe, and G. Yamamoto, *J. Am. Chem. Soc.*, **99**, 6527 (1977).
10) V. M. DePalma and E. M. Arnett, *J. Am. Chem. Soc.*, **100**, 3514 (1978).
11) M. Raban and D. P. Haritos, *J. Am. Chem. Soc.*, **101**, 5178 (1979).
12) W. C. Fernelius and L. G. Van Uitert, *Acta Chem. Scand.* **8**, 1726 (1954).
13) R. S. Drago, B. Wayland, and R. L. Carlson, *J. Am. Chem. Soc.*, **85**, 3125 (1963).
14) W. L. Reynolds, "Progress in Inorganic Chemistry," ed by S. J. Lippard, Interscience Publishers, John Wiley & Sons, New York (1970), Vol. 12, p. 16.
15) D. E. Arrington and E. Griswald, *J. Phys. Chem.*, **74**, 123 (1970).
16) J. S. Jha, S. Singh, and R. Gopal, *Bull. Chem. Soc. Jpn.*, **48**, 2782 (1975).
17) L. Onsager, *Physik. Z.*, **28**, 277 (1927).
18) Ref. 7, p. 126.
19) I. Yoshida, H. Kobayashi, and K. Ueno, *Bull. Chem. Soc. Jpn.*, **45**, 1411 (1972).
20) A Choplin-Gast and R. Hugel, *J. Inorg. Nucl. Chem.*, **34**, 2595 (1972).
21) L. G. Van Uitert, W. C. Fernelius, and B. E. Douglas, *J. Am. Chem. Soc.*, **75**, 457 (1953).
22) T. Inoue, *Rev. Polarogr. (Kyoto)*, **16**, 30 (1969).
23) B. Ćosović, M. Verži, and M. Branica, *J. Electroanal.*

Chem., **22**, 325 (1969).
24) T. E. Neal and R. W. Murray, *Anal. Chem.*, **42**, 1654 (1970).
25) D. Perrin, "Stability Constants of Metal-Ion Complexes, Part B," IUPAC Chemical Data Series (1979), No. 22, p. 719.
26) H. Imai, S. Inoue, and T. Shiraiwa, *Nippon Kagaku Kaishi*, **1980**, 1114.
27) R. W. Murray and L. K. Hiller, Jr., *Anal. Chem.*, **39**, 1221 (1967).
28) J. N. Burnett, L. K. Hiller, Jr., and R. W. Murray, *J. Electrochem. Soc.*, **117**, 1026 (1970).
29) S. Misumi, M. Aihara, and Y. Nonaka, *Bull. Chem. Soc. Jpn.*, **43**, 774 (1970).
30) M. Aihara and S. Misumi, *Memoirs of the Faculty of Science, Kyushu University, Ser. C*, **8**, 203 (1973).
31) G. Gritzner, H. Murauer, and V. Gutmann, *J. Electroanal. Chem.*, **101**, 185 (1979).

Isomerism of the Metal Complexes Containing Multidentate Ligands. IX. Structure of the *meso* Isomer of [Co(hexaen)]$^{3+}$ (hexaen=1,4,7,10,13,16-Hexaazacyclooctadecane)

Yuzo Yoshikawa,* Koshiro Toriumi,† Tasuku Ito,† and Hideo Yamatera

Department of Chemistry, Faculty of Science, Nagoya University, Chikusa-ku, Nagoya 464

†*Division of Applied Molecular Science, Institute for Molecular Science, Okazaki 444*

(Received May 21, 1981)

The crystal and molecular structure of *meso*-[Co(hexaen)]Cl_3 has been determined by single crystal X-ray diffractometry. The crystals are rhombohedral with space group $R\bar{3}$, $a=9.2976(10)$, $c=16.851(2)$ Å, and $Z=3$. The structure has been refined by least-squares calculations to an R value of 0.021 for 952 observed reflections. The complex ion has S_6 symmetry. The Co–N distance is 1.9966(8) Å and the N–Co–N angle in the chelate ring is 83.62(3)°. The molecular dimensions are in good agreement with those obtained from the conformational analysis.

An octahedral complex of a cyclic hexadentate ligand takes either *meso* or racemic form. Curry and Busch prepared an iron(III) complex with such kind of ligand, 2,16-dimethyl-3,6,9,12,15,21-hexaazabicyclo-[15.3.1]heneicosa-1(21),2,15,17,19-pentaene.[1] However, the complex of the *meso* form was not obtained on account of the rigidity of the ligand. Groth carried out an X-ray analysis on the complex between potassium *p*-toluenesulfonate and 1,4,7,10,13,16-hexaoxacyclooctadecane(18-crown-6).[2] The 18-crown-6 molecule in this compound, as well as those in most complexes of this crown and its derivatives,[3] have roughly S_6 symmetry (*meso* form). However, the crown complexes are labile in solution. It is stereochemically more interesting to investigate inert metal chelates with cyclic hexadentate ligands.

Recently we succeeded in isolating the *meso* isomer of [Co(hexaen)]$^{3+}$ as a minor reaction product, as well as a major product of the racemic one.[4] The conformational analysis of [Co(hexaen)]$^{3+}$ suggested that the *meso* isomer was much more unstable than the racemic one; that is, the calculated energy difference amounts to 15 kJ mol^{-1}. Searle *et al.* prepared the cobalt(III) complex of a very similar hexadentate ligand, 1,4,8,11,15,18-hexaazacycloheneicosane, but did not obtain the *meso* isomer.[5] Thus the title compound is the first example of the *meso* isomer of the inert complex with a cyclic hexadentate ligand.

In this study, the crystal structure of the title compound has been determined.

Experimental

Preparation of the Complex. To half a gram of hexaen·$3H_2SO_4$ suspended in 10 cm^3 of water, 1 cm^3 of concentrated aqueous ammonia was added. The mixture was diluted with water until the total volume of solution was about 500 cm^3. To the mixture was added a solution of 0.3 g of $[Co(H_2O)(NH_3)_5]_2(SO_4)_3\cdot 3H_2O$ in 500 cm^3 of water. The solution was heated and kept at 77 °C for 4 h. After standing overnight, the resulting orange-red solution was allowed to pass through a small column of SP-Sephadex C-25, which adsorbed cationic species. A portion of the mixture was subjected to the chromatographic separation described in a previous paper.[4] The effluents containing the *meso* isomer, which were obtained from several separations, were diluted with water and were adsorbed again by a small column of SP-Sephadex. The column was washed with a large amount of 10^{-2} mol dm^{-3} HCl, and then the complex was eluted with 1.0 mol dm^{-3} HCl. The effluent was evaporated to dryness in a vacuum desiccator over NaOH and P_2O_5. The resulting orange-red crystals were recrystallized from water. Crystals are orange-red square-plates. Found: C, 33.61; H, 7.21; N, 19.90%. Calcd for $C_{12}H_{30}N_6CoCl_3$: C, 34.02; H, 7.14; N, 19.83%. Absorption spectrum; $\bar{\nu}_{max}$/cm^{-1} (log ε), 20830 (2.33).

Table 1. Crystal data

Molecular formula	$C_{12}H_{30}N_6CoCl_3$
Formula weight	423.70
Crystal system	Rhombohedral
Cell dimensions (Hexagonal setting)	
	$a=9.2976(10)$ Å
	$c=16.851(2)$ Å
	$U=1261.6(3)$ Å^3
Space group	$R\bar{3}$
Z	3
Density	$D_m=1.67_7$ g cm^{-3}
	$D_x=1.67_3$ g cm^{-3}
μ(Mo $K\alpha$)	15.38 cm^{-1}

Physical Measurements. Electronic absorption and ^{13}C NMR spectra were recorded on a UNION SM-401 spectrophotometer and a JEOL JNM-FX60 spectrometer operating at 15.04 MHz, respectively.

X-Ray Structure Determination. A spherically shaped crystal of 0.43 mm in diameter was used for the X-ray experiment. Intensity data were collected up to $2\theta=65°$ on a Rigaku automated four-circle diffractometer AFC-5 with graphite-monochromatized Mo $K\alpha$ radiation, the θ-2θ scan technique being employed. 961 independent reflections with $|F_o|>3\sigma(|F_o|)$ were observed, and used in the structure analysis. No correction was made for absorption and extinction effect. The accurate cell dimensions were determined by a least-squares method from the θ values for 21 reflections in the range of $26°<2\theta<30°$ measured on the diffractometer. The crystallographic data are listed in Table 1.

The structure was solved by the heavy atom method and refined by the block-diagonal least-squares method with anisotropic temperature factors for non-hydrogen atoms. The scattering factors and the anomalous scattering corrections for non-hydrogen atoms were taken from International Tables for X-Ray Crystallography.[6] For hydrogen atoms, the values given by Stewart, Davidson, and Simpson

Table 2. Fractional coordinates, with their estimated standard deviations, multiplied by 10^5 for the non-hydrogen atoms and 10^3 for the hydrogen atoms

Atom	x	y	z	B or B_{eq}/Å^2 a)
Co	0	0	0	1.0
Cl(1)	0	0	50000	2.5
Cl(2)	0	0	22293(3)	2.0
N	21287(10)	11952(10)	6033(5)	1.4
C(1)	29154(12)	1391(13)	5946(6)	1.8
C(2)	32874(12)	28799(12)	2559(6)	1.8
H(1)	196(2)	125(2)	109(1)	1.7(0.2)
H(2)	229(2)	−75(2)	93(1)	2.0(0.3)
H(3)	409(2)	84(2)	76(1)	3.2(0.4)
H(4)	434(2)	307(2)	30(1)	2.1(0.3)
H(5)	318(2)	372(2)	56(1)	1.4(0.2)

a) The equivalent isotropic temperature factors as defined by W. C. Hamilton (*Acta Crystallogr.*, **12**, 609 (1959)).

were used.[7] The weighting scheme in the least-squares calculation was taken as $w=[\sigma_{count}^2+(0.015|F_o|)^2]^{-1}$. The R and R_w values were 0.024 and 0.040 for 961 independent reflections. The results at this stage revealed that nine strong, low-angle reflections (110, 300, 330, 011, 102, 003, 204, 014, $\bar{3}44$) were seriously affected by secondary extinction effect. The least-squares calculation for 952 intensities except for these nine reflections gave $R=0.021$ and $R_w=0.038$.

The final atomic parameters are listed in Table 2.[8] All the calculations were performed on a HITAC M-200H computer at the Computer Center of the Institute for Molecular Science with Universal Crystallographic Computational Program System UNICS III.[9]

Results and Discussion

Figure 1 shows a perspective drawing of *meso*-[Co(hexaen)]$^{3+}$ along the threefold axis. The bond lengths and angles are listed in Table 3. The cobalt atom lies at a crystallographic special position $\bar{3}$ and the complex ion has S_6 symmetry. The macrocyclic ligand, hexaen, is composed of six equivalent $-NHCH_2-CH_2-$ units. Six five-membered chelate rings are equivalent. This compound has very interesting structure containing both Δ- and Λ-[Co(en)$_3$]$^{3+}$ type chelate rings and was named "Cobalt Spinner" in a previous paper,[4] as it is suggestive of an old-fashioned spinning wheel which rotates about its threefold axis. The two methylene groups in each chelate ring are crystallographically independent. The five-membered ring adopts the unsymmetrical gauche conformation. The differences in the structural parameters of the two methylene carbon atoms are given in Table 3.

A Dreiding molecular model shows that the *meso* isomer may have a highly symmetrical and rigid D_{3d} structure with twelve equivalent methylene carbons. The D_{3d} structure, however, contains non-bonded hydrogen-hydrogen pairs which may have significantly large repulsive interactions. The conformational analysis of this compound, which was initiated from the

Table 3. Molecular geometries obtained from the X-ray and conformational analyses

Bond distances (l/Å) and angles (ϕ/°) with their e.s.d.'s.	X-Ray	Conformational analysis
Co–N	1.9966(8)	1.9925
N–C(1)	1.489(2)	1.489
N–C(2)	1.507(1)	1.503
C(1)–C(2)	1.515(2)	1.515
N–Co–N	83.62(4)	85.01
Co–N–C(1)	107.76(6)	106.88
Co–N–C(2)	110.49(8)	110.99
N–C(1)–C(2)	107.16(8)	108.22
N–C(2)–C(1)	108.73(7)	109.70
C(1)–N–C(2)	110.49(7)	109.38
Torsional angles (ϕ/°) with their e.s.d.'s.		
Co–N–C(1)–C(2)	−48.1(1)	−46.3
Co–N–C(2)–C(1)	−20.1(1)	−18.9
C(2)–N–C(1)–C(2)	74.6(1)	73.7
C(1)–N–C(2)–C(1)	100.1(1)	98.6
N–C(2)–C(1)–N	44.0(1)	42.8
Distances (l/Å) from the plane defined by Co, N, and N′ atoms.		
C(1)	0.704(1)	0.689
C(2)	0.127(1)	0.136

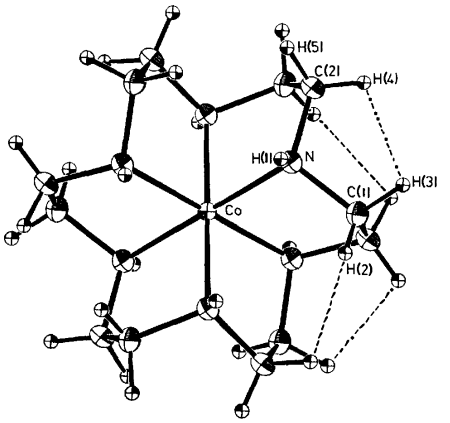

Fig. 1. A perspective drawing of the complex ion, *meso*-[Co(hexaen)]$^{3+}$, viewed down its threefold axis.

D_{3d} structure using the same parameters as in a previous report,[10] lead to the S_6 structure.[4] In Table 3, the molecular dimensions obtained from the conformational analysis are compared with those found in the X-ray crystal structure analysis. The agreement between them is excellent. In the energy minimized structure, the Co–N bond distance (1.993 Å) is longer than the initial one (1.970 Å) and almost the same as that found in the crystal (1.997(1) Å). The elongated coordination-bond distances are reflected on the red-shift of the absorption maximum as compared with that of [Co(en)$_3$]$^{3+}$. The two N–C

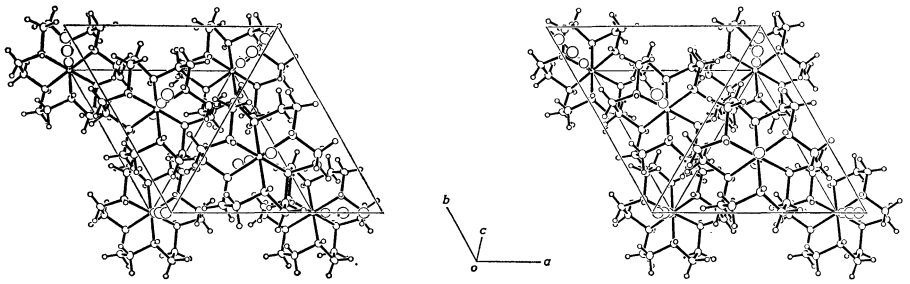

Fig. 2. Stereoscopic view of the crystal structure along the c axis.

Table 4. Relevant interatomic distances (*l*/Å) outside the complex ion with their e.s.d.'s

Cl(2)···N	3.234(1)
Cl(2)···H(1)	2.49(2)
Cl(2)···H(5)	2.82(2)
Cl(1)···H(3)	2.81(2)

bond distances in each chelate ring differ in such a way that large hydrogen-hydrogen repulsions inherent in the initial D_{3d} structure can be avoided. The relaxed hydrogen-hydrogen interactions are depicted as dotted lines in Fig. 1 (H(3)···H(4), 2.11(3) Å; H(2)···H(5), 2.11(2) Å). Although the two methylene carbons are crystallographically independent, they are equivalent in solution. The ^{13}C NMR spectrum of this compound shows only one resonance signal in an aqueous solution.[4] It is highly probable that the *meso* isomer undergoes a rapid interconversion between the two equivalent S_6 structures, resulting in an average structure of D_{3d} symmetry.

Figure 2 shows a stereoscopic view of the crystal structure. Close contact pairs in the crystal are listed in Table 4. All the chloride ions and the cobalt atoms are aligned on the same crystallographic threefold axis; Co and Cl(1) sit on the $\bar{3}$ special positions and Cl(2) on 3. The Cl(2) ion approaches a complex cation and makes hydrogen-bonds with three equivalent NH groups (N–H···Cl(2), 3.235(1) Å).

This work was supported by the Joint Studies Program (1979—1980) of the Institute for Molecular Science.

References

1) J. D. Curry and D. H. Busch, *J. Am. Chem. Soc.*, **86**, 592 (1964).
2) P. Groth, *Acta Chem. Scand.*, **25**, 3189 (1971).
3) a) D. L. Ward, H. S. Brown, and L. R. Sousa, *Acta Crystallogr., Sect. B*, **33**, 3537 (1977); b) D. Hlavatá, J. Hašek, and K. Huml, *Acta Crystallogr., Sect. B*, **34**, 416 (1978) and references cited therein.
4) Y. Yoshikawa, *Chem. Lett.*, **1978**, 109.
5) R. W. Hay, B Jeragh, S. F. Lincoln, and G. H. Searle, *Inorg. Nucl. Chem. Lett.*, **14**, 435 (1978).
6) "International Tables for X-Ray Crystallography," Kynoch Press, Birmingham (1974), Vol. IV.
7) R. F. Stewart, E. R. Davidson, and W. T. Simpson, *J. Chem. Phys.*, **42**, 3175 (1965).
8) Tables of anisotropic thermal parameters and a list of the observed and calculated structure factors are kept in the office of the Chemical Society of Japan (Document No. 8225).
9) T. Sakurai and K. Kobayashi, *Rikagaku Kenkyusho Hokoku (Rep. Inst. Phys. Chem. Res.)*, **55**, 69 (1979).
10) Y. Yoshikawa, *Bull. Chem. Soc. Jpn.*, **49**, 159 (1976).

Theoretical Signal-to-noise Ratio and Resolution in Ion-cyclotron-resonance Spectroscopy

Chikara Amano

Department of Engineering Physics, The University of Electro-Communications, 1-5-1 Chofugaoka, Chofu, Tokyo 182

(Received February 25, 1981)

A comparison is made theoretically of the signal-to-noise (S/N) ratio between the usual slow-sweep or the continuous-wave method and the pulsed Fourier-transform (FT) method in ion-cyclotron-resonance spectroscopy. Expressions of the maximum S/N ratio, as characterized by experimental parameters, are given in concrete form for both methods. Based on these expressions, it is shown that the FT method has a Fellgett S/N advantage when the resolution of a measurement is selected so as to be nearly equal to the true linewidth. A tradeoff between the S/N ratio and the resolution is discussed, and a possible reconciliation is suggested of inconsistent statements on a relation between the S/N and the resolution in the literature.

A physical system of spectroscopic interest can be considered to be an example of linear systems when the amplitude of excitation is small. According to the theory of linear systems, a spectrum of spectroscopy corresponds to what is called either a "system function" or "frequency response". There are several methods to obtain the system function.[1,2] One of them is the continuous-wave (CW) method, in which the amplitude and phase of a response are measured by sweeping frequencies of excitation. The name "frequency response" arose from this. Another one is the impulse-excitation method, in which the system function is obtained through the Fourier transformation of the response to a unit impulse excitation. The stochastic excitation method has also been proposed; in it the system function is evaluated through the Fourier transformation of the cross-correlation function of excitation and responce.

Of the many branches of spectroscopy, nuclear magnetic resonance (NMR), more specifically high-resolution NMR, which is a part of radio-frequency spectroscopy, is one of the most suitable for testing above ideas. This might be partly due to its spectroscopic characteristic that whole resonance lines concentrate within a narrow frequency range compared to the carrier frequencies, thus making it feasible to excite and detect a number of resonance lines at once. In NMR, of course, the CW method was employed first. Long after that, the impulse excitation method was applied by Ernst and Anderson, who noted that the method had an S/N advantage over the usual CW method.[3] An S/N gain of about one order was observed within a given experimental time. Spectrometers based on this principle are called "pulsed Fourier-transform spectrometers", and, because of their essential high sensitivity, they are now widely adopted in chemical and biological measurements. Soon after the advent of the FT method, the stochastic excitation method was also introduced; with pseudo-noise excitation, a similar S/N gain was obtained.[4,5] Meanwhile, in biological measurements a technique was required with which any portion of the whole spectrum could be excited and, at the same time, the S/N was high. The rapid scan or the correlation method was such a technique, in which excitation frequencies are swept fast linearly to time.[6,7] This may be considered to be another form of excitation for acquiring the system function.

The three relatively new methods have the common advantages over the CW method of a short observation time and, in consequence, a high sensitivity. These advantages essentially constitute a Fellgett advantage, which results from the simultaneous excitation and simultaneous detection of all spectral elements.[8] The Fellgett advantage may be described as follows. In spectroscopy, the frequency and amplitude of each frequency component are measured with a certain accuracy. The accuracy in frequency measurement defines the resolution. It is evident that it takes about $1/\Delta f$ to measure the frequency of a wave with an accuracy of Δf. This is a manifestation of the uncertainty principle between energy and time.[9] Thus, it takes $1/\Delta f$ to record one element of a spectrum with a resolution width of Δf. In the CW method, all the spectral elements are measured one by one, while in the other three methods they are obtained all at once. The former is a sequential method, while the latter three are simultaneous methods. The number of elements is $F/\Delta f$, where F is the whole spectral range of interest. Therefore, for the sequential method, the time required to record the whole spectrum is $F/(\Delta f)^2$. The band-width of noise superimposed on a spectral element is given by Δf. For the simultaneous method, on the other hand, the measurement time is only $1/\Delta f$, which is shorter by a factor of $(F/\Delta f)^{-1}$ than that for the sequential method. The band-width of noise is given again by Δf, though the band-width of the physical filter actually employed is F. Thus, S/N ratios are identical for the two methods if the magnitudes of the signals are assumed to be the same. Since S/N is improved as a square root of the measurement time[10], it is now evident that a Fellgett S/N gain of $(F/\Delta f)^{1/2}$ is obtained by the use of the simultaneous method. For radio-frequency spectroscopy, in which a coherent monochromatic excitation source is easily available, it is unclear why the sequential method is inefficient for utilizing signal energy, while it is evident for the infrared spectroscopy, in which only a small portion of the signal energy is utilized at one time by the use of a monochromator, the other big portion being wasted on the jaws of a slit, as Fellgett himself noted.

The pulsed-FT and rapid-scan methods have, in recent years, also been applied to ion cyclotron resonance (ICR), one branch of radio-frequency spec-

troscopy.[11,12] Besides the Fellgett advantage, the FT method as applied to ICR has an additional advantage of high resolution, which results essentially from the long observing time made possible by the use of ion-trapping cells.[13,14] Partly, however, it results from the characteristic of the FT method that the excitation period of ion motion is short; theoretically, high resolution may also be feasible for the CW method but experimentally it would be difficult since a very small amplitude of excitation is required. It was discussed by Marshall and Comisarow, by the use of analogy to optical multichannel spectrometers, how FT ICR has the Fellgett advantage.[15] There remains, however, some features to be clarified. First, in order to obtain the full Fellgett S/N gain it is necessary that the magnitude of a free decaying signal be the same as the signal magnitude for the CW method. This is not obvious, since the FT method utilizes transient responses, while the CW method treats steady-state responses. The second problem concerns noise levels. In the FT method, the band-width of a physical filter allowed is F, far broader than the band-width of the low-pass filter employed in the CW method. This may lead to an S/N disadvantage. Since a spectrum is obtained through the Fourier transformation of a time-domain signal, noise is also subjected to transformation, thus causing a frequency-domain noise. Third, it was stated by Marshall that there is a trade-off between the S/N and the resolution in the FT method.[16] More recently, however, a manuscript reporting contrary results has appeared.[14] In view of this situations, the present author felt that it was necessary to discuss S/N and resolution for the FT and the CW methods on a general basis. The ambiguities mentioned above will be made clear in this manuscript by evaluating S/N ratios at several stages involved in actual experiments.

Theoretical

We shall first describe some experimental conditions. The frequency range of a spectrum of interest is denoted by F. The resolution width of a measurement has the usual meaning that the width of a resonance line with a true width narrower than the resolution width may become widened through the measurement to the apparent magnitude of the resolution width; it is denoted by Δf. For the CW method, it is the reciprocal of the time spent to measure one frequency channel, and at the same time it is channel width. By using the scanning time, T_s, it is given thus;

$$\Delta f_{CW} = (F/T_s)^{1/2}. \tag{1}$$

For the FT method, on the other hand, it is given by the reciprocal of the sampling time, T_0, of free decaying (FD) signals:

$$\Delta f_{FT} = 1/T_0 \tag{2}$$

In order to obtain true line shapes determined by physical conditions, the resolution width of a measurement should be much narrower than the width of a resonance curve, $\Delta f_{1/2}$; *i.e.*

$$\Delta f \ll \Delta f_{1/2} \tag{3}$$

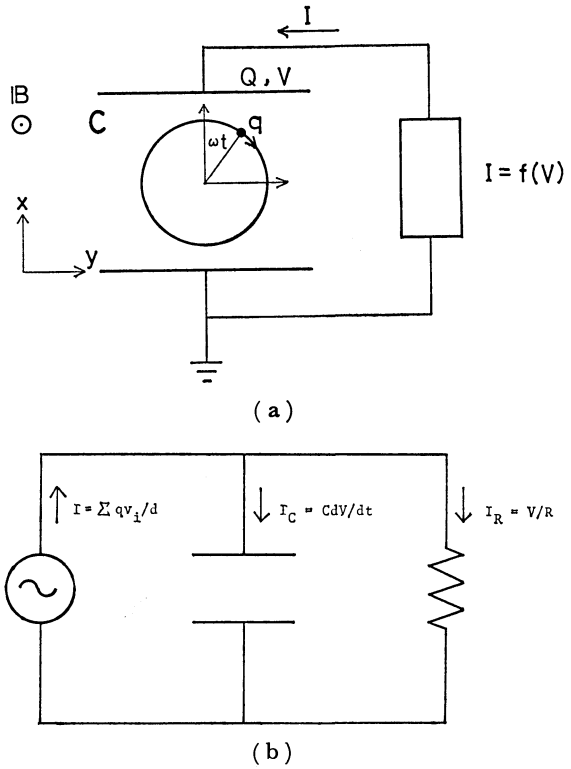

Fig. 1. (a): Moving ions in an ICR cell whose top and bottom plates form a capacitor C. The plates are connected with an outer circuit satisfying a current-voltage relation $I=f(V)$. Magnetic field is along z-axis, (b): current source equivalent to moving ions in a capacitor.

For the FT method, this is equivalent to a condition that the sampling time, T_0, should be much longer than the relaxation time. It should be noted that a so-called high resolution corresponds to a small resolution width in the present paper. The total experimental time is denoted by T_t. We assume ion-trapping cells,[17] since usual FT ICR experiments are done with such cells. With ion-drift cells, FT ICR experiments may be equally feasible, though greater experimental skill would be required. With a short burst of ionizing electrons, N numbers of ions are produced in a cell. If the trapping of ions is perfect, then only one burst of electrons will be sufficient for the whole experiment. Actually, however, the loss of ions from a cell can be significant after some time. Therefore, in order to enhance the S/N ratio through ensemble averaging, N ions must be produced afresh at every cycle after ejecting the ions of the previous cycle. For the CW and FT experiments, we assume a common detector which is equivalent to a pure resistance. It is realized either by the use of a parallel resonant circuit or by the use of a parallel CR combination when the circuit is essentially resistive, *i.e.*, $R \ll 1/j\omega C$. For the sake of simplicity, we shall limit considerations to a situation where only one resonance line is present in the whole spectrum range of interest. However, the following considerations may be easily extended to the case of N resonance lines.

Next, let us evaluate the maximum signal voltage obtained at a detector circuit. According to the signal

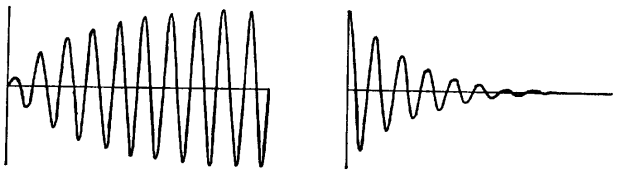

(a) (b)

Fig. 2. (a): Velocity component vertical to cell plates of an ion just at resonance condition for the initial condition $v=0$ at $t=0$ which is subjected to radio-frequency electric field with constant amplitude, (b): velocity component vertical to cell plates of an ion executing free decaying motion under no electric field after irradiation with a radio-frequency pulse.

theory,[18,19] moving ions are equivalent to a constant-current-source shunt across a cell whose top and bottom plates form a capacitor. This situation is illustrated in Fig. 1. There, the strength of the current source is:

$$I = \sum_{i=1}^{N} q_i v_i / d, \tag{4}$$

where q_i is the charge; v_i, a velocity component vertical to the plates and d, the distance between the two plates, and where summation is taken over the N ions in the cell. The velocity of the ion is given by the equation of motion for an average ion:

$$m d\boldsymbol{v}/dt = q(\boldsymbol{E} + \boldsymbol{v} \times \boldsymbol{B}) - mc\boldsymbol{v}, \tag{5}$$

where $\boldsymbol{E}$ is, as usual, the electric field; $\boldsymbol{B}$, the magnetic field, and c in the last term, a damping constant attributable to collisions with neutral atoms and molecules, which is usually called the reduced collision frequency.[20,21] Equations 4 and 5 form a pair of basic equations describing ICR phenomena. Equation 5 can be shown to be equivalent to the equation of motion for a harmonic oscillator with a friction. Thus, solutions of the latter problem are useful in ICR. Let us consider the ion motion under the condition of CW experiments in which ions are subjected to a radio-frequency electric field with a constant amplitude. The velocity of the ion at just the resonance for the initial condition, $v=0$ at $t=0$, is given by the form that increases with a time constant, $1/c$, and becomes nearly constant after some multiples of the time constant. This is shown in Fig. 2(a). The constant value depends on the amplitude of the rf electric field and on the collision frequency. The radius, r, of the ion orbit is limited within $d/2$ by the finite dimensions of a cell. Thus, when $r=d/2$, the ion velocity given by the $v=r\omega_c$ formula has as its maximum value $d\omega_c/2$, where ω_c is the cyclotron angular frequency. Since all ions subjected to an rf electric field rotate with the same radii and phases, Eq. 4 leads to:

$$I_{CW} = Nq\omega_c/2. \tag{6}$$

As we have assumed a pure resistance, R, for a detector, the maximum voltage is given simply as:

$$V_{CW} = Nq\omega_c R/2. \tag{7}$$

For FT experiments, on the other hand, ions are accelerated with a short rf pulse. The velocity of the ions quickly reaches its maximum value, $d\omega_c/2$, and thereafter decays exponentially with a time constant, $1/c$, under no external electric field. This free decaying motion is shown in Fig. 2(b). The maximum amplitude of the FD signal is again given by:

$$V_{FT} = Nq\omega_c/2. \tag{8}$$

It is evident that the maximum signal voltage for the FT method is the same as that for the CW method. We shall henceforth use V_m to denote it. It is worth noting that, for the latter, V_m corresponds to the peak value of a spectrum, while for the former it does not. For the FT method, the peak value of a spectrum is obtained after the Fourier transformation of an FD signal and it is given by the average amplitude of the FD signal. The FD signal decays exponentially with the time, as is illustrated in Fig. 2(b), so that the average amplitude over the sampling time decreases as the sampling time increases. We will see later that this feature leads to a serious tradeoff between the S/N and the resolution.

We shall next evaluate the maximum S/N ratio obtained for the CW method. Among various types of noise, we assume only thermal noise which appears across a resistor in a detector circuit. This is the so-called "detector limited-noise case". Thermal noise has a white power spectrum, and its rms voltage is:

$$\overline{(v_t^2)}^{1/2} = (4kTRf)^{1/2}, \tag{9}$$

where f is the band-width in which noise is measured. This form shows that, in order to get better S/N, the band-width should be made as narrow as possible by the use of a filter. However, the minimum width of a filter employed is determined by the condition that a measurement is carried out with a certain resolution. Considering a measurement by a point-by-point spectrometer, a predecessor of CW spectrometers, we see that the minimum width of a filter is equal to the resolution width, Δf. Then, the rms value of the noise voltage becomes $(4kTR\Delta f)^{1/2}$. In that condition, the signal of amplitude, V_m, can pass through the filter without appreciable decrease. Hence, the maximum S/N ratio for the CW method with the resolution width, Δf, is now obtained thus:

$$(S/N)_{CW} = V_m/(4kTR\Delta f)^{1/2}. \tag{10}$$

It is worth noting that S/N increases in proportion to the square root of the magnitude of resistance, R, since V_m in Eq. 10 is actually proportional to R, as can be seen in Eq. 7. The scanning time for the experiment is evidently given be:

$$T_s = F/(\Delta f)^2. \tag{11}$$

The result of Eq. 10, which has been obtained rather intuitively, can be obtained in a more rigorous fashion by the theory of the matched filter. This approach is the same as Ernst employed in the S/N analysis of FT NMR.[3] The matched filter may be defined to be a filter such as can give the maximum S/N ratio for a signal pulse superimposed with noise.[1] According to the theory of the matched filter, the muximum S/N ratio obtained by the use of the filter is given in the frequency domain as:

$$(S/N)^2 = (1/2\pi)\int_{-\infty}^{\infty} |S(\omega)|^2/N(\omega)d\omega, \quad (12)$$

where $S(\omega)$ is the Fourier transform of a time-domain signal, $s(t)$, and where $N(\omega)$ is power spectrum of the noise. For the white noise assumed here, $N(\omega)=$ const, which we denote by W. Equation 12 then reduces to:

$$(S/N)^2 = (1/2\pi W)\int_{-\infty}^{\infty} |S(\omega)|^2 d\omega. \quad (13)$$

Using Parceval's theorem:

$$(1/2\pi)\int_{-\infty}^{\infty} |S(\omega)|^2 d\omega = \int_{-\infty}^{\infty} s(t)^2 dt, \quad (14)$$

we move to a more convenient time-domain description to obtain:

$$(S/N)^2 = (1/W)\int_{-\infty}^{\infty} s(t)^2 dt. \quad (15)$$

Here, the term $\int_{-\infty}^{\infty} s(t)^2\,dt$ stands for the total energy of a signal, $s(t)$, and W stands for the noise energy per unit of time and unit angular frequency. Since we measure signals over the resistance, R, we must replace Eq. 15 with

$$(S/N)^2 = (1/WR)\int_{-\infty}^{\infty} V_s(t)^2 dt, \quad (16)$$

where $V_s(t)$ is the signal voltage measured over the resistance, R. By specifying the functional form of $V_s(t)$, S/N can thus be evaluated. The signal pulse corresponding to the ICR absorption may be described by the Lorentzian form:

$$V_s(t) = V_m c^2/\{(at - \omega_c)^2 + c^2\}, \quad (17)$$

where a is the scanning rate and is equal to $2\pi F/T_s$. The peak value of this signal is V_m, and the width is $2c$. Although the evaluation of Eq. 16 with this form is possible, we can employ an alternative form without introducing much error since we are deriving general results which depend not on the details of the line shape, but on the width:

$$V_s(t) = \begin{cases} 0 \text{ for } t < (\omega_c - c)/a \\ V_m \text{ for } (\omega_c - c)/a \leqq t \leqq (\omega_c + c)/a \\ 0 \text{ for } (\omega_c + c)/a < t. \end{cases} \quad (18)$$

This is a rectangular pulse with the same height and width as the Lorentzian pulse. The evaluation of Eq. 16 with this form easily gives:

$$(S/N)^2 = V_m^2/4kTR(a/2c). \quad (19)$$

Here, the relation $W=4kT$ has been used. By using $a=2\pi F/T_s$ and $T_s=F/(\Delta f)^2$, Eq. 19 is rewritten to

$$(S/N) = V_m/(4kTR\Delta f')^{1/2}, \quad (20)$$

$$\Delta f' = \pi(\Delta f)^2/c. \quad (21)$$

Here, $\Delta f'$ is the effective band-width of noise, which is determined by the band-width of the matched filter. As we are considering an experiment with a resolution of Δf, we must put the linewidth equal to the resolution width, *i.e.*, $c/\pi=\Delta f$. Then, the band-width of the matched filter also becomes equal to the resolution width. Moreover, S/N is again given by Eq. 10. The band-width of the matched filter and, in consequence, the effective band-width of noise have the following simple meanings. Note that the frequency components of a signal pulse with a certain duration, Δt, are contained mainly in a band-width of about $1/\Delta t$. Therefore, the minimum width of a filter which let pass through the main frequency components of the signal and, at the same time, reject noise is evidently $1/\Delta t$. By applying this result to the signal pulse with a duration of $2c/a$ considered above, the width of the filter is found to be $\pi(\Delta f)^2/c$, which agrees with Eq. 21.

Now let us evaluate the maximum S/N ratio for the FT method. For this case, the band-width of a filter applicable to FD signals is not Δf, but F. Actually, the filter is necessary only to guarantee that FD signals can be sampled at the Nyquist rate. Since usually $F \gg \Delta f$, the S/N of one FD transient is much worth than that of a spectrum of the CW method. As we have denoted the maximum amplitude of an FD signal by V_m, the S/N for one transient is:

$$(S/N)_{IFT} = V_m/(4kTRF)^{1/2}. \quad (22)$$

By requiring the resolution width of a spectrum to be Δf, the measurement time of the FD signals is set as $1/\Delta f$. This is equal to the measurement time of one frequency channel for the CW method with the same resolution width. Let us now consider the Fourier transformation of FD signals and noise. The FD signal is generally described by:

$$V_s(t) = V_m \cos(\omega_c t) \exp(-ct). \quad (23)$$

Assuming a finite sampling time, T_o, we may expand this in a Fourier series:

$$V_s(t) = \sum_{n=0}^{\infty} \{\alpha_n \cos(\omega_n t) + \beta_n \sin(\omega_n t)\}, \quad (24)$$

where $\omega_n=2\pi n/T_o$ and where n is an integer.[22] The Fourier coefficients α_n and β_n are given as usual:

$$\alpha_n = (2/T_o)\int_o^{T_o} V_s(t) \cos(\omega_n t)dt, \quad (25a)$$

$$\beta_n = (2/T_o)\int_o^{T_o} V_s(t) \sin(\omega_n t)dt. \quad (25b)$$

By substituting Eq. 23 into these forms, the absorption component, α_n, and the dispersion component, β_n, are obtained. The absorption gives the Lorentzian line shape of Eq. 17, and its peak amplitude is:

$$\alpha_n(\omega_n = \omega_c) = (V_m/cT_o)\{(1-\exp(-cT_o)\}. \quad (26)$$

This expression quantitatively describes how the peak amplitude varies with the sampling time: The amplitude decreases as the sampling time increases. The Fourier coefficients of noise are similarly obtained by substituting a random variable, $V_n(t)$, into Eq. 25. Then, α_n and β_n also become random variables; their dispersions are given by:

$$\overline{\alpha_n^2} = \overline{\beta_n^2} = N(f_n)/T_o, \quad (27)$$

where $N(f_n)$ is the power spectrum of the noise. This result can be directly derived from the definition of Eq. 25 by assuming that the correlation time of the noise is shorter than the sampling time, T_o.[10] Equation 27 shows that, through Fourier transformation, the band-width of the noise is reduced from F to Δf and that the rms value of the noise decreases with the square root of the reciprocal of the sampling time.

By combining Eqs. 26 and 27, the S/N ratio of a spectrum of the FT method is found to be:

$$(S/N)_{1FT} = (V_m/cT_o)\{1-\exp(-cT_o)\}/(4kTR)^{1/2}. \quad (28)$$

When the resolution of a measurement is nearly equal to the true width of a resonance line, *i.e.*, $1/T_o \sim c$, this reduces to:

$$(S/N)_{1FT} \simeq V_m/(4kTR\Delta f)^{1/2}.$$

This is the same form as Eq. 10 for the CW method. Therefore, when the resolution width of a measurement is nearly equal to the true linewidth, time is saved with the FT method by a factor of $\Delta f/F$. Through ensemble averaging of the coherent addition of $(F/\Delta f)$ samples which are obtained in the time equal to one scanning time, T_s, for the CW method, the S/N ratio can be enhanced by the factor of $(F/\Delta f)^{1/2}$. This is the Fellgett S/N gain. It should be noted, however, that the full Fellgett S/N gain can be obtained only if the condition $\Delta f \simeq c/\pi$ is satisfied. For usual experiments in which an accurate peak amplitude or linewidth is needed, the resolution width should be selected to be much smaller than the linewidth, *i.e.*, $\Delta f \ll c/\pi$. Therefore, the parameter of S/N enhancement is $(F\Delta f)^{1/2}/c$ rather than the Fellgett value $(F/\Delta f)^{1/2}$.

Finally, let us summarize the relations among the S/N, the resolution, the scanning time, and the total experimental time. For the CW method, the S/N and the resolution width are given in terms of the total spectral range of interest, F, and the scanning time, T_s:

$$S/N = V_m/(4kTR\Delta f)^{1/2} = V_m T_s^{1/4}/(4kTR)^{1/2}F^{1/4},$$
$$\Delta f = (F/T_s)^{1/2}.$$

When F is constant, these forms indicate that the S/N increases as the fourth root of the scanning time and that the so-called resolution appropriately given by $1/\Delta f$ also increases in accordance with the square root of the scanning time. Thus, there is no tradeoff between the S/N and the resolution. The fourth root law of the S/N seems curious, since it is inconsistent with the well-known fact that the accuracy of a measurement (S/N) increases with the square root of the measurement time.[10] Note, however, that, for the CW method, the increase in the scanning time inevitably results in an increase in the resolution. If an experiment in which the resolution is kept constant is considered, it can be shown that the usual square-root dependence of the S/N on the total time holds: by assuming a fixed resolution of Δf, the scanning time becomes $F/(\Delta f)^2$ and S/N is given by $\alpha T_s^{1/4}F^{-1/4}$, where α is a constant and is equal to $V_m/(4kTR)^{1/2}$. Consider the total experimental time, T_t, which is much longer than T_s. In that time, (T_t/T_s) times of scans are carried out. Through the ensemble averaging of the scans, the S/N can be enhanced by a factor of $(T_t/T_s)^{1/2}$, and the overall S/N ratio becomes $\alpha T_t^{1/2}T_s^{-1/4}F^{-1/4}$. By the use of the $T_s = F/(\Delta f)^2$ relation, this is rewritten to a convenient form:

$$(S/N)_{nCW} = \alpha T_t^{1/2}(\Delta f)^{1/2}F^{-1/2}, \quad (29)$$

where the subscript n stands for the number of scans and is equal to T_t/T_s. This shows the usual square root dependence of S/N ratio on the measurement time. It is also evident that in a given time, T_t, the tradeoff between the S/N and the resolution exists. This is the usual meaning of the tradeoff. For the FT method, on the other hand, the S/N and the resolution width are geven in terms of only the sampling time, T_o:

$$S/N = (V_m/cT_o^{1/2})\{1-\exp(-cT_o)\}/(4kTR)^{1/2},$$
$$\Delta f = 1/T_o.$$

These forms show that, as T_o increases, the resolution increases and the S/N decreases. This behavior is different from that in the case of the CW method, where both the S/N and the resolution increases with the scanning time. Consider also an experiment in this time where the resolution is held constant. In a given total experimental time, T_t, which is much longer than T_o, (T_t/T_o) times of FD signals are obtained, so that the S/N can be enhanced by a factor of $(T_t/T_o)^{1/2}$. Then, the overall S/N ratio becomes:

$$(S/N)_{nFT} = (V_m T_t^{1/2}\Delta f)\{1-\exp(-cT_o)\}/c(4kTR)^{1/2}, \quad (30)$$

where the subscript n is again the number of transients and is equal to T_t/T_o. This form again indicates the usual square root dependence of the S/N ratio on the total time and the tradeoff between the S/N and the resolution. However, the S/N is proportional to Δf for the FT method, so the tradeoff is more marked than for the CW method, where the S/N is proportional to the square root of Δf.

Discussion

We have shown in the previous section that the tradeoff between the S/N and the resolution is marked for the FT method. Marshall also discussed the tradeoff by considering the FD signals and the noise averaged over the sampling time, though he did not explicitly treat the Fourier transformation of the noise.[16] He obtained an expression describing the behavior of the relative S/N ratio vs. the sampling time, which is essentially the same as Eq. 30 in the present manuscript. More recently, however, a paper has appeared which reported that the tradeoff was not observed and that the S/N and the resolution simultaneously increased with the FT ICR.[14] Note that the simultaneous increase in the S/N and the resolution was obtained by lowering the sample pressure in that paper. The tradeoff should be referred to the method of measurements when the physical states of systems, for example, the sample pressure, are kept constant. It seems misleading to say that the S/N and the resolution simultaneously increase without the tradeoff, since the tradeoff between the S/N and the resolution has wide acceptance in physical measurements.

We shall next consider the so-called exponential filter. The operation of multiplying free-induction decay signals by an exponential function is called either "the exponential filter" or "the matched filter".[3,23,24] It seems inappropriate, however, to call such an operation a "filter" at all, since a filter is what carries out a convolution operation on time-domain signals to lower noise levels. Convolution in the time domain

corresponds to multiplication in the frequency domain. As we have seen in the previous section, through Fourier transformation the effective band-width of noise is reduced to a resolution width which is usually very narrow compared to the original band-width of noise in the time domain, so that the noise level is reduced. The so-called exponential filter carries out, on signals in each domain, the operation opposite to that of usual filters. It is evident that the convolution operation on a spectrum in which the noise level has already been reduced to a resolution width will not effectively improve the S/N ratio without leading to additional line-broadening.

Both ICR and NMR belong to radio-frequency spectroscopy, and there are many similarities between them. It would be useful to utilize such similarities. Among several techniques with the Fellgett advantage, the stochastic excitation method has not yet been applied to ICR. This method was, however, applied to NMR by Ernst, and thereby it was noted that it has a unique feature that the S/N and the resolution can be separately optimized.[4] Since the tradeoff between the S/N and the resolution seems general, however, it would be necessary to examine this method closely. The analysis of the S/N and the resolution in the present paper is general, and it can also be applied to NMR with a little modification. The Fellgett advantage can be obtained in various branches of spectroscopy, since it results essentially from the simultaneous excitation and simultaneous observation of all frequency channels.[25]

The author would like to thank Professor Masao Inoue for reading the manuscript. He also wishes to thank Professor Shizuo Fujiwara for his continuing interest and encouragement. Professor Yoji Arata offered many helpful discussions.

References

1) S. Goldman, "Information Theory," Prentice-Hall, New York (1953).
2) Y. W. Lee, "Statistical Theory of Communications," John Wiley and Sons, New York (1960).
3) R. R. Ernst and W. A. Anderson, *Rev. Sci. Instrum.* **37**, 93 (1966).
4) R. R. Ernst, *J. Magn. Reson.*, **3**, 10 (1970).
5) R. Kaiser, *J. Magn. Reson.*, **3**, 28 (1970).
6) J. Dadok and R. F. Sprecher, *J. Magn. Reson.* **13**, 243 (1974).
7) R. K. Gupta, J. A. Ferretti, and E. D. Becker, *J. Magn. Reson.*, **13**, 275 (1974).
8) P. Fellgett, *J. Phys. Radium*, **19**, 187 (1958).
9) L. Brilloin, "Science and Information Theory," Academic Press, New York (1962).
10) A. van der Ziel, "Noise," Prentice-Hall, New York (1954).
11) M. B. Comisarow and A. G. Marshall, *Chem. Phys. Lett.*, **25**, 282 (1974).
12) R. L. Hunter and R. T. McIver, Jr., *Chem. Phys. Lett.*, **49**, 577 (1977).
13) M. B. Comisarow, "Lecture Notes in Chemistry," H. Hartmann and K. -P. Wanczek, Springer, Berlin (1978), Vol. 7, p. 136.
14) R. L. White, E. B. Ledford, Jr., S. Ghaderi, C. L. Wilkins, and M. L. Gross, *Anal. Chem.*, **52**, 1527 (1980).
15) A. G. Marshall and M. B. Comisarow, *J. Chem. Educ.*, **52**, 639 (1975).
16) A. G. Marshall, *Anal. Chem.* **51**, 1710 (1979).
17) R. T. McIver, Jr., *Rev. Sci. Instrum.*, **41**, 555 (1970).
18) C. Amano, *Int. J. Mass Spectrom. Ion Phys.*, **35**, 47 (1980).
19) M. B. Comisarow, *J. Chem. Phys.*, **69**, 4097 (1978).
20) J. L. Beauchamp, *J. Chem. Phys.*, **46**, 1231 (1967).
21) D. Wobschall, J. R. Graham, and D. P. Malone, *Phys. Rev.*, **131**, 1565 (1963).
22) In the formal Fourier-series expansion of a function, the function is assumed to be periodic and Fourier coefficients which do not correspond to frequencies multiple of the fundamental become zero. Since we do not here assume that $V_s(t)$ is periodic, the Fourier coefficients usually have non-zero values at all frequencies below F (Hz).
23) R. R. Ernst, *Adv. Magn. Reson.*, **2**, 1 (1966).
24) E. D. Becker, J. A. Ferretti, and P. N. Gambhir, *Anal. Chem.*, **51**, 1413 (1979).
25) "Transform Techniques in Chemistry," ed by P. R. Griffiths, Plenum, New York (1978).

 © 1982 The Chemical Society of Japan Bull. Chem. Soc. Jpn., 55, 1431—1436 (1982)

Enthalpy of Oxidation-Reduction for the Ethylenediaminetetraacetatocobaltate(III/II) Couple Relative to the Hydrogen Ion Formation

Kunio Doi

Department of Synthetic Chemistry, Nagoya Institute of Technology, Showa-ku, Nagoya 466

(Received December 17, 1981)

Oxidation of ethylenediaminetetraacetatocobaltate(II) with permanganate ion has been studied spectrophotometrically. The first step in the oxidation is the rapid formation of $[Co^{III}(edta)(H_2O)]^-$, followed by the ring closure reaction of the complex to $[Co^{III}(edta)]^-$. On the basis of the spectrophotometric result, the enthalpies of the reactions, $[Co^{II}(edta)]^{2-}+1/5\ MnO^-_4+8/5\ H^+\rightarrow[Co^{III}(edta)(H_2O)]^-+1/5\ Mn^{2+}+4/5\ H_2O$ and $[Co^{III}(edta)(H_2O)]^-\rightarrow[Co^{III}(edta)]^-+H_2O$, have been determined at 25 °C and at an ionic strength of 0.1 by a direct thermometric titration procedure. The enthalpy of the reaction, $[Co^{III}(edta)]^-+1/2\ H_2\rightleftarrows[Co^{II}(edta)]^{2-}+H^+$, has been calculated by combining them with some other calorimetric data. The thermodynamic functions for formation of the $[Co^{III}(edta)]^-$ complex are estimated from the values so far reported. At 25 °C and at an ionic strength of 0.1 $\Delta G=-242$ kJ mol^{-1}, $\Delta H=-101$ kJ mol^{-1}, and $\Delta S=474$ J mol^{-1} K^{-1}.

The oxidation-reduction potential of a Co^{III}/Co^{II} system is reduced to a large extent in the presence of a complexing agent. It has been reported[1,2] that for the system in the presence of ethylenediaminetetraacetate(edta or L), the electrode reaction at a dropping mercury electrode is expressed by:

$$[Co^{III}(edta)]^- + e \rightleftharpoons [Co^{II}(edta)]^{2-},$$

its redox potential being reversible. The standard redox potential of the system has been determined by several authors[1-5] and furthermore, from information upon the stability constants of the Co(II)-edta complex and the standard redox potential of the $[Co(H_2O)_6]^{3+}/[Co(H_2O)_6]^{2+}$ couple,[6] the stability constant of the Co(III)–edta complex has been calculated. No thermodynamic function, however, has been reported for the $[Co^{III}(edta)]^-/[Co^{II}(edta)]^{2-}$ couple or the formation of the Co(III)–edta complex. Usually, the enthalpies of formation of Co(III) complexes can not be measured directly by a calorimetric method because they are substitution-inert. Cobalt(II) complexes are oxidized rapidly to form the corresponding Co(III) complexes. This is the case also for the edta complexes.[7,8] It is possible to measure heats of such rapid oxidation reactions by a calorimetric method and thus to obtain some information on the difference in enthalpies of the $[Co^{III}(edta)]^-/[Co^{II}(edta)]^{2-}$ couple, and thus, the enthalpy of formation of the Co(III)–edta complex. The present paper provides such information by determining the heat of oxidation of the Co(II)–edta complex with permanganate ion.

Experimental

Materials. The reagents used were Katayama super special grade potassium permanganate, Wako primary standard sodium oxalate, and Ventron iron(II) perchlorate. All other reagents used were of guaranteed reagent grade except for potassium nitrate and sodium perchlorate which were the same as described elsewhere,[9] while $K[Co^{III}(edta)]\cdot 2H_2O$[10] was prepared by the procedure described in the literature. The cobalt content of the complex was determined complexometrically[11] after thermal decomposition of the complex with perchloric and hydrochloric acids, the analytical value being 99.91% of the calculated value.

A stock solution of approximately 0.1 mol dm^{-3} in $Fe(ClO_4)_2$ and 0.2 mol dm^{-3} in $HClO_4$ was prepared and standardized against a 0.02 mol dm^{-3} solution of potassium permanganate, which was standardized against the primary standard sodium oxalate. Stock solutions of other metal ions were standardized by means of EDTA titrations.[11]

Measurements. All the measurements were made at 25.0 °C. The ionic strength of the solutions was maintained at 0.1 with potassium nitrate or sodium perchlorate. A Corning model 12 pH meter was used, the electrode system being standardized with the NBS standard buffer solutions. The pH values were converted to hydrogen ion concentrations by using an activity coefficient value of 0.782.[12]

Visible spectra were recorded on a Nippon Bunko UVIDEC-1 Spectrophotometer or a UNION High Sensitivity Spectrophotometer SM-401 with a thermostated cell compartment.

The titration calorimeter used was the same as described elsewhere.[13] The experimental procedure is described below with the treatment of thermograms. Once thermal equilibrium was established (temperature drift less than 2×10^{-4} °C for 10 min), a titrant (1—3 cm^3) was added to 130.0 cm^3 of a solution at a constant rate of 1.11 cm^3 min^{-1}, and the temperature change, ΔT, was recorded as a function of time, t. The ΔT *vs.* t curve recorded consisted of three parts: preperiod; titration period; afterperiod (for 10 min). Calibration was performed by using a standard heater set in the titration cell after each titration, the ΔT *vs.* t curve similarly consisting of three parts: preperiod; Joul heating period; afterperiod.

Upon heating by an electric heater at the rate of q' expressed in kJ s^{-1}, the ΔT *vs.* t curve is expressed by: $d(\Delta T)/dt=q'/C-\alpha(\Delta T)$ where α expressed in s^{-1} is Newton's cooling constant, which is considered to be constant during the heat measurements (for *ca.* 13 min), and C expressed in kJ K^{-1} is the heat capacity of the calorimeter vessel with its content of solution. The ΔT *vs.* t curve for the afterperiod is expressed by: $d(\Delta T)/dt=-\alpha(\Delta T)$. Solving two differential equations mentioned above, we obtained the following equation for the afterperiod: $\Delta T=q'(1-e^{-\alpha t_1})\times e^{-\alpha t}/\alpha C$, where t_1 is heating time. The values of α and C were refined by means of a least-squares method with a successive approximation. Reproducibilities of α and C obtained by analysis of the ΔT *vs.* t curve for 10 min of the afterperiod were within ±1.5% and ±0.2%, respectively.

The enthalpy of formation of the 1:1 Mn(II) acetato complex was estimated by titration of Mn(II) with edta in an acetate buffer solution. A 0.153 mol dm^{-3} solution of the tetrasodium salt of EDTA was added at the rate of

p' expressed in mol s^{-1} to solutions containing manganese(II) nitrate (1.12×10^{-2} mol dm^{-3}) and an acetate buffer (0.1 mol dm^{-3}) in the pH range from 3.7 to 5.0, the ionic strength being kept at 0.1 (=[AcOK]+[KNO_3]). EDTA was added in each run to be 2.89×10^{-3} mol dm^{-3} at the final concentration. The ΔT *vs.* t curve for the afterperiod was obtained in a similar manner as mentioned above: $\Delta T=-\Delta H_{obsd}\times p'(1-e^{-\alpha t_2})e^{-\alpha t}/\alpha C$, where t_2 was titration time, ΔH_{obsd} expressed in kJ mol^{-1} was the observed heat change, and the C value determined by the calibration was used. The values of ΔH_{obsd} and α were refined as for calibration. The treatment of ΔH_{obsd} will be described later in more detail. The values of ΔH_{obsd} and α for titration of Co(II) with edta in an acetate buffer solution and for titration of iron(II) perchlorate with permanganate ion in 0.1 mol dm^{-3} perchloric acid were also determined by the same method.

The heat of oxidation of the Co(II)-edta complex with permanganate ion was measured on adding freshly prepared potassium permanganate solution (0.02 mol dm^{-3}) at the rate of p' (mol s^{-1}) to solutions containing edta (2.5×10^{-3} mol dm^{-3}) and Co(II) nitrate in a 1:1.1 ratio and an acetate buffer (0.1 mol dm^{-3}) in the pH range from 3.6 to 5.8, the ionic strength being kept at 0.1 (=[AcOK]+[KNO_3]). Potassium permanganate was added in each run to give a 7:1 mole ratio of edta to MnO^-_4. The observed heat change results from dilution(ΔH_D), rapid oxidation(ΔH^c_{ox}), and slow ring closure reaction(ΔH_{el}) taking place in a Dewar vessel (see below about the definition in Eqs. 1, 2, and 9). The ΔT *vs.* t curve for the titration period is expressed by: $d(\Delta T)/dt=(q'_{ox}+q'_{el})/C-\alpha(\Delta T)$ where $q'_{ox}=-(\Delta H_D+\Delta H^c_{ox})\times p'$, $q'_{el}=-\Delta H_{el}\times d\{D[Co^{III}(edta)^-]\}/dt$, and $D[Co^{III}(edta)^-]$ is the change in moles of $[Co^{III}(edta)]^-$ formed. $D[Co^{III}(edta)^-]$ was calculated from a titration speed, p', and $d[Co^{III}(edta)^-]/dt=k[Co^{III}(edta)(H_2O)^-]$ in which the rate constant of k had been determined spectrophotometrically. The ΔT *vs.* t curve for the afterperiod is expressed by: $d(\Delta T)/dt=q'_{el}/C-\alpha(\Delta T)$. The differential equations were solved by the same treatment as described elsewhere.[14] Consequently, the ΔT *vs.* t curve for the afterperiod is expressed in a simple form: $\Delta T=-\Delta H_{mes}\times f(t)-\Delta H_{el}\times g(t)$, where $\Delta H_{mes}=\Delta H_D+\Delta H^c_{ox}$ and both $f(t)$ and $g(t)$ are a function of time. The values of ΔH_{mes} and ΔH_{el} were refined by means of a least-squares method. The values of C and α determined by calibration were used in the calculation of $f(t)$ and $g(t)$. The effective enthalpy of the oxidation, ΔH^c_{ox}, was obtained by subtracting ΔH_D from ΔH_{mes}.

Results

Oxidation of Co(II)–edta Complex with Permanganate Ion. Equilibrium data[15–17] so far reported indicate that the oxidation of the Co(II)–edta complex with permanganate ion or manganese dioxide in an acetate buffer solution produces the Co(III)–edta complex and Mn(II) ion as the final products. In the present reaction systems the following equilibrium is anticipated:

$$[Co^{II}(edta)]^{2-} + [Mn^{III}(edta)(H_2O)]^- \rightleftharpoons [Co^{III}(edta)]^- + Mn^{2+} + edta.$$

Judging from the equilibrium constant obtained for the reaction, the Mn(III)–edta complexes could be excluded under our experimental conditions. It is well known, however, that permanganate ion is powerful enough to oxidize EDTA molecules directly. For example, the absorbance at 527 nm of permanganate ion (0.3 mol cm^{-3}) was reduced to 70% of its initial value after 1 h at 25 °C and pH 4.5 in the presence of an excess EDTA (1.0 mol cm^{-3}). The decrease in absorbance, however, was little affected by the further addition of Zn(II) or Ni(II) to excess (3.0 mol cm^{-3}), where the absorbance decreased by less than 1.5% after 1 h. It is apparent that the addition of Zn(II) and Ni(II) prevent the oxidation of EDTA by forming edta complexes. The Co(III)–edta complexes were formed immediately when the reactants were mixed and thus, there would not occur the oxidation of, at least, free EDTA with permanganate ion under our experimental conditions.

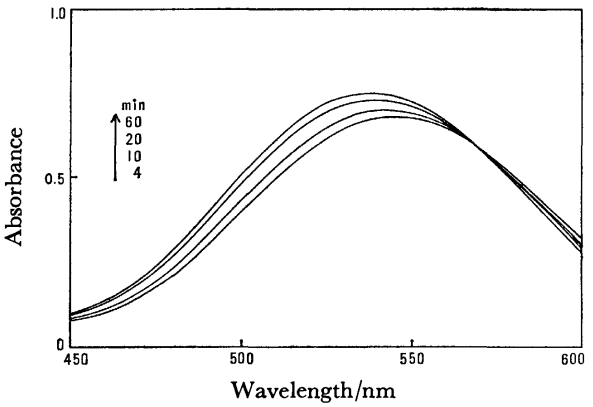

Fig. 1. The change of absorption spectrum with time after mixing Co(II)–edta complex with permanganate ion at pH 4.0.
$C_{Co(II)}=2.7$ mol cm^{-3}; $C_{EDTA}=2.5$ mol cm^{-3}; $C_{MnO_4}=0.47$ mol dm^{-3}.

The change in the absorption spectrum with time after mixing of the reactants is shown in Fig. 1. The wavenumbers of the absorption maxima at time zero and infinite time coincided with those of $[Co^{III}(edta)(H_2O)]^-$ ($\lambda_{max}=550$ nm)[8] and $[Co^{III}(edta)]^-$ ($\lambda_{max}=538$ nm),[18] respectively. The plot of the absorbance (538 nm) at infinite time against $5\times[MnO^-_4]/[Co(II)L]$ obtained under the condition as for Fig. 1 gave an inflection point at a ratio of 1.00 where minimum amounts of hydroxylamine required to reduce excess permanganate ions were added at the ratio more than 1.00. This indicates that little of the EDTA is lost and thus the following stoichiometry of the oxidation is held: 5Co(II)L+Mn(VII)→5Co(III)L+Mn(II). In addition, the molar absorptivity of the final product was derived to be 320 mol^{-1} dm^3 cm^{-1} by correcting for remaining reactants, the value being in agreement with that of $K[Co^{III}(edta)]\cdot2H_2O$ prepared in this work ($\varepsilon_{max}=320$ mol^{-1} dm^3 cm^{-1}) and reported by Ogino, *et al.*[18] ($\varepsilon_{max}=321$ mol^{-1} dm^3 cm^{-1}). It is concluded that the oxidation of Co(II)–edta complex with permanganate ion rapidly proceeds to give $[Co^{III}(edta)(H_2O)]^-$ in quantitative yields and then the five-coordinate edta in the complex slowly becomes six-coordinate in the final product:

$$[Co^{II}(edta)]^{2-} + \tfrac{1}{5}MnO_4^- + \tfrac{1}{5}H^+ \longrightarrow [Co^{III}(edta)(H_2O)]^- + \tfrac{1}{5}Mn^{2+} + \tfrac{4}{5}H_2O \quad \Delta H_{ox}, \quad (1)$$

$$[Co^{III}(edta)(H_2O)]^- \xrightarrow{k} [Co^{III}(edta)]^- + H_2O \quad \Delta H_{el}, \quad (2)$$

where ΔH_{ox} is the enthalpy of Reaction 1 expressed in kJ mol^{-1} of [Co (edta)(H_2O)]$^-$, and ΔH_{el} the enthalpy of Reaction 2 expressed in kJ mol^{-1} of [Co^{III}-(edta)]$^-$. Reaction 2 is first order in [Co^{III}(edta)-(H_2O)]$^-$ concentration. Shimi and Higginson[19] determined the first-order rate constant, k, in the range of 0—15 °C. The rate constant of 1.6×10^{-3} s^{-1} estimated by extrapolation of the plot of k *vs.* $1/K$ to 25 °C was in good agreement with that determined in the present reaction systems (1.61×10^{-3} s^{-1} at 25 °C).

Treatment of Observed Heat Change. Reaction 1 occurs accompanying the following side reactions:

$$[Co^{II}(edta)^{2-} + H^+ \rightleftharpoons [Co^{II}(Hedta)]^- \quad K=10^{3.0},\ \Delta H_3=-8.0, \quad (3)^{16}$$

$$Mn^{2+} + AcO^- \rightleftharpoons [Mn(AcO)]^+ \quad K=10^{0.5},\ \Delta H_4, \quad (4)^{20}$$

$$[Mn(AcO)]^+ + AcO^- \rightleftharpoons Mn(AcO)_2 \quad K=10^{0.9}, \quad (5)^{20}$$

$$Co^{2+} + AcO^- \rightleftharpoons [Co(AcO)]^+ \quad K=10^{1.1},\ \Delta H_6, \quad (6)^{20}$$

$$[Co(AcO)]^+ + AcO^- \rightleftharpoons Co(AcO)_2 \quad K=10^{0.4}, \quad (7)^{20}$$

$$H^+ + AcO^- \rightleftharpoons AcOH \quad K=10^{4.54},\ \Delta H_8=-0.17, \quad (8)^{13}$$

where K represents the equilibrium constant for the relevant reaction expressed in dm^3 mol^{-1} and ΔH the enthalpy expressed in kJ mol^{-1}. The values of K and ΔH reported in the relevant literature are used in this calculation, except for ΔH for Reactions 4—7 which are mentioned below. The measured heat, ΔH^c_{ox}, is given by:

$$\Delta H^c_{ox} = \Delta H_{ox} + \Delta H^c_3 + \Delta H^c_4 + \Delta H^c_6 + \Delta H^c_8, \quad (9)$$

where

$$\Delta H^c_3 = \Delta H_3 \times D[Co^{II}(Hedta)^-]/D[Co^{III}(edta)(H_2O)^-], \quad (10)$$

$$\Delta H^c_4 = \Delta H_4 \times \{D[Mn(AcO)^+] + D[Mn(AcO)_2]\}/D[Co^{III}(edta)(H_2O)^-], \quad (11)$$

$$\Delta H^c_6 = \Delta H_6 \times \{D[Co(AcO)^+] + D[Co(AcO)_2]\}/D[Co^{III}(edta)(H_2O)^-], \quad (12)$$

$$\Delta H^c_8 = \Delta H_8 \times D[AcOH]/D[Co^{III}(edta)(H_2O)^-], \quad (13)$$

and $D[\ ]$ is the change in moles of species given in brackets for each titrant addition and is calculated from the stoichiometric relationships by using equilibrium constants for Reactions 3—8. Thus, the heat contribution due to Reaction 1 is calculated:

$$\Delta H_{ox} = \Delta H^c_{ox} - \Delta H^c_3 - \Delta H^c_4 - \Delta H^c_6 - \Delta H^c_8. \quad (14)$$

A typical thermogram for titration of the Co(II)–edta complex with permanganate ion is shown in Fig. 2. In this case, ΔH^c_{ox} of -100.8 kJ mol^{-1} and ΔH_{el} of 4.4 kJ mol^{-1} were obtained. A plot of ΔH^c_{ox} *vs.* the final pH of the solution for each titration is shown in Fig. 3. The ΔH_{ox} values obtained over the pH range from 3.9 to 5.8 average -101.4 kJ mol^{-1} (solid line 1). Solid line 2 for ΔH^c_{ox} is the best fit line recalculated by using the average value of ΔH_{ox}. The calculated values of ΔH^c_8 were less than 0.03 kJ mol^{-1} over the pH range shown in Fig. 3. The broken line for ΔH^c_{ox}, which was measured at an ionic strength of 0.1 (=[AcONa]+[$NaClO_4$]), was lower than the solid line 2 by only *ca.* 0.5 kJ. In a solution of a low acetate concentration and an ionic strength, the effect of supporting electrolytes on ΔH^c_{ox} seems unimportant. The pH dependence of the ΔH_{el} values obtained at the same time could not be found in the pH region of 4.0 to 5.8 owing to the experimental errors. The ΔH_{el} value was determined to be 4.4 ± 0.8 kJ mol^{-1}.

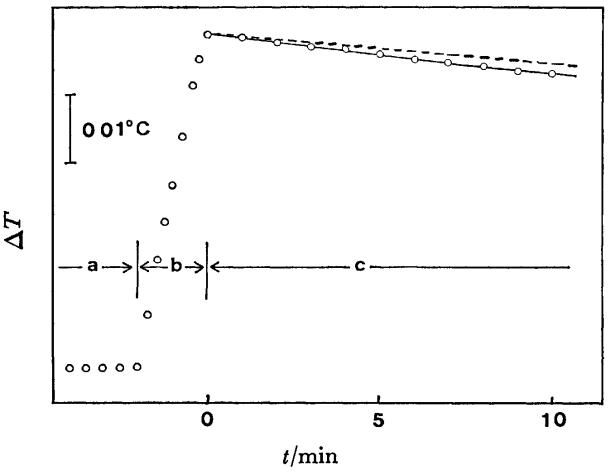

Fig. 2. Thermogram for the addition of permanganate ion to Co(II)–edta complex at pH 5.09. $C_{Co(II)}=2.8$ mol cm^{-3}, $C_{EDTA}=2.5$ mol cm^{-3}; $C_{MnO_4}=0.38$ mol cm^{-3}. a: Preperiod, b: titration period, c: afterperiod. $\alpha=1.74\times10^{-4}$ s^{-1}; $k=1.61\times10^{-3}$ s^{-1}. Solid line is the best fit one calculated from the enthalpies ΔH_{mes} and ΔH_{el}. Broken line is the presumed curve calculated with $\Delta H_{el}=0$.

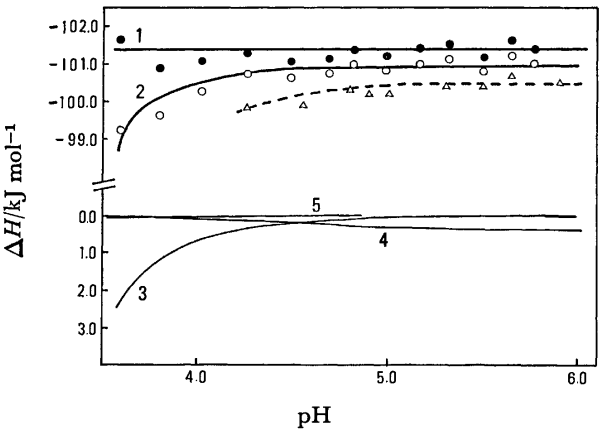

Fig. 3. ΔH^c_{ox} *vs.* the final pH of solution. Conditions as for Fig. 2.
○: ΔH^c_{ox} measured at $\mu=0.1$ (=[AcOK]+[KNO_3]), △: ΔH^c_{ox} measured at $\mu=0.1$ (=[AcONa]+[$NaClO_4$]), ●: ΔH_{ox} calculated according to Eq. 14. The solid lines represent: (1) the average value of ΔH_{ox}; (2) ΔH^c_{ox} recalculated with the average value of ΔH_{ox}; (3) ΔH^c_3; (4) ΔH^c_4; (5) ΔH^c_8.

The enthalpies of formation of the acetato complexes were mostly determined at an ionic strength of 1.0 or 3.0. As little knowledge of the enthalpy values determined in lower ionic media is available, the value for Mn(II) acetato complexes was estimated by titration of Mn(II) in 0.1 mol dm^{-3} acetate buffer solutions with the tetrasodium salt of EDTA. The observed heat, ΔH_{obsd}, refers to the process:

$$Mn^{2+\prime} + L(titrant) \longrightarrow Mn(II)L' \quad \Delta H_{obsd}, \quad (15)$$

where $[Mn^{2+\prime}]=[Mn^{2+}]+[Mn(AcO)^+]+[Mn(AcO)_2]$ and $[Mn(II)L']=[Mn^{II}(edta)^{2-}]+[Mn^{II}(Hedta)^-]$. The process of Eq. 15 comprises that of dilution of 0.153 mol dm^{-3} Na_4edta (Eq. 16) and formation of $[Mn^{II}(edta)]^{2-}$ complex (Eq. 17):

$$L(titrant) \longrightarrow edta \quad \Delta H_D, \quad (16)$$

$$Mn^{2+} + edta \rightleftharpoons [Mn^{II}(edta)]^{2-} \quad \Delta H_{17}, \quad (17)$$

in which Reaction 17 accompanies Reactions 4, 5, and 8 and furthermore the following side reaction:

$$[Mn^{II}(edta)]^{2-} + H^+ \rightleftharpoons [Mn^{II}(Hedta)]^- \quad K=10^{3.1},\ \Delta H=-5.0, \quad (18)^{16}$$

where K and ΔH are defined as for Eqs. 3—8. In such solutions containing 0.1 mol dm^{-3} acetate buffer, the 1:2 acetato complex is not present in amounts sufficient enough to permit the determination of the enthalpy value. Thus, the heat contribution due to stepwise formation of the 1:2 acetato complex is neglected as for Eq. 9 (*cf.* Eq. 11). The observed heat is corrected for ΔH_D, the value of which has been determined by the same method as described elsewhere.[9] Then, the following equations are obtained:

$$\begin{aligned}\Delta H_{cor} &= \Delta H_{obsd} - \Delta H_D \\ &= \Delta H_{17} + \Delta H_4^\circ + \Delta H_{18}^\circ + \Delta H_8^\circ \\ &= \Delta H_{17} + \Delta H_4 \times \{D[Mn(AcO)^+] \\ &\quad + D[Mn(AcO)_2]\}/D[Mn(II)L'] + \Delta H_{18}^\circ + \Delta H_8^\circ, \end{aligned} \quad (19)$$

where

$$\Delta H_4^\circ = \Delta H_4 \times \{D[Mn(AcO)^+] + D[Mn(AcO)_2]\}/D[Mn(II)L'],$$

$$\Delta H_{18}^\circ = \Delta H_{18} \times D[Mn^{II}(Hedta)^-]/D[Mn(II)L'],$$

$$\Delta H_8^\circ = \Delta H_8 \times D[AcOH]/D[Mn(II)L'],$$

$$D[Mn(II)L'] = D[Mn^{II}(edta)^{2-}] + D[Mn^{II}(Hedta)^-].$$

A least-sequares analysis is performed to provide ΔH_{17} and ΔH_4 in Eq. 19. A plot of ΔH_{cor} *vs.* the final pH of the solution for each titration is shown in Fig. 4. The best fit line was calculated by using the values, $\Delta H_{17}=-18.7$ kJ mol^{-1} and $\Delta H_4=6.3$ kJ mol^{-1}. The broken lines are for each ΔH on the right hand side of Eq. 19. The ΔH_8° values were less than 0.05 kJ mol^{-1} over the pH range shown in Fig. 4. The enthalpy of formation of the 1:1 Co(II) acetate complex was estimated to be 2.3±0.3 kJ mol^{-1} by the same method as above, from which the ΔH_6° values in Eq. 9 were calculated to be less than 0.07 kJ mol^{-1}.

The heat of oxidation of iron(II) ion with permanganate ion was measured in 0.1 mol dm^{-3} $HClO_4$. For the reaction

$$Fe^{2+} + \tfrac{1}{5}MnO_4^- + \tfrac{8}{5}H^+ \longrightarrow Fe^{3+} + \tfrac{1}{5}Mn^{2+} + \tfrac{4}{5}H_2O \quad \Delta H_{20}, \quad (20)$$

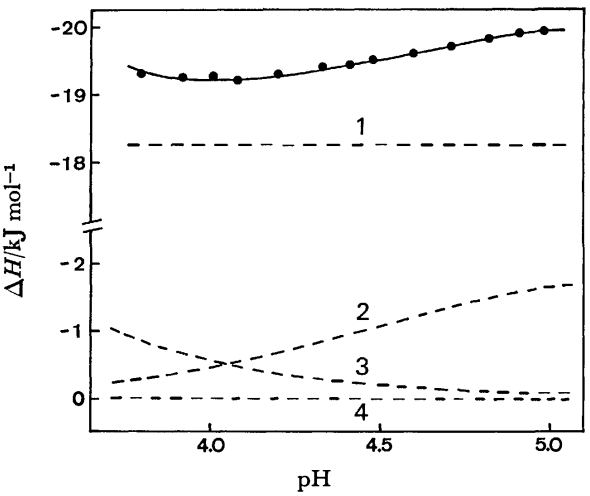

Fig. 4. ΔH_{cor} *vs.* the final pH of solution. $C_{Mn(II)}=11.0$ mol cm^{-3}; $C_{EDTA}=2.9$ mol cm^{-3}. ●: ΔH_{cor} measured at $\mu=0.1$ (=[AcOK]+[KNO_3]). Solid line is the best fit one calculated from the enthalpies ΔH_{17} and ΔH_4. The broken lines represent: (1) ΔH_{17}; (2) ΔH_4°; (3) ΔH_{18}°; (4) ΔH_8°.

we determined $\Delta H_{20}=-123.9\pm0.7$ kJ mol^{-1} of Fe^{3+}, in which the following side reaction was considered:

$$Fe^{3+} + H_2O \rightleftharpoons FeOH^{2+} + H^+ \quad K=10^{-2.50},\ \Delta H=42.3. \quad (21)^{13}$$

Discussion

A solution containing $[Co^{II}(edta)]^{2-}$ and $[Co^{III}(edta)]^-$ exhibits a reversible potential at a dropping mercury electrode.[2] It is possible to measure the standard redox potential, E°, with the solutions containing varied concentrations of $[Co^{II}(edta)]^{2-}$ and $[Co^{III}(edta)]^-$ complexes. For the reaction

$$[Co^{III}(edta)]^- + \tfrac{1}{2}H_2 \rightleftharpoons [Co^{II}(edta)]^{2-} + H^+, \quad (22)$$

the ΔG value is calculated from E° value determined by several authors[1-5] by use of the relation, $\Delta G=nFE^\circ$. On the other hand, the products formed by oxidation of the Co(II)–edta complexes with a variety of oxidants are not always the same as that by the electrode oxidation; the Co(II)–edta complexes are oxidized to form Co(III)–edta complexes containing five- or six-coordinate edta, or their mixture.[7,8] It was found that the oxidation by permanganate ion produced $[Co^{III}(edta)(H_2O)]^-$ under our experimental conditions, followed by the ring closure reaction of the complex to $[Co^{III}(edta)]^-$. For the reaction

$$[Co^{II}(edta)]^{2-} + \tfrac{1}{5}MnO_4^- + \tfrac{8}{5}H^+ \longrightarrow [Co^{III}(edta)]^- + \tfrac{1}{5}Mn^{2+} + \tfrac{4}{5}H_2O, \quad (23)$$

at an ionic strength of 0.1, therefore, we obtained $\Delta H=-97.0$ kJ mol^{-1} from the sum of ΔH values for Reactions 1 and 2. In order to convert a ΔH for the reaction to one for Reaction 22, the ΔH and ΔH_f° values mentioned below were adopted. For the reaction

$$Fe^{2+} + \tfrac{1}{2}H_2O_2(aq) + H^+ \longrightarrow Fe^{3+} + H_2O, \quad (24)$$

in 0.1 mol dm^{-3} $HClO_4$, Irving, *et al.*[21] obtained

$\Delta H = -146.0 \pm 0.8$ kJ mol^{-1}. Correcting it for the side reaction 21, we obtained $\Delta H = -147.3$ kJ mol^{-1}. Combination of this value with the standard enthalpies of formation of $H_2O(l)$ and $H_2O_2(aq)$ listed in N. B. S. Technical Notes[22] leads to $\Delta H = -43.0$ kJ mol^{-1} for the following reaction:

$$Fe^{3+} + \tfrac{1}{2}H_2(g) \rightleftharpoons Fe^{2+} + H^+. \quad (27)$$

A $\Delta H°$ of -42 kJ mol^{-1} or -40.6 kJ mol^{-1} for the reaction was recommended without consideration of ionic strength by Hepler, *et al.*[23] and in N. B. S. Technical Notes,[22] respectively. It is still difficult to estimate the effect of ionic strength on ΔH for the reaction from data so far reported. A ΔH of -69.9 kJ mol^{-1} for Reaction 22 was obtained from ΔH for Reactions 20, 23, and 27. ΔG for Reaction 22 was calculated to be -37.1 kJ mol^{-1} by use of $E° = 0.384$ V[1] (*vs.* NHE) measured at an ionic strength of 0.1 and then, the ΔS value was calculated to be -110 J mol^{-1} K^{-1}.

Reaction 22 comprises the following reactions:

$$Co^{3+} + \tfrac{1}{2}H_2 \rightleftharpoons Co^{2+} + H^+, \quad (28)$$

$$Co^{2+} + \text{edta} \rightleftharpoons [Co^{II}(\text{edta})]^{2-} \quad K = 10^{16.23},\ \Delta H = -17.6, \quad (29)[16]$$

$$Co^{3+} + \text{edta} \rightleftharpoons [Co^{III}(\text{edta})]^-. \quad (30)$$

Thus, it is possible to calculate the ΔH value for Reaction 30 by use of the ΔH values for Reactions 22, 28, and 29. But the exact values of ΔG and ΔH at low ionic strengths for Reaction 28 have not been yet estimated from the appropriate data. For the reaction

$$Co^{3+} + Fe^{2+} \longrightarrow Co^{2+} + Fe^{3+}, \quad (31)$$

in 4 mol dm^{-3} $HClO_4$ at 15 °C, Johnson and Sharpe[24] determined $\Delta H = -110$ kJ mol^{-1} by a direct calorimetric measurement. They combined it with the estimated entropy change (13 J mol^{-1} K^{-1}) to obtain ΔG of -114 kJ mol^{-1} at 15 °C. Neglecting a temperature dependence of ΔH, we obtained ΔG of -114 kJ mol^{-1} ($\Delta E = E°_{28} - E°_{27} = 1.18$ V) at 25 °C by the same manner. Combining it with the formal Fe^{3+}/Fe^{2+} potential of 0.749 V[25] at 25 °C and at an ionic strength of 0.1, we obtained the formal Co^{3+}/Co^{2+} potential of 1.93 V (*vs.* NHE) and thus ΔG of -186 kJ mol^{-1} for Reaction 28. Similarly the variation of ΔH for two half cell reactions involved in Eq. 31 with ionic strengths would adequately compensate each other because of the close similarity in size and charge of the pair of ions. Thus, the ΔH value for Reaction 28 was obtained to be -153 kJ mol^{-1} by summation of the ΔH values for Reactions 27 and 31 and thus the ΔS value was calculated to be -111 J mol^{-1} K^{-1}. The entropy change accompanying Reaction 28 can be represented by:

$$\Delta S° = \bar{S}°_{Co^{2+}} + \bar{S}°_{H^+} - \bar{S}°_{Co^{3+}} - \tfrac{1}{2}\bar{S}°_{H_2}, \quad (32)$$

where $\bar{S}°$ is the standard partial molal entropy of the species involved. $\Delta S°$ is approximate to ΔS and thus the $\bar{S}°_{Co^{3+}}$ values is calculated to be -290 J mol^{-1} K^{-1} by combining ΔS with $\bar{S}°_{Co^{2+}}$ and $\bar{S}°_{H_2}$ listed in N. B. S. Technical Notes.[22] The formal Co^{3+}/Co^{2+} potential of 1.84 V (*vs.* NHE) was determined at 25 °C and 3 mol dm^{-3} HNO_3 by use of a gold electrode,[26] the value being commonly used as that at ionic strengths of 0.1—0.2 in calculations[1-5] of the formation constants of the Co(III)-aminopolycarboxylate complexes. Combination of the ΔG value calculated from the potential with the ΔH value selected for Reaction 28 leads to the $\bar{S}°_{Co^{3+}}$ value of -260 J mol^{-1} K^{-1}. This value seems to be too low compared with the $\bar{S}°$ values of Fe^{3+} ion, which is similar to the size, mass, and charge of Co^{3+} ion, currently accepted: -316 (N. B. S.),[22] -293 (Latimer),[27] and -280 J mol^{-1} K^{-1} (Hepler).[23] From the ΔG and ΔS values determined for Reaction 22 and selected for Reactions 28 and 29, we obtained ΔG of -242 kJ mol^{-1} and ΔH of -101 kJ mol^{-1} as the most probable values for Reaction 30. Thus, the ΔS value was calculated to be 474 J mol^{-1} K^{-1}.

It was reported by Staveley[28] that a plot of ΔS for the formation of the metal(III)-edta complexes against the reciprocal of the ionic radius, r, of metal ion gave a curve with upward curvature. The ΔS values selected by Martell and Smith[16] were replotted against $1/r$, taken from Ahren's table,[29] the value for the Co(III) complex being situated upward the curvature only by *ca.* 30 J mol^{-1} K^{-1}. On the other hand, the ΔH value for the Co(III)-edta complex is much more exothermic than that for the metal(III)-edta complexes so far reported; ΔH of -30.1 kJ mol^{-1} for the In(III)-edta complex has been reported as the most exothermic ΔH value. It is reasonable to conclude, therefore, that the formation of the Co(III)-edta complex exhibits a normal entropy change, which is explained by the size and charge of the ion, together with that of other metal(III) complexes, whereas the enthalpy change for formation of the Co(III)-edta complex causes the complex to be the most stable of the metal(III)-edta complexes.

In a previous paper[13] ΔH of -11.5 kJ mol^{-1} and ΔS of 440 J mol^{-1} K^{-1} were reported for the formation of the Fe(III)-edta complex. The ΔS value for the Co(III) complex is somewhat higher than that for the Fe(III) complex. This would arise from the difference in the number of water molecules displaced from the coordination sphere of the aqua ion by the complex formation; Co^{3+} ion forms hexacoordinate complex, $[Co^{III}(\text{edta})]^-$, with edta, while Fe^{3+} ion forms heptacoordinate complex, $[Fe^{III}(\text{edta})(H_2O)]^-$.[30,31] The favorable enthalpy effect for formation of the Co(III)-edta complex is compatible with the facts that in the solid state the Co(III)-N bond-length (1.93 Å)[32] of the hexacoordinate Co(III)-edta complex is much shorter than the Fe(III)-N bond-length (2.32 Å)[33] of the heptacoordinate Fe(III)-edta complex and that Co^{3+} forms a low-spin complex with edta,[34] while Fe^{3+} forms a high-spin complex in weakly acid solution.[35] The redox potentials of the Co^{III}/Co^{II} and Fe^{III}/Fe^{II} systems are reduced from 1.93 V to 0.38 V and from 0.749 V to 0.12 V,[36] respectively, in the presence of EDTA. The larger decrease in the potential of the Co^{III}/Co^{II} system is caused by the enthalpy effect for formation

of the Co(III)–edta complex because the thermodynamic functions for formation of the Co(II)– and Fe(II)–edta complexes are similar to each other.[16]

References

1) C. N. Reilley, W. G. Scribner, and C. Temple, *Anal. Chem.*, **28**, 450 (1956).
2) N. Tanaka and H. Ogino, *Bull. Chem. Soc. Jpn.*, **38**, 1054 (1965).
3) G. Schwarzenbach and J. Heller, *Helv. Chim. Acta*, **34**, 574 (1951).
4) L. Hin-Fat and W. C. E. Higginson, *J. Chem. Soc., A*, **1967**, 298.
5) J. Bond and D. B. Hobson, *J. Chem. Soc., A*, **1969**, 2155.
6) A. A. Noyes and T. J. Deahl, *J. Am. Chem. Soc.*, **59**, 1337 (1937).
7) R. G. Wilkins and R. Yelin, *J. Am. Chem. Soc.*, **89**, 5496 (1967).
8) W. H. Woodruff, D. W. Margerum, M. J. Milano, H. L. Pardue, and R. E. Santini, *Inorg. Chem.*, **12**, 1490 (1973).
9) K. Doi, *J. Inorg. Nucl. Chem.*, **40**, 1639 (1978).
10) E. P. Dwyer, E. C. Gyarfas, D. P. Mellor, *J. Phys. Chem.*, **59**, 296 (1955).
11) K. Ueno, "Chelatometric Titration (reprinted 14)," Nankodo, Tokyo (1972).
12) H. S. Harned and W. J. Hamer, *J. Am. Chem. Soc.*, **55**, 2194 (1933).
13) K. Doi, *Talanta*, **25**, 97 (1978).
14) K. Doi, 24th Meeting of the Japan Society for Analytical Chemistry, Sapporo, October 1975. In this work, all the differential equations involved can be solved without numerical integration.
15) G. Milazzo and S. Caroli, "Tables of Standard Electrode Potentials, Wiley, New York (1978), pp. 302 and 336.
16) A. E. Martell and R. M. Smith, "Critical Stability Constants, Vol. 1; Amino Acids," Plenum Press, New York (1974), p. 206.
17) G. Anderegg, "Critical Survey of Stability Constants of EDTA Complexes," Pergamon Press, New York (1977), pp. 23—26.
18) H. Ogino, A. Masuko, T. Shirakashi, and N. Tanaka, *Nippon Kagaku Kaishi*, **1977**, 377.
19) I. A. W. Shimi and W. C. E. Higginson, *J. Chem. Soc.*, **1958**, 260.
20) A. Ringbom, "Complexation in Analytical Chemistry," Wiley-Interscience, New York (1963).
21) A. Sousa-Alonso, I. Chadwick, and R. J. Irving, *J. Chem. Soc., A*, **1968**, 2364.
22) "Selected Values of Chemical Thermodynamic Properties," National Bureau of Standard, Technical Notes 270-3 (1968).
23) J. W. Larson, P. Cerutti, H. K. Garber, and L. G. Hepler, *J. Phys. Chem.*, **72**, 2902 (1968).
24) D. A. Johnson and A. G. Sharpe, *J. Chem. Soc.*, **1964**, 3490.
25) W. C. Schumb, M. S. Sherrill, and S. B. Sweetser, *J. Am. Chem. Soc.*, **59**, 2360 (1937).
26) A. A. Noyes and T. J. Deahl, *J. Am. Chem. Soc.*, **59**, 1337 (1937).
27) R. E. Powell and W. M. Latimer, *J. Chem. Phys.*, **19**, 1139 (1951).
28) L. A. K. Staveley and T. Randall, *Discuss. Faraday Soc.*, **26**, 157 (1958).
29) "Landolt-Börnstein Zahlenwerte und Funktionen," I Band, Atom und Molekularphysik, 4 Teil, Kristalle, Springer-Verlag, Berlin (1955), p. 522.
30) M. D. Lind, M. J. Hamor, T. A. Hamor, and J. L. Hoard, *Inorg. Chem.*, **3**, 34 (1964).
31) E. L. Muetterties and C. M. Wright, *Quart. Rev. (London)*, **21**, 109 (1967).
32) H. A. Weakliem and J. L. Hoard, *J. Am. Chem. Soc.*, **81**, 549 (1959).
33) J. J. Steyowski, R. Countryman, and J. L. Hoard, *Inorg. Chem.*, **12**, 1749 (1973).
34) W. Klemm, *Z. Anorg. Chem.*, **252**, 225 (1944).
35) H. Schugar, C. Walling, R. B. Jones, and H. B. Gray, *J. Am. Chem. Soc.*, **89**, 3712 (1967).
36) G. Schwarzenbach and J. Heller, *Helv. Chim. Acta*, **34**, 576 (1951).

The Sensitization Effect in the Laser-induced Infrared Fluorescence Spectroscopy by Addition of a Second Component. II

Yasuhiro KAGAWA, Seiichiro HIGUCHI,* and Shigeyuki TANAKA

Department of Industrial Chemistry, Faculty of Engineering, The University of Tokyo, Hongo, Bunkyo-ku, Tokyo 113

(Received August 3, 1981)

A considerable degree of the sensitization is realized in the laser-induced infrared fluorescence spectra when some of the alkene compounds are mixed with an objective sample in the gas phase. This sensitization effect has been examined quantitatively for diethyl ether when ethylene or propylene is added as a second component. The 8.7 μm band of ether is used as a key band. The degree of sensitization is abruptly enhanced with lowering the concentration of diethyl ether, and at about 0.1 Torr† of the sample the intensities per unit concentration become about 150 and 50 times greater for ether–ethylene and ether–propylene systems, respectively compared with that without ethylene or propylene. A possibility of a new vibrational spectroscopy with high sensitivity and its applications to microanalysis are suggested.

Recently we have developed a measurement system for the laser-induced infrared fluorescence (IR-F) spectra, and begun to examine its analytical applications.[1] During this investigation, the intensities of IR-F bands of some organic compounds were found to be enhanced remarkably when propylene was added as a second component. In a previous paper,[2] we made a preliminary report on the experimental evidence of this sensitization effect. Since this effect comes out as the increase of the intensities per unit concentration, the phenomenon in question is interesting and attractive in view of not only pure scientific aspects but also analytical applications of the IR-F spectroscopy.

The IR-F spectroscopy is a new technique for measurements of vibrational spectra. Experimentally, it is based on the irradiation of a sample by a monocharomatic or quasi-monochromatic laser light. The sample is vibrationally excited to the various vibrational levels through some mechanisms. Thus, the IR-F spectrum which is a kind of infrared emission spectrum, is obtained. It is to be noted that the IR-F spectra are different from the usual fluorescence spectra based on the electronic transitions in that the signals of IR-F appear not only in the longer wavelength region but also in the shorter one than the wavelength of the exciting laser lines. This specific character of the IR-F has not completely been elucidated, though several possible mechanisms are proposed.[3,4] The main reason is that the emission mechanism of the IR-F spectrum is not fully explained at present.

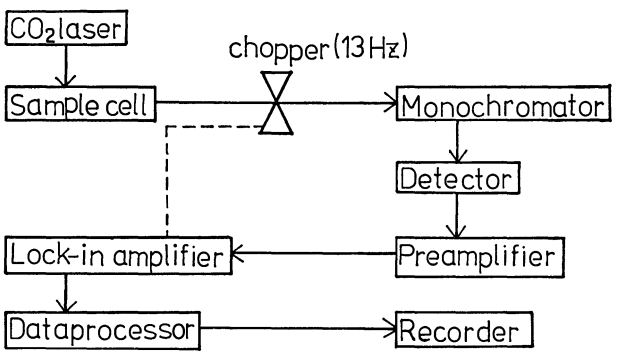

Fig. 1. The block diagram of the measurement system of IR-F spectra.

† 1 Torr≈133.322 Pa.

Under these circumstances, we are not in a position to make a satisfactory explanation about the phenomenon either. Therefore, only the experimental results are presented and they are discussed from the viewpoint of analytical utility. That is, after presenting a preliminary paper,[2] we have made a more detailed and quantitative experimental investigation on the sensitization effects of ethylene and propylene as the second component, which will be described in this paper.

Experimental

In Fig. 1 is shown the block diagram of the measurement system for IR-F spectroscopy, developed in our laboratory. The details for the essential elements composing this system were described in the previous paper.[1]

In this system, the sample in the sample cell is irradiated with the 10.6 μm lines from a CO_2 laser (output power: about 3 W). Then, the vibrationally excited sample emits the fluorescence light, and a part of this light going out from the cell in the direction perpendicular to that of the laser beam is modulated with a chopper of the frequency of 13 Hz. This frequency, which is adopted in commonly used infrared spectrophotometers, is selected rather arbitrarily and it is not certain whether it is optimal or not. This problem is left to be examined in the future. This chopped emission is sent into a monochromator and spectrally measured. The signals from a detector (MCT semiconductor detector) are discriminated and amplified with a lock-in amplifier. Finally, the signals are processed with a data processor containing a microcomputer, and then, they are recorded out. The IR-F spectra are all measured with the mechanical slit width fixed at 3.0 mm. The resolutions are 0.05, 0.06, 0.07, 0.08, and 0.08 μm at the wavelengths, 12.0, 10.0, 8.0, 6.0, and 5.0 μm, respectively. The scanning speed was about 5 μm/min, and the number of the repetitive scans was 16 or 32.

All of the spectra were measured for the samples in the gaseous state. The pressures or the partial pressures of samples were from a few hundred to about 0.1 Torr. The lower limit of sample pressures is determined mainly by the sample preparation apparatus, not by the sensitivity of the instrument. This fact needs to be borne in mind when the sensitivity of the IR-F spectroscopy is discussed in the later section of this paper.

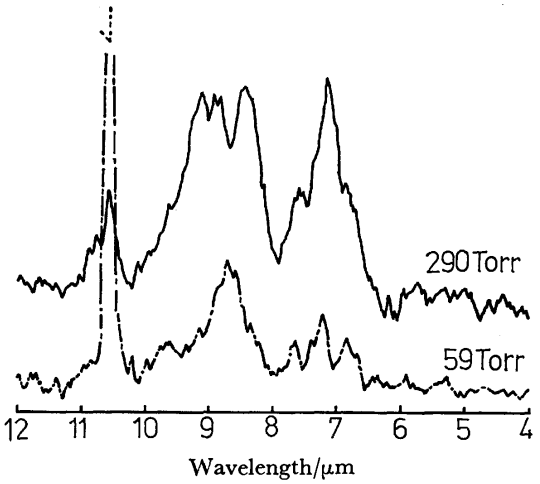

Fig. 2. IR-F spectra of diethyl ether at two different pressure.
——: 290 Torr, ————: 59 Torr.
The sharp band at 10.6 μm is considered to be due to the scattering of laser light in the sample cell.

Results and Discussion

The IR-F Spectra of the Sample Compound and the Sensitizing Agents. In the present investigation, we have selected diethyl ether as an objective sample, and the IR-F spectra for the mixed samples consisting of diethyl ether and some of the alkene compounds have been examined.

In Fig. 2 are shown the spectra of diethyl ether alone at the two different pressures. As is seen from this figure, the spectral patterns of ether in the 8—9 μm region are different for each pressure. That is, the 8.7 μm band, which can be assigned to the C–O–C stretching vibration, splits apparently into two peaks for the higher pressure, while the spectrum for the lower pressure exhibits only one band. This is considered to be due to the self-absorption.[1,5] Such phenomenon often occurs in the IR-F spectra when the pressures of gaseous samples are relatively high. This type of the band splitting is considered to be realized when the absorptions of samples are strong and the widths of the absorption bands are comparatively narrower than those of the corresponding IR-F bands.

In Figs. 3 and 4 are shown the IR-F spectra of ethylene and propylene, which are used as the main sensitizing agents in the present study. As can be seen from these figures, the IR-F spectra of these compounds exhibit no marked signal in the 7—9 μm region. Therefore, the influence of the presence of ethylene or propylene can be favorably examined, using the 8.7 μm band of diethyl ether as a key band. Thus, we deal with the intensity changes of this band in the range of the partial pressures of diethyl ether where no influence of the self-absorption appears.

The IR-F Spectra of Mixed Samples. Next we show the spectral evidence of the sensitization effect observed when some alkene compounds are added as the second component. The examples are shown in Figs. 5—7. Obviously the intensities of the 8.7 μm band of diethyl ether are enhanced considerably for the mixed samples, compared with those without a second component. All of the alkene compounds examined in the present study, *i.e.*, ethylene, propylene, 1-butene, 1-pentene, 1-hexene, have been found to induce the sensitization effect, though its degree is different among them.

We will examine the experimental results more quantitatively. Figure 5 shows the IR-F spectrum of diethyl ether alone (19.2 Torr) and that of a mixture of diethyl ether (19.9 Torr)–propylene (425 Torr).

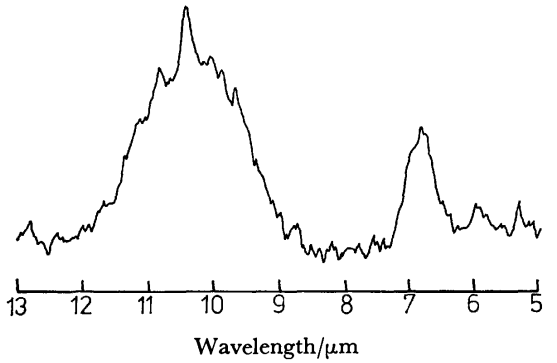

Fig. 3. IR-F spectra of ethylene (191 Torr).

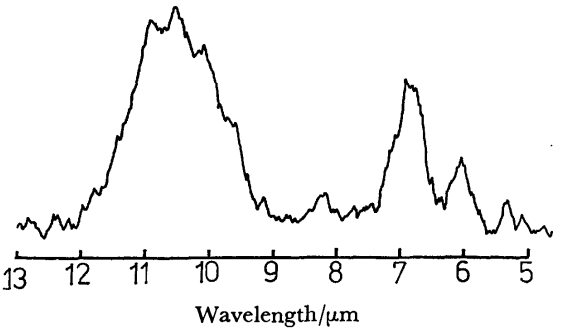

Fig. 4. IR-F spectra of propylene (260 Torr).

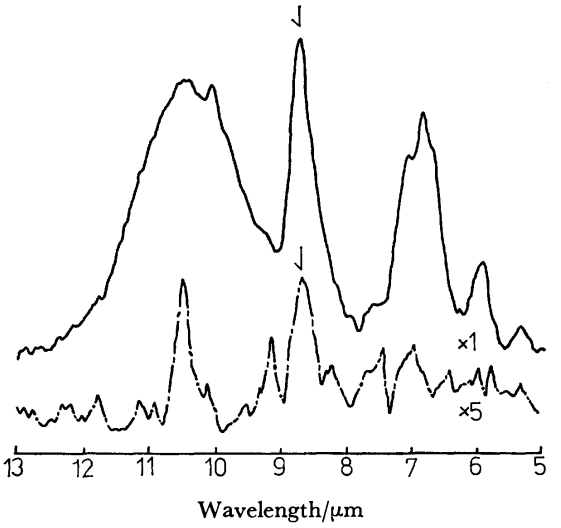

Fig. 5. IR-F spectra of diethyl ether only (19.2 Torr) and of diethyl ether (19.9 Torr)–propylene (425 Torr) mixed sample.
——: Mixed sample, ——: diethyl ether only.
Arrows show the 8.7 μm band of diethyl ether.

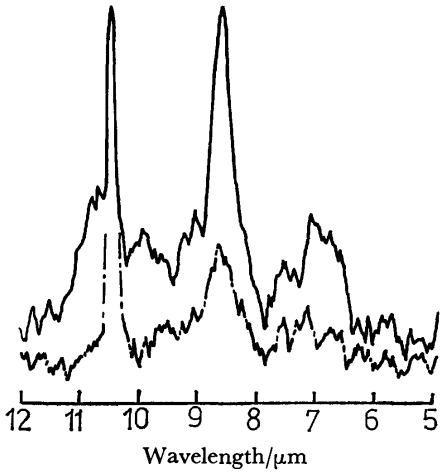

Fig. 6. IR-F spectra of diethyl ether only (59 Torr) and of diethyl ether (20 Torr)–1-butene (100 Torr) mixed sample.
——: Mixed sample, ———: diethyl ether only.

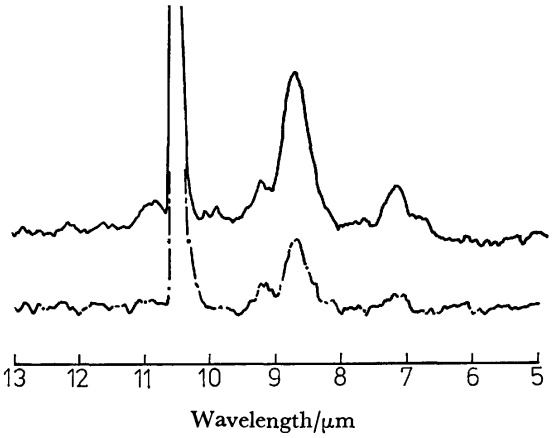

Fig. 7. IR-F spectra of diethyl ether only (37 Torr) and of diethyl ether (37 Torr)–1-hexene (37 Torr) mixed sample.
——: Mixed sample, ———: diethyl ether only.

The spectrum of ether alone has been measured with the instrumental sensitivity set five times higher than for the mixed sample. The sensitization of about one order of magnitude is realized in this particular case.

The Relation between the Degrees of the Sensitization and the Partial Pressures of Diethyl Ether. As was mentioned briefly in the previous paper,[2] the degrees of the sensitization were found to increase when the partial pressures of objective sample became smaller. In the present investigation, we have examined this phenomenon in more detail and quantitatively.

Theoretically, the experimental fact in question can be explained qualitatively in terms of the absorption of the laser light by ethylene, propylene or other sensitizing components, which is followed by inter- and intramolecular energy transfer, though the details of such mechanism remain obscure. In view of such mechanism, the above-mentioned experimental fact seems to be natural, since the probability of the intermolecular energy transfer between the sensitizing agent and diethyl ether is considered to increase when the concentration of the sensitizer relative to that of ether becomes greater. From such viewpoint, we have

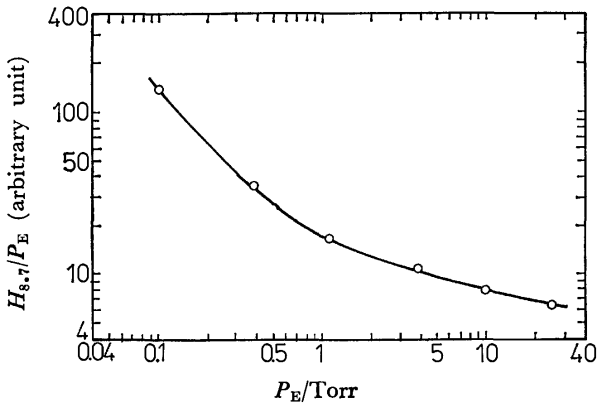

Fig. 8. Plots of value of $H_{8.7}/P_E$ *vs.* P_E on diethyl ether–ethylene mixed sample.
$H_{8.7}$: Peak height of 8.7 μm band of diethyl ether, P_E: partial pressure of diethyl ether.

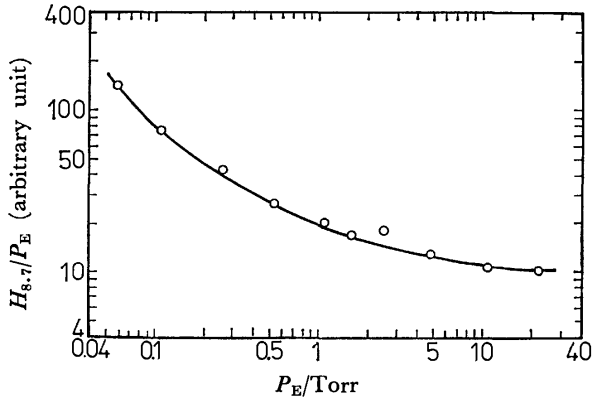

Fig. 9. Plots of value of $H_{8.7}/P_E$ *vs.* P_E on diethyl ether–propylene mixed sample.

examined experimentally the changes of the sensitization degree with the concentrations of ether. Since the effect in question comes out as the increase of the intensities, such results have direct relation to the microanalytical utility of the IR-F spectroscopy.

In the examinations described in the following, we have fixed the partial pressure of the sensitizing components at 100 Torr rather arbitrarily, and the effect of the concentrations of diethyl ether on the degrees of the sensitization has been examined for ethylene and propylene as the second components. The results are shown in Figs. 8 and 9. In these figures, we have plotted the values of $H_{8.7}/P_E$ ($H_{8.7}$: the peak height of the 8.7 μm band of diethyl ether, P_E: its partial pressure) against P_E. The value $H_{8.7}/P_E$ is considered to be the peak intensity per unit concentration of ether. Thus, this variable can be regarded as a measure of the degree of the sensitization effect. Moreover, the data are plotted in a logarithmic scale. This is not based on any theoretical consideration, but we have done it to show the sensitization changes more distinctly.

As is seen from these figures, the intensity per unit concentration is enhanced to a great extent for both of the sample systems when the partial pressures of diethyl ether become lower. For ethylene as a second component the values of $H_{8.7}/P_E$ become about

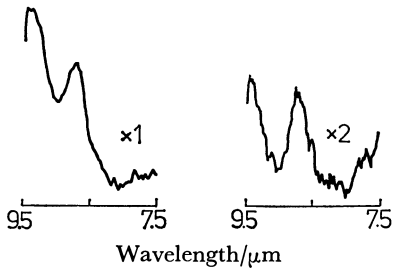

Fig. 10. The 8.7 μm bands of diethyl ether for the lowest concentrations.
Left side: diethyl ether (0.1 Torr)–ethylene (100 Torr) mixed sample, right side: diethyl ether (0.06 Torr)–propylene (100 Torr) mixed sample.

22 times greater when the pressures of ether change from 20 to 0.1 Torr. Since the intensity of the 8.7 μm band increases about 7 times when 100 Torr of ethylene is added to 20 Torr of diethyl ether, the sensitivity becomes about 150 times greater at 0.1 Torr of ether compared with that without ethylene. The value of 150 is to be considered the minimum, since this is estimated on the assumption that the relation between the pressures of diethyl ether and the peak heights is linear. In IR-F spectroscopy the relation is not always linear, but the one such as $H=\text{const}\times P^x$ ($X\geqq 1.0$) is often observed.[1,6] Thus, the sensitivity increase becomes greater than 150 when X is larger than unity.

For propylene as a sensitizing agent the same tendency of the changes of intensity per unit concentration of diethyl ether is realized. However, the types of the curves shown in Figs. 8 and 9 are obviously different. Quantitatively, for propylene, $H_{8.7}/P_E$ increases about 7 times when the pressure of ether changes from 20 to 0.1 Torr. Since the intensity of the 8.7 μm band is enhanced also about 7 times at the sample pressure of 20 Torr when 100 Torr of propylene is added, the minimum sensitivity enhancement is about 50 times, about one third of the value for ethylene. This fact indicates that the effectiveness of the alkenes as sensitizers is widely different among them.

In Fig. 10 are shown the 8.7 μm bands of diethyl ether for the lowest concentrations so far studied. At present, the lower limit of concentration is determined by the apparatus used for the sample preparation rather than by the sensitivity of the measurement system. The spectrum on the right side of this figure has been measured with the instrumental sensitivity set twice higher than that on the left. Considering the sensitivity changes shown in Figs. 8 and 9, and that the spectra for the lower concentrations were not measured, we cannot estimate the detection limits in the strict sense of the word from the spectra shown in Fig. 10. However, as a measure of the detection limits, we have estimated the concentrations at S/N=2 from these spectra. The results are the same for both spectra and about 0.01 Torr. This value corresponds to the concentration of about 12 ppm (1.2×10^{-5} ml/ml). It should be emphasized that we can say at most from this result that the detection limit is lower than 12 ppm for the sample system treated here.

Conclusion

In the present investigation, we have examined the sensitization effect observed in the IR-F spectra under the presence of some alkene compounds. The experimental results prove that the alkene compounds generally induce the enhancement of the IR-F intensities for the bands of samples. The quantitative discussions about the degrees of sensitization have been given for the diethyl ether–ethylene and diethyl ether–propylene systems in terms of the concentrations of ether.

The authors realize that there remain some important problems left unsolved. The first of them is the details of the mechanism of the phenomenon presented here. The second is where is the extremes of the improvement of the sensitivity, including the sensitizers other than ethylene and propylene. The third is related to the second problem. That is, from the viewpoint of the instrumental aspects, much of the emissions from samples is not effectively utilized in the present sample cell.[1] Thus, we are going to examine the sensitivity by use of a sample cell which contains the mirror system focusing the emitted light as much as possible into the detection system. The fourth is a rather important one, that is, the influence of the quantities of sensitizing agents, which is now under the examination as the next step of this investigation.

For all the above-mentioned problems left unsolved, we believe that the results obtained here suggest that the presented method greatly improves the sensitivity of the IR-F, and there is a possibility that the IR-F spectroscopy becomes an useful tool of microanalysis based on the vibrational spectra. The further examination in line with this purpose is proceeding in our laboratory.

The present work was supported by a Grant-in-Aid for Scientific Research No. 443014 from the Ministry of Education, Science and Culture.

References

1) S. Higuchi, N. Kihara, H. Waki, S. Tanaka, and N. Sakayanagi, *Bunko Kenkyu*, **30**, 250 (1981).
2) S. Higuchi, N. Kihara, H. Waki, and S. Tanaka, *Chem. Lett.*, **1981**, 609.
3) J. W. Robinson and J. D. Dake, *Anal. Chim. Acta*, **71**, 277 (1974).
4) J. W. Robinson, D. Nettles, and L. H. Jowett, *Anal. Chim. Acta*, **92**, 13 (1977).
5) D. M. Hailey, H. M. Barnes, and J. W. Robinson, *Anal. Chim. Acta*, **56**, 175 (1971).
6) J. W. Robinson and J. D. Dake, *Spectrosc. Lett.*, **6**, 685 (1973).

 © 1982 The Chemical Society of Japan Bull. Chem. Soc. Jpn., 55, 1441—1446 (1982)

The Effects of Multivalent Anions on the Aluminium Ion-assisted Aquation of the Pentaamminefluorocobalt(III) Complex**

Masayasu IIDA,* Mieko ANDO, and Hideo YAMATERA†

Department of Chemistry, Faculty of Science, Nara Women's University, Nara 630

†*Department of Chemistry, Faculty of Science, Nagoya University, Nagoya 464*

(Received August 28, 1981)

The presence of multivalent anions, such as sulfate, oxalate, and malonate ions, accelerated the aluminium ion-assisted aquation of $CoF(NH_3)_5^{2+}$ and gave the anionopentaamminecobalt(III), along with the aqua complex. The competition reaction for the sulfate ion showed a saturation of the product percentage (33% $CoSO_4(NH_3)_5^+$) at nearly $[SO_4^{2-}]_{total}=0.1$ mol dm^{-3}, while the saturation of the reaction rate was observed at a higher sulfate concentration. This difference can be explained by a scheme in which the reaction proceeds through two intermediates, $CoF(NH_3)_5^{2+}\cdot SO_4^{2-}\cdot Al^{3+}$ and $SO_4^{2-}\cdot CoF(NH_3)_5^{2+}\cdot SO_4^{2-}\cdot Al^{3+}$. The reaction for the oxalate and malonate ions gave extremely large yields (more than 90%) of $CoA(NH_3)_5^+$ (A^{2-}=oxalate ion or malonate ion) when $[A^{2-}]_{total}/[Al^{3+}]_{total}>2$, and the reaction rates showed a maximum at approximately $[A^{2-}]_{total}/[Al^{3+}]_{total}=2$. These specific effects can be attributed both to the strong affinities of the dicarboxylate ions for the aluminium ion and to the residual capacity of the aluminium-bonded dicarboxylate ions for coordinating with cobalt(III).

Our previous studies of $CrF(NH_3)_5^{2+}$–Al^{3+} [1] and $CoF(NH_3)_5^{2+}$–Al^{3+} [2] reactions have revealed that the reaction rates are approximately first-order with respect to each reactant and that the effects of ClO_4^- and $Co(CN)_6^{3-}$ on the former reaction can be explained from a purely electrostatic point of view. The assisted aquations in the presence of competing nucleophiles have been widely studied[3–8] and have thrown light on the reaction mechanism, in particular on the reaction intermediate. Among others, Posey and Taube[3] and Buckingham *et al.*[8] have explained the results in terms of the formation of ion pairs between the reactants and the nucleophiles. The ion pair formed in the intermediate step has, however, not been well characterized.

The present study has been undertaken in order to obtain information about the competition in the $CoF(NH_3)_5^{2+}$–Al^{3+} reaction. The nucleophilic anions used were sulfate, oxalate, and malonate ions. As they strongly interact with the reactant cations, they are useful in helping to see the role of the ion pair or complex formation in the reaction. The relationship between the product percentages and the reaction rates will be clarified by observing the effect of the sulfate ion in the pH range where the formation of HSO_4^- is slight. The strong affinities of the dicarboxylate ions(oxalate ion=ox^{2-}, or malonate ion=mal^{2-}) to the aluminium ion will give their specific behavior in the reaction.

Experimental

Materials. The preparation and confirmation of the $[CoF(NH_3)_5](ClO_4)_2$ crystals, $NaClO_4$ crystals, $Al(ClO_4)_3$ solution, and $Na_3[Co(CN)_6]\cdot 2H_2O$ crystals were made as has previously been described.[1,2] The anhydrous sodium oxalate was a guaranteed reagent from Wako Pure Chemicals Industries, Ltd., and was dried at 300 °C for one hour before use. Anhydrous sodium malonate, an extra pure reagent from Nakarai Chemicals Industries, was recrystallized from a water–methanol (1:1) solution, dried *in vacuo* at 60 °C, and then used. (Found: C, 24.00, H, 1.44%. Calcd for $Na_2C_3H_2O_4$: C, 24.34, H, 1.36%).

Kinetic Measurements. The sample solutions contained the anion and the aluminium ion in different concentrations and had different pH values, while they contained the complex ion in a constant concentration of 5.0×10^{-3} mol dm^{-3}. The kinetics were studied spectrophotometrically. Absorbance changes were followed at 480 nm in the cases of $Co(CN)_6^{3-}$ and SO_4^{2-} and at 500 nm in the cases of ox^{2-} and mal^{2-}. The pseudo-first-order rate constants, k_{obsd}, were determined by plotting $\ln|D_t-D_\infty|$ *vs.* t, where D_t and D_∞ are the absorbances at the time t and at the time when the absorbance becomes almost constant respectively. The kinetic studies were made at 25.0±0.1 °C unless otherwise stated.

Competition in the Formation of Products. After the reaction had been completely terminated, the reaction solution was added to a column of SP-Sephadex and eluted with a 0.15 mol dm^{-3} sodium-sulfate solution. Two bands were observed; the first was assigned to the aniono complex, and the second, to the aqua complex. The concentration ratios of the two complexes can be calculated by means of the following equation:

$$\frac{c_X}{c_A}=\frac{\varepsilon_A}{\varepsilon_X}\frac{D_X V_X}{D_A V_A},$$

where ε and D are the molar absorption coefficients and the absorbances at the absorption maxima respectively, where V is the volume of the eluate, and where the subscripts, X and A, indicate the aniono complexes and the aqua complex respectively. The ε values used are 47.5 at 492 nm for the aqua complex, 59.3 at 515 nm for the sulfato complex, 78.0 at 503 nm for the oxalato complex, and 74.9 at 503 nm for the malonato complex. We here use the product percentages defined as:

$$F=\frac{c_X}{c_X+c_A}\times 100\%.$$

Measurements of the pH and of the ^{19}F NMR followed previous studies;[1,2] the observed pH values were used without correction.

Results and Discussion

In a previous study, hexacyanocobaltate(III) ions have been shown to accelerate the $CrF(NH_3)_5^{2+}$–Al^{3+}

** A preliminary report on this work has been published in *Chem. Lett.*, **1981**, 781.

TABLE 1. EFFECTS OF $[Co(CN)_6^{3-}]$ ON THE REACTION RATES
(The ionic strength was not controlled. pH: 1.76±0.02. Runs 1—6 were made at 35 °C, and Runs 7—11, at 25 °C.)

Run	$[Al^{3+}]$/mol dm^{-3}	$[Co(CN)_6^{3-}]$/mol dm^{-3}	k_{obsd}/s^{-1}
1	0.10	0	2.6×10^{-4}
2	0.10	0.025	3.9×10^{-4}
3	0.10	0.050	5.5×10^{-4}
4	0.10	0.10	8.1×10^{-4}
5	0.10	0.20	8.9×10^{-4}
6	0.10	0.30	8.7×10^{-4}
7	0.051	0	3.3×10^{-5}
8	0.051	0.050	9.8×10^{-5}
9	0.051	0.10	1.2×10^{-4}
10	0.051	0.15	1.2×10^{-4}
11	0.051	0.20	1.3×10^{-4}

TABLE 2. DEPENDENCE OF THE RATE CONSTANTS ON THE CONCENTRATION OF SULFATE IONS
($[Al^{3+}]_{total}=0.051$ mol dm^{-3}, $[CoF(NH_3)_5^{2+}]_{initial}=5.0\times10^{-3}$ mol dm^{-3}, pH 2.9±0.1.)

$[SO_4^{2-}]$/mol dm^{-3}	$k_{obsd}\times10^4$/s^{-1}	I_{calcd}[a]
0	0.33	0.321
0.010	0.80	0.295
0.025	1.93	0.270
0.050	4.98	0.258
0.075	6.50	0.290
0.10	8.54	0.345
0.20	14.0	0.616
0.30	15.0	0.906

a) The ionic strengths are the values calculated considering the formation of ion pairs, $Al^{3+}\cdot SO_4^{2-}$.

reaction.[1] A similar acceleration effect was shown by the same anion on the $CoF(NH_3)_5^{2+}$–$Al(ClO_4)_3$ reaction systems. This is shown in Table 1, in which the reaction rate approaches saturation above the concentration ratio of $[Co(CN)_6^{3-}]/[Al^{3+}]\approx2$. These results can be understood from the formation of ion-pairs between the anions and the reacting cations.

TABLE 3. THE YIELDS OF $CoSO_4(NH_3)_5^+$
($[Al^{3+}]_{total}=0.051$ mol dm^{-3}, $[CoF(NH_3)_5^{2+}]_{initial}=5.0\times10^{-3}$ mol dm^{-3}, pH 2.9±0.1.)

$[SO_4^{2-}]_{total}$/mol dm^{-3}	F/%
0.010	19.8
0.025	26.4
0.050	29.6
0.075	31.7
0.10	32.5
0.20	32.4
0.30	32.7

Effects of Sulfate Ions. The results of the competition study of the sulfate ion are listed in Tables 2 and 3. A comparison of these tables shows a significant difference between the saturation of the rate constant and that of the yield of $CoSO_4(NH_3)_5^+$; thus, the saturation of the product percentage (33%) for $CoSO_4(NH_3)_5^+$ appears at nearly $[SO_4^{2-}]_{total}=0.1$ mol dm^{-3}, while the reaction rate reaches saturation at the higher sulfate concentration of $[SO_4^{2-}]_{total}>0.2$ mol dm^{-3}. The relation between the reaction rate and the product percentage has not yet been discussed for the competition reactions hitherto studied. In order to explain the relation, we shall describe the rate constants and the yields of $CoSO_4(NH_3)_5^+$ from the reaction scheme containing the sulfate ion. As both the anation,

$$CoOH_2(NH_3)_5^{3+} + SO_4^{2-} \xrightarrow{k_{an}} CoSO_4(NH_3)_5^+ + H_2O,$$

and the aquation,

$$CoSO_4(NH_3)_5^+ + H_2O \xrightarrow{k_{aq}} CoOH_2(NH_3)_5^{3+} + SO_4^{2-},$$

are known to be very slow ($k_{an}=1.49\times10^{-5}$ mol^{-1} dm^3 s^{-1} and $k_{aq}=1.20\times10^{-6}$ s^{-1} at 25 °C, I=0.5 mol dm^{-3}),[9] the formation of a considerable quantity of sulfato-complex ions can be attributed to the entry of sulfate ions into the inner sphere of the cobalt(III) ion immediately after the rate-determining step. The following scheme can be considered for the reaction in the presence of the sulfate ion:

$$CoF^{2+} + SO_4^{2-} \overset{K_1^{ip}}{\rightleftharpoons} CoF^{2+}\cdot SO_4^{2-}$$

$$Al^{3+} + SO_4^{2-} \overset{K_2^{ip}}{\rightleftharpoons} Al^{3+}\cdot SO_4^{2-}$$

$$\text{I}\quad CoF^{2+} + Al^{3+} \overset{K_I}{\rightleftharpoons} CoF^{2+}Al^{3+} \xrightarrow{k_I} CoFAl^{5+} \xrightarrow{\text{fast}} CoOH_2(NH_3)_5^{3+}$$

$$\text{II}\quad CoF^{2+} + Al^{3+}SO_4^{2-} \overset{K_{II}}{\rightleftharpoons} CoF^{2+}Al^{3+}SO_4^{2-} \xrightarrow{k_{II}} CoFAl^{5+}SO_4^{2-}$$

$$\text{III}\quad CoF^{2+}SO_4^{2-} + Al^{3+} \overset{K_{III}}{\rightleftharpoons} CoF^{2+}SO_4^{2-}Al^{3+} \xrightarrow{k_{III}} CoFAl^{5+}SO_4^{2-}$$

$$\left.\begin{matrix}\text{II}\\ \text{III}\end{matrix}\right\} \xrightarrow{\text{fast}} \left\{\begin{matrix}CoOH_2(NH_3)_5^{3+}\\ +\\ CoSO_4(NH_3)_5^+,\end{matrix}\right.$$

$$\text{IV}\quad CoF^{2+}SO_4^{2-} + Al^{3+}SO_4^{2-} \overset{K_{IV}}{\rightleftharpoons} SO_4^{2-}\text{–}CoF^{2+}SO_4^{2-}\text{–}Al^{3+} \xrightarrow{k_{IV}} SO_4^{2-}\text{–}CoFAl^{5+}SO_4^{2-} \xrightarrow{\text{fast}} \left\{\begin{matrix}CoOH_2(NH_3)_5^{3+}\\ +\\ CoSO_4(NH_3)_5^+,\end{matrix}\right.$$

where $CoF(NH_3)_5^{2+}$ is abbreviated as CoF^{2+} and where $CoFAl^{5+}$ indicates that F and Al are bonded more strongly than in $CoF^{2+}Al^{3+}$. The following conditions will be used in the discussion below:

1) The ion association of sulfate ions with the cobalt-complex ions had only a negligible effect on the sulfate-ion concentration, as the concentration of the cobalt complex was very low.

2) The formation of HSO_4^- ($\log K=1.36$, I=0.5 mol dm^{-3})[10] was not significant, as the experiments were carried out in the $(pH)_{obsd}$ range of 2.8—3.0.

3) As soon as the fluoride ligand was extracted by the aluminium ion, a sulfate ion or a water molecule rapidly entered the coordination sphere of the cobalt(III) ion; thus, the extraction of the fluoride ligand is the rate-determining step for the formation

of either the aqua or the sulfato complex.

4) The formation constants (K_I—K_{IV}) of the precursors of the reaction intermediates are small enough in comparison with the ion-pair formation constants, K_1^{ip} and K_2^{ip}.

Letting a, b, and c represent the total initial concentrations of $CoF(NH_3)_5^{2+}$, Al^{3+}, and SO_4^{2-} respectively, the reaction rate can be expressed as:

$$\begin{aligned}\text{Rate} &= k_{obsd}\,a = k_I K_I[CoF^{2+}][Al^{3+}] \\ &\quad + (k_{II}K_{II}K_2^{ip} + k_{III}K_{III}K_1^{ip})[CoF^{2+}][Al^{3+}][SO_4^{2-}] \\ &\quad + k_{IV}K_{IV}K_1^{ip}K_2^{ip}[CoF^{2+}][Al^{3+}][SO_4^{2-}]^2 \\ &= k_0(a-x_1)(b-x_2) + k_1[x_2(a-x_1)+x_1(b-x_2)] \\ &\quad + k_2x_1x_2, \qquad (1)\end{aligned}$$

where x_1 and x_2 denote the concentrations of two ion-pairs, $CoF^{2+}SO_4^{2-}$ and $Al^{3+}SO_4^{2-}$ respectively, and where the rate constants,

$$k_0 = k_I K_I,\ k_1 = \frac{k_{II}K_{II}K_2^{ip} + k_{III}K_{III}K_1^{ip}}{K_1^{ip}+K_2^{ip}},$$

and

$$k_2 = k_{IV}K_{IV},$$

have identical dimensions of $mol^{-1}\,dm^3\,s^{-1}$. The value of k_0 in Eq. 1 should be equal to the k_{obsd} value at $c=0$ ($6.6\times10^{-4}\,mol^{-1}\,dm^3\,s^{-1}$). The other rate constants, k_1 and k_2, can be determined from the results given in Table 2 by the use of the x_1 and x_2 values, which were calculated for each run by the method of successive approximations in the following way. The ion-pair formation constants are:

$$K_1^{ip} = \frac{x_1}{(a-x_1)(c-x_2)}, \qquad (2)$$

$$K_2^{ip} = \frac{x_2}{(b-x_2)(c-x_2)}, \qquad (3)$$

where $c-x_1-x_2$ has been approximated by $c-x_2$. As suming provisionally the ionic strength based on the analytical concentrations, the known values of the constants, $\log K_1^{ip}=2.46$ ($I=0$)[11] and $\log K_2^{ip}=3.73$ ($I=0$),[12] were corrected for the ionic strength by using the Davies equation:

$$\log y_i = -0.512\,z_i^2\left(\frac{\sqrt{I}}{1+\sqrt{I}} - 0.3I\right). \qquad (4)$$

The concentrations of the ion pairs, x_1 and x_2, were calculated by the use of Eqs. 2 and 3, and the ionic strength was re-evaluated. The final values of x_1 and x_2 were obtained by repeating such calculations until their values became unchanged within 0.01% of their respective values. Using x_1 and x_2 for each run, one can determine the rate constants, k_1 and k_2, from Eq. 1 so as to fit the observed rate constants, k_{obsd}: $k_1=(4.0\pm0.2)\times10^{-3}\,mol^{-1}\,dm^3\,s^{-1}$ and $k_2=(3.0\pm0.2)\times10^{-2}\,mol^{-1}\,dm^3\,s^{-1}$. These constants were obtained at the ionic strengths of 0.32 for k_0, 0.26—0.34 for k_1, and 0.3—0.9 for k_2 (Table 2); the effective charge of one of the reactants participating in each of the II—IV paths is low (+1 for II, and 0 for III and IV), so that the values of k_1 and k_2 will not be appreciably affected by the ionic-strength change.

The expression for the yields of $CoSO_4(NH_3)_5^+$, F (in %) on the basis of the reaction scheme given above is:

$$F/100 = [r_1k_1\{x_2(a-x_1)+x_1(b-x_2)\} + r_2k_2x_1x_2]/(k_{obsd}a), \qquad (5)$$

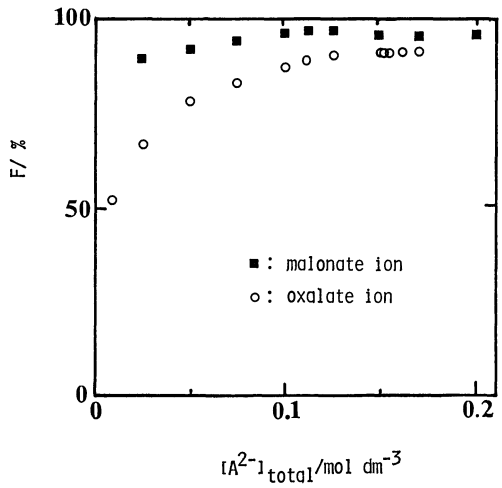

Fig. 1. The yield of $CoA(NH_3)_5^+$ depending on the concentration of the anions.
$[CoF(NH_3)_5^{2+}]_{initial}=5.0\times10^{-3}$ mol dm^{-3}, $[Al^{3+}]_{total}=5.1\times10^{-2}$ mol dm^{-3}.

where r_1 and r_2 are the fractions of SO_4^{2-} entering into the coordination sphere of cobalt(III) in competition with the H_2O solvent when AlF^{2+} leaves $CoF(NH_3)_5^{2+}SO_4^{2-}$-$Al^{3+}$ and SO_4^{2-}-$CoF(NH_3)_5^{2+}SO_4^{2-}$-$Al^{3+}$ respectively. In Eq. 5, all the parameter values except for r_1 and r_2 have been obtained in the analysis of the reaction rates. The value of r_2 can be taken as 0.33, which is the F/100 value at the saturation (Table 3). Then, $r_1=0.27\pm0.02$ results, thus fitting the experimental F values listed in Table 3. The r_1 and r_2 values are of comparable magnitude, in contrast to the significant difference between the k_1 and k_2 values. Thus, the reaction through Path IV is very important in determining the reaction rates, while Path IV only slightly increases the fraction of SO_4^{2-} entering into the coordination sphere of the cobalt(III). The second sulfate ion contained in the reaction intermediate assists the two reactant cations in approaching each other, but it rarely enters the coordination sphere of the cobalt(III) in the intermediate step.

Effects of Oxalate and Malonate Ions. The competition reactions were also examined in the presence of oxalate ions and of malonate ions. The product percentages and the rate constants are shown in Figs. 1 and 2 respectively. The effects of these ions distinctly differ from that of the sulfate ion in both the reaction rates and the products: (1) The reactions are more effectively accelerated by the dicarboxylate anions, but at high concentrations of the anions the reaction rate decreases instead of reaching saturation, and (2) the yields of the anionopentaamminecobalt(III) ions are unusually high. These specific effects of the anions have not so far been reported for the competition reactions accompanying the assisted aquations of the pentaamminecobalt(III) complexes.[3-8]

As the dicarboxylate ions tend to form complexes with the aluminium ion,[13,14] the present reactions can be regarded as reactions between $CoF(NH_3)_5^{2+}$ and AlA_n^{3-2n}. In order to confirm the stoichiometry, we made a ^{19}F NMR study of the final products existing

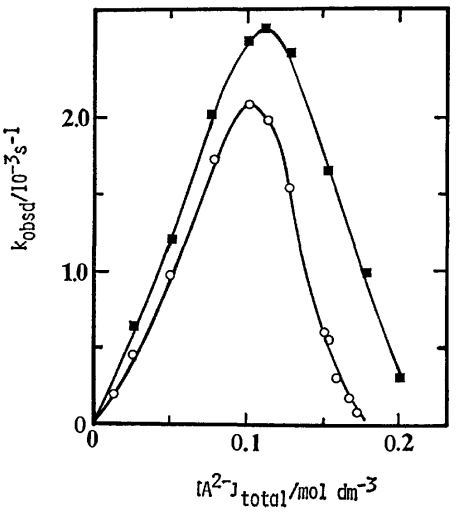

Fig. 2. Dependence of the rate constant on the concentration of the anions.
○: Oxalate ion, ■: malonate ion. $[CoF(NH_3)_5^{2+}]_{initial}=5.0\times10^{-3}$ mol dm^{-3}, $[Al^{3+}]_{total}=5.1\times10^{-2}$ mol dm^{-3}.

in the reaction solutions. The measurements were made for three samples varying in their concentrations of the added sodium oxalate, but with unchanged conditions of $[CoF(NH_3)_5^{2+}]_{initial}=0.050$ mol dm^{-3} and $[Al^{3+}]_{total}=0.20$ mol dm^{-3}. The values of the chemical shift (δ) of the main peak with reference to F^- were −35.2, −38.4, and −38.8 for $[ox^{2-}]_{total}=$ 0.20, 0.41, and 0.61 mol dm^{-3} respectively; the signal of $CoF(NH_3)_5^{2+}$ could not be detected. A solution of [NaF]=0.050 mol dm^{-3}, $[Al^{3+}]_{total}=0.20$ mol dm^{-3}, and $[ox^{2-}]_{total}=0.41$ mol dm^{-3} was also measured as a reference; it gave a peak at −38.5 from F^-. As the chemical shift of the AlF^{2+} peak is −36.1 from F^-,[2] the above results suggest the formation of the Al–F bonding. (The small differences among them may be due to the effect of oxalate ligands in the aluminium complexes.) A comparison of the peak areas between the samples and the reference reveals that most of the fluoride ions in the initial $CoF(NH_3)_5^{2+}$ had moved to the aluminium ions in every case. The ^{19}F NMR results, together with the results shown in Fig. 2, lead to the conclusion that the reaction:

$$CoF(NH_3)_5^{2+} + AlA_n^{3-2n} \longrightarrow CoA(NH_3)_5^{+} + AlFA_{n-1}^{4-2n},$$

produced about a 90% yield when $[A^{2-}]_{total} > [Al^{3+}]_{total} \gg [CoF(NH_3)_5^{2+}]_{initial}$.[15]

The mechanism of the reaction will be considered next. It is very improbable that the oxalate or the malonate ion enters into the coordination sphere of cobalt(III) after the formation of the aquapentaamminecobalt(III) ion, because the anation reaction of the aqua complex by these anions proceeds much more slowly than the present reaction.[16,17] This was confirmed by examining the reaction of the aqua complex with an excess of the oxalato- or the malonato-aluminium complex. The spectrum of the mixed solution remained unchanged for several days at 25 °C, and only the aqua complex was detected by means of a chromatographic technique using an SP-Sephadex column and a 0.15 mol dm^{-3} sodium-sulfate solution. It can, therefore, be concluded that the anion directly enters into the coordination sphere of cobalt(III) as soon as the aluminium ion extracts the fluoride ion from $CoF(NH_3)_5^{2+}$. The present reaction seems to be interesting as an extreme case of a competition reaction and can be classified as a double-ligand-exchange reaction, which is a very rare type of the reactions of the octahedral inert complexes.[18] This specific reaction will arise from the strong affinity of the aluminium ion to the dicarboxylate ions, combined with the residual capacity of the aluminium-bonded dicarboxylate ions for coordinating with cobalt(III). The latter factor is probably important, for the yield of the acetatopentaamminecobalt(III) in the $CoBr(NH_3)_5^{2+}$–$Hg(CH_3CO_2)_2$ system[7] was low (18.0 or 19.0%) in spite of the large formation constants of mercury–acetate complex. ($\log K_1=5.55$, $\log \beta_2=$ 9.30, at $I=1.0$ mol dm^{-3}).[19] A general rule for a high yield of the anionopentaamminecobalt(III) to be obtained in the competition reactions will be found by further studies of various systems.

An attempt was made to detect the formation of an intermediate in the present reaction. A binuclear complex such as $[(NH_3)_5Co\cdot\overset{F}{\underset{A}{\cdot}}\cdot Al]^{3+}$ might be present in the intermediate step. A rapid-scan spectrophotometer was used to follow the absorption change in the $CoF(NH_3)_5^{2+}$–Al^{3+}–ox^{2-} system (1:10:20, concentration ratio) in the wavelength region of about 290 to 350 nm, where $Coox(NH_3)_5^{+}$ or $CoHox(NH_3)_5^{2+}$ has a specific charge-transfer band originating in the Co–ox bonding. No species other than reactants and products were, however, detected in the time scale of 10 ms—10 s. This experiment was not able to distinguish between the dissociative and associative mechanisms.

The rate constants shown in Fig. 2 have a maximum approximately at the position of $[A^{2-}]_{total}/[Al^{3+}]_{total}=$ 2, decreasing on both sides with a less steep slope on the left side. These characteristics of the curve may result from different reactivities of the AlA_n^{3-2n} complexes with different n values. Thus, the concentrations of a series of aluminium–dicarboxylate species in each solution were calculated on the basis of the literature values of the successive formation constants, K_n and the acid dissociation constants, K_{a1} and K_{a2}, of the dicarboxylic acid: $\log K_1=6.06$, $\log K_2=5.03$, and $\log K_3=4.03$ for the Al^{3+}–ox^{2-} system ($I=$ 1.0 mol dm^{-3}),[13] $\log K_1=5.24$, $\log K_2=4.16$, and $\log K_3=4.06$ for the Al^{3+}–mal^{2-} system ($I=0.2$ mol dm^{-3}),[14] $pK_{a1}=3.5$ and $pK_{a2}=1.1$ for oxalic acid, and $pK_{a1}=5.1$ and $pK_{a2}=2.6$ for malonic acid at $I=1.0$ mol dm^{-3}.[20] The results are listed in Table 4, together with the kinetic results and the observed pH value. For $[A^{2-}]_{total}/[Al^{3+}]_{total}=1.0$ and 2.0, the calculated concentration of each aluminium complex and the observed rate constant vary in proportion to $[Al^{3+}]_{total}$ or $[A^{2-}]_{total}$, while the pH value changes without affecting their proportionality. From Fig. 2, the reactivities of the aluminium species can be expected to decrease in this order: $AlA_2^{-} > AlA^{+} > AlA_3^{3-}$

TABLE 4. DEPENDENCE OF THE RATE CONSTANTS ON THE CONCENTRATION OF THE ALUMINIUM COMPLEX ($[CoF(NH_3)_5^{2+}]=5.0\times10^{-3}$ mol dm^{-3}, $I^{a)}=0.80\pm0.02$ mol dm^{-3}; 25 °C.)

(I) A=ox	$[Al^{3+}]$	$[Alox^+]$	$[Alox_2^-]$	$[Alox_3^{3-}]$	k_{obsd}/s^{-1}	$(pH)_{obsd}$
(a) $[Al^{3+}]^{b)}_{total}=[ox^{2-}]_{total}$						
0.202	4.34×10^{-2}	1.18×10^{-1}	3.92×10^{-2}	1.73×10^{-3}	3.46×10^{-3}	1.70
0.101	2.18×10^{-2}	5.88×10^{-2}	1.95×10^{-2}	8.56×10^{-4}	1.72×10^{-3}	1.80
0.0505	1.09×10^{-2}	2.94×10^{-2}	9.79×10^{-3}	4.29×10^{-4}	9.28×10^{-4}	2.10
0.0303	6.54×10^{-3}	1.76×10^{-2}	5.85×10^{-3}	2.56×10^{-4}	5.54×10^{-4}	2.20
(b) $[Al^{3+}]_{total}=\frac{[ox^{2-}]_{total}}{2.0}$						
0.202	2.15×10^{-3}	4.50×10^{-2}	1.16×10^{-1}	3.92×10^{-2}	5.68×10^{-3}	1.51
0.101	8.67×10^{-4}	2.02×10^{-2}	5.80×10^{-2}	2.19×10^{-2}	2.75×10^{-3}	3.88
0.0505	4.34×10^{-4}	1.01×10^{-2}	2.90×10^{-2}	1.10×10^{-2}	1.38×10^{-3}	3.97
	4.40×10^{-4}	1.02×10^{-2}	2.90×10^{-2}	1.09×10^{-2}	1.35×10^{-3}	3.07
0.0303	2.61×10^{-4}	6.08×10^{-3}	1.74×10^{-2}	6.56×10^{-3}	7.61×10^{-4}	4.07
(c) $[Al^{3+}]_{total}=\frac{[ox^{2-}]_{total}}{3.0}$						
0.0909	8.51×10^{-8}	6.74×10^{-5}	6.56×10^{-3}	8.43×10^{-2}	3.22×10^{-4}	3.10
0.0505	1.07×10^{-7}	6.42×10^{-5}	4.72×10^{-3}	4.57×10^{-2}	1.43×10^{-4}	3.12
	2.16×10^{-7}	1.01×10^{-4}	5.85×10^{-3}	4.45×10^{-2}	2.32×10^{-4}	2.89
0.0303	1.31×10^{-7}	6.14×10^{-5}	3.53×10^{-3}	2.67×10^{-2}	1.01×10^{-4}	3.13

(II) A=mal	$[Al^{3+}]$	$[Almal^+]$	$[Almal_2^-]$	$[Almal_3^{3-}]$	k_{obsd}/s^{-1}	$(pH)_{obsd}$
(a) $[Al^{3+}]_{total}=[mal^{2-}]_{total}$						
0.182	5.97×10^{-2}	1.08×10^{-1}	1.34×10^{-2}	1.11×10^{-3}	6.01×10^{-3}	1.83
0.101	2.87×10^{-2}	6.21×10^{-2}	9.31×10^{-3}	9.22×10^{-4}	3.42×10^{-3}	2.33
0.0505	1.26×10^{-2}	3.17×10^{-2}	5.52×10^{-3}	6.35×10^{-4}	1.76×10^{-3}	2.68
0.0303	6.89×10^{-3}	1.92×10^{-2}	3.71×10^{-3}	4.74×10^{-4}	1.09×10^{-3}	3.02
(b) $[Al^{3+}]_{total}=\frac{[mal^{2-}]_{total}}{2.0}$						
0.182	5.25×10^{-3}	7.06×10^{-2}	6.57×10^{-2}	4.04×10^{-2}	8.31×10^{-3}	2.50
0.101	3.03×10^{-3}	3.99×10^{-2}	3.63×10^{-2}	2.18×10^{-2}	4.10×10^{-3}	2.75
0.0505	8.28×10^{-4}	1.50×10^{-2}	1.89×10^{-2}	1.57×10^{-2}	1.76×10^{-3}	4.09
	1.69×10^{-3}	2.09×10^{-2}	1.79×10^{-2}	1.01×10^{-2}	1.95×10^{-3}	2.90
	7.70×10^{-3}	3.18×10^{-2}	1.09×10^{-2}	7.52×10^{-5}	1.97×10^{-3}	1.98
0.0303	9.34×10^{-4}	1.21×10^{-2}	1.08×10^{-2}	6.42×10^{-3}	1.24×10^{-3}	3.13
(c) $[Al^{3+}]_{total}=\frac{[mal^{2-}]_{total}}{3.0}$						
0.0909	5.43×10^{-6}	9.05×10^{-4}	1.04×10^{-2}	7.95×10^{-2}	1.70×10^{-3}	3.96
0.0505	4.99×10^{-7}	1.55×10^{-4}	3.32×10^{-3}	4.70×10^{-2}	5.04×10^{-4}	4.95
	6.25×10^{-6}	8.07×10^{-4}	7.20×10^{-3}	4.25×10^{-2}	9.25×10^{-4}	3.99
	2.13×10^{-3}	2.29×10^{-2}	1.71×10^{-2}	8.40×10^{-3}	1.92×10^{-3}	2.39
0.0303	7.46×10^{-6}	7.53×10^{-4}	5.26×10^{-3}	2.43×10^{-2}	5.85×10^{-4}	4.00

a) The ionic strength was controlled with $NaClO_4$, considering the formation of the Al^{3+}-A^{2-} complexes shown in this table. b) All brackets denote the concentration in mol dm^{-3}.

and Al^{3+}. Therefore, when $[A^{2-}]_{total}/[Al^{3+}]_{total}=1.0$ and 2.0, the contribution of AlA_3^{3-} and Al^{3+} to the reaction can be neglected, and the observed rate constant can be expressed as: $k_{obsd}=k_1[AlA^+]+k_2[AlA_2^-]$. The values of k_1 and k_2 can be obtained so as to fit the experimental values, starting from the first approximate value of $k_2=k_{obsd}/[AlA_2^-]$ for the case of $[A^{2-}]_{total}/[Al^{3+}]_{total}=2.0$. The k_1 and k_2 values thus obtained are: $(1.5\pm0.1)\times10^{-2}$ mol^{-1} dm^3 s^{-1} and $(4.5\pm0.3)\times10^{-2}$ mol^{-1} dm^3 s^{-1} for A=ox, and $(4.2\pm0.3)\times10^{-2}$ mol^{-1} dm^3 s^{-1} and $(7.5\pm0.5)\times10^{-2}$ mol^{-1} dm^3 s^{-1} for A=mal. When $[A^{2-}]_{total}/[Al^{3+}]_{total}=3.0$, the concentrations of the aluminium complexes are more sensitive to the pH value; therefore, the calculated concentrations may be accompanied by considerable errors resulting from possible errors in the equilibrium constants and in the pH values. The gross rate constants calculated with the k_1 and k_2 values obtained above are 10—50% larger than the experimental values for A=ox, even when $Alox_3^{3-}$ is assumed to be nonreactive, while, for A=mal, they are 10—50% smaller than the experimental values

TABLE 5. DEPENDENCE OF THE RATE CONSTANTS ON THE TEMPERATURES

([cobalt complex] $=5.0\times10^{-3}$ mol dm^{-3}, $I_{app}=0.61$ mol dm^{-3}.)

(I) $[Al^{3+}]_{total}=\frac{1}{2.0}[ox^{2-}]_{total}=0.051$ mol dm^{-3}

T/°C	$10^3\times xk_{obsd}$/s^{-1}
20	1.17
25	1.97
30	3.02
35	4.17

(II) $[Al^{3+}]_{total}=\frac{1}{2.0}[mal^{2-}]_{total}=0.051$ mol dm^{-3}

T/°C	$10^3\times k_{obsd}$/s^{-1}
20	1.73
25	2.35
30	3.58
35	5.37

when calculated on the assumption that $Almal_3^{3-}$ is not reactive. It may, therefore, be said that the reactivity of $Alox_3^{3-}$ is low, while $Almal_3^{3-}$ is reactive to some extent.

The fact that the reactivity of AlA_2^- is the largest among the consecutive complexes can be attributed to the favorable characteristics that the complex electrostatically assists the two reactant cations in approaching each other and that it can easily react with the fluoride ligand of the cobalt complex. On the other hand, in spite of its larger negative charge, AlA_3^{3-} is not so reactive, probably because the aluminium ion is masked by the ligands in this complex. The malonate ion more effectively accelerates the reaction and increases the yield of $CoA(NH_3)_5^+$. This may be attributable to the flexibility of the chelate ring formed by malonate ligands; the central aluminium ion of the more flexible malonato complex may more easily come in contact with the fluoride ligand of the cobalt(III) complex, and the malonate ion may be more easily transferred to the cobalt(III).

The yields of $CoA(NH_3)_5^+$ are not listed in Table 4, because they scarcely depended at all on the concentration of the aluminium complex (varying only within 1%); they depended only on the $[A^{2-}]_{total}/[Al^{3+}]_{total}$ ratio (see Fig. 1).

Table 5 shows the rate constants at different temperatures with $[A^{2-}]_{total}/[Al^{3+}]_{total}=2.0$ (the ionic strength is given in the analytical concentration). They give the values of ΔH^* and ΔS^* as 57 ± 3 kJ mol^{-1} and -92 ± 14 J K^{-1} mol^{-1} respectively for A=ox, and as $\Delta H^*=55\pm2$ kJ mol^{-1} and $\Delta S^*=-110\pm11$ J K^{-1} mol^{-1} respectively for A=mal. These values approximately agree with each other, but they are significantly different from the values, $\Delta H^*=74$ kJ mol^{-1} and $\Delta S^*=-72$ J K^{-1} mol^{-1}, for the reaction in the $CoF(NH_3)_5^{2+}$–Al^{3+} system ($I=0.61$ mol dm^{-3}).[2] The activation enthalpies are depressed by the electrostatic attraction of the anions to both the reactant cations, while the activation entropies decrease as a result of a stringent geometrical condition to form the activated complex. These effects are similar to that of added salts on the activation parameters in a cation-cation reaction.[21]

References

1) M. Iida and H. Yamatera, *Bull. Chem. Soc. Jpn.*, **54**, 441 (1981).
2) M. Iida, E. Kai, K. Nishimoto, and H. Yamatera, *Bull. Chem. Soc. Jpn.*, **54**, 1818 (1981).
3) F. A. Posey and H. Taube, *J. Am. Chem. Soc.*, **79**, 255 (1957).
4) D. A. Buckingham, I. I. Olsen, A. M. Sargeson, and H. Satrapa, *Inorg. Chem.*, **6**, 1027 (1967).
5) W. L. Reynolds and E. R. Alton, *Inorg. Chem.*, **17**, 3355 (1978).
6) W. L. Reynolds, S. Hafezi, A. Kessler, and S. Holly, *Inorg. Chem.*, **18**, 2860 (1979).
7) W. G. Jackson, G. A. Lawrance, and A. M. Sargeson, *Inorg. Chem.*, **19**, 1001 (1980).
8) D. A. Buckingham, C. R. Clark, and W. S. Webley, *J. Chem. Soc., Dalton Trans.*, **1980**, 2255.
9) H. Taube and F. A. Posey, *J. Am. Chem. Soc.*, **75**, 1463 (1953).
10) G. G. Davis and W. M. Smith, *Can. J. Chem.*, **40**, 1836 (1962).
11) The value used here was obtained for the $CoCl(NH_3)_5^{2+}$–SO_4^{2-} system; D. W. Archer, D. A. East, and C. B. Monk, *J. Chem. Soc.*, **1965**, 720.
12) T. Nishide and R. Tsuchiya, *Bull. Chem. Soc. Jpn.*, **38**, 1398 (1965).
13) E. Bottari and L. Ciavatta, *Gazz. Chim. Ital.*, **98**, 1004 (1968).
14) a) V. T. Athavale, N. Mahadevan, P. K. Mathur, and R. M. Sathe, *J. Inorg. Nucl. Chem.*, **29**, 1947 (1967); b) N. K. Dutt and P. Bose, *Z. Anorg. Allg. Chem.*, **295**, 131 (1958).
15) Under the present conditions, the products of the cobalt complexes will be protonated to some extent.[16,17] The present discussion will, however, not be influenced by the protonation.
16) C. Andrade and H. Taube, *Inorg. Chem.*, **5**, 1087 (1966).
17) A. C. Dash and R. K. Nanda, *J. Inorg. Nucl. Chem.*, **38**, 119 (1976).
18) D. W. Margerum, "Coordination Chemistry," ed by A. E. Martell, American Chemical Society, Washington, D. C. (1978), Vol. 2, p. 190.
19) D. Banerjea and I. P. Singh, *Z. Anorg. Allg. Chem.*, **331**, 225 (1964).
20) D. D. Perrin, "Stability Constants of Metal-Ion Complexes," Pergamon, Oxford (1979), Part B, pp. 26 and 98.
21) The effect of the ionic strength on the activation parameters for a cation-cation reaction has not been well established. As an example, our results for the *cis*-$CoClOH_2(phen)_2^{2-}$–Hg^{2+} system were $\Delta H^*=107\pm5$ kJ mol^{-1} and $\Delta S^*=41\pm10$ J K^{-1} mol^{-1} when only the reactants are present in the reaction solution ($I=0.03$ mol dm^{-3}) and $\Delta H^*=55\pm3$ kJ mol^{-1} and $\Delta S^*=-122\pm15$ J K^{-1} mol^{-1} when $I=1.0$ mol dm^{-3}, controlled by $NaClO_4$. (unpublished result)

 © 1982 The Chemical Society of Japan Bull. Chem. Soc. Jpn., 55, 1447—1453 (1982)

Reactivity of Fe_2O_3 and Fe_2O_3–Al_2O_3 Mixture for Reduction of SO_2 with CO

Tadao Ishii,* Ryusaburo Furuichi, and Koji Shikano

Department of Applied Chemistry, Faculty of Engineering, Hokkaido University, Kita-ku, Sapporo 060

(Received August 31, 1981)

Catalytic reactivities of α-Fe_2O_3 powder (−200 mesh) and a α-Fe_2O_3–γ-Al_2O_3 powder mixture prepared by mechanical mixing, which were preheated at 360—700 °C, were studied for the reduction of SO_2 with CO by means of both a reaction gas-chromatographic technique using CO, SO_2, and 2CO–SO_2 pulses and the powder X-ray analysis. The reactivity of Fe_2O_3 decreases with increasing preheating temperature, which is explained on the basis of redox reactions between Fe_2O_3 and nascent (Fe_3O_4): $6Fe_2O_3+2CO\rightarrow4(Fe_3O_4)+2CO_2$ and $4(Fe_3O_4)+SO_2\rightarrow6Fe_2O_3+1/2S_2$. It is considered that the reactivity of Fe_2O_3 is attributable to the activity of (Fe_3O_4). The lifetime of active (Fe_3O_4) is within about 1 min, and the activity and lifetime of (Fe_3O_4) is increased by interfacial reaction between Fe_2O_3 and Al_2O_3 at 700 °C. The activity maximum in the Fe_2O_3–Al_2O_3 system preheated at 700 °C is attained at 70—75 wt% Fe_2O_3.

The catalytic reduction of sulfur dioxide by carbon monoxide has been extensively investigated. It is generally accepted that the reduction proceeds in the range of about 300 to 600 °C in the following way:

$$SO_2 + 2CO \longrightarrow 2CO_2 + 1/2S_2, \quad (1)$$

$$1/2S_2 + CO \longrightarrow COS. \quad (2)$$

Many catalysts, such as metals, metal oxides, and their mixtures, have been used in the study. Few papers have been published on the use of Fe_2O_3 for preparing the catalyst. Khalafalla *et al.*[1-3] used a catalyst prepared by reducing mixtures of hematite and γ-Al_2O_3 at 600 °C for 1 h with H_2. The hematite constituent of the catalyst was completely reduced to iron. Clay and Lynn[4] reported that iron oxide supported on alumina is a promising catalyst/adsorbent for use in the simultaneous removal of NO_x and SO_x from power plant stack gases. Iron oxide is converted to the iron(II) state, and SO_2 is removed as iron(II) sulfide or sulfate. Kasaoka *et al.*[5] used the coprecipitated metal oxides, Fe_2O_3–Al_2O_3, Fe_2O_3–Cr_2O_3, Fe_2O_3–CuO–Al_2O_3, and Fe_2O_3–Cr_2O_3–Al_2O_3, which were reduced with H_2 at 550 °C. However, studies on catalysts prepared by mechanically mixing Fe_2O_3 and metal oxide powders are rarely found for the SO_2–CO reaction.

In a previous work,[6] Ishii *et al.* examined the reactivity of powder mixtures of α-Fe_2O_3 and metal oxide, α-Al_2O_3, γ-Al_2O_3, MgO, or CaO, on the basis of their catalytic behavior, in the reduction of SO_2 with CO at 300 °C, as characterized by means of reaction gas-chromatography and X-ray analysis. A maximum catalytic activity for reaction (1) was obtained at a specific mixing ratio for each mixture. In a pure pulse of CO, Fe_2O_3 was easily reduced to Fe_3O_4, but in a mixed pulse of $2CO+SO_2$, no change of Fe_2O_3 resulted. This behavior was discussed in connection with the redox reaction between Fe_2O_3 and (Fe_3O_4) in the following way:

$$6Fe_2O_3 + 2CO \longrightarrow 4(Fe_3O_4) + 2CO_2, \quad (3)$$

$$4(Fe_3O_4) + SO_2 \longrightarrow 6Fe_2O_3 + 1/2S_2, \quad (4)$$

where (Fe_3O_4) means nascent Fe_3O_4. The unique catalytic behavior of this powder mixture appeared to be related to a reaction at the interface between Fe_2O_3 and oxide, which occurred during preheating the mixture.

In the present paper, on the basis of reactions (3) and (4) proposed, reactivities of α-Fe_2O_3 powder and a α-Fe_2O_3–γ-Al_2O_3 powder mixture prepared by mechanical mixing, which were preheated at various temperatures, were studied in detail for the reduction of SO_2 with CO.

Experimental

Materials. Reagent grade commercial α-Fe_2O_3 (Kanto) and γ-Al_2O_3 (Merck), which are hereinafter written as Fe_2O_3 and Al_2O_3, respectively, were used without further purification. All starting materials were ground so as to pass a 200 mesh sieve. The powder mixture was prepared by mixing Fe_2O_3 and Al_2O_3 powders for 2 h by means of a rotating-V-type micro mixer (Tsutsui Rikagaku). Commercial SO_2 (Teikoku), CO (Nissan), and CO_2 (Hokusan) were used without further purification.

Preliminary Calcining (Preheating). Prior to reactivity tests, powder samples were preheated at various temperatures, 360, 600, and 700 °C, for 1 h in a flowing He (25 cm³/min) in the same reactor as was used for testing the reactivity. It was confirmed from X-ray analysis that, by these preheating processes, neither new products are formed in the Fe_2O_3–Al_2O_3 system nor any change in γ-Al_2O_3 is shown.

Apparatus and Procedures. A pulse method using a reaction gas-chromatograph (Hitachi, K-23 type) was applied to study of the adsorption of SO_2 and CO and of the catalytic reduction of SO_2 with CO. The standard experimental conditions were as follows: pulse interval, 25 min; pulse volume, 0.5 cm³ of SO_2 and 1 cm³ of CO; carrier gas, 25 cm³/min of He; reaction temperature, 360±5 °C; reactor, a quartz tube of 5.5 mm diameter; separating column, a stainless steel tube of 3 mm diameter; packing, Porapak-QS 80—100 mesh (Gasukuro Kogyo) at 60 °C. Eighty mg of a Fe_2O_3–Al_2O_3 powder mixture with a mixing ratio in the range 0—100% and 24—80 mg of Fe_2O_3 were packed in the reactor. Both sides of these packed samples were fixed by glass wool. A glass injection-syringe of 1 cm³ was used for injecting SO_2 and CO gases into the reactor. In order to inject the mixture of CO (1 cm³) and SO_2 (0.5 cm³), these gases were simultaneously injected by use of two syringes. After preheating the catalyst sample, the temperature of the reactor was adjusted to the reaction temperature 360 °C without lowering the sample temperature to room temperature. The time required for lowering the preheating temperature (600—700 °C) to the reaction

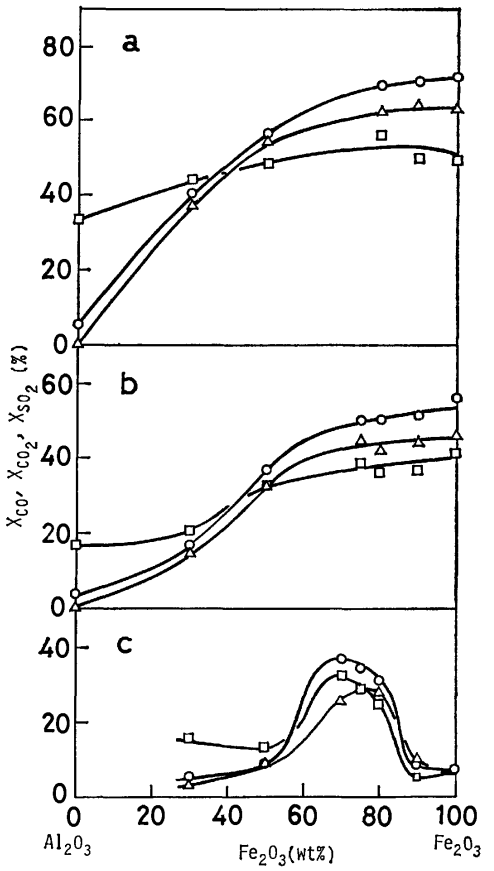

Fig. 1. Per cent conversions of CO and SO_2 (X_{CO} and X_{SO_2}), and % formation of CO_2 (X_{CO_2}) in $2CO+SO_2$ pulse for Fe_2O_3–Al_2O_3 systems with various mixing ratios and preheating temperatures.
Preheating temperature; (a): 360 °C, (b): 600 °C, (c): 700 °C. ○: X_{CO}, △: X_{CO_2}, □: X_{SO_2}.

temperature 360 °C was about 20—30 min. X-Ray analysis of samples before and after tests was carried out with a diffractometer (Geigerflex type-2004, Rigaku Denki) under the conditions: Co target, Fe filter, 35 kV, 10 mA, count full scale 1000 c/s, and scanning speed 1°/min.

Conversion of CO and SO_2 (X_{CO} and X_{SO_2}) and Formation of CO_2 (X_{CO_2}). For pulses of CO or SO_2 alone, areas of chromatographic peaks of CO, SO_2, and CO_2 at the outlet of reactor, relative to those for a blank test with no powder sample, were used for the determination of per cent conversions of CO (X_{CO}) and SO_2 (X_{SO_2}) and per cent formation of CO_2 (X_{CO_2}). The blank test for X_{CO_2} was carried out by using CO_2 gas.

For pulses of the mixture of CO and SO_2 ($2CO+SO_2$ pulse), the area of chromatographic peak of CO_2 at the outlet of reactor, relative to that of a blank test carried out using $2CO_2+SO_2$ pulse instead of $2CO+SO_2$ pulse, was used for the determination of per cent formation of CO_2 (X_{CO_2}) on the basis of reaction (1). Per cent conversions of CO (X_{CO}) and SO_2 (X_{SO_2}) were determined in the same way as for pulses of CO or SO_2 alone. Unless otherwise noted, arithmetic mean of five pulses was used as the value of X_{CO}, X_{SO_2}, or X_{CO_2}.

Results and Discussion

Fe_2O_3–Al_2O_3 System. Various pulse tests were carried out for the Fe_2O_3–Al_2O_3 system.

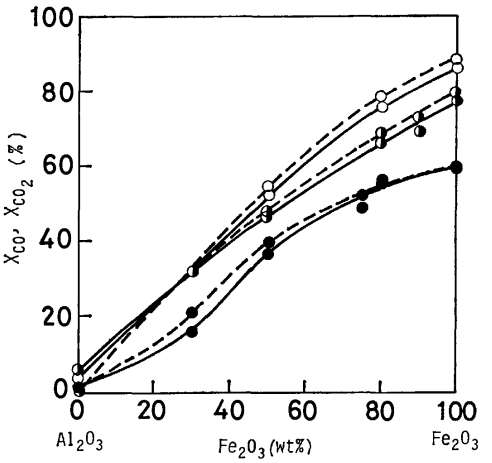

Fig. 2. Per cent conversion of CO (X_{CO}) and formation of CO_2 (X_{CO_2}) in CO pulse for Fe_2O_3–Al_2O_3 systems with various mixing ratios and preheating temperatures.
Preheating temperature: ○: 360 °C, ◑: 600 °C, ●: 700 °C. ——: X_{CO}, – – –: X_{CO_2}.

$2CO+SO_2$ Pulse: Figures 1(a)—(c) show per cent conversions of CO and SO_2 (X_{CO} and X_{SO_2}) and per cent formation of CO_2 (X_{CO_2}) in $2CO+SO_2$ pulse for the Fe_2O_3–Al_2O_3 systems with various mixing ratios (wt% of Fe_2O_3). (a) is the result of the sample preheated at 360 °C. The value of X_{CO} increases from 4.8% for Al_2O_3 alone (adsorption of CO) to 71.5% for Fe_2O_3 alone with increasing Fe_2O_3 content. The value of X_{CO_2} increases similarly to X_{CO}, but it is generally several per cents lower than the X_{CO} value. This seems to be due to occurrence of a side reaction such as reaction (2). Al_2O_3 alone does not show any activity for reaction (1). The value of X_{SO_2} increases from 33.2% for Al_2O_3 alone (adsorption of SO_2) to 49.2% for Fe_2O_3 alone with increasing Fe_2O_3 content. The fact that the X_{SO_2} value for Fe_2O_3 alone is lower than that of X_{CO_2} may be due to a lowering of activity of nascent (Fe_3O_4) on reaction (4) as will be considered later. Compared with (a), all the values in (c) for the samples preheated at 700 °C are significantly low, and the maximum X_{CO}, X_{SO_2}, and X_{CO_2} values are attained at their respective specific mixing ratios at about 70—75 wt% of Fe_2O_3 contents. The samples preheated at 600 °C on (b) show an intermediate behavior between (a) and (c).**

CO Pulse: Figure 2 shows the result of a CO pulse for the Fe_2O_3–Al_2O_3 systems with various mixing ratios and preheating temperatures. The value of X_{CO} increases in an approximately linear relationship with increasing ratio of Fe_2O_3, but it decreases with increasing preheating temperature. CO_2 is formed on all of samples except for Al_2O_3 alone, and X_{CO_2} is approximately the same as X_{CO}. These results show occurrence of reaction (5) without adsorption of CO:

$$3Fe_2O_3 + CO \longrightarrow 2F_3O_4 + CO_2. \quad (5)$$

** In a previous paper,[6] an activity maximum was attained at 80—90 wt% Fe_2O_3 preheated at 600 °C. This is probably due to the use of different lot No. of commercial Fe_2O_3 sample and different reaction temperature (300 °C).

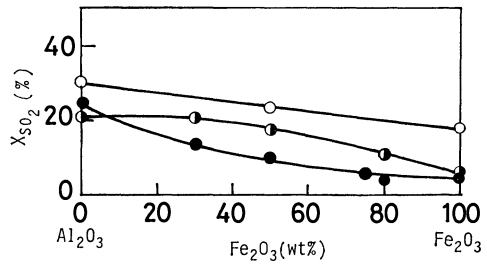

Fig. 3. Per cent conversion of SO_2 (X_{SO_2}) in SO_2 pulse for Fe_2O_3–Al_2O_3 systems with various mixing ratios and preheating temperatures.
Preheating temperature: ○: 360 °C, ◑: 600 °C, ●: 700 °C.

SO_2 Pulse: Figure 3 shows that the value of X_{SO_2} decreases with increasing ratio of Fe_2O_3 and preheating temperature. The values of X_{SO_2} for Al_2O_3 alone and Fe_2O_3 alone are 20—30 and 5—20%, respectively. It is thought that these values of X_{SO_2} may be due to irreversible adsorption of SO_2, because the experiments were carried out at 25-min pulse intervals in a flowing He gas.

Fe_2O_3 System. The effect of Al_2O_3 in the Fe_2O_3–Al_2O_3 systems of Figs. 1 and 2 on the reactions was examined by comparison with the results of the pure Fe_2O_3 system, of which the amounts of Fe_2O_3 correspond to those in the Fe_2O_3–Al_2O_3 systems (*e.g.*, 40 mg Fe_2O_3 corresponds to 50 wt% Fe_2O_3 in the Fe_2O_3–Al_2O_3 system).

$2CO+SO_2$ Pulse: Figures 4(a)—(c) show results of Fe_2O_3 preheated at 360, 600, and 700 °C in the pulse of $2CO+SO_2$, respectively. In the case of (a), the curves of X_{CO} and X_{CO_2} are similar to that in Fig. 1(a). Consequently, it is thought that no cooperative action between Fe_2O_3 and Al_2O_3 takes place during the preheating of the Fe_2O_3–Al_2O_3 system at 360 °C, and the behavior in the Fe_2O_3–Al_2O_3 system of Fig. 1(a) is attributable to that of Fe_2O_3 itself. Khalafalla *et al.*[1] reported that results in the Fe–Al_2O_3 system for reaction (1) are best explained on the basis of a dual-site mechanism with both iron and alumina augmenting their specific-site activities at their interparticle contacts. However, the present results indicate no action of bifunctional catalyst. Furthermore, on the basis of a comparison between X_{CO} or X_{CO_2} of Fig. 1(a) and that of Fig. 4(a), it is considered that there is no problem with respect to the contact between gas and powder arising from the small packing amount of powder used. On the other hand, the value of X_{SO_2} greatly differs from that in the Fe_2O_3–Al_2O_3 system, especially in the low Fe_2O_3 content region. This is due mainly to the adsorption of SO_2 on Al_2O_3.

In the case of Fig. 4(c), the curves differ greatly from that in Fig. 1(c). Consequently, it can be considered with regard to the unique catalytic behavior of Fig. 1(c) that some interfacial reactions between Fe_2O_3 and Al_2O_3 occurred during the preheating process at 700 °C. Figure 4(b) shows an intermediate behavior between (a) and (c).

CO Pulse: Figure 5 shows the result of Fe_2O_3 alone with various Fe_2O_3 amounts and preheating temperatures. The results obtained are approximately the same as that of the Fe_2O_3–Al_2O_3 systems in Fig. 2. This means that there is no significant effect of Al_2O_3 on reaction (5) in the Fe_2O_3–Al_2O_3 systems for all

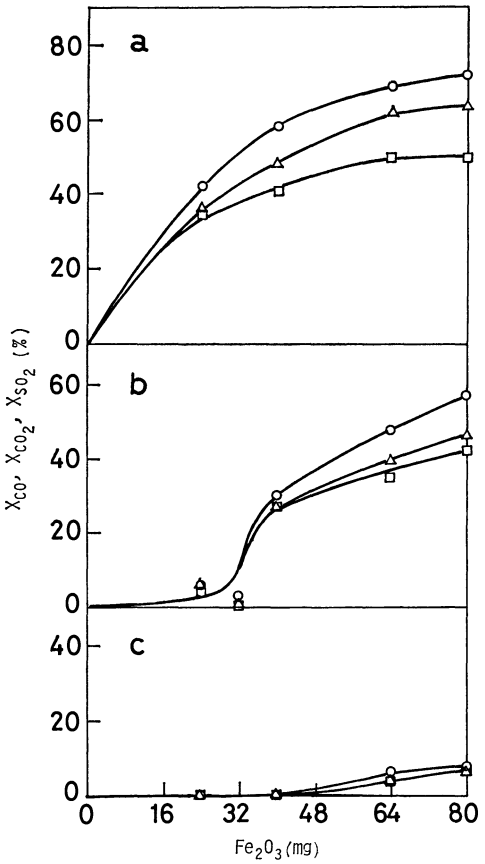

Fig. 4. Per cent conversions of CO and SO_2 (X_{CO} and X_{SO_2}),a nd % formation of CO_2 (X_{CO_2}) in $2CO+SO_2$ pulse for Fe_2O_3 systems with various Fe_2O_3 amounts and preheating temperatures.
Preheating temperature: (a): 360 °C, (b): 600 °C, (c): 700 °C. ○: X_{CO}, △: X_{CO_2}, □: X_{SO_2}.

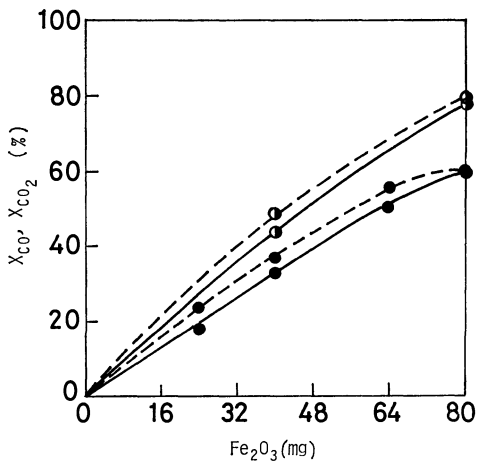

Fig. 5. Per cent conversion of CO (X_{CO}) and % formation of CO_2 (X_{CO_2}) in CO pulse for Fe_2O_3 systems wit hvarious Fe_2O_3 amounts and preheating temperatures.
Preheating temperature: ◑: 600 °C, ●: 700 °C.
——: X_{CO}, ----: X_{CO_2}.

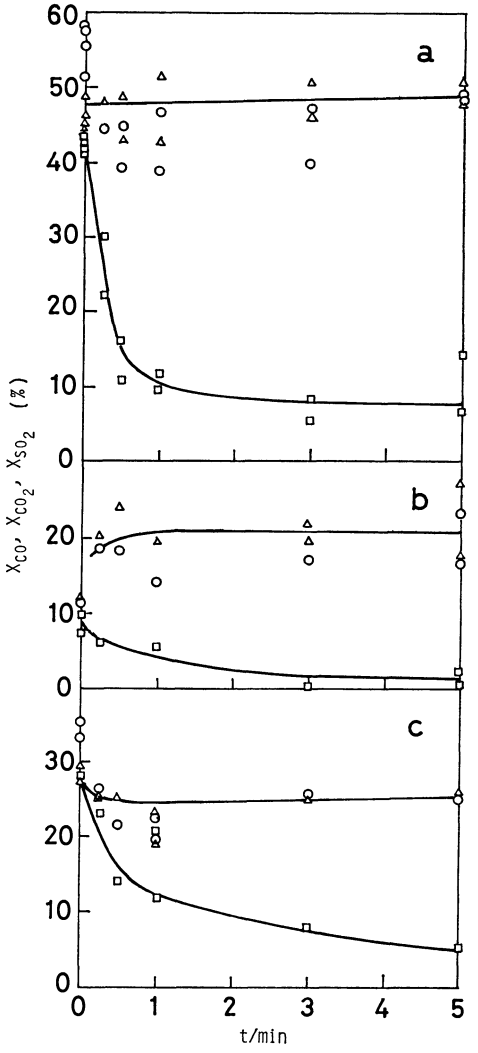

Fig. 6. Per cent conversions of CO and SO_2 (X_{CO} and X_{SO_2}), and % formation of CO_2 (X_{CO_2}) in $CO \xrightarrow{t} SO_2$ (t=0—5 min) pulses for Fe_2O_3 and F_2O_3–Al_2O_3 systems.
Powder system and preheating temperature: (a): Fe_2O_3, 600 °C, (b): Fe_2O_3, 700 °C, (c): Fe_2O_3–Al_2O_3 (75:25), 700 °C. ○: X_{CO}, △: X_{CO_2}, □: X_{SO_2}.

of the preheating temperatures.

Catalytic Mechanism. In order to determine, on the basis of reactions (3) and (4) which are proposed in the previous paper,[6] mechanism of the reduction of SO_2 with CO for the Fe_2O_3 and Fe_2O_3–Al_2O_3 systems, a pulse method (with varying pulse intervals), different from the above-described, was applied, and the composition of samples before and after the pulse experiment was identified by X-ray analysis.

$CO \xrightarrow{t} SO_2$ Pulse: Figures 6(a)—(c) show results of experiments where the first CO pulse was injected, followed by a SO_2 pulse, with varying pulse intervals t (min). Figure 6(a) shows that, for Fe_2O_3 preheated at 600 °C, reaction (3) proceeds with approximately constant value of X_{CO_2} regardless of t. The value of X_{CO} is similar to that of X_{CO_2}, although the data show some scatter (the curve of X_{CO} is not shown). In contrast to these results, the curve of X_{SO_2} decreases rapidly within t=1 min and then approaches the values

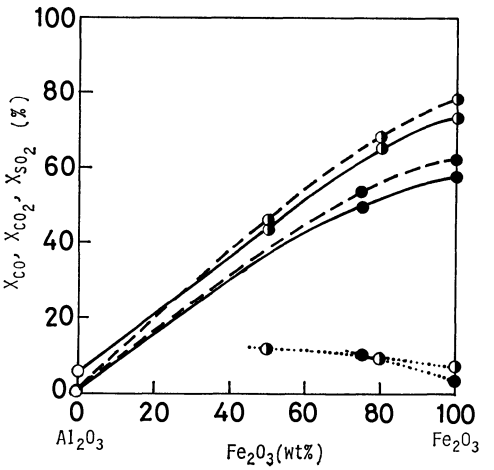

Fig. 7. Per cent conversions of CO and SO_2 (X_{CO} and X_{SO_2}), and % formation of CO_2 (X_{CO_2}) in $CO \times 5 \xrightarrow{t} SO_2 \times 5$ (t=25 min) pulse for Fe_2O_3–Al_2O_3 systems with various mixing ratios and preheating temperatures.
Preheating temperature: ◑: 600 °C, ●: 700 °C.
——: X_{CO}, – – –: X_{CO_2}, ·····: X_{SO_2}.

of X_{SO_2} for Fe_2O_3 (in Fig. 3) and Fe_3O_4 (commercial reagent) in the SO_2 pulse. From these results, it is thought that the activity of the nascent (Fe_3O_4) for reaction (4) decreases rapidly within 1 min of t. Figure 6(b) shows the result of Fe_2O_3 preheated at 700 °C. A behavior similar to (a) is shown, but all values of X_{CO}, X_{CO_2} and X_{SO_2} are significantly lower than (a). This is assumed to be due to a decrease in the reactivity of Fe_2O_3 caused by the preheating at higher temperature.

Figure 6(c) shows the result of the Fe_2O_3–Al_2O_3 (75:25) system preheated at 700 °C. The vaule of X_{SO_2} generally increases compared with (b), and the decreasing tendency of X_{SO_2} curve is mild compared with (a), while the values of X_{CO} and X_{CO_2} do not increase very much compared with (b) except for that of t=0 min. These probably mean the reactivity of nascent (Fe_3O_4) for reaction (4) become high and stable with addition of Al_2O_3 with Fe_2O_3, which results from interfacial reaction between Fe_2O_3 and Al_2O_3 caused by the preheating treatment at 700 °C.

$CO \times 5 \xrightarrow{t} SO_2 \times 5$ (t=25 min) Pulse: Figure 7 shows that, for the Fe_2O_3–Al_2O_3 system preheated at 600 and 700 °C, the first five CO pulses (25 min intervals) are injected, followed by five SO_2 pulses (25 min intervals) with 25 min of t. The curves of X_{CO} and X_{CO_2} are similar to that of Fig. 2, but the values of X_{SO_2} are greatly lower than that of Fig. 1, and approximately the same as that of the SO_2 pulse in Fig. 3. This means that the active nascent (Fe_3O_4) was changed to inactive Fe_3O_4 during the interval of 25 min and that the activity of (Fe_3O_4) for reaction (4) disappeared.

$SO_2 \xrightarrow{t} CO$ (t=5 min) Pulse: For the samples of Fe_2O_3 preheated at 360 and 600 °C, first a SO_2 pulse was injected, followed by a CO pulse with t of 5 min. The values of X_{CO_2}, X_{CO}, and X_{SC_2} were 0, 0.2, and 11.4% for the 360 °C preheating and 0, 1.1, and 4.6%

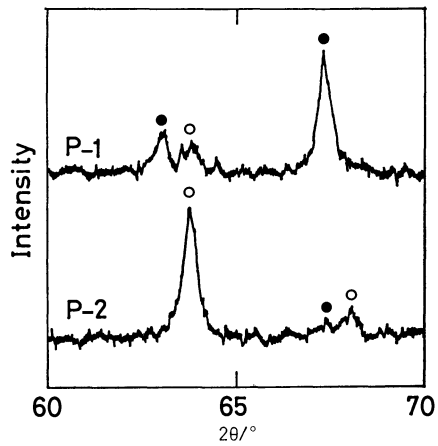

Fig. 8. X-Ray diffraction patterns after pulse experiments for Fe_2O_3 system preheated at 360 °C.
P-1: Fe_2O_3 in CO pulse, P-2: Fe_2O_3 in $2CO+SO_2$ pulse. ○: Fe_2O_3, ●: Fe_3O_4.

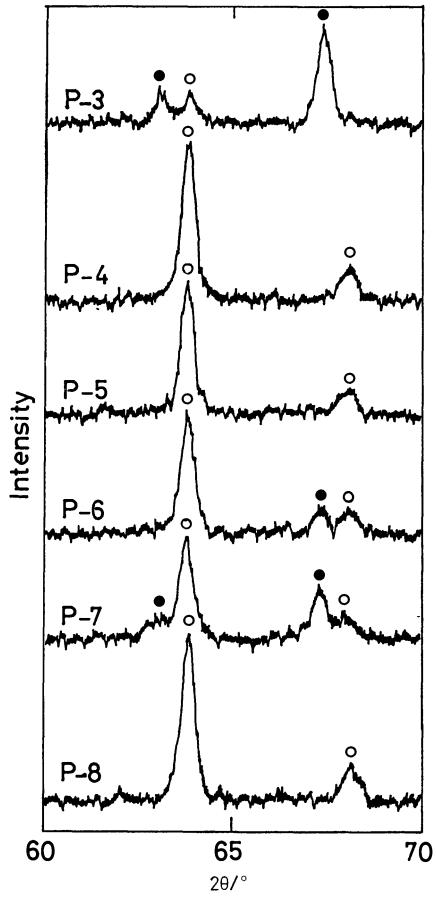

Fig. 9. X-Ray diffraction patterns after pulse experiments for Fe_2O_3 and Fe_2O_3-Al_2O_3 systems preheated at 600 °C.
P-3: Fe_2O_3 in CO pulse, P-4: Fe_2O_3 in $2CO+SO_2$ pulse, P-5: Fe_2O_3-Al_2O_3 (80:20) in $2CO+SO_2$ pulse, P-6: Fe_2O_3 in $CO \xrightarrow{t} SO_2$ (t=0.25 min) pulse, P-7: Fe_2O_3 in $CO \xrightarrow{t} SO_2$ (t=5 min) pulse, P-8: Fe_2O_3 in $SO_2 \xrightarrow{t} CO$ (t=5 min) pulse. ○: Fe_2O_3, ●: Fe_3O_4.

for the 600 °C preheating, respectively. These mean that reaction (5) is hindered by the SO_2 adsorbed on the surface of Fe_2O_3 particle and that the surface reaction between adsorbed SO_2 and gas phase CO did not occur.

X-Ray Analysis: On the basis of the results described above, it is considered that the reactivity of Fe_2O_3 for the reduction of SO_2 to S_2 is governed by the activity and lifetime of nascent (Fe_3O_4) with respect to the redox reactions (3) and (4). In order to confirm this consideration, X-ray analyses of samples were done after these experiments. These results are partly shown in Figs. 8—10 by using diffraction patterns at 2θ=60—70° (Co $K\alpha$). The ASTM cards (13—534 and 11—614) show that 2θ=63.8 and 68.0° (I/I_o=60 and 16) correspond to α-Fe_2O_3 and that 2θ=63.0 and 67.3° (I/I_o=60 and 85) correspond to Fe_3O_4.

Figure 8 shows the result of Fe_2O_3 preheated at 360 °C. Pattern 1 (noted as P-1) in CO pulse shows the formation of Fe_3O_4 on reaction (5) and the presence of small amounts of α-Fe_2O_3 remaining. P-2 in $2CO+SO_2$ pulse shows Fe_2O_3 with trace amounts of Fe_3O_4, which resulted from reaction (3) and (4).

Figure 9 shows the result of both the Fe_2O_3 and Fe_2O_3-Al_2O_3 (80:20) systems which were preheated at 600 °C. P-3 in CO pulse for Fe_2O_3 shows a pattern similar to P-1. P-4 in $2CO+SO_2$ pulse for Fe_2O_3 shows Fe_2O_3 formed as a result of reactions (3) and (4). P-5 in $2CO+SO_2$ pulse for the Fe_2O_3-Al_2O_3 system is the same as P-4. P-6 in $CO \xrightarrow{t} SO_2$ (t=0.25 min) pulse for Fe_2O_3 shows Fe_2O_3 with small amounts of Fe_3O_4. P-7 in $CO \xrightarrow{t} SO_2$ (t=5 min) pulse for Fe_2O_3 shows that Fe_3O_4 increases with increasing t and that active (Fe_3O_4) changes to inactive Fe_3O_4. These results (P-4, P-6, and P-7) support the consideration with Fig. 6(a). P-8 in $SO_2 \xrightarrow{t} CO$ (t=5 min) pulse for Fe_2O_3 shows Fe_2O_3 only, in supports of the consideration with the $SO_2 \xrightarrow{t} CO$ pulse tests shown above.

Figure 10 shows the result of both the Fe_2O_3 and Fe_2O_3-Al_2O_3 (75 : 25) systems which were preheated at 700 °C. P-9 in CO pulse for Fe_2O_3 shows a pattern similar to P-3. In a comparison of P-1, P-3, and P-9, relative intensities of Fe_2O_3 increase with increasing preheating temperature. This means that the reactivity of Fe_2O_3 decreases with increasing preheating temperature. P-10 in $2CO+SO_2$ pulse for Fe_2O_3 shows Fe_2O_3 only in analogy with P-4. P-11 in $2CO+SO_2$ pulse for the Fe_2O_3-Al_2O_3 system is similar to P-10. P-12 in $CO \xrightarrow{t} SO_2$ (t=0.25 min) pulse for Fe_2O_3 shows Fe_2O_3 only, but P-13 in $CO \xrightarrow{t} SO_2$ (t=5 min) pulse for Fe_2O_3 shows the presence of Fe_3O_4. This means that active (Fe_3O_4) changes to inactive Fe_3O_4 with increasing t, in a similar manner with P-7. P-14 in $CO \xrightarrow{t} SO_2$ (t=0.25 min) pulse for the Fe_2O_3-Al_2O_3 system shows Fe_2O_3 only, but P-15 in $CO \xrightarrow{t} SO_2$ (t=5 min) pulse for the Fe_2O_3-Al_2O_3 system shows the presence of Fe_3O_4 in analogy with P-13.

X-Ray patterns, in $CO \times 5 \xrightarrow{t} SO_2 \times 5$ (t=25 min)

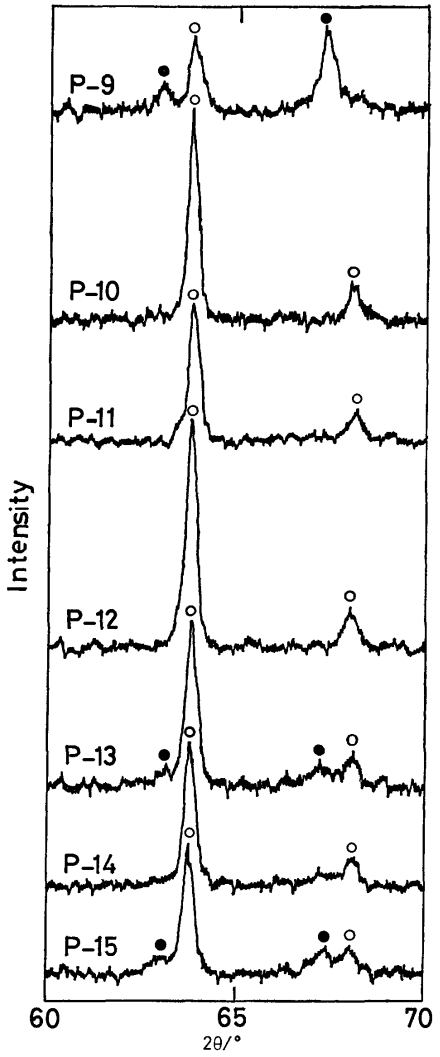

Fig. 10. X-Ray diffraction patterns after pulse experiments for Fe_2O_3 and Fe_2O_3–Al_2O_3 systems preheated at 700 °C.
P-9: Fe_2O_3 in CO pulse, P-10: Fe_2O_3 in $2CO+SO_2$ pulse, P-11: Fe_2O_3–Al_2O_3 (75:25) in $2CO+SO_2$ pulse, P-12: Fe_2O_3 in $CO \xrightarrow{t} SO_2$ (t=0.25 min) pulse, P-13: Fe_2O_3 in $CO \xrightarrow{t} SO_2$ (t=5 min) pulse, P-14: Fe_2O_3–Al_2O_3 (75:25) system in $CO \xrightarrow{t} SO_2$ (t=0.25 min) pulse, P-15: Fe_2O_3–Al_2O_3 (75:25) system in $CO \xrightarrow{t} SO_2$ (t=5 min) pulse. ○: Fe_2O_3, ●: Fe_3O_4.

pulse, for the same samples with of P-3 and P-5 in Fig. 9 and with P-9 and P-11 in Fig. 10, showed the same results as P-3 and P-9 in CO pulse. These results also support the consideration of $CO\times5 \xrightarrow{t} SO_2\times5$ (t=25 min) pulse in Fig. 7.

In order to test the reactivity of magnetite, pulse tests of $2CO+SO_2$ and SO_2 pulses were carried out for commercial Fe_3O_4 (Kanto) preheated at 360 °C. No reactivity for reaction (1) and no change in X-ray pattern for reaction (4) were shown.

From these discussions described above, the catalytic action may be explained on the basis of redox reaction between Fe_2O_3 and nascent (Fe_3O_4), which has been shown in reactions (3) and (4).

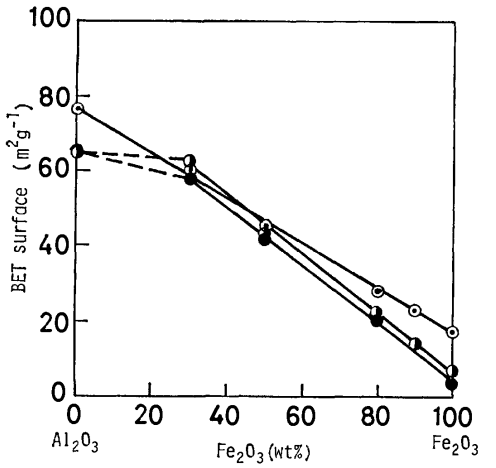

Fig. 11. BET surface of Fe_2O_3–Al_2O_3 systems with various mixing ratios and preheating temperatures.
Preheating temperature: ⊙: non-preheating, ◑: 600 °C, ●: 700 °C.

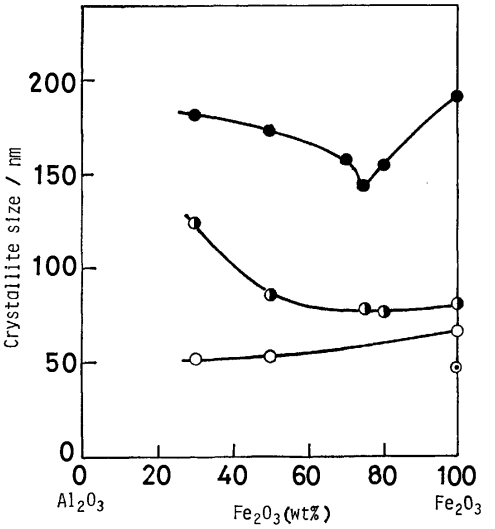

Fig. 12. Crystallite size of Fe_2O_3 (D_{104}) in Fe_2O_3–Al_2O_3 systems with various mixing ratios and preheating temperatures.
Preheating temperature: ⊙: non-preheating, ○: 360 °C, ◑: 600 °C, ●: 700 °C.

BET Surface and Crystallite Size. In order to examine the effect of Al_2O_3 on the reactivity of Fe_2O_3, some considerations were also attempted. Figure 11 shows the relationship between BET surface and Fe_2O_3 contents for the Fe_2O_3–Al_2O_3 systems with various mixing ratios and preheating temperatures. BET surface decreases with increasing Fe_2O_3 content in approximately a linear relationship. No good correlation is obtained between the reactivity of Fe_2O_3–Al_2O_3 mixture for the reduction of SO_2 (in Fig. 1) and BET surface. This is probably due to the sequence that the BET surface of inactive Al_2O_3 would govern that of the Fe_2O_3–Al_2O_3 mixture.

Figure 12 shows the relationship between the crys-

tallite size of Fe_2O_3 as calculated from Scherrer's equation and the Fe_2O_3 content in the Fe_2O_3–Al_2O_3 system. There are some interesting correlations between the crystallite size and the reactivity behavior in Fig. 1, especially at 700 °C of preheating temperature. If the minimum crystallite size value suggests the maximum distortion of the Fe_2O_3 lattice at 700 °C for preheating, it can be presumed that the occurrence of the maximum peak in Fig. 1(c) may be due to the distortion of the Fe_2O_3 lattice, which results from the interfacial reaction with surface diffusion between Fe_2O_3 and Al_2O_3. Furthermore, it is speculated that the activity of (Fe_3O_4) should be enhanced and the lifetime of active (Fe_3O_4) prologened by the interfacial reaction with Al_2O_3, as indicated by a comparison of Figs. 6(b) and (c).

References

1) S. E. Khalafalla, E. F. Foerster, and L. A. Hass, *Ind. Eng. Chem., Prod. Res. Dev.*, **10**, 133 (1971).
2) S. E. Khalafalla and L. A. Hass, *J. Catal.*, **24**, 115 (1972).
3) L. A. Hass and S. E. Khalafalla, *J. Catal.*, **29**, 264 (1973).
4) D. T. Clay and S. Lynn, *AIChE J.*, **21**, 466 (1975).
5) S. Kasaoka, H. Tsumaki, and T. Kochihira, *Nippon Kagaku Kaishi*, **1973**, 413.
6) T. Ishii, R. Furuichi, and K. Takamatsu, *Nippon Kagaku Kaishi*, **1980**, 1685.

Preparation and Spectroscopic Studies of Stereoisomers of the Tris[(*S*)-1-phenyl-1,3-propanediamine]cobalt(III) Complex

Masaaki KOJIMA and Junnosuke FUJITA*

Department of Chemistry, Faculty of Science, Nagoya University, Chikusa-ku, Nagoya 464

(Received September 8, 1981)

Three, *fac*-*Λ*, *fac*-*Λ*, and *mer*-*Λ*, of four possible diastereomers of the $[Co(S\text{-phtn})_3]^{3+}$ complex (*S*-phtn= (*S*)-1-phenyl-1,3-propanediamine) were obtained by two methods, a reaction between *trans*-$[CoCl_2(S\text{-phtn})_2]^+$ and *S*-phtn in DMSO (dimethyl sulfoxide), and oxidation of a DMSO solution containing Co(II) ions and *S*-phtn with air in the presence of active charcoal. Neither method yielded the *mer*-*Λ* isomer. The absorption and circular dichroism spectra of the isomers were recorded in water in the absence and presence of Na_2SO_4, and in DMSO. The shifts of the first absorption bands caused by changing solvents and the changes of circular dichroism spectra caused by the addition of sulfate ions seem to be related with the conformational instability of the flexible six-membered chelate ring in the complexes. The tetraammine complex of *S*-phtn was also prepared.

In the previous papers, we reported that the circular dichroism (CD) spectra of some cobalt(III) complexes containing six-membered diamine chelate rings such as trimethylenediamine (tn),[1] (*R*,*R*)-2,4-pentanediamine (*RR*-ptn),[1] or (*S*)-1,3-butanediamine (*S*-bn)[2] vary remarkably with changes in counter ions and solvents. Such CD variations were accounted for by conformational interconversions of the flexible six-membered chelate rings caused by ion-pair formation. Conformational flexibility of a 1,3-diamine chelate ring would depend on the nature of substituents on the chelate ring. In order to investigate the effect of a bulky substituent on conformational stability of a chelate ring, we have prepared cobalt(III) complexes containing (*S*)-1-phenyl-1,3-propanediamine (*S*-phtn) and measured their absorption and CD spectra under various conditions. The skeletal structure of the *S*-phtn chelate ring is similar to that of the *S*-bn one, although these (*S*)-diamines form stable *skew* conformations of different chirality;[3] the former with the equatorial phenyl group is either the *chair* or the *λ*-*skew* form, while the latter with the same equatorial methyl group is the *chair* or *δ*-*skew* form (Fig. 1).

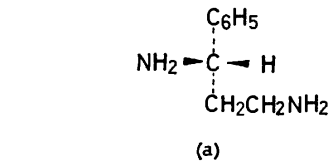

(a)

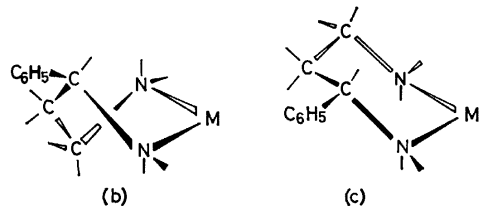

(b) (c)

Ligand	conformation δ-skew	λ-skew	chair
S-phtn	a	e	e(a)
S-bn	e	a	e(a)
RR-ptn	aa	ee	ae
meso-ptn	ae	ae	ee(aa)
SS-dppn	aa	ee	ae

e: substituent equatorial
a: substituent axial

Fig. 1. (a) Absolute configuration of *S*-phtn, (b) *λ*-skew and (c) chair conformations of the *S*-phtn chelate ring, and relationship between conformations of 1,3-diamine chelate rings and dispositions of substituent(s).

Experimental

Ligand. 3-Phenyl-3-aminopropionic acid[4] was converted into the amide by the method of Yang and Rising.[5] The amide was reduced with $LiAlH_4$ in dry tetrahydrofuran to give 1-phenyl-1,3-propanediamine (phtn) according to a method similar to that for 2-methyl-1,4-butanediamine.[6] The rac-diamine thus obtained was resolved by the following method. To an aqueous solution (30 cm³) of the diamine (13.5 g, 0.09 mol) was added an aqueous solution (50 cm³) of (+)-tartaric acid (27.5 g, 0.18 mol), and the solution was allowed to stand overnight at 5 °C. White crystals thus obtained were collected, washed with ethanol–water (1:1), and recrystallized from water (50 cm³). One careful recrystallization was sufficient to obtain the optically pure isomer. Yield: 8.3 g. To an aqueous solution (10 cm³) of the diastereomer (8.3 g, 18 mmol) was added an aqueous solution (15 cm³) of KCl (2.7 g, 36 mmol). Potassium hydrogen (+)-tartrate was precipitated, filtered off, and washed with cold water (10 cm³). The combined filtrate and washing were concentrated to a small volume under reduced pressure. White needles of (*S*)-1-phenyl-1,3-propanediamine dihydrochloride were formed by the addition of ethanol and acetone, filtered, and washed with acetone. Yield: 3.7 g. $[\alpha]_D^{25}=+9.06°$ (*c* 0.0136, H_2O).

The absolute configuration of the diamine was determined by preparing (−)-3-phenyl-3-aminopropionic acid of the known absolute configuration (*S*). *N*-Formyl-3-phenyl-3-aminopropionic acid was prepared by the method of Fischer *et al.*,[7] and the diastereomer with quinidine was prepared by the method of Cohen *et al.*[4] (−)-3-Phenyl-3-aminopropionic acid derived from the more soluble diastereomer is known to have the (*S*) configuration.[8] Since the (*S*)-diamine dihydrochloride obtained from the (*S*)-(−)-amino acid by the same method as that for the racemate was dextrorotatory, (+)-phtn·2HCl was determined to have

the (*S*) configuration.

trans-[*CoCl*$_2$(S-*phtn*)$_2$]*Cl*·*H*$_2$*O*. A methanol solution (30 cm^3) containing sodium methoxide (1.89 g, 35 mmol) and *S*-phtn·2HCl (4.0 g, 18 mmol) was stirred for about 1 h, and then filtered to remove sodium chloride precipitated. The filtrate was added to a methanol solution (170 cm^3) of $CoCl_2 \cdot 6H_2O$ (2.0 g, 8.5 mmol). The solution was aerated for 2.5 h at room temperature and then mixed with concd HCl (10 cm^3). Green crystals were obtained by concentrating the solution to a small volume under reduced pressure, filtered, and washed with a small amount of water. Yield: 0.7 g. The second crop was obtained by the addition of water to the filtrate. Yield: 1.1 g. The complex was recrystallized from methanol. Found: C, 44.45; H, 5.92; N, 11.60%. Calcd for $C_{18}H_{30}N_4Cl_3OCo$=*trans*-[$CoCl_2$-(*S*-phtn)$_2$]Cl·H_2O: C, 44.69; H, 6.25; N, 11.58%.

[*Co*(S-*phtn*)$_3$]$^{3+}$. *Method 1*: To a dimethyl sulfoxide (DMSO) solution (40 cm^3) of *trans*-[$CoCl_2$(*S*-phtn)$_2$]Cl·H_2O (0.097 g, 2 mmol) was added a suspension of *S*-phtn·2HCl (0.53 g, 2.4 mmol) and sodium methoxide (0.23 g, 4.2 mmol) in methanol (2 cm^3). The mixture was stirred for 2.5 h at 70 °C, diluted with 1 dm^3 of water, and acidified (pH 2) with hydrochloric acid. The solution was passed through an SP-Sephadex column (ϕ2.7×5 cm). A small portion of the Sephadex charged with the product was placed on the top of the adsorbent layer of an SP-Sephadex column (ϕ2.7×120 cm), and the adsorbed complexes were eluted with a 0.5 M Na_2SO_4 (1 M=1 mol/dm^3) solution adjusted to pH 2 with hydrochloric acid. The column showed four bands, I(pink, very small amount), II(orange, very small amount), IIIA(orange-red, large amount), and IIIB(red, small amount) from bottom to top of the column. Bands IIIA and IIIB were eluted much slower than bands I and II. The effluent of band IIIA was diluted with 10^{-2} M HCl and loaded again on an SP-Sephadex column. The adsorbed band was eluted with a 0.25 M sodium (+)-tartratoantimonate(III) solution. The column showed two bands, *mer*-*Λ*(IIIA-1) and *fac*-*Λ*(IIIA-2) in the order of elution. Band IIIB was the *fac*-*Λ* isomer. The formation ratio, *mer*-*Λ*(IIIA-1) : *fac*-*Λ*(IIIA-2) : *fac*-*Λ*(IIIB) was 8 : 5 : 1. No indication of the presence of the *mer*-*Λ* isomer was observed.

Method 2: To a stirred suspension of *S*-phtn·2HCl (2.0 g, 9.0 mmol) and sodium methoxide (0.92 g, 17 mmol) in methanol (8.5 cm^3) were added a DMSO solution (35 cm^3) of $Co(NO_3)_2 \cdot 6H_2O$ (0.73 g, 2.5 mmol), and active charcoal (0.5 g). The mixture was aerated for 4 h at room temperature, and filtered. The filtrate was diluted with 10^{-2} M HCl and passed through an SP-Sephadex column. The product adsorbed on SP-Sephadex was chromatographed by the same method as that for Method 1. Only two isomers, *mer*-*Λ* and *fac*-*Λ* were yielded, their formation ratio being 1.0:1.4.

mer-Δ[*Co*(S-*phtn*)$_3$](*ClO*$_4$)$_3$·*6H*$_2$*O*, fac-Δ-[*Co*(S-*phtn*)$_3$]-(*ClO*$_4$)$_3$·*2H*$_2$*O*, *and* fac-Λ-[*Co*(S-*phtn*)$_3$](*ClO*$_4$)$_3$·*4H*$_2$*O*. Each eluate of the isomers was diluted with 10^{-2} M HCl and passed through an SP-Sephadex column (ϕ1.5×3 cm). After the column had been washed with 10^{-2} M HCl (*ca.* 100 cm^3), the adsorbed complex was eluted with a 1.5 M $NaClO_4$ ethanol–water (1:1) solution. The eluate was acidified (pH 2) with $HClO_4$ and concentrated to a small volume in a vacuum desiccator over P_2O_5 to yield orange-red crystals. They were filtered, washed with a small amount of water, and recrystallized from 10^{-2} M $HClO_4$. *mer*-*Λ* isomer, Found: C, 35.35; H, 6.18; N, 8.80%. Calcd for $C_{27}H_{54}N_6Cl_3O_{18}Co$=[Co(*S*-phtn)$_3$](ClO$_4$)$_3$·$6H_2O$: C, 35.40; H, 5.94; N, 9.17%. *fac*-*Λ* isomer, Found: C, 38.20; H, 5.28; N, 9.98%. Calcd for $C_{27}H_{46}N_6Cl_3O_{14}Co$=[Co(*S*-phtn)$_3$](ClO$_4$)$_3$·$2H_2O$: C, 38.42; H, 5.49; N, 9.96%. *fac*-*Λ* isomer, Found: C, 37.09; H, 5.75; N, 9.33%. Calcd for $C_{27}H_{50}N_6Cl_3O_{16}Co$=[Co(*S*-phtn)$_3$](ClO$_4$)$_3$·$4H_2O$: C, 36.85; H, 5.73; N, 9.54%.

[*Co*(*NH*$_3$)$_4$(S-*phtn*)](*ClO*$_4$)$_3$·*H*$_2$*O*. A methanol solution (5 cm^3) of *S*-phtn (0.57 g, 5 mmol) was prepared by the same method as that described for *trans*-[$CoCl_2$(*S*-phtn)$_2$]Cl·H_2O. This was added to a DMSO solution (40 cm^3) of [Co(NH$_3$)$_5$(H$_2$O)](ClO$_4$)$_3$ (2.3 g, 5 mmol). The solution was stirred for 3 d at room temperature. The resulting red solution was diluted with 10^{-2} M HCl and passed through an SP-Sephadex column (ϕ2.7×5 cm). The product adsorbed was chromatographed by a method similar to that for [Co(*S*-phtn)$_3$]$^{3+}$ with 0.2 M Na_2SO_4 adjusted to pH 2 with hydrochloric acid. Six bands were eluted in the order of orange-red ([Co(NH$_3$)$_5$(H$_2$O)]$^{3+}$), yellow-orange ([Co(NH$_3$)$_6$]$^{3+}$), purple ([Co(NH$_3$)$_5$(DMSO)]$^{3+}$), orange ([Co(NH$_3$)$_4$(*S*-phtn)]$^{3+}$), orange (probably [Co(NH$_3$)$_5$(*S*-Hphtn)]$^{4+}$),[9] and pink (small amount, not characterized) bands. The eluate of the fourth band was diluted with 10^{-2} M HCl and passed through an SP-Sephadex column (ϕ1.5×3 cm). The adsorbed complex was eluted with 1.5 M $HClO_4$, and the eluate was concentrated to a small volume in a vacuum desiccator over P_2O_5 to yield orange needles, which were filtered and washed with ethanol. Found: C, 18.12; H, 5.07; N, 14.03%. Calcd for $C_9H_{29}N_6Cl_3O_{13}Co$=[Co(NH$_3$)$_4$(*S*-phtn)](ClO$_4$)$_3$·H_2O: C, 18.18; H, 4.75; N, 14.13%.

Attempts to Equilibrate [*Co*(S-*phtn*)$_3$]$^{3+}$. The *mer*-*Λ*-[Co(*S*-phtn)$_3$](ClO$_4$)$_3$·$6H_2O$ (0.3 g) isomer was refluxed in water (50 cm^3) in the presence of active charcoal (0.1 g) for 3—8 h. The equilibrium process was accompanied by decomposition of the complex to reduce Co(III) to Co(II). A similar experiment was carried out in DMSO, but neither equilibration nor decomposition of the complex occured.

Measurements. Absorption and CD spectra were recorded on a Hitachi 323 spectrophotometer and a JASCO J-20 spectropolarimeter, respectively. Optical rotations at 589 nm were measured with a JASCO DIP-4 polarimeter at 25 °C. ^{13}C NMR spectra were obtained in DMSO solutions with a JEOL FX-60 spectrometer using dioxane as an external reference.

Results and Discussion

[*Co*(*NH*$_3$)$_4$(S-*phtn*)]$^{3+}$. Figure 2 compares CD spectra of the tetraammine complexes of *S*-phtn, *S*-bn, and *RR*-ptn in aqueous solutions. The CD pattern of the *S*-phtn complex is enantiomeric to that of the *S*-bn complex in the first absorption band region. Since the *S*-phtn and *S*-bn chelate rings will be stabilized with the equatorially disposed substituent in the *chair* and/or the *λ*-*skew*, and in the *chair* and/or the *δ*-*skew* conformations, respectively (Fig. 1), it is possible to attribute these CD patterns to the presence of *skew* conformers of the diamines. However, the signs of main CD bands of the complexes are opposite to those reported for the vicinal effect of many chiral, *gauche* and *skew* conformers of diamine chelates; a *λ*(*δ*)-conformer gives the positive (negative) vicinal effect in the first absorption band region. Therefore, it appears that the *S*-phtn and *S*-bn chelates in the tetraammine complexes have the achiral *chair* conformation, and that the weak CD peaks are those related essentially to the vicinal effect of the chiral

Table 1. Absorption and CD spectral data

Complex	Absorption $\tilde{\nu}_{max}/cm^{-1}(\log \varepsilon)$	CD $\tilde{\nu}/cm^{-1}(\Delta\varepsilon)$	Concentration C/mol dm^{-3}
$[Co(NH_3)_4(S\text{-phtn})](ClO_4)_3\cdot H_2O$	20830 (1.89)	18620 (+0.0052) 21980 (−0.027)	7.17×10^{-3}
mer-Λ-$[Co(S\text{-phtn})_3](ClO_4)_3\cdot 6H_2O$	20200 (2.04) 28000 (2.34) sh	19920 (−0.698) 27800 (+0.070)	2.51×10^{-3}
	35200 (4.09) 43100 (4.46)	35000 (−1.9) 41300 (+9.7) 45500 (−1.9) 48500 (+13.5)	1.00×10^{-4}
fac-Λ-$[Co(S\text{-phtn})_3](ClO_4)_3\cdot 2H_2O$	20320 (2.04)	18800 (−0.226) 21000 (+0.311)	2.79×10^{-3}
	28000 (2.35) sh		
	35200 (4.0) sh 43500 (4.44)	35700 (−5.3) 41000 (+5.5) 46100 (−12) 48100 (+4.5)	1.12×10^{-4}
fac-Λ-$[Co(S\text{-phtn})_3](ClO_4)_3\cdot 4H_2O$	20040 (2.05) 28000 (2.4) sh	19880 (+1.39) 27800 (−0.07)	2.63×10^{-3}
	35200 (4.0) sh 42700 (4.45)	40000 (−12) 45100 (+7.7) 46900 (+11)	1.05×10^{-4}

sh: Shoulder.

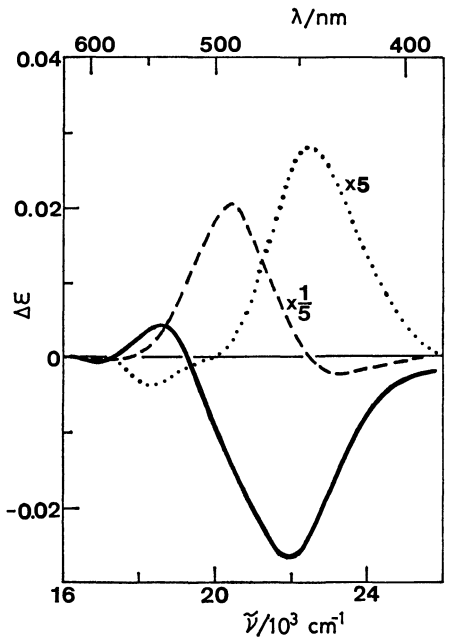

Fig. 2. CD spectra of $[Co(NH_3)_4(1,3\text{-diamine})]^{3+}$ in water. 1,3-Diamine: *S*-phtn (——), *RR*-ptn (----), and *S*-bn (·····).

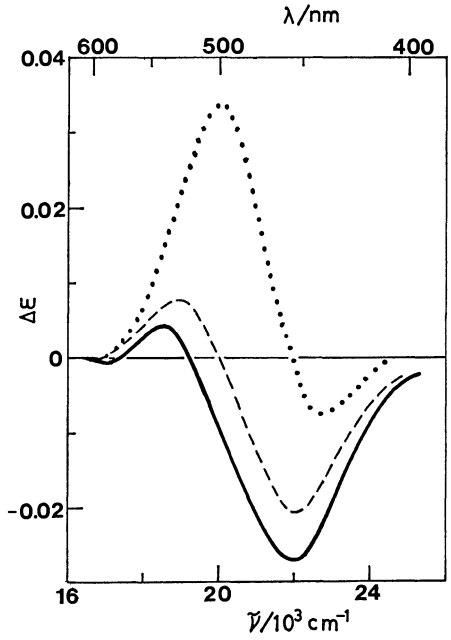

Fig. 3. CD spectra of $[Co(NH_3)_4(S\text{-phtn})]^{3+}$ in water (——), in 0.2 M Na_2SO_4 (----), and in DMSO–H_2O (1:1) (·····).

carbon atom. The CD strength of the *S*-phtn complex is about six times as large as that of the *S*-bn complex (Table 1). The CD of a tetraammine complex with a bulky phenyl-substituted diamine chelate seems to be larger than that of the corresponding methyl-substituted complex. For example, $[Co(NH_3)_4(R\text{-pen})]^{3+}$ (*R*-pen = (*R*)-1-phenyl-1,2-ethanediamine, $\Delta\varepsilon = +0.465$, 21600 cm^{-1})[10] and $[Co(NH_3)_4(R\text{-pn})]^{3+}$ (*R*-pn = (*R*)-1,2-propanediamine, $\Delta\varepsilon = +0.326$, 21690 cm^{-1});[10] $[Co(NH_3)_4(SS\text{-dpen})]^{3+}$ (*SS*-dpen = (*S*,*S*)-1,2-diphenyl-1,2-ethanediamine, $\Delta\varepsilon = -0.75$, 21370 cm^{-1})[11] and $[Co(NH_3)_4(SS\text{-2,3-bn})]^{3+}$ (*SS*-2,3-bn = (*S*,*S*)-2,3-butanediamine, $\Delta\varepsilon = -0.35$, 21740 cm^{-1}).[10]

The *S*-phtn complex increases the CD strength of the positive component and decreases complementarily that of the negative one in 0.2 M Na_2SO_4 and in DMSO–H_2O (1:1) (Fig. 3). The CD pattern in the latter solvent quite resembles that of $[Co(NH_3)_4(RR\text{-ptn})]^{3+}$ in water. The stable conformer of the *RR*-ptn chelate ring will be the *λ-skew* form in which the

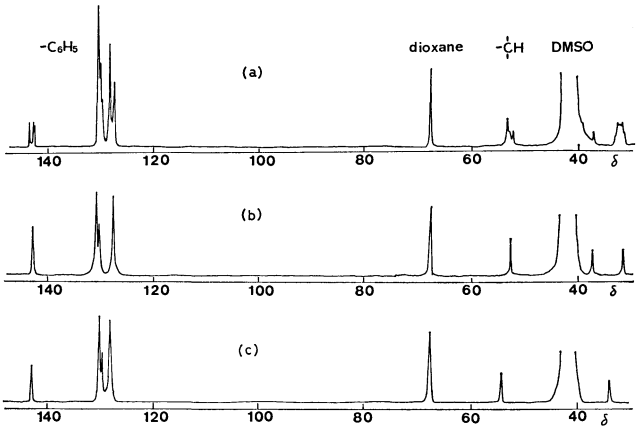

Fig. 4. ^{13}C NMR spectra of the three isomers of [Co(*S*-phtn)$_3$]$^{3+}$ in DMSO; (a) IIIA-1 (*mer*-*Δ*), (b) IIIA-2 (*fac*-*Δ*), and (c) IIIB (*fac*-*Λ*).

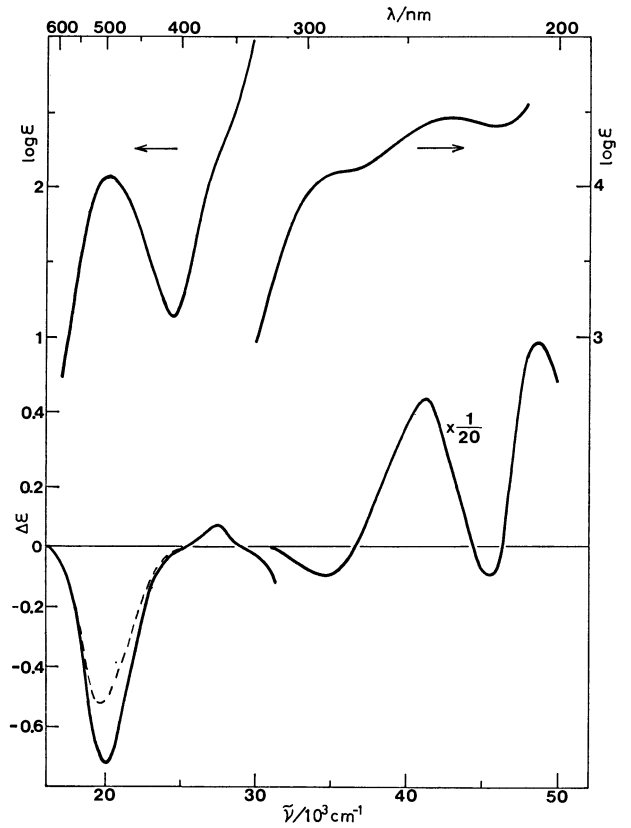

Fig. 5. Absorption and CD spectra of *mer*-*Δ*-[Co(*S*-phtn)$_3$]$^{3+}$ (IIIA-1) in water (——) and in 0.2 M Na_2SO_4 (----).

two methyl groups are disposed equatorially.[1] Thus the *S*-phtn complex is suggested to involve the *λ*-*skew* conformer stabilized under the conditions given. When the *S*-phtn chelate ring adopts the *λ*-*skew* form, the complex ion has a set of three N–H bonds suitable for hydrogen bonds with a sulfate or a perchlorate ion, the N–H bonds being provided by two ammonia molecules and the *S*-phtn chelate.[1] The N–H bonds of the diamine in the *chair* form are not directed properly for such hydrogen bonding. A perchlorate ion could form an ion-pair with the complex ion in DMSO–

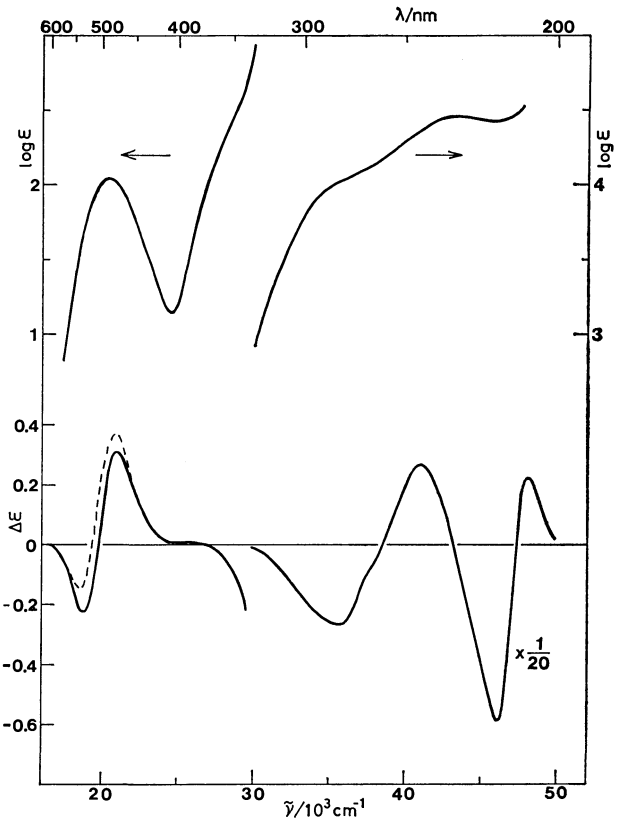

Fig. 6. Absorption and CD spectra of *fac*-*Δ*-[Co(*S*-phtn)$_3$]$^{3+}$ (IIIA-2) in water (——) and in 0.05 M Na_2SO_4 (----) (The complex is hardly soluble in 0.2 M Na_2SO_4.).

H_2O (1:1).[1]

[*Co*(S-*phtn*)$_3$]$^{3+}$. *Characterization and Formation Ratio of the Isomers*: The [Co(*S*-phtn)$_3$]$^{3+}$ complex can have four diastereomers, *mer*-*Δ*, *mer*-*Λ*, *fac*-*Δ*, and *fac*-*Λ*. ^{13}C NMR spectroscopy was used to distinguish between the *mer* and *fac* isomers (Fig. 4). The spectra of isomers IIIA-2 and IIIB give one and four resonances for the methine and the phenyl carbons, respectively, while that of isomer IIIA-1 shows complicated signals, indicating the presence of nonequivalent methine and phenyl groups. From symmetry argument (*fac*(C_3), *mer*(C_1)), isomers IIIA-1, IIIA-2, and IIIB can be assigned to the *mer*, *fac*, and *fac* configurations, respectively. Figures 5—7 show CD spectra of the three isomers in aqueous solutions in the absence and presence of sulfate ions. On the basis of the CD patterns in the first absorption band region, isomers IIIA-1, IIIA-2, and IIIB can be assigned to the *Δ*, *Δ*, and *Λ* configurations, respectively. For a cobalt(III) complex containing 1,3-diamine chelates, the CD pattern in this region often depends greatly on conditions measured, so that the use of the sign of the lowest energy CD band appearing in the Co(III)–diamine charge-transfer region has been recommended for assigning the absolute configuration;[12] the *Λ*-[Co(diamine)$_3$]$^{3+}$ complex shows a negative CD band at the lowest energy in this region. All the isomers give such a band at *ca.* 40000 cm^{-1}. The negative CD bands at *ca.* 35000 cm^{-1} of isomers IIIA-1 and

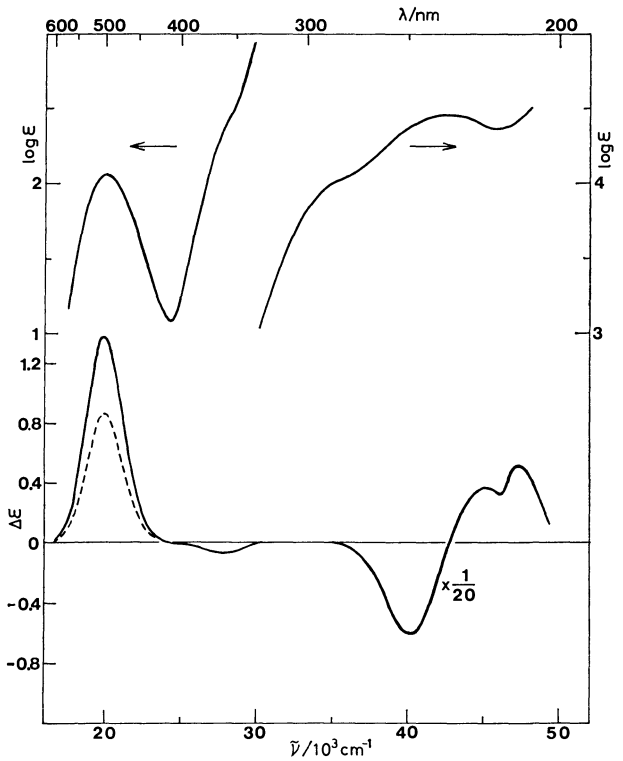

Fig. 7. Absorption and CD spectra of *fac*-*Λ*-[Co(*S*-phtn)$_3$]$^{3+}$ (IIIB) in water (——) and in 0.2 M Na_2SO_4 (----).

IIIA-2 should correspond to transitions of the phenyl group. Thus two isomers IIIA-1 and IIIA-2, and isomer IIIB which show a positive and negative CD band, respectively, at *ca.* 40000 cm^{-1} are assigned to *Δ* and *Λ* configurations, respectively. This assignment agrees with that based on the CD pattern in the first absorption band region. Thus it is concluded that isomers IIIA-1, IIIA-2, and IIIB are the *mer*-*Δ*, *fac*-*Δ*, and *fac*-*Λ* configurations, respectively.

The [Co(*S*-phtn)$_3$]$^{3+}$ complex was prepared by two methods. Method 1 is a substitution reaction between *trans*-[$CoCl_2$(*S*-phtn)$_2$]$^+$ and *S*-phtn in DMSO, and Method 2 oxidation of a DMSO solution containing Co(II) ions and *S*-phtn with air in the presence of active charcoal (Experimental). The formation ratios of the isomers, *mer*-*Δ*:*fac*-*Δ*:*mer*-*Λ*:*fac*-*Λ*, by Methods 1 and 2 were 8:5:0:1, and 1.0:1.4:0:0, respectively. Neither method yielded the *mer*-*Λ* isomer. A molecular model indicates that this isomer involves two phenyl groups situated very close to each other regardless of the conformation of the chelate rings. Although attempts to equilibrate the isomers were unsuccessful, the ratio obtained by Method 2 might be close to that at equilibrium, since the method was carried out in the presence of active charcoal. No *Λ* isomers were formed by Method 2. The *S*-phtn chelate ring can take the *λ*-*skew* conformation. When the diamines are in this conformation, the *Δ*- and *Λ*-[Co(*S*-phtn)$_3$]$^{3+}$ isomers form the *lel*$_3$ and *ob*$_3$ structures, respectively.[13] For [Co(tn)$_3$]$^{3+}$, the *ob*$_3$ isomer has been calculated by conformational analysis to have a substantially higher energy than the *lel*$_3$ and *chair*$_3$ isomers.[14] No formation of the *Λ* isomers might be related to the unstable structure of the *ob*$_3$ isomer. The formation ratio of the isomers, *mer*-*Δ*, *fac*-*Δ*, *mer*-*Λ*, and *fac*-*Λ*, in the corresponding [Co(*S*-bn)$_3$]$^{3+}$ complex was obtained as 1:2:1:14 by a method similar to Method 2 in this study. The *S*-bn complex gives all of the four possible isomers, although it also yields the *Λ* isomers to a greater extent than the *Δ* isomers. Since the chiralities of the *S*-bn and *S*-phtn chelates in the *skew* form are opposite to each other, the structure of *Λ*(*Δ*)-[Co(*S*-bn)$_3$]$^{3+}$ corresponds to that of *Δ*(*Λ*)-[Co(*S*-phtn)$_3$]$^{3+}$. The *Λ*-[Co(*S*-bn)$_3$]$^{3+}$ complex favors greatly the *fac* isomer over the *mer* one, while the *Λ*-[Co(*S*-phtn)$_3$]$^{3+}$ complex gives nearly the same amount of the *mer* and *fac* isomers. The stabilities of these isomers depend largely on the size of the substituent on the 1,3-diamine chelate ligand.

Absorption Spectra: The maximum positions of the first absorption bands of the [Co(*S*-phtn)$_3$]$^{3+}$ isomers differ considerably from each other (Table), in contrast to the case of [Co(*S*-bn)$_3$]$^{3+}$ in which the absorption maxima are in a small range of 20430 to 20370 cm^{-1}.[2] In a previous paper,[2] we reported that a [Co(1,3-diamine)$_3$]$^{3+}$ complex in the *skew* conformation gives the first absorption band at higher energy than that of the complex in the *chair* conformation. The fairly large energy difference in the absorption maixma among the isomers of [Co(*S*-phtn)$_3$]$^{3+}$ seems to be related with the difference in the conformation of chelate rings among the isomers.

When the *S*-phtn chelate ring adopts the *λ*-*skew* conformation, the *fac*-*Λ* and the *fac*-*Δ* isomers form the *ob*$_3$ and the *lel*$_3$ structures, respectively. Since the *ob*$_3$ structure should be less stable than the *chair*$_3$ one,[14] the *fac*-*Λ* isomer would be stabilized in the *chair*$_3$ form. On the other hand, the chelate rings in the *fac*-*Δ* isomer would be able to interchange between the chair and the *λ*-*skew* (*lel*) conformations, since the stability difference between the *chair*$_3$ and the *lel*$_3$ forms would be small.[14] The fact that the *fac*-*Δ* isomer gives the first absorption maximum (20230 cm^{-1}) at fairly higher energy than does the *fac*-*Λ* isomer (20040 cm^{-1}) indicates that the predominant conformation in the *fac*-*Δ* isomer is the *λ*-*skew* form. This isomer shows the blue shift in the first absorption band in DMSO (20410 cm^{-1}). The shift can be interpreted as the result of stabilization of the *lel*$_3$(*Δ*(*λ*-*skew*$_3$)) conformer in this solvent by ion-pair formation between the complex ion and the counter ion (*vide infra*). No solvent effect was observed for the *fac*-*Λ* isomer, suggesting the stability of the *chair*$_3$ structure.

The *mer*-*Δ* isomer shows the first absorption maximum at 20200 cm^{-1} in water. The two *S*-phtn chelate rings in the *mer*(C_1) configuration approach very close to each other, when they adopt the *chair* conformation. As suggested for the *mer* isomers of [Co(*S*-bn)$_3$]$^{3+}$,[2] the close approach of two chelate rings can be avoided when one of these rings takes the *λ*-*skew* conformation. Thus the stable structure of the *mer*-*Δ* isomer would be the (*chair*)$_2$(*λ*-*skew*) form in water. In fact, the first absorption maximum of the isomer is between those of the *fac*-*Δ* and *fac*-*Λ* isomers, in which the predominant conformers of *S*-

phtn have been assigned to the *λ-skew* and *chair* forms, respectively. The first absorption band of the *mer-Δ* isomer shows a small red shift in DMSO (20140 cm^{-1}), but the reverse shift in DMSO–H_2O (1:1) (20280 cm^{-1}). Although the reason for this is not clear, the complex might be stabilized in the lel_3-$(\lambda\text{-}skew)_3$ structure in the latter solvent. In the case of the *fac-Δ* isomer, the band shifts monotonously depending upon the ratio of DMSO to water.

Circular Dichroism Spectra: The study of absorption spectra suggested that the predominant conformer in one isomer differs from that in another. Such conformational flexibility of the *S*-phtn chelate ring is also reflected on the CD spectra. For example, the additive law[16] for the configurational and the vicinal (conformational) effects does not hold for the diastereomeric pair, *fac-Δ*- and *fac-Λ*-$[Co(S\text{-phtn})_3]^{3+}$. The lack of such additivity has also been found for the *RR*-ptn and *S*-bn complexes, and ascribed to the conformational flexibility of the six-membered chelate rings.

The CD pattern of *fac-Δ*-$[Co(S\text{-phtn})_3]^{3+}$ in water is very similar to that of *Δ*-$[Co(RR\text{-ptn})_3]^{3+}$ in 0.1 M Na_2SO_4. The latter has been considered to be stabilized in the $lel_3(\Delta(\lambda\text{-}skew)_3)$ form in the presence of sulfate ions.[1] Thus it is suggested that the stable structure of the *fac-Δ* isomer in water is the $\lambda\text{-}skew_3$-(lel_3) form. This suggestion agrees with that obtained from absorption studies. The corresponding *S*-bn complex, *fac-Λ*-$[Co(S\text{-bn})_3]^{3+}$, on the other hand, is stabilized in the $chair_3$ structure in water.[2] On addition of sulfate ions, *fac-Λ*-$[Co(S\text{-phtn})_3]^{3+}$ diminishes the CD strength of the negative component, and complementarily enhances that of the positive component. Such a change is known to be caused by an increase in the amount of the $lel_3(\Delta(\lambda\text{-}skew)_3)$ conformer due to ion-association between the complex ion and a sulfate ion; the lel_3 form is the most effective structure in forming an ion-pair through hydrogen bonding between the amino protons and a sulfate ion, and the increase in the positive CD component is caused by the increasing amount of the λ-conformer, since the vicinal effect of a λ-conformer is positive.[16] The lel_3 conformer of the *fac-Δ* isomer would be stabilized more in the presence of sulfate ions.

The *fac-Λ* isomer shows only one positive CD band in the first absorption band region, and the CD strength diminishes considerably on addition of sulfate ions. Both of these characteristics have been observed for *fac-Λ*-$[Co(RS\text{-ptn})_3]^{3+}$ (*RS*-ptn=(*R*,*S*)-2,4-pentanediamine), in which the *RS*-ptn chelate ring should be stabilized in the *chair* conformation with the two equatorial methyl groups. Thus the stable structure of *fac-Λ*-$[Co(S\text{-phtn})_3]^{3+}$ would be the $chair_3$ form as suggested from absorption studies.

The CD changes caused by the addition of sulfate ions for *fac-Δ*- and *fac-Λ*-$[Co(S\text{-phtn})_3]^{3+}$ correspond to those for *fac-Δ*- and *fac-Λ*-$[Co(S\text{-bn})_3]^{3+}$, respectively. On the other hand, the effect of sulfate ions on the CD of *mer-Δ*-$[Co(S\text{-phtn})_3]^{3+}$ differs significantly from that of *mer-Λ*-$[Co(S\text{-bn})_3]^{3+}$. By the addition of sulfate ions, the *S*-bn complex shows a fairly strong negative CD band with the decrease in strength of the positive CD band, suggesting the stabilization of the lel_3 form due to ion-pair formation with a sulfate ion.[2] However, the *S*-phtn complex diminishes only the strength of the negative CD band and shows no indication of appearance of a positive CD band. Thus no stabilization to the lel_3 form seems to occur in the *mer-Δ*-$[Co(S\text{-phtn})_3]^{3+}$ isomer. This might be related with the difficulty in forming an ion-pair with a sulfate ion. In the *mer-Δ* isomer, the bulky phenyl groups are disposed on either side of the pseudo-C_3 axis of the complex ion, and would hinder a sulfate ion from approaching the complex ion along the axis. Thus the complex will not be stabilized in the lel_3 form in the presence of sulfate ions.

Each of the three isomers of $[Co(S\text{-phtn})_3]^{3+}$ exhibits a characteristic CD change by the addition of sulfate ions, and all the CD changes can be interpreted on the basis of those of the corresponding *S*-bn complexes taking the steric effect of the bulky phenyl group into consideration.

This work was partly supported by a Grant-in-Aid for Scientific Research No. 243013 from the Ministry of Education, Science and Culture.

References

1) M. Kojima, M. Fujita, and J. Fujita, *Bull. Chem. Soc. Jpn.*, **50**, 898 (1977).
2) M. Kojima and J. Fujita, *Bull. Chem. Soc. Jpn.*, **50**, 3237 (1977).
3) R. S. Cahn, C. K. Ingold, and V. Prelog, *Angew. Chem., Int. Ed. Engl.*, **5**, 385 (1966).
4) S. G. Cohen and S. Y. Weinstein, *J. Am. Chem. Soc.*, **86**, 725 (1964).
5) P. S. Yang and M. M. Rising, *J. Am. Chem. Soc.*, **53**, 3183 (1931).
6) M. Kojima, K. Morita, and J. Fujita, *Bull. Chem. Soc. Jpn.*, **54**, 2947 (1981).
7) E. Fischer, H. Scheibler, and R. Groh, *Chem. Ber.*, **43**, 2020 (1910).
8) B. Sjöberg, B. Hansson, and R. Dahlbom, *Acta Chem. Scand.*, **16**, 1057 (1962).
9) H. Ogino, *Bull. Chem. Soc. Jpn.*, **50**, 2459 (1977).
10) M. Kojima and J. Fujita, *Bull. Chem. Soc. Jpn.*, **54**, 2691 (1981).
11) S. Arakawa, K. Kashiwabara, J. Fujita, and K. Saito, *Bull. Chem. Soc. Jpn.*, **50**, 2331 (1977).
12) M. Kojima and J. Fujita, *Chem. Lett.*, **1976**, 429.
13) J. Corey and J. C. Bailar, Jr., *J. Am. Chem. Soc.*, **81**, 2620 (1959).
14) S. R. Niketic and F. Woldbye, *Acta Chem. Scand.*, **27**, 621 (1973).
15) S. Arakawa, K. Kashiwabara, J. Fujita, and K. Saito, *Bull. Chem. Soc. Jpn.*, **50**, 2108 (1977).
16) C. T. Liu and B. E. Douglas, *Inorg. Chem.*, **3**, 1356 (1964); K. Ogino, K. Murano, and J. Fujita, *Inorg. Nucl. Chem. Lett.*, **4**, 351 (1968).

Reactions of the Bis(β-diketonato)platinum(II) Complexes with Various Nitrogen Bases**

Seichi OKEYA,*,† Yukio NAKAMURA, and Shinichi KAWAGUCHI*

Faculty of Science, Osaka City University, Sumiyoshi-ku, Osaka 558

†*Faculty of Education, Wakayama University, Masago-cho, Wakayama 640*

(Received September 16, 1981)

The bis(β-diketonato)platinum(II) complexes react with various nitrogen bases (L) to afford [Pt(β-dik)L_2]-(β-dik), [Pt(β-dik-*O*)$_2L_2$], [PtL_4](β-dik)$_2$, and [Pt(β-dik)(β-dik-*C*)L] depending on the natures of the β-diketonate anions and L. All of these complexes are stable in solution, showing no sign of isomerization and dissociation of L. The platinum(II) complexes containing the *O*-unidentate β-diketonate ligand are much more stable than the corresponding palladium(II) complexes and [Pt(acac)(piperidine)$_2$](acac) and [Pt(acac-*O*)$_2$(piperidine)$_2$] constitute a pair of linkage isomers. The complexes containing the 2,4-pentanedionate anion (acac) in the outer sphere readily undergo the H-D exchange of the methine proton of acac and the NH protons of coordinated amines with $CDCl_3$.

Bis(β-diketonato)palladium(II) complexes [Pd(β-dik)$_2$] are labile and undergo facile substitution reactions with ammonia, alkylamines, and heterocyclic nitrogen bases (L)[1,2] to afford complexes of the type [Pd(β-dik)L_2](β-dik) (**4**), [PdL_4](β-dik)$_2$ (**5**), [Pd(β-dik)(β-dik-*C*)L] (**7**), and [Pd(β-dik-*C*)$_2L_2$] (**8**), whereas reactions with aniline and its derivatives give rise to the anilide-bridged dinuclear complexes.[3] The reactions of [M(β-dik)$_2$] (M=Pd and Pt) with tertiary phosphines have also been studied and five-coordinate complexes [M(hfac)$_2$(PR_3)] (**2**)[4] as well as the complexes containing *O*-unidentate β-dik ligands [M(β-dik)(β-dik-*O*)(PR_3)] (**3**) and [M(β-dik-*O*)$_2$(PR_3)$_2$] (**6**) were isolated and characterized[5] besides complexes **4**, **5**, and **7**. This investigation demonstrated some differences between palladium(II) and platinum(II) in preference of the coordination modes of β-dik anions, and the present paper reports the supplementary study on the reactions of [Pt(β-dik)$_2$] with nitrogen bases which are to be compared with those of the corresponding [Pd(β-dik$_2$)] complexes.

Experimental

Preparation of Complexes. The starting [Pt(β-dik)$_2$] complexes inclusive of [Pd(acac)(tfac)] were prepared by the methods reported recently.[6] Gaseous methylamine was evolved from its aqueous solution by addition of potassium hydroxide and condensed in a trap cooled with Dry Ice–methanol. The other amines, pyridines, and ammonia were used as supplied without further purification.

*2,4-Pentanedionatobis(piperidine)platinum(II) 2,4-Pentanedionate, [Pt(acac)(pip)$_2$](acac) (**4a**), and Bis(2,4-pentanedionato-O)-bis(piperidine)platinum(II), [Pt(acac-O)$_2$(pip)$_2$] (**6a**)*: [Pt(acac)$_2$] (**1a**) (306 mg, 0.778 mmol) was placed in piperidine (519 mg, 6.10 mmol) and stirred at 70 °C for 15 min. The complex was dissolved gradually to produce a new white precipitate of **6a**, which was filtered and washed with benzene followed by dichloromethane. The yield was 86 mg (20%). Compound **6a** is hardly soluble in usual solvents such as benzene, chloroform, methanol, and dimethyl sulfoxide, but can be recrystallized from a mixture (1:1 by volume) of chloroform and methanol.

The filtrate was concentrated by evaporation at 50—60 °C under reduced pressure to leave a pale yellow oil, which, on standing in the atmosphere, crystallized in plates. The solid mass was washed several times with small portions of hexane to obtain a white powder of **4a** (329 mg) in a 75% yield. Contrary to **6a**, compound **4a** is soluble in various solvents such as benzene, dichloromethane, diethyl ether, and acetone. Recrystallization from hexane gave the monohydrate as white needles, while an acetone solution produced anhydrous crystals.

*[Pt(hfac)(Et$_2$NH)$_2$](hfac) (**4b**) and [Pt(hfac)(pip)$_2$](hfac) (**4c**)*: Diethylamine (44 mg, 0.60 mmol) was added to a diethyl ether solution (3 cm^3) of [Pt(hfac)$_2$] (**1b**) (122 mg, 0.200 mmol) and the solvent was evaporated spontaneously at room temperature to leave yellow plates on the wall of reaction vessel. The yield of **4b** was 144 mg (95%). A similar reaction of **1b** with a twice molar amount of piperidine in diethyl ether gave yellow plates of **4c** in a 95% yield.

*[Pt(hfac)(2-$CH_3C_6H_4NH_2$)$_2$](hfac) (**4d**)*: A mixture of **1b** (72 mg, 0.12 mmol) and 2-methylaniline (25 mg, 0.23 mmol) was allowed to react in benzene (3 cm^3) at ambient temperature for two days. The solvent was then removed under reduced pressure and the residue was extracted with dichloromethane. Hexane was added to the extract and the mixture was kept in a refrigerator to deposit yellow cubes (63 mg) in a 64% yield.

*[Pt(hfac)(Ph$_2$en)](hfac) (**4e**)*: On addition of an equimolar amount of *N,N'*-diphenylethylenediamine to a solution of **1b** in dichloromethane, a white crystalline precipitate of **4e** appeared immediately in a quantitative yield. Compound **4e** is sparingly soluble in usual solvents.

*[Pt(acac)(Et$_2$NH)$_2$](tfac) (**4f**) and [Pt(acac)(pip)$_2$](tfac) (**4g**)*: A mixture of [Pt(acac)(tfac)] (50 mg, 0.11 mmol) and diethylamine (3 cm^3) was heated under reflux for 2 h, when a tiny amount of white precipitate appeared, which was separated by filtration but was insufficient to be identified. The solvent was removed under reduced pressure to leave a yellow crystalline solid, which was recrystallized from a mixture (1:1 by volume) of dichloromethane and petroleum ether to afford colorless columns (20 mg) of **4f** in a 31% yield. Complex **4g** was also prepared in a manner similar to **4f** and recrystallization from benzene–petroleum ether gave colorless plates in a 22% yield.

*Tetrakis(propylamine)platinum(II) 2,4-Pentanedionate Monohydrate, [Pt(n-$PrNH_2$)$_4$](acac)$_2$·H_2O (**5a**)*: A mixture of **1a**

** In this paper the chelated, single oxygen bonded, and central carbon bonded anions of β-diketones (β-dikH) such as 2,4-pentanedione (acacH), 1,1,1-trifluoro-2,4-pentanedione (tfacH), and 1,1,1,5,5,5-hexafluoro-2,4-pentanedione (hfacH) are represented by β-dik, β-dik-*O*, and β-dik-*C*, respectively, and β-dik in the outer sphere shows a counter ion. Other abbreviation: pip, piperidine; Ph_2en, *N,N'*-diphenylethylenediamine; $CyNH_2$, cyclohexylamine.

(200 mg, 0.509 mmol) and propylamine (5 cm^3) was heated under reflux for 10 min and cooled then to −5 °C to deposit colorless plates, which were filtered and washed with diethyl ether. The yield was 155 mg (47%).

[Pt(en)$_2$](acac)$_2$·H$_2$O (5b): When a mixture of **1a** (168 mg, 0.427 mmol) and ethylenediamine (3 cm^3) was heated to about 80 °C for 3 h, a white precipitate appeared and increased gradually. The mixture was cooled spontaneously to room temperature and acetone (5 cm^3) was added to it. The precipitate was filtered and washed with acetone. Recrystallization from methanol–acetone gave white needles (163 mg) in a 72% yield.

[Pt(CyNH$_2$)$_4$](tfac)$_2$ (5c) and [Pt(CyNH$_2$)$_4$](hfac)$_2$ (5e): After the reaction of [Pt(tfac)$_2$] (**1c**) (50 mg, 0.10 mmol) with cyclohexylamine (0.5 cm^3) at about 80 °C for 10 min, diethyl ether (1 cm^3) was added to the cooled reaction mixture to deposit a white precipitate, which was filtered and washed with diethyl ether. The yield was 33 mg (37%). A similar reaction between **1b** and cyclohexylamine gave a white powder of **5e** in a 40% yield. Compounds **5c** and **5e** are both sparingly soluble in usual solvents.

[Pt(py)$_4$](tfac)$_2$·3H$_2$O (5d): A white precipitate appeared immediately after dissolution of **1c** (46 mg, 0.092 mmol) in pyridine (0.5 cm^3). A small portion of hexane was added to the mixture, which was cooled to −5 °C. The precipitate was filtered and washed with diethyl ether. The yield was 79 mg (74%). Recrystallization from dichloromethane–petroleum ether gave white needles.

[Pt(2-CH$_3$C$_6$H$_4$NH$_2$)$_4$](hfac)$_2$·(CH$_3$)$_2$CO (5f): 2-Methylaniline (32 mg, 0.30 mmol) was added to a solution of **1b** (45 mg, 0.074 mmol) in benzene (1 cm^3) and the mixture was stirred for 3 h. The solvent was removed under reduced pressure to leave a yellow crystalline solid, which was washed with diethyl ether. The yield was 69 mg (90%). Recrystallization from acetone–hexane gave white needles which contain an acetone molecule per platinum in crystals.

[Pt(py)$_4$](hfac)$_2$ (5g): Complex **1b** (80 mg, 0.13 mmol) reacted with pyridine (0.3 cm^3) in an exothermic fashion to result in an orange solution. Gradual addition of diethyl ether (1 cm^3) followed by hexane (5 cm^3) to the solution precipitated white needles, which were filtered and washed with a mixture (1:1 by volume) of diethyl ether and hexane. The yield was 103 mg (86%).

[Pt(4-CN-py)$_4$](hfac)$_2$ (5h): On addition of eight times molar 4-cyanopyridine to a benzene solution of **1b**, a yellow crystalline precipitate appeared immediately, which was filtered and washed with diethyl ether. The yield was almost quantitative. Compound **5h** is sparingly soluble in usual solvents.

[Pt(bpy)$_2$](hfac)$_2$ (5i): 2,2′-Bipyridine (54 mg, 0.35 mmol) was added to a solution of **1b** (104 mg, 0.171 mmol) in dichloromethane (2 cm^3) and the mixture was left to stand to deposit a yellow crystalline precipitate, which was filtered and washed with diethyl ether. The yield was 123 g (78%).

Bis(diethylamine)bis(1,1,1-trifluoro-2,4-pentanedionato-O)platinum(II), [Pt(tfac-O)$_2$(Et$_2$NH)$_2$] (6b), and [Pt(tfac-O)$_2$(pip)$_2$]·H$_2$O (6c): A twice molar amount of diethylamine or piperidine was added to a dichloromethane solution of **1c** and the solvent was evaporated spontaneously. The residue was washed with dichloromethane to leave a white crystalline solid. The yields of **6b** and **6c** were 14 and 19%, respectively. Solubilities of both complexes in usual solvents are low.

1,1,1-Hexafluoro-2,4-pentanedionato(1,1,1-hexafluoro-2,4-pentanedionato-C^3)(2-methylaniline)platinum(II), [Pt(hfac)(hfac-C^3)(2-CH$_3$C$_6$H$_4$NH$_2$)] (7a): 2-Methylaniline (24 mg, 0.22 mmol) was added to a solution of **1b** (120 mg, 0.200 mmol) in benzene (5 cm^3) and the mixture was refluxed for 8 h. The solvent was then removed under reduced pressure and the residue was recrystallized from hexane to give yellow cubes (45 mg) in a 31% yield.

Bis(4-methylamino-1,1,1,5,5,5-hexafluoro-3-penten-2-onato)platinum(II), [Pt{N(CH$_3$)C(CF$_3$)=CHCOCF$_3$}$_2$] (11): When methylamine (3 cm^3) was added to a solution of **1b** (120 mg, 0.200 mmol) in diethyl ether (5 cm^3), color of the solution changed from orange to red. The solvent was evaporated spontaneously to leave a red oil and a red crystalline solid. The mixture was dissolved in dichloromethane and recrystallized by addition of petroleum ether to give red needles (32 mg) in a 25% yield. Found: C, 22.70; H, 1.30; N, 4.51%. Calcd for $C_{12}H_8N_2O_2F_{12}Pt$: C, 22.69; H, 1.27; N, 4.41%. Sublimation temp: *ca.* 120 °C. IR in Nujol (cm^{-1}): ν(C=O)+ν(C=C)+ν(C=N), 1627 vs, 1602 s, 1545 vs, 1515 m; ν(C–F), 1230 vs, 1195 vs, 1138 vs. ^{1}H NMR in $CDCl_3$ (δ, ppm from internal Me_4Si): 3.45 q (3H, NCH_3, ^5J(F–H)=2 Hz, ^3J(Pt–H)=27 Hz), 5.99 s (1H, CH, ^4J(Pt–H)=6 Hz).

Measurements. IR spectra were recorded in Nujol mull on Hitachi EPI-S2 and 295 spectrophotometers. NMR spectra were measured with JEOL JNM-C60HL and -MH100 (for ^{1}H), FX60Q (for ^{1}H and ^{13}C), and PS-100 (for ^{19}F) instruments.

Results and Discussion

Reactions of [Pt(β-dik)$_2$] (β-dik=acac (**1a**), hfac (**1b**), and tfac (**1c**)) inclusive of [Pt(acac)(tfac)] with several kinds of nitrogen bases have been examined. In general primary amines and pyridines gave complexes of type **5**, while secondary amines **4** and/or **6**. The reaction between **1b** and 2-methylaniline was exceptional, giving three types of complexes **7a**, **4d**, and **5f** depending on the reactants mole ratio, but did not produce the anilide-bridged dinuclear complexes in contrast with the reactions of [Pd(hfac)$_2$] with aniline and its derivatives.[3]

Complexes **1a** and **1c** did not react with bubbling ammonia in dichloromethane solutions, while **1b** gave a minute amount of unidentified product. A solution of **1a** in methylamine showed no sign of reaction up to the boiling point. When **1b** and **1c** were dissolved in methylamine and propylamine, red solutions resulted indicating occurrence of reactions, but no reproducible product has been obtained except **11**. A Schiff base complex [Pt{N(CH$_3$)C(CF$_3$)=CHCOCF$_3$}$_2$] (**11**) was isolated from the reaction mixture of **1b** and methylamine in diethyl ether and characterized as described in the Experimental Section. A similar palladium(II) Schiff base complex was also obtained by the reaction of [Pd(tfac)$_2$] with aniline.[3]

Table 1 presents the analytical data for newly prepared complexes and Table 2 the IR data for representative ones among them. Similarly to the case of palladium(II) complexes,[1] the ν(C=O)+ν(C=C) bands in the 1800—1500-cm^{-1} region are helpful in diagnosing the bonding modes of the β-dik anions. Thus complexes **5** exhibit bands caused by β-dik anions in the outer sphere, but **4** additional bands assignable to the chalating β-dik ligands. Complexes

TABLE 1. NEWLY PREPARED COMPLEXES, [Pt(β-dik)L_2](β-dik) (**4**), [PtL_4](β-dik)$_2$ (**5**), [Pt(β-dik-*O*)$_2L_2$] (**6**), AND [Pt(β-dik)(β-dik-*C*)L] (**7**)

Compd	β-dik	L	Decomp temp °C	Found (Calcd) (%) C	H	N
4a	acac	pip	*ca.* 169	42.68(42.62)	6.50(6.44)	4.92(4.97)
4a[a]	acac	pip	69— 70 (mp)	41.32(41.30)	6.49(6.59)	4.56(4.82)
4b	hfac	Et_2NH	*ca.* 65	28.94(28.62)	3.33(3.20)	3.92(3.71)
4c	hfac	pip	161—162	30.59(30.82)	3.00(3.10)	3.52(3.59)
4d	hfac	ma[b]	*ca.* 135	34.99(35.00)	2.44(2.45)	3.33(3.40)
4e	hfac	½Ph_2en	195—200	35.04(35.09)	2.20(2.21)	3.57(3.41)
4f[c]	acac / tfac	Et_2NH	*ca.* 100 (mp)	35.95(36.42)	5.58(5.60)	4.48(4.72)
4g[c]	acac / tfac	pip	175—177	38.91(38.89)	5.32(5.39)	4.37(4.54)
5a[a]	acac	*n*-$PrNH_2$	184—186	42.32(41.96)	8.18(8.00)	9.38(8.90)
5b[a]	acac	½en	*ca.* 205	31.06(31.63)	6.03(6.07)	10.55(10.54)
5c	tfac	$CyNH_2$	183—185	44.99(45.48)	6.90(6.74)	6.34 (6.24)
5d[d]	tfac	py	*ca.* 132	41.36(41.33)	3.81(3.93)	6.30 (6.43)
5e	hfac	$CyNH_2$	197—200	41.21(40.60)	5.62(5.41)	5.14 (5.57)
5f[e]	hfac	ma[b]	*ca.* 151	44.99(44.93)	4.02(4.05)	5.12 (5.11)
5g	hfac	py	*ca.* 195	39.15(38.93)	2.52(2.40)	6.06 (6.06)
5h	hfac	4-CN-py	*ca.* 185	39.97(39.81)	1.76(1.77)	11.02(10.93)
5i	hfac	½bpy	157—164	38.62(39.10)	2.08(1.97)	6.06 (6.08)
6a	acac	pip	*ca.* 150	42.45(42.62)	6.53(6.44)	4.70 (4.97)
6b	tfac	Et_2NH	167—171	33.10(33.28)	4.70(4.97)	4.14 (4.34)
6c[a]	tfac	pip	*ca.* 180	34.90(34.94)	4.40(4.69)	3.97 (4.07)
7a	hfac	ma[b]	134—135	28.56(28.50)	1.60(1.55)	2.02 (1.96)

a) Monohydrate. b) 2-Methylaniline. c) The acac anion chelating. d) Trihydrate. e) Containing one acetone molecule per metal atom.

TABLE 2. CHARACTERISTIC IR BANDS OF REPRESENTATIVE COMPLEXES IN NUJOL MULL

Compd	ν(NH)/cm^{-1}	ν(C=C)+ν(C=O)/cm^{-1}
4a	3057 s	1610 vs, 1570 vs, 1550 s, 1525 vs, 1503 vs
4d	3180m, 3050 s	1670 s, 1600 vs, 1553 m, 1535 s
4g	3100 s	1640 s, 1565 vs, 1540 vs, 1520 vs
5a	3150 s, 3100 s	1602 vs, 1504 vs
5d		1635 vs, 1550 vs, br
5f	3210 s, 3020 s	1670 vs, 1520 vs
5g		1676 vs, 1573 m, 1530 vs, br
6a[a]	3170 vs,	1621 vs, 1583 w
6b[b]	3200 vs,	1649 vs
7a	3226m, 3148w	1752 vs, 1703 m, 1598 vs, 1573 s, 1560 s, 1536 m, 1505 m

a) The 1621 and 1583 cm^{-1} bands are assigned to vibrations of the localized C=O and C=C bonds, respectively. The ν(C-O) band is observed at 1165 cm^{-1} (vs). b) The 1649 cm^{-1} band is assigned to ν(C=O). The ν(C-O) band is indiscernible because of overlapping with strong ν(C-F) bands.

6a—c are the first examples of complexes composed of the *O*-unidentate β-dik and amines. The ν(C=O) frequencies for **6a** and **6b** are lower by about 30 and 10 cm^{-1}, respectively, than those for the corresponding triethylphosphine complexes, *trans*-[Pt(acac-*O*)$_2$(PEt_3)$_2$] (1650 cm^{-1})[7] and *trans*-[Pt(tfac-*O*)$_2$(PEt_3)$_2$] (1660 cm^{-1}).[5] The intramolecular or intermolecular hydrogen-bonding interaction between the dangling acetyl or trifluoroacetyl group and the amine group might be responsible for the lower frequency shift of the ν(C=O) band for the present complexes **6**.

^{1}H and ^{13}C NMR Spectra. Tables 3 and 4 list the ^{1}H NMR data for the present complexes except sparingly soluble ones. The ^{13}C NMR data for representative complexes are given in Table 5. They are quite similar to those for the corresponding palladium(II) complexes,[1] and couplings of ^{1}H and ^{13}C atoms to ^{195}Pt are very helpful in diagnosing the bonding states of β-dik anions in the present case. Complexes **5** exhibit each one set of ^{1}H and ^{13}C NMR signals from β-dik anions. All signals lack coupling to ^{195}Pt, indicating that the β-dik anions are involved as counter anions in the outer sphere. Complexes **4**, on the other hand, show each two sets of ^{1}H and ^{13}C signals from β-dik anions. Signals from the chelating β-dik are flanked by the ^{195}Pt satellites and easily distinguished from those assignable to β-dik in the outer sphere. The ^{13}C shieldings and the ^1J(C-H) and J(C-F) values for hfac anions in the outer sphere of **4c** and **5g** are quite similar to those obtained for [K(18-crown-6)](hfac)[1] and [{1,8-bis(dimethylamino)-naphthalene}H](hfac).[3] The ^{19}F NMR spectrum of **5g** in dichloromethane shows a singlet at 4.70 ppm downfield from external CF_3COOH without coupling to ^{195}Pt.

In spite of the salt-like compositions, complexes **4** and **5** as well as the corresponding palladium(II) complexes[1] are generally more soluble in aprotic or-

TABLE 3. ^{1}H NMR DATA FOR [PtL$_4$](β-dik)$_2$ (**5**) AND [Pt(acac-*O*)$_2$(pip)$_2$] (**6a**)[a]

Compd	Solvent	β-dik		L	
		CH_3	CH	NH_2	Other
5a	$CDCl_3$	1.70	5.06[b]	6.29 br {59}	*n*-Pr: 2.54 m, br, 1.59 m, 0.86 t(7)
	C_6D_6	1.91	5.40	6.76 br {*ca.* 60}	*n*-Pr: 2.69 m, br, 1.8 m, 0.95 t(7)
5b	D_2O	2.07	b)	b)	CH_2: 2.64{41}
5d	$CDCl_3$	2.23	5.62		py: 9.70 dd(6 and 2){41}, 7.4 br (H_2O: 2.50)
5f	$(CD_3)_2CO$		5.67	7.65 br {c)}	CH_3: 2.23, Ph: 6.96, 6.91
5g	$CDCl_3$		5.95		py: 9.72 dd(6 and 2){41}, 7.3—7.8 m
5i	$(CD_3)_2CO$		5.45		bpy: $H^{3,3'}$ 8.76 dd, $H^{4,4'}$ 8.41 dt, $H^{5,5'}$ 7.73 ddd, $H^{6,6'}$ 9.26 d{28} ($J_{3,4}$=8, $J_{3,5}$=*ca.* 2, $J_{4,5}$=8, $J_{4,6}$=*ca.* 1, and $J_{5,6}$=6)
6a	$CDCl_3$+CD_3OD (1:1 by volume)	2.34 {5} 2.25	6.92 {12}	4.1_3 br[d]	pip: $H^{2,6}$(eq) 3.1_3 br, $H^{2,6}$(ax) 2.7_4 br, $H^{3,4,5}$ 1.58 br

a) Chemical shifts in ppm from internal Me_4Si except those in D_2O from internal sodium 2,2-dimethyl-2-silapentane-5-sulfonate. Figures in parentheses and braces give J(H-H) and J(Pt-H) in Hz, respectively. d=Doublet, dd=doublet of doublets, ddd=doublet of double doublets, dt=doublet of triplets, m=multiplet, and br=broad. b) The H-D exchange occurs with the solvent. c) Indiscernible. d) NH proton.

TABLE 4. ^{1}H NMR DATA FOR [Pt(β-dik)L$_2$](β-dik) (**4**) AND [Pt(hfac)(hfac-*C*^{3})(2-$CH_3C_6H_4NH_2$)] (**7a**)[a]

Compd	Solvent	β-dik(IS)		β-dik(OS)		L[c]	
		CH_3	CH	CH_3	CH	NH	Other
4a	$CDCl_3$	1.88{*ca.* 4}	5.38{8}	1.84	5.13[b]	b)	pip: 3.4, 2.7, 1.5
	CD_2Cl_2	1.84{4}	5.45{8}	1.80	5.11	8.21{78}	pip: 3.6, 2.7, 1.5
	$(CD_3)_2CO$	1.83{4}	5.59{8}	1.72	4.99[b]	8.4_2[b]	pip: 3.3, 2.6, 1.4
	C_6D_6	1.44{*ca.* 3}	4.97{8}	2.12	5.52	8.85{*ca.* 80}	pip: 3.7, 2.7, 1.9, 1.2
4b	$CDCl_3$		6.29{7}		5.70	7.8_3{*ca.* 70}	Et: *ca.* 2.8 m, 1.43 t(7)
4c	$CDCl_3$		6.34{7}		5.91	7.75{78}	pip: 3.4, 2.6, 1.50
	C_6D_6		5.85{7}		6.36	7.77{83}	pip: 3.23, 2.31, 1.4_8, 1.11
4d	$CDCl_3$		6.03{8}		5.79	7.3_3{75}	CH_3: 2.33, Ph: 7.1 m
4f	$CDCl_3$	1.83{4}	5.44{8}	2.06	5.37	$7._5${*ca.* 80}	Et: 2.7 m, 1.44 t(7)
4h[d]	$CDCl_3$	1.96{4}	5.68{8}	2.32	5.20		py: $H^{2,6}$ 8.46 dd(6 and 2){44}, H^4 8.0 m, br, $H^{3,5}$ 7.5 m, br
7a	$CDCl_3$		6.21{7}		5.99[e] {120}	5.72 {*ca.* 80}	CH_3: 2.28, Ph: 7.1 m

a, b) Same as footnotes a) and b) for Table 3. IS and OS abbreviate inner and outer spheres, respectively. c) The NH-proton signals are all broad. Chemical shifts for the piperidine protons refer to $H^{2,6}$(equatorial), $H^{2,6}$(axial), and $H^{3,5}$(equatorial) plus H^4 in this sequence and those for $H^{3,5}$(axial) are indiscernible except in the case of **4a** (δ 1.9) and **4c** (δ 1.4_8) in C_6D_6. d) [Pt(acac)(py)$_2$](tfac) (**4h**) was obtained as an oily substance from the reaction of [Pt(acac)(tfac)] with twice molar pyridine in dichloromethane at room temperature. e) Methine of the carbon-bonded hfac.

ganic solvents such as dichloromethane and benzene rather than in water. The amine groups which are the most hydrophilic part in the complex cations might be shielded by the hydrocarbon moiety of the β-dik anion in the outer sphere *via* the hydrogen bonding with the carbonyl oxygens as revealed by the X-ray analysis of [Pd(acac)(Et$_2$NH)$_2$](acac) at −170 °C.[8] The fact that the NH proton of piperidine in **4a** resonates at downfield by 4 ppm as compared with that in **6a**, isomer of **4a**, also reflects the effect of hydrogen bonding with the acac anion in the outer sphere which is much stronger than the intramolecular interaction in **6a**. Complex **5b** as well as [Pd(NH$_3$)$_4$](β-dik)$_2$[1] is exceptional, which is readily soluble in water but not in organic solvents. In these complexes the ammine and amine protons may not be sufficiently shielded by the counter anions.

As is noticed in Tables 3 and 4, C_6D_6 exhibits a remarkable effect on the ^{1}H NMR spectra of complexes **4** and **5**. Signals from the chelating β-dik are shifted upfield by about 0.5 ppm and those from β-dik in the outer sphere are shifted downfield by

Table 5. ^{13}C NMR data for some representative complexes[a)]

Compd	Solvent	β-dik(IS)			β-dik(OS)			L		
		CH_3 or CF_3	CH	CO	CH_3 or CF_3	CH	CO	C^α	C^β	C^γ
4a	$CDCl_3$	26.6 (128) {33}	102.5 (159) {57}	184.3 {21}	29.0 (125)	97.5 (149)	187.7	53.4 (140) {30}	26.2 (127) {47}	24.3 (126) {8}
4c	$CDCl_3$	116.8q [283] {b)}	95.6 (168) {66}	170.8q [36] {b)}	118.0q [290]	86.3 (161)	175.4q [32]	54.1 (141) {32}	25.9 (128) {47}	23.5 (129) {7}
	C_6D_6	117.3q [283] {b)}	95.7 (168) {66}	170.3q [36] {*ca.* 20}	119.0q [290]	87.0 (161)	176.1q [32]	54.3 (141) {32}	26.2 (130) {51}	23.6 (130) {7}
5a	$CDCl_3$				28.6 (125)	97.4 (152)	187.3	50.2 (139) {23}	24.0 (128) {53}	11.6 (127)
5b	D_2O				28.1 (126)	c)	195.5	47.6 (143) {5}		
5g	$CDCl_3$				118.6 [292]	84.9 (160)	174.3q [30]	153.0 (185)	126.9 (170) {44}	139.5 (189) {12}

6a in a mixture (1:1 by volume) of $CDCl_3$ and CD_3OD

β-dik[d)]					pip		
C^1	C^2	C^3	C^4	C^5	C^α	C^β	C^γ
23.9 {b)}	188.7 {21}	103.3 {22}	196.8	30.6	53.4 {*ca.* 19}	26.7 {32}	23.9

a) Chemical shifts in ppm from internal Me_4Si except those for **5b** in D_2O which are referred to internal dioxane (δ 67.4). Figures in parentheses, braces, and brackets give J(C-H), J(Pt-C), and J(F-C) in Hz, respectively. q=Quartet. b) Indiscernible. c) Indiscernible because of H-D exchange. d) Numbering of the carbon atoms: $PtOC^2(C^1H_3)C^3HC^4OC^5H_3$.

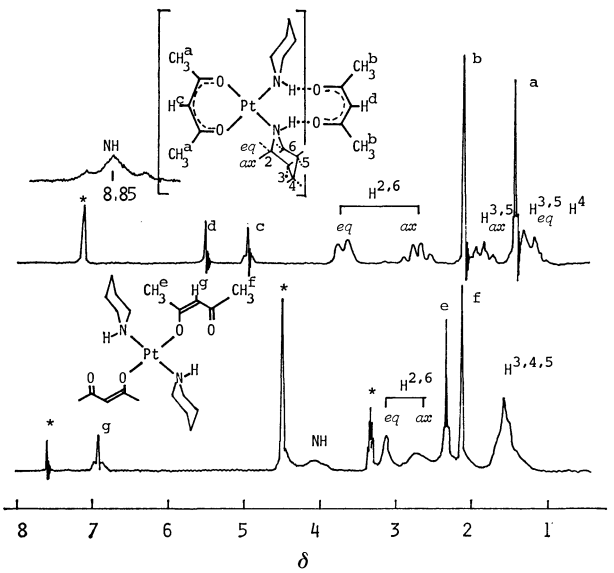

Fig. 1. The proposed structures and the ^1H NMR spectra of [Pt(acac)(pip)$_2$](acac) (**4a**) in C_6D_6 and [Pt(acac-*O*)$_2$(pip)$_2$] (**6a**) in $CDCl_3$+CD_3OD (1:1 by volume) at 100 MHz with internal Me_4Si. The asterisks denote the peaks due to solvent impurities.

0.2—0.5 ppm as compared with those in other solvents. Thus the methine signals for β-dik anions in the inner and outer spheres of **4a** and **4c** interchange their relative positions in $CDCl_3$ and C_6D_6. On the other hand, such a kind of solvent effect is not observed for ^{13}C NMR spectra of **4c** (Table 5). Similar phenomena were found for the corresponding palladium(II) complexes and attributed to the anisotropic magnetic effect of benzene molecules.[1)]

Solubilities of complexes **6** in organic solvents are very low but fortunately **6a** dissolves in a mixture (1:1 by volume) of $CDCl_3$ and CD_3OD sufficiently to allow NMR measurements. The ^1H NMR spectrum of **6a** is compared with that of its isomer **4a** in Fig. 1. The spectrum of **4a** involves two methine and two methyl signals, demonstrating that the two acac anions exist in different and both symmetric environments. On the other hand **6a** exhibits one methine signal and two methyl signals, of which the lower-field one is flanked by ^{195}Pt satellites but the higher-field one is not, indicating that the two acac anions in **6a** are environmentally equivalent, but two halves of each acac are not. The ^{13}C NMR spectrum of **6a** (Table 5) also contains only one set of acac signals and three carbons of each acac ligand couple to ^{195}Pt in accordance with the proposed *O*-unidentate structure. Furthermore, these features of NMR spectra indicate that the *O*-unidentate acac ligand has the stereochemically rigid cis configuration around the C=C bond, although $(CH_3)_3Si$(acac-*O*) molecules have either trans or cis enolate acac anion, the latter undergoing rapid head-to-tail fluxional motion.[9)] As to the geometrical structure of **6a**, the trans arrangement as depicted in Fig. 1 is tentatively assigned by the analogy with *trans*-[Pt(acac-

$O)_2(PEt_3)_2]$[7] and *trans*-[Pt(tfac-$O)_2(PEt_3)_2$].[5] The trans structure of the phosphine complexes was indicated by the characteristic quintet resonance of the methyl protons of PEt_3 and is also supported by small ^1J(Pt–P) values of 2657 and 2646 Hz observed for [Pt(tfac-$O)_2(PR_3)_2$] (R=Et and Cy), respectively.[10]

Complex **4a** is very stable and shows no change on being heated in benzene under reflux for 10 h, whereas complex **6a** decomposes gradually when heated in a chloroform–methanol solution. Thus, though **4a** and **6a** constitute a pair of isomers, interconversion between each other has not been realized. Linkage isomerism is the most interesting and important isomerism in coordination chemistry and a large number of examples have been reported.[11] Each of **4a** and **6a** is composed of two acac anions and two piperidine molecules. In complex **6a** both acac anions act as the *O*-unidentate ligand, whereas in **4a** one is serving as a bidentate ligand and the other as a counter ion. Thus the couple of **4a** and **6a** presents a novel type of linkage isomerism.

The ^{1}H NMR spectrum of **7a** in $CDCl_3$ closely resembles that of [Pd(hfac)(hfac-C^3)(2,4,6-$(CH_3)_3C_6H_2NH_2$)].[3] Although the J(Pt–H) value (7 Hz) of a methine signal at 6.21 ppm is similar to values observed for chelating β-dik anions in complexes **4** (Table 4), J(Pt–H) for the methine signal at 5.99 ppm is as large as 120 Hz, unequivocally indicating that one hfac anion is carbon-bonded to the metal atom. Metal complexes containing a carbon-bonded hfac anion as a ligand are quite rare,[5] but similar J(Pt–H) values have been reported for the methine protons of carbon-bonded acac ligands in [Pt(acac)(acac-C^3)L] (110 and 129 Hz for L=PPh_3[12] and py,[13] respectively) and [Pt(acac-$C^3)_2(py)_2$] (102 Hz).[13]

The H-D Exchange Reactions of Complexes 4 and 5 with $CDCl_3$. Change with time of ^{1}H NMR spectra of **4a** and **5a** in $CDCl_3$ solutions was followed. Intensities of signals assigned to the acac-methine and NH protons decreased gradually and the $CHCl_3$ signal increased instead to attain equilibria in 30 min (**4a**) and 1 d (**5a**). The corresponding palladium(II) complexes **4a** and **5a** react more rapidly, attaining equilibria in 13 min and several hours, respectively.[1] The key step of the H-D exchange was supposed to be the proton transfer from the coordinated amine to the acac anion in the outer sphere.[1] Deprotonation of coordinated amines might be more difficult in the platinum(II) complexes than in the corresponding palladium(II) complexes. The fact that contrary to the case of [Pd(hfac)$_2$],[3] the reaction of [Pt(hfac)$_2$] with 2-methylaniline in refluxing benzene does not afford the anilide-bridged dinuclear complex but result in **7a** might reflect the same trend. Other complexes **4** and **5** containing tfac and hfac as counter ions do not undergo the H-D exchange in $CDCl_3$ probably because of lower basicities of these anions.

Relative Stabilities in Various Bonding Modes of β-Diketonate Anions. The palladium(II) complexes of the types **4**, **5**, **7**, and **8**, which were prepared by the reactions of [Pd(β-dik)$_2$] with a variety of nitrogen and phophorus bases, are rather substitution labile in solution and attain interconversion equilibria such as **4**⇄**7**+L, **5**⇄**7**+3L, **7**⇄**1**+L, **27**⇄**4**+**1**, and **8**⇄**7**+L.[1,5] On the contrary, the platinum(II) complexes obtained in this study showed no sign of transformation on being kept in solution for a long time or on being heated. It may not be due to the extraordinary inertness, but be ascribed to thermodynamic stability of each platinum(II) complex, since the interconversion between [Pt(acac)(acac-C^3)(py)] and [Pt(acac-$C^3)_2(py)_2$] was studied at 40—80 °C.[13]

Although the reactions between [Pd(β-dik)$_2$] and secondary amines yield only the type-**4** complexes, [Pt(β-dik)$_2$] can afford **6** besides **4**. The *O*-unidentate linkage of β-dik anions seems to be more favorable to platinum(II) than palladium(II). The same trend was also noticed for reactions of [M(β-dik)$_2$] with tertiary phosphines.[5] [Pd(hfac)$_2$] reacts with 2,2′-bipyridine (bpy) to produce a type-**4** complex but does not give **5** probably because of the steric requirement of bpy.[1] On the contrary, [Pt(hfac)$_2$] affords **5i** solely. The discrepancy can not be reasonably rationalized, since the bond radii of palladium(II) and platinum(II) are not appreciably different as shown by X-ray analyses of [Pd(acac)$_2$][14] and [Pt(acac)$_2$].[15] It is not certain either why [Pt(tfac)$_2$] does not react with bpy despite that palladium gives [Pd(tfac)(bpy)](tfac).

Preference of the bonding mode is also influenced by the nature of β-dik itself. Piperidine produces both **4a** and **6a** in its reaction with [Pt(acac)$_2$], but gives only **6c** with [Pt(tfac)$_2$] and **4c** with [Pt(hfac)$_2$]. Thus preference of the *O*-unidentate bonding seems to be in the sequence tfac>acac>hfac. Since tfac is unsymmetric and the charge density may be larger on the acetyl oxygen than on the trifluoroacetyl oxygen, the *O*-unidentate bonding *via* the acetyl oxygen may not be so unfavorable compared with chelation especially when a good ancillary ligand coexists. On the other hand, chelates of symmetric β-dik anions are much more stable than the *O*-unidentate state because of not only the chelate effect but also the large electron delocalization effect compared with the case of tfac. Furthermore the least basic hfac anion is a weak ligand and prone to go out of the coordination sphere, the tendency being in the sequence, hfac>tfac>acac. The reactions of [Pt(acac)(tfac)] with secondary amines and pyridine clearly demonstrate this trend, displacing tfac exclusively into the outer sphere to afford [Pt(acac)L$_2$](tfac) (**4f**, **4g**, and **4h**). In a similar way, although pyridine reacts with [Pt(tfac)$_2$] and [Pt(hfac)$_2$] to give **5d** and **5g**, respectively, less basic 4-cyanopyridine can not displace tfac in the former chelate, but does remove hfac ligands in the latter chelate to result in **5h**.

The authors wish to thank Mr. Junichi Gohda for elemental analyses. S. O. and S. K. are grateful to the Ministry of Education, Science and Culture for Grants-in-Aid for Scientific Research, No. 454196 and 243014, respectively.

References

1) S. Okeya, H. Sazaki, M. Ogita, T. Takemoto, Y. Onuki, Y. Nakamura, B. K. Mohapatra, and S. Kawaguchi,

Bull. Chem. Soc. Jpn., **54**, 1978 (1981).
2) S. Okeya and S. Kawaguchi, *Inorg. Chem.*, **16**, 1730 (1977).
3) S. Okeya, H. Yoshimatsu, Y. Nakamura, and S. Kawaguchi, *Bull. Chem. Soc. Jpn.*, **55**, 483 (1982).
4) S. Okeya, T. Miyamoto, S. Ooi, Y. Nakamura, and S. Kawaguchi, *Inorg. Chim. Acta*, **45**, L147 (1980); *Bull. Chem. Soc. Jpn.*, to be submitted for publication.
5) S. Okeya, Y. Nakamura, and S. Kawaguchi, *Bull. Chem. Soc. Jpn.*, **54**, 3396 (1981).
6) S. Okeya and S. Kawaguchi, *Inorg. Synth.*, **20**, 65 (1980); S. Okeya, S. Ooi, K. Matsumoto, Y. Nakamura, and S. Kawaguchi, *Bull. Chem. Soc. Jpn.*, **54**, 1085 (1981).
7) T. Ito, T. Kiriyama, and A. Yamamoto, *Chem. Lett.*, **1976**, 835.
8) S. Kotake, T. Sei, K. Miki, Y. Kai, N. Yasuoka, and N. Kasai, *Bull. Chem. Soc. Jpn.*, **53**, 10 (1980).
9) J. J. Howe and T. J. Pinnavaia, *J. Am. Chem. Soc.*, **91**, 5378 (1969); T. J. Pinnavaia, W. T. Collins, and J. J. Howe, *ibid.*, **92**, 4544 (1970).
10) S. Okeya, unpublished data.
11) A. H. Norbury and A. I. P. Sinha, *Quart. Rev.*, **24**, 69 (1970); R. A. Bailey, S. L. Kozak, T. W. Michelsen, and W. N. Mills, *Coord. Chem. Rev.*, **8**, 407 (1971); A. H. Norbury, *Adv. Inorg. Chem. Radiochem.*, **17**, 232 (1975); R. J. Balahura and N. A. Lewis, *Coord. Chem. Rev.*, **20**, 109 (1976).
12) T. Ito, T. Kiriyama, and A. Yamamoto, *Bull. Chem. Soc. Jpn.*, **49**, 3250 (1976).
13) T. Ito, T. Kiriyama, Y. Nakamura, and A. Yamamoto, *Bull. Chem. Soc. Jpn.*, **49**, 3257 (1976).
14) M. Sato, K. Miki, Y. Kai, M. Tanaka, N. Yasuoka, and N. Kasai, referred to in 7).
15) S. Onuma, K. Horioka, H. Inoue, and S. Shibata, *Bull. Chem. Soc. Jpn.*, **53**, 2679 (1980); M. Katoh, K. Miki, N. Tanaka, and N. Kasai, *ibid.*, **54**, 611 (1981).

Di- and Trinuclear Metal Complexes Containing a β-Diketonate Dianion as a Bridging Ligand†

Yukie Otani, Yukio Nakamura,* Shinichi Kawaguchi, Seichi Okeya,†† and Tetsu Hinomoto†††

Faculty of Science, Osaka City University, Sumiyoshi-ku, Osaka 558

††*Faculty of Education, Wakayama University, Masago-cho, Wakayama 640*

†††*Japan Electron Optics Laboratories, Ltd., Akishima, Tokyo 196*

(Received October 16, 1981)

The dinuclear palladium(II) complexes $[(PP)Pd(C^1—C^3\text{-}\beta\text{-dik}(2-)\text{-}O,O')Pd(PP)](ClO_4)_2$ containing a β-diketonate dianion as a bridging ligand were prepared by the reactions of the mononuclear complexes $[Pd(\beta\text{-dik}(2-)\text{-}C^1—C^3)(PP)]$ with $[Pd(PP)(H_2O)_2](ClO_4)_2$. In the reactions of $[Pd(etac(2-)\text{-}C^1—C^3)(dpe)]$ with $[Pt(PPh_3)_2(H_2O)_2](ClO_4)_2$ and $[Ni(acac)_2]$ in the 1:1 mole ratio, similar dinuclear complexes $[(dpe)Pd(C^1—C^3\text{-}etac(2-)\text{-}O,O')Pt(PPh_3)_2](ClO_4)_2$ and $[(dpe)Pd(C^1—C^3\text{-}etac(2-)\text{-}O,O')Ni(acac)_2]$ were produced, respectively, while the reactions of $[Pd(\beta\text{-dik}(2-)\text{-}C^1—C^3)(PP)]$ with $Ni(ClO_4)_2\cdot 6H_2O$ and $Mg(ClO_4)_2$ in the 2:1 mole ratio afforded the trinuclear complexes $[M\{O,O'\text{-}\beta\text{-dik}(2-)\text{-}C^1—C^3Pd(PP)\}_2](ClO_4)_2$ (M=Ni(II) and Mg(II)). The trihapto coordination to palladium(II) and O,O'-chelation to another metal atom of the β-diketonate dianion in these complexes were deduced mainly by IR and NMR spectroscopy.

The terminal-carbon-bonded 2,4-pentanedionato and ethyl acetoacetato complexes with palladium(II), [PdCl(acac-C^1)(bpy)] and [PdCl(etac-C^1)(bpy)], were derived from the trihapto carbon-bonded complexes, $[PdCl(acac\text{-}C^1—C^3)]_2$ (**1a**)[1] and $[PdCl(etac\text{-}C^1—C^3)]_2$ (**1b**),[2] by the bridge-splitting reactions with 2,2'-bipyridine, and reacted with thallium(I) 2,4-pentanedionate to afford the trihapto complexes containing dianions of these β-dicarbonyl compounds [Pd(acac(2−)-$C^1—C^3$)(bpy)] (**2a**) and [Pd(etac(2−)-$C^1—C^3$)(bpy)] (**2b**).[3]

Each of dianion complexes **2a** and **2b** still possesses uncoordinated oxygen atoms, suggesting the possibility of coordination with another metal ion. In fact the reaction of **2a** with an equimolar amount of [Pd(hfac)(bpy)](hfac) (hfac=1,1,1,5,5,5-hexafluoro-2,4-pentanedionate anion) afforded a yellow precipitate which gave satisfactory analysis as $[Pd_2(acac(2-))(bpy)_2](hfac)_2$.[3] Although the IR spectral data of this compound strongly suggested that the 2,4-pentanedionate dianion is bridging two palladium(II) ions by the trihapto coordination and O,O'-chelation, insolubility of the compound in common organic solvents precluded satisfactory characterization. The present paper is concerned with this kind of dinuclear and trinuclear palladium(II) complexes of bridged β-dicarbonyl dianions containing phosphine ligands in place of 2,2'-bipyridine to increase solubility in organic solvents.[4] The C,O,O'-bridging of 2,4-pentanedionate dianions in the dinuclear and trinuclear complexes was previously reported,[5] and the second type of bridging is presented in this paper.

Experimental

Materials. Diphosphines, *cis*-1,2-bis(diphenylphosphino)ethylene(dpe), and 1,2-bis(diphenylphosphino)ethane (dppe), were purchased from Alfa division, Ventron, U.S.A. Dichloro(diphosphine)palladium(II) complexes $[PdCl_2(dpe)]$ and $[PdCl_2(dppe)]$ were prepared according to the literature method[6] (Anal. Found for $[PdCl_2(dpe)]$: C, 54.23; H, 3.86% and Found for $[PdCl_2(dppe)]$: C, 54.51; H, 4.20%). Diaquabis(triphenylphosphine)platinum(II) perchlorate $[Pt(PPh_3)_2(H_2O)_2](ClO_4)_2$ was prepared as follows:[7] a methanol solution (10 cm³) of silver(I) perchlorate (0.250 g, 1.19 mmol) was added to a suspension of *cis*-dichlorobis(triphenylphosphine)platinum(II) (0.470 g, 0.60 mmol) in chloroform at 0 °C. After stirring of the mixture for 5 min, silver(I) chloride precipitated was filtered off and the filtrate was evaporated to dryness under reduced pressure. These operations were performed at 0 °C. The crude product thus obtained was reprecipitated from dichloromethane–diethyl ether to obtain a white solid. The yield was 0.280 g (49%). Found: C, 45.05; H, 3.64%. Calcd for $C_{36}H_{34}O_{10}Cl_2P_2Pt$: C, 45.30; H, 3.59%. Perchlorate salts $Ni(ClO_4)_2\cdot 6H_2O$ and $Mg(ClO_4)_2$ were obtained from Mitsuwa Chemicals and Kishida Chemicals, respectively and used without further purification.

Mononuclear Trihapto Complexes of β-Diketonate Dianions with Palladium(II). η^3-3-Acetyl-2-oxidoallyl(2,2'-bipyridine)palladium(II) [Pd(acac(2−)-$C^1—C^3$)(bpy)] (**2a**) and η^3-3-ethoxycarbonyl-2-oxidoallyl(2,2'-bipyridine)palladium(II), [Pd(etac(2−)-$C^1—C^3$)(bpy)] (**2b**) were prepared by the reported method.[3] The corresponding diphosphine derivatives were prepared by simple displacement of the 2,2'-bipyridine ligand in **2a** and **2b** by diphosphines as follows.

*η^3-3-Acetyl-2-oxidoallyl{cis-1,2-bis(diphenylphosphino)ethylene}palladium(II) [Pd(acac(2−)-C¹—C³)(dpe)] (**3a**) and the Corresponding dppe Derivative [Pd(acac(2−)-C¹—C³)(dppe)] (**3b**)*: A dichloromethane solution (20 cm³) of dpe (0.522 g, 1.32 mmol) or dppe (0.573 g, 1.46 mmol) was added drop by drop to a suspension of **2a** (0.432 g, 1.20 mmol) in dichloromethane (15 cm³) with stirring at room temperature. After being stirred for 30 min, the mixture was passed through a glass filter and the filtrate was concentrated to *ca.* 5 cm³ by evaporation under reduced pressure. Diethyl ether (20 cm³) was added to the concentrate to obtain **3a** (0.654 g) and **3b** (0.640 g) as pale yellow precipitates in 91 and 87% yields, respectively.

*[Pd(etac(2−)C¹—C³)(dpe)] (**3c**), [Pd(etac(2−)-C¹—C³)(dppe)] (**3d**), and [Pd(etac(2−)-C¹—C³)(PPh₃)₂]·CH₂Cl₂ (**3e**)*: In a similar manner as above, η^3-3-ethoxycarbonyl-2-oxidoallyl derivatives **3c**, **3d**, and **3e** were prepared using a dichloromethane solution of **2b** instead of a suspension

† In this paper, β-dik(2−) represents a dianion of 2,4-pentanedione (acac(2−)) or ethyl acetoacetate (etac(2−)) and PP a bidentate phosphine such as *cis*-1,2-bis(diphenylphosphino)ethylene(dpe) and 1,2-bis(diphenylphosphino)ethane(dppe) or two molecules of triphenylphosphine.

of **2a** in the same solvent, as pale yellow powders in 87, 93, and 86% yields, respectively. Inclusion of one mole of solvent of crystallization in **3e** was confirmed by the elemental analysis and NMR spectroscopy.

Dinuclear Complexes Containing a β-Diketonate Dianion as a Bridging Ligand between Two Palladium(II) Ions. *[(dpe)Pd(C¹—C³-acac(2−)-O,O′)Pd(dpe)](ClO₄)₂ (4a)*: An acetone solution (10 cm³) of silver(I) perchlorate (0.234 g, 1.13 mmol) was added to a suspension of [$PdCl_2$(dpe)] (0.322 g, 0.562 mmol) in the same solvent (20 cm³) with stirring at room temperature. After stirring of the mixture for *ca.* 1 h, silver(I) chloride precipitated was filtered off and the filtrate was evaporated to dryness under reduced pressure, leaving diaquadiphosphinepalladium(II) perchlorate on the bottom and a trace of silver(I) chloride which had passed through the glass filter on the wall of the vessel. To obtain a transparent solution freed of silver(I) chloride, the residue was redissolved in a minimum amount of methanol (*ca.* 10 cm³) and the solution was filtered again, and then the filtrate was added drop by drop to a solution (15 cm³) of **3a** (0.308 g, 0.512 mmol) with stirring at 0 °C. The mixture was further stirred for 20 min and a yellow precipitate produced was filtered, washed with cold methanol and diethyl ether successively, and dried *in vacuo*. The yield was 0.380 g (57%). Crystallization from acetone–diethyl ether (1:2 by volume) gave transparent crystals which turned opaque on standing in air. Similarly, the corresponding dppe complex [(dppe)Pd(*C¹—C³*-acac(2−)-*O,O′*)Pd(dppe)]-$(ClO_4)_2$ (**4b**) was obtained as a yellow precipitate in a 55% yield, using [$PdCl_2$(dppe)] as a starting material instead of [$PdCl_2$(dpe)].

[(dpe)Pd(C¹—C³-etac(2−)-O,O′)Pd(dpe)](ClO₄)₂ (4c), *[(dppe)Pd(C¹—C³-etac(2−)-O,O′)Pd(dppe)](ClO₄)₂ (4d)*, *and [(PPh₃)₂Pd(C¹—C³-etac(2−)-O,O′)Pd(dppe)](ClO₄)₂ (4e)*: These 3-ethoxycarbonyl-2-oxidoallyl derivatives **4c**, **4d**, and **4e** were produced as pale yellow powders from **3c**, **3d**, and **3e**, respectively, by the reactions with appropriate diphosphine complexes in a similar fashion as above. The yields of **4c**, **4d**, and **4e** were 83, 71, and 70%, respectively.

Dinuclear Complexes Containing an Ethyl Acetoacetate Dianion as a Bridging Ligand between Palladium(II) and Another Metal Ion. *[(dpe)Pd(C¹—C³-etac(2−)-O,O′)Pt(PPh₃)₂](ClO₄)₂·0.72CH₃NO₂ (5a)* *and [(PPh₃)₂Pd(C¹—C³-etac(2−)-O,O′)-Pt(PPh₃)₂](ClO₄)₂·1.15CH₃NO₂ (5b)*: A nitromethane solution (20 cm³) of [$Pt(PPh_3)_2(H_2O)_2$]$(ClO_4)_2$ (0.372 g, 0.389 mmol) was added dropwise to a solution of **3c** (0.258 g, 0.409 mmol) or **3e** (0.340 g, 0.410 mmol) in methanol (15 cm³) with stirring at room temperature. After being stirred for *ca.* 40 min, the solution was concentrated to *ca.* 5 cm³ by evaporation under reduced pressure. Diethyl ether (20 cm³) was added to the concentrate to obtain **5a** and **5b** as yellow precipitates. The yields were 0.446 g (74%) and 0.484 g (74%), respectively. Inclusion of nitromethane which could not be removed by pumping was confirmed only by nitrogen analysis of **5a** and **5b**, since these complexes were not stable in solution.

[(dpe)Pd(C¹—C³-etac(2−)-O,O′)Ni(acac)₂] (6): An acetone solution (5 cm³) of [$Ni(acac)_2$] (0.140 g, 0.545 mmol) was added drop by drop to a solution of **3c** (0.320 g, 0.507 mmol) in the same solvent (10 cm³) with stirring at room temperature, and then the solution was heated to *ca.* 50 °C. After *ca.* 30 min, a pale yellow precipitate began to appear and the amount increased with continued stirring of the mixture at 50 °C for additional 2 h. The pale yellow product was then filtered, washed with diethyl ether, and dried *in vacuo*. The yield was 0.361 g (80%). The crude product was recrystallized from chloroform–diethyl ether.

Trinuclear Complexes Containing Bridging β-Diketonate Dianions between Two Palladium(II) Ions and Another Metal Ion. *[Ni{(O,O′-acac(2−)-C¹—C³)Pd(dpe)}₂](ClO₄)₂ (7a)*: An acetone solution (7 cm³) of $Ni(ClO_4)_2 \cdot 6H_2O$ (0.061 g, 0.17 mmol) was added dropwise to a solution of **3a** (0.200 g, 0.333 mmol) in dichloromethane (15 cm³) with stirring at room temperature. The mixture was filtered after *ca.* 1 h of stirring and the filtrate was concentrated to *ca.* 3 cm³ by evaporation under reduced pressure. Diethyl ether (15 cm³) was added slowly to the concentrate to obtain **7a** as a pale green precipitate. The yield was 0.223 g (92%). The product was reprecipitated from dichloromethane–diethyl ether.

[Ni{O,O′-etac(2−)-C¹—C³)Pd(dpe)}₂](ClO₄)₂ (7b) *and [Ni{(O,O′-etac(2−)-C¹—C³)Pd(dppe)}₂](ClO₄)₂ (7c)*: In a similar manner as above, **7b** and **7c** were prepared as pale green powders by reactions of $Ni(ClO_4)_2 \cdot 6H_2O$ with **3c** and **3d**, respectively. The yields were 0.251 g (87%) and 0.237 g (98%), respectively.

[Mg{(O,O′-acac(2−)-C¹—C³)Pd(dpe)}₂](ClO₄)₂ (8a): A methanol solution (5 cm³) of $Mg(ClO_4)_2$ (0.054 g, 0.25 mmol) was added drop by drop to a solution of **3a** (0.308 g, 0.512 mmol) in dichloromethane (20 cm³) with stirring at room temperature. After being stirred for *ca.* 40 min, the solution was concentrated to *ca.* 4 cm³ by evaporation under reduced pressure. Diethyl ether (10 cm³) was added to deposit a pale yellow powder of **8a**, which was filtered, washed with diethyl ether, and dried *in vacuo*. The yield was 0.328 g (93%). The product was reprecipitated from dichloromethane–diethyl ether. Pale yellow crystals of **8a** were obtained by careful crystallization from dichloromethane–acetone but they are not stable and turned opaque on standing in air. Similarly, the corresponding etac(2−) derivative, [Mg{(*O,O′*-etac(2−)-*C¹—C³*)Pd(dpe)}₂]$(ClO_4)_2$ (**8b**) was obtained as a pale yellow powder in a 93% yield by the reaction of $Mg(ClO_4)_2$ with **3c**.

Measurements. Infrared spectra were obtained in Nujol mull with a JASCO DS 701G (4000—200 cm^{-1}) infrared spectrophotometer. Absorption spectra were measured in CH_2Cl_2 with a Hitachi EPS-3T spectrophotometer. NMR spectra were recorded on JEOL JNM MH-100 (for ^1H), FX-60Q (for ^{13}C and ^{31}P), and FX-90Q (for ^{31}P) instruments. Molecular weights were determined with a vapor pressure osmometer manufactured by Knauer, West Berlin, West Germany. Magnetic susceptibility of **7b** was determined by the Faraday method using a balance manufactured by Shimadzu with $[Cr(NH_3)_6]Cl_3$ as a standard.

Results and Discussion

The dinuclear palladium(II) complexes of a novel type, [(PP)Pd(*C¹—C³-β*-dik(2−)-*O,O′*)Pd(PP)]$(ClO_4)_2$ (**4a—e**) containing dianions of 2,4-pentanedione and ethyl acetoacetate as a bridging ligand and diphosphines (PP), were prepared by the simple reactions of the η^3 complexes of β-diketonate dianions, [Pd(β-dik(2−)-*C¹—C³*)(PP)] (**3a—e**) with diaquadiphosphinepalladium(II) perchlorate in methanol at 0 °C.

These reactions were successfully extended to obtain dinuclear and trinuclear complexes containing a β-diketonate dianion which bridges palladium(II) and platinum(II), nickel(II), or magnesium(II) ions in the same way as above. Thus the mononuclear complexes **3c** and **3e** reacted with [$Pt(PPh_3)_2(H_2O)_2$]-$(ClO_4)_2$ in a mixture of nitromethane and methanol (2:1 by volume) at room temperature to give the

Table 1. Analytical data for the newly prepared complexes

	Complex	Found(Calcd)(%) C	H	P	Mol wt[a]
3a	[Pd(acac(2−)-C^1—C^3)(dpe)]	61.87(61.96)	4.69(4.70)	10.31(10.31)	617(601)
3b	[Pd(acac(2−)-C^1—C^3)(dppe)]	61.71(61.75)	5.04(5.02)		611[b] (603)
3c	[Pd(etac(2−)-C^1—C^3)(dpe)]	59.98(60.92)	4.73(4.79)	9.88(9.82)	638(631)
3d	[Pd(etac(2−)-C^1—C^3)(dppe)]	59.94(60.72)	5.07(5.10)		627[b] (633)
3e	[Pd(etac(2−)-C^1—C^3)$(PPh_3)_2$]·CH_2Cl_2	60.83(61.19)	4.78(4.78)		779[b] (759)
4a	[(dpe)Pd(C^1—C^3-acac(2−)-O,O')Pd(dpe)]$(ClO_4)_2$	52.20(52.48)	3.88(4.02)	9.32(9.50)	1347(1305)
4b	[(dppe)Pd(C^1—C^3-acac(2−)-O,O')Pd(dppe)]$(ClO_4)_2$	51.92(52.40)	4.15(4.17)	9.26(9.48)	1369(1307)
4c	[(dpe)Pd(C^1—C^3)-etac(2−)-O,O')Pd(dpe)]$(ClO_4)_2$	52.19(52.20)	3.90(4.08)	9.46(9.28)	1379(1335)
4d	[(dppe)Pd(C^1—C^3-etac(2−)-O,O')Pd(dppe)]$(ClO_4)_2$	51.54(52.12)	4.26(4.22)	8.58(8.47)	1445(1337)
4e	$[(PPh_3)_2$Pd(C^1—C^3-etac(2−)-O,O')Pd(dppe)]$(ClO_4)_2$	55.75(55.83)	4.34(4.27)		1419(1463)
5a	[(dpe)Pd(C^1—C^3-etac(2−)-O,O')Pt$(PPh_3)_2$]$(ClO_4)_2$·$0.72CH_3NO_2$	53.00(51.80)	4.03(3.93)	0.63[c] (0.63)	1318(1550)
5b	$[(PPh_3)_2$Pd(C^1—C^3-etac(2−)-O,O')Pt$(PPh_3)_2$]$(ClO_4)_2$·$1.15CH_3NO_2$	54.18(54.39)	4.22(4.12)	0.92[c] (0.92)	1591(1678)
6	[(dpe)Pd(C^1—C^3-etac(2−)-O,O')Ni$(acac)_2$]	56.49(56.82)	4.94(5.00)		841(888)
7a	[Ni{(O,O'-acac(2−)-C^1—C^3)Pd(dpe)}$_2$]$(ClO_4)_2$	49.61(51.03)	4.03(3.87)		1992(1459)
7b	[Ni{(O,O'-etac(2−)-C^1—C^3)Pd(dpe)}$_2$]$(ClO_4)_2$	48.97(50.93)	4.13(3.98)		1357(1519)
7c	[Ni{(O,O'-etac(2−)-C^1—C^3)Pd(dppe)}$_2$]$(ClO_4)_2$	50.29(50.46)	4.31(4.23)		1484(1523)
8a	[Mg{(O,O'-acac(2−)-C^1—C^3)Pd(dpe)}$_2$]$(ClO_4)_2$	51.57(52.60)	4.08(3.96)		
8b	[Mg{(O,O'-etac(2−)-C^1—C^3)Pd(dpe)}$_2$]$(ClO_4)_2$	51.46(51.76)	4.29(4.07)		

a) In CH_2Cl_2 at 27 °C unless otherwise stated. b) In $(CH_3)_2CO$ at 45 °C. c) N%.

Table 2. ^{13}C NMR data for mononuclear complexes **3a**, **3c**, and **3e** in $CDCl_3$[a]

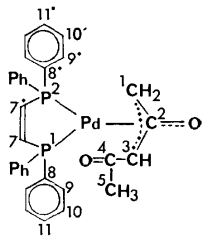

3a

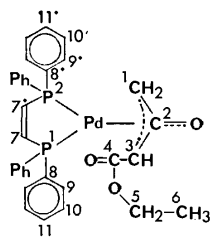

3c

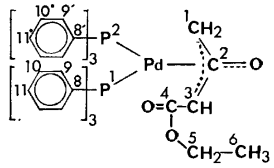

3e

		C^1	C^2	C^3	C^4	C^5	C^6	C^7,$C^{7'}$	C^8,$C^{8'}$	C^9,$C^{9'}$	C^{10},$C^{10'}$	C^{11},$C^{11'}$
3a	δ	48.4 d	177.0 t	75.9 d	203.7 dd	29.6		145.9 m		132.4 d	129.3 d 129.1 d	≈131.2
	$J(P^1$-C)	52.7	5.5	≈0	2	0				13.2	10.6	0
	$J(P^2$-C)	≈0	5.5	40	5	0					10.3	
	J(C-H)	149		145		127		165		≈161	164	≈161
3c	δ	48.3 d	176.4 dd	62.5 dd	171.1 dd	58.5	14.0	146.0 m		132.5 d	129.2 d 129.0 d	≈131.1
	$J(P^1$-C)	52.0	6.2	1.8	1.2	0	0			13.4	10.5	0
	$J(P^2$-C)	≈0	5.5	46.5	5.9	0	0				10.3	
	J(C-H)	150		152		146	126	165		≈161	163	≈161
3e	δ	54.1 dd	174.5 t	68.4 dd	170.1 dd	58.8	14.0		130.7 d 130.6 d	133.8 d 133.7 d	128.3 d 128.1 d	130.0 br
	$J(P^1$-C)	48	5	4	1	0	0		4	13	10	
	$J(P^2$-C)	2.5	5	45	6	0	0		5			
	J(C-H)	153		155		146	126			161	163	163

a) Chemical shift (δ) in ppm from internal Me_4Si and coupling constant (J) in Hz. d=Doublet, dd=doublet of doublets, t=triplet, m=multiplet, and br=broad.

Table 3. ^{1}H NMR data for mono- and dinuclear complexes[a]

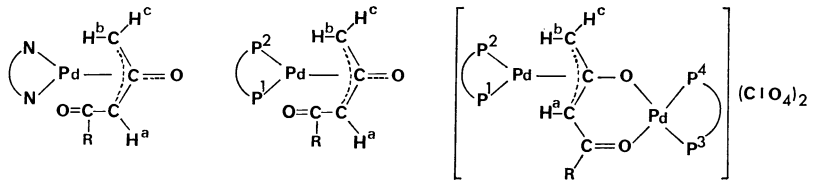

R=CH_3 (**2a**) OCH_2CH_3 (**2b**) R=CH_3 (**3a**, **3b**) OCH_2CH_3 (**3c**—**e**) R=CH_3 (**4a**) OCH_2CH_3 (**4c**)

	CH_3	CH_3——CH_2		H^a	H^b	H^c	Coupling constants in Hz
2a[b]	2.40			3.71 d	2.71 d	2.55 dd	J(bc)=4.4, J(ac)=1.5
2b[b]		1.23 t	4.07 q	3.53 d	3.02 d	2.27 dd	J(bc)=4.4, J(ac)=2.3
3a	1.78			4.27 d	≈3.0 br		$J(P^2-H^a)$=9.5
3b	1.70			4.35 d	2.96 m		$J(P^2-H^a)$=8.0
3c		0.83 t	3—4[c]	4.28 dd	3—4		$J(P^2-H^a)$=8.0, J(ac)=*ca.* 2.0
3d		0.81 t	3—5 br	4.38 d	3—4		$J(P^2-H^a)$=7.2
3e		0.86 t	3.4—3.5[c]	4.03 t	3.4—3.5	2.74 br	$J(P^2-H^a)$=5.4, J(ac)=5.4
4a	d)			5.25 d	d)	d)	$J(P^2-H^a)$=6.8
4c		0.81 t	3.78 br	4.78 d	3.7 br 3.0 br		$J(P^2-H^a)$=9.0

a) Same as footnote a) for Table 2. q=Quartet. In CD_2Cl_2 (**2a**, **2b**, **3a**, and **3c**) and in $(CD_3)_2CO$ (**3b**, **3d**, **3e**, **4a**, and **4c**). b) Ref. 3. c) Not assignable due to overlapping with H^b and H^c signals. d) Not assignable due to diethyl ether impurity.

ionic dinuclear mixed-metal complexes [(PP)Pd(C^1–C^3-etac(2—)-*O*,*O*′)Pt(PPh_3)$_2$](ClO_4)$_2$ (**5a**, PP=dpe; **5b**, PP=2PPh_3), whereas the reaction of **3c** with [Ni(acac)$_2$] in acetone at 50 °C afforded the neutral complex [(dpe)Pd(C^1—C^3-etac(2—)-*O*,*O*′)Ni(acac)$_2$] (**6**). Contrary to all these reactions in the mole ratio of 1:1, the reactions of **3a**, **3c**, and **3d** with Ni(ClO_4)$_2$·6H_2O and of **3a** and **3c** with Mg(ClO_4)$_2$, in the 2:1 mole ratio produced the ionic trinuclear mixed-metal complexes [M{*O*,*O*′-β-dik(2—)-C^1—C^3)Pd(PP)}$_2$](ClO_4)$_2$ (**7a**—**c**, M=Ni(II); **8a** and **8b**, M=Mg(II)), which contain two bridged β-diketonate dianions connecting two different metal ions.

All of the newly prepared complexes inclusive of the trinuclear ionic complexes are moderately soluble in usual organic solvents, and their analytical and molecular weight data are listed in Table 1. Except **7a** and **7b** which give somewhat abnormal molecular weights, each of almost all complexes does not dissociate in nonpolar organic solvents such as CH_2Cl_2.

Mononuclear Trihapto Complexes of β-Diketonate Dianions with Palladium(II). The ^{13}C NMR data for the mononuclear complexes **3a**, **3c**, and **3e** in $CDCl_3$ are listed in Table 2. The dpe complexes are more stable than the corresponding dppe and PPh_3 complexes, exhibiting very good ^{13}C NMR spectra. Assignment of the three sets of higher-field signals in the spectrum of **3a** to the methyl, methylene, and methine carbons was made on the basis of the ^{1}H non-decoupled data, and other signals were assigned as listed in Table 2 by comparison with the spectra for **2a**[3] and [Pt(acac(2—)-C^1—C^3){P(*p*-ClC_6H_4)$_3$}$_2$],[8] of which the trihapto structures were confirmed by the NMR spectra. Four carbons (C^1—C^4) of the acac(2—) skeleton couple to the ^{31}P atom(s), strongly suggesting the trihapto coordination of the ligand to palladium(II). Of these, the terminal methylene (C^1) and methine (C^3) carbons couple strongly to the ^{31}P atom situated at the trans position, each resonating as a doublet, whereas the central carbonyl carbon (C^2) resonates as a triplet, indicating that the coupling constants to both ^{31}P atoms are nearly equal in spite of their environmental nonequivalence. The other carbonyl carbon (C^4) is remote from the coordination sites and weakly couples to both P^1 and P^2. The ^{13}C NMR spectral data for [Pd(etac(2—)-C^1—C^3)-(Me_2bpy)][3] (**2c**) were also helpful for signal assignment of **3c** listed in Table 2. Compared with the ^{13}C NMR signals of the allylic moiety in **2a** and **2c**,[3] the methylene and methine carbons of **3a** and **3c** resonate at the lower field by 10—20 ppm. Such a deshielding of these carbon atoms is presumably due to the larger back-donation of palladium(II) to diphosphine than 2,2′-bipyridine. The same situation is also seen for the shielding of allylic protons (*vide infra*).

Contrary to **3a**, the terminal methylene (C^1) and methine (C^3) carbons of the allylic moiety in the PPh_3 complex **3e** resonate as a doublet of doublets due to the couplings to both P^1 and P^2. The coupling constants (Table 2) are quite similar to those in [Pt(acac-(2—)-C^1—C^3){P(*p*-ClC_6H_4)$_3$}$_2$][8] ($J(P^1-C^1)$=55, $J(P^2-C^1)$=5; $J(P^1-C^3)$=5, $J(P^2-C^3)$=52 Hz). Although the central carbonyl carbon (C^2) in **3e** does not discriminate both P atoms as in the case of **3a**, the environmental nonequivalence of both P atoms (*vide infra*) is shown by slightly different coupling constants of C^2 in the case of **3c**, the signal appearing as a doublet of doublets.

The ^{1}H NMR data for the mononuclear and dinuclear palladium(II) complexes containing β-diketonate dianions and diphosphines are listed in Table

Table 4. $^{31}P\{H\}$ NMR data for mononuclear (**3a**, **3c**, and **3e**) and dinuclear (**4a** and **4c**) complexes[a]

	P^1, P^2		$J(P^1-P^2)$	P^3, P^4	
3a[b]	52.8 d	60.2 d	11		
3c[b]	54.0 d	59.4 d	9		
3e[b]	24.5 d	30.3 d	27		
4a[c]	60.9 d	66.6 d	18	66.2 br	68.2 br
4c[c]	60.7 d	64.1 d	16	69.0 br	71.6 br

a) Chemical shift (δ) in ppm from external H_3PO_4 and coupling constant (J) in Hz. d=Doublet, br=broad. b) In $CDCl_3$. c) In $(CD_3)_2CO$ at 30 °C.

3, and compared with those for the analogous 2,2′-bipyridine complexes **2a** and **2b**.[3] Complexes **2a** and **2b** showed four and five signals with the area ratios of 3:1:1:1 and 3:1:1:1:2, respectively and these signals were reasonably interpreted on the basis of the trihapto structures of acac(2−) and etac(2−) as listed in Table 3.

On the other hand, the ^1H NMR spectra of the newly prepared diphosphine complexes are not conclusive for such a structure assignment, since the signals ascribable to H^b and H^c overlap with each other and with other signals. However, the signal from H^a is useful. Thus, H^a of complex **3c** resonates at 4.28 ppm from internal Me_4Si in $CDCl_3$ as a doublet of doublets due to coupling to P^2 (J=8 Hz) in the trans position and to H^c (J=2 Hz). The latter interaction between H^a and H^c appears as a coupling across four bonds constituting a planar zig-zag configuration (the so-called W rule),[9] suggesting the anti structure of the η-allylic etac(2−) ligand in **3c**. The H^a signal of the diphosphine complexes other than **3c** looks just like a doublet, but this may be attributed to low sensitivity of the NMR instrument used for the measurements. In the case of the triphenylphosphine complex **3e**, the 4.03-ppm signal probably assignable to H^a appears as a triplet, indicating same coupling constants (J=5.4 Hz) of H^a to each of H^c and P^2, accidentally. When one drop of D_2O was added to a $CDCl_3$ solution of **3e** and the mixture was left to stand for 30 min, the signal diminished remarkably, confirming assignment of the signal to an exchangeable unique proton H^a. The fact that the ^{13}C signal from the methine carbon (C^3) at 68.4 ppm decreased by the D_2O treatment also certifies that the methine proton was deuterated. The downfield shift of the H^a signal is generally observed in the present case for displacement of the 2,2′-bipyridine ligand in **2a** and **2b** by diphosphines, again indicating the difference in back-donation of palladium(II) to diphosphines and 2,2′-bipyridine (*vide supra*).

The $^{31}P\{H\}$ NMR spectra of the mononuclear (**3a**, **3c**, and **3e**) and dinuclear (**4a** and **4c**) complexes are recorded and listed in Table 4. The spectra of the mononuclear complexes in $CDCl_3$ are quite simple; for example, complex **3a** shows two signals as an AB quartet at 52.8 and 60.2 ppm downfield from external H_3PO_4 with $J(P^1-P^2)$=11 Hz. The spectrum indicates that the two phosphorus atoms are not equivalent and the difference in their environments is larger than that of two phosphorus atoms in [Pt(acac(2−)-C^1-C^3)-{P(*p*-$ClC_6H_4)_3$}$_2$],[8] of which signals appeared at 18.6 and 19.3 ppm as an AB quartet. In the platinum case, the signal at 19.3 ppm with larger ^1J(Pt-P) was assigned to P situated at the site trans to the allylic methine carbon, since the dangling acetyl moiety was thought to be electron attracting and the acetyl-substituted methylene group to exert slightly smaller trans influence than the unsubstituted methylene end. Although unequivocal discrimination of phosphorus atoms is not possible in the present case, the lower-field signal at 60.2 ppm might be assigned to P^2 situated at the site trans to the methine carbon (C^3). Other complexes **3c** and **3e** also give two doublets with $J(P^1-P^2)$=9 and 27 Hz, respectively. For two cis couplings of ^{31}P atoms in [PdCl(dppe){P(*n*-$Pr)_3$}]$^+$, similar values 11 and 21 Hz were reported, in contrast to 408 Hz for trans coupling.[10]

Here, it should be noticed that [Pd(acac(2−)-C^1—C^3)(NN)] (NN=bpy (**2a**), 4,4′-Me_2bpy, and phen) were always contaminated with the *C,O*-chelated acac(2−) complexes [Pd(acac(2−)-*C,O*)(NN)] in 20—25% proportions which were determined by ^1H NMR spectra.[3] However, none of NMR data in the present diphosphine complexes **3a** and **3b** show evidence for contamination with the *C,O*-chelated acac(2−) complex with diphosphinepalladium(II). Moreover, **3a** and **3b** are produced in high yields of 87—91% which exceed contents of **2a** (75—80%) in the starting complex. These facts suggest that the transformation of the bonding mode from *C,O*-chelation to trihapto coordination occurs during the preparation. Other

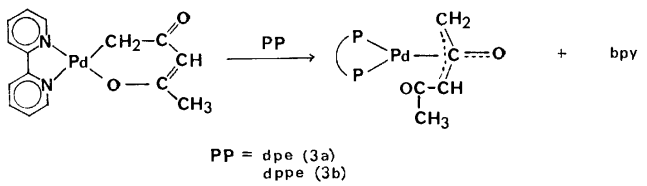

complexes [Pt(tfac(2−)-*C,O*)L_2] which contain a *C,O*-chelated 1,1,1-trifluoro-2,4-pentanedionate dianion with PPh_3, P(*p*-$ClC_6H_4)_3$, or $AsPh_3$ as L were isolated and characterized.[11]

Infrared spectra of the mononuclear complexes **3a**—**e** in the 1500—1700 cm^{-1} region are quite similar to those of **2a** and **2b**, exhibiting a medium ν(C=O) band at 1630—1670 cm^{-1} and a very strong and broad band at 1530—1560 cm^{-1} assignable to the ν(C=O) and/or ν(C=C) vibration. The weak bands due to δ(CCC) of the allylic skelton are not discernible owing to overlapping with strong bands from the diphosphine ligands in the region of 500—600 cm^{-1}.

Dinuclear Complexes Containing a β-Diketonate Dianion as a Bridging Ligand between Two Palladium(II) Ions. Only the ketonic carbonyl band at higher frequency (1633—1667 cm^{-1}) mentioned above is lost and the ν(C=O) and/or ν(C=C) band is shifted to higher frequency (1550—1590 cm^{-1}) more or less in the dinuclear complexes **4a**—**e** without noticeable change in the other part, suggesting that the free carbonyl oxygens coordinated to another palladium ion by *O,O′*-chelation to make dinuclear complexes.

Table 5. ^{13}C NMR data for β-diketonate dianions in dinuclear complexes **4a** and **4c** in $(CD_3)_2CO$

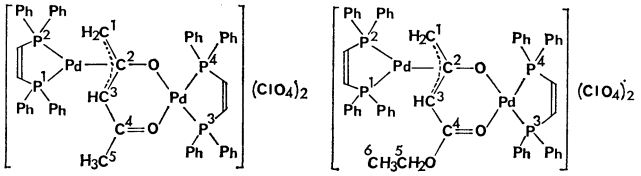

4a **4c**

		C¹	C²	C³	C⁴	C⁵	C⁶
4a	δ	53.4 d, br	166.7 t	76.9 d	208.4	≈29.4	
	Δδ	+5.0	−10.3	+1.0	+4.7	≈+0.2	
	$J(P^1\text{-C})$	43	6	≈0	≈0	≈0	
	ΔJ	−10	0	0	−2	0	
	$J(P^2\text{-C})$	≈0	6	28	≈0	≈0	
	ΔJ	0	0	−12	−5	0	
	J(C-H)	≈153		158		≈131	
4c	δ	53.5 d, br	170.1 t	63.7 d	180.5 br	64.7	13.7
	Δδ	+5.2	−6.3	+1.2	+9.4	+6.2	−0.3
	$J(P^1\text{-C})$	43	6	0	≈0	0	0
	ΔJ	−9	≈0	−2	−1	0	0
	$J(P^2\text{-C})$	≈0	6	33	≈0	0	0
	ΔJ	≈0	≈0	−14	−6	0	0
	J(C-H)	154		157		150	127

a) Same as footnote a) for Table 2. $\Delta\delta=\delta(\mathbf{4a})-\delta(\mathbf{3a})$, $\delta(\mathbf{4c})-\delta(\mathbf{3c})$. $\Delta J=J(\mathbf{4a})-J(\mathbf{3a})$, $J(\mathbf{4c})-J(\mathbf{3c})$.

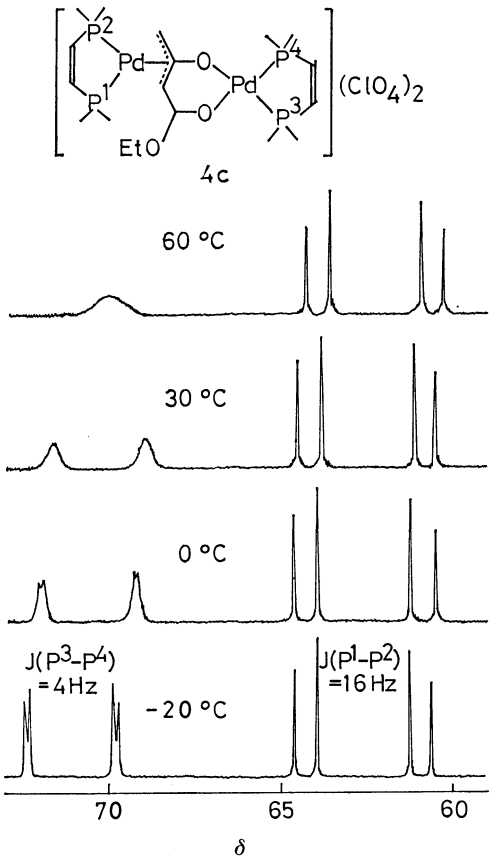

Fig. 1. Temperature dependence of the 24.2 MHz $^{31}P\{H\}$ NMR spectrum of [(dpe)Pd(*O,O'*-etac(2−)-*C*¹—*C*³)Pd(dpe)]$(ClO_4)_2$ (**4c**) in $(CD_3)_2CO$ with H_3PO_4 as an external reference.

Similarly, ^1H NMR spectrum of **4c** (Table 3) resembles as a whole that of the mononuclear complex **3c**, except the H^a signal which appears as a doublet at 4.78 ppm with $J(P^2\text{–}H^a)=9$ Hz. The downfield shift seems to be caused by coordination to the second palladium ion *via* the oxygen atoms and loss of coupling to H^c by violence of the W rule due to transposition of H^a from syn in **3c** to anti in **4c**.

The $^{31}P\{H\}$ NMR spectrum of **4a** in $(CD_3)_2CO$ at 30 °C shows two broader signals at 66.2 and 68.2 ppm besides two doublets at 60.9 and 66.6 ppm with $J(P^1\text{–}P^2)=18$ Hz (Table 4). A similar situation also appears in the spectrum of **4c** which shows two broader signals at 69.0 and 71.6 ppm apart from the two sharp doublets at 60.7 and 64.1 ppm with $J(P^1\text{–}P^2)=16$ Hz. The latter doublets are assigned to P^1 and P^2 by reference to the spectra of **3a** and **3c**. As Fig. 1 shows, the former signals which are assigned to P^3 and P^4, become broader with increasing temperature and coalesce at about 60 °C, indicating occurrence of the coordination site exchange between P^3 and P^4. On the other hand, these two signals sharpen as the temperature is lowered, giving two doublets with $J(P^3\text{–}P^4)=4$ Hz at −20 °C. This also reflects unsymmetric coordination of the etac(2−) anion to another palladium ion *via* oxygen atoms, although individual assignment of the signals to P^3 and P^4 is not possible. The coordination-site exchange may be assisted by solvent molecules.[12]

Table 5 lists the ^{13}C NMR data for the dinuclear complexes **4a** and **4c** in $(CD_3)_2CO$. It can be seen from Tables 2 and 5 that the trihapto coordination of the β-dik(2−) ligands with palladium(II) in the mononuclear complexes is still retained in the dinu-

clear complexes. Again, C^1 and C^3 signals in the dinuclear complexes **4a** and **4c** appear as doublets due to coupling to ^{31}P situated at the trans position. However, the coupling constants are smaller than those in the mononuclear complexes **3a** and **3c** as shown by ΔJ in Table 5, indicating that the allylic carbons-palladium bond became weaker on chelation to another metal ion *via* oxygen atoms. Each carbonyl carbon (C^2) in **4a** and **4c** resonates as a triplet like that in **3a** and **3e**. Contrary to couplings of these allylic carbons, the double doublet of ketonic carbonyl carbon (C^4) signal in the mononuclear complexes disappears in the dinuclear complexes and the C^4 carbon in **4a** and **4c** resonates as a broad singlet. Loss of the couplings indicates the transposition of the carbonyl group from the anti to syn position far apart from P^1 and P^2 in order to coordinate with another metal atom.

It is also worth noting that signals from C^1, C^3, and C^4 are shifted downfield more or less on chelation, while only C^2 shows substantial upfield shift, as shown by $\Delta\delta$ in Table 5. It might be caused by the change in the bonding mode around C^2 from $\rangle C{=}O$ to $\rangle C{-}O\diagdown$. In the case of neat 2,4-pentanedione, the carbonyl carbon of keto tautomer resonates at 202.6 ppm, while that of enol one resonates at 191.8 ppm,[13] making the upfield shift by $\Delta\delta = -10.8$ ppm from $\rangle C{=}O$ to $\rangle C{-}O\diagdown$ which is comparable to $\Delta\delta(C^2) = -10.3$ ppm from **3a** to **4a**.

Di- and Trinuclear Complexes Containing a β-Diketonate Dianion as a Bridging Ligand between Palladium(II) and Another Metal Ion. Except **6** which shows a ν(C=O) band at 1677 cm^{-1} and four strong to medium bands in the region of 1510—1610 cm^{-1}, IR spectra of **5a–8b** again exhibit no ketonic carbonyl band at higher frequency but only a strong and broad band assignable to the $\nu(C{=}O)$ and/or $\nu(C{=}C)$ vibration in the region of 1560—1640 cm^{-1}. Although the spectral region is a little higher than 1550—1590 cm^{-1} for **4a—e**, these features resemble those of dipalladium(II) complexes **4a—e**, suggesting that the bonding mode of β-dik(2—) ligands in **5a–8b** is similar to that in **4a—e**.

Contrary to dipalladium(II) complexes **4a—e**, these mixed-metal dinuclear and trinuclear complexes with palladium(II) and platinum(II), nickel(II), or magnesium(II) are less stable in usual organic solvents, and do not give good ^1H and ^{13}C NMR spectra. For instance, the dinuclear complex with platinum(II), **5a**, decomposes in $CDCl_3$ gradually during the spectral measurement, exhibiting free-ester signals and depositing a white precipitate on the wall of the NMR tube. The trinuclear complex with magnesium(II), **8b**, is rather stable in haloalkanes and gives somewhat broad ^{13}C signals in $CDCl_3$. However, signal assignment is unequivocal: C^1 (terminal methylene), 51.6d ($J(P^1{-}C) = ca.$ 51 Hz); C^2 (central carbonyl), 172.3; C^3 (methine), 60.0d ($J(P^2{-}C) = ca.$ 53); C^4 (ester carbonyl), 177.6; C^5 (ethoxy methylene), 60.5 and C^6 (ethoxy methyl), 13.3 ppm from internal Me_4Si. These chemical shifts are comparable to those for **4c**, suggesting that the etac(2—) ligands in **8b** are working as a bridging ligand through trihapto bonding to palladium(II) and *O,O'*-chelation to magnesium(II) as follows.

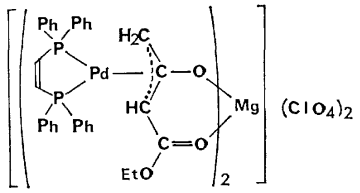

8b

Although the NMR data for all nickel(II) complexes, unfortunately, can not be obtained because of their paramagnetic characters, nickel(II) complexes **7a—c** seem to contain the β-dik(2—) ligands of bonding mode analogous to that in **8b** on the basis of the similarity of IR spectra between nickel(II) and magnesium(II) complexes. The above-mentioned higher-frequency shift of the $\nu(C{=}O)$ and/or $\nu(C{=}C)$ vibrations in **5a–8b** by *ca.* 10—50 cm^{-1} compared with those in **4a—e** might reflect the weaker metal-oxygen bonds in the mixed-metal complexes in conformity with instability of these complexes in solution.

In this connection, it is meaningful to remember that the dinuclear complex with $Ni(acac)_2$, **6**, shows a ν(C=O) band at 1677 cm^{-1} in addition to bands in the 1510—1610-cm^{-1} region, The absorption spectrum of **6** in CH_2Cl_2 exhibits two bands at 9100 cm^{-1} ($^3A_{2g} \rightarrow {}^3F_{2g}$, $\varepsilon = 7.7$) and at 15200 cm^{-1} ($^3A_{2g} \rightarrow {}^3T_{1g}(F)$, $\varepsilon = 8.6$), typical of the octahedral arrangement around the nickel(II) ion, although the third band is obscured by a higher-intensity ligand band. Hence, the higher-frequency carbonyl band in the IR spectrum of **6** might suggest the very weak bonding of the ketonic carbonyl oxygen to occupy the sixth coordination site around the nickel(II) ion, presumably due to the simple adduct formation between neutral molecules in this special case. In the addition compound, $[NiBr_2(C_5H_8O_2)_2]$, of anhydrous nickel bromide with two molecules of 2,4-pentanedione,[14] the ν(C=O) band appeared at 1693 cm^{-1} very near to 1677 cm^{-1}.

On the other hand, the stereochemistry around the nickel(II) ion in **7a—c** and the magnesium(II) ion in **8a** and **8b** seems to be tetrahedral and not planar. For instance, complex **7b** is paramagnetic as shown by the μ_{eff}^{Corr} value of 3.3 BM, and shows a shoulder band assignable to a spin-allowed transition ($^3T_1(F) \rightarrow {}^3T_1(P)$) at 22200 cm^{-1} ($\varepsilon = ca.$ 65) together with two weak bands at 16100 ($\varepsilon = 9.3$) and 8900 cm^{-1} ($\varepsilon = 5.5$).

We wish to thank Mr. Junichi Gohda for the elemental analysis and also grateful to the Ministry of Education, Science and Culture for the Grant-in-Aid for Scientific Research, No. 243014.

References

1) Z. Kanda, Y. Nakamura, and S. Kawaguchi, *Inorg. Chem.*, **17**, 910 (1978).

2) Y. Tezuka, T. Ogura, and S. Kawaguchi, *Bull. Chem. Soc. Jpn.*, **42**, 443 (1969); K. Oda, N. Yasuoka, T. Ueki,

N. Kasai, and M. Kakudo, *ibid.*, **43**, 362 (1970).

3) N. Yanase, Y. Nakamura, and S. Kawaguchi, *Inorg. Chem.*, **19**, 1575 (1980).

4) A short communication appeared in *Chem. Lett.*, **1981**, 11.

5) N. Yanase, Y. Nakamura, and S. Kawaguchi, *Inorg. Chem.*, **17**, 2874 (1978).

6) J. A. Davies, F. R. Hartley, and S. G. Murray, *J. Chem. Soc., Dalton Trans.*, **1979**, 1705.

7) F. Sasakura, K. Isobe, and S. Kawaguchi, 41st National Meeting of the Chemical Society of Japan, Osaka, April 1980, Abstr. No. 4L24.

8) The complex was prepared by the reaction of [Pt(acac)$_2$] with tris(*p*-chlorophenyl)phosphine in chloroform: S. Okeya, Y. Nakamura, S. Kawaguchi, and T. Hinomoto, *Bull. Chem. Soc. Jpn.*, **55**, 477 (1982).

9) L. M. Jackman and S. Sternhell, "Applications of Nuclear Magnetic Resonance Spectroscopy in Organic Chemistry," 2nd ed, Pergamon Press, London (1969), p. 334.

10) J. A. Davies, F. R. Hartley, and S. G. Murray, *Inorg. Chem.*, **19**, 2299 (1980).

11) S. Okeya, Y. Nakamura, S. Kawaguchi, and T. Hinomoto, *Inorg. Chem.*, **20**, 1576 (1981).

12) H. Tanaka, K. Isobe, and S. Kawaguchi, *Inorg. Chim. Acta*, **54**, L201 (1981).

13) J. B. Stothers and P. C. Lauterbur, *Can. J. Chem.*, **42**, 1563 (1964).

14) Y. Nakamura, K. Isobe, H. Morita, S. Yamazaki, and S. Kawaguchi, *Inorg. Chem.*, **11**, 1573 (1972).

Solvent Extraction Study on the Hydrolysis of Tracer Concentrations of Bismuth(III) in Perchlorate and Nitrate Solutions

Itsuhachiro HATAYE,* Hideo SUGANUMA, Hisashi IKEGAMI, and Takashi KUCHIKI

Radiochemistry Research Laboratory, Shizuoka University, Ooya, Shizuoka 422

(Received October 21, 1981)

The backward solvent extraction with dithizone-carbon tetrachloride solutions was used to examine the chemical species of Bi(III). A tracer concentration of Bi(III) ($<10^{-7}$ mol dm^{-3}) was found to exist in the form of Bi^{3+}, $Bi(OH)^{2+}$, $Bi(OH)_2^+$, and $Bi(OH)_3$ in 1.0 mol dm^{-3} (H,Na)ClO_4, and $Bi(NO_3)_n^{3-n}$, $Bi(OH)(NO_3)_n^{2-n}$, $Bi(OH)_2(NO_3)_n^{1-n}$, and $Bi(OH)_3(NO_3)_n^{n-}$ in 1.0 mol dm^{-3} (H,Na)NO_3 solutions depending on the acidity of the solutions. The constants of successive hydrolysis, β_1, β_2, and β_3, were calculated by using the distribution data. The resulting log β_1, log β_2, and log β_3 values were 12.0, 22.9, and 33.9 for 1.0 mol dm^{-3} (H,Na)ClO_4 solution, and 11.9, 22.7, and 33.2 for 1.0 mol dm^{-3} (H,Na)NO_3 solution, respectively. The chemical composition of the extracted species was most probably $Bi(HDz)_3$.

The hydrolysis of Bi(III) in solution has been extensively studied. The most significant early work on the identification of the polynuclear species formed as a result of hydrolysis of Bi(III) was the potentiometric study of Graner and Sillén.[1] The hydrolysis of Bi(III) was further studied by the absorption spectrophotometry,[2] the ultracentrifugation,[3] the potentiometry,[4] the light scattering measurements,[5] the X-ray diffraction,[6] the vibration spectrum,[7] the relaxation techniques,[8] and the spectrophotometric measurements.[9] These studies dealt with the polynuclear species of Bi(III) in regions of macro amounts of bismuth (10^{-4}—0.5 M; 1 M=1 mol dm^{-3}). On the other hand, Bidleman[10] studied the mononuclear species formed in minor concentrations of Bi(III) ($<10^{-4}$ M), based on the solvent extraction using dithizone (H_2Dz). In his work, the equilibrium constants for the Bi–H_2Dz system and the formation constants for the species $Bi(OH)^{2+}$, $Bi(OH)_3$, and $Bi(OH)_4^-$ have been determined. However, the hydrolysis of bismuth ion in more dilute aqueous solution and the formation constants of the species $Bi(OH)_2^+$ has not been well studied. Because the Bi–H_2Dz system has been well defined by many authors,[11–15] we studied on the hydrolysis of bismuth ion in a tracer concentration of $<10^{-7}$ M by using the backward extraction method,[16] by means of which the difficulties due to the anomalous chemical behavior of a tracer scale of substances could be avoided.

Experimental

Reagents. Water and reagents used were all purified to the highest degree, especially to overcome the difficulty due to contaminations. All the aqueous solutions used were finally purified by extraction with H_2Dz–CCl_4 solution. The H_2Dz–CCl_4 solution was prepared according to the method recommended by Sandell.[17] The concentration of H_2Dz–CCl_4 solutions purified was determined by the complexometric titration using a standard $AgNO_3$ solution. Lead (^{210}Pb) containing an equilibrium amount of ^{210}Bi in 3 M HNO_3, imported from the Radiochemical Centre, Amersham, England, was used by diluting it into the appropriate concentration with 3 M HNO_3. A ^{210}Bi tracer solution was prepared by milking to extract from the diluted ^{210}Pb–^{210}Bi solution (pH<3) with H_2Dz–CCl_4 solution. Bismuth nitrate was employed as a carrier of ^{210}Bi tracer.

Initial Organic Solution of Bismuth Dithizonate. A portion of bismuth stock solution was pipetted into a separatory funnel containing water and the bismuth was extracted with a definite concentration of H_2Dz solution at 2<pH<3. The stock solution thus prepared in a lower concentration, less than 10^{-5} M of H_2Dz, showed practically no change within 3 h after preparation against any possible decomposition of H_2Dz.

Measurements of Radioactivity. The radioactivity (β-rays) of ^{210}Bi was counted with a G.M. counter (Aloka Co., Ltd.), with an Al foil absorber (1.84 mg/cm^2) put on the sample planchet in which the bismuth extract was evaporated, by which the α-activity due to ^{210}Po contained in the bismuth extracts could be discriminated. The decay of ^{210}Bi activity ($t_{1/2}$=5.01 d) was compensated for by obtaining the activity relative to a standard specimen prepared at the same time.

Measurements of the Distribution Ratio. One ml (1 ml=1 cm^3) of the organic phase containing a definite amount of bismuth was mixed with 10 ml of 1.0 M (H,Na)-ClO_4 or 1.0 M (H,Na)NO_3 solution; the mixture was shaken at room temperature until the partition equilibrium was attained. After the completion of the equilibrium, a 0.5 ml portion of the organic phase was pipetted into a stainless steel planchet, evaporated, and subjected to the measurements of the β-activity (A_{org}). Because it is difficult to count the activity of the aqueous phase in the same geometrical form as the organic phase in the planchet, it was calculated using $A_{aq}=A^0{}_{org}-A_{org}$, where A_{aq} is the activity of a 5 ml portion of the aqueous phase and $A^0{}_{org}$ is the initial activity of a 0.5 ml portion of the organic phase before shaking. The distribution ratio of bismuth, D, is given as follows;

$$D = 10\times A_{org}/(A^0{}_{org}-A_{org}).$$

In each case, the multiple extraction procedures were repeated under conditions of a definite hydrogen ion concentration and definite amounts of bismuth in aqueous phase; the data obtained in the first half were all discarded and only the reproducible data in the other half were taken.

Measurements of Hydrogen Ion Concentration. As for acidic media (pH<1), the hydrogen ion concentration was calculated from the acidity of the $HClO_4$ or HNO_3 used. In other cases, it was measured with a pH meter (TŌA Electronics Ltd.) at room temperature as soon as possible after shaking.

Results and Discussion

Time Necessary for the Partition Equilibrium. As shown in Fig. 1, the partition of bismuth between

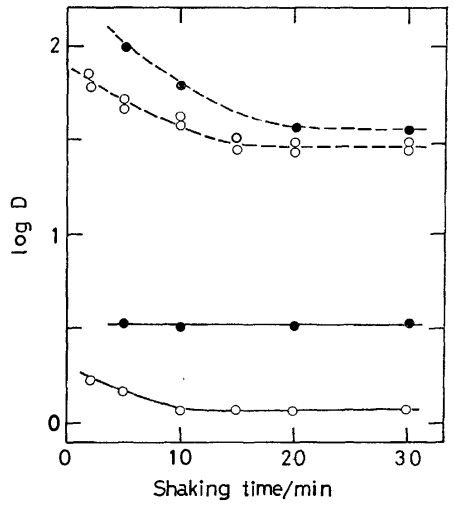

Fig. 1. The effect of shaking time on the distribution ratio in the backward extraction.
—●—: 1.0 M $HClO_4$ solution, $\log[H_2Dz]_{org} = -3.64$, --●--: 1.0 M (H,Na)$ClO_4$ solution ($-\log[H^+] = 3.80$), $\log[H_2Dz]_{org} = -5.77$, —○—: 1.0 M HNO_3 solution, $\log[H_2Dz]_{org} = -3.40$, --○--: 1.0 M (H,Na)$NO_3$ solution ($-\log[H^+] = 3.46$), $\log[H_2Dz]_{org} = -5.51$.

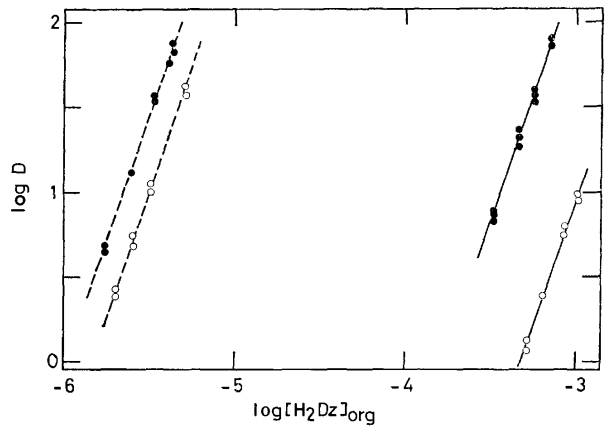

Fig. 2. The dependence of the distribution ratio on the concentration of dithizone in the organic phase.
—●—: 1.0 M $HClO_4$ solution, --●--: 1.0 M (H,Na)ClO_4 solution ($-\log[H^+] = 2.53$), —○—: 1.0 M HNO_3 solution, --○--: 1.0 M (H,Na)NO_3 solution ($-\log[H^+] = 3.01$).

two phases reaches equilibrium within 10 minutes for a high acidity (1.0 M $HClO_4$ and 1.0 M HNO_3) and in about 20 min for a weak acidity (1.0 M (H,Na)ClO_4, $-\log[H^+] = 3.80$; 1.0 M (H,Na)NO_3, $-\log[H^+] = 3.46$). Accordingly, the partition system was shaken for 25 min in all experiments to attain the equilibrium.

Dependence of the Distribution Ratio on the Bismuth Concentration. Table 1 shows the distribution ratios measured as a function of the amount of bismuth carrier in the tracer concentration ($<10^{-7}$ M). The bismuth concentration of the original tracer solution prepared in a carrier-free state was examined substoichiometrically with dithizone extraction. No effects of the bismuth concentration were observed for either 1.0 M $HClO_4$ media or 1.0 M (H,Na)ClO_4 solutions of $-\log[H^+] = 3.84$, nor for either 1.0 M HNO_3 or 1.0 M (H,Na)NO_3 solutions of $-\log[H^+] = 3.46$. These results suggest that there is no difference in the degree of polymerization of bismuth species between aqueous and organic phases. On the other hand, since it is improbable that any polymerized species remain stable in both phases, we may safely assume that the monomers are the main species involved in the solvent extraction of tracer concentrations of bismuth.

Dependence of the Distribution Ratio on the Dithizone Concentration in Organic Phase. The distribution ratio, D, was plotted as a function of the H_2Dz concentration at different hydrogen ion concentrations. Figure 2 shows that the plots of $\log D$ *vs.* $\log[H_2Dz]_{org}$ show a slope of $+3$ independent of the acidity and the media, where H_2Dz denotes a neutral dithizone molecule. In general, the slope of $\log D$ *vs.* $\log[H_2Dz]_{org}$, or $\partial \log D/\partial \log[H_2Dz]_{org}$, indicates the difference in the average number of univalent dithizone ions (HDz^-) attached to a bismuth atom between the organic and aqueous phases. It is generally accepted that the coordination number of Bi(III) is six, so the total number of ligands (as univalent) combined to a bismuth atom can be reasonably assumed not to exceed six, and the extracted species must be electrically neutral. Since HDz^- ion is a bidentate ligand, our results shown in Fig. 2 lead to the conclusion that bismuth exists in the chemical form of $Bi(HDz)_3$ in the organic phase. It also means that the concentration of Bi–HDz^- complex species is negligibly low in the aqueous phase of 1.0 M (H,Na)ClO_4 and 1.0 M (H,Na)NO_3.

The distribution ratio, D, is expressed as follows:

$$D = [Bi(HDz)_3]_{org}/\{\sum_{n=0}^{6-x}\sum_{x=0}^{6-n}[Bi(OH)_nX_x^{3-n-x}]\} \quad (1)$$

$$= \{K_3[H_2Dz]^3_{org}[H^+]^{-3}\}/\{\sum_{n=0}^{6-x}\sum_{x=0}^{6-n}\beta_{n,x}Q_w{}^n[H^+]^{-n} \times [X^-]^x\}, \quad (2)$$

where

$$K_3 = [Bi(HDz)_3]_{org}/\{[Bi^{3+}][H_2Dz]^3_{org}[H^+]^{-3}\}, \quad (3)$$

$$\beta_{n,x} = [Bi(OH)_nX_x^{3-n-x}]/\{[Bi^{3+}][OH^-]^n[X^-]^x\}, \quad (4)$$

$Q_w = [H^+][OH^-]$, and also X^- denotes ClO_4^- or NO_3^-.

D should be written in terms of the hydrolysis of bismuth in case of $[X^-] = 1.0$ M, as follows:

$$D/[H_2Dz]^3_{org} = K_3/(\sum_{n=0}^{6-x}\sum_{n=0}^{6-n}\beta_{n,x}Q_w{}^n[H^+]^{3-n}). \quad (5)$$

In the present case, $\sum_{n=0}^{6-x}\sum_{n=0}^{6-n}\beta_{n,x}$ is denoted by $\sum_{n=0}^{6}\beta_n$, because each $\beta_{n,x}$ can not be measured and the $\sum_{x=0}^{6}\beta_{0,x}$ is regarded as unity. Accordingly, Eq. 5 should be rewritten as follows:

$$D/[H_2Dz]^3_{org} = K_3/(\sum_{n=0}^{6}\beta_nQ_w{}^n[H^+]^{3-n}). \quad (6)$$

Dependence of the Distribution Ratio on the Hydrogen Ion Concentration. In Fig. 3, we plot $\log(D/[H_2Dz]^3_{org})$ as a function of $-\log[H^+]$ in 1.0 M

Table 1. The dependence of the distribution ratio on the bismuth concentration

Aqueous phase	$-\log[H^+]$	$[H_2Dz]_{org}$/M	$[Bi(III)]_{org}$[a]/M	$\log D$
1.0 M (H, Na)ClO_4	0.0	3.98×10^{-4}	Carrier free($<10^{-9}$)	1.15±0.11
			0.92×10^{-9}	1.18±0.09
			0.92×10^{-7}	1.22±0.15
	3.84	2.06×10^{-6}	Carrier free($<10^{-9}$)	1.75±0.05
			0.84×10^{-9}	1.76±0.15
			0.84×10^{-7}	1.78±0.11
1.0 M (H, Na)NO_3	0.0	5.08×10^{-4}	Carrier free($<10^{-9}$)	0.45±0.15
			0.84×10^{-9}	0.44±0.12
			0.84×10^{-7}	0.40±0.12
	3.46	3.40×10^{-6}	Carrier free($<10^{-9}$)	1.60±0.15
			0.84×10^{-9}	1.59±0.09
			0.84×10^{-7}	1.62±0.10

a) Initial concentration of Bi(III) in H_2Dz-CCl_4 solution.

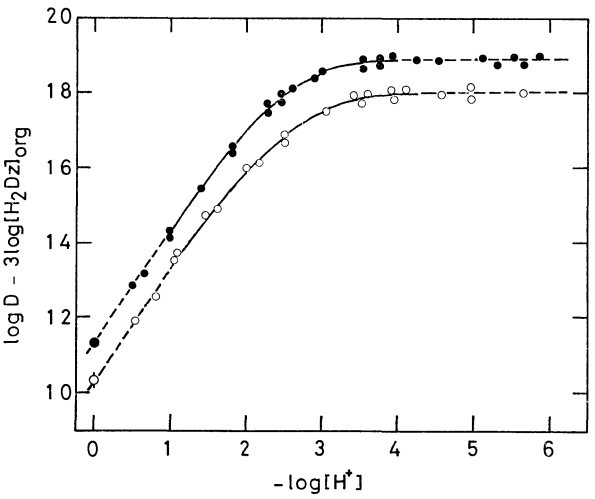

Fig. 3. The dependence of the distribution ratio on the hydrogen ion concentration.
●: 1.0 M (H,Na)ClO_4 solution, ○: 1.0 M (H,Na)-NO_3 solution.

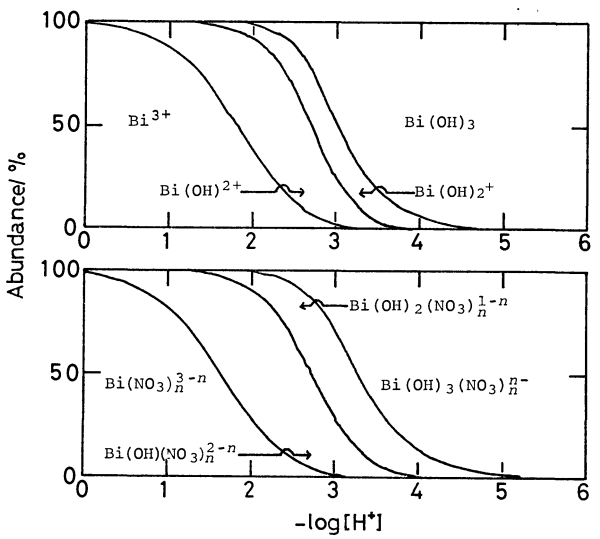

Fig. 4. The chemical species of the bismuth ion in 1.0 M (H,Na)ClO_4 solution (upper) and 1.0 M (H,Na)NO_3 solution (lower).

(H,Na)ClO_4 and 1.0 M (H,Na)NO_3 solutions. Since it is difficult to determine the distribution ratio by using only a single H_2Dz solution with a definite concentration in all regions of hydrogen ion concentration, $\log(D/[H_2Dz]^3_{org})$ is plotted instead of $\log D$. As shown in the figure, the slope seems to be +3 for the region of $-\log[H^+]<1.5$ in both 1.0 M (H,Na)-ClO_4 and 1.0 M (H,Na)NO_3 solutions, while it is 0 for $-\log[H^+]=4.0$—5.7. Therefore, there exist few hydroxo-compounds of Bi(III) in high acidity, while hydroxo-compounds such as $Bi(OH)_3X_x$ are predominant in the weakly acidic to neutral solutions. The distribution ratio in Eq. 6 can be expressed in terms of hydrolysis constants β_n as follows:

$$D/[H_2Dz]^3_{org} = K_3/([H^+]^3+\beta_1Q_w[H^+]^2 +\beta_2Q_w^2[H^+]+\beta_3Q_w^3), \quad (7)$$

where

$$\beta_1 = [Bi(OH)X_x^{2-x}]/([Bi^{3+}][OH^-][X^-]^x), \quad (8)$$

$$\beta_2 = Bi(OH)_2X_x^{1-x}]/([Bi^{3+}][OH^-]^2[X^-]^x), \quad (9)$$

$$\beta_3 = [Bi(OH)_3X_x^{x-}]/([Bi^{3+}][OH^-]^3[X^-]^x). \quad (10)$$

Estimation of K_3, $\beta_3Q_w^3$, $\beta_2Q_w^2$, *and* β_1Q_w. Figure 3 shows that the slope of $(\log D-3\log[H_2Dz]_{org})$ *vs.* $-\log[H^+]$ at $-\log[H^+]=0$ is nearly 3, so Eq. 7 can be simplified as $D/[H_2Dz]^3_{org}\approx K_3$. Consequently, the approximate values of K_3 were obtained from Figs. 1 and 3 and Table 1 to be $K_3=(2.40\pm0.33)\times10^{11}$ for 1.0 M (H,Na)ClO_4 solution and $K_3=(2.34\pm0.60)\times10^{11}$ for 1.0 M (H,Na)NO_3 solution. Furthermore, since Fig. 3 shows that the slope of $(\log D-3\log[H_2Dz]_{org})$ *vs.* $-\log[H^+]$ ($-\log[H^+]>4$) is zero, independent of the acidity, Eq. 7 can be simplified as $D/[H_2Dz]^3_{org}\approx K_3/(\beta_3Q_w^3)$. Consequently, the approximate value of $\beta_3Q_w^3$ was obtained from Fig. 3 to be $\beta_3Q_w^3=(3.02\pm1.01)\times10^{-8}$ for 1.0 M (H,Na)-ClO_4 solution and $\beta_3Q_w^3=(2.24\pm0.86)\times10^{-8}$ for 1.0 M (H,Na)NO_3 solution. By using the set of K_3 and $\beta_3Q_w^3$ obtained, the approximate values of a set of β_1Q_w and $\beta_2Q_w^2$ were obtained by least squares fit from the data in the region of $-\log[H^+]=1.5$—4 in Fig. 3; the values are $\beta_1Q_w=1.44\times10^{-2}$ and $\beta_2Q_w^2=1.81\times10^{-5}$ for 1.0 M (H,Na)ClO_4 solution, and also $\beta_1Q_w=2.13\times10^{-2}$ and $\beta_2Q_w^2=3.09\times10^{-5}$

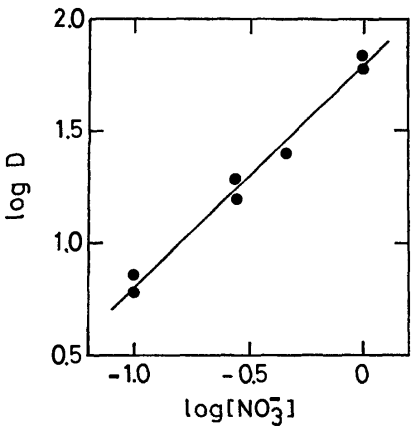

Fig. 5. The influence of the concentration of the nitrate ion on the distribution ratio at $-\log[H^+]=1.0$ ($\log[H_2Dz]_{org}=-3.87$).

for 1.0 M (H,Na)NO_3 solution, respectively. Equation 7 is third order with respect to the hydrogen ion concentration; therefore, no meaningful error in $\beta_1 Q_w$ and $\beta_2 Q_w^2$ calculations could be obtained. The values obtained of $\log \beta_1$, $\log \beta_2$, and $\log \beta_3$ are 12.0, 22.9, and 33.9 for 1.0 M (H,Na)ClO_4, when $\log Q_w$ is -13.80,[18] and 11.9, 22.7, and 33.2 for 1.0 M (H,Na)NO_3 solutions, when $\log Q_w$ is -13.61.[19] Per cent abundances of the chemical species of bismuth calculated from each β value at different hydrogen ion concentrations in 1.0 M (H,Na)ClO_4 and 1.0 M (H,Na)NO_3 solutions are represented in Fig. 4. In the latter case, because of possible coordination of nitrate ions to the bismuth atom in 1.0 M (H,Na)NO_3 solution, we have taken into consideration the contribution of nitrate ions to the bismuth species.

The Effect of Nitrate and Perchlorate Ion Concentration on the Distribution Ratio. The extractability of bismuth increased with an increasing nitrate ion concentration; this might be attributed to a salting-out effect of $NaNO_3$ as an electrolyte. Kapantsyan and Nabivanets[20] reported on the nitrate complexes of bismuth in the solution. Bismuth nitrate complexes may be present in 1.0 M (H,Na)NO_3 solution, because the values of $\log(D/[H_2Dz]^3_{org})$ for 1.0 M (H,Na)NO_3 solution are always smaller than those for the corresponding 1.0 M (H,Na)ClO_4 solution in all regions of $0 \leq -\log[H^+] \leq 5.7$, as shown in Fig. 3. This also implies that some effect opposing the bismuth extraction arises from the complexation of bismuth with the nitrate ion. Consequently, each β value obtained for 1.0 M (H,Na)NO_3 solution should be considered as conditional constants obtained under our experimental conditions. The effect of perchlorate ion concentration on the distribution ratio of Bi(III) was examined in the concentration of 0.1—1.0 M at $-\log[H^+]=1.0$, where little effect was observed in the concentration range of ClO_4^- examined. It is difficult to assume the presence of bismuth perchlorate complexes on a tracer scale in 1.0 M (H,Na)ClO_4 solution because of the less-complexing perchlorate ion, but in the macro region the formation of $Bi_6(OH)_{12}(ClO_4)_2^{4+}$ was reported by Johnson *et al.*[21] It can be said, nevertheless, that the effect of perchlorate ion concentration in the present study may be negligibly small, since the ionic concentration in the aqueous phase was kept constant to 1.0 M in all experiments.

Graner and Sillén[1] reported that Bi(III) was unhydrolyzed at acid concentrations greater than 0.5 M, and that the number of hydroxides bound per bismuth atom appeared to approach asymptotically the value 2 in titration experiments on 0.01, 0.025, and 0.05 M Bi(III) in 3 M $NaClO_4$ solutions. They proposed a species of polymeric hydrolysis products with the general formula $Bi_nO_{n-1}^{n+2}$ to account for their observations. Olin[4] extended the measurements to a broader range of Bi(III) concentrations, 10^{-4}—0.05 M Bi(III), and his more precise data from an amalgam electrode were analyzed in terms of two species $Bi(OH)^{2+}$ and $Bi_6(OH)_{12}^{6+}$. The mononuclear species was formed only in minor amounts. The vibration spectrum of $Bi_6(OH)_{12}^{6+}$ in very high concentrations of Bi(III) (up to 8.41 M Bi(III) in 8.85 M ClO_4^- solution) was reported by Maroni and Spiro.[7] Bidleman[10] studied the hydrolysis of bismuth ions in dilute ($<10^{-4}$ M) aqueous solution by the extraction measurements using dithizone, and obtained the equilibrium constants for the bismuth–dithizone system and the formation constants of the $Bi(OH)^{2+}$, $Bi(OH)_3$, and $Bi(OH)_4^-$, where the values of $\log \beta_1$, $\log \beta_3$, and $\log \beta_4$ are 12.4, 31.9, and 32.9 (μ(ionic strength)=0.1), respectively. In tracer concentrations of bismuth in 1.0 M (H,Na)ClO_4 and 1.0 M (H,Na)NO_3 solutions in the region of $0 \leq -\log[H^+] \leq 5.7$, our results showed the presence of Bi^{3+}, $Bi(OH)^{2+}$, $Bi(OH)_2^+$, and $Bi(OH)_3$, and/or $Bi(NO_3)_n^{3-n}$, $Bi(OH)(NO_3)_n^{2-n}$, $Bi(OH)_2(NO_3)_n^{1-n}$, and $Bi(OH)_3(NO_3)_n^{n-}$. For this latter group a further study on the mean charge of each species should be made. At the same time, no evidence for the existence of any polymerized species was found in the present conditions of aqueous media. However, in the stored and/or more concentrated bismuth solution, some polymerized species may be formed.

The value of $\log K_3$ (11.4) for 1.0 M (H,Na)ClO_4 found in this work is larger than those reported by Bidleman (10.9 at $\mu=0.1$ and 10.8 at $\mu=1.0$),[10] Busev and Bazhanova (10.0 at $\mu=0.2$),[14] Koroleff (9.7),[12] and Pilipenko (10.6 at $\mu=0.5$).[13] This fact may suggest that the formation of extracted species ($Bi(HDz)_3$) is depressed by forming polynuclear complexes in macro concentrations of bismuth solution. Another reason why the value of $\log K_3$ (10.4) for 1.0 M (H,Na)NO_3 is smaller than that for 1.0 M (H,Na)ClO_4 solution may be complex-formation with nitrate ion.

References

1) F. Graner and L. G. Sillén, *Acta Chem. Scand.*, **1**, 631 (1947).
2) P. Souchay and D. Peschanski, *Bull. Soc. Chim. Fr.*, **1948**, 439.
3) R. W. Holmberg, K. A. Kraus, and J. S. Johnson, *J. Am. Chem. Soc.*, **78**, 5506 (1956).
4) A. Olin, *Acta Chem. Scand.*, **11**, 1445 (1957).
5) R. S. Tobias and S. Y. Tyree, Jr., *J. Am. Chem. Soc.*,

82, 3244 (1960).
6) H. A. Levy, M. D. Danfold, and P. A. Agron, *J. Chem. Phys.*, **31**, 1458 (1959).
7) V. A. Maroni and T. G. Spiro, *J. Am. Chem. Soc.*, **88**, 1410 (1966).
8) V. Frei, G. Mages, and H. Wendt, *Ber. Bunsenges. Phys. Chem.*, **77**(**4**), 243 (1973).
9) C. Dragulescu, A. Nimaro, and I. Julean, *Rev. Roum. Chim.*, **7**, 1181 (1972).
10) T. F. Bidleman, *Anal. Chim. Acta*, **56**, 221 (1971).
11) J. Reith and C. Van Dijk, *Chem. Weekblad*, **36**, 343 (1939).
12) F. Koroleff, Thesis, Univ. of Helsingfors, Helsinki, Finland, 1950.
13) A. Pilipenko, *Zh. Anal, Khim.*, **8**, 256 (1963).
14) A. Busev and L. Bazhanova, *Russ. J. Inorg. Chem.*, **6**, 1128 (1961).
15) T. Ashizawa, K. Nagasawa, and K. Haruyama, *Bunseki Kagaku*, **13**, 1011 (1964).
16) I. Hataye, H. Suganuma, M. Sakata, and Y. Nagame, *J. Inorg. Nucl. Chem.*, **43**, 2101 (1981).
17) E. B. Sandell, "Colorimetric Determination of Traces of Metals," Interscience, New York (1964), p. 170.
18) F. Fischer and J. Byé, *Bull. Soc. Chim. Fr.*, **1964**, 2970.
19) V. P. Vasilév and G. A. Lovanov, *Zh. Fiz. Khim.*, **41**, 838 (1967).
20) E. E. Kapantsyan and B. I. Nabivanets, *Ukr. Khim. Zh.*, **33**, 961 (1967).
21) J. S. Johnson, G. Scatchard, and K. A. Kraus, *J. Phys. Chem.*, **63**, 787 (1959).

The Formation Process of Cobalt Sulfide from Tricobalt Tetraoxide Using Sulfur Dioxide as a Sulfidizing Agent

Ryoko MATSUZAKI, Akimasa YAJIMA, Motonori EGUCHI, and Yuzo SAEKI*

Research Laboratory of Resources Utilization, Tokyo Institute of Technology, 4259, Nagatsuta-cho, Midori-ku, Yokohama 227

(Received October 24, 1981)

The products obtained by heating a mixture of Co_3O_4 and carbon in a SO_2 stream were CoO and $CoSO_4$ at 400—600 °C, $Co_{1-x}S$ and CoO at 650—700 °C, and $Co_{1-x}S$ ($Co_{0.90}S$) at 750—800 °C. Sulfur was obtained outside the heating zone throughout the temperature range. The possible reactions during the above process were also examined. Further, thermodynamical consideration was made of the formation of $Co_{1-x}S$. The formation process of $Co_{1-x}S$ ($Co_{0.90}S$) from Co_3O_4 can be represented as follows: The reaction of carbon with SO_2 occurs at first to form sulfur. Above *ca.* 400 °C, the reaction of Co_3O_4 with SO_2 occurs to form CoO and $CoSO_4$. Above *ca.* 500 °C, the reductions of Co_3O_4 with carbon and with sulfur also occur to form CoO. Above *ca.* 600 °C, the reduction of $CoSO_4$ with carbon occurs to form CoO. Above *ca.* 650 °C, $Co_{1-x}S$ is formed by the reaction of CoO with sulfur, both of which had been formed by the above reactions.

There have been several reports on the formation of cobalt sulfide by the reaction of cobalt with sulfur[1] or hydrogen sulfide,[2] and by the reaction of cobalt monooxide (CoO) with hydrogen sulfide.[3] Regarding the synthesis of cobalt sulfide using sulfur dioxide (SO_2) as a sulfidizing agent, however, little information has been available apart from the report of Pechkovskii and Mal'tseva.[4] They performed the differential thermal analysis of a mixture of tricobalt tetraoxide(Co_3O_4) and carbon (Co_3O_4:C=1:5 by molar ratio) in a SO_2 stream. They observed the formation of cobalt(II) sulfate($CoSO_4$) and CoO above 450 °C and of cobalt sulfide in addition to these products above 600 °C. The sample which they obtained after heating up to about 970 °C was a mixture of cobalt sulfide and CoO containing no residual carbon. They also reported that the cobalt sulfide formed was CoS below 700 °C and Co_9S_8 at 750—1000 °C. But, the formation process of cobalt sulfide from Co_3O_4 using SO_2 has not yet been revealed. This process is not only interesting from the viewpoint of the synthesis of the sulfide itself, but is also important for the further utilization of SO_2.

In this work, the reactions of Co_3O_4 with SO_2 and of Co_3O_4 with SO_2 in the presence of carbon were examined. In order to elucidate the formation process of cobalt sulfide from Co_3O_4, the reactions of Co_3O_4 with carbon and with sulfur were examined. Also, the reaction of $CoSO_4$, formed during the reaction process of Co_3O_4 with SO_2 in the presence of carbon, with carbon and the reaction of CoO, formed during the reaction process, with sulfur in a SO_2 stream were examined. Further, thermodynamical consideration was made of the Co–S–C–O system.

Experimental

The Co_3O_4 used was prepared at 800 °C by the thermal decomposition in the air of pentacobalt(II) dicarbonate hexahydroxide($Co_5(CO_3)_2(OH)_6$), which had been prepared by adding sodium carbonate solution to cobalt(II) nitrate solution.[5] The CoO was prepared by the thermal decomposition of the $Co_5(CO_3)_2(OH)_6$ at 800 °C in an argon stream.[5] The $CoSO_4$ was prepared by the dehydration of the guaranteed reagent cobalt(II) sulfate heptahydrate at 400 °C and was β-form(orthorhombic: low-temperature form).[6] The carbon was prepared by the thermal decomposition of the guaranteed reagent D-glucose. The above materials were used as powders under 150 mesh.

A mixture of Co_3O_4 and carbon at a specified ratio in a quartz boat (length: 72 mm, width: 16 mm, depth: 9 mm) was placed in a transparent, quartz reaction tube (inner diameter: 28 mm, length: 1000 mm). Gaseous SO_2 was then introduced into the reaction tube at a flow-rate of 100 cm³/min. The sample part was positioned in the middle of the tubular electric furnace (heating length: 300 mm) maintained at a specified temperature for 1 h. The temperature of the sample part was controlled within ±2 °C. After heating, the sample was quenched rapidly, and then heated at 100 °C for 1 h in an argon stream in order to release the SO_2 adsorbed on unreacted carbon.[7] The reactions of Co_3O_4 with carbon and with sulfur and of $CoSO_4$ with carbon in an argon stream, and the reaction of CoO with gaseous sulfur in a SO_2 stream were examined in a similar manner.

The X-ray analysis of the sample was performed with an X-ray powder diffractometer equipped with a proportional counter using Ni filtered Cu radiation. The thermogravimetry (TG) was performed by using a thermal balance with a quartz helix. The sensitivity of the quartz helix used was approximately 94 mm/g. The heating rate of 2.5 °C/min was employed, and a flow-rate of SO_2 was maintained at 50 cm³/min.

Concerning the chemical analysis of the cobalt sulfide formed, the sample was oxidatively decomposed in HNO_3 with $KClO_3$. Then, the cobalt content was determined by the chelatometric titration[8] and sulfur content by the gravimetric method as $BaSO_4$. In the case of a mixture of cobalt sulfide, unreacted carbon, and sulfur adsorbed on the carbon, the sample was oxidatively decomposed, and the contents of cobalt and total sulfur were determined by the above techniques. Then, after dissolving the cobalt sulfide in the sample selectively with dilute HNO_3, the undissolved residue, which consisted of unreacted carbon and the sulfur adsorbed on it, was oxidatively decomposed in HNO_3 with $KClO_3$, and the amount of sulfur adsorbed on the carbon was gravimetrically determined. The amount of sulfur due to the cobalt sulfide in the sample was calculated as the difference between the above total sulfur and the sulfur adsorbed on the carbon.

Results and Discussion

Reaction of Co_3O_4 with SO_2. The TG of Co_3O_4 (0.3 g) in a SO_2 stream was carried out. The TG

Table 1. Products obtained by heating a mixture of Co_3O_4 and carbon in a SO_2 stream at various temperatures

Temp °C	Sample in the boat	Amount of sulfur obtained outside the heating zone/g
350	Co_3O_4	Trace
400	$Co_3O_4 > CoO > CoSO_4[\beta]$	Trace
450	$Co_3O_4 > CoO > CoSO_4[\beta]$	Trace
500	$CoO > Co_3O_4 > CoSO_4[\beta]$	Trace
550	$CoO > CoSO_4[\beta > \alpha]$	Trace
600	$CoO \gg CoSO_4[\alpha]$	Trace
650	$CoO > Co_{1-x}S$	Trace
700	CoO, $Co_{1-x}S$	0.01
750	$Co_{1-x}S$	0.55
800	$Co_{1-x}S$	2.40

curve showed that the sample weight increased continuously above about 400 °C and reached a constant value at about 670 °C. The sample heated up to 700 °C was found to be a mixture of CoO[9] and α-$CoSO_4$ (orthorhombic: high-temperature form)[10] by X-ray analysis. The final weight gain was 26.5%. This value was in good agreement with the value, 26.60%, which was calculated based on the reaction: $Co_3O_4(s)+SO_2(g) \rightarrow 2CoO(s)+CoSO_4(s)$. These results indicate that Co_3O_4 reacts with SO_2 above about 400 °C to form CoO and $CoSO_4$.

Reaction Products of Co_3O_4 with SO_2 in the Presence of Carbon. The reaction products of Co_3O_4 with SO_2 in the presence of carbon as a reducing agent were examined. Based on the results of preliminary experiments on the suitable amount of carbon to be mixed, the products obtained by heating a mixture of 2.00 g of Co_3O_4 and 2.00 g of carbon at various temperatures for 1 h in a SO_2 stream at a flow-rate of 100 cm^3/min were examined. The results are shown in Table 1. The sample in the boat was identified by X-ray analysis.[6,9-13] The modification of the $CoSO_4$ formed is represented in the brackets.

The formation of CoO and $CoSO_4$ was observed above 400 °C. Above 650 °C, the formation of $Co_{1-x}S$ was observed in addition to that of CoO. $Co_{1-x}S$ was obtained at 750—800 °C. Sulfur was obtained outside the heating zone throughout the temperature range in this experiment, and the amount of sulfur markedly increased above about 750 °C.

The X-ray diffraction data of the $Co_{1-x}S$ obtained are shown in Table 2. The $Co_{1-x}S$ phase is known to have a NiAs structure. The lattice constants of the $Co_{1-x}S$ formed were calculated from the X-ray diffraction data, shown in Table 2, to be $a_0=3.380$ Å and $c_0=5.185$ Å. The composition of the $Co_{1-x}S$ formed was determined by chemical analysis. The analysis gave Co 42.5%; S 25.7% for the sample obtained at 750 °C, and Co 61.3%; S 37.2% at 800 °C. From these results, the composition of the $Co_{1-x}S$ formed was determined to be $Co_{0.90}S$.

The formation of $Co_{1-x}S$ with the Co/S atomic ratio of 0.90 by the reaction of Co_3O_4 with SO_2 in the presence of carbon at 650—800 °C seems to be

Table 2. X-Ray diffraction data of the $Co_{1-x}S$ formed

d/Å	I/I_1	hkl
2.927	60	100
2.549	70	101
1.941	100	102
1.689	45	110
1.489	5	103
1.410	10	201
1.297	5	004
1.274	40	202
1.117	<5	203
1.082	10	211
1.028	15	114
1.017	20	212

Table 3. Experimental results for the reaction of Co_3O_4 with carbon in an argon stream

Temp °C	Weight loss/%	Sample in the boat
450	—	Co_3O_4
500	0.2	$Co_3O_4 \gg CoO$
600	1.3	$Co_3O_4 > CoO$
700	4.3	$CoO \gg Co_3O_4$
750	6.3	$CoO \gg Co[\beta]$
800	15.4	$Co[\beta] > CoO$

reasonable in terms of the phase diagram for the Co–S system, reported recently by Rau.[14] As mentioned before, Pechkovskii and Mal'tseva[4] described that Co_9S_8 was formed by heating a mixture of Co_3O_4 and carbon in a SO_2 stream at 750—1000 °C. But Co_9S_8 is unstable above 830 °C according to the above phase diagram.[14]

Reaction Process of Co_3O_4 with SO_2 in the Presence of Carbon. To elucidate the reaction process of Co_3O_4 with SO_2 in the presence of carbon, the following experiments were carried out under conditions similar to those described above.

Reaction of Co_3O_4 with Carbon: The products formed by heating a mixture of Co_3O_4 (2.00 g) and carbon (2.00 g) at various temperatures in an argon stream (100 cm^3/min) for 1 h were examined by X-ray analysis.[9,11,15] The results are shown in Table 3.

These results indicate that the reduction of Co_3O_4 with carbon proceeds above about 500 °C to form CoO, and that above about 750 °C CoO formed is further reduced with carbon to β-cobalt.

Reaction of Co_3O_4 with Sulfur: As seen from Table 1, when the mixture of Co_3O_4 and carbon was heated in a SO_2 stream, sulfur was formed. The reaction of carbon with SO_2 occurs even at 350 °C to form sulfur and this reaction proceeds markedly above about 700 °C, as reported by the present authors.[7] Therefore, the reaction of Co_3O_4 with gaseous sulfur was examined.

Co_3O_4(2.00 g) was heated in a stream of argon (100 cm^3/min) containing a specified amount of gaseous sulfur at various temperatures for 1 h. Prior to

Table 4. Products obtained by heating Co_3O_4 in a stream of argon containing gaseous sulfur

Temp °C	Weight loss/%	Sample in the boat
450	—	Co_3O_4
500	0.1	$Co_3O_4 \gg CoO$
550	0.2	$Co_3O_4 \gg CoO$
600	0.5	$Co_3O_4 > CoO$

Table 5. Experimental results for the reaction of $CoSO_4$ with carbon in an argon stream

Temp °C	Weight loss/%	Sample in the boat
500	—	$CoSO_4[\beta]$
550	—	$CoSO_4[\beta > \alpha]$
600	12.6	$CoSO_4[\beta > \alpha]$, CoO
650	27.8	CoO
700	28.7	CoO

this experiment, the amounts of sulfur formed by heating 2.00 g of carbon at various temperatures for 1 h in a SO_2 stream at a flow-rate of 100 cm³/min were measured. Based on these experimental results, the amount of sulfur introduced at various temperatures was controlled to be 0.01 g for the experiments below 550 °C, and 0.04 g at 600 °C. The experimental results are shown in Table 4.

These results indicate that the reduction of Co_3O_4 with gaseous sulfur proceeds gradually above about 500 °C to form CoO.

Reaction of $CoSO_4$ with Carbon: As seen from Table 1, when the mixture of Co_3O_4 and carbon was heated in a SO_2 stream, $CoSO_4$ was formed above about 400 °C. Therefore, the reaction of $CoSO_4$ with carbon was examined.

The products obtained by heating a mixture of $CoSO_4$ (2.00 g) and carbon (2.00 g) in an argon stream (100 cm³/min) for 1 h were examined. The results are shown in Table 5.

These results indicate that the reduction of $CoSO_4$ with carbon occurs above about 600 °C to form CoO.

The process of formation of the CoO on heating the mixture of Co_3O_4 and carbon in a SO_2 stream can be explained as follows: The reaction of Co_3O_4 with SO_2 occurs above about 400 °C to form CoO and $CoSO_4$. Above about 500 °C, the reductions of Co_3O_4 with carbon and with sulfur also occur to form CoO. Above about 600 °C, the $CoSO_4$ formed is reduced with carbon to CoO.

Formation Reaction of $Co_{1-x}S$ from CoO: As seen from Table 1, when the mixture of Co_3O_4 and carbon was heated in a SO_2 stream, $Co_{1-x}S(Co_{0.90}S)$ was formed above about 650 °C. Above this temperature, Co_3O_4 was reduced to CoO. Therefore, the reaction of CoO with gaseous sulfur in a SO_2 stream was examined.

The products formed by heating CoO (2.00 g) for 1 h in a stream of SO_2 (100 cm³/min) containing a specified amount of gaseous sulfur at various temperatures were examined. The amounts of sulfur introduced were controlled to be 0.04 g for the experiment at 600 °C, 0.12 g at 650 °C, 0.58 g at 700 °C, 1.62 g at 750 °C, and 3.34 g at 800 °C, based on the results obtained for the amounts of sulfur formed by heating 2.00 g of carbon at various temperatures for 1 h in a SO_2 stream at a flow-rate of 100 cm³/min. The experimental results are shown in Table 6.

Table 6. Products obtained by heating CoO in a stream of SO_2 containing gaseous sulfur

Temp °C	Weight gain/%	Sample in the boat
600	—	CoO
650	2.2	$CoO \gg Co_{1-x}S$
700	7.5	$CoO > Co_{1-x}S$
750	15.4	CoO, $Co_{1-x}S$
800	19.4	$Co_{1-x}S > CoO$

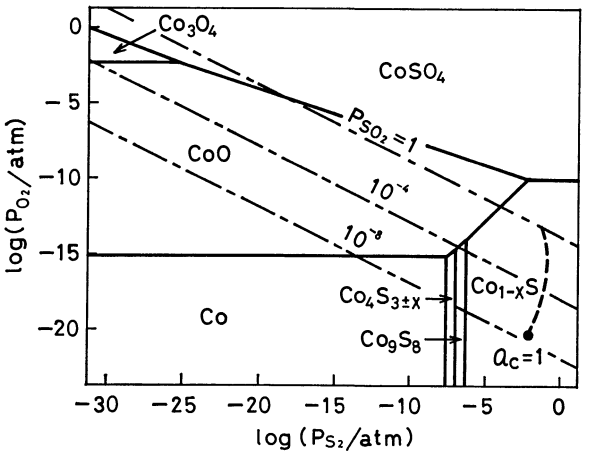

Fig. 1. Chemical potential diagram for the Co–S–C–O system at 800 °C (1 atm=101325 Pa).

These results indicate that the reaction of CoO with gaseous sulfur proceeds above about 650 °C to form $Co_{1-x}S$. The composition of the $Co_{1-x}S$ formed was evaluated to be $Co_{0.90}S$ by X-ray analysis (Table 2) and chemical analysis.

As seen from Table 3, CoO was reduced with carbon above about 750 °C to cobalt. In the Co–S system, the presence of Co_9S_8 and $Co_4S_{3\pm x}$ in addition to $Co_{1-x}S$ has been known as the lower sulfides. Therefore, thermodynamical consideration was made of the Co–S–C–O system, in order to discuss whether CoO was converted to $Co_{1-x}S$ *via* $Co_4S_{3\pm x}$, Co_9S_8 or cobalt, or without the formation of the lower sulfides or cobalt. The chemical potential diagrams for the Co–S–C–O system were constructed in a manner similar to that described by Yazawa[16] on the basis of the available thermodynamic data[17,18] and phase relations.[14] As an example, the diagram at 800 °C is shown in Fig. 1. The broken curved line shows the oxygen and sulfur potentials in the gas phase formed by the reaction of carbon with SO_2, depending on the carbon content in the gas phase. The activity of carbon, a_c, is unity at the dot mark. In these calculations, CO, CO_2, O_2, COS, CS_2, SO_2, SO_3, S_2, S_4, S_6, and S_8

were assumed to be gaseous products of carbon with SO_2.

The results shown in Fig. 1 indicate that CoO is converted to $Co_{1-x}S$ *via* cobalt, $Co_4S_{3\pm x}$, and Co_9S_8 under a pressure of SO_2 below *ca.* 10^{-5} atm, *via* $Co_4S_{3\pm x}$ and Co_9S_8 under a pressure of SO_2 at *ca.* 10^{-5}—10^{-4} atm, and *via* Co_9S_8 under a pressure of SO_2 at *ca.* 10^{-4}—10^{-3} atm, and that CoO is converted to $Co_{1-x}S$ without any formation of cobalt, $Co_4S_{3\pm x}$, and Co_9S_8 under a pressure of SO_2 above *ca.* 10^{-3} atm. Considering the experimental conditions in this work, the results in Fig. 1 show that $Co_{1-x}S$ is formed from CoO without any formation of the lower sulfides and cobalt.

From the results mentioned above, the process of formation of $Co_{1-x}S(Co_{0.90}S)$ by the reaction of Co_3O_4 with SO_2 in the presence of carbon can be represented as follows: On heating a mixture of Co_3O_4 and carbon in a SO_2 stream, the reaction of carbon with SO_2 occurs at first to form sulfur. Above about 400 °C, the reaction of Co_3O_4 with SO_2 occurs to form CoO and $CoSO_4$. Above about 500 °C, the reductions of Co_3O_4 with carbon and with sulfur also occur to form CoO. Above about 600 °C, the reduction of $CoSO_4$ with carbon occurs to form CoO. Above about 650 °C, $Co_{1-x}S$ is formed by the reaction of CoO with sulfur, both of which had been formed by the above reactions.

The present work was partially supported by a Grant-in-Aid for Scientific Research No. 555306 from the Ministry of Education, Science and Culture.

References

1) B. Morris, V. Johnson, and A. Wold, *J. Phys. Chem. Solids*, **28**, 1565 (1967); M. Brieu, R. Calsou, and L. Lafourcade, *C. R. Acad. Sci., Ser. B*, **264**, 1300 (1967).
2) J.-C. Colson, *C. R. Acad. Sci.*, **259**, 3261 (1964).
3) P. Barret, J.-C. Colson, and D. Delafosse, *C. R. Acad. Sci., Ser. C*, **262**, 83 (1966).
4) V. V. Pechkovskii and T. G. Mal'tseva, *Izv. Vssh. Uchebn. Zaved., Tsvetn. Metall.*, **7** (5), 45 (1964).
5) "Mukikagôbutsu No Gôsei [I], Shin-Zikkenkagaku-Kôza 8," ed by the Chemical Society of Japan, Maruzen, Tokyo (1976), pp. 297, 298; *ibid.*, [II], (1977), p. 889.
6) JCPDS Powder Data File, 28-386.
7) H. Araki, Y. H. Ryoo, M. Eguchi, R. Matsuzaki, and Y. Saeki, *Bull. Chem. Soc. Jpn.*, **53**, 2271 (1980).
8) R. Pribil, *Talanta*, **13**, 1223 (1966).
9) ASTM Powder Diffraction File, 9-402.
10) JCPDS Powder Diffraction File, 11-125.
11) ASTM Powder Diffraction File, 9-418.
12) JCPDS Powder Data File, 25-1081.
13) JCPDS Powder Diffraction File, 19-366.
14) H. Rau, *J. Phys. Chem. Solids*, **37**, 931 (1976).
15) JCPDS Powder Diffraction File, 15-806.
16) A. Yazawa, *Metall. Trans.*, **10B**, 307 (1979).
17) T. Rosenqvist, *J. Iron Steel Inst.*, **176**, 37 (1954).
18) O. Kubaschewski, E. Ll. Evans, and C. B. Alcock, "Metallurgical Thermochemistry," 4th ed, Pergamon Press (1967); H. H. Kellogg, *Trans. Metall. Soc. AIME*, **230**, 1622 (1964).

Photo-induced Ring-opening Reactions of 1-(2-Naphthoyl)aziridine in Various Solvents

Sei-ichi Nishimoto, Tsukuru Izukawa, and Tsutomu Kagiya*
Department of Hydrocarbon Chemistry, Faculty of Engineering, Kyoto University, Sakyo-ku, Kyoto 606

(Received February 9, 1981)

Photoreactions of 1-(2-naphthoyl)aziridine (NAz) have been investigated in various solvents under the deaerated conditions at room temperature. The photo-irradiation of NAz in halogenated hydrocarbons afforded halogen substituted secondary amides such as *N*-(2-chloroethyl)-2-naphthamide (CENA) or *N*-(2-bromoethyl)-2-naphthamide (BENA), a ring-expanded isomer of 2-(2-naphthyl)-2-oxazoline (NOz) and the NAz oligomer containing a chlorine atom. Secondary amides such as *N*-(2-methoxyethyl)-2-naphthamide (MENA) and *N*-ethyl-2-naphthamide (ENA) were obtained together with NAz oligomer in methanol and 2-propanol, respectively. The formation of *N*-(2-phenoxyethyl)-2-naphthamide (PENA), phenyl-2-naphthoate (PN) and NAz oligomer was observed in phenol (72 vol%)-acetonitrile mixture.

Extensive studies have been accomplished on the photochemical reactions of three-membered ring compounds such as cyclopropanes[1] and cyclopropenes.[2] The photochemistry of three-membered heterocycles has also received considerable attention.[3,4] A common feature of these photoreactions is ring-opening in the initial step, leading to cis-trans isomerization, acyclic compound formation, or rearrangement to ring-expanded products.

Although three-membered aziridines have been well characterized with respect to the thermal reactivities,[5] the photoreactions of these compounds have been little reported.[4] In this paper, the photochemical behavior of 1-(2-naphthoyl)aziridine (NAz) in various solvents was studied. Particular attention has been paid to the role of solvent molecules on the photochemical ring-opening of the aziridinyl group.

Experimental

General Methods. Melting points of all the products obtained are uncorrected. IR spectra were recorded on a JASCO DS-403 spectrophotometer, UV spectra on a Shimadzu UV-200S spectrophotometer, and ^{1}H NMR spectra on a JOEL PMX-60 spectrometer using tetramethylsilane as an internal standard. High speed liquid phase chromatography (HLPC) was carried out with a TOYO SODA HLC-802UR apparatus (gel permeation type column: TSK-GEL GMH6 and G2000H, 600 mm × 7.5 mm × 2, eluted with tetrahydrofuran at a flow rate of 1 cm^3 min^{-1} at 40 °C), using benzene as an internal standard.

Materials. Aziridine supplied from Nippon Shokubai Kagaku Kogyo Co. Ltd. was used after distillation. 2-Naphthoyl chloride (Tokyo Kasei Kogyo) was used without further purification. Acetonitrile was dried with calcium carbonate and distilled from phosphorus pentaoxide before use. Dibromomethane was dried with calcium chloride and distilled before use. Gaseous hydrogen chloride was prepared by the reaction of concentrated sulfuric acid (75 cm^3) with concentrated hydrochloric acid (40 cm^3).[6] The other solvents obtained commercially were used without further purification.

Preparation of 1-(2-Naphthoyl)aziridine (NAz). A solution of 2-naphthoyl chloride (53 mmol) in acetone (70 cm^3) was added to the equimolar (53 mmol) mixture of aziridine and triethylamine in acetone (200 cm^3) cooled in an ice bath. Triethylamine hydrochloride formed was removed as powder by filtration from the reaction mixture. The residue obtained by the evaporation of acetone was washed with methanol, followed by recrystallization three times from carbon tetrachloride to afford NAz (46% in yield), mp 82—83 °C. Found: C, 79.24; H, 5.56; N, 7.22; O, 7.90%. Calcd for $C_{13}H_{11}NO$: C, 79.19; H, 5.58; N, 7.11; O, 8.12%.

Photoreactions. Solutions of NAz in various solvents were deaerated by several freeze-pump-thawing cycles under vacuum in a Vycor or Pyrex glass tube (6 mmϕ) and sealed off. The photo-irradiation was carried out at room temperature, using a merry-go-round apparatus equipped with a high-pressure mercury lamp (EIKOSHA 500 W). After the irradiation, solvent was removed with a rotary evaporator under reduced pressure. The residual reaction mixture was subjected to the spectroscopic analyses. The conversion of NAz and the product yields were determined by the simultaneous use of ^{1}H NMR and HLPC measurements.

The photo-irradiation of a large amount of NAz solution was also carried out in order to identify the reaction products, using an immersion-type irradiation apparatus. The resulting reaction mixture was concentrated with a rotary evaporator and chromatographed on a silica gel column. The crude reaction mixture was also separated by repeated liquid phase chromatographies using the same column as mentioned above. The structures of the products were confirmed by the following data.

N-Ethyl-2-naphthamide (ENA). Mp 129.5—130 °C; IR ($CHCl_3$): 3420 (NH), 1510 and 1500 (NH), 1430, 1280, and 1230 (C–N) cm^{-1}; ^{1}H NMR ($CDCl_3$): δ 1.29 (3H, t, J=7.2 Hz), 3.60 (2H, q, J=6.6 Hz), 6.78 (1H, br), 7.68 (2H, m), 8.00 (4H, m), and 8.36 (1H, s). Found: C, 78.44; H, 6.70; N, 6.99; O, 7.89%. Calcd for $C_{13}H_{13}NO$: C, 78.39; H, 6.53; N, 7.04; O, 8.04%.

An identical product was obtained by the following procedures. 2-Naphthoyl chloride (14 mmol) dissolved in a minimum amount of acetone was added dropwise to a cooled aqueous solution (100 cm^3) containing ethylamine (14 mmol) and sodium hydroxide (31 mmol) under vigorous stirring. The white precipitate was purified from methanol (28% in yield).

N-(2-Chloroethyl)-2-naphthamide (CENA). Mp 135—136 °C; IR ($CHCl_3$): 3440 (NH), 1660 (C=O), 1519 and 1508 (NH), and 1285 (C–N) cm^{-1}; ^{1}H NMR ($CDCl_3$): δ 3.73 (4H, s), 6.83 (1H, br), 7.60 (2H, m), 7.83 (4H, m), and 8.27 (1H, s). Found: C, 66.70; H, 5.19; N, 5.84; O, 6.89; Cl, 15.11%. Calcd for $C_{13}H_{12}NOCl$: C, 66.81; H, 5.14; N, 6.00; O, 6.85; Cl, 15.20%.

An identical product was obtained when gaseous hydrogen chloride was bubbled through a solution of NAz (90 mmol)

Table 1. Photochemical reactions of NAz in various solvents[a)]

Run	Solvent	Glass tube	$[NAz]_0$ mmol dm^{-3}	Conversion %	Products (Yield[b)]/%) Secondary amide	Esters	NOz	Oligomer
1	Hexane	V	26	9	4 (ENA)		0	5
2	Benzene	V	156	7	2 (ENA)		0	5
3	Diethyl ether	V	105	6	1 (ENA)		0	5
4	Acetone	V	100	10	3 (ENA)		0	7
5	CH_3CN	V	91	10	3 (ENA)		0	7
6	CCl_4	V	91	84	57 (CENA)		2	25
7	CCl_4	P	91	13	10 (CENA)		0	3
8	$CHCl_3$	V	91	62	55 (CENA)		5	2
9	$CHCl_3$	P	91	4	4 (CENA)		0	0
10	CH_2Br_2	V	90	89	84 (BENA)		0	5
11	CH_2Br_2	P	90	70	17 (BENA)		52	1
12	CH_3OH	V	47	49	31 (MENA)	0	0	18
13	CH_3OH	P	47	31	18 (MENA)	0	0	11
14	$(CH_3)_2CHOH$	V	47	29	20 (ENA)	0	0	7
15	$(CH_3)_2CHOH$	P	47	13	10 (ENA)	0	0	3
16	Phenol/CH_3CN[c)]	V	91	100	38 (PENA)	19 (PN)	0	42
17	Phenol/CH_3CN[c)]	P	91	100	42 (PENA)	23 (PN)	0	35

a) Under the photo-irradiation in a Vycor (V) or Pyrex (P) glass tube for 200 min. b) Yields based on NAz were determined by ^1H NMR and HLPC. c) 72 vol% of phenol.

in chloroform (1 cm^3) at 0 °C (quantitative yield).

N-(2-Bromoethyl)-2-naphthamide (BENA). Mp 147.5—149 °C (lit,[7] mp 152 °C); IR (KBr): 3220 (NH), 1620 (C=O), 1535 (NH), 1310 (C–N), and 480 (C–Br) cm^{-1}; ^1H NMR (CD_2Cl_2): δ 3.71 (4H, q, J=4.8 Hz), 6.70 (1H, br), 7.50 (2H, m), 7.67 (4H, m), and 8.20 (1H, s).

The IR and ^1H NMR spectral data were identical with those of an authentic sample prepared by the reported method.[7]

Oligomer Obtained in Carbon Tetrachloride. IR (KBr): 1715, 1644, 1520, 1400, 1110, and 620 cm^{-1}; ^1H NMR ($CDCl_3$): δ 3.79 (3H, br), 7.56, 7.89, and 8.34 (7H, broad signals corresponding to the naphthyl group). Found: C, 46.52; H, 3.27; N, 3.33; O, 6.14; Cl, 35.00%.

2-(2-Naphthyl)-2-oxazoline (NOz). Mp 85.5—86.5 °C; IR ($CHCl_3$): 1645 (C=N), 1275 (=C–O–C), 1068 (C–O–C), 983, 961, and 943 cm^{-1}; ^1H NMR (CD_2Cl_2): δ 4.29 (4H, quartet, J=7.4 Hz), 7.60 (2H, m), 7.93 (4H, m), and 8.47 (1H, s). Found: C, 79.38; H, 5.59; N, 7.05; O, 8.19%. Calcd for $C_{13}H_{11}NO$: C, 79.19; H, 5.58; N, 7.11; O, 8.12%.

The IR and ^1H NMR spectral data were identical with those of an authentic sample prepared by the reported method.[7]

N-(2-Methoxyethyl)-2-naphthamide (MENA). Mp 86.5—87.5 °C; IR (CCl_4): 3440 (NH), 2975 (CH_3), 2820 (CH_3), 1664 (C=O), 1504 (NH), and 1068 (C–O–C) cm^{-1}; ^1H NMR ($CDCl_3$): δ 3.42 (3H, s), 3.61 (4H, m), 7.59 (2H, m), 7.89 (4H, m), and 8.29 (1H, s). Found: C, 72.61; H, 6.62; N, 5.94; O, 13.70%. Calcd for $C_{14}H_{15}NO_2$: C, 73.36; H, 6.55; N, 6.11; O, 13.97%.

An identical product was obtained when a solution of NAz (0.24 mmol) in methanol (40 cm^3) was permitted to stand for 30 min at room temperature in the presence of a catalytic amount of boron trifluoride under an argon atmosphere (quantitative yield).

Oligomer Obtained in Methanol. IR ($CHCl_3$): 3420 and 3300 (NH), 1760, 1650 (C=O), 1520 (NH), 1430, 1290 (C–N), and 1150 cm^{-1}; ^1H NMR ($CDCl_3$): δ 3.46 (5H, br), 3.73 (0.3H, singlet signal corresponding to the methoxyl group), and 7.53—8.28 (7H, br). Found: C, 52.79; H, 5.48; N, 5.03; O, 12.16%.

N-(2-Phenoxyethyl)-2-naphthamide (PENA). Mp 73—74 °C; IR (KBr): 3320 (NH), 1638 and 1625 (C=O), 1545 (NH), and 1081 (C–O–C) cm^{-1}; ^1H NMR ($CDCl_3$): δ 4.03 (4H, q, J=4.7 Hz), 6.63 (1H, br), 6.88—7.20 (5H, phenyl group), 7.61 (2H, m), 7.87 (4H, m), and 8.30 (1H, s). Found: C, 78.19; H, 6.39; N, 4.27; O, 10.61%. Calcd for $C_{19}H_{17}NO_2$: C, 78.35; H, 5.84; N, 4.81; O, 11.00%.

Phenyl-2-naphthoate (PN). Mp 90—90.5 °C (lit,[8] 96 °C); IR (KBr): 1732 (C=O), 1280 and 1228 (C–O–C) cm^{-1}.

The IR spectrum was identical with that of an authentic sample prepared by the reported method.[8]

N-(2-Acetoxyethyl)-2-naphthamide (AENA). Mp 78—79 °C; IR ($CHCl_3$): 3420 (NH), 1725 (C=O), 1648 (C=O), and 1500 (NH) cm^{-1}; ^1H NMR ($CDCl_3$): δ 2.09 (3H, s), 3.83 (2H, t, J=5.0 Hz), 4.36 (2H, t, J=5.0 Hz), 7.63 (2H, m), 7.87 (4H, m), and 8.32 (1H, s). Found: C, 69.10; H, 5.78; N, 5.54; O, 18.72%. Calcd for $C_{15}H_{15}NO_3$: C, 70.03; H, 5.84; N, 5.45; O, 18.68%.

Results and Discussion

UV Absorption Characteristics of NAz. The solution of NAz in hexane exhibited ultraviolet absorption maxima at 337 nm (ε; 1310), 282 nm (ε; 8320), and 245 nm (ε; 51800). These absorption bands may be attributed to the π-π^* transitions of naphthyl group of NAz in view of the similarity to those of naphthalene.[9] No absorption bands were observed in the wavelength region longer than these principal absorption bands. It thus seems that the carbonyl n-π^* band lies behind the intense π-π^* bands of the naphthyl group.[10]

Photoreactions of NAz in Non-halogenated Aprotic Solvents. The photo-irradiations of NAz in various solvents were carried out for 200 min at room temperature under deaerated conditions, using Vycor and Pyrex glass

tubes which transmit the light with wavelength longer than 215 and 286 nm, respectively. The results are summarized in Table 1.

It is apparent from Table 1 that NAz exhibits less photoreactivity in non-halogenated aprotic solvents such as hexane, benzene, diethyl ether, acetone and acetonitrile, in which the overall conversion of NAz did not exceed 10% (Runs 1—5). *N*-Ethyl-2-naphthamide (ENA) was afforded in low yield as a common ring-opened product in these solvents, accompanied by NAz oligomer.

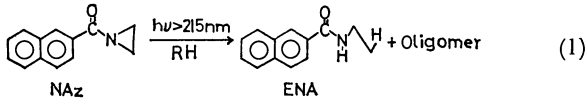

NAz ENA (1)

This photochemical ENA formation suggests that the hydrogen abstraction by NAz in the electronically excited state from a solvent molecule occurs to bring about α-cleavage of the aziridine ring. In this regard, it was confirmed that acetone is afforded along with the photochemical ENA formation in $(CH_3)_2CHOH$, as shown below (Eq. 10). Accordingly, the ENA formation in these solvents is expected to proceed by a radical mechanism in a similar manner to that in $(CH_3)_2CHOH$.

The low yield of ENA in these solvents may be attributed to the requirement of high activation energy for the hydrogen abstraction from solvent molecule. In the present systems, the hydrogen abstraction from either aziridinyl or naphthyl groups of NAz seems minor for the ENA formation because of the low reactivities of hydrogen atoms on these groups.[11]

On the other hand, ENA as a photoproduct was found to initiate oligomerization of NAz slowly in a similar manner to the ring-opening polymerization of most 1-acylaziridines by various amides.[12]

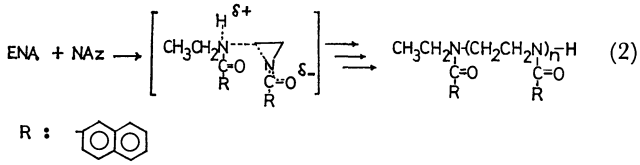

Photoreactions of NAz in Halogenated Hydrocarbons. The photo-irradiation of NAz in halogenated hydrocarbons through a Vycor glass tube (>215 nm) resulted in α-cleavage of the aziridine ring to afford halogen substituted secondary amide, *N*-(2-chloroethyl)-2-naphthamide (CENA) in CCl_4 and $CHCl_3$ or *N*-(2-bromoethyl)-2-naphthamide (BENA) in CH_2Br_2 with high yields above 55% (Runs 6, 8, 10).

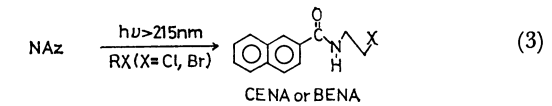

CENA or BENA

It was confirmed by a separate experiment that the photolysis of $CHCl_3$ occurs in a Vycor glass tube to afford HCl. Moreover, NAz was converted quantitatively into CENA without oligomerization by bubbling gaseous HCl through a solution of NAz in $CHCl_3$ in the dark. Such a ring-opening reaction by hydrogen halide would proceed *via* the following reactive intermediate of aziridinium salt:[13]

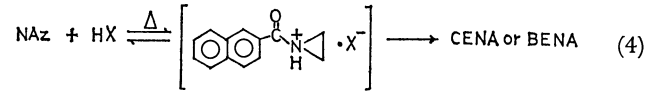

Under the conditions of the irradiation with light of wavelength longer than 215 nm, it is likely that a halogen atom such as Cl or Br is formed as a primary intermediate by the photolyses of halogenated hydrocarbon solvents and subsequently abstracts a hydrogen atom from a solvent molecule to afford a hydrogen halide, HCl or HBr. The hydrogen abstraction from NAz would be minor because of the low reactivities of hydrogen atoms on NAz, in a similar manner to the ENA formation in non-halogenated aprotic solvents.

It should be noted that, although CCl_4 does not contain any hydrogen atoms, CENA was obtained in the dark by the addition of NAz (90 mmol dm^{-3}) to a pre-irradiated CCl_4 under the same conditions as in the Vycor system. Furthermore, the yield of CENA (53%) in this post-reaction agreed closely with that (57%) in the in-source photoreaction (Run 6). It has been well known that Cl_2 is formed by the photolysis of CCl_4 at wavelengths shorter than 253.7 nm.[14] Therefore, the reaction of NAz with Cl_2 is presumed to afford HCl in the CCl_4 system.

The oligomer of NAz with a high content of chlorine atoms (35%) was also obtained along with CENA in CCl_4. The yield of this oligomer (25% based on NAz) was much higher than those (less than 5%) in hydrogen-containing $CHCl_3$ and CH_2Br_2. This would also be associated with the reaction between NAz and Cl_2.

On the other hand, the photo-irradiation of NAz in CCl_4 or $CHCl_3$ through a Pyrex glass tube (>286 nm) led to the same product, CENA, as afforded in the Vycor system (Runs 7, 9). Here the yields were reduced to one-sixth in CCl_4 and one-tenth in $CHCl_3$, respectively, and very little oligomerization of NAz occurred (<1%).

$$\text{NAz} \xrightarrow[CCl_4 \text{ or } CHCl_3]{h\nu>286\text{ nm}} \text{CENA} \qquad (5)$$

On the contrary, the product distribution in CH_2Br_2 was affected remarkably by the wavelength of irradiation. The photo-irradiation of NAz in CH_2Br_2 through a Pyrex glass tube resulted in a ring-expanded isomer of 2-(2-naphthyl)-2-oxazoline (NOz) as a major product, along with BENA (Run 11), in contrast to the exclusive BENA formation in the Vycor system (Run 10).

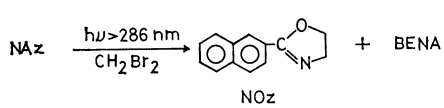

NOz 52% BENA 17%

Although BENA was readily converted into NOz at 70 °C in the presence of potassium hydroxide in CH_3OH (72% in yield), the photocyclization of BENA into NOz did not occur in CH_2Br_2 under the present conditions. Furthermore, BENA was obtained in 18% yield by the addition of NAz (90 mmol dm^{-3}) in the dark to a pre-irradiated CH_2Br_2 under the same con-

ditions as above. The good agreement with the yield of BENA in this post-reaction indicates that the BENA formation in the in-source photoreaction system can be attributed to the reaction of NAz with HBr formed by the photolysis of CH_2Br_2.

It may be presumed for the photo-isomerization that the dipole-dipole interaction of NAz in the electronically excited state with CH_2Br_2 promotes the ionic ring-opening of aziridinyl group, followed by the cyclization into oxazoline due to the stabilization of four center transition state.[5f]

Photoreactions of NAz in Alcohols and Phenol. The photochemical ring-opening reactions of NAz also occurred in CH_3OH, $(CH_3)_2CHOH$, and phenol (72 vol%)–CH_3CN mixture.

The photo-irradiation of NAz in CH_3OH afforded *N*-(2-methoxyethyl)-2-naphthamide (MENA) accompanied by NAz oligomer, whereas the dark reaction was not observed under the same conditions. As shown in Table 1, the product yields in the Pyrex system decreased compared with those in the Vycor system, but no appreciable difference was observed in the ratio of yields between MENA and oligomer (Runs 12, 13).

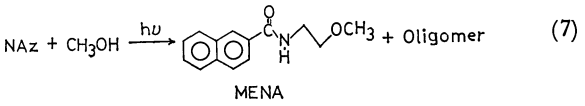

(7)

It seems possible that the MENA formation arises from the methanolysis of the aziridine ring of NAz in the electronically excited state in a similar manner to that in the photo-induced alcoholysis of three-membered ring compounds such as cyclopropanes,[1] oxiranes,[3d] 1,2,3-triphenylaziridine,[4b] and 1-(dimethylcarbamoyl)-2,3-diphenylaziridine.[4c]

Since the O–H bond (418 K J mol^{-1}) is stronger than the C–H bond (386 K J mol^{-1}) in CH_3OH,[15] radical cleavage of polar O–H bond seems not to be involved in the MENA formation. The addition of CH_3OH to aziridine ring may therefore occur by an ionic mechanism. It is also likely that the hydrogen bonding of CH_3OH to carbonyl oxygen of NAz facilitates the nucleophilic attack of the methoxide ion on the aziridinyl carbon due to the stabilization of a polar transition state.

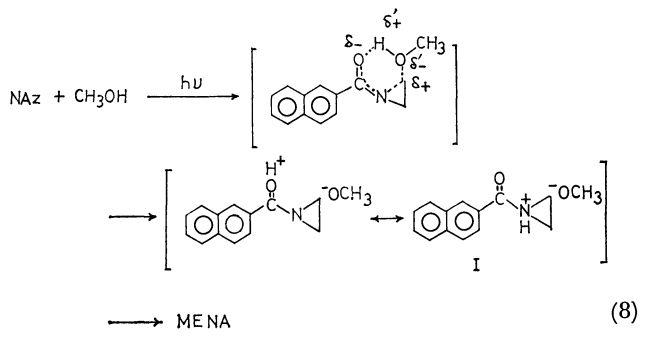

(8)

It has been well known that protonated aziridines are readily attacked by various nucleophiles on the aziridinium carbon.[5a] Consequently, the formation of aziridinium ion intermediate (I) would account for the relatively high yield of NAz oligomer in CH_3OH due to the polymerization faster than that initiated by the amide (Eq. 2).[16] The propagation may proceed by the cationic ring-opening of NAz as a nucleophile *via* aziridinium ion at the growing chain end. This scheme is consistent with the fact that the NAz oligomer contains a methoxyl group.

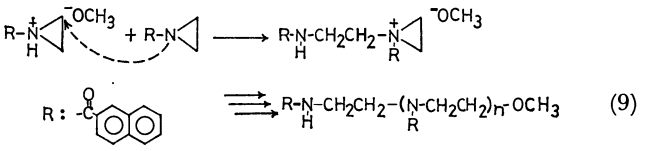

(9)

In $(CH_3)_2CHOH$, on the other hand, the photochemical behavior of NAz was markedly different from that in CH_3OH. The ring-opening reaction due to the addition of alcohol to NAz did not occur in $(CH_3)_2CHOH$, but the formation of an equimolar mixture of ENA and acetone was observed (Runs 14, 15).

(10)

It has been well established that $(CH_3)_2CHOH$ readily undergoes oxidation into acetone *via* hydrogen abstraction by various radical species. In view of such a characteristic reactivity of $(CH_3)_2CHOH$, the ring-opening of NAz by a radical mechanism seems to be involved in the photochemical ENA formation. The exclusive formation of ENA without *N*-(2-isopropoxyethyl)-2-naphthamide analogous to MENA may be attributed to the fact that the nucleophilicity of $(CH_3)_2CHOH$ is lower than that of CH_3OH.

In order to clarify the effect of nucleophilicity of alcohol on the photo-induced ring-opening of NAz, the photoreaction of NAz in phenol (72 vol%)–CH_3CN mixture was further examined. Under the irradiation through a Vycor or a Pyrex glass tube, NAz was converted quantitatively to afford *N*-(2-phenoxyethyl)-2-naphthamide (PENA), phenyl-2-naphthoate (PN), and NAz oligomer (Runs 16, 17).

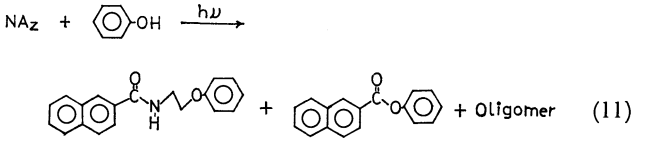

(11)

An identical reaction occurred in the dark to afford PENA and PN with 6% and 2% yields, respectively, but the conversion of NAz was low (8%) relative to the photoreaction. This result shows that the phenolysis of NAz is accelerated by the photo-irradiation.

The formation of PENA accompanied by NAz oligomer is apparently analogous to the photoreaction observed in CH_3OH (Eq. 7). In the phenol system, however, it is characteristic that the phenolysis of the carbonyl-aziridinium nitrogen bond of NAz leading to PN occurs simultaneously with that of the aziridine ring. These results suggest that phenol is capable of nucleophilic attack not only on the aziridinyl carbon but also the carbonyl carbon of NAz in the excited state because the nucleophilicity is higher than that of CH_3OH.

Furthermore, in the relatively strong acidic medium of acetic acid, the quantitative acetolysis of aziridine

ring of NAz was observed even in the dark to afford *N*-(2-acetoxyethyl)-2-naphthamide (AENA), which is essentially the same reaction as shown in Eq. 4 for the ring-opening by hydrogen halide. It is likely

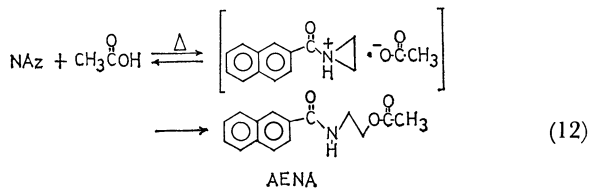

(12)

that the protonation to NAz occurs rapidly in the presence of protonic acids such as hydrogen halide and acetic acid to form an aziridinium ion intermediate, which undergoes nucleophilic addition by halide ion or acetate ion selectively to the aziridinium carbon.

These results seem to be consistent with the scheme postulated for the photochemical MENA formation (Eq. 8).

On the basis of the results presented in this paper, it may be concluded that NAz exhibited dual reactivity for the ring-opening reaction in the electronically excited state. In this reaction, solvent molecules play important roles in determining whether radical or ionic reaction occurs. Details of the reactivity of solvent molecule toward NAz in the excited state leading to ring-opening of the aziridinyl group will be reported in a subsequent paper.

References

1) a) S. S. Hixon, *Org. Photochem.*, **4**, 191 (1979); b) C. S. Irving, R. C. Petterson, I. Sarkar, H. Kristtinsson, C. S. Aaron, G. W. Griffin, and G. J. Boudreaux, *J. Am. Chem. Soc.*, **88**, 5675 (1966).

2) a) A. Padwa, *Acc. Chem. Res.*, **12**, 310 (1979); b) A. Padwa, *Org. Photochem.*, **4**, 261 (1979).

3) a) N. R. Bertoniere and G. W. Griffin, *Org. Photochem.*, **3**, 115 (1973); b) A. Padwa, *Acc. Chem. Res.*, **9**, 371 (1976); c) K. Tokumaru, *Bull. Chem. Soc. Jpn.*, **40**, 242 (1967).

4) a) A. Padwa and L. Hamilton, *J. Am. Chem. Soc.*, **89**, 102 (1967); b) H. Nozaki, S. Fujita, and R. Noyori, *Tetrahedron*, **24**, 2193 (1968); c) A. G. Anastassiou and R. B. Hammer, *J. Am. Chem. Soc.*, **94**, 303 (1972).

5) a) O. C. Dermer and G. F. Hamm, "Ethylenimine and Other Aziridines," Academic Press, New York (1969); b) C. U. Pittman, Jr., S. P. McManus, and J. W. Larsen, *Chem. Rev.*, **72**, 357 (1972); c) H. W. Heine, *Angew. Chem.*, **74**, 772 (1962); d) S. P. McManus, R. A. Hearn, and C. U. Pittman, Jr., *J. Org. Chem.*, **41**, 1895 (1976); e) H. W. Heine, W. G. Kenyon, and E. M. Johnson, *J. Am. Chem. Soc.*, **83**, 2570 (1961); f) H. W. Heine and Z. Proctor, *J. Org. Chem.*, **23**, 1554 (1958); g) P. E. Fanta and E. N. Walsh, *ibid.*, **31**, 59 (1966).

6) R. N. Maxson, "Inorganic Syntheses," ed by H. S. Booth, McGraw-Hill, New York (1939), Vol. 1, p. 147.

7) F. Saulmann, *Ber.*, **33**, 2637 (1900).

8) G. S. Saharia, *J. Sci. Ind. Research*, **13B**, 544 (1954).

9) a) J. R. Platt, *J. Chem. Phys.*, **17**, 484 (1949); b) S. F. Mason, *Quart. Rev.*, **15**, 287 (1961).

10) H. H. Jaffé and M. Orchin, "Theory and Applications of Ultraviolet Spectroscopy," John Wiley & Sons, New York (1962), p. 179.

11) a) J. W. S. Jamieson and C. A. Winkler, *J. Phys. Chem.*, **60**, 1542 (1956); b) A. Beckett and G. Porter, *Trans. Faraday Soc.*, **59**, 2038 (1963).

12) See p. 332 of Ref. 5a.

13) See p. 107 and p. 249 of Ref. 5a.

14) a) J. G. Calvert and J. N. Pitts, "Photochemistry," John Wiley & Sons, New York (1966), p. 522; b) H. Okabe, "Photochemistry of Small Molecules," John Wiley & Sons, New York (1978), p. 306.

15) J. A. Kerr, *Chem. Rev.*, **66**, 465 (1966).

16) a) W. G. Barb, *J. Chem. Soc.*, **1955**, 2564; b) T. Kagiya, T. Kondo, and K. Fukui, *Bull. Chem. Soc. Jpn.*, **41**, 2473 (1968).

 © 1982 The Chemical Society of Japan Bull. Chem. Soc. Jpn., 55, 1489—1492 (1982)

Quantitative Structure-activity Relations in Pyrazolylpyrimidine Derivatives for Their Analgesic Activities

Yoshikatsu Miyashita, Tomoko Seki, Yasuhiko Yotsui†, Ken-ichi Yamazaki,†
Mitsuji Sano,† Hidetsugu Abe, and Shin-ichi Sasaki*

School of Materials Science, Toyohashi University of Technology, Tempaku-cho, Toyohashi 440
†Research Institute, Daiichi Seiyaku Co. Ltd., Edogawa-ku, Tokyo 132

(Received March 17, 1981)

Statistically significant correlations have been demonstrated between analgesic activities of a series of pyrazolylpyrimidine derivatives and molecular properties. The structural parameters are partition coefficients, molar refractivities, an indicator variable, and MO indices obtained from the CNDO/2 method. The influence of the torsional angle between the pyrazole and pyrimidine rings on the electronic state was examined. The correlations indicate that transport and partition processes and electronic factors play a major part in determining the analgesic activity. In particular, of electronic parameters MO indices on the pyrazole ring are significant. These structure-activity relationships can be used to estimate the analgesic activities with some degree of confidence.

It is known that non-narcotic analgesics, including the derivatives of pyrazole, salicylic acid and acetanilide, have antipyretic and antiinflammatory properties. The most popular pyrazole compounds are antipyrine and aminopyrine.

Many attempts[1,2] have been carried out to develop new drugs by modification of existing pyrazole compounds, *e.g.*, antipyrine as a lead compound. The Hansch analysis has been applied to the studies of quantitative structure-activity relationships (QSAR) of antipyrine derivatives.[3] These studies revealed that pyrazoles having an alicyclic or heterocyclic group instead of a phenyl ring in antipyrine are potentially active.

Naito *et al.*, therefore, synthesized pyrazolylpyrimidine derivatives to find a highly potent drugs.[4,5] As a result it has been found that 4-methoxy-2-(5-methoxy-3-methyl-1*H*-pyrazol-1-yl)-6-methylpyrimidine (mepirizole) is the most potent compounds having an analgesic effect. In the QSAR studies it is important to ascertain if metabolites of the drug are not potent. It has been found that the metabolites of mepirizole have little effect.[6,7]

In an attempt to further investigate analgesic activities of pyrazole compounds, correlation between the activities of pyrazolylpyrimidine derivatives and the molecular structure is studied using the QSAR techniques in this paper. The structural parameters to establish QSAR are hydrophobic parameters, molar refractivities, an indicator variable and a variety of MO indices obtained from the CNDO/2 method.

Experimental

Data Set. The data used in this study were taken from the studies on a series of 44 pyrazolylpyrimidine compounds.[5] The analgesic activities are expressed as $\log A$, where A is relative potency compared with equimolar amounts of aminopyrine measured by the pressure method in mice. These values are given in Table 1. The fragments involving pyrazole R_i and pyrimidine P_j are shown in Fig. 1 to represent the compounds in Table 1.

The forty-four compounds are divided into two groups, (N^1 and N^2). Groups N^1 and N^2 contain subgroups A, B and C, D, respectively. Subgroups A and B contain series

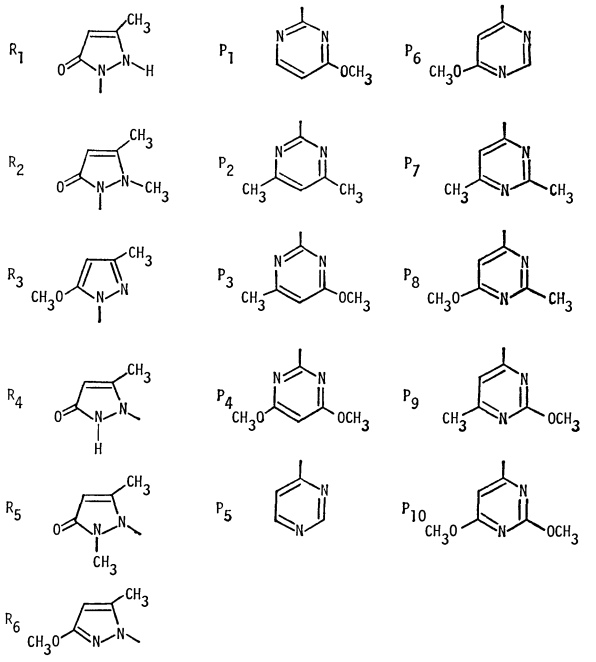

Fig. 1. The chemical structures of pyrazole R_i and pyrimidine P_j fragments.

R_1, R_2, and R_3 and subgroups C and D contain series R_4, R_5, and R_6, respectively. The numbers of active compounds in each group and series are shown in Table 2.

Structural Parameters of Pyrazoles. The hydrophobic parameters are determined experimentally or estimated using the observed data. 1-Octanol/water partition coefficients P for 23 compounds were measured at pH 7 and at room temperature by the flask shaking method. Table 1 shows the observed log P values. The fragment addition model, which is a similar procedure to the Free-Wilson method, is used to calculate the log P values for the remaining 15 compounds. This model is given by the following equation:

$$\log P = \sum_i R_i X_i + \sum_j P_j Y_j + \mu, \quad (1)$$

where R_i is the fragment contribution of a pyrazole ring, P_j is that of a pyrimidine ring, and μ is the overall average of the observed log P values ($X_i=1$ if the pyrazole ring is the i-th fragment, otherwise $X_i=0$, $Y_j=1$ if the pyrimidine ring is the j-th fragment, otherwise $Y_j=0$). Further the

Table 1. Analgesic activities, log P and MR values for pyrazolylpyrimidine derivatives

No.	Structure R_i	Structure P_j	log A	log P Obsd[a]	log P Calcd	MR
1	R_1	P_1	−0.18	—	0.645	52.83
2	R_1	P_2	−0.48	0.720	0.497	55.70
3	R_1	P_3	0.15	—	0.898	57.48
4	R_1	P_4	−0.48	1.158	1.158	59.26
5	R_1	P_5	−0.50	—	0.414	46.40
6	R_1	P_6	−0.59	0.987	0.992	52.83
7	R_1	P_7	−0.15	0.894	0.883	55.70
8	R_1	P_8	0.30	0.718	0.947	57.48
9	R_1	P_9	−0.46	1.030	1.030	57.48
10	R_1	P_{10}	−0.37	—	1.500	59.26
11	R_2	P_1	Inactive	—	0.119	57.67
12	R_2	P_2	−1.37	—	−0.028	60.53
13	R_2	P_3	−1.16	—	0.372	62.32
14	R_2	P_4	−0.57	—	0.632	64.10
15	R_2	P_5	Inactive	—	−0.112	51.24
16	R_2	P_6	−0.38	0.297	0.466	57.67
17	R_2	P_7	−0.61	0.244	0.357	60.53
18	R_2	P_8	−0.21	0.704	0.421	62.32
19	R_2	P_9	−0.54	—	0.504	62.32
20	R_2	P_{10}	−0.09	—	0.974	64.10
21	R_3	P_1	−0.12	1.007	1.007	58.05
22	R_3	P_2	−0.04	0.730	0.860	60.91
23	R_3	P_3	0.33	1.260	1.260	62.70
24	R_3	P_4	0.19	—	1.520	64.48
25	R_3	P_5	0.19	0.497	0.776	51.62
26	R_3	P_6	0.17	1.528	1.354	58.05
27	R_3	P_7	−0.12	—	1.245	60.91
28	R_3	P_8	0.10	1.544	1.309	62.70
29	R_3	P_9	0.04	—	1.392	62.70
30	R_3	P_{10}	−0.11	1.862	1.862	64.48
31	R_4	P_2	−0.03	1.291	1.387	55.70
32	R_4	P_3	−0.11	—	1.788	57.48
33	R_4	P_5	−1.18	1.400	1.304	46.40
34	R_4	P_7	Inactive	—	1.770	55.70
35	R_4	P_8	Inactive	—	1.837	57.48
36	R_5	P_2	−0.59	0.510	0.221	60.53
37	R_5	P_3	Inactive	—	0.622	62.32
38	R_5	P_7	Inactive	—	0.607	60.53
39	R_5	P_8	−0.46	0.382	0.671	62.32
40	R_6	P_2	−0.41	1.822	2.107	60.91
41	R_6	P_3	−0.21	—	2.507	62.70
42	R_6	P_5	−0.40	2.206	2.023	51.62
43	R_6	P_7	−0.42	2.595	2.493	60.91
44	R_6	P_8	−0.51	—	2.556	62.70

a) A dash indicates no data.

Table 2. Groups and series of pyrimidine compounds

Group	$N^1(28)$[a]			$N^2(10)$		
Subgroup	A(18)		B(10)	C(5)		D(5)
Series	$R_1(10)$	$R_2(8)$	$R_3(10)$	$R_4(3)$	$R_5(2)$	$R_6(5)$

a) Values in parentheses are the numbers of active compounds in the groups or series.

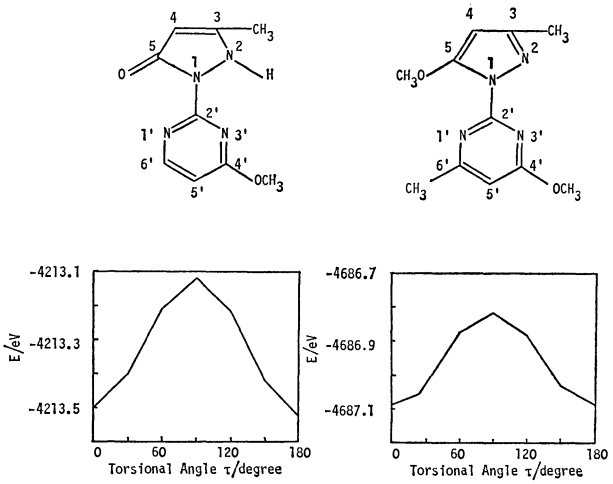

Fig. 2. Pyrazole numbering system ($\tau=0°$) and total energies of compound **1** (left) and mepirizole *vs.* rotation around N^1–$C^{2'}$ bond.

symmetry relations are given by the following equations:

$$\sum_i n_i R_i = 0, \qquad \sum_j n_j P_j = 0, \tag{2}$$

where n_i is the number of i-th pyrazole rings and n_j is that of the j-th pyrimidine rings for 23 compounds.

Combining Eqs. 1 and 2, the symmetry constraints vanish. The resulting simultaneous equations are solved by the least squares method to obtain the fragment contributions. The regression equation is

$$\begin{aligned}\log P = &-0.305X_1 - 0.831X_2 + 0.057X_3 + 0.585X_4 \\ &- 0.581X_5 + 1.305X_6 - 0.154Y_1 - 0.301Y_2 \\ &+ 0.099Y_3 + 0.359Y_4 - 0.385Y_5 + 0.193Y_6 \\ &+ 0.084Y_7 + 0.148Y_8 + 0.231Y_9 + 0.701Y_{10} \\ &+ 1.104 \end{aligned} \tag{3}$$

The correlation coefficient between observed and calculated log P values for 23 compounds is 0.965. The log P values for other compounds were calculated by this equation. These log P values are shown in Table 1.

In order to represent the steric feature, molar refractivities MR were calculated from bond refractivites.[8] The values are shown in Table 1. Seventeen varieties of MR values exist for all compounds.

Quantum mechanical indices were determined from the CNDO/2 method to explain electronic aspects of drug-acceptor interactions. They are energies of the highest occupied molecular orbital HOMO, the lowest unoccupied molecular orbital LUMO, the energy difference GAP between LUMO and HOMO, and total electron densities associated with the atoms on pyrazole ring (q_1—q_5). The numbering system for pyrimidine derivatives is shown in Fig. 2.

Molecular geometries are determined from the X-ray crystallographic data for pyrazole,[9] pyrimidine[10] and antipyrine.[11] The torsional angle τ between the pyrazole and pyrimidine rings in mepirizole(compound **23**) was determined as 20.5° from X-ray crystallographical data. The details of the characteristic feature of the geometry of pirizole will be published in the near future, and not demescribed in the present paper. The torsion of pyrimidine ring toward the pyrazole ring is most likely to have the most influence on the electronic state. In order to investigate

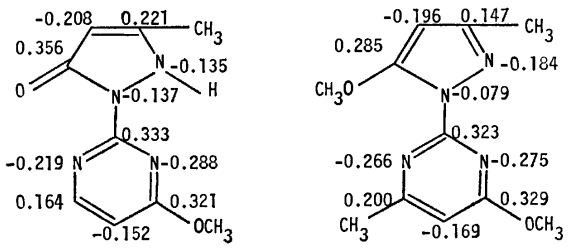

Fig. 3. Charge distribution of compound **1** (left) and mepirizole.

the effect of conformational alternations on the electronic states of these compounds, the rotation around the N^1–$C^{2'}$ bond were carried out with 30° increments for the typical compounds, compound **1** and mepirizole.

Conformation and Electronic State. The total energies of compound **1** and mepirizole vary in accordance with increment of the torsional angle (Fig. 2). The lowest energies are obtained at $\tau=0°$ and 180°, where pyrazole and pyrimidine situate on the same plane and electronic delocalization may occur over two rings. The highest energy is obtained at $\tau=90°$ for both compounds. The energy at 20.5° is a little higher than the lowest energy. The value is 0.04 eV which is near to the thermal energy and the torsion of that extent may easily occur. On the other hand, that the difference between the highest and lowest energy is more than 0.3 eV indicates the presence of the high energy barrier for the free rotation around the N^1–$C^{2'}$ bond. HOMO, LUMO, and GAP of the two compounds at 20.5° are slightly higher than the corresponding lowest energies.

Total electron densities on the pyrazole ring indicate the slight change in charge distribution for both compounds at 20.5° and 0°. The patterns of charge distribution at 20.5° are similar for both compounds (Fig. 3). All the pyrazole derivatives used in this study have similar patterns of charge distribution when the torsional angle is 20.5°. The rotational angles for all compounds are fixed at 20.5° to calculate the MO indices since the electronic state at 20.5° of torsional angle resembles that of the lowest energy.

Results and Discussion

By expressing the analgesic activity as the logarithm of relative potency log A, a systematic search of various parameters for pyrazole derivatives revealed statistically significant relationships. Linear regression analysis for 18 compounds in subgroup A yielded the following equations:

$$\log A = -0.906(\log P)^2 + 1.548(\log P) - 0.700\mathrm{HOMO} - 8.159, \quad (4)$$
$$n = 18,\ r = 0.798,\ s = 0.633,\ F = 8.21,$$

$$\log A = -0.608(\log P)^2 + 1.204(\log P) + 51.949Q_1 - 34.503Q_3 + 13.484, \quad (5)$$
$$n = 18,\ r=0.892,\ s=0.516,\ F=12.71.$$

In this report n represents the number of data points upon which the equation is based, s is the standard deviation, and F is the F ratio. Q_k is the net charge associated with the atom k on the pyrazole ring. These correlations, involving partition coefficients and MO parameters, indicate the importance of transport and electronic properties. By combining net charges on the pyrazole ring with hydrophobic parameters, 80% of the variation in the observed analgesic activities can be explained. Since Q_3 and Q_4 have a high negative correlation coefficient of −0.81, it seems that the substituents would have a similar effect on the net charges on these atom positions, which might play an important role for the analgesic activity.

Using similar approach, more extended relationships which include the entire members of group N^1 (subgroup A, B) were developed. The following equations are generated,

$$\log A = -0.532(\log P)^2 + 1.044(\log P) - 0.797\mathrm{HOMO} - 9.029, \quad (6)$$
$$n = 28,\ r = 0.842,\ s = 0.572,\ F = 19.51,$$

$$\log A = -0.666(\log P)^2 + 1.450(\log P) - 15.329Q_4 + 2.020, \quad (7)$$
$$n = 28,\ r = 0.835,\ s = 0.584,\ F = 18.40.$$

The hydrophobic parameters and HOMO or Q_4 correlated well with the activities of these derivatives as well as only with that of the subgroup B derivatives. This suggests that the mechanism of action of the subgroup B derivatives seems to be similar to that of the subgroup A derivatives.

The parabolic relationships of hydrophobic parameters in Eqs. 4—7 indicate that the optimal log P value for activity is about one. The log P values for the compounds having higher activity (compounds **3, 8, 23**) are close to this value, on the other hand, that for the compounds having low activities (**12, 13**) and inactive compounds are far from this value. However, the electronic factor is also important. Since the correlation between Q_3 and Q_4 is high in group N^1, Eq. 5 is closely related to Eq. 7. Therefore these positions of the pyrazole ring are considered to be fairly important for the group N^1 derivatives. No improvement is obtained by adding other parameters because MO parameters are relatively well correlated with each other.

The negative sign of the coefficients associated with HOMO in Eqs. 4 and 6 indicates that the more electron-donating ability, the lower activity becomes. In contrast with this result, Neely *et al.*[12] reported the positive sign of the coefficient with HOMO in the studies of a series of imidazole derivatives, that leads to a charge transfer complex model. Neither *MR* nor total electron density on the atom of the pyrimidine ring were of significant value in correlating the activity.

An analysis of the analgesic activities of 10 compounds in group N^2 revealed that *MR*, LUMO and GAP are significant parameters.

$$\log A = -0.009MR^2 + 1.051MR - 29.963, \quad (8)$$
$$n = 10,\ r = 0.879,\ s=0.542,\ F = 11.84,$$

$$\log A = 0.690\mathrm{LUMO} - 0.144\mathrm{IV} - 2.33, \quad (9)$$
$$n = 10,\ r = 0.842,\ s=0.612,\ F = 8.54,$$

$$\log A = 0.867\mathrm{GAP} - 0.907\mathrm{IV} - 11.535, \quad (10)$$
$$n = 10,\ r = 0.954,\ s = 0.341,\ F = 35.09,$$

where IV is an indicator variable with a value of

Table 3. Predicted log A values for Inactive compounds

No.	Predicted				No.	Predicted		
	Eq. 4	Eq. 5	Eq. 6	Eq. 7		Eq. 8	Eq. 9	Eq. 10
11	−0.95	−1.22	−0.90	−0.94	**34**	−0.17	−1.05	−1.14
15	−1.25	−0.98	−1.08	−1.23	**35**	−0.17	−1.10	−1.11
					37	−0.46	−0.31	−0.63
					38	−0.30	−0.40	−0.43

1 for the subgroup C derivatives and 0 for the subgroup D derivatives. The introduction of hydrophobic parameters into each regression in no case produced a significant improvement.

Equation 8 indicates that there exists an optimal MR value; a proper steric feature would be required for drug-acceptor interactions. The positive coefficient with LUMO in Eq. 9 indicates that the activity increases with the stability of electronic state. The indicator variable IV highly correslates with the net charges on the atoms of the pyrazole ring and reflects these electronic features. GAP, concerning with the transition energy, also correlates well with activity. Another regression analysis combining the other series compounds $R_i(i=1, 2,\cdots 6)$ in no case produced a significant correlation.

In order to examine the reliability of the results obtained above, the activities were predicted from Eqs. 4—10 for those compounds which are found to be inactive. The predicted activities are shown in Table 3. The analgesic activities for the group N^1 compounds were successfully predicted to be inactive from Eqs. 4—7. On the other hand, the group N^2 compounds were predicted to be not inactive from Eq. 8. This failure may be due to some unexplained factors. However, it is expected that observed relationships aid the development of understanding of the analgesic activities for these compounds.

The authors thank the Computer Center, Institute for Molecular Science for affording facilities for computation.

References

1) A. Ebnöther, E. Jucker, and A. Lindemann, *Helv. Chim. Acta*, **42**, 1201 (1959).
2) J. Büchi, P. Fabiani, H. U. Frey, A. Hofstetter, and A. Schorono, *Helv. Chim. Acta*, **49**, 272 (1966).
3) J. Okada, T. Esaki, and K. Fujieda, *Chem. Pharm. Bull.*, **24**, 61 (1976).
4) T. Naito, T. Yoshikawa, S. Kitahara, and N. Aoki, *Chem. Pharm. Bull.*, **17**, 1467 (1969).
5) Y. Oshima, T. Akimoto, W. Tsukada, T. Yamasaki, K. Yamaguchi, and H. Kojima, *Chem. Pharm. Bull.*, **17**, 1492 (1969).
6) E. Takabatake, R. Kodama, Y. Tanaka, R. Dohmori, H. Tachizawa, and T. Naito, *Chem. Pharm. Bull.*, **18**, 1900 (1970).
7) R. Dohmori, R. Yoshimura, S. Kitahara, Y. Tanaka, and T. Naito, *Chem. Pharm. Bull.*, **18**, 1908 (1970).
8) A. I. Vogel, W. T. Cresswell, G. W. Feffery, and J. Leicester, *Chem. Ind.*, **1950**, 358.
9) J. Berthou, J. Elguero, and C. Rérat, *Acta Crystallogr., Sect. B*, **26**, 1880 (1970).
10) P. J. Wheatley, *Acta Crystallogr.*, **13**, 80 (1960).
11) T. P. Singh and M. Vijayan, *Acta Crystallogr., Sect. B*, **29**, 714 (1973).
12) W. B. Neely, H. C. White, and A. Rudzik, *J. Pharm. Sci.*, **57**, 1176 (1968).

Reactions of Thiols with Phenylglyoxal to Give Thiomandelic *S*-Esters. Formation of Hemithioacetals and Their Rearrangement

Tadashi Okuyama,* Kazumasa Kimura, and Takayuki Fueno
Faculty of Engineering Science, Osaka University, Toyonaka, Osaka 560

(Received April 30, 1981)

Equilibrium constants K_h for the addition of 2-mercaptoethanol and glutathione to phenylglyoxal to form hemithioacetals were determined spectrophotometrically over the pH range 7—10. The observed K_h values decrease sigmoidally with pH as the thiol ionizes. Rearrangement of hemithioacetals formed from phenylglyoxal and various thiols was kinetically investigated. The rates increase with thiol concentration following a saturation curve to give K_h identical with the spectrophotometric value. The rearrangement is subject to general base catalysis. The solvent isotope effect on the rate of the rearrangement, k^{H_2O}/k^{D_2O}, is nearly 1.0; that on the equilibrium, $K_h^{H_2O}/K_h^{D_2O}$, is 0.38. The results strongly support the mechanism involving proton transfers through an enediol intermediate.

Glutathione (GSH), a tripeptide thiol, has been well known as a coenzyme which constitutes the glyoxalase enzyme system.[1] The enzyme catalyzes the Cannizzaro-type rearrangement of methylglyoxal to lactic acid. The suggestion that this action is related closely to the regulation of cell division[2] has stimulated interest in this enzyme system and its mechanism. The reaction proceeds through nonenzymatic formation of hemithioacetal and its rearrangement to α-hydroxy thiocarboxylic *S*-ester which is catalyzed by glyoxalase I:[1,3,4]

$$\begin{aligned} &CH_3\text{-}\overset{O}{\overset{\|}{C}}\text{-}\overset{O}{\overset{\|}{C}}\text{-}H + GSH \rightleftharpoons CH_3\text{-}\overset{O}{\overset{\|}{C}}\text{-}\overset{OH}{\overset{|}{C}}\text{H-SG} \\ &\xrightarrow{\text{glyoxalase I}} CH_3\text{-}\overset{OH}{\overset{|}{C}}\text{H-}\overset{O}{\overset{\|}{C}}\text{-SG} \\ &\xrightarrow{\text{glyoxalase II}} CH_3\text{-}\overset{OH}{\overset{|}{C}}\text{H-}\overset{O}{\overset{\|}{C}}\text{-OH} + GSH. \end{aligned} \quad (1)$$

Results of solvent isotope incorporation experiments led earlier investigators to conclude a mechanism involving an intramolecular hydride shift,[5,6] while recent NMR evidence of temperature-dependent incorporation of solvent protons suggested a mechanism of fast-shielded enediol proton transfer:[7]

$$\begin{aligned} R\text{-}\overset{O}{\overset{\|}{C}}\text{-}\overset{OH}{\overset{|}{C}}\text{H-SG} &\longrightarrow R\text{-}\overset{OH}{\overset{|}{C}}\text{=}\overset{OH}{\overset{|}{C}}\text{-SG} \\ &\longrightarrow R\text{-}\overset{OH}{\overset{|}{C}}\text{H-}\overset{O}{\overset{\|}{C}}\text{-SG}. \end{aligned} \quad (2)$$

Franzen[5,8] showed that certain 2-(dialkylamino)-ethanethiols are efficient nonenzymatic catalysts for rearrangement of a glyoxal which mimicks the glyoxalase reaction. Hall and Poet[9] found that some α-keto hemithioacetals rearrange to α-hydroxy thiocarboxylic *S*-esters under catalysis of such bases as sodium acetate and tertiary amines in *N*,*N*-dimethylformamide solution. Shinkai *et al.*[10] have recently demonstrated the intermediacy of enediol in reactions of some thiols with methyl- and phenylglyoxals by the flavin-trapping experiments. However, the kinetic phase of this reaction has been examined only briefly[7b] and has not well been characterized.

In the present investigation, we examined reactions of various thiols with phenylglyoxal (PG) in aqueous solution. Equilibrium constants for formation of hemithioacetals were determined in a wide pH range and their rearrangement was kinetically characterized.

Experimental

Materials. Phenylglyoxal (PG) hydrate was prepared according to the literature.[11] 2-Mercaptoethanol (ME), 1-butanethiol, ethyl mercaptoacetate, and 3-mercaptopropionic acid were distilled and stored under nitrogen. Sodium mercaptoacetate (Wako Pure Chemicals) was used without further purification. Glutathione (GSH) was a gift from Ajinomoto Co. 1,4-Diazabicyclo[2.2.2]octane (DABCO) and imidazole were recrystallized from ligroine and benzene, respectively. *N*-Methylmorpholine, 1,1,1,3,3,3-hexafluoro-2-propanol, 2-(dimethylamino)ethanol, and *N*-methylpiperidine were distilled before use. The other inorganic chemicals were used as received. Glass-distilled water, which was freshly boiled under nitrogen and contained 10^{-4} M (1 M = 1 mol dm^{-3}) disodium dihydrogen ethylenediaminetetraacetate (EDTA), was used throughout. The ionic strength of solutions was always maintained with KCl.

Buffer Preparations. Buffer solutions for reaction were prepared immediately before use by mixing equal volumes of a stock buffer solution (μ=0.50) and a stock solution of thiol in 10% aqueous acetonitrile (μ=0.45). Concentrations of thiols were assayed by the Ellman method.[12,13] All the flasks for solution preparation and cuvettes for spectrophotometry were flushed with nitrogen. A Shimadzu UV 200 spectrophotometer was used for spectrophotometric determination. Measurements of pH of buffer and reaction solutions were carried out with a Hitachi-Horiba F-7 pH meter.[14]

Equilibrium Constants. Equilibrium constants K_h for hemithioacetal formation were determined by measuring increase in UV absorbance at 280 nm that occurs when PG is added to buffer solutions containing varying concentrations (0.001—0.01 M) of thiol at constant pH. The equilibrium was attained by addition of 0.030 cm^3 of aqueous solution of PG hydrate (1.3×10^{-2} M) to 3.0 cm^3 of the buffer solution which was equilibrated at 30±0.1 °C in a stoppered quartz cuvette inserted in a water-jacketed cell holder. The blank solution in the spectrophotometer was identical with the reaction solution, except that water was added in place of aliquot of the PG solution. Change in absorbance with time was followed until the absorbance remained constant at lower pH. Since at higher pH (>8) the absorbance decreased slowly after initial rapid increase, the reading was extrapolated to the time of PG addition. In some cases, measurements were carried out of absorbance decrease at 250 nm with $[PG]_0 \simeq 7\times10^{-5}$ M.

Equilibrium constants K_h were calculated from absorbance

change according to

$$K_h = \frac{[\text{hemithioacetal}]}{[PG][RSH]} = \frac{\Delta A}{(\Delta A_{max} - \Delta A)[RSH]}, \quad (3)$$

where ΔA is the difference between the equilibrium absorbance of PG alone and that of PG plus thiol; ΔA_{max} is a hypothetical absorbance change when all the PG is transformed to hemithioacetal.

$$\Delta A_{max} = (\varepsilon_p - \varepsilon_h)[PG]_0, \quad (4)$$

where ε_p and ε_h are the extinction coefficients of PG and hemithioacetal, respectively. Equation 3 is transformed into

$$\frac{\Delta A}{[RSH]} = K_h \Delta A_{max} - K_h \Delta A. \quad (5)$$

Plots of $\Delta A/[RSH]$ against ΔA (the Scatchard plot)[15,16] give $-K_h$ as a slope and ΔA_{max} as an intercept of abscissa. Here, [RSH] is essentially equal to $[RSH]_0$ since $[RSH]_0 \gg [PG]_0$, but it was corrected for the hemithioacetal formation when necessary.

Kinetic Measurements. Rates of rearrangement were measured by following decrease in the absorption in the 280 nm region. The reaction was started in the same way as in the equilibrium measurement. Pseudo-first-order plots were usually linear over two lifetimes except for an initial short induction period due to the hemithioacetal formation. For slow reactions, a modified Guggenheim treatment[17] was employed.

Products of Reaction of 1-Butanethiol with PG. A sample of PG hydrate (0.5 g) was dissolved in 1 dm^3 of 0.1 M $(CF_3)_2$-CHOH–0.1 M $(CF_3)_2CHONa$ buffer solution containing 0.005 M 1-butanethiol and 10 vol% acetonitrile (pH 9.4). After standing overnight at 30 °C the solution was neutralized and the volume was reduced to 100 cm^3 under reduced pressure. The remaining solution was acidified and extracted with ether. The extract was dried over $MgSO_4$ and the ether was evaporated. The residues were dissolved in D_2O. The ^1H NMR spectrum showed two singlet signals at 7.43 and 5.26 ppm from DSS in intensity ratio of 5:1, which is identical with the spectrum of an authentic sample of mandelic acid.

The reaction in D_2O–CH_3CN solution was carried out on a 100-cm^3 scale in the same way as above. Isotopic purity of the deuterium buffer solution was about 95%. The ^1H NMR spectrum of the products showed formation of mandelic acid but the signal of benzylidene α-hydrogen (5.26 ppm) was hardly perceived.

Results

Hemithioacetal Formation. Phenylglyoxal (PG) is almost completely hydrated in aqueous solution with absorption maximum at 250 nm (ε_{250} 11900, ε_{280} 1550). When PG hydrate is dissolved in a buffer solution containing an appropriate amount of thiol, the absorption spectrum changes rapidly with an isosbestic point at 267 nm due to formation of an adduct, hemithioacetal. The spectrum of the hemithioacetal had an absorption maximum at 250 nm and a shoulder at 280 nm. Extinction coefficients for the hemithioacetal of 2-mercaptoethanol (ME) were found to be ε_{250}=9600 and ε_{280}=3150 by extrapolation. Those for glutathione (GSH) were ε_{250}=10100 and ε_{280}=3400.

Table 1. Formation constants of hemithioacetals of PG[a]

$HOCH_2CH_2SH$		GSH	
pH	K_h/M^{-1}	pH	K_h/M^{-1}
6.65	(752±73)[b]	6.67	603±31 (625±71)[b]
7.13	740±36	7.68	572±39
7.67	794±39	7.92	593±48
7.98	784±19	8.23	571±27
8.59	782±67	8.54	438±13
9.00	607±47	9.02	315±18
9.50	474±57	9.48	179±17
9.95	277±27	9.95	88±65
10.50	149±18		

a) Errors given are standard deviations. b) Measured at 250 nm.

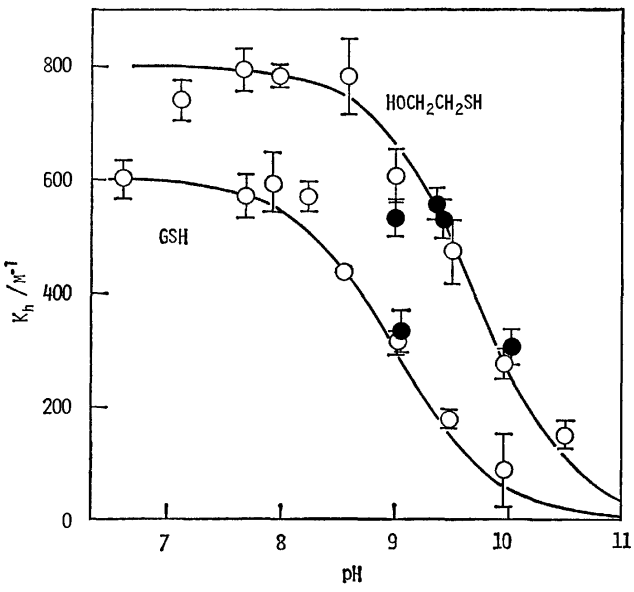

Fig. 1. pH dependence of the equilibrium constants K_h for hemithioacetal formation of ME and GSH. Closed circles are values obtained kinetically.

$$\text{Ph-C(=O)-C(H)(OH)-OH} + \text{RSH} \overset{K_h}{\rightleftharpoons} \text{Ph-C(=O)-C(H)(OH)-SR} + H_2O \quad (6)$$

Equilibrium constants for the hemithioacetal formation of PG with ME and GSH were determined by measuring increase in absorbance at 280 nm of PG of constant concentration in the presence of increasing concentration of thiol. Least-squares treatments of the Scatchard plots (Eq. 5) gave the equilibrium constants K_h summarized in Table 1. Values of K_h obtained from decreasing absorbance at 250 nm are included in Table 1. They agree well with those obtained at 280 nm.

The K_h values are not constant but seem to change sigmoidally with pH as shown in Fig. 1. The closed circles in the plots of Fig. 1 are the K_h values obtained kinetically as will be mentioned later. The sigmoid curves shown are those of pK_a=9.7 and 9.0

Table 2. Rates of the rearrangement of hemithioacetals of various thiols[a)]

Thiol	pK_a[b)]	$10^3k_{obsd}/s^{-1}$[c)]	$10^3k_{max}/s^{-1}$[d)]	K_h/M^{-1}[d)]
$EtOCOCH_2SH$	7.95	1.78	3.75±0.70	187± 55[e)]
GSH	8.7	3.10	4.96±0.50	331± 46
$HO(CH_2)_2SH$	9.7	1.29	1.80±0.06	533± 35
$DO(CH_2)_2SD$[f)]		1.60	1.89±0.11	1410±159
n-BuSH	10.7	(1.40)[g)]	1.69±0.14	1020± 80
$^-OCOCH_2SH$	10.7	1.11	1.28±0.30	1300±210
$^-OCO(CH_2)_2SH$	10.8	1.12		

a) 5% CH_3CN-H_2O (μ=0.475); [DABCO]=0.2 M; pH 9.0±0.5; 30 °C. b) pK_a of thiol taken from "CRC Handbook of Biochemistry," ed by H. A. Sober, Chem. Rubber Co., Cleveland (1968). c) k_{obsd} at [RSH]=0.005 M. d) Errors given are standard deviations. e) Value 1000±44 M^{-1} at pH 5.8 was obtained spectrophotometrically. f) 5% CH_3CN-D_2O; pD 9.74. g) Calculated value.

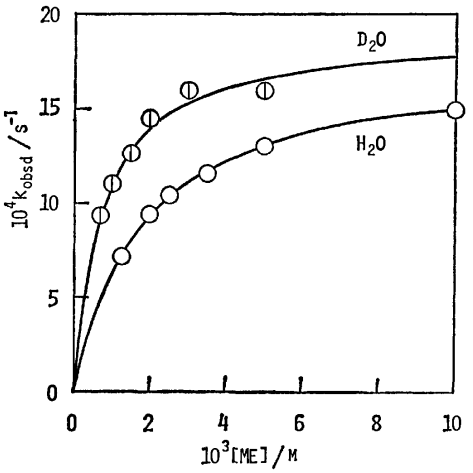

Fig. 2. Dependence of rates of the rearrangement of hemithioacetal upon thiol concentrations in 5% CH_3CN-H_2O (○) and 5% CH_3CN-D_2O (◑) at 30 °C. $[DABCO]_t$=0.2 M, buffer ratio=1, μ=0.475 (KCl).

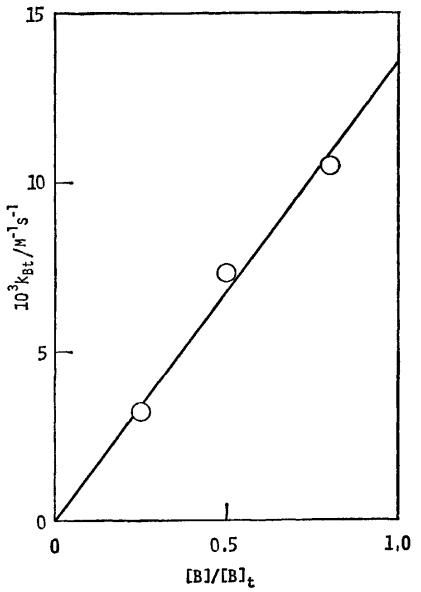

Fig. 3. Buffer-dependent rate constants k_{Bt} *vs.* base fraction of DABCO buffers. $[ME]_0$=0.05 M, 5% CH_3CN-H_2O (μ=0.475), 30 °C.

for ME and GSH, respectively. Ultimate K_h values at lower pH were taken to be 800 and 600 M^{-1} for ME and GSH, respectively, and those at higher pH to be zero.

Rearrangement. On addition of PG in a thiol-containing buffer solution, the absorbance in the 280 nm region decreases slowly after the initial rapid increase due to the formation of hemithioacetal. The slow decrease in absorbance is ascribed to rearrangement of the hemithioacetal to an α-hydroxy thiocarboxylic *S*-ester. The thioester is further hydrolyzed to mandelic acid in much smaller rate.[18)] The ultimate product obtained in the reaction with 1-butanethiol was identified by ^1H NMR spectroscopy. The product obtained from the reaction in deuterium media (D_2O-CH_3CN) showed incorporation of deuterium at the benzylidene α-position:

$$\mathrm{Ph\text{-}\overset{O}{\overset{\|}{C}}\text{-}\overset{OD}{\overset{|}{C}}\text{-}SR \xrightarrow{D_2O} Ph\text{-}\overset{OD}{\overset{|}{C}}\text{-}\overset{O}{\overset{\|}{C}}\text{-}SR.} \qquad (7)$$

The time-dependent absorbance change (decrease) in the second phase of reaction gave linear pseudo-first-order plots, from which rates of the rearrangement were obtained. The observed rate constants k_{obsd} showed saturation with increasing thiol concentration [RSH] as shown in Fig. 2 in accord with the rate equation

$$k_{obsd} = \frac{k_{max}K_h\,[RSH]}{1+K_h\,[RSH]}. \qquad (8)$$

Parameters k_{max} and K_h were determined from linear plots of the Scatchard-type (Eq. 9) or double reciprocal plots (Eq. 10):

$$\frac{k_{obsd}}{[RSH]} = K_hk_{max} + K_hk_{obsd}, \qquad (9)$$

$$\frac{1}{k_{obsd}} = \frac{1}{k_{max}} + \frac{1}{k_{max}K_h}\frac{1}{[RSH]}. \qquad (10)$$

Kinetic parameters k_{max} and K_h in a DABCO buffer of pH 9 are summarized in Table 2 for various thiols. Results in D_2O are also included. The equilibrium constants K_h obtained here agree very well with those obtained spectrophotometrically for the formation of hemithioacetal as illustrated in Fig. 1.

At constant [RSH], rates increase linearly with buffer concentration:

Table 3. Rate constants for the reaction of PG and ME in various buffer solutions[a]

pH	Buffer	10^4k_0 [b] / s^{-1}	10^3k_{Bt} [b] / $M^{-1}s^{-1}$	10^3k_B [b,c] / $M^{-1}s^{-1}$	10^3k_{max} [d] / s^{-1}	K_h [d] / M^{-1}
8.30	*N*-Methylmolpholine	0.21	0.337	0.45		
8.48	DABCO	1.02	3.20			
9.00	DABCO	1.62	7.48	13.5	1.80 ±0.06	533±35
9.36	$(CF_3)_2CHOH$	(4.0)	(6.83)	(13.7)	1.71 ±0.04	558±28
9.48	$(CH_3)_2N(CH_2)_2OH$	3.10	2.90	5.8	0.752±0.072	529±31
9.62	DABCO	7.42	10.5			
10.03	Carbonate	(6.5)	(10.6)	(21.2)	2.67 ±0.23	306±30
10.32	*N*-Methylpiperidine	16.3	10.7	21.4		

a) In 5% CH_3CN-H_2O (μ=0.475) at 30 °C. b) [ME]=0.05 M. Values in parentheses are those calculated from data of buffer dependence at [ME]=0.005 M. c) Estimated from k_{Bt} for OH^- is estimated to be 8.0 $M^{-1}s^{-1}$ from k_0 values. d) $[B]_t$=0.2 M. Errors given are standard deviations.

$$k_{obsd} = k'_0 + k'_{Bt}[B]_t \quad (11)$$

or

$$k_{max} = k_0 + k_{Bt}[B]_t. \quad (12)$$

Since $k_{obsd} \simeq k_{max}$ at $[RSH] \gg 1/K_h$, k_0, and k_{Bt} can be evaluated from buffer-dependence data obtained by keeping [RSH] large enough and constant. Table 3 summarizes kinetic results for the reaction of ME with PG under various conditions. Constants k_0 and k_{Bt} were obtained mostly by keeping [RSH]=0.05 M. Buffer-dependent rate constants k_{Bt} increase with increasing base fraction of the buffer (Fig. 3); the reaction is catalyzed by general bases. Catalytic constants k_B of some general bases estimated from results of one buffer ratio are included in Table 3.

Discussion

Reaction of thiols with aldehydes to form hemithioacetals has been well-known and some hemithioacetals of α-keto aldehydes have been even isolated.[19] However, equilibrium and kinetic studies are limited only in a few cases.[20-23] Equilibrium constants for the formation of hemithioacetals from GSH and various α-keto aldehydes were measured in relation to the glyoxalase reaction.[23] Values K_h were found to be essentially constant in the pH range 5—9.

The present results clearly show that K_h values sharply change in the pH range 8—10 for GSH and 9—11 for ME. The changes seem to follow sigmoid curves of pK_a=9.0 and 9.7 for GSH and ME, respectively. These pK_a values correspond to those of the respective thiols; that is, only the neutral form of the thiol contributes to the formation of hemithioacetal at equilibrium but the thiolate ion is hardly effective. This is reasonable when we consider an equilibrium cycle:

$$\begin{array}{ccc} RSH + R'CH(OH)_2 & \overset{K_h}{\rightleftharpoons} & R'CH(OH)(SR) + H_2O \\ K_a \downarrow\uparrow & & K'_a \downarrow\uparrow \\ RS^- + R'CH(OH)_2 & \overset{K'_h}{\rightleftharpoons} & R'CH(O^-)(SR) + H_2O. \end{array} \quad (13)$$

The ratio K_h/K'_h should be equal to K_a/K'_a which must be greater than 10^2.[24]

Rates of the rearrangement are dependent on [RSH] with saturation as seen in Fig. 2. Analysis of the curve gives the equilibrium constant K_h and the maximum rate constant k_{max}. The K_h values agree very well with those obtained independently by the spectrophotometric method. This observation firmly indicates that the hemithioacetal is a true intermediate of the reaction.

The rate constants k_{max} correspond to those of the rearrangement when all the PG is transformed into the hemithioacetal. The k_{max} values increase with buffer concentrations and the buffer-dependent rate constants k_{Bt} were found to be ascribed to a base form of the buffer (Fig. 3); the reaction is confirmed to be catalyzed by general bases.[26] The catalytic constants k_B summarized in Table 3 are not precise enough for further analysis but Brønsted β of about 0.45 may be estimated including k_{OH^-} value of 8 $M^{-1}s^{-1}$. The latter value involves another uncertainty owing to the k_0 values influenced by the term of general-base catalysis due to 0.05 M ME.

General base catalysis established here is consistent with a mechanism involving the enediol proton transfer.[7] This mechanism was concluded from the observation that the solvent proton is incorporated into the product for the glyoxalase reaction[7a] as well as a model reaction with 2-(diethylamino)ethanethiol.[7b] Similar results were obtained in the present reaction with a simple thiol. The product mandelic acid formed by the reaction of 1-butanethiol with PG in D_2O was found to have lost a proton at the benzylidene α-position.

Solvent isotope effects observed in a DABCO buffer are $k^{H_2O}_{max}/k^{D_2O}_{max}$=0.95±0.09 and $K^{H_2O}_h/K^{D_2O}_h$=0.38±0.07. The rate constant k_{max} is little affected by solvent isotopes.

$$\begin{array}{l} Ph\text{-}\overset{O}{\overset{\|}{C}}\text{-}\overset{OH}{\overset{|}{C}}\text{-}SR \longrightarrow Ph\text{-}\overset{O^-}{\overset{|}{C}}\text{=}\overset{OH}{\overset{|}{C}}\text{-}SR \\ \quad\quad H\ \ B \quad\quad\quad\quad HB^+ \\ Ph\text{-}\overset{O^-}{\overset{|}{C}}\text{=}\overset{OH}{\overset{|}{C}}\text{-}SR \rightleftharpoons Ph\text{-}\overset{OH}{\overset{|}{C}}\text{=}\overset{OH}{\overset{|}{C}}\text{-}SR \\ \quad\quad HB^+ \quad\quad\quad\quad B \end{array} \quad (14)$$

$$\rightleftharpoons Ph\text{-}\overset{OH}{\overset{|}{C}}\text{=}\overset{O^-}{\overset{|}{C}}\text{-}SR \longrightarrow Ph\text{-}\overset{OH}{\overset{|}{C}}\text{—}\overset{O}{\overset{\|}{C}}\text{-}SR \quad (15)$$
$$HB^+ \quad\quad\quad\quad H\ \ B$$

The rate-determining step must be proton transfer from the hemithioacetal to the base (DABCO) to form an enediol (Eq. 14). Protonation of the enediol at the β position (Eq. 15) should be faster than that at the α position (reverse of Eq. 14). The primary isotope effect of $k_H/k_D=2.3$ observed with PhCOCDO[7b] is also in accord with this mechanism. Inverse solvent isotope effects on the equilibrium constant K_h are not unreasonable on the basis of the isotopic fractionation factor of about 0.4—0.5 of thiol hydrogen.[27,28] Similar isotope effects of $K_h^{H_2O}/K_h^{D_2O}=0.44$ were found for the formation of hemithioacetal of acetaldehyde.[20a]

Kinetic parameters summarized in Table 2 were obtained with various thiols at pH 9 in DABCO buffers. Rates of rearrangement (k_{max}) show a tendency to decrease with increasing pK_a of the thiol. This is consistent with the mechanism involving the rate-determining deprotonation to form the enediol intermediate. Electron-withdrawing effects which lower pK_a of the thiol may ease the deprotonation of the hemithioacetal. Effective catalytic function of an intramolecular general base group of the thiol was found with *N*-(2-mercaptoethyl)piperidine and -morpholine in aqueous solution as will be reported in a separate paper.[29] However, the carboxylato group of mercaptoacetate and 3-mercaptopropionate does not seem to show any effective catalytic activity. Enhanced reactivity of GSH might be due partly to such intramolecular effects of the amino group. Shinkai *et al.*[10] noted low catalytic efficiency of GSH contrary to our observation. This is probably due to their use of borate buffers. Borate forms adducts with PG in aqueous solution[29] to retard the rearrangement. Furthermore, GSH itself may form some adduct with boric acid.

Magnitudes of K_h depend largely on the degree of ionization of the thiol in such a way that the ionization results in small value of K_h, but the thiol structure shows minor influence on the K_h value. As a whole, the catalytic efficiency of simple thiols in the rearrangement is not largely dependent on their structure unless the thiol is ionized under the reaction conditions. All the rearrangement reactions of α-keto hemithioacetals proceed through proton transfers involving the enediol as an intermediate.

We thank Mr. H. Nagamatsu for his assistance in kinetic measurements.

References

1) S. G. Waley, *Adv. Protein Chem.*, **21**, 1 (1966); A. Meister, "Metabolic Pathways," 3rd ed, ed by D. M. Greenberg, Academic Press, New York (1975), Vol. 7, Chap. 5.

2) A. Szent-Györgyi, L. G. Együd, and J. A. McLaughlin, *Science*, **155**, 539 (1967).

3) E. E. Cliffe and G. R. Waley, *Biochem. J.*, **79**, 475 (1961).

4) K. A. Davis and G. R. Williams, *Can. J. Biochem.*, **47**, 553 (1969).

5) V. Franzen, *Chem. Ber.*, **89**, 1020 (1956).

6) I. A. Rose, *Biochim. Biophys. Acta*, **25**, 214 (1957).

7) a) S. S. Hall, A. M. Doweyko, and F. Jordan, *J. Am. Chem. Soc.*, **98**, 7460 (1976); b) **100**, 5934 (1978).

8) V. Franzen, *Chem. Ber.*, **88**, 1361 (1955); **90**, 623 (1957).

9) S. S. Hall and A. Poet, *Tetrahedron Lett.*, **1970**, 2867.

10) S. Shinkai, T. Yamashita, Y. Kusano, and O. Manabe, *Chem. Lett.*, **1979**, 1323; *J. Am. Chem. Soc.*, **103**, 2070 (1981).

11) H. A. Riley and A. R. Gray, *Org. Synth.*, Coll. Vol. II, 509 (1953).

12) G. L. Ellman, *Arch. Biochem. Biophys.*, **82**, 70 (1959).

13) M. J. Fernandez Diez, D. T. Osuga, and R. E. Feenay, *Arch. Biochem. Biophys.*, **107**, 449 (1964).

14) Since thiol-containing solutions easily deteriorate a silver–silver chloride electrode of the pH meter especially at higher pH, care was taken to permit a short contact and the electrode was soaked in a 1.0 M HCl solution for a while after each measurement.

15) G. Scatchard, *Ann. N. Y. Acad. Sci.*, **51**, 660 (1949).

16) D. A. Deranleau, *J. Am. Chem. Soc.*, **91**, 4044 (1969).

17) E. S. Swinbourne, *J. Chem. Soc.*, **1960**, 2371.

18) T. Okuyama, H. Nagamatsu, and T. Fueno, *J. Org. Chem.*, **46**, 1336 (1981).

19) M. P. Schubert, *J. Biol. Chem.*, **111**, 671 (1935); B. Holmberg, *Ark. Kemi*, **14A**, No. 9, 1 (1940).

20) a) G. E. Lienhard and W. P. Jencks, *J. Am. Chem. Soc.*, **88**, 3982 (1966); b) R. E. Barnett and W. P. Jencks, *ibid.*, **91**, 6758 (1969).

21) H. F. Gilbert and W. P. Jencks, *J. Am. Chem. Soc.*, **99**, 7931 (1977).

22) M. S. Kanchuger and L. D. Byers, *J. Am. Chem. Soc.*, **101**, 3005 (1979).

23) D. L. Vander Jagt, L.-P. B. Han, and C. H. Lehman, *Biochemistry*, **11**, 3735 (1972); D. L. Vander Jagt, E. Daub, J. A. Krohn, and L.-P. B. Han, *ibid.*, **14**, 3669 (1975).

24) The pK_a' value must be greater than that of the hydrate ($pK_a \approx 11.2$[25]) since S is less electronegative than O.

25) J. Hine and G. F. Koser, *J. Org. Chem.*, **36**, 3591 (1971).

26) General base catalysis was suggested but not established.[7b]

27) R. L. Schowen, *Prog. Phys. Org. Chem.*, **9**, 275 (1972).

28) F. W. Hobden, E. F. Johnston, L. H. P. Weldon, and C. L. Wilson, *J. Chem. Soc.*, **1939**, 61.

29) T. Okuyama, S. Komoguchi, and T. Fueno, *J. Am. Chem. Soc.*, in press.

The Reaction of Bis(dimethylglyoximato)(pyridine)cobalt(I), Cobaloxime(I), with 2-(Allyloxy)ethyl Halides and the Photolysis of the Resulting Organo-cobaloximes[1]

Masami Okabe and Masaru Tada*

Department of Chemistry, School of Science and Engineering, Waseda University, Shinjuku-ku, Tokyo 160

(Received May 8, 1981)

The reactions of 2-(allyloxy)ethyl halides with cobaloxime(I) gave (tetrahydro-3-furanyl)methylcobaloximes *via* an electron transfer from cobaloxime(I) to the halides to give radical anions. The rupture of a halide ion to give an organic radical and the ring closure to give a (tetrahydro-3-furanyl)methyl radical are followed by the radical coupling between the organic radical and the cobaloxime(II). The structures of the organo-cobaloximes were determined by the analyses of the photolysis products under aerobic or anaerobic conditions.

The formation of organo-cobalt complexes by the reaction of cobalamin(I) or bis(dimethylglyoximato)-(pyridine)cobalt(I), hereafter cobaloxime(I) or $(Co^{I})^{-}$, with alkyl halides has been claimed to proceed by an S_N2 mechanism, an electron transfer mechanism, a four centered *syn*-substitution, and an S_Ni reaction with retention of configuration. The possibility of the last two mechanisms has been claimed as an interpretation of the reactions of 1-adamantyl bromide and 1-norbornyl bromide.[2] The S_N2 mechanism has been proposed based on a kinetic study[3] and the stereochemistry of products,[4] and the electron transfer mechanism has been proposed by the indication of the radical intermediate.[5-7]

In this paper we would like to report the experimental results supporting the electron transfer mechanism and the photolyses of the organo-cobaloximes which define the structures of the organo-cobaloximes. We used the cyclization of 2-(allyloxy)ethyl radical to (tetrahydro-3-furanyl)methyl radical as a probe of the radical intermediate (R·) formed by the rupture of halide ion (X^-) from the radical anion ($RX^{\cdot-}$) (Eq. 1).

$$(Co^{I})^- + RX \longrightarrow (Co^{II}) + RX^{\cdot-} \longrightarrow (Co^{II}) + R\cdot + X^- \longrightarrow (Co)R + X^- \quad (1)$$

Results

The Reaction of Cobaloxime(I) with Tosylates or Halides. 2-(Allyloxy)ethyl tosylates or 2-(allyloxy)ethyl halides were reacted with cobaloxime(I) in methanol under nitrogen; the results are summarized in Table 1. 2-(Allyloxy)ethyl tosylate (**1a**) gave a direct substitution product, 2-(allyloxy)ethylcobaloxime (**4a**) but 2-allyloxy-2-phenylethyl tosylate (**1b**) did not show any reactivity toward cobaloxime(I). The cobaloxime(I) anion reacted with 2-(allyloxy)ethyl bromide (**2a**) to give **4a** and (tetrahydro-3-furanyl)methylcobaloxime (**5a**). The reaction of cobaloxime(I) with 2-allyloxy-2-phenylethyl bromide (**2b**) and 2-allyloxy-2,2-diphenylethyl bromide (**2c**) gave (5-phenyltetrahydro-3-furanyl)methylcobaloxime (**5b**) and (5,5-diphenyltetrahydro-3-

Table 1. Reaction of cobaloxime(I) anion, $(Co^{I})^-$, with tosylates and halides in methanol[a]

Substrate	R^1	R^2	R^3	X	Product[b] composition	Yield[c] %
					4a : **5a**	
1a	H	H	H	OTs	100 : 0	47
2a	H	H	H	Br	71 : 29	60
3a	H	H	H	I	35 : 65	66
					4b : **5b**	
1b	Ph	H	H	OTs	— : —	0
2b	Ph	H	H	Br	0 : 100	38
3b	Ph	H	H	I	0 : 100	55
					4c : **5c**	
2c	Ph	Ph	H	Br	0 : 100	40
					4d : **5d**[d]	
1d	H	$-(CH_2)_4-$		OTs	— : —	0
2d	H	$-(CH_2)_4-$		Br	0 : 100	55
3d	H	$-(CH_2)_4-$		I	0 : 100	51
					7 : **8**	
6	—	—	—		35 : 65	55

a) See the general procedure in the experimental section for reaction conditions. b) Determined by the amount of isolated organo-cobaloximes. c) (**4**+**5**) or (**7**+**8**). d) Consisting of two stereo-isomers.

furanyl)methylcobaloxime (**5c**), respectively. Similarly the cyclic halides, *trans*-2-(allyloxy)cyclohexyl bromide (**2d**) and iodide (**3d**), gave (7-oxabicyclo[4.3.0]non-9-yl)methylcobaloxime (**5d**) but no direct substitution product **4d**. The corresponding tosylate **1d** did not show any reactivity toward cobaloxime(I). 2,2-Diphenyl-2-(2-methyl-2-propenyloxy)ethyl bromide (**6**) gave both a non-cyclized organo-cobaloxime, 2,2-diphenyl-2-(2-methyl-2-propenyloxy)ethylcobaloxime (**7**), and a cyclized organo-cobaloxime, (5,5-diphenyl-3-methyltetrahydro-3-furanyl)methylcobaloxime (**8**).

In seeking by-products from bromide **2d**, 3-(allyloxy)cyclohexene (**9**), 9-methylene-7-oxabicyclo-[4.3.0]nonane (**10**), and another by-product, which was anticipated to be 9-methyl-7-oxabicyclo[4.3.0]-nonane (**11**) from NMR data, were obtained in 5, 3, and 1% yields, respectively. Similarly 4-methyl-2-phenyltetrahydrofuran (**12**) and 4-methylene-2-phenyltetrahydrofuran (**13**) were formed from bromide **2b**.

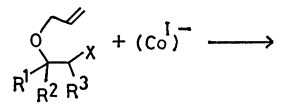

1a, **b**, and **d** (X=OTs)
2a, **b**, **c**, and **d** (X=Br)
3a, **b**, and **d** (X=I)

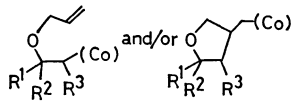

(2)

4a—d **5a—d**

a: $R^1=R^2=R^3=H$ **b**: $R^1=Ph$, $R^2=R^3=H$
c: $R^1=R^2=Ph$, $R^3=H$ **d**: $R^1=H$, $R^2+R^3=-(CH_2)_4-$

Photolyses of Organocobaloximes. The photolytic cleavage of the carbon-cobalt bond of an organocobaloxime gave an alkyl radical and cobaloxime(II) as primary products. Molecular oxygen inserts between the two radical species to give an alkyldioxycobaloxime under aerobic conditions (Eq. 3).[8] Under anaerobic conditions, however, the radical collapses into an olefin or a saturated compound depending upon the hydrogen-donating ability of the solvent used (Eqs. 4 and 5).[9,10]

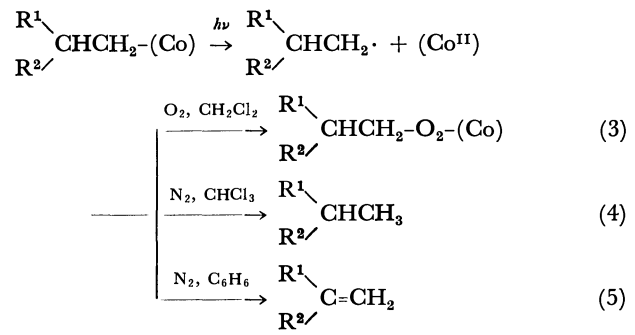

The analyses of the photolysis products, therefore, can define the structures of the cyclized organocobaloximes. The aerobic photolysis of **5a** gave a peroxide and the $NaBH_4$-reduction of the peroxide gave 3-(hydroxymethyl)tetrahydrofuran (**14**), which was identical to the authentic sample.[11] Anaerobic photolyses of organocobaloximes **5b**, **5c**, and **8** in chloroform gave **12** (98%), 2,2-diphenyl-4-methyltetrahydrofuran (**15**) (78%), and 4,4-dimethyl-2,2-diphenyltetrahydrofuran (**16**) (70%), respectively. On the other hand, anaerobic photolyses of **5b** and **5c** in benzene gave **13** and 2,2-diphenyl-4-methylenetetrahydrofuran (**17**), respectively. The hydrogenolysis of **12** over Pd–C gave 2-methyl-4-phenyl-1-butanol which was identified with the authentic sample.[12] The structures of all other tetrahydrofuran derivatives were deduced unequivocally from elemental analyses and spectral data, especially from NMR spectra. Similarly the anaerobic photolysis of **5d** in benzene gave **10**, which became 9-methylene-7-oxabicyclo[4.3.0]nonan-8-one (**18**) by CrO_3-oxidation; **18** was identified by comparison with the authentic sample.[13]

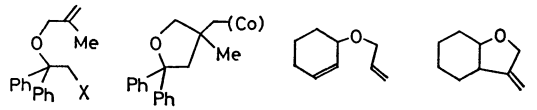

6 (X=Br) 8 9 10
7 (X=(Co))

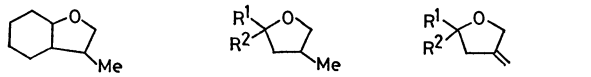

11 12 (R^1=Ph, R^2=H) 13 (R^1=Ph, R^2=H)
15 ($R^1=R^2$=Ph) 17 ($R^1=R^2$=Ph)

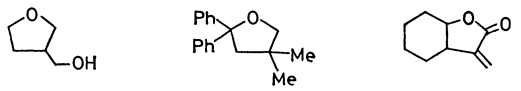

14 16 18

Discussion on Reaction Mechanism

In the reaction of cobaloxime(I) with halides, a carbenium ion intermediate has been excluded by the lack of a solvolysis product in methanol and also by the lack of a tetrahydropyran derivative which is expected to form *via* a more stable secondary cation.[14] A carbanion intermediate has been also excluded by the fact that the reaction in protic media, methanol or ethanol containing water, did not give a saturated product as a major one.

5-Hexenyl radical has a strong tendency to give cyclopentylmethyl radical irreversibly unless the radical center has an electron-attracting substituent.[15] The ring closure of 3-oxa-5-hexenyl radical, 2-(allyloxy)ethyl radical ($k=1.2\times10^6$ s^{-1}, 25 °C),[16] is faster than that of 5-hexenyl radical ($k=1.0\times10^5$ s^{-1}, 25 °C).[17] The oxa-system is, therefore, a better probe of a radical intermediate than the hydrocarbon system which is popular in radical chemistry.

Cobaloxime(I) anion and cobalamin(I) are strong nucleophiles in the reaction with methyl iodide and are called "supernucleophiles,"[18] but the bulky ligands in those cobalt complexes hinder the reaction with sterically bulky halides. Though we do not deny a normal S_N2 mechanism for simple halides such as methyl iodide, a four centered mechanism or a *syn*-displacement of halogen and bulky cobaloxime(I)[2]

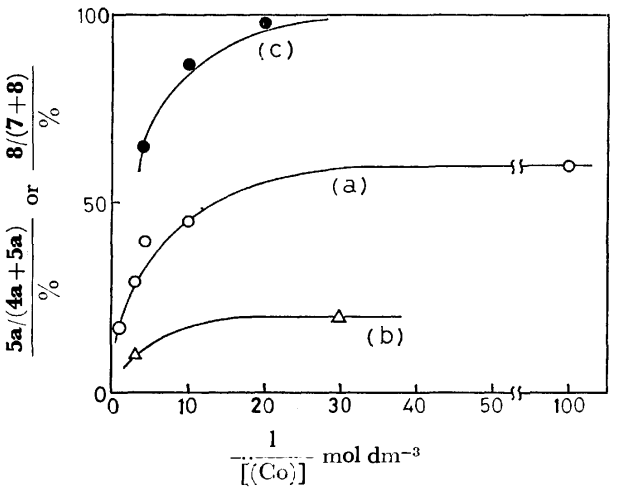

Fig. 1. Dependence of the formation of **5a** from **2a** (1.0×10^{-3} mol) and **8** from **6** (1.0×10^{-3} mol) on the concentration of cobaloxime [(Co)].
(a): Formation of **5a** in MeOH, (b): formation of **5a** in EtOH, (c): formation of **8** in MeOH.

is hardly acceptable as the mechanism of the reactions of sterically hindered halides and cobaloxime(I). The present experimental results clearly show the intervention of a radical species which is evidenced by the formation of tetrahydrofuran derivatives. The formation of a radical from an organic halide is expected by the single electron transter from cobaloxime(I) to the organic halide followed by the rupture of a halide ion. The radical intermediate is further supported by the formation of **10**, **11**, **12**, and **13** as minor products. The electron transfer process should be sensitive to the polarity of the solvent, and indeed the reaction in ethanol produced less cyclized product **5a** from bromide **2a** than the reaction in methanol (see Fig. 1).

The formation of the non-cyclized organo-cobaloxime **7** from bromide **6** must be entirely due to the electron transfer mechanism, since the S_N2 mechanism must not be operative in the reactions of the β,β-disubstituted halides such as bromide **2c**. The substantial formation of the non-cyclized organo-cobaloxime **7**, therefore, must be due to the retardation of radical cyclization by the methyl substitution at the reaction center. The cyclization rate of 5-methyl-5-hexenyl radical to (1-methylcyclopentyl)methyl radical is *ca.* 1/50 to that of 5-hexenyl radical.[19] 2-(Allyloxy)ethyl halides (**2b**, **2c**, **2d**, **3b**, and **3d**) having the substituents at the β-position give only the cyclized organo-cobaloximes (**5b**, **5c**, and **5d**) due to the inhibition of the direct substitution. This steric hindrance must inhibit both S_N2 and the direct radical coupling process to give non-cyclized organo-cobaloximes.

2-(Allyloxy)ethyl tosylate (**1a**) gave only the direct substitution product **4a**. This result suggests the lack of a radical intermediate in the reaction of **1a**. The tosylates (**1b** and **1d**) which have substituents at 2-position did not react with cobaloxime(I) due to the steric inhibition. Compared to a halogen, a tosyl group is a hard leaving group and the S_N2 reaction with the soft and bulky nucleophile, cobaloxime(I), is sluggish even in the case of tosylate **1a**. The reaction is slowered by the steric hindrance in the case of tosylates **1b** and **1d**, and no organo-cobaloxime is obtained.

The reaction scheme is summarized below (Scheme 1). The proportion of **4** and **5** from the radical intermediate **20** can be expressed by $[\mathbf{4}]/[\mathbf{5}]=k_1[(Co^{II})]/k_2$ and depends on the concentration of the (Co^{II}) intermediate. By carrying out the reaction in diluted state, we can decrease [(Co^{II})] and retard the formation of **4**, as shown in Fig. 1. Similarly, the formation of **8** from bromide **6** increases and overcomes completely the formation of **7** in diluted state. The radical coupling between the less hindered redical **20a** and (Co^{II}) is substantial but the radicals (**20b**, **20c**, and **20d**) having bulky substituents, from **2b**, **2c**, **2d**, **3b**, and **3d**, lack its reactivity to (Co^{II}) and only cyclized organo-cobaloximes (**5b**, **5c**, and **5d**) were obtained. The reaction of cobaloxime(I) with less hindered bromides may take an S_N2 process competitively with an electron transfer process. In high dilution state (total cobaloxime: 1.0×10^{-2} mol dm^{-3}), the non-cyclized organo-cobaloxime **4a** (40% from **2a**) must be formed by S_N2 mechanism, since the formation of **4a** by radical coupling is negligible under these reaction conditions (see Fig. 1). The variation in product ratio **4**/**5** from **1a**, **2a**, and **3a** indicates that the initial step (**2a** or **3a**→**19**) is a rate determining step, since iodide **3a** gives more cyclyzed product **5a** than bromide **2a**. The reaction of **2a** in polar methanol gives more cyclyzed product **5a**, formed by electron transfer mechanism, than in less polar ethanol.

In conclusion the reaction of cobaloxime(I) with organic halides takes place *via* an electron transfer mechanism as the most important one and the reaction with less hindered tosylates proceeds by an S_N2 mechanism.

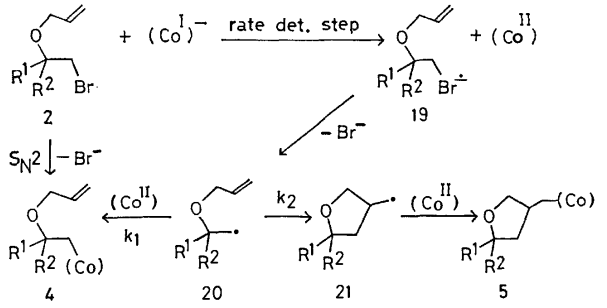

Scheme 1.

Experimental

Syntheses of 2-(Allyloxy)ethyl Tosylates. 2-(Allyloxy)ethyl Tosylate (1a): 2-(Allyloxy)ethyl tosylate was prepared by Bergman's method.[16] Tosylation of 2-(allyloxy)ethanol was carried out in a conventional manner with tosyl chloride in pyridine overnight at 0 °C and the purification by chromatography on silica gel gave tosylate **1a**, oil. NMR (CCl_4): δ 2.43 (s, 3H), 3.53 (t, 2H, J=5 Hz), 3.81—3.95 (m, 2H), 4.02 (t, 2H, J=5 Hz), 4.99—5.27 (m, 2H), 5.52—5.98 (m, 1H), 7.23 (d, 2H, J=8 Hz), and 7.68 (d, 2H, J=8 Hz).

2-Allyloxy-2-phenylethyl Tosylate (1b): Phenyloxirane (11.63 g, 0.097 mol) was added dropwise to a mixture of 70 cm^3 of allyl alcohol and 0.13 cm^3 of concd sulfuric acid during 5 min. The mixture was stirred for 30 min at room temperature and refluxed for 1 h. After being cooled, the mixture was treated with 0.2 g of sodium hydroxide and excess allyl alcohol was removed under reduced pressure. Ethereal solution of the residue was washed with water (50 $cm^3 \times 2$) and dried over sodium sulfate. Distillation of the product after removal of the ether gave 2-allyloxy-2-phenylethanol (65%), bp 114—115 °C/627.0 Pa. Tosylation of the alcohol in the same manner as in the case of **1a** gave tosylate **1b**,[20] oil. NMR(CCl_4): δ 2.40 (s, 3H), 3.71—3.86 (m, 2H), 3.87—4.00 (m, 2H), 4.46 (t, 1H, J=6 Hz), 4.92—5.20 (m, 2H), 5.48—5.85 (m, 1H), 7.05—7.21 (m, 7H), and 7.54 (d, 2H, J=8 Hz).

2-(Allyloxy)cyclohexyl Tosylate (1d): 2-(Allyloxy)cyclohexanol was prepared by the acid catalyzed addition of allyl alcohol to 1,2-epoxycyclohexane in the manner mentioned above, bp 93 °C/1067 Pa.[21] Tosylation of the alcohol in the same manner as in the case of **1a** gave tosylate **1d** (70%), oil. NMR (CCl_4): δ 1.10—2.20 (m, 8H), 2.46 (s, 3H), 3.15—3.41 (m, 1H), 3.82—3.94 (m, 2H), 4.39 (double triplet, 1H, J=4 and 7 Hz, $W_{1/2}$=19 Hz), 5.02—5.30 (m, 2H), 5.56—6.00 (m, 1H), 7.45 (d, 2H, J=8 Hz), and 7.96 (d, 2H, J=8 Hz). The tosylate **1d** was transformed by a simple substitution into 2-allyloxy-1-iodocyclohexane (**3d**) whose structural evidence will be described later, in the section for **3d**.

Syntheses of 2-(Allyloxy)ethyl Halides. 2-(Allyloxy)ethyl Bromide (2a): Bromide **2a** was prepared from tosylate **1a** (0.69 g) by the displacement of the tosyl group with a bromide ion. The displacement was carried out by the active magnesium bromide, prepared *in situ* from 1.92 g (1.2×10^{-2} mol) of 1,2-dibromoethane and 0.244 g (1.0×10^{-2} mol) of magnesium in 15 cm^3 of ether.[22] After stirring overnight at room temperature, the reaction mixture was diluted with water and extracted with ether. The ethereal extract gave 0.267 g (60%) of bromide **2a** on distillation. **2a**, bp 85—95 °C/13400 Pa.[23] NMR(CCl_4): δ 3.34 (t, 2H, J=6 Hz), 3.63 (t, 2H, J=6 Hz), 3.86—4.00 (m, 2H), 5.02—5.30 (m, 2H), and 5.59—6.01 (m, 1H).

2-Allyloxy-2-phenylethyl Bromide (2b): A solution of 13.2 g (5.0×10^{-2} mol) of 1,2-dibromo-1-phenylethane and 5 cm^3 of pyridine in 200 cm^3 of allyl alcohol was refluxed for 4 h. After removal of excess allyl alcohol under reduced pressure and addition of water (100 cm^3), the mixture was extracted by ether–benzene (1:1). Chromatography of the extract on silica gel gave the starting dibromide and 2.6 g (21%) of bromide **2b**, bp 78 °C/20.00 Pa.[23] NMR (CCl_4): δ 3.23—3.60 (m, 2H), 3.70—4.08 (m, 2H), 4.99 (dd, 1H, J=6 and 8 Hz), 5.04—5.35 (m, 2H), 5.65—6.05 (m, 1H), and 7.30 (s, 5H).

2-Allyloxy-2,2-diphenylethyl Bromide (2c): A solution of 1.60 g (1.0×10^{-2} mol) of bromine in 10 cm^3 of methanol-free dichloromethane was added to a cooled (−5 °C) solution of 1.80 g (1.0×10^{-2} mol) of 1,1-diphenylethylene in 20 cm^3 of methanol-free dichloromethane. After stirring for 30 min at 0 °C, the solvent was removed under reduced pressure at 0 °C and 15 cm^3 of allyl alcohol was added to the residue. To the cooled mixture (−5 °C) was added 0.66 g of potassium hydroxide and the reaction mixture was stirred for 1 h at 0 °C and for an additional hour at room temperature. Dichloromethane was added to the mixture and the solution was washed with water and dried over calcium chloride. Removal of the solvent gave the crude product and recrystallization from methanol gave 1.70 g (55%) of bromide **2c**, mp 66—67 °C; Found: C, 64.30; H, 5.42%. Calcd for $C_{17}H_{17}BrO$: C, 64.37; H, 5.40%. NMR (CCl_4): δ 3.59—3.71 (m, 2H), 4.00 (s, 2H), 4.90—5.32 (m, 2H), 5.56—5.94 (m, 1H), and 6.98—7.30 (m, 10H).

2-(2-Methyl-2-propenyloxy)-2,2-diphenylethyl Bromide (6): The same procedure for the preparation of bromide **2c** was employed by using 2-methyl-2-propen-1-ol instead of allyl alcohol. **6**, oil. NMR (CCl_4): δ 1.77 (s, 3H), 3.67 (s, 2H), 4.23 (s, 2H), 4.90 (br. s, 1H), 5.13 (br. s, 1H), and 7.24—7.53 (m, 10H).

The bromide **6** was treated with an excess amount of tributylstannane to give a mixture of 1-(2-methyl-2-propenyloxy)-1,1-diphenylethane and 4,4-dimethyl-2,2-diphenyltetrahydrofuran (**16**) (described later) in 1:3 ratio. The structure of the former compound, and therefore the structure of **6**, was evidenced by an unequivocal synthesis from 2-methyl-2-propenyl chloride and sodium 1,1-diphenylethoxide in THF. 1-(2-Methyl-2-propenyloxy)-1,1-diphenylethane, oil. IR (CCl_4): 1662, 901, and 700 cm^{-1}; NMR (CCl_4): δ 1.72 (s, 3H), 1.85 (s, 3H), 3.59 (br. s, 2H), 4.78 (br. s, 1H), 5.01 (br. s, 1H), and 7.06—7.40 (m, 10H).

2-Allyloxy-1-bromocyclohexane (2d): The same procedure for the preparation of bromide **2a** was employed by using 2-(allyloxy)cyclohexyl tosylate (**1d**) instead of tosylate **1a**. **2d**, bp 100—105 °C/1600 Pa.[24] NMR (CCl_4): δ 1.16—2.44 (m, 8H), 3.41 (double triplet, 1H, J=4 and 7 Hz, $W_{1/2}$=18 Hz), 3.90—4.17 (m, 3H), 5.03—5.40 (m, 2H), and 5.70—6.12 (m, 1H).

2-(Allyloxy)ethyl Iodide (3a): A mixture of 5.12 g (2.0×10^{-2} mol) of **1a** and 15.0 g (1.0×10^{-1} mol) of sodium iodide in 80 cm^3 of acetone was refluxed for 24 h. After cooling, 100 cm^3 of ether was added to the mixture and the resulting salts were filtered off. The filtrate was concentrated and dissolved in 100 cm^3 of ether. The ethereal solution was washed with aqueous sodium thiosulfate and dried over sodium sulfate. Distillation of the residue gave 2.78 g (65%) of iodide **3a**, bp 84 °C/4533 Pa.[17] NMR (CCl_4): δ 3.08 (t, 2H, J=7 Hz), 3.52 (t, 2H, J=7 Hz), 3.77—3.98 (m, 2H), 4.90—5.22 (m, 2H), and 5.48—5.90 (m, 1H).

2-Allyloxy-2-phenylethyl Iodide (3b): The tosyl group of **1b** was replaced by iodide by a similar procedure for the preparation of **2a** from **1a**, but active magnesium iodide was prepared from magnesium and iodine in ether.[22] The product was worked up as in the case of bromide **2a** but additional washing by aqueous sodium thiosulfate. Distillation gave iodide **3b** (27%), bp 110 °C/86.66 Pa. NMR (CCl_4): δ 3.17—3.35 (m, 2H), 3.65—4.07 (m, 2H), 4.40 (dd, 1H, J=6 and 8 Hz), 5.02—5.35 (m, 2H), 5.65—6.07 (m, 1H), and 7.30 (s, 5H). The iodide **3b** was transformed into its quarternary salt, 2-allyloxy-2-phenylethylpyridinium iodide.[20]

2-Allyloxy-1-iodocyclohexane (3d): The same procedure for the preparation of iodide **3b** gave iodide **3d** (53%), bp 82 °C/120.0 Pa. NMR(CCl_4): δ 1.15—2.50(m, 8H), 3.41(double triplet, 1H, J=4 and 7 Hz, $W_{1/2}$=19 Hz), 3.92—4.30 (m, 3H), 5.02—5.41(m, 2H), and 5.70—6.15(m, 1H). The iodide **3d** was treated with potassium *t*-butoxide in THF to give 3-(allyloxy)cyclohexene (**9**), which was synthesized unequivocally from 3-bromocyclohexene and sodium allylate in THF. **9**, bp *ca.* 60 °C/2780 Pa. NMR(CCl_4): δ 1.45—2.70(m, 6H), 3.74—3.92(m, 1H), 3.93—4.11(m, 2H), 5.04—5.40(m, 2H), and 5.65—6.15(m, 3H).

Reaction of Cobaloxime(I) with 2-(Allyloxy)ethyl Tosylates or 2-(Allyloxy)ethyl Halides. General Procedure: To a mixture of 0.238 g (1.0×10^{-3} mol) of cobalt(II) chloride hexahydrate and 0.233 g (2.0×10^{-3} mol) of dimethylglyoxime in 3 cm^3 of methanol was added 0.2 cm^3 of 10 mol dm^{-3}

aq sodium hydroxide (2.0×10^{-3} mol) and 0.1 cm^3 (1.2×10^{-3} mol) of pyridine. The mixture was stirred under nitrogen for 15 min at 0 °C and treated with 0.1 cm^3 (1.0×10^{-3} mol) of 10 mol dm^{-3} aq sodium hydroxide and 0.046 g (1.25×10^{-3} mol) of sodium borohydride. After stirring for 5 min the resulting methanol solution of cobaloxime (I)[25] (1.0×10^{-3} mol) was treated with one of the 2-(allyloxy)-ethyl tosylates or halides (1.0×10^{-3} mol) and the reaction mixture was stirred under nitrogen for 4—6 h at room temperature. The mixture was extracted with benzene (10 $cm^3\times4$) after addition of 40 cm^3 of water and the extract was washed with water, dried over sodium sulfate, and concentrated under reduced pressure. The residue was placed on Florisil column and elution with chloroform–ethyl acetate (1:1) gave orange eluate. Evaporation of the solvent gave organo-cobaloximes in the yields listed in Table 1. All the organo-cobaloximes have strong absorptions at *ca.* 1600, 1500—1560, *ca.* 1235, 1100—880 cm^{-1} (several bands) and the absorptions due to the alkyl ligands are weak. IR data therefore are omitted from the spectral data in the following description of this section.

4a, Mp 175 °C(decomp); Found: C, 47.17; H, 6.10; N, 15.55%. Calcd for $C_{18}H_{28}N_5O_5Co$: C, 47.68; H, 6.23; N, 15.45%. NMR($CDCl_3$): δ 1.58 (t, 2H, J=8 Hz), 2.07(s, 12H), 3.10(t, 2H, J=8 Hz), 3.74—3.86(m, 2H), 4.90—5.22(m, 2H), 5.58—6.00(m, 1H), 7.10—7.27(m, 2H), 7.49—7.70(m, 1H), and 8.40—8.50(m, 2H).

5a, Mp 185 °C(decomp); Found: C, 47.36; H, 6.23; N, 15.52%. Calcd for $C_{18}H_{28}N_5O_5Co$: C, 47.68; H, 6.23; N, 15.45%. NMR($CDCl_3$): δ 1.20—2.00(m, 5H), 2.11(s, 12H), 2.90—3.10(m, 1H), 3.46—3.73(m, 3H), 7.15—7.31(m, 2H), 7.54—7.73(m, 1H), and 8.42—8.53(m, 2H).

5b, Mp 175 °C(decomp); Found: C, 54.18; H, 6.07; N, 13.59%. Calcd for $C_{24}H_{32}N_5O_5Co$: C, 54.44; H, 6.09; N, 13.23%. NMR($CDCl_3$): δ 1.55—2.20(m, 5H), 2.01(s, 6H), 2.08(s, 6H), 3.18—3.36(m, 1H), 3.95—4.13(m, 1H), 4.86(t, 1H, J=7 Hz), 7.18—7.40(m, 7H), 7.60—7.80(m, 1H), and 8.43—8.60(m, 2H).

5c, Mp 205 °C(decomp); Found: C, 59.14; H, 6.02; N, 11.63%. Calcd for $C_{30}H_{36}N_5O_5Co$: C, 59.50; H, 5.99; N, 11.56%. NMR($CDCl_3$): δ 1.40—1.72(m, 3H), 1.90—2.12(m, 1H), 1.93(s, 6H), 2.00(s, 6H), 2.77(dd, 1H, J=6 and 11 Hz), 3.40(t, 1H, J=7 Hz), 3.97(t, 1H, J=7 Hz), 7.00—7.37(m, 12H), 7.47—7.66(m, 1H), and 8.39—8.51(m, 2H).

Organo-cobaloxime **7** decomposed quickly on Florisil to give 1,1-diphenylethylene and could not be isolated in pure form. This is a common property for 2-alkoxy-2,2-diphenylethylcobaloxime. The NMR data of **7** were read from those of the mixture of **7** and **8**. **7**, NMR($CDCl_3$): δ 1.75 (s, 3H), 1.85(s, 12H), 2.61(s, 2H), 3.50(s, 2H), 4.95(br. s, 1H), 5.32(br. s, 1H), 7.00—7.56(m, 12H), 7.60—7.88 (m, 1H), and 8.55—8.70(m, 2H).

8, Mp 180 °C(decomp); Found: C, 59.94; H, 6.16; N, 11.33%. Calcd for $C_{31}H_{38}N_5O_5Co$: C, 60.09; H, 6.18; N, 11.30%. NMR($CDCl_3$): δ 0.82(s, 3H), 1.75(s, 2H), 2.07(s, 12H), 2.47(s, 2H), 3.50(d, 1H, J=8 Hz), 3.58(d, 1H, J=8 Hz), 7.10—7.56(m, 12H), 7.63—7.85(m, 1H), and 8.58—8.70(m, 2H).

5d, Mp 175 °C(decomp); Found: C, 52.02; H, 6.91; N, 13.84%. Calcd for $C_{22}H_{34}N_5O_5Co$: C, 52.07; H, 6.75; N, 13.80%. NMR($CDCl_3$): δ 1.14—1.95(m, 12H), 2.15(s, 12H), 3.04—3.32(m, 1H), 3.70—4.15(m, 2H), 7.35—7.52 (m, 2H), 7.75—7.96(m, 1H), and 8.66—8.78 (m, 2H).

General Procedure of the Photolyses of Organo-cobaloximes under Anaerobic Conditions. *Photolyses in Chloroform*: An appropriate amount of an organo-cobaloxime (0.1—2.0 g) was dissolved in chloroform (20—100 cm^3) and the dissolved oxygen was purged by bubbling nitrogen from a syringe needle. The solution was irradiated with two circle-type fluorescent lamps (30 W×2) until the starting organo-cobaloxime disappeared (5—12 h). The concentrate of the reaction mixture was subjected to a Florisil chromatography and a 3-methyltetrahydrofuran derivative was isolated from colorless chloroform eluate in a high yield (see text). In the case of 9-methyl-7-oxabicyclo[4.3.0]nonane (**11**), Kugel-Rohr distillation (100—200 °C/13322 Pa) yielded **11**, which consists of two isomers with different configurations of the methyl group, in a poor yield (8%) due to the volatility.

11, Oil. NMR(CCl_4): δ 0.93 and 1.00(d, total 3H, J=7 Hz), 1.13—2.12(m, 10H), 3.13—3.49(m, 1H), and 3.70—4.26(m, 2H). One component of **11** was identified with the hydrogenation product of **10**.

12,[26] Oil. NMR(CCl_4): δ 1.05(d, 3H, J=7 Hz), 1.89 (t, 2H, J=7 Hz), 2.16—2.50(m, 1H), 3.32(t, 1H, J=8 Hz), 4.05(t, 1H, J=8 Hz), 4.86(t, 1H, J=7 Hz), and 7.15 (s, 5H). **12** was hydrogenolyzed over Pd–C in ethanol and the product was identified by comparison with the authentic sample of 2-methyl-4-phenyl-1-butanol.[12]

15, Mp 49 °C; Found: C, 85.65; H, 7.68%. Calcd for $C_{17}H_{18}O$: C, 85.67; H, 7.61%. IR(CCl_4): 1025 and 695 cm^{-1}; NMR(CCl_4): δ 1.00(d, 3H, J=6 Hz), 2.00(t, 1H, J=11 Hz), 2.10—2.53(m, 1H), 2.75(dd, 1H, J=6 and 11 Hz), 4.04(t, 1H, J=8 Hz), 4.42(t, 1H, J=8 Hz), and 6.85—7.40(m, 10H).

16, Mp 44.5 °C; Found: C, 85.78; H, 8.07%. Calcd for $C_{18}H_{20}O$: C, 85.67; H, 7.99%. IR(CCl_4): 1062 and 703 cm^{-1}; NMR(CCl_4): δ 1.00(s, 6H), 2.44(s, 2H), 3.55(s, 2H), and 6.96—7.42(m, 10H).

Photolyses in Benzene: An appropriate amount of an organo-cobaloxime (30—50 mg) in benzene (20 cm^3) was irradiated in the same manner as in the case of the photolyses in chloroform. The same work-up gave the products **10**, **13**, and **17** from **5d**, **5b**, and **5c**, respectively.

10, Oil. IR(CCl_4): 1670, 1050, 1030, and 885 cm^{-1}; NMR(CCl_4): δ 1.10—2.00(m, 8H), 2.26—2.60(m, 1H), 3.83—4.01(m, 1H), 4.25(d, 1H, J=14 Hz), 4.45(d, 1H, J=14 Hz), and 4.83—5.01(m, 2H). **10** was oxidized by chromic trioxide in dichloromethane containing pyridine to give *cis*-9-methylene-7-oxabicyclo[4.3.0]nonan-8-one (**18**).[13]

13, Oil. MS: (*m/e*) 160(M^+); IR(CCl_4): 1054, 883, and 695 cm^{-1}; NMR(CCl_4): δ 2.24(dd, 1H, J=7 and 16 Hz), 2.85(dd, 1H, J=6 and 16 Hz), 4.23(d, 1H, J=13 Hz), 4.42(d, 1H, J=13 Hz), 4.71—5.00(m, 3H), and 7.23 (m, 5H). Hydrogenolysis of **13** over Pd–C in ethanol gave 2-methyl-4-phenyl-1-butanol which was identified by comparison with the authentic sample.[12]

17, Mp 51—51.5 °C; Found: C, 86.21; H, 6.80%. Calcd for $C_{17}H_{16}O$: C, 86.40; H, 6.83%. MS: (*m/e*) 236(M^+); IR(CCl_4): 1670, 1046, 883, and 698 cm^{-1}; NMR(CCl_4): δ 3.10—3.20(m, 2H), 4.27—4.36(m, 2H), 4.72—4.80(m, 1H), 4.85—4.96(m, 1H), and 7.00—7.40(m, 10H).

*Photolysis of Organo-cobaloxime **5a** under Aerobic Conditions.* A solution of 4.70 g (1.0×10^{-2} mol) of **5a** in 600 cm^3 of dichloromethane was irradiated for 7 h in the same manner for the photolysis under anaerobic conditions, but the solution was bubbled with air during the irradiation. The concentrate of the reaction mixture was chromatographed on Florisil. The first orange band (chloroform–ethyl acetate, 1:1) contained the starting organo-cobaloxime (70%) and the second brown band (chloroform–ethyl acetate–methanol, 2:2:1) yielded the oxygenated product, (tetrahydro-3-furanyl)methyl cobaloximato peroxide, in 20% yield; NMR ($CDCl_3$): δ 1.20—2.20(m, 3H), 2.30(s, 12H), 3.20—3.50

(m, 3H), 3.53—3.79(m, 3H), 7.14—7.30(m, 2H), 7.59—7.78(m, 1H), and 8.31—8.42(m, 2H). The peroxide (0.960 g, 2.0×10^{-3} mol) in 40 cm^3 of methanol was reduced by sodium borohydride (92 mg, 2.5×10^{-3} mol) in the presence of 0.3 cm^3 of 10 mol dm^{-3} aq sodium hydroxide. After the mixture was stirred overnight, the methanol was evaporated and the residue was extracted with ether (10 $cm^3\times4$). The combined extracts were passed through a short column of silica gel. Kugel-Rohr distillation of the eluate with dichloromethane gave 106 mg (52%) of (tetrahydro-3-furanyl)-methanol (**14**), bp 120—140 °C (bath temperature)/2666 Pa. NMR(CCl_4): δ 1.38—1.74(m, 1H), 1.75—2.16(m, 1H), 2.20—2.51(m, 1H), 2.77(br. s, 1H), and 3.30—3.95(m, 6H). 3,5-Dinitrobenzoate of **14**, mp 80.5—81.0 °C.[11]

References

1) A part of this work has been published as preliminary reports. M. Tada and M. Okabe, *Chem. Lett.*, **1980**, 201 and 831.

2) H. Eckert, D. Lenoir, and I. Ugi, *J. Organomet. Chem.*, **141**, C23 (1977).

3) G. N. Schrauzer and E. Deutsch, *J. Am. Chem. Soc.*, **91**, 3341 (1969).

4) F. R. Jensen, V. Madan, and D. H. Buchanan, *J. Am. Chem. Soc.*, **92**, 1414 (1970).

5) R. Breslow and P. L. Khanna, *J. Am. Chem. Soc.*, **98**, 1297 (1976).

6) A. I. Scott, J. B. Hansen, and S.-K. Chung, *J. Chem. Soc., Chem. Commun.*, **1980**, 388.

7) J. Schaeffler and J. Rétey, *Angew. Chem., Int. Ed. Engl.*, **17**, 845 (1978).

8) F. R. Jensen and R. C. Kiskis, *J. Am. Chem. Soc.*, **97**, 5825 (1975).

9) M. C. Baird, *J. Organomet. Chem.*, **64**, 289 (1974).

10) M. Tada, M. Okabe, and K. Miura, *Chem. Lett.*, **1978**, 1135.

11) J. Bogner, J.-C. Duplan, Y. Infarnet, J. Delmau, and J. Huet, *Bull. Soc. Chim. Fr.*, **1972**, 3616.

12) J. V. Brawn and G. K. Kirschbaum, *Ber.*, **47**, 264 (1914).

13) A. D. Harmon and C. R. Hutchinson, *J. Org. Chem.*, **40**, 3474 (1975).

14) P. D. Bartlett, W. D. Closson, and T. J. Cogdell, *J. Am. Chem. Soc.*, **87**, 1308 (1965); W. S. Johnson, D. M. Bailey, R. Owyang, R. A. Bell, B. Jaques, and J. K. Crandall, *ibid.*, **86**, 1959 (1964).

15) M. Julia, *Acc. Chem. Res.*, **4**, 386 (1971); C. Walling and A. Cioffari, *J. Am. Chem. Soc.*, **94**, 6059 (1972).

16) R. J. Kinney, W. D. Jones, and R. G. Bergman, *J. Am. Chem. Soc.*, **100**, 7902 (1978).

17) D. Lal, D. Griller, S. Husband, and K. U. Ingold, *J. Am. Chem. Soc.*, **96**, 6355 (1974).

18) G. N. Schrauzer, *Angew. Chem., Int. Ed. Engl.*, **15**, 417 (1976).

19) A. L. Beckwith, I. A. Blair, and G. Phillipou, *Tetrahedron Lett.*, **1974**, 2251.

20) F. N. Hayes and C. Gutberlet, *J. Am. Chem. Soc.*, **72**, 3321 (1950).

21) G. H. Posner and D. Z. Rogers, *J. Am. Chem. Soc.*, **99**, 8202 (1977).

22) P. Place, M.-L. Roumestant, and J. Gore, *Bull. Soc. Chim. Fr.*, **1976**, 196.

23) C. D. Hurd and M. A. Pollack, *J. Am. Chem. Soc.*, **60**, 1908 (1938).

24) E. Schmidt, W. Bartholome, and A. Lübke, *Ber.*, **55**, 2105 (1922).

25) G. N. Schrauzer, *Inorg. Synth.*, **11**, 65 (1968).

26) G. Dana and J. P. Giraut, *Bull. Soc. Chim. Fr.*, **1972**, 1650.

The Reaction Involving One Electron Transfer in Key Step. NO_2-Catalyzed Halogenation of Polycyclic Aromatic Compounds with Metal Halides

Takashi SUGIYAMA

Institute for Chemical Research, Kyoto University, Uji, Kyoto 611

(Received July 17, 1981)

In the co-existence of catalytic amount of nitrogen dioxide and oxygen, aluminum halide, titanium(IV) halide, and some other metal halides have been found to be highly selective and regiospecific halogenating agents for polycyclic aromatic compounds, including anthracene, pyrene, benz[*a*]anthracene, chrysene, phenanthrene, naphthalene, triphenylene, fluoranthene, benzo[*b*]thiophene, and dibenzothiophene.

Aromatic nuclei have been halogenated with quite a few methods.[1] The methods could be classified into four groups. They are; (1) reaction of electron-rich aromatic nucleus with a molecular halogen; (2) reaction of less-activated nucleus with a molecular halogen in the presence of a catalyst such as a Lewis acid; (3) reaction of aromatic nucleus with a positive halogen; and (4) halogenation by a metal halide as a halogen-source.[2]

Extensive investigation has been done on the reactions in groups (1), (2), and (3). On the contrary, reactions that belong to the fourth group have received little attention. In many cases, the reaction of aromatic nucleus with a metal halide[3] results in metallation,[4] isomerization,[5] polymerization,[6] or disproportionation[5] rather than halogenation. Therefore, metal halides that have been employed for halogenation have been restricted to halides of copper(II),[7] iron(III),[8] tin(IV),[9] titanium(IV),[2] antimony(V),[10] vanadium(V),[2] and (nonmetallic) phosphorus(V).[9,11] Namely, the reaction with copper(II) chloride is known as Nonhebel's chlorination and has synthetic utility.[12] Side-reactions dominate with other metal halides.

Characteristic of the halogenation with these metal halides are that these metal ions are reduced to their low-valency states during the reaction according to Eq. 1 or 2.

$$ArH + 2M^{n+}X_n^- \longrightarrow ArX + 2M^{(n-1)+}X_{n-1}^- + HX \quad (1)$$

$$ArH + M^{n+}X_n^- \longrightarrow ArH + M^{(n-2)+}X_{n-2}^- + HX \quad (2)$$

It is plausible that the halogenation may take place with a metal halide whose metal ion cannot change its valency, provided a suitable electron-source is supplied to the reaction system. Indeed, the author has reported chlorination of anthracene with aluminum (III) chloride in the presence of catalytic amount of nitrogen dioxide under aerobic conditions (Eq. 3).[13]

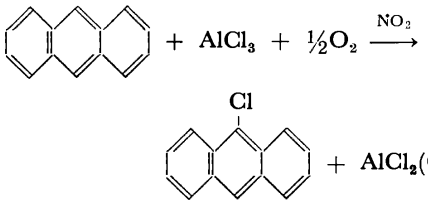

(3)

This novel chlorination method is superior to conventional ones in intermolecular selectivity, yield of the product, and reaction conditions.

In the present paper, the author wishes to report the scope and limitation of the halogenation which couples with a series of successive electron transfer systems, an electron-bridge.

Results and Discussion

Appropriate amounts of a polycyclic aromatic hydrocarbon and metal halide were allowed to react in toluene or in 1,2-dichloroethane at 0—30 °C. Benzene, nitromethane, acetonitrile, or carbon disulfide could also be used as a solvent. Although toluene was a suitable solvent for most halogenations, the reaction with less reactive aromatics afforded, sometimes, benzylated compounds in this solvent.

The products were isolated and identified by melting points as well as by comparing their spectroscopic properties with those of the corresponding authentic samples. The results are summarized in Table 1 for the chlorination and in Table 2 for the bromination.

The regioselectivity of chlorination is satisfactorily high; GLC-analyses showed that the chlorination of anthracene (**1**) and naphthalene (**2**) afforded 9-chloroanthracene and 1-chloronaphthalene, respectively, as monochlorinated compounds. Other isomeric products were scarcely recognized (2%). Only one monochlorinated product was detected in chlorination of phenanthrene (**4**), benz[*a*]anthracene (**5**), chrysene (**6**), or triphenylene (**7**). The reaction site is indicated in Scheme 1 by an arrow.

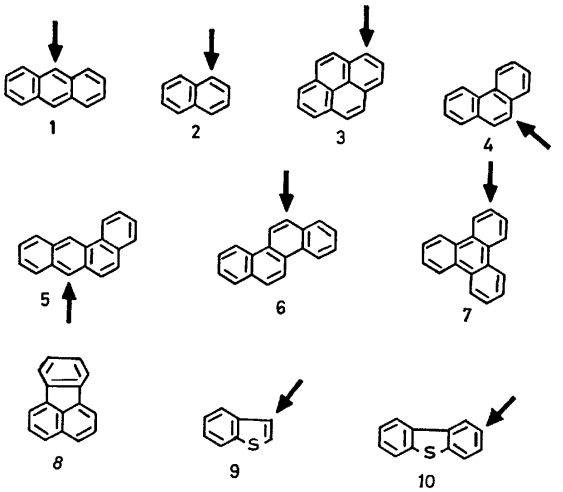

Scheme 1. Arrows indicate the position susceptible to monohalogenation. For compound **8**, the position is not identified. For compound **3**, significant amount of the other isomer is formed.

Table 1. Chlorination of polycyclic aromatics[a]

Substrate ArH_2	MX_n	NO_2[b] (mol%)	Time min	Consumed ArH_2 (%)	Yield of ArHCl[c] %	Yield of $ArCl_2$[c] %
1[d]	$AlCl_3$	13	30	100	86	0
	$AlCl_3$[e]	13	30	51	90	0
	$TiCl_4$	13	30	100	0	91
	$TiCl_4$[e]	13	30	100	91	Trace
	$SnCl_4$[e]	13	30	91	82	0
3	$AlCl_3$	13	20	33	79	0
	$TiCl_4$	20	5	100	Trace	92
	$TiCl_4$[e]	8	10	91	89	Trace
5	$AlCl_3$	13	20	71	65	3
	$TiCl_4$	13	10	98	80	2
6	$TiCl_4$	6	20	95	71	0
4[f]	$TiCl_4$	22	30	96	52	0
2[f]	$TiCl_4$	26	1440	95	53	0
7	$TiCl_4$	13	1200	92	67	0
8[i]	$TiCl_4$	10	120	—[g]	21[h]	0
9[i]	$TiCl_4$	10	120	—[g]	47[h]	0
10	$TiCl_4$	10	120	—[g]	40[h]	0

a) $MX_n/ArH_2=1.0$. Solvent: toluene. Temp: room temp. b) Mol% is based on substrate used. c) Yield is based on ArH_2 consumed. d) Data from Ref. 13. Temp: 0 °C. e) $MX_n/ArH_2=0.5$. f) Solvent: 1,2-dichloroethane. g) Consumed ArH_2 was not determined. h) Yield is based on ArH_2 used. i) Significant amounts of dimer and trimer were obtained.

Bromination takes place with less selectivity than the chlorination; 5—10% of 2-bromonaphthalene was detected on GLC in addition to the major product, 1-bromonaphthalene. However, the bromination of other substrates gave as good regioselectivity as the chlorination.

It should be noted that the ratio of mono-/dihalogenated product is extremely high in the present reaction, which is a marked contrast to the reaction with, for example, copper(II) chloride.[7] Most of the present reactions gave traces of, if any, or no dihalogenated product, when the relative amounts of the reagents were appropriate. On the other hand, dihalogenated compound was obtained as a sole product under appropriate reaction conditions.

Intermolecular selectivity is also seen in competitive chlorination of anthracene, pyrene (**3**), and triphenylene as listed in Table 3.

Further advantage of the present halogenation lies in its reactivity: Whereas it has been reported that a substrate which has ionization potential of less than 7.55 eV is unreactive toward the chlorination with copper(II) chloride,[14] in the present halogenation phenanthrene (IP; 8.03),[15] naphthalene (IP; 8.10),[15] and triphenylene (IP; 8.09)[15] are susceptible to the reaction.

It is interesting to point out that the number of halide ion available for the halogenation depends on the reactivities of both metal halide and substrate; as can be seen in Tables 1 and 2, only one of three chlorine atoms in aluminum(III) chloride is available for the chlorination of anthracene, whereas two of three bromine atoms in aluminum(III) bromide react with anthracene. On the other hand, two of four chlorine atoms in titanium(IV) chloride react in the chlorination of reactive substrates such as pyrene and benz[*a*]anthracene, but only one is reactive toward the chlorination of relatively less reactive substrates such as phenanthrene, naphthalene, and triphenylene. Therefore, one can obtain either mono- or dihalogenated compound depending on the substrate/metal halide molar ratio employed for the reaction (*vide supra*). In general, bromides are more reactive than the corresponding chlorides, and a substrate of low ionization potential is more reactive than that of high ionization potential.

Now, the author wishes to demostrate catalytic activity of nitrogen dioxide.[13] As listed in Table 4, practically no halogenation takes place with these metal halides when nitrogen dioxide is absent in the reaction system. Even titanium(IV), and tin(IV) bromides require nitrogen dioxide in order to undergo the reaction, though these metal ions have stable lower-valency states. Thus, it is apparent that the reaction with these metal halides is not of the types shown in Eqs. 1 and 2 under the present reaction conditions. Boron tribromide is an exception. Although the effect of catalyst is significant, bromination with boron tribromide proceeds in some extent without the catalyst. Since boron cannot change its valency, the author has no idea on a plausible mechanism.

In the absence of a reactive substrate, toluene is also susceptible to the halogenation and a 1:1 mixture of *ortho*- and *para*-bromotoluenes is obtained in the total yield of 81%.

Benzo[*b*]thiophene (**7**) and dibenzothiophene (**10**) can also be subjected to the halogenation. However, oxygen-containing compounds such as benzofuran and dibenzofuran do not undergo the reaction, probably because lone-pair electrons on the oxygen atom in-

Table 2. Bromination of polycyclic aromatics[a]

Substrate ArH_2	Metal halide MX_n (MX_n/ArH_2)	Time min	Consumed ArH_2 (%)	Yield of ArHBr[b] %	Yield of $ArBr_2$[b] %
1	$AlBr_3$ (0.5)	60	100	86	3
	$AlBr_3$ (1.0)	1020	100	1	82
	$AlBr_3$ (2.0)[c]	30	100	2	79
	$TiBr_4$ (0.5)	30	94	92	3
	$TiBr_4$ (1.0)	1020	100	0	87
	BBr_3 (0.5)	1020	100	63	26
	BBr_3 (1.0)	1020	100	1	85
	$CuBr_2$ (1.0)[d]	1020	100	74	Trace
	$SbBr_3$ (1.0)	1020	100	Trace	55
	$SnBr_4$ (1.0)	1020	100	18	15
	$SnBr_4$ (1.0)	1020	100	13	14
3	$AlBr_3$ (0.5)	30	84	76	5
	$AlBr_3$ (1.0)	30	100	61	6
	$AlBr_3$ (2.0)	30	100	0	69
	$AlBr_3$ (1.0)[e]	30	86	75	5
	$TiBr_4$ (1.0)	30	100	5	74
	$SnBr_4$ (1.0)	60	81	61	0
5	$AlBr_3$ (0.5)	10	75	92	0
	$AlBr_3$ (1.0)	10	99	94	0
	$TiBr_4$ (1.0)	10	96	96	0
	$SnBr_4$ (1.0)	20	95	75	0
6	$AlBr_3$ (1.0)	180	77	73	Trace
	$AlBr_3$ (2.0)	180	100	45	40
	$AlBr_3$ (1.0)[f]	180	100	72	28
	$AlBr_3$ (1.0)[f]	30	80	91	9
	$SnBr_4$ (1.0)	180	98	68	23
4	$AlBr_3$ (0.5)	60	53	47	0
	$AlBr_3$ (1.0)	60	88	64	0
	$AlBr_3$ (2.0)	60	100	69	13
	$TiBr_4$ (1.0)	180	99	69	Trace
	$SnBr_4$ (1.0)	60	59	39	0
	$SnBr_4$ (1.0)	180	100	33	Trace
2	$AlBr_3$ (1.0)[g]	180	84	56	Trace
	$AlBr_3$ (2.0)	180	100	49	Trace
	$TiBr_4$ (1.0)	180	86	71	Trace
	$SnBr_4$ (1.0)	180	95	63	0

a) Reaction conditions: See the experimental section. Solvent: toluene for **1**, **3**, **5**, and **6**, 1,2-dichloroethane for **4** and **2**. b) Yield is based on ArH_2 consumed. c) Reaction temp: 0 °C. d) Anthraquinone was obtained as a side-product. e) Solvent: acetonitrile. f) Solvent: 1,2-dichloroethane. g) Product: 1-bromonaphthalene/2-bromonaphthalene=93/7.

Table 3. Competitive chlorination

Substrate ArH_2	Yield of ArHCl[a] after 1 min/%	Yield of ArHCl[a] after 3 min/%
Anthracene	20	40
Pyrene	4	10
Triphenylene	—	0

a) Yield is based on substrate used.

teract with positive metal ion decreasing the reactivity of metal halide.

Unfortunately, attempts to iodinate aromatic hydrocarbons were found unsuccessful.

Although detailed mechanism of the reaction is under investigation, nucleophilic character of the halogenation as well as the following evidence allows the author to speculate the formation of an aromatic radical cations as an intermediate of the reaction: It is well known that polycyclic aromatic hydrocarbon forms a charge-transfer complex with Lewis acids.[16] The aromatic radical cation thus formed may abstract a halide ion. When the reaction is carried out in the presence of trichlorosilane, chlorinated product is obtained.[13] A hydrogen atom should be abstracted from trichlorosilane, if a free-radical mechanism governed the reaction. In addition, the fact that silicon tetrachloride cannot give the chlorinated products,[13] suggests the polar nature of the reaction.

At least a part of catalytic effect of nitrogen dioxide is exerted by the formation of an electron-bridge.

Table 4. Effect of NO_2 in bromination of anthracene[a)]

Metal halide MX_n	Solvent	Atmospheric condition	Consumed anthracene ArH_2 (%)	Yield of ArHBr[b)] %	Yield of $ArBr_2$[b)] %
$AlBr_3$[c)]	Toluene	N_2	29	Trace	0
$AlBr_3$[c)]	Toluene	O_2	38	Trace	0
$AlBr_3$[d)]	Toluene	NO_2-O_2	100	88	0
$TiBr_4$	Nitromethane	O_2	4	Trace	0
$TiBr_4$	Nitromethane	NO_2-O_2	100	0	0
BBr_3	Toluene	N_2	12	5	0
BBr_3	Toluene	O_2	52	31	0
BBr_3	Toluene	NO_2-O_2	100	1	86
$SbBr_3$	Acetonitrile	O_2	3	0	0
$SbBr_3$	Acetonitrile	NO_2-O_2	100	Trace	55
$SnBr_4$	Nitromethane	O_2	5	Trace	Trace
$SnBr_4$	Nitromethane	NO_2-O_2	100	18	15

a) Reaction time: 17 h. MX_n/Anthracene=1.0. Temp: room temp. Anthracene/NO_2=1.0/0.13 (mol/mol). NO_2 was used as a 10% solution. b) Yield is based on anthracene used. c) Reaction time: 30 min. d) Reaction time: 5 min. Temp: 0 °C. $AlBr_3$/Anthracene=0.5.

Table 5. Effect of solvent in bromination of polycyclic aromatics with $AlBr_3$[a)]

Substrate ArH_2	Solvent	Time min	Consumed ArH_2 (%)	Yield of ArHBr[b)] %	Yield of $ArBr_2$[b)] %
1		10	100	79	15
	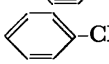	10	100	65	19
	$ClCH_2CH_2Cl$	10	100	63	23
	CS_2	10	100	75	17
	CH_3CN	10	37	41	0
	CH_3NO_2	10	64	64	0
3	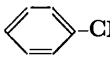	30	84	77	5
	CH_3NO_2	30	99	55	6
5	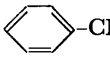	10	99	94	0
	$ClCH_2CH_2Cl$	10	100	91	0
	CH_3CN	10	25	32	0
6	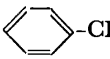	180	74	77	Trace
	$ClCH_2CH_2Cl$	180	100	72	28
	CH_3CN	180	88	80	21
	CS_2	180	80	88	8
4	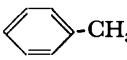	30	64	23	0
	$ClCH_2CH_2Cl$	30	84	63	0
	CH_3NO_2	30	23	9	0
2	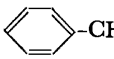	180	44	55	0
	$ClCH_2CH_2Cl$	180	86	55	0

a) Reaction conditions: See the experimental section. $AlBr_3$/ArH_2=1/1. b) Yield is based on ArH_2 consumed.

The halogenation without oxygen proceeds in the presence of equimolar amount of nitrogen dioxide, which implies that oxygen reproduces nitrogen dioxide from its reduced form, nitrogen monoxide. The formation of nitrogen monoxide may couple with the oxidation of aromatic hydrocarbon to its cationic form. Thus, the author prefers to propose that an electron-bridge is constructed in the present reaction, in which an electron migrates from a substrate to nitrogen dioxide and to oxygen molecule.

Experimental

Instruments. The IR, ^{1}H-NMR, and mass spectra were recorded on a Hitachi EPI-S2, Varian T60, and JEOL JMS-01SG spectrometers, respectively. Analytical GLC was carried out with a Yanaco G-1800 gas chromatograph using

a 1.5 m—0.3 cm o.d. stainless column packed with 5% Silicone OV-17 on Chromosorb W. The preparative GLC was carried out with a Varian aerograph model 920 instrument using a 1.0 m—0.45 cm o.d. stainless column packed with 10% Silicone OV-17 on Chromosorb W. The column chromatography was carried out on active alumina Woelm N. Akt. I with solvents of hexane and benzene.

Materials. All the chemicals except for triphenylene were obtained from commercial sources (Nakarai Chemical Co. and Wako Pure Chemical Industries, Ltd.) and used after purification by distillation or column chromatography. Commercial nitrogen dioxide was cooled to liquid in a Dry Ice–acetone bath, weighed, and used as a 5% solvent solution. Triphenylene was prepared from *o*-bromoaniline according to the method of Heaney and Millar[17] mp 198 °C (lit,[17] 199 °C). Found: C, 94.42; H, 5.31%. Calcd for $C_{18}H_{12}$: C, 94.70; H, 5.30%.

Product Analysis. Into a solution (100 ml) or a suspension (100 ml) of 5.0 mmol of an aromatic compound, were added 5.5 mmol of anhydrous metal halide and 460 mg of toluene containing 23 mg of NO_2 (0.5 mmol). The mixture was stirred for appropriate time interval under atmosphere of oxygen at room temperature, and the amount of oxygen absorbed was measured on a gas-buret connected to the reaction vessel. The reaction mixture was poured into dilute hydrochloric acid, and extracted with toluene (3×50 ml). The combined toluene layer was washed with water, neutralized with sodium hydrogencarbonate, dried over $CaCl_2$, and the toluene was removed under reduced pressure. The residue was separated, and purified with column chromatography, and/or with recrystallization. The isolated products were identified by comparing thier IR, ^{1}H-NMR, and mass spectra with those of the corresponding authentic samples. Elemental analyses gave satisfactory results.

Quantitative Analyses. A same experiment as mentioned above was carried out in 1/10 scale. The combined toluene layer was quantitatively analyzed by GLC, after a usual work-up.

Bromination of Toluene. Anhydrous aluminum tribromide (2050 mg, 7.6 mmol) in nitromethane (18.5 g) and nitrogen dioxide (12.5 mg, 0.27 mmol) in nitromethane (250 mg) were added into toluene (25 ml). The mixture was stirred for 24 h under atmosphere of oxygen at room temperature, and poured into dilute hydrochloric acid. Work-up of the mixture by separation of toluene layer, washing with water, drying over $CaCl_2$, and evaporation of toluene yielded a mixture of crude bromotoluenes, which were purified on a preparative gas chromatograph (column temp: 120 °C), and the structure was identified. Quantitative analysis was carried out by GLC (column temp: 120 °C).

Chlorination of Anthracene with Trichlorosilane. Into toluene (10 ml) saturated with BF_3, were added 100 mg (0.56 mmol) of anthracene, toluene (1.4 ml) containing 76 mg (0.56 mmol) of trichlorosilane, and nitromethane (0.15 ml) containing 7.5 mg (0.16 mmol) of NO_2. The mixture was stirred overnight under atmosphere of oxygen at room temperature. After usual work-up, 72 mg (72%) of anthracene and 24.6 mg (74% based on consumed anthracene) of 9-chloroanthracene were obtained on GLC.

Competitive Chlorination. Into a mixture of anthracene (89 mg, 0.5 mmol), pyrene (101 mg, 0.5 mmol) or triphenylene (120 mg, 0.5 mmol), and eicosane (50.8 mg) as an internal standard material for gas chromatographical analysis in dry toluene (10 ml), were added titanium(IV) chloride (142.5 mg, 0.75 mmol) in nitromethane (0.28 ml) at 0 °C, and stirred. After 1 min and 3 min, 1 ml aliquots of the reaction mixture were taken out, respectively. The aliquot was quenched, and after usual work-up, analyzed by GLC.

The author thanks Professor S. Oka and Dr. A. Ohno for useful discussions.

References

1) For general reviews of aromatic halogenation, see R. O. C. Norman and R. Taylor, "Electrophilic Halogenation," in "Electrophilic Substitution in Benzenoid Compounds," Elsevier Publishing Company, Amsterdam (1965), Chap. 5, pp. 119—156; H. P. Braendlin and E. T. McBee, "Halogenation," in "Friedel-Crafts and Related Reactions," ed by G. A. Olah, John Wiley and Sons, Inc., New York (1964), Vol. III, Part 2, Chap. 46, pp. 1517—1593.

2) G. K. Chip and J. S. Grossert, *Can. J. Chem.*, **50**, 1233 (1972).

3) P. Kovacic, "Reactions of Aromatics with Lewis Acid Metal Halides," in "Friedel-Crafts and Related Reactions," ed by G. A. Olah, John Wiley and Sons, Inc., New York (1964), Vol. IV, Chap. 48, pp. 111—126.

4) R. O. C. Norman and R. Taylor, "Electrophilic Metallation," in "Electrophilic Substitution in Benzenoid Compounds," Elsevier Publishing Company, Amsterdam (1965), Chap. 7, pp. 194—202.

5) D. A. McCaulay, "Isomerization of Aromatic Hydrocarbons," in "Friedel-Crafts and Related Reactions," ed by G. A. Olah, John Wiley and Sons, Inc., New York (1964), Vol. II, Chap. 24, pp. 1049—1073.

6) P. Kovacic and C. Wu, *J. Polym. Sci.*, **47**, 45 (1960); E. B. Mano and L. A. Alves, *ibid.*, *Part A-1*, **10**, 655 (1972); P. Kovacic, F. W. Koch, and C. E. Stephan, *ibid.*, *Part A-2*, 1193 (1964); G. G. Engstrom and P. Kovacic, *ibid.*, **15**, 2453 (1977).

7) A. W. Fort, *J. Org. Chem.*, **26**, 765 (1961); J. C. Ware and E. E. Borchert, *ibid.*, **26**, 2263, 2267 (1961); H. P. Crocker and R. Walser, *J. Chem. Soc., C*, **1970**, 1982.

8) References in Ref. 3, pp. 111—118.

9) P. Kovacic and C. Wu, *J. Org. Chem.*, **26**, 214 (1961).

10) P. Kovacic and A. K. Sparks, *J. Am. Chem. Soc.*, **82**, 5740 (1960); P. Kovacic and N. O. Brace, *ibid.*, **76**, 5491 (1954); P. Kovacic and A. K. Sparks, *J. Org. Chem.*, **26**, 1310 (1961).

11) D. P. Wyman, J. Y. C. Wang, and W. R. Freeman, *J. Org. Chem.*, **28**, 3173 (1963).

12) D. C. Nonhebel, *Org. Synth.*, **43**, 15 (1963).

13) T. Sugiyama, K. Tanioka, A. Ohno, and S. Oka, *Chem. Lett.*, **1976**, 307.

14) I. Tanimoto and K. Maruyama, 31st National Meeting of the Chemical Society of Japan, Sendai, October 1974, Abstr. Vol. 1, p. 439.

15) J. B. Birks and M. A. Slifkin, *Nature*, **101**, 761 (1961).

16) C. Dijikgraaf, *J. Phys. Chem.*, **69**, 660 (1965); L. A. Burkardt, P. R. Hamond, R. H. Knipe, and R. R. Lake, *J. Chem. Soc., A*, **1971**, 3789.

17) H. Heaney and I. T. Millar, *Org. Synth.*, Coll. Vol. V, 1120 (1973).

 © 1982 The Chemical Society of Japan Bull. Chem. Soc. Jpn., 55, 1509—1513 (1982)

An MO Theoretical Study of the Photochemical Reaction of Alkanenitronate Anions to Form Hydroxamic Acids

Osamu Kikuchi,*,† Takazumi Kanekiyo, Seiji Tanaka, Kiyoshi Naruchi, and Kazutoshi Yamada*

Department of Industrial Chemistry, Faculty of Engineering, The University of Chiba, Yayoi-cho, Chiba 280

†*Department of Chemistry, The University of Tsukuba, Sakura-mura, Ibaraki 305*

(Received July 23, 1981)

The reaction mechanism of the photochemical reaction of alkanenitronate anions to form hydroxamic acids was explored on the basis of the potential energy curves obtained by means of MINDO/3 CI calculations. The *O*-oxaziridine was calculated to be not an intermediate, but an unstable transient species in this photoreaction. This is different from the photoisomerization of methyleneamine *N*-oxide derivatives into the corresponding amides, in which the oxaziridine is considered to be an intermediate. The proposed reaction mechanism elucidates well the regioselectivity observed in the photochemical formation of hydroxamic acids from nitronate anions.

Although the photochemical reactions of aliphatic nitro compounds have been investigated extensively,[1] the photochemical reactions of alkanenitronate anions, which are formed from aliphatic nitro compounds in an alkaline solution, has not been reported before our recent studies.[2] The photolyses of nitronate anions, **1**, give hydroxamic acids, **2**. Since methyleneamine *N*-oxide derivatives, **3**, give, photochemically, the corresponding amides, **5**,[3] the **1**→**2** reaction may

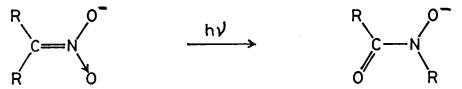

1 **2**

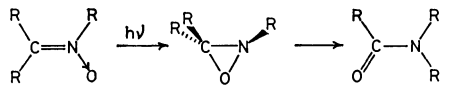

3 **4** **5**

be considered to proceed by means of a mechanism similar to that of the **3**→**5** reaction. In the **3**→**5** reaction, the oxaziridine, **4**, is considered to be an intermediate; some oxaziridines have been isolated.[3] In the case of the nitronate anions, however, the corresponding *O*-oxaziridines are too unstable to be observed by spectroscopic methods.[2] Moreover, the regioselectivity observed in the photolysis of **6** is different from that observed in the **8**→**9** reaction. Thus, the **1**→**2** reaction mechanism can not be sufficiently understood by analogy with that of the **3**→**5** reaction; we therefore decided to perform MO theoretical calculation along the **1**→**2** reaction process to explore the reaction mechanism and to complement our experimental studies.

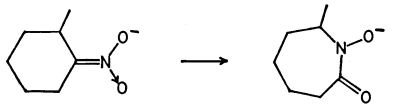

6 **7**

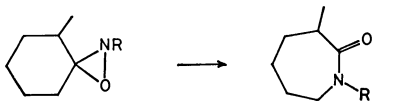

8 **9**

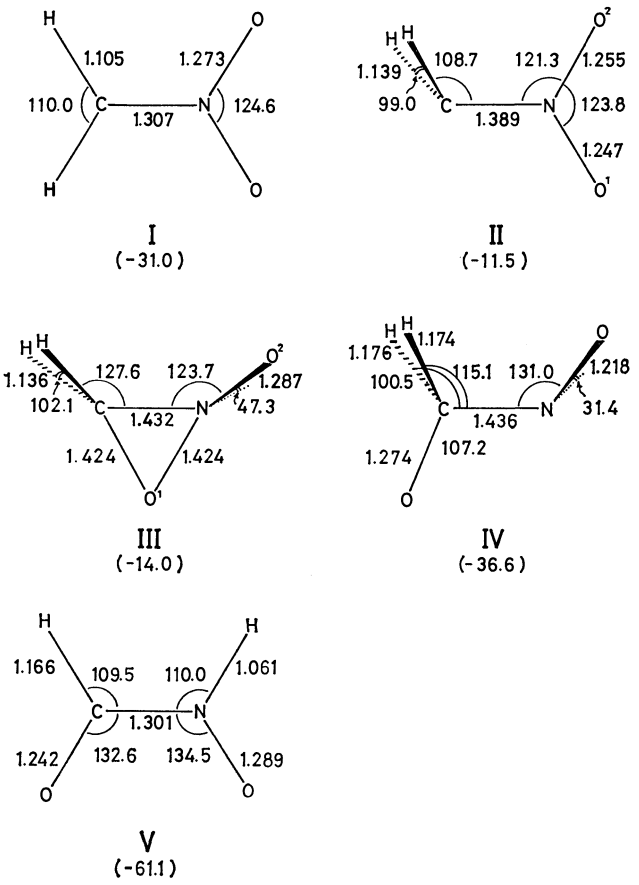

Fig. 1. Molecular structures and heats of formation (in parentheses) of the anions I—V obtained by MINDO/3. Bond lengths are in Å, bond angles in degrees, and heats of formations in kcal/mol (1 kcal=4.184 kJ).

Method and Results

The unsubstituted compound, I, was employed as the model nitronate anion. The molecular structures of the anions, I—V, were optimized by MINDO/3[5]

SCF (without CI) calculation. The configuration of the H atoms in II and III was restricted to symmetrical with respect to the CNO^1 plane. The calculated structures and the heats of formation of these anions are shown in Fig. 1. The energy difference between I and II, 81.6 kJ/mol, agrees well with the STO-3G value (64.9 kJ/mol).[6]

The HOMO of II is the CH_2 σ lone-pair orbital (carbanion type), while the LUMO of II is the NO_2 *anti*-bonding π orbital. The closed-shell configuration is the ground state of this twisted structure, and the HOMO→LUMO diradical structure is the excited state, as will be shown below. The CN bond of nitronate anions has a double-bond character. As may be expected from the electronic structure of the twisted ethylene,[7] the lowest singlet state of the species obtained by 90° rotation about a double bond is the diradical state. The lowest state of the twisted methyleneamine *N*-oxide was calculated to be the diradical state.[8] It is thus very interesting that the lowest singlet state of the twisted nitronate anion has a closed-shell electron configuration.

In the optimization of the bridged structure, III, the C–O^1 and N–O^1 distances were resticted to $R_{CO^1}=R_{NO^1}$. If this restriction is removed, the N–O^1 bond breaks spontaneously during the geometry optimization process, and the stable bridged structure cannot be obtained; the optimization gives an open structure, IV. Since the stable bridged structure is obtained for VI by the same optimization procedure,[8]

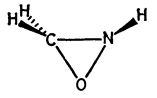

VI

the instability of III may be said to be characteristic of the *O*-oxaziridine derived from nitronate anions. The reaction product V is very stable (105 kJ/mol more stable than IV), and the transformation from IV to V can be expected to occur very easily.

The photochemical formation of V from I involves the methylene rotation, the oxygen migration from the nitrogen to carbon atoms, and the hydrogen migration in the reverse direction. The I→V process is thus too complex to be analyzed by the MO method. We restricted ourselves to considering three processes successively:

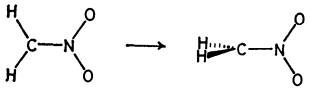

(1)

I II'

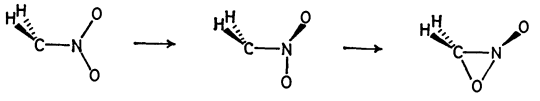

II VII III

TABLE 1. LOWER ELECTRONIC STATES OF THE PLANAR $CH_2=NO_2$ ANION

States	Energy/eV	Main configurations[a]
$^1A_1$	0.000	Ground conf. (97%)
$^1B_2$	3.68	12→13 (98%)
$^1A_1$	4.11	12→14 (58%), 11→13 (35%)
$^1B_2$	4.72	11→14 (53%), 12→16 (39%)
$^3A_1$	2.78	12→14 (98%)
$^3B_2$	2.83	12→13 (99%)
$^3A_1$	4.26	11→13 (85%), 11→16 (9%)

a) The highest occupied ϕ_{12} orbital is the C–N π orbital, the ϕ_{13} and ϕ_{16} orbitals are unoccupied σ orbitals, ϕ_{11} is the oxygen lone-pair σ orbital, and ϕ_{14} is the unoccupied π orbital.

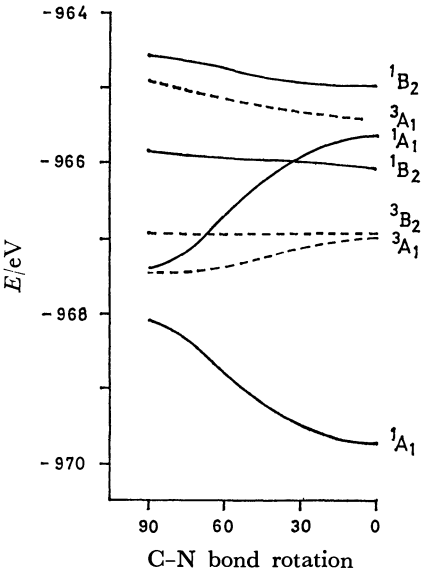

Fig. 2. Energy variations of several lower electronic states of the nitronate anion I along the rotation about the CN bond.

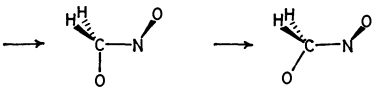

(2)

VIII IV

(3)

IV V

The potential curves along the methylene rotation, Eq. 1, were calculated by means of the CI method, in which 30 and 27 configuration functions were selected from singly- and doubly-excited configurations for the singlet and triplet states respectively. Several lower states of I are listed in Table 1, while their energy variations along the methylene rotation are shown in Fig. 2.

In order to determine the potential curves for the oxygen-migration reaction, the CI calculations were

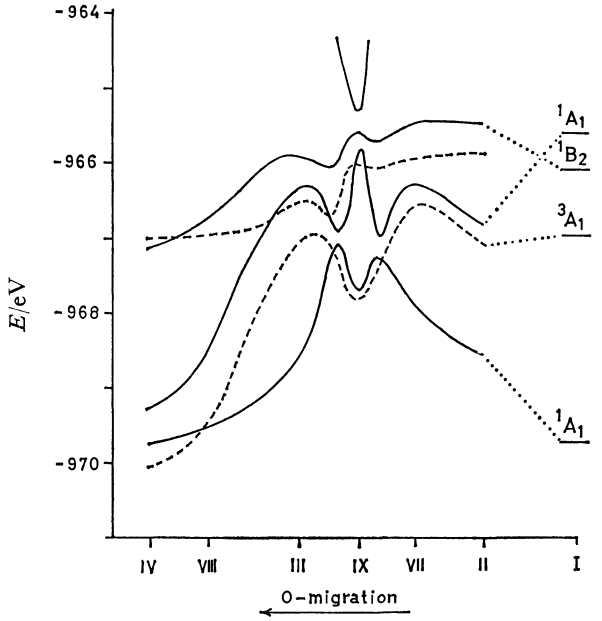

Fig. 3. Energy variation of lower electronic states along the oxygen migration process II→IV.

carried out for the five optimized structures involved in Eq. 2, as well as for several intermediate structures between VII and III. The potential curves obtained are shown in Fig. 3. An interesting shape of potential curves was observed between VII and III. In this region, two occupied orbitals, the carbanion-type σ lone-pair orbital on the carbon atom and the in-plane oxygen one-pair orbital, interact with each other to form the C–O^1 ϕ_σ and ϕ_{σ^*} occupied orbitals. When

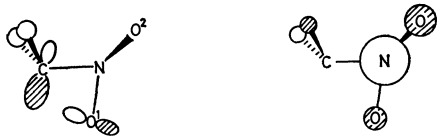

this interaction increases, the orbital energy of the occupied ϕ_{σ^*} orbital increases rapidly and crosses with the unoccupied ϕ_{π^*} orbital of the NO_2 group. Since the O^1 migration is accompanied by the deviation of the NO bond out of the CNO^1 plane, the ϕ_{σ^*} and ϕ_{π^*} orbitals mix to give the HOMO and LUMO in this region (Eqs. 4 and 5). According to Salem,[7]

$$\Psi_{12}(\text{HOMO}) = \frac{1}{\sqrt{2}}(\phi_{\sigma^*}+\phi_{\pi^*}) \quad (4)$$

$$\Psi_{13}(\text{LUMO}) = \frac{1}{\sqrt{2}}(\phi_{\sigma^*}-\phi_{\pi^*}) \quad (5)$$

the lowest singlet state in this region is a diradical state whose electron configuration is $(\phi_{\sigma^*})^1(\phi_{\pi^*})^1$. The wavefunction of the pure diradical singlet state of this electron configuration is:

$$\frac{1}{\sqrt{2}}(\Psi^1_{12}-\Psi^1_{13}).$$

Thus, the lowest singlet state in this region should be expressed by the two-configuration wavefunction. The CI calculation in this region was carried out for the

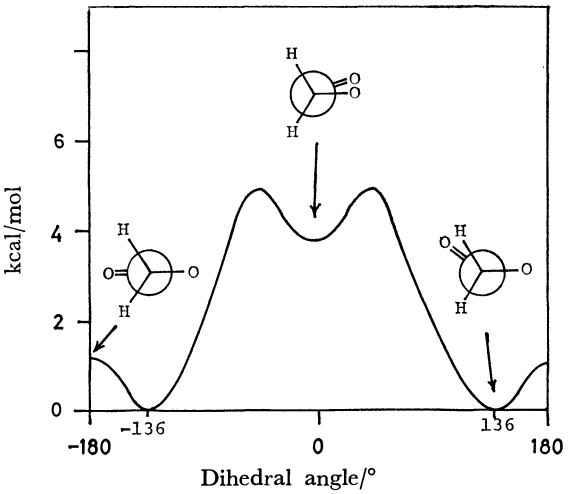

Fig. 4. Energy variation of IV along the rotation about the C–N bond. The structure is optimized at each rotational angle.

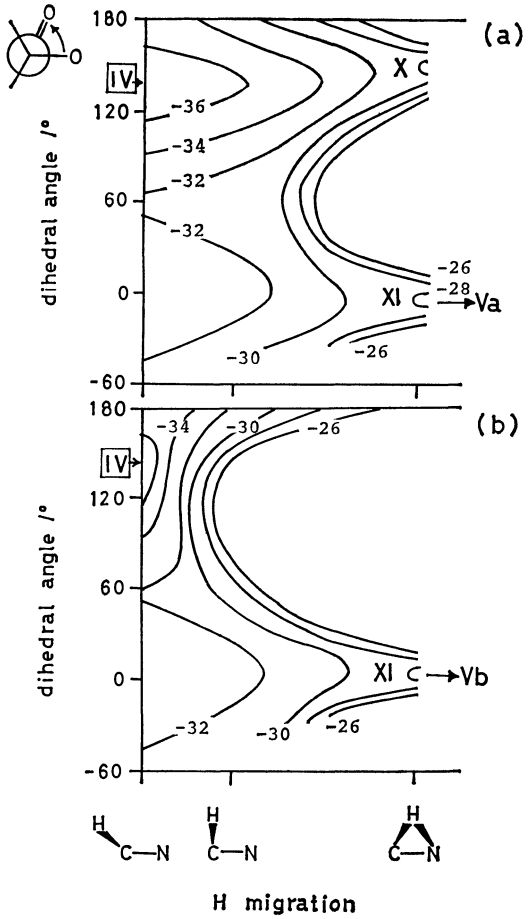

Fig. 5. Potential energy surfaces for the H-migration reaction from IV to the bridged structure. a) H^t migration. b) H^c migration. The values are heats of formation in kcal/mol (1 kcal=4.184 kJ).

diradical IX, whose molecular structure was optimized by using the double-configuration wavefunction. The IX structure corresponds to the deep minimum point in Fig. 3, and the CI wavefunction of the lowest singlet

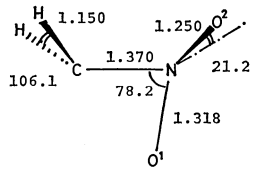

IX

state of IX is $0.759\Psi^2_{12}-0.569\Psi^2_{13}+\cdots$.

The hydrogen migration and the N=O group rotation are involved in Eq. 3. Figure 4 shows the energy variation in IV with respect to the dihedral angle between the OCN and CNO planes. Figure 5 shows the potential energy curves as a function of the dihedral angle and the H-migration coordinate. Two bridged structures, X and XI, were predicted for the transition states; X and XI give the *trans* and

X XI

cis isomers of the final product respectively. As may be seen from Fig. 4, the two hydrogen atoms in IV are not equivalent; one is *trans*, and the other is *cis*, with respect to the N=O bond. There are two possible paths leading to the *cis* isomer of the final product which corresponds to **7**. The potential energy surfaces in Fig. 5 indicate that the H^t migration is preferable to the H^c migration.

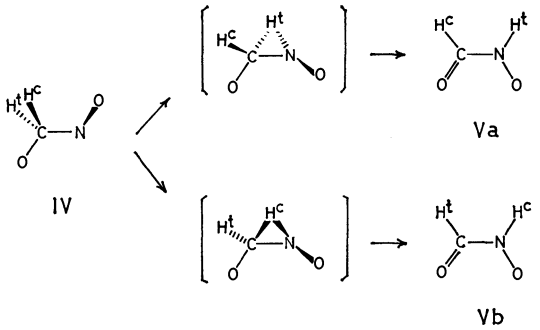

IV Va Vb

Discussion

The strong absorption of alkanenitronate anions observed in the 230—240 mμ region[2] can be assigned to the transition from the ground state to the $^1A_1(\pi\rightarrow\pi^*)$ excited state, since this is a symmetry-allowed transition. The rotation of the methylene group about the CN bond of I can occur in this excited state (Fig. 2). The nitronate anions can undergo photochemical isomerization from their $\pi\rightarrow\pi^*$ excited state. In the present calculation, two processes, the rotation of methylene and the oxygen migration, were treated separately; a concerted path of these two processes may be possible in the actual system. These steps do not occur from the ground state, since the activation energy required is more than 210 kJ/mol (Figs. 2 and 3).

The most clear-cut finding is the unstable property of the *O*-oxaziridine. In the photochemical **3**→**5** process, the oxaziridine, **4**, is an intermediate.[3] The difference in stability between III and VI originates

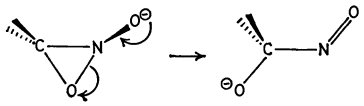

from the difference in their electronic structures. In the case of III, the electron migration occurs very easily to give the stable structure IV, while this type of electron migration is not expected in the oxaziridine, VI.

In the photochemical isomerization of cyclic oxaziridines into amides, **10**→**11**, an alkyl migration after the N–O bond cleavage has been proposed.[9] This mechanism is not applied to the present system, however, since the bridged structure, **12**, is a transient species. The ionic mechanism, in which **13** is an intermediate, is more appropriate for the present system. The alkyl migration, **13**→**14**, involved in this step is similar to the benzilic acid rearrangement[10] in an alkaline solution.

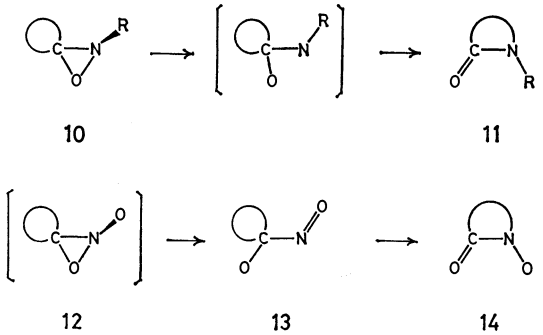

10 11 12 13 14

The photochemical reaction mechanism of nitronate anions can be understood by the schematic representation of the reaction process (Fig. 6). The CN bond rotation and the oxygen migration occur from the $\pi\rightarrow\pi^*$ excited state. The transition from the excited state to the ground state occurs near the diradical structure (XI), and the stable anion (IV) is produced

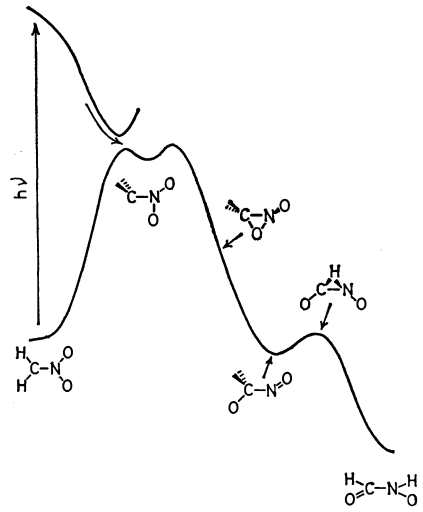

Fig. 6. Schematic representation of the photochemical process of alkanenitronate anions to form hydroxamic acids.

very easily. The oxaziridine is not an intermediate in this step. The alkyl migration requires only a small activation energy to form the final reaction product.

Oliveros *et al.*[9] have well explained the regioselectivity observed in the **8**→**9** reaction on the basis of theoretical calculations for the model system, **15**→**16**.

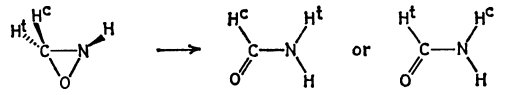

15 16a 16b

Their results indicated that the CH bond in the *cis* position with respect to the N–H hydrogen atom breaks easier than that in the *trans* position. In the case of nitronate anions, the nitroso compound, **13**, is an intermediate, and the regioselectivity observed in the **6**→**7** reaction may be explained by the selectivity expected in the **13**→**14** reaction. The model calculation for the IV→Va and IV→Vb processes suggested that the migration of the *trans* alkyl group is preferable to that of the *cis* one (Fig. 5). In the IV→V step, the hydrogen atom bearing a pair of electrons migrates to the nitrogen atom, and the interaction between the C–H bond and the N=O *anti*-bonding π orbital is very important. This stereoelectronic effect is why the H^t hydrogen atom migrates more

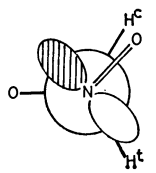

easily than the H^c atom. If the XII conformation, in which the steric interaction between the N=O oxygen atom and the ring substituent is minimized, is assumed to hold for the anion derived from **6**, the present model calculation predicts the formation of **7**, which is observed experimentally.

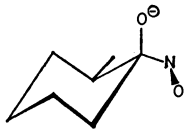

XII

References

1) H. A. Morrison, "The Photochemistry of the Nitro and Nitroso Groups," Interscience Publ., New York (1969), p. 165.

2) T. Kanekiyo, Thesis, Chiba Univ. (1981); T. Kanekiyo, S. Tanaka, K. Naruchi, and K. Yamada, *J. Am. Chem. Soc.*, **103**, 7003 (1981).

3) G. G. Spence, E. C. Taylor, and O. Buchardt, *Chem. Rev.*, **70**, 231 (1970); A. Lablache-Combier, "Photochemistry of Heterocyclic Compounds," ed by O. Buchardt, John Wiley & Sons, New York (1976), p. 207.

4) E. Oliveros, M. Riviere, and M. Parello, *Tetrahedron Lett.*, **1975**, 851; E. Oliveros, H. Antoun, M. Riviere, and A. Lattes, *J. Heterocycl. Chem.*, **13**, 623 (1976).

5) R. C. Bingham, M. J. S. Dewar, and D. H. Lo, *J. Am. Chem. Soc.*, **97**, 1285 (1975).

6) P. G. Mezey, A. J. Kresge, and I. G. Csizmadia, *Can. J. Chem.*, **54**, 2526 (1976).

7) L. Salem and C. Rowland, *Angew. Chem., Int. Ed. Engl.*, **11**, 92 (1972).

8) O. Kikuchi, K. Morihashi, and K. Suzuki, *Bull. Chem. Soc. Jpn.*, **55**, 1133 (1982).

9) E. Oliveros, M. Riviere, J. P. Malrieu, and Ch. Teichteil, *J. Am. Chem. Soc.*, **101**, 318 (1979).

10) T. H. Lowry and K. S. Richardson, "Mechanism and Theory in Organic Chemistry," Harper & Row, New York (1976), p. 317.

 © 1982 The Chemical Society of Japan Bull. Chem. Soc. Jpn., 55, 1514—1521 (1982) [Vol. 55, No. 5

Reactivities of Stable Rotamers. VIII. Difference in Reactivities of 1,2,3,4-Tetrachloro-9-(2-halo-1,1-dimethylethyl)triptycene Rotamers in Lewis Acid-catalyzed Reactions[1,2]

Hiromi KIKUCHI, Shigetaka SEKI, Gaku YAMAMOTO, Tsutomu MITSUHASHI, Nobuo NAKAMURA, and Michinori ŌKI*

Department of Chemistry, Faculty of Science, The University of Tokyo, Bunkyo-ku, Tokyo 113

(Received July 30, 1981)

±*sc*-1,2,3,4-Tetrachloro-9-(2-chloro-1,1-dimethylethyl)triptycene was found to react in the presence of titanium(IV) chloride at room temperature to give an isomeric mixture of 1,2-dimethyl-7,8,9,10-tetrachloro-1,2,6,10b-tetrahydro-6,10b-*o*-benzenoaceanthrylenes. The structure of the latter was confirmed by independent syntheses. In contrast, the *ap* conformer of the former did not give any sign of the reaction under the same conditions but reacted when antimony(V) chloride was added to give the same mixture. Careful examination of the reaction mixture suggests that the starting material was rapidly converted to (*E*)-1,2,3,4-tetrachloro-9-(1-methyl-1-propenyl)triptycene and cyclization followed. Action of silver nitrate on ±*sc*-9-(2-bromo-1,1-dimethylethyl)-1,2,3,4-tetrachlorotriptycene afforded a mixture of the stereoisomers of the olefin while the *ap* form remained intact.

Since we were able to show recently that methyls in a *t*-butyl group could behave differently in radical halogenations, when the rotation of the *t*-butyl group was frozen,[3] we naturally wished to extend the work on the reactivities of rotamers to see those of the halogenated compounds. Because 9-(2-halo-1,1-dimethylethyl)triptycenes possess the structure of neopentyl halide, their S_N2 type substitution was expected to be very slow.[4] However, we happened to find that the ±*sc* conformer of 1,2,3,4-tetrachloro-9-(2-chloro-1,1-dimethylethyl)triptycene (**1a**) was partially destroyed if purification was attempted by chromatography on alumina, whereas the *ap* form was eluted intact.[3] This suggests that ionization reactions of the halide may be facile in general, especially in the ±*sc* conformation. Thus we decided to investigate the reactivities of ±*sc*- and *ap*-**1a** in ionization reactions. This paper reports the difference in reactivities of the rotamers, when they are treated with a Lewis acid. The structure of the products was confirmed by independent syntheses. The possible mechanisms of the reaction are also discussed.

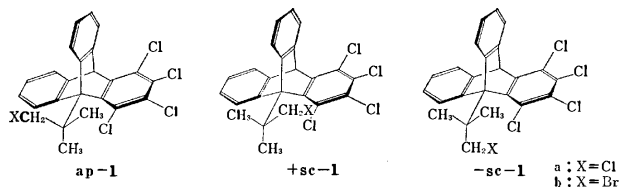

Results and Discussion

*Reactivities of 1,2,3,4-Tetrachloro-9-(2-chloro-1,1-dimethylethyl)triptycene (**1a**) Rotamers.* Since the barrier to rotation of the 2-chloro-1,1-dimethylethyl group about the C_9–C_{subst} bond is known to be *ca.* 37 kcal/mol (1 cal=4.18 J),[3] it is certain that we are looking at the reactivity of each isomer. The treatment of a mixture of **1a** rotamers with a large excess of titanium(IV) chloride caused the reaction of the ±*sc* form but the *ap* form remained unreacted. The pseudo-first order reaction rate constant for the ±*sc* form was obtained as 5.3×10^{-4} s^{-1} at 41 °C. Under the same conditions, the *ap* form did not give any sign of the reaction even after 164 h. This indicates that the rate constant of the reaction of *ap*-**1a** under the conditions is 8.7×10^{-8} s^{-1} at the most. (We took 5% of the material reacted since the error in integration of ^{1}H NMR spectra may be estimated at this level.) Then the relative reaction rate of ±*sc*-**1a** is $>6\times10^3$ if that of *ap*-**1a** is unity. The pseudo-first order rate constant of *ap*-**1a** in the presence of antimony(V) chloride was 8.8×10^{-4} s^{-1} at 39.8 °C, whereas the reaction of ±*sc*-**1a** was too fast to measure the rate by conventional methods under the conditions.

This large difference in reactivities of ±*sc*-**1a** and *ap*-**1a** must be derived by the presence of a chloro group in a peri-position. Since titanium(IV) chloride and antimony(V) chloride act as Lewis acids, it is expected that these coordinate with the chloro group in the 9-substituent and help ionization of the compound. Then the developed cation (**2**) can be stabilized by the presence of a chloro group in proximity in the ±*sc* conformation, since neighboring participation of the chloro group is well documented[5]

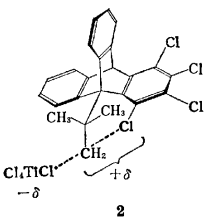

2

and chloronium ion is also known.[6] There is a possibility that the ground state of this molecule is so congested that the steric acceleration of ionization[7] ensues. However, if it were the main cause, the *ap*-form as well as the ±*sc* form should have ionized with comparable rates. It is especially noteworthy that titanium(IV) chloride, which is known to be a weak catalyst for the Friedel-Crafts reaction of primary organic halides,[8] does cause the reaction under mild conditions: Participation of the chloro group seems strong in this case. Indeed, several examples of strong participation of the peri-chloro group in triptycenes have been reported.[9] Another interesting

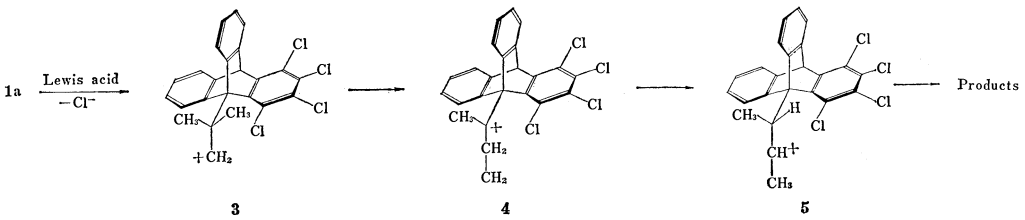

Scheme 1.

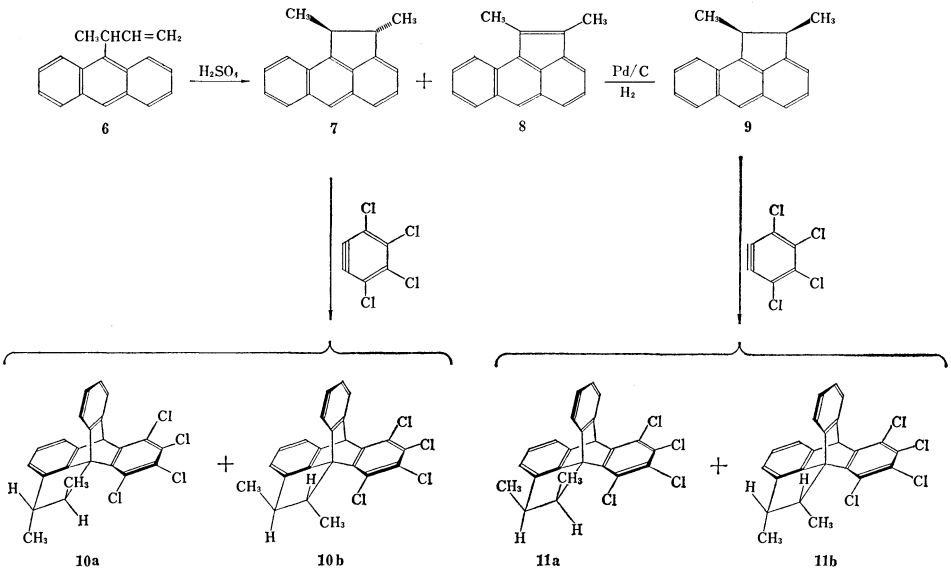

Scheme 2.

point is that the intermolecular Friedel-Crafts reaction with the solvent molecule has not been detected. This is probably because the intermolecular reaction is prohibited due to the steric factor.

Antimony(V) chloride is known to be a stronger Lewis acid than titanium(IV) chloride.[10] Therefore it is reasonable that this reagent caused the reaction of even *ap*-**1a**.

Structures of the Products. Both of the reactions catalyzed by Lewis acids afforded almost the identical mixture of the products. On standing, a part of the product solidified. After purification, the solid product showed ^{1}H NMR signals of two kinds of methyls, each coupled with a proton. A mass spectrum of the compound indicated that a molecule of hydrogen chloride was eliminated from the starting material. These results suggest that an extensive rearrangement has taken place in the 9-substituent of **1a**. Since the cation (**3**) originally formed from **1a** can undergo a series of Wagner-Meerwein rearrangements and finally the cation undergoes intramolecular cyclization (Scheme 1),[11,12] the most probable structure of the pure material seemed to be one of possible isomers of **10** and **11**.

It is not possible to assign the structure of the solid product from ^{1}H NMR spectral data only, because there are four possible stereoisomers. Thus independent syntheses of the products were performed (Scheme 2). 9-(1-Methyl-2-propenyl)anthracene (**6**) was treated with concentrated sulfuric acid to afford a mixture of *trans*-1,2-dimethylaceanthrene (**7**), 1,2-dimethylaceanthrylene (**8**), and a small amount of *cis*-1,2-dimethylaceanthrene (**9**). Compound **8** was separated by chromatography and hydrogenated over palladium–charcoal to afford **9**. The *cis*-dimethylaceanthrene **9** was treated with tetrachlorobenzyne to afford two isomers (**11**) which were formed by the different directions of attack by the benzyne. One of the products crystallized out and it was found to be identical with the solid product which was obtained above. Another isomer was purified by high pressure liquid chromatography to give a solution of the almost pure substance. Thus the original solid product has a *cis*-structure at the newly formed 5-membered ring. Likewise, *trans*-1,2-dimethylaceanthrene (**7**) was treated with tetrachlorobenzyne to give a mixture of stereoisomers of **10**. One of the products crystallized out from the mixture. Thus ^{1}H NMR spectra of two isomers each of **10** and **11** have become available.

The next step for the identification is to assign structures **10a** and **10b**, and structures **11a** and **11b**. We took advantage of two pieces of information available from the ^{1}H NMR spectra. The first is the chemical shift of the aromatic protons. Since 9-substituted triptycenes are highly congested, strong van der Waals interactions are due between the 9-substituent and the peri-proton. Accumulated data in this laboratory suggest that if the substituent in the 9-position is tertiary, the peri-proton gives rise to a multiplet signal at a far downfield of the aromatic region. The data may further be interpreted that if a proton in the peri-position is flanked by two methyl

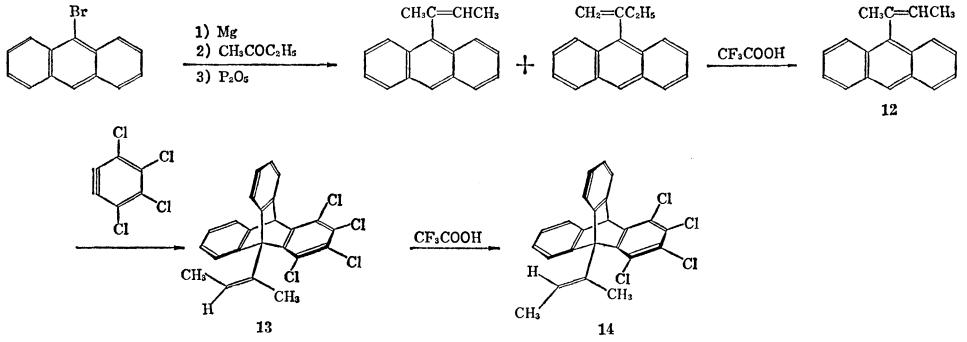

Scheme 3.

groups, it gives a signal at a considerably low field. Indeed, we have succeeded in assigning stereostructures of adducts between 9-(1,1-dimethyl-2-phenylethyl)anthracene and dimethyl acetylenedicarboxylate by this method.[13] Inspecting the molecular models, we notice that **10a** and **11a** possess a peri-hydrogen which is very close to a methyl, whereas **10b** and **11b** have that which is far from any of methyls. Therefore, if one of the two isomers of **10** and **11** gives an aromatic proton signal at a low field apart from others, then it is very likely to be **10a** and **11a**. Inspection of the NMR data suggests that, of the trans isomers, that which was obtained as crystals gives a low field signal and is likely to be **10a**. In contrast, a cis isomer which was obtained as crystals has no such low-field signal for the aromatic protons but that obtained as a solution exhibited a low-field signal. Thus the crystalline compound of the cis configuration is assigned to **11b**. These assignments are further confirmed by NOE experiments. An NOE experiment of the crystalline form of **10**, irradiating the methyl signal at δ 2.19 and observing the intensity of the signal at δ 7.90 showed 19% increase in intensity. Likewise, irradiation of the methyl proton signal at δ 2.11 of the isomer of **11**, which was obtained as a solution, showed 23% increase in intensity of the aromatic proton signal at δ 7.87, whereas no such enhancement of the signal was observed in the NOE experiment of the crystalline product of *cis*-structure or the crystalline product of the original cyclization reaction. Thus the structural assignment is now confirmed as follows.

10a: A crystalline product from the Diels-Alder reaction of *trans*-1,2-dimethylaceanthrene.

10b: Another product from the above reaction which was not purified completely.

11a: A compound which was obtained as an almost pure solution by high pressure liquid chromatography from the product of the Diels-Alder reaction of *cis*-1,2-dimethylaceanthrene.

11b: A crystalline product from the above reaction and also a crystalline product from the treatment of **1a** with Lewis acids.

Using the ^{1}H NMR signals of these compounds, we can now analyze the composition of the products obtained by the reactions of $\pm$*sc*-**1a** and *ap*-**1a**. The ratios were constant at **10a**:**10b**:**11a**:**11b**=45:$\approx$0:10:45 within the error of $\pm$5%.

Mechanisms of the Reaction. If we neglect the presence of a counterion, the mechanisms of cyclization may be shown as those in Scheme 1 as a first approximation. However, there are a few points we wish to mention here. The first is the intervention of an olefin (**13** and/or **14**). While, when a large excess of titanium(IV) chloride was used in the reaction of $\pm$*sc*-**1a** for a long time, only the cyclized products were detected, an olefin was a major product together with a small amount of the cyclized products when the reaction was conducted for a shorter period in the presence of a relatively small excess of the catalyst.

The structure of the olefin was determined by independent syntheses as follows (Scheme 3). A Grignard reagent prepared from 9-bromoanthracene was added to 2-butanone and the resulted alcohol was dehydrated with phosphorus(V) oxide to give a mixture of olefins. Treatment of the mixture of olefins with trifluoroacetic acid yielded a mixture of (*Z*)- and (*E*)-9-(1-methyl-1-propenyl)anthracene (**12**) in which the *Z*-form predominated. Treatment of the mixture of *Z*- and *E*-forms with tetrachlorobenzyne followed by chromatography gave (*Z*)-1,2,3,4-tetrachloro-9-(1-methyl-1-propenyl)triptycene (**13**). Isomerization of **13** to its *E*-isomer (**14**) was effected by trifluoroacetic acid.

The structures of olefins of the triptycenes (**13** and **14**) and those which were found during the synthesis of the former were elucidated by considering the ring current effect of the benzene rings in ^{1}H NMR spectra. Of the two 9-(1-methyl-1-propenyl)anthracenes, one gives a methyl signal at δ 1.98 and the other at δ 1.23. The space-filling models of these compounds suggest that, as are expected from analogy of mesitylene derivatives,[14] the two planes made by the olefin and the anthracene cannot be coplanar. Thus the methyl group at the far end in the *Z*-olefin is located over the anthracene ring. In contrast, in the *E*-form, the methyl is far from the anthracene. Therefore, it is reasonable to assign the *Z*-structure for a compound which shows its NMR signal of the methyl group at a higher field than the counterpart. Similarly, the *E* and *Z* structures of the olefin in triptycenes (**13** and **14**) were assigned by taking advantage of the geometry of molecules which is suggested by molecular models: in the *Z*-conformation of the olefinic triptycene, the methyl group at the end of the 9-sub-

stituent should be in the shielding zone of the flanking benzeno bridges, whereas it is in the deshielding zone of the benzeno bridges in the *E*-conformation. The fact that, while the anthracene gave a mixture of *Z* and *E* forms of the olefin on equilibration, the triptycenes gave the almost pure *E*-olefins on equilibration, may be rationalized by considering the steric factor: Since the end-methyl group directs inside of the triptycene skeleton in the *Z*-conformation, its thermodynamic stability must be low.

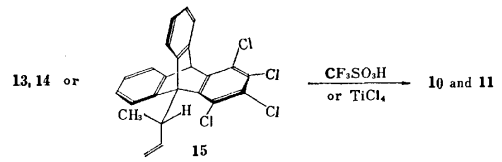

Cyclization of olefins (**13** and **14** as well as **15**) gives almost the identical mixture of isomers of the cyclized products (**10** and **11**) when they were treated with titanium(IV) chloride or trifluoromethanesulfonic acid. This may be taken as evidence that the cation (**4** and/or **5**) are really involved in the process of the cyclization. An interesting point is that, although the cyclization did occur under these conditions, no cyclization was observed if trifluoroacetic acid was used. The acid must be a strong one for the cyclization to occur. The failure of cyclization in the presence of sulfuric acid may be ascribed to the presence of a basic solvent molecule (CD_3CN). This will mean that the concentration of the protonated species **5** must be high for the cyclization to occur which is rather slow. The slow cyclization can be expected since the formation of the 5-membered ring proceeds in the conformation in which the fully eclipsed interactions between the benzo groups and the methyl or the hydrogen of the forming 5-membered ring develop.

It is questionable to say that the olefin (**13** or **14**) is the real intermediate of the reaction which gives the cyclized products (**10** and **11**), whereas it is certain that the cyclization which affords **10** and **11** is slow and the olefin is formed rapidly from the halogen compound (**1a**), because, should the cation be formed, it will rearrange rapidly to **4** to release the strain. We see that there are two possibilities (Scheme 4): One is that the reaction proceeds in the sequential manner where the olefin **14** is formed from either **4** or **5**, but on protonation, the olefin goes back to the cation (**4** and **5**). An alternative is the sequence

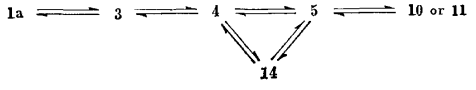

Scheme 4.

in which **14** becomes a real intermediate which on protonation gives the cation **5**. We cannot rule out any of the two processes at present. Probably the both processes contribute to the total reaction.

It is interesting that both *ap*-**1a** and ±*sc*-**1a** reacted to give almost identical mixtures of the cyclized products, although their reactivities differed to a great

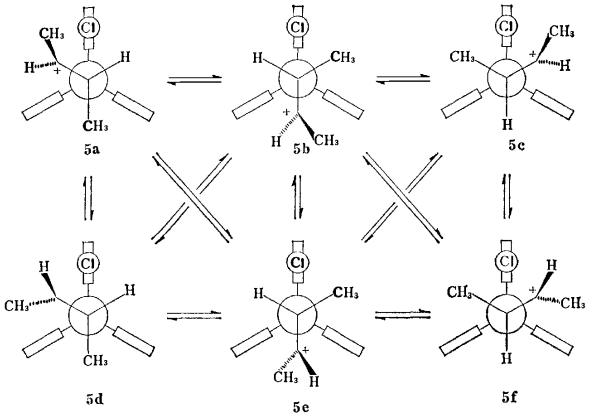

Scheme 5.

extent. This must mean that, although the ionization reaction of isomers of **1a** differes in their rates, the subsequent steps should involve at least a same intermediate. In addition, we could not find any of the intermediates other than the olefin **14** when the Lewis acids were used. The results can be accommodated if the Wagner-Meerwein rearrangement is fast: it is reasonable to assume so because the Wagner-Meerwein rearrangements were known to be very fast in various systems,[15] and the steric strain in the cation **3**, which is close to 1,2,3,4-tetrachloro-9-*t*-butyltriptycene[16] or 1,2,3,4-tetrachloro-9-(1-cyano-1,1-dimethylethyl)triptycene,[17] must be the driving force for the rearrangement, as discussed above (see also note 12). Thus the isomers of **3** are formed from *ap*- and ±*sc*-**1a** but they are transformed into **4** very rapidly. There are rotational isomers of **4** also. Therefore isomers of **4** may be formed from the rotamers of **1a**. However, the barriers to rotation of triptycenes carrying an sp^2-hybridized carbon at the bridgehead are known to be rather low.[18] The common intermediate is probably formed in this stage, although there is a possibility that, in the olefin **14**, the stereochemistry is scrambled. The final intermediate (**5**) should have a high barrier to rotation since its analogous compound, 1,2,3,4-tetrachloro-9-(1-methyl-2-propenyl)triptycene, has a high barrier and the rotation occurs slowly at room temperature.[19]

Since the cation **5** is the direct precursor for the cyclization, the discussion of the possible conformation leading to **10** and **11** may deserve further mention. There are various conformations possible for **5** (Scheme 5).[20] Since the conformational energy of C^+–CH_3 inside forms (**5d—f**) are very high from the steric grounds,[21] their concentrations should be very low. In addition, the reactivities of the C^+–CH_3 inside forms are not apparently higher than the C^+–CH_3 outside conformations (**5a—c**). Thus the reaction paths through C^+–CH_3 inside conformations (**5d—f**) may be neglected. Of the important conformations (**5a—c**), **5a** leads to **11a** when it cyclizes and **5c** to **10b**, whereas **5b** conformation gives rise to **10a** and **11b**. On the grounds of the interaction between a cation and a peri-substituent (chloro group in this case),[9] the conformations **5a** and **5c** are considered to be more stable than **5b**. However, in

practice, **10b** has not been observed in the products. We may have to assume that the cyclization from conformation **5c** is extremely unfavorable. In contrast, **11a** was formed, although the yield was lower than those of **10a** and **11b**. This is probably attributed to two factors. The first is the fact that, in the transition state for the cyclization, the methyl and the chloro groups are eclipsing with each other for the formation of **10b**, whereas the eclipsing is between the chloro and hydrogen for the formation of **11a**. The second factor is that the conformation **5c** is so energy-rich, because two bulky groups are flanking the chloro group in the peri-position, that its population is scarce.[22] Conformation **5b**, on the other hand, is not stabilized by any of the apparent intramolecular interaction. Since the products which are led from this intermediate are main, the reaction rates of **5b** should be very large relative to others.

*Reactions of 1,2,3,4-Tetrachloro-(2-bromo-1,1-dimethylethyl)triptycene (**1b**) Rotamers.* Although a bromo compound is known to be a little more reactive than a corresponding chloro compound in substitution reactions, the *ap* form of **1b** also failed to give any reaction product when it was treated with titanium(IV) chloride. ±*sc*-**1b** reacted normally to give the *E*-olefin (**14**) and cyclized products (**10** and **11**). The reaction is considered to proceed as was discussed in that of **1a**.

Likewise, a reaction of *ap*-**1b** with silver nitrate in acetonitrile failed to give any product after heating at 50—60 °C for 3 h, whereas ±*sc*-**1b** was completely converted to olefins (**13** and **14**) under the conditions. It is interesting to note that an almost 1:1 mixture of *E* and *Z* olefins was formed by the action of silver nitrate on **1b**, whereas the action of titanium(IV) chloride afforded the *E*-olefin exclusively. The cause for this phenomenon is not well understood at the moment but the weak basicity[23] and the bulkiness of the pentachlorotitanate anion must be responsible for the observed results. In contrast the smaller size and the stronger basicity[23] of the nitrate anion in addition to the higher temperature used for the reaction would give less selectivity of the reaction.

Experimental

*9-(1-Methyl-1-propenyl)anthracene (**12**).* A solution of 10 g (39 mmol) of 9-bromoanthracene and 7.7 g (41.2 mmol) of 1,2-dibromoethane in 150 mL of ether was added 2.95 g (123 mmol) of magnesium, activated by iodine, in 20 mL of ether. The addition required 24 h. The reaction mixture was boiled for further 24 h and then a solution of 2.9 g (40.3 mmol) of 2-butanone in ether was added to the mixture over a period of 4 h. The mixture was stirred for 24 h and decomposed with aqueous ammonium chloride. The organic layer was separated, washed, dried, and then evaporated. After removing anthracene by taking up the mixture in benzene, the soluble part was chromatographed on silica gel (10:1 hexane-benzene) to afford 9-(1-hydroxy-1-methylpropyl)anthracene in 20.3% yield. ^{1}H NMR ($CDCl_3$, δ): 0.89 (3H, t, J=7.4 Hz), 1.95 (3H, s), 2.12 (1H, s), 0.98—2.02 (2H, m), 7.08—7.46 (4H, m), 7.65—8.06 (2H, m), 8.19 (1H, br s), 8.61—8.95 (2H, m).

The crude alcohol (1.0 g or 4.0 mmol) was heated with 1.0 g of phosphorus(V) oxide in 50 mL of carbon tetrachloride. The mixture was filtered and the filtrate was evaporated. The residue (0.75 g) consisted of 33:22:45 (*E*)- and (*Z*)-9-(1-methyl-1-propenyl)anthracenes and 9-(1-ethylvinyl)anthracene, as judged from a ^{1}H NMR spectrum. The mixture in 50 mL of carbon tetrachloride was boiled with 1 mL of trifluoroacetic acid for 2 d, washed with water and then with aqueous sodium hydrogencarbonate, and dried over magnesium sulfate. Evaporation of the solvent gave a 3.7:1 mixture of (*Z*)- and (*E*)-9-(1-methyl-1-propenyl)-anthracene (**12**), recrystallization of which from tetrahydrofuran–hexane afforded a 1.6:1 mixture of the *Z*- and *E*-olefins, mp 70—73 °C. Found: C, 93.24; H, 6.70%. Calcd for $C_{18}H_{16}$: C, 93.06; H, 6.94%. The following ^{1}H NMR data ($CDCl_3$, δ) have been recorded. *E*-isomer: 1.98 (3H, d, J=7.1 Hz), 2.14 (3H, d, J=1 Hz), 5.62 (1H, dq, J=7.1 and 1 Hz), 7.3—7.6 (4H, m), 7.8—8.3 (4H, m), 8.32 (1H, s). *Z*-isomer: 1.23 (3H, br d, J=7.0 Hz), 2.07 (3H, d, J=1 Hz), 6.08 (1H, dq, J=7.0 and 1 Hz), 8.35 (1H, s) and other aromatic protons (8H). The following ^{1}H NMR data of 9-(1-ethylvinyl)anthracene were obtained by subtracting the data of *E*- and *Z*-olefins from those of the mixture ($CDCl_3$, δ): 1.15 (3H, t, J=7.5 Hz), 2.55 (2H, br q, J=7.5 Hz), 5.18 (1H, m), 5.78 (1H, m), and aromatic protons (8H).

trans-*1,2-Dimethylaceanthrene (**7**) and 1,2-Dimethylaceanthrylene (**8**).* A mixture of 20 mL of concentrated sulfuric acid and a solution of 3.95 g of 9-(1-methyl-2-propenyl)anthracene[19] in 50 mL of carbon tetrachloride was stirred at room temperature for 1 h. The organic layer was washed with water and then with aqueous sodium hydrogencarbonate, and evaporated. The residue was chromatographed on silica gel with the use of hexane as an eluent. Crude *trans*-1,2-dimethylaceanthrene (**7**), which was contaminated by a small amount of *cis*-isomer, and 1,2-dimethylaceanthrylene (**8**) were obtained in 28.4 and 18.9% yields, respectively.

trans-*1,2-Dimethylaceanthrene (**7**).* High resolution MS exhibited a molecular ion peak at *m/e* 232.1247. $C_{18}H_{16}$ requires 232.1248. ^{1}H NMR ($CDCl_3$, δ): 1.29 (3H, d, J=7 Hz), 1.42 (3H, d, J=7 Hz), 3.18 (1H, q, J=7 Hz), 3.59 (1H, q, J=7 Hz), 8.10 (1H, s), 6.9—8.2 (7H, m).

*1,2-Dimethylaceanthrylene (**8**).* Mp 112.5—113.0 °C. Found: C, 93.94; H, 5.85%. Calcd for $C_{18}H_{14}$: C, 93.87; H, 6.12%. ^{1}H NMR ($CDCl_3$, δ): 2.32 (3H, d, J=1 Hz), 2.64 (3H, d, J=1 Hz), 8.25 (1H, s), 7.2—8.6 (7H, m).

cis-*1,2-Dimethylaceanthrene (**9**).* A solution of 0.7 g of 1,2-dimethylaceanthrylene (**8**) in 30 mL of ethyl acetate was shaken with 50 mg of 5% palladium on charcoal under a hydrogen atmosphere. The theoretical amount of hydrogen was absorbed within 3 h. The mixture was filtered and the filtrate was evaporated. Recrystallization of the residue from ethanol–hexane gave pure product, mp 79—80 °C, in 65% yield. Found: C, 93.06; H, 6.85%. Calcd for $C_{18}H_{16}$: C, 93.06; H, 6.94%. ^{1}H NMR ($CDCl_3$, δ): 1.26 (3H, d, J=7 Hz), 1.45 (3H, d, J=7 Hz), 3.77 (1H, quintet, J=7 Hz), 4.07 (1H, quintet, J=7 Hz), 8.09 (1H, s), 7.0—8.1 (7H, m).

9-(1-Methyl-1-propenyl)triptycene. A solution of 360 mg (2.0 mmol) of anthranilic acid in 10 mL of acetone was added in 1 h to 9-(1-methyl-1-propenyl)anthracene (*Z*/*E*=1.6) and 0.5 mL of isopentyl nitrite in 20 mL of dichloromethane under a nitrogen atmosphere. The solvents were removed by evaporation and 5 mL of ethanol was added to induce crystallization. The crystals were recrystallized from acetone–hexane. The product, mp 185—192 °C, consisted of 1:1.6 of *E* and *Z* isomers. Found: C, 93.49; H, 6.32%. Calcd for $C_{24}H_{20}$: C, 93.46; H, 6.54%. The

following ^{1}H NMR ($CDCl_3$, δ) spectral data were obtained. *E*-isomer: 2.07 (3H, br d, J=6.9 Hz), 2.25 (3H, br s), 5.29 (1H, s), 6.55 (1H, br q, J=6.9 Hz), 6.78—7.10 (6H, m), 7.25—7.63 (6H, m). *Z*-isomer: 0.95 (3H, dq, J=6.9 and 1 Hz), 2.73 (3H, br s), 5.27 (1H, s), 6.18 (1H, br q, J=6.9 Hz), 6.83—7.10 (6H, m), 7.22—7.73 (6H, m).

(Z)-1,2,3,4-Tetrachloro-9-(1-methyl-1-propenyl)triptycene (13). A similar treatment of 9-(1-methyl-1-propenyl)anthracene with tetrachlorobenzyne, generated from tetrachloroanthranilic acid,[24] afforded the crude triptycene. Column chromatography on alumina (10:1 hexane–dichloromethane) followed by recrystallization of the eluted product from acetone–hexane gave 100 mg of pure (*Z*)-1,2,3,4-tetrachloro-9-(1-methyl-1-propenyl)triptycene, mp 239.5—240.5 °C. Found: C, 64.39; H, 3.34; Cl, 31.87%. Calcd for $C_{24}H_{16}Cl_4$: C, 64.61; H, 3.61; Cl, 31.78%. ^{1}H NMR ($CDCl_3$, δ): 0.91 (3H, br d, J=7.2 Hz), 2.68 (3H, br s), 5.89 (1H, s), 6.09 (1H, br q, J=7.2 Hz), 6.77—7.12 (4H, m), 7.22—7.51 (2H, m), 7.60—7.90 (2H, m).

trans-*1,2-Dimethyl-7,8,9,10-tetrachloro-1,2,6,10b-tetrahydro-6,10b-o-benzenoaceanthrylene (10).* This compound was prepared similarly from *trans*-1,2-dimethylaceanthrene (**7**) and tetrachlorobenzyne. After rough chromatography, the product consisted of 6:5 (1*SR*,2*SR*,10b*SR*) and (1*RS*,2*RS*,10b*SR*) isomers. Out of the mixture, one isomer crystallized out on standing. It was purified by recrystallization from hexane–ethanol. The pure compound, mp 265—266 °C, was assigned a (1*SR*,2*SR*,10b*SR*)-structure (**10a**) due to the NOE experiment. Found: C, 64.82; H, 3.42%. Calcd for $C_{24}H_{16}Cl_4$: C, 64.60; H, 3.62%. High resolution MS (M^+): 444.0011, 445.9942, 447.9951, 449.9950. $C_{24}H_{16}Cl_4$ requires 444.0002, 445.9973, 447.9943, and 449.9914. Intensities of the peaks agreed well with those calculated from natural abundance of ^{35}Cl and ^{37}Cl. ^{1}H NMR ($CDCl_3$, δ): 1.50 (3H, d, J=7 Hz), 2.19 (3H, d, J=7 Hz), 3.21 (1H, q, J=7 Hz), 3.83 (1H, q, J=7 Hz), 5.97 (1H, s), 6.8—7.5 (6H, m), 7.90 (1H, m). The (1*RS*,2*RS*,10b*RS*)-isomer (**10b**) could not be separated even by high performance liquid chromatography because its R_f value was too close to that of the (1*SR*,2*SR*,10b*SR*)-isomer. ^{1}H NMR ($CDCl_3$, δ): 1.40 (3H, d, J=7 Hz), 2.00 (3H, d, J=7 Hz), 6.05 (1H, s).

cis-*1,2-Dimethyl-7,8,9,10-tetrachloro-1,2,6,10b-tetrahydro-6,10b-o-benzenoaceanthrylene (11).* This compound was prepared as described in the preparation of the *trans*-isomer (**10**). One of the products crystallized out from the mixture, purified by recrystallization from hexane–ethanol and found to be (1*RS*,2*SR*,10b*SR*)-isomer (**11b**), mp 272.5—274.5 °C. Found: C, 64.63; H, 3.37; Cl, 31.68%. Calcd for $C_{24}H_{16}Cl_4$: C, 64.60; H, 3.62; Cl, 31.78%. ^{1}H NMR ($CDCl_3$, δ): 1.40 (3H, d, J=7 Hz), 1.55 (3H, d, J=7 Hz), 3.35 (1H, quintet, J=7 Hz), 3.83 (1H, quintet, J=7 Hz), 5.90 (1H, s), 6.8—7.6 (7H, m). The structural assignment based on the NOE experiment. The (1*SR*,2*RS*,10b*SR*)-isomer (**11a**) was separated as above and obtained as a solution of an almost pure material. ^{1}H NMR ($CDCl_3$, δ): 1.12 (3H, d, J=7 Hz), 2.11 (3H, d, J=7 Hz), 3.63 (1H, quintet, J=7 Hz), 4.48 (1H, quintet, J=7 Hz), 6.02 (1H, s), 6.8—7.5 (6H, m), 7.87 (1H, m). The original reaction mixture contained 3:2 (1*RS*,2*SR*,10b*SR*)- and (1*SR*,2*RS*,10b*SR*)-isomers.

Isomerization of 9-(1-Methyl-1-propenyl)triptycenes. A solution of 30 mg of 9-(1-methyl-1-propenyl)triptycene and 1 mmol of trifluoroacetic acid in 0.5 mL of chloroform-*d* was heated in a sealed tube at 90 °C. The isomerization was followed by ^{1}H NMR to show that the content was almost pure *E*-form after 50 h. The solvent was evaporated and the residue was purified by TLC (silica gel, 20:1 hexane–dichloromethane) to afford the pure *E*-form, mp 228 °C. Found: C, 93.28; H, 6.27%. Calcd for $C_{24}H_{20}$: C, 93.46; H, 6.54%.

Similarly the isomerization of (*Z*)-1,2,3,4-tetrachloro-9-(1-methyl-1-propenyl)triptycene (**13**) was carried out. It took 30 days to obtain *E*/*Z* ratio of 10. The *E*-isomer (**14**) was obtained as a pure form on recrystallization from the tetrahydrofuran–hexane, mp 222—223 °C. High resolution MS (M^+): 443.9990, 445.9969, 447.9919, 449.9889. $C_{24}H_{16}Cl_4$ requires 444.0002, 445.9973, 447.9943, and 449.9914. Intensity ratios of these peaks were in good agreement with those calculated from the natural abundance of ^{35}Cl and ^{37}Cl. ^{1}H NMR ($CDCl_3$, δ): 2.00 (3H, br d, J=6.9 Hz), 2.11 (3H, br s), 5.85 (1H, s), 6.50 (1H, br q, J=6.9 Hz), 6.8—7.1 (4H, m), 7.2—7.5 (2H, m), 7.6—7.9 (2H, m).

Reaction of 1,2,3,4-Tetrachloro-9-(2-chloro-1,1-dimethylethyl)triptycene (1a) Rotamers in the Presence of a Large Excess of Lewis Acids. To a solution of 0.13 mmol of a mixture of ±*sc*- and *ap*-**1a** in 10 mL of benzene was added 0.2 mL (3.3 mmol) of titanium(IV) chloride and the mixture was left to stand for 18 h. The mixture was washed with water and the solvent was evaporated. A ^{1}H NMR spectrum of this residue showed that, whereas the ±*sc* form had completely reacted, the *ap* form remained almost unaltered. The residue was purified by thin layer chromatography on silica gel, hexane being used as an eluent, to give a mixture of stereoisomers of 1,2-dimethyl-7,8,9,10-tetrachloro-1,2,6,10b-tetrahydro-6,10b-*o*-benzenoaceanthrylene (**10** and **11**) in 52% yield. On standing the product fraction, a part solidified which was purified by recrystallization from hexane–ethanol, mp 272.5—274.5 °C. MS showed M^+ peaks at *m/e* 452, 450, 448, 446, and 444 to indicate that a hydrogen chloride molecule was lost from the starting material. It was identical with (1*RS*,2*SR*,10b*SR*)-1,2-dimethyl-7,8,9,10-tetrahydro-1,2,6,10b-tetrahydro-6,10b-*o*-benzenoaceanthrylene (**11b**). The original mixture of the product contained 45:≈0:10:45 **10a**, **10b**, **11a**, and **11b** as judged from its ^{1}H NMR spectrum.

ap-**1a** was treated similarly with an excess of antimony(V) chloride in benzene. The cyclized product was obtained in 71% yield and the composition of isomers was very close to, if not identical with, that obtained from the ±*sc* form of **1a**. Antimony(V) chloride also effected the same reaction of a mixture of ±*sc* and *ap*-**1a** to give the same mixture.

Reaction of 1,2,3,4-Tetrachloro-9-(2-chloro-1,1-dimethylethyl)triptycene (1a) with Relatively Small Excess of Lewis Acid. A mixture (3:1) of ±*sc*- and *ap*-**1a** (60 mg or 0.12 mmol) in 0.4 mL of benzene-d_6 was mixed with 0.07 mL (1.1 mmol) of titanium(IV) chloride and the reaction was followed by ^{1}H NMR. It took 100 min for the reaction of ±*sc* form to proceed almost completely at room temperature under the conditions. The main product of the reaction was (*E*)-1,2,3,4-tetrachloro-9-(1-methyl-1-propenyl)triptycene (**14**) in addition to a small amount of cyclized compounds (**10** and **11**).

Reaction of 1,2,3,4-Tetrachloro-9-(2-bromo-1,1-dimethylethyl)triptycene (1b) with Lewis Acids. A mixture of ±*sc*- and *ap*-**1b** (25.6 mg, *sc*/*ap* 6.0) in 10 mL of benzene was treated overnight with 0.05 mL of titanium(IV) chloride as above. The reaction gave the *E*-olefin (**14**) in addition to a small amount of the cyclized compounds (**10** and **11**). The *ap* form of **1b** was recovered over 90%.

A mixture (50 mg or 0.095 mmol) of ±*sc*- and *ap*-**1b** with 0.17 mmol of silver nitrate in 0.05 mL of acetonitrile-d_3 was heated at 50—60 °C for 3 h because the reaction

was slow at room temperature. The reaction mixture gave the olefins (**13**/**14**=1) and recovered *ap*-**1b**.

Cyclization of Olefins with Acids. A mixture (30 mg) of (*E*)- and (*Z*)-1,2,3,4-tetrachloro-9-(1-methyl-1-propenyl)-triptycene was dissolved in 0.4 mL of chloroform-*d* and 0.05 mL of trifluoromethanesulfonic acid was added to the solution. The reaction was followed by ^{1}H NMR to show that it was complete within 5 min at room temperature. The product was a mixture of cyclized compounds (**10** and **11**) and the composition was quite similar with those obtained by other methods. The yield was *ca.* 70%.

Similarly 1,2,3,4-tetrachloro-9-(1-methyl-2-propenyl)triptycene (**15**) was treated with trifluoromethanesulfonic acid to afford 67% cyclized products (**10** and **11**). Titanium(IV) chloride could also effect cyclization of the olefin to give 71% cyclized products.

However, treatment of (*Z*)-1,2,3,4-tetrachloro-9-(1-methyl-1-propenyl)triptycene with trifluoroacetic acid resulted in formation of the *E*-form as stated above but failed to give cyclized products. Sulfuric acid-d_2 also failed to give cyclization products, although a mixture of the olefin and sulfuric acid-d_2 in $CDCl_3$–CD_3CN (3:1) was heated up to 90 °C.

Determination of Rates of Reactions. Reactions of 1,2,3,4-tetrachloro-9-(2-chloro-1,1-dimethylethyl)triptycene (**1a**) were carried out similarly as were described above, except using benzene-d_6 as a solvent and dioxane in a capillary tube as an external standard. Decrease in the amount of the starting material was followed by ^{1}H NMR spectroscopy. The data were treated by assuming that the reaction was of pseudo-first order since a large excess of the catalyst was employed.

Spectral Measurements. The normal ^{1}H NMR spectra were measured on either a Hitachi R-20B or Varian EM 390 spectrometer, operating at 60 and 90 MHz, respectively. With dilute solutions, a JEOL FX60 machine was used which was equipped with the FT facilities. For the NOE measurements of ordinary concentrations, the EM 390 spectrometer was used. A sample (25 mg) was dissolved in 0.3 mL of chloroform-*d*. Air in the sample tube was replaced by argon. The methyl signal appearing at a lower field was irradiated and the integration of a signal which was at the lowest field of the aromatic region was carried out. The integrated area was compared with that due to bridgehead proton appearing at δ *ca.* 6. For dilute solutions, data were accumulated for 500 times. Mass spectra were obtained with a Hitachi RMU-6L instrument and high resolution mass spectra with a JEOL JMS-D300.

High Pressure Liquid Chromatography. It was carried out with a Waters Model 6000A apparatus equipped with a UV detector. A microporasil column of 4 mm × 30 cm was used. The eluent was hexane. Although the peaks due to two isomers of **11** were not separated clearly, it was possible to shave the front part to give almost pure **11a**, as far as ^{1}H NMR spectra concerned. The overlap of peaks due to two isomers of **10** was so severe that it was impossible to concentrate **10b** by this method.

This work was supported by a grant from Toray Science Foundation to which our thanks are due.

References

1) For Part VII, see M. Ōki and R. Saito, *Chem. Lett.*, **1981**, 649.

2) A preliminary note has been published: H. Kikuchi, T. Mitsuhashi, N. Nakamura, and M. Ōki, *Chem. Lett.*, **1980**, 209.

3) T. Morinaga, S. Seki, H. Kikuchi, G. Yamamoto, and M. Ōki, *J. Am. Chem. Soc.*, **102**, 1173 (1980); S. Seki, T. Morinaga, H. Kikuchi, T. Mitsuhashi, G. Yamamoto, and M. Ōki, *Bull. Chem. Soc. Jpn.*, **54**, 1465 (1981).

4) F. C. Whitmore and G. H. Fleming, *J. Am. Chem. Soc.*, **55**, 4161 (1933); F. C. Whitmore, E. L. Wittle, and A. H. Popkin, *ibid.*, **61**, 1586 (1939).

5) A. Streitwieser, Jr., *Chem. Rev.*, **56**, 571 (1956).

6) P. E. Peterson and E. V. P. Tao, *J. Am. Chem. Soc.*, **86**, 4503 (1964); G. A. Olah and P. E. Peterson, *ibid.*, **90**, 4675 (1968).

7) H. C. Brown and R. S. Fletcher, *J. Am. Chem. Soc.*, **71**, 1845 (1949).

8) a) N. M. Cullinane and D. M. Leyshon, *J. Chem. Soc.*, **1954**, 2942; b) P. Mastagli, P. Lambert, and C. Hirigoyen, *C. R. Acad. Sci.*, **249**, 1964 (1959); c) G. A. Olah, S. Kobayashi, and M. Tashiro, *J. Am. Chem. Soc.*, **94**, 7448 (1972).

9) G. Izumi, G. Yamamoto, and M. Ōki, *Bull. Chem. Soc. Jpn.*, **54**, 3064 (1981).

10) O. C. Dermer, D. M. Wilson, and V. H. Dermer, *J. Am. Chem. Soc.*, **63**, 2881 (1941); Ref. 8c.

11) σ-Participation in isomerization of neopentyl type cation now seems to be established: T. Ando, H. Yamataka, H. Morisaki, J. Yamawaki, J. Kuramochi, and Y. Yukawa, *J. Am. Chem. Soc.*, **103**, 430 (1981); V. J. Shiner, Jr., and J. J. Tai, *ibid.*, **103**, 436 (1981). However, we show the scheme with classical cations for the sake of simplicity.

12) The possibility that the triptycyl group migrates at the first stage cannot be ruled out, since **1a** takes most probably, the conformation in which the chloro group in the 9-substituent takes an outward position of the triptycyl group and a group anti to the leaving group is prone to migration in Wagner-Meerwein rearrangement. However, this is not our first choice for the mechanism for the following reasons. If it is the case the cation formed at the initial stage may be approximated by **16** which does not easily cyclize because of the steric effect of the *gem*-dimethyl group but isomerizes to **17** and then to **5**. If **16** were to intervene, there should be a strong possibility that a proton is lost from one of the methyls to lead to 9-(2-methyl-2-propenyl) compound, which was not actually found in the olefinic products.

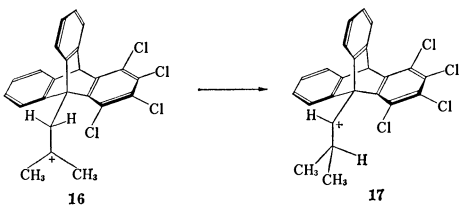

16 17

13) G. Yamamoto and M. Ōki, *Bull. Chem. Soc. Jpn.*, **48**, 3686 (1975).

14) L. L. Ingraham, "Steric Effects on Certain Physical Properties," in "Steric Effects in Organic Chemistry," ed by M. S. Newman, John Wiley & Sons, New York (1956), pp. 479—522.

15) M. Saunders, P. von R. Schleyer, and G. A. Olah, *J. Am. Chem. Soc.*, **86**, 5680 (1964); D. M. Brouwer, C. MacLean, and E. L. Mackor, *Discuss. Faraday Soc.*, **39**, 129 (1965); G. J. Karabatsos, R. A. Mount, D. O. Rickter, and S. Meyerson, *J. Am. Chem. Soc.*, **88**, 5651 (1966); M. Saunders and M. R. Kates, *ibid.*, **100**, 7082 (1978).

16) M. Mikami, K. Toriumi, M. Konno, and Y. Saito, *Acta Crystallogr., Sect. B*, **31**, 2427 (1975).

17) S. Otsuka, T. Mitsuhashi, and M. Ōki, *Bull. Chem. Soc. Jpn.*, **52**, 3663 (1979); S. Otsuka, G. Yamamoto, T. Mitsuhashi, and M. Ōki, *ibid.*, **53**, 2095 (1980).

18) M. Nakamura and M. Ōki, *Bull. Chem. Soc. Jpn.*, **48**, 2106 (1975).
19) H. Kikuchi, S. Hatakeyama, G. Yamamoto, and M. Ōki, *Bull. Chem. Soc. Jpn.*, **54**, 3832 (1981).
20) For the sake of simplicity of the scheme, some of the possible paths of interconversion were omitted.
21) M. Ōki, G. Izumi, G. Yamamoto, and N. Nakamura, *Bull. Chem. Soc. Jpn.*, **55**, 159 (1982); G. Yamamoto and M. Ōki, *ibid.*, **54**, 481 (1981); N. Nogami, Ph. D. Thesis, The University of Tokyo (1978).
22) F. Suzuki, M. Ōki, and H. Nakanishi, *Bull. Chem. Soc. Jpn.*, **47**, 3114 (1974).
23) Direct evidence that the proton affinity of pentachlorotitanate anion is less than that of nitrate anion is not available in literature. However, the relative acidity is apparent if one considers the strong reactivity of a complex between acetyl chloride and titanium(IV) chloride (A. Bertrand, *Bull. Soc. Chim. Fr.*, **1880**, 403: Gmelins Handbuch der Anorganischen Chemie, Titan, p. 320) and acetyl nitrate which is more or less covalent (H. Burton and P. F. G. Praill, *J. Chem. Soc.*, **1955**, 729).
24) V. Villiger and L. Blangey, *Ber.*, **42**, 3549 (1909).

Reactivities of Stable Rotamers. IX. Ionizing Reactions of 9-(2-Bromomethyl-6-methylphenyl)fluorene Rotamers[1]

Shigeru MURATA, Seiichiro KANNO, Yo TANABE, Mikio NAKAMURA, and Michinori ŌKI*

Department of Chemistry, Faculty of Science, The University of Tokyo, Bunkyo-ku, Tokyo 113

(Received October 6, 1981)

Ionizing reactions of *ap*-9-(2-bromomethyl-6-methylphenyl)fluorene in ionizing solvents afforded 12-methyl-8,12b-dihydrobenz[*a*]aceanthrylene and its dehydrogenated compound, whereas the *sp* isomer remained intact. Forced ionization of the *sp* isomer with silver salts afforded products originated from the corresponding cation and either the anion of the salt or the solvent, whereas the *ap* isomer gave cyclized product under the same conditions, if the nucleophilicity of the solvent was poor. The reaction of the *sp* isomer was faster than the *ap* in nucleophilic solvents, whereas the reverse was true for poorly nucleophilic solvents. Solvolysis of the rotamers in formic acid yielded the corresponding formates, the *sp* isomer reacting faster than the *ap*. The results are discussed on the basis that the solvation shell in the *ap* form is completed by the participation of the fluorene ring whereas in the *sp* form the shell is completed by the solvent molecules.

Some years ago successful isolation of *sp*- and *ap*-rotamers of 9-(2-bromomethyl-6-methylphenyl)fluorene (**1**) was reported from this laboratory.[2] Since then, reactivities of stable rotamers both in 9-arylfluorenes[3] and 9-substituted triptycenes[1,4] have been investigated. Some of the rotamers show striking differences in reactivities, although some showed differences by only small factors. These findings aroused our interests in investigating the differences in reactivities of *sp*-**1** and *ap*-**1**. Preliminary experiments of heating the isomers of **1** in trifluoroacetic acid revealed that the *ap* form reacted with a measurable rate at 62 °C whereas the *sp* remained intact.[5] In order to get into further insight, we have carried out a series of ionizing reactions of rotamers of **1**. This paper reports and discusses the results of such investigations, which show dramatic changes according to solvents used, in addition to the rotational barrier in **1**.

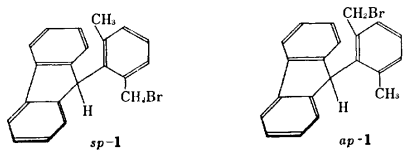

Experimental

9-(2-Bromomethyl-6-methylphenyl)fluorene Rotamers (1). To a boiling solution of 2.5 g (9.3 mmol) of 9-(2,6-dimethylphenyl)fluorene[6] in 100 mL of benzene was added 2.5 g (14 mmol) of *N*-bromosuccinimide and 170 mg of benzoyl peroxide in small portions during a period of 17 h. After filtration, the solvent was removed by evaporation and the residue was submitted to chromatography on silica gel, which used hexane as an eluent. The *sp* form was eluted first and the *ap* form followed. The separation of the isomers was more conveniently performed by using a Waters System 500 preparative liquid chromatographic apparatus, μ-porasil and hexane. In a typical run, 17% of *sp* and 6% of *ap* forms were obtained with 40% of the recovered starting material. The *sp* form, mp 115.0—115.5 °C. Found: C, 72.37; H, 4.76; Br, 23.06%. Calcd for $C_{21}H_{17}Br$: C, 72.22; H, 4.91; Br, 22.88%. ^{1}H NMR ($CDCl_3$, δ): 1.12 (3H, s), 4.83 (2H, s), 5.60 (1H, s), 6.8—7.9 (11H, m). The *ap* form, mp 125.0—126.0 °C. Found: C, 72.40; H, 4.74; Br, 23.06%. Calcd for $C_{21}H_{17}Br$: C, 72.22; H, 4.91; Br, 22.88%. ^{1}H NMR ($CDCl_3$, δ): 2.70 (3H, s), 3.37 (2H, s), 5.52 (1H, s), 7.0—8.0 (11H, m).

9-[2,6-Bis(bromomethyl)phenyl]fluorene, mp 143—144 °C, was obtained as a byproduct which was eluted later than the monobromo compounds in the chromatography. Found: C, 58.83; H, 3.54; Br, 37.65%. Calcd for $C_{21}H_{16}Br_2$: C, 58.91; H, 3.77; Br, 37.32%. ^{1}H NMR (CCl_4, δ): 3.22 (2H, s), 4.72 (2H, s), 5.50 (1H, s), 7.0—8.0 (11H, m).

Rates of Rotation. Either one of pure *sp* and *ap* isomers was dissolved in hexachlorobutadiene and the solution was heated by immersing it in an appropriate boiling solvent bath. The decrease in the amount of the starting material and/or the increase in the amount of the other isomer was monitored by ^{1}H NMR spectroscopy. Equilibrium constants were obtained at the temperature by heating the solution for a long enough time and were found to be invariant at $sp/ap = 3.6 \pm 0.2$ throughout the temperature range examined. The same equilibrium constants were obtained by starting from either of the isomers. The rate constants were obtained by utilizing the following equation (1), where K is now known, a is the initial amount and x the amount at time t, by assuming the first order reaction. The plot gave very good straight lines.

$$\ln\left\{1-\left(1+\frac{1}{K}\right)\frac{a}{x}\right\} = -k\left(1+\frac{1}{K}\right)t \qquad (1)$$

Putting these k's into the Arrhenius and the Eyring equations, we obtained the activation parameters.

Reaction of 1 with Silver Nitrate in Acetonitrile. To a solution of 22 mg (0.06 mmol) of *sp*-**1** in 2 mL of acetonitrile, 10 mg (0.06 mmol) of silver nitrate in 1.0 mL of acetonitrile was added. The whole was allowed to react for 30 min at 50 °C. The reaction mixture was filtered and the filtrate was evaporated. Recrystallization of the residue from ethanol afforded 20 mg (90%) of *sp*-2-(9-fluorenyl)-3-methylbenzyl nitrate, mp 104 °C. Found: C, 76.19; H, 5.03; N, 4.18%. Calcd for $C_{21}H_{17}NO_3$: C, 76.12; H, 5.17; N, 4.23%. ^{1}H NMR ($CDCl_3$, δ): 1.16 (3H, s), 5.32 (1H, s), 5.80 (2H, s), 7.0—7.9 (11H, m). IR (KBr disk): 1628, 1278, 842 cm^{-1}.

ap-**1** similarly gave *ap*-2-(9-fluorenyl)-3-methylbenzyl nitrate, mp 128 °C. Found: C, 75.97; H, 4.97; N, 4.30%. Calcd for $C_{21}H_{17}NO_3$: C, 76.12; H, 5.17; N, 4.23%. ^{1}H NMR ($CDCl_3$, δ): 2.75 (3H, s), 4.22 (2H, s), 5.56 (1H, s), 7.0—8.0 (11H, m). IR (KBr disk): 1617, 1280, 875 cm^{-1}.

Reaction of 1 with Silver Perchlorate in Acetonitrile. The reaction was carried out similarly as above except using silver perchlorate instead of silver nitrate and treating the reaction mixture as follows. The reaction mixture was

treated with 5% aqueous lithium chloride. Ether was added and the mixture was filtered to remove insoluble materials. The ether layer was separated and the aqueous layer was extracted with ether. The combined ether layer was washed, dried, and evaporated. The residue was recrystallized from hexane–ethanol.

sp-**1** gave *sp*-9-(2-acetamidomethyl-6-methylphenyl)-fluorene, mp 194 °C, in 70% yield. Found: C, 84.17; H, 6.31; N, 4.29%. Calcd for $C_{23}H_{21}NO$: C, 84.37; H, 6.46; N, 4.28%. ^{1}H NMR ($CDCl_3$, δ): 1.13 (3H, s), 1.96 (3H, s), 4.76 (2H, d, J=5.4 Hz), 5.37 (1H, s), 5.7 (1H, br s), 6.8—8.0 (11H, m). IR (KBr disk): 3240, 1635, 1550 cm^{-1}.

ap-**1** gave *ap*-9-(2-acetamidomethyl-6-methylphenyl)-fluoene, mp 188 °C, in 50% yield. Found: C, 84.23; H, 6.24; N, 4.37%. Calcd for $C_{23}H_{21}NO$: C, 84.37; H, 6.46; N, 4.28%. ^{1}H NMR ($CDCl_3$, δ): 1.46 (3H, s), 2.73 (3H, s), 3.23 (2H, d, J=6.3 Hz), 4.1 (1H, br s), 5.54 (1H, s), 7.0—8.0 (11H, m). IR (KBr disk): 3270, 1640, 1550 cm^{-1}.

Reaction of **1** *with Silver Perchlorate in Benzene.* The reaction was carried out similarly with that in acetonitrile except that benzene was used as a solvent and the reaction mixture was allowed to stand overnight at 22 °C.

sp-**1** afforded *sp*-9-(2-benzyl-6-methylphenyl)fluorene, mp 105 °C, as a sole product in 64% yield. Found: C, 93.50; H, 6.20%. Calcd for $C_{27}H_{22}$: C, 93.60; H, 6.40%. ^{1}H NMR ($CDCl_3$, δ): 1.10 (3H, s), 4.37 (2H, s), 5.45 (1H, s), 6.8—7.9 (16H, m).

Formation of bis[*sp*-2-(9-fluorenyl)-3-methylbenzyl] ether (see below) was detected during the reaction but this compound subsequently reacted under the reaction conditions to afford *sp*-9-(2-benzyl-6-methylphenyl)fluorene.

ap-**1** afforded 12-methyl-8,12b-dihydrobenz[*a*]aceanthrylene, which was characterized in the section of the reaction in trifluoroacetic acid, and *ap*-9-(2-benzyl-6-methylphenyl)-fluorene, mp 143 °C, in 1:12 ratio. Found: C, 93.76; H, 6.22%. Calcd for $C_{27}H_{22}$: C, 93.60; H, 6.40%. ^{1}H NMR ($CDCl_3$, δ): 2.67 (2H, s), 2.69 (3H, s), 5.54 (1H, s), 6.5—7.9 (16H, m).

Bis[sp-*2-(9-fluorenyl)-3-methylbenzyl*] *Ether.* A mixture of 15 mg of *sp*-**1** in 2.6 mL of benzene and 17.8 mg of silver perchlorate in 1.7 mL of benzene containing *ca.* 10 μL of water was stirred for 30 h at room temperature and then was heated at 50 °C for 30 min. To the cooled mixture, 3.5 mL of methanol and then 5% aqueous lithium chloride were added. Silver salts were removed by filtration and the organic products were collected. Preparative TLC on silica gel (3:1 hexane–benzene) afforded *ca.* 4 mg of the desired ether, which was recrystallized from benzene–ethanol, mp 192—193 °C, and small amounts each of *sp*-9-(2-methoxymethyl-6-methylphenyl)fluorene (see below) and *sp*-(2-benzyl-6-methylphenyl)fluorene. Found: C, 91.23; H, 5.88%. Calcd for $C_{42}H_{34}O$: C, 90.94; H, 6.18%. MS (M$^+$): 554. ^{1}H NMR ($CDCl_3$, δ): 1.12 (6H, s), 4.98 (4H, s), 5.64 (2H, s), 6.8—7.9 (22H, m).

9-(2-Hydroxymethyl-6-methylphenyl)fluorene. To a solution of 60 mg (0.17 mmol) of *sp*-**1** in 6 mL of acetone was added a solution of 106 mg (0.51 mmol) of silver perchlorate in 1 mL of water. The mixture was stirred for 10 min at room temperature in dark, and then warmed at 50 °C for 10 min. After silver bromide was removed by filtration, the reaction product was precipitated by addition of water and extracted with ether. The extract was washed with water, dried, and evaporated. The residue was developed on a preparative TLC plate (1:4 hexane–benzene) to give 40 mg (81%) of *sp*-9-(2-hydroxymethyl-6-methylphenyl)-fluorene, mp 74—75 °C, which was recrystallized from hexane. Found: C, 88.17; H, 6.21%. Calcd for $C_{21}H_{18}O$: C, 88.08; H, 6.34%. ^{1}H NMR ($CDCl_3$, δ): 1.12 (3H, s), 1.8 (1H, br s), 5.02 (2H, s), 5.59 (1H, s), 6.8—7.9 (11H, m).

Solvolysis of **1** *in Formic Acid.* A solution of 29 mg of *sp*-**1** in 3 mL of chloroform and 20 mL of formic acid was heated at 50—60 °C for 24 h and poured into water. The organic materials were extracted with ether and the ether extract was washed and dried. After evaporation of the solvent, the residue was developed on a preparative TLC plate (1:2 hexane–benzene) to give *ca.* 80% *sp*-2-(9-fluorenyl)-3-methylbenzyl formate, oil. High resolution MS (M$^+$): 314.1314. Calcd for $C_{22}H_{18}O_2$: 314.1307. ^{1}H NMR ($CDCl_3$, δ): 1.12 (3H, s), 5.37 (1H, s), 5.54 (2H, s), 6.8—8.0 (11H, m), 8.14 (1H, s). IR (neat): 1722, 1150 cm^{-1}.

Similarly, *ap*-**1** afforded *ca.* 80% *ap*-2-(9-fluorenyl)-3 methylbenzyl formate, mp 106 °C, which was recrystallized from pentane–ethanol. Found: C, 84.02; H, 5.50%. Calcd for $C_{22}H_{18}O_2$: C, 84.05; H, 5.77%. ^{1}H NMR ($CDCl_3$, δ): 2.75 (3H, s), 3.97 (2H, s), 5.53 (1H, s), 6.9—8.0 (12H, m). IR (KBr disk): 1716, 1178 cm^{-1}.

Reaction of **1** *Caused by Heating a Trifluoroacetic Acid (TFA) Solution.* A solution of 33 mg of *ap*-**1** in 1.5 mL of chloroform was added to 25 mL of TFA. The whole solution was heated at 60 °C for 6 h. The mixture was poured into water and then extracted with chloroform. After the usual treatment, the products were purified by silica gel TLC (hexane) to afford 8 mg (32%) of 12-methyl-8,12b-dihydrobenz[*a*]aceanthrylene, mp 180—181 °C, after recrystallization from benzene–ethanol. Found: C, 94.23; H, 5.78%. Calcd for $C_{21}H_{16}$: C, 93.99; H, 6.01%. ^{1}H NMR ($CDCl_3$, δ): 2.48 (3H, s), 3.99 (1H, d, J=16.4 Hz), 4.14 (1H, dd, J=16.4 and 2.3 Hz), 4.80 (1H, d, J=2.3 Hz), 6.9—8.1 (10H, m). MS (M$^+$): 268.

The product was always accompanied by 12-methylbenz[*a*]aceanthrylene which was eluted before the dihydro compound. Preparation of the dehydrogenated compound is described below. This dehydrogenation seemed to be effected by atmospheric oxygen, since careful exclusion of oxygen decreased the amount of this product, increasing the yield of the dihydro compound.

The concentration of *ap*-**1** in trifluoroacetic acid plays an important role in determining the yield of the cyclized product. Heating a solution of 80 mg of *ap*-**1** in 5 mL of chloroform and 15 mL of TFA gave at least 10 spots in TLC, although the cyclized product was main, and a more concentrated solution, which was convenient for the routine ^{1}H NMR measurement, than this afforded only polymers.

sp-**1** did not apparently react under the similar conditions. Heating a solution of 20 mg of *sp*-**1** in 0.1 mL of chloroform and 0.4 mL of TFA at 62 °C for 40 h gave only the recovered starting material.

12-Methylbenz[a]*aceanthrylene.* A solution of 6 mg of 12-methyl-8,12b-dihydrobenz[*a*]aceanthrylene in 1 mL of benzene was mixed with 6 mg of 2,3-dichloro-5,6-dicyano-*p*-benzoquinone in benzene. The mixture was stirred for 1 h at room temperature and then heated at 50 °C for 1 h. The hydroquinone produced in the reaction was removed by passing the solution through a column of 200 mg of silica gel. The filtrate and washings (1:1 hexane–benzene) were combined and evaporated to give the desired compound, orange oil, in an almost quantitative yield. High resolution MS (M$^+$): 266.1106. $C_{24}H_{14}$ requires M$^+$ 266.1095. ^{1}H NMR ($CDCl_3$, δ): 3.17 (3H, s), 7.2—8.5 (11H, m). UV (EtOH, λ_{max} in nm and log ε in parentheses): 430 (3.65), 366 (3.40), 260 (4.54).

Reaction of **1** *Caused by Heating a 1,1,1,3,3,3-Hexafluoro-2-propanol (HFP) Solution.* A solution of 10 mg of *ap*-**1**

in 0.3 mL of chloroform and 15.6 mL of HFP was heated at 50—55 °C for 4 h. The reaction product was similarly treated as above to give 65—75% 12-methyl-8,12b-dihydrobenz[*a*]aceanthrylene. The dehydrogenated product was detected only in a trace amount.

Under the similar conditions, *sp*-**1** was completely recovered.

Reaction of **1** *in HFP with Silver Perchlorate.* A heterogeneous mixture of 10 mg of *ap*-**1** in 0.6 mL of chloroform and 15.6 mL of HFP and *ca.* 3 equiv. of silver perchlorate was stirred at 20 °C for 5 h. The mixture was treated with methanol to decompose any of the possible perchlorate still present. After the usual treatment, 3 mg (40%) of 12-methyl-8,12b-dihydrobenz[*a*]aceanthrylene was obtained. No methoxy compound was detected.

Similar treatment of *sp*-**1** afforded 30% *sp*-(2-methoxymethyl-6-methylphenyl)fluorene (for the characterization, see below). No cyclized product was obtained.

Reaction of **1** *in TFA with Silver Perchlorate.* This reaction was performed similarly as above. The *ap* form gave the cyclized product, whereas the *sp* form afforded the methoxy compound only.

9-(2-Methoxymethyl-6-methylphenyl)fluorene Rotamers. To a solution of 25 mg (0.07 mmol) of *sp*-**1** in 0.4 mL of chloroform and 5 mL of methanol, was added a solution of 56 mg (0.27 mmol) of silver perchlorate in 2 mL of methanol. The mixture was allowed to stand for 10 min at room temperature in dark. Silver bromide was removed by filtration and the filtrate was poured into water. The mixture was extracted with dichloromethane. The extract was washed, dried, and evaporated to give a colorless oil. High resolution MS (M^+): 300.1497. $C_{22}H_{20}O$ requires 300.1512, ^{1}H NMR ($CDCl_3$, δ): 1.12 (3H, s), 3.44 (3H, s), 4.76 (2H. s), 5.56 (1H, s), 6.8—7.9 (11H, m).

Similarly, *ap*-9-(2-methoxymethyl-6-methylphenyl)fluorene (recrystallized from ethanol), mp 118 °C, was obtained from *ap*-**1**. Found: C, 88.11; H, 6.66%. Calcd for $C_{22}H_{20}O$: C, 87.96; H, 6.71%. ^{1}H NMR ($CDCl_3$, δ): 2.56 (3H, s), 2.71 (3H, s), 3.14 (2H, s), 5.48 (1H, s), 6.9—8.0 (11H, m).

Reaction of **1** *in TFA–CH_3OH–$CHCl_3$ or HFP–CH_3OH–$CHCl_3$.* The reaction was similarly carried out as for those without methanol, except 3 (v/v)% methanol was added to TFA or HFP prior to the mixing. *ap*-**1** afforded 12-methyl-8,12b-dihydrobenz[*a*]aceanthrylene and its dehydrogenated compound in both systems. *sp*-**1** was recovered unchanged in TFA, whereas it gave *sp*-9-(2-methoxymethyl-6-methylphenyl)fluorene in HFP. When *sp*-**1** in TFA–CH_3OH–$CHCl_3$ was heated, only polymers were obtained.

Competitive Reactions. A typical procedure follows. To a solution of 6.0 mg (17 μmol) of *sp*-**1**, the same amount of *ap*-**1** and 2.9 mg of fluorene in 1 mL of acetonitrile was added a solution of 3.0 mg (17 μmol) of silver nitrate. The mixture was stirred for 40 min at 25 °C. An excess amount of aqueous lithium chloride was added and the precipitate was removed by filtration. The amount of unreacted material was measured with the use of a Waters M-6000A high pressure liquid chromatograph which was equipped with a UV detecter. Fluorene which had been added to the original mixture served as an internal standard. The relative reactivity was calculated by applying the following equation (2).

$$k_{sp}/k_{ap} = \log \frac{[sp]}{[sp]_0} \Big/ \log \frac{[ap]}{[ap]_0}, \qquad (2)$$

where subscript 0 denotes the initial concentration.

In the cases of other competitive reactions, the solvent systems quoted in the independent reactions for the respective rotamers were used. The amount of the substrate and a silver salt was kept equimolar in every reaction. Solvolytic reactions were also carried out similarly.

Spectral Measurements. ^{1}H NMR spectra were recorded on a Hitachi R-20B spectrometer operating at 60 MHz or on a Varian EM390 spectrometer operating at 90 MHz. A detailed spectrum of 12-methyl-8,12b-dihydrobenz[*a*]aceanthrylene was obtained with a Bruker 270 MHz machine. IR and UV spectra were obtained with a Hitachi IR-260-30 spectrometer and a Hitachi UV-340 spectrometer, respectively. High resolution mass spectra were recorded on a JEOL D-300 machine.

Table 1. Rate constant for isomerization of 9-(2-bromomethyl-6-methylphenyl)fluorene rotamers in hexachlorobutadiene

Temperature/°C	$k_{sp\to ap}/10^{-6}$ s^{-1}	$k_{ap\to sp}/10^{-5}$ s^{-1}
80	1.0	0.36
100	6.4	2.3
111	19	6.9
121	57	21

Table 2. Activation parameters for internal rotation in 9-(2-bromomethyl-6-methylphenyl)-fluorene and in 9-(2-methyl-1-naphthyl)fluorene

	9-(2-Bromomethyl-6-methylphenyl)-fluorene[c]		9-(2-Methyl-1-naphthyl)-fluorene[d] (both direction same)
	sp→*ap*	*ap*→*sp*	
E_a/kcal mol^{-1} [a]	27.0	27.1	29.8
log A/s^{-1}	10.7	11.3	12.9
ΔH^*/kcal mol^{-1} [a]	26.2	26.3	29.9
ΔS^*/e. u.[b]	−12.2	−9.3	0.4
ΔG^*_{373}/kcal mol^{-1} [a]	30.7	29.8	29.8

a) 1 cal=4.18 J. b) 1 e. u.=4.18 J K^{-1} mol^{-1}. c) Hexachlorobutadiene solvent. d) Tetrachloroethylene solvent.

Results and Discussion

Rotational Barriers and Rotamer Populations. Assignment of the stereochemistry of the rotamers were performed by taking the ring current effect of the fluorene ring in ^{1}H NMR spectra into account. In the *sp* conformation, the CH_2Br group is in the shielding zone of the benzene ring, whereas the methyl group is in the deshielding zone. In contrast, the CH_2Br group in the *ap* conformation is in the deshielding zone and the methyl group is in the shielding. Thus the methyl and the methylene protons in the *ap* form show a very large difference in chemical shifts, whereas those in the *sp* show a small chemical shift difference.

Results of the kinetic measurements are summarized in Table 1. Putting these rate constants into the Arrhenius equation, we obtain E_a and log A as shown in Table 2 which summarizes ΔH^* and ΔS^* obtained by putting the rate constants into the Eyring equation as well, together with the free energies of activation for rotation at 373 K. Table 2 also contains activation parameters for rotation in 9-(2-methyl-1-

naphthyl)fluorene (**2**) for comparison: the data by the Arrhenius plot were obtained by Siddall and Stewart[6b] and those by the Eyring plot were calculated by us, using the reported rate constants.[6b]

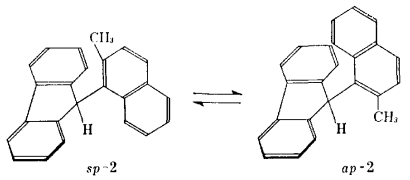

sp-2 *ap*-2

The barrier to rotation in 9-(2,6-dimethylphenyl)-fluorene was predicted to be over 25 kcal/mol on the basis of dynamic NMR study.[7] The present results conform with this expectation. Comparison of the rate constants of internal rotation in compound **2** with those in compound **1** shows interesting trends: At low temperatures, the rotation in compound **2** is relatively slow whereas that in compound **1** is definitely slower than that in the naphthyl compound (**2**) at higher temperatures. On close examination, one notices that the enthalpy of activation and Arrhenius activation energy are definitely larger for compound **2** than those for compound **1**. The slow rotation in compound **1** at the higher temperature is attributed to large negative entropy of activation. This point deserves further mention.

The steric effect of a methyl group given to its ortho position in a substituted phenyl system is often comparable with that of the peri-CH group given to the 1-position of a naphthalene system. As far as we discuss the enthalpy of activation and the Arrhenius activation energy, this general trend is not held here. We may have to admit that the rigidity of the molecule has a profound effect on the enthalpy of activation in 9-arylfluorene systems: Being more rigid than the 2,6-dimethylphenyl group, the 2-methyl-1-naphthyl group will give severer interactions in the transition state for rotation with the fluorene. The effect of the bromo group in **1** may be neglected in discussion, since substitution of a substituent for hydrogen in a methyl group is normally quoted as increasing the size of the whole substituent (however, *vide infra*).

The role of entropy of activation in realizing almost the same free energies of activation for rotation for both systems in the vicinity of 100 °C is thus important. Namely, the negative entropy of activation for rotation in compound **1** makes a contrast with the entropy of activation for **2** which is almost zero. On one hand, we may attribute this outcome to the effect of solvation: in the ground state, the solvation is more difficult than in the transition state for rotation in **1** because of the steric effect. Thus entropy is decreased in the transition state relative to the ground state due to the loss of freedom in the motion of solvent molecules.

On the other hand, the freedom of internal rotation of the CH_2Br group must be considered. Entropy will be decreased when the *sp* form approaches the transition state for rotation from the ground state, because the conformation in the transition state is limited whereas the conformations in the ground state are not. But the decrease in entropy is not certain in the *ap* conformation, because, in its ground state, the possible conformations are also limited due to the steric interaction between the bromo group in the CH_2Br and the fluorene moiety: If the bromo group takes certain positions in possible conformations, the strain will be prohibitively strong.

Summation of these effects together with other unknown factors contributes to the observed entropy change. The results suggest therefore that comparison of the amount of free energies should be made carefully when hydrocarbons and their substituted derivatives are involved.

As for the distribution of *sp* and *ap* conformers at equilibrium, the *sp* form is favored by a factor of 3.6. This is usually attributed to the size of the substituent by saying that the bromomethyl group is larger than a methyl. However, if one compares the size of CH_2Br with CH_3 in the part of direct interactions, one notices that it is the CH_2 in both cases that is responsible because, in the CH_2Br group, the bromine atom is too large to direct toward the fluorene ring. We may attribute this difference in populations to the effect of entropy and/or the solvation effect. Entropy in the *ap* does decrease relative to the *sp* form because of the restriction of some rotamers. Formation of a solvation shell cannot be completed with the solvent molecules only in the *ap* conformation because of the steric effect. The invariance in the equilibrium constants throughout the temperature range suggests that the entropy factor controls equilibrium.

From the barriers to rotation, one calculates that the time necessary for conversion of 5% of the *sp* isomer to the *ap* at 80 °C is *ca.* 1×10^4 s: The limit of errors in NMR spectroscopy to detect a molecular species is considered to be at this level. The reaction conditions used in bromination exceed this limit, yet the reaction period is not long enough to reach equilibrium. Therefore the formation ratio (*sp*/*ap*=2.2—2.7) clearly shows that the *sp* methyl is kinetically favored in bromination. Since there is no apparent strong electronic effects which favor the bromination of the *sp*-methyl, we may attribute this result to the steric effects: the direction of attack on the *ap*-methyl is limited because, at least, one side of the methyl group is blocked by the fluorenyl group.

Products from ap-**1** *Heated in Trifluoroacetic Acid (TFA).* When a solution of *ap*-**1** in TFA–$CHCl_3$ was heated at 62 °C, the products were dependent on the concentration. If the concentration was high, the products were polymer mixtures. If the concentration was lowered, however, a compound was obtained in a pure state. Its MS and elemental analyses were consistent with the formula in that a molecule of hydrogen bromide was lost from the starting material. The most probable structure of the product is 12-methyl-8,12b-dihydrobenz[*a*]aceanthrylene (**3**), of

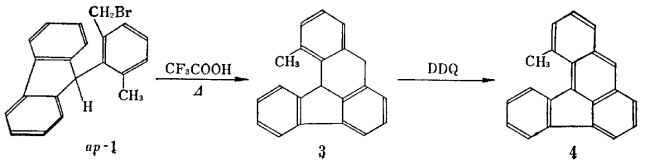

ap-1 3 4

TABLE 3. DEPENDENCE OF DISTRIBUTION OF PRODUCTS IN THE REACTION OF *ap*-**1** WITH SILVER PERCHLORATE IN BENZENE

Reaction conditions		Products[a]			**7**/(**3**+**4**)
Temperature/°C	Duration/h	*ap*-**7**	**3**	**4**	
70	0.7	4.22	1.0	0.28	3.2
50	2.0	5.23	1.0	0.07	4.9
20	23	13.1	1.0	0.14	11.5

a) The product distribution is shown in relative amounts, taking the amount of **3** as reference.

which formation is rationalized by considering the ionization at the CH_2Br group followed by a Friedel-Crafts type cyclization.

^1H NMR spectral data are consistent with the structure. Long-range couplings in the 9,10-dihydroanthracene structure have been known,[8] and the coupling constants are in the order $J_{aa}>J_{ae}>J_{ee}$, where subscripts a and e denote axial and equatorial hydrogens, respectively. In the present compound, the hydrogen in the 12b position is fixed in the axial direction because of the ring structure. Therefore the proton signal which is located at a lower field and shows a coupling constant 2.3 Hz is assigned to the axial proton in the 8-position, as shown in the scheme.

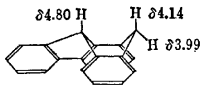

a perspective of 3

When **3** was dehydrogenated with DDQ, a colored hydrocarbon was obtained. This latter compound (**4**) showed absorption maxima at 260, 366, and 430 nm in a UV-VIS spectrum which are very close to those of a known benz[*a*]aceanthrylene skeleton.[9] The UV-VIS data give further confirmation of the structure of the product in the TFA treatment.

Compound **3** was always accompanied by **4** in the reaction in TFA. However, the amount of **4** could be reduced appreciably when atmospheric oxygen was carefully purged.

Reaction of ***1*** *with Silver Salts.* In the heating experiment of a TFA solution of *sp*-**1** no reaction was detected although the solution was heated at 62 °C for 40 h. If the ring system is rigid, there should be formed a diastereomer from the *sp* form by a similar ring closure. In order to explore the possibility, several reactions of *sp*-**1** and *ap*-**1** with silver salts were investigated.

Silver salts are often used for forced ionization of organic halides. Because of the complexity derived by the catalytic action of silver halide, the reaction machanism is not well understood: Pocker *et al.* found the reaction of silver nitrate to be of 2.5th order[10] and Kevill *et al.* carried out some detailed investigations on the reaction of allyl chlorides with silver nitrate.[11] These authors suggest that the reaction proceeds with the intermediacy of ion pairs. In spite of these difficulties, silver nitrate is the most handy reagent for the ionization of organic halides from the stand point of synthesis. We therefore used silver nitrate at the outset.

To our surprise, both isomers gave the corresponding nitrate esters (**5**) in good yields. It is especially interesting in that the *ap* isomer gave the nitrate instead of the cyclized product (**3**). Probably the nucleophilicity of the nitrate anion is so high[12] that the ion pair collapses before the internal rotation, which is necessary for the ring closure, takes place.

In order to lower the nucleophilicity of the anion present in the system, silver perchlorate was used, although we cannot avoid the complexity of the reaction mechanism by using the perchlorate salt.[13]

The reaction of *sp*-**1** and *ap*-**1** with silver perchlorate in acetonitrile gave, after treatment of the reaction mixture with water, the corresponding acetamido derivatives (**6**) which were expected if the Ritter type reaction[14] should take place. The results suggest that acetonitrile is nucleophilic enough to react with carbocations in this system. Since no cyclization product was found from *ap*-**1**, the reaction of the carbocation with acetonitrile is by far the more favored process than the cyclization to afford **3**.

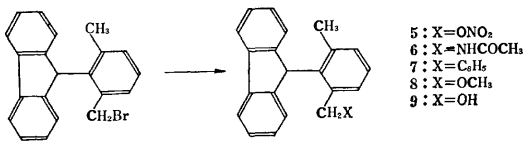

The reaction of *ap*-**1** with silver perchlorate in benzene afforded *ap*-9-(2-benzyl-6-methylphenyl)fluorene (*ap*-**7**) and the cyclized product (**3**) in a 12:1 ratio; apparently the intermolecular Friedel-Crafts reaction is favored over the intramolecular reaction. The intermediacy of a common species is apparent from the temperature dependence of the product ratio. As shown in Table 3, the formation of the cyclized product (**3**) becomes relatively favored as the temperature is raised, though it does never become a main reaction.

Although Pocker and Kevill[15] showed that organic perchlorate can survive for some time in a nonpolar solvent such as benzene, no trace of a product which might be derived from the perchlorate and water was detected under the conditions. However, the long lifetime of the perchlorate could be reproduced as follows. Whereas both *ap*-**1** and *sp*-**1** in benzene reacted very rapidly with silver perchlorate at room temperature to produce silver bromide precipitate, 9-(2-methoxymethyl-6-methylphenyl)fluorene (**8**) with retention of the stereochemistry was formed on addition of methanol after 2—3 h together with 9-(2-benzyl-6-methylphenyl)fluorene (**7**).

Table 4. Relative reactivity of *sp*-**1** and *ap*-**1** under ionizing conditions

Silver salt	Solvent	Concn/mM		Temp °C	Reaction period	k_{sp}/k_{ap}	k_{bz}/k_{sp}[c]
		Substrate	Silver salt				
$AgNO_3$	CH_3CN	9	9	25	40 min	5.9	0.36
$AgClO_4$	CH_3CN	9	9	60	20 h	1.3	0.21
$AgClO_4$	C_6H_6	10	20	22	2 h	1.6	*ca.* 34
$AgClO_4$	HFP[a]	0.8	b)	14	72 min	0.78	—
$AgClO_4$	TFA[a]	0.8	b)	25	13 min	0.94	—

a) These solvents contain *ca.* 5 (v/v)% chloroform. b) Heterogeneous reactions. c) k_{bz}/k_{sp} denotes the relative reactivity of benzyl bromide, taking the reactivity of *sp*-**1** as a reference.

Though not found after the reaction period of 23 h, bis[*sp*-2-(9-fluorenyl)-3-methylbenzyl] ether (**10**) was detected when the reaction mixture from *sp*-**1** and silver perchlorate was treated with methanol after a few hours. This product is derived from water which is present within the reaction system, because careful drying of the reagent and the solvent decreased the amount of the ether (**10**). No such ether was detected when *ap*-**1** was treated similarly. This difference, together with the unusuality discussed below, led us to believe that water or the benzyl alcohol (**9**) derived from *sp*-**1** and water is strongly adsorbed on the silver bromide surface where the formation reaction of **10** takes place.

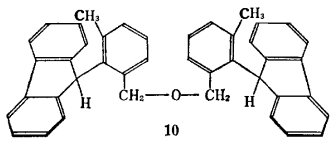

10

During the reaction of *sp*-**1** with silver perchlorate in benzene, the formation of the corresponding benzyl alcohol (**9**) was detected, if water was intentionally added. However, an attempted coupling of the benzyl alcohol (**9**) in the presence of concentrated sulfuric acid did not give any of **10** but led to the formation of polymers. Neither an attempted Williamson synthesis of **10** from *sp*-**1** and the *sp*-alcohol (**9**) in DMF in the presence of silver oxide succeeded. Feasibility of the reaction occurring on the surface of silver bromide is supported also if one considers the concentration of water or the benzyl alcohol (**9**) in the system: if the reaction is to occur in solution, the concentration of the substrate may be prohibitively low. The disappearance of the ether (**10**) in the reaction products after 23 h must be ascribed to the possibility that the ether (**10**) is cleaved by perchloric acid which is formed as a result of the Friedel-Crafts reaction.

TFA is known to be little nucleophilic[16] and 1,1,1,3,3,3-hexafluoro-2-propanol (HFP) is even less nucleophilic.[17] Therefore, in these solvents, the reaction with solvent molecules is practically prohibited. In order to explore further the feasibility of the ring closure of *sp*-**1**, the ionization of *sp*-**1** in these solvents were investigated with the aid of silver perchlorate. Silver perchlorate is not appreciably soluble in these solvents: the reaction had to be carried out in heterogeneous systems. If the reaction was carried out at room temperature, the corresponding perchlorate ester (or perchlorate ion pair or trifluoroacetate ion pair) survived until more nucleophilic reagent was added. Thus the *sp* isomer of the methoxy compound (**8**) was the sole product when methanol was added. When the reaction mixture was heated, only polymers resulted. *ap*-**1**, under the similar conditions, reacted to give the cyclic compound (**3**) in good yields. Thus it becomes apparent that the *ap* isomer cyclized easily whereas the *sp* isomer gave only polymers if the cation is forced to develop.

A rationale for the apparent difference in reactivity of *ap*-**1** and *sp*-**1** may be given in the following way. As has been pointed out, the internal rotation is necessary to form the cyclized product (**3**): The barrier to rotation is over 25 kcal/mol. This may be the reason why even poorly nucleophilic benzene can react with *ap*-**1** to produce *ap*-**7** in the presence of silver perchlorate, in competition with the benzene ring in the fluorene moiety, to consitute the main process at 20 °C. A precise estimation of the barriers to rotation in the *ap* cation (or the ion pair) is not possible at present, but the barrier should be lowered in the cation relative to the parent compound because the barrier to rotation in 9-(2-formyl-1-naphthyl)fluorene,[18] a model compound with an sp^2-carbon as a substituent, is known to be appreciably lower than that in 9-(2-methyl-1-naphthyl)fluorene,[6b] that has an sp^3-hybridized carbon as a substituent in the 2 position of the naphthalene ring: The substituent in the 2 position of the naphthalene ring is responsible in determining the barrier to rotation. Molecular models suggest that it is the substituent in the *ap* position, with respect to the 9-H, rather than the substituent in the *sp* that determines the sharpness of the rising of the potential curve at the early stage of rotation from the ground state. Then in *sp*-**1**, the ease of rotation may not be changed on ionization to an appreciable extent, whereas the ease of rotation is increased in *ap*-**1** on ionization. Thus the polymerization is the preferred process in *sp*-**1** under the conditions examined. At extreme dilution, the cyclization of *sp*-**1** may be possible in principle, but it is not practicable.

Competitive Reactions between sp-*1 and* ap-*1*. In order to see whether the large difference in reactivity of the diastereomers of **1** in TFA is peculiar in that solvent, competitive reactions of *sp*-**1** and *ap*-**1** with silver salts in various solvents were carried out. The results are summarized in Table 4 together with the relative reactivity of benzyl bromide used as a reference compound under the same conditions. We may compare the reactivity of *sp*-**1** and *ap*-**1**, although the

products are formed by different mechanisms after ionization, because the initial ionization can be considered as the rate determining step in both isomers.

Of silver nitrate and silver perchlorate, the former gave a larger k_{sp}/k_{ap} value than the latter in acetonitrile. As has been noticed, the corresponding perchlorate ester is formed, though its lifetime is short, in the reaction with silver perchlorate, which then reacts with the solvent molecule. This will be the main source of difference between the perchlorate and nitrate cases, in the latter of which the collapse of the ion pair gives directly the product. At any rate, the *sp* form is more reactive than the *ap*, making a contrast to the reactivity in TFA.

It is interesting to note that, while the relative reactivity of *sp*-**1** is larger than that of *ap*-**1** in acetonitrile and in benzene, the reverse is true in TFA and HFP. However, the reactivity ratio is not so large as that obtained by heating a TFA solution. The difference may again reflect that in silver perchlorate cases the rate of decomposition of the perchlorate ester is important, whereas the ionization in TFA occurs from the bromide.

In acetonitrile, benzyl bromide is less reactive than *sp*-**1**, while the former is more reactive by a large factor than the latter in benzene. We wish to attribute these phenomena tentatively to the steric effects within the substrates and to those in solvation. On one hand, because of the molecular shape and the fact that the molecule coordinates to a cation with its nitrogen, the steric effect in the solvation with acetonitrile may not play an important role for retardation in the ionization of the CH_2Br group in *sp*-**1**. On the other, the steric interaction in the ground state of *sp*-**1** is relieved to some extent on its ionization. Thus the steric acceleration is operative in the ionization of *sp*-**1** in acetonitrile. In contrast, the completion of the solvation shell for the cation derived from *sp*-**1** requires extra energy in benzene because of the space-demanding molecular shape of the solvent molecule. Therefore the cation derived from *sp*-**1** in benzene is much more unstable than that derived from benzyl bromide. This solvation effect rather than the steric acceleration seems to be a ruling factor in the reactions in benzene.

Solvolytic Reactions. In the foregoing section, the role of solvent is found to be important in determining the relative reactivity. To shed light further on this point, it may be necessary to keep the leaving group constant. Thus we have investigated the solvolytic reactions of *sp*-**1** and *ap*-**1** in various ionizing solvents.

The first choice was formic acid in which solvolytic reactions are close to S_N1.[19] Solvolysis of *sp*-**1** and *ap*-**1** in formic acid gave the corresponding formate to indicate that formic acid is nucleophilic enough to win the competition with cyclization in *ap*-**1**. The first order rate constants of the reaction of *sp*-**1** and *ap*-**1** in formic acid containing *ca.* 8 (v/v)% chloroform at 42 °C were obtained as 7.6×10^{-4} min^{-1} and 4.6×10^{-4} min^{-1}, respectively. Thus the relative rate k_{sp}/k_{ap} is 1.6: The *sp* form is more reactive than the *ap* under these conditions.

In a 1:1 (v/v) mixture of TFA and chloroform, the rate of disappearance of *ap*-**1** was determined at two concentrations. At 86 mM, the first order rate constant was 8.5×10^{-4} min^{-1} at 60 °C, whereas it was 5.6×10^{-4} min^{-1} at 48 mM at the same temperature. At this level of concentration, the products were polymers which were undoubtedly formed by intermolecular Friedel-Crafts reactions. The results suggest that the solute in TFA assists ionization in some ways. Under the similar conditions, *sp*-**1** was always recovered as well as benzyl bromide. The relative rate (k_{sp}/k_{ap}) is less than 0.05.

At 2 mM in TFA containing 3 (v/v)% chloroform, the half life of *ap*-**1** at 60 °C was 50—60 min. Heating a 2 mM HFP (containing 2 (v/v)% chloroform) solution of *ap*-**1** at 55 °C showed the disappearance of the solute with a half life of 30—40 min. Under the same conditions, *sp*-**1** was completely recovered, the relative reactivity (k_{sp}/k_{ap}) being less than 0.05. The main product in these reactions was **3**. The formation of **4** was diminished when HFP was used as a solvent and only a trace amount of **4** was usually detected.

Considering the ionizing ability of formic acid, TFA, and HFP,[20] one may wonder why the more ionizing solvents show no reaction of *sp*-**1** while the less ionizing solvent gives the solvolysis product. The key to solve this problem can be the fact that the more ionizing solvents are less nucleophilic. Namely, *sp*-**1** may ionize to contact ion pairs or to solvent separated ion pairs in TFA or HFP: It is more reasonable to assume so when one considers the ionizing power of these solvents. However, the nucleophilicity of TFA and HFP is so low that the ion pairs return to the covalent species rather than to give a reaction product. In contrast, formic acid is nucleophilic enough to give the formate if *sp*-**1** ionizes either to the contact ion pair or to the solvent separated ion pair.

If the above mentioned idea is correct, a TFA or HFP solution containing a nucleophile should show some reactivity of *sp*-**1**. Thus the reaction in HFP containing 5 (v/v)% chloroform and 3 (v/v)% methanol was investigated. As expected, *sp*-**1** afforded the corresponding methoxy compound (**8**) in a good yield, whereas *ap*-**1** afforded the cyclized products (**3** and **4**). The rates of decrease in the amount of *sp*-**1** and *ap*-**1** were treated as first order reactions. The rate constants were 1.5×10^{-3} and 8.4×10^{-3} min^{-1} for *sp*-**1** and *ap*-**1**, respectively, at 1.8 mM and at 40 °C. The rate constants may again be compared directly because in both cases the ionization is the rate determining step. Then the relative rate (k_{sp}/k_{ap}) is 0.18. It is striking to note that *ap*-**1** did not give *ap*-**8** to a measurable degree, because methanol is more nucleophilic than formic acid in which the solvolysis afforded the formate. We may have to assume that the ion pairs formed from *ap*-**1** in HFP are so tight that they react intramolecularly with the benzene ring of the fluorene rather than with external methanol.

Under the same conditions in TFA (TFA–$CHCl_3$–CH_3OH, 40 °C, 18 mM) the rate constants of the reaction were 3.1×10^{-4} and 1.5×10^{-3} min^{-1}, respectively, for *sp*-**1** and *ap*-**1**, as measured by the decrease

in the amount of the substrates. The relative reactivity k_{sp}/k_{ap} is calculated to be 0.19. The TFA–$CHCl_3$–CH_3OH system did not give the corresponding methoxy compound (*sp*-**8**) from *sp*-**1**, however, although *ap*-**1** gave the cyclized products (**3** and **4**). The behaviors of the products from *sp*-**1** on a TLC plate were similar to those of the polymers obtained by heating a mixture of *sp*-**1** in TFA or HFP and silver perchlorate. We abandoned attempts to prepare the methoxy compound (*sp*-**8**) from *sp*-**1** under similar conditions for the following reasons. The apparent failure in affording *sp*-**8** in the TFA–$CHCl_3$–CH_3OH system must be attributed to the reduction in effective concentration of methanol in the system owing to protonation. Although we could have made *sp*-**8** by increasing the molar fraction of methanol in the system, the increase in the concentration of methanol also increases the reaction rate of *sp*-**1** with methanol in S_N2 fashion. It would become difficult to tell the extent of contributions of S_N1 and S_N2 reactions.

Role of Solvent Molecules in Ionization. At any rate, the above results suggest that in TFA and in HFP, ionization of *sp*-**1** is slower than that of *ap*-**1**. We have attributed this difference to π-participation of the fluorene system.[5] However, having additional experimental data in hand, we notice that the situation is not so simple as we have thought: Solvent plays an important role in controlling the rates of reaction.

The first we notice is that the ionization reaction of *sp*-**1** is faster than in *ap*-**1** in acetonitrile, in benzene, and in formic acid, whereas the reverse is true in TFA and in HFP. We wish to postulate, in summarizing the results described above, that the completion of the solvation shell is important in determining the ease of ionization.

Let us assume that free carbocations are formed by the ionization reaction. Then the cation must be surrounded by solvent molecules to form a solvation shell as depicted by **11** and **12**.[21] A main difference

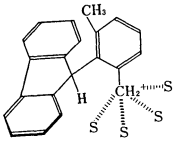

11

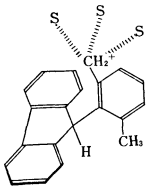

12

here is that, while the solvent molecules form a solvation shell in the *sp* conformation, at least one of the solvent molecule cannot participate in the solvation of the cation derived from the *ap* form because of the steric effect of the fluorene ring. In other words, the benzene ring of the fluorene moiety participate in completing the solvation shell (This can be viewed as π-participation.). Mere consideration of this situation leads to a conclusion that if a solvent molecule is more basic than the benzene ring in fluorene, then *sp*-**1** can be more reactive than *ap*-**1**. Similarly *ap*-**1** can be more reactive than *sp*-**1**, if the basicity of the solvent molecule is lower than the benzene ring in fluorene.

The general tendency seen in the experimental results conform with this expectation: in more basic solvents, the *sp* form is more reactive, while the *ap* form is more reactive in poorly basic solvents. One might argue that if we admit the hypothesis we must consider that benzene and formic acid must be more basic than the benzene in fluorene, contrary to the common belief.[22] We consider that this result is derived because the relative arrangement, in space, of the fluorene ring and the cation derived from *ap*-**1** is limited and is not optimum for the interaction between them. Thus the benzene ring in the fluorene moiety is not as effective as it should be. Free benzene molecules can assume optimum arrangement to stabilize the cation. The case of formic acid can be understood similarly.

We wish to thank Professor T. Miyazawa of this University for measuring the ^1H NMR spectrum at 270 MHz. This work was supported by a grant from Toray Science Foundation to which our thanks are due.

References

1) Preceding paper: H. Kikuchi, S. Seki, G. Yamamoto, T. Mitsuhashi, and M. Ōki, *Bull. Chem. Soc. Jpn.*, **55**, 1514 (1982).

2) M. Nakamura and M. Ōki, *Tetrahedron Lett.*, **1974**, 505.

3) M. Nakamura, N. Nakamura, and M. Ōki, *Bull. Chem. Soc. Jpn.*, **50**, 1097 (1977).

4) S. Seki, T. Morinaga, H. Kikuchi, T. Mitsuhashi, G. Yamamoto, and M. Ōki, *Bull. Chem. Soc. Jpn.*, **54**, 1465 (1981).

5) S. Murata, S. Kanno, Y. Tanabe, M. Nakamura, and M. Ōki, *Angew. Chem.*, **93**, 579 (1981).

6) a) R. Adams and J. Campbell, *J. Am. Chem. Soc.*, **72**, 153 (1950); b) T. H. Siddall, III, and W. E. Stewart, *J. Org. Chem.*, **34**, 233 (1969).

7) A. Rieker and H. Kessler, *Tetrahedron Lett.*, **1969**, 1227.

8) P. W. Rabideau, *Acc. Chem. Res.*, **11**, 141 (1978); A. W. Brinkman, M. Gordon, R. G. Harvey, P. W. Rabideau, J. B. Stothers, and A. L. Ternay, *J. Am. Chem. Soc.*, **92**, 5912 (1970).

9) E. Clar and W. Willicks, *J. Chem. Soc.*, **1958**, 942.

10) Y. Pocker and W. H. Wong, *J. Am. Chem. Soc.*, **97**, 7097, 7105 (1975).

11) D. N. Kevill and C. R. Degenhart, *J. Am. Chem. Soc.*, **101**, 1465 (1979).

12) The nucleophilic strength of nitrate anions is definitely larger than that of water. J. O. Edwards, *J. Am. Chem.* **76**, 1540 (1954).

13) Y. Pocker and D. N. Kevill, *J. Am. Chem. Soc.*, **87**, 4771 (1965).

14) J. J. Ritter and P. P. Minieri, *J. Am. Chem. Soc.*, **70**, 4045 (1948).

15) Y. Pocker and D. N. Kevill, *J. Am. Chem. Soc.*, **87**, 5060 (1965).

16) P. v. R. Schleyer, J. L. Fry, L. K. M. Lam, and C. J. Lancelot, *J. Am. Chem. Soc.*, **92**, 2542 (1970).

17) T. W. Bentley, C. T. Bowen, W. Parker, and C. I. F. Watt, *J. Am. Chem. Soc.*, **101**, 2486 (1979).

18) M. Ōki and R. Saito, *Chem. Lett.*, **1981**, 649,

19) F. L. Schadt, T. W. Bentley, and P. v. R. Schleyer, *J. Am. Chem. Soc.*, **98**, 7667 (1976).
20) F. L. Schadt, P. v. R. Schleyer, and T. W. Bentley, *Tetrahedron Lett.*, **1974**, 2335.
21) Real species present in the reaction system must be ion pairs rather than free ions but the following discussion does not make much difference by the change in the species. Likewise, we use four ligands to complete the solvation shell to show our idea only. The number of ligands around the carbocation may be different.
22) T. W. Bentley and P. v. R. Schleyer, *Adv. Phys. Org. Chem.*, **14**, 1 (1977).

Enzymatic Synthesis of Pyridine Nucleotides. Structural Property of Some New NAD-analogs, and Base Conditions Available for the Analog Formation[1)]

Shuichi TONO-OKA

Institute of Immunological Science, Hokkaido University, Kita 15-jo, Nishi 7-chome, Kita-ku, Sapporo 060

(Received August 3, 1981)

Some new β-NAD-analogs were prepared by a base-exchange reaction catalyzed by pig-brain NADase. The analogs produced from methyl 4-(methylamino)- and 4-(dimethylamino)nicotinates were proved to be 1,4-dihydropyridine form. On the contrary, the analog obtained from 4-(acetylamino)nicotinamide was shown to be a quaternary pyridinium form. Moreover, an unexpected analog of 1,4-dihydro-4-pyridinone form was given by 4-methoxynicotinamide. It was shown to be indispensable for the formation of NAD-analog that the ring nitrogen of pyridine bases concerned should at least be free from protonation around pH 7. Interestingly nicotinic acids with 4-amino, methylamino, and dimethylamino groups were found to be much more basic for the ring nitrogen atom than their respective methyl esters.

Previously we have reported[2,3)] the enzymatic synthesis of new pyridine nucleosides utilizing the corresponding NAD-analogs (**2** and **3**) as intermediates, which were prepared from β-NAD (**1**) and 4-amino derivative of methyl nicotinate or nicotinamide by a NADase-catalyzed base-exchange reaction (Scheme 1). These analogs were proved to take a 1,4-dihydropyridine form instead of a quaternary pyridinium one.

Now our attention has been extended to investigate the structural property of pyridine moiety of NAD-analogs which will be produced from other *N*-substituted 4-amino derivatives (methylamino, dimethylamino, *etc.*) of methyl nicotinate or nicotinamide. Moreover, these analogs are also of interest in connection with their possible efficiency as competitive inhibitors[4)] for NAD. On the other hand, it comes to be an important problem whether the pyridine bases concerned bring about the corresponding NAD-analog or not, when this method is utilized for the synthesis of pyridine nucleosides. As previously reported,[3)] nicotinic acids with 4-amino, methylamino, and dimethylamino functions produced no detectable amount of analog unless the 3-carboxyl group was pre-transformed into a methoxycarbonyl or carbamoyl one. In view of these facts, the spectroscopic behaviors of pyridine bases were examined with alterations in pH to clarify the relationship between their reactivity and chemical property.

The present paper describes the structural properties of newly prepared NAD-analogs and necessary conditions of pyridine bases for the analog formation in the base-exchange reaction.

Results and Discussion

Preparation and Structural Property of NAD-analogs. On the basis of the results described in the previous paper,[3)] various NAD-analogs were prepared under the following conditions: Base concentration was more than 25 mM (1 M=1 mol dm^{-3}) if possible, and the base/NAD molar ratio was about 4:1. The yield and some spectral data of the analogs obtained were summarized in Table 1.

In the UV spectra (pH 7), although the replacing base, methyl 4-(methylamino)nicotinate and ADP-ribose have an absorption at 260 (log ε 4.08) and 259 nm (log ε 4.20), respectively, methylamino analog (**4**) obtained showed its maximum at 268 nm (log ε 4.27) with a bathochromic shift, suggesting the structural change of pyridine chromophore. In the ^{1}H-NMR spectra, a methyl group adjacent to the nitrogen atom of the replacing base showed a doublet in DMSO-d_6 with the vicinal coupling of J_{NH,CH_3}=5.2 Hz, which collapsed by the addition of deuterium oxide. In contrast, compound **4** showed a singlet for the methyl group in the same solvent. From these observations, the 4-nitrogen atom of pyridine moiety in **4** proved to bear no proton, indicating 1,4-dihydropyridine structure of **4**.

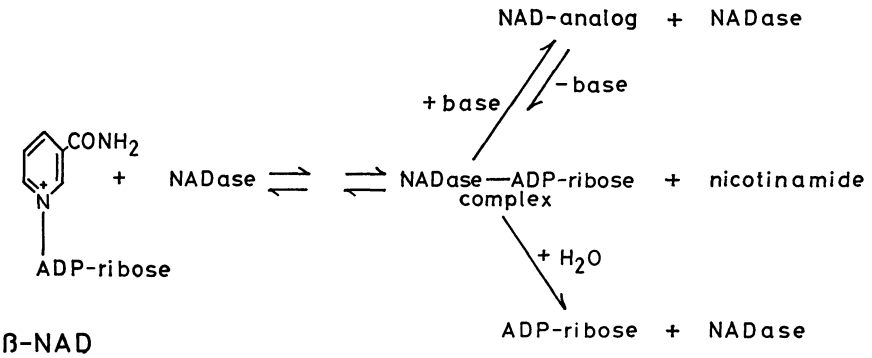

Scheme 1.

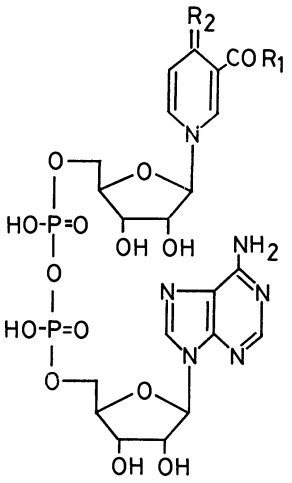

2: $R_1=OCH_3$ $R_2=NH$
3: $R_1=NH_2$ $R_2=NH$
4: $R_1=OCH_3$ $R_2=NCH_3$
5: $R_1=OCH_3$ $R_2=\overset{+}{N}(CH_3)_2$
8: $R_1=OCH_3$ $R_2=O$
9: $R_1=NH_2$ $R_2=O$

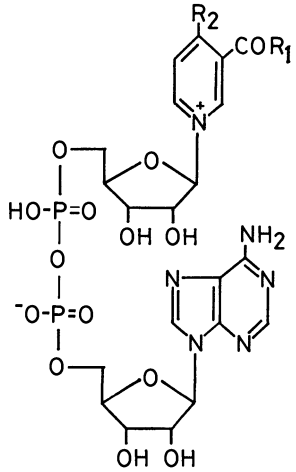

1: $R_1=NH_2$ $R_2=H$
6: $R_1=NH_2$ $R_2=NHCOCH_3$
7: $R_1=OH$ $R_2=NHCOCH_3$
10: $R_1=NH_2$ $R_2=CH_3$
11: $R_1=OH$ $R_2=CH_3$

Dimethylamino analog (**5**), produced from methyl 4-(dimethylamino)nicotinate which bears no proton at the nitrogen atom to participate in tautomerism, was anticipated to take a pyridinium form instead of a 1,4-dihydropyridine one. However, compound **5** was shown to be the dihydropyridine structure of 4-dimethyliminium type from the following findings. The ^{1}H-NMR spectrum of **5** exhibited a six-proton singlet at δ 3.11 due to the two methyl groups, and the anomeric proton of pyridine side appeared at δ 5.62 accompanying 0.4 ppm higher field resonance compared with that of adenine side. Moreover, the $H_{5,6}$ coupling of pyridine moiety was estimated to be 8.2 Hz, indicating the olefinic character of C_5–C_6 bond. Its UV spectral behavior was also compatible with the structure of **5** (Table 1).

Acetylamino analogs (**6** and **7**) were remarkably different from **4** and **5** in some respects in the ^{1}H-NMR spectra. Both the two anomeric protons appeared as a broad two-proton doublet at δ 6.0, and the $H_{5,6}$ coupling of pyridine ring was 6.0 Hz, the value of which was distinctly smaller than for **4** and **5**. In addition, its pyridine protons showed the lower field shift of 0.4—0.6 ppm as a whole compared with those of the acetylamino bases alone. The UV spectrum of these analogs nearly corresponded with the sum absorptions of acetylamino base and ADP-ribose. These observations indicated the quaternary pyridinium form of **6** and **7**.

Table 1. Yields and spectral properties of analogs obtained from various pyridine bases

Compd No.	Yield [a] %	^{1}H-NMR [b] C_1' (δ)	^{1}H-NMR [b] $J_{5,6}$/Hz	UV$_{max}$ (λ/nm) [c] Bases	UV$_{max}$ (λ/nm) [c] Analogs [d]
4	76	5.63	8.0	260	268
5	58	5.62	8.2	273	296
6	72	6.00	6.0	272	268
7	50	6.01	6.0	268	266
8	64	5.60	8.0	233	265
9	73	5.60	8.0	234	266
10	68	6.00	6.0	261	260
11	48	5.98	6.0	261	260

a) Analog/(analog + ADP-ribose) × 100. b) Measured in deuterium oxide. c) Measured in water. d) All the compounds showed the ε-value of more than 1.6×10^4.

It has thus been shown that even if the amino group was methylated, its lone pair electrons contributed to the 1,4-dihydropyridine structure, and that when it was acetylated, its resonance effect on pyridine nucleus was prevented by the electron-withdrawing acetyl group in spite of possessing a proton at the nitrogen atom.

In connection with dimethylamino base in which an amino group is methylated, it seems of deep significance to investigate methyl 4-methoxynicotinate and 4-methoxynicotinamide in which a hydroxyl group is methylated. If they bring about a similar type of analog as described for **5**, the formation of the system $-N-C=C-C=\overset{+}{O}CH_3$ must be expected. However, the oxonium form is generally unstable compared with the ammonium or iminium one,[5] whereby the above system with methoxonium ion can hardly be considered. The analogs formed were thus anticipated to have the alternative pyridinium system $-\overset{+}{N}=C-C=C-OCH_3$ instead. They, however, exhibited an unexpected UV absorption at 266 nm ($\log\varepsilon$ 4.24), accompanying a large bathochromic shift of more than 30 nm from that of the methoxy bases alone. The ^{1}H-NMR spectra of these analogs (**8** and **9**) showed the absence of a three-proton singlet due to a methoxyl methyl group. The anomeric proton in question exhibited a similar behavior to that of **4** and **5**, and the $H_{5,6}$ coupling was observed to be 8.0 Hz. These facts demonstrate the 1,4-dihydro-4-pyridinone form of **8** and **9**, which would probably be brought about from once formed 4-methoxypyridinium compound by demethoxylation subsequent to undergoing the nucleophilic attack of water at the 4-position (Scheme 2).

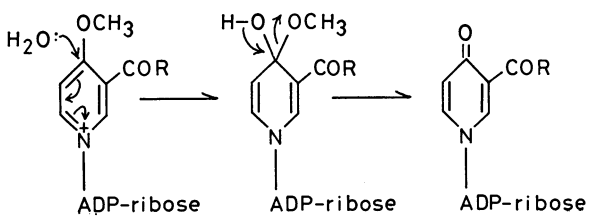

Scheme 2.

Table 2. Susceptibility of NAD-analogs to the hydrolase action of NADase

Compd No.	Hydrolysis rate (%)		
	3 h	6 h	18 h
1 (NAD)	76	100	—
2	0	5	9
3	0	0	5
4	0	4	8
5	0	5	10
6	25	42	68
7	24	36	52
8	0	4	6
9	0	0	4
10	34	56	74
11	26	45	60
12[a)]	58	80	100

a) NAD-analog of INH.

By using 4-methylnicotinamide as a replacing base, which has an UV maximum at 261 nm (log ε 3.60), 4-methyl analog (**10**)[6] was obtained which showed the absorption at 260 nm (log ε 4.26). In the ^{1}H-NMR spectrum of **10**, the methyl protons were clearly observed at δ 2.62 as a three-proton singlet and the $H_{5,6}$ coupling was 6.0 Hz, indicating a quaternary pyridinium form of **10** rather than 1,4-dihydro-4-methylenepyridine one. Such was also found to be the case of the analog (**11**) obtained from 4-methylnicotinic acid.

As previously suggested,[2] the susceptibility of NAD-analogs to the hydrolase action of NADase might be employed as an indication of their pyridinium ion character. In order to clarify this assumption more precisely, the above obtained analogs were incubated with NADase, and the amount of ADP-ribose liberated was examined with elapse of time on TLC in comparison with NAD itself and its isonicotinic acid hydrazide (INH) analog (**12**),[7] which is a typical NAD-analog of pyridinium form (Table 2). All the analogs (**6**, **7**, and **10**—**12**) which exist in pyridinium form underwent hydrolysis more or less, though not so fast as NAD. On the other hand, the analogs (**2**—**5**, **8**, and **9**) which exist in dihydropyridine form were little susceptible to the enzyme, indicating that their glycosyl bonds were much more stable than those of the former analogs. These results strongly supported the validity of the assumption.

Necessary Conditions of Bases for the Analog Formation. This base-exchange reaction can be assumed to proceed through the nucleophilic attack of pyridine base on an enzyme–ADP-ribose complex. From this point of view, the reactivity of pyridine base was considered to be notably affected by the nucleophilicity of ring nitrogen. As previously described, nicotinic acids with 4-amino group inclusive of methyl- and dimethylamino ones were found to produce no NAD-analog, although nicotinic acid itself and its 4-methyl derivative produced successfully the corresponding analogs. In order to infer the chemical property of analog-productive pyridine bases and non productive ones around pH

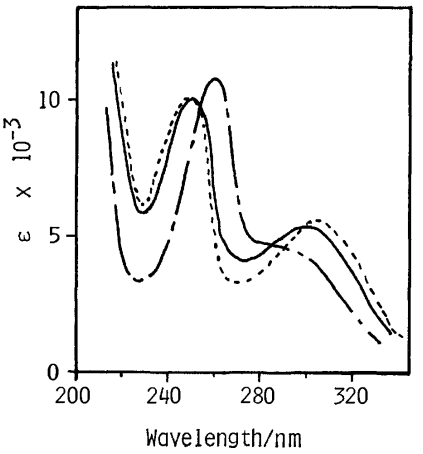

Fig. 1. Absorption spectra of methyl 4-aminonicotinate (**13**) at some values of pH.
— — —: pH 2, ——: pH 7, ----: pH 12.

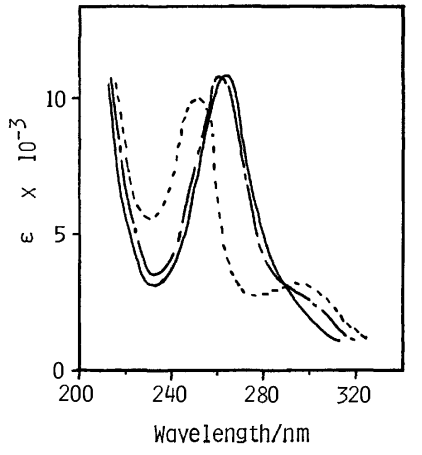

Fig. 2. Absorption spectra of 4-aminonicotinic acid (**16**) at some values of pH.
— — —: pH 2, ——: pH 7, ----: pH 12.

7 wherein the NADase-catalyzed reaction proceeds, their UV spectra were firstly examined at some different pHs.

In the case of methyl 4-aminonicotinate (**13**) which gives rise to a NAD-analog in good yield, its absorption maximum at pH 7 approximated closely to that at pH 12 (Fig. 1). A similar spectral pattern was also observed for 4-aminonicotinamide. On the other hand, in the case of 4-aminonicotinic acid (**16**) which gives rise to no NAD-analog, its absorption maximum approximated closely to that at pH 2 (Fig. 2). The same spectral correlations were also recognized in a pair of corresponding 4-methylamino compounds (**14** and **17**) and 4-dimethylamino ones (**15** and **18**). The structure of now described compounds (**13**—**18**) are summarized in Table 3.

Brown and Plasz[8] have previously reported that the first protonation of 4-aminopyridine occurred at the ring nitrogen and not at the substituent amino group. Since the primary amino function is a very weak base, the second protonation occurs only in more strongly acidic solutions ($pH \lesssim -3$) like 2 M sulfuric acid.[9] In the acidic solution of pH 2, therefore, the

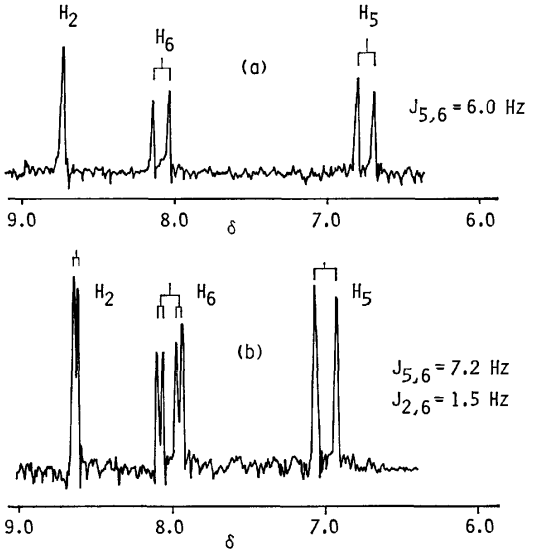

Fig. 3. ^{1}H-NMR spectral patterns of **13** (a) and **16** (b) at pH 7.

pyridine bases dealt with here should be protonated at the ring nitrogen. In the alkaline solution, on the contrary, the nitrogen should be completely free from protonation. It is accordingly suggested that the ester bases (**13**—**15**) would mainly exist in a free form, whereas the carboxyl bases (**16**—**18**) suffer a protonation in the neutral solution.

When ^{1}H-NMR spectra were measured for these two kinds of bases, their spectroscopic differences were revealed more clearly. The signal pattern of **13** in the neutral solution was substantially identical with that of pH 12, and the $H_{5,6}$ coupling was 6.0 Hz (Fig. 3a). In contrast, **16** showed a different signal pattern almost identical with that of pH 2; the $H_{5,6}$ coupling became larger ($J_{5,6}$=7.2 Hz) and the $H_{2,6}$ long range coupling appeared clearly ($J_{2,6}$=1.5 Hz) (Fig. 3b). These spectroscopic behaviors were also observed for the couples of **14** and **17** as well as **15** and **18**.

Craig *et al.*[10] have previously found in the structural studies of 4-aminoquinoline derivatives that a coupling constant between H_2 and H_3 of the quinoline ring could be an indication of the extent of aromaticity. This concept was well applicable to the 3,4-disubstituted pyridine compounds now dealt with. If the ring nitrogen was protonated, the cation formed could be stabilized by resonance, such as that between the cannonical forms (**a**) and (**b**) (Scheme 3). The C_5–C_6 bond should then come to have an olefinic character due to the contribution of the structure **b**. It is well known that the vicinal coupling of olefines is usually larger than that of aromatic environment, and the $H_{2,6}$ coupling is increased by *ca.* 1 Hz on undergoing a protonation.[11]

Thus, the ring nitrogen of ester bases were proved to be essentially free around pH 7, whereas that of carboxyl bases suffered a protonation under the same conditions. On acetylation of **16**, however, its spectral properties came to be similar to those of **13**, and the acetyl compound (**19**) certainly provided a NAD-analog in 50% yield (Table 1). Apart from this,

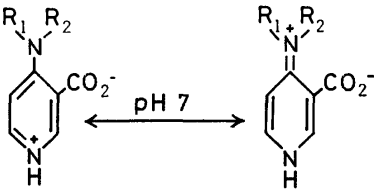

(a) **16** $R_1=R_2=H$ (b)
17 $R_1=H$, $R_2=CH_3$
18 $R_1=R_2=CH_3$

Scheme 3.

TABLE 3. pK_a VALUES FOR PYRIDINE BASES IN AQUEOUS SOLUTION AT 25 °C

Base No.	X	Y	pK_a (proton gained)
13	NH_2	CO_2CH_3	6.6
14	$NHCH_3$	CO_2CH_3	6.6
15	$N(CH_3)_2$	CO_2CH_3	6.9
16	NH_2	CO_2H	9.1
17	$NHCH_3$	CO_2H	9.2
18	$N(CH_3)_2$	CO_2H	9.4
19	$NHCOCH_3$	CO_2H	6.2
20	H	CO_2CH_3	3.1[a]
21	H	CO_2H	2.1[a]
22	NH_2	H	9.2[a]
23	$NHCH_3$	H	9.4[b]
24	$N(CH_3)_2$	H	9.6[b]

a) A. Albert, "Physical Methods in Heterocyclic Chemistry," ed by A. R. Katritzky, Academic Press, New York (1963), Vol. I, p. 72. b) A. Albert, *ibid.*, (1971), Vol. IV, p. 9.

other analog-productive 4-methyl- and 4-methoxynic otinic acids were also found to be free from protonation at pH 7.

These observations demonstrated that the mostly free state of ring nitrogen in the pyridine bases concerned is at least necessary for the formation of NAD analog.

Basicity of Pyridine Bases. To undergo an easy protonation implies the high basicity of ring nitrogen. Strangely, there has so far been no report on the basicity of pyridine bases here dealt with. Therefore, their pK_a values were determined by the convenient spectrometric method of Albert *et al.*[12] Contrary to our intuitional expectation, carboxyl bases (**16**—**18**) ($pK_a \geq 9$) proved much more basic than corresponding ester bases (**13**—**15**) ($pK_a \leq 7$) and showed no significant difference in basicity compared with 4-aminopyridines (**22**—**24**) (Table 3). This fact indicates that the presence of 3-carboxyl group has no special influence on the basicity of ring nitrogen, whereas 3-methoxycarbonyl group has an effect to reduce it, unlike the

correlation of nicotinic acid (**21**) and its methyl ester (**20**). The lower basicity of **19** compared to **16** should be considered due to the inhibitory effect of electron-withdrawing acetyl group on the dispersal of lone pair electrons of amino function into the ring nitrogen. In view of this explanation, the unexpected decrease of basicity by esterification of carboxyl group seems possibly dependent on an intermolecular non-bonded interaction between the amino nitrogen and the carbonyl carbon of ester group. On that account, the lone pair electrons of amino function can hardly contribute to the resonance effect, resulting in the reduced basicity of ring nitrogen. On the other hand, there would occur no appreciable interaction in the case of carboxyl bases, presumably due to the deficiency of carbonium ion character in the carboxyl group.

In conclusion, the basicity of pyridine bases is surely an important factor for the formation of NAD-analogs. However, since the enzymatic reaction must be carried out around pH 7, highly basic pyridine bases can no longer function as nucleophiles because of suffering a protonation. Thus, the suitable basicity ($pK_a \lesssim 7$) was shown to be one of the necessary conditions for enough nucleophilicity of replacing bases.

The biological activity of here prepared pyridine nucleotides will be reported elsewhere.[13]

Experimental

All the melting points are uncorrected. The UV spectra were measured on a Hitachi 200-20 spectrophotometer, and the ^{1}H-NMR spectra were determined on a Hitachi R-20B (60 MHz) spectrometer in deuterium oxide with sodium 2,2-dimethyl-2-silapentane-5-sulfonate (DSS) as an internal standard unless otherwise stated. The abbreviations "s, d, dd, br, bs, and bd" denote "singlet, doublet, double doublet, broad, broad singlet, and broad doublet," respectively. Optical rotations were measured with a Union PM 101 digital polarimeter. Ionic strength and pH measurements were made on an Emuesu CD-35M II conductivity meter and a Radiometer pHM-26 pH meter equipped with a G-202 glass electrode, respectively. Thin layer chromatographies (TLC) were carried out on silica gel 60 F_{254} HPTLC plates (Merck, 10 cm × 10 cm) using 2-propanol–0.2% aqueous ammonia (7 : 3, v/v) as the developing system. The analysis of chromatograms were performed by a Shimadzu CS-910 scanner equipped with a chromatopack C-R1A. Column chromatographies[14] were carried out on DEAE-Sephadex (A-25, 3.5 mequiv./g) connected to LKB Uvicord II (254 nm). β-NAD (Grade III) was purchased from Sigma Chemical Co.

Pig-brain NADase (EC 3.2.2.5). The crude particulate enzyme was prepared by the method of Zatman *et al.*[7a] The colloidal supernatant fluid containing *ca.* 0.4 U/ml[15] of NADase activity was used without further purification.

4-(Methylamino)nicotinic Acid. Prepared from 4-chloronicotinic acid 1-oxide[16] and methylamine in two steps, and recrystallized from aqueous methanol: mp 277—279 °C (decomp) [lit,[17] 274—276 °C (decomp)].

Methyl 4-(Methylamino)nicotinate. Prepared by esterification of the above compound, and recrystallized from dichloromethane–petroleum benzine: mp 71—73 °C. Found: C, 57.86; H, 6.04; N, 16.76%. Calcd for $C_8H_{10}N_2O_2$: C, 57.82; H, 6.07; N, 16.86%.

4-(Dimethylamino)nicotinic Acid. Prepared from 4-chloronicotinic acid 1-oxide[16] and dimethylamine in two steps, and recrystallized from aqueous ethanol: mp 223—225 °C (decomp). Found: C, 57.74; H, 6.21; N, 16.65%. Calcd for $C_8H_{10}N_2O_2$: C, 57.82; H, 6.07; N, 16.86%.

Methyl 4-(Dimethylamino)nicotinate. Prepared by the esterification of the above compound, and recrystallized from dichloromethane–petroleum benzine: mp 75—77 °C. Found: C, 60.07; H, 6.61; N, 15.55%. Calcd for $C_9H_{12}N_2O_2$: C, 59.99; H, 6.71; N, 15.55%.

4-(Acetylamino)nicotinic Acid. Prepared by the acetylation of 4-aminonicotinic acid[18] with acetic anhydride, and recrystallized from water: mp 252—254 °C (decomp). Found: C, 53.45; H, 4.37; N, 15.82%. Calcd for $C_8H_8N_2O_3$: C, 53.32; H, 4.43; N, 15.55%.

4-(Acetylamino)nicotinamide. Prepared by the acetylation of 4-aminonicotinamide,[19] and recrystallized from ethanol: mp 223—225 °C (decomp). Found: C, 53.76; H, 4.98; N, 23.71%. Calcd for $C_8H_9N_3O_2$: C, 53.63; H, 5.03; N, 23.47%.

Methyl 4-Methoxynicotinate. Prepared from 4-nitronicotinic acid 1-oxide[18] in two steps, and recrystallized from benzene: mp 85—87 °C (lit,[20] 83—84 °C).

4-Methoxynicotinamide. Prepared by ammonolysis of the above compound, and recrystallized from benzene: mp 155—157 °C (lit,[20] 153—154 °C).

4-Methylnicotinic Acid. Prepared from 4-methylquinoline in two steps, and recrystallized from water: mp 215—217 °C (decomp) (lit,[21] 215—217 °C).

4-Methylnicotinamide. Prepared by the ammonolysis of the above compound, and recrystallized from methanol: mp 167—169 °C (lit,[19] 165—167 °C).

Methyl 1,4-Dihydro-4-(methylimino)nicotinate Adenine Dinucleotide (4). Methyl 4-(methylamino)nicotinate (1.6 mmol, 265 mg) and NAD (0.4 mmol, 280 mg, neutralized with 2M NaOH to pH 7) were incubated with pig-brain NADase (6 U, 15 ml) in 0.1 M Tris–HCl (pH 7.2, 30 ml) at 37 °C for 5 h. The incubation mixture was treated with 70% trichloroacetic acid (1 ml) and the precipitated protein was removed by centrifugation. To the clear supernatant thus obtained, cold acetone (300 ml) was added to give yellowish hygroscopic powder (235 mg) as the crude product. It was dissolved in water (20 ml) and then applied to a column of DEAE-Sephadex (HCO_3^--form) (column size; 2.5 cm × 45 cm). The column was washed with 0.02 M NH_4HCO_3 (250 ml) to remove the included free bases and then eluted with 300 ml portions of 0.2, and 0.5 M NH_4HCO_3 (pH 7.8), successively. The first major component showing UV-absorbing peak at 268 nm was eluted with the 0.2 M solution. The eluate (50 ml) was immediately collected and lyophilized repeatedly to give **4** (186 mg) as the ammonium salt. An analytical sample of **4** was obtained by rechromatography and drying over P_2O_5 *in vacuo* for 12 h at 40 °C: $[\alpha]_D^{20}$ −60.9° (*c* 0.92, H_2O); UV (H_2O), λ_{max} 268 nm (log ε 4.26); ^{1}H-NMR (δ, D_2O), 3.05 (3H, s, $NC\underline{H}_3$), 3.98 (3H, s, $CO_2C\underline{H}_3$), 4.2—4.6 (10H, br, riboses), 5.63 (1H, bd, J=5 Hz, py-C$_5'$-$\underline{H}$), 6.01 (1H, d, J=5.5 Hz, ad-C$_1'$-$\underline{H}$), 6.87 (1H, d, J=8.0 Hz, py-$\underline{H}_5$), 8.03 (1H, s, ad-$\underline{H}_2$), 8.15 (1H, dd, J=1.5, 8.0 Hz, py-$\underline{H}_6$), 8.28 (1H, s, ad-$\underline{H}_8$), 8.67 (1H, d, J=1.5 Hz, py-$\underline{H}_2$). Found: C, 34.05; H, 5.71; N, 15.79%. Calcd for $C_{23}H_{31}N_7O_{15}P_2 \cdot 2NH_3 \cdot 4H_2O$: C, 33.95; H, 5.53; N, 15.50%.

Methyl 1,4-Dihydro-4-(dimethyliminio)nicotinate Adenine Dinucleotide (5). Methyl 4-(dimethylamino)nicotinate (1.5 mmol, 270 mg) and NAD (0.4 mmol, 275 mg) were incubated with NADase (6 U, 15 ml) in 0.1 M Tris–HCl (pH 7.2, 30 ml) at 37 °C for 5 h. The incubation mix-

ture was treated in a similar manner to that described above to give the crude product (228 mg), which was dissolved in water (20 ml) and applied to a column (HCO_3^--form). The column was eluted with aqueous NH_4HCO_3 similarly as described above. The first major component was eluted with the 0.2 M solution. The eluate (40 ml) showing the UV maximum at 266 and 296 nm was immediately collected and lyophilized repeatedly to give **5** (113 mg) as the ammonium salt: $[\alpha]_D^{20}$ −46.3° (*c* 0.76, H_2O); UV (H_2O), λ_{max} 266 nm (log ε 4.23), 296 nm (log ε 4.24); ^{1}H-NMR (δ, D_2O), 3.11 (6H, s), 3.96 (3H, s), 4.2—4.6 (10H, br), 5.62 (1H, bd, J=5 Hz), 6.00 (1H, d, J=5.5 Hz), 7.02 (1H, d, J=8.2 Hz), 8.04 (1H, s), 8.12 (1H, dd, J=1.5, 8.2 Hz), 8.31 (1H, s), 8.44 (1H, d, J=1.5 Hz). Found: C, 35.34; H, 5.52; N, 14.18%. Calcd for $C_{24}H_{33}N_7O_{15}P_2 \cdot NH_3 \cdot 4H_2O$: C, 35.52; H, 5.42; N, 13.81%.

4-(Acetylamino)nicotinamide Adenine Dinucleotide (6). A mixture of 4-(acetylamino)nicotinamide (2 mmol, 355 mg) and NAD (0.6 mmol, 390 mg) was incubated with NADase (6 U, 15 ml) in 0.1 M Tris–HCl (40 ml) for 7 h. The incubation mixture was treated as described for **4** to give the crude hydroscopic product (408 mg), which was purified by the chromatographic procedures using aqueous HCO_2NH_4 (pH 6.8) as eluent in the manner as described for **4** to provide **6** (332 mg) as the hygroscopic ammonium salt: $[\alpha]_D^{20}$ −12.4° (*c* 0.64, H_2O); UV (H_2O), λ_{max} 268 nm (log ε 4.07), 340 nm (log ε 3.77); ^{1}H-NMR (δ, D_2O), 2.35 (3H, s), 4.25—4.65 (10H, br), 6.00 (2H, bd), 7.43 (1H, d, J=6.0 Hz), 7.95 (1H, s), 8.21 (1H, s), 8.62 (1H, dd, J=1.5, 6.0 Hz), 9.15 (1H, d, J=1.5 Hz). Found: C, 35.15; H, 5.15; N, 18.12%. Calcd for $C_{23}H_{30}N_8O_{15}P_2 \cdot 2NH_3 \cdot H_2O$: C, 35.70; H, 4.92; N, 18.11%.

4-(Acetylamino)nicotinic Acid Adenine Dinucleotide (7). A mixture of 4-(acetylamino)nicotinic acid (2.9 mmol, 523 mg) and NAD (1.3 mmol, 935 mg) was incubated with NADase (8 U, 20 ml) in 0.1 M Tris–HCl (70 ml) for 12 h. The crude product (776 mg) obtained was purified by the chromatographic procedures to give **7** (372 mg): $[\alpha]_D^{20}$ −44.5° (*c* 1.1, H_2O); UV (H_2O), λ_{max} 266 nm (log ε 4.18), 283 nm (log ε 4.18); ^{1}H-NMR (δ, D_2O), 2.39 (3H, s), 4.3—4.7 (10H, br), 6.01 (2H, bd), 8.15 (1H, s), 8.35 (1H, s), 8.63 (2H, bs), 9.05 (1H, bs). Found: C, 35.39; H, 4.88; N, 14.73%. Calcd for $C_{23}H_{29}N_7O_{16}P_2 \cdot NH_3 \cdot 2H_2O$: C, 35.66; H, 4.65; N, 14.47%.

Methyl 1,4-Dihydro-4-oxonicotiate Adenine Dinucleotide (8). Methyl 4-methoxynicotinate (6.5 mmol, 1080 mg) and NAD (1.6 mmol, 1050 mg) were incubated with NADase (12 U, 30 ml) in 0.1 M Tris–HCl (120 ml) for 6 h. The crude product (852 mg) obtained by treating the reaction mixture as described for **4** was purified by column chromatography on DEAE-Sephadex (HCO_2^--form) as described for **6** to give **8** (546 mg): $[\alpha]_D^{20}$ −29.6° (*c* 1.05, H_2O); UV (H_2O), λ_{max} 265 nm (log ε 4.26); ^{1}H-NMR (δ, D_2O), 3.90 (3H, s), 4.2—4.6 (10H, br), 5.60 (1H, bd, J=5 Hz), 5.97 (1H, d, J=5.5 Hz), 6.85 (1H, d, J=8.0 Hz), 7.95 (1H, s), 8.02 (1H, dd, J=1.5, 8.0 Hz), 8.24 (1H, s), 8.68 (1H, d, J=1.5 Hz). Found: C, 34.28; H, 5.11; N, 11.24%. Calcd for $C_{22}H_{28}N_6O_{16}P_2 \cdot 2NH_3 \cdot 2H_2O$: C, 34.55; H, 4.97; N, 10.99%.

1,4-Dihydro-4-oxonicotinamide Adenine Dinucleotide (9). In 0.1 M Tris–HCl (80 ml), 4-methoxynicotinamide (6.6 mmol, 998 mg) and NAD (1.7 mmol, 1140 mg) were incubated with NADase (12 U, 30 ml) for 6 h. The reaction mixture was treated in a similar manner as described for **4** to give **9** (770 mg): $[\alpha]_D^{20}$ −37.9° (*c* 0.69, H_2O); UV (H_2O), λ_{max} 266 nm (log ε 4.24); ^{1}H-NMR (δ, D_2O), 4.25—4.65 (10H, br), 5.60 (1H, bd, J=5 Hz), 6.04 (1H, d, J=5.5 Hz), 6.90 (1H, d, J=8.0 Hz), 8.12 (1H, dd, J=1.5, 8.0 Hz), 8.15 (1H, s), 8.44 (1H, s), 8.60 (1H, d, J=1.5 Hz). Found: C, 34.14; H, 4.47; N, 17.41%. Calcd for $C_{21}H_{27}N_7O_{15}P_2 \cdot 2NH_3 \cdot H_2O$: C, 34.44; H, 4.78; N, 17.24%.

4-Methylnicotinamide Adenine Dinucleotide (10).[6] A mixture of 4-methylnicotinamide (2.8 mmol, 380 mg) and NAD (0.7 mmol, 475 mg) was incubated with NADase (8 U, 20 ml) in 0.1 M Tris–HCl (60 ml) for 6 h. The reaction mixture was treated as described for **4** to give **10** (324 mg): $[\alpha]_D^{20}$ −24.8° (*c* 0.85, H_2O); UV (H_2O), λ_{max} 260 nm (log ε 4.27); ^{1}H-NMR (δ, D_2O), 2.66 (3H, s), 4.1—4.6 (10H, br), 6.0 (2H, bd), 7.65 (1H, d, J=6.0 Hz), 8.05 (1H, s), 8.40 (1H, s), 8.70 (1H, dd, J=1.5, 6.0 Hz), 8.82 (1H, d, J=1.5 Hz). Found: C, 34.86; H, 5.04; N, 15.22%. Calcd for $C_{22}H_{29}N_7O_{14}P_2 \cdot NH_3 \cdot 3H_2O$: C, 35.29; H, 5.08; N, 14.97%.

4-Methylnicotinic Acid Adenine Dinucleotide (11). A mixture of 4-methylnicotinic acid (2.4 mmol, 330 mg) and NAD (0.6 mmol, 404 mg) was incubated with NADase (8 U, 20 ml) in Tris–HCl (50 ml) for 5 h. The reaction mixture was treated as described for **4** to give **11** (196 mg): $[\alpha]_D^{20}$ −36.1° (*c* 0.90, H_2O); UV (H_2O), λ_{max} 260 nm (log ε 4.23); ^{1}H-NMR (δ, D_2O), 2.62 (3H, s), 4.1—4.6 (10H, br), 5.98 (2H, bd), 7.78 (1H, d, J=6.0 Hz), 8.02 (1H, s), 8.33 (1H, s), 8.63 (1H, dd, J=1.5, 6.0 Hz), 8.75 (1H, d, J=1.5 Hz). Found: C, 35.48; H, 5.16; N, 12.94%. Calcd for $C_{22}H_{28}N_6O_{15}P_2 \cdot NH_3 \cdot 3H_2O$: C, 35.24; H, 4.94; N, 13.08%.

Susceptibility of NAD-analogs to the Hydrolase Action of NADase. A series of mixtures (0.6 ml) containing 30 mM NAD-analog (pH 7, 0.2 ml), NADase (0.12 U, 0.3 ml), and 0.5 M Tris–HCl (pH 7.2, 0.1 ml) was incubated at 37 °C for 18 h. In the course of incubation, the aliquot (1 μl) of the resulting mixture was analyzed by TLC using a thin layer scanner with a chromatopack. Based on the chromatograms thus obtained the amount of ADP-ribose produced was estimated semi-quantitatively. The data in Table 2 show the averages of three measurements.

pK_a *Values of Pyridine Bases.* The values were determined by the spectrometric method of Albert and Phillips[12] using the following series of 0.01 M buffers; glycine–hydrochloric acid (pH 2.00), acetate (pH 5.00), phosphate (pH 7.00), borate (pH 9.00), and glycine–sodium hydroxide (pH 12.00).

The author wishes to thank Prof. T. Masamune (Department of Chemistry, Faculty of Science) and Prof. I. Azuma (Institute of Immunological Science) for their encouragement and useful suggestions during this work.

References

1) Partly presented at the 43rd Annual Meeting of the Chemical Society of Japan, Tokyo 1981.

2) S. Tono-oka, A. Sasaki, H. Shirahama, T. Matsumoto, and S. Kakimoto, *Chem. Lett.*, **1977**, 1449.

3) S. Tono-oka, Y. Sasahara, A. Sasaki, H. Shirahama, T. Matsumoto, and S. Kakimoto, *Bull. Chem. Soc. Jpn.*, **54**, 212 (1981).

4) A. C. Lovesey, *J. Med. Chem.*, **13**, 693 (1970).

5) U. E. Wiersum and H. Wynberg, *Tetrahedron Lett.*, **1967**, 2951.

6) This compound was previously synthesized by a chemical method, and its biochemical properties were examined: M. Jarman and F. Searle, *Biochem. Pharmacol.*, **21**, 455 (1972).

7) a) L. J. Zatman, N. O. Kaplan, S. P. Colowick,

and M. M. Ciotti, *J. Biol. Chem.*, **209**, 467 (1954); b) J. K. Seydel, S. Tono-oka, K. -J. Schaper, L. Bock, and M. Wiencke, *Arzneim. -Forsch.*, **26**, 477, (1976).
8) E. V. Brown and A. C. Plasz, *J. Heterocycl. Chem.*, **7**, 335 (1970).
9) A. Albert and E. P. Serjeant, "Ionization Constants of Acids and Bases," John Wiley & Sons, New York (1962).
10) J. C. Craig and D. E. Pearson, *J. Heterocycl. Chem.*, **5**, 631 (1968).
11) A. R. Katritzky, "Physical Methods in Heterocyclic Chemistry," Academic Press, New York (1971), Vol. IV, p. 196.
12) A. Albert and J. N. Phillips, *J. Chem. Soc.*, **1956**, 1294.
13) I. Saiki, S. Tono-oka, and I. Azuma, *Int. J. Vitam. Nutr. Res.*, in press.
14) S. Tono-oka, A. Sasaki, and S. Kakimoto, *Bull. Inst. Immun. Sci. Hokkaido Univ.*, **38**, 46 (1978).
15) The 1 U is the amount of enzyme which will cleave 1 μmol of β-NAD to nicotinamide and ADP-ribose per min.
16) E. C. Taylor and J. S. Driscoll, *J. Am. Chem. Soc.*, **82**, 3141 (1960).
17) G. M. Badger and R. P. Rao, *Aust. J. Chem.*, **17**, 1399 (1964).
18) W. Herz and D. R. K. Murty, *J. Org. Chem.*, **26**, 122 (1961).
19) T. Wieland and H. Biener, *Chem. Ber.*, **96**, 266 (1963).
20) W. C. J. Ross, *J. Chem. Soc., C*, **1966**, 1816.
21) J. M. Bobbit and D. A. Scola, *J. Org. Chem.*, **25**, 560 (1960).

Unusual Reaction of Azoxybenzenes with *p*-Toluenesulfonic Acid in Acetic Anhydride

Ichiro SHIMAO,* Ken FUJIMORI,† and Shigeru OAE†

Department of Industrial Chemistry, Faculty of Engineering, Toyama University, Takaoka, Toyama 933

†*Department of Chemistry, The University of Tsukuba, Sakura-mura, Ibaraki 305*

(Received August 10, 1981)

Treatment of azoxybenzene with *p*-toluenesulfonic acid in acetic anhydride gave tosylates of 4- and 2-(phenylazo)phenols, and the corresponding acetates as by-product, besides azobenzene. However, a similar reaction of 4,4′-difluoroazoxybenzene gave 2-tosyloxy-4,4′-difluoroazobenzene as rearrangement product, besides 4-fluorophenyl tosylate and 4-fluorophenyl acetate. Meanwhile, the reaction of 4,4′-diacetoxyazoxybenzene afforded 4-acetoxyphenyl tosylate and hydroquinone diacetate in high yields. These unique reactions involve C–N bond cleavage, and may proceed through a pathway involving formation of benzenediazonium ion as the key intermediate.

In the Wallach rearrangement of azoxybenzenes, concentrated sulfuric acid has generally been used.[1] Meanwhile, treatment of azoxybenzene with chlorosulfuric acid[2] yielded chlorosulfate of *p*-hydroxyazobenzene. Similarly, in the reaction with fluorosulfuric acid,[3] the corresponding fluorosulfate of *p*-hydroxyazobenzene was obtained. Recently, the reaction of azoxybenzene with arenesulfonyl chloride[4] and tosyl anhydride[5] have also been found to give the arenesulfonates of *o*- and *p*-hydroxyazobenzene.

In the ordinary Wallach rearrangement of azoxybenzene with sulfuric acid, hydrogen sulfate ester of *p*-hydroxyazobenzene is formed as the rearrangement product, which is then rapidly hydrolyzed to give *p*-hydroxyazobenzene as the final product.[6] However, the sulfonic acid esters of hydroxyazobenzene do not hydrolyze under the reaction conditions. Recently, Yamamoto *et al.* reported that the treatment of azoxybenzene with trichloroacetic acid in acetic anhydride afforded hydroxyazobenzene,[7] *via* forming the corresponding ester, which is however unstable and hydrolyzed during the isolation of the reaction product.

Earlier, we reported that azoxybenzene reacts with an equimolar amount of acetic anhydride only upon heating at such a high temperature as 190 °C for a long hour, affording a mixture of azobenzene, acetanilide and acetic acid along with carbon dioxide, carbon monoxide and methane.[8] We then suggested that the initial slow step is the acetylation to give the *N*-acetoxyazobenzene, which undergoes homolytic fission of N–O bond shown below.

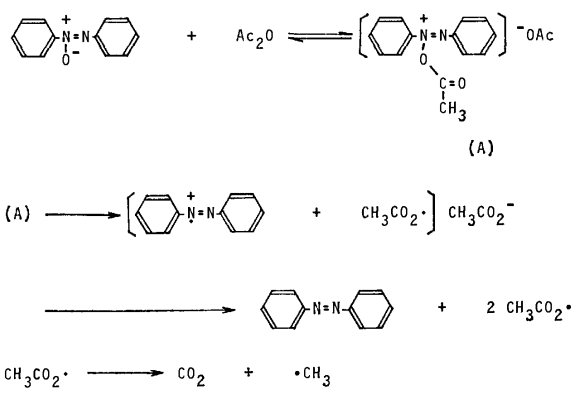

Since acetylation of *N*-oxides or sulfoxides is markedly accelerated by acid catalysis, it was anticipated that the reaction of azoxybenzene with acetic anhydride would proceed under mild conditions in the presence of a strong acid such as *p*-toluenesulfonic acid, and gives the rearranged ester, because water is absent under the conditions and hence the esters would not be hydrolyzed. Indeed the reaction between azoxybenzene and a mixture of acetic anhydride and *p*-toluenesulfonic acid was found to proceed smoothly even at 100 °C, and gave both tosyl and acetyl esters of hydroxyazobenzene. This paper is concerned with the reaction of some azoxybenzenes with *p*-toluenesulfonic acid in acetic anhydride.

Results and Discussion

Treatment of azoxybenzene (**1**) with excess *p*-toluenesulfonic acid (TsOH) in excess acetic anhydride at 100 °C for 12 h gave 2-tosyloxyazobenzene (**2**) (5%) and 4-isomer (**3**) (20%), 2-acetoxyazobenzene (**4**) (0.3 %) and 4-isomer (**5**) (2%) as rearrangement products, along with azobenzene (**6**) (7.5%).

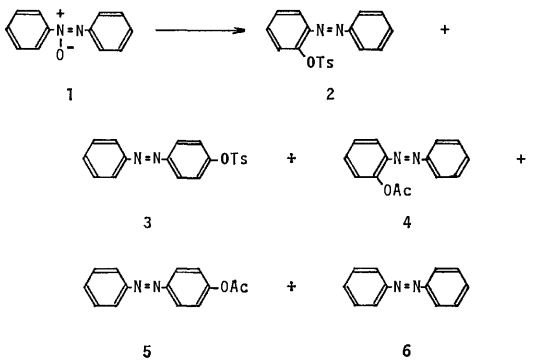

These rearrangement products may be formed through a mechanistic pathway similar to that proposed for the reaction of **1** with arenesulfonyl chloride,[3] as illustrated in the following sequential scheme: (i) Formation of the mixed acid anhydride, (ii) reaction of **1** with TsOAc to form *O*-tosylated intermediate (**7**), (iii) migration of tosyloxyl group to *o*-position, (iv) deprotonation to give eventually **2**, or (v) nucleophilic attack of tosylate ion (or acetate ion) at *p*-position of **7**, and (vi) subsequent elimination of tosyloxyl group bonded to azo nitrogen and deprotonation

to give **3** (or **5**).

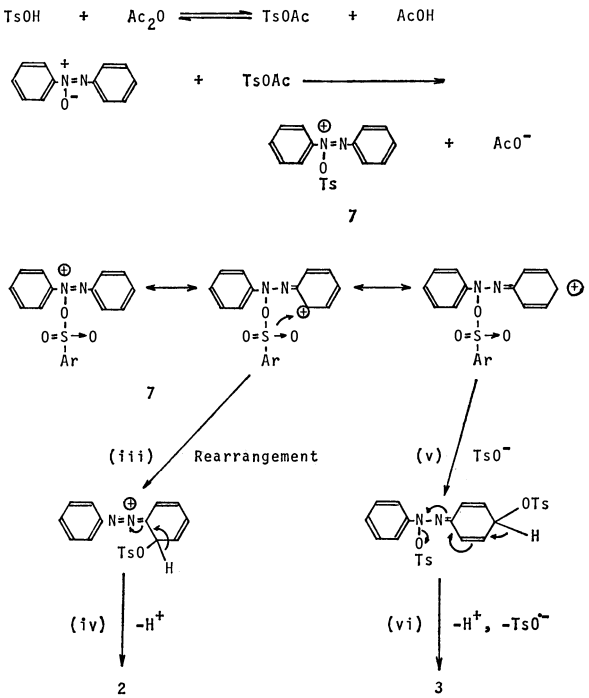

In the step (iii), the intermediate, **7**, may dissociate to form an intimate ion pair (**8**), prior to migration. When acetoxyl group migrates to the *o*-position, compound **4** is formed, though the yield is so low. In addition, there might be an alternative pathway to form a dication intermediate directly by cleavage of tosylate ion from **7**.

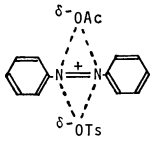

8

Here again, the formation of azobenzene may be rationalized in terms of incipient formation of azobenzene cation radical similarly as in the reaction of azoxybenzene with acetic anhydride at 190 °C.

The ratio of *o*-rearrangement to *p*-rearrangement is higher (1:4) than that of the reaction of **1** with sulfuric acid ($o:p=1:26$).[9] Probably, unlike the rearrangement in polar sulfuric acid, in which dissociation of water from azo group is more complete and hence the intermolecular migration to *p*-position predominates, that of the intermediate, **7**, in less polar acetic anhydride is more prone to proceed intramolecularly to *o*-position (step iii). This may be the reason why the *o*/*p* product ratio is a little higher in the reaction with acetic anhydride–TsOH system than with sulfuric acid.

The yield of acetate, **5**, was low, despite more nucleophilic character of acetate ion than tosylate ion. However, in the presence of TsOH, acetate ion, if formed, would be completely protonated to form acetic acid which is no longer nucleophilic enough to compete with tosylate ion to attack the *p*-position. The ester exchange reaction between tosylate, **3**, and acetate, **5**, was not observed under the above reaction conditions.

Table 1. Reaction of 4-bromo-ONN- and 4-bromo-NNO- azoxybenzenes

Compound	Yield/%					
	16	**17**	**18**	**19**	Acetate[a]	Recovery
15*α*	4.0	2.5	1.3	0.7	1.3	80
15*β*	4.8	3.3	1.6	0.8	1.3	73

a) 4-(*p*-Bromophenylazo)phenyl acetate contaminated by small amounts of the 2-isomer.

Treatment of 4,4′-difluoroazoxybenzene (**9**) with a mixture of TsOH and acetic anhydride gave in poor yield, ortho rearrangement product, 2-tosyloxy-4,4′-difluoroazobenzene (**10**) (yield 4%) and 2-(*p*-fluorophenylazo)-5-fluorophenol (**11**) (yield 1.5%) which is undoubtedly formed by hydrolysis of 2-acetoxy-4,4′-difluoroazobenzene during the isolation process of the reaction products. However, *p*-fluorophenyl tosylate (**12**) (yield 12%) and *p*-fluorophenyl acetate (**13**) (yield 5%) formed by the cleavage[16] of azoxy N and phenyl C bond were obtained, besides 4,4′-difluoroazobenzene (**14**) (yield 4.5%).

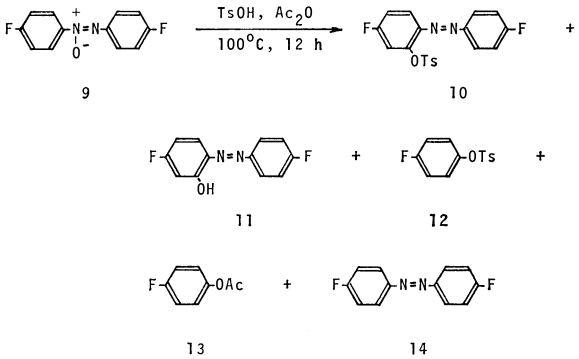

The reaction of 4,4′-dichloroazoxybenzene with a mixture of TsOH and acetic anhydride was relatively slow, and only after heating at 100 °C for 50 h, 2-tosyloxy-4,4′-dichloroazobenzene (3%), 2-(*p*-chlorophenylazo)-5-chlorophenol (0.4%), *p*-chlorophenyl tosylate (0.5%), and 4,4′-dichloroazobenzene (5.5%) were obtained.

Meanwhile, the reaction of 4,4′-dichloroazoxybenzene with sulfuric acid yielded abnormal rearrangement products, *e.g.* 2-chloro-4-(*p*-chlorophenylazo)phenol and 4-(*p*-chlorophenylazo)phenol, in which chlorine is migrated or lost.[10] However, these abnormal products were not observed at all in the reaction of 4,4′-dichloroazoxybenzene with a mixture of TsOH and acetic anhydride. The *O*-tosylated intermediate, **7**, did not accept the nucleophilic attack of tosylate ion at ipso position but preferentially rearranged to form the ester of *o*-hydroxyazobenzene. In addition, the formation of dicationic intermediate ($Ar-\overset{+}{N}\equiv\overset{+}{N}-Ar$) may be suppressed by low acidity under this reaction conditions. Consequently, the ipso attack of tosylate ion did not occur.

The reaction of 4-bromo-ONN-azoxybenzene (**15*α***) and the NNO-isomer (**15*β***) with a mixture of TsOH and acetic anhydride gave 4-(*p*-bromophenylazo)phen-

yl tosylate (**16**), 2-(phenylazo)-5-bromophenyl tosylate (**17**), 2-(*p*-bromophenylazo)phenyl tosylate (**18**), and 2-bromo-4-(phenylazo)phenyl tosylate (**19**) (Table 1).

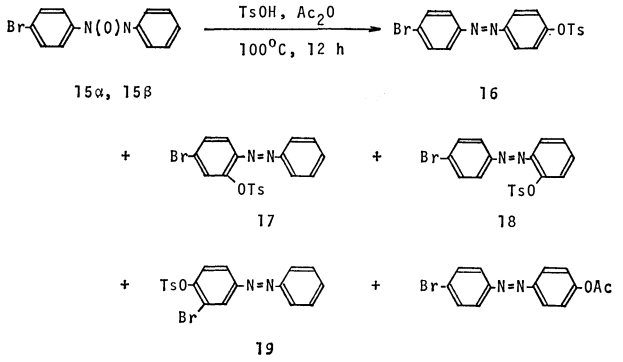

Azophenol tosylates, **16**—**19**, could not be isolated in this reaction. Therefore, the mixture was analyzed by gas chromatography. The mixture was hydrolyzed further with sodium hydroxide solution to isolate the corresponding azophenols.

The reaction products obtained from α-isomer of 4-bromoazoxybenzene (**15α**) were practically similar to those formed from the β-isomer (**15β**). It appears that the reaction proceeds *via* a common intimate ion pair intermediate (**20**). The product, **19**, is considered to be formed by rearrangement accompaning the migration of bromine. The similar rearrangement was observed in the reaction of 4,4'-dibromoazoxybenzene with sulfuric acid.[10] Thus, the rearrangement may be interpreted by the following mechanistic scheme in which the intimate ion pair, **20**, is the common intermediate in the rearrangement to both *o*- and *p*-positions and also in the migration of bromine, similar to that proposed previously.

The reaction of 4,4'-diacetoxyazoxybenzene(**21**)

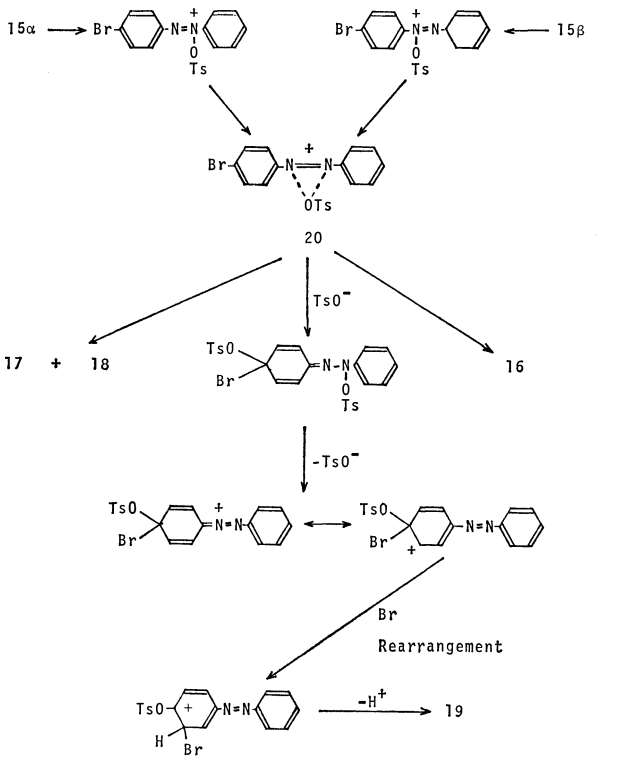

Table 2. Reaction of 4-acetoxyazoxybenzenes with TsOH in acetic anhydride (100 °C, 2 h)

Compound	Yield/%				
	22	**23**	**26**	**27**	**25β**
25α	77	9	18	72	
25β	33	4	8	30	60

gave mainly unique 1-ipso substitution products, *i.e.* 4-acetoxyphenyl tosylate (**22**) (yield 51%) and hydroquinone diacetate (**23**) (yield 47%), in high yield with evolution of nitrogen. The expected rearrangement products (the corresponding azophenol esters) were not obtained.

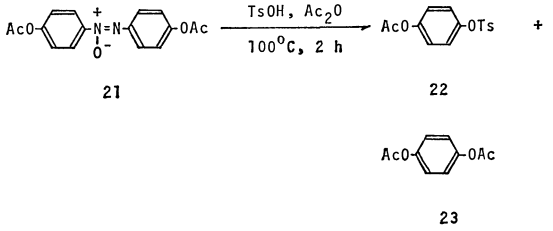

The reaction may be nicely explained by the following mechanistic scheme: (i) The initial formation of *O*-tosylated azoxybenzene (**24**), (ii) cleavage of the C–N bond and simultaneous attack to the tosyloxy oxygen (*i.e.* formation of **22** and the diazonium ion), (iii) decomposition of the diazonium ion to form **22** and **23** with evolution of nitrogen. Step (ii) may be attributed to the resonance effect of acetoxyl group to facilitated the cleavage of C–N bond. In this process, there might be a possibility that tosyloxyl group is alternated to acetoxyl group to give **23**.

In analogy with the reaction, when a solution of **21** and tosyl anhydride in acetonitrile was refluxed for 2 h, **22** was obtained in yield of 16%. Also the reaction of **21** with sulfuric acid in acetic anhydride (100 °C, 1 h) afforded **23** (yield 35%).

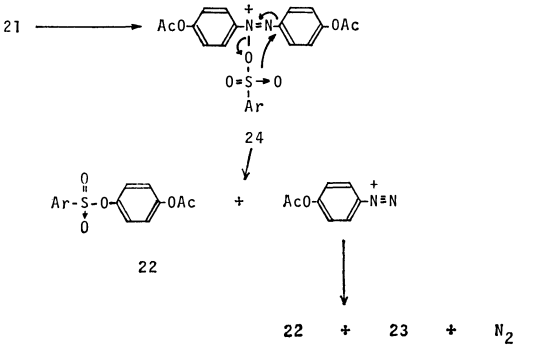

On the other hand, 2,2'-diacetoxyazoxybenzene gave also 2-acetoxyphenyl tosylate (41%), cathecol diacetate (18%), and 2,2'-diacetoxy-4-tosyloxyazobenzene (16%). In this reaction, the rearrangement product was obtained to a considerable extent.

The C–N bond cleavage was also found to occur in the reaction of 4-acetoxyazoxybenzene. Compounds, **22** and **23**, as well as, phenyl tosylate (**26**) and phenyl acetate (**27**) were obtained in the reaction of 4-acetoxy-ONN-azoxybenzene (**25α**) and 4-acetoxy-

NNO-azoxybenzene (**25β**). The results are shown in Table 2.

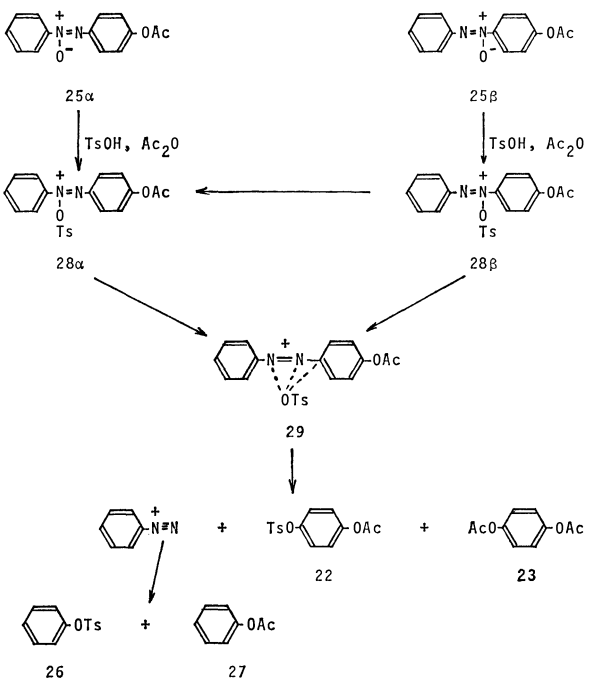

The α-isomer (**25α**) was found to react more rapidly than the β-isomer (**25β**). Accordingly, when the mixture of α- and β-isomers was used, the β-isomer was isolated as recovered material. Thus this procedure can be applied to prepare the β-isomer.

Both **25α** and **25β** gave the products nearly in the same ratio. Therefore, the reaction is presumed to proceed *via* a same common transient intermediate, perhaps a symmetrical ion pair (**29**). Alternatively, there is a possibility that **28β** rearranges to **28α** before undergoing the C–N bond cleavage.

The yield of tosylate, **22**, was higher than that of acetate, **23**, and while the yield of **27** was higher than that of **26**. Therefore, the first C–N bond cleavage would occur on the carbon atom of benzene ring having *p*-acetoxyl group, to give benzenediazonium ion and **22** (and **23**). In this step, tosyloxyl oxygen attacks the C_1 atom of benzene ring in preference to acetoxyl oxygen, since acetoxyl group would be completely protonated and lack enough nucleophilicity to attack ipso C_1. Benzenediazonium ion thus formed is reactive and hence would react readily with acetoxyl group present in a large exess.

In the presence of toluene, the reaction of **25** (α- and β-isomer) with TsOH and acetic anhydride afforded methylbiphenyl (yield 9%), as well as **22**, **23**, **26**, and **27**. Gas chromatographic analysis showed

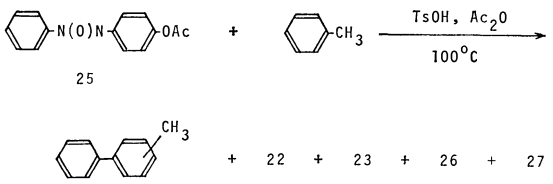

that the isomer distribution of methylbiphenyl was *o*: 57%, *m*: 21%, *p*: 22%. This ratio is close to that obtained by the reaction of toluene with benzenediazoniom ion in the presence of TsOH (*o*: 61%, *m*: 16%, *p*: 23%). The formation of methylbiphenyl demonstrates the participation of benzenediazonium ion as the intermediate.

Formation of arenediazonium ion from azoxyarene is not entirely unprecedented. The photo-rearrangement of 2,2′-dimethylazoxybenzene was reported to give a diazonium ion as an intermediate which eventually yielded abnormal by-product.[11]

Similarly, 4-chloro-4′-acetoxyazoxybenzene (a mixture of α- and β-isomer) yielded **22** (52%), **23** (5%), *p*-chlorophenyl tosylate (13%), and *p*-chlorophenyl acetate (45%). The recovered azoxy compound (37%) was almost 4-(*p*-chlorophenylazoxy)-NNO-phenyl acetate (β-isomer).

Experimental

Melting points are uncorrected. GLC analyses were performed on a Shimadzu GC-6A (column: 1.5% Silicone OV-17, 1 m or 2% Silicone OV-225, 3 m). Other instruments used are the same as those previously described.[10]

The reaction products were identified by comparison with samples prepared independently.

Material. 4,4′-Difluoro- and 4,4′-dichloro-azoxybenzenes and *p*-bromoazoxybenzenes were prepared according to the method given in the previous paper.[10] 4,4′-Diacetoxyazoxybenzene (**21**) was obtained as described by Jeonard and Curry,[12] mp 169—170 °C (from benzene). 2,2′-Diacetoxyazoxybenzene, *p*-acetoxyazoxybenzene, and *p*-acetoxy-*p*′-chloroazoxybenzene were prepared by oxidation of the corresponding azo compound with 30% H_2O_2 in AcOH. 2,2′-Diacetoxyazoxybenzene, mp 115—116 °C. Found: C, 61.35; H, 4.60; N, 8.72%. Calcd for $C_{16}H_{14}N_2O_5$: C, 61.14; H, 4.50; N, 8.91%. 4-Acetoxyazoxybenzene was a mixture of α-isomer 61% and β-isomer 39% (GLC). 4-Acetoxy-4′-chloroazoxybenzene was a mixture of α-isomer 57% and β-isomer 43% (HPLC). 4-Phenylazoxy-ONN-phenyl acetate (**25α**) and its NNO-isomer (**25β**) were prepared by acetylation of the corresponding phenylazoxyphenol with acetic anhydride and pyridine, **25α**, mp 93—95 °C (lit,[13] 89—90 °C), **25β**, mp 80—81 °C (lit,[13] 79—80 °C).

Reaction of Azoxybenzene (1). *p*-Toluenesulfonic acid (TsOH) monohydrate (5.0 g) was heated at 140 °C under reduced pressure to remove the crystalline water. To a solution of TsOH in acetic anhydride (12.5 ml) was added **1** (0.5 g). The solution was heated at 100 °C for 12 h. The reaction mixture was poured into cold water, and extracted with benzene. The extract was washed with $NaHCO_3$ solution, dried over Na_2SO_4, and evaporated. The residue was chromatographed on silica gel (benzene). Each fraction was analyzed by GLC. First fraction was a mixture of azobenzene (**6**) (0.034 g) and **1** (0.156 g). Second fraction was a mixture of 2-tosyloxyazobenzene (**2**) (0.045 g) and 4-tosyloxyazobenzene (**3**) (0.178 g). Third fraction was a mixture of 2-acetoxyazobenzene (**4**) (1.7 mg) and 4-acetoxyazobenzene (**5**) (12 mg).

Reaction of 4,4′-Difluoroazoxybenzene (9). Compound, **9**, (0.2 g) was treated with a mixture of TsOH and Ac_2O similarly, and worked up according to the procedure described above. The reaction product was chromatographed on silica gel (benzene). First fraction was a mixture o 4,4′-difluoroazobenzene (**14**) (9 mg) and **9** (82 mg). Second fraction was distilled under reduced pressure to give 4-fluorophenyl acetate (**13**) (7 mg), and the residue was chromato-

graphed on alumina.[15] Elution with benzene gave a mixture of 4-fluorophenyl tosylate (**12**) (27 mg) and 2-tosyloxy-4,4'-difluoroazobenzene (**10**) (13 mg). Recrystallization from hexane gave **10**, mp 116—117 °C, and the mother liquor was evaporated and distilled *in vacuo* to give **12**, mp 56—58 °C) from hexane). The residue on alumina column was eluted with EtOH–H_2O to give 2-(*p*-fluorophenylazo)-5-fluorophenol (**11**), mp 126 °C (from hexane).

Reaction of 4,4'-Diacetoxyazoxybenzene (21). TsOH monohydrate (5.0 g) was dehydrated at 140 °C under reduced pressure. A solution of **21** (0.5 g) and TsOH in Ac_2O (12.5 ml) was then heated at 100 °C for 2 h. The solution was poured into cold water. The precipitate was filtered off and purified by column chromatography on silica gel (benzene) to give 4-acetoxyphenyl tosylate (**22**) (0.50 g), mp 77.5—78 °C (from hexane-benzene). The mother liquor was extracted with benzene. The extract gave hydroquinone diacetate (**23**) (0.29 g), mp 122—123 °C (from hexane).

Reaction of 2,2'-Diacetoxyazoxybenzene. 2,2'-Diacetoxyazoxybenzene (0.2 g) was treated with a mixture of TsOH and Ac_2O similarly according the method described above. The reaction product was chromatographed on silica-gel column (benzene). First fraction was 2-acetoxyphenyl tosylate (0.16 g), mp 90—91 °C (from hexane). Second fraction was cathecol diacetate (0.044 g), mp 61—62 °C (from hexane). Third fraction (0.05 g) gave 2,2'-diacetoxy-4-tosyloxyazobenzene, mp 97—98 °C (from EtOH). Found: C, 59.02; H, 4.37; N, 6.00%. Calcd for $C_{23}H_{20}N_2O_7S$: C, 58.97; H, 4.30; N, 5.98%. The authentic sample was prepared by acetylation of 2,2'-dihydroxy-4-tosyloxyazobenzene (mp 223—225 °C).

Reaction of 4-Acetoxyazoxybenzene (25). 4-Acetoxyazoxybenzene (0.5 g) was treated with a similar mixture of TsOH and Ac_2O at 100 °C for 1 h according to the procedure described above. The reaction mixture was poured into cold aqueous $NaHCO_3$ solution, and then extracted with ether. The extract was distilled to give phenyl acetate (0.09 g). The residue was chromatographed on silica gel (benzene). First fraction gave phenyl tosylate (0.06 g), mp 94—95 °C (from hexane). Second fraction was the unchanged azoxy compound (0.16 g) (α-isomer 13.5% and β-isomer 86.5%). Third fraction gave 4-acetoxyphenyl tosylate (0.29 g) mp 79—80 °C (from hexane-benzene). Fourth fraction gave hydroquinone diacetate (0.019 g), mp 122—123 °C.

Authentic Sample of Tosylate Derivatives. The corresponding phenol was treated with tosyl chloride and pyridine by conventional method. **2**, mp 84—85 °C (lit,[4] 85—86 °C). **3**, mp 164—165 °C (lit,[4] 159—160 °C). 2-Tosyloxy-4,4'-dichloroazobenzene, mp 136—138 °C (from benzene-hexane). Found: C, 54.22; H, 3.14; N, 6.39%. Calcd for $C_{19}H_{14}Cl_2N_2O_3S$: C, 54.16; H, 3.33; N, 6.65%. **10**, mp 115—116 °C (from EtOH). Found: C, 58.88; H, 3.50; N, 7.22%. Calcd for $C_{19}H_{14}F_2N_2O_3S$: C, 58.76; H, 3.63; N, 7.21%. **16**, mp 157—159 °C. Found: C, 53.22; H, 3.33; N, 6.71%. **17**, mp 132—133 °C. Found: C, 52.83; H, 3.47; N, 6.75%. **18**, mp 123—124 °C. Found: C, 53.14; H, 3.40; N, 6.63%. **19**, mp 78—79 °C. Found: C, 52.63; H, 3.51; N, 6.52%, (from benzene-hexane). Calcd for $C_{19}H_{15}BrN_2O_3S$: C, 52.91; H, 3.51; N, 6.50%.

12, mp 58—59 °C (from hexane), Found: C, 58.45; H, 3.98%. Calcd for $C_{13}H_{11}FO_3S$: C, 58.64; H, 4.16%. *p*-Chlorophenyl tosylate, mp 68—70 °C, (from hexane). Found: C, 55.22; H, 3.92%. Calcd for $C_{13}H_{11}ClO_3S$: C, 55.23; H, 3.96%. **22**, mp 76.5—77.5 °C (from hexane-benzene). Found: C, 58.94; H, 4.83%. Calcd for $C_{15}H_{14}O_5S$: C, 58.81; H, 4.61%. 2-Acetoxyphenyl tosylate, mp 91—92 °C. Found: C, 58.65; H, 4.78%. Calcd for $C_{15}H_{14}O_5S$: C, 58.81; H, 4.61%. **26**, mp 94—95 °C (lit,[14] 94—95 °C).

References

1) R. A. Cox and E. Buncel, "The Chemistry of the Hydrazo, Azo and Azoxy Groups," ed by S. Patai, John Wiley & Sons, New York (1975), p. 808.
2) V. O. Lukashevich and T. N. Kurdyumova, *Zh. Obshch. Khim.*, **18**, 1963 (1948); *Chem. Abstr.*, **43**, 3800f (1949).
3) T. E. Stevens, *J. Org. Chem.*, **33**, 2667 (1968).
4) S. Oae, T. Maeda, S. Kozuka, and M. Nakai, *Bull. Chem. Soc. Jpn.*, **44**, 2495 (1971).
5) S. Oae and T. Maeda, *Tetrahedron*, **28**, 2127 (1972).
6) E. Buncel and W. M. J. Strachen, *Can. J. Chem.*, **47**, 911 (1969).
7) J. Yamamoto, N. Sato, M. Koshikawa, Y. Isoda, and M. Umezu, *Yuki Gosei Kagaku Kyokai Shi*, **33**, 270 (1975).
8) S. Oae, T. Maeda, and S. Kozuka, *Bull. Chem. Soc. Jpn.*, **44**, 442 (1971).
9) I. Shimao and S. Matsumura, *Bull. Chem. Soc. Jpn.*, **49**, 2294 (1976).
10) I. Shimao, K. Fujimori, and S. Oae, *Bull. Chem. Soc. Jpn.*, **55**, 546 (1982).
11) N. J. Bunce, *Bull. Chem. Soc. Jpn.*, **47**, 725 (1974); *Can. J. Chem.*, **55**, 383 (1977).
12) N. J. Jeonard and J. W. Curry, *J. Org. Chem.*, **17**, 1071 (1952).
13) A. Risaliti, *Gazz. Chim. Ital.*, **93**, 583 (1963); *Chem. Abstr.*, **59**, 13850 g (1963).
14) R. Otto, *Ber.*, **19**, 1833 (1886).
15) In this process, aryl acetate was hydrolyzed to give the corresponding phenol.
16) The resonance effect of fluorine is more suitable on the C–N bond cleavage than that of chlorine, however, acetoxyl group serves more effectively on the cleavage reaction than fluorine.

A Stereoselective One-stage α-Glucosylation with 2,3,4,6-Tetra-*O*-benzyl-α-D-glucopyranose and a Mixture of Methanesulfonic Acid, Cobalt(II) Bromide, and Tetraethylammonium Perchlorate

Shinkiti Koto,* Naohiko Morishima, and Shonosuke Zen

School of Pharmaceutical Sciences, Kitasato University, Shirokane, Minato-ku, Tokyo 108

(Received September 5, 1981)

A one-stage procedure for the stereoselective α-glucosylation of alcohol with 2,3,4,6-tetra-*O*-benzyl-α-D-glucopyranose and a mixture of methanesulfonic acid, cobalt(II) bromide, and tetraethylammonium perchlorate is described. The mechanism of the glucosylation reaction is discussed.

Continuing effort has been dedicated to developing a variety of stereoselective α-glucosylation methods.[1] The methods employing various kinds of glucosyl halides and equivalents with a non-participating benzyloxyl group at C-2 are most often used for the synthesis of α-glucosides.[2] However, they always require the preparation of the moisture-sensitive glucosylating precursors. Even the one-pot method starting from the stable glucosylating precursor, 2,3,4,6-tetra-*O*-benzyl-α-D-glucopyranose (**1**), involves a two-stage treatment of activation and condensation.[2e]

The glucosylation of alcohol with **1** readily proceeds in one-stage fashion in the presence of methanesulfonic acid ($MeSO_3H$) and $CoBr_2$ in CH_2Cl_2 at 25 °C.[3a] The later improvement[3b] of the stereoselectivity of this reaction using the additive tetraethylammonium perchlorate (Et_4NClO_4) enabled us to develop a simple method for the highly stereoselective α-glucosylation of alcohol with **1** (In Eq. 1, G denotes the 2,3,4,6-tetra-*O*-benzyl-D-glucopyranosyl group).

$$\alpha\text{GOH} + \text{ROH} \xrightarrow{MeSO_3H/CoBr_2/Et_4NClO_4} \alpha\text{GOR}\ (+\beta\text{GOR}) \quad (1)$$

The method is as handy as the modified Fischer method[4] and is practically free from the moisture problem often encountered in the usual glucosylation, since $CoBr_2$ is a strong desiccant.

Results and Discussion

Glucosylation with $MeSO_3H$ and $CoBr_2$.[3a] When an equimolar mixture of **1**, cyclohexylmethanol, and $CoBr_2$ in CH_2Cl_2 was treated with $MeSO_3H$ at 25 °C, the glucosylation reaction (In Eq. 2, R=cyclohexylmethyl, X=$MeSO_3$) was found to proceed smoothly to give the anomeric glucosides (**2a** and **2b**)

$$\alpha\text{GOH} + \text{ROH} \xrightarrow{HX/CoBr_2} \alpha\text{GOR} + \beta\text{GOR} \quad (2)$$

(Table 1). The yield of the glucosides **2a** and **2b** was maximized at 0.5 h (Runs 1—6). The yield was very dependent on the amount of $MeSO_3H$ (Runs 1, 3, and 5) and moderately dependent on that of $CoBr_2$ (Runs 2, 3, and 4) and of the alcohol (Runs 3 and 6). Too much use of $MeSO_3H$ and the alcohol decreased yields of the glucosides (Runs 5 and 6). No other salts examined so far showed such acceleration effects.[5] Acid such as *p*-toluenesulfonic acid and 2,4,6-trimethylbenzenesulfonic acid were of use, but trifluoroacetic acid was not. As for the solvent, benzene was useful for the reaction. Nitromethane ($MeNO_2$) brought about the stereoselective formation of the α-glucoside **2a**, but the yield was not satisfactory because de-*O*-benzylation reactions occurred concurrently. Even in the use of CH_2Cl_2, trace amounts of by-products such as the de-*O*-benzylation products, cyclohexylmethyl 3,4,6-tri-*O*-benzyl-α- and -β-D-gluco-

Table 1. Results of glucosylation of cyclohexylmethanol (CmOH) with 2,3,4,6-tetra-*O*-benzyl-α-D-glucopyranose (**1**), $MeSO_3H$, and $CoBr_2$ at 25 °C

Run	$MeSO_3H$ equiv.	$CoBr_2$ equiv.	CmOH equiv.	Solvent	Time / h	Yield of the glucosides **2a** and **2b**/%(α/β)	Recovery of **1**/%
1	0.1	1.0	1.0	CH_2Cl_2	0.5	27 (44/56)	68
2	0.3	0.5	1.0	CH_2Cl_2	0.5	29 (55/45)	67
3	0.3	1.0	1.0	CH_2Cl_2	0.5	72 (49/51)	14
4	0.3	2.0	1.0	CH_2Cl_2	0.5	72 (47/53)	15
5	1.0	1.0	1.0	CH_2Cl_2	0.5	51 (59/41)	25
6	0.3	1.0	2.0	CH_2Cl_2	0.5	64 (59/41)	14
7	0.3	1.0	1.0	CH_2Cl_2	2.0	85 (52/48)	1
8	0.3	1.0	1.0	C_6H_6	2.0	82 (54/46)	—[d]
9	0.3	1.0	1.0	CH_3NO_2	2.0	60 (72/28)	—[d]
10[a]	0.3	1.0	1.0	CH_2Cl_2	2.0	75 (53/47)	—[d]
11[b]	0.3	1.0	1.0	CH_2Cl_2	2.0	71 (51/49)	—[d]
12[c]	0.3	1.0	1.0	CH_2Cl_2	2.0	13 (46/54)	39

a) *p*-Toluenesulfonic acid (0.3 equiv.) used instead of $MeSO_3H$. b) 2,4,6-Trimethylbenzenesulfonic acid (0.3 equiv.) used instead of $MeSO_3H$. c) CF_3CO_2H (0.3 equiv.) used instead of $MeSO_3H$. d) Not determined.

Table 2. Results of glucosylation of cyclohexylmethanol with 2,3,4,6-tetra-*O*-benzyl-α-D-glucopyranose (1), $MeSO_3H$, $CoBr_2$, and an additive in CH_2Cl_2[a]

Run	Additive	Equiv.	Time / h	Yield of the glucosides, **2a** and **2b**/%(α/β)	Recovery of **1**/%
13[b]	Bu_4NBr	0.5	2.0	65 (52/48)	—
14[b]	Bu_4NBr	1.0	2.0	62 (74/26)	27
15[b]	Bu_4NBr	1.0	4.0	62 (77/23)	30
16[b]	Bu_4NBr	2.0	2.0	5 (80/20)	88
17[b]	$BnEt_3NBr$[c]	1.0	2.0	69 (61/39)	20
18[b]	EtPyBr[c]	1.0	2.0	76 (55/45)	14
19[b]	KBr	1.0	2.0	70 (59/41)	—
20[c]	Et_4NClO_4	0.5	2.0	87 (75/25)	—
21[b]	Et_4NClO_4	1.0	2.0	75 (76/24)	—
22[d]	Et_4NClO_4	1.3	2.0	83 (76/24)	—
23[b]	$LiClO_4$	1.0	2.0	75 (53/47)	—
24[b]	$Et_4NCF_3SO_3$	1.0	2.0	50 (61/39)	—
25[b]	Et_4NBF_4	1.0	2.0	69 (60/40)	—

a) The reaction was conducted at 25 °C. Yields are based on the weight of glucosides obtained compared to the weight of alcohol charged. b) The mole ratio of **1**, $MeSO_3H$, and $CoBr_2$ to alcohol was 1.0, 0.3, and 1.0, respectively. c) The mole ratio of **1**, $MeSO_3H$, and $CoBr_2$ to alcohol was 1.3, 0.3, and 1.0, respectively. d) The mole ratio of **1**, $MeSO_3H$, and $CoBr_2$ to alcohol was 1.3, 0.4, and 1.3, respectively. e) Bn denotes benzyl group and EtPy means *N*-ethylpyridinium ion.

pyranosides (**3a** and **3b**), and the self-condensation products (**4a** and **4b**) of **1**[6a] were isolated from the reaction mixture.[6b]

When the glucosylation of methanol (MeOH) with **1** was carried out at 0 °C, the transient accumulation of the glucosyl bromide (**5**) was observed by means of TLC at the beginning of the reaction (<0.5 h). The ^1H NMR spectrum of the filtrate of the mixture of **1**, $MeSO_3H$, and $CoBr_2$ in CH_2Cl_2 was essentially superimposable with that of the authentic **5** in CH_2Cl_2. Therefore, **5** evidently intervenes in the glucosylation reaction.

The IR spectrum of the solid material recovered from the glucosylation mixture had the characteristic absorption of the salt of $MeSO_3H$ at ν=1180 and 1060 cm^{-1} and the ^1H NMR spectrum of the supernatant of the glucosylation mixture did not show the signal of the methyl group of $MeSO_3H$ near at δ 3.2. Moreover, it was found that $MeSO_3H$ and $CoBr_2$ reacted to afford the solid material whose composition was $CoBr_{2-x}(CH_3SO_3)_x$. Consequently, $MeSO_3H$ surely reacts with $CoBr_2$ to generate HBr (Eq. 3) during the glucosylation reaction.

$$CoBr_2 + xMeSO_3H \longrightarrow CoBr_{2-x}(MeSO_3)_x + xHBr \quad (3)$$

It was then confirmed that the glucosylation of MeOH with **1** proceeds well in the presence of $CoBr_2$ and HBr (In Eq. 2, R=Me, X=Br) and $CoBr_2$ accelerates the alcoholysis of **5** with cyclohexylmethanol.[7a] It is concluded that HBr generated *in situ* cooperates with $CoBr_2$ to convert **1** efficiently into **5** (Eq. 4a), which then undergoes alcoholysis (Eq. 4b). Figure 1 presents a summarized scheme for the one-stage glucosylation of alcohol using **1** and the mixture of $MeSO_3H$ and $CoBr_2$.[7b]

$$\alpha GOH \xrightarrow[-H_2O]{\text{a) HBr/CoBr}_2} \alpha GBr \xrightarrow[-HBr]{\text{b) ROH/CoBr}_2} \alpha GOR + \beta GOR \quad (4)$$

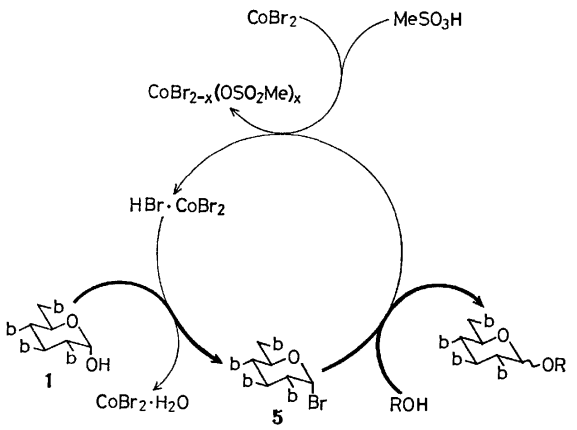

Fig. 1. Summarized scheme of the glucosylation reaction of alcohol with 2,3,4,6-tetra-*O*-benzyl-α-D-glucopyranose using the mixture of methanesulfonic acid and cobalt(II) bromide.

Improvement of the Stereoselectivity of the Glucosylation.[3b] Since the glucosyl bromide **5** intervenes in the glucosylation reaction (Fig. 1), tetrabutylammonium bromide (Bu_4NBr) and relatives were added into the reaction mixture, because it was anticipated that they cause the bromide ion-catalyzed stereoselective α-glucosylation[2c] (Table 2). The addition of Bu_4NBr caused the predominant formation of the α-glucoside **2a**, but with a decrease of the yields of **2a** and **2b** (Runs 13—15). Excessive use of Bu_4NBr sharply decreased the yield of glucosides; two molar amounts of Bu_4NBr almost inhibited the reaction (Run 16). This is attributable to the fact that two molar amounts of Bu_4NBr interrupts the formation of **5** from **1**, because the bromide anion strongly coordinates with $CoBr_2$ to form $[CoBr_3]^-$ and/or $[CoBr_4]^{2-}$, in competition with $MeSO_3H$ (*cf.* Eq. 2).[8] Other bromides showed simi-

lar tendencies, but the effects were weaker than for Bu_4NBr.

Next, effects of Et_4NClO_4 and related substances on the selectivity of the glucosylation were examined, because the perchlorate anion has poor coordinating ability to $CoBr_2$[9] and the glucosyl perchlorates with a benzyloxyl group at C-2 undergo the stereoselective α-glucosylation[2b] (Runs 20—25). Among the salts used, Et_4NClO_4 sharply increased the proportion of the α-anomer **2a** without serious decrease of the yield of the glucosides. The difference in the coordinating ability to $CoBr_2$ between perchlorate anion (weaker) and bromide anion (stronger)[7b] promotes the formation of the glucosyl perchlorate as in Eq. 5, so that the perchlorate anion does not interrupt the whole reaction. The effect of other salts was similar but feeble (Runs 23—25).

$$\alpha GOH + Et_4N^+//ClO_4^- + CoBr_2 \longrightarrow G^+//ClO_4^- + Et_4N^+//[CoBr_3]^- \quad (5)$$

Finally, the extent of the anomerization of the β-glucoside **2b** was determined under the three glucosylation conditions described above (Table 3). Because **2b** did not anomerize into **2a** so much in the presence of $MeSO_3H$, $CoBr_2$, and Bu_4NBr (Run 27), most of **2a** seems to be formed *via* the bromide ion-catalyzed alcoholysis of **5**, in the glucosylation (Run 14) of cyclohexylmethanol with **1** and this reagent mixture. In contrast to this, the mixture of $MeSO_3H$, $CoBr_2$, and Et_4NClO_4 in CH_2Cl_2 anomerized **2b** into **2a** efficiently (Run 28) (Eq. 6). The composition of the anomeric glucosides of the anomerization mixture was almost identical with that of the glucosylation mixture of the alcohol with **1** and this ternary mixture (Run 21). Therefore, this glucosylation furnishes an equilibrium mixture of the anomeric glucosides like the Fischer glucosylation does. It is noted that the mixture of $MeSO_3H$ and $CoBr_2$ in $MeNO_2$ smoothly anomerized **2b** and the composition of the anomeric glucosides was equal to that of the glucosylation mixture in $MeNO_2$ containing this binary mixture (Run 9). In this case, the high solubility of $CoBr_2$ in $MeNO_2$ may greatly enhance the polarity of the medium. This promotes the formation of the glucosyl cation G^+ to attain the anomerization of **2b** with $MeSO_3H$. Based on the results described so far, the mechanism of the stereoselective α-glucosylation affording the equilibrium mixture of the anomeric glucosides is postulated in Fig. 2.

$$\beta GOR \xrightarrow{MeSO_3H/CoBr_2/Et_4NClO_4} \alpha GOR \quad (6)$$

Table 3. Anomerization of cyclohexylmethyl 2,3,4,6-tetra-*O*-benzyl-β-D-glucopyranoside (**2b**) in various conditions[a]

Run	Additive, equiv.	Solvent	Yield of glucosides (**2a**, **2b**) %	(α/β)
26	None	CH_3NO_2	54	(74/26)
27	Bu_4NBr, 1.0	CH_2Cl_2	74	(12/88)
28	Et_4NClO_4, 1.0	CH_2Cl_2	74	(78/22)

a) The reaction was conducted for 2 h at 25 °C. The mole ratios of $MeSO_3H$ and $CoBr_2$ to the glucoside **2b** were 0.3 and 1.0.

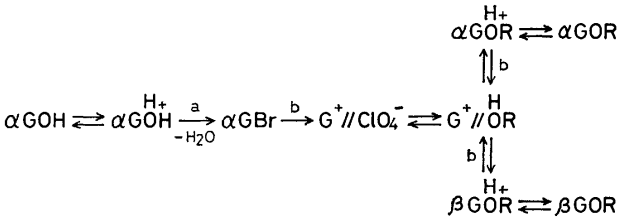

Fig. 2. Scheme of the stereoselective α-glucosylation of alcohol with 2,3,4,6-tetra-*O*-benzyl-α-D-glucopyranose using the mixture of methanesulfonic acid, cobalt(II) bromide, and tetraethylammonium perchlorate (**a** denotes the step which may be assisted by $CoBr_2$ and **b** does the one which may be promoted be $CoBr_2$ and ClO_4^-).

Table 4. Results of glucosylation of various alcohols through the ternary system[a]

Alcohol	Glucosides obtained	Yield of glucosides %	(α/β)
1-Hexanol[b]	**7a, 7b**	83	(73/27)
1-Octanol[b]	**8a, 8b**	82	(75/25)
1-Dodecanol[b]	**9a, 9b**	80	(77/23)
Cyclohexylmethanol[b,d]	**2a, 2b**	83	(76/24)
6-(2,4-Dinitroanilino)-1-hexanol[b,d]	**10a, 10b**	88	(71/29)
Cyclopentanol[c]	**11a, 11b**	85	(72/28)
Cyclohexanol[c,d]	**12a, 12b**	83	(80/20)
Cyclooctanol[d]	**13a, 13b**	78	(77/23)
Cyclododecanol[c]	**14a, 14b**	80	(74/26)
5α-Cholestan-3β-ol[c,d]	**15a, 15b**	63	(79/21)

a) The reaction was conducted on a 0.5 mmol scale in CH_2Cl_2 for 2 h at 25 °C. Yields were based on the weight of glucosides compared to the weight of alcohol charged. b) Mole ratios of **1**, $MeSO_3H$, $CoBr_2$, and Et_4NClO_4 to alcohol were 1.3, 0.4, 1.3, and 1.3. c) Mole ratios of **1**, $MeSO_3H$, $CoBr_2$, and Et_4NClO_4 to alcohol were 1.3, 0.3, 1.3, and 0.5. d) Anomeric glucosides obtained were identified with the samples prepared by alternative methods (Ref. 11).

This one-stage stereoselective α-glucosylation was applied to several alcohols to give the results summarized in Table 4. For practical use, slightly excess amounts of **1**, $CoBr_2$, and Et_4NClO_4 were charged in the case of primary alcohols (Runs 22, 29—32). Because of the high susceptibility of the glucoside of secondary alcohols to the anomerization,[10] smaller amounts of Et_4NClO_4 was used in the glucosylation of such alcohols (Runs 33—37).

Experimental

Instruments used are identical with those described previously.[6a] Green-colored anhydrous $CoBr_2$ (Wako) was stored over P_2O_5. The acid $MeSO_3H$ (Tokyo Kasei) was used without any pretreatments. The additives Et_4NClO_4 (Tokyo Kasei) and Bu_4NBr (Tokyo Kasei), recrystallized from acetonitrile containing hexane, were used after being stored *in vacuo* over P_2O_5 for several days. The pre-distilled

Table 5. Physical and analytical data of alkyl D-glucoside derivatives

Compd	Mp θ_m/°C	$[\alpha]_D^{20}$/° (c, $CHCl_2$)	Found (%) C	Found (%) H	Molecular formula	Calcd (%) C	Calcd (%) H
7a	—	+32 (0.5)	76.71	7.76	$C_{40}H_{48}O_6$	76.89	7.74
7b	35—37	+6 (0.6)	76.97	7.68			
8a	—	+32 (0.7)	77.24	8.01	$C_{42}H_{52}O_6$	77.27	8.03
8b	30—32	+8 (0.9)	77.43	8.13			
9a	—	+30 (0.6)	77.82	8.63	$C_{46}H_{60}O_6$	77.93	8.53
9b	—	+5 (0.5)	77.79	8.70			
11a	—	+41 (1.8)	76.76	7.33	$C_{39}H_{44}O_6$	76.94	7.29
11b	102—103	+9 (0.6)	76.72	7.29			
13a	—	+50 (2.0)	77.39	7.72	$C_{42}H_{50}O_6$	77.51	7.74
13b	87—88	+6 (0.7)	77.46	7.81			
14a	—	+49 (2.0)	78.05	8.40	$C_{46}H_{58}O_6$	78.15	8.27
14b	96—97	+3 (1.0)	78.13	8.21			

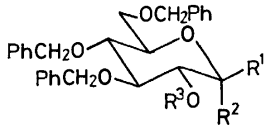

Compd	R^1	R^2	R^3	Compd	R^1	R^2	R^3
1	H	OH	Bn	**9a**	H	ODd	Bn
2a	H	OCm	Bn	**9b**	ODd	H	Bn
2b	OCm	H	Bn	**10a**	H	ODh	Bn
3a	H	OCm	H	**10b**	ODh	H	Bn
3b	OCm	H	H	**11a**	H	OCp	Bn
4a	H	OαG	Bn	**11b**	OCp	H	Bn
4b	OαG	H	Bn	**12a**	H	OCh	Bn
5	H	Br	Bn	**12b**	OCh	H	Bn
6a	H	OMe	Bn	**13a**	H	OCoc	Bn
6b	OMe	H	Bn	**13b**	OCoc	H	Bn
7a	H	OHx	Bn	**14a**	H	OCdd	Bn
7b	OHx	H	Bn	**14b**	OCdd	H	Bn
8a	H	OOc	Bn	**15a**	H	OCt	Bn
8b	OOc	H	Bn	**15b**	OCt	H	Bn

Bn = benzyl, Ch = cyclohexyl, Cm = cyclohexylmethyl, Coc = cyclooctyl, Cp = cyclopentyl, Ct = 5α-cholestan-3β-yl, Dd = dodecyl, Dh = 6-(2,4-dinitroanilino)-1-hexyl, αG = 2,3,4,6-tetra-*O*-benzyl-α-D-glucopyranosyl, Hx = hexyl, Me = methyl, Oc = octyl.

solvents were stored over Molecular Sieve (Linde 3A). Tetraethylammonium trifluoromethanesulfonate and tetrafluoroborate were prepared by the treatment of Et_4NBr with CF_3SO_3Ag (Alpha) and with $AgBF_4$ (Wako), respectively, in dry MeOH followed by evaporation *in vacuo*. Compound **1**, 6-(2,4-dinitroanilino)-1-hexanol, 5α-cholestan-3β-ol (Tokyo Kasei) were stored *in vacuo* over P_2O_5. Column chromatography of the pre-processed mixture of products was done on silica gel (Kanto Kagaku) using the solvent system of hexane and ethyl acetate, unless otherwise stated; each fraction was examined by TLC on silica gel (Merck, 7731). Evaporation was carried out under reduced pressure at 35—40 °C, unless otherwise stated. Table 5 summarized the physical and analytical data of newly synthesized compounds.

The Procedure for the Glucosylation with 2,3,4,6-Tetra-O-benzyl-α-D-glucopyranose (1), $MeSO_3H$, and $CoBr_2$. The acid $MeSO_3H$ (3.2 μl, 0.05 mmol) was added to a stirred mixture of **1** (90 mg, 0.17 mmol), $CoBr_2$ (36.5 mg, 0.17 mmol) and cyclohexylmethanol (20.5 μl, 0.17 mmol) in CH_2Cl_2 (0.45 ml). After being vigorously stirred at 25 °C for 2 h, the mixture was diluted with benzene, followed by the addition of powdered $NaHCO_3$ with agitation. The filtrate was evaporated and chromatographed to give cyclohexylmethyl 2,3,4,6-tetra-*O*-benzyl-α- and -β-D-glucopyranoside (**2a** and **2b**) and the by-products.[6] The glucosides (**2a** and **2b**) and the self-condensation products (**4a** and **4b**) were identified by comparison with those reported.[6a,11] Yields are based on the weight of products obtained, with reference to the weight of **1** charged. The results are summarized in Table 1.

The Glucosylation of MeOH with the Benzylated Glucose 1, $MeSO_3H$, and HBr. A cooled saturated solution of HBr in CH_2Cl_2 (0.64 M, 0.28 ml) was added into a stirred mixture of **1** (90 mg, 0.17 mmol), $CoBr_2$ (36.5 mg, 0.17 mmol), and MeOH (7 μl, 0.17 mmol) in CH_2Cl_2 (0.45 ml). After being agitated for 2 h at 25 °C, the mixture was processed as above to afford methyl 2,3,4,6-tetra-*O*-benzyl-α-D-glucopyranoside (**6a**) (30 mg, 33%) and the β-anomer **6b** (26 mg, 28%), identified with those reported.[6a] Some unchanged **1** was recovered (21 mg, 23%).

Without $CoBr_2$, the anomeric mixture of **6a** and **6b** was obtained in 15% yield (α/β = 70/30) and **1** was recovered (83%).

The Formation of 2,3,4,6-Tetra-O-benzyl-α-D-glucopyranosyl Bromide (5) from the Benzylated Glucose 1 with $MeSO_3H$ and $CoBr_2$. A mixture of **1** (90 mg, 0.17 mmol), $MeSO_3H$ (11 μl, 0.17 mmol), and $CoBr_2$ (36.5 mg, 0.17 mmol) in CH_2Cl_2 (0.45 ml) was stirred for 1 h at 25 °C. The insoluble material was filtered, washed with CH_2Cl_2, and ignited at 110 °C *in vacuo*; IR (KBr) 1345 (Me), 1180, 1060 cm^{-1} (SO_3). Found: C, 7.07; H, 2.08; Br, 18.07%. Calcd for $CoBr_{0.55}(CH_3SO_3)_{1.45}$: C, 7.23; H, 1.82; Br, 18.25%. The ^1H NMR of the filtrate was essentially the same as that of **5** prepared *via* the treatment of ethyl 2,3,4,6-tetra-*O*-benzyl-1-thio-α-D-glucopyranoside[12] (49 mg, 0.083 mmol) in CH_2Cl_2 (0.5 ml) with a solution of Br_2 in CH_2Cl_2 (60% w/v, 27 μl) for 10 min in the dark, followed by the quick evaporation at 60 °C; δ = 6.59 (d, J = 4.0 Hz, H-1 of **5**).

When Bu_4NBr (107 mg, 0.33 mmol) was added to the reaction mixture prior to the addition of $MeSO_3H$, ^1H NMR of the filtrate indicated that **5** did not form (the signal at δ 6.59 was absent).

The Procedure for the Glucosylation with the Benzylated Glucose 1, $MeSO_3H$, $CoBr_2$, and Additive. To a mixture of **1** (90 mg, 0.17 mmol), $CoBr_2$ (36.5 mg, 0.17 mmol), an additive, and an alcohol (0.17 mmol) in a solvent (0.45 ml), $MeSO_3H$ (3.3 μl, 0.050 mmol) was added under stirring. After agitation for 2 h at 25 °C, the mixture was processed

and then chromatographed as described above. The results are summarized in Tables 2 and 4.

*Synthesis of Cyclohexylmethyl 3,4,6-Tri-O-benzyl-α- and -β-D-glucopyranose(**3a** and **3b**), Which Were Isolated from the Reaction Mixture of the Glucosylation of Cyclohexylmethanol with the Benzylated Glucose **1**.* 3,4,6-Tri-*O*-benzyl-α-D-glucopyranose[13] (450 mg, 1.0 mmol) was condensed with cyclohexylmethanol (124 μl, 1.0 mmol) in CH_2Cl_2 (2.5 ml) in the presence of $MeSO_2H$ (20 μl, 0.3 mmol) and $CoBr_2$ (219 mg, 1.0 mmol) at 25 °C for 2 h. After processing, the mixture was chromatographed (benzene–2-butanone, gradient, 100:1→10:1) to afford the β-anomer **3b** (107.5 mg, 20%); colorless needles, mp 89.5—91 °C, $[\alpha]_D^{20}$ −8° (*c* 1.0, $CHCl_3$), and then the α-anomer **3a** (199.5 mg, 37%); $[\alpha]_D^{20}$ +84° (*c* 1.0, $CHCl_3$). Found: (**3a**) C, 74.03; H, 7.74%. (**3b**) C, 75.00; H, 7.83%. Calcd for $C_{34}H_{42}O_6$: C, 74.70; H, 7.74%.

The Reaction of $CoBr_2$ with $MeSO_3H$ in CH_2Cl_2. A suspension of $CoBr_2$ (43.6 mg, 0.2 mmol) in CH_2Cl_2 (0.54 ml) was treated with $MeSO_3H$ (0.2—0.4 mmol) at 25 °C for 1 h under vigorous stirring. The solid material was collected, washed with dry CH_2Cl_2 (0.3 ml×7), and ignited *in vacuo* at 110 °C over P_2O_5. In each case, the evolution of HBr was seen at the removal of the stopper of the vessel and the filtrate precipitated AgBr on addition of aq $AgNO_3$. The solid material obtained was analyzed to afford the following data [the amount of $MeSO_3H$ (mmol), analysis]: 13 μl (0.2). Found: C, 5.08; H, 1.36; Br, 30.37%. Calcd for $CoBr_{0.92}(CH_3SO_3)_{1.08}$: C, 5.52; H, 1.39; Br, 31.29%. 26 μl (0.4). Found: C, 7.47; H, 2.14; Br, 17.19%. Calcd for $CoBr_{0.50}(CH_3SO_3)_{1.50}$: C, 7.46; H, 1.89; Br, 16.54%.

References

1) A. F. Bochkov and G. E. Zaikov, "Chemistry of the *O*-Glycosidic Bond, Formation and Cleavage," Translated by C. Schuerch, Pergamon Press (1979), Chap. 2.

2) a) P. W. Austin, F. E. Hardy, J. G. Buchanan, and J. Baddiley, *J. Chem. Soc.*, **1964**, 2128; R. Eby and C. Schuerch, *Carbohydr. Res.*, **34**, 79 (1974); b) K. Igarashi, J. Irisawa, and T. Homma, *ibid.*, **39**, 213 (1975); c) R. U. Lemieux, K. B. Hendriks, R. V. Stick, and K. James, *J. Am. Chem. Soc.*, **97**, 4056 (1975); d) J.-R. Pougny, J.-C. Jaquinet, M. Nassr, D. Duchet, M. L. Milat, and P. Sinaÿ, *J. Am. Chem. Soc.*, **99**, 6762 (1977); e) J. Leroux and A. S. Perlin, *Carbohydr. Res.*, **67**, 163 (1978), T. Mukaiyama, T. Nakatsuka, and S. Shoda, *Chem. Lett.*, **1979**, 487.

3) a) S. Koto, N. Morishima, and S. Zen, *Chem. Lett.*, **1976**, 1109; b) S. Koto, N. Morishima, S. Inada, and S. Zen, IXth Intern. Symp. Carbohydr. Chem., 1978, Apr. 10—14, London, B-27.

4) R. E. Wing and J. N. BeMiller, *Carbohydr. Res.*, **10**, 441 (1969); A. Klemer and R. Kutz, *Tetrahedron Lett.*, **1969**, 1693; F. Micheel and E.-D. Pick, *ibid.*, **1969**, 1695; A. Klemer and B. Kraska, *Carbohydr. Res.*, **32**, 400 (1974).

5) The following salts gave **2a** and **2b** in, at best, poor yields (<10%) when the equimolar mixture of **1**, $MeSO_3H$, a salt, and cyclohexylmethanol in CH_2Cl_2 was stirred for 2 h at 25 °C: $CoCl_2$, $CoSO_4$, $Co(MeSO_3)_2$, $NiBr_2$, $CuBr_2$, $HgBr_2$, $CdBr_2$, $ZnBr_2$, $CaBr_2$, $MnBr_2$, $MgSO_4$, and $CaSO_4$.

6) a) S. Koto, N. Morishima, and S. Zen, *Bull. Chem. Soc. Jpn.*, **52**, 784 (1979); b) For example, the isolated by-products of Run 7 were **4a**(5%), **4b**(2.6%), **3a**(3.8%), and **3b**(0.8%).

7) a) Stirring the equimolar mixture of $CoBr_2$, cyclohexylmethanol, and the glucosyl bromide **5** in CH_2Cl_2 for 2 h at 25 °C gave **2a** and **2b** in a 70% yield (α/β=54/46) and the de-*O*-benzylation products; b) The fact that $CoBr_2$ coordinates reversibly with alcohol but irreversibly with H_2O [K. Sone, T. Fukuda, J. Mizusaki, and K. Moriyama, *Monatsh. Chem.*, **107**, 271 (1976)] and selectively coordinates with Br^- in the presence of alcohol [D. L. Wertz and R. F. Kruh, *Inorg. Chem.*, **9**, 595 (1970); S. Buffagni and R. M. Dunn, *J. Chem. Soc.*, **1961**, 5105] appears important for the glucosylation to proceed. The order of the affinity of nucleophiles to $CoBr_2$ in CH_2Cl_2 may be: $H_2O \gg Br^- > ROH > ClO_4^-$.

8) F. A. Cotton, D. M. L. Goodgame, and M. Goodgame, *J. Am. Chem. Soc.*, **83**, 4690 (1961).

9) K. Sawada and M. Tanaka, *J. Inorg. Nucl. Chem.*, **39**, 339 (1977).

10) S. Koto, *et al.*, *Bull. Chem. Soc. Jpn.*, to be submitted.

11) S. Koto, T. Sato, N. Morishima, and S. Zen, *Bull. Chem. Soc. Jpn.*, **53**, 1761 (1980).

12) F. Weygand and H. Ziemann, *Justus Liebigs Ann. Chem.*, **657**, 179 (1962).

13) G. Ekborg, B. Lindberg, and J. Lönngren, *Acta Chem. Scand.*, **26**, 3287 (1972); P. A. Gent and R. Gigg, *Carbohydr. Res.*, **49**, 325 (1976).

Oxidation of Lipids. I. Quantitative Determination of the Oxidation of Methyl Linoleate and Methyl Linolenate

Yorihiro YAMAMOTO, Etsuo NIKI,* and Yoshio KAMIYA

Department of Reaction Chemistry, Faculty of Engineering, The University of Tokyo, Hongo, Bunkyo-ku, Tokyo 113

(Received August 12, 1981)

The extent of oxidation of methyl linoleate and methyl linolenate has been measured quantitatively by several methods such as oxygen uptake, substrate disappearance, and formation of conjugated diene, TBA-reactive material and of hydrocarbon gas. In the early stage of oxidation of methyl linoleate, oxygen uptake, substrate disappearance, peroxide and conjugated diene formation were all quantitative and their results agreed well each other. Little TBA-reactive material and hydrocarbons were observed. In the oxidation of methyl linolenate, however, no product was formed quantitatively, and the extent of oxidation estimated decreased in the order, oxygen uptake>substrate disappearance>peroxide>conjugated diene>TBA-reactive material.

Oxidation of unsaturated fatty acids has been the subject of research since the onset of studies on autoxidation in 1940's.[1,2] It has recently received renewed attention, especially in relevance to the oxidation of lipids in biological systems as well as the oxidative deterioration of fats and oils.[2]

It is important and crucial to know how much oxidative deterioration has occured, but it is usually quite difficult to evaluate it, especially the oxidation *in vivo*. The oxidation reactions of saturated hydrocarbons are rather simple; they give hydroperoxides as the primary product in a substantially quantitative yield at moderate temperatures and low conversion. Thus, under these conditions, oxygen uptake, substrate disappearance, and hydroperoxide formation are all quantitative and their results agree well each other. The oxidations of olefins are more complicated: The addition to the double bond and abstraction of allylic hydrogen by peroxyl radicals compete. The addition mechanism gives primarily polyperoxides and epoxide, while the abstraction mechanism gives hydroperoxide as a major product.[3]

Oxidations of polyunsaturated fatty acids, major components of lipids, are more complicated, and usually many reactions proceed simultaniously and competitively. Thus, some criteria for accessing the extent of oxidation are required.

The extent of oxidation has been measured by several criteria such as oxygen uptake, peroxide value, conjugated diene formation, TBA-value, ethane and pentane formation, chemiluminescence, and development of fluorescence.[4,5] These methods have been applied by many investigators and are now well accepted. However, only one or two of these methods are usually used for each system, and little work has been done to examine the quantitative interrelationship between these methods.

Moreover, although many works have been done on the oxidation of unsaturated fatty acid, most of them are only qualitative or semi-quantitative; in other words, the oxidation is not measured quantitatively, but only a portion, sometimes a minor portion of these oxidation reactions is followed. Another question is that the ratio of measured oxidation to total oxidation depends on the substrate and experimental variables.

In this study, we intended to measure the oxidation of methyl linoleate and methyl linolenate by various analytical methods in order to find out how quantitative these methods are and what method is suitable for the specific reaction system.

Experimental

Methyl linoleate((*Z,Z*)-9,12-octadecadienoate) and methyl linolenate((*Z,Z,Z*)-9,12,15-octadecatrienoate) were obtained from Sigma Chemical Company and used as received. Prior to the oxidation, it was ascertained that neither conjugated diene nor peroxide was detected in the substrates. The oxidation was carried out in acetonitrile solvent using an ampoule of approximately 30 ml volume, which was immersed in a carefully temperature-controlled oil bath. 2,2'-Azobis(2,4-dimethylvaleronitrile) (AMVN) was used as a radical initiator. The rate of inhibition was measured from the induction period observed in the presence of inhibitor, 2,6-di-*t*-butyl-4-methylphenol (BMP).[6]

The rate of oxygen absorption was measured by following the pressure decrease using a pressure transducer. The oxygen uptake was calculated from the difference between initial and final oxygen amounts measured by Toepler

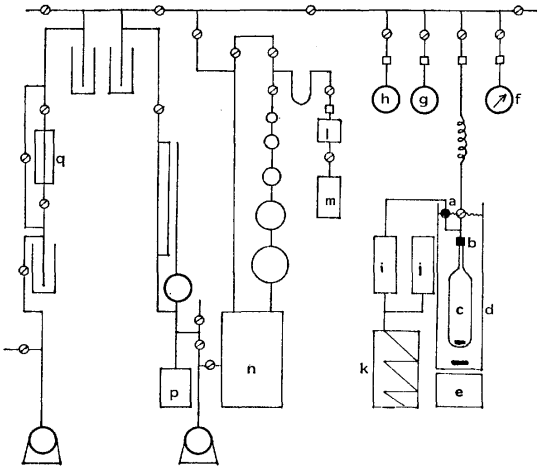

Fig. 1. Oxidation apparatus.
a: Pressure transducer, b: Swagelok teflon fittings, c: ampoule, d: Silicone oil bath, e: magnetic stirrer, f: pressure gauge, g: oxygen, h: nitrogen, i: bridge circuit, j: standard mV supply, k: recorder, l: gas sampler, m: gas chromatography, n: Toepler pump, p: Mcleod gauge (10^{-2}—10^{-6} Torr, 1 Torr≈133.32 Pa), q: mercury diffusion pump.

Table 1. Oxidation of methyl linoleate(LH) at 50 °C in acetonitrile, concentrations in μmol

Run No.	1	2	3	4	5
$(LH)_0$(μmol)	2096	2313	2039	2085	2082
$(LH)_0$(mM)	368	402	360	367	367
$(AMVN)_0$[a](mM)	12.6	11.9	12.1	12.4	12.5
Time/min	10	20	30	60	90
Initial O_2(μmol)	724.1	678.0	1166.7	1157.7	1067.6
Initial O_2(Torr)	591	555	951	975	871
Final O_2(μmol)	656.8	587.0	998.3	719.3	592.4
Final O_2(Torr)	536	480	806	612	483
O_2 uptake(μmol)	67.3	91.0	178.4	438.4	475.2
$(-dO_2/dt\times10^6)$/M s^{-1}			17.0	18.3	19.1
k.c.l.[b]			62.6	66.0	68.3
$[k_p/(2k_t)^{1/2}\times10^3]$/(M s)$^{-1/2}$			90.9	95.1	98.7
ΔLH(μmol)	68	87	238	402	483
$\Delta LH/(LH)_0\times10^2$(%)	3.2	3.8	11.7	19.3	31.3
Peroxide(μmol)	70	90	165	320	360
$(C=C)_2$(μmol)	74	98	139	243	328
TBA(μmol)	trace	trace	trace	trace	trace
$\Delta LH/\Delta O_2$	1.01	0.96	1.33	1.13	1.37
Peroxides/ΔO_2	1.04	0.99	0.92	0.90	0.76
$(C=C)_2/\Delta O_2$	1.10	1.08	0.78	0.68	0.69
TBA/ΔO_2	0	0	0	0	0

a) 2,2′-Azobis(2,4-dimethylvaleronitrile). b) Kinetic chain length.

pump.[7] A schematic diagram of oxidation apparatus is shown in Fig. 1.

The consumption of the substrate was measured by GLC. Peroxide formation was measured by iodometric titration and/or by formation of triphenylphosphine oxide by the reduction of peroxide with triphenylphosphine. Conjugated diene was measured by the absorbance at 230—236 nm, $\varepsilon=28000$ M^{-1} cm^{-1} (1 M = 1 mol dm^{-3}). TBA value was estimated by the conventional photometric method, $\lambda_{max}=$ 531 nm and $\varepsilon=1.17\times10^5$ M^{-1} cm^{-1}. Hydrocarbon gas formation was analyzed by GLC.

Results and Discussion

Tables 1 and 2 show some pertinent data for the AMVN-initiated oxidation of methyl linoleate and methyl linolenate, respectively in acetonitrile at 50 °C. The oxidation of methyl linoleate proceeded at 50 °C even in the absence of a radical initiator, but the rate was very slow. In the presence of AMVN, it was oxidized faster and the plot of oxygen uptake as a function of time gave a good straight line at the initial stage.

Under such mild conditions that the primary products are stable and their secondary oxidation is negligible, the oxidation proceeds virtually by the following scheme.

Initiation: $IN_2I \longrightarrow 2I\cdot + N_2$

$I\cdot \xrightarrow{O_2, LH} IOOH + LO_2\cdot$

Propagation: $LO_2\cdot + LH \xrightarrow{k_p} LOOH + L\cdot$

$L\cdot + O_2 \longrightarrow LO_2\cdot$

Termination: $2LO_2\cdot \xrightarrow{k_t}$ non-radical products

IN_2I and LH are azo initiator and substrate, respectively. The chain carrying peroxyl radicals abstract doubly allylic hydrogen exclusively from methyl linoleate or methyl linolenate, whereas abstraction of other hydrogen and addition to a double bond are quite

Table 2. Oxidation of methyl linolenate(LH) at 50 °C in acetonitrile, concentrations in μmol

Run No.	6	7	8	9
$(LH)_0$(μmol)	2056	2068	2181	1020
$(LH)_0$(mM)	360	365	382	191
$(AMVN)_0$[a](mM)	12.0	13.6	11.8	12.2
Time/min	20	30	40	60
Initial O_2(μmol)	793.2	989.3	1235.2	1190.7
Initial O_2(Torr)	631	807	1009	956
Final O_2(μmol)	567.3	627.1	769.9	654.0
Final O_2(Torr)	451	511	629	606
O_2 uptake(μmol)	225.9	362.2	465.3	436.7
$(-dO_2/dt\times10^6)$/M s^{-1}	34.8	34.3	36.8	23.3
k.c.l.[b]	130	113	140	85.4
$[k_p/(2k_t)^{1/2}\times10^3]$/(M s)$^{-1/2}$	188	171	188	234
ΔLH(μmol)	180	260	299	261
$\Delta LH/(LH)_0\times10^2$(%)	8.8	12.6	13.7	25.6
Peroxide(μmol)	129	176	208	
$(C=C)_2$(μmol)	33	46	58	27
TBA(μmol)	33	46	61	60
$\Delta LH/\Delta O_2$	0.80	0.72	0.64	0.60
Peroxide/ΔO_2	0.57	0.49	0.45	
$(C=C)_2/\Delta O_2$	0.15	0.13	0.12	0.06
TBA/ΔO_2	0.15	0.13	0.13	0.14

a) 2,2′-Azobis(2,4-dimethylvaleronitrile). b) Kinetic chain length.

scarce.[8]

Under these conditions, the rate of oxidation is expressed by

$$\text{rate of oxidation} = R_o = k_p(R_i/2k_t)^{1/2}[LH],$$

where k_p, k_t, and R_i are the rate constants for propagation and termination, and the rate of initiation, respectively. The ratio of the rate constants $k_p/(2k_t)^{1/2}$ gives the relative reactivity of the substrate. Tables 1 and 2 show that $k_p/(2k_t)^{1/2}$ for methyl linoleate and methyl linolenate is 0.0949 and 0.182 $(M\ s)^{-1/2}$, respectively, indicating that methyl linolenate is approximately twice as reactive as methyl linoleate.

It should be noted that this value does not always indicate the relative reactivities of the substrates, or more strictly of C–H bonds, toward peroxyl radicals. The rate and oxidizability are determined not only by k_p but also by k_t. Howard and Ingold[8] found that k_p (per reactive C–H bond) and k_t for methyl linolenate are about two and four times, respectively, larger than those for methyl linoleate at 30 °C.

Methyl linoleate was subjected to oxidation for different reaction times and conversions. As shown in Table 1, kinetic chain length was long, and oxygen uptake and reaction products increased as the oxidation proceeded. A small increase with reaction time in the ratio of rate constants, $k_p/(2k_t)^{1/2}$, was observed, indicating that this oxidation is slightly autocatalytic.

Peroxides were analyzed by high pressure liquid chromatography after reduction with triphenylphosphine, and as reported previously[9,10] four isomeric methyl hydroxylinoleates were found: (9*Z*,11*E*)-13-hydroxy-, (9*E*,11*E*)-13-hydroxy-, (10*E*,12*Z*)-9-hydroxy-, and (10*E*, 12*E*)-9-hydroxyoctadecadienoic acid methyl esters.

Table 1 shows that, at early stages where conversion is low, the values of substrate disappearance, peroxide and conjugated diene formation agreed well. As the oxidation proceeded, however, the amount of the conjugated diene formed became smaller than oxygen uptake. On the other hand, only a trace amount of TBA-reactive material was found and neither pentane nor ethane was observed. It has been pointed out that the TBA-reactive materials are formed from olefins with three or more double bonds.[11]

The oxidation of methyl linolenate exhibited a somewhat different pattern from that of methyl linoleate. Methyl linolenate was oxidized faster than methyl linoleate and $k_p/(2k_t)^{1/2}$ increased with increasing conversion, again suggesting autocatalytic oxidation. The most interesting point is that the amount of substrate reacted, and peroxides and conjugated diene formed were considerably smaller than oxygen uptake, whereas some TBA-reactive materials were observed, although they were 15% of oxygen uptake. Pryor[12] also observed in the oxidation of methyl linolenate by air containing 1.5 ppm ozone that the formation of peroxide was larger than that of conjugated diene which was still larger than TBA-reactive material.

The results given above demonstrate that none of the presently accepted tests is quantitative and that the validity of each method for measuring the extent of oxidation of lipids and tissues depend on the profile of unsaturated fatty acids existing in each sample. Care should be taken in the application of methods suitable for the specific system. For example, the oxidation may have proceeded considerably even if the TBA value is small. The oxygen uptakde must be the most useful, versatile and quantitative measure, but it should be emphasized that the oxidation should be followed by as many approaches as possible. Which the best criterion relevant to pathological effect is, remains, of course, as another question.

The support of the Toyota Foundation is hereby gratefully acknowledged.

References

1) W. O. Lundberg, "Autoxidation and Antioxidants," Interscience, New York (1962).
2) "Free Radicals in Biology," ed by W. A. Pryor, Academic Press, New York (1976), Vol. I, and subsequent series.
3) F. R. Mayo, *Acc. Chem. Res.*, **1**, 193 (1968).
4) For example, A. L. Tappel, "Free Radicals in Biology," ed by W. A. Pryor, Academic Press, New York (1976), Vol. IV, pp. 1—47.
5) J. I. Gray, *J. Am. Oil Chem. Soc.*, **55**, 539 (1978).
6) C. E. Boozer, G. S. Hammond, C. E. Hamilton, and J. N. Sen, *J. Am. Chem. Soc.*, **77**, 3233 (1955).
7) E. Niki, Y. Takaishi, and Y. Kamiya, *Nippon Kagaku Kaishi*, **1975**, 1559.
8) J. A. Howard and K. U. Ingold, *Can. J. Chem.*, **45**, 793 (1967).
9) H. W. S. Chan and G. Levett, *Lipids*, **12**, 99 (1977).
10) N. A. Porter, B. A. Weber, H. Weenen, and J. A. Khan, *J. Am. Chem. Soc.*, **102**, 5597 (1980).
11) L. K. Dahle, E. G. Hill, and R. T. Holman, *Arch. Biochem. Biophys.*, **98**, 253 (1962).
12) W. A. Pryor and J. P. Stanley, *J. Org. Chem.*, **40**, 3615 (1975).

Oxidation of Lipids. II. Rate of Inhibition of Oxidation by α-Tocopherol and Hindered Phenols Measured by Chemiluminescence

Etsuo NIKI,* Ritsuko TANIMURA, and Yoshio KAMIYA

Department of Reaction Chemistry, Faculty of Engineering, The University of Tokyo, Hongo, Bunkyo-ku, Tokyo 113

(Received September 11, 1981)

The rate constants for the interactions of peroxyl radicals with α-tocopherol and hindered phenols were determined by chemiluminescence method. The thermal decomposition of di-*t*-butyl diperoxyoxalate in *o*-dichlorobenzene with and without ethylbenzene was found to give chemiluminescence under oxygen. 9,10-Dibromoanthracene was an effective activator. The addition of 1-tetralyl hydroperoxide gave chemiluminescence both in the presence and absence of oxygen, while the addition of *t*-butyl hydroperoxide suppressed the chemiluminescence almost completely even under oxygen. The addition of α-tocopherol and phenols also diminished the chemiluminescence, but after reaching the minimum intensity it again increased as the inhibitors were consumed. The rate constants for the scavenging of 1-phenylethylperoxyl radical by α-tocopherol, 2,4,6-tri-*t*-butylphenol and 2,6-di-*t*-butyl-4-methylphenol were obtained as 1.5×10^5, 1.2×10^4, and 1.0×10^4 M^{-1} s^{-1} (1 M= 1 mol dm^{-3}) respectively.

α-Tocopherol **1**, the major component of vitamin E, is known to contribute in biological systems as an inhibitor of lipid peroxidation.[1,2] α-Tocopherol is

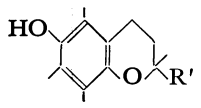

1

R′: $(CH_2CH_2CH_2\underset{\displaystyle CH_3}{\underset{|}{CH}})_3CH_3$

also used as an added antioxidant for foods and oils. It has been reported that α-tocopherol scavenges not only peroxyl radicals but also singlet oxygen[3-7] and superoxide anion radical.[8-12] However, trapping of peroxyl radicals must be the most important function of vitamin E, and to know the reactivity of α-tocopherol toward peroxyl radicals is important in understanding the antioxidizing behavior of vitamin E.

The rate constant for the interaction of α-tocopherol with peroxyl radicals has been determined recently.[13-15] The reported values range from 2×10^5 to 5×10^8 M^{-1} s^{-1}. Kharitonova *et al.*[13] obtained k_{inh} as 2×10^5

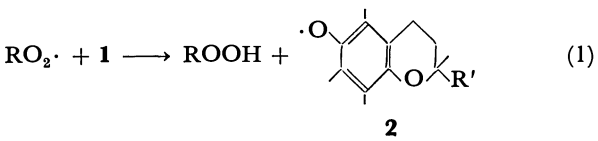

$RO_2\cdot + 1 \longrightarrow ROOH +$ **2** (1)

M^{-1} s^{-1} at 60 °C from the rate of inhibited oxidation of cumene. Ingold and his coworkers[15] also determined k_{inh} as 2.3×10^6 M^{-1} s^{-1} from the rate of inhibited oxidation of styrene. On the other hand, Packer, Slater, and Willson[14] obtained k_{inh} for trichloromethylperoxyl radical as 5×10^8 M^{-1} s^{-1} spectrometrically.

We have measured this rate constant k_{inh} for **1** by the chemiluminescence method. Since the first finding by Vassilev and Vichutinskii[16] that the oxidation of organic compounds is accompanied by the emission of weak chemiluminescence, the rate constants for autoxidation have been determined by measuring the chemiluminesence intensity.[17,18] This chemiluminescence method has been also applied recently to estimate the extent of oxidation of fats, oils and biological systems.[19-26]

Experimental

Materials. Natural *d*-α-tocopherol was kindly supplied from Eisai Co. Ltd. 2,4,6-Tri-*t*-butylphenol (TBP) and 2,6-di-*t*-butyl-4-methylphenol (BMP) were recrystallized from methanol. 2,6-Di-*t*-butylphenol was used as received. Di-*t*-butyl diperoxyoxalate (DBPO) was synthesized from *t*-butyl hydroperoxide and oxalyl chloride by the method of Bartlett *et al.*[27] Commercial 9,10-dibromoanthracene was recrystallized from methanol. 1-Tetralyl hydroperoxide (TOOH) was prepared by the air oxidation of tetralin in the presence of azobisisobutyronitrile, followed by recrystallization from heptane. Commercial *t*-butyl hydroperoxide was distilled under reduced pressure prior to use 42 °C/24 Torr (1 Torr ≈ 133.322 Pa). Ethylbenzene was washed with acid, water, alkaline and water, dried and distilled. *o*-Dichlorobenzene was used as received.

Apparatus and Procedure. The emission intensity of chemiluminescence was measured by the single photon counting apparatus, type OX-7, manufactured by Tohoku Elec-

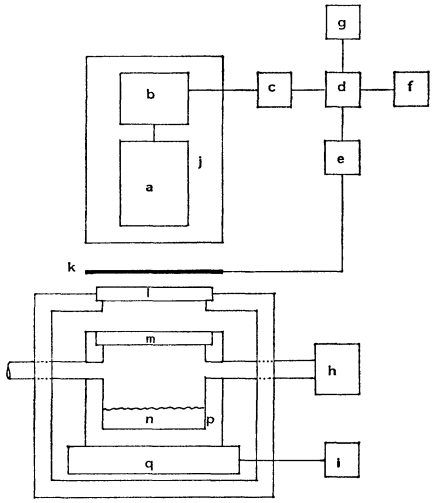

Fig. 1. Schematic diagram of the single photon counting apparatus, OX-7.
a: Photomultiplier, b: amplifier, c: gain thresh, d: counter, e: controller, f: printer, g: recorder, h: pump, i: temperature controller, j: cooler, k: shutter, l: filter, m: quartz window, n: sample, p: cell, q: heater.

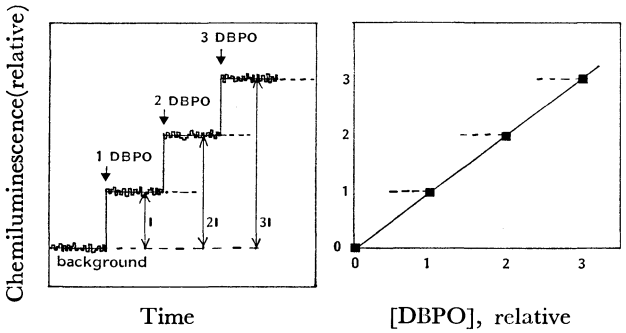

Fig. 2. Chemiluminescence intensity as a function of DBPO concentration.

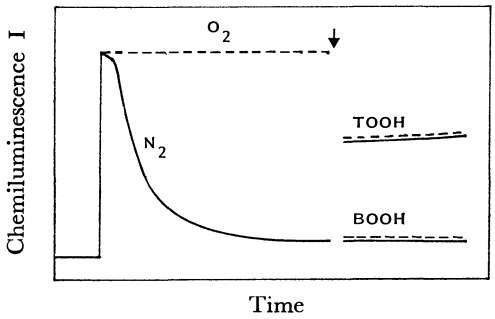

Fig. 3. Effect of atmosphere and addition of tetralyl (TOOH) and *t*-butyl (BOOH) hydroperoxides on the chemiluminescence, [DBPO]=0.10 M in *o*-dichlorobenzene at 25 °C.

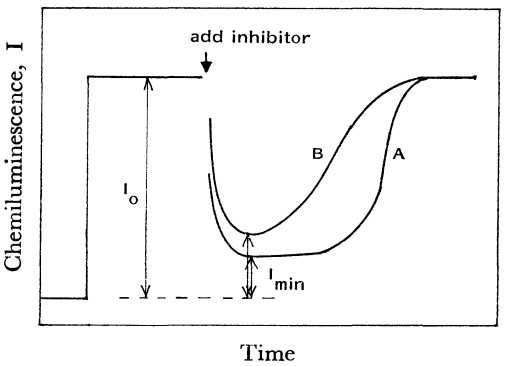

Fig. 4. Effect of addition of α-tocopherol (A) and TBP (B) on the chemiluminescence, [DBPO]=0.10 M in *o*-dichlorobenzene-ethylbenzene, 25 °C.

tronic Industries. The schematic diagram of the apparatus is shown in Fig. 1. The cell temperature was kept at 25 °C and the photomultiplier, Hamamatsu TV Co. type R878, was cooled to −20 °C.

In general, 2 or 3 ml of appropriate solution was taken into the stainless steel cell and the chemiluminescence intensity was measured every 10 second and recorded. Neat *o*-dichlorobenzene or a mixture of *o*-dichlorobenzene and ethylbenzene (1/1 by v/v) was usually used as solvent. No filter was used.

Results

A strong chemiluminescence was observed when DBPO was thermally decomposed in *o*-dichlorobenzene or *o*-dichlorobenzene-ethylbenzene at 25 °C under air. As shown in Fig. 2, the chemiluminescence intensity

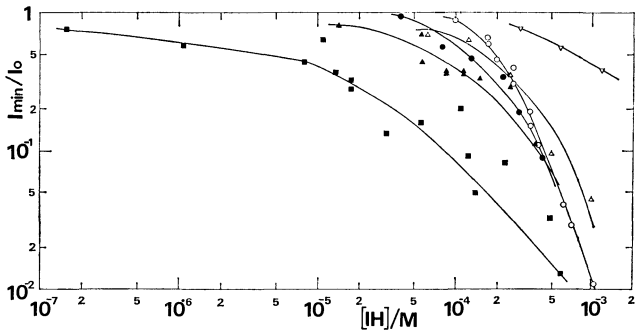

Fig. 5. Plot of I_{min}/I_o as a function of inhibitor concentration in the thermal decomposition of DBPO at 25 °C in *o*-dichlorobenzene (open) and *o*-dichlorobenzene-ethylbenzene (solid).
■: α-Tocopherol, △,▲: TBP, ○,●: BMP, ▽: 2,6-di-*t*-butylphenol.

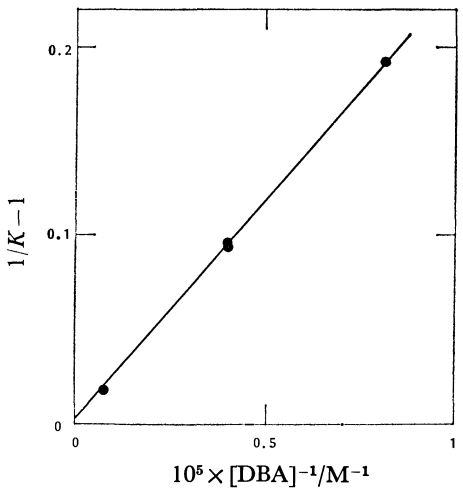

Fig. 6. Plot of $1/K-1$ against 1/[DBA] in the thermal decomposition of DBPO at 25 °C in *o*-dochlorobenzene.

I was proportional to the concentration of DBPO, or more strictly, to the absolute amount of DBPO. The concentration of DBPO was chosen so that the chemiluminescence intensity was several times larger than the background. Under nitrogen, however, little chemiluminescence was observed. Furthermore, as shown in Fig. 3, the addition of tetralyl hydroperoxide to the above solution gave chemiluminescence and its intensity was the same irrespective of the presence or absence of oxygen. On the other hand, the addition of *t*-butyl hydroperoxide did not give appreciable chemiluminescence even in the presence of oxygen.

Figure 4 shows that the addition of phenolic inhibitors to the DBPO solution diminished the chemiluminescence sharply and that, after reaching the minimum intensity I_{min}, it increased again as the inhibitors were consumed. Figure 5 shows the plot of I_{min}/I_o as a function of inhibitor concentration. Similar phenomenon was observed when cobalt(II) acetylacetonate was added to the DBPO solution as observed by Gal and his colleagues.[18]

The addition of 9,10-dibromoanthracene (DBA) increased the chemiluminescence intensity markedly.

As shown in Fig. 6, the plot of $1/K-1$ as a function of 1/[DBA] gave a straight line, where $K=I_A/I_o$, and I_A and I_o are the chemiluminescence intensity in the presence and absence of 9,10-dibromoanthracene respectively.

Discussion

Upon thermal decomposition, DBPO gives two molecules each of *t*-butoxyl radical and carbon dioxide. The rate constant for unimolecular decomposition of DBPO is $k_d=1.6\times10^{-5}$ s^{-1} at 25 °C and its half life is $\tau_{1/2}=12$ h.[27] Therefore, it may be safely considered that DBPO gives *t*-butoxyl radical at constant rate under the present reaction conditions.

$$\mathrm{DBPO} \xrightarrow{k_d} 2(\mathrm{CH_3})_3\mathrm{CO}\cdot + 2\mathrm{CO_2} \quad (1)$$

$$(\mathrm{CH_3})_3\mathrm{CO}\cdot \longrightarrow (\mathrm{CH_3})_2\mathrm{CO} + \mathrm{CH_3}\cdot \quad (2)$$

$$\mathrm{CH_3}\cdot + \mathrm{O_2} \longrightarrow \mathrm{CH_3O_2}\cdot \quad (3)$$

$$2\mathrm{CH_3O_2}\cdot \xrightarrow{k_t} \mathrm{CH_3OH} + {}^3\mathrm{CH_2O}^* + {}^1\mathrm{O_2} \quad (4)$$

$${}^3\mathrm{CH_2O}^* \longrightarrow {}^1\mathrm{CH_2O} + h\nu \quad (5)$$

$${}^1\mathrm{O_2} \longrightarrow {}^3\mathrm{O_2} + h\nu \quad (6)$$

Chemiluminescence arises at the expense of the energy released by exothermic reaction and in the liquid phase oxidation only the chain terminating recombination of peroxyl radicals are sufficiently exothermic for ensuring luminescence in the visible region.[17] About 100 kcal/mol of energy is liberated in the recombination of peroxyl radicals and it is distributed among the products. It has been known that the bimolecular interactions of primary and secondary peroxyl radicals yield triplet carbonyl compound and singlet oxygen[17,28-31] and that these two species emit the chemiluminescence.

Thus, the chemiluminescence observed in the decomposition of DBPO must arise from triplet formaldehyde and/or singlet oxygen formed in Reaction 4. That there was little chemiluminescence in the absence of oxygen suggests that acetone formed in Reaction 2 does not give chemiluminescence.

The steady state treatment for Reactions 1 to 6 gives

$$[\mathrm{CH_3O_2}\cdot] = (k_d[\mathrm{DBPO}]/k_t)^{1/2}. \quad (7)$$

Therefore, the chemiluminescence intensity I is directly proportional to the concentration of DBPO as observed experimentally (Fig. 2).

$$I = a[\mathrm{CH_3O_2}\cdot]^2 = ak_d[\mathrm{DBPO}]/k_t \quad (8)$$

It has been reported that species such as oxygen[31,32] and di-*t*-butyl peroxide[33,34] quench the chemiluminescence. Especially, the quenching by oxygen may be important since oxygen molecule is formed in the bimolecular termination reactions of peroxyl radicals in the close neighborhood of the excited product and may cause its deactivation. The effect of these adventitious quenchers must be small, however, when the ratio of intensity I/I_o is considered rather than the absolute intensity. The luminescence yield is independent of the radical concentration.[35] Phenols are known as photoluminescence quencher, but it was established that the chemical reaction between phenols and peroxyl radicals is of major importance and the physical effect, if any, is negligibly small.[17]

The effect of addition of tetralyl and *t*-butyl hydroperoxides supports the above conclusion. *t*-Butoxyl radical formed from DBPO abstracts readily the hydroperoxidic hydrogens to yield peroxyl radicals. The bimolecular interactions of tetralylperoxyl radicals are terminating and give tetralol, tetralone, and oxygen.

$$(\mathrm{CH_3})_3\mathrm{CO}\cdot + \mathrm{ROOH} \longrightarrow (\mathrm{CH_3})_3\mathrm{COH} + \mathrm{RO_2}\cdot \quad (9)$$

The triplet tetralone and/or singlet oxygen give chemiluminescence irrespective of the presence or absence of oxygen. On the other hand, the bimolecular interactions of *t*-butylperoxyl radicals proceed differently.[36] The *t*-butoxyl radical formed in Reaction 11

$$2(\mathrm{CH_3})_3\mathrm{CO_2}\cdot \longrightarrow [(\mathrm{CH_3})_3\mathrm{COOOOC}(\mathrm{CH_3})_3]$$

$$\longrightarrow (\mathrm{CH_3})_3\mathrm{COOC}(\mathrm{CH_3})_3 + \mathrm{O_2} \quad (10)$$

$$\longrightarrow 2(\mathrm{CH_3})_3\mathrm{CO}\cdot + \mathrm{O_2} \quad (11)$$

again reacts with added *t*-butyl hydroperoxide. Therefore, the addition of *t*-butyl hydroperoxie suppresses the formation of triplet carbonyl and singlet oxygen, and hence the chemiluminescence as well.

The activation of chemiluminescence by 9,10-dibromoanthracene (DBA) in DBPO–ethylbenzene system may be explained by the following scheme, where A represents DBA. *t*-Butoxyl radical attacks ethylbenzene to give 1-phenylethyl radical, which reacts with oxygen and then gives 1-phenylethanol, acetophenone, and oxygen.

$$\mathrm{DBPO} \longrightarrow 2(\mathrm{CH_3})_3\mathrm{CO}\cdot + 2\mathrm{CO} \quad (1)$$

$$(\mathrm{CH_3})_3\mathrm{CO}\cdot + \mathrm{PhCH_2CH_3} \longrightarrow (\mathrm{CH_3})_3\mathrm{COH} + \mathrm{PhC}\dot{\mathrm{H}}\mathrm{CH_3} \quad (12)$$

$$\mathrm{PhC}\dot{\mathrm{H}}\mathrm{CH_3} + \mathrm{O_2} \longrightarrow \mathrm{PhCH(OO}\cdot)\mathrm{CH_3} \quad (13)$$

$$2\mathrm{PhCH(OO}\cdot)\mathrm{CH_3} \xrightarrow{k_t'} \mathrm{PhCH(OH)CH_3} + \mathrm{PhC(=O)CH_3}^* + \mathrm{O_2} \quad (14)$$

$$\mathrm{PhC(=O)CH_3}^* \xrightarrow{f_P} \mathrm{PhC(=O)CH_3} + h\nu \quad (15)$$

$$\mathrm{PhC(=O)CH_3}^* + \mathrm{A} \longrightarrow \mathrm{PhC(=O)CH_3} + \mathrm{A}^* \quad (16)$$

$$\mathrm{A}^* \xrightarrow{f_A} \mathrm{A} + h\nu \quad (17)$$

Under these circumstances, Eq. 18 holds,[17]

$$\frac{1}{K-1} = \frac{\eta_P}{\eta_A-\eta_P} + \frac{1}{\eta_A-\eta_P}\cdot\frac{f_P}{k_{PA}}\cdot\frac{1}{[\mathrm{DBA}]} \quad (18)$$

where η_P, η_A, f_P, and k_{PA} represent, respectively, quantum yields for chemiluminescence of activated acetophenone and activator, probability of radiative transitions and the rate constant for energy transfer from triplet carbonyl to activator. From the intercept of Fig. 6, $\eta_P/(\eta_A-\eta_P)=1.09\times10^{-3}$, and hence, $\eta_A/\eta_P\approx10^3$, suggesting that 9,10-dibromoanthracene has much higher quantum yield than excited acetophenone.

In the presence of phenolic inhibitors IH, the reaction proceeds by the steps 1, 12, 13, 14, 15, 19, and 20, where $\mathrm{RO_2}\cdot$ denotes the 1-phenylethylperoxyl radical.

$$\mathrm{RO_2}\cdot + \mathrm{IH} \xrightarrow{k_{inh}} \mathrm{ROOH} + \mathrm{I}\cdot \quad (19)$$

$$\mathrm{RO_2}\cdot + \mathrm{I}\cdot \xrightarrow{k_0} \mathrm{ROOI} \quad (20)$$

Table 1. Rate constants for the trapping of peroxyl radicals by inhibitors measured by chemiluminescence method, 25 °C

Inhibitor	$k_{inh}/M^{-1}\,s^{-1}$		
	DBPO-IH	DBPO-IH-PhC_2H_5	Literature values
BMP	3.6×10^4	1.0×10^4	7.95×10^3,[a] 1.0×10^4,[b] 1.58×10^4,[c] 2.5×10^4,[d]
TBP	3.1×10^4	1.2×10^4	7.30×10^3,[a] 6.8×10^3,[b] 1.3×10^4 [d]
2,6-Di-*t*-butylphenol	6.0×10^3		2.25×10^3,[a] 9.5×10^3 [d]
α-Tocopherol		1.5×10^5	2.0×10^5,[e] 2.3×10^6,[f] 5×10^8 [g]

a) From the rate of inhibited oxidation of styrene at 65 °C, Ref. 39. b) From the ESR method and extraporated to 25 °C, Ref. 40. c) From the rate of inhibited oxidation of styrene at 50 °C, Ref. 41. d) At 60 °C, Ref. 42. e) From the inhibited rate of oxidation of cumene at 60 °C, Ref. 13. f) From the rate of inhibited rate of oxidation of styrene at 30 °C, Ref. 15. g) From pulse radiolysis and spectrometrical determination for trichloromethylperoxyl radical, Ref. 14.

In the absence of inhibitor,

$$-d[RO_2\cdot]/dt = R_i - 2k_t'[RO_2\cdot]_0^2 \quad (21)$$

and hence,

$$[RO_2\cdot]_0 = (R_i/2k_t')^{1/2}, \quad (22)$$

where $R_i=2k_d[DBPO]$ is the rate of initiation and $[RO_2\cdot]_0$ is the steady state concentration of 1-phenylethylperoxyl radical in the absence of the inhibitor. When the inhibitor is added, the concentration of the inhibitor and so that of the peroxyl radical also changes with time, and the steady state treatment can not be applied. The concentration of the peroxyl radical is given by

$$d[RO_2\cdot]/dt = R_i - 2k_t'[RO_2\cdot]^2 - k_{inh}[RO_2\cdot][IH] - k_0[RO_2\cdot][I\cdot]. \quad (23)$$

Since $k_0 \gg k_{inh}$,

$$d[I\cdot]/dt = k_{inh}[RO_2\cdot][IH] - k_0[RO_2\cdot][I\cdot] = 0. \quad (24)$$

Therefore,

$$d[RO_2\cdot]/dt = R_i - 2k_t'[RO_2\cdot]^2 - 2k_{inh}[RO_2\cdot][IH]. \quad (25)$$

At the time when the chemiluminescence intensity is the minimum, I_{min},

$$d[RO_2\cdot]/dt = R_i - 2k_t'[RO_2]_{min}^2 - 2k_{inh}[RO_2\cdot]_{min}[IH] = 0. \quad (26)$$

Then

$$\frac{I_{min}}{I_0} = \frac{[RO_2\cdot]_{min}^2}{[RO_2\cdot]_0^2} = \frac{R_i-2k_{inh}[RO_2\cdot]_{min}[IH]}{2k_t'}\frac{1}{(R_i/2k_t')} = 1 - \frac{2k_{inh}[IH]}{(2k_t'R_i)^{1/2}}\left(\frac{I_{min}}{I_0}\right)^{1/2}, \quad (27)$$

and

$$\frac{1}{Q} - Q = \frac{2k_{inh}}{(2k_t'R_i)^{1/2}}[IH], \quad (28)$$

where $Q=(I_{min}/I_0)^{1/2}$.[37] Similarly, in the system of DBPO and inhibitor in *o*-dichlorobenzene without ethylbenzene,

$$\frac{1}{Q} - Q = \frac{2k_{inh}}{(2k_tR_i)^{1/2}}[IH]. \quad (29)$$

Figures 7 and 8 show the plot of $Q^{-1}-Q$ as a function of inhibitor concentration for the systems DBPO-inhibitor and DBPO-inhibitor-ethylbenzene respectively. Some scatters are observed, but from the slope and the rate constants $k_t=10^8\ M^{-1}\,s^{-1}$ and $k_t'=2\times10^7\ M^{-1}\,s^{-1}$ from the literature,[36] the rate constants for the trapping of peroxyl radicals by an inhibitor are calculated as summarized in Table 1.

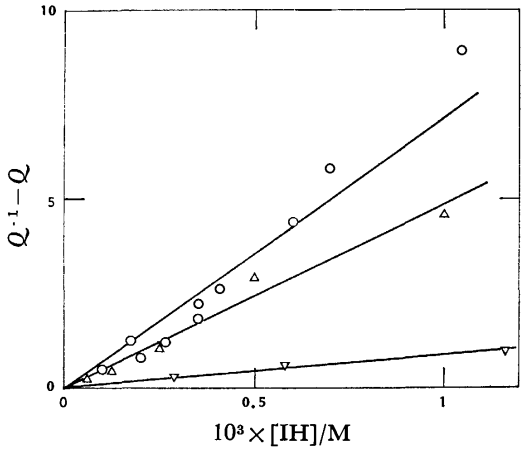

Fig. 7. Plot of $Q^{-1}-Q$ as a function of inhibitor concentration in *o*-dichlorobenzene.
△: TBP, ○: BMP, ▽: 2,6-di-*t*-butylphenol.

The rate constants measured in this study for hindered phenols are in reasonable agreement with literature values. The higher k_{inh} in the absence of ethylbenzene must be ascribed to the contribution of faster interaction of *t*-butoxyl radical with phenols. The high k_{inh}, $5\times10^8\ M^{-1}\,s^{-1}$, for α-tocopherol toward trichloromethylperoxyl radical[14] must be due to a higher reactivity of trichloromethylperoxyl radical than normal alkylperoxyl radicals.[43] Those for α-tocopherol toward arylalkylperoxyl radicals are in fair agreement ranging from 1.5×10^5 to $2\times10^6\ M^{-1}\,s^{-1}$. The reason of this discrepancy is not clear at present. It may be in part due to the different attacking peroxyl radicals: The polymeric peroxyl radical in the oxidation of styrene may have higher reactivity toward α-tocopherol than simple alkylperoxyl radicals as it has toward hydrocarbons.[36,44]

In Figs. 7 and 8, $Q^{-1}-Q$ was plotted against the initial concentration of the inhibitor assuming the loss of inhibitor by the time the chemiluminescence intensity reached minimum was negligibly small. Ac-

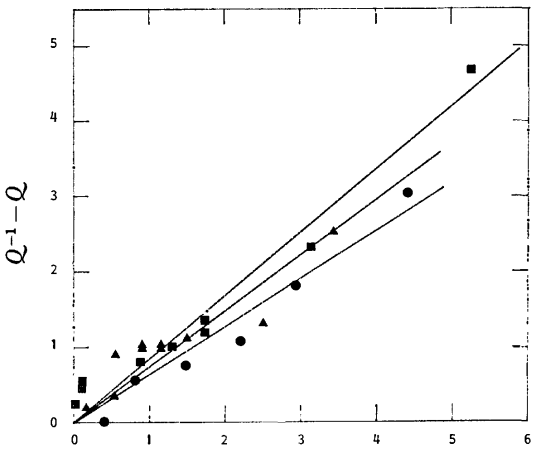

Fig. 8. Plot of $Q^{-1}-Q$ as a function of inhibitor concentration in *o*-dichlorobenzene-ethylbenzene.
■: α-Tocopherol, ▲: TBP, ●: BMP.

cordingly, the k_{inh} we obtained for α-tocopherol may be lower slightly than it should be.

Figures 5 and 8 show that α-tocopherol has higher reactivity than TBP and BMP. Ingold and collaborators[15] argue that higher reactivity of α-tocopherol than simple hindered phenols toward peroxyl radicals arises from the fused chroman ring system that maintains a near-optimal orientation of the ethereal oxygen *p*-type lone pair with respect to the aromatic ring.

As reported previously,[45] the 6-chromanyloxyl radical **2** formed from α-tocopherol seems to have different reactivity toward peroxyl radical from the hindered phenoxyl radicals. We are currently extending our study on the antioxidizing behavior of tocopherols.

This work was partly supported by The Toyota Foundation. A gift of α-tocopherol from Eisai Co. Ltd. is also gratefully acknowledged.

References

1) "Tocopherol, Oxygen and Biomembranes," ed by C. de Duve and O. Hayaishi, Elsevier, Amsterdam (1978).
2) "Vitamin E," ed by L. J. Machlin, Marcel Dekker, New York (1980).
3) S. R. Fahrenholtz, F. H. Doleiden, A. M. Trozzolo, and A. A. Lamola, *Photochem. Photobiol.*, **20**, 505 (1974).
4) C. S. Foote, T. Y. Ching, and G. G. Geller, *Photochem. Photobiol.*, **20**, 511 (1974).
5) B. Stevens, R. Small, and S. Perez, *Photochem. Photobiol.*, **20**, 515 (1974).
6) S. Matsushita, J. Terao, and R. Yamauchi, in Ref. 1, p. 23.
7) R. L. Clough, B. G. Yee, and C. S. Foote, *J. Am. Chem. Soc.*, **101**, 683 (1979).
8) M. Nishikimi and L. J. Machlin, *Arch. Biochem. Biophys.*, **170**, 684 (1975).
9) M. Nishikimi and K. Yagi, "Biochemical and Medical Aspects of Active Oxygen," ed by O. Hayaishi and K. Asada, Japan Sci. Soc. Press, Tokyo (1977), pp. 79—87.
10) S. Matsumoto and M. Matsuo, *Tetrahedron Lett.*, **1977**, 1999.
11) T. Ozawa, A. Hanaki, S. Matsumoto, and M. Matsuo, *Biochem. Biophys. Acta*, **531**, 72 (1978).
12) M. Matsuo, S. Matsumoto, Y. Iitaka, A. Yanaki, and T. Ozawa, *J. Chem. Soc., Chem. Commun.*, **1979**, 105.
13) A. A. Kharitonova, Z. G. Kozlova, V. F. Tsepaolv, and G. P. Gladyshev, *Kinet. Katal.*, **20**, 593 (1979).
14) J. E. Packer, T. F. Slater, and R. L. Willson, *Nature*, **278**, 737 (1979).
15) G. W. Burton, Y. Le Page, E. J. Gabe, and K. U. Ingold, *J. Am. Chem. Soc.*, **102**, 7791 (1980).
16) R. F. Vassilev and A. A. Vichutinskii, *Nature*, **194**, 1276 (1962).
17) R. F. Vassilev, *Prog. Reaction Kinet.*, **4**, 305 (1967).
18) V. M. Goldberg. J. Lukacs, G. Vasvari, and D. Gal, *Oxidation Commun.*, **1**, 189 (1980).
19) R. Usuki, T. Kaneda, A. Yamagishi, C. Takyu, and H. Inaba, *J. Food Sci.*, **44**, 1573 (1979).
20) R. Usuki, N. Takaso, and T. Kaneda, *Nippon Shokuhin Kogyo Gakkaishi*, **27**, 332 (1980).
21) T. Miyazawa and T. Kaneda, *Proc. Jpn. Conf. Biochem. Lipids*, **23**, 121 (1981).
22) K. Sugioka and M. Nakano, *Biochim. Biophys. Acta*, **423**, 203 (1976).
23) M. Nakano, K. Takayama, Y. Shimidzu, Y. Tsuji, H. Inaba, and T. Migita, *J. Am. Chem. Soc.*, **98**, 1974 (1976).
24) T. Soshimoto, S. Yamamoto, K. Sugioka, M. Nakano, C. Takyu, A. Yamagishi, and H. Inaba, *J. Biol. Chem.*, **255**, 10199 (1980).
25) K. Naito and T. K. Kwei, *J. Polym. Sci., Polym. Chem. Ed.*, **17**, 2935 (1979).
26) I. Kamiya and T. Sugimoto, *Bull. Chem. Soc. Jpn.*, **54**, 25 (1981).
27) P. D. Bartlett, E. P. Benzing, and R. E. Pincock, *J. Am. Chem. Soc.*, **82**, 1762 (1960).
28) G. A. Russell, *J. Am. Chem. Soc.*, **79**, 3871 (1957).
29) J. A. Howard and K. U. Ingold, *J. Am. Chem. Soc.*, **90**, 1056 (1968).
30) T. Mill and R. S. Stringham, *J. Am. Chem. Soc.*, **90**, 1062 (1968).
31) R. E. Kellog, *J. Am. Chem. Soc.*, **91**, 5433 (1969).
32) R. F. Vassilev, *Nature*, **196**, 668 (1962).
33) D. Griller, K. U. Ingold, and J. C. Scaiano, *J. Magn. Reson.*, **38**, 169 (1980).
34) J. C. Scaiano and G. G. Wubbels, *J. Am. Chem. Soc.*, **103**, 640 (1981).
35) A. A. Vichutinskii, *Nature*, **206**, 292 (1965).
36) J. A. Howard, *Adv. Free Radical Chem.*, **4**, 49 (1972).
37) Similar but somewhat different equation has been derived by Karpukhin *et al.*[38]
38) O. N. Karupkhin, V. Ya. Shlyapintokh and N. V. Zolotova, *Izv. Akad. Nauk SSSR, Otd. Khim. Nauk*, **1963**, 1718.
39) J. A. Howard and K. U. Ingold, *Can. J. Chem.*, **41**, 2800 (1963).
40) J. A. Howard and E. Furimsky, *Can. J. Chem.*, **51**, 3738 (1973).
41) Y. Ohkatsu, T. Haruna, and T. Osa, *J. Macromol. Sci.*, **A11**, 1975 (1977).
42) O. N. Karupukhin, V. Ya. Shlyapintokh, I. F. Rusina, and N. V. Zolotova, *Izv. Akad. Nauk SSSR*, **1963**, 1718.
43) J. E. Packer, R. L. Willson, D. Bahnemann, and K. D. Asmus, *J. Chem. Soc., Perkin Trans. 2*, **1980**, 296.
44) E. Niki, Y. Kamiya and N. Ohta, *Bull. Chem. Soc. Jpn.*, **42**, 2312 (1969).
45) J. Tsuchiya, E. Niki, and Y. Kamiya, in contribution.

Solid-phase Synthesis of Substrate Model Peptides and Their Hydroxylation with Collagen Lysyl Hydroxylase

Yasuo KIKUCHI* and Nobuo TAMIYA

Department of Chemistry, Faculty of Science, Tohoku University, Aobayama, Sendai 980

(Received July 24, 1981)

The peptides, (Ala–Lys–Gly)$_{10}$–Phe, (Ile–Lys–Gly)$_3$–Phe, and (Ile–Lys–Gly)$_5$–Phe, were synthesized by solid-phase fragment condensation method. The contaminating shorter peptides and branched chain peptides were removed by CM-cellulose column chromatography. The peptides were useful as synthetic model substrates for collagen lysyl hydroxylase. The –Ile–Lys–Gly– units in (Ile–Lys–Gly)$_5$–Phe showed a higher affinity to the enzyme than those in (Ile–Lys–Gly)$_3$–Phe. A strong substrate inhibition was observed with highly basic peptide, (Ala–Lys–Gly)$_{10}$–Phe.

Hydroxylysine and hydroxyproline are synthesized *in vivo* by enzymic hydroxylation of lysyl and prolyl residues in the peptide chain of procollagen.[1] The proline hydroxylation involves an oxygenation mechanism: The atmospheric ^{18}O is incorporated into hydroxyl group of collagen hydroxyproline.[2-4] On the other hand, hydroxylysine isolated from the chick embryos incubated in ^{18}O-enriched atmosphere did not contain ^{18}O.[4] There are two possibilities to explain the absence of ^{18}O in hydroxylysine: (1) Hydroxylation of lysyl residues involves a non-oxygenation mechanism, (2) The oxygen atom incorporated into hydroxyl group through an oxygenation mechanism is equilibrated with water oxygen by an enzymic process.

More recently the purified enzymes, lysyl hydroxylase and prolyl hydroxylase, were shown to require the same cosubstrates, namely, O_2, α-oxoglutarate, Fe^{2+} and ascorbic acid with similar K_m values.[5-7] During the enzymic hydroxylation, α-oxoglutarate is decarboxylated into CO_2 and succinate stoichiometrically to the formation of hydroxylysine or hydroxyproline.[8,9] The kinetic studies elucidated the same reaction scheme for the two hydroxylases involving an ordered binding of substrates to enzyme and an ordered release of products.[10,11] These results strongly suggest an oxygenation mechanism for lysine hydroxylation and support the second possibility mentioned above; *i.e.* an oxygenetic hydroxylation of lysyl residues is followed *in vivo* by an enzymic equilibration of hydroxyl group with water. The lysine hydroxylation will be studied separately from the oxygen equilibration and the oxygen source of hydroxyl group will be demonstrated for the first time if a synthetic substrate is subjected to the action of purified lysyl hydroxylase *in vitro*. Since the minimum sequence requirement for substrate is known as X–Lys–Gly[12] tripeptide,[9] the present paper describes the syntheses of substrate model peptides, (X–Lys–Gly)$_n$–Phe (X= Ala or Ile) and their enzymic hydroxylation with purified lysyl hydroxylase.

Experimental

Protected Tripeptides. The protected tripeptides, Boc–Ala–Lys(Z)–Gly[12] (**9**) and Boc–Ile–Lys(ZCl_2)–Gly (**11**), were synthesized by the solution method of peptide synthesis as shown in Scheme 1. The yields, melting points, and elemental analyses are shown in Table 1.

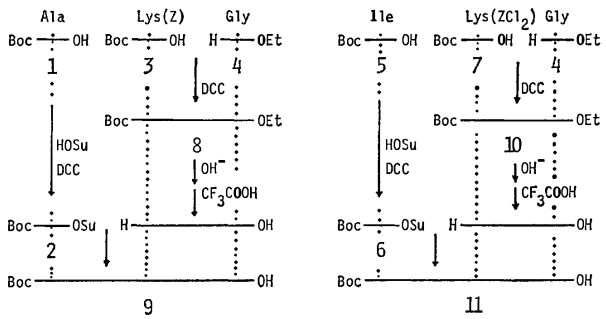

Scheme 1. Syntheses of Boc-Ala-Lys(Z)-Gly (**9**) and Boc-Ile-Lys(ZCl_2)-Gly (**11**).

Aoc–Phe–Resin.[12] Aoc–Phe–resin (0.3 mmol of Phe per g of resin) was prepared from Aoc–Phe (5 mmol) and chloromethylated copoly(styrene – 2%divinylbenzene)(Cl : 1 mmol per g resin, Protein Research Foundation, Osaka, Japan) (10 g) by the method of Loffet.[19] The unreacted chloromethyl sites were acetylated by the same method using acetic acid (20 mmol).

Solid-phase Syntheses. (Ala–Lys–Gly)$_{10}$–Phe (12): The Aoc–Phe–resin (2 g, 0.6 mmol of Phe) was placed in a 20 ml reaction vessel and converted into Boc–(Ala–Lys(Z)–Gly)$_{10}$–Phe–resin by manual additions of **9** in ten cyclic steps as follows; (1) deprotection for 60 min with 33% (by vol) trifluoroacetic acid in dichloromethane (15 ml), (2) washing for 5 min with dichloromethane (20 ml × 3) and DMF[12] (20 ml × 2), (3) neutralization for 5 min with 5% (by vol) triethylamine in DMF (20 ml), (4) washing for 5 min with DMF (20 ml × 2) and dichloromethane (20 ml × 3), (5) condensation for 20 h with **9** (0.65 g, 1.28 mmol) and DCC[12] (0.28 g, 1.28 mmol) in dichloromethane (20 ml) and (6) washing for 5 min with dichloromethane (20 ml × 5). After ten cycles, the resin was dried (4.25 g, 100%). An aliquot (0.85 g) of the peptidyl resin was treated with anhydrous HF (15 ml) and anisole (1 ml) for 60 min at 0 °C and dried.[20] The peptide was extracted into 1% (by vol) acetic acid (10 ml × 1, 45 min, and 2.5 ml × 3, 15 min each) and the extract passed through a column (1 cm × 3 cm) of Amberlite IRA-400 (acetate form). The eluate was washed with ethyl acetate (10 ml) and freeze-dried to afford (Ala–Lys–Gly)$_{10}$–Phe (**12**) (244 mg, 77%).

(Ile–Lys–Gly)$_3$–Phe (13) and (Ile–Lys–Gly)$_5$–Phe (14): Aoc–Phe–resin (2 g, 0.6 mmol of Phe) was subjected to the condensation cycles with **11** (0.8 g, 1.29 mmol) instead of **9** as described above except that THF[12]–dichloromethane (1:4 by vol) mixture was used as a solvent for the condensation reactions. After three cycles, about a half of the peptidyl resin was removed and dried to give Boc–(Ile–Lys(ZCl_2)–Gly)$_3$–Phe–resin (1.4 g, approx. 94%). The rest

Table 1. Synthesis of amino acid derivatives and peptides

	Compound	Yield %	Mp θ_m/°C	Elemental analysis (%)			Ref.
				C	H	N	
1	(DCHA[12] salt)	62	147—148	C. 64.8 F. 64.5	10.3 10.3	7.6 7.5	13
2		87	161—163	C. 50.3 F. 50.3	6.3 6.4	9.8 9.6	14
3	(DCHA salt)	65[a]	112—113	C. 66.3 F. 66.5	9.2 9.3	7.5 7.7	15, 16, 17
4	(Hydrochloride)	95	144—145	C. 34.4 F. 34.1	7.2 7.6	10.0 10.0	18
5	(DCHA salt)	93	126—126.5	C. 67.0 F. 66.8	10.8 10.8	6.8 6.9	17
6		Approx. 100	Oil				14
7		Approx. 100[a]	Oil				16, 17
8		72	68—68.5	C. 59.3 F. 59.6	7.6 7.8	9.0 9.2	
9		83	77—80	C. 56.2 F. 56.7	7.2 7.1	10.8 11.0	
10		87	94.5—95.5	C. 51.7 F. 51.9	6.2 6.4	7.9 7.7	
11		76	97—97.5	C. 52.3 F. 52.0	6.5 6.5	9.0 8.9	

a) Yield for *t*-butyloxycarbonylation.

of the resin was subjected to two more cycles with **11** (0.4 g, 0.65 mmol) and dried to give Boc–(Ile–Lys(ZCl_2)–Gly)$_5$–Phe–resin (1.7 g, approx. 96%). The peptidyl resin preparations were treated with anhydrous HF as above and the peptides extracted into 2% (by vol) acetic acid were passed through an Amberlite IRA-400 (acetate form) column as above and freeze-dried (324 mg and 360 mg, respectively).

Fractionation of the Peptide Preparations. The preparations of **12**, **13**, and **14** were fractionated on a CM-cellulose[12] column by linear gradient elutions of NaCl concentration. Fractions were pooled as shown in Fig. 1. The peptides in the fractions were desalted by gel filtrations on a Sephadex G-10 column (1.9 cm × 100 cm) equilibrated with 5 mM HCl and freeze-dried.

Collagen Lysyl Hydroxylase. The enzyme was extracted from 13-day-old chick embryos (312 g) and purified by ammonium sulfate fractionation and affinity chromatography on a column (1.5 cm × 12 cm) of concanavaline-A-Sepharose 4B (Pharmacia) as described by Turpeennien *et al.*[21] except that the buffer solution used in the affinity chromatography did not contain $MnCl_2$. The protein concentration of the enzyme solution (12 ml) was 1.2 mg/ml.

Assay Procedures. The enzymic hydroxylation of lysyl residues in substrate model peptides was assayed by the stoichiometric release of $^{14}CO_2$ from [1-^{14}C]-α-oxoglutarate as described by Rhoads and Udenfriend[8] and Kivirikko *et al.*[9] The incubation was carried out at 37 °C and $^{14}CO_2$ released was captured and counted with liquid scintillation counter as described by Ichiyama *et al.*[22]

Results

Synthetic Peptides. The preparations of **12**, **13**, and **14** were fractionated by CM-cellulose column chromatography (Figs. 1-a, b, and c). The yields and amino acid compositions are shown in Table 2. The peptides in the fraction of A-10, B-2, and C-4, namely (Ala–Lys–Gly)$_{10}$–Phe (**12**), (Ile–Lys–Gly)$_3$–Phe (**13**), and (Ile–Lys–Gly)$_5$–Phe (**14**), were used as substrates in the following enzymic reactions.

Enzymic Reactions. The time course of the reaction is shown in Fig. 2. The double reciprocal plots of the radioactivity of $^{14}CO_2$ released during 60 min incubations against the substrate concentration are shown in Fig. 3. A linear relationship was observed with **13** over the whole range of concentration examined. With **14**, a substrate inhibition was observed, however, at higher concentration than 0.5 mM of –Ile–Lys–Gly– unit. The apparent values of K_m and V_{max} were estimated by extrapolation of the linear part obtained in the lower concentration range, where the inhibition was not so significant. The values for **12** could not be obtained because of its strong substrate inhibition.

Discussion

The lysyl and prolyl residues at Y-position of –X–Y–Gly– tripeptide units in procollagen can be hydroxylated by the hydroxylases specific to them, respectively. In the present work, the peptides, (X–Lys–Gly)$_n$–Phe, were synthesized and subjected to the action of collagen lysyl hydroxylase. The syntheses were carried out by successive condensations of protected tripeptide units to phenylalanine linked to an insoluble supporting resin. Because of the incomplete reaction in the deprotection and/or condensation steps, the products were mixtures of peptides with varying number of repeating units. The peptides were separated from one another by CM-cellulose column chromatography making use of varying lysine content (Figs. 1-a, b, and c). The main component of A-10 (Fig. 1-a) was characterized as the designed peptide (Ala–Lys–Gly)$_{10}$–Phe (**12**) by amino acid composition (Table 2). Most of the other components, A-1 to A-9, were shorter peptides. The relatively low phen-

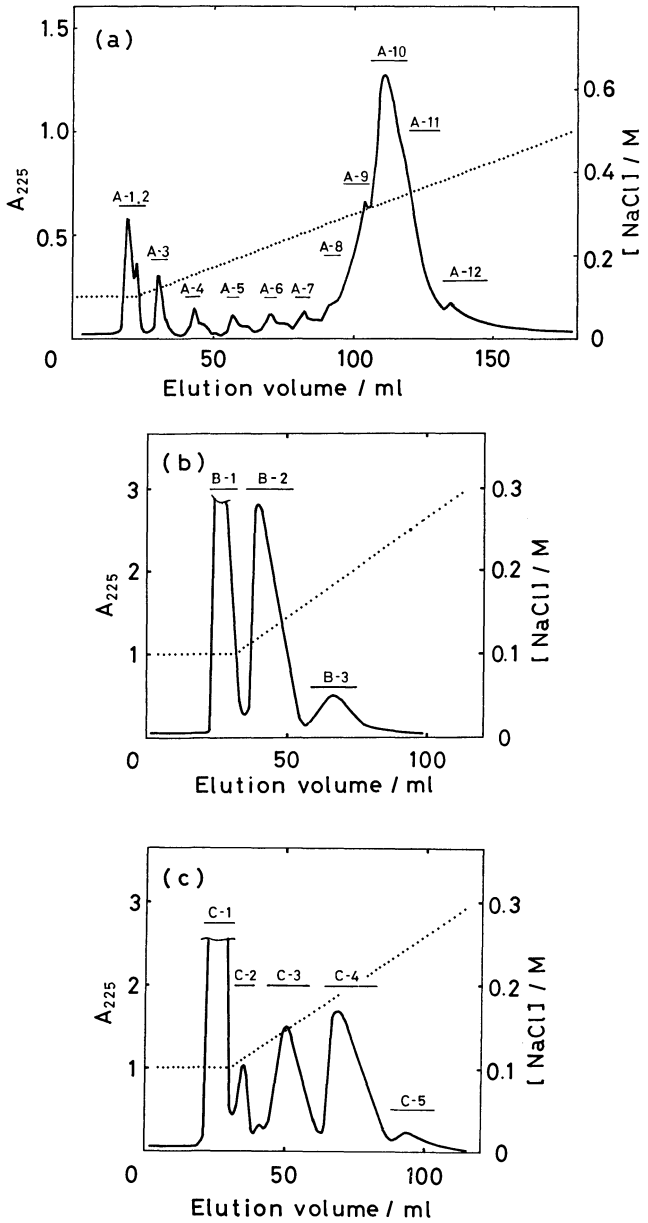

Fig. 1. CM-cellulose column chromatography of peptides prepared by fragment condensation in solid-phase method.
Crude preparations of (a) (Ala–Lys–Gly)$_{10}$–Phe (**12**), 185 mg; (b) (Ile–Lys–Gly)$_3$–Phe (**13**), 195 mg; and (c) (Ile–Lys–Gly)$_5$–Phe (**14**), 203 mg, were dissolved in 0.05 M NaCl (20 ml) and applied on a CM-cellulose column (2.6 cm × 50 cm) equilibrated with 0.1 M NaCl. The column was eluted with 0.1 M NaCl (70 ml) and with 0.1 M to 0.6 M NaCl (linear gradient, total 2000 ml) at 150 ml/h. Fractions of 15 ml were collected. —: Absorbance at 225 nm, ·····: concentration of NaCl.

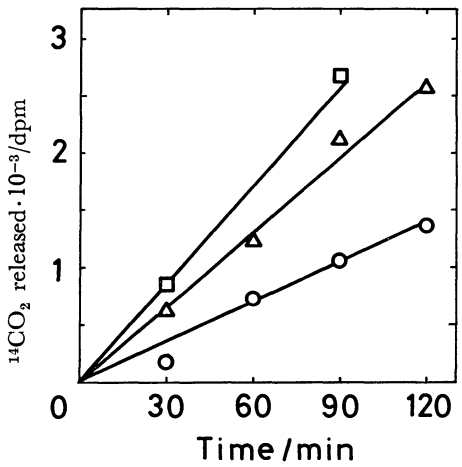

Fig. 2. Time course of the enzymic reaction.
Peptide (Ala–Lys–Gly)$_{10}$–Phe (**12**) (0.31 mg/ml) (○), (Ile–Lys–Gly)$_3$–Phe (**13**) (0.32 mg/ml) (△), or (Ile–Lys–Gly)$_5$–Phe (**14**) (0.32 mg/ml) (□) was incubated with the enzyme (0.06 mg protein/ml) and [1-^{14}C]-α-oxoglutarate (60000 dpm/ml) at 37 °C in 3 ml of reaction mixture.

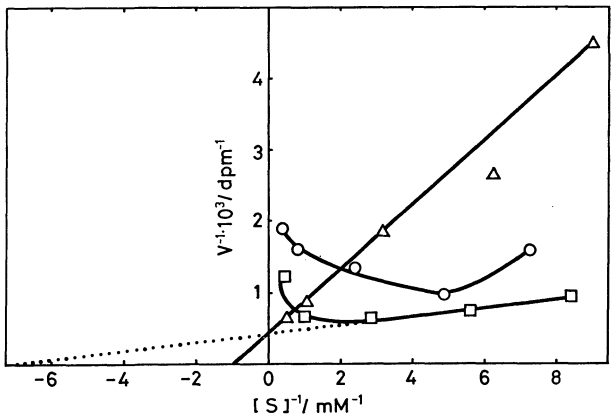

Fig. 3. Double reciprocal plot of initial rate of enzymic hydroxylation against the substrate concentration.
The initial rate is expressed as dpm of $^{14}CO_2$ released from [1-^{14}C]-α-oxoglutarate (9×10^4 dpm) during the incubation (60 min) with the enzyme (0.22 mg protein/ml) and varying amount of substrate peptide in 1 ml of the reaction mixture. Substrate concentration, [S], is expressed as mM of –X–Lys–Gly– unit. —○—: (Ala–Lys–Gly)$_{10}$–Phe (**12**), —△—: (Ile–Lys–Gly)$_3$–Phe (**13**), —□—: (Ile–Lys–Gly)$_5$–Phe (**14**).

ylalanine content in the fractions A-3 to A-7 is probably due to the contamination of peptides without phenylalanine at C-termini. A very small extent of contamination of such peptides (1 to 2% by weight) produced by random cleavage of peptide bond during the HF treatment will affect the amino acid composition. Fraction A-11 was a tailing part of A-10 and fraction A-12 contained branched-chain peptides which resulted from the deprotection of N$^{\varepsilon}$-group on exposures to 33% trifluoroacetic acid. Although a more acid-stable 2,4-dichlorobenzyloxycarbonyl (ZCl_2) group[16] was used for the protection of N$^{\varepsilon}$-group in the syntheses of **13** and **14**, the branched-chain peptides, B-3 and C-5, were produced (Figs. 1-b and c). The presence of considerable amount of shorter peptides besides (Ile–Lys–Gly)$_5$–Phe (Fig. 1-c) reflects the low reaction yield in the solid-phase fragment condensation of **11**. The large absorption values observed with peptide B-1 and C-1 are mainly due to the presence of anisole in these fractions. The

Table 2. Yields[a] and amino acid compositions[b] of fractionated pfptides

Fraction	Yield wt%	Amino acid composition[c]			Fraction	Yield wt%	Amino acid composition			
		Ala	Gly	Phe			Ile	Lys	Gly	Phe
A-1, 2	1.4				B-1	16.9	2.0	2.1	2.2	1
A-3	1.1	3.5	3.7	1	B-2	70.0	2.9	2.8	3.0	1
A-4	1.3	6.4	6.5	1	B-3	4.7	3.9	4.8	4.8	1
A-5	0.8	6.2	6.2	1						
A-6	1.1	8.3	8.3	1	C-1	6.3	2.1	2.2	2.1	1
A-7	1.5	9.9	10.0	1	C-2	10.3	3.3	3.2	3.4	1
A-8	2.5	7.9	8.0	1	C-3	36.9	4.1	4.0	4.3	1
A-9	13.2	9.5	9.6	1	C-4	31.8	4.8	4.9	5.2	1
A-10	43.0	10.3	10.3	1	C-5	4.5	5.4	6.0	6.2	1
A-11	12.1	10.4	10.6	1						
A-12	5.0	12.1	12.9	1						

a) Yields are based on the amount of peptides subjected to the fractionation. b) Peptides were hydrolyzed with 6 M HCl at 105 °C for 24 h in evacuated tubes and the resulting amino acid mixtures were subjected to amino acid analysis with JLC 8AH amino acid analyzer (JEOL). Amino acid compositions are expressed as molar ratios to phenylalanine content. c) The lysine contents were not determined.

Table 3. Comparison of model peptides as substrate for collagen lysyl hydroxylase

Substrate	Relative V_{max}	K_m	
		mg/ml	mM of -X-Lys-Gly-
$(Ile\text{-}Lys\text{-}Gly)_2$		1.2[a]	4[a]
$(Ile\text{-}Lys\text{-}Gly)_3$-Phe	1	0.35	1
$(Ile\text{-}Lys\text{-}Gly)_5$-Phe	1[b]	0.05[b]	0.14[b]
L-III[c]		0.7[a]	0.2[a]

a) Values reported by Kivirikko *et al.*[9] b) Values obtained by extrapolation (see Experimental). c) synthetic peptide; $(Pro\text{-}Pro\text{-}Gly)_4$-Ala-Arg-Gly-Met-Lys-Gly-His-Arg-Gly-$(Pro\text{-}Pro\text{-}Gly)_4$.[9]

amino acid compositions of B-2 and C-4 agreed with those expected for **13** and **14**, respectively.

The lysyl residues in the model substrates were hydroxylated by collagen lysyl hydroxylase. When K_m values of various synthetic substrates are compared on molar basis of -X-Lys-Gly- unit (Table 3), the longer is a peptide, the higher is the affinity per unit to the enzyme. The average K_m value (0.14 mM) per -Ile-Lys-Gly- unit in **14** is almost equal to the K_m value (0.2 mM) reported for -Met-Lys-Gly- unit in a synthetic model peptide of collagen.[9] The effect of the chain length is obvious merely on the affinity of the peptide to the enzyme. No difference was observed between the V_{max} values of **13** and **14** (Fig. 3 and Table 3).

The substrate inhibition observed for **12** over the whole range of the concentration examined here and for **14** at higher concentration may be due to a high basicity of the peptides because the positive charges per molecule increase with increasing n value of $(X\text{-}Lys\text{-}Gly)_n$-Phe. A highly basic peptide may inactivate the enzyme which is charged negatively at pH 7.4.[21]

The authors are grateful to Dr. Haruhiko Aoyagi of Kyushu University for practical suggestions in the synthesis of $Lys(ZCl_2)$ and for providing an authentic preparation of it and to Mr. Chikahisa Takasaki of this laboratory for providing Aoc-Phe. The present work was supported in part by the fund from the Ministry of Education, Science and Culture.

References

1) K. I. Kivirikko and D. J. Prockop, *Proc. Natl. Acad. Sci. U.S.A.*, **57**, 782 (1967).
2) D. Fujimoto and N. Tamiya, *Biochem. J.*, **84**, 333 (1962).
3) D. J. Prockop, A. Kaplan, and S. Udenfriend, *Biochem. Biophys. Res. Commun.*, **9**, 192 (1962).
4) D. Fujimoto and N. Tamiya, *Biochem. Biophys. Res. Commun.*, **10**, 498 (1963).
5) K. I. Kivirikko and D. J. Prockop, *Biochim. Biophys. Acta*, **258**, 366 (1972).
6) L. Tuderman, R. Myllylä, and K. I. Kivirikko, *Eur. J. Biochem.*, **80**, 341 (1977).
7) U. Puistola, T. M. Turpeennien-Hujanen, R. Myllylä, and K. I. Kivirikko, *Biochim. Biophys. Acta*, **611**, 40 (1980).
8) R. E. Rhoads and S. Udenfriend, *Proc. Natl. Acad. Sci. U.S.A.*, **60**, 1473 (1968).
9) K. I. Kivirikko, K. Shudo, S. Sakakibara, and D. J. Prockop, *Biochemistry*, **11**, 122 (1972).
10) R. Myllylä, L. Tuderman, and K. I. Kivirikko, *Eur. J. Biochem.*, **80**, 349 (1977).
11) U. Puistola, T. M. Turpeennien-Hujanen, R. Myllylä, and K. I. Kivirikko, *Biochim. Biophys. Acta*, **611**, 51 (1980).
12) Abbreviations for amino acids are according to the IUPAC-IUB Commission on Biochemical Nomenclature, *J. Biol. Chem.*, **247**, 977 (1972). All amino acids except for glycine are of L configuration. Other abbreviations used: Aoc, *t*-pentyloxycarbonyl; Boc, *t*-butyloxycarbonyl; CM, carboxymethyl; DCC, dicyclohexylcarbodiimide; DCHA, dicyclohexylamine; DMF, *N*,*N*-dimethylformamide; HOSu, *N*-hydroxysuccinimide; Z, benzyloxycarbonyl; $Z(Cl_2)$, 2,4-dichlorobenzyloxycarbonyl.
13) R. Schwyzer, P. Sieber, and H. Kappler, *Helv. Chim. Acta*, **42**, 2622 (1959).
14) G. W. Anderson, J. E. Zimmerman, and F. M.

Callhan, *J. Am. Chem. Soc.*, **86**, 1839 (1964).
15) A. Neuberger and F. Sanger, *Biochem. J.*, **37**, 515 (1943).
16) B. W. Erickson and R. B. Merrifield, *J. Am. Chem. Soc.*, **95**, 3757 (1973).
17) E. Schnabel, *Ann. Chim.*, **702**, 188 (1967).
18) R. W. Chambers and F. H. Carpenters, *J. Am. Chem. Soc.*, **77**, 1522 (1955).
19) A. Loffet, *Int. J. Pept. Protein Res.*, **3**, 297 (1971).
20) S. Sakakibara, Y. Shimonishi, Y. Kishida, M. Okada, and H. Sugihara, *Bull. Chem. Soc. Jpn.*, **40**, 2164 (1967).
21) T. M. Turpeennien, U. Puistola, H. Anttinen, and K. I. Kivirikko, *Biochim. Biophys. Acta*, **438**, 215 (1977).
22) A. Ichiyama, S. Nakamura, Y. Nishizuka, and O. Hayaishi, *J. Biol. Chem.*, **245**, 1699 (1970).

 © 1982 The Chemical Society of Japan Bull. Chem. Soc. Jpn., 55, 1561—1563 (1982)

Six New Sesquiterpenoids from the Red Alga *Laurencia nipponica* Yamada[1)]

Teruaki Suzuki, Hajime Kikuchi, and Etsuro Kurosawa*

Department of Chemistry, Faculty of Science, Hokkaido University, Sapporo 060

(Received October 1, 1981)

Six new laurane-type sesquiterpenoids were isolated from the red alga *Laurencia nipponica* Yamada and their structures were established on the basis of spectral and chemical evidence.

In the course of our investigation on the constituents from the red alga *L. nipponica* Yamada (Rhodophyta, Rhodomelaceae, Urasozo in Japanese), we have reported[2)] many halogenated or non-halogenated sesquiterpenoids and non-terpenoids consisting of C_{15}-straight carbon skeleton with terminal conjugated enyne or allene moiety. The diversity of terpenoids and non-terpenoids biosynthesis in this alga is found to be greatly dependent upon its growth localities. We wish to report here that this species, collected at Atsuta in the vicinity of Sapporo, Ishikari Bay, Hokkaido, produces six new sesquiterpenoids (**1**, **2**, **3**, **4**, **5**, and **6**) together with already chemically synthesized halochamigrene epoxide (**7**)[3)] as the major component (27% of the neutral essential oil) and the other four known compounds, laurene[4)] (**8**, 1.4%), halochamigrene[3,5)] (**9**, 2.0%), *trans*-phytol (**10**, 2.5%), and *trans*-phytol acetate[6)] (**11**, 0.8%) as the minor components. But surprisingly, this alga does not show the presence of C_{15} non-terpenoids, which are found to be biogenetically derived from laurediol (**12**)[2c)] and have been usually isolated as the major components (20—40%) from this species collected at the several different locations in Japan Sea, including Ishikari Bay.

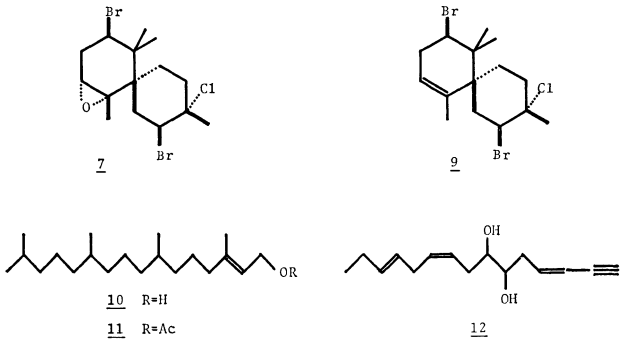

Half-dried algae[7)] were extracted with methanol and the neutral fraction was obtained from the methanol extract by the usual method. Then the neutral fraction was subjected to separation on a combination of column chromatography over neutral alumina and HPLC to give six new terpenoids (**1**, **2**, **3**, **4**, **5**, and **6**) and five known compounds (**7**, **8**, **9**, **10**, and **11**). Five known compounds were identified by the comparison of IR, ^1H and ^{13}C NMR spectra and the optical rotation with those of the authentic specimens.

*The Structure of Isodihydrolaurene (**1**).*[8)] Isodihydrolaurene (**1**); colorless oil, $C_{15}H_{22}$ *m/e* 202 (M^+), $[\alpha]_D$ +33.5° (*c* 1.24, $CHCl_3$), λ_{max}^{EtOH} 205 nm (ε 4,000); had characteristic IR bands at 1655 and 875 cm^{-1} due to an exocyclic methylene group, and it was further supported by ^1H and ^{13}C NMR spectra at δ 4.70 (1H, br.s), 4.77 (1H, br.s), and 105.3 (t). Moreover, the NMR spectra showed signals due to a secondary methyl at δ 0.76 (3H, d, J=7 Hz), a tertiary methyl at 0.98 (3H, s), an olefinic methyl at 1.63 (3H, br.s) and two olefinic protons at 5.34 (2H, m), and 117.8 (d) and 118.8 (d). Treatment of **1** with DDQ in refluxing dioxane resulted in quantitative aromatization to give laurene (**8**), which was identified by the comparison of IR, ^1H and ^{13}C NMR spectra and the optical rotation with those of the authentic specimen. Since the UV spectrum of **1** did not exhibit an absorption due to 1,3-cyclohexadiene moiety,[9)] the

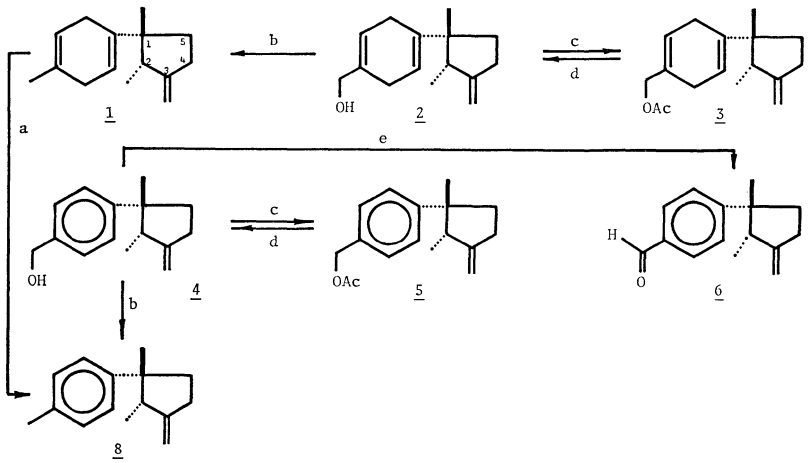

Fig. 1. a) DDQ-dioxane, reflux 80 min; b) 1) MsCl-Et_3N, 0 °C, 1 h; 2) $LiAlH_4$-THF, reflux 0.5 h; c) Ac_2O-Py, room temp, 18 h; d) K_2CO_3-MeOH, room temp, 1.5 h; e) CrO_3-2Py, CH_2Cl_2, room temp, 5 min.

structure of isodihydrolaurene, including the absolute configuration, should be represented by the formula **1**.

The Structures of Isodihydrolaurenol (2) and Isodihydrolaurenol Acetate (3). The ^{1}H NMR spectrum of **2** was almost identical with that of **1** except for an olefinic methyl at δ 1.63 in **1** and, instead of it, showed signals due to a hydroxymethyl group at 2.26 (1H, br.s, -O<u>H</u>) and 3.85 (2H, br.s, -C<u>H</u>$_2$OH). The structure of **2** was confirmed by the chemical correlation with **1**. When alcohol (**2**) was treated with MsCl and Et_3N in CH_2Cl_2 followed by reduction with LAH, **2** was converted to **1**. The spectral evidence and chemical correlation reaction defined the structure of isodihydrolaurenol as shown in the formula **2**. Moreover acetylation of **2** with acetic anhydride and pyridine generated the natural product (**3**) in quantitative yield.

The Structures of Laurenol (4) and Laurenol Acetate (5). Laurenol (**4**); colorless oil, $[\alpha]_D$ +34.7° (*c* 0.26, $CHCl_3$), $C_{15}H_{20}O$ *m/e* 216 (M^+), λ_{max}^{EtOH} 257 nm (ε 290), ν_{max}^{film} 3340 cm^{-1}; showed in ^{1}H NMR spectrum signals due to a secondary methyl at δ 0.67 (3H, d, J=7 Hz), a tertiary methyl at 1.23 (3H, s), a hydroxymethyl at 4.44 (2H, s), an exocyclic methylene at 4.77 (2H, br.s) and four aromatic protons at 7.05 (4H, br.s), and the signals were found to be well corresponding with the structure **4**. The structure of **4** was further confirmed by chemical correlation with **8** as shown in Fig. 1. The structure of **5** was established by acetylation of **4** with acetic anhydride in pyridine.

The Structure of Laurenal (6). Laurenal; colorless oil, $[\alpha]_D$ +33.2° (*c* 0.23, $CHCl_3$), $C_{15}H_{18}O$ *m/e* 214 (M^+), λ_{max}^{EtOH} 258 (ε 12700) and 205 nm (17500), ν_{max}^{film} 2820, 2730, and 1700 cm^{-1}; exhibited the presence of an aromatic aldehyde group in ^{1}H NMR at δ 9.88 (1H, s), IR and UV spectra. Collins oxidation[10] of **4** gave an aldehyde in 85% yield, whose spectral data and the optical rotation were identical with those of natural aldehyde (**6**).

Experimental

The IR and UV spectra were recorded on a JASCO model A-102 and Hitachi model 134 spectrophotometers, respectively. The ^{1}H NMR spectra were determined using a JEOL JNM-PS-100 spectrometer in CCl_4 solution with TMS as an internal standard and the ^{13}C NMR spectra were obtained with a Bruker SXP4-100 spectrometer in $CDCl_3$. A JASCO model DIP-SL was used for the measurement of the optical rotation in $CHCl_3$. Alumina (Merck, activity II—III) and silica gel (Merck, Kieselgel 60) were used for the column chromatography and HPLC was performed on a JASCO Finpac SIL-C$_{18}$.

Isolation. Half-dried algae (4.6 kg), collected at Atsuta in Ishikari Bay, Hokkaido, in July 1980, were extracted with 10 L of methanol for two weeks and the methanol solution was concentrated to about 1.5 L under reduced pressure and the residue was percolated with ether. The ether solution was shaken with 5% NaOH for removing acidic part and then dried over anhydrous Na_2SO_4. After evaporation of solvent, the dark greenish neutral oil (52 g) was obtained and then subjected to column chromatography over neutral alumina. The fraction eluted with hexane gave pure laurene (**8**, 1.4% of the neutral fraction) and halochamigrene (**9**, 2.0%), and crude isodihydrolaurene (**1**), and the last was further purified on HPLC with CH_3CN–H_2O (95:5) to give the pure material of **1** (2.5%). The fraction eluted with hexane–benzene (1:1) yielded halochamigrene epoxide (**7**, 27%). The fraction eluted with benzene–ethyl acetate (10:1) was further subjected to HPLC with MeOH–H_2O (80:20) to give isodihydrolaurenol (**2**, 0.51%), isodihydrolaurenol acetate (**3**, 0.2%), laurenol (**4**, 0.51%), laurenol acetate (**5**, 0.2%), laurenal (**6**, 0.03%), *trans*-phytol (**10**, 2.5%), and *trans*-phytol acetate (**11**, 0.8%).

Isodihydrolaurene (1). Colorless oil; $[\alpha]_D$ +33.5° (*c* 1.24, $CHCl_3$); λ_{max}^{EtOH} 205 nm (ε 4000); ν_{max}^{film} 3070, 3020, 1655, 1370, 1165, 1090, 1020, 950, 875, and 775 cm^{-1}; ^{1}H NMR (CCl_4) δ 0.76 (3H, d, J=7 Hz), 0.98 (3H, s), 1.39 (1H, ddd, J=11, 6, 6, α-H on C-5), 1.63 (3H, br.s), 1.8—2.5 (3H), 2.19 (1H, br.q, J=7), *ca.* 2.5 (4H, m), 4.70 (1H, br.s), 4.77 (1H, br.s), and 5.34 (2H, m, W_H=9); ^{13}C NMR ($CDCl_3$) δ 17.5 (q), 22.8 (q), 25.8 (q), 27.4 (t), 28.6 (t), 31.8 (t), 32.8 (t), 48.8 (d), 49.5 (s), 105.3 (t), 117.8 (d), 118.8 (d), 130.9 (s), 139.2 (s), and 157.9 (s). Found: *m/e* 202.1714. Calcd for $C_{15}H_{22}$: M, 202.1719.

Isodihydrolaurenol (2). Colorless oil; $[\alpha]_D$ +40.0° (*c* 1.52, $CHCl_3$); λ_{max}^{EtOH} 205 nm (ε 6000); ν_{max}^{film} 3300, 3070, 3020, 1690, 1655, 1425, 1370, 1095, 1055, 1030, 1005, 960, 880, 810, 785, and 755 cm^{-1}; ^{1}H NMR (CCl_4) δ 0.77 (3H, d, J=7 Hz), 0.99 (3H, s), 1.42 (1H, ddd, J=12.5, 5.5, 5.5), 1.8—2.6 (4H), 2.26 (1H, br.s, -O<u>H</u>), 2.62 (4H, m), 3.85 (2H, br.s, -C<u>H</u>$_2$OH), 4.73, 4.78, 5.42, and 5.59 (1H each, br.s). Found: *m/e* 218.1643. Calcd for $C_{15}H_{22}O$: M, 218.1668.

Isodihydrolaurenol Acetate (3). Colorless oil; $[\alpha]_D$ +40.0° (*c* 0.21, $CHCl_3$); λ_{max}^{EtOH} 206 nm (ε 9700); ν_{max}^{film} 3080, 3030, 1740, 1655, 1370, 1245, 1230, 1025, 960, 887, and 802 cm^{-1}; ^{1}H NMR (CCl_4) δ 0.77 (3H, d, J=7 Hz), 0.99 (3H, s), 1.43 (1H, ddd, J=12, 5, 5), 1.9—2.6 (3H), 1.97 (3H, s), 2.13 (1H, br.q, J=7), 2.65 (4H, m), 4.37 (2H, br.s), 4.71, 4.78, 5.39 and 5.66 (1H each, br.s). Found: *m/e* 260.1782. Calcd for $C_{17}H_{24}O_2$: M, 260.1776.

Laurenol (4). Colorless oil; $[\alpha]_D$ +34.7° (*c* 0.26, $CHCl_3$); λ_{max}^{EtOH} 257 (ε 290), 263 (ε 330) and 272 nm (ε 230); ν_{max}^{film} 3340, 3060, 3020, 1655, 1615, 1515, 1415, 1370, 1030, 1020, 880, 840, 815 and 805 cm^{-1}; ^{1}H NMR (CCl_4) δ 0.67 (3H, d, J=7 Hz), 1.23 (3H, s), 1.6—2.6 (5H), 2.06 (1H, br.s, -O<u>H</u>), 4.44 (2H, s, -C<u>H</u>$_2$OH), 4.77 (2H, br.s), and 7.05 (4H, br.s). Found: *m/e* 216.1496. Calcd for $C_{15}H_{20}O$: M, 216.1511.

Laurenol Acetate (5). Colorless oil; $[\alpha]_D$ +23.6° (*c* 0.42, $CHCl_3$); λ_{max}^{EtOH} 255 (ε 300), 261 (ε 330), 267 (ε 270), and 271 nm (ε 200); ν_{max}^{film} 3070, 3020, 1740, 1655, 1615, 1515, 1430, 1375, 1360, 1225, 1075, 1030, 1020, 965, 880, 825, and 815 cm^{-1}; ^{1}H NMR (CCl_4) δ 0.69 (3H, d, J=7 Hz), 1.26 (3H, s), 1.6—2.6 (5H), 2.00 (3H, s), 4.81 (2H, br.s), 4.94 (2H, s), and 7.12 (4H, br.s). Found: *m/e* 258.1626. Calcd for $C_{17}H_{22}O_2$: M, 258.1620.

Laurenal (6). Colorless oil; $[\alpha]_D$ +33.2° (*c* 0.23, $CHCl_3$); λ_{max}^{EtOH} 258 (ε 12700) and 205 nm (ε 17500); ν_{max}^{film} 3070, 3030, 2820, 2730, 1700, 1655, 1605, 1570, 1415, 1385, 1370, 1310, 1215, 1175, 1075, 1015, 880, and 825 cm^{-1}; ^{1}H NMR (CCl_4) δ 0.69 (3H, d, J=7 Hz), 1.28 (3H, s), 1.8—2.8 (5H), 4.85 (2H, m), 7.29 (2H, br.d, J=8), 7.71 (2H, br.d, J=8) and 9.88 (1H, s). Found: *m/e* 214.1371. Calcd for $C_{15}H_{18}O$: M, 214.1358.

Aromatization of 1. A mixture of **1** (16 mg) and DDQ (24 mg) in freshly distilled dioxane (2 ml) was refluxed under nitrogen atmosphere. After cooling, the resulting

suspension was filtered through a column of neutral alumina (2 g) and eluted with hexane to give colorless oil (15 mg), whose spectral data and optical rotation were identical with those of the authentic specimen of laurene (**8**).[4]

*Conversion of Isodihydrolaurenol (**2**) into **1**.* To a cooling solution of **2** (10 mg) in dry CH_2Cl_2 containing dry Et_3N (10 μl) was gradually added distilled MsCl (5 μl). The mixture was stirred for 1 h at 0 °C, and then poured into ice water. Ether-extract was successively washed with 1 M HCl, 5% $NaHCO_3$, and brine, and then dried over anhydrous Na_2SO_4. After evaporation of the solvent, the resulting crude mesylate (12 mg), colorless oil, was reduced with LAH (20 mg) in refluxing THF (1 ml) for 0.5 h under nitrogen atmosphere. Ice was added to the cooled solution at 0 °C to decompose the excess of LAH. After the usual work-up, the resulting oily material was purified by column chromatography over silicic acid to give pure **1** (9 mg).

*Acetylation of **2**.* A solution of **2** (20 mg) in acetic anhydride (0.2 ml) and pyridine (0.2 ml) was allowed to stand overnight at room temperature and then worked up in the usual way to give monoacetate (**3**) (22 mg).

*Transformation of **4** into **8**.* To a cooling solution of **4** (12 mg) in dry CH_2Cl_2 (0.3 ml) containing dry Et_3N (10 μl) at 0 °C was gradually added distilled MsCl (6 μl) and stirred for 1 h at 0 °C. The reaction mixture was poured into ice–water and extracted with ether. After the usual work-up, the resulting crude mesylate (17 mg) was treated with LAH (20 mg) in refluxing THF (1 ml) for 0.5 h under nitrogen atmosphere. After usual manner for separation, the resulting oily material was chromatographed over silicic acid to give hydrocarbon (**8**) (11 mg).

*Acetylation of **4**.* Acetylation of **4** (20 mg) was carried out in the same manner as that of **2** to give **5** (22 mg).

*Collins Oxidation of **4** into **6**.* Dry CrO_3 (15 mg) was added to the solution of dry CH_2Cl_2 (0.5 ml) and dry pyridine (23 μl) in a dried two necked flask and the mixture was stirred at room temperature under nitrogen atmosphere for 5 min. Then a solution of **4** (6 mg) in dry CH_2Cl_2 (0.25 ml) was added to the resulting burgundy colored solution and it was stirred for an additional 5 min. After addition of ether, filtration and washing with ether, the ethereal solution was shaken with 5% $NaHCO_3$ and dried over anhydrous Na_2SO_4. After removal of the solvent, the oily substance (5 mg) was obtained, whose spectral data and the optical rotation were identical with those of natural aldehyde (**6**).

References

1) Part 47 of "Constituents of Marine Plants." Part 46; M. Suzuki and E. Kurosawa, *Tetrahedron Lett.*, in press.

2) a) T. Irie, A. Fukuzawa, M. Izawa, and E. Kurosawa, *Tetrahedron Lett.*, **1969**, 1343; b) T. Irie, M. Izawa, and E. Kurosawa, *Tetrahedron*, **26**, 851 (1970); c) E. Kurosawa, A. Fukuzawa, and T. Irie, *Tetrahedron Lett.*, **1972**, 2121; d) E. Kurosawa, A. Fukuzawa, and T. Irie, *ibid.*, **1973**, 4135; e) A. Furusaki, E. Kurosawa, A. Fukuzawa, and T. Irie, *ibid.*, **1973**, 4579; f) T. Suzuki, M. Suzuki, and E. Kurosawa, *ibid.*, **1975**, 3057; g) T. Suzuki, A. Furusaki, N. Hashiba, and E. Kurosawa, *ibid.*, **1977**, 3731; h) T. Suzuki and E. Kurosawa, *Chem. Lett.*, **1979**, 301; i) A. Fukuzawa and E. Kurosawa, *Tetrahedron Lett.*, **1979**, 2797; j) A. Fukuzawa and E. Kurosawa, *ibid.*, **21**, 1471 (1980); k) T. Suzuki, *Chem. Lett.*, **1980**, 541; l) T. Suzuki, H. Kikuchi, and E. Kurosawa, *ibid.*, **1980**, 1267; m) K. Kurata, A. Furusaki, C. Katayama, H. Kikuchi, and T. Suzuki, *ibid.*, **1981**, 773; n) T. Suzuki, A. Furusaki, H. Kikuchi, E. Kurosawa, and C. Katayama, *Tetrahedron Lett.*, in press.

3) a) B. M. Howard and W. Fenical, *Tetrahedron Lett.*, **1975**, 1687; b) The absolute stereostructure has been confirmed as the formula **7** by the X-ray crystallographic study, unpublished result; c) This compound has been also isolated from *L. okamurai* Yamada, M. Ojika, Y. Shizuri, and K. Yamada, 43rd National Meeting of the Chemical Society of Japan, 1981.

4) a) T. Irie, T. Suzuki, Y. Yasunari, E. Kurosawa, and T. Masamune, *Tetrahedron*, **25**, 459 (1969); b) J. E. McMurry and L. A. von Beroldingen, *ibid.*, **30**, 2027 (1974).

5) M. Suzuki and E. Kurosawa, *Tetrahedron*, **35**, 823 (1979).

6) J. J. Sims and J. A. Pettus, Jr., *Phytochemistry*, **15**, 1076 (1976).

7) The algae were identified as *L. nipponica* Yamada by Dr. Yuzuru Saito, a specialist of *Laurencia* Taxonomy, Faculty of Fisheries, Hokkaido University, Japan.

8) Dihydrolaurene has been isolated from *L. filiformis*, R. Kazlauskas, P. T. Murphy, R. J. Quinn, and R. J. Wells, *Aust. J. Chem.*, **29**, 2533 (1976).

9) W. G. Dauben and P. Oberhänsli, *J. Org. Chem.*, **31**, 315 (1966).

10) J. C. Collins, W. W. Hess, and F. J. Frank, *Tetrahedron Lett.*, **1968**, 3363.

Infrared Spectra and Intramolecular Hydrogen Bonding of Some Salicylanilides of Pharmaceutical Interest

Hiroko Endo, Minoru Hirota,* Yoshio Ito,† Isao Takeuchi,† and Yoshiki Hamada†

Department of Applied Chemistry, Faculty of Engineering, Yokohama National University, Hodogaya-ku, Yokohama 240

†Faculty of Pharmacy, Meijo University, Tempaku-ku, Nagoya 468

(Received October 2, 1981)

Intramolecular hydrogen bonding of the title compounds was investigated by measuring their infrared spectra in the OH, NH, and C=O stretching regions. The results showed that the intramolecular hydrogen bonding in the salicyloyl moiety plays an important role in the antibacterial activities of these salicylanilides.

As a part of a series of investigations to correlate the biological and pharmaceutical activities to their structures and physical properties, the intramolecular hydrogen bonding and the conformations of salicylanilides (**1**) were studied by infrared spectroscopy.

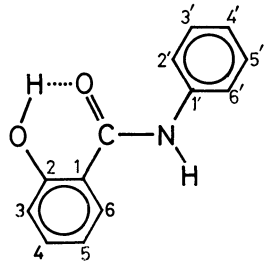

1

Intramolecular hydrogen bonds affect remarkably the associative properties and the solubilities of these compounds, thereby influencing on their biological activities in different ways. These anilides have coplanar chelate rings made up of very strong OH···O=C intramolecular hydrogen bonds of hexagonal arrangement. In turn, the amide moiety of the anilide usually takes a planar *s-trans* conformation as illustrated by **1**. In this connection, it is interesting to examine how the hydrogen bonding and the conformations of these anilides are affected with the steric effect caused by the substituents located ortho to either or both of amide and salicyloyl groups. For this purpose, the OH, NH, and C=O stretching absorptions of these anilides were measured and discussed.

Experimental

Preparation of the materials were reported elsewhere.[1] Infrared spectra were obtained in carbon tetrachloride solutions using a Hitachi 225 infrared spectrophotometer. The concentration of the solution was kept below 3×10^{-3} mol/l (usually at about 1×10^{-3} mol/l) in order to prevent the effect of the associated species.

Results and Discussion

Infrared spectra of the anilides are given in Table 1. In general, the *s-trans* conformer is known to be 4—8 kJ/mol more stable than the *cis*. Thus the salicylanilides without ortho (3, 6, 2′, and 6′) substituents absorb at about 3450 cm^{-1} in the NH stretching region, which was assigned to the *s-trans* conformation by Suzuki and co-workers.[2] Besides this band, they have absorption bands at *ca.* 1660 cm^{-1} in the carbonyl stretching region and broad bands around 3000 cm^{-1} due to chelated OH group, both of them suggesting the presence of intramolecularly hydrogen-bonded chelate rings. These facts support the *s-trans* conformation with chelated salicyloyl group as illustrated in **1**.

Effect of 2- (and 6-) Substituents on the Conformation and the Hydrogen Bonding. The substituent at the positions ortho to the amide group (on the anilino ring) may affect considerably the conformations of the amide groups of the salicylanilides. The effect can be classified as i) that from steric hindrance and ii) that from hydrogen bond formation. Since the planar conformation of the amide group is rather rigid, the bulky group at the ortho positions causes almost exclusively a torsion around the C_{Ar}–N bond. However, the effect on the NH frequency is not predominant. In short, the steric effect by the 2′- (and 6′-)substituent does not perturb the conformation of the amide group considerably.

The substituents capable of forming hydrogen bonds with the NH group investigated are aryloxyl, halo, and arylthio groups, all of them behaving as hydrogen acceptors in hydrogen bonding. With three anilides (**9**—**11**) carrying 2′-aryloxyl groups, their NH stretching absorptions tend to shift towards lower frequencies only slightly. The very small but definite low frequency shifts suggest the existence of very weak hydrogen bonding. The absorptions in the carbonyl and hydroxyl stretching regions also coincide with those of the parent salicylanilide (**1**), showing no indication for the substituent effect. The 2′-chloro substituted anilides **6** and **7** absorb at 3433 and 3432 cm^{-1} in the NH stretching region, which are somewhat 20 cm^{-1} lower than those of the parent anilide (**1**). Infrared spectral shifts due to intramolecular hydrogen bonding ($\Delta\nu_{NH}=\nu_f-\nu_b$) are again rather small. However, Welti[3] has measured the infrared spectra of some halogenated salicylanilides and concluded the existence of intramolecular hydrogen bonding from the $\Delta\nu_{NH}$ values of similar magnitudes for 2′-chlorinated derivatives and from considerably larger $\Delta\nu_{NH}$ values for 2′-brominated derivatives. The absorption due to chelated salicyloyl group is again similar to the parent salicylanilide (**1**).

The most intense ν_{NH} bands of 2′-arylthiosalicyl-

TABLE 1. INFRARED ABSORPTIONS IN THE OH, NH, AND C=O STRETCHING REGIONS OF SALICYLANILIDES

No.	Substituent on		ν_{OH}/cm^{-1}	ν_{NH}/cm^{-1}			$\nu_{C=O}/cm^{-1}$	
	Anilino moiety	Salicyloyl moiety		*s-trans*	*s-cis*	H-bonded	Amide (chelate)	Others
1	None	None		3454 (67)			1657 (373)	
2	3-Cl-4-(*p*-ClC_6H_4S)	5-Cl		3450 (110)			1663 (350)	
3	3-Cl-4-(*p*-ClC_6H_4S)	3,5-Cl_2	3511 (56)	3449 (104)		3398 (67)	1659 (254)	1686 (85) free
4	2-CH_3-4-Cl	5-Cl		3466 (40) 3442 (40)			1659 (201)	
5	2-CH_3-4-Cl	2-*O*-Ac-5-Cl	3538 (36)	3440 (82)	3405 (sh)			1697 (320) free 1792 (157) Ac 1768 (210) Ac
6	2,4-Cl_2	5-Cl		3433 (113)			1659 (325)	
7	2,4-Cl_2	3,5-Cl_2	3516 (43)	3432 (108)		3362 (42)	1660 (350)	1684 (111) free
8	2,4-Cl_2	2-*O*-Ac-5-Cl		3425 (sh)	3399 (148)			1692 (242) free 1792 (233) Ac 1772 (157) Ac
9	2-(*p*-FC_6H_4O)-5-Cl	5-Cl		3443 (122)			1659 (372)	
10	2-(*p*-ClC_6H_4O)-5-Cl	5-Cl		3443 (130)			1660 (281)	
11	2-(*p*-ClC_6H_4O)-5-Br	5-Cl		3444 (124)			1660 (275)	
12	2-(*p*-ClC_6H_4O)-5-Br	2-*O*-Ac-5-Cl			3406 (103)			1689 (273) free 1791 (229) Ac 1769 (167) Ac
13	2-(*p*-ClC_6H_4O)-5-CF_3	5-Cl		3444 (72)			1660	[1752] [1702]
14	2-(α-$C_{10}H_7O$)-5-Br	5-Cl		3439 (120)			1659 (277)	
15	2-(β-$C_{10}H_7O$)-5-Br	5-Cl		3439 (120)			1659 (293)	
16	2-(α-$C_{10}H_7O$)-5-CF_3	5-Cl		3443 (78)	3420 (sh)		1660 (248)	1686 (sh) [1753 (125)] [1705 (40)]
17	2-(β-$C_{10}H_7O$)-5-CF_3	5-Cl		3442 (93)	3419 (sh)		1659 (174)	[1757 (94)] [1702 (74)]
18	2-(α-$C_{10}H_7O$)-5-CF_3	2-*O*-Ac-5-Cl			3405 (87)			1686 (252) free 1790 (185) Ac 1765 (170) Ac [1705 (sh)]
19	2-(β-$C_{10}H_7O$)-5-CF_3	2-*O*-Ac-5-Cl		3441 (sh)	3408 (57)			1687 (200) free 1789 (121) Ac 1777 (148) Ac [1750 (200)] [1700 (220)]
20	2-(*p*-ClC_6H_4S)-5-Cl	5-Cl	3525 (14)	3434 (sh)	3406 (sh)	3353 (90)	1661 (306)	[1701 (47)]
21	2-(*p*-ClC_6H_4S)-5-Cl	3,5-Cl_2	3516 (22)	3434 (sh)	3406 (sh)	3353 (80)	1659 (137)	1685 (21) free
22	2-(*p*-ClC_6H_4S)-5-Br	5-Cl			3402 (sh)	3360 (82)	1663 (227)	
23	2-(*p*-ClC_6H_4S)-5-CF_3	5-Cl			3402 (sh)	3362 (66)	1662 (283)	[1751 (20)] [1703 (107)]

a) Broad band due to chelated OH (at *ca.* 3000 cm^{-1}) is omitted. b) Bands in brackets are assigned to the intensified overtones of CF absorptions.

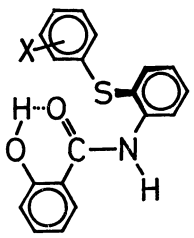

(I)

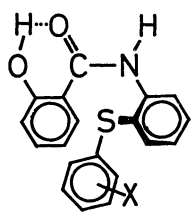

(II)

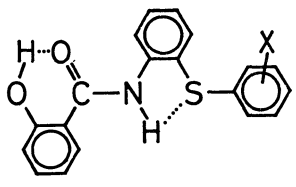

(III)

	(I)	(II)	(III)
	s-trans(free)	*s-cis*(free)	H-bonded
ν_{NH}/cm^{-1}	3434	3402	3360
Abundance	Less	Least	Most predominant

Table 2. NH and C=O stretching frequencies of some 2-substituted 5-chloroacetanilides

X	ν_{NH}/cm^{-1}	$\nu_{C=O}/cm^{-1}$
H	3440	1714
p-ClC_6H_4O	3435	1712
p-ClC_6H_4S	3366	1715 1698.5

anilides **20**—**23** are located at around 3350 cm^{-1}, which is a remarkably lower frequency than those of the other 2′-substituted derivatives discussed above. Besides this band, two additional absorption bands are observed at 3434 and 3402 cm^{-1}. The larger $\Delta\nu_{NH}$ suggests the presence of a hydrogen bond stronger than those in 2′-aryloxy and 2′-chloro derivatives (**7**—**13**). Similarly, NH···S intramolecular hydrogen bond is stronger than NH···O hydrogen bond in the series of the corresponding acetanilides given in Table 2. The other two NH bands were assigned to the free *s-trans* (I) and *s-cis* (II) conformers of the salicylanilides **20**—**23**. These 2′-arylthiosalicylanilides have weak bands at 1700 cm^{-1} of the $\nu_{C=O}$ region in addition to the strong bands at about 1660 cm^{-1}. This may be an indication of an unchelated structure for the *s-cis*(free) conformer absorbing at 3402 cm^{-1} in ν_{NH} region. If the chelated conformation (III) is assumed for the cis conformer, the molecule is expected to be considerably crowded sterically. Therefore an unchelated conformer may appear in a small amount.

Effect of Substituents on 3- and Other Positions on the Salicyloyl Residue. The 3-chloro derivatives (**3**, **7**, **21**) have two absorption bands in the ν_{NH} region; the one at a higher frequency (*ca.* 3430 cm^{-1}) may be assignable to the free *s-trans* amide group, while the other at a lower frequency (3400—3350 cm^{-1}) should arise from an intramolecularly hydrogen-bonded NH group. According to Welti,[3] these absorption bands are assigned properly to the conformer (IV) and (V), respectively. The former is estimated to be more predominant from the intensities of their characteristic absorption bands.

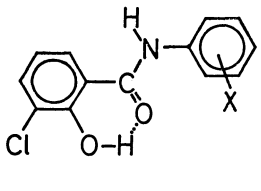

(IV)

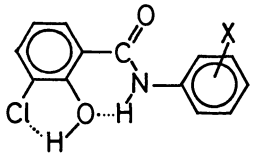

(V)

	(IV)	(V)
ν_{OH}/cm^{-1}	3000 (broad)	3516
$\nu_{C=O}/cm^{-1}$	1660	1685
ν_{NH}/cm^{-1}	3430	3400—3350
Abundance	More predominant	Less predominant

The conformations of the salicylanilides might be perturbed seriously by the acetylation of the 2-hydroxyl functional groups, since the intramolecular hydrogen bond participating in the formation of the chelate ring and keeping the carbonyl and the hydroxyl groups close is no longer persistent. The acetyl derivatives (**5**, **8**, **12**) have NH absorption bands at approximately 3400 cm^{-1}, which can be assigned to the NH···O(Ac) hydrogen bonded conformers (VI). The considerably small $\Delta\nu_{NH}$ values in these compounds are reasonable since the acetoxyl group is in general a hydrogen acceptor weaker than the hydroxyl groups.[4] The conformer (VI) become less

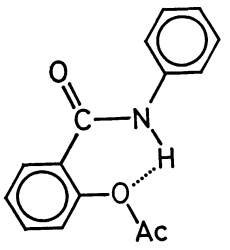

(VI)

favorable by the introduction of 2′-substituent, and the 3440 cm^{-1} band due to the free *s-trans* conformer appears. The low frequency shift of this band in **8** is ascribable to the intramolecular hydrogen bonding with 2′-chloro substituent. The acetyl derivatives usually have three absorptions at about 1690, 1770, and 1790 cm^{-1} in the $\nu_{C=O}$ region; the former band is assigned to the amide and the latter two to the acetyl group.

5′-Trifluoromethylsalicylanilides (**13** and **23**) have two unusual absorption bands at 1750 and 1700 cm^{-1}. These bands are interpreted as the intensified overtone vibrations, by Fermi resonance, of strong C–F stretching vibrations in 850—900 cm^{-1} region, since the intensities of the carbonyl band at *ca.* 1690 cm^{-1} is remarkably reduced, and since the corresponding trifluoromethyl substituted aniline has no such bands.

Table 3. Antibacterial activities of some substituted salicylanilides

Compound	Antibacterial activity (MIC: μg/ml)	
	S. aureus (A)	*B. subtilis* (B)
2	10	10
3	0.16	0.16
10	0.8	0.8
11	0.8	0.8
12	0.16	0.16
13	0.8	0.8
14	50	10
15	50	10
16	1	1
17	1	1
18	0.16	0.16
22	0.8	0.8
23	5	0.8

Preliminary Results on the Correlation with Their Antibacterial Activities. The six-membered hydrogen bonding in salicyloyl moiety is hereby shown to be perturbed when 3-chloro or 2-*O*-acetyl substituent is introduced to the salicylanilide molecule. The antibacterial activities towards *Staphyrococcus aureus* FDA 209-P (A) and *Bacillus subtilis* PCI-219 (B) are remarkably high with the compounds carrying the above substituents (**3**, **12**, and **18**) as given in Table 3. Thus, the structural and conformational change in the sali-

cyloyl moiety might play an important role in the biological activities of these salicylanilides. On the other hand, the activity is not affected considerably by the conformational change in the amide moiety. However, further informations on a wider range of the anilides and the bacteria is necessary in order to conclude the structure-activity relationship confidently.

The authors are grateful to Prof. T. Ito, Kansai Medical University, for the examination of the antibacterial activity.

References

1) Y. Hamada, I. Takeuchi, Y. Ito, S. Matsui, and T. Ito, *Yakugaku Zasshi*, **101**, 633 (1981).
2) I. Suzuki, M. Tsuboi, T. Shimanouchi, and S. Mizushima, *Spectrochim. Acta*, **16**, 471 (1960).
3) D. Welti, *Spectrochim. Acta*, **22**, 281 (1966).
4) An alternative explanation that the 3400 cm^{-1} band arises from the free *s-cis* conformer cannot be excluded.

Optical Resolution of 2-Amino-1,2-diphenylethanol by Preferential Crystallization and Its Utilization in Fractional Crystallization and Enantioselective Reduction of Prochiral Ketones

Kazuhiko SAIGO,*,† Shigeo OGAWA, Shigetoshi KIKUCHI, Atsushi KASAHARA, and Hiroyuki NOHIRA

Department of Applied Chemistry, Faculty of Engineering, Saitama University, Shimo-ohkubo, Urawa 338

(Received October 8, 1981)

(±)-*erythro*-2-Amino-1,2-diphenylethanol prepared from benzoin oxime by catalytic reduction was successfully resolved into a pair of optically active forms by preferential crystallization. The optically active amino alcohol was found to be useful as a basic resolving agent for the optical resolution of tartaric acid, *trans*-2,3-oxiranedicarboxylic acid, 2-hydroxy-2-phenylpropionic acid, and 3-*endo*-benzamido-5-norbornene-2-*endo*-carboxylic acid. Chiral hydrides prepared from lithium aluminium hydride and optically active *threo*- or *erythro*-2-amino-1,2-diphenylethanol derivatives were applied to the enantioface differentiating reduction of prochiral ketones to give the corresponding optically active alcohols in 26—72% optical purities.

In contrast to ephedrine which is widely used in fractional crystallization as a resolving agent[1] and in asymmetric synthesis as a chiral source,[2] *erythro*-2-amino-1,2-diphenylethanol having similar configuration to ephedrine is little applied to fractional crystallization and asymmetric synthesis except for the synthesis of optically active asparic acid.[3] The preparation of optically active *erythro*-2-amino-1,2-diphenylethanol in a preparative quantity was considered to be troublesome because it is obtained by the fractional crystallization of diastereomeric salts with L-glutamic acid.[4] These prompted us to study on the optical resolution of *erythro*-2-amino-1,2-diphenylethanol by preferential crystallization, which gives preparatively both enantiomers by simple operation, and on the application of itself or its derivative to fractional crystallization of chiral carboxylic acids as a resolving agent and to asymmetric reduction of prochiral ketones as a modifier for lithium aluminium hydride.

In the previous papers, it was reported that 2-amino-2-phenylethanol (**1**)[5] and cinnamic acid salts of 1-phenylethylamine (**2**) and 1-phenyl-2-(*p*-tolyl)ethylamine (**3**)[6] were successfully resolved into pairs of enantiomers by preferential crystallization. Based on these results, *erythro*-2-amino-1,2-diphenylethanol (**4**) was considered to be also resolvable by preferential crystallization of itself or its cinnamic acid salt because **4** has α-aminobenzyl group in the structure in analog with **1**, **2**, and **3**.

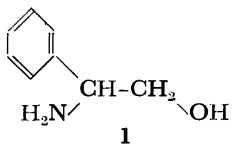

1

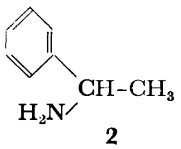

2

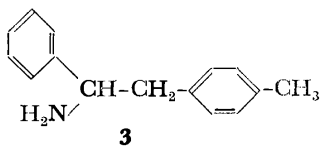

3

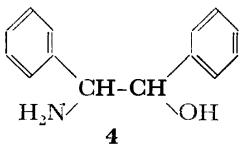

4

Comparing physical properties such as melting point and solubility, infrared spectrum, and X-ray diffraction pattern of optically active form with those of racemate is efficient and appropriate to ensure the possibility of optical resolution by preferential crystallization. Then, to obtain optically active **4**, the fractional crystallization of diastereomeric salts of (±)-**4** with L-glutamic acid was initially tried according to the method described in the literature.[4] The fractional crystallization of diastereomeric salts of (±)-**4** with optically active *trans*-2-benzamidocyclohexanecarboxylic acid (**5**)[7] was found to be more convenient. Thus, the fractional crystallization of the diastereomeric salts of (±)-**4** with (+)-**5** gave (−)-**4**·(+)-**5** salt in a high optical purity, and a similar treatment of **4** recovered from the mother liquor with (−)-**5** gave highly optically pure (+)-**4**·(−)-**5** salt.

Table 1. Properties of **4** and its salts

		Optically active form		Racemate
4	Mp θ_m/°C	142—143		163—164
	Solubility[a]	5.64		3.73
	IR Spectrum		Different	
4·6 Salt	Mp θ_m/°C	172—173		172—173
	Solubility[a]	0.25		0.41
	IR Spectrum		Identical	
	X-Ray Diffraction Pattern		Identical	
4·7 Salt	Mp θ_m/°C	159—160		162—163
	Solubility[a]	0.71		1.71
	IR Spectrum		Different	
4·8 Salt	Mp θ_m/°C	131—132		165—167
	Solubility[a]	1.38		0.92
	IR Spectrum		Different	

a) g/100 ml of 99% EtOH at 15 °C.

Physical properties, infrared spectrum, and X-ray diffraction pattern of optically active **4** obtained as above or of its salt with an achiral carboxylic acid such as cinnamic acid (**6**), benzoic acid (**7**), or *cis*-1,2-cyclohexanedicarboxylic acid (**8**) were compared with those of the corresponding racemate. As shown in Table 1, optically active **4·6** salt has the same melting point as the racemate and is less soluble in ethanol than the racemate, and their infrared spectra and X-ray diffraction patterns are identical. These results indicate that crystals of **4·6** salt are deposited as con-

† Present address: Department of Synthetic Chemistry, Faculty of Engineering, The University of Tokyo, Hongo, Bunkyo-ku, Tokyo 113.

Table 2. Preferential crystallization of **4·6** salt on standing

Run	(±)-**4·6** Salt added (g)	Seed	Cooling		Yield	$[\alpha]_{435}$[a]/°	Optical purity[b]
			Temp °C	Time min	g		%
1	—	(+)	7	250	0.32	+53.5	31
2	0.40	(−)	5	250	0.40	−97.6	57
3	0.50	(+)	6	250	0.48	+120.4	71
4	0.70	(−)	5	180	0.77	−167.8	98
5	0.70	(+)	6	160	0.45	+161.2	94
6	0.80	(−)	6	180	0.76	−162.1	95
7	0.90	(+)	5	180	0.84	+167.8	98

The initial composition of the mother liquor: (±)-**4·6** salt (4.30 g) and (±)-**4**·lactic acid salt (6.00 g) in 99% methanol (110 ml). In all runs, 0.02 g of seed was added.
a) (*c* 0.60, 99% MeOH). b) Based on $[\alpha]_{435}^{30}$ + and −170.7°.

Table 3. Preferential crystallization of **4·6** salt under stirring

Run	(±)-**4·6** Salt added (g)	Seed	Cooling		Yield	$[\alpha]_{435}$[a]/°	Optical purity[b]
			Temp °C	Time min	g		%
1	—	(+)	8	75	5.11	+164.3	96
2	5.50	(−)	9	80	4.99	−161.6	95
3	5.00	(+)	6	60	4.99	+169.6	99
4	5.00	(−)	6	85	4.58	−167.7	98
5	6.00	(+)	6	35	4.80	+156.2	92
6	5.00	(−)	7	35	5.11	−166.8	98
7	5.00	(+)	8	35	4.78	+160.7	94
8	5.00	(−)	7	40	5.40	−155.7	91

The initial composition of the mother liquor: (±)-**4·6** salt (22.40 g), (+)-**4·6** salt (2.17 g), which was added to facilitate the prefcrential crystallization from the first stage, and (±)-**4**·lactic acid salt (30.00 g) in 99% methanol (550 ml). In all runs, 0.04 g of seed was added.
a) (*c* 0.60, 99% MeOH). b) Based on $[\alpha]_{435}^{30}$ + and −170.7°.

glomerate and that **4·6** salt is resolvable by preferential crystallization in a similar manner as **2·6** and **3·6** salts.

Actually, (+)-**4·6** salt was obtained from a supersaturated solution of (±)-**4·6** salt in methanol when (+)-**4·6** salt, which was prepared from equimolar amounts of (+)-**4** and **6** followed by recrystallizations for several times, was seeded to the solution, and the solution was stood for 2.5 h at around 5 °C. Alternate seeding of (−)- or (+)-**4·6** salt to the solution supersaturated in a similar magnitude gave (−)- or (+)-**4·6** salt in a moderate to high optical purity.

The procedure is inapplicable to the optical resolution of (±)-**4·6** salt in a preparative scale because it is difficult to obtain optically active **4·6** salt in a constant yield. The problem was overcome by coexisting the readily soluble (±)-lactic acid salt of (±)-**4** in the mother liquor, which decreased the concentration change of 2-hydroxy-1,2-diphenylethylammonium ion in the solution during crystallization to stabilize the preferential crystallization (Table 2). Moreover, gentle stirring of the supersaturated solution in the course of crystallization was found to be effective to shorten the cooling time. Stirring made the solution uniform and accelerated the crystal growth from seed surface. But, the nucleation of the unseeded antipode crystals of **4·6** salt occured when the solution was stirred too vigorously. The result is summarized in Table 3.

The crystals having the same sign of optical rotation were combined and recrystallized from methanol to give highly purified (+)- and (−)-**4·6** salts. They seemed to be almost optically pure because the values of their specific rotations were almost same to those of recrystallized **6** salts of (+)- and (−)-**4** obtained by the fractional crystallization with L-glutamic acid or *trans*-2-benzamidocyclohexanecarboxylic acid (**5**).

Decomposition of purified (+)- and (−)-**4·6** salts with an alkali solution gave (+)- and (−)-**4**, of which the specific rotations at 589 nm in absolute ethanol were +7.7° and −7.6°, respectively. Weijland *et al.* reported that the specific rotations were +10.2° and −10.1°, respectively.[4] Attempts to get (+)- and (−)-**4** which have the specific rotations of the values were unsuccessful. No drop of the specific rotations under the conditions of the liberation of (+)- or (−)-**4** was observed. Recent literatures reported that the specific rotations were +6.8°[3] and −6.4°,[8] respectively. Based on the data, (+)- and (−)-**4** obtained as above were considered to be almost optically pure.

Then, we applied optically active **4** to the optical resolution of chiral carboxylic acids such as tartaric acid (**9**), *trans*-2,3-oxiranedicarboxylic acid (**10**), 2-hydroxy-2-phenylpropionic acid (**11**), and 3-*endo*-5-nor-

Table 4. Resolution of chiral carboxylic acids using **4**

Salt	Recrystallization: Solvent	Recrystallization: Time	Yield[a] %	Specific rotation
(−)-**9**·(+)-**4**	H_2O	1	64	$[\alpha]_{435}^{32}$ +155.9° (*c* 0.30, H_2O)
(+)-**9**·(−)-**4**	H_2O	1	69	$[\alpha]_{435}^{34}$ −157.1° (*c* 0.30, H_2O)
(−)-**10**·(−)-**4**	90% EtOH[b]	2	56	$[\alpha]_{435}^{24}$ −190.9° (*c* 0.68, 2 M HCl)
(−)-**11**·(−)-**4**	99% MeOH	2	63	$[\alpha]_{435}^{22}$ −235.4° (*c* 0.51, 99% MeOH)
(−)-**12**·(+)-**4**	95% EtOH	3	41	$[\alpha]_{435}^{33.5}$ −56.3° (*c* 0.61, 99% MeOH)

The specific rotations of (+)- and (−)-**4** used as resolving agent: $[\alpha]_{589}^{30}$ +7.4° and −7.1° (*c* 0.60, abs. EtOH), respectively.

a) Based on half the amount of (±)-carboxylic acid used. b) Extraction of more soluble salt under refluxing.

Table 5. Liberation of carboxylic acids resolved

Acid	Total yield[a]/%	Mp θ_m/°C	Specific rotation	Optical purity/%
(−)-**9**	54	167.5—168	$[\alpha]_{589}^{24}$ −14.4° (*c* 1.04, H_2O)	91[b]
(+)-**9**	60	166—167	$[\alpha]_{589}^{29}$ +14.1° (*c* 1.02, H_2O)	89[b]
(−)-**10**	40	177—178	$[\alpha]_{589}^{24}$ −117.4° (*c* 2.58, 99% EtOH)	100[c]
(−)-**11**	52	116.5—117	$[\alpha]_{589}^{30.5}$ −49.3° (*c* 1.00, H_2O)	92[d]
(−)-**12**	36	179—180	$[\alpha]_{435}^{33}$ −251.3° (*c* 1.00, 99% MeOH)	99[e]

a) Based on half the amount of (±)-carboxylic acid used. b) Based on the specific rotation of commercial (+)-tartaric acid: $[\alpha]_{589}^{25}$ +15.9° (*c* 1.01, H_2O). c) Based on $[\alpha]_{589}^{25}$ +117.8° (*c* 2.6, EtOH).[1c] d) Based on $[\alpha]_{589}^{20}$ +53.5° (*c* 1.591, H_2O).[10] e) Based on $[\alpha]_{435}^{20}$ −254° (*c* 1.00, 99% MeOH).[11]

bornene-2-*endo*-carboxylic acid (**12**) by fractional crystallization. As shown in Tables 4 and 5, they were resolved in moderate to high optical purities, and optically active **4** was found to be useful as a resolving agent. The results indicate that **4** is as effective as 2-amino-2-phenylethanol (**1**)[5] in the resolution of **9** and **11** and is superior to **1** with regard to the resolution of **10** which could not be resolved with **1**.

Next stage, derivatives of **4** were applied to asymmetric reduction of prochiral ketones as modifiers of lithium aluminium hydride. (−)-*threo*-2-Amino-1,2-diphenylethanol ((−)-**13**) was obtained from (−)-**4** *via* *N*-formylation, cyclization, and hydrolysis according to the procedure in the literatures.[4,9] The Eschweiler-Clarke reaction of (−)-**13** gave (−)-*threo*-2-dimethylamino-1,2-diphenylethanol ((−)-**14**). The reaction of (+)- and (−)-**4** also yielded (+)- and (−)-*erythro*-2-dimethylamino-1,2-diphenylethanol ((+)- and (−)-**15**), respectively (Scheme 1).

Acetophenone was chosen as a model substrate, and the reduction with lithium aluminium hydride modified by (−)-**14** or (+)-**15** was carried out in ether at −78 °C. As shown in Table 6 (Exp. 1 and 2), lithium aluminium hydride treated with 2.2 molar amounts of (+)-**15** was found to be more effective than that treated with (−)-**14**.

Contrary to the reduction with lithium aluminium hydride–(−)-**14** complex, which gave (*R*)-(+)-1-phenylethanol, the reduction with lithium aluminium hydride–(+)-**15** complex yielded (*S*)-(−)-1-phenylethanol. The result was considered to indicate that the configuration of the product was influenced by the configuration of C2 (the carbon atom carrying amino group) of 2-amino-1,2-diphenylethanol. The consideration is supported by the fact that the absolute configuration of (−)-**14** and (+)-**15**, derived from

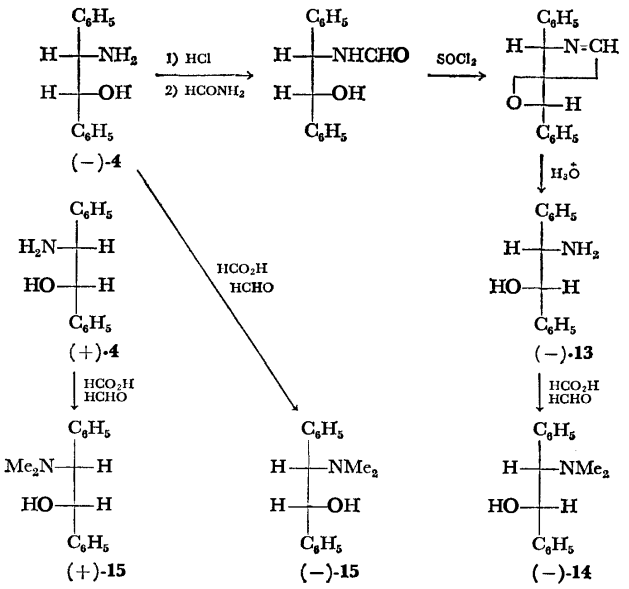

Scheme 1.

(*1S,2S*)-(−)-**13**[4,9] and (*1S,2R*)-(+)-**4**,[4] are (*1S,2S*) and (1*S*,2*R*), respectively.

A similar optical purity was achieved when lithium aluminium hydride was treated with 1.1 molar amount of (+)-**15** and 2.2 molar amounts of ethanol (Table 6. Exp. 10), but in the other cases no improvement was obtained by adding an achiral alcohol such as 2,4-xylenol and ethanol in several molar ratios (Table 6. Exp. 5—9). Moreover, lithium aluminium hydride modified with (+)-**15** and ethanol as mentioned above was found to be less effective for the asymmetric reduction of propiophenone (Table 6. Exp. 11).

Utilizing lithium aluminium hydride treated with 2.2 molar amounts of (+)- or (−)-**15**, the reduction

Table 6. Asymmetric reduction of prochiral ketones with $LiAlH_4$-chiral amino alcohol complex

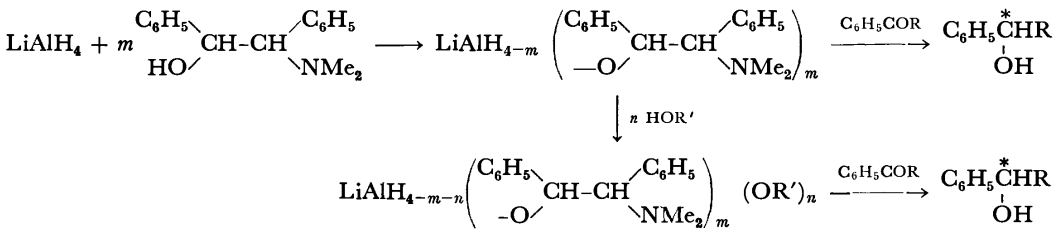

Exptl	R of ketone	Amino alcohol	Achiral alcohol	Molar ratio[a]	Reaction[b] time/h	Yield %	$[\alpha]_{589}$/° (c, solvent, T/°C)	Optical purity/%
1	CH_3	(−)-**14**	—	A	5	55	+19.3 (6.71, C_5H_{10}, 23)	45[c]
2	CH_3	(+)-**15**	—	A	5	92	−29.0 (7.21, C_5H_{10}, 30)	67[c]
3	C_2H_5	(+)-**15**	—	A	5	83	−32.5 (5.14, $CHCl_3$, 32)	72[d]
4	n-C_3H_7	(−)-**15**	—	A	5	94	+29.9 (4.28, C_6H_6, 33)	69[e]
5	CH_3	(+)-**15**	Xylenol	B	5	83	−17.9 (7.31, C_5H_{10}, 32)	42[c]
6	CH_3	(+)-**15**	Xylenol	C	10	54	−16.3 (3.94, C_5H_{10}, 26)	38[c]
7	CH_3	(+)-**15**	Xylenol	D	10	94	−11.8 (7.22, C_5H_{10}, 35)	27[c]
8	CH_3	(+)-**15**	Ethanol	B	5	91	−11.1 (7.20, C_5H_{10}, 28)	26[c]
9	CH_3	(+)-**15**	Ethanol	C	10	52	−14.4 (5.60, C_5H_{10}, 27)	33[c]
10	CH_3	(+)-**15**	Ethanol	D	10	82	−26.6 (7.11, C_5H_{10}, 32)	62[c]
11	C_2H_5	(+)-**15**	Ethanol	D	10	99	−16.6 (5.19, $CHCl_3$, 34)	37[d]

a) $LiAlH_4$: Amino alc. : Achiral alc. : Ketone

A	2.0	4.4	0	1.0
B	2.0	2.2	2.0	1.0
C	2.0	4.4	2.0	1.0
D	2.0	2.2	4.0	1.0

b) The reactions were carried out in ether at −78 °C. c) Based on $[\alpha]_{589}^{21}$ −43.1° (c 7.19, cyclopentane).[12] d) Based on $[\alpha]_{589}$ −45.45° (c 5.15, $CHCl_3$).[13] e) Based on $[\alpha]_{589}$ +43.6° (c 4.18, C_6H_6).[14]

of propiophenone and butyrophenone was carried out to give 1-phenyl-1-propanol in 72% optical purity and 1-phenyl-1-butanol in 69% optical purity, respectively.

In conclution, it is noteworthy that both enantiomers of **4** become obtainable in high optical purities by the preferential crystallization of (±)-**4**·**6** salt and that it or its derivative is useful as a synthetic basic resolving agent for the optical resolution of chiral carboxylic acids or as a modifier of lithium aluminium hydride for asymmetric reduction of prochiral ketones.

Experimental

The melting points were determined on a Laboratory Devices Mel-Temp apparatus and are uncorrected. The values of specific rotation were measured on JASCO DIP-181 digital polarimeter. The ^{1}H-NMR spectra were recorded in $CDCl_3$ solution at 60 MHz on Varian A-60 Spectrometer using TMS as an internal standard. The IR spectra were determined on JASCO IR-2A Spectrophotometer.

*Synthesis of (±)-*erythro*-2-Amino-1,2-diphenylethanol ((±)-4).* To a solution of benzoin α-oxime (50.30 g, 0.22 mol) in 90% ethanol (530 ml) was added 5% palladium–chacoal catalyst (5.00 g), and the suspension was stirred at 51—52 °C under a hydrogen atmosphere using an ordinary pressure hydrogenation apparatus. After the required amount of hydrogen (about 10 l) has been absorbed, hydrogen absorption abruptly slowed. At this point, the hydrogenation was stopped, and concd HCl (40 ml) was added to the reaction mixture. After the mixture was stirred at around 60 °C for 1.5 h, the solvent was evaporated. To the residue was added boiling water (500 ml), and the catalyst was filtered off from the hot aqueous solution. The catalyst was washed twice with boiling water (500 ml). The filtrate and the washings were combined, basified with concd aqueous ammonia, and cooled with ice bath to give white precipitates. The precipitates were collected by filtration and recrystallized from 99% methanol to yield 41.81 g of (±)-**4**: mp 163—164 °C (lit,[4] 163 °C).

Optical Resolution of (±)-4 with Optically Active trans*-2-Benzamidocyclohexanecarboxylic Acid (5) by Fractional Crystallization.* A clear solution of (±)-**4** (7.64 g) and (+)-**5**[7] (9.51 g) in a mixture of 99% ethanol and ethyl acetate (1:1) (200 ml) at an elevated temperature was allowed to cool slowly at room temperature and stood overnight. The white precipitates were collected by filtration to give 5.76 g (67%) of crude (−)-**4**·(+)-**5** salt: $[\alpha]_{435}^{30}$ −68.6° (c 1.01, 99% MeOH). The mother liquor was reserved for later use. Recrystallization of the crude salt (5.66 g) from a 99% ethanol–ethyl acetate (1:1) mixture (150 ml) gave 3.85 g (46% total yield) of pure (−)-**4**·(+)-**5** salt: mp 187.5—188 °C; $[\alpha]_{435}^{26}$ −80.9° (c 1.17, 99% MeOH).

To a solution of the salt (3.85 g) in 99% methanol (50 ml) was added 3 M NaOH solution at 0 °C to basify the solution. After evaporation of the solvent, water (50 ml) was added to the white mass remained, and the suspension was vigorously stirred for 1 h. The precipitates were collected by filtration to yield 1.62 g of (−)-**4**. Recrystallization from 95% ethanol gave 1.05 g (28% total yield based on half the amount of (±)-**4** used) of pure (−)-**4**: mp 141—142 °C; $[\alpha]_{589}^{30}$ −7.3° (c 0.63, abs. EtOH) (lit,[8] mp 141—144 °C; $[\alpha]_{589}^{24}$ −6.4° (c 1.25, abs. EtOH)).

The mother liquor from the original crystallization was

concentrated under reduced pressure, and a similar treatment of the remained residue gave 4.50 g of **4** which contained (+)-**4** in excess. The recovered amino alcohol (4.50 g) and (−)-**5**[7] (5.21 g) were dissolved in a 99% ethanol–ethyl acetate (1:1) mixture (210 ml) under refluxing, and the solution was allowed to cool slowly at room temperature to give 7.66 g of crude (+)-**4**·(−)-**5** salt. Recrystallization of the salt (7.66 g) from a 99% ethanol–ethyl acetate (1:1) mixture gave 5.54 g of the pure salt: mp 187—188 °C; $[\alpha]^{27}_{435}$ +79.0° (*c* 1.04, 99% MeOH).

Decomposition of the salt in a similar manner to the case of (−)-**4**·(+)-**5** salt yielded 2.28 g of (+)-**4**. Recrystallization from 95% ethanol gave 1.77 g (46% total yield based on half the amount of (±)-**4** used) of pure (+)-**4**: mp 142—143 °C; $[\alpha]^{30}_{589}$ +7.1° (*c* 0.60, abs. EtOH) (lit,[3] $[\alpha]^{22}_{589}$ +6.8° in abs. EtOH).

Preferential Crystallization of (±)-4·Cinnamic Acid (6) Salt. Racemic **4·6** salt was prepared from equimolar amounts of (±)-**4** and **6** in methanol. For instance, a boiled solution of (±)-**4** (19.20 g) and **6** (13.33 g) in 99% methanol was cooled slowly and stood overnight at room temperature to give 24.57 g (76%) of (±)-**4·6** salt: mp 172—173 °C; IR (KBr) 3425, 3250, 3050, 2925, 1640, 1500, 1395, 1380 (shoulder), and 700 cm^{-1}. Found: N, 3.60%. Calcd for $C_{23}H_{23}NO_3$: N, 3.88%.

Optically active **4·6** salts for seeds in the preferential crystallization were also prepared from (+)- and (−)-**4** in a similar manner followed by twice recrystallizations from 99% methanol: mp 172—173 °C; $[\alpha]^{30}_{435}$ + and −170.7° (*c* 0.60, 99% MeOH); IR (KBr) 3425, 3250, 3050, 2925, 1640, 1500, 1395, 1380 (shoulder), and 700 cm^{-1}.

A refluxed solution of (±)-**4·6** salt (22.40 g), (+)-**4·6** salt (2.17 g), which was added to facilitate the preferential crystallization from the first stage, and (±)-**4**·lactic acid salt (30.00 g) in 99% methanol (550 ml) was cooled at about 35 °C to give a supersaturated solution. To the solution was added (+)-**4·6** salt (0.04 g) as a seed, and the solution was stirred gently (about 25 rpm) by a mechanical stirrer for 75 min at about 8 °C. The white precipitates deposited were collected by filtration, washed with 99% methanol (8 ml), and dried over P_2O_5 to yield 5.11 g of (+)-**4·6** salt: $[\alpha]^{27.5}_{435}$ +164.3° (*c* 0.60, 99% MeOH); 96% optical purity.

To the filtrate was added (±)-**4·6** salt (5.50 g) and dissolved at an elevated temperature. In a similar manner, the solution was cooled, seeded with (−)-**4·6** salt, and stirred gently at about 9 °C for 80 min to give 4.99 g of (−)-**4·6** salt: $[\alpha]^{26}_{435}$ −161.5° (*c* 0.60, 99% MeOH); 95% optical purity.

After several stages of the preferential crystallization as shown in Table 3, the crystals having the same sign of optical rotation were combined and recrystallized from 99% methanol to yield almost optically pure (+)- and (−)-**4·6** salts, respectively. For example, recrystallization of (+)-**4·6** salt (36.78 g, 91% optical purity on the average) from 99% methanol (440 ml) gave 24.25 g (66%) of (+)-**4·6** salt: mp 172—173 °C; $[\alpha]^{25}_{435}$ +168.5° (*c* 0.60, 99% MeOH); 99% optical purity. Found: N, 3.68%. Calcd for $C_{23}H_{23}NO_3$: N, 3.88%.

Similar recrystallization of (−)-**4·6** salt (34.40 g, 90% optical purity on the average) from 99% methanol (400 ml) gave 21.12 g (61%) of (−)-**4·6** salt: mp 172—173 °C; $[\alpha]^{26}_{435}$ −169.6° (*c* 0.60, 99% MeOH), 99% optical purity. Found: N, 3.61%. Calcd for $C_{23}H_{23}NO_3$: N, 3.88%.

Liberation of (+)- and (−)-4 from the Cinnamic Salts. To a hot solution of (−)-**4·6** salt (10.65 g) in 99% methanol (200 ml) was added 10% NaOH solution (50 ml) to decompose the salt. After evaporation of the solvent, water (200 ml) was added to the remained residue and the suspension was stirred for 40 min. The precipitates were collected by filtration and recrystallized from 95% ethanol (50 ml) to give 4.89 g (78%) of (−)-**4**: mp 143—144 °C; $[\alpha]^{32}_{589}$ −7.6° (*c* 0.60, abs. EtOH) (lit,[8] mp 141—144 °C; $[\alpha]^{24}_{589}$ −6.4° (*c* 1.25, abs. EtOH)). Found: N, 6.28%. Calcd for $C_{14}H_{15}NO$: N, 6.57%.

In a similar manner, (+)-**4** (8.26 g) was obtained from (+)-**4·6** salt (19.16 g): mp 143—144 °C; $[\alpha]^{24}_{589}$ +7.7° (*c* 0.63, abs. EtOH) (lit,[3] $[\alpha]^{22}_{589}$ +6.8° in abs. EtOH). Found: 6.78%. Calcd for $C_{14}H_{15}NO$: N, 6.57%.

Resolution of (±)-Tartaric Acid ((±)-9) with (+)-4. A solution of (±)-**9** (1.50 g, 10 mmol) and (+)-**4** (2.13 g, 10 mmol) in water (75 ml) was refluxed to give a clear solution. The solution was allowed to cool and stood overnight at room temperature. The white precipitates were collected by filtration and dried over P_2O_5 to yield 1.16 g (64%) of (−)-**9**·(+)-**4** salt: $[\alpha]^{32}_{435}$ +155.9° (*c* 0.30, H_2O).

To a suspension of the salt (1.06 g) was added 2 M NaOH (5 ml), and the precipitates appeared were filtered off. The aqueous solution was charged on an ion exchange column (Amberlite IR 120B, 35 ml) and the product was eluted with water (200 ml). The eluate was concentrated under reduced pressure. The mass remained was ground to a powder and dried over P_2O_5 to give 0.37 g (54% total yield based on half the amount of (±)-**9** used) of (−)-**9**: mp 167.5—168 °C; $[\alpha]^{24}_{589}$ −14.4° (*c* 1.04, H_2O), 91% optical purity based on the specific rotation of commercial (+)-tartaric acid.

When (−)-**4** was used as a resolving agent instead of (+)-**4**, similar treatment gave 2.51 g of (+)-**9**·(−)-**4** salt $[\alpha]^{34}_{435}$ −157.1° (*c* 0.30, H_2O). The salt (1.26 g) was similarly decomposed with 2 M NaOH to yield 0.45 g of (+)-**9**: mp 166—167 °C; $[\alpha]^{20}_{589}$ +14.1° (*c* 1.02, H_2O); 89% optical purity.

In a similar fashion, *trans*-2,3-oxiranedicarboxylic acid (**10**), 2-hydroxy-2-phenylpropionic acid (**11**), and 3-*endo*-benzamido-5-norbornene-2-*endo*-carboxylic acid (**12**) were resolved by fractional crystallization using (+)- or (−)-**4** as a resolving agent as shown in Tables 4 and 5.

Synthesis of (−)-threo-2-Amino-1,2-diphenylethanol (13). The compound was prepared from 8.54 g of (−)-**4**·HCl salt (mp 212—214 °C; $[\alpha]^{28}_{589}$ −61.3° (*c* 1.00, H_2O)) according to the procedure in the literature[4,9] without the purification of the products in each steps. Recrystallization of crude (−)-**13** from 70% ethanol gave pure (−)-**13**: yield 3.24 g (44% total yield); mp 115—116 °C; $[\alpha]^{23}_{589}$ −125° (*c* 1.00, 99% EtOH) (lit,[4] mp 115.2—115.8 °C; $[\alpha]^{22}_{589}$ −123.7° (*c* 1.2, abs. EtOH).

The Eschweiler-Clarke Reaction of (−)-threo-, (+)-erythro-, and (−)-erythro-2-Amino-1,2-diphenylethanol ((−)-13, (+)-4, and (−)-4). The reaction was carried as follows: To a solution of 2-amino-1,2-diphenylethanol (8.0 g, 37.5 mmol) in 99% formic acid (16.0 g, 342 mmol) was added dropwise 35% aq formalin (8.0 g, 93 mmol) in a period of 15 min, and the mixture was refluxed for 20 h with stirring. After cooling at room temperature, concd HCl solution (28 ml) was added to the reaction mixture. The solution was concentrated under reduced pressure, treated with 10% NaOH solution at 0 °C (pH≃10), and extracted with ether (3×180 ml). The ethereal extracts were combined, washed with saturated NaCl solution, and dried with $MgSO_4$. Concentration of the solution followed by recrystallization from hexane gave pure 2-dimethylamino-1,2-diphenylethanol.

(−)-*threo*- ((−)-**14**): yield 6.72 g (74%): mp 57—58 °C; $[\alpha]^{29}_{589}$ −124.7° (*c* 1.00, 99% EtOH); IR (KBr) 3450, 750, and 700 cm^{-1}; NMR ($CDCl_3$) δ=2.20 (s, 6H), 3.53

(d, 1H, J=10 Hz), 5.00 (d, 1H, J=10 Hz), 4.95 (s, 1H), and 6.9—7.4 (m, 10H). Found: N, 5.74%. Calcd for $C_{16}H_{19}NO$: N, 5.80%.

(+)-*erythro*- ((+)-**15**): yield 8.27 g (91%); mp 90—91 °C; $[\alpha]_{589}^{24}$ +123° (*c* 1.00, 99% EtOH); IR (KBr) 3510, 770, 750, and 700 cm^{-1}; NMR ($CDCl_3$) δ=2.30 (s, 6H), 3.20 (d, 1H, J=4.5 Hz), 3.30 (s, 1H), 5.27 (d, 1H, J=4.5 Hz), and 6.8—7.2 (m, 10H). Found: N, 6.01%. Calcd for $C_{16}H_{19}NO$: N, 5.80%.

(−)-*erythro*- ((−)-**15**): yield 7.84 g (87%); mp 90—91 °C; $[\alpha]_{589}^{27}$ −123° (*c* 1.01, 99% EtOH); IR (KBr) 3510, 770, 750, and 700 cm^{-1}; NMR ($CDCl_3$) δ=2.30 (s, 6H), 3.20 (d, 1H, J=4.5 Hz), 3.30 (s, 1H), 5.27 (d, 1H, J=4.5 Hz), and 6.8—7.2 (m, 10H). Found: N, 5.91%. Calcd for $C_{16}H_{19}NO$: N, 5.80%.

General Procedure for Asymmetric Reduction of Ketone. To a standardized ethereal solution of $LiAlH_4$ (8.90 ml, 4.0 mmol) were added successively dry ether (8.0 ml) and 2-dimethylamino-1,2-diphenylethanol (2123.8 mg, 8.8 mmol) in dry ether (8.0 ml) at room temperature in a period of 30 min, and the suspension was stirred for an additional hour. Ketone (2.0 mmol) in ether (8.0 ml) was added to the suspension, cooled at −78 °C, with stirring in a period of 1 h. After the reaction mixture was stirred for 5—10 h at that temperature, water (1 ml) was added to hydrolyze $LiAlH_4$ complex, and a cooling bath was removed. To the mixture was added 6 M HCl solution (20 ml) followed by ether (50 ml), and the precipitates appeared were filtered off and washed with ether (3×20 ml). The filtrate and washings were combined, and the ethereal layer was separated. The ethereal solution was dried with Na_2SO_4 and concentrated under reduced pressure to give crude product. The product was purified by preparative TLC to give the corresponding alcohol. Further, it was purified for the measurement of specific rotation by bulb to bulb distillation. The chiral amino alcohol was recovered by usual work up from the aqueous layer and the precipitates filtered off.

References

1) For example: W. M. Cumming, I. V. Hopper, and T. S. Wheeler, "Systematic Organic Compound," 4th ed, Longmanns, Green and Company Ltd., (1950), p. 415; E. Walton, A. F. Wagner, F. W. Bachelar, L. H. Peterson, F. W. Holly, and K. Folker, *J. Am. Chem. Soc.*, **77**, 5145 (1955); J. Oh-hashi and K. Harada, *Bull. Chem. Soc. Jpn.*, **40**, 2977 (1967).

2) For example: I. Jacquet and J.-P. Vigneron, *Tetrahedron Lett.*, **1974**, 2065; J.-P. Vigneron and V. Bloy, *ibid.*, **1979**, 2683; T. Mukaiyama, T. Takeda, and K. Fujimoto, *Bull. Chem. Soc. Jpn.*, **51**, 3368 (1978); T. Mukaiyama, K. Fujimoto, and T. Takeda, *Chem. Lett.*, **1979**, 1207; T. Mukaiyama, K. Fujimoto, T. Hirose, and T. Takeda, *ibid.*, **1980**, 635; H. Takahashi, K. Tomita, and H. Otomasu, *J. Chem. Soc., Chem. Commun.*, **1979**, 668.

3) J.-P. Vigneron, H. Kagan, and A. Horeau, *Tetrahedron Lett.*, **1968**, 5681.

4) J. Weijland, K. Pfister, 3rd, E. F. Swanezy, C. A. Robinson, and M. Tishler, *J. Am. Chem. Soc.*, **73**, 1216 (1951).

5) K. Saigo, H. Miura, K. Ishizaki, and H. Nohira, *Bull. Chem. Soc. Jpn.*, **55**, 1188 (1982).

6) H. Nohira, M. Kai, M. Nohira, J. Nishikawa, T. Hoshiko, and K. Saigo, *Chem. Lett.*, **1981**, 951.

7) H. Nohira and H. Miura, *Nippon Kagaku Kaishi*, **1975**, 1122; H. Nohira, K. Ehara, and A. Miyashita, *Bull. Chem. Soc. Jpn.*, **43**, 2230 (1970).

8) M. Nakazaki, *Bull. Chem. Soc. Jpn.*, **36**, 1204 (1963).

9) G. G. Lyle and W. Lacroix, *J. Org. Chem.*, **28**, 900 (1963).

10) L. Smith, *J. Prakt. Chem.*, **84**, 731 (1911).

11) K. Saigo, Y. Okuda, S. Wakabayashi, T. Hoshiko, and H. Nohira, *Chem. Lett.*, **1981**, 857.

12) S. Yamaguchi and H. S. Mosher, *J. Org. Chem.*, **38**, 1970 (1973).

13) R. H. Pickard and J. Kenyon, *J. Chem. Soc.*, **99**, 45 (1911).

14) J. Kenyon and S. M. Portridge, *J. Chem. Soc.*, **1936**, 128.

Synthetic Approach toward Antibiotic Tunicamycins. 3. Methyl 3,4,7,8-Tetra-*O*-acetyl-10-*O*-benzyl-2-benzyloxycarbonylamino-2,6-dideoxy-11,12-*O*-isopropylidene-β-L-dodecodialdo-(12*R*)-furanose-(12,9)-pyranosides-(1,5)

Yoshimasa FUKUDA, Hiroaki SASAI, and Tetsuo SUAMI*

Department of Applied Chemistry, Faculty of Science and Technology, Keio University, Hiyoshi, Kohoku-ku, Yokohama 223

(Received October 13, 1981)

Higher carbon carbohydrates, dodecose derivatives have been synthesized by the base-catalyzed addition of nitro sugar to sugar aldehyde. The addition reaction of methyl 2-benzyloxycarbonylamino-2,6,7-trideoxy-3,4-*O*-isopropylidene-7-nitro-α-D-*galacto*-heptopyranoside to 3-*O*-benzyl-1,2-*O*-isopropylidene-α-D-ribodialdofuranose-(1,4) yielded nitro-dodecose derivatives. The nitro-dodecose derivatives were then converted into the corresponding hydroxy and acetoxy derivatives.

The nucleoside antibiotic tunicamycins are found in a fermentation broth of a strain of *streptomyces* and exhibit a broad spectrum of antitumor activity.[1] Their structures were established by Ito *et al.* in 1980 by chemical degradation.[2] The structures of tunicamycins consist of uracil, a novel higher-carbon carbohydrate named tunicamine, fatty acid, and *N*-acetyl-D-glucosamine. The tunicamine is an undecose derivative which, in turn, is bound to uracil to form tunicaminyl uracil. Analogous higher-carbon carbohydrates have been found in other nucleoside antibiotics, such as anthelmycin (hikizimysin),[3] sinefungin,[4] ezomycin,[5] and mildiomycin.[6]

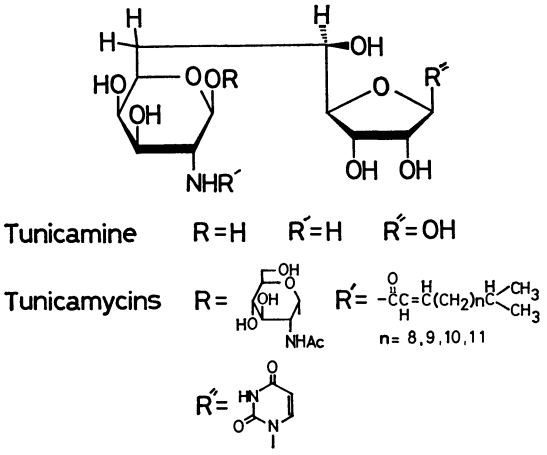

Scheme 1.

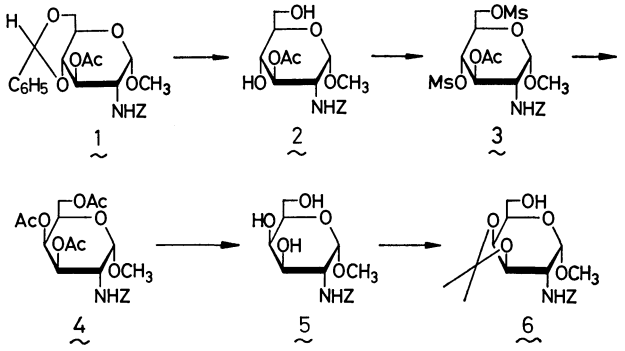

Scheme 2.

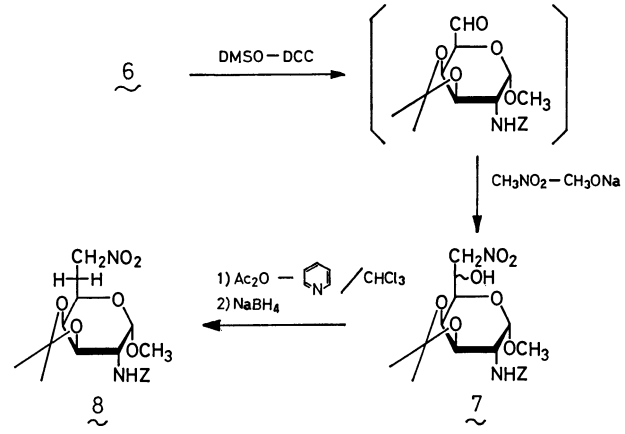

Scheme 3.

In preceding papers,[7] the base-catalyzed addition of nitro sugar to sugar aldehyde has been developed as a generally applicable method for the synthesis of higher-carbon complex carbohydrates. For a synthetic approach to tunicamine in the present study, the base-catalyzed addition of methyl 2-benzyloxycarbonylamino-2,6,7-trideoxy-3,4-*O*-isopropylidene-7-nitro-α-D-*galacto*-heptopyranoside (**8**) to 3-*O*-benzyl-1,2-*O*-isopropylidene-α-D-ribodialdofuranose-(1,4) (**9**) has been investigated. Then the nitro-dodecose derivatives were converted into the corresponding hydroxy and acetoxy derivatives to afford the four theoretically possible diastereoisomers of dodecose derivatives.

Results and Discussion

The hydrolysis of methyl 3-*O*-acetyl-2-benzyloxycarbonylamino-4,6-*O*-benzylidene-2-deoxy-α-D-glucopyranoside (**1**)[8] in warm aqueous acetic acid gave the hydrolyzate (**2**). The mesylation of **2** with an excess amount of mesyl chloride in pyridine afforded the dimesylate (**3**). The displacement of the mesyloxy groups of **3** by acetate ions occurred with an epimerization of the configuration on C-4, giving the methyl α-D-galactoside derivative (**4**) in a yield of 59%. The deacetylation of **4** in methanolic ammonia, followed by acetonation, gave the 3,4-*O*-isopropylidene derivative (**6**) in 53% yield. The oxidation of the hydroxyl group on C-6 of **6** by the Pfitzner-Moffatt oxidation method,[9] followed by addition with nitromethane in the presence of sodium methoxide, afforded a mixture of two diastereoisomers of 7-nitroheptopyranosides (**7**) in 46% yield. The dehydroxylation of the hydroxyl group on C-6 of **7** with acetic anhydride and pyridine in chloroform, followed by

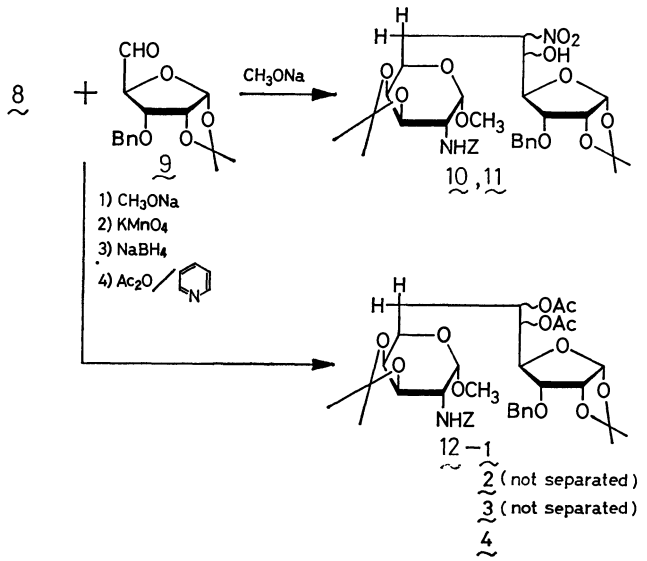

Scheme 4.

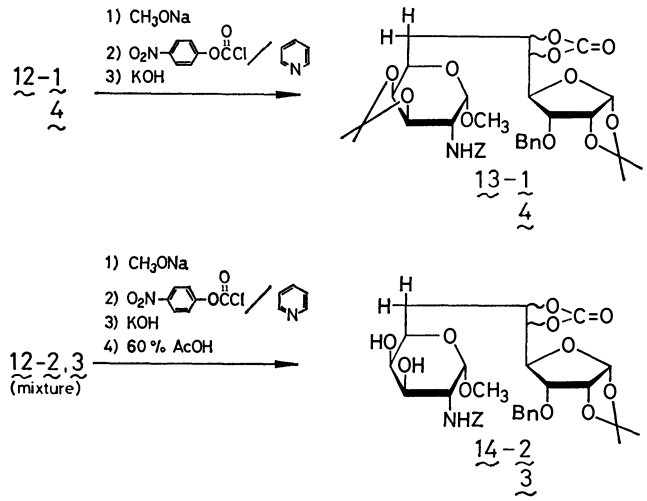

Scheme 5.

the hydrogenation of a double bond between C-6 and C-7 with sodium borohydride, afforded the 6-deoxy derivatives (**8**) in 78% yield.

On the other hand, 3-*O*-benzyl-1,2-*O*-isopropylidene-α-D-ribodialdofuranose-(1,4) (**9**) was prepared by the periodate oxidation of 3-*O*-benzyl-1,2-*O*-isopropylidene-α-D-allofuranose.[10]

When the nitro-heptoside, **8**, reacted with the ribodialdofuranose-(1,4) derivative, **9**, in the presence of sodium methoxide, a mixture of diastereomers was obtained in a yield of 92%. The TLC and ^{1}H NMR of the intact mixture revealed the presence of the four theoretically possible diastereoisomeric nitrodocecose derivatives, from which only two compounds (**10**) and (**11**) were obtained in homogeneous states by repeated chromatographic fractionations. The structures of **10** and **11** were established, by means of their ^{1}H NMR and IR spectra, as methyl 10-*O*-benzyl-2-benzyloxycarbonylamino-2,6,7-trideoxy-3,4:11,12-di-*O*-isopropylidene-7-nitro-β-L-dodecodialdo-(12*R*)-furanose-(12,9)-pyranosides-(1,5), but the absolute configurations on C-7 and C-8 have not yet been established.

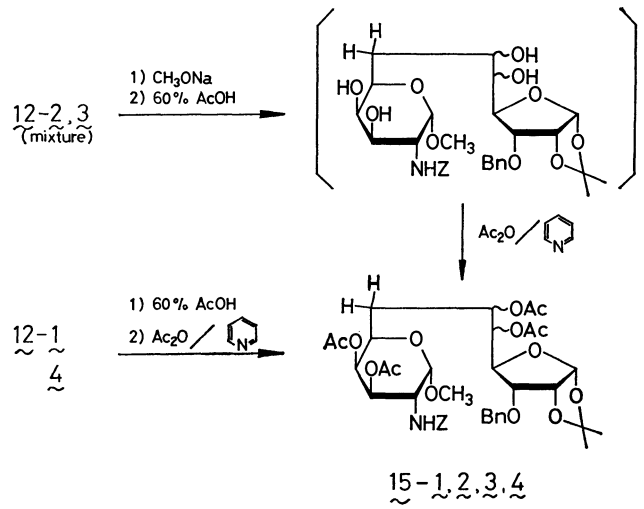

Scheme 6.

On the other hand, the oxidation of the intact mixture of the nitro-dodecoses with potassium permanganate[11] in water, followed by reduction with sodium borohydride and conventional acetylation, afforded a mixture of 7,8-di-*O*-acetyl derivatives in 43% yield. Chromatographic fractionations of the mixture gave two compound (**12-1** and **12-4**) as homogeneous products and the rest as a mixture of (**12-2**) and (**12-3**). The deacetylation of **12-1**, followed by carbonylation, gave a cyclic 7,8-*O*-carbonyl derivative (**13-1**) in 52% yield. By analogous reactions, the diastereomer (**13-4**) was obtained from **12-4**. The mixture of **12-2** and **12-3**, by analogous reactions plus mild hydrolysis in aqueous acetic acid, yielded two compounds (**14-2** and **14-3**), which were subsequently succesfully separated by column chromatography. The coupling constant of $J_{7,8}$ in the ^{1}H NMR spectrum of **14-2** was 8.0 Hz, suggesting the existence of vicinal cis protons on C-7 and 8.[12] That of **13-4** was 5.0 Hz, which showed trans protons on C-7 and 8. Those of **13-1** and **14-3** were 7.3 Hz and 6.4 Hz; their configurations have not yet been designated.

Finally, an intact mixture of **12-1** **12-2**, **12-3**, and **12-4** was hydrolyzed in 58% aqueous acetic acid at 40 °C for 1.5 h. The 3,4-*O*-isopropylidene group was selectively hydrolyzed under those conditions without a cleavage of the 11,12-*O*-isopropylidene group (another *O*-isopropylidene group on C-11 and 12). The product was acetylated to give four tetra-*O*-acetyl derivatives (**15-1**, **15-2**, **15-3**, and **15-4**), which were subsequently isolated by means of column chromatography. These compounds are important intermediates for further studies of the synthesis of tunicamine; that is, the selective removal of the 11,12-*O*-isopropylidene group, followed by oxidation (the cleavage of the C–C bond between C-11 and 12 by periodate oxidation) with sodium metaperiodate and deacylation, may provide undecose derivatives. However, it is still unknown which intermediate has the same configurations on C-7 and 8 as those of tunicamine.

Experimental

General Methods. The melting points were taken in capillary tubes in a liquid bath and are uncorrected. The solutions were concentrated under reduced pressure below 50 °C. The IR spectra were measured with a Hitachi 225 spectrophotometer and are expressed in reciprocal centimeters. The ^{1}H NMR spectra were obtained on a Varian EM-390 apparatus (90 MHz) and are reported as δ values in parts per million relative to tetramethylsilane as an internal standard. The TLC was performed on precoated silica-gel 60 F-254 (Merck, Darmstadt; Art. 5715; 0.25-mm thickness). The silica-gel columns used for chromatography utilized Wako gel C-200 or C-300 (Wako Pure Chemical Industries, Ltd.).

Methyl-3-O-acetyl-2-benzyloxycarbonylamino-2-deoxy-α-D-glucopyranoside (2). A stirred solution of methyl 3-*O*-acetyl-2-benzyloxycarbonylamino-4,6,-*O*-benzylidene-2-deoxy-α-D-glucopyranoside (**1**)[8] (76.7 g) in 70% aqueous acetic acid (1000 ml) was heated at 60—70 °C for 1 h. The solution was then concentrated to dryness. The residue was purified on a silica-gel column [C-300, 250 g, toluene–ethyl acetate 8:1—1:1 (v/v)] to give 58.2 g (94%) of **2**; R_f 0.39 [benzene–ethanol 5:1 (v/v)], $[\alpha]_D^{21}$ +75.5° (*c* 1.0, chloroform), ^{1}H NMR ($CDCl_3$) δ 1.93 (3H, s, Ac), 3.36 (3H, s, OCH_3), 7.27 (5H, s, C_6H_5). Found: C, 55.28; H, 6.32; N, 3.62%. Calcd for $C_{17}H_{23}NO_8$: C, 55.28; H, 6.28; N, N, 3.79%.

Methyl 3-O-Acetyl-2-benzyloxycarbonylamino-2-deoxy-4,6-di-O-methylsulfonyl-α-D-glucopyranoside (3). To a solution of **2** (58.2 g) in pyridine (450 ml) was added methanesulfonyl chloride (29.3 ml) under ice cooling. After 18 h in a refrigerator, the reaction mixture was poured into ice and water (8 l), and then extracted with chloroform (500 ml). The chloroform layer was washed with water, a $NaHSO_4$ solution, water, a saturated $NaHCO_3$ solution, and water, and then concentrated to give an oily crude residue (76.5 g) which showed a single spot on TLC in 5:1 (v/v) benzene–ethyl acetate. A part (869.8 mg) of the crude residue was purified on a silica-gel column [C-300, 73 g, 3:1 (v/v) benzene–ethyl acetate] to give **3** (836.4 mg) as a homogeneous syrup in 89% yield from **2**. **3**; R_f 0.53 [5:1 (v/v) benzene–ethanol], $[\alpha]_D^{21}$ +77.3° (*c* 1.1, chloroform), ^{1}H NMR ($CDCl_3$) δ 1.91 (3H, s, Ac), 3.01, 3.05 (3H×2, s×2, CH_3SO_3), 3.39 (3H, s, OCH_3), 7.27 (5H, s, C_6H_5). Found: C, 43.39; H, 5.21; N, 2.48; S, 12.06%. Calcd for $C_{19}H_{27}NS_2O_{12}$: C, 43.42; H, 5.18; N, 2.67; S, 12.20%.

Methyl 3,4,6-Tri-O-acetyl-2-benzyloxycarbonylamino-2-deoxy-α-D-galactopyranoside (4). To a stirred solution of **3** (4.64 g) in acetic acid (35 ml) was added water (1.8 ml) and sodium acetate (29.3 g). After 24 h at 130—135 °C, acetic anhydride (25 ml) was added to the reaction mixture. After 2 h at 130 °C, the mixture was cooled to room temperature. The reaction mixture was then poured into a mixture of ice (500 g), chloroform (300 ml), and sodium carbonate (60 g). The chloroform layer was separated, washed with a saturated $NaHCO_3$ solution and water, and concentrated. The residue was purified on a silica-gel column [C-200, 25 g, 5:1 (v/v) toluene–ethyl acetate] to give oily **4** (2.69 g, 59% yield); R_f 0.28 [3:1 (v/v) toluene–ethyl acetate], $[\alpha]_D^{21}$ +86.6° (*c* 1.1, chloroform), IR ($CHCl_3$ solution) 3435 (NH), 1740 cm^{-1} (C=O), ^{1}H NMR ($CDCl_3$) δ 1.86, 2.01, 2.12 (3H×3, s×3, Ac), 3.36 (3H, s, OCH_3), 7.26 (5H, s, C_6H_5). Found: C, 55.71; H, 5.81; N, 2.85%. Calcd for $C_{21}H_{27}NO_{10}$: C, 55.87; H, 5.81; N, 3.10%.

Methyl 2-Benzyloxycarbonylamino-2-deoxy-α-D-galactopyranoside (5). A solution of **4** (26.8 g) in methanolic ammonia (11%) was left to settle in a refrigerator for 18 h. The reaction mixture was then concentrated, and the residue was recrystallized from water to give 11.4 g (58.8%) of **5**; R_f 0.22 [5:1 (v/v) benzene–ethanol]; mp 197—197.5 °C, $[\alpha]_D^{20}$ +131° (*c* 0.5, methanol), ^{1}H NMR (CD_3OD) δ 7.37 (5H, s, C_6H_5), 3.30 (3H, s, OCH_3). Found: C, 55.17; H, 6.43; N, 4.18%. Calcd for $C_{15}H_{21}NO_7$: C, 55.04; H, 6.47; N, 4.28%.

Methyl 2-Benzyloxycarbonylamino-2-deoxy-3,4-O-isopropylidene-α-D-galactopyranoside (6). To a suspension of **5** (5.01 g) in acetone (80 ml) was added acetone (200 ml) containing concentrated sulfuric acid (0.1 ml). After 2.5 h at the ambient temperature, the reaction mixture was neutralized with Amberlite IRA-400(OH^-) resin; the resin was then filtered off. The filtrate was concentrated, and toluene (100 ml) was added to the residue. The insoluble matter was removed by filtration, and the filtrate was concentrated to *ca.* 30 ml, and then left for 1 d. The precipitate was collected to give 2.13 g (38.2%) of **6** as crystals. The filtrate was repeatedly worked-up as has been described above to give 0.81 g (14.6%) of **6**. Total yield, 2.94 g (53%). **6**; R_f 0.53 [5:1 (v/v) benzene–ethanol], mp 105—105.5 °C, $[\alpha]_D^{23}$ +131° (*c* 1.0, methanol), ^{1}H NMR ($CDCl_3$) δ 3.32 (3H, s, OCH_3), 1.57, 1.32 (3H×2, s×2, isopropylidene). Found: C, 59.03; H, 6.85; N, 3.74%. Calcd for $C_{18}H_{25}NO_7$: C, 58.85; H, 6.86; N, 3.80%.

Methyl 2-Benzyloxycarbonylamino-2,7-dideoxy-3,4-O-isopropylidene-7-nitro-DL-glycero-D-galacto-heptopyranoside (7). To a stirred solution of **6** (4.07 g) in benzene (8 ml) and dimethyl sulfoxide (26 ml) were added pyridine (0.2 ml), phosphoric acid (0.1 ml), and dicyclohexylcarbodiimide (7.2g) under ice cooling. After stirring for 4 h at the ambient temperature, a suspension of oxalic acid (5 g) in methanol (5 ml) was added to the solution. After 1 h, the mixture was extracted with ethyl acetate (150 ml). The ethyl acetate layer was washed with a $NaHCO_3$ solution and water dried over Na_2SO_4 and concentrated. To a solution of the residue in methanol (35 ml) was added nitromethane (8.55 ml) and 1 M methanolic sodium methoxide (9.54 ml). After 1 h at the ambient temperature, the solution was neutralized with Amberlite IR-120B(H^+) resin and concentrated. The residue was chromatographed on a silica-gel column [C-200, 2:1 (v/v) chloroform–ethyl acetate]. The product was then recrystallized from toluene to give 2.18 g (46%) of **7**; mp 115—117 °C, $[\alpha]_D^{23}$ +96.8° (*c* 1.0, methonol), IR (KBr) 3510 (OH), 3360 (NH), 1698 (C=O), 1555, 1530, 1390 cm^{-1} (NO_2), ^{1}H NMR ($CDCl_3$) δ 1.34, 1.56 (3H×2, s×2, isopropylidene), 3.29 (3H, s, OCH_3), 7.26 (5H, s, C_6H_5). Found: C, 53.70; H, 6.16; N, 6.56%. Calcd for $C_{19}H_{26}N_2O_9$: C, 53.52; H, 6.15; N, 6.57%.

Methyl 2-Benzyloxycarbonylamino-2,6,7-trideoxy-3,4-O-isopropylidene-7-nitro-α-D-galacto-heptopyranoside (8). To a solution of **7** (2.1 g) in chloroform (50 ml) were added acetic anhydride (2.8 ml) and pyridine (1.6 ml) under ice cooling. After 22 h at the ambient temperature, the reaction mixture was washed with water, a saturated $NaHCO_3$ solution, and water, then chloroform layer was concentrated. The residue was dissolved in ethanol (50 ml) and toluene (20 ml), and to the solution was added a suspension of sodium borohydride (0.56 g) in ethanol (30 ml). After 1 h at the ambient temperature, the reaction mixture was neutralized with Amberlite IR-120B(H^+) resin; the resin was then filtered off. The filtrate was concentrated, and the residue was recrystallized from ethanol to give 1.58 g (77.8%) of **8**; R_f 0.44 [3:1 (v/v) toluene–ethyl acetate], $[\alpha]_D^{19}$ +140.6° (*c* 0.5, chloroform), IR (KBr) 1690 (C=O), 1550, 1386, 1375

cm^{-1} (NO_2), ^1H NMR ($CDCl_3$) δ 1.27, 1.52 (3H×2, s×2, isopropylidene), 3.32 (3H, s, OCH_3), 7.18 (5H, s, C_6H_5). Found: C, 55.74; H, 6.42; N, 6.66%. Calcd for $C_{19}H_{26}N_2O_8$: C, 55.60; H, 6.38; N, 6.83%.

*Methyl 10-O-Benzyl-2-benzyloxycarbonylamino-2,6,7-trideoxy-3,4:11,12-di-O-isopropyridene-7-nitro-β-L-dodecodialdo-(12R)-furanose-(12,9)-pyranosides-(1,5) (**10** and **11**).* To a solution of **9** (300 mg) in ethanol (15 ml) were added **8** (305.4 mg) and 1 M methanolic sodium methoxide (0.74 ml) under ice cooling. After 18 h at the ambient temperature, the reaction mixture was neutralized with Amberlite IR-120B (H^+) resin; the resin was then filtered off. The filtrate was concentrated, and the residue was purified on a silica-gel column [C-300:C-200 1:5, 30 g, 7:1 (v/v) toluene–ethyl methyl ketone] to give a mixture of nitrododecose derivatives; 437.2 mg (92.3% yield from **8**). The mixture was repeatedly chromatographed analogously to the method described above to afford two homogeneous nitrododecose isomers, **10** and **11**. However, the other two isomers could not separated. **10**; syrup, R_f 0.58 [1:1 (v/v) toluene–ethyl acetate], $[\alpha]_D^{19}$ +107° (*c* 1.0, chloroform), IR (chloroform solution) 3570 (OH), 3430 (NH), 1720 (C=O), 1567, 1386 cm^{-1} (NO_2), ^1H NMR ($CDCl_3$) δ 7.25, 7.23 (5H×2, s×2, C_6H_5), 5.64 (1H, d, $J_{11,12}$=3 Hz, H-12), 3.23 (3H, s, OCH_3), 1.56, 1.38, 1.36, 1.23 (3H×4, s×4, isopropylidene). Found: C, 59.05; H, 6.37; N, 4.14%. Calcd for $C_{34}H_{44}N_2O_{13}$: C, 59.29; H, 6.44; N, 4.07%.

11; Mp 182—183.5 °C, R_f 0.37 [1:1 (v/v) toluene–ethyl acetate], $[\alpha]_D^{19}$ +111° (*c* 0.4, chloroform), IR (chloroform solution) 3530 (OH), 3435 (NH), 1740 (C=O), 1550, 1385 cm^{-1} (NO_2), ^1H NMR ($CDCl_3$) δ 7.25 (10H, s, C_6H_5×2), 5.62 (1H, d, $J_{11,12}$=3.5 Hz, H-12), 3.26 (3H, s, OCH_3), 1.53, 1.33, 1.29 (6H and 3H×2, s×3, isopropylidene). Found: C, 59.50; H, 6.47; N, 4.25%.

*Methyl 7,8-Di-O-acetyl-10-O-benzyl-2-benzyloxycarbonylamino-2,6-dideoxy-3,4:11,12-di-O-isopropylidene-β-L-dodecodialdo-(12R)-furanose-(12,9)-pyranosides-(1,5) (**12-1**, **12-2**, **12-3**, and **12-4**).* 1 M methanolic sodium methoxide (2.2 ml) was added to a solution of **8** (900 mg) and **9**, obtained from 3-*O*-benzyl-1,2-*O*-isopropylidene-α-D-allofuranose (672 mg), in methanol (30 ml). After 18 h at the ambient temperature, methanol (45 ml) was added to the reaction mixture, which was then poured into ice-cold water (300 ml). To the solution was added a solution of magnesium sulfate (450 mg) in water (50 ml); subsequently, a solution of potassium permanganate (630 mg) in water (120 ml) was added, drop by drop, to the stirred mixture under ice cooling. After 1 h at the ambient temperature, acetic acid (2.7 ml) and chloroform (150 ml) were added to the solution and inorganic precipitates were removed by filtration. The chloroform layer was separated, and the aqueous layer was extracted with chloroform (50 ml×4). The organic layers were combined and concentrated. The residue was dissolved in ethanol (80 ml), and sodium borohydride (460 mg) was added to the solution under ice cooling. After 2 h at the ambient temperature, the mixture was concentrated. Water (30 ml) was added to the residue, and the mixture was extracted with ethyl acetate (45 ml×2). The organic solution was concentrated. The oily residue was acetylated by acetic anhydride (4.5 ml) in pyridine (35 ml) for 18 h. The reaction mixture was concentrated, and the residue was purified on a silica-gel column (C-200, 65 g), using 4:1 (v/v) toluene–ethyl acetate, to give 185.8 mg of a mixture of **12-1**, **12-2**, and **12-3** 128.1 mg of a mixture of **12-2** and **12-3**, 48 mg of a mixture of **12-2**, **12-3**, and **12-4**, and 389 mg of only **12-4** as crystals. Total yield, 650.9 mg (43.1% from **8**).

The mixture of **12-1**, **12-2**, and **12-3**, (185.8 mg) obtained above, was chromatographed again on a silica-gel column [C-200, 18 g, 4:1 (v/v) toluene–ethyl acetate] to give 28.1 mg of only **12-1**, 75.6 mg of a mixture of **12-1**, **12-2**, and **12-3**, and 56.7 mg of a mixture of **12-2** and **12-3**. Total yield, 160.4 mg (86.3% recovery). However **12-2** and **12-3** could not be separated, as their R_f values on TLC were the same in several solvent systems.

12-1: R_f 0.61 [1:1 (v/v) toluene–ethyl acetate], mp 78—81 °C, $[\alpha]_D^{19}$ +104° (*c* 0.3, chloroform), ^1H NMR ($CDCl_3$) δ 7.25 (10H, s, C_6H_5×2), 5.65 (1H, d, $J_{11,12}$=3.5 Hz, H-12), 3.20 (3H, s, OCH_3), 1.97, 1.91 (3H×2, s×2, Ac), 1.55, 1.33 (6H×2, s×2, isopropylidene), IR (KBr) 1735 cm^{-1} (C=O). Found: C, 61.22; H, 6.77; N, 1.70%. Calcd for $C_{38}H_{49}NO_{14}$: C, 61.36; H, 6.64; N, 1.88%.

12-2 and **12-3**: R_f 0.55 [1:1 (v/v) toluene–ethyl acetate].

12-4: R_f 0.44 [1:1 (v/v) toluene–ethyl acetate], mp 192—193 °C, $[\alpha]_D^{21}$ +123° (*c* 1.0, chloroform), ^1H NMR ($CDCl_3$) δ 7.33 (10H, s, C_6H_5×2), 5.70 (1H, d, $J_{11,12}$=3.5 Hz, H-12), 3.25 (3H, s, OCH_3), 2.05 (6H, s, Ac×2), 1.58 1.57, 1.35, 1.31 (3H×4, s×4, isopropylidene), IR (KBr) 1740, 1690 cm^{-1} (C=O). Found: C, 61.23; H, 6.69; N, 2.06%.

*Methyl 10-O-Benzyl-2-benzyloxycarbonylamino-7,8-O-carbonyl-2,6-dideoxy-3,4:11,12-di-O-isopropylidene-β-L-dodecodialdo-(12R)-furanose-(12,9)-pyranosides-(1,5) (**13-1** and **13-4**).* To a solution of **12-1** or **12-4** (20 mg) in methanol (10 ml) was added 1 M methanolic sodium methoxide (0.2 ml). After 3 h at the ambient temperature, toluene (30 ml) was added to the reaction mixture, which was then concentrated to *ca.* 20 ml. To the solution were added water (10 ml) and ethyl acetate (30 ml). The organic layer was separated, dried, and concentrated. The residue was reacted with *p*-nitrophenoxycarbonyl chloride (30 mg) in pyridine (2 ml) and tetrahydrofuran (0.5 ml). After 18 h at the ambient temperature, water (20 ml) was added to the reaction mixture, which was then extracted with ethyl acetate (30 ml). The ethyl acetate layer was washed with a saturated $NaHCO_3$ solution and water, and then concentrated. The residue was purified on a silica-gel column (C-200, 2 g), using 1:1 (v/v) toluene–ethyl acetate, to give **13-1** or **13-4**.

13-1: Yield, 52%, R_f 0.67 [1:1 (v/v) toluene–ethyl acetate], mp 179.5—180 °C, IR (KBr) 1808 cm^{-1} (C=O), ^1H NMR ($CDCl_3$) δ 7.34 (10H, s, C_6H_5×2), 5.72 (1H, d, $J_{11,12}$=3.5 Hz, H-12), 5.08 (1H, m, $J_{7,8}$=7.3 Hz, H-7), 3.35 (3H, s, OCH_3), 1.60, 1.57, 1.27, 1.28 (3H×4, s×4, isopropylidene). Found: C, 61.04; H, 6.33; N, 1.83%. Calcd for $C_{35}H_{43}NO_{13}$: C, 61.31, H, 6.32, N, 2.04%.

13-4: Yield, 48%, R_f 0.69 [1:1 (v/v) toluene–ethyl acetate], mp 87.5—88.5 °C (amorphous solid), IR (KBr) 1805 cm^{-1} (C=O), ^1H NMR ($CDCl_3$) δ 7.35, 7.34 (5H×2, s×2, C_6H_5), 5.73 (1H, d, $J_{11,12}$=3.5 Hz, H-12), 4.94 (1H, m, $J_{7,8}$=5.0 Hz, H-7), 3.34 (3H, s, OCH_3), 1.62, 1.60, 1.36, 1.34 (3H×4, s×4, isopropylidene). Found: C, 61.48; H, 6.49; N, 2.06%.

*Methyl 10-O-Benzyl-2-benzyloxycarbonylamino-7,8-O-carbonyl-2,6-dideoxy-11,12-O-isopropylidene-β-L-dodecodialdo-(12R)-furanose-(12,9)-pyranosides-(1,5) (**14-2** and **14-3**).* A mixture of **12-2** and **12-3** (110.8 mg) was hydrolyzed in 0.1 M methanolic sodium methoxide (17.9 ml) for 1 h at the ambient temperature. The reaction mixture was then neutralized with Amberlite IR-120B (H^+) resin and the resin was filtered off. The fitrate was subsequently concentrated. To a solution of the residue in pyridine (6 ml) was added *p*-nitrophenoxycarbonyl chloride (300 mg).

After 18 h, the reaction mixture was extracted with chloroform, and the chloroform layer was washed with saturated $NaHCO_3$ solution and water. The solution was concentrated to give an oily residue, which contained *p*-nitrophenoxycarbonyl derivatives. The residue was treated with methanol (4 ml) containing potassium hydroxide (9.4 mg) at the ambient temperature for 3 h, then the reaction mixture was concentrated. To the residue was added water, which was then extracted with ethyl acetate (20 ml×3). The ethyl acetate layers were combined and concentrated. The oily product, without purification, was treated with 60% acetic acid at 40 °C for 3 h. The reaction mixture was concentrated, and the residue was purified on a silica-gel column [C-300, 5 g, 2:1 (v/v) toluene–ethyl methyl ketone] to give **14-2** and **3**, each as a homogenous amorphous solid.

14-2: Mp 96—98 °C, R_f 0.52 [1:1 (v/v) toluene–ethyl methyl ketone], IR (KBr) 1805, 1705 cm^{-1} (C=O), ^1H NMR ($CDCl_3$) δ 7.35 (10H, s, $C_6H_5\times2$), 5.73 (1H, d, $J_{11,12}$= 3.8 Hz, H-12), 4.94 (1H, m, $J_{7,8}$=8.0 Hz, H-7), 3.33 (3H, s, OCH_3), 2.33 (2H, m, H-6) 1.55, 1.35 (3H×2, s×2, isopropylidene). Found: C, 59.30; H, 6.25; N, 2.36%. Calcd for $C_{33}H_{39}NO_{13}$: C, 59.53; H, 6.09; N, 2.17%.

14-3: Mp 81—84 °C, R_f 0.45 [1:1 (v/v) toluene--ethyl methyl ketone], IR (KBr) 1805, 1705 cm^{-1} (C=O), ^1H NMR ($CDCl_3$) δ 7.35 (10H, s, $C_6H_5\times2$), 5.73 (1H, d, $J_{11,12}$= 3.8 Hz, H-12), 4.82 (1H, m, $J_{7,8}$=6.4 Hz, H-7), 3.34 (3H, s, OCH_3), 1.59, 1.36 (3H×2, s×2, isopropylidene). Found: C, 59.53; H, 6.19; N, 2.16%.

*Methyl 3,4,7,8-Tetra-O-acetyl-10-O-benzyl-2-benzyloxycarbonylamino-2,6-dideoxy-11,12-O-isopropylidene-β-L-dodecodialdo-(12R)-furanose-(12,9)-pyranoside-(1,5) (**15**).* *a) **15-1** and **15-4***: Compound **12-1** or **12-4** (200 mg) was treated with acetic acid (70 ml) and water (50 ml) at 40 °C for 1.5 h. The reaction mixture was concentrated to dryness. The residue was purified on a silica-gel column [C-200, 20 g, 1:1 (v/v) toluene–ethyl acetate] to afforded a diol derivative. The diol derivative was reacted with acetic anhydride (0.7 ml) in pyridine (10 ml) for 2 d. The reaction mixture was co-evaporated with toluene, and the residue was extracted with chloroform. The chloroform layer was washed with water, a saturated $NaHCO_3$ solution, and water, dried and cocentrated. The residue was purified on silica-gel column [C-200, 15 g, 2:1 (v/v) toluene–ethyl acetate] to give **15-1** or **4**.

15-1: Yield, 70%, R_f 0.62 [1:1 (v/v) toluene–ethyl acetate] mp 84—86 °C, $[\alpha]_D^{23}$ +98.4° (*c* 0.5, chloroform), ^1H NMR ($CDCl_3$) δ 7.20 (10H, s, $C_6H_5\times2$), 5.57 (1H, d, $J_{11,12}$=3.5 Hz, H-12), 3.18 (3H, s, OCH_3), 2.07, 1.95, 1.86, 1.78 (3H×4, s×4, Ac), 1.52, 1.30 (3H×2, s×2, isopropylidene). Found: C, 59.20; H, 6.29; N, 1.87%. Calcd for $C_{39}H_{49}NO_{16}$: C, 59.46; H, 6.27; N, 1.78%.

15-4: Yield, 80%, R_f 0.49 [1:1 (v/v) toluene–ethyl acetate] mp 130.5—131.5 °C, $[\alpha]_D^{28}$ +125.4° (*c* 0.5, chloroform), ^1H NMR ($CDCl_3$) δ 7.22 (10H, s, $C_6H_5\times2$), 5.53 (1H, d, $J_{11,12}$=3.5 Hz H-12), 3.23 (3H, s, OCH_3), 2.08, 1.96, 1.94, 1.82 (3H×4, s×4, Ac), 1.49, 1.28 (3H×2, s×2, isopropylidene). Found: C, 59.65; H, 6.37; N, 1.79%.

*b) **15-2** and **15-3***: A mixture of **12-2** and **12-3** (128.1 mg) was hydrolyzed in 0.1 M methanolic sodium methoxide (20 ml) for 3 h. To the reaction mixture was added toluene (30 ml), which was subsequently concentrated to *ca.* 20 ml. To the solution was added water (10 ml) and ethyl acetate (20 ml). The organic layer was separated and cocentrated. The residue was treated with 60% acetic acid (10 ml) at 40 °C for 2 h. The reaction mixture was co-evaporated with toluene, and the residue was purified on a silica-gel column [C-200, 20 g, 30:1 (v/v) chloroform–methanol] to give the tetrahydroxy derivative, 13.4 mg (10.3%) with an R_f value of 0.30 [10:1 (v/v) chloroform–methanol], 14.9 mg (12.4%) with an R_f value of 0.32 in the same solvent system, and 39.1 mg of a mixture of them. Total yield, 67.4 mg (55%). Each tetrahydroxy derivative obtained above was reacted with acetic anhydride (0.3 ml) in pyridine (2 ml) for 18 h. The reaction mixture was then co-evaporated with toluene, and the residue was purified on a silica-gel column [C-200, 4 g, 3:1 (v/v) toluene–ethyl acetate] to give 14.3 mg (76%) of **15-2** and 13.7 mg (81%) of **15-3**.

15-2: R_f 0.52 [1:1 (v/v) toluene–ethyl acetate], mp 77—78 °C $[\alpha]_D^{28}$ +102.4° (*c* 0.5, chloroform), ^1H NMR ($CDCl_3$) δ 7.24 (10H, s, $C_6H_5\times2$), 5.50 (1H, d, $J_{11,12}$=3.5 Hz, H-12), 3.33 (3H, s, OCH_3), 2.04, 1.97, 1.87, 1.83 (3H×4, s×4, Ac), 1.62, 1.30 (3H×2, s×2, isopropylidene). Found: C, 59.24; H, 6.26; N, 1.76%. Calcd for $C_{39}H_{49}NO_{16}$: C, 59.46; H, 6.27; N, 1.78%.

15-3: R_f 0.54 [1:1 (v/v) toluene–ethyl acetate], mp 81.5—83.5 °C, $[\alpha]_D^{23}$ +101° (*c* 0.5, chloroform), ^1H NMR ($CDCl_3$) δ 7.20 (10H, s, $C_6H_5\times2$), 5.55 (1H, d, $J_{11,12}$= 3.5 Hz, H-12), 3.25 (3H, s, OCH_3), 1.97, 2.10, 1.83 (6H and 3H×2, s×3, Ac), 1.53, 1.30 (3H×2, s×2, isopropylidene). Found: C, 59.44; H, 6.33; N, 1.84%.

The authors wish to thank Professor Gakuzo Tamura, Tokyo University, for his helpful suggestions. They also wish to express their appreciation to Pharmaceutical Development Laboratories, Meiji Seika Kaisha, Ltd., for the NMR spectral data; to Mr. Saburo Nakada for the elemental analyses, and to Mr. Masazumi Kameda for the IR spectral data.

References

1) T. Ito, Y. Kodama, K. Kawamura, K. Suzuki, A. Takatsuki, and G. Tamura, *Agric. Biol. Chem.*, **41**, 2303 (1977).

2) T. Ito, A. Takatsuki, K. Kawamura, K. Sato, and G. Tamura, *Agric. Biol. Chem.*, **44**, 695 (1980).

3) P. L. Hamill and M. M. Hoehn, *J. Antibiot., Ser. A*, **17**, 100 (1964); M. Vuilhrgne, S. Ennifar, B. P. Das, J. W. Pascal, R. Nagarajan, E. W. Hagman, and E. Wenkert, *J. Org. Chem.*, **42**, 3289 (1977).

4) R. Nagarajan, B. Chao, D. E. Dorman, S. M. Nash, L. Occolwitz, and A. Schabei, 17th International Conference on Antimicrobial Agents and Chemotherapy, New York, N. Y., 1977, Abstract 50.

5) K. Sakata, A. Sakurai, and S. Tamura, *Tetrahedron Lett.*, **1974**, 4327; *Agric. Biol. Chem.*, **40**, 1933 (1976).

6) S. Harada, E. Mizuta, and T. Kishi, *J. Am. Chem. Soc.*, **100**, 4895 (1978).

7) Y. Fukuda, H. Sasai, and T. Suami, *Bull. Chem. Soc. Jpn.*, **54**, 1830 (1981); Y. Fukuda, H. Kitasato, H. Sasai, and T. Suami, *ibid.*, **55**, 880 (1982).

8) K. Z-Yoong, *Sci. Sinica (Peking)*, **5**, 461 (1956).

9) K. E. Pfitzner and J. G. Moffatt, *J. Am. Chem. Soc.*, **85**, 3027 (1963); **87**, 5661 (1965).

10) J. S. Brimacombe, *Carbohydr. Res.*, **8**, 82 (1968).

11) S. M. Gunner, R. D. King, W. G. Overend, and N. R. Williams, *J. Chem. Soc., C*, **1970**, 1954; W. P. Blackstock, C. C. Kuenzle, and C. H. Eugster, *Helv. Chem. Acta*, **57**, 1003 (1974); H. Shechter and F. T. Williams, Jr., *J. Org. Chem.*, **27**, 3699 (1962).

12) P. J. L. Daniels, "Drug Action and Drug Resistance on Bacteria," ed by S. Mitsuhashi, Tokyo Univ. Press, Tokyo (1975), pp. 88—89; J. E. Herweh, T. A. Folglia, and D. Swern, *J. Org. Chem.*, **33**, 4029 (1968).

Synthesis of Biotin-containing Peptides Representing the Biotin Binding Site of *E. coli* Acetyl-CoA Carboxylase†

Hiroki KONDO,* Fumio MORIUCHI, and Junzo SUNAMOTO
Department of Industrial Chemistry, Faculty of Engineering, Nagasaki University, Nagasaki 852
(Received October 19, 1981)

Two biotin-containing peptides, Ac-Met-Bct-Met-Met-OMe (**1**) and Boc-Met-Bct-Met-Met, that correspond to the local sequence of biotin carboxyl carrier protein subunit of *E. coli* acetyl-CoA carboxylase have been synthesized. The precursor tetrapeptide Boc-Met-Lys(Cbz)-Met-Met-OMe was prepared first by the stepwise elongation method and biotin was incorporated subsequently by the active ester method. Another biotin-containing peptide, HCO-Met-Bct-Met-Met-OMe, has also been prepared. Magnesium ion binding to peptide **1** in acetonitrile has been studied by means of ^{13}C NMR spectroscopy. The metal interacts principally with the amide carbonyls rather than sulfide moieties, as deduced from a significant downfield shift of the former carbon signals in ^{13}C NMR.

In biotin-requiring carboxylases the prosthetic group biotin (**4**) is attached to the ε-amino moiety of a certain lysine residue on the so-called BCCP (biotin carboxyl carrier protein) subunit.[1] The binding of BCCP to other subunits directly involved in the transformation of biotin and substrates is very tight. In some instances biotin itself can bind to the enzyme with a high K_m value relative to that for BCCP.[2,3] It is, hence, clear that the polypeptide part of BCCP contributes much to the binding of biotin, but what part of the amino acid sequence is required remained to be clarified. In light of the accumulating knowledge on the primary structure around biocytin (biotinyllysine, **5**) of several biotin enzymes,[4-6] Bodanszky

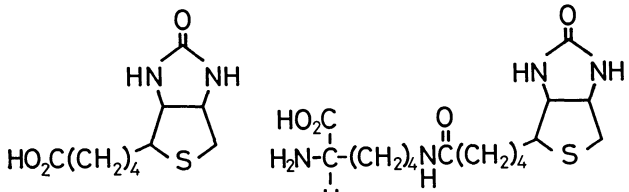

4 5

and Fagan were the first to undertake this subject.[7] They prepared biotin-containing peptides such as **6**, that corresponds to the local structure adjacent to biocytin of transcarboxylase. Unfortunately, however, the peptides failed to restore enzymic activity. It was later reported that the amino acid sequence of transcarboxylase on which their model peptides based was in error.[8]

Boc-Ala-Met-Bct-Thr-Gly-OEt **6**

According to the known primary structure of biotin enzymes, they have a unique structure in that biocytin is flanked by methionines. In the case of acetyl-CoA carboxylase from *E. coli*, an additional Met is placed at the C terminal side of the sequence (**7**). Since

-Met-Bct-Met-Met- **7**

each amino acid residue in **7** carries a sulfide moiety, we have speculated that these four sulfide groups may be playing an important role in the binding of biotin to the enzyme. If one recalls that the enzyme requires metal ions such as Mn^{2+} and Mg^{2+} for activity, this might be performed through chelate formation. Hence, we have prepared model peptides **1**—**3**, analogous to **7**, and studied their interaction with metal ions by means of ^{13}C NMR spectroscopy.[9]

Results and Discussion

Synthesis. The liquid phase synthesis of **1** and **2** has been achieved according to the routes shown in Fig. 1 and Scheme 1. The basic strategy was to prepare the tetrapeptide Boc-Met-Lys(Cbz)-Met-Met-OMe **8** first and biotin was incorporated to the peptide subsequently. This should help avoid possible side reactions on the biotin moiety and interference of the biotin's urea group with amino acid coupling.[7] The α-amino function of both Met and Lys was protected with Boc, while the ε-amino moiety of Lys was with Cbz. An alternate combination of protecting groups may appear equally well as long as special care is taken for the removal of Cbz groups. One of the most popular methods of doing this, hydrogenolysis, did not work even in the presence of boron trifluoride etherate even at the dipeptide level.[10] So, this approach was abandoned and switched to the alternative one without testing extensively other deprotection methods. The Boc group was removed

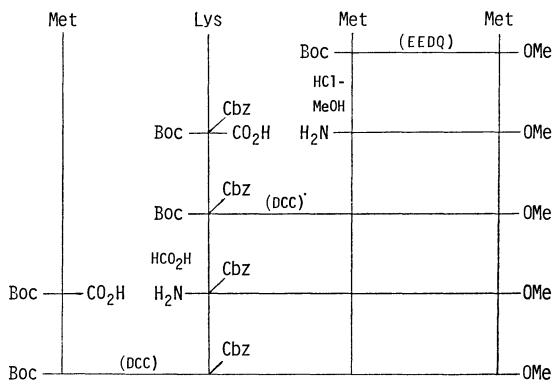

Fig. 1. Synthetic route to **8**.

† The abbreviations used in this article follow the nomenclature recommended by the IUPAC-IUB Commission of Biochemical Nomenclature: Met, L-methionine; Lys, L-lysine; Bct, biotinyl-L-lysine; Cbz, benzyloxycarbonyl; Boc, *t*-butoxycarbonyl; EEDQ, *N*-ethoxycarbonyl-2-ethoxy-1,2-dihydroquinoline; DCC, dicyclohexylcarbodiimide; HOBt, 1-hydroxybenzotriazole; NEM, *N*-ethylmorpholine; TEA, triethylamine.

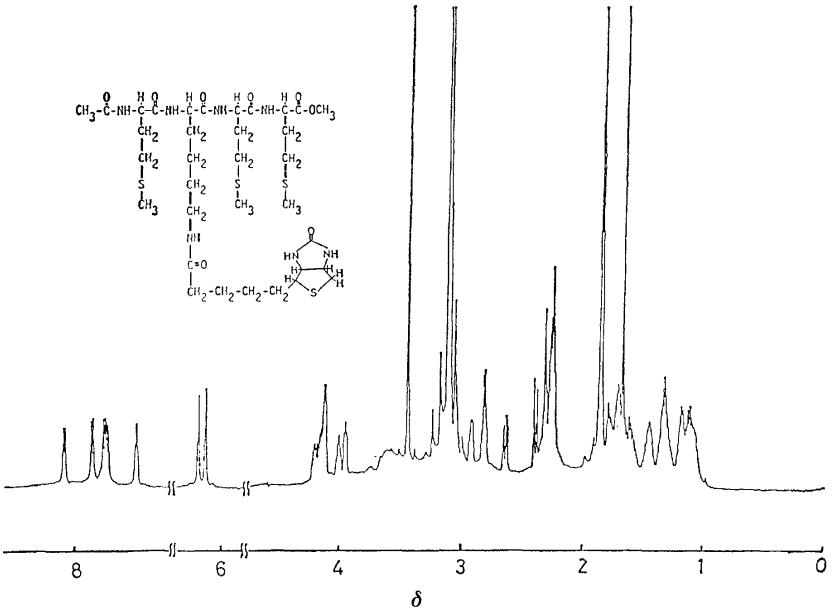

Fig. 2. 500 MHz NMR spectrum of **1** in DMSO-d_6.

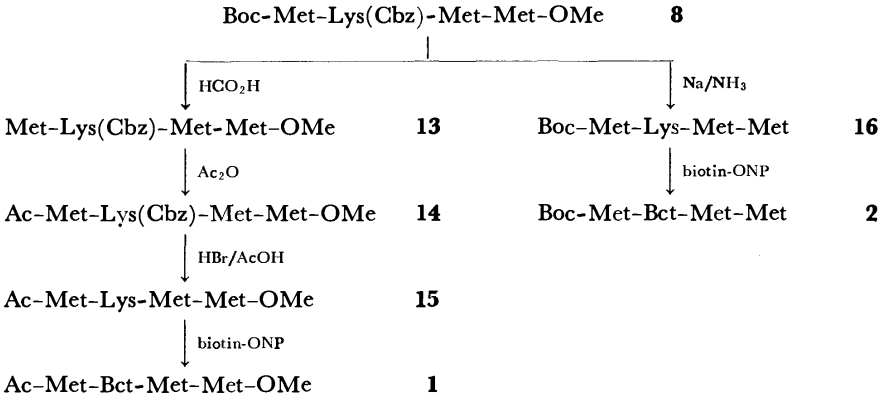

Scheme 1.

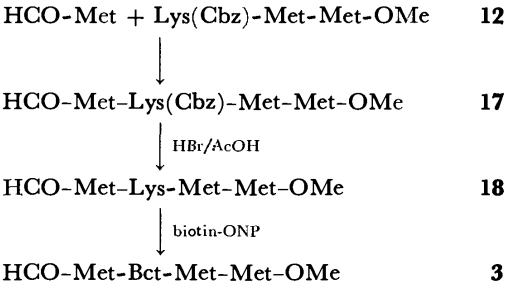

Scheme 2.

from Boc–Met–Met–OMe with 10 M HCl in methanol and from Boc–Lys(Cbz)–Met–Met–OMe and Boc–Met–Lys(Cbz)–Met–Met–OMe with formic acid.

The tetrapeptide **8** was derivatized to the final products according to the synthetic routes shown in Scheme 1. Removal of Boc in **8** with formic acid followed by acetylation gave **14**, whose Cbz was removed with 25% HBr in acetic acid to give **15**. Treatment of **8** with sodium in liquid ammonia provided **16** smoothly. Introduction of biotin into **15** and **16** was accomplished by the active ester method. In view of the fact that *N*-hydroxysuccinimide ester of biotin is successfully employed for the covalent attachmen of biotin to the affinity adsorbents,[11] we have tested this method first. The reaction was carried out in DMF in the presence of TEA or NEM at temperatures ranging from room temperature to 50 °C with total failure. Subsequently, the *N*-hydroxysuccinimide ester was replaced by *p*-nitrophenyl ester of biotin,[7] and its reaction with **15** or **16** at ambient temperatures gave **1** or **2**, respectively, but in low yields (28—38%). Coupling of **15** with biotin acid chloride has also been tried,[12] but this method did not work either. The synthesis of **3** has also been done according to the route shown in Scheme 2.

The structure of biotin-containing peptides **1**—**3** has been ascertained by the following criteria. All the peptides gave a characteristic pink color upon reaction with *p*-dimethylaminocinnamaldehyde, indicating the presence of a biotinyl moiety.[13] In Fig. 2 is shown the 500 MHz NMR spectrum of **1** in DMSO-d_6. Two singlets are clearly observable for the biotin N–H protons at 6.14 and 6.20 ppm as well as five signals for the amide protons at 7.5—8.1 ppm. Other peaks are also reasonably assignable to individual protons of **1**. There are six amide carbonyl signals in

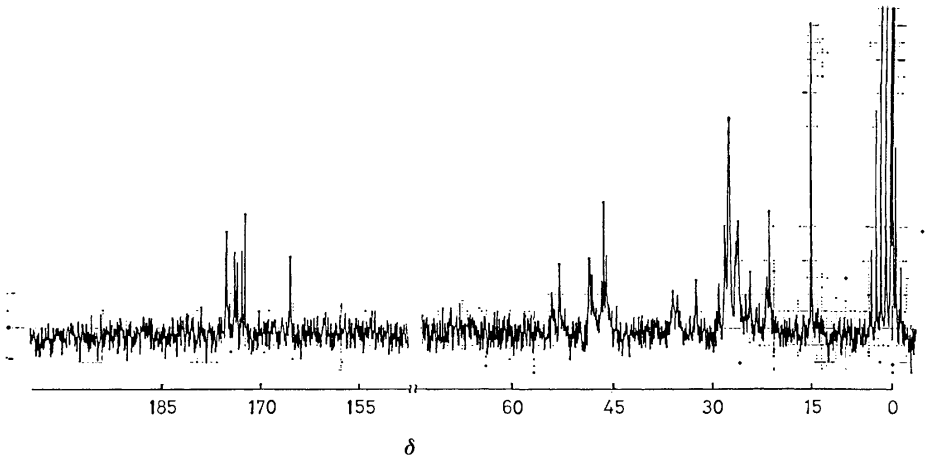

Fig. 3. ^{13}C NMR spectrum of **1** in CD_3CN in the presence of 4 mol of magnesium perchlorate.

Table 1. ^{13}C NMR chemical shifts of carbonyl carbons of **1** and **8** in CD_3CN in the absence or presence of 4 mol of $Mg(ClO_4)_2$

8	**8**+Mg^{2+}	$\Delta\delta$[a]	**1**+Mg^{2+}	$\Delta\delta'$[b]
174.6	176.5	1.9	176.4	1.8
173.8	176.4	2.6	176.2	2.4
172.5	174.4	1.9	174.7	2.2
172.1	173.6	1.5	174.2	2.1
172.0	173.0	1.0	173.4	1.4
157.4	158.5	1.1	172.8	—
164.3[c]			164.4	0.1

a) $\Delta\delta$=column 2 - column 1. b) $\Delta\delta'$=column 4 - column 1. c) Value for biotin *p*-nitrophenyl ester.

the 172—177 ppm region as well as one urea carbonyl signal at 164.4 ppm in the ^{13}C NMR spectrum of **1** in CD_3CN in the presence of magnesium perchlorate (Fig. 3). Results of elemental analysis are also satisfactory (see Experimental), establishing the purity and structure of these compounds.

Magnesium Ion Binding. All the biotin-containing peptides (**1**—**3**) are sparingly soluble in acetonitrile but they become considerably soluble in the presence of magnesium perchlorate, suggesting that the peptides interact with magnesium ion. In order to prove this, further studies were done by using ^{13}C NMR spectroscopy. Because of the poor solubility of **1**, **8** was chosen as a reference compound. As seen in Table 1, all five amide carbonyls of **8** show a considerable downfield shift (average 1.8 ppm) in the presence of 4 mol of magnesium perchlorate. This is true for **1**: five amide carbonyls show a downfield shift of 2.0 ppm on the average, compared to the amide carbonyls of **8** in the absence of magnesium perchlorate. On the other hand, the ureido carbonyl of biotin suffers little effect, in line with our previous finding that this moiety of 2-imidazolidinones is a poor ligand to magnesium.[9] In contrast to the carbonyl signals, other carbon signals including those of *S*-methyl carbons of methionines were not affected by magnesium perchlorate. This indicates that the metal coordinates to the carbonyls rather than the sulfides. It is plausible that the magnesium ion plays its role through association with ATP or its conjugate with hydrogencarbonate in enzymatic carboxylations. In order for biotin to be carboxylated the coenzyme must come into contact with other reactants at the enzyme active site. This might be made possible through coordination of peptide carbonyls adjacent to the biotin in BCCP to form a ternary complex composed of BCCP, Mg^{2+} and ATP or its conjugate with hydrogencarbonate.

Experimental

^1H NMR spectra were taken on a JEOL JNM-MH-100 spectrometer. ^{13}C NMR spectra were obtained on a JEOL JNM-FX-90Q spectrometer operating at 22.50 MHz. Parameters for these experiments were the following: spectral width 5000 Hz with acquisition of 8 K data points, 7 μs pulse, and a recovery time of 3 s. The numbers of spectral accumulations were in the range 2000—5000. Samples were dissolved in CD_3CN for measurements at 25.0 °C and chemical shifts are given in ppm downfield from internal TMS. Optical rotation was determined on a JASCO DIP-4 digital polarimeter.

TLC on silica gel was run in the following solvent systems: ethyl acetate (A), CH_2Cl_2–ethyl acetate (5:1, B), ethyl acetate–methanol (4:1, C), and ethyl acetate–methanol (5:1, D). Spots on the TLC plate were detected with either I_2 vapor or ninhydrin. Biotin-containing peptides gave a pink color upon spraying of *p*-dimethylaminocinnamaldehyde.[13]

L-Methionine, L-lysine, EEDQ, DCC, *N*-hydroxysuccinimide, 25% HBr/AcOH, CbzCl, and *O*-*t*-butyl *S*-4,6-dimethyl-2-pyrimidinyl thiocarbonate were obtained from Protein Research Foundation. Trimethylacetyl chloride was purchased from Aldrich Co. Ltd. *d*-Biotin and other reagents were obtained from Wako Pure Chemical Co.

Boc–Met–Met–OMe (9). *N*-(*t*-Butoxycarbonyl)methionine and Met–OMe were coupled by the EEDQ method.[14] After the usual work-up, a crude product was obtained as a syrup. This was purified by chromatography on silica gel with ethyl acetate as an eluent, followed by recrystallization from ether and petroleum ether. Yield 68%, mp 67—69 °C (lit,[15] 66—67 °C), $[\alpha]_D^{25}$ −30.5° (*c* 3.1, CH_3OH), R_f 0.90 (A). Found: C, 48.34; H, 7.67; N, 7.16%. Calcd for $C_{16}H_{30}N_2O_5S_2$: C, 48.71; H, 7.66; N, 7.10%.

*Met-Met-OMe·HCl (**10**·HCl).* A 2.0 g (5.0 mmol) sample of **9** was dissolved in 10 ml of 10 M HCl in methanol. The mixture was stirred at room temperature for 1 h. The solvent was removed *in vacuo* and then 100 ml of ether was added. After allowing the suspension to stand at −5 °C for 1 d, the supernatant was discarded. The same procedure was repeated twice more. The oily residue was dried *in vacuo* at room temperature to give a very hygroscopic product. Yield 1.3 g (87%). R_f 0.40 (A). Complete removal of the protecting group was confirmed by NMR.

*Boc-Lys(Cbz)-Met-Met-OMe (**11**).* A solution of N^{α}-Boc-N^{ε}-Cbz-Lys[16] (1.0 g, 2.6 mmol), DCC (0.54 g, 2.6 mmol), and HOBt (0.35 g, 2.6 mmol) in 15 ml of DMF was mixed with a solution of **10**·HCl (0.76 g, 2.6 mmol) and NEM (0.30 g, 2.6 mmol) in 15 ml of DMF. The reaction mixture was stirred at room temperature for 8 h and the precipitate formed was filtered off. The filtrate was concentrated *in vacuo* to about 5 ml, and then diluted with 100 ml of ethyl acetate. The solution was washed successively with the following solvents: 4% $NaHCO_3$, saturated NaCl, 10% citric acid, and saturated NaCl. After drying over sodium sulfate at −5 °C (to effect complete precipitation of DCUrea), the solution was concentrated to about 50 ml, and kept overnight in a freezer. The crystalline mass formed was collected by filtration. Yield 1.2 g (71%), mp 105—106 °C, $[\alpha]_D^{25}$ −18.7° (*c* 3.2, CH_2Cl_2), R_f 0.92 (A), 0.88 (B). Found: C, 54.94; H, 7.52; N, 8.60%. Calcd for $C_{30}H_{48}N_4O_8S_2$: C, 54.86; H, 7.37; N, 8.53%.

*Lys(Cbz)-Met-Met-OMe·HCO$_2$H (**12**·HCO$_2$H).* A 1.2 g (1.8 mmol) sample of **11** was dissolved in 10 ml of formic acid and stirred at room temperature. The reaction was complete in 3 h, as inspected by TLC. The mixture was diluted with 100 ml of methanol and the solvents were evaporated *in vacuo*. The product was precipitated by addition of ether. Yield 0.82 g (84%). R_f 0.25 (A). Complete removal of the protecting group was confirmed by NMR.

*Boc-Met-Lys(Cbz)-Met-Met-OMe (**8**).* In 30 ml of DMF were dissolved 5.0 g (92 mmol) of **12**·HCO_2H, 1.1 g (92 mmol) of NEM, 2.3 g (92 mmol) of Boc-Met, 1.9 g (92 mmol) of DCC, and 1.4 g (92 mmol) of HOBt. The mixture was stirred overnight at room temperature. The DCUrea formed was filtered off. After removal of the solvent *in vacuo*, the residue was taken up in 1 L of ethyl acetate. The solution was washed as for **11** and then dried over sodium sulfate. Concentration of the solution to about 300 ml gave precipitates of crude product. They were recrystallized from ethyl acetate. Yield 4.5 g (63%), mp 172—173 °C, $[\alpha]_D^{25}$ −22.7° (*c* 2.6, CH_2Cl_2). R_f 0.61 (B). Found: C, 53.22; H, 7.33; N, 8.84%. Calcd for $C_{35}H_{57}N_5O_9S_3$: C, 53.34; H, 7.29; N, 8.89%.

*Met-Lys(Cbz)-Met-Met-OMe·HCO$_2$H (**13**·HCO$_2$H).* A sample of **8** (4.8 g, 4.2 mmol) was dissolved in 50 ml of formic acid and the solution was stirred for 4 h at room temperature. After addition of 100 ml of methanol, the solvents were evaporated *in vacuo*. The same procedure was repeated twice more. Addition of ether to the syrupy residue gave precipitates of the product (4.2 g, 95%).

*Ac-Met-Lys(Cbz)-Met-Met-OMe (**14**).* To a DMF solution (10 ml) containing 0.90 g (1.2 mmol) of **13**·HCO_2H and 0.14 g (1.2 mmol) of NEM were added slowly 8 ml of acetic anhydride. The whole mixture was stirred for 3 h. The precipitates formed were collected by filtration and washed with ether. Yield 0.82 g (91%), mp 213—214 °C. R_f 0.26 (C), 0.86 (D). $[\alpha]_D^{25}$ −27.5° (*c* 2.0, DMF). Found: C, 52.22; H, 7.07; N, 9.48%. Calcd for $C_{32}H_{51}N_5O_8S_3$: C, 52.65; H, 7.04; N, 9.59%.

*Ac-Met-Lys-Met-Met-OMe·CH$_3$CO$_2$H (**15**·AcOH).* A sample of **14** (1.0 g, 1.4 mmol) was dissolved in 30 ml of 25% HBr/AcOH with 5 ml of dimethyl sulfide. The mixture was stirred for 3 h and then 50 ml of dichloromethane and 400 ml of ether were added. The precipitates formed were filtered off to give 0.85 g (92%) of the product.

*Ac-Met-Bct-Met-Met-OMe (**1**).* **15**·AcOH (0.17 g, 0.26 mmol), TEA (2.6 mg, 0.26 mmol), and biotin *p*-nitrophenyl ester[7,17] in 4 ml of DMF were allowed to react at room temperature for 15 h. The solution was first clear but precipitates gradually formed. They were filtered off and washed with water, methanol, and ether. Yield 60 mg (28%), mp 231 °C (dec). Found: C, 48.84; H, 7.22; N, 11.88%. Calcd for $C_{34}H_{59}N_7O_8S_4\cdot H_2O$: C, 48.61; H, 7.32; N, 11.67%.

*Boc-Met-Lys-Met-Met (**16**).* **8** (1.0 g, 1.3 mmol) was dissolved in 100 ml of liq. ammonia. Sodium was added in small portions until the blue color was retained for 5 min. Ammonium chloride was added until the blue color disappeared. Ammonia was evaporated off and 50 ml of methanol was added to the residue. The suspension was warmed at 40 °C for 30 min. The insoluble material was removed by filtration and evaporation of the filtrate *in vacuo* gave 0.60 g (71%) of the product. Removal of the Cbz and ester groups was confirmed by NMR.

*Boc-Met-Bct-Met-Met (**2**).* To a methanol solution (3 ml) of **16** (0.60 g, 0.92 mmol) and 92 mg (0.92 mmol) of TEA were added 80 mg (2 mmol) of biotin *p*-nitrophenyl ester.[7,17] The mixture was stirred at room temperature for 15 h, whereupon 80 ml of ether was added. The precipitates formed were filtered off and then washed with water. Yield 0.30 g (38%), mp 174—176 °C. R_f 0.45 (C). Found: C, 48.14; H, 7.43; N, 10.92%. Calcd for $C_{36}H_{63}N_7O_9S_4\cdot 2H_2O$: C, 47.92; H, 7.48; N, 10.86%.

*HCO-Met-Lys(Cbz)-Met-Met-OMe (**17**).* To a cold (−10 °C) solution of HCO-Met[18] (0.48 g, 2.7 mmol), pyridine (0.2 ml, 2.7 mmol), and *N*-ethylpiperidine (0.4 ml, 2.7 mmol) in CH_2Cl_2 (10 ml) was added a CH_2Cl_2 solution (2 ml) of trimethylacetyl chloride (0.33 g, 2.7 mmol). The mixture was allowed to react at −10 °C for 20 min, whereupon a CH_2Cl_2 solution of **12**·HCO_2H (1.5 g, 2.7 mmol) and NEM (0.3 g, 2.7 mmol) was added. The whole solution was stirred for 15 min at −10 °C and then for 1 h at room temperature. The solvent was removed *in vacuo* and the solid material left was filtered and washed with 10% citric acid, water, and 5% $NaHCO_3$. Yield 1.8 g (93%), mp 204—205 °C. R_f 0.35 (D). $[\alpha]_D^{26}$ −14.8° (*c* 1, CH_3OH). Found: C, 51.59; H, 6.98; N, 9.69%. Calcd for $C_{31}H_{49}N_5O_8S_3\cdot 0.5H_2O$: C, 51.36; H, 6.95; N, 9.66%.

*HCO-Met-Lys-Met-Met-OMe·HBr (**18**·HBr).* **17** (1.5 g, 2.1 mmol) was dissolved in 10 ml of 25% HBr/AcOH with 0.62 g (10 mmol) of dimethyl sulfide. The mixture was stirred for 3 h and then concentrated *in vacuo*. The residue was purified by reprecipitation from methanol–ether three times. Yield 1.3 g (94%). R_f 0.15 (C). The structure was confirmed by NMR.

*HCO-Met-Bct-Met-Met-OCH$_3$ (**3**).* **18**·HBr (1.3 g, 1.9 mmol), TEA (0.19 g, 1.9 mmol), and biotin *p*-nitrophenyl ester[7,17] (1 g, 2.8 mmol) were dissolved in 4 ml of DMF. Two ml of water were added and the solution was stirred at room temperature for 4 h. The precipitates formed were filtered and washed with water, methanol, and ether. Yield 0.5 g (35%), mp 205—206 °C. R_f 0.04 (D). Found: C, 48.27; H, 7.12; N, 11.85%. Calcd for $C_{32}H_{57}N_7O_8S_4$: C, 48.28; H, 7.22; N, 12.32%.

The authors are indebted to Prof. E. T. Kaiser

of the University of Chicago for the determination of 500 MHz ^{1}H NMR spectra. Thanks are also due to Dr. S. Shinkai for the use of polarimeter. This work was supported by a Grant-in-Aid (No. 521325) for Scientific Research from the Ministry of Education, Science and Culture.

References

1) M. C. Scrutton and M. R. Young, "The Enzymes," Academic Press, New York (1972), Vol. VI, Chap. 1.
2) P. Dimroth, R. B. Guchhait, E. Stoll, and M. D. Lane, *Proc. Natl. Acad. Sci. U.S.A.*, **67**, 1353 (1970).
3) A. M. Nervi, A. W. Alberts, and P. R. Vagelos, *Arch. Biochem. Biophys.*, **143**, 401 (1971).
4) M. R. Sutton, R. R. Fall, A. M. Nervi, A. W. Alberts, P. R. Vagelos, and R. A. Bradshaw, *J. Biol. Chem.*, **252**, 3934 (1977).
5) D. B. Rylatt, D. B. Keech, and J. C. Wallace, *Arch. Biochem. Biophys.*, **183**, 113 (1977).
6) W. L. Malog, B. U. Bowien, G. K. Zwolinski, K. G. Kumar, H. G. Wood, L. H. Ericsson, and K. A. Walsh, *J. Biol. Chem.*, **254**, 11615 (1979).
7) M. Bodanszky and D. T. Fagan, *J. Am. Chem. Soc.*, **99**, 235 (1977).
8) H. G. Wood and R. E. Barden, *Ann. Rev. Biochem.*, **46**, 385 (1977).
9) H. Kondo, D. Horiguchi, S. Ikeda, J. Sunamoto, and K. Tsujii, *J. Org. Chem.*, **44**, 4430 (1979).
10) H. Yajima, K. Kawasaki, Y. Kinomura, T. Oshima, S. Kimoto, and M. Okamoto, *Chem. Pharm. Bull.*, **16**, 1342 (1968).
11) E. A. Bayer and M. Wilchek, *Methods Enzymol.*, **34**, 265 (1974).
12) D. E. Wolf, J. Valiant, and K. Folkers, *J. Am. Chem. Soc.*, **73**, 4142 (1951).
13) D. B. McCormick, *J. Heterocycl. Chem.*, **10**, 235 (1973).
14) D. Belleau and G. Malek, *J. Am. Chem. Soc.*, **90**, 1651 (1968).
15) F. Naider and J. M. Bekar, *Biopolymers*, **13**, 1011 (1974).
16) E. Bayer, G. Jung, and H. Hagenmaier, *Tetrahedron*, **24**, 4853 (1968).
17) E. A. Bayer and M. Wilchek, *Methods Enzymol.*, **46**, 613 (1977).
18) J. C. Sheehan and D. D. H. Young, *J. Am. Chem. Soc.*, **80**, 1154 (1958).

The Biosynthesis of Protoanemonin in *Ranunculus glaber*. The Pivotal Biosynthetic Intermediate and the Stereospecific Hydrogen Elimination from the Intermediate

Takayuki SUGA* and Toshifumi HIRATA

Department of Chemistry, Faculty of Science, Hiroshima University, Higashisenda-machi, Naka-ku, Hiroshima 730

(Received October 22, 1981)

The pivotal biosynthetic intermediate directly leading to protoanemonin was established to be 2-oxoglutarate on the basis of the labeling patterns in protoanemonin biosynthesized from sodium acetate-1-^{14}C, sodium malonate-2-^{14}C, sodium succinate-2,3-$^{14}C_2$, sodium glutamate-5-^{14}C, and sodium 2-oxoglutarate-5-^{14}C by *Ranunculus glaber*. Also the $^{3}H/^{14}C$ ratio in protoanemonin biosynthesized from (3*R*)-2-oxoglutaric-3-$^{3}H_1$-3,4-$^{14}C_2$ and 2-oxoglutaric-3-$^{3}H_2$-3,4-$^{14}C_2$ acids demonstrated that the formation of the double bond at the 3-position of protoanemonin involves the stereospecific elimination of the *pro*-3*S* hydrogen atom from 2-oxoglutaric acid.

It has been well known that many of the plants belonging to Ranunculaceae family show antimicrobial activities and, in some cases, the bruised tissues of the plants cause an intense burn or blister to the skin.[1-5] Such properties of the plants are described to be owing to protoanemonin (**1**), which is probably enzymatically liberated from ranunculin (**2**) by crushing the tissues of the *Ranunculus* plants.[6] It is documented that many C_5 compounds similar to protoanemonin have been found in the form of a glycoside in *Ranunculus* species.[7] Although the biosynthetic pathway of such a simple lactone is of considerable interest, it has not been investigated yet. We have performed feeding experiments of the radioisotopically labeled compounds into protoanemonin (**1**) with the intact plant of *Ranunculus glaber* Makino for clarifying the pivotal biosynthetic intermediate directly leading to the formation of protoanemonin (**1**) and then the stereospecificity in the hydrogen elimination from the intermediate at the stage of the double bond formation in **1**. The findings of the feeding experiments have been partly outlined in preliminary communications.[8-10] We here wish to describe, *en bloc*, details of the results.

Results and Discussion

Biosynthetic Pathway of Protoanemonin (1) in R. glaber. The feeding experiments were carried out on the sprigs of *R. glaber*. The radioisotopically labeled compounds used for the feeding experiments were sodium acetate-1-^{14}C, sodium malonate-2-^{14}C, sodium succinate-2,3-$^{14}C_2$, sodium glutamate-5-^{14}C, and sodium 2-oxoglutarate-5-^{14}C. After the incorporation of the respective precursors, the sprigs were subjected to steam-distillation to give protoanemonin (**1**). Since protoanemonin (**1**) is unstable, it was immediately converted to pentanoic acid by hydrogenation in the presence of PtO_2.[3] All the above-described labeled compounds were incorporated into protoanemonin (**1**) to the extent as shown in Table 1. This indicates that these labeled compounds are of the biosynthetic precursors for protoanemonin (**1**) in a wide sence.

In order to elucidate a pivotal biosynthetic intermediate for protoanemonin (**1**), the labeling pattern in protoanemonin (**1**) biosynthesized from the above-described labeled compounds was determined by subjecting the pentanoic acid derived from the labeled protoanemonin (**1**) to degradation to each carbon atom as follows. The labeled pentanoic acid on Schmidt's reaction[11] gave carbon dioxide and butylamine, which was further converted to butyric acid by potassium permanganate oxidation. Such procedures as described above were repeated in the same manner, but with the acid obtained in the just former procedure. The degradation involving the procedure as above gave carbon dioxide originating from each carbon atom of C-1—C-3 of the pentanoate. On the

Table 1. The incorporation of the radioisotopically labeled precursors into protoanemonin (**1**) in *R. glaber*

Exptl No.	Precursors	Radioactivities of precursors used / mCi	Feeding time[a] / d	Sp. act. of **1**[b] / (dpm/mmol) × 10^{-4}	Incorp. / %
1	Sodium acetate-1-^{14}C	0.1	2	3.34±0.04	0.063
2	Sodium malonate-2-^{14}C	0.015	1	7.10±0.15	0.37
3	Sodium molonate-2-^{14}C	0.015	2	10.5 ±0.13	0.60
4	Sodium succinate-2,3-$^{14}C_2$	0.05	1	8.85±0.21	0.48
5	Sodium succinate-2,3-$^{14}C_2$	0.05	2	10.5 ±0.11	0.61
6	Sodium 2-oxoglutarate-5-^{14}C	0.025	1	12.0 ±0.22	0.21
7	Sodium 2-oxoglutarate-5-^{14}C	0.025	2	21.8 ±0.39	0.35
8	Sodium glutamate-5-^{14}C	0.025	1	13.2 ±0.25	0.24
9	Sodium glutamate-5-^{14}C	0.025	2	8.31±0.24	0.15

a) Metabolic period after uptake of the precursors. b) The specific radioactivity of **1** was determined on the basis of the radioactivity of pentanoic acid obtained from **1** by its hydrogenation.

Table 2. The distribution of radioactivity in protoanemonin (1) after uptake of the radioisotopically labeled precursors

Exptl No.[a]	Precursors	The distribution of radioactivity on the carbon atoms originating from **1** (%)				
		C-1	C-2	C-3	C-4	C-5
1	Sodium acetate-1-^{14}C		5.9±0.4		3.1±0.4	91.0±1.1
3	Sodium malonate-2-^{14}C	11.4±0.5	12.2±0.5	12.0±0.7	60.8±3.1	3.6±0.1
5	Sodium succinate-2,3-$^{14}C_2$	21.2±0.8	30.2±0.1	34.1±1.3	7.4±0.3	7.1±0.2
6	Sodium 2-oxoglutarate-5-^{14}C		5.8±0.2			94.2±2.7
7	Sodium 2-oxoglutarate-5-^{14}C	18.9±0.9	2.6±0.1	2.2±0.1		76.3±2.8
9	Sodium glutamate-5-^{14}C	19.2±0.9	6.0±0.3	5.4±0.3		69.4±3.0

a) "Exptl No." correspond to the number in Table 1.

other hand, the oxidative degradation of the radioactive pentanoic acid by the Kuhn-Roth oxidation[12] gave acetic acid involving the C-4 and C-5 carbon atoms of the pentanoic acid. The acetic acid on Schmidt's reaction gave carbon dioxide and methylamine, which was further converted into carbon dioxide by the Van Slyke-Folch oxidation.[13] Carbon dioxide obtained by the degradation as above was converted into barium carbonate for the determination of its radioactivity. The distribution of radioactivity on each carbon atom of **1** is shown in Table 2.

In the administration of sodium acetate-1-^{14}C, about 90 percent of the total radioactivity in protoanemonin (**1**) was located on its C-5 carbon atom.[14] The uptake of sodium malonate-2-^{14}C resulted in the location of about 60 percent of the radioactivity on C-4 of **1**. The malonate-2-^{14}C would biologically yield acetate-2-^{14}C by the action of acetyl-CoA carboxylase. The incorporation of the acetate-2-^{14}C into **1** results in the location of radioactivity on its C-4 carbon atom. Accordingly, the above-described labeling pattern indicates that the C-4 and C-5 carbon atoms of **1** came from the C_2-unit of acetate. However, the incorporation of these precursors resulted in the random distribution of the low radioactivity on the C-1—C-3 carbon atoms of **1**. This random labeling seems to indicate that the C-1—C-3 carbon atoms of **1** arise from a source differing from the acetate. In order to clarify the source, the feeding experiment of sodium succinate-2,3-$^{14}C_2$ was carried out, and 64 percent of the radioactivity was found to be located on the C-2 and C-3 carbon atoms of **1**. This demonstrated clearly that the C-1—C-3 carbon atoms of **1** came from succinic acid. From the results obtained in the uptake of acetate, malonate, and succinate, it was found that these precursors participate in the biosynthesis of protoanemonin (**1**) through the tricarboxylic acid cycle. This finding suggests a possibility that a pivotal intermediate for the biosynthesis of **1** might be 2-oxoglutarate.

This possibility was proved by the preferential location of almost all the radioactivity on the C-5 carbon atom in **1** biosynthesized by incorporation of 2-oxoglutarate-5-^{14}C for a 1-d period. In the incorporation of this precursor for a 2-d period, the location of radioactivity on C-5 resulted in 76 percent, and 19 percent of the radioactivity was newly located on C-1 of **1**; this suggests occurrence of the randomization of the ^{14}C-label from C-5 of 2-oxoglutarate to its C-1 by turn around of the tricaboxylic acid cycle. These facts indicate that the pivotal intermeidate for the biosynthesis of **1** is 2-oxoglutarate (**3a**). This was supported by the fact that the distribution of radioactivity in **1** biosynthesized from glutamate-5-^{14}C is similar to that observed in the uptake of 2-oxoglutarate-5-^{14}C during a 2-d period, since the interconversion of the glutamate and 2-oxoglutarate is of wide occurrence in a biological system. Thus, it was established that the pivotal intermediate for the biosynthesis of protoanemonin (**1**) is 2-oxoglutarate (**3a**). We will here propose that the biological formation of protoanemonin (**1**) from the 2-oxoglutarate (**3a**) may involve the lactonization between the 5-carboxyl and the 2-carbonyl groups of **3a** as well as the hydrogen elimination from **3a** for the formation of the C–C double bond.

Stereospecific Hydrogen-loss of 2-Oxoglutarate in the Biosynthesis of Protoanemonin (1). The hydrogen elimination in the formation of double bond at the 3-position of protoanemonin (**1**) was, therefore, investigated by examining the $^3H/^{14}C$ ratio in **1** biosynthesized from the $^3H/^{14}C$-labeled 2-oxoglutarate. 2-Oxoglutaric-3-$^3H_2$ acid (**3b**) was prepared by exchanging the hydrogen atoms at the 3-position of sodium 2-oxoglutarate by treatment with tritiated water.[15] (3*R*)-2-Oxoglutaric-3-$^3H_1$ acid (**3c**) was prepared by incubation of the tritiated 2-oxoglutaric acid (**3b**) with isocitrate dehydrogenase.[16] 2-Oxoglutaric-3,4-$^{14}C_2$ acid (**3d**) was prepared by condensation of dimethyl succinate-2,3-$^{14}C_2$ with diethyl oxalate.[17] The (3*R*)-2-oxoglutaric-3-$^3H_1$-3,4-$^{14}C_2$ and 2-oxoglutaric-3-$^3H_2$-3,4-$^{14}C_2$ acids, (**3e** and **3f**), were prepared by mixing the above-described singly labeled 2-oxoglutaric acids.

Table 3 shows the incorporations of the doubly labeled precursors into protoanemonin (**1**). The $^3H/^{14}C$ ratios in protoanemonin (**1**) thus biosynthesized are shown in Table 4. The $^3H/^{14}C$ ratio in **1** biosynthesized from 2-oxoglutaric-3-$^3H_2$-3,4-$^{14}C_2$ acid (**3f**) resulted in a half of the $^3H/^{14}C$ ratio in **3f**, whereas the $^3H/^{14}C$ ratio in **1** was retained in the feeding of

TABLE 3. THE INCORPORATION OF (3*R*)-2-OXOGLUTARIC-3,4-$^{14}C_2$ ACID (**3e**) AND 2-OXOGLUTARIC-3-$^{3}H_2$-3,4-$^{14}C_2$ ACID (**3f**) INTO PROTOANEMONIN (**1**) BY *R. glaber*

Exptl No.	Precursors	Radioactivities of precursors used[b] μCi	Feeding time[c] h	Sp. act. of **1**[a,b] (dpm/mmol)×10^{-2}	Incorp.[d] %
10	**3e**	0.249	12	7.40±0.22	0.61
11	**3e**	0.015	12	1.83±0.12	0.47
12	**3f**	0.066	12	2.32±0.18	0.52
13	**3f**	0.059	12	2.76±0.18	0.73

a) The specific radioactivity of **1** was determined on the basis of the radioactivity of pentanoic acid obtained from **1** by its hydrogenation. b) The radioactivity of the doubly labeled compounds refers to only ^{14}C. c) Metabolic period after uptake of the precursors. d) The incorporation is calculated with respect to only ^{14}C.

TABLE 4. THE $^{3}H/^{14}C$ RATIOS IN PROTOANEMONIN (**1**) AFTER UPTAKE OF (3*R*)-2-OXOGLUTARIC-3-$^{3}H_1$-3,4-$^{14}C_2$ ACID (**3e**) AND 2-OXOGLUTARIC-3-$^{3}H_2$-3,4-$^{14}C_2$ ACID (**3f**)

Exptl No.[a]	Precursors			Protoanemonin (**1**)	
	The acids	$^{3}H/^{14}C$ Ratio	$^{3}H:^{14}C$ (Normalized)[b]	$^{3}H/^{14}C$ Ratio	$^{3}H:^{14}C$ (Normalized)[c]
10	**3e**	1.96±0.01	1:1	1.89±0.07	0.96:1
11	**3e**	6.21±0.31	1:1	6.01±0.66	0.97:1
12	**3f**	13.9 ±0.22	2:1	6.18±0.51	0.89:1
13	**3f**	12.8 ±0.98	2:1	6.56±0.45	1.03:1

a) "Exptl No." corresponds to the numbers in Table 3. b) This is the normalized ratio as related to the number of ^{3}H-label at C-3 of 2-oxoglutaric acid. c) The normalized $^{3}H:^{14}C$ ratio was obtained by dividing the $^{3}H/^{14}C$ ratio of **1** by the $^{3}H/^{14}C$ ratio of 2-oxoglutaric acid and multiplying the answer by the number of ^{3}H-label at C-3 of the acid.

(3*R*)-2-oxoglutaric-3-$^{3}H_1$-3,4-$^{14}C_2$ acid (**3e**). These results demonstrate clearly that (i) the formation of double bond at the 3-position of protoanemonin (**1**) results from the elimination of the hydrogen atom at the 3-position of 2-oxoglutaric acid and (ii) the hydrogen elimination involves the stereospecific loss of the *pro*-3*S* hydrogen atom (R_S) and the retention of the *pro*-3*R* hydrogen atom (R_R) of 2-oxoglutaric acid (**3a**).

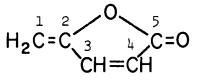

1

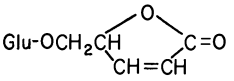

2

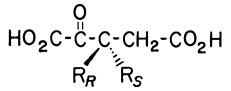

3a: R_R=R_S=H
3b: R_R=R_S=^{3}H
3c: R_R=^{3}H, R_S=H

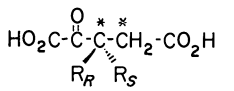

3d: R_R=R_S=H
3e: R_R=^{3}H, R_S=H
3f: R_R=R_S=^{3}H

Experimental

All the radioisotopically labeled compounds derived from radioactive protoanemonin (**1**) were purified to a constant specific radioactivity by a combination of preparative TLC with silica-gel plates (Kieselgel GF_{254}; 0.75 mm thick) and/or repeated recrystallization. All the compounds showed ^{1}H NMR and IR spectra identical with those of authentic samples. The radioactivity was counted on a liquid-scintillation spectrometer using Bray's scintillation solvent[18] and/or a 2π-gas flow low-back counter on $BaCO_3$ planchets at an infinite thickness.

Plant Material and Labeled Precursors. The sprigs of *Ranunculus glaber* Makino were collected in May at the damp ground in the suburbs of Hiroshima City. Each sprig used for the feeding experiments was about 20 cm in length and about 15 g in fresh wt. The singly labeled precursors, such as sodium 2-oxoglutarate-5-^{14}C (13 mCi/mmol), sodium acetate-1-^{14}C (23 mCi/mmol), sodium malonate-2-^{14}C (15 mCi/mmol), sodium succinate-2,3-$^{14}C_2$ (33 mCi/mmol), and sodium glutamate-5-^{14}C (68 mCi/mmol), were the products of the Daiichi Pure Chemicals Co., Ltd, Tokyo and used for the feeding experiments without purification. The doubly labeled precursors were prepard as described below.

Feeding of the Labeled Precursors to R. glaber. The labeled precursor (Tables 1 and 3) dissolved in a phosphate-buffered soln (2.0 cm^3; pH 7.0—7.4) was fed to the fresh-collected sprigs (*ca.* 70 g in total wt) through their cut-stem in a glass tube, and then the phosphate-buffered soln was soaked into the sprigs several times to force the uptake of the labeled precursor to completion. At the end of the metabolic periods shown in Tables 1 and 3, the sprigs were subjected to the following procedure to isolate the radioisotopically labeled protoanemonin (**1**).

*Isolation of the Radioisotopically Labeled Protoanemonin (**1**).* The sprigs (*ca.* 70 g) were steam-distilled. The distillate was extracted with five 50-cm^3 portions of ether. The removal of the solvent from the ether soln at temp below 25 °C under a reduced pressure in a current of nitrogen gave protoanemonin (**1**) (*ca.* 100 mg), which was then, without purification, converted into pentanoic acid [95 mg; IR (liq) 3300—2500 and 1710 cm^{-1} (COOH)] by hydrogenation in MeOH (10 cm^3) in the presence of Adam's

platinum oxide (5 mg).[3] A portion (20 mg) of the sample of pentanoic acid was treated with *p*-bromophenacyl bromide to give the *p*-bromophenacyl derivative (45 mg): mp 65—67 °C; IR (KBr) 1740 cm^{-1} (ester); ^1H NMR (60 MHz, CCl_4) δ=1.03 (3H, t, Me), 1.59 (4H, bs, $-CH_2-CH_2-$), 2.52 (2H, t, $-CO-CH_2-$), 5.33 (2H, s, $-CH_2-O-$), and 7.80 (4H, m, arom. H); MS (70 eV), *m/z* (rel intensity), 300 and 298 (6%, M^+), 185 and 183 (100), 85 (42), 57 (36), and 28 (51). Found: C, 51.98; H, 4.89%. Calcd for $C_{13}H_{15}O_3Br$: C, 52.19; H, 5.05%. The specific radioactivities of **1** were determined by measuring the specific radioactivities of the *p*-bromophenacyl derivatives; they are shown in Tables 1 and 3.

Labeling Pattern of Radioactive Pentanoic Acid. After radioactive pentanoic acid (50 mg) resulted from **1** as described above was diluted 10 times with the carrier, the pentanoic acid was converted into its silver salt (800 mg) by adding a 5% $AgNO_3$ soln to it. The silver pentanoate (200 mg) on the Schmidt reaction[11] yielded carbon dioxide and butylamine (62 mg). Carbon dioxide was absorbed in a $Ba(OH)_2$ soln and converted into $BaCO_3$ (88 mg). Butylamine (60 mg) was oxidized with a 5% $KMnO_4$ soln for 30 min at 100 °C, and the reaction mixture, after the decomposition of the remaining oxidant with sodium hydrogensulfite, was extracted with Et_2O by a continuous liquid-liquid extractor. The removal of the solvent from the ethereal soln gave butyric acid, which was then converted to the silver salt (92 mg). The oxidative degradation of this silver butyrate (80 mg) by the Schmidt reaction was repeated as described above, giving $BaCO_3$ (86 mg) and propionic acid (57 mg as the silver salt). Silver propionate (50 mg) was again subjected to the degradation in the same manner as above to give $BaCO_3$ (36 mg) and silver acetate (11 mg). On the other hand, the radioactive silver pentanoate (100 mg) on the Kuhn-Roth oxidation[12] afforded sodium acetate (17 mg). This acetate was then subjected to the Schmidt reaction[11] to give carbon dioxide and methylamine, which were then converted into $BaCO_3$ (21 mg) and methylamine hydrochloride (4 mg), respectively. This methylamine hydrochloride was then further converted into $BaCO_3$ (12 mg) by the Van Slyke-Folch oxidation.[13]

The distribution of radioactivity in each carbon atom originating from **1** was determined on the basis of the radioactivities of $BaCO_3$ obtained by the Schmidt reaction and the Kuhn-Roth oxidation; they are shown in Table 2.

Preparation of 2-Oxoglutaric-3-$^3H_2$ *Acid (3b).* On reference to the method described in the literature,[15] sodium 2-oxoglutarate (50 mg) dissolved in tritiated water (0.16 cm^3; 160 μCi) was heated at 120 °C for 30 min in a sealed glass tube. The reaction mixture was put on an Amberlite IR-45 column. After the column was washed thoroughly with H_2O to remove the tritiated water, elution of the column with 0.3% HCl (50 cm^3) gave 2-oxogutaric-3-$^3H_2$ acid (**3b**) (31 mg; 12.5 μCi) as an eluate.

Preparation of (3R)-2-Oxoglutaric-3-$^3H_1$ *Acid (3c).* Following the method described in the literature,[15,16] the tritiated 2-oxoglutaric acid (**3b**) (7.5 mg; 3.0 μCi) was incubated with isocitrate dehydrogense (50 units; Sigma Chemical Company) in the presence of NADPH (25 mg) and $MgCl_2$ (3.6 mg) in a triethanolamine hydrochloride buffered soln (50 cm^3; pH 7.1) at 30 °C for 6 h. The reaction mixture was subjected to column chromatography using Amberlite IR-45 as an ion exchange resin and 0.3% HCl as an eluent to afford (3*R*)-2-oxoglutaric-3-$^3H_1$ acid (**3c**) (5.9 mg; 1.1 μCi).

Preparation of 2-Oxoglutaric-3,4-^{14}C *Acid (3d).* On reference to the method described in the literature,[17] dimethyl succinate-2,3-$^{14}C_2$ (0.26 mg; 50 μCi) was added to a suspension of diethyl oxalate (2.0 mg) and potassium ethoxide [potassium (10 mg) in EtOH (0.1 cm^3)] in Et_2O (1.0 cm^3) with stirring at room temp. After 10 min, a precipitated yellow mass (5.1 mg) was filtered and dissolved in concd HCl. The soln obtained was extracted with Et_2O to give an oily product (2.3 mg), which was then refluxed with concd HCl (1 cm^3) for 1 h. The mixture was left to stand at room temp for 12 h and then extracted with Et_2O to give a crude sample of 2-oxoglutaric-3,4-$^{14}C_2$ acid (**3d**). Purification of this crude sample by preparative TLC (cellulose; 0.5 mm thick) with *n*-BuOH–$CHCl_3$ (1:19, v/v) and then *n*-BuOH–AcOH–H_2O (12:3:5, v/v/v) afforded the pure sample of 2-oxoglutaric-3,4-$^{14}C_2$ acid (**3d**) (3.0 μCi).

The authors wish to thank Misses Yoko Okamoto, Tomoko Horikawa, Noriko Waki, and Emiko Okamoto and Mr. Makio Kataoka, who assisted them in a part of the experimental work.

References

1) Y. Asahina, *Yakugaku Zasshi*, **396**, 81 (1915).
2) Y. Asahina and A. Fujita, *Yakugaku Zasshi*, **455**, 1 (1920).
3) F. B. Kipping, *J. Chem. Soc.*, **1935**, 1145.
4) E. Shaw, *J. Am. Chem. Soc.*, **68**, 2510 (1946).
5) G. H. Mahran, A. H. Saber, and T. El-Alfy, *Planta Med.*, **16**, 323 (1968).
6) R. Hill and R. V. Heyningen, *Biochem. J.*, **49**, 332 (1951).
7) R. Tshesche, K. Welmer, G. Wulff, and G. Snatzke, *Chem. Ber.*, **105**, 290 (1972).
8) T. Suga and T. Hirata, *Chem. Lett.*, **1973**, 637.
9) T. Suga, T. Hirata, T. Horikawa, and N. Waki, *Chem. Lett.*, **1974**, 1201.
10) T. Suga, T. Hirata, E. Okamoto, and M. Kataoka, *Chem. Lett.*, **1977**, 709.
11) K. F. Schmidt, *Chem. Ber.*, **57**, 704 (1924).
12) R. Kuhn and H. Roth, *Chem. Ber.*, **66**, 1274 (1933).
13) D. D. Van Slyke and J. Folch, *J. Biol. Chem.*, **136**, 509 (1940).
14) In this report, for convenience, the carbon atoms of protoanemonin (**1**) are numbered as shown in structural formula **1** as related with those of 2-oxoglutaric acid (**3a**).
15) Z. B. Rose, *J. Biol. Chem.*, **235**, 928 (1960).
16) A. C. Stoolmiller and R. H. Abeles, *J. Biol. Chem.*, **241**, 5764 (1966).
17) L. Friedman and E. Kosower, *Org. Synth.*, **26**, 42 (1946).
18) G. A. Bray, *Anal. Biochem.*, **1**, 279 (1960).

The Total Syntheses of (−)-Occidentalol and Its C_7-Epimer. The Stereochemical Assignment of (+)-Occidentalol[1,2]

Masayoshi Ando,* Toyonobu Asao,† Toru Nakagawa, Ken Nanaumi, and Kahei Takase

Department of Chemistry, Faculty of Science, Tohoku University, Aramaki-aza-Aoba, Sendai 980

(Received October 23, 1981)

The total syntheses of (−)-occidentalol and its C_7-epimer are reported with the object of establishing the structure of naturally occurring (+)-occidentalol.

The sesquiterpene alcohol (+)-occidentalol was first isolated from the wood of Eastern white cedar (*Thuja occidentalis* L.) by Nakatsuka and Hirose.[3] Subsequent reports from various laboratories lead to the acceptance of the structure **1**.[4–7] In 1969, Hortmann and De Roos reported a careful analysis of 100 MHz NMR spectrum of (+)-occidentalol and suggested the structure **2** for (+)-occidentalol.[8] In 1970, we established the structure **2** for (+)-occidentalol by the syntheses of compound **1** and (−)-occidentalol (**3**).[2] After our syntheses had been completed, several other syntheses of (+) or (±)-occidentalol were reported.[9–14] Recent isolation and characterization of dehydrochamaecynenol[15] and dictyolene,[16] which possess similar structures to compound **1**, is interesting matter from the biosynthetic point of view. This paper details the total syntheses of **1** and (−)-occidentalol (**3**) with the object of establishing the structure of naturally occurring (+)-occidentalol and the stereochemical consideration of their related compounds.

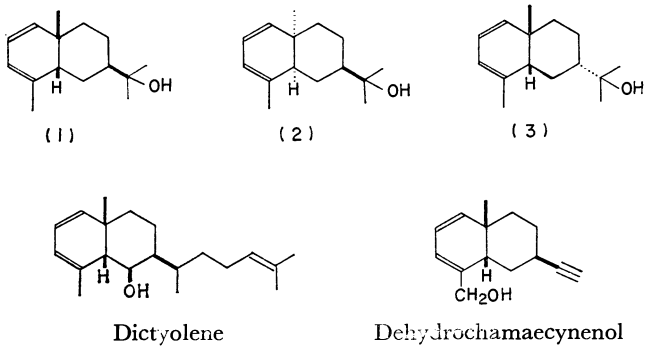

Dictyolene Dehydrochamaecynenol

Syntheses

We chose an olefinic ketone (**4**) as the starting material since **4** was easily available from l-α-santonin by means of the previously reported method[17] and conveniently functionalized as the starting material of both **1** and **3**. We envisioned an approach which consisted of the transformation of the terminal olefine at C_7 of **4** to a methoxycarbonyl group (**4**→**7**), the introduction of a homoannular 1,3-diene unit (**7**→**14**), and its transformation to **1**, or the epimerization of the methoxycarbonyl group from β to α (**14**→**17**), and its transformation to **3**.

The treatment of **4** with four equivalent of $NaIO_4$ in the presence of a catalytic amount of OsO_4 gave

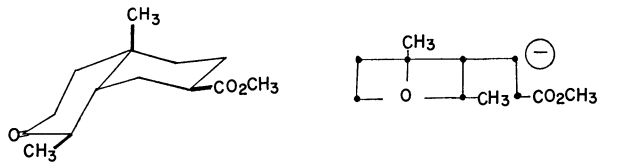

7 Steroid conformation $[\theta]_{270} = -1980$

Fig. 1.

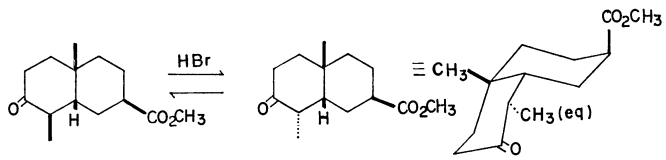

7 **18** Non-steroid conformation

Fig. 2.

a 1:1 mixture of a carboxylic acid (**6**) and an aldehyde (**5**). The latter was oxidized with Ag_2O to **6**. The compound (**6**) was methylated with CH_2N_2 to give the ester (**7**). In agreement with the structure of a *cis*-decalin derivative possessing the steroid conformation, the CD curve exhibited a negative Cotton effect.[18]

The bromination of **7** with Br_2 in acetic acid in the presence of HBr afforded two kinds of oily monobromides (**8** and **9**). The splitting patterns of the NMR signals due to the bromomethine protons, δ 4.72 (q, J=6.0 and 14.0 Hz) and δ 4.73 (q, J=6.0 and 12.0 Hz) for **8** and **9** respectively, indicated that both **8** and **9** were α-bromo ketones bearing the equatorial bromine atoms. Judging from the reaction conditions, both C_4–Me groups of **8** and **9** were deduced to be thermodynamically the more stable equatorial configuration. In addition, the β(*eq*)-configuration of the C_4–Me group of **8** and the α(*eq*)-configuration of the C_4–Me group of **9** were confirmed by the transformation of these compounds to the α,β-unsaturated ketones, **10** and **11**, respectively. The formation of the bromides **8** and **9** starting from **7** can be reasonably explained as follows. The ketone **7** was epimerized at C_4 in the presence of HBr to give an equilibrium mixture of **7** and its C_4-epimer, **18**. The bromination of **7** and **18** in the reaction mixture at the C_2-position gave **8** and **9**, respectively.

The dehydrobromination of **8** with LiBr–Li_2CO_3 in DMF produced an oily α,β-unsaturated ketone (**10**). In accordance with the stereo-structure **10** with the steroid conformation, as is shown in Fig. 3, the NMR spectrum (CCl_4, 100 MHz) did not show a long-range coupling between C_1–H and C–H.[19,20] The half-

† Present address: Department of Chemistry, College of General Education, Tohoku University, Kawauchi, Sendai 980.

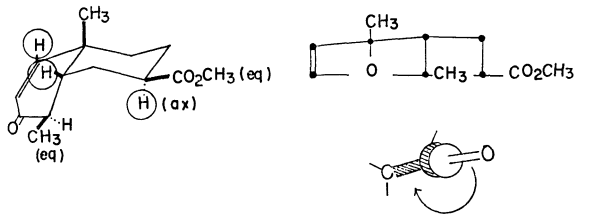

10 Steroid conformation $n\rightarrow\pi^*$ $[\theta]_{320}=-2580$ $\pi\rightarrow\pi^*$ $[\theta]_{225}=+33900$

Fig. 3.

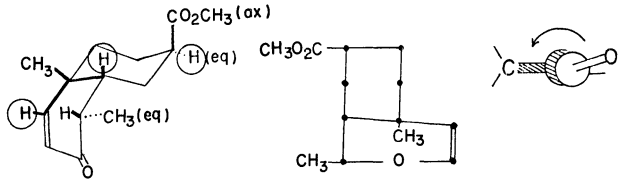

11 Non-steroid conformation $n\rightarrow\pi^*$ $[\theta]_{310}=+1200$ $\pi\rightarrow\pi^*$ $[\theta]_{225}=-12600$

Fig. 4.

band width of C_7–H was *ca.* 20 Hz, which agreed with the expected value of $\alpha(ax)$ C_7–H.[19] The β-equatorial configuration of the C_4–Me group of **10** was suggested from the solvent effect in the NMR spectrum on passing from CCl_4 to benzene ($\delta_{CCl_4}-\delta_{C_6H_6}=+0.01$ ppm)[21] and was confirmed from the coupling constant between C_4–H and C_5–H ($J=12.5$ Hz). The CD curve of **10** showed a negative Cotton effect at 320 nm for the $n\rightarrow\pi^*$ transition and a positive Cotton effect at 225 nm for the $\pi\rightarrow\pi^*$ transition[22] which agreed with the signs expected from the stereo-structure **10** with the steroid conformation bearing a $\beta(eq)$-methyl group at C_4 and a $\beta(eq)$-methoxycarbonyl group at C_7.

The dehydrobromination of **9** with LiBr–Li_2CO_3 in DMF gave an oily α,β-unsaturated ketone (**11**). In agreement with the stereo-structure **11**, as is shown in Fig. 4, the NMR (CCl_4, 100 MHz) spectrum showed a long-range coupling ($J=2.5$ Hz) between C_1–H and C_5–H.[19,20] The half-band width of C_7–H was *ca.* 10 Hz which agreed with the expected value of $\alpha(eq)$ C_7–H.[19] The α-equatorial configuration of the C_4–Me group of **11** was suggested from the solvent effect in the NMR spectrum on passing from CCl_4 to benzene ($\delta_{CCl_4}-\delta_{C_6H_6}=-0.09$ ppm)[21] and was confirmed from the coupling constant between C_4–H and C_5–H ($J=3.8$ Hz). The CD curve of **11** showed a positive Cotton effect at 310 nm for $n\rightarrow\pi^*$ transition and a negative Cotton effect at 225 nm for $\pi\rightarrow\pi^*$ transition[22] which agreed with the signs expected from the stereo-structure **11** with the non-steroid conformation bearing an $\alpha(eq)$-methyl group at C_4 and a $\beta(ax)$-methoxycarbonyl group at C_7.

The reduction of **10** and **11** with $NaBH_4$ gave an oily mixture of epimeric alcohols (**12**) and of epimeric alcohols (**13**), respectively. On being heated at 210 °C in the presence of alumina containing 4% of pyridine,[23] both mixtures of alcohols gave the same oily diene (**14**). The diene (**14**) was conveniently prepared from **7** by the same method described above, without the

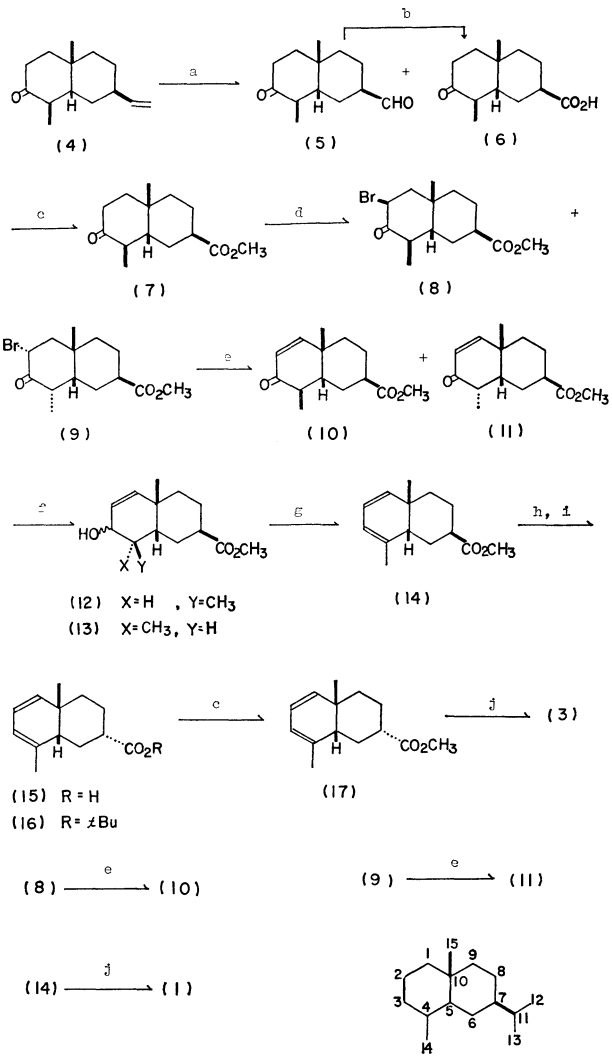

a: OsO_4, $NaIO_4$; b: Ag_2O; c: CH_2N_2; d: HBr, Br_2; e: LiBr, Li_2CO_3, DMF; f: $NaBH_4$; g: Al_2O_3–Py; h: *t*-BuOK/*t*-BuOH; i: hydrolysis; j: MeMgI

Scheme 1.

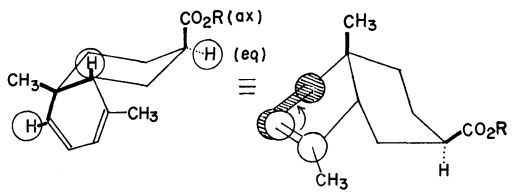

14 R=CH_3 $[\theta]_{259}=-33800$
19 R=$CH(CH_3)_2$ $[\theta]_{260}=-34200$
Non-steroid conformation

Fig. 5.

separation of the epimers in each step. The non-steroid conformation bearing the $\beta(ax)$-methoxycarbonyl group at C_7 for **14**, as is shown in Fig. 5, was revealed from the NMR spectrum which showed the long-range coupling between C_1–H and C_5–H ($J=1.0$ Hz)[8,19,20] and a rather small magnitude of the half-band width ($W_{h/2}=11$ Hz) of C_7–H.[19] The CD curve of **14** showed a negative Cotton effect at 259 nm due to the skewing of the *s-cis* butadiene moiety in the sense of a left-hand helix[24] which agreed with

Table 1. The NMR spectral data of *s-cis* diene derivatives

Compound	Conformation	Chemical shifts of hydrogens (δ)						The orientation of the functional groups at C_7
		C_1-H	C_2-H	C_3-H	C_7-H	C_4-CH_3	C_{10}-CH_3	
1	Steroid	5.2—5.8 (3H, m)				1.80	1.10	β (*eq*)
2, 3	Non-steroid	5.21 (d)	5.74 (dd)	5.49 (m)		1.79	0.85	α (*eq*)
14	Non-steroid	5.22 (d)	5.76 (dd)	5.52 (m)	2.49 ($W_{h/2}$=11 Hz)	1.80	0.86	β (*ax*)
16	Non-steroid	5.27 (d)	5.80 (dd)	5.55 (m)		1.79	0.85	α (*eq*)
17	Non-steroid	5.28 (d)	5.81 (dd)	5.50 (m)		1.79	0.86	α (*eq*)
19[25]	Non-steroid	5.22 (d)	5.75 (dd)	5.51 (m)	2.44 ($W_{h/2}$=12 Hz)	1.79	0.85	β (*ax*)

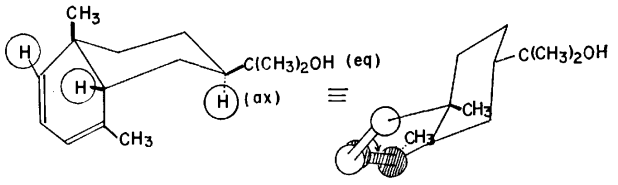

1 Steroid conformation $[\theta]_{261}$= +27600

Fig. 6.

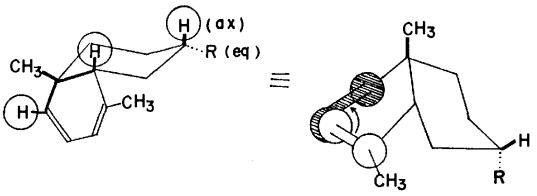

17 R=CO_2Me $[\theta]_{262}$= −49200
3 R=$C(CH_3)_2OH$ $[\theta]_{260}$= −56900
Non-Steroid conformation

Fig. 7.

the stereo-structure **14** with the non-steroid conformation bearing a β(*ax*)-methoxycarbonyl group at C_7.

The treatment of **14** with methylmagnesium bromide gave an unstable oily alcohol (**1**), which exhibited completely different IR (in $CHCl_3$), NMR (in CCl_4), CD (in MeOH), and MS (at 70 eV) from those of naturally occurring occidentalol. In accordance with the stereo-structure **1** with the steroid conformation, as is shown in Fig. 6, the CD curve of **1** showed a positive Cotton effect due to the skewing of *s-cis* butadiene moiety in the sense of right-hand helix.[24]

Since the structure **1**, the Rudloff's structure of (+)-occidentalol, was not identical with naturally occurring "(+)-occidentalol", our attention was focused on the synthesis of **3**, the C_7-epimer of **1**.

The treatment of **14** with 1 M (1 M=1 mol dm^{-3}) *t*-BuOK in *t*-BuOH under refluxing temperature for 2 h gave a mixture of a carboxylic acid (**15**) and the corresponding *t*-butyl ester (**16**). The hydrolysis of the latter with aqueous alkali and the combined acidic part was methylated subsequently with diazomethane to give a 1:22 mixture of **14** and **17**. The NMR spectrum of **17** was quite similar to that of **14** except the signal of C_7-H which was shifted to higher field than the corresponding signal of **14** and was overlapped with those of other protons. These NMR data

Steroid conformation Non-steroid conformation

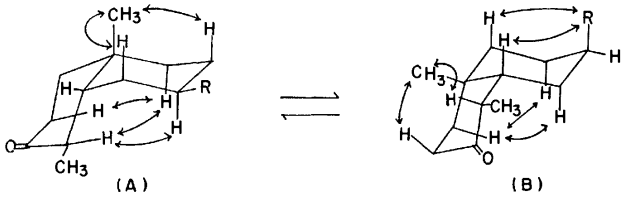

Fig. 8.

Table 2. Equilibration data for the **A**⇌**B** reaction at 25 °C

R	K (**B**/**A**)	ΔG/kcal mol^{-1}
-C≡CH	1.58	−0.27[17]
$-CO_2CH_3$	0.45	0.46
$-CH=CH_2$	0.16	1.09[17]
$-CH_2-CH_3$	(0)	[17]

strongly suggest that compounds **14** and **17** are stereoisomeric at C_7 position with each other and have the same non-steroid conformation. The CD curve of **17** showed a negative Cotton effect at 262 nm due to the skewing of the *s-cis* butadiene moiety in the sense of a left-hand helix[24] which agreed with the conclusion from the NMR data.

The treatment of **17** with methylmagnesium bromide gave an alcohol (**3**), which was identical with naturally occurring (+)-occidentalol in the NMR, IR, and MS but showed the opposite sign in the CD curves. These results indicate that the structure of naturally occurring "(+)-occidentalol" must be represented by the structure (**2**) and the alcohol (**3**) is its antipodal (−)-occidentalol (**3**).

The Stereochemical Studies of the Synthetic Intermediates

Equilibration of 7⇌18 and 10⇌11. The keto ester (**7**) was treated with a 2% KOH solution of ethanol for 6 h at 25 °C and then quenched by the use of aqueous acetic acid solution to give a 2.2:1.0 equilibrium mixture of **7** and **18**. The ΔG value of this equilibration at 25 °C was determined to be 0.46 kcal mol^{-1}. This ΔG value was compared with those of three pairs of *cis*-decalone derivatives possessing the different functional groups at C_7-position and summarized in Table 2. The examination of Dreiding models showed that the observed ΔG values

Steroid conformation Non-steroid conformation

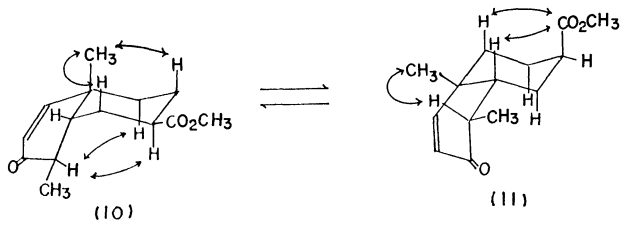

Fig. 9.

Steroid conformation Non-steroid conformation

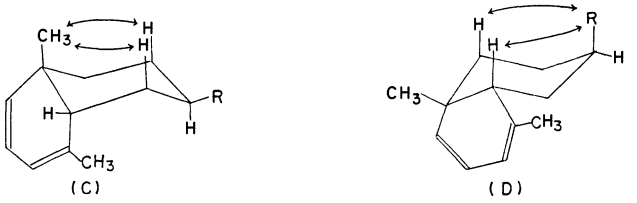

Fig. 10.

should reflect the difference between the one inner H–H interaction in the A-series compounds and the two R–H 1,3-diaxial interactions in the B-series compounds since two Me–H 1,3-diaxial interactions and two inner H–H interactions existed in both series compounds, as depicted in the stereo-structures **A** and **B**. Actually, the observed ΔG values, summarized in Table 2, reflect well the order of the bulkiness of R at C_7, $-CH_2CH_3 \gg -CH{=}CH_2 > -CO_2Me > -C{\equiv}CH$. The equilibrium reaction of α,β-unsaturated ketones **10** and **11** gave a tendency similar to that of the equilibrium reaction of **7** and **18**. The ΔG value is 0.37 kcal mol^{-1}, smaller than the latter case, because in **11** one Me–H interaction and two inner H–H interactions are eliminated compared with **18** by the introduction of a double bond at C_1, whereas in **10** one inner H–H interaction is eliminated compared with **7**.

The Stereochemistry of s-cis *Diene Derivatives.* For *s-cis* diene derivatives (**1**, **14**, and **19**) bearing a β-oriented substituent at C_7 there are two possible conformations, steroid conformation (**C**) and non-steroid conformation (**D**). The examination of Dreiding models showed there to be two Me–H 1,3-diaxial interactions in the conformer (**C**) as depicted by the arrows. On the other hand, in the conformer (**D**) there are two R–H 1,3-diaxial interactions as depicted by the arrows. Since the R–H 1,3-diaxial interaction is far bigger than that of Me–H in the case of R=–C-$(CH_3)_2OH$, the compound (**1**) exists exclusively in the steroid conformation (**C**).

When R is methoxycarbonyl or isopropoxycarbonyl group, the non-steroid conformation **D** may be expected to be the favored conformer by the following reasons. The methoxycarbonyl and isopropoxycarbonyl groups are planar and the magnitudes of the 1,3-diaxial interactions of these groups at C_7 and the two hydrogen atoms at C_5 and C_9 in the conformer **D** are smaller than those of the angular methyl group and two hydrogen atoms at C_6 and C_8 in the conformer (**C**). Actually **14** and the corresponding isopropyl ester (**19**)[25] exist exclusively in the non-steroid conformation (**D**).

Steroid conformation Non-steroid conformation

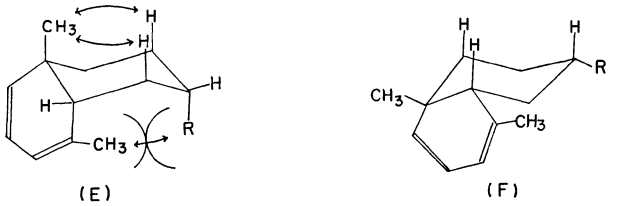

Fig. 11.

For *s-cis* diene derivatives (**3**, **16**, and **17**) bearing an α-oriented substituent at C_7 there are two possible conformations, the steroid conformation (**E**) and the non-steroid conformation (**F**). In the conformer **E** there is a big interaction between the axial substituent at C_7 and the A-ring in addition to two Me–H 1,3-diaxial interactions as depicted by the arrows, whereas there is no remarkable interaction in the conformer **F**. Actually all of the compounds **3**, **16**, and **17** exist exclusively in the non-steroid conformation (**F**).

Experimental

All the melting points are uncorrected. The IR spectra were recorded on Shimadzu IR-27 spectrophotometers. The NMR spectra were recorded on Varian A-60, Nichiden-Varian T-60, and Varian HA-100 spectrometers, employing tetramethylsilane as the internal reference. The CD spectra were recorded on a Nihonbunko ORD/UV-5 spectrometer. Mass spectra were recorded on a Hitachi RMu-6D spectrometer with a direct inlet system operating at 70 eV.

*Methyl 3-Oxo-4α*H*,5β-12,13-bisnoreudesman-11-oate (7).* A mixture of *4α*H*,5β*-13-noreudesm-11-en-3-one (**4**, 2.90 g, 14.1 mmol), $NaIO_4$ (12.1 g, 56.6 mmol), and OsO_4 (13.3 mg, 0.05 mmol) in 50 ml of dioxane–H_2O (4:1) was stirred for 2 h at room temperature and filtered. The filtrate was poured into a saturated aq soln of NaCl (200 ml) and extracted with ether (100 ml×3). The combined extracts were washed successively with a 2 M aq soln of Na_2CO_3 (20 ml×3), and a saturated aq soln of NaCl, dried and concentrated to give an oily neutral product (1.94 g). The combined washings of Na_2CO_3 were acidified with 6 M HCl and extracted with ether (50 ml×3). The combined extracts were washed with a saturated soln of NaCl, dried ($MgSO_4$), and concentrated to give 745 mg of an oily acidic product. The neutral part was stirred with Ag_2O, which was freshly prepared from 17 g of $AgNO_3$, in 50 ml of THF–H_2O (4:1) for 70 h at room temperature to give further 785 mg of acidic part. The combined acidic product (1.52 g) was methylated with 12 ml of CH_2N_2–ether soln (0.6 mmol/ml) to give 1.62 g of crude methyl ester, which was chromatographed over silica gel (Merck, finer than 230 mesh, 80 g) and eluted with CCl_4–$CHCl_3$ (1:1) to give 804 mg (24%) of spectroscopically pure **7**. This was recrystallized from pentane to give colorless prisms; mp 71 °C. IR (KBr): 1730 and 1698 cm^{-1}. NMR (CCl_4): δ 0.97 (3H, d, J=6.5 Hz, C_4–Me), 1.07 (3H, s, C_{10}–Me), and 3.61 (3H, s, –OMe) ppm. CD (MeOH): $[\theta]_{270} = -1980$. Found: C, 70.54; H, 9.26%. Calcd for $C_{14}H_{22}O_3$: C, 70.55; H, 9.31%.

Methyl 5β-12,13-Bisnoreudesma-1,3-dien-11-oate (14) from **7** *without Separation of Stereoisomers in Each Step.* Into a solution of **7** (1.645 g, 6.90 mmol) and HBr (0.1 ml) in AcOH

(15 ml) was added a solution of Br_2 (1.20 g, 7.5 mmol) in AcOH (5 ml). The mixture was stirred for 30 min at room temperature, poured into a saturated aq soln of NaCl (200 ml) and extracted with ether (50 ml×3). The combined extracts were washed successively with a saturated aq soln of Na_2CO_3 and a saturated aq soln of NaCl dried ($MgSO_4$), and concentrated to give 2.26 g of the crude bromides as the epimeric mixture of C_2 and C_4, which was employed in the following reaction without any purification.

A mixture of the crude bromides (2.26 g), dry DMF (30 ml), LiBr (2.36 g, 27.2 mmol), and Li_2CO_3 (2.36 g, 31.9 mmol) was heated at 153 °C under stirring for 8 h. The mixture was poured into a saturated aq soln of NaCl (200 ml) and extracted with ether (50 ml×3). The combined extracts were washed successively with a 2 M aq soln of HCl (30 ml) and a saturated aq soln of NaCl, dried and concentrated to give a mixture of **10** and **11** (2:1, 863 mg), which was employed in the next step without any purification.

The mixture of **10** and **11** (863 mg) was reduced with $NaBH_4$ (140 mg, 3.70 mmol) in ether–MeOH (2:1, 27 ml) and treated in the usual way to give a mixture of allylic alcohols as a epimeric mixture at C_3 and C_4, which was employed without any purification in the next step.

The resultant allylic alcohols were passed through the column packed with basic alumina†† (2.6 g), which was preheated at 220 °C, with the flow of nitrogen. The product was trapped in a flask cooled with Dry Ice–acetone bath to give spectroscopically pure **14** (264 mg, 17.4% overall yield from **7**) as an oily material, which was chromatographed over silica gel (Merck, finer than 230 mesh) and eluted with $CHCl_3$–CCl_4 (1:1) to give the analytical sample as an oil. IR (neat): 1730 and 1645 cm^{-1}. NMR (CCl_4): δ 0.86 (3H, s, C_{10}–Me), 1.80 (3H, broad s, C_4–Me), 2.49 (1H, m, $W_{h/2}$=11.0 Hz, C_7–H), 3.64 (3H, s, –OMe), 5.22 (1H, ddd, $J_{1,3}$=1.0 Hz, $J_{1,5}$=1.0 Hz, and $J_{1,2}$=9.5 Hz, C_1–H), 5.52 (1H, dqd, $J_{1,3}$=1.0 Hz, $J_{3,14}$=1.8 Hz, and $J_{2,3}$=5.0 Hz, C_3–H), and 5.76 (1H, dd, $J_{2,3}$=5.0 Hz and $J_{1,2}$=9.5 Hz, C_2–H) ppm. CD (MeOH): $[\theta]_{259}=-33800$. MS (70 eV) *m/e* (rel intensity): 220 (19, M^+), 173 (15), 160 (24), 145 (100), 119 (35), 105 (23), 91 (20). Found: C, 76.12; H, 9.27%. Calcd for $C_{14}H_{20}O_2$: C, 76.32; H, 9.15%.

Methyl 2β-Bromo-3-oxo-4αH,5β-12,13-bisnoreudesman-11-oate (8) and Methyl 2α-Bromo-3-oxo-4βH,5β-12,13-bisnoreudesman-11-oate (9). A mixture of the crude bromide (253 mg) which was prepared from **7** was chromatographed over silica gel (Merck, finer than 230 mesh) and eluted with CCl_4–$CHCl_3$ (2:1) to give 19 mg of spectroscopically pure **9** from the first fraction and 42 mg of spectroscopically pure **8** from the last fraction. NMR (CCl_4) of **8**: δ 1.05 (3H, d, J=6.5 Hz, C_4–Me), 1.10 (3H, s, C_{10}–Me), 3.58 (3H, s, –OMe), and 4.72 (1H, q, J=6.0 and 14.0 Hz, C_2–H) ppm. NMR (CCl_4) of **9**: δ 1.03 (3H, d, J=6.5 Hz, C_4–Me), 1.33 (3H, s, C_{10}–Me), 3.61 (3H, s, –OMe), and 4.73 (1H, q, J=6.0 and 12.0 Hz) ppm.

Methyl 3-Oxo-4αH,5β-12,13-bisnoreudesm-1-en-11-oate (10) and Methyl 3-Oxo-4βH,5β-12,13-bisnoreudesm-1-en-11-oate (11). The crude mixture of α,β-unsaturated ketones (**10** and **11**, 572 mg) which was prepared by the previously mentioned method was chromatographed over silica gel (60 g, Merck, finer than 230 mesh) and eluted with CCl_4–$CHCl_3$ (1:1). The first fraction gave **11** (85 mg). IR (neat): 1732 and 1680 cm^{-1}. NMR (CCl_4): δ 1.05 (3H, d, J=7.0 Hz, C_4–Me), 1.24 (3H, s, C_{10}–Me), 2.63 (1H, m, $W_{h/2}$=*ca.* 10 Hz, C_7–H), 2.88 (1H, dq, J=3.8 and 7.0 Hz, C_4–H), 3.65 (3H, s, –OMe), 5.79 (1H, d, J=10.0 Hz, C_2–H), and 6.34 (1H, dd, J=2.5 and 10.0 Hz, C_1–H) ppm. NMR (C_6H_6): δ 0.88 (3H, s, C_{10}–Me) and 1.14 (3H, d, J=7.0 Hz, C_4–Me). CD (MeOH): $[\theta]_{225}=-12600$, $[\theta]_{310}=+1200$. MS (70 eV) *m/e* (rel intensity): 236 (91, M^+), 221 (21), 189 (32), 177 (34), and 161 (100). The second fraction gave a mixture of **10** and **11**. The third fraction gave **10** (120 mg). IR (neat): 1736 and 1680 cm^{-1}. NMR (CCl_4): δ 1.10 (3H, d, J=6.5 Hz, C_4–Me), 1.23 (3H, s, C_{10}–Me), 2.34 (1H, m, $W_{h/2}$=*ca.* 20 Hz, C_7–H), 2.42 (1H, qd, J=6.5 and 12.5 Hz, C_4–H), 3.62 (3H, s, –OMe), 5.76 (1H, d, J=10.0 Hz, C_2–H), and 6.45 (1H, d, J=10.0 Hz, C_1–H) ppm. NMR (C_6H_6): δ 0.80 (3H, s, C_{10}–Me) and 1.09 (3H, d, J=6.5 Hz, C_4–Me). CD (MeOH): $[\theta]_{225}=+33900$, $[\theta]_{320}=-2580$. MS (70 eV): *m/e* (rel intensity), 236 (97, M^+), 221 (28), 189 (28), 177 (44), 161 (79), 82 (100).

Preparation of 11 from 9. A mixture of **9** (19 mg, 0.06 mmol), LiBr (20 mg, 0.23 mmol), Li_2CO_3 (24 mg, 0.32 mmol) in dry DMF was stirred at 160 °C for 6 h and treated in a usual way to give spectroscopically pure **11** (8 mg, 57%).

Preparation of 10 from 8. A mixture of **8** (42 mg, 0.13 mmol), LiBr (20 mg, 0.23 mmol), Li_2CO_3 (24 mg, 0.32 mmol) was stirred at 160 °C for 6 h and treated in a usual way to give spectroscopically pure **10** (22 mg, 70%).

Preparation of 14 from 10. The α,β-unsaturated ketone **10** (100 mg, 0.42 mmol) was reduced with $NaBH_4$ (16 mg, 0.42 mmol) in ether–MeOH (2:1, 1.5 mmol) and treated in a usual way to give methyl 3-hydroxy-4α*H*,5β-12,13-bisnoreudesm-1-en-11-oate (**12**) as an epimeric mixture at C_3. This mixture was passed through the column packed with basic alumina (300 mg), which was preheated at 220 °C, with N_2 flow to give **14** (31 mg, 33%).

Preparation of 14 from 11. The α,β-unsaturated ketone **11** (40 mg, 0.17 mmol) gave **14** (12 mg, 33%) in the same procedure above mentioned.

5β-Eudesma-1,3-dien-11-ol (1). Into a dry ether solution of methylmagnesium iodide [prepared from magnesium (73 mg, 3.00 mmol), methyl iodide (426 mg, 3.00 mmol), and dry ether (4 ml)] was added **14** (150 mg, 0.68 mmol) in dry ether (2 ml). This mixture was refluxed under N_2 for 1 h, poured into an aq soln of ammonium chloride, and extracted with ether (20 ml×3). The combined extracts were washed with a saturated aq soln of NaCl, dried ($MgSO_4$) and concentrated to give **1** (110 mg, 73%). IR (neat): 3350, 756, and 732 cm^{-1}. NMR (CCl_4): δ 1.10 (3H, s, C_{10}–Me), 1.13 (6H, s, C_{11}–Me), 1.80 (3H, broad s, C_4–Me), and 5.2—5.8 (3H, m) ppm. CD (MeOH): $[\theta]_{261}=27600$. MS (70 eV): *m/e* 220.

Methyl 5β,7βH-12,13-Bisnoreudesma-1,3-dien-11-oate (17). A mixture of **14** (80 mg, 0.36 mmol) and 1 M *t*-BuOK/*t*-BuOH (5 ml) was refluxed for 1.5 h under N_2, allowed to stand at room temperature for 2 h, poured into a saturated aq soln of NaCl, and extracted with ether (15 ml×3). The combined extracts were washed with a saturated aq soln of NaCl, dried ($MgSO_4$) and concentrated to give 57 mg of oily material as a neutral part, which mainly consisted of *t*-butyl 5β,7β*H*-12,13-bisnoreudesma-1,3-dien-11-oate (**16**). NMR (CCl_4): δ 0.85 (3H, s, C_{10}–Me), 1.39 (9H, s, *t*-Bu), 1.79 (3H, broad s, C_4–Me), 5.27 (1H, broad d, J=9.5 Hz, C_1–H), 5.55 (1H, m, C_3–H), 5.80 (1H, dd, J=5.0 and 9.5 Hz, C_2–H) ppm.

The aq layer was acidified by 2 M HCl and extracted with ether (15 ml×3). The combined extracts were wash-

†† The mixture of neutral alumina (active grade I, 5 g) and pyridine (0.4 ml) was shaken and evaporated at room temperature under reduced pressure (20 mmHg) for 7 h to give 5.23 g of basic alumina.

ed with a saturated aq soln of NaCl, dried ($MgSO_4$) and concentrated to give 28 mg of crystalline material, which mainly consisted of 5β,7βH-12,13-bisnoreudesma-1,3-dien-11-oic acid (**15**).

The neutral part was dissolved in a mixture of MeOH (5 ml) and a 10% aq soln of NaOH (2 ml). The mixture was refluxed for 40 min under N_2, cooled, poured into a saturated aq soln of NaCl, and extracted with ether. The aq layer was acidified by 2 M HCl and extracted with ether (15 ml×3). The combined ether layer was treated in a usual way to give 24 mg of a crystalline material, which mainly consisted of **15**.

The combined acidic part (52 mg) was methylated with a slight excess of diazomethane in ether to give 55 mg of oily material, which was ascertained to be a mixture of **14** and **17** (1:22) by the analysis of GLPC.

In another experiment a mixture of **14** (50 mg, 0.23 mmol) and 1 M *t*-BuOK/*t*-BuOH (3 ml) was refluxed for 2 h under N_2, poured into a saturated aq soln of NaCl, and extracted with ether to eliminate the neutral part. The aq layer was acidified by 2 M hydrochloric acid and extracted with ether (15 ml×3). The combined extracts were washed with a saturated aq soln of NaCl, dried ($MgSO_4$) and concentrated to give a crystalline material, which was recrystallized from ether to give 37 mg of **15** (mp 113 °C). This material was methylated by diazomethane to give **17** (40 mg, 80%). IR (neat): 1735, 1705 (sh), and 728 cm^{-1}. NMR (CCl_4): δ 0.86 (3H, s, C_{10}–Me), 1.79 (3H, broad s, C_4–Me), 3.57 (3H, s, –OMe), 5.28 (1H, broad d, J= 9.5 Hz, C_1–H), 5.50 (1H, m, C_3–H), and 5.81 (1H, dd, J=5.5 and 9.5 Hz, C_2–H) ppm. CD (MeOH): $[\theta]_{262}$= −49200. Found: C, 76.75; H, 9.11%. Calcd for $C_{14}H_{20}O_2$: C, 76.32; H, 9.15%.

(−)-Occidentalol (3). Into an ether solution of methylmagnesium iodide [prepared from magnesium powder (25 mg, 1.0 mmol) and methyl iodide (182 mg, 1.0 mmol) in dry ether (10 ml)] was added **17** (37 mg, 0.17 mmol) in dry ether (7 ml). The solution was stirred at room temperature for 40 min, then refluxed for 30 min under N_2. The reaction mixture was poured into a saturated aq soln of NH_4Cl, and extracted with ether. The combined extracts was washed with a saturated aq soln of NaCl, dried ($MgSO_4$) and concentrated to give an oily material (34 mg), which was purified by preparative TLC (silica gel GF_{254}, thickness 0.25 mm, $CHCl_3$) to give 20 mg (54%) of spectroscopically pure (−)-occidentalol (**3**), mp 83—85 °C.

References

1) The Synthetic Studies of the Sesquiterpenes with the *cis*-Fused Decalin System. III. Part I: M. Ando, T. Asao, N. Hiratsuka, K. Takase, and T. Nozoe, *Bull. Chem. Soc. Jpn.*, **53**, 1425 (1980). Part II: M. Ando, T. Asao, and K. Takase, *Bull. Chem. Soc. Jpn.*, **53**, 1039 (1980).

2) Preliminary report of this work: M. Ando, K. Nanaumi, T. Nakagawa, T. Asao, and K. Takase, *Tetrahedron Lett.*, **1970**, 3891.

3) T. Nakatsuka and Y. Hirose, *Bull. Agric. Chem. Soc. Jpn.*, **20**, 215 (1956).

4) Y. Hirose and T. Nakatsuka, *Bull. Agric. Chem. Soc. Jpn.*, **23**, 140 (1959).

5) E. von Rudloff and H. Ertmann, *Tetrahedron*, **18**, 1315 (1962).

6) K. Mislow and A. Moscowitz, *Tetrahedron Lett.*, **1963**, 699.

7) H. Ziffer, T. J. Batterham, U. Weiss, and E. von Rudloff, *Tetrahedron*, **20**, 67 (1964).

8) A. G. Hortmann and J. B. De Roos, *J. Org. Chem.*, **34**, 736 (1969).

9) M. Sergent, M. Mongrain, and P. Deslongchamps, *Can. J. Chem.*, **50**, 336 (1972).

10) Y. Amano and C. H. Heathcock, *Can. J. Chem.*, **50**, 340 (1972).

11) D. S. Watt and E. J. Corey, *Tetrahedron Lett.*, **1972**, 4651.

12) A. G. Hortmann, D. S. Daniel, and J. E. Martinelli, *J. Org. Chem.*, **38**, 728 (1973).

13) J. A. Marshall and P. G. M. Wuts, *J. Org. Chem.*, **42**, 1794 (1977).

14) Y. Mizuno, M. Tomita, and H. Irie, *Chem. Lett.*, **1980**, 107.

15) T. Asao, S. Ibe, K. Takase, Y. S. Cheng, and T. Nozoe, *Tetrahedron Lett.*, **1968**, 3639.

16) H. H. Sun, S. M. Waraszkiewicz, K. L. Erickson, J. Finer, and J. Clardy, *J. Am. Chem. Soc.*, **99**, 3516 (1977).

17) M. Ando, T. Asao, N. Hiratsuka, K. Takase, and T. Nozoe, *Bull. Chem. Soc. Jpn.*, **53**, 1425 (1980).

18) W. Moffitt, R. B. Woodward, A. Moscowitz, W. Klyne, and C. Djerassi, *J. Am. Chem. Soc.*, **83**, 4013 (1961).

19) N. S. Bhacca and D. H. Williams, "Applications of NMR Spectroscopy in Organic Chemistry," Holden-Day, San Fransisco (1964).

20) T. Toda, M. C. Woods, and K. Takahashi, *Tetrahedron*, **27**, 5391 (1971).

21) D. H. Williams and N. S. Bhacca, *Tetrahedron*, **21**, 2021 (1965).

22) C. Djerassi, R. Records, E. Bunnenberg, K. Mislow, and A. Moscowitz, *J. Am. Chem. Soc.*, **84**, 870 (1962); G. Snatzke, *Tetrahedron*, **21**, 413, 421, and 439 (1965); M. Legrand and R. Viennet, *C. R. Acad Sci.*, **261**, 1667 (1965); L. Velluz and M. Legrand, *Angew. Chem.*, **77**, 842 (1965).

23) E. von Rudloff, *Can. J. Chem.*, **39**, 1860 (1961).

24) A. Moscowitz, E. Charney, U. Weiss, and H. Ziffer, *J. Am. Chem. Soc.*, **83**, 4661 (1961).

25) The isoproyl ester (**19**) was prepared in 47% yield as the following procedures.

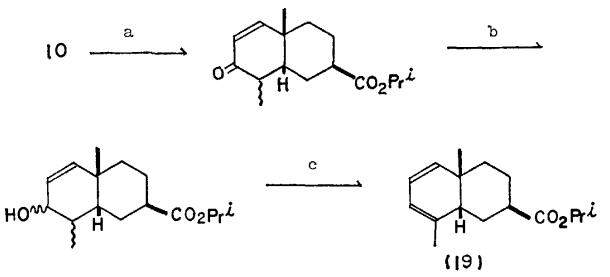

a: $Al(i\text{-}PrO)_3$, *i*-PrOH; b: $NaBH_4$; c: Al_2O_3–Py

A Convenient Synthesis of 4- and 5-Acetyltropolone

Hiroshi YAMAMOTO,* Atsushi HARA, Ayashi NOGUCHI, Heizan KAWAMOTO, Saburo INOKAWA, and Tetsuo NOZOE†

Department of Chemistry, Faculty of Science, Okayama University, Tsushima, Okayama 700

(Received October 24, 1981)

4-Acetyltropolone is derived from hinokitiol (β-thujaplicin) in four steps, with an overall yield of 60%, *via* readily available 8-azidohinokitiol. γ-Thujaplicin almost quantitatively forms its difluoroboron complex, which, upon bromination, provides an 85% yield of the 8-bromo-γ-thujaplicin difluoroboron complex. This bromo compound readily gives γ-dolabrin (87% with triethylamine) and 8-azido-γ-thujaplicin (88% with sodium azide), from which 5-acetyltropolone is derived in an 80% yield by ozonolysis or in a 40% yield with sulfuric acid. The considerable differences in the reactivities observed between these 4- and 5-substituted tropolones are discussed. The pK_a values of 4- and 5-acetyltropolone and 4- and 5-(3,4,5-trimethoxycinnamoyl)tropolones are also reported.

The tropolone nucleus is well known to be susceptible to many electrophilic substitution reactions, but does not undergo the Friedel-Crafts-type alkylation or acylation.[1-4] Several examples of direct carbon-carbon bond formation on the tropolone nucleus by various methods under basic conditions (*e.g.*, the Reimer-Tiemann reaction, hydroxymethylation, and the Mannich reaction) have been reported. These reactions, however, have drawbacks either with respect to the preparative yield or the regioselective control.[1-5] Organometallic reagents, such as Grignard or lithium reagents, give rise to the alkyl- or aryl-substitution products only at the 2-position of the tropolone nucleus.[1] Therefore, one of the present authors (T.N.) and his co-workers utilized naturally occurring β-dolabrin[6] (**8**) or 3-carboxy-4-carboxymethyltropolone derived from natural purpurogallin[1-3] as the starting material in preparing tropolones bearing a *C*-substituent at the 4-position.[7] For example, **8** was oxidatively converted[6b] into 4-acetyltropolone (**1**), which subsequently afforded a wide variety of the cinnamoyltropolones (**3**) and their derivatives (**5**) for the attempted synthesis of colchicine analogs,[1,8] although the detailed experimental results have remained unpublished[7] (Scheme 1). 5-Acetyltropolone (**2**) was also derived from **8** by a multi-step conversion in a 10—15% overall yield and likewise afforded the 5-cinnamoyltropolones[9] (**4**).

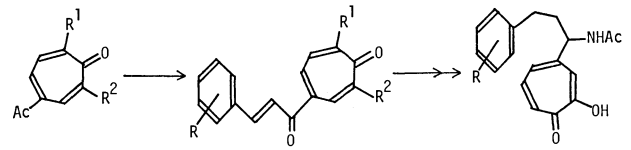

	R^1	R^2
1	H	OH
2	OH	H

	R^1	R^2
3	H	OH
4	OH	H

5

Scheme 1.

Renewed interest in the pharmacology of colchicine, particularly concerning the binding sites of the microtuburins in the muscle and nerve cells,[8] led us to reinvestigate our old synthetic scheme involving **3** or **4** as an intermediate. However, the extremely limited supply of the natural β-dolabrin necessitated a search for an alternative, efficient method of preparing two acetyltropolones, **1** and **2**. Although two practically valuable methods have been reported recently for the preparation of **8** starting from troponetricarbonyliron[4] or quinone monoacetals,[8a] the conversion of hinokitiol[1] (**6a**) and γ-thujaplicin[10] (**10a**) into **1** and **2** appeared to be more preparative value, since these isopropyltropolones are easily available from an isopropylcyclopentadiene–dichloroketene adduct by applying the Stevens method.[11,12] We wish to describe herein the effective synthesis of two acetyltropolones **1** and **2** as the initial part of a reinvestigation of the synthesis of various 4- and 5-substituted tropolones including colchicine analogs.

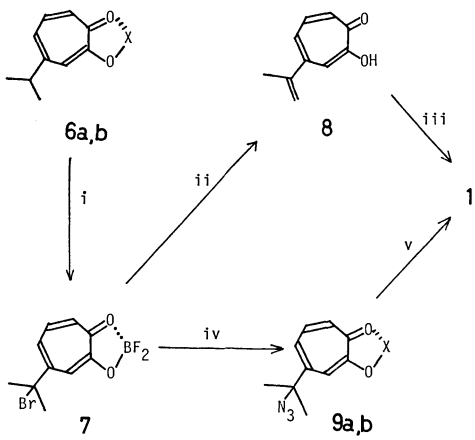

Scheme 2. a: X=H, b: $X=BF_2$. Reagents: i, Ref. 13; ii, n-$Bu_4N^+Br^-$–0.5 M NaOH–CH_2Cl_2; iii, Ref. 6b, 16; iv, NaN_3; v, H_2SO_4.

Seto *et al.*[13] reported an efficient conversion of **6a** into the bromo compound (**7**), which in turn was dehydrobrominated to afford a 30% yield of **8** (Scheme 2). Since the above elimination reaction with potassium *t*-butoxide in *t*-butyl alcohol failed to produce **8** in our experiment, we examined the conversion of **7** to **8** using various other bases, such as triethylamine in chloroform, 1,8-diazabicyclo[5.4.0]undec-7-ene (DBU) in DMF, or 0.5 mol dm^{-3} sodium hydroxide–dichloromethane with tetrabutylammonium bromide as a phase-transfer catalyst. Among these, only the last procedure afforded a 20—25% yield of **8**; the major products under these conditions were an intractable, polymerized substance and 8-hydroxyhinoki-

† 811, 2-5-1, Kamiyoga, Setagaya-ku, Tokyo 158.

Table 1. Ionization constants and UV spectra[a)]

Compd	Species[c)]	Ionization in water (25 °C)			Spectroscopy[b)] in water		
		pK_a	Concn/M	A.w.l.[d)]	λ_{max}/nm	log ε	pH
1	0				251, 318, 382	4.50, 3.75, 3.76	1.0
	—	6.23±0.06	3.09×10^{-5}	436	267, 344, 436	4.33, 4.02, 3.77	9.1
2	0				226, 257, 342	4.57, 4.39, 4.34	1.0
	—	4.97±0.05	1.43×10^{-5}	389	237, 270, 389	4.59, 4.00, 4.66	9.1
3[e)]	0				255, 342	4.41, 4.31	MeOH[f)]
	0				254, *340*, 370	4.34, *4.14*, 4.15	1.0
	—	6.08±0.07	1.19×10^{-5}	348	222, 262, *275*, 348, *425*	4.27, 4.16, *4.14*, 4.34, *3.60*	9.1
4[e)]	0				228, 259, 358	4.47, 4.23, 4.32	1.0
	—	4.85±0.06	1.19×10^{-5}	425	230, *240*, *272*, *388*, 425	4.50, *4.43*, *4.03*, *4.33*, 4.51	9.1

a) Measured with a Hitachi EPS 3T Recording Spectrophotometer. b) Inflections in italics. c) Neutral species (0) and monoanion (−). d) Analytical wavelength in nm (*cf.* Ref. 19). e) R=3,4,5-$(MeO)_3$ (*cf.* Refs. 1, 7, 9). f) From Ref. 7c.

tiol.[14)] Because of the fluctuation in the yield and the difficulties in optimizing the conditions of the above reaction, we sought for a more reliable alternative route to 4-acetyltropolone (**1**).

Thus, the treatment of **7** with 1.3 equivalent sodium azide in DMF produced an 85% yield of the boron complex (**9b**), which in turn was directly transformed into **1** (82%) with concd sulfuric acid, apparently by means of a Schmidt reaction[15)] (Scheme 2). The structure of the hitherto unreported intermediate, **9b**, was based on the elementary analysis and the spectroscopic data (see Experimental section). The mild alkaline hydrolysis of **9b** readily afforded crystalline 8-azidohinokitiol (**9a**; 88% yield), which had been postulated by Doi[16)] as an intermediate during the conversion of **8** into **1** with hydrazoic acid. The free tropolone (**9a**) indeed produced **1** in an 80% yield when similarly subjected to the Schmidt reaction. The overall yield of **1** from **6a** (*via* **9b**) was *ca.* 60%, which far exceeds that obtained through the formerly employed route *via* **8** (10—15%).[6b,16)]

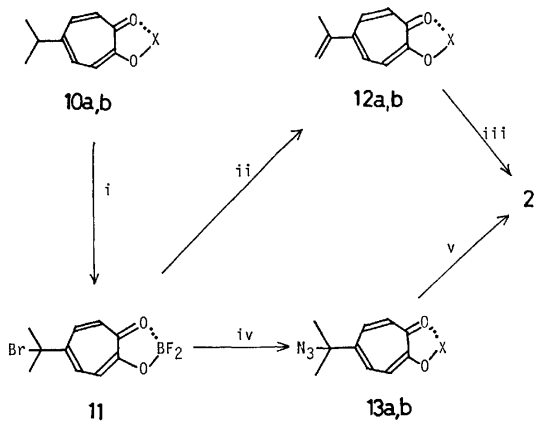

Scheme 3. a: X=H, b: $X=BF_2$. Reagents: i, $BE_3\cdot OEt_2$; ii, Et_3N; iii, O_3–Me_2S; iv, NaN_3; v, H_2SO_4.

This convenient synthetic method of preparing **1** led us to examine an analogous approach in preparing 5-acetyltropolone (**2**) (Scheme 3). Thus, γ-thujaplicin (**10a**) was almost quantitatively converted into its difluoroboron complex (**10b**), and then into the 8-bromo derivative (**11**) in an 85% yield, by employing a slight modification of the procedure described above. Compound **11** was found to undergo surprisingly facile dehydrobromination with triethylamine in chloroform at 15 °C to furnish γ-dolabrin (**12a**) in an 85% overall yield after the hydrolysis of the intermediate boron complex (**12b**). This was in striking contrast with the results for its β-isomer (**7**), which gave mostly a polymerized product and 8-hydroxyhinokitiol. Since **12a** had been prepared[9)] either from the octyl ester of 5-carboxytropolone (7% overall) or β-dolabrin (**8**) by a three-step conversion (15%), the above method is obviously of some value for preparing **12a**.

Although 5-acetyltropolone (**2**) was obtained from **12a** through oxidative cleavage (60—70% overall yield with HCO_3H, NaOH, and HIO_4),[9)] the ozonolysis of **12a** at −70 °C was found to provide **2** more conveniently in an 80—85% yield. Alternatively, a similar application of the Schmidt reaction on either 8-azido-γ-thujaplicin (**13a**) or its difluoroboron complex (**13b**), both of which are readily available from **11**, as in the case of the β-isomer, produced only a moderate yield (40%) of 5-acetyltropolone (**2**), together with a minor amount of 5-aminotropolone.[17)] This result was again different from that for the β-isomer (**9a,b**), which prodived **1** exclusively. 5-Acetyltropolone (**2**) was thus found to be synthesized from γ-thujaplicin (**10a**) more satisfactorily through γ-dolabrin (**12a**) in an overall yield of 70%.

Scheme 4. X=Br, N_3.

Considerable differences in various reactivities were observed between the 4- and 5-positions in the tropolone nucleus. The extremely facile dehydrobromination in **11** and the increased migratory aptitude of tropolone ring in **13** to produce a considerable amount of 5-aminotropolone could be explained in terms of

a very limited contribution of a polar resonance form **14** to the actual ground state of the 5-substituted tropolones (**11** and **13**) compared with that of **15** to the 4-substituted tropolones **7** and **9b** (Scheme 4). On the other hand, the presence of an appreciable cationic charge at Position 4, as is shown in **15**, would suppress the elimination reaction in **7** and promote the polymerization of the side-chain of the β-dolabrin difluoroboron complex formed. Formula **15** is also compatible with the suppressed migratory aptitude of the tropolone nucleus in the Schmidt reaction of **9**. However, a closer mechanistic study with regard to these interesting differences is currently in progress.

A significant positional difference was also observed in the pK_a values of 4- and 5-acetyltropolone and the readily obtainable 4- and 5-(3,4,5-trimethoxycinnamoyl)tropolones [**3**,**4**; R=3,4,5-(MeO_3)]; these hitherto unreported values are recorded in Table 1, along with their UV-spectral values in aqueous buffers. The pK_a value of **2** fits this relation:

$$pK_a = 6.42 - 3.10\sigma$$

if the σ_p constant for phenol is used (predicted: 4.8).[18] These values, therefore, appear to be in conformity with the generally observed feature that Positions 4 and 5 in tropolones are approximately to be equated with Positions 3 and 4 in phenols.

The 4- and 5-acetyltropolone (**1** and **2**), thus synthesized easily from the readily available starting materials, **6a** and **10a**, are considered to be valuable intermediates in synthesizing various 4- and 5-substituted troponoids, including colchicine analogs, which are under investigation.

Experimental

The ^{1}H-NMR spectra were measured in $CDCl_3$ with a Hitachi High-resolution NMR Spectrometer, R-20A (60 MHz) at 30 °C. The chemical shifts are reported as δ values in ppm relative to TMS (δ 0.0) as the internal standard. The IR spectra were taken with a Nihon-Bunko IR-S spectrometer. The microanalysis was carried out in this department using a Yanagimoto CHN Corder, MT-2. Substances stated to be identical were compared by means of their IR and ^{1}H-NMR spectra, TLC (silica gel), HPLC (Hitachi gel #3011, with 0.1% AcOH/MeOH as a solvent), and paper chromatography (developed in 7:3 *n*-BuOH/5 M (1 M=1 mol dm^{-3}) AcOH or 2:1 *n*-PrOH/1% aq ammonia).

Difluoro(3-isopropyl-7-oxo-1,3,5-cycloheptatrienyloxy)borane (Hinokitiol Difluoroborane; ***6b***). The procedure of Seto *et al.*[13] was followed, but on a much larger scale, using an overhead mechanical stirrer, a three-necked flask fitted with a dropping funnel, and a condenser. Thus, 18.0 g (0.11 mol) of **6a** and 15.6 g (0.11 mol) of freshly distilled boron trifluoride etherate gave 22.2 g (96%) of the difluoroborane (**6b**) after recrystallization from chloroform–benzene (*ca.* (4:7); mp 171—172 °C (lit,[13] 178—179 °C). Further purification by silica-gel chromatography with 5% AcOEt/C_6H_6 and recrystallization did not raise the melting point. NMR 1.37 (6H, d, J=7.0), 3.20 (1H, sept, J=7.0), and 7.35—8.1 (4H, m).

[3-(1-Bromo-1-methylethyl)-7-oxo-1,3,5-cycloheptatrienyloxy]difluoroborane (8-Bromohinokitiol Difluoroborane; ***7***). This material was also prepared according to the procedure of Seto *et al.*,[13] but on a larger scale and with a slight modification. Thus, 15.0 g (0.094 mol) of freshly distilled bromine was slowly added to a refluxing solution of 15.0 g (0.071 mol) of **6b** dissolved in 150 ml of dry chloroform under a tungsten light with mechanical stirring. The mixture was refluxed for 6 h with stirring, with protection against moisture being provided by a $CaCl_2$ tube. The precipitate was filtered off and washed with chloroform, giving 18.3 g (89%) of **7**; mp 176—180 °C dec (from $CHCl_3$) (lit,[13] 188—189 °C). NMR (DMSO-d_6/$CDCl_3$, 1:2) 2.30 (6H, s) and 7.8—8.4 (4H, m).

4-Isopropenyl-2-hydroxy-2,4,6-cycloheptatrien-1-one (β-Dolabrin; ***8***). A suspension of 0.29 g (1.0 mmol) of **7** in 20 ml of dichloromethane was added at 40 °C to a stirred mixture of 20 ml of 0.5 mol dm^{-3} NaOH and 5 ml of CH_2Cl_2 containing 70 mg (0.21 mmol) of tetrabutylammonium bromide over a period of 50 min; then the mixture was stirred under N_2 at 40—45 °C for 12 h. After separation, the aq layer was washed with CH_2Cl_2, carefully brought to pH 3 at 5 °C with 6 mol dm^{-3} HCl, and extracted with CH_2Cl_2. The dried (over Na_2SO_4) extracts were evaporated *in vacuo*, and the residue was flash-distilled at 85 °C (bath)/7 Torr (1 Torr≈133.322 Pa), giving 40 mg (25%) of **8** as a pale yellow liquid which slowly solidified on standing and which was identical with an authentic specimen. No appreciable amount of **8** was obtained when other bases were used *e.g.*, triethylamine in chloroform (50 °C, 6 h; 60% recovery, 15% of 8-hydroxyhinokitiol), *t*-BuOK/*t*-BuOH[13] (10—20 °C, 1.5 h; 30% recovery of **7**, 10% of 8-hydroxyhinokitiol, and 5% of **8**), DBU/DMF (0 °C, 1.5 h; 40% of **7**, 10% of 8-hydroxyhinokitiol). In all cases, the residue was an intractable gummy substance, apparently a polymerized product.

[3-(1-Azido-1-methylethyl)-7-oxo-1,3,5-cycloheptatrienyloxy]difluoroborane (8-Azidohinokitiol Difluoroborane; ***9b***). A solution of 4.11 g (14.1 mmol) of **7** and 1.18 g (18.2 mmol) of sodium azide in 40 ml of dry DMF was stirred under N_2 at 15 °C for 15 h. The solvent was then removed *in vacuo* (pump), and the residue, diluted with water, was extracted with benzene. The combined extracts were dried over Na_2SO_4 and evaporated *in vacuo*. The residue was purified by passing it through a short column of silica gel with 5% AcOEt–C_6H_6, thus affording 3.04 g (85%) of **9b** as colorless crystals; mp 71—73 °C (from benzene–light petroleum). NMR 1.74 (6H, s, 2CH_3-8) and 7.6—8.2 (4H, m, aromatic). IR ($CHCl_3$) 2150 (N_3) and 1615 cm^{-1} (C=O). Found: C, 47.25; H, 4.11; N, 16.49%. Calcd for $C_{10}H_{10}N_3O_2BF_2$: C, 47.47; H, 3.98; N, 16.61%.

4-(1-Azido-1-methylethyl)-2-hydroxy-2,4,6-cycloheptatrien-1-one (8-Azidohinokitiol; ***9a***). A mixture of 46 mg of **9b**, 2 ml of *t*-butyl alcohol, and 2 ml of 1 mol dm^{-3} KOH was stirred at 20 °C for 5 h. The alcohol was then removed *in vacuo*, and the remaining aq layer was taken to pH 4 with 2 mol dm^{-3} HCl at 5 °C and extracted with CH_2Cl_2. The combined organic layers were dried over Na_2SO_4 and evaporated *in vacuo*, giving 33 mg (88%) of **9a** as colorless prisms (from ether–light petroleum); mp 45—46 °C. NMR 1.68 (6H, s, 2CH_3-8), 7.2—7.45 (3H, m, H-5,6,7), 7.56 (1H, bs, H-3), and 8.0 (1H, bm, HO-2, D_2O exchangeable). IR ($CHCl_3$) 3450 (OH), 2150 (N_3), and 1610 cm^{-1} (C=O). Found: C, 58.65; H, 5.62; N, 20.15%. Calcd for $C_{10}H_{11}N_3O_2$: C, 58.53; H, 5.40; N, 20.48%.

4-Acetyl-2-hydroxy-2,4,6-cycloheptatrien-1-one (4-Acetyltropolone; ***1***). Three milliliters of concd sulfuric acid were added dropwise to a solution of 3.84 g (15.2 mmol) of **9b** in 6 ml of chloroform at 0 °C; the mixture was then stirred at 0 °C for 15 min and at 20 °C for 2 h. After the $CHCl_3$ layer

had then been removed, the acid layer was diluted with 15 ml of cold water, brought to pH 3 by adding solid $NaHCO_3$, and extracted with $CHCl_3$. The combined extracts were dried over Na_2SO_4 and evaporated *in vacuo*, giving 2.04 g (82%) of **1** as yellow crystals; mp 125—127 °C (from 70% aq ethanol). The product was identical with an authentic specimen[6] (mp 129 °C). 8-Azidohinokitiol (**9a**) produced **1** in 80% and 64% yields when similarly treated with concd sulfuric acid and polyphosphoric acid (at 55 °C) respectively.

*Difluoro(4-isopropyl-7-oxo-1,3,5-cycloheptatrienyloxy)borane (γ-Thujaplicin Difluoroborane; **10b**).* The procedure for the β-isomer was followed. Thus, 5.3 g (31 mmol) of trifluoroboron etherate, dissolved in 10 ml of dry ether, was added dropwise to a solution of 4.59 g (28 mmol) of **10a** in 80 ml of dry ether–benzene (1:1) at 5 °C over a period of 1 h with stirring under the protection of a $CaCl_2$ tube. After being stirred at 5 °C for 4 h, the mixture was concentrated *in vacuo*, and the residue was recrystallized from benzene/light petroleum to give 5.05 g of **10b** as white needles; mp 104—105 °C. The filtrate was concentrated *in vacuo*, and the residue was chromatographed over silica gel with 5% ether–benzene, thus affording 0.50 g more of **10b**; mp 103 °C (from the same mixed solvent); thus, the combined yield of **10b** was 5.55 g (94%). NMR 1.35 (6H, d, J=6.5, $2CH_3$-8), 2.13 (1H, sept, J=6.5, H-8), 7.75 (2H, d, J=11, H-2,6), and 8.00 (2H, d, J=11, H-3,5). Found (for material dried at 40 °C/15 Torr): C, 56.43; H, 5.11%. Calcd for $C_{10}N_{11}O_2BF_2$: C, 56.60; H, 5.18%.

*[4-(1-Bromo-1-methylethyl)-7-oxo-1,3,5-cycloheptatrienyloxy]difluoroborane (8-Bromo-γ-thujaplicin Difluoroborane; **11**).* To a stirred suspension of 6.78 g (32 mmol) of **10b** in 250 ml of dry CCl_4 was added dropwise 5.2 g (32.5 mmol) of bromine dissolved in 20 ml of dry CCl_4 at 20 °C over a period of 90 min under a tungsten light and a slow stream of N_2; the mixture was subsequently stirred at room temperature for 4 h. The precipitate was filtered off and washed with CCl_4, thus giving 7.82 g (85%) of **11** as colorless crystals; mp 116—119 °C. Recrystallization from benzene–light petroleum raised the melting point to 119—120 °C. A lesser yield of **11** was obtained when chloroform was used as the solvent or when the reaction mixture was refluxed. NMR 2.28 (6H, s, $2CH_3$-8), 7.81 (2H, d, J=12, H-2,6), and 8.51 (2H, d, J=12, H-3,5). Found: C, 41.01; H, 3.25%. Calcd for $C_{10}H_{10}O_2BrBF_2$: C, 41.24; H, 3.42%.

*Difluoro(4-isopropenyl-7-oxo-1,3,5-cycloheptatrienyloxy)borane (γ-Dolabrin Difluoroborane: **12b**).* To a solution of 200 mg (0.69 mmol) of **11** in 3 ml of dry CH_2Cl_2 was added 73 mg (1.37 mmol) of triethylamine under N_2 at 0 °C. The mixture was stirred at 15 °C for 7 h, and then a 3-ml portion of cold water was added. After separation, the aq layer was extracted with CH_2Cl_2. The combined organic layers were dried over Na_2SO_4 and evaporated *in vacuo*, thus giving 130 mg (90%) of **12b** as colorless needles; mp 148—149 °C (from benzene–light petroleum). NMR 2.26 (3H, bs, CH_3-8), 5.40 (2H, bs, CH_2=C-8), 7.84 (2H, d, J=12, H-2,6), and 8.17 (2H, d, J=12, H-3,5). Found: C, 57.51; H, 4.48%. Calcd. for $C_{10}H_9O_2BF_2$: C, 57.17; H, 4.76%.

*5-Isopropenyl-2-hydroxy-2,4,6-cycloheptatrien-1-one (γ-Dolabrin; **12a**).* A mixture of 4.40 g (15 mmol) of **11** and 3.50 g (35 mmol) of triethylamine in 60 ml of dry $CHCl_3$ was stirred under N_2 at 20 °C for 3 h and then concentrated *in vacuo*. The residue was stirred with a mixture of 50 ml of *t*-butyl alcohol and 260 ml of 1.3 mol dm^{-3} KOH at 20 °C for 30 min. The alcohol was removed *in vacuo*, and the residue was carefully taken to pH 3 with 2 mol dm^{-3} HCl at 5 °C. The precipitate was filtered off and washed with water, thus giving 1.88 g of **12a** as pale yellow crystals; mp 98—100 °C (lit,[9] 100—101 °C). From the filtrate, 0.25 g more of **12a** was obtained after extraction with $CHCl_3$, sublimation at 80 °C/0.01 Torr, and recrystallization from cyclohexane; thus, the total yield of **12a** from **11** was 2.13 g (87%). NMR 2.15 (3H, bs, CH_3-8), 5.20 and 5.28 (1H, each, m, CH_2=C-8), 7.33 (2H, d, J=11, H-3,7), 7.49 (2H, d, J=11, H-4,6), and 7.80 (1H, bs, HO-2, D_2O exchangeable). The product was identical with an authentic specimen.[9]

*[4-(1-Azido-1-methylethyl)-7-oxo-1,3,5-cycloheptatrienyloxy]difluoroborane (**13b**) and 8-Azido-γ-thujaplicin (**13a**).* A mixture of 20 mg (0.069 mmol) of **11** and 6 mg (0.092 mmol) of sodium azide in 0.5 ml of dry DMF was stirred under N_2 at 50 °C for 1.5 h. The solvent was then evaporated at 20 °C/0.3 Torr. The residue was dissolved in benzene, washed with water, dried over Na_2SO_4, and evaporated *in vacuo*, thus giving 10 mg (57%) of **13b** as pale yellow needles; mp 81—83 °C (from ether–light petroleum). NMR 1.75 (6H, s, $2CH_3$-8), 7.86 (2H, d, J=12, H-2,6), and 8.32 (2H, d, J=12, H-3,5). IR ($CHCl_3$) 2150 (N_3) and 1615 cm^{-1} (C=O). Found: C, 47.25; H, 4.16; N, 16.32%. Calcd for $C_{10}H_{10}N_3O_2BF_2$: C, 47.47; H, 3.98; N, 16.61%.

When the reaction was carried out using 116 mg of **11** at 20 °C for 16 h, 89 mg (88%) of a *ca.* 2:1 mixture of **13b** and **13a** (see below) were produced as an amber liquid.

A mixture of 17 mg (0.066 mmol) of **13b**, 1 ml of 1 mol dm^{-3} KOH, and 1 ml of *t*-BuOH was stirred under N_2 at 20 °C for 3 h. The alcohol was then removed *in vacuo*, and the remaining aq solution was taken to pH 4 with 2 mol dm^{-3} HCl and extracted with $CHCl_3$, thus giving 11 mg (80%) of **13a** as a pale amber oil. NMR 1.58 (6H, s, $2CH_3$-8), 7.30 (2H, d, J=12, H-3,7), 7.64 (2H, d, J=12, H-4,6), and 7.7 (1H, bm, OH). IR ($CHCl_3$) 3450 (OH), 2150 (N_3), and 1610 cm^{-1} (C=O).

*5-Acetyl-2-hydroxy-2,4,6-cycloheptatrien-1-one (5-Acetyltropolone; **2**).* *A)*: Into a stirred solution of 0.50 g (3.9 mmol) of **12a** in 50 ml of dry CH_2Cl_2 was passed 42 mg (8.5 mmol) of ozone at −70 °C over a period of 1 h; then 0.6 ml of dimethyl sulfide was added. The mixture was gradually warmed, and the stirring was continued at 15 °C for 3 h. The solvent was evaporated *in vacuo*, and the residue, diluted with brine, was extracted with $CHCl_3$, thus giving 0.43 g (85%) of **2** as pale yellow crystals after recrystallization from $CHCl_3$–ethanol (with carbon); mp 179—181 °C (lit,[9] 182—183 °C). NMR 2.63 (3H, s, Ac), 6.1 (1H, bs, OH, D_2O exchangeable), 7.37 (2H, d, J=12, H-3,7), and 8.11 (2H, d, J=12, H-4,6). The product was identical with an authentic specimen.[9]

B): To a cold solution of 36 mg of crude **13b** in 1.5 ml of $CHCl_3$ was added 1.5 ml of concd sulfuric acid at 0 °C. The mixture was stirred at 20 °C for 1 h, after which the organic layer was separated. The aq layer was diluted with 4 ml of cold water, taken to pH 3 with $NaHCO_3$, and extracted with $CHCl_3$, thus giving 10 mg (40%) of **2** as pale yellow crysals; mp 175—178 °C (from $CHCl_3$–EtOH). The above aq layer (after $CHCl_3$ extraction at pH 3) was found to contain 5-aminotropolone (by HPLC and paper chromatography), which was subsequently isolated and identified as the picrate: yellow crystals, mp 220—225 °C dec (lit,[17] 225—226 °C dec). Almost the same result was obtained by using **13a** as the starting material or by employing polyphosphoric acid as the reaction medium.

The present work was partially suppoted by a Research Grant from the Suntory Institute of Bioorganic

Research, Osaka, to which we wish to express our thanks.

References

1) a) T. Nozoe, *Experientia*, Suppl. VII, 306 (1957); b) T. Nozoe, *Prog. Org. Chem.*, **5**, 132 (1961); c) T. Nozoe, K. Takase, and H. Matsumura, "Dai Yuki Kagaku (Comprehensive Organic Chemistry)," ed by M. Kotake, Asakura, Tokyo (1960), Vol. 13, pp. 1—437.

2) D. Lloyd, "Carbocyclic Non-benzenoid Aromatic Compounds," Elsevier, Amsterdam (1966), pp. 135—144.

3) F. Pietra, *Chem. Rev.*, **73**, 293 (1973).

4) The 2-acetyltropone-tricarbonyliron complexes were prepared by the Friedel-Crafts acylation of tropone-tricarbonyliron: M. Frank-Neumann, F. Brion, and D. Martina, *Tetrahedron Lett.*, **1978**, 5033.

5) An indirect C–C bond formation has recently been reported for the synthesis of 3-, 4-, and 5-(substituted vinyl)-tropolones from the corresponding halotropolones by means of palladium-catalyzed vinylic substitution; H. Horino, N. Inoue, and T. Asao, *Tetrahedron Lett.*, **1980**, 741.

6) a) T. Nozoe, *Fortsch. Chem. Org. Naturstoffe*, **13**, 232 (1956); b) T. Nozoe, K. Takase, and M. Ogata, *Chem. Ind.*, **1957**, 1070; c) J. A. F. Gardner and G. M. Barton, *Can. J. Chem.*, **36**, 1612 (1958); d) E. Zavarin, R. M. Smith, and A. B. Anderson, *J. Org. Chem.*, **24**, 1318 (1959).

7) a) T. Nozoe, K. Takase, and T. Asao, unpublished results; b) K. Suzuki, M. Sc. Thesis, Tohoku Univ. (1959); c) N. Kawabe, M. Sc. Thesis, Tohoku Univ. (1965).

8) For the synthesis and pharmacology of colchicine, see a) D. A. Evans, D. J. Hart, and P. M. Koelsch, *J. Am. Chem. Soc.*, **100**, 4594 (1978), and the references cited therein; b) D. A. Evans, D. J. Hart, P. M. Koelsch, and P. A. Cain, *Pure Appl. Chem.*, **51**, 1285 (1979); c) C. -P. Mak and G. Büchi, *J. Org. Chem.*, **46**, 1 (1981).

9) T. Nozoe, T. Mukai, and T. Asao, *Bull. Chem. Soc. Jpn.*, **33** 1452 (1960).

10) H. Erdtman and J. Gripenberg, *Nature*, **161**, 719 (1948); *Acta Chem. Scand.*, **2**, 625 (1948).

11) H. C. Stevens, J. K. Rinehart, J. M. Lavanish, and G. M. Trenta, *J. Org. Chem.*, **36**, 2780 (1971) and the references cited therein.

12) K. Tanaka and A. Yoshikoshi, *Tetrahedron*, **27**, 4889 (1971).

13) S. Seto, S. Matsumura, and K. Ro, *Chem. Pharm. Bull. (Tokyo)*, **10**, 901 (1962).

14) H. Yamamoto, M. Sc. Thesis, Tohoku Univ. (1965); NMR δ 1.68 (6H, s, $2CH_3$-8), 2.8 (1H, bm, OH, D_2O exchangeable), and 7.1—7.7 (5H, m, ring protons and OH) IR (neat) 3450 (OH) and 1610 cm^{-1} (C=O).

15) For reviews of the Schmidt reaction, see a) H. Wolff, "Organic Reactions," ed by R. Adams, Wiley, New York (1946), Vol. 3, p. 307; b) P. A. S. Smith, "Molecular Rearrangements," ed by P. de Mayo, Wiley, New York (1963), pp. 457—527.

16) K. Doi, *Bull. Chem. Soc. Jpn.*, **34**, 501 (1961).

17) T. Nozoe, S. Seto, S. Ito, and M. Sato, *Proc. Jpn. Acad.*, **27**, 426 (1952).

18) a) Y. Oka, M. Umehara, and T. Nozoe, *Nippon Kagaku Zasshi*, **83**, 1197 (1962); b) G. B. Barlin and D. D. Perrin, *Quart. Rev.*, **20**, 75 (1966).

19) A. Albert and E. P. Serjeant, "Ionization Constants of Acids and Bases," Methuen, London (1962).

Total Synthesis of (±)-Pisiferic Acid, Methyl (±)-Pisiferate, and (±)-Pisiferol

Takashi MATSUMOTO* and Shuji USUI

Department of Chemistry, Faculty of Science, Hiroshima University, Higashisenda-machi, Naka-ku, Hiroshima 730

(Received October 26, 1981)

Acid catalyzed cyclization of 4-(3-isopropyl-4-methoxyphenethyl)-3,5,5-trimethyl-2-cyclohexen-1-one afforded 12-methoxyabieta-8,11,13-trien-2-one and its *cis*-isomer. Both compounds were further converted into 12-methoxyabieta-8,11,13-trien-2β-ol, which was treated with lead tetraacetate in the presence of iodine to yield 2β,20-epoxy-12-methoxyabieta-8,11,13-triene. Ether cleavage of the 2β,20-epoxy compound with acetyl *p*-toluenesulfonate, followed by catalytic hydrogenation, afforded 20-acetoxy-12-methoxyabieta-8,11,13-triene (**23**). This was then converted into methyl 12-methoxyabieta-8,11,13-trien-20-oate (**27**) *via* methyl 12-methoxy-7-oxoabieta-8,11,13-trien-20-oate. Demethylation of **27** with $AlBr_3$–EtSH gave pisiferic acid, but with $AlCl_3$–EtSH **27** was partially demethylated to give methyl pisiferate. The acetate **23** was also converted into pisiferol by demethylation and reduction.

Recently three new ferruginol type diterpenes, pisiferic acid (**1**), methyl pisiferate (**2**), and pisiferol (**3**), have been isolated from the leaves of *Chamaecyparis pisifera* by Yatagai *et al.*[1] All these compounds are are tricyclic diterpenes possessing an oxidized angular methyl group. As an extension of our previous studies[2,3] of the syntheses of natural tricyclic diterpenes possessing an oxygen function in the ring A, we have attempted the syntheses of these rare natural compounds. This paper[4] describes the total syntheses of (±)-pisiferic acid (**1**), methyl (±)-pisiferate (**2**), and (±)-pisiferol (**3**), starting from (±)-12-methoxyabieta-8,11,13-trien-2-one (**4**),[3] which was prepared from (±)-4-(3-isopropyl-4-methoxyphenethyl)-3,5,5-trimethyl-2-cyclohexen-1-one (**5**).

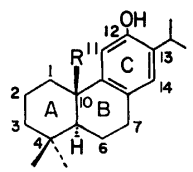

1 R = CO_2H
2 R = CO_2Me
3 R = CH_2OH

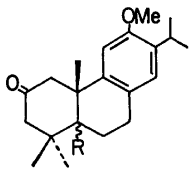

4 R = α-H
6 R = β-H

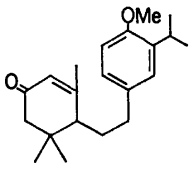

5

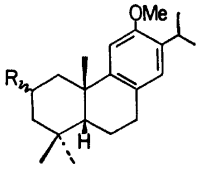

7 R = β-OAc
8 R = α-OAc

Cyclization of **5** in hexane with boron trifluoride etherate in the presence of 1,2-ethanedithiol, followed by hydrolysis with mercury (II) chloride in aqueous acetonitrile, gave **4** (28%) and its *cis*-isomer (**6**: 16%).[3] Since all natural compounds (**1**, **2**, and **3**) possess a trans A/B ring junction, conversion of the *cis*-isomer **6** into the trans compounds was carried out as follows. Reduction of **6** with lithium aluminium hydride in THF, followed by acetylation, gave two epimeric acetates, **7** (32%) and **8** (52%). The ^1H NMR spectrum of **7** showed signals at δ 0.35, 0.98, and 1.18 due to the C-4 dimethyl and C-10 methyl groups. The steroidal conformation (**7a**) of **7** was suggested by the appearance of the signal due to one of two C-4 methyl groups in very high field (δ 0.35), owing to the shielding effect of the aromatic C-ring. The ^1H NMR spectrum of **8** showed the corresponding signals at δ 1.02, 1.26, and 1.49. The appearance of these three tertiary methyl signals in a lower field than those in **7** suggested that **8** exists in a nonsteroidal conformation (**8a**).[5] The stereochemistry of the acetoxyl group at C-2 in **7** and **8** was assigned respectively to be β- and α-configuration by their ^1H NMR spectra, each of which showed a broad signal due to the C-2 proton at δ 4.4—5.1 in **7** and at δ 4.6—5.4 in **8**, suggesting the presence of an axial hydrogen. The acetate **7** in acetone was oxidized with Jones reagent to give the corresponding 7-oxo compound (**9**: 60%) along with the 6,7-dioxo compound (**10**: 13%). Bromination of **9** with pyridinium tribromide in dichloromethane afforded the 6β-bromo derivative (**11**: 91%), which was converted into 2β-acetoxy-12-methoxyabieta-5,8,11,13-tetraen-7-one (**12**: 86%) by treatment with lithium carbonate and lithium bromide in *N*,*N*-dimethylformamide at 110—130 °C. The tetraene **12** in ethyl acetate was catalytically hydrogenated with Pd–C in the presence of perchloric acid to yield 2β-acetoxy-12-methoxyabieta-8,11,13-triene (**13**: 72%) and **9** (17%). Treatment of **13** in THF with lithium aluminium hydride gave 12-methoxyabieta-8,11,13-trien-2β-ol (**14**). Similarly, the acetate **8** was also oxidized with Jones reagent to give the corresponding 7-oxo (**15**: 53%) and 6,7-dioxo (**16**: 16%) compounds. The 7-oxo compound **15** was further converted into 2α-acetoxy-12-methoxyabieta-5,8,11,13-tetraen-7-one (**18**) *via* the corresponding 6β-bromo derivative (**17**). The β-configuration of the bromine atom in **11** and **17** was supported by their ^1H NMR spectra, which showed signals due to the C-10 methyl group in low field (δ 1.57 in **11** and δ 1.68 in **17**), owing to the 1,3-diaxial interaction between the bromine atom and the C-10 methyl group. Catalytic hydrogenation of **18** in ethyl acetate over Pd–C afforded 2α-acetoxy-12-methoxyabieta-8,11,13-triene (**19**: 70%) and **8** (25%). The acetate **19** in THF was reduced with lithium aluminium hydride

and the resulting alcohol was immediately oxidized with pyridinium chlorochromate in dichloromethane to afford **4** (88%), which was then converted into **14**[3] by reduction with lithium aluminium hydride in THF.

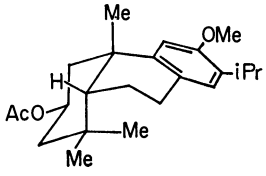

7a

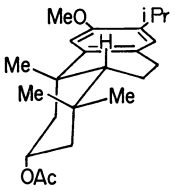

8a

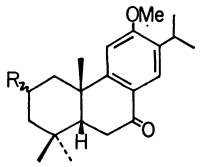

9 R=β-OAc
15 R=α-OAc

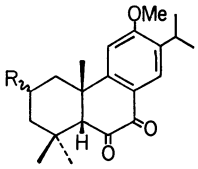

10 R=β-OAc
16 R=α-OAc

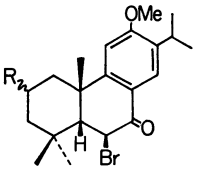

11 R=β-OAc
17 R=α-OAc

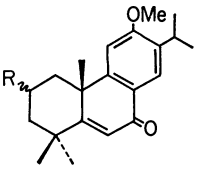

12 R=β-OAc
18 R=α-OAc

In order to oxidize the angular methyl group by transannular oxidation, the alcohol **14** in hexane was treated with lead tetraacetate in the presence of iodine at room temperature. Purification of the crude product by column chromatography on silica gel afforded 2β,20-epoxy-12-methoxyabieta-8,11,13-triene (**20**: 51 %). The structure of **20** was supported by the appearance of signals in its ^{1}H NMR spectrum due to methylene protons (ABq at δ 3.78) and by the disappearance of the signal due to angular methyl group. Treatment of **20** with acetyl *p*-toluenesulfonate[6] in dichloromethane gave an olefinic acetate (**21**: 83%) and a tosyloxy acetate (**22**: 11%). The ^{1}H NMR spectrum of **21** showed signals due to two vinylic protons at δ 5.55 (2H, m), methylene protons at δ 4.27 (2H, bs), an acetoxyl group at δ 1.90 (3H, s), and two tertiary methyl groups at δ 1.03 and 1.08 (each 3H and s). From these spectral data, the structure of **21** was assigned to be 20-acetoxy-12-methoxyabieta-2,8,11,13-tetraene. The spectrum of **22** showed the presence of a tosyloxyl group [δ 2.48 (3H, s), 7.34 and 7.83 (each 2H, d, and J=8 Hz)] and no vinylic proton. The α-configuration of the tosyloxyl group was supported by the broad signal at δ 4.2—4.9 (1H, m) due to the C-2 proton, suggesting the presence of an axial β hydrogen. Treatment of **22** with potassium carbonate in refluxing aqueous methanol yielded **20**. The olefinic acetate **21** in ethanol was submitted to catalytic hydrogenation over PtO_2 to afford 20-acetoxy-12-methoxyabieta-8,11,13-triene (**23**: 93%)

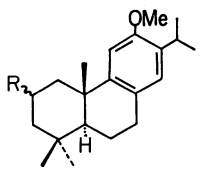

13 R=β-OAc
14 R=β-OH
19 R=α-OAc

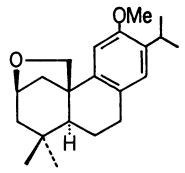

20

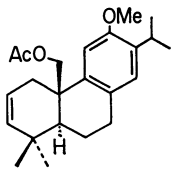

21

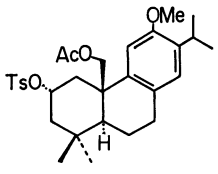

22

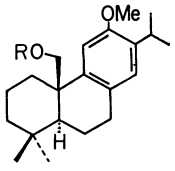

23 R=Ac
24 R=H

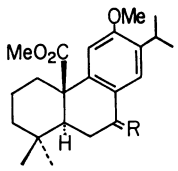

25 R=O
27 R=H$_2$

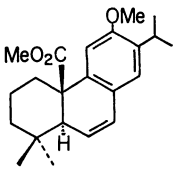

26

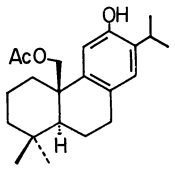

28

which, on reduction with lithium aluminium hydride in THF, gave the corresponding alcohol (**24**: 95%). Oxidation of **24** in acetone with Jones reagent, followed by methylation with diazomethane, afforded methyl 12-methoxy-7-oxoabieta-8,11,13-trien-20-oate (**25**: 40%). The structure of **25** was supported by its IR (1720 and 1660 cm^{-1}) and ^{1}H NMR [δ 3.57 (CO_2CH_3), 6.70 (C_{11}–H), and 7.79 (C_{14}–H)] spectra. The 7-oxo compound **25** was then reduced with sodium borohydride in ethanol and the resulting mixture of epimeric alcohols was immediately dehydrated[7] with acetyl *p*-toluenesulfonate in dichloromethane to give methyl 12-methoxyabieta-6,8,11,13-tetraen-20-oate (**26**: 71%). Catalytic hydrogenation of **26** in ethanol over PtO_2 afforded methyl 12-methoxyabieta-8,11,13-trien-20-oate (**27**: 99%). Demethylation of **27** with anhydrous aluminium bromide and ethanethiol[8] at room temperature for 13 h gave pisiferic acid (12-hydroxyabieta-8,11,13-trien-20-oic acid) (**1**: 93%). Similar treatment of **27** with anhydrous aluminium chloride and ethanethiol[9] in dichloromethane at 0—5 °C for 4 h yielded methyl pisiferate (methyl 12-hydroxyabieta-8,11,13-trien-20-oate (**2**: 97%). Subsequently, the acetate **23** was demethylated with anhydrous aluminium chloride and ethanethiol in dichloromethane to give 20-acetoxyabieta-8,11,13-trien-12-ol

(**28**: 74%) which, on reduction with lithium aluminium hydride in THF, afforded pisiferol (abieta-8,11,13-triene-12,20-diol) (**3**: 88%). The IR and ^{1}H NMR spectra of the synthetic **1**, **2**, and **3** were identical with those of natural products.

Experimental

All melting points are uncorrected. The IR spectra were measured in chloroform, and the ^{1}H NMR spectra in carbon tetrachloride at 60 MHz, with tetramethylsilane as an internal standard, unless otherwise stated. The chemical shifts are presented in terms of δ values; s: singlet, bs: broad singlet, d: doublet, bd: broad doublet, dd: double doublet, t: triplet, bt: broad triplet, m: multiplet. Column chromatography was performed using Merck silica gel (0.063 mm).

*Cyclization of 4-(3-Isopropyl-4-methoxyphenethyl)-3,5,5-trimethyl-2-cyclohexen-1-one (**5**).* A stirred mixture of **5**[3] (5.03 g), 1,2-ethanedithiol (1.4 ml), boron trifluoride etherate (6.1 ml), and dry hexane (50 ml) was refluxed for 6 h. The mixture was cooled, poured into aqueous sodium hydroxide, and extracted with ether. The ether extract was washed with brine, dried over sodium sulfate, and evaporated *in vacuo*. The residue was refluxed for 3 h with mercury(II) chloride (13 g) in a mixture of acetonitrile (50 ml) and water (5.0 ml), filtered, and the filtrate was concentrated *in vacuo*. The residue was extracted with ether and the ether extract was washed with brine, dried over sodium sulfate, and evaporated *in vacuo*. The crude products were purified by column chromatography on silica gel (Merck, 0.063—0.200 mm, 400 g), using ether–hexane (7:93 and then 1:9) as the eluent, to give 12-methoxyabieta-8,11,13-trien-2-one (**4**) (1.40 g: 28 %). Subsequent elution gave 12-methoxy-5βH-abieta-8,11,13-trien-2-one (**6**) (0.78 g: 16%). Further elution with ether–hexane (3:7) gave 12-methoxy-5β-methyl-18-norabieta-8,11,13-trien-2-one (1.02 g: 20%). The IR and ^{1}H NMR spectra of these products were identical with those of the authentic samples.[3]

*Reduction and Acetylation of **6**.* A mixture of **6** (2.051 g) and lithium aluminium hydride (200 mg) in dry tetrahydrofuran (30 ml) was stirred at room temperature for 3 h. To the mixture was added successively water (0.20 ml), 10% aqueous sodium hydroxide (0.20 ml), and water (0.60 ml). The precipitate was removed by filtration and the filtrate was evaporated *in vacuo*. The residue was acetylated with acetic anhydride (0.70 ml) and pyridine (2.0 ml) at room temperature for 13 h. After the usual work-up, the crude products were purified by column chromatography on silica gel (200 g), using ether–benzene (1:99) as the eluent, to give 2β-acetoxy-12-methoxy-5βH-abieta-8,11,13-triene (**7**) (749 mg: 32%). IR: 1718 cm^{-1}; ^{1}H NMR: 0.35 (3H, s, $C_{4\alpha}$–CH_3), 0.98 (3H, s, $C_{4\beta}$–CH_3), 1.18 (3H, s, C_{10}–CH_3), 1.18 (6H, d, J=7 Hz, –CH(CH_3)$_2$), 2.00 (3H, s, –OCOCH_3), 3.92 (3H, s, –OCH_3), 4.4—5.1 (1H, m, C_2–H), 6.68 and 7.04 (each 1H and s, C_{11}–H and C_{14}–H). Found: C, 76.83; H, 9.66%. Calcd for $C_{23}H_{34}O_3$: C, 77.05; H, 9.56%.

Further elution gave 2α-acetoxy-12-methoxy-5βH-abieta-8,11,13-triene (**8**) (1.225 g: 52%). IR: 1720 cm^{-1}; ^{1}H NMR: 1.02 and 1.26 (each 3H and s, –C(CH_3)$_2$), 1.16 (6H, d, J=7 Hz, –CH(CH_3)$_2$), 1.49 (3H, s, C_{10}–CH_3), 1.85 (3H, s, –OCOCH_3), 3.77 (3H, s, –OCH_3), 4.6—5.4 (1H, m, C_2–H), 6.63 (2H, bs, C_{11}–H and C_{14}–H). Found: C, 77.34; H, 9.76%. Calcd for $C_{23}H_{34}O_3$: C, 77.05; H, 9.56%.

*Oxidation of **7**.* Jones reagent (2.5 M: 0.72 ml) was added dropwise at 0—5 °C to a stirred solution of **7** (427 mg) in acetone (8.0 ml). The mixture was further stirred at room temperature for 2 h, diluted with water, and extracted with ether. The ether extract was washed with brine, dried over sodium sulfate, and evaporated *in vacuo*. The residue was purified by column chromatography on silica gel (40 g), using ether–benzene (3:97) as the eluent, to give the starting **7** (63 mg: 15%) and 2β-acetoxy-12-methoxy-5βH-abieta-8,11,13-trien-7-one (**9**) (264 mg: 60%), which was recrystallized from methanol. Mp 163—164 °C; IR: 1720, 1655 cm^{-1}; ^{1}H NMR: 0.36 (3H, s, $C_{4\alpha}$–CH_3), 1.04 (3H, s, $C_{4\beta}$–CH_3), 1.25 (6H, bd, J=7 Hz, –CH(CH_3)$_2$), 1.34 (3H, s, C_{10}–CH_3), 2.03 (3H, s, –OCOCH_3), 4.03 (3H, s, –OCH_3), 4.4—5.1 (1H, m, C_2–H), 7.09 (1H, s, C_{11}–H), 7.75 (1H, s, C_{14}–H). Found: C, 74.42; H, 8.87%. Calcd for $C_{23}H_{32}O_4$: C, 74.16; H, 8.66%.

Further elution gave 2β-acetoxy-12-methoxy-5βH-abieta-8,11,13-triene-6,7-dione (**10**) (60 mg: 13%), which was recrystallized from methanol. Mp 180—182 °C; IR: 1720, 1667 cm^{-1}; ^{1}H NMR: 0.48 (3H, s, $C_{4\alpha}$–CH_3), 1.06 (3H, s, $C_{4\beta}$–CH_3), 1.27 (6H, d, J=7 Hz, –CH(CH_3)$_2$), 1.31 (3H, s, C_{10}–CH_3), 2.08 (3H, s, –OCOCH_3), 2.57 (1H, s, C_5–H), 4.11 (3H, s, –OCH_3), 4.5—5.3 (1H, m, C_2–H), 7.25 (1H, s, C_{11}–H), 7.86 (1H, s, C_{14}–H). Found: C, 71.50; H, 7.83%. Calcd for $C_{23}H_{30}O_5$: C, 71.48; H, 7.82%.

*2β-Acetoxy-6β-bromo-12-methoxy-5βH-abieta-8,11,13-trien-7-one (**11**).* A mixture of **9** (420 mg) and 80% pyridinium tribromide (450 mg) in dichloromethane (8.0 ml) was stirred at room temperature for 1 h. The mixture was diluted with water and extracted with ether. The ether extract was washed with water, dried over sodium sulfate, and evaporated *in vacuo*. The crude product was purified by column chromatography on silica gel (50 g), using ether–benzene (3:97) as the eluent, to give **11** (463 mg: 91%), which was recrystallized from benzene. Mp 212—213 °C; IR: 1720, 1663 cm^{-1}; ^{1}H NMR ($CDCl_3$): 0.31 (3H, s, $C_{4\alpha}$–CH_3), 1.18 (3H, s, $C_{4\beta}$–CH_3), 1.24 (6H, d, J=7 Hz, –CH(CH_3)$_2$), 1.57 (3H, s, C_{10}–CH_3), 2.10 (3H, s, –OCOCH_3), 2.47 (1H, s, C_5–H), 4.07 (3H, s, –OCH_3), 4.5—5.2 (1H, m, C_2–H), 4.84 (1H, s, C_6–H), 7.18 (1H, s, C_{11}–H), 7.86 (1H, s, C_{14}–H). Found: C, 61.43; H, 7.00%. Calcd for $C_{23}H_{31}O_4Br$: C, 61.20; H, 6.92%.

*2β-Acetoxy-12-methoxyabieta-5,8,11,13-tetraen-7-one (**12**).* A mixture of **11** (210 mg), lithium carbonate (103 mg), and lithium bromide (81 mg) in *N,N*-dimethylformamide (3.0 ml) was stirred at 110—130 °C for 4 h in a stream of nitrogen. The mixture was cooled, poured into ice-dilute hydrochloric acid, and extracted with ether. The ether extract was washed with brine, dried over sodium sulfate, and evaporated *in vacuo*. The crude product was purified by column chromatography on silica gel (20 g), using ether–benzene (3:97) as the eluent, to give **12** (149 mg: 86%), which was recrystallized from ethanol. Mp 134—135 °C; IR: 1725, 1645 cm^{-1}; ^{1}H NMR: 1.23 and 1.26 (each 3H, d, and J=7 Hz, –CH(CH_3)$_2$), 1.33, 1.46, and 1.66 (each 3H and s, –C(CH_3)$_2$ and C_{10}–CH_3), 2.07 (3H, s, –OCOCH_3), 3.92 (3H, s, –OCH_3), 5.10 (1H, m, $W_{1/2}$=17 Hz, C_2–H), 6.32 (1H, s, C_6–H), 6.77 (1H, s, C_{11}–H), 7.83 (1H, s, C_{14}–H). Found: C, 74.50; H, 8.14%. Calcd for $C_{23}H_{30}O_4$: C, 74.56; H, 8.16%.

*Catalytic Hydrogenation of **12**.* A mixture of **12** (120 mg), 10% Pd–C (100 mg), and 70% perchloric acid (4 drops) in ethyl acetate (6.0 ml) was stirred at room temperature for 9 h in an atmosphere of hydrogen. After the usual work-up, the crude products were purified by column chromatography on silica gel (15 g), using ether–benzene (1:99) as the eluent, to give 2β-acetoxy-12-methoxyabieta-8,11,13-triene (**13**) (83 mg: 72%), whose IR and ^{1}H NMR spectra were identical with those of the authentic sample.[3]

Further elution with ether–benzene (5: 95) gave **9** (21 mg: 17%).

*12-Methoxyabieta-8,11,13-trien-2β-ol (**14**).* A mixture of **13** (83 mg) and lithium aluminium hydride (10 mg) in dry tetrahydrofuran (2.0 ml) was stirred at room temperature for 1.5 h. The mixture was poured into dilute hydrochloric acid and extracted with ether. The ether extract was washed with brine, dried over sodium sulfate, and evaporated *in vacuo*. The crude product was purified by column chromatography on silica gel (10 g), using ether–benzene (5:95) as the eluent, to give **14** (70 mg: 95%), whose IR and ^{1}H NMR spectra were identical with those of the authentic sample.[3]

*Oxidation of **8**.* A solution of **8** (978 mg) in acetone (20 ml) was oxidized with Jones reagent (2.5 M: 2.20 ml) at *ca.* 10 °C for 30 min and then at room temperature for 2 h. The mixture was diluted with water and extracted with ethyl acetate. The organic solution was washed with brine, dried over sodium sulfate, and evaporated *in vacuo*. The residue was purified by column chromatography on silica gel (100 g), using ether–benzene (3: 97) as the eluent, to give the starting **8** (141 mg: 14%) and 2α-acetoxy-12-methoxy-5β*H*-abieta-8,11,13-trien-7-one (**15**) (541 mg: 53%), which was recrystallized from methanol. Mp 162.5—163 °C; IR: 1720, 1660 cm^{-1}; ^{1}H NMR: 0.68 (3H, s, $C_{4\alpha}$–CH_3), 1.03 (3H, s, $C_{4\beta}$–CH_3), 1.19 and 1.23 (each 3H, d, and J= 7 Hz, –CH($C\underline{H}_3$)$_2$), 1.37 (3H, s, C_{10}–CH_3), 1.53 (3H, s, –OCOCH_3), 3.88 (3H, s, –OCH_3), 4.88 (1H, m, $W_{1/2}$= 9 Hz, C_2–H), 6.65 (1H, s, C_{11}–H), 7.75 (1H, s, C_{14}–H). Found: C, 74.04; H, 8.73%. Calcd for $C_{23}H_{32}O_4$: C, 74.16; H, 8.66%.

Further elution with ether–benzene (5: 95) gave 2α-acetoxy-12-methoxy-5β*H*-abieta-8,11,13-triene-6,7-dione (**16**), which was recrystallized from methanol. Mp 193—196 °C (changed the crystalline form at 140—145 °C); IR: 1725, 1670 cm^{-1}; ^{1}H NMR ($CDCl_3$): 0.79 (3H, s, $C_{4\alpha}$–CH_3), 1.02 (3H, s, $C_{4\beta}$–CH_3), 1.23 and 1.26 (each 3H, d, and J=7 Hz, –CH($C\underline{H}_3$)$_2$), 1.32 (3H, s, C_{10}–CH_3), 1.69 (3H, s, –OCOCH_3), 2.72 (1H, s, C_5–H), 3.96 (3H, s, –OCH_3), 5.10 (1H, m, $W_{1/2}$=8 Hz, C_2–H), 6.82 (1H, s, C_{11}–H), 7.99 (1H, s, C_{14}–H). Found: C, 71.51; H, 7.92%. Calcd for $C_{23}H_{30}O_5$: C, 71.48; H, 7.82%.

*2α-Acetoxy-6β-bromo-12-methoxy-5βH-abieta-8,11,13-trien-7-one (**17**).* A mixture of **15** (541 mg) and 80% pyridinium tribromide (610 mg) in dichloromethane (5.0 ml) was treated as described for the preparation of **11**. The crude product was purified by column chromatography on silica gel (70 g), using ether–benzene (3: 97) as the eluent, to give **17** (639 mg: 93%), which was recrystallized from benzene. Mp 201—202 °C; IR: 1725, 1662 cm^{-1}; ^{1}H NMR ($CDCl_3$): 0.63 (3H, s, $C_{4\alpha}$–CH_3), 1.15 (3H, s, $C_{4\beta}$–CH_3), 1.19 and 1.24 (each 3H, d, and J=7 Hz, –CH($C\underline{H}_3$)$_2$), 1.68 (6H, s, C_{10}–CH_3 and –OCOCH_3), 2.47 (1H, s, C_5–H), 3.91 (3H, s, –OCH_3), 5.00 (1H, s, C_6–H), 5.03 (1H, m, $W_{1/2}$=7 Hz, C_2–H), 6.75 (1H, s, C_{11}–H), 7.92 (1H, s, C_{14}–H). Found: C, 61.26; H, 7.02%. Calcd for $C_{23}H_{31}O_4Br$: C, 61.20; H, 6.92%.

*2α-Acetoxy-12-methoxyabieta-5,8,11,13-tetraen-7-one (**18**).* A mixture of **17** (226 mg), lithium carbonate (111 mg), and lithium bromide (87 mg) in *N,N*-dimethylformamide (3.0 ml) was stirred at 120—130 °C for 1.5 h in a stream of nitrogen. After the same work-up as described for the preparation of **12**, the crude product was purified by column chromatography on silica gel (20 g), using ether–benzene (5:95) as the eluent, to give **18** (178 mg: 96%), which was recrystallized from ethanol. Mp 134—135 °C; IR: 1725, 1645 cm^{-1}; ^{1}H NMR: 1.22 and 1.26 (each 3H, d, and J= 7 Hz, –CH($C\underline{H}_3$)$_2$), 1.32, 1.48, and 1.62 (each 3H and s, –$\underline{C}$(CH_3)$_2$ and C_{10}–CH_3), 2.03 (3H, s, –OCOCH_3), 3.92 (3H, s, –OCH_3), 4.9—5.7 (1H, m, C_2–H), 6.29 (1H, s, C_6–H), 6.77 (1H, s, C_{11}–H), 7.84 (1H, s, C_{14}–H). Found: C, 74.52; H, 8.24%. Calcd for $C_{23}H_{30}O_4$: C, 74.56; H, 8.16%.

*Catalytic Hydrogenation of **18**.* A mixture of **18** (178 mg), 10% Pd–C (150 mg), and 70% perchloric acid (4 drops) in ethyl acetate (7.0 ml) was treated as described in the hydrogenation of **12**. The crude products were purified by column chromatography on silica gel (20 g), using benzene as the eluent, to give 2α-acetoxy-12-methoxyabieta-8,11,13-triene (**19**) (97 mg: 56%). IR: 1720 cm^{-1}; ^{1}H NMR: 1.06 (6H, s, –$\underline{C}$(CH_3)$_2$), 1.17 (6H, d, J=7 Hz, –CH($C\underline{H}_3$)$_2$), 1.29 (3H, s, C_{10}–CH_3), 2.03 (3H, s, –OCOCH_3), 3.79 (3H, s, –OCH_3), 4.8—5.4 (1H, m, C_2–H), 6.57 and 6.71 (each 1H and s, C_{11}–H and C_{14}–H). Further elution gave a mixture (*ca.* 1:1) of acetates (**19** and **8**) (48 mg: 28%) and pure **8** (18 mg: 11%).

*12-Methoxyabieta-8,11,13-trien-2-one (**4**).* A mixture of **19** (97 mg) and lithium aluminium hydride (10 mg) in dry tetrahydrofuran (2.0 ml) was stirred at room temperature for 1 h. After the same work-up as described for the preparation of **14**, the crude product was immediately oxidized with pyridinium chlorochromate (90 mg) in dichloromethane (2.0 ml) at room temperature for 1.5 h. The mixture was poured into aqueous sodium carbonate and extracted with ether. The ether extract was washed successively with brine, dilute hydrochloric acid, and brine. The dried extract was evaporated *in vacuo* to give a crude product, which was purified by column chromatography on silica gel (10 g), using ether–benzene (1: 99) as the eluent, to give **4** (75 mg: 88%). The IR and ^{1}H NMR spectra of **4** were identical with those of the authentic sample.[3] Reduction[3] of **4** with lithium aluminium hydride in dry tetrahydrofuran gave **14**.

*2β,20-Epoxy-12-methoxyabieta-8,11,13-triene (**20**).* A mixture of **14** (250 mg), lead tetraacetate (90%: 390 mg), iodine (200 mg), and dry hexane (10 ml) was stirred at room temperature for 2 h and more lead tetraacetate (390 mg) was added. The mixture was stirred for an additional 4 h and diluted with ether. The organic solution was separated and washed successively with aqueous sodium hydrogencarbonate, aqueous sodium thiosulfate, and brine. The dried solution was evaporated *in vacuo*. The crude product was purified by column chromatography on silica gel (30 g), using ether–benzene (1: 99) as the eluent, to afford **20** (126 mg: 51%), which was recrystallized from hexane. Mp 159—160 °C; ^{1}H NMR: 1.00 and 1.10 (each 3H and s, –$\underline{C}$(CH_3)$_2$), 1.16 (6H, d, J=7 Hz, –CH($C\underline{H}_3$)$_2$), 3.17 (1H, m, –$C\underline{H}$(CH_3)$_2$), 3.47 and 4.06 (each 1H, d, and J=9 Hz, –OCH_2–), 3.75 (3H, s, –OCH_3), 4.42 (1H, bt, J=5 Hz, C_2–H), 6.65 and 6.72 (each 1H and s, C_{11}–H and C_{14}–H). Found: C, 80.27; H, 9.72%. Calcd for $C_{21}H_{30}O_2$: C, 80.21; H, 9.62%.

*Ether Cleavage of **20**.* A mixture of **20** (145 mg) and acetyl *p*-toluenesulfonate (290 mg) in dichloromethane (2.0 ml) was stirred at room temperature for 2 h and then diluted with ether. The ether solution was washed successively with aqueous sodium carbonate and brine, dried over sodium sulfate, and evaporated *in vacuo*. The residue was purified by column chromatography on silica gel (15 g), using ether–benzene (1: 99 and then 5: 95) as the eluent, to give 20-acetoxy-12-methoxyabieta-2,8,11,13-tetraene (**21**) (137 mg: 83 %), which was recrystallized from methanol. Mp 116—117 °C; IR: 1727 cm^{-1}; ^{1}H NMR: 1.03 and 1.08 (each

3H and s, $-C(CH_3)_2$), 1.16 and 1.19 (each 3H, d, and J= 7 Hz, $-CH(CH_3)_2$), 1.90 (3H, s, $-OCOCH_3$), 3.79 (3H, s, $-OCH_3$), 4.27 (2H, bs, $-CH_2O-$), 5.55 (2H, m, C_2–H and C_3–H), 6.68 and 6.77 (each 1H and s, C_{11}–H and C_{14}–H). Found: C, 77.22; H, 9.10%. Calcd for $C_{23}H_{32}O_3$: C, 77.49; H, 9.05%.

Further elution gave 20-acetoxy-12-methoxy-2α-tosyloxyabieta-8,11,13-triene (**22**) (28 mg: 11%). IR: 1733 cm^{-1}; ^1H NMR: 0.96 and 0.99 (each 3H and s, $-C(CH_3)_2$), 1.16 (6H, bd, $-CH(CH_3)_2$), 2.00 (3H, s, $-OCOCH_3$), 2.48 (3H, s, $-C_6H_4CH_3$), 3.75 and 4.62 (each 1H, d, and J=11 Hz, $-CH_2O-$), 3.78 (3H, s, $-OCH_3$), 4.2—4.9 (1H, m, C_2–H), 6.55 and 6.75 (each 1H and s, C_{11}–H and C_{14}–H), 7.34 and 7.83 (each 2H, d, and J=8 Hz, $-C_6H_4CH_3$).

*Conversion of **22** into **20**.* A mixture of **22** (59 mg), potassium carbonate (10 mg), methanol (3.0 ml), and water (2 drops) was refluxed for 2.5 h. The mixture was cooled, diluted with water, and extracted with ether. The ether extract was washed with brine, dried over sodium sulfate, and evaporated *in vacuo*. The crude product was chromatographed on silica gel (5.0 g), using ether–benzene (1:99) as the eluent, to give **20** (24 mg: 69%).

*20-Acetoxy-12-methoxyabieta-8,11,13-triene (**23**).* A mixture of **21** (191 mg) and PtO_2 (20 mg) in ethanol (6.0 ml) was subjected to catalytic hydrogenation at room temperature for 70 min. After the usual work-up, the crude product was purified by column chromatography on silica gel (20 g), using ether–benzene (1:99) as the eluent, to give **23** (178 mg: 93%). IR: 1725 cm^{-1}; ^1H NMR: 1.00 (6H, s, $-C(CH_3)_2$), 1.14 and 1.17 (each 3H, d, and J=7 Hz, $-CH(CH_3)_2$), 1.85 (3H, s, $-OCOCH_3$), 3.76 (3H, s, $-OCH_3$), 4.01 and 4.51 (each 1H, d, and J=10 Hz, $-CH_2O-$), 6.60 and 6.72 (each 1H and s, C_{11}–H and C_{14}–H). Found: C, 77.19; H, 9.58%. Calcd for $C_{23}H_{34}O_3$: C, 77.05; H, 9.56%.

*12-Methoxyabieta-8,11,13-trien-20-ol (**24**).* A mixture of **23** (178 mg) and lithium aluminium hydride (20 mg) in dry tetrahydrofuran (4.0 ml) was stirred at room temperature for 2.5 h. The mixture was poured into ice-dilute hydrochloric acid and extracted with ether. The ether extract was washed with brine, dried over sodium sulfate, and evaporated *in vacuo*. The residue was purified by column chromatography on silica gel (20 g), using ether–benzene (3:97) as the eluent, to give **24** (149 mg: 95%). IR: 3585 cm^{-1}; ^1H NMR: 0.98 (6H, s, $-C(CH_3)_2$), 1.18 (6H, d, J=7 Hz, $-CH(CH_3)_2$), 3.53 and 3.80 (each 1H, d, and J=11 Hz, $-CH_2OH$), 3.79 (3H, s, $-OCH_3$), 6.63 and 6.79 (each 1H and s, C_{11}–H and C_{14}–H).

*Methyl 12-Methoxy-7-oxoabieta-8,11,13-trien-20-oate (**25**).* Jones reagent (2.5 M: 1.1 ml) was added to a stirred solution of **24** (176 mg) in acetone (3.5 ml) at 5 °C. The mixture was stirred at this temperature for 30 min and then at room temperature for 1.5 h, diluted with water, and extracted with ether. The ether extract was washed with brine, dried over sodium sulfate, and evaporated *in vacuo*. The residue was methylated with diazomethane at room temperature. The crude product was purified by column chromatography on silica gel (20 g), using ether–benzene (1:99) as the eluent, to give **25** (80 mg: 40%), which was recrystallized from methanol. Mp 168.5—169 °C; IR: 1720, 1660 cm^{-1}; ^1H NMR: 0.83 and 0.98 (each 3H and s, $-C(CH_3)_2$), 1.20 and 1.25 (each 3H, d, and J=7 Hz, $-CH(CH_3)_2$), 3.57 (3H, s, $-CO_2CH_3$), 3.89 (3H, s, $-OCH_3$), 6.70 (1H, s, C_{11}–H), 7.79 (1H, s, C_{14}–H). Found: C, 73.85; H, 8.72%. Calcd for $C_{22}H_{30}O_4$: C, 73.71; H, 8.44%.

*Methyl 12-Methoxyabieta-6,8,11,13-tetraen-20-oate (**26**).* A mixture of **25** (80 mg) and sodium borohydride (20 mg) in ethanol (2.0 ml) was stirred at room temperature for 4 h. The mixture was diluted with aqueous ammonium chloride and extracted with ether. The ether extract was washed with brine, dried over sodium sulfate, and evaporated *in vacuo*. The residue was dissolved in dichloromethane (1.0 ml) and acetyl *p*-toluenesulfonate (140 mg) was added. The reaction mixture was stirred at room temperature for 30 min, diluted with aqueous sodium hydrogencarbonate, and extracted with ether. The ether extract was washed successively with aqueous sodium hydrogencarbonate and brine, dried over sodium sulfate, and evaporated *in vacuo*. The residue was chromatographed on silica gel (10 g), using benzene as the eluent, to give **26** (55 mg: 71%), which was recrystallized from methanol. Mp 135—136 °C, IR: 1705 cm^{-1}; ^1H NMR: 0.85 and 1.03 (each 3H and s, $-C(CH_3)_2$), 1.16 and 1.19 (each 3H, d, and J=7 Hz, $-CH(CH_3)_2$), 2.42 (1H, t, J=3 Hz, C_5–H), 3.43 (3H, s, $-CO_2CH_3$), 3.82 (3H, s, $-OCH_3$), 5.87 and 6.28 (each 1H, dd, and J=3, 9 Hz, C_6–H and C_7–H), 6.69 and 6.77 (each 1H and s, C_{11}–H and C_{14}–H). Found: C, 76.99; H, 9.06%. Calcd for $C_{22}H_{30}O_3$: C, 77.15; H, 8.83%.

*Methyl 12-Methoxyabieta-8,11,13-trien-20-oate (**27**).* A mixture of **26** (23 mg) and PtO_2 (5.0 mg) in ethanol (6.0 ml) was subjected to catalytic hydrogenation at room temperature for 1.5 h. After the usual work-up, the crude product was purified by column chromatography on silica gel (Merck, 0.063—0.200 mm, 5.0 g), using benzene as the eluent, to give **27** (23 mg: 99%), which was recrystallized from methanol. Mp 111—112 °C, IR: 1710 cm^{-1}; ^1H NMR ($CDCl_3$): 0.79 and 0.98 (each 3H and s, $-C(CH_3)_2$), 1.19 (6H, d, J=7 Hz, $-CH(CH_3)_2$), 3.57 (3H, s, $-CO_2CH_3$), 3.76 (3H, s, $-OCH_3$), 6.74 and 6.88 (each 1H and s, C_{11}–H and C_{14}–H). Found: C, 76.43; H, 9.35%. Calcd for $C_{22}H_{32}O_3$: C, 76.70; H, 9.36%. The ^1H NMR spectrum of **27** was identical with that[1] of methyl pisiferate methyl ether.

*Pisiferic Acid (12-Hydroxyabieta-8,11,13-trien-20-oic Acid) (**1**).* A mixture of **27** (33 mg) and anhydrous aluminium bromide (250 mg) in ethanethiol (1.0 ml) was stirred at room temperature for 13 h. The mixture was poured into dilute hydrochloric acid and extracted with ether. The ether extract was washed with brine, dried over sodium sulfate, and evaporated *in vacuo*. The residue was chromatographed on silica gel (Mallinckrodt, Silic AR CC-4, 5.0 g), using ether–benzene (1:9) as the eluent, to give **1** (28 mg: 93%), which was recrystallized from ether–hexane. Mp 226—227 °C (sublimed); IR: 3600, 3500—2400, 1690 cm^{-1}; ^1H NMR ($CDCl_3$: 90 MHz): 0.84 and 0.97 (each 3H and s, $-C(CH_3)_2$), 1.21 (6H, d, J=7 Hz, $-CH(CH_3)_2$), 6.68 and 6.89 (each 1H and s, C_{11}–H and C_{14}–H). Found: C, 76.19; H, 9.19 %. Calcd for $C_{20}H_{28}O_3$: C, 75.91; H, 8.92%. The IR and ^1H NMR spectra of the synthetic **1** were identical with those of natural pisiferic acid.

*Methyl Pisiferate (Methyl 12-Hydroxyabieta-8,11,13-trien-20-oate) (**2**).* A mixture of **27** (20 mg), anhydrous aluminium chloride (54 mg), ethanethiol (0.2 ml), and dichloromethane (1.0 ml) was stirred at 0—5 °C for 4 h. After the same work-up as described for the preparation of **1**, the crude product was chromatographed on silica gel (Merck, 0.063—0.200 mm, 5.0 g), using ether–benzene (5:95) as the eluent, to give **2** (19 mg: 97%), which was recrystallized from ether–hexane. Mp 170—171.5 °C; IR: 3610, 3350br, 1719 cm^{-1}; ^1H NMR ($CDCl_3$: 90 MHz): 0.74 and 0.93 (each 3H and s, $-C(CH_3)_2$), 1.18 (6H, d, J=7 Hz, $-CH-$

($C\underline{H}_3)_2$), 3.12 (1H, m, $-C\underline{H}(CH_3)_2$), 3.53 (3H, s, $-CO_2CH_3$), 5.39 (1H, bs, -OH), 6.71 and 6.88 (each 1H and s, C_{11}–H and C_{14}–H). Found: C, 76.32; H, 9.36%. Calcd for $C_{21}H_{30}O_3$: C, 76.32; H, 9.15%. The IR and ^{1}H NMR spectra of the synthetic **2** were identical with those of natural methyl pisiferate.

20-Acetoxyabieta-8,11,13-trien-12-ol (28). A mixture of **23** (121 mg), anhydrous aluminium chloride (270 mg), ethanethiol (0.2 ml), and dichloromethane (2.0 ml) was stirred at 0—5 °C for 6.5 h. After the same work-up as described for the preparation of **1**, the crude product was purified by column chromatography on silica gel (15 g), using ether–benzene (5:95) as the eluent, to give **28** (87 mg: 74%); IR: 3610, 3375br, 1726 cm^{-1}; ^{1}H NMR: 0.99 (6H, s, $-\overset{|}{C}(CH_3)_2$), 1.21 (6H, d, J=7 Hz, $-CH(C\underline{H}_3)_2$), 1.85 (3H, s, $-OCOCH_3$), 4.10 and 4.50 (each 1H, d, and J=11 Hz, $-CH_2O-$), 5.85 (1H, s, -OH), 6.53 and 6.73 (each 1H and s, C_{11}–H and C_{14}–H).

Pisiferol (Abieta-8,11,13-triene-12,20-diol) (3). A mixture of **28** (87 mg) and lithium aluminium hydride (20 mg) in dry tetrahydrofuran (1.0 ml) was stirred at room temperature for 1 h. The mixture was poured into dilute hydrochloric acid and extracted with ether. The ether extract was washed with brine, dried over sodium sulfate, and evaporated *in vacuo*. The residue was chromatographed on silica gel (10 g), using ether–benzene (1:9) as the eluent, to give **3** (67 mg: 88%), which was recrystallized from benzene. Mp 185—188 °C (softened at *ca.* 82 °C); IR: 3590, 3325br cm^{-1}; ^{1}H NMR ($CDCl_3$: 90 MHz): 0.91 and 0.93 (each 3H and s, $-\overset{|}{C}(CH_3)_2$), 1.22 (6H, d, J=7 Hz, $-CH(C\underline{H}_3)_2$), 3.17 (1H, m, $-C\underline{H}(CH_3)_2$), 3.61 and 3.97 (each 1H, d, and J=11 Hz, $-C\underline{H}_2OH$), 6.10 (1H, bs, -OH), 6.63 and 6.89 (each 1H and s, C_{11}–H and C_{14}–H). Found: C, 79.62; H, 10.23%. Calcd for $C_{20}H_{30}O_2$: C, 79.42; H, 10.00%. The IR and ^{1}H NMR spectra of the synthetic **3** were identical with those of natural pisiferol.

The authors are grateful to Dr. M. Yatagai, Forestry and Forest Products Research Institute, for kindly supplying the natural pisiferic acid and spectral data. This work was partially supported by Grant-in-Aid for Scientific Research No. 56540324 from the Ministry of Education, Science and Culture.

References

1) M. Yatagai, T. Shirato, Y. Hayashi, N. Fukuhara, and T. Takahashi, *Mokuzai Gakkaishi*, **24**, 267 (1978); M. Yatagai and T. Takahashi, *Phytochemistry*, **18**, 176 (1979).

2) T. Matsumoto, S. Usui, H. Kawashima, and M. Mitsuki, *Bull. Chem. Soc. Jpn.*, **54**, 581 (1981).

3) S. Usui, *J. Sci. Hiroshima Univ., Ser. A*, **44**, 353 (1981).

4) Although the nomenclature and formulas represent only one enantiomer, they should be taken to indicate racemates.

5) E. Wenkert, A. Afonso, P. Beak, R. W. J. Carney, P. W. Jeffs, and J. D. McChesney, *J. Org. Chem.*, **30**, 713 (1965).

6) M. H. Karger and Y. Mazur, *J. Org. Chem.*, **36**, 528 (1971).

7) When the alcohol was dehydrated with dilute hydrochloric acid, the yields of the tetraene (**26**) were only 10—30%.

8) M. Node, K. Nishide, M. Sai, K. Fuji, and E. Fujita, *J. Org. Chem.*, **46**, 1991 (1981).

9) M. Node, K. Nishide, M. Sai, K. Ichikawa, K. Fuji, and E. Fujita, *Chem. Lett.*, **1979**, 97.

Photochemical Reactions of Aromatic Compounds. XXXVII.[1] Solvent Effects on Fluorescence Quenching and Photoreactions of Naphthonitrile–Olefin and Furan Systems. Qualitative Consideration on Electronic Structures and Reactivities of Nonemissive Exciplexes

Chyongjin PAC,* Masahide YASUDA, Kensuke SHIMA,† and Hiroshi SAKURAI

Department of Chemical Process Engineering, Faculty of Engineering, Osaka University, Suita, Osaka 565

†*Department of Industrial Chemistry, Faculty of Engineering, Miyazaki University, Miyazaki 880*

(Received October 29, 1981)

Solvent effects on the fluorescence-quenching rate constants (γk_c) as well as on the quantum yields ($\phi^{\infty}{}_{-A}$) of photoreactions have been investigated for the nonemissive exciplex systems in which 1- or 2-naphthonitrile is the electron acceptor whereas the donors are some enol ethers, a few simple alkenes, furan, 2-methylfuran, and ethyl phenyl ether. On the basis of the assumption of the solvent as a continuous dielectric medium, the relationships between electronic structures and reactivities of nonemissive exciplexes have been qualitatively estimated from the plots of log γk_c and log $[\phi^{\infty}{}_{-A}/(1-\phi^{\infty}{}_{-A})]$ *vs.* $(\varepsilon-1)/(2\varepsilon+1)$. In nonpolar and moderately polar aprotic solvents, the nonemissive exciplexes have low charge-transfer contributions but relatively high reactivities in the cycloaddition while much larger charge-transfer contributions are induced in more polar alcoholic solvents; the reactivities in the protic solvents decrease with the increase of solvent polarity. For some exciplexes, the occurrence of complete electron transfer in very polar solvents such as ethanol, methanol, and acetonitrile is strongly suggested from the product distributions. The possible availability of $E_T(30)$ or Z value as a scale of solvent polarity has been tested for the solvent effects on the processes from the nonemissive exciplexes.

It is now widely accepted that the exciplex formation is a general mechanistic pathway for interactions between electronically excited and ground-state molecules involving luminescence quenching[2] as well as photoreactions,[3] especially photocycloadditions.[3–5] We have extensively investigated photocycloadditions of aromatic nitriles to olefinic and furan compounds,[4] most of which proceed *via* totally or virtually nonemissive exciplexes.[4f–k,6] Scheme 1 shows the major mechanistic pathways for the photoreactions of aromatic nitriles (electron acceptors, A) with olefinic and furan compounds (electron donors, D), where $^1[A\cdot D]^*$ and $(A^{\mp}\cdots D^{\pm})$ represent an exciplex and an ion-radical pair respectively. The complete electron-transfer process (k_e) is negligeble in nonpolar solvents but may be important in very polar solvents such as acetonitile and methanol.[2,4f,4k,7]

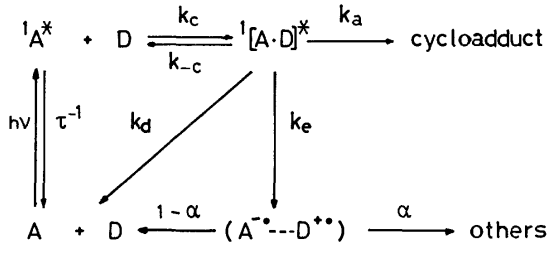

Scheme 1.

These dynamic processes probably depend on the electronic nature of exciplexes that can be simply represented by

$$^1[A\cdot D]^* \equiv {}^1A^*D \leftrightarrow A^-D^+.$$

A stimulating problem in the chemistry of exciplex is to establish the relationships between reactivities and electronic structures of exciplexes.[2b,5] Although exciplex emissions can provide a direct clue to the estimation of the electronic structures,[2c–e,8] the exciplex intermediates postulated in numerous photoreactions are very often nonemissive. In these cases, the charge-transfer (CT) nature of nonemissive exciplexes has been usually discussed from the linear correlations between the logarithm of luminescence-quenching rate constants and ionization potentials of D or electrochemical reduction potentials of A for a family of similar A-D pairs.[9–12] However, the linear correlations can reveal only the linear free-energy relationships in the quenching process.[11,13]

In order to establish structure-reactivity relationships in the chemistry of nonemissive exciplexes, therefore, it is required to find suitable phenomena that allow us to estimate their electronic structures. Since exciplexes are more or less polar, their physical and chemical consequences should be affected by the sorrounding medium, depending on the CT nature. Therefore, solvent effects on kinetics may be diagnostic for the estimation of the CT nature of nonemissive exciplexes. We have found that the naphthonitrile-olefin and furan systems reveal remarkable solvent dependences of both fluorescence-quenching rate constants and quantum yields of the photoreactions. In the present work, we have performed qualitative, steady-state analyses of the solvent effects on the basis of the dielectric continuum model[14] and have tested the applicability of E_T (30),[15] an empirical scale of solvent polarity.

Results

Reaction Systems. Chart 1 lists the electron acceptors (A) and the donors (D) employed in the present work. Table 1 shows the selected A-D pairs that

TABLE 1. SELECTED EXCIPLEX-FORMING SYSTEMS

Classification	A[a]	D[b]	Cycloadduct (isomer ratio)[c,d]	Reference
Case I	**1a**	**2a**	**3a** : **4a** ($\approx$1 : 1)	4c
		2c	**3c** : **4c** ($\approx$1 : 1)	Present work
	1b	**2a**	**5a**	4i, 4j
		2c	n.d.[e]	
Case II	**1a**	**2b**	**3b** : **4b** ($\gtrsim$95 : $\lesssim$5)	4e
		2f	**7**	4a
	1b	**2d**	**5d**	f)
		2g	**8** : **9** (1 : 4)	g)
Case III	**1a**	**2e**	**3e** : **4e** ($\approx$1 : 1)	h)
Case IV	**1a**	**2h**	No adduct	

a) **1a** : 1-Naphthonitrile and **1b** : 2-naphthonitrile. b) **2a** : Ethyl vinyl ether, **2b** : phenyl vinyl ether, **2c** : 2-methyl-2-butene, **2d** : 2,3-dimethyl-2-butene, **2e** : 2,3-dihydropyran, **2f** : furan, **2g** : 2-methylfuran, and **2h** : ethyl phenyl ether. c) See abbreviations in Scheme 1. d) In benzene solutions. e) Not determined. f) T. S. Cantrell, *J. Am. Chem. Soc.*, **94**, 5929 (1972). g) C. Pac, T. Sugioka, and H. Sakurai, unpublished results. See also Ref. 4b. h) C. Pac, K. Mizuno, and H. Sakurai, unpublished results. See also Ref. 4c.

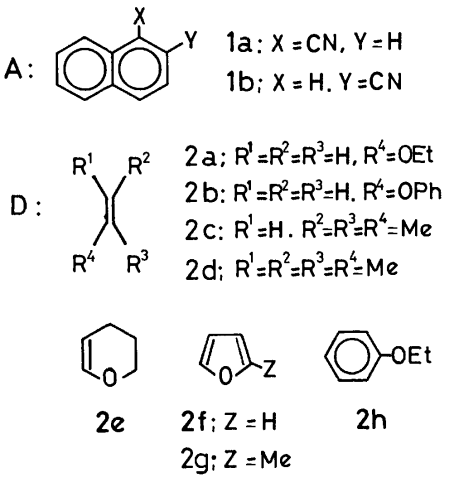

Chart 1.

are classified into the four cases. Case I is the reaction system that gives only the cycloadduct(s) irrespective of solvent polarity when photoreactions occur. The photoreactions of case II give again the cycloadducts in nonpolar and moderately polar solvents while other products are formed in very polar solvents (*vide infra*). In both cases, exciplex emissions

TABLE 2. SCALES OF SOLVENT POLARITY AND FLUORESCENCE LIFETIMES OF 1- AND 2-NAPHTHONITRILES (**1a** AND **1b**) IN VARIOUS SOLVENTS

	Solvent										
	CH[a]	BZ[b]	BE[c]	DO[d]	THF[e]	EA[f]	TB[g]	IP[h]	ET[i]	ME[j]	AN[k]
ε[l]	2.02	2.28	3.08	2.21	7.58	6.02	12.47	19.92	24.55	32.7	37.5
$f(\varepsilon)$[m]	0.20	0.23	0.29	0.22	0.41	0.39	0.44	0.46	0.47	0.48	0.48
$E_T(30)$/kcal mol^{-1}	31.2	34.5	33.4	36.0	37.1	38.1	43.9	48.6	51.9	55.5	46
τ_F[n]/ns; **1a**	18.5	12.3	12.7	11.3	11.1	12.3	10.2	9.7	9.4	8.4	9.3
τ_F[n]/ns; **1b**	30.3	24.9	17.7	24.3	21.9	22.9	21.8	21.4	20.6	19.7	21.8
τ_F[air o]/ns; **1a**	11.1	8.8	7.7	9.3	8.4	7.6	8.1	7.4	7.0	6.3	6.8
τ_F[air o]/ns; **1b**	13.6	12.4	10.0	16.4	16.7	10.4	14.0	12.6	11.6	10.3	10.6

a) Cyclohexane. b) Benzene. c) Di-*n*-butyl ether. d) Dioxane. e) Tetrahydrofuran. f) Ethyl acetate. g) *t*-Butyl alcohol. h) 2-Propanol. i) Ethanol. j) Methanol. k) Acetonitrile. l) Dielectric constant. m) $f(\varepsilon)=(\varepsilon-1)/(2\varepsilon+1)$. n) Fluorescence lifetimes in degassed solutions; $\pm$0.3 ns. o) Fluorescence lifetimes in aerated solutions; $\pm$0.5 ns.

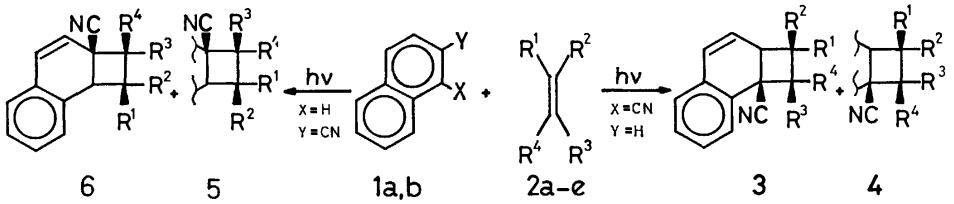

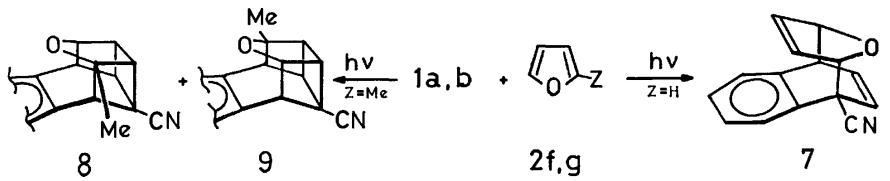

Scheme 2.

Table 3. Logarithm of fluorescence-quenching rate constants for naphthonitrile–olefin and -furan pairs[a)]

A	D	log γk_c[b)] CH	BZ	BE	DO	THF	EA	TB	IP	ET	ME	AN
1a	**2a**	8.95	9.10	9.07	9.08	9.23	9.30	9.05	9.45	9.64	9.82	9.83
	2b	8.88	8.75	8.81	8.93	9.02	9.14	9.21	9.37	9.57	9.95	9.82
	2c	8.02	8.27	8.21	8.62	8.69	8.60	9.11	9.26	9.63	9.89	9.58
	2f	7.40	7.96	7.86	8.18	8.38	8.42	9.24	9.48	9.83	10.31	9.45
	2h	8.61	8.73	8.90	8.93	9.11	9.30	9.72	9.77	10.0	10.05	10.09
1b	**2a**	7.28	7.57	7.38	7.62	7.58	7.70	8.11	8.20	8.32	8.53	8.39
	2c	7.22	7.47	7.32	7.44	7.45	7.69	8.10	8.34	8.56	8.96	8.81
	2d	8.35	8.66	8.62	8.84	8.69	8.50	9.04	9.16	9.49	9.83	10.09
	2g	7.91	8.13	8.12	8.41		8.52	9.09	9.33	9.74	10.14	9.89

a) For aerated solutions; [**1a** and **1b**] = 3—6 × 10^{-4} mol dm^{-3}. See abbreviations in Chart 1 and Table 2. b) Averaged values for three or four runs; uncertainties ±0.05.

Table 4. Solvent effects on isomer ratios of [2+2] photocycloadducts of **1a-2a** and **1a-2c** pairs[a,b)]

A-D pair	**3**/**4**[c)] BZ	EA	TB	IP	ET	ME	AN
1a-2a	0.96	1.11	1.33	1.23	1.22	1.23	1.11
1a-2c	1.30	1.29	1.26	1.45	1.45	1.41	1.42

a) Solutions containing ≈0.05 mol dm^{-3} in **1a** and ≈1.0 mol dm^{-3} in the olefins were irradiated at 313 nm under cooling with water; conversions were 10—30%. b) See abbreviations in Chart 1, Scheme 1, and Table 2. c) *Endo*-to-*exo* isomer ratios determined by GLC and NMR.

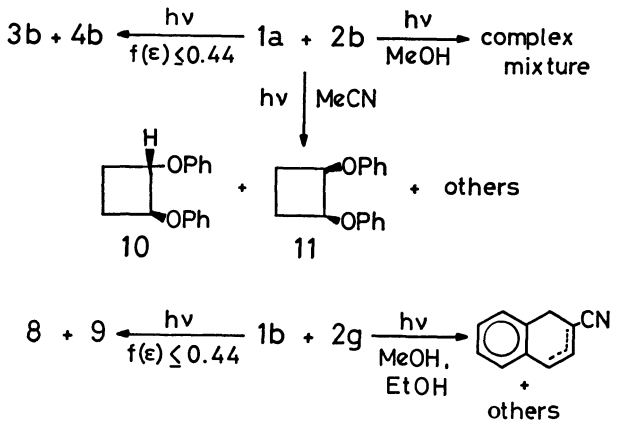

Scheme 3.

are not detectable or, if any, negligebly weak in any solvent at room temperature. The **1a-2e** pair (case III) was employed as a typical reactive exciplex that is emissive in measurable intensities at room temperature. The **1a-2h** pair (case IV) is a reference exciplex that is fairly emissive but undergoes no net photoreaction. The types of photocycloadditions are shown in Scheme 2. Most of the cycloadducts are known compounds,[4)] and the structures of a few unknown adducts were readily determined by comparison of their spectroscopic data with those of similar known compounds.

The obligatory intermediacy of singlet exciplexes in these photocycloadditions has been established by the oxygen-quenching method for the **1a-2a** and **1a-2e** pairs,[16)] by negative temperature effects on the photoreaction of **1a** and **2f**,[6a)] and by exciplex quenching by pyridine for the **1b-1a**, **1b-2d**, **1b-2e**, and **1b-2g** pairs.[4j,6b,6c)] The *endo* selective nature of the photocycloaddition of **1a** to **2b** strongly suggests the intervention of an exciplex intermediate which determines the stereoselectivity.

Fluorescence Quenching in Various Solvents. Table 2 lists fluorescence lifetimes of **1a** and **1b** in deaerated and aerated solutions (τ_F and τ_F^{air}) and the parameters of solvent polarity including dielectric constant (ε), its function [$f(\varepsilon)=(\varepsilon-1)/(2\varepsilon+1)$], and the $E_T(30)$ values in kcal mol^{-1}. Quenching of the fluorescence of **1a** or **1b** by **2a**—**h** was performed for air-saturated solutions, the quenching rate constants (γk_c) being thus determined from the linear Stern-Volmer plots using Eq. 4. Table 3 summarizes the logarithm of γk_c for the selected A-D pairs.

Solvent Effects on Product Distribution. Table 4 lists the *endo*/*exo*-isomer ratios (**3**/**4**) of the cycloadducts in the photoreactions of the **1a-2a** and **1a-2c** pairs (case I) in various solvents. There can be seen a tendency that the ratios in the alcoholic solvents are slightly, but significantly, higher than those in the less polar aprotic solvents. Other products than the cycloadducts were not formed even in acetonitrile and methanol.

On the other hand, irradiation of the A-D pairs of case II commonly gave complex mixtures of other products than the cycloadducts in the solvents of $f(\varepsilon)>0.46$; an increase of solvent polarity results in an increase of formation of complex mixtures. In the case of the **1a-2f** pair, irradiation of ethanol, methanol, and acetonitrile solutions gave complex mixtures involving oligomeric and polymeric compounds and a small amounts of **7**, as demonstrated by GLC, GPC, and NMR (see Fig. 8). In contrast the photoproduct in ethyl acetate and *t*-butyl alcohol is exclusively **7**.

The photoreaction of **1a-2b** pair in either *t*-butyl alcohol or ethyl acetate gave exclusively the cyclo-

TABLE 5. QUANTUM YIELDS FOR DISAPPEARANCE OF 1-NAPHTHONITRILE IN THE PHOTOREACTIONS WITH ETHYL VINYL ETHER (**2a**), 2-METHYL-2-BUTENE (**2c**), 2,3-DIHYDROPYRAN (**2e**), AND FURAN (**2f**)

	ϕ_{-A}[b] (ϕ^{∞}_{-A})[c]									
D	CH	BZ	BE	DO	EA	TB	IP	ET	ME	AN
2a	0.47	0.50	0.44	0.47	0.37	0.34	0.19	0.22	0.14	0.30
	(0.52)	(0.55)	(0.49)	(0.51)	(0.40)	(0.38)	(0.20)	(0.23)	(0.14)	(0.30)
2c	0.34	0.58	0.35	0.52	0.52	0.79	0.30	0.13	0.08	0.25
	(0.64)	(0.93)	(0.62)	(0.66)	(0.69)	(0.87)	(0.35)	(0.13)	(0.08)	(0.25)
2e[d]	0.57	0.46	0.53	0.40	0.06	0.03	0.014	<0.01	<0.01	<0.01
2f	0.21	0.39	0.37	0.40	0.34	0.22	0.15[e]	0.14[e]	0.08[e]	0.08[e]
	(0.50)	(0.58)	(0.62)	(0.51)	(0.41)	(0.23)	(0.15)	(0.14)	(0.08)	(0.08)

a) See abbreviations in Chart 1 and Table 2. b) Determined at 313 nm for aerated solutions containing 3.5—4.5 × 10^{-4} mol dm^{-3} in **1a** and 1.0 mol dm^{-3} in the olefins or 2.6 mol dm^{-3} in furan; averaged values for three runs with uncetainties of ±(8—15)%. c) Calculated by multiplying ϕ_{-A} by $(1+K_{SV}[D])/K_{SV}[D]$; see text. d) It is assumed that $\phi_{-A} \simeq \phi^{\infty}_{-A}$, since $K_{SV}[D](=51—95) \gg 1$ in all the solvents. e) Other products than the cycloadduct (**7**) were formed.

adduct (**3b**), while the dimers of **2b** (**10** and **11**)[17] were formed in acetonitrile as the major detectable products. The irradiation of a methanolic solution gave complex mixtures involving **3b**, **10**, and **11** in small amounts. The photoreaction of the **1b-2g** pair in *t*-butyl alcohol or in less polar solvents gave again the cage compounds (**8** and **9**) in >80% yields while the irradiation in methanol or ethanol gave complex mixtures from which 1,2- and 1,4-dihydro-2-naphthonitriles were obtained. Scheme 3 summarizes the photoreactions of the **1a-2b** and **1b-2g** pairs in different solvents.

Quantum Yields in Various Solvents. Table 5 shows the quantum yields (ϕ_{-A}) for disappearance of **1a** and the calculated limiting quantum yields (ϕ^{∞}_{-A}) for some selected A-D pairs in aerated solutions. The ϕ^{∞}_{-A} values were calculated by multiplying ϕ_{-A} by $(K_{SV}[D]+1)/K_{SV}[D]$; K_{SV} and [D] represent, respectively, the slopes of the Stern-Volmer plots for the fluorescence quenching and the concentration at which ϕ_{-A} was determined. This method was confirmed to be approximately valid since the calculated values of ϕ^{∞}_{-A} in cyclohexane for the **1a-2a** and **1a-2f** pairs are almost identical to the observed values (0.51 and 0.49 respectively) obtained from the intercepts of the usual plots of ϕ_{-A}^{-1} *vs.* $[D]^{-1}$. In cases where $K_{SV}[D] \gg 1$, it was assumed that $\phi_{-A} \simeq \phi^{\infty}_{-A}$. In the quantum-yield measurements, concentrations of **1a** were set very similar to those used in the fluorescence-quenching experiments.

Discussion

Kinetic Representation and Free-energy Relationships. On the basis of Scheme 1, steady-state analysis gives the Stern-Volmer equation for fluorescence quenching (Eq. 3) and the rate equation for ϕ_{-A} (Eq. 4); Eq. 5 represents the rate equation of the limiting quantum yield for disappearance of A. In these equations, the quenching of both $^1A^*$ and $^1[A\cdot D]^*$ by molecular oxygen (Eqs. 1 and 2) has been taken into consideration since both the fluorescence-quenching and quantum-yield measurements were performed for aerated solutions. However, both $k_q[O_2]$ and $k^c_q[O_2]$ are probably almost constant independently on solvent polarity since the reported solubilities of O_2 upon air saturation into the solvents employed are in the rage of (2—3) × 10^{-3} mol dm^{-3} at 25 °C[18] and since it is reasonable to assume that $k_q \simeq k^c_q \simeq 2 \times 10^{10}$ dm^3 mol^{-1} s^{-1}.[16b,c,19] Moreover, it was confirmed that the presence of O_2 diminishes ϕ_{-A} in cyclohexane and ethyl acetate for the A-D pairs employed in the quantum-yield measurements; the irradiation in these solvents under air saturation gave no other products than the cycloadducts in significant amounts. Therefore, chemical processes involving O_2 can be safely neglected.

$$^1A^* + O_2 \xrightarrow{k_q} A + O_2 \quad (1)$$

$$^1[A\cdot D]^* + O_2 \xrightarrow{k^c_q} A + D + O_2 \quad (2)$$

$$\frac{I^{\circ}_F}{I^{D}_F} = 1 + K_{SV}[D] = 1 + \gamma k_c \tau_F^{air}[D] \quad (3)$$

$$\frac{1}{\phi_{-A}} = \frac{1}{\phi^{\infty}_{-A}}\left(1 + \frac{1}{\gamma k_c \tau_F^{air}[D]}\right) \quad (4)$$

$$\frac{1}{\phi^{\infty}_{-A}} = \frac{k_a + \alpha k_e}{k_a + k_d + k_e + k^c_q[O_2]} \quad (5)$$

$$\frac{1}{\tau_F^{air}} = \frac{1}{\tau_F} + k_q[O_2] \quad (6)$$

$$\gamma = \frac{k_a + k_d + k_e + k^c_q[O_2]}{k_a + k_d + k_e + k^c_q[O_2] + k_{-c}} \quad (7)$$

It is well established that $k_c \simeq (1—2) \times 10^{10}$ dm^3 mol^{-1} s^{-1} for a variety of exciplex-forming systems.[2,6b,20,21] In cases where $\gamma k_c \ll 10^{10}$ dm^3 mol^{-1} s^{-1}, therefore, it is reasonable to assume that $\gamma \ll 1$, *i.e.* $(k_a + k_d + k_e + k^c_q[O_2]) \ll k_{-c}$. If this is the case, γk_c can be simplified to Eq. 8 which is then rewritten as Eq. 9; ΔG_c is the free-energy change associated with exciplex formation.

$$\gamma k_c \simeq \frac{k_c}{k_{-c}}(k_a + k_d + k_e + k^c_q[O_2]) \quad (8)$$

$$\log \gamma k_c \simeq -\frac{\Delta G_c}{2.3RT} + \log (k_a + k_d + k_e + k^c_q[O_2]) \quad (9)$$

If an exciplex is a solute that has a dipole moment

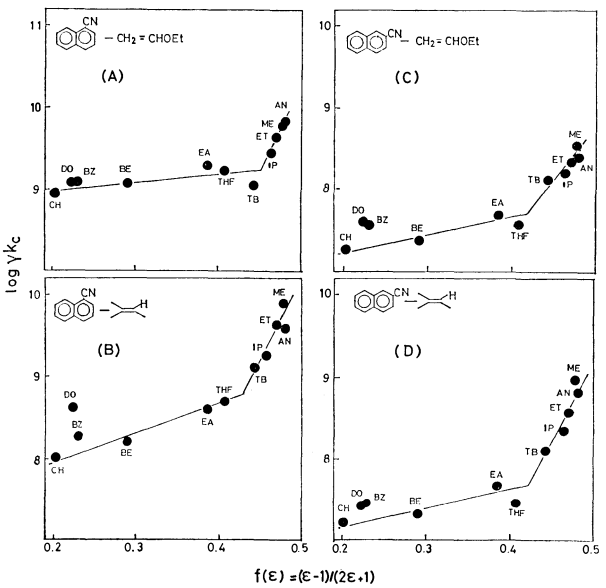

Fig. 1. Plots of log γk_c *vs.* $f(\varepsilon)$ [$=(\varepsilon-1)/(2\varepsilon+1)$] for A-D pairs of case I; (A) **1a-2a**, (B) **1a-2c**, (C) **1b-2a**, and (D) **1b-2c** pairs; see abbreviations in Chart 1 and Table 2.

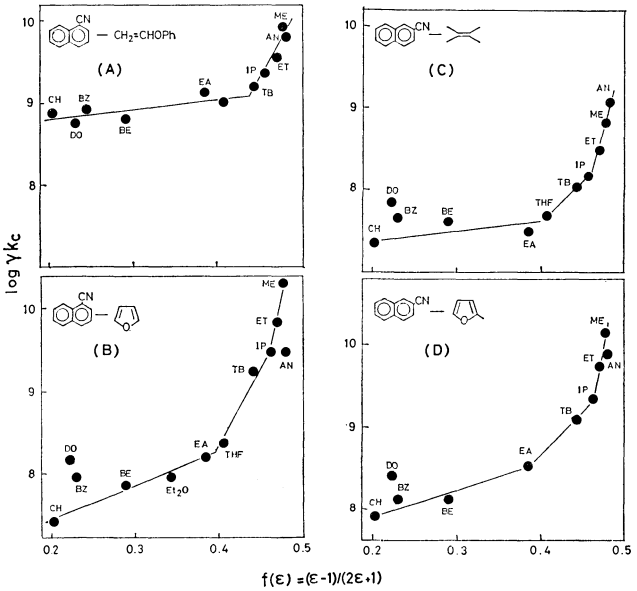

Fig. 2. Plots of log γk_c *vs.* $f(\varepsilon)$ [$=(\varepsilon-1)/(2\varepsilon+1)$] for A-D pairs of case II; (A) **1a-2b**, (B) **1a-2f**, (C) **1b-2d**, and (D) **1b-2g** pairs; see abbreviations in Chart 1 and Table 2.

of μ_c with a separation of R_c Å, the treatment of the solvent as a continuous dielectric medium gives Eq. 10 for the difference of ΔG_c between the reference solvent (*e.g.* cyclohexane) and the medium of dielectric constant ε.[14,22] Thus Eq. 9 coupled with Eq. 10 gives Eq. 11, predicting that the slope of the plot of log γk_c *vs.* $f(\varepsilon)$ may reflect the dipole moment of an exciplex, if the solvent dependence of k_{-c} is much greater than that of the other rate constants.[20]

$$\Delta\Delta G_c = -\frac{{\mu_c}^2}{{R_c}^3} f(\varepsilon) + \text{constant} \tag{10}$$

$$\Delta \log \gamma k_c = \frac{1}{2.3RT} \times \frac{{\mu_c}^2}{{R_c}^3} f(\varepsilon) + \Delta \log (k_a + k_d + k_e + k_q^c[O_2]) + \text{constant} \tag{11}$$

$$\left[f(\varepsilon) = \frac{\varepsilon - 1}{2\varepsilon + 1} \right]$$

Equation 7 can be rewritten as Eq. 12. It has been reported that the complete electron-transfer process is negligeble in the decay pathways of **1a**——1,2-dimethylcyclopentene exciplex in ethyl acetate,[20] *i.e.* $(k_a + k_d + k_q^c[O_2]) \gg k_e$. This is probably true for the present nonemissive exciplexes in the solvents of $f(\varepsilon) \leq 0.44$, since the cycloadducts are commonly the exclusive products in these solvents and since the ionization potentials of the present donors are higher than that of 1,2-dimethylcyclopentene(7.84 eV);[23] see Table 7. In this case, therefore, Eq. 12 can be reduced to Eq.13. If the cycloaddition occurs from an ex-

$$\frac{\phi^{\infty}_{-A}}{1-\phi^{\infty}_{-A}} = \begin{cases} \dfrac{k_a + \alpha k_e}{k_d + (1-\alpha)k_e + k_q^c[O_2]} & (12) \\ \dfrac{k_a}{k_d + k_q^c[O_2]} & (13) \end{cases}$$

Table 6. Slopes of the plots of log γk_c *vs.* $(\varepsilon-1)/(2\varepsilon+1)$ for the naphthonitrile-olefin, furan, and ethyl phenyl ether pairs[a,b]

			Slopes	
	A	D	$f(\varepsilon)^{c)} < \approx 0.4$	$f(\varepsilon)^{c)} > \approx 0.4$
Case I	**1a**	**2a**	1.0	20
		2c	1.4	21
	1b	**2a**	0.9	13
		2c	1.0	17
Case II	**1a**	**2b**	1.2	18
		2f	2.3	$\gtrsim$21
	1b	**2d**	0.6	$\gtrsim$10
		2g	1.3	$\gtrsim$10
Case IV	**1a**	**2e**	2.9	11.2

a) Values obtained by a rough estimate from the plots in Figs. 1, 2, and 3(B). b) See abbreviations in Chart 1. c) $(\varepsilon-1)/(2\varepsilon+1)$.

$$\log\left(\frac{\phi^{\infty}_{-A}}{1-\phi^{\infty}_{-A}}\right) = -\frac{\Delta G_{sol}^{*}}{2.3RT} - \log (k_d + k_q^c[O_2]) + \text{constant}$$

$$\left[\Delta G_{sol}^{*} = \left(\frac{{\mu_c}^2}{{R_c}^3} - \frac{{\mu_*}^2}{{R_*}^3}\right) f(\varepsilon)\right] \tag{14}$$

ciplex of dipole moment μ_c to a transition state of dipole moment μ_* in the medium of dielectric constant ε, the dielectric continuum assumption gives Eq. 14 where ΔG_{sol}^{*} is the electrostatically induced free-energy change for the cycloaddition process.

Solvent Effects on Fluorescence Quenching. Estimation of Electronic Nature of Nonemissive Exciplex: As can be seen in Table 3, the fluorescence-quenching rate constants are much lower than the diffusion-controlled limits except for those in very polar solvents for

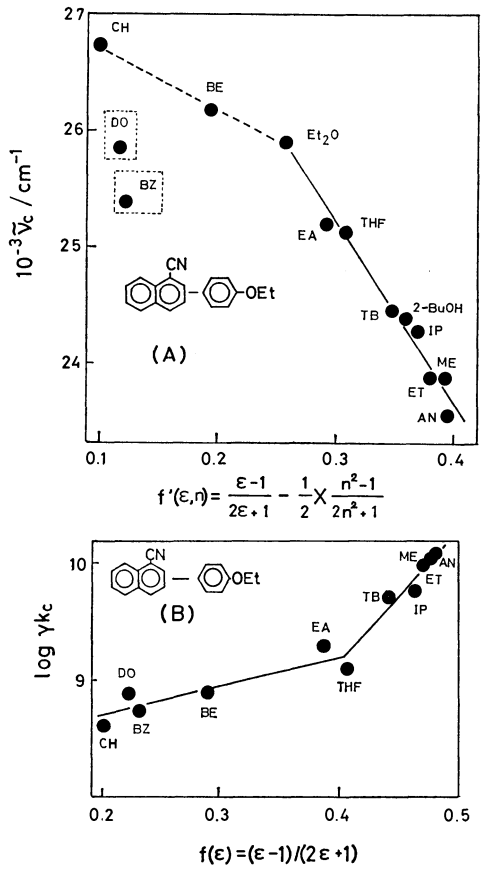

Fig. 3. (A) Plot of $\tilde{\nu}_c$ *vs.* $f'(\varepsilon,n)$ $[=(\varepsilon-1)/(2\varepsilon+1)-(n^2-1)/2(2n^2+1)]$ and (B) plot of log γk_c *vs.* $f(\varepsilon)$ $[=(\varepsilon-1)/(2\varepsilon+1)]$ for **1a-2h** pair; see abbreviations in Chart 1 and Table 2.

Table 7. Reduction potentials of 1- and 2-naphthonitriles, oxidation potentials, and ionization potentials of electron donors (D), and calculated free-energy changes for complete electron transfer[a)]

	A	$-E^{red}_{p/2}$ [b)] / V	D	$E^{ox}_{p/2}$ [b)] / V	*IP* / eV	$-\Delta G_{ET}$ [c)] / kcal mol^{-1}
Case I	**1a**	2.06	**2a**	1.35	8.49[d)]	10.5
			2c	1.47	8.85[e)]	7.7
	1b	2.18	**2a**			5.2
			2c			2.5
Case II	**1a**		**2b**	1.37		10.0
			2f	1.40	8.89[f)]	9.3
	1b		**2d**	1.13	8.30[g)]	9.7
			2g	1.14	8.39[f)]	10.1
Case III	**1a**		**2e**	1.12	8.34[f)]	15.8

a) See abbreviations in Chart 1. b) Determined by cyclic voltammetry for dry acetonitrile solutions *vs.* $Ag/AgNO_3$. c) Calculated according to the following equation; $\Delta G_{ET}=23.06[E^{ox}_{p/2}-E^{red}_{p/2}-e^2/\varepsilon a]-E_{0\text{-}0}(^1A^*)$. For $E_{0\text{-}0}(^1A^*)$, see Ref. 18, p. 19. d) N. E. Shore and N. J. Turro, *J. Am. Chem. Soc.*, **97**, 2482 (1975). e) W. C. Price, R. Bralsford, and P. V. Harris, *Spectrochimica Acta*, **14**, 45 (1959). f) K. Watanabe, T. Nakayama, and J. Mottl, *J. Quant. Spectrosc. Radiat. Transfer*, **2**, 369 (1962). g) W. C. Price, *Chem. Rev.* **47**, 257 (1947).

some A-D pairs. Therefore, Eqs. 8 and 9 hold for the fluorescence quenching of the present A-D pairs in most solvents. Figures 1 and 2 show the plots of log γk_c *vs.* $f(\varepsilon)$ for the 8 A-D pairs; the following common features should be noted. (1) The plots give, at least, two linear lines with a break at $f(\varepsilon)\simeq 0.4$. It is therefore suggested that the simple dielectric continuum approximation (Eq. 11) is applicable to the fluorescence-quenching process *via* the nonemissive exciplexes within the limited regions of solvent polarity, *i.e.* at $f(\varepsilon)<0.4$ (nonpolar and moderately polar solvents) and at $f(\varepsilon)>0.4$ (polar alcoholic solvents and acetonitrile). (2) The slopes of the plots at the lower region of $f(\varepsilon)$ are much smaller than those at the higher region (Table 6). On the basis of Eq. 11, therefore, μ_c^2/R_c^3 is much greater in the polar solvents of $f(\varepsilon)>0.4$ than that in the less polar solvents, suggesting that the electronic structures of the nonemissive exciplexes are changed from minor CT contributions in the nonpolar and moderately polar solvents to much larger CT contributions in the polar solvents. Such solvent-induced changes in the electronic nature have been demonstrated for a few emissive exciplexes.[20,24,25] (3) Benzene and dioxane which are nonpolar but polarizable are the out-of-line solvents in most cases. The nonemissive exciplexes would be specifically solvated by these solvents.

In order to obtain further insight into solvent effects on the electronic nature of exciplexes, we have investigated both the solvent-induced shifts of the emission maximum ($\tilde{\nu}_c$, cm^{-1}) and the solvent dependence of γk_c for the emissive **1a-2h** exciplex (case IV). The dipole moment (μ_c) of the exciplex was estimated as usual using Eq. 15. As is shown in Fig. 3A, the plot of $\tilde{\nu}_c$ *vs.* $f'(\varepsilon,n)$ gives a linear correlation at $f'(\varepsilon,n)>0.25$ with a slope of -1.3×10^4 cm^{-1} which corresponds to >10D of μ_c taking $R_c=4.5$—5 Å. This large dipole moment demonstrates the dominant CT contributions in the solvents of $f'(\varepsilon,n)>0.25$. Unfortunately, the plot at $f'(\varepsilon,n)<0.25$ is poorly correlated because of the substantial deviations of $\tilde{\nu}_c$ in benzene and dioxane, though a smaller value of μ_c in the less polar solvents might be suggested (*vide infra*).

$$\tilde{\nu}_c = -\frac{2\mu_c^2}{hcR_c^3}\left(\frac{\varepsilon-1}{2\varepsilon+1}-\frac{n^2-1}{4n^2+2}\right)+\text{constant}$$
$$= -\frac{2\mu_c^2}{hcR_c^3}f'(\varepsilon,n)+\text{constant} \quad (15)$$

Figure 3B shows a plot of log γk_c *vs.* $f(\varepsilon)$ that again consists of two linear lines with a break at $f(\varepsilon)\simeq 0.4$. From these slopes calculations based on Eq. 11 taking $T=298$ K give the values of μ_c^2/R_c^3 that are 1.5×10^4 J mol^{-1} at $f(\varepsilon)<0.4$ and 6.3×10^4 J mol^{-1} at $f(\varepsilon)>0.4$. The latter value is similar to that separately calculated from the linear portion in Fig. 3A (7.8×10^4 J mol^{-1}). Since the slope at $f(\varepsilon)<0.4$ is only one-fourth that at $f(\varepsilon)>0.4$, the CT contributions are perhaps much lower in the less polar solvents. It is thus suggested that Eq. 11 can be used as a convenient basis for qualitative estimation of electronic

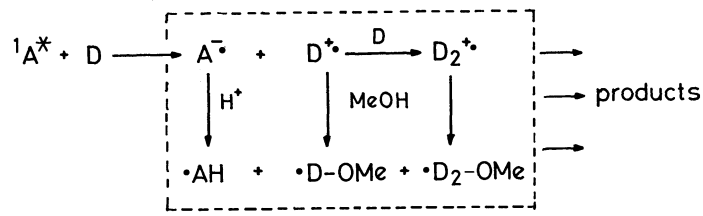

Scheme 4.

structures of nonemissive exciplexes, though other physical and chemical properties of solvent should be taken into consideration for sophisticated interpretations of the solvent effects. At any rate the electronic nature of the nonemissive exciplexes seems to be inherently sensitive to the sorrounding medium.

Occurrence of Complete Electron Transfer in Very Polar Solvents: Complete electron transfer from D to $^1A^*$ may occur in very polar solvents as has been established for a variety of exciplex-forming systems.[2,5f,5k,7] Table 7 lists the observed anodic half-peak potentials ($E_{P/2}^{ox}$) and reported ionization potentials of D, the cathodic half-peak potentials of A, and the calculated free-energy changes (ΔG_{ET}) in acetonitrile associated with the complete electron-transfer process. According to the Rehm-Weller treatment,[26] the net rate constant for complete electron transfer reaches the diffusion-controlled limits in cases where $\Delta G_{ET} < -5$—-6 kcal mol^{-1}, *i.e.* $k_{-c} \ll k_e$. Since the calculated values of ΔG_{ET} are substantially negative in most cases, complete electron transfer can, but not necessarily, occur in acetonitrile and probably also in methanol.

In particular, the occurrence should be taken into consideration for the A-D pairs of case II in the polar solvents of $f(\varepsilon) > 0.44$ as indicated by the photoproducts in these solvents. The photoreaction of the **1a-2b** pair in acetonitrile clearly indicates the occurrence of complete electron transfer since the photodimerization of **2b** *via* the cation radical has now been well established.[27] The attenuation of the dimerization of **2b** in methanol can be interpreted in terms of the nucleophilic addition of methanol to the cation radical of **2b** since it is now well-known that alcohols can attack on cation-radical species of olefinic and furan compounds.[4k,28] Therefore, formation of complex mixtures in the photoreactions of methanolic solutions of the **1a-2b**, **1a-2f**, and **1b-2g** pairs can be considered to be initiated by complete electron transfer from D to $^1A^*$ followed by complex reactions involving a variety of reactive species such as $A^{\cdot-}$, its protonated species, $D^{+\cdot}$, dimer cation radicals of D, and methoxylated species of the cation radicals (Scheme 4).[4k] Moreover, McCullough *et al.* reported that the photoreactions of **1a** and **1b** with **2d** in such very polar solvents as acetonitrile and methanol proceeds by way of complete electron transfer.[7]

In this regard, it should be noted that sharp increases of log γk_c can be seen at $f(\varepsilon) > 0.46$ in the plots for the **1a-2f**, **1b-2d**, and **1b-2g** pairs, presumably arising from increasing contributions of k_e to γ. In case I, however, the occurrence of complete electron transfer is questionable even in acetonitrile since the cycloadditions exclusively occurred in any solvent.

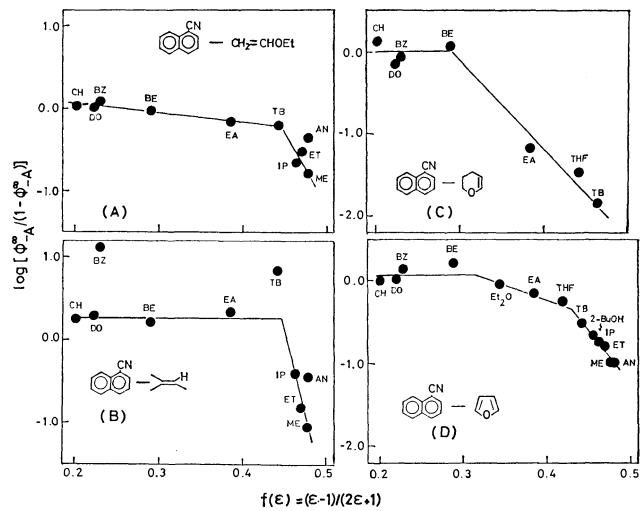

Fig. 4. Plots of $\log[\phi^{\infty}_{-A}/(1-\phi^{\infty}_{-A})]$ *vs.* $f(\varepsilon)$ [$=(\varepsilon-1)/(2\varepsilon+1)$] for (A) **1a-2a**, (B) **1a-2c**, (C) **1a-2e**, and (D) **1a-2f** pairs; see abbreviations in Chart 1 and Table 2.

Solvent Effects on Reactivities of Nonemissive Exciplexes. Figure 4 shows the plots of $\log[\phi^{\infty}_{-A}/(1-\phi^{\infty}_{-A})]$ *vs.* $f(\varepsilon)$ for the **1a-2a**, **1a-2c**, **1a-2f**, and **1a-2e** pairs. Since the complete electron-transfer process (k_e) can be neglected for these A-D pairs, at least, in solvents of $f(\varepsilon) < 0.44$, Eq. 13 can be used for analyses of the plots as a basis for the estimation of exciplex reactivities. In case of the **1a-2f** pair (case II), however, Eq. 12 should be used at $f(\varepsilon) > 0.44$ where complete electron transfer may occur as a competitive or dominant pathway.

For the **1a-2a** pair, k_a and k_d in cyclohexane have been determined by the oxygen-quenching method to be $\approx 10^8$ s^{-1} and $\approx 5 \times 10^7$ s^{-1} respectively.[16d] Since $k_q^c[O_2]$ approximately equals $(4—6) \times 10^7$ s^{-1} independently on solvent polarity, Fig. 4A suggests that both k_a and k_d do not greatly depend on solvent polarity at $f(\varepsilon) < 0.44$. On the other hand, the increase of solvent polarity at $f(\varepsilon) > 0.44$ leads to a decrease of k_a and/or an increase of k_d. A similar conclusion appears to be obtainable from Fig. 4B for the **1a-2c** pair, though the ϕ^{∞}_{-A} values in benzene and *t*-butyl alcohol are unusually high relative to those in the other solvents. On the other hand, the plot for the **1a-2e** pair (Fig. 4C) demonstrates drastic changes of k_a and/or k_d at $f(\varepsilon) > 0.3$.

Lewis and Hoyle reported that the k_a values for the diphenylvinylene carbonate–2,5-dimethyl-2,4-hexadiene exciplex remarkably decrease with solvent polarity.[24] This solvent dependence of k_a has been interpreted on the basis of the Michl's theory;[29] this

theory predicts that k_a is the rate constant for the adiabatic process of avoided crossing from the polar exciplex minimum on the singly excited hypersurface to the less polar or nonpolar doubly excited state. Activation barriers for the adiabatic process should therefore be higher in more polar solvents since an exciplex of polar CT nature is more stabilized by solvation than the less polar transition state. A similar conclusion was put forth by Caldwell and Creed who observed the dependence of k_a and the independence of k_d on the degrees of CT contributions for some emissive cyanophenanthrene–styrene exciplexes.[5f,30]

On the basis of the Michl's theory, therefore, the solvent-dependent changes in ϕ^{∞}_{-A} can be expected to arise mainly from the changes in k_a.[31] If this is the case, the plots of $\log[\phi^{\infty}_{-A}/(1-\phi^{\infty}_{-A})]$ *vs.* $f(\varepsilon)$ are thus diagnostic for the elucidation of the observed solvent effects on reactivities of the nonemissive exciplexes. For example, the large negative slope of the plots at $f(\varepsilon)>0.3$ in Fig. 4C for the **1a-2e** exciplex can be interpreted to reflect large electronic changes in the cycloaddition process which presumably occur from the very polar exciplex state to the much less polar transition state. The very polar nature of the **1a-2e** exciplex was confirmed by the plot of $\bar{\nu}_c$ *vs.* $f'(\varepsilon,n)$ that gives a linear correlation with a slope of $-(1.5\pm0.2)\times10^4$ cm^{-1} at $f'(\varepsilon,n)>0.2$.[32a] The adiabatic process in which large electronic changes occur probably requires larger reorganization of the surrounding slovent molecules in more polar solvents at $f(\varepsilon)>0.3$, thus leading to greater ΔG_{sol}^{*}. In the much less polar and nonpolar solvents ($f(\varepsilon)<0.3$), however, solvation shells round the exciplex would be so weak that ΔG_{sol}^{*} might not significantly contribute to the total activation energies of the cycloaddition process.

Thus the plots in Figs. 4A and 4B suggest that electronic changes are only minor in the adiabatic process from the **1a-2a** or **1a-2c** exciplex to the transition state even in the moderately polar solvents of $f(\varepsilon)\leq0.44$. In other words, these nonemissive exciplexes seem to be almost nonpolar in these less polar solvents. On the other hand, substantial CT nature might be induced by specific solute-solvent interactions in the polar solvents of $f(\varepsilon)>0.44$, thus leading to greater ΔG_{sol}^{*} with higher solvent polarity. Moreover, conformational changes of the exciplexes would also occur on going from the aprotic solvents to the protic solvents since the *endo*/*exo*-isomer ratios are changed; the increase of solvent polarity at $f(\varepsilon)>0.44$ would make conformations of the exciplexes less favorable for the cycloaddition; solvent-dependent changes in R_c have been suggested.[20,25]

The **1a-2f** exciplex (case II) reveals different behaviors in the solvent dependence of ϕ^{∞}_{-A} as shown in Fig. 4D. Since the plot gives a linear line with a low negative slope at the region of $f(\varepsilon)$ from 0.3 to 0.44, this exciplex seems to be significantly, but slightly, ionic in these solvents. On the other hand, the greater negative slope at $f(\varepsilon)>0.44$ presumably arises from changes in the electronic and steric configuration of the exciplex as well as from the participation of complete electron transfer. Since both k_e and

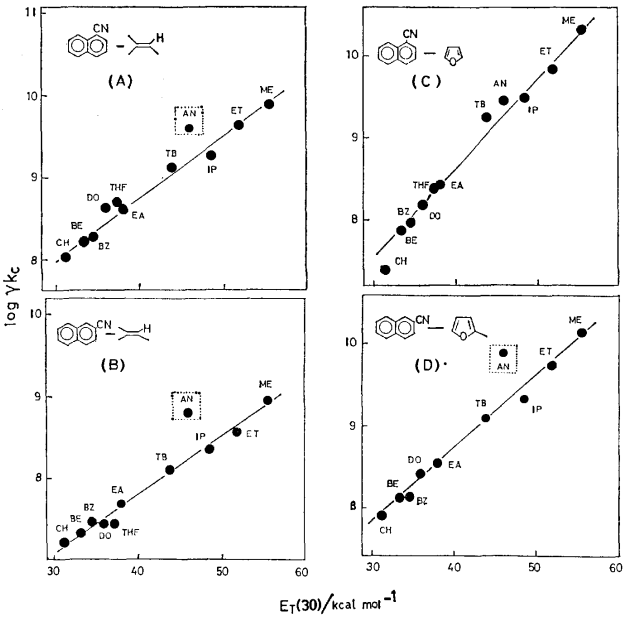

Fig. 5. Plots of $\log \gamma k_c$ *vs.* $E_T(30)$ for (A) **1a-2c**, (B) **1b-2c**, (C) **1a-2f**, and (D) **1b-2g** pairs; see abbreviations in Chart 1 and Table 2.

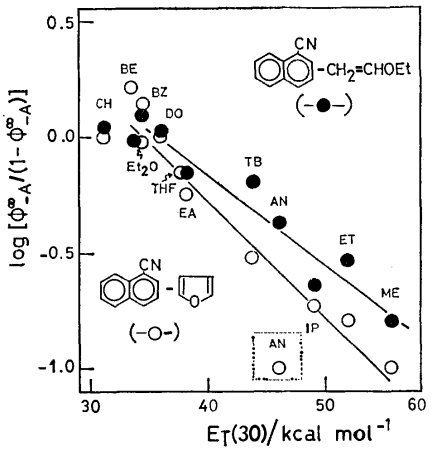

Fig. 6. Plots of $\log[\phi^{\infty}_{-A}/(1-\phi^{\infty}_{-A})]$ *vs.* $E_T(30)$ for **1a-2f** (—○—) and **1a-2a** (—●—) pairs; see abbreviations in Chart 1 and Table 2.

α probably increase with the increase of solvent polarity, the decrease of k_a would be, at least in part, cancelled out. In the extreme case where complete electron transfer is dominant, ϕ^{∞}_{-A} should be α, probably the value in acetonitrile or methanol that is very low (≈0.08). Since k_a is comparable with or much smaller than αk_e at $f(\varepsilon)>0.44$, the decrease of k_a with the increase of solvent polarity might be much more remarkable than that expected from the slope of the plot at $f(\varepsilon)>0.44$.

Applicability of $E_T(30)$ to the Solvent Effects on the Nonemissive Exciplexes. Kosower recomended the use of the $E_T(30)$ or Z value as a suitable scale of solvent polarity for exciplex systems.[33] In keeping this in mind, moreover, the finding that the logarithmic values of product ratio are linearly correlated with the Z scale for the naphthalene–acrylonitrile system in protic media[34] prompts us to investigate the availability of

$E_T(30)$ for elucidation of solvent effects on the processes from the exciplexes. Figure 5 shows typical plots of $\log \gamma k_e$ *vs.* $E_T(30)$ for the four selected A-D pairs; similar plots which are not shown here were also obtained for the other A-D pairs. Each plot gives a single linear line with a relatively good correlation irrespective of the solvent nature throughout the full range of solvent polarity employed; acetonitrile is the only out-of-line solvent. Figure 6 shows the plots of $\log[\phi^{\infty}_{-A}/(1-\phi^{\infty}_{-A})]$ *vs.* $E_T(30)$ for the **1a-2a** and **1a-2f** pairs, both of which reveal linear correlations with negative slopes at $E_T(30)>38$ kcal mol^{-1} but tend to level off at the lower region of $E_T(30)$; a remarkable deviation can be observed for the value of **1a-2f** pair in acetonitrile.

The $E_T(30)$ scale is based on the solvatochromic shifts of the longest absorption band of *p*-(1-pyridinio)-phenoxide **30** whose electronic structures are more polar like **30a** in the ground state and less polar like **30b** in the excited state;[15,35] the increase of solvent

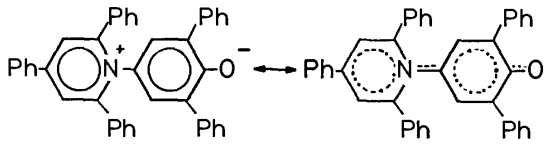

30a 30b

polarity causes stabilization of the ground state and destabilization of the excited Franck-Condon state, thus leading to the increase in the excitation energies. Therefore, the linear plots in Figs. 5 and 6 indicate the involvement of consequential changes from a less polar state to a more polar one in the fluorescence-quenching pocess and from a more polar intermediate to a less polar transition state in the cycloaddition process.

From these plots alone, however, it is hard to perceive any solvent-induced changes in the electronic structures of the exciplexes or in the mechanisms of the fluorescence quenching and photoreactions, an observation which is inconsistent with the discussions based on the dielectric continuum assumption. Since **30** is a polar solute of the mobile π electronics, the excitation energies, $E_T(30)$, may be perturbed by a variety of solute-solvent interactions involving hydrogen bonding in protic solvents. Taft, Abboud, and Kamlet recently reported that the $E_T(30)$ scale can be expressed by a multiple linear regression equation of the solvent dipole moment and $(n^2-1)/2(2n^2+1)$ for nonhydrogen-bonding solvents;[36] combined contributions of dipole-dipole interactions and solvent polarizability are involved in this scale unlike the electrostatic model. Therefore, the linear plots in Figs. 5 and 6 can not be simply interpreted but should be regarded to reflect only the parallel relationships in the solvent dependencies between the excitation energies of **30** and the free-energy changes in the fluorescence-quenching and cycloaddition processes.

Finally the plot of $\bar{\nu}_e$ *vs.* $E_T(30)$ for the **1a-2h** exciplex is shown in Fig. 7, which gives two linear lines with a break at $E_T(30)\approx 38$ kcal mol^{-1}, suggesting a solvent-induced change in the electronic nature of the

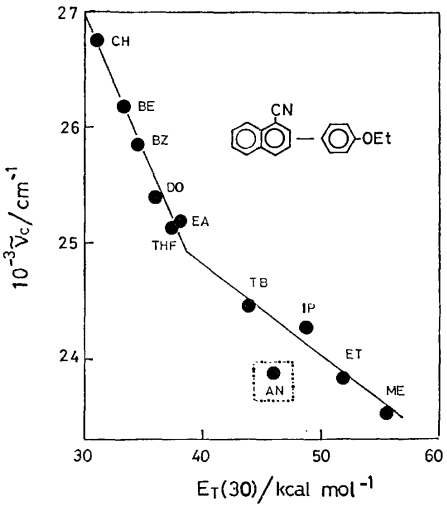

Fig. 7. Plot of $\bar{\nu}_e$ *vs.* $E_T(30)$ for **1a-2h** pair; see abbreviations in Chart 1 and Table 2.

exciplex. A similar plot which is not shown here was also obtained for the **1a-2e** exciplex.[32b] Since the linearity is strikingly good, the solvatochromic shifts of the exciplex emission is probably again very similar to those of the absorption band of **30** in the origin. At any rate, it should be emphasized that solvent effects on the processes from exciplexes involving reversible dissociation, cycloaddition, and emission parallel those on the electronic excitation of **30**. The good linearity of the plots using $E_T(30)$ as a scale of solvent polarity seems to indicate something essential though detailed discussions can not be made because of the lack of information concerning the physical and chemical entities involved in $E_T(30)$.

Conclusion

Solvent effects on the reversible dissociation and cycloaddition processes from the nonemissive naphthonitrile-olefin and furan exciplexes have been qualitatively analyzed by steady-state kinetics based on the assumption of the solvent as a continuous dielectric medium. The nonemissive exciplexes are commonly changed in both the electronic structures and the reactivities when the medium is changed from a nonpolar or moderately polar aprotic solvent to a polar protic solvent. In the less polar aprotic solvents, CT contributions are low but reactivities in the cycloadditions are relatively high. On the other hand, considerable degrees of CT contributions are induced in the more polar protic solvents, and the reactivities decrease with the increase of solvent polarity. Our results concerning CT contribution-reactivity relationships in either the [2+2] or [4+4] cycloaddition *via* an exciplex are in line with the Lewis[24] and Caldwell's[30] interpretations based on the Michl's theory.[29]

Dimroth and Reichardt's $E_T(30)$ has been found to be a suitable scale of solvent polarity for linear free-energy relationships associated with the solvent dependences in the reversible dissociation, cycloaddition, and emission processes from exciplexes. The

good linearity in the plots with $E_T(30)$ may originate from internal correction of specific solute-solvent interactions. Unfortunately, implications of the linear relationships can not be sufficiently uncovered with regard to electronic structures and reactivities of exciplexes as well as the mechanisms in fluorescence quenching and photoreactions owing to umbiguities of the physical definition of $E_T(30)$.

The present treatments on solvent effects on fluorescence-quenching rate constants and quantum yields of photoreactions can thus provide a convenient, useful basis for qualitative estimations of electronic structures and reactivities of nonemissive exciplexes and will be applicable to other similar nonemissive exciplex systems, though the application is limited to such A-D pairs for which $\gamma k_c \ll 10^{10}$ dm^3 mol^{-1} s^{-1} in nonpolar and moderately polar solvents.

Experimental

Materials. An ethereal solution of the naphthonitriles (Tokyo Kasei) was washed three times with dilute hydrochloric acid and then with water, saturated sodium hydrogencarbonate, and water, dried, filtered, and evaporated. Pale yellow solids which had been obtained by vacuum distillation were purified by column chromatography on silica gel (Merck, 70—230 mesh) followed by repeated recrystallization from hexane; the pure 1- and 2-naphthonitriles were thus obtained as white flakes. The electron donors (**2a** and **2c—h**) were commercially obtained (Tokyo Kasei and Nakarai Chemicals) while **2b** was prepared according to the literature method.[37] The electron donors were distilled from sodium under a nitrogen atmosphere before use.

All the solvents were spectrograde (Tokyo Kasei and Nakarai Chemicals). Cyclohexane was used as received. Ethyl acetate and benzene were distilled. Diethyl ether, dibutyl ether, and tetrahydrofuran were distilled from lithium aluminium hydride. Dioxane, *t*-butyl alcohol, 2-butanol, 2-propanol, and ethanol were distilled from sodium. Methanol and acetonitrile were distilled from calcium hydride. All the distillations were performed under a nitrogen atmosphere before use.

Anayltical methods. A Hitachi MPF-4 spectrofluorometer equipped with a data processor (612-0085) was used for the fluorescence-quenching experiments and the measurements of emission spectra; all the fluorescence spectra were recorded after correction of specral response of the photomultiplier. The fluorescence lifetimes of 1- and 2-naphthonitriles were determined on the Hitachi MPF-4 spectrofluorometer equipped with a Hitachi time-resolved photometer. Concentrations of the naphthonitriles were set to $(3—6)\times10^{-4}$ mol dm^{-3} in all the spectroscopic measurements.

Proton nuclear magnetic resonance (NMR) spectra were recorded at 100 MHz on a JEOL JNM-PS-100 spectrometer or at 60 MHz on a JEOL JNM-60 spectrometer. Ultraviolet (UV) spectra were obtained on a Hitachi 124 spectrophotometer. Gas-liquid chromatography (GLC) was performed on a Shimadzu GC-3BF dual-column instrument with flame ionization detectors using 75 cm×4 mm columns packed with 5% SE-30 on Celite 545 and 10% PEG 20M on Shimalite W. Gel permeation chromatography (GPC) was carried out on a Toyosoda HLC-801 using a column of G-1000H6 polystyrene gel; tetrahydrofuran was used as eluant at an elution rate of 1.1 cm^3 min^{-1}.

Oxidation and reduction potentials were measured for

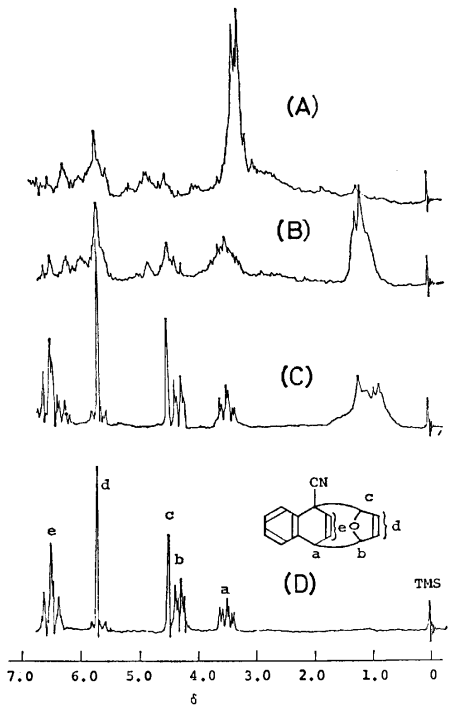

Fig. 8. NMR spectra ($CDCl_3$ solution) of photolysates of **1a-2f** pair in (A) methanol, (B) ethanol, (C) 2-butanol, and (D) benzene; the spectra were taken after thorough removal of both solvent and **2f** from the corresponding solutions irradiated at 313 nm; 30—40% conversions.

N_2-saturated acetonitrile solutions ($\approx10^{-3}$ mol dm^{-3}) *vs.* an $Ag/AgNO_3$ reference electrode by cyclic voltammetry. Tetraethylammonium tetrafluoroborate (0.1 mol dm^{-3}) was used as supporting electrolyte. The scan speed was 0.2 V s^{-1} and the temperature was kept at 23±0.1 °C. No cyclic voltammograms showed reversible peaks corresponding to oxidation of anion radicals and reduction of cation radicals. Therefore, half-peak values ($<\pm0.015$ V) were employed as oxidation and reduction potentials. Details of measurements were identical to those described previously.[38]

Determination of Quantum Yields for Disappearance of 1-Naphthonitrile. Monochromatic light at 313 nm was isolated from a high-pressure mercury lamp (Eikosha, POH-450) by passage through a Toshiba UV-D25 glass filter and an aqueous potassium chromate solution (0.2 g dm^{-3}, 10 mm path length). The intensity (I_0) of incident light was determined by potassium trioxalatoferrate(III) actinometry to be 2.01×10^{-7} einstein cm^{-3} min^{-1}. A solution (4 cm^3) containing **1a** ($(3.5—4.5)\times10^{-4}$ mol dm^{-3}) and an olefin (1.0 mol dm^{-3}) or furan (2.6 mol dm^{-3}) was introduced into an optical cell and then irradiated with the 313-nm light at 20±1 °C. The decrease in the absorbance (OD) of **1a** at 307 nm was monitored at appropriate intervals of time; ln ($e^{OD}-1$) was plotted against irradiation time (*t*, min). The plots were linear up to 20—40% conversions of **1a**. Quantum yields (ϕ_{-A}) for disappearance of **1a** were thus obtained by applying the slopes of the plots to Eq. 16, where κ is the observed molar absorption coefficient of **1a** at 307 nm for each solution in the optical cell used.

$$\ln(e^{OD}-1) = -1000\kappa I_0\phi_{-A}t + \text{constant} \quad (16)$$

Photoreaction of 1-Naphthonitrile with Ethyl Vinyl Ether or 2-Methyl-2-butene in Various Solvents. Solutions containing **1a** (70—80 mg/10 cm^3, ≈0.05 mol dm^{-3}) and the olefin ($\approx$ 1.0 mol dm^{-3}) were irradiated with a high-pressure mercury

lamp (Eikosha, PIH-300) through an aqueous potassium chromate solution (0.2 g dm^{-3}, 10 mm path length) under cooling with water. The progress of the photoreaction was followed by GLC, and it was confirmed that the cycloadducts (**3** and **4**) were the exclusive products without any change in the isomer ratios up to ≈50% conversion of **1a**. After ≈40% of **1a** had been consumed, the irradiated solutions were thoroughly evaporated under a high vacuum below 40 °C. The remaining oils were subjected to NMR. The isomer ratios were thus determined by both NMR and GLC and are listed in Table 4.

Photoreaction of 1-Naphthonitrile with Furan in Various Solvents. Solutions containing **1a** (70—80 mg/10 cm^3, ≈0.05 mol dm^{-3}) and **2f** (≈1.0 mol dm^{-3}) were irradiated in a similar way. The progress of the photoreaction was followed by GPC, and it was confirmed that product distributions were almost constant up to ≈40% conversion of **1a**. After 30—40% of **1a** had been consumed, the irradiated solutions were thoroughly evaporated under a high vacuum below 30 °C, and then the remaining oils were subjected to NMR. The NMR spectra are shown in Fig. 8.

Photoreaction of 1-Naphthonitrile with Phenyl Vinyl Ether in Acetonitrile. An acetonitrile solution (200 cm^3) containing **1a** (0.75 g, 0.005 mol) and **2b** (6 g, 0.05 mol) was irradiated for 20 h at 313 nm under cooling with water. After the removal of the solvent, vacuum distillation gave 2.5 g of **2b**. The distillation residue was chromatographed on silica gel (Merck, 70—230 mesh). Elution with 10% benzene in hexane gave *cis*-1,2-diphenoxycyclobutane[17] (0.42 g, 12% yield based on unrecovered **2b**) and the *trans* isomer[17] 0.42 g, 12%); 0.51 g of **1a** was recovered by elution with 30% benzene in hexane. Further elution gave untractable heavy oils.

This work was partially supported by a Grant-in-Aid No. 56550590 from the Ministry of Education, Science and Culture.

References

1) Part XXXVI: M. Yasuda, C. Pac, and H. Sakurai, *Bull. Chem. Soc. Jpn.*, **54**, 2352 (1981).

2) a) A. Weller, *Pure Appl. Chem.*, **16**, 115 (1968); b) L. M. Stephenson and G. S. Hammond, *ibid.*, **16**, 125 (1968); c) J. B. Birks, "Photophysics of Aromatic Molecules," Wiley-Interscience, New York (1970); d) P. Froehlich and E. L. Wehry, "Modern Fluorescence Spectroscopy," ed by E. L. Wehry, Plenum Press, New York (1976), Vol. 2, p. 319; e) N. Mataga and M. Ottolenghi, "Molecular Association," ed by R. Foster, Academic Press, New York (1979), Vol. 2, p. 1.

3) a) R. S. Davidson, "Molecular Association," ed by R. Foster, Academic Press, New York (1975), Vol. 1, p. 215; b) S. G. Cohen, A. Parola, and G. H. Parson, *Chem. Rev.*, **73**, 141 (1973).

4) a) C. Pac, T. Sugioka, and H. Sakurai, *Chem. Lett.*, **1972**, 39; b) T. Sugioka, C. Pac, and H. Sakurai, *ibid.*, **1972**, 791; c) C. Pac, T. Sugioka, K. Mizuno, and H. Sakurai, *Bull. Chem. Soc. Jpn.*, **46**, 238 (1973); d) K. Mizuno, C. Pac, and H. Sakurai, *Chem. Lett.*, **1973**, 309; e) C. Pac, K. Mizuno, T. Sugioka, and H. Sakurai, *ibid.*, **1973**, 187; f) K. Mizuno, C. Pac, and H. Sakurai, *J. Am. Chem. Soc.*, **96**, 2993 (1974); g) K. Mizuno, C. Pac, and H. Sakurai, *J. Chem. Soc. Perkin Trans. 1*, **1974**, 2360; h) K. Mizuno, C. Pac, and H. Sakurai, *J. Chem. Soc., Chem. Commun.*, **1974**, 648; i) K. Mizuno, C. Pac, and H. Sakurai, *J. Chem. Soc., Perkin Trans. 1*, **1975**, 2221; j) K. Mizuno, C. Pac, and H. Sakurai, *J. Org. Chem.*, **42**, 3313 (1977); k) M. Yasuda, C. Pac, and H. Sakurai, *Bull. Chem. Soc. Jpn.*, **53**, 502 (1980).

5) a) F. D. Lewis, *Acc. Chem. Res.*, **12**, 152 (1979); b) R. A. Caldwell and D. Creed, *ibid.*, **13**, 45 (1980); c) N. C. Yang, R. L. Yates, J. Masnovski, D. M. Shold, and W. Chiang, *Pure Appl. Chem.*, **51**, 173 (1979).

6) a) T. Sugioka, C. Pac, and H. Sakurai, *Chem. Lett.*, **1972**, 667; b) C. Pac and H. Sakurai, *ibid.*, **1976**, 1067; c) T. Majima, C. Pac, and H. Sakurai, *Bull. Chem. Soc. Jpn.*, **51**, 1811 (1978).

7) a) J. J. McCullough, R. C. Miller, D. Fuang, and W. -S. Wu, *J. Am. Chem. Soc.*, **97**, 5942 (1975); b) J. J. McCullough and W. -S. Wu, *J. Chem. Soc., Chem. Commun.*, **1972**, 1136.

8) a) H. Knibbe, D. Rehm, and A. Weller, *Ber. Bunsenges. phys. Chem.*, **73**, 839 (1969); b) H. Knibbe and A. Weller, *Z. Phys. Chem. N. F.*, **56**, 99 (1967) and *Acta Phys. Polon.*, **34**, 593 (1968).

9) T. R. Evans, *J. Am. Chem. Soc.*, **93**, 208 (1971).

10) B. S. Solomon, C. S. Steel, and A. Weller, *Chem. Commun.*, **1968**, 927.

11) D. A. Labianca, G. N. Taylor, and G. S. Hammond, *J. Am. Chem. Soc.*, **94**, 3679 (1972).

12) a) M. P. Niemczyk, N. E. Shore, and N. J. Turro, *Mol. Photochem.*, **5**, 69 (1973); b) N. E. Shore and N. J. Turro, *J. Am. Chem. Soc.*, **97**, 2482 (1975); c) B. M. Monroe, C. -G. Lee, and N. J. Turro, *Mol. Photochem.*, **6**, 271 (1974); d) J. B. Guttenplan and S. G. Cohen, *J. Am. Chem. Soc.*, **94**, 4040 (1972).

13) M. E. R. Morcondes, V. G. Toscano, and R. G. Weiss, *J. Am. Chem. Soc.*, **97**, 4485 (1975).

14) J. Kirkwood, *J. Chem. Phys.*, **2**, 351 (1934).

15) C. Reichardt, "Lösungsmittel-Effekte in der organischen Chemie," Verlag Chemie, GmbH (1969), pp. 141—149.

16) a) The oxygen-quenching method has been reported to be useful for the detection of a nonemissive exciplex[16b] as well as for the determination of lifetimes of emissive exciplexes;[16c] b) J. L. Charlton, D. E. Townsend, B. D. Watson, P. Shanon, J. Kowalruska, and J. Saltiel, *J. Am. Chem. Soc.*, **99**, 5992 (1977); c) R. A. Caldwell, D. Creed, and H. Ohta, *ibid.*, **97**, 3246 (1975); R. A. Caldwell, D. Creed, D. C. DeMarco, L. A. Melton, H. Ohta, and P. H. Wine, *ibid.*, **102**, 2369 (1980); R. A. Caldwell and T.-S. Maw, *J. Photochem.*, **11**, 165 (1979); d) The limiting quantum yield of the disappearance of **1a** for a degassed cyclohexane solution of the **1a-2a** pair is 0.63, significantly greater than that for aerated solution (0.51). The limiting quantum yields for degassed and aerated solutions can be represented by $k_a/(k_a+k_d)$ and $k_a/(k_a+k_d+k_q^c[O_2])$ respectively. Therefore, both k_a and k_d can be calculated, provided $k_q^c[O_2] \simeq 4\times 10^7\ s^{-1}$; C. Pac, K. Mizuno, and H. Sakurai, unpublished results.

17) S. Kuwata, Y. Shigemitsu, and Y. Odaira, *J. Org. Chem.*, **38** 3803 (1973).

18) S. L. Murov, "Handbook of Photochemistry," Marcel Dekker, New York (1973), p. 89.

19) J. B. Berlman, "Handbook of Fluorescence Spectra of Aromatic Molecules," Academic Press, New York (1965).

20) D. V. O'Connor and W. R. Ware, *J. Am. Chem. Soc.*, **101**, 121 (1979).

21) C. Lewis and W. R. Ware, *Mol. Photochem.*, **5**, 261 (1973).

22) Y. Taniguchi, Y. Nishina, and N. Mataga, *Bull. Chem. Soc. Jpn.*, **45**, 764 (1972).

23) G. N. Taylor, *Chem. Phys. Lett.*, **10**, 355 (1971).

24) F. D. Lewis and L. E. Hoyle, *J. Am. Chem. Soc.*, **99**,

2779 (1977).
25) a) N. Mataga, T. Okada, and N. Yamamoto, *Bull. Chem. Soc. Jpn.*, **39**, 2562 (1966); b) *Chem. Phys. Lett.*, **1**, 119 (1967).
26) D. Rehm and A. Weller, *Isr. J. Chem.*, **8**, 259 (1970).
27) T. R. Evans, R. W. Wake, and O. Jaenicke, "The Exciplexes," ed by M. Gordon and W. R. Ware, Academic Press, London (1975), p. 345.
28) a) R. A. Neunteufel and D. R. Arnold, *J. Am. Chem. Soc.*, **95**, 4080 (1973); b) Y. Shigemitsu and D. R. Arnold, *J. Chem. Soc., Chem. Commun.*, **1975**, 407; c) A. J. Maroulis, Y. Shigemitsu, and D. R. Arnold, *J. Am. Chem. Soc.*, **100**, 535 (1978); d) T. Majima, C. Pac, A. Nakasone, and H. Sakurai, *ibid.*, **103**, 4499 (1981).
29) W. Gerhartz, R. D. Poshusta, and J. Michl, *J. Am. Chem. Soc.*, **98**, 6427 (1976); J. Michl, *Photochem. Photobiol.*, **25**, 141 (1977).
30) R. A. Caldwell and D. Creed, *J. Am. Chem. Soc.*, **101**, 6960 (1979).
31) Strictly speaking, the k_a should be replaced by $\beta k_a'$; k_a' and β represent, respectively, the true rate constant for the adiabatic process and the partition coefficient for crossing to cycloadduct(s) from the pericyclic minimum.[5b] However, the use of "k_a" does not alter the qualitative discussions and conclusions concerning reactivities of the non-emissive exciplexes at all.
32) a) The $\tilde{\nu}_c$ values in benzene and dioxane are again much lower than those expected from the linear plot against $f'(\varepsilon,n)$. b) Acetonitrile is again the only out-of-line solvent in the plot of $\tilde{\nu}$.
33) E. M. Kosower, "An Introduction to Physical Organic Chemistry," John Wiley and Sons, New York (1968).
34) R. M. Bowman, T. R. Chamberlain, C. -W. Huang, J. J. McCullough, *J. Am. Chem. Soc.*, **96**, 672 (1974).
35) a) K. Dimroth, C. Reichardt, T. Seipman, and F. Bohlmann, *Justus Liebigs Ann. Chem.*, **661**, 1 (1963); b) C. Reichardt, *Angew. Chem., Int. Ed. Engl.*, **18**, 98 (1979).
36) R. W. Taft, J.-L. M. Abboud, and M. J. Kamlet, *J. Am. Chem. Soc.*, **103**, 1080 (1981).
37) S. M. McElvain and B. Fajardo-Pinzon, *J. Am. Chem. Soc.*, **67**, 650 (1945).
38) T. Majima, C. Pac, and H. Sakurai, *J. Am. Chem. Soc.*, **102**, 5265 (1980).

 © 1982 The Chemical Society of Japan Bull. Chem. Soc. Jpn., 55, 1617—1619 (1982)

Room-temperature Fluorine Addition to Fluoro-substituted Naphthalene Derivative Using Xenon Difluoride

Barbara ZAJC and Marko ZUPAN*

"Jozef Stefan" Institute and Department of Chemistry, "E. Kardelj" University of Ljubljana, Ljubljana, Yugoslavia

(Received November 5, 1980)

Room-temperature boron trifluoride catalyzed addition of fluorine to octafluoronaphthalene with xenon difluoride proceeds as 1,4- and 1,2-addition, giving decafluoro-1,4-dihydronaphthalene and decafluoro-1,2-dihydronaphthalene. Fluorine addition to 2-methoxy- and 2-ethoxyheptafluoronaphthalene gave only 1,4-adducts, while reaction with 2-isopropoxyheptafluoronaphthalene resulted in octafluoro-1,2-dihydronaphthalene-2-one and 6-isopropoxynonafluoro-1,4-dihydronaphthalene.

Perfluoroaromatic molecules react with electrophilic reagents under rigorous experimental conditions, while reactions with nucleophiles are typical examples of this class of compound.[1] Hexafluorobenzene reacted with fluorine at 0 °C giving a complex reaction mixture,[2] while reaction with a mixture of cobalt(III) fluoride and calcium fluoride could be adjusted so that only octafluorocyclohexa-1,4-diene and decafluorocyclohexane were formed.[3] Recently we have found that fluorine addition to fluoro substituted benzene derivatives could be carried out at room temperature using xenon difluoride in the presence of boron trifluoride as catalyst.[4] Reaction with hexafluorobenzene proceeded regiospecifically as 1,4-addition, thus forming octafluoro-1,4-cyclohexadiene. We now report further studies on the regioselectivity of room-temperature fluorine addition to fluorosubstituted naphthalene derivatives.

Results and Discussion

Xenon difluoride represents an easy handling, mild reagent for the fluorination of alkenes, acetylenes, aromatic and heteroaromatic molecules and some organic molecules containing hetero atoms, and has recently been reviewed.[5] Fluorinations with xenon difluoride are usually successful in the presence of a catalyst and the following substrates proved to be convenient catalyst: HF, HF/pyridine, CF_3COOH, Br_2, pentafluorothiophenol, BF_3/etherate, and BF_3. The choice of catalyst depends on the structure of the organic molecule, its reactivity and its sensitivity to the reaction conditions.

In a typical experiment, 1 mmol of fluoro-substituted naphthalene was dissolved in 2 ml of dichloromethane, 1.1 mmol of xenon difluoride was added at room temperature and BF_3 was introduced into the reaction mixture. The reaction was complete in 30—60 min, the solvent was removed under reduced pressure, the crude reaction mixture was analyzed by ^{19}F NMR spectroscopy and the products were isolated by preparative GLC. After analysis of the crude reaction mixture obtained by fluorination of octafluoronaphthalene (**1**, Scheme 1), we concluded that two products were formed in the ratio 1: 6.7.

The products were separated by preparative GLC and the major product showed the following singals in its ^{19}F NMR spectrum: $\delta = -99.6$ (F_1, F_4, m, 4F), -137.6 (F_5, F_8, m, 2F), -147.2 (F_6, F_7, m, 2F), and

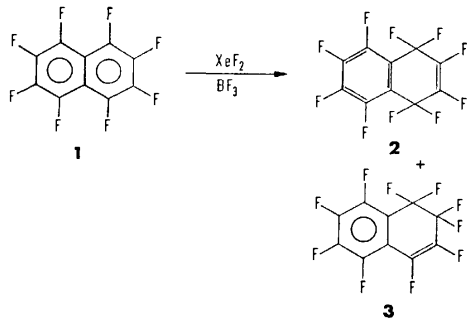

1 **2** **3**

Scheme 1.

-155.8 (F_2, F_3, m, 2F). On the basis of the spectroscopic data we established that decafluoro-1,4-dihydronaphthalene (**2**) was formed.[7] The minor product had the following signals in its ^{19}F NMR spectrum: $\delta = -118.5$ (F_1, m, 2F), -126.7 (F_2, m, 2F), -136.7 (F_8, m, 1F), -159.8 (F_3, m, 1F), δF_4, $F_5 = -140$ (dm, $J = 63$ Hz), -141.8 (dm, $J = 63$ Hz), and δF_6, $F_7 = -147$ (m, 1F), -150 (m, 1F).

From these spectroscopic data we established that decafluoro-1,2-dihydronaphthalene (**3**) was formed.[7,8] The mass spectra of both products (**2** and **3**) are also of interest, the loss of a CF_3-radical being the most notable at 70 eV. Similar fragmentation has also been observed by 9,9,10,10-tetrafluoro-9,10-dihydrophenanthrene.[6] The three possible pathways leading to the fragment $M^{+\cdot}-CF_3$ are presented in Scheme 2, all of them being confirmed by metastable fragments (values noted in Scheme 2).

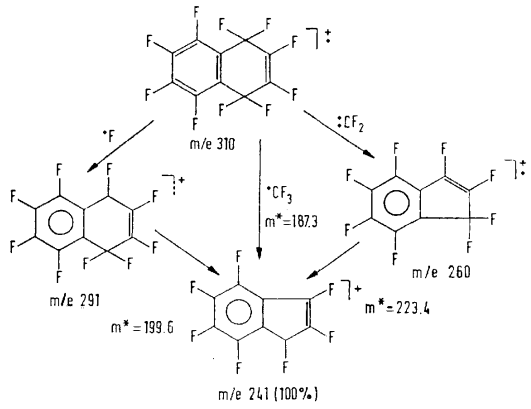

Scheme 2.

Further, we have studied the regioselectivity of fluorine addition to various alkoxy-substituted heptafluoronathalenes and found that fluorination of 2-methoxy (**4a**, Scheme 3) and 2-ethoxy (**4b**) derivatives resulted in the formation of only one product to each. In the case of **4a** the ^{19}F NMR signals are the following: $\delta=-97.2$ (F_1, m, 2F), -98.6 (F_4, m, 2F), -140 (F_5, F_8, m, 2F), -150.4 (F_6, F_7, m, 2F), and -163.1 (F_3, m, 1F), with the following coupling constants: $4J_{F_4F_5}=4J_{F_1F_8}=17$ Hz, $4J_{F_1F_3}=12$ Hz, $3J_{F_3F_4}=24$ Hz, and $5J_{F_3CH_3}=4$ Hz. On the basis of the spectroscopic data, we established that 2-methoxynonafluoro-1,4-dihydronaphthalene (**5a**) was formed.

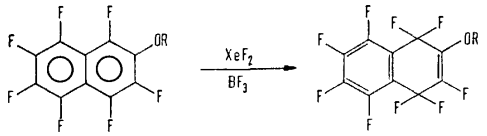

4a: R=CH_3
4b: R=CH_2CH_2

Scheme 3.

1,4-Addition of fluorine with xenon difluoride had also been observed in the case of the 2-ethoxy derivative (**4b**), while reaction with 2-isopropoxyheptafluoronaphthalene (**6**) gave two products in the ratio 1:6.7, which could be separated by preparative GLC. The major product formed (**7**) shows a peak in its IR spectrum at 1715 cm^{-1}, characteristic of the CO group, and the following signals in its ^{19}F NMR spectrum: $\delta=-100.5$ (F_1, m, 2F), -123 (F_4, dm), -135.8 (F_8, tddd), -139 (F_5, dddd), -148.5 (F_6, F_7, m, 2F), and -157.8 (F_3, dt), with the following coupling constants: $4J_{F_1F_8}=18$ Hz, $4J_{F_1F_3}=7.5$ Hz, $3J_{F_3F_4}=15$ Hz, $4J_{F_4F_5}=81$ Hz, $3J_{F_5F_6}=18$ Hz, $4J_{F_5F_7}=7.5$ Hz $5J_{F_5F_8}=18$ Hz, $3J_{F_7F_8}=18$ Hz, and $4J_{F_6F_8}=8$ Hz.

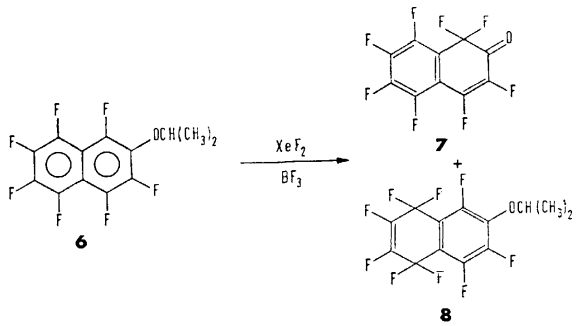

6 **7** **8**

Scheme 4.

On the basis of the spectroscopic data, we established that octafluoro-1,2-dihydronaphthalene-2-one (**7**) was formed. The second product formed (**8**) shows the following signals in its ^{19}F NMR spectrum: $\delta=-99.8$ (F_1, F_4, m, 4F), -132.8 (F_5, tdd), -141.8 (F_8, dtd), -144 (F_7, dd), -156.8 (F_2, F_3, m, 2F), with coupling constants: $3J_{F_7F_8}=20$ Hz, $4J_{F_1F_8}=15$ Hz, $5J_{F_5F_8}=15$ Hz, $4J_{F_5F_7}=12$ Hz, and $4J_{F_4F_5}=15$ Hz. On the basis of spectroscopic data we established that 6-iso-propoxynonafluoro-1,4-dihydronaphthalene was formed.

Experimental

IR spectra were recorded using a Perkin-Elmer 727 B spectrometer and ^1H and ^{19}F NMR spectra with a JEOL-JNM-PS 100 from CCl_4 or $CDCl_3$ solutions with Me_4Si or CCl_3F as internal reference. Mass spectra and high resolution measurements were taken on a CEC 21-110 spectrometer. Gas liquid partition chromatography was carried out on a Varian Aerograph Model 1800.

Fluorination of Octafluoronaphthalene (1). Yield: 279 mg of oily products, separated by GLC (10% SE-30 Chromosorb A 45/60, $T=80$ °C).

Decafluoro-1,4-dihydronaphthalene (2). Yield: 113.8 mg (36.5%), mp 31.5—32 °C (mp[7] 33—34 °C). Found: *m/e* 309.9840. Calcd for $C_{10}F_{10}$: 309.9840. MS, *m/e* (rel intensity): 310 (M^+, 34), 291(26), 272(9), 260(20), 242(10), 241 (100), 222(6), 210(12), and 141(9).

Decafluoro-1,2-dihydronaphthalene (3) Yield: 10.1 mg (3.3%) of oily product. Found: *m/e* 309.9841. Calcd for $C_{10}F_{10}$: 309.9840. MS, *m/e* (rel intensity): 310 (M^+, 34), 291(28), 272(8), 260(21), 242(12), 241(100), 210(15), and 141(13).

Fluorination of 2-Methoxyheptafluoronaphthalene(4a). Yield: 264 mg of crude reaction mixture; separation by preparative GLC (12% DDP Chromosorb Regular 100, $T=135$ °C).

2-Methoxynonafluoro-1,4-dihydronaphthalene (5a). Yield: 112 mg (35%), bp 212—213 °C. Found: *m/e* 322.0030. Calcd for $C_{11}H_3F_9O$: 322.0024. MS, *m/e* (rel intensity): 323 (M^++1, 13), 322(M^+, 100), 307(13), 303(40), 292(10), 291(72), 279(70), 272(32), 260(25), 257(14), 253(14), 241(74), 229(66), 223(25), 222(10), 210(37), 203(10), 179(25), 160(10), 141(27), 117(17), 93(18), 81(75), and 69(13). Found: C, 41.0; H, 0.8%. Calcd for $C_{11}H_3F_9O$: C, 41.0; H, 0.9%.

Fluorination of 2-Ethoxyheptafluoronaphthalene (4b). Yield: 296 mg of crude reaction mixture, separated by preparative GLC (12% DDP Chromosorb Regular 100, $T=135$ °C).

2-Ethoxynonafluolo-1,4-dihydronaphthalene (5b). Yield: 133.8 mg (39.8%), bp 220—221 °C. ^{19}F NMR: -96.9 (F_1, m, 2F), -98.6 (F_4, m, 2F), -140.3 (F_5, F_8, m, 2F), -150.4 (F_6, F_7, m, 2F), and -162.4 (F_3, m, 1F) with the following coupling constants: $4J_{F_1F_8}=17$ Hz, $4J_{F_1F_3}=12$ Hz, $3J_{F_3F_4}=24$ Hz, $4J_{F_4F_5}=17$ Hz, and $5J_{F_3CH_2}=3$ Hz. Found: *m/e* 336.0200. Calcd for $C_{12}H_5F_9O$: 336.0197. MS, *m/e* (rel intensity): 336 (M^+, 30), 309 (11), 308 (100), 289 (25), 288 (28), 272 (24), 269 (12), 260 (82), 258 (18), 242 (11), 241 (91), 239 (37), 229 (15), 222 (14), 210 (29), 179 (16), 141 (22), 117 (12), 93 (12), 86 (23), and 84 (38). Found: C, 42.2, H, 1.7%. Calcd for $C_{12}H_5F_9O$: C, 42.7, H, 1.5%.

Fluorination of 2-Isopropoxyheptafluoronaphthalene (6). Yield: 244 mg of the crude reaction mixture. The products were separated by preparative GLC (10% SE-30 Chromosorb A 45/60, $T=130$ °C).

Octafluoro-1,2-dihydronaphthalene-2-one (7). Yield: 145 mg (50.3%), mp 33—34.5 °C. Found: *m/e* 287.9800. Calcd for $C_{10}F_8O$: 287.9805. MS, *m/e* (rel intensity): 288 (M^+, 39), 260 (48), 242 (10), 241 (100), 210 (50), 160 (11), 141 (33), 122 (12), 117 (17), 93 (14), and 79 (12). IR; 1715 cm^{-1} (C=O).

6-Isopropoxynonafluoro-1,4-dihydronaphthalene (8). Yield: 22 mg (6.3%), mp 35—38.5 °C. Found: *m/e* 350.0350. Calcd for $C_{13}H_7F_9O$: 350.0353. MS, *m/e* (rel intensity): 350 (M^+, 8), 335 (20), 309 (12), 308 (100), 289 (30), 288 (12), 260 (13), 258 (12), 241 (33), 239 (30), 210 (25), 179 (10), 141 (17), 119 (15), and 117 (18).

We thank Professor J. Slivnik for xenon difluoride.

References

1) R. D. Chambers, "Fluorine in Organic Chemistry," John Wiley and Sons, New York (1973).
2) I. J. Hotchkins, R. Stephens, and J. C. Tatlow, *J. Fluorine Chem.*, **6**, 135 (1975).
3) R. D. Chambers, D. T. Clark, T. F. Holmes, W. Kenneth, and R. Musgrave, *J. Chem. Soc., Perkin Trans. 1*, **1974**, 114.
4) S. Stavber and M. Zupan, *J. Chem. Soc., Chem. Commun.*, **1978**, 969.
5) R. Filler, *Isr. J. Chem.*, **17**, 71 (1978).
6) M. Zupan and A. Pollak, *J. Org. Chem.*, **40**, 3794 (1975).
7) T. W. Bastock, A. E. Pedler, and J. C. Tatlow, *J. Fluorine Chem.*, **8**, 11 (1976).
8) V. D. Shteingarts and B. G. Oksenenko, *Zh. Org. Khim.*, **6**, 1611 (1970).

A New Method for the Determination of Equilibrium Constant and Molar Extinction Coefficient of 1 : 1 Type Complex

Bejoy Kumar SEAL,* Harideb SIL, Manas BANERJEE, and Dulal Chandra MUKHERJEE†
Department of Chemistry, Burdwan University, Burdwan 713104, West Bengal, India
†*Department of Chemistry, University College of Science and Technology, Calcutta 700009, India*
(Received February 20, 1981)

Job's method of continuous variation has been reinvestigated with respect to the formation of 1 : 1 type complex from the view point of (i) geometrical significance of the Job curve, (ii) developing a method for determining the equilibrium constant and molar extinction coefficient of the complex. A mathematical analysis of the method of continuous variation as applied to the formation of strictly 1 : 1 type complex shows that the Job curve is a hyperbola obeying the equation

$$\frac{(d-\beta)^2}{a^2} - \frac{(C_M^\circ/\lambda - 1/2)^2}{b^2} = 1,$$

where d is the corrected optical density, C_M° is the initial concentration of the metal ion in solution, λ is a constant equal to the sum of the concentrations of the metal and the ligand in solution, β is the ordinate of the local origin of the hyperbola referred to the conventional framework of the Job curve, a and b represent respectively the semi-major and semi-minor axes of the hyperbola. The equation has been recast into the form $x = A_3d^2 + A_2d + A_1$, where $x = (C_M^\circ/\lambda - 1/2)^2$ and A_3, A_2, and A_1 are the appropriate coefficients. A parabolic fit of this equation between x and d by the least square deviation method using the computer B-6800 system enables one to find the coefficients A_3, A_2, and A_1 from which K and ε are evaluated. This equation has been tested with literature data on a variety of 1 : 1 type metal complexes whose formation constants and extinction coefficients as calculated by the present method agree closely with those determined by other methods. The promising features of the equation have been discussed.

There are various methods for ascertaining the composition of complexes, of which the most noteworthy is the method of continuous variation introduced by Job.[1] The simplicity of the method has made it very attractive and it is widely used in the evaluation of spectrophotometric data. Beck[2] has listed several limitations of the method and has cautioned that they have to be considered before it is applied to the study of complexes. The method works well if only one complex is formed in the system, although Voshburgh and Cooper[3] as well as Katzin and Gebert[4] applied it to the study of stepwise complex formation. For a very stable complex the curve of absorbance (or other suitable measured property) *versus* mole fraction (X) of one of the two components of the complex consists of two strictly linear intersecting portions.[2] In the case of moderately stable complexes there is no such linearity, and from the deviation of the curve and that constructed by extrapolation from the slopes near the extreme values of x, the value of the equilibrium constant can be calculated. There are, however, other methods[2,5,6] for determining the equilibrium constant of metal-chelate formation reactions from spectral data. A critical analysis of the principle of continuous variation method shows that the geometrical significance of the Job curve as observed in the case of 1:1 complex has not been elucidated, not to mention of those found in the case of higher order complexes. The purpose of the present investigation is to elucidate the geometrical nature of the conic, and to develop therefrom a general method for determining the stability constant and molar extinction coefficient of 1: 1 complexes.

Principle

The stability constant for an 1: 1 type complex, ML, formed between a metal ion and a ligand is given by

$$K_c = \frac{C_{ML}}{(C_M^\circ - C_{ML})(C_L^\circ - C_{ML})}, \quad (1)$$

where C's are the concentrations of the various species at equilibrium, the superscript zero refers to the initial concentrations. The optical density (corrected for absorption, if any, by the metal and the ligand) of a solution containing the complex, the free metal and the ligand is

$$d = \frac{1 + K_c(C_L^\circ + C_M^\circ) - [\{K_c(C_L^\circ - C_M^\circ)\}^2 + 2K_c(C_L^\circ + C_M^\circ) + 1]^{1/2}\varepsilon l}{2K_c}, \quad (2)$$

where ε is the effective extinction coefficient of the complex ($\varepsilon = \varepsilon_{ML}$ only when the complex alone absorbs at the wavelength of measurement), l is the path length. In Job type experiment the sum total of the concentrations of the metal and the ligand is held constant, *i.e.*, $C_M^\circ + C_L^\circ = \text{constant} = \lambda$ (say). Under this condition Eq. 2 reduces to the equation of the hyperbola

$$\frac{(d-\beta)^2}{a^2} - \frac{(C_M^\circ/\lambda - 1/2)^2}{b^2} = 1, \quad (3)$$

where $a^2 = \frac{1+2K_c\lambda}{m^2}$, $b^2 = \frac{1+2K_c\lambda}{4K_c^2\lambda^2}$, $\beta = \frac{1+K_c\lambda}{m}$, and $m = \frac{2K_c}{\varepsilon l}$.

Here a and b represent respectively the semi-major and semi-minor axes of the hyperbola; β is the ordinate of the local origin of the hyperbola referred to the conventional framework of the Job curve.

In Job type experiment we plot customarily d along the y-axis and C_M°/λ in the abscissa. According to Eq. 3 a plot of d against C_M°/λ should be a hyperbola and it is evident that the axes of the hyperbola are not the axes in our original framework of the coordinate system but some axes which are parallel and interchanged with respect to the original axes.

The eccentricity of the hyperbola is related to a and b of the hyperbola and to the physical parameters of the complex by the relation

$$e^2 = 1 + \frac{b^2}{a^2} = 1 + \frac{1}{\lambda^2\varepsilon^2 l^2}, \quad (4)$$

which shows that the nature of the hyperbola depends on the extinction coefficient and on the total molar concentration of the solution but not on the equilibrium constant of the complex.

Determination of K_c and ε. Equation 3 can be written in the following form

$$x = A_3 d^2 + A_2 d + A_1, \quad (5)$$

where $x = (C_M^\circ/\lambda - 1/2)^2$, $A_3 = \frac{b^2}{a^2}$, $A_2 = -2\left(\frac{b^2}{a^2}\right)\beta$, and

$$A_1 = b^2\left(\frac{\beta^2}{a^2} - 1\right).$$

The coefficients A_3, A_2, and A_1 of Eq. 5 can be found out by making a parabolic fit between x and d by the least square deviation method. The extinction coefficient, ε, of the complex is evaluated from A_3 by using the relation

$$\varepsilon = \frac{1}{\lambda l A_3^{1/2}}. \quad (6)$$

The stability constant K_c of the complex is determined from a knowledge of all three coefficients using Eq. 7

$$K_c = \frac{1 \pm (1+4S)^{1/2}}{4\lambda S}, \quad (7)$$

where $S = (A_2^2/4A_3) - A_1$. Only the admissible value of K_c is accepted. K_c can also be calculated by utilizing A_2 and A_3 only. This yields a unique value of K_c since the equation in K_c is not quadratic in nature. K_c obtained by this method agrees with that calculated from Eq. 7.

For a very stable complex the curve of absorbance *vs.* mole fraction of one of the two components of the complex consists of two strictly linear intersecting portions. This can be explained with the help of Eq. 5 which can be written in the following form

$$x = \left[A_3^{1/2} d + \frac{A_2}{2A_3^{1/2}}\right]^2 - b^2, \quad (8)$$

where $b^2 = A_1 - (A_2^2/4A_3)$ and is negligible for a complex of high stability constant so that Eq. 8 splits into Eqs. 9 and 10 respectively.

$$d = \frac{1}{A_3^{1/2}}\left(\frac{C_M^\circ}{\lambda}\right) - \left[\frac{A_3^{1/2} + A_2}{2A_3}\right], \quad (9)$$

$$\text{and} \quad d = -\frac{1}{A_3^{1/2}}\left(\frac{C_M^\circ}{\lambda}\right) + \left[\frac{A_3^{1/2} - A_2}{2A_3}\right]. \quad (10)$$

Equation 9 describes the left hand portion of the Job curve and for a complex with very high formation constant it represents a straight line passing through the origin since the term $\frac{A_3^{1/2} + A_2}{2A_3}$ is practically zero. Similarly Eq. 10 describes the right hand portion of the Job curve and represents a straight line with negative slope and positive intercept.

The principle of the method as embodied in Eq. 5 is valid for complexes whose stoichiometry is strictly 1:1 (*i.e.*, $m=n=1$ where m and n refer to the mole numbers of the metal and the ligand respectively).

Results and Discussion

The principle of the method, *viz.*, Eq. 5 has been tested with literature data on a variety of 1:1 metal complexes formed by Al^{3+}, Ga^{3+}, Fe^{3+}, La^{3+}, Cu^{2+}, and Pd^{2+} with one or more of the following ligands such as salicylic acid (SA), sulfosalicylic acid (SSA), *p*-aminosalicylic acid (PAS), 2-quinizarinsulfonic acid, 1-(*p*-nitrophenylazo)chromotropic acid, and Chromeazurol S. The compositions of the complexes were ascertained by Job's method of continuous variation. The optical density data necessary for our purpose have, therefore, been read from the Job curves of the complexes available in the literature. A perusal of the literatures concerned reveals that Job's experiments involving these complexes were performed at constant pH's and at constant values of λ but not at constant ionic strength. The ligand Chromeazurol S forms with Pd^{2+} a violet coloured 1:1 chelate which is stable between pH 3.5 and 8.0 with an absorption maxima at 585 nm.[7] 2-Quinizarinsulfonic acid forms a blackish violet water soluble complex with Fe^{3+} in 1:1 mole ratio.[8] La^{3+} forms with 1-(*p*-nitrophenylazo)chromotropic acid (abbreviated as CTB) a reddish violet chelate which is stable between pH 5 and 12.5 and has an absorption maxima at 340 nm.[9] In these three cases metal ion was used as its chloride salt. Iron(III) forms a violet complex with PAS at pH 2.5.[10] While Al^{3+} and Ga^{3+} form colourless complexes with SA and SSA,[11,12] complexes of copper with these reagents[13] are olivegreen in colour. In the study of these latter complexes perchlorates of the respective metals were used. The violet complex of Fe^{3+} with PAS has been reinvestigated by us. Stability constants and molar extinction coefficients of the complexes have been calculated from the Job data with the help of Eq. 5. A special computer program has been written to solve Eq. 5. In solving Eq. 5 two additional points corresponding to mole-fractions of zero and unity have been considered. Experience suggests that inclusion of these two points improves the final results appreciably. The computer Burroughs 6800 has been used for the purpose. The results are shown in Table 1 where other experimental details such as wavelength of measurement, total molarity of the solution, pH values, *etc.*, are also recorded. The formation constants recorded in column 5 and extinction coefficients shown in column 7 of the complexes calculated by Eq. 5 agree fairly well with those (vide columns 6 and 7 of Table 1) determined by other methods. The agreement is noticeable, particularly, in the case of iron (III) *p*-aminosalicylate complex. The variations in K_c values noted in some cases, particularly with wavelength, may be traced to the fact that ionic strength of the medium was not maintained constant in Job's experiments done at constant pH's and at constant values of λ.

An attempt has been made to test approximately the validity of Eqs. 9 and 10 with data on complexes which are not very strong. According to these equations the magnitude of the slope of the plot d *vs.* C_M°/λ is

TABLE 1.

System	Wavelength / nm	Total molarity / mol l^{-1}	pH	K_c / l mol^{-1}	K_c / l mol^{-1} (Reported)	ε / l mol^{-1} cm^{-1}
Iron(III)	500	3.596×10^{-4}	2.5	3.07×10^{4}	$(2.21—3.06)\times10^{4}$	
p-aminosalicylate		4.795×10^{-4}		2.4×10^{4}		1606 (1675)
		7.192×10^{-4}		2.5×10^{4}		
—[a]		7.0×10^{-4}		2.5×10^{4}		1589
Iron(III)	570	1.0×10^{-3}	2.45	1.02×10^{3}	$(4.34—5.41)\times10^{3}$	796 (726)
2-quinizarinsulfonate		5.0×10^{-4}		7.57×10^{3}		
complex	580	1.0×10^{-3}		2.78×10^{3}		
		5.0×10^{-4}		2.85×10^{3}		728
		6.66×10^{-4}		3.89×10^{3}		(602)
Aluminium	310	2.0×10^{-4}	4.0	6.46×10^{4}	$(1.68—7.04)\times10^{4}$	2282
sulfosalicylate		3.0×10^{-4}		3.22×10^{4}		(2277)
	320	2.0×10^{-4}		6.44×10^{4}	$(1.73—7.31)\times10^{4}$	3015
		3.0×10^{-4}		4.5×10^{4}		(2716)
Gallium sulfosalicylate	315	3.0×10^{-4}	3.0	5.76×10^{4}	2.43×10^{4} at 310 nm	1666 (1564)
Gallium salicylate	310	3.0×10^{-4}	3.5	6.46×10^{4}	$(1.34—9.43)\times10^{4}$	1304 (1355)
Copper(II) sulfosalicylate	750	9.0×10^{-3}	4.5	5.82×10^{2}	$(1.07—3.88)\times10^{2}$	47 (34)
		1.2×10^{-2}		1.54×10^{2}		
Copper(II) salicylate	750	1.287×10^{-2}	4.5	1.32×10^{2}	$(1.52—2.04)\times10^{2}$	20 (21)
		1.716×10^{-2}		0.86×10^{2}		
Lanthanum(III) 1-(*p*-nitrophenylazo) chromotropate complex	590	2.0×10^{-4}	6.0 ± 0.2	2.26×10^{4}	3.162×10^{4}	5226 (—)
Palladium(II) chromeazurol S Complex	585	1.66×10^{-4}	4.0	1.56×10^{5}	1.58×10^{5}	—

a) Investigated by us.

$1/A_3^{1/2}$ from which the extinction coefficient of the complex can be estimated. With iron(III) *p*-aminosalicylate complex studied by Das and Aditya[10] the extreme left and right wings of the Job curve correspond approximately to straight lines from whose slopes the average extinction coefficient of the complex is found to be 1634 which is in fairly good agreement with the reported value, considering the approximations made in deriving Eqs. 9 and 10.

Furthermore, the formation constant of the iron(III) *p*-aminosalicylate complex calculated from the intercept of the straight line drawn through the right wing portion of the Job curve for the system is 5.13×10^{4} which is in fairly good agreement with the value obtained by using Eq. 7.

The present treatment of the principle of continuous variation has several promising features of which the most important is that it determines simultaneously the relative composition, the stability constant and the extinction coefficient of a complex from the same experimental data by considering all the points of the Job curve. In this respect the present method is advantageous over the one based on the measurement of the deviation between the experimental Job curve and that constructed by extrapolation from the slopes near the extreme values of mole-fraction.[14] The latter method considers only a single point corresponding to the maximum in the Job curve and it involves an element of arbitrariness in drawing tangents to the Job curve because experimental data near the extreme values of mole-fraction which should be most imprortant in drawing tangents to the Job curve are wanting in most cases. These demerits are obviously absent in Eq. 5. Moreover, the proposed method does not require a prior knowledge of extinction coefficient of a complex, which is required in other methods[2,5,6,14] for computing the formation constant of a complex. Another fruitful result obtained from Eq. 5 is that it explains quantitatively the nature of the Job curve in the case of complexes with very high formation constant. It yields two Eqs. 9 and 10 which can profitably be used to compute the stability constant and extinction coefficient of such complexes.

The errors in A_1, A_2, and A_3 have been calculated for the various systems investigated. The sequence of errors is $\Delta A_1<\Delta A_2<\Delta A_3$. The error in A_1 hardly exceeds 4%, that in A_2 is within 10%, while the error in A_3 is somewhat large. In some cases it is observed to be about 16 to 20%. The estimated error in ε in such cases hardly exceeds 10%, particularly, when the extinction coefficient of the complex is large. The error in K, however, lies within 10% in any case. The

analysis of errors in A_1, A_2, and A_3 does not warrant the presence in solution of complexes having stoichiometries other than 1:1. It is felt that the theory developed here be tested with precise Job data on many more systems.

References

1) P. Job, *Ann. Chim. Phys.*, **9**, 113 (1928).
2) M. T. Beck, "Chemistry of Complex Equilibria," Van Nostrand Reinhold, London (1970), Chap. 5, pp. 86—89.
3) W. C. Voshburgh and G. R. Cooper, *J. Am. Chem. Soc.*, **63**, 427 (1941).
4) L. J. Katzin and E. Gebert, *J. Am. Chem. Soc.*, **72**, 5455 (1950).
5) S. K. Banerjee and A. K. Dey, *Z. Anorg. Allg. Chem.*, **309**, 226 (1961).
6) J. H. Yoe and A. L. Jones, *Ind. Eng. Chem., Anal. Ed.*, **16**, 111 (1944).
7) S. P. Sangal and A. K. Dey, *J. Indian Chem. Soc.*, **40**, 464 (1963).
8) D. P. Joshi and D. V. Jain, *J. Indian Chem. Soc.*, **41**, 33 (1964).
9) S. P. Sangal, S. C. Srivastava, and A. K. Dey, *J. Indian Chem. Soc.*, **40**, 275 (1963).
10) R. C. Das and S. Aditya, *J. Indian Chem. Soc.*, **37**, 557 (1960).
11) R. K. Nanda and S. Aditya, *J. Indian Chem. Soc.*, **40**, 660 (1963).
12) R. C. Das, R. K. Nanda, and S. Aditya, *J. Indian Chem. Soc.*, **40**, 739 (1963); R. K. Nanda and S. Aditya, *ibid.*, **40**, 755 (1963).
13) R. C. Das and S. Aditya, *J. Indian Chem. Soc.*, **42**, 15 (1965); R. C. Das, R. K. Nanda, and S. Aditya, *ibid.*, **42**, 307, (1965).
14) F. J. C. Rossotti and H. Rossotti, "The Determination of Stability Constants and other Equilibrium Constants in Solution," McGraw-Hill, London (1961), Chap. 3, pp. 47—53.

Study of Molecular Complexes by Refractometry

Ram Adhar SINGH† and Subray Narayan BHAT*
Department of Chemistry, North-Eastern Hill University, Shillong-793003, India
†*Chemistry Department, Banaras Hindu University, Varanasi, India*

(Received April 17, 1981)

The refractive index measurement technique is used to investigate molecular complex formation in liquid solutions and the association constants are determined directly. The association constants at 25 °C and heats of complexation for naphthalene–phenol, benzene–tetracyanoethylene, *p*-xylene–tetracyanoethylene, hexamethylbenzene–tetracyanoethylene, and triethylamine–iodine in cyclohexane are 8.2, 2.2, 8.6, 231, and 4620 $dm^3\ mol^{-1}$ and 19.25, 11.30, 18.00, 32.21, and 51.46 kJ/mol, respectively. These values agree well with the literature data obtained by spectroscopic methods.

The Benesi-Hildebrand equation[1] and their modified equations[2,3] have been widely used in the study of molecular complexes. However, these methods were subject to criticism, particularly in the case of weakly interacting systems, as the valid separation of K and ε from $K\varepsilon$ product may be difficult to attain, the error increasing with the decrease in the strength of the complexes.[4–6] So if one wants to have accurate values of $K\varepsilon$, K, and ε, which are essential in developing and testing theories[7] of electron donor-acceptor interactions, one has to supplement the results obtained by the non-spectral methods to the one obtained by spectral methods. Recently we have shown that the equilibrium constant, K, can be determined directly by the non-spectral methods like surface tension[8] and refractive index measurements[9] and we have felt that in order to establish the suitability of refractometry in obtaining reliable value of K directly, an extensive studies on the applications of this method to various systems is worthwhile to carry out. In the present paper the studies of naphthalene–phenol, methylbenzenes–tetracyanoethylene, and triethylamine–iodine in cyclohexane have been reported as they represent weak, moderate and strong interactions between electron donors and acceptors.

Experimental

Materials. Triethylamine (Riedel de Hainay) was treated with acetic anhydride to remove primary and secondary amines.[10] It was then dried over anhydrous KOH pellets and fractionally distilled (bp 89.5 °C). Iodine (BDH, A.R. grade) was purified by sublimation from a mixture of iodine and potassium iodide (in the ratio of 2.5 : 1). Phenol was crystallized from cyclohexane–ethanol mixture (mp 42.8 °C). Nephthalene, *p*-xylene, and hexamethylbenzene were purified by the standard procedures.[11] Tetracyanoethylene (Du Pont) was purified by crystallization (from chlorobenzene solution) and vacuum sublimation (mp 199.5°C in sealed tube). Benzene and cyclohexane (BDH Spectro quality) were used as such.

Method. The refractive index of solution was measured using Pulfrich refractometer (Adam Hilger No. M 48302/20210).[9] A mercury vapor lamp was used as source of light. The refractive index was obtained by measuring the angle of refraction (θ) for green (546 nm) and yellow (578 nm) lines of mercury, using the formula

$$\eta^2 = \eta_0^2 - \sin^2\theta, \qquad (1)$$

where η_0 is the prism constant for a particular wavelength at a particular temperature.

The refractive indices of triethylamine, iodine, benzene, *p*-xylene, hexamethylbenzene, tetracyanoethylene, naphthalene, and phenol in cyclohexane and those of "mixed solutions," keeping the total concentration constant were measured at 25, 30, 35, 40, and 45 °C. The temperature of solution was maintained constant (±0.1 °C) by circulating water from a thermostat. The refractive index could be determined with an accuracy of ±0.00002.

The refractive index at infinite wavelength can be calculated using Couchy's approximation,[12]

$$n_\infty = \frac{n_y\lambda_y^2 - n_g\lambda_g^2}{\lambda_y^2 - \lambda_g^2}, \qquad (2)$$

where n_y, λ_y and n_g, λ_g are refractive index and wavelength of yellow and green line of mercury respectively. The experiments were repeated at least twice and the values obtained were within the experimental error.

The stoichiometry of the complexes was determined by the continuous variation method.[13]

Determination of Equilibrium Constant

The non-linear plot of any physical property of the "mixed solution" against the concentration of pure components, *i.e.*, the deviation from ideal behaviour of the pure components in solution, is an indication of the interaction between the two species, namely the donor D, and the acceptor A, (neglecting the solvent effect). If we can assume that the deviation is entirely due to the complex alone, then the deviation should be proportional to the concentration of the complex. Baur and his co-workers[14] had developed a procedure by which deviations from additivity of the total polarization and refraction of a binary solution can be related to the association constant of a complex (AD) formed from two non-polar molecules. However, the equilibrium constant can be calculated for ternary systems, using the equation proposed by Yoshida and Osawa,[15]

$$K = \frac{2\sqrt{k}[\sqrt{k}(C+C') - (C+kC')]}{(C-kC')^2}, \qquad (3)$$

where K is equilibrium constant in $dm^3\ mol^{-1}$, k is the ratio of the maximum deviations for total concentrations of C and C' in two different sets. Here we should note that the results obtained by the continuous variation method must be taken with caution since with this method it is not always possible to observe all the complexes present in the solution, and in such cases the titration method should be followed.[16]

The equilibrium constant, K, can also be obtained as described earlier.[8]

Consider the interaction of A with D,

$$A + D \rightleftharpoons AD.$$

Let C_A, C'_A, C_D, and C'_D be the initial concentrations of the acceptor and donor respectively for the two sets of solutions, and C_{AD}, C'_{AD} be the concentration of the complexes. For the first set,

$$K = \frac{C_{AD}}{[(C_D - C_{AD})(C_A - C_{AD})]}, \quad (4)$$

and for the second set,

$$K = \frac{C'_{AD}}{[(C'_D - C'_{AD})(C'_A - C'_{AD})]}, \quad (5)$$

therefore,

$$\frac{C_{AD}}{[(C_D - C_{AD})(C_A - C_{AD})]} = \frac{C'_{AD}}{[(C'_D - C'_{AD})(C'_A - C'_{AD})]}. \quad (6)$$

If there is a linear relationship between Δn and the concentration of the complex (*i.e.*, similar to the test of Beer's law), we can conclude that if the two solutions show the same deviations of refractive indices, then they must have the same concentration of the complex. Therefore if

$$\Delta n_1 = \Delta n_2, \text{ then } C_{AD} = C'_{AD}.$$

From the above equations, we get

$$K = \frac{(C'_A C'_D - C_A C_D)[(C'_A + C'_D) - (C_A + C_D)]}{[(C'^2_A + C_A C_D) - C'_A(C_A + C_D)][(C'^2_D + C_A C_D) - C'_D(C_A + C_D)]}. \quad (7)$$

The K values thus calculated agree well with the values calculated using Eq. 3.

Results and Discussion

Naphthalene–Phenol System. The refractive indices of naphthalene and phenol in cyclohexane increase linearly with the increase in concentration of the solute in the experimental range of concentrations (0.01—0.10 mol dm^{-3}). The plot of n^2_∞ against the concentration of naphthalene in the "mixed solutions" of naphthalene–phenol shows only one maximum at a position

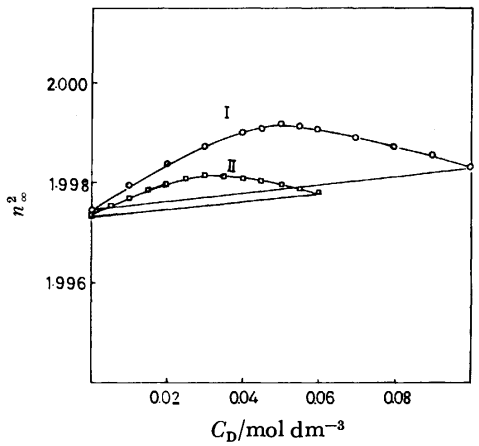

Fig. 1. Plot of n^2_∞ *vs.* concentration of naphthalene in naphthalene–phenol system (solvent : cyclohexane). Total concentration: I: 0.10 mol dm^{-3}, II; 0.06 mol dm^{-3}.

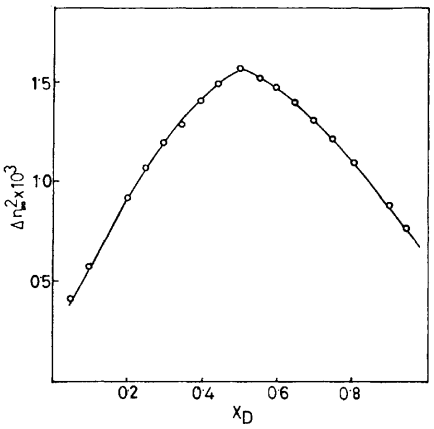

Fig. 2. Plot of Δn^2 *vs.* mole fraction of naphthalene in naphthalene–phenol in cyclohexane.

Table 1. Square of refractive indices, n^2_∞, of naphthalene–phenol system of different compositions in cyclohexane

Concentration/mol dm^{-3}		Square of refractive indices, n^2_∞,		
Naphthalene	Phenol	Obsd	Calcd	Difference ($\Delta n^2 \times 10^3$)
1st set: Total concentration=0.10 mol dm^{-3}.				
0.000	0.100	2.03528	—	—
0.005	0.095	2.03551	2.03514	0.37
0.010	0.090	2.03570	2.03514	0.56
0.020	0.080	2.03604	2.03514	0.90
0.025	0.075	2.03620	2.03514	1.06
0.030	0.070	2.03633	2.03514	1.19
0.035	0.065	2.03644	2.03514	1.30
0.040	0.060	2.03654	2.03514	1.40
0.045	0.055	2.03661	2.03514	1.47
0.050	0.050	2.03670	2.03514	1.56
0.055	0.045	2.03664	2.03514	1.50
0.060	0.040	2 03661	2.03514	1.47
0.065	0.035	2.03653	2.03514	1.37
0.070	0.030	2.03644	2.03514	1.30
0.075	0.025	2.03633	2.03514	1.19
0.080	0.200	2.03622	2.03514	1.08
0.090	0.100	2.03602	2.03514	0.88
0.095	0.005	2.03590	2.03514	0.76
0.100	0.000	2.03579	—	—
2nd set: Total concentration=0.06 mol dm^{-3}				
0.000	0.060	2.03494	—	—
0.005	0.055	2 03522	2.03496	0.26
0.010	0.050	2.03550	2.03497	0.53
0.015	0.045	2.03570	2.03497	0.73
0.020	0.040	2.03592	2.03496	0.96
0.025	0.035	2.03610	2.03496	1.14
0.030	0.030	2.03627	2.03496	1.31
0.035	0.025	2.03616	2.03497	1.19
0.040	0.020	2.03607	2.03497	1.10
0.045	0.015	2.03593	2.03496	0.97
0.050	0.010	2.03579	2.03497	0.82
0.055	0.005	2.03563	2.03497	0.66
0.060	0.000	2.03545	—	—

of half the concentration of naphthalene (Fig. 1; Table 1); similarly the plot of Δn^2, difference in square of refractive indices of the calculated and observed values against the concentration of donor (in mole fraction) shows only one maximum at 0.5 mole fraction (Fig. 2). These indicate that naphthalene forms only 1 : 1 complex with phenol in the experimental range of concentrations.

By knowing the maximum deviation in Δn^2 for two sets of different total concentrations (10.0 and 6.0×10^{-2} mol dm^{-3}) the equilibrium constants for different temperatures were calculated. The equilibrium constant at 25 °C and the enthalpies are 8.20 ± 0.50 mol dm^{-3} and 19.25 ± 1.25 kJ/mol respectively (Table 2). These data indicate that equilibrium constant and enthalpy obtained by the above mentioned procedure are reasonably in good agreement with the literature values.

Methyl Benzenes–Tetracyanoethylene Systems. The refractive indices of benzene, *p*-xylene, hexamethylbenzene, and tetracyanoethylene in cyclohexane increase linearly with an increase in concentration of the solute in the experimental concentration range (0.01—0.15 mol dm^{-3}). When tetracyanoethylene is mixed with benzene, *p*-xylene or hexamethylbenzene solutions, stable neutral complex is formed, A plot of Δn, the difference in refractive indices of the calculated and observed values against the calculated concentration of the complex is linear; this indicates that there is no interaction between the complex and the individual species. A plot of n_∞^2 against the concentration of the donor shows only one maximum at a position of half the donor concentration, indicating that there is predominantly one type of complex, *i.e.* 1 : 1, when the donor concentration is comparable to that of the acceptor. Higher order molecular complexes may be formed only when the concentration of either one of the two components is very high.[17]

The values of K_c and $-\Delta H^\circ$ thus obtained are summarised in Table 2 along with the literature data. In the case of benzene–TCNE, the literature data are under different conditions. From the data, it is evident that the values of K_c and $-\Delta H^\circ$ obtained by refractometry are in good agreement with the literature data except for the HMB–TCNE system. It has been shown recently that the value of K_c, based on the assumption that only 1 : 1 complex is formed in HMB–TCNE, is much lower than the value of K_c reported earlier in the literature, which includes other types of complexes.[17] Here it must be noted that the literature data are under different sets of conditions,[3,18] and that the value of K_c depends on the experimental conditions such as whether A$\gg$D, D$\gg$A, or A$\approx$D, and also on the nature of solvents.

The values of K_c (at only one temperature, for the sake of brievity), ΔH° and the other thermodynamic parameters thus obtained for methylbenzenes–tetracyanoethylene in cyclohexane are given in Table 2 along with the literature data. From the data, it is evident that the relative enthalpies and free energies obtained from a series of donors, increase with the increased methylation of the donor. These observations are consistent with charge-transfer theory[7] and go in parallel with the literature data for similar π-π complexes and the values of K_c and ΔH° obtained by refractometry are thus in good agreement with the data obtained by spectroscopic methods. Here it must be worth mentioning that ΔH° values are more reliable than the equilibrium constants obtained by separating K and ε from $K\varepsilon$. As ΔH° values which are more reliable than K values, are in very good agreement with the literature data, we feel our values of K which are obtained directly, are probably more acceptable than the literature data.

Triethylamine–Iodine System. The refractive index of triethylamine in cyclohexane decreases whereas that of iodine increases with the concentration of solute in the experimental range of concentration ($0.5—10.0\times 10^{-3}$ mol dm^{-3}). The total concentrations of triethylamine–iodine (6.0 and 10.0×10^{-3} mol dm^{-3}) are such that when they are mixed, neutral complex is formed which was confirmed spectroscopically.[19]

The plot of n_∞^2 against the concentration of triethylamine in triethylamine–iodine, shows one maximum at a position of half the donor concentration; similarly the plot of Δn^2, difference in square of refractive indices of the calculated and observed values against the concentration of donor (in mole fraction) shows only one maximum at 0.5 mole fraction. These indicate that

TABLE 2. EQUILIBRIUM CONSTANT, K_C, AND OTHER THERMODYNAMIC PARAMETERS FOR NAPHTHALENE–PHENOL, METHYLBENZENES–TETRACYANOETHYLENE, AND TRIETHYLAMINE–IODINE IN CYCLOHEXANE

System	K(25 °C) / dm^3 mol^{-1}	$-\Delta H^\circ$ / kJ mol^{-1}	$-\Delta G^\circ$ / kJ mol^{-1}	$-\Delta S^\circ$ / J K^{-1} mol^{-1}
Naphthalene–Phenol	8.2 ± 0.5 (5.0[a])	19.25 ± 1.25	5.02	47.7
Benzene–TCNE	2.2 ± 0.2 (2.0[b])	11.30 ± 1.25 (10.46[c])	2.10	30.9
p-Xylene–TCNE	8.6 ± 0.5 (7.6[c])	18.00 ± 2.10 (14.22[b])	5.02	43.5
Hexamethylbenzene–TCNE	231 ± 10 (263[c]) (417[d]) (219[e])	32.21 ± 2.10 (32.2[b])	12.55	66.6
Triethylamine–Iodine	4620 ± 50 (4690[f])	51.46 ± 0.6 (51.04[f])	20.50	103.8

The values in the parentheses refer to the literature data. Solvent : CH_2Cl_2 a) A. S. N. Murthy and C. N. R. Rao, *Appl. Spectrosc. Revs.*, **2**, 69 (1969). b) P.H. Emslie and R. Foster, *Tetrahedron*, **21**, 2851 (1965). c) R. E. Merrifield and W. D. Phillips, *J. Am. Chem. Soc.*, **80**, 2778 (1958). d) D. Dodson, R. Foster, A. A. S. Bright, M. I. Foreman, and J. Gorton, *J. Chem. Soc., B*, **1971**, 1283. e) R. A. Singh, S. P. Mishra, and S. N. Bhat, *Proc. Ind. Acad. Sci.*, **89**, 139 (1980). f) S. Nagakura, *J. Am. Chem. Soc.*, **80**, 520 (1958).

triethylamine forms only 1 : 1 complex with iodine in the experimental range of concentrations. From this it appears that triethylamine forms only one 1 : 1 complex with iodine and not any other complexes as suggested by Schmulback.[20] The higher order complexes are invariably formed only when the concentration of one of the two components is in very much excess (*i.e.* D⋙A or A⋙D), but in the present case, as the concentration of donor and acceptor are comparable, the higher order complexes seem to be improbable.

The plot of Δn^2 against the concentration of complex (calculated using the equilibrium constant for different initial donor and acceptor concentrations in all the cases) is linear. This justifies the assumption that the deviation is proportional to the concentration of the complex and there is no interaction between the complex and individual species.

The equilibrium constant and enthalpy value for triethylamine–iodine system are given in Table 2. It is evident from the data that the equilibrium constant and other thermodynamic parameters determined from refractometry are in very good agreement with the literature data.

The increment in the dipole moment is directly related to charge-transfer and the dipole moment of a complex depends on the total polarizability of the complex. However, in the calculation of the dipole moment of complex, so far, the electronic and atomic (which is about 5—10% of electronic) polarizability has been neglected on the ground that the electronic and atomic polarization of the complex is equal to the sum of the electronic and atomic polarization of individual molecules.[17,21,23] As can be seen from the above data and figures, whenever there is any interaction between the molecules, the electronic polarizability exceeds the additive value. Therefore the contribution of the electronic polarizability cannot be neglected if one wants to determine the exact dipole moment of the complex.

Thus as shown earlier, our present observations confirm our earlier suggestive evidences that the refractive index measurement method can be used for not only detecting the formation of the complex but also to determine its equilibrium constants directly even in the case of very weak complexes

Financial assistance from U.G.C. is acknowledged.

References

1) H. A. Benesi and J. H. Hildebrand, *J. Am. Chem. Soc.*, **71**, 2703 (1949).
2) C. N. R. Rao, S. N. Bhat, and P. C. Dwivedi, *Appl. Spectrosc. Revs.*, **5**, 1 (1972).
3) R. Foster, "Organic Charge Transfer Complexes," Academic Press, New York (1969).
4) S. D. Christian, J. D. Childs, and E. H. Lane, *J. Am. Chem. Soc.*, **94**, 6861 (1972); J. D. Childs, S. D. Christian, and J. Grundness *ibid.*, **94**, 5657 (1972).
5) M. Tamres and S. N. Bhat, *J. Am. Chem. Soc.*, **94**, 2577 (1972).
6) W. B. Person, *J. Am. Chem. Soc.*, **87**, 167 (1965).
7) R. S. Mulliken and W. B. Person, "Molecular Complexes," Wiley-Interscience, New York (1969); A. K. Colter and E. Grunwald, *J. Phys. Chem.*, **74**, 3637 (1970).
8) R. A. Singh, S. P. Mishra, and S. N. Bhat, *Proc. Indian Acad. Sci.*, **89**, 139 (1980).
9) R. A. Singh and S. N. Bhat, *Indian J. Chem.*, **15A**, 1106 (1977); R. A. Singh and S. N. Bhat, *J. Phys. Chem.*, **82**, 2323 (1978).
10) "Techniques of Chemistry, Vol. IV, Organic Solvents," ed by A. Weissberger, Wiley-Interscience, New York (1970).
11) A. I. Vogel, "A Text Book of Practical Organic Chemistry," ELBS, London (1973).
12) V. I. Minkin, O. A. Osipov, and Y. A. Zhdanov, "Dipole Moments in Organic Chemistry," Plenum Press, New York (1970).
13) P. Job, *Ann. Chim. (Paris)*, **9**, 113 (1928).
14) M. E. Baur, D. A. Horsma, C. M. Knobler, and P. Perez, *J. Phys. Chem.*, **73**, 641 (1969).
15) Z. Yoshida and E. Osawa, *Bull. Chem. Soc. Jpn.*, **38**, 140 (1965); F. M. Arshid, G. M. Giles, E. C. Molure, A. Ogilvie, and T. J. Rose, *J. Chem. Soc.*, **1955**, 67.
16) E. N. Guryanova, I. P. Goldshtein, and I. P. Romm, "Donar-Acceptor Bond," John Wiley & Sons, New York (1975).
17) R. Foster and N. Kulevsky, *J. Chem. Soc., Faraday Trans.*, **69**, 1427 (1973).
18) M. Muanda, J. B. Nagy, and O. B. Nagy, *Tetrahedron Lett.*, **38**, 3421 (1974).
19) S. Nagakura, *J. Am. Chem. Soc.*, **80**, 520 (1958).
20) C. D. Schmulback and D. M. Hart, *J. Am. Chem. Soc.*, **86**, 2347 (1964).
21) N. Kulevsky, "Molecular Association," ed by R. Foster, Academic Press, New York (1975), Vol. I.
22) S. N. Bhat and C. N. R. Rao, *J. Am. Chem. Soc.*, **80**, 6008, (1968).

A Perturbative Study of Medium and Long Range Interactions between Some Characteristic Fragments of Lipid-Protein Systems

Antonio RAUDINO,* Felice ZUCCARELLO, Giuseppe BUEMI, and Carmelo RIGANO†

Istituto Dipartimentale di Chimica e Chimica Industriale, Università di Catania, Viale A. Doria 8, 95125, Catania, Italy

†*Seminario Matematico, Università di Catania, Viale A. Doria 8, 95125, Catania, Italy*

(Received February 10, 1981)

An intermolecular perturbation theory, originally presented by Murrell and developed by use of the LCAO approximation, was applied to a theoretical study on the interaction of a hydrogen-bonded dimer of formamide with ethane molecule or ammonium ion in order to simulate interaction between characteristic frameworks of proteins and lipids. Ethane has a preferential orientation parallel to the carbonyl bond supported by the prevailing charge-transfer contribution. Ammonium ion has preferential interaction regions dependent on the balance between the charge-transfer and coulombic forces along the NH···OC axis.

Essentially biological membranes are built up from lipid bilayers in which proteins are imbedded. Therefore, to study lipid protein interaction is an interesting task, but hampered by the complexity arising from the size of isolated molecules.[1] One of possible ways to overcome this difficulty is to construct more simplified models describing relevant interactions. From study of these model systems it is possible to get information on the nature of forces and on the spatial preference in interaction between more complex systems. At this stage we examine interaction between fragments of lipids and the polypeptide chain, but for simplicity it is here simulated by using two H-bonded formamide molecules spatially arranged in such a way that the geometry of α-helix may be reproduced. In biological membranes lipids are essentially arranged in such a way that two ranges of interactions are possible to be separated, in one of which the protein interacts with the hydrophobic chain and in the other it interacts with the ionic heads. For the sake of computational economy we selected ethane as a model of the aliphatic chain of lipid and ammonium ion as a simplified model of ionic head. The latter constitutes the simplest model of known lipid heads, *e.g.*, the positive end of phosphatidylethanolamines.

We inspect medium and long range interactions between these fragments along the axis of the H-bonding existing in the pitch of α-helix in order to evaluate i) the entity of interaction energies, ii) the spatial specificity and anisotropy of interactions, and iii) the origin of intermolecular forces.

The energies were evaluated by means of the perturbation theory, following Murrell's approach[2] developed in the LCAO approximation by Fueno *et al.*[3]

Calculations

Interaction energy calculations were performed following the second order perturbation theory put forward by Murrell *et al.*[2] and developed by Fueno *et al.*[3] in the usual LCAO approximation. We adopted the ZDO approximation within single molecules, but retained the overlap integral between interacting molecules. Therefore, coefficients of wave function and transition energies relative to isolated molecules were calculated following the CNDO method.[4] Moreover, intermolecular three- and four-center integrals were approximated by Mulliken's equation:[5]

$$V_{a,rs} \simeq (V_{a,rr} + V_{a,ss})\frac{S_{rs}}{2},$$

$$(rs|tu) \simeq [(rr|tt) + (rr|uu) + (ss|tt) + (ss|uu)]\frac{S_{rs}S_{tu}}{4}.$$

Following the scheme presented by Fueno *et al.*,[3] the intermolecular interaction energy was divided into five contributions: coulombic (E_Q), exchange (E_k), induction (E_I), dispersion (E_D), and charge-transfer (E_{CT}) energies.

Preliminarily, we have considered several approaches in calculating the electron core attraction and the interelectronic repulsion intermolecular integrals. We first calculated both $V_{a,rr}$ and (rr|ss) integrals theoretically by using an STO basis set, then considered the point charge approximation as suggested by Suzuki and Iguchi,[6] and finally considered the CNDO approximations: $(rr|ss)=\gamma_{ab}$ and $V_{a,rr}=-Z_a\gamma_{ab}$. We have found that, at distances greater than 3.5 Å, all these approximations give convergent values of energy; however, the present figures come from the last approximation. It is to be borne in mind that the present perturbation approach cannot be utilized in calcuating reliable equilibrium distances, many terms being uncorrectly calculated at short distances (*e.g.*, double excharge terms are lacking in the calculation of the exchange energy[7]). However, this method gives good information about preferential approaching pathways at large distances,[3] for which the simplified SCF-MO methods are ineffective.

The geometries of ethane molecule and ammonium ion were taken from the literature.[8] The geometry of the formamide dimer was determined by adopting the standard bond lengths and bond angles,[9] and by choosing the distance and dihedral angle between the two planar molecules so that the standard geometry of the α-helix[9] might be reproduced (see Fig. 1).

One of us (C.R.) has worked out a program in FORTRAN IV for the CDC 6600 computer, such that perturbation energies may be calculated in a step on the basis of the CNDO/2 program. This CNDO/2 program is the Del Bene-Jaffè version[10,11] modified so that it may calculate, for a given geometry, first the electron structure of two isolated molecules, then intermolecular

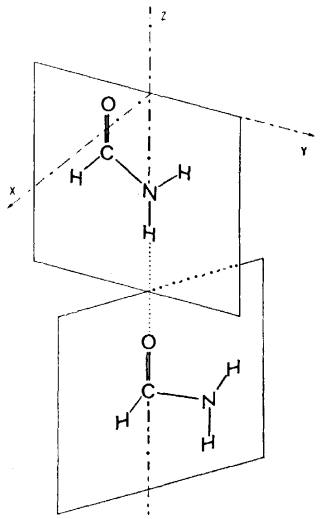

Fig. 1. Spatial conformation of formamide dimer reproducing the framework of protein α-helix.

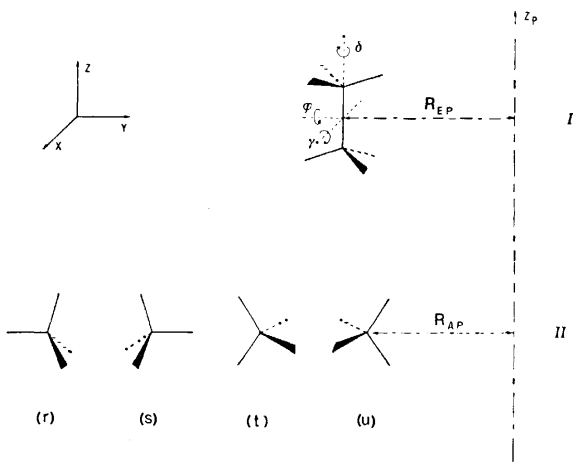

Fig. 2. Approaching pathways for ethane and ammonium ion. Z_P represents the z axis (NH···OC axis) of formamide dimer.

integrals, and finally intermolecular energies.

Figure 2 shows approach pathways between the NH··· OC axis and each of ethane (I) and ammonium ion (II, r, s, t, u) and defines the rotation angles (ϕ, γ, and δ) for ethane. Three relative positions were considered for the set of ethane and NH···OC zxis: (1) ethane placed in front of the N–H bond (A_I); (2) ethane placed in front of the C=O (C_I); and (3) ethane placed in an intermediate region (B_I). The ethane–protein axis (R_{EP}) was held perpendicular to the plane of the nearest amide molecule and the intermediate region (B_I) had an averaged orientation imposed.

Five relative positions were considered for ammonium ion in view of its greater specificity for intermolecular interaction. They describe the positioning of the ion in front of atoms N, H, O, and C and in the intermediate (H-bridge) region (A_{II}, B_{II}, D_{II}, E_{II}, and C_{II} regions, respectively). The same criterion as for the ethane–protein axis was adopted also for the orientation of the ammonium–protein axis (R_{AP}).

Results and Discussion

Interaction energies for the set of ethane and formamide dimer, located in the three significant regions along the NH···OC axis, are given in Table 1. Rotation angle ϕ is defined in Fig. 2. The data indicate

Table 1. Energies for interaction between ethane and formamide dimer

Conformation		E_Q	E_K	E_I	E_D	E_{CT}	E_{TOTAL}
R_{EP}	φ	kcal mol^{-1}	kcal mol^{-1}	kcal mol^{-1}	kcal mol^{-1}	kcal mol^{-1}	kcal mol^{-1}
				Region A_I			
4.5	0	−0.001	−0.002	−0.002	−0.098	−0.080	−0.184
	45	−0.002	−0.003	−0.003	−0.099	−0.076	−0.183
	90	0.006	−0.003	−0.002	−0.098	−0.070	−0.167
5.5	0	≈0	≈0	−0.001	−0.034	−0.002	−0.038
	45	≈0	≈0	−0.001	−0.035	−0.002	−0.037
	90	0.002	≈0	−0.001	−0.033	−0.002	−0.034
				Region B_I			
4.5	0	0.003	−0.002	−0.002	−0.087	−1.216	−1.305
	45	0.002	−0.003	−0.002	−0.084	−0.681	−0.768
	90	≈0	−0.001	−0.003	−0.085	−0.213	−0.302
5.5	0	≈0	≈0	−0.001	−0.032	−0.026	−0.059
	45	≈0	≈0	−0.001	−0.032	−0.016	−0.048
	90	≈0	≈0	−0.001	−0.033	−0.006	−0.039
				Region C_I			
4.5	0	≈0	−0.002	−0.009	−0.101	−3.208	−3.319
	45	0.001	0.001	−0.010	−0.109	−2.086	−2.203
	90	0.008	0.001	−0.006	−0.092	−1.936	−2.026
5.5	0	≈0	≈0	−0.003	−0.033	−0.072	−0.107
	45	≈0	≈0	−0.003	−0.035	−0.047	−0.085
	90	0.003	≈0	−0.002	−0.031	−0.046	−0.076

that in the proximity of the N-H bond the ethane molecule is isotropic both at R_{EP}=4.5 and 5.5 Å. For the other two positions (C=O and H···O), we can note isotropy at 5.5 Å, while at 4.5 Å a preferential orientation of the C–C axis of ethane along the NH···OC axis occurs. In any cases preferred intermolecular binding is in the neighborhood of the C=O bond. This trend is justifiable if we look at the dispersion and charge-transfer contributions to the total energy, the other contributions (E_Q, E_K, and E_I) being nearly zero. Dispersion energy is about −0.03 kcal mol^{-1} at 5.5 Å, independent of the position along the NH···OC axis. Analogously an isotropy appears at 4.5 Å with a value of about −0.1 kcal mol^{-1}. These figures are probably underestimated because of the limited set of excited states; however, since the dispersion results are nearly isotropic along the protein axis (see Table 1), this fact will little affect our future conclusions. The charge-transfer contribution shows a non-isotropic trend. In fact, it is very small in the neighborhood of the N-H bond, so that at 5.5 Å it is nearly zero; a large CT contribution has been evidenced in the H···O region at 4.5 Å, while it is very small at 5.5 Å. The largest CT energy is observed in the proximity of the C=O bond; in fact at 4.5 Å the total interaction energy is due mainly to it, and at 5.5 Å the CT energy appears com-

TABLE 2. ENERGIES FOR INTERACTION BETWEEN AMMONIUM ION AND FORMAMIDE DIMER

Conformation		E_Q	E_K	E_I	E_D	E_{CT}	E_{TOTAL}
R_{AP}	Path	kcal mol^{-1}	kcal mol^{-1}	kcal mol^{-1}	kcal mol^{-1}	kcal mol^{-1}	kcal mol^{-1}
				Region A_{II}			
4.5	r	−2.173	0.020	−0.341	−0.033	−0.051	−2.582
	s	−2.129	0.011	−0.335	−0.032	−0.022	−2.507
	t	−2.132	0.031	−0.350	−0.037	−0.070	−2.558
	u	−2.174	0.007	−0.334	−0.037	−0.017	−2.555
5.5	r	−1.730	≈0	−0.173	−0.011	−0.002	−1.916
	s	−1.711	≈0	−0.171	−0.011	≈0	−1.894
	t	−1.715	≈0	−0.176	−0.012	−0.002	−1.905
	u	−1.725	≈0	−0.171	−0.013	≈0	−1.910
				Region B_{II}			
4.5	r	−1.678	0.016	−0.490	−0.035	−0.059	−2.245
	s	−1.644	0.007	−0.480	−0.032	−0.024	−2.173
	t	−1.670	0.018	−0.502	−0.046	−0.096	−2.296
	u	−1.690	0.005	−0.476	−0.031	−0.023	−2.215
5.5	r	−1.826	≈0	−0 229	−0.012	−0.002	−1.529
	s	−1.273	≈0	−0.226	−0.012	≈0	−1.511
	t	−1.286	≈0	−0.225	−0.016	−0.003	−1.537
	u	−1.288	≈0	−0.233	−0.012	≈0	−1.525
				Region C_{II}			
4.5	r	−1.053	0.004	−0.535	−0.039	−0.214	−1.837
	s	−1.059	0.002	−0.532	−0.037	−0.170	−1.796
	t	−1.137	0.004	−0.550	−0.049	−0.503	−2.235
	u	−1.029	0.002	−0.521	−0.026	−0.202	−1.775
5.5	r	−0.560	≈0	−0.241	−0.014	−0.005	−0.820
	s	−0.561	≈0	−0.240	−0.014	−0.004	−0.819
	t	−0.588	≈0	−0.245	−0.017	−0.012	−0.862
	u	−0.548	≈0	−0.236	−0.010	−0.004	−0.798
				Region D_{II}			
4.5	r	0.208	0.004	−0.327	−0.035	−0.731	−0.881
	s	0.107	0.012	−0.341	−0.041	−2.439	−2.702
	t	0.135	0.007	−0.333	−0.033	−1.639	−1.863
	u	0.215	0.007	−0.331	−0.039	−0.985	−1.133
5.5	r	0.440	≈0	−0.162	−0.013	−0.015	0.250
	s	0.406	≈0	−0.166	−0.014	−0.051	0.176
	t	0.416	≈0	−0.163	−0.012	−0.034	0.207
	u	0.441	≈0	−0.163	−0.013	−0.021	0.243
				Region E_{II}			
4.5	r	1.722	0.009	−0.196	−0.037	−1.390	0.108
	s	1.758	0.027	−0.202	−0.034	−3.996	−2.447
	t	1.751	0.018	−0.198	−0.029	−3.215	−1.673
	u	1.725	0.008	−0.201	−0.045	−1.695	−0.208
5.5	r	1.363	≈0	−0.109	−0.012	−0.029	1.212
	s	1.370	≈0	−0.111	−0.011	−0.090	1.158
	t	1.372	≈0	−0.109	−0.010	−0.068	1.186
	u	1.363	≈0	−0.111	−0.015	−0.030	1.208

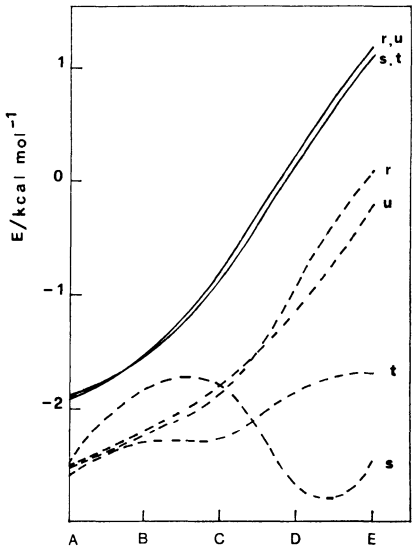

Fig. 3. Interaction energy curves for approaching pathways of ammonium ion in various regions of the NH··· OC axis. r, s, t, and u are defined in Fig. 2.
A, B, D, and E correspond to z coordinates of atoms N, H, O, and C, respectively. C corresponds to the intermediate region. ·····: R_{AP}=4.5 Å, ——: R_{AP}=5.5 Å.

parable with the dispersion term. This behaviour is well justified if we bear in mind that the HOMO of formamide dimer is essentially located on the carbonyl group. Calculations were also undertaken for various angles of rotation (δ) around the C–C axis of ethane. The results indicate a small anisotropy, of about 0.5 kcal mol^{-1}, at 4.5 Å and in the proximity of the carbonyl group. Further calculations were carried out at 3.5 Å. The results are not reliable because of the large overlap which limits the validity of the present perturbation approach. However, even if the results are numerically unacceptable (essentially the CT contribution is overestimated at short distances), the figures are sure to follow the same trend.

As far as the charged molecule NH_4^+ is concerned, a large anisotropy is evidenced in the neighborhood of the C=O group at 4.5 Å, as we can see from Fig. 3 (region E) and Table 2, which summarizes results for the five positions of the ion located at 4.5 and 5.5 Å in front of the NH···OC axis. Moreover, a complete isotropy is found in correspondence with the N–H bond, and only a little preference for *t* conformation is found in the intermediate region. At 5.5 Å the four orientations (r, s, t, and u) of the ion are isoenergetic; the minimum potential is found in correspondence with the N–H bond. Even if the energy scale is not so accurate owing to the underestimation of dispersion forces, the trend may be considered reliable since the dispersion term is isotropic as observed for ethane. The overall trend is dependent essentially on the balance between the electrostatic and CT contributions since the other terms are almost constant or zero. At 4.5 Å the total energy curves have such trends as are highly differentiated for the various orientations of ammonium ion with respect to the protein z axis (see Fig. 2) as a consequence of the trend of the CT contribution, which, in the neighborhood of the carbonyl group, can be predominant when an optimum overlap is attained (pathways s and t). At 5.5 Å the curves for the total energy nearly match the trend of the electrostatic term.

From the present results we can argue that an aliphatic chain prefers to locate itself in the proximity of, and parallel to the carbonyl group of the polypeptide chain. The ammonium ion at 5.5 Å shows a preference for the N atom lone pair, while at shorter distances (in the range of experimental equilibrium distances) a competitive attraction of the N atom and of the C=O bond appears. From a study on formamide interacting with metal ions, a preferential binding of the ion along the C=O bond axis was found.[12] In our case, even if the C=O group is bound to the N–H bond by an H-bridge, we are still to find this tendency of the carbonyl group to attract the positive ion. However, it is to be pointed out that energies in balance are so small that the steric and/or solvent effects may also be competitive.

The present results, which may be considered as a good description of lipid systems with poly-L-glycine, suggest that in proteins with nonpolar side residues, the field experienced by the molecules adjacent to the polyamidic α-helix is nearly isotropic. Consequently, we may conclude that, for proteic systems without ionic or highly polar side residues, the approximation which simulates the protein as a dielectric cylinder[13] is reasonably applicable. However, effects of hydrophobic and/or polar residues and of the solvent on lipid–protein interactions are a matter of further investigation.

References

1) D. F. Bocian and S. I. Chan, *Ann. Rev. Phys. Chem*, **29**, 307 (1978) and references cited.
2) J. N. Murrell, M. Randic, and D. R. Williams, *Proc. R. Soc. London, Ser. A*, **284**, 566 (1965).
3) T. Fueno, S. Nagase, K. Tatsumi, and K. Yamaguchi, *Theor. Chim. Acta (Berl.)*, **26**, 43 (1972).
4) J. A. Pople and D. L. Beveridge, "Approximate Molecular Orbital Theory," McGraw-Hill, New York (1970).
5) R. S. Mulliken, *J. Chim. Phys.*, **46**, 497 (1949).
6) K. Suzuki and K. Iguchi, *J. Chim. Phys.*, **75**, 779 (1978).
7) P. Hobza and R. Zahradnik, "Weak Intermolecular Interactions in Chemistry and Biology," Elsevier, Amsterdam (1980).
8) L. E. Sutton, "Intermolecular Distances," The Chem. Soc., Spec. Publ., London (1965).
9) G. E. Schulz and R. H. Schirmer, "Principles of Protein Structure," Springer-Verlag, New York (1979).
10) a) J. DelBene and H. H. Jaffé, *J. Chem. Phys.*, **48**, 1807 (1968); b) G. Kuehnlenz and H. H. Jaffé, *ibid.*, **58**, 2238 (1973).
11) J. DelBene, H. H. Jaffé, R. L. Ellis and G. Kuehnlenz, "CNDOS-CI Molecular Orbital Calculations with the Complete Neglect of Differential Overlap and Configuration Interaction," Program No. 174, Quantum Chemistry Program Exchange, Indiana University, Bloomington, IN.
12) R. Fussenegger and B. M. Rode, *Chem. Phys. Lett.*, **44**, 95 (1976).
13) J. Mahanty and B. W. Ninham, "Dispersion Forces," Academic Press, London (1976).

Electron Spin Resonance Studies of Manganese(II) Doped in $Cd(NH_3)_2Ni(CN)_4 \cdot 2C_6H_6$. Angular and Temperature Dependency of Fine Structures

Taku NAKANO

Department of Pharmaceutical Sciences, Toyama Medical and Pharmaceutical University, Toyama 930-01

(Received April 30, 1981)

ESR measurements on Mn(II) ion doped in single crystals of $Cd(NH_3)_2Ni(CN)_4 \cdot 2C_6H_6$ confirmed the structure of the Hofmann-type clathrate predicted before. Spin Hamiltonian parameters obtained are $g=2.0033\pm 0.0010$, $A=(-84.9\pm1.0)\times10^{-4}$ cm^{-1} (123 K) and $(-84.3\pm1.0)\times10^{-4}$ cm^{-1} (room temp), $D=(67.5\pm1.0)\times10^{-4}$ cm^{-1} (123 K) and $(17.3\pm1.0)\times10^{-4}$ cm^{-1} (room temp), and $a=(16.5\pm1.0)\times10^{-4}$ cm^{-1}. The environment of Mn(II) ion has a tetragonally distorted cubic symmetry. While the parameter a is independent of temperature, the parameter D is found to be dependent on temperature obeying to $D\propto(T_0-T)^2$ where T_0 is 473 K. The nuclear forbidden lines, $\Delta m=\pm1$, were also detected, intensities of which vary in terms of D squared.

The series of Hofmann-type clathrates has the general formula of $M(NH_3)_2M'(CN)_4 \cdot 2G$, (M–M'–G), where M is a divalent metal ion such as Mn(II), Fe(II), Co(II), Ni(II), Cu(II), Zn(II), and Cd(II), and M' is Ni(II), Pd(II), or Pt(II).[1–3] G represents an aromatic molecule such as benzene (Bz), aniline *etc.* The inorganic part of the compound, $M(NH_3)_2M'(CN)_4$, forms a two-dimensional network which clathrate aromatic molecules between them as shown in Fig. 1.[4–6]

X-Ray crystallographic investigations have been reported in cases of Mn–Ni–Bz,[6] Ni–Ni–Bz,[4] Cu–Ni–Bz,[7] and Cd–Ni–Bz.[5] The compounds have an isomorphous structure with a space group of P4/m.

Magnetic properties of the clathrates have been reported for Mn–Ni–G,[8] Ni–Ni–G,[9] and Cu–Ni–G.[10] The ^{1}H NMR of ammonia molecules, which coordinate to metal ion M, is also reported in both diamagnetic[11] and paramagnetic[12,13] compounds. ESR study of copper(II) has shown the Jahn-Teller distortion around the copper(II) ion which reveals that d_{z^2} orbital is the ground state.[7,14,15]

The manganese(II) ion in Hofmann-type clathrate has a high spin d^5 structure and the orbital angular momentum is quenched. The purpose of this study is to clarify the behavior of the paramagnetic manganese(II) ion which will reflect the fundamental characters of Hofmann-type clathrates by means of ESR spectroscopy.

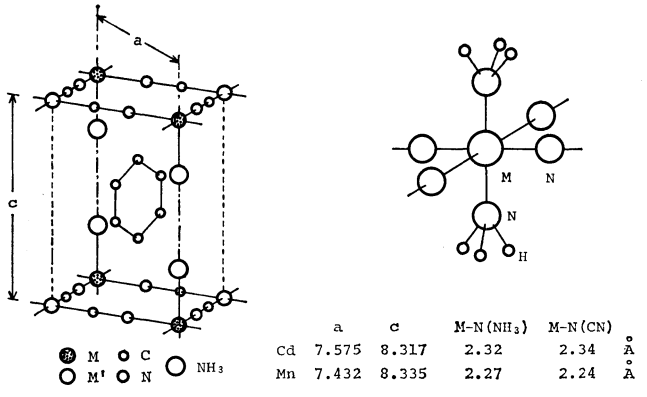

	a	c	M-N(NH$_3$)	M-N(CN)	
Cd	7.575	8.317	2.32	2.34	Å
Mn	7.432	8.335	2.27	2.24	Å

Fig. 1. The structure of Hofmann-type clathrates, $M(NH_3)_2M'(CN)_4 \cdot 2C_6H_6$.

Experimental

The single crystals of Cd–Ni–Bz which contain 0.1% of manganese(II) were prepared from an aqueous layer of an ammoniacal solution containing 1×10^{-2} mol dm^{-3} $Cd(NO_3)_2$, 1×10^{-5} mol dm^{-3} $MnCl_2$, 1×10^{-2} mol dm^{-3} $K_2Ni(CN)_4$, and 0.5 mol dm^{-3} NH_4Cl: pH adjusted to 8—9 using ammonia, and an organic layer of toluene containing benzene. The crystals grew at the interface between the aqueous and organic layers and on the bottom of the vessel. The dimension of the single crystal investigated in the present study is *ca.* $0.5\times0.5\times1.0$ mm^3 of the form of a square pillar, having ends in the form of pyramids.

The preparation of the crystals and the measurements of the ESR were done under a nitrogen atmosphere to prevent manganese(II) ions from being oxidized.

The ESR spectra were recorded using JES-FE-3X spectrometer at an X band frequency: 9.2 GHz, and a field modulation of 100 KHz and modulation widths of 0.4 mT. The field was calibrated with signals of manganese(II) doped in MgO. The crystal was rotated about the [001] and [110] axes and the temperature was varied with a stream of cold nitrogen, measured by a copper-constantan thermocouple.

Results and Discussion

The ESR spectra were recorded at various temperatures and at various angles, θ and φ; θ is the angle between the field and the [001] axis of the crystal and φ is that between the field in the (001) plane and [110] axis.

Figure 2 shows the ESR spectra recorded at various angles, θ, at 123 K. The spectral change when the magnetic field rotated about [001] axis at 123 K reveals the fourfold symmetry, on the other hand that about [110] axis reveals the twofold symmetry. The symmetry indicated above confirms the structure of the Hofmann-type clathrates.

It is reasonable to assume that the manganese(II) ions are located at the same positions as the cadmium(II) ions in Cd–Ni–Bz crystals. The X-ray crystallographic investigations have shown that the environment of manganese(II) in Mn–Ni–Bz[6] as well as that of cadmium(II) in Cd–Ni–Bz[5] has D_{4h} symmetry. The detailed structural parameters, the lattice con-

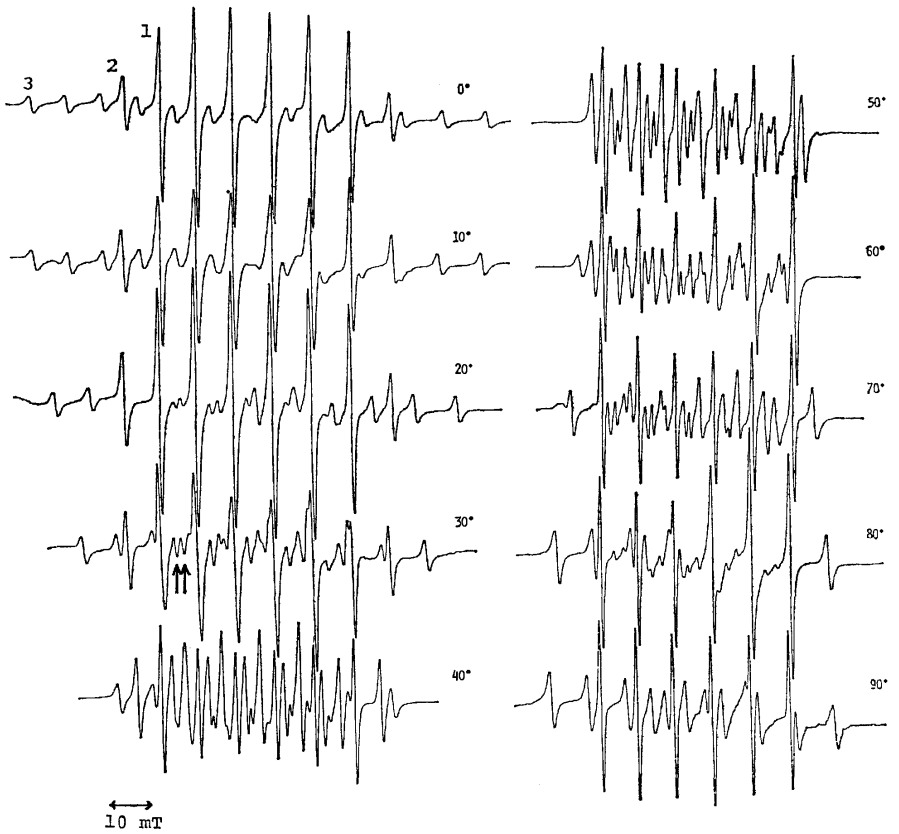

Fig. 2. ESR spectral change on angle θ at 123 K and $\varphi=0°$.
1: $|M,m>=|1/2,5/2>\leftrightarrow|-1/2,5/2>$, 2: $|M,m>=|1/2,5/2>\leftrightarrow|3/2,5/2>$, 3: $|M,m>=|3/2,5/2>\leftrightarrow|5/2,5/2>$. Arrows in the spectrum at $\theta=30°$ indicate the nuclear forbidden transitions: see text.

stants and the metal-nitrogen distances, are quoted in Fig. 1 to compare both compounds.[5,6]

The comparison of the metal-nitrogen distances has permitted us to assume the conservation of symmetry D_{4h} about manganese(II) ions doped in Cd-Ni-Bz. Thus the magnanese(II) ion was treated as having a nearly cubic but slightly tetragonally distorted structure of a weak crystalline field, and the assumption was revealed to be good.

The explanation of the spectra and the spectral changes can be made with a spin Hamiltonian of the form:

$$\mathcal{H} = \beta \boldsymbol{H}\cdot\boldsymbol{g}\cdot\boldsymbol{S} + D[S_z^2 - S(S+1)/3] + E(S_x^2 - S_y^2) + \frac{1}{6}a\left[S_x^4+S_y^4+S_z^4-\frac{1}{5}S(S+1)(3S^2+3S-1)\right] + \boldsymbol{S}\cdot\boldsymbol{A}\cdot\boldsymbol{I} - g_n\beta_n\boldsymbol{H}\cdot\boldsymbol{I}, \quad (1)$$

where D and E are axial and rhombic distortion parameters, respectively. The quantity a is a cubic parameter of the fourth order. Other symbols have their ordinary meanings.

The fields of the allowed transitions that are used for a high spin d^5 system of manganese(II) assuming the spin Hamiltonian (1) are calculated by the following equations:[16] it is also assumed that g and A are isotropic according to the results shown later.

$$M=\left|\pm\frac{5}{2}\right>\leftrightarrow\left|\pm\frac{3}{2}\right>:\ H = H_0 \mp 2\left(\frac{D}{g\beta}\right)(3\cos^2\theta-1) - \frac{32}{H_0}\left(\frac{D}{g\beta}\right)^2\cos^2\theta\sin^2\theta + \frac{1}{H_0}\left(\frac{D}{g\beta}\right)^2\sin^4\theta \mp 2p\left(\frac{a}{g\beta}\right) + f(M,m),$$

$$M=\left|\pm\frac{3}{2}\right>\leftrightarrow\left|\pm\frac{1}{2}\right>:\ H = H_0 \mp \left(\frac{D}{g\beta}\right)(3\cos^2\theta-1) + \frac{4}{H_0}\left(\frac{D}{g\beta}\right)^2\cos^2\theta\sin^2\theta - \frac{5}{4H_0}\left(\frac{D}{g\beta}\right)^2\sin^4\theta \pm \frac{5}{2}p\left(\frac{a}{g\beta}\right) + f(M,m),$$

$$M=\left|+\frac{1}{2}\right>\leftrightarrow\left|-\frac{1}{2}\right>:\ H = H_0 + \frac{16}{H_0}\left(\frac{D}{g\beta}\right)^2\cos^2\theta\sin^2\theta - \frac{2}{H_0}\left(\frac{D}{g\beta}\right)^2\sin^4\theta + f(M,m), \quad (2)$$

where M and m mean electron and nuclear(^{55}Mn) magnetic quantum numbers respectively, and $p=1-5(l^2m^2+m^2n^2+n^2l^2)$ and l, m, and n are direction cosines of the magnetic field with respect to the x, y, and z axes, respectively. The last terms correspond to a hyperfine splitting for the transition $|M>\leftrightarrow|M-1>$, $\Delta m=0$, to be expressed as;

$$f(M,m) = -\left(\frac{A}{g\beta}\right)m - \frac{1}{2H_0}\left(\frac{A}{g\beta}\right)^2\times\left[\frac{35}{4}-m^2+m(2M-1)\right]. \quad (3)$$

TABLE 1. SPIN HAMILTONIAN PARAMETERS

	Parameters	T/K
$g(g_{//}=g_{\perp})$	2.0033 ± 0.0010	
$A(A_{//}=A_{\perp})/cm^{-1}$	$(-84.9\pm1.0)\times10^{-4}$	123
	$(-84.3\pm1.0)\times10^{-4}$	room
D/cm^{-1}	$(67.5\pm1.0)\times10^{-4}$	123
	$(17.3\pm1.0)\times10^{-4}$	room
E/cm^{-1}	0	
a/cm^{-1}	$(16.5\pm1.0)\times10^{-4}$	

In Fig. 2, the most intense sextet is assigned to be $|-1/2>\leftrightarrow|1/2>$ transition, the middle ones are $|\pm1/2>\leftrightarrow|\pm3/2>$ transitions and the weakest are $|\pm3/2>\leftrightarrow|\pm5/2>$ transitions.

The Hamiltonian parameters were obtained from the spectra both at room temperature and at 123 K and are listed in Table 1. The shifts of signal positions *versus* angle θ arise from D and a terms and those *versus* φ only from a term. The g value and the hyperfine constant A are isotropic namely $g=g_{//}=g_{\perp}$ and $A=A_{//}=A_{\perp}$ within the experimental error.

The absolute signs of the parameters were determined by considering the angular dependency of the signal positions according to Eqs. 2 and 3, where the second order approximation was dealt with. If $D\cdot A<0$, for the sextet of the transition of $M>0$, the splitting caused by Eq. 3 is smaller, and the position at $\theta=0°$ is at a lower field than that of $M<0$ or *vice versa*. This is the case. The change of the signal positions on angle θ make it clear that the parameters D and a have the same sign. When A is assumed to be negative, as general, the sign of a is positive being consistent with Watanabe's theory.[17] The signs of the parameters thus obtained are shown in Table 1. Other sets of signs do not explain the change of the signal positions.

The thirty angular dependence curves calculated according to Eq. 2 using the parameter values in Table 1 are in a good agreement with the experimental results shown in Figs. 3 and 4, where the assignments are indicated.

Temperature Dependency of the Fine Structures. As reported in many cases of manganese(II) ESR, the parameter D has non-zero values also in the Hofmann-type clathrate, though g and A are isotropic. Here, it is noteworthy that the D value is dependent on temperature. The changes of the signal positions due to temperature are shown in Fig. 5 in the temperature region from 123 to 433 K. Above room temperature the signals were irreversibly broadened because of an escape of benzene molecules from the surface of the crystal.

While the signal positions of the sextet $M=|1/2>\leftrightarrow|-1/2>$ do not vary with temperature, those of the sextets $M=|\pm1/2>\leftrightarrow|\pm3/2>$ and $M=|\pm3/2>\leftrightarrow|\pm5/2>$ shift outwards with decreasing temperature. The values of the parameters D and a are plotted in Fig. 6.

As shown clearly in Fig. 6, the cubic parameter a is independent of temperature. Since the parameter a relates closely with the strength of the cubic crystalline field parameter Dq, as indicated by Watanabe,[17] the constancy of the parameter a suggests that the crystalline field does not vary as the results of the structural change around manganese(II) ions in the temperature region studied here.

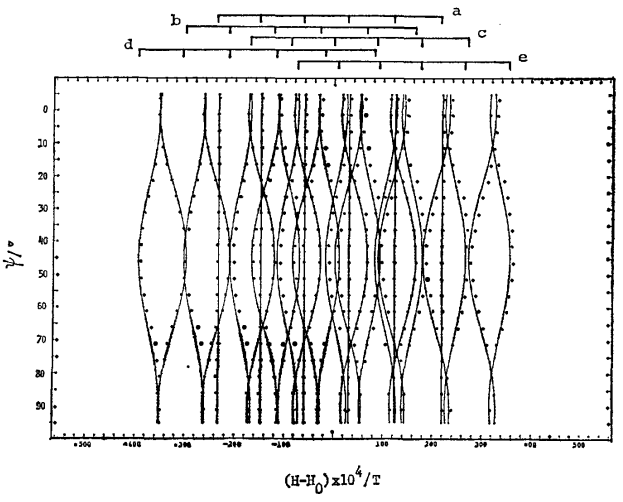

Fig. 3. Angular dependence of ESR signals on angle φ at $\theta=90°$.
$H_0=3274\times10^{-4}$ T. Dots are the experimental results and the solid lines are calculated curves using the parameter values at 123 K in Table 1. The signal positions are assigned at $\varphi=45°$. a: $|M>=|1/2>\leftrightarrow|-1/2>$, b: $|M>=|-1/2>\leftrightarrow|-3/2>$, c: $|M>=|1/2>\leftrightarrow|3/2>$, d: $|M>=|-3/2>\leftrightarrow|-5/2>$, e: $|M>=|3/2>\leftrightarrow|5/2>$. As for m, the lowest is assigned to be $m=-5/2$ and the highest 5/2 for all five sextets.

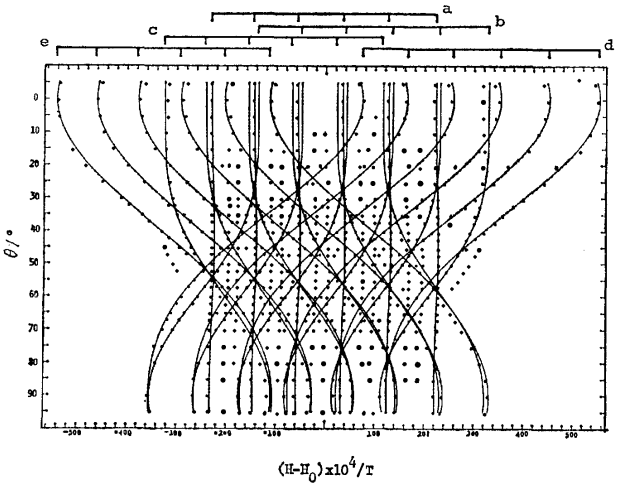

Fig. 4. Angular dependence of ESR signals on angle θ at $\varphi=0°$.
$H_0=3274\times10^{-4}$ T. Dots are the experimental results and the solid lines are calculated curves using the parameter values at 123 K in Table 1. The signal positions are assigned at $\theta=0°$. a: $|M>=|1/2>\leftrightarrow|-1/2>$, b: $|M>=|-1/2>\leftrightarrow|-3/2>$, c: $|M>=|1/2>\leftrightarrow|3/2>$, d: $|M>=|-3/2>\leftrightarrow|-5/2>$, e: $|M>=|3/2>\leftrightarrow|5/2>$. As for m, the lowest is assigned to be $m=-5/2$ and the highest 5/2 for all five sextets.

According to Watanabe,[17] the crystalline field parameter Dq is estimated to be 1407 cm^{-1}. Unfortunately the spectroscopic data was not available for comparison with the theoretical value in this stage.

On the other hand, the parameter D increases with decreasing temperature as shown in Figs. 6 and 7. In Fig. 7 the square root of D is plotted and has a linear relation to temperature. Thus the temperature dependency of D was found experimentally to be

$$D(T) = k(T_0 - T)^2, \quad (4)$$

where T is the absolute temperature and T_0 and k were found to be 473 K and $5.2_7 \times 10^{-8}$ cm^{-1} K^{-2} respectively.

The temperature dependence of D has been found for example in cases of nickel(II) ESR in $NiSnCl_6 \cdot 6H_2O$,[18] and $NiSiF_6 \cdot 6H_2O$,[19] manganese(II) ESR in K_2SO_4,[20] and iron(III) ESR in $BaTiO_3$;[21] in the latter two cases the changes of D are attended on phase transitions. However the clear elucidation of these phenomena has not been given until now. In the case of manganese(II) in the Hofmann-type clathrate, any structural change has not been reported in the temperature region studied here and moreover the invariability of the parameter a does not suggest any phase transitions. Though the reason for the temperature dependency cannot be elucidated in this stage, this phenomenum would add a new characteristic feature on the Hofmann-type clathrates. Further investigation of the structure will be necessary.

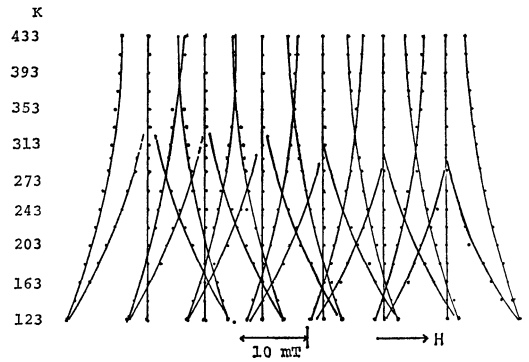

Fig. 5. Temperature dependence of the ESR signals at $\theta=90°$ and $\varphi=0°$.

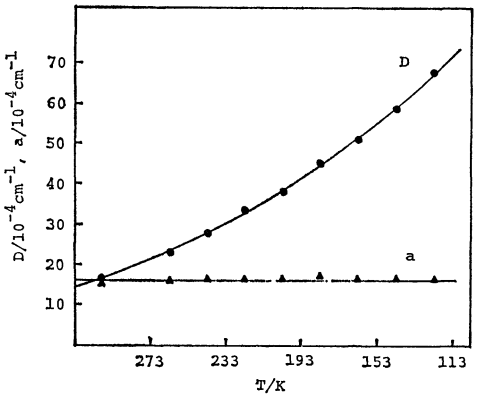

Fig. 6. Relations between D and a parameters and temperature.

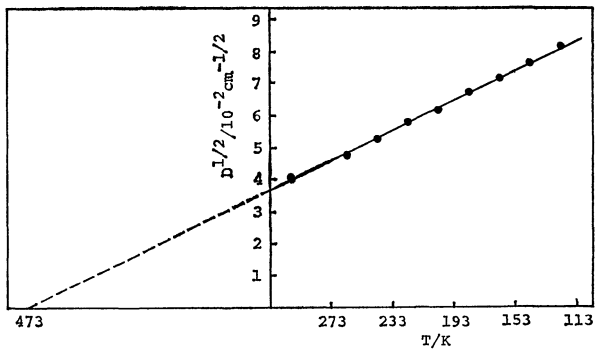

Fig. 7. Temperature dependence of D parameter.

The Nuclear Forbidden Lines. The arrows in the spectra in Figs. 2 and 8 indicate the nuclear forbidden lines, $\Delta m = \pm 1$. The intensities of these lines found here do change with temperature. The number of theoretically predicted forbidden lines is thirty, but in this case we could find the relatively intense five doublets that appear among the sextet of allowed transitions $|1/2> \leftrightarrow |-1/2>$, and others that are barely recognizable outside the intensive allowed signals near $\theta=50°$. In Fig. 4, the dots aside from the solid lines mark the positions of the forbidden lines.

The forbidden lines appear when the magnetic field

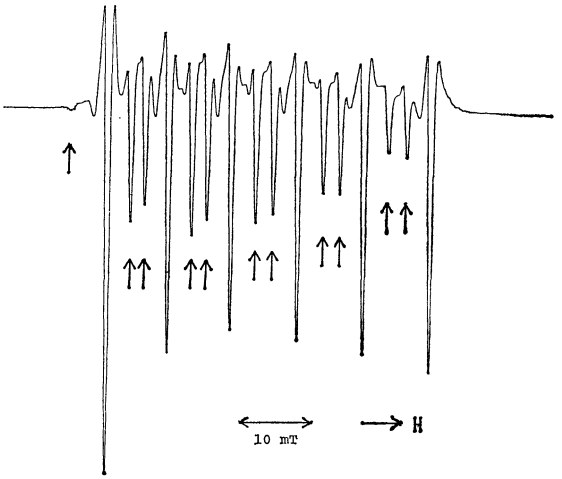

Fig. 8. Nuclear forbidden lines at $\theta=55°$ and $\varphi=0°$, and at 113 K. The spectrum is a second derivative curve. Five doublets are assigned to be $M=|1/2> - |-1/2>$, $\Delta m=\pm 1$, and the arrow at the lowest field indicates the one not assigned.

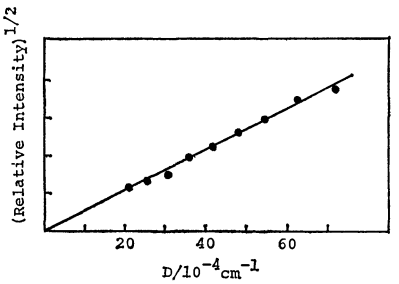

Fig. 9. Relation between D and intensity of the forbidden lines: $\Delta M=\pm 1$ and $\Delta m=\pm 1$.

is rotated about the [110] axis, disappearing at $\theta=0°$ and 90°, and not observed when the field is rotated about the [001] axis. The signals have maximum intensities near $\theta=55°$. Unfortunately the precise determination of the change of intensity with rotation was impossible since the strong signals of the allowed transitions superimpose on the forbidden lines.

The relative intensity increases with decreasing temperature, suggesting that it is related closely with the D value. Figure 9 shows the relation between the intensity of one of the pairs of the doublets and the axial parameter D at $\theta=55°$, at which angle the forbidden lines clearly appear separated from the allowed transitions. The intensity is proportional to D^2;

$$I(1/2) = k(\theta)D^2, \quad (5)$$

where $I(1/2)$ is the intensity of the forbidden line $M=|1/2>\leftrightarrow|-1/2>$, and $k(\theta)$ is a function of angle θ.

The intensity of the forbidden lines will vary as $A\cdot D^2(\sin 2\theta)^2+B\cdot a^2(\sin 4\theta)^2$, when the parameters D and a have non-zero values.[22,23] However the relation revealed in this compound between the intensity and the parameter D suggests that the mixing of the energy states may arise from the second order perturbation only with the D term, and those with the a term would be too small to be detected here.

The positions of the forbidden lines $M=|1/2>\leftrightarrow|-1/2>$ and the separations of the doublets were independent of temperature. The separations of doublets obtained experimentally are 18.7, 20.6, 23.4, 23.4, and 25.3×10^{-4} cm^{-1} for $m=|-5/2>\leftrightarrow|-3/2>$, $m=|-3/2>\leftrightarrow|-1/2>$, $m=|-1/2>\leftrightarrow|+1/2>$, $m=|1/2>\leftrightarrow|3/2>$, and $m=|3/2>\leftrightarrow|5/2>$, respectively. The calculated values according to Bleaney and Rubins[22] are 18.8, 20.7, 22.3, 23.9, and 25.8×10^{-4} cm^{-1}, respectively. The detailed work about the seperation will give the precise values of g_n and Q (quadrapole moment) of ^{55}Mn.

Conclusion

From the parameter values obtained, manganese(II) ion has a g value which is almost the same as that of a free electron, and slightly tetragonally distorted cubic symmetry, D_{4h}. It is noteworthy that the axial parameter D is dependent on the temperature. This suggests a new characteristic feature in this compound, while the cubic parameter a does not change. The forbidden transitions arise from the D term and are also dependent on temperature.

The work was supported by a Grant-in-Aid for Scientific Research No. 474265 from the Ministry of Education, Science and Culture.

References

1) T. Nakano, T. Miyoshi, T. Iwamoto, and Y. Sasaki, *Bull. Chem. Soc. Jpn.*, **40** 1297 (1967).
2) M. Morita, T. Miyoshi, T. Iwamoto, T. Miyamoto, and Y. Sasaki, *Bull. Chem. Soc. Jpn.*, **40** 1556 (1967).
3) T. Iwamoto, T. Nakano, M. Morita, T. Miyoshi, T. Miyamoto, and Y. Sasaki, *Inorg. Chim. Acta*, **2**, 313 (1968).
4) J. H. Rayner and H. M. Powell, *J. Chem. Soc.*, **1959**, 319.
5) Y. Sasaki, *Bull. Chem. Soc. Jpn.*, **42**, 2412 (1969).
6) R. Kuroda and Y. Sasaki, *Acta Crystallogr., Sect. B*, **30**, 687 (1974).
7) T. Miyoshi, T. Iwamoto, and Y. Sasaki, *Inorg. Chim. Acta*, **7**, 97 (1973).
8) H. Kitaguchi, S. Nagata, and T. Watanabe, *J. Phys. Soc. Jpn.*, **41**, 1159 (1976).
9) S. Takayanagi and T. Watanabe, *J. Phys. Soc. Jpn.*, **28**, 296 (1970).
10) H. Kitaguchi, S. Nagata, and T. Watanabe, *J. Phys. Soc. Jpn.*, **38**, 998 (1975).
11) T. Miyamoto, *Inorg. Chim. Acta*, **3**, 511 (1969).
12) T. Nakano, *Bull. Chem. Soc. Jpn.*, **46**, 2124 (1973).
13) S. Takayanagi and T. Watanabe, *J. Phys. Soc. Jpn.*, **31**, 109 (1971).
14) R. Murugesan and S. Subramanian, *J. Magn. Reson.*, **36**, 389 (1979).
15) S. Nagata, Y. Miyako, and T. Watanabe, *J. Phys. Soc. Jpn.*, **34**, 1158 (1973).
16) B. Bleaney and D. J. E. Ingram, *Proc. R. Soc. London, Ser. A*, **205**, 336 (1951).
17) H. Watanabe, *Prog. Theor. Phys.*, **18**, 405 (1957).
18) Y. Ajiro, S. A. Friedberg, and N. S. VanderVen, *Phys. Rev. B*, **12**, 39 (1975).
19) R. P. Penrose and K. W. H. Stevens, *Proc. Phys. Soc. London*, **A63**, 29 (1950).
20) B. V. R. Chowdari and P. Venkateswarlu, *J. Chem. Phys.*, **48**, 318 (1968).
21) A. W. Hornig, R. C. Rempel, and H. E. Weaver, *J. Phys. Chem. Solids*, **10**, 1 (1959).
22) B. Bleaney and R. S. Rubins, *Proc. Phys. Soc. London*, **77**, 103 (1961).
23) J. E. Drumheller and R. S. Rubins, *Phys. Rev. A*, **133**, 1099 (1964).

© 1982 The Chemical Society of Japan

NOTES

Bull. Chem. Soc. Jpn., 55, 1637—1638 (1982)

Pyrene-cation Formation on Reactions of Pyrene Triplet State with Metal Ions in Caffeine-solubilized Aqueous Solution

Yoshio NOSAKA,* Akira KIRA, and Masashi IMAMURA

The Institute of Physical and Chemical Research, Wako, Saitama 351

(Received August 7, 1981)

Synopsis. Quenching of triplet states of pyrene and other aromatic hydrocarbons by metal ions in caffeine-solubilized aqueous solution was investigated. The concomitant formation of aromatic cations was observed on quenching of triplet pyrene by Hg^{2+} and Fe^{3+} and triplet phenanthrene and benz[*a*]anthracene by Hg^{2+}.

To the reactions between excited states of aromatic hydrocarbons and metal ions have been paid attention from the viewpoint of their application to solar energy conversion based on the photo-induced electron transfer reactions. However, such charge separation with metal ions was known only for the triplet states of thiazine dyes.[1-4] Recently, we have reported reduction of metal ions with the excited singlet state of pyrene solubilized in aqueous solution of caffeine.[5] The experiments performed in aqueous solution are of greater advantage than those in organic solvents in regard to dissolving various metal ions. In the present paper, we report a study on quenching of triplet states of pyrene and other aromatic hydrocarbons by metal ions in caffeine-solubilized aqueous solution. The results indicate that electron transfer occurs from the triplet state of pyrene to Hg^{2+} and Fe^{3+} whose reduction potentials are rather low. Other metal ions were not reduced, although they quenched the triplet state of pyrene to a certain extent.

The apparatus using a frequency doubled Q-switched ruby laser and experimental procedures have been described in the previous paper.[5] Figure 1 exhibits oscilloscope profiles representing the decay of the pyrene triplet state and concomitant growth of pyrene cations on quenching by Hg^{2+}. The assignment of the growing species to the pyrene cation was based on its absorption spectrum.[6] The concentrations of pyrene cations and pyrene triplet states were estimated from the absorbances at 450 and 414 nm using reported values of extinction coefficient.[7,8] The yields of the cation originating in the excited singlet state, which also contribute to the observed cation yields in the time region of Fig. 1, were given in the previous report.[5]

The bimolecular rate constant for triplet-quenching (k_q) was obtained from the observed pseudo-first-order rate constants;

$$k_{obsd} = k_o + k_q[M^{n+}],$$

where $[M^{n+}]$ is the concentration of metal ions. The reaction of the triplet state (^3P) with metal ions is expressed by Reactions 1 and 2.

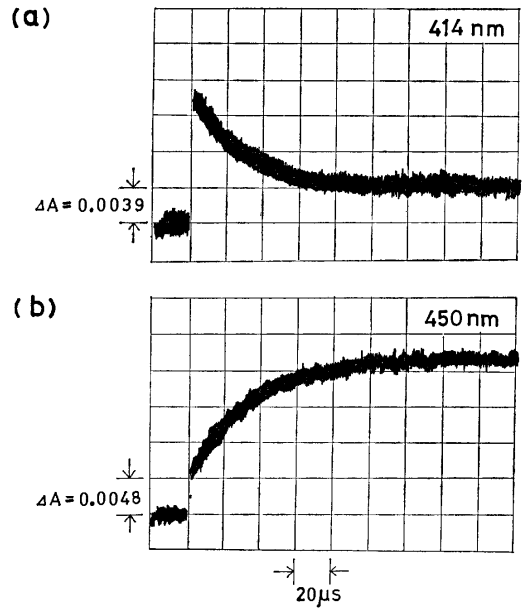

Fig. 1. Oscilloscope traces after laser excitation observed at 414 and 450 nm, which correspond to absorption peaks for pyrene triplet state and pyrene cation, respectively. [Pyrene]=0.04 mM, [Hg$(NO_3)_2$]=1.0 mM, and [caffeine]=60 mM.

$$^3P + M^{n+} \xrightarrow{k_{1q}} P + M^{n+}, \quad (1)$$

$$^3P + M^{n+} \xrightarrow{k_{2q}} P^+ + M^{(n-1)+}, \quad (2)$$

for which

$$k_q = k_{1q} + k_{2q}.$$

Quenching rate constants k_q measured for the reactions of the triplet state of pyrene with some metal ions and for the reactions of the triplet states of phenanthrene (^{3}Phe) and benz[*a*]anthracene (^{3}BA) with Hg^{2+} are shown in Fig. 2 as a function of the free-energy change (ΔG°)[5,9] of the charge transfer reaction (Eq. 2). For Eu^{3+}, Zn^{2+}, Cd^{2+}, Tl^+, and Tb^{3+}, the experimental values for k_q were less than 10^6 M^{-1} s^{-1}. Rate constants for pyrene fluorescence quenching as well as a theoretical curve which has been discussed in the previous report[5] are also shown in Fig. 2. The theoretical curve implies that electron transfer occurs with an activation energy of 0.75 eV in the case of $\Delta G^\circ = 0$ eV.[9]

The fraction of charge transfer, which is expressed by the ratio of the rate constants, k_{2q}/k_q, is calculated as the ratio of an increment of the pyrene cations to a decrement of the triplet state in the quenching process. The charge transfer fractions were more than 0.9 for Hg^{2+} and Fe^{3+}, and less than 0.1 for Cu^{2+},

* Present address: Department of Materials Science and Technology, The Technological University of Nagaoka, Nagaoka, Niigata 949-54.

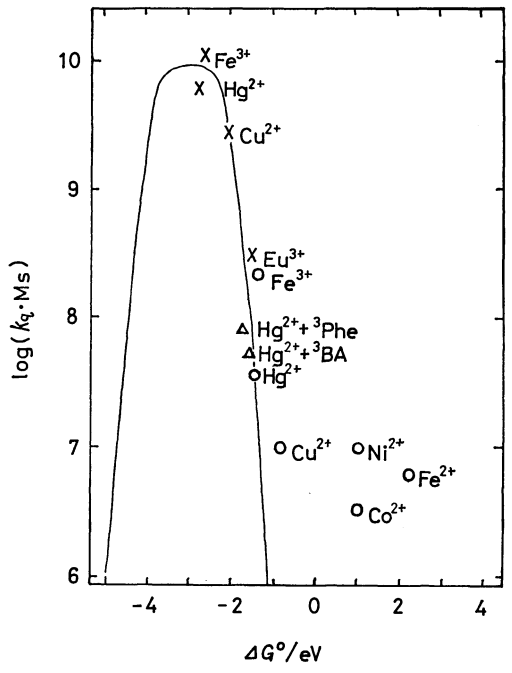

Fig. 2. Plot of log k_q as a function of the free energy change($\Delta G°$) for electron transfer reaction from excited states of pyrene to metal ions. Open circles and crosses show the reaction rates for triplet state and excited singlet state[5] of pyrene, respectively. ^{3}Phe and ^{3}BA are triplet states of phenanthrene and benz[*a*]anthracene.

Ni^{2+}, Fe^{2+}, and Co^{2+}. For metal ions by which hydrocarbon cations were formed, the experimental points for triplet excited states are located on the theoretical curve presented for singlet excitated states.[5] For the other metal ions, the experimental points are not located on the curve but above it, indicating existence of some efficient quenching mechanisms other than the electron transfer mechanism. The mechanism presented previously[5] for triplet state formation on fluorescence quenching may also be applicable to the mechanism of singlet state formation on phosphorescence quenching in this case. Further experiments for various metal ions will afford much information concerning the quenching mechanism which is applicable to both singlet and triplet excited states.

References

1) S. A. Alkaitis, R. Beck, and M. Grätzel, *J. Am. Chem. Soc.*, **97**, 5723 (1975).
2) Y. Moroi, A. M. Braun, and M. Grätzel, *J. Am. Chem. Soc.*, **101**, 567 (1979).
3) E. Pelizzetti and E. Pramauro, *Ber. Bunsenges. Phys. Chem.*, **83**, 996 (1979).
4) T. Ohno and N. N. Lichtin, *J. Am. Chem. Soc.*, **102**, 4636 (1980).
5) Y. Nosaka, A. Kira, and M. Imamura, *J. Phys. Chem.*, **85**, 1353 (1981).
6) T. Shida and S. Iwata, *J. Am. Chem. Soc.*, **95**, 3473 (1973).
7) G. E. Hall and G. A. Kenny-Wallace, *Chem. Phys.*, **32**, 313 (1978).
8) W. Heinzelmann and H. Labhart, *Chem. Phys. Lett.*, **4**, 20 (1969).
9) D. Rehm and A. Weller, *Isr. J. Chem.*, **8**, 259 (1970).

Solvent Effect on the Nonradiative Deactivation of the Excited State of Tris(2,2'-bipyridyl)ruthenium(II) Ion

Katsumi NAKAMARU

Department of Chemistry, Faculty of Science, Hirosaki University, Bunkyo, Hirosaki, Aomori 036

(Received September 21, 1981)

Synopsis. Emission quantum yields and lifetimes of the $[Ru(bpy)_3]^{2+}$ ion were measured in various solvents at 25 °C. Nonradiative rate constants (k_{nr}) were calculated from these data. A plot of k_{nr} *vs.* the Gutmann's acceptor number was found to be linear. This result can be explained in terms of the contributions of charge transfer to solvent (CTTS).

The well-known luminescence of the tris(2,2'-bipyridyl)ruthenium(II) ion, $[Ru(bpy)_3]^{2+}$, has been extensively studied. It has been generally accepted that the luminescence at 77 K arises from a charge transfer to ligand (CTTL) excited state.[1] Houten and Watts,[2,3] however, studied effects of ligand and solvent deuteration on the luminescence quantum yields and lifetimes in aqueous solution between 0 and 100 °C. They concluded that in this temperature range charge transfer to solvent (CTTS) configurations contribute to the luminescence in addition to the CTTL configuration. This conclusion suggests that complex-solvent interactions in fluid solutions are important in the deactivation processes of the CTTL excited state. So it is surprising that there have been few photophysical and systematic studies of the $[Ru(bpy)_3]^{2+}$ complex in organic solvents. In this paper the author reports the emission quantum yields and lifetimes measured in various solvents and also some information on the contributions of CTTS to the nonradiative deactivation of the CTTL excited state.

Experimental

Tris(2,2'-bipyridyl)ruthenium(II) chloride pentahydrate, $[Ru(bpy)_3]Cl_2 \cdot 5H_2O$, was prepared according to the method described in the literature.[4] Found: C, 48.88; H, 4.51; N, 11.67%. Calcd for $C_{30}H_{34}O_5N_6RuCl_2$: C, 49.32; H, 4.69; N, 11.50%. All solvents were reagent grade and used without further purification. Absorption and emission spectra were measured with a Hitachi 124 double-beam spectrophotometer and a Hitachi MPF-4 fluorescence spectrophotometer, respectively. Emission quantum yields were determined at the excitation wavelength of 436 nm by the modified Parker and Rees method[5] using fluorescein purified by the reported procedures[6] in 0.1 mol dm^{-3} NaOH (yield, 0.90) or $[Ru(bpy)_3]Cl_2$ in aerated aqueous solution (yield, 0.028[7]) as the standards. Lifetimes were measured using an apparatus with a pulsed nitrogen laser as the exciting light source. All samples were prepared immediately prior to use and the complex solutions were nitrogen-saturated for 15—20 min. All measurements were carried out at 25 °C.

Results and Discussion

The absorption maxima in the visible CTTL band of the $[Ru(bpy)_3]^{2+}$ ion show only slighter shifts than the emission maxima upon changes of solvents (Table 1). However, the efforts to relate the tendency in the spectral shifts with solvent parameters such as dielectric constants were unsuccessful, although it was seen that both absorption and emission spectra shifted to red in alcohols having a longer carbon-carbon bond chains. The latter observation has been reported by Meisel *et al.*[8]

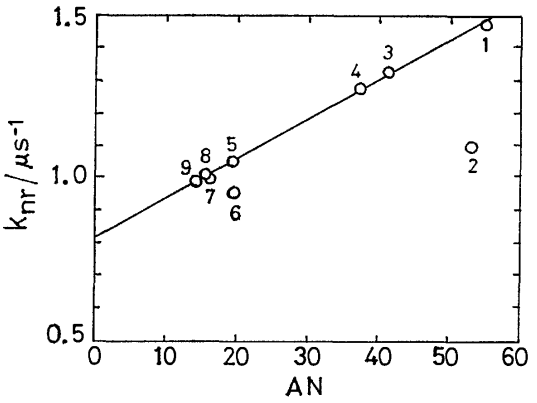

Fig. 1. Plot of k_{nr} *vs.* acceptor number(AN) for $[Ru(bpy)_3]Cl_2$ in various solvents at 25 °C. Solvent: 1, water; 2, acetic acid; 3, methanol; 4, ethanol; 5, acetonitrile; 6, dimethyl sulfoxide; 7, *N*,*N*-dimethylformamide; 8, benzonitrile; 9, pyridine.

The results of the emission quantum yields listed in Table 1 may be explained this way. If CTTS actually contributes to the CTTL excited state, it may safely be said that the higher electron-attractive power a solvent has (that is, the more electrophilic a solvent is), the more easily the charge transfers to the solvent. Such a state is unlikely to be stable and thus would lead to a fast nonradiative deactivation. Taking account of the fact that the so-called Gutmann's acceptor number[9] adequately fits the solvent properties described above, the nonradiative rate constant for the CTTS deactivation, k_{CTTS}, can be considered to be proportional to the acceptor number (AN). Hence the following expression:

$$k_{nr} = k^{\circ}_{nr} + k_{CTTS} = k^{\circ}_{nr} + k'[AN],$$

can be derived, where k_{nr}, k°_{nr}, and k' denote the total nonradiative rate constant, the nonradiative rate constant independent of CTTS, and a rate constant dependent on AN, respectively. The value of k_{nr} can be calculated from the emission quantum yields (Q) and measured lifetimes (τ_m) by the equation, $k_{nr}=\tau_m^{-1}-k_r$, where k_r is the radiative rate constant calculated from Q/τ_m. The results are also tabulated in Table 1. The plot of k_{nr} *vs.* the acceptor number, AN, is illustrated in Fig. 1, which clearly shows a linear dependence of k_{nr} on AN with a slope of 0.012

Table 1. Absorption and emission spectral data, emission quantum yields, lifetimes, and solvent parameters for $[Ru(bpy)_3]Cl_2$ in various solvents at 25 °C

Solvent	Ab[a] λ_{max}/nm	Em[b] λ_{max}/nm	Q[c]	$\frac{\tau_m}{\mu s}$[d]	$\frac{k_{nr}}{\mu s^{-1}}$	AN	Dielectric constant[e]	R/%[f]
Methanol	449	609	0.045±0.002	0.72±0.03	1.33	41.3	32.6	38
Acetonitrile	450	611	0.059±0.002	0.89±0.03	1.06	19.3	38.0	23
Ethanol	450	608	0.052±0.004	0.74±0.02	1.28	37.1	24.3	36
Acetic anhydride	451	611	0.075±0.003				20.7	
Acetic acid	451	619	0.065±0.003	0.85±0.05	1.10	52.9	6.13	26
Ethylene glycol	452	611	0.070±0.003				40.75	
Water	452	628	0.042±0.002	0.65±0.02	1.47	54.8	78.3	45
1-Pentanol	452	610	0.059±0.003				13.9	
DMF[g]	453	628	0.068±0.006	0.93±0.04	1.00	16.0	36.1	18
Benzyl alcohol	454	610	0.078±0.002				13.1	
1-Octanol	454	628	0.061±0.002				10.34	
1-Decanol	454	630	0.056±0.002					
Pyridine	454	619	0.087±0.003	0.92±0.05	0.99	14.2	12.3	18
DMSO[h]	454	630	0.077±0.005	0.96±0.02	0.96	19.3	46.6	15
Benzonitrile	454	609	0.073±0.002	0.92±0.02	1.01	15.5	25.2	19

a) Absorption maxima. b) Emission maxima. c) Excited at 436 nm. d) Excited at 337 nm. e) Ref. 10. f) See text. g) *N,N*-Dimethylformamide. h) Dimethyl sulfoxide.

μs^{-1} except in the case of the acidic solvent, acetic acid. Using the value of the intercept, 0.82 μs^{-1} (= k_{nr}°), the percentages, R, for the contributions of CTTS to the total nonradiative rate constant can be evaluated (Table 1). As was expected, in a solvent with a large acceptor number such as water, about half of the CTTL excited state of the $[Ru(bpy)_3]^{2+}$ ion deactivate through the contributions of CTTS, whereas in solvents such as *N,N*-dimethylformamide, benzonitrile, and pyridine the percentages are only about 20%. Unfortunately the experiments in other solvents could not be carried out because of the solubility problem or the lack of the knowledge of the acceptor number, but the general features obtained in this work seem to be unchanged.

The author wishes to thank Associate Professor Hiroshi Kokubun and Dr. Koichi Kikuchi of Tohoku University for their kindness in allowing use of their apparatus for lifetime measurements.

References

1) J. N. Demas and G. A. Crosby, *J. Am. Chem. Soc.*, **93**, 2841 (1971).
2) J. Van Houten and R. J. Watts, *J. Am. Chem. Soc.*, **97**, 3843 (1975).
3) J. Van Houten and R. J. Watts, *J. Am. Chem. Soc.*, **98**, 4853 (1976).
4) I. Fujita and H. Kobayashi, *J. Chem. Phys.*, **59**, 2902 (1973).
5) C. A. Parker and W. T. Rees, *Analyst (London)*, **85**, 587 (1960).
6) W. R. Orndorff and A. J. Hemmer, *J. Am. Chem. Soc.*, **49**, 1272 (1927).
7) K. Nakamaru, K. Nishio, and H. Nobe, *Sci. Rep. Hirosaki Univ.*, **26**, 57 (1979).
8) D. Meisel, M. S. Matheson, and J. Rabani, *J. Am. Chem. Soc.*, **100**, 117 (1978).
9) V. Gutmann, *Electrochim. Acta*, **21**, 661 (1976).
10) "Lange's Handbook of Chemistry," 11th ed, ed by J. A. Dean, McGraw-Hill, New York (1973), Sect. 10.

Apparent Molar Volumes of Water in Methanol and Tetrahydrofuran at 298.15 K

Masao SAKURAI* and Tsurutaro NAKAGAWA

Department of Polymer Science, Faculty of Science, Hokkaido University, Sapporo 060

(Received October 7, 1981)

Synopsis. The densities of water–methanol(MeOH) and water–tetrahydrofuran(THF) mixtures have been measured at 298.15 K. The apparent molar volumes of water, $V_{\phi,w}$, have been derived as a function of concentration. The values of $V_{\phi,w}$ in MeOH increase monotonously with the concentration, while for THF solutions the $V_{\phi,w}$ curve passes through a minimum at low mole fraction of water. These are interpreted in terms of the formation of water–organic solvent and water–water hydrogen bonding.

Previously, we have reported that the apparent molar volumes of water, $V_{\phi,w}$, are almost independent of the concentration in very dilute solutions of water in benzene and in methanol.[1] In this paper we will report the density data for water–methanol(MeOH) and water–tetrahydrofuran (THF) mixtures over a wide range of concentration, and will compare the results with those reported by Benson and his coworkers.[2-4]

Experimental

The MeOH and THF were dried over anhydrous calcium sulfate and then fractionally distilled. The water was deionized and distilled using a quartz still. The mole fractions of water, X_w, of the mixtures in the organic solvent-rich region (*ca.* $X_w<0.1$) were determined with an automatic Karl Fischer titration apparatus (Hiramuma, AQ-3). In most cases the error in the mole fraction was estimated to be less than 1×10^{-4}. The densities, ρ, of the mixtures relative to pure water at 298.15 K were determined with an oscillating tube densimeter (Paar, DMA 60/601). The density of water was taken as 0.997045 g cm^{-3}.[5] Details of the apparatus and its operating procedure have been described previously.[1]

Results and Discussion

The experimental results are summarized in Table 1. The apparent molar volume of water is given by:

$$V_{\phi,w} = (\rho^*-\rho)/c\rho^* + M_w/\rho^*, \quad (1)$$

where ρ^* is the density of pure solvent, c is molar concentration, and M_w is the molar mass of water. Since we could not obtain any sample of solvents completely free from water, the value of ρ^* was estimated by the extrapolation of the solution densities to $c=0$, as will be described below.

For dilute solutions the apparent molar volume of nonelectrolytes can be represented in terms of molarity:

$$V_\phi = V^\infty + b_v c, \quad (2)$$

where V^∞ is partial molar volume at infinite dilution. From Eqs. 1 and 2, the density of the solution is given by:

$$\rho = \rho^* + (M_w-\rho^*V_w^\infty)c-\rho^*b_v c^2. \quad (3)$$

Table 1. Densities of the MeOH and THF solutions of water at 298.15 K

X_w	ρ / g cm^{-3}	X_w	ρ / g cm^{-3}
	MeOH solutions		
0.0169	0.789234	0.0903	0.801739
0.0208	0.789857	0.0953	0.802677
0.0247	0.790546	0.1074	0.804863
0.0256	0.790677	0.1077	0.804816
0.0303	0.791498	0.1305	0.808860
0.0339	0.792131	0.1347	0.809728
0.0415	0.793381	0.1487	0.812227
0.0433	0.793734	0.1827	0.818221
0.0487	0.794575	0.2545	0.831852
0.0488	0.794555	0.3565	0.851527
0.0556	0.795801	0.5142	0.884120
0.0574	0.796085	0.5963	0.901940
0.0676	0.797883	0.6975	0.924446
0.0770	0.799434	0.7917	0.945453
0.0875	0.801317		
	THF solutions		
0.0019	0.882014	0.0343	0.883377
0.0036	0.882077	0.0426	0.883783
0.0040	0.882109	0.0930	0.886363
0.0057	0.882174	0.1363	0.888838
0.0070	0.882220	0.1426	0.889158
0.0097	0.882325	0.1753	0.891182
0.0108	0.882363	0.2363	0.895218
0.0111	0.882374	0.2606	0.896978
0.0157	0.882568	0.3077	0.900397
0.0189	0.882690	0.3467	0.903528
0.0254	0.882982	0.5623	0.924206

Table 2. Densities[a] and partial molar volumes for the MeOH and THF solutions of water at 298.15 K

	ρ^* / g cm^{-3}	V_w^∞ / cm^3 mol^{-1}	b_v / cm^3 dm^3 mol^{-2}
MeOH[b]	0.786427	14.42	0
THF	0.881950	17.00	−0.8

a) Values of ρ^*/g cm^{-3} from the literature are: 0.786350,[4] 0.78660,[6] 0.78636,[7] 0.78686[8] for pure MeOH; 0.88195,[2] 0.881968,[3] 0.88194[9] for pure THF. b) Ref. 1.

Previously we have found that the densities of MeOH solutions of water increase linearly with the molarity in the concentration range less than about 0.7 mol dm^{-3} ($X_w<0.027$), that is, $b_v\simeq0$.[1] On the other hand, no linearity was found for the THF solutions. In Table 2 are given the values of ρ^*, V_w^∞, and b_v determined by the method of least squares in the concentration range less than about 0.5 mol dm^{-3}

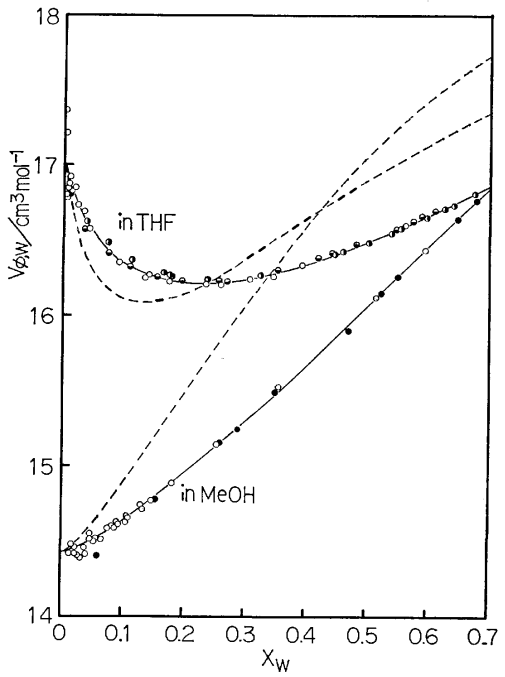

Fig. 1. Concentration dependence of the apparent (solid lines) and partial(dotted lines) molar volumes of water in MeOH and THF solutions at 298.15 K. ○: This work, ◑: Ref. 2, ◒: Ref. 3, ●: Ref. 4.

($X_w<0.04$), along with the values for the MeOH solutions.[1]

The V_w^∞ values in both the solvents, as well as in other polar solvents,[10–12] are less than the molar volume of pure water (18.07 cm^3 mol^{-1}). This decrease in volume may be related to the loss of the open structure of bulk water and to the formation of hydrogen bonds between water molecules and the solvent molecules. The smaller V_w^∞ value in MeOH can be attributed mainly to the strong hydrogen bond formation between water and MeOH molecules.

Using the ρ^* values obtained, we can estimate the $V_{\phi,w}$ at finite concentrations. The results are shown in Fig. 1. The closed and half-closed circles represent the values calculated from excess volumes reported by Benson and his co-workers.[2–4] These are in fair agreement with our results. The dotted lines are the partial molar volumes of water estimated by the relation:

$$V_w = V_{\phi,w} + X_w(1-X_w)\partial V_{\phi,w}/\partial X_w. \quad (4)$$

The values of $V_{\phi,w}$ (or V_w) in MeOH increase monotonously with the increase in X_w, while for THF solutions the $V_{\phi,w}$ *vs.* X_w curve passes through a broad minimum at near 0.25 mole fraction of water ($X_w \simeq$ 0.13 for minimum V_w).

It is well known that the partial molar volumes of various nonelectrolytes and organic electrolytes in water have a characteristic minimum in the water-rich region. The occurrence of this minimum has been ascribed to a balance between the enhancement of water structure by the solutes and the breaking of the structure with further increase in the concentration.[13] The minimum in the $V_{\phi,w}$ curve shown in Fig. 1, on the other hand, could not be attributed to such a structural influence because the open structure of water no longer exists in the THF-rich region. At present the molecular significance of the minimum is not clear but it may be related to the fact that THF–water hydrogen bonding is weaker than water–water hydrogen bonding.[2] The addition of water to THF will result in the formation of stronger hydrogen bonds between water molecules that would bring about volume contraction. Further increase in X_w may result in the formation of the well-known, three-dimensional open structure of water and the $V_{\phi,w}$ (or V_w) would increase to 18 cm^3 mol^{-1} in pure water.

This work was supported by Grant-in-Aid for Scientific Research No. 474195 from the Japanese Ministry of Education, Science and Culture.

References

1) M. Sakurai and T. Nakagawa, *J. Chem. Thermodyn.*, **14**, 269 (1982).
2) O. Kiyohara and G. C. Benson, *Can. J. Chem.*, **55**, 1354 (1977).
3) O. Kiyohara, P. J. D'Arcy, and G. C. Benson, *Can. J. Chem.*, **56**, 2803 (1978).
4) G. C. Benson and O. Kiyohara, *J. Solution Chem.*, **9**, 791 (1980).
5) G. S. Kell, *J. Chem. Eng. Data*, **20**, 97 (1975).
6) D. Hamilton and R. H. Stokes, *J. Solution Chem.*, **1**, 213 (1972).
7) J. L. Hales and J. H. Ellender, *J. Chem. Thermodyn.*, **8**, 1177 (1976).
8) M. Diaz Pena and G. Tardajos, *J. Chem. Thermodyn.*, **11**, 441 (1979).
9) W. Hayduk, H. Laudie, and O. H. Smith, *J. Chem. Eng. Data*, **18**, 373 (1973).
10) C. de Visser, W. J. M. Heuvelsland, L. A. Dunn, and G. Somsen, *J. Chem. Soc., Faraday Trans. 1*, **74**, 1159 (1978).
11) A. D'Aprano, I. D. Donato, E. Caponetti, and V. Agrigento, *Gazz. Chim. Ital.*, **108**, 601 (1978).
12) Y. Baratoux and J. Juillard, *Talanta*, **27**, 427 (1980).
13) F. Franks and D. S. Reid, "Water, A Comprehensive Treatise," ed by F. Franks, Plenum Press, New York (1973), Vol. 2, Chap. 5.

The Crystal Structure of *o*-Fluorobenzamide

Yoshihiro KATO* and Kiichi SAKURAI

Department of Physics, Osaka Kyoiku University, Tennoji-ku, Osaka 543

(Received October 17, 1981)

Synopsis. The crystal of the title compound is monoclinic, with space group $P2_1/a$, $a=12.695$, $b=20.534$, $c=5.133$ Å, $\beta=97.80°$, $Z=8$. The molecules are connected by one pair of hydrogen bonds to form asymmetric dimers and these dimers are further linked by two kinds of hydrogen bonds into endless chains along the c axis.

The crystals of *m*- and *p*-fluorobenzamides[1,2] contain four molecules per unit cell and the molecules are connected by hydrogen bonds to form centrosymmetric dimers. These dimers are linked by two kinds of hydrogen bonds into one-dimensional chains (*m*-fluorobenzamide) and two-dimensional networks (*p*-fluorobenzamide). The present study was undertaken to determine the type of hydrogen bonds and the molecular arrangement in the crystal of *o*-fluorobenzamide which has eight molecules in a unit cell.

Experimental

Crystals were grown from a hot aqueous solution by slow cooling to room temperature. The cell dimensions and reflection intensities were measured on a Rigaku automated four-circle diffractometer using monochromatized Mo $K\alpha$ radiation. The crystal data are as follows: $a=12.695(2)$, $b=20.534(2)$, $c=5.133(1)$ Å, $\beta=97.80(1)°$, $P2_1/a$, $Z=8$.

The intensity data were collected by the 2θ-ω scan technique with a speed of $8°(2\theta)$ min^{-1} up to $2\theta=58°$. The crystal used had approximate dimensions of $0.4\times0.4\times0.5$ mm^3. A total of 1953 reflections were obtained, of which 1471 were non-zero reflections. No corrections for absorption and extinction were made.

Structure Determination and Refinement

The structure was solved by the direct method with the MULTAN program.[3] All the non-hydrogen atoms appeared clearly in the *E* map, and the hydrogen atoms were found on difference Fourier maps. The *R* value was finally reduced to 0.076 by the block-diagonal least-squares refinement using the program *HBLS V*[4] with anisotropic thermal parameters for non-hydrogen atoms and an isotropic one ($B=3.7$ Å^2) for hydrogen atoms. The weighting scheme of the type $w=1-\exp(-15s^2)$ with $s=\sin\theta/\lambda$ was used. The final positional parameters and equivalent isotropic temperature factors for non-hydrogen atoms are listed in Table 1.[5]

Discussion

The bond lengths and bond angles are shown in Fig. 1. The molecular arrangement projected along the c axis is shown in Fig. 2. The least-squares plane through the six carbon atoms of the benzene ring and the plane through the C, N, and O atoms of the carbamoyl group for molecules I and II are given

Table 1. Final positional parameters with their standard deviations ($\times10^4$) and B_{eq}[a] for non-hydrogen atoms

	x	*y*	*z*	B_{eq}/Å^2
F (1)	3531 (3)	0213 (2)	3094 (5)	6.0
O (1)	1417 (3)	0196 (2)	−3505 (7)	4.5
N (1)	1413 (4)	0346 (2)	0788 (8)	4.6
C (11)	1820 (4)	0092 (2)	−1260 (9)	3.4
C (12)	2777 (4)	−0332 (2)	−0759 (9)	3.3
C (13)	3581 (4)	−0276 (3)	1327 (10)	4.0
C (14)	4459 (4)	−0678 (3)	1680 (12)	5.1
C (15)	4520 (4)	−1170 (3)	−0052 (12)	5.2
C (16)	3743 (5)	−1251 (3)	−2184 (12)	4.9
C (17)	2897 (4)	−0830 (3)	−2550 (10)	4.3
F (2)	−0226 (3)	2522 (2)	−6347 (9)	6.6
O (2)	−0376 (4)	1286 (2)	−0381 (7)	5.2
N (2)	−0180 (3)	1237 (2)	−4655 (9)	4.0
C (21)	−0546 (4)	1506 (2)	−2627 (9)	3.7
C (22)	−1199 (4)	2117 (2)	−3106 (10)	3.7
C (23)	−1031 (4)	2592 (2)	−4939 (11)	4.5
C (24)	−1633 (6)	3149 (3)	−5252 (15)	6.1
C (25)	−2450 (7)	3225 (4)	−3846 (17)	7.5
C (26)	−2659 (6)	2768 (4)	−2050 (16)	7.2
C (27)	−2028 (5)	2213 (3)	−1682 (12)	5.5

a) $B_{eq}=8\pi^2(u_1^2+u_2^2+u_3^2)/3$, where u_i is the root-mean-square deviation in the *i*-th principal axis of the thermal ellipsoid.

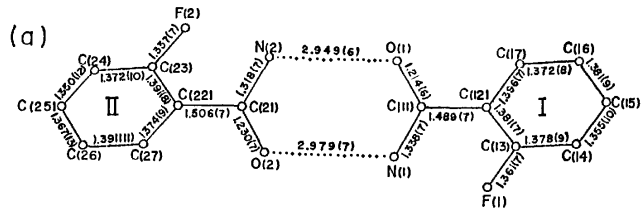

Fig. 1. a) Bond lengths (l/Å) and b) bond angles (ϕ/°).

by the following equations:

molecule I

benzene ring $0.577X+0.612Y-0.541Z=1.864$,

carbamoyl group $0.588X+0.808Y-0.032Z=1.583$,

molecule II

benzene ring $0.527X+0.471Y+0.707Z=0.240$,

carbamoyl group $0.813X+0.555Y+0.179Z=1.064$,

where *X*, *Y*, and *Z* are coordinates measured in Å

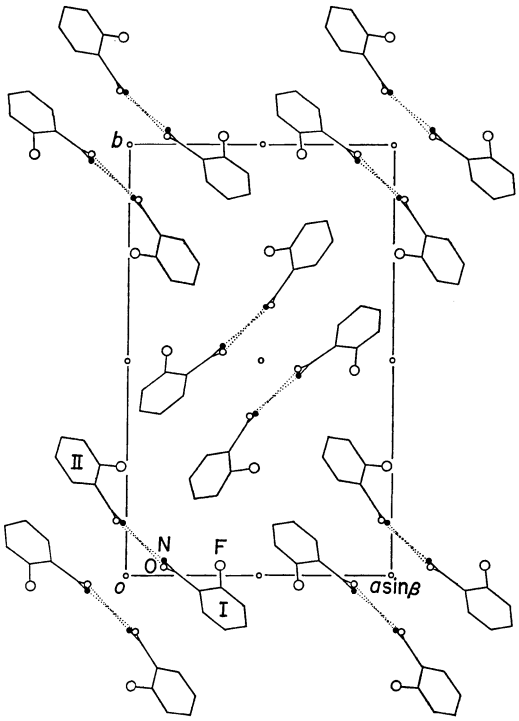

Fig. 2. The crystal structure viewed along the c axis.

along the orthogonal axes a, b, and c* respectively. The dihedral angles between the plane of the carbamoyl group and the mean plane of the benzene ring are 31.7° for molecule I and 35.4° for molecule II, which are rather small as compared with those of other ortho-substituted benzamides.[6] This can be explained from the fact that the van der Waals radius of the F atom is close to that of the H atom. It is interesting that the F atom lies on the side of N atom of the carbamoyl group for both of molecules I and II, while in the crystals of other *o*-halogenobenzamides[6] the halogen atoms lie on the side of O atom of the carbamoyl group. It is also noticeable that in the crystal of *o*-fluorobenzamide the unit cell contains eight molecules, which are linked in pairs by NH···O hydrogen bonds (2.949, 2.979 Å) to form asymmetric dimers. These dimers are further linked by the other NH···O hydrogen bonds (2.917, 2.945 Å) to form one-dimensional chains along the c axis. A pair of such chains related by a center of symmetry forms a double-chain having an enantiometric configuration.

X-Ray data collection was carried out on a Rigaku automated four-circle diffractometer at Crystallographic Research Center, Institute for Protein Research, Osaka University.

References

1) T. Taniguchi, Y. Takaki, and K. Sakurai, *Mem. Osaka Kyoiku Univ.*, **24**, Ser. III, 119 (1975).

2) Y. Takaki, T. Taniguchi, and K. Sakurai, *Mem. Osaka Gakugei Univ.*, **14**, 48 (1965).

3) P. Main, S. E. Hull, L. Lessinger, G. Germain, J. P. Declercq, and M. M. Woolfson, A System of Computer Programs for the Automatic Solution of Crystal Structures from X-Ray Diffraction Data, MULTAN 78, University of York, 1978.

4) T. Ashida, HBLS V, The Universal Crystallographic Computing System-Osaka, p. 53. The Computation Center, Osaka University (1979).

5) The lists of anisotropic thermal parameters for non-hydrogen atoms, positional parameters for hydrogen atoms, and structure factors are kept as Document No. 8224 at the Office of the Bulletin of the Chemical Society of Japan.

6) K. Sakurai, *Mem. Osaka Kyoiku Univ.*, **30**, Ser. III 119 (1982).

Anomalous Crystallization Behavior in the Glass Forming Composition Region of the H_2O-HNO_3 System

Kenji SATOH and Hitoshi KANNO*

Department of Chemistry, Meisei University, Hino, Tokyo 191

(Received November 20, 1981)

Synopsis. Glass formation composition region of aqueous HNO_3 solution is determined. Anomalous crystallization behavior was observed for the solution having the composition near $HNO_3 \cdot 3H_2O$. From T_g data, T_g for a bulk glassy water is estimated to be -144 ± 2 °C.

Glass forming composition regions in aqueous solution systems have recently been determined for a relatively large number of both inorganic salt–water and binary organic compound mixture systems.[1-3] From these studies, it has become evident that glass transition temperature (T_g) can be a useful parameter for characterizing thermodynamic and transport properties of a liquid at low temperatures.[1-4]

In this note, we report an anomalous crystallization behavior of an aqueous HNO_3 solution in the composition near $HNO_3 \cdot 3H_2O$, which is very suggestive for clarifying both glass formation mechanism and structure changes of the solution with composition.

All solutions were made by weighing out and mixing required amounts of a commercially available guaranteed-grade ≈62 wt% nitric acid and distilled water. The glass transition temperature of each solution was measured by a conventional, simple DTA method. The details of the experiment were essentially the same as previously reported.[3] Overall cooling rate of the sample solution contained in a 2 mm i.d. Pyrex glass cell was about 10^3 K/min. The T_g value was obtained at a heating rate of about 5 K/min in the warm-up DTA trace using chromel-alumel thermocouples.

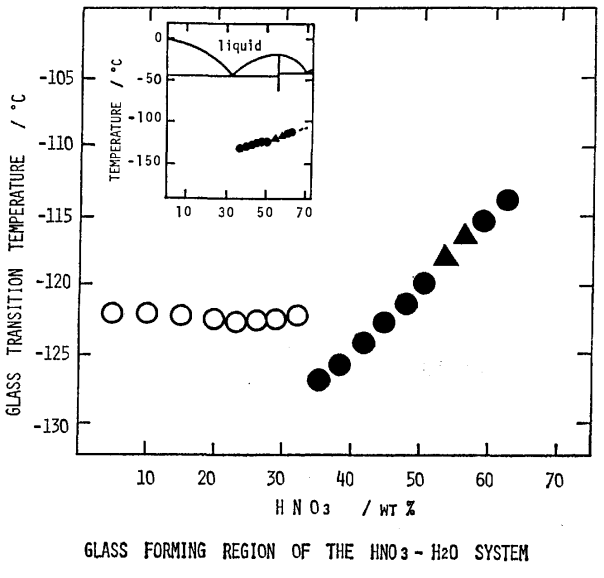

GLASS FORMING REGION OF THE HNO3 - H2O SYSTEM

Fig. 1. Variation of T_g with solution composition. The inset shows the phase diagram of the HNO_3–H_2O system [from J. Timmermans, "Physico Chemical Constants of Binary Systems," Interscience Publishers, Inc., New York (1960), Vol. 4, p. 466]. ●: T_g in the glass-forming composition region, ○: T_g of the portion remained uncrystallized in the non-glass-forming composition region, ▲: the expected glass transition temperature if the solution was glass-forming.

The results obtained are plotted in Fig. 1 together with the phase diagram as an inset. Glass formation was visually checked and it began from the composition of about 35 wt% HNO_3 up to about 62 wt% HNO_3 (above which measurements were not made because of non-availability of a higher cocentration in this study). The solutions having the composition of less than 35 wt% HNO_3 are only partially glass-forming, therefore giving a glass transition as seen in the DTA trace A in Fig. 2.

An interesting point is the existence of a very narrow window (≈54 wt% HNO_3 region) where no glass transition is observed, indicating that the whole body of the solution crystallizes in the quenching rate of about 10^3 K/min. This is peculiar because most aqueous solutions which have a glass forming composition region are partially glass forming even in the non-glass forming composition region.[4,5] As the composition of the non-glass forming solution is very near 54 wt%, we consider that an additive compound of the composition $HNO_3 \cdot 3H_2O$ was formed in the cooling process. This is supported by the DTA trace C shown in Fig. 2. The fact that an appreciable part (about 5%) of the 53.8% HNO_3 solution crystallized in the eutectic composition, as evidenced with

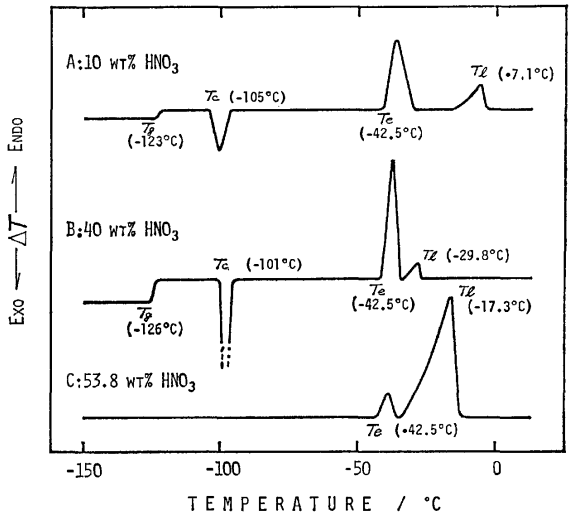

Fig. 2. DTA traces of several quenched HNO_3 solution.
T_c: Crystallization temperature, T_e: eutectic temperature of the HNO_3–H_2O system, T_l: liquidus temperature of the HNO_3–H_2O solution.

the DTA peak at −42 °C, suggests that there exists a considerable concentration fluctuation about 53.8 wt% HNO_3 in the solution in the liquid state.

Linear variation of T_g with solution composition indicates that the structure of the HNO_3 solution varies smoothly with the composition in the glass-forming composition region (≈35 to 62 wt% HNO_3). Thus, the existence of the narrow non-glass forming region can not be ascribed to a sudden change of the solution structure. It is considered that whether or not a given liquid crystallizes during cooling before a glass transition is reached is purely a kinetic problem.[6-8] Taking account of various factors appearing in the kinetic theories of glass formation developed by Turnbull *et al.*[7,9] and Uhlmann,[8] we consider that a geometrical factor, which has not been properly incorporated in the current kinetic theories despite of the fact that its importance has often been noted in various qualitative criteria for the glass-forming of a liquid,[10,11] is a main cause for the anomalous crystallization behavior. In other words, the structure of the ≈54 wt% HNO_3 solution at low temperature is expected to resemble that of the $HNO_3 \cdot 3H_2O$ crystal so that the barrier to nucleation is low as compared with that in other glass-forming concentration region.

Estimation of T_g for a pure non-glass forming liquid has often been made by the extrapolation of T_g data for binary mixtures.[1,2,12] A simple least-squares curve fitting for the present T_g data yields the following formula for the concentration dependence of T_g for the HNO_3 solution:

$$T_g = 0.48X - 144, \quad (1)$$

where X in HNO_3 wt% and T_g in °C. From Eq. 1, we estimate that the T_g value for a glassy bulk water will be −144±2 °C if water is successfully made a glassy state by a rapid cooling. This value is a little lower than those (−134——138 °C) estimated from other T_g data for several aqueous solutions[1,12] and that (−139 °C) obtained for amorphous ice made by a vapor deposition method.[13] We consider that this low value is presumably due to hydronium ions in the glassy HNO_3 solution though an explicit interpretation is at present difficult. However, a plausible, though indirect, evidence for the above speculation comes from the observation that the mobility of H_3O^+ ions in ice is faster than that in aqueous solution (at room temperature) by about two order of magnitude.[14] Another supporting experimental evidence is that glass transition in a glassy crystal ice, which is claimed to be related to proton disordering, occurs at −173 °C.[15]

This work was in part assisted by a Grant-in-Aid for Scientific Research from the Ministry of Education, Science and Culture.

References

1) C. A. Angell and E. J. Sare, *J. Chem. Phys.*, **52**, 1058 (1970); C. A. Angell, J. M. Sare, and E. J. Sare, *J. Phys. Chem.*, **82**, 2622 (1978).
2) A. V. Lesikar, *J. Chem. Phys.*, **63**, 2297 (1975); **66**, 4263 (1977); *J. Phys. Chem.*, **80**, 1005 (1976); *J. Solution Chem.* **6**, 81, 839 (1977).
3) H. Kanno, I. Shirotani, and S. Minomura, *Bull. Chem. Soc. Jpn.*, **53**, 2079 (1980); **54**, 2607 (1981).
4) S. Blaser, P. B. Macedo and R. Weiler, *J. Phys. Chem.*, **73**, 4147 (1969).
5) H. Rawson, "Inorganic Glass Forming System," Academic Press, London (1967), Chap. 13.
6) W. B. Hillig and D. Turnbull, *J. Chem. Phys.*, **24**, 914 (1956); D. Turnbull and M. H. Cohen, *ibid.*, **29**, 1049 (1958); "Modern Aspects of the Vitreous State," ed by V. D. Mackenzie, Butterworth, London (1960), Vol. 1, pp. 38—62.
7) D. Turnbull, *Trans. AIME*, **221**, 422 (1961); *J. Phys. Chem.*, **66**, 609 (1962).
8) D. Uhlmann, *J. Non-Cryst. Solids*, **7**, 337 (1972).
9) D. Turnbull, *Contemp. Phys.*, **10**, 473 (1972).
10) A. Smekal, *J. Soc. Glass Technol.*, **35**, 411 (1951).
11) Ref. 5, Chaps. 1 and 2.
12) D. H. Rasmussen and A. P. Mackenzie, *J. Phys. Chem.*, **75**, 967 (1971).
13) M. Sugisaki, H. Suga, and S. Seki, *Bull. Chem. Soc. Jpn.*, **41**, 2591 (1968).
14) N. H. Fletcher, "The Chemical Physics of Ice," Cambridge Univ. Press, London (1970), Chap. 7.
15) H. Suga and S. Seki, *J. Non-Cryst. Solids*, **16**, 171 (1974).

Adsorption of Electron Acceptors on Titania

Kunio Esumi* and Kenjiro Meguro

Department of Applied Chemistry, Faculty of Science, Science University of Tokyo, Kagurazaka, Shinjuku-ku, Tokyo 162

(Received June 23, 1981)

Synopsis. Four electron acceptors with electron affinities ranging from 1.26 to 2.84 eV were adsorbed from acetonitrile solution on to a titania sample. On adsorption, radical anions were formed on the titania surface as a result of electron transfer to the acceptors from the surface of the titania. The concentration of radical anions thus formed decreased with the decreasing electron affinity of the acceptors; the decrease is steep between 1.26 and 1.77 eV. These results suggest that the limit of electron transfer from the titania surface to the acceptor ranges between 1.77 and 1.26 eV in the electron affinity of the acceptor.

Recently, the adsorption of electron acceptors on metal oxides has been investigated to estimate electron donor properties of metal oxides and their characterization.[1-3] Flockhart *et al.*[4] studied the electron donor properties of alumina surface by the adsorption of tetracyanoethylene (TCNE) and they concluded that the electron donor sites originated from unsolvated hydroxide ions for the samples activated at lower temperatures, but from defect centers involving oxide ions for the samples activated at higher temperatures.

In this work we report the adsorption of some electron acceptors on titania in order to evaluate the limit of the electron transfer. For this purpose, the following electron acceptors were employed as adsorbates: 7,7,8,8-tetracyanoquinodimethan (TCNQ), 2,5-dichloro-*p*-benzoquinone (DCQ), *p*-dinitrobenzene (PDNB), and *m*-dinitrobenzene (MDNB), whose electron affinity ranges between 2.84 and 1.26 eV.

The preparation of titania has been described elsewhere.[3] The specific surface area of the sample measured by the BET method was about 47 m^2/g. The sample was found to be anatase by X-ray diffractometry. TCNQ was supplied by Dainippon Ink Chemical, Ltd, and recrystallized from acetonitrile. DCQ, PDNB and MDNB were supplied by Tokyo Kasei, Ltd., and were purified by recrystallization from ethanol, chloroform and carbon tetrachloride, respectively. The acetonitrile used as solvent was of reagent grade supplied by Kokusan Chemical Works, Ltd. The apparatus and procedure used in this study have been described previously.[1]

Figure 1 shows the adsorption isotherms of TCNQ, DCQ, PDNB, and MDNB from their acetonitrile solutions at 25 °C on the titania surface. All the isotherms except MDNB are of Langmuir type. In the case of MDNB, the amount adsorbed was so small that it was hard to estimate. The limiting amounts of TCNQ, DCQ and PDNB adsorbed on the surface estimated from the Langmuir plots, are given in the second column of Table 1. As shown in Table 1, it is noticeable that the limiting amount decreases with the decreasing electron affinity[5,6] of the acceptors.

When the electron acceptors were adsorbed from the solution in acetonitrile on the surface of titania, the surface showed a remarkable coloration characterized with the kind of acceptors: violet for TCNQ, brown for DCQ and PDNB, and colorless for MDNB. It has been reported by some workers[1-4] that the adsorption of acceptors on metal oxides produces a surface coloration due to the interaction between acceptor molecules adsorbed and metal oxide surfaces. To study the nature of the interaction the electronic spectrum of colored samples was measured, as illustrated in Fig. 2. The bands appearing below 400

Table 1. Summary of the electron acceptor adsorption

Electron acceptor	Electron affinity / eV	Adsorbed amount / mol $m^{-2} \times 10^{-7}$	Radical concentration / spins m^{-2}
TCNQ	2.84	6.0	3.1×10^{16}
DCQ	2.30	5.0	1.5×10^{15}
PDNB	1.77[a]	2.0	7.1×10^{13}
MDNB	1.26	Negligible	0

a) The value given by Briegleb[5] plus 1.07 eV.

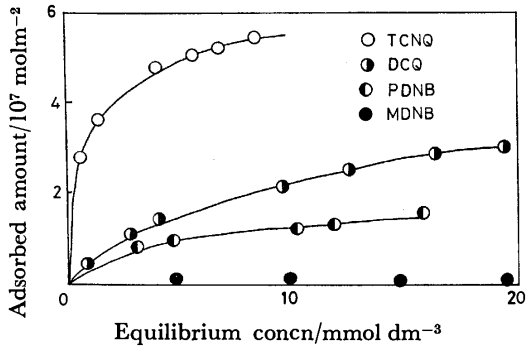

Fig. 1. Adsorption isotherms of electron acceptors on titania (at 25 °C).

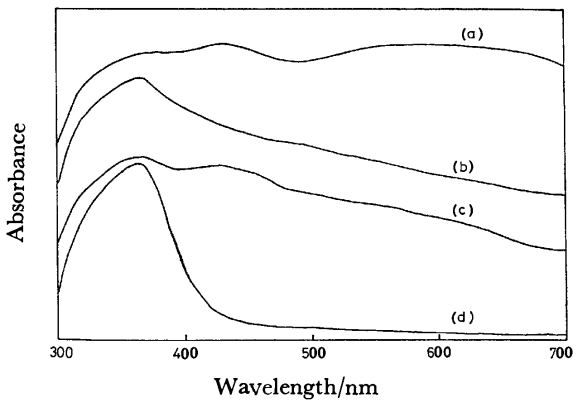

Fig. 2. Electronic spectra from electron acceptors on titania: (a) TCNQ; (b) DCQ; (c) PDNB; (d) MDNB.

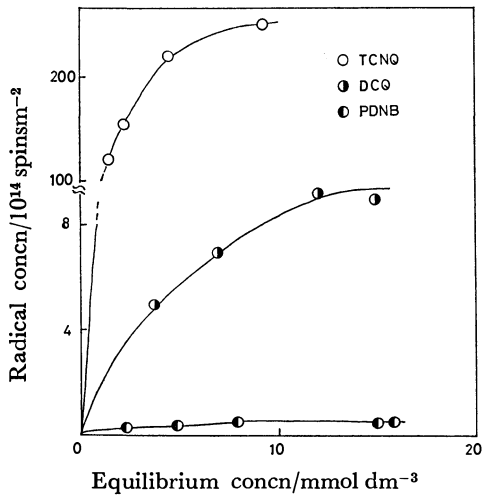

Fig. 3. Radical concentration on titania *vs.* equilibrium concentration of electron acceptor (at 25 °C).

nm are common to all the samples and could not be assigned specifically to any adsorption state because titania alone has a characteristic band in the same region. The absorption band near 600 nm observed in Fig. 2(a) can be attributed to the dimer TCNQ anion radical which absorbs light at 643 nm.[7] In Fig. 2(b), a broad tail band extending to 700 nm was observed and may be supposed to correspond to the DCQ anion radical.[8] The spectrum shown in Fig. 2(c) has a maximum absorption at about 420 nm and the band may be attributed to the PDNB anion radical. In the case of MDNB as shown in Fig. 2(d), no new band was observed on adsorption. If the acceptor anion radicals are formed by the adsorption on the titania surface, the adsorbed species obtained will show ESR signals. Indeed, the colored species gave an unresolved ESR spectrum with a g-value of 2.003 for TCNQ, 2.005 for DCQ and 2.004 for PDNB, respectively. However, the sample of adsorbed MDNB showed no ESR signal. These phenomena confirm the formation of TCNQ, DCQ, and PDNB anion radicals as a result of electron transfer from titania surface to each acceptor.

The nature of the sites responsible for the electron transfer process is not well understood. However, it might be suggested that two possible electron sources exist on the titania surface. One of these is Ti^{3+} ions and the other is surface hydroxide ions.[9]

Figure 3 shows the radical concentration on the surface of titania plotted against the equilibrium concentration of electron acceptor. All the isotherms are of Langmuir type. The limiting radical concentration of TCNQ, DCQ, and PDNB adsorbed on the titania surface estimated by the Langmuir plot is given in the third column of Table 1. It is found that the limiting radical concentration decreases with decreasing electron affinity of the acceptors and steeply between PDNB and MDNB. This suggests that adsorption sites of titania act as electron donors to the adsorbed molecules with electron affinity larger than 1.77 eV but not to those smaller than 1.26 eV. Accordingly, the limit of electron transfer from electron donor sites of titania to electron acceptor molecules is located between 1.77 and 1.26 eV in the electron affinity of the acceptors.

References

1) K. Meguro and K. Esumi, *J. Colloid Interface Sci.*, **59**, 93 (1977).
2) K. Esumi and K. Meguro, *J. Colloid Interface Sci.*, **66**, 192 (1978).
3) H. Hosaka, T. Fujiwara, and K. Meguro, *Bull. Chem. Soc. Jpn.*, **44**, 2616 (1971).
4) B. D. Flockhart, I. R. Leith, and R. C. Pink, *Trans. Faraday Soc.*, **65**, 542 (1969).
5) G. Briegleb, *Angew. Chem.*, **76**, 326 (1964).
6) E. C. M. Chen and W. E. Wentworth, *J. Chem. Phys.*, **63**, 3183 (1975).
7) R. H. Boyd and W. D. Phillips, *J. Chem. Phys.*, **43**, 2927 (1965).
8) R. Foster and T. J. Thomson, *Trans. Faraday Soc.*, **58**, 860 (1962).
9) M. Che and B. Imelik, *J. Catal.*, **24**, 328 (1972).

The Effect of Ultraviolet Radiation on Wettability of Polymer Surfaces

Kunio Esumi,* Kenjiro Meguro, A. M. Schwartz,† and A. C. Zettlemoyer†

Department of Applied Chemistry, Science University of Tokyo, Kagurazaka, Shinjuku-ku, Tokyo 162

† *Center for Surface and Coatings Research, Sinclair Laboratory, Lehigh University, Bethlehem, Pa 18015, U. S. A.*

(Received September 25, 1981)

Synopsis. The wettability of polystyrene and poly(methyl vinyl ketone) surface can be markedly changed by ultraviolet irradiation in air. The contact angle of water on both polymers decreases dramatically as a function of exposure time. This effect is mainly due to increase in the polar component of surface energy. The wettability of irradiated polymers goes back to near original values due to soluble photooxidation products into water after the water extraction.

Polymers, under normal conditions, are in contact with atmospheric oxygen and are subjected to varying temperatures, humidities and exposures to light. A polymer is expected to undergo photochemical induced change at or near its surface.

The wettability of surfaces by liquids of known surface tensions has been determined by many investigators. Contact angle measurements, in particular, have been used to evaluate changes in a surface composition. Fox *et al.*[1] have reported that with a number of amorphous polymers the changes in contact angles for various liquids with ultraviolet radiation time, not surprisingly, are a function of the nature of the polymers. According to Fox's study, it might be expected that by ultraviolet radiation the wettability of polymer surfaces can be changed from hydrophobic to hydrophilic.

This study describes the effect of ultraviolet radiation on the wettability of two polymers.

The liquids used for contact angle measurements were deionized water and diiodomethane.

Polymers used were polystyrene supplied by Monomer-Polymer and Dajac Laboratories, Inc. and poly(methyl vinyl ketone) by Polyscience, Inc. Films of each polymer were prepared by the evaporation of 2 wt% dichloromethane solution on aluminum plate.

Exposures were carried out in air in a hood with the unfiltered radiation from 55.1 W low pressure mercury lamp supplied by Oriel Co. The distance between the sample and the lamp was 5 cm.

Contact angles were measured with a goniometer at 20 °C. Three drops for a given liquid were measured on both sides of the drops and the six values were averaged. The overall variation in the contact angle measurement was about ±3°.

To evaluate surface energy, the interfacial term γ_{ab} by theory (Owens and Wendt,[2] Kaelble and Uy,[3] Wu[4]), is given as follows:

$$\gamma_{ab} = \gamma_a + \gamma_b - 2(\gamma_a^d\gamma_b^d)^{1/2} - 2(\gamma_a^p\gamma_b^p)^{1/2}, \quad (1)$$

where γ is the respective surface energy and the dispersive(d) and polar(p) components of the surface energies for solid a and liquid b are considered to interact only with their own kind. To obtain values

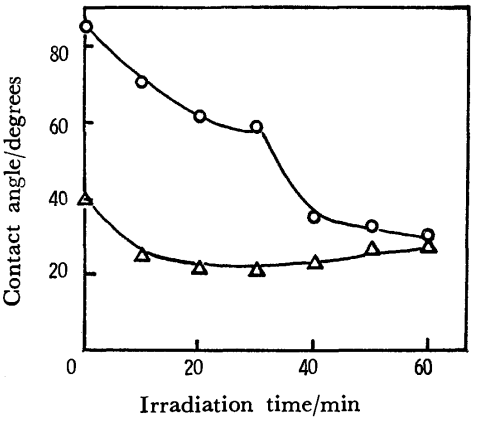

Fig. 1. Irradiation time *vs.* contact angles on polystyrene.
○: Water contact angle, △: diiodomethane contact angle.

for the dispersive and polar components of the solid surface energies, Eq. 1 is combined with the Young equation to give for a solid(a)/liquid(b) pair,

$$\text{Cos}\,\theta + 1 = \frac{2}{\gamma_b}[(\gamma_a^d\gamma_b^d)^{1/2} + (\gamma_a^p\gamma_b^p)^{1/2}], \quad (2)$$

where θ is the contact angle. If the dispersive and polar components of the surface energies of the various liquids are known,[5,6] each pair of equations of the form of Eq. 2 yields solutions for γ_a^d, γ_a^p. In this study, by using Eq. 2, values of γ_a^d and γ_a^p for polymers were calculated as a function of ultraviolet irradiation time. Here, literature values of γ_b^d and γ_b^p for water and diiodomethane are applied in the surface energy analysis:[5,6] γ_b^d=21.8 erg/cm², γ_b^p=50.8 for H_2O, γ_b^d=50.8, γ_b^p=0 for CH_2I_2.

The wettability of polystyrene and poly(methyl vinyl ketone) was evaluated as a function of exposure time of ultraviolet irradiation. The results for contact angle measurements are shown in Figs. 1 and 2. Compared with the original polymers, oxygenated moieties in the surfaces would be expected to interact more strongly with polar liquid like water, but might be less wet by a nonpolar liquid like diiodomethane. From these figures, it can be seen that the contact angles of water decreased with increase in the exposure time on both polystyrene and poly(methyl vinyl ketone). On the other hand, the contact angles of diiodomethane remained constant as irradiation progressed.

Furthermore, γ_a^d and γ_a^p are calculated as a function of exposure time, shown in Figs. 3 and 4. For both polymers, the dispersion component of surface energy did not change significantly with exposure time, but the polar component increased remarkably as irra-

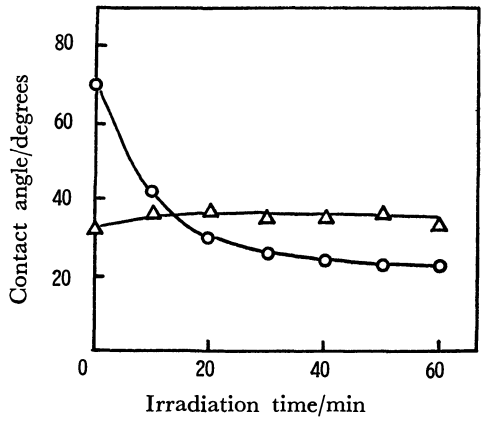

Fig. 2. Irradiation time *vs.* contact angles on poly(methyl vinyl ketone).
○: Water contact angle, △: diiodomethane contact angle.

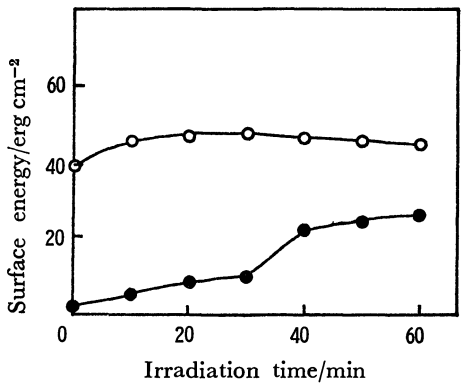

Fig. 3. Irradiation time *vs.* surface energy on polystyrene.
○: γ_s^d, ●: γ_s^p.

diation progressed. This increase means that during irradiation the surface of the polymers were photooxidated to yield hydrophilic products on the surface. Also, by means of multiple internal reflectance spectra of irradiated polystyrene film, the carbonyl band due to photooxidation near 1725 cm^{-1} has been observed.[1)]

As a next step, to study the stability of irradiated

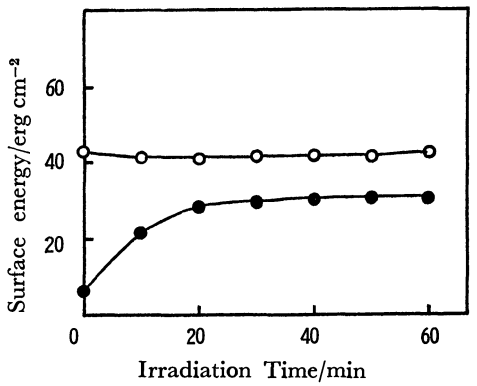

Fig. 4. Irradiation time *vs.* surface energy on poly(methyl vinyl ketone).
○: γ_s^d, ●: γ_s^p.

polymer surfaces, two tests were carried out. One was that after irradiation, the samples were kept in a desiccator for 2 d and then contact angles were measured. The other was a water extraction test. The irradiated samples were immersed in distilled water for 15 min and dried *in vacuum*, then the contact angles for the samples were measured. For both polystyrene and poly(methyl vinyl ketone), the contact angles of water after 2 d storage were almost the same as the immediate results. On the other hand, the contact angles of water after the water extraction increased significantly, although they did not come back to the original unexposed values. The increase of the water contact angles might be attributed to water-soluble photooxidation products.

References

1) R. B. Fox, T. R. Price, and D. S. Cain, *Adv. Chem. Ser.*, **87**, 72 (1968).
2) D. K. Owens and R. C. Wendt, *J. Appl. Polym. Sci.*, **13**, 1741 (1969).
3) D. H. Kaelble and K. C. Uy, *J. Adhesion*, **2**, 50 (1970).
4) S. Wu, *J. Adhesion*, **5**, 39 (1973).
5) F. M. Fowkes, *Treatise of Adhesion and Adhesives*, ed by R. L. Patrick, Marcel Dekker, New York (1967).
6) J. R. Dann, *J. Colloid Sci.*, **32**, 302 (1970).

Effect of the Chlorine Contents on the Lattice Constants of β-FeOOH

Matashige OHYABU and Yusuke UJIHIRA*

Department of Industrial Chemistry, Faculty of Engineering, The University of Tokyo, 7-3-1 Hongo, Bunkyo-ku, Tokyo 113

(Received September 16, 1981)

Synopsis. The lattice constants of β-FeOOH including chlorine and fluorine, were determined by X-ray diffractometry. The chlorine-content dependence of the lattice constants showed that chlorine ions are distributed at random, occupying certain sites of β-FeOOH.

β-FeOOH, also known as akaganeite, is a kind of iron(III) oxide hydroxide. It is formed as a hydrolysis product from iron(III) salt solutions containing Cl^- or F^- ions. It is well known that Cl^- or F^- ions are necessary for the formation of β-FeOOH and that the β-FeOOH thus produced contains Cl or F in the crystal without exception. Recently, Mossbauer spectroscopic studies have indicated that iron atoms exist in two or three different chemical states in the β-FeOOH crystal.[1-4] In a previous paper,[5] we reported on the synthesis of β-FeOOH from various solutions containing different concentrations of Cl^- and F^-, and proposed the possibility that Cl^- and F^- ions are directly bound to Fe^{3+} ions in β-FeOOH.

The present paper reports the variation in the lattice constants of β-FeOOH determined by X-ray diffractometry and its correlation to the difference in Cl and F concentrations in the crystal.

Experimental

Preparation of β-FeOOH. β-FeOOH was prepared by heating Fe(III) solutions containing various concentrations of Cl^- and F^- ions. The details were described previously.[5] The X-ray diffraction patterns and the electron micrographs proved the purity of the β-FeOOH thus synthesized.

Measurement of X-Ray Diffraction Patterns. An X-ray diffractometer was operated with an Fe tube. The powder and the scan speed were 28 kV (6 mA) and 0.25° min^{-1}, respectively.

Analysis of Diffraction Data. The lattice constants were calculated from the 2θ values of the (211) and (400) diffraction lines. The peak positions were determined by drawing the tangent lines on both sides of the diffraction profiles. The diffraction lines of α-Fe_2O_3[6] were used for the correction of the diffraction angle.

Results and Discussion

The structure of β-FeOOH is tetragonal,[7,8] and several observed values of the lattice constants have been reported (*e.g.*, a=10.48 Å, and c=3.023 Å).

Since Mackay's studies of the crystal,[7] Cl^- and F^- ions have been believed to occupy the hole site in β-FeOOH, but no experimental confirmation has yet been made. We proposed that Cl^- and F^- ions are directly bound to the Fe^{3+} ion in the β-FeOOH crystal.[5] The expansion or the contraction of the lattice in the crystal can be expected without any contradiction if Cl^- and F^- ions are located at certain sites in β-FeOOH.

TABLE 1. CHLORINE AND FLUORINE CONTENTS AND THE OBSERVED LATTICE CONSTANTS

Sample	Cl/Fe[a]	F/Fe[a]	a[b] / Å	c[b] / Å
A	0.148	0	10.56	3.035
B	0.143	0	10.54	3.034
C	0.110	0.113	10.51	3.033
D	0.056	0.197	10.48	3.023
E	0.031	0.281	10.46	3.030
F	0.023	0.332	10.46	3.026
G	0.014	0.384	10.46	3.023

a) Cl/Fe and F/Fe are represented as atomic ratios; the error is below 5%. b) The errors are ±0.01 Å and 0.001 Å for a and c, respectively.

Table 1 shows the Cl and F contents in synthesized β-FeOOH and the observed lattice constants. If β-FeOOH is regarded as non-stoichiometric, the variation in the lattice constants will follow Vegard's law.[9]

$$a = a_0 + px_{Cl} + qx_F, \quad (1)$$

where x_{Cl}=Cl/Fe, x_F=F/Fe, and p and q are the coefficients concerned with the ion radii and chemical nature of the Cl^- and F^- ions. a_0 is the expected lattice constant of β-FeOOH free from Cl^- or F^-. Practically the estimation of p and q is difficult because of the absence of a compound where the certain sites are completely replaced by Cl^- or F^- ions.

Here, $|p| \gg |q| \approx 0$ can be assumed, since the ionic radius of F^- is almost identical with that of OH^-/O^{2-}. Equation 1 can be reduced as follows:

$$a \fallingdotseq a_0 + px_{Cl}. \quad (2)$$

The Cl content dependence of the lattice constants is shown in Fig. 1. It is found that the liner relationship is nearly satisfied and that the variation in the lattice constants follows Vegard's law. Namely,

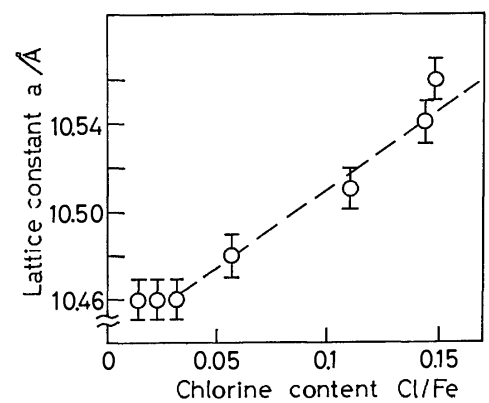

Fig. 1. Chlorine content dependence of the lattice constants a of β-FeOOH. p in Eq. 2 is estimated to be 0.8 Å.

it is confirmed that, in the β-FeOOH crystal, Cl^- ions are not localized, forming such compound as $FeCl_3$, but the distributed at random, occupying certain sites.

This confirmation is in accordance with the experimental finding that neither the diffraction lines nor the Mössbauer resonant peaks of the Fe(III) compounds were observed other than in the case of β-FeOOH.[10]

References

1) D. Chambaere, A. Govaert, J. de Sitter, and E. de Grave, *Solid State Commun.*, **26**, 657, (1978).
2) J. H. Johnston and N. E. Logan, *J. Chem. Soc., Dalton. Trans.*, **1979**, 13.
3) E. Murad, *Clay Miner.*, **14**, 273 (1979).
4) D. Chambaere, A. Govaert, E. de Grave, G. Harts, and G. Robbrecht, *J. Phys. (Paris), Colloq.*, C2-350 (1979).
5) M. Ohyabu and Y. Ujihira, *J. Inorg. Nucl. Chem.*, **43**, 3125 (1981).
6) ASTM, Powder Diffraction File, 13-534.
7) A. L. Mackay, *Miner. Mag.*, **32**, 545 (1960).
8) A. Szytula, M. Balanda, and Ž. Dimitrijevic, *Phys. Status Solidi A*, **3**, 1033 (1970).
9) H. P. Klug and L. E. Alexander, "X-Ray Diffraction Procedures," John Wiley & Sons, New York and London (1974), p. 562.
10) M. Ohyabu and Y. Ujihira, *Nippon Kagaku Kaishi*, **1979**, 634.

Photo- and Thermally-induced Radical Rearrangements of 6-Methyl- and 4,4,6-Trimethylcholest-5-en-3β-ol

Hiroshi SUGINOME,* Norio MAEDA,† Yoshikatsu SEKI, and Kazuhiko ORITO

Organic Synthesis Division, Department of Chemical Process Engineering, Faculty of Engineering, Hokkaido University, Sapporo 060

† *Department of Chemistry, Faculty of Science, Hokkaido University, Sapporo 060*

(Received June 5, 1981)

Synopsis. The irradiation of 6-methylcholest-5-en-3β-ol in benzene containing mercury(II) oxide and iodine gave 3α,5-epoxy-6-methylene-*A*-homo-4-oxa-5α-cholestane (23%) and 2-iodo-6-methyl-*A*-nor-2,3-secocholest-5-en-3-yl formate (32%). The thermally-induced reaction at 55—60 °C gave the former in a 16% yield. The corresponding photo-reaction of 4,4,6-trimethylcholest-5-en-3β-ol, however, gave 4,6-dimethyl-4-methylene-3,4-secocholest-5-en-3-al.

Earlier parts of this series[1–5] have described the results of the photo- and thermally-induced rearrangements of a number of cholest-5-en-3-ols[1–4] and *C*-nor-*D*-homosteroid-5-en-3β-ols[5] in the presence of mercury(II) oxide and iodine. In either a photo- or thermally-induced reaction, 3β,5-epoxy-*A*-homo-4-oxa-5α-cholestanes or the *C*-nor-*D*-homo analogue, among others, were common products. The introductions of methyl substituents at the C-3 or C-4[2–4] position or of an oxo group at the C-7[1] position, and changing the C-ring from 6-membered to 5-membered[5] were found appreciably to affect the relative yields of the products and even to lead to an additional formation of 3-oxacholest-5-enes.[3,4]

In this paper, the photo- and thermally-induced rearrangement of two cholest-5-en-3β-ols, 6-methylcholest-5-en-3β-ol(**1**),[6] and 4,4,6-trimethylcholest-5-en-3β-ol(**4**), will be reported. The work was undertaken in order to gain more information concerning the effect of alkyl groups on the products of this reaction. The reactions were conducted under the conditions reported previously.[2] Thus, the irradiation of **1** in benzene containing iodine and mercury(II) oxide with a 100-W high pressure mercury arc for 6 h under an atmosphere of nitrogen gave a mixture of products. The separation of the products by preparative TLC gave two products, (**2**) (32%) and (**3**) (23%) (Scheme 1).

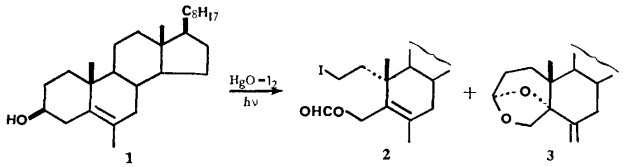

1 2 3

Scheme 1.

The molecular formula of the crystalline product **2** was determined to be $C_{28}H_{47}O_2I$ by means of high-resolution mass spectrometry, while its structure as a formate, 2-iodo-6-methyl-*A*-nor-2,3-secocholest-5-en-3-yl formate, was immediately made apparent by the IR and NMR spectra[2] (see Experimental). The molecular formula, $C_{28}H_{46}O_2$, of **3** was also determined by high-resolution mass spectrometry. The IR and NMR spectra were in agreement with the 3α,5-epoxy-6-methylene-*A*-homo-4-oxa-5α-cholestane structure (see Experimental).

The product **3** was also obtained in a 16% yield in the thermally-induced reaction of **1** conducted at 55—60 °C.

The reactions of another 6-methylcholest-5-ene **4**[7] carrying a *gem*-dimethyl group at the C-4 positions, were then undertaken in order to confirm whether or not they give an oxabicyclic compound of type 3 and substituted 3-oxacholest-5-ene. The irradiation of **4** in benzene containing mercury(II) oxide and iodine for 4 h under an atmosphere of nitrogen gave a mixture of products, from which only one product (**5**) was isolated in a pure form (39% yield) (Scheme 2). A careful examination of the reaction

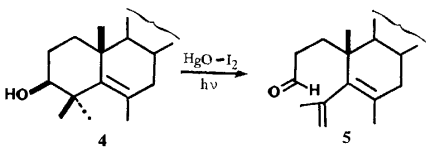

4 5

Scheme 2.

products indicated the absence of any oxabicyclic compounds or substituted 3-oxacholest-5-enes. The molecular formula ($C_{30}H_{52}O$) of **5** was determined by means of high-resolution mass spectrometry. On the basis of the IR, UV, and NMR spectra (see Experimental), the 4,6-dimethyl-4-methylene-3,4-secocholest-5-en-3-al structure is assigned to this compound.[8] The absorption maximum (205 nm) in the UV spectrum of **5** shows a considerable deviation from the value predicted by means of the Woodward diene rule[9] (Calculated value, 237 nm). This deviation is attributable to the loss of planarity of the diene system in **5** due to overcrowding caused by the 6-methyl group. The thermally-induced reaction was also attempted, but this reaction led only to an intractable mixture, and none of the products were identified.

The results obtained from the reactions of **1** also indicate the generality of the formation of oxabicyclic compounds (*e.g.*, **3**), the pathway of which has been discussed in the previous paper.[2] However, the methyl group at the C-6 position hinders the reaction of the hypothetical carbocation (**6**) with the iodine source,

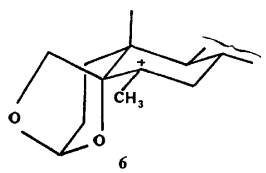

6

thus leading to the formation of the olefin, **3**.

The experiments on cholest-5-en-3β-ol **4** confirm that the introduction of three methyl groups at the C-4 and C-6 positions hinders the formation of both oxabicyclic compounds (*e.g.*, **3**) and substituted 3-oxacholest-5-enes; the latter was found to be formed particularly in the reaction of cholest-5-en-3β-ol car-

rying *gem*-dimethyl groups on the C-4.[2,4] The methyl groups destabilize the conformations of the intervening allyl radical and the successive intermediates required for the intramolecular radical additions, and also retard the combination of iodine or iodine oxide with the radical intermediates.[2]

Experimental

For the instruments used and general procedures, see Ref. 2 unless otherwise stated. The low-resolution mass spectra of **1**, **2**, and **3** and the high-resolution mass spectra of **2**, **3**, and **5** were recorded by Miss Yuko Chiba of the Faculty of Agriculture of this university with a JEOL JMS-D 300 spectrometer. The mass spectra of **4** and **5** were recorded by the staff of the Faculty of Pharmaceutical Sciences of this University with a JEOL JMS-D 300 spectrometer.

6-Methylcholest-5-en-3β-ol (1). **1** was prepared by the previously described procedure.[6] NMR, 9.33 (3H, s, 18-H), 9.02 (3H, s, 19-H), 8.40 (3H, s, 6-CH_3), 7.02 (1H, dd, J=12.0 and 4.5 Hz, 7β-H); MS (70 eV), (rel intensity) 400 (M^+, 79.5), 385 (M^+-CH_3, 100), 382 (M^+-H_2O, 46.8), 367 ($M^+-CH_3-H_2O$, 59.5), 159 (39.4), 95 (37.0), 81 (35.1), 55 (37.3), and 43 (35.9).

The Rearrangement of the Hypoiodite of 6-Methylcholest-5-en-3β-ol in the Presence of Mercury(II) Oxide and Iodine. By Irradiation. **1** (300 mg, 0.75 mmol), mercury(II) oxide (488 mg, 2.25 mmol), and iodine (570 mg, 2.24 mmol) in benzene (38 ml) were irradiated for 6 h with a 100-W high-pressure Hg arc under a nitrogen atmosphere. The solution was then filtered, and the filtrate was washed with 5% aq sodium hydrogensulfite and water successively, and then dried (Na_2SO_4). The subsequent romoval of the solvent left a product mixture (414 mg) which was subjected to preparative TLC with benzene to give five fractions: A (10 mg), B (132 mg), C (71 mg), D (89 mg), and E (87 mg) in the order of decreasing mobility. B Fraction was a formate, **2**, and after recrystallization from methanol it had a mp 64.0—66.0 °C. $[\alpha]_D^{18}$ −4.2° (*c*, 0.8 $CHCl_3$); (Found: M^+ 542.2626. Calcd for $C_{28}H_{47}O_2I$ 542.2621); IR, 1733 (OCHO), 1188, and 1163 cm^{-1} (OCHO); NMR, τ 9.34 (3H, s, 18-H), 9.11 (3H, s, 19-H), 8.31 (3H, s, 6-CH_3), 6.98 (2H, m, 2-H), 5.31 (2H, s, 3-H), and 1.83 (1H, s, OCHO): MS (70 eV), *m/e* (rel intensity), 542 (M^+, 1.0), 496 (1.4), 415 (1.2), 387 (16.5), 341 (100), and 133 (27.2). C Fraction was Compound **3** (Found: M^+ 414.3454. Calcd for $C_{28}H_{46}O_2$, M, 414.3496); IR, 1377, 1123, 1114, 998, and 901 cm^{-1}; NMR, 9.33 (3H, s, 18-H), 9.24 (3H, s, 19-H), 6.24 and 5.85 (each 1H, d, J=7.5 Hz, 4a-H), 5.45 and 5.12 (each 1H, s, 6-CH_2), and 4.48 (1H, broad s, 3β-H); MS (70 eV), *m/e* (rel intensity) 414 (M^+, 2.7), 398 (100), 383 (32.4), 133 (53,6), 107 (49.7), 95 (61.9), 81 (55.5), 69 (46.1), 57 (57.7), 55 (66.0) and 43 (72.9).

By Thermal Reaction. A thermal reaction conducted at 55—60 °C under a nitrogen atmosphere for 3 h gave a crude product (348 mg), which was then subjected to preparative TLC to afford seven fractions: A (36 mg), B (12 mg), C (4 mg), D (16 mg), E (51 mg), F (47 mg), and G (154 mg), in the order of decreasing mobility. E Fraction was identified as product **3** by a comparison of its IR, NMR, and mass spectra with those of the specimen obtained from the photo-reaction.

4,4,6-Trimethylcholest-5-en-3β-ol (4). 4,4,6-Trimethylcholest-5-en-3-one[7] (1.78 g) and lithium aluminum hydride (1 g) in dry diethyl ether (100 ml) under a nitrogen atmosphere were stirred for 10 min at 0 °C and then for 50 min at room temperature. After the addition of ethyl acetate, methanol, and water were added to the solution. The solution was then extracted with diethyl ether. The organic layer was worked-up in the usual way. Recrystallization from methanol gave **1** (1.4 g, 83%); mp 155—158 °C. An analytical specimen (mp 160.5—161 °C) was obtained by recrystallization from diethyl ether–methanol. $[\alpha]_D^{20}$ −5.3° (*c*, 1.1 $CHCl_3$) (Found: C, 83.83; H, 12.06%. Calcd for $C_{30}H_{52}O$: C, 84.04; H, 12.23%); IR, 3422 (OH), and 1036 cm^{-1}; NMR, 9.33 (3H, s, 18-H), 8.98 (3H, s, 19-H), 8.83 (3H, s, 4α-CH_3), 8.59 (3H, s, 4β-CH_3), and 6.68 (1H, dd, J=8.3 and 9.8 Hz); MS (70 eV), *m/e* (rel intensity), 428 (M^+-H_2O, 58.4). 359 ($M^+-H_2O-CH_3$, 100), 345 (89.9), 187 (26.2), 95 (52.6), 81 (38.2), 69 (43.2), 55 (50.2), and 43 (54.1).

The Rearrangement of the Hypoiodite of 4,4,6-Trimethylcholest-5-en-3β-ol in the Presence of Mercury(II) Oxide and Iodine. By Irradiation. **4** (322 mg, 0.75 mmol), mercury(II) oxide (488 mg, 2.25 mmol), and iodine (570 mg, 2.25 mmol) in benzene (38 ml) were irradiated for 4 h under a nitrogen atmosphere. The solution was then worked-up as usual, and the product was subjected to preparative TLC with benzene to yield seven fractions: A (48 mg), B (78 mg), C (24 mg), D (20 mg), E (38 mg), F (62 mg), and G (122 mg), in the order of decreasing mobility. Fractions A and B were aldehyde. The aldehyde was purified by preparative TLC, but we failed to induce crystals. (Found: M^+, 426.3877. Calcd for $C_{30}H_{50}O$. M, 426.3862); $[\alpha]_D^{21}$ −18.3 (*c*, 1.0 $CHCl_3$); IR, (neat), 908 (-C=CH_2), 1626, 1728 (CHO), and 2715 (CHO); NMR, τ 9.32 (3H, s, 18-H), 8.95 (3H, s, 19-H), 8.41 (3H, s, 6-CH_3 or 4-CH_3), 8.17 (3H, s, 6-CH_3 or 4-CH_3), 5.64 and 4.93 (each 1H, br.s, $W_{1/2}$= 0.6 Hz, 4-CH_2) and 0.09 (1H, t, J=0.3 Hz, CHO); UV_{max} (C_2H_5OH) 205 nm (ε 6700); MS (70 eV), *m/e* (rel intensity), 426 (M^+, 15.5), 411 ($M^+-CH_2CH_2CHO$, 100), 161 (27.5), 95 (33.9), 57 (37.7), and 43 (38.0).

By Thermal Reaction. A thermal reaction in the same scale conducted at 55—60 °C under a nitrogen atmosphere for 3 h in the dark gave a crude product (374 mg), which was then subjected to preparative TLC to give six fractions; A (67 mg), B (27 mg), C (23 mg), D (31 mg), E (51 mg), and F (156 mg), in the order of decreasing mobility. Fraction D was found to be identical with **5** by a comparisons of the IR, UV, NMR and mass spectra.

References

1) Photo-induced Transformations. Part 62. Part 61: H. Suginome, T. Yabe, and E. Osawa, *J. Chem. Soc., Perkin Trans. 1*, **1982**, 931.

2) H. Suginome, A. Furusaki, K. Kato, N. Maeda, and F. Yonebayashi, *J. Chem. Soc., Perkin Trans. 1*, **1981**, 236.

3) H. Suginome and N. Maeda, *Bull. Chem. Soc. Jpn.*, **53**, 2621 (1980).

4) H. Suginome and N. Maeda, *Bull. Chem. Soc. Jpn.*, **53**, 2626 (1980).

5) H. Suginome, K. Kato, and T. Masamune, *Bull. Chem. Soc. Jpn.*, **54**, 3181 (1981).

6) L. F. Fieser and J. Rigaudy, *J. Am. Chem. Soc.*, **73**, 4660 (1951).

7) R. J. Abraham and J. S. E. Holker, *J. Chem. Soc.*, **1963**, 806; S. Julia and B. Decouvelaere, *Bull. Soc. Chem. Fr.*, **1964**, 2476; H. Suginome, N. Maeda, Y. Takahashi, and N. Miyata, *Bull. Chem. Soc. Jpn.*, **54**, 846 (1981).

8) An alternative structure, 4,4-dimethyl-6-methylene-3,4-secocholest-4-en-3-al (A), is also consistent with the observed IR, UV, NMR, and mass spectra, and therefore cannot definitely be excluded:

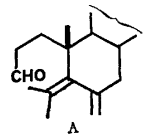

A

9) R. B. Woodward, *J. Am. Chem. Soc.*, **64**, 72 (1942).

Studies of Aromatic Sesquiterpenes. III. The Synthesis of 4-Methoxyisocadalene[1]

Kazuo ADACHI* and Naoki TANIGUCHI
Osaka Institute of Technology, Omiya, Asahi-ku, Osaka 535
(Received August 5, 1981)

Synopsis. Starting from *p*-cresol, the title sesquiterpene was synthesized through 4-methoxy-1,6-dimethylnaphthalene as a key intermediate.

The new aromatic sesquiterpene ether, 4-methoxyisocadalene, was recently isolated,[2] along with cadalene and other substances, from the aerial parts of Mexican *Heterotheca inuloides* Cass. (Compositae). 2-Isopropyl-1-methoxy-4,7-dimethylnaphthalene (**1**) was proposed as the structure of this sesquiterpene on the basis of comprehensive spectral studies.[2] In this paper the synthesis of **1** through the acetylation of 4-methoxy-1,6-dimethylnaphthalene (**2**) will be described.

2-Methoxy-5-methylpropiophenone (**3**) was converted to ethyl 2-(2-methoxy-5-methylbenzoyl)propionate (**4**), which, on reduction with $NaBH_4$ and subsequent chlorination, afforded ethyl 3-chloro-2-methyl-3-(2-methoxy-5-methylphenyl)propionate (**6**). The reduction of **6** with $LiAlH_4$ gave 2-methyl-3-(2-methoxy-5-methylphenyl)-1-propanol (**7**), from which 3,4-dihydro-5-methoxy-3,8-dimethyl-1(2*H*)-naphthalenone (**11**) was prepared in 4 steps. The aromatization of **11** produced a key intermediate (**2**), which, on acetylation, resulted in a mixture of 2-acetyl-4,7-dimethyl-1-naphthol (**14**) and other acetyl compounds (**15**—**17**). The title compound was synthesized from the reaction product of the methyl ether (**18**) with methylmagnesium iodide.

The structure of the synthesized product (**1**) was confirmed by a comparison of its NMR data with those reported in the literature.[2] The complexes of **1** with picric acid and 1,3,5-trinitrobenzene showed mp 90.5—91.5 °C and 104.5—105.5 °C respectively.

1: R=*i*-Pr
2: R=H

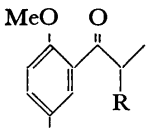

3: R=H
4: R=CO_2Et

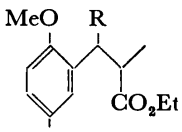

5: R=OH
6: R=Cl

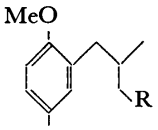

7: R=OH
8: R=Br
9: R=CN
10: R=CO_2H

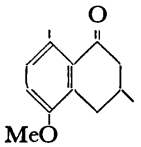

11

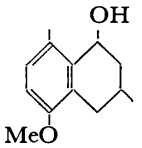

12

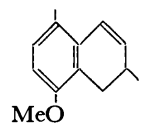

13

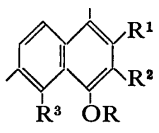

	R	R^1	R^2	R^3
14:	H	H	Ac	H
15:	Me	H	H	Ac
16:	Me	Ac	H	H
17:	H	H	Ac	Ac
18:	Me	H	Ac	H

Experimental

2-Methoxy-5-methylpropiophenone (3). The condensation of *p*-methylanisole (122.2 g) and propionyl chloride (97.3 g) by $AlCl_3$ (140 g) in CS_2 (370 ml) gave **3** (173.8 g) in a 97.5% yield; bp 128—130 °C/10 mmHg (1 mmHg≈133.322 Pa); IR: 1675, 810 cm^{-1}; NMR: δ 1.08 (t, 3H, CH_3), 2.23 (s, 3H, CH_3), 2.86 (q, 2H, CH_2), 3.78 (s, 3H, OCH_3), 6.71 (d, 1H, J=9 Hz), 7.08 (dd, 1H, J=9 and 2 Hz), 7.35 (d, 1H, J=2 Hz).

2,4-Dinitrophenylhydrazone: Yellow needles; mp 112.0—112.5 °C. Found: C, 57.24; H, 5.03; N, 15.84%. Calcd for $C_{17}H_{18}N_4O_5$: C, 56.98; H, 5.06; N, 15.64%.

Ethyl 2-(2-Methoxy-5-methylbenzoyl)propionate (4). A reaction product of diethyl oxalate (76.7 g) and a sodio-derivative of **3** prepared from **3** (89.0 g) and Na (12.1 g) in ethanol (160 ml) was decarbonylated (2 h, 180 °C) to give **4** (113.1 g) in a 90.5% yield; bp 144—145 °C/3 mmHg; IR: 1735, 1675, 810 cm^{-1}; NMR: δ 1.15 (t, 3H, CH_3), 1.43 (d, 3H, CH_3), 2.25 (s, 3H, CH_3), 3.82 (s, 3H, OCH_3), 4.09 (q, 2H, CH_2), 4.33 (q, 1H, >CH–), 6.85 (d, 1H, J=8 Hz), 7.27 (dd, 1H, J=8 and 2 Hz), 7.57 (d, 1H, J=2 Hz).

Ethyl 3-Hydroxy-2-methyl-3-(2-methoxy-5-methylphenyl)propionate (5). The reduction of **4** (25.0 g) with $NaBH_4$ (1.4 g) in methanol (100 ml) (3 h, 25 °C) furnished **5** (24.2 g) in a 96.0% yield; bp 143—144 °C/6 mmHg; IR: 3450, 1730, 805 cm^{-1}; NMR: δ 1.03 (d, 3H, CH_3), 1.20 (t, 3H, CH_3), 2.27 (s, 3H, CH_3), 2.78 (m, 1H, >CH–), 3.20 and 3.32 (1H, OH), 3.77 (s, 3H, OCH_3), 4.08 (q, 2H, CH_2), 4.87 (m, 1H, >CH–), 6.63 (d, 1H, J=9 Hz), 6.85 (d, 1H, J=2 Hz), 7.09 (dd, 1H, J=9 and 2 Hz).

Ethyl 3-Chloro-2-methyl-3-(2-methoxy-5-methylphenyl)propionate (6). A mixture of **5** (77.2 g) and concd HCl (450 ml) was stirred for 1 h at 20 °C to give **6** (77.2 g) in a 93.2% yield as a mixture consisting of two diastereomers (1:1); bp 148—148.5 °C/7 mmHg.

dl-erythro-*Isomer of* **6**: Prisms, mp 75—76 °C; IR 1735, 1040, 1035, 805 cm^{-1}; NMR: δ 0.94 (d, 3H, CH_3), 1.27 (t, 3H, CH_3), 2.27 (s, 3H, CH_3), 3.12 (dq, 1H, >CH–, J=11 and 7 Hz), 3.77 (s, 3H, OCH_3), 4.16 (q, 2H, CH_2), 5.51 (d, 1H, >CH–, J=11 Hz), 6.73 (d, 1H, J=9 Hz), 7.03 (dd, 1H, J=9 and 2 Hz), 7.20 (br, 1H). Found: C, 62.24; H, 6.83%. Calcd for $C_{14}H_{19}ClO_3$: C, 62.11; H, 7.07%.

dl-threo-*Isomer of* **6**: Oil, bp 135—136 °C/5 mmHg; IR: 1735, 1030, 810 cm^{-1}; NMR: δ 1.05 (t, 3H, CH_3), 1.26 (d, 3H, CH_3), 2.27 (s, 3H, CH_3), 3.17 (qin, 1H, >CH–, J=7 Hz), 3.77 (s, 3H, OCH_3), 3.98 (q, 2H, CH_2), 5.66 (d, 1H, >CH–, J=7 Hz), 6.69 (d, 1H, J=9 Hz), 7.03 (dd, 1H, J=9 and 2 Hz), 7.27 (br, 1H). Found: C, 62.16; H, 7.22%. Calcd for $C_{14}H_{19}ClO_3$: C, 62.11; H, 7.07%.

3-Methyl-4-(2-methoxy-5-methylphenyl)butyric Acid (10). The reduction of **6** (9.2 g) with $LiAlH_4$ (4.0 g) in ether (60 ml) gave 2-methyl-3-(2-methoxy-5-methylphenyl)-1-propanol (**7**); yield, 5.7 g (86.4%); bp 124—126 °C/7 mmHg; IR: 3350, 800 cm^{-1}.

The reaction of **7** (19.4 g) with PBr_3 (11.7 g) in CCl_4 (60 ml) gave 2-methyl-3-(2-methoxy-5-methylphenyl)propyl bromide (**8**); yield, 12.1 g (47.1%); bp 118—119.5 °C/4

mmHg.

A solution of **8** (42.9 g), KCN (32.2 g) and water (60 ml) in ethanol (386 ml) was refluxed for 20 h to give 3-methyl-4-(2-methoxy-5-methylphenyl)butanenitrile (**9**); yield, 29.8 g (87.9%); bp 130—132 °C/7 mmHg; IR: 2240, 805 cm^{-1}.

A mixture of **9** (29.8 g), concd H_2SO_4 (60 ml), acetic acid (60 ml), and water (60 ml) was refluxed for 5 h to give **10**; yield, 23.4 g (71.8%); bp 164—167 °C/8 mmHg, mp 53.5—54.5 °C; IR: 1690, 805 cm^{-1}. Found: C, 70.21; H, 8.37%. Calcd for $C_{13}H_{18}O_3$: C, 70.24; H, 8.16%.

*3,4-Dihydro-5-methoxy-3,8-dimethyl-1(2H)-naphthalenone (**11**).* The reaction of **10** (19.2 g) and thionyl chloride (30.9 g) in benzene (50 ml) gave the acid chloride of **10**; yield, 19.7 g (94.7%); bp 137 °C/5 mmHg. The cyclization of this acid chloride (11.2 g) by $SnCl_4$ (36.5 g) in benzene (50 ml) gave 9.0 g (94.7%) of **11**; bp 140—142 °C/8 mmHg, mp 38—39 °C; IR: 1670, 810 cm^{-1}; NMR: δ 1.10 (m, 3H, CH_3), 2.03—3.25 (m, 5H), 2.48 (s, 3H, CH_3), 3.78 (s, 3H, OCH_3), 6.74 (d, 1H, J=9 Hz), 6.94 (d, 1H, J=9 Hz). Found: C, 76.41; H, 8.03%. Calcd for $C_{13}H_{16}O_2$: C, 76.44; H, 7.90%.

2,4-Dinitrophenylhydrazone: Red needles, mp 196.5—197.0 °C. Found: C, 59.37; H, 5.19; N, 14.71%. Calcd for $C_{19}H_{20}N_4O_5$: C, 59.37; H, 5.24; N, 14.58%.

*4-Methoxy-1,6-dimethylnaphthalene (**2**) and Its Acetylation.* The reduction of **11** (15.6 g) with $NaBH_4$ (1.5 g) in methanol (60 ml) produced 15.7 g (99.3%) of 1,2,3,4-tetrahydro-5-methoxy-3,8-dimethyl-1-naphthol (**12**), needles; mp 107.0—107.5 °C; IR: 3350, 800, 790 cm^{-1}. Found: C, 75.46; H, 8.93%. Calcd for $C_{13}H_{18}O_2$: C, 75.69; H, 8.80%.

The dehydration of **12** (15.0 g) with $KHSO_4$ (3.0 g) gave 12.3 g (89.9%) of 1,2-dihydro-8-methoxy-2,5-dimethylnaphthalene (**13**); bp 103—105 °C/4 mmHg; NMR: δ 1.09 (d, 3H, CH_3), 2.22 (s, 3H, CH_3), 2.4—3.0 (m, 3H, CH_2 and >CH–), 3.70 (s, 3H, OCH_3), 5.82 (dd, 1H, J=9 and 3 Hz), 6.48 (d, 1H, J=9 Hz), 6.49 (d, 1H, J=9 Hz), 6.81 (d, 1H, J=9 Hz).

A dehydrogenation product of **13** (12.3 g) upon heating with 5% Pd–C (2.5 g) (5 h, 230 °C) was distilled to give two fractions. The fore-run (3.1 g) was a mixture of 1.6-dimethylnaphthalene (48.3%), **2** (36.8%) and other substances. The main fraction was 7.9 g (64.9%) of **2**; bp 123—125 °C/5 mmHg; IR: 1600, 1580, 1380, 1355, 1270, 1090, 815 cm^{-1}; NMR: δ 2.48 (s, 3H, CH_3), 2.53 (s, 3H, CH_3), 3.87 (s, 3H, OCH_3), 6.58 (d, 1H, J=8 Hz), 7.08 (d, 1H, J=8 Hz), 7.29 (dd, 1H, J=9 and 2 Hz), 7.78 (d, 1H, J=9 Hz), 8.08 (br, 1H). *Picrate*: Red needles; mp 158.0—158.5 °C. Found: C, 55.00; H, 3.93; N, 10.02%. Calcd for $C_{19}H_{17}N_3O_8$: C, 54.94; H, 4.13; N, 10.12%.

The reaction of **2** (3.0 g) and acetyl chloride (2.3 g) with $AlCl_3$ (4.8 g) in CS_2 (40 ml) gave acetyl compounds (3.4 g), a mixture of **14** (45.5%), **15** (8.9%), **16** (23.4%), and **17** (18.2%). Each component was isolated by elution with CH_2Cl_2 through a silica-gel column.

*2-Acetyl-4,7-dimethyl-1-naphthol (**14**)*: Yellow needles; mp 124.0—124.5 °C; IR: 1615, 815 cm^{-1}; NMR: δ 2.48 (br, 6H, two CH_3), 2.58 (s, 3H, CH_3), 7.27 (br, 1H), 7.41 (dd, 1H, J=9 and 2 Hz), 7.71 (d, 1H, J=9 Hz), 8.22 (br, 1H), 13.77 (s, 1H, OH). Found: C, 78.67; H, 6.43%. Calcd for $C_{14}H_{14}O_2$: C, 78.48; H, 6.59%.

*1-Acetyl-8-methoxy-2,5-dimethylnaphthalene (**15**)*: Needles; mp 65.0—66.5 °C; IR: 1695, 820, 780 cm^{-1}. Found: C, 78.86; H, 7.19%. Calcd for $C_{15}H_{16}O_2$: C, 78.92; H, 7.06%.

*2-Acetyl-4-methoxy-1,6-dimethylnaphthalene (**16**)*: Micro crystals; mp 71.5—72.5 °C; IR: 1675, 810 cm^{-1}. Found: C, 78.84; H, 7.19%. Calcd for $C_{15}H_{16}O_2$: C, 78.92; H, 7.06%.

*2,8-Diacetyl-4,7-dimethyl-1-naphthol (**17**)*: Yellow micro crystals; mp 172.0—173.5 °C; IR: 1695, 1615, 870 cm^{-1}. Found: C, 75.02; H, 6.29%. Calcd for $C_{16}H_{16}O_3$: C, 74.98; H, 6.29%.

*2-Acetyl-1-methoxy-4,7-dimethylnaphthalene (**18**).* The methylation of **14** (0.4 g) with dimethyl sulfate (0.3 g) and K_2CO_3 (0.4 g) in acetone (20 ml) gave 0.4 g of **18**; IR: 1670, 815 cm^{-1}; NMR: δ 2.50 (s, 6H, two CH_3), 2.60 (s, 3H, CH_3), 3.85 (s, 3H, OCH_3), 7.26 (dd, 1H, J=9 and 2 Hz), 7.37 (br, 1H), 7.71 (d, 1H, J=9 Hz), 7.90 (br, 1H). *2,4-Dinitrophenylhydrazone*: Yellow needles; mp 230—231 °C (dec). Found: C, 61.84; H, 4.91; N, 13.55%. Calcd for $C_{21}H_{20}N_4O_5$: C, 61.76; H, 4.94; N, 13.72%.

*4-Methoxyisocadalene (**1**).* The reaction product of **18** (0.5 g) and the Grignard reagent prepared from Mg (0.5 g) and methyl iodide (2.2 g) in ether (40 ml) were stirred with concd HCl (10 ml) for 30 min. Then the reaction product was stirred with $LiAlH_4$ (1.0 g) in ether (20 ml) at 40 °C for 4 h. The resulting product was hydrogenated in ethanol (50 ml) over Pd–C (5%, 0.5 g) and then chromatographed over silica-gel, eluting with CH_2Cl_2, to give 0.4 g (75.0%) of **1**; IR: 1625, 1605, 1380, 1350, 1095, 995, 875, 810 cm^{-1}; NMR: δ 1.28 (d, 6H, $<^{CH_3}_{CH_3}$), 2.52 (s, 3H, CH_3), 2.57 (s, 3H, CH_3), 3.52 (m, 1H, >CH–), 3.83 (s, 3H, OCH_3), 7.03 (br, 1H), 7.16 (dd, 1H, J=9 and 2 Hz), 7.71 (d, 1H, J=9 Hz), 7.80 (br, 1H). *Picrate*: Orange brown needles; mp 90.5—91.5 °C. Found: C, 58.00; H, 5.21; N, 8.92%. Calcd for $C_{22}H_{23}N_3O_8$: C, 57.76; H, 5.07; N, 9.19%. *1,3,5-Trinitrobenzene complex*: Yellow orange needles; mp 104.5—105.5 °C. Found: C, 60.05; H, 5.40; N, 9.35%. Calcd for $C_{22}H_{23}N_3O_7$: C, 59.86; H, 5.25; N, 9.52%.

References

1) Preceding paper: J. Tanaka and K. Adachi, *Nippon Kagaku Kaishi*, **1981**, 994.

2) F. Bohlmann and C. Zdero, *Chem. Ber.*, **109**, 2021 (1976).

The Racemization of Glutamic Acid Induced by Aliphatic Aldehydes

Mihoko YAMAMOTO, Hiroshi OZAKI, Akira TAI,* and Yoshiharu IZUMI
Division of Organic Chemistry, Institute for Protein Research, Osaka University, 3-2 Yamada-oka, Suita, Osaka 565
(Received July 20, 1981)

Synopsis. The real catalytic species in the racemization of glutamic acid induced by acetaldehyde was investigated and found to be 2-butenal produced *in situ* from acetaldehyde.

It has been reported that the catalytic species of the racemization of alanine induced by Cu_2O was acetaldehyde produced in alanine and Cu_2O–O_2 system.[1] In the course of a study of the racemization of glutamic acid with acetaldehyde, it has also been made clear that acetaldehyde functions not only as a moderately active racemization catalyst, but also as a precursor of the highly active racemization catalyst produced in the course of the reaction. In a patent, aliphatic aldehydes have been reported to be a good catalyst for the racemization of amino acid.[2] However, no systematic study has been carried out. In this paper, the function of aliphatic aldehydes in the racemization of glutamic acid will be discussed.

The racemizations of glutamic acid with various aliphatic aldehydes were carried out in the presence of Cu^{2+} ions. The time courses of the racemization yield and the consumption of aldehyde are shown in Fig. 1. The time courses of racemization with different aldehydes showed different features. The activity induced by acetaldehyde was much higher than that induced by the other aldehydes. The order of activity was: acetaldehyde>propionaldehyde>formaldehyde>isobutyraldehyde.

As may be found in Fig. 1, the racemization induced by acetaldehyde proceeds with the consumption of acetaldehyde. The high rate of racemization was unchanged even after 90% of the acetaldehyde has disappeared in the reaction mixture. This result strongly suggests that, although acetaldehyde itself may have some catalytic activity, another compound having a much higher racemization activity than acetaldehyde is produced *in situ* at an early stage of the reaction.

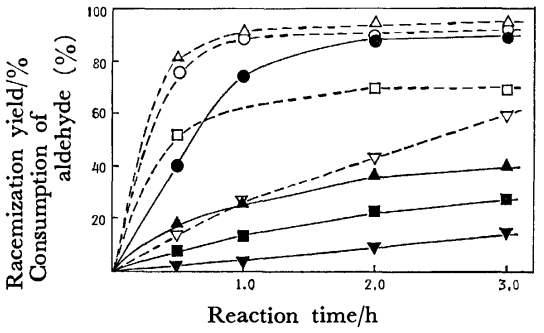

Fig. 1. Time course of racemization with acetaldehyde (—●—), propionaldehyde (—▲—), formaldehyde (—■—), and isobutyraldehyde (—▼—), and time course of consumption of acetaldehyde (—○—), propionaldehyde (—△—), formaldehyde (—□—), and isobutyraldehyde (—▽—).

Propionaldehyde shows the same consumption curve as acetaldehyde. However, the rate of racemization with propionaldehyde was found to be slow. That is, the racemization activity of the compound produced from propionaldehyde *in situ* was not expected to be so strong as that produced from acetaldehyde. When isobutyraldehyde was used, the consumption of the aldehyde was very slow, and the rate of racemization was almost negligible compared to that with acetaldehyde.

In the case of formaldehyde, the rate of racemization was unexpectedly slow, and the consumption of aldehyde was also slow.

The analyses of carbonyl compounds in the reaction mixture indicated that 2-butenal (I), 3-hydroxybutanal (II), and 2-oxoglutaric acid (III) were formed even at an early stage of the reaction. I and II were the products of the aldol condensation of acetaldehyde, while III was the product of the oxidative deamination of glutamic acid. As may be found in Fig. 2, the products of the aldol condensation showed a high racemization activity, while III showed no appreciable activity. Thus, the aldol condensation of acetaldehyde in the reaction system was expected to play a major role in giving a highly active catalyst for the racemization *in situ*. The order of the activity

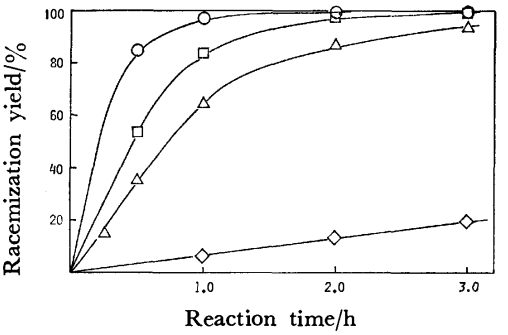

Fig. 2. Time course of racemization (at 56 °C) with acetaldehyde (—△—), II (—□—), I (—○—), and III (—◇—).

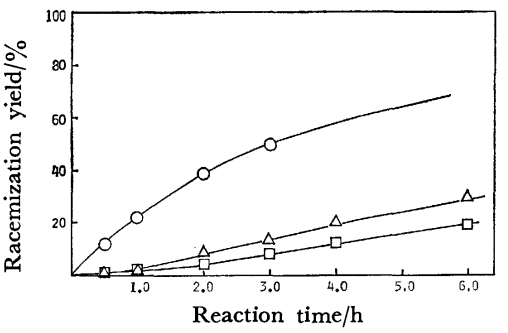

Fig. 3. Time course of racemization (at 25 °C) with acetaldehyde (—△—), II (—□—), and I (—○—).

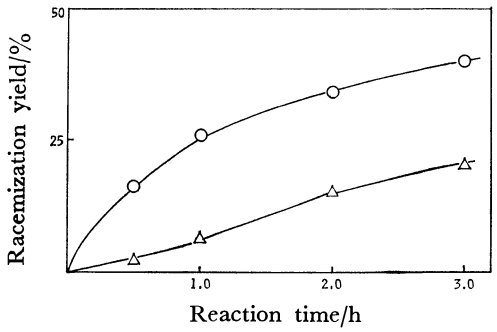

Fig. 4. Time course of racemization with propionaldehyde (—○—) and 2-methyl-2-pentenal (—△—).

at 50 °C was as follows: acetaldehyde<II<I. However, at 25 °C (Fig. 3), the order of II and acetaldehyde was reversed (II<acetaldehyde<I). Since the conversion of acetaldehyde and II to I must be slow at a lower reaction temperature, the order of the catalytic activities at 25 °C is considered to reflect the order of the intrinsic racemization activity of each compound. On the other hand, at a higher reaction temperature, 56 °C, II and acetaldehyde are converted to I. Since I is produced from II (one-step reaction) much more easily than from acetaldehyde (two-step reaction), a higher racemization rate was attained by the use of II than that of acetaldehyde. From the fact that I exhibited the highest activity both at a low and at a high reaction temperature, it is clear that the real active species in the racemization induced by acetaldehyde at a high temperature is I.

It is possible to convert propionaldehyde to 2-methyl-2-pentenal through aldol condensation and successive dehydration in the reaction system. However, the racemization activity of this compound was found to be lower than that of propionaldehyde itself (Fig. 4). Thus, the overall rate of the racemization induced by propionaldehyde was not enhanced by the accumulation of α,β-unsaturated aldehyde.

Both isobutyraldehyde, which does not afford α,β-unsaturated aldehyde, and formaldehyde, which does not produce an aldol-type compound, were found to induce a poor racemization activity.

These findings also support the idea that the high rate of racemization induced by acetaldehyde is attributable to the formation and to the accumulation of the I produced in a reaction system.

Experimental

The colorimetric determination was performed using a Hitachi 124 spectrometer. Thin-layer chromatography was carried out with a precoated plate of silica gel (E. Merck) with Solvent 1 (diethyl ether/cyclohexane=10/2.5) or Solvent 2 (1-butanol/1-propanol/benzene/conc. ammonia/water =3/10/3/0.5/3.5). The optical rotation was measured by the use of Perkin-Elmer 241 Polarimeter.

Materials. The (*S*)-glutamic acid and copper(II) sulfate pentahydrate were obtained from commercial sources. The acetaldehyde was generated by the decomposition of paraldehyde in the presence of sulfuric acid. The propionaldehyde, isobutyraldehyde, II, and I were distilled immediately before use.

Racemization. Into a slurry of (*S*)-glutamic acid (30 mmol) and $CuSO_4 \cdot 5H_2O$ (3 mmol) in 10 ml of water, was added a 7 M (1 M=1 mol dm^{-3}) NaOH solution until the pH of the solution became 10.4. Then the mixture was made up to 30 ml with water.

In a shaker flask, a 25-ml portion of the solution and 2.5 mmol of aldehyde were placed, after which the mixture was shaken at the temperature stated in the text. At specific time intervals, a small portion of the reaction mixture was taken out for analysis.

Determination of the Racemization Yield. A 3-ml portion of the reaction mixture at each reaction time was acidified with 6 ml of 6 M HCl. After the removal of Cu^{2+} from the 3-ml portion of the acidified reaction mixture by treatment with H_2S, the resulting solution was made up to 5 ml with water and subjected to the determination of the optical rotation (α_D^{20}). The degree of racemization was calculated from the ratio of α_D^{20} at each reaction time to the α_D^{20} at the beginning of the reaction.

Determination of Aldehydes. A 3-ml portion of the acidified reaction mixture was mixed with 3 ml of a 1.5% aqueous solution of 4-nitrophenylhydrazine hydrochloride. The reaction product was extracted with 10 ml of ethyl butyrate.

A 100-μl portion of the extract was submitted to chromatography on a TLC plate with Solvent 1. The 4-nitrophenylhydrazone of aldehyde was recovered by scraping the corresponding part of the silica gel and eluting with 5 ml of ethanol. The amount of 4-nitrophenylhydrazone of aldehyde in the elute was determined by colorimetry with the absorbances at 380 nm (acetaldehyde), 390 nm (propionaldehyde and isobutyraldehyde), and 345 nm (formaldehyde).

Identification of Carbonyl Compounds. From the acidified reaction mixture induced by acetaldehyde, yellow products were obtained by a reaction with 4-nitrophenylhydrazine. The yellow crystals were found to contain 4-nitrophenylhydrazone derivatives of II, I, and III by a comparison of their Rf values and UV absorption spectra (λ_{max}) with those of authentic samples. The Rf values of the 4-nitrophenylhydrazone derivatives were found to be 0.095 for II, 0.47 for I, and 0.12 for III by the use of Solvent 1, while their λ_{max} values were 380 nm for II, 395 nm for I, and 383 nm for III.

The authors wish to express their thanks to Dr. Katsumoto Yamanouchi for his helpful suggestions. This work was supported in part by a Scientific Research Grant from the Ministry of Education, Science and Culture Japan (411108).

References

1) A. Tai, K. Okada, T. Masuda, and Y. Izumi, *Bull. Chem. Soc. Jpn.*, **49**, 310 (1976).

2) T. Ogasawara, H. Tachimichi, and S. Suzuki, Japan Patent 13445 (1967).

A Mild Silver Salt-induced Oxidation of Dibromo-5-hydroxytropolones to Dibromo-*p*-tropoquinones

Hitoshi TAKESHITA,* Tomoyuki KUSABA,† and Akira MORI

Research Institute of Industrial Science, 86, Kyushu University, Hakozaki, Fukuoka 812

† *Graduate School of Engineering Sciences, 39, Kyushu University, Hakozaki, Fukuoka 812*

(Received July 24, 1981)

Synopsis. The treatment of 3,6-dibromo-, 3,7-dibromo, 4,6-dibromo-, and unsubstituted 5-hydroxytropolones with silver acetate in acetone gave the corresponding *p*-tropoquinones in good yields. When this reaction was carried out in protic solvents, some of these tropoquinones underwent further attack by solvent nucleophiles to give Michael-adducts or ring-contracted cyclohexadienones.

Some years ago, Itô *et al.* reported the first synthesis of *p*-tropoquinone, 3,6-cycloheptadiene-1,2,5-trione (**1**), from 5-hydroxytropolone (**2**),[1] and a hydrated *o*-tropoquinone, 2,2-dihydroxy-4,6-cycloheptadiene-1,3-dione (**A**),[2] and subsequent papers described the remarkable physical and chemical properties of these basic nonbenzenoid quinones.[3,4] We will herein describe an alternative synthesis of **1** and its bromo derivatives.

When an acetone solution of 3,6-dibromo-5-hydroxytropolone (**3**) and silver acetate was kept at room temperature, metallic silver was precipitated after 15 min. From the supernatant organic layer, pale yellow crystals (**4**) were obtained by means of brief silica-gel chromatography. The **4** retained two bromine atoms intact, and the NMR data were in accord with 3,6-dibromo-*p*-tropoquinone [δ:[5] 7.59 (1H, s) and 7.72 (1H, s)]. Similarly, 3,7-dibromo-5-hydroxytropolone (**5**), 4,6-dibromo-5-hydroxytropolone (**6**), and the bromine-free **2** gave the *p*-tropoquinones, 3,7-dibromo-*p*-tropoquinone (**7**), 4,6-dibromo-*p*-tropoquinone (**8**), and **1**, respectively in good yields.

On the other hand, silver salt-induced oxidation in a protic solvent gave no tropoquinone derivative; the oxidation of **3** in acetic acid gave a Michael-type adduct of **4**, 3-acetoxy-4,7-dibromo-6-cycloheptene-1,2,5-trione (**9**), while the oxidation of **3** in ethanol gave a ring-contraction product, 2,5-dibromo-4-ethoxycarbonyl-4-hydroxy-2,5-cyclohexadien-1-one (**10**). The Michael addition must be catalyzed by the silver ion exemplified in the case of authentic **4**, changing to **9**. As expected, one 4,6-disubstituted quinone, **8**, gave no Michael adduct. Furthermore, **5** in ethanol gave 3,5-dibromo-4-ethoxycarbonyl-4-hydroxy-2,5-cyclohexadien-1-one (**11**), and the ring-contraction occurred only with the 3-bromo-*p*-tropoquinones; from the parent compound (**2**) or **6**, no cyclohexadienone was isolated.

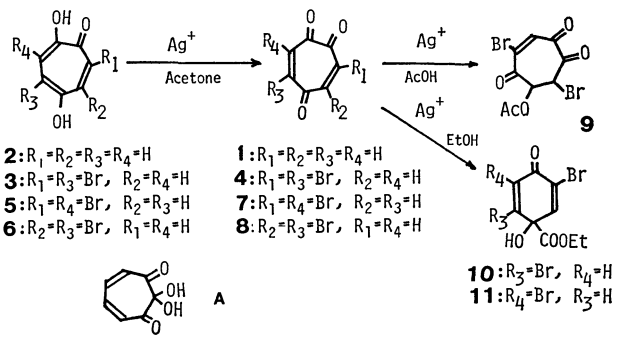

The results of an early attempt at synthesizing **1** by an iron(III) chloride or silver nitrate oxidation of **2**,[6] should be, in view of the present results, explained in terms of the protic solvents used in the reaction.

Experimental

Preparation of the Dibromo Derivatives of ***2***. To a refluxing AcOH solution (300 cm³) containing **2** (5.42 g), an AcOH solution (200 cm³) of Br_2 (13.7 g, 2.2 mol equiv.) was added, drop by drop. After the evaporation of the solvent, the residue was separated by fractional recrystallizations; from the least soluble fractions, **5** was obtained as pale yellow needles (mp 166—167 °C (from MeOH); 356 mg (3%) [Found: C, 28.30; H, 1.64%. Calcd for $C_7H_4O_3Br_2$: C, 28.41; H, 1.36%. δ^{MeOD}: 7.68 (2H, s). δ(C): 128.1(2C), 130.3(2C), 154.3, 162.8(2C). ν: 1605, 1570, 920, 870 cm^{-1}. λ_{max}^{MeOH}: 261 nm (ε=25000), 350 (7400), 412 (7600)]), followed by other pale yellow needles, **6** (mp 146—147 °C (from MeOH); 2420 mg (21%) [Found: C, 28.61; H, 1.54%. δ^{MeOD}: 8.20 (2H, s). δ(C): 131.0(2C), 134.6(2C), 151.3, 168.7(2C). ν: 1605, 1530, 960, 930 cm^{-1}. λ_{max}^{MeOH}: 263 nm (ε=14000), 386 (6300), 406 (6900)]). From the most soluble fractions, **3** was obtained as pale yellow needles; mp 166—168 °C (from EtOAc–CCl_4); 700 mg (6%) [Found: C, 28.90; H, 1.62%. δ^{MeOD}: 7.76 (1H, s), 8.08 (1H, s). δ(C): 120.6, 126.5, 131.5, 132.0, 153.6, 158.4, 169.5. ν: 1590, 1520, 990, 920 cm^{-1}. λ_{max}^{MeOH}: 251 nm (ε=13000), 334 (4300), 400 (550)].

AgOAc-oxidation of ***3*** *in Acetone.* To an acetone solution (6 cm³) of **3** (44 mg), AgOAc (50 mg) was added all at once. After magnetical stirring for 10 h at room temperature, the deposited Ag was filtered off; the filtrate was evaporated *in vacuo* and chromatographed on a short silica-gel column with benzene to give yellow crystals (**4**) (35 mg, 80%), which after recrystallizations from benzene showed a mp of 146—150 °C [Found: C, 28.74; H, 0.93; Br, 53.80%. Calcd for $C_7H_2O_3Br_2$: C, 28.60; H, 0.69; Br, 54.37%.[7] δ: 7.72 (1H, s), 7.59 (1H, s). δ(C): 135.5, 136.1, 139.3, 140.8, 178.1, 179.6, and 181.8. ν: 1700, 1680, 1640, 1600 cm^{-1}].

Catalytic Hydrogenation of ***4***. An EtOAc solution of **4** (50 mg) was hydrogenated with 5%-Pd-on-carbon (50 mg) at room temperature under an H_2-atmosphere for 10 min. After the filtration of the catalyst, the yellow needles obtained by the removal of the solvent were identical with **3** (45 mg, 89.4%).

AgOAc-oxidation of ***5*** *in Acetone.* Similarly, an acetone solution (4 cm³) of **5** (99 mg) was treated with AgOAc (51 mg) for 1 h at room temperature to give yellow needles (**7**); mp 96—97 °C (from benzene); 79 mg (81%) [Found: C, 28.64; H, 1.02%. δ: 7.51 (2H, s). δ(C): 134.9(2C), 140.6(2C), 181.8(2C), 181.9. ν: 1695, 1685 cm^{-1}].

AgOAc-oxidation of ***6*** *in Acetone.* Similarly, an acetone

solution (10 cm³) of **6** (550 mg) was oxidized with AgOAc (630 mg) at room temperature. The yellow needles obtained from the benzene fraction by silica-gel-column chromatography consisted of 480 mg (87%) of **8**; mp 146—150 °C [Found: C, 28.66; H, 0.94%. δ: 7.58 (2H, s). δ(C): 136.1(2C), 138.5(2C), 176.1(2C), and 180.7. ν: 1660, 1595 cm^{-1}].

AgOAc-oxidation of ***2*** *in Acetone.* An acetone solution (3 cm³) of **2** (100 mg) was similarly oxidized by AgOAc (245 mg) for 1.5 h. The yellow needles, 45 mg (46%), obtained by a similar work-up were identical with the authentic **1**[1] in every respect.

AgOAc-oxidation of ***3*** *in Acetic Acid.* To an AcOH solution (2 cm³) of **3** (95 mg), AgOAc (108 mg) was added at room temperature, after which the mixture was stirred for 1.5 h. The mixture was then heated *in vacuo* (below 60 °C) to remove the AcOH, and the residue was fractionated by preparative thin-layer chromatography (PTLC) to give a colorless oil (**9**); 12.6 mg (13.3%) [Found: *m/e*, 352, 353.8579 (M^+, Calcd for $C_9H_6O_5{}^{79}Br^{81}Br$: 353.8562), 356. δ: 2.18 (3H, s), 4.16 (1H, d, J=3 Hz), 5.22 (1H, d, J=3 Hz), and 6.70 (1H, s) for *cis*-**9**; 2.13 (3H, s), 4.48 (1H, d, J=9 Hz), 5.17 (1H, d, J=9 Hz), and 6.72 (1H, s) for *trans*-**9**. *cis*/*trans*=1/2. ν: 1750, 1700 cm^{-1}].

Treatment of ***4*** *with Acetic Acid.* An AcOH solution (4 cm³) of **4** (42 mg) was kept under magnetical stirring at room temperature until all of the starting **4** had been consumed (for 20 h). By PTLC fractionation, 11 mg (21%) of a colorless oil was then obtained from the mixture; it was identical with respect to the NMR spectroscopy with the **9** prepared from **3**. The rest of the material was insoluble to most ordinary organic solvents, and no further attempt at its fractionation was made.

AgOAc-treatment of ***1*** *in Acetic Acid.* To an AcOH solution (0.5 cm³) of **1** (44.4 mg), AgOAc (54.5 mg) was added all at once, after which the mixture was stirred at room temperature for 24 h. The PTLC of the reaction mixture afforded only the recovered **1** (23.9 mg, 54%), although some minor spots due to other products were detectable.

AgOAc-treatment of ***8*** *in Acetic Acid.* To an AcOH solution of **8** (34 mg), AgOAc (19 mg) was added all at once, after which the mixture was stirred at room temperature for 24 h. The PTLC resulted in the recovery of **8** (22.4 mg, 66%); no other compound was isolable.

AgOAc-oxidation of ***3*** *in Ethanol.* An EtOH solution (2 cm³) of **3** (11 mg) was stirred at room temperature with AgOAc (15 mg) for 10 h. After the filtration of the deposited Ag, the mixture was heated *in vacuo* to remove the solvent and separated by PTLC to give a colorless oil (**10**); 5.3 mg (42%) [Found: C, 32.07; H, 2.59%. Calcd for $C_9H_8O_4Br_2$: C, 31.80; H, 2.37%. δ: 1.28 (3H, t), 4.36 and 4.33 (2H, AB-part of ABX_3), 6.84 (1H, s), and 7.18 1H, s)].

AgOAc-treatment of ***4*** *in Ethanol.* An EtOH solution (4 cm³) of **4** (23.7 mg) was treated with AgOAc (14 mg) at room temperature for 20 h. The reaction mixture was then separated on PTLC to give **10** (17.3 mg, 64%).

AgOAc-oxidation of ***5*** *in Ethanol.* To an EtOH solution (1.5 cm³) of **5** (32 mg), AgOAc (37 mg) in EtOH (1.5 cm³) was added at room temperature, after which the mixture was kept for 10 h. After the filtration of metallic Ag, the mixture was separated by PTLC to give colorless crystals, mp 104—105 °C (from $CHCl_3$); 14.2 mg (38%) of **11** [Found: C, 31.91; H, 2.48%. δ: 1.33 (3H, t), 4.47 (2H, q), 6.96 (2H, s). δ(C): 13.8, 65.2, 132.8, 142.8, 167.8, 180.8. ν: 1760, 1740 cm^{-1}].

An Attempted Ring Contraction of ***6****.* An EtOH solution (4 cm³) of **6** (50 mg) was treated with AgOAc (85 mg) for 24 h. The PTLC of the reaction mixture revealed the very slow development of a new spot, but no product was isolable other than the quinone, **8** (31 mg, 63%).

AgOAc-treatment of ***1*** *in Ethanol.* An ethanol solution (2 cm³) of **1** (80.1 mg) was similarly treated with AgOAc (97.5 mg) for 24 h. The recovered **1** (52.1 mg, 65%) was the sole isolable compound in the PTLC fractionation.

References

1) S. Itô, Y. Shoji, H. Takeshita, M. Hirama, and K. Takahashi, *Tetrahedron Lett.*, **1975**, 1075.

2) M. Hirama and S. Itô, *Tetrahedron Lett.*, **1975**, 1071. For the synthesis of anhydrous **A**, see M. Hirama, Y. Fukazawa, and S. Itô, *Tetrahedron Lett.*, **1978**, 1299.

3) H. Sakurai, A. Okada, Y. Shoji, and S. Itô, *Tetrahedron Lett.*, **1978**, 2289.

4) M. Hirama, Y. Koyama, Y. Shoji, and S. Itô, *Tetrahedron Lett.*, **1978**, 2289.

5) The NMR spectra were measured in $CDCl_3$ unless otherwise stated, and the chemical shifts were expressed in δ units from the internal standard, Me_4Si. For the NMR solvent, MeOD should be read as methanol-d_4.

6) T. Nozoe, S. Seto, S. Itô, M. Sato, and T. Katono, *Proc. Jpn. Acad.*, **28**, 488 (1952).

7) The determination of the bromine content has been carried out by The Kyoto University Station of Elemental Analyses. We thank Dr. T. Otsuki, Kyoto University, for his arrangement of this measurement.

The Cheletropic Addition of Dichlorocarbene to 2-Phenylsulfonyl-2-azabicyclo[3.2.1]octa-3,6-diene and Its 8-Substituted Derivatives

Hiroo Inoue,* Kazuhiko Tokisato, and Katsumi Umano

Department of Applied Chemistry, College of Engineering, University of Osaka Prefecture, Sakai, Osaka 591

(Received August 31, 1981)

Synopsis. It was found that dichlorocarbene undergoes *exo* addition preferentially on the C_3–C_4 double bond of 2-phenylsulfonyl-2-azabicyclo[3.2.1]octa-3,6-diene and *endo* addition on that of 2-phenylsulfonyl-syn-8-benzoyloxy-2-azabicyclo[3.2.1]octa-3,6-diene.

Recently we have discovered that the 1,3-dipolar cycloadditions of phenylglyoxylonitrile oxide to 2-phenylsulfonyl-2-azabicyclo[3.2.1]octa-3,6-diene (**1**) and 2-phenylsulfonyl-syn-8-benzoyloxy-2-azabicyclo[3.2.1]-octa-3,6-diene (**3**) take place selectively with an *exo* attack on the C_6–C_7 double bond.[1] In order to explore further the reactivity of the C_3–C_4 and C_6–C_7 double bonds, particularly in their *exo* and *endo* sides, the addition of dichlorocarbene was investigated with azabicyclic dienes, **1**—**3**. Herein, we wish to report our findings on these reactions.

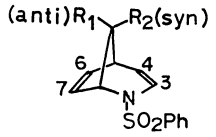

1; $R_1=R_2=H$
2; $R_1=PhCOO$, $R_2=H$
3; $R_1=H$, $R_2=PhCOO$

The reaction of diene **1** with dichlorocarbene, generated by the usual phase-transfer method,[2] afforded the 1:1 *exo* adduct (**4**) in a high yield after 30 min, as Table 1 shows. In a prolonged reaction, the 1:2 adduct (**5**) was produced by the subsequent addition of dichlorocarbene to adduct **4**. The reaction with diene **2**, in which the *exo* side of the C_6–C_7 double bond was blocked by the benzoyloxyl group, resulted in the formation of only the 1:1 *exo* adduct (**6**), even after 72 h, and the 1:2 adduct (**6'**) was not obtained at all. This indicates that the *endo* side of the C_6–C_7 double bond is much less reactive. On the other hand, when the *exo* side of the C_3–C_4 double bond was blocked by the benzoyloxyl group, the addition of dichlorocarbene was diverted to the *endo* side to afford the 1:1 *endo* adduct (**7**), together with the 1:2 adduct (**8**), as Table 1 shows.

Table 1. The yields of the products in the addition of dichlorocarbene to dienes **1**—**3**

Dienes	Time/h	Adduct(yield/%)[a]
1	0.5	**4** (84), **5** (5)
1	3	**4** (65), **5** (23)
1	72	**4** (33), **5** (45)
2	3	**6** (91)
2	72	**6** (85)
3	3	**7** (77), **8** (20)
3	72	**7** (47), **8** (30)

a) Based on the dienes.

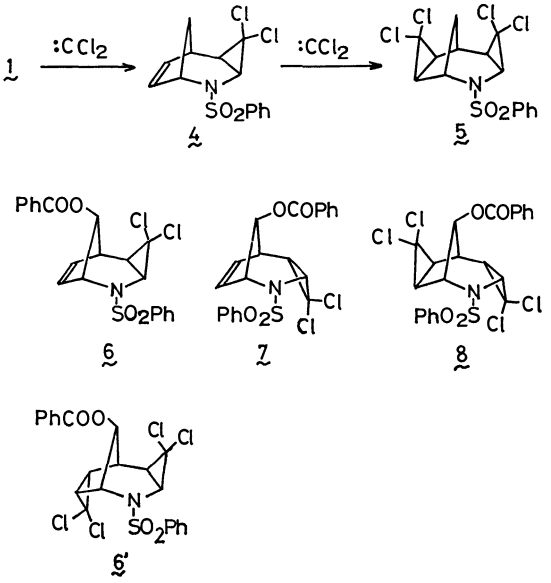

Next, the reactions of dienes **1**—**3** with dichlorocarbene were compared with those with phenylglyoxylonitrile oxide as a 1,3-dipole. The 1,3-dipolar addition to **2** in tetrahydrofuran at 0 °C afforded two *exo* adducts, **9** and **10**, in 47 and 22% yields respectively after 3 h. This phenomenon of the *exo* prevalence, which is observed even in the existence of the benzoyloxyl group in the C_6–C_7 side of **2**, agreed with the results in the cases of **1** and **3** reported previously.[1] As has been described above, we have found that dichlorocarbene exhibits an *exo* or *endo* attack preferentially on the C_3–C_4 double bond of dienes **1**—**3**, while phenylglyoxylonitrile oxide exhibits an *exo* attack on their C_6–C_7 double bonds, and that the *endo* side of the C_3–C_4 double bond is less reactive to dichlorocarbene than its *exo* side. Thus, the addition of dichlorocarbene to dienes **1**—**3** is governed by the steric effect of hydrogen or the substituent at the 8-position.

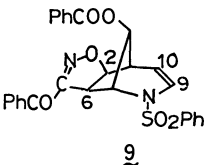

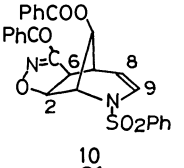

Experimental

The melting points are uncorrected. The ^1H NMR spectra were taken at room temperature with a Hitachi R-24A spectrometer, using tetramethylsilane as the internal standard. The IR spectra were taken with a Hitachi 216 grating infrared spectrometer.

Materials. Dienes **1**—**3** were prepared from nor-

bornadiene and 7-benzoyloxynorbornadiene according to the published procedures.[3] **2**: mp 121.5—122 °C; IR (KBr) 1715 cm^{-1} (CO), 1345, 1180 cm^{-1} (SO_2); ^1H NMR ($CDCl_3$) δ 2.76 (m, 1H, 5-H), 4.82 (brs, 2H, 1-H and 8-H), 5.15 (m, 2H, 4-H and 7-H), 6.09 (dd, 1H, $J_{6,7}$=5.3 Hz, $J_{5,6}$=2.3 Hz, 6-H), 6.28 (d, 1H, $J_{3,4}$=9.0 Hz, 3-H), 6.88—8.02 (m, 10H, aromatic). Found: C, 65.67; H, 4.63; N, 4.08%. Calcd for $2_{20}H_{17}NO_4S$: C, 65.40; H, 4.63; N, 3.81%. **3**: mp 114.5—115 °C; IR (KBr) 1710 cm^{-1} (CO), 1340, 1165 cm^{-1} (SO_2); ^1H NMR ($CDCl_3$) δ 2.75 (m, 1H, 5-H), 4.71 (m, 1H, 1-H), 5.07 (m, 2H, 4-H and 8-H), 5.39 (dd, 1H, $J_{6,7}$=6.0 Hz, $J_{1,7}$=3.0 Hz, 7-H), 6.09 (dd, 1H, $J_{6,7}$=6.0 Hz, $J_{5,6}$=3.3 Hz, 6-H), 6.57 (d, 1H, $J_{3,4}$=8.0 Hz, 3-H), 6.92—8.00 (m, 10H, aromatic). Found: C, 65.41; H, 4.64; N, 4.11%. Calcd for $C_{20}H_{17}NO_4S$: C, 65.40; H, 4.63; N, 3.81%.

General Procedure for the Addition of Dichlorocarbene to Dienes ***1—3***. A 50% aqueous sodium hydroxide solution (6.5 g) was stirred, drop by drop, into a solution of dienes (2.72 mmol) in chloroform (10 g) with benzyltriethylammonium chloride (50 mg) for 30 min at room temperature. After a definite period of stirring, the reaction mixture was diluted with water and extracted with chloroform. After the removal of the chloroform *in vacuo*, the residue was chromatographed on a silica-gel column, using benzene, hexane, or ethyl acetate as the eluant.

Reaction with ***1***. Two adducts, **4** and **5**, were obtained. **4**: mp 132.5—134 °C; IR (KBr) 1335 and 1168 cm^{-1} (SO_2); ^1H NMR (C_6D_6) δ 1.10 (m, 1H, 9-H_{anti}), 1.48 (dd, 1H, $J_{3,5}$=10.0 Hz, $J_{5,6}$=3.0 Hz, 5-H), 2.3 (d, 1H, $J_{9s,9a}$=11.3 Hz, 9-H_{syn}), 2.32 (m, 1H, 6-H), 3.2 (d, 1H, $J_{3,5}$=10.0 Hz, 3-H), 4.48 (m, 1H, 1-H), 5.40 (dd, 1H, $J_{7,8}$=5.7 Hz, $J_{1,8}$=2.7Hz, 8-H), 5.64 (dd, 1H, $J_{7,8}$=5.7 Hz, $J_{7,9}$=2.3 Hz, 7-H), 6.75—8.00 (m, 5H, aromatic). Found: C, 51.07; H, 3.96; N, 4.55%. Calcd for $C_{14}H_{13}NO_2SCl_2$: C, 50.92; H, 3.97; N, 4.24%. **5**: mp 165—166.5 °C; IR (KBr) 1360 and 1172 cm^{-1} (SO_2); ^1H NMR (C_6D_6) δ 1.24 (d, 1H, $J_{3,5}$=10.7 Hz, 5-H), 1.32 (d, 1H, $J_{7,9}$=7.3 Hz, 7-H), 1.69 (d, 1H, $J_{7,9}$=7.3 Hz, 9-H), 1.80 (m, 2H, 10-CH_2), 2.17 (m, 1H, 6-H), 3.13 (d, 1H, $J_{3,5}$=10.7 Hz, 3-H), 4.38 (m, 1H, 1-H), 6.67—8.10 (m, 5H, aromatic). Found: C, 43.41; H, 2.91; N, 3.36%. Calcd for $C_{15}H_{13}NO_2SCl_4$: C, 43.61; H, 3.17; N, 3.39%.

Reaction with ***2***. The adduct **6** was obtained: mp 136—137 °C; IR (KBr) 1720 cm^{-1} (CO), 1355, 1170 cm^{-1} (SO_2); ^1H NMR ($CDCl_3$) δ 2.22 (dd, 1H, $J_{3,5}$=10.0 Hz, $J_{5,6}$=3.0 Hz, 5-H), 3.27 (d, 1H, $J_{3,5}$=10.0 Hz, 3-H), 3.30 (m, 1H, 6-H), 4.91 (m, 1H, 1-H), 5.80 (m, 2H, 8-H and 9-H), 6.35 (dd, 1H, $J_{7,8}$=5.3 Hz, $J_{6,7}$=2.3 Hz, 7-H), 7.09—8.20 (m, 10H, aromatic). Found: C, 56.17; H, 3.66; N, 3.10%. Calcd for $C_{21}H_{17}NO_4SCl_2$: C, 56.01; H, 3.78; N, 3.11%. The small values of the coupling constants between H-5 and H-6 for **4** and **6** and between H-1 (H-6) and H-9 (H-7) for **5** indicated the *exo* configurations of **4**, **5**, and **6**.

Reaction with ***3***. The adducts **7** and **8** were obtained. **7**: mp 130—130.5 °C; IR (KBr) 1720 cm^{-1} (CO), 1355, 1170 cm^{-1} (SO_2); ^1H NMR ($CDCl_3$) δ 1.93 (dd, 1H, $J_{5,6}$=8.0 Hz, $J_{3,5}$=10.7 Hz, 5-H), 3.66 (d, 1H, $J_{3,5}$=10.7 Hz, 3-H), 3.48 (m, 1H, 6-H), 4.49 (m, 1H, 1-H), 5.11 (t, 1H, $J_{1,8}$=$J_{7,8}$=4.7 Hz, 8-H), 6.00 (m, 2H, 7-H and 9-H), 6.94—8.00 (m, 10H, aromatic). Found: C, 56.13; H, 3.65; N, 3.11%. Calcd for $C_{21}H_{17}NO_4SCl_2$: C, 56.01; H, 3.78; N, 3.11%. **8**: mp 185—186 °C; IR (KBr) 1720 cm^{-1} (CO), 1360, 1170 cm^{-1} (SO_2); ^1H NMR [(2:1)C_6D_6–$CDCl_3$] δ 1.67 (dd, 1H, $J_{3,5}$=10.7 Hz, $J_{5,6}$=9.3 Hz, 5-H), 2.21 (d, 1H, $J_{7,9}$=8.0 Hz, 7-H), 2.41 (d, 1H, $J_{7,9}$=8.0 Hz, 9-H), 2.91 (dd, 1H, $J_{6,10}$=4.7 Hz, $J_{5,6}$=9.3 Hz, 6-H), 3.14 (d, 1H, $J_{3,5}$=10.0 Hz, 3-H), 4.36 (d, 1H, $J_{1,10}$=4.7 Hz, 1-H), 5.67 (t, 1H, $J_{1,10}$=$J_{6,10}$=4.7 Hz, 10-H), 6.74—7.90 (m, 10H, aromatic). Found: C, 49.55; H, 3.09; N, 2.65%. Calcd for $C_{22}H_{17}NO_4SCl_4$: C, 49.55; H, 3.19; N, 2.63%. The large values of the coupling constants between H-5 and H-6 for **7** and **8** indicated the *endo* configurations of **7** and **8**.

Reaction of ***2*** *with Phenylglyoxylonitrile Oxide*. A solution of a mixture of **2** (1.63 mmol) and α-chloro-α-(hydroxyimino)acetophenone (1.63 mmol) was cooled in an ice bath. Into the cooled solution, a solution of triethylamine (2.12 mmol) in tetrahydrofuran (20 cm^3) was then added and stirred. After 2 h, a precipitate was removed by filtration, and the filtrate was evaporated to dryness under reduced pressure. The residue was chromatographed on a silica-gel column, using (40:1) benzene–ethyl acetate as the eluant, to give two adducts, **9** (0.39 g, 47%) and **10** (0.19 g, 22%), puls a 23% recovery of **2**. **9**: mp 164—165 °C; IR (KBr) 1730 cm^{-1} (CO), 1355, 1170 cm^{-1} (SO_2); ^1H NMR ($CDCl_3$) δ 3.04 (d, 1H, $J_{1,10}$=7.3, 1-H), 3.96 (d, 1H, $J_{2,6}$=9.3 Hz, 6-H), 5.07 (m, 4H, 2-H, 7-H, 10-H, and 11-H), 6.51 (d, 1H, $J_{9,10}$=7.7 Hz, 9-H), 6.88—8.17 (m, 15H, aromatic). Found: C, 65.14; H, 4.22; N, 5.25%. Calcd for $C_{28}H_{22}N_2O_6S$: C, 65.37; H, 4.28; N, 5.44%. **10**: mp 147—148 °C; IR (KBr) 1725 cm^{-1} (CO), 1360, 1175 cm^{-1} (SO_2); ^1H NMR ($CDCl_3$) δ 3.18 (d, 1H, $J_{7,8}$=7.7 Hz, 7-H), 4.38 (d, 1H, $J_{2,6}$=9.3 Hz, 6-H), 4.86 (m, 2H, 1-H and 11-H), 5.10 (d, 1H, $J_{2,6}$=9.3 Hz, 2-H), 5.29 (dd, 1H, $J_{7,8}$=7.7 Hz, $J_{8,9}$=8.0 Hz, 8-H), 6.41 (d, 1H, $J_{8,9}$=8.0 Hz, 9-H), 6.98—8.11 (m, 15H, aromatic). Found: C, 65.18; H, 4.12; N, 5.27%. Calcd for $C_{28}H_{22}N_2O_6S$: C, 65.37; H, 4.28; N, 5.44%. The large difference in the chemical shifts between 2-H and 6-H indicated the orientation of adduct **9**.[4]

References

1) K. Umano, S. Mizone, K. Tokisato, and H. Inoue, *Tetrahedron Lett.*, **1981**, 73.

2) G. C. Joshi, N. Singh, and L. M. Pande, *Tetrahedron Lett.*, **1972**, 1461.

3) A. C. Oehlschlager and L. H. Zalkow, *J. Org. Chem.*, **30**, 4205 (1965); M. Klaus and H. Prinzbach, *Angew. Chem., Int. Ed. Engl.*, **10**, 273 (1971); K. Umano, H. Taniguchi, H. Inoue, and E. Imoto, *Tetrahedron Lett.*, **1979**, 247.

4) H. Taniguchi, T. Ikeda, and E. Imoto, *Bull. Chem. Soc. Jpn.*, **51**, 1859 (1978).

A New Synthesis of Aldehydes and Aldehydes-*d* from Grignard Reagents

Masakazu YAMASHITA,* Kanako MIYOSHI, Yutaka NAKAZONO, and Rikisaku SUEMITSU

Department of Applied Chemistry, Faculty of Engineering, Doshisha University, Kamikyo-ku, Kyoto 602

(Received September 10, 1981)

Synopsis. Aldehydes were prepared from Grignard reagents in high yields using pentacarbonyliron as the carbonylating agent. This reaction was also found to be applicable to the synthesis of aldehydes-*d*.

Although there have been some reports on the synthesis of aldehydes by the use of Grignard reagents, these processes have been restricted to the hydrolysis of an intermediate derived from the reagent, and it is impossible to synthesize an aldehyde-*d*.[1] In this note, we wish to report an alternative and useful method for synthesizing aldehydes and aldehydes-*d* from Grignard reagents using pentacarbonyliron.

A representative reaction procedure was as follows. To a tetrahydrofuran solution of hexylmagnesium bromide derived from hexyl bromide and magnesium, an equimolar amount of pentacarbonyliron was injected by means of a syringe, after which the mixture was stirred for 2 h at room temperature under an argon atmosphere. Acetic acid was then added to the solution, and stirring was continued for a further 5 min. The mixture was washed with 1 mol dm^{-3} hydrochloric acid and then 0.1 mol dm^{-3} aqueous sodium hydroxide saturated with sodium chloride; it was subsequently extracted with diethyl ether, dried, and filtered, and the ether was removed with a rotary evaporator. The residue was purified by distillation under reduced pressure. The product was identified as heptanal by means of IR, NMR, MS, and GLC. The yield was 91% on the basis of the Grignard reagent (GLC). When CH_3COOD was used instead of CH_3COOH, heptanal-1-*d* was obtained in the same yield. The results are listed in Table 1.

In these reactions, the acyltetracarbonylferrates **1** are assumed to be intermediates,[2] which are hydrogenated or deuterated to give aldehydes or aldehydes-*d* (Eq. 1).

$$\text{R-MgBr} \xrightarrow{\text{Fe(CO)}_5} \left[\text{R-C(=O)-Fe(CO)}_4\right]^- \xrightarrow{\text{H}^+ \text{ or } \text{D}^+} \underset{\mathbf{1}}{} \text{R-CHO or R-CDO} \quad (1)$$

The ease of the reaction procedure, the mildness of the reaction conditions, and the high yields of the products may make it possible to utilize this reaction for the syntheses of aldehydes and aldehydes-*d* from Grignard reagents.

Experimental

The infrared spectra were recorded on a Hitachi 260-10 Infrared Spectrophotometer, the NMR spectra were measured on a Hitachi R-600 FT-NMR Spectrometer, and the mass spectra were measured on a Hitachi RM-50 GC-MS. Gas chromatography was carried out on a Yanagimoto G-8 Model equipped with a stainless column packed with Silicone gum SE-30 on chromosorb. All the experiments were carried out under an atmosphere of argon. The tetrahydrofuran was dried by distillation from lithium aluminum hydride. The pentyl bromide, hexyl bromide, bromobenzene, and cyclohexyl bromide were all commercial products and were distilled before use. The pentacarbonyliron was purchased from a commercial source and was used without further purification. The acetic acid, acetic acid-*d*, and magnesium for the Grignard reaction were also commercial products of the highest available purity.

TABLE 1. SYNTHESIS OF ALDEHYDES FROM GRIGNARD REAGENTS

Run	RMgBr R	AcOH or AcOD	Product	Yield/%[a]
1	$CH_3(CH_2)_5$-	AcOH	$CH_3(CH_2)_5CHO$	91 (44)
2		AcOD	$CH_3(CH_2)_5CDO$	(43)
3	$CH_3(CH_2)_4$-	AcOH	$CH_3(CH_2)_4CHO$	99
4	C_6H_5-	AcOH	C_6H_5CHO	94
5		AcOD	C_6H_5CDO	(33)
6	C_6H_{11}-[b]	AcOH	$C_6H_{11}CHO$	40
7		AcOD	$C_6H_{11}CDO$	(14)

a) Determined by GLC. Yields in parentheses are those of substances isolated by fractional distillation. b) Cyclohexyl.

Representative Synthesis of Heptanal-d. Into the tetrahydrofuran solution (30 ml) of hexylmagnesium bromide derived from hexyl bromide (22 mmol) and magnesium (44 mg-atom), pentacarbonyliron (3 ml, 22 mmol) was injected by means of a syringe, after which the mixture was stirred for 2 h at room temperature under argon. Acetic acid-*d* (26 mmol) was then added to the solution, and stirring was continued for further 5 min. The mixture was washed with 1 mol dm^{-3} hydrochloric acid and then 0.1 mol dm^{-3} aqueous sodium hydroxide saturated with sodium chloride, and subsequently extracted with diethyl ether. The organic layer was dried over sodium sulfate, and the solvent was removed with a rotary evaporator. The residue thus obtained was purified by distillation *in vacuo*, giving heptanal-1-*d* (1.09 g): bp 46—49 °C/17 Torr (1 Torr≈133.322 Pa); NMR ($CDCl_3$) δ 0.93 (3H, t, $-CH_3$), 1.13—2.07 (8H, m, $-(CH_2)_4-$), 2.48 (2H, t, $-CH_2CO-$); IR (neat) 2070, 1710 cm^{-1}; MS *m/e* (%) 115 (M^+, 4), 97 (27), 85 (27), 82 (23), 70 (100).

Benz(aldehyde-d*)*. Bp 70 °C/17 Torr; NMR ($CDCl_3$) δ 7.42—8.16 (5H, C_6H_5-); IR (neat) 2110, 1695 cm^{-1}; MS *m/e* (%) 107 (M^+, 100), 105 (96), 77 (89).

Cyclohexane(carboaldehyde-d*)*. Bp 45 °C/10 Torr; NMR ($CDCl_3$) δ 0.82—2.83 (11H, m, $C_6H_{11}-$); IR (neat) 2050, 1710 cm^{-1}; MS *m/e* (%) 113 (M^+, 8), 95 (21), 83 (56), 71 (21), 68 (36), 55 (100).

The hexanal, heptanal, benzaldehyde, and cyclohexane-

carboaldehyde were identified by a comparison of their IR, NMR, and mass spectra with those of authentic samples.

References

1) L. I. Smith and M. Bayliss, *J. Org. Chem.*, **6**, 437 (1941); L. I. Smith and J. Nichol, *ibid.*, **6**, 489 (1941); W. J. Dole, L. Starr, and C. W. Strobel, *ibid.*, **26**, 2225 (1961); M. Hojo, R. Masuda, T. Saeki, K. Fujimori, and S. Tsutsumi, *Tetrahedron Lett.*, **1977**, 3883; F. Sato, K. Oguro, H. Watanabe, and M. Sato, *ibid.*, **1980**, 2869.

2) M. Yamashita and R. Suemitsu, *Tetrahedron Lett.*, **1978**, 761, 1477.

^{13}C and ^{19}F Chemical Shifts Induced by C-H···Base Hydrogen Bonding. Particular Polarizations of C-Halogen and C=C Bonds

Shinichi UEJI,* Michiko NAKAMURA,† Masayuki KITADANI, and Akira SERA*,†

Department of Chemistry, College of General Education, Kobe University, Nada, Kobe 657

† *Department of Chemistry, Faculty of Science, Kobe University, Nada, Kobe 657*

(Received September 21, 1981)

Synopsis. The ^{13}C and ^{19}F chemical shifts induced by C-H···Base hydrogen bonding were measured for dichlorofluoromethane, chloroform, pentachloroethane, and trichloroethylene. These chemical shifts were shown to be linear using the β scale of hydrogen-bond acceptor basicities proposed by Kamlet and Taft. The analysis of the linear solvation energy relationships reveals that the particular polarizations of the C-halogen and C=C bonds play an important role in the C-H···Base hydrogen-bond formation.

The participation of C-H groups of haloforms in hydrogen bonding has been recognized for a long time.[1] The C-H hydrogen bonds with bases (C-H···Base hydrogen bonds) have been extensively investigated by means of IR and ^1H NMR spectroscopies. However, comparatively little attention has been paid to the chemical shifts of other nuclei.

Here, we wish to report on the ^{13}C and ^{19}F chemical shifts of haloforms and related compounds induced by the C-H···Base hydrogen bonding. The mode and mechanism of the inductive electronic effects will be discussed on the basis of the linear solvation energy relationships between the observed chemical shifts and the β scale of the hydrogen-bond acceptor basicities.

Results and Discussion

The ^{13}C chemical shifts of **1**—**4** and the ^{19}F chemical shifts of **1** were measured in a variety of solvents which can act as proton acceptors (Table 1). The β scale

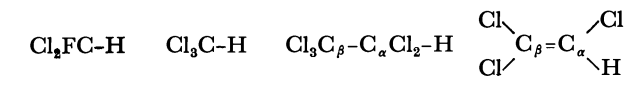

1 **2** **3** **4**

for the solvents listed in Table 1 is the measure of the hydrogen-bond acceptor basicities recently proposed by Kamlet and Taft.[2] Both the ^{13}C and ^{19}F chemical shifts are very sensitive to the change in solvent. In order to clarify the origin of the solvent shifts observed, the concept of the linear solvation energy relationship (LSER)[3] is applied to these chemical-shift data. Then, a good LSER is obtained for each compound [δ(ppm) = (slope)β + (intercept)].[4] Table 2 summarizes the magnitudes and signs of the slopes for these LSER's. The success of the LSER means that both the ^{13}C and ^{19}F chemical shifts are mainly controlled by the strength of the C-H···Base hydrogen bonds. Since the corresponding fully halogenated compounds were used as internal references, other solvent effects should be largely canceled out.[5]

An inspection of the chemical-shift data (Table 1) shows that the C-H···Base hydrogen-bond formations induce downfield shifts of the C_α-(H) atoms of **1**—**4**. This observation is consistent with those of Morishima *et al.*[6] and Lichter and Roberts.[7] However, no definite information about the behavior of halogen atoms and carbon atoms other than C_α in such hydrogen bonding has yet been established.

As is shown in Table 2, the magnitudes and signs of the slopes for the LSER's are characteristic of each carbon atom of each compound. The slope is related to the sensitivity to the inductive electronic effects, and the (+) and (−) signs of the slopes should correspond to the positive and negative charge densities induced on the carbon (or the fluorine) atom respectively. Therefore, the magnitudes and signs of the slopes serve as a probe for studying the mode and mechanism of the transmission of the inductive electronic effects.

For **1**, it should be noted that the sign (+) of the slope for the carbon atom is opposed to that (−) for the fluorine atom, thus suggesting the existence of the $\overset{+}{C}$–$\overset{-}{F}$ bond polarization. According to a recent theoretical study on hydrogen bonds,[8] the C-H···Base hydrogen bond is well represented by this electrostatic model:

$$\text{C-H···Base} \longleftrightarrow \bar{C}: \quad \overset{+}{H}: \text{Base}$$
$$(1) \qquad\qquad (2)$$

The observed ^{13}C downfield shifts seem to be incon-

Table 1. ^{13}C chemical shifts[a] of **1**—**4** and ^{19}F chemical shifts[a] of **1** in various solvents

Solvent β Scale		Anisole 0.247	Dioxane 0.368	Acetone 0.499	Cyclohexanone 0.534	DMF 0.710	DMSO 0.752	HMPA[b] 0.990
1	^{13}C	−13.59	−13.01	−12.75	−12.89	−11.98	−11.95	−11.28
	^{19}F	−80.35	−80.55	−80.70	−80.81	−80.84	−81.07	−80.93
2	^{13}C	−19.39	−18.45	−17.90	−17.50	−16.95	−16.40	−15.36
3	$^{13}C(\alpha)$	−17.13	−16.80	−16.25	−16.10	−15.49	−15.91	−15.54
	$^{13}C(\beta)$	+2.86	+3.26	+3.68	+3.90	+4.08	+4.08	+4.51
4	$^{13}C(\alpha)$	−3.66	−3.30	−2.70	−2.50	−2.07	−1.71	−0.36
	$^{13}C(\beta)$	+2.80	+2.43	+2.48	+2.62	+2.19	+1.88	+1.16

a) The (+) and (−) signs indicate the downfield and upfield shifts from the internal reference respectively. b) Hexamethylphosphoric triamide.

Table 2. Magnitudes and signs of slopes in linear solvation energy relationships

	1		2	3		4	
	^{13}C	^{19}F	^{13}C	$^{13}C(\alpha)$	$^{13}C(\beta)$	$^{13}C(\alpha)$	$^{13}C(\beta)$
Slope	+3.21	−1.11	+5.41	+2.32	+2.31	+4.46	−2.40
r[a)]	0.988	0.872	0.994	0.953	0.965	0.988	0.930

a) Correlation coefficient.

sistent with the structure (2) having a localization of electrons on the carbon atom. Lichter and Roberts[7] reported that the ^{13}C downfield shifts for chloroform hydrogen-bonded with bases are attributable to the change in the average distance of bonding electrons in the C–H bond of chloroform. Here, we wish to propose a new concept of bond polarizations to explain the electronic structure in the hydrogen-bonded systems. The electronic structure of **1** can be explained by assuming that the localized electrons on the carbon atom are transmitted through the $\overset{+}{C}$–$\overset{-}{F}$ bond polarization onto the fluorine atom, thus resulting in the ^{13}C downfield and ^{19}F upfield chemical shifts. Furthermore, the holding of the LSER shows that the degree of the $\overset{+}{C}$–$\overset{-}{F}$ bond polarization increases with the increase in the strength of the hydrogen bonding.

Similar ^{13}C downfield shifts are observed for **2**; they can also be interpreted in terms of the $\overset{+}{C}$–$\overset{-}{Cl}$ bond polarization. However, the magnitude of the slope for **2** is larger than that for **1**. This experimental result can be nicely explained by the fact that the longitudinal polarizability[9] of the C–Cl bond (3.2×10^{-24} cm^3) is larger than that of the C–F bond (1.2×10^{-24} cm^3); hence, the carbon atom of **2** becomes more positive than does that of **1**.

For **3**, both the C_α and C_β atoms show the positive sign arising from the $\overset{+}{C}$–$\overset{-}{Cl}$ bond polarization. The small slope for the C_α atom is attributable to the smaller polarizability of the C–C bond (0.99×10^{-24} cm^3).[9] On the other hand, the slope for the C_β atom is larger than that which might be predicted from a simple attenuate transmission mode of the inductive effects in the C_α–C_β saturated bond. However, the polarization effect of three C–Cl bonds reinforces the positive charge on the C_β atom; this makes the magnitude of the slope larger than expected.

In the system containing the C_α=C_β bond, **4**, the sign of the slope for the C_α atom is opposite to that for the C_β atom. This sign alternation can be attributed to the polarization of the $\overset{+}{C}_\alpha$=$\overset{-}{C}_\beta$ bond, because the C=C bond is significantly more polarizable (2.8×10^{-24} cm^3)[9] than the C–C bond. At the same time, the $\overset{+}{C}_\beta$–$\overset{-}{Cl}$ bond polarization should be considered; it will partially reduce the negative charge induced on the C_β atom. In fact, this idea agrees well with the experimental result.

Experimental

The ^{13}C spectra were obtained under proton-decoupled conditions in the pulse FT mode at 25.03 MHz (45° pulse width of 10 μs; 8 K data points; resolution of 0.06 ppm) with a JEOL PS-100 spectrometer. The ^{19}F spectra were measured with the same spectrometer operating at 94.10 MHz in the frequency sweep mode with an external lock. The ^{13}C and ^{19}F chemical shifts of **1**, **2** and **3**, and **4** were determined with reference to internal $CFCl_3$, CCl_4, and Cl_2C=CCl_2 respectively. The concentration of the sample was *ca.* 1.5 M.[10]

The authors are indebted to Dr. T. Satokawa of Daikin Industry Co., Ltd, for a gift of dichlorofluoromethane.

References

1) "Hydrogen Bonding by C–H Groups," ed by R. D. Green, The Macmillan Press, London (1974).
2) M. J. Kamlet and R. W. Taft, *J. Am. Chem. Soc.*, **98**, 377 (1976).
3) Recently, Kamlet and Taft have reported a number of successful applications of LSER's to the problems of solvent effects in organic chemistry; *e.g.*, R. W. Taft, J. M. Abboud, and M. J. Kamlet, *J. Am. Chem. Soc.*, **103**, 1080 (1981).
4) These ^1H chemical shifts also show rough correlations in the LSER's. The deviations from the correlations are attributable to the solvent anisotropy.
5) In fact, the lack of any correlation between our chemical-shift data and the solvent parameter, $(\varepsilon-1)/(\varepsilon+1)$, indicates that the reaction field effect is not a major contribution to the origin of the solvent shift.
6) I. Morishima, K. Endo, and T. Yonezawa, *J. Am. Chem. Soc.*, **93**, 2048 (1971).
7) R. L. Lichter and J. D. Roberts, *J. Phys. Chem.*, **74**, 912 (1970).
8) P. A. Kollman and L. C. Allen, *Chem. Rev.*, **72**, 283 (1972).
9) R. J. W. LeFèvre, *Adv. Phys. Org. Chem.*, **3**, 50 (1965).
10) At this concentration, the solute-solute interaction may occur. The slope in the LSER increases slightly with the decrease in the solute concentration, but the trend is almost the same.

The Reaction of 1-Methoxycarbonyl-2-imidazolidone with Phenylmagnesium Bromide

Noboru MATSUMURA,* Kimihiro MATSUKAWA, Yujiro SAKAGUCHI, and Hiroo INOUE

Department of Applied Chemistry, College of Engineering, University of Osaka Prefecture, Sakai, Osaka 591

(Received September 22, 1981)

Synopsis. It is found that 1-methoxycarbonyl- or 1-phenoxycarbonyl-2-imidazolidone reacts with phenylmagnesium bromide to afford benzophenone and triphenylmethanol, together with 2-imidazolidone, by nucleophilic attack on the carbonyl group at the side chain.

The reaction of 1-methoxycarbonyl- or 1-phenoxycarbonyl-2-imidazolidone (**1a** or **1b**) with nucleophiles is of interest in relation to the reactivity of a carboxylated biotin coenzyme transferring the carboxylato group to Ac–CoA in a biological system.[1] Recently we have reported that the reaction of Compound **1a** with butylamine proceeds via the formation of an isocyanate intermediate (**2**) by ring opening to afford *N*-butylcarbamoyl-*N'*-methoxycarbonylethylenediamine (**3a**) in a quantitative yield.[2] In the course of our studies of the reactivity of Compound **1**, we have found that phenylmagnesium bromide undergoes nucleophilic attack on the carbonyl group of **1a** and **1b** to afford benzophenone, triphenylmethanol, and 1-benzoyl-2-imidazolidone (**5**). Herein, we wish to report our findings on these reactions.

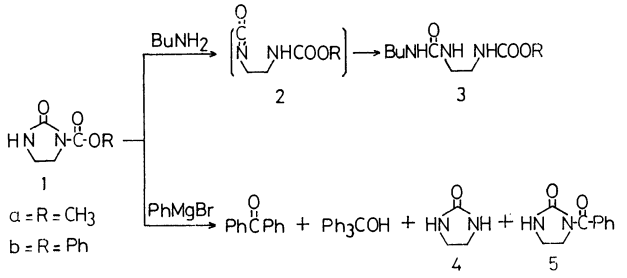

Scheme 1.

The reactions of Compounds **1a** and **1b** with phenylmagnesium bromide in tetrahydrofuran were carried out by stirring under argon at room temperature for 2 h. At the **1a**/phenylmagnesium bromide molar ratio of 1:1, benzophenone, triphenylmethanol, 2-imidazolidone and **5** were obtained in low yields, with an almost entire recovery of **1a**, as Table 1 shows. The low yields of the products is caused by the consumption of phenylmagnesium bromide for abstracting the hydrogen of the NH group of **1**. This was established by the fact that, in the reaction of 1-methoxycarbonyl-2-imidazolidone-3-*d* (**6**) with 1-naphthylmagnesium bromide in the molar ratio of 1:1, naphthalene-1-*d* is produced in a 90% yield. When the **1a**/phenylmagnesium bromide molar ratio of 1:3 was used, benzophenone and triphenylmethanol were obtained in higher yields, without the formation of any methyl benzoate, as Table 1 shows. No products by ring opening were obtained at all. The formation of benzophenone was observed also in the reaction with **1b**. However, it was difficult to isolate Compound **4**

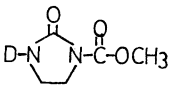

6

in amounts corresponding to those of benzophenone and triphenylmethanol, since it was very soluble in water. In addition to these products, Compound **5** was obtained, though in a low yield. Thus, it became apparent that the reactions of Compounds **1a** and **1b** with phenylmagnesium bromide result in the fission of the N–COOMe bond.

The difference in reactivity between butylamine and phenylmagnesium bromide led us to consider that the chelation of the Mg^{2+} ion after the abstraction of the hydrogen of the NH group of **1** prevents ring opening and brings about the nucleophilic attack of phenylmagnesium bromide on the side chain (Scheme 2). Furthermore, benzophenone is regarded as being formed *via* the intermediary formation of Compound **5** rather than methyl benzoate on the basis of the following results: 1) Methyl benzoate is not detected in the reaction of **1** with phenylmagnesium bromide; 2) the reaction of Compound **5** with phenylmagnesium bromide under similar conditions affords benzophenone and triphenylmethanol in good yields, together with the formation of Compound **4**, as Table 1 shows; 3) the reaction of a mixture (1:1) of **1a** and methyl benzoate with phenylmagnesium bromide (3 equiv.) affords benzophenone, triphenylmethanol, **4**, and **5** in 42, 1, 17, and 7% yields respectively, with a 94% recovery of methyl benzoate.

As has been described above, it became apparent that phenylmagnesium bromide can cleave the N–COOR bond by the assistance of the Mg^{2+} ion, unlike the behavior of butylamine, and that this behavior of the Mg^{2+} ion is similar to that in the butylamine/Mg^{2+}-ion system, bringing about the cleavage of the N–COOR bond.[3]

TABLE 1. THE YIELDS OF THE PRODUCTS IN THE REACTIONS OF **1** AND **5** WITH PHENYLMAGNESIUM BROMIDE[a]

Compd	Compd/PhMgBr Molar ratio	Yield/% PhCOPh	Ph_3COH	**4**	**5**
1a[b]	1 : 1	6	1	11	5
1a	1 : 3	42	15	22	4
1b[c]	1 : 3	63	5	35	6
5	1 : 2	75	8	40	

a) Concentration of Compounds **1** and **5**: 6.81 mmol in 25 cm^3 of tetrahydrofuran. b) Recovery %=81%. c) Phenol was obtained in a 56% yield.

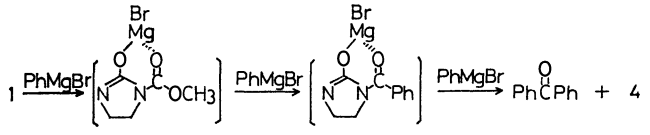

Scheme 2.

Experimental

Materials. *1-Methoxycarbonyl-2-imidazolidone (**1a**)*: Compound **1a** (mp 178—179 °C) was prepared by the method described in our previous paper.[2]

*1-Benzoyl-2-imidazolidone (**5**)*: A solution of 16.3 g (0.116 mol) of benzoyl chloride in 20 cm³ of dry benzene was added, under nitrogen, to a solution of 10 g (0.116 mol) of **4** in 50 cm³ of dry benzene at room temperature; the solution was stirred under reflux for 20 h and then cooled to room temperature. The crystals thus deposited were collected by filtration, washed with water, and recrystallized from chloroform to give 19.9 g (90%) of **5**: mp 167—168 °C; IR (KBr) 3220 (NH), 1733, 1670 cm^{-1} (C=O); ^{1}H NMR ($CDCl_3$) δ=3.62(t, 2H, $-CH_2-$), 4.25(t, 2H, $-CH_2-$), 5.78 (bs, 1H, NH), and 7.29—7.8 (m, 5H, aromatic); Found: C, 63.12; H, 5.18; N, 14.69%, Calcd for $C_{10}H_{10}N_2O_2$: C, 63.15; H, 5.30; N, 14.73%.

*1-Methoxycarbonyl-2-imidazolidone-3-*d *(**6**)*: A mixture of 2 g (13.9 mmol) of **1a** and 20 cm³ of D_2O was refluxed for 2 h and then evaporated to dryness under reduced pressure. The white residue was dried again under reduced pressure at 100 °C to yield **6**. The **6** exhibited an IR (KBr) peak at 2480 cm^{-1} (N–D) and 1760, 1670 cm^{-1} (C=O) and the complete disappearance of the NMR ($CDCl_3$) signal of N–H at δ 6.45, although the other signals were the same as those of **1a**.

*Reaction of 1-Methoxycarbonyl-2-imidazolidone-3-*d *with 1-Naphthylmagnesium Bromide.* A solution of 1.576 g (6.81 mmol) of 1-naphthylmagnesium bromide in 10 cm³ of tetrahydrofuran was added, drop by drop and at room temperature, to a solution of 0.988 g (6.81 mmol) of 1-methoxycarbonyl-2-imidazolidone-3-*d* in 15 cm³ of tetrahydrofuran, and then the mixture was stirred for 2 h. The resulting mixture was treated by a method similar to that used in the case of **1a** to yield 0.791 g (90%) of naphthalene-1-*d* (**7**). The IR (KBr) signals of **7** coincided with those of the authentic specimens. MS *m/e*, 129 (M^+). Another product, **1a**, was isolated from the acidic solution in an 87% yield.

Reaction with Phenylmagnesium Bromide. *Compound **1a***: A solution of 3.7 g (20.43 mmol) of phenylmagnesium bromide in 10 cm³ of tetrahydrofuran was added under argon to a solution of 0.982 g (6.81 mmol) of **1a** in 15 cm³ of tetrahydrofuran, after which the mixture was stirred at room temperature for 2 h. The resulting mixture was acidified with a dilute hydrochloric acid with ice, and the solution was extracted with ether and then chloroform. The ether and chloroform solutions were combined and dried over magnesium sulfate. After the removal of the ether and chloroform *in vacuo*, the residue was chromatographed on a silica-gel column, using chloroform as the eluent, to give 0.521 g (42%) of benzophenone, 0.266 g (15%) of triphenylmethanol, and 0.052 g (4%) of **5**. The aqueous layer was evaporated *in vacuo*, and the residue was chromatographed on a silica-gel column, using methanol and ethanol as the eluents, to give 0.127 g (13%) of **1a** and 0.129 g (22%) of **4**. The products were identified by a comparison of their melting points and IR, ^{1}H NMR, and mass spectra with those of the respective authentic specimens.

*Compounds **1b** and **5***: The reaction of **1b** and **5** with phenylmagnesium bromide and the isolation of the reaction products were carried out by a method similar to that used in the case of **1a**.

References

1) a) J. Moss and M. D. Lane, *Adv. Enzymol.*, **35**, 321 (1971), and the references cited therein; b) M. C. Scrutton and M. R. Young, "The Enzymes," ed by P. D. Boyer, Academic Press, New York (1972), Vol. 6, pp. 1—35, and the references cited therein.

2) N. Matsumura, Y. Yagyu, H. Kawai, Y. Otsuji, and E. Imoto, *Nippon Kagaku Kaishi*, **1977**, 362.

3) N. Matsumura, H. Kawai, Y. Otsuji, and E. Imoto, *Bull. Chem. Soc. Jpn.*, **50**, 2417 (1977).

An MO Study of the Photochemical Electrocyclic Isomerization between Vinylketene and Cyclobutenone

Osamu KIKUCHI

Department of Chemistry, The University of Tsukuba, Sakura, Ibaraki 305

(Received September 26, 1981)

Synopsis. The MINDO/3 CI potential energy surfaces of the vinylketene–cyclobutenone system suggest that the cyclization of vinylketene occurs from the $\pi\rightarrow\pi^*$ state *via* the zwitterion, in which the negative charge is located on the 90°-twisted methylene carbon atom, while the reverse reaction proceeds *via* a diradical structure.

It was shown in previous papers[1] that the photochemical electrocyclic reaction mechanism of hetero-atom-conjugated systems is very different from that of the corresponding all-hydrocarbon conjugated systems; there is no distinction between conrotatory and disrotatory modes in the former systems. In the photocyclization of hetero-atom-conjugated systems, the rotation of the terminal methylene group occurs from the $\pi\rightarrow\pi^*$ excited state to give the twisted structure, and the ring closing occurs from the Z_+ zwitterion,

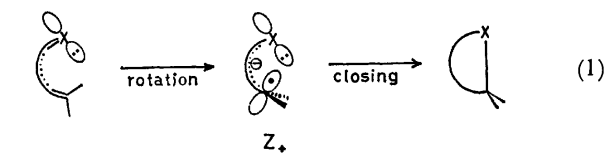

(1)

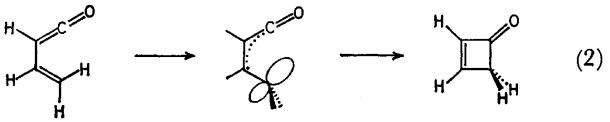

(2)

1 2 3

in which the positive charge is located on the carbon atom of the twisted methylene group.[1] The vinylketene–cyclobutenone isomerization is another example in which the conrotatory/disrotatory dichotomy is meaningless, and its mechanistic examination is of much interest.[2]

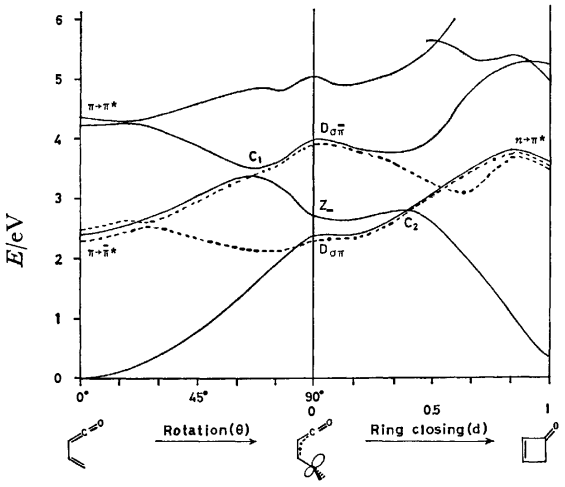

Fig. 1. Potential energy curves of lower four singlet states (solid lines) and two triplet states (broken lines) along the step-by-step path.[4]

Figure 1 shows the MINDO/3[3]-CI potential energy curves[4] along the step-by-step path of the vinylketene–cyclobutenone system, (2), in which the rotation of the methylene group and the ring closing occur independently. The lower singlet electronic states of the twisted structure, **2**, are the $D_{\sigma\pi}$, Z_-, and $D_{\sigma\bar{\pi}}$ states.[5] The lowest singlet state is the diradical one in which the $\sigma(CH_2)$ and π^* orbitals are occupied by unpaired electrons. The Z_- excited state has a pair of electrons

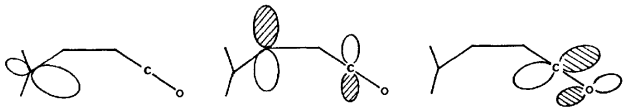

$\sigma(CH_2)$ π^* $\bar{\pi}^*$

in the $\sigma(CH_2)$ orbital, and it is a polarized zwitterion; the negative charge on the terminal carbon atom was calculated to be −0.70. As may be seen from Fig. 1, the excited Z_- state correlates directly with the ground state of cyclobutenone, and it can be generated from the $\pi\rightarrow\pi^*$ excited state of vinylketene. Thus, the following reaction path appears to exist in the **1**→**3** photocyclization: The rotation of the terminal methylene group occurs in the $\pi\rightarrow\pi^*$ excited state of vinylketene to give the Z_- zwitterion, after which this zwitterion undergoes cyclization without any activation energy to form cyclobutenone.

The electrocyclic reaction of vinylketene has been shown to proceed *via* the Z_- zwitterion. This is an interesting contrast with Reaction 1, which proceeds *via* the Z_+ zwitterion. In the hetero-atom-conjugated system, the in-plane lone-pair electrons of the terminal hetero atom are consumed in the new σ bond formation, while in the case of the ketene conjugated system, the anti-bonding $\bar{\pi}^*$ orbital of the carbonyl group receives an electron from the terminal carbon atom to form the new σ bond. This is the reason why the Z_- zwitterion is involved in the **1**→**3** photochemical process.

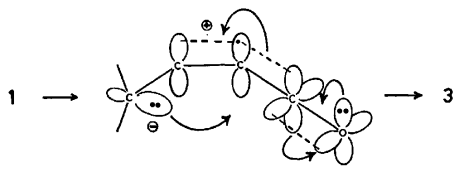

The $D_{\sigma\pi}$ twisted diradical correlates with the ground state of vinylketene, and it is derived easily from the $n\rightarrow\pi^*$ excited state of cyclobutenone (Fig. 1). Thus, the ring opening of cyclobutenone is expected to proceed from the singlet (or triplet) $n\rightarrow\pi^*$ excited state of cyclobutenone *via* the $D_{\sigma\pi}$ diradical.[6]

Figure 2 shows the two-dimensional potential energy surfaces of three lower singlet states. The symbols W and H indicate the potential minimum and maxi-

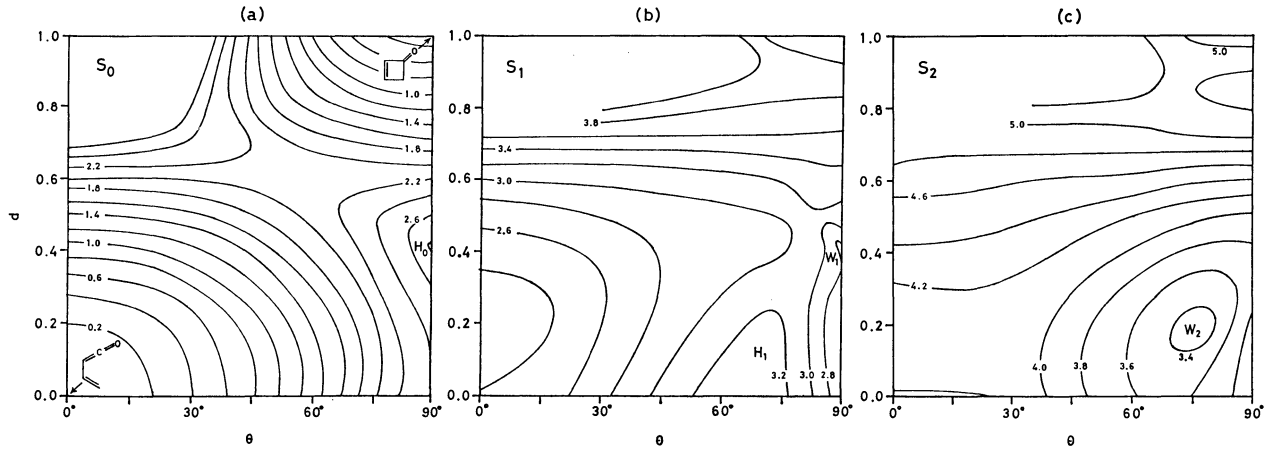

Fig. 2. Two-dimensional potential energy surfaces for three singlet states.[4] The values indicated on the potential curves are energies(eV) relative to the ground state structure of the vinylketene.

mum points respectively. The W_1 and W_2 regions correspond to the C_2 and C_1 crossing regions respectively, shown in Fig. 1. The W_1 well is a pin hole which can be a leakage channel from the S_1 state to the S_0 state. As may be seen from Fig. 2-b, the $n\rightarrow\pi^*$ state of cyclobutenone undergoes bond-breaking with a small activation energy, forming the S_0 vinylketene *via* the W_1 pin hole. The rotation of the methylene group of the $n\rightarrow\pi^*$ vinylketene requires an appreciable activation energy (Fig. 2-b), while it occurs very easily on the S_2 surface (Fig. 2-c). The W_2 well on the S_2 surface interacts strongly with the potential height, H_1, on the S_1 surface. Thus, the two dimensional potential energy surfaces also support the reaction paths described above.

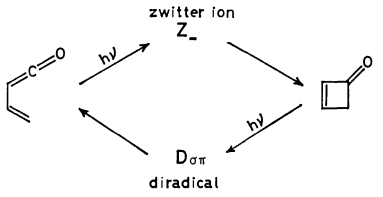

References

1) O. Kikuchi, H. Kubota, and K. Suzuki, *Bull. Chem. Soc. Jpn.*, **54**, 1126 (1981); O. Kikuchi, *Tetrahedron Lett.*, **22**, 859 (1981).

2) Vinylketenes are very reactive with nucleophiles or with olefins, and their photochemical behavior has not been clarified. The thermal and photochemical isomerization of cyclobutenone derivatives into vinylketenes has, however, been reported: J. E. Baldwin and M. C. McDaniel, *J. Am. Chem. Soc.*, **90**, 6118 (1968); O. L. Chapman and J. D. Lassila, *ibid.*, **90**, 2449 (1968); A. Krantz, *ibid.*, **96**, 4992 (1974); R. Huisgen, and H. Mayr, *J. Chem. Soc., Chem. Commun.*, **1976**, 55; H. Mayr, *Angew. Chem., Int. Ed. Engl.*, **14**, 499 (1975).

3) R. C. Bingham, M. J. S. Dewar, and D. H. Lo, *J. Am. Chem. Soc.*, **97**, 1285 (1975).

4) In the calculation of the potential energy curves, the molecular structures of **1** and **3** were optimized by the use of MINDO/3 (without CI). The structural change involved in the isomerization between **1** and **3** was expressed by two parameters: the rotation angle of the terminal methylene group, θ, which expresses the structure of the CH_2 fragment, and the d parameter, which indicates the linear change in the structural parameters, x_1, associated with a substructure other than that of the methylene group; $x_1 = x_1^{\text{initial}} + d(x_1^{\text{final}} - x_1^{\text{initial}})$. In the CI calculation, 42 and 41 configuration functions were selected for the singlet and triplet states respectively.

5) The electronic states of the twisted structure were calculated by the closed-shell SCF method, followed by CI; geometry optimization was not performed for any electronic state. The results shown in Fig. 1 are not fit for a quantitative discussion of the relative energy levels of the electronic states of the twisted structure.

6) The photochemical α-cleavage of 2,4-cyclohexadienones from the $n\rightarrow\pi^*$ manifold *via* the $D_{\sigma\pi}$ diradical has been well explained; W. G. Dauben, L. Salem, and N. J. Turro, *Acc. Chem. Res.*, **8**, 41 (1975).

A Facile One-pot Synthesis of *N*-Substituted Phthalimides Using a Catalytic Amount of Crown Ether

Kenso Soai,* Atsuhiro Ookawa, and Kyoko Kato

Department of Applied Chemistry, Faculty of Science, Science University of Tokyo, Kagurazaka, Shinjuku-ku, Tokyo 162

(Received October 19, 1981)

Synopsis. *N*-Substituted phthalimides, intermediates of the Gabriel synthesis, were obtained in high yields (84—100%) by the addition of a *catalytic* amount of 18-crown-6 to the reaction of potassium phthalimide and alkyl halides in toluene.

During these several years, increasing interest has been centered upon crown ethers.[1] However, possibilities of their use in phase transfer catalysis (PTC) in organic synthesis have not been so fully documented as those of onium salts.[2]

Though it is one of the major advantages of PTC that a *catalytic* (small) amount of the reagent can promote the reaction, no report has been appeared, to the best of our knowledge, on the alkylation of imides using a *catalytic* amount of crown ethers. Meanwhile, *N*-substituted phthalimides have been known as intermediates of the Gabriel synthesis of primary amines.[3] Moreover, ethoxycarbonyl and sulfonyl derivaties are used in phthaloylation of amines and amino acids.[4] Synthesis of *N*-substituted phthalimides by the alkylation of potassium phthalimide is usually run in dipolar aprotic solvents or in the presence of onium salts as PTC.[5]

Concerning the synthesis of *N*-substituted phthalimides using crown ether, it is reported that halides react with *stoichiometric* amounts of the complex (**1**) of crown ether–potassium phthalimide–water.[6] However, examples of halides are limited to only a few activated aromatic ones, and the synthesis has following shortcomings from the standpoint of preparative organic synthesis. (1) Use of *stoichiometric* amounts of crown ether. It is desirable to find a process in which a *catalytic* amount of crown ether promotes the reaction. (2) Prior to the reaction with halides, it is necessary to prepare **1**. (3) Since **1** contains *stoichiometric* amounts of water, competing reaction of water especially with aliphatic halides with functional groups may occur. (4) Potential suppression of anion activation by water in the medium because of anion solvation.

We wish to describe the results of our method which avoids all of these shortcomings. We have found that by the addition of a catalytic amount (10 mol%) of 18-crown-6 (**2**) an increase in the reaction rate of potassium phthalimide (**3**) and alkyl halides (**4**) was brought about in toluene and that *N*-substituted phthalimides (**5**) were obtained in high yields (Eq. 1).

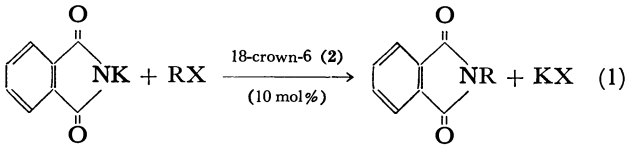

(1)

3 **4** **5**

In the first place, we examined the effect of solvents on the reaction of **3** and **4** in the presence of 10 mol% of **2**. Results are summarized in Table 1. As is shown in Table 1, the overall reaction rate is

Table 1. Solvent effects on the alkylation of **3** with **4** in the presence of **2**

Entry	RX(**4**)[a]	Solvent[b]	**5** Yield/%[c]
A	$PhCH_2Br$	Toluene	98
B	$PhCH_2Br$	Toluene containing a trace amount of water	13[d]
C	n-$C_8H_{17}Br$	Toluene	94
D	n-$C_8H_{17}Br$	3-Pentanol	83

a) Molar ratio of **3** : **4** : **2** was 1.2 : 1.0 : 0.1. b) Reactions were run at 100 °C for 6 h. c) Isolated yield. d) By-product was benzyl alcohol(14%).

Table 2. Preparation of *N*-substituted phthalimides(**5**) from **3** and **4** using a catalytic amount of **2**

Entry	**4**	Molar ratio[a] **3** : **4** : **2**	**5** Yield/%[b]		Mp θ_m/°C	Mp θ_m/°C lit.	Procedure
A	n-$C_8H_{17}Br$	1.2 : 1.0 : 0	0				A
B		1.2 : 1.0 : 0.1	94		48—49	48—49[e]	A
C	$PhCH_2Cl$	0.8 : 1.0 : 0.1	89		113—114	115—116[e]	A
D		1.2 : 1.0 : 0.1	100		113—114	115—116[e]	A
E	$PhCH_2Br$	1.2 : 1.0 : 0.1	98		115	115—116[e]	A
F	$BrCH_2CH_2Br$	1.2 : 0.5 : 0.1	84	45[c]	81	82—83[f]	A
				39[d]	225—227	233—234[g]	
G	CH_3- -SO_2Cl	1.2 : 1.0 : 0.1	100		231	235[h]	B
H	C_2H_5OCOCl	1.2 : 1.0 : 0.1	96		79—81	80[h]	B

a) Reactions were carried out at 90 °C or 100 °C for 0.5—6 h. b) Isolated yields. All compounds gave satisfactory NMR and IR spectra. c) *N*-(2-Bromoethyl)phthalimide. d) *N,N'*-Ethylenediphthalimide. e) See Ref. 7. f) *Org. Synth.*, Coll. Vol. I, 119 (1932). g) E. J. Sakellarious, *Helv. Chim. Acta*, **29**, 1675 (1946). h) See Ref. 4a.

larger in aprotic solvent than in protic solvent (Entries A, B, C, and D). Especially the presence of a trace amount of water lowered the reaction rate of alkylation considerably (Entry B), and caused the side reaction of benzyl bromide. It was concluded that absence of water was essential to accelerate the alkylation reaction and to avoid side reactions of halides.

Results of the alkylation of **3** with various kinds of **4** in the presence of 10 mol% of **3** in toluene are shown in Table 2.

Following conclusions may be drawn from the data in Table 2: (1) A *catalytic* amount of **2** was essentially necessary. This showed that crown ether behaved as a solid-liquid PTC (Entries A and B), (2) Both chloride and bromide gave high yields of **5** (Entries D and E), (3) Slight excess of **3** was required to complete the reaction (Entries C and D), (4) **4** with functional groups such as sulfone and ester gave high yields of **5** (Entries G and H).

As described above, this one-pot reaction afforded high yields of *N*-substituted phthalimides (**5**) and required only a *catalytic* amount of crown ether and avoided hydrolysis of alkyl halides.

Experimental

Procedure A. N-*Octylphthalimide*: To a mixture of **3** (0.222 g, 1.2 mmol) and 1-bromooctane (0.193 g, 1.0 mmol) in 1.3 ml of toluene was added **2** (0.1 mmol, 10 mol%). After the mixture was heated at 100 °C for 6 h with stirring under an argon atmosphere, water was added to the mixture. Organic layer was separated and aq layer was extracted with dichloromethane. Combined organic layer was dried over sodium sulfate, and then solvent was evaporated under reduced pressure. Purification on silica-gel TLC(dichloromethane–hexane 1:1 as eluent) afforded *N*-octylphthalimide (0.243 g, 94%, mp 48—49 °C[7]).

Procedure B. N-*(Ethoxycarbonyl)phthalimide*: **3** (0.222 g, 1.2 mmol) and ethyl chloroformate (0.109 g, 1.0 mmol) were allowed to react in toluene (1.3 ml) in the presence of **2** (0.1 mmol, 10 mol%) at 90 °C for 1 h. Precipitate was filtered off, and filtrate was evaporated under reduced pressure. Crystallization from hexane–chloroform afforded *N*-(ethoxycarbonyl)phthalimide (followed by two additional crops for a total of 0.210 g, 96% yield) mp 79—81 °C, (lit, mp 80 °C[4a]).

References

1) G. Gokel and H. D. Dures, *Synthesis*, **1976**, 168.
2) E. V. Dehmlow and S. S. Dehmlow, "Phase Transfer Catalysis," Verlag Chemie, Weinheim, (1980).
3) M. S. Gibson and R. W. Bradshaw, *Angew. Chem.*, **80**, 986 (1968).
4) a) G. H. L. Nefkens, G. I. Tesser, and R. J. F. Nivard, *Recl. Trav. Chim. Pays-Bas*, **79**, 688 (1960); b) Y. Imai and M. Ishimori, *Nippon Kagaku Kaishi*, **1973**, 1729.
5) D. Landini and F. Rolla, *Synthesis*, **1976**, 389; J. Palecek and J. Kutham, *ibid.*, **1976**, 550.
6) V. W. Rasshofer and F. Voegtle, *Tetrahedron Lett.*, **1979**, 1217; W. Rasshofer, G. Oepen, and F. Voegtle, *Isr. J. Chem.*, **18**, 249 (1979).
7) "Dictionary of Organic Compounds," ed by J. R. A. Pollock and R. Stevens, Eyre and Spottiswoode (Publishers) Ltd., London (1965).

Electrosynthesis of 2-Methyl-1,4-naphthoquinone (Vitamin K_3) Directly from 2-Methyl-5,8-dihydro-1,4-naphthalenediol by a Four-electron Oxidation Procedure

Sigeru Torii,* Hideo Tanaka, and Shoji Nakane

Department of Industrial Chemistry, School of Engineering, Okayama University, Okayama 700

(Received October 22, 1981)

Synopsis. A straightforward synthesis of Vitamin K_3 was performed by electrolysis of 2-methyl-5,8-dihydro-1,4-naphthalenediol in a MeCN–*t*-BuOH (9/1)–$LiClO_4$–(Pt or C electrodes) system. The use of perchlorate salts or tetrafluoroborate salts as supporting electrolytes in various electrolysis systems, such as AcOH–*t*-BuOH (9/1)–$LiClO_4$–(Pt) and AcOEt–*t*-BuOH (9/1)–Bu_4NClO_4–(Pt), also provided good results, while the use of Et_4NOTs in MeOH afforded 2-methyl-5,8-dihydro-1,4-naphthoquinone, preferentially.

2-Methyl-1,4-naphthoquinone (vitamin K_3) (**2**) and its homologs constitute a class of biologically active quinones as well as precursors in the synthesis of vitamin K series.[1] Many efforts have been made to devise a simple route to **2** based on the oxidation of 2-methyl-5,8-dihydro-1,4-naphthalenediol (**1**),[2a] 2-methyl-1,4-naphthalenediol (**4**),[2b] 2-methylnaphthalene,[2c] and related compounds[2d] with oxidizing agents *i.e.*, CrO_3, $Mn_2(SO_4)_3$, H_2O_2, $Ce(NH_4)_2(NO_3)_6$, and so on. The lack of product-selectivity in the oxidation of 2-methylnaphthalene to **2**[2a,3] as well as the disadvantages of using stoichiometric amounts of the oxidizing agents spurred us to develop the present procedure.

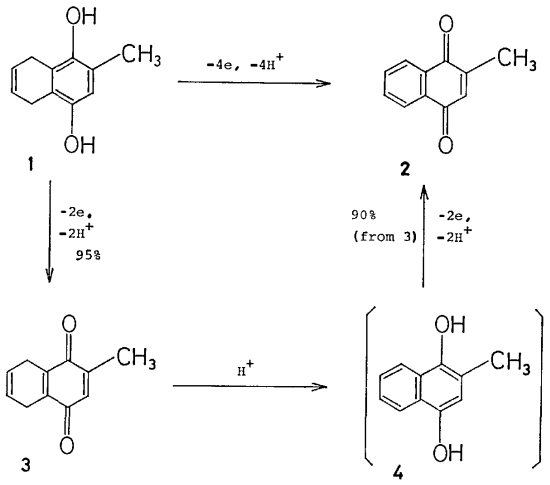

Here, we wish to report a clean and straightforward electrosynthesis of **2** from 2-methyl-5,8-dihydro-1,4-naphthalenediol (**1**) without isolating the intermediate, 2-methyl-5,8-dihydro-1,4-naphthoquinone (**3**), which can also be obtained by the choice of another electrolysis system.

Electrooxidation of **1** to the desired **2** was carried out by employing a MeCN–*t*-BuOH (9/1)–$LiClO_4$–(Pt or C electrodes) system at a constant current of 1.67 mA/cm^2 in a divided cell. As shown in the Table (entries 1 and 2), passage of 9 F/mol of electricity yielded **2** in 91—94% yields. The two systems of AcOH–*t*-BuOH (9/1)–$LiClO_4$–(Pt) and AcOEt–*t*-BuOH (9/1)–Bu_4NClO_4–(Pt) also provided good results (entries 9 and 12). Interestingly, the presence of *t*-BuOH in acetic acid can suppress the formation of by-products (*cf.* entry 10),[4] in contrast to the result obtained in MeCN–$LiClO_4$ system (entry 3).

Particularly noteworthy is the effect of the supporting electrolytes. As shown in entries 1—7, use of perchlorate salts, lithium tetrafluoroborate, and lithium trifuloroacetate, as supporting electrolytes facilitated the formation of **2**. However, use of tetraethylammonium *p*-toluenesulfonate (Et_4NOTs) in various electrolysis systems (entries 8, 11, and 14) mainly afforded **3** (70—84%) along with **2** (7—13%) after passage of 8—9 F/mol of electricity. The selective formation of **3** was achieved in a MeOH–Et_4NOTs–(Pt) system by passage of 2—4 F/mol of electricity (entries 15 and 16). Most of the starting material **1** was converted into **3** in each case when *ca.* 2 F/mol of electricity were passed. However, efficient conversion of **3** into **2** took place smoothly in the MeCN–*t*-BuOH (9/1)–$LiClO_4$–(Pt) system.

Transformation of **3** into **2** can be reasonably explained by assuming the acid-catalyzed isomerization of **3** to 2-methyl-1,4-naphthalenediol (**4**) with strong acid in the vicinity of the electrode and a subsequent two-electron oxidation of **4** at the anode.[5] The isomerization of **3** into **4** takes place more effectively in the anode compartment, in which most of counter ions, *i.e.*, ClO_4^-, BF_4^-, and $CF_3CO_2^-$, of strong acids are concentrated by the electrolysis.[6] In contrast, TsOH arising from Et_4NOTs, seems less effective in catalyzing this isomerization.[7]

Experimental[8]

Materials. 2-Methyl-5,8-dihydro-1,4-naphthalenediol (**1**) was obtained by the acid-catalyzed isomerization of Diels-Alder adduct of 2-methyl-1,4-benzoquinone and butadiene.[2a] Authentic samples of **3** and **4** were derived from **1** according to reported procedures.[2a] Commercially available vitamin K_3 (**2**) was used as an authentic sample. Acetic acid, methanol, *t*-butyl alcohol, and acetonitrile were distilled before use. Reagent-grade supporting electrolytes were used.

Electrolysis Procedure. A conventional H-type cell divided with fritted glass was used, which was fitted with two platinum or carbon electrodes (1.5×2 cm^2). Regurated DC power was supplied by Kowa Electronics model PGS-1550 potentio-galvanostat. The conditions and results are summarized in Table 1. A typical electrolysis procedure is as follows.

Electrooxidation of 2-Methyl-5,8-dihydro-1,4-naphthalenediol (1) in MeCN–t-BuOH(9/1)–$LiClO_4$–(Pt electrodes) System (Entry 1 in Table 1). A solution of **1** (30 mg, 0.17 mmol) and $LiClO_4$ (600 mg) in MeCN (13.5 ml) and *t*-BuOH (1.5 ml) was charged into the anode compartment fitted

Table 1. Electrooxidation of 2-methyl-5,8-dihydro-1,4-naphthalenediol[a)]

Entry	Electrolysis system Solvent-Electrolyte-(Electrodes)[b)]	Electricity F/mol	Products yields/%[c)]	
			Compd **3**	Compd **2**
1	MeCN-*t*-BuOH[d)]-$LiClO_4$-(Pt)	9		94
2	MeCN-*t*-BuOH[d)]-$LiClO_4$-(C)	9		91
3	MeCN-$LiClO_4$-(Pt)	6		90
4	MeCN-*t*-BuOH[d)]-Et_4NClO_4-(Pt)	9	Trace	88
5	MeCN-*t*-BuOH[d)]-Bu_4NClO_4-(Pt)	8.5		81
6	MeCN-*t*-BuOH[d)]-$LiBF_4$-(Pt)	7.5		93
7	MeCN-*t*-BuOH[d)]-$LiOCOCF_3$-(Pt)	9		66
8	MeCN-*t*-BuOH[d)]-Et_4NOTs-(Pt)	9	74	7
9	AcOH-*t*-BuOH[d)]-$LiClO_4$-(Pt)	9	7	92
10	AcOH-$LiClO_4$-(Pt)	6		57[e)]
11	AcOH-*t*-BuOH[d)]-Et_4NOTs-(Pt)	9	70	13
12	AcOEt-*t*-BuOH[d)]-Bu_4NClO_4-(Pt)	9		92
13	MeOH-$LiClO_4$-(Pt)	9	18	68
14	MeOH-Et_4NOTs-(Pt)	8[f)]	84	11
15	MeOH-Et_4NOTs-(Pt)	4[f)]	95	
16	MeOH-Et_4NOTs-(Pt)	2.25[f)]	89[g)]	

a) Carried out at a constant current density (1.67 mA/cm²) at 16—22 °C. b) Pt: platium foil electrodes (1.5×2 cm²); C: carbon plate electrodes (1.5×2 cm²). c) Isolated yields. d) Containing 10% (v/v) of *t*-BuOH. e) Tarry materials were obtained. f) Current density: 10 mA/cm². g) Monomethyl ether of **1** (11%) was recovered.

with Pt electrode (1.5×2 cm²) and a thermometer. A solution of $LiClO_4$ (400 mg) in MeCN (9 ml) and *t*-BuOH (1 ml) was charged into the cathode compartment fitted with Pt electrode (1.5×2 cm²). Nine F/mol of electricity was passed at a constant current of 1.67 mA/cm² at 16—18 °C for 8.6 h.[9)] The anode solution was concentrated *in vacuo* and the residue was taken up in CH_2Cl_2. The extracts were washed with brine, dried (Na_2SO_4), concentrated *in vacuo*, and chromatographed on silica gel with hexane/ether (5/1) to give **2** (28.9 mg, 94%): mp 102—103.5 °C (lit,[2a)] 105—106 °C).

Electrooxidation of 2-Methyl-5,8-dihydro-1,4-naphthalenediol (1) in MeOH-Et_4NOTs-(Pt) System (Entry 16). In a similar manner, a solution of **1** (67 mg, 0.38 mmol) and Et_4NOTs (600 mg) in MeOH (15 ml) [catholyte: MeOH (10 ml)-Et_4NOTs (400 mg)] was electrolyzed at 10 mA/cm² at 20—22 °C for 1.35 h (4 F/mol of electricity passed). Usual workup of the anolyte gave **3** (63 mg, 95%): mp 83—85 °C (lit, mp 91—92 °C[2a)] 82—84 °C,[10)] 86 °C[11)]).

Electrooxidation of 2-Methyl-5,8-dihydro-1,4-naphthoquinone (3) in MeCN-$LiClO_4$-(Pt) System. A solution of **3** (30 mg, 0.17 mmol) and $LiClO_4$ (600 mg) in MeCN [catholyte: MeCN (10 ml)-$LiClO_4$ (400 mg)] was electrolyzed at 1.67 mA/cm² at 16—17 °C. After passage of 3.5 F/mol of electricity (3.2 h), usual workup of the anolyte gave **2** (26.5 mg, 90%) and **3** (1 mg, 4%).

References

1) K. Sato, S. Inoue, and K. Saito, *J. Chem. Soc., Perkin Trans. 1*, **1973**, 2289; Y. Naruta and K. Maruyama, *Chem. Lett.*, **1979**, 881; Y. Naruta, *J. Org. Chem.*, **45**, 4097 (1980), and references cited therein.

2) a) K. Okahara and K. Murata, *Nippon Kagaku Zasshi.*, **63**, 1354 (1942); b) M. Wakae and K. Konishi, *Repts. Ind. Research Inst., Osaka Prefect. 7/2* **1955**, 59; *Chem. Abstr.*, **50**, 12005c (1956); V. A. Zagorevskii and D. A. Zykov, *Zh. Prikl. Khim.*, **32**, 2815 (1959): *Chem. Abstr.*, **54**, 9818e (1960); c) M. Periasamy and M. V. Bhatt, *Tetrahedron Lett.*, **1978**, 4561; L. F. Fieser, *J. Biol. Chem.*, **133**, 391 (1940); R. T. Arnold and R. Larson, *J. Org. Chem.*, **5**, 250 (1940); d) L. Syper, K. Kloc, J. Mlochowski, and Z. Sulc, *Synthesis*, **1979**, 521; M. Shimizu and G. Ouchi, *J. Pharm. Soc. Jpn.*, **71**, 963 (1951).

3) Vapor-phase oxidation of 2-methylnaphthalene with various catalysts has been investigated. However, the yields of the desired product **3** are not necessarily satisfactory: S. K. Ray, G. S. Murty, and H. S. Rao, *Proc. Symp. Chem. Oil Coal*, **1969**, 320; *Chem. Abstr.*, **80**, 135736s (1974).

4) The significant effect of *t*-BuOH in the electrolysis media has been mentioned in the previous papers: S. Torii, H. Tanaka, T. Shiroi, and M. Akada, *J. Org. Chem.*, **44**, 3305 (1979); S. Torii, H. Tanaka, and T. Mandai, *ibid.*, **40**, 2221 (1975).

5) G. Cauquis and G. Marbach, *Experientia Suppl.*, **1971**, 205.

6) The pH value of the electrolysis solution was more acidic than pH 1, after the electrolysis.

7) Exposure of **3** in MeOH (2 ml)-TsOH (40 mg) at 24 °C for 7 h resulted in the recovery of **2** (≈90%) along with monomethyl ether of **1** (≈2%) and **3** (≈5%).

8) All melting points are uncorrected.

9) The anode potential of 0.40—0.45 V *vs.* Ag/Ag^+ at the initial stage of the electrolysis shifted up to 2—2.1 V vs. Ag/Ag^+ after passing 2 F/mol of electricity.

10) E. W. J. Butz and L. W. Butz, *J. Org. Chem.*, **8**, 497 (1943).

11) A. N. Grinew and A. P. Terentév, *Zh. Obshch. Khim.*, **26**, 560 (1956): *Chem. Abstr.*, **50**, 13860d (1956).

Synthesis of Cyclic Silyl Diazo Compounds

Akira SEKIGUCHI and Wataru ANDO*

Department of Chemistry, The University of Tsukuba, Niiharigun, Ibaraki 305

(Received October 23, 1981)

Synopsis. Cyclic silyl diazo compounds, 1-diazo-2,2-diphenyl-4-bromo-1,2-dihydro-2-silanaphthalene, 6-diazo-1,1-dimethyl-2,3,4,5-tetraphenylsilacyclohexa-2,4-diene, and 10-diazo-9,9-dimethyl-9,10-dihydro-9-silaanthracene, were prepared and their spectroscopic properties were determined.

In recent years, interest in the chemistry of silylcarbenes has remarkably increased for the formation of silicon-carbon double bonded intermediates.[1] Simple silyl diazo compounds such as trimethylsilyldiazomethane,[2] ethyl trimethylsilyldiazoacetate,[3] bis(trimethylsilyl)diazomethane,[4] and their derivatives have been synthesized and studied. However, cyclic silyl diazo compounds like 1-diazo-1,2-dihydro-2-silanaphthalene, 6-diazosilacyclohexa-2,4-diene, and 10-diazo-9,10-dihydro-9-silaanthracene, have not been prepared so far. We now wish to report here synthesis of 1-diazo-2,2-diphenyl-4-bromo-1,2-dihydro-2-silanaphthalene (**1**), 6-diazo-1,1-dimethyl-2,3,4,5-tetraphenylsilacyclohexa-2,4-diene (**2**), and 10-diazo-9,9-dimethyl-9,10-dihydro-9-silaanthracene (**3**).

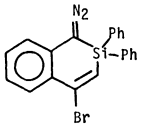

1

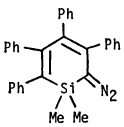

2

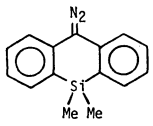

3

Diazo compound **1** was prepared by the conversion of the silyl ketone **4** to the hydrazone **5** followed by the oxidation with mercury(II) oxide in petroleum ether and benzene in 69% yield (Eq. 1). The spectroscopic data are given in Table . Silyl diazo compound **2** was obtained by a modification of the method of Doering and DePuy.[5] Direct diazo transfer by *p*-toluenesulfonyl azide to the silacyclohexadienyl anion **7** produced the silyl diazo compound **2** as yellow crystals in 36% yield (Eq. 2). Both **1** and **2** are relatively stable enough to be recrystallyzed. Diazo compound **3** was prepared as described in Eq. 3. Tosylhydrazone **9** was synthesized by the reaction of the ketone **8** with tosylhydrazine in ethanol in the presence of $BF_3 \cdot Et_2O$. The reaction is too slow in the absence of the catalyst. Treatment of the hydrazone **9** with sodium methoxide in pyridine afforded the diazo compound **3** in 90% yield as purple crystals.

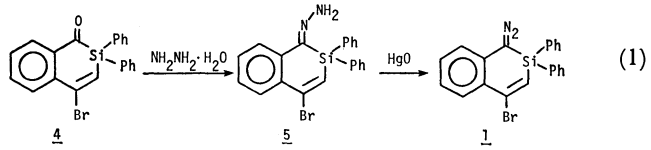

(1)

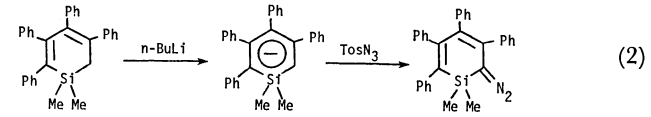

(2)

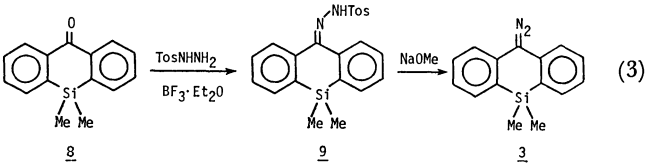

(3)

TABLE 1. SPECTROSCOPIC DATA OF CYCLIC SILYL DIAZO COMPOUND

Diazo compd	NMR (CCl_4, δ)	IR (KBr, $\nu(N_2)/cm^{-1}$)	UV λ_{max}/nm (C_6H_6, ε)
1	6.70—8.17 (m, ArH and BrC=CHSi)	2030	318 (4.69×10^3) 333 (4.78×10^3) 360 (6.96×10^3)
2	0.43(s, 6H, $SiMe_2$), 6.37—7.33(m, 20H, ArH)	2025	377 (1.17×10^4)
3	0.43(s, 6H, $SiMe_2$), 6.90—7.70(m, 8H, ArH)	2030	297 (1.73×10^4) 309 (1.87×10^4) 537 (52.0)

Experimental

General. NMR spectra were recorded on a Varian EM 360A spectrometer. IR and UV spectra were obtained by a Hitachi 260-50 spectrometer and a Shimadzu UV-365 spectrometer, respectively.

Materials. 2,2-Diphenyl-4-bromo-1,2-dihydro-2-silanaphthalene-1-one (**4**),[6] 1,1-dimethyl-2,3,4,5-tetraphenylsilacyclohexa-2,4-diene (**6**),[7] and 9,9-dimethyl-9,10-dihydro-9-silaanthracene-10-one (**8**),[8] were prepared by known procedures as referenced.

Synthesis of Hydrazone ***9***. Tosylhydrazone **9** was prepared in 32% yield by dissolving the ketone **8** (4.76 g, 20.0 mmol) in ethanol, adding excess tosylhydrazine (8.44 g, 45.4 mmol) and *ca.* 1 mL of $BF_3 \cdot Et_2O$ and refluxing for 3 h. The reaction mixture was concentrated, and the residue was chromatographed on silica gel with benzene/chloroform. Evaporation of the solvent afforded crude product **9** which was recrystallyzed from ethanol to give white crystals (2.63 g, 6.48 mmol), mp 168—169.5 °C. Found: C, 65.01; H, 5.44; N, 6.94%. Calcd for $C_{22}H_{22}N_2O_2SSi$: C, 64.99; H, 5.45; N, 6.89%.

Synthesis of ***1***. Hydrazine hydrate (16 g, 320 mmol) was added to a mixture of ethanol and benzene containing the silyl ketone **4** (10 g, 25.6 mmol) and a few drops of acetic acid at 0 °C. After stirring for 1.5 h, the reaction mixture was poured into water, and extracted with benzene. Hydrazone **5** was used without isolation. The benzene solution of **5** was diluted with petroleum ether, and then mercury(II) oxide (20 g, 92.3 mmol) was added. After stirring for 24 h, precipitated mercury was filtered off and the filtrate was concentrated. The residue was chromatographed on silica gel containing 10% water at 0 °C with petroleum ether/carbon tetrachloride. Evaporation of the solvent gave crude product **1** which was recrystallyzed from benzene/ethanol to give yellow-orange crystals (7.1 g, 69%), mp 129—130

°C. Found: C, 62.47; H, 3.69; N, 7.05; Br, 20.10%. Calcd for $C_{21}H_{15}N_2SiBr$: C, 62.53; H, 3.74; N, 6.94; Br, 19.81%.

Synthesis of ***2***. 1,1-Dimethyl-2,3,4,5-tetraphenylsilacyclohexa-2,4-diene (**6**) (7.0 g, 16.4 mmol) was treated with equimolar amount of butyllithium in THF at 0 °C. The red silacyclohexadienyl anion **7** was formed immediately. The anion was slowly added to a solution of *p*-toluenesulfonyl azide (3.9 g, 19.8 mmol) in THF at −78 °C, and the reaction mixture was slowly warmed to room temperature. The mixture was poured into water, and extracted with hexane. Chromatography on silica gel containing 10% water at 0 °C with hexane/benzene gave crude product **2** which was recrystallyzed from ethanol/benzene to give yellow crystals (2.7 g, 36%), mp(decomp) 134.5—135.5 °C. Found: C, 81.90; H, 5.65%. Calcd for $C_{31}H_{26}N_2Si$: C, 81.89; H, 5.76%.

Synthesis of ***3***. Tosylhydrazone **9** (1.00 g, 2.46 mmol) was dissolved in pyridine, and sodium methoxide (0.278 g, 5.15 mmol) was added to the solution. The mixture was heated at 70 °C for 15 min. The resulting red solution was poured into water, and extracted with hexane. Chromatography on silica gel containing 10% water at 0 °C with hexane gave purple crystals (0.554 g, 90%), mp 96—97 °C. Found: C, 72.07; H, 5.64; N, 11.05%. Calcd for $C_{15}H_{14}N_2Si$: C, 71.95; H, 5.63; N, 11.18%.

References

1) A. Sekiguchi and W. Ando, *J. Am. Chem. Soc.*, **103**, 3579 (1981), and references cited therein.

2) D. Seyferth, A. W. Dow, H. Menzel, and T. C. Flood, *J. Am. Chem. Soc.*, **90**, 1080 (1968).

3) U. Schöllkopf and N. Rieber, *Angew. Chem.*, **79**, 906 (1967).

4) D. Seyferth and T. C. Flood, *J. Organomet. Chem.*, **29**, C25 (1971).

5) W. E. Doering and C. H. DePuy, *J. Am. Chem. Soc.*, **75**, 5955 (1953).

6) R. Corriu and J. P. Masse, *J. Organomet. Chem.*, **22**, 321 (1970).

7) G. Märkl and P. L. Merz, *Tetrahedron Lett.*, **1971**, 1303.

8) J. Y. Corey, M. J. Dye, R. L. Farrell, and M. V. Mitchell, *J. Organomet. Chem.*, **153**, 127 (1978).

Absolute Configurations of α-Substituted Glycidates. (−)-(*R*)-Ethyl 2-Methyl-1-oxaspiro[2.5]octane-2-carboxylate and (−)-(*R*)-Ethyl 2,3-Dimethyl-2,3-epoxybutanoate

Toshio SUGITA,* Nobuyuki NISHIO, and Katsuhiko ICHIKAWA

Department of Hydrocarbon Chemistry, Faculty of Engineering, Kyoto University, Sakyo-ku, Kyoto 606

(Received October 24, 1981)

Synopsis. The absolute configurations of the title compounds were determined by chemical correlation and by asymmetric syntheses.

In the course of stereochemical studies of the Darzens reaction, it has been necessary to distinguish the stereoisomerism of the α-carbon of glycidates from the geometrical isomerism. No model compound with a known absolute configuration at the α-carbon of glycidate has, however, been reported, to our knowledge. Thus, we determined the absolute configurations of some α-substituted glycidates, which were symmetrically β,β-disubstituted: (−)-ethyl 2-methyl-1-oxaspiro-[2.5]octane-2-carboxylate (**3a**) and (−)-ethyl 2,3-dimethyl-2,3-epoxybutanoate (**3b**).

The potassium *t*-butoxide-catalyzed Darzens reactions of (−)-menthyl 2-chloropropanoate (**2**) and cyclohexanone (**1a**) or acetone (**1b**), followed by sodium ethoxide-catalyzed transesterification, afforded **3a** or **3b** respectively, each of which was exceeded in the (−)-isomer.

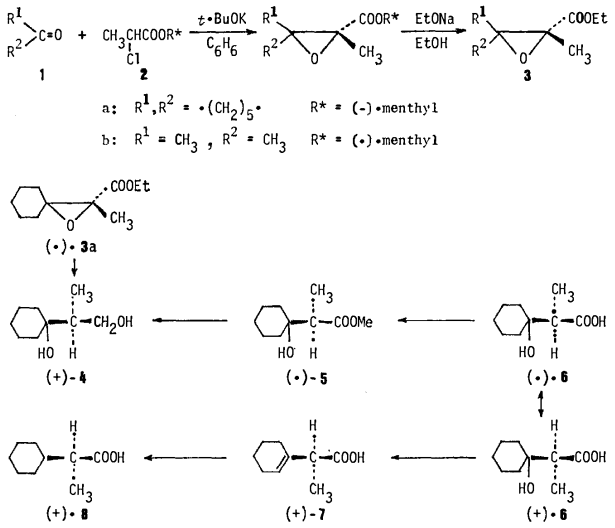

The (−)-**3a** was reduced by lithium aluminium hydride to give a mixture of 1,2- and 1,3-glycols. By periodic acid oxidation, the 1,2-glycol was cleaved to cyclohexyl methyl ketone, while 2-(1-hydroxycyclohexyl)-1-propanol (**4**) was left unaffected, indicating dextrorotation. (−)-2-(1-Hydroxycyclohexyl)propanoic acid (**6**), prepared by the Reformatsky reaction of cyclohexanone and ethyl 2-bromopropanoate, followed by hydrolysis and resolution with (−)-1-phenylethylamine, was converted with diazomethane to its (−)-methyl ester (**5**). The lithium aluminium hydride reduction of (−)-**5** afforded (+)-**4**. On the other hand, (+)-**6** was dehydrated by heating with 10% sulfuric acid to give (+)-2-(1-cyclohexenyl)propanoic acid (**7**). The catalytic hydrogenation of (+)-**7** gave (+)-2-cyclohexylpropanoic acid (**8**), the absolute configuration of which had been established as *S*.[1] It has been known that the lithium aluminium hydride reductions of oxirane rings accompany inversion of configuration at the reduced carbon.[2] In the other steps of the reaction sequence, the chiral carbon is not subjected to chemical changes; thus, the absolute configuration of (−)-**3a** is established to be *R*.

The asymmetric Darzens syntheses of **3a** and **3b** were carried out under the same conditions, and both products were exceeded in the (−)-isomers. Thus, (−)-**3b** is expected to have the same *R* configuration as (−)-**3a**.

Experimental

The ^{1}H-NMR spectra (in $CDCl_3$ using TMS as an internal standard) were taken on a JEOL PMX-60 spectrometer. The optical rotations were obtained on a Zeiss polarimeter or a JASCO DIP-180 polarimeter in chloroform solutions, unless otherwise mentioned.

A Typical Asymmetric Synthesis of the Glycidates (3). To a well-stirred solution of **1a** (20 g, 0.20 mol) and (−)-**2** (bp 111—113 °C/4 mmHg (1 mmHg≈133.322 Pa); $[\alpha]_D^{31}$ −71.03° (*c* 5.56); 50 g, 0.20 mol) in 200 ml of benzene, powdered potassium *t*-butoxide, freshly prepared from potassium (7.8 g, 0.20 mol) and *t*-butyl alcohol, was added, portion to portion, over 30 min at 10—15 °C under a nitrogen atmosphere. The mixture was stirred for an additional 2 h and then allowed to stand overnight at room temperature. Water was added to the reaction mixture, and extracted with ether. The extract was washed with aqueous NaCl and dried ($MgSO_4$). By removal of the solvents, crude (−)-menthyl 2-methyl-1-oxaspiro[2.5]octane-2-carboxylate (63.3 g) was obtained. The crude menthyl ester was refluxed with a solution of sodium ethoxide, prepared by dissolving sodium (2.0 g, 87 mmol) in 150 ml of ethanol, for 10 h. The mixture was neutralized with acetic acid, concentrated, and extracted with ether. The extract was washed with aqueous $NaHCO_3$ and with aqueous NaCl, dried ($MgSO_4$), and distilled by means of a Vigreaux-column to give (−)-menthol (bp 91.5—101 °C/9 mmHg, 26.5 g (85%)) and **3a** (bp 101.5—117.5 °C/9 mmHg, 16.8 g (42%)), which was found by vpc analysis to contain a small amount of (−)-menthol. After repeated distillations (3 times), pure ethyl 2-methyl-1-oxaspiro[2.5]octane-2-carboxylate (**3a**) (bp 122—123 °C/12 mmHg (lit,[3] bp 154—156 °C/40 mmHg), $[\alpha]_D^{33}$ −4.10° (*c* 10.71)) was obtained.

From 12 g (0.21 mol) of **1b** and 37 g (0.15 mol) of **2**, (−)-menthyl 2,3-dimethyl-2,3-epoxybutanoate (bp 100—137 °C/15 mmHg, 34.8 g (64.2%)) was obtained. The menthyl ester was transesterified to **3b** (bp 95.5—100 °C/66 mmHg, 9.4 g (40% from **2**)), which was found by vpc to contain a small amount of ethyl 2-chloropropanoate and a trace of (−)-menthol. Pure ethyl 2,3-dimethyl-2,3-epoxybutanoate (**3b**) (bp 100 °C/66 mmHg (lit,[4] bp 80—82 °C/20 mmHg);

$[\alpha]_D^{17}$ −1.32° (*c* 12.21); Found: C, 61.16; H, 9.44%) was obtained after repeated distillations.

(+)-2-(1-Hydroxycyclohexyl)-1-propanol (4) from (−)-3a. A solution of (−)-**3a** ($[\alpha]_D^{12}$ −3.13° (*c* 8.69), 9.9 g, 50 mmol) in 60 ml of ether was added to a stirred suspension of $LiAlH_4$ (2.3 g, 60 mmol) in 100 ml of ether. The mixture was stirred for 2.5 h, and then worked-up as usual. By the distillation of the reaction product, a mixture of **4** and 2-cyclohexyl-1,2-propanediol (bp 117—120.5 °C/3 mmHg, 5.7 g (72.2%)) was obtained. To the glycol mixture was added 130 ml of a 0.2 M (1 M=1 mol dm^{-3}) aqueous HIO_4 solution; this mixture was kept at an ambient temperature for 4 h with occasional shaking. After the duration, the mixture was extracted with ether, the extract was washed with a small amount of cold aqueous $Na_2S_2O_3$ and with aqueous NaCl, dried ($MgSO_4$), and distilled to give cyclohexyl methyl ketone (bp 53—58 °C/9 mmHg, 1.5 g (36.1%)) and (+)-**4** (bp 103.5—104 °C/2 mmHg (lit,[5] bp 106—110 °C/1 mmHg); $[\alpha]_D^{13}$ +2.24° (*c* 4.29); 1.1 g (21.2%); ^{1}H-NMR: δ=0.9 (d, J=8, 3H), 1.5 (broad s, 11H), 2.5—3.3 (2H), 3.7 (d, J=5, 2H)).

(−)-Methyl 2-(1-Hydroxycyclohexyl)propanoate (5). An ether solution of diazomethane was added until the mixture turned pale yellow to (−)-**6** ($[\alpha]_D^{28}$ −2.58°; 1.5 g, 8.7 mmol), prepared by the Reformatsky reaction of **1a** and ethyl 2-bromopropanoate,[6] followed by hydrolysis with ethanolic KOH and resolution with (−)-1-phenylethylamine. The mixture was distilled to give (−)-**5** (bp 121—122 °C/17 mmHg (lit,[7] bp 132 °C/18 mmHg); $[\alpha]_D^{29}$ −3.41° (*c* 10.14); 1.3 g (80%); ^{1}H-NMR: δ=1.18 (d, 3H), 1.48 (broad s, 10H), 2.50 (q, 1H), 2.75 (s, 1H), 3.70 (s, 3H); Found: C, 64.76; H, 9.92%).

(+)-2-(1-Hydroxycyclohexyl)-1-propanol (4) from (−)-5. (−)-**5** ($[\alpha]_D^{20}$ −30.3° (*c* 0.957); 1.5 g, 8.1 mmol) in 20 ml of ether was added to a stirred suspension of $LiAlH_4$ (0.5 g, 13 mmol) in 20 ml of ether, then the mixture was refluxed for 2.5 h. After the usual work-up, **4** was obtained: bp 119—120.5 °C/4 mmHg, $[\alpha]_D^{21}$ +10.69° (*c* 4.66), 0.7 g (56%). (Found: C, 67.84; H, 11.50%). The IR and ^{1}H-NMR spectra of **4** obtained from (−)-**3a** and (−)-**5** were completely superimposable.

(+)-2-(1-Cyclohexenyl)propanoic Acid (7). (+)-**6** ($[\alpha]_D^{20}$ +5.89°; 1.3 g, 7.6 mmol) was suspended to 10 ml of 10% sulfuric acid and stirred at 95—100 °C for 5.25 h. The mixture was extracted with ether, the ethereal extract was washed with aqueous NaCl, dried ($MgSO_4$), and distilled to give crude **7** (bp 140—144 °C/11 mmHg, 0.8 g (80%)). The NMR data indicated that the product contained a small amount of **6**. The product was chromatographed on a silica-gel (Wakogel C-200) column, using hexane–benzene (1:1) as the eluent, to give **7** (bp 150—153 °C/21 mmHg (lit,[8] bp 154—156 °C/26 mmHg); $[\alpha]_D^{28}$ +20.84° (*c* 3.03); ^{1}H-NMR: δ=1.27 (d, 3H), 1.65 (broad s, 4H), 2.06 (broad s, 4H), 3.18 (q, 1H), 5.89 (broad s, 1H), 10.4 (s, 1H); Found: C, 70.38; H, 9.40%).

(+)-2-Cyclohexylpropanoic Acid (8). (+)-**7** ($[\alpha]_D^{28}$ +39.27°; 1.05 g, 6.8 mmol) in 40 ml of methanol was hydrogenated over a 5% Pd–$BaSO_4$ catalyst (2.3 g) at atmospheric pressure and at room temperature. The reduction product was freed from the catalyst and the solvent, and distilled to give (+)-**8** (bp 122—123 °C/6 mmHg; $[\alpha]_D^{22}$ +10.10° (*c* 1.248, ethanol) (lit,[9,1] bp 121—123 °C/5 mmHg; $[\alpha]_D^{25}$ +18.9°)). ^{1}H-NMR δ=1.18 (d) and 0.7—2.6 (broad). (Found: C, 69.39; H, 10.64%).

References

1) D. J. Cram and F. D. Greene, *J. Am. Chem. Soc.*, **75**, 6005 (1953).
2) L. W. Trevoy and W. G. Brown, *J. Am. Chem. Soc.*, **71**, 1675 (1949); R. E. Parker and N. S. Isaacs, *Chem. Rev.*, **59**, 737 (1959).
3) G. Darzens, *C. R. Acad. Sci.*, **144**, 1123 (1907).
4) G. Darzens, *C. R. Acad. Sci.*, **141**, 766 (1905).
5) H. M. Walborsky and C. Colombini, *J. Org. Chem.*, **27**, 2387 (1962).
6) R. L. Shrinar, *Org. React.*, **1**, 1 (1942).
7) K. Auwers and P. Ellinger, *Justus Liebigs Ann. Chem.*, **387**, 228 (1912).
8) P. Rajzman, *Bull. Soc. Chim. Fr.*, **1948**, 754.
9) A. Maccioni, *Boll. Sci. Fac. Chim. Ind. Bologna*, **23**, 41 (1965); *Chem. Abstr.*, **63**, 8239 (1965).

Chemical Property of 1-Dialkylamino-2-phenylthioethylene

Toshio AGAWA,* Minori ISHIKAWA, Mitsuo KOMATSU, and Yoshiki OHSHIRO

Department of Petroleum Chemistry, Faculty of Engineering, Osaka University, Yamada-oka 2-1, Suita, Osaka 565

(Received October 28, 1981)

Synopsis. The olefins which are vicinally substituted by amino and phenylthio groups showed the reactivity as an enamine in the reactions with heterocumulenes and in cycloadditions with a 1,3-dipole and a 2-propenimine, giving a pyrazole derivative and a pyridine derivative, respectively.

Hetero-atom substituted olefins such as enamines, vinyl sulfides, and nitrogen and sulfur analogs of ketene acetals are versatile synthons in organic synthesis. However, utility of vicinally dihetero-atom substituted olefins has not been known so well.[1] Recently we developed a new synthetic method for the ethylenes which are vicinally substituted by dialkylamino and phenylthio (or methylthio) groups.[2] To clarify their chemical properties, we report here several reactions of 1-dialkylamino-2-phenylthioethylenes **1**.

The olefins **1** are highly sensitive to hydrolysis and, for example, β-phenylthio-α-piperidinostyrene (**1a**) was easily converted to α-phenylthioketone **2** under acidic conditions.

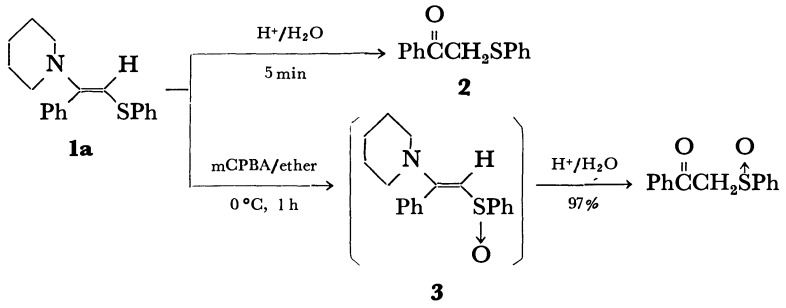

Oxidation of the olefin **1a** with *m*-chloroperbenzoic acid (mCPBA) gave β-phenylsulfinyl-α-piperidinostyrene (**3**) in 56% yield by NMR. It was difficult to isolate the sulfoxide **3** which was hydrolyzed to afford α-phenylsulfinylacetophenone.

Reaction of the olefins **1** with methyl iodide or benzyl bromide afforded salt-like materials which could be neither isolated nor identified. As a hydrolyzed product, benzyl phenyl sulfide was isolated by chromatographic treatment of the reaction mixture of **1a**

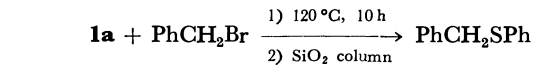

with benzyl bromide. The result implied a considerable extent of nucleophilic attack from the sulfur atom to the bromide. On the contrary, the reaction of **1a** with benzoyl chloride gave *N*-benzoylpiperidine in 34% yield as a hydrolyzed product, and 1-dimethylamino-2-phenylthioethylene (**1b**) gave *N*,*N*-dimethylbenzamide in 60% yield. Thus the reaction on the nitrogen atom is predominant in these reactions. However, no C–C bond forming reactions were observed for the reactions with the alkyl and acyl halides.

Diphenylketene is a highly reactive dipolarophile and smoothly reacted with the olefin **1a** at 20 °C to give the butenone derivative **4a** and with **1b** to give the butenone **4b**. Similarly, **1a** reacted with phenyl isocyanate to afford α-phenylthio-β-piperidinocinnamanilide (**5**) in 54% yield. These products are considered to be formed *via* 1:1 cycloadducts which rearrange to the linear 1:1 adducts.[3] Thus formation of the carbonyl compounds **4** and **5** would provide us a preparative method for highly functionalized olefins.

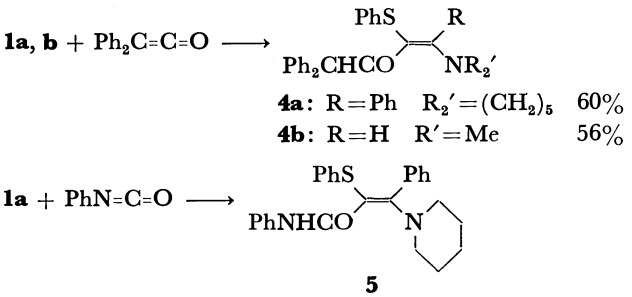

Cycloaddition reactions were also studied. The olefin **1b** reacted with the nitrilimine **6** to give the pyrazole derivative **7** in 40% yield. The formation of **7** is elucidated by elimination of dimethylamine from a 1:1 cycloadduct. As a dienophile the olefins

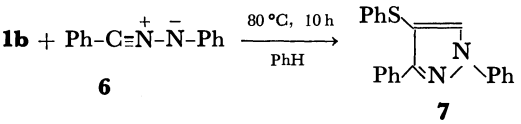

1 were not so reactive with cyclopentadiene and ethyl sorbate. However, **1b** reacted with a heterodiene, *N*-*t*-butyl-2-ethyl-2-propenimine (**8**), to give 3-ethyl-5-phenylthiopyridine (**9**) in 51% yield when heated at

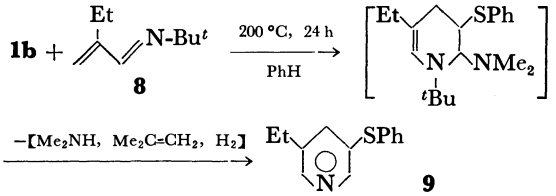

200 °C for 24 h. The reaction is assumed to proceed *via* cycloaddition followed by elimination of dimethylamine and isobutylene and successive oxidative aromatization.

As these addition products **7** and **9** are suggested to be similar to 1:1 cycloaddition products of phenylthioacetylene with the 1,3-dipole **6** and the diene **8**, respectively, the olefins of type **1** are expected to become a reagent equivalent to arylthioacetylenes[4] in cycloadditions. In conclusion the olefins **1** show chemical property as an enamine rather than a vinyl sulfide but lower reactivity than usual enamines.

Experimental

Materials. Commercially available reagents were used unless otherwise noted. The olefins **1a** and **1b** were prepared by the reported method.[2] Diphenylketene was prepared by dehydrochlorination of diphenylacetyl chloride. The propenimine **8** was obtained by the reaction of *N-t*-butylmethanimine and 1-piperidino-1-butene at 150 °C for 6 h; bp 55—57 °C/4000 Pa; NMR ($CDCl_3$) δ 1.10(3H, t), 1.19(9H, s), 2.4(2H, m), 5.33(1H, broad s), 5.51(1H, m), 7.90(1H, s).

Hydrolysis. To a solution of **1a** (1.26 g, 4.3 mmol) in EtOH (5 ml) was added 12 mol dm^{-3} HCl (2 ml) and allowed to stand for 5 min. Extraction (ether), drying ($CaSO_4$), and concentration gave 725 mg (74%) of α-phenylthioacetophenone (**2**) which was identified with an authentic sample.

Oxidation. To a solution of **1a** (1.48 g, 5.0 mmol) in ether (5 ml) containing 1.06 g (10 mmol) of Na_2CO_3 was added mCPBA (1.08 g, 6.0 mmol) in ether (20 ml) and the mixture was stirred at 0 °C for 1 h. The reaction mixture was worked up as usual to give the crude oil containing the sulfoxide **3** (56% yield by NMR); IR (neat) 1580 (C=C) and 1030 cm^{-1} (S→O); NMR ($CDCl_3$) δ 5.4 (s, =CH). The oil (164 mg) was hydrolyzed in EtOH (5 ml) containing 12 mol dm^{-3} HCl (2 ml) to afford 97% of α-phenylsulfinylacetophenone which was identified with an authentic sample prepared by oxidation of **2**.

Reactions with Halides. A benzene solution (6 ml) of **1a** (1.48 g, 5.0 mmol) and benzyl bromide (0.85 g, 5.0 mmol) was heated at 120 °C for 10 h in a sealed tube. The reaction mixture was chromatographed (SiO_2–hexane) to give benzyl phenyl sulfide (0.35 g, 35%).

A solution of **1a** (5.0 mmol) and benzoyl chloride (703 mg, 5.0 mmol) in ether (10 ml) containing K_2CO_3 (2.0 g) was stirred for 20 h at 20 °C. Chromatographic treatment (SiO_2–benzene) of the filtrate gave 322 mg (34%) of *N*-benzoylpiperidine which was identified with an authentic sample. Similarly, 0.90 g (60%) of *N,N*-dimethylbenzamide was obtained from 1.79 g (10 mmol) of **1b**, the chloride (1.41 g, 10 mmol) and triethylamine (1.01 g, 10 mmol) using DMF as a solvent.

Reactions with Diphenylketene and Phenyl Isocyanate. To a solution of **1** (5.0 mmol) in ether (10 ml) was added the ketene (0.97 g, 5.0 mmol) and the mixture was stirred for 3 h at 20 °C. A crystalline product was obtained by concentration in the case of **1a** and an oily product by column chromatography (SiO_2–EtOH) in the case of **1b**. 1,1,4-Triphenyl-3-phenylthio-4-piperidino-3-buten-2-one (**4a**): yield 1.47 g (60%); mp 163—164 °C; IR (Nujol) 1600 cm^{-1} (C=O); NMR ($CDCl_3$) δ 1.4—1.8 (6H, m), 2.9—3.3 (4H, m), 6.20 (1H, s), 6.8—7.5 (20H, m); MS *m/e* 489 (M^+). Found: C, 81.22; H, 6.25; N, 2.83; S, 6.31%. Calcd for $C_{33}H_{31}NOS$: C, 80.95; H, 6.38; N, 2.86; S, 6.53%. 4-Dimethylamino-1,1-diphenyl-3-phenylthio-3-buten-2-one (**4b**): yield 1.17 g (56%); IR (Nujol) 1640 cm^{-1} (C=O); NMR ($CDCl_3$) δ 3.10(6H, s), 6.13(1H, s), 6.9—7.3(15H, m), 8.18(1H, s); MS *m/e* 373 (M^+).

A mixture of **1a** (5.0 mmol) and the isocyanate (0.60 g, 5.0 mmol) in ether (10 ml) was stirred for 20 h at 20 °C. Concentration of the mixture gave solid material which was recrystallized from CH_2Cl_2 to give 1.12 g (54%) of β-phenylthio-α-piperidinocinnamanilide (**5**): mp 160 °C; IR (Nujol) 1620 cm^{-1} (C=O); NMR ($CDCl_3$) δ 1.4—1.9(6H, m), 3.0—3.5(4H, m), 6.9—7.6 (15H, m), 8.5—8.8(1H, broad s); MS *m/e* 414 (M^+).

Reaction with N-Phenylbenzonitrilimine (6). A mixture of **1b** (1.79 g, 10 mmol), *N*-anilinobenzimidoyl chloride[5] (2.3 g, 10 mmol) and triethylamine (3.0 g, 30 mmol) in benzene (20 ml) was heated at reflux for 10 h. The reaction mixture was chromatographed (SiO_2–benzene) to give 1.31 g (40%) of 1,3-diphenyl-4-phenylthiopyrazole (**7**): mp 80—82 °C; IR (Nujol) 1600 cm^{-1} (C=C, C=N); NMR ($CDCl_3$) δ 6.8—7.7(13H, m), 7.81(1H, s), 8.0—8.2(2H, m); MS *m/e* 328 (M^+). Found: C, 76.78; H, 4.75; N, 8.52; S, 9.66 %. Calcd for $C_{21}H_{16}N_2S$: C, 76.81; H, 4.91; N, 8.53; S, 9.75%.

Reaction with the Propenimine 8. A mixture of **1b** (1.60 g, 8.9 mmol) and the imine (1.24 g, 8.9 mmol) in benzene (10 ml) was heated at 200 °C for 24 h in a sealed tube. The reaction mixture was extracted ($CHCl_3$), dried (Na_2CO_3), and chromatographed (SiO_2–benzene) to give 3-ethyl-5-phenylthiopyridine (**7**, 51%), whose analytical sample was obtained as a picrate: mp 141.5—142.5 °C (picrate); NMR ($CDCl_3$) δ 7.1—7.4 (5H, m), 7.45(1H, dd), 8.30 (1H, d), 8.37(1H, d); MS *m/e* 215 (M^+). Found: C, 50.71; H, 3.37; N, 12.64; S, 7.13%. Calcd for $C_{19}H_{16}N_4O_7S$ (picrate): C, 51.35; H, 3.63; N, 12.61; S, 7.20%.

References

1) H. Matsuda, K. Hirai, and Y. Kishida, *Ann. Rep. Sankyo Res. Lab.*, **24**, 96 (1972).

2) T. Agawa, M. Ishikawa, M. Komatsu, and Y. Ohshiro, *Chem. Lett.*, **1980**, 335.

3) H. Urlich, "Cycloaddition Reactions of Heterocumulenes," Academic Press, New York (1967), pp. 51—56 and 139—141.

4) H. Groen and J. F. Arens, *Recl. Trav. Chim. Phys-Bas.*, **80**, 879 (1961); E. Angeletti, F. Montanari, and A. Negrini, *Gazz. Chim. Ital.*, **87**, 1115 (1957).

5) A. Eckell, R. Huisgen, R. Sustman, G. Wallbilich, D. Grashey, and E. Spindler, *Chem. Ber.*, **100**, 2192 (1967).

Heterocylic Studies. Synthesis of 9-Hydroxybenzimidazo[2,1-*b*]-benzothiazoles and Their Quaternary Derivatives

R. P. Soni and J. P. Saxena*
Department of Chemistry, University of Jodhpur, Jodhpur, India
(Received September 22, 1980)

Synopsis. A series of substituted 9-hydroxybenzimidazo[2,1-*b*]benzothiazoles has been synthesized. The position of phenolic hydroxyl group in these compounds has been ascertained on the basis of spectral data.

Benzimidazole derivatives exhibit pronounced antiviral activity.[1] Thiabendazole[2-(4-thiazolyl)benzimidazole] is well known for its use as the leading anthelmintic for the control of most gastrointestinal nematodes of man, with exception of Trichuris species.[2-4] It was therefore worthwhile to synthesize some new compounds containing benzimidazole moiety and study their mode of formation through spectral data.

Recently we have reported the synthesis of 6-hydroxy [1,3,4]thiadiazolo[2,3-*b*]benzimidazoles.[5] In this paper we report the synthesis of some new 9-hydroxybenzimidazo[2,1-*b*]benzothiazoles (**2**), obtained by the reaction of 2-aminobenzothiazoles (**1**) with *p*-benzoquinone.

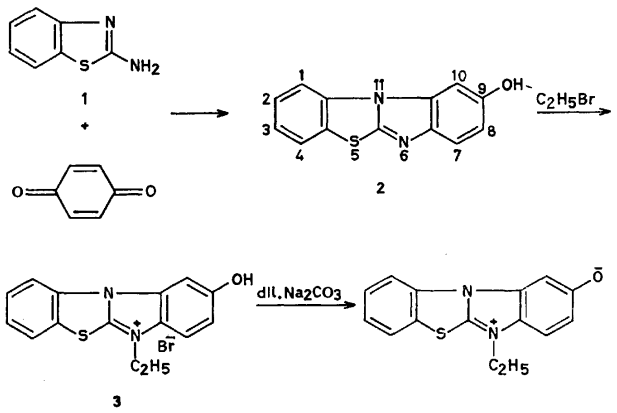

Quaternization of **2** with ethyl bromide yields 6-ethyl-9-hydroxybenzimidazo[2,1-*b*]benzothiazolium bromide (**3**), as evidenced by the work of Paudler and Blewitt for the site of protonation and *N*-methylation of imidazo-[1,2-*a*]pyridines.[6] Compound **3** gave intense yellow color with dil alkali due to the formation of the phenol betaines.[7,8]

Experimental

All the reagents were thoroughly dried and purified before use. All melting points were determined on Kofler instrument and were uncorrected. IR spectra were recorded on a Perkin-Elmer 577 spectrophotometer in KBr. UV absorption spectra were scanned on a Beckman spectrophotometer, Model DU-2.

6-Hydroxybenzimidazo[2,1-b]benzothiazoles (2). A solution of *p*-benzoquinone (0.01 mol) in glacial acetic acid (10 ml) was added in small portions to the substituted 2-aminobenzothiazoles (0.01 mol) in glacial acetic acid (10 ml) with constant shaking. The mixture was refluxed for 2 h and left aside for 5—7 d. To the reaction mixture 20 ml of 50% HCl was added and the solution was diluted with water, and then extracted with ether to remove any unreacted quinone and hydroquinone. The resulting solution was just neutralized with aq sodium carbonate. A crude solid product was obtained. It was filtered, washed well with water, and then recrystallized from an appropriate solvent after decolorizing with charcoal in ethanol till it gave a single spot on TLC with aq ethanol.

6-Ethyl-9-hydroxybenzimidazo[2,1-b]benzothiazolium Bromides (3). A mixture of **2** (0.01 mol) and ethyl bromide (0.01 mol) was taken in minimum quantity of acetone. The reaction mixture was boiled under reflux on a water bath for 1 to 2.5 h. The solvent was evaporated to dryness under reduced pressure. The residue was recrystallized from ethanol–ether mixture.

Table 1. 9-Hydroxybenzimidazo[2,1-*b*]benzothiazoles (**2**)

Starting thiazole	Molecular formula	Mp θ_m/°C	Yield %	Calcd (%)	Found (%)	UV Spectra: Ethanol λ_{max}/nm	log ε	0.1 M HCl λ_{max}/nm	log ε	0.1 M NaOH λ_{max}/nm	log ε
2-Amino-benzothiazole[9]	$C_{13}H_8N_2OS$	321—322	53	C, 65.0	64.7	245	3.60				
				H, 3.3	3.1	271	3.97	326	3.71	315	3.51
				N, 11.6	11.5	341	3.86	374	3.81	442	3.43
2-Amino-6-methoxy benzothiazole[10]	$C_{14}H_{10}N_2O_2S$	307	45	C, 66.1	65.9	248	3.61				
				H, 3.9	3.6	279	4.00	330	3.67	322	3.59
				N, 11.0	10.8	348	3.82	273	3.91	451	3.47
2-Amino-5,5-dimethyl-4,5,6,7-tetrahydro-benzothiazol-7-one[11]	$C_{15}H_{14}N_2O_2S$	345 (decomp)	35	C, 62.8	62.6	250	3.86				
				H, 4.9	4.7	292	4.05	335	3.57	325	3.47
				N, 9.7	9.6	364	3.74	391	3.81	483	3.34
2-Amino-4,5,6,7-tetra-hydrobenzothiazole[12]	$C_{13}H_{12}N_2OS$	297	33	C, 63.1	62.9	257	3.51				
				H, 4.9	4.6	305	4.15	321	3.41	315	3.61
				N, 11.0	10.7	357	4.07	401	3.76	476	3.54
2-Amino-6-methyl-4,5,6,7-tetrahydro-benzothiazole	$C_{14}H_{14}N_2OS$	314	38	C, 65.1	64.8	254	3.67				
				H, 5.4	5.3	301	4.09	318	3.56	310	3.57
				N, 10.8	10.5	352	4.10	397	3.82	471	3.42

TABLE 2. 6-ETHYL-9-HYDROXYBENZIMIDAZO[2,1-*b*]-BENZOTHIAZOLIUM BROMIDE (**3**)

Molecular formula	Mp θ_m/°C	Yield %	Calcd (%)	Found (%)	UV Spectra Ethanol λ_{max}/nm	log ε
$C_{15}H_{13}N_2OSBr$	274	41	N, 8.0 Br, 22.9	7.9 22.6	260 507	3.41 3.66
$C_{16}H_{15}N_2O_2SBr$	287	37	N, 7.7 Br, 22.0	7.4 21.7	263 512	3.81 3.75
$C_{17}H_{19}N_2O_2SBr$	337	25	N, 7.2 Br, 21.4	6.9 21.2	268 517	3.34 3.75
$C_{15}H_{17}N_2OSBr$	256	38	N, 7.9 Br, 22.6	7.7 22.5	275 542	3.64 3.51
$C_{16}H_{19}N_2OSBr$	304	42	N, 7.6 Br, 21.7	7.3 21.4	272 548	3.91 3.72

Discussion

The structure of compounds **2** has been determined on the basis of IR, UV spectra, and elemental analysis. The IR spectra of these compounds showed bands at 3340, 1210 (phenolic OH), 1625 (C=N), 1315 (C–N), and 1450 cm^{-1} (aromatic ring). Electronic absorption spectra of **2** have been studied which have a bearing on their finer structure, particularly with regards to the position of phenolic hydroxyl group which could be either on 9th or 8th carbon atom.

Compounds **2** show the characteristic bathochromic shifting of the absorption maximum in the longer wavelengths in both acid and alkaline medium.

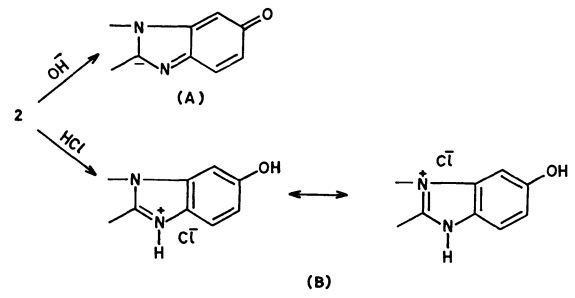

In alkaline medium this red shift of about 100 nm is more pronounced and is ascribed to the quinonoid structure (A) as one of the contributing form to the total structure. In acid medium (about 40 nm) it should be due to the salt formation (B).

The quaternary compounds **3** show a further red shifting of absorption maxima in the visible region (λ_{max}>500 nm) (Table 2). This may be attributed to salt formation and contribution of the dipolar betaine structure in ethanol.

The formation of **2** can be explained by the following mechanisms.

Whichever of the two mechanisms cited here may be taking place, the position of phenolic hydroxyl group remains ascertained as meta to the bridgehead nitrogen atom and para to second imidazole nitrogen, through either of these routes.

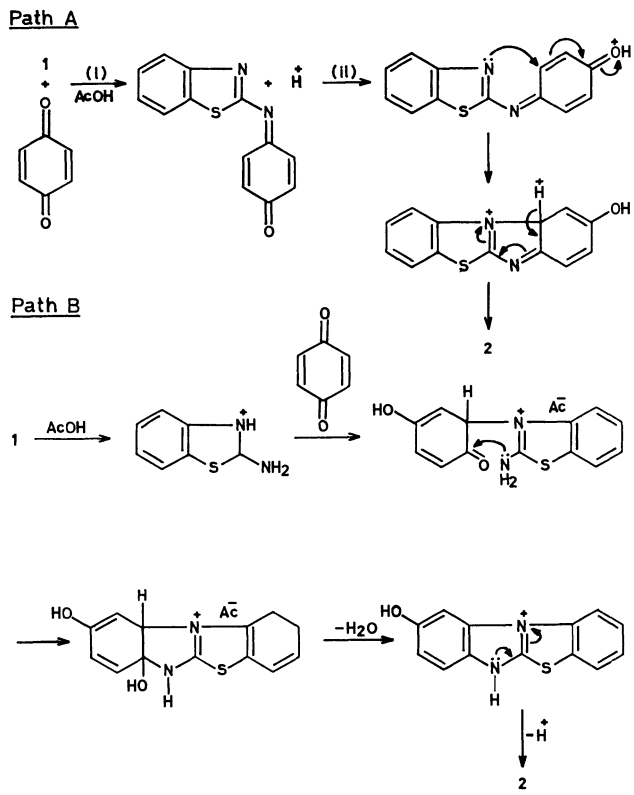

Thanks are due to the U.G.C., New Delhi for the award of a Junior Research Fellowship to R.P.S. and to the Director, C.D.R.I., Lucknow for the IR spectra and elemental analysis.

References

1) H. J. Eggers and I. Tamm, *J. Exp. Med.*, **113**, 657 (1961).
2) H. D. Brown, A. R. Matzuk, I. R. Ilves, L. H. Peterson, S. A. Harris, L. A. Sarett, J. R. Egerton, J. J. Yakstis, W. C. Campbell, and A. C. Cuckler, *J. Am. Chem. Soc.*, **83**, 1764 (1961).
3) J. R. Douglas and N. F. Baker, *Ann. Rev. Pharmacol.*, **8**, 213 (1968).
4) A. C. Cuckler and K. C. Mezey, *Arzneim.-Forsch.*, **190**, 852 (1964).
5) R. P. Soni and J. P. Saxena, *Bull. Chem. Soc. Jpn.*, **52**, 2033 (1979).
6) W. W. Paudler and H. L. Blewitt, *J. Org. Chem.*, **31**, 1295 (1961).
7) J. P. Saxena, *J. Sci. Ind. Res.*, **22**, 8 (1963).
8) J. P. Saxena, W. H. Stafford, and W. L. Stafford, *J. Chem. Soc.*, **1959**, 1579.
9) S. Hugerschoff, *Ber.*, **36**, 3121 (1903); **34**, 3130 (1901).
10) C. G. Stuckwisch, *J. Am. Chem. Soc.*, **71**, 3417 (1949).
11) J. Mohan and H. K. Pujari, *Indian J. Chem.*, **13**, 871 (1975).
12) H. Erlenmeyer and W. Schoenauer, *Helv. Chim. Acta*, **24**, 172 (1941).

Atropisomerism in Metal Chelates. The Crystal Structure and Absolute Configuration of $(-)_{589}$-3-(2,4-Dinitro-1-naphthyl)-2,4-pentanedionato[tris(2-aminoethyl)amine]cobalt(III) Dibromide

Yoshiharu NAKANO*,† and Shoichi SATO

The Institute for Solid State Phisics, The University of Tokyo, Roppongi 7-22-1, Minato-ku, Tokyo 106

(Received June 8, 1981)

The crystal structure and the absolute configuration of $(-)_{589}$-3-(2,4-dinitro-1-naphthyl)-2,4-pentanedionato-[tris(2-aminoethyl)amine]cobalt(III) dibromide were determined by X-ray diffraction. The complex crystallizes as the orthorhombic space group $P2_12_12_1$, with $a=13.738(2)$, $b=15.446(1)$, $c=12.243(1)$ Å, and $Z=4$. The structure was solved by the Patterson-Fourier method and refined to a final R_1 value of 0.038 for the 3347 observed reflections with $|F_o|>3\sigma(|F_o|)$. The acetylacetonate (acac) ring adopts a more deformed boat conformation than that in 3-(6-methyl-2,4-dinitrophenyl)-2,4-pentanedionato analogue. The three chelate rings of tris(2-aminoethyl)amine (tren) have envelope conformations and adopt λ, λ, and δ conformations. The absolute configuration of the title compound can be designated as *R*.

One of the present authors (Y. N.) has synthesized and resolved a series of optically active complexes whose optical activity arises from the restricted rotation of an aromatic ring system. The crystal structure of a member of the series has been determined by X-ray diffraction (Complex II in Fig. 1).[1] In this complex, the $[CoN_4O_2]$ chromophore possesses approximately the C_{2v} symmetry, while the two apical five membered chelate rings formed by tren have enantiomeric conformations. Although the 6-methyl-2,4-dinitrophenyl group is, as expected, almost perpendicular to the acac ring, the acac ring bends slightly toward the 2-nitro group.

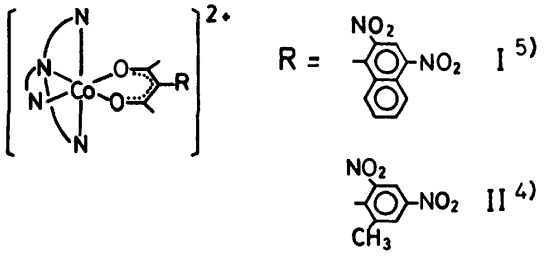

Fig. 1. Skeletal stucture of 3-aryl-2,4-pentanedionato-[tris(2-aminoethyl)amine]cobalt(III) cation.

Since the title complex has the same chromophore as Complex II, except for its π-electronic system of the aromatic ring, almost all the transitions in the CD spectrum of Complex II should also appear in that of Complex I. In fact, the CD spectrum of the title complex showed the same sign and reasonable rotational strength compared to that of $(-)_{589}$-complex II in the first absorption region. Accordingly, the following structural features, observed in Complex II, were also expected for Complex I: (1) The relative configuration of the 2-nitro group with respect to the tren chain, (2) the bent structure of the acac ring, and (3) the disposition of the aromatic system relative to the acac ring.

The authors' interest lies in clarifying the structural details, such as those described above and other structural factors which may contribute to the rotatory strength.

Experimental

The present complex[2] consists of orange-red plates. The crystal data and data collection detailes are summarized in Table 1. The intensities were corrected for Lorentz and polarization effects and for absorption. The structure was solved by the heavy-atom method. All the parameters for non-hydrogen atoms were refined by a block-diagonal least-squares method with anisotropic thermal parameters. The weights for the refinement were $w=1/[\sigma^2(|F_o|)+(0.015|F_o|)^2]$. The refinement converged to $R_1=0.038$ and $R_2=0.042$. The final positional parameters shift of C(2) was 1.5σ, those of the other non-hydrogen atoms were less than their σ. The final difference Fourier maps showed no peaks greater than 0.6 e/Å^3.

Table 1. The crystal data[a] and data collection

$C_{21}H_2Br_2CoN_6O_6$	
Orthorhombic	$P2_12_12_1$
$a=13.738(2)$ Å, $b=15.446(1)$ Å, $c=12.243(1)$ Å, $V=2598.1(4)$ Å^3	
$D_x=1.74$, $D_m=1.73$ g cm^{-3}; $Z=4$, $\mu=40.0$ cm	
Crystal used	A sphere 0.35 mm in diameter
Diffractometer	Rigaku AFC-3 automated four-circle diffractometer
Radiation	Mo $K\alpha$ (monochromated with graphite), $\lambda=0.71069$ Å
Data-collection range	$3<2\theta<60°$
Scan mode	θ-2θ scan(2°/min in θ)
Total data collected	4375
Data with $|F_o|>3\sigma(|F_o|)$	3347

a) The lattice constants were obtained by a least-squares calculation based on 31 reflections with $12.1<\theta<21.3°$.

† Present address: Department of Chemistry, Ibaraki University, Bunkyo 2-1-1, Mito 310.

TABLE 2. ATOMIC PARAMETERS, WITH THEIR STANDARD DEVIATIONS IN PARENTHESES

Atom	x	y	z	U_{eq}/Å^2 a) or U_{iso}/Å^2
Co	0.35086(4)	0.20621(4)	0.90118(5)	0.0210(3)
Br(1)	0.56479(5)	0.17166(4)	1.22141(5)	0.0462(3)
Br(2)	0.12908(4)	0.12748(4)	1.17904(5)	0.0480(3)
C(1)	0.3975(4)	0.0287(3)	0.9186(5)	0.037(3)
C(2)	0.3418(4)	0.0344(3)	1.0239(4)	0.036(3)
C(3)	0.4915(4)	0.1395(3)	0.8160(5)	0.040(3)
C(4)	0.5492(4)	0.1696(3)	0.9145(5)	0.040(3)
C(5)	0.3195(4)	0.1091(3)	0.7665(4)	0.038(3)
C(6)	0.2193(4)	0.1103(4)	0.8170(5)	0.044(3)
C(7)	0.3711(4)	0.4142(3)	0.7377(4)	0.034(3)
C(8)	0.3546(3)	0.3681(3)	0.8446(4)	0.024(2)
C(9)	0.3417(3)	0.4132(3)	0.9420(4)	0.024(2)
C(10)	0.3118(3)	0.3701(3)	1.0385(4)	0.025(2)
C(11)	0.2770(4)	0.4225(3)	1.1328(4)	0.037(3)
C(12)	0.3492(3)	0.5097(3)	0.9479(4)	0.026(2)
C(13)	0.4316(4)	0.5524(3)	0.9811(4)	0.031(2)
C(14)	0.4389(5)	0.6433(3)	0.9846(4)	0.040(3)
C(15)	0.3597(5)	0.6917(3)	0.9592(4)	0.041(3)
C(16)	0.2710(4)	0.6553(3)	0.9265(4)	0.037(3)
C(17)	0.1870(5)	0.7035(4)	0.8956(5)	0.053(4)
C(18)	0.1036(5)	0.6634(4)	0.8662(5)	0.057(4)
C(19)	0.0968(4)	0.5729(4)	0.8665(5)	0.050(4)
C(20)	0.1773(4)	0.5234(3)	0.8930(4)	0.034(3)
C(21)	0.2661(4)	0.5628(3)	0.9212(4)	0.029(2)
N(1)	0.3928(3)	0.1136(2)	0.8557(3)	0.028(2)
N(2)	0.3514(3)	0.1230(2)	1.0690(3)	0.028(2)
N(3)	0.4882(3)	0.2339(3)	0.9737(3)	0.029(2)
N(4)	0.2179(3)	0.1755(3)	0.9055(3)	0.029(2)
N(5)	0.5186(3)	0.5069(3)	1.0204(4)	0.041(3)
N(6)	0.3720(5)	0.7856(3)	0.9747(4)	0.064(3)
O(1)	0.3524(2)	0.2855(2)	0.8335(2)	0.024(1)
O(2)	0.3077(2)	0.2887(2)	1.0521(3)	0.026(2)
O(3)	0.5102(3)	0.4378(3)	1.0676(4)	0.052(2)
O(4)	0.5971(3)	0.5430(3)	1.0067(5)	0.071(3)
O(5)	0.4502(5)	0.8170(3)	0.9525(5)	0.093(4)
O(6)	0.3050(5)	0.8262(3)	1.0138(6)	0.108(5)
H(C1A)	0.454(4)	0.015(3)	0.928(4)	0.044(16)
H(C1B)	0.376(4)	−0.018(4)	0.865(5)	0.060(19)
H(C2A)	0.365(4)	−0.005(3)	1.071(4)	0.038(15)
H(C2B)	0.277(4)	0.022(3)	1.011(4)	0.041(15)
H(N2A)	0.403(3)	0.123(3)	1.108(4)	0.019(12)
H(N2B)	0.306(4)	0.132(4)	1.099(5)	0.054(18)
H(C3A)	0.482(3)	0.190(3)	0.768(4)	0.022(12)
H(C3B)	0.521(4)	0.092(3)	0.777(4)	0.041(15)
H(C4A)	0.606(4)	0.194(3)	0.892(4)	0.041(15)
H(C4B)	0.562(5)	0.120(4)	0.951(5)	0.066(20)
H(N3A)	0.500(3)	0.284(3)	0.952(4)	0.029(13)
H(N3B)	0.502(4)	0.224(3)	1.058(4)	0.043(16)
H(C5A)	0.330(3)	0.155(2)	0.720(3)	0.008(10)
H(C5B)	0.333(3)	0.061(3)	0.739(4)	0.027(13)
H(C6A)	0.175(3)	0.124(3)	0.758(4)	0.027(13)
H(C6B)	0.202(4)	0.059(3)	0.842(4)	0.040(16)
H(N4A)	0.188(4)	0.224(3)	0.881(4)	0.035(15)
H(N4B)	0.186(4)	0.154(3)	0.963(4)	0.041(15)
H(C7A)	0.334(3)	0.393(3)	0.693(4)	0.026(13)
H(C7B)	0.355(4)	0.473(3)	0.744(5)	0.046(16)
H(C7C)	0.422(4)	0.402(4)	0.708(5)	0.053(17)
H(C11A)	0.218(4)	0.468(3)	1.112(4)	0.041(16)
H(C11B)	0.249(4)	0.390(4)	1.190(5)	0.055(18)
H(C11C)	0.326(3)	0.453(3)	1.154(4)	0.027(13)
H(C14)	0.493(4)	0.664(3)	1.011(4)	0.037(15)
H(C17)	0.197(4)	0.763(3)	0.891(4)	0.042(16)
H(C18)	0.051(5)	0.693(4)	0.835(6)	0.073(21)
H(C19)	0.035(4)	0.539(3)	0.837(4)	0.037(15)
H(C20)	0.168(4)	0.462(3)	0.883(4)	0.032(14)

a) $U_{eq}=(U_{11}+U_{22}+U_{33})/3$.

The positional parameters of all the atoms with their standard deviations, are listed in Table 2. The thermal parameters[3] and observed and calculated structure factors[3] are kept in the office of the Chemical Society of Japan. The atomic-scattering factors were taken from Ref. 4. The calculations were performed on a FACOM 230-48 computer of this Institute with a local version of UNICS.[5]

The absolute configuration was determined by anomalous-scattering techniques. Some Friedel pairs were examined on equi-inclination Weissenberg photographs taken with Cu $K\alpha$ radiation. Observed and calculated intensities are compared, for which $|F_c(hkl)|$ and $|F_c(h\bar{k}\bar{l})|$ differd by more than 35%.[3] The concordance of the intensities indicated that the absolute configuration of this complex is R, according to the Cahn-Ingold-Prelog notation.[6] When the enantiomeric structure was refined under identical conditions, it converged to $R_1=0.056$ and $R_2=0.058$. An application of the residual-index-ratio-test[7] showed that this structure could be rejected at the 0.005 significance level in favor of the R configuration.

Description of Structure and Discussion

Figures 2 and 3 show the projection of the crystal structure along the c and b axes respectively. The complex cations are linked through N–H···Br hydrogen bonds to form zigzag chains along the a axis. The

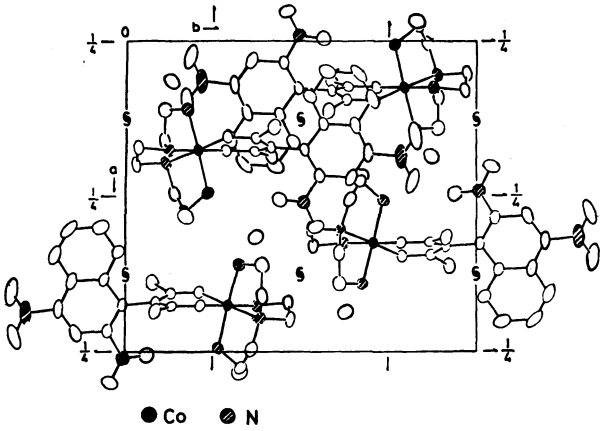

Fig. 2. A projection of the unit cell along the c axis.

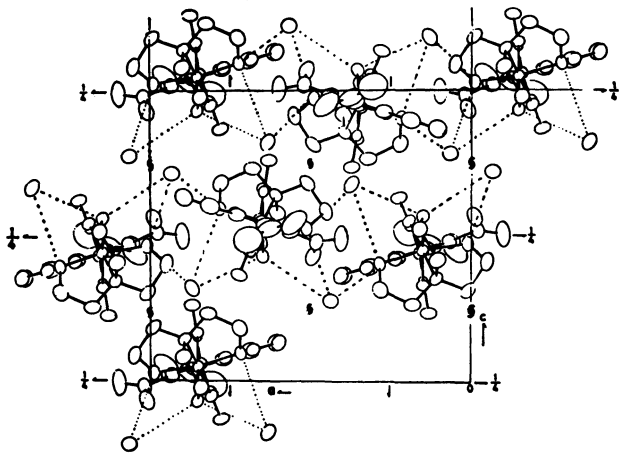

Fig. 3. A projection of the unit cell along the b axis. Broken lines indicate hydrogen bonds.

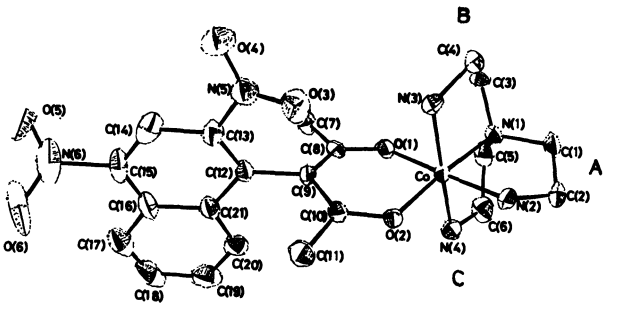

Fig. 4. A perspective drawing of the complex cation and the numbering scheme of the atoms. The three chelate rings are denoted by A, B, and C.

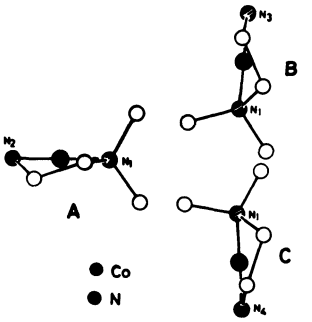

Fig. 5. Conformation of the tren chain.

interatomic distances and bond angles of the hydrogen bonds[3] and the short intermolecular distances[3] are listed in the supplementary materials.

A perspective drawing of the complex ion is shown in Fig. 4. In contrast to the case of Complex II, neither disorder in the chelate-A ring nor a large libration of the aromatic ring was observed. The chelate rings of tren (labeled A, B, and C, as are shown in Fig. 5) adopt the envelop conformation. The B and C rings are almost enantiomeric, and their conformations are λ and δ respectively, whereas A ring takes a λ conformation. The conformation of the rings favors the formation of hydrogen bonds between the primary amino groups and bromide ions (see Fig. 3).[3] Bond distances and angles in the cation are listed in Table 3.[3] The Co–N(1) and Co–N(2) bonds in the chelate ring A are significantly shorter than the other two, Co–N(3) and Co–N(4) (see Table 3). The Co–N(3) and Co–N(4) bonds are not colinear, the N(3)–Co–N(4) angle being 171.4(2)°. Such a deformation is attributable to the strain due to fused chelate-ring formation. Similar distortions are observed in Complex II and other related chelate complexes.[8,9]

Figure 6 shows a projection of the complex cation along the line through the two oxygen atoms of the acac ring. The ring assumes a boat conformation similar to that in Complex II.[1] This seems to be due to electrostatic interaction between the amino and 2-nitro groups as will be described below. The deformation of the acac ring in this complex is larger than that in Complex II. The mean plane of O(1), O(2), C(8), and C(10) makes dihedral angles of 15.3° with respect to the coordination plane of the acac ring and 7.9° with respect to the plane of C(8), C(9), and C(10). The bonds around the atoms

TABLE 3. BOND LENGTHS AND ANGLES; WITH THEIR STANDARD DEVIATIONS

	Bond lengths(l/Å)		
Co–N(1)	1.936(4)	Co–N(2)	1.933(4)
Co–N(3)	1.954(4)	Co–N(4)	1.968(4)
Co–O(1)	1.891(3)	Co–O(2)	1.871(3)
C(7)–C(8)	1.507(6)	C(8)–C(9)	1.393(6)
C(9)–C(10)	1.415(6)	C(8)–O(1)	1.284(5)
C(10)–O(2)	1.270(5)	C(10)–C(11)	1.489(7)
C(9)–C(12)	1.497(6)	C(13)–N(5)	1.468(7)
N(5)–O(3)	1.218(6)	N(5)–O(4)	1.225(6)
	Bond Angles(ϕ/°)		
N(1)–Co–N(2)	87.6(2)	N(1)–Co–N(3)	87.7(2)
N(1)–Co–N(4)	85.8(2)	N(3)–Co–N(4)	171.4(2)
N(3)–Co–O(1)	87.4(2)	N(4)–Co–O(1)	87.1(2)
O(1)–Co–O(2)	93.8(1)	Co–O(1)–C(8)	124.3(3)
Co–O(2)–C(10)	125.0(3)	O(1)–C(8)–C(7)	112.4(4)
O(2)–C(10)–C(11)	115.0(4)	O(1)–C(8)–C(9)	125.8(4)
O(2)–C(10)–C(9)	126.0(4)	C(8)–C(9)–C(10)	121.1(4)
C(8)–C(9)–C(12)	122.0(4)	C(10)–C(9)–C(12)	116.6(4)
C(12)–C(13)–N(5)	122.6(5)	O(3)–N(5)–O(4)	123.2(5)

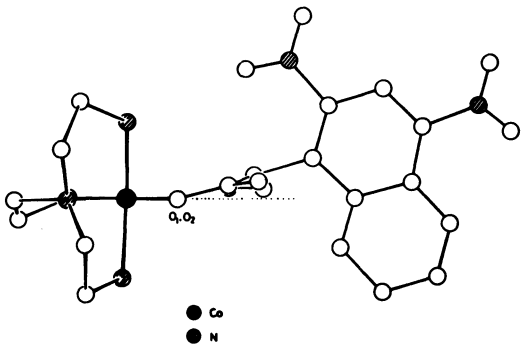

Fig. 6. A projection of the complex cation along the line of two oxygen atoms, O(1) and O(2).

of C(8) and C(10) have the sp^2 character. Thus, the two sets of groups, O(1), C(7), C(8), and C(9), and O(2), C(9), C(10), and C(11), are almost planar. The maximum shifts of the atoms from the least-squares planes of the two groups are 0.01 and 0.02 Å respectively. The former plane makes dihedral angles of 4.2° with respect to the plane of O(1), O(2), C(8), and C(10), and the latter, 8.0°. Consequently, the C(7) and C(11) atoms shift from the plane of O(1), O(2), C(8), and C(10) to the opposite side of the C(9) atom.

The two coordination bonds of the acac ring differ significantly from each other. Such a difference was also observed in Complex II. The bond distance, Co–O(2), is shorter than Co–O(1) by 0.020 Å. Mitsui observed a similar shortening in an analogous glycine chelate.[8] The pivot bond, C(9)–C(12), tilts by 5.1(4)° from the plane of C(8), C(9), and C(10). The aromatic system tilts slightly around the pivot bond, so that the 2-nitro group approaches the O(2) atom. The direction of the tilt is opposite to that found in Complex II. The angle between the O(1)–Co–O(2) plane and the mean plane of the aromatic system is 85.4°. In this complex, the distances between the amino nitrogen atom, N(3), and the oxygen atom of the 2-nitro, is 3.367(6) Å, while that between O(3) and H(N3A) is 2.77(5) Å. The bond angle of N(3)–H(N3A)–O(3) is 130(4°). These values suggest that the formation of a strong hydrogen bond between N(3) and O(3) is not favored. Electrostatic interaction between the amino and 2-nitro groups may force the acac ring to adopt a boat conformation.

In an aqueous solution, all the polar groups and the bromide ions will be solvated; interactions between the 2-nitro group and the amino group will diminish, and the hydrogen bonds between the bromide ions and the amino groups will be broken. These changes will lead to random conformations of the tren instead of rigid dissymmetric conformations. Therefore, the disposition and configuration of the aromatic system relative to the tren chain seems to contribute most to the rotational strength in the present complex.

In the resolution chromatography of the complexes, I and II, *R* isomers are eluted faster than *S* isomers. The *R* isomers associate with the $(+)_{589}$-tartratoantimonate(III) ion more strongly than the *S* isomers, and they can be dissociated more easily from the sulfonate groups of SP-Sephadex resin.[10] Furthermore, the pair of elution bands in Complex I are more separated than those in Complex II; the pair of the elution bands are completely separated in Complex I, but the tail of the *R*-isomer band overlaps the S isomer in Complex II. These facts suggest that the π-electronic system may play a role in discriminating the enantiomers. The associative complex of the *S* isomer with tartratoantimonate(III) ion are probably less stable than that of the *R* isomer because of the steric hindrance of the benzo moiety in the associative complex. A crystallographic study of the tartratoantimonate salt of the title complex would shed light on the problem.

Part of the cost of this research was met by a Grant-in-Aid for Scientific Research (No. 364206) from the Ministry of Education, Science and Culture, to which the authors' thanks are due.

References

1) Y. Nakano and S. Sato, *Inorg. Chem.*, **19**, 3391 (1980).
2) Y. Nakano and H. Seki, *Chem. Lett.*, **1976**, 611.
3) Supplementary materials (Document No. 8221) have been deposited at the office of the Chemical Society of Japan: a) Thermal parameters of non-hydrogen atoms; b) Table of $|F_o|$ and $|F_c|$; c) Observations of some Bijvoet pairs; d) Interatomic distances and angles of the hydrogen bonds; e) Table of close interatomic distances outside the complex ion; f) Non-essential data of bond length and angles.
4) "International Tables for X-Ray Crystallography," Kynoch Press, Birmingham (1974), Vol. IV, p. 71.
5) UNICS (1967). Universal Crystallographic Computation Program System, ed by T. Sakurai, The Crystallographic Society of Japan, Tokyo (1967).
6) R. S. Cahn, C. K. Ingold, and V. Prelog, *Angew. Chem., Int. Ed. Engl.*, **5**, 385 (1966).
7) W. C. Hamilton, *Acta Crystallogr.*, **18**, 502 (1965).
8) Y. Mitsui, J. Watanabe, Y. Harada, T. Sakai, Y. Iitaka, and E. Kimura, *J. Chem. Soc., Dalton Trans.*, **1976**, 2095.
9) K. Okiyama, S. Sato, and Y. Saito, *Acta Crystallogr., Sect. B*, **35**, 2389 (1977).
10) H. Nakazawa and H. Yoneda, A. symposium on Stereochemistry of Chiral Metal Complexes held at the University of Tsukuba (1978), p. 71.

Photocatalytic Dehydrogenation of 2-Propanol over TiO_2 and Metal/TiO_2 Powders

Shousuke TERATANI, Junichi NAKAMICHI,† Kazuo TAYA,† and Kazunori TANAKA*
The Institute of Physical and Chemical Research, Wako, Saitama 351
†*Tokyo Gakugei University, Koganei, Tokyo 184*

(Received June 29, 1981)

A series of TiO_2 catalysts loaded with transition metals were prepared by photodeposition. The activity order for these catalysts in the title reaction was as follows: $Pt/TiO_2 > Rh/TiO_2 > Pd/TiO_2 > Ru/TiO_2 > Ir/TiO_2 > TiO_2$. Upon heat treatment the activities of all the metal/TiO_2 catalysts were enhanced, but the above sequence was unaltered.

The recent and on-going concern with photocatalytic production of hydrogen from water or organic materials is related to solar energy conversion and storage. Among the catalysts used in this type of reactions are metal-loaded oxides[1,2] such as Pt/TiO_2 and $Rh/SrTiO_3$ as well as binary oxides[3,4] such as $NiO–SrTiO_3$ and $RuO_2–TiO_2$. In our laboratory we prepared a series of polycrystalline metal/TiO_2 powders (metal=Ru, Rh, Pd, Ir, Pt), and compared their photocatalytic activities, relative to TiO_2, for dehydrogenation of 2-propanol. A few related experiments were also made to gain a better understanding of this reaction. This paper reports the results of these experiments.

Experimental

Materials. Anatase was purchased from Kanto Chemical Co., Inc.: the absence of rutile was confirmed by X-ray powder diffraction, and the BET surface area was determined to be 11.5 m^2/g. Metal salts (H_2PtCl_6, $RhCl_3$, $IrCl_4$, $PdCl_2$, $RuCl_3$) used for catalyst preparation were also commercially obtained. 2-Propanol (Wako Pure Chemical Ind., Guaranteed grade) was used without further purification. All aqueous solutions or suspensions of these chemicals were prepared using distilled water.

Apparatus. Figure 1 illustrates the photochemical reaction vessel used for both catalyst preparation and kinetic studies. The reaction vessel consists of two parts separable at joint J. There are two interchangeable inner parts of an identical shape and size, one made of pyrex glass and the other of quartz. Unless otherwise stated, the experiments in this report were conducted using the quartz unit. An irradiation lamp can be placed inside the innermost wall A. Water from a thermostatically controlled bath can flow through the thin space between A and B, cutting off the thermall energy from the irradiation lamp. The outer part is a three side-necked flask, one sideneck connected to a cooler, a second used for sampling, and the other (not indicated in the figure) for bubbling of N_2 or Ar to purge air before reaction. During reaction the third sideneck was sealed with a pinchcock. The outermost space D between walls B and C is the reaction region. The whole reaction vessel is immersed in a thermostatted water bath. The reaction temperatures recorded are those of this bath.

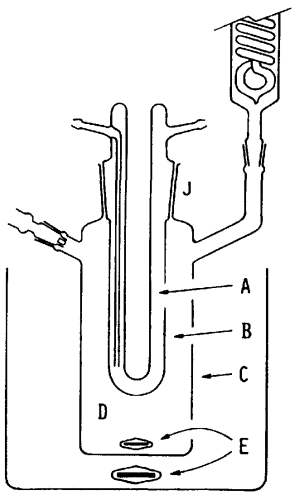

Fig. 1. Reaction vessel.
A—D: See text, E: Teflon-coated magnetic bars.

Catalyst Preparation. Three metal/TiO_2 catalysts (metal=Ru, Pd, Pt) were prepared by photodeposition of the metal on TiO_2 according to a method similar to that of Kraeutler and Bard.[5] As a typical example, anatase powders (3 g) were homogenized in water (50 ml) for 1 h in a Mitamura Riken ultrasonic cleaner (70 W). To the resulting slurry was added an aqueous solution of an appropriate concentration of H_2PtCl_6, a $CH_3COOH–CH_3COONa$ buffer (pH=4, *ca.* 10 ml), and water to adjust the whole volume to *ca.* 250 ml. The whole mixture was transferred to space D of the reaction vessel, and N_2 was bubbled for 20 min to eliminate dissolved air. To commence the photocatalytic deposition of the metal, a 30-W low-pressure Hg lamp was switched on, and irradiation was carried out at 40 or 55 °C under continued stirring and N_2 bubbling until metal deposition was complete (1 h for Pd; 2.5 h for Ru and Pt). After irradiation, the mixture was filtered off through a Gelman Membrane Filter DM-450 (pore size 0.45 μm), washed with water until the washings were neutral. The precipitate collected was dried first at 45 °C overnight between filter papers in an electric oven and then under reduced pressure for several days at room temperature, and finally stored in a vial under a nitrogen atmosphere.

The above procedure was not applicable to the preparation of Rh/TiO_2 and Ir/TiO_2 because of the difficulty to achieve complete reduction of $RhCl_3$ and $IrCl_4$ to the metallic state. The following modifications were thus made: methanol was used instead of the $CH_3COOH–CH_3COONa$ buffer, and the irradiation source was replaced by a more intense 100-W high-pressure Hg lamp.

Air treatment of the metal/TiO_2 catalysts was conducted by heating for 2 h at 380 °C under a stream of air in an electric furnace. Before heat treatment, all the metal/TiO_2 catalysts were off-white. Upon heat treatment, Ru/TiO_2 acquired a slightly blueish tint, while there was no significant variation in appearance for the other metal/TiO_2 catalysts.

Kinetic Procedure. The photocatalytic dehydrogenation of 2-propanol was conducted as follows. To space D of the reaction vessel were introduced a metal/TiO_2 catalyst (0.1 g)

and a water–2-propanol mixture (1 : 1 by vol., 200 ml). Argon was bubbled through the suspension for 30 min, then the photocatalyzed dehydrogenation was started by irradiating at 40 °C with the 100-W high-pressure Hg lamp. Small portions of the reaction solution were withdrawn at intervals and analyzed for product acetone by a gas chromatograph using a 2 m × 3 mm i.d. column of 30% PEG 20 M on 30—60 mesh chromosorb WAW at 60 °C. The gas evolved was led through the cooler-attached sideneck into water or aqueous $Ba(OH)_2$ solution, and collected in a gas burette.

Results and Discussion

Stoichiometry and Reaction Profile. The gas evolved under irradiation in the presence of metal/TiO_2 catalysts did not make the aqueous $Ba(OH)_2$ solution turbid, and consisted almost exclusively of hydrogen, judged from mass spectral data. It has been confirmed with Pt/TiO_2 that acetone and H_2 are produced in nearly equal amounts by photocatalytic dehydrogenation of 2-propanol (Inset a, Fig. 2). A small amount of 2,3-dimethyl-2,3-butanediol (pinacol) was detected as the only by-product (Inset b). Pinacol formation was completely suppressed upon replacing the quartz inner part of the reaction vessel by the pyrex glass one. Thus it is very likely that pinacol is produced by the reaction of 2-propanol with ultraviolet-excited acetone. No reaction occurred at all with the mercury lamp switched off. The rates of acetone formation in duplicate experiments conducted under identical conditions were reproducible within 5%.

At the beginning of the reaction, as seen from Fig. 2, the amount of acetone produced increased almost

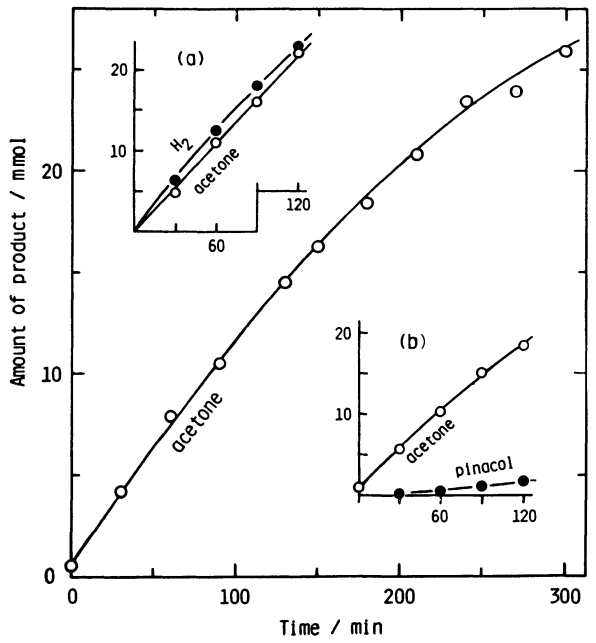

Fig. 2. A typical reaction profile for photocatalytic dehydrogenation of 2-propanol on Pt/TiO_2.
Catalyst: 1%-Pt/TiO_2 (100 mg), reactant: H_2O+2-propanol (1 : 1 by volume, 200 ml as the mixture), reaction temperature: 40 °C. Inset (a): near molar equivalence of produced H_2 and acetone. Inset (b): slight formation of pinacol as the by-product.

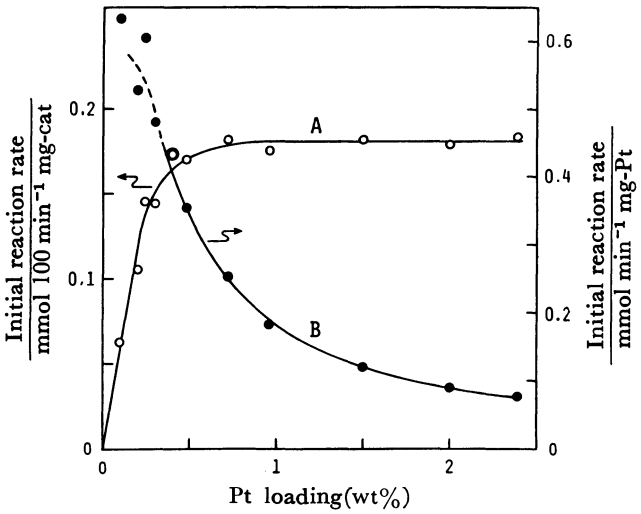

Fig. 3. The reaction rate for photocatalytic dehydrogenation per 100 mg of catalyst (Pt/TiO_2) (curve A) and that per mg of Pt (curve B).

Table 1. Activities of TiO_2 and metal/TiO_2 catalysts for photocatalytic dehydrogenation of 2-propanol to acetone

Catalyst	V [a] / μmol min^{-1}	R_1^{rel} [b]	R_2^{rel} [c]
	Before heat treatment		
TiO_2	1.6(V_0)	1	—
Ru/TiO_2	7.6	4.7	0.076
Rh/TiO_2	38.4	24	0.37
Pd/TiO_2	13.1	8.2	0.12
Ir/TiO_2	4.0	2.5	0.021
Pt/TiO_2	194	121	1
	After heat treatment		
Ru/TiO_2	12.6	7.8	0.12
Rh/TiO_2	51.1	32	0.48
Pd/TiO_2	15.1	9.4	0.14
Ir/TiO_2	6.9	4.3	0.035
Pt/TiO_2	200	124	1

a) Obtained using 0.1 g of each catalyst. b) $R_1^{rel} \equiv V/V_0$, the activity relative to TiO_2. c) $R_2^{rel} \equiv \{V(\text{metal})/M(\text{metal})\}/\{V(\text{Pt})/M(\text{Pt})\}$, where M is the molecular weight. Thus, R_2^{rel} represents the activity relative to Pt/TiO_2, referred to unit molar quantity of the loaded metal.

linearly with time, and then gradually leveled off. With the metal/TiO_2 catalysts containing 1 wt% metal, the extent of the initial linear region ranged from *ca.* 1 h (Pd, 0.05% conversion) to 2.5 h (Pt, 1.2% conversion). The photocatalytic dehydrogenation rates of a series of Pt/TiO_2 catalysts were estimated from the initial slope, and are plotted in Fig. 3 (curve A) as a function of Pt content. It is seen that as the Pt loading increases, the rate increases almost linearly and then approaches a constant value. The rate per mg Pt (curve B) remains almost constant in the low Pt loading region, and then decreases with increasing Pt loading.

Catalytic Activity. The activities of these metal-loaded catalysts diminished somewhat during storage in a vial; rather rapidly in the first few days (*e.g.*, by

20—30%), and then quite slowly (*e.g.*, by a further 20—30% after storage for a few months). The activity data of Table 1 were obtained with those metal/TiO_2 catalysts that had been loaded with 1% metal and stored for about a week. The values of V for the catalyst samples before heat treatment indicate that the activities fall in the sequence

$$Pt/TiO_2 > Rh/TiO_2 > Pd/TiO_2 > Ru/TiO_2 > Ir/TiO_2 > TiO_2. \quad (1)$$

In accord with this sequence, Kawai and Sakata[1] have shown recently that Pt/TiO_2 is twice as active as Pd/TiO_2 in photocatalyzed dehydrogenation of methanol. A comparison of the V values between the heat-treated and untreated catalysts shows that the heat treatment somewhat enhanced the activity for all the metal/TiO_2 catalysts, but did not alter sequence (1). The cause of the activity enhancement due to heat treatment is not clear at present: It could be (i) the rearrangement of surface metal atoms, (ii) the burning-off of undetected surface impurities, or (iii) the partial oxidation of the loaded metal.

In connection with item (i), it is interesting to refer to Johnson and Keith's paper[6] dealing with the state of platinum in Pt/Al_2O_3 catalysts. They have found that air or O_2 treatment of the catalysts at high temperatures (427—650 °C) followed by reduction leads to a high dispersion of the platinum. In relation to item (iii), it is to be noted that the metal in metal/semiconductor catalysts acts as the pool of electrons photogenerated under irradiation. Partial oxidation of the platinum possibly increases the capacity of the pool, thereby also increases the concentration of positive holes in the TiO_2 phase.

Additional Remarks. A fundamental question about any photocatalytic phenomenon is whether it is really catalytic. To answer this question, let us estimate "the turnovers accomplished."[7] This quantity represents the total number of molecules reacted per surface site. The rough numerical calculations were made based on the acetone formation over the initial 2h-period of reaction; a surface area for TiO_2 of 11.5 m^2/g was used and a catalytic site concentration of $5 \times 10^{14}/cm^2$ was assumed. The turnovers accomplished thus estimated are listed in Table 2. The quite large values for Pt/TiO_2 and Rh/TiO_2 indicate clearly that the dehydrogenation of 2-propanol was really photocatalytic on these two catalysts. The reaction on Ru/TiO_2 and Pd/TiO_2 is also likely to be photocatalytic.

Lehn *et al.*[2] compared a variety of metal/$SrTiO_3$ catalysts for water splitting under illumination. Since these catalysts and the reaction resemble ours, it seems worthwhile to compare the activities. The activity sequence they observed was

$$Rh/SrTiO_3 > Ru/SrTiO_3 > Re/SrTiO_3 > Ir/SrTiO_3 = Pt/SrTiO_3 > Pd/SrTiO_3 > Os/SrTiO_3 > Co/SrTiO_3 > SrTiO_3. \quad (2)$$

As far as the loaded metals are concerned, sequence (1) does not conform to sequence (2). This discord might stimulate further studies in this area.

TABLE 2. THE TURNOVERS ACCOMPLISHED FOR EACH CATALYST

Catalyst	Turnovers accomplished / molecules site^{-1}	
	Before heat treatment	After heat treatment
TiO_2	2	—
Ru/TiO_2	9	16
Rh/TiO_2	46	57
Pd/TiO_2	11	11
Ir/TiO_2	5	5
Pt/TiO_2	247	266

We thank Dr. Y. Takagi for valuable discussions, Mr. A. Ikuo and M. Watanabe for their technical assistance, and Mrs. N. Tejima for her BET measurement of the TiO_2 catalyst. This work was supported by a grant from the Science and Technology Agency towards the Solar Energy Reseach Project.

References

1) T.Kawai and T. Sakata, *J. Chem. Soc., Chem. Commun.*, **1980**, 694.
2) J.-M. Lehn, J.-P. Sauvage, and R. Ziessel, *Nuouvo. J. Chim.*, **4**, 623 (1980).
3) K. Domen, S. Naito, M. Soma, T. Onishi, and K. Tamaru, *J. Chem. Soc., Chem. Commun.*, **1980**, 543.
4) S. Arimitsu, Japanese Published Unexamined Patent Application, No. 57-35525 and No. 57-63132.
5) B. Kraeutler and A. J. Bard, *J. Am. Chem. Soc.*, **100**, 4317 (1978).
6) M. F. L. Johnson and C. D. Keith, *J. Phys. Chem.*, **67**, 200 (1963).
7) L. P. Childs and D. F. Ollis, *J. Catal.*, **66**, 383 (1980).

ESR Studies of Cobalt(II) in $[TMPD^+]_2[Ni(mnt)_2]$ and $[TMPD^+]_2[Pt(mnt)_2]$ ($TMPD^+$: *N,N,N′,N′*-Tetramethyl-*p*-phenylenediamine Cation, mnt: 1,2-Dicyano-1,2-ethylenedithiolato)

Tomoyoshi SETOI,† Motomich INOUE,†† and Daiyu NAKAMURA*
Department of Chemistry, Nagoya University, Chikusa-ku, Nagoya 464
(Received July 27, 1981)

The Co(II) and triplet exciton ESR spectra of Co(II)-doped $[TMPD^+]_2[Ni(mnt)_2]$ and $[TMPD^+]_2[Pt(mnt)_2]$ were observed at different temperatures. The triplet exciton signals of the solid solutions yielded practically the same ESR parameters as those of the pure Ni(II) and Pt(II) complexes. The Co(II) spectra showed a well-resolved hyperfine structure, each component line of which became broad with increasing temperature. This can be interpreted in terms of exciton transfer from $TMPD^+$ lattices to the metal ions.

The compound $[TMPD^+]_2[Ni(mnt)_2]$ consisting of planar organic radical cations and also planar metal-chelate anions has recently attracted considerable attention because of its novel crystal structure[1] schematically shown in Fig. 1. In this structure, $TMPD^+$ radicals form alternating chains whereas $[Ni(mnt)_2]^{2-}$ ions are stacked equidistantly to construct regular chains. The intradimer spin interaction of $TMPD^+$ radicals ($2J_1=-0.23$ eV) is strong enough, as compared with the interdimer one in a $TMPD^+$ chain ($|J_2/J_1|\approx 0.1$), to generate triplet excitons which migrate throughout in the chain.[1,2]

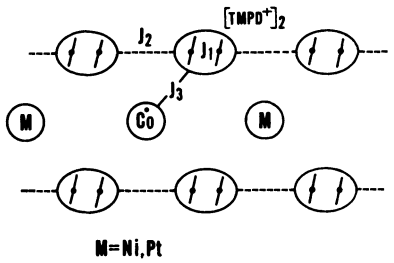

Fig. 1. Structure of $[TMPD^+]_2[M(mnt)_2]$ (M=Ni or Pt) depicted schematically.

Previously, we studied the ESR of the solid solution $[TMPD^+]_2[Cu_xNi_{1-x}(mnt)_2]$ and found the existence of magnetic interaction between Cu(II) ions and $TMPD^+$ dimers. This can be interpreted in terms of the partial migration of triplet excitons onto neighboring metal chelate chains.[2,3] It is known that Co(II) ions usually have an electron-spin relaxation time shorter than that of Cu(II) ions. Therefore, we can expect to obtain further information about the exciton-metal interaction by use of Co(II) ions as a probe to detect it. The present ESR investigation has been undertaken on Co(II) ions and triplet excitons in Co(II)-doped $[TMPD^+]_2[Ni(mnt)_2]$ and $[TMPD^+]_2[Pt(mnt)_2]$, both pure complexes of which are known to be isostructural to each other from our previous ESR study.[3]

Experimental

A boiling ethanol solution of $(Et_4N)_2[Co(mnt)_2]$ and $(Et_4N)_2[Ni(mnt)_2]$ mixed in an appropriate ratio was added all together to a boiling ethanol solution of $[TMPD^+]ClO_4$.[2] On cooling, the resulting solution separated black needle crystals having the crystal form identical with that of the pure Ni(II) complex. The crystals were identified as $[TMPD^+]_2[Co_xNi_{1-x}(mnt)_2]$. The solid solution of $[TMPD^+]_2[Co_xPt_{1-x}(mnt)_2]$ was synthesized in a similar manner from $(Et_4N)_2[Pt(mnt)_2]$, $(Et_4N)_2[Co(mnt)_2]$, and $[TMPD^+]ClO_4$.[2,3] Black needle crystals were obtained. All preparative experiments were carried out under a dry-nitrogen atmosphere.

The ESR spectra of the crystalline powders prepared were recorded by means of a JEOL ES-SCXA X-band spectrometer in a temperature range of 80—300 K. Mn^{2+}/MgO was employed as a marker. The sample temperature was controlled by use of a cold-gas flow system. Two copper *vs.* constantan thermocouples were mounted near either side of the sample tube along the stream of cold nitrogen gas for the determination of sample temperatures. The observed temperature was estimated to be accurate within ±2 K.

Results

Figure 2 shows the ESR spectra of $[TMPD^+]_2[Co_xNi_{1-x}(mnt)_2]$ ($x\approx 0.02$) recorded at different tem-

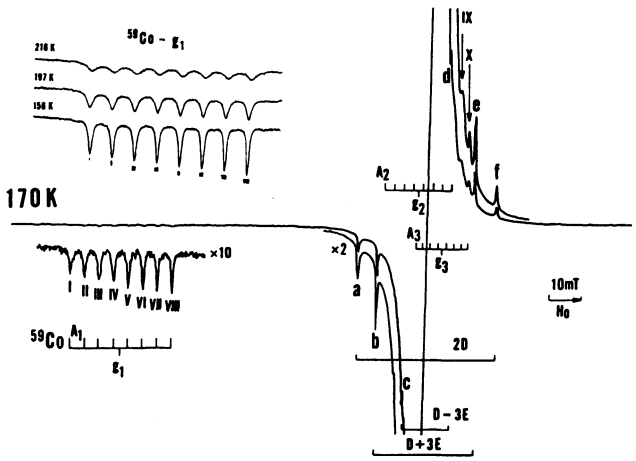

Fig. 2. ESR spectrum of $[TMPD^+]_2[Co_xNi_{1-x}(mnt)_2]$ ($x\approx 0.02$) recorded at 170 K. The hyperfine peaks I—VIII due to ^{59}Co are shown for the temperatures 156, 197, and 216 K. g_2 and A_2 determined for the Bu_4N^+ salt are shown for reference.

† Present address: Escuela de Informática, Universidad Autónoma de Guadalajara, Guadalajara, Jal., México.

†† Present address: Centro de Investigación sobre Polímeros y Materiales, Escuela de Ingeniería, Universidad de Sonora, Hermosillo, Sonora, México.

peratures. In the temperature range 160—200 K, signals assignable to Co(II) (indicated by Roman numerals) were observed well separately from triplet exciton signals (indicated by the alphabet) arising from $TMPD^+$ dimers. With decreasing temperature, the $TMPD^+$ signals became weak whereas the Co(II) signals increased their intensity in conformity with the Curie law. Below 160 K, only the latter signals were observed. The ESR spectra of $[TMPD^+]_2[Co_xPt_{1-x}(mnt)_2]$ are given in Fig. 3. These spectra closely resemble those of the Co(II)-doped Ni(II) analogue.

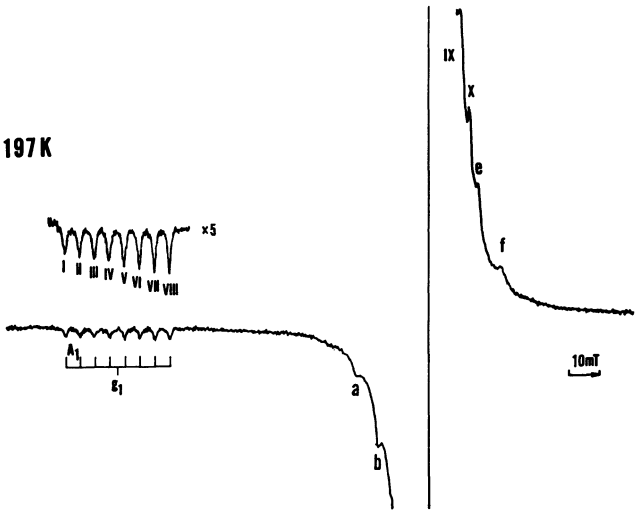

Fig. 3. ESR spectrum of $[TMPD^+]_2[Co_xPt_{1-x}(mnt)_2]$ ($x\approx0.01$) recorded at 197 K.

The triplet exciton signals are interpreted in terms of a fine structure represented by

$$\mathcal{H}_{fs} = D[S_z^2 - S(S+1)/3] + E(S_x^2 - S_y^2). \quad (1)$$

The zero splitting parameters (D and E) obtained from the spectra of the Ni(II) and Pt(II) solid solutions agree well with those of the pure Ni(II) and Pt(II) complexes, respectively, as given in Table 1. The well resolved hyperfine structure due to ^{59}Co nuclei yields the g_1 value and the corresponding hyperfine coupling constant A_1 as indicated in Table 2. The peaks IX and X can be assigned to the component lines of the g_3 signal by comparing them to the ESR spectrum of Co(II) ions diluted in $(Bu_4N)_2[Ni(mnt)_2]$.[4] The separation between the two peaks is nearly equal to the A_3 value of Co(II) in the butylammonium salt. If the equal separation is assumed for the eight component lines, the g_3 value can be evaluated as given in Table 2 in agreement with the value of Co(II) in the butylammonium salt. In each spectrum of the Ni(II) and Pt(II) solid solutions, an extra strong signal attributable to $TMPD^+$ monomers unavoidably involved as an impurity appeared at $g=2.006$, where the g_2 signals of Co(II) should be observed. Therefore, we could not determine the g_2 and A_2 values of the present compounds. The values of g_2 and A_2 in Fig. 2 show the data reported for Co(II) diluted in $(Bu_4N)_2[Ni(mnt)_2]$.[4] These g_2 and A_2 values are thought not to be much different from the respective inherent values of the $TMPD^+$ complex. All of the ESR parameters thus determined were independent of the concentration of Co(II) ions.

Table 1. TRIPLET EXCITON ESR PARAMETERS D AND E AND THE EXCHANGE INTEGRAL J_1 OF $[TMPD^+]_2[Co_xNi_{1-x}(mnt)_2]$ ($x\approx0.02$) AND $[TMPD^+]_2[Co_xPt_{1-x}(mnt)_2]$ ($x\approx0.01$)

Compound	D/mT	E/mT	$-2J_1$/eV
$[TMPD^+]_2[Co_xNi_{1-x}(mnt)_2]$	21.6	2.8	0.19
$[TMPD^+]_2[Co_xPt_{1-x}(mnt)_2]$	23.0	2.9	0.23
$[TMPD^+]_2[Ni(mnt)_2]$[a]	21.6	2.9	0.23
$[TMPD^+]_2[Pt(mnt)_2]$[b]	22.9	2.9	0.21

a) Refs. 1 and 2. b) Ref. 3.

With increasing temperature above 160 K, the signals of $TMPD^+$ in the Ni(II) solid solution become gradually strong. The intensity I of the triplet exciton ESR signal should increase in proportion to the triplet density ρ and also to reciprocal temperature. Accordingly, one can obtain the following equation when $2|J_1| \geqq kT$.

$$I \propto \rho/T = 3[\exp(2J_1/kT)]/T. \quad (2)$$

From the temperature dependence of the exciton signal intensity, the exchange integral J_1 of $TMPD^+$ dimers was determined as $2J_1 = -0.19$ eV. Above 200 K, the $TMPD^+$ signals gradually broaden owing to the migration of triplet excitons within $TMPD^+$ chains. It is interesting to note that the Co(II) signals also gradually broaden above 200 K. This indicates that the triplet excitons have some magnetic interaction with the Co(II) ions.

Since the peaks I—VIII are separated well from each other, we can determine the temperature dependence of the half-height width. When the line broadening is assumed to be caused by a thermal activation process with an activation energy ΔE, the linewidth W can be expressed as[2,5]

$$W = W_0 + W_1 \exp(-\Delta E/kT). \quad (3)$$

Here, W_0 denotes the linewidth at the low temperature limit, and can be regarded, in the present problem, as that observed at 78 K. Figure 4 shows the semilogarithmic plot of $(W-W_0)$ against T^{-1} for the Ni(II) solid solution. The experimental results deviate from

Table 2. Co(II) ESR SIGNAL PARAMETERS OF $[TMPD^+]_2[Co_xNi_{1-x}(mnt)_2]$ ($x\approx0.02$) AND $[TMPD^+]_2[Co_xPt_{1-x}(mnt)_2]$ ($x\approx0.01$)

Compound	g_1	g_2	g_3	A_1/mT	A_2/mT	A_3/mT
$[TMPD^+]_2[Co_xNi_{1-x}(mnt)_2]$	2.847	—[b]	1.98_3	4.6	—[b]	2.3
$[TMPD^+]_2[Co_xPt_{1-x}(mnt)_2]$	2.871	—[b]	1.97_6	4.7	—[b]	2.5
$(Bu_4N)_2[Co_xNi_{1-x}(mnt)_2]$[a]	2.798	2.025	1.977	3.8	3.0	2.5

a) Ref. 4. b) Unable to observe the signals because of a strong impurity signal.

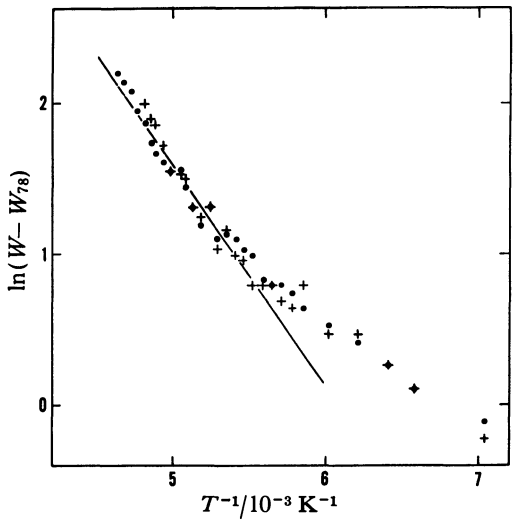

Fig. 4. Temperature dependence of the half-height width of the ^{59}Co hyperfine peaks I (+) and VIII (●) observed for the Co(II)-doped $[TMPD^+]_2[Ni(mnt)_2]$. The straight line shows the best fit of Eq. 3 to the peak VIII above 185 K. W_{78} in the ordinate denotes the linewidth at 78 K.

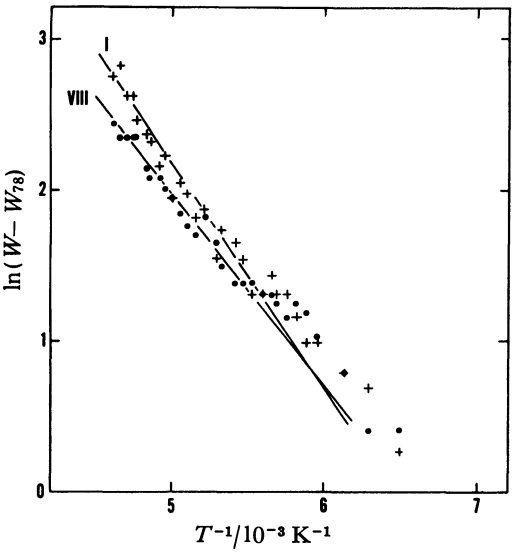

Fig. 5. Temperature dependence of the half-height width of the ^{59}Co hyperfine peaks I (+) and VIII (●) observed for Co(II) in $[TMPD^+]_2[Pt(mnt)_2]$. The straight lines show the best fits of Eq. 3 to the peaks I and VIII. The slopes of the lines give different activation energies, but the difference is smaller than the experimental errors.

Eq. 3 in the low temperature region. However, the linear relation is satisfied above 200 K yielding $\Delta E = 0.15 \pm 0.04$ eV.

The Co(II)-doped platinum salt yielded the ESR parameters very similar to those of the Ni(II) solid solution as given in Tables 1 and 2. The temperature dependence of the Co(II) linewidth in the Pt(II) complex (shown in Fig. 5) gave the ΔE value equal to that of the Ni(II) solid solution.

Discussion

Since the $TMPD^+$ signal parameters D, E, and J_1 of the present solid solutions agree with the corresponding values of the pure Ni(II) or Pt(II) salt, it is thought that the crystal lattices remain almost unchanged even in the solid solutions. Therefore, the ESR results can be discussed on the basis of the structure of the respective pure salts. The Co(II) signals of the solid solutions yield similar ESR parameters to those of Co(II) in $(Bu_4N)_2[Ni(mnt)_2]$. This indicates that magnetic interaction operating between organic radicals and metal chelates is weak enough to permit one its quantitative evaluation with ESR experiments. It is interesting to note that Co(II) ions diluted in $(Et_4N)_2[Ni(mnt)_2]$ yielded Co(II) ESR signals showing no line broadening in the temperature range in which the line broadening was observed for the $TMPD^+$ salt. Therefore, the line broadening of the Co(II) signals observed is ascribable to the triplet excitons.

When magnetic interaction between Co(II) ions and triplet excitons is a main cause for the Co(II) electron spin relaxation, the linewidth W of Co(II) ESR signals can be written as[2,6]

$$W = W_0 + W'\rho = W_0 + 3W' \exp(2J_1/kT). \quad (4)$$

On comparing the functional form of this equation with that of Eq. 3, ΔE is apparently equal to $2|J_1|$. The magnetic interaction of triplet excitons is accompanied by their migration over a barrier into adjacent sites. If this effect is taken into account, the ΔE value should be greater than $2|J_1|$. In the present solid solutions, however, the value of ΔE determined from the data at higher temperatures is certainly smaller than $2|J_1|$. This clearly indicates that the relaxation mechanism of Co(II) ESR given by Eq. 4 is inadequate for the interpretation of the present results. It is known that an electron spin on an isolated Co(II) ion can easily relax through *IS*- and/or *LS*-coupling.[7] In our previous experiments,[2,3] Cu(II) ESR signals in both Et_4N^+ and $TMPD^+$ salts showed a remarkable saturation effect, whereas no such effect was detectable for the Co(II) signals even at the highest power level ($\approx$100 mW) of our microwave oscillator. Accordingly, we have to take into account another relaxation mechanism for the Co(II) ESR of the present compounds such as modulation of *IS*- and/or *LS*-coupling through field fluctuation induced by the motion of $TMPD^+$ triplet excitons.

Figures 2 and 3 obviously show that the Co(II) signals I—VIII carefully taken at a given temperature for finely powdered samples have different linewidths from each other, whereas the component lines of Co(II) in the Et_4N^+ salt showed practically the same half-height width. The electronic state of the Co(II) ions can be fluctuated by exciton transfer from the $TMPD^+$ lattices to the metal ions. This transfer is accompanied by the so-called partial oxidation of the Co(II) ions in solids. This is considered to take place without difficulty, since the ligand mnt forms stable metal complexes with high oxidation states of the central metals.[8] The fluctuated electronic state of Co atoms induces the fluctuation of the g and A values. Owing to this effect,

the ESR Hamiltonian for the peaks I—VIII is given by the time dependent g and A:

$$\mathcal{H} = g_1(t)\mu_B HS_1 + A_1(t)I_1S_1. \quad (5)$$

The fluctuation in the present complexes is slow enough as compared with the ESR frequency, because the hyperfine lines are well separated. Under this condition, the linewidth W is[7]

$$W \approx \frac{1}{T_2}$$
$$= \frac{1}{2\hbar}\int_{-\infty}^{\infty} \overline{[H_{\alpha\alpha}(t+\tau) - H_{\beta\beta}(t+\tau)][H_{\alpha\alpha}(t) - H_{\beta\beta}(t)]}\,d\tau, \quad (6)$$

where $H_{\alpha\alpha}$ and $H_{\beta\beta}$ are the matrix elements of the above Hamiltonian. The values $g_1(t)$ and $A_1(t)$ can be reasonably assumed to be fluctuated with the same time constant τ_c, because the fluctuation comes from the same origin. Under this assumption along with $\omega\tau_c \gg 1$, we obtain

$$\frac{1}{T_2} = \frac{\tau_c}{\hbar^2}(g_1\mu_B H + A_1 M_I)^2, \quad (7)$$

where g_1 and A_1 are time independent. The ratio of the linewidths of the peaks $M_I = 7/2$ and $-7/2$ is evaluated as $(225+4.6\times 7/2)^2/(225-4.6\times 7/2)^2 = 1.3$, which agrees well with the observed ratio 1.5 of the half-height widths of the peaks I and VIII. Thus, the difference of linewidth among the peaks I—VIII at an arbitrary temperature can be interpreted in terms of a random modulation of the *IS* coupling by the motion of triplet excitons.

Since the linewidth of each Co(II) peak broadens with increasing temperature, τ_c in Eq. 7 should be temperature dependent. If we assume that the aforementioned triplet-exciton transfer is thermally activated with an energy ε, the correlation time τ_c may be written as,

$$\tau_c \propto \frac{1}{|J_3|}\exp(-\varepsilon/kT), \quad (8)$$

where J_3 denotes the exchange integral between $[TMPD^+]_2$ and Co(II) ions. In this mechanism, the linewidth can be given by the same functional form as Eq. 3. Accordingly, the triplet excitons in the present solid solutions transfer onto the metal lattices with the activation energy of $\Delta E \approx 0.15$ eV and result in the relaxation of the Co(II) electron spin through its *IS*-coupling. The relaxation is correlated only in the indirect process to the triplet excitons activated thermally with $2|J_1|$. The activation energy does not depend on the kind of the host crystals. The interaction between the metal chelates is so weak that an exciton transferred to a Co(II) chelate undergoes no further transfer to the adjacent metal chelates.

References

1) M. J. Hove, B. M. Hoffman, and J. A. Ibers, *J. Chem. Phys.*, **56**, 3490 (1972).
2) M. Inoue, H. Kuramoto, and D. Nakamura, *J. Magn. Reson.*, **33**, 409 (1979).
3) M. Inoue, *J. Magn. Reson.*, **38**, 481 (1980).
4) A. H. Maki, N. Edelstein, A. Davison, and R. H. Holm, *J. Am. Chem. Soc.*, **86**, 4580 (1964).
5) P. L. Nordio, Z. G. Soos, and H. M. McConnell, *Ann. Rev. Phys. Chem.*, **17**, 237 (1966).
6) J. S. Valentine, A. J. Silverstein, and Z. G. Soos, *J. Am. Chem. Soc.*, **96**, 97 (1974).
7) G. E. Pake and T. L. Estle, "The Physical Principles, of Electron Paramagnetic Resonance," W. A. Benjamin, Inc., London (1973).
8) R. P. Burns and C. A. McAuliffe, *Adv. Inorg. Chem. Radiochem.*, **22**, 303 (1979).

Static and Dynamic Properties of Quinoxalines in the Phosphorescent Triplet State from Optically Detected Magnetic Resonance

Kazuhiko SUGA and Minoru KINOSHITA*

The Institute for Solid State Physics, The University of Tokyo, Roppongi, Minato-ku, Tokyo 106

(Received August 27, 1981)

The static and dynamic properties of the phosphorescent triplet states of quinoxaline and 2,3-disubstituted derivatives in hexane have been studied at 1.4 K using the methods of optically detected magnetic resonance. In addition, the absorption and phosphorescence excitation spectra have also been measured to attain the information about the low lying excited states. A systematic comparison has been made for the purpose of examining the effect of substitution. A significant enhancement of the pumping rates for the y spin sublevel observed in the chlorine-substituted derivatives is concluded to be due to the additional indirect process of intersystem crossing which occurs from S_1 of n,π^* to T_1 passing through the intermediate triplet state of π,π^*. A detailed discussion on the observed phosphorescence spectra originating from the three sublevels has achieved a satisfactory success in understanding the mechanisms responsible for the radiative decay processes. It is concluded that the mechanisms due to vibronic coupling with closely lying n,π^* triplet states are of little importance in the systems studied here.

Quinoxaline is one of the most widely studied aza-aromatics from a variety of viewpoints. In particular, the properties of the lowest excited triplet state have attracted considerable attention[1-13] since the method of optically detected magnetic resonance (ODMR) was successfully applied to organic compounds.

Optical and magnetic resonance studies[5-13] have revealed that the interaction between the lowest π,π^* triplet state and low lying n,π^* states plays an important role in the decay and populating processes. However, with a few exceptions[12,13] the studies reported so far have little information on the detailed mechanisms, which give rise to the radiative decay from the individual spin sublevels.

Commonly, in order to obtain much information about the radiative activity of the spin sublevels at the vibronic bands, it is desirable to measure the phosphorescence spectra coming from the sublevels separately. Microwave-induced delayed phosphorescence (MIDP) method provides a useful procedure to obtain a sublevel emission spectrum. A set of three sublevel emission spectra makes it possible to discuss in detail the radiative properties even for the vibronic bands of small intensity.

In addition to quinoxaline, three 2,3-disubstituted quinoxalines are studied here in order to obtain closer insight into static and dynamic properties of the phosphorescent states by a systematical comparison. Besides the sublevel emission spectra, the kinetic rate constants are measured by means of the conventional MIDP method. The results are discussed in terms of the possible mechanisms of radiative transitions. The mechanisms operative in the intersystem crossing process are also discussed. The transition energies of the excited states are determined from the absorption and phosphorescence excitation spectra to provide supplementary information.

Experimental

Quinoxaline, 2,3-dimethylquinoxaline, 2-chloro-3-methylquinoxaline, and 2,3-dichloroquinoxaline were purified by recrystallization and vacuum sublimation. Hexane of spectroscopic grade obtained from Tokyo Kasei Co., Ltd. was used as received. The equipment and procedure for the optical and magnetic resonance experiments are essentially the same as described in previous papers.[14] The molecular structures and axis system for the compounds studied are shown in Fig. 1.

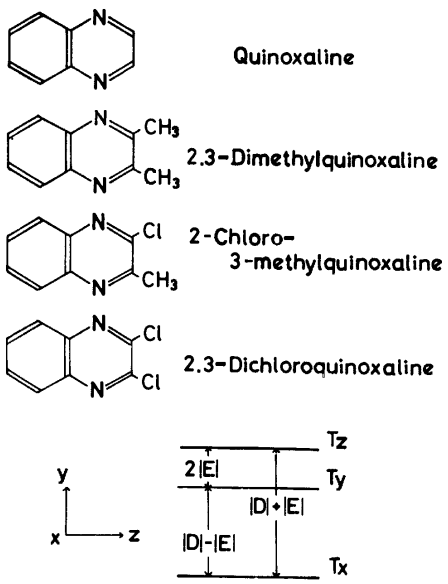

Fig. 1. Molecular structure and choice of axis system.

Absorption Spectra

The absorption spectra of quinoxaline and the three derivatives were measured in hexane at room temperature. The spectra are shown in Fig. 2.

Quinoxaline. As concerns quinoxaline, the analysis was based on the theoretical prediction about the transition energies and the moments for the transitions to the π,π^* excited singlet states reported in the literature.[15,16]

The first $^1A_1(\pi,\pi^*)$ band is observed with onset at 31490 cm^{-1}, and shows a slow decline, extending to $\cong$40000 cm^{-1}, which could be attributed to the presence of the second allowed π,π^* transition of B_2 symmetry. Accordingly, the peak found at 32780 cm^{-1} may be assigned as $^1B_2(\pi,\pi^*)$ band, predicted to lie at $\cong$32750 cm^{-1}.[15]

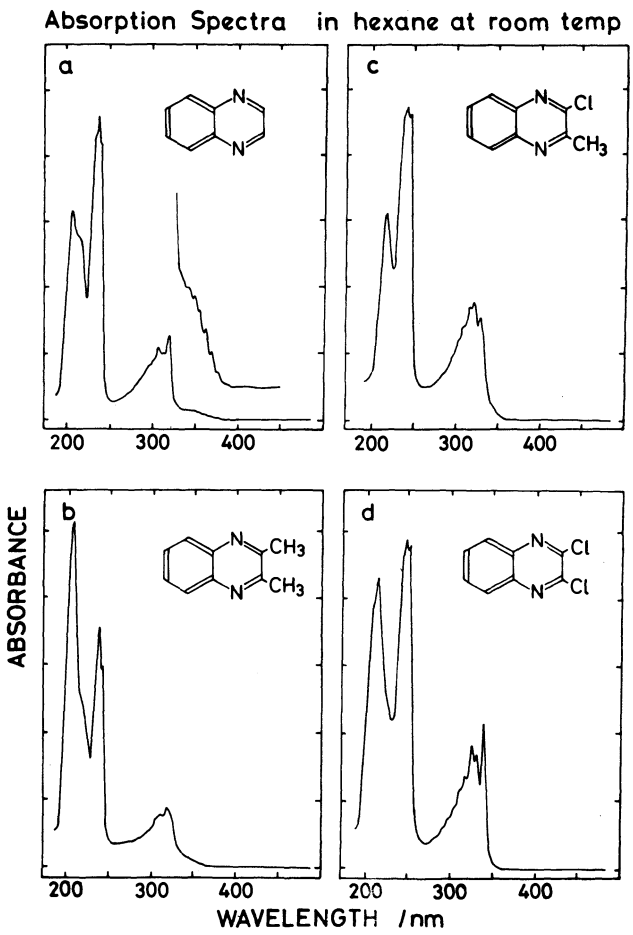

Fig. 2. The absorption spectra of quinoxalines in hexane at room temperature.
(a) Quinoxaline, (b) 2,3-dimethylquinoxaline, (c) 2-chloro-3-methylquinoxaline, and (d) 2,3-dichloroquinoxaline.

The second distinct structure is seen at 42720 cm^{-1} and, with reason, associated with the $^1A_1(\pi,\pi^*)$, which has been calculated to lie at 42670 cm^{-1}.[16] A more diffuse maximum is noted at ≅46930 cm^{-1} and followed by intense band with maximum at ≅49250 cm^{-1}. The former is likely attributed to the transition to the $^1B_2(\pi,\pi^*)$ state suggested to lie at ≅47200 cm^{-1} [15] and the latter to the $^1A_1(\pi,\pi^*)$ predicted at 49500 cm^{-1} [15] from the results of calculations.

In addition, the spectrum of quinoxaline contains a $^1B_1(n,\pi^*)$ transition at about 26300 cm^{-1}, which is in good agreement with the calculated value of 26382 cm^{-1}.[16] The electronic origin of this transition has been reported previously to lie at 25825 cm^{-1} in a naphthalene host crystal by Clarke *et al.*,[17] and at 27071 cm^{-1} in vapor phase by Glass *et al.*[18]

Substituted Quinoxalines. It is seen from Fig. 2 that the absorption spectra of the substituted quinoxalines are similar to that of quinoxaline. This apparent similarity permits the analysis to be made easily by comparison. The effect of substitution shifts the π,π^* excited singlet states to the red by a considerable amount.

It is to be noted that in the case of chloro-substituted quinoxalines, the absorption bands corresponding to the band at 46930 cm^{-1} of quinoxaline reduce the intensity significantly. In fact, the band in the spectrum of 2-chloro-3-methylquinoxaline is buried in the subsequent intense band, and the band in 2,3-dichloroquinoxaline is recognized only as a weak shoulder.

Phosphorescence Excitation Spectra

The phosphorescence excitation spectra of the four compounds were observed in hexane at 4.2 K. The spectra are shown in Fig. 3. It is seen from Figs. 2 and 3 that the lowest excited singlet states of all the three substituted quinoxalines are also of n,π^* character in hexane.

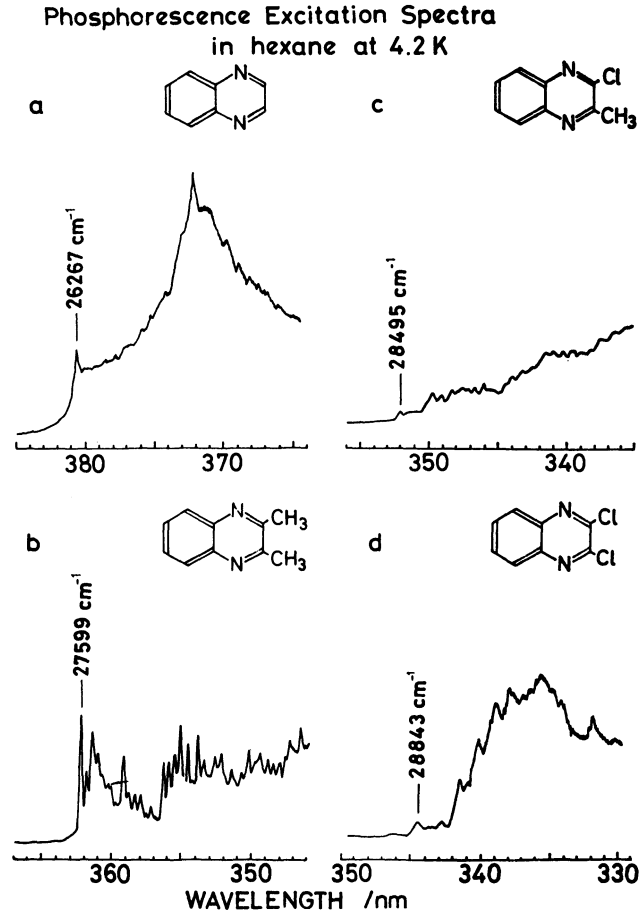

Fig. 3. The phosphorescence excitation spectra of quinoxalines in hexane at 4.2 K.
(a) Quinoxaline, (b) 2,3-dimethylquinoxaline, (c) 2-chloro-3-methylquinoxaline, and (d) 2,3-dichloroquinoxaline.

The phosphorescence excitation spectra of the neat crystals of quinoxaline and 2,3-dimethylquinoxaline were also measured as shown in Fig. 4. The first absorption bands in these excitation spectra correspond to the $^3B_2(\pi,\pi^*)\leftarrow S_0$ transitions. The absorption bands found at 24032 cm^{-1} in the spectrum of quinoxaline and at 25182 cm^{-1} in that of 2,3-dimethylquinoxaline are assigned to the $^3B_1(n,\pi^*)\leftarrow S_0$ transitions.

The energy separations between the $^1B_1$ and $^3B_1(n,\pi^*)$ states are very similar in these two compounds, and about 2350 cm^{-1}. By assuming that these states of all the compounds studied here are separated by the

Table 1. The energy levels of the excited electronic states of quinoxaline and the derivatives (in units of cm^{-1})

	Quinoxaline	2,3-Dimethyl-quinoxaline	2-Chloro-3-methyl-quinoxaline	2,3-Dichloro-quinoxaline
$^3B_2(\pi,\pi^*)$	21 325[a]	22 149[a]	21 885[a]	21 523[a]
$^3B_1(n,\pi^*)$	(23 920)[b]	(25 250)[b]	(26 150)[b]	(26 500)[b]
$^1B_1(n,\pi^*)$	26 267[c]	27 599[c]	28 495[c]	28 843[c]
$^1A_1(\pi,\pi^*)$	31 490	31 440	30 480	29 660
$^1B_2(\pi,\pi^*)$	32 780	32 250	31 790	31 000
$^1A_1(\pi,\pi^*)$	42 720	42 180	41 310	40 150
$^1B_2(\pi,\pi^*)$	46 930	46 280		45 440
$^1A_1(\pi,\pi^*)$	49 250	48 650	46 500	46 930

a) Obtained from the phosphorescence spectra at 4.2 K. b) The values in the parentheses are estimated ones, see text. c) Obtained from the phosphorescence excitation spectra at 4.2 K. Others were determined from the absorption spectra at room temperature.

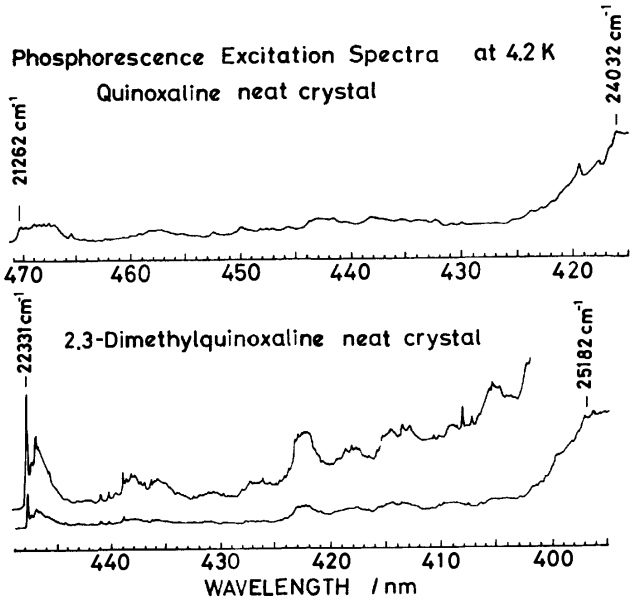

Fig. 4. The phosphorescence excitation spectra of (a) the quinoxaline neat crystal and (b) the 2,3-dimethyl-quinoxaline neat crystal at 4.2 K.

amount of 2350 cm^{-1}, the locations of $^3B_1(n,\pi^*)$ states are estimated. All the data for the locations of the excited states obtained from the absorption, phosphorescence excitation, and phosphorescence spectra are listed in Table 1.

ODMR Results

The zero-field (zf) transitions among the spin sublevels were measured to determine the zf splitting parameters D and E by means of the steady state phosphorescence microwave double resonance (PMDR) technique and/or the MIDP technique. The zf splitting parameters D and E are defined in a similar manner used commonly for naphthalene (Fig. 1). The total decay rates, k_i, steady state populations, N_i^0, and relative populating rates, P_i, for the spin sublevels (i=x, y, z) were also obtained by the MIDP method. The results for all the compounds are summarized in Table 2 for the sake of comparison.

Quinoxaline. Only two strong zf ODMR signals were observed by monitoring the phosphorescence emission in hexane. The signal at 1.157 GHz is assigned to the $T_z \leftrightarrow T_y$ transition, which has been observed at 1.187 GHz in a durene host[9] and at 1.132 GHz in a naphthalene-d_8 host.[9,13] The signal at 3.557 GHz is referable to the $T_z \leftrightarrow T_x$ transition, which has been found at 3.641 GHz in durene[9] and at 3.480 GHz in naphthalene-d_8.[9] The total decay rates obtained here are similar to those in durene[9] and naphthalene-d_8[9,13] reported by other authors.

2,3-Dimethylquinoxaline. The zf transitions are observed at 1.239 GHz for the $T_z \leftrightarrow T_y$ transition and at 3.731 GHz for $T_z \leftrightarrow T_x$. The total decay rates for all the three sublevels of 2,3-dimethylquinoxaline are

Table 2. The zero field splitting and kinetic parameters of quinoxaline and the derivatives

	Quinoxaline	2,3-Dimethyl-quinoxaline	2-Chloro-3-methyl-quinoxaline	2,3-Dichloro-quinoxaline
$\lvert D\rvert/cm^{-1}$	0.0993	0.1075	0.1017	0.1017
$\lvert E\rvert/cm^{-1}$	0.0193	0.0207	0.0189	0.0179
k_z/s^{-1}	12.3±0.3	7.23±0.14	3.54±0.09	3.29±0.12
k_y/s^{-1}	1.14±0.06	0.67±0.06	5.04±0.10	6.18±0.10
k_x/s^{-1}	0.86±0.02	0.34±0.03	0.45±0.03	0.38±0.01
N_z^0	1	1	1	1
N_y^0	0.90±0.08	0.99±0.06	0.80±0.05	0.78±0.05
N_x^0	0.64±0.07	1.61±0.15	0.82±0.06	0.48±0.03
P_b	1	1	1	1
P_y	0.084	0.091	1.14	1.45
P_x	0.045	0.075	0.10	0.055

smaller by a factor of about 0.6 than those of quinoxaline.

2,3-Dichloroquinoxaline. The observed zf transitions at 2.510 and 3.586 GHz can be assigned to the $T_y \leftrightarrow T_x$ and $T_z \leftrightarrow T_x$ transition, respectively, which have been reported to be at 2.467 and 3.515 GHz in a durene host crystal.[19,20] The total decay rates of the sublevels determined here are somewhat smaller than those obtained in other crystal systems.[19-22] It is to be noted that the relative populating rate of the y sublevel is as large as that of the z sublevel.

2-Chloro-3-methylquinoxaline. As in the case of 2,3-dichloroquinoxaline, the zf ODMR signals found at 2.483 and 3.616 GHz are attributed to the $T_y \leftrightarrow T_x$ and $T_z \leftrightarrow T_x$ transition, respectively. The total decay rate for the y sublevel is smaller to a certain extent than that of 2,3-dichloroquinoxaline, while with respect to the z and x sublevels, there is little difference between these compounds. The pattern of populating process is also characterized by high selectivity for both the z and y sublevels, as in the case of 2,3-dichloroquinoxaline.

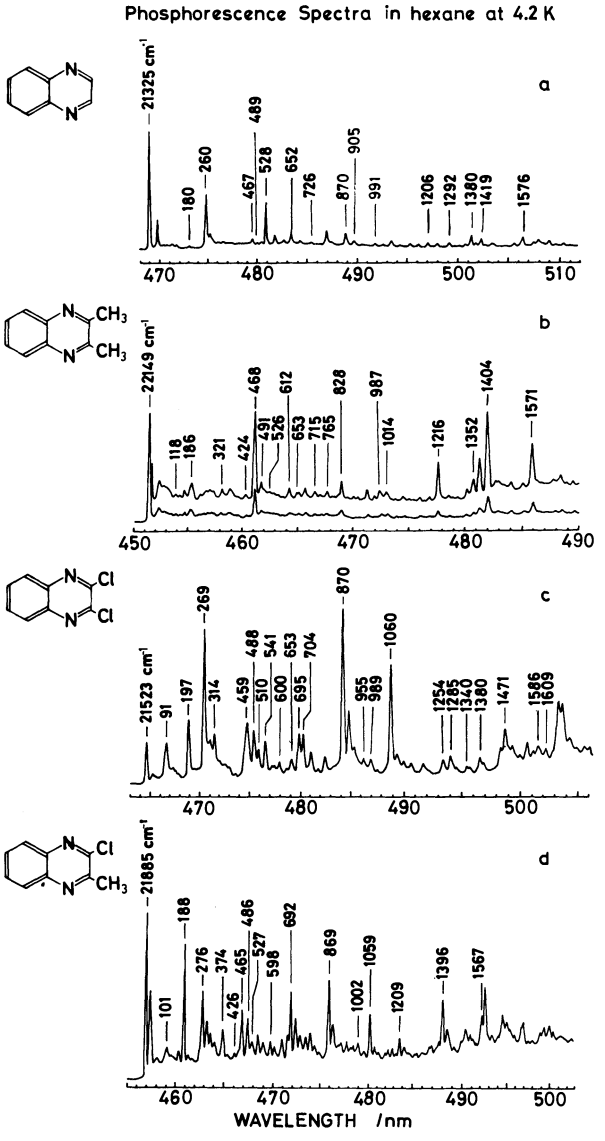

Fig. 5. The phosphorescence spectra in hexane at 4.2 K. (a) Quinoxaline, (b) 2,3-dimethylquinoxaline, (c) 2,3-dichloroquinoxaline, and (d) 2-chloro-3-methylquinoxaline.

Phosphorescence Spectra

The phosphorescence spectra of quinoxaline and the three derivatives in hexane are characterized by well resolved feature (FWHM=0.3 nm). The spectra obtained at 4.2 K are presented in Fig. 5. Assignments of the vibronic bands in the spectra were made in reference to the vibrational assignments of the IR and Raman spectra reported in the literature.[23-25]

Quinoxaline. The spectrum obtained in hexane differs from those observed in the naphthalene-d_8[13] and durene[7,10,12] host crystals. The vibronic bands at 180, 260, and 904 cm^{-1} from the origin appear with considerable intensity in hexane. However, the corresponding bands are far from being observable in the other host crystal systems.[7,10,12,13]

2,3-Dimethylquinoxaline. There is noticeable difference between quinoxaline and 2,3-dimethylquinoxaline. The intensity of the vibronic band at 0−467 cm^{-1} exceeds those of the vibronic bands such as 0−525 cm^{-1} involving totally symmetric vibrations, in contrast with quinoxaline.

2,3-Dichloroquinoxaline. There is some difference between the spectra obtained in hexane and in durene.[19,22] The vibronic bands observed at 197, 459, 510, and 695 cm^{-1} from the origin appear with considerable intensity in hexane, whereas in the durene host, these bands appear as nothing more than weak traces. The vibronic bands found at 0−197 and 0−695 cm^{-1} are due to the b_1 vibrations, corresponding probably to the frequencies of 180 and 725 cm^{-1} of quinoxaline. The band at 0−459 cm^{-1} is attributed to the vibronic band involving a_2 vibration corresponding to that of 647 cm^{-1} of quinoxaline. The remaining band at 0−510 cm^{-1} is assigned to the vibronic band due to totally symmetric vibration.

2-Chloro-3-methylquinoxaline. The frequencies of the vibrations appearing in the spectrum of 2-chloro-3-methylquinoxaline are in excellent correspondence to those in that of 2,3-dichloroquinoxaline. This enables one to readily analyze the vibrational structure by comparing the spectra of these compounds. It is to be noted that the origin band appears intensely in the spectrum of 2-chloro-3-methylquinoxaline, whereas in 2,3-dichloroquinoxaline, the intensity of the 0,0 band is quite small.

Sublevel Emission Spectra

The sublevel emission spectra of all the four molecules measured by means of the MIDP method are shown in Fig. 6. The relative radiative decay rates for the 0,0 and some vibronic bands of interest were also determined. The results are shown in Table 3, where experimental errors are estimated to be about ±20% for the k_x^r and k_y^r values larger than 0.02 and about +100—−50% for those less than 0.02. It is to be noted that the sublevel spectra in Fig. 6 show only the qualitative feature of the spin selectivity of each sublevel; in other

Table 3. Relative radiative decay rate constants for some vibronic bands

Band $\Delta\nu$/cm^{-1}	k_z^r	k_y^r	k_x^r	Assignment
		(a) Quinoxaline		
0	1	0.008	0.011	0,0
260	1	0.024	0.012	a_2 γ skel. dist.
467	1	0.013	0.018	a_2 γ skel. dist.
489	1	0.014	0.015	b_1 γ skel. dist.
528	1	0.007	0.015	a_1 β skel. dist.
652	1	0.012	0.020	a_2 γ skel. dist.
870	1	0.013	0.015	b_1 γ CH bend.
1056	1	0.009	0.018	528×2
		(b) 2,3-Dimethylquinoxaline		
0	1	0.032	0.049	0,0
186	1	0.024	0.059	b_1 ring wag.
424	1	0.031	0.064	b_1 γ skel. dist.
467	1	0.025	0.057	a_2 γ skel. dist.
612	1	0.039	0.060	a_1 β skel. dist.
828	1	0.033	0.061	b_2 β skel. dist.
1216	1	0.026	0.056	a_1 β CH bend.
1375	1	0.028	0.054	a_1 CH_3 sym. dist.
1404	1	0.029	0.046	a_1 β CH bend.
1571	1	0.032	0.032	a_1 β ring str.
		(c) 2,3-Dichloroquinoxaline		
0	1	0.29	0.07	0,0
91	1	10.2	0.30	a_2
197	1	0.35	0.09	b_1 ring wag.
269	1	12.7	0.26	a_2 γ skel. dist.
314	1	2.85	0.32	b_1
459	1	1.65	0.20	a_2 γ skel. dist.
488	1	1.17	0.26	b_1 γ skel. dist.
510	1	1.59	0.28	a_1 β skel. dist.
541	1	7.12	0.24	a_2
600	1	0.97	0.12	a_1 β skel. dist.
653	1	3.67	0.14	a_2
695	1	2.00	0.13	b_1 γ CH bend.
870	1	11.7	0.29	a_2 γ CH bend.
895	1	4.18	0.19	
1060	1	1.99	0.20	
		(d) 2-Chloro-3-methylquinoxaline		
0	1	1.56	0.13	0,0
101	1	5.00	0.35	a″(a_2)
188	1	1.39	0.19	a″(b_1) ring wag.
276	1	5.88	0.35	a″(a_2) γ skel. dist.
465	1	2.17	0.17	a″(a_2) γ skel. dist.
486	1	2.44	0.24	a″(b_1) γ kel. dist.
598	1	2.33	0.21	a′(a_1) β skel. dist.
692	1	0.56	0.11	a″(b_1) γ CH bend.
869	1	1.89	0.21	a″(a_2) γ CH bend.
1059	1	1.20	0.20	
1396	1	1.56	0.14	a′(a_1) β CH bend.
1567	1	0.79	0.13	a′(a_1) β ring str.

a) The correlation of species of the C_s and C_{2v} symmetry groups is shown in the parentheses.

words, the spectra are not compatible with the data in Table 3, because some of the spectra were taken with different slit widths.

Brief comments on some of the specific experimental findings are described in the following.

Quinoxaline. It is clearly seen in Fig. 6(a) that the intensity of the vibronic bands such as 0—260, 0—904, 0—1380, and 0—1618 cm^{-1} relative to the 0,0 band is significantly larger in the y and x sublevel spectra than z. On the other hand, no spin state selectivity is noted with regard to the intensity of the bands such as 0—467, 0—527, 0—651, and 0—1576 cm^{-1}. The vibronic bands involving b_2 vibrations have a certain intensity in the y and x sublevel spectra.

2,3-Dimethylquinoxaline. The emission spectra of the spin sublevels resemble each other. It is found that the vibronic bands due to the b_1 vibrations such as 185, 424, and 490 cm^{-1} appear more intensely in all the three sublevel spectra in comparison with those of quinoxaline.

2,3-Dichloroquinoxaline. The vibronic bands involving a_2 or b_1 vibrations appear more strongly in all the three sublevel spectra than those of quinoxaline. On the other hand, the vibronic bands due to the b_2 vibrations have a considerable intensity only in the y sublevel spectrum. By examining carefully the change in the intensity, it is found that as concerns the y sublevel spectrum, the bands such as 0—269 cm^{-1} are affected by chlorine substitution to a more extent than the bands such as 0—459 cm^{-1}, although these vibrations are classified into the same species of a_2. With respect to the vibronic bands due to b_1 vibrations, a similar situation is found by comparing, for example, the bands at 0—197 and 0—488 cm^{-1}. This can be seen more clearly in Table 3(c).

2-Chloro-3-methylquinoxaline. Although both the a_2 and b_1 species in C_{2v} point group are reduced to the a″ species in C_s, the distinction between these species remains with regard to the radiative decay process, with an exception that the y sublevel emits strongly at the 0,0 band. This indicates clearly that the radiative decay process of 2-chloro-3-methylquinoxaline is governed by the mechanisms similar to those of 2,3-dichloroquinoxaline.

Assignments of Some Vibrations

Most of the vibronic bands in the phosphorescence spectra are assigned on the basis of the vibrational data reported previously[23-25] and confirmed by the experimental findings in the sublevel spectra. Several vibronic bands, however, are assigned anew. The bands such as 0—197 and 0—695 cm^{-1} of 2,3-dichloroquinoxaline are assigned only in view of the observed sublevel spectra. Here, the reasons for the assignments of the bands of importance are commented briefly.

Although no data of the vibrational assignments from IR and Raman spectra are available concerning the vibrations of 197 and 695 cm^{-1} of 2,3-dichloroquinoxaline, the vibronic bands due to these vibrations can be assigned to those of b_1 symmetry for the following reasons. First, the 0—197 cm^{-1} band appears with more intensity than the 0,0 band in the phosphorescence spectrum. Therefore, it is reasonable to leave the possibility of a_1 or b_2 species out of consideration. In fact, there are no vibrational modes of a_1 or b_2 species with such low frequency. Second, the behavior of this

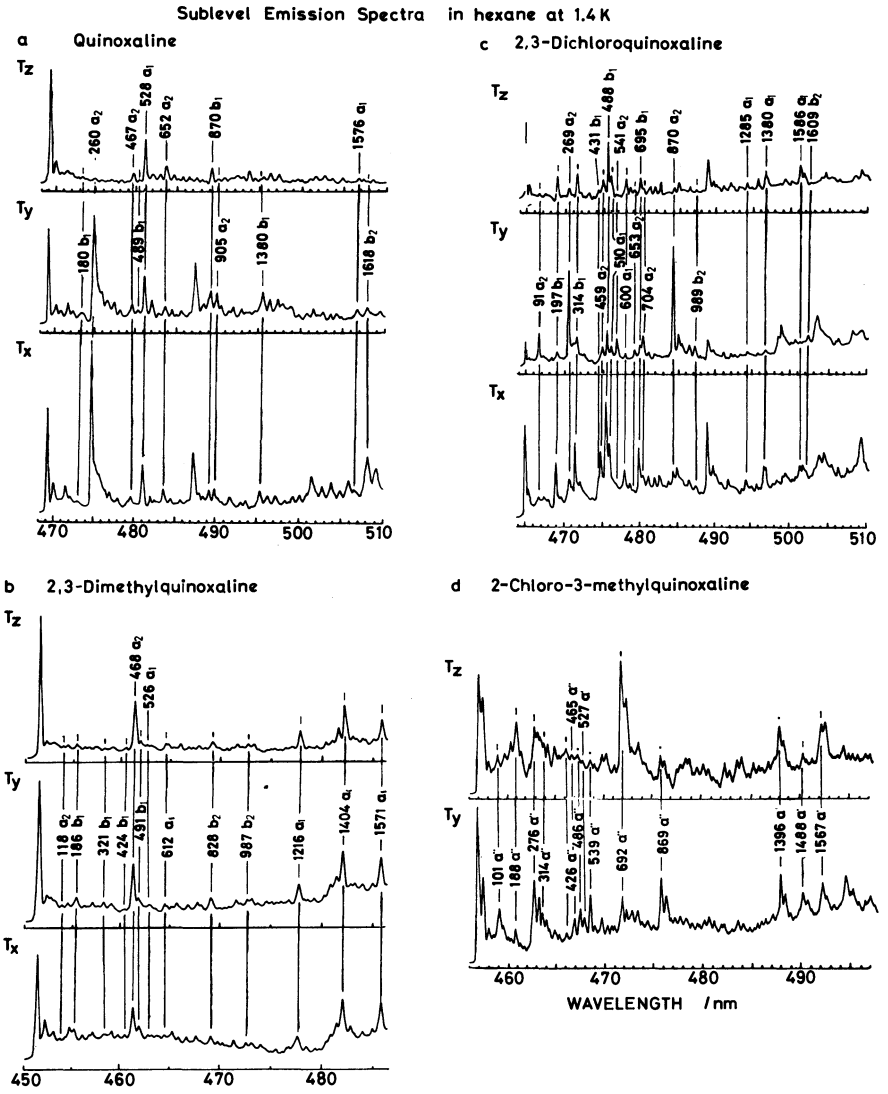

Fig. 6. The sublevel emission spectra in hexane at 1.4 K. (a) Quinoxaline, (b) 2,3-dimethylquinoxaline, (c) 2,3-dichloroquinoxaline, and (d) 2-chloro-3-methylquinoxaline.

band in the sublevel spectra is different from that of the vibronic band due to a_2 vibration such as 0—269 cm^{-1}, but rather similar to that of the band due to b_1 such as 0—488 cm^{-1}. The 0—695 cm^{-1} band can also be assigned to the band due to b_1 vibration in view of intensity behavior in the sublevel spectra. In fact, the corresponding band, 0—692 cm^{-1}, of 2-chloro-3-methylquinoxaline appears with much intensity in the z sublevel spectrum as well as the 0—188 cm^{-1} band corresponding to the 0—197 cm^{-1} band of 2,3-dichloroquinoxaline, but in contrast to the 0—276 cm^{-1} band corresponding to the 0—269 cm^{-1} band of 2,3-dichloroquinoxaline.

Electronic States

Some comments on the assignment of the low lying electronic states may be added, although the absorption and excitation spectra have been discussed briefly above. The absorption spectra of quinoxaline and 2,3-dichloroquinoxaline in hexane have been reported previously by another author.[26] The band at 42720 cm^{-1} of quinoxaline and the corresponding band at 40150 cm^{-1} of 2,3-dichloroquinoxaline have been assigned to the $^1B_2 \leftarrow S_0$ transition in the earlier works.[18,26] In the present study, however, these bands are assigned to the $^1A_1 \leftarrow S_0$ transition. This assignment is in good agreement with the theoretical predictions.[15,16]

It is again emphasized that the lowest excited singlet state is the $^1B_1(n,\pi^*)$ state for all the compounds studied here. Yamauchi and Azumi[22] have suggested that in a durene host the $^1B_1(n,\pi^*)$ state of 2,3-dichloroquinoxaline lies at 29520 cm^{-1}, higher by 1210 cm^{-1} than the $^1A_1(\pi,\pi^*)$ state, even though the transition monent for the transition to the $^1B_1$ state is considered to be much smaller than that to the $^1A_1$. On the other hand, the phosphorescence excitation spectrum of 2,3-dichloroquinoxaline in hexane obtained here shows that the $^1B_1(n,\pi^*)$ state lies lower than the $^1A_1$ state and is the lowest excited singlet state without question.

All the results for 2,3-dimethylquinoxaline and 2-chloro-3-methylquinoxaline are determined anew. The

locations of the $^3B_1$ states of quinoxaline and 2,3-dimethylquinoxaline are also determined from the present observation of the excitation spectra of the neat crystals.

The values of D are all very similar. They differ from each other only within 4%. The same holds true for the values of E. The methyl group and chlorine atom seem to have a little influence on the lowest excited triplet state with regard to the stationary properties of the wave function. Thus, it is reasonably assumed that (1) all the molecules studied here have essentially the same type of orbital wave function as that of the parent molecule, quinoxaline, and (2) there occurs no significant rotation of spin axes by going from the molecules with C_{2v} symmetry to the molecule with C_s. This latter point is strongly corroborated by the dynamic measurements. In fact, 2-chloro-3-methylquinoxaline shows the decay pattern similar to that of 2,3-dichloroquinoxaline.

Total Decay Rates

As for the z sublevel of aza-aromatics, the low lying n,π^* states are known to be of importance in the interactions relevant in causing both the radiative and radiationless decays.[1-5] Therefore, the decrease in k_z on substitution is presumably due to the reduction of the interaction with n,π^* states, resulting from the increased energy separations.

Quinoxaline and 2,3-dimethylquinoxaline show the relation of $k_z > k_y$. The decay process from the y sublevel is expected to be determined mainly by the interactions with n,π^* states.

On the other hand, in the case of chloro-substituted quinoxalines, the relation of $k_z < k_y$ indicates that there exists an additional mechanism for the decay from the y sublevel. The π electrons are likely to delocalize onto the chlorine atom(s) in some degree, so that one center integrals at the chlorine atom are expected to mean something to the spin orbit coupling matrix elements. Hence, the y sublevel can mix significantly with the $^1\sigma,\pi^*$ state *via* a one-center spin orbit coupling matrix element, in addition to the mixing with the ^{1}n,π^* state *via* a two-center spin orbit coupling matrix element. Accordingly, the large activity of the y sublevel in the decay process observed in 2-chloro-3-methylquinoxaline is also ascribed to the influence of chlorine substitution on the spin orbit interaction as stated before for 2,3-dichloroquinoxaline.[19,22]

Intersystem Crossing

It is seen from Table 2 that in the case of quinoxaline and 2,3-dimethylquinoxaline, the z sublevel is populated in much preference to the other sublevels *via* intersystem crossing from S_1. Considering that the lowest excited singlet states of these compounds are n,π^* states of B_1 symmetry, the high selectivity for the z sublevel with respect to the intersystem crossing process must be, as stated before,[8,9] a consequence of the efficient spin orbit coupling between the $^1B_1$(n,π^*) and $^3B_2$(π,π^*) states, by way of which only the z sublevel is coupled directly.

The situation is quite different for the chlorosubstituted quinoxalines. The populating pattern of these compounds is characterized by highly selective intersystem crossing to both of the z and y sublevels. Seeing that the $^1B_1$(n,π^*) is the lowest excited singlet state, as observed above, the direct spin orbit coupling with S_1 accounts for P_z. The value of P_y is quite large for the chlorosubstituted derivatives as compared with that for quinoxaline and 2,3-dimethylquinoxaline. For a similar enhancement in the system of 2,3-dichloroquinoxaline in durene, Tinti and El-Sayed have suggested two possible mechanisms which differ depending on the assignment of the nature of the lowest excited singlet state.[19] On the basis of the present n,π^* assignment, these mechanisms can be discriminated unambiguously. The $^3A_1$(π,π^*) state is expected to lie lower in energy than the $^1B_1$(n,π^*) state in the case of 2,3-dichloroquinoxaline, because chlorine substitution shifts π,π^* states to the red and n,π^* states to the blue, as mentioned above. Further, considering the n orbitals to be mixed with other σ orbitals of the aromatic frame (delocalization) to a certain extent, $^3A_1$(π,π^*) state could couple with $^1B_1$(n,π^*) state appreciably. If this is the case, it is necessary to take into account an indirect process, which goes from S_1 through the intermediate triplet state, $^3A_1$(π,π^*), and then to T_1. This process can populate only the y sublevel. Thus, the large value of P_y observed in 2,3-dichloroquinoxaline is surely ascribed to this additional intersystem crossing mechanism. The same holds true for 2-chloro-3-methylquinoxaline.

Mechanisms of Radiative Decay

As described above, all the molecules studied here are considered to have essentially the same type of orbital wave function. In the following discussion, therefore, it is assumed that all the molecules can well be characterized by C_{2v} point group symmetry for the purpose of avoiding unnecessary complications. Including up to the second order perturbations, the possible mechanisms, which are group-theoretically predicted, are divided into the following classes.[27]

(I) Spin orbit coupling.

(II) Vibronic coupling in the singlet manifold with spin orbit coupling.

(III) Spin orbit coupling with vibronic coupling in the triplet manifold.

(IV) Spin vibronic coupling.

Among a number of the mechanisms group-theoretically allowed, the mechanisms of little importance are excluded in view of the following criteria:

(1) Spin orbit, spin vibronic, and vibronic coupling operators are considered as the sum of one-electron operators in good approximation;

(2) As concerns mechanisms of types (II) and (III), the perturbing singlet configurations, which have allowed transitions to the ground state, are limited to π,π^*;

(3) With respect to mechanisms of type (IV), the contribution of the mechanisms involing $^3\pi,\pi^*$ and $^1\pi,\pi^*$ states is neglected because of the vanishingly small magnitude of the matrix elements between these states.

TABLE 4. ALL THE POSSIBLE MECHANISMS FOR THE RADIATIVE DECAY PROCESS

Species[a]		Mechanism[b]
a_1	I.1	$T_z \leftarrow so \rightarrow {}^1B_1(n,\pi^*)$
	I.2	$T_z \leftarrow so \rightarrow {}^1B_1(\sigma,\pi^*)$
	I.3	$T_y \leftarrow so \rightarrow {}^1A_2(n,\pi^*)$
	I.4	$T_y \leftarrow so \rightarrow {}^1A_2(\sigma,\pi^*)$
	I.5	$T_x \leftarrow so \rightarrow {}^1A_1(\pi,\pi^*)$
a_2	II.1	$T_z \leftarrow so \rightarrow {}^1B_1(n,\pi^*) \leftarrow v \rightarrow {}^1B_2(\pi,\pi^*)$
	II.2	$T_z \leftarrow so \rightarrow {}^1B_1(\sigma,\pi^*) \leftarrow v \rightarrow {}^1B_2(\pi,\pi^*)$
	III.1	$T_z \leftarrow v \rightarrow {}^3B_1(n,\pi^*) \leftarrow so \rightarrow {}^1B_2(\pi,\pi^*)$
	III.2	$T_z \leftarrow v \rightarrow {}^3B_1(\sigma,\pi^*) \leftarrow so \rightarrow {}^1B_2(\pi,\pi^*)$
	II.3	$T_y \leftarrow so \rightarrow {}^1A_2(n,\pi^*) \leftarrow v \rightarrow {}^1A_1(\pi,\pi^*)$
	II.4	$T_y \leftarrow so \rightarrow {}^1A_2(\sigma,\pi^*) \leftarrow v \rightarrow {}^1A_1(\pi,\pi^*)$
	III.3	$T_y \leftarrow v \rightarrow {}^3B_1(n,\pi^*) \leftarrow so \rightarrow {}^1A_1(\pi,\pi^*)$
	III.4	$T_y \leftarrow v \rightarrow {}^3B_1(\sigma,\pi^*) \leftarrow so \rightarrow {}^1A_1(\pi,\pi^*)$
b_1	II.5	$T_z \leftarrow so \rightarrow {}^1B_1(n,\pi^*) \leftarrow v \rightarrow {}^1A_1(\pi,\pi^*)$
	II.6	$T_z \leftarrow so \rightarrow {}^1B_1(\sigma,\pi^*) \leftarrow v \rightarrow {}^1A_1(\pi,\pi^*)$
	III.5	$T_z \leftarrow v \rightarrow {}^3A_2(n,\pi^*) \leftarrow so \rightarrow {}^1A_1(\pi,\pi^*)$
	III.6	$T_z \leftarrow v \rightarrow {}^3A_2(\sigma,\pi^*) \leftarrow so \rightarrow {}^1A_1(\pi,\pi^*)$
	II.7	$T_y \leftarrow so \rightarrow {}^1A_2(n,\pi^*) \leftarrow v \rightarrow {}^1B_2(\pi,\pi^*)$
	II.8	$T_y \leftarrow so \rightarrow {}^1A_2(\sigma,\pi^*) \leftarrow v \rightarrow {}^1B_2(\pi,\pi^*)$
	III.7	$T_y \leftarrow v \rightarrow {}^3A_2(n,\pi^*) \leftarrow so \rightarrow {}^1B_2(\pi,\pi^*)$
	III.8	$T_y \leftarrow v \rightarrow {}^3A_2(\sigma,\pi^*) \leftarrow so \rightarrow {}^1B_2(\pi,\pi^*)$
	IV.1	$T_x \leftarrow sv \rightarrow {}^1B_1(n,\pi^*)$
	IV.2	$T_x \leftarrow sv \rightarrow {}^1B_1(\sigma,\pi^*)$
b_2	IV.3	$T_y \leftarrow sv \rightarrow {}^1B_1(n,\pi^*)$
	IV.4	$T_y \leftarrow sv \rightarrow {}^1B_1(\sigma,\pi^*)$
	II.9	$T_x \leftarrow so \rightarrow {}^1A_1(\pi,\pi^*) \leftarrow v \rightarrow {}^1B_2(\pi,\pi^*)$
	III.9	$T_x \leftarrow v \rightarrow {}^3A_1(\pi,\pi^*) \leftarrow so \rightarrow {}^1B_2(\pi,\pi^*)$

a) The first column shows the coupled vibrational species.
b) The interaction is indicated by the following notations: so, spin orbit coupling; v, vibronic coupling; sv, spin vibronic coupling.

Accordingly, the mechanisms, which are listed in Table 4, remain to be taken into consideration.

In the case of chloro-substituted quinoxalines, the π electron orbitals of the aromatic frame are mixed in some degree with the out-of-plane atomic orbital on the chlorine atom. This is responsible for the large red-shift of the π,π^* excited singlet states. This also causes the matrix elements of the spin orbit coupling to contain integrals over the chlorine atomic orbitals. Since σ orbitals are easily mixed with the in-plane orbitals of the chlorine atom, the matrix elements between π,π^* and σ,π^* states become large through one-center integrals on the chlorine atom. In view of the localized character of n orbitals, the integrals over the chlorine atomic orbitals make relatively small contribution to the matrix elements between π,π^* and n,π^* states. These points are to be kept in mind in the following discussion.

The 0,0 Band and Vibronic Bands Involving a_1 Vibrations. As seen in Table 3(a), the z sublevel has the largest radiative activity at the 0,0 band in the phosphorescence spectrum of quinoxaline. As suggested by other authors,[5-8,10-13] there is no doubt to conclude that the main mechanism, which accounts for the activity of the z sublevel at the 0,0 band, is mechanism (I.1). This is a consequence of not only the efficient spin orbit coupling from the one-center terms on the N atom, but also rather small energy separation between the ${}^3B_2(\pi,\pi^*)$ and ${}^1B_1(n,\pi^*)$ states.

In the case of substituted quinoxalines, the spin orbit interaction between the ${}^3B_2(\pi,\pi^*)$ and ${}^1B_1(n,\pi^*)$ states is expected to be reduced in response to the increase in the energy separation, ΔE_{ST}. If the magnitude of the spin orbit matrix element is assumed to be affected by no means on substitution, the mixing coefficient, $(<|H_{SO}|>/\Delta E_{ST})^2$, is predicted to decrease by factors of 0.81, 0.56, and 0.46 for 2,3-dimethyl-, 2-chloro-3-methyl-, and 2,3-dichloroquinoxaline, respectively. Although the radiative and radiationless parts in the total decay rates can not be strictly separated for the lack of quantum yield data for phosphorescence and triplet formation, the degree of reductions of the total decay rates k_z appears to be in good correlation with the values estimated above, presumably indicating that the mixing with the ${}^1B_1(n,\pi^*)$ state is also the main source of the radiative activity of substituted quinoxalines.

In the x sublevel spectrum, the 0,0 band can gain radiative character through the interaction with ${}^1A_1(n,\pi^*)$ state; mechanism (I.5). In view of the ratio k_x^x/k_z^x, the radiative decay rate constants of the x sublevel for the 0,0 band are found to increase to some degree on chlorine substitution. This increase is mainly a consequence of the decrease in the energy difference between ${}^3B_2(\pi,\pi^*)$ and ${}^1A_1(\pi,\pi^*)$, and the increase in the probability of the transition between the ${}^1A_1(\pi,\pi^*)$ and the ground state (see Fig. 2).

On the other hand, the influence of chlorine substitution significantly enhances the radiative activity of the y sublevel at the 0,0 band. Therefore, in the case of chloro-substituted quinoxalines, the major source, which gives rise to the radiative activity at the 0,0 band, is concluded to be mechanism (I.4), of which the matrix element contains one-center integrals over the chlorine atomic orbitals. The same explanation has been suggested by other authors for 2,3-dichloroquinoxaline.[22] The large intensity of the 0,0 band in the y sublevel spectrum of 2-chloro-3-methylquinoxaline is attributable to the reduction in molecular symmetry to C_s, where A_2 symmetry is reduced to A''. Unlike the chloro-substituted quinoxalines, mechanism (I.4) is expected to make a minor contribution, and mechanism (I.3) is likely to be the main one in the case of 2,3-dimethylquinoxaline, as stated for quinoxaline.[13] In fact, the rather small energy denominator and the large contribution of the N atomic orbital to the matrix element are in favor of mechanism (I.3).

The Vibronic Bands Involving a_2 Vibrations. For the vibronic bands due to a_2 vibrations, mechanisms (II.1), (II.2), (III.1), and (III.2) may contribute to the z sublevel emission. In the case of naphthalene, the bands of this type, which are exclusively due to the interaction involving σ,π^* states; mechanisms (II.2) and (III.2), have a negligible intensity in the spectrum.[28] Thus, it is reasonable to leave mechanisms (II.2) and (III.2) out of consideration.

If mechanism (III.1) plays an important role, the

intensity of these bands in the z sublevel spectrum in comparison to that of the 0,0 bands is expected to decrease significantly in response to the increase in the energy difference between the $^3B_2(\pi,\pi^*)$ and $^3B_1(n,\pi^*)$ states. If mechanism (II.1) is the case, in contrast, these bands will increase intensity to a certain extent.

It is easily seen that the bands due to a_2 vibrations appear in the z sublevel spectra of substituted quinoxalines with somewhat more intensity than those of quinoxaline. In an instant, this leads to the conclusion that mechanism (II.1) is the main source in producing the radiative activity of the z sublevel at the bands involving a_2 vibrations. The fact that the vibronic bands due to a_2 vibrations appear also in the $^1B_1(n,\pi^*)\leftarrow S_0$ absorption spectrum of quinoxaline in a naphthalene host crystal[17] strongly supports the validity of the inference described above.

With respect to the y sublevel, mechanisms (II.3), (II.4), (III.3), and (III.4) may make a contribution. An argument similar to that made concerning the z sublevel emission may explain the increase in intensity on chlorine substitution. The increase in intensity clearly indicates that mechanism (III.3) can not be of importance.

By examining the experimental results in detail, it is noticed that the vibronic bands such as 0−269, 0−541, and 0−870 cm^{-1} are enhanced by chlorine substitution more largely than the bands such as 0−459 and 0−653 cm^{-1}. This can also be seen from the relative radiative decay rate constants (see Table 4(c)). This difference in the enhancement can be understood in the following way. The former bands can be associated with mechanisms (II.4) and/or (III.4), in which the spin orbit matrix elements between σ,π^* and π,π^* states are affected strongly by the large one-center terms on the chlorine atom(s), whereas the latter bands can be due to mechanism (II.3), in which the contribution from the chlorine atom(s) is rather small.

The Vibronic Bands Involving b_1 Vibrations. The fact that naphthalene has no activity at the bands due to b_1 vibrations[28] evidently allows one to limit the possibility to mechanisms (II.5) and (III.5) with respect to the z sublevel. Since the bands of this type appear strongly in the chloro-substituted quinoxalines as compared with quinoxaline, there is no doubt to conclude that the z sublevel gains activity at these bands by mechanism (II.5). The increase in intensity can be ascribed to the decrease in the energy difference between the $^1B_1(n,\pi^*)$ and $^1A_1(\pi,\pi^*)$ states. In addition, the manifest evidence for the strong vibronic interaction between the $^1B_1$ and $^1A_1$ states has been found in the $^1B_1(n,\pi^*)\leftarrow S_0$ absorption spectrum reported previously.[17]

The detailed examination of the y sublevel emission reveals that the vibronic bands such as 0−197 cm^{-1} behave in different way from the bands such as 0−488 cm^{-1} with regard to the effect of chlorine substitution. Accordingly, by an argument similar to that made for the a_2 vibrations, it is possible to conclude that mechanisms (II.8) and/or (III.8) as well as (II.7) make a contribution toward producing the radiative activity at the bands due to b_1 vibrations.

The x sublevel emission is ascribed to either mechanisms (IV.1) or (IV.2). The experimental finding that the chlorine substitution affects the intensity to a great extent assuredly indicates that the x sublevel gains the radiative activity through mechanism (IV.2) in preference to (IV.1).

The Vibronic Bands Involving b_2 Vibrations. The vibronic bands due to b_2 vibrations are observable in the y and x sublevel emission. With regard to the y sublevel, mechanisms (IV.3) and (IV.4) may contribute. Of the two mechanisms, the former seems to be more favorable in view of the energy denominators. The intensity of the bands due to b_2 vibrations in the y sublevel emission is by no means affected by chlorine substitution. This seems to take a side with mechanism (IV.3).

Mechanisms (II.9) and (III.9) are predicted group-theoretically to contribute to the x sublevel emission. It is worthy to note that the configuration of the perturbing $^1B_2$ state is probably $\pi(b_1),\pi^*(a_2)$. Accordingly, the experimental finding that the bands due to b_2 vibrations appear in the spectrum of 2,3-dichloroquinoxaline with less intensity than in that of quinoxaline can be attributed to the decrease in the transition moment for the transition to the $^1B_2$ state, which is readily seen from the absorption spectra.

This work was partly supported by a Gran-in-Aid for Scientific Research from the Ministry of Education, Science and Culture (No. 510205).

References

1) M. S. de Groot, I. A. M. Hesselmann, J. Schmidt, and J. H. van der Waals, *Mol. Phys.*, **15**, 17 (1968).
2) D. M. Burland and J. Schmidt, *Mol. Phys.*, **22**, 19 (1971).
3) R. H. Clarke and J. M. Hayes, *J. Chem. Phys.*, **57**, 569 (1972); **59**, 3113 (1973).
4) D. A. Antheunis, J. Schmidt, and J.H. van der Waals, *Mol. Phys.*, **27**, 1521 (1974).
5) M. A. El-Sayed and R. G. Brewer, *J. Chem. Phys.*, **39**, 1623 (1963).
6) E. C. Lim and J. M. H. Yu, *J. Chem. Phys.*, **49**, 3878 (1968).
7) Y. Nakano and T. Azumi, *Bull. Chem. Soc. Jpn.*, **43**, 985 (1970).
8) S. M. Ziegler and M. A. El-Sayed, *J. Chem. Phys.*, **52**, 3257 (1970).
9) J. Schmidt, D. A.Antheunis, and J. H. van der Waals, *Mol. Phys.*, **22**, 1 (1971).
10) K. Ikegami and M. Ito, *Bull. Chem. Soc. Jpn.*, **45**,297 (1972).
11) R. Li and E. C. Lim, *J. Chem. Phys.*, **57**, 605 (1972).
12) S. Yamauchi and T. Azumi, *Chem. Phys. Lett.*, **21**, 603 (1973).
13) S. Yamauchi and T. Azumi, *J. Chem. Phys.*, **67**, 7 (1977).
14) E. Kanezaki, N. Nishi, and M. Kinoshita, *Bull. Chem. Soc. Jpn.*, **52**, 2836 (1979); K. Suga and M. Kinoshita, *ibid.*, **54**, 1651 (1981).
15) H. Baba and I. Yamazaki, *J. Mol. Spectrosc.*, **44**, 118 (1972).
16) J. E. Ridley and M. C. Zerner, *J. Mol. Spectrosc.*, **50**, 457 (1974).
17) R. H. Clarke, R. M. Hochstrasser, and C. J. Marzzacco, *J. Chem. Phys.*, **51**, 5015 (1969).

18) R. W. Glass, L. C. Robertson, and J. A. Merritt, *J. Chem. Phys.*, **53**, 3857 (1970).
19) D. S. Tinti and M. A. El-Sayed, *J. Chem. Phys.*, **54**, 2529 (1971).
20) D. Schweitzer, J. Zuclich, and A. M. Maki, *Mol. Phys.*, **25**, 197 (1973).
21) C. B. Harris and R. J. Hoover, *J. Chem. Phys.*, **56**, 2194 (1973).
22) S. Yamauchi and T. Azumi, *J. Chem. Phys.*, **68**, 4138 (1978).
23) W. L. F. Armerego, C. B. Barlin, and E. Spinner, *Spectrochim. Acta*, **22**, 17 (1966).
24) R. W. Mitchell, R. W. Glass, and J. A. Merritt, *J. Mol. Spectrosc.*, **36**, 310 (1970).
25) G. Peyronel, A. Pignedoli, and W. Malavosi, *Spectrochim. Acta, Part A*, **32**, 1015 (1976).
26) H. H. Perkampus, *Z. Naturforsch., A*, **17**, 614 (1962).
27) A. C. Albrecht, *J. Chem. Phys.*, **38**, 354 (1963).
28) D. M. Hanson, *J. Chem. Phys.*, **51**, 5063 (1969).

ESR Studies on the Free Radical Intermediates in the Photoreduction of Duroquinone in Alcohol Solutions

Shoji NODA,* Kiyoshi SANEHIRA, Takahisa DOBA, and Hiroshi YOSHIDA
Faculty of Engineering, Hokkaido University, Kita-ku, Sapporo 060

(Received September 9, 1981)

ESR measurements during photolysis of duroquinone (DQ) solutions in ethanol and 2-propanol have revealed the generation of both durosemiquinone anion (DQ^-) and durosemiquinone radicals (DQH·). Correspondingly, alkoxyl radicals have been detected from the photolyzed solutions by the spin trapping-ESR technique, though the quantum yield of their formation is very low (10^{-3} for the ethanol solution). Main conclusions deduced from the present work are (1) that DQ^- is generated through the one-electron reduction of DQ by α-hydroxyalkyl radical and through the photodissociation of ($DQ-DQH_2$) complex, and (2) that DQH· is generated through the hydrogen abstraction of $^3DQ^*$ either from solvent alcohols or from photoproduct durohydroquinone (DQH_2). The one-electron reduction in alcohol solution previously reported for *p*-benzoquinone is a minor pathway of chemical quenching of $^3DQ^*$. The quantum yield of the DQH_2 formation in an early period of photolysis of a dilute DQ in methanol, ethanol, and 2-propanol has been observed to be 0.12, 0.23, and 0.36 respectively. These values are discussed in terms of the mechanism of the quinone photoreduction.

Despite extensive studies[1-9] on the photochemistry of duroquinone (DQ) in alcohol solutions, there still remains a controvery about the initial photochemical reaction, the chemical quenching of triplet excited duroquinone ($^3DQ^*$). This reaction can be explained either as a hydrogen abstraction (reaction (1))[1-8] giving a durosemiquinone radical (DQH·), or as a one-electron transfer (reaction (2))[9] giving a durosemiquinone anion (DQ^-):

$$^3DQ^* + RR'CHOH \longrightarrow DQH\cdot + RR'\dot{C}OH, \quad (1)$$

$$^3DQ^* + RR'CHOH \longrightarrow DQ^- + RR'CH\dot{O} + H^+. \quad (2)$$

DQ^- should also be generated through the reduction of DQ by α-hydroxyalkyl radical:[10]

$$DQ + RR'\dot{C}OH \longrightarrow DQ^- + RR'C{=}O + H^+. \quad (3)$$

The formation of DQ^- is thus expected by either mechanism of the chemical quenching. However, no definite detection of DQ^- by electron spin resonance (ESR) technique has been reported for the photolysis of DQ in alcohol solutions. The ESR detection of DQH· has been reported by several research groups,[11-13] but an efficient chemical quenching of $^3DQ^*$ by durohydroquinone (DQH_2), a main photoproduct,

$$^3DQ^* + DQH_2 \longrightarrow 2\,DQH\cdot \quad (4)$$

may be a dominant source of the detected DQH·. The ESR observations do not seem to have been well explained in the mechanism of photoreduction of DQ in alcohols.

We have demonstrated in the previous ESR study during the photolysis of *p*-benzoquinone in ethanol that the yields of semiquinone radical and semiquinone anion depend on the flow rate of the solution and *p*-benzoquinone concentration.[14] We have also detected ethoxyl and 1-hydroxyethyl radicals by the spin trapping-ESR technique.[14] In contrast, no α-hydroxyalkyl radical has been detected by this technique from the photoreduction of DQ in several alcohols.[15] The spin trapping-ESR detection of α-hydroxyalkyl radicals will depend on the efficiency of the reduction of quinones with the radicals, such as reaction (3).

In order to give further insight into the generation and behavior of semiquinone intermediates, the steady-state ESR measurements during photolysis combined with the spin trapping-ESR measurements are extended in the present investigation to DQ in ethanol and 2-propanol.

Experimental

Chemicals. DQ and DQH_2 from Tokyo Chemical Industry Co. were purified by repeated sublimation. Methanol, ethanol, and 2-propanol of 99.5% purity from Wako Pure Chemical Ind. were used without further purification. Occasionally the effects of purifying the alcohols were examined, but no significant difference was observed in the results. α-Phenyl-*N*-butylnitrone (PBN) was synthesized as described previously[14] and was used as a spin trap.

ESR Measurements during Photolysis. The transient semiquinone intermediates were observed by ESR measurements with a Varian E-109 spectrometer during continuous photolysis of the DQ solution in ethanol or 2-propanol flowing through a quartz flat cell in the resonant cavity, as described in detail elsewhere.[16] The photolysis was carried out with light from a supper-high pressure mercury lamp (Philips, SP-500) or from a mercury-xenon lamp (Conrad-Hanovia 941B0010). Occasionally degassed solutions in a quartz ESR tube were photolyzed in the resonant cavity.

Spin Trapping-ESR Measurements. The DQ solutions in ethanol or 2-propanol containing a small amount of PBN were degassed, sealed in a rectangular quartz optical cell (optical path of 1.0 cm) connected with a Pyrex tube (0.2 cm i.d.) for ESR measurements, and photolyzed with light of 436 nm from a high pressure mercury lamp (Toshiba, SHL-100UV) through filters (Toshiba VY-42 and VV-42).

Optical Absorption Measurements. The decay of DQ and the formation of DQH_2 were followed by observing their absorption spectra with a recording spectrophotometer (Shimadzu, MPS-5000) before and after an intermittent photolysis of the DQ solutions in methanol, ethanol, and 2-propanol sealed in a rectangular quartz optical cell (optical path of 1.0 cm) under a pressure of 10^{-3} Pa. The photolysis was carried out with the light of a sharp resonance line at 254 nm from a low pressure mercury lamp (Toshiba, GL-15) through a glass filter (Toshiba, UVD33S) and an aqueous solution of $NiSO_4 \cdot H_2O$ (500 g dm^{-3}) of 1 cm path length. The intensity of the incident light was calibrated by actinometry with potassium trioxalatoferrate(III).

Results

ESR Detection of Semiquinone Intermediates. ESR spectra observed during photolysis show only semiquinone intermediate(s) as shown in Figs. 1A and B. Dilute DQ solutions ($\leq 10^{-4}$ mol dm^{-3}) in ethanol and 2-propanol flowing in the cell gave only the spectrum of $DQ^{\cdot}$ with thirteen hyperfine lines equally separated with a splitting constant of 0.19 mT (Fig. 1A). Its intensity increased with increasing resident time of the solutions in the resonant cavity up to 1s (with decreasing flow rate of the solutions). This increase is probably due to the accumulation of $DQ^{\cdot}$ during the photolysis of the solution within the effective volume of the cell, and give a rough estimate of the lifetime of $DQ^{\cdot}$ of 1s. The estimated value is of the same order of magnitude as that expected by combining an observed steady-state concentration ($\approx 5\times 10^{-8}$ mol dm^{-3}) and a reported second order rate constant for bimolecular decay of $DQ^{\cdot}$, 3.5×10^{6} mol^{-1} dm^{3} s^{-1}.[2] When the DQ concentration is high, a weak spectrum due to DQH· ($7\times 7\times 2$ line spectrum with hyperfine splittings of 0.48, 0.07, and 0.03 mT)[17] was superimposed on the intense spectrum of $DQ^{\cdot}$. Both spectra decreased in intensity with increase of the resident time.

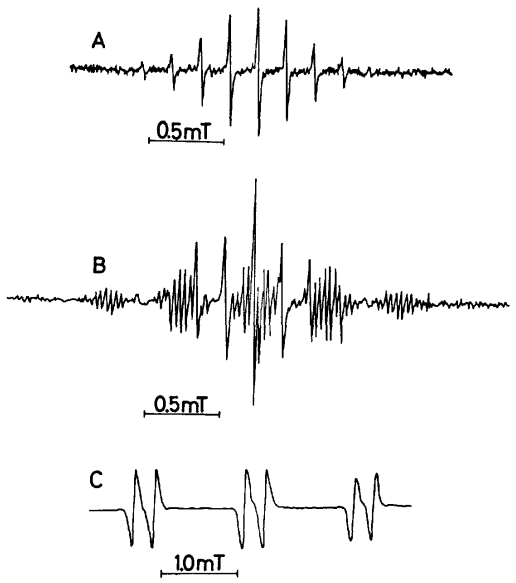

Fig. 1. A: ESR spectrum of a continuously photoirradiated flowing solution of DQ in ethanol. [DQ]$=5\times 10^{-5}$ mol dm^{-3} and resident time was one second. B: ESR spectrum of a continuously photoirradiated sealed solution of DQ in ethanol. [DQ]$=50$ mmol dm^{-3}. C: ESR spectrum of spin-adduct radical. [DQ]$=1$ mmol dm^{-3}, [PBN]$=0.1$ mol dm^{-3}.

The concentration ratio of DQH·to $DQ^{\cdot}$ depends on the flow rate of the solutions and the DQ concentration. This varying ratio indicates neither that the acid-base equilibrium between DQH· and $DQ^{\cdot}$ is reached rapidly compared with their lifetime nor that the ratio is determined by the branching ratio of the chemicalquenching pro cesses, (1) and (2). There will

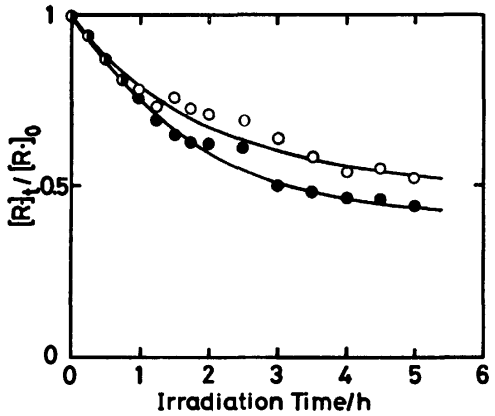

Fig. 2. The variation of $DQ^{\cdot}$ and DQH· yields with irradiation time.
$[DQ]_0=20$ mmol dm^{-3}, ○: $DQ^{\cdot}$, ●: DQH·.

exist reaction pathway(s) of generating semiquinone intermediates other than reactions (2) and (3).

When the solution of high DQ concentration (50 mmol dm^{-3}) sealed in a quartz sample tube was continuously photolyzed, DQH· was observed with comparatively intense spectral intensity, as shown in Fig. 1B. The ratio of steady-state concentration of DQH· to that of $DQ^{\cdot}$ was initially about 2. As the photolysis was prolonged, both the DQH· and the $DQ^{\cdot}$ gradually decrease in their spectral intensity, and the concentration ratio also decreased as shown in Fig. 2. The former observation is due to the decrease in the DQ concentration. The quenching of ^{3}DQ* by diduroquinone, one of photoproducts in the solution of a high DQ concentration, may also contribute to it.[4,5] The latter observation is not compatible with the rapid acid-base equilibrium. It is interpreted by the quenching of ^{3}DQ* by DQH_2, which competes with the quenching by solvent alcohols, and by the more efficient ionic dissociation of directly photoexcited CT complex (DQ–DQH_2) in the later period of photolysis.

The influence of DQH_2 was examined by photolyzing a flowing 2-propanol solution of a fixed DQ concentration with DQH_2 added to it with various concentrations. The $DQ^{\cdot}$ formation was enhanced in the presence of

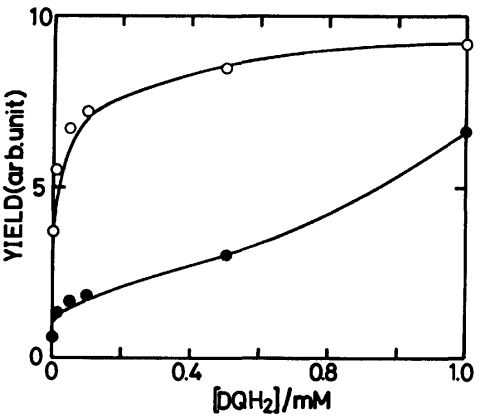

Fig. 3. Effects of DQH_2 on the yields of $DQ^{\cdot}$ and DQH· in ethanol solution of DQ.
[DQ]$=1$ mmol dm^{-3}, ○: $DQ^{\cdot}$, ●: DQH·.

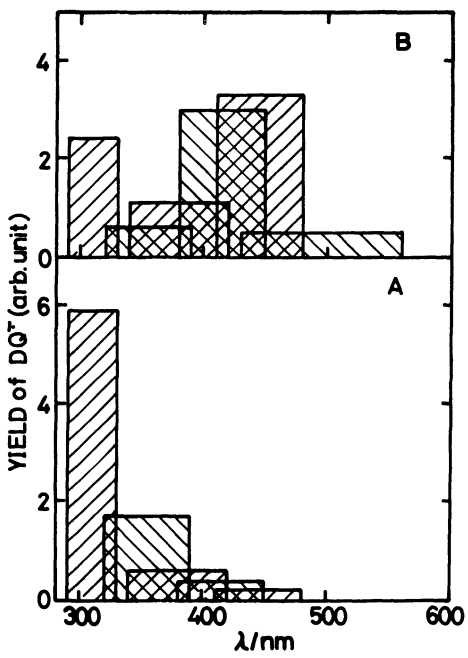

Fig. 4. Wavelength dependence of $DQ^{\cdot}$ yield in a flowing solutions (A) of 1 mmol dm^{-3} DQ and (B) of 1 mmol dm^{-3} DQ+1 mmol dm^{-3} DQH_2.

DQH_2 at low concentration, whereas the DQH· yield increased steadily with DQH_2 concentration throughout its concentration range studied, as shown in Fig. 3. DQH· is generated by the quenching of $^3DQ^*$ by DQH_2 in its presence.

In order to see the origin of $DQ^{\cdot}$, its yield was examined for the solutions of 1 mmol dm^{-3} DQ with and without 1 mmol dm^{-3} DQH_2 in ethanol and in 2-propanol by photolyzing the light successively cut off with a long-wave pass filter whose 50% transmission wavelength was 310, 350, 390, 420, 450, 480, or 580 nm. The dependence of the yield on the wavelength without DQH_2 agreed qualitatively with the absorption spectrum of DQ, but the dependence of the yield with DQH_2 showed an additional peak of the action spectrum at 400—450 nm, as shown in Fig. 4, for the ethanol solutions. Correspondingly, the ethanol solution of equimolar DQ and DQH_2 showed a weak, broad absorption band extending from 380 to 600 nm with λ_{max} of 410 nm, which is attributed to a (DQ–DQH_2) complex. $DQ^{\cdot}$ is generated by the direct excitation of DQ followed by the reactions (1) and (3) or the reaction (2), or by the photodissociation of the complex into ions,

$$(DQ\text{–}DQH_2) \xrightarrow{h\nu} DQ^{\cdot} + DQH_2^{+} \qquad (5)$$

depending on the wavelength of light and on the concentration of the coexisting DQH_2. The solutions containing 50 mmol dm^{-3} DQ and 50 mmol dm^{-3} DQH_2 gave no $DQ^{\cdot}$ spectrum at all for any wavelength of light between 254 and 600 nm. This will be discussed later.

Spin Trapping of Free Radicals from Alcohols. Although α-hydroxyalkyl radicals have been detected together with benzophenone ketyl radicals from the photoreduction of benzophenone in alcohols by ESR,[16] no ESR spectrum of free radicals generated from solvent alcohols has been observed from the photoreduction of quinones in alcohol solutions. This may be due to the efficient oxidation of α-hydroxyalkyl radicals by quinones (such as reaction (3)). Alkoxyl radicals, if generated, will be rapidly transformed into the α-hydroxyalkyl radicals by the hydrogen abstraction reactions. The alkoxyl radicals, if any, will be difficult to detect, because their spectra are broadened with their short T_1.[18] The spin trapping-ESR technique is useful to detect the transient free radicals generated from alcohols. The technique was first utilized successfully for the photoreduction of quinones in alcohols by McLauchlan and Sealy.[15] The present authors have studied in detail by the same technique the free radicals from solvent ethanol for the photoreduction of *p*-benzoquinone, and observed the formation of both α-hydroxyethyl and ethoxyl radicals.[14] The study has been extended here to the photoreduction of DQ in ethanol and in 2-propanol. PBN has been used as a spin trap, because it reacts efficiently with both α-hydroxyalkyl and alkoxyl radicals.[14]

In the photoreduction of DQ, the observed ESR spectrum is exclusively due to the spin adduct of ethoxyl or isopropoxyl radical, as reported previously.[15] Figure 1C shows the spectrum of the ethoxyl radical adduct with hyperfine constants of 1.46 mT for a nitrogen nucleus and 0.26 mT for a proton, which is the same as that reported previously.[14,15,19] The quantum yield of the spin adduct was determined to be 10^{-3} or less for the ethanol solution, by examining the intensity of the ESR spectrum as a function of the PBN concentration. These quantum yields are much lower than the quantum yield for the conversion of DQ into DQH_2 described later. The quantum yield was still lower for the 2-propanol solution. The dependence of the spin adduct yield on the wavelength was examined by cutting off the photolyzing light in the same way as for the $DQ^{\cdot}$ yield, and it was found to agree qualitatively with the absorption spectrum of DQ. The above observations lead to the conclusion that the alkoxyl radicals are generated by the reaction of photoexcited duroquinone, $^3DQ^*$, with solvent alcohols, *i.e.*, *via* reaction (2), though it is a minor pathway for the chemical quenching of $^3DQ^*$.

Yield of DQH_2. In order to compare with the kinetic behavior of the transient intermediates, the conversion of DQ into a major final product DQH_2 was examined by photolyzing dilute solutions of DQ in methanol, ethanol, and 2-propanol with light of 254 nm. The decay of DQ and the formation of DQH_2 were monitored with the intensity of their optical absorption using the reported molar absorptivities.[5] Isosbestic points observed at 233, 279, and 320 nm for the spectral curves during the photolysis indicate that the simple conversion of DQ into DQH_2 is the major consequence of the photolysis. The conversion proceeded linearly with the number of absorbed photons in the very early period of the photolysis, and then the conversion rate gradually decreased as demonstrated previously by Nafisi-Movaghar and Wilkinson for DQ in 2-propanol.[5] The initial quantum yield of the DQH_2 formation was

determined from the conversion curves to be 0.12, 0.23, and 0.36 for the methanol, ethanol, and 2-propanol solutions of 8×10^{-5} mol dm^{-3} DQ. This quantum yield determination will be discussed further in the following section.

Discussion

The present investigation was motivated by the following two questions: what is the role of semiquinone anions which we detected by ESR from the photoreduction of quinones in alcohols, and why have the semiquinone anions (especially $DQ^{\cdot}$) been unobserved in most of the previous photolysis-ESR studies?

The present results clearly show that $DQ^{\cdot}$ is generated in alcohol solutions either directly from the photoexcited DQ through its chemical quenching with solvent alcohols (reaction (2)) or indirectly from α-hydroxyalkyl radicals through a one-electron transfer (reaction (3)). The former is, however, a minor pathway for the $DQ^{\cdot}$ formation, because the quantum yield of alkoxyl radicals, the counterproduct of the reaction (2), is much lower than the quantum yield for the disappearance of DQ. Therefore, the $DQ^{\cdot}$ formation observed significantly in the present ESR study is attributed to the latter reaction pathway. Scheer and Grätzel[9] have reported that in a more polar solvent, *i.e.*, water–ethanol mixed solvent, the chemical quenching of $^3DQ^*$ leads almost exclusively to the formation of $DQ^{\cdot}$, as the solvation of ions favors the ionic dissociation of encounter exciplexes.

In aqueous solution, the acid-base equilibrium

$$DHQ\cdot \rightleftharpoons DQ^{\cdot} + H^+ \qquad (6)$$

is reached very quickly. The $DQ^{\cdot}$ observed in the flash photolysis-optical absorption study has been attributed to the dissociation of DQH·.[2] However, the forward reaction (6) is not significant in alcohols as a reaction pathway for the $DQ^{\cdot}$ formation. From the acid-base equilibrium of phenol and its analogues in water and in methanol, the relationship of pK_a (methanol)$=pK_a$ (water)$+4.4$ has been found experimentally and rationalized theoretically.[20] Provided that this relationship holds for DQH·, the pK_a of DQH· in methanol is estimated to be 9.4 from the reported pK_a of 5 in water.[21,22] The pK_a value will be somewhat larger in ethanol and in 2-propanol. Provided further that the reverse reaction (6) is diffusion-controled ($k_{-6}=10^{10}$ mol^{-1} dm^3 s^{-1}), 4×10^{-10} mol dm^{-3} of K_a leads to the rate of the forward reaction, k_6, being as low as 4 s^{-1}. The dissociation of DQH· is too slow to account for the present ESR observation of $DQ^{\cdot}$ in the alcohol solutions. The delayed formation of $DQ^{\cdot}$ in ethanol observed in the previous flash photolysis study cannot be due to the reaction (6) but due to the reaction (3), as pointed out by Amoyal and Bensasson.[8]

An additional path opens for the $DQ^{\cdot}$ formation, when DQH_2 either accumulates in the photolyzed DQ solution or is intentionally added and the absorption band of the (DQ–DQH_2) complex is excited. As the pK_a of DQH_2 in water is 11.3,[23] the pK_a in methanol will be 15.7. This gives rough estimates of pH, 9.3 and 8.4 for 1 and 50 mmol dm^{-3} DQH_2 present in the

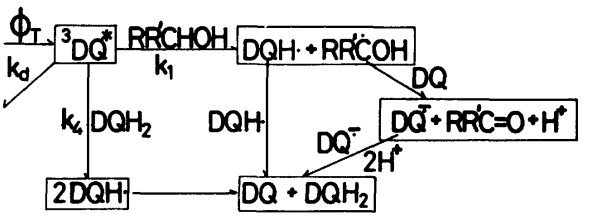

Fig. 5. A photoreduction scheme of DQ in alcohol.

alcohol solution. Comparison of these values with the pK_a of DQH·, the equilibrium (6) favors very much to the left at the higher concentration of DQH_2, so that $DQ^{\cdot}$ will be readily transformed into DQH·. This is consistent, though qualitatively, with the ESR observation during the photolysis of ethanol solutions of DQ and DQH_2 sealed in ESR sample tubes.

The reaction mechanism of major significance for the formation of the final product, DQH_2, has been proposed as shown in Fig. 5 based on the flash photolysis and product analysis results.[5] The quenching of $^3DQ^*$ by DQH_2 results in the DQH· formation but gives effectively no net chemical change. The steady-state treatment gives the following relationship:

$$\frac{I_T}{[DQH_2]} = \frac{k_4[DQH_2]}{2k_1\phi_T[RR'CHOH]} + \frac{k_d+k_1[RR'CHOH]}{k_1\phi_T[RR'CHOH]}, \qquad (7)$$

where I_T is the number of photons absorbed in the unit volume of the solution, ϕ_T is the quantum yield of $^3DQ^*$ generation, and k_d is the rate constant of deexcitation of $^3DQ^*$ to the ground state.[5] Actually, the present results of the DQH_2 formation follow the expected linear relationship between $I_T/[DQH_2]$ and $[DQH_2]$, as shown in Fig. 6. The quantum yield of the DQH_2 formation in the absence of DQH_2 is determined, from the inverse of the intercept, to be 0.12, 0.23, and 0.36 in methanol, ethanol, and 2-propanol, respectively. The result for

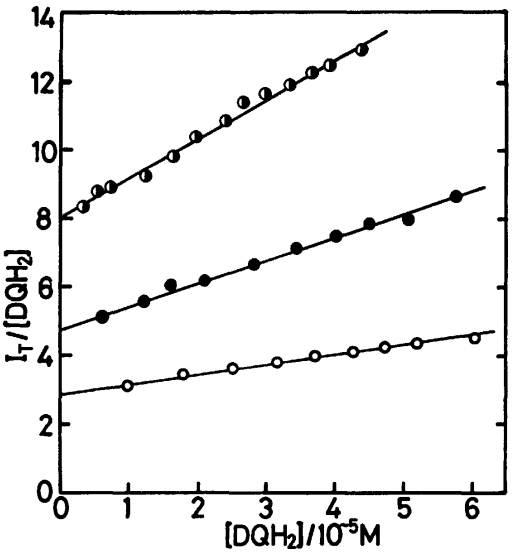

Fig. 6. A kinetic plots of DQH_2 formation (see text in detail).
○: 2-Propanol, ●: ethanol, ◑: methanol.

the 2-propanol solution agrees with the previous result obtained in the same way.[5] Combining these values with the pseudo-first order decay rate of $^3DQ^*$, $k_d+k_1[RR'CHOH]$, determined by the laser-flash photolysis experiment, 6.6×10^4 s^{-1} in ethanol[8] and 1×10^5 s^{-1} in 2-propanol,[3] k_d and k_1 can be determined separately, as $\phi_T=1.0$.[5,6,8] The results are $k_d=5.2\times10^4$ and 6×10^4 s^{-1}, and $k_1=8.1\times10^2$ and 3×10^3 mol^{-1} dm^3 s^{-1} for ethanol and 2-propanol. The chemical quenching of $^3DQ^*$ is three times as efficient in 2-propanol as in ethanol, whereas the physical quenching is independent of the alcohols.

According to the reaction scheme, $DQ^{\cdot}$ and DQH· should be generated with an identical yield during the photoreduction of DQ into DQH_2 in alcohols, if the efficient chemical quenching of $^3DQ^*$ by DQH_2 is not predominant. Actually, $DQ^{\cdot}$ could be detected by the present steady-state ESR measurements, when photolyzed solutions were refreshed by flowing. The comparatively weak ESR spectrum due to DQH· (or its absence) is attributed to the lifetime of DQH· much shorter than that of $DQ^{\cdot}$: The steady-state concentration of DQH· in the fresh DQ solutions is too low for its ESR detection. The rate constant for the disproportionation of DQH· has been reported to be 3.7×10^8 mol^{-1} dm^3 s^{-1} which is larger by two order of magnitude than that of $DQ^{\cdot}$.[2] The previous ESR studies of DQ in alcohols have shown the spectrum to be due exclusively to DQH·. The $DQ^{\cdot}$ spectrum has not been observed even in the absence of a hydrogen donor. This seems to have been caused by the inevitable contamination with DQH_2 of the solution photolyzed for a long time. A small amount of oxygen in a solution resulting from an insufficient degassing should reduce the $DQ^{\cdot}$ yield because of an efficient electron transfer from $DQ^{\cdot}$ to O_2.[21] The ESR observations on DQH· cannot necessarily be a proof for the hydrogen abstraction of $^3DQ^*$ from alcohols (reaction (1)) before excluding a possible occurrence of reaction (4).

In conclusion, the present investigation has shown the correct location of the semiquinone intermediates observed by ESR in the reaction scheme of the DQ photoreduction in alcohol solutions. In addition, the present ESR study has indicated three reaction pathways for the $DQ^{\cdot}$ formation: The photoinduced one-electron transfer from alcohol to DQ, though the quantum yield for it is very small, the one-electron transfer from α-hydroxyalkyl radical to DQ, and the ionic dissociation of a photoexcited CT-complex (DQ–DQH_2), which becomes important at high DQH_2 concentrations with irradiation by an incandescent light.

References

1) N. K. Bridge and G. Porter, *Proc. R. Soc. London, Ser. A*, **244**, 259 (1958).
2) N. K. Bridge and G. Porter, *Proc. R. Soc. London, Ser. A*, **244**, 276 (1958).
3) F. Wilkinson, G. M. Seddon, and K. Tickle, *Ber. Bunsenges. Phys. Chem.*, **72**, 315 (1968).
4) H. Hermann and G. O. Schenck, *Photochem. Photobiol.*, **8**, 255 (1968).
5) J. Nafisi-Movaghar and F. Wilkinson, *Trans. Faraday Soc.*, **66**, 2257 (1970).
6) J. Nafisi-Movaghar and F. Wilkinson, *Trans. Faraday Soc.*, **66**, 2268 (1970).
7) D. R. Kemp and G. Porter, *Proc. R. Soc. London, Ser. A*, **326**, 117 (1971).
8) E. A. Amouyal and R. Bensasson, *Trans. Faraday Soc.*, **72**, 1274 (1976).
9) R. Scheere and M. Grätzel, *J. Am. Chem. Soc.*, **99**, 865 (1977).
10) R. L. Willson, *Trans. Faraday Soc.*, **67**, 3020 (1971).
11) A. J. Elliot and J. K. S. Wan, *J. Phys. Chem.*, **82**, 444 (1978).
12) A. D. Trifunac and J. R. Norris, *Chem. Phys. Lett.*, **59**, 140 (1978).
13) Y. Kambara and H. Yoshida, *Bull. Chem. Soc. Jpn.*, **50**, 1367 (1978).
14) S. Noda, T. Doba, T. Mizuta, M. Miura, and H. Yoshida, *J. Chem. Soc., Perkin Trans. 2*, **1980**, 61.
15) K. A. McLauchlan and R. C. Sealy, *J. Chem. Soc., Chem. Commun.*, **1976**, 115.
16) H. Yoshida and T. Warashina, *Bull. Chem. Soc. Jpn.*, **44**, 2950 (1971).
17) T. Warashina, O. Edlund, and H. Yoshida, *Bull. Chem. Soc. Jpn.*, **48**, 636 (1975).
18) B. Brocklehurst, *J. Chem. Soc., Faraday Trans. 2*, **75**, 123 (1979).
19) A. Ledwith, P. J. Russel, and L. H. Sutcliffe, *Proc. R. Soc. London, Ser. A*, **332**, 151 (1973).
20) C. H. Rochester and B. Rossal, *J. Chem. Soc., B*, **1967**, 986.
21) K. B. Patel and R. L. Willson, *J. Chem. Soc., Faraday Trans. 1*, **1973**, 814.
22) R. L. Willson, *J. Chem. Soc., Chem. Commun.*, **1971**, 1249.
23) G. Kortüm, W. Vogel, and K. Andrussow, "Dissociation Constants of Organic Acids in Aqueous Solutions," Butterworth, London (1961).

Liquid Crystal Formation in Binary Systems. V.[1] Liquid Crystals Induced in *N*-[4-(Dimethylamino)benzylidene]-4-ethoxyaniline-*N*-(4-Nitrobenzylidene)-4-nitroaniline and Related Mixtures

Kotaro Araya and Yoshio Matsunaga*
Department of Chemistry, Faculty of Science, Hokkaido University, Sapporo 060
(Received September 10, 1981)

The induction of liquid crystals was demonstrated with binary mixtures comprising *N*-(4-nitrobenzylidene)-4-nitroaniline and *N*-[4-(dimethylamino)benzylidene]-4-alkoxyaniline or *N*-(4-alkoxybenzylidene)-4-(dimethylamino)aniline. Both nematic and smectic phases were observed with the ethoxy derivatives, but only a smectic A phase with the propoxy derivatives. The mesophases appear in the region centered around 30 mol% of the dinitro compound. Similarly, liquid crystals could be induced in several mixtures of *N*-[4-(dialkylamino)benzylidene]-4-(dialkylamino)aniline with *N*-(4-nitrobenzylidene)-4-alkoxyaniline or *N*-(4-alkoxybenzylidene)-4-nitroaniline. The bis(dialkylamino) and dinitro derivatives of azoxybenzene were also shown to be efficient as one of the component compounds in producing binary liquid crystals.

As we reported earlier, nematic and smectic liquid crystals can be induced by mixing a nonmesogenic electron donor and a nonmesogenic electron acceptor of the type 4-X-C_6H_4-Z-C_6H_4-Y-4.[2,3] Donor molecules having a dimethylamino group on one end and acceptor molecules having a nitro group on one end were employed in those works. The donor and acceptor molecules each had a short alkoxyl group of the same kind on the other end. The central double bond linkages were chosen from -CH=CH-, -CH=N-, and -N=N- groups. Although the component compounds themselves form no mesophase, they may be considered potentially mesogenic, because the molecules are elongated and lath-liked in shape. The induction or the enhancement of the thermal stability of liquid crystals in the above-mentioned mixtures is maximized when the mole ratio is near 1 : 1. The orientational cohesive force arising from the interaction of the electron donor-acceptor type may be responsible for the ordered arrangement of the molecules in liquid crystals. In ordinary crystals, this sort of intermolecular interaction is known to result in the parallel alignment of the planar component molecules.

As the molecules of *N*-benzylideneanilines are generally nonplanar, the intermolecular interaction in the induced liquid crystals may be more or less localized between the benzene ring with a dimethylamino group in the donor molecule and that with a nitro group in the acceptor molecule. If so, each benzene ring in the dinitro derivative may be able to interact with a molecule of the dimethylamino derivative. Similarly, a molecule of the bis(dimethylamino) derivative may associate with two molecules of the mononitro derivative. In this paper, we wish to report that liquid crystalline phases are really induced with such combinations.

Experimental

Materials. The *N*-benzylideneanilines were prepared

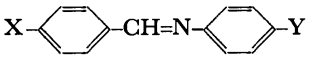

by a condensation reaction between a *p*-Y derivative of benzaldehyde and a *p*-X derivative of aniline, and were purified by repeated recrystallizations from a suitable solvent. Hereafter, they are represented by the terminal groups in parentheses, (X, Y). 4,4'-Dinitroazoxybenzene (DNAO)

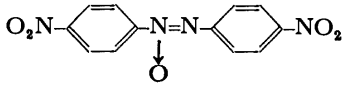

was obtained by the oxidation of *p*-nitroaniline with ammonium peroxodisulfate, as described by Witt and Kopetschni.[4] The crude product was treated with fuming nitric acid and then recrystallized from benzene.[5] 4,4'-Bis-(dimethylamino)azoxybenzene (BDMAAO) was synthesized by the catalytic reduction of *p*-nitroso-*N*,*N*'-dimethylaniline with hydrazine hydrate, following the method reported by Busch and Schulz.[6] 4,4'-Bis(diethylamino)azoxybenzene (BDEAAO) was analogously prepared. The procedure of preparing binary mixtures was given in our previous paper.[2]

Measurements. The calorimetric and spectroscopic measurements were carried out as described in Part II of this series.[2]

Results and Discussion

N-(4-Nitrobenzylidene)-4-nitroaniline (NO_2, NO_2) as an Electron Acceptor. The following four donor Schiff bases were found to form liquid crystals when mixed with this acceptor: (NMe_2, EtO), (EtO, NMe_2), (NMe_2, PrO), and (PrO, NMe_2). As the acceptor has a melting point of 200 °C, which is higher by 53 to 85 °C than those of the donors, and the observation of liquid crystals is limited to the composition range from 15 to 40 mol% of (NO_2, NO_2), we studied the phase diagrams only up to 50 mol%.

In the (NMe_2, EtO)-(NO_2, NO_2) system, the nematic and smectic liquid crystals appear from the supercooled isotropic melt (see Fig. 1a). The former phase exists as a single phase only below 20 mol%. When the temperature drops, two transitions associated with liquid crystals were detected at the composition of 25 mol%. The first transition is found at 127 °C and is ascribed to the appearance of a metastable smectic phase accompanied by the isotropic melt; the second one, at 120 °C, is ascribed to the transformation into a metastable nematic phase in equilibrium with the smectic phase. The latter temperature is that of the intersection between the isotropic liquid-smectic liquid crystal (I-S) transition curve and the isotropic liquid-

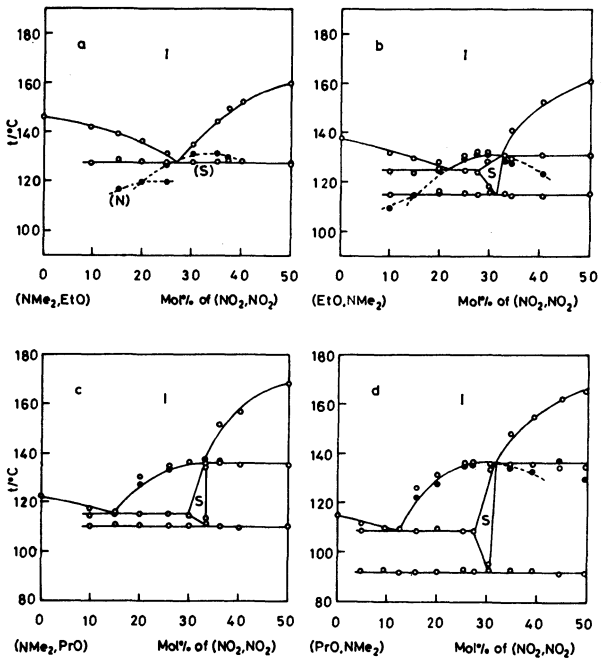

Fig. 1. Phase diagrams of the systems of (NO_2, NO_2) with (a) (NMe_2, EtO), (b) (EtO, NMe_2), (c) (NMe_2. PrO), and (d) (PrO, NMe_2). The open and shaded circles are transitions observed in the processes of heating and cooling respectively.

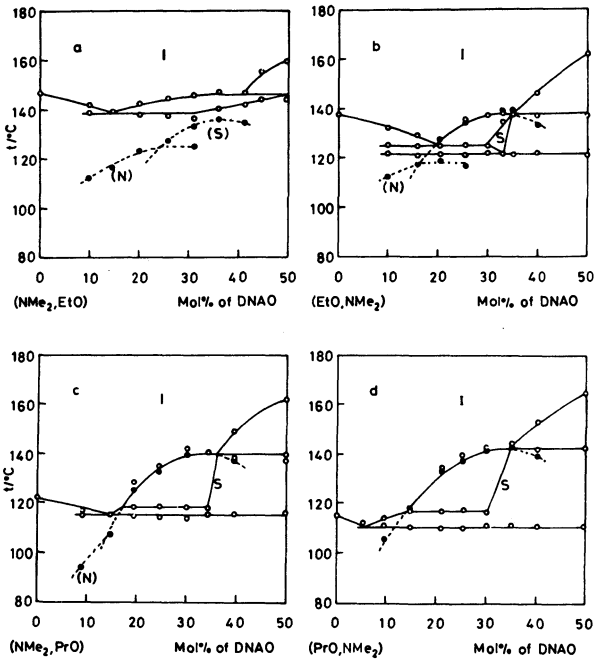

Fig. 2. Phase diagrams of the systems of DNAO with (a) (NMe_2, EtO), (b) (EtO, NMe_2), (c) (NMe_2, PrO), and (d) (PrO, NMe_2). As to the open and shaded circles, see the caption of Fig. 1.

nematic liquid crystal (I-N) transition curve. The maximum of the I-S transition occurs at 131.5 °C and 33 mol%.

The phase diagram of the (EtO, NMe_2)–(NO_2, NO_2) system shown in Fig. 1b is more complicated than that described above. Enhancement of the smectic phase is so pronounced that the I-S transition curve encounters the freezing point curve of the donor compound at 125 °C and 22 mol% and also another freezing point curve at 131 °C and 32.5 mol% of (NO_2, NO_2). The horizontal line at 125 °C terminates at 27.5 mol%, indicating that the isotropic melt and a smectic liquid crystal are in equilibrium with each other in the temperature range specified by the I-S transition curve and this line. This smectic phase is stable above 115 °C with the coexisting solid. The region of existence of this mesophase as a single phase is represented by a triangle in the diagram and lies in the composition range between 27.5 and 32.5 mol%. The intersection between the I-S and I-N transition curves is at 115 °C and 14.7 mol%. Below this composition, the metastable nematic liquid crystal may be observed without any coexisting phase.

Figure 1c presents the diagram of the (NMe_2, PrO)–(NO_2, NO_2) system. The area bounded by the following points represents the condition for the stable existence of the induced liquid crystal as a single phase: 115 °C and 30 mol%, 136 °C and 33.3 mol%, and 110 °C and 33.3 mol% of (NO_2, NO_2). The mesophase appearing at 33 mol% was identified as a smectic A phase by the miscibility test with *N*-(4-phenylbenzylidene)-4-(ethoxycarbonyl)aniline, which exhibits a smectic A phase stable between 121.6 and 131 °C.[7]

The diagram of the (PrO, NMe_2)–(NO_2, NO_2) system shown in Fig. 1d is also of the same type. The corners of the region for a stable smectic phase existing without any other phase are located at 108.5 °C and 27.5 mol%, 136.5 °C and 31.8 mol%, and 92 °C and 30.5 mol% of (NO_2, NO_2).

4,4'-Dinitroazoxybenzene (DNAO) as an Electron Acceptor. This compound has a melting point of 192 °C. All the four donors employed for the systems shown in Fig. 1 can produce mesophases by mixing with DNAO. Their phase diagrams are given in Fig. 2. Again, the induction of the smectic liquid crystal in the combination with (NMe_2, EtO) is not sufficient to make the phase enantiotropic (see Fig. 2a). The maximum temperature of the induced smectic phase is 136 °C. The I-S and I-N transition curves meet each other at 125 °C and 24 mol%. The presence of a horizontal line extending from this intersection to 31 mol% is indicative of the coexistence of the smectic phase and the isotropic melt above this line and that of the smectic phase and the nematic phase below this line.

The diagram for the (EtO, NMe_2)–DNAO system bears some similarity to that for the (EtO, NMe_2)–(NO_2, NO_2) system (compare Figs. 1b and 2b). The I-S transition curve intersects the freezing point curve of the donor compound at 125 °C and 20 mol% of DNAO and the other freezing point curve at 138 °C and 35 mol%. The triangle for the stable single smectic phase is specified by the latter intersection and the following two: 125 °C and 30 mol% and 121.5 °C and 32 mol%. The intersection between the I-S and I-N transition curves occurs at 118 °C and 16 mol%.

The (NMe_2, PrO)–DNAO and (PrO, NMe_2)–DNAO systems yield diagrams greatly different from the preceding cases. The S-I transition curve encounters

Table 1. The maximum temperature of the smectic liquid crystal-isotropic liquid transition/°C

Acceptor	Donor			
	(NMe_2, EtO)	(EtO, NMe_2)	(NMe_2, PrO)	(PrO, NMe_2)
(NO_2, NO_2)	131.5	131	136	136.5
DNAO	136	139	140	143

the freezing point curve twice on the acceptor-rich side. The points of intersection are found at 118 °C and 17 mol% and at 140 °C and 36 mol% in the former system. As is evident from the presence of a horizontal line at 118 °C, the induced smectic phase and the isotropic melt are involved in the composition range from 17 to 34 mol%.

Similarly, the diagram of the (PrO, NMe_2)–DNAO system has two intersections between the S-I transition curve and the freezing point curve. They are located at 117 °C and 15 mol% and at 143 °C and 35 mol%. At the latter composition, the solid is wholly transformed into the mesophase at 110.5 °C and then into the isotropic melt at 143 °C. The horizontal line separating the solid and the smectic liquid crystal, both of which coexist with the isotropic melt, appears at 117 °C and below 30 mol%.

The maximum temperatures of the S-I transition in the eight systems described above are summarized in Table 1. For a given electron donor, DNAO gives consistently higher transition temperatures, but only by several degrees, than (NO_2, NO_2) does. It is not clear whether the differences are attributable to the effect of the central double bond linkage on the induction of mesophase or on the latent transition temperature of the acceptor compound. Nevertheless, it may be added that the same sequence has been found for the N-I transition temperatures.[8] As to the donor compounds, the smectic phases induced by the propoxy derivatives are more thermally stabilized than those induced by the ethoxy derivatives. This effect of terminal substituents is in agreement with our observation made in an earlier work.[2]

The donor and acceptor compounds employed in the present work are yellow, while their combinations are reddish brown or dark red, suggesting the formation of solid molecular complexes of the electron donor-acceptor type. The phase diagrams suggest that the solid complex is formed at the composition of 50 mol% or higher of the dinitro compound. The electronic spectrum of (NMe_2, PrO)–(NO_2, NO_2) at 50 mol% is shown in Fig. 3, along with those of the solid component compounds. New absorption bands undoubtedly appear and are located at about 18 and 22×10^3 cm^{-1}. They may be assigned to the charge-transfer transitions from (NMe_2, PrO) to (NO_2, NO_2). The spectrum of (NMe_2, PrO)–DNAO at 50 mol% is very much like the aforementioned, but the first band is shifted further to the low-energy side, by $(1.5—2)\times10^3$ cm^{-1}. This shift may imply that the electron affinity of DNAO is larger by about this extent than that of (NO_2, NO_2). This postulate is not unreasonable if one compares the electronegativities of the atoms in the central linkages. As the color of the mesophases is similar to that of the corresponding solid complex, it is very likely that the unusually pronounced nonlinear behavior of smectic liquid crystals is caused by the complexation between the donor and acceptor molecules in appropriate mole ratios.

N-[*4-(Dimethylamino)benzylidene*]-*4-(dimethylamino) aniline* (*NMe_2, NMe_2*) *as an Electron Donor.* Smectic phase is produced when (NO_2, PrO) is combined with this donor compound. As is shown in Fig. 4a, the induced mesophase is entirely metastable. The maximum of the I-S transition curve is located at 121 °C near 30 mol% of (NMe_2, NMe_2).

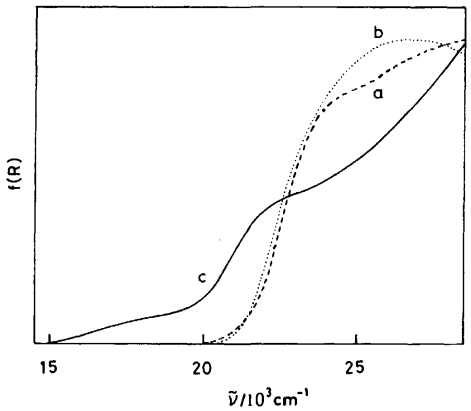

Fig. 3. Diffuse reflection spectra of (a) (NMe_2, PrO), (b) (NO_2, NO_2), and (c) the binary system at 50 mol%.

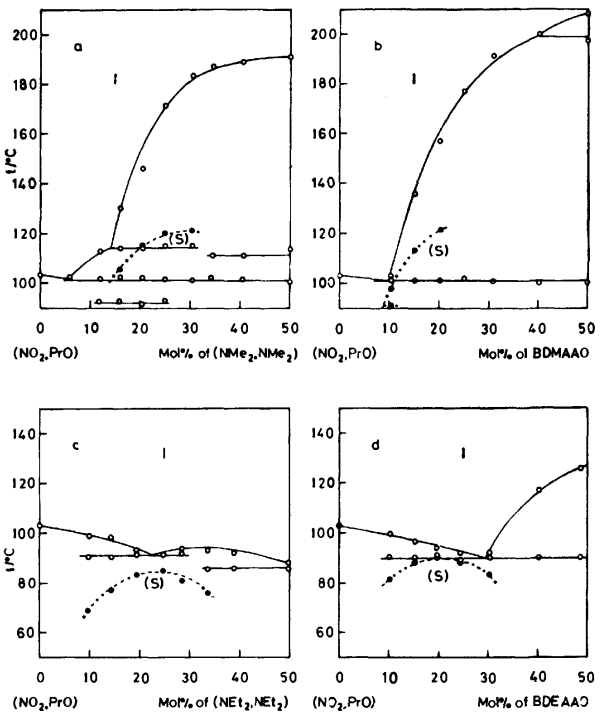

Fig. 4. Phase diagrams of the (a) (NMe_2, NMe_2)–(NO_2, PrO), (b) BDMAAO–(NO_2, PrO), (c) (NEt_2, NEt_2)–(NO_2, PrO), and (d) BDEAAO–(NO_2, PrO) systems. As to the open and shaded circles, see the caption of Fig. 1.

Metastable nematic liquid crystals appear when the donor compound is mixed with (NO_2, EtO) and also with (PrO, NO_2). In the former combination, the mesophase is observable in the composition range from 10 to 20 mol% of (NMe_2, NMe_2) and at temperatures between 105 and 113 °C. The mesophase relatively rich in the donor compound can persist only within a few degrees below the transition curve. The nematic liquid crystal in the latter system can be found below 25 mol%. The curve extends from the I-N transition point of (PrO, NO_2) and reaches 112 °C by the said composition.

4,4'-Bis(dimethylamino)azoxybenzene (BDMAAO) as an Electron Donor. According to our survey, made by the contact method,[9] the induction of mesophase occurs only in the system with (NO_2, PrO). The metastable smectic phase is observed in the range from 10 to 20 mol% of BDMAAO (see Fig. 4b). The transition temperature at the former composition is 98 °C, while that at the latter is 122 °C. The coexistence of smectic and nematic liquid crystals is found at 10 mol% and below 91 °C.

In contrast to the mesophases obtained with the dinitro compounds shown in Figs. 1 and 2, the liquid crystals induced with the bis(dimethylamino) compounds are not very stable. The melting point of (NMe_2, NMe_2) is as high as 234.5 °C and that of BDMAAO is even higher: *i.e.*, 244 °C. Because of the large differences in melting point between the donor and acceptor compounds, the major part of the induced mesophases is far below the freezing point curve on the donor-rich side. In such a situation, it is hard to suspend the solidification down to the I-S transition temperature. Consequently, we tried the bis(diethylamino) compounds, the melting points of which are expected to be appreciably lower, as electron donors.

N-[4-(Diethylamino)benzylidene]-4-(diethylamino)aniline (NEt_2, NEt_2) as an Electron Donor. This compound melts at 118 °C. Nevertheless, liquid crystal can be produced only when the compound is mixed with (NO_2, PrO) and exists as a metastable phase (see Fig. 4c). The smectic phase is induced in the range from 10 mol% of (NEt_2, NEt_2) to the composition of the solid complex. The maximum of the I-S transition curve lies at 85 °C and about 25 mol%. This temperature is markedly lower than that found in the (NMe_2, NMe_2)–(NO_2, PrO) system.

4,4'-Bis(diethylamino)azoxybenzene(BDEAAO) as an Electron Donor. The melting point of this compound is 158 °C, which is lower by 86 °C than that of BDMAAO. Smectic liquid crystals could be observed in the mixtures not only with (NO_2, PrO) but also with (PrO, NO_2). The diagram of the former system is presented in Fig. 4d. The mesophase is seen in the range from 10 to 30 mol% of BDEAAO. The maximum transition temperature is almost in coincidence with the eutectic temperature and is found at about 20 mol%. The smectic phase induced by mixing with (PrO, NO_2) is less stable; the maximum lies at 71 °C and about 20 mol%.

Thus, the lowering of the melting point by the replacement of dimethylamino groups with diethylamino groups is appreciable; however, the observation of induced mesophases is not made much easier. It seems highly likely that the latent I-S transition temperature is also lowered by this replacement, as we suggested in our earlier work on the *N*-benzylidene-4-aminoazobenzenes.[1] The latter effect may be, at least partly, lifted if the *N*-benzylideneanilines carrying a dimethylamino group on one end and a diethylamino group on the other end are employed. Indeed, (NEt_2, NMe_2) is known to melt at 140—141 °C.[10] This temperature is only 22 °C higher than the melting point of (NEt_2, NEt_2).

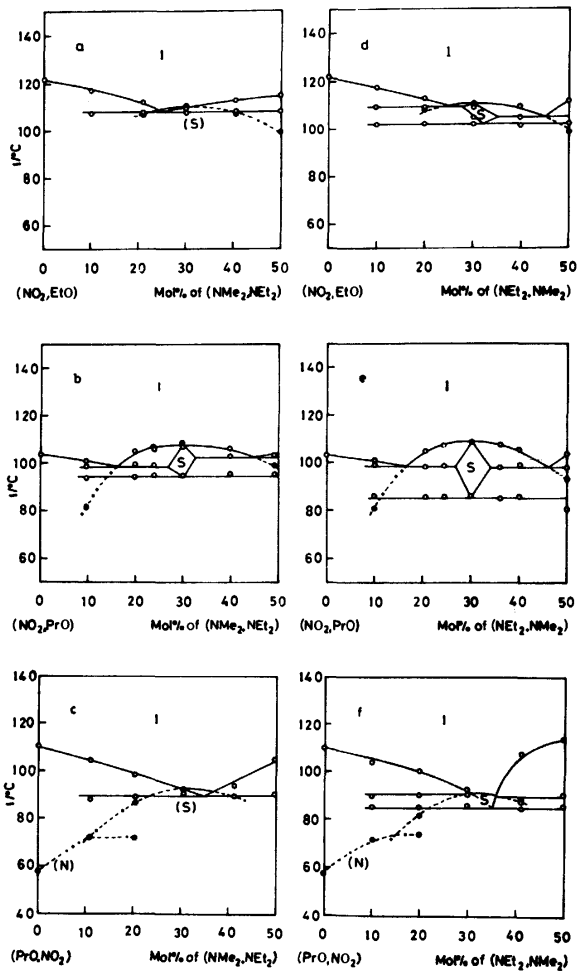

Fig. 5. Phase diagrams of the (a) (NMe_2, NEt_2)–(NO_2, EtO), (b) (NMe_2, NEt_2)–(NO_2, PrO), (c) (NMe_2, NEt_2)–(PrO, NO_2), (d) (NEt_2, NMe_2)–(NO_2, EtO), (e) (NEt_2, NMe_2)–(NO_2, PrO), and (f) (NEt_2, NMe_2)–(PrO, NO_2) systems. As to the open and shaded circles, see the caption of Fig. 1.

N-[4-(Dimethylamino)benzylidene]-4-(diethylamino)aniline (NMe_2, NEt_2) as an Electron Donor. The acceptors, (NO_2, EtO), (NO_2, PrO), and (PrO, NO_2) were found to produce smectic liquid crystals when combined with this donor, the melting point of which is 136 °C. Their phase diagrams are given in Figs. 5a, b, and c. In all the cases, the induced mesophase has an area where it can exist as a single stable phase. The system with (NO_2, EtO) produces a mesophase observable in the range from 20 to 50 mol% of (NMe_2,

NEt_2). The maximum of the transition curve lies at 111 °C and about 30 mol%.

The smectic phase is most stabilized in the system with (NO_2, PrO). The I-S transition curve is met by the freezing point curve of (NO_2, PrO) at 98 °C and 16 mol% and by that on the (NMe_2, NEt_2)-rich side at 102 °C and 44.5 mol%. The maximum of the transition curve is found at 107 °C. The composition is not distinguishable from that of the eutectic point, 94 °C and 30 mol%.

The mesophase induced in mixtures with (PrO, NO_2) is metastable except for the small area above the eutectic point. The enantiotropic I-S transition is seen only between 31 and 36.5 mol%. The maximum is located at 92 °C. Below 72 °C and 11 mol%, the nematic phase can exist as a single phase.

N-[4-(Diethylamino)benzylidene]-4-(dimethylamino)aniline (NEt$_2$, NMe$_2$) as an Electron Donor. Smectic liquid crystals are induced in the systems with (NO_2, EtO), (NO_2, PrO), and (PrO, NO_2) and are generally more stable than those induced with the isomeric donor compound, (NMe_2, NEt_2) (see Figs, 5d, e, and f).

The diagrams in Figs. 5d and e are similar to that given in Fig. 5b. With (NO_2, EtO), the I-S transition curve intersects the freezing point curve of (NO_2, EtO) at 109.5 °C and 25 mol% and that on the donor-rich side at 105 °C and 45 mol%. The maximum temperature of 111.5 °C is found around 30 mol%. The smectic phase and the isotropic melt coexist in most of the area below the I-S transition curve. The lower temperature limit as a single stable mesophase is 102 °C located at 32 mol%.

The enantiotropic I-S transition curve in the system with (NO_2, PrO) covers the composition range from 16.5 to 46 mol% of (NEt_2, NMe_2), passing through a maximum at 109 °C and about 30 mol%. The area in which the induced smectic phase appears as the sole stable phase covers the temperature range from 85 to 109 °C and the composition range from 27 to 34 mol%.

When mixed with (PrO, NO_2), the mesophase is stable in the area specified by the intersections between the I-S transition curve with the freezing point curves at 91 °C and 31 mol% and at 90 °C and 36 mol% and by the eutectic point at 85 °C and 35 mol%. The metastable I-S transition curve encounters the metastable I-N transition curve at 74 °C and 15 mol%.

The upper temperature limits of the smectic phases induced with the six donor compounds are compared in Table 2. As to the donors, the temperature changes in this order:

Table 2. The maximum temperature of the smectic liquid crystal-isotropic liquid transition/°C

Donor	Acceptor		
	(NO_2, EtO)	(NO_2, PrO)	(PrO, NO_2)
(NMe_2, NMe_2)	—	121	—
BDMAAO	—	122	—
(NMe_2, NEt_2)	111	107	92
(NEt_2, NMe_2)	111.5	109	92
(NEt_2, NEt_2)	—	84	—
BDEAAO	—	90	71

$$\text{BDMAAO} \simeq (NMe_2, NMe_2) > (NEt_2, NMe_2) \simeq (NMe_2, NEt_2) > \text{BDEAAO} > (NEt_2, NEt_2).$$

As the melting point follows the same order except for the last two, it is not possible to compare the stabilization of the induced phases based on this order.

The color developed with these bis(dialkylamino) compounds is not so deep as that developed with the dinitro compounds. For example, the 1:2 (NMe_2, NMe_2)–(NO_2, PrO) complex is brown. Comparison of the diffuse reflectance spectrum of the complex with those of the components reveals the occurrence of a weak absorption around 19×10^3 cm^{-1}. This energy value is only a little bit lower than that found in the combination of (NMe_2, EtO) and (NO_2, EtO) reported earlier.[2] The shift arises from the rather small improvement of the donor strength by the replacement of an electron-donating alkoxyl group with another electron-donating dialkylamino group. In contrast, the shift found in Fig. 3 is large. The increase in the acceptor strength is due to the replacement of an alkoxyl group with an electron-withdrawing nitro group. The thermal stabilization of smectic liquid crystals induced by the dinitro compounds is more extensive than that induced by the mononitro compounds. This observation may be also attributed to the rather large difference in the acceptor strength.

The composition at the maximum of the I-S transition curve varies with the combination of electron donor and acceptor but, without exception, occurs near 30 mol% of the dinitro or bis(dialkylamino) compound. The exact composition is supposed to depend not only on the extent of the formation of 2 : 1 or 1 : 2 molecular complexes in the mesophases but also on the difference in the latent I-S transition temperature between the component compounds. The above-mentioned compositions suggest that the temperatures of the dinitro and bis(dialkylamino) compounds are considerably lower than those of the other component compounds employed in this work.

The authors wish to express their sincere thanks to Mr. Nobuhiko Miyajima for the preparation of 4,4'-bis(dimethylamino)azoxybenzene. The present work was partly supported by a Grant-in-Aid for Scientific Research from the Ministry of Education, Science and Culture (No. 543001).

References

1) Part IV: M. Fukui and Y. Matsunaga, *Bull. Chem. Soc. Jpn.*, **54**, 3137 (1981).
2) K. Araya and Y. Matsunaga, *Bull. Chem. Soc. Jpn.*, **53**, 3079 (1980).
3) K. Araya and Y. Matsunaga, *Bull. Chem. Soc. Jpn.*, **54**, 2430 (1981).
4) O. N. Witt and E. Kopetschni, *Ber.*, **45**, 1134 (1912).
5) A. Werner, *Ber.*, **32**, 3256 (1899).
6) M. Busch and K. Schulz, *Ber.*, **62**, 1458 (1929).
7) D. Demus and H. Sackmann, *Z. Phys. Chem. (Leipzig)*, **222**, 127 (1963).
8) L. E. Knaak, H. M. Rosenberg, and M. P. Serve, *Mol. Cryst. Liq. Cryst.*, **17**, 171 (1972).
9) H. Sackmann and D. Demus, *Z. Phys. Chem. (Leipzig)*, **222**, 143 (1963).
10) R. Mohlau, *Ber.*, **31**, 2250 (1898).

Electron Spin Resonance of X-Irradiated Single Crystals of Dicyclohexyldiazene 1,2-Dioxide

Yoshihisa FUJII, Michio KASHIWAGI,†,†† Hideki NAKADA,†,††† and Yukio KURITA*
Department of Materials Chemistry, Faculty of Engineering, Yokohama National University, Hodogaya-ku, Yokohama 240
†*Basic Research Laboratory, Toray Industries, Inc., Tebiro, Kamakura 248*
(Received September 11, 1981)

ESR studies of X-irradiated single crystals of dicyclohexyldiazene 1,2-dioxide, $(C_6H_{11}NO)_2$, revealed the generation of the stably trapped radicals $C_6H_{11}N(O)N'H''(O')C_6H_{11}$. The principal elements of the g value were found to be 2.0030, 2.0060, and 2.0086. The principal elements of the hyperfine coupling constants were found to be 3.88, 1.53, and 1.38 mT for N, and 1.53, 1.41, and 1.14 mT for H''. The direction cosines of these principal elements, when compared with those of the bonds in the parent molecule, indicate that the radical is formed by addition of a hydrogen atom to the N=N' double bond without causing a large change in the molecular framework. The spin densities for this radical were calculated to be 0.041 and 0.47 in the 2s and 2p orbitals of the atom N, respectively.

C-Nitroso compounds in solution produce nitroxide radicals by photochemical or thermal decomposition. It is well established that the radical formation takes place through the nitroso monomer:[1]

$$(RNO)_2 \underset{\text{or } \Delta}{\overset{h\nu}{\rightleftharpoons}} 2RNO \xrightarrow[\text{or } \Delta]{h\nu} R\cdot + NO\cdot$$

$$+ RNO \longrightarrow R_2NO\cdot + NO\cdot$$

However, little is known about the decomposition of *C*-nitroso compounds in the solid state, where they exist as dimers.

Nitrosocyclohexane has industrial significance as a precursor of cyclohexanone oxime, which is used to give poly(ε-caprolactam). X-Ray analysis revealed that nitrosocyclohexane exists as a dimeric form, dicyclohexyldiazene 1,2-dioxide (**1**), in the crystalline state.[2] This paper will report the ESR study of X-irradiated single crystals of **1**.

Experimental and Results

Compound **1**, $(C_6H_{11}NO)_2$, mp 117—118 °C, was prepared according to the method of Okamura *et al.*[3] Single crystals were grown by the slow evaporation of a saturated methanol solution in a refrigerator at 5 °C. The crystals obtained were thin plates (8 mm × 3 mm × 1 mm, Fig. 1) with well developed planes: {100}, {010}, and {001}.

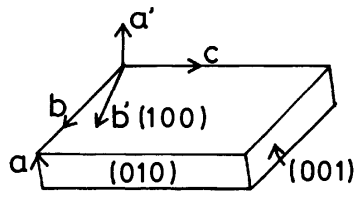

Fig. 1. The crystal form of **1** and the crystallographic axes abc and the rectangular coordinate axes a'b'c employed for analysis of the ESR spectra.

The crystal structure has been determined by Tanimura *et al.* using X-ray methods.[2] The crystal is triclinic and the space group is $P\bar{1}$ with the unit cell of dimensions: $a_0=1.0133$, $b_0=0.6758$, $c_0=0.5583$ nm, $\alpha=121°42'$, $\beta=96°50'$, $\gamma=78°06'$. The unit cell contains one molecule, which has a center of symmetry at the midpoint of the N=N' bond.

A rectangular coordinate system a'b'c was chosen for the ESR measurements. The c axis is the same as the crystal c axis. The b' axis is selected in the bc plane, perpendicular to the c axis, and the a' axis is perpendicular to the bc plane. The crystal axes were determined by comparing interfacial angles calculated from the lattice constants with those measured with an optical goniometer. The results are shown in Fig. 1.

Single crystals were irradiated with X-rays of 180 keV to a dose of about 1 Mrad (10^4 J/kg) at 77 K. The ESR spectra were measured using a Varian Model V4501 X-band spectrometer.

The ESR spectra measured at 77 K immediately after X-ray irradiation at 77 K were impossible to analyze, since they consisted of a broad, almost featureless

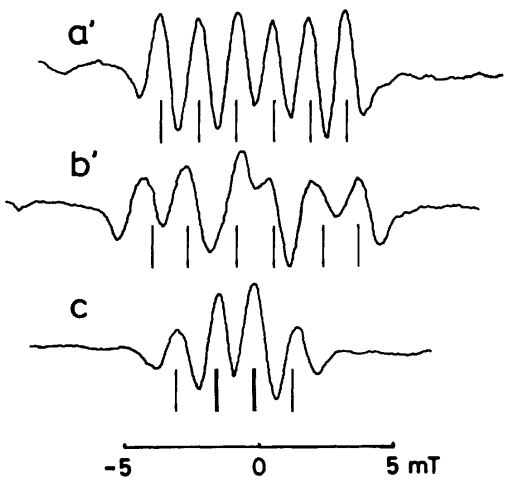

Fig. 2. Second derivative ESR spectra of a single crystal of **1**, which was measured at room temperature after X-Rays irradiation at 77 K. The magnetic filed was applied parallel to the a', b', or c axis, and measured relative to the reference DPPH signal ($g=2.0036$).

†† Present address: Engineering Research Laboratories, Toray Industries, Inc., Sonoyama, Otsu 520.

††† Present address: Aichi Plant, Toray Industries, Inc., Nishi-ku, Nagoya 451.

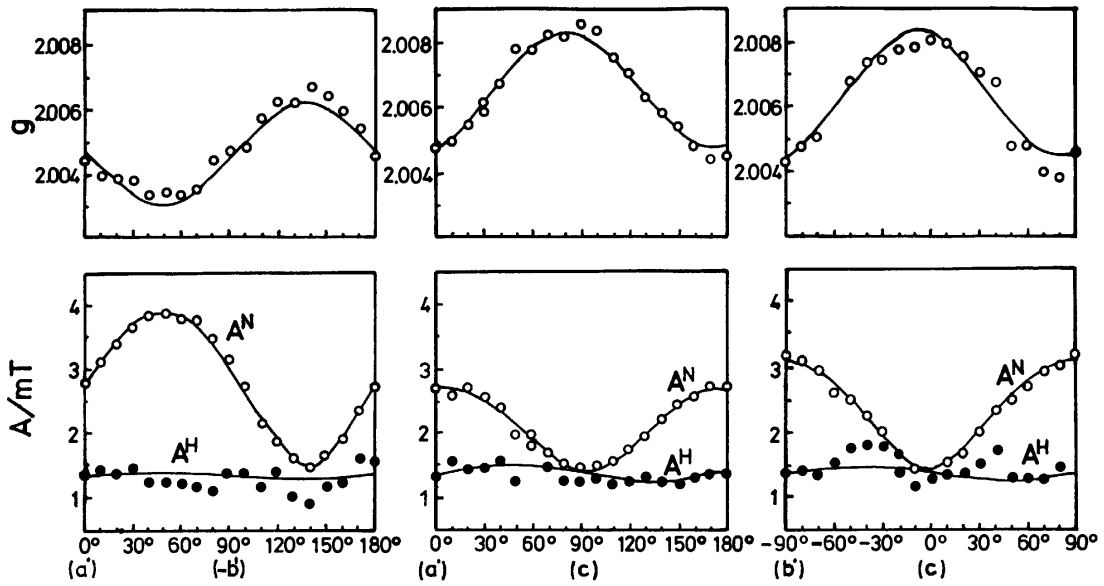

Fig. 3. Angular dependencies of A^N, A^H, and g in an X-irradiated single crystal of **1**. The magnetic field is in the a'b', a'c, and b'c planes. The circles indicate the observed values and the solid lines indicate the theoretical curves.

Table 1. The principal values of g, A^N, and A^H and their direction cosines with regard to the a'b'c system

g, A^N, and A^H	Principal values	Direction cosines with regard to the a'b'c system		
g_1	2.0030	0.670	−0.743	0.018
g_2	2.0060	0.709	0.631	−0.314
g_3	2.0086	0.222	0.223	0.949
A_1^N/mT	3.88	0.643	−0.765	0.023
A_2^N/mT	1.53	0.659	0.569	0.492
A_3^N/mT	1.38	0.389	0.301	−0.871
A_1^H/mT	1.53	0.539	0.309	0.784
A_2^H/mT	1.41	0.639	−0.756	−0.141
A_3^H/mT	1.14	0.549	0.577	−0.605

absorption. However, the spectra measured at room temperature became simple after storage at room temperature. Some typical spectra are shown in Fig. 2. Each spectrum, consisting of six lines with equal intensity, can be interpreted in terms of one anisotropic nitrogen hyperfine coupling constant A^N and one nearly isotropic proton hyperfine coupling constant A^H. Each component line is broad, having about 0.7 mT of maximum slope width.

The observed angular dependencies of A^N, A^H, and g values are plotted in Fig. 3. Principal elements of A^N-, A^H-, and g-tensors are determined using the least-squares method and are given in Table 1. The solid lines in Fig. 3 are the theoretical angular variations calculated from the principal elements in Table 1.

Discussion

The observed coupling constants clearly show that the free radical contains a nitrogen atom having a large fraction of unpaired electrons and β-type hydrogen atom with nearly isotropic coupling constant. Table 1 shows that the nitrogen coupling tensor has almost cylindrical symmetry about the A_1^N direction. This symmetry is to be expected for the unpaired electron in a nitrogen orbital aligned in this direction when the contribution from unpaired electrons on other orbitals is negligible. The analysis of coupling tensors of this type has been fully discussed in a previous paper.[4] The results are summarized as follows.

The molecular orbital containing the unpaired electron can be written as

$$\phi = C_s\phi_{2s}{}^N + C_p\phi_{2p}{}^N + C_h\phi_{1s}{}^H\ C_x\phi^X,$$

where $\phi_{2s}{}^N$, $\phi_{2p}{}^N$, and $\phi_{1s}{}^H$ are the 2s, 2p atomic orbitals of the nitrogen atom and the 1s atomic orbital of the hydrogen atom, respectively, and ϕ^X is a normalized orbital of a group of atoms that makes negligible contribution to the hyperfine structure. Coefficients are obtained from the relations:

$$C_s{}^2 = a^N/A_{2s}{}^N,$$
$$C_p{}^2 = (A_1{}^N - a^N)/(2B_{2p}{}^N),$$
$$C_h{}^2 = a^H/A_{1s}{}^H,$$
$$C_x{}^2 = 1 - C_s{}^2 - C_p{}^2 - C_h{}^2,$$

where

$$a^N = (A_1{}^N + A_2{}^N + A_3{}^N)/3,$$
$$a^H = (A_1{}^H + A_2{}^H + A_3{}^H)/3.$$

The 2p orbital is parallel to the direction of $A_1{}^N$(maximum) and g_1(minimum).

With the observed values in Table 1 and $A_{2s}{}^N$=55.0 mT, $B_{2p}{}^N$=1.71 mT, and $A_{1s}{}^H$=50.8 mT,[5] one finds $C_s{}^2$=0.041, $C_p{}^2$=0.47, $C_h{}^2$=0.027, and $C_x{}^2$=0.462; the total spin density on the nitrogen atom is 0.51. The directions of g_1 and $A_1{}^N$ are calculated to be 1.6° apart; they are parallel within the experimental error.

The spin densities and g values of this radical are compared in Table 2 with those of nitroxide and iminoxyl radicals, which are typical π- and σ-radicals, respectively. The comparison suggests that this radical

Table 2. Spin densities and g factors of radicals containing N–O group

	Nitroxyl radical[a,b]	The radical in this work	Iminoxyl radical[c]
C_s^2	0.027	0.041	0.050
C_p^2	0.50	0.47	0.36
g_1	2.0027	2.0030	2.0025
g_2	2.0061	2.0060	2.0064
g_3	2.0089	2.0086	2.0118

a) Ref. 7. b) The isotropic proton coupling constant of dimethyl nitroxide radical was 1.23 mT: J. Q. Adams, S. W. Nicksic, and J. R. Thomas, *J. Chem. Phys.*, **45**, 654 (1966). c) Ref. 4.

has an electronic structure similar to that of nitroxide radical except for the high spin density on the 2s atomic orbital of the nitrogen atom.

Stable radicals trapped in irradiated organic crystals at room temperature include the following types: (1) The primary free radicals formed by dissociation of the undamaged molecules; (2) the secondary free radicals formed by addition of the primary radicals of small size to the undamaged molecule or to diamagnetic molecular fragments that are produced by the dissociation of the undamaged molecules. There are seven possible radicals (**2**—**8**) of this type that can be produced from **1** and have a coupling nitrogen atom with the spin density of about one half. All the radicals except **2** will be readily excluded from the canditates for the observed radical since these radicals cannot be reconciled with the observed coupling constants.

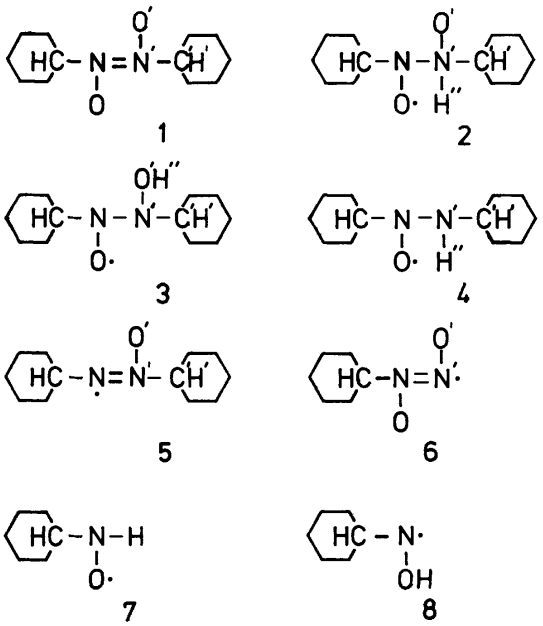

Radical **7** has an anisotropic coupling proton of the NH group. The anisotropy of the coupling constant, $A_{max}^{H}-A_{min}^{H}$, for an α proton of an >N̈–H π radical is proportional to the spin density on the nitrogen 2p orbital (ρ_π^N) with a proportional constant of 3.2 mT.[6] With the spin density of 0.47, the anisotropy in **7** is estimated to be 1.5 mT; this is different from the observed anisotropy of 0.39 mT. It is shown in the same way that the proton coupling of the OH group of **8** has an anisotropy different from the observed one. Thus **7** and **8** are excluded.

Radicals **5** and **6** probably give rise to two discernible couplings due to N and N′ atoms, because spin densities on these atoms do not seem to differ too much. Because only one nitrogen coupling was observed, **5** and **6** can be excluded.

Radicals **2**, **3**, and **4** can be formed from the parent molecule as a result of hydrogen addition or hydrogen addition after oxygen abstraction. Therefore, it can be assumed that all atoms in these radicals except O′ and H″ occupy the same positions in the lattice as those in the parent molecule. The isotropic coupling constant of H, a^H(CH), can be expressed by McConnell's $\cos^2\theta$ rule:

$$a^H(CH) = Q_N^{CH}\rho_\pi^N \cos^2\theta,$$

where θ is a dihedral angle between the C–H bond in the parent molecule and the unpaired electron orbital (parallel to A_1^N and g_1) in the observed radical, and $\rho_\pi^N=(C_{2p}^N)^2$. The orientation of the parent molecule in the crystal, determined by X-ray analysis, is given in Table 3. Using the value of 76—77° for θ calculated from Tables 1 and 3, 0.47 for ρ_π^N from Table 2, and 5.0 mT for Q_N^{CH}, one obtains 0.2 mT for a^H(CH). Because this value is much smaller than the observed isotropic proton coupling of 1.36 mT, the observed one is not attributable to the hydrogen atom of the CH group.

Table 3. Orientation of the parent molecule with regard to the a′b′c system

Bond and normal	Direction cosines with regard to the a′b′c system		
	a′	b′	c
C–H	−0.445	−0.151	−0.882
N–C	0.551	0.379	−0.743
N–O	0.164	0.256	0.952
N–N′	−0.720	−0.655	−0.228
n_1[a]	0.478	−0.874	−0.091
n_2[b]	0.646	−0.758	0.093

a) n_1: The normal to the plane HCN of **1**. b) n_2: The normal to the plane CNO of **1**.

The ESR of *t*-butyl cyclohexylamino nitroxide analogous to **4**, has been studied in solution; its isotropic couplings were 1.86 mT for N(NO), 0.09 mT for N(NH), H(CH), and H(NH).[8] The isotropic coupling constant of H(NH) of **4** is probably close to 0.09 mT; this value cannot account for the observed value of 1.36 mT. In nitroxide radicals, the unpaired electron is mainly localized on the >N–O moiety; hence the proton coupling constant of H(OH) in **3** will be too small to explain the observed constant. Thus there remains only **2** as a candidate. The following discussion will show that **2** is consistent with the ESR data of the trapped radical.

In the parent molecule **1**, six atoms CNOC′N′O′ are almost planar and oxygen atoms are placed *trans*

with regard to the N=N′ bond. Radical **2** is produced by the rupture of this π bond with the addition of H″ at N′. For the time being, we shall assumed that CNON′ in **2** occupies the same position in the lattice as in the parent molecule. Then, the unpaired electron occupies a molecular orbital composed of the p_π orbitals of N and O, which are perpendicular to the CNO plane. This can explain the result that the normal to the CNO plane was calculated from the direction cosines in Tables 1 and 3 to make an angle of 4° with the directions of g_1 and A_1^N, therefore with the direction of the p_π orbital. On addition of H″ to N′, the hybridization of the nitrogen orbitals changes from sp^2 to sp^3. Then O′ is moved and N′–H″ uses one of the sp^3 hybrid orbitals, making a dihedral angle of 30° with the p_π orbital of the unpaired electron. Though nitroxide radicals with –N(O·)NH(O)– moiety have not been reported, a radical $HN^{\cdot}$–NH_3^+ somewhat analogous to **2** was reported by Shrivastava and Anderson[9] and extensively discussed by Gordy.[6] The resultant parameters are $a^N(NH_3)=0.4$ mT, $a^H(NH_3)=1.50$ mT, $\rho_\pi^N=0.97$, $Q_N^{NH}=3.09$ mT, where Q_N^{NH} is the coefficient in

$$a^H(NH_3) = Q_N^{NH}\rho_\pi \cos^2\theta.$$

Applying this relation to **2** with $\rho_\pi^N=0.47$ and $\theta=30°$, we obtain 1.09 mT for the coupling constant of H″, which agrees well with the observed one of 1.36 mT.

The hydrogen atom H″ added at N′ will occupy two positions in the lattice; one lies above the NN′C′ plane, the other below the plane. The anisotropic coupling tensor of each hydrogen atom is calculated and compared with the observed coupling tensor of A^H. The position of H″ was not determined with assurance because of the relatively large angular error in the observed coupling tensor.

The coupling of β-nitrogen is supposed to be proportional to the spin density on the α-nitrogen. The coupling constant of 0.4 mT for $\rho_\pi^N=0.97$ in HN–NH_3^+ predicts that of **2** to be about 0.2 mT from $\rho_\pi^N=0.47$. This is within the observed line width of 0.7 mT.

If the nitroxide moiety of **2** is perfectly planar, it will have the spin density on the nitrogen 2s orbital approximately equal to that of ordinary nitroxide radicals. However, Table 2 shows that the former (0.041) is appreciably larger than the latter (0.027). The difference suggests a change of nitroxide moiety from planar configuration. Experimental and theoretical studies have shown that the methyl radical is planar and the radicals CF_3, CHF_2, and CH_2F are pyramidal.[10,11] Pauling has shown by a simple quantum-mechanical argument that the electronegativity difference of the atom is the major factor in determining the configuration of these radicals.[11] For a radical $\dot{M}X_3$, as X is more electronegative than M, the unpaired electron orbital will contain more charactor of M and the radical will have a pyramidal structure. This explains the configuration change in nitroxide radicals: If one replaces an alkyl group in the dialkyl nitroxide radical with a nitrogen function, the spin density on the nitrogen 2s orbital of the nitroxide moiety will increase.

We therefore conclude that the radical stably trapped in the solid state is **2**.

References

1) For a review of the literature on C-nitroso compounds, see B. G. Gowenlock and W. Lüttke, *Quart. Rev.*, **12**, 321 (1958).
2) M. Tanimura, K. Kobori, M. Kashiwagi, and Y. Kinoshita, *Bull. Chem. Soc. Jpn.*, **43**, 1962 (1970).
3) I. Okamura, R. Sakurai, and T. Tanabe, *Kobunshi Kagaku*, **9**, 279, 284 (1952).
4) Y. Kurita, M. Kashiwagi, and H. Saisho, *Nippon Kagaku Zasshi*, **86**, 578 (1965).
5) J. R. Morton, *Chem. Rev.*, **62**, 453 (1964).
6) W. Gordy, "Theory and Applications of Electron Spin Resonance," Wiley-Interscience, New York (1980), pp. 230—238.
7) O. H. Griffith, D. W. Cornell, and H. M. McConnell, *J. Chem. Phys.*, **43**, 2909 (1965).
8) I. I. Bilkis and S. M. Shein, *Tetrahedron*, **31**, 969 (1975).
9) K. H. Shrivastava and R. S. Anderson, *J. Chem. Phys.*, **48**, 4599 (1968).
10) J. K. Koichi, "Advances in Free-Radical Chemistry," ed by G. H. Williams, Elek Science, London (1975), Vol. V, Chap. 4.
11) L. Pauling, *J. Chem. Phys.*, **51**, 2767 (1969).

 © 1982 The Chemical Society of Japan Bull. Chem. Soc. Jpn., 55, 1719—1726 (1982)

Selective Reduction of Nitrogen Monoxide with Hydrogen on Pt/Al_2O_3 Containing a Metal Oxide

Yukio Kosaki,* Akira Miyamoto, and Yuichi Murakami
Department of Synthetic Chemistry, Faculty of Engineering, Nagoya University, Furo-cho, Chikusa-ku, Nagoya 464
(Received September 18, 1981)

By using a three-way catalyst containing a metal oxide, NO can be selectively converted to N_2 and N_2O without the formation of NH_3 even at the "rich" side of the air/fuel ratio. In order to elucidate the mechanism of this action of the added metal oxide, the NO–H_2 reaction on $Pt–V_2O_5/Al_2O_3$ catalyst was investigated using the pulse reaction technique. In the NO–H_2 reaction on Pt/Al_2O_3 catalyst, a significant amount of NH_3 was formed in the "rich" region of the reactants ($H_2/NO>1$), although NO was completely removed. In the NO–H_2 reaction on the $Pt–V_2O_5/Al_2O_3$ catalyst, on the other hand, no NH_3 was formed even in the "rich" region of the reactants; in addition, NO was completely removed. During the NO–H_2 reaction on the $Pt–V_2O_5/Al_2O_3$ catalyst, the V_2O_5 in the catalyst was found to be reduced from V^{5+} to V^{4+}. The reaction of NO with NH_3 and the reaction of NH_3 or H_2 with $Pt–V_2O_5$ mixed catalysts for various states of mixing were also investigated. From these results, the NO–H_2 reaction on the $Pt–V_2O_5/Al_2O_3$ catalyst has been shown to be composed of the following three main steps: Step I, the formation of NH_3 by the reduction of NO with H_2 on Pt; Step II, the NO–NH_3 reaction on Pt to form N_2 or N_2O; and Step III, the reduction of V_2O_5 in the catalyst by H_2 which is accelerated by the "hydrogen spillover." In the NO–H_2 reaction on Pt/Al_2O_3 catalyst, NO is first reduced to NH_3 in Step I and the NO–NH_3 reaction in Step II follows. In the "rich" region, the formation of NH_3 takes place more readily than the subsequent NO–NH_3 reaction. In the NO–H_2 reaction on the $Pt–V_2O_5/Al_2O_3$ catalyst, the formation of excess NH_3 is suppressed by the removal of hydrogen from Pt in Step III, and the NH_3 thus produced reacts with NO to form N_2 or N_2O selectively in Step II. The rates of Steps I, II, and III were also discussed in terms of the structure of the catalysts and composition of the reactants.

The three-way catalyst system is used for the simultaneous removal of nitrogen monoxide, carbon monoxide, and hydrocarbons in the automotive exhaust emissions.[1–5] This is done in a single bed of catalyst by controlling the air/fuel ratio within a region near the stoichiometric point, which is called the "window." The width of the "window" is usually very narrow; therefore, in order to control the air/fuel ratio within the "window," a feedback control system of the air/fuel ratio has been developed using an oxygen sensor.[3,6–14] The three-way catalyst coupled with this feedback control system, however, cannot fully control the fluctuation of the air/fuel ratio within the "window," and this brings about the incomplete removal of NO, CO, and hydrocarbons, and also the formation of NH_3. The development of a three-way catalyst with a broad "window" is therefore highly desirable. Although the supported Rh or Rh–Pt catalyst has a "window" with a broader width than the supported Pt or Pd catalyst,[15–19] a large demand for Rh cannot be met by supply because of the limited reserve of the resources.[4,20]

The three-way catalyst containing a metal oxide such as V_2O_5,[21] Re_2O_7,[22,23] MoO_3,[24] or CeO_2[25,26] has been shown to deal effectively with the fluctuation of the air/fuel ratio; thereby, the width of the "window" has been markedly broadened. The role of the added metal oxide has been considered as "oxygen storage."[27–29] However, further details of the mechanism of the action of the metal oxide added to the three-way catalyst have not been clarified. This may be due to the complexity of the system: (i) The automative exhaust gas contains many components, including NO, CO, H_2, hydrocarbons, SO_2, and water, which lead to very complex networks of elementary reactions on the catalyst, and (ii) the three-way catalyst containing the metal oxide has not been well characterized.

As a first step to the investigation of the mechanisms of the reactions involved in the automotive exhaust emissions control using a three-way catalyst containing a metal oxide, the purposes of this study were (i) to investigate whether the action of the added metal oxide for the selective reduction of NO can also be observed in the NO–H_2 reaction on $Pt–V_2O_5/Al_2O_3$ catalyst—a system which is much simpler than the real three-way catalyst system, and (ii) to reveal the action of the metal oxide in the NO–H_2 reaction on the $Pt–V_2O_5/Al_2O_3$ catalyst. The NO–H_2 reaction was investigated, since this reaction is one of the most important reactions in the "rich" region for the removal of NO,[30,31] and is mainly responsible for the formation of NH_3.[32] It should be noted that the rate of the reaction in the "rich" region is considered to be much slower than that in the "lean" region.[28] V_2O_5 was chosen as the metal oxide because (i) the structure of V_2O_5 on Al_2O_3 support has been well characterized[33] and (ii) it is one of the metal oxides which have been known to be excellent additives to the three-way catalyst.[21] A pulse reaction technique was employed in this study because this technique is useful for investigating the kinetic behavior of the reduction or oxidation process involved in the redox cycles of a catalyst.[34–36]

Experimental

Catalysts. Pt/Al_2O_3 catalyst (Pt loading was 0.5 wt%) was purchased from Nippon Engelhard Ltd. $Pt–V_2O_5/Al_2O_3$ catalyst was prepared by impregnating the Pt/Al_2O_3 particles (0.3—0.6 mm) with an oxalic acid solution of ammonium metavanadate, followed by drying and subsequent heating in a stream of O_2 at 773 K for 3 h. Unless otherwise specified, the content of V_2O_5 in the $Pt–V_2O_5/Al_2O_3$ catalyst was 9 wt%, although $Pt–V_2O_5/Al_2O_3$ with 36 wt% V_2O_5 loading was also

used. A V_2O_5 was prepared by the thermal decomposition of ammonium metavanadate in an O_2 stream at 773 K for 3 h. A Pt/Al_2O_3–metal oxide(M) catalyst (the ratio of Pt/Al_2O_3 to the metal oxide was 1/1 in weight)was prepared by mixing powders of Pt/Al_2O_3 and the metal oxide in a mortar for 20 min without water. A Pt/Al_2O_3–V_2O_5(P) catalyst was obtained by mixing Pt/Al_2O_3 particles (0.3—0.6 mm) with an equal weight of V_2O_5 particles (0.3—0.6 mm) with a spatula, followed by shaking in a pulse reactor.

Reagents. Commercial NO (more than 99.5% purity), H_2 (99.99% purity), and NH_3 (99.9% purity) were used without further purification. He or Ar as a carrier gas was purified with a titanium metal sponge heated at 1023 K and a Molecular Sieve at room temperature.

Apparatus and Procedures. Experiments were conducted using a pulse reaction apparatus, the reactor consisting of a Pyrex glass tube (4 mm i.d.). Unless otherwise specified, experiments were carried out under the following conditions: The carrier gas flow rate was 87 cm³-STP/min; the reaction temperature was 573 K; the total amount of a single pulse was 5 cm³-STP; the concentration of NO in pulse was 2.3% which corresponded to the amount of NO 5.1 μmol; the concentration of H_2 was varied over the range 1.15—4.6%, which corresponded to the amounts of H_2 2.25—10.2 μmol; catalyst weights were 5—218 mg. Before introducing the reactant pulse, all catalysts containing a metal oxide were treated with an O_2 stream at 773 K for 30 min. Columns used for gas-chromatographic analysis were tetraethylenepentamine on Difron for NH_3, silica gel for N_2O, and Molecular Sieve type 13X for H_2, N_2, and NO; they were connected in an intermediate cell system.[37] Ar (in the case of He carrier) or N_2 (in the case of Ar carrier) was used as an internal standard.

Converions of NO (X_{NO}) and H_2 (X_{H_2}), yields of NH_3 (Y_{NH_3}), N_2 (Y_{N_2}), and N_2O (Y_{N_2O}), and selectivities to NH_3 (S_{NH_3}), N_2 (S_{N_2}), and N_2O (S_{N_2O}) were calculated from outlet amounts of NO (Q_{NO}), H_2(Q_{H_2}), NH_3 (Q_{NH_3}), N_2 (Q_{N_2}), and N_2O (Q_{N_2O}) as follows:

$$X_{NO} = 1 - Q_{NO}/Q^\circ_{NO}, \quad (1)$$

$$X_{H_2} = 1 - Q_{H_2}/Q^\circ_{H_2}, \quad (2)$$

$$Y_{NH_3} = Q_{NH_3}/Q^\circ_{NO}, \quad (3)$$

$$Y_{N_2} = 2Q_{N_2}/Q^\circ_{NO}, \quad (4)$$

$$Y_{N_2O} = 2Q_{N_2O}/Q^\circ_{NO}, \quad (5)$$

$$S_{NH_3} = Y_{NH_3}/(Y_{NH_3} + Y_{N_2} + Y_{N_2O}), \quad (6)$$

$$S_{N_2} = Y_N/(Y_{NH_3} + Y_{N_2} + Y_{N_2O}), \quad (7)$$

$$S_{N_2O} = Y_{N_2O}/(Y_{NH_3} + Y_{N_2} + Y_{N_2O}), \quad (8)$$

where Q°_{NO} and $Q^\circ_{N_2}$ are the amounts of NO and H_2 injected into the reactor.

The oxidation state of V_2O_5 in the catalysts before and after the pulse reaction was studied by ESR spectroscopy, using a JEOL ME 1X spectrometer.

Results

Effect of the H_2/NO Ratio on the NO–H_2 Reaction on Pt/Al_2O_3 and Pt–V_2O_5 Mixed Catalysts. Figures 1 and 2 show results of the NO–H_2 reaction on the Pt/Al_2O_3, Pt–V_2O_5/Al_2O_3, Pt–Al_2O_3/V_2O_5(M), and Pt/Al_2O_3–V_2O_5(P) catalysts at various inlet H_2/NO ratios. As is evident from Figs. 1 and 2, the catalytic properties of these catalysts changed significantly depending on the kind of catalysts and composition of the reactants. As shown in Fig. 1, X_{NO} varied with the

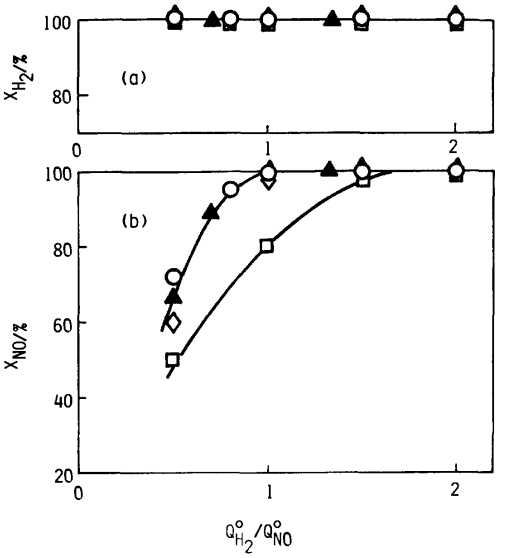

Fig. 1. Effect of the H_2/NO ratio on the conversions of NO (X_{NO}) and H_2 (X_{H_2}) in the NO–H_2 reaction on the Pt/Al_2O_3 and Pt–V_2O_5 mixed catalysts.
Catalyst weight: Pt/Al_2O_3=100 mg, Pt–V_2O_5/Al_2O_3 =109 mg, Pt/Al_2O_3–V_2O_5 (M)=200 mg, Pt/Al_2O_3–V_2O_5 (P)=200 mg (Pt weight in catalysts=500 μg). ▲: Pt/Al_2O_3, ○: Pt–V_2O_5/Al_2O_3, □: Pt/Al_2O_3–V_2O_5 (M), ◇: Pt/Al_2O_3–V_2O_5 (P).

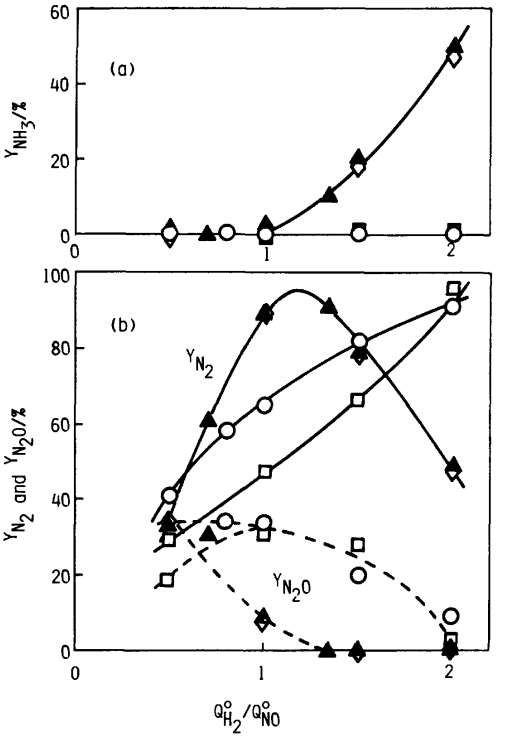

Fig. 2. Effect of the H_2/NO ratio on the yields of NH_3 (Y_{NH_3}), N_2 (Y_{N_2}), and N_2O (Y_{N_2O}) in the NO–H_2 reaction on the Pt/Al_2O_3 and Pt–V_2O_5 mixed catalysts.
Catalyst weight: Pt/Al_2O_3=100 mg, Pt–V_2O_5/Al_2O_3= 109 mg, Pt/Al_2O_3–V_2O_5(M)=200 mg, Pt/Al_2O_3–V_2O_5-(P)=200 mg (Pt weight in catalysts=500 μg). ▲: Pt/Al_2O_3, ○, Pt–V_2O_5/Al_2O_3, □: Pt/Al_2O_3–V_2O_5(M), ◇: Pt/Al_2O_3–V_2O_5(P), —: Y_{N_2}, ···: Y_{N_2O}.

$Q^\circ_{H_2}/Q^\circ_{NO}$ and the kind of catalysts, while the X_{H_2} was 100% for all of the catalysts indicated. X_{NO} for the Pt/Al_2O_3 catalyst was 100% when $Q^\circ_{H_2}/Q^\circ_{NO}$ was more than unity; that is, when $Q^\circ_{H_2}$ was greater than the stoichiometry ($Q^\circ_{H_2}/Q^\circ_{NO}=1$, that is, $H_2+NO=H_2O+1/2N_2$). As $Q^\circ_{H_2}$ decreased from the stoichiometry, X_{NO} for the Pt/Al_2O_3 catalyst decreased. X_{NO} for the $Pt-V_2O_5/Al_2O_3$ or $Pt/Al_2O_3-V_2O_5$(P) catalyst was almost equal to X_{NO} for the Pt/Al_2O_3 catalyst at any $Q^\circ_{H_2}/Q^\circ_{NO}$, while X_{NO} for the $Pt/Al_2O_3-V_2O_5$(M) catalyst was slightly lower than that for the Pt/Al_2O_3, $Pt/Al_2O_3-V_2O_5$(P), or $Pt-V_2O_5/Al_2O_3$ catalyst especially in the "lean" region, *i.e.* $Q^\circ_{H_2}/Q^\circ_{NO}<1$. As shown in Fig. 2, in the "rich" region, *i.e.* $Q^\circ_{H_2}/Q^\circ_{NO}>1$, a considerable amount of NH_3 was produced in the NO–H_2 reaction on the Pt/Al_2O_3 catalyst, and Y_{NH_3} increased markedly with increasing $Q^\circ_{H_2}/Q^\circ_{NO}$. In the NO–$H_2$ reaction on the $Pt-V_2O_5/Al_2O_3$ and $Pt/Al_2O_3-V_2O_5$(M) catalysts, no NH_3 was produced independent of the value of $Q^\circ_{H_2}/Q^\circ_{NO}$, while NO was almost selectively reduced to N_2 or N_2O as shown in Fig. 2(b). It should be emphasized that no NH_3 was produced even in the "rich" region, *i.e.* $Q^\circ_{H_2}/Q^\circ_{NO}>1$. Y_{NH_3}, Y_{N_2}, and Y_{N_2O} for the $Pt/Al_2O_3-V_2O_5$(P) catalyst were almost the same as those for the Pt/Al_2O_3 catalyst. The V_2O_5 alone was not active for the NO–H_2 reaction under the experimental conditions of the present study.

ESR spectra of all the $Pt-V_2O_5$ mixed catalysts were measured before and after the reaction at $Q^\circ_{H_2}/Q^\circ_{NO}=1.5$ or 2.0. For the $Pt-V_2O_5/Al_2O_3$ and $Pt/Al_2O_3-V_2O_5$(M) catalysts, the ESR intensity of V^{4+} ions in the used catalyst increased markedly compared with that in the fresh catalyst. For the $Pt/Al_2O_3-V_2O_5$(P), on the other hand, the ESR intensity of V^{4+} ions in the used catalyst was the same as that in the fresh catalyst. The fresh $Pt-V_2O_5$ mixed catalysts were all yellow in color. The color of the used $Pt-V_2O_5/Al_2O_3$ and $Pt/Al_2O_3-V_2O_5$(M) catalyst changed to black, but the color of the used $Pt/Al_2O_3-V_2O_5$(P) catalyst remained yellow. These data indicate that the V_2O_5 in the $Pt-V_2O_5/Al_2O_3$ and $Pt/Al_2O_3-V_2O_5$(M) catalysts was reduced during the NO–H_2 reaction in the "rich" region, *i.e.* at $Q^\circ_{H_2}/Q^\circ_{NO}=1.5$ or 2.0, while the V_2O_5 in the $Pt/Al_2O_3-V_2O_5$(P) catalyst was not reduced.

Effect of the Catalyst Weight on the NO–H_2 Reaction. The NO–H_2 reaction in the "rich" region ($Q^\circ_{H_2}/Q^\circ_{NO}=1.5$) on the Pt/Al_2O_3, $Pt-V_2O_5/Al_2O_3$, and $Pt/Al_2O_3-V_2O_5$(M) catalysts was investigated using various amounts of the catalysts. The results are shown in Figs. 3 and 4. Here, the weight of Pt in the catalyst gave the measure of the catalyst weight, since V_2O_5 was not active for the NO–H_2 reaction. Figure 3(a) shows the results of the Pt/Al_2O_3 catalyst. The maximum yield of NH_3 was attained when the Pt weight in the catalysts was *ca.* 25 μg, then Y_{NH_3} decreased gradually up to 50 μg, and it remained unchanged even with further increase of the Pt weight in catalyst. X_{NO} and X_{H_2} increased monotonically with increasing Pt weight in the catalyst, and attained 100% when the Pt weight was 50 μg. Figure 3(b) shows the results of the Pt–

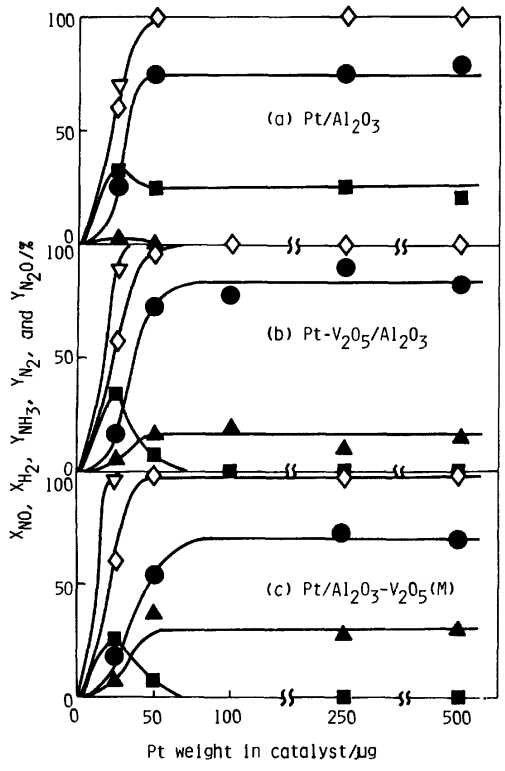

Fig. 3. Relationship between the Pt weight in the Pt/Al_2O_3 and $Pt-V_2O_5$ mixed catalysts and the activities and yields in the NO–H_2 reaction in the "rich" region ($Q^\circ_{H_2}/Q^\circ_{NO}=1.5$).
◇: X_{NO}, ▽: X_{H_2}, ■: Y_{NH_3}, ●: Y_{N_2}, ▲: Y_{N_2O}.

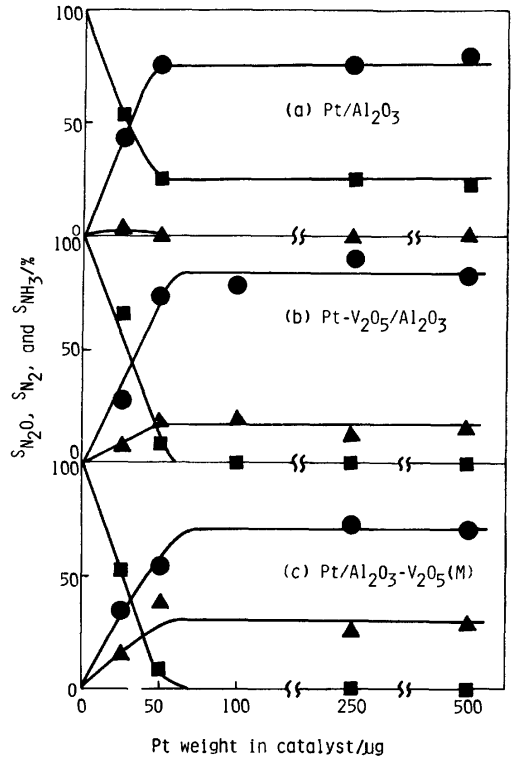

Fig. 4. Relationship between the Pt weight in the Pt/Al_2O_3 and $Pt-V_2O_5$ mixed catalysts and the selectivities in the NO–H_2 reaction in the "rich" region ($Q^\circ_{H_2}/Q^\circ_{NO}=1.5$).
■: S_{NH_3}, ●: S_{N_2}, ▲: S_{N_2O}.

V_2O_5/Al_2O_3 catalyst. Y_{NH_3} attained its maximum, which was almost the same Y_{NH_3} value as that for the Pt/Al_2O_3 catalyst when the Pt weight in the catalyst was *ca.* 25 μg, then decreased significantly with increasing Pt weight in the catalyst, and finally reached 0% when the Pt weight in the catalyst was 75 μg. The relationship between X_{NO} and the Pt weight was the same as that for the Pt/Al_2O_3 catalyst. However, X_{H_2} for the $Pt–V_2O_5/Al_2O_3$ catalyst was higher than that for the Pt/Al_2O_3 catalyst at the same Pt weight: For example, when the Pt weight in the catalyst was 25 μg, X_{H_2} for the $Pt–V_2O_5/Al_2O_3$ catalyst was about 90%, while X_{H_2} for the Pt/Al_2O_3 catalyst was about 70%. Figure 3(c) shows the results of the $Pt/Al_2O_3–V_2O_5$(M) catalyst. X_{NO}, X_{H_2}, Y_{NH_3}, Y_{N_2}, and Y_{N_2O} for the $Pt/Al_2O_3–V_2O_5$(M) were respectively in accord with those for the $Pt–V_2O_5/Al_2O_3$ catalyst. Figure 4 shows the results of S_{NH_3}, S_{N_2}, and S_{N_2O} at various catalyst weights. It is interesting to note that S_{NH_3} increased markedly with decreasing Pt weight in the catalyst in the region of low Pt weight (50 μg) and it was extrapolated to almost 100% when the Pt weight decreased to 0 μg. A similar relationship was also observed for the reaction in the "lean" region, while S_{NH_3} became 0 when the Pt weight in the catalyst was 50 μg.

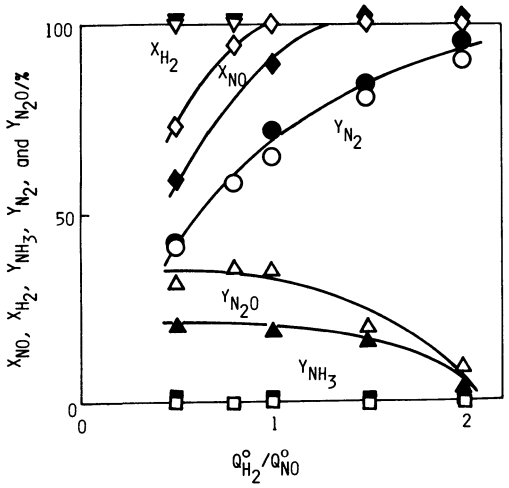

Fig. 5. Effect of the loading of V_2O_5 in the $NO–H_2$ reaction on various $Pt–V_2O_5/Al_2O_3$ catalysts.
Catalyst weight: $Pt–V_2O_5/Al_2O_3$ (9 wt% V_2O_5) = 109 mg, $Pt–V_2O_5/Al_2O_3$ (36 wt% V_2O_5) = 136 mg (Pt weight in catalysts = 500 μg). ◇, ◆: X_{NO}, ▽, ▼: X_{H_2}, □, ■: Y_{NH_3}, ○, ●: Y_{N_2}, △, ▲: Y_{N_2O}. Open symbols: $Pt–V_2O_5/Al_2O_3$ (9 wt% V_2O_5); closed symbols: $Pt–V_2O_5/Al_2O_3$ (36 wt% V_2O_5).

Effect of V_2O_5 Loading on the $NO–H_2$ Reaction on the $Pt–V_2O_5/Al_2O_3$ Catalyst. Figure 5 shows the results of the $NO–H_2$ reaction on the $Pt–V_2O_5/Al_2O_3$ catalysts with two different loadings of V_2O_5, 9 and 36 wt%. X_{H_2} was 100% irrespective of the V_2O_5 loading. X_{NO} for the $Pt–V_2O_5/Al_2O_3$ (36 wt% V_2O_5) was slightly lower than that for the $Pt–V_2O_5/Al_2O_3$ (9 wt% V_2O_5) when $Q^\circ_{H_2}/Q^\circ_{NO}$ was less than 1.5. NH_3 was not produced with either of the catalysts. Y_{N_2} was not significantly changed with the V_2O_5 loading, while Y_{N_2O} for the

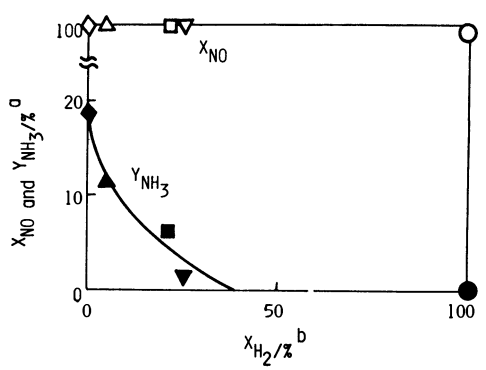

Fig. 6. Relationship between the conversion of NO (X_{NO}) and the yield of NH_3 (Y_{NH_3}) in the $NO–H_2$ reaction on various Pt–metal oxide(M) catalysts and the conversion of H_2 (X_{H_2}) in the reaction of H_2 with catalysts.
a: The $NO–H_2$ reaction, $Q^\circ_{H_2}/Q^\circ_{NO} = 1.5$, b: the reaction of H_2 with catalysts, concentration of H_2 in pulse = 3.7%. Catalyst weight; Pt/Al_2O_3 = 100 mg, Pt/Al_2O_3–metal oxide(M) = 200 mg (Pt weight in catalysts = 500 μg). ◇, ◆: Pt/Al_2O_3, △, ▲: $Pt/Al_2O_3–SnO_2$(M), □, ■: $Pt/Al_2O_3–WO_3$(M), ▽, ▼: $Pt/Al_2O_3–MoO_3$(M), ○, ●: $Pt/Al_2O_3–V_2O_5$(M). Open symbols: X_{NO}, closed symbols: Y_{NH_3}.

$Pt–V_2O_5/Al_2O_3$ (36 wt% V_2O_5) was slightly lower than that for the $Pt–V_2O_5/Al_2O_3$ (9 wt% V_2O_5).

The $NO–H_2$ Reaction on Various Pt/Al_2O_3–Metal Oxide(M) Catalysts. Figure 6 shows the results of the $NO–H_2$ reaction on various Pt/Al_2O_3–metal oxide(M) catalysts at $Q^\circ_{H_2}/Q^\circ_{NO} = 1.5$; under this condition, X_{NO} was 100% for all of the catalysts and the metal oxide itself was inactive for either the $NO–H_2$ reaction or the reaction of H_2 (or NH_3) with the catalyst. Here, the results are represented as a relationship between Y_{NH_3} in the $NO–H_2$ reaction and X_{H_2} for the reaction of H_2 with the catalyst. As shown, Y_{NH_3} for the $NO–H_2$ reaction decreased monotonically with increasing X_{H_2} for the reaction of H_2 with the catalyst and it was 0% for the $Pt/Al_2O_3–V_2O_5$(M) catalyst.

The $NO–NH_3$ Reaction, and the Reaction of H_2 or NH_3 with the Catalysts. Table 1 shows the results of the $NO–NH_3$ reaction and those of the reaction of H_2 or NH_3 with the catalysts. These experiments were

Table 1. Activities of $Pt–V_2O_5$ mixed catalysts for various reactions at 573 K

Catalyst	Weight / mg	Reaction: $NO–NH_3$[b] X_{NO}/%	H_2-catal[c] X_{H_2}/%	NH_3-catal[d] X_{NH_3}/%
Pt/Al_2O_3	100[a]	89	0	0
$Pt–V_2O_5/Al_2O_3$	109[a]	88	100	57
$Pt/Al_2O_3–V_2O_5$(M)	200[a]	87	100	2
$Pt/Al_2O_3–V_2O_5$(P)	200[a]	85	0	2
V_2O_5	100	57	0	2

a) Pt weight in catalyst = 500 μg. b) The inlet NO/NH_3 ratio = 1/1 (the inlet concentration of NO in pulse = 2.5%). c) The reaction of H_2 with the catalyst; the inlet concentration of H_2 in pulse = 3.7%. d) The reaction of NH_3 with the catalyst; the inlet concentration of NH_3 in pulse = 2.5%.

Table 2. Conversion of H_2 in the reaction of H_2 with various Pt-V_2O_5 mixed catalysts at 573 K

Catalyst	Pt weight	V_2O_5 weight	X_{H_2} a)
	μg	mg	%
Pt-V_2O_5/Al_2O_3(9 wt%V_2O_5)	25	0.5	12
Pt-V_2O_5/Al_2O_3(36 wt%V_2O_5)	25	1.8	14
Pt/Al_2O_3-V_2O_5(M)	25	5.0	19

a) The concentration of H_2 in pulse=10% (22 μmol).

made because these reactions are considered to be important steps in the NO-H_2 reaction. As shown in Table 1, X_{NO} in the NO-NH_3 reaction was almost constant for the Pt/Al_2O_3, Pt-V_2O_5/Al_2O_3, Pt/Al_2O_3-V_2O_5(M), and Pt/Al_2O_3-V_2O_5(P) catalysts, while X_{NO} for the V_2O_5 was considerably lower than those for the former catalysts. This indicates that the activity of the Pt/Al_2O_3 catalyst for the NO-NH_3 reaction is not markedly increased by the addition of V_2O_5. X_{H_2} in the reaction of H_2 with the catalyst was 100% for both the Pt-V_2O_5/Al_2O_3 and Pt/Al_2O_3-V_2O_5(M) catalysts, while it was 0% with the Pt/Al_2O_3, Pt/Al_2O_3-V_2O_5(P), or V_2O_5 catalyst. Table 2 also shows the results of X_{H_2} in the reaction of H_2 with the catalyst; the catalyst weight was considerably decreased in order to decrease the value of X_{H_2}. As shown, X_{H_2} was almost constant for the Pt-V_2O_5/Al_2O_3 (9 wt% V_2O_5), Pt-V_2O_5/Al_2O_3 (36 wt% V_2O_5), and Pt/Al_2O_3-V_2O_5(M) catalysts. These data indicate that the V_2O_5 in the Pt-V_2O_5/Al_2O_3 and Pt/Al_2O_3-V_2O_5(M) catalysts was reduced by H_2, while the V_2O_5 in the Pt/Al_2O_3-V_2O_5(P) or V_2O_5 catalyst was not reduced. The data of X_{NH_3} for the reaction of NH_3 with the catalyst (Table 1) indicate that this reaction occurred with the Pt-V_2O_5/Al_2O_3 catalyst, but NH_3 was not decomposed very much on the Pt/Al_2O_3, Pt/Al_2O_3-V_2O_5(M), Pt/Al_2O_3-V_2O_5(P), or V_2O_5 catalyst.

Discussion

Selective Reduction of NO with H_2 on the Pt-V_2O_5/Al_2O_3 Catalyst. A large amount of NH_3 is formed in the NO-H_2 reaction on Pt/Al_2O_3 catalyst.[32] The production of a large amount of NH_3 has also been confirmed in the NO-H_2-O_2 reaction on Pt/Al_2O_3 catalyst in the "rich" region.[31] These results are undesirable from the viewpoint of the selective reduction of NO to N_2 or N_2O. As shown in Fig. 2, for the NO-H_2 reaction on the Pt/Al_2O_3 catalyst, also, a significant amount of NH_3 was produced in the "rich" region of the reactant ($Q^\circ_{H_2}/Q^\circ_{NO}>1$), and the yield of NH_3 increased significantly with increasing $Q^\circ_{H_2}/Q^\circ_{NO}$. This is in accordance with the behavior in the NO-H_2 reaction[32] and in the NO-H_2-O_2 reaction[31] on Pt-Al_2O_3 catalyst. It is interesting that no NH_3 was produced in the NO-H_2 reaction on the Pt-V_2O_5/Al_2O_3 catalyst even in the "rich" region of the reactants; in addition, the conversion of NO was 100%. This behavior of the NO-H_2 reaction on the Pt-V_2O_5/Al_2O_3 catalyst is similar to that of the reaction of the synthetic exhaust gas on a three-way catalyst containing a metal oxide.[28] This indicates that the action of the added metal oxide for the selective reduction of NO to N_2 or N_2O can also be observed in the NO-H_2 reaction on Pt/Al_2O_3 catalyst containing V_2O_5—a system which is much simpler than the real three-way catalyst system.

Reaction Scheme. Although the scheme of the NO-H_2 reaction on the Pt/Al_2O_3 or Pt-V_2O_5/Al_2O_3 has not been well established, the previous data of the NO-H_2 reaction and NO-NH_3 reaction on Pt/Al_2O_3 and metal oxide catalysts lead to the reaction steps shown in Scheme I. Here, Step I is a process where NH_3

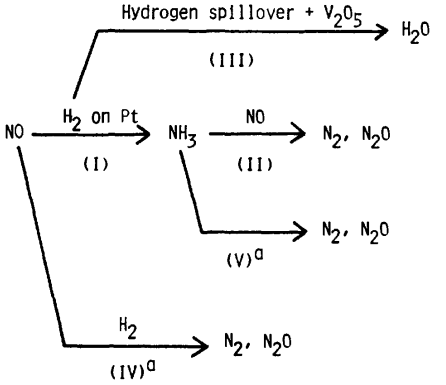

Scheme 1. Mechanism of the NO-H_2 reaction on the Pt/Al_2O_3 and Pt-V_2O_5/Al_2O_3 catalysts. a: Step IV or V does not play an important role in the NO-H_2 reaction under the conditions of this study.

is produced by the NO-H_2 reaction on Pt.[32] Step II is a process where N_2 or N_2O is formed by the NO-NH_3 reaction on Pt/Al_2O_3[38,39] and V_2O_5.[40,41] Step III is a process where V_2O_5 is reduced by the reaction with hydrogen spilled over from Pt.[42-44] Step IV is a process where NO is directly reduced to N_2 or N_2O without the formation of NH_3 as an intermediate, and it is observed in the NO-H_2 reaction on some metal oxides.[41,45-47] Step V is a process where NH_3 is decomposed to N_2 on Pt or is oxidized by V_2O_5 to N_2 or N_2O and the latter is observed on Pt-V_2O_5/$BaSO_4$[48] and metal oxides.[49] Scheme 1 merely indicates some possible steps for the NO-H_2 reaction on the Pt/Al_2O_3, and Pt-V_2O_5/Al_2O_3 catalysts; therefore, it is necessary to investigate which of these Steps I—V play the main role in the NO-H_2 reaction on the Pt/Al_2O_3 and Pt-V_2O_5/Al_2O_3 catalysts.

First, the scheme of the NO-H_2 reaction on the Pt/Al_2O_3 catalyst is discussed: Step III cannot play an important role on the Pt/Al_2O_3 catalyst because of the absence of the metal oxide. Step V is also negligible, since the decomposition of NH_3 did not occur on the Pt/Al_2O_3 (Table 1). According to Scheme 1, the primary products of the NO-H_2 reaction are determined by the relative rate of Step I to that of Step IV. From the results of S_{NH_3}, S_{N_2}, and S_{N_2O} shown in Fig. 4(a), Step IV is not considered to play a significant role in the NO-H_2 reaction on the Pt/Al_2O_3 catalyst. This is because S_{NH_3} is extrapolated to almost 100% when the Pt weight is decreased to 0. In other words, NH_3 formed by Step I is the main primary product of the NO-H_2 reaction on the Pt/Al_2O_3 catalyst. The formation of NH_3 for the reaction even in the "lean"

region supports the validity of this conclusion. As the catalyst weight increases, Y_{NO} and S_{N_2} increase, while S_{NH_3} decreases [Fig. 4(a)]. According to Scheme 1, this is ascribable to the formation of N_2 by the reaction of the unreacted NO with the formed NH_3, that is, Step II. It is therefore considered that Steps I and II proceed successively in the NO–H_2 reaction on the Pt/Al_2O_3 catalyst. This agrees with the previous inference that NH_3 is an important intermediate for the reduction of NO in the synthetic exhaust emissions[50] or for the NO–H_2–O_2 reaction[31] on the Pt/Al_2O_3 catalyst.

Next, the scheme of the NO–H_2 reaction on the Pt–V_2O_5/Al_2O_3 catalyst is discussed. As mentioned above, the V_2O_5 in the Pt–V_2O_5/Al_2O_3 and Pt/Al_2O_3–V_2O_5(M) catalysts was reduced from V^{5+} to V^{4+} during the NO–H_2 reaction in the "rich" region; and these catalysts were effective for the selective reduction of NO to N_2 or N_2O in the "rich" region. On the other hand, the V_2O_5 in the Pt/Al_2O_3–V_2O_5(P) was not reduced during the NO–H_2 reaction; and this catalyst was not effective for the selective reduction of NO. From these results coupled with the data of the reaction of H_2 with the catalyst (Table 1), Step III is considered to proceed readily in the NO–H_2 reaction on the Pt–V_2O_5/Al_2O_3 and Pt/Al_2O_3–V_2O_5(M) catalysts. Similar to the case of the Pt/Al_2O_3 catalyst, S_{NH_3} for the Pt–V_2O_5/Al_2O_3 and Pt/Al_2O_3–V_2O_5(M) catalysts is extrapolated to almost 100% when the catalyst weight decreases to 0. This indicates that Step IV does not play an important role in the NO–H_2 reaction on the Pt–V_2O_5/Al_2O_3 or Pt/Al_2O_3–V_2O_5(M) catalyst; in other words, NH_3 is the main primary product of the NO–H_2 reaction. From the data of the reaction of NH_3 with the catalyst (Table 1), Step V can take place for the Pt–V_2O_5/Al_2O_3, but it proceeds on neither the Pt/Al_2O_3–V_2O_5(M) nor Pt/Al_2O_3–V_2O_5(P) catalyst. However, Step V also does not play an important role in the selective reduction of NO to N_2 or N_2O.[51]

Rates of Steps I and III. As mentioned above, the NO–H_2 reaction on the Pt–V_2O_5/Al_2O_3 catalyst is composed of Steps I, II, and III, and the consumption of hydrogen by Step III proceeding competitively with Step I at the upper part of the catalyst bed is the main factor for the selective reduction of NO in the "rich" region. According to Scheme 1, if the rate of Step III is much slower than that of Step 1, an excess amount of NH_3 is formed in Step I. Even if a part of the excess NH_3 is converted to N_2 or N_2O in Step II, a considerable amount of NH_3 is exhausted from the catalyst bed. According to Scheme 1, also, if the rate of Step III is much faster than that of Step I, the amount of NH_3 produced in Step I is not enough to convert NO completely to N_2 or N_2O in Step II; therefore, the unreacted NO is emitted from the outlet of the catalyst bed. If the rate of formation of NH_3 in Step I is successfully controlled by Step III, the NH_3 produced in Step I reacts with the unreacted NO to form N_2 or N_2O selectively (Step II). Therefore, it is important to investigate the rates of Steps I and III in terms of the composition of the reactants and structures of the catalysts. Although we have not conducted experiments to determine the rates of Steps I and III, $Q_{H_2}(I)$ and $Q_{H_2}(III)$ defined by Eqs. 9 and 10 would be useful as measures of the rates of Steps I and III.

$$Q_{H_2}(I) = Q^\circ_{NO}(5/2\ Y_{NH_3} + Y_{N_2} + 1/2\ Y_{N_2O}), \quad (9)$$

$$Q_{H_2}(III) = Q^\circ_{H_2} \cdot X_{H_2} - Q_{H_2}(I). \quad (10)$$

Each coefficient of Y_{NH_3}, Y_{N_2}, or Y_{N_2O} in Eq. 9 is determined by the stoichiometry of the formation of each product. As is evident from Eqs. 9 and 10, $Q_{H_2}(I)$ and $Q_{H_2}(III)$ are respectively the amounts of H_2 consumed by Steps I and III during the NO–H_2 reaction. Under the experimental conditions shown in Figs. 1, 2, and 5, X_{H_2} is 100%; therefore, Eq. 10 leads to Eq. 11 under the stated conditions.

$$Q_{H_2}(III) = Q^\circ_{H_2} - Q^\circ_{H_2}(I). \quad (11)$$

$Q_{H_2}(I)$ and $Q_{H_2}(III)$ are calculated from the data of the NO–H_2 reaction shown in Figs. 1, 2, and 5. As shown in Figs. 7 and 8, $Q_{H_2}(I)$ for the Pt/Al_2O_3 is almost equal to $Q^\circ_{H_2}$ at any $Q^\circ_{H_2}/Q^\circ_{NO}$, while $Q_{H_2}(III)$ for the Pt/Al_2O_3 is very small, which means that almost all of the H_2 in the reactants are consumed by Step I. This is reasonable since Step III occurs only very slightly on the Pt/Al_2O_3 catalyst. As for the results of the Pt–V_2O_5/Al_2O_3 catalysts, $Q_{H_2}(I)$ is almost equal to $Q^\circ_{H_2}$ in the "lean" region of the reactants ($Q^\circ_{H_2}/Q^\circ_{NO}<1$). Correspondingly, the value of $Q_{H_2}(III)$ is very small in this region. In other words, in the "lean" region of the reactants, little H_2 is consumed in Step III but most of the H_2 is consumed in Step I. In the "rich" region of the reactants ($Q^\circ_{H_2}/Q^\circ_{NO}>1$), $Q_{H_2}(I)$ for the Pt–V_2O_5/Al_2O_3 catalyst is almost independent of $Q^\circ_{H_2}/Q^\circ_{NO}$, while $Q_{H_2}(III)$ increases markedly with increasing $Q^\circ_{H_2}/Q^\circ_{NO}$. This means that excess H_2 in the "rich" region is almost selectively removed by Step III, and hence the formation of excess NH_3 in Step I is suppressed. Such changes of $Q_{H_2}(I)$ and $Q_{H_2}(III)$ with $Q^\circ_{H_2}/Q^\circ_{NO}$ for the Pt–V_2O_5/

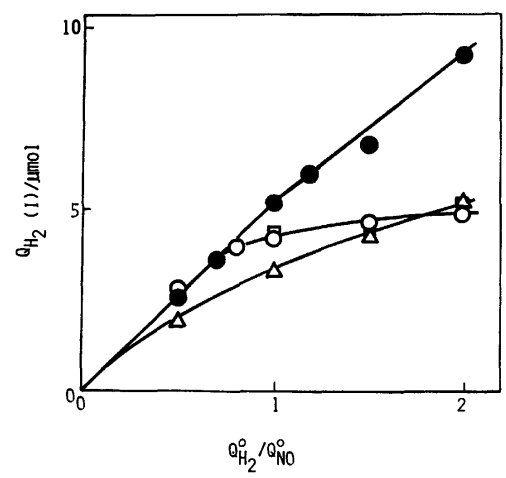

Fig. 7. Consumption of H_2 in Step I in the NO–H_2 reaction on the Pt/Al_2O_3 and various Pt–V_2O_5 mixed catalysts.
Catalyst weight: Pt/Al_2O_3=100 mg, Pt–V_2O_5/Al_2O_3 (9 wt% V_2O_5)=109 mg, Pt–V_2O_5/Al_2O_3 (36 wt% V_2O_5)=136 mg, Pt/Al_2O_3–V_2O_5(M)=200 mg (Pt weight in catalysts=500 μg). ●: Pt/Al_2O_3, ○: Pt–V_2O_5/Al_2O_3 (9 wt% V_2O_5), □: Pt–V_2O_5/Al_2O_3 (36 wt% V_2O_5), △: Pt/Al_2O_3–V_2O_5(M).

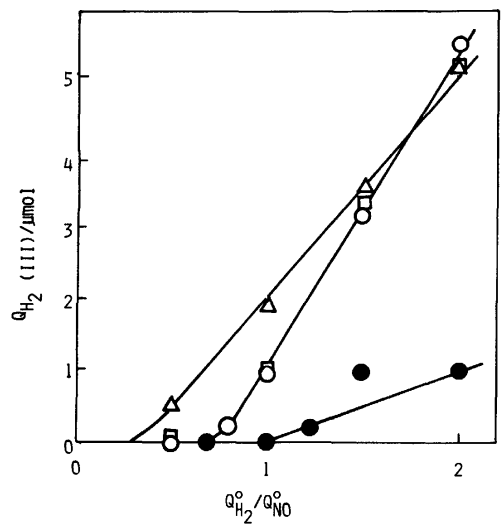

Fig. 8. Consumption of H_2 in Step III in the NO–H_2 reaction on the Pt/Al_2O_3 and various Pt–V_2O_5 mixed catalysts.
Catalyst weight: Pt/Al_2O_3=100 mg, Pt–V_2O_5/Al_2O_3 (9 wt% V_2O_5)=109 mg, Pt–V_2O_5/Al_2O_3 (36 wt% V_2O_5)=136 mg, Pt/Al_2O_3–V_2O_5(M)=200 mg (Pt weight in catalysts=500 μg). ●: Pt/Al_2O_3, ○: Pt–V_2O_5/Al_2O_3 (9 wt% V_2O_5), □: Pt–V_2O_5/Al_2O_3 (36 wt% V_2O_5), △: Pt/Al_2O_3–V_2O_5(M).

Al_2O_3 catalyst are desirable from the viewpoint of the selective reduction of NO. The reason for this is that, in the "lean" region, a reducing agent (H_2) is effectively used for the reduction of NO, whereas, in the "rich" region, an excess amount of reducing agent is removed by Step III and the formation of excess NH_3 is suppressed. In this manner, selective reduction of NO to N_2 or N_2O is warranted for a broad composition of the reactants. As shown in Fig. 7, Q_{H_2}(I) for the Pt–V_2O_5/Al_2O_3 is almost independent of $Q^{\circ}_{H_2}/Q^{\circ}_{NO}$ in the "rich" region of the reactants. This is in accordance with the behavior of the reduction of NO in the NO–H_2–O_2 reaction on Pt/Al_2O_3 catalyst.[31] According to the computer simulation of the NO–H_2–O_2 reaction on the Pt/Al_2O_3 catalyst,[31] the rate of the reduction of NO with H_2 is only slightly decreased even if the amount of adsorbed hydrogens on Pt surface is decreased by the addition of O_2 to the system.

References

1) M. Shelef, *Catal. Rev.*, **11**, 1 (1975).
2) J. Wei, *Adv. Catal.*, **24**, 57 (1975).
3) T. Ono, *Shokubai*, **19**, 142 (1977).
4) H. Ohara, S. Kondo, and Y. Fujitani, *Papers Soc. Automotive Eng. Jpn.*, **16**, 9 (1978).
5) W. M. Wang, *SAE Paper*, 800052 (1980).
6) J. G. Riverd, *SAE Paper*, 730005 (1973).
7) R. Zechnall, G. Baumann, H. Eisele, and R. Bosch, *SAE Paper*, 730566 (1973).
8) W.E. Bernhardt, "The Catalytic Chemistry of Nitrogen Oxides," ed by R. L. Klimisch and J. G. Larson, Plenum Press, New York, N.Y. (1975), p. 297.
9) S. Nakagawa and T. Yamaguchi, *J. Soc. Automotive Eng. Jpn.*, **31**, 1175 (1977).
10) M. Konno, *J. Soc. Automotive Eng. Jpn.*, **31**, 1182 (1977).
11) M. Kawai and H. Watanabe, *J. Soc. Automotive Eng. Jpn.*, **32**, 122 (1978).
12) R. P. Canale, C. R. Carlson, S. R. Winegarden, and D. L. Miles, *SAE Paper*, 780205 (1978).
13) R. E. Seiter and R. J. Clark, *SAE Paper*, 780203 (1978).
14) C. D. Falk and J. J. Mooney, *SAE Paper*, 800462 (1980).
15) G. L. Beuerle, G. R. Service, and K. Nobe, *Ind. Eng. Chem. Prod. Res. Dev.*, **11**, 54 (1972).
16) D. R. Ashmead, J. S. Campbell, P. Davies, and K. Famery, *SAE Paper*, 740249 (1974).
17) K. C. Taylor, "The Catalytic Chemistry of Nitrogen Oxides," ed by R. L. Klimisch and J. G. Larson, Plenum Press, New York, N.Y. (1975), p. 173.
18) J. C. Schlatter, *SAE Paper*, 780199 (1978).
19) P. Oser, *SAE Paper*, 790306 (1979).
20) F. Morikawa, *Kagaku To Kogyo*, **34**, 203 (1981).
21) H. Ohara, Y. Miura, and Y. Fujitani, *Preprints Meeting Soc. Automotive Eng. Jpn.*, **1978**, 629.
22) H. S. Gandhi and M. Shelef, *Patent Application*, No. 607660 (1975).
23) H. C. Yao and M. Shelef, *J. Catal.*, **44**, 392 (1976).
24) H. S. Gandhi, H. C. Yao, Y. K. Steipein, and J. T. Kummer, 2nd Chem. North Am. Continent, San Francisco, 1980, No. 150.
25) J. C. Summers and S. A. Ausen, *J. Catal.*, **58**, 131 (1979).
26) J. C. Schlatter and P. J. Mitchell, *Ind. Eng. Chem. Prod. Res. Dev.*, **19**, 288 (1980).
27) J. E. Hunter, *SAE Paper*, 720122 (1972).
28) H. S. Gandhi, A. G. Piken, M. Shelef, and R. G. Delosh, *SAE Paper*, 760210 (1976).
29) S. Nakagawa and A. Tamano, *J. Soc. Automotive Eng. Jpn.*, **32**, 1025 (1978).
30) J. H. Jones, J. T. Kummer, K. Otto, M. Shelef, and E. E. Weaver, *Environ. Sci. Technol.*, **5**, 790 (1971).
31) A. Miyamoto, B. Inoue, and Y. Murakami, *Ind. Eng. Chem. Prod. Res. Dev.*, **18**, 104 (1979).
32) M. Schelef and H. S. Gandhi, *Ind. Eng. Chem. Prod. Res. Dev.*, **11**, 393 (1972).
33) Y. Murakami, M. Inomata, A. Miyamoto, and K. Mori, *Proc. 7th Int. Congr. Catal.*, Tokyo, 1980, Kodansha (Tokyo) and Elseiver (Amsterdam-Oxford-New York) (1981), p. 1344.
34) M. Niwa and Y. Murakami, *J. Catal.*, **26**, 359 (1972).
35) M. Niwa and Y. Murakami, *J. Catal.*, **27**, 26 (1972).
36) Y. Murakami, "Some Theoretical Problems of Catalysis," ed by T. Kwan, G. K. Boreskov, and K. Tamaru, University of Tokyo Press, Tokyo (1973), p. 203.
37) Y. Murakami, *Bull. Chem. Soc. Jpn.*, **32**, 316 (1959).
38) T. Otto, M. Shelef, and J. T. Kummer, *J. Phy. Chem.*, **74**, 2690 (1970).
39) T. Otto, M. Shelef, and J. T. Kummer, *J. Phy. Chem.*, **75**, 875 (1971).
40) A. Miyamoto, Y. Yamazaki, and Y. Murakami *Nippon Kagaku Kaishi*, **1977**, 619.
41) Y. Murakami, K. Hayashi, K. Yasuda, T. Ito, T, Minami, and A. Miyamoto, *Nippon Kagaku Kaishi*, **1977**, 173.
42) Since V_2O_5 alone was not reduced by H_2 (Table 1), one can neglect a mechanism that V_2O_5 is directly reduced by H_2.
43) P. A. Sermon and G. C. Bond, *Catal. Rev.*, **8**, 211 (1973).
44) K. Fujimoto and S. Asaoka, *Sekiyu Gakkai Shi*, **19**, 837 (1976).
45) E. Echigoya, H. Niiyama, and A. Ebitani, *Nippon Kagaku Kaishi*, **1974**, 222.
46) A. Ebitani, H. Niiyama, and E. Echigoya, *Nippon Kagaku Kaishi*, **1974**, 1185.

47) E. Echigoya, H. Niiyama, A. Ebitani, and H. Iida, *Bull. Jpn. Petrol. Inst.*, **17**, 232 (1975).
48) N. I. Il'chenko, *Kinet. Katal.*, **17**, 380 (1976).
49) Y. Kosaki, A. Miyamoto, and Y. Murakami, *Bull. Chem. Soc. Jpn.*, **52**, 617 (1979).
50) R. L. Klimisch and K. C. Taylor, *Environ. Sci. Technol.*, **7**, 12 (1973).
51) (i) The activity of the $Pt-V_2O_5/Al_2O_3$ catalyst for the reaction with NH_3 was considerably lower than that for the reaction with H_2 (Table 1). (ii) Although the activity of the $Pt-V_2O_5/Al_2O_3$ catalyst for the reaction with NH_3 was much higher than that of the $Pt/Al_2O_3-V_2O_5$ (M) catalyst, the behavior of Y_{NH_3} in the $NO-H_2$ reaction on the $Pt/Al_2O_3-V_2O_5$ (M) catalyst at various catalyst weights was almost the same as that on the $Pt-V_2O_5/Al_2O_3$ catalyst (Fig. 3).

Electric Birefringence and Electric Dichroism of Sonicated DNA in Aqueous Solutions with Various Additives. Electro-optical and Hydrodynamic Properties

Koichiro MATSUDA and Kiwamu YAMAOKA*
Faculty of Science, Hiroshima University, Higashisenda-machi, Naka-ku, Hiroshima 730
(Received October 2, 1981)

Electric birefringence (EB) and electric linear dichroism (ED) of a sonicated DNA ($M_w = 1.24 \times 10^5$) sample were studied in solutions containing various additives at 7 °C. Signals of EB at 535 nm and of ED at 260 nm were measured in the electric field range 0—*ca.* 19 kV/cm. Both signals obeyed the Kerr law at low field strengths ($E <$ *ca.* 5 kV/cm) and showed a saturating trend at high fields. The mean relaxation time, $\langle\tau\rangle_{EB}$, obtained from the decay of EB, was field-strength dependent, indicating the effect of the polydispersity of sDNA. The field strength dependence of steady-state EB signals was nearly identical with that of ED signals. These results were analyzed with the "classical" orientation functions derived for mono- and polydisperse systems. The optical anisotropy factor ($g_3 - g_1$) of sDNA was *ca.* -2.0×10^{-2}, while the average angle between the orientation axis of sDNA and the transition moment of the base pair was *ca.* 70° at 260 nm. The electric moment of sDNA was influenced by ionic strength, counterions, and other additives. The weight-average length l_w of sDNA decreased in this order: 0.2 mM NaCl**>9-aminoacridinium chloride ($P/D = 10$)>1.0 mM NaCl>0.33 mM $MgCl_2$> 20 vol% glycerol. Values of l_w/base pair were 2.8—2.7 Å in the glycerol and 3.6—3.4 Å in the 1.0 mM NaCl.

Electric dipole moments of DNA in solutions have been investigated by various methods, *e.g.*, electric birefringence (EB),[1-16] electric dichroism (ED),[3-5,17-27] and dielectric relaxation.[28-33] Both EB and ED are powerful techniques for studying the optical, electric, and hydrodynamic properties of DNA in aqueous solutions. With reversing-pulse electric birefringence, Greve and Heij[7] and Yamaoka and Matsuda[15] recently demonstrated that DNA fragments have no permanent dipole moment. Hogan *et al.*[21] found that an apparent dipole moment of DNA is inversely proportional to the square-root of ionic strength. There have been numerous observations that the electro-optical property of DNA is very sensitive to its molecular weight and to external conditions such as ionic strength and small molecular weight additives in solutions.[5,11,13-16,19,21,23] Stellwagen[16] recently studied the electro-optical and hydrodynamic properties of restriction enzyme fragments of DNA whose lengths vary widely, exposing a number of interesting points to be clarified. The decay process of birefringence, for example, could not be explained by a monodisperse system when the DNA fragments are larger than 217 base pairs (bp). The previous studies[1-33] are unanimous in pointing out that native DNA in solution can be oriented by an external electric field, but they also indicate that the nature of the electric moments responsible for field orientation remains to be clarified. Sustained efforts are needed for resolving this problem. For this purpose, the intrinsic effects of the polydispersity of DNA length and the flexibility of DNA chain, and the external effects of the various ionic additives must be considered on a systematic basis.

The present study is the first of a series of work on the electro-optical properties of DNA and related biopolymers. In this paper, the electric field strength dependence of steady-state signals of EB and ED was examined with a sonicated rodlike DNA (sDNA) sample under various ionic conditions. The decay curve of the EB signal was also measured an a function of field strength. This is a result that cannot be explained if the sample is monodisperse. Hence, tan analytical method for the polydisperse system was utilized to compare the observed EB and ED data with theoretical orientation functions. The length of sDNA in solutions with various additives was not constant, but was influenced by external factors. The applicability of the "classical" mixed orientation function $\Phi(\beta, \gamma)$[34] was tested for the sDNA system.

** 1 mM = 10^{-3} mol dm^{-3}.

Experimental

Materials. A calf thymus DNA sample was purchased from Worthington Biochemical Corp (USA). The sonication procedure for sDNA was described elsewhere.[26] The protein content was determined to be less than 0.01 mg/1 mg DNA by the microbiuret method. The weight-average molecular weight was determined to be *ca.* 1.24×10^5 by ultracentrifugation.[26] (The ratio of the weight-average to the number-average molecular weight for sonicated DNA samples is known to be in the range between 1.02 and 1.11.[35]) The cationic dye, 9-aminoacridinium chloride (AA), was described in previous papers.[36-38] Other chemicals used were of reagent grade.

Preparation of Sample Solutions. The stock sDNA solution (*ca.* 1 mg cm^{-3}) containing *ca.* 1 mM NaCl was prepared in an ice bath. The solutions were unbuffered to avoid any effect of buffer cations.[37] Each stock DNA solution was diluted ten-fold and dialyzed against NaCl or $MgCl_2$ solutions of desired ionic strength at 4 °C for *ca.* 48 h. The concentration of AA was determined by using a molar absorption coefficient, ε, of 1.03×10^4 M^{-1} cm^{-1} at 401 nm.[37] The sDNA–AA solution was prepared by adding the dye solution to the sDNA solution at a molar mixing ratio of DNA-phosphate residue-to-dye (P/D) of 10, the final concentration of AA being 10 μM. The concentration of sDNA solution was determined photometrically with a molar absorption coefficient of 6400 M^{-1} cm^{-1} at 258.5 nm.[39] The sDNA in a 20 vol% glycerol–0.8 mM NaCl solution was prepared in an ice bath by adding glycerol to the aqueous sDNA solution. The hyperchromicity of the denatured sDNA solution containing either 1.0 mM NaCl or 0.2 mM NaCl was higher than 30%.[39,40] Absorption spectra were measured at 7 °C on a

Hitachi EPS-3T double-beam recording spectrophotometer equipped with a thermostated cell holder.

Measurements of Electric Birefringence and Electric Linear Dichroism. An EB apparatus constructed in our laboratory was used.[41] The voltage and the duration of a single square-wave electric pulse field were continuously varied between 0.248 and 3.24 kV and between *ca.* 40 and 150 μs, respectively. The instrumental response time for a transient birefringence signal was usually faster than 0.5 μs; this was checked with nitrobenzene.[42] The linear response between the transmitted light intensity and the output voltage generated across a load resistor was verified by testing the Malus law.[42] In order to determine the sign of the birefringence and to increase the sensitivity of the signal, a quarter-wave plate was placed before the analyzer. The phase retardation was measured at 535 nm and at 7 °C with the procedure described previously.[4,5,42] An electric linear dichroism apparatus was also built in our laboratory and has been described in detail.[24,38] Both the parallel dichroism ($\Delta A_{\parallel}/A$) and the perpendicular dichroism ($\Delta A_{\perp}/A$)[24,25,38] were measured at 7 °C and at 260 nm. The voltage and the duration of a single square-wave electric pulse field were varied between 0.455 and 3.91 kV and between 50 and 200 μs. The linear response between the photocurrent and the incident light intensity was checked with a metal mesh of a known absorbance (= 1.20),[24] the deviation being always kept less than 1%. For both EB and ED, optical path lengths of the "Kerr" cell were 2 cm (electrode gap 0.33 cm) and 1 cm (electrode gap 0.207 cm).[38] Two electric pulses were usually applied to each fresh solution, but the sample solution was discarded after a single high-field pulse to avoid denaturation of sDNA.

Method of Data Analysis

Analysis of Steady-state. For a monodisperse system, the steady-state birefringence (Δn) of a rodlike polymer of axial symmetry (the 3-axis) may be given as[34]

$$\Delta n = \frac{\lambda}{d}\cdot\frac{\delta}{2\pi} = \frac{2\pi C_v}{n}(g_3-g_1)\Phi, \tag{1}$$

where λ is the wavelength of light *in vacuo*, d is the path length, δ is the phase retardation of solution, n is the refractive index of the solution, C_v is the volume fraction of solute, (g_3-g_1) is the optical anisotropy factor, and Φ is the orientation function. Correspondingly, the steady-state reduced dichroism ($\Delta A/A$) is given as[4,38,43]

$$\frac{\Delta A}{A} = \frac{A_{\parallel}-A_{\perp}}{A} = \frac{\Delta A_{\parallel}}{A} - \frac{\Delta A_{\perp}}{A} = \frac{3}{2}(3\cos^2\theta - 1)\Phi, \tag{2}$$

where $\Delta A_{\parallel}/A$ and $\Delta A_{\perp}/A$ are the specific parallel and perpendicular dichroisms, respectively. A is the isotropic absorbance of the solution in the absence of an electric field. θ is the angle between the transition moment of a chromophoric group and the orientation axis of sDNA.

For a polydisperse system, the molecular weight (or the length for rodlike molecules) distribution of a polymer sample must be considered. For this purpose, the Schulz-Zimm function was assumed;[44,45] then, the number-average length distribution density function $f_n(l)$ is given as[38]

$$f_n(l) = \frac{(ym_0)^k}{\Gamma(k)} l^{k-1}e^{-ym_0 l}, \tag{3}$$

where y and k are related to the number-average and the weight-average molecular weights (M_n and M_w) as $M_n = k/y$ and $M_w = (k+1)/y$. The conformation of sDNA is a rigid double-stranded helix and is approximated by a cylindrical model. The molecular weight M of an sDNA molecule may be equated to $m_0 l$, where l is the contour length and m_0 is the molecular weight per unit length. The ratio M_w/M_n may be equated to the ratio of weight-average length to number-average length, *i.e.*, l_w/l_n. According to the analytical method devised for the polydisperse system,[27] Eqs. 1 and 2 may be expressed in terms of the sum of the contributions from component species of heterogeneous lengths, for which the length distribution density function is defined by Eq. 3:[38]

$$\Delta n = \frac{2\pi(g_3-g_1)\bar{C}_v}{n}\cdot\frac{\int_{L_1}^{L_2} l f_n(l)\Phi dl}{\int_{L_1}^{L_2} l f_n(l) dl} \equiv \frac{2\pi(g_3-g_1)\bar{C}_v}{n}\langle\Phi\rangle_w, \tag{4}$$

and similarly,

$$\frac{\Delta A}{A} \equiv \frac{3}{2}(3\cos^2\theta - 1)\langle\Phi\rangle_w, \tag{5}$$

where $\bar{C}_v$ is the total volume of all solute molecules with various chain lengths divided by the volume of solution and $\langle\Phi\rangle_w$ is the weight-average orientation function. Both L_1 and L_2 are the lower and upper limits of l.

The field strength dependence of the steady-state EB or ED for many DNA systems[5,13,14,16,18,19,21,25,27] has been described by the "classical" orientation function, $\Phi(\beta,\gamma)$, where $\beta = \mu E/kT$ and $\gamma = \Delta\alpha E^2/2kT$ (≥ 0).[34] Notations are the same as those in Refs. 34 and 38.

Analysis of Decay Process. The electric birefringence-average relaxation time $\langle\tau\rangle_{EB}$ and initial slope $\langle S\rangle_{EB}$ of the decay process of EB for the polydisperse system are given as[27,46,47]

$$\langle\tau\rangle_{EB} = \int_0^{\infty}\frac{\Delta n(t)}{\Delta n(0)}dt = \frac{\int_{L_1}^{L_2}\tau(l) l f_n(l)\Phi dl}{\int_{L_1}^{L_2} l f_n(l)\Phi dl}, \tag{6}$$

$$\langle S\rangle_{EB} = -\int_{L_1}^{L_2}\tau(l)^{-1} l f_n(l)\Phi dl \Big/ \int_{L_1}^{L_2} l f_n(l)\Phi dl, \tag{7}$$

where $\Delta n(t)$ is the birefringence at time t after removal of an electric field, $\Delta n(0)$ is the birefringence of the steady-state. $\tau(l)$ is the relaxation time for a cylindrical molecule of length l and may be calculated from the Broersma equation:[48]

$$\tau(l) = \frac{\pi\eta_0 l^3}{18kT}\left[\ln\frac{l}{b} - 1.57 + 7\left(\frac{1}{\ln(l/b)} - 0.28\right)^2\right]^{-1}, \tag{8}$$

where η_0 is the viscosity of the solvent and b is the radius of the cylinder.

At infinitely high field strength, Φ approaches unity.[34,43] Then, Eqs. 6 and 7 become the weight-average relaxation time,

$$\langle\tau\rangle_w = \int_{L_1}^{L_2}\tau(l) l f_n(l) dl \Big/ \int_{L_1}^{L_2} l f_n(l) dl, \tag{9}$$

and the weight-average initial slope,

$$\langle S\rangle_w = -\left\langle\frac{1}{\tau}\right\rangle_w = -\int_{L_1}^{L_2}\tau(l)^{-1} l f_n(l) dl \Big/ \int_{L_1}^{L_2} l f_n(l) dl, \tag{10}$$

respectively. These quantities are independent of the electric parameters, β and γ, since the orientation function is not involved. Once $\langle\tau\rangle_w$ and $\langle S\rangle_w$ are obtained from the experimental data, the ratio l_w/l_n and the length l_w can be evaluated;[27] with these values, the most likely Schulz-Zimm function may be determined.

Results and Discussion

Electric Field Strength Dependence of the Steady-state Birefringence and Linear Dichroism. Figure 1 shows the field strength dependence of the birefringence ($\Delta n/C$) of sDNA in solutions with various additives. Values of $\Delta n/C$ tend to saturate at high field strengths. The sign of Δn is negative in all cases. No positive or peculiar signal of Δn could be observed at low fields, contrary to the report by Colson *et al.*[6] At a given field strength, *e.g.*, 10 kV/cm, values of $-\Delta n/C$ of sDNA decrease with solvent compositions in this order: 0.2 mM NaCl>AA(P/D=10)–1.0 mM NaCl>1.0 mM NaCl>0.33 mM $MgCl_2$>20 vol% glycerol–0.8 mM NaCl. This result does not necessarily indicate a difference in the degree of orientation of sDNA in solutions with various additives. The birefringence at an electric field strength and at a wavelength is given by the product of the orientation factor and the optical factor (*cf.* Eq. 1). Hence, the different values of Δn arise from the differences in these factors. In order to obtain values of (g_3-g_1), μ, and $\Delta\alpha$ of sDNA, the experimental points will be compared with the theoretical orientation functions (see Discussion, together with Fig. 5).

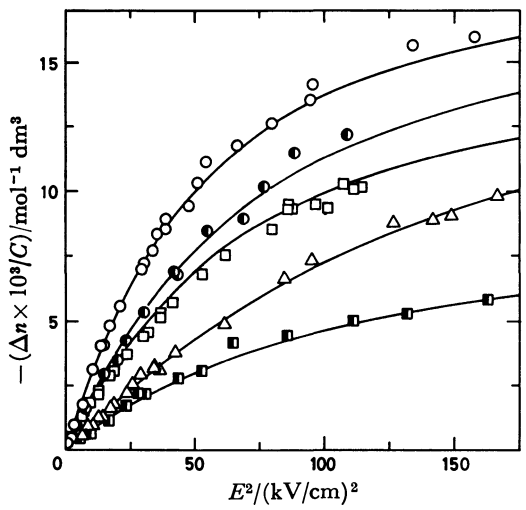

Fig. 1. The field strength dependence of the birefringence ($\Delta n/C$) of sDNA at 535 nm and at 7 °C in solutions with various additives. The residue concentration of sDNA (C) and the concentration of additives are: C=0.165 mM and [NaCl]=0.2 mM (○); C=0.10 mM, [AA]=0.01 mM, and [NaCl]=1.0 mM (◐); C=0.171 mM and [NaCl]=1.0 mM (□); C=0.22 mM and [$MgCl_2$]=0.33 mM (△); C=0.10 mM, [NaCl]=0.8 mM, and 20 vol% glycerol (◧). Symbols indicate experimentally determined points, while solid curves are the theoretical ones calculated by using the orientation function $\langle\Phi(\beta,\gamma)\rangle_w$ for the polydisperse system.

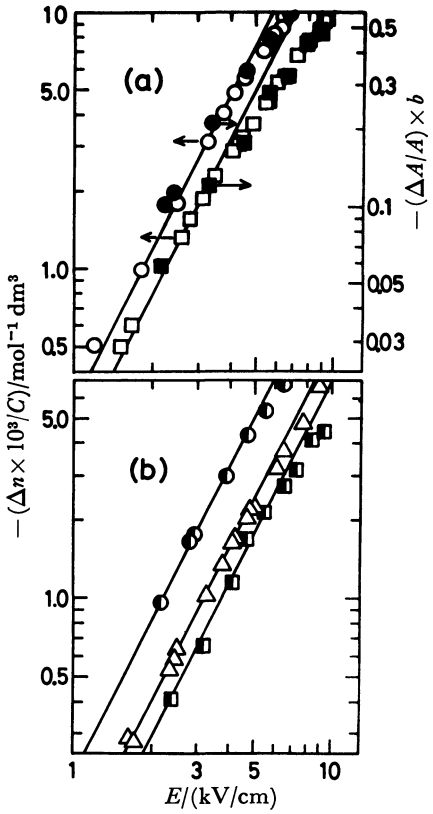

Fig. 2. The double-logarithmic plots of the field-strength dependence of both $\Delta n/C$ and $\Delta A/A$ of sDNA in the low field strength region. The slope of the straight lines is 2. The right ordinate refers to values of $\Delta A/A$ of sDNA at 260 nm and at 7 °C in 0.2 mM NaCl (●), for which b=1.1, and in 1.0 mM NaCl (■) for which b=1.0. Other symbols and conditions are the same as in Fig. 1.

Figure 2 shows the double logarithmic plots of $\Delta n/C$ against E. In the low field strength region, the experimental points follow a straight line with a slope of 2; thus, the Kerr law holds for sDNA in various solvents (E<5 kV/cm). The field strength dependence of reduced dichroism ($\Delta A/A$) of sDNA in 0.2 and 1.0 mM NaCl solutions is also shown in Fig. 2(a) (closed symbols). The sign of $\Delta A/A$ is negative for both cases. In the same low field strength region (E<5 kV/cm), the Kerr law holds for sDNA. This quadratic field strength dependence of EB and ED has been predicted by the electro-optical theories for molecules with cylindrical symmetry.[34,43,49] Hence, the dependence of EB and ED on the first power of electric field in the low field region, as was observed by Sokerov and Weill for the aqueous sDNA solution,[12] must be considered rather anomalous. From our result in Fig. 2, it is now verified that the Kerr law holds for the low molecular weight, rodlike sDNA in diverse cases. The fact that the straight lines of $\Delta n/C$ and $\Delta A/A$ in Fig. 2(a) are superimposed upon each other is reasonable, considering that the orientation function Φ in Eqs. 1 and 2 must be the same for a given sDNA solution provided that the backbone conformation of the sDNA molecule is rigid.

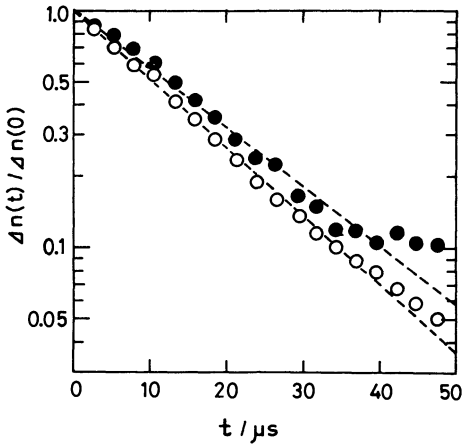

Fig. 3. The semi-logarithmic plots of the field-free decay curves of EB for sDNA in a 20 vol% glycerol–0.8 mM NaCl solution at a low field strength (E=6.45 kV/cm) (●) and at a high field strength (E=10.5 kV/cm) (○). Dashed lines (------) are straight lines.

Electric Field Strength Dependence of the Relaxation Time of sDNA. As a precautionary example, two normalized decay curves of birefringence, $(\Delta n(t)/\Delta n(0))$, are shown in Fig. 3 for sDNA in a 20 vol% glycerol–0.8 mM NaCl solution. The field-free decay curve (open circles) of EB after removal of a high electric field yields a nearly straight line (dashed line) on a semilogarithmic plot, whereas the curve displayed by a solution subjected to a low electric field (filled circles) deviates slightly from the straight line, being larger than the former. This example clearly indicates that a single decay curve of EB at a relatively high electric field may often result in an ambiguity over whether or not a polymer system is monodisperse. In order to determine whether the polymer system is polydisperse, the electric field strength dependence of relaxation times must be examined. The field-free relaxation time of sDNA from a low electric field should be larger than that of sDNA from a high electric field, if the sample is polydisperse.

Figure 4 shows the electric field dependence of birefringence-average relaxation time $\langle\tau\rangle_{EB}$. The persistence length of DNA is generally 1.5×10^3 Å in 5 mM NaCl[50] or 1.3×10^3 Å in 30 mM NaCl.[51] These values are much larger than the contour length of an sDNA molecule of 1.24×10^5 daltons. Therefore, the present sDNA sample is probably a rigid rod with little

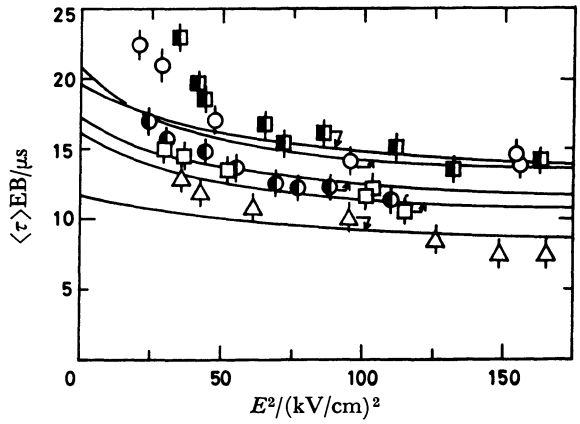

Fig. 4. The dependence of birefringence-average relaxation times, $\langle\tau\rangle_{EB}$, of sDNA solutions obtained from the field-free decay curves on the applied electric field strength. Symbols and conditions are the same as in Fig. 1. Solid lines are theoretical curves calculated by the use of Eq. 6 with the parameters (l_w/l_n, l_w, $\beta_w^2/2\gamma_w$). These values for each curve are: l_w/l_n=1.16, l_w=742 Å, and $\beta_w^2/2\gamma_w$=2 (—○—); l_w/l_n=1.16, l_w=674 Å, and $\beta_w^2/2\gamma_w$=2 (—□—); l_w/l_n=1.16, l_w=533 Å, and $\beta_w^2/2\gamma_w$=4 (—■—); l_w/l_n=1.16, l_w=682 Å, and $\beta_w^2/2\gamma_w$=4 (—◐—); l_w/l_n=1.16, l_w=596 Å, and $\beta_w^2/2\gamma_w$=2 (—△—).

flexibility at low ionic strengths. The results in Fig. 4 may be best explained by the effect of the length polydispersity of sDNA. An analytical method for treating the decay process of the polydisperse rigid rodlike system was recently developed.[27] According to this method, the values of l_w/l_n and l_w for a given sDNA sample can be determined from the weight-average relaxation time $\langle\tau\rangle_w$ and the weight-average initial slope $\langle S\rangle_w$ at infinitely high field, provided that an appropriate length distribution is assumed. The best values of l_w/l_n and l_w can be determined by comparing experimental values of $\langle\tau\rangle_w$ and $\langle S\rangle_w$ with the theoretical values of $\langle\tau\rangle_w$ and $\langle S\rangle_w$ which were calculated from Eqs. 9 and 10. In this work, the Schulz-Zimm function (Eq. 3) was used for the length distribution density function, together with two values of 10 Å[52] and 13 Å[16,21] for the radius b of the cylinder assumed for sDNA. Two sets of parameters (l_w/l_n, l_w) thus determined are given in Table 1. The theoretical relaxation times calculated from Eq. 6 with the experi-

TABLE 1. THE WEIGHT-AVERAGE RELAXATION TIME, $\langle\tau\rangle_w$, THE WEIGHT-AVERAGE LENGTH, l_w, AND THE WEIGHT-AVERAGE LENGTH PER BASE PAIR FOR sDNA IN SOLUTIONS CONTAINING DIFFERENT COUNTERIONS

sDNA in	$I\times10^3$ [a]	$\langle\tau\rangle_w$ [b]	b[c]=10 Å (l_w/l_n=1.16)[d]		b[c]=13 Å (l_w/l_n=1.17)[d]	
		μs	l_w[d]/Å	(l_w/bp)[e]/Å	l_w[d]/Å	(l_w/bp)[e]/Å
0.2 mM NaCl	0.2	12.5	742	3.9	712	3.8
1.0 mM NaCl	1.0	9.7	674	3.6	645	3.4
20 vol% glycerol, 0.8 mM NaCl	0.8	11.4	533	2.8	509	2.7
AA(P/D=10), 1.0 mM NaCl	1.0	10.0	682	3.6	635	3.4
0.33 mM $MgCl_2$	1.0	7.0	596	3.2	569	3.0

a) I is the ionic strength. b) Values obtained from the relaxation time $\langle\tau\rangle_{EB}$ which is extrapolated to infinitely high field strength. c) b is the radius of the cylinder for sDNA in Å (1 Å=0.1 nm). d) Values of l_w were evaluated from Eqs. 9 and 10 with experimental values of $\langle\tau\rangle_w$ and $-\langle S\rangle_w^{-1}$(=4.68μs) by using a constant value of l_w/l_n. e) bp is the number of base pairs, which is 188 for sDNA.

mentally obtained parameters (l_w/l_n, l_w, and $\beta_w^2/2\gamma_w$) for each sDNA solution are also shown by solid curves in Fig. 4. The "classical" mixed orientation function $\langle\Phi(\beta, \gamma)\rangle_w$ was utilized for the calculation of the theoretical relaxation times (the reason is given later). Except for the low field strength region, the experimental points are in fairly good agreement with the theoretical curve in each case.

The weight-average length (l_w) of sDNA given in Table 1 decreases with the increase of the ionic strength or the valence of counterion. The value of $\langle\tau\rangle_{EB}$ or $\langle\tau_w\rangle$ for the sDNA in the 20 vol% glycerol–0.8 mM NaCl solution is almost equal to that for the sDNA in the 0.2 mM NaCl solution. However, the values of l_w are very different. This is because the solvent viscosity of the former solution is about 2.2 times larger than that of the latter. The weight-average length per base pair (l_w/bp) is also given in Table 1; it decreases in the order: 0.2 mM NaCl>AA ($P/D=10$)–1.0 mM NaCl> 1.0 mM NaCl>0.33 mM $MgCl_2$>20 vol% glycerol–0.8 mM NaCl. The value of l_w/bp in 1.0 mM NaCl is 3.4—3.6 Å, which is close to that for B-form DNA, whereas it is 2.7—2.8 Å in 20 vol% glycerol–0.8 mM NaCl, which is close to that of A-form DNA. The latter value appears to support the proposals by Nelson and Johnson[53] and Ivanov *et al.*[54,55] that the A-form DNA exists in water–alcohol solutions.

The decay curve of ED was not analyzed in the present work, because the time constant for the signal detector of our ED apparatus was *ca.* 2.7 μs (with a load resister of 12 kΩ) for good signal-to-noise ratios. The good transient signals of EB could be measured with the instrumental decay time less than 0.5 μs (at a load resister of 2 kΩ) for the same sDNA solutions under the identical experimental conditions; therefore, the analysis of decay curves was possible in this case. Since the field strength dependence of the steady-state EB and ED is superimposable upon each other (*vide post*), the mean relaxation times of EB and ED may be the same for a given sDNA solution.

Electro-optical Properties of sDNA. Figure 5 shows the field strength dependence of the steady-state EB and ED signals of sDNA in 0.2 mM (circles) and 1.0 mM (squares) NaCl solutions. In order to obtain both the electric dipole moments responsible for field orientation and the intrinsic birefringence and dichroism (Δn_s and $(\Delta A/A)_s$), the experimental data may be compared with the theoretical orientation function. The orientation function $\Phi(\kappa)$ proposed by Kikuchi and Yoshioka,[49]

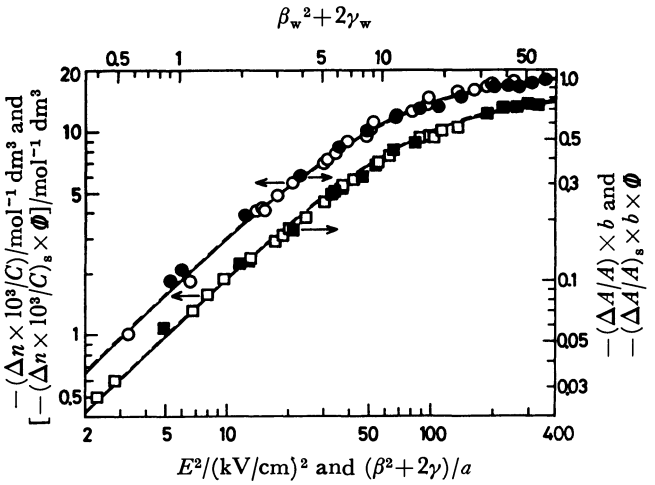

Fig. 5. Comparison of experimental values of birefringence and reduced dichroism for sDNA in 0.2 mM NaCl (○ for EB and ● for ED) and 1.0 mM NaCl (□ for EB and ■ for ED) solutions with the theoretical orientation functions, Φ, for the monodisperse and polydisperse systems. Two sets of the double-logarithmic plots are shown: $\Delta n/C$ against E^2 (○, □); $(\Delta n/C)_s\,\Phi(\beta, \gamma)$ against $(\beta^2+2\gamma)/a$ (——); $(\Delta n/C)_s\,\langle\Phi(\beta, \gamma)\rangle_w$ against $(\beta_w^2+2\gamma_w)$ (----); $\Delta A/A$ against E^2 (●, ■); $(\Delta A/A)_s\,\Phi(\beta, \gamma)$ against $(\beta^2+2\gamma)/a$ ¦(——); $(\Delta A/A)_s\,\langle\Phi(\beta, \gamma)\rangle_w$ against $\beta_w^2+2\gamma_w$ (----). The intrinsic values of $(\Delta n/C)_s$ and $(\Delta A/A)_s$ are given in Table 2. The factor a is 0.192, while the factor b is 1.0 for (■) and 1.1 for (●). Symbols and experimental conditions are the same as in Fig. 2 (a).

in which ion-atmosphere polarization is considered, seems to be the most reasonable one for the polyelectrolyte with axial symmetry. The applicability of $\Phi(\kappa)$ has been already tested for sodium poly(*p*-styrenesulfonate) (NaPSS) and NaPSS–AA systems.[38] It was, however, found that the fitting of $\Phi(\kappa)$ to the experimental data is good only in the low field strength range. In view of this fact, the function $\Phi(\beta, \gamma)$ has been employed for many DNA systems.[5,13,14,16,18,19,21,25,27] It will be also used in this work, although it was originally derived for nonionized polymers.

The experimental points in Fig. 5 (open symbols for EB and closed symbols for ED) fit not only the theoretical curves for monodisperse system, $\Phi(\beta, \gamma)$.[34] but also those for polydisperse system, $\langle\Phi(\beta, \gamma)\rangle_w$, fairly well over a wide range of field strength, provided that values of the interaction terms, β and γ, or, β_w and γ_w, are

Table 2. Electro-optical properties of sDNA in solutions of different counterions

sDNA in	$I\times10^3$	$\mu_w\times10^{-3}$ [a] / D [b]	μ_w/bp / D	$\langle\Delta\alpha\rangle_w\times10^{16}$ [a] / $\mathrm{cm^3}$ [b]	$-(\Delta n/C)_s$ [c] / $\mathrm{mol^{-1}\,dm^3}$	$-(g_3-g_1)$	$-(\Delta A/A)_s$
0.2 mM NaCl	0.2	4.5	24	2.6	0.023	0.027	1.0(70)[d]
1.0 mM NaCl	1.0	4.0	21	2.0	0.016	0.018	0.88(68)
20 vol% glycerol, 0.8 mM NaCl	0.8	3.3	18	0.7	0.009	0.011	
AA($P/D=10$), 1.0 mM NaCl	1.0	3.8	20	0.9	0.019	0.022	
0.33 mM $MgCl_2$	1.0	2.7	14	0.9	0.018	0.021	

a) The number-average distribution density function $f_n(l)$ with the parameters ($l_w/l_n=1.16$, l_w in Table 1) was used. b) 1 D$=3.336\times10^{-30}$ C m, and 1 $\mathrm{cm^3}=1.113\times10^{-16}$ F $\mathrm{m^2}$. c) C stands for the residue concentration of sDNA. d) Values in parentheses are the angles θ in degrees.

adjusted. This is because the curve of $\Phi(\beta, \gamma)$ for the monodisperse system differs only slightly from that of $\langle\Phi(\beta, \gamma)\rangle_w$, if $l_w/l_n<1.3$. Hence, it is difficult to determine uniquely the exact electric property of sDNA in solutions from the field strength dependence of Δn (or $\Delta A/A$). Nevertheless, $\langle\Phi(\beta, \gamma)\rangle_w$ should be employed because, as noted in the preceding section, it was verified that the sDNA sample is a polydisperse system. The best values of β_w ($=\mu_o l_w E/kT$) and γ_w ($=\Delta\alpha_o l_w E^2/2kT$), where $\mu_w=\mu_o l_w$ and $\Delta\alpha_w=\Delta\alpha_o l_w$, were read by the curve fitting method[25,34,38,42] and are given in Table 2. It has been shown by reversing-pulse electric birefringence that sDNA has no appreciable permanent dipole moment, but has only a pseudo-permanent dipole moment.[15] It is clear that this moment depends strongly on the ionic strength and the species of counterions and decreases in the order (*cf.* Table 2): 0.2 mM NaCl>1.0 mM NaCl>AA ($P/D=10$)-1.0 mM NaCl>20 vol% glycerol-0.8 mM NaCl>0.33 mM $MgCl_2$. In conclusion, the electric dipole moment of sDNA may be accounted for by the counterion-induced dipole moment which originates from the interaction between the counterions of sDNA and the applied external field.

From values of Δn_s at infinitely high field strength, together with the partial specific volume of 0.55 cm^3/g in 1 mM NaCl (Emonds-Alt *et al.*),[13] the optical anisotropy factor (g_3-g_1) was estimated to be $-(2.7-1.1)\times10^{-2}$ for sDNA at 535 nm. This result is in good agreement with the values of $-(2.0-0.5)\times10^{-2}$ at 550 nm (Houssier *et al.*)[5,13] and $-(2.8-2.3)\times10^{-2}$ at 633 nm (Stellwagen).[16] These values are much larger than $-(7.1-6.4)\times10^{-4}$ for high molecular weight DNA at 633 nm (Marion *et al.*).[14]

The apparent angle θ between the plane of base pair and the orientation axis of sDNA helix was estimated from Eq. 5 and is given in Table 2. It is in good agreement with the θ value of $73°\pm3°$ at 265 nm obtained for digested fragment DNA by Hogan *et al.*[22] It is very close to the value for A-form DNA or the revised B-form DNA,[56] but differs from that for the original B-form DNA. The apparent tilt angle remains unchanged by a 5-fold increase in NaCl concentration, while the weight-average length per base pair, l_w/bp, decreases about 10% (*cf.* Table 1). In 1.0 mM NaCl, however, the value of l_w/bp is 3.6 Å, which is close to that of B-form DNA (l_w/bp=3.4 Å). The value of $(\Delta A/A)_s$ should represent the true tilt angle of *ca.* 70° between the plane of the bases and the orientation axis of the sDNA helix, only if no out-of-plane transition (such as the n-π^* transition) is involved in the 260 nm band of the bases. In order to determine the exact conformation of rigid rodlike DNA in solutions with various additives, we should study the wavelength dependence of reduced dichroism spectra of DNA over the entire UV region.

Conclusion

The field strength dependence of both the steady-state EB and the field-free relaxation time of sDNA in solutions with various additives can be described over a wide range of field strength by the "classical" mixed-dipole orientation function $\langle\Phi(\beta, \gamma)\rangle_w$ for the polydisperse system. Similarly, the dependence of steady-state ED of sDNA is fitted by this orientation function with the same electric and distribution parameters (β_w, γ_w, l_w/l_n, and l_w). The weight-average length and the electric dipole moment for sDNA are strongly influenced by the ionic strength, the species of counterions, and additives, while the optical properties such as the apparent tilt angle (*ca.* 70°) and the optical anisotropy factor (*ca.* −0.02) are constant. The value of l_w/bp for sDNA in 20 vol% glycerol is close to 2.5 Å for A-form DNA, but that of l_w/bp for sDNA in 1 mM NaCl is close to 3.4 Å for B-form DNA.

We are deeply indebted to Mr. K. Fukudome for the use of his original computer program for calculating the polydispersity parameters, for participating in many discussions, and for determining the protein content of a DNA sample. We also thank Mr. K. Takarada for measuring the ED data.

References

1) M. L. Allais, *J. Chim. Phys. Phys.-Chim. Biol.*, **59**, 873 (1962).
2) M. Shirai, *Nippon Kagaku Zasshi*, **86**, 18 (1965).
3) T. Soda and K. Yoshioka, *Nippon Kagaku Zasshi*, **87**, 1326 (1966).
4) K. Yamaoka and E. Charney, *Macromolecules*, **6**, 66 (1973).
5) E. Fredericq and C. Houssier, "Electric Dichroism and Electric Birefringence," Clarendon Press, Oxford (1973), pp. 129—159.
6) P. Colson, C. Houssier, E. Fredericq, and J. A. Bertolotto, *Polymer*, **15**, 396 (1974).
7) J. Greve and M. E. de Heij, *Biopolymers*, **14**, 2441 (1975).
8) C. Houssier, J. Bontemps, X. Emonds-Alt, and E. Fredericq, *Ann. N. Y. Acad. Sci.*, **303**, 170 (1977).
9) B. Roux, J. C. Bernengo, C. Marion, and M. Hanss, *J. Colloid Interface Sci.*, **66**, 421 (1978).
10) N. C. Stellwagen, "Molecular Electro-Optics," ed by C. T. O'Konski, Marcel Dekker, Inc., New York (1978), Part 2, Chap. 18, pp. 645—683.
11) D. C. Rau and V. A. Bloomfield, *Biopolymers*, **18**, 2783 (1979).
12) S. Sokerov and G. Weill, *Biophys. Chem.*, **10**, 161 (1979).
13) X. Emonds-Alt, C. Houssier, and E. Fredericq, *Biophys. Chem.*, **10**, 27 (1979).
14) C. Marion, B. Roux, J. C. Bernengo, and M. Hanss, *Int. J. Biol. Macromol.*, **2**, 235 (1980).
15) K. Yamaoka and K. Matsuda, *Macromolecules*, **13**, 1558 (1980).
16) N. C. Stellwagen, *Biopolymers*, **20**, 399 (1981).
17) G. A. Dvorkin, *Dokl. Akad. Nauk. SSSR*, **135**, 739 (1960).
18) M. Shirai, *Nippon Kagaku Zasshi*, **86**, 1115 (1965).
19) D. W. Ding, R. Rill, and K. E. Van Holde, *Biopolymers*, **11**, 2109 (1972).
20) J. Ramstein, C. Houssier, and M. Leng, *Biochim. Biophys. Acta*, **335**, 54 (1973).
21) M. Hogan, N. Dattagupta, and D. M. Crothers, *Proc. Natl. Acad. Sci. U.S.A.*, **75**, 195 (1978).
22) M. Hogan, N. Dattagupta, and D. M. Crothers, *Biochemistry*, **18**, 280 (1979).

23) E. Charney, K. Yamaoka, and G. S. Manning, *Biophys. Chem.*, **11**, 167 (1980).
24) K. Yamaoka and K. Matsuda, *J. Sci. Hiroshima Univ., Ser. A*, **43**, 185 (1980).
25) K. Yamaoka and K. Matsuda, *Macromolecules*, **14**, 595 (1981).
26) E. Charney and K. Yamaoka, *Biochemistry*, **21**, 834 (1982).
27) K. Yamaoka and K. Fukudome, manuscript in preparation.
28) S. Takashima, *J. Mol. Biol.*, **7**, 455 (1963).
29) M. Sakamoto, H. Kanda, R. Hayakawa, and Y. Wada, *Biopolymers*, **15**, 879 (1976).
30) M. Sakamoto, R. Hayakawa, and Y. Wada, *Biopolymers*, **17**, 1507 (1978).
31) M. Sakamoto, R. Hayakawa, and Y. Wada, *Biopolymers*, **18**, 2769 (1979).
32) M. Sakamoto, R. Hayakawa, and Y. Wada, *Biopolymers*, **19**, 1039 (1980).
33) M. Sakamoto, T. Fujikado, R. Hayakawa, and Y. Wada, *Biophys. Chem.*, **11**, 309 (1980).
34) C. T. O'Konski, K. Yoshioka, and W. H. Orttung, *J. Phys. Chem.*, **63**, 1558 (1959).
35) J. E. Godfrey, *Biophys. Chem.*, **5**, 285 (1976).
36) K. Yamaoka, *Biopolymers*, **11**, 2537 (1972).
37) M. Takatsuki, *Bull. Chem. Soc. Jpn.*, **53**, 1922 (1980).
38) K. Matsuda and K. Yamaoka, *Bull. Chem. Soc. Jpn.*, **55**, 69 (1982).
39) K. Yamaoka and R. A. Resnik, *J. Phys. Chem.*, **70**, 4051 (1966).
40) K. Yamaoka and M. Masujima, *Biopolymers*, **17**, 2485 (1978).
41) K. Yamaoka, T. Ichibakase, K. Ueda, and K. Matsuda, *J. Am. Chem. Soc.*, **102**, 5109 (1980).
42) K. Yamaoka, Ph. D. Thesis, University of California, Berkeley, U. S. A., 1964.
43) K. Yamaoka and E. Charney, *J. Am. Chem. Soc.*, **94**, 8963 (1972).
44) G. V. Schulz, *Z. Phys. Chem.*, **B43**, 25 (1939).
45) B. H. Zimm, *J. Chem. Phys.*, **16**, 1099 (1948).
46) K. Yoshioka and H. Watanabe, *Nippon Kagaku Zasshi*, **84**, 626 (1963).
47) K. Yoshioka and H. Watanabe, "Physical Principles and Techniques of Protein Chemistry," ed by S. J. Leach, Academic Press, New York (1969), Part A, Chap. 7, pp. 335—367.
48) S. Broersma, *J. Chem. Phys.*, **32**, 1626 (1960).
49) K. Kikuchi and K. Yoshioka, *Biopolymers*, **15**, 583 (1976).
50) R. E. Harrington, *Biopolymers*, **17**, 919 (1978).
51) C. Frontali, E. Dore, A. Ferrauto, E. Gratton, A. Bettini, M. R. Pozzen, and E. Valdevit, *Biopolymers*, **18**, 1353 (1979).
52) R. T. Kovacic and K. E. Van Holde, *Biochemistry*, **16**, 1490 (1977).
53) R. G. Nelson and W. C. Johnson, Jr., *Biochem. Biophys. Res. Commun.*, **41**, 211 (1970).
54) V. I. Ivanov, L. E. Minchenkova, A. K. Schyolkina, and A. I. Poletayev, *Biopolymers*, **12**, 89(1973).
55) V. I. Ivanov, L. E. Minchenkova, E. E. Minyat, M. D. Frank-Kamenetskii, and A. K. Schyolkina, *J. Mol. Biol.*, **87**, 817 (1974).
56) M. Levitt, *Proc. Natl. Acad. Sci. U.S.A.*, **75**, 640 (1978).

Conformational Analysis of Stilbenes by Photoelectron Spectroscopy

Tsunetoshi KOBAYASHI,* Hiroshi SUZUKI,† and Keiichiro OGAWA†
The Institute of Physical and Chemical Research, Wako, Saitama 351
The Institute for Solid State Physics, The University of Tokyo, Roppongi, Minato-ku, Tokyo 106
†*Department of Chemistry, College of General Education, The University of Tokyo, Komaba, Meguro-ku, Tokyo 153*
(Received October 13, 1981)

Conformations of (*Z*)-stilbene, (*E*)-stilbene, and various methyl-substituted (*E*)-stilbenes were discussed from the standpoint of photoelectron spectroscopy. Photoelectron spectral data of (*Z*)-stilbene and (*E*)-stilbene were found to be perfectly consistent with the results by the gas electron diffraction method concerning the twist angles of the phenyl groups. The twist angles of the phenyl groups in various methyl-substituted (*E*)-stilbenes were estimated using the photoelectron spectral data by the new method presented recently. These estimated values correspond well to those obtained from the standpoint of the electronic absorption spectra.

Steric hindrance and molecular conformation are important subjects in organic chemistry. We have been studying the steric hindrance effect on photoelectron spectra[1] and the application of photoelectron spectroscopy to conformational analysis[2] of various types of organic compounds. In this paper we investigate the conformations of some stilbenes from the standpoint of photoelectron spectroscopy.

Conformations of stilbenes have long been and are still attracting great interests from the structural chemical and reaction mechanistic standpoints.[3] Although (*Z*)-stilbene (ZS) has mostly and reasonably been regarded or concluded to be nonplanar or twisted because of the steric hindrance effect between the two phenyl groups, (*E*)-stilbene (ES) has often been presumed on the basis of the x-ray crystallographic analysis,[4] or concluded to be essentially planar even in the fluid phases (see, however, Ref. 5, for example). However, according to the recent gas electron diffraction study,[6] ES is not planar but its two phenyl groups are twisted by 32.2° from the olefinic group plane, and this value is rather close to that of ZS, 43.2°.[7]

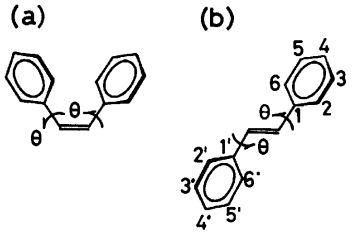

Fig. 1. Twisted conformations of (*Z*)-stilbene (a) and (*E*)-stilbene (b).

In this work, at first we examine if the photoelectron spectral data of ZS and ES are consistent with the gas electron diffraction results[6,7] concerning the twist angles of the phenyl groups, θ, and then we carry out the conformational analysis of various methyl-substituted ES's. In the conformational analysis we use the new technique developed in our recent paper.[2c] Concerning the photoelectron spectra of stilbenes, formerly we[1e] and Maier and Turner[8] studied both ZS and ES regarding ES as (nearly) planar in the vapors. Dewar and Goodman[9] reported the ionization energy values of ES by a low-resolution instrument, and Kricka *et al.*[10] those of ZS without interpretation. Afterwards Hudson *et al.*[11] treated the photoelectron spectra of ES and diphenylpolyenes regarding these as planar, and McAlduff and Chan[12] those of ES, (*E*)-4-methylstilbene (E4MS), and other 4-substituted ES's, concluding that these are planar.

Previously one of us (H.S.) developed a method for conformational analysis using electronic absorption spectra on the HMO level and discussed the conformations of various stilbenes in detail.[5,13] In this paper the conformational analysis by photoelectron spectroscopy is compared with that by this electronic absorption spectroscopic method.

Experimental

Materials. (*E*)-2,2′-Dimethylstilbene (E22′ DMS) (mp 81.0—82.0 °C, from hexane), (*E*)-3,3′-dimethylstilbene (E33′-DMS) (mp 58.0—58.5 °C, from ethanol), and (*E*)-2,2′,5,5′-tetramethylstilbene (E22′55′TMS) (mp 161.0—162.0 °C, from hexane) were prepared according to the procedure of Mukaiyama *et al.*[14] (Melting points are uncorrected.) Found for E22′55′TMS: C, 91.31; H, 8.70%; M+, 236. Calcd for $C_{18}H_{20}$: C, 91.47; H, 8.53%; M, 236. Preparations of (*E*)-4-methylstilbene (E4MS), (*E*)-4,4′-dimethylstilbene (E44′DMS), and (*E*)-2,2′,4,4′,6,6′-hexamethylstilbene (E22′44′66′HMS) were reported previously,[13c] and ZS was a commercial product of Aldrich Chemical Co.

Measurements. The HeI photoelectron spectra of the methyl-substituted ES's were measured using the photoelectron spectrometer described formerly.[1c] The sample inlet and target chamber systems were heated and kept at 131 °C for E4MS and E44′DMS, at 115 °C for E22′DMS, at 111 °C for E33′DMS and E22′55′TMS, and at 134 °C for E22′44′-66′HMS.

The electronic absorption spectra of ZS, E22′DMS, E33′-DMS, and E22′55′TMS in heptane were newly measured on a Hitachi EPS-3T spectrometer.

Computational

The CNDO/S calculations of ZS and ES were carried out with a FACOM 230-75 computer at the Institute of Physical and Chemical Research. All the necessary atomic integrals and parameters were taken from or estimated according to Ref. 15.

The geometrical structural parameters of ES and ZS necessary for the CNDO/S calculations were taken from or properly assumed based on Refs. 6 and 7. Their values are as follows:

The C=C–C bond angles, the C=C and the C–C bond lengths are 129.5°, 1.334 Å, and 1.489 Å for ZS, and 127.0°, 1.332 Å, and 1.483 Å for ES, respectively. The C=C–H bond angles, the C=C and the C–H bond lengths were taken to be 129.4°, 1.398 Å, and 1.095 Å, respectively, commonly both for ZS and ES.

Results and Discussion

(Z)- and (E)-Stilbene. The photoelectron spectra of ZS and ES were formerly studied by us[1e] in detail and also by Maier and Turner.[8] According to these former researches the first and the fifth bands of each compound are the so-called conjugation π bands and correspond to the ionizations from the π molecular orbitals delocalized over the entire molecular carbon frameworks, and the energy difference between these two molecular orbitals is quite sensitive to the change in θ. We use, therefore, the differences between the first and the fifth vertical ionization energies, $\Delta E_{IV}^{1,5}$, of these compounds to estimate θ from the photoelectron spectra.

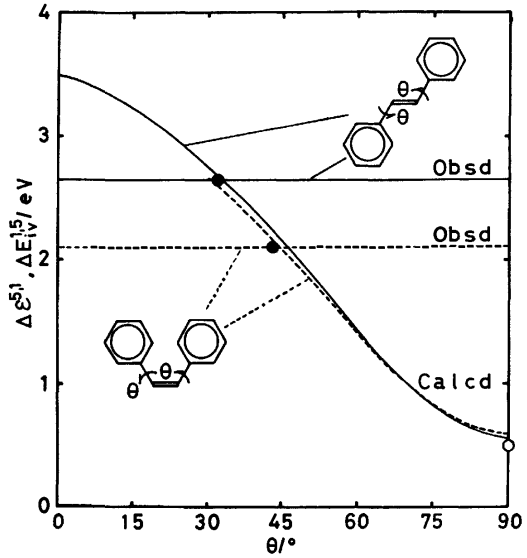

Fig. 2. Twist angle, θ, dependences of calculated energy differences between fifth and first highest occupied π molecular orbitals, $\Delta\varepsilon^{5,1}$, for (*Z*)- and (*E*)-stilbene with observed differences between first and fifth vertical ionization energies, $\Delta E_{IV}^{1,5}$.
The solid circles denote the gas electron diffraction results combined with the observed $\Delta E_{IV}^{1,5}$ values and the open one the estimated $\Delta E_{IV}^{1,5}$ for $\theta=90°$.

In Fig. 2 are shown the energy differences between the fifth and the first highest occupied π molecular orbitals, $\Delta\varepsilon^{5,1}$, for ZS and ES calculated by the CNDO/S method against θ. In the calculations the twist angles θ of the two phenyl groups of ZS or ES were assumed to be the same as each other. The $\Delta E_{IV}^{1,5}$ values at the twist angles of 90° for ZS and ES are commonly estimated to be 0.49 eV by using the first and the second ionization energies of ethylbenzene, 8.78 and 9.27 eV,[2c] and the first ones of (*Z*)- and (*E*)-1,2-dimethylethylene, 9.12 eV.[16] The calculated $\Delta\varepsilon^{5,1}$ *vs.* θ curve for ZS or ES passes the point very close to this estimated value at 90°. This fact suggests that the calculated $\Delta\varepsilon^{5,1}$ *vs.* θ curves in Fig. 2 simulate well the real $\Delta E_{IV}^{1,5}$ *vs.* θ curves for ZS and ES in the large θ region.

At first as a test case we treat ZS which is apparently a heavily sterically hindered compound. If we compare the observed difference between the first and the fifth vertical ionization energies, 2.10 eV, with the $\Delta\varepsilon^{5,1}$ *vs.* θ curve for ZS, we get 45° as the estimation for the θ value of ZS. This estimated value is very close to that observed by the gas electron diffraction method, 43.2°.[7] This satisfactory result and the point that ZS is structurally closely related with ES may guarantee the applicability of the same procedure to ES to estimate θ.

By applying the above procedure to ES we get 33° as θ. This estimated value is again very close to the one determined by the gas electron diffraction method, 32.2°.[6] From this result we can say that the photoelectron spectra of ZS and ES are perfectly consistent with the gas electron diffraction results concerning the twist angles, and that the phenyl groups of ES are considerably twisted in the gas phase from the photoelectron spectral point of view also.

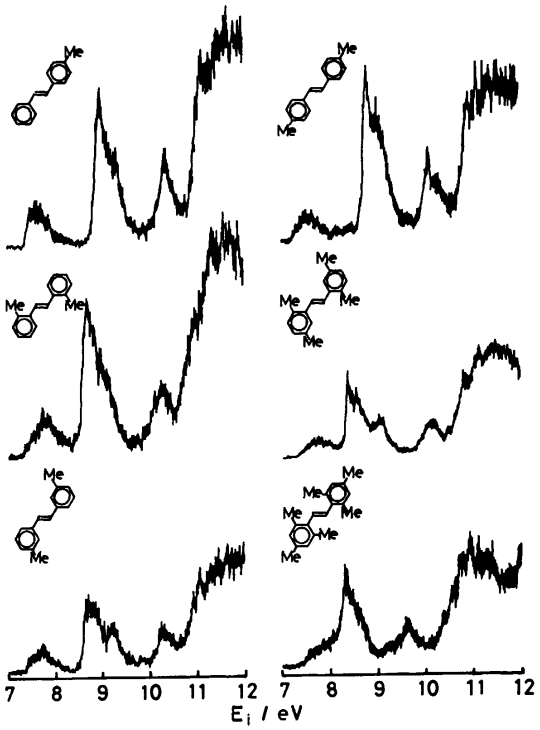

Fig. 3. Photoelectron spectra of methyl-substituted (*E*)-stilbenes.

Methyl-substituted (E)-Stilbenes. Now let us move to the conformational analysis of various methyl-substituted ES's. The photoelectron spectra of various methyl-substituted ES's are shown in Fig. 3. The vertical ionization energies obtained from these spectra are summarized in Table 1.

Judging from the vertical ionization energy values the first five bands of the methyl-substituted ES's are safely correlated with those of ES,[1e] respectively, that is, the first and the fifth bands correspond to the ioniza-

TABLE 1. VERTICAL IONIZATION ENERGIES, E_{iv}, OF STILBENES

Compound	E_{iv}/eV					
	Band					
	1	2	3	4	5	6
(*Z*)-Stilbene (ZS)[a)]	8.17	8.99	9.22	9.36	10.27	11.3
(*E*)-Stilbene (ES)[a)]	7.87	9.08	9.08	9.50	10.51	11.3
(*E*)-4-Methylstilbene (E4MS)	7.63	9.02	9.02	9.33	10.33	11.1
(*E*)-2,2′-Dimethylstilbene (E22′DMS)	7.83	8.72	8.72	9.17	10.27	11.0
(*E*)-3,3′-Dimethylstilbene (E33′DMS)	7.74	8.73	8.73	9.20	10.25	11.1
(*E*)-4,4′-Dimethylstilbene (E44′DMS)	7.54	8.82	8.82	9.0	10.12	11.0
(*E*)-2,2′,5,5′-Tetramethylstilbene (E22′55′TMS)	7.63	8.37	(8.6)	9.02	10.06	10.8
(*E*)-2,2′,4,4′,6,6′-Hexamethylstilbene (E22′44′66′HMS)	7.9	8.29	8.29	8.8	9.61	10.5

a) Ref. 1e.

tions from the π molecular orbitals delocalized over the entire molecular carbon frameworks. The second and the third bands of each compound correspond to the ionizations from the π molecular orbitals formed by the combinations between the two benzene ring e_{1g}(A) type orbitals, and the fourth band to the ionization from the π molecular orbital formed mainly by the out-of-phase type of combination between the two benzene ring e_{1g}(S) type orbitals slightly mixed with the olefinic anti-bonding π orbital. Here the e_{1g}(S) orbital denotes one of the degenerate $e_{1g}\pi$ orbitals of benzene ring and is symmetric against the mirror plane passing the 1- and the 4-position and perpendicular to the benzene ring plane, and the e_{1g}(A) orbital denotes the other e_{1g} orbital orthogonal to the e_{1g}(S) orbital mentioned above.

Now we estimate the θ values of these methyl-substituted ES's using the energy differences between the first and the fifth π bands. We have already seen the fact that the $\Delta\varepsilon^{5,1}$ *vs.* θ curves for ZS and ES pass the points very close to the experimentally estimated point for $\theta=90°$, and the fact that the comparison of the $\Delta\varepsilon^{5,1}$ *vs.* θ curves for ZS and ES with the observed energy differences between the first and the fifth vertical ionization energies give very good estimates for θ in these compounds. Judging from these facts we can safely say that the calculated $\Delta\varepsilon^{5,1}$ *vs.* θ curves simulate very well the real $\Delta E_{iv}^{1,5}$ *vs.* θ curves in the case of ZS and ES. Therefore, we use the calculated $\Delta\varepsilon^{5,1}$ *vs.* θ curve for ES as the starting point for the estimation of θ of the methyl-substituted ES's.

In order to estimate the θ values of the methyl-substituted ES's we use the essentially same procedure as developed in our recent paper,[2c)] that is, we correct the $\Delta\varepsilon^{5,1}$ *vs.* θ curve of ES for the methyl-substituent effect by the first order perturbation theory regarding the methyl substitutions as perturbations, and get the estimated $\Delta E_{iv}^{1,5}$ *vs.* θ curves for the methyl-substituted ES's. In the perturbation theoretic calculations we use the parameters evaluated in the preceding paper.[2c)] By comparing the estimated $\Delta E_{iv}^{1,5}$ *vs.* θ curves for the methyl-substituted ES's with the observed $\Delta E_{iv}^{1,5}$ values we can estimate the twist angles. As an example, the estimated $\Delta E_{iv}^{1,5}$ *vs.* θ curve for E44′DMS is shown in Fig. 4. By comparing the observed $\Delta E_{iv}^{1,5}$ value of this compound with the curve in Fig. 4, we get 36° as

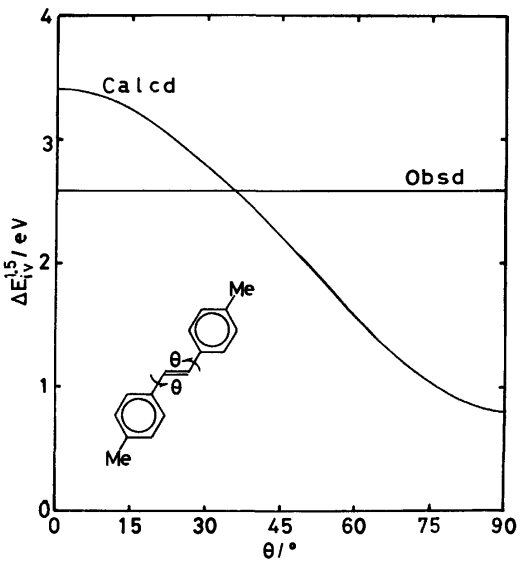

Fig. 4. Estimated θ dependence of $\Delta E_{iv}^{5,2}$ for (*E*)-4,4′-dimethylstilbene with observed $\Delta E_{iv}^{1,5}$.

θ. The θ values estimated for the various methyl-substituted ES's in this manner are summarized in Table 2 with those by other methods. In the case of E22′DMS the estimated θ values for the three main types of conformers, the (*E*)-2,2′-, (*E*)-6,6′-, and (*E*)-2,6′-dimethyl conformers, were the same. This was also the case for E33′DMS. In the case of E22′55′-TMS the estimated θ values for the (*E*)-2,2′,5,5′-, (*E*)-3,3′,6,6′-, and (*E*)-2,3′,5,6′-tetramethyl conformers were 41, 40, and 40°, respectively.

The estimated θ value of E4MS, 32°, that of E33′DMS, 37°, and that of E44′DMS, 36°, are very close to that of and the observed one of ES, 33° and 32.2°, as seen in Table 2. This is reasonable because the methyl groups can not cause any steric hindrance in these molecules.

In the case of E22′DMS and E22′55′TMS the estimated θ values are 40 and 40—41°, respectively, and these are slightly larger than that for ES. This suggests the presence of slight steric hindrance by the 2- and 2′-methyl groups. In the case of E22′44′66′HMS, the estimated value is considerably larger than that of E22′DMS or E22′55′TMS, and this is reasonable

Table 2. Twist angles, θ, in stilbenes[a)]

Compound	θ/°							
	UPS (gas)		EAS[d)] (solution)		ED[f)] (gas)	XD[g)] (solid)	NDDO[h)]	MM[i)]
	This work[b)]	HMO[c)]	I[e)]	II[e)]				
ZS	45	35	29.4	42.2	43.2±1.3		38	35—40
ES	33	(0)	(0)	(32.2)	32.2±2.1	3.4, 6.9	20	0—15
E4MS	32		(0)	(32.2)				
E22'DMS	40[e)]		20.2	37.3				
E33'DMS	37[e)]		(0)	(32.2)				
E44'DMS	36		(0)	(32.2)				
E22'55'TMS	40—41[e)]		24.4	39.4				
E22'44'66'HMS	60		54.3[j)]	59.7				50—55

a) The values in the parentheses are the assumed ones. b) The estimated error range for θ is around ±5° in the case of E22'44'66'HMS and ±4° in the case of the other methyl-substituted ES's. c) The HMO level method, Ref. 8. d) The electronic absorption spectral method on the HMO level, this work except for E22'44'66'HMS. e) See the text. f) The electron diffraction method, Refs. 6 and 7 for ES and ZS, respectively. g) The x-ray diffraction method, Ref. 4d. h) The NDDO method, Ref. 17. i) The molecular mechanics method, Ref. 18. j) Ref. 13c.

because the 2-, 2'-, 6-, and 6'-methyl groups are expected to cause greater steric hindrance than the pair of the 2- and 2'-methyl groups only.

As discussed above the estimated θ values show very reasonable tendency, and this fact supports the validity of the method used here.

Comparison with the Electronic Absorption Spectroscopic and Other Approaches. Formerly one of us (H.S.) developed a method on the HMO level to estimate the twist angles using the energies of the longest-wavelength electronic absorption spectral band maxima and discussed the conformations of various stilbenes in detail.[5,13)] We now compare the conformation analytical results obtained by photoelectron spectroscopy with those by electronic absorption spectroscopy.

For this purpose the electronic absorption spectra of ZS, E22'DMS, E33'DMS, and E22'55'TMS were newly measured in heptane and are shown in Fig. 5.

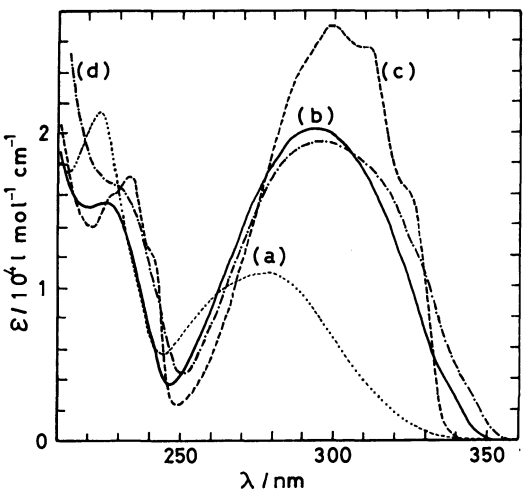

Fig. 5. Electronie absorption spectra of (*Z*)-stilbene (a), (*E*)-2,2'-dimethylstilbene (b), (*E*)-3,3'-dimethylstilbene (c), and (*E*)-2,2',5,5'-tetramethylstilbene (d) in heptane.

The wavelengths and the molar absorption coefficients at the absorption maxima of the longest-wavelength intense bands of these compounds are as follows:
ZS, 278.7 nm, 1.031×10^4 l/mol cm; E22'DMS, 293.6 nm, 2.022×10^4 l/mol cm; E33'DMS, 299.5 nm, 2.699×10^4 l/mol cm; E22'55'TMS, 295.4 nm, 1.945×10^4 l/mol cm.
The spectra of the other stilbenes treated in this study were reported formerly.[5,13c)]

The twist angles of the stilbenes estimated by using the energies of the first conjugation bands according to the method described formerly in detail[5,13c)] are summarized in Table 2. The electronic bathochromic effects of the methyl substituents located on the benzene nuclei were taken into account by adequately choosing the reference compounds for correlation between the calculated transition energies and the observed ones as described in Ref. 13c. The θ values of the entry I in Table 2 were estimated on the assumption that ES, E4MS, E33'DMS, and E44'DMS are completely planar, and those of the entry II on the assumption that the θ values for these compounds are commonly 32.2°, adopting the gas electron diffraction result for ES.[6)]

The θ values estimated from the photoelectron spectral data of these stilbenes are consistent in the tendency with those of the entry I in Table 2 and are almost quantitatively consistent with those of the entry II. These facts support the validities of the both methods which are independent of each other and suggest that the relative conformational situations are similar to each other between the gas and the solution phases.

In Table 2 are also given the θ values calculated by other authors for the sake of comparison. The recent NDDO result[17)] seems to be fair as for the θ value of ES. The empirical molecular mechanics type calculation[18)] underestimated the θ value for ES though the method is for free molecules.

Electronic Absorption Spectral Band Features. Finally let us examine the band features of the electronic

absorption spectra of some stilbenes from the conformational standpoints briefly. Formerly it has been pointed out and discussed in detail[13c,19] that the longest-wavelength absorption band of an apparently sterically hindered stilbene such as E22'44'66'HMS is considerably weaker in intensity than that of a sterically (almost) unhindered one such as ES, E4MS, or E44'DMS, and that the former is almost structureless while the latter shows well-resolved fine structures.

Keeping this point in mind let us see the electronic spectra of E22'DMS and E22'55'TMS shown in Fig. 5. The first bands of these spectra are almost structureless, almost equal to each other in intensity, and considerably weaker in intesity than that of E33'DMS shown in Fig. 5 which is reasonably regarded to be sterically unhindered. These facts mean clearly that the θ values of E22'DMS and E22'55'TMS are almost equal to each other and larger than that of E33'DMS. And this is consistent with the tendency of the θ values for these compounds estimated in this paper.

The longest-wavelength electronic absorption band of E33'DMS is quite similar in intensity and in fine structures to those of ES,[5] E4MS,[13c] and E44'DMS.[13c] These facts mean that E33'DMS is unhindered and support the validity of the mutual closeness of the θ values for these compounds estimated from the photoelectron spectra in this study. However, the fine structures of the longest-wavelength band of E33'DMS are slightly blurred compared to that of ES, E4MS, or E44'DMS, and this point may reflect the fact that the three main conformers, which may be designated as (*E*)-3,3'-, (*E*)-5,5'-, and (*E*)-3,5'-dimethylstilbene and are almost energetically equivalent to one another, are contributing to the ground state of E33'DMS in the fluid phases.

References

1) a) T. Kobayashi and S. Nagakura, *Chem. Lett.*, **1972**, 903; b) T. Kobayashi and S. Nagakura, *ibid.*, **1972**, 1013; c) T. Kobayashi, K. Yokota, and S. Nagakura, *J. Electron Spectrosc. Relat. Phenom.*, **2**, 449 (1973); d) T. Kobayashi and S. Nagakura, *Bull. Chem. Soc. Jpn.*, **47**, 2563 (1974); e) T. Kobayashi, K. Yokota, and S. Nagakura, *ibid.*, **48**, 412 (1975).

2) a) R. Nakagaki, T. Kobayashi, and S. Nagakura, *Bull. Chem. Soc. Jpn.*, **53**, 901 (1980); b) R. Akaba, K. Tokumaru, T. Kobayashi, and C. Utsunomiya, *ibid.*, **53**, 2002 (1980) and see also, R. Akaba, K. Tokumaru, and T. Kobayashi, *ibid.*, **53**, 1993 (1980); c) T. Kobayashi, T. Arai, H. Sakuragi, K. Tokumaru, and C. Utsunomiya, *ibid.*, **54**, 1658 (1981).

3) For example, A. R. Gregory and D. F. Williams, *J. Phys. Chem.*, **83**, 2652 (1979) and references cited therein.

4) a) J. M. Robertson and I. Woodward, *Proc. R. Soc. London, Ser. A*, **162**, 568 (1937). For the refined crystal structural analyses, see the followings: b) C. J. Finder, M. G. Newton, and N. L. Allinger, *Acta Crystallogr., Sect. B*, **30**, 411 (1974); c) J. Bernstein, *ibid.*, **31**, 1268 (1975); d) A. Hoekstra, P. Meertens, and A. Vos, *ibid.*, **31**, 2813 (1975).

5) H. Suzuki, *Bull. Chem. Soc. Jpn.*, **33**, 379 (1960).

6) M. Trætteberg, E. B. Frantsen, F. C. Mijlhoff, and A. Hoekstra, *J. Mol. Struct.*, **26**, 57 (1975).

7) M. Trætteberg and E. B. Frantsen, *J. Mol. Struct.*, **26**, 69 (1975).

8) J. P. Maier and D. W. Turner, *J. Chem. Soc., Faraday Trans. 2*, **69**, 196 (1973).

9) M. J. S. Dewar and D. W. Goodman, *J. Chem. Soc., Faraday Trans. 2*, **68**, 1784 (1972).

10) L. J. Kricka, M. C. Lambert, and A. Ledwith, *J. Chem. Soc., Perkin Trans. 1*, **1974**, 52.

11) a) B. S. Hudson, J. N. A. Ridyard, and J. Diamond, *J. Am. Chem. Soc.*, **98**, 1126 (1976); b) K. L. Yip, N. O. Lipari, C. B. Duke, B. S. Hudson, and J. Diamond, *J. Chem. Phys.*, **64**, 4020 (1976).

12) E. J. McAlduff and T. Chan, *Can. J. Chem.*, **56**, 2714 (1978).

13) a) H. Suzuki, *Bull. Chem. Soc. Jpn.*, **25**, 145 (1952); b) H. Suzuki, *ibid.*, **33**, 396 (1960); c) H. Suzuki, *ibid.*, **33**, 406 (1960); d) H. Suzuki, "Electronic Absorption Spectra and Geometry of Organic Molecules," Academic Press Inc., New York, N.Y. (1967), Chap. 14 and references cited therein.

14) T. Mukaiyama, T. Sato, and J. Hanna, *Chem. Lett.*, **1973**, 1041.

15) R. L. Ellis, G. Kuehnlenz, and H. H. Jaffé, *Theor. Chim. Acta*, **26**, 131 (1972).

16) P. Masclet, D. Grosjean, G. Mouvier, and J. Dubois, *J. Electron Spectrosc. Relat. Phenom.*, **2**, 225 (1973).

17) H.-J. Hofmann and P. Birner, *J. Mol. Struct.*, **39**, 145 (1977).

18) A. Bromberg and K. A. Muszkat, *Tetrahedron*, **28**, 1265 (1972).

19) H. Suzuki, *Bull. Chem. Soc. Jpn.*, **35**, 1715 (1962).

 © 1982 The Chemical Society of Japan Bull. Chem. Soc. Jpn., 55, 1739—1742 (1982)

The Insertion Reaction of NH Singlet Radicals into the C-H Bonds of Cyclopropane and Isobutane in the Liquid Phase

Jun-ich HAMADA, Shigeru TSUNASHIMA,* and Shin SATO

Department of Applied Physics, Tokyo Institute of Technology, Ookayama, Meguro-ku, Tokyo 152

(Received October 21, 1981)

Hydrogen azide was photolyzed in liquid cyclopropane at the temperature of Dry Ice–methanol. The main products observed were nitrogen, cyclopropylamine, and ammonia. The relative yields of the products depended slightly on the concentration of hydrogen azide. The results were then compared with those obtained with paraffin and olefin. The isobutane solution of hydrogen azide was photolyzed at 0 °C. The products observed were the same as those obtained at the temperature of Dry Ice–methanol. The relative yields of the products and the concentration dependence, however, were different.

In spite of many investigations of the reactions of $O(^1D)$ and $CH_2(^1A_1)$, only a few investigations have been reported of the reactions of the NH singlet ($a^1\Delta$), which is isoelectronic with O and CH_2.[1] Recently, we have photolyzed hydrogen azide in liquid ethane, propane, isobutane, ethylene, and propene at the temperature of Dry Ice–methanol.[2-4] In the case of paraffin, the main basic products were ammonia and amines, *i.e.*, ethylamine from ethane, propyl- and isopropylamine from propane, and isobutyl- and *t*-butylamine from isobutane. The amine formations were explained by the insertion reaction of the NH singlet into the C–H bonds of paraffin. In the case of olefin, aziridines were found to be formed; they were explained by the addition reaction of the NH singlet to the double bond of olefin. When hydrogen azide was photolyzed in liquid carboxylic acid, the formation of amino acids was observed.[5,6] Recently, Kajimoto and Fueno studied the photolysis of a mixture of hydrogen azide and ethane in the gas phase at room temperature.[7] They showed that the reactions of the NH singlet with ethane give insertion, abstraction, and deactivation products with branching ratios of 60%, 10%, and 30% respectively. These studies have shown that the main reaction of the NH singlet is the insertion reaction into the C–H bond.

In the case of the paraffin solution at the temperature of Dry Ice–methanol, the relative yield of amine decreased, and that of ammonia increased, with an increase in the concentration of hydrogen azide.[2,3] In the case of olefin, however, no concentration dependence was observed.[4] The difference was tentatively explained by a "solvent effect" on Reaction 1:

$$NH(a^1\Delta) + HN_3 \rightarrow NH_2 + N_3. \quad (1)$$

In order to get further information about the reactions of the NH singlet, hydrogen azide was photolyzed in the liquid cyclopropane at the temperature of Dry Ice–methanol, since cyclopropane is known as a hydrocarbon which shows a property intermediate between paraffin and olefin. The isobutane solution of hydrogen azide was also photolyzed at 0 °C in order to study the effects of the temperature on the reactions.

Experimental

The experimental methods were essentially the same as those described in the previous papers.[2-4] Hydrogen azide was prepared *in vacuo* by heating a mixture containing sodium azide and an excess amount of stearic acid, and was used after having been dried with phosphorus pentaoxide and degassed at −120 °C. Research-grade ethane, cyclopropane, and isobutane (Takachiho Shoji Co.) were purified by repeated trap-to-trap distillation. The mixture of hydrogen azide and hydrocarbon was prepared in a quartz tube with an o.d. of 8 mm and irradiated with a medium-pressure mercury lamp (Wako Denki Co.) through a filter (Toshiba UV 27) at the temperature of Dry Ice–methanol or 0 °C. The amount of the solution was about 1 cm^3.

After the irradiation, non-condensable products at −196 °C were analyzed with a combination of a Toepler pump, a gas burette, and a CuO furnace at 300 °C. The solvent was evacuated at about −80 °C. Less volatile products, including unreacted hydrogen azide, were passed through a trap packed with NaOH-coated glass wool. The products thus obtained were analyzed with GLC, using columns packed with Amipack 124 (Gasukuro Kogyo Co.) and with Porapak Q. For the identification of the products, a mass spectrometer and an NMR spectrometer were used. D_2O was used as a solvent for the NMR analysis.

Results

Cyclopropane–Hydrogen Azide Solution. When hydrogen azide was photolyzed in liquid cyclopropane at the temperature of Dry Ice–methanol, the formation of a white precipitant was observed, much as in the cases of paraffin and olefin.[2-4] The non-condensable products at −196 °C were nitrogen and hydrogen. No methane formation was observed. The H_2/N_2 ratio was 0.015 ± 0.004, independent of the changes in the concentration of hydrogen azide. Among the less volatile products, ammonia and cyclopropylamine were found. Allylamine, which is expected to be formed by the isomerization of the vibrationally excited cyclopropylamine, was not found. The yields of ammonia and cyclopropylamine relative to nitrogen are plotted in Fig. 1 as a function of the concentration of hydrogen azide. For comparison, previous results obtained with propane and propene are also included in Fig. 1.[3,4] The concentration dependence obtained with cyclopropane shows behavior intermediate between that obtained with propane and with propene. The sum of the relative yields of the products, $(c\text{-}C_3H_5NH_2 + 3H_2 + 4NH_3)/N_2$, was 0.95 ± 0.06 for the concentration range examined.

Cyclopropane–Ethane–Hydrogen Azide Solution. When ethane was added to a cyclopropane solution of hydrogen

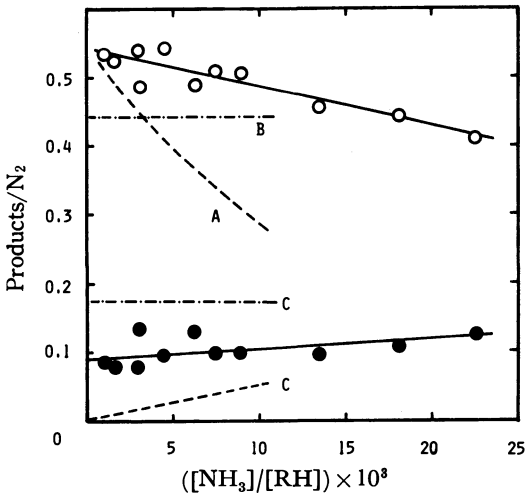

Fig. 1. Yields of cyclopropylamine (○) and ammonia (●) relative to nitrogen as a function of the concentration of hydrogen azide. (------) and (-·-·-) show the results obtained in the propane and propene solutions (from Refs. 3 and 4). A: (propyl- and isopropylamine)/N_2, B: (methylaziridine+allylamine)/N_2, C: NH_3/N_2.

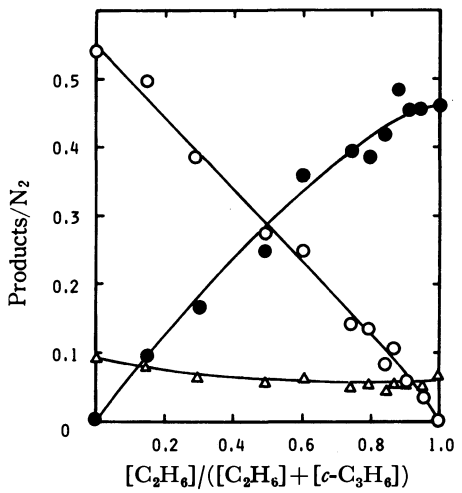

Fig. 2. Effects of ethane on the photolysis of cyclopropane solution of hydrogen azide as a function of the mole fraction of ethane. The $[HN_3]/([C_2H_6]+[c\text{-}C_3H_6])$ ratio is 2.07×10^{-3}. ○: $c\text{-}C_3H_5NH_2/N_2$, ●: $C_2H_5NH_2$, △: NH_3/N_2.

azide, the relative yield of cyclopropylamine decreased, while the yield of ethylamine increased. The results obtained at the constant concentration of hydrogen azide, $[HN_3]/([C_2H_6]+[c\text{-}C_3H_6])=2.07\times10^{-3}$, are plotted in Fig. 2 as a function of the mole fraction of ethane, X.

Isobutane–Hydrogen Azide Solution at 0 °C. In order to investigate the effects of the reaction temperature, hydrogen azide was photolyzed in liquid isobutane at 0 °C. The products obtained at 0 °C were essentially the same as those obtained at the temperature of Dry Ice–methanol. Figure 3 shows the concentration dependence of the relative yields of ammonia and amines (the sum of isobutyl- and *t*-butylamine). The results

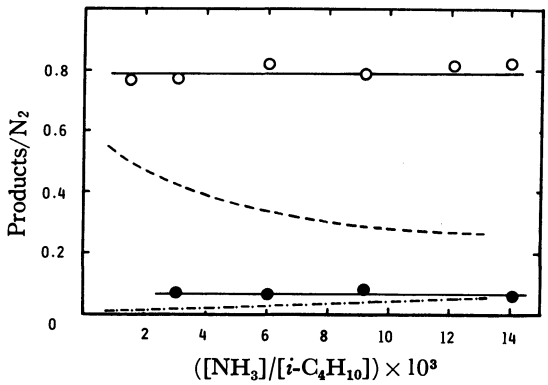

Fig. 3. Yields of isobutyl- and *t*-butylamines (○) and ammonia (●) relative to nitrogen as a function of the concentration of hydrogen azide at 0 °C. The results obtained at the temperature of Dry Ice–methanol are also shown for the amines (------) and ammonia (-·-·-) (from Ref. 3).

obtained at the temperature of Dry Ice–methanol are also included for comparison.[3] The relative yields of the products were independent of the changes in the concentration of hydrogen azide at 0 °C: $(i\text{-}C_4H_9NH_2+t\text{-}C_4H_9NH_2)/N_2=0.79\pm0.03$, $NH_3/N_2=0.06\pm0.01$, $H_2/N_2=0.03\pm0.01$, and $i\text{-}C_4H_9NH_2/t\text{-}C_4H_9NH_2=4.3\pm0.03$. The $i\text{-}C_4H_9NH_2/t\text{-}C_4H_9NH_2$ ratio obtained at 0 °C is almost equal to that obtained at the temperature of Dry Ice–methanol. The sum of the relative yields, $(i\text{-}C_4H_9NH_2+t\text{-}C_4H_9NH_2+3H_2+4NH_3)/N_2$, was close to unity, and thus different from that obtained at a lower temperature.

Discussion

Cyclopropane–Hydrogen Azide Solution. As has been discussed in previous papers,[2-4] the following general reaction mechanism can also be considered in the case of cyclopropane:

$$HN_3 + h\nu \rightarrow {}^1NH + N_2, \quad (2)$$
$$\rightarrow H + N_3, \quad (3)$$
$${}^1NH + HN_3 \rightarrow NH_2 + N_3 \quad k_a, \quad (4)$$
$${}^1NH + RH \rightarrow RNH_2 \quad k_i, \quad (5)$$
$$\rightarrow {}^3NH + RH \quad k_d, \quad (6)$$
$${}^3NH + HN_3 \rightarrow NH_2 + N_3, \quad (7)$$
$$NH_2 + HN_3 \rightarrow NH_3 + N_3, \quad (8)$$
$$H + HN_3 \rightarrow H_2 + N_3, \quad (9)$$
$$2NH_2 \rightarrow N_2H_4, \quad (10)$$
$$2N_3 \rightarrow 3N_2, \quad (11)$$

where ^1NH and ^3NH represent the NH radicals in the first excited singlet state ($a^1\Delta$) and the ground triplet state ($X^3\Sigma^-$) respectively. RH and RNH_2 are cyclopropane and cyclopropylamine respectively.

Since the $(RNH_2+3H_2+4NH_3)/N_2$ ratio was close to unity, Reaction 10 can be neglected in the case of cyclopropane, much as in the case of propene. In the case of propane, however, Reaction 10 was important to explain the facts that (1) the $(RNH_2+3H_2+4NH_3)/$

N_2 ratio was less than unity and (2) the NH_3/N_2 ratio approached zero when the concentration of hydrogen azide approached zero (*cf.* Fig. 1).

In the above reaction mechanism, the hydrogen-atom abstraction by the NH triplet is neglected;

$$^3NH + RH \rightarrow NH_2 + R, \quad (12)$$

because the reaction is about 36 kJ mol^{-1} endothermic. Reaction 13 may also be unimportant at a low temperature because of its large activation energy.[8] If Reactions

$$NH_2 + RH \rightarrow NH_3 + R \quad (13)$$

12 and 13 were important in the present system, the cyclopropyl radical, R, would abstract a hydrogen atom from hydrogen azide:

$$R + HN_3 \rightarrow RH + N_3. \quad (14)$$

As it is, it is difficult to distinguish these reactions from Reactions 7 and 8.

Kajimoto and Fueno have proposed that a part of the reaction of the NH singlet with ethane in the gas phase at room temperature is a hydrogen-atom abstraction.[7] A similar reaction is expected to occur in the present system because the reaction is about 115 kJ mol^{-1} exothermic:

$$^1NH + RH \rightarrow NH_2 + R. \quad (15)$$

If NH_2 and R abstracted a hydrogen atom from hydrogen azide, Reaction 15 would be indistinguishable from Reaction 6. In the liquid phase, however, NH_2 and R recombine because of the cage effect:

$$NH_2 + R \rightarrow RNH_2. \quad (16)$$

In this case, Reaction 15 is indistinguishable from Reaction 5. If Reaction 16 competed with Reactions 8 and 14, the NH_3/N_2 ratio would increase and the RNH_2/N_2 ratio would decrease with an increase in the concentration of hydrogen azide. This is consistent with the results obtained in the paraffin and cyclopropane solutions at the temperature of Dry Ice–methanol. This assumption, however, cannot explain the concentration dependence of the products obtained in the cases of the olefin solutions at the temperature of Dry Ice–methanol and isobutane solution at 0 °C.

Since Reaction 5 is about 460 kJ mol^{-1} exothermic, a vibrationally excited cyclopropylamine is formed; this will be isomerized to allylamine unless stabilized by a collision. In the cases of CH_2 reactions with cyclopropane, the isomerization of the initially formed vibrationally excited methylcyclopropane has been observed in the gas phase at room temperature.[9] Since no allylamine formation could be observed, the stabilization of the vibrationally excited cyclopropylamine must be efficient under the present experimental conditions.

Assuming the above reaction mechanism, Reactions 2—11, the rate constant ratios, k_a/k_i and $k_i/(k_i+k_d)$, can be estimated to be 6.4 ± 1.1 and 0.83 ± 0.01 respectively by the method described in the previous papers.[3,4] Here, the a, i, and d subscripts denote the abstraction reaction of hydrogen atom from hydrogen azide, the insertion reaction, and the deactivation of the singlet NH respectively. McDonald *et al.* have estimated the values of k_a and k_i+k_d in the gas phase at room temperature.[10] Their $k_a/(k_i+k_d)$ ratio was 2.6, about a half of the present results.

The k_a/k_i ratio was 49 in the case of propane.[3] In the case of propene, no concentration dependence was observed;[4] this means that the k_a/k_i ratio was less than unity. Thus, the difference in the concentration dependence of the yields of amine and ammonia may be explained by the difference in the k_a/k_i ratio.

Relative Rate of the Insertion. Using the results shown in Fig. 2, the relative rate can be estimated for the insertion of the NH singlet into ethane (k_{ei}) and cyclopropane (k_{ci}):

$$^1NH + C_2H_6 \rightarrow C_2H_5NH_2 \quad k_{ei}, \quad (17)$$

$$^1NH + c\text{-}C_3H_6 \rightarrow c\text{-}C_3H_5NH_2 \quad k_{ci}. \quad (18)$$

Assuming Reactions 17 and 18, the following relation can be obtained:

$$C_2H_5NH_2/(C_2H_5NH_2 + c\text{-}C_3H_5NH_2) = X/(f(1-X) + X), \quad (19)$$

where X is the mole fraction of ethane and where f is the k_{ci}/k_{ei} ratio. The left-hand-side of Eq. 19 is plotted against the weighted mole fraction, assuming various values for f. When f is assumed to be $1.0_5\pm0.1$, a good linearity is obtained, as is shown in Fig. 4; the insertion rate of the NH singlet into the C–H bond of cyclopropane is almost equal to that of ethane. Incidentally, Cvetanović and his co-workers estimated the relative rate of the reactions of $O(^1D)$ with cyclopropane and ethane to be 1.0_5 in the gas phase.[11]

As Fig. 2 shows, the relative yields of ethylamine were almost constant for the mole fractions of ethane larger than 0.85. This behavior may be explained by Reactions 2—11 under the assumption that the value of k_a depends on the mole fraction of ethane. The following relation is obtained for the yields of ethylamine:

$$C_2H_5NH_2/(C_2H_5NH_2 + c\text{-}C_3H_5NH_2 + H_2 + NH_3 + 2N_2H_4) = C_eX/(C_eA\,k_a/k_i + X + (1-X)fC_e/C_c, \quad (20)$$

where C_e and C_c are the fractions of the insertion of the NH singlet into ethane and cyclopropane respectively. A is the mole fraction of hydrogen azide; $2.0_7\times10^{-3}$. The left-hand-side of Eq. 20 is plotted in Fig. 5 as a function of the mole fraction of ethane. The amount of

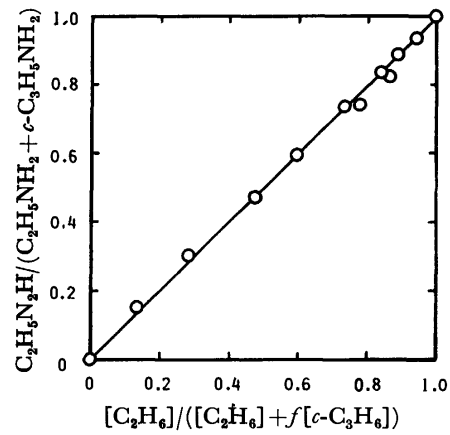

Fig. 4. Plots of $C_2H_5NH_2/(C_2H_5NH_2+c\text{-}C_3H_5NH_2)$ as a function of the weighted mole fraction of ethane, $f=1.05$. See the text for detail.

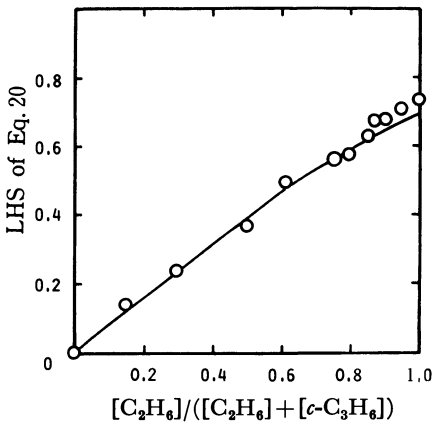

Fig. 5. Plots of the left-hand-side of Eq. 20 (○) as a function of the mole fraction of ethane. The solid curve shows the calculated ones. See the text for detail.

$$N_2H_4 = (1/5)(N_2 - C_2H_5NH_2 - c\text{-}C_3H_5NH_2 - 3H_2 - 4NH_3). \quad (21)$$

N_2H_4 was estimated using Eq. 21, as was done in a previous paper.[3] The right-hand-side of Eq. 20 is estimated by assuming Eq. 22 for the values of k_a/k_i at various mole fractions of ethane:

$$k_a/k_i = (k_a/k_i)_e^{x}(k_a/k_i)_c^{(1-x)}, \quad (22)$$

where the e and c subscripts mean the values obtained in a pure ethane solution and in a pure cyclopropane solution respectively. The results are shown in Fig. 5 as a solid curve. As Fig. 5 shows, the agreement is satisfactory.

Effects of Reaction Temperature. As Fig. 3 shows, the relative yields of the products were independent of the changes in the concentration of hydrogen azide in the case of isobutane at 0 °C. These observations may be explained by assuming a small value of k_a/k_i (less than unity) under the assumed reaction mechanism. As was shown in a previous paper,[3] the k_a/k_i ratio was 40 in liquid isobutane at the temperature of Dry Ice–methanol. If the decrease in the k_a/k_i ratio can be explained by the temperature dependence on k_i, the insertion reaction should have an activation energy larger than 21 kJ mol^{-1}. The effect of the reaction temperature was also observed in the k_d/k_i ratio, which is equal to $NH_3/(i\text{-}C_4H_9NH_2+t\text{-}C_4H_9NH_2)$ at 0 °C under the assumed reaction mechanism; *i.e.*, k_d/k_i= 0.08 at 0 °C and 0.33 at the temperature of Dry Ice–methanol.[3] From these values, the activation energy of k_i can be estimated to be about 8 kJ mol^{-1} larger than that of k_d.

In the case of O(^{1}D), no temperature effect has been observed for the insertion reaction.[12] For the reactions of the NH singlet, the temperature effect on the rate has not been studied. If the rate is independent of the changes in the reaction temperature, much as in the case of O(^{1}D), it is necessary to assume that k_a will decrease with an increase in the reaction temperature. As has been discussed above, we had to assume various values of k_a for different solutions and different temperatures. This might be due to the status of hydrogen azide in the hydrocarbon solutions. If hydrogen azide molecules were determined in isobutane to be in the form of a "cluster" at low temperatures, a large k_a value can be expected; hydrogen azide molecules are always present near the NH singlet formed by photolysis in a solution. At higher temperatures, this "cluster" may be decomposed by the motion of the solvent molecule, and a small k_a value can be expected. The size of the "cluster" may also depend on the solvent. If such a "cluster" was formed, the photolysis would take place inhomogeneously in the solution, and the recombination of NH_2 would become important. Such a "cluster," if formed, will play a significant role in the ethane, propane, and isobutane solutions at the temperature of Dry Ice–methanol.

As has been discussed above, the reactions of the NH singlet in liquid hydrocarbons are complicated. Further studies are necessary to elucidate the complete reaction mechanism.

The authors are much obliged to Professor Takeshi Nakai of this Institute for the NMR analysis.

References

1) R. S. Berry, "Nitrenes," ed by W. Lwowski, Interscience Publishers, New York (1970), p. 13.
2) S. Tsunashima, M. Hotta, and S. Sato, *Chem. Phys. Lett.*, **64**, 435 (1979).
3) S. Tsunashima, J. Hamadam, M. Hotta, and S. Sato, *Bull. Chem. Soc. Jpn.*, **53**, 2443 (1980).
4) T. Kitamura, S. Tsunashima, and S. Sato, *Bull. Chem. Soc. Jpn.*, **54**, 55 (1981).
5) S. Sato, T. Kitamura, and S. Tsunashima, *Chem. Lett.*, **1980**, 687.
6) S. Tsunashima, T. Kitamura, and S. Sato, *Bull. Chem. Soc. Jpn.*, **54**, 2869 (1981).
7) O. Kajimoto and T. Fueno, *Chem. Phys. Lett.*, **80**, 484 (1981).
8) P. V. Khe and R. Lesclaux, *J. Phys. Chem.*, **83**, 1119 (1979).
9) J. N. Butler and G. B. Kistiakowsky, *J. Am. Chem. Soc.*, **82**, 759 (1960); **83**, 1324 (1961).
10) J. R. McDonald, R. G. Miller, and A. P. Baronavski, *Chem. Phys.*, **30**, 133 (1978).
11) P. Michaud, G. Paraskevopoulos, and R. J. Cvetanović, *J. Phys. Chem.*, **78**, 1457 (1974).
12) K. Schofield, *J. Photochem.*, **9**, 55 (1978).

Multi-ionic Potential and Membrane Permeability Matrix. I. NaCl-CsCl Bi-ionic System with a Cation Exchange Membrane

Kozue KAIBARA* and Hideo KIMIZUKA
Department of Chemistry, Faculty of Science, Kyushu University, Hakozaki, Higashi-ku, Fukuoka 812
(Received October 23, 1981)

This paper is concerned with analysis of membrane transport processes on the basis of nonequilibrium thermodynamics. Inter-ionic correlations between permeating ions are quantitatively estimated by applying the membrane permeability matrix theory to the system in which the NaCl and CsCl solution phases are divided by a highly selective cation exchange membrane. The membrane permeability matrix of the system may be expressed by four ionic correlation terms concerning with Na^+ and Cs^+. The electroconductive and diffusional membrane permeabilities are expressed as a function of the matrix elements having the dimension of permeating speed of ions. The conductive and diffusional permeabilities as well as the matrix elements are estimated from membrane potential, conductance, and ionic flux data. The external electrolyte concentration dependence of these permeability parameters is discussed. The conductive and diffusional permeabilities considerably differ from each other and their ratio changes with the external electrolyte concentration, whereas the permeability ratio of Na^+ to Cs^+ is constant. Electroconductive and diffusional characteristics of membrane transport processes are consistently analyzed in terms of the membrane permeability matrix theory.

The membrane permeability matrix theory was presented as an application of the nonequilibrium thermodynamics to the analysis of transport phenomena of ions across membrane.[1] The fundamental idea of the theory is an estimation of permeability coefficients to offer a consistent explanation for membrane properties such as membrane potential, conductance, and ionic flux. In this context, the membrane permeability matrix was introduced as a fundamental parameter characterizing membrane properties. Each matrix element possesses the dimension of permeating speed of ions across membrane and represents a partial correlation between movements of migrating ions. The membrane permeability matrix can be regarded as a modified set of coefficients in the linear phenomenological equations describing membrane transport processes.

The commonly used membrane permeability theories formulated on the basis of the Nernst-Planck equation provide only one permeability coefficient for an ion (see, for example, Refs. 2—5), but any consistent explanation for membrane phenomena cannot be presented by these theories, since membrane permeabilities estimated from diffusional and electroconductive data are remarkably different as described later. In the preceding paper,[6] an experimental verification of the permeability matrix theory was presented by using a cation exchange membrane-aqueous calcium chloride solution system and it was pointed out that the theory is advantageous for a better understanding of ionic memberane transport.

In the present paper, a bi-ionic system in which NaCl and CsCl aqueous solutions are divided by a cation exchange membrane is studied by measurement of membrane potential, membrane conductance, and ionic flux. The membrane permeability matrix is estimated from observed data and discussed in relation to membrane transport processes.

Experimental

A "CK-1, 1.0 t" cation exchange membrane (Asahi Chemical Industry Co., Ltd.) was employed throughout the experiment with aqueous NaCl and CsCl solutions prepared from conductivity water and extra pure salts. The "CK-1, 1.0 t" membrane is composed of a styrene–divinylbenzene copolymer with ion exchange group of sulfonic acid type and its basic physicochemical properties are as follows: exchange capacity, 2.8 mequiv. (g dry-resin)$^{-1}$; water content, 38%; thickness, 1.09 mm. This membrane exhibits an ideal permselectivity to monovalent cations in single electrolyte systems (concentration cells), since apparent transport numbers to Na^+ and Cs^+ estimated from potential data are almost unity. The tracers used in the flux measurements, ^{22}Na and ^{137}Cs in chloride form, were obtained from the Japan Radioisotope Association.

Membrane potentials and conductances were measured by the ordinary method and ionic fluxes were estimated by measuring ^{22}Na and ^{137}Cs radioactivities transferred across membrane from one side of the solution chamber to the

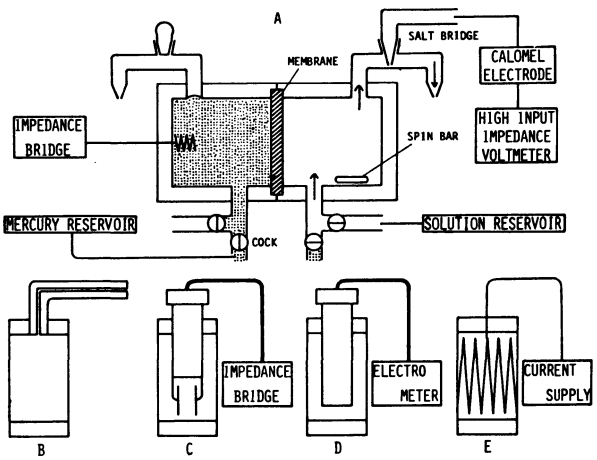

Fig. 1. Schematic representation of experimental assemblies. A shows the basic arrangement for the electrochemical measurements: potential measurements are performed by perfusing the chambers with electrolyte solutions (right-side diagram); conductance measurements are performed by means of filling the chamber with mercury as a conductivity electrode (left-side diagram). Accessary attachements B, C, and D (ion sensitive electrode) are employed to measure the volume flow, conductivity of solution, and ionic activity of solution, respectively. Attachement E is used when electric currents are applied externally.

other.[6-8] The schematic representation of experimental assemblies is given in Fig. 1. A high input impedance integrating voltmeter (Takeda Riken TR6856) and an impedance bridge circuit (Yokogawa-Hewlett-Packard 4255A and 4440B) were used to measure electrochemical properties. The detections of γ-activities of ^{22}Na and ^{137}Cs were performed by a γ-ray scintillation counter (Aloka Nd-151D). All experiments were carried out at a regulated room temperature, 20.0 ± 1.0 °C.

Results and Discussion

Experimental data are summarized in Figs. 2 and 3; measurements were carried out on the systems in which the NaCl or CsCl concentration of phase II was kept constant at 10^{-1}, 10^{-2}, or 10^{-3} mol dm^{-3}, while the CsCl or NaCl concentration of phase I was varied from 10^{-1} to 10^{-3} mol dm^{-3}. As illustrated in Fig. 2A, the membrane potential changed by about 58 mV for the tenfold alteration in electrolyte activity of phase I, whether NaCl or CsCl concentration was varied. Fig. 2A also shows that the system composed of NaCl and CsCl solutions of the same concentration generates a membrane potential of 8.7 mV where the NaCl side is positive. Membrane conductance *vs.* external salt concentration curves are given in Fig. 2B. Ionic fluxes estimated by means of the radiotracer method are plotted against the geometrical mean of NaCl and CsCl activities of external solutions in Fig. 3. These experimental results indicate that the Cl^- flux is negligibly small as compared with cationic fluxes. Thus, the ionic fluxes in the present system can be expressed by only those of Na^+ and Cs^+ as a reasonable approximation. The membrane permeability matrix for the present system can be estimated from the above electrochemical and ionic flux data on the basis of the previous theory.[1]

The membrane transport process in the present system can be characterized by the following modified phenomenological equation:

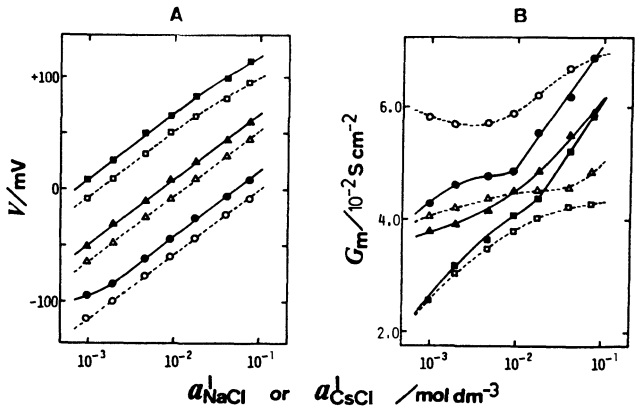

Fig. 2. Electrochemical data. Membrane potentials (A) and membrane conductances (B).
CsCl(I)-NaCl(II) systems, NaCl(II): ●; 10^{-1} mol dm^{-3}, ▲; 10^{-2} mol dm^{-3}, ■; 10^{-3} mol dm^{-3}. NaCl-(I)-CsCl(II) systems, CsCl(II): ○; 10^{-1} mol dm^{-3}, △; 10^{-2} mol dm^{-3}, □; 10^{-3} mol dm^{-3}.

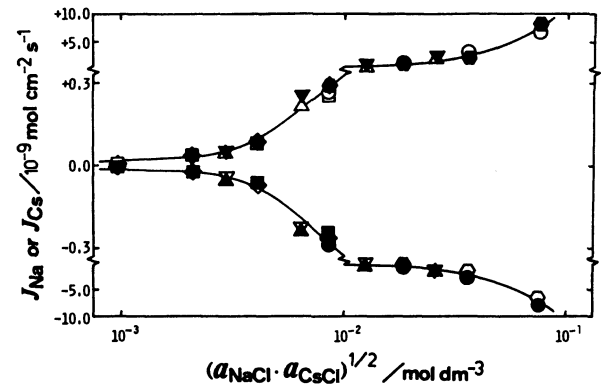

Fig. 3. Cationic flux data as a function of the geometrical mean of external NaCl and CsCl activities.
The closed and open symbols indicate J_{Na} and J_{Cs}, respectively. CsCl(I)-NaCl(II) systems, NaCl(II): (●, ○); 10^{-1} mol dm^{-3}, (▲, △); 10^{-2} mol dm^{-3}, (■, □); 10^{-3} mol dm^{-3}. NaCl(I)-CsCl(II) systems, CsCl(II): (●, ○); 10^{-1} mol dm^{-3}, (▼, ▽); 10^{-2} mol dm^{-3}, (◆, ◇); 10^{-3} mol dm^{-3}.

$$\begin{bmatrix} J_{Na} \\ J_{Cs} \end{bmatrix} = -\begin{bmatrix} P_{Na,Na} & P_{Na,Cs} \\ P_{Cs,Na} & P_{Cs,Cs} \end{bmatrix} \times \begin{bmatrix} a^{II}_{Na}\exp(FV/2RT) - a^{I}_{Na}\exp(-FV/2RT) \\ a^{II}_{Cs}\exp(FV/2RT) - a^{I}_{Cs}\exp(-FV/2RT) \end{bmatrix}, \quad (1)$$

where J is the ionic flux, a is the activity, and V is the membrane potential; F, R, and T have the usual physical meanings; the subscripts Na and Cs refer to Na^+ and Cs^+; the superscripts I and II denote the solution phases I and II divided by the membrane, respectively. The 2×2 membrane permeability matrix in the right hand side of Eq. 1 is a principal parameter to describe membrane phenomena for the present system. Each matrix element represents the partial contribution to the ionic transport caused by the inter-ionic correlation denoted by the subscript. The participation of volume flow in the mebrane transport process was neglected in the present study, since the assumption of zero volume flow was experimentally verified for the studied electrolyte concentration range with the CK-1, 1.0t membrane in a previous paper.[9] At low electrolyte concentrations less than 10^{-1} mol dm^{-3}, the estimated changes in phenomenological coefficients were so small as to be within the experimental error, whether the volume flow was taken into account or not. This may be due to the low water content and high fixed charge density of the CK-1, 1.0t cation exchange membrane.[6]

From Eq. 1, the total membrane current, I, is expressed as:

$$I = -F\{P_{Na}[a^{II}_{Na}\exp(FV/2RT) - a^{I}_{Na}\exp(-FV/2RT)] + P_{Cs}[a^{II}_{Cs}\exp(FV/2RT) - a^{I}_{Cs}\exp(-FV/2RT)]\}, \quad (2)$$

where P_{Na} and P_{Cs} are the electroconductive membrane permeabilities to Na^+ and Cs^+ defined as a function of the permeability matrix elements, respectively:

$$P_{Na} = P_{Na,Na} + P_{Cs,Na},\ P_{Cs} = P_{Na,Cs} + P_{Cs,Cs}. \quad (3)$$

On the other hand, Eq. 1 is reduced to the next form when the membrane current is absent:

$$\begin{bmatrix} J_{Na} \\ J_{Cs} \end{bmatrix} I=0 = - \begin{bmatrix} P^0_{Na} & 0 \\ 0 & P^0_{Cs} \end{bmatrix} \times \begin{bmatrix} a^{II}_{Na} \exp(FV_0/2RT) & -a^{I}_{Na} \exp(-FV_0/2RT) \\ a^{II}_{Cs} \exp(FV_0/2RT) & -a^{I}_{Cs} \exp(-FV_0/2RT) \end{bmatrix}, \quad (4)$$

where V_0 is the membrane potential at zero membrane current. P^0_{Na} and P^0_{Cs} are the diffusional membrane permeabilities which are defined as a function of the matrix elements and differ from the electroconductive permeabilities defined by Eq. 3:

$$P^0_{Na} = |P|/P_{Cs}, \quad P^0_{Cs} = |P|/P_{Na} \; ; \; |P| = \begin{vmatrix} P_{Na,Na} & P_{Na,Cs} \\ P_{Cs,Na} & P_{Cs,Cs} \end{vmatrix}. \quad (5)$$

As pointed out in the preceding paper,[1,6] the conductive and diffusional membrane permeabilities are transport parameters which represent electronductive and diffusional characteristics of membrane systems. From Eqs. 3 and 5, relationships between these permeabilities are obtained as:

$$P^0_{Na}/P_{Na} = P^0_{Cs}/P_{Cs} = 1-(P_{Cs,Na}/P_{Na}) - (P_{Na,Cs}/P_{Cs}). \quad (6)$$

The conductive permeability can be discriminated from the diffusional permeability only on the basis of nonequilibrium thermodynamical theory and it should be noted that both the permeabilities are identical when the ionic correlation between Na^+ and Cs^+ is absent. The diffusional membrane permeability can be estimated according to Eq. 4 by using the ionic flux and potential data. The conductive permeability can be calculated from the electrochemical data using the following relations:[4,7]

$$P_{Na}a^{II}_{Na} + P_{Cs}a^{II}_{Cs} = (RT/F^2)G_m \exp(-FV_0/2RT),$$
$$P_{Na}a^{I}_{Na} + P_{Cs}a^{I}_{Cs} = (RT/F^2)G_m \exp(FV_0/2RT), \quad (7)$$

where G_m is the membrane conductance.

Four elements of the membrane permeability matrix, $P_{Na,Na}$, $P_{Na,Cs}$, $P_{Cs,Na}$, and $P_{Cs,Cs}$, characterizing the present system were estimated from Eqs. 3 and 6 with the following relation between the cross matrix elements:[1]

$$\frac{P_{Na,Cs}}{P_{Cs,Na}} = \frac{(a^{I}_{Na}a^{II}_{Na})^{1/2} \sinh[F(V-V_{Na})/2RT]/[F(V-V_{Na})/2RT]}{(a^{I}_{Cs}a^{II}_{Cs})^{1/2} \sinh[F(V-V_{Cs})/2RT]/[F(V-V_{Cs})/2RT]}, \quad (8)$$

where V_{Na} and V_{Cs} are the Nernst equilibrium membrane potentials for Na^+ and Cs^+, respectively, which are defined as:

$$V_{Na} = -(RT/F)\ln(a^{II}_{Na}/a^{I}_{Na}),$$
$$V_{Cs} = -(RT/F)\ln(a^{II}_{Cs}/a^{I}_{Cs}). \quad (9)$$

In the present study, Eq. 8 must be modified under the limited experimental conditions; the relation, $-V_{Na} = V_{Cs} = \infty$, would be satisfied in the CsCl(I)–NaCl(II) system where $a^{I}_{Na} = a^{II}_{Cs} = o$, and the relation, $V_{Na} = -V_{Cs} = \infty$, in the NaCl(I)–CsCl(II) system where $a^{II}_{Na} = a^{I}_{Cs} = o$. In these limiting cases, the following relations can be obtained from Eq. 8:

$$P_{Na,Cs}/P_{Cs,Na} = \begin{cases} a^{II}_{Na}/a^{I}_{Cs} \text{ for the CsCl(I)-NaCl(II) system} \\ a^{I}_{Na}/a^{II}_{Cs} \text{ for the NaCl(I)-CsCl(II) system.} \end{cases} \quad (10)$$

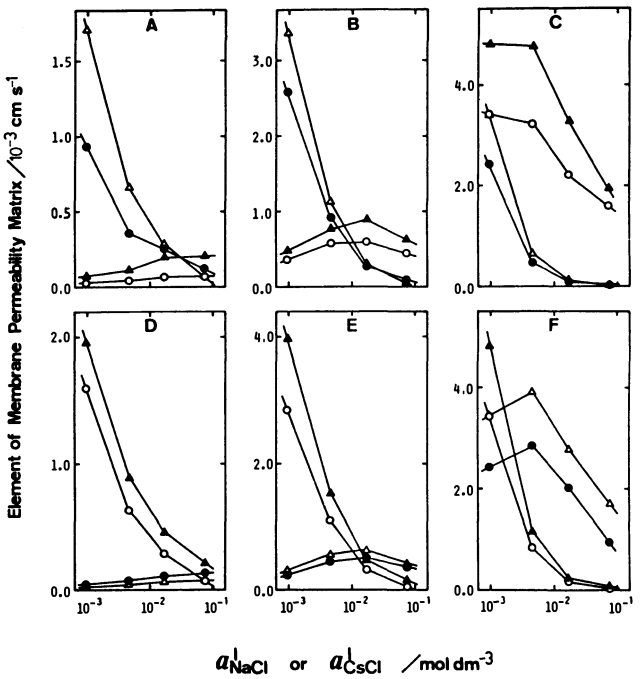

Fig. 4. Membrane permeability matrix elements as a function of mean electrolyte activity of phase I.
CsCl(I)–NaCl(II) systems, NaCl(II): A; 10^{-1} mol dm^{-3}, B; 10^{-2} mol dm^{-3}, C; 10^{-3} mol dm^{-3}. NaCl(I)–CsCl(II) systems, CsCl(II): D; 10^{-1} mol dm^{-3}, E; 10^{-2} mol dm^{-3}, F; 10^{-3} mol dm^{-3}. ●; $P_{Na,Na}$, ○; $P_{Ca,Na}$, ▲; $P_{Cs,Cs}$, △; $P_{Na,Cs}$.

Calculated transport parameters are summarized in Figs. 4 and 5. The membrane permeability matrix elements estimated for the six studied systems are plotted, in Fig. 4, against the mean electrolyte activity of phase I. From this figure, effects of inter-ionic correlations on the membrane ionic transport processes can be quantitatively evaluated. In Fig. 5, the conduc-

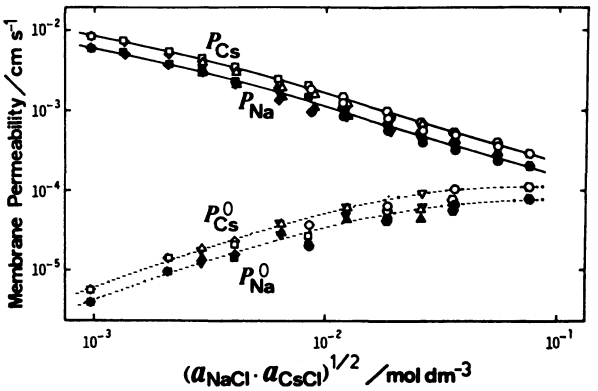

Fig. 5. Conductive and diffusional membrane permeabilities as a function of the geometrical mean of external NaCl and CsCl activities.
Solid and broken lines refer to the conductive and diffusional permeabilities; the closed and open symbols indicate the permeabilities to Na^+ and Cs^+, respectively. CsCl(I)–NaCl(II) systems, NaCl(II): (●, ○); 10^{-1} mol dm^{-3}, (▲, △); 10^{-2} mol dm^{-3}, (■, □); 10^{-3} mol dm^{-3}. NaCl(I)–CsCl(II) systems, CsCl(II): (⬢, ⬡); 10^{-1} mol dm^{-3}, (▼, ▽); 10^{-2} mol dm^{-3}, (◆, ◇); 10^{-3} mol dm^{-3}.

tive and diffusional membrane permeabilities are plotted as a function of the geometrical mean of NaCl and CsCl activities of phases I and II. As can be seen in this figure, the two types of the permeabilities are considerably different from each other and exhibit an opposite dependence upon the external electrolyte activity. The disagreement between the electroconductive and diffusional characteristics in the membrane transport processes indicates the failure of the Nernst-Einstein equation which relates the diffusion coefficient to the mobility. The deviation from the Nernst-Einstein equation has hitherto been interpreted as a contribution of electroosmotic effects (see, for example, Refs. 10 and 11). However, this effect seems to be minor especially in a highly permselective membrane system such as the CK-1, 1.0t membrane as suggested in the preceding papers.[6,9] These results showed that only a quite small electroosmotic effect is operative for the membrane having both a low water content and a homogeneous highly-charged polymer structure. In addition, the discrepancy between the diffusional and conductive permeabilities was also observed for a liquid ion exchange membrane system where no charged pores exist and accordingly where the electroosmotic permeation mechanism of solvent is not conceivable.[12,13] Moreover, the transport processes can be affected by the inter-ionic correlations even in a simple aqueous electrolyte system.[14–18] Thus, it is quite reasonable that the interaction between permeating ions should be taken into consideration as an origin for the failure of th Nernst-Einstein equation. Only when the cross terms of the permeability matrix are zero, the conductive and diffusional membrane permeabilities to ions coincide with each other; namely, the conductive and diffusional characteristics of the membrane system are consistently explained based on the classical Nernst-Einstein relation.

In Fig. 6, ratios of the diffusional to conductive membrane permeabilities, P^0_{Na}/P_{Na} and P^0_{Cs}/P_{Cs}, are plotted together with the permeability ratios,

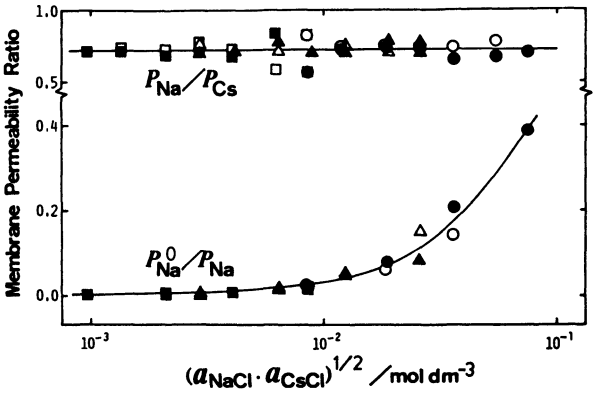

Fig. 6. Membrane permeability ratios as a function of the geometrical mean of external NaCl and CsCl activities.
Upper and lower traces indicate the values of P_{Na}/P_{Cs} and P^0_{Na}/P_{Na} $(=P^0_{Cs}/P_{Cs})$, respectively. CsCl(I)-NaCl(II) systems, NaCl(II): ●; 10^{-1} mol dm^{-3}, ▲; 10^{-2} mol dm^{-3}, ■; 10^{-3} mol dm^{-3}. NaCl(I)-CsCl(II) systems, CsCl(II): ○; 10^{-1} mol dm^{-3}, △; 10^{-2} mol dm^{-3}, □; 10^{-3} mol dm^{-3}.

$P_{Na}/P_{Cs}(=P^0_{Na}/P^0_{Cs})$. In the present system, the membrane potentials are determined by Na^+ and Cs^+ excluding Cl^-, so the following equations may be termed as the cationic pseudo-equilibrium potential:

$$V_{Na-Cs} = \begin{cases} -(RT/F)\ln(P_{Na}a^{II}_{Na}/P_{Cs}a^{I}_{Cs}) \\ \text{for the CsCl(I)-NaCl(II) system} \\ -(RT/F)\ln(P_{Cs}a^{II}_{Cs}/P_{Na}a^{I}_{Na}) \\ \text{for the NaCl(I)-CsCl(II) system.} \end{cases} \quad (11)$$

This equation suggests that the membrane potential possesses the Nernstian slope against the logarithmic activity of phase I, in the case of a constant permeability ratio, P_{Na}/P_{Cs}. As illustrated in Figs. 2A and 6, the potential data show the characteristics described above and the average value of P_{Na}/P_{Cs} is 0.72. This fact also verifies the approximation that the system is characterized by Na^+ and Cs^+ excluding the effect of Cl^-.

The significance of constant permeability ratio in the ionic membrane transport phenomena was studied from experimental and theoretical points of views.[5,7,19–21] According to the preceding paper, the following relations are satisfied:[4,6]

$$(P_{Na})^{-1} = \exp(-FV/2RT)\times \int (RTU_{Na})^{-1}\exp[(F\phi/RT) + \zeta_{Na}]dx$$
$$(P^0_{Na})^{-1} = \exp(-FV/2RT)\times \int (D_{Na})^{-1}\exp[(F\phi/RT) + \zeta_{Na}]dx, \quad (12)$$

where U_{Na} and D_{Na} are the ionic mobility and diffusion coefficient of Na^+ within the membrane phase, ϕ is the electrical potential, and ζ_{Na} is the partition factor of Na^+ between the membrane and solution phases. The integration is carried out with respect to the membrane phase. An identical relation is also satisfied for Cs^+. Since the ionic mobilities, diffusion coefficients, and partition factors of Na^+ and Cs^+ are considered to be constant, the next relation is obtained from Eq. 12:

$$\begin{aligned} P_{Na}/P_{Cs} &= (U_{Na}/U_{Cs})\exp(\zeta_{Na} - \zeta_{Cs}) \\ &= (U_{Na}/U_{Cs})K_{Na-Cs} \\ &= (D_{Na}/D_{Cs})K_{Na-Cs} \\ &= P^0_{Na}/P^0_{Cs}, \end{aligned} \quad (13)$$

where K_{Na-Cs} is the equilibrium constant for the exchange reaction between Na^+ and Cs^+ in the membrane system. This equation suggests that the ratio of diffusion coefficients as well as that of ionic mobilities takes a constant value, since the observed permeability ratios are constant. The diffusional to conductive membrane permeability ratios are indications of the interaction between Na^+ and Cs^+. The values of $P^0_{Na}/P_{Na}(=P^0_{Cs}/P_{Cs})$ increase with increasing electrolyte activity as shown in Fig. 6.

To examine the dependence of the inter-ionic correlation on the external electrolyte activity, $P_{Na\cdot Na}/P_{Na}$ and $P_{Cs\cdot Cs}/P_{Cs}$ are plotted against the external NaCl/CsCl activity ratio in Fig. 7. The Na^+ contributions to the conductive permeabilities, $P_{Na\cdot Na}/P_{Na}$ and $P_{Na\cdot Cs}/P_{Cs}$, increase as the relative activity of Na^+ to Cs^+ increases. For usual cation exchange membranes such as CK-1, 1.0t, the NaCl/CsCl concentration ratio in the membrane phase is approximately the same as that

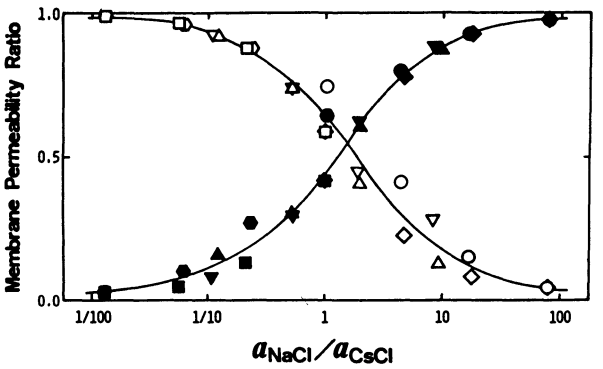

Fig. 7. $P_{Na.Na}/P_{Na}$ and $P_{Cs.Cs}/P_{Cs}$ *vs.* NaCl/CsCl activity ratio of external solutions I and II relations.
The closed and open symbols refer to the ratios for Na^+ and Cs^+. CsCl(I)–NaCl(II) systems, NaCl(II): (●, ○); 10^{-1} mol dm^{-3}, (▲, △); 10^{-2} mol dm^{-3}, (■, □); 10^{-3} mol dm^{-3}. NaCl(I)–CsCl(II) systems, CsCl(II): (●, ○); 10^{-1} mol dm^{-3}, (▼, ▽); 10^{-2} mol dm^{-3}, (◆, ◇); 10^{-3} mol dm^{-3}.

in the solution phase when the membrane is equilibrated with the electrolyte solution (unpublished data). The degree of participation of cations in the membrane transport processes would be parallel to their concentrations within the membrane phase. In the present system, the cross elements of the permeability matrix, $P_{Na.Cs}$ and $P_{Cs.Na}$, are positive quantities, so Eq. 6 leads to:

$$0 \leq 1 - (P_{Cs.Na}/P_{Na}) - (P_{Na.Cs}/P_{Cs}) \leq 1. \quad (14)$$

which is equivalent to the next relation:

$$1 \leq P_{Na.Na}/P_{Na} + P_{Cs.Cs}/P_{Cs} \leq 2. \quad (15)$$

As a limiting case, the equal signs in the right hand side of these inequalities are satisfied when the ionic interactions between Na^+ and Cs^+ are absent, *i.e.*, $P_{Na.Cs}=P_{Cs.Na}=0$. In this case, the system is characterized by:

$$P_{Na} = P^0_{Na} = P_{Na.Na}P_{Cs} = P^0_{Cs} = P_{Cs.Cs}. \quad (16)$$

Such a situation is equivalent to that of an electrolyte solution at infinite dilution where no inter-ionic interactions exist. On the other hand, the equal signs in the left hand sides are realized in the case of the situation expressed as:

$$P_{Na.Na}/P_{Na} = P_{Na.Cs}/P_{Cs}, \quad P_{Cs.Na}/P_{Na} = P_{Cs.Cs}/P_{Cs}. \quad (17)$$

But, the situation of this limiting case where $P^0_{Na}=P^0_{Cs}=0$ is physically meaningless, although P^0_{Na}/P_{Na} is very small and close to zero for lower concentrations.

These results suggest that the transport of cations takes place through the inter-ionic exchange of Na^+ and Cs^+. The participation of the rate of inter-exchange of ions in the bi-ionic systems was discussed on the basis oft he Nernst-Planck approach.[22] However, it may be pointed out that only with the aid of the membrane permeability matrix the conductive and diffusional permeabilities can be related directly to the electrical mobility and diffusion coefficient, respectively, therefore, the movement of ions in the membrane system should be interpreted on the basis of nonequilibrium thermodynamics.

References

1) H. Kimizuka and K. Kaibara, *J. Colloid Interface Sci.*, **52**, 516 (1975).
2) D. E. Goldman, *J. Gen. Physiol.*, **27**, 37 (1943).
3) A. L. Hodgkin and B. Katz, *J. Physiol. (London)*, **108**, 37(1949).
4) H. Kimizuka and K. Koketsu, *J. Theor. Biol.*, **6**, 290 (1964).
5) J. P. Sandblom and G. Eisenman, *Biophys. J.*, **7**, 217 (1967).
6) H. Kimizuka, K. Kaibara, E. Kumamoto, and M. Shirōzu *J. Membr. Sci.*, **4**, 81 (1978).
7) K. Kaibara, A. Yamauchi, and H. Kimizuka, *Mem. Fac. Sci., Kyushu Univ., Ser. C*, **8**, 247 (1973).
8) K. Kaibara, K. Saito, and H. Kimizuka, *Bull. Chem. Soc. Jpn.*, **46**, 3712 (1973).
9) E. Kumamoto and H. Kimizuka, *J. Phys. Chem.*, **85**, 635 (1981).
10) A. Despic and G. J. Hills, *Discuss. Faraday Soc.*, **21**, 150 (1956).
11) M. H. Gottlieb and K. Sollner, *Biophys. J.*, **8**, 515 (1968).
12) K. Nomura, A. Matsubara, and H. Kimizuka, *Bull. Chem. Soc. Jpn.*, **51**, 1037 (1978).
13) K. Nomura, A. Matsubara, and H. Kimizuka, *Bull. Chem. Soc. Jpn.*, **54**, 1324 (1981).
14) A. Katchalsky and P. F. Curran, "Nonequilibrium Thermodynamics in Biophysics," Harvard University Press, Cambridge, Mass. (1965), Chap. 9.
15) S. R. De Groot and P. Mazur, "Non-equilibrium Thermodynamics," North-Holland Publishing Co.,Amsterdam (1969), Chap. 11.
16) H. Fujita and L. J. Gosting, *J. Phys. Chem.*, **64**, 1256 (1960).
17) D. G. Miller, *J. Phys. Chem.*, **71**, 616 (1967).
18) E. Kumamoto and H. Kimizuka, *Bull. Chem. Soc. Jpn.*, **52**, 2145 (1979).
19) A. Yamauchi and H. Kimizuka, *J. Theor. Biol.*, **30**, 285 (1971).
20) H. Kimizuka, *J. Theor. Biol.*, **13**, 145 (1966).
21) K. Kaibara, H. Ito, N. Inoue, and H. Kimizuka, *Mem. Fac. Sci., Kyushu Univ. Ser. C*, **12**, 125 (1980).
22) M. H. Gottlieb, *Biophys. J.*, **8**, 1413 (1968).

The Nature of Oxygen Species Responsible for Propene Oxidation over V-Mo and V-Sn Oxides

Takehiko ONO* and Yutaka KUBOKAWA
Department of Applied Chemistry, University of Osaka Prefecture, Sakai, Osaka 591
(Received September 7, 1981)

The rate of oxidation of C_3H_6 has been investigated over V–Mo oxides using $^{18}O_2$(99%) tracer. The extent of participation of lattice oxygen in the oxidation increases with increasing MoO_3 content, showing a maximum at V–Mo (33 mol% of MoO_3) oxide. The rate of oxidation of C_3H_6 varies parallel to the extent of participation of lattice oxygen. A marked dependence of the rate of oxidation upon oxygen pressure observed with V–Mo(33) oxide is attributed to its high reducibility. Similar experiments have been carried out with V–Sn (94 mol% of SnO_2) oxide. The rate of reduction of the oxide with C_3H_6 is about ten times smaller than that of the corresponding catalytic oxidation of C_3H_6, suggesting the participation of adsorbed oxygen in the oxidation. The results of ^{18}O tracer experiments show participation of lattice oxygen in the oxidation. A mechanism which explains such conflicting results has been proposed.

We have recently investigated the rate of oxidation over V–Sn oxides of various compositions.[1] The rate shows two maxima at V–Sn (50 mol% of SnO_2) and V–Sn (94 mol%). It has been concluded that the rate maximum with V–Sn(50) arises from the formation of amorphous material from which lattice oxygen is easily released, participating in the oxidation. However, with V–Sn(94) oxide it is still unclear what oxygen species is responsible for the C_3H_6 oxidation.

There have been a number of work made on the oxidation reaction over V–Mo oxide catalysts.[2–9] It is well known that the rate of oxidation passes through a maximum at 10—30 mol% of MoO_3 and that such maximum activities are often observed under the conditions of high oxygen concentration.[2–6] On the other hand, several workers have observed no maximum activity at these compositions.[7–9] Whether or not the rate maximum is observed appears to be associated with the concentration of oxygen in the reaction mixture. Furthermore, Takita *et al.*[6] have attributed the rate maximum to formation of adsorbed oxygen species which is facilitated by the presence of V^{4+} ions. These appear to remain problems unsolved.

^{18}O Tracer studies appear to be appropriate for the purpose of solving both problems. In the present work, therefore, these studies together with comparison of the rate of oxidation of C_3H_6 in the presence and absence of oxygen have been carried out.

Experimental

Materials. *V–Mo-450 Catalyst*: The solution containing desired quantities of hexaammonium heptamolybdate and ammonium metavanadate was evaporated with constant stirring, and the dried product was calcined in air at 450 °C.

V–Mo-680 Catalyst: A mechanical mixture of V_2O_5 and MoO_3 powders in a desired ratio was melted at 680 °C for 0.5 h, and the melt was ground to powder after cooling. The method of preparation of V–Sn (94) was described previously.[1] $^{18}O_2$ (99.1%) was obtained from B. O. C. Limited (U. K.).

Apparatus and Procedure. The catalytic oxidation and the reduction of the oxides were carried out in a closed circulation system (290 cm^3). The reaction products such as acryladehyde, CO_2, and CO were analyzed by gas chromatography.

X-Ray diffraction patterns of the catalysts were obtained on a Rigaku Denki D-3F X-ray diffractometer using Cu $K\alpha$ radiation with a Ni filter. IR spectra of the catalysts were recorded on a Hitachi G2 spectrometer. The samples were prepared by the KBr pellet technique. The ^{18}O% in the reaction products were determined with a Hitachi RMU-6E mass spectrometer using the following ionization voltage; 80 V for CO and CO_2, 16.5 V for H_2O, and 15 V for CH_2=CHCHO. The BET surface area, the IR spectra, and the results of X-ray diffraction analysis are shown in Table 1.

Results and Discussion

C_3H_6 Oxidation over V–Mo Oxides and Their Reduction with C_3H_6. The rates of reduction of V–Mo oxides with C_3H_6 were determined at 320 °C in the range where the plot of the amount reacted *vs.* time is linear (0.5—3 min). The amount of oxygen removed under these conditions corresponded to one or two oxide layers, the distribution of the reaction products being 50% for CO, 35—30% for CO_2, 15—20% for CH_2=CHCHO,

TABLE 1. STRUCTURE OF CATALYSTS

	MoO_3 (mol%)	Area/$m^2\,g^{-1}$	IR spectra (ν/cm^{-1})	X-Ray diffraction
V–Mo-450	(0)	2.1	1020, 818	V_2O_5
	(33)	3.5	1012, 830, 960	V_2O_5, $Mo_6V_9O_{40}$ [a]
	(50)	4.2	1018, 830, 995, 965	V_2O_5, $Mo_6V_9O_{40}$
V–Mo-680	(0)	1.8	1028, 800	V_2O_5 [b]
	(33)	1.6	1015, 810	V_2O_5 [c], $Mo_6V_9O_{40}$
	(50)	1.0	—, 990—965, 880, 810	$Mo_6V_9O_{40}$
V–Sn(94, SnO_2 mol%)		43	620	SnO_2

a) See Ref. 10. b) Strongly oriented in the direction perpendicular to c axis. c) The distance between the (001) plane was contracted from 4.38 Å to 4.30 Å.

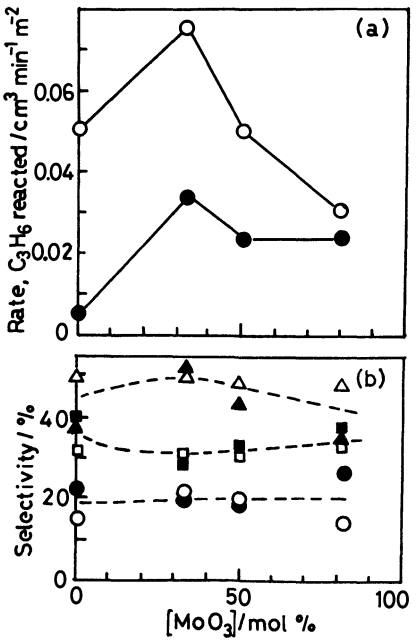

Fig. 1. Reduction of V–Mo oxides with C_3H_6.
(a) Rate. ○: V–Mo-450, ●: V–Mo-680. (b) Selectivity. △, ▲: CO, □, ■: CO_2, ○, ●: CH_2=CHCHO. Closed symbols refer to V–Mo-680. Temp 320 °C, $P_{C_3H_6}$=23 Torr (1 Torr=133.3 N m^{-2}).

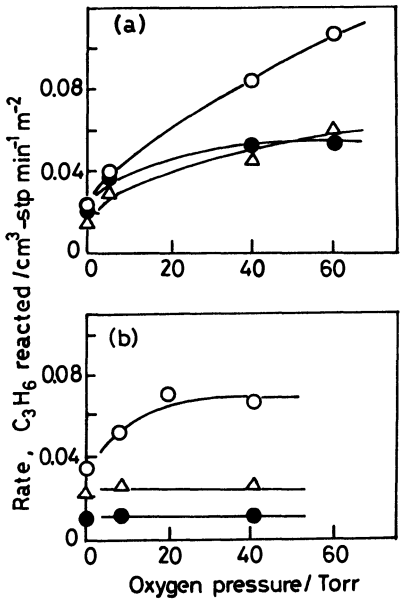

Fig. 2. C_3H_6 oxidation over V–Mo oxides at various oxygen pressures.
Temp 320 °C, ●: V_2O_5, ○: V–Mo (33), △: V–Mo (50). (a) V–Mo-450, $P_{C_3H_6}$=6 Torr. (b) V–Mo-680, $P_{C_3H_6}$=23 Torr.

below 2—3% for CH_3CHO and CH_3COCH_3. Figure 1 shows the rate of reduction thus obtained as a function of MoO_3. With V–Mo-450 as well as V–Mo-680, the rate of reduction passes through a maximum at V–Mo-(33) as reported by several workers.[2-6] The product distribution is the same throughout all the catalysts, suggesting that the reduction of vanadium ions is the main reaction. It should be noted that the preparation temperature affects the reducibility of the oxides markedly, *i.e.*, V_2O_5-450 is almost 10 times more reactive than V_2O_5-680, although the V–Mo oxides exhibit no such a marked difference in their reducibility according to their preparation temperature.

Table 2. ^{18}O contents in the products of C_3H_6 oxidation over V–Mo oxides
$P_{C_3H_6}$=23 Torr, $P_{^{18}O_2}$=8 Torr, and temp 320 °C.

Catalyst[a]	Reaction time / min	Yield[b] of each product and its ^{18}O content (%)[c]				Total yield[e] / μmol-oxygen atoms	Average[f] ^{18}O/%	Lattice oxygen[g] participated / μmol m^{-2} (layer)
		CO_2	CO	H_2O	CH_2=CHCHO			
V_2O_5-680	3	1.6	1.6	2.4	0.3	6	8—11	35
		(4.6)	(14)	(—)	(24)			(≈2)
	15	13	6.4	12.5	1.2	33	28	
		(25)	(31)	(—)	(35)			
V–Mo(33)-680	1	5.7	7.5	10.6	0.8	25	5	600
		(4.6)	(5)	(—)	(11)			(≈30)
	3	22	26	37	1.3	90	7	
		(6)	(7)	(3)	(8)			
V–Mo(50)-680	3	11	10	16	0.7	38	8	230
		(6.5)	(6)	(8)	(13)			(≈11)
V_2O_5-450	1	14	15	22	0.9	53	13	180
		(12)	(13)	(11)	(25)			(≈9)
	3	29	32	47	1.5	110	25	
		(25)	(25)	(20)	(31)			
V–Mo(33)-450	1	19	20	29	0.7	70	9	370
		(9)	(8)	(10)	(15)			(≈19)
V–Mo(50)-450	1	14	11	18	1.1	45	8	270
		(8)	(8)	(6)	(14)			(≈13)

a) 2 m^2 of catalyst was used. b) Expressed as μmol of oxygen atoms in each product. c) Values in parentheses. d) Calculated from hydrogen balance. e) This value was nearly the same as that obtained from the amount of $^{18}O_2$ consumed in the oxidation. f) (Total amount of ^{18}O/total amount of oxygen) × 100. g) See Ref. 13.

Figure 2 shows the dependence of the rate of the catalytic oxidation of C_3H_6 over V–Mo oxides upon oxygen pressure. In the oxidation at high pressure of oxygen (<40 Torr), the rate of oxidation is higher for V–Mo(33)-450 than for other V–Mo-450 oxides, although the situation is not clear in the low pressure region (>6 Torr). Such a behavior reflects the high dependence of the rate of oxidation for V–Mo(33)-450 upon oxygen pressure, *i.e.*, the order of the reaction in oxygen is about 0.4 for V–Mo(33)-450, while 0.3 for other V–Mo oxides. A similar situation is observed with V–Mo-680; The order of the reaction is 0.2 for V–Mo-(33)-680, but zero for other V–Mo-680 oxides. As is shown in Table 2, the product distribution for catalytic oxidation of C_3H_6 is essentially the same as that for the reduction of oxides with C_3H_6, *i.e.*, the oxidation of C_3H_6 in the absence of gaseous oxygen.

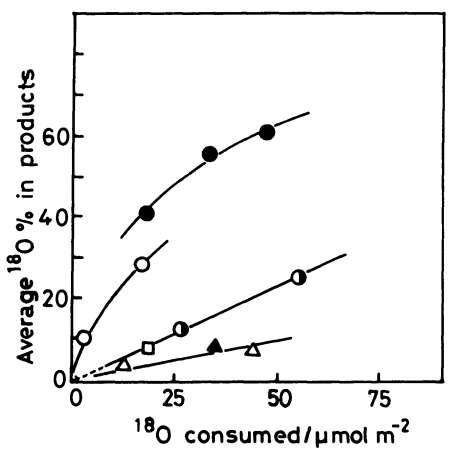

Fig. 3. Average ^{18}O%[a] in the products *vs.* amounts of oxygen consumed[b] in the oxidation.
○: V_2O_5-680, ◑: V_2O_5-450, △: V–Mo(33)-680, ▲: V–Mo(33)-450, □: V–Mo(50)-680, ●: V–Sn(94). Experimental conditions are the same as in Table 2. a), b) see Table 2.

C_3H_6 Oxidation over V–Mo Oxides Using $^{18}O_2$ Tracer. Table 2 and Fig. 3 show the results of the oxidation experiments using $^{18}O_2$ tracer. The product selectivities towards CO_2, CO, and CH_2=CHCHO are nearly the same as those of the reduction experiments (Fig. 1). No change in the ^{18}O content of the oxygen occurred during the reaction, i.e., no formation of $^{16}O^{18}O$ took place. This suggests that the heterophase exchange[11] of oxygen with the catalyst did not take place. According to the work of Blanchared *et al.*,[12] the exchange of oxygen through CO_2 appears to be negligible under the present experimental conditions.

The ^{18}O content in the products ranges from 5 to 10% at the initial stage of the reaction (Table 2 and Fig. 3), in spite of the use of 99% of $^{18}O_2$ as the reactant. This suggests that lattice oxygen participates in the oxidation. Since the anion vacancies formed by the reduction with C_3H_6 are refilled by gaseous oxygen, the ^{18}O content in the lattice oxygen increases with progress of the oxidation. If only the surface layer of the oxides participates in the oxidation, the increase of the ^{18}O content in the products with progress of the oxidation will be very rapid. On the other hand, if many sublayers participate in the oxidation, the reverse situation will result owing to the dilution of the incorporated ^{18}O with lattice oxygen. Accordingly, the feature of the increase of ^{18}O% in the products provides information to what extent the lattice oxygen participates in the reaction. Furthermore, if only the surface layer of the oxide participates in the oxidation, the surface anion vacancies formed by the reduction are refilled directly by gaseous oxygen without diffusion of the oxide ions in the lattice. On the other hand, when the extent of participation of lattice oxygen is high, most of the surface anion vacancies are refilled by diffusion of oxide ions. This suggests that whether or not the diffusion of the oxide ions is easy appears to be important for determining the extent of participation of lattice oxygen in the oxidation. As has been done by Keulks *et al.*,[13] assuming uniform distribution of the incorporated ^{18}O among the sublayers of the oxides and the number of oxygen atoms in unit area of the surface, the extent of participation of lattice oxygen in the reaction has been calculated (Table 2).

As regards V–Mo-680, the extent of participation of lattice oxygen increases with increasing MoO_3 content, showing a maximum at V–Mo(33), and then it decreases. As shown in Table 1, V–Mo(33) and V–Mo(50) consist of V_2O_5 as well as $Mo_6V_9O_{40}$, and $Mo_6V_9O_{40}$ alone, respectively. It is well known that addition of MoO_3 to V_2O_5 leads to formation of V^{4+},[2] which increases the concentration of anion vacancy in V_2O_5, *i.e.*, makes the diffusion of the oxide ions in the lattice easy. Thus, a marked increase in the participation of lattice oxygen observed with V–Mo(33)-680 is explicable, since the extent of participation of lattice oxygen is associated with the rate of diffusion of the oxide ions as described above. The decrease in the participation of lattice oxygen observed with V–Mo(50) seems to be attributed to formation of $Mo_6V_9O_{40}$ where the diffusion of oxide ions will be more difficult than with V_2O_5.

A similar situation is observed with V–Mo-450. The extent of participation of lattice oxygen is higher for V–Mo(33)-450 than for V–Mo(50)-450. Furthermore, a marked difference between the extent of lattice oxygen participation for V_2O_5-680 and -450 appears to be attributed to a higher concentration of V^{4+} for V_2O_5-450.

It is seen from Table 2 that for both V–Mo-680 and -450 oxides the extent of participation of lattice oxygen runs parallel with the rate of catalytic oxidation of C_3H_6, *i.e.*, for both series of V–Mo oxides the order V_2O_5<V–Mo(50)<V–Mo(33) holds. Such feature is in agreement with that observed with Bi–Mo oxides by Keulks *et al.*[13]

As will be shown later, the participation of lattice oxygen in the oxidation does not always exclude the possibility that adsorbed oxygen participates in the oxidation. Comparison of the rates of C_3H_6 oxidation in the presence and absence of gaseous oxygen is expected to provide information on such possibility (Fig. 2). Since the rates of catalytic oxidation of C_3H_6 over V–Mo oxides vary with the pressure of oxygen, it is difficult to compare both rates of oxidation quantita-

tively. However, as is seen in Fig. 2, there appears to be no marked difference between both rates of oxidation, suggesting that no adsorbed oxygen plays a significant role in the oxidation over V–Mo oxides.

As has been proposed by a number of workers[15] with Bi–Mo oxides, the reduction of the oxides with C_3H_6 and its oxidation by gaseous oxygen occur in different regions on the surface, A and B, respectively. The surface anion vacancies formed in the region A are refilled by diffusion of the oxide ions in the bulk, which results in formation of the surface anion vacancies in the region B. These vacancies bring about the oxygen uptake. Under such situation, the following equation holds:

$$k_A N_A P_{C_3H_6} \theta_A = k_B N_B P_{O_2}^{1/2} (1 - \theta_B),$$

where θ and 1-θ refer to the surface oxide ions and anion vacancies, respectively.

Similar situation will be expected for V–Mo oxides. Since the rate of oxidation for V–Mo oxides is not independent of oxygen pressure (Fig. 2), the values of θ_A and θ_B are less than unity, in contrast with the case of Bi–Mo oxides where $\theta_A = \theta_B = 1$ holds. There appears to be no marked difference between the values of θ_A and θ_B, since the diffusion of the oxide ions will be rapid as compared to the surface reduction. Accordingly, the above equation is transformed as follows:

$$k_1 P_{C_3H_6} \theta = k_2 P_{O_2}^{1/2} (1 - \theta),$$

where k_1 is rate constant for reduction step and k_2 for reoxidation step. The following rate equation results:

$$r = k_1 k_2 P_{C_3H_6} P_{O_2}^{1/2} / (k_1 P_{C_3H_6} + k_2 P_{O_2}^{1/2}).$$

This equation has been found to be applicable to the results shown in Fig. 2 with the values of k_1 and k_2 in

Table 3. Values of k_1 and k_2 at 320 °C

	V–Mo-450			V–Mo-680		
MoO_3 (mol%)	(0)	(33)	(50)	(0)	(33)	(50)
k_1[a]	0.01	0.03	0.01	0.0002	0.003	0.001
k_2[b]	0.04	0.025	0.03	0.04	0.10	0.10

a) $cm^4\ Torr^{-1}\ min^{-1}\ m^{-2}$. b) $cm^3\ Torr^{-1/2}\ min^{-1}\ m^{-2}$.

Table 3. It is seen that with V–Mo-680 as well as V–Mo-450 k_1 is higher for V–Mo(33) than for V–Mo(50) and V_2O_5, while no marked difference in the value of k_2 is observed for all catalysts. Such a high value of k_1 for V–Mo(33) is expected from the order of increasing reducibility of V–Mo oxides, V_2O_5<V–Mo(50)<V–Mo(33) (Fig. 1). Furthermore, it is to be noted that a marked dependence of the rate of oxidation upon oxygen pressure observed with V–Mo(33) is explicable in terms of the concept that the value of k_2/k_1 for V–Mo-(33) is smaller than the corresponding value for other catalysts.

The above considerations suggest that the rate maximum for V–Mo(33) oxide results from the weakening of V=O bond[2] and is not attributable to the fact that formation of adsorbed oxygen is facilitated by the presence of V^{4+} ions. In fact, the shifts of the V=O absorption band occur for V–Mo(33)-680 (1028→1015 cm^{-1}) and V–Mo(33)-450(1020→1012 cm^{-1}). The change in the lattice constant of V_2O_5 (d_{001}: 4.38→4.30 Å) has been observed with V–Mo(33)-680 alone. No change in the lattice constant with V–Mo(33)-450 may be attributed to the fact that dissolution of Mo ions into V_2O_5 is confined to the surface region alone.

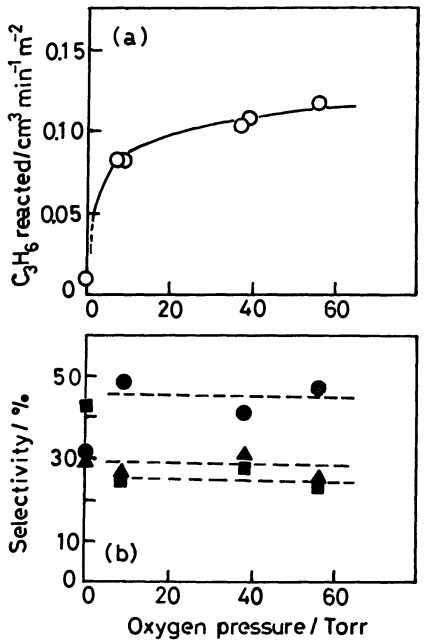

Fig. 4. C_3H_6 oxidation over V–Sn(94) oxide at various oxygen pressures.
(a) Rate. (b) Selectivity. ●: CH_2=CHCHO ▲: CO, ■: CO_2. Temp 320 °C, $P_{C_3H_6}$=23 Torr.

C_3H_6 Oxidation over V–Sn Oxides. Figure 4 shows the rate of C_3H_6 oxidation over V–Sn(94) oxide as a function of oxygen pressure. The rate of oxidation increases slightly with increasing oxygen pressure, the order of the reaction being about 0.1 in oxygen. The rate of reduction of V–Sn(94) oxide with C_3H_6, *i.e.*, the rate of oxidation of C_3H_6 in the absence of oxygen shown in Fig. 4 is 10—12 times smaller than the corresponding catalytic oxidation at 8—60 Torr of oxygen, in contrast with the results for V–Mo oxides where a slight difference is observed between both rates of oxidation. Such a marked difference in the rate of oxidation of C_3H_6 in the presence and absence of oxygen suggests that some active oxygen species may be formed in the presence of gaseous oxygen over V–Sn(94) oxide. Such an active oxygen species may be referred to adsorbed oxygen. As regards adsorbed oxygen, the following case should be mentioned. Some fraction of surface lattice oxygen is more reactive than the remainder; the redox cycle taking place in the presence of oxygen will be limited to such a small fraction. In the absence of oxygen the reaction will occur on the whole surface, including inactive regions. In this case, the enhancement of the rate of oxidation by the presence of oxygen similar to that observed for adsorbed oxygen is expected. Here, such a special type of lattice oxygen is included in the adsorbed oxygen, since it is very difficult to distinguish between both types of oxygen species. The rate of oxidation of C_3H_6 over V–Sn(94) oxide was

Table 4. ^{18}O contents in the products of C_3H_6 oxidation over V–Sn(94) oxide
Experimental conditions are the same as Table 2.

Catalyst[a]	Reaction time / min	Yield[b] of each product and its ^{18}O content (%)[c]				Total yield[e] / μmol-oxygen atoms	Average[f] ^{18}O/%
		CO_2	CO	H_2O[d]	CH_2=CHCHO		
V–Sn(94)	0.5	12	6.2	14.2	1.8	35	40
		(38)	(40)	(—)	(40)		
	1.0	27.6	9.8	27.6	4.0	69	57
		(57)	(50)	(—)	(57)		
	2.0	33	20	37	2.6	92	61
		(59)	(62)	(—)	(61)		

a)—f) See Table 2.

found to be independent of C_3H_6 in the range 8—60 Torr. Accordingly, the following rate expression holds $r=kp^0_{C_3H_6}P^{0.1}_{O_2}$. Such a low order of the reaction in oxygen as well as in C_3H_6 is different from the feature of the reaction order observed with V_2O_5 and V–Mo oxides.

C_3H_6 Oxidation over V–Sn(94) Oxide Using $^{18}O_2$ Tracer. Table 4 and Fig. 3 show the results of C_3H_6 oxidation using $^{18}O_2$ tracer for V–Sn(94) oxide. The ^{18}O content in the reaction products ranges from 40 to 60%, being much higher than those for V–Mo oxides. There is little or no difference in the ^{18}O content among CO, CO_2, and CH_2=CHCHO. The increase in the ^{18}O content with progress of the reaction is similar to that with V–Mo oxides.

If only adsorbed oxygen participated in the reaction, no incorporation of lattice oxygen in the oxidation would take place, *i.e.*, the ^{18}O content in the products would reach 100%. Such feature has been found by Morooka *et al.*[14] who investigated the oxidation of C_3H_6 over Cu_2O. The observed ^{18}O content in the products for V–Sn(94) oxide (Table 4) suggests that in addition to adsorbed oxygen, lattice oxygen participates in the oxidation. From the data at the reaction time of one minute it is concluded that the rate of incorporation of lattice oxygen (^{16}O) into the oxidation products is about 15 μmol/min m^2, being much larger than the corresponding rate of the oxidation in the absence of oxygen, *i.e.*, the reduction of the oxide with C_3H_6 which is only 2—3 μmol/min m^2 (Fig. 4). Such a marked enhancement of the rate of incorporation of lattice oxygen by the presence of gaseous oxygen suggests that the oxidation by lattice oxygen and by adsorbed oxygen do not proceed independently, *i.e.*, both oxidations are combined with each other in some way. If adsorbed oxygen attacks propene to form a reaction intermediate, which is easily oxidized by lattice oxygen, it would be possible to explain such an enhancement of the rate of incorporation of lattice oxygen by the presence of oxygen. At present, the nature of the reaction intermediate is unclear. A possible adsorbed oxygen appears to be oxygen anion radicals. Kazanskii *et al.*[16] have proposed that the O^- anion radicals can initiate an effective catalytic oxidation of CO over V_2O_5 supported on silica gel. Further study is necessary to clarify the true nature of adsorbed oxygen as well as the reaction intermediate.

The authors wish to thank Messrs. Hazime Nakazawa and Tadashi Terasaki for carrying out part of the experiments.

References

1) T. Ono, Y. Nakagawa, and Y. Kubokawa, *Bull. Chem. Soc. Jpn.*, **54**, 343 (1981).
2) K. Tarama, S. Teranishi, S. Yoshida, and N. Tamura, *Proc. 3rd Int. Congr.Catal.*, Amsterdam, 1964, Vol. 1, p. 282; S. Yoshida, *Shokubai* **10**, 90 (1968).
3) I. I. Ioffe, Z. I. Fzhkova, and A. G. Lyubarskii, *Kinet. Catal.*, **3**, 165 (1962).
4) M. Ai and S. Suzuki, *Nippon Kagaku Kaishi*, **1973**, 260.
5) N. I. Il'chenko, G. I. Golodets, and Yu. I. Pyatuitskii, *Kinet. Catal.* **14**, 312 (1971).
6) Y. Takita, K. Iwanaga, N. Yamazoe, and T. Seiyama, *Oxidation Commun.*, **1**, 137 (1979); K. Nitta, Y. Takita, N. Yamazoe, and T. Seiyama, Catal. Sympo. Catal. Soc. Japan, Prepr., No. 3H12 (1976).
7) K. Wakabayashi and Y. Kamiya, *Bull. Chem. Soc. Jpn.*, **40**, 401 (1967).
8) D. J. Cole, C. F. Culles, and D. J. Hucknall, *J. Chem. Soc., Faraday Trans. 1*, **1976**, 2744.
9) L. N. Kutsena and L. Ya. Margolis, *J. Gen. Chem.*, **32**, 100 (1962).
10) R. H. Munch and E. D. Pierron, *J. Catal.*, **3**, 406 (1964).
11) E. R. S. Winter, *J. Chem. Soc., A*, **1968**, 2889.
12) M. Blanchard and G. Louguet, *Kinet. Catal.*, **14**, 20 (1973).
13) G.W. Keulks and L. D. Krenzke, *Proc. 6th Int. Congr. Catal.*, London, 1976, Vol. 2, p. 806; L. D. Krenzke and G. W. Keulks, *J. Catal.*, **61**, 316 (1980).
14) Y. Morooka, W. Ueda, S. Tanaka, and T. Ikawa, *Proc. 7th Int. Congr. Catal.*, Tokyo, 1980, Vol. 2, p. 1086.
15) *E. g.*, J. Haber and B. Grzybowska, *J. Catal.*, **28**, 489 (1973); I. Matsuura and G. C. A. Schuit, *ibid.*, **25**, 314 (1972); T. Otsubo, H. Miura, Y. Morikawa, and T. Shirasaki, *ibid.*, **36**, 240 (1975).
16) V. B. Kazanskii, *Kinet. Catal.*, **14**, 72 (1973); V. A. Shvets, V. M. Vorotyntsev, and V. B. Kazanskii, *ibid.*, **10**, 287 (1969).

 © 1982 The Chemical Society of Japan Bull. Chem. Soc. Jpn., 55, 1753—1755 (1982)

Kinetic Studies of Spin Trapping Reactions. III. Rate Constants for Spin Trapping of the Cyclohexyl Radical

Takahisa DOBA† and Hiroshi YOSHIDA*
Faculty of Engineering, Hokkaido University, Kita-ku, Sapporo 060
(Received October 19, 1981)

In order to give a quantitative basis for the spin trapping technique, the spin trapping rate constants for the reactions between commonly-used spin traps and cyclohexyl radicals have been determined. The cyclohexyl radicals were generated by γ-irradiating cyclohexane solutions of the spin traps. The rate constants for nitrosobenzene, nitrosodurene, pentamethylnitrosobenzene, 2,4,6-tri-*t*-butylnitrosobenzene, and α-phenyl-*N*-*t*-butylnitrone at 299 K are 9×10^7, 1.4×10^7, 1.6×10^7, 2.4×10^4, and 8×10^3 mol^{-1} dm^3 s^{-1}, respectively. The results are qualitatively in accordance with previous data for *t*-butyl, 1-methyl-5-hexenyl, and 5-hexenyl radicals.

The spin trapping technique, that is, the transformation of short-lived free radicals into stable, persistent radicals by a reaction with a spin trap, such as a nitroso compound, and the subsequent observation of these persistent radicals by means of conventional electron spin resonance (ESR) measurements, has proved to be useful for the detection and indentification of free radical intermediates in liquid and gas-phase reaction systems. Before the method is utilized in mechanistic and kinetic studies of free radical reactions, its quantitative aspects should be further explored. The yields of the free radical intermediates, for example, cannot be derived by this technique without a knowledge of the rate constant for the spin trapping reaction between the spin trap used and the free radical in question. There has been relatively few rate date available for spin trapping reactions.

We have reported the first systematic study on the spin trapping rate constants for reactions between several spin traps (mostly nitroso compounds) and the *t*-butyl radical.[1] It was found that the rate constant varies over a wide range, from 10^4 to 10^8 mol^{-1} dm^3 s^{-1}, depending on the spin trap. Later, Ingold *et al.* have reported investigations on the spin trapping rate constant with 5-hexenyl[2] and 1-methyl-2-hexenyl radicals,[3] and have shown a general trend in the reactivity of several spin traps toward primary, secondary, and tertiary alkyl radicals.

In the present investigation, we have determined the spin trapping rate constants for reactions of commonly-used spin traps and another secondary alkyl radical, the cyclohexyl radical. We recently found that γ-radiolysis of cyclohexane containing a spin trap gave ESR spectra which were exclusively due to a cyclohexyl radical spin adduct.[4,5] This radiation-chemical technique has been used to generate authentic cyclohexyl radical spin adducts in the present investigation.

Experimental

Spectro-grade cyclohexane was used without further purification. Pentamethylnitrosobenzene (PMNB)[6] and α-phenyl-*N*-*t*-butylnitrone (PBN, *N*-*t*-butyl-α-toluenimine *N*-oxide)[7] were synthesized as has been described previously. Nitrosobenzene (NB) and 2-methyl-2-nitrosopropane (BNO) were purchased commercially and used as received. Nitrosodurene (ND) and 2,4,6-tri-*t*-butylnitrosobenzene (BNB) were kindly donated by Dr. R. Konaka of Shionogi Pharm. Co. Ltd. and Dr. S. Moriuchi of Mitsui Petrochemical Ind. Ltd.

Sample solutions of spin traps in cyclohexane were degassed by freeze-pump-thaw cycles nder a vacuumu of 10^{-5} Torr** and sealed in quartz ESR tubes. They were irradiated with ^{60}Co γ-rays at a dose rate of about 0.5 krad/min at 289—1 K, and subjected to ESR measurement with a Varian E-109 X-band spectrometer at the ambient temperature. Decay of the spin adducts during storage was avoided by freezing the irradiated samples at 77 K.

If the concentration of the spin traps was too low to be determined by weighing, it was determined from the intensity of their optical absorption. The optical absorption data which were used are summarized in Table 1.

Results and Discussion

When the sample solution contains one kind of spin trap, it generally shows an ESR spectrum which is due exclusively to a cyclohexyl radical spin adduct, as reported previously for PMNB.[4] An exception is BNO, which gave an ESR spectrum with 3×9 hyperfine lines. This spectrum cannot be due to the cyclohexyl radical spin adduct, but is probably due to the spin adduct of a secondarily generated free radical. Although BNO is one of the most commonly used spin adducts, it was omitted from the present investigation.

When two kinds of spin traps are present, the two corresponding spin adducts of the cyclohexyl radical are observed by ESR. This is shown in Fig. 1 for a pair of spin traps, PBN and BNB. The ESR signal is comprised of a triple doublet spectrum with a nitrogen hyperfine coupling, a_N, of 1.35 mT and a proton hyperfine coupling, a_H, of 0.25 mT and a triple quartet spectrum with a_N of 1.10 mT and a_H of 0.20 mT. The former spectrum is due to a nitroxide-type cyclohexyl radical-PBN spin adduct (*N*-*t*-butyl-α-cyclohexylbenzylaminoxyl), whereas the latter is due to an anilino-type cyclohexyl radical-BNB spin adduct (*O*-cyclohexyl-*N*-(2,4,6-tri-*t*-butylphenyl)hydroxylaminyl). This assignment is based on reported hyperfine coupling data.[8,9]

Assuming the absence of decay of the spin adducts once these have been generated, the relative yields of the spin adducts should be determined by a competition between the spin trapping reactions of the coexisting

† Present address: Institute of Polymer Technology, Royal Institute of Technology, S-1000 44 Stockholm 70, Sweden.

** 1 Torr ≈ 133.322 Pa.

Table 1. Optical absorption data and monomer-dimer equilibrium constants of spin traps in benzene determined at 299 K

Spin trap	Optical absorption[a] λ_{max}/nm	Optical absorption[a] ε/mol^{-1} dm^3 cm^{-1}	Monomer-dimer equilibrium const.[b] K/mol^{-1} dm^3
Nitrosobenzene (NB)	770	53[c]	0
Nitrosodurene (ND)	800	36[d]	1000[d]
Pentamethylnitrosobenzene (PMNB)[e]	790	52.6	1300
2,4,6-Tri-*t*-butylnitrosobenzene (BNB)	750	13	0
2-Methyl-2-nitrosopropane (BNO)	680	20	0.52
α-Phenyl-*N*-*t*-butylnitrone (PBN)	295	2.5×10^4	0

a) Absorption band due to $n\pi^*$ transition of the –NO group of monomeric form. b) Determined as [dimer]/[monomer]^2. c) Ref. 15. d) According to a recent experiment in a wider concentration range, values reported in Ref. 1 should be revised. e) Ref. 4.

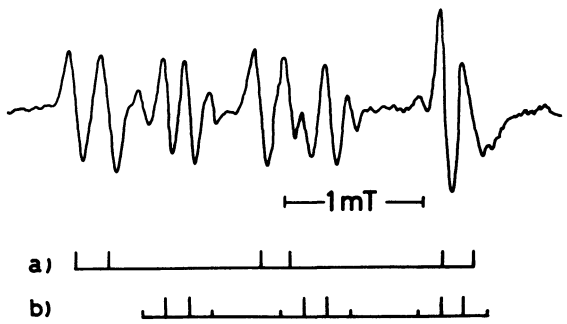

Fig. 1. ESR signal observed from γ-irradiated cyclohexane containing BNB and PBN. The stick diagrams show (a) the cyclohexyl radical-PBN spin adduct and (b) the cyclohexyl radical-BNB (anilino-type) spin adduct.

spin traps (denoted as 1 and 2). This means that the relationship

$$\frac{d[A_1]/dt}{d[A_2]/dt} = \frac{k^T_1[T_1]}{k^T_2[T_2]} \qquad (1)$$

should hold between the concentrations of spin traps and spin adducts, T_i and A_i. k^T_i is the spin trapping rate constant of the i-th spin trap, and t is the time of the γ-irradiation. The rate constant ratio k^T_1/k^T_2 has been determined for several pairs of spin traps at 289 K by irradiating the sample solutions to a low dose so that $[A_i]$ increased linearly with the irradiation time.[4] Pairs of spin traps were chosen for which overlapping spectra of spin adducts can be separated from each other. A typical example of the observed results, that of the PMNB-BNB pair, is shown in Fig. 2.

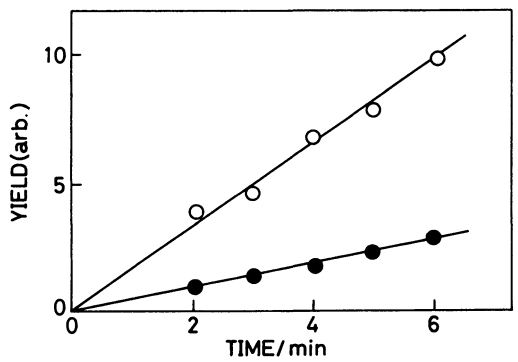

Fig. 2. Yields of (○) cyclohexyl radical-PMNB and (●) cyclohexyl radical-BNB spin adducts as a function of γ-irradiation time observed from cyclohexane containing 1.9×10^{-4} mol/dm^3 PMNB and 5×10^{-2} mol/dm^3 BNB.

The rate constant ratio was determined according to the following scheme, where arrows connect the pairs of the spin traps examined, pointing from the more reactive to the less reactive trap. The observed ratio is given above each arrow. It is the average of two to five individual competitive measurements at various trap concentrations. The numbers in parentheses show the relative spin trapping rate constants determined with respect to PMNB by averaging all possible paths with a weight factor inversely proportional to the number of arrows along the path. For example, the rate constant for NB is $100\times[(4.2\times10^3\ 8.7\times10^2+1.0\times10^4/1.7\times10^3)/2+(1.0\times10^4/3.6\times8.4\times10^2+3.6\times4.2\times10^3/1.7\times10^3)/3]\times(6/10)=560$. The values thus determined show the validity of the scheme by their internal consistency. These values seem to be correct with an uncertainty of 20%.

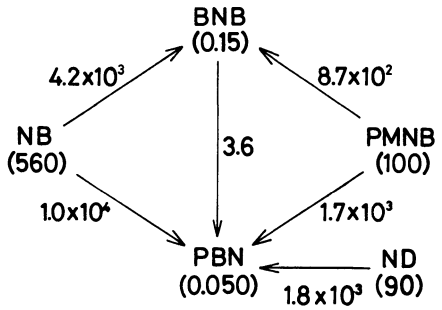

The absolute value of the spin trapping rate constant can generally be determined from competition experiments using a reference reaction with a known rate constant. We previously determined the spin trapping rate constant for the reaction of PMNB and the cyclohexyl radical to be 1.6×10^7 mol^{-1} dm^3 s^{-1} at 299 K. This was done by using

$$\dot{C}_6H_{11} + (C_4H_9)_3SnH \longrightarrow C_6H_{12} + (C_4H_9)_3\dot{S}n, \qquad (2)$$

as a reference reaction.[10] The temperature was 10 K higher than that in the present experiment. The activation energy of k^T has been reported to be so small (1—3 kcal/mol)[2] that the experimental k^T_1/k^T_2 ratio

TABLE 2. SUMMARY OF RATE CONSTANTS FOR THE SPIN TRAPPING OF ALKYL RADICALS

Spin trap	$k^T/10^5$ mo^{-1} dm^3 s^{-1}			
	t-Butyl[a] (299 K)	Cyclohexyl[b] (299 K)	1-Methyl-5-hexenyl[c] (313 K)	5-Hexenyl[c] (313 K)
Nitrosobenzene (NB)	>2000	900	—	—
Nitrosodurene (ND)	900[d]	140	406	407
Pentamethylnitrosobenzene (PMNB)	900[e]	160	—	—
2,4,6-Tri-*t*-butylnitrosobenzene (BNB)	2.3[f]	0.24[f]	3.3[g]	4.7
2-Methyl-2-nitrosopropane (BNO)	33	—	61	90
α-Phenyl-N-*t*-butylnitrone (PBN)	<0.1	0.08	0.68	1.3

a) Reference 1. b) This work. c) Refs. 2 and 3. d) Revised value, see Ref. 4. e) Recalculated using the revised value of $\varepsilon=36$ mol^{-1} dm^3 cm^{-1}. f) Anilino-type spin adduct is generated. g) 3.1 and 0.18 for anilino- and nitroxide-type spin adduct formations.

is expected to be almost temperature-independent in a small temperature range, such as that from 289 to 299 K. A difference of 1 kcal/mol in activation energy leads to a difference of 12% in the ratio. Actually, no temperature-dependence could be found experimentally for the PBN-ND pair. The spin trapping rate constant for each spin trap was calculated from the rate constant ratio determined in the present study and the absolute rate constant for PMNB reported previously.[4]

The results of the present study are shown in Table 2 together with the rate constants for spin trapping primary (5-hexenyl), secondary (1-methyl-5-hexenyl), and tertiary (*t*-butyl) radicals as reported by Ingold *et al.*[2,3] and by ourselves.[1] Alkyl radicals are efficiently spin-trapped by all of the aromatic nitroso compounds examined except BNB. The rate constants for the spin trapping reactions of the different nitroso compounds decrease in the order $k^T_{NB}>k^T_{ND}\approx k^T_{PMNB}\gg k^T_{BNB}$. This shows that substituting ortho hydrogens in the aromatic ring for bulky groups has a significant effect on the spin trapping reactions. It also supports the previous suggestion[2] that the spin trapping reaction of BNB is slow because formation of the adduct requires a fairly exact configuration of the reactions, even though the potential energy barrier to be surmounted is small. The type of trapping reaction BNB undergoes depends on the free radical trapped. For primary alkyl radicals, the result is a nitroxide-type spin adduct which many other spin traps also give. But for tertiary alkyl radicals the results is an anilino-type spin adduct. Secondary alkyl radicals are on the borderline between these two types of the trapping reactions. For the 1-methyl-5-hexenyl radical, both the anilino- and nitroxide-type spin adducts are found,[3] whereas for the cyclohexyl radical only the anilino-type spin adduct is observed.[4,9] Although the nitrone is not an efficient spin trap for alkyl radicals, including the cyclohexyl radical, it is efficient in trapping phenyl[11] and alkoxyl radicals.[12–14] It should be stressed that the spin trapping rate constants of commonly-used spin traps differ over a wide range of four orders of magnitude.

Although the overall picture for primary, secondary, and tertiary alkyl radicals has revealed that $k^T_{prim}>k^T_{sec}>k^T_{tert}$,[3] the spin trapping rate constants determined for the cyclohexyl radical in this paper are generally smaller than those for *t*-butyl radical as previously determined by ourselves.[1] This unexpected result may stem from an experimental artifact caused by an improper choice of reference reactions. Nevertheless, the results summarized in this paper gives a clue to the quantitative application of the spin trapping technique to mechanistic and kinetic studies of free radical reactions.

The authers wish to thank Dr. R. Konaka of Shionogi Pharm. Co. Ltd. and Dr. S. Moriuchi of Mitsui Petrochemical Ind. Ltd. for their kindness in donating spin traps, and Dr. K. U. Ingold of the National Research Council, Canada, for the suggestion, which enabled us to improve the data shown in Table 1.

References

1) T. Doba, T. Ichikawa, and H. Yoshida, *Bull. Chem. Soc. Jpn.*, **50**, 3158 (1977).
2) P. Schmid and K. U. Ingold, *J. Am. Chem. Soc.*, **100**, 2493 (1978).
3) Y. Maeda and K. U. Ingold, *J. Am. Chem. Soc.* **101**, 4975 (1979).
4) T. Doba, S. Noda, and H. Yoshida, *Bull. Chem. Soc. Jpn.*, **52**, 21 (1979).
5) T. Doba, S. Nishimura, T. Ichikawa, S. Noda, and H. Yoshida, *Bull. Chem. Soc. Jpn.*, **53**, 3711 (1980).
6) T. Doba, T. Ichikawa, and H. Yoshida, *Bull. Chem. Soc. Jpn.*, **50**, 3124 (1977).
7) W. D. Emmons and A. S. Pagano, *Org. Syntheses*, **49**, 13 (1969); W. D. Emmons, *J. Am. Chem. Soc.*, **79**, 5739 (1957).
8) H. Iwahashi, Y. Ishikawa, S. Sato, and K. Koyano, *Bull. Chem. Soc. Jpn.*, **50**, 1278 (1977).
9) S. Terabe and R. Konaka, *J. Chem. Soc., Perkin Trans. 2*, 369 (1973).
10) D. J. Carlsson and K. U. Ingold, *J. Am. Chem. Soc.*, **90**, 7047 (1968).
11) E. G. Janzen and C. A. Evans, *J. Am. Chem. Soc.*, **97**, 205 (1975).
12) E. G. Janzen and C. A. Evans, *J. Am. Chem. Soc.*, **95**, 8205 (1973).
13) V. E. Zubarev, V. N. Belevskii, and V. T. Bugaenko, *Dokl. Phys. Chem. (Eng. Trans.)*, **226**, 9 (1976).
14) S. Noda, T. Doba, T. Mizuta, M. Miura, and H. Yoshida, *J. Chem. Soc., Perkin Trans. 2*, **1980**, 61.
15) B. G. Gowenlock and W. Lüttke, *Quart. Rev. (London)*, **12**, 321 (1958).

Solvent Effects on the Fluorescence Quantum Yields and Lifetimes of 1- and 2-Acetyl- or Benzoylanthracenes

Takashi TAMAKI
Research Institute for Polymers and Textiles, Yatabe-Higashi 1-1-4, Tsukuba, Ibaraki 305

(Received October 22, 1981)

The fluorescence quantum yields and lifetimes of 1- and 2-acetyl- or benzoylanthracenes were measured in various degassed solvents at room temperature. The natural fluorescence lifetime was evaluated to be 30—40 ns, depending a little on the compounds, but little on the solvent. This strongly supports the recent finding that the lowest excited singlet state of the acylanthracenes is of a $\pi\pi^*$ character. On the basis of triplet-yield measurements, it was also confirmed that the low fluorescence yield in nonpolar solvents is due to an efficient intersystem crossing to an upper triplet state.

It is well established that an intersystem crossing (ISC) is the dominant nonradiative decay pathway for the lowest excited singlet state (S_1) of aromatic hydrocarbons. In the case of anthracene, the lowest triplet state (T_1) lies much lower in energy than S_1, so that the direct ISC to T_1 is incapable of competing with rapid fluorescence. Instead, the ISC to an upper triplet state (T_x) lying slightly below S_1 is favored.[1] On the other hand, it has been widely accepted for 9-methyl-, phenyl-, or haloanthracene that the ISC occurs dominantly from a thermally activated level of S_1 into T_x lying above S_1.[2] This temperature-dependent ISC well explains the considerable fluorescence variation with the temperature.[3—6]

The fluorescence of 1- or 2-acetylanthracenes is significantly dependent on the solvent. As a general trend, the fluorescence yield increases, with a concomitant red-shift of the peak maximum, as the solvent polarity increases.[7,8] The possible mechanisms for this solvent variation in the fluorescence yield are as follows; (I) a change in the thermal barrier of the temperature-dependent ISC due to the displacement of the S_1 level, and (II) an inversion of the excited electronic configuration from $n\pi^*$ to $\pi\pi^*$, as in the case of 3-pyrenecarbaldehyde.[9] Recently, Hirayama has pointed out that the S_1 of acylanthracenes has a $\pi\pi^*$ electronic configuration.[10] His conclusion was supported for 9-acylanthracenes by the external-pressure effect on the fluorescence.[11] If this is so also for 1- or 2-acylanthracenes, the (II) mechanism can be excluded.

This paper will describe the results of the fluorescence-quantum-yield, lifetime, and triplet-yield measurements for 1- and 2-acetyl- or benzoylanthracenes in various degassed solvents at room temperature, these findings are consistent with the (I) mechanism.

Experimental

1-Acetyl- (**1A**), 1-benzoylanthracene (**1B**), and their 2-isomers (**2A** and **2B** respectively) were the same as those used before.[8] The cyclohexane (Cy), dipropyl ether (DPE), tetrahydrofuran (THF), 1,2-dichloroethane (DCE), acetone (AC), acetonitrile (ACN), *t*-butyl alcohol (*t*-BuOH), 2-propanol (*i*-PrOH), ethanol (EtOH), and methanol (MeOH) were GR- or Spectro-grade reagents. For all optical measurements except for that of phosphorescence, the sample solutions were degassed by the freeze-thaw method ($<5\times10^{-5}$ Torr; 1 Torr$\approx$133.32 Pa).

The corrected fluorescence spectra were measured by using a Hitachi MPF 4 spectrofluorometer, and the observed spectra on the wavelength scale were transformed into those on the wave-number scale. The fluorescence spectra of the samples were independent of the excitation wavelength. The fluorescence intensities calculated from the trapezoid rule were corrected for the refractive index of the solvent and for the sample absorbance at the exciting wavelength (385 nm for **1A** and **1B** and 360 nm for **2A** and **2B**). The fluorescence quantum yields were based on that of 9,10-diphenylanthracene in EtOH (0.76[12]).

The fluorescence lifetime measurements were done using an Ortec SP-3 nanosecond fluorometer. A nanosecond flash lamp filled with 0.5 atm of air was operated at 5 kV at a frequency of 100 kHz, the half-bandwidth of the light pulse being 6 ns. A band-pass filter (Corning 3-73) was inserted between the flash lamp and the sample cell in order to excite the sample by nitrogen-line outputs at 300—400 nm effectively. The monitoring wavelengths were selected by means of a monochrometor; 430 nm for aprotic solutions and 500 nm for alcoholic solutions.

The analogous technique developed by Grinvald and Steinberg[13] was applied to the deconvolution of the fluorescence time evolution $\{f(t)\}$, which has this form:

$$f(t) = \int_0^t g(t-s)i(s)\mathrm{d}s,$$

where $g(t)$ is the response of the detection system to the excitation flash and where $i(t)$ is the required fluorescence decay function. $g(t)$ was experimentally determined after Wahl *et al.*[14] by using 2,5-bis[5-*t*-butylbenzoxazol-2-yl]thiophene (BBOT) as a fluorophore. $i(t)$ was assumed to be mono- and biexponential; thus:

$$i(t) = \sum_j^{1,2} C_j \exp(-\lambda_j t),$$

where C_j and λ_j are unknown parameters. The convolution product of $i(t)$ with $g(t)$ was iteratively calculated by Marquardt's least-squares method[15] to fit the decay curves observed. The calculation was terminated whenever

$\Delta C_j/C_j \leq 0.001$ and $\Delta\lambda_j/\lambda_j \leq 0.001$ for all j,

where ΔC_j and $\Delta\lambda_j$ are the increments in the parameters at the last iteration. In order to judge whether or not the curve smoothing is good, the autocorrelation function and the residuals between observed and calculated curves were calculated.[13] If theobserved decay data scatter randomly about the calculated curve, the autocorrelation function fluctuates near the zero line with a high frequency and a low amplitude.[13] A typical example of the computer-simulated decay curve is shown in Fig. 1.

The triplet-triplet absorption measurements were done using a Ushio UFP-105 microsecond flash apparatus. The sample concentrations were prepared to be $1—2\times10^{-4}$ mol

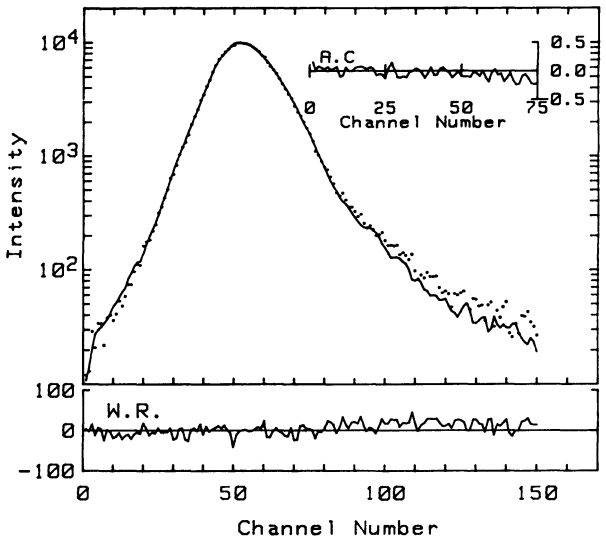

Fig. 1. Observed and simulated fluorescence decay curves of 2-acetylanthracene in cyclohexane.
W. R.: Weighted residual, A. C.: autocorrelation function.

dm^{-3}, so that the samples absorbed almost all the incident light selected by a Corning 3-73 filter. The relative triplet yields were determined from the initial absorbances of the maximum band lying at 485 nm for **1A**, at 437 nm for **2A**, at 422 nm for **1B**, and at 450 nm for **2B**, since the absorption spectra were little dependent on the solvent. The phosphorescence measurements were done in rigid methylcyclohexane glasses at 77 K.

Results

The absorption and fluorescence spectra of **1A** and **2A** in Cy are shown in Figs. 2a and 2b respectively. The general forms of the absorption and fluorescence spectra are little dependent on the substituent (acetyl and benzoyl) groups, but on the C-position of an anthryl ring, at which the substitution occurs. The fluorescence spectra of all the compounds examined are remarkably dependent on the solvent, while the absorption spectra undergo no corresponding change.[8] As the solvent polarity increases, the fluorescence spectra become more structureless and the peak maxima move to lower energies. Concomitantly, significant variations in the fluorescence quantum yield (ϕ_f) and the actual lifetime (τ_f) are observed. These values for **1A** and **2A** in several aprotic and alcoholic solvents, together with the energy of the fluorescence maxima ($\tilde{\nu}_f$), are listed in Table 1. In aprotic solvents, ϕ_f increases with an increase in the solvent polarity, but such a simple relation breaks in alcohols. From *t*-BuOH through MeOH, the ϕ_f value for **1A** increases, remains practically the same for **2A**, and considerably decreases for **1B** and **2B**. The observed solvent dependence of τ_f is similar to that of ϕ_f. Table 1 also shows the values of the radiative and nonradiative rate constants (k_f and k_{nr} respectively) evaluated from the observed ϕ_f and τ_f values for **1A** and **2A**.

It should be noted that the best fit to the fluorescence decay curves observed for **1B** and **2B** in alcohols was obtained by taking the biexponential function as $i(t)$; this is in contrast with the other cases, for which the observed decay curves were satisfactorily simulated with the monoexponential. The C_j and λ_j values for **2B**, together with the observed $\tilde{\nu}_f$ and ϕ_f values, are

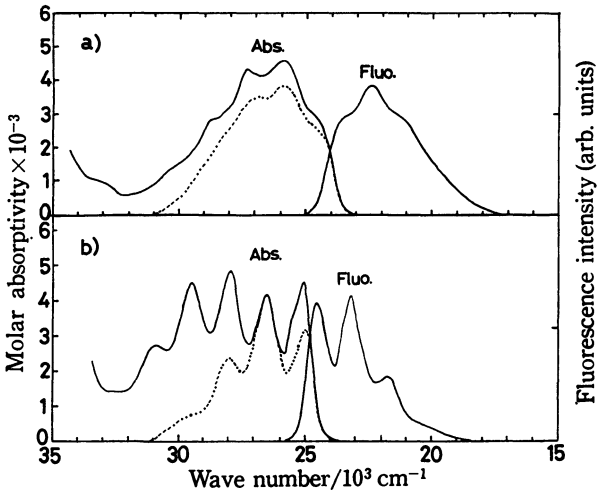

Fig. 2. Absorption and fluorescence spectra in cyclohexane.
a) 1-Acetylanthracene, b) 2-acetylanthracene. The broken curves are the mirror reflection of the fluorescence spectrum.

Table 1. Fluorescence maxima ($\tilde{\nu}_f$), quantum yields (ϕ_f), lifetimes (τ_f), radiative rate constants (k_f), and nonradiative rate constants (k_{nr}) of 1- and 2-acetylanthracenes in various degassed solvents

Solvents	1-Acetylanthracene					2-Acetylanthracene				
	$\tilde{\nu}_f$/cm^{-1}	ϕ_f	τ_f/ns	k_f/10^7 s^{-1}	k_{nr}/10^7 s^{-1}	$\tilde{\nu}_f$/cm^{-1}	ϕ_f	τ_f/ns	k_f/10^7 s^{-1}	k_{nr}/10^7 s^{-1}
Cy	21978	0.002	0.2	1.0	500	23419	0.035	1.6	2.2	59
DPE	21739	0.003	0.4	0.8	250	23095	0.073	3.2	2.3	29
THF	21413	0.014	0.6	2.3	160	22779	0.24	8.7	2.7	8.8
DCE	20964	0.046	1.9	2.5	51	22523	0.43	15	2.8	3.7
AC	20921	0.028	1.2	2.3	81	22676	0.36	13	2.8	4.9
ACN	20790	0.055	2.5	2.2	38	22472	0.49	18	2.7	2.9
t-BuOH	20243	0.35	9.1	3.9	7.1	21459	0.78	22	3.5	0.97
i-PrOH	19881	0.45	12	3.7	4.4	20661	0.82	22	3.8	0.81
EtOH	19531	0.50	13	3.8	3.9	20284	0.76	22	3.5	1.1
MeOH	19120	0.54	15	3.7	3.1	19802	0.77	23	3.4	0.99

TABLE 2. FLUORESCENCE MAXIMA ($\tilde{\nu}_f$), QUANTUM YIELDS (ϕ_f), C_j, AND λ_j FOR 2-BENZOYLANTHRACENE IN SEVERAL DEGASSED ALCOHOLS

Solvents	$\tilde{\nu}_f$/cm^{-1}	ϕ_f	$C_1/10^7$	$C_2/10^7$	$\lambda_1/10^7$ s^{-1}	$\lambda_2/10^7$ s^{-1}
t-BuOH	19920	0.63	6.9	6.9	4.8	4.8
i-PrOH	19268	0.57	9.2	5.7	7.4	4.1
EtOH	18553	0.37	9.0	9.7	18	6.0
MeOH	18051	0.10	29	1.3	24	5.9

TABLE 3. RELATIVE TRIPLET YIELDS (ϕ_T)

Solvents	ϕ_T[a]			
	1A	**2A**	**1B**	**2B**
Cy	1.0	1.0	1.0	1.0
THF	1.0	0.6		0.7
ACN	0.6	0.3	0.8	0.2
t-BuOH	0.6	0.03		0.1
MeOH	0.04	0.01	0.01	0.01

a) Relative to the triplet yield in cyclohexane.

listed in Table 2. Since the apparent lifetime of **1B** was very short, the C_j and λ_j values obtained were less reproducible.

The relative triplet yields (ϕ_T) in several solvents are listed in Table 3. An inverse relationship is observed between ϕ_T and ϕ_f as the solvent polarity increases in going from Cy through *t*-BuOH. It appears likely that the ϕ_T values in MeOH are too low to cover all of the nonradiative decay probability. This is of particular interest in the case of **1B** and **2B**, since the ϕ_f values of these compounds are also very low in the same solvent. On the other hand, the triplet lifetime was observed to be 0.2—0.4 ms, slightly dependent on the compound, but less sensitive to the solvent. The phosphorescence was detected except for **2A** (λ_{max}=684, 680, and 675 nm for **1A**, **1B**, and **2B** respectively).

Discussion

Red Shift of the Fluorescence Peak Maxima. The solvent dependence of $\tilde{\nu}_f$, as listed in Table 1, can be interpreted in terms of the nonspecific and specific solvent-solute interactions. In aprotic solvents, $\tilde{\nu}_f$ is well correlated with the macroscopic solvent polarity, which is itself associated with the dielectric constant and the refractive index.[8] This may suggest that the higher the solvent polarity, the greater the contribution of the charge-transfer (CT) resonance form in the excited state, in which positive and negative charges are localized in the anthryl and acyl moieties respectively. In reality, the excited-state dipole moments in polar solvents were measured to be 7D for **1A** and **1B** and 10D for **2A** and **2B**.[8] On the other hand, the red shift of $\tilde{\nu}_f$ in alcohols is extraordinarily larger than that to be expected from the solvent polarity. For example, $\tilde{\nu}_f$ in MeOH is lower in energy by *ca.* 2000 cm^{-1} than that in ACN, though these two solvents have quite similar polarities. The excess of the red shift in MeOH agrees with the stabilization energy due to the specific formation of hydrogen-bonded complex(es) in a hexane–MeOH mixture solution.[16]

Electronic Configuration of S_1 and ISC to the Upper Triplet State. As is shown in Table 1, k_f is little dependent on the solvent, whereas k_{nr} undergoes significant variation with the solvent. The k_f values observed in all solvents used are in an order of 2—3 $\times 10^7$ s^{-1},[17] suggesting that the electronic configuration of the compounds concerned in the S_1 state is of the $\pi\pi^*$ type, even in a very nonpolar solvent (Cy) where ϕ_f is quite low. The result is consistent with a recent conclusion.[10] The $\pi\pi^*$ nature of the fluorescence can be further confirmed by a comparison of the observed k_f value with that alternatively calculated from the observed absorption and fluorescence spectra. Unfortunately, the two $\pi\pi^*$ transition bands ascribed to ^1L_a and ^1L_b are largely overlapping in the long-wavelength absorption spectra of the compounds concerned,[8] and no mirror-symmetry relation is seen between the absorption and fluorescence spectra, as is shown in Fig. 2. Therefore, the calculation of k_f was done using the long-end absorption band obtained from the mirror-symmetry reflection of the fluorescence spectrum according to this equation:

$$\varepsilon(\tilde{\nu})/\tilde{\nu} = F(2\tilde{\nu}_0 - \tilde{\nu})/(2\tilde{\nu}_0 - \tilde{\nu})^3, \quad (1)$$

where $\varepsilon(\tilde{\nu})$ and $F(2\tilde{\nu}_0-\tilde{\nu})$ are the molar absorptivity and the fluorescence intensity as a function of the wave number respectively, and where $\tilde{\nu}_0$ is the mirror-symmetry frequency.[18] The transition band thus assumed for **1A** and **2A** is shown in Fig. 2. In such cases, k_f can be calculated from the following equation:[18]

$$k_f = 2.88 \times 10^9 n^2 \int \varepsilon(\tilde{\nu})(2\tilde{\nu}_0 - \tilde{\nu})^3 / \tilde{\nu} d\tilde{\nu}, \quad (2)$$

where n is the refractive index of the solvent. The value of k_f was obtained as 4×10^7 s^{-1} for **1A** and as 3×10^7 s^{-1} for **2A**. These values are rather close to those experimentally determined from ϕ_f and τ_f, in spite of the rough estimation of $\varepsilon(\tilde{\nu})$.

Clearly, the solvent variation in both ϕ_f and τ_f in aprotic solvents is predominantly due to the solvent variation in k_{nr}. From the inverse relation between ϕ_f and ϕ_T, it appears probable that the ISC plays an important role in the nonradiative deactivation. Furthermore, it is shown that k_{nr} decreases with a decrease in the $\tilde{\nu}_f$ value. The plot of log k_{nr} *vs.* $\tilde{\nu}_f$ for **2A** is shown in Fig. 3. A linear relation is observed between

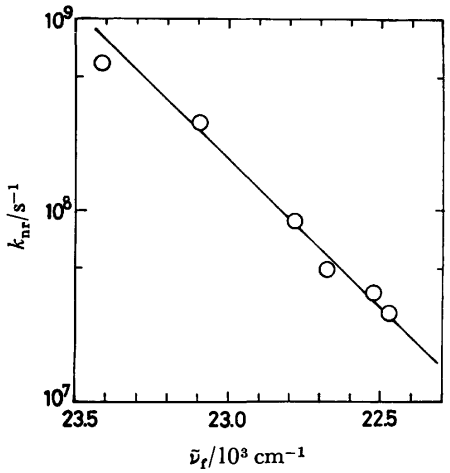

Fig. 3. Plots of log k_{nr} *vs.* $\tilde{\nu}_f$ for 2-acetylanthracene.

them. This striking relation may most reasonably be explained in terms of the (I) mechanism describing the validity of the thermally activated ISC, as in the cases of 9-haloanthracene derivatives, for which a direct correlation has been shown between the activation energy of the ISC and the solvent shift of S_1.[6] The situation is common to all the compounds examined, but it appears likely that not only the thermally activated ISC, but also the temperature-independent ISC, is operative for **1A**, **1B**, and **2B**, since these compounds exhibit the phosphorescence at 77 K, where the former ISC is inhibited. On the other hand, the temperature-independent ISC may be less important for **2A**, which emits no phosphorescence.

It was suggested for acylanthracenes that the triplet states of both $\pi\pi^*$ (T_2) and $n\pi^*$ ($T_{n\pi^*}$) are lying near S_1 and that, on the basis of the photoreduction and oxetane formation reaction, the reactive $T_{n\pi^*}$ lies above the nonreactive T_2 for the photostable derivatives.[10] The compounds concerned in this study are just like this. Combining these results with our data, the relative energy levels of relevant excited states in such noninteracting solvents as Cy may be deduced as follows; $T_{n\pi^*}>T_2>S_1$ for **2A** and $T_{n\pi^*}>S_1\geqslant T_2$ for **1A**, **1B**, and **2B**. Thus, the temperature-independent ISC to T_2 occurs only in the latter cases, but the temperature-dependent ISC to $T_{n\pi^*}$ occurs commonly in both cases.

Nonradiative Decay Pathways in Alcohols. It is clear that the fluorescence of the acylanthracenes in alcohols is perturbed by the hydrogen-bond interaction with the solvent. The very low ϕ_T values in such powerful hydrogen-donating solvents as MeOH may be due to the fact that a solvent-induced internal conversion pathway replaces ISC as the major nonradiative decay pathway.[19] However, the anomaly of the fluorescence decay kinetics observed for **1B** and **2B** cannot be explained by this mechanism alone. An explanation is, however, given by the following reaction scheme:

$$B \xrightarrow{h\nu} B^{*1} \underset{k_{-r}}{\overset{k_r}{\rightleftharpoons}} X \xrightarrow{k_d} B$$

$$B^{*1} \xrightarrow{k_f} B + h\nu' \quad B \text{ or } {}^3B^*$$

$$B^{*1} \xrightarrow{k_{nr}} {}^3B^*$$

where the k's are the rate constants, where B, $^1B^*$, and $^3B^*$ are the aromatic carbonyl compounds in the ground, excited singlet, and triplet states respectively, and where it is assumed that $^1B^*$ is reversibly converted into a nonfluorescent X. The identification of X remains ambiguous at this stage of our investigation. In this respect, it was suggested that the nonradiative decay due to intramolecular charge sepearation is responsible for the observed decrease in ϕ_f.[8] The decrease in the delocalization interaction between the anthryl and benzoyl moieties may be associated with a noncoplanar geometry between the anthryl and phenyl rings. If so, the torsional isomer appears a likely possible model for X.

The reaction scheme leads to the following equations;

$$C_1 = (\lambda_2 - Z)(C_1 + C_2)/(\lambda_2 - \lambda_1), \quad (3)$$

$$C_2 = (Z - \lambda_1)(C_1 + C_2)/(\lambda_2 - \lambda_1), \quad (4)$$

Table 4. Rate parameters for 2-benzoylanthracene

Solvents	$k_f/10^7\ s^{-1}$	$(k_f+k_{nr}+k_r)/10^7\ s^{-1}$	$(k_{-r}+k_d)/10^7\ s^{-1}$
t-BuOH	3.0	4.8	4.8
i-PrOH	3.2	6.2	5.4
EtOH	3.3	12	12
MeOH	2.1	24	6.6

$$Z = k_f + k_{nr} + k_r, \quad (5)$$

$$\lambda_1 + \lambda_2 = k_f + k_{nr} + k_r + k_{-r} + k_d, \quad (6)$$

$$\lambda_1\lambda_2 = (k_f + k_{nr})(k_{-r} + k_d) + k_r k_d. \quad (7)$$

In the photostationary state, ϕ_f is given in the form:

$$\phi_f = k_f\,(k_{-r} + k_d)/\lambda_1\lambda_2. \quad (8)$$

By using the values of C_j, λ_j, and ϕ_f observed experimentally, the values of $k_f+k_{nr}+k_r$, $k_{-r}+k_d$, and k_f can be evaluated from Eqs. 3 or 4, 6, and 8 respectively. The results for **2B** are listed in Table 4. It is noteworthy that the k_f values thus obtained are of a similar magnitude with those observed in polar aprotic solvents ($k_f \simeq 3\times10^7\ s^{-1}$). This result may support the validity of the reaction scheme postulated. It is observed that either k_{nr} or k_r, or both, increases in going from *t*-BuOH to MeOH, while the sum of k_{-r} and k_d is less variant. It appears likely that the nonradiative decay due to the solvent-induced geometry change as well as to the solvent-induced internal conversion is important for **1B** and **2B** in polar protic solvents.

References

1) R. E. Kellogg, *J. Chem. Phys.*, **44**, 411 (1966).
2) J. B. Birks, "Organic Molecular Photophysics," ed by J. B. Birks, John Wiley and Sons, New York (1973), Vol. 1, p. 35.
3) E. J. Bowen and J. Sahu, *J. Phys. Chem.*, **63**, 4 (1959).
4) R. G. Bennett and P. J. McCartin, *J. Chem. Phys.*, **44**, 1969 (1966).
5) E. L. Lim, J. D. Laposa, and J. M. H. Yu, *J. Mol Spectrosc.*, **19**, 412 (1966).
6) A. Kearvell and F. Wilkinson, "Transitions Non-Radiatives dans les Molecules," Paris (1969); *J. Chim. Phys.*, **1970**, 125 (1970).
7) A. S. Cherkasov, *Opt. Spectrosc.*, **9**, 285 (1960).
8) T. Tamaki, *Bull. Chem. Soc. Jpn.*, **51**, 2817 (1978).
9) K. Bredereck, Th. Förster, and H.-G. Oesterlin, "Luminescence of Organic and Inorganic Materials," ed by H. P. Kallmann and G. M. Spruch, John Wiley and Sons, New York (1962), p. 161.
10) a) S. Hirayama, *Rev. Phys. Chem. Jpn.*, **42**, 49 (1972); b) S. Hirayama, *Bull. Chem. Soc. Jpn.*, **48**, 1127 (1975).
11) D. J. Mitchell, G. B. Schuster, and H. G. Drickamer, *J. Am. Chem. Soc.*, **99**, 1145 (1977).
12) J. B. Birks, "Photophysics of Aromatic Molecules," Wiley Interscience, London (1970), p. 128.
13) A. Grinvald and I. Z. Steinberg, *Anal. Biochem.*, **59**. 583 (1974).
14) Ph. Wahl, J. C. Auchet, and B. Donzel, *Rev. Sci. Instrum.*, **45**, 28 (1974).
15) N. R. Draper and H. Smith, "Applied Regression Analysis," John Wiley and Sons, New York (1966).
16) T. Tamaki, *Bull. Chem. Soc. Jpn.*, **55**, 1761(1982).

17) The reproducibility for the τ_f values of **1A** in Cy and DPE is doubtful, since they are very short. This may affect the reliability of the k_f and k_{nr} values. We believe, however, that the k_f values for these solvents are of the same magnitude as that of the k_f values for the other solvents.

18) Ref. 12, pp. 85—88.

19) T. C. Werner, T. Matthews, and B. Soller, *J. Phys. Chem.*, **80**, 533 (1976).

The Photoassociation of 1- and 2-Acetylanthracenes with Methanol

Takashi TAMAKI
Research Institute for Polymers and Textiles, Yatabe-Higashi 1-1-4, Tsukuba, Ibaraki 305

(Received October 22, 1981)

The effect of small amounts of methanol ($\lesssim$0.34 mol dm^{-3}) upon the absorption and fluorescence spectra of 1- and 2-acetylanthracenes in hexane was investigated. While the formation of a 1 : 1 hydrogen-bonded complex in the ground state was revealed by the isosbestic points of the absorption spectra, the change in the fluorescence spectra was indicative of the photogeneration of a highly associated complex which includes at least two alcohol molecules. On the assumption that the excited 1 : 1 complex further associates with an alcohol molecule, the computer simulation by the least-squares method provided a good fit of the observed concentration dependence of methanol upon the fluorescence quantum yield. The photokinetic parameters and the thermodynamic quantities were evaluated from the simulated parameter values.

The fluorescence spectra of aromatic compounds are, in general, sensitive to solvent polarity, because the electrostatic solvent-solute interaction (dipole-dipole and dipole-induced dipole interactions) perturbs the excited singlet states of the compounds. On the other hand, the fluorescence spectra of some aromatic compounds, such as heterocycles, ketones, and amines, in nonpolar solvents are significantly affected by the addition of small amounts of a protic solvent, which are insufficient to alter the dielectric properties of the solvents.[1-4] This specific perturbation of the fluorescence is due to the formation of a hydrogen-bonded (H-bonded) complex. Recently, the photodynamics of the complex formation has been investigated by using nanosecond fluorescence spectroscopy.[5-7] In their study of time-resolved emission measurements for aminophthalimides in alcohol solvents at low temperatures, Ware and his co-workers found that the spectral shift due to the complex formation occurs in a subnanosecond, preceding the spectral shift associated with the nonspecific dipolar relaxation.[5] DeToma and Brand studied the interaction of 2-anilinonaphthalene in cyclohexane with alcohol at the ambient temperature and presented direct kinetic evidence that this system results in stoichiometric complex formation at a low alcohol concentration, followed by the reorientation of the solvent cage when the concentration of alcohol is high.[6] For the *m*-aminoacetophenone-alcohol-viscous nonpolar solvent system, Itoh and his co-workers reported the formation of an exciplex including two alcohol molecules.[7]

In a previous study of the time-dependent spectral shifts of 1- and 2-acylanthracenes in alcohols at low temperatures,[8] it was suggested that the perturbation of alcohol on the fluorescence of these compounds is caused by a combination of the specific H-bond interaction and a nonspecific dipole reorientation of the solvent, as in the case of aminophthalimide. This paper will describe the photokinetics of the complex formation for 1- (**1A**) and 2-acetylanthracenes (**2A**) with methanol in hexane.

Experimental

The acetylanthracenes (**1A** and **2A**) were the same as those used before.[8] The hexane and methanol were Spectro- and GR-grade reagents respectively and were used without further purification.

The absorption measurements were done using a Cary 17D spectrophotometer equipped with a thermostated cell holder. The concentration of the samples used was 3×10^{-5} mol dm^{-3}. Methanol was added to the sample solutions by up to 0.34 mol dm^{-3}, at which point the dielectric property of the hexane–methanol mixture solution corresponds approximately to that of dipropyl ether (ε=3.4). For the Scott plots,[9] the absorption changes in the presence of methanol were monitored by using 10-cm cylindrical cells at 440 nm for **1A** and at 424 nm for **2A**, where the absorption of uncomplexed ketones is negligible. The absorption spectra of the complex between the aromatic ketones and methanol were determined by means of the following equation:

$$\varepsilon_C(\lambda) = \varepsilon_A(\lambda)\{d(\lambda) - \alpha d_0(\lambda)\}/(1-\alpha)d_0(\lambda),$$

where $\varepsilon_A(\lambda)$ and $\varepsilon_c(\lambda)$ are the molar absorptivities of the ketones and the complex at λ nm respectively, where $d(\lambda)$ and $d_0(\lambda)$ are the absorbances in a unit of the light path at λ nm in the presence and in the absence of methanol respectively, and where α is the mole fraction of the uncomplexed ketones to the total ketones, which can be evaluated from the equilibrium constant.

The corrected fluorescence spectra were measured using a Hitachi MPF 4 spectrofluorometer. The concentrations of the samples and of methanol were the same as those used for the absorption measurements. A 1-cm square cell was placed on a thermostated cell holder connected with a Haake FK constant-temperature circulator. The excitation was done at 350 nm for **1A** and at 368 nm for **2A**, at these points the absorption spectra show their isosbestic points, so that the relative fluorescence intensities correspond directly to the relative fluorescence quantum yields. The steady-state fluorescence data were manipulated by the aid of an HP 9845B desk-top computer. Firstly, the fluorescence spectra on the wavelength scale were transformed into those on the wave-number scale, and the relative fluorescence intensities were calculated from the trapezoid rule. Secondly, the data on the fluorescence quantum yields were analyzed by the use of a software file (09845-15140) programing the nonlinear regression analysis. The initial values of the free parameters were set as 10, and the calculation was iterated until the value of each parameter converged into (1$\pm$0.1) times the preceding value.

The nanosecond fluorescence measurements and the deconvolution analysis were done in ways similar to those described elsewhere.[10] Since the fluorescence lifteime of **1A** in hexane is too short ($<$1 ns) to be detected by our apparatus, no experimental result for this compound is presented.

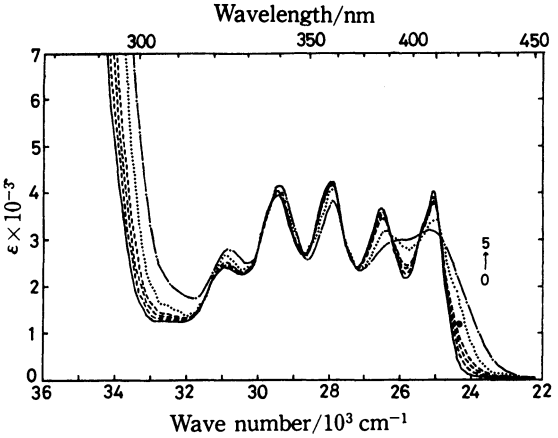

Fig. 1. Absorption spectra of 2-acetylanthracene in the binary mixture of methanol–hexane. Concentrations of methanol/mol dm^{-3}: 0) 0, 1) 0.1, 2) 0.2, 3) 0.29, 5) 24.7 (pure methanol). Spectrum 4 refers to an H-bonded complex.

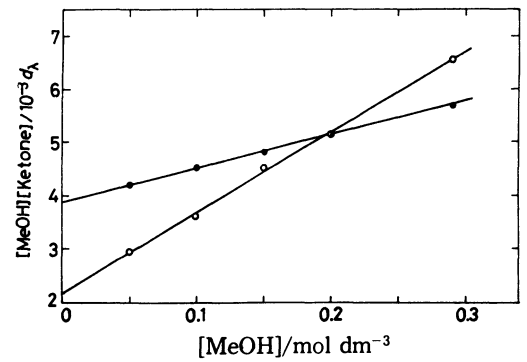

Fig. 2. Scott plots for 1- (—○—) and 2-acetylanthracene (—●—) in the binary mixture of methanol–hexane at 20 °C.

Results

The absorption spectra of **2A** in hexane in the presence and in the absence of methanol (M) are shown in Fig. 1. The apparent isosbestic points in the spectra are indicative of the formation of the complex. The Scott plots for **1A** and **2A** are shown in Fig. 2. The linearity of the plots is gratifying. The equilibrium constant (K_g) was evaluated to be 6.8 mol^{-1} dm^3 for **1A** and 2.7 mol^{-1} dm^3 for **2A** at 20 °C, only slightly dependent on the temperature. The absorption spectrum of the complex for **2A** is also shown in Fig. 1. The general form of this spectrum is close to that in pure methanol, which is also shown for the sake of comparison. The two vibrational bands lying at 376 and 388 nm in hexane are deformed, and the long wavelength edge extends to the red region. The red shift of the peak maximum amounts to *ca.* 100 cm^{-1} for **2A**. On the other hand, the spectral shift for **1A** is very small, and the peak maxima of the perturbed and unperturbed spectra are practically the same.

1A and **2A** emit a weak and structured fluorescence in hexane. The addition of small amounts of M induces a significant change in these fluorescence spectra. A typical example is shown in Fig. 3. The fluorescence spectra in the presence of M become intensive and move to the red area with an increase in the concentration of M ([M]). The [M] dependence of the total fluorescence quatum yield (Φ), divided by the fluorescence quantum yield (ϕ_A°) in the absence of M at several temperatures, is shown in Fig. 4.

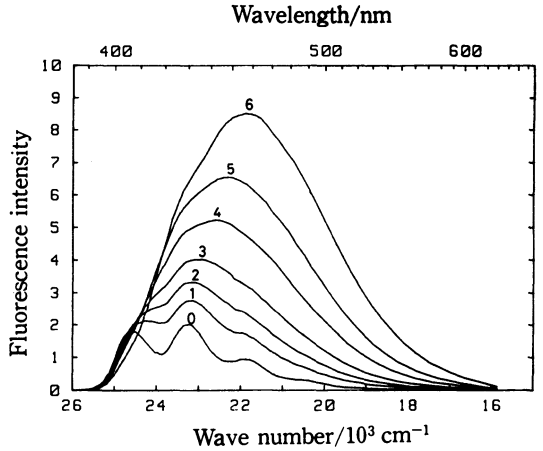

Fig. 3. Fluorescence spectra of 2-acetylanthracene in the binary mixture of methanol–hexane at 20 °C. Concentrations of methanol/mol dm^{-3}: 0) 0, 1) 0.03, 2) 0.05, 3) 0.075, 4) 0.12, 5) 0.2, 6) 0.34.

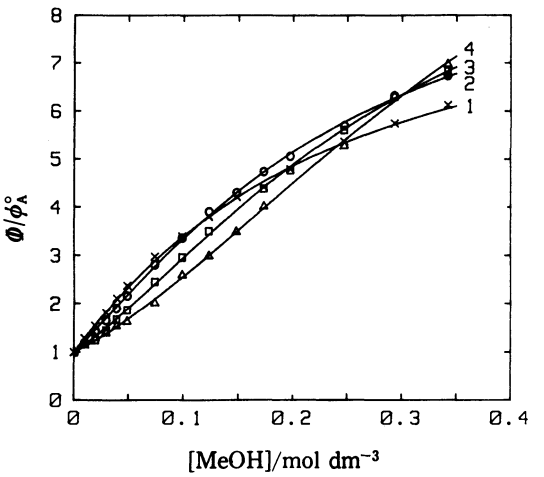

Fig. 4. Observed and simulated concentration dependence of methanol upon the relative fluorescence yield of 2-acetylanthracene. Temperature/°C: 1) 12, 2) 20, 3) 30, 4) 40.

Discussion

Reaction Scheme for the Specific Interaction of Acetylanthracenes with Methanol. The red shift of the fluorescence peak maxima for **1A** and **2A** in the presence of small amounts of M is much larger than that to be expected from the nonspecific solvent-solute interaction. As is shown in Fig. 3, the amounts of the red shift span about 30 nm under our conditions, whereas the relevent increase in the solvent polarity causes the fluorescence spectra of **1A** and **2A** to shift toward the red region by only several nm. Therefore, it appears probable that

the observed change in the fluorescence spectra is mainly due to the specific interaction between the aromatic ketones and M. The effect of added M on the fluorescence spectra is not only the red shift of the peak maxima, but also the broadening of the bandwidth, indicating the appearance of the emission band which can be ascribed to the H-bonded complex. Furthermore, the fluorescence spectra for **2A** show that an isoemissive point near 410 nm does not come out until [M] reaches *ca.* 0.05 mol dm^{-3}. This suggests that a highly associated complex, that is, one in which at least two alcohol molecules are intimately associated with the aromatic ketone, is photogenerated at a relatively high [M].

Consequently, the following reaction scheme can be postulated for the specific interaction of **1A** and **2A** with M:

$$A \underset{-M}{\overset{+M,\,K_g}{\rightleftharpoons}} C, \tag{1}$$

$$A \xrightarrow{h\nu} A^*, \tag{2}$$

$$C \xrightarrow{h\nu} C^*, \tag{3}$$

$$A^* \underset{-M,\,k_4}{\overset{+M,\,k_8}{\rightleftharpoons}} C^* \underset{-M,\,k_5}{\overset{+M,\,k_7}{\rightleftharpoons}} E^* \qquad (k_1,\ k_2,\ k_3,\ k_6,\ k_9,\ k_{10}) \tag{4}$$

$$A + h\nu'\ A \quad C + h\nu''\ C \quad C + M + h\nu'''\ C + M,$$

where A is the uncomplexed ketones, where C and E are the complexes including one and two alcohol molecules respectively, where the superscript asterisk represents the excited singlet state, and where the k's are the rate constants of the respective processes.

There is a possibility that the more highly associated complexes other than E are successively photogenerated at a high [M]. However, such a situation, requiring more sophisticated kinetic treatments, is not considered in this work. In fact, the fluorescence data observed are well consistent with the reaction kinetics to be described below.

Kinetic Treatments for Steady-state Fluorescence. In the photostationary state, the fluorescence quantum yields (ϕ) of A, C, and E relative to $\phi_A^\circ = k_1/(k_1+k_2)$ are given by the following equations:

$$\phi_A/\phi_A^\circ = \frac{\{1+P_3(1+P_1[M])+P_6[M]\}}{(\text{Denominator})}, \tag{5}$$

$$\phi_C/\phi_A^\circ = \frac{P_4[M]\{P_1+P_2(1+P_1[M])\}}{(\text{Denominator})}, \tag{6}$$

$$\phi_E/\phi_A^\circ = P_5[M](\phi_C/\phi_A^\circ), \tag{7}$$

where the ϕ's are defined as $\phi_A = k_1[A^*]/\{\varepsilon_A(\lambda)[A]+\varepsilon_C(\lambda)[C]\}$ *etc.*, (Denominator)$=(1+P_1[M])\{(1+P_2[M])\times(1+P_6[M])+P_3\}$, and

$$P_1 = K_g\varepsilon_C(\lambda)/\varepsilon_A(\lambda),$$
$$P_2 = k_3/(k_1+k_2),$$
$$P_3 = k_4/(k_5+k_6),$$
$$P_4 = k_5(k_1+k_2)/k_1(k_5+k_6),$$
$$P_5 = k_7k_9/k_5(k_8+k_9+k_{10}),$$
$$P_6 = k_7(k_9+k_{10})/(k_5+k_6)(k_8+k_9+k_{10}).$$

If these three fluorescence quantum yields could be separately determined, it would be possible to ascertain whether or not the parameter values evaluated from these experimental runs were consistent with each other. Previously, we tried to divide the perturbed fluorescence spectra into the component spectra arising from the uncomplexed ketone and the complex by subtracting the unperturbed spectra from the perturbed spectra, those which were normalized on the short wavelength side where the contribution of the complex is negligible.[8] This technique is, however, not practical in quantitative kinetic treatments, for the low fluorescence intensity at the normalized wavelength makes the errors in the subtraction procedure considerable. Moreover, it can not be applied to the **1A**–M system, for the fluorescence intensities, even on the short-wavelength side, show a monotonous increase with an increase in [M], presumably because of the large overlapping of the component spectra. Therefore, we directly analyzed the data observed for Φ/ϕ_A°, which should conform to this equation:

$$\Phi/\phi_A^\circ = 1 + [M]\{P_4(1+P_5[M]) - (1+P_6[M])\}\times \{P_1+P_2(1+P_1[M])\}/(\text{Denominator}). \tag{8}$$

Since P_1 can be independently determined from the absorption measurements, the fitting of the plots by the nonlinear regression analysis was done by holding P_1 fixed and by treating the others (P_2—P_6) as free parameters. The results for the computer simulation are shown in Fig. 4, while the values of the parameters obtained are listed in Table 1. Although the apparent dependencies of [M] on Φ/ϕ_A° are different from temper-

Table 1. Calculated parameter values

Temperature °C	P_1	P_2	P_3	P_4	P_5	P_6	SSR[a]
			1-Acetylanthracene				
12	6.8	11.1	3.0	10.5	4.0	0.6	0.087
20	6.7	10.7	4.8	11.4	5.0	0.7	0.16
30	6.6	8.6	7.0	11.4	8.6	2.3	0.037
40	6.5	5.7	10.1	11.0	12.6	4.7	0.038
			2-Acetylanthracene				
12	2.7	2.1	0.5	10.7	5.8	7.6	0.023
20	2.7	4.9	1.7	9.2	7.5	7.2	0.029
30	2.6	6.8	4.3	9.5	8.6	7.6	0.027
40	2.6	9.8	11.3	12.2	6.8	5.6	0.044

a) Sum of squared residuals.

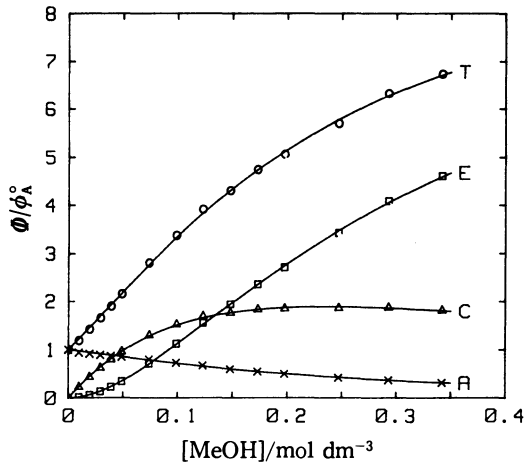

Fig. 5. Simulated concentration dependence of methanol upon the relative fluorescence yield of three emissive components for 2-acetylanthracene: A) an uncomplexed ketone, C) a 1 : 1 complex, E) a 1 : 2 complex, T) A+C+E.

ature to temperature, the simulated curves satisfactorily smooth the observed plots with the order of 10^{-2} of the sum of the squared residuals for all the experimental runs. This strongly supports the validity of the reaction scheme postulated. Particularly, the sigmoid and upward dependencies of [M] revealed at relatively high temperatures are characteristic of the formation of a highly associated complex; the formation of C alone results in no such dependencies.

The functions $\{\phi_A([M])/\phi_A^\circ$, *etc.*$\}$ predicted from Eqs. 5—7 for **2A** at 20 °C are shown in Fig. 5. It can be seen that, as [M] increases, ϕ_A decreases; ϕ_C, which increases at first, decreases slightly, and ϕ_E increases at the expense of ϕ_C. On the assumption that the only emissive species at very low [M] values are A and C, and that the peak maxima and the forms of these two fluorescence spectra do not change at higher [M] values, the perturbed fluorescence spectra can be divided into their three component spectra by using the predicted fluorescence quantum yields. The fluorescence spectra of E thus obtained were found to be invariant in general form and peak maximum at [M]$\leqslant$0.25 mol dm^{-3}. An example of such a spectral division for **2A** at [M]=0.12 mol dm^{-3} at 20 °C is shown in Fig. 6. The fluorescence spectra of the H-bonded complexes (C and E) become structureless and move to the red with an increase in the number of the associated alcohol molecule. The energies of the fluorescence peak maxima of A, C, and E for **1A** and **2A** at 20 °C, together with the amounts of the red shift relative to A, are listed in Table 2.

Photokinetics for Pulse Excitation at Low [M]. At low [M] values, where the perturbed fluorescence spectra consist of A and C, the contribution of E being negligible, the observed time evolution of the fluorescence is the convolution of a lamp decay profile, with the true fluorescence decay function given in this form:

$$F(t) = C_1 \exp(-\lambda_1 t) + C_2 \exp(-\lambda_2 t) \quad (9)$$

where:

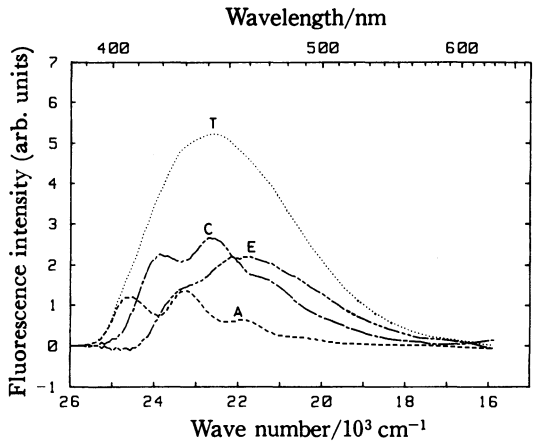

Fig. 6. Division of the fluorescence spectrum of 2-acetylanthracene in the presence of methanol (0.12 mol dm^{-3}) into three component spectra: T) the fluorescence spectrum as observed, A) an uncomplexed ketone, C) a 1 : 1 complex, E) a 1 : 2 complex.

TABLE 2. FLUORESCENCE PEAK MAXIMA OF THE UNCOMPLEXED KETONE (A), 1 : 1 COMPLEX (C), AND 1 : 2 COMPLEX (E)

Compound	λ_A/nm	λ_C/nm ($\Delta\tilde{\nu}_{A-C}$/cm^{-1})[a]	λ_E/nm ($\Delta\tilde{\nu}_{A-E}$/cm^{-1})[a]
1-Acetylanthracene	449	465 (767)	483 (1568)
2-Acetylanthracene	431	440 (475)	460 (1463)

a) The amounts of the red shift relative to A.

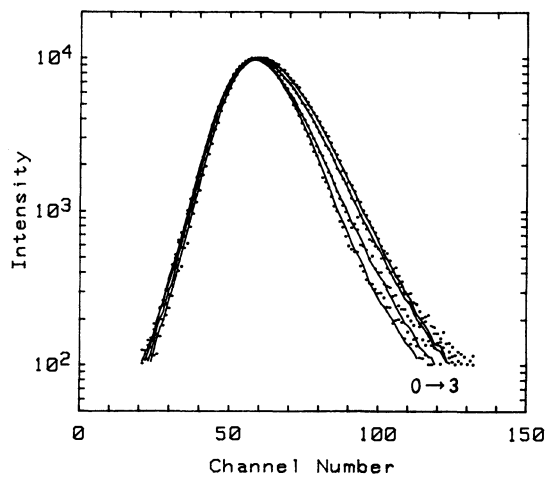

Fig. 7. Observed and simulated time evolution of the fluorescence of 2-acetylanthracene in the binary mixture of methanol–hexane at 20 °C. Concentrations of methanol/mol dm^{-3}: 0) 0, 1) 0.01, 2) 0.03, 3) 0.05.

$$\lambda_{1,2} = (1/2)(k_1 + k_2 + k_3[M] + k_4 + k_5 + k_6) \pm \sqrt{(k_1+k_2+k_3[M]-k_4-k_5-k_6)^2+4k_3k_4[M]},$$

and:

$$\lambda_1 + \lambda_2 = k_1 + k_2 + k_3[M] + k_4 + k_5 + k_6, \quad (10)$$

$$\lambda_1\lambda_2 = (k_1 + k_2)(k_4 + k_5 + k_6) + k_3(k_5 + k_6)[M]. \quad (11)$$

The related photokinetics for the time evolution of the

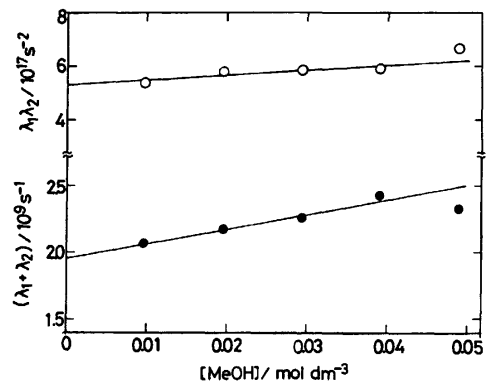

Fig. 8. Plots of $\lambda_1+\lambda_2$ and $\lambda_1\lambda_2$ *vs.* [methanol] for 2-acetylanthracene.

fluorescence at high [M] values remains unresolved in this paper, since the luminescent system involving ternary components makes the kinetic analysis extremely complex.

Figure 7 shows the actual time evolution of the fluorescence monitored at 430 nm for **2A** in the presence of M ($\leqslant$0.05 mol dm^{-3}) at 20 °C, together with the decay curves calculated by the method of convolution, assuming Eq. 9. The observed decay curves are well simulated by the biexponential decay function. The plots for $\lambda_1+\lambda_2$ and $\lambda_1\lambda_2$ *vs.* [M] are shown in Fig. 8. From the slopes of these two linear plots, the values of k_3 and k_5+k_6 are obtained as 1.1×10^{10} mol^{-1} dm^3 s^{-1} and 1.8×10^8 s^{-1} respectively. The intercepts of these plots at [M]=0 give $k_1+k_2+k_4+k_5+k_6=1.9\times10^9$ s^{-1} and $(k_1+k_2)(k_4+k_5+k_6)=5.4\times10^{17}$ s^{-1}, yielding $k_1+k_2=1.6\times10^9$ s^{-1} and $k_4+k_5+k_6=3.4\times10^8$ s^{-1}; the value of k_1+k_2 is within the limits of experimental error, proximate to the reciprocal of the fluorescence lifetime independently measured for **2A** in the absence of M at 20 °C ($1/\tau_A^\circ=1/(k_1+k_2)=1.4\times10^9$ s^{-1}). The values of the other rate constants (k_3—k_6) are in line with those evaluated from the steady-state measurements, as will be described below.

Evaluation of Photokinetic Parameters. By analogy with ϕ_A° and τ_A°, the intrinsic fluorescence efficiencies (ϕ°) and lifetimes (τ°) for C and E are written as follows; $\phi_C^\circ=k_5/(k_5+k_6)$, $\tau_C^\circ=1/(k_5+k_6)$, $\phi_E^\circ=k_9/(k_9+k_{10})$, and $\tau_E^\circ=1/(k_9+k_{10})$. One can derive the following equations;

$$\phi_C^\circ/\phi_A^\circ = (k_5/k_1)(\tau_C^\circ/\tau_A^\circ) = P_4, \quad (12)$$

$$\phi_E^\circ/\phi_A^\circ = (k_9/k_1)(\tau_E^\circ/\tau_A^\circ) = P_4P_5/P_6. \quad (13)$$

The parameter values on the right-hand side of these equations (P_4 and P_4P_5/P_6) were evaluated to be in the order of 10 (Table 1), indicating that ϕ_C° and ϕ_E° are an order of magnitude greater than ϕ_A°. The low ϕ_A° values for **1A** and **2A** are mainly due to an intersystem crossing to an upper triplet state lying near the singler state.[10] The fluorescence intensity of acylanthracenes involving **1A** and **2A** is sensitive to external variables, which induce the displacement of the excited singlet level, such as the solvent polarity,[10] the temperature,[8] and the pressure.[11] It generally increases with a decrease in the excited singlet level, which is interpreted as a result of the inhibition of the intersystem crossing due to the increase in the energy separating the singlet and triplet levels.[12] From the fact that the fluorescence spectra of C and E are sufficiently red-shifted (Fig. 6 and Table 2), the fluorescence enhancement due to the H-bond interaction may be explained by a related mechanism. This would require a decrease in the nonradiative rate constant (k_6, $k_{10}\ll k_2$). On the other hand, the alternative possibility that the increase in the radiative rate constant plays a role can be excluded for the following reasons: (1) $\tau_C^\circ/\tau_A^\circ$ for **2A** at 20 °C was obtained from the pulse-excitation measurements to be 8.9, a value which agrees well with that of P_4 (Table 1). This immediately leads to $k_5/k_1\simeq1$; *i.e.*, the radiative rate constants of A and C are almost the same. (2) This consequence is also suggested by the close simmilarity between the oscillator strengths calculated from the long-wavelength absorption bands of these emissive species (Fig. 1). With these points in mind, it appears likely that k_5 and, presumably, k_9 are approximately equal to k_1, though no specific information about k_9 was obtained.

The values of ϕ_C° and ϕ_E° were evaluated from the observed ϕ_A° values, and, on the assumption of $k_1\simeq k_5\simeq k_9$, the values of τ_C° and τ_E° were obtained from the observed τ_A° values. The results for **2A** are listed in Table 3. The values of k's except k_7 and k_8, to which there is no satisfactory route, were determined as follows; the radiative rate constants (k_1, k_5, and k_9) from the corresponding ϕ° and τ° values, the nonradiative rate constants (k_2, k_6, and k_{10}) from the corresponding $1-\phi^\circ$ and τ° values, k_3 from P_2 and τ_A°, and k_4 from P_3 and τ_C°. The results for **2A** are also listed in Table 3. The values of k_3, k_4, and k_5+k_6 at 20 °C are comparable with the

Table 3. Fluorescence efficiencies (ϕ°) and lifetimes (τ°) of the uncomplexed (A), 1 : 1 complex (C), and 1 : 2 complex (E), and rate constants for 2-acetylanthracene

Temp/°C	ϕ_A°	τ_A°/ns			ϕ_C°	τ_C°/ns	ϕ_E°	τ_E°/ns
12	0.023	0.91			0.25	9.7	0.19	7.4
20	0.020	0.73			0.18	6.7	0.19	7.0
30	0.018	0.68			0.17	6.5	0.19	7.3
40	0.016	0.57			0.20	7.0	0.24	8.4
	$k_1/10^7$ s^{-1}	$k_2/10^8$ s^{-1}	$k_3/10^9$ M^{-1} s^{-1}	$k_4/10^8$ s^{-1}	$k_5/10^7$ s^{-1}	$k_6/10^8$ s^{-1}	$k_9/10^7$ s^{-1}	$k_{10}/10^8$ s^{-1}
12	2.5	11	2.3	0.51	2.5	0.8	2.5	1.1
20	2.7	13	6.7	2.5	2.7	1.2	2.7	1.2
30	2.7	14	10	6.7	2.7	1.3	2.7	1.1
40	2.8	17	17	16	2.8	1.2	2.8	0.9

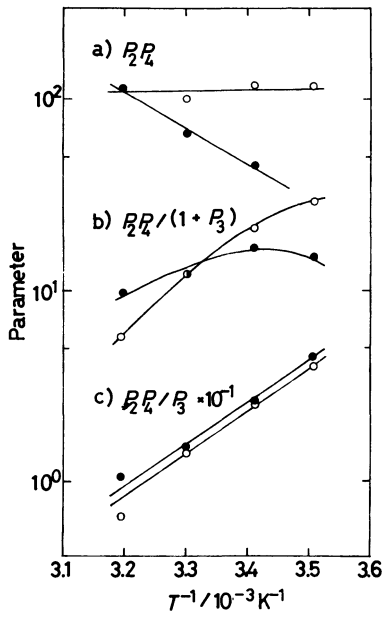

Fig. 9. Temperature dependence of a) $\log P_2P_4$, b) $\log P_2P_4/(1+P_3)$, and c) $\log P_2P_4/P_3$, for 1-(—○—) and2-acetylanthracene (—●—).

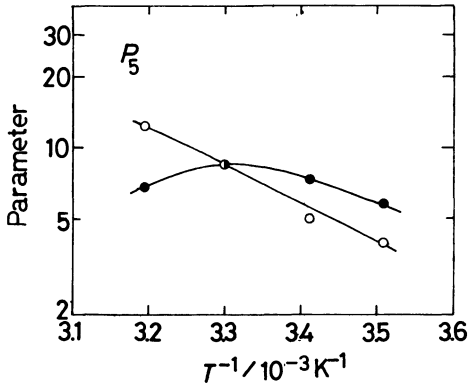

Fig. 10. Plots of $\log P_5$ *vs.* T^{-1} for 1-(—○—) and 2-acetylanthracene (—●—).

respective values determined independently from the pulse-excitation measurements at the same temperature.

The thermodynamic quantities associated with the complex formation in the excited state were determined by using the following equations:

$$\log P_2P_4/(1 + P_3) \simeq \log k_3\tau_C^\circ/(1 + k_4\tau_C^\circ), \quad (14)$$

$$\log P_5 \simeq \log k_7\tau_E^\circ/(1 + k_8\tau_E^\circ), \quad (15)$$

where $k_1 \simeq k_5 \simeq k_9$ is assumed. The experimental curves of the left-hand sides in Eqs. 14 and 15 against T^{-1} (T: absolute temperature) are plotted in Figs. 9b and 10 respectively. The slopes of these curves are negative and/or positive with respect to T. In the case of Fig. 9b, the negative temperature dependence is realized when $k_4\tau_C^\circ$ $(=P_3)>1$. Eventually, Eq. 14 can be reduced to this equation; $\log P_2P_4/P_3 \simeq \log k_3/k_4$, suggesting that the limiting temperature coefficient is consistent with the slope of the plots for $\log P_2P_4/P_3$, which can be ascribed to the enthalpy change (ΔH_C°) for the photoassociation of C. From the linear relationship obtained for $\log P_2P_4/P_3$ *vs.* T^{-1} (Fig. 9c), the value of ΔH_C° was found to be -9 kcal mol^{-1} for **1A** as well as for **2A**. The ΔH_C° values estimated from the extrapolation of the slopes shown in Fig. 9b agreed with this value within ± 2 kcal mol^{-1}. The entropy change (ΔS_C°) was calculated as -26 cal deg^{-1} mol^{-1} for **1A** and as -24 cal deg^{-1} mol^{-1} for **2A**, suggesting a rather rigid and tight complex. On the other hand, it appears likely that $k_4\tau_C^\circ$ $(=P_3)<1$ holds for the positive slope of the plots for $\log P_2P_4/(1+P_3)$, though there are few data on this side. At this time, Eq. 14 can be rewritten as $\log P_2P_4 \simeq \log k_3\tau_C^\circ$, suggesting that a thermally activated process (k_3) is responsible for the positive temperature dependence. The plots of $\log P_2P_4$ *vs.* T^{-1} are shown in Fig. 9a. The temperature coefficient for **2A** was found to be about 8 kcal mol^{-1}, ascribable to the activation energy for k_3 (ΔE_3), since τ_C° is little dependent on T (Table 3). The value of ΔE_3 obtained is larger than that to be expected from a diffusion-controlled reaction in hexane (*ca.* 2 kcal mol^{-1} [13]). The curve for **1A** is practically temperature-independent; this may be due to the fact that the negative temperature dependence of τ_C° cancels out the positive temperature dependence of k_3, but the details remain uncertain.

In substantially similar ways, the results shown in Fig. 10 can be analyzed to give the enthalpy change (ΔH_E°) and the activation energy (ΔE_7) associated with the formation of E. The plots of $\log P_5$ *vs.* T^{-1} for **2A** give the curve with $\Delta H_E^\circ \simeq -10$ kcal mol^{-1} at low temperatures and with $\Delta E_7 \simeq 5$ kcal mol^{-1} at high temperatures (the evaluation of these values is only approximate, because there are few data on either side). From the curve for **1A**, which has a positive slope over the temperature range employed, the value of ΔE_7 was evaluated to be 7 kcal mol^{-1} on the assumption that τ_E° is temperature-independent.

Conclusively, the fluorescence change observed can be explained as stoichiometric complex formation in the ground and excited states. It is striking that the steady-state fluorescence data are well simulated by the highly-associated-complex model. In the study of the time-resolved fluorescence measurements for *m*-aminoacetophenone–alcohol–viscous nonpolar solvent systems, Itoh and his co-workers observed the time-dependent fluorescence shift associated with the formation of E.[7] In contrast with their observations, no time-dependent spectral shift could be detected in the present cases using our detecting system. However, this is not necessarily in contradiction with our model, because it appears likely that, under the present experimental conditions, the relaxation by the H-bond interaction is so rapid that the time-resolved fluorescence observed is distorted by the convolution of the light pulse, which has a definite duration (half bandwidth $\simeq 6$ ns), with the decay of the sample.

On the other hand, time-resolved fluorescence measurements in viscous alcohol at low temperatures are informative from the viewpoint of complex formation. It was shown that the fluorescence spectrum of **2A** in propylene glycol undergoes time-dependent changes even at -125 °C, where the solvent relaxation time is much slower than the fluorescence decay time. This

spectral change may be ascribed to the specific solvent-solute interaction, since a general solvent relaxation would induce a more drastic change in the fluorescence spectrum of this compound.[8] Moreover, the fluorescence spectra monitored at zero- and several-ten-ns delay times at −125 °C (*cf.* Fig. 4 in Ref. 8) are quite similar to those of C and E respectively (Fig. 4). These results may support the conclusion reached in this study.

It appears probable that the complex formation is facilitated in the excited state, since the photoexcitation leads to preferential electron migration from the anthryl ring to the carbonyl group, resulting in an increase in the carbonyl basicity.[8] Therefore, the formation of the highly associated complex is electronically reasonable, but the conformation of this complex remains uncertain at this stage of the investigation.

References

1) N. Mataga and S. Tsuno, *Bull. Chem. Soc. Jpn.*, **30**, 368 (1957).
2) H. Kokubun, *Z. Phys. Chem. N. F.*, **17**, 281 (1958); **101**, 137 (1976).
3) K. Bredereck, Th. Förster, and H.-G. Oesterlin, "Luminescence of Organic and Inorganic Materials," ed by H. P. Kallmann and G. M. Spruch, John Wiley and Sons, New York (1962), p. 161.
4) M. Kitamura and H. Baba, *Bull. Chem. Soc. Jpn.*, **48**, 1191 (1975).
5) W. R. Ware, S. K. Lee, G. J. Brant, and P. P. Chow, *J. Chem. Phys.*, **54**, 4729 (1971).
6) R. P. DeToma and L. Brand, *Chem. Phys. Lett.*, **47**, 231 (1977).
7) Y. Tanimoto, K. Inoue, Y. Furukawa, Y. Segawa, and M. Itoh, *Bull. Chem. Soc. Jpn.*, **52**, 1601 (1979).
8) T. Tamaki, *Bull. Chem. Soc. Jpn.*, **53**, 577 (1980).
9) R. L. Scott, *Rec. Trav. Chim.*, **75**, 787 (1956).
10) T. Tamaki, *Bull. Chem. Soc. Jpn.*, **55**, 1756(1982).
11) D. J. Mitchell, G. B. Schuster, and H. B. Drickamer, *J. Am. Chem. Soc.*, **99**, 1145 (1977).
12) S. Hirayama, *Rev. Phys. Chem. Jpn.*, **42**, 49 (1972).
13) J. B. Birks, M. D. Lumb, and I. H. Munro, *Proc. R. Soc. London, Ser. A*, **280**, 289 (1964).

The Decomposition of Water on the CO- or H_2-reduced Indium Oxide

Kiyoshi Otsuka,* Takao Yasui, and Akira Morikawa
Department of Chemical Engineering, Tokyo Institute of Technology, Ookayama, Meguro-ku, Tokyo 152
(Received October 28, 1981)

The reduction of In_2O_3 by H_2 or CO and the reoxidation of the reduced oxide by water, accompanying the formation of hydrogen, have been investigated at $\geq$673 K. The reduction of In_2O_3 and the decomposition of water have been expressed by the forward reaction and the backward reaction respectively of this equation: $In_2O_3(s)+xH_2(g)\rightleftarrows In_2O_{3-x}(s)+xH_2(g)$, where $In_2O_{3-x}(s)$ is a mixture of indium metal and In_2O_3. Surface oxygen atoms of fresh In_2O_3 are easily removed by H_2- or CO-reduction at 673 K, but they can not be reformed by oxidation with water. This explains the observation that the quantity of hydrogen produced in the oxidation step was somewhat deficient compared to that consumed by the reduction. The maximum rate of the decomposition of water is observed when the oxide has been reduced up to a 50% reduction-level. However, an excessive reduction (greater than 85%) results in a sharp decrease in the rate of the decomposition of water, probably because of the isolation of metallic indium from the host In_2O_3.

Recently we have proposed a simple two-step water-decomposition process which uses a reduction-oxidation cycle of In_2O_3.[1] In Step 1, the oxide is reduced by various reductants at a high temperature. In Step 2, the reduced oxide is reoxidized by water at a low temperature, producing hydrogen. Since Steps 1 and 2 are carried out separately, pure hydrogen can be obtained in Step 2. Various reducing agents, such as diluted hydrogen, carbon monoxide or light hydrocarbons in waste gas from chemical plants, may be used as reductants in Step 1.

It has also been reported[2] that the reduction of In_2O_3 by hydrogen and the subsequent decomposition of water over the reduced oxide proceed smoothly at 673 K. However. more fundamental studies of the reduction-oxidation cycles are needed in order to develop the two-step hydrogen-production process. This report will present the results of kinetic studies of the reduction of In_2O_3 by hydrogen and carbon monoxide and of the oxidation of the reduced oxide by water. The conditions required for the hydrogen-production and the nature of the reduced In_2O_3 are also discussed.

Experimental

Materials. The In_2O_3 used was a reagent-grade powder (purity$>$99.9%) obtained from the Wako Pure Chemical Co. The surface area of the fresh In_2O_3, as measured by means of the nitrogen adsorption (BET method), was 13.9 $m^2 g^{-1}$. The hydrogen and carbon monoxide used as reducing gases were purified by passing them through a silica-gel adsorbent cooled at 77 or 195 K. The water was purified three times by trap-to-trap distillation in a vacuum apparatus. The dissolved gases in the water were removed by repeated freeze-degassing-thaw procedures.

Procedure. The apparatus employed was a conventional mercury-free static gas-circulation system with a volume of $\approx$320 ml. Before each run of the experiment, the sample oxide (0.10—0.50 g) in a U-shaped quartz reactor was degassed at 773 K for 2 h. The reduction of the sample was initiated by adding H_2 and CO to the system at 473—773 K. During the reduction, the H_2O and CO_2 produced were removed from the gaseous phase by condensing them into a trap which had been placed in the gas-circulation line and cooled by means of liquid nitrogen. Kinetic curves of the reduction were obtained by measuring the pressure drop of the reducing gas or the change in the gas-chromatographic peak. After In_2O_3 had been reduced to a certain extent, the gases in the reaction system were pumped out; the reoxidation of the reduced oxide was then started by adding and circulating a mixture of water vapor (2.1×10^3 Pa) and nitrogen (1.33×10^4 Pa, added to ensure the gas-circulation). The quantity of hydrogen produced was measured by means o gas chromatography.

Results

Reduction of In_2O_3. The reductions of In_2O_3 by H_2 and CO occur at temperatures greater than 573 and 473 K respectively under 6.7×10^3 Pa of the reducing gases. Figure 1-a indicates the temperature effect on the kinetics of the consumption of hydrogen during the reduction of In_2O_3. Although the initial pressure of hydrogen was kept constant ($6.74\pm0.08\times10^3$ Pa), the final pressure of hydrogen depended on the reaction temperature (3.02×10^3 Pa at 623 K to 0.76×10^3 Pa at 773 K). The marked decrease in the hydrogen pressure

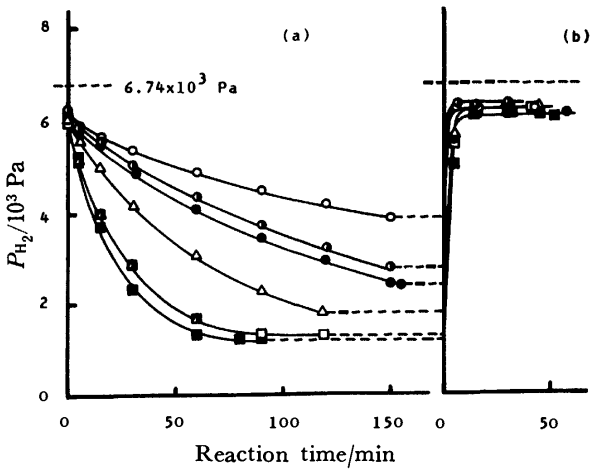

Fig. 1. (a) Kinetic curves of hydrogen-consumption during the reduction of In_2O_3 at 623—773 K. Temperature of reduction: ○: 623 K, ◑: 648 K, ●: 673 K, △: 698 K, □: 723 K, ▲: 748 K, ■: 773 K. The weight of In_2O_3 was 0.50 g. (b) Subsequent reoxidation of the reduced oxide with water accompanying hydrogen-production at 673 K. The symbols in (b) correspond to the samples of the same symbols in (a).

explained the rapid decrease in the reduction rate, especially for the high-temperature runs. For every kinetic curve, a very rapid consumption of hydrogen ($\approx$200 μmol g^{-1}) was observed at the very first contact with the oxide. After the hydrogen and water had been outgassed from the system, the addition of fresh water vapor to the reduced oxide at 673 K caused a rapid formation of hydrogen, as is shown in Fig. 1-b. The decomposition of water finished within 15 min. The amount of hydrogen produced for every kinetic curve was 200 ± 50 μmol g^{-1} less than that of the hydrogen consumed in the preceding reduction. The apparent activation energy of the reduction, as obtained from the initial rates at a 5% degree of reduction, was 72.4 kJ mol^{-1}. The degree of reduction was determined on the basis of the percentage of oxygen atoms removed from the original In_2O_3. Figure 2 shows the effect of pressure of hydrogen on the rate of reduction at 673 K as observed at different degrees of reduction. The rate increases linearly with the pressure of hydrogen, irrespective of the degree of reduction.

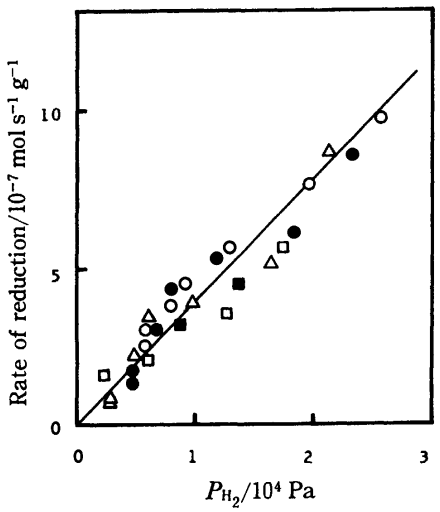

Fig. 2. The effect of pressure of hydrogen on the rate of reduction of In_2O_3 at 673 K.
Degree of reduction of In_2O_3: ○: 2%, ●: 5%, △: 10%, □: 20%, ■: 30%.

The initial rate of reduction of In_2O_3 by carbon monixide is one order of magnitude greater than that by hydrogen at the temperatures of 473—773 K under a pressure of 6.7×10^3 Pa. This fact shows that carbon monoxide is a stronger reducing agent for In_2O_3 than is hydrogen. The deficiency of $\approx$200 μmol g^{-1} in the amount of produced hydrogen compared to that of the consumed carbon monoxide in the preceding reduction was also observed in this case. The apparent activation energy of the reduction by carbon monoxide at a 2% degree of reduction was obtained as 59.4 kJ mol^{-1}.

Decomposition of Water. The decomposition of water on the H_2- or CO-reduced indium oxide occurs at temperatures higher than $\simeq$423 K. Figure 3 shows the kinetic curves of the formation of hydrogen at different temperatures for the sample with a 14% degree of reduction. The reaction at >673 K was to rapid to

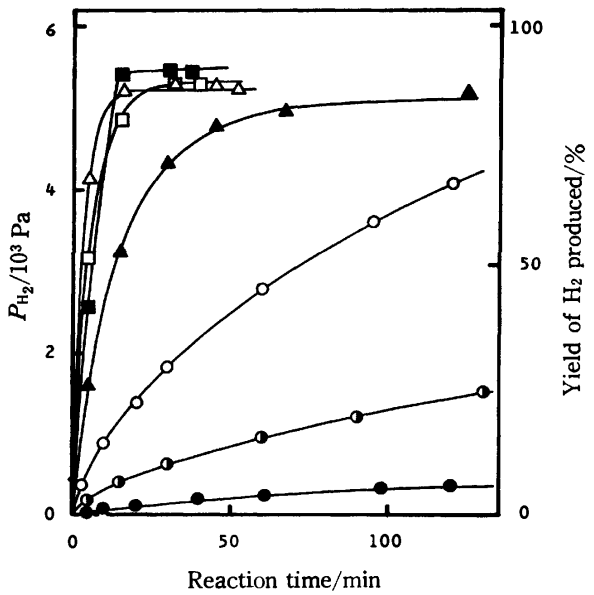

Fig. 3. Kinetic curves of the formation of hydrogen at different temperatures.
□: 873 K, ■: 773 K, △: 673 K, ▲: 573 K, ○: 523 K, ◑: 473 K, ●: 423 K. The weight of In_2O_3 used was 0.50 g.

be measured accurately. The vertical axis of the right-hand side indicates the yield of hydrogen production on the basis of the quantity of oxygen atoms transferred from water to the reduced oxide compared to that removed from In_2O_3 during the preceding reduction. The decomposition of water was completed within 15 min when the temperature was higher than 673 K. The yield of hydrogen production never reached 100%, not even at 873 K. The Arrhenius plot of the initial rate of hydrogen production, as evaluated from the slopes of the kinetic curves (423—573 K) in Fig. 3, gave the apparent activation energy of 50.1 kJ mol^{-1}.

All the results described above have been obtained for the oxide with a degree of reduction of less than 30%.

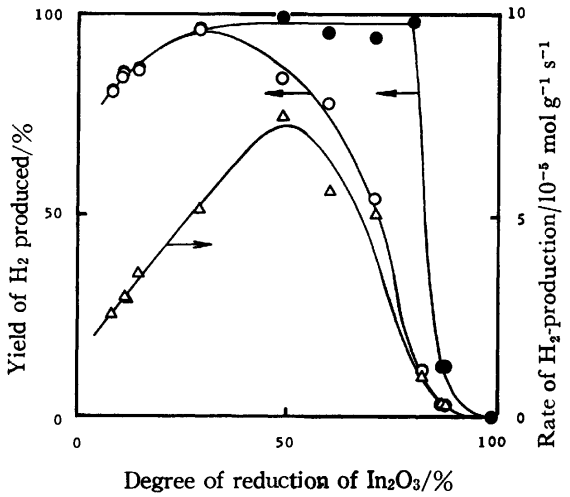

Fig. 4. The yield and rate of H_2-production as functions of the degree of reduction of In_2O_3.
○: Yield at 20 min, ●: yield at 100 min, △: initial rate of H_2-production.

Figure 4 shows the yield of water decomposition as a function of the degree of reduction. The pre-reduction of In_2O_3 had been carried out by the use of hydrogen at 673 K, and the subsequent oxidation by water was conducted at the same temperature. The triangles in Fig. 4 indicate the initial rate of water-decomposition: The quantity of hydrogen produced in 5 min divided by the time. The open and closed circles are the yields of the production of hydrogen at 20 and 100 min respectively. The results in the figure show that the maximum in the rate of hydrogen-production lies at a ≈50% degree of reduction. Although the rate of reaction decreases as the degree of reduction increases above the 50% level, the reaction is complete within 100 min when the reduction-level is lower than 85% (closed circles).

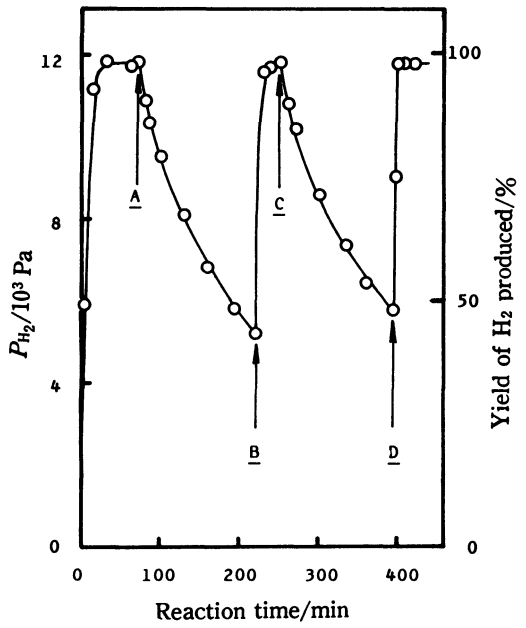

Fig. 5. Reproducible oxidation and reduction of indium oxide at 673 K.
The weight of In_2O_3 used was 0.50 g.

Figure 5 shows the progress of the oxidation-reduction cycles at 673 K: the sample oxide had been reduced by hydrogen to the degree of 29.2% before the experiments. The condensation of water vapor in the circulating gas at 77 K (Point A) caused the backward reaction; *i.e.*, the reduction of the oxide was initiated. The evaporation of the condensed water at Point B caused the decomposition of water to be resumed. The subsequent reduction and oxidation were recommenced at C and D respectively. The results shown in Fig. 5 show that smooth and repeating reduction-oxidation cycles can be operated at 673 K.

The ratio of the pressure of the water vapor to that of hydrogen under apparent equilibrium conditions has been measured using two initial systems: a partially reduced In_2O_3–water system and an In_2O_3–hydrogen system. The ratio obtained after 200 min standing at 673 K was in the range of 0.011 ± 0.003.

Discussion

The Reduced State of the Oxide. The lower valent oxides of indium than In_2O_3 suggested their existence are InO and In_2O. InO is very unstable and has been detected spectroscopically under indium-arc burning in air.[3] There is no clear evidence for the existence of InO under mild conditions. The formation of In_2O by the reduction of In_2O_3 with hydrogen was reported by Klemm and Vogel.[4] The existence of crystalline In_2O was suggested by several workers.[5,6] However, Brewer[7] concluded in his review that the supposedly crystalline In_2O is a stoichiometric mixture of indium and In_2O_3 or is a metastable homogeneous phase. Broch and Christensen[8] attempted to prepare crystalline In_2O; they came to the conclusion, after a detailed X-ray analysis of the products, that no proof for the existence of crystalline In_2O could be given. Wit *et al.*[9] commented, with regard to the existence of crystalline In_2O, that an indium suboxide like In_2O exists only as a parasitic phase, in combination with the contacting indium metal and In_2O_3, and is highly nonstoichiometric. Thus, there is still controversy with regard to the existence of crystalline In_2O. Our X-ray spectroscopic studies of the partially reduced In_2O_3 could establish only the existence of In_2O_3 and indium metal.

Therefore, let us tentatively write the following equation for the reduction of In_2O_3:

$$In_2O_3(s) + xH_2(g) \longrightarrow In_2O_{3-x}(s) + xH_2O(g), \quad (1)$$

where $In_2O_{3-x}(s)$ might be a crystalline In_2O or mixture of indium metal and In_2O_3. The ratio (0.011 ± 0.003) of the equilibrium pressure of water vapor to that of hydrogen over the oxide at 673 K observed in this work is very close to the value (0.0091) from the table[10] for the following equilibrium:

$$In_2O_3(s) + 3\,H_2(g) \rightleftarrows 2\,In(l) + 3\,H_2O(g). \quad (2)$$

This fact supports the idea that the $In_2O_{3-x}(s)$ in Eq. 1 is a mixture of indium metal and In_2O_3 under the experimental conditions applied in this work. When the sample was reduced excessively (>≈85%-degree of reduction), the formation of indium metal particles was observed at the bottom of the reactor.

The Presence of Highly Reducible Surface Oxygen Atoms. In the case of the reduction of fresh In_2O_3, a very rapid initial consumption of hydrogen was always observed, irrespective of the pressures and temperatures for the reduction. The quantity of the initial hydrogen-consumption and the BET surface area of the sample have been measured after each reduction-oxidation cycle. The results showed that the quantity of the initial rapid consumption of hydrogen decreased from 200 ± 20 (fresh sample) to 20 (second reduction) and 16 μmol g^{-1} (third reduction). The surface areas of the sample before each reduction were 13.9 (fresh sample), 5.3 (after the first oxidation), and 3.6 $m^2\,g^{-1}$ (after the second oxidation). The decrease in the quantity of the initial rapid consumption of hydrogen is too large to be explained by the decrease in the surface area of the sample. Let us assume that there are highly reactive surface oxygen atoms on fresh In_2O_3 and that, by

the use of hydrogen, they are rapidly removed as water from the surface at the very first stage of the reduction; the oxygen atoms, however, can not be recovered after the oxidation with water. This assumption explains the remarkable decrease in the quantity of the initial rapid consumption of hydrogen observed in the second and third reduction experiments compared to that for the fresh sample. The quantity of hydrogen produced on the first water-decomposition was deficient by the quantity of 200 ± 50 μmol g^{-1} compared to that consumed in the first reduction of fresh In_2O_3 (Figs. 1 and 3). The deficiency corresponds approximately to the quantity of hydrogen which had been consumed by fresh In_2O_3 at the very first stage of the reduction. Thus, the deficiency in the yield of hydrogen for the first cycle can be ascribed to the surface oxygen atoms, which are not regenerated by oxidation with water. Further studies are, however, needed to clarify the state and the nature of the active surface oxygen atoms (or might be molecules) described above.

Information from Kinetic Studies. In general, the rate of the reduction of crystalline metallic oxides to their lower oxidized states or metals is a function of three quantities: the rate of nucleation, the rate of the propagation of the interface between the reduced states and the oxide, and the size and shape of the particles. The energetics (*i.e.*, the activation energy) of the reduction process are primarily dependent upon the second of these quantities. However, the results in this work can shed little light on these factors. The rate of the reduction of In_2O_3 did not decrease, but increased for the second reduction compared to the first reduction, despite the fact that the surface area of the sample had decreased from 13.9 to 5.3 m^2 g^{-1}. The fact that the reduction rate increases in proportion to the pressure of hydrogen, irrespective of the degree of reduction (Fig. 2), indicates that the change in the surface area of the sample does not influence the rate of reduction. These observations can not yet be explained satisfactorily.

The kinetic curves of the oxidation of reduced-In_2O_3 by water did not obey a simple rate law, such as logarithmic, linear, parabolic, or cubic. Therefore, no simple oxidation mechanism can be applied for the oxidation of the reduced-In_2O_3.

Conditions Required for the Hydrogen Production. The findings on the temperature effect on the rates of reduction of In_2O_3 (Fig. 1) and of hydrogen-production (Fig. 3) show that both the reactions proceed rapidly at $\geq$673 K. This has been confirmed by the smooth and repeated cycles of the reactions at 673 K (Fig. 5). The results of Fig. 4 show that the reduction level around 50% is suitable for the hydrogen-production as far as the rate of reaction is concerned. The lower yield of hydrogen-production at a reduction level lower than 30% can be ascribed to the non-recovery of the surface oxygen atoms, as has been described earlier. The ratio of the quantity of surface oxygen atoms to that of the total hydrogen consumed for the reduction of In_2O_3 becomes smaller as the reduction level increases, which explains the $\simeq$100% yield of hydrogen at higher reduction levels. When the oxide experienced too much reduction ($>\approx$85% degree of reduction), the rate of reoxidation of the reduced oxide decreased sharply (Fig. 4). The formation of indium metal particles shows a clear separation of the metal phase from In_2O_3 at >85%-degree of reduction. The drop in the rate of recovery of In_2O_3 above an 85%-degree of reduction might be ascribed to the change in the physical or chemical nature of the reduced phase due to the isolation of the metal phase from the oxide.

References

1) K. Otsuka, Y. Takizawa, S. Shibuya, and A. Morikawa, *Chem. Lett.*, **1981**, 347.
2) K. Otsuka, T. Yasui, and A. Morikawa, *J. Catal.*, **72**, 392 (1981).
3) W. W. Watson and A. Shambon, *Phys. Rev.*, **50**, 607 (1936).
4) W. Klemm and H. U. V. Vogel, *Z. Anorg. Chem.*, **219**, 45 (1934).
5) K. A. Klinedinst and D. A. Stevenson, *J. Chem. Thermodyn.*, **5**, 21 (1973).
6) T. J. Anderson and L. F. Donaghey, *J. Chem. Thermodyn.*, **9**, 617 (1977).
7) L. Brewer, *Chem. Rev.*, **52**, 38 (1953).
8) N. C. Broch and A. N. Christensen, *Acta Chem. Scand.*, **20**, 1996 (1966).
9) A. J. Van Dillen, J. W. Geus, and J. H. W. de Wit, *J. Chem. Thermodyn.*, **10**, 895 (1978).
10) I. Barin and O. Knacke, "Thermochemical Properties of Inorganic Substances," Springer-Verlag, Berlin (1973 and 1977).

The Kinetics of Bromate-Cerium(III) and -Iron(II) Reactions

Toshihisa YOSHIDA* and Yataro USHIKI
Department of Chemistry, Faculty of Education, Saitama University, Urawa, Saitama 338
(Received October 31, 1981)

The bromate-cerium(III) and -iron(II) reactions in acidic media were examined with special reference to their induction periods and reaction rates. In the bromate-cerium(III) reaction, the induction period is followed by a burst of cerium(IV) formation and then a gradual formation of cerium(IV). In the bromate-iron(II) reaction, a slow decrease occurs only in acidic media, even without bromate, so it may differ from the decrease in the tris(1,10-phenanthroline)iron(II) concentration based on the oxidation by bromate. It was interpreted as the dissociation from $[Fe(phen)_3]^{2+}$ to $[Fe(phen)_2]^{2+}$ and phen. This is the induction period for iron(III) formation, which follows as the burst. The induction period and the rates of cerium(IV) or iron(III) formation can be interpreted on the basis of the mechanism for the Belousov oscillatory and the present redox reactions proposed by Noyes and his co-workers.

The Belousov reaction,[1,2] a typical oscillating reaction, is the oxidation of malonic acid with potassium bromate catalyzed by cerium(III) and (IV) ions. The mechanism of the reaction was investigated by Field and Noyes,[3] who suggested that the reaction involves both the oxidation of the cerium(III) ion by potassium bromate and an autocatalytic reaction with respect to bromous acid. This suggestion has led us to take an interest in the redox reactions between potassium bromate and cerium(III) sulfate or tris(1,10-phenanthroline)iron(II).[4]

The reactions between bromate and various reducing agents, Ce(III), $[Fe(phen)_3]^{2+}$, Co(II), Mn(II), Np(V), and V(V), had been examined qualitatively.[3,5,6] The kinetic behaviour of these systems could be described experimentally by this rate law: $-d[BrO_3^-]/dt = k_0[BrO_3^-]^2$. However, to date all attempts to understand these systems adequately in this quantitative aspect have been unsuccessful.

If the mechanism suggested by Noyes and his co-workers[3] is applied to the oxidation of cerium(III) and iron(II) with no bromide ion involved, the following set of elementary reactions are obtained:

$$BrO_3^- + HBrO_2 + H^+ \rightleftharpoons 2BrO_2^\cdot + H_2O, \quad (1)$$

$$BrO_2^\cdot + M^{n+} + H^+ \rightleftharpoons HBrO_2^\cdot + M^{(n+1)+}, \quad (2)$$

$$BrO_2^\cdot + M^{(n+1)+} + H_2O \rightleftharpoons BrO_3^- + M^{n+} + 2H^+, \quad (3)$$

$$2\,HBrO_2 \rightleftharpoons BrO_3^- + HOBr + H^+, \quad (4)$$

where M^{n+} and $M^{(n+1)+}$ are the reducing agent and its oxidized form respectively.

The observation that an induction period is followed by a burst of oxidation suggests that there is at least one elementary autocatalytic reaction, and that it corresponds to the following reaction (5). It is obtainable from two of the elementary reactions above, (1) and (2), and it contains $HBrO_2$ as the vital species:

$$BrO_3^- + HBrO_2 + 2M^{n+} + 3H^+ = 2HBrO_2 + 2M^{(n+1)+} + H_2O. \quad (5)$$

Considering that the bromate-cerium(III) and -iron(II) reactions are characterized by an induction period, the rapid formation of cerium(IV) or iron(III) at the inflection point on a kinetic curve and the slow formation of cerium(IV) had been examined in connection with the above suggestion by Noyes *et al.*[3] The purposes of this paper are to present our results on the reduction of bromate by cerium(III) or $[Fe(phen)_3]^{2+}$ ions and to explain these systems, as in a previous paper.[7]

Experimental

The potassium bromate, $Ce_2(SO_4)_3 \cdot 8H_2O$, $FeSO_4 \cdot 7H_2O$, and 1,10-phenanthroline monohydrate of a guaranteed reagent grade were obtained from the Wako Pure Chemical Industries, Ltd., Japan. Especially, the $[Fe(phen)_3]^{2+}$ stock solution was prepared by mixing $FeSO_4 \cdot 7H_2O$ and 1,10-phenanthroline monohydrate in a 1 : 3 mole ratio. The ionic strengths of the aqueous reaction solutions were usually controlled by means of a 1.5 mol dm^{-3} portion of sulfuric acid for cerium(III) and a 0.5 mol dm^{-3} portion of sulfuric acid for iron(II) in such a way that their concentrations were far higher than the concentration of either the potassium bromate or the cerium sulfate and $[Fe(phen)_3]^{2+}$ employed. Each sulfuric acid solution was degassed before use.

The bromate-cerium(III) reaction was allowed to run in a nitrogen atmosphere and in the dark; the potassium bromate and cerium(III) sulfate were each dissolved in a degassed sulfuric acid solution. Mixing the two solutions initiated the bromate-cerium(III) reaction, the progress of which was followed by recording the absorbance at 320 nm for the cerium(IV) ion, the molar absorptivity at this wavelength being 5520 mol^{-1} dm^3 cm^{-1}.[8] The bromate-iron(II) reaction was also allowed to run in a nitrogen atmosphere and in the dark; the $[Fe(phen)_3]^{2+}$ stock solution was diluted in a degassed sulfuric acid solution. The mixing of the bromate and the iron(II) solutions initiated the bromate-iron(II) reaction. The concentration of the $[Fe(phen)_3]^{2+}$ stock solution was determined spectrophotometrically at 509 nm, at which point the molar absorptivity of $[Fe(phen)_3]^{2+}$ is 11100 mol^{-1} dm^3 cm^{-1},[9] but some correction of this molar absorptivity was needed based on that of $[Fe(phen)_3]^{3+}$, about 500 mol^{-1} dm^3 cm^{-1}. The wavelength of the maximum absorption of $[Fe(phen)_3]^{3+}$ was found to be 590 nm.[10] The progress of this reaction was followed by recording the absorbance at 509 nm for the iron(II) ion. A Hitachi Model 125 spectrophotometer equipped with a temperature controller was used. The reaction vessel was directly connected to the cell of this spectrophotometer by tubing with a circulating pump.

The duration of the induction period was highly dependent on the ages of both the bromate- and cerium(III)-sulfuric acid solutions, but after the induction the change in cerium(III) was almost independent of the ages of either solution. Reproducible results for the duration of the induction period were obtained by the use of a cerium(III)-sulfuric acid solution which had been aged for 1 h and a potassium bromate-sulfuric

acid solution which had been aged for 24 h. On the other hand, the dilution of the $[Fe(phen)_3]^{2+}$ stock solution was carried out before use. All these solutions were prepared in a nitrogen atmosphere and in the dark. The reaction rate was not affected by stirring.

Results and Discussion

The progress of the bromate-cerium(III) reaction consists of three stages: (1) An induction period, (2) a burst in cerium(IV) formation, and (3) a gradual formation of cerium(IV).[7,11] The duration of the induction period is inversely proportional to the initial bromate concentration, and the rate of the fast formation of cerium(IV) is proportional to the square of the initial bromate concentration, whereas both quantities are independent of the initial cerium(III) concentration. In the slow formation of cerium(IV), the steady-state treatment can be applied with success, even to the concentration of the bromous ion, as well as to those of radical species.[7] The details of the kinetic behaviour of the bromate-cerium(III) reaction were reported in a previous paper.[7]

Dissociation of $[Fe(phen)_3]^{2+}$. After the mixing of the bromate and the iron(II) solution, a slow decrease of the absorbance at 509 nm occurs in the beginning only in acidic media, and this decrease occurs also without bromate. If only $[Fe(phen)_3]^{2+}$, without bromate, is left alone in acidic media for 22 h at 25 °C, the absorbance in the range from 800 to 370 nm disappears completely. The spectra of the products in the reaction without bromate and in the reaction with bromate were identical. This decrease is independent of the acid concentration, at least in the range from 0.1 to 1.0 mol dm^{-3} sulfuric acid.[10,12] It has been postulated as the dissociation from $[Fe(phen)_3]^{2+}$ to $[Fe(phen)_2]^{2+}$ and phen,[5,10] and its mechanism has been postulated to be the step-by-step dissociation of the ligand from the complex. For the bromate-iron(II) reaction, this dissociation is considered to be in progress during the burst of $[Fe(phen)_3]^{3+}$ formation. Therefore, it must be considered to be parallel to the $[Fe(phen)_3]^{3+}$ formation. This rate of decrease based on the dissociation to $[Fe(phen)_2]^{2+}$ is proportional to the concentration of $[Fe(phen)_3]^{2+}$ and is independent of the bromate and acid concentrations. The rate-determining step for the dissociation of the complex can be postulated to be the loss of the first ligand molecule.[10]

Table 1. The dissociation rate constants to $[Fe(phen)_2]^{2+}$ from $[Fe(phen)_3]^{2+}$ in 0.10 mol dm^{-3} aq H_2SO_4

$[Fe(phen)_3]^{2+}_0$ / mol m^{-3}	$k \times 10^5$ / s^{-1}		Temperature / °C
0.153	7.45		25.1
0.118	7.03		25.1
0.101	7.77	7.51±0.35	25.1
0.0512	7.28		25.1
0.0242	8.02		25.1
0.150	16.2		30.7
0.151	4.22		21.7
0.150	0.999		14.7

The details of the dissociation rate are summarized in Table 1. Körös[5] and Shakhashiri[10] had reported this dissociation rate constant at 25 °C (k; first-order dependency to $[Fe(phen)_3]^{2+}$ concentration) to be $(7.54 \pm 0.42) \times 10^{-5}$ and 7.50×10^{-5} s^{-1} respectively. Our constant is in good agreement with their values. It is much smaller than the following burst-rate constant for the oxidation to $[Fe(phen)_3]^{3+}$. The activation energy for this dissociation is 123 kJ/mol.

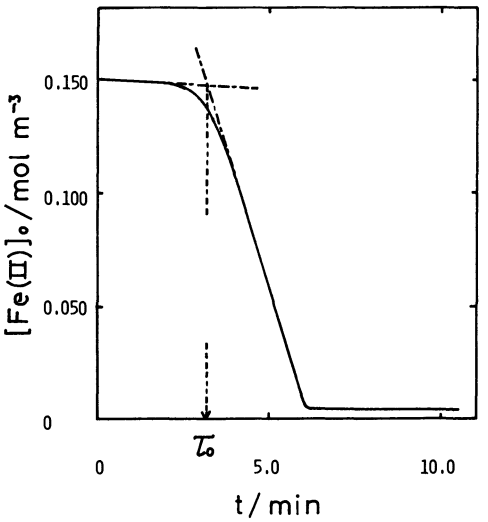

Fig. 1. Kinetic behavior of the bromate–iron system. Reaction-temperature 25 °C, $[BrO_3^-]_0 = 1.53$ mol m^{-3}, $[Fe(II)]_0 = 0.151$ mol m^{-3}, $[H^+] = 1.0$ mol dm^{-3}. Induction period (time, τ_0) defined by a dotted line.

Figure 1 shows the typical behaviour of $[Fe(phen)_3]^{2+}$ concentration with time. Let the induction period, τ_0, be defined as the time of intercept on the initial, slow and decreasing slope (dissociation) by the tangent (burst of iron(III) formation) drawn at the inflection point on the kinetic curve, as is shown in Fig. 1.

Induction Period. For the bromate-cerium(III) reaction, Thompson[6] and Kasperek[11] obtained a similar but qualitative dependence of the induction period on the initial bromate and acid concentrations. We have previously attempted to explain our quantitative results on the basis of the elementary steps given above.[3] The following steps may be considered:

$$BrO_3^- + HBrO_2 + H^+ \xrightarrow{k_1} 2BrO_2^\cdot + H_2O, \qquad (1')$$

$$BrO_2^\cdot + M^{n+} + H^+ \underset{k_{-2}}{\overset{k_2}{\rightleftharpoons}} HBrO_2 + M^{(n+1)+}, \qquad (2)$$

$$2HBrO_2 \xrightarrow{k_4} BrO_3^- + HOBr + H^+, \qquad (4')$$

where $BrO_2^\cdot$ is a radical species. As the amount of unstable $BrO_2^\cdot$ is assumed to be extremely small in comparison with those of the other species, the reverse of Step (1) and the slow Step (3) can be disregarded.[3] In acidic solutions, HOBr easily converts to Br^-, so the reverse of Step (4) can also be disregarded.[12] Moreover, the steady-state treatment is applied to the concentration of unstable $BrO_2^\cdot$ for the bromate-iron(II) reaction as:

$$\frac{d[BrO_2^\cdot]}{dt} = 2k_1[H^+][HBrO_2][BrO_3^-] - k_2[H^+][BrO_2^\cdot][Fe(II)] + k_{-2}[HBrO_2][Fe(III)] = 0. \quad (6)$$

The rate equations for the increase in the iron(III) concentration, the decrease in the bromate concentration, and the change in the bromous concentration are formulated as:

$$\frac{d[Fe(III)]}{dt} = k_2[H^+][BrO_2^\cdot][Fe(II)] - k_{-2}[HBrO_2][Fe(III)] = 2k_1[H^+][BrO_3^-][HBrO_2], \quad (7)$$

$$-\frac{d[BrO_3^-]}{dt} = k_1[H^+][BrO_3^-][HBrO_2] - k_4[HBrO_2]^2, \quad (8)$$

$$\frac{d[HBrO_2]}{dt} = k_1[H^+][BrO_3^-][HBrO_2] - 2k_4[HBrO_2]^2. \quad (9)$$

The concentration of $BrO_2^\cdot$ can be neglected as compared with those of the other species.[3] The following relations are assumed to hold for the initial stage, as based on the simple material and valency balances:

$$[BrO_3^-]_o + [HBrO_2]_o = [BrO_3^-] + [HBrO_2], \quad (10)$$

$$[Fe(III)] = 2\{[BrO_3^-]_o - [BrO_3^-]\}, \quad (11)$$

where the subscript o indicates the initial value.

The integration of Eq. 7 gives:

$$\ln\left\{\frac{[BrO_3^-]_o(2[HBrO_2]_o + [Fe(III)])}{[HBrO_2]_o(2[BrO_3^-]_o - [Fe(III)])}\right\} = k_1[H^+]\{[BrO_3^-]_o + [HBrO_2]_o\}t. \quad (12)$$

The concentration of the initial bromous acid is negligible as compared with that of the bromate and is at a steady value ($[HBrO_2]_o/[BrO_3^-]_o = C_1$; constant), as established through the aging adopted in the preparation of the reactions.

The induction period is obtained as follows. The relation between the time, t_f, and the concentration, $[Fe(III)]_f$, at the inflection point on the kinetic curve in Fig. 1 is obtainable from Eq. 12. On the other hand, $[BrO_3^-]_f$ and $[HBrO_2]_f$ may be obtained on the basis of $d^2[Fe(III)]/dt^2 = 0$ at the inflection point:

$$[HBrO_2]_f = C_2[BrO_3^-]_f = \frac{C_2}{C_2+1}[BrO_3^-]_o, \quad (13)$$

where the subscript f denotes the value for the inflection point and where:

$$C_2 = 1 + \frac{k_1[H^+]}{2k_4} - \sqrt{1 + \left(\frac{k_1[H^+]}{2k_4}\right)^2}. \quad (14)$$

The slope of the tangent drawn at the inflection point on the kinetic curve is determined from Eq. 7 as:

$$\frac{d[Fe(III)]_f}{dt} = 2k_1[H^+]_f \frac{C_2}{(C_2+1)^2}[BrO_3^-]_o^2. \quad (15)$$

Now, we obtain τ_0 from t_f, $[BrO_3^-]_f$, $[HBrO_2]_f$, $[Fe(III)]_f$, and the above tangent as follows:

$$\tau_o = \frac{1}{k_1[H^+][BrO_3^-]_o}\{\ln(C_2/C_1) - (C_2 + 1)\}, \quad (16)$$

which calls for τ_0 being inversely proportional to both $[H^+]$ and $[BrO_3^-]_o$; this is in good agreement with the experimental results shown in Fig. 2. In Fig. 2, results

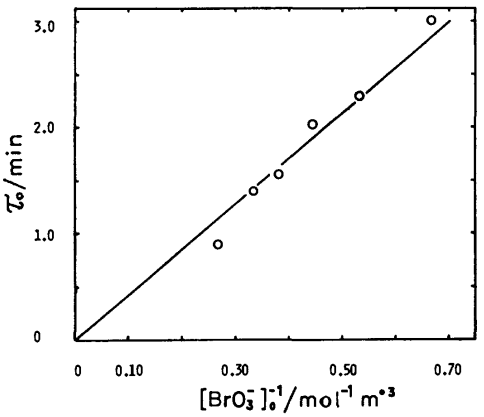

Fig. 2. Kinetic relation between τ_0 and the inverse of the initial $KBrO_3$ concentration.
Reaction-temperature 25 °C, $[Fe(II)]_o = 0.15$ mol m^{-3}, $[H^+] = 1.0$ mol dm^{-3}.

are shown for runs of the reaction with the initial iron(II) concentration of 0.150 mol m^{-3}. The induction period for a burst of iron(III) formation is inversely proportional to the initial bromate concentration, such as that of the cerium(IV) formation.[7] The induction period is independent of the initial iron(II) concentration.

The Burst of Iron(III) Formation. For the burst of iron(III) formation, the rate of iron(III) formation (R) is defined as the corrected slope of the tangent drawn at the inflection point on the kinetic curve. Figure 3 shows the relation between the corrected slope of the tangent and the square of the initial bromate concentration. The rates of iron(III) formation at 20, 25, and 30 °C are completely proportional to the square of the initial bromate concentration, whereas they are almost independent of the initial iron(II) concentration, shown in Fig. 4. These results are consistent with the interpretation based on Eq. 15. Similar results and a

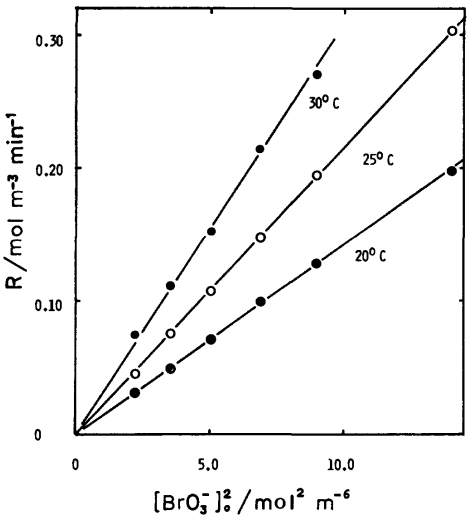

Fig. 3. Kinetic relation between the rate of burst Fe(III) formation (R) and the square of the initial $KBrO_3$ concentration.
$[Fe(II)]_o = 0.15$ mol m^{-3}, $[H^+] = 1.0$ mol dm^{-3}. Different reaction-temperatures shown above.

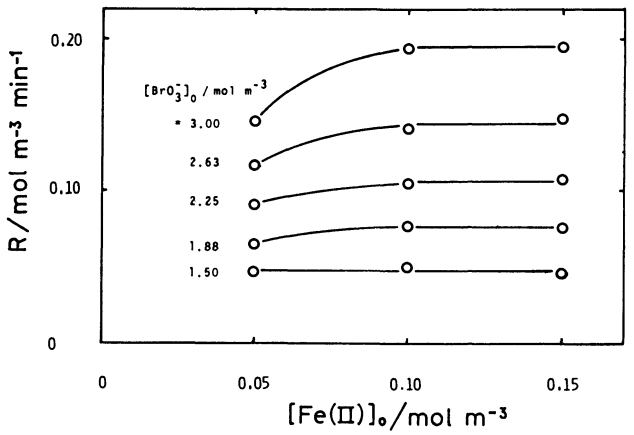

Fig. 4. Kinetic relation between the rate of burst Fe(III) formation (R) and the initial Fe(II) concentration. Reaction-temperature 25 °C, $[H^+]=1.0$ mol dm^{-3}. Various initial $KBrO_3$ concentrations shown above.

similar interpretation have been obtained for the burst of cerium(IV) formation in the previous paper.[7]

Comparison between Bromate-Cerium and -Iron Reactions. For the bromate-cerium(III) reaction, there is an induction period, followed by a burst of cerium(IV) formation, and then a gradual formation of cerium(IV). For the bromate-iron(II) reaction, a slow dissociation to $[Fe(phen)_2]^{2+}$ is observed in the beginning. It is the duration of the induction period for the iron(III) formation, which is followed by the burst of iron(III) formation.

Table 2. Apparent kinetic constants of k_r and k_r for iron and cerium systems

	k_r[a] s^{-1} mol^{-2} dm^6	k_r s^{-1} mol^{-2} dm^6	Temperature °C
Iron(II)	3.22	0.118	20
reaction	3.93	0.180	25
	4.68	0.257	30
Cerium(III)	—	5.44	20
reaction	0.772	7.44	25
	1.98	11.0	30

a) k_r is equal to $k_1/\{\ln(C_2/C_1)-(C_2+1)\}$. b) k_r is equal to $k_1C_2/(C_2+1)^2$.

For the bromate-cerium(III) and -iron(II) reactions, the details of the apparent kinetic constants are summarized in Table 2: k_r for the induction period and k_r for the burst oxidation of metal ions, based on Eqs. 16 and 15 respectively. Now, we obtain:

$$k_r = \frac{k_1}{\ln(C_2/C_1)-(C_2+1)}, \tag{17}$$

and:

$$k_r = \frac{k_1C_2}{(C_2+1)^2}. \tag{18}$$

The apparent activation energies of k_r are 27.5 for iron and 140 kJ/mol for cerium. This large difference may result from the different standard electrode potential, the E° values for the $[Fe(phen)_3]^{2+}/[Fe(phen)_3]^{3+}$ and Ce(III)/Ce(IV) couples, and the different ligands of the reaction complexes, which cause dissociation in the iron complex, but not in the cerium one. On the other hand, the apparent activation energies of k_r are 57 for iron and 52 kJ/mol for cerium. These are the same values as we obtained in neptunium from Knight's data (57—70 kJ/mol).[13] This fact may be interpreted well by the behaviour of the $BrO_2^\cdot$ radical if the oxidation rate of metal complex is controlled by the formation of the radical, as is shown in Eq. 1. Since the rate of the bromate-iron(II) ion reaction is faster than that of $[Fe(phen)_3]^{2+}$ dissociation to $[Fe(phen)_2]^{2+}$, we can also conclude that electrode transfer takes place *via* an outer-sphere path.[10]

Let us now consider how the hydrogen ion influences the burst formation of the oxidized metal ion. Knight and Thompson[13] obtained an empirical formation which summarized the variation in $2k_r[H^+]$ with the change in the hydrogen-ion concentration. The two-parameter expression, compared with Eq. 15:

$$2k_r[H^+] = \alpha[H^+]^2/(1+\beta[H^+]), \tag{19}$$

fits the data much better for the bromate-Np(V) reaction.[13]

If the $C_2(\simeq k_1[H^+]/2k_4)$ quantity is sufficiently smaller than unity, we obtain, instead of Eq. 15:

$$\frac{d[Fe(III)]_f}{dt} = \frac{\frac{k_1^2}{k_4}[H^+]^2}{1+\frac{k^1}{k^4}[H^+]}[BrO_3^-]_0^2. \tag{20}$$

In the bromate-cerium system, Noyes and his co-workers[3] reported k_1 and k_4 to be 1.0×10^4 mol^{-2} dm^6 s^{-1} and 4.0×10^7 mol^{-1} dm^3 s^{-1} respectively. Therefore, the above assumption seems to be reasonable. Equation 20 is completely consistent with Eq. 19.

The authors wish to express their cordial thanks to Professor Tominaga Keii, Science University of Tokyo, and Professor Isao Matsuzaki, Shinshu University, for their discussions, and acknowledge the help in this work by Mr. Toshio Iizuka and Mr. Hiroshi Izumi.

References

1) B. P. Belousov, *Sb. Ref. Radiats. Med., Moscow*, **1958**, 145.
2) A. W. Zhabotinskii, "Oscillatory Process in Biological and Chemical Systems," Science Publ., Moscow (1967).
3) R. M. Noyes, R. J. Field, and R. C. Thompson, *J. Am. Chem. Soc.*, **93**, 7315 (1971); R. M. Noyes, R. J. Field, and E. Koros, *ibid.*, **94**, 1394, 8649 (1972); R. J. Field and R. M. Noyes, *ibid.*, **60**, 1877, (1974); S. Barkin, M. Bixon, R. M. Noyes, and K. Bar-Eli, *Int. J. Chem. Kinet.*, **11**, 841 (1977); K. Bar-Eli and R. M. Noyes, *J. Phys. Chem.*, **82**, 1352 (1978); R. M. Noyes, *J. Am. Chem. Soc.*, **102**, 4644 (1080).
4) Hereafter $Fe(phen)_3^{2+}$.
5) E. Koros, M. Burger, and A. Kis, *React. Kinet. Catal. Lett.*, **1**, 475 (1974).
6) R. C. Thompson, *J. Am. Chem. Soc.*, **93**, 7315 (1971).
7) T. Yoshida, *React. Kinet. Catal. Lett.*, **14**, 451 (1980).
8) M. M. Hsu, H. G. Kruzyna, and R. M. Meiburn, *Inorg. Chem.*, **8**, 2201 (1969).
9) D. H. Wilkins, A. A. Schilt, and G. F. Smith, *Anal. Chem.*, **27**, 1574 (1955).

10) B. Z. Shakhashiri and G. Gordon, *J. Am. Chem. Soc.*, **91**, 1103 (1969).
11) G. J. Kasperek and T. C. Bruice, *Inorg. Chem.*, **10**, 382 (1971).
12) T. S. Lee, I. M. Kolthoff, and D. L. Leussing, *J. Am. Chem. Soc.*, **70**, 2348, 3596 (1948).
13) G. C. Knight and R. C. Thompson, *Inorg. Chem.*, **12**, 63 (1973).

 © 1982 The Chemical Society of Japan Bull. Chem. Soc. Jpn., 55, 1777—1781 (1982)

Correlation between Critical Solution Phenomena and Ultralow Interfacial Tensions in a Surfactant/Water/Oil System

Hironobu KUNIEDA* and Kōzō SHINODA

Department of Applied Chemistry, Faculty of Engineering, Yokohama National University, Tokiwadai 156, Hodogaya-ku, Yokohama 240

(Received November 4, 1981)

A three-phase region consisting of surfactant (D), water (W), and oil (O) phases appeared due to the superposition of two critical phenomena of D–W and O–D in a nonionic surfactant/water/oil system. Three interfacial tensions, γ_{O-W}, γ_{O-D}, and γ_{D-W}, among the three phases were determined at various temperatures. The generalized Antonoff's rule ($\gamma_{O-W}=\gamma_{O-D}+\gamma_{D-W}$) holds approximately in the three-phase region. γ_{O-D} and γ_{D-W} disappear at the respective critical solution temperatures, and ultralow interfacial tensions are attained in the vicinity of both critical temperatures. The oil–water interfacial tension, γ_{O-W}, reaches its minimum in the midst of the temperature range of the three-phase region, and the narrower the temperature range of the three-phase region, the lower the interfacial tension. The correlation between the interfacial tensions and the types of emulsions is also discussed.

There exists a three-phase region consisting of surfactant, water, and oil phases around the transition-temperature range at which the surfactant changes from water-soluble to oil-soluble in a nonionic surfactant/water/oil system.[1] A similar three-phase region has been observed in an ionic surfactant system in the presence of salt and a co-surfactant.[2–6] Saito and Shinoda found very low interfacial tensions in a three-phase region of a nonionic surfactant system.[7] Later Healy *et al.* found ultralow interfacial tensions between a surfactant phase (they called it a middle-phase microemulsion) and a water (or oil) phase in a petroleum sulfonate system.[3,8] On the other hand, ultralow interfacial tensions in very dilute systems of ionic surfactants were reported by Wade *et al.*[9–11]

In a previous paper,[12] it was clarified that a three-phase region appears due to the superposition of three miscibility gaps *i.e.*, surfactant–oil, surfactant–water, and oil–water phases, at a constant temperature. Furthermore, it was made clear that the lower (or upper) limiting temperature of the three-phase region corresponds to the lower (or upper) critical solution temperature of surfactant–water (or surfactant–oil) phases in a nonionic surfactant system. Interfacial tensions can be expected to be very small in the vicinity of the respective critical solution temperature. Since the emulsion type changes from O/W to W/O around the three-phase region,[1] the phase inversion in emulsion may be directly related to the balance of two interfacial tensions, *i.e.*, the oil–surfactant and water–surfactant interfaces, in the three-phase region. In this context, the correlation among the phase behavior, the ultralow interfacial tensions, and the phase-inversion in emulsions has been studied.

Experimental

Materials. Pure $C_8H_{17}(OCH_2CH_2)_3OH$ was kindly donated by POLA Chemicals, while pure $C_{12}H_{25}(OCH_2CH_2)_4OH$ was obtained from Nikko Chemicals; the purities (above 98%) were confirmed by gas-chromatographic analysis. Extra-pure-grade heptane, octane, nonane, dodecane, tetradecane, hexadecane, and 2-butoxyethanol were obtained from the Tokyo Kasei Kogyo Co. and were used without further purification.

Procedures. The interfacial tensions were measured by a sessile-drop method.[13,14] After attaining equilibrium, a drop of a high-density phase was placed on a Teflon film immersed in a low-density phase. The maximum height of the sessile drop above the equator, y, was measured by means of a cathetometer. The interfacial tension was calculated by a large drop approximation as follows:

$$\gamma = gy^2\Delta\rho/2,$$

where γ is the interfacial tension; g, the gravitational acceleration, and $\Delta\rho$, the density difference between two liquids.[14] In order to reduce error, x/y (x is the radius of the sessile drop at the equator) has to be at least more than 10. The density was measured by means of a digital density meter (Anton Paar DMA 40). The procedures of the determination of phase volumes and cream volumes has been described elsewhere.[15–17]

Results and Discussion

Phase Behavior of Nonionic Surfactant in Oil–Water. A schematic ternary phase diagram for a nonionic surfactant/water/oil system at the temperature range around the three-phase region is shown in Figs. 1(a)—(c).[12] The water, surfactant and oil phases are indicated by W, D, and O respectively. The compositions of the three coexisting liquids at a constant temperature and pressure are indicated by invariant points, α (D phase), β (O phase), and γ (W phase). There is a plait point (isothermal critical point), L, in the D+O region, but not in the D+W region in Figs. 1(b) and (c), because a lower critical solution temperature on a water-nonionic surfactant axis is usually lower than this temperature. Point α shifts toward the water apex with a decrease in the temperature, and finally Points α and γ coincide with each other at the critical end point Kc ($\alpha=\gamma$) and the three-phase region disappears, as is shown in Fig. 1(a). On the Kc-β line, the critical mixture ($\alpha=\gamma$) is in equilibrium with the oil phase, β. In this case, the D+W region usually remains in the vicinity of the water-surfactant axis.[12] The boundary between D+O and O+W regions at this temperature is the Kc-β line, but we can not draw the boundary at temperatures below that of the critical end point, Kc. Therefore, the D($\simeq$W)+O notation is used for the two-phase

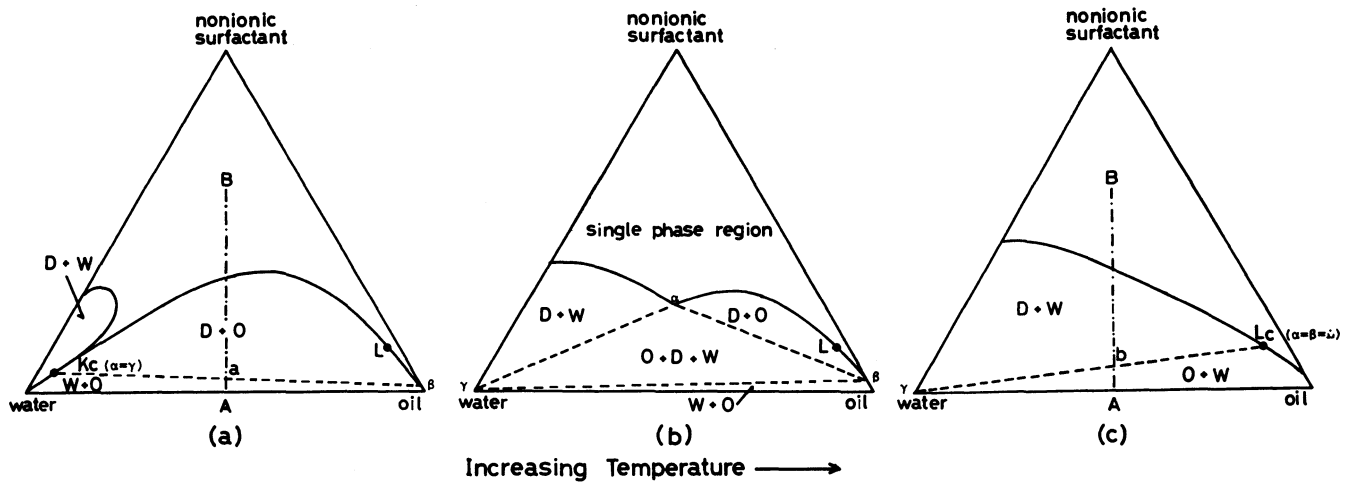

Fig. 1. Schematic phase diagram for a nonionic surfactant/water/oil system at the temperatures of a lower critical end point (Fig. 1(a)), in the midst of two critical end points (Fig. 1(b)), and of a upper critical end point (Fig. 1(c)). Kc and Lc are the lower and upper critical end points. α, β, and γ are the invariant points forming the three-phase region. O, D, and W are an oil, a surfactant, and a water phases. Points a and b correspoind to those in Fig. 2.

region at lower temperatures (*cf.* Fig. 2). D($\simeq$W) is usually called the aqueous micellar solution phase, which solubilizes oil. On the other hand, Point α shifts toward the oil apex with an increase in the temperature, and finally Points α, β, and L become identical at another critical end point, Lc ($\alpha=\beta=$L), as is shown in Fig. 1(c). Therefore, the three-phase and D+O regions disappear at this temperature, leaving the D+W and O+W regions. The W phase is nearly pure water; its composition is indicated by γ. Since we can not draw the boundary between the D+W and O+W regions at temperatures above that of the critical end point, Lc, the D($\simeq$O)+W notation is used for the two-phase region (*cf.* Fig. 2). D($\simeq$O) is usually called the nonaqueous reversed micellar solution phase, which solubilizes water.

A phase diagram consisting of equal weights of hydrocarbon and water as functions of the concentration of $C_8H_{17}(OCH_2CH_2)_3OH$ and the temperature is shown in Fig. 2. Point a in the tetradecane system, corresponds to that in Fig. 1(a), so it seems that the meniscus separating the D and W phases has just disappeared at Point a. Figure 3 shows the change in the volume fractions of respective phases as a function of the temperature in the $C_8H_{17}(OCH_2CH_2)_3OH$/water/tetradecane system. The concentration of the surfactant changes along with the broken line, a-b, in Fig. 2. The densities of the respective phases along the same line are also shown in Fig. 4. The densities of the O and W phases are almost equal to those of the pure components in the three-phase region. Accordingly, it is considered that the surfactants are singly dispersed in both phases.[7] However, the solubility of the surfactant in the O or W phase seems to increase abruptly in the vicinity of Points a and b as is shown in Fig. 4. As a

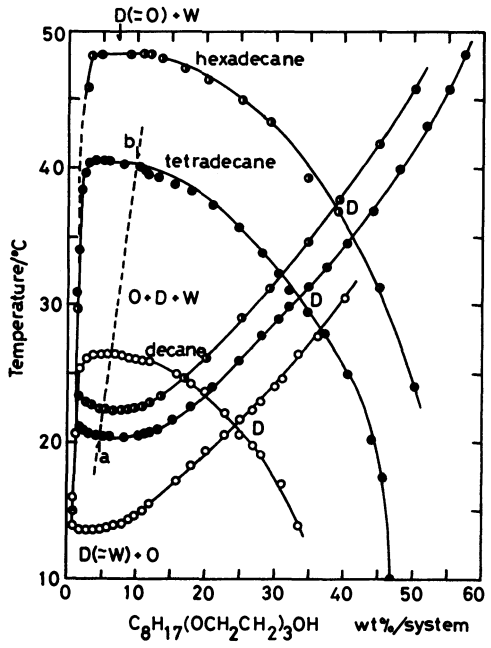

Fig. 2. Phase diagram of equal weight of water–oil containing $C_8H_{17}(OCH_2CH_2)_3OH$ as a function of temperature. The compositions correspond to the line A-B in Fig. 1.

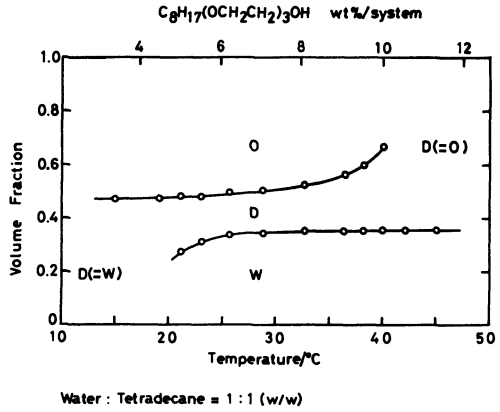

Fig. 3. The volume fractions of respective phases on the line a-b in Fig. 2.

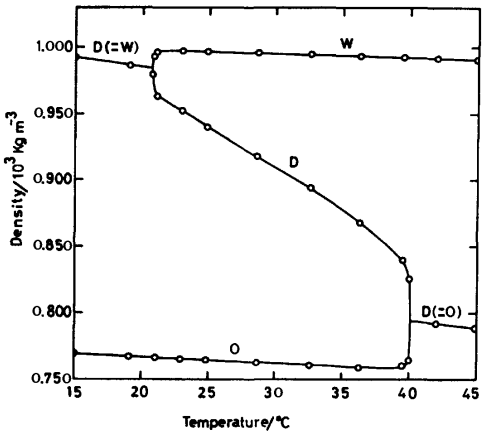

Fig. 4. The densities of respective phases on the line a-b in Fig. 2.

result, it is obvious that a three-phase region consisting of the O, W, and D phases appears in the range of two critical end temperatures, *i.e.*, a lower critical solution temperature (LCST) of the D and W phases, at which Kc exists, and an upper critical solution temperature (UCST) of the D and O phases, at which Lc exists. A similar result was obtained in an ionic surfactant system.[4,12] In the system, in which the LCST coincides with the UCST, there is a tricritical point at which the three coexisting liquids become identical.[18,19]

Correlation between Critical Solution Phenomena and Ultralow Interfacial Tensions in a Surfactant System. Since the interfacial tension becomes zero at a critical point,[20,21] and since the change in the activity of a surfactant with the concentration is very small,[22] the change in the concentration has scarcely no effect on chemical potential or interfacial tension, which is a function of the chemical potential; *i.e.*, ultralow interfacial tensions are attained in the vicinity of Point a or b in Fig. 2. Interfacial tensions between respective phases along the a-b line in Fig. 2 are shown in Fig. 5. $\gamma_{O\text{-}W}$, $\gamma_{O\text{-}D}$, and $\gamma_{D\text{-}W}$ are the interfacial tensions at the O–W, O–D, and D–W interfaces in the three-phase regions. $\gamma_{D(\simeq O)\text{-}W}$ and $\gamma_{O\text{-}D(\simeq W)}$ are the interfacial tensions at the D(≃O)–W and O–D(≃W) interfaces at temperatures above and below the critical temperatures. Naturally, $\gamma_{O\text{-}W}$, $\gamma_{O\text{-}D}$, and $\gamma_{O\text{-}D(\simeq W)}$ coincide with one another at the LCST (at Point a), while $\gamma_{O\text{-}W}$, $\gamma_{D\text{-}W}$, and $\gamma_{D(\simeq O)\text{-}W}$ coincide with one another at the UCST (Point b). $\gamma_{O\text{-}D}$ decreases with an increase in the temperature and becomes zero at Point b. On the other hand, $\gamma_{D\text{-}W}$ decreases with a decrease in the temperature and becomes zero at Point a. Accordingly, the ultralow interfacial tensions at surfactant–oil and surfactant–water interfaces are attained at temperatures in the vicinity of each critical temperature, *i.e.*, on the Lc-γ and Kc-β lines in Fig. 1. The critical point in a surfactant system usually exists in a solvent-rich region.[4,12,22,23] This is very important for such a practical purpose as the tertiary oil recovery,[8] for the amount of surfactant used to reduce the inter-

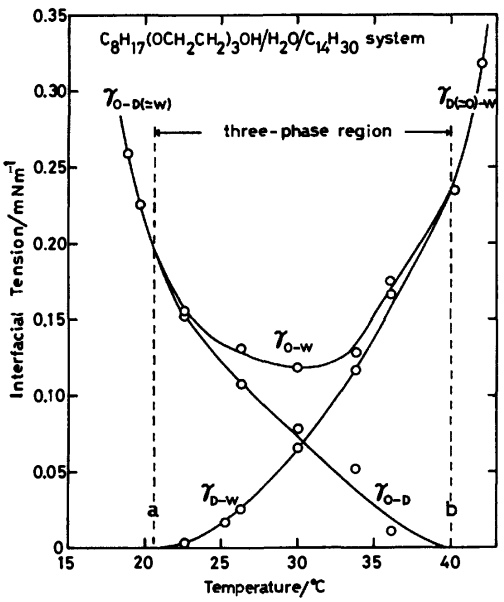

Fig. 5. The interfacial tensions between O–W, W–D, and O–D as a function of temperature on the line a-b in Fig. 2.

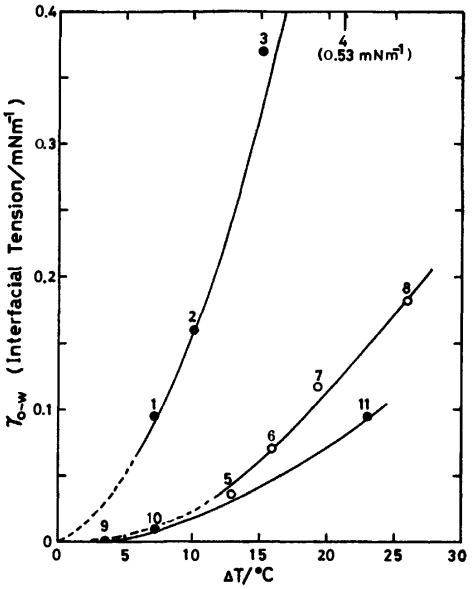

	system		
1	$C_4H_9OCH_2CH_2OH/H_2O/C_7H_{16}$	at	9.0 °C
2	$C_4H_9OCH_2CH_2OH/H_2O/C_8H_{18}$		17.3
3	$C_4H_9OCH_2CH_2OH/H_2O/C_9H_{20}$		26.4
4	$C_4H_9OCH_2CH_2OH/H_2O/C_{10}H_{22}$		34.4
5	$C_8H_{17}(OCH_2CH_2)_3OH/H_2O/C_{10}H_{22}$		20.1
6	$C_8H_{17}(OCH_2CH_2)_3OH/H_2O/C_{12}H_{26}$		26.2
7	$C_8H_{17}(OCH_2CH_2)_3OH/H_2O/C_{14}H_{30}$		30.0
8	$C_8H_{17}(OCH_2CH_2)_3OH/H_2O/C_{16}H_{34}$		35.5
9	$C_{12}H_{25}(OCH_2CH_2)_4OH/H_2O/C_{12}H_{26}$		22.2
10	$C_{12}H_{25}(OCH_2CH_2)_4OH/H_2O/C_{16}H_{34}$		31.1
11	$C_{12}H_{25}(OCH_2CH_2)_4OH/H_2O$/squalane		47.3

Fig. 6. Correlation between the difference in two critical end temperatures ($\Delta T = T_{UCST} T_{LCST}$) and the minima of O–W interfacial tensions in various nonionic surfactant systems. The interfacial tensions were measured at $(T_{UCST} + T_{LCST})/2$.

facial tension to the ultralow range has to be small.

At each critical temperature, a generalized Antonoff's rule, $\gamma_{O-W}=\gamma_{O-D}+\gamma_{D-W}$, automatically holds on the Lc-γ and Kc-β lines in Fig. 1,[24] because:

$$\gamma_{D-W}=0,\ \gamma_{O-W}=\gamma_{O-D} \quad \text{at LCST,} \tag{1}$$

$$\gamma_{O-D}=0,\ \gamma_{O-W}=\gamma_{D-W} \quad \text{at UCST.} \tag{2}$$

In the three-phase region, Antonoff's rule holds approximately, but, strictly speaking, γ_{O-W} is slightly smaller than $\gamma_{O-D}+\gamma_{D-W}$ as is shown in Fig. 5. A reverse inequality does not hold at true equilibrium.[24-27]

$$\gamma_{O-W}<\gamma_{O-D}+\gamma_{D-W} \quad \text{in the three-phase region} \tag{3}$$

Since a stable lens of the surfactant phase was formed at the water–oil interface after equilibrium was attained at 30 °C (50/50 water/tetradecane, $C_8H_{17}(OCH_2CH_2)_3$-OH 1.5 wt%/system), the (3) relation surely holds. The minimum was observed on the γ_{O-W} *versus*-temperature curve in the three-phase region, as is shown in Fig. 5. It is obvious from Relations 1—3 that this minimum becomes ultralow when the two critical end temperatures approach each other. If the LCST coincides with the UCST completely, γ_{O-W} becomes zero at the tricritical point at which three coexisting phases become identical, as has been described before. The correlation between the temperature difference at two critical end points ($\Delta T=T_{UCST}-T_{LCST}$) and the minima of γ_{O-W} in various nonionic surfactant systems is shown in Fig. 6. The interfacial tensions were measured at temperatures in the midst of the three-phase region. It is clear from Fig. 6 that the ultralow interfacial tension at an oil–water interface is attained in the system in which the difference in two critical temperatures is very small, and that the longer the hydrocarbon chain length of a surfactant, the lower the oil–water interfacial tension. In this case, both the oil phase and the water phase contain only a small amount of a surfactant, *i.e.*, cmc or so, as is shown in Figs, 1, 2, and 4. Therefore, the concentration of a surfactant required to reduce the interfacial tension to the ultralow range is very small.

Correlation between the Emulsion Type and Interfacial Tension. Since the three-phase region appears in the temperature range between the two critical points of the O–D and D–W phases, the interfacial tensions at the respective interfaces will be directly relevant to the inversion of the emulsion type. If γ_1 is the interfacial tension between a water phase and a surfactant monolayer adsorbed on the O–W interface, and γ_2 that between an oil phase and a surfactant monolayer, $\gamma_{O-W}=\gamma_1+\gamma_2$ holds in the three-phase region (*cf.* Fig. 7.) $\gamma_{O-D(\simeq W)}=\gamma_1+\gamma_2$ and $\gamma_{D(\simeq O)-W}=\gamma_1+\gamma_2$ also hold at temperatures below the LCST and above the UCST. As has been described before, $\gamma_{O-D(\simeq W)}$ is the interfacial tension between an aqueous micellar solution phase and an excess oil, and $\gamma_{D(\simeq O)-W}$ that between a reversed micellar solution phase and excess water. Since Antonoff's rule holds approximately in the three-phase region, the O–W interface can be regarded as a thin film of the D phase. However, strictly,

$$\gamma_{O-D}=\gamma_2+\gamma_1',\ \gamma_{D-W}=\gamma_1+\gamma_2', \tag{4}$$

where γ_1' and γ_2' are the correction terms which are not negative, judging from Eq. 3. Since Antonoff's rule holds strictly at each critical temperature, *i.e.*, $\gamma_1'=\gamma_2'=0$, the following relations hold:

$$\gamma_1=0,\ \gamma_{O-W}=\gamma_2 \quad \text{at LCST,} \tag{5}$$

$$\gamma_2=0,\ \gamma_{O-W}=\gamma_1 \quad \text{at UCST.} \tag{6}$$

γ_{D-W} may be zero or negative at a flat interface below the LCST, because the D–W interface is not stable at equilibrium. Therefore, $\gamma_1\leq 0$ and $\gamma_{O-D(\simeq W)}\leq\gamma_2$ hold below the LCST. Similarly, $\gamma_2\leq 0$ and $\gamma_{D(\simeq O)-W}\leq\gamma_1$ hold above the UCST. These relations are shown schematically in Fig. 8. The interface on the oil side of the surfactant monolayer tends to shrink, while that on the water side of the surfactant monolayer tends to expand, at temperatures below the LCST, because $\gamma_1\leq 0$ and $\gamma_2>0$, as is shown in Fig. 8. Therefore, in this temperature range, an O/W-type emulsion is formed. The case is the reverse above the UCST, so that a W/O-type emulsion is formed. $\gamma_1=\gamma_2$ holds at the temperature in the midst of a three-phase region. This temperature is the Hydrophile-Lipophile-Balanced (HLB) temperature and may correspond to the phase inversion temperature in emulsion. Since the interfacial tension curve is almost symmetrical, as is shown in Fig. 5, the phase inversion temperature (PIT) may be close to

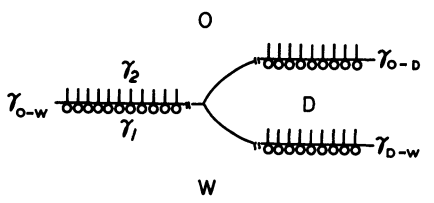

Fig. 7. Schematic O–W, O–D, and D–W interfaces. γ_1 and γ_2 are the interfacial tensions on the two sides of surfactant monolayer at O–W interface.

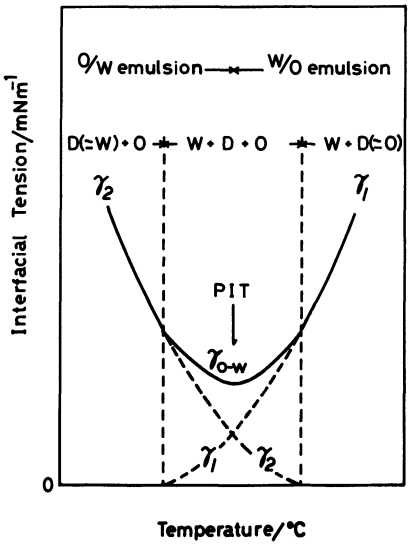

Fig. 8. Schematic change of the two interfacial tensions on the two sides of surfactant monolayer, γ_1 on the water side and γ_2 on the oil side as a function of temperature. A real curve corresponds to the interfacial tension of oil–water emulsion system.

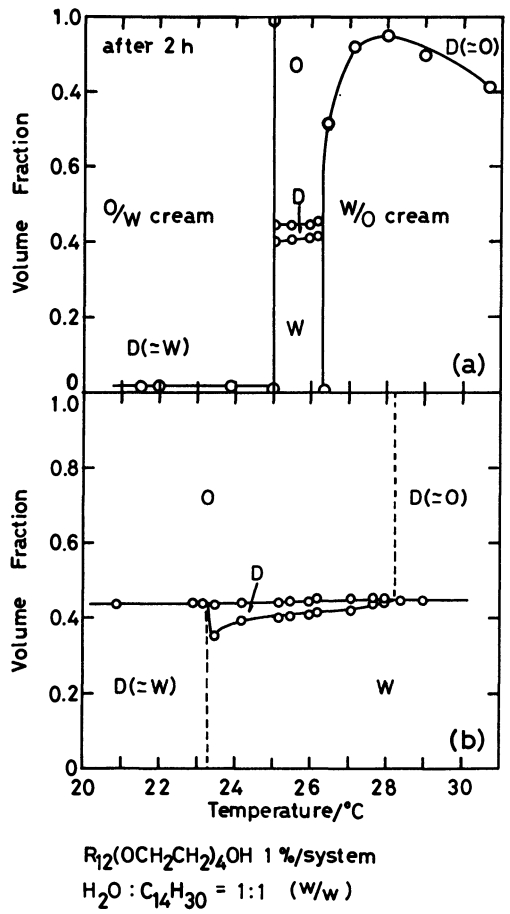

Fig. 9. The effect of emulsification temperature on the type of emulsion (a) and the volume fractions of O, W, and D phases at equilibrium (b) in $C_{12}H_{25}(OCH_2CH_2)_4$-OH/water/tetradecane system.

the temperature at which γ_{O-D} and γ_{D-W} become equal. In order to confirm this reasoning, the effect of the temperature on the emulsion type was carefully determined; it is shown in Fig. 9.[28,29] It is obvious that PIT is in the midst of the three-phase region.

References

1) K. Shinoda and H. Saito, *J. Colloid Interface Sci.*, **26**, 70 (1968).
2) P. A. Winsor, "Solvent Properties of Amphiphilic Compounds," Butterwoeths, London (1954), p. 68.
3) R. N. Healy, R. L. Reed, and D. G. Stenmark, *Soc. Pet. Eng. J.*, **16**, 147 (1976).
4) H. Kunieda and K. Shinoda, *J. Colloid Interface Sci.*, **75**, 601 (1980).
5) K. Shinoda, H. Kunieda, N. Obi, and S. E. Friberg, *J. Colloid Interface Sci.*, **80**, 304 (1981).
6) A. M. Bellocq, D. Bourbon, and B. Lemanceau, *J. Colloid Interface Sci.*, **79**, 419 (1981).
7) H. Saito and K. Shinoda, *J. Colloid Interface Sci.*, **32**, 647 (1970).
8) R. N. Healy and R. L. Reed, "Improved Oil Recovery by Surfactant and Polymer Flooding," ed by D. O. Shah and R. S. Schechter, Academic Press, New York (1977), p. 383.
9) J. L. Cayias, R. S. Schechter, and W. H. Wade, *J. Colloid Interface Sci.*, **59**, 31 (1977).
10) L. Cash, J. L. Cayias, G. Fournier, D. Macallister, T. Schares, R. S. Schechter, and W. H. Wade, *J. Colloid Interface Sci.*, **59**, 39 (1977).
11) P. H. Doe, M. El-Emary, W. H. Wade, and R. S. Schechter, *J. Am. Oil Chem. Soc.*, **55**, 505 (1978).
12) H. Kunieda and S. E. Friberg, *Bull. Chem. Soc. Jpn.*, **54**, 1010 (1981).
13) G. Quincke, *Pogg. Ann.*, **160**, 337 (1877).
14) A. W. Adamson, "Physical Chemistry of Surfaces," 3rd ed John Wiley and Sons, New York (1976), p. 31.
15) K. Shinoda and H. Saito, *J. Colloid Interface Sci.*, **30**, 258 (1969).
16) K. Shinoda and H. Kunieda, *J. Colloid Interface Sci.*, **42**, 381 (1973).
17) H. Kunieda and K. Shinoda, *J. Phys. Chem.*, **82**, 1710 (1978).
18) R. B. Griffiths, *J. Chem. Phys.* **60**, 195 (1974).
19) J. C. Lang, Jr., and B. Widom, *Physica*, **81A**, 190 (1975).
20) M. P. Brun, *C. R., Acad. Sci.*, **184**, 966 (1927).
21) D. Atack and O. K. Rice, *Discuss. Faraday Soc.*, **15**, 210 (1953).
22) K. Shinoda, M. Hanrin, H. Kunieda, and H. Saito, *Colloids Surfaces*, **2**, 301 (1981).
23) J. C. Lang and R. D. Morgan, *J. Chem. Phys.* **73**, 5849 (1980).
24) J. C. Lang, Jr., P. K. Lim, and B. Widom, *J. Phys. Chem.*, **80**, 1719 (1976).
25) B. Widom, *J. Chem. Phys.*, **62**, 1332 (1975).
26) Ref. 14, p. 109.
27) P. D. Fleming, III, and J. E. Vinatieri, *J. Colloid Interface Sci.*, **81**, 319 (1981).
28) K. Shinoda and H. Saito, *J. Colloid Interface Sci.*, **30**, 258 (1969).
29) K. Shinoda and H. Sagitani, *J. Colloid Interface Sci.*, **64**, 68 (1978).

Spin Density Distribution and Energy Stabilization in the Cation Radicals of Multilayered Compounds

Hiroaki OHYA-NISHIGUCHI,* Atsushi TERAHARA, Noboru HIROTA, Yoshiteru SAKATA,† and Soichi MISUMI†

Department of Chemistry, Faculty of Science, Kyoto University, Kyoto 606

†The Institute of Scientific and Industrial Research, Osaka University, Osaka 565

(Received November 6, 1981)

The spin density distributions and the energy stabilizations in the polymer cation radicals ($R_n^{+\cdot}$) have been investigated by measuring the oxidation potentials ($E^\circ_{1/2}$) and the electron spin resonance (ESR) spectra of the cation radicals generated by the electrochemical oxidations of some multilayered compounds. $E^\circ_{1/2}$ decreased monotonically as the number of layers increased. The spin densities on the aromatic rings have been estimated from the hyperfine coupling constants with the help of the McLachlan's and INDO calculation. It was found that the spin density tends to localize in the central moieties in $R_n^{+\cdot}$. The localization of the spin density and the energy stabilization are interpreted with a simple theoretical model of $R_n^{+\cdot}$, which takes into accounts the repulsion integral (γ_1) and resonance integral (ζ) between the nearest neighbor molecules. The comparison with the experimental data has lead to the numerical estimates of $\gamma_1=0.1$ eV and $\zeta=0.4$ eV.

The dimer cation radicals ($R_2^{+\cdot}$) of some aromatic hydrocarbons are known to be formed by the reaction

$$R^{+\cdot} + R \rightleftharpoons R_2^{+\cdot}, \quad (1)$$

when R are partly oxidized chemically in liquid solution,[1] by high energy irradiation in solid solution,[2] or by chemical reaction in gaseous state.[3] Such dimer cations have been characterized by negative enthalpies of formation, spin densities equally distributed over the two moieties, and eclipsed configurations in the dimers. The negative enthalpies are possibly due to the transannular interaction between the moieties which stabilizes the dimer species.

Higher polymeric radical species $R_n^{+\cdot}$ may be formed successively by the reaction scheme

$$R_{n-1}^{+\cdot} + R \rightleftharpoons R_n^{+\cdot}, \quad (2)$$

if the enthalpy difference between $R_n^{+\cdot}$ and $R_{n-1}^{+\cdot}$ is much larger than kT and sufficient concentration of R is present. In agreement with this expectation we previously succeeded in obtaining the ESR spectrum of coronene trimer cation radical $C_3^{+\cdot}$.[1m] It was shown from the spectrum analysis that the ratio between the spin densities in the central molecule and those in the side molecules is 6 : 1 in contrast to the 2 : 1 ratio predicted by the HMO calculation. This difference was attributed to the effect of transannular interaction.

The cation radicals of multilayered compounds such as paracyclophanes can be regarded as suitable model compounds for $R_n^{+\cdot}$ in clarifying characteristic features of $R_n^{+\cdot}$ arising on polymer formation. Anthracenophane cation radical, for example, was found to be a good model of anthracene dimer cation radical.[1k]

For an ESR study of the cation radicals of multilayered compounds, electrochemical generation has some advantages over the usual chemical methods or high energy irradiation: One is that the radical generation can easily be controlled by application of a proper voltage comparable to $E^\circ_{1/2}$ of the compound under consideration from outside the ESR system. One of the present authors (H.O.) recently developed a simple two-electrode cell using a helix which is very advantageous over the commonly used electrolysis cell in obtaining the spectra of unstable radical cations.[4] In this work, we have used this cell in studying ESR spectra of the radical cations of some multilayered compounds.

Although the ESR study of the multilayered compounds provide valuable information about their electronic wave functions constructed from those of constituting moieties, the information about their orbital energies is not obtained directly. On the other hand, cyclic voltammetry (CV) is an efficient and convenient method in obtaining the oxidation and reduction potentials associated with removal of an electron from the highest occupied molecular orbital (HOMO) and addition to the lowest unoccupied molecular orbital (LUMO), respectively. We have attempted to estimate the magnitude of transannular interactions from measurements of redox potentials.

In this paper we first report the results of electrochemical measurements of the several compounds **1** to **5** in Fig. 1 in relation to the dependence of the oxidation

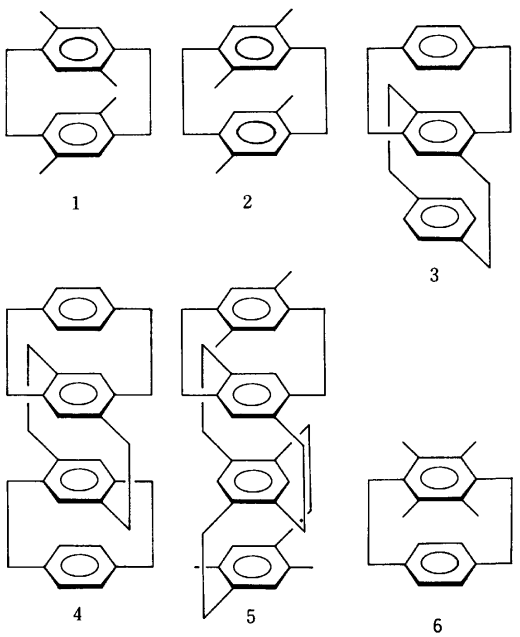

Fig. 1. Molecular structures of the multilayered compounds investigated.

potentials on the number of aromatic layers. Secondly, the ESR results of the cation radicals of these compounds are shown, and compared with those of $R_2^{+\cdot}$ and $R_3^{+\cdot}$ so far investigated. The MO calculations of the multilayered compounds were carried out using McLachlan's and INDO methods in order to interpret the observed spectra. Thirdly, we present a theoretical treatment of the spin distribution and energy stabilization in the multilayered aromatic systems, which takes into account repulsion and resonance integrals between the nearest neighbor molecules.

The model compounds such as those treated here are more amenable to detailed ESR investigations than the clustering intermediates produced in the course of chemical and biochemical reactions. Therefore, definitive ESR characterization of the multilayered compounds provides a framework for further understanding of the clustering intermediates in the chemical reactions.

Experimental

Substances shown in Fig. 1 were synthesized according to the methods described previously.[5,6] Commercially available hexamethylbenzene (**H**) and durene (**D**) were used without further purification. Purified and dried dichloromethane (CH_2Cl_2) or butyronitrile (BuCN) and tetrabutylammonium tetrafluorobotate (TBFB) of special grade for polarography were used as solvents and a supporting electrolyte, respectively. The cyclic voltammograms of the compounds, **1** to **5**, **H**, and **D**, were measured using a PAR 173 potentio/galvanostat equipped with an I/V converter, PAR 176, in conjunction with a Hewlett-Packard 3310A function generator. As a pseudo reference electrode a silver wire was used. In order to avoid the ambiguity of the potential of the reference electrode, a small amount of ferrocene was added and the position of the waves of the compounds under consideration were directly compared to that of ferrocenium/ferrocene (Fc^+/Fc) couple (0.400 V *vs.* NHE) used as an internal standard.[7] The electrochemical oxidation of the compounds for ESR measurements was carried out in the cavity using a helical working electrode made of gold wire. The details of the cell construction and the experimental procedure were given previously.[4] The appearance voltage, V_a, at which the ESR signal with modiulation amplitude of 1 G†† appears, was measured before the observation of high resolution spectra. The ESR spectra were measured with a JEOL FE-3X spectrometer, equipped with a temperature controller. Potassium nitrosylbis(sulfate) was used as a standard sample for the calibration of the magnitude and interval of the magnetic field, the accuracy of the latter being 0.005 G.

Results

The Appearance Voltages and the Oxidation Potentials of the Multilayered Compounds. V_a were measured at low temperatures at which the ESR spectra were also obtained (−70 °C to −90 °C). On the other hand, the $E^\circ_{1/2}$ were estimated from the peak potentials appeared on the anodic and cathodic sweeps (100 mV/s) by the usual method. V_a and $E^\circ_{1/2}$ of **3** to **5** nicely coinsided with each other in the range of experimental errors, but V_a of **1** and **2** become appreciably high compared with the corresponding $E^\circ_{1/2}$. This is probably due to the instability of the cation radicals produced, as pointed out in the previous paper.[4] It can be seen from Table 1 that both V_a and $E^\circ_{1/2}$ decrease as the number of the aromatic rings in the molecule n increases. In addition, $E^\circ_{1/2}$ of **1** showed an appreciable decrease from $E^\circ_{1/2}$ of **D**. This suggests the importance of the transannular interaction between the two moieties in spite of their configulation with a small overlap integral.

ESR Spectra of $1^{+\cdot}$ and $2^{+\cdot}$. After the temperature of the solution of **1** was decreased as low as −85 °C, the voltage applied between the two electrodes was increased step by step, while observing the ESR signal on an oscilloscope or a recorder. At 1.6±0.1 V well separated 13 lines with the relative intensity ratios of combinations of $_{12}C_r$ appeared. When the modulation amplitude was decreased as low as 0.063 G, each line was further split into well resolved 25 lines as shown in Fig. 2a. The analysis of this spectrum and assignment of the hfcc obtained were straight forward because of different

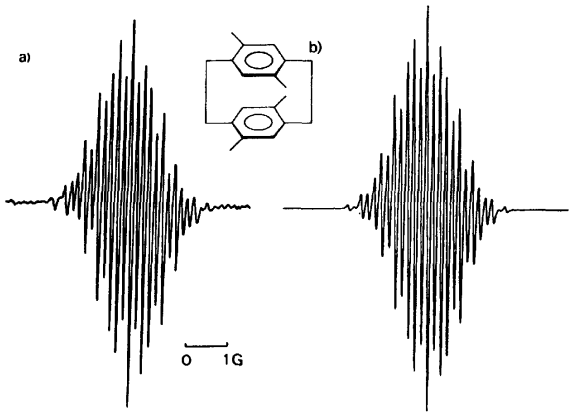

Fig. 2. One of well separated 13 groups due to the methylgroups in the ESR spectra of $1^{+\cdot}$; (a): observed (b): simulated.

Table 1. The appearance voltages (V_a) and the oxidation potentials of **1** to **5** in addition to those of durene (**D**), hexamethyl benzene (**H**), and paracyclophane (**P**)

	D	**H**	**P**	**1**	**2**	**3**	**4**	**5**
$V_a/V^{a)}$	—	—	—	1.6	1.4	1.1	0.8	0.8
$E^\circ_{12}/V^{b)}$	1.67[c)]	1.52[c)]	1.40[c)]	1.24[d)]	1.13[e)]	1.07[e)]	0.83[e)]	0.80[e)]

a) Voltages at which the ESR signals appear at −70 °C to − 90 °C. Solvent: $CH_2Cl_2+CF_3COOH$ (10 : 1), with $TBAPF_6$. b) ($E^\circ_{1/2}$ *vs.* NHE)/V were estimated from $(V^O+V^R)/2$ *vs.* the peak potential of ferrocene (0.400 V *vs.* NHE). Solvents: BuCN or CH_2Cl_2, with $TBAPF_6$. c) Irreversible. d) Quasireversible. e) Reversible.

†† 1 G=10^{-4} T.

numbers of the equivalent protons: 6.486 G for twelve methyl-protons, 0.486 G for eight bridge-protons, and 0.334 G for four ring-protons.

The ESR signals of $\mathbf{2}^{+\cdot}$ similar to that of $\mathbf{1}^{+\cdot}$ appeared at -70 °C at 1.4 ± 0.1 V which was 0.2 V lower than that of **1**. The resolution of each group of lines is poorer than in the case of $\mathbf{1}^{+\cdot}$ because of the small difference between the two small hfcc: 6.365 G for twelve methyl-protons, 0.41 G for eight bridge-protons, and 0.43 G for four ring-protons.

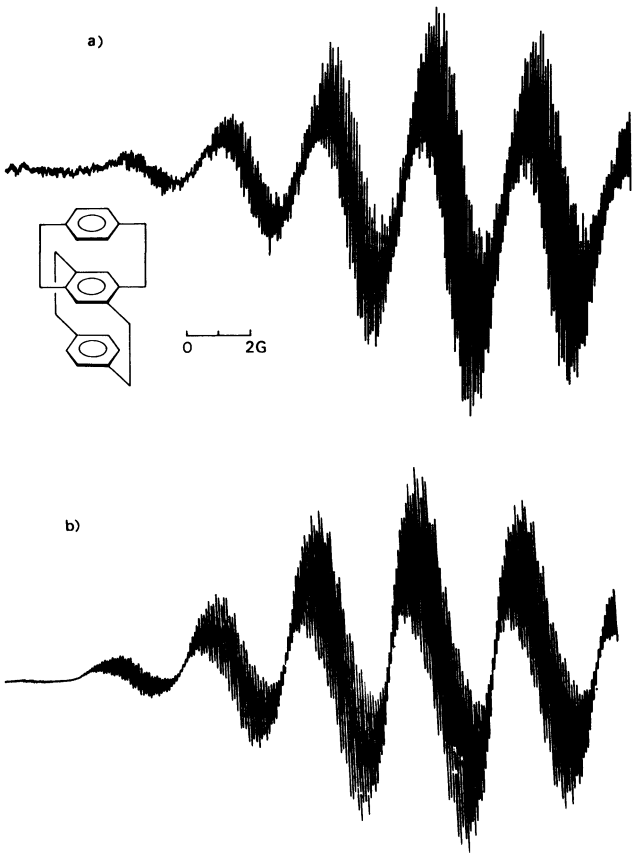

Fig. 3. The observed (a) and simulated (b) ESR spectra of $\mathbf{3}^{+\cdot}$.

The ESR Spectrum of $\mathbf{3}^{+\cdot}$. The well resolved spectrum of $\mathbf{3}^{+\cdot}$ was obtained at -56 °C (Fig. 3a). V_a (1.1 V) was lower than those of **1** and **2**. The obtained spectrum was very complex, but resolved well enough to be analyzed completely by computer simulation (Fig. 3b). 0.789 G due to two equivalent protons can be assigned unequivocally to the ring protons in the central ring in **3**. The larger hfcc, 3.279 and 3.049 G, due to two groups of equivalent four protons were not assigned uniquely, but assigned tentatively to the two four-equivalent bridge protons close to the central ring. The other hfcc can be attributable to the protons attached to the two side rings.

The ESR Spectra of $\mathbf{4}^{+\cdot}$ *and* $\mathbf{5}^{+\cdot}$. At -85 °C the ESR signals of both compounds appeared at 0.8 ± 0.1 V, which is 0.3 V lower than that of $\mathbf{3}^{+\cdot}$. They showed only one broad Gaussian-type line with the linewidths of 5.6 and 4.5 G, respectively. These radical species were very stable compared with the other species described above.

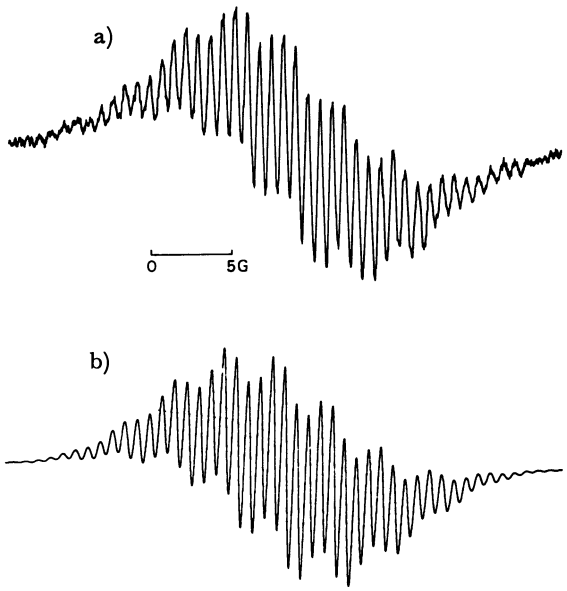

Fig. 4. The observed (a) and simulated (b) ESR spectra due to $\mathbf{1}_2^{+\cdot}$ at -112 °C.

The ESR Spectrum of $\mathbf{1}_2^{+\cdot}$. When a solution of **1** was oxidized at higher concentration and the lowest temperature available, -112°C, we observed a spectrum different from that of $\mathbf{1}^{+\cdot}$ (Fig. 4a). The conditions for obtaining this spectrum, a) high concentration, b) low temperature, and c) the beginning of the electrolysis, coincided with those for production of the dimers of typical aromatic hydrocarbons.[4] Figure 4b was obtained by the coupling constants: 3.074 G and 0.768 G for twelve-equivalent protons, and the additional unresolved couplings, 0.177 and 0.138 G for eight- and four-equivalent protons, respectively, using the Lorential lines of the widths of 0.380 G. The agreement between the simulated spectrum and the observed one is good enough to conclude that the spectrum is due to the dimer cation radical $\mathbf{1}_2^{+\cdot}$, formed according to Eq. 1. The hfcc of 3.074 G and 0.768 G are due to two different types of methyl protons, which indicates that spin densities on the central and the side rings are very different; the ratio being 4.0 : 1.

Comparison of the Hfcc with MO Calculations. Detailed molecular orbital calculations of paracyclophane and related compounds have been reported by many investigators.[8] In order to interpret the observed spectra, we have calculated hfcc by the McLachlan's and INDO methods. The usefulness of the McLachlan's method in calculating the hfcc of ordinary aromatic radical ions is well established. We have applied this method to the multilayered compounds taking into account of inter-ring interactions.

In Fig. 5 are shown the simplified molecular models (**1′** to **3′**) for **1** to **3**, used for calculation. Effects of the ethylene bridges are taken into consideration by changing the Coulomb integrals of the carbons in the rings as $\alpha(C')=\alpha_C-0.1\beta$. In our case the observed hfcc due to the methyl protons suggest a large effect of hyperconjuga-

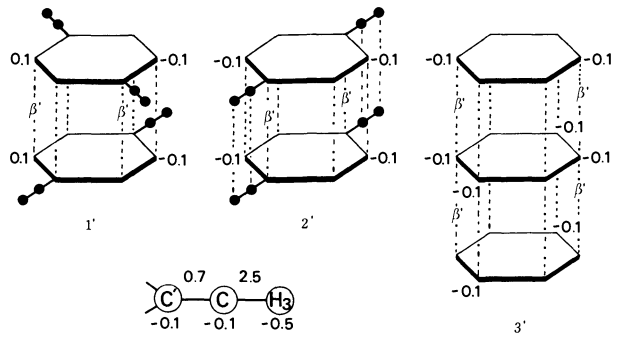

Fig. 5. The simplified molecular models, **1'**, to **3'**, for **1** to **3**, used for McLachlan's MO calculation.

tion. Therefore, the values of the Coulomb and resonance integrals of the methyl group C'–C≡H_3 were chosen as $\alpha(C')=\alpha(C)=\alpha_C-0.1\beta$, $\alpha(H_3)=\alpha_C-0.5\beta$, $\beta(C'-C)=0.7\beta$, and $\beta(C-H_3)=2.5\beta$ (hyperconjugation model[9]). In addition to those values the resonance integrals between the atoms of the upper and lower moieties in the molecule (β') were included only for pairs of carbon atoms C^l and C^u that lie on top of one another, as shown in Fig. 5. The interactions between the methyl groups in **2'** were also included.

Q values for estimating the hfcc from the calculated spin densities are somewhat ambiguous because 1) the layered configurations of the π-orbitals yield direct overlap of H atoms in the one moiety with the π-electron cloud of the other moiety, 2) each moiety does not have a planer structure, and 3) the exact configurations of the bridge protons are not known. In Table 2 are listed the hfcc calculated by this method using the following equations;

$$a_H = -24\rho_{C'} \quad \text{for ring protons,}$$

$$a_H^{CH_3} = 170\rho_{H_3} + 25\rho_{C'} \quad \text{for methyl protons, and}$$

$$a_H^{CH_2} = 6.3\rho_{C'} \quad \text{for bridge protons.}$$

The Q values for the bridge protons were estimated by $Q=50\cos\theta$,[10] where θ was calculated based on the crystallographic data of paracyclophane.[11]

Figure 6 shows the hfcc of $\mathbf{1}^{+\cdot}$ and $\mathbf{2}^{+\cdot}$ calculated as functions of β'. The dependences of the hfcc on β' are remarkably different in the two molecules. It can be seen that the hfcc of the ring protons in $\mathbf{1}^{+\cdot}$ drastically changes from 0.65 to −3.10 G as β' increases. At $\beta'=0.03\,\beta$ the theoretical hfcc due to three kinds of protons are all in reasonably good agreements with the experimental values given in Table 2. On the other hand, the hfcc of $\mathbf{2}^{+\cdot}$ are independent of the variation of β'. Calculated values are in good agreement with the observed ones.

The hfcc of $\mathbf{3}^{+\cdot}$ were calculated in the similar manner as in the case of $\mathbf{1}^{+\cdot}$ and $\mathbf{2}^{+\cdot}$. The best fit was obtained at $\beta'=0.04\,\beta$. The calculated values are also shown in Table 2. The largest and the second largest hfcc in the experimental data were well reproduced by those due to the bridge protons close to the central ring in spite of many ambiguities described above. The spin density is extremely localized on the central ring to those on the side rings being about 15 : 1.

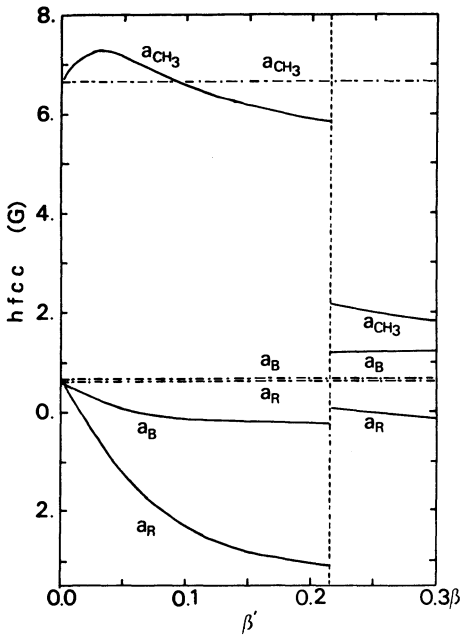

Fig. 6. The β' dependences of the hfcc of $\mathbf{1}^{+\cdot}$ and $\mathbf{2}^{+\cdot}$. ——: $\mathbf{1}^{+\cdot}$, -·-·-: $\mathbf{2}^{+\cdot}$.

Table 2. The observed and calculated hyperfine coupling constants of $\mathbf{1}^{+\cdot}$, $\mathbf{2}^{+\cdot}$, $\mathbf{3}^{+\cdot}$, and $\mathbf{1}_2^{+\cdot}$

	Obsd (G)	Calcd (G)		
		McLachlan		INDO
$\mathbf{1}^{+\cdot}$	(12H) 6.486	7.254		8.772
	(8H) 0.486	−0.569		−0.353
	(4H) 0.334	0.279		0.769
$\mathbf{2}^{+\cdot}$	(12H) 6.365	6.668		
	(8H) 0.41	0.662		
	(4H) 0.43	0.646		
			(Case 1)[a]	(Case 2)[a]
$\mathbf{3}^{+\cdot}$	(4H) 3.279	3.201	6.330	4.910
	(4H) 3.039		4.672	3.462
	(2H) 0.789	1.487	2.563	1.660
	(4H) 0.320	−0.858	−0.468	−0.706
	(4H) 0.238		−0.620	−0.859
	(8H) 0.091	1.410	−0.023	0.031
		0.772	−0.018	0.141
$\mathbf{1}_2^{+\cdot}$	(12H) 3.074			
	(12H) 0.768			
	(8H) 0.177			
	(4H) 0.138			

a) See text.

The hfcc of $\mathbf{1}^{+\cdot}$ and $\mathbf{2}^{+\cdot}$ were also calculated by the INDO method. The positions of the atoms in **1** were derived from the crystallographic data of paracyclophane.[11] In addition, we adopted a trial configuration in which the C–C bond connecting the methyl groups to the aromatic rings are parallel to the C–H bond of paracyclophane and one of the C–H bonds in the methyl group is equatorial about the rings. The hfcc of the methyl protons are averaged after the calculation because the rotations of the methyl groups about the C–C bonds are usually fast. The INDO calculation also gives the same trend of the spin distribution as

obtained by the McLachlan's method, but the numerical agreements are somewhat poorer. The main cause of the discrepancy may be due to the difference between the actual structure of $\mathbf{1}^{+\cdot}$ and that of paracyclophane.

In the INDO calculation of $\mathbf{3}^{+\cdot}$ the positions of the atoms in **3** were first derived from the crystallographic data of brominated **3** (Case 1).[12] In the second trial we used a structure in which the distance between the central moiety and the side ones were shortened by 0.2 Å (Case 2). The 1.25 A C–H bond length of the central ring protons derived crystallographically was also changed to the usual C–H bond distance of 0.98 Å in Case 2. The agreements between the experimental and calculated hfcc are poor in Case 1, but considerable improvement was achieved in Case 2. Although the largest hfcc obtained in Case 2 is large, the INDO result is in agreement with the result obtained by the McLachlan's calculation with $\beta'=0.04\,\beta$. The INDO result in Case 1 resembles to the McLachlan's result with β' smaller than $0.01\,\beta$. This may suggest that on the formation of the cation radical two side moieties are contracted to the central moiety, leading to the increased spin densities on the side moieties. The number of the atoms in **4** and **5** were too large to carry out the INDO calculations.

Theoretical Model of $R_n^{+\cdot}$

When two or more aromatic rings are stucked face to face, some transannular interactions are expected between π-electronic systems. As the whole they constitute an aggregate R_n. The spin density of $R_n^{+\cdot}$ is related to the highest occupied molecular orbital (HOMO) of R_n which are constructed by the HOMO of constituting molecules. In the following, therefore, we only consider the HOMO $\phi_i(i=1$ to $n)$ of i-th molecule in R_n, which is doubly occupied by π-electrons. The total energy of R_n can be generally given by

$$E_0^n = \int \boldsymbol{\Psi}_0 \boldsymbol{H} \boldsymbol{\Psi}_0 d\tau = 2\sum_i^n H_{ii} + \sum_i^n \sum_j^n (2J_{ij} - K_{ij}), \quad (3)$$

where H_{ij}, J_{ij}, and K_{ij} have the usual meanings.[13] Assuming that an electron is removed from ϕ_i, a configuration $\boldsymbol{\Psi}_i$ of $R_n^{+\cdot}$ is written as $\boldsymbol{\Psi}_i=|\phi_1^2\phi_1^2\cdots\phi_i^1\cdots\phi_n^2|$ and the ground state wave function $\boldsymbol{\Psi}_G^n$ of $R_n^{+\cdot}$ is expressed by a linear combination of n configurations:

$$\boldsymbol{\Psi}_G{}^n = \sum_{i=1}^n C_i \boldsymbol{\Psi}_i, \quad (4)$$

where C_i is the coefficient of the linear combination, and C_i^2 corresponds to the spin density on the i-th molecule. In order to derive the ground state energy $E_G{}^n$, one need to solve

$$(\boldsymbol{H} - E\boldsymbol{I})\boldsymbol{C} = 0, \quad (5)$$

where $\boldsymbol{H}$ is the hamiltonian matrix defined by

$$H_{ij} = \langle \boldsymbol{\Psi}_i | \boldsymbol{H} | \boldsymbol{\Psi}_j \rangle. \quad (6)$$

$\boldsymbol{I}$ is the unit matrix, and $\boldsymbol{C}$ is the column vector which consists of C_i $(i=1$ to $n)$. The diagonal elements of the matrix H_{ii} can be simply expressed in reference to $E_0{}^n$ as

$$H_{ii} = E_0{}^n - H_{ii} - \sum_j^n \{2J_{ij} - K_{ij}\}. \quad (7)$$

We assume that J_{ij} and K_{ij} have non zero values only when $j=i$ $(i=1$ to $n)$ and $j=i\pm1$ $(i=2$ to $n-1)$ and replace J_{ii} and $J_{i\,i+1}$ by γ_0 and γ_1. Then

$$H_{ii} = E_0{}^n - H_{ii} - \gamma_0 - 2\gamma_1 \quad \text{for } i = 1 \text{ and } n, \quad (8)$$

$$H_{ii} = E_0{}^n - H_{ii} - \gamma_0 - 4\gamma_1 \quad \text{for } i = 2 \text{ to } n-1. \quad (9)$$

The off diagonal elements H_{ij} is also assumed as

$$H_{ij} = \zeta \quad \text{for } j = i \pm 1, \quad (10)$$

$$H_{ij} = 0 \quad \text{for others.} \quad (11)$$

By substituting H_{ij} into Eq. 5, one can derive the determinant D_n as

$$D_n = \begin{vmatrix} -2\gamma_1-\varepsilon & \zeta & 0 & \cdots & 0 \\ \zeta & -4\gamma_1-\varepsilon & \zeta & \cdots & 0 \\ 0 & \zeta & -4\gamma_1-\varepsilon & \cdots & 0 \\ \cdots & \cdots & \cdots & \cdots & \cdots \\ 0 & 0 & 0 & & -2\gamma_1-\varepsilon \end{vmatrix} = 0, \quad (12)$$

where

$$\varepsilon = -E_0{}^n + H_{ii} + \gamma_0 - E. \quad (13)$$

It is convenient to rewrite D_n by using θ and α defined by

$$-4\gamma_1 - \varepsilon = \zeta \cdot 2\cos\theta, \quad (14)$$

$$\gamma_1 = \alpha\zeta. \quad (15)$$

Then

$$D_n = \zeta^n \begin{vmatrix} 2\cos\theta + 2\alpha & 1 & 0 & \cdots & 0 \\ 1 & 2\cos\theta & 1 & \cdots & 0 \\ 0 & 1 & 2\cos\theta & \cdots & 0 \\ \cdots & \cdots & \cdots & \cdots & \cdots \\ 0 & 0 & 0 & \cdots & 2\cos\theta+2\alpha \end{vmatrix} = 0. \quad (16)$$

D_n can be expanded into a polynomial of $\cos\theta$ expressed as

$$D_n = \frac{\zeta^n(-1)^{n-2}}{\sin\theta} \times \{\sin(n+1)\theta - 4\alpha\sin n\theta + 4\alpha^2\sin(n-1)\theta\} = 0. \quad (17)$$

From this equation one can obtain n solutions $\theta_k(k=1$ to $n)$ which lead to

$$E_G{}^n = E_0 - H_{ii} - \gamma_0 - 4\gamma_1 + 2\zeta\cos\theta_1, \quad (18)$$

$$\boldsymbol{\Psi}_G{}^n = A\sum_i \{\sin i\theta_1 - 2\alpha\sin(i-1)\theta_1\}\phi_i. \quad (19)$$

It should be noted that the transannular interaction $(E_G^n - E_G^1)$ is given as a sum of the repulsion and the resonance integrals.[14] The spin density distribution at the i-th molecule is finally derived as

$$\rho_i = A^2\{\sin i\theta_1 - 2\alpha\sin(i-1)\theta_1\}^2. \quad (20)$$

In Fig. 7 the ratio of the spin densities of the central moieties to those of the side ones plotted as functions of α for the cases of $n=3$ and $n=4$.

As $n\to\infty$, the stabilization energy in reference to $R_1^{+\cdot}$, $H_n=E_G{}^n-E_G{}^1$, converges to $-4\gamma_1+2\zeta$. In Fig. 8 $2\cos\theta_1$ is plotted as a function of n. As n approaches infinity this quantity converges to 2, as can be seen from Eq. 18. On the other hand, in the limit of $\zeta=0$, Eqs. 18 and 19 are reduced to the following equations which

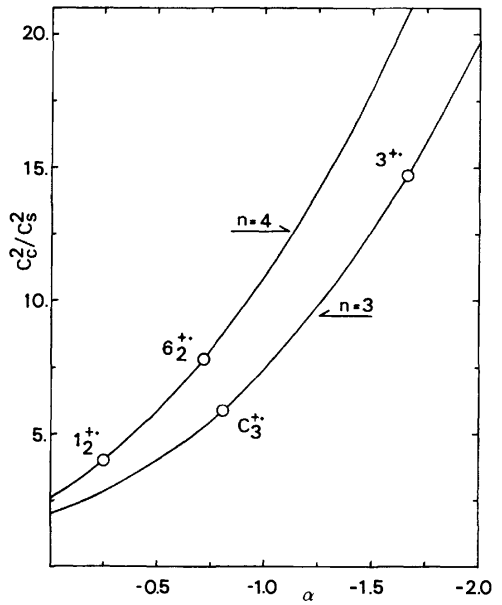

Fig. 7. The ratio of the spin densities of the central moieties to those of the side ones plotted as functions of α for the cases of $n=3$ and $n=4$.

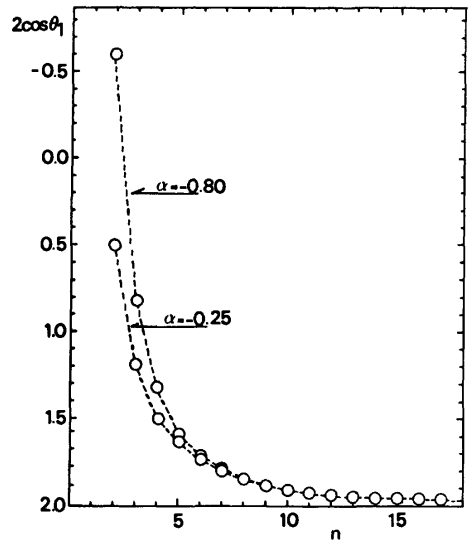

Fig. 8. $2\cos\theta_1$ plotted as functions of n for $\alpha=-0.25$ and -0.80.

are derived for the chain molecules in the Hückel treatment:[15]

$$E_j = \gamma_0 + 2\zeta\cos\theta_j, \tag{22}$$

$$\Psi_j = A\sum_i \sin i\theta_j\cdot\phi_i, \tag{23}$$

with

$$\theta_j = \frac{\pi\cdot j}{n+1}. \tag{23}$$

It should be noted in Eq. 16 that even in the case of $R_n^{+\cdot}$ in which two end molecules are different from others the determinant similar to Eq. 16 can be derived. Therefore, one can use Eqs. 18 and 19 even in the case of **3**, adjusting the parameter which includes the energy difference $H_{ii}-H_{jj}$.

Discussion

The Energy Stabilization. V_a and $E^\circ_{1/2}$ of **1** to **5** decrease in the order of **1** to **5**. This trend is consistent with that of Fig. 8 derived theoretically from Eq. 18. It is of interest to examine the magnitude of the transannular interaction of each compound in relation to this trend.

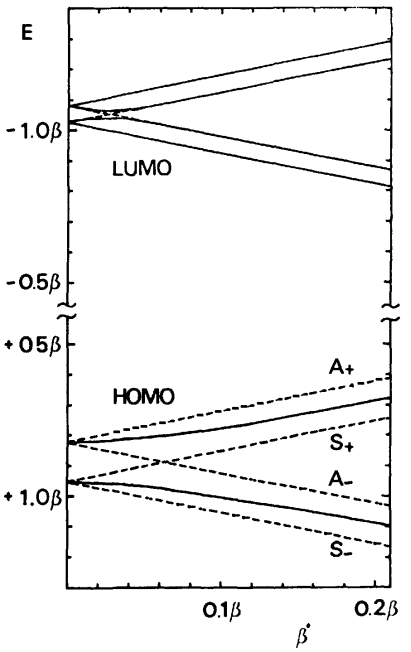

Fig. 9. β' dependences of some orbital energies including the HOMO and the LUMO calculated by HMO method; for **1** (——) and **2** (------).

Figure 9 shows β' dependence of some orbital energies including the HOMO and the LUMO of **1** and **2** calculated by the HMO method. The degenerate benzene orbitals, A and S (e_{1u}), have nodal planes perpendicular to each other, which are also perpendicular to the benzene plane. These orbital energies are split into two by substituting methyl and methylene groups to two benzene rings which results in **1** or **2**. The orbital energy of A is higher than that of S. As the transannular interaction between the two moieties M_u and M_l increases, each orbital of **2** splits further into two orbitals which are given as

$$A^{\pm} = (A^u \pm A^l)/2,$$

$$S^{\pm} = (S^u \pm S^l)/2. \tag{24}$$

The HMO and McLachlan's calculations of $\mathbf{2}^{+\cdot}$ show constant hfcc (Fig. 6) and linear change of the HMO energy with respect to the increase of β'. $\mathbf{2}^{+\cdot}$ corresponds to the usual dimeric species $R_2^{+\cdot}$ of the typical aromatic hydrocarbons with eclipsed configuration.

On the other hand, the energies of A^+ and A^- (S^+ and S^-) of **1** are almost degenerate in all range below 0.2 β, because the twisting configuration of the two moieties reduces the resonance energy between the moieties,

but an orbital mixing between $A^{\pm}$ and $S^{\pm}$ occurs through the transannular interaction. Such a mixing in **1** causes the spin density redistribution in each moiety and the lifting of the HOMO energy, as shown in Fig. 9.

The oxidation potential of durene was measured as 1.67 V. **1** consists of two durene moieties rotated each other by about 60°. Since the resonance stabilization of **1** is almost zero, one can roughly estimate the value of γ_1 using Eq. 18. As the measured value of $E^{\circ}_{1/2}$ of **1** is 1.24 V, the difference with that of durene, 0.43 V, is equal to $4\gamma_1$. Then γ_1 is estimated to be 0.11 eV. Since the interlayer distance of the compounds measured here do not change much, γ_1 of these compounds may be regarded to be the order of this magnitude.

$E^{\circ}_{1/2}$ of **2** is 0.11 V lower than that of **1**. This means that the eclipsed configuration of drurene in **2** results in an appreciable resonance interaction between the two moieties. Using Eq. 18, the difference between $E^{\circ}_{1/2}$ of **1** and that of **2** is given to be $2\zeta \cos\theta_1$, from which we can derive the numerical value of ζ provided that $2\cos\theta_1$ is estimated experimentally.

The dimeric species of **1**, $\mathbf{1}_2^{+\cdot}$, exhibited clear hf splittings with the ratio of two kinds of hfcc due to the methyl groups being 4 : 1. Assuming that the four aromatic rings in $\mathbf{1}_2^{+\cdot}$ are stacked face to face and the interactions among four moieties are equal, we obtain $\alpha=-0.25$ from this ratio with $n=4$ in Eq. 20. As γ_1 is of the order of 0.1 eV, ζ is estimated to be 0.4 eV from Eq. 15. Alternatively, the difference between $E^{\circ}_{1/2}$ of **1** and that of **2**, 0.11 V corresponds to $2\zeta\cos\theta_1$. Substituting $\alpha=-0.25$ into Eq. 18, we obtain $2\cos\theta_1=0.50$ and $\zeta=0.22$ eV. ζ estimated by these two different methods are in the same order of magnitude.

The π system of **3** consists of one durene at the center and two *p*-xylenes at both sides. The HOMO of *p*-xylene and durene are A and S respectively, each of which has a nodal plane rotated by 30° from each other. Therefore the resonance interaction is to be rather small, but $E^{\circ}_{1/2}$ of **3**, 1.08 V, is about 0.6 V lower than that of durene. This mean that the repulsion integral $4\gamma_1$ in Eq. 18 contributes considerably to the stabilization. If we adopt here $\gamma_1=0.1$ eV, the difference 0.2 eV can be regarded as the contribution from the resonance interaction.

The energy stabilization of **4** and **5** is further enhanced by the eclipsed configuration of the two durene moieties in the center of **4** and orbital mixings of the four durene moieties in **5**, as in the cases of **1** and **2**. $E^{\circ}_{1/2}$ of **4** and **5** clearly show the energy stabilization of the order of 0.9 V.

Spin Density Distribution. The transannular interaction in the staggered configuration in **1** does not so much stabilize the system, but induces the mixing between A and S, which results in the spin density redistribution. From the comparison of the observed hfcc with those of the calculated ones, we can estimate β' as 0.03 β. In the previous work,[1m] we also obtained $\beta'=0.03\,\beta$ in the case of coronene trimer cation radical $C_3^{+\cdot}$. It is remarkable that β' estimated in the two different systems coincide with each other in spite of the difference of the compounds.

About 0.5 G splittings due to the ring protons in **1** is the same magnitude as that in **2**, but the theoretical calculations (McLachlan and INDO) indicate the opposite sign. This is probably due to the fact that the small transannular interaction between the two moieties induces the spin density redistribution which converts accidentally the sign of usually negative hfcc of −0.5 G.

From the hfcc due to $\mathbf{3}^{+\cdot}$ it was found that the spin density is localized on the central moiety of durene, the ratio of the spin density in the central moiety to that of the side moieties being about 15 : 1. The theoretical treatment of such a mixed layer compound leads to a large apparent a, as indicated in Fig. 8. Dessau *et al.* obtained the hfcc of $\mathbf{D}^{+\cdot}$: 10.7 G for the twelve methyl protons and 0.8 G for the two ring protons.[16] The latter is very close to that of the central ring protons in $\mathbf{3}^{+\cdot}$ (0.789 G). Both McLachlan's and INDO calculations support such localization of the spin density, although the hfcc of the side moieties do not agree with the experimental values so well. This probably due to the fact that the hfcc of the side moieties are very sensitive to the distance between the central and side moieties. It is appropriate to conclude that most of the spin density is localized on the central durene moiety in $\mathbf{3}^{+\cdot}$.

The linewidths of $\mathbf{4}^{+\cdot}$ and $\mathbf{5}^{+\cdot}$ show only indirect evidence that the spin density localizes at the central two moieties. The four methyl substitution to **4**, which leads to **5**, produced only a small variation to the linewidth. This suggests small spin distribution on the both side rings and large spin localization on the two central rings of **4**.

The authors wish to express their thanks to Professor Suehiro Iwata of Keio University for his kind suggestions concerning the theoretical treatment of the polymer cation radicals.

References

1) a) I. C. Lewis and L. C. Singer, *J. Chem. Phys.*, **43**, 2712 (1965); b) O. Howarth and G. K. Fraenkel, *J. Am. Chem. Soc.*, **88**, 4514 (1966); *J. Chem. Phys.*, **52**, 1371 (1970); c) H. van Willigen, E. de Boer, J. T. Cooper, and W. F. Forbes, *ibid.*, **49**, 1190 (1968); d) W. F. Forbes and J. T. Cooper, *Can. J. Chem.*, **46**, 1158 (1968); e) T. C. Chiang and A. H. Reddoch, *J. Chem. Phys.*, **52**, 1371 (1970); f) S. Shih and R. M. Dessau, *ibid.*, **55**, 3757 (1971); g) H. Yoshimi and K. Kuwata, *Mol. Phys.*, **23**, 297 (1972); h) O. Edlund, P. Kinell, A. Lund, and A. Shimizu, *J. Chem. Phys.*, **46**, 3679 (1967); i) P. Kinell and A. Lund, *Acta Chem. Scand*, **26**, 444 (1972); j) T. Ichikawa and P. K. Ludwig, *J. Am. Chem. Soc.*, **91**, 1024 (1969); k) J. Bruhin, F. Gerson, and H. Ohya-Nishiguchi, *Helv. Chim. Acta*, **60**, 2471 (1977); l) F. Gerson, G. Kaupp, and H. Ohya-Nishiguchi, *Angew. Chem., Int. Ed. Engl.*, **16**, 657 (1977); m) H. Ohya-Nishiguchi, H. Ide, and N. Hirota, *Chem. Phys. Lett.*, **66**, 581 (1979).

2) a) B. Badger, B. Brocklehurst, and R. D. Russel, *Chem. Phys. Lett.*, **1**, 122 (1967); b) B. Badger and B. Brocklehurst, *Nature*, **219**, 263 (1968); c) B. Badger and R. D. Russel, *Trans. Faraday Soc.*, **65**, 2159 (1969); d) B. Badger and B. Brocklehurst, *ibid.*, **65**, 2576, 2582, 2588 (1969); **66**, 2939 (1970); e) S. Arai, A. Kira, and M. Imamura, *J. Chem. Phys.*, **56**, 1777 (1972); f) A. Kira, S. Arai, and M. Imamura, *J.*

Phys. Chem., **76**, 1119 (1972); g) M. A. J. Rogers, *Chem. Phys. Lett.*, **9**, 107 (1971); h) M. A. J. Rogers, *J. Chem. Soc., Faraday Trans. 1*, **68**, 1278 (1972).

3) a) M. Meot-Ner(Mautner), P. Hamlet, E. P. Hunter, and F. H. Field, *J. Am. Chem. Soc.*, **100**, 5466 (1978); b) M. Meot-Ner(Mautner), *J. Phys. Chem.*, **84**, 2724 (1980).

4) H. Ohya-Nishiguchi, *Bull. Chem. Soc. Jpn.*, **52**, 2064 (1979).

5) T. Otsubo, S. Mizogami, I. Otsubo, Z. Toyoda, A. Sakagami, Y. Sakata, and S. Misumi, *Bull. Chem. Soc. Jpn.*, **46**, 3519 (1973).

6) T. Otsubo, S. Mizogami, Y. Sakata, and S. Misumi, *Chem. Commun.*, **1971**, 678; *Tetrahedron Lett.*, **1971**, 4803.

7) R. R. Gagne, C. A. Coval, and G. C. Lisensky, *Inorg. Chem.*, **19**, 2854 (1980).

8) B. Kovac, M. Mohraz, E. Heilbronner, V. Boeckelheide, and H. Hopf, *J. Am. Chem. Soc.*, **102**, 4314 (1980), and other references cited therein.

9) F. Gerson, "High Resolution E. S. R. Spectroscopy," John Wiley and Sons Lts. Verlag Chemie (1970), p. 50.

10) N. M. Atherton, "Electron Spin Resonance; Theory and Applications," John Wiley and Sons Inc. New York (1973), p. 105.

11) D. K. Lonsdale, F. R. S., H. J. Milledge, and K. V. K. Rao, *Proc. R. Soc. London, Ser. A*, **255**, 82 (1960).

12) Y. Koizumi, T. Toyoda, H. Horita, and S. Misumi, presented at the 22nd National Meeting of the Chemical Society of Japan, Tokyo, April 1975, Summary I, p. 184.

13) For example, J. A. Pople and D. L. Beveridge, "Approximate Molecular Orbital Theory," McGraw-Hill Inc. (1970).

14) S. Iwata, private communication.

15) E. Hückel, *Z. Phys.*, **76**, 628 (1932).

16) R. M. Dessau, S. Shih, and E. I. Heiba, *J. Am. Chem. Soc.*, **92**, 412 (1970).

Translational Energy Distribution and Relative Emission Cross Section of Excited Hydrogen Atom Produced in Electron-chloroform Collisions

Teiichiro OGAWA,* Fumihiro MIYOSHI,† and Morihide HIGO††
Department of Molecular Science and Technology, Kyushu University, Kasuga, Fukuoka 816
(Received Nobember 13, 1981)

Dissociative excitation of $CHCl_3$ and $CDCl_3$ has been investigated by means of the controlled electron impact and the high resolution emission spectroscopy. The emission spectrum shows such excited species as H, CH, CH^+, Cl^+, CCl, and HCl^+. The excitation function of H* has two thresholds, 20.5 and 41.0 eV. The emission cross spections of H* and D* reveal an isotope effect, which is dependent on the excitation energy and the principal quantum number. Translational energy distributions of H* and D* have been determined from the Doppler line shape of the Balmer-β line, and average translational energies from the half-width of the Balmer-α, β, γ, and δ lines. There are no noticeable isotope effect for the translational energy; their major peaks lie at 0—1, 4, and 6—12 eV. These findings indicate that there are at least three major processes for the formation of the excited hydrogen atom. They are assigned to dissociative excitation through the Rydberg states converging to the $(2a_1)^1$ ionic states and through doubly excited Rydberg states.

An excited molecule may decompose by itself to give an excited fragment atom. An electron-molecule collision is an efficient method to trigger dissociative excitation of the molecule. A detailed elucidation of this process has become possible through the investigation of the translational energy distributions of H* and D* obtained from the analysis of the Doppler line shape of their Balmer lines.[1,2] It has been found that there are two or more processes for dissociative excitation of H_2,[3] D_2,[4] HCl,[2] and CH_4[5] to produce the excited hydrogen atom from such molecules. The high resolution spectroscopy of H* is equally important with the mass spectroscopy of H^+ for a detailed analysis of the dissociation mechanism of highly-excited molecules.

Dissociation mechanism of chloroform has been investigated under the controlled electron impact excitation of $CHCl_3$ and $CDCl_3$.[6] The photoelectron spectrum of chloroform has been measured and discussions on the excited electronic states have been given.[7-9]

The relative value of the emission cross sections of H* to those of D* produced in the collision process is also useful for the investigation of the dissociation mechanism and is related to competition among various dissociation and ionization processes of the highly-excited molecule.[10]

In the present paper, the emission spectra of $CHCl_3$ and $CDCl_3$ have been measured with a high resolution by using a Fabry-Perot interferometer. The translational energy distributions of H* and D*, the excitation function and the relative emission cross sections have been obtained in order to discuss the mechanism of dissociative excitation of chloroform.

Experimental

The apparatus has been described previously.[2,3] The very high resolution spectrum was obtained with a Fabry-Perot interferometer (Mizojiri Optics). The $CDCl_3$ (99.8 D atom %) was obtained from Aldrich Chemical. The chloroform was used as supplied and subjected to several freeze-pump-thaw cycles before use.

Results and Discussion

Spectrum. Collisions between a chloroform molecule and an electron give photoemissions of several fragments, as are shown in Fig. 1. They are the excited hydrogen atoms (n=3,4,5,6,7,8), CH(A–X, B–X, C–X), CH^+(A–X, B–A, b–a), Cl^+, CCl(A–X), and HCl^+(A–X). The spectrum of $CDCl_3$ is similar; however, the Balmer lines are relatively weaker.

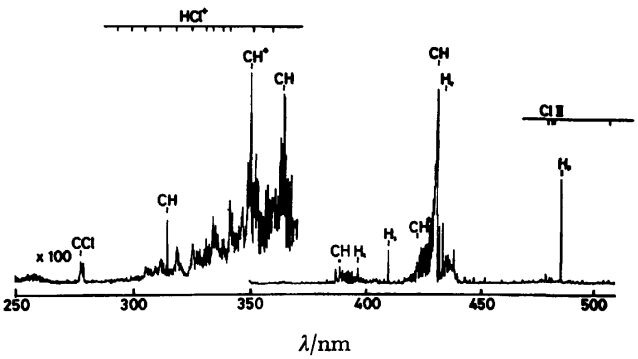

Fig. 1. Emission spectrum of chloroform by controlled electron impact. Electron energy 100 eV, electron-beam current 800 μA, spectral resolution 2 Å.

The intensities of the Balmer lines and bands of CH(A–X), CH^+(B–A), and CCl(A–X) are proportional to the electron-beam current and the gas pressure. Thus, these species should be produced in a one-electron-one-molecule primary collision. On the other hand, the square root of the emission intensity of HCl^+(A–X) is proportional to the electron-beam current (Fig. 2), although this intensity is directly proportional to the gas pressure. These results indicate that HCl^+ is produced in a two-step molecular elimination mechanism as in the case of CH_2Cl_2.[6]

Thresholds. The excitation functions of CH(A–X)

† Present address: Chiba works, Kawasaki Steel Co., Kawasaki, Chiba 260.

†† Present address: Faculty of Engineering, Kagoshima University, Korimoto, Kagoshima 890.

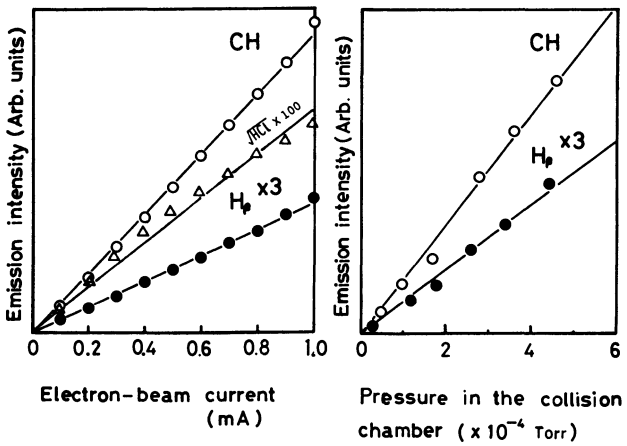

Fig. 2. Dependence of emission intensities on the electron-beam current and the gas pressure. Electron energy 100 eV.

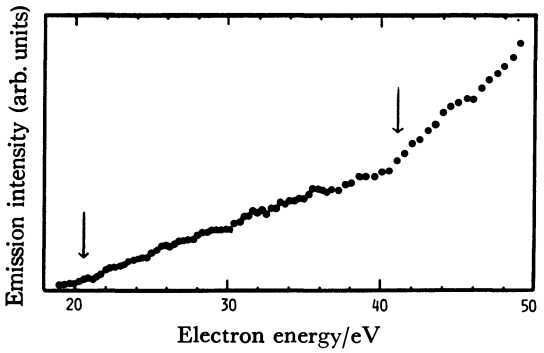

Fig. 3. Excitation function of the dissociative excitation of chloroform to yield the excited hydrogen atom (n=4).
Thresholds are indicated by arrows. The electron-beam current is 1 μA.

and H(n=4) have been measured and the latter is shown in Fig. 3. The threshold energies for the formation of CH(A) lie at 16.8±1.0 and 34.0±2.5 eV, and those of H(n=4) lie at 20.5±1.7 and 41.0±2.5 eV. These values are shown in Table 1, together with the previous results[6] and several possible dissociation processes.

The first threshold of CH(A) at 16.8 eV can be assigned to some of the processes (a), (b), or (c) in Table 1. The first threshold of H*(n=4) at 20.5 eV can be assigned to process (f), since the excited hydrogen atom carries some translational energy. The excess energy above the dissociation limit is partitioned into the translational, vibrational and rotational energies of the fragments. For the process (f), the law of conservation of momentum requires that H*(n=4) carries 99% of the total translational energy, and the residual energy should be the vibrational and rotational energies of CCl_3.

Isotope Effect. The emission cross sections of the excited hydrogen atom produced in electron-hydrogen and electron-hydrogen chloride collisions have isotope effects.[10-12] One of the main sources of this isotope effect is competition between dissociation and autoionization of superexcited states produced in the collision process.[13]

The emission spectra of H* and D* have been measured for mixtures of $CHCl_3$ and $CDCl_3$ in the equal amount; typical spectra of the Balmer-α line are shown in Fig. 4.

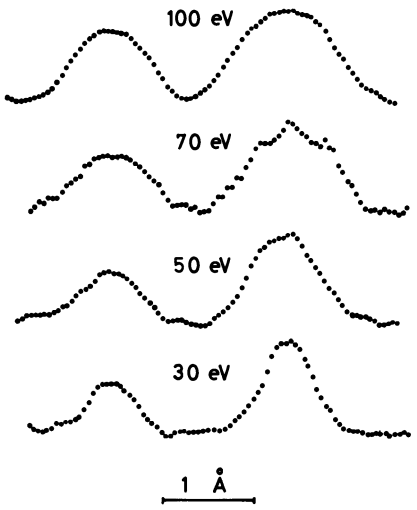

Fig. 4. High resolution spectra of the Balmer-α lines of H* and D* measured for mixtures of $CHCl_3$ and $CDCl_3$ in the equal amount. The left peak (smaller) is D* at 6561.0 Å and the right one (taller) is H* at 6562.8 Å. The resolution was 0.08—0.15 Å (Spex 1269 monochromator).

Table 1. Threshold energies for dissociative excitation of chloroform

	Process	Calculated dissociation limit	Observed threshold energy: This work	Observed threshold energy: Toyoda *et al.*[6]
(a)	$CHCl_3 \xrightarrow{e} CH(A)+Cl_2(X)+Cl(3P^5\ ^2P)$	12.0	16.8±1.0	17.6±1.0
(b)	$CH(A)+Cl_2(A)+Cl(3P^5\ ^2P)$	14.2		
(c)	$CH(A)+3Cl(3P^5\ ^2P)$	14.4		
(d)	$CH(A)+Cl_2(C)+Cl(3P^5\ ^2P)$	19.1		
(e)	$CH(A)+Cl_2(X)+Cl(4S^1\ ^4P)$	20.9		
(f)	$CHCl_3 \xrightarrow{e} H(n=4)+CCl_3(X)$	16.7	20.5±1.7	
(g)	$H(n=4)+CCl_2(X)+Cl(3P^5\ ^2P)$	19.0		
(h)	$H(n=4)+CCl(X)+Cl_2(X)$	20.0		
(i)	$H(n=4)+CCl(X)+Cl_2(A)$	22.2		
(j)	$H(n=4)+CCl(X)+2Cl(3P^5\ ^2P)$	22.5		

TABLE 2. RELATIVE EMISSION CROSS SECTIONS (σ_D/σ_H) OF THE BALMER LINES OF THE EXCITED HYDROGEN ATOMS IN ELECTRON-CHLOROFORM COLLISIONS

Electron energy/eV		Balmer-α $n=3$	Balmer-β $n=4$	Balmer-γ $n=5$	Balmer-δ $n=6$
100		0.61±0.07	0.61±0.07	0.65±0.09	0.72±0.09
70		0.63±0.07	0.54±0.07	0.59±0.09	0.68±0.08
50		0.56±0.07	0.61±0.07	0.58±0.10	0.66±0.08
40		—	0.51±0.08	0.53±0.11	0.62±0.09
30		0.50±0.08	0.52±0.08	—	0.60±0.09
Optical resolution used/Å	above 50 eV	0.13	0.08	0.08	0.08
	30, 40 eV	0.15	0.11	0.11	0.11

The relative emission cross sections (σ_D/σ_H) have been determined from the relative area of the Balmer lines; the area was measured with a planimeter. The optical resolution of the measurements is so good that we can ignore the distortion of the line shape. The relative emission cross sections are dependent on the excitation energy and the principal quantum number of the excited hydrogen atom, as are shown in Table 2.

The electron energy dependence of the relative cross sections indicates that there are two or more processes for the formation of the excited hydrogen atom and that their relative contribution is dependent on the electron energy, since the value of a single dissociation process is expected to be independent of the excitation energy.[10]

Dissociation through a repulsive potential curve has a smaller isotope effect than that through a bound potential curve, since the former is expected to be faster than the latter and, as a result, affects a smaller competition with preionization. The difference of the Franck-Condon region may be important for the dissociation through a bound curve.[14] The decrease of the observed isotope effect (approach of the value of σ_D/σ_H to 1.0) indicates that dissociation through a repulsive curve becomes more important at higher electron energies.

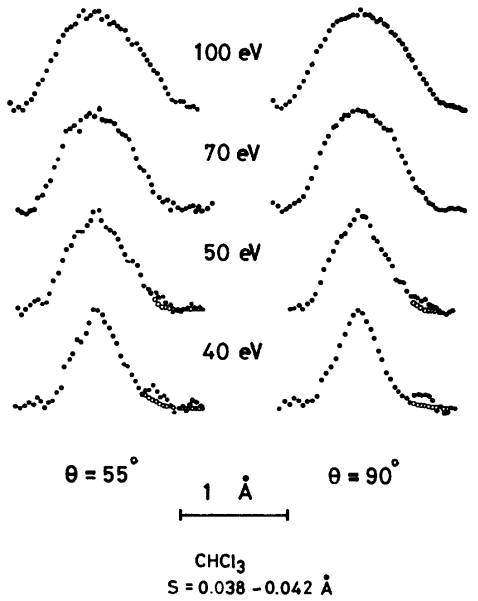

Fig. 5. Very high resolution spectra of the Balmer-β lines of H* obtained by a Fabry-Perot interferometer at a optical resolution of 0.038—0.042 Å.
Solid dots: experimental data, open circles: corrected for background radiation. Electron-beam current 800 μA.

Translational Energy Distribution. Translational energy distribution of the fragment atom has much to do with the shape of the potential curve for the formation of this fragment atom. Dissociation through a repulsive curve results in fragments with high velocity, and that through a bound curve with low velocity.

The high resolution spectra of H* from $CHCl_3$ taken with a Fabry-Perot interferometer are shown in Fig. 5. The lines are distorted by some background lines, possibly, of Cl or Cl^+. This distortion was manually corrected as shown in the Figure.

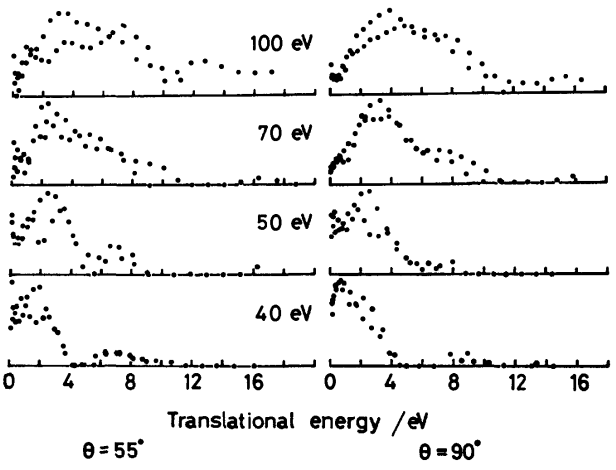

Fig. 6. The translational energy distribution of H* produced in electron-$CHCl_3$ collisions. Distributions were taken at 55° and 90° and they agree within experimental uncertainty.

The line shapes taken at 90° and 55° with respect to the electron-beam are in agreement with each other; thus, the effect of anisotropy is smaller than the experimental uncertainty. The differentiation of the line shape gives the translational energy distribution.[1,2] The results are shown in Fig. 6 for H* from $CHCl_3$ and in Fig. 7 for D* from $CDCl_3$.

The translational energy distribution excited by 100 eV electrons has a peak at about 4 eV. Upon decreasing the electron energy, the distribution shifts toward the lower energy and it has another peak at 0—1 eV when

TABLE 3. THE CORRECTED HALF-WIDTH ($\delta\lambda_t$) (Å) OF THE BALMER LINES OF THE EXCITED HYDROGEN AND DEUTERIUM ATOMS IN ELECTRON-CHLOROFORM COLLISIONS

Electron energy/eV	Balmer-α $n=3$	Balmer-β $n=4$	Balmer-γ $n=5$	Balmer-δ $n=6$
$CHCl_3$				
300	1.17±0.08	0.88±0.05	0.76±0.05	0.71±0.08
100	1.19±0.06	0.89±0.05	0.77±0.06	0.77±0.07
70	0.96±0.07	0.78±0.05	0.67±0.06	0.68±0.07
50	0.84±0.07	0.62±0.05	0.58±0.06	0.59±0.07
40	—	0.44±0.07	0.43±0.07	0.42±0.07
30	0.59±0.08	0.47±0.09	0.39±0.08	0.38±0.08
$CDCl_3$				
300	0.87±0.07	0.64±0.04	0.56±0.06	0.56±0.06
100	0.85±0.06	0.64±0.04	0.53±0.06	0.60±0.06
70	0.82±0.06	0.54±0.04	0.44±0.07	0.48±0.07
50	0.64±0.07	0.42±0.04	0.32±0.07	0.46±0.08
40	—	0.30±0.07	0.28±0.08	0.29±0.09
30	0.50±0.09	0.34±0.09	—	0.35±0.10

The optical resolution (s) is 0.04—0.20 Å.

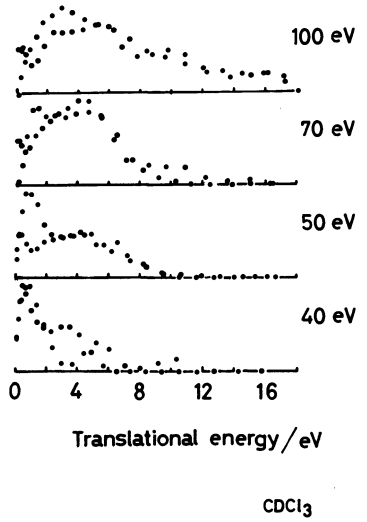

Fig. 7. The translational energy distribution of D* produced in electron-$CDCl_3$ collisions. The data were taken at 90°.

excited at 40 eV electrons. The distributions of H* and D* are, on the whole, similar; accordingly, the dissociation processes are qualitatively equal for two molecules. Furthermore, it is noteworthy that the distributions are similar to those of methane;[5] this finding suggests that dissociation processes of hydrogen from chloroform and from methane are similar. Molecules of similar structure and similar chemical bond may dissociate similarly.

Average Translational Energy. The translational energy distribution gives detailed and precise information of the kinetic character of the fragment produced in the collision processes. However, requirement of very high resolution makes it very difficult to apply the method for a weak line. Balmer-α, γ, and δ lines from chloroform are such cases. Thus, instead of the translational energy distribution, an average translational energy has been obtained through the measurement of the half-width of the Balmer lines by use of a grating monochromator.

There are two methods to take the average of the translational energy; one assumes a Maxwell distribution[15,16] and the other a δ-function distribution.[17,18] The value of the average depends substantially on the method used.[19]

$$E\,(\text{Av. }\delta\text{-function}) = 0.462\,E\,(\text{Av. Maxwell})$$

We have calculated the average translational energy with both methods and found that the average obtained by assuming a δ-function distribution agrees more with the peak of the translational energy distribution shown in Figs. 6 and 7 than the average obtained by another method does.

The observed half-widths are shown in Table 3 and the average translational energies obtained by assuming a δ-function distribution in Table 4. The results indicate that there seems no isotope effect in the average translational energy just as in the case of the distribution. This is superficially evident since the potential energy diagram should be identical for isotopic molecule; a

TABLE 4. AVERAGE TRANSLATIONAL ENERGIES (eV) OF THE EXCITED HYDROGEN AND DEUTERIUM ATOMS PRODUCED IN ELECTRON-CHLOROFORM COLLISIONS

Electron energy/eV	Balmer-α $n=3$	Balmer-β $n=4$	Balmer-γ $n=5$	Balmer-δ $n=6$
$CHCl_3$				
300	3.7±0.5	3.8±0.5	3.6±0.5	3.5±0.7
100	3.8±0.4	3.9±0.5	3.7±0.6	4.1±0.7
70	2.5±0.4	3.0±0.4	2.8±0.5	3.2±0.7
50	1.9±0.3	1.9±0.3	2.1±0.5	2.4±0.6
40	—	1.0±0.3	1.2±0.4	1.2±0.4
30	0.9±0.3	1.1±0.4	1.0±0.4	1.0±0.4
$CDCl_3$				
300	4.1±0.7	4.0±0.5	3.9±0.8	4.4±0.9
100	3.9±0.6	4.0±0.5	3.5±0.8	4.9±1.0
70	3.6±0.5	2.9±0.4	2.4±0.8	3.2±0.9
50	2.2±0.5	1.7±0.3	1.3±0.6	2.9±0.9
40	—	0.9±0.4	1.0±0.5	1.2±0.7
30	1.4±0.5	1.1±0.6	—	1.7±0.9

difference, however, has been found for hydrogen molecules.[4]

Dissociation Process. The translational energy distributions and the average translational energies of the excited hydrogen atoms produced in electron-chloroform collisions show that there are more than one major dissociation processes just as in the case of methane. Methane has the fourth component, which is very fast.[5] The translational energy distribution of chloroform (Figs. 6 and 7) may have a corresponding component at 6—12 eV region. Thus, there are at least three major components of the excited hydrogen atom from chloroform with peaks of the distribution at 0—1, 4, and 6—12 eV, respectively.

The $2a_1$ molecular orbital of chloroform, which is C–H bonding, is located at 19.8—20.8 eV vertically above the ground state.[7,8] The corresponding molecular orbital of methane lies at 22.4 eV and is concluded to play an important role for the formation of the component with the peak of the translational energy distribution at about 3 eV and with the threshold at 21.6 eV.[5] Since the first threshold of H* from chloroform is 20.5 eV, we can conclude that one of the components of H* from chloroform is produced through excitation to Rydberg states converging to the $(2a_1)^1$ ionic state, just as in the case of methane. This component has the average translational energy of about 1 eV (Table 4); this component may be different from the one which has the peak at 0—1 eV at the excitation of 40 eV.

Higher doubly excited states have been found to be important for molecular dissociation and formation of the excited hydrogen atom.[3-5] There seems to be few reports on such excited states of chloroform and neither their location nor their electronic configuration are clear. However, similarity of the translational energy distribution with that of methane suggests that similar doubly excited states with those of methane play important roles in the formation of other components of H*(D*) from $CHCl_3$ ($CDCl_3$). One of the components with the peak of translational energy distribution at 4 eV may correspond to the excited hydrogen atom with the threshold at 41.0 eV.

Concluding Remarks. The translational energy distribution of the fragment atom gives useful information of the highly excited states and their dissociation. The detailed understanding, however, becomes possible by combining various information on highly excited states, which is in serious lack for chloroform.

The authors thank professor Nobuhiko Ishibashi for encouragement. The present study was partially supported by a Grant-in-Aid for Special Project Research from the Ministry of Education, Science and Culture.

References

1) T. Ogawa and M. Higo, *Chem. Phys. Lett.*, **65**, 610 (1979).
2) M. Higo and T. Ogawa, *Chem. Phys.*, **44**, 279 (1979).
3) T. Ogawa and M. Higo, *Chem. Phys.*, **52**, 55 (1980).
4) M. Higo and T. Ogawa, *Chem. Phys.*, **56**, 15 (1981).
5) T. Ogawa, J. Kurawaki, and M. Higo, *Chem. Phys.*, **61**, 181 (1981).
6) M. Toyoda, T. Ogawa, and N. Ishibashi, *Bull. Chem. Soc. Jpn.*, **49**, 384 (1976).
7) A. W. Potts, H. J. Lempka, D. G. Street, and W. C. Price, *Phil. Trans. Roy. Soc.*, **A268**, 59 (1970).
8) T. Ohta and H. Kuroda, *Bull. Chem. Soc. Jpn.*, **49**, 2939 (1976).
9) K. Kimura, S. Katsumata, T. Yamazaki, and S. Iwata, "Handbook of HeI Photoelectron Spectra of Fundamental Organic Mölecules," Jpn. Sci. Soc. Press, Tokyo (1981), p. 91.
10) M. Higo and T. Ogawa, *Chem. Phys. Lett.*, **75**, 271 (1980).
11) G. R. Möhlmann, F. J. de Heer, and J. Los, *Chem. Phys.*, **25**, 103 (1977); C. Karolis and E. Harting, *J. Phys. B*, **11**, 357 (1978).
12) T. Ogawa, M. Higo, M. Toyoda, and N. Ishibashi, *Chem. Lett.*, **1978**, 493.
13) R. L. Platzman, *Vortex*, **23**, 372 (1962).
14) M. Higo, S. Kamata, and T. Ogawa, unpublished.
15) T. Ogawa, F. Masumoto, and N. Ishibashi, *Chem. Lett.*, **1976**, 207.
16) I. Tokue, I. Nishiyama, and K. Kuchitsu, *Chem. Phys. Lett.*, **35**, 69 (1975).
17) K. Ito, N. Oda, Y. Hatano, and T. Tsuboi, *Chem. Phys.*, **17**, 35 (1976); **21**, 203 (1977).
18) R. S. Freund, J. A. Schiavone, and D. F. Brader, *J. Chem. Phys.*, **64**, 1122 (1976).
19) I. Nishiyama, T. Kondow, and K. Kuchitsu, *Chem. Phys. Lett.*, **68**, 333 (1979).

Nanosecond Laser Flash Photolysis of 1-Anilinonaphthalene

Hiroki NAKAMURA,* Jiro TANAKA, Nobuaki NAKASHIMA, and Keitaro YOSHIHARA
Department of Chemistry, Faculty of Science, Nagoya University, Chikusa-ku, Nagoya 464
†*Institute for Molecular Science, Okazaki 444*

(Received December 2, 1981)

The photoionization mechanism of 1-anilinonaphthalene (1-AN) was investigated by a nanosecond laser flash photolysis and the result was compared with that of 8-anilino-1-naphthalenesulfonate (ANS). The photoionization of 1-AN in polar solvent is shown to occur through a biphotonic process *via* a triplet state; the mechanism is different from those of ANS, in which an intermediate of a charge transfer to solvent (CTTS) state was observed. Thus the major deactivation process of the lowest excited singlet state is an intersystem crossing in 1-AN, while it is a transition to the CTTS state in ANS which might be stabilized by the sulfonato group.

The fluorescence spectra, quantum yields, and lifetimes of naphthylamine derivatives, especially 8-anilino-1-naphthalenesulfonate (ANS) and 6-(*p*-toluidino)-2-naphthalenesulfonate (TNS) are extremely sensitive to their environment.[1-6] For example, ANS shows a dramatic decrease in fluorescence lifetime by increasing the solvent polarity (ethanol (12.5 ns) and water (0.2 ns)).[6] These properties have been used as probes for structural studies of biological molecules for many years.[1,3,7] Fleming *et al.*[8] proposed that the major deactivation process of the excited singlet state of ANS and 1-anilinonaphthalene (1-AN) in polar solvents may be a monophotonic ionization from their excited singlet state with a result of nanosecond laser flash photolysis. We reported that the photoionization of ANS is a biphotonic process *via* a charge transfer to solvent (CTTS) state.[9] It has been recognized that 1-AN, which has no sulfonato group, shows the red shift of fluorescence spectrum accompanying with the increase of the solvent polarity;[10] the behavior is analogous to ANS and TNS. However, 1-AN does not show a drastic decrease of fluorescence lifetime by increasing the solvent polarity.[11] It is conceivable that the sulfonato group of anilinonaphthalenesulfonate plays an important role in the deactivation process of the lowest excited singlet state in polar solvents. We studied the mechanism of photoionization of 1-AN, which has no sulfonato group, by comparing it with that of ANS.

Experimental

1-AN obtained from Nakarai Chemical Ltd. was used after twice recrystallizations from ethanol. *trans*-Stilbene and potassium iodide were used as received from Nakarai Chemical Ltd. Spectroscopic grade water, methanol, ethanol, and cyclohexane were used as solvents. The degassed samples were sealed after repeated freeze-pump-thaw degassing cycles. Fluorescence spectra were measured on a Hitachi MPF-2A spectrofluorometer located at Chemical Instrument Center of Nagoya University. Details of the laser flash photolysis and the fluorescence lifetime measurement were described previously.[6,9] The exciting source for the laser flash photolysis was a XeF excimer laser (Lambda Physik EMG-500) with an emission line at 351 nm and a pulse width of 12 ns.

Results and Discussion

Fleming *et al.*[8] found a transient absorption spectrum of 1-AN in methanol–water (1 : 1) mixed solvent which is similar to that of ANS in an aqueous solution. They proposed that the major deactivation process of 1-AN in polar solvent is a photoionization because of a similarity of transient spectrum. We also measured the transient absorption spectrum of 1-AN in a degassed methanol–water (1 : 1) mixed solvent. The spectrum which we obtained is somewhat different from that reported by Fleming *et al.* in the longer wavelength region than 580 nm as shown in Fig. 1 (curve A). Both the 420 and 800 nm bands are similar to the absorption of ANS radical which has peaks at 450 and 800 nm, respectively. These bands are assigned to the absorption of 1-AN cation radical. Furthermore we observed a transient absorption of 1-AN having a decay time identical with the fluorescence lifetime in the wavelength region above 700 nm, and these absorptions are assigned to the $S_n \leftarrow S_1$ absorption of 1-AN (Fig. 1 (curve B)).

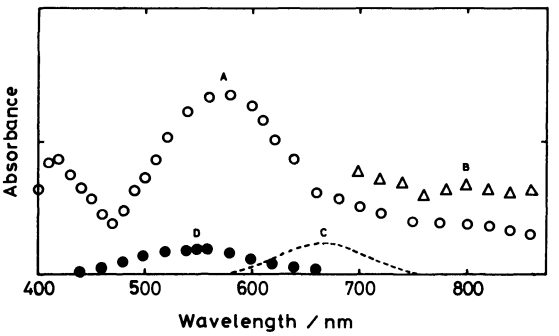

Fig. 1. Transient absorption spectra of 1-AN.
A: 70 ns after the laser pulse in a degassed methanol–water (1 : 1) mixed solvent, B: the $S_n \leftarrow S_1$ absorption, C: the absorption spectrum of solvated electron, D: the $T_n \leftarrow T_1$ absorption in cyclohexane.

The strongest absorption band with the maximum at 580 nm is not assigned to that of solvated electron because the peaks of solvated electron in water and methanol appear at 720 and 640 nm,[12,13] respectively. Moreover, we measured the transient spectrum in solution containing an electron scavenger (N_2O), which will diminish the absorption of solvated electron. The differential transient spectrum between the solution in a degassed and N_2O saturated methanol–water (1 : 1) mixed solvent gives the absorption spectrum of solvated electron with a maximum at about 670 nm as shown in Fig. 1 (curve C). Since the peak of solvated electron

is found at normal wavelength region, the absorption band at 580 nm is regarded as the $T_n \leftarrow T_1$ absorption. Furthermore the following reasons are available to support the $T_n \leftarrow T_1$ assignment.

(1) The absorption maximum lies in the position of the $T_n \leftarrow T_1$ absorption observed in cyclohexane (Fig. 1 (curve D)). The latter spectrum agreed with that reported by Fleming *et al.*[8]

(2) The dependence of the absorbance at 580 nm on the light intensity shows a linear relationship. It shows that the absorption at 580 nm is produced by a monophotonic process.

(3) The transient absorption at 580 nm is extensively quenched by adding a triplet quencher such as oxygen and *trans*-stilbene into solution. The quenching by *trans*-stilbene was investigated with varying concentration in methanol–water (4 : 1) mixed solvent. Figure 2 shows the Stern-Volmer relationship of the decay time of the absorption at 580 nm. The quenching rate obtained from the slope of this plot is 4.5×10^9 ($mol^{-1}\ s^{-1}$). The relation shows that the quenching is a diffusion-controlled process.

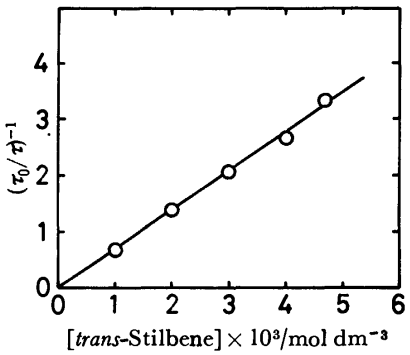

Fig. 2. Stern-Volmer plot of the decay time of the $T_n \leftarrow T_1$ absorption at 580 nm against the concentration of *trans*-stilbene in a methanol–water (4 : 1) mixed solvent.

In order to find whether the photoionization process occurs through the monophotonic or biphotonic one, we measured the dependence of the yield on the light intensity. The photoionization yield was monitored by the absorbance of 1-AN cation radical at 420 nm and the absorbance was plotted against the square of the light intensity in Fig. 3. The plot shows a linear relation, indicating that the photoionization is a biphotonic process.

Three species are conceivable as the intermediate of the biphotonic ionization; (1) the CTTS state, (2) the lowest excited singlet state, and (3) the triplet state. The CTTS state seems to be not involved because no evidence is obtained about the transient spectrum with a short lifetime. In order to find which of the singlet or the triplet excited state is the intermediate, we measured the change of the photoionization yield by adding different kind of quenchers.

The fluorescence of 1-AN was quenched by potassium iodide and we obtained the value of the quenching rate k_q from the Stern-Volmer plot ($k_q = 2.6 \times 10^8$ $mol^{-1}\ s^{-1}$). We also observed that both absorbances of the $T_n \leftarrow T_1$

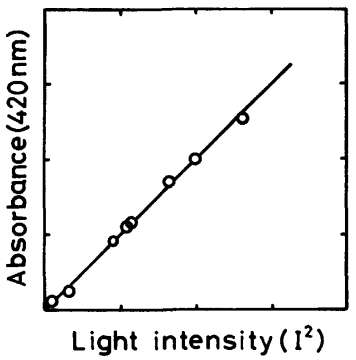

Fig. 3. Dependence of the absorbance at 420 nm on the square of the exciting light intensity in a degassed methanol–water (1 : 1) mixed solvent.

absorption and 1-AN cation radical are intensified with a linear relation by increasing the concentration of potassium iodide. This shows that potassium iodide enhances the intersystem crossing from the excited singlet state to the triplet state and the yield of the biphotonic ionization is increased. Therefore the photoionization process *via* the lowest triplet state is more probable.

Then, the change of the yield with the triplet quencher is investigated. The absorbance of 1-AN cation radical at 420 nm and the $T_n \leftarrow T_1$ absorption at 580 nm are decreased accompanying with the increase of the concentration of *trans*-stilbene. *trans*-Stilbene is a triplet quencher, therefore the photoionization is considered to take place through the triplet state. Following this result, the photoionization of 1-AN is given by the following scheme.

$$\text{1-AN}^* \xrightarrow{k_{isc}} \text{1-AN}^T \xrightarrow{h\nu} \text{1-AN}^+ + e^-_{sol}$$

$$\text{1-AN} \quad \overset{h\nu}{\underset{F}{\rightleftarrows}} \quad \text{1-AN}^* \xrightarrow{k_{isc}} \text{1-AN}^T$$

To distinguish the reaction mechanism of ANS and 1-AN in the excited singlet state, the fluorescence properties are measured and compared. Table 1 shows the fluorescence maxima and the fluorescence lifetimes of ANS and 1-AN in several solvent. The fluorescence maximum of 1-AN is shifted to the longer wavelength by increasing the solvent polarity as well as ANS. DeToma and Brand[14] reported the shift of the fluorescence maximum of 2-anilinonaphthalene in cyclo-

Table 1. Uncorrected fluorescence maxima and lifetimes in several solvent at 25°C

Solvent	ANS		1-AN			
	λ_{max} nm	τ_f ns	λ_{max} nm	τ_f ns	τ_f[a] ns	τ_f[b] ns
Water	514	0.20	461	2.6		5.0
Methanol–Water (1 : 1)			450	5.4		
Methanol	473	8.5	419	7.4	5.3	
Ethanol	466	12.5	412	7.6	5.6	5.75
Cyclohexane			374	5.8	4.1	4.1

a) For non-degassed samples. b) Ref. 11.

hexane–ethanol (<0.2 mol dm^{-3}) mixed solvent and we also observed the red shift of the fluorescence spectrum of 1-AN in mixed solvent of the same composition. It appears that the red shift is due to the solvent relaxation through the dipole-dipole interaction between the excited molecule and the polar solvent molecules during the lifetime of the excited singlet state, because the dipole moment of the first excited singlet state is greater than that of the ground state.[2,15]

We reported that the major deactivation process of ANS in polar solvent is the transition from the excited singlet state to the CTTS state and the $T_n \leftarrow T_1$ absorption is not detected.[9] The fluorescence lifetime of ANS is dramatically decreased by increasing the solvent polarity because the CTTS state is formed and the transition to it is enhanced in polar solvents. On the other hand the major deactivation process of the excited singlet state of 1-AN is shown to be the intersystem crossing to the triplet state, and it is less dependent on the polarity of the solvent. Hence the fluorescence lifetime of 1-AN is not shrunk significantly in polar solvent.

The biphotonic ionization occurs through the CTTS state in ANS, while it takes place *via* the triplet state in 1-AN. The difference of the photoionization mechanism between ANS and 1-AN is distinct. The presence of the sulfonato group in ANS may be connected with the formation of the CTTS state. Sadkowski and Fleming[11] suggested that the SO_3^- group of ANS forms a solvent trap through the hydrogen bond with the solvent molecules and the photoionization process from the excited ANS molecule could be interpreted by an electron transfer to the solvent trap. However we proposed the electron is transfered to the CTTS state rather than to bulk solvents before the photoionization and the SO_3^- group may stabilize the CTTS state by forming a zwitter-ion like structure. The zwitter-ion like structure is supported from the similarity of the transient absorption spectra between ANS radical and 1-AN cation radical. A similar phenomenon was reported in pyrene and pyrenesulfonic acid by Grätzel *et al.*[16]

References

1) L. Stryer, *J. Mol. Biol.*, **13**, 482 (1965).
2) D. C. Turner and L. Brand, *Biochemistry*, **7**, 3381 (1968).
3) J. Yguerabide, *Meth. Enzymol.*, **26**, 498 (1972).
4) E. M. Kosower, H. Dudiuk, K. Tanizawa, M. Ottolenghi, and N. Orbach, *J. Am. Chem. Soc.*, **97**, 2167 (1975).
5) G. W. Robinson, R. J. Robbins, G. R. Fleming, J. M. Morris, A. E. W. Knight, and R. J. S. Morrison, *J. Am. Chem. Soc.*, **100**, 7145 (1978).
6) H. Nakamura and J. Tanaka, *Chem. Phys. Lett.*, **78**, 57 (1981).
7) L. Brand and J. R. Gohlke, *Ann. Rev. Biochem.*, **41**, 843 (1972).
8) G. R. Fleming, G. Porter, R. J. Robbins, and J. A. Synowiec, *Chem. Phys. Lett.*, **52**, 228 (1977).
9) H. Nakamura, J. Tanaka, N. Nakashima, and K. Yoshihara, *Chem. Phys. Lett.*, **77**, 419 (1981).
10) A. Kawski and C. Strzalkowska, *Z. Naturforsch., Teil A*, **27**, 916 (1972).
11) P. J. Sadkowski and G. R. Fleming, *Chem. Phys.*, **54**, 79 (1980).
12) L. M. Dorfman, F. Y. Jou, and R. Wageman, *Ber. Bunsenges. Phys. Chem.*, **75**, 681 (1971).
13) R. R. Hentz and G. Kenney-Wallace, *J. Phys. Chem.*, **76**, 2931 (1972).
14) R. P. DeToma and L. Brand, *Chem. Phys. Lett.*, **47**, 231 (1977).
15) A. Kawski, B. Bortoszewicz, and C. Stralkowska, *Z. Chem.*, **12**, 275 (1972).
16) M. Grätzel, K. Kalyanasundaram, and J. K. Thomas, *J. Am. Chem. Soc.*, **96**, 7869 (1974).

A Co-59 Nuclear Magnetic Resonance Study of the Interaction of Lanthanoid Shift Reagents with Tris(β-diketonato)-cobalt(III) Complexes

Masatoshi HIRAYAMA,* Yoshimichi KAWAMATA, Yuki FUJII, and Yoshiharu NAKANO
Department of Chemistry, Faculty of Science, Ibaraki University 2-1-1 Bunkyo, Mito 310
(Received November 19, 1981)

$Ln(fod)_3$ (Ln=La, Pr, Nd, Sm, and Eu)-induced ^{59}Co shifts (δ_{Co}) for a series of tris(β-diketonato)Co(III) complexes were determined directly from separate observations of the free complexes and 1 : 1 adducts with $Ln(fod)_3$ at room temperature (25 °C) in $CHCl_3$; $Ln(dpm)_3$-induced shifts were also observed in CCl_4. Values of δ_{Co} corrected for the adduct-formation shifts (δ'_{Co}) are separated into contact and pseudo-contact contributions by using the intercept and slope in a linear plot of $\delta'_{Co}/\langle S_z\rangle$ *vs.* $D/\langle S_z\rangle$. It is suggested from the estimated hfs constant of ^{59}Co (≈ -0.2 G, 10^{-4} T) that the spin polarization mechanism may be predominant for the electron spin transfer from Ln ion into Co ion.

The lanthanoid shift reagents (LSR) have been extensively used for structural studies of organic substrates, but on their application to inorganic coordination complexes only a few investigations have so far been reported.[1-4] It has been found from ^1H or ^{13}C NMR studies by Lindoy *et al.*[2-4] that Ni(II) complexes of O_2N_2-donor quadridentate ligands coordinate to $Eu(fod)_3$[5] *via* two bridging donor oxygens and rapidly exchange between their free forms and 1 : 1 adducts with $Eu(fod)_3$ in $CDCl_3$ solution at room temperature,[2] while tris(β-diketonato)Co(III) complexes are bound to $Eu(fod)_3$ *via* three bridging oxygens and their exchange rates are very slow.[3,4]

These investigations prompted us to examine whether or not lanthanoid-induced shifts (LIS) can be detected at the nucleus of central metal ion of such complexes. This paper reports on LIS's of ^{59}Co measured for adducts of a series of tris(β-diketonato)Co(III) complexes with $Ln(fod)_3$ and $Ln(dpm)_3$.[5] Some of the results have been reported in a preliminary paper.[6]

Experimental

$Co(acac)_3$[5] was obtained from Tokyo Kasei Kogyo Co., Ltd. and used without further purification. Benzoylacetone was obtained commercially and *p*-methoxybenzoylacetone synthesized from *p*-methoxyacetophenone and acetic anhydride under boron trifluoride. $Co(bzac)_3$[5] and $Co(mbzac)_3$[5] were prepared according to the published method.[7] $CHCl_3$ and CCl_4 as a solvent were dried with molecular sieves before use. Eu- and $Pr(fod)_3$ were obtained from Merck Sharp and Dohme Canada Ltd. La-, Nd-, and $Sm(fod)_3$ and $Ln(dpm)_3$ (Ln= La, Pr, Nd, Sm, and Eu) were synthesized according to the literatures.[8] All the LSR's were used after being dried over P_2O_5 in a vacuum desiccator.

^{59}Co NMR spectra were recorded on a Varian CFT-20 spectrometer, equipped with a broad band accessory, at 19.104 MHz at room temperature (25 °C) using an external deuterium field-lock system. The aquisition time was taken as 0.05 s for the spectral width of 8065 Hz, the number of data points being 807. The number of transients was 100—500.

Results and Discussion

^{59}Co NMR of the Adducts of $Co(acac)_3$ with $Ln(fod)_3$. Figure 1 shows the ^{59}Co NMR spectra observed with a 0.085 mol dm^{-3} $Co(acac)_3$ solution in $CHCl_3$ at room temperature (25 °C) at a molar ratio (ρ) of $Ln(fod)_3$ (Ln=La, Pr, Nd, Sm, and Eu) to $Co(acac)_3$ of about 0.5. These spectra can be interpreted by analogy with the ^1H spectra of the $Co(acac)_3$–$Eu(fod)_3$ system measured by Lindoy *et al.*[3,4] as follows: The lower- and higher-field resonances in each spectrum can be determined to arise from the free form of $Co(acac)_3$ and its 1 : 1 adduct with $Ln(fod)_3$, respectively, by observing the change in intensity ratios of these with changing ρ. Such a separate observation of ^{59}Co shifts indicates that the chemical exchange of $Co(acac)_3$ between its free form and its 1 : 1 adduct with $Ln(fod)_3$ under these experimental conditions is very slow on the NMR time scale. No ^{59}Co resonance lines of the adducts with the later members of lanthanoid series (Gd—Yb) could be detected owing to the long T_1 of electron spin in addition to the slow exchange rate.

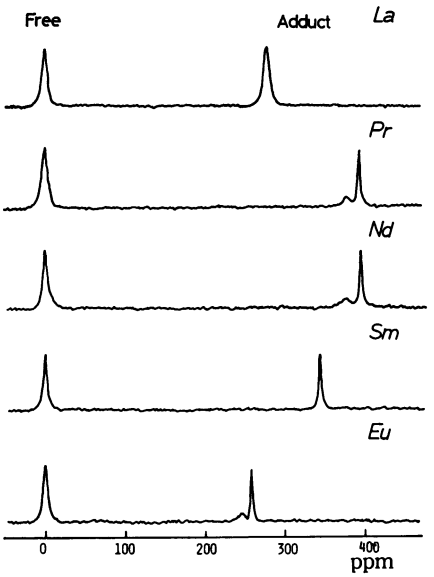

Fig. 1. The ^{59}Co NMR of free $Co(acac)_3$ and its adducts with $Ln(fod)_3$ in $CHCl_3$ at 25 °C. $\rho \approx 0.5$. High-field shifts are given as positive.

A considerable amount of large high-field shift was observed with diamagnetic $La(fod)_3$. This may not be surprising considering that the paramagnetic term of ^{59}Co shift (σ_{para}) is greatly sensitive to variation in ligand

and ligand field symmetry.[9] Thus, this high-field shift can be ascribed to a slight distortion of ligand field symmetry arising from the geometric distortion of oxygen donor atoms[3] and small changes in electron densities on these oxygens by the adduct formation. On the other hand, one may consider that this diamagnetic high-field shift corresponds to an increase in ΔE, the energy separation between the ground state and the excited $^1T_{1g}$ level of Co^{3+},[9] on going from free $Co(acac)_3$ to the adduct.

Each of the adducts with Pr-, Nd-, and $Eu(fod)_3$ gave rise to a peak of weak intensity at a slightly lower field ($\approx$20 ppm) than the main peak. The ratios of this satellite to the main peak were unchanged with changing ρ. These satellites may not be considered to arise from any impurities in $Co(acac)_3$, from the experimental result that the remaining Sm- and La-adducts studied here do not exhibit such a satellite. It has been confirmed by Lindoy *et al.* that symmetrical adducts are formed in these systems, that is, coordination of $Ln(fod)_3$ occurs *via* three β-diketone oxygen atoms at one available octahedral-face of $Co(acac)_3$ along the C_3 axis to form a 1 : 1 adduct. Thus, the possibility of coordination *via* one or two donor oxygens may be excluded and these satellites can, therefore, be presumed to be due to a small amount of geometrical isomer appearing on the adduct formation. It is generally presumed that the intramolecular rapid exchange between the *fac-* and *mer*-isomers of $Ln(fod)_3$ occurs at room temperature in $CDCl_3$ solution.[10] With the adduct formation, however, this exchange rate may be anticipated to become so slow that different effects of these isomers of $Ln(fod)_3$ on ^{59}Co shifts may separately be observed. Since the *fac*-isomer is more stable from the view of steric hindrance than the *mer*-isomer, the larger main peak may correspond to the adduct containing *fac*-$Ln(fod)_3$. The ^{59}Co shifts of these peaks relative to that of its free form (δ_{Co}) are shown in Table 1 together with its line widths ($\Delta\omega$). It is very interesting that the line widths of adducts are fairly smaller than those of free complexes for all the adducts except for the $La(fod)_3$-adduct.[11]

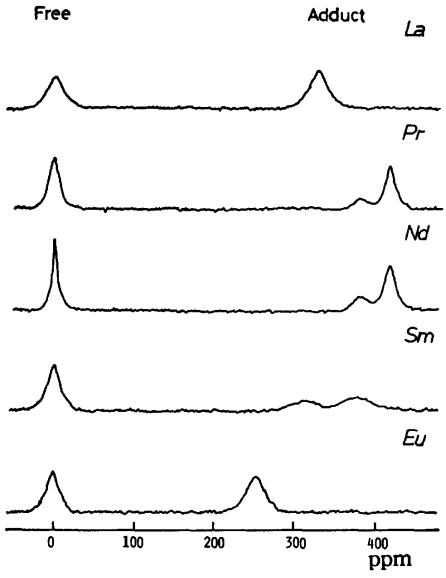

Fig. 2. The ^{59}Co NMR of free $Co(acac)_3$ and its adducts with $Ln(dpm)_3$ in CCl_4 at 25 °C. $\rho\approx0.5$. High-field shifts are given as positive.

^{59}Co NMR of the Adducts of $Co(acac)_3$ with $Ln(dpm)_3$. It was found that in $CHCl_3$ $Co(acac)_3$ is not bound to $Ln(dpm)_3$ at 25 °C, but that in CCl_4 the adducts with $Ln(dpm)_3$ are formed. This may be ascribed to the larger dielectric constant of $CHCl_3$ than that of CCl_4. The ^{59}Co spectra and LIS's of the adducts are shown in Fig. 2 and Table 1, respectively. The chemical exchange of $Co(acac)_3$ between its free form and its 1 : 1 Ln-$(dpm)_3$-adduct in CCl_4 is considerably slow, as with the $Co(acac)_3$–$Ln(fod)_3$ adduct in $CHCl_3$. In contrast to the $Ln(fod)_3$-adducts, the line widths are comparable in magnitude with those of corresponding free complexes, except for that of the $Sm(dpm)_3$-adduct which is about twice as broad as that of the free form. Furthermore, the high-field shift induced by $La(dpm)_3$ is larger by $\approx$50 ppm than that by $La(fod)_3$. This may be due to the difference in distortion of the octahedral ligand-field of Co^{3+} between these two La-adducts, which may arise from the difference in Lewis acidities and geometries of adducts.[12]

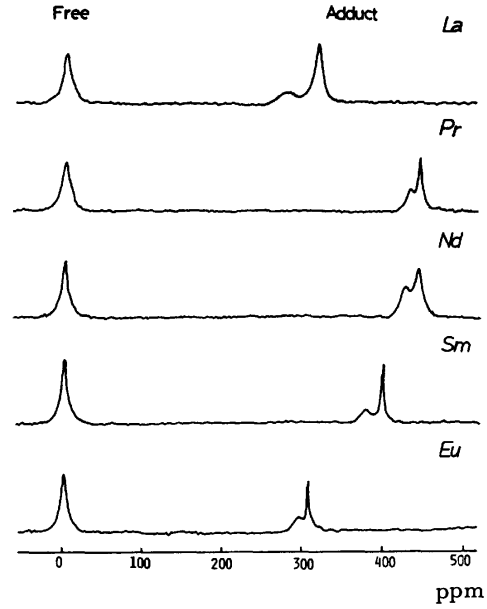

Fig. 3. The ^{59}Co NMR of free $Co(bzac)_3$ and its adducts with $Ln(fod)_3$ in $CHCl_3$ at 25 °C. $\rho\approx0.5$. High-field shifts are given as positive.

^{59}Co NMR of the Adducts of $Co(bzac)_3$ and $Co(mbzac)_3$ with $Ln(fod)_3$. Also from $Co(bzac)_3$ and $Co(mbzac)_3$ with $Ln(fod)_3$ in $CHCl_3$ at 25 °C, ^{59}Co signals assignable to the free complex and the corresponding 1 : 1 adduct with $Ln(fod)_3$ were separately observed. The spectra obtained from $Co(bzac)_3$ are shown in Fig. 3. Both of the free complexes exhibited only one line, though slightly broarder than that of $Co(acac)_3$ in $CHCl_3$, and this suggests that the shift differences between the *fac-* and *mer*-isomers of these complexes are essentially small within the line widths observed or that only the isomer of *fac*-type may exist.[13] The adduct resonances have patterns similar to those from

TABLE 1. ^{59}Co LIS OF TRIS(β-DIKETONATO)Co(III)–Ln(fod)$_3$ AND –Ln(dpm)$_3$ ADDUCTS AND ITS SEPARATION INTO CS AND PCS[a]

Complex						Calculated		
		δ_{Co}[b]	$\Delta\omega$[c]	AFS[d]	δ_{Co}[e]	pcs	cs	Total
Co(acac)$_3$	La(fod)$_3$	281	202	281	0			
	Pr(fod)$_3$	394(376)	126	305	89	62.8	27.7	90.5
	Nd(fod)$_3$	396(375)	76	317	79	24.0	41.8	65.8
	Sm(fod)$_3$	344	50	341	3	3.6	−0.6	3.0
	Eu(fod)$_3$	257(247)	50	353	−96	−22.8	−99.6	−122.4
Co(acac)$_3$	La(dpm)$_3$	332	680	332	0			
	Pr(dpm)$_3$	416(383)	450	350	66	34.2	31.9	66.1
	Nd(dpm)$_3$	417(381)	400	359	58	13.1	48.1	61.2
	Sm(dpm)$_3$	378(317)	875	376	2	2.2	−0.7	1.5
	Eu(dpm)$_3$	252	600	385	−133	−12.4	−114.6	−127.0
Co(bzac)$_3$	La(fod)$_3$	326(287)	180	326	0			
	Pr(fod)$_3$	446(435)	173	354	92	74.0	21.7	95.7
	Nd(fod)$_3$	445(430)	250	368	77	28.3	32.7	61.0
	Sm(fod)$_3$	400(378)	130	396	4	4.7	−0.5	4.2
	Eu(fod)$_3$	308(299)	90	410	−102	−26.9	−77.9	−104.8
Co(mbzac)$_3$	La(fod)$_3$	332	160	332	0			
	Pr(fod)$_3$	460(445)	220	361	99	81.0	22.5	103.5
	Nd(fod)$_3$	462(442)	160	376	86	30.9	33.9	64.8
	Sm(fod)$_3$	409(395)	80	405	4	5.2	−0.5	4.7
	Eu(fod)$_3$	318(301)	100	419	−101	−29.4	−80.0	−109.4

a) In ppm. Down-field shifts are given as negative. The accuracy of the observed shifts is ± 1 ppm for all the adducts except for that of Co(acac)$_3$ with Ln(dpm)$_3$ (± 2 ppm). b) Relative to free complex. Values in parentheses are for the small peaks (see text). c) The line widths of adduct peaks in Hz. d) $\delta_{Co}(La)+\alpha\cdot N$, where α is 12 ppm (Co(acac)$_3$ with Ln(fod)$_3$), 8.9 ppm (Co(acac)$_3$ with Ln(dpm)$_3$), 14.0 ppm (Co(bzac)$_3$ with Ln(fod)$_3$), and 14.5 ppm (Co(mbzac)$_3$ with Ln(fod)$_3$).

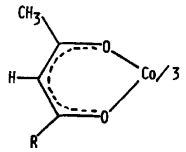

R=CH$_3$ Co(acac)$_3$
R=C$_6$H$_5$ Co(bzac)$_3$
R=*p*-CH$_3$O–C$_6$H$_5$ Co(mbzac)$_3$

Co(acac)$_3$, except for the adduct of Co(mbzac)$_3$ with La(fod)$_3$ which has only one line; that is, a satellite appears at a lower-field (15—20 ppm) than the main peak, though its intensity relative to the main peak is larger than that for Co(acac)$_3$. This two-line pattern can, therefore, be interpreted as arising from the *fac*- and *mer*-isomers of Ln(fod)$_3$-part in the adduct exchanging each other very slowly on the NMR time scale.[14] For comparison with the adduct of Co(acac)$_3$ with Ln(fod)$_3$, the larger peaks at higher-field are taken as δ_{Co}, which are listed in Table 1.

Separation of ^{59}Co LIS's into Contact (cs), Pseudo-contact (pcs), and Adduct-formation Shifts (AFS). Since it was found from an X-ray analysis of the Co(acac)$_3$–Eu(fod)$_3$ crystal[3] that this adduct has a C_3 axis, the approximation of magnetic axial symmetry can be applied to the analyses of the δ_{Co} observed above. Furthermore, the hyperfine splitting constant (A) and the geometric factor, $(3\cos^2\theta-1)r^{-3}$, (G) of ^{59}Co nucleus in the adduct are assumed to be constant along the lanthanoid series, on the basis of the reasonable expectation that the bonding nature and geometries of these adducts are almost independent of the lanthanoid metal. Thus, δ_{Co} can be expressed as

$$\delta_{Co} = A\cdot\langle S_z\rangle + G\cdot D'\cdot D + \text{AFS}, \quad (1)$$

where AFS is a diamagnetic adduct-formation shift, $\langle S_z\rangle$[15] is the projection of the total electron spin magnetization of lanthanoid ion in the direction of the external magnetic field, D'[16] is the product of the first and the third term in Bleaney's equation

$$\Delta\nu/\nu_0 = \beta^2/(60(kT)^2)\cdot(3\cos^2\theta-1)/r^3\cdot 2A_2^0\langle r^2\rangle \times g^2J(J+1)(2J-1)(2J+3)\langle J\|\alpha\|J\rangle \quad (2)$$

(a constant for a given temperature and ligand field), and D[16] is the fourth term in the above equation (a constant for a given lanthanoid). When δ_{Co} corrected for AFS is denoted as δ'_{Co},

$$\delta'_{Co} = A\cdot\langle S_z\rangle + G\cdot D'\cdot D \quad (3)$$

is obtained. By rearrangement of Eq. 3, one obtains

$$\delta'_{Co}/\langle S_z\rangle = A + G\cdot D'\cdot(D/\langle S_z\rangle). \quad (4)$$

If the assumption of constant A and G is reasonable, the $\delta'_{Co}/\langle S_z\rangle$ *vs.* $D/\langle S_z\rangle$ plot should be linear. For several systems consisting of an organic substrate and Ln(fod)$_3$, good linear relations have been obtained by several workers.[17]

An use as AFS of the La(fod)$_3$-induced shift, $\delta_{Co}(La)$, gave no linear relation in Eq. 4 for Co(acac)$_3$ with Ln(fod)$_3$. On the other hand, for the Al(acac)$_3$–Ln(fod)$_3$ system similar in structure to the present adduct,

$\delta'_{Al}/\langle S_z\rangle$ *vs.* $D/\langle S_z\rangle$ plot has given a good linearity on the use of La(fod)$_3$-induced ^{27}Al shifts as AFS.[18] This result leads us to anticipate that, in contrast to ^{27}Al shifts, ^{59}Co shifts (mainly σ_{para}) are very sensitive to even a slight change in diamagnetic electron-densities on the bridging oxygen atoms. Then, by taking δ_{Co}(La) $+a\cdot N$ as AFS where N is the number of 4f-electrons and a the contribution of a 4f-electron to AFS, a was decided so that the best linearity may be obtained. Consequently, satisfactory values for correlation coefficients were obtained by using the tabulated values for $\langle S_z\rangle$[15] and D.[16] The plot obtained is shown in Fig. 4, together with correlation coefficients (R). Also for δ_{Co} of Co(acac)$_3$ with Ln(dpm)$_3$ and Co(bzac)$_3$ and Co(mbzac)$_3$ with Ln(fod)$_3$, the same process gave good results (Figs. 4 and 5). Thus, by using the slope and intercept of the linear relation, δ'_{Co} was successfully separated into cs and pcs terms. The results are listed in Table 1.

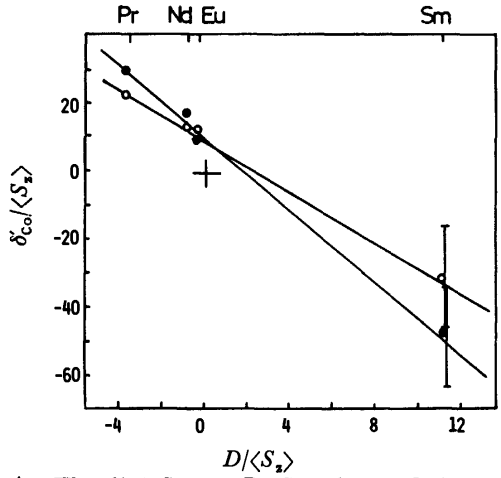

Fig. 4. The $\delta'_{Co}/\langle S_z\rangle$ *vs.* $D/\langle S_z\rangle$ plots. Co(acac)$_3$–Ln(fod)$_3$ and –Ln(dpm)$_3$ adducts are denoted by filled and open symbols, respectively.
●: R=0.980, ○: R=0.998.

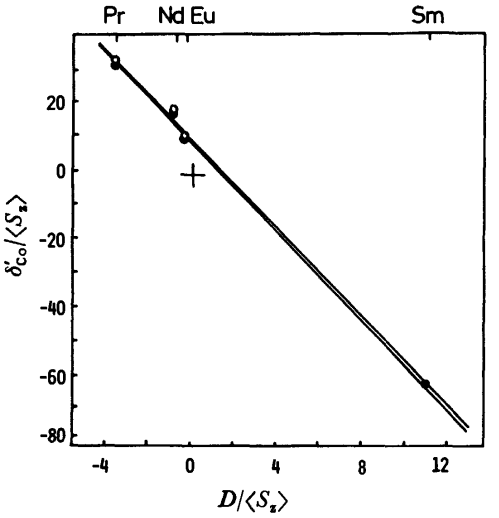

Fig. 5. The $\delta'_{Co}/\langle S_z\rangle$ *vs.* $D/\langle S_z\rangle$ plots. Co(bazc)$_3$– and Co(mbzac)$_3$–Ln(fod)$_3$ adducts are denoted by filled and open symbols, respectively.
●: R=0.987, ○: R=0.991.

Considering the use of theoretical values of $\langle S_z\rangle$ and D for the above treatment of experimental data, one cannot discuss the details of adduct geometries by comparing the slight differences between the slopes estimated for several complexes. However, it may roughly be said that the slope for the adduct of Co(acac)$_3$ with Ln(fod)$_3$ is larger than that with Ln(dpm)$_3$. The magnitude of slope estimated from Fig. 4 contains the crystal field parameter $A_2^0\langle r^2\rangle$. Since values of $A_2^0\langle r^2\rangle$ for the present systems are unknown, G cannot be estimated directly from the slope. However, if $A_2^0\langle r^2\rangle$ for Ln(fod)$_3$- and Ln(dpm)$_3$-adducts of Co(acac)$_3$ were similar in magnitude, G for the former would be larger than that for the latter. On the other hand, in the former, the coordination interaction *via* three bridging oxygens may be more pronounced because of the strong Lewis-acidity of Ln(fod)$_3$ and the Co–Ln distance can thus be expected to be shorter than the latter. The G value was calculated to be 0.0543 Å^{-3} (the distance of Co to Ln is 3.33 Å) from the X-ray crystal data,[3] on the assumption that the Co atom is located on the principal magnetic axis, as deduced on the basis of the approximation of magnetic axial-symmetry. From this value of G and the slope for the Ln(fod)$_3$-adduct given in Fig. 4, $A_2^0\langle r^2\rangle$ is calculated to be 175 cm^{-1}. This value is comparable in magnitude to those estimated for several other adducts, *e.g.*, 200—500 cm^{-1} for the γ-picoline–Ln(fod)$_3$ system in $CDCl_3$[19] and 100—150 cm^{-1} for the aniline–Ln(fod)$_3$ system in CCl_4.[20] If 175 cm^{-1} is taken also for the Co(acac)$_3$–Ln(dpm)$_3$ adduct, the Co–Ln distance for this adduct would be about 1.1 times as long as that of Ln(fod)$_3$-adduct.

A_{Co} for the Co(acac)$_3$–Ln(fod)$_3$ adduct was estimated to be about −0.2 G from Fig. 4. The amount of electron spin transferred from Ln ion into Co ion is estimated to be $\approx 2\times 10^{-4}$. The minus sign of A_{Co} and the very small amount of spin detected at the Co nucleus may imply that the spin polarization mechanism is predominant for electron spin transfer.

References

1) G. R. Tauszik, G. Pellizer, and G. Costa, *Inorg. Nucl. Chem. Lett.*, **9**, 717 (1973); S. J. Anderson and A. H. Norbury, *J. Chem. Soc., Chem. Commun.*, **1975**, 48; A. R. Hendrickson, J. M. Hope, and R. L. Martin, *J. Chem. Soc., Dalton Trans.*, **1976**, 2032.

2) L. F. Lindoy and W. E. Moody, *J. Am. Chem. Soc.*, **97**, 2275 (1975); **99**, 5863 (1977); J. K. Beattie, L. F. Lindoy, and W. E. Moody, *Inorg. Chem.*, **15**, 3170 (1975).

3) L. F. Lindoy, H. C. Lip, H. W. Louie, M. G. B. Drew, and M. J. Hudson, *J. Chem. Soc., Chem. Commun.*, **1977**, 778.

4) L. F. Lindoy and H. W. Louie, *J. Am. Chem. Soc.*, **101**, 841 (1979).

5) fod=6,6,6,7,7,8,8-heptafluoro-2,2-dimethyloctane-3,5-dionate ion; dpm=dipivaloylmethanate ion; acac=acetylacetonate ion; bzac=benzoylacetonate ion; mbzac=*p*-methoxybenzoylacetonate ion.

6) M. Hirayama and Y. Kawamata, *Chem. Lett.*, **1980**, 1295.

7) H. F. Bauer and W. C. Drinkard, *J. Am. Chem. Soc.*, **82**,

5031 (1960).

8) C. S. Springer, Jr., D. W. Meek, and R. E. Sievers, *Inorg. Chem.*, **6**, 1105 (1967); K. J. Eisentraut and R. E. Sievers, *Inorg. Syn.*, **11**, 94 (1968).

9) J. W. Emsley, J. Feeney, and L. H. Sutcliffe, "High Resolution Nuclear Magnetic Resonance Spectroscopy," Pergamon Press, New York, N. Y. (1965), p. 1080.

10) The observation of only one ^{1}H line arising from *t*-butyl protons was confirmed by a simultaneous ^{1}H NMR experiment. This is consistent with a rapid exchange between the isomers. Although it is also possible that only one of the two isomers exists, this model may be ineffective for interpretation of these satellites.

11) Two relaxation mechanisms of ^{59}Co nucleus due to quadrapole interaction and electron spins seem to be influenced each other. A discussion on this problem is in progress.

12) It may be reasonable to consider that when $CHCl_3$ or CCl_4 is used as a solvent, the difference of these solvent effects on the ^{59}Co shifts of a free complex and a corresponding adduct is similar in magnitude. Thus, for interpreting this shift difference, the solvent effect need not be taken into account.

13) Since the rate of isomerization for tris(β-diketonato)Co-(III) is generally said to be slow, it may not be considered that the observed one line corresponds to averaging *fac-* and *mer-*isomers.

14) It may not be considered that these satellites arise from the *mer*-isomer of Co-complex-part of the adduct, because of steric hindrance on the adduct formation.

15) R. M. Golding and M. P. Halton, *Aust. J. Chem.*, **25**, 2577 (1972).

16) B. Bleaney, C. M. Dobson, B. A. Levine, R. B. Martin, R. J. P. Williams, and A. V. Xavier, *J. Chem. Soc., Chem. Commun.*, **1972**, 791; B. Bleaney, *J. Magn. Reson.*, **8**, 91 (1972).

17) C. N. Reilly, B. W. Good, and R. D. Allendoerfer, *Anal. Chem.*, **48**, 1446 (1976); G. A. Elgavish and J. Reuben, *J. Am. Chem. Soc.*, **99**, 5590 (1977); J. Reuben and G. A. Elgavish, *J. Magn. Reson.*, **39**, 421 (1980); A. D. Sherry, P. P. Yang, and L. O. Morgan, *J. Am. Chem. Soc.*, **102**, 5755 (1980).

18) M. Hirayama and K. Kitami, *J. Chem. Soc., Chem. Commun.*, **1980**, 1030.

19) K. Ajisaka and M. Kainosho, *J. Am. Chem. Soc.*, **97**, 330 (1975).

20) M. Hirayama, M. Sato, M. Takeuchi, and M. Saito, *Bull. Chem. Soc., Jpn.* **48**, 2690 (1975).

A Proton Magnetic Resonance Study of Dialkyl Terephthalate Dianions

Masatoshi HIRAYAMA* and Mitsuo KANEKO
Department of Chemistry, Faculty of Science, Ibaraki University, 2-1-1 Bunkyo, Mito 310
(Received December 14, 1981)

NMR spectra were observed for green solutions formed from dimethyl, diethyl, and diisopropyl terephthalates in contact with sodium metal in THF-d_8 *in vacuo* at ambient probe temperature. A comparison of proton chemical shifts with excess charge densities calculated by the CNDO MO method supports that the green species are disodium salts of π-dianions.

It has been demonstrated by observation of NMR spectra that several unsubstituted aromatic compounds are reduced into their dianions by alkali metal *in vacuo* in aprotic solvent.[1] However, for aromatic compounds containing N- or O-hetero atom and electron-withdrawing substituents, the formation of their dianions has not so far been ascertained, probably because of their instability in solution.

Dimethyl terephthalate (DMTP), when brought into contact with Na metal in THF *in vacuo*, is at first converted into its purple-red anion radical[2] and then into a diamagnetic green species (G-species) within several minutes even if kept separated from Na metal; this species is stable for several months at room temperature even with a high concentration of starting substance of *ca.* 0.5 mol dm^{-3}. Kowata and Koizumi[3] interpreted this phenomenon in terms of UV investigation as follows: The G-species is the disodium salt $Na^+DMTP^{2-}Na^+$ of DMTP dianion formed from the sodium salt $DMTP^-Na^+$ of DMTP anion radical by the disproportionation

$$2(DMTP^-\,Na^+) \rightleftharpoons Na^+\,DMTP^{2-}\,Na^+ + DMTP.$$

Their interpretation was supported by an experimental result that the G-species has a powerful agency capable of reducing aromatic compounds such as trinitrobenzene stronger in electron affinity than DMTP. We now report ^{1}H NMR spectra successfully observed for this system.

Experimental

DMTP and diethyl terephthalate (DETP) obtained from Tokyo Kasei Kogyo Co. were used after recrystallization from benzene, and diisopropyl tetrephthalate (DPTP) was synthesized from DMTP by the exchange reaction of ester groups. THF-d_8 (Merck Sharp and Dohm Canada Ltd.) was purified by vacuum distillation after contact with Na–K alloy *in vacuo*.

^{1}H NMR spectra were measured on a Hitachi R-20A spectrometer at ambient probe temperature (34 °C) at 60 MHz in a frequency-swept mode. MO calculations were performed on HITAC-8250 at the Computer Center of Ibaraki University and on Hitachi M-200H at the Computer Center of the University of Tokyo. The program used for CNDO MO calculations is Y4CB04[4] from the library programs collected in the Computer Center of the University of Tokyo.

Results and Discussion

A 0.3 mol dm^{-3} THF-d_8 solution of DMTP was kept in contact with Na metal for 10 min *in vacuo* at room temperature and 24 h after separation from the Na metal an NMR spectrum was measured for the resulting green solution, which is shown in Fig. 1a. New resonance lines A′ and B′ appeared at higher-fields of corresponding ring (A) and methyl proton peaks (B) of unreduced DMTP, respectively, and furthermore, the intensity ratio A′/B′ was nearly equal to A/B, hence A′/A≈B′/B. On introducing air into the sample tube, the solution was caused to turn light yellow with formation of a white precipitate and the lines A and B disappeared. When methyl *p*-nitrobenzoate was introduced into the sample tube containing the G-species *in vacuo*, the formation of sodium salt of the anion radical of this ester was confirmed by observation of ESR. Also in the spectra obtained from DETP and DPTP in contact with Na in THF-d_8, the expected higher-field lines corresponding to the neutral molecule were observed and the intensity ratios A′/A, B′/B, and C′/C for ring,

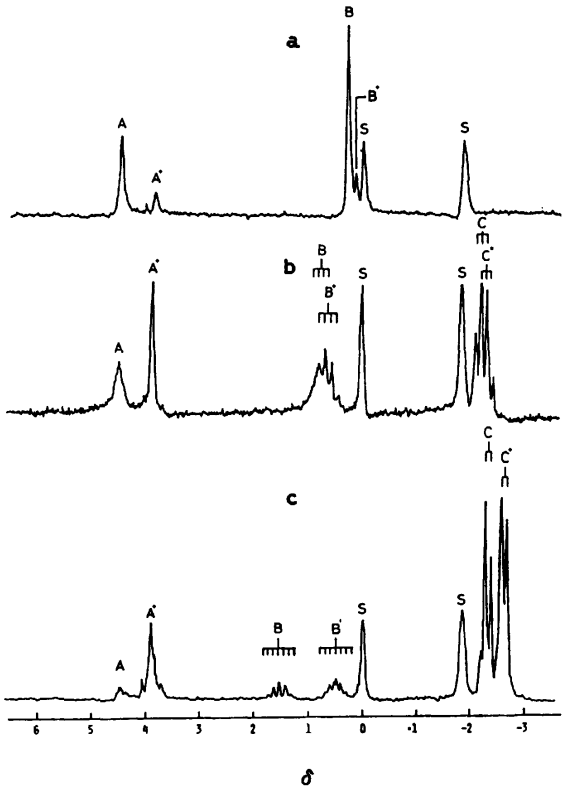

Fig. 1. NMR spectra of the dianion disodium salts of dialkyl terephthalates accompanied by the unreduced neutral molecule in THF-d_8 at 60 MHz and 34 °C. (a) DMTP, (b) DETP, (c) DPTP. The shifts are measured from the lower-shielding peak of THF. A: Ring-H, B: α-H, C: β-H, S: the solvent as an isotopic impurity. The prime letters indicate the dianion peaks.

α-, and β-protons, respectively,[5] were nearly equal to one another for both the systems, except that the intensity of A for DPTP is too small (Figs. 1b and 1c).

With all the samples, for several minutes after separation from Na metal an extensive line broadening was observed only for the peak A and then the line width became gradually sharper, while for the other protons line broadening was negligible due to smaller hfs constants than those of ring protons. These results may suggest that electron spin rapidly exchanges between the neutral molecule and the anion radical sodium salt still remaining owing to slow disproportionation. On the other hand, the line A′ remained sharp under the same conditions and this may then be considered to be ascribed to a very slow exchange of electron spin between the anion radical sodium salt and the G-species in solution.

These features of NMR spectra together with the interpretation of this reaction system based on UV spectra[3] indicate that all the lines denoted by prime letter in Fig. 1 result from dianion disodium salts. This is supported also by the fact that the lines B′ and C′ assume the same coupling patterns as those of B and C, respectively. The magnitude of $J_{\alpha\beta}$ is unchanged on going from the neutral to dianion molecule.

It has previously been decided from an ESR investigation[2] that the ester groups in the terephthalate anion radicals are fixed on the benzene plane, and this situation should also be applied to the dianion molecules. Actually, the line A′ is composed of several lines, though not completely resolved, as seen from Fig. 1 and this should be a superposition of two slightly different AA′BB′ patterns arising from *cis* and *trans* rotational isomers (Fig. 2). The center of these superposed lines is taken as the average shift of the ring protons of dianion. The shift values measured from the lower-shielding methylene peak of THF as an isotopic impurity are listed in Table 1.

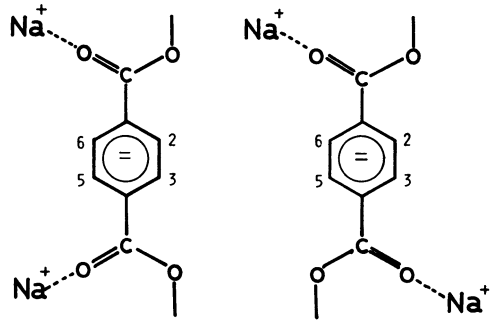

Fig. 2. The proposed structures of disodium salts of dianions of dialkyl terephthalates.

Table 1. The observed ^1H shifts of dianions

Compound		Ring-H	α-H	β-H
DMTP	Neutral[a]	4.45	0.30	
	Dianion[a]	3.84	0.16	
	$\Delta\delta_H$(obsd)[b]	−0.61	−0.14	
DETP	Neutral	4.52	0.76	−2.23
	Dianion	3.90	0.65	−2.33
	$\Delta\delta_H$(obsd)	−0.62	−0.11	−0.10
DPTP	Neutral	4.54	1.55	−2.35
	Dianion	3.89	0.53	−2.64
	$\Delta\delta_H$(obsd)	−0.65	−1.02	−0.29

a) Measured in ppm from the lower-shielding methylene peak of THF as an isotopic impurity. Negative sign denotes high-field shift. b) Shift of the dianion relative to its corresponding neutral molecule.

It has previously been established[1c,6,7] that, in simple aromatic systems, the proton chemical shift ($\Delta\delta_H$) is directly proportional to the excess π-electron density (Δq) on the carbon atom to which the proton is bonded. This may be empirically expressed by the simple linear relationship

$$\Delta\delta_H = k\,\Delta q,$$

where the constant k has been experimentally found to have a value of 10 to 11 ppm per electron.[1c,6,7] Then, proton chemical shifts provide reliable information about charge density distributions, provided that there exists no interfering effect such as the magnetic anisotropy of neighboring atoms or substituent groups. It has been predicted from theoretical consideration that the two excess electrons in the lowest vacant π-orbital of the dianion do not contribute to the ring current.[8] Therefore, no correction of the observed shift for the ring current effect is required for comparing the observed with calculated shifts. Although the anisotropy of C=O and C–O bonds for the dianion is considered to be different in magnitude from that for the neutral molecule, this effect may be neglected since these bonds are remote from the ring protons.

Thus, the π-charge densities on the carbon 2p orbitals, ρ^{π}_{2p}, were calculated by using both the CNDO and semiempirical SCF π-MO (ppp) methods. Several geometric parameters used were taken from the literature.[9] MO calculations were made for the *cis* and *trans* rotational conformers for the ester groups (Fig. 2) and ρ^{π}_{2p} was averaged over positions 2 and 6 and over the two conformers. The increase in the resulting average ρ^{π}_{2p} on going from the neutral to dianion molecule is taken as the excess charge, $\Delta\rho^{\pi}_{2p}$. The increases in the ring proton shifts corresponding to $\Delta\rho^{\pi}_{2p}$, $\Delta\delta_H$, were then calculated from $\Delta\rho^{\pi}_{2p}$ by using 10.7 ppm as k and are compared with the observed ones

Table 2. Comparison of observed shifts ($\Delta\delta_H$(obsd)) with those predicted from MO calculations ($\Delta\delta_H$(calcd)) for dimethyl terephthalate dianion[a]

		Ring-H	α-H
$\Delta\delta_H$(obsd)		−0.61	−0.14
$\Delta\delta_H$(calcd)	CNDO	−1.14(0.106)[b]	
	PPP	−1.29(0.121)[c]	
	CNDO	−1.6(0.095)[d]	−0.8(0.05)[d]

a) In ppm relative to the corresponding neutral molecule. Negative sign denotes high-field shift. b) The figure in parentheses is $\Delta\rho^{\pi}_{2p}$ (CNDO) (see text). c) The figure in parentheses is $\Delta\rho^{\pi}_{2p}$ (ppp) (see text). d) The figure in parentheses is $\Delta\rho^{H}_{1s}$ (CNDO) (see text).

($\Delta\delta_H$(obsd)) in Table 2. The result shows that $\Delta\delta_H$ (calcd) is about twice as much as $\Delta\delta_H$(obsd) for both the cases using the MO methods.

On the other hand, it has been predicted theoretically that a 6% increment of electron density on a hydrogen 1s orbital (ρ^H_{1s}) corresponds to 1 ppm high-field shift of the hydrogen. Using this relation, an attempt was made to estimate, though roughly, $\Delta\delta_H$ of ring protons from the excess charge on its 1s orbital estimated by the CNDO method, $\Delta\rho^H_{1s}$. ρ^H_{1s} was obtained from the averaging mentioned above. As shown in Table 2, the result indicates a further larger high-field shift than $\Delta\delta_H$(obsd). The same process was applied to the α-protons of methyl group but resulted in too large high-field shift.[10]

It may be resonable to consider that the counter ion effect of Na ions is responsible for this discrepancy: The hfs patterns in ESR spectra of terephthalate anion radicals have excellently been interpreted in terms of MO calculations performed on the ion pair model based on the interaction of Na ion with a carbonyl oxygen of one ester group.[2] By analogy with anion radicals, one may expect that the two Na ions bind to each of the two carbonyl oxygens of ester groups in the dianion disodium salt (Fig. 2). In this model, the bonding of Na ion to the carbonyl oxygen may increase the π-densities on the ester groups and hence may decrease those on the ring. This model is thus possibly effective for elucidation of the above discrepancy for the ring protons. However, the much larger value of CNDO $\Delta\rho^H_{1s}$ for the methyl protons than expected is difficult to be explained from this consideration and appears to be associated with the change in the anisotropy of C=O and C–O bonds on going from the neutral to dianion molecule. $\Delta\delta_H$(obsd) of the α-protons for DPTP is much larger than those for the other two compounds and this may suggest that the C–H bond of the isopropyl group in this dianion trends to be perpendicular to the molecular plane, in contrast to the case of the anion radical of this compound where this bond has been determined to be fixed on the benzene plane.[2]

It is known that for actual charged molecules the excess charge trends to be somewhat more uniformly distributed over the molecule than indicated by simple MO calculations.[1b] This effect is in competition with the trend of electron localization toward the ester groups by the bonding of Na ion. Another possible explanation for such discrepancy between the observed and calculated $\Delta\delta_H$ is related to the formation of π-π dimer dianion proposed on the basis of much larger concentrations of the starting aromatic compound than that suitable for the observation of ESR. This model is attractive since this might lead to about half $\Delta\rho$(calcd).

References

1) a) T. J. Katz, *J. Am. Chem. Soc.*, **82**, 3784 (1960); T. J. Katz, M. Yoshida, and L. C. Siew, *ibid.*, **87**, 4516 (1965); C. S. Baxter, P. J. Garratt, and K. P. C. Vollhardt, *ibid.*, **91**, 7783 (1969); B. M. Trost and P. L. Kinson, *ibid.*, **92**, 2591 (1970); J. F. M. Oth, K. Mullen, H. Konigshofen, J. Wassen, and E. Vogel, *Helv. Chim. Acta*, **57**, 2387 (1974); G. L. B. Lundgren, M. Mohammad, and M. Szwarc, *J. Am. Chem. Soc.*, **98**, 1461 (1976); L. A. Paquette, F. D. Ewing, S. Traynor, and J. M. Gardlik, *ibid.*, **99**, 6155 (1977); K. Mullen, *Helv. Chim. Acta*, **61**, 1296 (1978); M. Hirayama and M. Endo, *J. Chem. Res. (S)*, **1979**, 1 78. b) R. G. Lawler and C. V. Ristagno, *J. Am. Chem. Soc.*, **91**, 1535 (1969); K. Mullen, *Helv. Chim. Acta*, **59**, 1357 (1976). c) T. Schaefer and W. G. Schneider, *Can. J. Chem.*, **41**, 966 (1963).

2) M. Hirayama, *Bull. Chem. Soc. Jpn.*, **40**, 2234 (1967).

3) T. Kowata and M. Koizumi, *Bull. Chem. Soc. Jpn.*, **42**, 3352 (1969).

4) This program was prepared according to J. A. Pople, D. L. Beveridge, and P. A. Dobosh, *J. Chem. Phys.*, **47**, 2026 (1967).

5) The proton position is defined by

$$O=\underset{1}{C}-O-\underset{\alpha}{CH_2}-\underset{\beta}{CH_3}.$$

6) G. Fraenkel, R. E. Carter, A. McLachlan, and J. H. Richards, *J. Am. Chem. Soc.*, **82**, 5846 (1960).

7) H. Spiesecke and W. G. Schneider, *Tetrahedron Lett.*, **1961**, 468.

8) J. A. Pople, *Mol. Phys.*, **1**, 175 (1958).

9) M. Bailey, *Acta Crystallogr.*, **2**, 120 (1949).

10) CNDO calculations were made for two rotational conformers for methyl groups in which one C–H bond is perpendicular and coplanar to the benzene plane. The excess ρ^H_{1s} for the dianion, $\Delta\rho^H_{1s}$, was estimated through the averaging of ρ^H_{1s} over the three methyl protons in each conformer.

The Estimation of the Liquid-Liquid Distribution Coefficients of Acetylacetone by Means of the Group Solution Theory

Masanao KATO*

Department of Chemistry, Faculty of Science, Tohoku University, Sendai 980

(Received June 27, 1981)

The estimation of the liquid-liquid distribution coefficients of acetylacetone tautomers was attempted on the basis of the UNIFAC equation, and it was found that the calculated values of the reciprocals of the activity coefficients of tautomers in organic phases were linearly related to the distribution coefficients. It was verified that the estimation by the UNIFAC equation could be extended to the organic solvents with no characteristic parameter.

Acetylacetone (2,4-pentanedione), a well-known extractant, is extensively employed in the solvent extraction of various matallic elements. In the scheme of the extraction, the distribution of acetylacetone between two liquid phases plays an important role. The distribution ratio of metal elements is represented as a function of the partition coefficient of acetylacetone, the dissociation constant of acetylacetone in the aqueous phase, the formation constant of the metal acetylacetone complex, and the partition coefficient of the complex. From this point of view, the distribution of acetylacetone and its thermodynamic properties have been thoroughly investigated.

As a thermodynamic study, an interpretation of the distribution coefficients on the basis of the regular solution theory has been reported by Wakahayashi *et al.*;[1] they found a good correlation between the distribution coefficient of acetylacetone and the solubility parameter of organic solvents. The determination of the activity coefficients of each tautomer has also been tried in terms of the Wilson equation[2] and the UNIFAC equation[3] in our laboratory.[4,5] By the use of these analytical equations, the activity coefficients of tautomers could clearly be determined. Inoue *et al.* had also compared the activity coefficients of the tautomers with the distribution coefficients; they found a qualitative agreement between them.[4] For practical use, the Wilson parameters are required for all of the binary mixtures cencerned in the distribution experiments. That is, the vapor pressures of all the acetylacetone+organic solvent mixtures must be measured.

On the other hand, the calculation by the UNIFAC equation requires a smaller amount of parameters than those by the regular solution theory and the Wilson equation. Once the parameters are determined, these parameters can be employed for all the calculations for mixtures containing the same functional groups. In this study, the applicability of the UNIFAC equation to the estimation of the liquid-liquid distribution coefficients of acetylacetone was examined.

Theory

The UNIFAC Equation. The UNIFAC equation[3] consists of Eqs. 1 to 4. Eq. 1 represents the contribution of the size difference of the substances in the mixtures to the activity coefficients. In the original paper, it is named the combinatorial part, γ_i^C:

$$\ln \gamma_i^C = \ln \frac{\phi_i}{x_i} + \frac{z}{2} \ln \frac{\theta_i}{\phi_i} + l_i - \frac{\phi_i}{x_i} \sum x_j l_j, \quad (1)$$

and:

$$\theta_i = q_i x_i / (\sum_j q_j x_j), \quad \phi_i = r_i x_i / (\sum_j r_j x_j),$$
$$l_i = z(r_i - q_i)/2 - (r_i - 1), \quad (1a)$$

where x_i denotes the mole fraction of the i-th species; z, the coordination number; q_i, the parameter concerning the molecular surface area, and r_i, the parameter of the molecular volume. The q_i and r_i values are represented by the summation of the corresponding parameters, Q_k and R_k, for the functional groups by the following equations:

$$q_i = \sum_k \nu_k^{(i)} Q_k,$$
$$r_i = \sum_k \nu_k^{(i)} R_k, \quad (1b)$$

and

$$Q_k = A_{w,k}/(2.5 \times 10^9),$$
$$R_k = V_{w,k}/15.17, \quad (1c)$$

where $\nu_k^{(i)}$ is the number of the k group in the i-th species. $A_{w,k}$ and $V_{w,k}$ denote the van der Waals surface area and volume of the k group respectively. In Eq. 1, the required parameters are Q_k's and R_k's, and x_i is determined by the experimental conditions.

The following equations, Eqs. 2 and 3, represents the contribution of intermolecular interaction to the activity coefficients, in which γ_i^R is called the residual part, in the original paper:

$$\ln \gamma_i^R = \sum_k \nu_k^{(i)} [\ln \Gamma_k - \ln \Gamma_k^{(i)}], \quad (2)$$

$$\ln \Gamma_k = Q_k \left[1 - \ln \left(\sum_m \theta_m \Psi_{mk} \right) - \sum_m \frac{\theta_m \Psi_{km}}{\sum_n \theta_n \Psi_{nm}} \right], \quad (3)$$

where

$$\theta_m = Q_m X_m / (\sum_n Q_n X_n),$$
$$\Psi_{mn} = \exp(-a_{mn}/RT). \quad (3a)$$

The Γ_k represents the group-activity coefficient, and the additivity is postulated. The $\Gamma_k^{(i)}$ is the group-activity coefficient in the pure i species, and normalizes the activity coefficient to be unity in the pure state. The a_{mn} assesses the inter-group interaction between m and n groups; these values were summarized in the original paper in the form of a_{mn}/R. R and T are the gas constant and the temperature respectively. X_m denotes the mole

* Present address: Department of Material Science, Toyohashi University of Technology, Tempaku-cho, Toyohashi 440.

fraction of the m group in the given mixtures. In Eqs. 2 and 3, the required parameters are Q_k's and a_{mn}'s.

The activity coefficient of the i-th species, γ_i, is represented by the summation of Eqs. 1 and 2 as follows:

$$\ln \gamma_i = \ln \gamma_i^{C} + \ln \gamma_i^{R}. \quad (4)$$

The Q_k and R_k values have been determined for a variety of group; the a_{mn} values have also been evaluated for the pair of principal groups. The activity coefficient in mixtures composed of well-known substances are calculated from the values of the parameters determined by Fredenslund *et al.*[6]

Distribution Coefficients. The distribution ratio, D, is generally defined by the concentration ratio of a solute in two liquid phases, ordinarily aqueous and organic phases:

$$D = C_{org}/C_{aq}. \quad (5)$$

The subscripts "org" and "aq" denote the organic and aqueous phases respectively. The distribution coefficients of tautomers of acetylacetone are represented as follows:

$$D = K_D^{E} f_{aq}/f_{org} = K_D^{K}(1-f_{aq})/(1-f_{org}), \quad (6)$$

where K_D^{E} and K_D^{K} denote the distribution coefficients of the enol and keto tautomers respectively, and where f is the enol content.

The chemical potentials, μ, of a solute in both phases are represented as follows:

$$\mu_{org} = \mu^{\circ} + RT \ln x_{org}\gamma_{org}, \quad (7)$$

$$\mu_{aq} = \mu^{\circ} + RT \ln x_{aq}\gamma_{aq}. \quad (8)$$

As the UNIFAC equation is defined for a symmetric ideal reference system, the μ°'s in Eqs. 7 and 8 are equal. The chemical potentials in both phases are equal in an equilibrium state:

$$\mu_{org} = \mu_{aq}. \quad (9)$$

Accordingly, the following relation is obtained:

$$K_{D,x} = \frac{x_{org}}{x_{aq}} = \frac{\gamma_{aq}}{\gamma_{org}}. \quad (10)$$

Equation 10 is a desirable equation, as it shows that the distribution coefficient in the symmetric ideal reference system is represented by the ratio of the activity coefficients of the solute in both phases. The distribution coefficient in molarity, K_D, is transformed to that in the mole fraction, $K_{D,x}$, by means of Eq. 11:

$$K_{D,x} = K_D v_{org}/v_{aq}, \quad (11)$$

where v denotes the molar volume of the solvents. From the above equations, it is possible to compare the activity coefficients of a given solute, calculated from the UNIFAC equation with the observed distribution coefficients.

Experimental

The acetylacetone and chlorobenzene (guaranteed reagents of commercial origin) were distilled with a distillator with 80 to 100 theoretical plates, and the middle portions were submitted to vapor-pressure measurements. Redistilled water was used. No signal due to impurities was detected on a gas chromatogram.

The apparatus for the vapor pressure measurements was previously reported by our laboratory.[7] The thermostat was controlled at 298.15±0.001 K.

The enol content of acetylacetone in water and chlorobenzene was determined from the signal area of the terminal methyl groups of each tautomer in an NMR spectrogram at 298±1 K.

The concentrations of the liquid and vapor phases were determined from their densities.

Results

The observed vapor pressures are listed in Table 1, along with the activity coefficients of the component substances. In this table, x_{acac} denotes the mole fraction of acetylacetone in the liquid phase; y_{acac}, that in the vapor phase, and p, the total pressure. Table 2 summarizes the dependence of the enol content, f, on the concentration of acetylacetone. The enol content in chlorobenzene mixtures was smoothed by the least-squares method as follows:

$$10^2 f = 2\ 538 x_{acac}^2 + 7.393 x_{acac} + 8\ 525. \quad (12)$$

No concentration dependence of the enol content in the mixtures containing water was found in diluted solutions.

Table 1. Observed activity coefficients of the tautomers of acetylacetone, γ^{E} and γ^{K} and a solvent, $\gamma^{solvent}$, at 298.15 K

x_{acac} [a]	y_{acac} [b]	p [c] / mmHg [d]	γ^{E}	γ^{K}	$\gamma^{solvent}$
Acetylacetone+Chlorobenzene					
0.0	0.0	11.64	—	—	1.0
0.103	0.099	11.47	1.038	2.118	0.990
0.219	0.194	11.45	0.965	1.768	1.015
0.345	0.293	11.41	0.934	1.523	1.058
0.420	0.355	11.21	0.920	1.405	1.071
0.519	0.440	10.90	0.907	1.268	1.090
0.635	0.558	10.87	0.951	1.201	1.131
0.734	0.657	10.38	0.937	1.086	1.150
0.846	0.789	9.97	0.952	1.003	1.174
0.936	0.897	9.69	0.963	0.941	1.340
1.0	1.0	9.67	1.013	0.936	—
Acetylacetone+Water					
0.0	0.0	23.41	—	—	1.0
0.0022	0.057$_4$	24.44	300.8	13.94	0.986
0.0070	0.138	25.30	235.2	10.90	0.938
0.0114	0.149	26.49	163.3	7.57	0.974

a) Mole fraction of acetylacetone in the liquid phase. b) Mole fraction of acetylacetone in the vapor phase. c) Total pressure. d) 1 mmHg≈133.322 Pa.

Table 2. Dependence of the enol fraction, f, upon the concentration of acetylacetone at 298 K

x_{acac}	$10^2 f$ [a]	x_{acac}	$10^2 f$ [a]	x_{acac}	$10^2 f$ [a]
Acetylacetone+Chlorobenzene					
0.151	90.3	0.498	83.6	0.787	85.4
0.294	90.2	0.729	85.5	0.845	84.5
0.422	88.5				
Acetylacetone+Water					
0.0078	15.8	0.863	82.0	0.923	81.9
0.0146	16.9	0.869	81.9	0.928	80.4
0.0207	17.3				

a) f=[enol]/[acac].

TABLE 3. INTER-GROUP INTERACTION ENERGY PARAMETERS, a_{mn}/R, ALONG WITH QUOTED VALUES FROM REF. 6

a_{mn}/R	CH_2	CH_2CO	E.R.[a]	ACH	$ACCH_2$	ACCl	$CHCl_3$	CCl_4
CH_2	0	476.4[b]	610	61.13[b]	76.50[b]	321.5[b]	24.90[b]	104.3[b]
CH_2CO	26.77[b]	0	−130	140.1[b]	365.8[b]	150.0	−354.6[b]	−39.20[b]
E.R.[a]	570	310	0	220	70	150	−160	10
ACH	−11.12[b]	25.77[b]	190	0	167.0[b]	538.2[b]		
$ACCH_2$	−69.70	−52.10[b]	600	−146.8[b]	0			
ACCl	−141.3[b]	60	280	−237.7[b]		0		
$CHCl_3$	36.7[b]	552.1[b]	240				0	
CCl_4	−78.45[b]	372[b]	550					0

a) Denotes the enol ring. b) Quoted from Ref. 6.

Discussion

In applying the UNIFAC equation to the mixtures containing acetylacetone, the parameters for the enol tautomer should be defined as a modified value. Because the enol ring forms a resonance structure, it is reasonable to consider that it should be treated as one functional group. The details of the definition were described in Ref. 3. As more accurate data for the temperature dependence of the vapor pressure of acetylacetone were reported by Inoue *et al.*,[4] the values of a_{mn}/R were recalculated; they are listed in Table 3, along with the values reported by Fredenslund *et al.*[6] An example of the analysis by means of the UNIFAC equation is shown in Fig. 1 for acetylacetone+chlorobenzene mixtures.

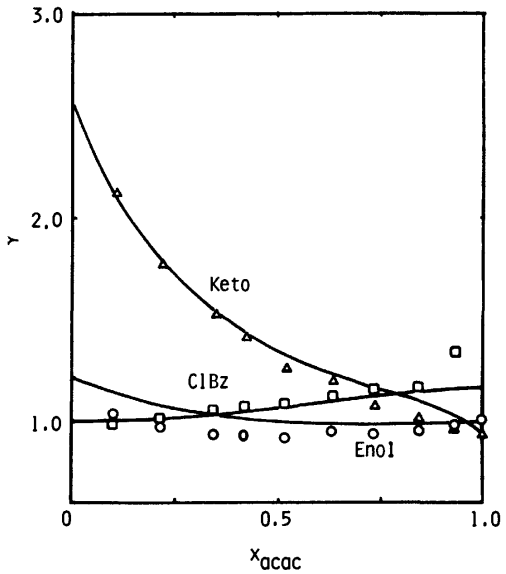

Fig. 1. Activity coefficients of the components in acetylacetone+chlorobenzene mixture at 298.15 K. ○ denotes enol tautomer, △ is keto tautomer, and □ is chlorobenzene. Solid lines represent the values calculated from the UNIFAC equation.

Correlation between $K_{D,x}$ and the Ratio of γ. As has been described above, the distribution coefficients, $K_{D,x}$, are represented as a ratio of the activity coefficients of a solute in two phases. In this study, the dependence of the distribution coefficients upon the activity coefficient in organic phases was considered.

When the activity coefficients of acetylacetone tautomers in several organic solvents were calculated by the UNIFAC equation, the concentration of acetylacetone was determined to be 10^{-3} in the mole fraction. This concentration nearly corresponds to 10^{-2} mol dm^{-3}. It has been found that the distribution coefficients of acetylacetone are independent of the concentration of acetylacetone in this concentration range.[1]

The calculated activity coefficients are listed in Table 4. In this table, D denotes the distribution coefficients of acetylacetone reported by Johansson and Rydberg.[8] The f_{org} values estimated from the equation reported by Pawling and Bernstein[9] are used because of the scarcity of experimental data. $K^{E}_{D,x}$ and $K^{K}_{D,x}$ denote the distribution coefficients of enol and keto tautomers respectively in the mole fraction. In Table 4, the systems containing benzene, toluene, chloroform, carbon tetrachloride, and chlorobenzene were used for the determination of the a_{mn}/R values. However, the activity coefficients in the mixtures of xylene, mesitylene, ethylbenzene, and some alkanes were calculated without any characteristic parameter for solvent molecules.

Figure 2 shows the correlation between $K^{E}_{D,x}$ and the

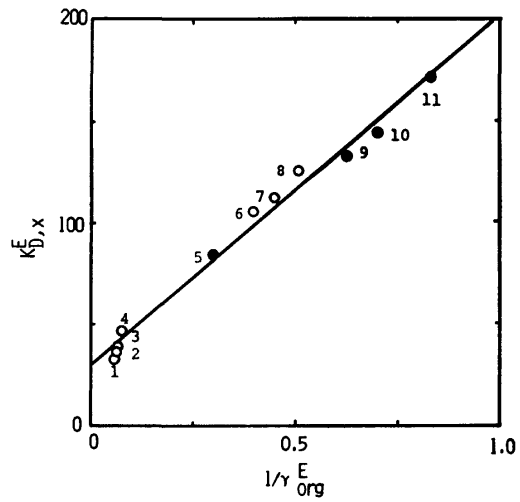

Fig. 2. Correlation between $K^{E}_{D,x}$ and $1/\gamma^{E}_{org}$ at 298.15 K. The open circles denote the systems having no characteristic parameters for solvent. (1-cyclohexane, 2-hexane, 3-heptane, 4-dodecane, 5-carbon tetrachloride, 6-mesitylene, 7-ethylbenzene, 8-xylene, 9-toluene, 10-benzene, and 11-chlorobenzene).

TABLE 4. DISTRIBUTION COEFFICIENTS AND ACTIVITY COEFFICIENTS OF TAUTOMERS OF ACETYLACETONE AT 298.15 K

Solvent	D	f_{org}	$K^{E}_{D,x}$ a)	$1/\gamma^{E}_{org}$ b)	$K^{K}_{D,x}$ a)	$1/\gamma^{K}_{org}$ b)
Benzene	5.93	0.89	144.3	0.70	3.94	0.31
Toluene	4.57	0.89	132.9	0.63	3.63	0.27
Xylene	3.69	0.89c)	124.0	0.51	3.39	0.27
Mesitylene	2.73	0.89c)	103.7	0.40	2.83	0.28
Ethylbenzene	3.31	0.89c)	110.8	0.45	3.03	0.21
Cyclohexane	1.03	0.96	32.8	0.059	0.303	0.0098
Hexane	0.95	0.95	36.3	0.061	0.422	0.0104
Heptane	0.89	0.97	38.8	0.063	0.265	0.0106
Dodecane	0.69	0.97c)	46.7	0.076	0.320	0.0126
Chlorobenzene	5.98	0.92	170.8	0.83	3.51	0.39
Chloroform	23.80	0.87	507.2	4.12	17.51	5.24
Carbon tetrachloride	3.31	0.96	94.2	0.30	0.87	0.058

a) Calculated from Eqs. 6 and 11. b) Calculated from the UNIFAC equation. c) Estimated from the equation proposed by Pawling and Bernstein.[9]

reciprocal of the activity coefficient of the enol tautomer, $1/\gamma^{E}_{org}$. The open circles denote a system with no characteristic parameter. The linearity of this figure is satisfactory. The correlation is represented by the least-squares method as follows:

$$K^{E}_{D,x} = 171.04/\gamma^{E}_{org} + 30.69. \quad (13)$$

The correlation coefficient was 0.992, omitting the chloroform system. Figure 3 shows the similar plots for the keto tautomer. The correlation by the least-squares method, except for chlorobenzene, mesitylene and chloroform, was as follows:

$$K^{K}_{D,x} = 12.43/\gamma^{K}_{org} + 0.20. \quad (14)$$

The correlation coefficient was 0.997. When only the data for chloroform were excluded,

$$K^{K}_{D,x} = 11.75/\gamma^{K}_{org} + 0.22. \quad (15)$$

The correlation coefficient was 0.986. As the amounts of the keto tautomer were very small in an organic solvent, the inaccuracy in enol contents strongly contributed to the calculated results. These two figures show that a good linear correlation exists between the

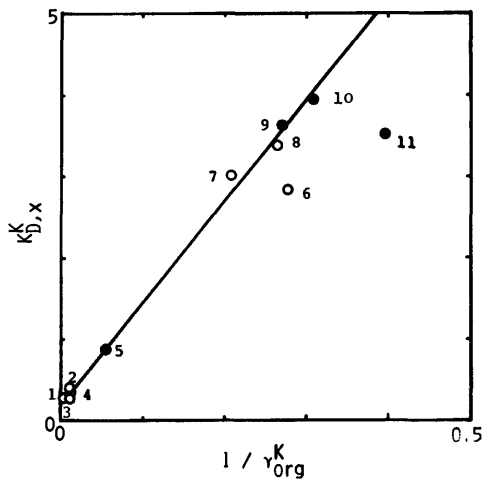

Fig. 3. Correlation between $K^{K}_{D,x}$ and $1/\gamma^{K}_{org}$ at 298.15 K. The open circles denote the systems having no characteristic parameters for solvent. The numbers are corresponding to that in Fig. 2.

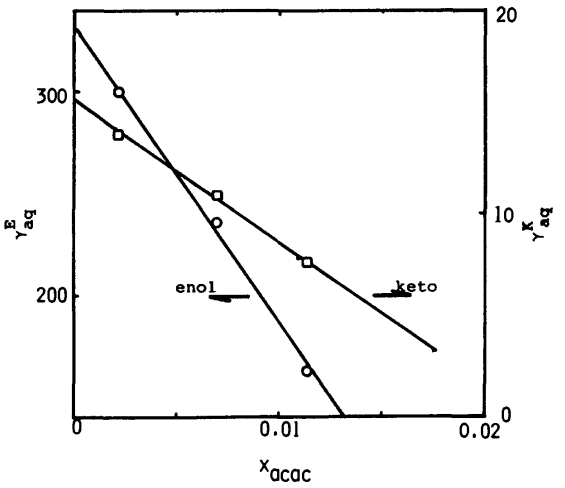

Fig. 4. Activity coefficients of acetylacetone tautomers in water at 298.15 K.

distribution coefficient and the reciprocal of the activity coefficient in the organic phase.

Comparing Eqs. 13 to 15 with Eq. 10, it is found that the slopes in Figs. 2 and 3 correspond to the activity coefficients of tautomers in the aqueous phase. As is shown in Fig. 4, the observed activity coefficient of the enol tautomer in an aqueous mixture was about 330, while that of the keto tautomer was 15.6 at an infinite dilution. The slope for the enol tautomer in Fig. 2 remarkably disagreed with the observed activity coefficient, and an intercept appeared. The disagreement of slopes indicates a smaller distribution coefficient than that calculated from the activity coefficient. The activity coefficients calculated from the UNIFAC equation were slightly greater than the observed values. The plots of Fig. 2 obtained by the use of the observed activity coefficients show a small intercept, but the same slope. As the concentration of electrolytes in the aqueous phase was 10^{-3} mol dm^{-3} of $HClO_4$,[8] it is considered that the activity coefficient of the enol tautomer takes the same value as the value in Fig. 4. In the experiment of distribution, small amounts of water were found in the organic phase. Recently, it has been found that acetylacetone, particularly its enol tautomer, associates

with water in a benzene solution.[10] This fact supports the greater activity coefficient in distribution experiments than that in vapor-pressure measurements, and smaller distribution coefficients than those calculated from the activity coefficients.

Conclusion

The activity coefficients of tautomers of acetylacetone were clearly determined by the UNIFAC equation, and it was found that the distribution coefficients were linearly related to the calculated activity coefficients. This fact shows that the UNIFAC equation is applicable to the estimation of the liquid-liquid distribution coefficients. As the UNIFAC equation can be easily extended to multi-component mixtures, it is expected that the foregoing presentation can be extended to the distribution by mixed solvents. The estimation of distribution coefficients by the UNIFAC equation can be considered to be a very useful method.

References

1) T. Wakahayashi, S. Oki, T. Omori, and N. Suzuki, *J. Inorg. Nucl. Chem.*, **26**, 2255 (1964).
2) G. M. Wilson and G. Scatchard, *J. Am. Chem. Soc.*, **86**, 127 (1964).
3) A. Fredenslund, R. L. Jones, and J. M. Prausnitz, *AIChE J.*, **21**, 1086 (1975).
4) M. Inoue, Y. Arai, S. Saito, and N. Suzuki, *J. Chem. Eng. Data*, **26**, 287 (1981).
5) M. Kato, *Ind. Eng. Chem., Fundam.*, **19**, 253 (1980).
6) A. Fredenslund, J. Gmehling, M. Michelsen, P. Rasmussen, and J. M. Prausnitz, *Ind. Chem., Process Des. Dev.*, **16**, 450 (1977).
7) M. Inoue, K. Azumi, and N. Suzuki, *Ind. Eng. Chem., Fundam.*, **14**, 312 (1975).
8) H. Johanssen and J. Rydberg, *Acta Chem. Scand.*, **23**, 2797 (1969).
9) J. Pawling and H. J. Bernstein, *J. Am. Chem. Soc.*, **73**, 4353 (1951).
10) M. Kato, H. Watarai, and N. Suzuki, *Can. J. Chem.*, **55**, 1473 (1977).

 © 1982 The Chemical Society of Japan Bull. Chem. Soc. Jpn., 55, 1811—1819 (1982)

Electron Spin Resonance and Some Spectral Studies on Coordination Behaviors of Paramagnetic Metal Ions for Chelating Resins

Akira NAKASHIMA, Toshiyuki ISOBE,* and Toshikazu TARUTANI
Department of Chemistry, Faculty of Science, Kyushu University 33, Hakozaki, Fukuoka 812
(Received August 28, 1981)

Coordination behaviors of VO(II), Cr(III), Mn(II), Fe(III), Cu(II), and Gd(III) ions for the iminodiacetato group in the chelating ion-exchange resin Dowex A-1 were studied with the aid of ESR, infrared absorption, and Mössbauer spectroscopies. A comparative investigation also was made with the *o*-hydroxybenzyliminodiacetato group in the chelating resin Unicellex UR-50. The iminodiacetato group in Dowex A-1 is considered to coordinate as a tridentate ligand and form 1 : 1 chelates with metal ions, whereas the *o*-hydroxybenzyliminodiacetato group in Unicellex UR-50 coordinates as a quadridentate ligand in alkaline media and forms 1 : 1 chelates. Elucidation of spin-spin exchange interaction has led to a conclusion that the iminodiacetato groups present in the coordination pore of Unicellex UR-50 are closer to one another than those of Dowex A-1. For Fe(III) ions adsorbed in concentrated HCl media, besides the species $[FeCl_4]^-$, lower symmetric species are considered to be adsorbed with the anion exchange effect, from results of resin phase ESR and Mössbauer spectra.

Recently, new type chelating resins which are highly selective for certain metal ions have been synthesized and selective separation of metal ions has been investigated. As the selectivity is considered to depend on the chelating functional group, an investigation of the coordination behavior of metal ions for the group is of great importance in synthesis of metal ion specific resin. Commercially-available resins, Dowex A-1 and Unicellex UR-50, have different functional groups and show different coordination behaviors.

The chelating resin Dowex A-1 consists of a styrene–divinylbenzene copolymer to which iminodiacetato group is attached as chelating group. Cohen and Heitner-Wirguin suggested Cu(II) ion species adsorbed on Dowex A-1 by infrared and ESR measurements.[1,2] They assumed that Dowex A-1 acts only as an anion exchanger in concentrated HCl media and Cu(II) ion is adsorbed as $[CuCl_4]^{2-}$ or $[CuCl_3(H_2O)]^-$. In neutral and alkaline solution the functional group acts as bidentate and tridentate ligands, respectively. Their assumption was supported by Umezawa and Yamabe[3] considering the mobility of Cu(II) ions adsorbed on the resin phase and the effect of the water molecules involved in the resin phase by means of ESR spectroscopy. More recently, Hoek and Reedijk[4] suggested from ESR and electronic spectra measurements that the iminodiacetato group in Chelex 100 (analytical grade Dowex A-1) coordinates as a tridentate chelating ligand to metal ions, such as Co(II), Ni(II), and Cu(II), and that the distorted octahedral is completed by either water molecules or by carboxylate oxygens from excess neighboring iminodiacetato groups.

The chelating resin Unicellex UR-50 was made by polycondensation of *N*-(*o*-hydroxybenzyl)iminodiacetic acid with phenol and formaldehyde. Tomoshige *et al.*[5] compared the coordination behavior of the resin with that of Chelex 100 and suggested, by considering chelate stability constants of the resin with metal ions, that the phenolic hydroxyl group plays an important role in the chelating behavior. However, they gave no discussion of the adsorption structure of metal ions on the resin phase. To investigate the adsorption structure of metal ions on the resin phase would give significant information about the coordination behavior of the resin. Thus, we have made a comparison of coordination behaviors of Dowex A-1 and Unicellex UR-50 in connection with the adsorption structure of metal ions on the resins from the viewpoint of synthesis of metal ion specific resin. This paper presents a study of resin phase ESR spectra of paramagnetic metal ions, such as VO(II), Cr(III), Mn(II), Fe(III), Cu(II), and Gd(III) ions, distributions of these metal ions between the resin and solution phases, and adsorption structures of these metal ions. Furthermore, chelating behaviors of monomers, such as iminodiacetic acid (IDA) and *N*-benzyliminodiacetic acid (BIDA), are also compared with those of the resins.

Experimental

Reagents and Materials. All reagents used were of analytical grade. Stock solutions of VO(II), Cr(III), Mn(II), Fe(III), and Cu(II) ions were prepared by dissolving vanadyl dichloride, chromium(III) nitrate, manganese(II) chloride, iron(III) chloride, and copper(II) chloride in dilute hydrochloric acid solution, respectively. Their concentrations were standardized by EDTA titration. Standard solution of metal ions of desired concentration were prepared by diluting the stock solutions. The buffer solutions were as follows: pH 1 to 2, potassium chloride–hydrochloric acid; pH 3 to 6, sodium acetate–acetic acid; pH 7 to 9, tris(hydroxymethyl)-aminomethane–hydrochloric acid; pH 10, ammonium chloride–ammonia water. Deionized distilled water was used. The chelating ion-exchange resins used were Dowex A-1 (Dow Chemical Co.) in the sodium form as 50—100 mesh beads and Unicellex UR-50 (Unitika, Ltd.) in the hydrogen form as 20—50 mesh beads. The resins were conditioned and transformed into the hydrogen and sodium forms in a conventional manner, respectively. The cation exchange capacities of Dowex A-1 and Unicellex UR-50 were 3.74 and 3.57 mequiv. per g of dry resin, based upon the uptake of tetraamminecopper(II) ion which was formed in 2 mol dm^{-3} ammonia water. Nonaqueous ion-exchanger Amberlyst A-26 (Rohm and Haas) in the chloride form was used without further treatment.

Preparation of Samples and Reference Compounds. About 500 mg of dry resin, 10 cm^3 of metal ion solution and 40 cm^3 of 0.1 mol dm^{-3} buffer solution were placed in a flask and

agitated for 24 h at 20±1 °C. Metal ion concentration was 100 μg/cm³. After equilibration, the pH value was measured, the solution was filtered, and the wet resin phase (dried in a silica gel desiccator for 12 h) and the dry resin phase (dried for 2 d) were subjected to ESR spectral measurements. Only for estimation of distribution ratio the resin was rinsed rapidly with deionized distilled water except resins immersed in concentrated HCl media, then the solution and rinse were combined and analyzed for metal ion concentration by atomic absorption spectrometry except Gd(III) ion (colorimetry). Distribution ratio, D, is defined as follows and evaluated by determining the metal ion concentration in an equilibrated solution:

$$D = \frac{\text{amt. of metal ion per g of dry resin}}{\text{amt. of metal ion per cm}^3\text{ of solution}}.$$

The amount of metal ions adsorbed on the resin phase was also analyzed after elution with 2 mol dm^{-3} HCl except Cr(III) ion. The amount of Cr(III) ions on the resin phase was analyzed after ashing the resin.

$[FeCl_4]^-$ ion was prepared by extraction into diisopropyl ether from aqueous acidic chloride solution.[6] This chloro-complex was adsorbed on the anion exchanger Amberlyst A-26 in diisopropyl ether media and compared with that on Dowex A-1 in concentrated HCl media. Other reference compounds such as $(CH_3NH_3)_2[MnCl_4]$, $[(CH_3)_4N]_2[MnCl_4]$, $(CH_3NH_3)_3[FeCl_6]\cdot CH_3NH_3Cl$, $(NH_4)_2[FeCl_5(H_2O)]$, and $(CH_3)_4N[FeCl_4]$ were prepared by addition of counter ion's chloride to a concentrated HCl solution containing chloro-complex of Mn(II) or Fe(III).[7,8] IDA and BIDA complexes of Cu(II) ion were prepared by the following method: To 50 cm³ of solution containing 0.01 mol of $CuCl_2\cdot 2H_2O$ was added 100 cm³ of solution containing 0.01 or 0.02 mol of IDA or BIDA. The resulting solution was adjusted to pH 7 with 0.02 mol of $NaHCO_3$ and HCl and warmed nearly to boiling point and then absolute ethanol was added until a slight turbidity appeared. Finally, the solution was cooled in an ice-bath. The resulting crystalline material was filtered and recrystallized from a water–ethanol mixture. The obtained complexes were identified by elemental analysis as $CuIDA\cdot 3H_2O$ (Found: C, 19.39; H, 4.87; N, 5.59%. Calcd for complex: C, 19.32; H, 4.45; N, 5.63%), $Na_2Cu(IDA)_2\cdot 2.5H_2O$ (Found: C, 23.00; H, 3.36; N, 6.62%. Calcd for complex: C, 23.06; H, 3.62; N, 6.72%), and $Na_2Cu(BIDA)_2\cdot 2H_2O$ (Found: C, 44.54; H, 4.09; N, 4.74%. Calcd for complex: C, 44.94; H, 4.46; N, 4.76%).

Physical Methods and Analysis. The pH value of equilibrated solutions was measured on a Hitachi-Horiba D-5 pH meter. A Nippon Jarrell-Ash AA-781 atomic absorption and flame emission spectrophotometer was used in determination of metal ion concentration. First derivative ESR spectra were recorded on a JEOL JES-ME-3X spectrometer at X-band frequencies at room and liquid nitrogen temperatures. Resin particle samples without grinding were packed in JEOL quartz cells and their ESR spectra were measured. No change in ESR spectral shape between the wet and dry resin phases was observed, hence it follows that resin phase spectra can be obtained with the equilibrium state kept. As the amount of metal ion in the solution phase in the resin can be neglected, ESR spectra obtained are regarded as corresponding to the metal ion on the resin phase. For measurement of solution ESR spectra, a JEOL capillary cell (0.05 cm³) was used. Care was taken to keep all settings of the spectrometer knobs unchanged within a series of intensity measurements except for receiver gain amplitude.[9] Relative ESR signal intensity is defined by $(R.I.)=h_{pp}(\Delta H_{pp})^2/\text{Gain}$, where h_{pp} is peak-to-peak height in dm and ΔH_{pp} is peak-to-peak width in mT. Magnetic field was reassessed by DPPH or Mn^{2+}/MgO powder marker. Mössbauer spectra were measured by the constant acceleration method on an Austin Science Associates, Inc. Mössbauer spectrometer at room and liquid nitrogen temperatures, with a source of cobalt-57 (5 mCi) diffused into a palladium foil. The scan speed of spectrometer was calibrated using a pure iron foil, which was also used as a reference for isomer shift. All spectra were fitted to Lorentzian line shapes by computer calculation. Infrared spectra were measured in KBr pellets on a JASCO Model DS-403 G grating infrared spectrophotometer in the range 4000—200 cm^{-1}.

Results and Discussion

General. pH dependences of distribution ratio, amount of metal ions adsorbed on the resin phase, and ESR signal intensity of metal ions for Dowex A-1 and Unicellex UR-50 are shown in Fig. 1. The variation in D values with pH for Dowex A-1 is in the same tendency as that obtained by Leyden and Underwood and obviously different from that for Unicellex UR-50.[10] This difference seems to reflect the effect of the phenolic hydroxyl group at *o*- or *p*-position in Unicellex UR-50. Amounts of metal ions adsorbed on the resin phase are expressed in $(M)_R$, metal ion μg per g dry resin. With Dowex A-1 the decrease in $(Mn)_R$ values above pH 9 may suggest an inhibition of adsorption due to hydrolysis, and on the contrary, the increase in $(Fe)_R$ values above pH 8 may suggest adsorption or adherence of hydroxyl complexes and hydroxide due to hydrolysis. With Unicellex UR-50, however, the variation in $(M)_R$ values due to hydrolysis was found in higher pH regions than that for Dowex A-1. ESR signal intensities are expressed in $(R.I.)_m$, signal intensity per g of metal ion in the dry resin. The following signals were used for the estimation of h_{pp} and ΔH_{pp}: The $M_I=-1/2$ line for VO(II), the $g_{eff}\triangleq 2$ signal for Cr(III), Mn(II), and Gd(III), the $g_{eff}\triangleq 4$ signal for Fe(III), and the $g_\perp$ line for Cu(II). The order of signal intensities was Mn(II)> Cu(II)>VO(II)≈Cr(III)≈Fe(III)≈Gd(III) in all of the pH regions. For each metal ion, there was no marked difference in signal intensity between Dowex A-1 and Unicellex UR-50, except for Gd(III) ion.

Table 1 shows infrared spectral data, of which assignments were made according to the literature.[11] The method is based on the simple rule that the unionized and uncoordinated COO stretching band occurs at 1750—1700 cm^{-1} and 1200—1220 cm^{-1}, whereas the ionized and coordinated COO stretching band is at 1650—1590 cm^{-1}. For example, sodium form resin was suggested to be Type III+Type IV, having a strong absorption band at 1585 cm^{-1} and a weak absorption band at 1210 cm^{-1}. The acting resin forms are found to transform from Type I to Type IV depending on the pH of media. As described above, resin phase infrared spectra are very efficient in suggesting the acting resin form. It should be noted that all infrared spectra have the absorption due to H_2O molecule around 3400 cm^{-1}. From the weight loss after drying at 100 °C, the water content of hydrogen form Dowex A-1 was found to be 11.03%. These H_2O molecules may influence adsorption behaviors of the metal ions, together with the buffer salts, onto the resin phase.

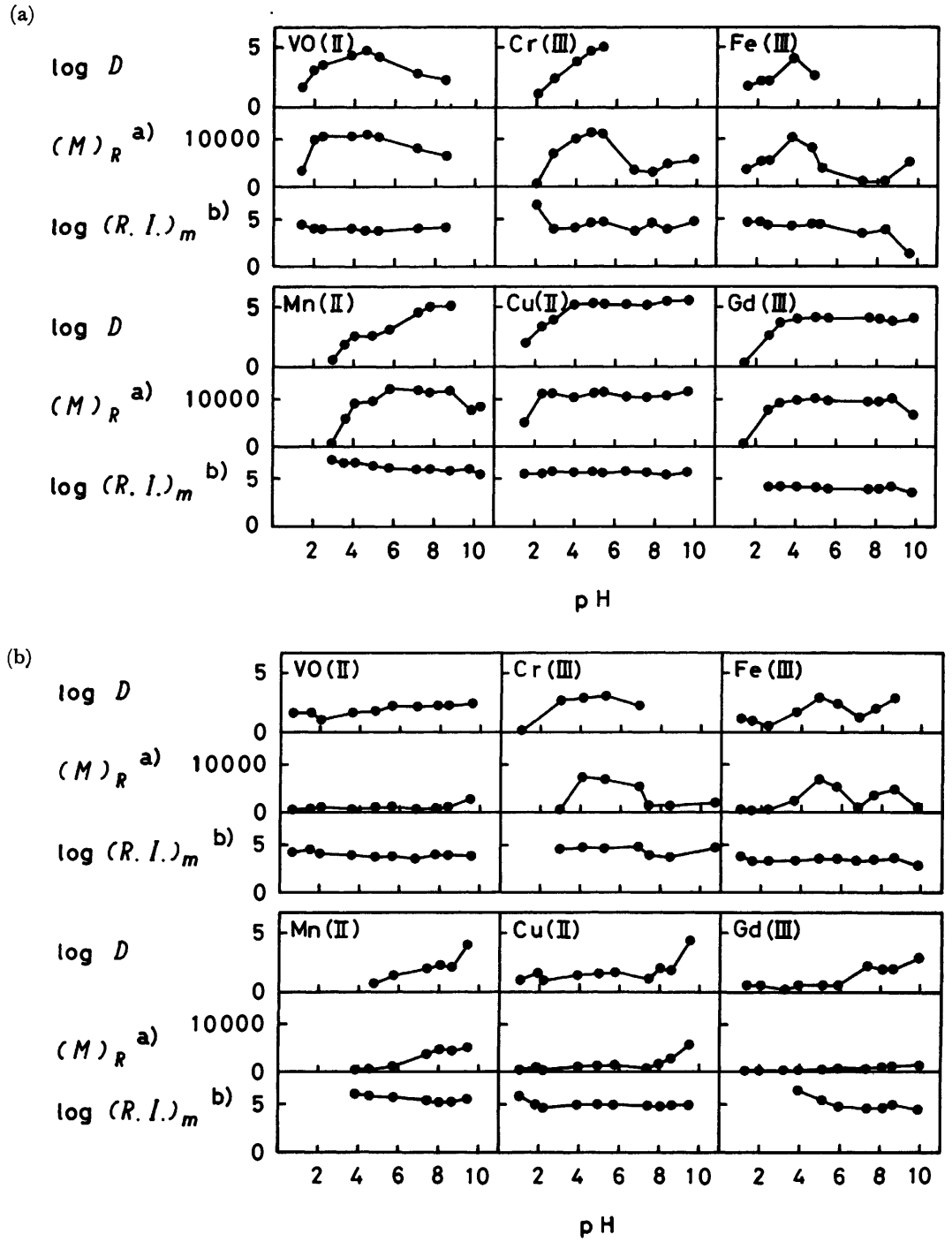

Fig. 1. pH Dependences of distribution ratios, amounts of metal ions adsorbed on (a) Dowex A-1 and (b) Unicellex UR-50 and their ESR signal intensities. a): Metal ion μg per g dry resin, b): signal intensity per g of metal ion in the dry resin.

Cu(II) Ions Adsorbed on the Resin Phase. From the results of infrared absorption bands, with both Dowex A-1 and Unicellex UR-50 acting resin forms were suggested to be Type I in concentrated HCl media, Type II+Type III in the media of pH 4, and Type III+Type IV in the media of pH 9. ESR spectra and parameters of Cu(II) ions adsorbed on the resin phase and of some reference compounds are shown in Fig. 2 and Table 2.

In concentrated HCl media, the suggested resin form of Type I is supported by the similarity of the resin phase ESR spectra to those of anion exchanger Dowex 1×4.[2] Comparing ESR spectra of Cu(II) ions adsorbed on Dowex A-1 and Unicellex UR-50 in concentrated HCl media, we find no significant change except for the free radical signal of Unicellex UR-50. Although the cation exchange capacities of these resins are approximately the same, the amount of Cu(II) ions adsorbed on Unicellex UR-50 is about one seventieth that on Dowex A-1. This fact seems to reflect the steric

TABLE 1. INFRARED ABSORPTION BANDS (cm^{-1}) OF DRY RESIN PHASES

Sample	Equilibration conditions[a)]	Carboxyl group[b)]			Suggested resin forms[c)]
		-COOH	COO-M	-COOH	
A-1	Na-form		1585	1210_{vw}	III+IV
A-1	blank, concd HCl	1730_{s}	1600	1200_{s}	I
A-1	blank, pH 4.40	1720	1620	1210_{w}	II+III
A-1	blank, pH 8.58		1630_{vs}	1215_{vw}	III+IV
A-1	metal, concd HCl	$1730—1710_{s}$	1610—1600	$1210—1180_{s}$	I
A-1	metal, ≈pH 4	1720—1210	1625—1600	$1210—1200_{w}$	II+III
A-1	metal, ≈pH 9		$1625—1600_{vs}$	$1210—1200_{vw}$	III+IV
UR-50	H-form	1700_{s}	1620	1210_{s}	I
UR-50	blank, concd HCl	1725_{s}	1590	1190_{s}	I
UR-50	blank, pH 4.01	1700	1620	1200_{w}	II+III
UR-50	blank, pH 8.08		1610_{vs}	1210_{vw}	III+IV
UR-50	metal, concd HCl	$1725—1720_{s}$	1600—1590	$1200—1180_{s}$	I
UR-50	metal, ≈pH 4	1720—1690	1620—1590	$1210—1190_{w}$	II+III
UR-50	metal, ≈pH 9		$1620—1590_{vs}$	$1210—1200_{vw}$	III+IV

a) Metal: VO(II), Cr(III), Mn(II), Fe(III), Cu(II), and Gd(III). b) vs: Very strong, s: strong, w: weak, vw: very weak.

c)

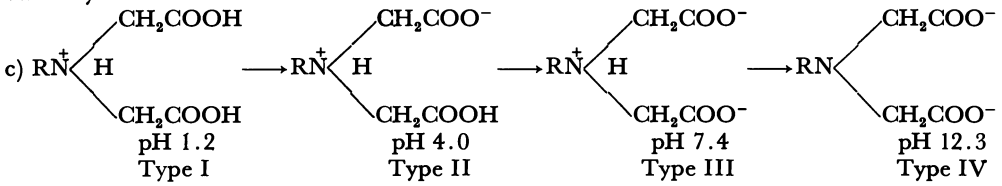

R: Resin polymer matrix.

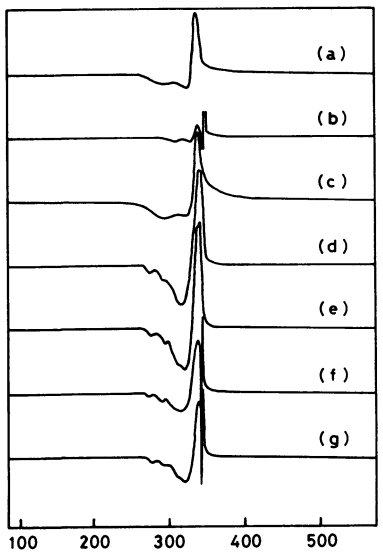

Fig. 2. ESR spectra of Cu(II) ions adsorbed on the resin phases.
(a): A-1, concd HCl, dry, (b): UR-50, concd HCl, dry, (c): 1×4, concd HCl, dry, (d): A-1, pH 4.32, dry, (e): A-1, pH 9.30, dry, (f): UR-50, pH 3.87, dry, (g): UR-50, pH 8.60, dry.

TABLE 2. ESR PARAMETERS FOR Cu(II) IONS ADSORBED ON THE RESIN PHASES

Sample	$(Cu)_R$[a)]	Parameter		
		$A_{//}$/mT	$g_{//}$	$g_{\perp}$
A-1, concd HCl, wet			2.27	2.09
dry	0.29×10^{4}		2.29	2.08
1×4, concd HCl, wet			2.32	2.09
dry	0.14×10^{4}		2.31	2.09
UR-50, concd HCl, wet			2.25	2.08
dry	0.004×10^{4}		2.23	2.08
A-1, pH 4.32, wet		18.6	2.29	2.07
dry	1.58×10^{4}	18.4	2.31	2.09
A-1, pH 9.30, wet		18.0	2.27	2.08
dry	1.09×10^{4}	19.1	2.29	2.08
UR-50, pH 3.87, wet		16.9	2.30	2.08
dry	0.09×10^{4}	16.1	2.31	2.08
UR-50, pH 8.60, wet		15.0	2.28	2.07
dry	0.25×10^{4}	16.9	2.28	2.07

a) Cu(II) ion μg per g dry resin.

hindrance of the phenolic hydroxyl group in Unicellex UR-50. Waki *et al.*[12] suggested from distribution measurements that $[CuCl_3(H_2O)]^-$ and $[Cu_2Cl_7]^{3-}$ species are present in Dowex 1 resin phases in concentrated HCl media. However, on the basis of the ESR spectra of Cu(II) ions adsorbed on the resin phase in concentrated HCl media in this work, it is not possible to differentiate $[CuCl_3(H_2O)]^-$ and $[Cu_2Cl_7]^{3-}$ species. ESR spectra of Cu(II) ions adsorbed on the resin phase in concentrated HCl media are different from powder ESR spectra of $[CuCl_4]^{2-}$ species in solid samples.

In the media of pH 4 and pH 9, no conclusive difference in the dependence of chelation on the transformation of acting resin forms was indicated in the resin phase ESR spectra. The resin phase ESR spectra of Cu(II) ions exhibited axial spectra with $g_{//}$ and $g_{\perp}$ parts and Cu(II) ions on the resin phase were expected to be of distorted tetragonal structure. ESR parameters of the wet resin phase are almost identical with those of the dry resin phase, independent of the pH of media

Table 3. ESR parameters of the resin phases and the powders and frozen solutions of Cu(II) complexes with IDA and BIDA

Sample	Parameters g values (ΔH_{pp}/mT)
A-1, pH10.00, $(Cu)_R=8.93\times10^4$ a)	$g_{iso}=2.12(13.4)$
UR-50, pH10.00, $(Cu)_R=1.90\times10^4$ a)	$g_{iso}=2.10(19.6)$
$CuIDA\cdot3H_2O$ powder	$g_{iso}=2.14(17.7)$
$Na_2Cu(IDA)_2\cdot2.5H_2O$ powder	$g_{//}=2.27$, $g_{\perp}=2.07$
Cu(II) : IDA=1 : 1 frozen solution	$g_{iso}=2.12(13.4)$
1 : 2 frozen solution	$g_{//}=2.29$, $g_{\perp}=2.07$
$Na_2Cu(BIDA)_2\cdot2H_2O$ powder	$g=2.08(9.3)$
Cu(II) : BIDA=1 : 1 frozen solution	$g_{iso}=2.10(14.6)$
1 : 2 frozen solution	$g_{//}=2.24$, $g_{\perp}=2.05$

a) Cu(II) ion μg per g dry resin.

and different from those of aqua complex and cation exchange resin phase.

Other comparative investigations with some reference compounds were done. Chelating behaviors of monomers, such as iminodiacetic acid (IDA) and *N*-benzyliminodiacetic acid (BIDA), were compared with those of the resins. ESR parameters of Cu(II) ion on the resin phase and of powders and frozen solutions of Cu(II) complexes with the monomers are listed in Table 3. The chelate stability constants of IDA with Cu(II) ions were reported as $\log K_1=10.55$ and $\log K_2=5.65$, and structures of the chelates were assumed.[13] The 1 : 1 Cu–IDA chelate shows an isotropic ESR spectrum and the 1 : 2 chelate shows an anisotropic ESR spectrum. Since the resin phase ESR spectra of Cu(II) ions are similar to the powder and frozen solution ESR spectra of the 1 : 1 chelate, the iminodiacetato group in Dowex A-1 was concluded to form the 1 : 1 chelate with Cu(II) ion.

From the above results, it seems that the iminodiacetato group must chelate as a tridentate ligand to Cu(II) ions to form the 1 : 1 chelate in all of the pH regions. However, no conclusive evidence is found for chelation through the nitrogen atom. Although coordination of the phenolic hydroxyl group in Unicellex UR-50 was indicated from the increase in $(Cu)_R$ values above pH 8, the resin phase ESR spectra seemed unchange. Thus, it may be suggested that the phenolic hydroxyl group does not contribute so significantly to the structure of Cu(II) ions on the resin phase.

The hyperfine structure of the $g_{//}$ part became obscure with the increase in $(Cu)_R$ values and the isotropic spectra with $g_{iso}=2.12$ and $\Delta H_{pp}=13.4$ mT for Dowex A-1 and $g_{iso}=2.10$ and $\Delta H_{pp}=19.6$ mT for Unicellex UR-50 were observed. In the isotropic spectra, when the gain became 100 times, the peak presumably based on $\Delta M_s=\pm2$ could be observed at $g=4.38$ and $g=4.60$ for Dowex A-1 and Unicellex UR-50, respectively. This fact clearly indicates that exchange interaction must be present.

Spin-spin interaction affect the line width either as broadening (dipole-dipole interaction) or as narrowing (exchange interaction). For purely dipolar interactions between identical spins in the field of cubic symmetry, the expected line width for polycrystalline powder is

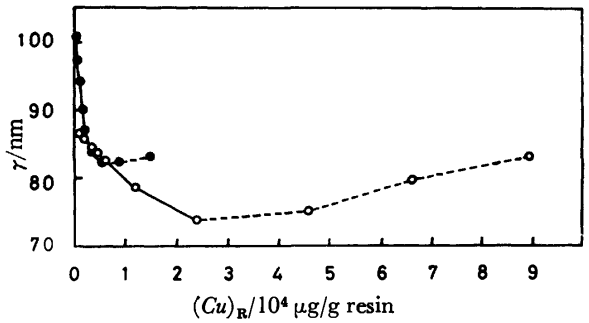

Fig. 3. Variation of distance between the neighboring spins with amount of Cu(II) ions adsorbed on the resin phases.
○: Dowex A-1, ●: Unicellex UR-50.

given by the expressions:[14]

$$r^6=\frac{3}{5}S(S+1)g^2\beta^2\frac{8.5}{\langle\Delta H^2\rangle},$$

and

$$\langle\Delta H^2\rangle=\frac{1}{4}(\Delta H_{pp})^2,$$

where, r is the distance between the neighboring spins. On the basis of the above discussion and on the assumption that the expressions be applicable to the resin phase, the distance between the neighboring spins for Cu(II) ions on the resin phase may be estimated. The variation in the distance with $(Cu)_R$ values is shown in Fig. 3. Exchange interactions may be concluded to be present above $(Cu)_R=2.4\times10^4$ μg/g resin phase for Dowex A-1 and above 0.6×10^4 μg/g resin phase for Unicellex UR-50. As previously described, nearly the same cation exchange capacities of these resins mean that the resins have almost the same amount of iminodiacetato groups. Therefore, the difference in $(Cu)_R$ value between Dowex A-1 and Unicellex UR-50 is demonstrated to be attributable mainly to the polymer matrix, that is to say, the iminodiacetato groups present in a coordination pore of Unicellex UR-50 are closer to one another than those of Dowex A-1.

Mn(II) Ions Adsorbed on the Resin Phase. In concentrated HCl media, Mn(II) ion is considered to be adsorbed on the resins with anion exchange effect in the same way as Cu(II) ion. From a comparison of resin phase ESR spectra of Mn(II) ions with powder ESR spectra of $[(CH_3)_4N]_2[MnCl_4]$ and $(CH_3NH_3)_2[MnCl_4]$,[15] of which ESR parameters are listed in Table 4, Mn(II) ions adsorbed on the resin phase in concentrated HCl media were suggested to be predominantly tetrahedral $[MnCl_4]^{2-}$.

ESR spectra of Mn(II) ions adsorbed on Dowex A-1 and Unicellex UR-50 in the media of pH 4 and pH 9 are shown in Fig. 4. In the resin phase ESR spectra of Mn(II) ions adsorbed in the media of pH 4, peaks with $g=5$ and $g=3$ were observed besides the sextet lines with $g=2$, whereas in the media of pH 9, the sextet ones smeared out and signal intensities of the peak resulting from the zero-field splitting increased. This change in ESR spectra means that Mn(II) ions in low symmetry sites increased with increasing pH of the media. The resin phase ESR spectra of Mn(II) ions

TABLE 4. ESR PARAMETERS FOR Mn(II) IONS ADSORBED ON DOWEX A-1, DOWEX 1×4, AND UNICELLEX UR-50 IN CONCENTRATED HCl MEDIA AND SOME REFERENCE COMPOUNDS

Sample	$(Mn)_R$ a)	Parameters	
		g	ΔH_{pp}/mT
Mn(II)-A-1, wet		2.00	47.4
dry	0.01×10^4	2.00	47.2
Mn(II)-1×4, wet		2.00	44.6
dry	0.07×10^4	2.00	43.8
Mn(II)-UR-50, wet		2.00	49.3
dry	n.d.	2.00	49.8
$[(CH_3)_4N]_2[MnCl_4]$ powder		2.02	22.8
$(CH_3NH_3)_2[MnCl_4]$ powder		2.01	3.3

a) Mn(II) ion μg per g dry resin.

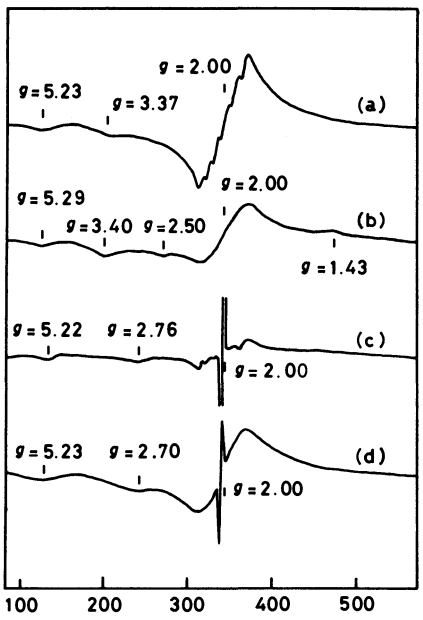

Fig. 4. ESR spectra of Mn(II) ions adsorbed on Dowex A-1 and Unicellex UR-50.
(a): A-1, pH 4.33, dry, (b): A-1, pH 9.65, dry, (c): UR-50, pH 3.83, dry, (d): UR-50, pH 8.59, dry.

adsorbed in the media above pH 4 show very interesting patterns. Dowsing *et al.*[16-19] interpreted several ESR spectra of high-spin d^5 system in terms of a spin Hamiltonian of the form

$$\mathcal{H} = g\beta\boldsymbol{HS} + D[S_z^2-\frac{1}{3}S(S+1)] + E(S_x^2-S_y^2),$$

theoretically discussed the change of ESR spectra according to the distortion parameters, D and λ (E/D), and compared with observed spectra. Through analysis of the resin phase ESR spectra of Mn(II) ions in the media above pH 4, distortion parameters D and λ were tentatively assigned by their energy diagram. The data may fit $D=0.17$ cm^{-1} and $\lambda=0.167$ cm^{-1} for Mn(II) ions on Dowex A-1, and $D=0.29$ cm^{-1} and $\lambda=0.244$ cm^{-1} on Unicellex UR-50. Blumberg[20] showed that if $\lambda=0$ represents axial symmetry, $0<\lambda<1/3$ represents a departure toward rhombic symmetry, $\lambda=1/3$ represents the maximum possible rhombic symmetry, $1/3<\lambda<1$ represents a convergence toward axial symmetry again and $\lambda=1$ represents entirely axial symmetry. On the basis of the above discussion, therefore, Mn(II) ions adsorbed on the resin phase in the media above pH 4 were suggested to be of rhombic symmetry lowered from octahedral and axial symmetries perhaps by the substitution of coordinated H_2O molecules for hydroxide ions. The difference between the ESR spectra of Dowex A-1 and Unicellex UR-50 resin phases shows that the phenolic hydroxyl group in Unicellex UR-50 strongly influences the coordination structure of Mn(II) ions.

Fe(III) Ions Adsorbed on the Resin Phase. The dry resin phase ESR spectra of Fe(III) ions adsorbed in concentrated HCl media and $[FeCl_4]^-$ adsorbed on Amberlyst A-26 in diisopropyl ether media are shown in Fig. 5 and the analyzed data are listed in Table 5. For comparison, powder ESR spectral parameters of $(CH_3NH_3)_3[FeCl_6]\cdot CH_3NH_3Cl$, $(NH_4)_2[FeCl_5(H_2O)]$, and $(CH_3)_4N[FeCl_4]$ and solution ESR spectral parameters of $[FeCl_4]^-$ in diisopropyl ether media are included in Table 5. The resin phase ESR spectra of Fe(III) ions adsorbed on Dowex A-1 in concentrated HCl media seem to have patterns with $g_{eff}=4$ and $g_{eff}\triangleq2$ similar to those on Dowex 1×4 and of $[FeCl_4]^-$ adsorbed on Amberlyst A-26. The $g_{eff}\triangleq2$ signal is

TABLE 5. ESR PARAMETERS FOR Fe(III) IONS ADSORBED ON THE RESIN PHASES IN CONCENTRATED HCl MEDIA AND $[FeCl_4]^-$ ADSORBED ON AMBERLYST A-26 IN DIISOPROPYL ETHER MEDIA

Sample	$(Fe)_R$ a)	Parameters
		g values (ΔH_{pp}/mT)
Fe(III)-A-1, dry	0.68×10^4	4.41(18.1), 2.02(24.4)
Fe(III)-A-1, dry b)	4.80×10^4	4.36(19.0), 2.03(73.1)
Fe(III)-1×4, dry	0.74×10^4	4.42(20.0), 2.00(32.5)
Fe(III)-1×4, dry b)	8.80×10^4	4.45(5.2), 2.04(70.9)
Fe(III)-UR-50, dry	0.31×10^4	4.17(22.6), 2.02(55.8)
$[FeCl_4]^-$-A-26, dry	0.47×10^4	4.32(16.9), 2.02(62.4)
$H[FeCl_4]$ diisopropyl ether solution		2.02(25.2)
$(CH_3)_4N[FeCl_4]$ powder		2.02(21.3)
$(NH_4)_2[FeCl_5(H_2O)]$ powder		2.02(25.1)
$(CH_3NH_3)_3[FeCl_6]\cdot CH_3NH_3Cl$ powder		2.02(8.8)

a) Fe(III) ion μg per g dry resin. b) The column method.

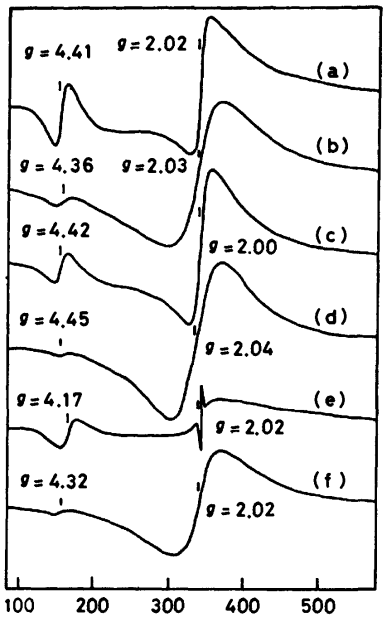

Fig. 5. ESR spectra of Fe(III) ions adsorbed on the resin phases in concentrated HCl media and $[FeCl_4]^-$ adsorbed on Amberlyst A-26 in diisopropyl ether media. (a): Fe(III)-A-1, dry, (b): Fe(III)-A-1, dry (column method), (c): Fe(III)-1×4, dry, (d): Fe(III)-1×4, dry (column method), (e): Fe(III)-UR-50, dry, (f): $[FeCl_4]^-$-A-26, dry.

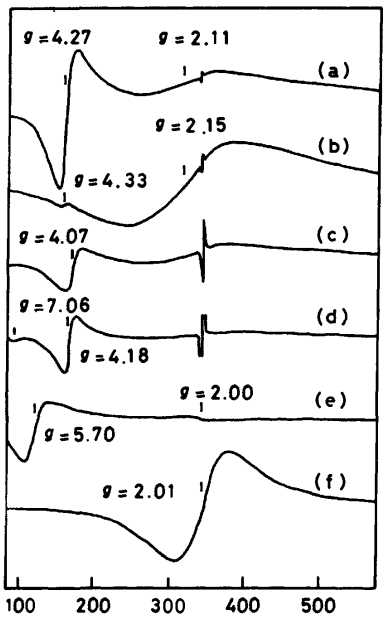

Fig. 6. ESR spectra of Fe(III) ions adsorbed on Dowex A-1 and Unicellex UR-50 and reference compounds. (a): A-1, pH 4.32, dry, (b): A-1, pH 10.05, dry, (c): UR-50, pH 5.00, dry, (d): UR-50, pH 8.80, dry, (e): Fe(III)-*meso*-tetraphenylporphine chloride, (f): Fe(III) hydroxide.

considered to be due to $[FeCl_4]^-$ species. On the other hand, with the resin phase ESR spectrum of Fe(III) ions adsorbed on Unicellex UR-50 in concentrated HCl media, the intensity of the $g_{eff}\triangleq 2$ signal is not so large as that of Dowex A-1. It is apparent that the $g_{eff}\triangleq 4$ signal is not attributable to the coordination by the iminodiacetato group because of the similarity to the resin phase ESR spectra of Fe(III) ions adsorbed on Dowex 1×4 in concentrated HCl media and on Amberlyst A-26 in diisopropyl ether media, as can be seen in Fig. 5.

ESR signals close to $g=4$ often occur in biological materials and clay minerals. Castner *et al.*[21] proposed $D=0$ and $E\neq 0$ to account for the $g=4.27$ spectrum found for iron(III) ions in glass. Griffith[22] showed that d^5 ion is in special environments, then D need not be zero but shall be small. The special environments are tetrahedral MA_2B_2, distorted octahedral MA_6, and octahedral MA_3B_3. Of these environments, the $g_{eff}\triangleq 4$ signal is attributable to tetrahedral MA_2B_2. From the above discussion, since the resin phase ESR spectrum of Fe(III) ions adsorbed in concentrated HCl media shows two signals with $g_{eff}\triangleq 4$ and $g_{eff}\triangleq 2$, the MA_2B_2 species, in addition to the MA_4 species, $[FeCl_4]^-$ is considered to be present. That is, besides the species $[FeCl_4]^-$ simply adsorbed with the anion exchange effect, lower symmetric anion species such as a mixed ion cluster bridging by Cl atoms may be considered to be adsorbed.

Figure 6 shows the ESR spectra of Fe(III) ions adsorbed on Dowex A-1 and Unicellex UR-50 in the media of pH 4 and pH 9. In the resin phase ESR spectra of Fe(III) ions adsorbed on Dowex A-1 in the media above pH 8, a broad signal with $g_{eff}\triangleq 2$ and $\Delta H_{pp}\triangleq 100$ mT and a weak signal with $g_{eff}\triangleq 4$ were observed. As this broad signal is similar to that of Fe(III) hydroxide powder, of which a spectrum is included in Fig. 6, most of Fe(III) ions on the resin phase are considered to exist as hydroxyl complex or hydroxide. In the resin phase ESR spectra of Fe(III) ions adsorbed on Unicellex UR-50, however, a broad signal with $g_{eff}\triangleq 2$ was not observed and the $g_{eff}\triangleq 4$ signal intensity increased in the pH region where hydroxide forms. The $g_{eff}\triangleq 4$ signal in the media of pH 4 was analyzed in the same way with Mn(II) ion. The data may be $D>0.23\ cm^{-1}$ and $\lambda=-1/3\ cm^{-1}$. Therefore, the Fe(III) ions adsorbed on the resin phase in the media of pH 4 are suggested to be of rhombic symmetry similarly to Mn(II) ions. For comparison, an ESR spectrum of Fe(III)-porphine complex, which is characterized by strong axial symmetry, is also shown in Fig. 6.[16] Although the $g_{eff}\triangleq 4$ signal for pH 4 is apparently similar to that for concentrated HCl media, it must be emphasized that the adsorbed species are different.

Especially for Fe(III) ions, resin phase Mössbauer spectra were observed by using metallic iron-57 and spectral parameters at room temperature are listed in Table 6. The Mössbauer parameters suggest that the iron adsorbed on the resin phase in concentrated HCl media is trivalent of high-spin configuration and of tetrahedral symmetry[23] and a small peak that shows lower symmetric species was observed in a Mössbauer spectrum at liquid nitrogen temperature, whereas those for the iron adsorbed in the media of pH 4 suggest that

TABLE 6. MÖSSBAUER PARAMETERS FOR IRON ADSORBED ON THE RESIN PHASES

Sample	I.S.[a] mm s^{-1}	Q.S.[a] mm s^{-1}	L.W.[a] mm s^{-1}
A-1, concd HCl	0.19	0.36	0.24
A-1, pH 4.00	0.37	0.65	0.72
A-1, pH 9.00	0.37	0.80	0.53
UR-50, concd HCl		n.d.	
UR-50, pH 4.00	0.45	0.82	0.76
UR-50, pH 9.00	0.41	0.87	0.56

a) I.S.: Isomer shift; Q.S.: quadrupole splitting; L.W.: line width.

the iron on the resin phase is trivalent of high-spin configuration and very distorted symmetry of tetrahedron rather than octahedron as judged from the value of isomer shift. In the media of pH 9 the parameters are similar to those of iron(III) hydroxide.[24] This fact suggests the adherence of hydroxide in addition to the adsorption of hydroxyl complex and accounts for the increase in $(Fe)_R$ values and for the appearance of the broad ESR signal with $g_{eff} \triangleq 2$.

The Mössbauer parameters at room temperature for the iron adsorbed on Unicellex UR-50 in the media of pH 4 suggest that the iron on the resin phase is trivalent of high-spin configuration and distorted octahedral symmetry. All Mössbauer spectra were also measured at the liquid nitrogen temperature but no significant suggestion was obtained.

From the above discussion, it may be concluded that the iminodiacetato group in Dowex A-1 coordinates as a tridentate ligand to Fe(III) ion and a distorted tetrahedron is completed by water molecules, whereas in Unicellex UR-50 the phenolic hydroxyl group also coordinates in alkaline media and a distorted octahedron is completed by water molecules.

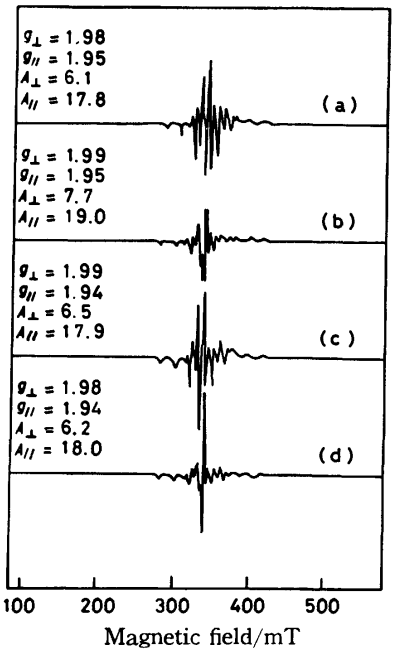

Fig. 7. ESR spectra of VO(II) ions adsorbed on Dowex A-1 and Unicellex UR-50.
(a): A-1, concd HCl, dry, (b): UR-50, concd HCl, dry, (c): A-1, pH 3.82, dry, (d): UR-50, pH 3.58, dry. A values are expressed in mT.

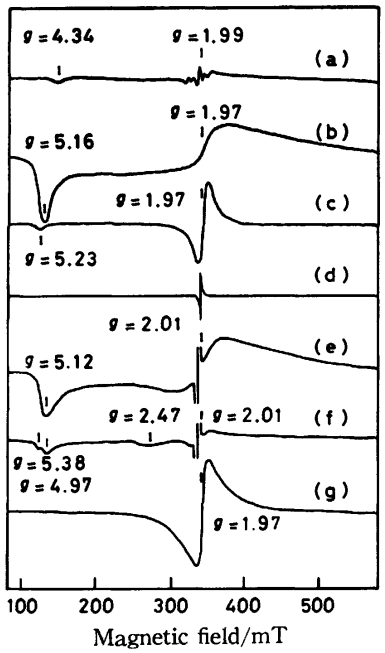

Fig. 8. ESR spectra of Cr(III) ions adsorbed on Dowex A-1 and Unicellex UR-50 and hydroxide.
(a): A-1, concd HCl, dry, (b): A-1, pH 3.90, dry, (c): A-1, pH 8.50, dry, (d): UR-50, concd HCl, dry, (e): UR-50, pH 4.04, dry, (f): UR-50, pH 8.38, dry, (g): Cr(III) hydroxide.

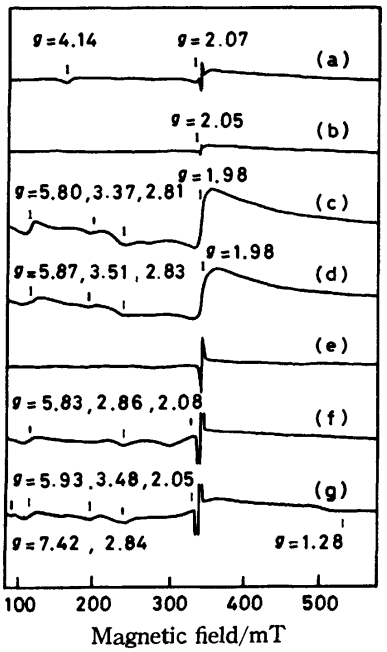

Fig. 9. ESR spectra of Gd(III) ions adsorbed on Dowex A-1, Dowex 1×4 and Unicellex UR-50.
(a): A-1, concd HCl, dry, (b): 1×4, concd HCl, dry, (c): A-1, pH 3.91, dry, (d): A-1, pH 8.55, dry, (e): UR-50, concd HCl, dry, (f): UR-50, pH 3.84, dry, (g): UR-50, pH 8.59, dry.

Other Paramagnetic Metal Ions Adsorbed on the Resin Phase. ESR spectra of VO(II), Cr(III), and Gd(III) ions adsorbed on the resin phase are shown in Figs. 7, 8, and 9. VO(II) ions adsorbed on the resin phase show anisotropic spectra and ESR parameters for VO(II) ions on Dowex A-1 and Unicellex UR-50 are virtually unchanged. In the resin phase infrared spectra of VO(II) ions adsorbed on Dowex A-1 and Unicellex UR-50 in the media of pH 9, V–O stretching bands were observed at 970 and 1010 cm^{-1}, respectively. This fact may reflect the coordination of the phenolic hydroxyl group in Unicellex UR-50. VO(II) ions adsorbed on Dowex A-1 and Unicellex UR-50 are considered to be of distorted tetragonal symmetry completed by water molecules.

In the resin phase ESR spectra of Cr(III) ions adsorbed on Dowex A-1 in the media of pH 4, signals with $g \triangleq 5$ and $g=1.97$ resulting from the zero-field splitting were observed. In the resin phase ESR spectra of Cr(III) ions adsorbed on Unicellex UR-50 in alkaline media, the $g \triangleq 5$ signal splitted into $g=5.28$ and $g=4.93$ and the $g \triangleq 2.5$ signal appeared. This fact may reflect the coordination of the phenolic hydroxyl group in Unicellex UR-50.

Gd(III) ions adsorbed on Dowex A-1 and Unicellex UR-50 also show signals resulting from the zero-field splitting. The difference in $(Gd)_R$ values and resin phase ESR spectral patterns between Dowex A-1 and Unicellex UR-50 also may reflect the coordination of the phenolic hydroxyl group in Unicellex UR-50.

The authors are grateful to Unitika Ltd, for the supply of Unicellex chelating resin.

References

1) C. Heitner-Wirguin, "Ion Exchange and Solvent Extraction," ed by J. A. Marinsky, Y. Marcus, Marcel Dekker. Inc., New York and Based (1977), Vol. 7, Chap. 3, pp. 141—148.

2) R. Cohen and C. Heitner-Wirguin, *Inorg. Chim. Acta*, **3 : 4**, 647 (1977).

3) K. Umezawa and T. Yamabe, *Bull. Chem. Soc. Jpn.*, **45**, 56 (1972).

4) P. J. Hoek and J. Reedijk, *J. Inorg. Nucl. Chem.*, **41**, 401 (1979).

5) S. Tomoshige, M. Hirai, H. Ueshima, and K. Ueno, *Anal. Chim. Acta*, **115**, 285 (1980).

6) G. R. Hertel and H. M. Clark, *J. Phys. Chem.*, **65**, 1930 (1961).

7) C. A. Clausen, III and M. L. Good, *Inorg. Chem.*, **7**, 2662 (1968).

8) D. Nicholls, "Comprehensive Inorganic Chemistry," ed by J. C. Bailar, H. J. Emeleus, Sir Ronald Nyholm, and A. F. Trotman-Dickenson, Pergamon Press, Ltd., London (1973), Vol. 3, pp. 979.

9) M. Ichiki, T. Isobe, and T. Tarutani, *Mem. Fac. Sci., Kyushu Univ., Ser. C*, **11**, 41 (1978).

10) D. E. Leyden and A. L. Underwood, *J. Phys. Chem.*, **68**, 2093 (1964).

11) K. Nakamoto, "Infrared Spectra of Inorganic and Coordination Compounds," John Willey and Sons (1963), pp. 205—210.

12) H. Waki, S. Takahashi, and S. Ohashi, *J. Inorg. Nucl. Chem.*, **35**, 1259 (1973).

13) S. Chaberek, Jr., and A. E. Martell, *J. Am. Chem. Soc.*, **74**, 5052 (1952).

14) S. A. Al'tshuler and B. M. Kozyrev, "Electron paramagnetic resonance," Translated by C. P. Poole, Jr., Academic Press, Inc., New York (1964).

15) J. J. Foster and Naida S. Gill, *J. Chem. Soc., A*, **1968**, 2625.

16) R. D. Dowsing and J. F. Gibson, *J. Chem. Phys.*, **50**, 294 (1969).

17) R. D. Dowsing, J. F. Gibson, M. Goodgame, and P. J. Hayward, *J. Chem. Soc., A*, **1969**, 187.

18) R. D. Dowsing, J. F. Gibson, D. M. L. Goodgame, M. Goodgame, and P. J. Hayward, *J. Chem. Soc., A*, **1969**, 1242.

19) R. D. Dowsing, J. F. Gibson, M. Goodgame, and P. J. Hayward, *J. Chem. Soc., A*, **1970**, 1133.

20) W. E. Blumberg, "Magnetic Resonance in Biological Systems," ed by A. Ehrenberg, B. E. Malmström, and T. Vänngard, Pergamon Press, Ltd., London (1967), p. 119.

21) T. Castner, Jr., G. S. Newell, W. C. Holton, and C. P. Slichter, *J. Chem. Phys.*, **32**, 668 (1960).

22) J. S. Griffith, *Mol. Phys.*, **8**, 213, 217 (1964).

23) Y. Takashima, Y. Maeda, and S. Umemoto, *Bull. Chem. Soc. Jpn.*, **42**, 1760 (1969).

24) H. Ujihira and J. Kitayama, *Analysis and Research*, **15 : 12**, 542 (1977).

Phase Equilibria in the Gd_2O_3–V_2O_3–V_2O_5 System at 1200 °C

Kenzo KITAYAMA* and Takashi KATSURA
Department of Chemistry, Faculty of Science, Tokyo Institute of Technology, Ookayama, Meguro-ku, Tokyo 152
(Received September 16, 1981)

The phase equilibria in the Gd_2O_3–V_2O_3–V_2O_5 system are studied at 1200 °C by changing the oxygen partial pressure from −0.68(air) to −12.50 in terms of log P_{O_2}. In this system, Gd_2O_3, $GdVO_4$, $GdVO_3$, $0.81Gd_2O_3 \cdot 0.19V_2O_5$, V_2O_3, V_3O_5, V_4O_7, V_5O_9, V_6O_{11}, V_7O_{13}, and VO_2 are stable. $GdVO_4$ and $0.81Gd_2O_3 \cdot 0.19V_2O_5$ have nonstoichiometric compositions. The crystallographic properties of the latter are determined with reference to the indices of a certain compound, $4Tm_2O_3 \cdot V_2O_5$. On the basis of the phase equilibria, the Gibbs free energy of these two reactions: $31/50\ Gd_2O_3 + 19/50\ GdVO_3 + 19/100\ O_2 = Gd_{1.62}V_{0.38}O_{3.38}$ and: $GdVO_3 + 1/2\ O_2 = GdVO_4$ are determined to be 57.0 and 127.8 kJ respectively.

The phase equilibria in the Ln_2O_3–V_2O_3–V_2O_5 systems (Ln=Sm, Lu, and Er) at 1200 °C have been established.[1–3] In these systems, the existence of V_nO_{2n-1}(n=3—7) was confirmed between V_2O_3 and VO_2. In addition to the above vanadium oxides, in the Sm_2O_3–V_2O_3–V_2O_5 system, $5Sm_2O_3 \cdot V_2O_5$ ($Sm_{10}V_2O_{20}$), $SmVO_3$, and $SmVO_4$; in the Lu_2O_3–V_2O_3–V_2O_5 system, $LuVO_3$, $LuVO_4$, $Lu_7V_3O_{16}$, $Lu_2V_2O_7$, and LuV_4O_8, and in the Er_2O_3–V_2O_3–V_2O_5 system, $ErVO_3$, $ErVO_4$, and $4Er_2O_3 \cdot V_2O_5$ ($Er_8V_2O_{17}$) were stable as the ternary compounds. Different patterns of the phase diagram were obtained as results of differences in the coexisting compounds.

In the present study, Gd_2O_3 was chosen as one of the Ln_2O_3 compounds, because Gd is the first one in the heavy-lanthanoid series from the viewpoint of the electron configuration.

In the Gd_2O_3–V_2O_3 system, only $GdVO_3$ is well known as a double-oxide phase. However, the system has not yet completely been studied because of the instability of V_2O_3 in an atmosphere of air. The crystallographic properties of $GdVO_3$ have been investigated by many researchers.[4–6] It is an orthorhombic system, like the other rare-earth vanadites except $LaVO_3$ and $CeVO_3$.[4,6]

The Gd_2O_3–V_2O_5 system was studied by Brusset *et al.*[7,8] in the temperature range from 600 to 1500 °C. They found two compounds, $4Gd_2O_3 \cdot V_2O_5$ and $5Gd_2O_3 \cdot V_2O_5$, as intermediate phases above 1150 °C in addition to $GdVO_4$. The spacing and relative intensities of the two compounds were also included in one of the reports,[7] but the assignment of the indices was not successful.

The objectives of the present study are: (1) to establish the detailed phase equilibria in the Gd_2O_3–V_2O_3–V_2O_5 system at 1200 °C in order to clarify the stable ternary compounds, (2) to calculate the Gibbs free energy of the reactions of the ternary compounds which were found in the phase diagram, and (3) to ascertain whether or not there exists a linear relationship between the Gibbs free energy of the reactions and the ionic radius of the lanthanoid, as is found in the Ln–Fe–O.[9]

Experimental

Analytical grades of Gd_2O_3 (99.9%) and V_2O_5, which had been obtained by heating guaranteed-grade NH_4VO_3 at 500 °C in air for about 24 h, were used as the starting materials. The desired ratios of Gd_2O_3/V_2O_5 were obtained by mixing the appropriate quantities thoroughly in an agate motar under ethyl alcohol. The mixtures thus made were treated by the procedures described previously.[1] The apparatus and procedures for controlling the oxygen partial pressures, keeping the furnace at a constant temperature, the method of thermogravimetry, the criterion for an equilibrium establishment, the method of identifing solid phases after quenching, the method of lattice-constant measurement, and the method of wet chemical analysis were the same as those described in previous papers.[1,10–13]

The oxygen partial pressure of −12.50 in terms of log P_{O_2} was chosen as the reference oxygen partial pressure, because even samples which contain less than 50% of Gd_2O_3 in mole are stable in composition in this reference atmosphere at 1200 °C.

Results and Discussion

Phase Equilibria. Ten samples with Gd_2O_3/V_2O_5 mole ratios of 86/14, 81/19, 76/24, 7/3, 6/4, 1, 4/6, 2/8, and 1/9 were prepared for use in the thermogravimetric experiment. In Fig. 1, the relationship between the oxygen partial pressure and the weight change, W_{O_2}/W_T, is shown; W_{O_2} is the weight gain of the sample from the reference-state atmosphere of log P_{O_2}=−12.50, and W_T is the total weight gain that the sample would get if the V_2O_3 in the sample changed to V_2O_5. The experimental results for four representative samples, 86/14, 8/2, 7/3, and 2/8, are shown in Fig. 1.

In Table 1, the results of the identification of the phases are shown: the first column shows the compositions of the starting materials; in the second and third are shown the experimental conditions of the oxygen partial pressure in terms of log P_{O_2} and the experimental duration respectively; in the fourth are shown the phases, as identified by means of an X-ray powder diffractometer using Cu $K\alpha$ radiation.

Based upon the above experimental results, a phase diagram of the system at 1200 °C is depicted in Fig. 2. The following phases are present under the present experimental conditions except in the V_2O_3–V_2O_5 system: Gd_2O_3(R), $Gd_{1.62}V_{0.38}O_{3.38}$(A), $GdVO_3$(L), and $GdVO_4$(K). The compounds in the V_2O_3–V_2O_5 system are the same as those in the previous report.[1]

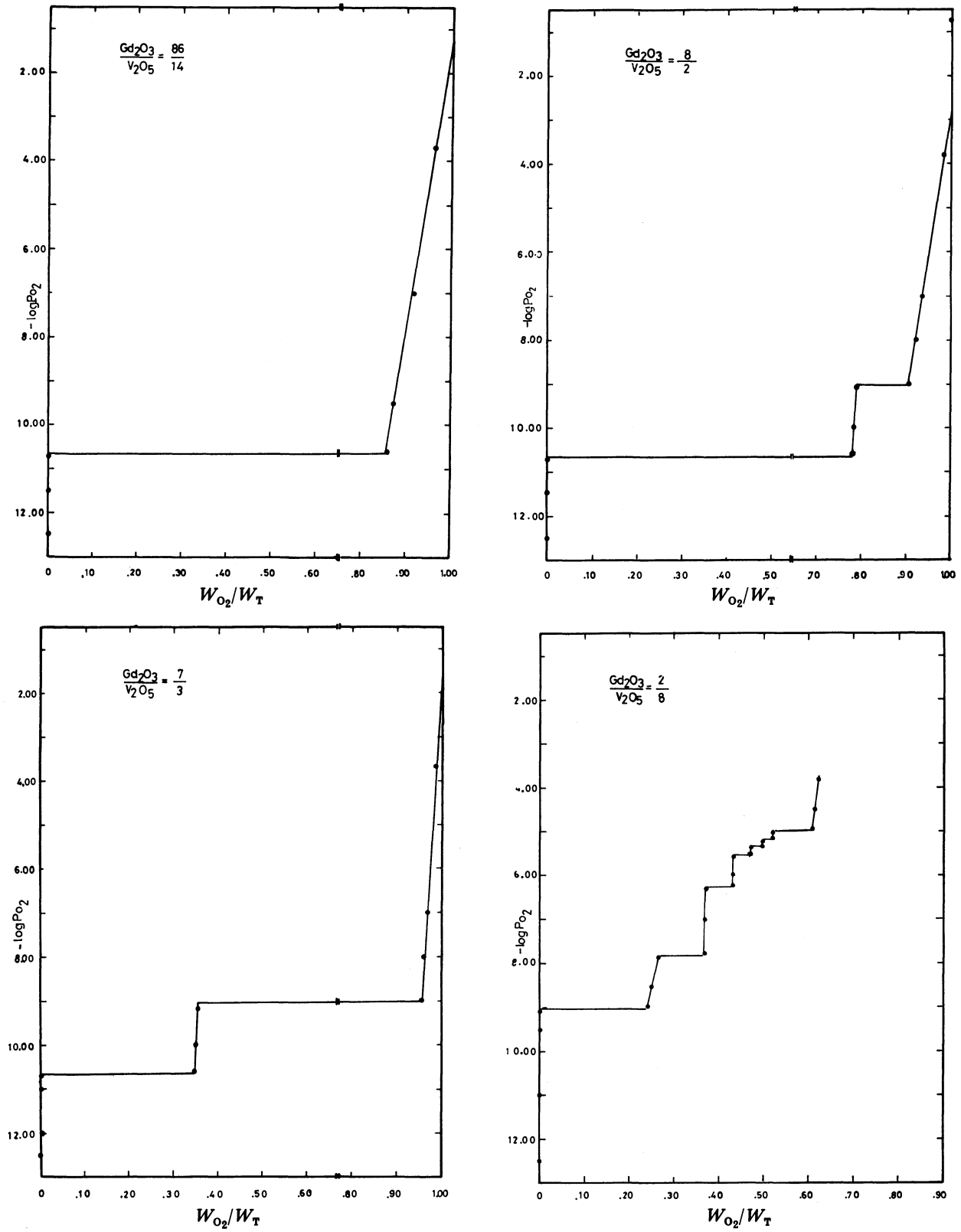

Fig. 1. The relationship between $-\log P_{O_2}$ and the weight gain (W_{O_2}/W_T) of the sample.
(a): Gd_2O_3/V_2O_5=86/14, (b): Gd_2O_3/V_2O_5=8/2, (c): Gd_2O_3/V_2O_5=7/3, (d): Gd_2O_3/V_2O_5=2/8.

Compound A has no round mole ratio such as the $4Gd_2O_3 \cdot V_2O_5$ reported by Brusset *et al.*[7,8] A straight line that connects the experimental points tends toward the $0.81Gd_2O_3 \cdot 0.19V_2O_5$ composition point rather than toward $4Gd_2O_3 \cdot V_2O_5$. This result is also supported by the results of the thermogravimetry of the sample 8/2 (Fig. 1-2). That is, the abrupt change occured at -9.06 in $\log P_{O_2}$. In order to support the fact by quenching method, we tried to make two phases quenched samples (A+$GdVO_3$) and (A+$GdVO_4$) at

TABLE 1. IDENTIFICATION OF PHASES

Starting material (mol%)		$-\log P_{O_2}$	Time / h	Phases[a)]
Gd_2O_3	V_2O_5			
86	14	11.00	10.0	$Gd_2O_3+GdVO_3$
		10.50	18.7	Gd_2O_3+A
		8.50	19.4	Gd_2O_3+A
		0.68	23.5	Gd_2O_3+A
70	30	11.00	10.0	$Gd_2O_3+GdVO_3$
		10.50	18.7	A+$GdVO_3$
		8.50	19.4	A+$GdVO_4$
		0.68	23.5	A+$GdVO_4$
20	80	11.00	10.0	$GdVO_3+V_2O_3$
		10.50	18.7	$GdVO_3+V_2O_3$
		8.50	19.4	$GdVO_4+V_2O_3$
		7.00	19.0	$GdVO_4+V_3O_5$
		5.75	28.0	$GdVO_4+V_4O_7$
		5.50	26.0	$GdVO_4+V_5O_9$
		5.30	41.5	$GdVO_4+V_6O_{11}$
		5.10	91.5	$GdVO_4+V_7O_{13}$
		4.50	39.0	$GdVO_4+VO_2$
10	90	11.00	10.0	$GdVO_3+V_2O_3$
		10.50	18.7	$GdVO_3+V_2O_3$
		8.50	19.4	$GdVO_4+V_2O_3$
		7.00	19.0	$GdVO_4+V_3O_5$
		5.75	28.0	$GdVO_4+V_4O_7$
		5.50	26.0	$GdVO_4+V_5O_9$
		5.30	41.5	$GdVO_4+V_6O_{11}$
		5.10	91.5	$GdVO_4+V_7O_{13}$
		4.50	39.0	$GdVO_4+VO_2$

a) A: $Gd_{1.62}V_{0.38}O_{3.38}$.

$\log P_{O_2}=-10.00$ and in air. However, peaks of $GdVO_3$ and $GdVO_4$ are too weak to identify the phases.

Compounds A and $GdVO_4$ have non-stoichiometric compositions. The relationship between the oxygen partial pressure and the compositions are represented by the following equations: $N_O/N_A=5.83\times10^{-3}\log P_{O_2}+8.83\times10^{-3}$ for Compound A and $N_O/N_K=1.50\times10^{-3}\log P_{O_2}+4.5\times10^{-3}$ for $GdVO_4$. Here, N_O/N_A and N_O/N_K denote the mole fraction ratio of the oxygen to the oxide component, shown by the letters A and K, and the deviation from the stoichiometry. Non-stoichiometry was not found for $GdVO_3$ under those experimental conditions.

In Table 2, the compositions of the compound, as calculated from the results of the thermogravimetry, the symbols of the compounds, the stability ranges of the compounds in terms of the oxygen partial pressure

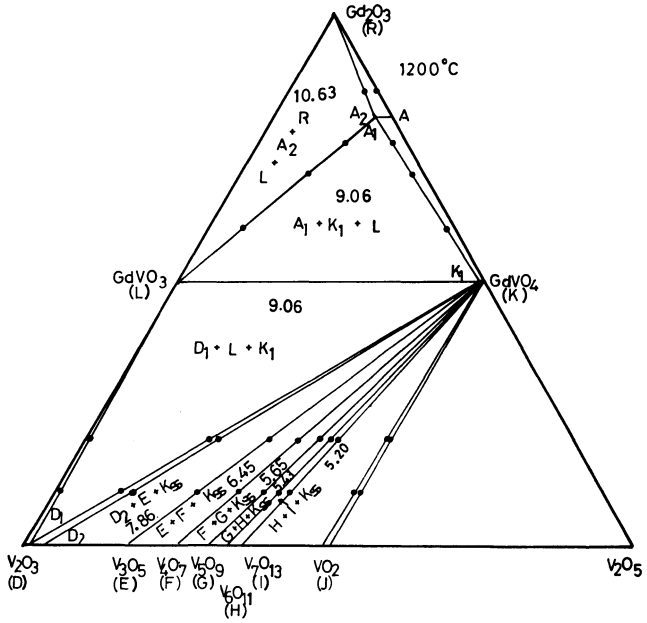

Fig. 2. Phase equilibria in the Gd_2O_3–V_2O_3–V_2O_5 system at 1200 °C. Numerical values in three solid phases regions are the oxygen partial pressure in $-\log P_{O_2}$ in equilibrium. Abbreviations are the same as those in Table 2.

TABLE 3. SPACINGS AND RELATIVE INTENSITIES OF A POWDER SAMPLE OF $Gd_{1.62}V_{0.38}O_{3.38}$ AND PREVIOUS DATA OF $Gd_8V_2O_{17}$

h	k	l	d(obsd)	d(calcd)	I/I_0	$Gd_8V_2O_{17}$ d	$Gd_8V_2O_{17}$ I/I_0
1	2	3	3.12	3.14	100	3.166	65
2	0	4	2.95	2.97	19	3.129	100
0	3	2	2.70	2.75	45	3.009	55
0	3	3	2.59	2.57	11	2.919	8
0	4	1	2.14	2.17	12	2.690	45
−5	2	2	1.912	1.916	51	1.941	25
−2	4	5	1.766	1.765	18	1.922	10
5	3	2	1.631	1.629	42	1.881	15
						1.870	15
						1.865	20
						1.655	10
						1.639	10
						1.625	10
						1.618	10
						1.589	10
						1.564	7

TABLE 2. COMPOSITIONS, STABILITY RANGES IN OXYGEN PARTIAL PRESSURES, AND ACTIVITIES IN SOLID SOLUTIONS

Component	Composition	Symbol	$-\log P_{O_2}$	$\log a_i$
$Gd_{1.62}V_{0.38}O_{3.38}$	$Gd_{1.62}V_{0.38}O_{3.38}$	A	1.52[b)]−0.68[a)]	0.121
	$Gd_{1.62}V_{0.38}O_{3.34}$	A_1	9.06	0.0381
	$Gd_{1.62}V_{0.38}O_{3.33}$	A_2	10.63	0
$GdVO_4$	$GdVO_4$	K	3.00[b)]−0.68[a)]	0.0138
	$GdVO_{3.99}$	K_1	9.06	0

a) The stability range in $\log P_{O_2}$ may be higher than −0.68. b) This value was obtained by extrapolation using the experimental values.

Table 4. Unit-cell dimensions of the compounds

Sample	$-\log P_{O_2}$	a/Å	b/Å	c/Å	β/°	V/Å^3	Ref.
$Gd_{1.62}V_{0.38}O_{3.38}$	10.00	10.69±0.06	8.70±0.05	16.4±0.3	99.5±0.7	1504±27	
	0.68	10.70±0.07	8.77±0.08	16.3±0.3	99.6±0.9	1503±35	
$GdVO_3$	12.00	5.341±0.003	5.605±0.003	7.634±0.003		228.5±0.2	
		5.341	5.606	7.630			5
		5.342	5.604	7.637		228.6	6
$GdVO_4$	8.50	7.210±0.001		6.347±0.001		330.0±0.1	
	0.68	7.207±0.001		6.344±0.001		329.5±0.1	
		7.216±0.003		6.351±0.003			8
		7.211		6.350		330.2	15

in $\log P_{O_2}$, and the activities of the components are tabulated. The activities of all the components in the solid solutions are calculated by using the Gibbs-Duhem equation. A detailed method of the calculation has been described in the paper of Kimizuka and Katsura.[13]

The assignment of indices for Compound A was tried with the aid of previous data on $4Tm_2O_3 \cdot V_2O_5$.[14] In Table 3, the results of the assignment of indices, the relative intensities, and the spacings of the sample are tabulated, together with the spacings and relative intensities of $4Gd_2O_3 \cdot V_2O_5$ obtained by Brusset *et al.*[7] There are other weak and broad peaks that are not shown in Table 3. Though Brusset *et al.* did not present the indices, the two substance have similar spacings.

The lattice constants of three samples, A, $GdVO_3$, and $GdVO_4$ are tabulated in Table 4. The figures in second column are the oxygen partial pressure used in preparation of the quenched samples. The present values are in good agreement with those of the previous reports. The experimental errors in the lattice constants of Compound A are, however, still large. Refinement will be done in the near future.

Calculation of Gibbs Free Energy of Reactions. On the basis of the phase equilibria, the Gibbs free energy of reactions, referred to the following equations:

$$31/50Gd_2O_3 + 19/50GdVO_3 + 19/100O_2 = Gd_{1.62}V_{0.38}O_{3.38} \quad (1)$$

and:

$$GdVO_3 + 1/2O_2 = GdVO_4 \quad (2)$$

can be calculated from this equation: $\Delta G^\circ = -RT \ln K$, where R is the gas constant; T, the absolute temperature, and K, the equilibrium constant of the reaction. The activities of $Gd_{1.62}V_{0.38}O_{3.38}$ and $GdVO_4$ at the A_2 and K_1 compositions (Table 2) in both solid solutions may be equal to unity. Values of 57.0 and 127.8 kJ were obtained for Reactions 1 and 2 respectively.

References

1) K. Kitayama and T. Katsura, *Bull. Chem. Soc. Jpn.*, **50**, 889 (1977).
2) K. Kitayama and T. Katsura, *Bull. Chem. Soc. Jpn.*, **51**, 1358 (1978).
3) K. Kitayama, T. Sugihara, and T. Katsura, *Bull. Chem. Soc. Jpn.*, **52**, 458 (1979).
4) B. Reuter, *Colloq. Int. C. N. R. S.*, **1965**, 1053.
5) H. Brusset, R. Mahe, and A. Deboiche, *C. R. Acad. Sci. Paris*, **274**, 1293 (1972).
6) G. J. McCarthy, C. A. Sipe, and K. E. McIlvried, *Mater. Res. Bull.*, **9**, 1279 (1974).
7) H. Brusset, F. Madaule-Aubry, B. Blanck, and A. Deboiche, *Bull. Soc. Chim. Fr.*, **1969**, 15.
8) H. Brusset, F. Madaule-Aubry, B. Blanck, J. P. Glaziou, and J. P. Laude, *Can. J. Chem.*, **49**, 3700 (1971).
9) T. Katsura, K. Kitayama, T. Sugihara, and N. Kimizuka, *Bull. Chem. Soc. Jpn.*, **48**, 1809 (1975).
10) T. Katsura and H. Hasegawa, *Bull. Chem. Soc. Jpn.*, **40**, 561 (1967).
11) N. Kimizuka and T. Katsura, *J. Solid State Chem.*, **13**, 176 (1975).
12) T. Katsura and A. Muan, *Trans. AIME*, **230**, 77 (1964).
13) N. Kimizuka and T. Katsura, *J. Solid State Chem.*, **15**, 151 (1975).
14) H. Brusset, R. Mahe, and J. P. Laude, *Bull. Soc. Chim. Fr.*, **1973**, 495.
15) H. Schwarz, *Z. Anorg. Allg. Chem.*, **223**, 44 (1963).

Anion Exchange Separation of Hard Acid-metals Using HF-H_3BO_3 Media

Takeo ADACHI

Analytical Chemistry Laboratory, Japan Atomic Energy Research Institute, Tokai, Ibaraki 319-11

(Received October 2, 1981)

The properties of HF–H_3BO_3 media and the distribution coefficients of eighteen metals have been investigated to achieve the separation of hard acid-metals by the anion exchange method. As the addition of boric acid to hydrofluoric acid solution reduces the free fluoride ion concentration to about one hundredth, it is possible to control the formation of metal fluoride complexes in a way favorable for the separation. The BF_4^- and BF_3OH^- produced in this media are adsorbed strongly to the resin and reduce the relative adsorbabilities of metal fluoride complexes remarkably. Using these properties of HF–H_3BO_3 media and the adsorbabilities of other anions, a new anion exchange method for the separation of hard acid-metals has been proposed. The new method is especially useful for the separation of titanium, zirconium, niobium, and tantalum. Distribution coefficients and elution behaviors of metal ions are not affected by the increase of the amount of metals because of the buffer action relating to the fluoride ion in HF–H_3BO_3 media.

Most ion exchange separations of hard acid-metals[1] such as titanium, zirconium, niobium, tantalum, tungsten, molybdenum, and tin have been done using anion exchange resins[2] (unless otherwise devised[3]), because these metals are easily hydrolysed in the absence of complexing agents and tend to form stable anion complexes in the presence of complexing agents.

As anion complexes of these metals have similar chemical properties, the separation of these metals is not easy, and many efforts have been attempted.[4–13] The following three points are considered to be essential for the satisfactory separation:

(1) Select a proper complexing agent forming metal complexes whose chemical properties depend on the kind of metals.

(2) Choose coexisting anions and their concentrations to control the relative adsorbabilities of metal anionic complexes on the resin.

(3) Control the concentration of complexing agents, to adjust the stage of complex formation.

As for point (1), such complexing agents as fluoride,[14,15] oxalate,[11–13] and thiocyanate[16–18] have been investigated. Fluoride has been most frequently adopted in the practical separations of hard acid-metals, probably because the stability constants of fluoride complexes depend on the kind of metals most strongly. Even in hydrofluoric acid (more than 0.1 M, 1 M=1 mol dm^{-3}), however, sufficient separation is not expected unless other anions are present, since the difference in the adsorbabilities of fluoride complexes on a fluoride-form resin are not large enough.[14]

As for point (2), such a mixed solvent as HF–HCl[4–7] or HF–HNO_3[8–10] has been proposed for the separation of hard acid-metals. The adsorbability of a chloride or nitrate ion on the anion exchange resin is much stronger than that of fluoride ion. With the strong adsorbability of chloride or nitrate, the relative adsorbabilities of metal fluoride complexes are weakened and the separation of hard acid-metals becomes possible.

As for point (3), Kraus *et al.*[19] controlled the stage of chloride complex formation by adjusting the concentration of hydrochloric acid suitably and proposed the anion exchange separation of transition metals (including a few hard acid-metals).

If one would apply point (3) to the separation of hard acid-metals in the media containing fluoride ions, the concentration of fluoride ion must be kept fairly low and constant, because these metals form fully fluorinated complexes such as ZrF_6^{2-} and TiF_6^{2-} in hydrofluoric acid more than 0.1 M. In solutions which contain fluoride ion in less than 10^{-4} M, partially fluorinated complexes such as ZrF_5^- and TiF_4 are expected to form.[3]

In hydrofluoric acid solution or HF–HCl and HF–HNO_3 mixtures, however, it is not easy to maintain the fluoride ion concentration low and constant all through the procedures, since fluoride ions may be consumed by the relatively large amounts of metal ions or supplied from metal fluoride complexes adsorbed on the resin and fluoride-form resin.

The author reported in a previous paper[3] that the fluoride ion concentration can be kept low (10^{-4} to 10^{-5} M) in HF–H_3BO_3 media according to the formation of fluoroboric acids, though the concentration of hydrofluoric acid is rather high (more than 0.1 M). In the media, the fluoride ion concentration is kept constant by the buffer action based on the dissociation of fluoroboric acids even when large amounts of metal ions are present.

In the present paper, the separation of hard acid-metals is discussed in HF–H_3BO_3 media in relation to the above mentioned properties of HF–H_3BO_3 media and the adsorbabilities of coexisting anions, while referring to points (2) and (3).

Experimental

Chemicals and Apparatus. Standard solutions of metal ions were prepared by the procedures mentioned in the previous paper.[3] Other chemicals and apparatus were also the same as used previously.

Ion Exchange Resin. A strongly basic anion exchange resin, Diaion SA # 100, product of Mitsubishi Chemical Ind. Ltd. (8% DVB, 75 to 150 μm, Cl^--form) was used. After washing the resin in a column with five times volume of 3 M HNO_3 and with distilled water untill the effluent was free from nitrate ions, the resin was dried to constant weight at 70 °C and stored in a vacuum desiccator.

Determination of Distribution Coefficient. *Method I*: Fifty ml of a definite concentration of hydrofluoric–nitric acid solution or hydrofluoric–boric–nitric acid solution containing 2×10^{-4} M of a metal ion was added to a 150 ml polyethylene

bottle containing 0.5 g of the dried resin. The bottle was then shaken gently for 24 h at room temperature (the equilibrium is attained within 4 h). After filtration of the resin, the metal ion concentration in the solution was determined by a suitable method as previously described.[3]

The distribution coefficient, K_d, was determined by the following equation:

$$K_d = (\text{Amount of metal ion in resin/Amount of metal ion in solution}) \times (\text{ml of solution/g of resin}) \quad (\text{ml/g})$$

Method II: Fifty ml of 0.2 M hydrofluoric acid solution containing 2×10^{-4} M of a metal ion was added to a 150 ml polyethylene bottle containing 0.5 g of the dried resin. The bottle was then shaken for 24 h at room temperature. After discarding the solution the resin was washed with 10 ml of 10^{-2} M HF, and 50 ml of a definite concentration of HF–HNO_3 solution or HF–H_3BO_3–HNO_3 solution was added to the bottle. Subsequent procedures were the same as in Method I.

Column Operation. About 4 g of the dried resin in NO_3^--form which had been swelled with distilled water was packed in a polyethylene column (8 mmϕ × 180 mm) and the column was conditioned with about 50 ml of 0.2 M HF. After addition of a test solution containing 1 mg of a metal ion in 0.2 M HF, an eluent of a definite composition was passed through the column. The effluent was collected with a fraction collector and the concentration of the metal ion in each fraction was determined by the methods previously mentioned.[3]

Results

The following experimental results were obtained in solutions containing more than 10^{-2} M in HNO_3 in order to prevent the hydrolysis of hard acid-metals, unless otherwise mentioned.

Distribution Coefficients. Distribution coefficients K_d of Ti(IV), Zr(IV), Nb(V), and Ta(V) were investigated by Method I in solutions which contained various concentrations of hydrofluoric acid (C_{HF}) both in the presence and in the absence of 0.5 M H_3BO_3. The results are illustrated in Fig. 1.

The K_d values of these metals in HF–H_3BO_3 media are smaller than those in HF. In both media, the K_d values of these metals are increased with the increase of C_{HF} up to 10^{-2} M. In solutions containing more than 10^{-2} M of HF, the K_d in HF–H_3BO_3 media are decreased with increasing C_{HF}, whereas those in HF are almost unchanged with C_{HF}. The K_d values in both media at any C_{HF} decrease with increasing nitric acid concentration (C_{HNO_3}).

The K_d values obtained by Method II are similar to those by Method I as shown in Fig. 2.

The K_d of other metals in HF–H_3BO_3 media containing HNO_3 are presented in Table 1. In the third and fourth columns in Table 1, K_d in solutions containing various concentrations of H_3BO_3 ($C_{H_3BO_3}$) and 0.1 M HF, and K_d in solutions containing various C_{HF} and 0.5 M H_3BO_3 are listed.

At constant C_{HF} (column 3 in Table 1), the K_d of W(VI), Nb(V), Hf(IV), Zr(IV), Mo(VI), Ti(IV), and Sn(IV) remarkably decrease when the $C_{H_3BO_3}$ is changed from 10^{-2} to 0.1 M. The decrease of K_d of Ta(V) with increasing C_{HF}, however, is not noticeable.

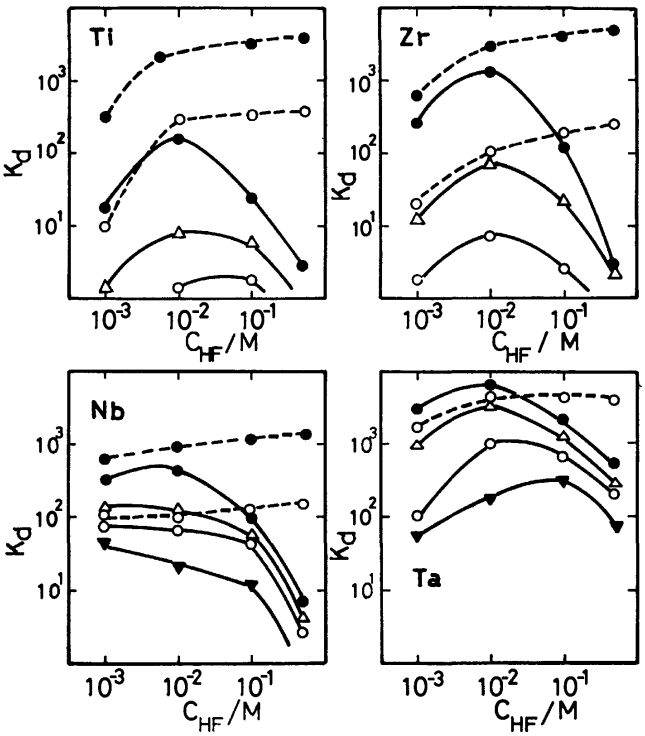

Fig. 1. Distribution coefficients of Ti(IV), Zr(IV), Nb(V), and Ta(V) in HF and HF–H_3BO_3 media containing HNO_3.
HF–0.5 M H_3BO_3–HNO_3 (——), HF–HNO_3 (------).
C_{HNO_3}; ●: 10^{-2} M, △: 0.03 M, ○: 0.1 M, ▼: 0.3 M.

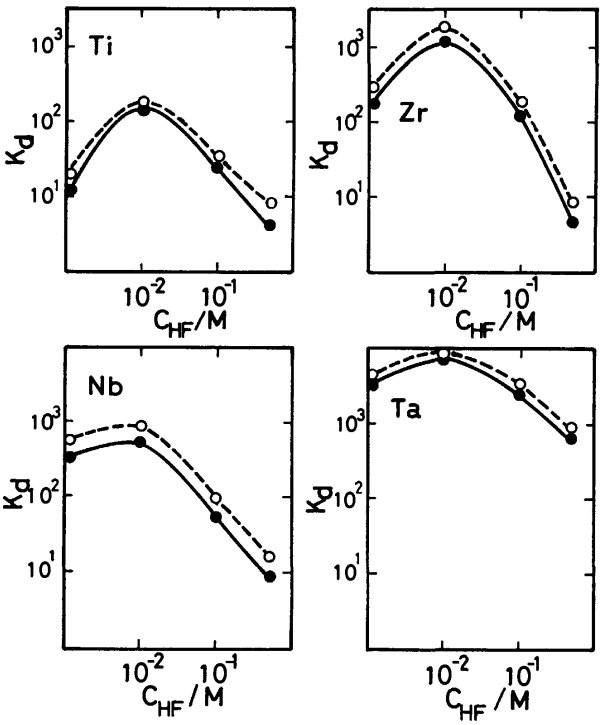

Fig. 2. Effect of equilibrating method on K_d of Ti(IV), Zr(IV), Nb(V), and Ta(V) in HF–0.5 M H_3BO_3–10^{-2} M HNO_3.
—●—: Method I, ---○---: Method II.

Table 1. Anion exchange distribution coefficients of metal ions in $HF-H_3BO_3$ media containing HNO_3

Ion	$[HNO_3]$/M	0.1 M HF–H_3BO_3 $[H_3BO_3]$/M 0	10^{-3}	10^{-2}	0.1	0.5	HF–0.5 M H_3BO_3 [HF]/M 10^{-3}	10^{-2}	0.1	0.5
Ta(V)	10^{-2}	$>5\times10^3$	5×10^3	4.1×10^3	2.4×10^3	2.3×10^3	3.3×10^3	5×10^3	2.3×10^3	606
	10^{-1}	4.0×10^3	1.5×10^3	1.2×10^3	1.0×10^3	790	102	955	790	315
W(VI)	10^{-2}	$>5\times10^3$	5×10^3	765	97	232	4.3×10^3	2.4×10^3	232	13
	10^{-1}	115	110	28	14	56	182	112	56	5
Nb(V)	10^{-2}	5×10^3	5.0×10^3	531	90	95	321	383	95	6
	10^{-1}	102	91	68	18	58	79	71	58	3
Hf(IV)	10^{-2}	4.2×10^3	2.2×10^3	1.4×10^3	181	152	1.0×10^3	1.6×10^3	152	19
	10^{-1}	360	320	245	7	<3	<3	10	<3	3
Zr(IV)	10^{-2}	$>5\times10^3$	$>5\times10^3$	5.0×10^3	162	140	306	1.3×10^3	140	4
	10^{-1}	375	346	282	6	<3	<3	8	<3	<3
Mo(VI)	10^{-2}	1.2×10^3	906	209	33	44	995	613	44	11
	10^{-1}	75	56	25	4	15	48	33	15	6
Ti(IV)	10^{-2}	$>5\times10^3$	$>5\times10^3$	3.8×10^3	70	15	18	150	15	3
	10^{-1}	405	355	302	18	<3	<3	<3	<3	<3
Sn(IV)	10^{-2}	$>5\times10^3$	$>5\times10^3$	5.0×10^3	57	15	39	141	15	14
	10^{-1}	420	390	322	15	<3	<3	<3	<3	<3
V(V)	10^{-2}	92	76	15	11	<3	4	3	<3	<3
	10^{-1}	4	<3	<3	<3	<3	<3	<3	<3	<3
U(VI)	10^{-2}	72	49	5	<3	<3	20	15	<3	<3
	10^{-1}	<3	<3	<3	<3	<3	<3	<3	<3	<3
V(IV)	10^{-2}	12	6	13	15	<3	6	10	<3	<3
	10^{-1}	<3	<3	<3	<3	<3	<3	<3	<3	<3
Al(III)	10^{-2}	30	20	12	10	7	8	5	7	3
	10^{-1}	<3	<3	<3	<3	<3	<3	<3	<3	<3
Cr(III)	10^{-2}	31	28	14	<3	5	3	14	5	<3
	10^{-1}	<3	<3	<3	<3	<3	<3	<3	<3	<3
Fe(III), Cu(II), Cd(II), Ni(II), Mn(II), Co(II)				<3				<3		

At constant $C_{H_3BO_3}$ (column 4 in Table 1), the K_d of Hf(IV) or Sn(IV) is at a maximum when C_{HF} is at around 10^{-2} M, but the K_d of W(VI) and Mo(VI) are large even when C_{HF} is at 10^{-3} M and decrease monotonously with the increase of C_{HF}. This is similar to the results for Ti(IV), Zr(IV), Nb(V), and Ta(V) (Fig. 1). The large K_d values of W(VI) and Mo(VI) at low C_{HF} may be due to the fact that these metals exist as such anions as WO_4^{2-} and $Mo_7O_{24}^{6-}$ even in the absence of complexing agents.

The K_d of V(V), V(IV), U(VI), Al(III), Cr(III), and Fe(III) are small at most of C_{HF} and $C_{H_3BO_3}$.

According to the Ringbom's criterion for ion exchange separation by column filtration (*i.e.* K_d of an adsorbed ion is larger than 10^2 to $10^{2.5}$ and that of the emerging ion is less than $10^{0.5}$ to 10^1),[20] the following results are expected from the K_d values in Fig. 1 and Table 1 for the column separation of hard acid-metals; (a) In 0.1 M HF–10^{-2} M HNO_3, hard acid-metals such as Ta(V), W(VI), Nb(V), Hf(IV), Zr(IV), Mo(VI), Ti(IV), Sn(IV), V(V), and U(VI) are retained in the column and V(IV) and Fe(III) are eluted from the column. Al(III) and Cr(III) are retained loosely or eluted slowly. (b) In 0.1 M HF–0.5 M H_3BO_3–10^{-2} M HNO_3, among the metals retained in the column in (a), V(V) and U(VI) are eluted and Ti(IV) and Sn(IV) are eluted slowly. Mo(VI) is retained loosely. (c) In 0.1 M HF–0.5 M H_3BO_3–0.1 M HNO_3, among the metals retained in (b), Hf(IV) and Zr(IV) are eluted and Mo(VI) is eluted slowly. W(VI) and Nb(V) are retained loosely. (d) In 0.5 M HF–0.5 M H_3BO_3–0.1 M HNO_3, among the metals retained in (c), W(VI) and Nb(V) are eluted. Ta(V) cannot be eluted by the media mentioned above.

Although the media mentioned in (a) to (d) are chosen as an example, other possibilities for separation are obtained by selecting C_{HF}, $C_{H_3BO_3}$, and C_{HNO_3} properly.

Effect of Concentrations of HCl, H_2SO_4, HNO_3, and $HClO_4$ on K_d of Metals in HF–H_3BO_3 Media. The effects of various acids and their concentrations on the K_d of Ti(IV), Zr(IV), Nb(V), and Ta(V) in 10^{-2} M HF–0.5 M H_3BO_3 are presented in Fig. 3. In this experiment the anion exchange resin used had been converted to the respective anion form, as in the coexisting acids (*e.g.* when coexisting acid is $HClO_4$, the resin was converted to the ClO_4^--form).

Although the K_d values of all metals examined decrease with increasing the acid concentration regardless of the kind of acids, the degree of the effect of coexisting acids on K_d depends on the kind of acids; the effect is most serious with $HClO_4$.

The effect of concentration of sulfuric acid on K_d is gentle compared with those of other acids.

The K_d values of Nb(V) and Ta(V) are decreased

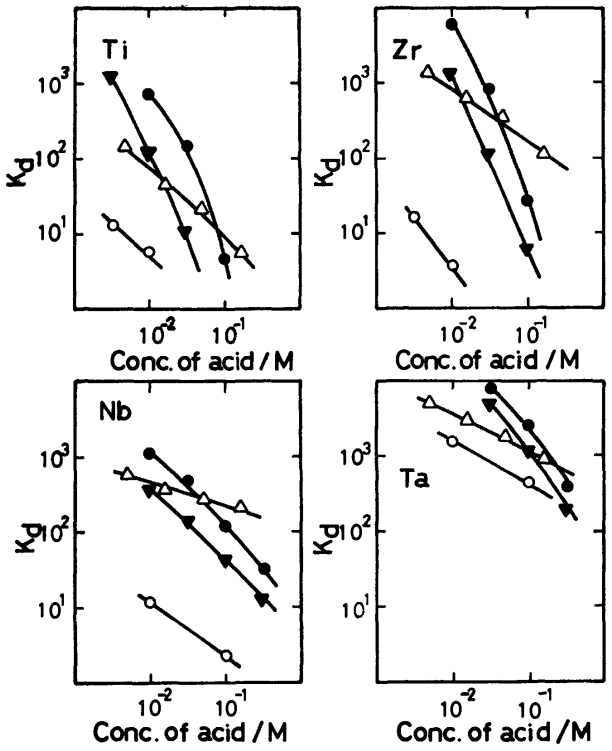

Fig. 3. Effect of concentration of coexisting acids on K_d of Ti(IV), Zr(IV), Nb(V), and Ta(V) in 10^{-2} M HF–0.5 M H_3BO_3.
●: HCl, △: H_2SO_4, ▼: HNO_3, ○: $HClO_4$.

more gently with the increase of acid concentration than those of Ti(IV) and Zr(IV).

Elution Behavior. In order to determine the practical conditions for the separation of Ti(IV), Zr(IV), Nb(V), and Ta(V), the elution behavior in HF–H_3BO_3 media was investigated after adsorption of these metals in a column (4 g of the dried resin, 8 mmϕ × 180 mm) in 0.2 M HF prior to the elution experiment. The flow rate of elution was adjusted to be 1.0 to 1.5 ml min^{-1}. The elution curves are shown in integrated form in Fig. 4.

As expected from the K_d values obtained by the batch method (Fig. 1 and Table 1), the mutual separation of these metals is possible by the column method as follows.

Ti(IV) is eluted when 100 ml of 10^{-2} M HF–0.5 M H_3BO_3–3×10^{-2} M HNO_3 or 0.1 M HF–0.5 M H_3BO_3–10^{-2} M HNO_3 is passed through the column, while Zr(IV), Nb(V), and Ta(V) are retained in the column even with 400 ml of these eluents (Fig. 4, (a)). Ti(IV) and Zr(IV) are eluted with 100 ml of 10^{-2} M HF–0.5 M H_3BO_3–0.1 M HNO_3 or 0.1 M HF–0.5 M H_3BO_3–0.1 M HNO_3, and Nb(V) is eluted with 300 ml of these eluents (Fig. 4, (b)). Ti(IV), Zr(IV), and Nb(V) are eluted with 100 ml of 0.5 M HF–0.5 M H_3BO_3–0.1 M HNO_3, while Ta(V) is not eluted with 300 ml of the eluent (Fig. 4, (c)). Ta(V) is eluted with 100 ml of 1 M HF–0.5 M H_3BO_3–5 M HNO_3 (Fig. 4, (d)-4), since the K_d value for Ta(V) in the medium is about 10.

The successive separation of Ti(IV), Zr(IV), Nb(V), and Ta(V) can be achieved when the media mentioned in (a) to (c) in Fig. 4 are properly combined as (d) in

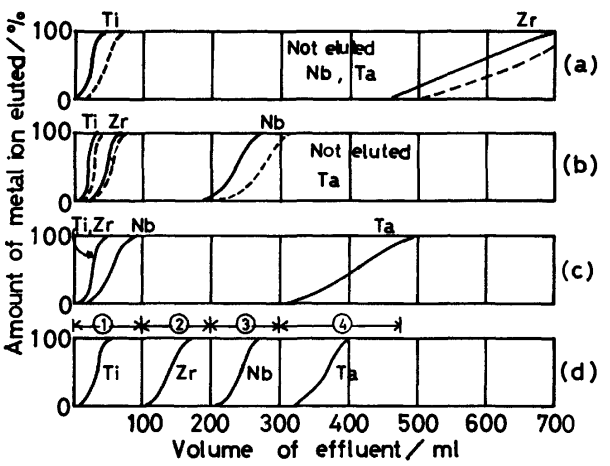

Fig. 4. Column elution behavior of Ti(IV), Zr(IV), Nb(V), and Ta(V) in HF–H_3BO_3 media containing HNO_3.
Diaion SA # 100: 4 g, flow rate: 1.0 ml/min. Concentration of HF–H_3BO_3–HNO_3 (M); (a) 0.1–0.5–10^{-2} (——), 10^{-2}–0.5–3×10^{-2} (------), (b) 0.1–0.5–0.1 (——), 10^{-2}–0.5–0.1 (------), (c) 0.5–0.5–0.1, (d) ①: 0.1–0.5–10^{-2}, ②: 0.1–0.5–0.1, ③: 0 5–0 5–0.1, ④: 1–0.5–5.

Fig. 4, as long as the amount of each metal is less than 1 mg.

Effect of Amount of Metal Ions on K_d and Elution Behavior of Metals. In HF–H_3BO_3 media, the free fluoride ion concentration is extremely low, as mentioned in the previous paper.[3] Therefore, the K_d values might be affected by the amount of metal ions owing to the deficiency of fluoride ions caused by the complex formation of large amount of metals with fluoride and/or the surplus of fluoride ions which are released from the large amount of metal fluoride complexes. This would occur especially when metals are adsorbed to the column in rather concentrated hydrofluoric acid in the beginning of the elution procedure.

The effect of the amount of Zr(IV) on K_d of Zr(IV) investigated by the batch method is summarized in Table 2. In this experiment, 2 g of the dried resin was used in order to keep the loading less than 0.1 and the solution of Zr(IV) was made free from fluoride ion. The C_{HF} was chosen so that the K_d of Zr(IV) is around 10^2 at 1 mg level of Zr(IV), *i.e.* 10^{-3} M C_{HF} in the absence of H_3BO_3 and 0.1 M C_{HF} in the presence of 0.5 M H_3BO_3.

The K_d obtained by equilibrating the media containing Zr(IV) with the resin (Method I in Table 2) is decreased by the increase of the amount of Zr(IV) from 0.25 to 50 mg, when 10^{-3} M HF–10^{-2} M HNO_3 is used as the medium. But the K_d is not changed with the amount of Zr(IV) up to 20 mg, when 0.1 M HF–0.5 M H_3BO_3–10^{-2} M HNO_3 is used as the medium.

The K_d obtained by equilibrating zirconium-free media with the resin on which Zr(IV) had been adsorbed in 0.2 M HF (Method II in Table 2) is extremely large compared with that by Method I and is more than 5×10^3 regardless of the amount of Zr(IV) when 10^{-3} M HF–10^{-2} M HNO_3 is used as the medium. On the other

Table 2. Effect of the amount of metal ions on distribution coefficients by batch method

Ion	Amount		K_d	
	mg	mmol	Method I[a]	Method II[b]
			(10^{-3} M HF–10^{-2} M HNO_3)	
Zr(IV)	0.25	2.7×10^{-3}	1.0×10^{3}	$>5\times10^{3}$
	1.0	1.1×10^{-2}	90	$>5\times10^{3}$
	10.0	0.11	6	$>5\times10^{3}$
	50.0	0.53	3	$>5\times10^{3}$
			(0.1 M HF–0.5 M H_3BO_3–10^{-2} M HNO_3)	
Zr(IV)	0.25	2.7×10^{-3}	145	165
	1.0	1.1×10^{-2}	142	160
	10.0	0.11	132	168
	20.0	0.21	126	162
	50.0	0.53	42	155
			(0.1 M HF–0.5 M H_3BO_3–0.1 M HNO_3)	
Nb(V)	1.0	1.1×10^{-2}	65	68
	10.0	0.11	66	82
	20.0	0.22	70	75

a) Determined by equilibrating the medium containing a metal ion with the resin. b) Determined by equilibrating the metal-free medium with the resin on which a metal ion had been adsorbed in 0.2 M HF.

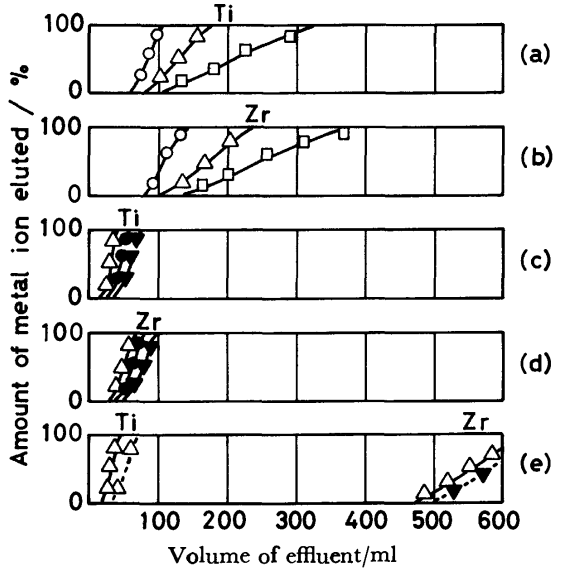

Fig. 5. Effect of amount of metal ions on elution behaviors of Ti(IV) and Zr(IV).
(a) and (b): 10^{-3} M HF–0.1 M HNO_3, (c) and (e): 0.1 M HF–0 5 M H_3BO_3–10^{-2} M HNO_3, (d): 0 1 M HF–0 5 M H_3BO_3–0.1 M HNO_3. Amount of metal ions; ○: 0.25 mg, △: 1 mg, □: 5 mg, ●: 10 mg, ▼: 50 mg.

hand, when 0.1 M HF–0.5 M H_3BO_3–10^{-2} M HNO_3 is used as the medium, the K_d by Method II is identical with that by Method I and is not affected by the amount of Zr(IV) up to 50 mg.

The reason why the K_d value in HF–H_3BO_3–HNO_3 media does not change may be attributed to the F^--buffer action of this media, as mentioned in the previous paper.[3]

The large K_d obtained by Method II in 10^{-3} M HF–10^{-2} M HNO_3 cannot be explained clearly, but it may be due to the irreversible adsorption of Zr(IV)–fluoride complexes and/or the change of C_{HF} caused by the partial dissociation of highly fluorinated zirconium complexes on the resin.

The K_d of Nb(V) in 0.1 M HF–0.5 M H_3BO_3–0.1 M HNO_3 is the same regardless of the equilibrating method used and the amount of Nb(V), up to 20 mg.

The effect of the amount of Zr(IV) or Ti(IV) on their column elution behavior is shown in Fig. 5. These metals had been adsorbed to the column in 0.2 M HF prior to this elution experiment. Though the elution of Ti(IV) or Zr(IV) was extremely retarded by the increase of metal ions in 10^{-3} M HF–0.1 M HNO_3 (Figs. 5(a) and (b)), the elution was hardly affected by increasing the amount of the metal ions up to 50 mg, when 0.1 M HF–0.5 M H_3BO_3–10^{-2} M HNO_3 or 0.1 M HF–0.5 M H_3BO_3–0.1 M HNO_3 was used as the eluent (Figs. 5(c) and (d)). Less than 50 mg of coexisting Zr(IV) hardly affected the elution behavior of 1 mg of Ti(IV) in 0.1 M HF–0.5 M H_3BO_3–10^{-2} M HNO_3 (Fig. 5(e)).

Discussion

The K_d values of metals for the anion exchange resin in solutions involving complexing agents are generally expressed by the equation presented by Helfferich.[21] The equation can be modified into Eq. 1, by considering the adsorption of a metal ion M^{n+} to A^{a-}-form anion exchange resin in a solution containing fluoride ions as a complexing agent:

$$K_d = \sum_{j=0}^{N}[x_j(K_A^{MF_j})^{1/a}([A^{a-}]_r/[A^{a-}])^{j-n/a}], \quad (1)$$

$$x_j = [F^-]^j\beta_j/(1+[F^-]\beta_1+\cdots+[F^-]^N\beta_N). \quad (2)$$

Here j is the number of fluoride ions complexed with the metal ion M^{n+}, N is the maximum coordination number of fluoride ion for M^{n+}, x_j is the molar fraction of MF_j to the total metal species in the solution, $K_A^{MF_j}$ is the selectivity coefficient of MF_j to A^{a-}, $[A^{a-}]_r$ and $[A^{a-}]$ are the concentration of anion A^{a-} in resin and solution and β_j is the cumulative stability constant of MF_j.

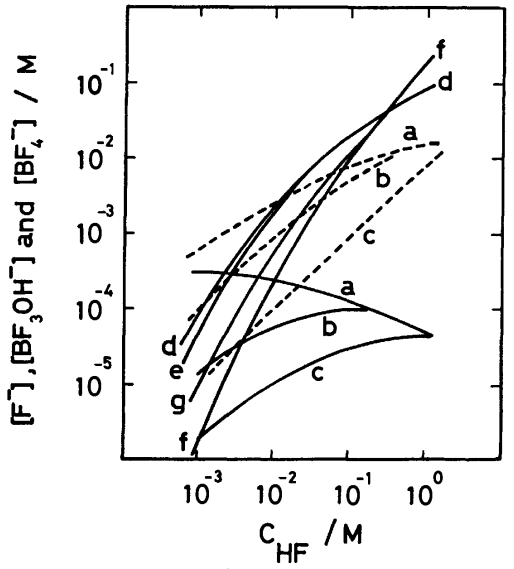

Fig. 6. Concentration of F^-, BF_3OH^-, and BF_4^- in HF and HF–H_3BO_3 media containing HNO_3.
——: HF–0.5 M H_3BO_3, ------: HF. a, b, and c: $[F^-]$ (a: without HNO_3, b: with 10^{-2} M HNO_3, c: with 0.1 M HNO_3), d and e: $[BF_3OH^-]$ (d: without HNO_3, e: with 0.1 M HNO_3), f and g: $[BF_4^-]$ (f: without HNO_3, g: with 0.1 M HNO_3).

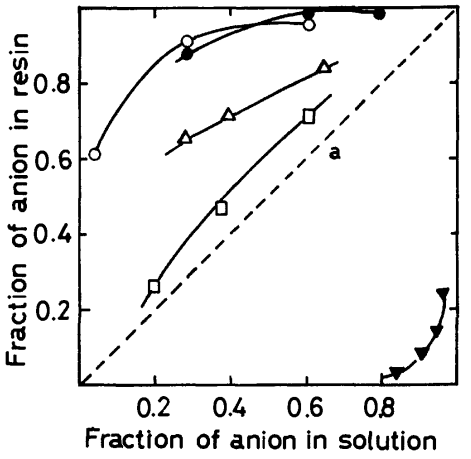

Fig. 7. Exchange of anions with Cl^- in the resin.
Diaion SA # 100: 1.0 g. Amount of acids: 0.5 to 20 mmol in 20 ml of solution. ○: BF_4^-, ●: ClO_4^-, △: NO_3^-, □: SO_4^{2-}, ▼: F^-.

As is evident from Eq. 1, the K_d value is a function of x_j, which is controlled by $[F^-]$ in the solution (Eq. 2), of $(K_A^{MF_j})^{1/a}$ which indicates the relative adsorbability of MF_j to A^{a-} (and hence, the value depends on the kind of anion), and of $([A^{a-}]_r/[A^{a-}])^{j-n/a}$, which depends on the valency and the concentration of anion A^{a-}.

Concentrations of free fluoride ion and other anions which exist in hydrofluoric acid and HF–H_3BO_3 media containing HNO_3 are calculated by the procedure described in the previous paper.[3] These are illustrated in Fig. 6; the dissociation constants of hydrofluoric acid and fluoroboric acids were used.

Figur 6 and the dependency of K_d on C_{HF} shown in Fig. 1 can be explained as follows: In solutions containing less than 10^{-2} M HF and 10^{-2} M HNO_3 with and without 0.5 M H_3BO_3, the resin stays as NO_3^-–form because the concentration of anions in solution other than nitrate is low and, hence, the second and third terms in Eq. 1 can be considered as constant at a definite C_{HNO_3}. Therefore, the increase of K_d with increasing C_{HF} up to 10^{-2} M may be ascribed to the change of x_j term, that is, to the increase of anionic metal fluoride complexes.

As an example, the species of Zr(IV) fluoride complexes and their fractions x_j in HF–H_3BO_3 media are calculated using the stability constants of Zr(IV) fluoride complexes.[22] The free fluoride ion concentration in the media of 0.5 M H_3BO_3–10^{-2} M HNO_3 containing 10^{-3} or 10^{-2} M HF is $10^{-5.0}$ or $10^{-4.3}$ M, respectively (see Fig. 6). The molar fraction of major species of Zr(IV) in solutions containing $10^{-5.0}$ M or $10^{-4.3}$ M of free fluoride ion are 35% of ZrF_4, 15% of ZrF_5^-, and 2% of ZrF_6^{2-} or 30% of ZrF_4, 55% of ZrF_5^-, and 15% of ZrF_6^{2-}, respectively. Consequently, the increase of the K_d of Zr(IV) with increasing C_{HF} is mainly due to the increase of the fraction of ZrF_5^- (and ZrF_6^{2-}).

The decrease of K_d with the increase of C_{HF} in HF–H_3BO_3 media containing more than 10^{-2} M HF (see Fig. 1) cannot be explained by the change of x_j because the free fluoride ion concentration slightly increases with the increase of C_{HF} (Fig. 6), but may be attributed to the change of the second and third terms in Eq. 1. Because the concentration of BF_4^- and BF_3OH^- increases remarkably with increasing C_{HF} in the solutions which are more than 10^{-2} M HF and 0.5 M H_3BO_3 (Fig. 6), it is suspected that BF_4^- and BF_3OH^- are adsorbed rather strongly on the resin, reducing the relative adsorbabilities of the metal fluoride complexes.

The adsorbability of BF_4^- was investigated and compared with the adsorbabilities of ClO_4^-, NO_3^-, SO_4^{2-}, and F^- according to Wheaton *et al.*[23] After equilibrating 1.0 g of Cl^--form dry anion exchange resin with 20 ml of various concentrations of HBF_4, $HClO_4$, HNO_3, H_2SO_4, or HF for 24 h at room temperature, the amount of chloride ion desorbed from the resin was determined by the Volhard method.[24] Assuming the amount of chloride desorbed is equivalent to the anions adsorbed, the molar fractions of the anion examined both in resin and solution are calculated (Fig. 7). In Fig. 7, the curve of an anion which lies above line (a) suggests the stronger adsorbability of the anion than that of chloride ion.[23] It is seen from Fig. 7 that the adsorbability of BF_4^- is very strong and is comparable to that of ClO_4^-. The order of adsorbabilities of anions is as follows:

$$BF_4^- \simeq ClO_4^- > NO_3^- > SO_4^{2-} > Cl^- > F^-. \quad (3)$$

Although the adsorbability of BF_3OH^- cannot be determined experimentally because of the difficulty of the preparation of BF_3OH^- free from BF_4^-,[25] it is considered that BF_3OH^- has the similar adsorbability to that of BF_4^- since the structure and the ionic charge of BF_3OH^- resemble those of BF_4^-.[25]

According to the considerations mentioned above, the decrease of K_d with the increase of C_{HF} in HF–H_3BO_3 media containing more than 10^{-2} M HF (Fig. 1) may

be attributed to the increase of BF_4^- and BF_3OH^- which are strongly adsorbed on the resin. And the decrease of K_d with the increase of $C_{H_3BO_3}$ in HF–H_3BO_3 media containing more than 10^{-2} M H_3BO_3 (column 3 in Table 1) may also be attributed to the increase of BF_4^- and BF_3OH^-.

The effects of coexisting acids and their concentrations on K_d (Fig. 3) may also be due to the difference in the adsorbabilities of the anions included in the coexisting acids. The different adsorbability given by various kinds of anions changes the second term in Eq. 1, $(K_A^{MF_j})^{1/a}$, and the concentrations of anions affect the third term in Eq. 1, $([A^{a-}]_r/[A^{a-}])^{j-n/a}$.

Based on the above discussions, the separation of Ti(IV), Zr(IV), Nb(V), and Ta(V) in HF–H_3BO_3 media shown in Fig. 4(d) is interpreted as follows: Metals in 0.2 M HF are adsorbed on the resin as fully fluorinated complexes. When the eluent, 0.1 M HF–0.5 M H_3BO_3–10^{-2} M HNO_3, is introduced to the column, metal complexes tend to be transformed to partially fluorinated complexes and the K_d values of these metals are reduced, because the concentration of free fluoride is extremely low in the medium. With this eluent Ti(IV), whose K_d is the smallest among these metals in this medium, is eluted from the column. With the increase of C_{HNO_3} in the eluent, the amount of NO_3^- adsorbed on the resin is increased, and Zr(IV) is eluted. When C_{HF} is increased from 0.1 M to 0.5 M, BF_4^- or BF_3OH^-, whose adsorbabilities are stronger than that of NO_3^-, is increased and Nb(V) is eluted. Since the adsorbability of Ta(V) fluoride complexes is extremely strong, a medium containing strong adsorptive anions in rather high concentration such as 1 M HF–0.5 M H_3BO_3–5 M HNO_3 is required to elute Ta(V).

Generally, in the separation of hard acid-metals by anion exchange, mixtures of HF (more than 0.1 M) and fairly concentrated HCl[4–7] or HNO_3[10] are used as eluents. Using these media, however, a separation such as that of Ti(IV) from Zr(IV) is difficult, because the adsorbabilities of fully fluorinated complexes of these metals resemble each other. Although for the elution of Ta(V) a solution of salt in high concentration such as 1 M NH_4F–4 M NH_4Cl[4,7] or a mixture of concentrated acids such as 5 M HF–12 M HNO_3[10] are employed in the works of HF–HCl or HF–HNO_3 media, it is difficult to remove the large amount of salts from the effluent and the concentrated acids decompose the resin. Using HF–H_3BO_3 media proposed in the present paper, these disadvantages are eliminated.

In conclusion, there is a buffer action relating to fluoride ion based on the dissociation of fluoroboric acids in HF–H_3BO_3 media, as discussed in the previous paper.[3] Therefore, despite the low fluoride ion concentration in HF–H_3BO_3 media, the separation can be attained without any effect of the amount of metal ions (up to 50 mg) as illustrated in Table 2 and Fig. 5.

The author wishes to thank Professor Taitiro Fujinaga, Drs. Tooru Kuwamoto, Kakuzo Tada, Hiroshi Hashitani, Sorin Kihara, and Mr. Hideyo Yoshida for their helpful discussions and useful suggestions.

References

1) R. G. Pearson, *J. Chem. Educ.*, **45**, 581, 643 (1968).
2) See, for example, S. Kallman, "Treatise on Analytical Chemistry," ed by I. M. Kolthoff and P. J. Elving, Interscience Publishers, New York (1964), Pt. II, Vol. 6, p. 241; W. Rieman and H. F. Walton, "Ion Exchange in Analytical Chemistry," Pergamon Press, London (1970), p. 140.
3) T. Adachi, *Bull. Chem. Soc. Jpn.*, **55**, 802 (1982).
4) K. A. Kraus and G. E. Moore, *J. Am. Chem. Soc.*, **73**, 9, 13, 2900 (1951); K. A. Kraus, F. Nelson, and G. E. Moore, *ibid.*, **77**, 3972 (1955).
5) D. H. Wilkins, *Talanta*, **2**, 355 (1959).
6) J. L. Hague, E. D. Brown, and H. A. Bright, *J. Natl. Bur. Stand.*, **53**, 261 (1954); J. L. Hague and L. A. Machlan, *ibid.*, **62**, 11, 53 (1959).
7) J. B. Headridge and E. J. Dixon, *Analyst*, **87**, 32 (1962); E. J. Dixon and J. B. Headridge, *ibid.*, **89**, 185 (1964).
8) E. A. Huff, *Anal. Chem.*, **36**, 1921 (1964).
9) L. Danielsson, *Acta Chem. Scand.*, **19**, 1859 (1965).
10) A. I. Williams, *Analyst*, **92**, 43 (1967).
11) A. Speecke and J. Hoste, *Talanta*, **2**, 332 (1959).
12) W. R. Bandi, E. G. Buyok, L. L. Lewis, and L. M. Melnick, *Anal. Chem.*, **33**, 1275 (1961).
13) F. W. E. Strelow, C. H. S. N. Weinert, and C. Eloff, *Anal. Chem.*, **44**, 2352 (1972).
14) J. P. Faris, *Anal. Chem.*, **32**, 521 (1960).
15) M. K. Nikitin, *Dokl. Acad. Nauk*, **148**, 595 (1963).
16) H. Grosse-Ruyken and H. G. Döge, *Talanta*, **12**, 73 (1965).
17) J. S. Fritz and E. E. Kaminski, *Talanta*, **18**, 541 (1971).
18) D. Singh and S. N. Tandon, *Talanta*, **26**, 163 (1979).
19) K. A. Kraus and F. Nelson, "Special Technical Publication," No. 195, American Society for Testing Materials, Philadelphia (1958), p. 27.
20) A. Ringbom, "Complexation in Analytical Chemistry," Interscience Publishers, New York (1963), p. 229.
21) F. Helfferich, "Ion Exchange," McGraw-Hill, New York (1962), p. 215.
22) L. G. Sillèn and A. E. Martell, "Stability Constants of Metal-Ion Complexes," Special Publication No. 17, The Chemical Society, London (1964), p. 259.
23) R. M. Wheaton and W. C. Bauman, *Ind. Eng. Chem.*, **43**, 1088 (1951).
24) I. M. Kolthoff, E. B. Sandell, E. J. Meehan, and S. Bruckenstein, "Quantitative Chemical Analysis," The Macmillan Co., New York (1969), p. 798.
25) R. E. Mesmer, K. M. Palen, and C. F. Baes, Jr., *Inorg. Chem.*, **12**, 89 (1973).

Separation and Quantification for Various Phosphorus Oxoacids by Isotachophoresis

Takao YAGI,† Kayoko KOJIMA,† Hiroyuki NARIAI, and Itaru MOTOOKA*
Department of Chemistry, Faculty of General Education, Kobe University, Nada-ku, Kobe 657
†*Analytical Application Laboratory, Shimadzu Corporation, Nakagyo-ku, Kyoto 604*
(Received October 5, 1981)

The analytical procedure for the separation and quantification of various phosphorus oxoacids was investigated by the capillary type isotachophoresis. The various phosphorus oxoacids, such as linear-, cyclic-, and lower phosphorus oxoacids, were separated at pH 5.5 with a 0.01 mol dm^{-3} hydrochloric acid–histidine–0.1% triton X-100 mixture as the leading electrolyte and a 0.01 mol dm^{-3} hexanoic acid as the terminating electrolyte. The PU value increased in the order of $P_{3m}<P_{4m}<P_3<P_2<\overset{1}{P}<\overset{3}{P}<P_1$. The calibration curves for the various phosphorus oxoacids were linear in the range of 0.5—3.5 μg as phosphorus oxoacids. Coefficients of variation for the measured phosphorus oxoacids were less than 2% except for P_3. Separation times were approximately 15 min. This procedure was applied to the ground phosphates.

Phosphorus oxoacids and their salts have an important role as fertilizers, detergents, watersofteners *etc.* As they have many varieties, paper- and ion exchange chromatography have been used for the separation and quantification of them. A disadvantage of these method is that they are laborious and time consuming.

Recently, more rapid and less laborious methods were developed by the use of a high liquid chromatography and an automatic phosphate analyzer.[1–4]

In the present paper, a procedure for the separation and quantification for chain-, cyclic-, and lower phosphorus oxoacids by isotachophoresis is described to remove the above disadvantage. It is applied to the ground phosphates.

Mikkers, *et al.*[5–7] have also attempted an isotachophoresis of phosphates, but they have only analyzed chain phosphates.

Experimental

Samples. Reagent-grade sodium phosphinate monohydrate ($NaPH_2O_2\cdot H_2O$; $\overset{1}{P}$) was used. Sodium phosphonate (Na_2PHO_3; $\overset{3}{P}$) and sodium dihydrogenorthophosphate (NaH_2PO_4; $\overset{5}{P}$ or P_1) were obtained by heating Wako's reagents to dehydrate water of crystallization. Tetrasodium pyrophosphate ($Na_4P_2O_7$; P_2), pentasodium triphosphate ($Na_5P_3O_{10}$; P_3) and trisodium *cyclo*-triphosphate ($Na_3P_3O_9$; P_{3m}) were prepared by heating sodium orthophosphate, purified by recrystallization, and dehydrated water of crystallization. Tetrasodium *cyclo*-tetraphosphate ($Na_4P_4O_{12}$; P_{4m}) was prepared according to the method of Bell *et al.*[8]

All phosphorus oxoanions were standardized by paper chromatography. The ground samples were obtained by grinding $Na_2H_2P_2O_7$ and $Na_5P_3O_{10}$, respectively, for the specified lengths of time in an AGA-type Ishikawa's mill with an agate mortor.

Apparatus and Procedure. A Shimadzu Capillary Tube Isotachophoretic Analyzer IP-2A was used. The isotachophoretic tubes for the separation composed of a main capillary column (0.5 mm i.d., 100 mm in length) and a pre-column (1.0 mm i.d., 100 mm in length). The conditions of the isotachophoretic analysis are given in Table 1. After the electric driving current of 200 μA was applied for 12 min to shorten the analytical time, that of 100 μA was done. The potential gradient detector was used. Paper chromatography was performed as reported previously.[9]

Table 1. Operational system for separation of phosphorus oxoacids

	Electrolyte	
	Leading	Terminating
Anion	0.01 mol dm^{-3} Cl^-	Hexanoate$^-$
Counterion	Histidine$^+$	H^+
pH	4.5—6.0	3.4
Additive	0.1% Triton X-100	
Solvent	Water	Water
Capillary tube	1.0×100 mm+0.5×100 mm	
Current	200 μA (12 min)→100 μA	
Detector	PGD	
Temperature	25 °C	
Chart speed	40 mm min^{-1}	

Results and Discussion

The separation of the various phosphorus oxoanions is affected by the pH of leading solution. The relationship between the pH of the leading solution and the *PU* value, which is an indicator in qualitative analysis, is shown in Fig. 1. When the *PU* values of oxoanions are close, a mixed zone of them is formed. It can be seen from Fig. 1 that the separation at pH 4.5, 5.5, and 6.0 is unfavourable, but good separation is obtained in the range of pH 5.3—5.7. Therefore, seven varieties of the phosphorus oxoacids were separated at pH 5.5.

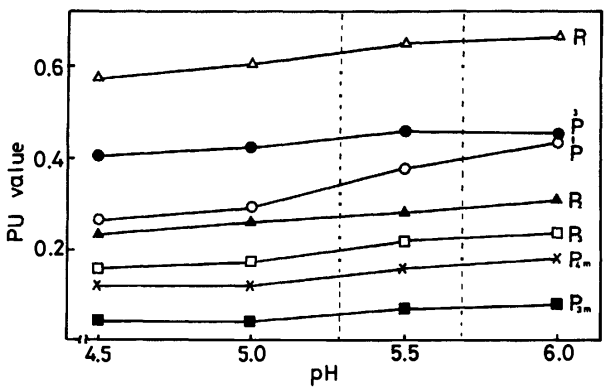

Fig. 1. Effect of pH of leading electrolyte on *PU* value.

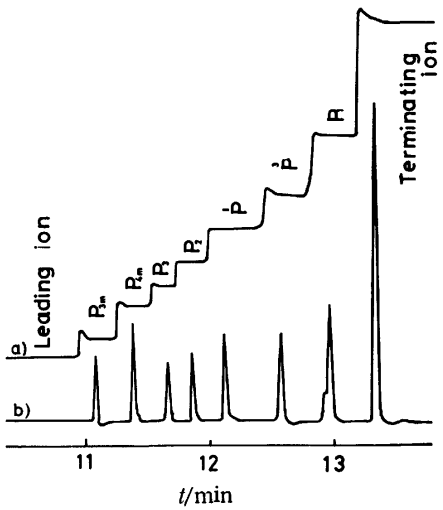

Fig. 2. Isotachopherogram of various phosphorus oxoacids.
a): Potential gradient, b): differential potential gradient.

Figure 2 shows the isotachopherogram of the various phosphorus oxoacids. An order of the *PU* value is $P_{3m}<P_{4m}<P_3<P_2<{}^{1}P<{}^{3}P<P_1$. These results indicate that the electrophoretic mobility of the chain phosphate ion increased with an increase in the number of phosphorus atoms, that of the cyclic phosphate ion decreased with an increase in the number of phosphorus atoms, and that of the lower phosphorus oxoanion with different oxidation numbers decreased with an increase of oxidation numbers.

TABLE 2. REPRODUCIBILITY AND MOLAR RESPONSE FOR VARIOUS PHOSPHORUS OXOACIDS

	PU value		Zone length		Molar response[c]
	$\bar{X}$[a](n=8)	*CV*[b] %	$\bar{X}$[a](n=8) mm	*CV*[b] %	10^8 mm mol^{-1}
${}^{1}P$	0.394	1.02	36.8	1.09	5.57(0.95)
${}^{3}P$	0.498	0.80	29.3	1.02	5.28(0.90)
${}^{5}P(P_1)$	0.661	0.76	34.1	1.76	5.85(1.00)
P_2	0.305	2.95	19.4	1.55	7.38(1.26)
P_3	0.233	2.58	15.2	5.26	7.79(1.33)
P_{3m}	0.074	1.35	24.2	0.83	10.57(1.81)
P_{4m}	0.170	2.35	22.1	0.90	12.85(2.20)

a) Average value. b) Coefficient of variation ($CV=\sigma/\bar{X}\times100$). c) Value in parentheses is relative molar response (as $P_1=1.00$).

Table 2 shows the reproducibilities of the *PU* value and the zone length, and molar response. All coefficients of variation (*CV*%) of the *PU* value were less than 3% and those of the zone length were less than 2% except for P_3. A high *CV* value (5.25%) of P_3 is due to only one abnormal data. If this abnormal data is removed, the *CV* value of P_3 is 2.22%. The molar response for the various phosphorus oxoacids in Table 2 was calculated from the zone length on the isotachopherogram and the amount of injected phosphorus oxoacids. The value in parentheses represents the relative molar response which is the value converted as that of P_1 is 1.00. It can be seen from these results that the relative molar response of both chain- and cyclic phosphates increased with an increase in the number of phosphorus atoms of the phosphates, that of the cyclic phosphates is higher value than that of the chain phosphates, and that of phosphorus oxoacids with different oxidation numbers doesn't depend on the oxidation numbers.

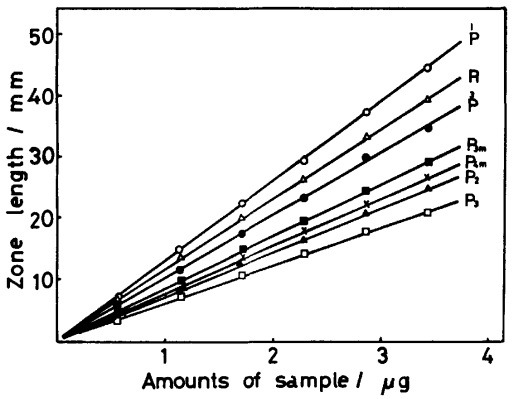

Fig. 3. Calibration curves of various phosphorus oxoacids.
Chart speed: 40 mm min^{-1}.

Figure 3 shows the calibration curves for seven varieties of phosphorus oxoacids. These phosphorus oxoacids were injected simultaneously. Linear relationship were obtained over the range of 0.5—3.5 μg of sodium salts of phosphorus oxoacids, but the calibration curve was nonlinear above 3.5 μg because the phosphorus oxoanions with adjacent *PU* values formed the mixed zone. When a single phosphorus oxoacid was injected, a linear relationship was obtained over a wide range of the amount of phosphorus oxoacids, 0.5—30.0 μg.

As the linear region of the calibration curve depends on the volume of the capillary tube, it is preferable to select an adequate capillary tube to obtain good results.

Application

The procedure mentioned above was applied to the separation and quantification of the ground phosphates.

The P–O–P linkages of the chain phosphates, such as pyro- and triphosphate, were severed to shorter chain

TABLE 3. ANALYTICAL RESULTS OF GROUND PYROPHOSPHATE

Grinding time/h	IP[a]		PC[b]	
	P_1(%)	P_2(%)	P_1(%)	P_2(%)
6	4.2	95.8	5.3	94.7
24	8.6	91.4	7.1	92.9
48	11.0	89.0	12.7	87.3
96	13.9	86.1	16.8	83.2
168	25.3	74.7	24.4	75.6

a) Isotachophoresis. b) Paper chromatography.

Table 4. Analytical results of ground triphosphate

Grinding time/h	IP[a]			PC[b]		
	P_1(%)	P_2(%)	P_3(%)	P_1(%)	P_2(%)	P_3(%)
6	6.5	26.0	67.5	8.7	26.2	65.1
48	10.4	46.3	43.3	11.1	46.2	42.7
72	12.2	60.0	27.8	14.5	57.4	28.1
168	17.4	72.7	9.9	19.1	72.7	8.2

a) Isotachophoresis. b) Paper chromatography.

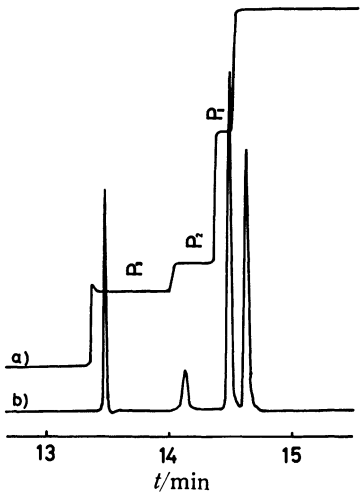

Fig. 4. Isotachopherogram of ground triphosphate.
a): Potential gradient, b): differential potential gradient.

phosphates due to grinding.[10] Therefore, the ground samples contained the different chain-length phosphates were obtained by grinding for different times.

Figure 4 is the representative isotachopherogram of the ground triphosphate. The results of the isotachophoresis of these ground samples have been summarized in Tables 3 and 4. These results are comparable with those of paper chromatography.

References

1) I. Motooka, K. Saeki, and M. Kobayashi, *Nippon Kagaku Kaishi*, **1976**, 1784.
2) H. Yamaguchi, T. Nakamura, Y. Hirai, and S. Ohashi, *J. Chromatogr.*, **172**, 131 (1979).
3) Y. Hirai, N. Yoza, and S. Ohashi, *Anal. Chem. Acta*, **115**, 269 (1980).
4) Y. Hirai, N. Yoza, and S. Ohashi, *Chem. Lett.*, **1980**, 499.
5) F. Mikkers, W. von Gils, and W. Roos, "Analytical Isotachophoresis," ed by F. M. Everaerts, Elsevier, Amsterdam (1981), p. 91.
6) D. Lúčanský, V. Bátora, J. Polonský, and J. Garaj, "Analytical Isotachophoresis," ed by F. M. Everaerts, Elsevier, Amsterdam (1981), p. 147.
7) J. Polonský, D. Lúčanský, and L. Repášová, "Analytical Isotachophoresis," ed by F. M. Everaerts, Elsevier, "Amsterdam(1981), p. 195.
8) R. N. Bell, L. F. Audrieth, and O. F. Hill, *Ind. Eng. Chem.*, **44**, 568 (1952).
9) I. Motooka, M. Ishizaki, H. Nozu, and M. Kobayashi, *Kogyo Kagaku Zasshi*, **69**, 2071 (1966).
10) I. Motooka and M. Kobayashi, "Topics in Phosphorus Chemistry," ed by M. Grayson and E. J. Griffith, John Wiley and Sons, New York (1980), Vol. 10, p. 171.

 © 1982 The Chemical Society of Japan Bull. Chem. Soc. Jpn., 55, 1834—1839 (1982) [Vol. 55, No. 6

The Crystal and Molecular Structure of (*N*-Benzyl-L-alaninato)-[*N,N'*-ethylenebis(α-methylsalicylideneaminato)]-cobalt(III) Trihydrate

Yoshihiko KUSHI,* Toshiji TADA, Yuki FUJII,† and Hayami YONEDA

Department of Chemistry, Faculty of Science, Hiroshima University, Higashi-senda-machi, Naka-ku, Hiroshima 730

†*Department of Chemistry, Faculty of Science, Ibaraki University, Bunkyo-cho, Mito, Ibaraki 310*

(Received October 7, 1981)

The crystal and molecular structure of the title complex $(-)_{435}$-Λ_{RS}-β_2(mer)-[Co(α-Me-sal$_2$en)(*N*-Bz-L-ala)]·3H$_2$O, has been determined by single crystal X-ray analysis. The crystals are orthorhombic, space group $P2_12_12_1$, with unit cell dimensions $a=19.247(8)$, $b=14.162(4)$, $c=10.329(4)$ Å, and $Z=4$. The structure was solved by the heavy-atom method and refined by block-diagonal least-squares technique, using 1624 independent reflections, to the final *R*-value of 0.080. The molecular structure is of a Λ_{RS}-*cis*-β_2(mer) type in which two coordination sites of a distorted octahedron are occupied by the *N*-Bz-L-ala group and the others by the quadridentate α-Me-sal$_2$en Schiff-base ligand in a nonplanar configuration. The Co–O and Co–N bon lengths, 1.938(12) and 1.989(15) Å respectively, of the *N*-Bz-L-ala group are significantly longer than the usual values. The molecule is distinctly strained as shown by the bond angles of the ligands and those of the cobalt(III) coordination polyhedron. The water molecules form a hydrogen bonded chain linking phenolate and carboxylate oxygens of different molecules along the crystallographic c axis.

The crystal structures of Schiff-base metal complexes have been studied extensively.[1] However, there are only a few structures in which the quadridentate Schiff-base ligands took a nonplanar configuration.[2-6] Recently, studies of several metal complexes with quadridentate Schiff-base ligands in *cis*-configuration have shown that they exhibit stereoselective effects in coordinating optically active amino acids.[7,8] In order to elucidate these effects more clearly, we have synthesized a series of mixed complexes of the type [Co(α-Me-sal$_2$en)(AA)] where α-Me-sal$_2$en is the dianion of the quadridentate *N,N'*-ethylenebis(α-methylsalicylideneaminato) ligand and AA is the anion of one of the following amino acids: *N*-methyl-L-alanine, *N*-benzyl-L-alanine (abbreviated as *N*-Bz-L-ala), and *N*-benzyl-*N*-methyl-L-alanine.[9] This paper reports the result of an X-ray diffraction study of the crystal and molecular structure of $(-)_{435}$-[Co(α-Me-sal$_2$en)(*N*-Bz-L-ala)]·3H$_2$O, which is the predominant isomer at equilibrium conditions.

Experimental

Preparation of Compound. $(-)_{435}$-*cis*-β_2(mer)-[Co(α-Me-sal$_2$en)(*N*-Bz-L-ala)]·3H$_2$O was prepared by a method described elsewhere.[9] From a mixed solution of methanol and water (1 : 1), dark green crystals were obtained. Found: C, 58.36; H, 6.10; N, 7.29%. Calcd for $C_{28}H_{30}CoN_3O_4$·2.5H$_2$O: C, 58.33; H, 6.12; N, 7.29% and for $C_{28}H_{30}CoN_3O_4$·3H$_2$O: C, 57.43; H, 6.20; N, 7.18%. From comparison with the X-ray result, these values suggest that a partial dehydration occurred. $(M)_{435}=-4.38\times10^4$° ($c=1.0\times10^{-3}$ mol dm^{-3}; chloroform solution).

Crystallographic-data Collection. The size of the crystal used for the X-ray measurement was $0.35\times0.28\times0.17$ mm^3. The systematic absences for $h00(h=2n+1)$, $0k0(k=2n+1)$, $00l(l=2n+1)$ indicated the space group $P2_12_12_1$. The determination of cell dimensions and the collection of intensity data were carried out on a Rigaku AFC-5 automated four-circle diffractometer with Mo *Kα* radiation ($\lambda=0.71069$ Å) monochromated by a graphite plate. The unit cell dimensions were refined by a least-squares method with 20 reflections ($2\theta>22$°). The crystal data were as follows: orthorhombic, space group $P2_12_12_1$, $a=19.247(8)$, $b=14.162(4)$, $c=10.329(4)$ Å, $D_m=1.35$ g cm^{-3} (by flotation in a $ZnCl_2$ solution), $Z=4$, and $D_c=1.38$ g cm^{-3}. The intensity data were collected in the ω-2θ scan mode up to $2\theta=50$° with the scan rate of 8°/min (50 kV, 170 mA). The scan range was $(1.2+0.5\tan\theta)$°. Of the 2119 unique observed reflections, 1624 reflections with $|F_o|\geq3\sigma(F_o)$ were used for the structure determination. Corrections for the absorption effect were neglected (μ(Mo *Kα*)=6.9 cm^{-1}).

Determination and Refinement of Crystal Structure

The structure was solved by the heavy-atom method and refined by the block-diagonal least-squares method. Three kinds of water molecules were found from a difference Fourier map after the other non-hydrogen atoms were located. The refinement using anisotropic

TABLE 1. POSITIONAL AND THERMAL PARAMETERS

Atom	*x*	*y*	*z*	B_{eq} or *B*/Å^2
Co	0.3644(1)	0.2109(1)	0.4979(2)	2.40
OA1	0.3222(6)	0.0981(8)	0.4266(11)	3.80
OA2	0.3292(7)	−0.0008(9)	0.2636(12)	4.73
OS1	0.2939(5)	0.2793(8)	0.4148(10)	3.28
OS2	0.4061(5)	0.3230(7)	0.5582(10)	2.64
NA1	0.4207(6)	0.2120(11)	0.3364(12)	3.11
NS1	0.3099(7)	0.1391(9)	0.5933(13)	2.80
CA1	0.3509(10)	0.0699(14)	0.3237(16)	4.19
CA2	0.4115(10)	0.1228(12)	0.2610(16)	3.66
CA3	0.4803(10)	0.0642(12)	0.2670(16)	4.93
CA4	0.4064(11)	0.2988(13)	0.2515(20)	2.91
CA5	0.4525(9)	0.3062(11)	0.1330(14)	2.34
CA6	0.4192(8)	0.2982(10)	0.0144(13)	3.66
CA7	0.4578(8)	0.3096(12)	−0.0988(15)	3.72
CA8	0.5256(9)	0.3282(12)	−0.0953(16)	3.62
CA9	0.5592(8)	0.3297(12)	0.0271(15)	3.52
CA10	0.5221(8)	0.3192(13)	0.1414(16)	3.64
CE1	0.3303(9)	0.1188(13)	0.7301(14)	3.37
CE2	0.3924(9)	0.0670(12)	0.6698(19)	3.88
CS11	0.2582(7)	0.3406(10)	0.4774(16)	2.74

TABLE 1. (Continued)

Atom	x	y	z	B_{eq} or B/Å^2
CS12	0.2323(9)	0.4194(12)	0.4066(19)	3.71
CS13	0.1917(11)	0.4829(14)	0.4608(19)	5.42
CS14	0.1721(11)	0.4834(13)	0.5938(24)	5.85
CS15	0.1960(9)	0.4067(14)	0.6618(19)	4.41
CS16	0.2383(8)	0.3365(12)	0.6122(15)	2.76
CS17	0.2595(8)	0.2531(13)	0.6887(15)	3.33
CS18	0.2228(9)	0.2348(13)	0.8113(16)	3.96
CS21	0.4754(9)	0.3304(12)	0.5550(14)	3.21
CS22	0.5022(10)	0.4204(12)	0.5343(13)	3.80
CS23	0.5737(9)	0.4321(13)	0.5239(17)	4.29
CS24	0.6178(9)	0.3528(13)	0.5370(17)	4.17
CS25	0.5909(8)	0.2689(15)	0.5625(17)	4.04
CS26	0.5192(8)	0.2511(13)	0.5731(18)	2.73
CS27	0.4935(8)	0.1629(11)	0.6196(14)	3.43
CS28	0.5391(10)	0.1019(14)	0.7028(25)	5.62
OW1	0.2618(7)	0.0577(9)	0.0360(12)	5.92
OW2	0.2291(10)	0.2365(14)	0.1545(15)	9.37
OW3	0.1523(12)	0.4080(20)	0.0377(25)	15.42
H(NA1)	0.468(7)	0.225(10)	0.355(13)	1.60
H(CA2)	0.405(7)	0.141(11)	0.148(15)	1.38
H1(CA3)	0.468(10)	0.000(14)	0.229(20)	5.54
H2(CA3)	0.501(8)	0.054(11)	0.357(15)	1.55
H3(CA3)	0.521(8)	0.106(12)	0.207(17)	2.77
H1(CA4)	0.351(8)	0.295(12)	0.218(15)	2.63
H2(CA4)	0.413(8)	0.352(12)	0.297(16)	1.24
H(CA6)	0.368(8)	0.286(11)	0.006(18)	3.03
H(CA7)	0.433(7)	0.311(10)	−0.171(13)	1.40
H(CA8)	0.561(10)	0.335(14)	−0.160(19)	4.97
H(CA9)	0.607(7)	0.328(10)	0.024(15)	1.83
H(CA10)	0.551(11)	0.319(15)	0.211(22)	6.75
H(CS12)	0.244(8)	0.423(11)	0.304(16)	2.47
H(CS13)	0.178(9)	0.529(13)	0.415(19)	4.71
H(CS14)	0.141(8)	0.520(11)	0.637(15)	2.22
H(CS15)	0.185(8)	0.403(12)	0.753(16)	2.93
H1(CS18)	0.243(10)	0.175(13)	0.853(18)	4.90
H2(CS18)	0.230(9)	0.291(13)	0.872(18)	4.64
H3(CS18)	0.175(10)	0.226(15)	0.798(20)	6.30
H1(CE1)	0.286(7)	0.075(10)	0.750(14)	1.31
H2(CE1)	0.348(7)	0.145(11)	0.828(15)	1.69
H1(CE2)	0.375(9)	0.007(12)	0.612(16)	2.85
H2(CE2)	0.423(9)	0.035(14)	0.749(18)	4.50
H(CS22)	0.467(8)	0.476(11)	0.526(16)	3.11
H(CS23)	0.597(8)	0.499(11)	0.506(18)	3.68
H(CS24)	0.670(8)	0.361(11)	0.533(15)	2.39
H(CS25)	0.623(7)	0.227(10)	0.573(14)	1.17
H1(CS28)	0.587(9)	0.124(14)	0.715(18)	3.81
H2(CS28)	0.522(9)	0.111(14)	0.807(19)	4.65
H3(CS28)	0.538(9)	0.034(13)	0.684(18)	4.29
H1(OW1)	0.283(9)	0.031(14)	0.113(19)	a)
H2(OW1)	0.246(10)	0.010(13)	−0.007(18)	a)
H1(OW2)	0.250(8)	0.248(12)	0.225(16)	a)
H2(OW2)	0.241(11)	0.173(15)	0.109(21)	a)
H1(OW3)	0.177(11)	0.345(15)	0.082(23)	a)
H2(OW3)	0.110(9)	0.402(13)	0.004(21)	a)

$B_{eq}=8\pi^2(U_{11}+U_{22}+U_{33})/3$. The anisotropic thermal parameters for the non-hydrogen atoms have been preserved by the Chemical Society of Japan.

a) These values were fixed at $B=6.0$/Å^2 during the least-squares calculations.

thermal parameters for the non-hydrogen atoms reduced the R value (defined as $\sum||F_o|-|\sum|F_c||/\sum|F_o|$) to 0.097. At this stage, all the hydrogen atoms were located from a difference Fourier map. The final refinement including the contribution of these hydrogen atoms with isotropic temperature factors converged to the R value of 0.080. The effect of the anomalous dispersion of the Co atom was included in the calculation.[10] The final difference map showed no peaks higher than 0.5 electrons/Å^3. Atomic scattering factors were taken from Ref. 10. All the computations were carried out by a HITAC M-180 computer at the Hiroshima University Information Processing Center. The computer programs used were FOUR-MMM[11] and HBLS-IV with a slight modification.[12] An ORTEP drawing was carried out by a computer system XTL in a Syntex R3 automated diffractometer.[13] The final atomic parameters are summarized in Table 1 with averaged isotropic temperature factors. The anisotropic thermal parameters and complete lists of the $|F_o|$ and $|F_c|$ values have been preserved by the Chemical Society of Japan (Document No. 8222).

Results and Discussion

The projections of the crystal structure along the c and b axes with the numbering scheme are shown in Figs. 1 and 2. The crystals are built up of discrete [Co(α-Me-sal$_2$en)(*N*-Bz-L-ala)] molecules and waters of crystallization.

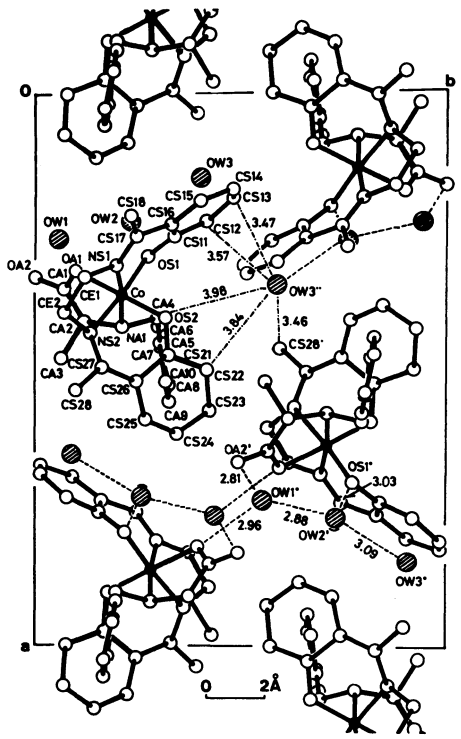

Fig. 1. A perspective drawing of the contents of the unit cell viewed down the c axis. The hydrogen bonds are indicated by bloken lines. Hydrogen atoms are omitted for clarity.

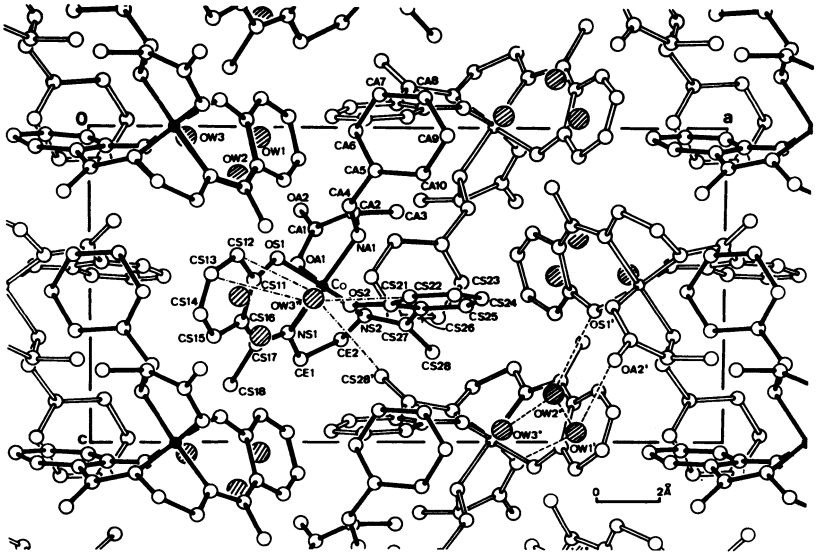

Fig. 2. A perspective drawing of the contents of the unit cell viewed down the b axis with the numbering scheme.

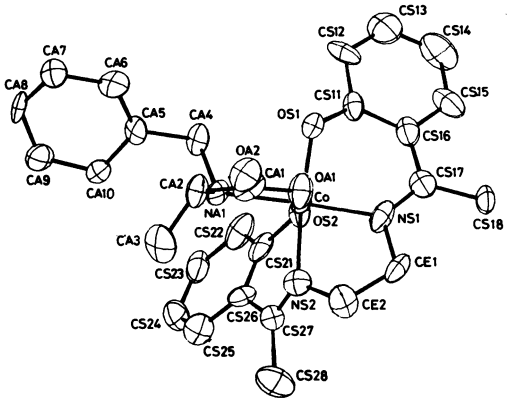

Fig. 3. An ORTEP drawing of the complex molecule. All atoms are drawn with 50% probability ellipsoids. Hydrogen atoms are omitted for clarity.

Molecular Structure. The ORTEP drawing of the complex molecule is shown in Fig. 3 where the thermal ellipsoids are depicted with a 50% probability. The molecular structure of [Co(α-Me-sal$_2$en)(*N*-Bz-L-ala)] has a close resemblance to that of [Co(α-Me-sal$_2$en)(L-isoleu)].[6] The *N*-benzyl-L-alaninate anion is nitrogen- and oxygen-bonded bidentate, and the α-methyl-sal$_2$en group has the *cis*-β_2 configuration[14] of a quadridentate ligand. The co-ordination polyhedron around the central cobalt atom is a meridional N_3O_3 structure in which the oxygen atom(OA 1) of the *N*-Bz-L-ala group is situated on the *trans* position of the oxygen atom(OS 2) of the phenolate moiety sal(2).

The absolute configuration of the complex molecule is *Λ*[15] as deduced from the known absolute configuration of the asymmetric carbon atom of the L-alaninato skeleton as an internal reference.[16] The arrangement of the group around the nitrogen atom(NA 1) of the *N*-benzyl-L-alaninato ligand is an *R* configuration and those around the asymmetric carbon atom(CA 2) is an *S* configuration. Thus, the structure of the complex molecule is denoted as *Λ*$_{RS}$-*cis*-β_2(mer) type.

Bond lengths and bond angles in the complex molecule are listed in Table 2 together with their estimated standard deviations. The Co–O and Co–N bond lengths of α-Me-sal$_2$en ligand are in agreement with those in the nonplanar [Co(salen)(acac)] derivatives within the experimental error.[2,3] The corresponding distances of the *N*-Bz-L-ala group, Co–OA1 1.938(12) and Co–NA1 1.989(15) Å, are significantly longer than those reported in Co(III) amino acidato chelates; Co–$O_{av.}$ 1.885(9) and Co–$N_{av.}$ 1.945(10) Å in (−)-mer-[Co(L-ala)$_3$][17] and Co–O 1.892(7) and Co–N 1.920(9) Å for L-phenylalaninato group in [Co(acac)$_2$(L-phala)].[18]

The bond angles around the cobalt atom are approximately in agreement with those in [Co(salen)(acac)][3] and [Co(salen)(bzacac)].[2] The chelate angle for the *N*-Bz-L-ala group, OA1–Co–NA1 85.2(6)°, is normal.

A perspective drawing of the complex molecule projected down the axis through the middle point of NS1-NS2 atoms and the cobalt atom is depicted in Fig. 4. Bailay *et al.* mentioned that the strain of the *cis*-β_2 type salen ligand is apparent in: (i) Angular strain in the "en" chelate ring, (ii) the nonplanar coordination geometry around the azomethine nitrogens, and (iii) the angular strain in the salicylideneamine moiety sal(2).[2] The highly strained conformational state about the "en" ring and the coordination geometry around the azomethine nitrogens (NS1 and NS2) are clearly shown in Fig. 4. The strain in the sal(2) moiety is also noticed by comparison with the sal(1) moiety in Fig. 4 and the sal(2) moiety in Fig. 3.

Calligaris *et al.* showed another representation for giving the degree of strain in these molecules.[3] Based on their representation, the angles between the planes passing through sal(1), sal(2), and the ala moieties, and the planes of the three equatorial planes of the octahedron around the cobalt atom are illustrated in Fig. 5.

TABLE 2. BOND DISTANCES AND ANGLES (e.s.d.'s IN PARENTHESES)

Bond distances (l/Å)							
Co–OA1	1.938(12)	CA4–NA1	1.535(22)	CS13–CS14	1.425(32)	CS27–CS28	1.503(31)
Co–OS1	1.872(12)	CA4–CA5	1.514(23)	CS14–CS15	1.372(32)	CS27–CS26	1.427(23)
Co–OS2	1.885(10)	CA5–CA6	1.388(24)	CS15–CS16	1.384(27)	CS26–CS21	1.418(23)
Co–NA1	1.989(15)	CA6–CA7	1.395(25)	CS16–CS11	1.445(24)	CS26–CS25	1.406(25)
Co–NS1	1.911(14)	CA7–CA8	1.332(25)	CS16–CS17	1.478(25)	CS25–CS24	1.323(28)
Co–NS2	1.887(13)	CA8–CA9	1.420(25)	CS17–CS18	1.472(26)	CS24–CS23	1.414(28)
CA1–OA1	1.263(23)	CA9–CA10	1.388(25)	CS17–NS1	1.303(23)	CS23–CS22	1.391(27)
CA1–OA2	1.250(24)	CA10–CA5	1.356(25)	CE1–NS1	1.440(23)	CS22–CS21	1.391(26)
CA1–CA2	1.530(27)	CS11–OS1	1.281(20)	CE1–CE2	1.535(26)	CS21–OS2	1.337(20)
CA2–CA3	1.564(28)	CS11–CS12	1.424(25)	CE2–NS2	1.473(23)		
CA2–NA1	1.494(24)	CS12–CS13	1.315(28)	CE27–NS2	1.310(22)		

Bond angles (ϕ/°)					
OA1–Co–NA1	85.2(6)	CA2–NA1–CA4	111.0(13)	CS17–NS1–CE1	120.3(15)
OS1–Co–NS1	91.8(6)	NA1–CA4–CA5	114.4(13)	Co–NS1–CS17	120.6(12)
OS2–Co–NS2	90.0(5)	CA4–CA5–CA6	115.9(15)	Co–NS1–CE1	113.1(11)
NS1–Co–NS2	83.0(6)	CA10–CA5–CA4	122.5(15)	NS1–CE1–CE2	110.9(15)
OA1–Co–OS1	87.1(5)	CA10–CA5–CA6	121.6(16)	CE1–CE2–NS2	105.1(14)
OA1–Co–NS1	90.4(6)	CA5–CA6–CA7	119.0(16)	CE2–NS2–CS27	121.4(14)
OA1–Co–NS2	91.8(6)	CA6–CA7–CA8	121.5(17)	Co–NS2–CE2	109.6(11)
OS1–Co–OS2	91.4(5)	CA7–CA8–CA9	118.3(16)	Co–NS2–CS27	126.4(12)
OS1–Co–NA1	90.4(6)	CA8–CA9–CA10	121.4(16)	NS2–CS27–CS28	121.5(17)
OS2–Co–NA1	92.2(5)	CA9–CA10–CA5	118.0(17)	NS2–CS27–CS26	118.9(15)
OS2–Co–NS1	92.3(5)	Co–OS1–CS11	120.4(11)	CS28–CS27–CS26	119.5(16)
NA1–Co–NS2	94.7(6)	OS1–CS11–CS12	117.3(15)	CS27–CS26–CS25	121.6(15)
OA1–Co–OS2	176.9(5)	OS1–CS11–CS16	126.9(15)	CS27–CS26–CS21	122.1(15)
OS1–Co–NS2	174.7(6)	CS16–CS11–CS12	115.7(15)	CS21–CS26–CS25	115.6(15)
NA1–Co–NS1	175.0(6)	CS11–CS12–CS13	121.7(18)	CS26–CS25–CS24	124.1(18)
Co–OA1–CA1	113.4(12)	CS12–CS13–CS14	124.8(20)	CS25–CS24–CS23	119.9(19)
OA1–CA1–OA2	121.7(18)	CS13–CS14–CS15	113.6(21)	CS24–CS23–CS22	119.5(18)
OA1–CA1–CA2	122.3(17)	CS14–CS15–CS16	125.2(20)	CS23–CS22–CS21	119.2(18)
OA2–CA1–CA2	116.0(17)	CS15–CS16–CS11	118.9(16)	CS22–CS21–CS26	121.7(16)
CA1–CA2–CA3	111.6(16)	CS15–CS16–CS17	122.6(16)	OS2–CS21–CS22	116.5(15)
CA1–CA2–NA1	106.5(15)	CS11–CS16–CS17	118.3(15)	OS2–CS21–CS26	121.9(14)
NA1–CA2–CA3	109.1(15)	CS16–CS17–CS18	118.0(16)	Co–OS2–CS21	118.9(10)
Co–NA1–CA2	111.5(11)	CS16–CS17–NS1	121.7(16)		
Co–NA1–CA4	112.8(10)	CS18–CS17–NS1	120.3(16)		

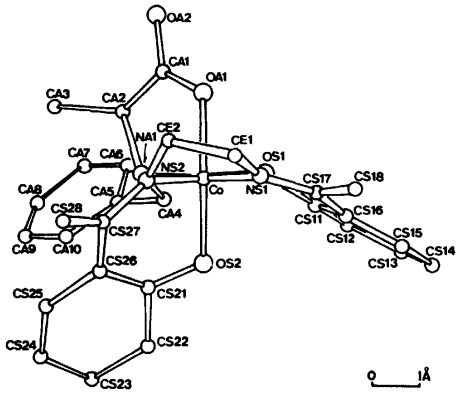

Fig. 4. Structure of the complex molecule viewed down the axis through the middle point of NS1-NS2 atoms and the cobalt atom.

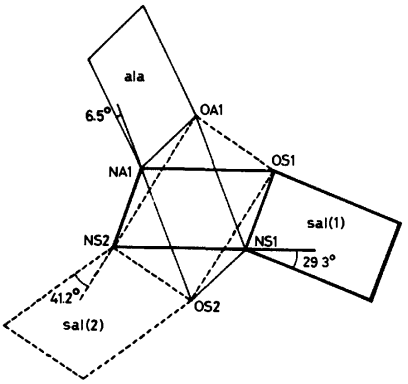

Fig. 5. A schematic drawing of the dihedral angles between the least-squares planes.

Comparison between these values, which are summarized in Table 3, and those found in [Co(salen)(acac)], 5.0, 29.3, and 17.9° for sal(1), sal(2), and acac respectively, indicates that the strain caused by the *cis*-β_2-salen skeleton in the present complex is distinctly higher than that in [Co(salen)(acac)].

The coordination of the bulky *N*-benzyl-L-alaninato ligand is probably responsible for this difference, as evidenced by the long Co–O and Co–N bond distances in the *N*-Bz-L-ala group. Two short intramolecular

TABLE 3. DISTANCES OF ATOMS FROM LEAST-SQUARES PLANES AND DIHEDRAL ANGLES BETWEEN THE PLANES

Least-aquares planes

Plane (1)		Plane (2)		Plane (3)	
Co	−0.040 Å	Co	−0.015 Å	Co	0.006 Å
OS1	−0.015	OA1	−0.037	OA1	0.034
NA1	0.035	OS1	0.087	OS2	0.029
NS1	0.039	OS2	−0.078	NA1	−0.034
NS2	−0.019	NS2	0.052	NS1	−0.034
Sal (1)		**Sal (2)**		**Ala**	
OS1	0.070 Å	OS2	0.027 Å	OA1	−0.020 Å
NS1	−0.146	NS2	0.159	OA2	0.059
CS11	0.001	CS21	0.001	NA1	0.058
CS12	−0.021	CS22	−0.047	CA1	−0.028
CS13	−0.008	CS23	−0.012	CA2	−0.067
CS14	−0.035	CS24	0.046		
CS15	0.009	CS25	0.032		
CS16	0.010	CS26	0.011		
CS17	0.127	CS27	−0.207		

Dihedral angles between the planes

Plane (1)	-Sal (1)	29.3°	Plane (2)	-Plane(3)	86.3°
	-Plane(2)	88.1		-Sal(1)	71.1
	-Plane(3)	88.6		-Ala	87.6
	-Sal(2)	60.5	Plane (3)	-Ala	6.5
	-Ala	89.5		-Sal(1)	67.2
Plane (2)	-Sal(2)	41.2		-Sal(2)	70.0

Plane equations: each plane is represented by $lx'+my'+nz'+p=0$ with respect to the orthogonal axes, where x', y', and z' are coordinates in Å.

	Plane(1)	Plane(2)	Plane(3)	Sal(1)	Sal(2)	Ala
l	−0.418	−0.608	−0.715	−0.808	−0.028	−0.665
m	−0.848	−0.043	0.547	−0.538	−0.192	0.522
n	−0.324	0.793	−0.435	−0.240	−0.981	−0.534
p	7.097	0.297	5.626	7.795	6.779	5.734

nonbonded contacts are found between the methylene carbon atom(CA4) of *N*-Bz-L-ala group and the oxygen atoms of the α-Me-sal$_2$en ligand: CA4–OS1 2.760(21) and CA4–OS2 3.187(20) Å.

A new question thus arises. Why the fairly bulky amino nitrogen atom of *N*-Bz-L-ala(NA1) coordinates in the somewhat crowded position which is *trans* to the nitrogen atom NS1 in the equatorial plane instead of in the less crowded position *trans* to the apical oxygen atom(OS2)?

In relation to this, it is noteworthy that the structure of chloro(pyridine)[*N*,*N*'-tetramethylenebis(salicylideneaminato)]rhodium(III), in which the sal$_2$trien group acts as a quadridentate chelated ligand and takes a common *cis*-β type structure, belongs to the meridional coordination about the arrangement of mononegative coordination atoms(Cl^-, O^-, O^-) and the neutral nitrogen atoms(N(py), N(sal$_2$trien), N(sal$_2$trien)).[5] In the structure of μ-peroxo-bis{[3,3'-bis(salicylideneamino)dipropylaminato]cobalt(III)}, again the coordination around the cobalt atom takes a meridional N_3O_3 type.[19] Moreover, our X-ray studies on (−)$_{435}$-(L-isoleucinato)[*N*,*N*'-ethylenebis(α-methylsalicylideneaminato)]cobalt(III) 1.5H_2O has clearly shown that the structure is Λ_L-*cis*-β_2-mer(N_3O_3) type.[6] Therefore, as far as we know, all the structures of the related complexes so far determined by X-ray analyses are of meridional type. Thus, it can be inferred that the preference for the meridional coordination plays an important role in determining the molecular structures of these complexes.

There were many studies on the stereoselectivity or stereospecificity of [Co(N_4)(AA)] complexes with a chiral amino acid.[20] In comparison with these *cis*-β_2-[Co(N_4)(AA)] complexes, the stereoselectivity of *cis*-β_2-type cobalt(III) Schiff-base complexes is surprisingly high: for example, in the present *N*-Bz-L-ala complex, the stereoselectivity for the Λ_{RS}-*cis*-β_2(mer) configuration is almost 100%.[9] Recently, Yamaguchi *et al.* reported that the structure of (+)$_{589}$-[Co(*R*-ala)(*SS*-pyht)]$^{2+}$, which is the predominant isomer at the equilibrium conditions, is a Λ_R-*cis*-β_2 type.[21] The complex has no significant nonbonded interaction between the tetramine moiety and the alaninato ligand. In contrast to this, our present cobalt(III) Schiff-base complex has several significant nonbonded interactions between the α-Me-sal$_2$en moiety and the *N*-Bz-L-ala group though this isomer is the most favorable one at the equilibrium conditions.[9] The intramolecular nonbonded distances are as follows: CA4–OS1 2.760(21), CA4–Co 2.947(17), CA4–OS2 3.187(20), NA1–CA10 3.190(24), NA1–CS21 3.003(23) and NA1–CS26 3.143(22) Å.

If the absolute configuration around the *N*-Bz-L-amino nitrogen atom(NA1) changes from *R* to *S* and remaining part of the molecule is fixed, several abnormally short contacts appear around the methylene

Table 4. Intermolecular distances and angles

D–H···A	D···A(*l*/Å)	H···A(*l*/Å)	D–H···A(*φ*/°)
Hydrogen bond distances and bonding modes			
OW1–H1(OW1)···OA2	2.81(2)	1.84(20)	171(18)
OW1–H2(OW1)···OA1^{i}	2.96(2)	2.14(19)	161(18)
OW2–H1(OW2)···OS1	3.03(2)	2.18(16)	174(15)
OW2–H2(OW2)···OW1	2.88(2)	1.85(22)	177(19)
OW3–H1(OW3)···OW2	3.09(3)	1.98(23)	175(19)

Selected intermolecular distances (*l*/Å)			
CS21···CA7^{ii}	3.60(3)	CS18···OA2^{iv}	3.50(2)
CS26···CA8^{ii}	3.60(2)	OA2···CS23^{v}	3.64(2)
CS27···CA7^{ii}	3.64(3)	CA3···CA10^{v}	3.60(3)
CS14···CA6^{iii}	3.65(3)	CS25···CS11^{vi}	3.60(3)
CE1···OA2^{iv}	3.51(2)	CS28···CS13^{vi}	3.60(3)
Selected intermolecular distances around OW3 atom (*l*/Å)			
OW3^{iii}···OS2	3.98(3)	OW3^{iii}···CS13	3.47(3)
···CS22	3.84(3)	···CS14	3.76(4)
···CS12	3.57(3)	···CS28^{vii}	3.46(4)

Roman numerals as superscripts refer to the following equivalent positions, relative to the reference atom at (x,y,z): i$(1/2-x, -y, -1/2+z)$, ii$(x, y, 1+z)$, iii$(1/2-x, 1-y, 1/2+z)$, iv$(1/2-x, -y, 1/2+z)$, v$(1-x, -1/2+y, 1/2-z)$, vi$(1/2+x, 1/2-y, 1-z)$, vii$(1-x, 1/2+y, 3/2-z)$. D; Hydrogen donor, A; hydrogen acceptor.

carbon atom(CA4) of the *N*-Bz moiety. The shortest intramolecular distance calculated in this Λ_{SS} model is only 2.10 Å for CA4–CS26(sal(2)). On contrast to this, the inversion of the absolute configuration around the α-carbon atom(CA2) of *N*-Bz-L-ala group from *S* to *R* introduces a fairly small repulsive effect. The shortest distance in this Λ_{RR} model is 2.64 Å for CA2(R)–CA4. Thus, our presumption about the thermodynamic stabilities among the diastereoisomers of the present complex,[9] $\Lambda_{RS} \gg \Lambda_{RR} > \Lambda_{SS}$, can be verified clearly.

Crystal Packing and Water of Crystallization. The selected intermolecular distances including the hydrogen bonding modes are summarized in Table 4. Three water molecules of crystallization(OW1, OW2, and OW3) make a columnar structure around the two-fold screw axis along the c-direction, and provide crystalline stability by forming strong hydrogen bonds. The hydrogen bonding network of these water molecules, including three other oxygen atoms(two(OA1 and OA2) come from the *N*-Bz-L-ala group and one(OS1) from the sal(1) moiety), is shown in Fig. 1 and Fig. 2 by the dotted lines.

Three benzene rings are present in this molecule. The packing modes around these benzene rings in the present crystal are as follows: (i) The benzene ring of the sal(1) moiety has close contacts with the water molecule OW3(see Table 4), and (ii) the remaining two benzene rings(one comes from the *N*-Bz-L-ala and the other from the sal(2) of the α-Me-sal$_2$en) are stacked nearly perpendicular to each other along the crystallographic c axis.

The intermolecular bond distances around the water molecule OW3 are summarized in Table 4. It is interesting to note that this water molecule lies nearly on a line which passes through the central cobalt atom and the middle point of the OS1 and OS2 oxygen atoms as shown in Fig. 2. Therefore, the central area of the OS1–Co–OS2 plane is covered with the water molecule OW3, and this water molecule prohibits other molecules from approaching along this direction.

The packing feature around the water molecule OW3 is also responsible for the thermal dehydration behavior of this crystal. The elemental analysis shows that partial dehydration should occur in this crystal. There are strong interactions around the water molecules OW1 and OW2 as shown in Table 4. In contrast, only one short contact is found around the OW3; OW3–OW2 3.09(3) Å. Additionally, the averaged isotropic temperature factor for OW3 (B_{eq}=15.4 Å^{-2}) is considerably larger than those obtained for OW1(5.9) and OW2(9.4). Thus, it can be concluded that the partial dehydration mainly occurs at the position of OW3.

The authors wish to acknowledge a Grant-in-Aid for Scientific Research from the Ministry of Education, Science and Culture.

References

1) M. Calligaris, G. Nardin, and L. Randaccio, *Coord. Chem. Rev.*, **7**, 385 (1972).
2) N. A. Bailey, B. M. Higson, and E. D. Mckenzie, *J. Chem. Soc., Dalton Trans.*, **1972**, 503.
3) M. Calligaris, G. Manzini, G. Nardin, and L. Randaccio, *J. Chem. Soc., Dalton Trans.*, **1972**, 543.
4) D. Cummins, E. D. McKenzie, and H. Milburn, *Inorg. Chim. Acta*, **12**, L17 (1975).
5) B. M. Gatehouse, B. E. Reichert, and B. O. West, *Acta Crystallogr., Sect. B*, **32**, 30 (1976).
6) Y. Kushi, R. Tamura, M. Kuramoto, T. Yoshizawa, H. Yoneda, and Y. Fujii, *J. Chem. Soc., Chem. Commun.*, **1978**, 266.
7) Y. Fujii, T. Isago, and M. Sano, *Chem. Lett.*, **1975**, 1299.
8) Y. Fujii, K. Shiono, K. Ezuka, and T. Isago, *Bull. Chem. Soc. Jpn.*, **53**, 3537 (1980).
9) Y. Fujii, M. Matsufuru, A. Saito, and S. Tsuchiya, *Bull. Chem. Soc. Jpn.*, **54**, 2029 (1981).
10) "International Tables for X-Ray Crystallography," Kynoch Press, Birmingham (1974), Vol. IV, pp. 49, 72—79.
11) Y. Kushi, unpublished work.
12) T. Ashida, "The Universal Crystallographic Computation Program System," ed by T. Sakurai, The Crystallographic Society of Japan (1967).
13) C. K. Johnson, ORTEP, Report ORNL-3794, Oak Ridge National Laboratory, Oak Ridge, Tennessee, U. S. A., 1965.
14) L. G. Marzilli and D. A. Buckingham, *Inorg. Chem.*, **6**, 1042 (1967): β_1 and β_2 refer to the two configurational isomers. For amino acidate, β_2 refers to the isomer with O atom trans to the apical O atom of the quadridentate Schiff base ligand.
15) IUPAC, *Inorg. Chem.*, **9**, 1 (1970).
16) K. E. Voss, R. J. Angelici, and R. A. Jacobson, *Inorg. Chem.*, **17**, 1922 (1978).
17) R. Herak, B. Prelesnik, and I. Krastanovic, *Acta Crystallogr. Sect. B*, **34**, 91 (1978).
18) R. Fink, D. Revus, and D. Holm, *Acta Crystallogr. Sect. B*, **33**, 1660 (1977).
19) L. A. Lindblom, W. P. Schaefer, and R. E. Marsh, *Acta Crystallogr., Sect. B*, **27**, 1461 (1971).
20) M. Yamaguchi, S. Yamamatsu, T. Furusawa, S. Yano, M. Saburi, and S. Yoshikawa, *Inorg. Chem.*, **19**, 2010 (1980), and references cited therein.
21) M. Yamaguchi, S. Yano, M. Saburi, and S. Yoshikawa, *Inorg. Chem.*, **19**, 2016 (1980).

X-Ray Structures of (−)$_{589}$-Bis(isothiocyanato)bis(1,3-propanediamine)-chromium(III) Bis[μ-(+)-tartrato(4−)]bis[antimonate(III)] Dihydrate and Its Cobalt(III) Analogue

Keiji MATSUMOTO,* Shun'ichiro OOI, Hiroshi KAWAGUCHI,† Mamoru NAKANO, and Shinichi KAWAGUCHI

Department of Chemistry, Faculty of Science, Osaka City University, Sumiyoshi-ku, Osaka 558

†*Department of Chemistry, Faculty of Science, Kochi University, Akebono-cho, Kochi 780*

(Received October 12, 1981)

The crystal structures of (−)$_{589}$-[Cr(NCS)$_2$(tn)$_2$]1/2[Sb$_2$(+)-tart$_2$]·2H$_2$O (**1**) and (−)$_{589}$-[Co(NCS)$_2$(tn)$_2$]1/2-[Sb$_2$(+)-tart$_2$]·2H$_2$O (**2**) have been determined from the X-ray diffraction data. The structures were solved by the Patterson-Fourier method and refined by the least-squares method to R=0.043 (**1**) and 0.070 (**2**) for 2659 and 1826 reflections respectively. The two crystals are isomorphous with each other. The complex cations in **1** and **2** have a similar geometry. Their absolute configuration is Λ, and agrees with that assigned from the CD spectra in comparison with those in the first d-d band region of bis(ethylenediamine)cobalt(III) complexes. The six-membered chelate rings are of chair conformation. The chairs are flattened more than expected from the conformational analysis.

As a part of studies of circular dichroism(CD)-structure correlation of metal complexes involving 1,3-propanediamine,[1,2] we describe here X-ray structure analyses of (−)$_{589}$-bis(isothiocyanato)bis(1,3-propanediamine)chromium(III) bis[μ-(+)-tartrato(4−)]-bis[antimonate(III)] dihydrate (−)$_{589}$-[Cr(NCS)$_2$(tn)$_2$]-1/2[Sb$_2$(+)-tart$_2$]·2H$_2$O (tn=1,3-propanediamine, [Sb$_2$(+)-tart$_2$]$^{2-}$=bis[μ-(+)-tartrato(4−)]-bis[antimonate(III)] anion) and its cobalt(III) analogue (−)$_{589}$-[Co(NCS)$_2$(tn)$_2$]1/2[Sb$_2$(+)-tart$_2$]·2H$_2$O. Preliminary communication on the cobalt(III) complex has already been reported.[3]

Experimental

X-Ray Data Collection. The crystal of (−)$_{589}$-[Cr(NCS)$_2$(tn)$_2$]1/2[Sb$_2$(+)-tart$_2$]·2H$_2$O (**1**) is red and hexagonal tablet. The (−)$_{589}$-[Co(NCS)$_2$(tn)$_2$]1/2[Sb$_2$(+)-tart$_2$]·2H$_2$O complex (**2**) crystallizes in dark red prisms. The compounds **1** and **2** were prepared and resolved by Kawaguchi and his co-workers.[4,5] Preliminary oscillation and Weissenberg photographs showed the space group and approximate unit-cell dimensions for each crystal. The unit-cell dimensions were refined by least-squares analyses of the θ values of 32 reflections for **1** and 23 for **2**. The crystal data for **1** and **2** are given in Table 1. Intensity data were collected at room temperature on a Philips PW1100 automated diffractometer, using graphite-monochromated Mo $K\alpha$ radiation. During the data collection, three standard reflections were monitored every 4 h to check the stability and orientation of each crystal. Both compounds remained quite stable. Each data set was corrected for Lorentz-polarization[6] and absorption effects.[7]

Structure Solution and Refinement. The structure of **2** was first solved by the Patterson-Fourier techniques. Since the two crystals **1** and **2** are isomorphous, the structure solution for **1** was straightforward. Refinement of the structures was carried out by using the block-diagonal least-squares method. The function minimized was $\sum w(F_o-|F_c|)^2$, where $w=1/\sigma^2(F_o)$ was used. In the final cycle of refinement, all the parameter shifts were less than 0.8σ for **1** and 0.4σ for **2**. Neutral-atom scattering factors for the Sb, Cr, Co, S, O, N, and C atoms were taken from Ref. 8, with anomalous dispersion corrections for Sb, Cr, and Co atoms. The final R values were 0.043 for **1** and 0.070 for **2**. No attempt was made to locate hydrogen atoms. No chemically significant peaks were observed on final difference Fourier maps for **1** and **2**. Maximum peaks were 1.0 e Å^{-3} for **1** and 1.5 e Å^{-3} for **2**.

The absolute configurations of (−)$_{589}$-[Cr(NCS)$_2$(tn)$_2$]$^+$ and (−)$_{589}$-[Co(NCS)$_2$(tn)$_2$]$^+$ were determined on the basis of the known configuration of the (+)-tartric acid. The $F_o-|F_c|$ Tables for **1** and **2** and the anisotropic temperature factors are preserved by the Chemical Society of Japan (Document No. 8223). The final atomic coordinates are given in Table 2. Figures 1 and 2 were drawn by the use of ORTEP.[9] All the computations were performed by a FACOM 230-60 computer at Osaka City University using programs in the UNICS.[10]

Results and Discussion

The perspective views of (−)$_{589}$-[Cr(NCS)$_2$(tn)$_2$]$^+$ and (−)$_{589}$-[Co(NCS)$_2$(tn)$_2$]$^+$ are given in Fig. 1. They have a similar structure and their absolute configuration is Λ, which is consistent with the assignment from the CD data obtained by Kawaguchi and his co-workers.[4,5] Each complex cation has an approximate two-fold axis of rotation passing through the central metal and bisecting the N(NCS)–M–N(NCS) (M=Cr, Co) angle. The six-membered chelate rings are of chair conformation. The chairs in each complex have the Λpa[11](BB)[12] conformation and fold apart from one another (Fig. 1). Geue and Snow[12] calculated that the Λpa(BB) conformer is energetically more stable than the Λap(AA)

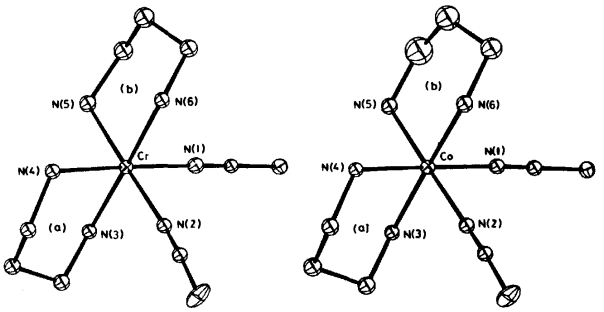

Fig. 1. The absolute configurations of the complex cations: (−)$_{589}$-[Cr(NCS)$_2$(tn)$_2$]$^+$ (left) and (−)$_{589}$-[Co(NCS)$_2$(tn)$_2$]$^+$ (right). The "a" ring is the "p" conformer and the "b" ring has the "a" form.

Table 1. Summary of crystal data and experimental details

Compound	**1** $(-)_{589}$-$[Cr(NCS)_2(tn)_2]$ $1/2[Sb_2(+)\text{-tart}_2]\cdot 2H_2O$	**2** $(-)_{589}$-$[Co(NCS)_2(tn)_2]$ $1/2[Sb_2(+)\text{-tart}_2]\cdot 2H_2O$
Crystal system	Orthorhombic	Orthorhombic
Space group	$P2_12_12$	$P2_12_12$
a/Å	12.121(5)	12.161(7)
b/Å	19.996(9)	19.502(24)
c/Å	9.240(6)	9.165(7)
$F(000)$	1140	1152
F.W.	594.05	600.98
U/Å^3	2239.5(16)	2173.5(33)
Z	4	4
D_m/g cm^{-3}	1.74	1.81
D_c/g cm^{-3}	1.76	1.84
μ(Mo $K\alpha$)/cm^{-1}	19.6	22.9
Crystal size/mm^3	$0.57\times0.39\times0.15$	$0.35\times0.11\times0.08$
Scan type	ω	ω
Scan speed/° s^{-1}	0.017	0.008
Scan range/°	$1.4+0.2\tan\theta$	$1.0+0.2\tan\theta$
$2\theta_{max}$/°	55	55
Background measurement/s	40	20
Maximum and minimum transmission factors	1.82, 1.31	1.20, 1.12
Number of unique reflections with $F_o^2\geq3\sigma(F_o^2)$	2659	1826
$R(R_w)$	0.043(0.055)	0.070(0.064)

Table 2. Positional and thermal parameters with their estimated standard deviations in parentheses

Atom	**1** $(-)_{589}$-$[Cr(NCS)_2(tn)_2]1/2[Sb_2(+)\text{-tart}_2]\cdot 2H_2O$ $10^4\times x$	$10^4\times y$	$10^4\times z$	$10\times B$/Å^2
Cr	2834.1(9)	1967.4(5)	8553.0(12)	21.5(3)[a]
S(1)	283(2)	1517(1)	12328(1)	29.8(5)[a]
S(2)	2460(3)	4310(1)	7967(4)	61.9(9)[a]
N(1)	1828(5)	1846(3)	10244(7)	33(1)
N(2)	2466(5)	2943(3)	8450(6)	27(1)
N(3)	1542(5)	1715(3)	7161(7)	27(1)
N(4)	3840(5)	2087(3)	6739(7)	29(1)
N(5)	3264(6)	956(3)	8701(8)	33(1)
N(6)	4153(5)	2190(3)	9940(7)	29(1)
C(1)	1174(6)	1705(3)	11124(8)	24(1)
C(2)	2461(6)	3515(4)	8276(8)	30(1)
C(3)	1370(7)	2128(4)	5824(9)	33(2)
C(4)	2347(7)	2132(4)	4828(9)	35(2)
C(5)	3391(7)	2452(4)	5432(9)	32(2)
C(6)	3586(8)	698(5)	10162(11)	46(2)
C(7)	4530(9)	1043(5)	10834(11)	50(2)
C(8)	4344(8)	1769(4)	11257(10)	39(2)
Sb(1)	5000.0	5000.0	485.3(6)	26.0(2)[a]
Sb(2)	5000.0	5000.0	5874.9(6)	21.6(2)[a]
C(9)	3847(6)	3853(3)	1778(8)	27(1)
C(10)	3240(6)	4488(3)	2339(8)	24(1)
C(11)	3288(6)	4439(3)	4002(8)	25(1)
C(12)	2794(6)	5116(3)	4567(7)	26(1)
O(1)	3718(4)	5076(2)	1834(5)	26(1)
O(2)	4755(4)	3975(3)	1121(6)	30(1)
O(3)	3456(5)	3292(3)	2007(6)	36(1)
O(4)	4360(4)	4350(2)	4479(5)	25(1)
O(5)	3436(4)	5482(2)	5283(6)	28(1)
O(6)	1831(5)	5251(3)	4255(7)	43(1)
O(7)	5122(14)	975(9)	5124(18)	156(5)
O(8)	1062(7)	3328(4)	2153(9)	62(2)

Table 2. (continued)

Atom	**2** $(-)_{589}$-$[Co(NCS)_2(tn)_2]1/2[Sb_2(+)\text{-tart}_2]\cdot 2H_2O$ $10^4\times x$	$10^4\times y$	$10^4\times z$	$10\times B/Å^2$
Co	2870.0(17)	1943.6(10)	8507.9(23)	21.8(6)[a]
S(1)	354(4)	1557(4)	12296(5)	30.6(12)[a]
S(2)	2458(5)	4303(3)	8136(8)	57.6(18)[a]
N(1)	1899(10)	1833(7)	10143(14)	27(3)
N(2)	2505(10)	2900(6)	8442(15)	27(3)
N(3)	1609(10)	1715(6)	7166(14)	25(3)
N(4)	3853(10)	2061(6)	6790(15)	25(2)
N(5)	3250(10)	957(7)	8607(15)	29(3)
N(6)	4105(11)	2191(7)	9833(15)	32(3)
C(1)	1263(13)	1722(8)	11032(18)	27(3)
C(2)	2506(12)	3479(8)	8341(19)	27(3)
C(3)	1380(15)	2138(9)	5887(20)	35(4)
C(4)	2398(15)	2120(9)	4835(21)	39(4)
C(5)	3482(15)	2441(9)	5497(18)	34(4)
C(6)	3693(26)	701(16)	9906(32)	92(8)
C(7)	4469(20)	1003(13)	10742(27)	70(6)
C(8)	4334(17)	1752(11)	11144(23)	54(5)
Sb(1)	5000.0	5000.0	515.7(14)	30.1(4)[a]
Sb(2)	5000.0	5000.0	5961.0(14)	22.3(4)[a]
C(9)	3883(14)	3829(9)	1818(22)	37(14)
C(10)	3234(12)	4474(8)	2377(18)	25(3)
C(11)	3313(13)	4411(8)	4047(18)	24(3)
C(12)	2784(12)	5109(8)	4623(13)	26(3)
O(1)	3725(7)	5086(5)	1908(10)	24(2)
O(2)	4779(9)	3959(5)	1156(11)	32(2)
O(3)	3495(9)	3247(6)	2061(14)	41(3)
O(4)	4374(9)	4323(5)	4541(12)	26(2)
O(5)	3447(9)	5488(5)	5330(13)	31(2)
O(6)	1822(11)	5243(6)	4309(14)	48(3)
O(7)	5130(21)	949(12)	5188(23)	135(7)
O(8)	1068(16)	3360(10)	2157(22)	105(6)

a) Equivalent isotropic temperature factor (W. C. Hamilton, *Acta Crystallogr.*, **12**, 609 (1959)).

Table 3. Comparison of the torsion angles, bond angles, and dihedral angles

Six-membered chelate ring	Torsion angle about N–C	(τ/°)	Bond angle (ϕ/°) N–M–N	M–N–C		Dihedral angle(ϕ/°) D_1[a]	D_2[a]
Ring A in Λ ap (AA)[b]	54.4	61.6	92.6	119.0			
Ring B in Λ pa (BB)[b]	67.2	68.6	87.7	113.3			
Ring (a) } (**1**)	59.7	57.9	88.4	119.1	118.6	37.8	56.1
Ring (b) } (**1**)	58.3	59.0	88.6	117.2	119.7	37.2	58.2
Ring (a) } (**2**)	57.5	61.4	90.0	120.8	120.7	38.1	56.8
Ring (b) } (**2**)	53.2	42.8	91.8	118.5	119.3	32.1	41.9

a) D_1 is the dihedral angle between the N–M–N and N–C–C–N planes and D_2 is that between the N–C–C–N and C–C–C planes. b) Ring A or Ring B in *cis*-$[Co(CO_3)(tn)_2]^+$ in Ref. 12.

and Λpp(AB) conformations. They also indicated that no flattening should occur for two rings in Λpa(BB) conformation. However, we observed the flattening of the chairs in the crystals. Table 3 compares the tortion angles and bond angles calculated by Geue and Snow with those of the present work. The chairs of (a) and (b) in **1** and (a) in **2** have a similar geometry and are flattened more than expected from the calculation. The chair (b) in **2** shows a much pronounced flattening in comparison with the former three, and consequently the geometries of two rings in **2** are significantly different from each other. Since these flattenings are not predicted by the conformational analysis, the chair conformation in the present complexes presumably results from the

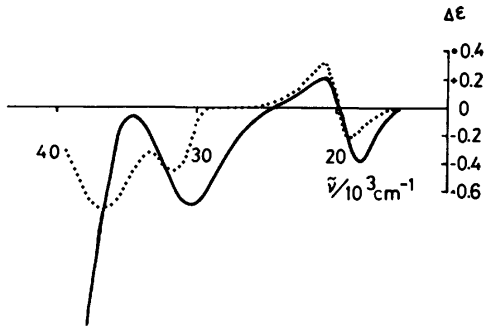

Fig. 2. The circular dichroism spectra of $(-)_{589}$-$[Cr(NCS)_2(tn)_2](NCS)$ (……) in methanol and $(-)_{589}$-$[Co(NCS)_2(tn)_2](ClO_4)$ (——) in water.

TABLE 4. INTERATOMIC DISTANCES AND BOND ANGLES WITH THEIR ESTIMATED STANDARD DEVIATIONS IN PARENTHESES

1 $(-)_{589}$-$[Cr(NCS)_2(tn)_2]1/2[Sb_2(+)\text{-tart}_2]\cdot 2H_2O$

Bond lengths (l/Å)		Bond angles (ϕ/°)	
Cr–N(1)	1.996(7)	Cr–N(1)–C(1)	170.7(6)
Cr–N(2)	2.003(6)	Cr–N(2)–C(2)	166.4(6)
Cr–N(3)	2.089(6)	N(1)–C(1)–S(1)	179.6(7)
Cr–N(4)	2.086(7)	N(2)–C(2)–S(2)	177.9(7)
Cr–N(5)	2.094(7)	N(3)–Cr–N(4)	88.4(3)
Cr–N(6)	2.097(7)	N(5)–Cr–N(6)	88.6(3)
N(1)–C(1)	1.17(1)	Cr–N(3)–C(3)	118.6(5)
N(2)–C(2)	1.16(1)	Cr–N(4)–C(5)	119.1(5)
C(1)–S(1)	1.595(7)	Cr–N(5)–C(6)	117.2(5)
C(2)–S(2)	1.615(8)	Cr–N(6)–C(8)	119.7(5)
N(3)–C(3)	1.50(1)	N(3)–C(3)–C(4)	113.5(7)
N(4)–C(5)	1.51(1)	N(4)–C(5)–C(4)	112.8(7)
N(5)–C(6)	1.50(1)	N(5)–C(6)–C(7)	114.9(8)
N(6)–C(8)	1.50(1)	N(6)–C(8)–C(7)	110.5(8)
C(3)–C(4)	1.50(1)	C(3)–C(4)–C(5)	115.7(7)
C(4)–C(5)	1.52(1)	C(6)–C(7)–C(8)	116.1(9)
C(6)–C(7)	1.47(2)	N(1)–Cr–N(2)	91.1(3)
C(7)–C(8)	1.52(2)		

Short contacts (l/Å)[a)]

$N(3)\cdots O(2)^{V}$	3.019(8)	$N(5)\cdots O(6)^{III}$	3.076(10)
$N(3)\cdots O(5)^{III}$	3.344(8)	$N(6)\cdots O(3)^{II}$	3.037(9)
$N(4)\cdots S(1)^{IV}$	3.407(7)	$O(8)\cdots O(7)^{V}$	3.093(21)
$N(4)\cdots O(7)^{I}$	3.095(20)		

2 $(-)_{589}$-$[Co(NCS)_2(tn)_2]1/2[Sb_2(+)\text{-tart}_2]\cdot 2H_2O$

Bond lengths (l/Å)		Bond angles (ϕ/°)	
Co–N(1)	1.920(15)	Co–N(1)–C(1)	173.1(13)
Co–N(2)	1.919(14)	Co–N(2)–C(2)	166.3(14)
Co–N(3)	2.015(13)	N(1)–C(1)–S(1)	179.6(16)
Co–N(4)	1.990(14)	N(2)–C(2)–S(2)	177.2(17)
Co–N(5)	1.980(14)	N(3)–Co–N(4)	90.0(6)
Co–N(6)	1.991(14)	N(5)–Co–N(6)	91.8(6)
N(1)–C(1)	1.15(2)	Co–N(3)–C(3)	120.7(2)
N(2)–C(2)	1.13(2)	Co–N(4)–C(5)	120.8(11)
C(1)–S(1)	1.633(17)	Co–N(5)–C(6)	118.5(11)
C(2)–S(2)	1.619(19)	Co–N(6)–C(8)	119.3(11)
N(3)–C(3)	1.46(2)	N(3)–C(3)–C(4)	109.3(14)
N(4)–C(5)	1.47(2)	N(4)–C(5)–C(4)	111.5(14)
N(5)–C(6)	1.40(3)	N(5)–C(6)–C(7)	126.5(26)
N(6)–C(8)	1.50(3)	N(6)–C(8)–C(7)	112.0(17)
C(3)–C(4)	1.57(3)	C(3)–C(4)–C(5)	114.4(15)
C(4)–C(5)	1.58(3)	C(6)–C(7)–C(8)	118.9(23)
C(6)–C(7)	1.35(4)	N(1)–Co–N(2)	89.5(6)
C(7)–C(8)	1.52(3)		

Short contacts (l/Å)[a)]

$N(3)\cdots O(2)^{V}$	3.008(17)	$N(5)\cdots O(6)^{III}$	3.015(19)
$N(3)\cdots O(5)^{III}$	3.312(17)	$N(6)\cdots O(3)^{II}$	2.994(19)
$N(4)\cdots S(1)^{IV}$	3.361(15)	$O(8)\cdots O(7)^{V}$	3.007(32)
$N(4)\cdots O(7)^{I}$	3.044(29)		

a) Roman numeral Superscripts refer to the following equivalent positions: I x, y, z; II $x, y, 1+z$; III $1/2-x, -1/2+y, 1-z$; IV $1/2+x, 1/2-y, 2-z$; V $-1/2+x, 1/2-y, 1-z$.

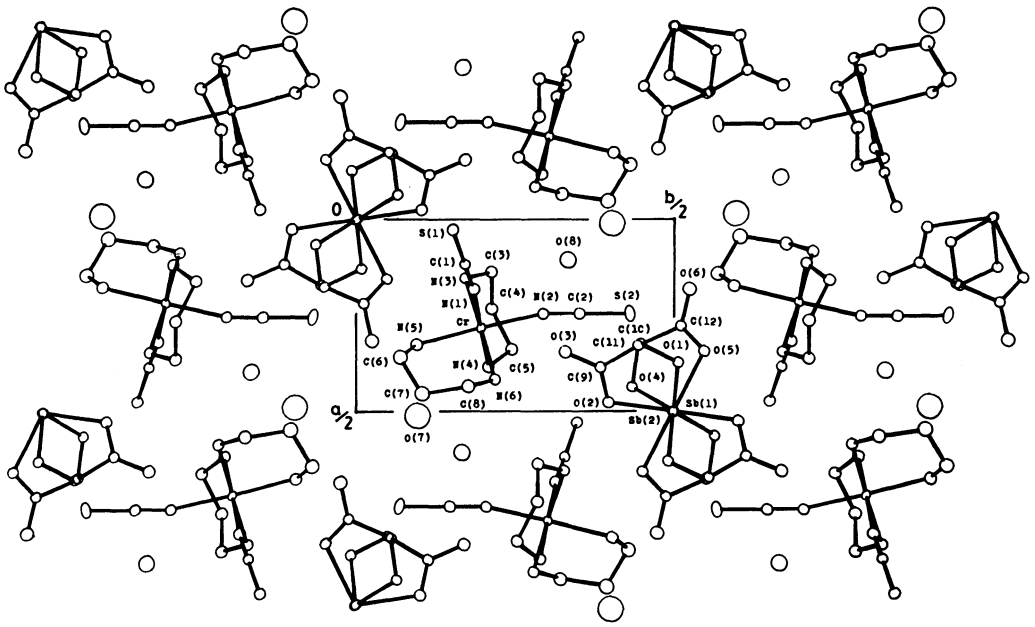

Fig. 3. The crystal structure of **1** viewed down the c axis, showing the atom numbering scheme.

crystal packing.

The bond distances between the metal ion and the ligator atoms are slightly larger in **1** than in **2**.[13] The average M–N bond distances are Cr–N(amine) 2.092 Å, Cr–N(NCS) 2.000 Å, Co–N(amine) 1.994 Å, and Co–N(NCS) 1.920 Å. These values are in agreement with those previously reported.[11–13] Deviations of the M–N(1)–C(1) bonds (Cr–N(1)–C(1)=170.7°, Co–N(1)–C(1)=173.1°) from 180° are less than the M–N(2)–C(2) bonds (Cr–N(2)–C(2)=166.4°, Co–N(2)–C(2)=166.3°). The isothiocyanato groups are approximately linear. The chelate bite angle (88.5°) in **1** is slightly less than 90°, but in **2** the value is 90.9° (Table 4).

The CD spectra of Λ-$(-)_{589}$-$[Cr(NCS)_2(tn)_2](NCS)$ and Λ-$(-)_{589}$-$[Co(NCS)_2(tn)_2](ClO_4)$ are given in Fig. 2. The CD pattern in the first d-d band region is

similar to each other and to the corresponding bis(ethylenediamine)cobalt(III) complexes.[14,15] Therefore, by analogy with bis(ethylenediamine)cobalt(III) complexes, each positive CD peak at higher wave-number could be assigned to the combined A and B components derived from the E_a component of the parent trigonal complex and each negative CD peak in the lower wave-number to the B component. Mason's criterion[16] that the absolute configuration of bis(ethylenediamine) cobalt(III) complex should be *Λ* if the CD of the combined A and B components are positive in sign, appears to hold in the present cases. It is noticed, however, that in *Λ*-$(-)_{589}$-$[Co(NCS)_2(tn)_2]^+$, the absolute configuration is related to the sign of the less dominant CD peak in the first absorption band region.

The $[Sb_2(+)\text{-tart}_2]^{2-}$ anion has a crystallographically imposed two-fold axis of rotation which passes through the two Sb atoms. The geometry of $[Sb_2(+)\text{-tart}_2]^{2-}$ anion is identical with those previously reported.[17]

Figure 3 gives the crystal structure of **1**. The crystals **1** and **2** are isomorphous. Each crystal consists of *Λ*-$(-)_{589}$-$[M(NCS)_2(tn)_2]^+$ cations, $[Sb_2(+)\text{-tart}_2]^{2-}$ anions, and water molecules, which are mainly bound by the N–H···O and N–H···S hydrogen bonds. Short contact distances are given in Table 4.

K. M. acknowledges the financial support of the Matsunaga Science Foundation.

References

1) K. Matsumoto, H. Kawaguchi, H. Kuroya, and S. Kawaguchi, *Bull. Chem. Soc. Jpn.*, **46**, 2424 (1973).

2) K. Matsumoto and S. Ooi, *Bull. Chem. Soc. Jpn.*, **52**, 3307 (1979).

3) K. Matsumoto, M. Yonezawa, H. Kuroya, H. Kawaguchi, and S. Kawaguchi, *Bull. Chem. Soc. Jpn.*, **43**, 1269 (1970).

4) M. Nakano and S. Kawaguchi, *Bull. Chem. Soc. Jpn.*, **52**, 3563 (1979).

5) H. Kawaguchi and S. Kawaguchi, *Bull. Chem. Soc. Jpn.*, **43**, 2103 (1970).

6) J. Hornstra and B. Stubbe, PW1100 Data Processing Programs, Philips Research Laboratories, Eindhoven, Holland.

7) L. Templeton and D. Templeton, *Am. Cryst. Assoc., Abstr. Papers*, 1973.

8) "International Tables for X-Ray Crystallography," Kynoch Press, Birmingham (1974), Vol. IV, pp. 71, 148.

9) C. K. Johnson, "ORTEP," Report ORNL-3794, Oak Ridge National Laboratory, Oak Ridge, Tenn., 1965.

10) "The Universal Crystallographic Computation Program System," The Crystallographic Society of Japan (1969).

11) F. A. Jurnak and K. N. Raymond, *Inorg. Chem.*, **11**, 3149 (1972).

12) R. J. Geue and M. R. Snow, *J. Chem. Soc., A*, **1971**, 2981.

13) F. A. Jurnak and K. N. Raymond, *Inorg. Chem.*, **13**, 2387 (1974), and references cited therein; E. N. Duesler and K. N. Raymond, *Inorg. Chim. Acta*, **30**, 87 (1978).

14) K. Yamasaki, J. Hidaka, and Y. Shimura, *Bull. Chem. Soc. Jpn.*, **49**, 3060 (1976).

15) D. A. House, *J. Inorg. Nucl. Chem.*, **35**, 3103 (1973).

16) A. J. McCaffery, S. F. Mason, and B. J. Norman, *J. Chem. Soc.*, **1965**, 5094.

17) M. E. Gress and R. A. Jacobson, *Inorg. Chim. Acta*, **8**, 209 (1974); R. E. Tapscott, R. L. Belford, and I. C. Paul, *Coord. Chem. Rev.*, **4**, 323 (1969).

Influences of the Lanthanoid Contraction on the Thermal Dehydration Reactions of Lanthanoid(III) Malonate Hydrates

Kazuo MURAISHI, Kenzo NAGASE,† Masae KIKUCHI,†† Kozo SONE,*,††† and Nobuyuki TANAKA††††

Department of Chemistry, Faculty of Science, Yamagata University, Koshirakawa-machi, Yamagata 990
†*College of General Education, Tohoku University, Kawauchi, Sendai 980*
††*Institute for Iron, Steel and Other Metals, Tohoku University, Katahiracho, Sendai 980*
†††*Department of Chemistry, Faculty of Science, Ochanomizu University, Otsuka, Bunkyo-ku, Tokyo 112*
††††*Department of Chemistry, Faculty of Science, Tohoku University, Aoba, Aramaki, Sendai 980*

(Received October 16, 1981)

The thermal dehydration reactions of lanthanoid(III) malonate hydrates $Ln_2mal_3 \cdot nH_2O$ (Ln=Ce—Lu; mal=$CH_2(COO)_2$; n=6 for Ce—Eu and 8 for Gd—Lu) were investigated mainly by the thermogravimetries under conventional conditions and in atmosphere of water vapor at a constant reduced pressure and a superslow heating rate. The latter conditions were useful especially to detect the formation of new intermediate hydrates, and to determine the dehydration temperatures with accuracy. The main features of the results could be reasonably understood in view of the effects of the lanthanoid contraction.

The lanthanoid elements (Ln) are characterized by an overall decrease in size of atoms or ions with increasing atomic number. In the case of Ln^{3+} ions, the effects of this "lanthanoid contraction" appear most dramatically, and its influences on the coordination number (C.N.) and geometry are the unifying concept in the chemistry of Ln(III) compounds.[1,2] Lanthanoid(III) ions have unoccupied inner orbitals, but the ligand field stabilization caused by their presence is said to be much smaller than in the case of 3d-transition metal ions.[3] The C.N. of Ln^{3+} is normally 6 to 9, and the metal-ligand bonds are mainly ionic.

In aqueous solutions, most of Ln^{3+} compounds are labile, but it is said that their coordination spheres seek to achieve a compromise between the most spherical shielding for Ln^{3+} and the minimum interligand repulsion.[2]

In the solid state, polymorphs are often formed because of the small energy differences among possible structures of high C.N., and it is known that, in certain cases, one or two of the ligands are in "partial coordination," to reduce the overcrowdedness of the coordination sphere.[4] Thus the influences of the lanthanoid contraction observed in the solid state may look quite different from those[5] observed in solution.

In the present paper, such influences upon the thermal dehydration reaction of Ln^{3+} malonate hydrates in the solid state will be discussed mainly on the basis of thermogravimetric data.

Experimental

Preparation of $Ln_2mal_3 \cdot nH_2O$. Aqueous solutions of $LnCl_3$ (0.24 mol dm^{-3}) and Na_2mal (0.36 mol dm^{-3}) were mixed quickly at room temperature. Each precipitate obtained was allowed to stand overnight in contact with the mother liquor, washed several times with water by decantation, and filtered. It was further washed with ethanol and ether, and dried at room temperature. Contents of Ln, C, and H in the samples are given in Table 1.

Themogravimetry (TG) and Differential Thermal Analysis (DTA). The TG and DTA curves were obtained with a Shinku Riko TGD-3000 differential thermal microbalance at a heating rate of 3 °C/min in a dry nitrogen stream of 30 cm^3/min, and also at a superslow heating rate of 2 °C/h in water vapor at 10 Torr (1 Torr≈133 Pa).[6] About 20 mg of the powdered sample was used for each run.

IR and X-Ray Diffraction. The infrared spectra in the frequency region of 400—4000 cm^{-1} were obtained by the

Table 1. Analytical data of the malonate hydrates prepared in the present work

Compound	Color	Metal[a](%) Found	Metal[a](%) Calcd	Carbon[a](%) Found	Carbon[a](%) Calcd	Hydrogen(%) Found	Hydrogen(%) Calcd
$Ce_2mal_3 \cdot 6H_2O$	white	40.18	40.35	15.99	15.57	2.88	2.61
$Pr_2mal_3 \cdot 6H_2O$	green	40.39	40.48	15.33	15.53	3.00	2.60
$Nd_2mal_3 \cdot 6H_2O$	violet	40.65	41.05	15.66	15.38	2.71	2.58
$Sm_2mal_3 \cdot 6H_2O$	white	41.96	42.07	15.51	15.12	2.57	2.54
$Eu_2mal_3 \cdot 6H_2O$	white	41.96	42.31	15.14	15.05	2.78	2.53
$Gd_2mal_3 \cdot 8H_2O$	white	41.30	41.13	13.98	14.14	3.08	2.90
$Tb_2mal_3 \cdot 8H_2O$	white	41.34	41.38	14.06	14.07	2.67	2.89
$Dy_2mal_3 \cdot 8H_2O$	white	41.86	41.90	13.96	13.94	2.87	2.86
$Ho_2mal_3 \cdot 8H_2O$	pink	42.19	42.26	13.56	13.86	3.06	2.84
$Er_2mal_3 \cdot 8H_2O$	pink	42.84	42.61	13.90	13.77	3.15	2.82
$Tm_2mal_3 \cdot 8H_2O$	white	43.21	42.82	13.74	13.72	2.86	2.81
$Yb_2mal_3 \cdot 8H_2O$	white	44.07	43.46	13.97	13.57	2.98	2.78
$Lu_2mal_3 \cdot 8H_2O$	white	43.57	43.73	13.67	13.51	2.73	2.77

a) The metal contents were determined by titration with EDTA and Xylenol Orange in the pH range of 5.1—5.6.

KBr disk method with a Hitachi 215 infrared spectrometer and the powder X-ray diffraction analysis was made with a Rigaku Denki DS X-Ray diffractometer.

Results and Discussion

The samples prepared can be formulated as $Ln_2mal_3 \cdot nH_2O$, where $n=6$ for Ce—Eu and 8 for Gd—Lu (*cf.* Table 1). Hansson has studied the crystal structures of $Nd_2mal_3 \cdot 6H_2O$,[7] $Nd_2mal_3 \cdot 8H_2O$,[8] and $Eu_2mal_3 \cdot 8H_2O$;[9] the hexahydrates and octahydrates prepared in the present study showed essentially the same X-ray diffraction patterns as those of Hansson's $Nd_2mal_3 \cdot 6H_2O$ and $Eu_2mal_3 \cdot 8H_2O$, respectively. The infrared spectra were also divided into two different groups of Ce—Eu and Gd–Lu.

It must be mentioned here that most of these hydrates were already prepared by Azikov *et al.*, who also obtained their TG curves, and stated that their infrared spectra can be divided into two proups of Ce—Gd and Tb—Lu.[10,11] The accuracy of their data, however, is seemingly not very high, and their classification of Gd is not very convincing. Therefore, the TG and DTA behaviors of these hydrates were studied in more detail to get better structural correlations.

TG and DTA in N_2 at the Heating Rate of 3 °C/min. Among the TG and DTA curves of all the samples obtained, those of Eu, Gd, Ho, and Lu are shown in Fig. 1 as typical examples. As seen in the curve of Eu, all the hexahydrates lose their waters in a single step, whereas the octahydrates lose them in two steps, which can be distinguished more clearly with the heavier lanthanoids.

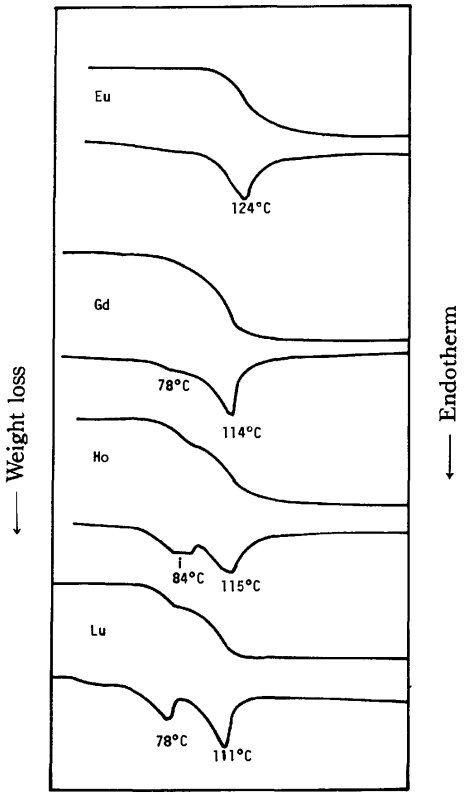

Fig. 1. TG and DTA curves of $Ln_2mal_3 \cdot nH_2O$ in N_2. The temperatures in the figure correspond to DTA peaks.

This difference in the mode of dehydration can be related with the structural data of these hydrates. It is known that the two Ln^{3+} in $Ln_2mal_3 \cdot 6H_2O$ are equivalent, and all the waters in them are coordinated to the Ln^{3+}, so that the hexahydrates can be represented as $[Ln_2mal_3(H_2O)_6]$ in which the C.N. of each Ln^{3+} is 9.[7] On the other hand, two waters in $Ln_2mal_3 \cdot 8H_2O$ are coordinated to one Ln^{3+} with C.N. 8, and three to another with C.N. 9, and the remaining three are held as lattice waters in two different ways.[9] Thus the octahydrates can be represented as $[Ln_2mal_3(H_2O)_5] \cdot 2H_2O \cdot \underline{H_2O}$.

Therefore, we can roughly say that, upon dehydration, the hexahydrates lose all of the coordination waters in a single step, but the octahydrates lose the lattice waters in the first step, and then the coordination waters in the second. Closer observations, however, reveal some more facts of interest.

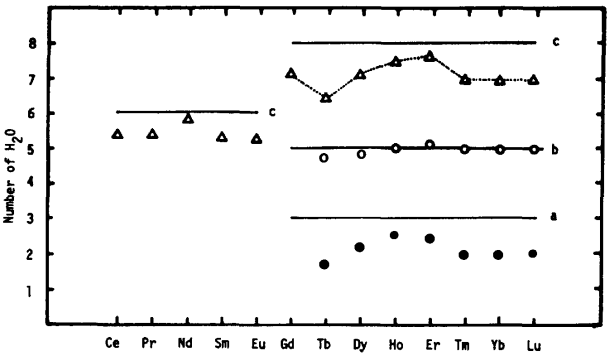

Fig. 2. Numbers of H_2O lost in the complete dehydration (△), and those lost in the first (●) and second (○) step, respectively, which were determined by TG in N_2. The solid lines indicate the theoretical values for lattice waters (a), coordination waters (b) and total waters (c).

When the numbers of H_2O lost by the complete dehydration are plotted against the symbols of Ln arranged in the order of increasing atomic number (Fig. 2), it is seen that they are somewhat smaller than expected; in the case of the octahydrates they are not exactly 8, and in most cases, nearly 7. This fact indicates that, among the waters in it, one of the lattice waters (the underlined one in the above formula) is held especially weakly, and easily lost from the sample in advance of the TG measurement.** So we represent the whole change as follows:

$$[Ln_2mal_3(H_2O)_5] \cdot 2H_2O \cdot H_2O \xrightarrow[I]{-H_2O}$$

$$[Ln_2mal_3(H_2O)_5] \cdot 2H_2O \xrightarrow[II]{-2H_2O}$$

$$[Ln_2mal_3(H_2O)_5] \xrightarrow[III]{-5H_2O} Ln_2mal_3.$$

** TG measurement on fresh samples in static air indicates, in all cases, an approximately quantitative loss of water.

Step I seems to occur very easily, so that it is either not observed on the TG curves (Lu, Yb, and Tm), or seemingly appears in combination with Step II (Ho and Er). The temperature difference between Steps II and III becomes smaller with the decrease of atomic number (or increase of ion size) of Ln as shown in Fig. 1, showing that the difference between the two kinds of waters in these hydrates decreases in the same way. We can imagine that, as the coordination sphere of Ln^{3+} expands in this direction, the lattice waters will gradually get involved in it, or get more "coordinated" in nature. This will be the reason why there is no distinct break between Steps II and III with Gd; when Ln^{3+} becomes still larger, all the waters get coordinated, forming the hexahydrates.

As to the hexahydrates, the numbers of waters lost by their complete dehydration are again somewhat smaller than expected, mostly being 5—5.5 instead of 6.** As mentioned above, all these hydrates contain their waters in a highly crowded coordination sphere (C.N. 9), and the energy difference between possible structures of C.N. 9 and C.N. 8 will be small. So it is conceivable that a small part of it is easily "squeezed out" of the coordination sphere and lost in advance of the TG study, as the case of the lattice water of the octahydrate. After this initial loss, however, the remaining waters are lost in a single step, as expected from their original formula $[Ln_2mal_3(H_2O)_6]$.

TG Analysis in Water Vapor of Constant Reduced Pressure at a Superslow Heating Rate. In order to see the nature of the steps in more detail, the TG curves were obtained in an atmosphere of water vapor at a constant reduced pressure (10 Torr) at a superslow heating rate of 2 °C/h. This technique, developed by us and reported in the preceding paper,[6] was found to be especially useful to study the dehydration of hydrated salts (such as $CuSO_4 \cdot nH_2O$), since (1) each of the dehydration steps becomes notably steeper, and more easily distinguishable, and (2) the whole pattern of the TG curve becomes remarkably similar to the true equilibrium weight-temperature relation under the specified water vapor pressure.

The comparison of the two curves in Fig. 3, which are given for examples, shows that this technique can be applied effectively to the present case. As expected, the steps of Curve A are very much steeper, in comparison with Curve B. The first step on A seems to correspond to the tail of Step I mentioned in the preceding section. Closer comparison of these curves shows that, although the total of the waters lost on Curve B is about 7(=2+5), those estimated from Curve A is about 6.7(=0.4+2.3+4). Under the present conditions, therefore, the eight waters are not lost in the order of (1)-2-5, but approximately (2)-2-4 by way of a tetrahydrate. Since the original hydrate contained only 3 lattice waters, a structural change is expected to occur when it is heated extremely slowly at a constant water vapor pressure (under quasi equilibrium conditions). In the course of the heating, a coordination water is squeezed out of the coordination sphere, and the dehydration proceeds as if the original complex should be formulated as $[Ln_2mal_3(H_2O)_4] \cdot 2H_2O \cdot 2H_2O$, losing $2H_2O$ at first,*** and then 2 and $4H_2O$ at the two main steps, respectively.

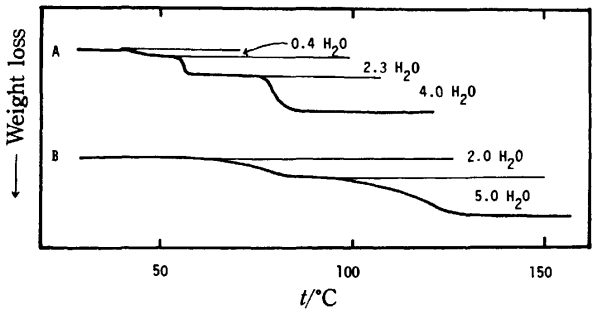

Fig. 3. TG curves of $Lu_2mal_3 \cdot 8H_2O$ obtained under two different conditions: (A) at a heating rate of 2 °C/h in water vapor at 10 Torr and (B) at a heating rate of 3 °C/min in N_2 stream of 30 cm^3/min. In both cases, some water molecules were lost before the TG measurements.**

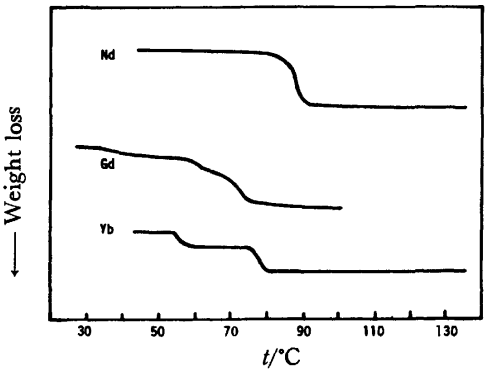

Fig. 4. TG curves of $Ln_2mal_3 \cdot nH_2O$ at the superslow heating rate in the water vapor.

Typical TG curves of other hydrates obtained under the same conditions are shown in Fig. 4. The curves of all the hexahydrates (Ce—Eu) are similar to that of Nd, in which all the coordination waters are lost in a single step. Stepwise release of waters is observed at Gd, but here the curve is dull. The curves of Tb—Yb are more or less similar, and show two clear steps as can be seen on the curve of Yb. Then comes Lu, with one more additional step as mentioned above.

The numbers of H_2O lost with each sample are now plotted in Fig. 5, just as in Fig. 2. The numbers corresponding to the complete dehydration of the octahydrates are 5 to 6, showing that they lose much of its lattice waters in advance of the TG measurement.*** About 2 H_2O among them are then lost in the first TG step, and 3 to 4 in the second. On the other hand, the hexahydrates lose about one of its coordination waters in advance, just as in the case of the TG in N_2, and then all the rest of it in a single step.

Although at present it is difficult to explain the

*** In the present case, these molecules seemingly escape from the sample during the preliminary evacuation which takes a few hours before the start of the TG measurement.

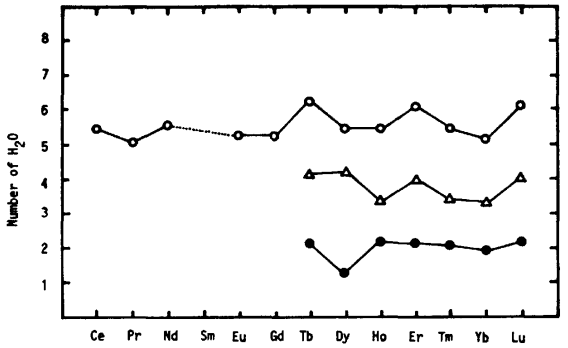

Fig. 5. Numbers of H_2O lost in the complete dehydration (○), and those lost in the first (●) and second (△) step, respectively, which were determined by TG with the superslow heating rate in the water vapor. The dehydration did not proceed completely with Sm, probably owing to the recombination of water vapor under these conditions.

complicated "ups and downs" among these numbers (see later), it is fairly certain that the mode of dehydration of the octahydrate is dependent on the atmosphere and heating rate, and the patient "squeezing" (*i.e.*, very slow heating in a diffuse water vapor) can release more water than the hasty one (*i.e.*, quick heating under 1 atm of N_2) which can only sweep out the lattice water.

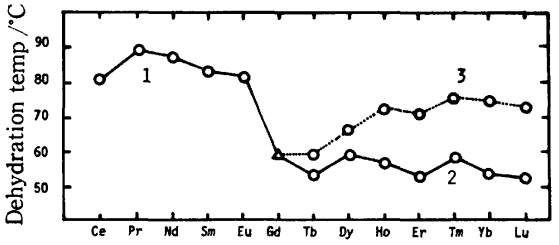

Fig. 6. Dehydration temperatures (t_i) obtained from TG with the superslow heating rate in the water vapor. As to the meaing of (1)—(3), see text. The value of Gd is given by (△), because here the two steps overlap.

The initial weight-loss temperature (t_i), or the temperature from which the TG curve begins to drop, may be taken as a measure of the relative strengths of Ln^{3+}–OH_2 bonds. In the TG studies in N_2, it was quite hard to determine exact t_i values, because all the steps observed were too dull (*cf.* Fig. 1). In the present case, the steps are much steeper (*cf.* Fig. 3), so we can quite accurately determine the t_i values for most of the steps observed, and plot them as shown in Fig. 6. The t_i values thus obtained can roughly be divided in three groups, *i.e.*: (1) Ce to Eu (hexahydrates); (2) Gd to Lu (octahydrates), 1st step; (3) Gd to Lu, 2nd step. The t_i's in the groups (1) and (3) are the temperatures at which the coordination waters hegin to escape. In both cases, in general, the t_i first rises, and then drops through a flat maximum, in the order of increasing atomic number. This can be understood as a balance between the two counteracting tendencies, *i.e.*, the strengthening of Ln^{3+}–OH_2 bond resulting from the decrease in size of Ln^{3+}, and the increase in interligand repulsion caused by the same effect. In previous studies[12,13] on lanthanoid dimethyl sulphoxide, tetrahydrothiophene 1-oxide and *N,N,N',N'*-tetramethylurea complexes, their general TG–DTA behaviours could also be explained by these two tendencies.

However, the sudden drop of the t_i at Gd (or the double periodicity between the former half and the latter half of the Ln sequence) can not be explained in such a simple way, because the lanthanoid contraction continues with little break from Ce to Lu.[14] Such "gadolinium break" has been often found among the thermodynamic data of lanthanoid complex formation in solution.[15] As one of the reasons for such a break, a change in C.N. has been suggested in the case of the formation constants of Ln^{3+} complexes with various amino polycarboxylates.[5] However, in the present case, this view is inconsistent with the trends of the t_i, since the ions of Gd—Lu with the smaller C.N. (see above) is expected to bind H_2O more strongly, and to bring about an elevation of t_i's.

By the way, among these hydrates, it is natural to suppose that the Ln^{3+}–OH_2 coordinate bonds will become weaker, when the Ln^{3+}–mal^{2-} bonds become stronger. By the X-Ray analysis,[7,9] it is known that there are two kinds of malonate ions in the hexahydrate, a chelated one and an open and bridging one, while all malonate ions in the octahydrate are chelated. These facts lead to the view that the ions of Gd—Lu are probably more suitable in size for the formation of chelate rings than those of Ce—Eu. The drop of the t_i for the malonate hydrates of the former ions thus may be due to the much more rigid Ln^{3+}–mal^{2-} bondings in them, which is reflected on the more pronounced chelation, in comparison with those in the hydrates of the latter ions.

The t_i's in the group(2) are the temperatures at which the waters squeezed out of the coordination sphere begin to escape, and generally drop from Gd to Lu, although some irregularities are observed. This kind of waters become more and more loosely held when the coordination waters lost at the last step become more and more firmly bound. The irregularities observed seem to be related to the number of H_2O contained in the hydrates, *i.e.*, the t_i's of the hydrates with more H_2O are relatively lower (*cf.* Fig. 5). These "ups and downs" may be related to the differences in the $4f^n$ electronic configurations, whose influences upon thermodynamic properties of Ln^{3+} were reviewed.[16]

In conclusion, we can say that, although the obtained results look highly complicated, their main features can be reasonably understood in view of the effects of the lanthanoid contraction.

Our cordial thanks are due to Mrs. Hiroko Yokobayashi, College of General Education, Tohoku University, for her great help in this work.

References

1) T. Moeller, *J. Chem. Educ.*, **47**, 417 (1970).
2) D. G. Karraker, *J. Chem. Educ.*, **47**, 424 (1970).
3) K. B. Yatsimirskii and N. A. Kostromina, *Zh. Neorg.*

Khim., **9**, 1793 (1964).
4) A. Zalkin and D. H. Templeton, *J. Am. Chem. Soc.*, **75**, 2453 (1953); M. Mansmann, *Z. Kristallogr.*, **122**, 375 (1965).
5) T. Moeller, D. F. Martin, L. C. Thompson, R. Ferrus, G. R. Feistel, and W. J. Randall, *Chem. Revs.*, **65**, 1 (1965).
6) K. Nagase, H. Yokobayashi, M. Kikuchi, and K. Sone, *Thermochim. Acta*, **35**, 99 (1980).
7) Eva Hansson, *Acta Chem. Scand.*, **27**, 2441 (1973).
8) Eva Hansson, *Acta Chem. Scand.*, **27**, 2813 (1973).
9) Eva Hansson, *Acta Chem. Scand.*, **27**, 2827 (1973).
10) B. S. Azikov and V. V. Serebrennikov, *Zh. Neorg. Khim.*, **12**, 445 (1967).
11) B. S. Azikov, S. E. Kharzeeva, Z. A. Grankina, and V. V. Serebrennikov, *Zh. Neorg. Khim.*, **13**, 1831 (1968).
12) K. Nagase, H. Yokobayashi, A. Iwase, and K. Sone, *Thermochim. Acta*, **17**, 335 (1976).
13) K. Sone, K. Nagase, M. K. Kuya, and E. Giesbrecht, *Bull. Chem. Soc. Jpn.*, **55**, 449 (1982).
14) D. H. Templeton and C. H. Duben, *J. Am. Chem. Soc.* **76**, 5237 (1954).
15) S. F. Ashcroft and C. T. Mortimer, "Thermochemistry of Transition Metal Complexes," Academic Press, London and New York (1970).
16) R. J. Ackermann and E. G. Rauh, *Rev. Int. Hautes Temp. Refract.*, **15**, 259 (1978).

Potentiometric Study of Thermodynamic Parameters of Complexing of Lithium Ion-Basic Aprotic Solvents and Sodium Ion-Macrocyclic Polyethers in Acetonitrile

Toshio NAKAMURA,* Yasuke YUMOTO, and Kosuke IZUTSU
Department of Chemistry, Faculty of Science, Shinshu University, Asahi, Matsumoto 390
(Received October 28, 1981)

Formation constants of the 1 : 1 complexes of lithium ion in acetonitrile (AN) with DMF, DMSO, DMA, and HMPA and of sodium ion in AN with 15-crown-5 (15C5), 18-crown-6 (18C6), dibenzo-18-crown-6 (DB18C6), and cryptand 211 (Cryp 211), were determined at 10, 25, and 40 °C by potentiometric methods with a cation-sensitive glass electrode. From the change of the formation constants with temperature, thermodynamic parameters ΔG°_{298}, ΔH°_{298}, and $-T\Delta S^\circ_{298}$, were obtained. ΔG°_{298}, ΔH°_{298}, and $-T\Delta S^\circ_{298}$, all in kJ mol^{-1}, for Li^+-solvent complexes were, respectively, -7.9, $-9._0$, $+1._1$ for DMF, -9.7, $-10._1$, $+0._5$ for DMSO, -10.0, $-9._9$, $-0._1$ for DMA, and -18.9, $-15._8$, $-3._1$ for HMPA, and those for Na^+-macrocyclic polyether complexes, -28.4, $-24._1$, $-4._5$ for 15C5, -27.2, $+1._6$, $-28._7$ for 18C6, -28.6, $-14._3$, $-14._2$ for DB18C6, and -51.9, $-53._8$, $+2._1$ for Cryp 211. Some features about the roles of enthalpy and entropy terms in complexing have been discussed.

In the previous papers,[1-5] we reported the successive formation constants of complexes of several univalent cations in acetonitrile (AN) with other donor solvents. They were obtained potentiometrically at 25 °C by using a univalent cation-sensitive glass electrode (Beckman 39047). In this paper, intending to understand the complexing phenomena in more detail, we have determined at several different temperatures the formation constants of lithium ion in AN with some basic aprotic solvents and obtained the values of ΔG°_{298}, ΔH°_{298}, and $-T\Delta S^\circ_{298}$ for the reaction shown by Eq. 1:

$$Li^+_S + D = Li^+_D, \tag{1}$$

where Li^+_S is the lithium ion solvated only by AN and Li^+_D that complexed by one molecule of solvent D. We have also obtained similar thermodynamic parameters for the complexing (Eq. 2) of the sodium ion in AN with some macrocyclic polyethers by a potentiometric method:

$$Na^+_S + L = Na^+_L, \tag{2}$$

where Na^+_S is the sodium ion solvated only by AN and Na^+_L that complexed by macrocyclic polyether L. The general construction of the cell used for the measurements was as follows:

$$\mathrm{Ag}\left|\begin{matrix}5\times10^{-3}\ \mathrm{M\ AgNO_3} + \\ 10^{-2}\ \mathrm{M\ Et_4NClO_4(AN)}\end{matrix}\right\|\begin{matrix}5\times10^{-2}\ \mathrm{M} \\ \mathrm{Et_4NClO_4(AN)}\end{matrix}\Bigg\|$$
$$10^{-3}\ \mathrm{M\ M^+ClO_4^-} + 10^{-2}\ \mathrm{M}\,\Big|\,\text{Cation-sensitive}$$
$$\mathrm{Et_4NClO_4(AN + D\ or\ L)}\,\Big|\,\text{glass electrode}$$
(Cell I)

where M^+ was Li^+_S for reaction (1) and Na^+ for reaction (2).

Complexing of the Lithium Ion in AN with Other Aprotic Solvents. The formation constant, K_1 in mol^{-1} dm^3, for reaction (1) is defined by

$$K_1 = \frac{(Li^+_D)}{(Li^+_S)[D]}, \tag{3}$$

where (Li^+_S) and (Li^+_D) are the activities of Li^+_S and Li^+_D, respectively, and [D] is the concentration of solvent D. The values of K_1 at 10, 25, and 40 °C were determined by the same method as those in the previous papers.[1-5] From the relation between $R\ln K_1$ and $1/T$, ΔH°_{298} was obtained using the SALS program of the Tokyo University Computer Center. The value of $-T\Delta S^\circ_{298}$ was obtained with the following relation:

$$-RT\ln K_1 = \Delta G^\circ_{298} = \Delta H^\circ_{298} - T\Delta S^\circ_{298}. \tag{4}$$

Complexing of the Sodium Ion in AN with Macrocyclic Polyethers. The formation constant, K in mol^{-1} dm^3, for the 1 : 1 complexing of the sodium ion in AN with a macrocyclic polyether L (Eq. 2) is defined by

$$K = \frac{(Na^+_L)}{(Na^+_S)_L[L]}, \tag{5}$$

where $(Na^+_S)_L$ and (Na^+_L) are the activities of Na^+_S and Na^+_L, respectively, and [L] is the concentration of L. Here, the activity coefficient of the sodium ion is assumed not to change on complexation. Then we may write Eq. 5 as follows:

$$K = \frac{[Na^+_L]}{[Na^+_S]_L[L]}, \tag{6}$$

There exist following relations:

$$[Na^+_L] = [Na^+_S]_{\mathrm{Init}} - [Na^+_S]_L, \tag{7}$$

$$[L] = C_L - [Na^+_L], \tag{8}$$

where $[Na^+_S]_{\mathrm{Init}}$ and $[Na^+_S]_L$ are the concentrations of Na^+_S before and after the addition of L to Cell I, and C_L shows the total concentration of L added. Equation 6 can then be written as follows:

$$K = \frac{[Na^+_S]_{\mathrm{Init}} - [Na^+_S]_L}{[Na^+_S]_L\{C_L - [Na^+_S]_{\mathrm{Init}} + [Na^+_S]_L\}}. \tag{9}$$

Here, $[Na^+_S]_{\mathrm{Init}}$ and $[Na^+_S]_L$ are related with the electrode potentials, E_{Init} before the addition of L and E_L after the addition of L, by the following equation:

$$E_L = E_{\mathrm{Init}} + \frac{RT}{F}\ln\frac{[Na^+_S]_L}{[Na^+_S]_{\mathrm{Init}}}. \tag{10}$$

To obtain K, the sodium ion in AN was titrated with a solution of L in AN up to about three times the equivalence point and the potential change during the titration was plotted. K-values which precisely fitted with the titration curves were obtained by successive approximation method. From the values of K at 10, 25, and 40 °C, values of ΔG°_{298}, ΔH°_{298}, and $-T\Delta S^\circ_{298}$ for Eq. 2 were obtained as above.

Experimental

The apparatus and experimental techniques were the same as those described before,[1,2] except that more effort was made to keep all parts of the cell assembly, including the reference electrode, precisely (within±0.2 °C) at the desired temperatures.

Nakarai's reagent grade dibenzo-18-crown-6 (DB18C6) was purified by extraction with chloroform and recrystallization from ethanol. 18-Crown-6 (18C6), 15-crown-5 (15C5), and cryptand 211 (Cryp 211) were the Merck products and were used without further purification. Hexamethylphosphoric triamide (HMPA) was a products of Johoku Chemical Industry Co. Ltd. and was purified by distilling three times under vacuum, first from barium oxide, second by the addition of small amount of sodium metal, and last without additives.[6] This HMPA was used within an hour after the purification. Other solvents and reagents were the same as those used in the previous reports.[1,2]

Results and Discussion

Before running the present experimental work, the cation-sensitive glass electrode was confirmed to respond in a Nernstian way to the activities of sodium and lithium ions in AN at 10, 25, and 40 °C. The value of the activity coefficient y used was calculated from the Debye-Hückel equation, $\log y = -AI_c^{1/2}/[1+BaI_c^{1/2}]$ ($A=1.82(\varepsilon T)^{-3/2}\times 10^6$ mol$^{-1/2}$ dm$^{3/2}$ (deg K)$^{3/2}$, $B=5.03(\varepsilon T)^{-1/2}\times 10^{10}$ dm$^{1/2}$ mol$^{-1/2}$ (deg K)$^{1/2}$, $a=5\times 10^{-9}$ dm, and I_c=ionic strength). As the dielectric constant at 10, 25, and 40 °C, respectively, 39.1, 36.7, and 34.3 were used.[7] The density of HMPA was measured to be 1.03_3, 1.02_1, and 1.00_7 g cm^{-3} at 10, 25, and 40 °C, respectively. For the densities of other solvents, we referred to literature values.[8]

Complexing of the Lithium Ion in AN with Other Aprotic Solvents. The values of K_1 for the complexing of *N,N*-dimethylformamide (DMF), dimethyl sulfoxide (DMSO), *N,N*-dimethylacetamide (DMA), and HMPA are shown in Table 1. Each value is the average of more than four determinations. Maximum concentrations of solvent D added to Cell I were 0.08 M for DMF, 0.045 M for DMSO, 0.05 M for DMA, and 0.005 M for HMPA. The relation between $R\ln K_1$ and $1/T$ for each solvent is linear, as shown in Fig. 1, and makes possible to obtain ΔH°_{298} and $-T\Delta S^\circ_{298}$. These values, calculated by using the SALS program and Eq. 4, are also shown in Table 1. It is interesting to note that, in each case, the enthalpy term plays an important role and the role of the entropy term is relatively small in determining the free energies. These results seem to be reasonable if the complexation reaction of Eq. 1 is considered to be the exchange of one solvated AN molecule with one molecule of added solvent D.

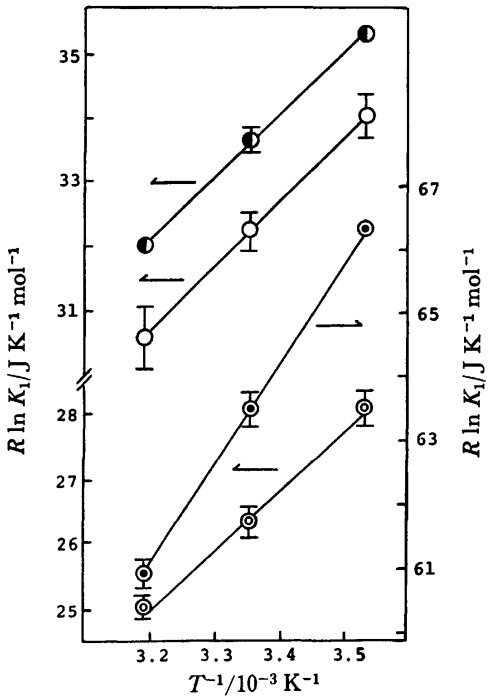

Fig. 1. Relation between $R\ln K_1$ for the reaction $Li^+ + D = Li_D^+$ and $1/T$.
D=DMF (◎), DMSO (○), DMA (◐), and HMPA (⊙).

To obtain reliable ΔH°_{298}, K_1 at each temperature should be determined at least within errors of several percent. The present potentiometric method could give such K_1-values for the complexing of lithium ion with

Table 1. Thermodynamic parameters for the complexing of lithium ion in acetonitrile with other aprotic solvents

Ligand D	K_1/mol^{-1} dm^3 (T/K)	$-\Delta G^\circ_{298}$ / kJ mol^{-1}	$-\Delta H^\circ_{298}$ / kJ mol^{-1}	$T\Delta S^\circ_{298}$ / kJ mol^{-1}
DMF	29.5±1.1(283)	+7.85±0.07	+9.0±1.0	−1.1±1.0
	23.7±0.7(298)			
	20.3±0.4(313)			
DMSO	59.8±2.9(283)	+9.70±0.09	+10.1±1.9	−0.5±1.9
	50.0±3.1(298)			
	39.7±2.5(313)			
DMA	70.1±1.5(283)	+10.04±0.06	+9.9±0.5	+0.1±0.5
	57.3±1.5(298)			
	47.0±0.3(313)			
HMPA	(2.87±0.04)×10^3(283)	+18.91±0.08	+15.8±0.8	+3.1±0.8
	(2.05±0.07)×10^3(298)			
	(1.51±0.04)×10^3(313)			

TABLE 2. THERMODYNAMIC PARAMETERS FOR THE COMPLEXING OF SODIUM ION WITH SEVERAL MACROCYCLIC POLYETHERS

Ligand L	K/mol^{-1} dm^3 (T/K)	$-\Delta G^\circ_{298}$ / kJ mol^{-1}	$-\Delta H^\circ_{298}$ / kJ mol^{-1}	$T\Delta S^\circ_{298}$ / kJ mol^{-1}
15C5	$1.7_2\times10^5$(283)	+28.4±0.1	+24.1±2.0	+4.5±2.0
	$9._5\times10^4$(298)			
	$6._4\times10^4$(313)			
18C6	$5._4\times10^4$(283)	+27.2±0.1	−1.6±0.4	+28.7±0.4
	$5._8\times10^4$(298)			
	$5._7\times10^4$(313)			
DB18C6	$1.3_4\times10^5$(283)	+28.6±0.2	+14.3±2.3	+14.2±2.4
	$1.0_1\times10^5$(298)			
	$7._4\times10^4$(313)			
Cryp 211	$3.7_5\times10^9$(283)	+51.9±0.4	+53.8±0.9	−2.1±1.0
	$1.2_3\times10^9$(298)			
	$4.2_0\times10^8$(313)			

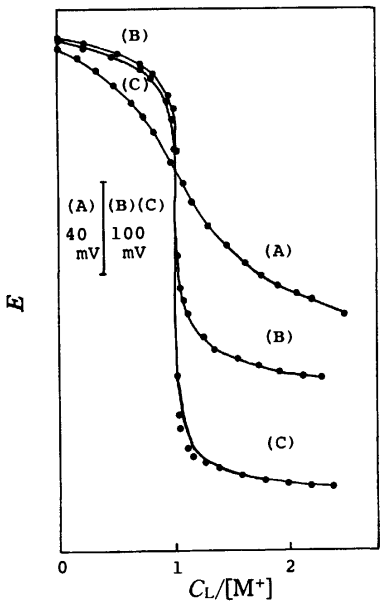

Fig. 2. Titration curves for the reaction $M^+ + L = M_L^+$: (A) M=Na and L=18C6; (B) M=Na and L=Cryp211; (C) M=Li and L=Cryp211 (at 25 °C).

basic aprotic solvents, as is apparent from Fig. 1 and Table 1. But the application of this method becomes somewhat difficult for the complexing of lower formation constants. We have run similar experiment for complexing of the sodium ion, but the precision of K_1 was not sufficiently good. Qualitatively, however, the smaller ΔG°_{298} for the sodium complexes could be attributed mainly to the smaller ΔH°_{298}. Work is now in progress for the complexing of other univalent cations.

Complexing of the Sodium Ion in AN with Macrocyclic Polyethers. Thermodynamic parameters for the complexing of sodium ion in AN with such macrocyclic polyethers as 15C5, 18C6, DB18C6, and Cryp211 were determined by titrating sodium ion in 0.01 M Et_4NClO_4–AN with 0.01 M Et_4NClO_4–AN solution containing 0.02—0.04 M of macrocyclic ligands. Titrations were carried out at 10, 25, and 40 °C. Some examples of the titration results are shown in Fig. 2. Curve(A) is for the titration with 18C6 and Curve(B) for that with Cryp211. In each case, the formation constant K, which fitted well with the titration results, could be found by the successive approximation method; the solid curves were obtained from Eqs. 9 and 10 using such K values. Thus the assumption of the 1 : 1 complexing is proved to be reasonable. Curve(C) in Fig. 2 is for the titration of lithium ion with Cryp211 In this case, the formation constant of Li^+–Cryp211, is expected to be larger than 10^{10} from the potential jump at the equivalence point, but it is impossible to find a K-value which fits exactly with the experimental results. This may be due to the fact that the response of the glass electrode deviates somewhat from the Nernstian one at such low activities of lithium ion in the presence of Cryp211. The values of K of the sodium complexes are shown in Table 2. log K for the complexes of Na^+–DB18C6 and Na^+–18C6 at 25 °C were 5.00 and 4.76, respectively, in good agreement with the literature values of 4.8_5—5.0_0 for Na^+–DB18C6 and 4.5_5 for Na^+–18C6.[9]

The relations between $R\ln K$ and $1/T$ are plotted in

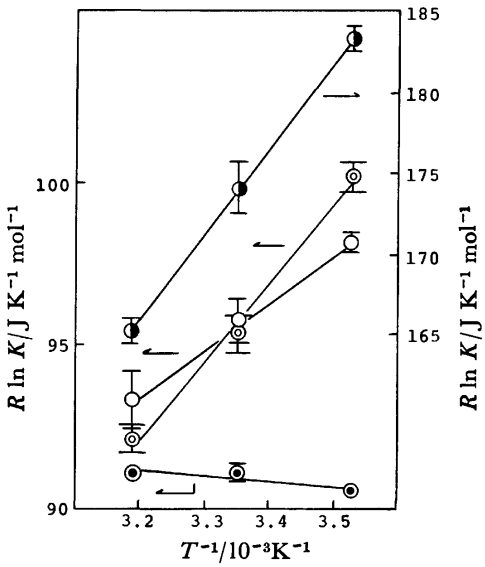

Fig. 3. Relation between $R\ln K$ for the reaction $Na^+ + L = Na_L^+$ and $1/T$.
L=15C5 (◎), 18C6 (◉), DB18C6 (○), and Cryp 211 (◑).

Fig. 3, and thermodynamic parameters obtained by the SALS program and Eq. 4 are shown in Table 2. Except for the complex with Cryp211, the formation constants are approximately the same order of magnitudes, but it is interesting to note that the factors determining the free energies of complex formation are quite different from one complex to another. For the complex with 15C5 the enthalpy term plays a predominant role, while for the complex with 18C6 the entropy term is predominant. For the complex with DB18C6, the contributions from both factors are approximately the same. The small contribution of the enthalpy term for the 18C6 complex has been found by Popov[10] in the calorimetric investigation of the lithium ion complexing ($\Delta H^\circ_{298} \approx 0$ and $-T\Delta S^\circ_{298} = 13.3$ kJ mol^{-1}). For Na^+–Cryp211, most of the free energy of formation was determined by the ethalpy term.

Because of the importance of complexes with macrocyclic polyethers, reports concerning the thermodynamic parameters of the complexing are recently increasing. Various methods, such as NMR,[10-12] conductometry,[13,14] potentiometry,[15] and calorimetry,[10,16] have been applied in several solvents. In order to discuss the mechanism of the complexing, however, the data are still too scarce. The present potentiometric method will be very convenient to obtain further information on this problem.

References

1) K. Izutsu, T. Nomura, T. Nakamura, H. Kazama, and S. Nakajima, *Bull. Chem. Soc. Jpn.*, **47**, 1657 (1974).
2) T. Nakamura, *Bull. Chem. Soc. Jpn.*, **48**, 1447 (1975).
3) T. Nakamura, *Bull. Chem. Soc. Jpn.*, **49**, 1304 (1976).
4) K. Izutsu, T. Nakamura, T. Murayama, and T. Fujinaga, *Bull. Chem. Soc. Jpn.*, **51**, 2905 (1978).
5) K. Izutsu, T. Nakamura, and K. Iwata, *Anal. Chim. Acta*, **117**, 329 (1980).
6) T. Fujinaga, K. Izutsu, and S. Sakura, *Pure Appl. Chem.* **44**, 117 (1975).
7) J. Timmermans, A. M. Piette, and R. Philippe, *Bull. Soc. Chim. Belg.*, **64**, 5 (1955).
8) *E. g.*, J. A. Riddick and W. B. Bunger, "Organic Solvents, (Techniques of Chemistry)," 3rd ed, ed by A. Weissberger, Wiley-Interscience, New York (1970), Vol. II, pp. 446, 450, 466.
9) I. M. Kolthoff and M. K. Chantooni, Jr., *Anal. Chem.*, **52**, 1039 (1980).
10) A. J. Smetana and A. I. J. Popov, *J. Solution Chem.*, **9**, 183, (1980).
11) M. Shamsipur and A. I. J. Popov, *J. Am. Chem. Soc.*, **101**, 4051 (1979).
12) M. Shamsipur, G. Rounaghi, and A. I. J. Popov, *J. Solution Chem.*, **9**, 701 (1980).
13) E. Shchori, J. Jagur-Grodzinski, Z. Luz, and M. Shporer, *J. Am. Chem. Soc.*, **93**, 7133 (1971).
14) Y. Takeda and H. Yano, *Bull. Chem. Soc. Jpn.*, **53**, 1720 (1980).
15) J. M. Lehn and J. P. Sauvage, paper presented at Conference de Theremodynamique Chimique, Societe Chimique of France, Bordeaux, France, Oct. 20, 1972; J. J. Christensen, D. J. Eatough, and R. M. Izatt, *Chem. Rev.*, **74**, 351 (1974).
16) R. M. Izatt, R. E. Terry, B. L. Haymore, L. D. Hansen, N. K. Dalley, A. G. Avondet, and J. J. Christensen, *J. Am. Chem. Soc.*, **98**, 7620 (1976).

The Flow-injection Analysis of D-Glucose Using a Flow-cell with Immobilized Peroxidase and Its Application to Serum

Tadashi HARA,* Motohiro TORIYAMA, and Masakatsu IMAKI†
Department of Chemical Engineering, Faculty of Engineering, Doshisha University, Karasuma Imadegawa, Kamigyo-ku, Kyoto 602
†*Horiba, Ltd., Kissyoin, Minami-ku, Kyoto 601*
(Received October 31, 1981)

The D-glucose concentration in a serum sample of less than 0.01 cm^3 could be continuously determined at the rate of about 20 samples/h by the use of a chemiluminescent reaction between luminol and hydrogen peroxide, a flow-cell with immobilized peroxidase, and a column with immobilized glucose oxidase. By immobilizing peroxidase as a chemiluminescent catalyst inside the flow-cell, simplification could be achieved with regard to apparatus, reagents and operation. The detection limit of hydrogen peroxide was about 5×10^{-6} mol dm^{-3}, and the calibration curves for both hydrogen peroxide and D-glucose were approximately linear in the range of 5×10^{-5}—1×10^{-3} mol dm^{-3}, a range which corresponded to the glucose concentration, 0.1—18 mg cm^{-3}, obtained by diluting serum to 50 times its initial volume.

The present study was carried out with the object of establishing a simple, rapid, and economical method by which D-glucose in a sample could be determined continuously by measuring the chemiluminescence (CL) emitted on a flow-cell with immobilized peroxidase (EC 1.2.1.7)(PO).

Generally speaking,[1] CL analysis is superior to fluorometric or absorptiometric analysis in the following points: 1) High sensitivity, 2) a wide dynamic range, 3) a simple apparatus (needs no spectrometer), and 4) an easy establishment of a continuous analysis system.

Several reports[2,3] on the chemiluminescent determination of glucose have, therefore, been published; in them, the glucose in a sample is first converted to hydrogen peroxide (H_2O_2) with fixed glucose oxidase (EC 1.1.3.4) (GO) and then determined by measuring the intensity of the CL emitted by the reaction between the H_2O_2 and 5-amino-2,3-dihydro-1,4-phthalazinedione(luminol) in the presence of potassium hexacyanoferrate(III) ($K_3[Fe(CN)_6]$) as a catalyst.

However, this method requires a considerable amount of $K_3[Fe(CN)_6]$, an environmental pollutant; moreover, it makes it imposible to recycle the used $K_3[Fe(CN)_6]$. These problems can, however, be overcome by the use of a flow-cell with immobilized PO, for PO acts on the reaction between H_2O_2 and luminol as a catalyst.[4] Though Freeman *et al.*[5] developed a CL fiber-optic probe for a batch-by-batch measurement of H_2O_2 by immobilizing the PO in a polyacrylamide gel on the end of a fiber-optic, the probe can not be used for a continuous measurement of H_2O_2 because the enzyme phase prepared by immobilizing PO and luminol by physical entrapment in a polyacrylamide gel has to be kept with a definite concentration of the luminol solution. With the use of the flow-cell with immobilized PO which has previously been proposed by the present authors, the following advantages can be expected: 1) A simple system for a how-injection analysis can be easily constructed; 2) the reagents necessary for an analysis can be minimized; 3) waste treatment becomes easier than in conventional methods in which $K_3[Fe(CN)_6]$, cupper(II), cobalt(II), and so on are used as catalysts, and 4) an improvement is made in the selective measurement of glucose because of the PO specificity for H_2O_2.

In the present paper, a flow-cell with immobilized PO has been successfully applied to the determination of glucose and then extended to serum.

Experimental

Immobilization of Glucose Oxidase. GO (Toyobo, grade II, 100 U/mg) was immobilized on 80—120 mesh of porous glass beads (CPG-10, pore size 7500 nm) in accordance with the diazotization method of Weetall[6] after the introduction of an aminoalkyl group[7] onto the porous glass beads.

Immobilization of Peroxidase. Five procedures were tried for the immobilization of PO, and the following procedure was found to be most satisfactory: A glass disk 12 mm in diameter and 1.8 mm thick, with one ground plane, was refluxed for 6 h in a 2% (3-aminopropyl)ethoxysilane solution in toluene. The glass-disk was dried at 60 °C after washing with toluene, and then refluxed for 6 h in a chloroform solution containing 5% triethylamine and 10% *p*-nitrobenzoyl chloride. The glass-disk was washed with chloroform and dried. The nitro group on the glass-disk was reduced by refluxing for 1 h with a 5% sodium dithionite solution. After the glass-disk has been washed with water, it was dipped in a 1 mol dm^{-3} hydrochloric acid solution, 3 cm^3 of a 0.5 mol dm^{-3} sodium nitrite solution was added at 0 °C over 15 min, and the mixture was reacted for an additional 15 min. The glass-disk was picked up, washed with a 5% sulfamic acid solution and water in that order, and immediately dipped in a 5 cm^3 solution of PO (Toyobo, grade III, 102 U/mg) at the concentration of 1 mg cm^{-3}, the PO have previously been made to react with

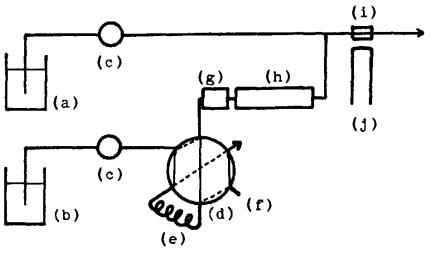

Fig. 1. Apparatus.
a: Luminol, b: buffer solution, c: pump, d: six-way cock, e: sampling loop, f: sample inlet, g: DEAE-cellulose column, h: immobilized glucose oxidase column, i: flow-cell with immobilized peroxidase, and j: photomultiplier.

the glass-disk for 48 h at 3 °C. Thus, the glass-disk with immobilized PO was obtained.

All the reagents were of an analytical grade and were used without further purification.

Procedure. The determination of glucose was done with the apparatus shown in Fig. 1. A Teflon-made tube (1 mm i. d.) and Teflon-made joints (GU-2F and GT-2F, Gasukuro Kogyo) are used for piping. The flow path between (d) and (i) is about 80 cm long. Figure 1(a) is filled with a 1.0×10^{-3} mol dm^{-3} luminol solution (pH 8.6) containing a 10^{-4} mol dm^{-3} EDTA solution and a boric acid–potassium chloride–sodium hydroxide buffer solution, and (b), with a potassium dihydrogenphosphate–sodium hydroxide buffer solution (pH 7.1). These solutions are both fed in at the rate of 0.99 cm^3 min^{-1} by means of a pump (c) (Tokyo Rikakikai, MP-12, Micro Tube Pump). By the use of the present pump, two flows can be driven simultaneously, and pulsation in a flow after mixing is minimized, thus resulting in the stabilization of a base line on a recorder chart. The capacity of the sampling loop (e) is about 0.2 cm^3, and each definite volume of the sample solution is injected into a column (g) by rotating a six-way cock (d). After being passed through a 100 mm × 3 mm i.d. column (g) charged with DEAE-cellulose (Nakarai Chemicals, 0.89 mequiv. g^{-1}), the sample solution is introduced into a 250 mm × 3 mm i.d. column (h) charged with the glass beads with immobilized GO; in this column, the β-D-glucose in a sample is converted to gluconic acid and H_2O_2 by means of an enzyme reaction. The H_2O_2 evolved is mixed with a luminol solution immediately before it enters the flow-cell (i) with immobilized PO, and the resulting solution is brought to pH 8.4 by means of the previous calibration. The CL emitted by the chemiluminescent reaction on the flow-cell with immobilized PO is converted to the photocurrent with a photomultiplier (j) (Hamamatsu TV, R-374), and the photocurrent is amplified with a Horiba OPE-402 amplifier, followed by recording with a recorder (Matsushita Communication Industrial, VP6521A). The determination of glucose in a sample is done from the peak height on a recorder chart.

The flow-cell with immobilized PO is shown in Fig. 2. The internal volume of the flow-cell is about 0.2 cm^3, and the glass-disk (d) with immobilized PO is installed as in Fig. 2.

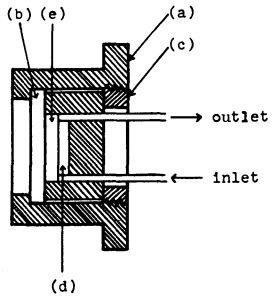

Fig. 2. Flow-cell.
a: Cell holder, d: window-glass, c: pressure screw, d: glass-disk with immobilized peroxidase, and e: flow-cell.

Results and Discussion

Immobilization of Peroxidase. In order to immobilize PO onto the flow-cell (Fig. 1(i)), an investigation was carried out with regard to the following five procedures: 1) Fixation onto the porous glass beads (CPG-10; 80—120 mesh; pore size, 7500 nm) by the glutaraldehyde method[8] after the introduction of an aminoalkyl group; 2) fixation onto the same aminoalkylated porous glass beads as 1) by the diazotization method;[6] 3) fixa tion onto the 6-Nylon disk by the glutaraldehyde method[9] after the partial hydrolysis of 6-Nylon; 4) fixation by physical entrapment[10] into a gel made of alubumin and glutaraldehyde, and 5) fixation onto the glass-disk by the diazotization method.

The glass beads with PO immobilized by Procedures 1) and 2) were charged respectively in Tygon tubes (2 mm i.d.); the tubes were subsequently coiled spirally and used as flow-cells. However, they were not sensitive enough for the present purpose, for the light generated by the chemiluminescent reaction was scattered to all directions. Both the 6-Nylon disk and the gel immobilized with PO by Procedures 3) and 4) were set as in Fig. 2(d) and used as flow-cells. They were first senstive enough, but rapidly became low in sensitivity with the lapse of time because of the lowering of the enzyme activity. The glass-disk with PO immobilized by procedure 5) was best in both the intensity of CL and its life, a and it still showed stable activity as a chemiluminescent catalyst even after analyses of up to 300 samples.

Effect of Luminol Concentration. The relationship between the luminol concentration and the CL intensity is shown in Fig. 3. As can be seen there, the maximum intensity of CL was obtained by the use of a 1.0×10^{-3} mol dm^{-3} luminol solution.

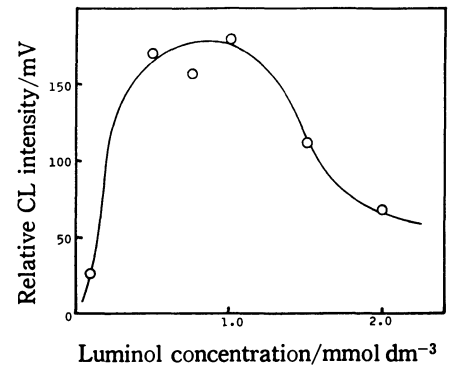

Fig. 3. Effect of luminol concentration on CL intensity.
Experimental conditions: flow rate 1.98 cm^3 min^{-1}; pH 7.8. Sample: 1.03×10^{-4} mol dm^{-3} H_2O_2.

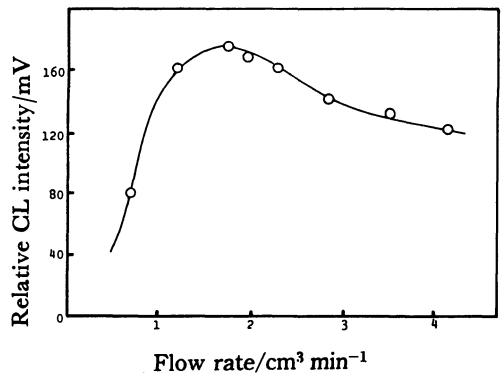

Fig. 4. Effect of flow rate on CL intensity.
Experimental conditions: 1.0×10^{-3} mol dm^{-3} luminol; pH 7.8. Sample: 1.03×10^{-4} mol dm^{-3} H_2O_2.

Effect of Flow Rate. The flow rate is an important parameter and has a close relation with the sensitivity, the precision, and the speed in flow-injection analysis. The relationship between the flow rate of a sample solution and the intensity of CL is shown in Fig. 4. The maximum in Fig. 4 is characteristic for the present flow-cell with immobilized PO, while the maximum intensity of CL appeared around a flow rate of 1.8 cm^3 min^{-1}. This phenomenon is explained as follows: 1) The intensity of CL at a flow rate less than about 1.8 cm^3 min^{-1} increases with an increase in the flow rate because the amounts of luminol and H_2O_2 fed into the flow-cell within a definite period increase with an increase in the flow rate, and the flow rate does not seriously affect the diffusion amounts of luminol and H_2O_2 to the enzyme phase, and 2) the intensity of CL at a flow rate of more than about 1.8 cm^3 min^{-1} decreases with an increase in the flow rate because the amounts of luminol and H_2O_2 fed into the flow-cell within a definite period increase with an increase in the flow rate, but the diffusion amounts of luminol and H_2O_2 into the enzyme phase are considerably lowered with an increase in the flow rate. The reaction rate between luminol and H_2O_2 on the present flow-cell with immobilized PO can be expected to be very large, since the reaction between luminol and H_2O_2 in the presence of free PO has been reported by Cormier *et al.*[4] to proceed to completion within 0.2 s. This confirms the usefulness of the present flow-cell with immobilized PO for the determination of glucose.

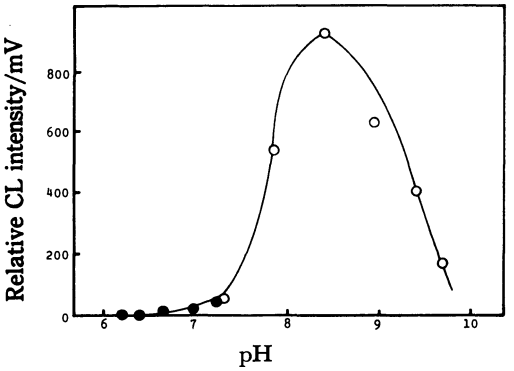

Fig. 5. Effect of pH on CL intensity.
Experimental conditions: 1.0×10^{-3} mol dm^{-3} luminol; flow rate 1.98 cm^3 min^{-1}; ●: KH_2PO_4–NaOH buffer solution, ○: H_3BO_3–KCl–NaOH buffer solution. Sample: 1.03×10^{-4} mol dm^{-3} H_2O_2.

Effect of pH. The catalytic activity of free PO shows its maximum around pH 6, whereas the quantum yield of CL between luminol and H_2O_2 shows its maximum around pH 11.[11] Therefore, the optimum pH for the maximum intensity of CL should be expected in the reaction between luminol and H_2O_2 in the presence of PO. The relationship between the pH of a solution and the intensity of CL is shown in Fig. 5. As can be seen from Fig. 5, the maximum intensity was obtained around pH 8.4.

On the basis of these experimental results, the experimental conditions for the maximum intensety of CL were chosen as follows: Flow rate, 1.98 cm^3 min^{-1}; luminol concentration, 1.0×10^{-3} mol dm^{-3}, and pH, 8.4.

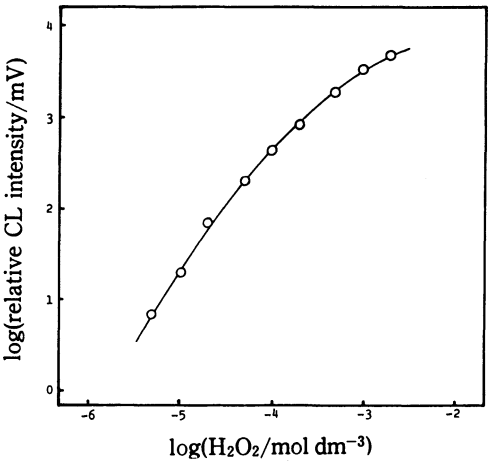

Fig. 6. Calibration curve for H_2O_2.

Calibration Curve of H_2O_2. The calibration curve of H_2O_2 as a sample is shown in Fig. 6. The time necessary for an analysis by means of the present apparatus with a DEAE-cellulose column and an immobilized GO column was about 3 min, while it was 30 s when an apparatus without the above columns was used. Since the band broadening of a sample was observed when it was passed through those columns, a sample was injected every 3 min to avoid overlapping of peaks. The detection limit for H_2O_2 was about 5×10^{-6} mol dm^{-3}, more or less inferior to that obtained by the use of $K_3[Fe(CN)_6]$ as a catalyst. The calibration curve was approximately linear between 5×10^{-5} mol dm^{-3} and 1×10^{-3} mol dm^{-3} H_2O_2. The intensity of CL at a H_2O_2 concentration of more than 1×10^{-3} mol dm^{-3} deviated from the straight line, but this was due to the fact that the experiment was carried out at a definite concentration of the luminol solution, while the chemiluminescent reaction gradually depended on the concentration of the luminol solution. At a H_2O_2 concentration of less than 5×10^{-5} mol dm^{-3}, the slope of the calibration curve shown by the log-log plot approaches 2, but this phenomenon is similar to that obtained by the CL fiber optic probe proposed by Freeman *et al.*[5]

Calibration Curve of D-*Glucose.* The calibration curve of D-glucose as a sample is shown in Fig. 7. The intensity of CL in Fig. 7 was smaller than the corresponding intensity in Fig. 6. This is mainly attributed to the fact that D-glucose is composed of about 66% of β-D-glucose, 34% of α-D-glucose, and a trace amount of aldehyde-type D-glucose, while only the β-D-glucose is made to react with GO. The large deviation from the straight line at a concentration of D-glucose of more than 1×10^{-3} mol dm^{-3} may be attributed to the treatment capacity of the column with immobilized GO. According to the present apparatus, an approximately linear calibration curve is obtained in the concentration range of 5×10^{-5}—1×10^{-3} mol dm^{-3} glucose.

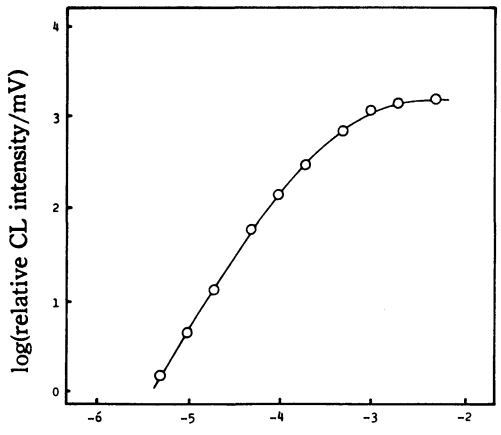

Fig. 7. Calibration curve for glucose.

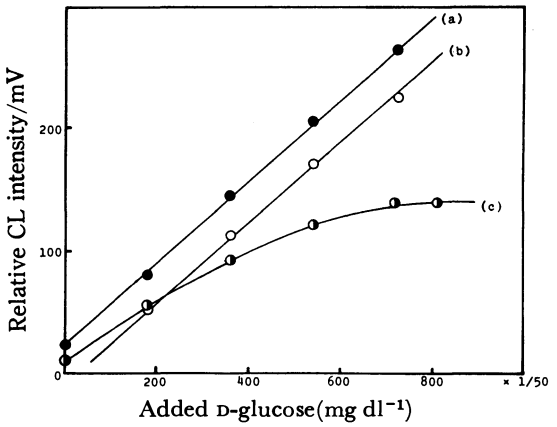

Fig. 8. Calibration curve for glucose added to serum. a: Serum+D-glucose, b: D-glucose, c: serum+D-glucose (without using a DEAE-cellulose column).

Determination of D-*Glucose in Serum.* About 1 mg cm^{-3} of glucose is contained in a normal human serum. Therefore, the concentration of glucose in a serum is brought to around 10^{-4} mol dm^{-3} by diluting it to 50 times its initial volume; it can be expected to be determined by the use of the linear part of the calibration curve in Fig. 7. Then, the relationship between the amount of glucose added and the intensity of the CL was examined after Hyland Control Serum I had been diluted to 50 times its initial volume. The results obtained are shown in Fig. 8. When an experiment was done without using a column(g) (Fig. 1), serum proteins were captured on the glass-disk with immobilized PO. This resulted in markedly lowering the intensity of CL (Fig. 8(c)), and no correlation was found between, the amount of glucose added and the intensity of the CL after analyses of 20 samples.

In order to avoid the capture of serum proteins on the above-mentioned glass-disk, a 100 mm × 3 mm i.d. column charged with various capturing agents was placed between a six-way cock (Fig. 1(d)) for sampling and a column (Fig. 1(h)) with immobilized GO. The efficiency of the capturing agents for the capture of serum proteins was examined by the use of: 1) Glass beads (80—120 mesh), 2) active charcoal (35—60 mesh), 3) silica gel (60—80 mesh), 4) activated alumina (about 200 mesh), and 5) DEAE-cellulose. Glass beads were not effective for the capture of serum proteins. Active charcoal captured serum proteins as well as glucose, and no serum proteins were observed on the glass-disk with immobilized PO. Here, the peak on a recorder chart showed tailing phenomenon and the intensity of the CL was considerably smaller than the expected value. Silica gel, activated alumina, and DEAE-cellulose were more or less effective for the removal of the interference of serum proteins, but DEAE-cellulose was most excellent in peak height and reproducibility (Fig. 8(a)).

The CL observed without adding glucose to serum in Fig. 8(a) is attributed to the glucose contained in Hyland Control Serum I. There was a parallel relationship between the calibration curve (Fig. 8(a)) obtained by adding glucose to Hyland Control Serum I and the calibration curve (Fig. 8(b)) obtained by glucose alone, where the difference between the intensities of the two lines corresponded approximately to a 1 mg cm^{-3} of glucose concentration in serum.

Judging from the complexity of serum composition, the standard addition method in which, for example, two serum samples are diluted to 50 times their initial volume with water and a definite concentration of a glucose solution respectively, seems to be most recommendable for the rapid and exact determination of glucose in serum by the present method.

It is concluded from the above results that a glucose concentration in serum of less than 0.01 cm^3 can be continuously determined at the rate of about 3 min/sample by the present method, in which a flow-cell with immobilized PO is used.

References

1) W. R. Seitz and M. P. Neary, *Anal. Chem.*, **46**, 188A (1974).
2) D. T. Bostick and D. M. Hercules, *Anal. Chem.*, **6**, 447 (1975).
3) D. C. Williams, G. F. Huff, and W. R. Seitz, *Clin. Chem.*, **22**, 372 (1976).
4) M. J. Cormier and P. M. Prichard, *J. Biol. Chem.*, **243**, 4706 (1968).
5) T. M. Freeman and W. R. Seitz, *Anal. Chem.*, **50**, 1242 (1978).
6) H. H. Weetall, *Biochim. Biophys. Acta*, **212**, 1 (1970).
7) M. K. Weibel, W. Dritschilo, H. J. Bright, and A. E. Humphrey, *Anal. Biochem.*, **52**, 402 (1973).
8) C. Yuan, S. S. Kuan, and G. G. Guilbault, *Anal. Chim. Acta*, **124**, 169 (1981).
9) D. J. Inman and W. E. Hornby, *Biochem. J.*, **129**, 255 (1972).
10) M. Mascini and G. G. Guilbault, *Anal. Chem.*, **49**, 795 (1977).
11) I. Kamitani, "Kagakuhakko," Kodansha, Tokyo (1972), p. 50.

A Calorimetric Study on the Relative Thermal Stability in Some Nickel(II) Complexes Containing *N,N'*- or *N,N*-Diethylethylenediamine

Ryokichi Tsuchiya,* Akira Uehara, and Yoshiyuki Ohtsuka
Department of Chemistry, Faculty of Science, Kanazawa University, Kanazawa 920
(Received November 24, 1981)

The enthalpy changes (ΔH) in the reaction of $Ni(AA)_2X_2 \cdot nH_2O$ type complexes with aqueous potassium cyanide were calorimetrically measured at 25 °C, where AA is *N,N'*-diethylethylenediamine (*NN'*-deen) or *N,N*-diethylethylenediamine (*NN*-deen); X is Cl^-, Br^-, I^-, or NO_3^- ion; and *n* is 0 or 2. On the basis of the enthalpy data measured, the thermal stability was compared among chloride, bromide, iodide, and nitrate in the following each group of compounds: $Ni(NN'\text{-deen})_2X_2 \cdot 2H_2O$, $Ni(NN'\text{-deen})_2X_2$, $Ni(NN\text{-deen})_2X_2 \cdot 2H_2O$, and $Ni(NN\text{-deen})_2X_2$. The thermal stability was found to decrease in the order, chloride>bromide>nitrate>iodide in each group. Comparison of the enthalpy data between the chlorides of the *NN'*-deen and *NN*-deen complexes revealed the difficulty of anation in the latter rather than in the former. $[Ni(NN\text{-deen})_2(H_2O)_2]Br_2$ was, when heated, converted into $[Ni(NN\text{-deen})_2]Br_2$ without anation differing from the chloride. The difference was also discussed on the basis of the enthalpy data.

Nickel(II) complexes are fascinating compounds from the viewpoint that they have a possibility to take various coordination structures easily capable of transforming to each other in the solution and in the solid phase.[1] The equilibria and mutual conversions are most familiarly investigated among their tetrahedral, square planar, and octahedral configurations.[2]

We have already reported that the compounds $[Ni(NN'\text{-deen})_2(H_2O)_2]X_2$ (*NN'*-deen: *N,N'*-diethylethylenediamine; X: Cl^-, Br^-, I^-, or NO_3^- ion) undergo anation to form $[NiX_2(NN'\text{-deen})_2]$ upon heating in the solid phase still keeping the octahedral environment.[3] On the other hand, the complexes $[Ni(NN\text{-deen})_2(H_2O)_2]X_2$ (*NN*-deen: *N,N*-diethylethylenediamine; X: Cl^- or Br^-) display some different thermal reactions from the *NN'*-deen complexes: *i.e.*, the chloride undergoes anation in a manner similar to the corresponding *NN'*-deen compounds, but the bromide deaquates to form square planar complexes. In addition, in the case of the iodide and nitrate, we always failed in attempting to prepare the octahedral diaqua complexes like the chloride or bromide, but exclusively obtained the square planar $[Ni(NN\text{-deen})_2]X_2$.[4]

It is therefore worthwhile to know why such differences take place in the thermal reaction. The present study was undertaken (1) to measure calorimetrically the enthalpy changes (ΔH) in the reaction of $Ni(AA)_2X_2 \cdot nH_2O$ (AA: *NN'*- or *NN*-deen; X: Cl^-, Br^-, I^-, or NO_3^- ion; *n*: 0 or 2) with aqueous potassium cyanide, (2) to compare the thermal stability of these complexes on the basis of the enthalpy changes obtained, and (3) to try to interprete the difference of the features appearing in the thermal reactions in the solid phase.

Experimental

Preparation of Complexes. $Ni(NN'\text{-deen})_2X_2 \cdot nH_2O$,[5] and $Ni(NN\text{-deen})_2X_2 \cdot nH_2O$[6] (X=$Cl^-$, Br^-, I^-, and NO_3^-; *n*=0 and 2) were prepared by the known method and identified by the chemical analysis and the electronic spectra.

Calorimetric Measurements. In order to discuss the thermal stability of these complexes, the enthalpy changes in the reaction of them in the powder state with potassium cyanide solution were measured with Tokyo-Riko twin isoperibol calorimeter TIC-2S at 25 °C. In each run, the diamine complexes employed were accurately weighed in the range of order of 1×10^{-4} mol and the aqueous potassium cyanide employed was 100 cm^3 of 6×10^{-2} mol dm^{-3} solution. The reactions proceeded quantitatively, for example, according to the Eqs. 1 and 2, and the enthalpy changes (ΔH) for each reaction were estimated as mentioned in the later section.

Results and Discussion

Thermal Stability in the NN'*-deen Complexes.* The enthalpy changes for the *NN'*-deen and *NN*-deen complexes measured are summarized in Table 1. The enthalpy changes for the reaction of diaquabis(*NN'*-deen)chromium(III) chloride and bromide with potassium cyanide solution are given as below,

$$[Ni(NN'\text{-deen})_2(H_2O)_2]Cl_2(s) + 4CN^-(aq) = Ni(CN)_4^{2-}(aq) + 2NN'\text{-deen}(aq) + 2Cl^-(aq) + 2H_2O(l) \quad \Delta H = -128\ 8\ kJ\ mol^{-1} \quad (1)$$

$$[Ni(NN'\text{-deen})_2(H_2O)_2]Br_2(s) + 4CN^-(aq) = Ni(CN)_4^{2-}(aq) + 2NN'\text{-deen}(aq) + 2Br^-(aq) + 2H_2O(l) \quad \Delta H = -103.3\ kJ\ mol^{-1}. \quad (2)$$

Table 1. Enthalpy changes for the reaction of nickel(II)-bis(diamine) complexes with CN^- (kJ mol^{-1})[a]

X^-	AA=*NN'*-deen		*NN*-deen	
Cl^-	Oh	Oh'	Oh	Oh'
	−128.8	−143.5	−121.4	−155.6
Br^-	Oh	Oh'	Oh	Sq
	−103.3	−128.3	−96.2	−102.0
I^-	Oh	Oh'	Sq	
	−81.6	−177.8	−111.6	
NO_3^-	Oh	Oh'	Sq	
	−91.3	−124.3	−113.6	

a) Oh designates the octahedral diaquabis(diamine) complexes $[Ni(AA)_2(H_2O)_2]X_2$, Oh', the octahedral diacidobis(diamine) complexes $[NiX_2(AA)_2]$produced by the anation of the former, and Sq means the square-planar bis(diamine) complexes $[Ni(AA)_2]X_2$.

By combining these two enthalpy changes with the following values,

$Cl^-(aq) = Cl^-(g)$ $\Delta H = -76.5$ kJ mol^{-1} [7]

$Br^-(aq) = Br^-(g)$ $\Delta H = -110.5$ kJ mol^{-1},[8]

the enthalpy change for the reaction,

$$[Ni(NN'\text{-deen})_2(H_2O)_2]Cl_2(s) + 2Br^-(g) = [Ni(NN'\text{-deen})_2(H_2O)_2]Br_2(s) + 2Cl^-(g),$$

was calculated as ΔH=42.5 kJ mol^{-1}. This value corresponds to the difference of lattice energy between the chloride and bromide: this result reflects that the bromide is thermally more unstable by this value than the chloride.

In the same way, by using the enthalpy data measured for the iodide (ΔH=$-$81.6 kJ mol^{-1}) and nitrate (ΔH=$-$91.3 kJ mol^{-1}) and those for the following changes,

$I^-(aq) = I^-(g)$ $\Delta H = -154.0$ kJ mol^{-1} [9]

$NO_3^-(aq) = NO_3^-(g)$ $\Delta H = -128.9$ kJ mol^{-1},[10]

the enthalpy changes for the substitution reaction of the chloride by iodide or nitrate ion were obtained as follows:

$$[Ni(NN'\text{-deen})_2(H_2O)_2]Cl_2(s) + 2X^-(g) = [Ni(NN'\text{-deen})_2(H_2O)_2]X_2(s) + 2Cl^-(g)$$

$\Delta H = 107.9$ kJ mol^{-1} for X = I^-

$\Delta H = 67.4$ kJ mol^{-1} for X = NO_3^-

These values are the difference of the lattice energies between the iodide or nitrate and the chloride.

As seen from Table 1, the enthalpy changes for the octahedral diacido complexes $[NiX_2(NN'\text{-deen})_2]$ formed by the anation of the octahedral diaqua complexes $[Ni(NN'\text{-deen})_2(H_2O)_2]X_2$ were measured as $-$143.5, $-$128.3, $-$117.8, and $-$124.3 kJ mol^{-1} for the chloride, bromide, iodide, and nitrate, respectively. By analogous calculations to the diaqua complexes, the enthalpy changes for the following substitution reactions were estimated. These values correspond to the

$$[NiCl_2(NN'\text{-deen})_2](s) + 2X^-(g) = [NiX_2(NN'\text{-deen})_2](s) + 2Cl^-(g)$$

$\Delta H = 52.8$ kJ mol^{-1} for X = Br^-

$\Delta H = 129.4$ kJ mol^{-1} for X = I^-

$\Delta H = 85.7$ kJ mol^{-1} for X = NO_3^-

decrements of lattice energy of the bromide, iodide, and nitrate from that of the chloride. As expected from the equation of lattice energy by Kapustinskii,[11] the lattice energy decreases as the radius of anion increases if the cation is the same. The radius of Cl^-, Br^-, I^-, and NO_3^- are 1.18,[12] 1.96,[12] 2.16,[13] and 1.89 Å,[14] respectively. The order of decrement of lattice energy observed in the diaqua and diacido complexes is, therefore, parallel to the increasing order of the radius except for the case of the nitrate.

The enthalpy level diagram for the *NN'*-deen complexes by using the enthalpy data obtained above is illustrated in Fig. 1. It is obvious from the figure that the thermal stability decreases in the order, chloride> bromide>nitrate>iodide, both in the diaqua and diacido series. The enthalpy changes in the dehydration

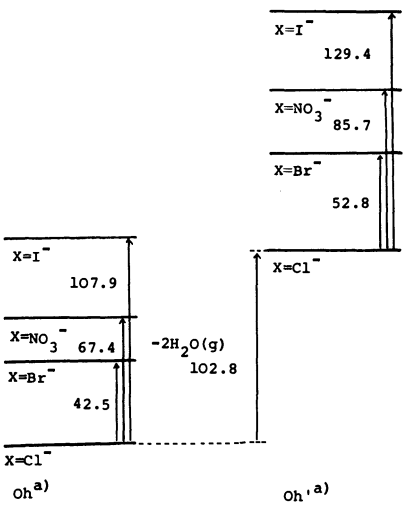

Fig. 1. Enthalpy level diagram for the *NN'*-deen complexes. The numerals are expressed by the unit of kJ mol^{-1}.
a) These designations are the same as those employed in Table 1.

followed by the anation were obtained by combining the heat of vaporization of water with the enthalpy changes measured for the reaction of $[Ni(NN'\text{-deen})_2(H_2O)_2]X_2$ or $[NiX_2(NN'\text{-deen})_2]$ type complexes with potassium cyanide solution. The value found in the dehydration of the chloride is 102.8 kJ mol^{-1} (Fig. 1).

Thermal Stability in the NN*-deen Complexes.* The enthalpy changes for the reaction of $[Ni(NN\text{-deen})_2(H_2O)_2]Cl_2$ and $[Ni(NN\text{-deen})_2(H_2O)_2]Br_2$ with aqueous potassium cyanide corresponding to Eqs. 1 and 2 were measured as ΔH=$-$121.4 kJ mol^{-1} and ΔH=$-$96.2 kJ mol^{-1}, respectively, in a manner similar to those for the *NN'*-deen complexes (Table 1). The difference of the lattice energy between the chloride

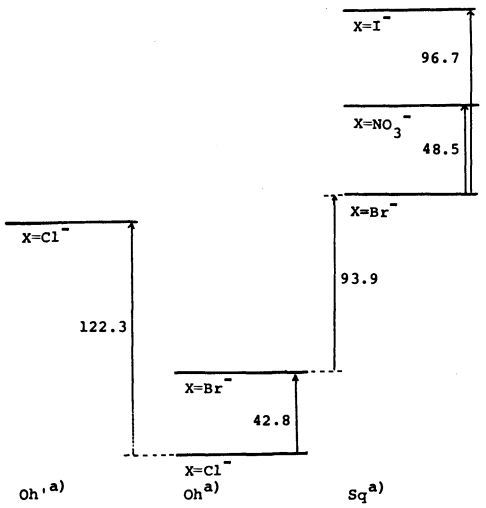

Fig. 2. Enthalpy level diagram for the *NN*-deen complexes. The numerals are expressed by the unit of kJ mol^{-1}.
a) These designations are the same as those employed in Table 1.

and bromide was estimated as ΔH=42.8 kJ mol^{-1}. The enthalpy level diagram for the *NN*-deen complexes, including the latter value, is presented in Fig. 2.

In the thermal reaction of the *NN'*-deen complexes in the solid phase, the anation was generally found, but only a slight difference was shown in ease of anation depending upon the kind of anations. It is probably due to the lesser steric effect of two equatorial ethyl groups in *NN'*-deen upon anation relative to *NN*-deen. On the contrary, the *NN*-deen complexes have at least one axial ethyl group in each *NN*-deen chelate ring, and hence notable steric effect may be expected. For example, as stated in the introduction, the chloride of the *NN*-deen complex undergoes anation, whereas the corresponding bromide is converted into square planar complex after losing the coordinated water.

The enthalpy change in the dehydration accompanied by the anation, from [Ni(*NN*-deen)$_2$(H_2O)$_2$]Cl_2 to [$NiCl_2$(*NN*-deen)$_2$], was obtained as ΔH=122.3 kJ mol^{-1} in the same way as that for the corresponding *NN'*-deen complex. In [Ni(*NN*-deen)$_2$(H_2O)$_2$]Br_2, on the other hand, the enthalpy change in the dehydration followed by the formation of square planar complex without anation was obtained as ΔH=93.9 kJ mol^{-1} by employing the measured value for [Ni(*NN*-deen)$_2$]-Br_2, ΔH=−102.0 kJ mol^{-1} (Table 1, Fig. 2). In the iodide and nitrate, the diaqua complexes were not obtained, but prepared only in anhydrous square planar configuration as mentioned in the introduction. For these square planar complexes, the differences of lattice energies of the iodide and the nitrate from the bromide were calculated as ΔH=96.7 and 48.5 kJ mol^{-1}, respectively. From Fig. 2, the thermal stability for the square planar complexes decreases in the order, bromide>nitrate>iodide.

Difference in Thermal Stability between the NN'*-deen and* NN*-deen Complexes.* The enthalpy change for the reaction of [Ni(NN'-deen)$_2$(H_2O)$_2$]Cl_2 with aqueous potassium cyanide expressed by Eq. 1, ΔH=−128.8 kJ mol^{-1}, and that for the reaction of the corresponding *NN*-deen complex, ΔH=−121.4 kJ mol^{-1} (Table 1), were combined with the following values:

NN'-deen(l) = *NN'*-deen(aq)	ΔH = −48.5 kJ mol^{-1}
NN'-deen(l) = *NN'*-deen(g)	ΔH = 37.6 kJ mol^{-1}
NN-deen(l) = *NN*-deen(aq)	ΔH = −44.0 kJ mol^{-1}
NN-deen(l) = *NN*-deen(g)	ΔH = 37.0 kJ mol^{-1}.

Here, the heats of dissolution of *NN'*-deen (ΔH=−48.5 kJ mol^{-1}) and *NN*-deen (ΔH=−44.0 kJ mol^{-1}) were measured with the calorimeter, and the heats of vaporization of *NN'*-deen (ΔH=37.6 kJ mol^{-1}) and *NN*-deen (ΔH=37.0 kJ mol^{-1}) were calculated from their boiling points and Trouton's constant. The enthalpy change in the reaction,

[Ni(*NN'*-deen)$_2$(H_2O)$_2$]Cl_2(s) + 2*NN*-deen(g)
= [Ni(*NN*-deen)$_2$(H_2O)$_2$]Cl_2(s) + 2*NN'*-deen(g),

was thus calculated as ΔH=2.8 kJ mol^{-1}. The enthalpy change for substituting *NN'*-deen by *NN*-deen in the bromide was obtained as ΔH=3.1 kJ mol^{-1} in the same way as that employed in the chloride.

Figure 3 illustrates the enthalpy level diagram for the

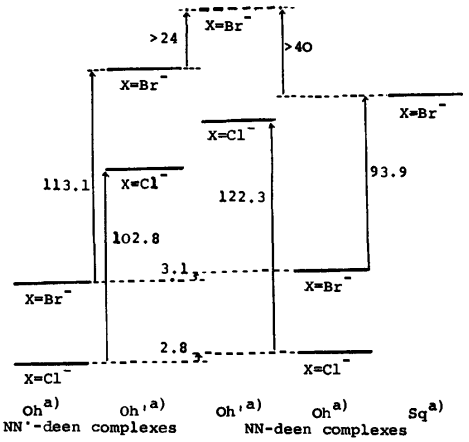

Fig. 3. Enthalpy level diagram for the chlorides and bromides of the *NN'*-deen and *NN*-deen complexes. The numerals are expressed by the unit of kJ mol^{-1}. a) These designations are the same as those employed in Table 1.

chlorides and bromides of the *NN'*-deen and *NN*-deen complexes. It is found from the figure that the enthalpy (ΔH=122.3 kJ mol^{-1}) required for [Ni(*NN*-deen)$_2$-(H_2O)$_2$]Cl_2 to form [$NiCl_2$(*NN*-deen)$_2$] is greater than that (ΔH=102.8 kJ mol^{-1}) for [Ni(*NN'*-deen)$_2$(H_2O)$_2$]-Cl_2 to form [$NiCl_2$(*NN'*-deen)$_2$]. This suggests that the former undergoes anation with more difficulty than the latter. It is probably due to the presence of an exial ethyl group in the *NN*-deen complex and its absence in the *NN'*-deen complex. Such a difference between *NN*-deen and *NN'*-deen complexes is also expected in the bromide, but we were unable to estimate the difference because [$NiBr_2$(*NN*-deen)$_2$] was not prepared. It is, however, assumed that the anation of [Ni(*NN*-deen)$_2$(H_2O)$_2$]Br_2 is not so easy as that of the corresponding chloride because bromide ion has larger radius than chloride ion. Therefore, the enthalpy level for the imaginary [$NiBr_2$(*NN*-deen)$_2$] may be expected to be higher by >24 kJ mol^{-1} than that of the corresponding *NN'*-deen complex as shown by a broken line (Fig. 3). In addition, as seen obviously in the diagram, the enthalpy level for the imaginary [$NiBr_2$(*NN*-deen)$_2$] is much higher (>40 kJ mol^{-1}) than that for [Ni(*NN*-deen)$_2$]Br_2. This might be the reason why [Ni(*NN*-deen)$_2$(H_2O)$_2$]Br_2 is, when heated in the solid phase, converted into the square planar complex without anation.

References

1) a) R. S. Nyholm, *Chem. Rev.*, **53**, 263 (1953); b) M. Ciampolini and G. P. Speroni, *Inorg. Chem.*, **5**, 45 (1966); c) J. R. Preer and H. B. Gray, *J. Am. Chem. Soc.*, **92**, 7306 (1970); d) I. Bertini, M. Ciampolini, P. Dapporto, and D. Gatteschi, *Inorg. Chem.*, **11**, 2254 (1972).

2) a) L. Sacconi, G. Lombardo, and P. Paoletti, *J. Am. Chem. Soc.*, **82**, 4185 (1960); b) H. C. Clark and R. J. O'Brien, *Can. J. Chem.*, **39**, 1030 (1961); c) G. W. Everett, Jr., and R. H. Holm, *J. Am. Chem. Soc.*, **87**, 2118 (1965).

3) Y. Ihara, E. Izumi, A. Uehara, R. Tsuchiya, S. Nakagawa, and E. Kyuno, *Bull. Chem. Soc. Jpn.*, **55**, 1028 (1982).

4) R. Tsuchiya, S. Joba, A. Uehara, and E. Kyuno, *Bull. Chem. Soc. Jpn.*, **46**, 1454 (1973).
5) D. M. L. Goodgame and L. M. Venanzi, *J. Chem. Soc.*, **1963**, 616.
6) D. M. L. Goodgame and L. M. Venanzi, *J. Chem. Soc.*, **1963**, 5909.
7) K. J. McCallum and J. E. Mayer, *J. Chem. Phys.*, **11**, 58 (1943).
8) P. M. Doty and J. E. Mayer, *J. Chem. Phys.*, **12**, 323 (1944).
9) F. D. Rossini, D. D. Wagman, W. H. Evans, S. Levine, and I. Jaffe, "Selected Values of Chemical Thermodynamic Properties," U. S. Governm. Printing Office, Washington, D. C. (1962), p. 31.
10) F. B. Bichowsky and F. D. Rossini, "The Thermochemistry," New York (1963); K. B. Yatsimirskii, *Izv. An. SSSR, Ohn.*, **6**, 590 (1948).
11) A. F. Kapustinskii, *Zh. Obshch. Khim.*, **13**, 497 (1943).
12) V. M. Goldschmidt, *Ber.*, **60**, 1263 (1927).
13) L. Pauling, *J. Am. Chem. Soc.*, **49**, 765 (1927).
14) K. B. Yatsimirskii, *Izv. Akad. Nauk SSSR, Otdel, Khim. Nauk*, **1948**, 398.

Solvent Dependence of the Circular Dichroism Spectra of Some *cis*-Dianionobis(ethylenediamine)cobalt(III) Complexes

Ushio SAKAGUCHI, Hiroshi NAKAZAWA, Kazuhisa SAKAI, and Hayami YONEDA*
Department of Chemistry, Faculty of Science, Hiroshima University, Naka-ku, Hiroshima 730
(Received December 17, 1981)

The circular dichroism spectra of some *cis*-bis(ethylenediamine)cobalt(III) complexes have been measured in several solvents. Among these complexes, the diisothiocyanato complex was found to exhibit a marked solvent dependence; the dominant circular dichroism band in the lowest energy spin-allowed transition region changed its sign upon going from, *e.g.*, water, dimethyl sulfoxide, methanol, or acetone to pyridine or its analogues. Coupled with the proton NMR spectra and a similar solvent dependence of the circular dichroism spectra of nitroisothiocyanatobis(ethylenediamine)cobalt(III) and diisothiocyanatobis(ethylenediamine)chromium(III) complexes, we ascribed the origin of the sign inversion of the diisothiocyanato complex to the stereoselective hydrogen bonding of *cis* N–H_B with pyridine-like molecules, where *cis* N–H_B is the hydrogen bonded to the nitrogen atom *cis* to NCS^- and directed off the molecular twofold axis.

It has been known for some time that the optical activity of some organic compounds is solvent dependent and this effect has been used, for example, for conformational analysis.[1] In the field of coordination chemistry, however, no systematic studies have been made on the effect of solvents upon the optical activity of metal complexes.[2] Recently, Bosnich and Harrowfield[3] found that the circular dichroism (CD) spectra of bobalt(III) complexes of the type *trans*-$[Co(N)_4(X)_2]^+$ are particularly sensitive to solvents, where $(N)_4$ represents chiral quadridentate amine ligands. Depending upon the solvent, some of these complexes changed even the sign of rotational strength of the lowest energy spin-allowed $^1A_{1g}$ to $^1T_{1g}(D_{4h})$ circular dichroism, which owes its origin to the so-called vicinal effect. Although they examined many closely related systems extensively, no definite conclusion was reached about the origin of the large CD variations observed. Subsequently, Hawkins *et al.*[4] investigated the CD and proton NMR spectra of some *trans*-$[Co(R\text{-pn})_2(X)_2]^{n+}$ and related complexes in several solvents, where *R*-pn is (*R*)-1,2-propanediamine. They ascribed the prominent solvent dependence of the CD spectra to the stereoselective hydrogen bonding that is formed between the equatorial amino hydrogens of the complex cation and the solvent molecule, rendering the coordinated nitrogens asymmetric.

Though several other scattered examples can be found in the literature[5] which describes significant solvent variation of CD spectra of metal complexes, no further attempt appears to be made at the elucidation of the solvent variation *per se*. In the above, we confined our interest to such systems that contain no chiral solvents, because in chiral solvents additional sources of complication might arise due to, *e.g.*, induced CD,[6] asymmetric transformation,[7] or the Pfeiffer effect.[8]

We have studied the CD spectra of some optically stable *cis*-dianionobis(ethylenediamine)cobalt(III) complexes, *cis*-$[Co(en)_2(X)_2]^{n+}$, in several solvents, where en=ethylenediamine and $(X)_2$=$(CN)_2$, $(NO_2)_2$, $(NCS)_2$, $(N_3)_2$, oxalate, acetylacetonate, $(NH_3)_2$, and en. These substituents range from strong- to weak-field ligands in the spectrochemical series. The diisothiocyanato and dicyano complexes were found to exhibit marked solvent dependences; the dominant and minor CD bands, respectively, changed their signs in some solvents. This paper describes the results of such studies and discusses, in particular, the origin of the CD variation of the diisothiocyanato complex with solvents.

Experimental

Materials. The literature methods were used for the preparation and optical resolution of *cis*-$[Co(en)_2(X)_2]^{n+}$ complexes, where $(X)_2$=$(CN)_2$,[9] $(NO_2)_2$,[10] $(NCS)_2$,[11] $(N_3)_2$,[12] en,[13] acetylacetonate,[14] $(NH_3)_2$,[15] and oxalate.[16] The methods for the preparation and optical resolution of the chromium(III) analogue *cis*-$[Cr(en)_2(NCS)_2]^+$ and *cis*-$[Co(en)_2(NO_2)(NCS)]^+$ were those of House[11] and Yamazaki *et al.*,[12] respectively. Each of these complexes was obtained in the form of chloride, bromide, iodide, perchlorate, and tetraphenylborate (BPh_4^-) by metathesis. For complexes containing monodentate ligands, ion-exchange chromatography with SP-Sephadex C-25 resin was used to confirm the absence of any *trans* impurities. The identity of these complexes was confirmed by unpolarized absorption spectra, proton NMR spectra, and CD spectra.

The nonaqueous solvents used for the CD measurements were of spectroscopic grade or of highest grade commercially available, mostly from Katayama Chemical Industries Co., Ltd. (Osaka) or Tokyo Kasei Kogyo Co., Ltd. (Tokyo), and used as supplied. Dimethyl-d_6 sulfoxide (DMSO-d_6, 99 atom% D minimum) and pyridine-d_5 (99 atom% D minimum) were purchased from E. Merck (Darmstadt).

Measurements. The CD spectra were obtained on a JASCO J-40CS recording spectropolarimeter at ambient temperature. Tetraphenylborate salts were used throughout for nonaqueous solvents and the complex concentration was typically 1.1×10^{-3} to 2.7×10^{-3} mol dm^{-3}.

Proton magnetic resonance spectra were run on a JEOL JNM-PMX60 spectrometer at 36 °C or on a JEOL PS-100 spectrometer at ambient temperature. Chemical shifts were referenced to internal tetramethylsilane (TMS).

Results and Discussion

The utility of CD spectra in assigning the stereochemistry and the absolute configuration of metal complexes relies upon the structure-spectrum correlation in the d-d transition and/or exciton band region.[17]

The correlation has now been believed to be well established both theoretically and experimentally, especially for configurational CD spectra. Usually, the configurational effects dominate over the conformational and vicinal effects for five-membered chelate ring systems.[17] The CD spectra due to the latter two effects have been shown,[3-5] in some complexes, to vary with solvents. For configurational CD spectra, however, no examples appear to be reported in which the sign of rotational strength changes with solvents. This spectral stability seems to be the basis of the utility of configurational CD spectra in the determination of absolute configuration. The absolute configuration of *cis*-$[Co(en)_2(X)_2]^+$ complexes has been determined based on the sign of the rotational strength of the dominant CD band in the first d-d transition region.[18] Thus, if the sign of the rotational strength of the dominant CD band changed with the environment or the medium for unknown reasons, it might lead to the undesired situation where CD spectra are unreliable and useless in the study of the stereochemistry and absolute configuration of metal complexes.

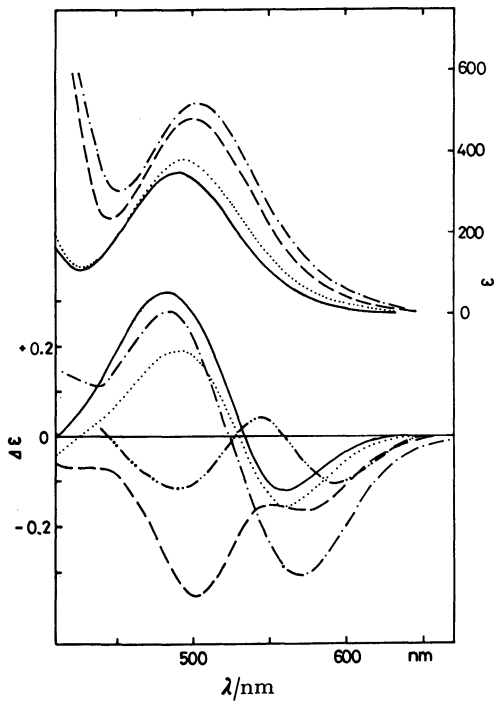

Fig. 1. The unpolarized absorption and CD spectra in the first d-d transition region of *Λ-cis*-$[Co(en)_2(NCS)_2]^+$ in water (——), DMSO (·····), THF (-·-·-·-), and pyridine (------), and the CD spectrum in nitrobenzene (-·-·-·-·-).

Diisothiocyanato Complex. Figure 1 shows the absorption and CD spectra of *Λ-cis*-$[Co(en)_2(NCS)_2]^+$ in several solvents, including water (solid curve) and pyridine (broken curve). The counter anions were chloride and BPh_4^- in water and nonaqueous solvents, respectively. In the absorption spectra, it is noted that the peak position and the intensity of the first d-d band are affected by solvents to some extent. Though the CD spectra in water, DMSO, and tetrahydrofuran (THF) differ in magnitude, their shapes are not so drastically different, as with ordinary solvents like methanol, acetone, and acetonitrile. The lowest energy CD peak, which was assigned[18] to the B_1 transition, has a minus sign in these solvents, while the higher energy component, assigned to the A_2+B_2 transition, is plus. These notations follow those of McCaffery, Mason, and Norman.[18] In contrast to these minus-plus couplets, the pyridine solution yielded a minus-minus couplet; the sign of the dominant CD band is changed from plus to minus, while leaving the minor CD band relatively unaffected. This may be the most spectacular example ever reported. If we judge simply from the sign of the dominant CD band, the pyridine spectrum is almost enantiomeric to the water or DMSO spectrum.

The CD variation shown in Fig. 1 does not seem to be primarily due to the counter anions. The CD spectrum in water did not show any noticeable change upon changing the counter anion from chloride to perchlorate. Also, addition of ten-fold excess of sodium perchlorate did not affect the spectrum in water. It is only addition of ten-fold excess of chloride to the DMSO solution that gave rise to measurable, though small, CD changes.[19] The tetraphenylborate anion is believed to show little tendency to ion association in nonaqueous solvents with bulk dielectric constants greater than 15.[20] Note that the dielectric constants of pyridine, THF, and DMSO are about 13, 7, and 47, respectively. Thus, we may safely eliminate the possibility of the counter anions generating these CD variations. That the observed CD change is not an artifact nor due to any chemical reactions was confirmed by the stability of the

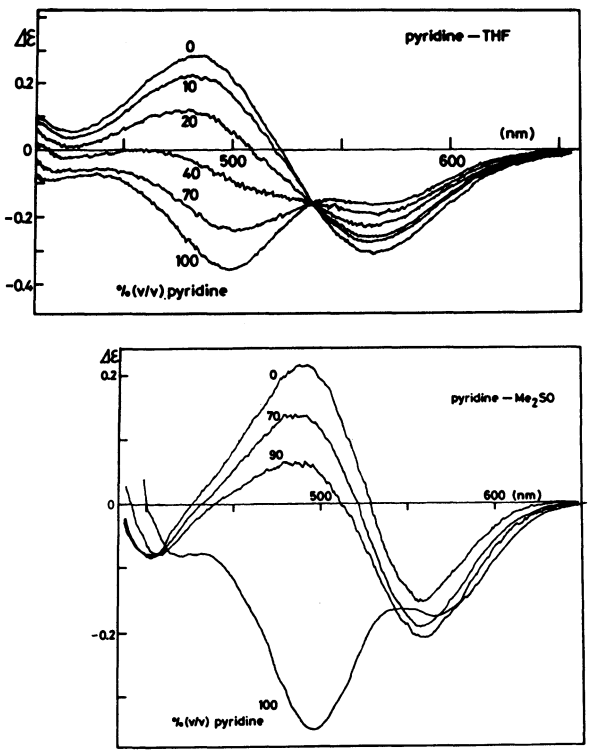

Fig. 2. The CD change of *Λ-cis*-$[Co(en)_2(NCS)_2]BPh_4$ as a function of the pyridine content in pyridine/THF (upper) and pyridine/DMSO (lower) mixed solvents.

spectra against time and by recovering the identical compound from the pyridine solution.

In order to see what type of spectrum is obtained in a mixed solvent, we measured the CD spectrum of the diisothiocyanato complex as a function of solvent composition. The results are given in Fig. 2 for the combination of pyridine/THF and pyridine/DMSO. The figure clearly indicates that the band positions are not affected greatly but the sign of the dominant CD band changed with the solvent composition. The change is, however, not a smoothly varying function of the solvent composition and a strong preference for one component can be recognized. For example, the 70%(v/v) pyridine solution in pyridine/DMSO systems yielded the CD spectrum similar to that of DMSO rather than the pyridine spectrum. This indicates that the immediate solvation sphere of the complex cation is not a smoothly varying function of the solvent composition, a phenomenon known as preferential solvation.[21] Thus, the observed CD changes are not primarily due to a change in the energy positions of the bands but due to the immediate solvation of the complex cation, causing the inversion of the intrinsic sign of the dominant band. Further, all the CD curves obtained for the pyridine/THF systems have isodichroic points, which is evidence for the presence of only two species in solution and therefore the presence of a substantial, well-defined entity that generates the sign inversion. Thus, the changes observed in Figs. 1 and 2 result most probably from some specific solute-solvent interaction. To see the nature of this interaction, we examined (i) the effect of other pyridine-like solvents, (ii) whether or not two isothiocyanato groups are essential to the sign inversion of the dominant band, and (iii) the effect of the central metal ion, by replacing cobalt(III) by chromium(III).

Figure 3 gives the CD spectra of the diisothiocyanato complex in various solvents, mostly nitrogen-containing heterocycles. From this figure, the following points will be noted. The solvents that cause the sign inversion of the dominant band are unsaturated *N*-heterocycles and the nitrogen center should not be sterically crowded.

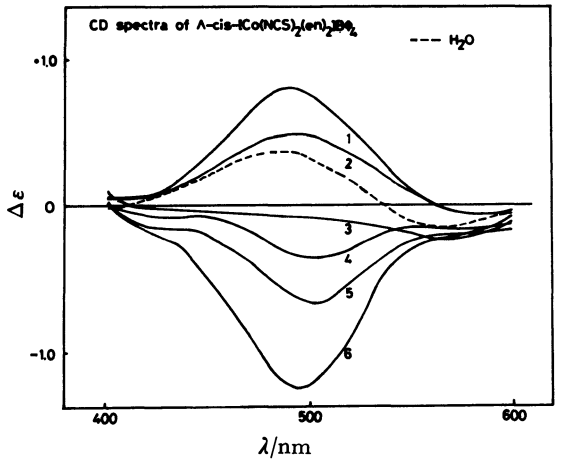

Fig. 3. The CD spectrum of *Λ-cis*-$[Co(en)_2(NCS)_2]BPh_4$ in piperidine (1), pyrrolidine (2), α-picoline (3), pyridine (4), 3,5-lutidine (5), and quinoline (6).

For example, solvents that contain a saturated nitrogen center, such as *N*-methylmorpholine, piperidine, pyrrolidine, and aniline, do not give rise to inversion. The sterically crowded 2,6-lutidine solvent behaves similarly, whereas the less crowded 3,5-lutidine solvent does cause the inversion. These structural features necessary for the inversion suggest that the nitrogen centers are interacting with the complex cation through their lone electron pairs. Further, since only unsaturated or aromatic solvents caused the inversion, these unsaturated parts of the solvent molecules too should be considered to interact with the complex cation. This latter point will be discussed later. The site of interaction with a lone electron pair may be either the isothiocyanato group or the N–H group of the complex cation. But the former group is anionic and its interaction with a lone electron pair is unlikely. Interaction with the N–H group(s) of the complex cation is thus the only possibility. The donor power of pyridine and its derivatives are rather large[22] and the acidity of the coordinated amino groups are also comparatively high, allowing for, *e.g.*, pK_a measurements,[23] electrophilic attach by several Lewis bases at deprotonated amino groups,[24] and the exchange with deuterium in neutral deuterium oxide solution.[25] Therefore, the hydrogen bonding between pyridine and coordinated amino group(s) is highly likely. In fact, the same type of interaction with pyridine has been postulated by Hawkins *et al.*[2,4] to play a major role in the solvent variations of the CD spectra of some *trans*-$[Co(N)_4(X)_2]^{n+}$ type of complexes.

TABLE 1. THE AMINE PROTON CHEMICAL SHIFTS (δ) OF *cis*-$[Co(en)_2(NCS)_2]X$ IN DMSO-d_6[a]

X	*cis* NH		*trans* NH	
BPh_4	(6.15)6.08	5.68(5.62)	4.48	
ClO_4	(6.08)6.00	5.67(5.55)	4.45	
I	(6.15)6.05	5.72(5.60)	4.55	
Br	(6.08)5.97	5.80(5.68)	5.37,5.27	4.57,4.47
Cl	(6.07)5.95	5.77(5.65)	5.90,5.80	4.53,4.42

a) From TMS internal standard. Numbers in parentheses refer to shoulders. Accuracy ±0.07 ppm.

In order to ascertain the actual site of hydrogen bonding with pyridine, we investigated the amine portion of the proton NMR spectrum of *cis*-$[Co(en)_2(NCS)_2]^+$. Table 1 lists the amine proton chemical shifts of *cis*-$[Co(en)_2(NCS)_2]X$ in DMSO-d_6, where X was varied from BPh_4^- through ClO_4^-, I^-, Br^- to Cl^-. We can note a particular hydrogen whose chemical shift is, among others, susceptible to the counter anion. As for other *cis*-$[Co(en)_2(X)_2]^+$ complexes with $(X)_2$= $(CN)_2$, $(NO_2)_2$, oxalate, malonate, $(Cl)_2$, and $(N_3)_2$, the chemical shift changes of this particular hydrogen brought about by the counter anions are considered to be due to the ion-pair formation with the counter anions *via* hydrogen bonding.[19,26] Thus, this hydrogen can be assigned to the amine hydrogen that is bonded to the nitrogen atom *trans* to NCS^- and pointing approximately parallel to the molecular C_2 axis. This hydrogen will be called *trans* H_A. The other *trans* hydrogen, *trans* H_B, is thus assigned to the peak at about δ 4.50 and the

Table 2. The amine proton chemical shifts (δ) of *cis*-$[Co(en)_2(NCS)_2]BPh_4$ in mixed pyridine-d_5/DMSO-d_6 solvents[a]

Pyridine %(v/v)	*cis* NH		*trans* NH
0	(6.15)6.08	5.68(5.62)	4.48
17	(6.20)6.08	5.77(5.67)	4.55
33	(6.43)6.33	5.98(5.87)	4.75
67	*ca.*6.7[b]	6.25(6.13)	5.00
83	*ca.*7.2[b]	6.43(6.30)	5.23
100	8.32, 8.27	6.33, 6.28	5.76

a) From TMS internal standard. Numbers in parentheses refer to shoulders. Accuracy ± 0.07 ppm. b) Overlapped with the phenyl resonances of BPh_4^-.

low field AB quartet to two *cis* hydrogens.

Table 2 gives the chemical shifts of amine hydrogens of *cis*-$[Co(en)_2(NCS)_2]BPh_4$ in mixed pyridine-d_5/DMSO-d_6 solvents. As the pyridine content in the solvent increases, *trans* hydrogens and one of the *cis* hydrogens move to low fields by about 1.28 and 0.64 ppm, respectively. In contrast, the other *cis* hydrogen suffers a downfield shift of as great as about 2.20 ppm by pyridine and it appears in neat pyridine at about δ 8.30, which is downfield of even the phenyl resonances of BPh_4^-. This may be taken as evidence for the stereoselective hydrogen bonding at *cis* N–H by pyridine. This *cis* hydrogen, pertaining to the stereoselective hydrogen bonding, may be *cis* $N-H_B$, the *cis* hydrogen directing off the molecular C_2 axis, in analogy with the assignment made previously for the acetylacetonato- and diazidobis(ethylenediamine)cobalt(III) complexes.[19,26] Comparison of the values of Table 2 and the CD variation of Fig. 2(b) provides additional evidence for the stereoselective hydrogen bonding. The chemical shifts of the other *cis* hydrogen, *cis* $N-H_A$, and the two *trans* hydrogens are monotonic functions of the pyridine content, whereas the *cis* $N-H_B$ hydrogen suffers downfield shifts from pyridine in a manner quite similar to the CD variation due to pyridine in pyridine/DMSO systems. The similarity of the chemical shift variation of *cis* $N-H_B$ and the CD variation in pyridine/DMSO systems suggests strongly that this hydrogen plays a key role in the sign inversion of the dominant CD band.

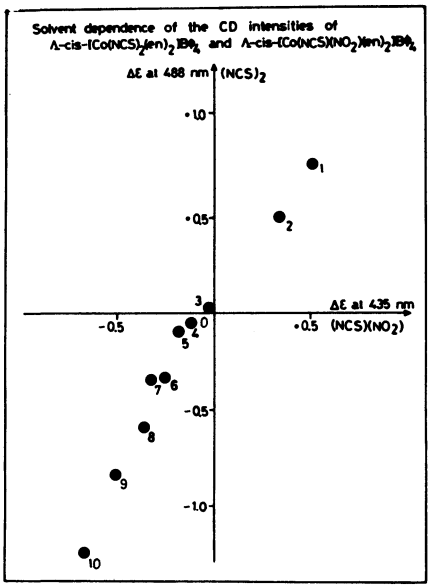

Fig. 4. The correlation of the CD intensities of *Λ-cis*-$[Co(en)_2(NCS)_2]BPh_4$ and *Λ-cis*-$[Co(en)_2(NO_2)(NCS)]BPh_4$ in various solvents, including piperidine (1), pyrrolidine (2), pyrrole (3), aniline (4), α-picoline (5), β-picoline (6), pyridine (7), 3,5-lutidine (8), isoquinoline (9), and quinoline (10).

Table 3 gives the CD data of the monoisothiocyanato complex, *Λ-cis*-$[Co(en)_2(NO_2)(NCS)]^+$, and the chromium(III) complex, *Λ-cis*-$[Cr(en)_2(NCS)_2]BPh_4$. The reason for substitution of one NCS^- by NO_2^- is that among several *Λ-cis*-$[Co(en)_2(X)_2]^{n+}$ complexes investigated, the CD spectrum of the dinitro complex was the least sensitive to the change in solvents (see below). The solvent dependence of the CD spectrum of the monoisothiocyanato complex is very similar to that of the diisothiocyanato complex. This correlation will be seen most clearly by Fig. 4, in which the CD intensity of the diisothiocyanato complex in a solvent is plotted against that of the monoisothiocyanato complex in the same solvent. In this plot, we used the wavelengths at which the CD intensities change significantly with solvents. As seen from Fig. 4, the correlation is very good and more importantly, the change in the CD intensity of the diisothiocyanato complex is

Table 3. CD peaks of *Λ-cis*-$[Co(en)_2(NO_2)(NCS)]BPh_4$ and *Λ-cis*-$[Cr(en)_2(NCS)_2]BPh_4$

Solvent	λ/nm	Δε	Solvent	λ/nm	Δε
		Λ-cis-$[Co(en)_2(NO_2)(NCS)]BPh_4$			
Piperidine	484	+0.829	β-Picoline	450	−0.178
Pyrrolidine	488	+0.659		526	+0.073
Pyrrole	496	+0.287	Pyridine	450	−0.407
Aniline	435	+0.161		525	+0.065
	500	−0.468	3,5-Lutidine	453	−0.472
α-Picoline	448	−0.277		557	+0.024
	507	+0.277	Quinoline	455	−0.953
		Λ-cis-$[Cr(en)_2(NCS)_2]BPh_4$			
Pyrrolidine	485	+0.93	3,5-Lut dine	460	+0.17
Pyridine	472	+0.34		525	−0.32
	486	+0.31	Quinoline	488	−0.27
				510	−0.27

approximately twice as large as that of the mono complex. This indicates (i) that the isothiocyanato group is essential to the CD change, as is also trivial from the fact that the CD changes of the other *cis*-$[Co(en)_2(X)_2]^+$ complexes examined here were much smaller, if any (see below), and (ii) that the two isothiocyanato groups interact independently with pyridine-like molecules. In the case of *Λ-cis*-$[Cr(en)_2(NCS)_2]$-BPh_4, the CD variation is not so drastic as to produce an enantiomeric spectrum but the essential features of the cobalt(III) complexes are retained; the order of increasing tendency to invert the dominant CD band observed here (pyrrolidine≪pyridine<3,5-lutidine< quinoline) parallels that of the di- and mono-isothiocyanato complexes of cobalt(III). This suggests that the sign inversion as observed for the cobalt(III) complexes is due to specific ligand-solvent interactions. It should be pointed out that the above order and a similar order in Fig. 4 can not be correlated in a simple way with common solvent parameters, such as the dielectric constant, dipole moment, E_T or Z value, or the basicity.[22]

From all the above observations, we propose a model for the interaction of the isothiocyanato complexes with pyridine-like molecules in solution, as illustrated schematically in Fig. 5. For convenience, this figure is drawn for pyridine and *Λ-cis*-$[Co(en)_2(NCS)_2]^+$. The nitrogen lone electron pair of pyridine is involved in the *cis* N–H_B···N type hydrogen bonding, as deduced from the NMR spectra. A crystal structure analysis[27] established that the Co(III)–NCS bond is linear, indicating Co–N≡C–S^- as the dominant resonance form. Molecular models show that the pyridine ring

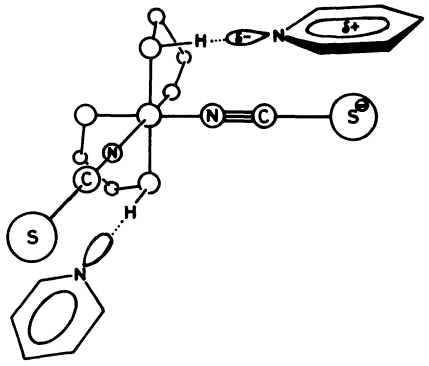

Fig. 5. The proposed model for the interaction of *Λ-cis*-$[Co(en)_2(NCS)_2]^+$ and pyridine.

TABLE 4. ABSORPTION AND CD PEAKS OF *Λ-cis*-$[Co(en)_2(X)_2]^{n+}$

$(X)_2$		Solvent			
		H_2O	DMSO	THF	Pyridine
$(CN)_2$	AB	400(78.3)	421(79.7)	416(79.7)	419(83.0)
	CD	443(+0.315)	447(+0.273)	443(+0.206)	433(+0.198)
		366(+0.206)	398(−0.154)	342(+0.095)	342(+0.062)
			337(+0.105)		
$(NO_2)_2$	AB	435(173)	438(201)	436(218)	440(227)
	CD	458(+1.66)	462(+1.68)	461(+1.49)	463(+1.01)
		405(−0.60)	410(−0.85)	405(−0.72)	410(−0.80)
$(N_3)_2$	AB	520(332)	523(394)	524(369)	525(397)
	CD	568(−0.80)	589(−0.92)	607(−0.86)	608(−0.77)
		501(+1.17)	508(+4.22)	516(+5.22)	517(+4.26)
$(NCS)_2$	AB	490(351)	493(380)	503(521)	499(482)
	CD	559(−0.12)	561(−0.16)	571(−0.31)	573(−0.16)
		483(+0.32)	495(+0.19)	484(+0.28)	501(−0.35)
$(Cl)_2$	AB	534(92.6)	539(104)		
	CD	613(−0.60)	622(−0.77)		
		538(+0.70)	540(+0.68)		
ox[a]	AB	496(118)	561(140)	C)	504(151)
		335(154)	363(154)		363(162)
	CD	523(+2.60)	530(+2.65)	C)	532(+2.52)
		385(+0.118)	383(+0.194)		386(+0.204)
		335(+0.212)	338(+0.164)		339(+0.135)
acac[b]	AB	498(138)	498(138)	490(250)	498(144)
	CD	495(+2.6)	530(+1.49)	490(+1.70)	489(+2.92)
		373(−1.3)	372(−0.90)	377(−0.75)	383(−1.28)
$(NH_3)_2$	AB	467(84)	470(87)	472(115)	
	CD	494(+0.49)	497(+0.49)	500(+0.32)	
		433(−0.03)	440(−0.08)	446(−0.10)	
en	AB	466(91)	468(97)	463(100)	469(106)
	CD	490(+1.89)	492(+1.88)	497(+1.26)	495(+1.28)
		429(−0.11)	433(−0.24)	441(−0.42)	425(−0.31)

a) ox: Oxalate. b) acac: Acetylacetonate. c) Insoluble.

can be situated over the sulfur atom, which carries a negative charge. In this model, the aromatic ring is tentatively assumed to interact with the negatively charged sulfur atom, which is reminiscent of the case of tetrabutylammonium bromide in nitrobenzene, where the bromide anion was assumed to be situated on the aromatic phenyl group.[28] The production of such a well-defined entity in solution may alter the CD spectrum of the complex cation either by rendering the hydrogen-bonded N–H center asymmetric (vicinal effects[17]) or by simply attaching a large "*N*-substituent" (regional rules[29]) which is orientated stereospecifically. Such a two-site interaction would be conceivable not only for pyridine but also for other aromatic molecules, if they satisfy steric requirements for this type of interaction. For example, nitrobenzene may interact in a similar fashion, though this molecule appears a little too large for such an interaction and its basicity is very much weaker than the basicity of pyridine.[22] In fact, the nitrobenzene solution gave the CD spectrum which is a weaker imitation of the pyridine spectrum rather than the water or DMSO spectrum, as shown in Fig. 1.

Other Complexes. We describe briefly the effect of solvents upon the CD spectra of the other complexes. Table 4 summarizes the absorption and CD data of all the bis(ethylenediamine) type of complexes examined here. The dicyano complex shows a relatively large CD variation especially for DMSO; the higher-energy B_1 transition, which was placed in water at 366 nm, appears to have shifted to a longer wavelength and changed the sign of its rotational strength in DMSO. The spectrum of the dinitro complex undergoes a comparatively small variation upon changing the solvents. The CD intensity of the higher-energy dominant band of the diazido complex[30] is enhanced by a factor of more than four upon going from water to DMSO, THF, or pyridine. For the oxalato and acetylacetonato complexes, prominent solvent effects are noted also for the higher-energy transitions rather than for the lower-energy ones. The peak positions and the intensities of the first d-d band of all the complexes are affected by these solvents. The origin and the nature of these spectral variations are not clear as yet.

This work was partially supported by a Grant-in-Aid for Scientific Research from The Ministry of Education, Science and Culture (B-547043).

References

1) M. Legrand, "Fundamental Aspects and Recent Developments in Optical Rotatory Dispersion and Circular Dichroism," ed by F. Ciardelli and P. Salvadori, Heyden and Sons, London (1973), Chap. 4.2, p. 285.

2) T. D. Bailey and C. J. Hawkins, "Stereochemistry of Optically Active Transition Metal Compounds," ed by B. E. Douglas and Y. Saito, ACS Symposium Series, No. 119, American Chemical Society (1980), p. 221.

3) B. Bosnich and J. M. Harrowfield, *J. Am. Chem. Soc.*, **94**, 989 (1972); B. Bosnich and J. M. Harrowfield, *Inorg. Chem.*, **14**, 828, 836, 847, 853, 861 (1975).

4) C. J. Hawkins, G. A. Lawrance, and R. M. Peachey, *Aust. J. Chem.*, **30**, 2115 (1977); C. J. Hawkins and M. L. McEniery, *ibid.*, **32**, 1433 (1979).

5) K. Kashiwabara, K. Igi, and B. E. Douglas, *Bull. Chem. Soc. Jpn.*, **49**, 1573 (1976); K. Kashiwabara, M. Kojima, and J. Fujita, *ibid.*, **52**, 772 (1979); S. Arakawa, K. Kashiwabara, J. Fujita, and K. Saito, *ibid.*, **50**, 2331 (1977); M. Kojima, M. Fujita, and J. Fujita, *ibid.*, **50**, 898 (1977).

6) H. Nakazawa, C. E. Oh, K. Miyoshi, and H. Yoneda, *Bull. Chem. Soc. Jpn.*, **53**, 273 (1980); Y. Taniguchi, J. Hidaka, and Y. Shimura, *ibid.*, **50**, 2093 (1977), and references therein.

7) See, *e.g.*; B. Bosnich, in "Fundamental Aspects and Recent Developments in Optical Rotatory Dispersion and Circular Dichroism," ed by F. Ciardelli and P. Salvadori, Heyden and Sons, London (1973), Chap. 3.8, p. 254.

8) K. Miyoshi, Y. Matsumoto, and H. Yoneda, *Chem. Lett.*, **1980**, 1319; K. Miyoshi, Y. Kuroda, J. Takeda, H. Yoneda, and I. Takagi, *Inorg. Chem.*, **18**, 1425 (1979).

9) K. Kuroda, *Nippon Kagaku Zasshi*, **89**, 720 (1968); S. C. Chan and M. L. Tobe, *J. Chem. Soc.*, **1963**, 966.

10) J. Springborg and C. E. Schäffer, *Inorg. Synth.*, **14**, 63 (1973); F. P. Dwyer and F. L. Garvan, *ibid.*, **6**, 195 (1960).

11) D. A. House, *J. Inorg. Nucl. Chem.*, **35**, 3103 (1973).

12) a) P. J. Staples and M. L. Tobe, *J. Chem. Soc.*, **1960**, 4812; b) K. Yamazaki, J. Hidaka, and Y. Shimura, *Bull. Chem. Soc. Jpn.*, **49**, 3060 (1976).

13) J. B. Work, *Inorg. Synth.*, **2**, 221 (1946); J. A. Broomhead, F. P. Dwyer, and F. W. Hogarth, *ibid.*, **6**, 183 (1960).

14) I. K. Reid and A. M. Sargeson, *Inorg. Synth.*, **9**, 167 (1967).

15) K. Garbett and R. D. Gillard, *J. Chem. Soc., A*, **1966**, 802.

16) W. T. Jordan, B. T. Brennan, L. R. Fröbe, and B. E. Douglas, *Inorg. Chem.*, **12**, 1827 (1973).

17) See for reviews; "Optical Activity and Chiral Discrimination," ed by S. F. Mason, D. Reidel, Dordrecht (Holland) (1979); C. J. Hawkins, "Absolute Configuration of Metal Complexes," Wiley-Interscience, New York (1971), Chap. 5; R. D. Gillard, *Prog. Inorg. Chem.*, **7**, 215 (1966); J. Fujita and Y. Shimura, "Spectroscopy and Structure of Metal Chelate Compounds," ed by K. Nakamoto and P. J. McCarthy, Wiley, New York (1968); L. I. Katzin and I. Eliezer, *Coord. Chem. Rev.*, **7**, 331 (1972).

18) A. J. McCaffery, S. F. Mason, and B. J. Norman, *J. Chem. Soc.*, **1965**, 5094.

19) H. Nakazawa, U. Sakaguchi, and H. Yoneda, *J. Am. Chem. Soc.*, in press.

20) M. Herlem and A. I. Popov, *J. Am. Chem. Soc.*, **94**, 1431 (1972); M. S. Greenberg, R. L. Bonder, and A. I. Popov, *J. Phys. Chem.*, **77**, 2449 (1973), and references therein.

21) H. Schneider, "Solute-Solvent Interactions," ed by J. F. Coetzee and C. D. Ritchie, Marcel Dekker, New York (1969), Vol. 2, Chap. 11; S. Behrendt, C. H. Langford, and L. S. Frankel, *J. Am. Chem. Soc.*, **91**, 2236 (1969).

22) See, for example: U. Mayer and V. Gutman, *Struct. Bonding (Berlin)*, **12**, 113 (1972); T. R. Griffiths and D. C. Pugh, *Coord. Chem. Rev.*, **29**, 129 (1979); U. Mayer, *Pure Appl. Chem.*, **51**, 1697 (1979).

23) A. A. Grinberg and K. I. Gildengershel, *Izv. Akad. Nauk SSSR*, **1948**, 479; F. P. Dwyer and J. W. Hogarth, *J. Am. Chem. Soc.*, **77**, 6152 (1955); B. P. Block and J. C. Bailar, Jr., *ibid.*, **73**, 4722 (1951); G. Navon, R. Panigel, and D. Meyerstein, *Inorg. Chim. Acta*, **6**, 299 (1972); D. A. Buckingham, C. R. Clark, and T. W. Lewis, *Inorg. Chem.*, **18**, 2041 (1979).

24) See, *e.g.*; A. M. Sargeson, *Pure Appl. Chem.*, **50**, 905 (1978).

25) U. Sakaguchi, K. Maeda, and H. Yoneda, *Bull. Chem. Soc. Jpn.*, **49**, 397 (1976).

26) H. Nakazawa, U. Sakaguchi, H. Yoneda, and Y. Morimoto, *Inorg. Chem.*, **20**, 973 (1981).

27) K. Matsumoto, M. Yonezawa, H. Kuroya, H. Kawaguchi, and S. Kawaguchi, *Bull. Chem. Soc. Jpn.*, **43**, 1269 (1970).
28) J. B. Hyne, *J. Am. Chem. Soc.*, **85**, 304 (1963).
29) B. Bosnich, *Acc. Chem. Res.*, **2**, 266 (1969).
30) Our recent crystal structure analysis revealed that the $(+)_{589}$ enantiomer of the diazido complex cation, which forms the less-soluble diastereoisomer, $(+)_{589}[Co(en)_2(N_3)_2]_2[Sb_2(d\text{-tart})_2]\cdot 2.5H_2O$, has the Λ absolute configuration, contrary to an earlier assignment[12b] based on the CD spectrum, where $[Sb_2(d\text{-tart})_2]^{2-}$ is the *d*-tartratoantimonate(III) ion. See; A. Miyanaga, Y. Kushi, and H. Yoneda, to be submitted.

Orbital Tilting Due to Destabilizing Four-electron and Stabilizing Two-electron Orbital Interactions. An Elucidation of *Exo-endo*-nonequivalency of π-MO Extension of Norbornene

Suketaka Ito* and Akikazu Kakehi
Department of Industrial Chemistry, Faculty of Engineering, Shinshu University, Wakasato, Nagano 380
(Received April 25, 1981)

A new concept, "Orbital Tilting," leading to hybridization change, was introduced on the basis of the destabilizing and the stabilizing secondary orbital interaction. The predominant π-MO extension of norbornene in the *exo*-direction was elucidated by application of the concept to the orbital system.

The *exo*-stereoselectivity in electrophilic addition to norbornene has been ascribed to π-HOMO extending predominantly in the *exo*-direction.[1] The nonequivalent orbital extension was rationalized in terms of the perturbation of etheno-π and -σ orbital through the orbital interaction with the methano-bridge.[1a,b] The orbital interaction results in the mixing between the unperturbed etheno-π and the etheno-σ MO or the basis 2p and 2s AO, which is the ground of the nonequivalency of the π-MO extension. Thus the *exo-endo*-nonequivalency of the π-MO extension can be understood as a problem of hybridization change.

According to Woodward and Hoffmann,[2] the cyclization of conjugated polyenes such as that of *s-cis*-butadiene to cyclobutene is represented in terms of the inclinations of both terminal methylenes. The inclination of methylene groups implies a tilt of orbitals, and the HOMO-LUMO interaction scheme[3] and other MO-theoretical treatments[2,4] rationalize the conrotatory cyclization of butadiene. In these treatments, however, only the tilt of p-π-type orbitals are considered; thus, the concomitant hybridization change is not handled in principle.[5]

In the present paper, on the basis of the HOMO-LUMO maximum overlapping principle,[3] we introduce a new concept, "Orbital Tilting," which involves the tilt of (s,p)-hybrid σ-type orbitals and leads to hybridization change.[6] The norbornene π-MO with predominant extension in the *exo*-direction is derived by application of the concept to an orbital system with an originally equivalent π-MO extension.

Results

Orbital Tilting and Hybridization Change. Let us consider a chemical system involving a methylene carbon (in sp^2 hybridization) bonded to another carbon in sp^2-sp^2 σ mode (χ_1 for the sp^2-hybrid AO of the methylene carbon, χ_2 for that of the other) and a group with an sp^2-hybrid orbital (χ_3) which is going to overlap in a σ symmetry with the p-type orbital (p) located in the methylene carbon (Fig. 1). Since a localized bonding σ_{CC} level is underlain by a bonding σ_{CH} level and the antibonding counterpart of σ_{CC} underlies that of σ_{CH} in ordinary hydrocarbons,[7] the order of orbital levels of the system under consideration is given as $\sigma^*_{CH}>\sigma^*_{CC}(=\chi_1-\chi_2)>p>\chi_3>\sigma_{CC}(=\chi_1+\chi_2)>\sigma_{CH}$. In this orbital system, χ_3 can interact with p upon approach and also with the localized σ-type orbitals. When the interaction between χ_3 and the σ orbitals located in the C–H bond regions is neglected as a first approximation,[8] the σ^*_{CC} orbital takes part as the next LUMO (NLUMO) or LUMO in the orbital interaction leading to hybridization change. According to the occupancy of p and χ_3,[9] four types of orbital interaction can be applied to the orbital system represented in Fig. 1: (1) A two-electron system (both χ_3 and p are unoccupied); (2) a four-electron system (χ_3 is occupied and p unoccupied); (3) a four-electron system (χ_3 is unoccupied and p occupied); (4) a six-electron system (both χ_3 and p are occupied).[10]

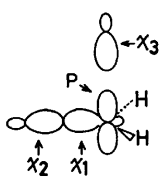

Fig. 1. Four-center orbital system leading to orbital tilting.

On the basis of the frontier orbital[3] or the perturbation concept,[11] these orbital systems can be treated in the following way. In Case 2, the interaction of χ_3 (HOMO) with p (LUMO) stabilizes the system, which is represented by the in-phase combination of χ_3 and p. Secondary stabilization may arise from the overlap between χ_3 (HOMO) and σ^*_{CC} (NLUMO). The orbital arrangement of σ^*_{CC} should be selected in such a way that χ_3 and χ_1 are in-phase (χ_3 and χ_2 are out-of-phase) (Fig. 2a); because χ_1 is located closer to χ_3 than χ_2 is and the in-phase overlap between χ_1 and χ_3 stabilizes the system. In this situation, as shown in Fig. 2a, the interaction of χ_1 with χ_3 and that of χ_2 with the bottom lobe of p are attractive. The HOMO-LUMO-NLUMO maximum overlap may be realized[12] by orbital tilting when the methylene group is inclined in the symmetrically bisecting plane to the configuration in which the two hydrogen atoms are more remote from the approaching group with local χ_3. Since χ_1 becomes orthogonal to the out-of-phase combination of χ_2 and χ_3 in the MO representation after orbital tilting (ϕ_2 in Fig. 2a), ϕ_2 should be revised to ϕ'_2, which is just the delocalized HOMO in the orbital system. In Case 3, the orbital system is occupied in the reverse manner of that in Case 2; however, since p (HOMO) interacts with σ^*_{CC} (NLUMO) through χ_3 (LUMO), the mode of orbital interaction should be equivalent to that of Case 2.

In Case 4, the interaction of χ_3 (NHOMO) with p

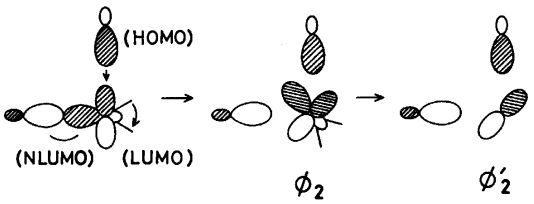

(a) Interaction of σ_{CC}* as NLUMO.

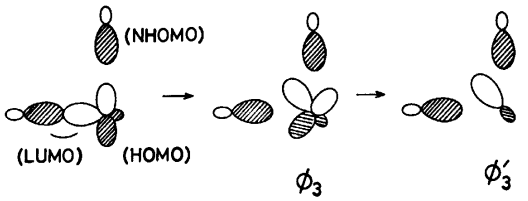

(b) Interaction of σ_{CC}* as LUMO (Type I).

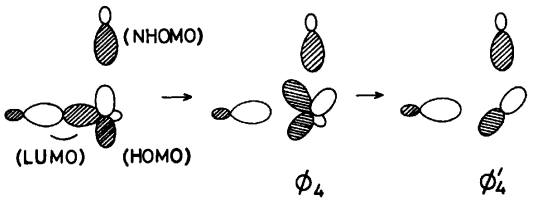

(c) Interaction of σ_{CC}* as LUMO (Type II).

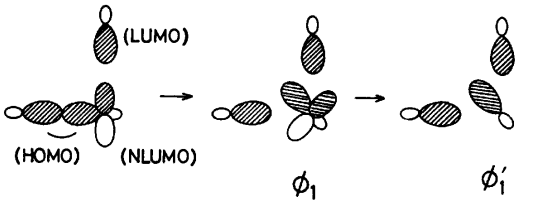

(d) Interaction of σ_{CC} as HOMO.

Fig. 2. Orbital tilting in the four-center orbital system.

(HOMO) destabilizes the system; this situation is represented by the out-of-phase combination of χ_3 and p. This representation is consistent with that of the semi-delocalized HOMO in the initial state. For stabilization, the following two alternative terms are available: One may arise from the overlap between p (HOMO) and σ^*_{CC} (LUMO), in which χ_2 and the bottom lobe of p are in-phase (Type I), and the other may arise from the overlap between χ_3 (NHOMO) and σ^*_{CC} (LUMO), in which χ_3 and χ_1 are in-phase (Type II). Since the magnitude of stabilization is dependent upon both the extent of orbital overlapping and the difference between the energy levels of orbitals, these circumstances are somewhat equivocal. However, the former stabilization term is probably dominant in view of the closer energy level of p to σ^*_{CC} and of the bonding character between χ_3 and χ_2. The situation of orbital interaction in this manner is given in Fig. 2b. The interaction of p with χ_2 becomes attractive; the HOMO-LUMO maximum and the HOMO-NHOMO minimum overlap may be achieved compatibly by orbital tilting in a manner similar to that of Cases 2 and 3. In the MO representation after orbital tilting (ϕ_3 in Fig. 2b), p is orthogonal to the in-phase combination of χ_2 and χ_3; accordingly, ϕ_3 should be revised to ϕ'_3, which is the delocalized HOMO in this orbital system. For this orbital system, the delocalized LUMO (ϕ'_4) can be derived in the same way from the alternative orbital representation in which σ^*_{CC} is given in such a way that χ_3 and χ_1 are in-phase (Fig. 2c).

For Case 1, σ_{CC} is the HOMO and χ_3 and p are the LUMO and the NLUMO, respectively. In the MO representation, χ_3 and σ_{CC} are in-phase; similarly, χ_3 and p are in-phase, for the in-phase combination of χ_3 and p designates the semi-delocalized LUMO. The orbital interaction can be treated analogously; this treatment is given in Fig. 2d. Since ϕ'_1 is the HOMO for the four-center two-electron system, it lies in the bottom level. Similarly, from the fact of electron occupation, it is evident that the energy ordering is $\phi'_1<\phi'_2<\phi'_3<\phi'_4$.[13]

On the one hand, since the constituent p and χ_1 in ϕ_1—ϕ_4 are based on the atomic p and the hybrid sp^2 orbital, they can be re-hybridized into a new equivalent basis set, $(\lambda\chi_1-p)/\sqrt{1+\lambda^2}$ $(=\chi_4)$ and $(\chi_1+\lambda p)/\sqrt{1+\lambda^2}$ $(=\chi_5)$. In the orbital system after re-hybridization, χ_4 overlaps with χ_2 and χ_5 with χ_3, where $\lambda\approx1$. The orbital system after re-hybrodization is represented schematically in Fig. 3 by an example.[14] Consequently, the two hybridization-changed C–C σ bonds are represented with the sets of bond orbitals, $(\chi_2+\chi_4)/\sqrt{2}$ and $(\chi_2-\chi_4)/\sqrt{2}$, and $(\chi_3+\chi_5)/\sqrt{2}$ and $(\chi_3-\chi_5)/\sqrt{2}$, respectively.

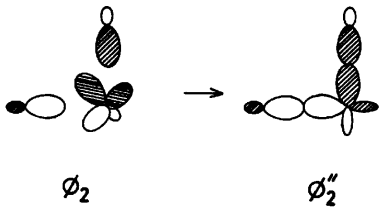

Fig. 3. Re-hybridization.

Predominant Extension of π-HOMO and π-LUMO in the Exo-direction in Norbornene System. We assume first a bicyclo[2.2.1]hept-2-ene structure in which its π-MO originally extends *exo-endo*-equivalently. For this system, the hyperconjugative four-electron interaction between the methano-bridge methylene and the double bond (through space) may be considered. As has been well known, the hyperconjugative effect of simple alkyl and alkylene groups is electron-donating.[15] The hypothetical unperturbed bicycloheptene system is represented in Fig. 4 with three localized π_{CH_2} orbitals (χ_{11}, χ_{12}, and χ_{13}) and one π orbital. In this orbital system, the three localized π_{CH_2} orbitals give a new set of semi-delocalized

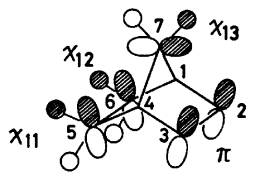

Fig. 4. Bicyclo[2.2.1]hept-2-ene system represented with unperturbed π and π_{CH_2} orbitals.

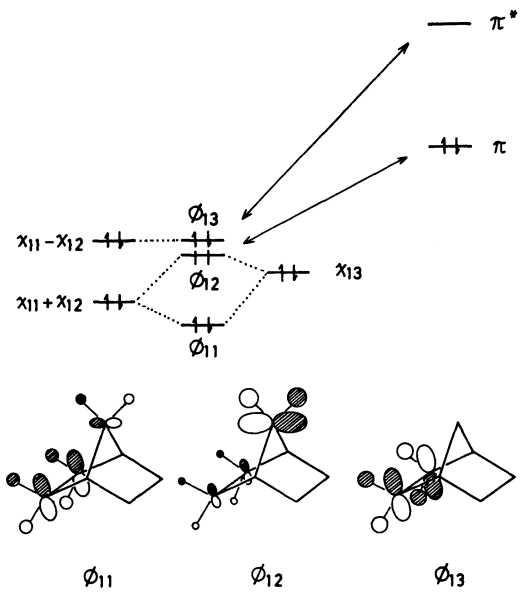

Scheme 1.

orbitals, ϕ_{11}, ϕ_{12}, and ϕ_{13}, according to the orbital interaction principle[11] (Scheme 1).

Since the orbital interaction between χ_{11} and χ_{12} is stronger than those of other combinations, ϕ_{13} should be underlain by ϕ_{12}, in which χ_{13} is the predominant contributor. According to the property of orbital symmetry, ϕ_{12} can interact with π in a four-electron fashion and ϕ_{13} with π^* in a two-electron fashion, and the interaction between ϕ_{11} and π can be considered weak and negligible in view of the difference in energy level.[16] The fact that the energy levels of ϕ_{12} and π are closer than the energy levels of ϕ_{13} and π^* suggests that the interaction of ϕ_{12} with π is dominant over that of ϕ_{13} with π^*. In this orbital system, the decrease of NHOMO (ϕ_{12})-HOMO (π) overlap and the increase of HOMO (ϕ_{13})-LUMO (π^*) overlap, both leading to the stabilization of the system, may be realized by orbital tilting, when the etheno group is inclined around the C_2–C_3 σ axis in the direction from the *exo-* to the *endo-*side to a certain extent keeping the C_2–C_3 and the two C–H σ bonds unchanged. The localized σ_{CC} bond orbitals located in C_1–C_2 and C_3–C_4 ought to be deformed by orbital tilting because, without this deformation, the etheno group cannot be inclined at all while the C_2–C_3 and the two C–H bonds are conserved.

When the σ orbitals located in C_1–C_2 and C_3–C_4 are represented in a semi-delocalized manner on the basis of sp^2 hybrids, the resulting low-lying vacant level (σ_{13}^*) may interact, upon orbital tilting, with ϕ_{12} in a stabilizing manner and with the low-lying filled level (σ_{11})[17] in a destabilizing manner. The stabilization arising from the interaction of ϕ_{12} with σ_{13}^* can be considered to dominate over the destabilization arising from that with σ_{11} in view of energy-level closing; however, both terms may be small because of their weak interaction. The MO representation for the orbital interaction between ϕ_{12} and π is given in Fig. 5, in which the low-lying vacant level (σ_{13}^*) is represented. The situation of orbital interaction resembles that of Case 4 described above, except that no formation of bond is involved; thus, the orbital system after tilting can be treated in the same manner and each constituent sp^2 hybrid and p orbital involved in σ_{13}^* and π are re-hybridized to give a new set of unequally hybridized orbitals. One pair of the new hybrids, consisting of a large fraction of the original sp^2 hybrids and a small fraction of the p orbital, lie in the $C_1C_2C_3C_4$ coplane and overlap with the local hybrid orbitals in C_1 and C_4 to lead to the generation of $\sigma_{13}^{*\prime}$ which corresponds to σ_{13}^*. The low-lying filled level, σ_{11}', is obtained analogously by considering the participation of σ_{11}. The other pair, consisting of a large fraction of p and a small fraction of sp^2 hybrids, should be in-phase and has its predominant extension in the exo-direction unquestionably, as seen in Fig. 5. This in-phase combination of the pair thus obtained (π' in Fig. 5) is the HOMO of norbornene system.

In a similar manner, the LUMO of norbornene with its predominant extension in the exo-direction can be derived from the orbital system involving ϕ_{13}, π^*, σ_{12}, and σ_{14}^*.[18]

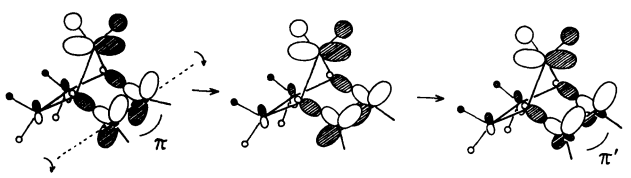

Fig. 5. Derivation of norbornene π-HOMO with predominant extension in the *exo*-direction.

Discussion

Orbital tilting does not mean the physical inclination of orbitals (only the shift of nuclei takes place actually), of course, but it merely an artificial device in analogy with orbital hybridization. However, orbital tilting is specified in such a way that the HOMO-HOMO minimum and the HOMO-LUMO maximum overlap may be realized; therefore, this method has its theoretical grounds in the perturbation or the frontier orbital theory. In this connection, it should be noted that the delocalized MO's, ϕ_1', ϕ_2', ϕ_3', and ϕ_4', obtained above by orbital tilting can be given alternatively by the qualitative LCAO method and that the relative energy levels are consistent with the assignment stated above (Scheme 2). As seen in Fig. 3, the re-hybrids by orbital tilting

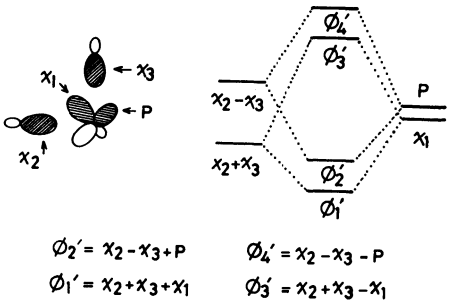

Scheme 2.

are in sp^5 hybridization, which are slightly different from the situation actually observed. This difference results from neglecting the interaction of σ orbitals located in the C–H bond regions, and is not serious.

In the method based on the orbital mixing rule, delocalized orbitals are considered for the purpose of predicting orbital extension[1a,b] or hybridization change,[6] which leads to configuration altering.[19] On the other hand, in the present method, the orbitals are represented in a localized manner and the configuration is altered so that the orthogonality of orbitals may be conserved approximately: The alteration of configuration results in hybridization change. A recognition of hybridization change on the basis of localized MO's may be feasible and reasonable;[20] for the localized MO's represented with bond orbitals correspond best with classical chemical structures and hybridization itself is based on local AO's. The merit of the concept of orbital tilting is the ease with which one can infer the alteration of configuration accompanied by hybridization change or molecular deformation.

As has been seen above, the norbornene π MO with predominant extension in the *exo*-direction can be derived from the unperturbed etheno-π MO involved in bicyclo[2.2.1]hept-2-ene structure by application of the concept of orbital tilting, due to the secondary interaction with the methano-bridge methylene as the main hyperconjugative entity.[21] Since it is generally accepted that the stability of norbornen-7-ylium ion and the instability of norbornen-7-ide ion are due to the homoconjugation[22] of the ion center with the double bond, the (homo)hyperconjugation of methano-bridge methylene with the double bond can be expected *a priori* in the bicycloheptene structure. On the other hand, if other conditions such as the extent of orbital overlapping can be regarded as equivalent, the hyperconjugative effect of the methano- and ethano-bridge in the neutral system may be dominant over that of methylenes because the energy level of a localized σ_{CC} orbital is higher than that of a localized σ_{CH}. However, from the view point of orbital symmetry, the hyperconjugative effect of methano- and ethano-bridging bond can be expected to operate in the same manner[23] as that of methylene C–H bonds.

The inclination of etheno group around the C_2–C_3 σ axis causes the hydrogen atoms attached to C_2 and C_3 to shift slightly downward from the $C_1C_2C_3C_4$ coplane (Fig. 5): This situation accords with the result of MO-theoretical calculation for norbornene[1c] and for bicyclo[2.2.1]hept-2-yl.[24]

The conformational properties and geometries of small and simple hydrocarbon molecules have been analyzed in terms of the four-electron destabilizing or the two-electron stabilizing interaction *via* hyperconjugation;[25] the same principle should be applicable also to more complex, rigid molecules. Thus, the hyperconjugative effect on the double bond results in the molecular deformation, which is the origin of the predominant extension in the *exo*-direction for π MO in norbornene system.

References

1) a) S. Inagaki and K. Fukui, *Chem. Lett.*, **1974**, 509; b) S. Inagaki, H. Fujimoto, and K. Fukui, *J. Am. Chem. Soc.*, **98**, 4054 (1976); c) G. Wipff and K. Morokuma, *Tetrahedron Lett.*, **21**, 4445 (1980).

2) R. B. Woodward and R. Hoffmann, "The Conservation of Orbital Symmetry," Academic Press, New York (1969).

3) K. Fukui, "Modern Quantum Chemistry," ed by O. Sinanoglu, Academic Press, New York (1965), Vol. I, p. 49; K. Fukui, *Fortschr. Chem. Forsch.*, **15**, 1 (1970); K. Fukui, *Acc. Chem. Res.*, **4**, 57 (1971).

4) H. Zimmerman, *Acc. Chem. Res.*, **4**, 272 (1971); M. J. S. Dewar, *Angew. Chem., Int. Ed. Engl.*, **12**, 36 (1971); W. A. Goddard III, *J. Am. Chem. Soc.*, **94**, 793 (1972).

5) In the reverse reaction (the ring opening), the rotation of sp^3 hydrids are considered, but their hybridization change has not also been dealt with.

6) The hybridization change in the nucleo- or electrophilic addition to an unsaturated carbon has been dealt with by Fukui (*Kagaku To Kogyo*, **29**, 470 (1976); "Kagaku-hanno To Denshi No Kido," Maruzen, Tokyo (1976), p. 188) on the basis of the sigma-pi interaction (K. Fukui and H. Fujimoto, *Bull. Chem. Soc. Jpn.*, **39**, 2116 (1966).

7) W. L. Jorgensen and L. Salem, "The Organic Chemist's Book of Orbitals," Academic Press, New York (1973), p. 14.

8) Neglecting the interaction of σ orbitals located in the C–H bonds implies that the two σ_{CH} and the two σ^*_{CH} levels are regarded as orthogonal to other levels throughout the course of reaction.

9) Single occupation is excluded from the scope of this argument.

10) In all cases, the number of electrons includes two electrons which occupy the σ_{CC} orbital.

11) Ref. 7, p. 10.

12) The destabilization arising from the decreased in-phase overlap between χ_3 and p is repaired by the stabilization arising from the increased in-phase overlap between χ_2 and p.

13) The energy ordering is in accord with that of group orbitals for CH_2: $\sigma_{CH_2}<\pi_{CH_2}<\sigma^*_{CH_2}<\pi^*_{CH_2}$. See Ref. 7, p. 7.

14) MO's ϕ_1''—ϕ_4'', which are equivalent to ϕ_1—ϕ_4, are formulated approximately as follows:

$$\phi_1'' = (\chi_3+\chi_5)/2 + (\chi_2+\chi_4)/2,$$
$$\phi_2'' = (\chi_3+\chi_5)/2 - (\chi_2+\chi_4)/2,$$
$$\phi_3'' = (\chi_3-\chi_5)/2 + (\chi_2-\chi_4)/2,$$
$$\phi_4'' = (\chi_3-\chi_5)/2 - (\chi_2-\chi_4)/2.$$

15) I. Fleming, "Frontier Orbitals and Organic Chemical Reactions," John Wiley and Sons, New York (1976), p. 48.

16) From the fact that ϕ_{12} has its largest amplitude in C_7, the hyperconjugative effect of methano-bridge methylene should predominate over that of ethano-bridge methylenes.

17) The high-lying counterparts, σ_{12} (filled) and σ_{14}^* (vacant), interact with π^* upon orbital tilting.

18) The σ type orbitals, σ_{12}' and $\sigma_{14}'^*$ corresponding to σ_{12} and σ_{14}^*, are also obtained.

19) That is to say, the alteration of configuration is treated as the result of a hybridization change.

20) Another advantage of identifying a chemical process on the basis of localized MO's has been in a method for predicting pericyclic reactions: S. Ito, A. Kakehi, and Y. Tanaka, *Bull. Chem. Soc. Jpn.*, **48**, 2855 (1975).

21) The predominant extension of bicyclo [2.1.0]pent-2-ene in the *exo*-direction[1a,b] can be likewise derived on the basis of the secondary four-electron interaction between π and the

Walsh σ_{CC} orbital extending in the *exo*-direction.

22) S. Winstein, *Quart. Revs.*, **23**, 141 (1969). See also: J. B. Grutzner and W. L. Jorgensen, *J. Am. Chem. Soc.*, **103**, 1372 (1981); E. Kaufmann, H. Mayr, J. Chandrasekhar, and P. v.R. Schleyer, *ibid.*, **103**, 1375 (1981); and references cited therein.

23) The same result can be obtained by orbital tilting, when the σ MO's for the methano- and the ethano-bridging bonds are represented with group-type orbitals (shown below) in a semi-delocalized manner, or with each (2s, 2p) hybrid located in C_5, C_6, and C_7 by postulating that the interaction between π MO and the local sp^2-type hybrids in C_1 and C_4 are very weak.

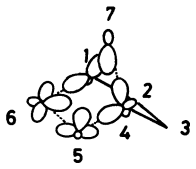

24) H. Fujimoto and K. Fukui, *Tetrahedron Lett.*, **1966**, 5551.

25) R. Hoffmann, L. Radom, J. A. Pople, P. v.R. Schleyer, W. J. Hehre, and L. Salem, *J. Am. Chem. Soc.*, **94**, 6221 (1972).

Photoreduction of Aminoanthraquinones by an Electron Transfer *via* the Upper Excited nπ* Triplet State

Haruo INOUE,* Kiyoshi KAWABE, Noboru KITAMURA, and Mitsuhiko HIDA

Department of Industrial Chemistry, Faculty of Technology, Tokyo Metropolitan University, Fukazawa, Setagaya-ku, Tokyo 158

(Received July 8, 1981)

The photoreduction of 2-piperidinoanthraquinone (**1**) by an electron transfer from hydroxide ion in aqueous 2-propanol was reinvestigated. The reaction proceeded actively on irradiation at 365 nm, but very weakly on irradiation at 420 nm. The fluorescence of **1** was not affected by hydroxide ion. 1,3-Cyclohexadiene as a triplet quencher retarded the photoreduction. All results revealed that the reactive state of **1** in the photoreduction is not the intramolecular excited CT state, but the upper excited nπ* triplet state. Kinetic studies indicated that the rate of deactivation from the $T_2(^3n\pi^*)$ level of **1** is unusually slow ($k_d = 1.7 \times 10^8\ s^{-1}$). The photoreduction *via* the upper excited $T_2(^3n\pi^*)$ level was also observed in 1-amino- and 1-piperidinoanthraquinone, while 2-aminoanthraquinone did not exhibit any reactivity. Wavelength-dependencies (313 nm, 365 nm, and >420 nm irradiations) of the photoreductions were also observed.

Anthraquinone derivatives have four ππ* absorption bands in the wavelength range between 220 nm and 350 nm, and also an nπ* band at longer wavelength near 400 nm. When electron donating substituents such as hydroxyl, amino, and methylamino groups are introduced into the nucleus, a new ππ* absorption band, an intramolecular charge transfer band, appears in the visible region.[1] In the photochemistry of anthraquinone derivatives, it has long been emphasized that the excited triplet nπ* state is very reactive, while the intramolecular CT state has little reactivity.[2] Recently we have found a new photosubstitution reaction of aminohaloanthraquinones with amines under irradiation with visible light and demonstrated that the intramolecular CT state is reactive in the reaction.[3] A. K. Davies *et al.* also postulated that the intramolecular CT state is reactive in the photoreduction of 2-piperidinoanthraquinone (**1**) by an electron transfer from hydroxide ion or alkoxide ion on irradiation with the light of $\lambda = 365$ nm.[4] However, an ambiguity remains in their conclusion about the reactive state; another possibility of the photoreduction *via* the upper excited $T_2(^3n\pi^*)$ level can not be excluded. The results of our reinvestigation of this photoreduction of **1** by hydroxide ion showed that the reaction proceeds not *via* the intramolecular CT state but *via* the upper excited $T_2(^3n\pi^*)$ state, contrary to Davies' conclusion. We also examined the photoreduction *via* the upper excited nπ* level of other anthraquinones (1-aminoanthraquinone (**2**), 2-aminoanthraquinone (**3**), 1-piperidinoanthraquinone (**4**) and we observed dramatic wavelength dependencies (313 nm, 365 nm, and >420 nm irradiations) on the photoreduction in these anthraquinones including 2-SO_3Na (**5**) and 1-SO_3Na (**6**) derivatives.

Experimental

Materials. *2-Piperidinoanthraquinone (1)*: 2-Chloroanthraquinone (10 g) and piperidine (150 ml) were heated to reflux for 8 h. The excess piperidine was evaporated from the reaction mixture and the residual red crystals of **1** were washed thoroughly with water and dried. The yield was 12.3 g. The crude **1** was purified by repeated recrystallizations from ethanol–benzene mixture (4 : 1 v/v); mp 164—165 °C; Found: C, 78.18%; H, 5.71%; N, 4.63%. Calcd for $C_{19}H_{17}NO_2$: C, 78.31%; H, 5.89%; N, 4.80%. 1-Aminoanthraquinone (**2**) (Sumitomo Chemical Co.) was purified by column chromatography (Al_2O_3/toluene) and repeated recrystallizations from benzene; mp 252—253 °C; Found: C, 75.31%; H, 3.86%; N, 6.44%. Calcd for $C_{14}H_9NO_2$: C, 75.32%; H, 4.06%; N, 6.27%. 2-Aminoanthraquinone (**3**) (Sumitomo Chemical Co.) was purified by the procedures recommended by Maki[5] using 82% aqueous sulfuric acid; mp 302 °C; Found: C, 75.24%; H, 3.78%; N, 6.02%. Calcd for $C_{14}H_9NO_2$: C, 75.32%; H, 4.06%; N, 6.27%. 1-Piperidinoanthraquinone (**4**): 1-Chloroanthraquinone (15 g) and piperidine (225 ml) were refluxed for 2.5 h. After evaporating off the excess piperidine, the red crystals of **4** were washed thoroughly with water and dried. The yield was 17.3 g. The crude **4** was passed through a silica-gel column (hexane–acetone, 3 : 1 v/v) and recrystallized repeatedly from ethanol; mp 124 °C; Found: C, 78.24%; H, 5.88%; N, 4.67%. Calcd for $C_{19}H_{17}NO_2$: C, 78.31%; H, 5.89%; N, 4.80%. Both sodium anthraquinone-2-sulfonate (**5**) and sodium anthraquinone-1-sulfonate (**6**) (Sumitomo Chemical Co.) were purified by respective salting-outs and repeated recrystallizations from water until molar absorption coefficients in their UV spectra became constant. 2-Propanol and methanol were purified as reported previously.[3] 1,3-Cyclohexadiene (Tokyo Kasei, GR) was further purified by fractional distillation before use.

Procedure. Each sample (4 ml) was degassed in a quartz cell by repeated freeze and thaw procedures and was irradiated with a high pressure mercury lamp (Toshiba H-400P or USHIO USH-500D) through the following filter systems; Toshiba UV-D25 glass filter and aqueous solution of K_2CrO_4 (0.27 g/dm³) Na_2CO_3 (1.0 g/dm³) (optical length: 1 cm) for the irradiation by monochromatic light of 313 nm; Toshiba UV-DIA glass filter and naphthalene (5.0×10^{-2} mol/dm³) in 2-propanol (optical length: 1 cm) for irradiation at 365 nm. The visible and UV absorption spectra of the irradiated reaction mixtures were recorded by a Shimadzu UV-200 spectrophotometer. The number of photons absorbed by each sample was determined by the use of a chemical actinometer of potassium tris(oxalato)ferrate(III).[6] In a typical case, the numbers of photons of the incident light of 313 nm and 365 nm were 3.2×10^{15} quanta/s and 1.6×10^{16} quanta/s, respectively.

Results

Photoreduction of 2-Piperidinoanthraquinone (1) in Alkaline

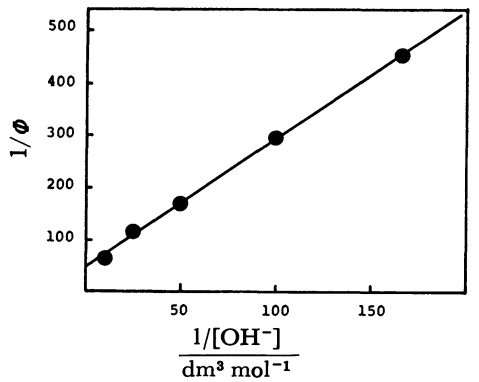

Fig. 1. Effect of the concentration of hydroxide ion on the quantum yield of the photoreduction of **1**; [**1**]: 1.00×10^{-4} mol/dm³ in 4 : 1 2-propanol–water mixture under nitrogen atmosphere; irradiation light: $\lambda=365$ nm.

Aqueous 2-Propanol. When **1** (1.00×10^{-4} mol/dm³) and sodium hydroxide (5.00×10^{-2} mol/dm³) in 4 : 1 2-propanol–water mixture was irradiated with monochromatic light of $\lambda=365$ nm under nitrogen atmosphere, the absorption bands at $\lambda=402$, 476, and >650 nm, assigned to the radical anion of **1**, increased. Isosbestic points were observed at $\lambda=377$, 498, and 570 nm. Introduction of air to the irradiated reaction mixture caused rapid disappearance of the radical anion of **1**, and **1** was recovered unchanged. A similar effective photoreduction was also observed in aqueous acetonitrile which is considered to have little reactivity toward a conventional hydrogen atom abstraction (Φ(in 4 : 1 acetonitrile–water)/Φ(in 4 : 1 2-propanol–water)=0.56 when [NaOH]=5×10^{-2} mol/dm³). As shown in Fig. 1, the reciprocal of the quantum yield for the production of the radical anion of **1** was found to be linear with the reciprocal of the total amount of hydroxide ion added to the reaction system. These results suggest that the radical anion of **1** is produced not by a conventional hydrogen abstraction by the excited **1** from the solvent followed by a deprotonation (Eqs. 2 and 3), but by a direct electron transfer from the hydroxide ion (Eq. 1).

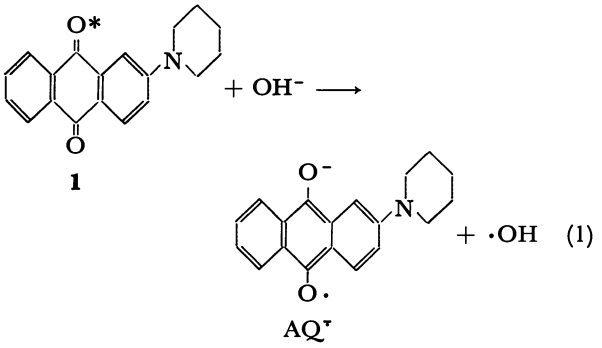

$$AQ^* + H\text{-}\underset{|}{\overset{|}{C}}\text{-} \longrightarrow AQH\cdot + \cdot\underset{|}{\overset{|}{C}}\text{-} \quad (2)$$

$$AQH\cdot + OH^- \longrightarrow AQ^- + H_2O \quad (3)$$

The radical anion of **1** was stable in the reaction system for more than 1d. Hence it was supposed that most of the hydroxyl radical, a powerful oxidizing agent, produced in the reaction system along with the radical anion of **1** (Eq. 1) would abstract a hydrogen atom from 2-propanol to produce water and acetone (Eq. 4). In the irradiated reaction mixture acetone was really detected by GLC analysis (column/PEG-20M; 40 °C).

$$OH\cdot + (CH_3)_2CHOH \longrightarrow H_2O + (CH_3)_2\dot{C}OH \quad (4)$$

$$(CH_3)_2\dot{C}OH + AQ \longrightarrow (CH_3)_2C{=}O + AQH\cdot \quad (5)$$

The radical anion of **1** is also produced by a deprotonation of the semiquinone radical (AQH·) generated in Eq. 5. If the photoreduction of **1** by hydroxide ion proceeds *via* the ^{1}CT level as proposed by Davies *et al.*,[4] **1** should be photoreduced on irradiation with light of $\lambda>420$ nm which excites **1** exclusively to its ^{1}CT level. The fluorescence of **1** should be quenched by the addition of hydroxide ion to an extent predicted from the linear plot of Fig. 1. However, as shown in Table 1, the radical anion of **1** was only very weakly produced on irradiation with light of $\lambda>420$ nm, and the fluorescence intensity of **1** was not affected by the presence of hydroxide ion to an extent predicted from the linear plot of Fig. 1. However, as shown in Table 1, the radical anion of **1** was only very weakly produced on irradiation with light of $\lambda>420$ nm, and the fluorescence intensity of **1** was not affected by the presence of hy-

Table 1. Effect of the wavelength of irradiating light on the photoreduction of **1**

Wavelength of irradiation/nm	Relative quantum yield
313	1.0
365	1.0
>420	0.003

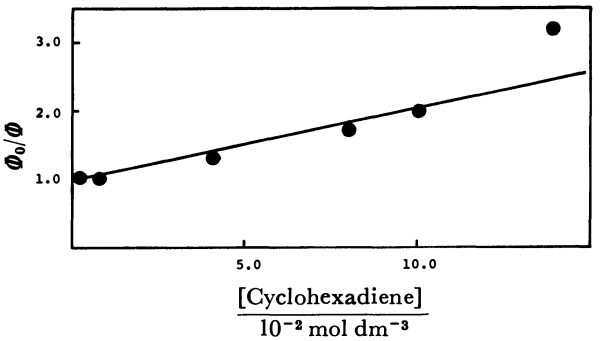

Fig. 2. Stern-Volmer plot for the quenching effect of 1,3-cyclohexadiene on the photoreduction of **1**; [**1**]: 1.00×10^{-4} mol/dm³ in 4 : 1 2-propanol–water mixture under nitrogen atmosphere; [OH⁻]: 0.1 mol/dm³; irradiation light: $\lambda=365$ nm.

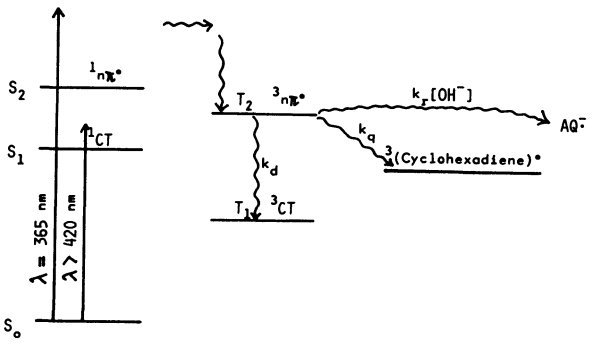

Fig. 3. Energy state diagram of **1** and the reaction scheme of the photoreduction by hydroxide ion.

droxide ion (1×10^{-3}—1×10^{-1} mol/dm^3). These results clearly indicate that the photoreduction of **1** does not proceed *via* the ^{1}CT level, but *via* the upper excited level. Moreover, the photoreduction was retarded by the addition of 1,3-cyclohexadiene as a triplet quencher[22] and a linear Stern-Volmer plot was obtained with the Stern-Volmer constant, $k_q\cdot\tau=20$ dm^3/mol (Fig. 2). Since the triplet level of 1,3-cyclohexadiene ($E_T=217$ kJ/mol) is higher than the $T_1(^3CT)$ of **1** and lower than the $T_2(^3n\pi^*)$,[7] 1,3-cyclohexadiene can be considered to quench the $T_2(^3n\pi^*)$ level of **1**. It is concluded that the photoreduction of **1** by an electron transfer from hydroxide ion proceeds *via* the $T_2(^3n\pi^*)$ level of **1**. These conclusions are schematized in Fig. 3. The quantum yield (Φ) for the production of the radical anion of **1** can be written as

$$\Phi = 2\Phi_T\,(365\text{ nm})\frac{k_r[OH^-]}{k_d+k_r[OH^-]}, \qquad (6)$$

and the Stren-Volmer equation is

$$\Phi_0/\Phi = 1 + \frac{k_q[CHD]}{k_d+k_r[OH^-]}, \qquad (7)$$

where $\Phi_T(365\text{ nm})$ denotes the triplet yield upon the irradiation of the light of $\lambda=365$ nm, k_i [i=r, d, and q] represents each rate constant in Fig. 3, and CHD refers to 1,3-cyclohexadiene. Equation 6 and the ratio of the slope to the intercept in the plot of Equation 1 indicate $k_d/k_r=5.0\times10^{-2}$ mol/dm^3. Equation 7 indicates that the Stern-Volmer cons tant in the plot of Fig. 2 is $k_q/(k_d+k_r[OH^-])=20$ dm^3/mol ($[OH^-]=0.1$ mol/dm^3). Supposing that the quenching rate constant k_q by 1,3-cyclohexadiene is diffusion controlled (10^{10} dm^3 mol^{-1} s^{-1}), the rate constants of $k_r=3.3\times10^9$ dm^3 mol^{-1} s^{-1} and $k_d=1.7\times10^8$ s^{-1} are obtained.[23] From the intercept in the linear plot of Fig. 1, $\Phi_T(365\text{ nm})$ is found to be 1.0×10^{-2}.

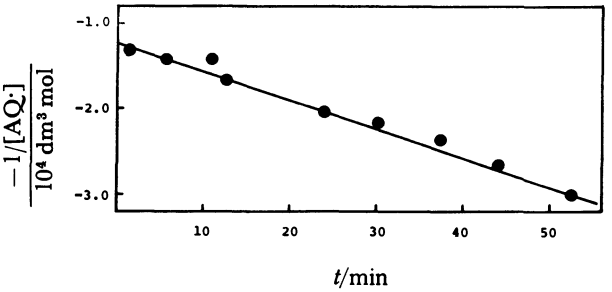

Fig. 4. Decay of the radical anion ($AQ^{\cdot}$) of **2** generated in the photoreduction by hydroxide ion; [**2**]: 1.00×10^{-4} mol/dm^3 in 4 : 1 2-propanol–water mixture under nitrogen atmosphere; [OH^-]: 5.0×10^{-2} mol/dm^3; irradiation light: $\lambda>300$ nm.

Photoreduction of other Anthraquinones in Alkaline Aqueous Alcohol. Such ready photoreduction of **1** by hydroxide ion *via* the upper excited $T_2(^3n\pi^*)$ level prompted our investigation of other anthraquinones such as **2**, **3**, **4**, **5**, and **6**. The results are summarized in Table 2. **2** (1.00×10^{-4} mol/dm^3) and sodium hydroxide (5.00×10^{-2} mol/dm^3) in 4 : 1 2-propanol–water mixture was irradiated with the light of $\lambda>300$ nm under nitrogen atmosphere. The corresponding radical anion of **2** ($\lambda_{max}=389$, 482 nm) was also readily produced with the irradiation, having isosbestic points

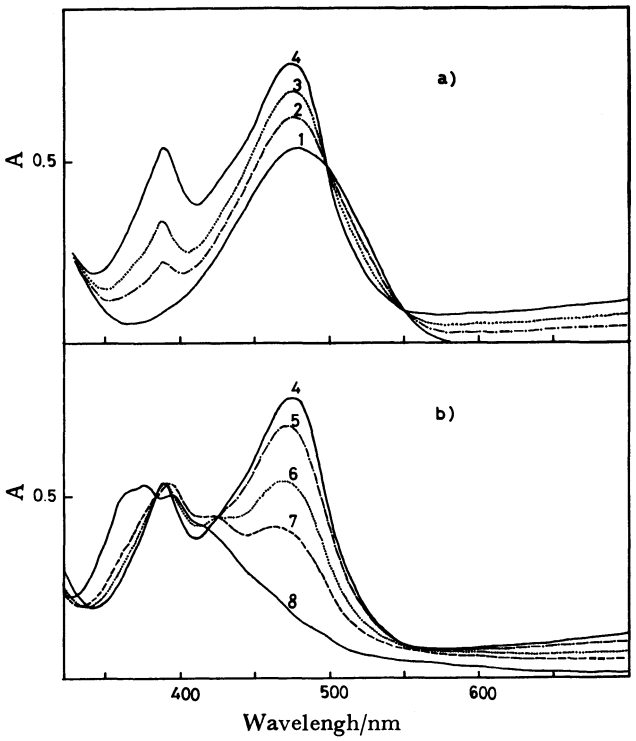

Fig. 5. Visible absorption spectra of the photoreduction of **2** by hydroxide ion in 1 : 1 methanol–water mixture under nitrogen atmosphere; [**2**]: 1.00×10^{-4} mol/dm^3; [OH^-]: 8.71×10^{-2} mol/dm^3; a) irradiation light: $\lambda>300$ nm; **1** (——): 0 min; **2** (·····): 70 min; **3** (·····): 210 min; **4** (——): 400 min; b) irradiation light: 280 nm$<\lambda<$400 nm; **5** (·····): 8 min after **4**; **6** (·····): 35 min after **4**; **7** (------): 60 min after **4**; **8** (——): 21 min irradiation without a glass filter after **7**.

Table 2. Photoreduction of aminoanthraquinones *via* the upper excited $n\pi^*$ triplet states

Anthraquiones	2-Piperidino (**1**)[a]	1-NH_2 (**2**)[b]	2-NH_2 (**3**)[b]	1-Piperidino (**4**)[a]	2-SO_3Na (**5**)[b]	1-SO_3Na (**6**)[b]
λ_{max}/nm	477,352	479,309	448,298	522,322	329	328
Φ365 nm/Φ313 nm	1.0	0.0	—	0.0	1.0	0.91
$\Phi>$420 nm/Φ313 nm	0.0	0.0	—	0.0	—	—
Φ_T(313 nm)/%	1.0	0.5	—	—	100	9.4
Φ_T(365 nm)/%	1.0	0.0	—	0.0	100	8.5
$[k_d/k_r]$/mol dm^{-3}	5.0×10^{-2}	1.5×10^{-2}	—	—	—	7.6×10^{-2}
Product	$AQ^{\cdot}$	$AQ^{\cdot}$	—	AQ^{2-}	$AQ^{\cdot}$	$AQ^{\cdot}$
Type of reaction	E.T,[c]	E.T.	—	H.A.[d], E.T.	H.A., E.T.	E.T.

a) In 4 : 1 2-propanol–water. b) In 1 : 1 methanol–water. c) E.T.: Electron transfer. d) H.A.: Hydrogen abstraction.

at λ=320, 510, 551 nm. Introduction of air to the irradiated reaction mixture also caused rapid disappearance of the radical anion of **2** and **2** was recovered unchanged. However the radical anion of **2** was unstable in 2-propanol–water and gradually disappeared with a second order decay constant of k=2.8 dm^3 mol^{-1} s^{-1} as shown in Fig. 4. This may be due to the following second order decay process of dismutation (Eq. 8). Of

$$AQ^{\cdot} + AQ^{\cdot} \xrightarrow{k} AQ^{2-} + AQ \quad (8)$$

the solvent compositions examined (aqueous solutions of methanol, ethanol, and 2-propanol), 1 : 1 methanol–water mixture was found to stabilize the radical anion for several hours. The visible absorption spectra of the reaction system in 1 : 1 methanol–water mixture are shown in Fig. 5. The corresponding radical anion of **2** alone was produced during the first 400 minutes of irradiation through a soda glass filter which only transmitted radiation of λ>300 nm (Fig. 5(a)). On prolonged irradiation the absorption intensities at λ=389 nm, 475 nm, and >650 nm gradually decreased and then, upon the irradiation through UVD-33S glass filter which transmitted radiation of 280 nm<λ<400 nm, the radical anion disappeared rapidly with the production of the dianion of **2** (λ_{max}=395 nm) having new isosbestic points at λ=388, 392, and 425 nm (Fig. 5(b)). Further irradiation of the reaction system by a 500 W high pressure mercury lamp without a glass filter also caused a disappearance of the dianion with an increment of the absorption intensity near 370 nm which might be characterized by the production of aminoanthrone derivative[8] (line(8) in Fig. 5(b)). As summarized in Eq. 9, the photochemical reduction of **2** proceeded *via* three steps. At an early stage of the photoreaction the radical anion of **2** is produced from **2** (Process I; Fig. 5(a)) and after the complete conversion of **2** into the radical anion, the dianion of **2** is produced from the radical anion (Process II; Fig. 5(b)). Finally, an end product which may be aminoanthrone is produced from the dianion of **2** (Process III). The

$$AQ \xrightarrow{h\nu} AQ^{\cdot} \xrightarrow{h\nu} AQ^{2-} \xrightarrow{h\nu} \text{aminoanthrone} \quad (9)$$

spectra in Fig. 5(a) indicate that the absorption coefficients of the radical anion of **2** at the λ_{max} of 389 and 475 nm in 1 : 1 methanol–water mixture are 53200 and 76000 dm^2/mol respectively. As is shown in Fig. 6, a plot of the reciprocal of the quantum yield of the photoreduction of process I versus the reciprocal of the concentration of hydroxide ion added to the reaction system gave a fairly straight line. The ratio of the slope to the intercept in the plot was found to be 1.5×10^{-2} mol/dm^3. Hence the radical anion of **2** is also supposed to be produced by a direct electron transfer from hydroxide ion to the excited **2** in a manner similar to the case of **1**. As mentioned above, irradiation with light of 313 nm was effective for the photoreduction of **2**. On the other hand, neither visible light irradiation (>420 nm), which excited **2** to ^{1}CT level, nor irradiation with light of 365 nm which excited **2** to $^1n\pi^*$ level induced photoreduction of **2**. Moreover the fluorescence intensity of **2** was hardly affected by hydroxide ion; the Stern-Volmer constant of the fluorescence quenching by hydroxide ion was smaller than 4 dm^3/mol. These results clearly indicate that the photoreduction of **2** by an electron transfer from hydroxide ion proceeds through the upper excited state which can be populated by 313 nm excitation. Though the quenching experiments by appropriate triplet quenchers could not be carried out because of their insolubilities in 1 : 1 methanol–water mixture, by analogy with the case of **1**, it is well supposed that the upper excited triplet $n\pi^*$ (T_2) level of **2** is responsible for the photoreduction. The value of the intercept in the plot of Fig. 6 indicates the triplet yield upon irradiation of the light of 313 nm, Φ_T(313 nm), to be 0.5×10^{-2}. A mixture of **3** (1.0×10^{-4} mol/dm^3) and sodium hydroxide (5.0×10^{-2} mol/dm^3) in 1 : 1 methanol–water mixture was irradiated with light of λ=313 nm, 365 nm and λ>420 nm under nitrogen atmosphere, respectively. Contrary to our expectation, in every case **3** did not react at all, even with prolonged irradiation at 313 nm. This unexpected result seems very interesting and will be discussed later.

The photoreduction of **4** (1.0×10^{-4} mol/dm^3) in 4 : 1 2-propanol–water mixture in the presence of hydroxide ion (5.0×10^{-2} mol/dm^3) gave its dianion (λ_{max}=408 and 493 nm) alone. Both quantum yields in the presence and the absence of hydroxide ion were almost the same to each other; in the latter case 1-piperidino-9,10-anthracenediol was produced. These results were in accord with those reported by Davies *et al.*[4] Since the production of 1-piperidino-9,10-anthracenediol from **4** at neutral conditions is believed to be due to hydrogen abstraction from 2-propanol, the dianion formation at alkaline conditions is also considered to be caused by hydrogen abstraction by the excited **4** in its triplet $n\pi^*$ state, followed by a deprotonation (Eqs. 2 and 3) in contrast to the reactions of **1** and **2**. The dianion of **4**, however, was produced effectively even in alkaline aqueous acetonitrile solution. This indicates that the electron transfer mechanism from hydroxide ion was also operating in the photoreduction of **4** along with the hydrogen abstraction mechanism. The dependency of the photoreduction of **4** on the wavelength of irradiation was similar to that of **2**: The reaction was only induced with irradiation of light of λ=313 nm and **4** did not react at all upon irradiation of the light of λ=365 nm

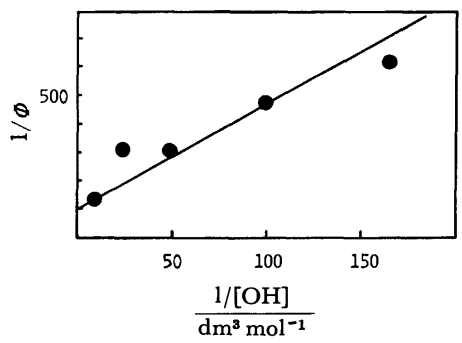

Fig. 6. Effect of the concentration of hydroxide ion on the quantum yield of the photoreduction of **2**; [**2**]: 1.00×10^{-4} mol/dm^3 in 1: 1 methanol–water mixture under nitrogen atmosphere; irradiation light: λ=313 nm.

and $\lambda>420$ nm, respectively. Hence the upper excited triplet $n\pi^*$ state (T_2), which can be populated by 313 nm excitation is probably responsible for the photoreduction of **4**. Compound **5** is a good sensitizer for the photosensitized oxidation and its photochemistry has been most intensively studied.[2] The triplet ($^3n\pi^*$) yield of **5** is known to be unity and the quantum yield for the formation of 9,10-dihydroxy-2-anthracenesulfonate from **5** by a hydrogen abstraction is also unity at neutral condition.[9] In alkaline solution or in the presence of an appropriate electron donor, photoreduction by an electron transfer mechanism is also significant.[10] Irradiation of **5** (1.0×10^{-4} mol/dm^3) in the presence of sodium hydroxide (5.0×10^{-2} mol/dm^3) in 1 : 1 methanol–water mixture with the light of $\lambda>300$ nm induced an effective formation of the radical anion of **5** ($\lambda_{max}=400$ and 502 nm) as a sole end product. The quantum yield for the formation of the radical anion of **5** was not affected by the concentration of hydroxide ion ($0.1—6\times10^{-3}$ mol/dm^3) and by the wavelength of irradiation ($\lambda=313$ and 365 nm). Compound **6** has been classified as a poor sensitizer.[11] When **6** (1.0×10^{-4} mol/dm^3) and sodium hydroxide (5.0×10^{-2} mol/dm^3) in 1 : 1 methanol–water mixture was irradiated with light of $\lambda>300$ nm, the radical anion of **6** ($\lambda_{max}=400$ and 497 nm) was produced at an early stage of the reaction. The radical anion produced was stable in the dark for several hours in 1 : 1 methanol–water. On prolonged irradiation, the dianion of **6** was further produced from the radical anion after the complete conversion of **6** into the radical anion. The spectral changes were similar to those of the reaction of **2**. The absorption coefficient of the radical anion of **6** at 497 nm in 1 : 1 methanol–water was estimated to be 45100 dm^2/mol. Studzinskii *et al.* reported that the quantum yield for the production of the radical anion was independent of the wavelength of irradiation in alkaline aqueous alcohols.[12] However, careful investigation revealed a slight wavelength dependency; Φ365 nm/Φ313 nm$=0.91\pm0.05$. A plot of the reciprocal of the quantum yield versus the reciprocal of the concentration of hydroxide ion added to the reaction system gave a fairly straight line with a value of 7.6×10^{-2} mol/dm^3 for the ratio of the slope to the intercept. This suggests that the radical anion formation in alkaline aqueous methanol is mainly induced by an electron transfer from hydroxide ion. The values of the intercept in the plot also indicate the triplet ($^3n\pi^*$) yield upon irradiation with light of 313 and 365 nm, Φ_T(313 nm) and Φ_T(365 nm) to be 9.4×10^{-2} and 8.5×10^{-2}, respectively. It is easily understood that the low reactivity of **6** (classified as a poor sensitizer) is mainly ascribable to such a low intersystem-crossing efficiency of $^1n\pi^*$ states.

Discussion

The energy state diagram of anthraquinone derivatives (**1**—**4**), having an electron-donating group, is depicted in Fig. 7.[2,13] The first absorption band in the visible region for each derivative corresponds to the lowest excited singlet state (S_1 : ^{1}CT) and the absorption band near $\lambda=300$ nm to the $\pi\pi^*$ singlet state overlying

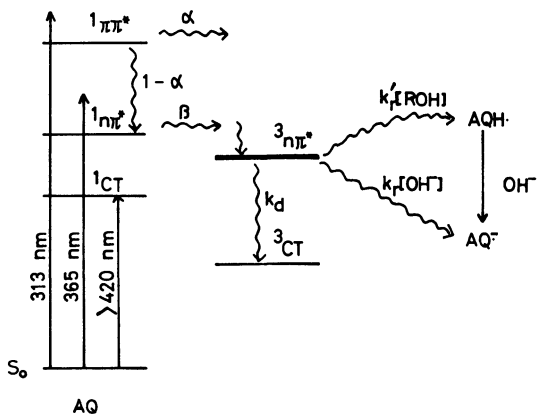

Fig. 7. Energy state diagram of the anthraquinone derivatives having electron donating substituents.

the $n\pi^*$ state. On the other hand the energy state diagram of **5** and **6** have no intramolecular CT level.[2,13] In the case of anthraquinone the $n\pi^*$ (^{1}U) and the higher $\pi\pi^*$ (^1L_b) levels have the energy of 24000 and 30000 cm^{-1}, respectively.[14] Taking account of both mechanisms of electron transfer from hydroxide ion and hydrogen abstraction from the solvent *via* the $n\pi^*$ level, the quantum yield of the photoreduction is given by Eq. 10.

$$\Phi \propto \Phi_T\left(\frac{k_r[OH^-]+k_r'[ROH]}{k_d+k_r[OH^-]+k_r'[ROH]}\right), \qquad (10)$$

where Φ_T denotes the $n\pi^*$ triplet yield upon the irradiation of the light of appropriate wavelength, k_d the rate constant of the deactivation of the $^3n\pi^*$, k_r the rate constant of electron transfer, and k_r' the rate constant of hydrogen abstraction. From Fig. 7 the triplet yields upon the irradiation of the light of $\lambda=313$ nm are expressed by Eqs. 11 and 12, respectively,

$$\Phi_T(313\text{ nm}) = \alpha + (1-\alpha)\beta, \qquad (11)$$

$$\Phi_T(365\text{ nm}) = \beta, \qquad (12)$$

where α and β denote the apparent individual intersystem crossing efficiencies of the higher $^1\pi\pi^*$ and $^1n\pi^*$ states respectively. By solving equations 11 and 12 the values of α and β can be estimated from the triplet yields summarized in Table 2. The values of α and β for **2** are 5×10^{-3} and zero, while those for **6** are 9.8×10^{-3} and 8.5×10^{-2}. High efficiency of the intersystem crossing of $^1n\pi^* \rightsquigarrow {}^3n\pi^*$ of **5** ($\beta=1.0$) renders it impossible to estimate the value of the intersystem crossing, α, from the higher level. The absence of the wavelength dependency between 313 and 365 nm in the case of **1** with low Φ_T value ($\Phi_T=1.0\%$) apparently indicates the absence of the intersystem crossing from the higher $^1\pi\pi^*$ state. However, as indicated in Table 2, the second absorption band ($\lambda_{max}=352$ nm) of **1** is largely red-shifted as compared with other derivatives. Hence the respective irradiation of the light of 313 and 365 nm may excite **1** to the same level of the higher $^1\pi\pi^*$ overlying the $^1n\pi^*$. More precise investigation on the wavelength dependency of the photoreduction of **1** may be required. The value of k_d of **1** indicates the lifetime of the $T_2(^3n\pi^*)$ state to be 5.9×10^{-9} s in 4 : 1 2-propanol–water mixture. The lifetime of the $T_2(^3n\pi^*)$

of **2** in 1 : 1 methanol–water is also estimated to be longer than 6.7×10^{-9} s from the value of $k_d/k_r = 1.5\times10^{-2}$ mol/dm^3, supposing k_r to be diffusion controlled (10^{10} dm^3/mol s) as a maximum limit. These values are longer as compared with those of T_2 of anthracenes (2—5×10^{-10} s),[15] naphthalene (1.7×10^{-11} s).[16] In the study of the photoreduction of 1-dimethylaminoanthraquinone by hydrogen abstraction, Davies *et al.* pointed out that anthraquinone derivatives might have a lifetime long enough to photoreact in their upper excited $T_2(^3n\pi^*)$ level.[17] 1-Amino-2,4-dibromoanthraquinone is also known to have a long-lived $T_2(^3n\pi^*)$ state in benzene.[18] These long lifetimes of $T_2(^3n\pi^*)$ in spite of upper excited levels are considered to be characteristic of aminoanthraquinones. The rate of internal conversion from T_2 with 0 vibrational level to T_1 with n isoenergetic vibrational levels, $k_{ic}(T_2\rightarrow T_1)$, which nearly equals the rate of deactivation, k_d, is theoretically given by Eq. 13.[19]

$$k_{ic}(T_2\rightarrow T_1) \propto \langle\psi_{T_2}|J|\psi_{T_1}\rangle^2\cdot|\textstyle\sum_n\langle\chi_{T_2 0}|\chi_{T_1 n}\rangle|^2, \qquad (13)$$

where ψ_{T2} and ψ_{T1} are the electronic wave functions of T_2 and T_1, J is the nuclear kinetic energy operator, and $\chi_{T_2 0}$ and $\chi_{T_1 n}$ are the nuclear wave functions of the corresponding states. The orthogonality between the $T_2(^3n\pi^*)$ and $T_1(^3CT)$ states can cause a poor electronic term in Eq. 13. The second term of Eq. 13 is the well known Franck-Condon factor and is largely affected by the energy gap between the two states.[20] Since the $T_2(^3n\pi^*)$ levels of aminoanthraquinones have been considered to have similar energies to that of the $^3n\pi^*$ of anthraquinone (259 kJ/mol)[2] and the $T_1(^3CT)$ levels were reported to lie in the range of 236—201 kJ/mol (**3**), 197—176 kJ/mol (**1** and **2**), and $<$123 kJ/mol (**4**),[7] the energy gaps between the T_2 and T_1 of these aminoanthraquinones are estimated to have larger values than 62 kJ/mol (**1** and **2**) and 136 kJ/mol (**4**), while that of **3** is in the range of 23—58 kJ/mol. These rather large energy gaps (except that of **3**) may also cause a poor Franck-Condon factor resulting in the long life of the $T_2(^3n\pi^*)$ levels. The lifetime of the $T_2(^3n\pi^*)$ of each derivative may be in the order of **4**$>$**1**$\approx$**2**$>$**3** in accord with the order of the energy gap. The lifetime of the $T_2(^3n\pi^*)$ of **3** may be too short for any reactions to be observed. While the $T_2(^3n\pi^*)$ of **1** and **2** may have moderate lifetimes to permit only rapid process of electron transfer to compete, the $T_2(^3n\pi^*)$ of **4** may have sufficient long one even for rather slow reaction of hydrogen abstraction[21] to proceed.

References

1) R. A. Morton and W. T. Earlman, *J. Chem. Soc.*, **1941**, 159; Z. Yoshida and F. Takabayashi, *Tetrahedron*, **24**, 933 (1968); H. Inoue, T. Hoshi, J. Yoshino, and Y. Tanizaki, *Bull. Chem. Soc. Jpn.*, **45**, 1018 (1972); **46**, 380 (1973).

2) H. Inoue and M. Hida, *Yuki Gosei Kagaku Kyokai Shi*, **32**, 348 (1974) and references cited therein. D. Schulte-Frohlinde and C. V. Sontag, *Z. Phys. Chem.*, **44**, 314 (1965), J. M. Bruce, *Quart. Rev.*, **21**, 405 (1967).

3) H. Inoue, T. D. Tuong, M. Hida, and T. Murata, *Chem. Commun.*, **1971**, 1347; H. Inoue, T. D. Tuong, M. Hida, and T. Murata, *Bull. Chem. Soc. Jpn.*, **46**, 1759 (1973); H. Inoue, K. Nakamura, S. Kato, and M. Hida, *ibid.*, **48**, 2872 (1975); H. Inoue and M. Hida, *ibid.*, **51**, 1793 (1978); H. Inoue, T. Shinoda, and M. Hida, *ibid.*, **53**, 154 (1980).

4) G. O. Phillips, A. K. Davies, and J. F. Mckeller, *Chem. Commun.*, **1970**, 519; A. K. Davies, J. F. Mckeller, and G. O. Phillips, *Proc. R. Soc. London, Ser. A*, **323**, 69 (1971).

5) Maki, *J. Soc. Chem. Ind. Jpn.*, **36**, 44 (1933).

6) C. G. Hatchard and C. A. Parker, *Proc. R. Soc. London*, **1956**, 518.

7) B. E. Hulme, E. J. Land, and G. O. Phillips, *J. Chem. Soc., Farady Trans. 1*, **68**, 2003 (1972).

8) G. S. Egerton, N. E. N. Assaad, and N. D. Uffindell, *J. Soc. Dyers and Colourists*, **1967**, 409.

9) C. F. Wells, *Trans. Farady Soc.*, **57**, 1703, 1719 (1961); H. R. Cooper and B. M. Talbot, *ibid.*, **61**, 506 (1965); G. O. Phillips, P. Barber, and T. Richards, *J. Chem. Soc.*, **1964**, 3443; C. F. Wells, *ibid.*, **1962**, 3100; F. Wilkinson *J. Phys. Chem.*, **66**, 2569 (1962).

10) G. Eigenmann, *Helv. Chim. Acta*, **46**, 864 (1963); V. A. Kuzmin and A. K. Chibisov, *J. Chem. Soc., D*, **1971**, 1559; V. A. Kuzmin, A. K. Chibisov, and A. V. Karyakin, *Int. J. Chem. Kinet.* **4**, 639 (1972).

11) F. Wilkinson, *J. Phys. Chem.*, **66**, 2569 (1962), G. O. Phillips, J. C. Arthur, Jr., *Text. Res. J.*, **34**, 497, 572 (1964).

12) O. P. Studzinskii, N. I. Rtisehev, A. V. Devekki, G. V. Fomin, L. M. Gurdzhinyan, and A. V. El'stov, *Zh. Org. Khim.*, **8**, 2130 (1972).

13) H. H. Dearman and A. Chan, *J. Chem. Phys.*, **44**, 416 (1966).

14) L. W. Sidman, *J. Am. Chem. Soc.*, **78**, 4567 (1956).

15) R. S. H. Liu and J. R. Edman, *J. Am. Chem. Soc.*, **91**, 1492 (1969); R. O. Cambell and R. S. H. Liu, *ibid.*, **95**, 6560 (1973).

16) C. C. Ladwig and R. S. H. Liu, *J. Am. Chem. Soc.*, **96**, 6210 (1974), **98**, 8093 (1976).

17) A. K. Davies, R. Ford, J. F. Mckeller and G. O. Phillips, *J. Chem. Soc., Perkin Trans. 2*, **1972**, 923.

18) H. Inoue and M. Hida, *Bull. Chem. Soc. Jpn.*, **51**, 1793 (1978).

19) J. B. Birks, "Organic Molecular Photophysics," Wiley-Interscience, New York, N. Y. (1975), Vol. 1. p. 32.

20) W. Siebrand, *J. Chem. Phys.*, **47**, 2411 (1967).

21) The rate of hydrogen abstraction from alcohols by the excited antraquinone in its $^3n\pi^*$ state has been reported to be in the range of *ca.* 10^6—10^7 dm^3/mol s.[2]

22) The fluorescence of **1** in 4 : 1 2-propanol–water mixture was not quenched by 1,3-cyclohexadiene (1×10^{-3}—0.5 mol/dm^3).

23) The observed rate constant ($k_r = 3.3\times10^9$ dm^3 mol^{-1} s^{-1}) of the electron transfer from hydroxide ion to **1** coincides reasonably with the calculated value (1.2×10^9 dm^3 mol^{-1} s^{-1}) with the aid of the Rehm and Weller's equation when the oxidation and reduction potentials of hydroxide ion and **1** are taken to be 2.0 and -0.80 V *vs.* NHE, respectively. (D. Rehm and A. Weller, *Isr. J. Chem.*, **8**, 259 (1970).

Photochemical Electron Transport from Water Layer to Organic Layer *via* Sodium Anthraquinone-2-sulfonate by Stepwise Two Photon Excitation†

Haruo INOUE* and Mitsuhiko HIDA
Department of Industrial Chemistry, Faculty of Technology, Tokyo Metropolitan University, Fukazawa, Setagaya-ku, Tokyo 158

(Received July 9, 1981)

Photochemical electron transport from hydroxide ion to organic acceptor molecule *via* an anthraquinone derivative as an electron carrier was investigated in homogeneous, cationic micellar, and cationic reversed micellar systems. In homogeneous alkaline aqueous ethanol, the photochemically generated radical anion of sodium anthraquinone-2-sulfonate (**1**) was stable against further irradiation with visible light (λ>450 nm), while the dianion of **1** was reversibly converted to the radical anion by visible light irradiation. The reversible conversion was accelerated by the addition of an organic acceptor molecule such as 1,4-dicyanobenzene. In a cationic hexadecyltrimethylammonium micellar system, an effective photoreduction of **1** by an electron transfer from hydroxide ion concentrated on the micellar surface to the excited **1** located in the surface area of the micelle was observed. In a reversed micellar system an electron was effectively transported from the water layer to the organic layer; an electron was transfered from hydroxide ion in the water layer incorporated in a benzylhexadecyldimethylammonium reversed micelle to **1** at the micellar surface by irradiation with light of λ=365 nm. Successive visible light irradiation (λ>450 nm) caused an electron ejection from the radical anion of **1** to benzonitrile as a bulk phase solvent. The possibility of the incorporation of carbon dioxide into the acceptor cycle of the electron transport system was also examined. In pyridine solution, carbon dioxide caused the disappearance of the reduced species of **1** on visible light irradiation (λ>450 nm). Trace amounts of dihydropyridinedicarboxylic acid derivatives were obtained.

Recently many intensive studies have been made on photochemical electron transport systems in relation to the photochemical conversion of solar energy.[1] Considerable attention has been paid to the photochemical splitting of water into hydrogen and oxygen using semiconductors,[2] metal complexes,[3] and chlorophylls.[4] Photochemical reductions of carbon dioxide[5] and nitrogen[6] have also been examined. Various different approaches to the photochemical electron transport system including water molecules are required in order to achieve more effective conversion of solar energy.

It is of interest to investigate the photochemical redox reactions including the water molecules as an electron donor and some quinone as an electron carrier with a view to approaching artificial photosynthesis. It is well known that anthraquinones are readily photoreduced by an electron transfer from hydroxide ion to produce the corresponding radical anion ($AQ^{\cdot-}$) as a stable product.[7,8,19] Then, it may be possible to formulate an electron transport system as depicted in Fig. 1; that is, light irradiation of the anthraquinones would evoke the oxidation of hydroxide ion equilibrated with water and successively the electron would be transfered from the radical anion ($AQ^{\cdot-}$) to another molecule step by step. The successive visible light irradiation of the resultant radical anion ($AQ^{\cdot-}$) is expected to raise the reductive power of $AQ^{\cdot-}$ itself and this photoredox system may cover a wide range of redox potential by stepwise two photon excitation. On the basis of this view point, we attempted to construct an electron transport system including anthraquinones as carrier of electron in homogeneous, cationic micellar, and cationic reversed micellar systems. The photoreduction by an electron transfer through the cationic micellar surface was actually observed to take place and an effective irreversible electron transport from the water layer to the organic layer could be attained in the cationic reversed micellar system. Furthermore, the possibility of the incorporation of carbon dioxide into the acceptor cycle of the electron transport system was examined.

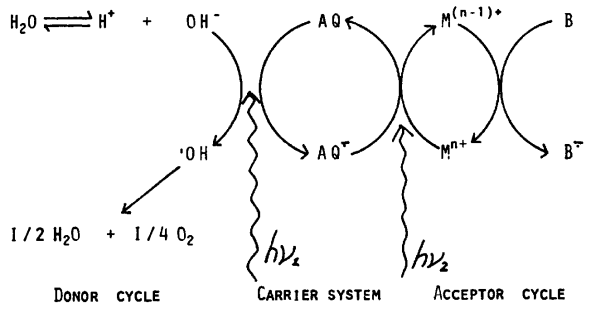

Fig. 1. Electron transport cycle including anthraquinone derivative (AQ) as a carrier and water as an electron donor by stepwise two photon excitation.

† A part of this study was presented in *Chem. Lett.*, **1979**, 107.

Experimental

Materials. Sodium anthraquinone-2-sulfonate (**1**),[19] sodium 1-aminoanthraquinone-2-sulfonate (**2**),[9] and 2-piperidinoanthraquinone (**3**)[19] were purified as reported elsewhere. Anthraquinone (**4**) (Sumitomo Chemical Co.) was passed through silica-gel column and recrystallized repeatedly from benzene; mp 285—286 °C, Found: C, 80.58%; H, 3.78%. Calcd for $C_{14}H_8O_2$: C, 80.76%; H, 3.87%. Sodium 1-amino-4-butylaminoanthraquinone-2-sulfonate (**5**) was obtained by the photoamination of sodium 1-amino-4-bromoanthraquinone-2-sulfonate with butylamine.[10] 1-Acetylaminoanthraquinone (**6**) was prepared by acetylation of 1-aminoanthraquinone with acetic anhydride and was purified by

repeated recrystallization from 1 : 1 toluene–ethanol mixture; mp 220—221 °C; Found: C, 72.42%; H, 3.95%; N, 5.27%. Calcd for $C_{16}H_{11}NO_3$: C, 72.47%; H, 4.15%; N, 5.28%. 1-Lauroylaminoanthraquinone (**7**) was prepared by the reaction between 1-aminoanthraquinone and lauroyl chloride in pyridine solution and was purified by passing through a silica, gel column and the repeated recrystallization from 2 : 5 benzene–ethanol; mp 132.5—133.5 °C; Found: C, 76.96%; H, 7.79%; N, 3.38%. Calcd for $C_{26}H_{31}NO_3$: C, 77.01%; H, 7.71%; N, 3.45%. Hexadecyltrimethylammonium bromide (CTAB) (Tokyo Kasei, EP) was recrystallized twice from water. Hexadecyltrimethylammonium hydroxide (CTAH) (10% in methanol; Tokyo Kasei) and benzylhexadecyldimethylammonium hydroxide (CDBAH) (10% in methanol; Tokyo Kasei) were used without further purification. Bis(ethylenediamine)copper(II) sulfate was prepared from copper(II) sulfate and ethylenediamine.[11] 1,4-Dicyanobenzene (Tokyo Kasei; G. R.) was used without further purification. Benzonitrile was dried with phosphorus pentoxide and fractionally distilled under a nitrogen atmosphere before use. Pyridine was refluxed with potassium hydroxide and fractionally distilled under a nitrogen atmosphere. Ion exchanged neutral water was used for the preparations of micellar solutions except where otherwise stated.

Procedures. Each sample of non-micellar and cationic micellar solution was degassed in a quartz cell by repeated freeze-thaw procedures. The reversed micellar reaction mixture was prepared by the following procedures; an appropriate amount of CDBAH methanol solution was placed in a Schlenck flask and the methanol was evaporated completely. Benzonitrile and **1** were added to the flask and the mixture was stirred vigorously. The suspension of the mixture was brought into solution by adding small amount of water (≈0.5 v/v%). The dissolved oxygen was removed by bubbling with nitrogen for at least 30 min or by the repeated freeze-thaw procedures. Monochromatic light of $\lambda=365$ nm and visible light of $\lambda>450$ nm were generated by a 500 W high pressure mercury lamp (USHIO USH-500D) through UV-DIA (Toshiba) and VY-45 (Toshiba) glass filters, respectively. The visible and UV absorption spectra of the irradiated reaction mixtures were measured by a Shimadzu UV-200 spectrophotometer. GC-Mass spectra were measured by a JMS D-100 (JEOL) mass spectrometer equipped with Thermon-100 and SE-30 columns.

Results and Discussion

Photochemical Electron Transport in Aqueous Alcohol. Sodium anthraquinone-2-sulfonate (**1**) (1.0×10^{-4} mol/dm^3) in the presence of hydroxide ion (NaOH=6.0×10^{-2} mol/dm^3) in 1 : 1 ethanol–water mixture was irradiated with monochromatic light of $\lambda=365$ nm under a nitrogen atmosphere. The visible absorption spectra of the reaction system are shown in Fig. 2. The radical anion ($AQ^{\cdot}$) of **1** alone was produced during the initial irradiation for 90s (Process I in Fig. 2). On prolonged irradiation the radical anion disappeared, along with the formation of the dianion of **1** (AQ^{2-}) (Process II in Fig. 2). The radical anion ($AQ^{\cdot}$) and dianion (AQ^{2-}) produced were stable for several hours in the dark. The spectral changes in the processes I and II had different isosbestic points. These results indicated that the dianion (AQ^{2-}) was produced by the further irradiation with light ($\lambda=365$ nm) to the radical anion ($AQ^{\cdot}$). Contrary to our expectation the radical anion

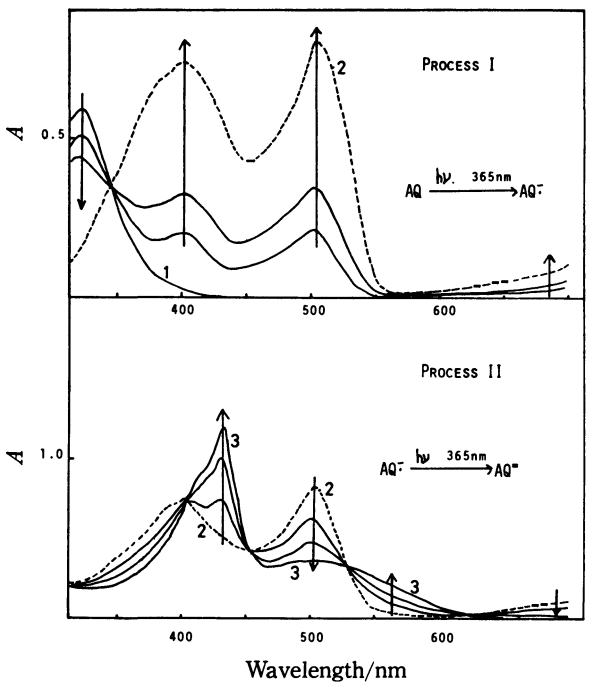

Fig. 2. Absorption spectra of the reaction system of the photoreduction of **1** under nitrogen atmosphere; [**1**]: 1.0×10^{-4} mol/dm^3 in 1 : 1 ethanol–water mixture; [OH$^-$]: 6.0×10^{-2} mol/dm^3; irradiation light: $\lambda=365$ nm; 1: 0 s; 2: 90 s; 3: 30 min.

($AQ^{\cdot}$) was stable against its selective excitation by further visible light irradiation ($\lambda>450$ nm) even in the presence of an acceptor molecule, such as 1,4-dicyanobenzene (DCB) (1×10^{-2} mol/dm^3). However, the dianion (AQ^{2-}) was reversibly reconverted to the radical anion ($AQ^{\cdot}$) on visible light irradiation ($\lambda>450$ nm) with the same isosbestic points in process II. Thus,

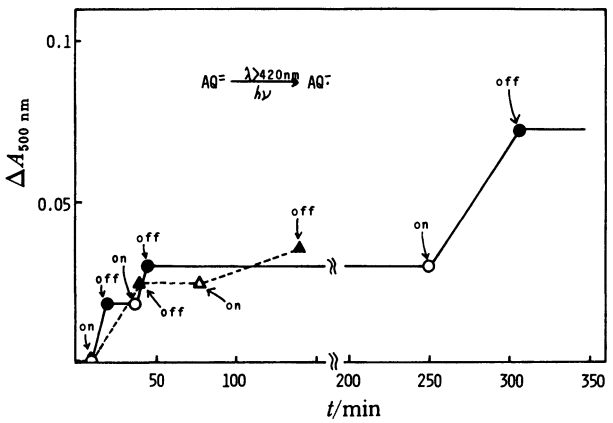

Fig. 3. Effect of the irradiation of visible light ($\lambda>420$ nm) on the reversible reconversion from the dianion (AQ^{2-}) to the radical anion ($AQ^{\cdot}$) of **1**; the amount of the reconversion was monitored at $\lambda=500$ nm; "on": light is on; "off": light is off;

	[**1**] mol/dm^3	[OH$^-$] mol/dm^3	[CN-⬡-CN] mol/dm^3
—○—●—	1.0×10^{-4}	6.0×10^{-2}	1.0×10^{-2}
---△---▲---	1.0×10^{-4}	6.0×10^{-2}	0

the photochemical ejection of an electron from the dianion (AQ^{2-}) was observed on the visible light irradiation. As indicated in Fig. 3, this reverse change from AQ^{2-} to $AQ^{\cdot}$ was accelerated by the addition of DCB as an electron acceptor; similar tendencies, though to a lesser extent, were also observed on the addition of benzonitrile, pyridine, and bromobenzene. Though it was revealed that under these conditions in 1 : 1 ethanol–water mixture the radical anion ($AQ^{\cdot}$) was mainly produced by a hydrogen abstraction from ethanol rather than an electron transfer from hydroxide ion,[12] the dianion (AQ^{2-}) was also produced from the radical anion ($AQ^{\cdot}$) in alkaline aqueous solution, indicating that hydroxide ion can also act as an electron donor in the process II. These results imply that an electron transport system including the reversible cycle $AQ^{\cdot} \rightleftharpoons AQ^{2-}$ can be constructed under appropriate conditions (Fig. 4). As a whole three photons are concerned with the electron transport.

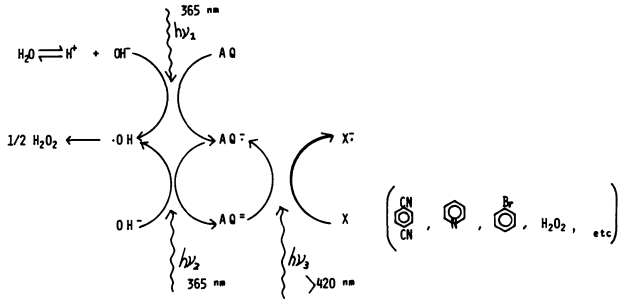

Fig. 4. Electron transport cycles including the reversible cycle of $AQ^{\cdot} \rightleftharpoons AQ^{2-}$.

Photochemical Electron Transport in Cationic Micellar System. It is most important to establish a suitable donor system in Fig. 1 for an effective electron transport. Since cationic micelles are known to concentrate hydroxide ion on their surface[13] and may be preferable for charge seperation,[14] the reactions in a cationic micelle were examined. When **1** (1.0×10^{-4} mol/dm^3) was irradiated with light of $\lambda = 365$ nm in a cationic hexadecyltrimethylammonium bromide (CTAB) (8.0×10^{-3} mol/dm^3) micelle[15] in water (pH 5.70) under a nitrogen atmosphere, effective simultaneous productions of both the radical anion ($AQ^{\cdot}$) and the dianion (AQ^{2-}) of **1** were observed on irradiation. On the other hand, the photoreaction in the same cationic micelle in phosphate buffer solution (pH 6.88) afforded the corresponding 9,10-anthracenediol (AQH_2) (Fig. 5). Since the equilibrium in Eq. 1 is well known to lie well over to the right in neutral and acidic media,[16] the difference between the reactions in water and phosphate buffer solution strongly indicated that the micro pH value around the micellar surface in phosphate buffer solution was kept neutral, while that in water was raised to that in an alkaline medium in spite of the bulk phase solvent being acidic. No hydroxylated compound

$$AQ^{2-} + 2H^+ \rightleftharpoons AQH_2 \qquad (1)$$

was observed in contrast to the reaction in aqueous solution.[17] The radical anion ($AQ^{\cdot}$) and the dianion (AQ^{2-}) of **1** in aqueous ethanol were rapidly oxidized to **1** in the instant of introducing air to the reaction system, while they are reasonably stable in the cationic micelle for *ca.* 30 min even with the vigorous stirring under an air atmosphere. A similar apparent protective effect of a micelle against the oxidation of the reduced species had also been observed in an anionic micellar system.[18] In a hexadecyltrimethylammonium hydroxide (CTAH 2×10^{-2} mol/dm^3) system in which the micellar surface is thought to be covered with hydroxide ion, the photoreduction was promoted by a factor of *ca.* 100 as compared with that in neutral aqueous solution

Table 1. Photoreduction in aqueous solution

	Surfactant	Product	Relative reactivity
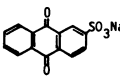	None	AQH_2	1.0
	CTAB (8×10^{-3} mol/dm)	$AQ^{\cdot}$,AQ^{2-}	5.5
	CTAH (2×10^{-2} mol/dm)	$AQ^{\cdot}$,AQ^{2-}	100
	CTAB (8×10^{-3} mol/dm^3)	AQH_2	$\ll 1.0$

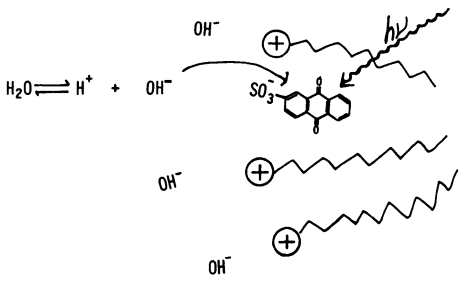

(Table 1). When anthraquinone (**4**), which was assumed to be incorporated in the micellar interior, was used in place of **1**, the photoreduction was hardly observed. CTAB formed 1 : 1 complex with **1** to precipitate quantitatively at the concentration below its cmc according to Eq. 2 (Found: C, 69.22%; H, 8.85%;

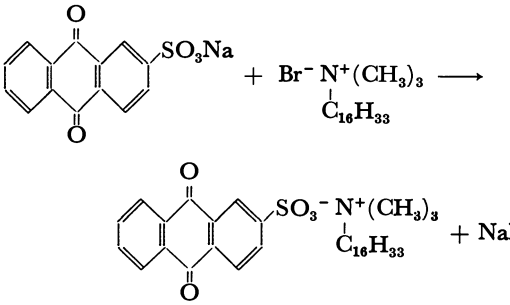

(2)

N, 2.42%. Calcd for $C_{23}H_{49}NSO_5$: C, 69.31%; H, 8.64%; N, 2.45%). These results indicated that an electron might be transfered effectively from the hydroxide ion concentrated at a micellar surface to the excited **1** located in the surface area of the cationic micelle. The production of the radical anion was not affected at all by addition of $Cu(en)_2^{+2}$ (3×10^{-4} mol/dm^3) that has lower reduction potential ($E_0 = -0.35$ V *vs.* NHE), but was completely suppressed by the addition of $CuSO_4$ (2×10^{-4} mol/dm^3) that has a higher reduction potential (E_0=through the micellar

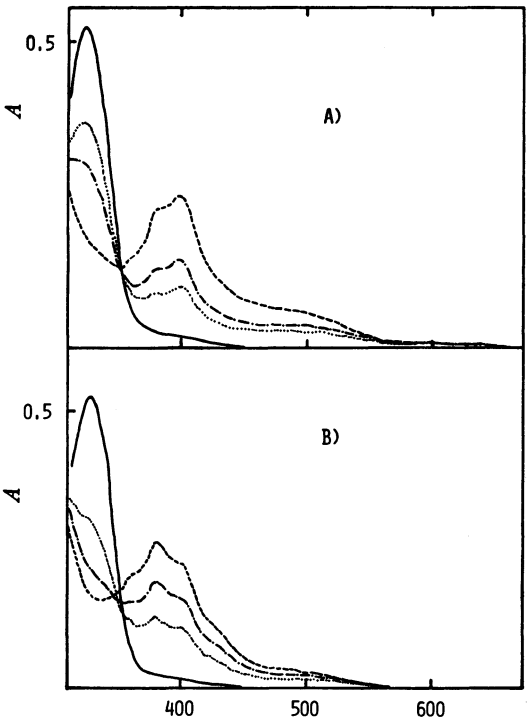

Fig. 5. Absorption spectra of the reaction system of the photoreduction of **1** in CTAB micelle; [**1**]: 1.0×10^{-4} mol/dm^3; [CTAB]: 8.0×10^{-3} mol/dm^3; irradiation light: $\lambda=365$ nm;
A) dispersed in aqueous solution (pH=5.70); irradiation time; (——): 0 min; (·····): 10 min; (-·-·-): 16 min; (------): 38 min; B) dispersed in phosphate buffer solution (pH=6.88); irradiation time; (——): 0 min; (·····): 7 min; (-·-·-): 13 min; (------): 23 min.

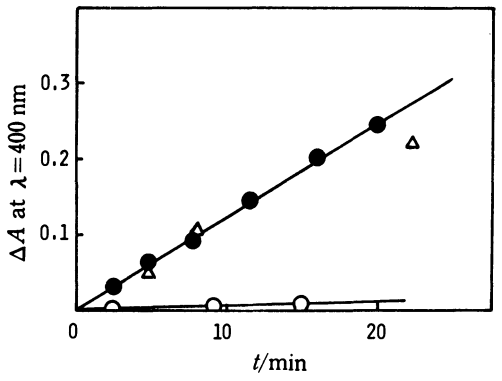

Fig. 6. Effect of cupric copper on the production of the radical anion ($AQ^{\cdot}$) of **1** in the photoreduction in CTAB micelle; irradiation light: $\lambda=365$ nm; the amount of $AQ^{\cdot}$ was monitored by the absorbance at $\lambda=400$ nm;

	[**1**] mol/dm^3	[CTAB] mol/dm^3	[$CuSO_4$] mol/dm^3	[$Cu(en)_2$]SO_4 mol/dm^3
—●—	1.0×10^{-4}	8.0×10^{-3}	0	0
—○—	1.0×10^{-4}	8.0×10^{-3}	2.0×10^{-4}	0
—△—	1.0×10^{-4}	8.0×10^{-3}	0	3.0×10^{-4}

0.159 V) (Fig. 6). This strongly suggested the presence of the electron transfer such as $OH^- \rightarrow AQ \rightarrow Cu^{2+}$ surface. When DCB (1×10^{-2} mol/dm^3) was added to the micellar system as an acceptor molecule, the photochemical ejection of an electron from the dianion (AQ^{2-}) was accelerated, indicating that an electron was irreversibly transported from hydroxide ion to an acceptor molecule *via* **1** or reduced **1** by the stepwise UV ($\lambda=365$ nm) and visible light ($\lambda>450$ nm) irradiations. Since aminoanthraquinones are known to be photoreduced by an electron transfer from hydroxide ion in their upper excited $n\pi^*$ triplet states in homogeneous solution,[19] their photoreduction in CTAB and CTAH micelles were also examined. However, sodium 1-aminoanthraquinone-2-sulfonate (**2**), 2-piperidinoanthraquinone (**3**), sodium 1-amino-4-butylaminoanthraquinone-2-sulfonate (**5**), 1-acetylaminoanthraquinone (**6**), and 1-lauloylaminoanthraquinone (**7**) were all ineffective for photoreduction. The reason for those inactivities is not clear. Small differences of their solubilization sites in the cationic micelle from that of **1** may cause the differences of the reactivities.

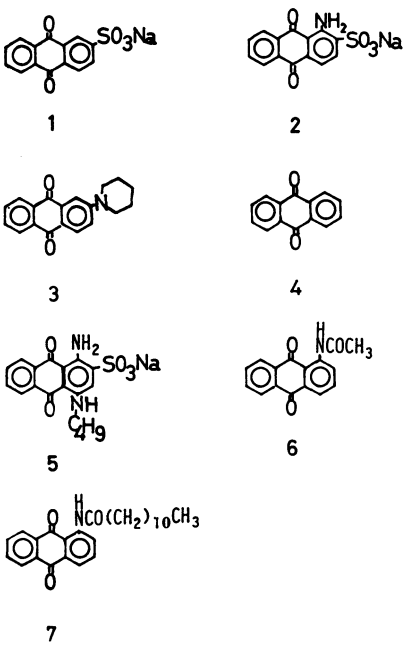

Electron Transport in Cationic Reversed Micelle. It is well known that some surfactant molecules in non-aqueous solutions form reversed micelles which can solubilize considerable quantities of water and have inverse structures from those formed in water.[20] In search of a more effective electron transport system, the reaction in a reversed micellar system was attemped, in which the bulk phase solvent itself was expected to act as an acceptor in high concentration. **1** (1×10^{-4} mol/dm^3) in the presence of benzylhexadecyldimethylammonium hydroxide (CDBAH) (1×10^{-2} mol/dm^3) and water (0.5 v/v%) in benzonitrile was irradiated by the monochromatic light of $\lambda=365$ nm. After sufficient formation of the radical anion ($AQ^{\cdot}$) was observed, the selective excitation of the radical anion by visible light ($\lambda>450$ nm) irradiation for about 3 min caused a rapid disappearance of the radical anion itself (Fig. 7). As indicated in Fig. 8, the radical anion again

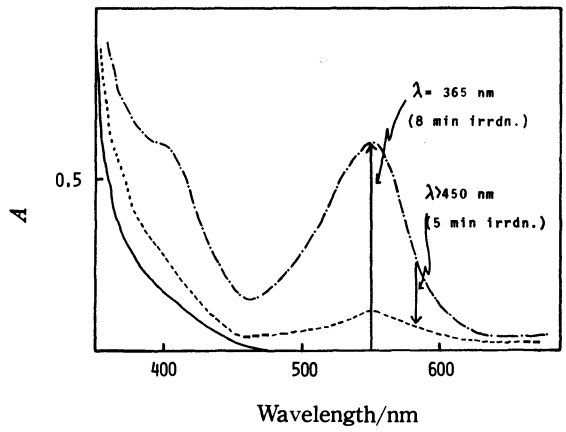

Fig. 7. Absorption spectra of the reaction system of the photoreduction of **1** in CDBAH reversed micelle dispersed in benzonitrile; [**1**]: 1.0×10^{-4} mol/dm^3; [CDBAH]: 2.5×10^{-2} mol/dm^3; [H_2O]: 0.5 v/v% in benzonitrile; (——): before irradiation; (·····): 8 min irradiation with the light of $\lambda=365$ nm; (------): 5 min irradiation with the light of $\lambda>450$ nm subsequently.

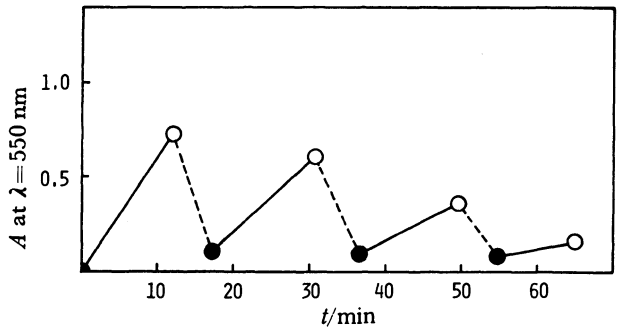

Fig. 8. Effect of the repeated irradiations of UV ($\lambda=365$ nm) and visible ($\lambda>450$ nm) light on the production of the radical anion ($AQ^{\cdot-}$) of **1** in CDBAH reversed micelle dispersed in benzonitrile; [**1**]: 1.0×10^{-4} mol/dm^3; [CDBAH]: 2.5×10^{-2} mol/dm^3; [H_2O]: 0.5 v/v % in benzonitrile; the absorbance at $\lambda=550$ nm was monitored; (●——): UV light ($\lambda=365$ nm) was irradiated; (○——): visible light ($\lambda>450$ nm) was irradiated.

appeared on 365 nm irradiation and disappeared on visible light ($\lambda>450$ nm) irradiation repeatedly. A small amount of hydrogen peroxide (5.4×10^{-5} mol/dm^3) was really detected in the reaction system after the photoreaction, suggesting that the greater part of the hydroxyl radical produced in the reaction system might abstract a hydrogen atom from the surfactant molecule. Moreover, a GC-Mass measurement (column; SE-30, 180 °C) of the irradiated reaction mixture indicated the presence of a trace amount of dihydrodimer (*m/e*; 208, 121, 103) and trimer (*m/e*; 309, 103) of benzonitrile which might be produced from the radical anion of benzonitrile as observed in electrochemical reduction.[21,22] These results strongly suggested that an effective irreversible electron transport was attained from the water layer incorporated in the reversed micelle to the organic layer benzonitrile as solvent and that **1** acted as an electron carrier at the micellar

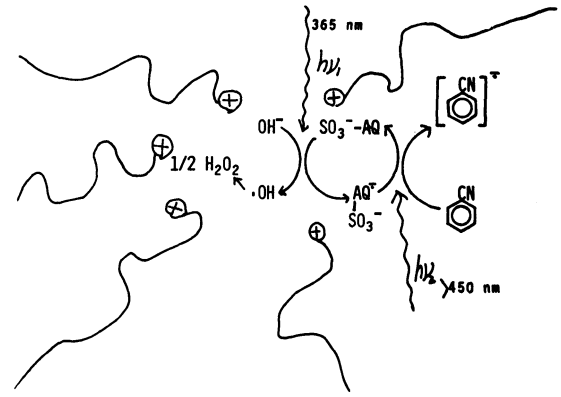

Fig. 9. Electron transport in reversed micellar system.

interface by the stepwise two photon excitation. These conclusions are illustrated in Fig. 9. However, the electron transfer cycle lost its ability to transfer an electron in the repeated cycles as observed in Fig. 8, though repeated short time irradiations seemed to improve the apparent number of transfer cycles. Side reactions such as photohydroxylation[17] and photodesulfonation[23] of **1** may cause this fatigue-like phenomenon. However, the fact that no hydroxylated compound was detected in the reaction system, and **4** as a possible product in the case of desulfonation *via* the radical anion ($AQ^{\cdot-}$) of **1**, also acted as a carrier, ruled out the above possibilities. The main reason may be that the hydroxide ion in the water layer incorporated in a reversed mecelle is consumed during the photoreduction and the resultant acidification renders the system inactive. Hence we attempted the reaction in a two phase system, in which benzonitrile solution of **1** and CDBAH was placed over the water layer including potassium hydroxide. In this two phase system, it is expected that the water core of the reversed micelle in the benzonitrile organic layer is always washed with fresh alkaline aqueous solution by vigorous stirring and the system is refreshed. In accordance with the expectation, the apparent number of transfer cycles was greatly improved to more than twenty in the two phase system. Though more detailed studies are required, it will be useful to carry out the reaction in such a two phase system.

The Possibility of the Incorporation of Carbon Dioxide into the Electron Transport. Next we examined the possibility that carbon dioxide might be incorporated into the electron transfer cycle. In order to obtain a high concentration and activation of carbon dioxide, pyridine was used as solvent. **1** and CTAB or CTAH (2.0×10^{-2} mol/dm^3) with a small amount of water (0.5 v/v%) in pyridine were irradiated by light of $\lambda=365$ nm. The radical anion and dianion of **1** were produced on irradiation. Then, visible light of $\lambda>450$ nm was irradiated successively. When the pyridine solution had been saturated with carbon dioxide, the reduced species decreased with visible light irradiation. On the other hand, under a nitrogen atmosphere without carbon dioxide, no such tendency for the disappearance of the reduced species of **1** was observed. After the photoreaction under carbon dioxide, potassium hydroxide was added to the reaction mixture and the solvent was evaporated. The residual mixture was then

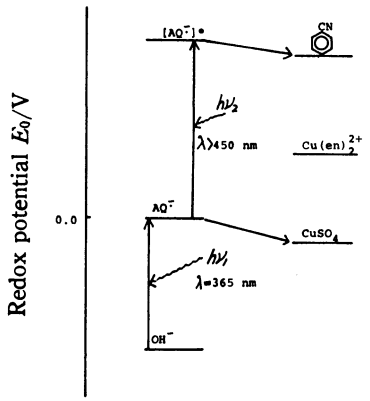

Fig. 10. Flow of electron in the electron transport system including **1** as a carrier by stepwise UV and visible light irradiations.

acidified with sulfuric acid and esterified with 1-butanol. GC-Mass spectra (column; Thermon 100, 150 °C) of the hexane solution extracted from the esterified reaction mixture indicated the presence of trace amounts of products (*m/e*; 281, 207, 57) which might be assigned to isomers of a dibutyl ester of dihydropyridinedicarboxylic acid. Since carbon dioxide did not affect the initial productions of the reduced species of **1**, carbon dioxide participated in the process after the photoreduction, that is, carbon dioxide could be incorporated in the acceptor cycle of the electron transport system to produce the addition products with pyridine.

In an attempt to establish an artificial photosynthesis which produces carbohydrate from water and carbon dioxide under illumination with sunlight, it is required to prepare a redox system which can cover a wide range of redox potential in order to carry an electron from hydroxide ion (E_0=2.0 V) to carbon dioxide (E_0 is in the neighborhood of −2 V) photochemically by one electron processes, if we use only organic materials without multi-electron conversion system such as semiconductors. As summarized in Fig. 10, the redox system including **1** as a carrier was demonstrated in this study to cover a wide range of redox potential (*ca.* 4 V) and may be useful for the purpose.

We would like to thank Dr. K. Anda and his colleagues of the Tokyo Metropolitan Industrial Technic Institute for their kind measurement of the GC-Mass spectra.

References

1) C. R. Bock, T. J. Meyer, and D. G. Whitten, *J. Am. Chem. Soc.*, **96**, 4710 (1974); V. Balzani, L. Maggi, M. F. Manfrin, F. Bolleta, and M. Gleria, *Science*, **189**, 852 (1975); Y. Tsutsui and T. Matsuo, *Photochem. Photobiol.*, **27**, 695 (1978); J. R. Bolton, *Science*, **202**, 705 (1978); M. Calvin, *Acc. Chem. Res.*, **11**, 369 (1978); I. Willner, W. E. Ford. J. W. Otvos, and M. Calvin, *Nature*, **280**, 823 (1979); A. F. Jantzen, J. R. Bolton, and M. J. Stillman, *J. Am. Chem. Soc.*, **101**, 6337 (1979).

2) A. Fujishima and K. Honda, *Nature*, **238**, 37 (1972).

3) K. Kalyansundaram, J. Kiwi, and M. Grätzel, *Helv. Chim. Acta*, **61**, 2720 (1978); K. Kalyansundaram and M. Grätzel, *Angew. Chem.*, **91**, 759 (1979); J. Kiwi and M. Gräzel, *Chimia*, **33**, 289 (1979); *Angew. Chem.*, **91**, 659 (1979); *J. Am. Chem. Soc.*, **101**, 7214 (1979); *Nature*, **281**, 657 (1979); J. M. Lehn, J. P. Sauvage, and R. Ziessel, *Nouv. J. Chem.*, **3**, 423 (1979); J. M. Lehn and J. P. Sauvage, *ibid.*, **1**, 449 (1977); A. Moradpour, E. Amouyal, P. Keller, and H. Kagan, *ibid.*, **2**, 547 (1978); B. V. Koryakin, T. S. Dzhabiev, and A. E. Shilov, *Dokl. Akad. Nauk SSSR*, **238**, 620 (1977).

4) L. Galloway, D. R. Fruge, G. M. Haley, A. B. Coddinglon, and F. K. Fong, *J. Am. Chem. Soc.*, **101**, 229 (1979); F. K. Fong and L. Galloway, *ibid.*, **100**, 3594 (1978).

5) J. C. Hemminger, R. Carr, and G. A. Somorjai, *Chem. Phys. Lett.*, **57**, 100 (1978); M. Halmann., *Nature*, **275**, 155 (1978); T. Inoue, A. Fujishima, S. Konishi, and K. Honda, *ibid.*, **277**; 637 (1979); D. R. Fruge, G. D. Fong, and F. K. Fong, *J. Am. Chem. Soc.*, **101**, 3694 (1979).

6) G. N. Schrauzer and T. D. Guth, *J. Am. Chem. Soc.*, **99**, 7189 (1977); C. R. Dickson and A. J. Nozik, *ibid.*, **100**, 8007 (1978).

7) V. A. Kuzmin and A. K. Chibisov, *Chem. Comm.*, **1971**, 1559.

8) H. Inoue, K. Kawabe, N. Kitamura, and M. Hida, *Chem. Lett.*, **1977**, 987.

9) T. D. Tuong, Thesis, The Univ. of Tokyo, 1970.

10) H. Inoue, M. Hida, T. D. Tuong, and T. Murata, *Bull. Chem. Soc. Jpn.*, **46**, 1759 (1973).

11) *Inorg. Synth.*, **5**, 19; H. Grossmann and B. Schük, *Z. Anorg. Allg. Chem.*, **50**, 16 (1906).

12) Detailed kinetic study indicated that the rate constant of electron transfer from hydroxide ion by the excited **1** was 40 times larger than that of hydrogen abstraction from ethanol and the actual rate of hydrogen abstraction in 1 : 1 ethanol-water in the presence of hydroxide ion (6.0×10^{-2} mol/dm^3) was estimated to be 3.6 times faster than that of electron transfer. (H. Inoue, K. Hirose, and M. Hida, unpublished results.)

13) J. H. Fendler and E. J. Fendler "Catalysis in Micellar and Macromolecular Systems," Academic Press Inc., New York and London (1975), Chap. 5.

14) K. Kano, Y. Takada, and T. Matsuo, *Bull. Chem. Soc. Jpn.*, **48**, 3215 (1975); R. Scheerer and M. Grätzel, *Ber. Bunsenges. Phys. Chem.*, **80**, 979 (1976).

15) The cmc of CTAB at 25 °C is known to be 9.2×10^{-4} mol/dm^3. (Ref. 13, p. 20).
(1975), p. 20)

16) K. Tickle and F. Wilkinson, *Trans. Farady Soc.*, **61**, 1981 (1965).

17) K. P. Clark and H. I. Stonehill, *J. Chem. Soc., Faraday Trans. 1*, **68**, 577, 1676 (1972).

18) K. Kano and T. Matsuo, *Bull. Chem. Soc. Jpn.*, **47**, 2836 (1974).

19) H. Inoue, K. Kawabe, N. Kitamura, and M. Hida, *Bull. Chem. Soc. Jpn.*, **55**, 1874 (1982).

20) U. K. A. Klein and M. Hauser, *Z. Phys. Chem. (Fremkfurt am Main)*, **90**, 215 (1974).

21) P. H. Rieger, I. Bernal, W. H. Reinmuth, and G. Fraenkel, *J. Am. Chem. Soc.*, **85**, 683 (1963).

22) M. R. Rifi and F. H. Covitz, "Introduction to Organic Electrochemistry," Marcel Dekker Inc., New York (1974), p. 238.

23) G. V. Fomin, L. M. Gurdzhiyan, O. P. Studzinskii, N. I. Rtischev, A. V. El'stov, and V. V. Buluscheva, *Zh. Fis. Khim.*, **47**, 470 (1973).

Interaction of Amylose with Iodine. I. Characterization of Cooperative Binding Isotherms for Amyloses

Masako YAMAMOTO, Takayuki SANO,† and Tatsuya YASUNAGA*,†
Department of Home Economics, Hiroshima Women's University, Hiroshima 734
†*Department of Chemistry, Faculty of Science, Hiroshima University, Hiroshima 730*
(Received July 20, 1981)

The interaction of amylose with iodine was investigated as a function of degree of polymerization (DP) of amylose by amperometric titration, and the binding isotherms were obtained. The intrinsic equilibrium constant and cooperative parameter were determined with a one-dimensional Ising model for amyloses of various DPs. The inflection of the plot of the intrinsic equilibrium constant *vs.* DP observed at about DP 60 suggests that a helical segment of amylose consists of anhydroglucose residues less than 60. The discontinuity of the cooperativity at about DP 60 was interpreted by two kinds of cooperative effects, intra- and interhelical effects. These results suggest that the interrupted helix is a good model for the amylose structure in aqueous solution. The temperature dependencies of the cooperative parameters show that the cooperativity of amylose-iodine complexation is entropy-controlled.

The structure of amylose in aqueous solution has not yet been established, in spite of its important role for food and industry. Figure 1 shows three representative structural models proposed for amylose in aqueous solution. Model A is a random coil structure,[1] model B is a deformed helix structure,[2,3] and model C is an interrupted helix structure composed of the helix regions with intervals of random coils between them.[4,5] These studies clarified that the iodine staining characteristics, *e.g.*, maximum wavelength λ_{max}, or iodine binding capacity I_b, increases with DP of amylose.[6,7] These results were interpreted by the increase of the affinity for iodine, which implies the existence of a cooperative effect for the complexation, *i.e.*, neighboring iodine forms a more stable complex.[8] A quantitative analysis of the cooperative effect was introduced by Schneider and Cronan.[9] They examined precisely the binding isotherms of iodine to high DP amylose from the standpoint of the cooperative phenomenon and determined the intrinsic equilibrium constant and cooperative parameters. However, no quantitative investigation of the effect of DP on these parameters has been performed.

In the present study, the effect of DP of amylose on the intrinsic equilibrium constant and the cooperative parameter was studied by the amperometric titration, with special emphasis on the change in cooperativity. These results are discussed from the point of view of the structure of amylose in aqueous solution.

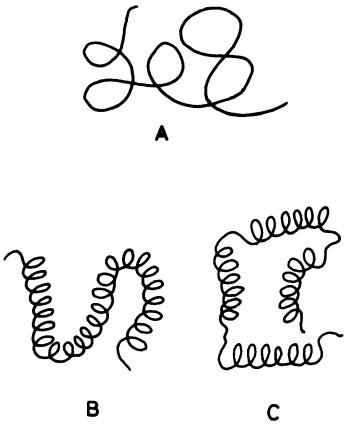

Fig. 1. Proposed models for amylose structure in aqueous solution. A) Random coil structure,[1] B) deformed helix structure,[2,3] and C) interrupted helix structure.[4,5]

Experimental

Materials. Potato amylose was purchased from Pierce Chemical and purified by precipitation three times from 1-butanol. The DP was evaluated to be 1100 by gel-filtration chromatography on Sepharose 4B gel. Degraded amyloses were obtained by hydrolysis of the above amylose with α-amylase[10] and fractionated in a dimethyl sulfoxide–ethanol solvent system. Further purification was done by gel chromatography[11] on Sephadex G-25 and G-75. The DP of each fraction was determined by the relationship between λ_{max} and DP reported by Banks *et al.*[12] The results are listed in Table 1 together with I_b. All solutions containing amylose were freshly prepared immediately before measurements.

Table 1. Properties of the amylose samples

DP	K_{av}[a]	λ_{max} / nm	I_b[b] / mg
27±2	0.24	510	1.5
32±1	0.31	530	4.7
42±3	0.41	545	8.6
57±5	0.51	570	12.6
76±3	0.65	588	15.0
142±20	0.88	610	18.1
1100±50	1.0	620	19.6

a) Elution constant[15] for a Sephadex G-75 gel. b) The amount of iodine binding to 100 mg of amylose.

Measurements. In the amperometric titration, an apparatus similar to that described by Kainuma *et al.*[13] was used in conjunction with two bright platinum electrodes. A solution of 50 cm^3 of amylose (0.5 mM** anhydroglucose) was titrated by adding 30 mm^3 portions of 10 mM iodine solution at constant concentrations of KI (50 mM) and KCl (50 mM) at 75 s intervals. The temperature was controlled at 20.0 °C by circulating thermostatically controlled water around the cell.

** In this paper 1 M = 1 mol dm^{-3}.

Results and Discussion

The binding isotherms of the amylose-iodine system were obtained for a series of amyloses, from DP 27 to 1100 by amperometric titration; these are shown in Fig. 2. As can be seen, the maximum amount of bound iodine increases with increase of DP of amylose.

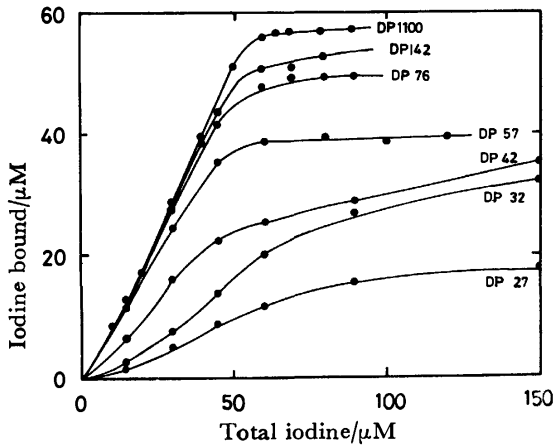

Fig. 2. Binding isotherms of iodine for a series of amyloses obtained by the amperometric titration at 20 °C. Concentration: amylose; 0.5 mM, and KI; 50 mM.

The binding equilibrium of amylose-iodine system is written as

$$A + (I_3^-)_f \rightleftarrows (I_3^-)_b, \quad (1)$$

where A is the binding site, and $(I_3^-)_f$ and $(I_3^-)_b$ are the free and bound triiodide, respectively.[14] The Scatchard equation for reaction (1) is given by

$$r/C_f = K_{app}(n-r), \quad (2)$$

where r and n are the amount of bound iodine and the maximum amount of bound iodine per glucose residue, respectively, C_f is the concentration of free iodine,[16] and K_{app} is the apparent equilibrium constant. Representative Scatchard plots are shown in Fig. 3. All of the amylose-iodine systems are indicative of the cooperativity in the complex formation.[18] If the complexation is independent of cooperativity, the plot

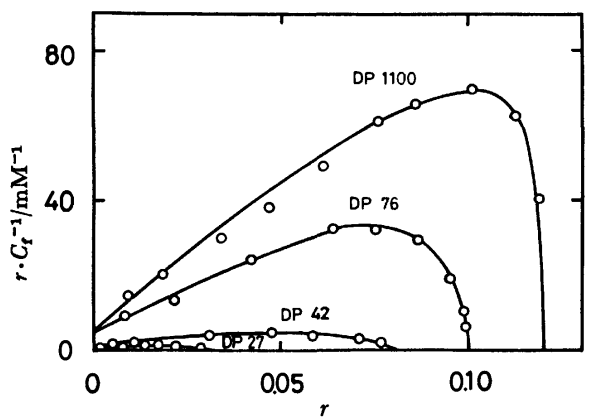

Fig. 3. Representative Scatchard plots of binding isotherms of iodine to amyloses. Solid lines show the theoretical curves obtained by Eq. 3.

Table 2. Binding parameters of the complex formation

DP	$\frac{n}{10^{-2}}$	$\frac{K_0}{10^3\ M^{-1}}$	K_{st}
27	3±1	4.7±0.2	5±1
32	7±1	4.9±0.1	6±1
42	8±2	7.9±0.1	7±1
57	9±1	15±5	9±2
76	10±2	14±1	40±5
142	10±1	14±1	50±10
1100	12±1	14±2	85±10

should show a straight line with negative slope, as can be seen in Eq. 2. The values of n were obtained from the intercept at $r/C_f=0$ in Fig. 3, and are listed in Table 2. The continuous elevation of n with DP will be due to the decrease of the "terminal effect" which means that each end of amylose does not make helix structure and so iodine can not bind there. According to the one-dimensional Ising model of McGhee and von Hippel,[19] the Scatchard equation (2) can be rewritten as

$$\frac{r}{C_f} = K_0(n-r)\left\{\frac{n-2r+R}{2(n-r)}\right\}^2, \quad (3)$$

with $R = \{(n-2r)^2+4K_{st}r(n-r)\}^{1/2}$,

where K_0 is the equilibrium constant for the intrinsic binding of iodine to amylose site (intrinsic equilibrium constant) and K_{st} is the cooperative parameter expressing the first nearest neighboring interaction between bound iodines.

The values of K_0 and K_{st} were determined so as to give the best fit of the data to the Scatchard equation, these are also listed in Table 2. The values of K_0 and K_{st} for amylose of DP 1100 were in good agreement with the corresponding values obtained by Schneider and Cronan.[9]

The value of K_0 increases with DP up to DP 60 and then remains constant, as shown in Fig. 4. With increase of a helical region, the iodine included in the center of a helix will be stabilized gradually, due to the interruption

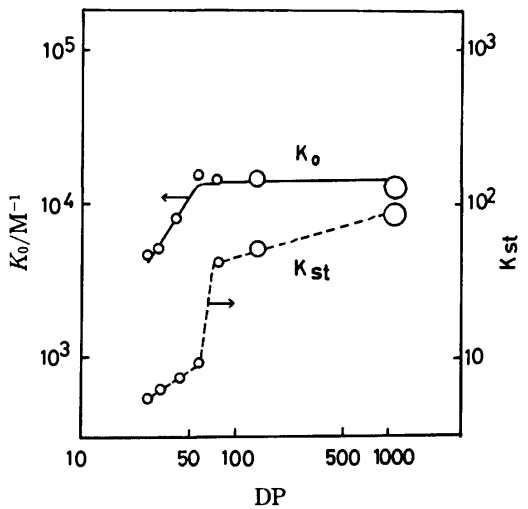

Fig. 4. The DP dependencies of the binding parameters of the amylose-iodine complex.

of the dissociation. According to this idea, the behavior of K_0 in Fig. 4 indicates that the length of a helix increases with DP up to a definite DP and then becomes constant, and suggests the model C in Fig. 1 as the amylose structure in aqueous solution. Furthermore, the length of the helical segment in the unit of DP (hereafter denoted by LHS) was estimated to be less than 60. Compared with the literature values of LHS, ranging from 66 to 140,[20-23] our value is smallest. Inconsistencies in the literature values have been ascribed mainly to the distribution of the DP of amylose.[23] However, some of them will be induced by the differences of the physical quantities used for the determination of the LHS.[24] Since the physical quantities which have been used so far were the values under the saturated condition of iodine, they should be affected significantly by the cooperativity. The value of K_0, on the contrary, does not contain any contribution from the cooperativity and is influenced only by the DP of amylose. Therefore, we believe that K_0 is the most preferable parameter for the determination of the LHS.

The value of K_{st} increases with DP of amylose up to DP 60, at this point it steeply jumps and then gradually increases, as shown in Fig. 4. Such discontinuous behavior of K_{st} can be interpreted by introducing two kinds of cooperative effects. One is the effect within a helical segment (intrahelical effect) which comes out in the region of DP up to 60, where amylose has only one helical segment. The other is the effect between different helical segments (interhelical effect) which comes out only above DP 60 where the amylose consists of more than two helical segments. This idea about cooperativity also supports the model C in Fig. 1 as the structure of amylose in aqueous solution.

Thermodynamic parameters for the intrinsic equilibrium constant and cooperativity were obtained for two kinds of amyloses (DP 42 and DP 1100). Figure 5 shows the Scatchard plots for the amylose of DP 1100

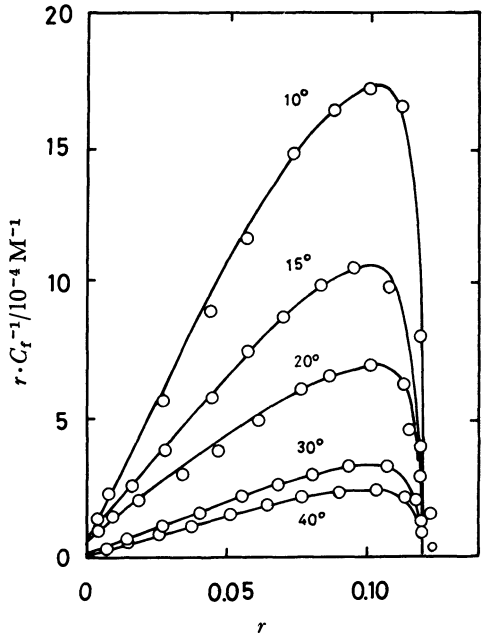

Fig. 5. The Scatchard plots of amylose (DP 1100)–iodine complex at different temperatures.

TABLE 3. EFFECT OF THE TEMPERATURE ON THE BINDING PARAMETERS OF THE COMPLEX FORMATION

Temp/°C	DP 42		DP 1100	
	K_0 / $10^3\,M^{-1}$	K_{st}	K_0 / $10^3\,M^{-1}$	K_{st}
10±0.1	16±3	7±1	24±1	85±10
15±0.1	10±1	7±1	15±1	85±10
20±0.1	7.9±0.1	7±1	14±1	85±10
30±0.1	3.9±0.7	7±1	4.7±0.3	85±10
40±0.1	—	—	3.5±0.3	85±10

TABLE 4. THERMODYNAMIC PARAMETERS OF THE COMPLEX FORMATION

Parameter	DP 42	DP 1100
ΔH_0/kJ mol^{-1}	−50	−50
ΔG_0/kJ mol^{-1}	−22	−37
ΔS_0/J K^{-1} mol^{-1}	−94	−42
ΔH_{st}/kJ mol^{-1}	0	0
ΔG_{st}/kJ mol^{-1}	−5.4	−11
ΔS_{st}/J K^{-1} mol^{-1}	19	38

measured at different temperatures. The magnitude of the plots decreases with increase of temperature, while the shape does not change. The values of K_0 and K_{st} for the two amyloses are listed in Table 3. From the temperature dependencies of K_0 and K_{st}, thermodynamic parameters were estimated, they are summarized in Table 4. It is noteworthy that the cooperative enthalpy change ΔH_{st} is zero for both amyloses and, therefore, the cooperativity is controlled not by enthalpy but by entropy.

References

1) W. Banks and C. T. Greenwood, *Staerke*, **23**, 300 (1971).
2) V. S. R. Rao and J. F. Foster, *Biopolymers*, **1**, 527 (1963).
3) Q. T. Nguyen, P. Aptel, and J. Neel, *Biopolymers*, **15**, 2097 (1976).
4) M. B. Senior and E. Hamori, *Biopolymers*, **12**, 65 (1973).
5) J. Hóllo and J. Szejtli, *Staerke*, **10**, 49 (1958).
6) J. Szejtli, M. Richter, and S. Augustat, *Biopolymers*, **5**, 5 (1967).
7) B. Pfannemüller, H. Mayerhöffer, and R. C. Schulz, *Makromol. Chem.*, **121**, 147 (1969).
8) J. A. Thoma and D. French, *J. Am. Chem. Soc.*, **83**, 1825 (1961).
9) F. W. Schneider and C. L. Cronan, *J. Phys. Chem.*, **72**, 4563 (1968).
10) D. L. Mould, *Biochemistry*, **58**, 593 (1954).
11) T. C. Laurent and J. Killander, *J. Chromatog.*, **14**, 317 (1964).
12) W.Banks, C.T. Greenwood, and K. M. Khan, *Carbohydr. Res.*, **17**, 25 (1971).
13) K. Kainuma, "Denpun Kagaku Handbook," ed by J. Nikuni, Asakura, Tokyo (1977), p. 178.
14) The bound species is I_3^- under the present experimental conditions, according to Cronan and Schneider.[15] Hence, in the present manuscript, iodine represents I_3^-.
15) C. L. Cronan and F. W. Schneider, *J. Phys. Chem.*, **73**, 3990 (1969).
16) The concentration of I_3^- is determined by considering

the reaction $I_2+I^- \rightleftharpoons I_3^-$, using $K'=[I_3^-]/[I_2][I^-]=866\ M^{-1}$ at 20 °C.[17]

17) A. D. Awtrey and R. E. Connick, *J. Am. Chem. Soc.*, **73**, 1842, 6417 (1954).
18) G. Schwarz, *Biophys. Chem.*, **6**, 65 (1977).
19) J. D. McGhee and P. H. von Hippel, *J. Mol. Biol.*, **86**, 469 (1974).
20) J. Szejtli, M. Richter, and S. Augustat, *Biopolymers*, **6**, 27 (1968).
21) T. Watanabe, K. Ogawa, and S. Ono, *Bull, Chem. Soc. Jpn.*, **43**, 950 (1970).
22) K. Hiromi, T. Shibaoka, and S. Ono, *J. Biochem.*, **68**, 205 (1970).
23) B. Pfannemüller, H. Mayerhöffer, and R. C. Schulz, *Biopolymers*, **10**, 243 (1971).
24) In fact, in the present study, if we use λ_{max} or I_b in Table 1, the value of LHS will be about 110, which is almost two times larger than that determined from K_0.

 © 1982 The Chemical Society of Japan Bull. Chem. Soc. Jpn., 55, 1890—1895 (1982) [Vol. 55, No. 6

The Preparation of Protoheme Mono-*N*-[5-(2-methyl-1-imidazolyl)pentyl]amide and Its Oxygenation

Eishun TSUCHIDA,* Hiroyuki NISHIDE, Yoshinori SATO, and Manabu KANEDA
Department of Polymer Chemistry, Waseda University, Tokyo 160
(Received August 5, 1981)

Iron(II)protoporphyrin IX *N*-[5-(2-methyl-1-imidazolyl)pentyl]amide ethyl ester (**1**) and its derivatives (**2**—**4**) were prepared. They predominantly form pentacoordinate heme complexes in organic and aqueous solutions, based on their 2-methylimidazole-ligand and spacer *N*-pentylamide groups. Oxygen adducts of **1**—**4** were rapidly formed on exposure to oxygen in *N*,*N*-dimethylformamide (DMF) at −30 °C, and their life-times were more than 30 min.

It is interesting to attempt to synthesize an iron–porphyrin complex with an oxygen-binding ability. Much recent work has been reported on such attempts, and two approaches have been partially successful. The first is the elegant steric modification of porphyrin: porphyrins have been replaced with "picket fence groups,"[1] "crown ether groups,"[2] "strap groups,"[3] *etc.*[4,5] The second approach is to attach the iron–porphyrin complex to a polymer chain.[6–8] By these means, a reversible oxygen bnding has been achieved in aprotic solvents or in the solid state, but in an aqueous medium all the iron–porphyrin derivatives have been irreversibly oxidized.

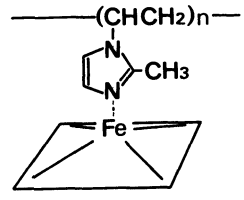

Scheme 1.

Recently, the present authors have found that the heme (iron(II)-protoporphyrin IX) complex with poly-(1-vinyl-2-methylimidazole) (PMI) (Scheme 1) forms the oxygen adduct even in an aqueous solution at −30 °C.[9] It is very important for oxygen binding in an aqueous solution that the heme complex has pentacoordinate structure the sixth coordination site of which is vacant to bind oxygen.[10]

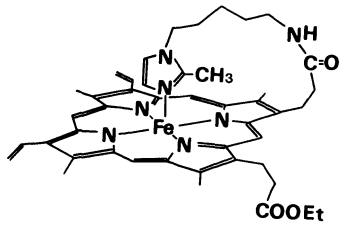

Scheme 2.

In this work, we synthesized heme derivatives having a 2-methylimidazole-ligand with *N*-pentylamide groups, **1**—**4**, which are expected to preferentially form the pentacoordinate heme complexes, as is shown in Scheme 2. A series of heme derivatives with covalently bound imidazole-ligands has already been studied by Traylor.[11–13] The mesoheme *N*-[3-(1-imidazolyl)propyl]amide ethyl ester derivative (**6**) is typical and forms the oxygen adduct in an aprotic, organic solvent.[12] However, the solution of **6** gave the visible spectrum of hexacoordinate heme, the sixth ligand having been derived from the solvent, and was irreversibly oxidized in aqueous media. On the other hand, the heme derivative with the 2-methylimidazole-ligand with an *N*-propylamide group has also been reported. However, the 2-methylimidazole-ligand could not coordinate to the central iron-ion because the *N*-propylamide group was too short, and the tetracoordinate heme complex was predominantly formed. From these results and the geometrical consideration of heme derivatives shown in Scheme 2, we selected the *N*-pentylamide group as a spacer group which bonds the 2-methylimidazole-ligand with heme and synthesized **1** and their derivatives: **2** as a water-soluble derivative, **3** as a bis(ligand)-type derivative, and **4** as a polymer-bound derivative. The coordination structure and oxygen binding ability of these heme derivatives (**1**—**4**)

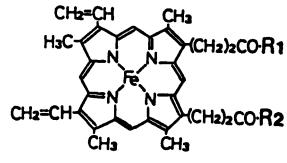

Compound	R_1	R_2
Heme	OH	OH
1	$NH(CH_2)_5$-(2-methylimidazolyl)	OC_2H_5
2	$NH(CH_2)_5$-(2-methylimidazolyl)	OH
3	$NH(CH_2)_5$-(2-methylimidazolyl)	$NH(CH_2)_5$-(2-methylimidazolyl)
4	$NH(CH_2)_5$-(2-methylimidazolyl)	Gly-PEG
5	$NH(CH_2)_3$-(2-methylimidazolyl)	OC_2H_5
6	$NH(CH_2)_3$-imidazolyl	OC_2H_5
7	$NH(CH_2)_3$-imidazolyl	$NH(CH_2)_3$-imidazolyl

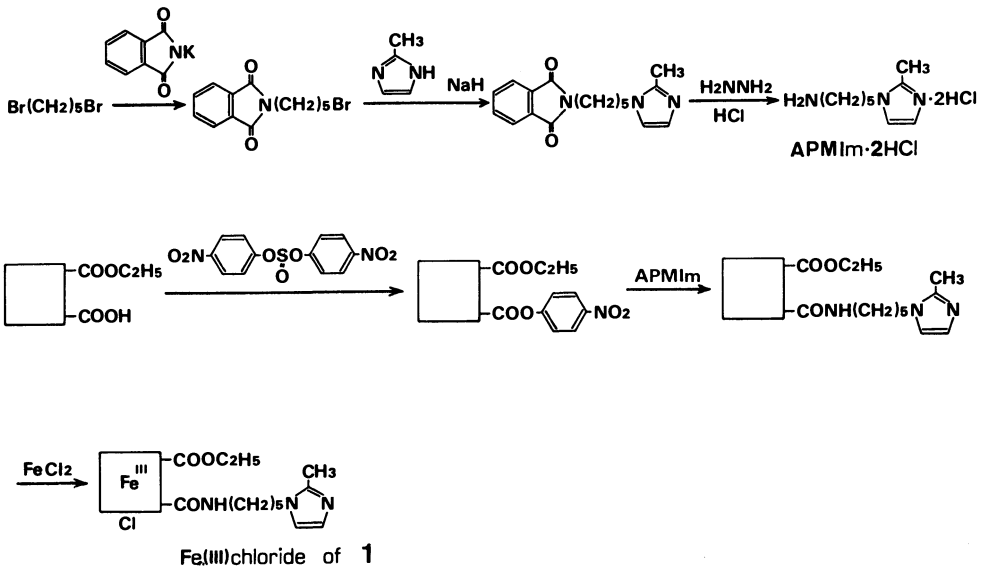

Scheme 3.

were studied in comparison with those of the previously reported Traylor's heme derivatives (**5**, **6**, and **7**) and with those of the polymer-heme complexes.

Results and Discussion

1 was obtained by the reaction of 1-(5-aminopentyl)-2-methylimidazole and the protoporphyrin IX monoethyl ester. The reaction process is illustrated in Scheme 3. **2** was obtained by hydrolyzing **1**. **3** was similarly prepared from 1-(5-aminopentyl)-2-methylimidazole and protoporphyrin IX, while **4** was obtained from **2** and poly(ethylene glycol)glycine[14] by using dicyclohexylcarbodiimide. The analytical data are given in the Experimental section.

The ultraviolet and visible absorption spectra of **1**, **5**, and **6** in the DMF solution (volume ratio DMF/H_2O= 9/1) are shown in Fig. 1. The visible spectrum of **1** was characterized by a single-peak absorption at 557 nm, the coordination structure of which was assigned to the pentacoordinate one; the iron(II) ion was in a high-spin state like myoglobin (557 nm). The molar absorption coefficients (ε) of **1** were 2.3×10^5 at 433 nm and 1.4×10^4 at 557 nm, nearly equal to those of the pentacoordinate heme complex with a large excess of 2-methylimidazole. On the other hand, the spectrum of **5** was broadened considerably, much like that of the tetracoordinate heme complex. This means that the 2-methylimidazole-ligand could not coordinate sufficiently to the central iron(II) ion, probably because of its shorter spacer group (*N*-propylamide group), and the pentacoordinate structure was not completed. **6** showed a double-peak absorption in the visible region (530 and 560 nm, Fig. 1) assigned to the hexacoordinate and low-spin heme complex, as had been reported by Traylor.[11] Although **6** formally has one imidazole-ligand, it forms the hexacoordinate heme complex in solution. The solvent molecule combines with the sixth coordination site of heme.[11] From these results, it may be concluded that **1** more predominantly forms the pentacoordinate heme complex than **5** and **6** do.

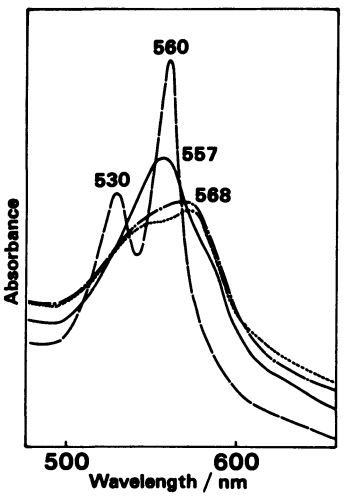

Fig. 1. Visible spectra of the deoxy heme complexes in DMF-H_2O(9/1) at −30 °C.
[Fe(II)]=0.1 mmol dm^{-3}, ——: **1**, —·—: **5**, -----: **6**, ·····: heme.

2 and **3** in aqueous solutions also showed the single-peak absorption at 557 nm, and the pentacoordinate structure was stable in the concentration range from about 0.01 to 10 mmol dm^{-3}. The visible spectrum of **3**, with two 2-methylimidazole-ligands, was identical to that of **1**. This means that one of the 2-methylimidazole pair coordinates to the central iron ion, while the other 2-methylimidazole-ligand can not coordinate to the sixth coordination site of heme. This behavior was like that of 2-methylimidazole-heme which took the pentacoordinate structure even if a large excess of 2-methylimidazole existed. This result was in contrast to that for **7**, which took the very stable hexacoordinate structure.

The oxygenation ability of each complex was measured in DMF-H_2O(9/1) at −30 °C. Except for **7**, all the heme complexes gave the oxygen adduct. As an

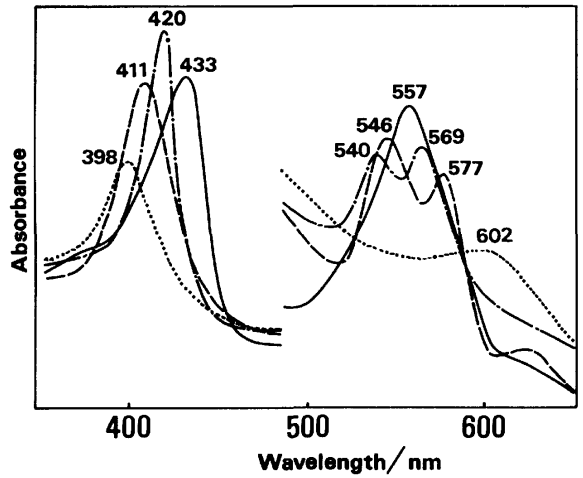

Fig. 2. Ultraviolet and visible spectra of **1** in DMF–H_2O(9/1) at −30 °C.
[**1**]=0.1 mmol dm^{-3}, ——: deoxy complex, ------: O_2-adduct, —·—: CO-adduct, ·····: oxidized complex.

example, the spectrum of the oxy-**1** complex (Fig. 2) was identified as that of the oxygen adduct by means of the following results: (i) The spectrum changed to that of the heme-CO complex when carbon monoxide was bubbled through the solution, and (ii) returned to the deoxy complex when nitrogen gas was introduced.

One must pay careful attention to the residue of the sodium dithionite which is used to prepare the heme complex (see Experimental section), because it often complicates the spectrum of the heme complex under aerobic conditions. The contribution of sodium dithionite and its residue to this reversible oxygenation was denied by the following results: (i) A small excess of sodium dithionite was used for reduction, and no trace of it remained before the oxygen exposure. (ii) The porphyrin ring of heme was degrated, and no oxygenation was observed in the presence of a large excess of dithionite. (iii) Organic reductants, such as L-ascorbic acid or D-glucose, were also effective reducing agents in forming an oxygen complex.

1—**4**, which took the pentacoordinate deoxy structure, immediately bound oxygen. Figure 3(a) shows the isosbestic spectral change in **1** after exposure to oxygen. In contrast, **6** reacted slowly with oxygen, while **7** did not react at all. It may be concluded from these results that the rate of the oxygenation reaction of the pentacoordinate heme complex is high, for the sixth coordination site, *i.e.*, the oxygen-binding site, is vacant.

The oxygen adduct of heme derivatives degraded to form a high-spin hemin complex (weak absorption at about 602 nm) through isosbestic points (528, 590 nm) as is shown in Fig. 4. The degradation obeyed first-order kinetics, and the life-time of the oxygen adduct was calculated by means of the following equation: $1/\tau=(1/t)\ln[(A_0-A_\infty)/(A_t-A_\infty)]$, where τ indicates the life-time of the oxygen adduct and where A_0, A_t, and A_∞ are the absorbance of the visible spectrum of heme-oxygen adduct at the beginning, at after time t, and when the degradation is complete respectively. The life-time is summarized in Table 1.

Table 1. Life-times of the oxygen adducts at −30 °C

Complex	Life-time/min	
	In DMF–H_2O (9/1)	In H_2O–ethylene glycol (1/1)
PMI-heme[a]	63	25
1	32	—
2	—	Oxidized
3	72	1
4	35	Oxidized
2-Methylimidazole-heme[b]	6	Oxidized
6	98	Oxidized
7	Oxidized	Oxidized

a) [2-Methylimidazole residue]/[heme]=500. b)[2-Methylimidazole]/[heme]=5000.

The life-time of oxy-**1** was much longer than that of the 2-methylimidazole-heme system; **1** could give oxygen adduct with not only a large formation rate, but also a long life-time. Table 1 shows that **3** and PMI-

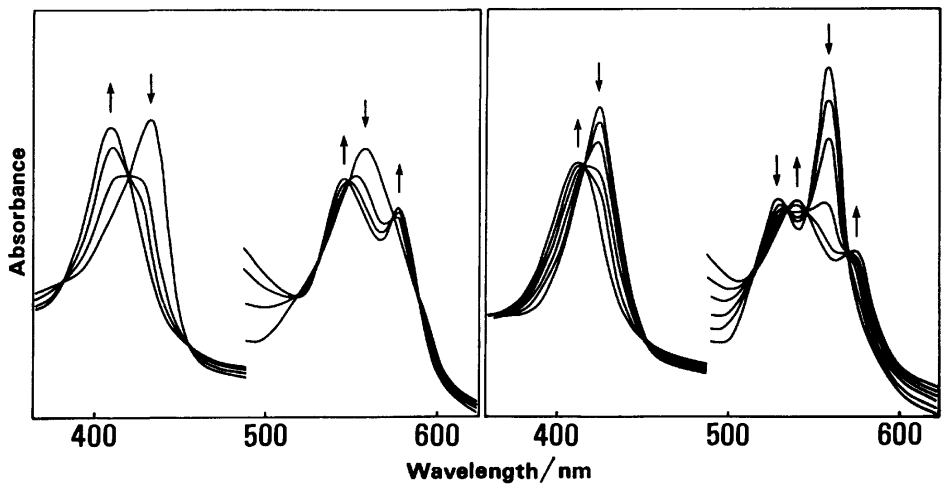

Fig. 3. Oxygenation of **1** (a) and **6** (b) in DMF–H_2O(9/1) at −30 °C. After exposing to oxygen: 0, 0.5, 1, and 2 min for (a); 0, 1, 2, 5, 10, and 15 min for (b).

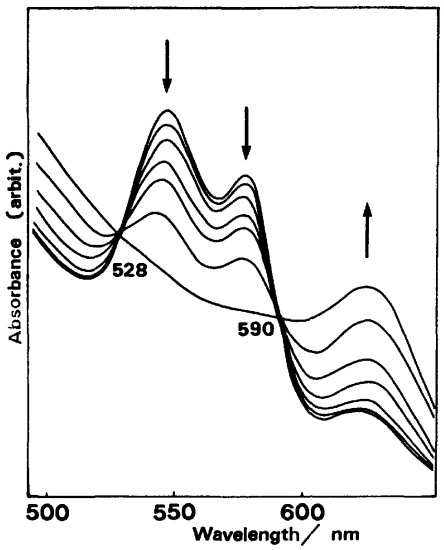

Fig. 4. Degradation of the oxygen adduct of **1** in DMF–H_2O(9/1) at −30°C. After 0, 5, 10, 20, 30, 60 min, and 1 d.

heme form more stable oxygen adducts, which approach the oxy-**6** studied by Traylor. 2-Methylimidazole residue that exists near the sixth coordination site of heme makes a good contribution to the stabilization of the oxygen adduct.

The oxygenation reaction was also checked in H_2O–ethylene glycol (1/1) at −30 °C. PMI-heme and **3**, which gave stable oxygen adducts in DMF–H_2O (9/1), could also form oxygen adducts even in an aqueous medium, though they were not so stable. The reasons for the oxygen-binding ability of PMI-heme and **3** in an aqueous medium are presumed to be as follows: (i) PMI-heme and **3** form pentacoordinate, high-spin-state complexes with large formation constants, and the rates of oxygenation are high, and (ii) the polymer-ligand, PMI, or the unchelated 2-methylimidazole sterically occludes heme and provides an effective hydrophobic environment which surrounds the oxygen adduct.

The synthesis and oxygen-binding ability of polymer-bound **1** will be presented in a subsequent paper.

Experimental

*Synthesis of Iron(III)protoporphyrin IX Mono-*N*-[5-(2-methyl-1-imidazolyl)pentyl]amide Ethyl Ester Chloride (Iron(III) Chloride of **1**) and the Corresponding Amide Acid (Iron(III) Chloride of **2**).* 1-(5-Aminopentyl)-2-methylimidazole (AMPIm) was prepared by a Gabriel reaction. Potassium phthalimide (74 g, 0.4 mol) was suspended in 1,5-dibromopentane (300 g, 1.3 mol), after which the mixture was allowed to react at 190—200 °C for 12 h. The mixture was steam-distilled to remove the unreacted 1,5-dibromopentane. *N*-(5-Bromopentyl)phthalimide (BPP) was extracted with chloroform, dried (Na_2SO_4), evaporated to dryness, and then recrystallized from ethanol; pale yellow crystals (yield, 59.8 g).

50% oily sodium hydride (4.80 g) was suspended in dry toluene (100 ml). 2-Methylimidazole (8.21 g, 0.10 mol) was added to this suspension, and the mixture was refluxed for 5 h under nitrogen. Then, BPP (29.6 g, 0.10 mol) was added, and the mixture was allowed to react for 15 h under reflux. After filtration, the solution was evaporated to dryness. The brown oily product was chromatographed on a silica-gel column (about 300 mesh, 5 cm × 45 cm for operating 1.5 g). The fourth fraction with chloroform–methanol (20 : 1) was collected (R_f=0.19 with chloroform–methanol (20 : 1)) and evaporated to dryness. *N*-(5-Phthalimidopentyl)-2-methylimidazole (PPIm): pale yellow powder; yield, 17.8 g (59.9%), IR; ν_{ring} 1621 (phenyl), 1620 (imidazole), $\nu_{C=O}$ 1780, 1720 cm^{-1}. Found: C, 69.1; H, 6.58; N, 13.9%. Calcd for $C_{17}H_{19}N_3O_2$: C, 68.7; H, 6.40; N, 14.1%.

PPIm (17.7 g, 59.5 mol) was dissolved in methanol (250 ml). Hydrazine monohydrate (2.98 g, 59.5 mol) was added to this solution, which was then refluxed for 15 h. Then water (200 ml) was added, and the methanol was removed by evaporation. Concd hydrochloric acid (200 ml) was added to this aqueous solution, and the mixture was refluxed for 2 h. After cooling to 0 °C, the white precipitate was filtered off. The filtrate was evaporated to dryness, and the crude product was recrystallized from ethanol. 1-(5-aminopentyl)-2-methylimidazole dihydrochloride (APMIm 2HCl): pale yellow crystals; yield 12.1 g (84.7%) ^1H NMR (DMSO-d_6, δ): imidazole C–H, 7.5, 7.7(2H); $-(CH_2)_5-$, 1.3—1.8(6H), 2.7(2H), 4.1(2H); $-CH_3$, 2.6(3H); $-NH_3^+$, 8.2(3H). Found: C, 45.1; H, 7.88; N, 17.4; Cl, 29.6%. Calcd for $C_9H_{19}N_3Cl_2$: C, 45.0; H, 7.92; N, 17.5; Cl, 29.6%. IR: ν_{ring} 1605 (imidazole), $\nu_{NH_3^+}$ 3000, 2510, 2420 cm^{-1}.

On the other hand, the protoporphyrin IX monoethyl ester (PMEE) was prepared as follows. Protoporphyrin IX sodium salt (4.5 g, 7.4 mmol) and phosphorus pentachloride (2.4 g, 11.5 mmol) were dissolved in chloroform (250 ml), and the mixture was stirred for 30 min at 30 °C. Ethanol (15 ml) was added, and this mixture was stirred for 30 min, after which more ethanol (15 ml) was added. The reaction was conveniently followed by examining the TLC (silica-gel, chloroform–methanol (10 : 1)). The amount of the second fraction, based on PMEE, increased as the esterification proceeded. The reaction was finished after 45 min, and chloroform (200 ml) and water (1.5 ml) were added to this solution. The pH was then controlled to 6.0 by adding triethylamine. After washing with water, the chloroform layer was filtered and concentrated. The crude product was chromatographed on a silica-gel column (5 cm × 20 cm for operating 2 g). The column was eluted with chloroform until the eluent was very pale. The PMEE was obtained with chloroform–methanol (15 : 1) as the first fraction; 30% yield.

Protoporphyrin IX mono-*N*-[5-(2-methyl-1-imidazolyl)-pentyl]amide ethyl ester (PMImPe) was synthesized as follows. PMEE (2.7 g, 4.5 mmol) was dissolved in a mixture of DMF (30 ml) and pyridine (30 ml), after which bis(*p*-nitrophenyl) sulfite (5.9 g, 18 mmol) was added . After stirring for 18 h at room temperature, the solution was concentrated by evaporation. The residue was dissolved in chloroform, and the insoluble part was removed by filtration. After concentration, PMImPe was precipitated from diethyl ether–petroleum ether (1 : 1). The brown, powdered product was chromatographed on a silica-gel column (4 cm × 20 cm for operating 1 g) eluted with benzene–acetone (25 : 1). The *p*-nitrophenyl ester was obtained as the main fraction in a 65.9% yield.

The *p*-nitrophenyl ester (0.85 g, 1.2 mmol) and PMEE (0.25 g, 1.5 mmol) were dissolved in chloroform (30 ml), and the mixture was stirred for 1 d at room temperature. After concentration, the residue was dissolved in chloroform, and the mixture was filtered. Then PMImPe was precipitated

from diethyl ether. PMImPe: brown powder; yield, 733 mg (83.6%). IR: $\nu_{C=O}$ 1640, 1550 (amide), 1730 (ester). Found: C, 73.1; H, 7.21; N, 13.2%. Calcd for $C_{45}H_{53}N_7O_3$; C, 73.1; H, 7.17; N, 13.3%. ^{1}H NMR ($CDCl_3$, δ): ring $-CH_3$, 3.55—3.80(12H); imidazole $-CH_3$, 0.30(3H), imidazole $-H$, 4.7(1H) propionic α-CH_2, 4.10(4H); propionic β-CH_2, 3.15 (4H); α-CH_2, 0.90(2H); β-CH_2, 0.20(2H); γ-CH_2, 2.35(2H); δ-CH_2, 1.95(2H); ε-CH_2, 2.83(2H); NH, 5.8(1H); *meso*-H, 9.6—9.9(4H); vinyl-H, 5.0—5.5, 6.9(3H); OC_2H_5, 4.10(2H), 2.05(3H); pyrrole-H, 4.50(2H).

By the incorporation of the iron ion in PMImPe, iron(III)-protoporphyrin IX mono-*N*-[5-(2-methyl-1-imidazolyl)pentyl]amide ethyl ester chloride (iron(III) chloride of **1**) was obtained. PMImPe (300 mg, 0.36 mmol) was dissolved in DMF (300 ml). $FeCl_2 \cdot nH_2O$ (180 mg) was added to this solution, and the mixture was heated to 70 °C under nitrogen for 1 h. The solvent was removed by evaporation, and the residue was extracted with a chloroform–methanol (3 : 1) mixture. The crude product was chromatographed on a basic alumina column (3 cm × 15 cm), eluted with chloroform–methanol (30 : 1). The first and second fractions (iron(III) chloride and μ-oxo dimer of **1**) were collected and brought to dryness. Iron(III) chloride of **1**: brown powder; yield, 172 mg (51.2%). Found: C, 65.1; H, 6.10; N, 11.8; Cl, 4.35%. Calcd for $C_{45}H_{51}N_7O_3FeCl$: C, 65.2; H, 6.16; N, 11.8; Cl, 4.29%.

By hydrolyzing PMImPe, iron(III) chloride of **2** was obtained. Iron(III) chloride of **1** (350 mg) was dissolved in methanol (15 ml). NaOH (2 mol dm^{-3}, 6 ml) was added to this solution, and the mixture was stirred for 12 h at room temperature. Water (10 ml) was added to this solution, and the methanol was removed by evaporation. The solution was acidified to pH 4.0 by adding dilute hydrochloric acid, and extracted with chloroform. The chloroform layer was dried (Na_2SO_4), and then the solvent was removed by evaporation. Iron(III) chloride of **2**: brown powder; yield, 280 mg (80%). IR: $\nu_{C=O}$ 1500, 1620 (amide), 1720 (carboxylic acid) cm^{-1}. Found: C, 64.7; H, 5.92; N, 12.1; Cl, 4.50%. Calcd for $C_{43}H_{47}N_7O_3FeCl$: C, 64.5; H, 5.87; N, 12.2; Cl, 4.44%.

Synthesis of Iron(III)protoporphyrin IX Bis[N-[*5-(2-methyl-1-imidazolyl)pentyl*]*amide*] *Chloride (Iron(III) Chloride of 3).* Protoporphyrin IX (1.12 g, 2 mmol) and bis(*p*-nitrophenyl) sulfite (4.0 g, 12.3 mmol) were dissolved in 50 ml of DMF–pyridine (1 : 1), after which the solution was allowed to react for 18 h at room temperature. After filtration, the solution was concentrated. The residue was dissolved in dichloromethane, and the insoluble part was removed by filtration; then the solution was poured into diethyl ether–petroleum ether (1 : 1). The crude product was chromatographed on a silica-gel column (3 cm × 20 cm for operating 1 g). The bis(*p*-nitrophenyl ester) was obtained in a 73% yield as the first fraction with dichloromethane–acetone (60 : 1).

The bis(*p*-nitrophenyl ester) (150 mg, 0.18 mmol) and APMIm (4.0 g, 12.3 mmol) were dissolved in a mixture of DMF–dichloromethane (1 : 1) (8 ml), after which the solution was allowed to react for 12 h at room temperature. The resulting solution was concentrated and washed with diethyl ether to remove the *p*-nitrophenol. The crude product was chromatographed on a silica-gel column (1.5 cm × 12 cm). The third fraction chloroform–methanol (4 : 1) was collected and brought to dryness. Protoporphyrin IX bis[*N*-[5-(2-methyl-1-imidazolyl)pentyl]amide] ($P(MImPe)_2$): Found: C, 72.7; H, 7.43; N, 16.3%. Calcd for $C_{52}H_{64}N_{10}O_2$: C, 72.6; H, 7.44; N, 16.3%. IR: $\nu_{C=O}$ 1650, 1555 (amide) cm^{-1}.

The corresponding iron(III) complex of $P(MImPe)_2$ (iron(III) chloride of **3**) was obtained by the above mentioned procedure in a 52% yield. Found: C, 65.7; H, 6.59; N, 14.7; Cl, 3.77%. Calcd for $C_{52}H_{62}N_{10}O_2FeCl$: C, 65.7; H, 6.53; N, 14.7; Cl, 3.74%.

Synthesis of Iron(III)protoporphyrin IX N-[*5-(2-Methyl-1-imidazolyl)pentyl*]*amide* N′-[*ω-Hydroxypoly(ethyleneoxy) carbonylmethyl*]*amide (Iron(III) Chloride of 4).* Iron(III) chloride of **2** was combined with $H_2NCH_2CO(OCH_2CH_2)_nOH$ (Gly-PEG) by the following procedure. Iron(III) chloride of **2** (120 mg, 0.15 mmol) and 1-hydroxybenzotriazole (30 mg, 0.22 mmol) were dissolved in DMF (4 ml). Dicyclohexylcarbodiimide (33 mg, 0.16 mmol) was added to this solution at 0 °C, after which the mixture was allowed to react for 30 min. Gly-PEG (0.5 g, 0.05 mmol of the functional group) and *N*-methylmorpholine (5.5 mg) were then dissolved in DMF (3 ml) and added to this solution. The mixture was stirred for 2 d at room temperature. After concentration, the residue was dissolved in chloroform, and the insoluble part was removed by filtration; then the solution was poured into diethyl ether–ethyl acetate (2 : 1). The crude product was chromatographed on a Sephadex LH-60 column (3 cm × 40 cm for operating 0.2 g). The first fraction with methanol was collected and brought to dryness. The product was reprecipitated from a chloroform–diethyl ether system twice. The degree of incorporation of the complex unit into the functional group of the polymer was determined to be 71% from the absorbance at 385 nm of a chloroform solution of iron(III) chloride of **4** referred to that of the iron(III) chloride of **1**.

Iron(III) chlorides of **5**, **6**, and **7** were synthesized according to Traylor's method.

Other Chemicals. The 2-methylimidazole was purified by recrystallization twice from benzene. The DMF for spectroscopic measurement was treated with molecular sieves (4 Å), and distilled under reduced pressure before use. The ethylene glycol added as antifreeze for spectroscopic measurement was distilled under reduced pressure before use.

Fe(II) Complex Solution. The Fe(III) complex was dissolved in a solvent (DMF/H_2O or pH 10 buffer/ethylene glycol). In the case of PMI-heme and 2-methylimidazole-heme, the ligand was added in this step. Nitrogen gas was bubbled through this solution, and an aqueous solution of sodium dithionite ($[Na_2S_2O_4]/[Fe(III)]=5$) was added to obtain the Fe(II) complex solution.

Measurements. The electronic absorption spectrum was measured with a Union Giken SM-401 spectrophotometer.

This work was partially supported by a Grant-in-Aid for Scientific Research No. 56209024 from the Ministry of Education, Science and Culture, Japan.

References

1) J. P. Collman, R. R. Gagne, T. R. Halbert, J. C. Marchon, and C. A. Reed, *J. Am. Chem. Soc.*, **95**, 7868 (1973).
2) C. K. Chang, *J. Am. Chem. Soc.*, **99**, 2819 (1977).
3) H. Ogoshi, H. Sugimoto, and Z. Yoshida, *Tetrahedron Lett.*, **1976**, 4477.
4) A. R. Battersby and A. D. Hamilton, *J. Chem. Soc., Chem. Commun.*, **1980**, 117.
5) T. G. Traylor, D. Campbell, and S. Tsuchiya, *J. Am. Chem. Soc.*, **101**, 4748 (1979).
6) J. H. Wang, *Acc. Chem. Res.*, **3**, 90 (1970).
7) O. Leal, D. L. Anderson, R. G. Bowman, F. Basolo, and R. L. Burwell, *J. Am. Chem. Soc.*, **97**, 5125 (1975).
8) E. Tsuchida, *J. Macromol. Sci. Chem.*, **13**, 545 (1979).
9) H. Nishide, H. Ohno, and E. Tsuchida, *Markomol. Chem. Rapid Commun.*, **2**, 55 (1981).

10) H. Nishide, H. Ohno, and E. Tsuchida, *Kobunshi Ronbunshu*, **37**, 641 (1980).
11) C. K. Chang and T. G. Traylor, *J. Am. Chem. Soc.*, **95**, 8475 (1973).
12) C. K. Chang and T. G. Traylor, *J. Am. Chem. Soc.*, **95**, 8477 (1973).
13) C. K. Chang and T. G. Traylor, *Proc. Natl. Acad. Sci. U.S.A.*, **72**, 1166 (1975).
14) E. Bayer and M. Mutter, *Chem. Ber.*, **107**, 1344 (1974).

 © 1982 The Chemical Society of Japan Bull. Chem. Soc. Jpn., 55, 1896—1900 (1982)

The Effect of Polyhydric Alcohols on the Thermal Denaturation of Lysozyme as Measured by Differential Scanning Calorimetry

Yukihisa FUJITA,* Yasuchika IWASA, and Yukinao NODA
Department of Chemistry, Hyogo College of Medicine, Mukogawa, Nishinomiya, Hyogo 663
(Received September 3, 1981)

The thermal denaturation of lysozyme in aqueous solutions of polyhydric alcohols at pH 2 was investigated by differential scanning calorimetry (DSC). The polyhydric alcohols employed were inositol, sorbitol, xylitol, erythritol, glycerol, and ethylene glycol. These alcohols tended to enhance the thermal stability of lysozyme; both the temperature and the enthalpy of denaturation increased almost linearly with increasing alcohol concentration. The increase in denaturation temperature at a given alcohol concentration was a linearly increasing function of the number of hydroxyl groups per alcohol molecule. The denaturation enthalpy at identical temperature increased only slightly by the addition of polyhydric alcohol. The hypothesis may be supported that the dominant mechanism by which polyhydric alcohols stabilize proteins to thermal denaturation is through their effect on the water structure, which determines the strength of the hydrophobic interactions between the nonpolar groups of the protein.

The folding, structural stability, and dynamics of globular proteins are thought to be extensively controlled by the interactions of the protein with water. Various substances affect the protein-water interactions when added to aqueous protein solutions and consequently alter the structural stability of proteins.[1-3] There have been many investigations which show the stabilizing effect of polyhydric alcohols and sugars on the native conformation of proteins. Simpson and Kauzmann[4] observed that the extent of denaturation of ovalbumin in urea solutions was reduced in the presence of glycerol or sucrose. The influence of polyhydric alcohols and sugars on the rate of subunit dissociation of tetrameric L-asparaginase in the presence of urea was investigated by Shifrin and Parrott.[5] Gerlsma and Stuur[6] showed by spectrophotometric measurements that polyhydric alcohols raised the thermal transition temperature of lysozyme and ribonuclease. A similar effect of polyhydric alcohols has also been observed for chymotrypsinogen.[7,8] However, the manner in which polyhydric alcohols and sugars induce the increased thermal stability of proteins or reduce the extent of denaturation by other reagents is poorly understood.

The application of differential scanning calorimetry (DSC) to the investigation of thermally induced conformational transitions of protein has provided valuable information on the mechanism of protein denaturation; this has been recently reviewed by Biltonen and Freire[9] and Privalov.[10] The extensive calorimetric investigation of the thermal denaturation of lysozyme has been reported by Privalov and Khechinashvili.[11] The reversible nature of the denaturation has been established. Recently, the DSC study of the thermal denaturation of lysozyme in sugar solutions has been reported by Uedaira and Uedaira.[12]

We have been investigating the effect of various substances on the thermal stability of globular proteins by means of DSC. In the previous paper,[13] the effect of monohydric alcohols on the thermal denaturation of lysozyme was reported. The denaturation temperature of lysozyme in monohydric alcohol solutions decreased gradually with increasing alcohol concentration, which became more pronounced with increasing hydrocarbon content of alcohol. On the other hand, the denaturation enthalpy passed through a maximum with increasing alcohol concentration and the maximal value decreased with increasing hydrocarbon content of alcohol. A similar behavior has been observed with sulfoxides.[14] These tendencies may be interpreted in terms of the mixed hydrophobic-hydrophilic character of monohydric alcohols and sulfoxides.

In the present paper, the effect of polyhydric alcohols on the thermal denaturation of lysozyme has been investigated by means of DSC and the results are compared with those of monohydric alcohols.

Experimental

Materials. The hen egg-white lysozyme used was a salt-free, six-times-recrystallized preparation obtained from Seikagaku Kogyo Co. The molecular weight of lysozyme was taken to be 14307. Analytical grade inositol, sorbitol, and xylitol were purchased from Nishio Kogyo Co. and reagent grade *meso*-erythritol from Merck. Spectral grade glycerol and ethylene glycol were obtained from Wako Pure Chemicals. These polyhydric alcohols were used without further purification.

Methods. The stock solution of lysozyme was prepared with 0.1 mol dm^{-3} glycine buffer at pH 2.0 containing 0.1 mol dm^{-3} NaCl and if necessary the pH was adjusted by adding HCl. The protein concentration was determined spectrophotometrically using an extinction of $E^{1\%}_{1cm}=26.9$ at 280 nm in 0.1 mol dm^{-3} glycine buffer at pH 3.0.[15] A Hitachi 323 automatic recording spectrophotometer was used. Polyhydric alcohol was added by weight.

Thermal measurements were performed with a Daini Seikosha SSC-560U differential scanning calorimeter (conduction type) at protein concentrations of 2.39—2.47%. The sample (0.06 cm^3) was hermetically sealed in a silver vessel. A heating rate of 1 K min^{-1} was typically used, although some measurements were performed at 0.2, 0.5, and 2.5 K min^{-1} to check the effect of the heating rate. The calorimeter was calibrated with indium, benzophenone, and benzoic acid.

Results and Discussion

Figure 1 shows the DSC curves for the thermal denaturation of lysozyme in aqueous solutions (pH 2) containing different amounts of sorbitol at a heating rate of 1 K min^{-1}. In every measurement, a reproducible

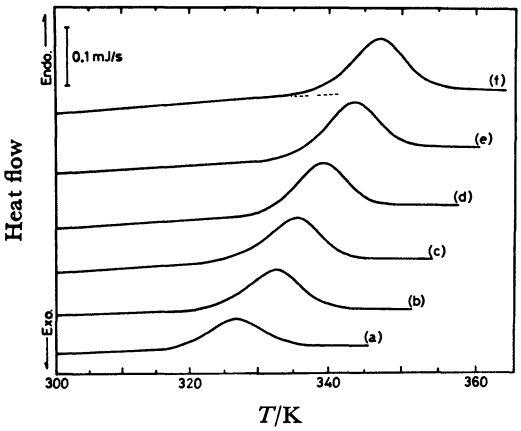

Fig. 1. DSC curves at heating rate of 1 K min^{-1} for the thermal denaturation of lysozyme in aqueous sorbitol solutions at pH 2.
The sorbitol concentrations are (a): 0, (b): 0.95, (c): 1.45, (d): 1.98, (e): 2.56, and (f): 3.04 mol dm^{-3}.

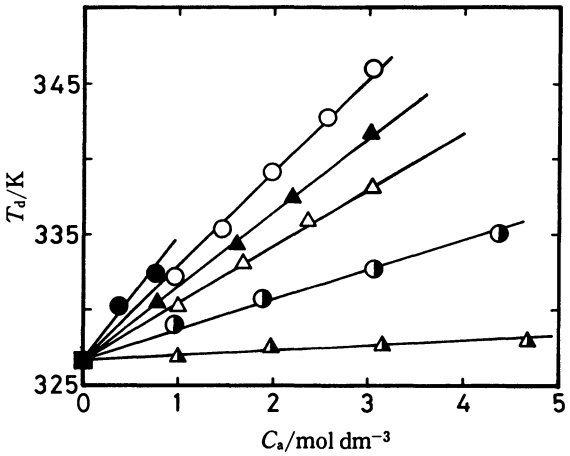

Fig. 2. The denaturation temperature of lysozyme as a function of concentration of polyhydric alcohol.
■: Aqueous, ●: inositol, ○: sorbitol, ▲: xylitol, △: erythritol, ◑: glycerol, ◭: ethylene glycol.

endothermic peak was observed occurring over a temperature width of 23—25 K. The endothermic peak shifted to higher temperature with increasing sorbitol concentration, while the peak area became larger and also the peak width slightly larger. The denaturation temperature, T_d, was estimated by assuming that the area under the thermogram was proportional to the amount denatured, and T_d defined as the temperature at which the protein is half-denatured. The difference between the estimated T_d and the peak temperature of the transition peak did not exceed 0.6 K in every measurement. The denaturation enthalpy, ΔH_d, was estimated by measuring the area between the transition peak and a base line fitted by inspection.

In order to check the effect of the heating rate, the thermal denaturation of lysozyme in aqueous solution and in aqueous sorbitol solutions was measured at heating rates of 0.2, 0.5, and 2.5 K min^{-1} other than 1 K min^{-1}. There was no significant difference in the denaturation enthalpies obtained at different heating rates. The denaturation temperature, however, showed a slight dependence on the heating rate; the denaturation temperature increased slightly with increasing heating rate. The values extrapolated to zero heating rate were lower than those obtained at a heating rate of 1 K min^{-1} by 0.4—0.6 K, which were in fair agreement with the denaturation temperature obtained by Gerlsma and Stuur[6] from spectrophotometric measurements.

The effect of polyhydric alcohols on the denaturation temperature of lysozyme is shown in Fig. 2. The T_d increased almost linearly with increasing concentration of alcohol and the increase became more pronounced with an increase in the number of hydroxymethyl groups in the alcohol. It is evident that these alcohols stabilize the protein against thermal denaturation. This tendency of polyhydric alcohols differ clearly from that of monohydric alcohols. As described in the previous paper,[12] monohydric alcohols lower the denaturation temperature of lysozyme, which becomes more pronounced with increasing alcohol concentration and increasing hydrocarbon content of the alcohol. That is, monohydric alcohols unstabilize the native structure of the protein. The unstabilizing effect of monohydric alcohols has been generally interpreted in terms of the hydrophobic interactions between the nonpolar groups of the protein and the alkyl chain of alcohol.[16,17]

The dependence of the denaturation enthalpy of lysozyme on the concentration of polyhydric alcohols is shown in Fig. 3. In every case studied, the ΔH_d was

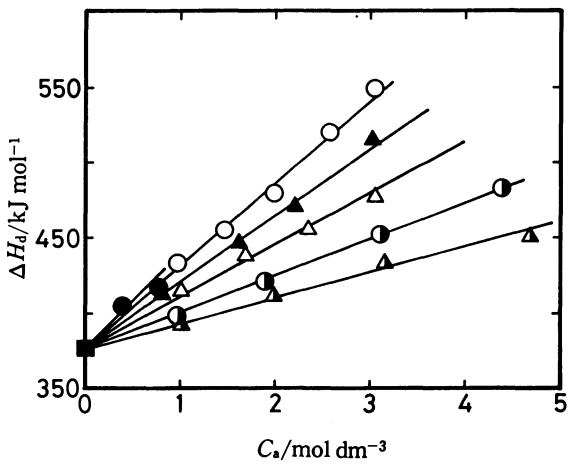

Fig. 3. The denaturation enthalpy of lysozyme as a function of concentration of polyhydric alcohol.
The symbols used are identical with those in Fig. 2.

enhanced by the addition of polyhydric alcohol. The ΔH_d increased almost linearly with increasing alcohol concentration. The increase in ΔH_d for a given concentration of alcohol becomes more pronounced as the number of hydroxymethyl groups of the added alcohol increase. The effect of the polyhydric alcohols on the denaturation enthalpy also differs from that of monohydric alcohols. As has been reported by Velicelebi and Sturtevant[17] and us,[13] the ΔH_d of lysozyme in the presence of monohydric alcohol shows a complex

dependence on the alcohol content; the ΔH_d passes through maximum with increasing alcohol concentration and the maximal value decreases with an increase in the hydrocarbon content of alcohol. A comparison between the results with polyhydric and monohydric alcohols suggests that the second and additional hydroxyl groups in the polyhydric alcohols play an important role in their stabilizing influence on the thermal denaturation of protein.

At a constant concentration of alcohol, the increase of T_d and ΔH_d with inositol were larger than those with sorbitol. This indicates that the stabilizing ability of inositol with a cyclic structure on the thermal denaturation of lysozyme is higher than that of sorbitol with a linear structure. This configuration effect may be analogous to the effect induced by branching the alkyl chain of monohydric alcohols. It has been established that the lowering of the denaturation temperature of globular proteins by monohydric alcohols with branched alkyl chain is smaller than that by the corresponding straight-chain alcohols.[13,18] It is possible that cyclization causes the increase in the content of hydroxymethyl groups per molecular chain and consequently brings about the high stabilizing ability of inositol on the thermal stability of lysozyme.

Figure 4 shows the plot of the increase in the denaturation temperature of lysozyme at an identical alcohol concentration of 1 mol dm^{-3}, ΔT_d, against the number of hydroxyl groups of the polyhydric alcohols used. As can been seen, the ΔT_d shows the linear dependence

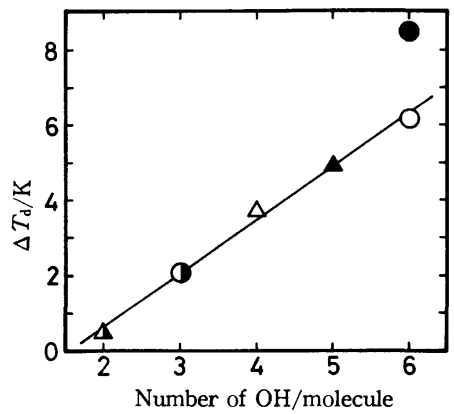

Fig. 4. Plot of the increase in the denaturation temperature of lysozyme at an identical alcohol concentration of 1 mol dm^{-3} against the number of hydroxyl groups of polyhydric alcohols.

on the number of hydroxyl groups of the polyhydric alcohols used with the exception of inositol. From the slope in Fig. 4, the T_d of lysozyme is raised by 1.4 K per hydroxyl group in the linear polyhydric alcohols, which is considerable larger than that measured by Gerlsma and Stuur.[6] A similar relation has been found with sugars as well as with polyhydric alcohols. Uedaira and Uedaira[12] have recently reported that the T_d of lysozyme in aqueous sugar solutions increases almost linearly with an increase in the number of equatorial hydroxyl groups in the sugar. From the direct dependence of ΔT_d on the number of hydroxyl groups of alcohols, it is presumed that there is no direct molecular interaction between the protein and the polyhydric alcohol, since any direct interaction would depend on the molar concentration.

The dependence of the denaturation enthalpy of lysozyme on the denaturation temperature in the presence of polyhydric alcohol is shown in Fig. 5. For

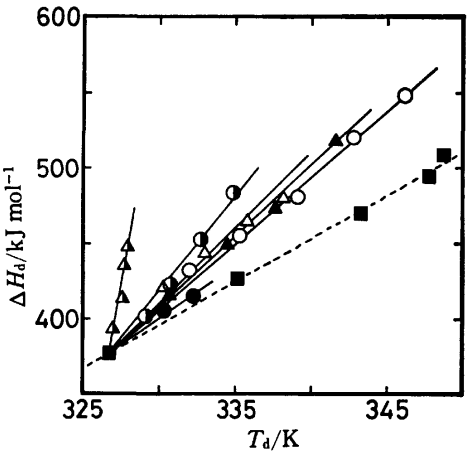

Fig. 5. The dependence of the denaturation enthalpy of lysozyme on the denaturation temperature.
The symbols used are identical with those in Fig. 2.

all the alcohols, the ΔH_d showed the linear function of T_d. This is similar to the behavior reported by Pfeil and Privalov[19] with variations of T_d produced by variation of the pH and addition of guanidinium chloride. However, there is a difference in the dependence of ΔH_d on T_d for each polyhydric alcohol. The slope of ΔH_d *vs.* T_d in the presence of alcohol decreased with an increase in the number of hydroxyl groups in the alcohol. This also suggests that the stabilizing effect of polyhydric alcohols on the thermal denaturation of protein is closely related to the number of hydroxyl groups in the alcohol.

Since ΔH_d is dependent on temperature, as mentioned above, the effect of polyhydric alcohols on ΔH_d must be estimated by comparison of the variation of ΔH_d with alcohols at identical temperature. In order to obtain the temperature dependence of ΔH_d in the absence of polyhydric alcohol, we also measured the thermal denaturation of lysozyme in glycine buffer solutions at different pH values and in acetate buffer solution at pH 5.0. These results are summarized in Table 1 together with those obtained by other investigators from calorimetric studies. Taking into account the difference in the measurement conditions such as heating rate, protein concentration, and ionic strength, our results are in good agreement with those obtained by other investigators. The dependence of ΔH_d on T_d in the absence of alcohol is shown in Fig. 5 together with that in the presence of alcohol. From the slope of this function, the temperature dependence of the denaturation enthalpy of lysozyme in the absence of alcohol, $(d\Delta H_d/dT_d)$, was obtained to be 5.6 kJ K^{-1} mol^{-1}, which was in rough agreement with that obtained from

Table 1. The denaturation temperatures and enthalpies of lysozyme at different pH values obtained by calorimetric studies

pH[a)]	T_d / K	ΔH_d / kJ mol^{-1}
1.0	319.2[b)]	234[b)]
2.0	326.7	377
	329.2[c)]	444[c)]
	325.2[d)]	382[d)]
2.5	335.2	427
3.0	343.2	470
	347.7[c)]	556[c)]
3.8	347.8	496
4.5	351.7[c)]	590[c)]
5.0	348.7	509
5.4	349.7[e)]	577[e)]

a) The following buffer solutions were used: 0.1 mol dm^{-3} glycine buffer for pH 2.0, 2.5, 3.0, and 3.8; 0.1 mol dm^{-3} acetate buffer for pH 5.0. b) O'Reilly and Karasz.[20)] c) Privalov and Khechinashvili.[11)] d) Velicelebi and Sturtevant.[17)] e) Delben and Crescenzi.[21)]

precision measurement by Pfeil and Privalov.[19)] Assuming that $(d\Delta H_d/dT_d)$ remains identical with the value in the absence of alcohol at all alcohol solutions used, the denaturation enthalpy of lysozyme in the presence of alcohol at a given temperature, $\Delta H_d°(a)$, is expressed as follows:

$$\Delta H_d°(a) = \Delta H_d + (d\Delta H_d/dT_d)(T_d° - T_d), \quad (1)$$

where ΔH_d and T_d are the observed enthalpy and temperature of denaturation in the presence of alcohol and $T_d°$ is a given temperature. Then, the variation of denaturation enthalpy by the addition of polyhydric alcohol at identical temperature, $\Delta(\Delta H_d°)$, can be evaluated by the following equation,

$$\Delta(\Delta H_d°) = \Delta H_d°(a) - \Delta H_d°(w), \quad (2)$$

where $\Delta H_d°(w)$ is the denaturation enthalpy in the absence of alcohol at same temperature.

Figure 6 shows the dependence of $\Delta(\Delta H_d°)$ on polyhydric alcohol concentration at 326.7 K which is the denaturation temperature of lysozyme in aqueous solution at pH 2.0. Although these plots show appreciable scatter, it is obvious that the $\Delta(\Delta H_d°)$ is a slight

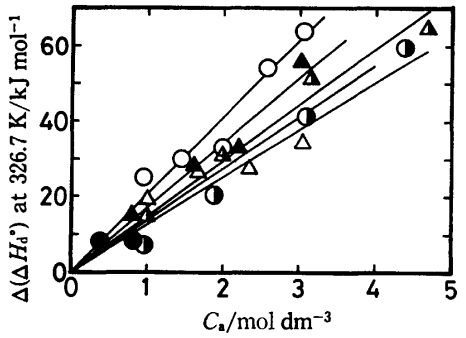

Fig. 6. The variation of the denaturation enthalpy of lysozyme with polyhydric alcohols at an identical temperature, 326.7 K, as a function of concentration of polyhydric alcohol.
The symbols used are identical with those in Fig. 2.

increasing function of alcohol concentration. However, the $\Delta(\Delta H_d°)$ value should be considerably smaller as compared with that presumed from the large increase in T_d. Substantially, the $\Delta(\Delta H_d°)$ values in the range of lower concentration of alcohol are within the experimental error in ΔH_d. Therefore, it is difficult to consider that the increase in the free energy change of denaturation by the addition of polyhydric alcohol results from only the slight increase of the denaturation enthalpy. These polyhydric alcohols for which data are available have lower dielectric constants than pure water.[22)] Thus, electrostatic interactions are stronger in these solutions than in water, which causes the denaturation enthalpy to increase. However, this contribution to the stabilizing effect appears to be relatively small.

It is interesting that the effect of polyhydric alcohols is different from that of monohydric alcohols. There have been many investigations which show the direct interaction of monohydric alcohols with protein.[23)] The unstabilizing effect of monohydric alcohols on the native structure of protein has been generally interpreted in terms of the interaction between protein and alcohol. Bull and Breese[24)] have reported from their study on the binding of alcohols to protein using equilibrium dialysis that monohydric alcohols are strongly bound to protein, but there is no direct binding of polyhydric alcohols to protein. Our presumption based on the direct dependence of ΔT_d on the number of hydroxyl groups of the added polyhydric alcohols is strongly supported by their observations. Therefore, it is conceivable that there exist other interactions which stabilize the native structure of protein in the system protein–alcohol–water. It is likely that polyhydric alcohols interact principally with the other component in the system, that is, water.

From thermodynamic studies of transfer of amino acids from water to aqueous solutions of polyhydric alcohols, Gekko and Noguchi[25)] have recently found that the enthalpy change of the transfer is positive for nonpolar side chains of amino acids and that polyhydric alcohols decrease the solubility of nonpolar groups by an unfavorable enthalpy effect. According to their findings, it is presumed that the added polyhydric alcohols dominantly affect the hydrophobic interactions between the nonpolar groups of protein. Back *et al.*[26)] have also reported that the hydrophobic interactions between pairs of hydrophobic groups are stronger in aqueous glycerol solutes than in pure water. Since hydrophobic interaction is a result of a rearrangement of the water molecules surrounding hydrophobic groups, it is likely that there is a relation between the effect of the added solutes on hydrophobic interaction and their effect on the structure of water. The effect of polyhydric alcohols on hydrophobic interaction and consequently on the thermal stability of protein may depend upon how they affect the structure of water.

There is no completely unambiguous numerical measure of "structure making" or "structure breaking" by a solute, but a change in the extent to which water is structured is accompanied by a volume change.[27)] According to Oakenfull and Fenwick,[28)] the effect of solute on the water structure is closely related with its

partial molar volume. The structure-making effect of polyhydric alcohols determined from their partial molar volume enhances in the order sorbitol>xylitol> erythritol>glycerol>ethylene glycol, that is, increasing number of hydroxyl groups per alcohol molecule. The structure-making effect of inositol, a cyclic alcohol, is larger than that of sorbitol. The stabilizing ability of polyhydric alcohols on the thermal denaturation of lysozyme also increases in the same order.

These results suggest the hypothesis that the dominant mechanism by which polyhydric alcohols stabilize protein against thermal denaturation is through their effect on the structure of the water, which, in turn, determines the strength of the hydrophobic interactions.

References

1) C. Tanford, *Adv. Protein Chem.*, **23**, 121 (1968).
2) F. Franks and D. Eagland, *CRC Crit. Rev. Biochem.*, **3**, 165 (1975).
3) D. Eagland, "Water: A Comprehensive Treatise," ed by F. Franks, Plenum Press, N. Y. (1975), Vol. 4, Chap. 5.
4) R. B. Simpson and W. Kauzmann, *J. Am. Chem. Soc.*, **75**, 5139 (1953).
5) S. Shifrin and C. L. Parrott, *Arch. Biochem. Biophys.*, **166**, 426 (1975).
6) S. Y. Gerlsma and E. R. Stuur, *Int. J. Peptide Protein Res.*, **4**, 377 (1972).
7) S. Y. Gerlsma, *Eur. J. Biochem.*, **14**, 150 (1970).
8) K. Gekko and T. Morikawa, *J. Biochem.* (*Tokyo*), **90**, 51 (1981).
9) R. L. Biltonen and E. Freire, *CRC Crit. Rev. Biochem.*, **1978**, 85.
10) P. L. Privalov, *Adv. Protein Chem.*, **33**, 167 (1979).
11) P. L. Privalov and N. N. Khechinashvili, *J. Mol. Biol.*, **86**, 665 (1974).
12) H. Uedaira and H. Uedaira, *Bull. Chem. Soc. Jpn.*, **53**, 245 (1980).
13) Y. Fujita, A. Miyanaga, and Y. Noda, *Bull. Chem. Soc. Jpn.*, **52**, 3659 (1979).
14) Y. Fujita, S. Izumiguchi, and Y. Noda, *Int. J. Peptide Protein Res.*, **19**, 25(1982).
15) K. Hamaguchi, *J. Biochem.* (*Tokyo*), **56**, 441 (1964).
16) R. M. Parodi, E. Bianchi, and A. Ciferri, *J. Biol. Chem.*, **248**, 4047 (1973).
17) G. Velicelebi and J. M. Sturtevant, *Biochemistry*, **18**, 1180 (1979).
18) E. E. Schrier, R. T. Ingwall, and H. A. Scheraga, *J. Phys. Chem.*, **69**, 298 (1965).
19) W. Pfeil and P. L. Privalov, *Biophys. Chem.*, **4**, 23, 33 (1976).
20) J. M. O'Reilly and F. E. Karasz, *Biopolymers*, **9**, 1429 (1970).
21) F. Delben and V. Crescenzi, *Biochim. Biophys. Acta*, **194**, 615 (1969).
22) G. Akerlof, *J. Am. Chem. Soc.*, **54**, 4125 (1932).
23) K. Ikeda and K. Hamaguchi, *J. Biochem.* (*Tokyo*), **68**, 785 (1970).
24) H. B. Bull and K. Breese, *Biopolymers*, **17**, 2121 (1978).
25) K. Gekko and H. Noguchi, 17th Annual Meeting of the Biophys. Soc. Japan, Nagoya, Oct. 1979, Abstr. p. 303.
26) J. F. Back, D. Oakenfull, and M. B. Smith, *Biochemistry*, **18**, 519 (1979).
27) F. Franks and D. S. Reid, "Water: A Comprehensive Treatise," ed by F. Franks, Plenum Press, N. Y. (1973), Vol. 2, Chap. 5.
28) D. Oakenfull and D. F. Fenwick, *J. Chem. Soc., Faraday Trans. 1*, **75**, 636 (1979).

Synthesis of [3.3](1,3)Ferrocenophane and Its Derivatives

Akira KASAHARA,* Taeko IZUMI, Yoshio YOSHIDA, and Iwao SHIMIZU
Department of Applied Chemistry, Faculty of Engineering, Yamagata University, Yonezawa 992
(Received September 22, 1981)

[3.3](1,3)Ferrocenophane-1,15-diene-3,14-dione was synthesized *via* the base-catalyzed condensation of 1,3-ferrocenedicarbaldehyde with 1,3-diacetylferrocene utilizing the high dilution technique. The reduction of the compound with $LiAlH_4$–$AlCl_3$ and the subsequent catalytic hydrogenation led to the formation of [3.3](1,3)-ferrocenophane. The transannular π-electronic interactions between the two ferrocene moieties in these compounds were examined on the basis of NMR and electronic spectra.

Recently, cyclophane compounds in which two or more aromatic rings are mutually stratified have been investigated, with emphasis on transannular π-electronic interactions.[1] However, there are only a few investigations of ferrocenophane having transannular π-electronic interactions: [2.2]Ferrocenophane-1,13-diyne,[2] [2.2]-ferrocenophane-1,13-diene,[3] [2]paracyclo[2]paracyclo-[2](1,1')ferrocenophane derivatives,[4] [3.3](1,1')-ferrocenophane-1,15-diene-3,14-dione,[5] [5.5](1,1')ferrocenophane derivatives,[5] and [0]metacyclo[2]-metacyclo[0](1,1')ferrocenophan-7-ene.[6] Benedikt and Schlögl[7] have recently reported on the synthesis of [2.2](1,2)ferrocenophane and Yamakawa *et al.*[8] have described the synthesis of [2.2.2](1,3)ferrocenophanetriene.

The synthetic methods and structures as well as chemical and physical properties of [2.2]metacyclophanes[9] and [3.3]metacyclophanes[10] have been widely investigated: Based on this and similar experiences in the metallocene field it seemed of considerable interest to prepare and study related metallocenophanes, especially in the ferrocenophane series. According to its molecular geometry, ferrocene cannot accommodate two ethylene bridges between two ferrocene units in the 1,3-positions such as in [2.2]metacyclophane; however, [3.3](1,3)ferrocenophane seemed to be —according to molecular models—a promising target for synthetic and structural investigations. This paper deals with the preparations of four [3.3](1,3)ferrocenophane derivatives (**1**, **2**, **3**, and **4**) having transannular π-electronic interactions.

Experimental

Materials and Measurement. Melting points were not corrected. All the reactions were performed under nitrogen. 1,3-Diacetylferrocene (**5**) was prepared according to the method described by Nesmeyanov *et al.*[11] The IR, NMR, mass, and electronic spectra were recorded with a Hitachi 215, a Hitachi R-22, a Hitachi RMU-6M, and a Hitachi EPS-

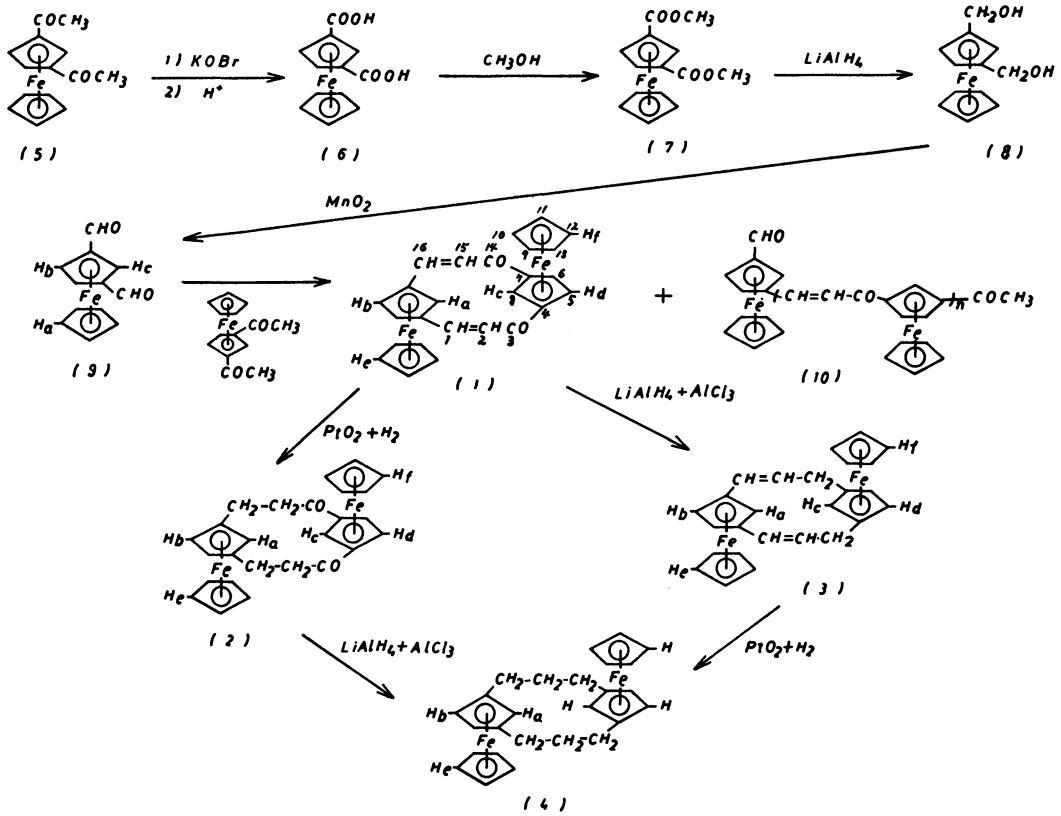

Scheme 1. Synthesis of [3.3]ferrocenophane derivatives.

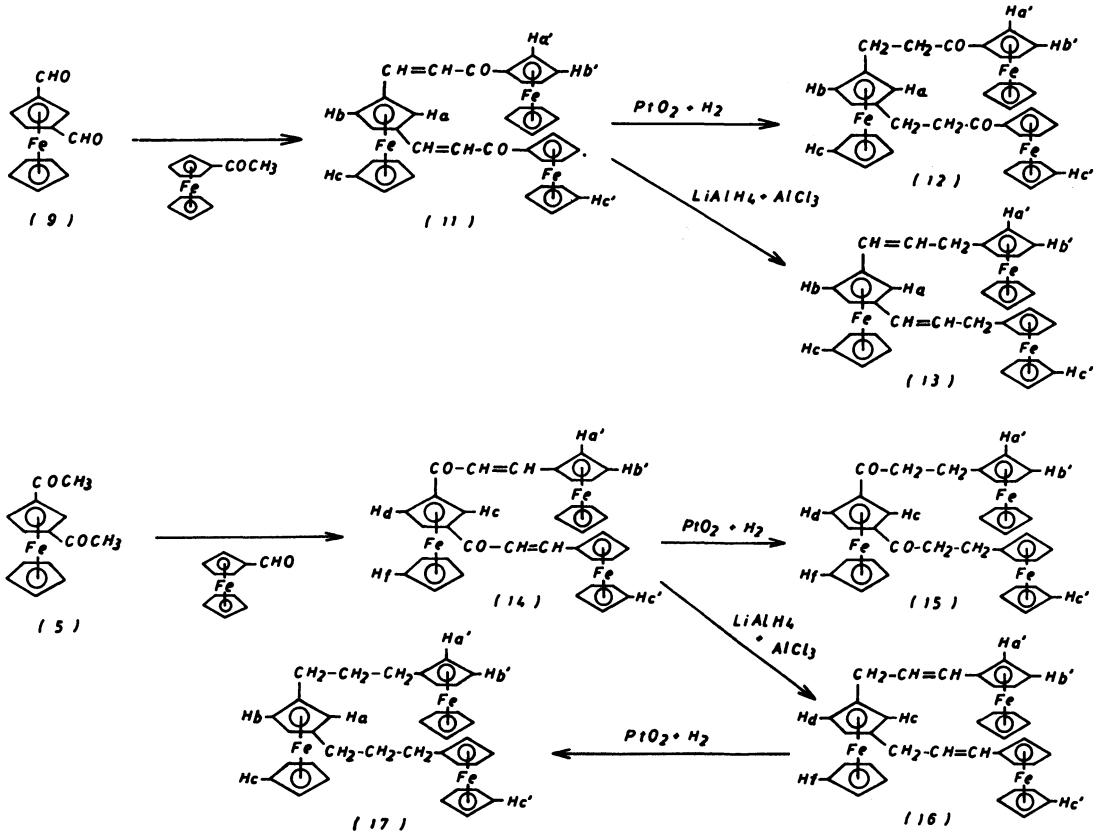

Scheme 2. Synthesis of the refernce compounds.

3T spectrometer, respectively.

Dimethyl 1,3-Ferrocenedicarboxylate (7). To a solution of 23 g (0.58 mol) of sodium hydroxide in 140 ml of water was dropwise added 26 g (0.16 mol) of bromine at 0—10 °C with stirring. Then 70 ml of dioxane was added in portions. At a temperature of 0—5°C, 7.0 g (0.026 mol) of **5** was added in small portions to the vigorously stirred solution. After the addition was over, stirring was continued for one additional hour at 0—5 °C. The reaction mixture was filtered, the filtrate was washed with CH_2Cl_2, and the aqueous layer was heated up to 80 °C. After cooling, acidification with 10% HCl gave orange red crystals, 1,3-ferrocenedicarboxylic acid (**6**) (3.6 g, 50% yield), mp 228 °C (decomp) (lit,[8] mp 227. 5 °C (decomp)). IR (KBr): 3100, 1675 (-C=O), 1100, 1000 cm^{-1}. MS: *m/e* 274 (M^+).

A suspension of 7.0 g of crude **6** in 150 ml of methanol containing 1 ml of concd H_2SO_4 was heated under reflux for 28 h. After removal of the solvent, the residue was taken up with $CHCl_3$ and chromatographed on silica gel with benzene. The crude product was recrystallized from benzene–hexane to give 6.9 g (90% yield) of **7**, mp 155—157 °C (lit,[8] mp 155—156 °C). IR (KBr): 3100, 1710 (ester), 1100, 1000 cm^{-1}. MS: *m/e* 302 (M^+).

1,3-Bis(hydroxymethyl)ferrocene (8). To a solution of 2.2 g (0.053 mol) of $LiAlH_4$ in 150 ml of dry diethyl ether was added dropwise a solution of 4.5 g (0.015 mol) of **7** in 50 ml of dry diethyl ether at room temperature with stirring. After the solution was heated under reflux for an additional 4 h, the reaction mixture was decomposed with a small amount of cold water. Yellow crystalline **8**, mp 115—116 °C (lit,[8] mp 115—117.5 °C), was obtained in 95% yield (3.5 g). IR (KBr): 3400, 3200, 3100, 1100, 1000, 905 cm^{-1}. MS: *m/e* 246 (M^+).

1,3-Ferrocenedicarbaldehyde (9). Active manganese(IV) dioxide (30 g) was added to a solution of **8** (3.0 g, 0.012 mol) in $CHCl_3$ (200 ml) and the resulting mixture was stirred in the dark for 12 h. After filtration, the red solution was evaporated and the dry residue was chromatographed on silica gel with benzene. Bright red crystals, mp 69—70 °C (lit,[8] yellow oil), were obtained in 91% yield (2.7 g). IR (KBr): 3100, 1670 (-C=O), 1100, 995, 920, 905 cm^{-1}. NMR ($CDCl_3$): δ=4.34 (5H, s, H_a), 5.13 (2H, m, H_b), 5.40 (1H, m, H_c), 10.03 (2H, s, -CHO). Found: C, 59.58; H, 4.25%; M^+, 242. Calcd for $C_{12}H_{10}O_2Fe$: C, 59.54; H, 4.16%; M, 242.

[3.3](1,3)Ferrocenophane-1,15-diene-3,14-dione (1). To a solution of **9** (2.4 g, 0.01 mol) in ethanol (150 ml) containing 15 g of potassium hydroxide was dropwise added a solution of 2.7 g (0.01 mol) of **5** in ethanol (160 ml) by a motor driven syringe pump over 4 h at room temperature. The resulting mixture was stirred at 55 °C for an additional 2 h, and then evaporated *in vacuo*. The residue was extracted with $CHCl_3$ (300 ml) to isolate the desired product from the polycondensation products (**10**). The $CHCl_3$ extracts were washed with brine to neutralize them and then dried over anhydrous $MgSO_4$. After removal of the solvents, the residue was chromatographed on silica gel with benzene–ether to give 0.6 g 10% yield of **1**, deep red crystals, mp 230—232 °C (decomp). IR (KBr): 3100, 1650 (-C=O), 1100, 995, 920, 905, 815 cm^{-1}. MS: *m/e* 476 (M^+), 238 (*m/2e*), 56 (Fe^+). Found: C, 65.51; H, 4.18%. Calcd for $C_{26}H_{20}O_2Fe_2$: C, 65.58; H, 4.23%; M, 476.

[3.3](1,3)Ferrocenophane-1,16-dione (2). An ethanol (100 ml) solution of **1** (0.5 g) was hydrogenated with PtO_2 at room temperature under ordinary pressure. The reaction mixture was filtered to remove the catalyst and the filtrate was evaporated. The residue was chromatographed over silica gel with benzene–hexane to give 0.45 g (90% yield) of **2**, orange red needles,mp 183—184 °C(decomp). IR(KBr): 3100,

1670 (-C=O), 1100, 1000, 920, 905 cm^{-1}. MS: *m/e* 480 (M^+), 240 (*m/2e*), 56 (Fe^+). Calcd for $C_{26}H_{24}O_2Fe_2$: C, 65.03; H, 5.03%; M, 480.

[3.3](1,3)Ferrocenophane-1,15-diene (3). A dry diethyl ether solution (100 ml) of **1** (0.40 g) was added to a suspension of $LiAlH_4$ (0.2 g) and $AlCl_3$ (0.8 g) in dry diethyl ether (50 ml). After refluxing for 4 h, the excess reagent was decomposed with moist ether and then with water. After the resulting reaction mixture was extracted with ether, the ether extracts were washed with water, saturated sodium hydrogencarbonate solution, and finally brine, and then dried over anhydrous $MgSO_4$. The removal of the solvent left 0.25 g (65% yield) of **3**, orange yellow crystals, mp 196—197 °C (decomp). IR (KBr): 3100, 1100, 1000, 925, 905, 800 cm^{-1}. MS: *m/e* 448 (M^+), 224 (*m/2e*), 56 (Fe^+). Found: C, 69.55; H, 5.23%. Calcd for $C_{26}H_{24}Fe$: C, 69.67; H, 5.38%: M, 448.

[3.3](1,3)Ferrocenophane (4). Reduction of **2** (0.20 g) with $LiAlH_4$–$AlCl_3$ in anhydrous diethyl ether was carried out in the the same way as described for **3**, and 0.11 g of **4** (60% yield), yellow crystals, mp 202—203 °C (decomp), was obtained. Catalytic hydrogenation of **3** with PtO_2 in ethanol also led to the formation of **4** in 75% yield. IR (KBr): 3100, 1100, 995, 925, 905 cm^{-1}. MS: *m/e* 452 (M^+), 226 (*m/2e*), 56 (Fe^+). Found: C, 68.91; H, 6.08%. Calcd for $C_{26}H_{28}Fe_2$: C, 69.05; H, 6.24%; M, 452.

1,3-Bis[2-(ferrocenylcarbonyl)vinyl]ferrocene (11). To a solution of **9** (2.4 g, 0.01 mol) in ethanol (150 ml) containing 15 g of potassium hydroxide was dropwise added a solution of acetylferrocene (4.6 g, 0.02 mol) in ethanol (150 ml). The resulting mixture was stirred at 55 °C for an additional 2 h, and then evaporated *in vacuo*. The extracts with $CHCl_3$ were washed with an aqueous solution of HCl, saturated sodium hydrogencarbonate solution, and brine, then dried and evaporated. The residue was chromatographed over silica gel with benzene–chloroform to afford **11**, red crystals, mp 220—221 °C (3.5 g, 53% yield). IR (KBr): 3100, 1650 (-C=O), 1590, 970 (*trans* -CH=CH-), 1100, 1000, 920, 905 cm^{-1}. Found: C, 65.21; H, 4.48%; M^+, 662. Calcd for $C_{36}H_{30}O_2Fe_2$: C, 65.29; H, 4.56%, M, 662.

1,3-Bis[2-(ferrocenylcarbonyl)ethyl]ferrocene (12). An ethanol–dioxane (200 ml, 1 : 1) solution of **11** (0.9 g) was hydrogenated with PtO_2 at room temperature. The reaction mixture was filtered to remove the catalyst, and the filtrate was evaporated. The residue was chromatographed over silica gel to give 0.8 g of **12** (92% yield), orange red crystals, mp 128—130 °C. IR (KBr): 3100, 1660 (-C=O), 1100, 1000, 920, 905 cm^{-1}. Found: C, 64.73; H, 5.05%; M^+, 666. Calcd for $C_{36}H_{34}O_2Fe_2$: C, 64.86; H, 5.14%; M, 666.

1,3-Bis(3-ferrocenyl-1-propenyl)ferrocene (13). The reduction of **11** with $LiAlH_4$–$AlCl_3$ was carried out in the same way as described for **3**, and orange yellow crystals of **13**, mp 113—115 °C, were obtained in 57% yield. IR (KBr): 3100, 1620, 960 (*trans* -CH=CH-), 1100, 1000, 925, 900 cm^{-1}. Found: C, 68.23; H, 5.48%; M^+, 634. Calcd for $C_{36}H_{34}Fe_2$: C, 68.11; H, 5.40; M, 634.

1,3-Bis(3-ferrocenylacryloyl)ferrocene (14). The base-catalyzed condensation reaction of ferrocenecarbaldehyde (4.3 g, 0.02 mol) with **5** (2.7 g, 0.01 mol) was carried out in the same way as described for **11**, and red crystals of **14**, mp 237—238 °C (decomp), were obtained in 60% yield. IR(KBr): 3100, 1645 (-C=O), 1600, 980 (*trans* -CH=CH-), 1100, 1000, 920, 905 cm^{-1}. Found: C, 65.17; H, 4.41%; M^+, 662. Calcd for $C_{36}H_{30}O_2Fe_2$: C, 65.29; H, 4.56%; M, 662.

1,3-Bis(3-ferrocenylpropionyl)ferrocene (15). The catalytic hydrogenation of **14** with PtO_2 in ethanol–dioxane was carried out in the same way as described for **12**, and orange yellow crystals of **15**, mp 188—190 °C, were obtained in 90% yield. IR (KBr): 3100, 1665 (-C=O), 1100, 1000, 920, 905 cm^{-1}. Found: C, 64.80; H, 5.02%; M^+, 666. Calcd for $C_{36}H_{34}O_2Fe$: C, 64.86; H, 5.14%; M, 666.

1,3-Bis(3-ferrocenylallyl)ferrocene (16). The reaction of **14** with $LiAlH_4$–$AlCl_3$ was carried out in the same way as described for **3**, and an orange yellow oil of **16** was obtained in 48% yield. IR (oil film): 3100, 1615, 955 (*trans* -CH=CH-), 1100, 1000, 925, 900 cm^{-1}. Found: C, 68.17; H, 5.45%; M^+, 634. Calcd for $C_{36}H_{34}Fe_2$: C, 68.11; H, 5.45%; M, 634.

1,3-Bis(3-ferrocenylpropyl)ferrocene (17). The catalytic hydrogenation of **16** was carried out in the same way as described for **3**, and a yellow oil of **17** was obtained in 94% yield. IR (oil film): 3100, 2950, 1100, 1000, 925,905 cm^{-1}. Found: C, 67.86; H, 6.11%; M^+, 638. Calcd for $C_{36}H_{38}Fe_2$: C, 67.74; H, 6.00%; M, 638.

Results and Discussion

Synthesis. All of the [3.3](1,3)ferrocenophanes (**1**, **2**, **3**, and **4**) were prepared by the synthetic sequence shown in Scheme 1. As spectral reference compounds, 1,3-disubstituted ferrocene derivatives (**11**—**17**) were synthesized (see Scheme 2).

In connection with the synthesis of the ferrocenophanes (**1**—**4**), it became desirable to synthesize 1,3-ferrocenedicarbaldehyde (**9**)[12] in quantity. A treatment of 1,3-diacetylferrocene (**5**) with sodium hypobromite in dioxane–H_2O below 10 °C, led to the formation of 1,3-ferrocenedicarboxylic acid (**6**) in 50% yield. Then, 1,3-bis(hydroxymethyl)ferrocene (**8**) was synthesized in 95% yield by the usual $LiAlH_4$ reduction of dimethyl ester (**7**), which was prepared by acid-catalyzed esterification of **6**. The oxidation reaction of **8** in chloroform with active manganese dioxide led to the formation of **9** in good yield.

Under high dilution conditions, a base-catalyzed (ethanolic KOH) condensation of **5** with **9** gave the desired [3.3](1.3)ferrocenophane-1,15-diene-3,14-dione (**1**), accompanied by polycondensation products (**10**). On the other hand, using potassium *t*-butoxide or potassium ethoxide as a base catalyst, the reaction led only to the formation of **10**. The catalytic hydrogenation of **1** afforded [3.3](1,3)ferrocenophane-1,16-dione (**2**) and the reduction of **1** with $LiAlH_4$–$AlCl_3$ gave [3.3](1,3)ferrocenophane-1,15-diene (**3**). Furthermore, both the reduction of **2** with $LiAlH_4$–$AlCl_3$ and the catalytic hydrogenation of **3** afforded the same product: [3.3](1,3)ferrocenophane (**4**).

Structures and Spectra. The NMR spectral data of **1**—**4** and the reference compounds (**11**—**17**) are summarized in Table 1. The structural assignment for **1** is based on spectral evidence and the elemental analyses. The mass spectrum shows two prominent peaks; a molecular ion at *m/e* 476 and a doubly charged ion at *m/2e* 238. This fragmentation pattern is normally observed in [2.2]- and [3.3](1,1')ferrocenophane.[2,3,5] The IR spectrum in **1** exhibits the characteristic absorptions of the carbonyl (1650 cm^{-1}) and *cis* olefinic groups (815cm^{-1}), and of the 1,3-disubstituted ferrocene ring (925 and 905 cm^{-1}).[13] The NMR spectrum of **1** is also consistent with a cyclophane structure and the *anti* orientation of the cyclopentadienyl rings. The chemical

TABLE 1. NMR DATA OF [3.3](1,3) FERROCENOPHANE DERIVATIVES (**1**—**4**) AND REFERENCE COMPOUNDS (**11**—**17**) IN $CDCl_3$ (δ)

Compound	Cyclopentadieny ring protons	Other protons
1	H_a 4.30(s,1H)	7.11(d,2H,J=10 Hz,-C=CH-CO-)
	H_b 4.83(b-s,2H)	7.81(d,2H,J=10 Hz,-CH=C-CO-)
	H_c 4.39(s,1H)	
	H_d 5.44(b-s,2H)	
	H_e 4.27(s,5H)	
	H_f 4.33(s,5H)	
2	H_a 3.87(s,1H)	2.67—2.75(m,8H,-CH_2CH_2CO-)
	H_b 4.08(s,2H)	
	H_c 3.91(s,1H)	
	H_d 4.93(b-s,2H)	
	H_e+H_f 4.12(s,10H)	
3	H_a 3.90(b-s,1H)	3.02(m,4H,-C=C-CH_2-Fc)
	H_b 4.33(b-s,2H)	5.75(m,2H,-C=CH-CH_2-)
	H_c 3.85(b-s,1H)	6.18(b-s,2H,-CH=C-CH_2-)
	H_d 4.08(b-s,2H)	
	H_e+H_f 4.02(s,10H)	
4	H_a 3.86(s,2H)	1.46—1.75(m,4H,-C-CH_2-C-)
	H_b 4.06(s,4H)	2.22(m,8H,-CH_2-Fc)
	H_e 4.00(s,10H)	
11	H_a 5.00(s,1H)	6.80(d,2H,J=16 Hz,-C=CH-CO-)
	H_b 4.89(b-s,2H)	7.69(d,2H,J=16 Hz,Fc-CH=C-CO-)
	$H_c+H_{c'}$ 4.18(b-s,15H)	
	$H_{a'}$ 4.84(t,4H)	
	$H_{b'}$ 4.57(t,4H)	
12	H_a 4.05(b-s,1H)	2.56—2.93(m,8H,-CH_2CH_2CO-)
	H_b 4.07(s,1H)	
	$H_{a'}$ 4.71(t,4H)	
	$H_{b'}$ 4.43(t,4H)	
	$H_c+H_{c'}$ 4.10(s,15H)	
13	H_a+H_b 4.15(m,3H)	3.01(d-d,4H,-CH_2-)
	$H_{a'}+H_{b'}$ 4.07(m,8H)	6.01(m,2H,-C=CH-C-)
	$H_c+H_{c'}$ 4.00(s,15H)	7.31(d,2H,-CH=C-C-)
14	H_c 5.56(s,1H)	6.81(d,2H,J=16 Hz,-C=CH-CO-)
	H_d 5.19(s,2H)	7.78(d,2H,J=16 Hz,-CH=C-CO-)
	$H_f+H_{c'}$ 4.18(s,15H)	
	$H_{a'}$ 4.64(t,4H)	
	$H_{b'}$ 4.51(t,4H)	
15	H_c 5.03(s,1H)	2.64—2.93(m,8H,-CH_2CH_2CO-)
	H_d 5.00(s,2H)	
	$H_f+H_{c'}$ 4.11(s,15H)	
	$H_{a'}+H_{b'}$ 4.07(s,8H)	
16	H_c+H_d 4.07(s,3H)	3.01(d-d),4H,-CH_2-)
	H_f+H_d 4.00(s,15H)	5.98(m,2H,-C=CH-C-)
	$H_{a'}$ 4.17(m,4H)	7.28(d,2H,-CH=C-C-)
	$H_{b'}$ 4.12(m,4H)	
17	H_a+H_b 4.08(m,3H)	1.66(m,4H,-C-CH_2-C-)
	$H_c+H_{a'}+H_{b'}$ 4.02(b-s,13H)	2.20—2.34(m,8H,Fc-CH_2-)
	$H_{c'}$ 3.96(s,10H)	

shifts for H_a and H_c protons of the cyclopentadienyl rings are found respectively at 0.70 and 1.17 ppm upfield relative to those (H_a and H_c) of the reference compounds, 1,3-bis(2-ferrocenylcarbonylvinyl)ferrocene (**11**) and 1,3-bis(3-ferrocenylacryloyl)ferrocene (**14**). These upfield shifts are expected due to the position of protons (H_a and H_c in **1**) relative to the shielding cone of the nearby cyclopentadienyl ring. On the other hand, the shifts of H_b (Δ, 0.06 ppm) and H_d (Δ, −0.25 ppm) in **1** are negligible, compared with those (H_b and H_d) in **11** or **14**. The smaller upfield shift of the H_b and H_d relative to the H_a and H_c protons is consistent with the *anti* structure for **1** (see Fig. 1). Figure 2 shows the electronic spectra of **1**, **11**, and **14**. In the spectrum of ferrocene itself, the long wavelength bands at 325 and 440 nm can be assigned with some certainty to (d-d) type transitions within the ligand field formalism.[14] The electronic spectrum of **1** is consistent with a cyclophane structure and exhibits three broadened maxima at λ_{max}(dioxane) 308, 422, and 504 nm. Similar to the

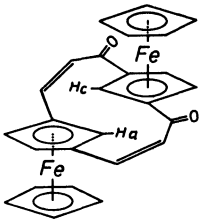

Fig. 1. Conformation of [3.3](1,3)-ferrocenophane (**1**).

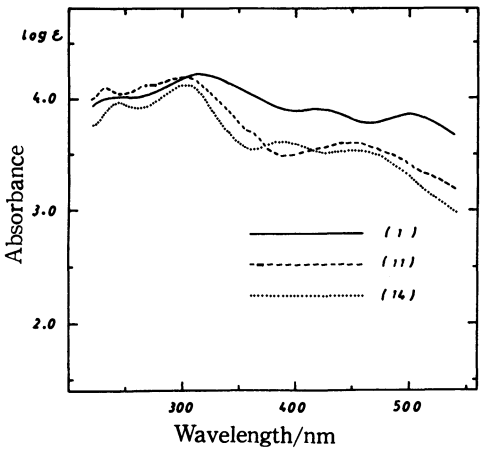

Fig. 2. Electronic spectra of **1**, **11**, and **14** in dioxane.

electronic spectra of other cyclophanes there are observed a general broadening of all bands in the spectrum and hyperchromic and bathochromic shifts of the long wavelength band relative to **11** or **14**. This is probably due to some transannular interaction between the two ferrocene moieties.

The structure of **2** can be assigned to *anti*-conformation by a comparison of its NMR data with those of the reference compounds: 1,3-Bis(2-ferrocenylcarbonylethyl)ferrocene (**12**) and 1,3-bis(3-ferrocenylpropionyl)ferrocene (**15**). Similar to the case of **1**, the upfield shifts of H_b (Δ, −0.01 ppm) and H_d protons (Δ, 0.07 ppm) in **2**, compared with those in **12** and **15**, are explained by the *anti*-structure, in which the internal cyclopentadienyl protons (H_a and H_c) lie in close proximity to the π-cloud (and the cone of shielding) of the opposed cyclopentadienyl moiety. Furthermore, the NMR spectrum of **2** contained H_a at δ 3.87 ppm, indicating an upfield shift (0.53 ppm) with respect to the diene **1** which is characteristic of such pairs of cyclophanes (with saturated and unsaturated bridges).[14] The IR spectrum of **2** also exhibits bands due to the carbonyl group (1670 cm^{-1}) and the 1,3-disubstituted ferrocene rings (920 and 905 cm^{-1}), and the mass spectrum shows two prominent peaks: one due to a molecular ion (*m/e* 480) and the other to a doubly-charged ion (*m/e* 240). In the electronic spectra of **2**, compared with those of **12** and **15**, all the absorption curves exhibit common features of cyclophane, *viz.*, broarding, bathochromic, and hyperchromic shifts, caused by the transannular electronic interaction (see Fig. 3).

In compound **3**, the IR spectrum reveals the presence

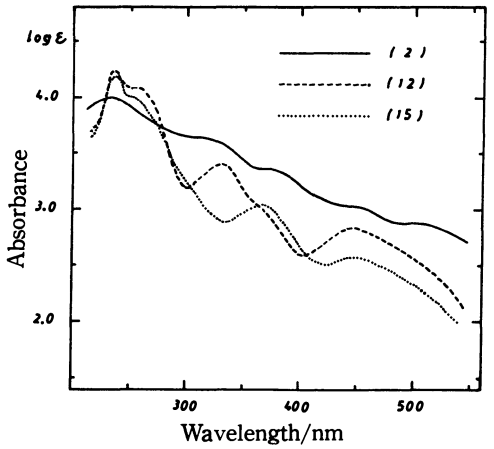

Fig. 3 Electronic spectra of **2**, **12**, and **15** in dioxane.

of *cis* olefinic bonds (800 cm^{-1}) and 1,3-disubstituted ferrocene ring (925 and 905 cm^{-1}), and in the mass spectrum, the most intense peaks is that due to the parent ion of *m/e* 448; the remaining two prominent peaks are *m/e* 224 and 56, corresponding to a doubly-charged ion and Fe^+. In the NMR spectrum of **3**, the upfield shifts of H_a (Δ, 0.25 ppm) and H_c protons (Δ, 0.22 ppm) and the downfield shifts of H_b (Δ, −0.18 ppm) and H_d protons (Δ, −0.01 ppm), compared with the corresponding ones in the reference compounds: 1,3-bis(3-ferrocenyl-1-propenyl)ferrocene (**13**) and 1,3-bis(3-ferrocenyl-2-propenyl)ferrocene (**16**), are also explained by the *anti*-structure. The upfield shifts of H_a and H_c protons in **3** are not marked, compared with those of compounds **1** and **2**. In Fig. 4, however, the electronic absorption curve becomes relatively structureless, with bathochromic shifts and increased intensity of the bands near 340 and 450 nm, compared with those of the reference compounds **13** and **16**. This indicates that the two ferrocene moieties in **3** interact strongly with each other.

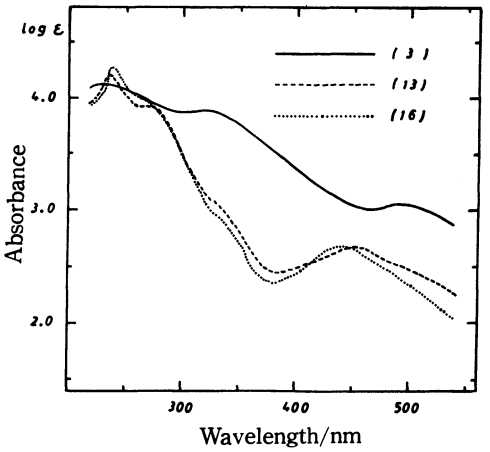

Fig. 4. Electronic spectra of **3**, **13**, and **16** in dioxane.

The spectrum of **4** exhibits bands at 925 and 905 cm^{-1}, which are characteristic of the 1,3-disubstituted ferrocene ring. By comparison with the NMR spectrum

of the reference compound, 1,3-bis(3-ferrocenylpropyl)-ferrocene (**17**), the upfield shifts of H_a protons (Δ, 0.22 ppm) and the small upfield shifts of H_b protons (Δ, 0.02 ppm) are consistent with the *anti*-structure for **4**, similarly to the cases of **1**, **2**, and **3**. The electronic spectrum of **4** (Fig. 5) exhibits two broadened maxima in the visible region, at λ_{max}(dioxane) 320 and 488 nm, and there is observed a general broadening and a bathochromic shift (48 nm) of the long wavelength band relative to **17**. These are probably due to some transannular π-electronic interactions between the two ferrocene moieties.

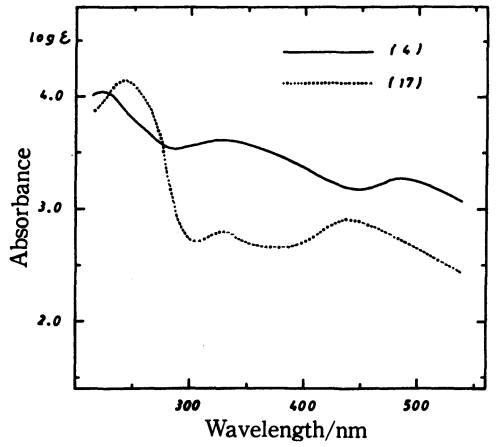

Fig. 5. Electronic spectra of **4** and **17** in dioxane.

Financial support by the Ministry of Education, Science and Culture, Japanese Government, (Grant-in-Aid No. 554137) is gratefully acknowledged.

References

1) S. Misumi and T. Otsubo, *Acc. Chem. Res.*, **11**, 251 (1978).
2) M. Rosenblum, N. M. Brawn, D. Clappenelli, and J. Tancrede, *J. Organomet. Chem.*, **24**, 469 (1970).
3) A. Kasahara and T. Izumi, *Chem. Lett.*, **1978**, 21.
4) A. Kasahara, T. Izumi, and I. Shimizu, *Chem. Lett.*, **1979**, 1119.
5) A. Kasahara, T. Izumi, and I. Shimizu, *Chem. Lett.*, **1979**, 1317.
6) A. Kasahara, T. Izumi, and H. Umezawa, *Chem. Lett.*, **1980**, 1039.
7) M. Benedikt and K. Schlögl, *Monatsh. Chem.*, **109**, 1805 (1978).
8) K. Yamakawa, O. Tachikawa, and M. Hisatome, The 12th Symposium on Non-benzenoid Aromatic Compounds, Matsumoto, Japan, September 1979, Abstr. p. 141.
9) S. Hayashi and T. Sato, *Nippon Kagaku Zasshi*, **91**, 950 (1970); T. Sato, *ibid.*, **92**, 277 (1971); F. Vögtle and P. Neumann, *Synthesis*, **1973**, 85.
10) T. Shinmyozu, T. Inazu, and T. Yoshino, *Chem. Lett.*, **1976**, 1405; **1979**, 541; H. A. Staab and A. Dohling, *Tetrahedron Lett.*, **1979**, 2019.
11) A. N. Nesmeyanov, E. V. Leonova, N. S. Kochetkova, A. I. Malkova, and A. G. Makarovskaya, *J. Organomet. Chem.*, **96**, 275 (1975).
12) The synthetic method of **9** has been briefly reported by Yamakawa *et al.*[8]
13) M. Rosenblum, "Chemistry of the Iron Group Metallocenes," Interscience Publishers, New York, Part 1, pp. 39, 85, and 211.
14) Ref. 13, p. 42.
15) R. H. Mitchell and V. Boekelheide, *J. Am. Chem. Soc.*, **96**, 1547 (1974); J. R. Davy and J. A. Reiss, *Aust. J. Chem.*, **29**, 163 (1976); J. R. Davy, M. N. Iskander, and J. A. Reiss, *ibid.*, **32**, 1067 (1979).

New Synthesis of Megastigma-4,6,8-trien-3-ones, 3-Hydroxy-β-ionol, 3-Hydroxy-β-ionone, 5,6-Epoxy-3-hydroxy-β-ionol, and 3-Oxo-α-ionol

Osamu TAKAZAWA,* Hiroshi TAMURA, Kunio KOGAMI, and Kazuo HAYASHI
Kawasaki Research Laboratories, T. Hasegawa Co. Ltd., 335 Kariyado, Nakahara-ku, Kawasaki 211
(Received October 5, 1981)

The Lewis acid-catalysed reaction of 1-trimethylsiloxy-1,3-cyclohexadienes with aldehydes and trialkyl orthoformates afforded the corresponding 4-substituted 2-cyclohexenones. A new reaction of 2,4,6-trienones with *m*-chloroperbenzoic acid followed by the reduction with zinc in acetic acid gave 7-hydroxy-3,5-dienones. Utilizing these efficient reactions, megastigma-4,6,8-trien-3-ones, 3-hydroxy-β-ionol, 3-hydroxy-β-ionone, 5,6-epoxy-3-hydroxy-β-ionol, and 3-oxo-α-ionol were successfully synthesized.

A large number of megastigmane derivatives, which are considered to be carotenoid metabolites having 13 carbon atoms, have been isolated successively from various tobacco leaves as neutral aroma constituents. Most of them have an oxygen function at the C-3 position in their cyclohexane rings, such as megastigma-4,6,8-trien-3-ones (**1**),[1] 3-hydroxy-β-ionol (**2**),[2] 3-hydroxy-β-ionone (**3**),[3] 5,6-epoxy-3-hydroxy-β-ionol (**4**),[4] and 3-oxo-α-ionol (**5**).[5] Recently, **1** and **3** were also found in Kudzu oil (Pueravia lobata Ohwi).[6] A number of synthetic methods for these megastigmane derivatives have been reported,[7] because they are considered to be potent flavoring components of tobacco and are frequently utilized as intermediates leading to carotenoids such as zeaxanthin. However, there still remain many problems, such as starting material, overall yield, and synthetic route.

In this paper, we will report a simple and efficient synthesis of **1** *via* the intermediate (**8a**) starting from readily available isophorone (**6a**), and an efficient conversion of **1** into **2**—**5** by way of an other intermediate (**13**).

Results and Discussion

The Lewis acid-catalysed aldol-type reactions of silyl enol ethers with various electrophiles such as carbonyl compounds, acetals, and trialkyl orthoformates were studied by Mukaiyama *et al.*[8] Recently, attention is focused on the reaction of dienoxysilanes with various electrophiles, which is a most useful means of organic synthesis because of its high selectivity of γ-attacking products. Mukaiyama and Ishida reported the $TiCl_4$-promoted reaction of 1-trimethylsiloxy-1,3-butadiene with acetals giving 5-alkoxy-2-enals.[9] In the course of our studies, some reports on the Lewis acid-catalysed reaction of dienoxysilanes with various electrophiles have appeared.[10]

In order to apply to the syntheses of the desired megastigmane derivatives, we attempted to react 1-trimethylsiloxy-1,3-cyclohexadienes (**7**) with aldehydes or trialkyl orthoformates in the presence of Lewis acid. As a method to synthesize **7**, the reaction of 3-cyclohexenones (**10**) with lithium diisopropylamide and subsequent trapping with trimethylchlorosilane has been known, we discovered a simple synthetic method of **7** from 2-cyclohexenones (**6**) by application of the method of Kharasch *et al.*[11] Consequently, 1-hydroxyalkylated cyclohexenones (**8**) or dialkoxymethylated cyclohexenones (**9**) could be regioselectively synthesized from **6** *via* **7** as in the following (Scheme 1):

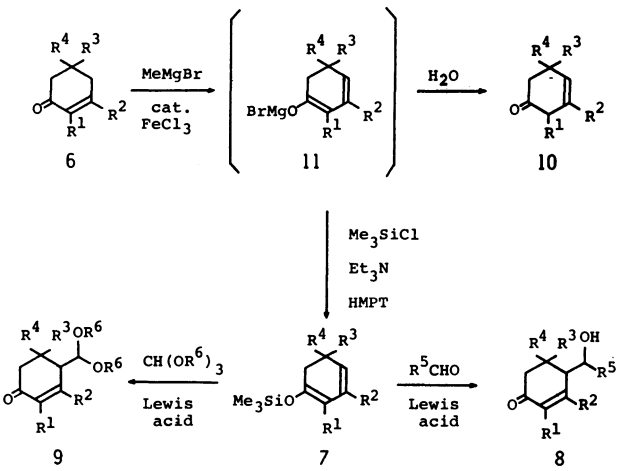

Scheme 1.

These results are listed in Tables 1 and 2.

3,5,5-Trimethyl-1-trimethylsiloxy-1,3-cyclohexadiene (**7a**) was employed to introduce an oxygen function into the C-3 position of the megastigmane skeleton. From **7a**, **1** was synthesized as in the following (Schemes 1 and 2):

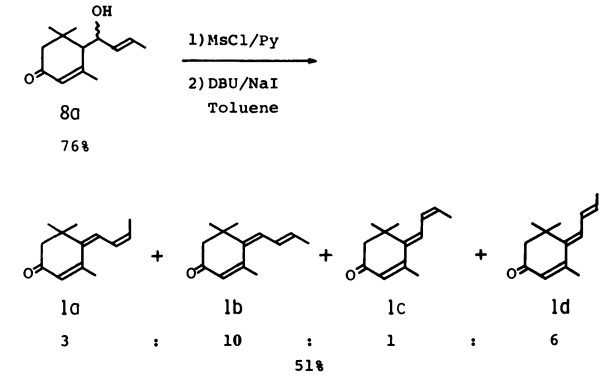

Scheme 2.

Table 1. Preparation of 1-trimethylsiloxy-1,3-cyclohexadienes (7) from 2-cyclohexenones (6)

2-Cyclohexenone (6)	Product (7)					Yield[a] %
		R^1	R^2	R^3	R^4	
Isophorone (**6a**)	**7a**	H	CH_3	CH_3	CH_3	80
l-Carvone (**6b**)	**7b**	CH_3	H	C(CH_3)CH_2	H	72

a) Isolated yields.

Treatment of 3-oxo-α-damascol (**8a**) with methanesulfonyl chloride and 1,8-diazabicyclo[5.4.0]undec-7-ene (DBU)[12] gave a mixture of **1a—d** in 51% total yield. The four isomers (**1a—d**), all of which occur in nature, were found in the ratio 3 : 10 : 1 : 6, determined by gas chromatography. All spectral data of the four isomers, isolated by means of preparative gas chromatography (20% PEG 20M), were consistent with those in the literature.[1]

In the process of transforming **1** to ionone-type compounds (**2—5**), there are two problems: the introduction of an oxygen function into the C-9 position and the isomerization of double bonds from the C-4 and C-6 positions to the C-5 and C-7 positions. We resolved the problems by the synthesis of a key intermediate (**13**), which was obtained by the regioselective epoxidation of **1** with *m*-chloroperbenzoic acid in dichloromethane, followed by the selective reduction with zinc in acetic acid in 65% yield (Scheme 3). The isomers of the epoxy compound (**12**) were not isolated, but the position of epoxy function was confirmed by measurement with NMR. (This was based upon the result that two olefin protons of the C-8 and C-9 positions of **1** disappeared). The epoxy ring cleavage accompanying isomerization of double bonds was caused by treatment of **12** with zinc in acetic acid. The isomerization of double bonds of **13** to conjugated system did not take place under these conditions. Concerning the similar reduction of 4,5-epoxy-2-enones under acidic conditions, two methods have been reported.[13] But their products were not unconjugated 5-hydroxy-3-enones but conjugated 5-hydroxy-2-enones, and the corresponding 2,4-dienones were also produced as by-products. In our synthesis of 7-hydroxy-3,5-dienone (**13**) from 6,7-epoxy-2,4-dienone (**12**), **13** could be selectively obtained as the sole product in good yield without any contamination of conjugated products. It is thought that this selectivity is due to either the conjugated effect of diene or the characteristic property of megastigmane skeleton.

The syntheses of **2—5** from **1** are shown in Scheme 3. Treatment of 3-oxo-β-ionol (**13**) with sodium borohydride in ethanol or sodium methoxide in methanol gave 3-hydroxy-β-ionol (**2**) or 3-oxo-α-ionol (**5**) in 91% or 93% yield, respectively. All spectral data of **2** and **5** were consistent with those in the literature.[2,5] 3-Hydroxy-β-ionone (**3**) and 4,5-epoxy-3-hydroxy-β-ionol (**4**) had been synthesized from **2** by Mori[14] and Takagi *et al.*,[4] respectively.

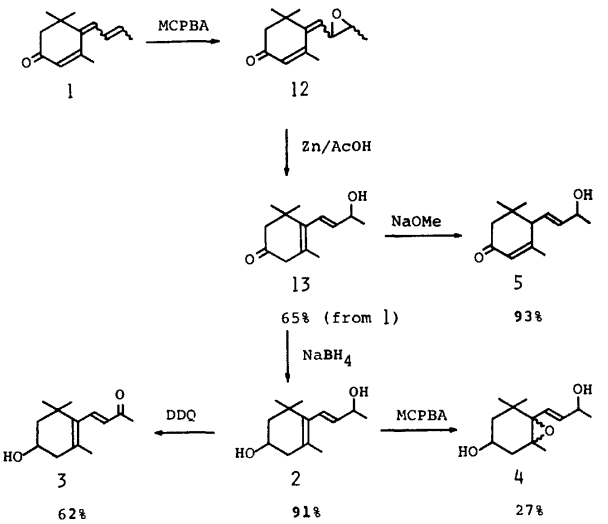

Scheme 3.

In conclusion, megastigmane derivatives oxidized at the C-3 position (**1—5**) were efficiently synthesized starting from readily available isophorone (**6a**) by using a regioselective aldol-type reaction of dienoxysilanes (**7**) and selective transformation of 2,4,6-trienone (**1**) into 7-hydroxy-3,5-dienone (**13**) in each key step.

Experimental

All the boiling points are uncorrected. The IR spectra were recorded with a JASCO IRA-2 spectrometer. The NMR spectra were measured with a Hitachi R-24A spectrometer, using tetramethylsilane as the internal standered. The mass spectra were determined with a Hitachi RMU-6E mass spectrometer.

Table 2. Preparation of 4-substituted 2-cyclohexenones, 8 and 9, from dienoxysilanes (7)

Dienoxysilane (7)	Electrophile	Lewis acid	Product (8 or 9)			Yield[a] %	Isomer ratio A/B
				R^5	R^6		
7a	$CH_3CH=CHCHO$	$TiCl_4$	**8a**	$CH=CHCH_3$	—	67	41/59[b]
7a	$CH_3CH=CHCHO$	$BF_3\cdot OEt_2$	**8a**	$CH=CHCH_3$	—	76	43/57[b]
7b	$(CH_3)_2CHCHO$	$BF_3\cdot OEt_2$	**8b**	$CH(CH_3)_2$	—	63	86/14[c]
7b	PhCHO	$BF_3\cdot OEt_2$	**8c**	Ph	—	60	93/7[c]
7a	$CH(OCH_3)_3$	$TiCl_4$	**9a**	—	CH_3	64	—
7a	$CH(OCH_3)_3$	$BF_3\cdot OEt_2$	**9a**	—	CH_3	61	—
7a	$CH(OCH_2CH_3)_3$	$TiCl_4$	**9b**	—	CH_2CH_3	62	—
7b	$CH(OCH_2CH_3)_3$	$BF_3\cdot OEt_2$	**9c**	—	CH_2CH_3	67	87/13[c]

a) Isolated yields. b) *Threo-erythro* isomers. c) *Cis-trans* isomers. A/B=*trans*/*cis*.

Preparation of 3,5,5-Trimethyl-1-trimethylsiloxy-1,3-cyclohexadiene (7a). To a mixture of 2 M (1 M = 1 mol dm^{-3}) ether solution of methylmagnesium bromide (400 ml, 0.8 mol) and iron(III) chloride (2.0 g), a solution of isophorone (**6a**) (83 g, 0.60 mol) in dry ether (100 ml) was added dropwise at −20 °C, and the mixture was stirred for 0.5 h at −20 °C. Trimethylchlorosilane (87 g, 0.80 mol), triethylamine (60 ml), and hexamethylphosphoric triamide (HMPT) (60 ml) were successively added at 0 °C and the mixture was stirred for 24 h at room temperature. The mixture was poured into cold water and extracted with hexane. The extract was washed with a saturated solution of $KHSO_4$, a saturated solution of $NaHCO_3$, and brine, and then dried over $MgSO_4$. After removal of the solvent, the residue was distilled to give **7a** (101 g, 80%). Bp 88—89 °C/16 Torr (1 Torr = 133.322 Pa); IR (neat) 1655, 1595, and 850 cm^{-1}; NMR ($CDCl_3$) δ=0.22 (9H, s), 0.99 (6H, s), 1.68 (3H, d, J=2.0 Hz), 2.03 (2H, d, J=1.0 Hz), 4.87 (1H, m), and 4.96 (1H, m); MS (70 eV), *m/e* (%), 210 (M^+, 24), 195 (100), 179 (45), 105 (26), 75 (31), 73 (69), and 45 (26). Found: C, 68.63; H, 10.38%. Calcd for $C_{12}H_{22}SiO$: C, 68.51; H, 10.54%.

Preparation of 5-Isopropenyl-2-methyl-1-trimethylsiloxy-1,3-cyclohexadiene (7b). In the same manner, *l*-carvone (**6b**) (57 g, 0.38 mol) was treated with methylmagnesium bromide (2 M ether solution, 225 ml, 0.45 mol), iron(III) chloride (1.0 g), trimethylchlorosilane (49 g, 0.45 mol), triethylamine (35 ml), and HMPT (35 ml). The work-up described above gave **7b** (61 g, 72%). Bp 111—112 °C/17 Torr; IR (neat) 1670, 1640, 1585, 920, 890, and 843 cm^{-1}; NMR ($CDCl_3$) δ=0.20 (9H, s), 1.65 (3H, m), 1.76 (3H, m), 2.18 (1H, m), 2.36 (1H, m), 3.13 (1H, m), 4.80 (2H, m), 5.37 (1H, dd, J=9.5, 3.0 Hz), and 5.80 (1H, dd, J=9.5, 2.4 Hz); MS (70 eV), *m/e* (%), 222 (M^+, 21), 207 (17), 181 (15), 165 (18), 91 (21), 75 (24), 73 (100), and 45 (35). Found: C, 70.24; H, 9.79%. Calcd for $C_{13}H_{22}SiO$: C, 70.21; H, 9.97%.

Reaction of Dienoxysilanes (7) with Aldehydes Using $TiCl_4$ or $BF_3 \cdot OEt_2$. *General Procedure*: A solution of $TiCl_4$ (3.80 g, 20 mmol) or $BF_3 \cdot OEt_2$ (2.84 g, 20 mmol) in dry dichloromethane (5 ml) was added dropwise to a cold solution (−60 °C) of **7** (20 mmol) and aldehyde (24 mmol) in dry dichloromethane (20 ml). After being stirred for 2 h at −60 °C, the mixture was quenched with water. The dichloromethane layer was further stirred with a 10% solution of $(CO_2H)_2$ for 24 h at room temperature and washed with a saturated solution of $NaHCO_3$ and brine, and then dried over $MgSO_4$. After evaporation of the solvent, the residue was subjected to silica-gel column chromatography (hexane–ether) to afford **8**.

3-Oxo-α-damascol (8a): Two stereoisomers (*threo-erythro*), **8aA** and **8aB**, were prepared. **8aA**: IR (neat) 3450, 1650, and 970 cm^{-1}; NMR ($CDCl_3$) δ=1.02 (3H, s,) 1.13 (3H, s), 1.64 (3H, d, J=5.0 Hz), 1.90 (1H, d, J=18.0 Hz), 2.11 (3H, d, J=1.5 Hz), 2.32 (1H, d, J=3.5 Hz), 2.45 (1H, d, J=18.0 Hz), 3.30 (1H, broad s), 4.57 (1H, dd, J=7.0, 3.5 Hz), 5.60 (2H, m), and 5.98 (1H, broad s); MS (70 eV), *m/e* (%), 208 (M^+, 3), 193 (3), 190 (3), 149 (9), 138 (47), 123 (45), 96 (69), 95 (51), 82 (35), 81 (61), 70 (45), 69 (42), 41 (100), and 39 (77). Found: C, 74.77; H, 9.87%. Calcd for $C_{13}H_{20}O_2$: C, 74.96; H, 9.68%. **8aB**: IR (neat) 3370, 1645, and 985 cm^{-1}; NMR ($CDCl_3$) δ=1.00 (3H, s), 1.16 (3H, s), 1.70 (3H, dd, J=5.0, 1.5 Hz), 1.8—2.0 (1H, m), 1.98 (3H, d, J=1.5 Hz), 2.05 (1H, d, J=1.5 Hz), 2.78 (1H, d, J=18.0 Hz), 3.42 (1H, broad s), 4.67 (1H, m), 5.60 (2H, m), and 5.98 (1H, broad s); MS (70 eV), *m/e* (%), 208 (M^+, 3), 193 (3), 190 (2), 149 (8), 138 (47), 123 (43), 96 (70), 95 (53), 82 (47), 81 (61), 70 (47), 69 (38), 41 (100), and 39 (81). Found: C, 74.68; H, 9.51%. Calcd for $C_{13}H_{20}O_2$: C, 74.96; H, 9.68%.

4-(1-Hydroxy-2-methylpropyl)-5-isopropenyl-2-methyl-2-cyclohexenone (8b): *Trans*-isomer (**8bA**) and *cis*-isomer (**8bB**) were separated. **8bA**: IR (neat) 3460, 1660, and 895 cm^{-1}; NMR ($CDCl_3$) δ=0.95 (3H, d, J=6.5 Hz), 0.99 (3H, d, J=6.5 Hz), 1.76 (6H, m), 2.0—3.1 (6H, m), 3.55 (1H, m), 4.85 (2H, m), and 6.73 (1H, m); MS (70 eV), *m/e* (%), 150 (M^+−72, 100), 135 (93), 109 (74), 108 (63), 107 (51), 73 (79), 55 (79), 43 (72), and 41 (60). Found: C, 75.48; H, 9.78%. Calcd for $C_{14}H_{22}O_2$: C, 75.63; H, 9.97%. **8bB**: IR (neat) 3500, 1660, and 890 cm^{-1}; NMR ($CDCl_3$) δ=0.96 (6H, d, J=6.5 Hz), 1.76 (3H, m), 1.86 (3H, m), 2.2—3.1 (6H, m), 3.56 (1H, m), 4.48 (2H, m), and 6.65 (1H, m); MS (70 eV), *m/e* (%), 204 (M^+−18, 4), 150 (M^+−72, 100), 135 (59), 109 (49), 108 (93), 107 (68), 73 (56), 55 (59), 43 (73), and 41 (51). Found: C, 75.83; H, 9.72%. Calcd for $C_{14}H_{22}O_2$: C, 75.63; H, 9.97%.

4-(α-Hydroxybenzyl)-5-isopropenyl-2-methyl-2-cyclohexenone (8c): *Trans*-isomer (**8cA**) and *cis*-isomer (**8cB**) were separated. **8cA**: IR (neat) 3450, 1665, and 895 cm^{-1}; NMR ($CDCl_3$) δ=1.70 (3H, m), 1.77 (3H, m), 2.3—3.2 (5H, m), 4.85 (1H, m), 4.94 (2H, m), 6.53 (1H, m), and 7.30 (5H, s); MS (70 eV), *m/e* (%), 257 (M^++1, 3), 256 (M^+, 1), 187 (5), 150 (100), 135 (43), 109 (40), 108 (31), 107 (100), 91 (21), 79 (79), and 77 (60). Found: C, 79.43; H, 7.66%. Calcd for $C_{17}H_{20}O_2$: C, 79.65; H, 7.86%. **8cB**: IR (neat) 3400, 1660, and 900 cm^{-1}; NMR ($CDCl_3$) δ=1.73 (6H, m), 2.2—3.1 (5H, m), 4.75—4.95 (3H, m), 6.82 (1H, m), and 7.25 (5H, s); MS (70 eV), *m/e* (%), 256 (M^+, 0.3), 255 (M^+−1, 1), 187 (2), 150 (96), 135 (41), 109 (35), 108 (27), 107 (100), 91 (22), 79 (75), and 77 (59), Found: C, 79.49; H, 7.70%. Calcd for $C_{17}H_{20}O_2$: C, 79.65; H, 7.86%.

Reaction of Dienoxysilanes (7) with Trialkyl orthoformates Using $TiCl_4$ or $BF_3 \cdot OEt_2$. *General Procedure*: To a cold solution (−60 °C) of **7** (20 mmol) and trialkyl orthoformate (26 mmol) in dry dichloromethane (20 ml), a solution of $TiCl_4$ (3.80 g, 20 mmol) or $BF_3 \cdot OEt_2$ (2.84 g, 20 mmol) in dry dichloromethane (5 ml) was added. After being stirred for 1 h at −60 °C, the mixture was quenched with methanol (5 ml). The mixture was poured into water and extracted with dichloromethane after separation of the organic layer. The extract was washed with a saturated solution of $NaHCO_3$ and dried over $MgSO_4$. After evaporation of the solvent, the residue was subjected to silica-gel column chromatography (hexane–ether) to afford **9**.

4-Dimethoxymethyl-3,5,5-trimethyl-2-cyclohexenone (9a): IR (neat) 1665, 1120, and 1075 cm^{-1}; NMR ($CDCl_3$) δ=1.02 (3H, s), 1.11 (3H, s), 1.95 (1H, d, J=17.0 Hz), 2.06 (3H, d, J=1.5 Hz), 2.24 (1H, d, J=3.0 Hz), 2.57 (1H, d, J=17.0 Hz), 3.39 (3H, s), 3.42 (3H, s), 4.53 (1H, d, J=3.0 Hz), and 5.95 (1H, broad s); MS (70 eV), *m/e* (%), 181 (M^+−31, 2), 180 (M^+−32, 4), 165 (5), 137 (7), 125 (7), 75 (100), 47 (15), 41 (12), and 39 (10). Found: C, 67.62; H, 9.70%. Calcd for $C_{12}H_{20}O_3$: C, 67.89; H, 9.50%.

4-Diethoxymethyl-3,5,5-trimethyl-2-cyclohexenone (9b): IR (neat) 1660, 1630, 1120, and 1065 cm^{-1}; NMR ($CDCl_3$) δ=1.04 (3H, s), 1.13 (3H, s), 1.16 (3H, t, J=7.0 Hz), 1.23 (3H, t, J=7.0 Hz), 1.95 (1H, d, J=17.0 Hz), 2.10 (3H, d, J=1.5 Hz), 2.23 (1H, d, J=3.0 Hz), 2.65 (1H, d, J=17.0 Hz), 3.3—4.0 (4H, m), 4.75 (1H, d, J=3.0 Hz), and 5.95 (1H, broad s); MS (70 eV), *m/e* (%), 195 (M^+−45, 6), 139 (8), 123 (10), 111 (15), 103 (88), 75 (81), and 47 (100). Found: C, 70.20; H, 9.88%. Calcd for $C_{14}H_{24}O_3$: C, 69.96; H, 10.07%.

4-Diethoxymethyl-5-isopropenyl-2-methyl-2-cyclohexenone (9c): GLC (10% PEG 20M) indicated two stereoisomers, **9cA** (*trans*-isomer) and **9cB** (*cis*-isomer). The analytically pure samples of both isomers were prepared by preparative GLC (20% PEG 20M). **9cA**: IR (neat) 1670, 1110, 1060, and 895 cm^{-1}; NMR ($CDCl_3$) δ=1.18 (3H, t, J=7.0 Hz), 1.25 (3H, t,

J=7.0 Hz), 1.76 (6H, m), 2.2—3.1 (4H, m), 3.3—4.0 (4H, m), 4.45 (1H, d, J=3.0 Hz), 4.85 (2H, m), and 6.88 (1H, m); MS (70 eV), *m/e* (%), 207 (M^+−45, 2), 135 (13), 103 (86), 75 (73), and 47 (100). Found: C, 71.11; H, 9.31%. Calcd for $C_{15}H_{24}O_3$: C, 71.39; H, 9.59%. **9cB**: IR (neat) 1670, 1110, 1060, and 895 cm^{-1}; NMR ($CDCl_3$) δ=1.17 (3H, t, J=7.0 Hz), 1.22 (3H, t, J=7.0 Hz), 1.80 (6H, m), 2.0—3.1 (4H, m), 3.2—4.0 (4H, m), 4.42 (1H, d, J=5.0 Hz), 4.84 (2H, m), and 6.80 (1H, m); MS (70 eV), *m/e* (%), 207 (M^+−45, 4), 135 (14), 103 (75), 75 (67), and 47 (100). Found: C, 71.15; H, 9.42%. Calcd for $C_{15}H_{24}O_3$: C, 71.39; H, 9.59%.

*Preparation of Megastigma-4,6,8-trien-3-ones (**1a**—**d**).* The reaction of **8a** (6.24 g, 30 mmol) with methanesulfonyl chloride (6.87 g, 60 mmol) was carried out in pyridine (25 ml) at 0 °C for 2 h. The mixture was quenched with cold 2 M HCl and extracted with ether. The extract was washed with a saturated solution of $NaHCO_3$ and brine, dried over $MgSO_4$, and then concentrated. The residue was added to a cold solution (0 °C) of DBU (9.12 g, 60 mmol), NaI (4.50 g, 30 mmol), and toluene (30 ml) and the mixture was refluxed for 1 h. The mixture was poured into cold 2 M HCl and extracted with ether. The extract was washed with a saturated solution of $NaHCO_3$ and brine, and then dried over $MgSO_4$. After removal of the solvent, the residue was distilled to give a mixture (2.90 g, bp 120—130 °C/4 Torr, 51%) of **1a**, **1b**, **1c**, and **1d** in *ca.* 3 : 10 : 1 : 6 ratio. The analytically pure samples of four isomers were prepared by preparative GLC (20% PEG 20M).

*(6Z, 8Z)-Megastigma-4,6,8-trien-3-one (**1a**)*: IR (neat) 1665, 1630, 1590, and 730 cm^{-1}; NMR ($CDCl_3$) δ=1.25 (6H, s), 1.82 (3H, dd, J=7.0, 1.5 Hz), 2.23 (3H, d, J=1.5 Hz), 2.30 (2H, s), 5.70 (1H, m), 5.90 (1H, broad s), and 6.2—6.8 (2H, m); MS (70 eV), *m/e* (%), 190 (M^+, 100), 175 (82), 148 (82), 147 (79), 133 (79), 122 (59), 119 (68), 105 (68), 91 (91), 79 (55), 77 (61), 69 (76), 55 (61), 41 (98), and 39 (82).

*(6Z, 8E)-Megastigma-4,6,8-trien-3-one (**1b**)*: IR (neat) 1665, 1635, 1595, and 970 cm^{-1}; NMR ($CDCl_3$) δ=1.19 (6H, s), 1.86 (3H, dd, J=7.0, 1.5 Hz), 2.28 (3H, d, J=1.5 Hz), 2.29 (2H, s), 5.89 (1H, dd, J=14.0, 7.0 Hz), 5.92 (1H, broad s), 6.25 (1H, d, J=11.0 Hz), and 6.55 (1H, dd, J=14.0, 11.0 Hz); MS (70 eV), *m/e* (%), 190 (M^+, 74), 175 (61), 148 (75), 147 (70), 133 (82), 122 (41), 119 (63), 105 (60), 91 (78), 79 (48), 77 (52), 69 (68), 55 (49), 41 (100), and 39 (59).

*(6E, 8Z)-Megastigma-4,6,8-trien-3-one (**1c**)*: IR (neat) 1665, 1582, and 725 cm^{-1}; NMR ($CDCl_3$) δ=1.36 (6H, s), 1.83 (3H, dd, J=7.0, 1.5 Hz), 2.13 (3H, d, J=1.5 Hz), 2.35 (2H, s), 5.92 (1H, broad s), and 5.5—7.0 (3H, m); MS (70 eV), *m/e* (%), 190 (M^+, 97), 175 (67), 148 (76), 147 (76), 133 (82), 122 (55), 119 (55), 105 (64), 91 (79), 79 (48), 77 (55), 69 (73), 55 (52), 41 (100), and 39 (73).

*(6E, 8E)-Megastigma-4,6,8-trien-3-one (**1d**)*: IR (neat) 1670, 1630, 1585, and 968 cm^{-1}; NMR ($CDCl_3$) δ=1.35 (6H, s), 1.89 (3H, dd, J=7.0, 1.5 Hz), 2.08 (3H, d, J=1.0 Hz), 2.35 (2H, s), 5.91 (1H, broad s), 5.94 (1H, dd, J=14.5, 7.0 Hz), 6.50 (1H, d, J=11.5 Hz), and 6.75 (1H, dd, J=14.5, 11.5 Hz). MS (70 eV), *m/e* (%), 190 (M^+, 100), 175 (81), 148 (98), 147 (92), 133 (98), 122 (54), 119 (77), 105 (65), 91 (94), 79 (52), 77 (63), 69 (81), 55 (60), 41 (100), and 39 (81).

*Preparation of 3-Oxo-β-ionol (**13**).* To a cold solution (0 °C) of **1** (2.25 g, 12 mmol) in dry dichloromethane (50 ml) was added *m*-chloroperbenzoic acid (2.59 g, 15 mmol) and the mixture was stirred at 0 °C for 2 h. The mixture was washed with a 1% solution of NaOH and brine, dried over $MgSO_4$, and concentrated. The residue was added to a mixture of zinc powder (3.92 g, 60 mg atom) and acetic acid (20 ml) at room temperature. After the mixture was stirred for 2 h at room temperature, the precipitate was filtered off and washed with ether (100 ml). The filtrate was washed with a saturated solution of $NaHCO_3$ and brine, dried over $MgSO_4$, and then concentrated. Purification by silica-gel column chromatography (hexane–ether) afforded **13** (1.61 g, 65%). IR (neat) 3400, 1720, 1660, and 975 cm^{-1}; NMR ($CDCl_3$) δ=1.06 (6H, s), 1.33 (3H, d, J=6.0 Hz), 1.76 (3H, s), 2.39 (2H, s), 2.86 (2H, s), 3.57 (1H, s), 4.43 (1H, quintet, J=6.0 Hz), 5.61 (1H, dd, J=16.0, 6.0 Hz), and 6.07 (1H, d, J=16.0 Hz); MS (70 eV), *m/e* (%), 208 (M^+, 5), 190 (15), 175 (12), 135 (30), 133 (24), 121 (26), 109 (29), 108 (46), 107 (34), 91 (36), and 43 (100).

*Reduction of **13** to 3-Hydroxy-β-ionol (**2**).* To a suspension of $NaBH_4$ (0.076 g, 2 mmol) in ethanol (10 ml) was added **13** (0.801 g, 3.9 mmol) at room temperature. After the mixture had been stirred for 1 h at room temperature, the mixture was quenched with cold 5% $(CO_2H)_2$ and extracted with ether. The extract was washed with a saturated solution of $NaHCO_3$ and brine, dried over $MgSO_4$, and then concentrated. Purification by silica-gel column chromatography (hexane–ether) afforded **2** (0.734 g, 91%).

*Isomerization of **13** to 3-Oxo-α-ionol (**5**).* To a solution of NaOMe (0.010 g) in methanol (5 ml) was added **13** (0.243 g, 1.2 mmol) at room temperature, then the mixture was stirred for 10 min at room temperature, poured into cold water, and extracted with ether. The extract was washed with brine, dried over $MgSO_4$, and then concentrated. Purification by silica-gel column chromatography (hexane–ether) afforded **5** (0.225 g, 93%).

The authors wish to express their thanks to Professor Teruaki Mukaiyama, The University of Tokyo, for his helpful discussions.

References

1) A. J. Aasen, B. Kimland, S. Almqvist, and C. R. Enzell, *Acta Chem. Scand.*, **26**, 2573 (1972); E. Demole and D. Berthet, *Helv. Chim. Acta*, **55**, 1866 (1972); D. L. Roberts and W. A. Rohde, *Tobacco Science*, **16**, 107 (1972); J. N. Schumacher and L. Vestal, *ibid.*, **18**, 43 (1974); T. Fujimori, R. Kasuga, H. Matsushita, H. Kaneko, and M. Noguchi, *Agric. Biol. Chem.*, **40**, 303 (1976).

2) T. Fujimori, R. Kasuga, H. Kaneko, and M. Noguchi, *Agric. Biol. Chem.*, **39**, 913 (1975).

3) T. Fujimori, R. Kasuga, M. Noguchi, and H. Kaneko, *Agric. Biol. Chem.*, **38**, 891 (1974).

4) Y. Takagi, T. Fujimori, H. Kaneko, T. Fukuzumi, and M. Noguchi, *Agric. Biol. Chem.*, **42**, 1785 (1978).

5) A. J. Aasen, B. Kimland, and C. R. Enzell, *Acta Chem. Scand.*, **25**, 1481 (1971); B. Kimland, A. J. Aasen, and C. R. Enzell, *ibid.*, **26**, 2177 (1972); A. J. Aasen, B. Kimland, and C. R. Enzell, *ibid.*, **27**, 2107 (1973); T. Fujimori, R. Kasuga, H. Matsushita, H. Kaneko, and M. Noguchi, *Agric. Biol. Chem.*, **40**, 303 (1976).

6) S. Shibata, A. Katsuyama, and M. Noguchi, *Agric. Biol. Chem.*, **42**, 195 (1978).

7) A. J. Aasen, B. Kimland, S. Almqvist, and C. R. Enzell, *Acta Chem. Scand.*, **26**, 2573 (1972); E. Demole and P. Enggist, *Helv. Chim. Acta*, **57**, 2087 (1974); B. M. Trost and J. L. Stanton, *J. Am. Chem. Soc.*, **97**, 4018 (1975); S. Torii, T. Inokuchi, and H. Ogawa, *Bull. Chem. Soc. Jpn.*, **52**, 1233 (1979); D. E. Loeber, S. W. Russell, T. P. Toube, B. C. L. Weedon, and (in part) J. Diment, *J. Chem. Soc., C*, **1971**, 404; A. J. Aasen, B. Kimland, and C. R. Enzell, *Acta Chem. Scand.*, **27**, 2107 (1973).

8) T. Mukaiyama, K. Banno, and K. Narasaka, *J. Am. Chem. Soc.*, **96**, 7503 (1974); T. Mukaiyama and M. Hayashi,

Chem. Lett., **1974**, 15; K. Narasaka, K. Soai, Y. Aikawa, and T. Mukaiyama, *Bull. Chem. Soc. Jpn.*, **49**, 779 (1976).
9) T. Mukaiyama and A. Ishida, *Chem. Lett.*, **1975**, 319.
10) M. Asaoka, N. Sugimura, and H. Takei, *Bull. Chem. Soc. Jpn.*, **52**, 1953 (1979); I. Fleming, J. Goldhill, and I. Paterson, *Tetrahedron Lett.*, **1979**, 3205; 3209.
11) M. S. Kharasch and P. O. Tawney, *J. Am. Chem. Soc.*, **63**, 2308 (1941).
12) T. Kitahara, Y. Takagi, and M. Matsui, *Agric. Biol. Chem.*, **43**, 2359 (1979).
13) W. S. Knowles and Q. E. Thompson, *J. Am. Chem. Soc.*, **79**, 3212 (1957); C. H. Robinson and R. Henderson, *J. Org. Chem.*, **37**, 565 (1972).
14) K. Mori, *Agric. Biol. Chem.*, **37**, 2899 (1973).

2-Methylamino-4,5-imidazoledione. A Revised Structure for Creatone, Methylparabanic Acid Imide, and (3-Methylguanidino)glyoxylic Acid

Hiroshi YAMAMOTO* and Wolfgang PFLEIDERER†
Department of Chemistry, Faculty of Science, Okayama University, Okayama 700
†Universität Konstanz, Fakultät für Chemie, D-7750 Konstanz, Germany
(Received November 18, 1981)

The previous structures presented for the $Hg(OAc)_2$ oxidation product of creatine, the condensation product of methylguanidine and diethyl oxalate, and the peracid oxidation product of 1-methyl-2-amino-dihydropyrimidines are all replaced by a revised formulation, 2-methylamino-1*H*-imidazole-4,5-dione on the basis of the pK_a values (0.62 and 7.87) and the spectra. The equilibria between this thermodynamically controlled product and the previous formulations are discussed.

Creatine (**1**) is present in the muscular tissue of many vertebrates, mostly as phosphocreatine, which plays an important role in energy transfer and storage.[1] It has been reported[2,3] that the action of mercury(II) acetate on **1** afforded a single product (creatone) (mp 203—204°C decomp), to which the structure of (1-methylguanidino)-glyoxylic acid (**3**) was assigned (Scheme 1). The same product was also isolated from beef and regarded as a constituent of muscle tissue.[4] Traube and Gorniak,[5] meanwhile, briefly reported a condensation product (mp 205—207 °C decomp) of methylguanidine and diethyl oxalate; the structure of "1-methylparabanic acid imide" (2-imino-1-methylimidazolidine-4,5-dione) (**4**) was simply presented for this product, without any proof.

During our study of the oxidative pyrimidine→1,3,5-triazine rearrangement, we found that the action of performic acid on 2,4-diamino-1-methyl-1,6-dihydro-pyrimidin-6-ones (**5**) and the 6-amino-4-oxo isomer (**6**) afforded a 20—25% yield of colorless needles (mp 200 °C decomp), to which the Zwitter ion structure, (3-methylguanidino)glyoxylic acid (**7**), was assigned on the evidences of the elemental analysis and spectral data

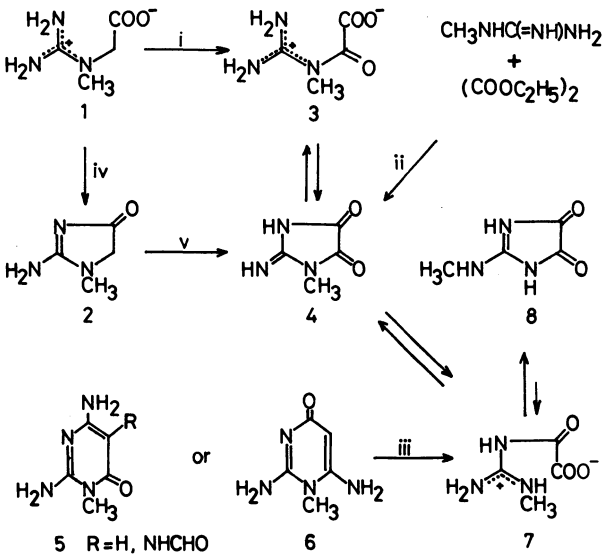

Scheme 1. Reaction pathways for the formation of **8** from **1**, **2**, **5**, **6**, and methylguanidine–diethyl oxalate. i, $Hg(OAc)_2$, Refs. 2, 3. ii, Ref 5. iii, H_2O_2/HCOOH. Ref. 6. iv, H^+. v, $Hg(OAc)_2$.

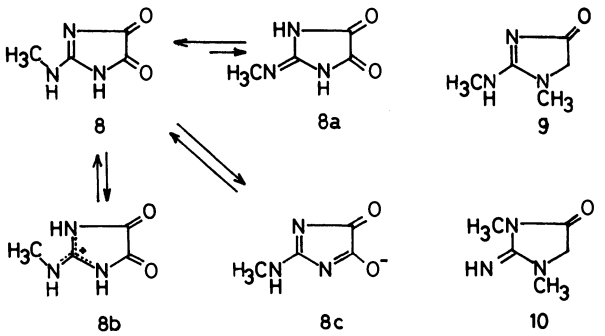

Scheme 2. Tautomeric forms and equilibria of **8**.

(UV, IR, and ^{1}H-NMR).[6] However, the close similarity of the melting points and the solubilities (in water) among the products, **3**, **4**, and **7**, led us to reinvestigate those structures.

We have now found that both creatone (**3**) prepared[3] from **1** and the condensation product[5] (**4**) were identical with our specimen,[6] derived from **5** and **6**, on the evidence of the spectroscopic data (IR, NMR) and the mixed melting points. Creatinine (**2**), an important end product of nitrogen metabolism,[7] also produced the identical substance more rapidly than **1** upon treatment with mercury(II) acetate. The revised structure of 2-methylamino-1*H*-imidazole-4,5-dione (**8**) was then assigned to the common product on the basis of the spectral data, as will be shown below.

The repeated elemental analysis of the specimen of **8** dried at 120 °C/0.05 Torr** over P_2O_5 showed an analytical figure corresponding to $C_4H_5N_3O_2$ instead of $C_4H_7N_3O_3$, which had previously been reported.[2,3,6] The EI high-resolution and chemical-ionization mass spectra clearly confirmed the molecular formula ($C_4H_5N_3O_2$), and the characteristic fragmentation peaks were those at *m/e* 99 and 71 due to the successive loss of two CO groups from the molecular ion. The presence of imino and two kinds of carbonyl groups were confirmed by the IR spectrum (3200, 1710, and 1630 cm^{-1}). Because of the sparing solubility in other suitable solvents (*e.g.*, DMSO-d_6, D_2O, or pyridine-d_5), the NMR spectrum of **8** was taken in trifluoroacetic acid (TFA); the signals are recorded in Table 1. In TFA-*d*, the doublet at 3.31 collapsed into a singlet,

** 1 Torr≈133.332 Pa.

Table 1. Physical properties of some imidazole derivatives

Compd	^{1}H-NMR parameters[a]				Ionization and UV spectra[l] in water (25 °C)			
	CH_3-1* or H-1	H_2N-2* or CH_3NH-2	H-3	2H-5	Species[l]	pK_a	λ_{max}/nm (ε)	pH
1[b]	3.37*s	6.54*bm	6.54bm[c]	4.54s	+	2.54[k]		
					−	14.28[k]		
2	3.37*s	8.03*bm	8.03bm[d]	4.66s	+	4.83[l]		
					0		235(7060)[m]	
8[e]	7.70bm	3.31d[f,g]	7.70bm	—	+	0.62±0.10[n]	212(9380)	−0.05
		8.65bq[f,h]			0		204(13600)	4.0
					−	7.87±0.04[n]	234(10100)[o]	9.8
9					+	4.55[p]		
					0		212(18400)[p]	
							235(shoulder)	
10					+	8.07[p]		
					0		205(13 600)[p]	

a) δ values in TFA at 30 °C, with TMS as the internal standard; s, singlet; d, doublet; q, quartet; m, multiplet; b, broad. b) The numbering of **1** corresponds to that of **2** for the purpose of comparison. On setting aside the sample solution in TFA at 25 °C, **1** gradually changes to **2** ($t_{1/2}$ *ca.* 3 d), which, in contrast, remains unchanged. c) 2H. d) The assignment has been made because **2** probably exists as the monocation in TFA. e) The spectra are of compounds, **3**, **4**, and **7**, all of which are identical and exist as the monocation **8b** in TFA. f) J=5.0 Hz. g) 3H. h) 1H. i) Measured with a Hitachi EPS 3T Recording Spectrophotometer. j) Monocation (+), neutral species (0), monoanion(−). k) From Ref. 17. l) From Ref. 8. m) From Ref. 9. n) Determined spectroscopically according to Ref. 16. o) Extrapolated value since the anionic species gradually decomposes during the measurement. p) From Ref. 10.

and the broad multiplet and the quartet disappeared, suggesting the presence of a CH_3NH– (or $CH_3\overset{+}{N}H$=) group in the molecule. Structures **3** and **4** were thus eliminated because their *N*-methyl signal may be expected to be a singlet, as was observed in the spectra of the two starting materials, **1** and **2**, in the same solvent (see Table 1).

Creatinine (**2**) was shown to exist mainly in the amino-oxo form rather than the universally written 2-imino-1-methylimidazolidin-4-one form by comparing the pK_a value and other physical properties with those of such related compounds as **9** and **10** (see Table 1).[8–11] The pK_a values and UV spectra of **8** were thus measured; the results are summarized in Table 1. Although the neutral species of **8** was completely stable in water at 25 °C, both cationic and anionic species were gradually degraded——*e.g.*, $t_{1/2}$ 3 d (in 1 mol dm^{-3} HCl) and 70 min (at pH 9—13). The extremely low value (0.6) of the basic pK_a of **8** and the stability of its neutral species in water point to the amino-oxo form (**8**) rather than the tautomeric imino form (**8a**) (Scheme 2), since the exocyclic imono group may be expected to be more basic and unstable in a protic solvent, as is shown in the case of **10**, which gradually isomerized to **9** in boiling methanol.[10] The UV absorption maximum of **8** in acid and the NMR doublet signal of the methyl group in TFA suggest the resonance-stabilized form **8b** for the monocation. The large bathochromic shift (30 nm) observed in the UV absorption maximum in alkaline solutions indicates that **8** probably becomes a fully conjugated diazacyclopentadienone form, **8c**, which in turn tends to decompose readily to oxalic acid and methylguanidine.

The oxidation of **1** and **2** with mercury(II) acetate presumably proceeds in a manner similar to that of the dehydrogenation of cyclic tertiary amines[12] to give **4**, which is in equilibrium with the ring-opened forms **3** and **7** (Scheme 1). The latter should provide **8** upon a recyclization similar to the Dimroth rearrangement,[13] and the predominant formation of the final product **8** could be explained by its thermodynamical stability compared with other isomers (**3**, **4**, and **7**). The formation of **8** from the pyrimidines, **5** and **6**, is initiated by the peroxy acid degradation to afford a common intermediate **4** or **7**, followed by a similar equilibrium transformation. The same equilibrium scheme was also applied to the condensation product of methylguanidine and diethyl oxalate, as is shown in Scheme 1.

Many rearrangements have been known[14] involving the fission of a heterocyclic ring and ring closure in the alternate direction catalyzed by acid, base, heat, light, or miscellaneous reagents. The present rearrangement at such a low temperature can be classified, to the best of our knowledge, as a rare example of thermodynamically controlled ring transformation of the imidazole-ring system.[15]

Experimental

The ^{1}H-NMR spectra were measured in TFA with a Hitachi High-resolution NMR Spectrometer, R-20A (60 MHz), at 30 °C. The IR spectra were taken with a Nihon-Bunko IR-S spectrometer. The mass spectra were measured at the Department of Chemistry, the University of Alberta, with an A. E. I. MS 50 ultra-high-resolution instrument (for the accurate mass measurement) and an A. E. I. MS 12 appararus (for the chemical ionization with NH_3). The measurements of the ionization constants were carried out spectrophotometrically in 0.01 mol dm^{-3} buffers by the usual method.[16]

The microanalyses were performed using a Yanagimoto CHN Corder, MT-2. Substances stated to be identical were compared by means of mixed-melting-point determinations, their spectra (IR, NMR), and TLC (silica gel; developed with DMF–MeOH–$CHCl_3$, 1 : 5 : 15). The melting points are uncorrected.

The Oxidation of Creatinine (2). To a solution of 1.13 g (10 mmol) of **2** in 80 ml of water was added 11.2 g (35 mmol) of mercury(II) acetate, after which the mixture was allowed to stand at room temperature; after *ca.* 3 h, colorless leaflets began to separate, and 4.82 g (15 mmol) more of $Hg(OAc)_2$ was added after 1 d. The precipitate was filtered off after 3 d and washed with a small amount of cold water; the pH of the supernatant solution was 3 throughout this period. The filter cake was suspended in 100 ml of water and saturated with hydrogen sulfide gas with stirring. The black mercury sulfide was filtered by gravity and washed with boiling water (20 ml). The combined filtrate and washings were evaporated to dryness *in vacuo*, and the residue was washed with 80% aq *t*-BuOH, giving 0.56 g (38%) of **8** as a colorless powder: mp 197—199 °C decomp (from 50% aq ethanol); IR (KBr), 3200 (NH), 1710 (C=O), 1630 (C=N–CO=), 1450, 1370, 1190, 1160, 790, and 680 cm^{-1}; EI high-resolution MS, *m/e* (rel intensity), 127 (89; M^+), 99 (100; M−CO), 71 (54; M−2CO), 58 (34), 56 (75; MeNHC≡N), and 55 (71; MeNCN); CI (NH_3) MS, *m/e* (rel intensity), 147 (0.8; P+2), 146 (5.5; P+1), 145 [100; P(M+NH_4^+)], 128 (2.8), 102 (1.0), and 86 (6.9).

Found (for material dried over P_2O_5 at 120 °C/0.05 Torr for 7 h): C, 37.42; H, 4.21; N, 32.83%; *m/e*, 127.0381. Calcd for $C_4H_5N_3O_2$: C, 37.81; H, 3.97; N, 33.06%; *m/e*, 127.0382.

The product was identical with the specimen[6] obtained from **5** and **6**.

The Oxidation of Creatine (1). The procedure fo Greenwald[3] was followed; after *ca.* 10 h, colorless leaflets began to separate. The product similarly obtainep after 8 d (20%yield, mp 197—199 °C decomp) was identical with **8**.

The Condensation of Methylguanidine and Diethyl Oxalate. Traube and Gorniak[5] reported the product **4** without describing the experimental procedure in detail. Thus, the reaction was carried out as follows: a solution of sodium ethoxide was prepared by dissolving 0.30 g (13 mmol) of sodium in 10 ml of absolute ethanol. To this were added, under argon at 5 °C, 1.42 g (13 mmol) of methylguanidine hydrochloride and 1.9 g (13 mmol) of diethyl oxalate. The resulting white suspension was stirred at 20 °C for 5 h. The mixture was taken to pH 4 by the careful addition of 5 mol dm^{-3} AcOH at 5 °C and subsequently concentrated *in vacuo*. The residue was suspended in methanol (20 ml) and filtered off, giving 0.80 g (47%) of **8** as colorless leaflets; mp 203—205 °C decomp (from 50% aq ethanol).

We wish to thank Dr. M.-A. Armour of the University of Alberta for the high-resolution mass spectra.

References

1) For reviews of the chemistry and biology of creatine, see a) S. Schipper and A. R. Day, "Hetetrocyclic Compounds," ed by R. C. Elderfield, Wiley, New York (1957), Vol. 5, p. 263; b) M. Cohn, *Quart. Rev. Biophys.*, **3**, 61 (1970).

2) L. Baumann and T. Ingvaldsen, *J. Biol. Chem.*, **35**, 277 (1918).

3) I. Greenwald, *J. Am. Chem. Soc.*, **41**, 1109 (1919).

4) V. S. Gulevich, *C. R. A. Sci. U. R. S. S.*, **1930A**, 559; *Z. Phys. Chem.*, **217**, 63 (1933).

5) W. Traube and K. Gorniak, *Z. Angew. Chem.*, **42**, 379 (1929).

6) H. Yamamoto and W. Pfleiderer, *Chem. Ber.*, **106**, 3194 (1973); the material dried at 100 °C/15 Torr gave an analytical figure corresponding to $C_4H_7N_3O_3$.

7) A. H. Ennor and J. F. Morrison, *Phys. Rev.*, **38**, 631 (1958).

8) A. K. Grzybowski and S. P. Datta, *J. Chem. Soc.*, **1964**, 187.

9) K. Matsumoto and H. Rapoport, *J. Org. Chem.*, **35**, 552 (1968).

10) G. L. Kenyon and G. L. Rowley, *J. Am. Chem. Soc.*, **93**, 5552 (1971).

11) J. Elguero, C, Marzin, A. R. Katritzky, and P. Linda, "The Tautomerism of Heterocycles," (Adv. Heterocyclic Chem. Supplement 1), Academic Press, New York (1976), pp. 479—481.

12) N. J. Leonard, L. A. Miller, and P. D. Thomas, *J. Am. Chem. Soc.*, **78**, 3463 (1956); J. Knabe and H. Roloff, *Chem. Ber.*, **97**, 3452 (1964).

13) See D. J. Brown, "Mechanisms of Molecular Migrations" ed by B. S. Thyagarajan, Interscience-Wiley, New York (1968), Vol. 1, p. 202.

14) H. C. van der Plas, "Ring Transformation of Heterocycles," Academic Press, New York (1973).

15) A closer mechanistic study is currently in progress.

16) A. Albert and E. P. Serjeant, "Ionization Constants of Acid and Base," Methuen, London (1962).

17) A. Hahn and H. Fasold, *Z. Biol.*, **82**, 473 (1925); C. F. Failey and E. Brand, *J. Biol. Chem.*, **102**, 767 (1933).

Oxidative *S*-Dealkylation Reaction of Sulfide Catalyzed by Co(II)(bzacen)

Yoshihito WATANABE, Tatsuo NUMATA, and Shigeru OAE*
Department of Chemistry, The University of Tsukuba, Niihari-gun, Sakura-mura, Ibaraki 305
(Received December 10, 1981)

In the oxygenation reaction of alkyl sulfides with Co(II)(bzacen)–O_2 system, oxidative S–C bond cleavage (*S*-dealkylation) was found to take place exclusively. The reactivity of *S*-dealkylation reaction was dependent markedly on both acidity of α-methylene and steric hindrance of alkyl sulfide. The peroxo-Co(III) species is presumed to be the intermediate in this *S*-dealkylation reaction.

Although mechanisms of many reactions with hydrolytic enzymes have been understood fairly well now, those of the reactions with both mono- and di-oxygenases are by no means well-understood,[1-3] since many of the oxygenation intermediates in the reactions with oxygenases are unstable and hence not well-characterized. Therefore, numerous nonenzymatic models have been designed to investigate the nature of many enzymatic oxygenations.[4,5]

Meanwhile, as a model of the active site of myoglobin and oxymyoglobin "picket fence porphyrin"–iron(II) complexes have been synthesized and fully characterized by Mössbauer spectroscopy, magnetic susceptibility, and X-ray crystallography analysis.[6-8] These picket fence porphyrin–iron complexes can bond with molecular oxygen to give endo-on type complexes. Model oxygenation systems of another types are cobalt–Schiff base complexes.[9,10] However, only a few oxygenation reactions of aromatic compounds with metal-molecular oxygen complexes have been examined.[11,12] Meanwhile, sulfides bearing electron-withdrawing group were found recently by us to be oxygenated in the presence of a Co(II)–Schiff base complex affording exclusively the *S*-dealkylation products.[13]

In the meantime, in the oxygenation of divalent sulfur compounds with cytochrome P-450 monooxygenase, we have demonstrated that both dealkylation and *S*-oxygenation reactions take place *via* the sulfenium radical as the common intermediate formed in the rate-determing one electron transfer from sulfur atom to the "oxenoid" intermediate.[14,15] The "oxenoid" intermediate is believed to be the metal–mono-oxygen complex ($Fe{=}O^{3+}$).[16] Thus, it is of interest to examine the nature of the reaction with metal-molecular oxygen complex as compared to that with cytochrome P-450 in the oxygenation of various sulfides.

This report described a detailed account on the oxygenation of divalent sulfur compounds with Co(II)-(bzacen), [*N*,*N*′-bis(2-benzoyl-1-methylethylidene)ethylenediamine], which is known to ninteract with molecular oxygen to give ligand–Co(II)–O_2 complex that was found to be the endo-on type complex by X-ray study (Eq. 1).[17]

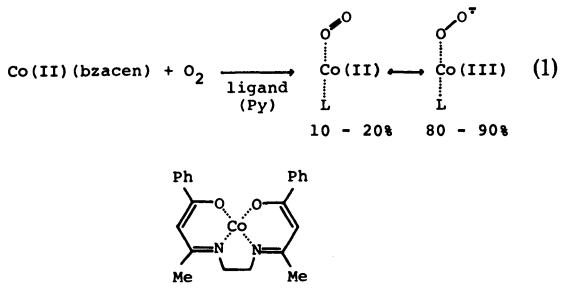

Results and Discussion

When a β-keto sulfide (**1a**, 0.40 mmol) was incubated aerobically in a 16 mL of methanol solution containing Co(II)(bzacen) (0.10 mmol) for 30 min at room temperature, the oxygenation was found to complete. The products were analyzed by GLC by removing the catalyst by adsorption through an ion exchange resin [Dowex 50W-8 (H^+ form)]. After GLC measurement and replacing methanol by dichloromethane, treatment of the mixture with an excess diazomethane to determine carboxylic acids gave methyl esters which were also analyzed by GLC (Scheme 1). In the oxygenation reaction, oxidative cleavage of S–C bond of the sulfide (**1a**) took place exclusively to afford only the corresponding carbonyl compound (**2a**) and diphenyl disulfide (**3**) in good yields (Scheme 1). The oxidative cleavage of other sulfides each having an acidic α-methylene (**1b—d**) was also found to proceed catalytically in methanol solution at room temperature but required a longer reaction time to complete the oxygenation reaction (Table 1). As shown in Table 1, the reaction proceeds faster with the sulfide bearing a higher acidic α-methylene group.[15] Benzyl phenyl sulfide (**1f**) and thioanisole (**1g**) were not oxygenated under these conditions. Thus, the reactivity of the oxidative *S*-dealkylation appears to depend strongly on the acidity of α-hydrogen of the alkyl sulfide.

$$\underset{\mathbf{1a}}{PhSCH_2COPh} + \text{cat. Co(II)(bzacen)} \xrightarrow[MeOH,\ r.t.]{O_2}$$

$$\underset{\mathbf{3}\ \text{quant}}{1/2PhSSPh} + \underset{\mathbf{2a}\ 81\%}{PhCOCHO} + PhCOCO_2H + PhCO_2H$$

$$+ \underset{1.2\%}{PhCO_2Me} \xrightarrow{CH_2N_2} \underset{13\%}{PhCOCO_2Me} + \underset{4.5\%}{PhCO_2Me}$$

Scheme 1.

Phenacyl phenyl ether (**6**), oxygen analogue of the keto sulfide (**1a**), was added into the methanol solution containing 1/2 equimolar amount of Co(II)(bzacen) was also found to be oxygenated aerobically and the corresponding phenol (**7**) and aldehyde (**2a**) were obtained (Table 2). The reactivity of ether (**6**) is quite

TABLE 1. THE OXYGENATION OF SULFIDES, SULFOXIDE, AND ETHER HAVING α-ACTIVE METHYLENES CATALYZED BY Co(II)(bzacen)

$$Ph\text{–}S\text{–}CH_2R + Co(II)(bzacen) \xrightarrow[r.t.]{O_2} PhSSPh + RCHO + RCO_2H$$

	1 R	(Equiv.)[a]	Time/h	Solvent	3	2 Yield/%[b]	
a	–COPh	1/4	30min	MeOH	quant[c]	81	13
b	–CN	1	15	MeOH	quant[c]	—[d]	
c	$-CO_2Et$	1/4	15	MeOH	52	—[d]	
d	$-C_6H_4NO_2$-*p*	1	72	MeOH	no reaction		
		1	48	MeOH–Py (1 : 1)	quant[c]	50	trace
e	$-CH_2CN$	1	120	MeOH (or MeOH–Py)	no reaction		
f	–Ph	1	120	MeOH	no reaction		
g	–H	1	120	MeOH	no reaction		
5	$PhS(O)CH_2CN$	1	120	MeOH	no reaction		
6	$PhOCH_2COPh$	1/2	16	MeOH	50	(PhOH) 93	

a) Based on the substrate used. b) Yield/% was calculated based on the substrate and was determined by GLC. c) Quantitative yield (>95%). d) Aldehyde was not observed in both TLC and GLC.

TABLE 2. PHYSICAL CONSTANTS OF α-SUBSTITUTED SULFIDES (4)

4	Bp θ_b/°C(mmHg)[b]	^{1}HNMR δ-values, *J*/Hz
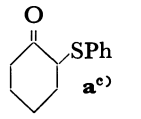 **a**[c]	145(2)[lit,[20] 150—153(5)]	1.5—2.5(7H,m) 2.5—3.1(1H,m) 3.75(1H,t,*J*=5.1) 7.1—7.5(5H,m)
PhCOCHSPh Ph **b**[c]	Mp 77—78 °C [lit,[21] 78—79]	5.85(1H,s) 7.0—7.53(8H,m) 7.8—8.05(2H,m)
PhCOCHSPh Me **c**[d]	195(3) [lit,[22] 110—115 (0.003)]	1.45(3H,d,*J*=6.6) 4.53(1H,q,*J*=6.6) 7.18—7.55(8H,m) 7.8—8.02 (2H,m)
PhCOCHSPh Et **d**[d,e]	181(2)	0.99(3H,t,*J*=7.2) 1.6—2.2(2H,m) 4.33(1H,t,*J*=7.8) 7.0—7.5(8H,m) 7.8—8.0(2H,m)
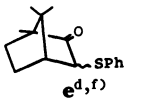 **e**[d,f]	180(2)	0.90(6H,s) 0.96(3H,s) 1.2—2.1(4H,m) 2.2(1H,brs) 3.2(0.9H, s,H_{endo}) 3.8(0.1H,d,*J*=4.6 H_{exo}) 7.1—7.6(5H,m)

a) Recrystallized from EtOH. b) Bath temperature. c) In $CDCl_3$. d) In CCl_4. e) Found: C 74.62, H 6.21%. Calcd for $C_{16}H_{16}OS$: C 74.96, H 6.29%. f) Found: C 73.54, H 7.71%. Calcd for $C_{15}H_{20}OS$: C 73.80, H 7.74%.

$$Ph\text{–}O\text{–}CH_2COPh + Co(II)(bzacen) \xrightarrow{O_2} PhOH + PhCOCHO \quad (2)$$
6 **7** **2a**

comparable to that of the sulfide (**1b**), seemingly supporting the hypothesis that one of the most important factors is the acidity of the α-methylene, since both pK_a's of methylene proton of **6** and **1b** are quite similar (pK_a; $PhCO\underline{CH_3}$ 24.7, $NC\underline{CH_3}$ 31.3, $PhS(O_2)\underline{CH_2}OPh$ 27.9, $PhS(O_2)CH_2SPh$ 20.3).[18,19]

Meanwhile, the steric effect on the reactivity has been examined systematically with various α-substituted β-, keto sulfides (**4**) which are listed in Table 2. When 2-(phenylthio)cyclohexanone (**4a**) was incubated for 16h diphenyl disulfide (**3**) and 1,2-cyclohexanedione (**8a**) were obtained in good yields. The oxygenation of 2-(phenylthio)propiophenone (**4c**) with the Co(II)-(bzacen)–O_2 system required 23 h to be completed in methanol, eventually affording diphenyl disulfide (**3**) quantitatively and 1-phenyl-1,2-propanedione (**8c**) in 50% yields, respectively. Although phenyl group would activate the α-proton of **4b** which would hence be more

TABLE 3. THE OXYGENATION REACTION OF α-SUBSTITUTED SULFIDE (4) CATALYZED BY Co(II)(bzacen)[a]

Sulfide 4	Co(II)(bzacen) (Equiv.)	Time h	PhSSPh 3 (%)[b]	RCOCOR′ 8
a	1/10	16	quant[c] (85)[d]	quant[c] (60)[d]
b	1/4	4	quant[c]	quant[c]
c	1	23	quant[c]	50
d	1/4	24	10	—
e	1	48	no reaction[e]	

a) The reaction was carried out in MeOH at room temperature. b) Determined by GLC. c) Quantitative yield (95%). d) Isolated yield. e) In MeOH–Py system, sulfide (**4e**) was recovered.

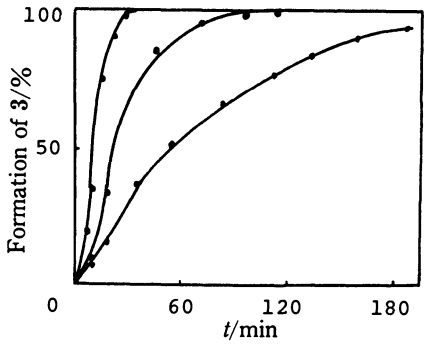

$$PhSCH_2COPh + Co(II)(bzacen) \xrightarrow{O_2} 1/2PhSSPh$$

Fig. 1. The effect of concentration of Co(II)(bzacen) on the formation of disulfide (**3**).
a: Co/**1a**=1/2, b: Co/**1a**=1/4, c: Co/**1a**=1/8, [**1a**]=2.5×10^{-2} mol/dm^3.

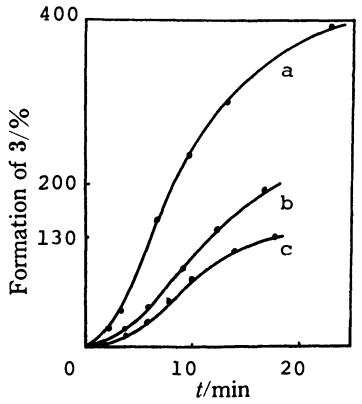

$$PhSCH_2COPh + Co(II)(bzacen) \xrightarrow{O_2} 1/2PhSSPh$$

Fig. 2. The effect of concentration of sulfides (**1a**) on the formation of disulfide (**3**).
a: Co/**1a**=1/4, b: Co/**1a**=1/2, c: Co/**1a** 1/1.3, [Co]=2.5×10^{-2} mol/dm^3.

acidic than α-proton of **1a**, the reactivity of *S*-dealkylation of **4d** is substantially decreased. In the case of a most crowded β-keto sulfide, *i.e.*, 3-(phenylthio)-*dl*-camphor (**4e**), which is an *endo* and *exo* mixture, the oxygenation was not found to proceed for both *endo* and *exo* sulfides even though the reaction mixture was incubated for 48 h (Table 3).

These observations clearly indicate that the steric hindrance is second important factor for the *S*-dealkylation reaction. As shown previously, oxygenations catalyzed by cobalt(salen) are related to the electron donor character of the substrate and the steric hindrance would reduce the donor character of the substrates.[11]

In order to understand the whole feature of oxidative *S*-dealkylation reaction, several experiments have been carried out.[13] In the kinetic experiments of oxygenation of **1a** with Co(II) (bzacen) in methanol, the rate of the reaction was found to be of first order dependence both on the concentration of the sulfide (**1a**) and that of the catalyst; the plot of the amounts of the formation of the diphenyl disulfide (**3**) against time gave a sigmoidal curve shown in Figs. 1 and 2. On the other hand, an equimolar amount of molecular oxygen was found to be consumed by the reaction (Fig. 3).

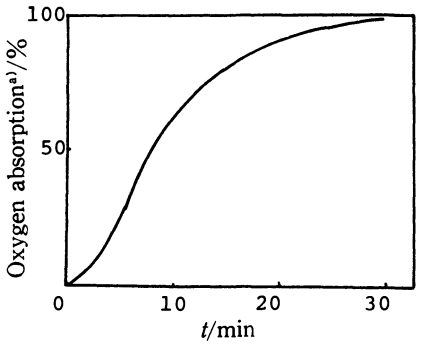

$$PhSCH_2COPh + Co(II)(bzacen) \xrightarrow{O_2} 1/2\ PhSSPh$$

Fig. 3. Oxygen uptake in the oxygenation reaction of **1a** with Co(II) (bzacen).
Co/**1a**=1/4, [Co]=2.5×10^{-2} mol/dm^3.
a) 100 (%) means 1 equiv. oxygen absorption to sulfide (**1a**).

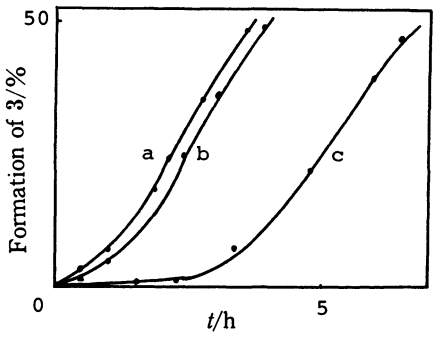

$$X\text{-}C_6H_4\text{-}SCH_2CN + Co(II)(bzacen) \xrightarrow{O_2} 1/2\ ArSSAr$$

Fig. 4. The effect of *para*-substituent on benzene ring of **1b** on the formation of disulfide (**3**).
a: X=CH_3, b: X=H, c: X=Cl, Co/**1b**=1, [Co]=5.0×10^{-1} mol/dm^3.

These results suggest that the oxygenation reaction catalyzed by Co(II)(bzacen) has a pre-equilibrium which may be the process of coordination of sulfide to cobalt like a ES complex in the actual enzymatic reaction.

We cannot conclude whether or not the formation of the first complex (S·Co) involves the coordination of molecular oxygen, however, Fig. 3 suggests the participation of molecular oxygen in a ES like complex which eventually gave the products.

$$\underset{(E)}{S + Co} \overset{O_2}{\rightleftharpoons} \underset{(ES)}{S\cdot Co\cdot O_2} \longrightarrow P + Co \qquad (3)$$

The effect of *p*-substituent on benzene ring of **1b** on this biomimetic oxygenation was examined to demonstrate the participation of divalent sulfur atom in the first equilibrium of the coordination. When the *p*-substituent was electron-donating group, the induction period of the oxygenation of **1b** was found to be shortened, however, the rate of formation of diaryl disulfide (**3**) after the induction period was not affected at all by the substituent. Meanwhile, an electron-withdrawing substituent prolonged only the induction period as shown in Fig. 4. The effect of *p*-substituent on benzene

ring may be explained in that the initial step of the oxygenation is the coordination of divalent sulfur atom to cobalt as an axial ligand.

Cyanomethyl phenyl sulfoxide (**5**) did not react at all under the same reaction conditions clearly suggesting that cobalt coordinates to divalent sulfur atom but not α-methylene position in the first step of oxygenation, since α-methylene proton is activated more by the sulfinyl group than sulfenyl group.

The effect of solvent was quite substantial; *e.g.*, the reaction in methanol was markedly faster than in pyridine. The reaction of **1a** in pyridine proceeded only 2% while the reaction in methanol was completed in the same period. These solvent and steric effects are similar to those in the oxygenation of indole derivatives by Co(II)(salen)–O_2 system.[11]

When the reaction of **1b** was carried out in methanol-d_1, the recovered sulfide was found to retain only 69% of deuterium at α-methylene carbon after 50% conversion of sulfide (**1b**) to diphenyl disulfide (**3**) (4 h, room temperature, Co(II)/**1b**=1). The H-D exchange reaction between the substrate and methanol-d_1 indicates that the reversible deprotonation step to give carbanion is involved in the oxygenation reaction. When an *endo* and *exo* mixture of very crowded 3-(phenylthio)-*dl*-camphor (**4e**) (*endo* : *exo*=1 : 9) was incubated with Co(II)(bzacen) in methanol-d_1 for 19 h to examine the H-D exchange, the starting sulfide (**4e**) was recovered quantitatively, however, 25% of *endo*-proton (less hindered proton) and 0% of *exo*-proton was deuterated (Scheme 2). The same reaction was found to take place when the reaction of sulfide (**4e**) with D_2O was carried out in the presence of pyridine as base, *i.e.*, only 28% of *endo*-proton was deuterated.

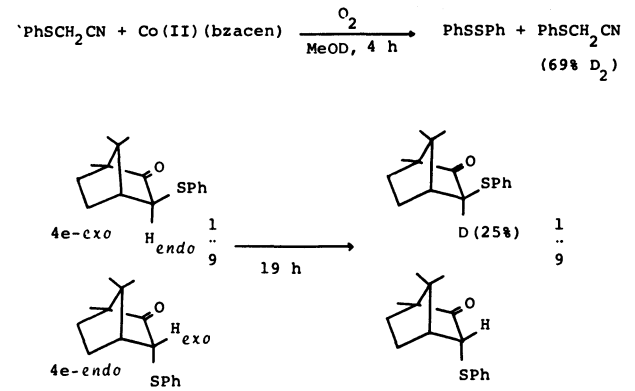

Scheme 2.

Meanwhile, oxidative dealkylation reaction of sulfides (**1a** and **1b**) was also found to take place with strong bases under oxygen atmosphere but very slowly without catalyst; *e.g.*, **1a** gave **2a** (10%), **3** (10%) and **1a** (85% recovered) upon treatment of **1a** with NaH in THF under oxygen atmosphere at room temperature for 20 min (Eq. 4).

In these reactions, peroxy intermediate (**9**) would be formed prior to give *S*-dealkylation products (Eq. 5). The products distribution in the autoxidation of sulfides supports that in the oxygenation of sulfides with Co(II)-(bzacen), a similar peroxy-intermediate (**10**) would be

$$\underset{\mathbf{1a}}{PhSCH_2COPh} + NaH \xrightarrow[\substack{THF,\ r.t.\\ 20\ min}]{O_2} PhSSPh + OHCCOPh + recov. \quad (4)$$

$$\mathbf{3}\ 10\% \qquad \mathbf{2a}\ 10\% \qquad 85\%$$

$$\underset{\mathbf{1b}}{PhSCH_2CN} + t\text{-}BuOK \xrightarrow[\substack{DMSO,\ r.t.\\ 30\ min}]{O_2} PhSSPh + recov.$$

$$\mathbf{3}\ 30\% \qquad 70\%$$

formed as described in other cobalt-Schiff base induced oxygenations of *t*-butylsubstituted phenols and indoles.[11,12,23]

$$PhSCH_2R + :B \xrightarrow{Ar} PhS\dot{C}HR \xrightarrow{O_2} [PhS\dot{C}HR\ O_2^{\cdot}] \longrightarrow \left[\begin{array}{l} PhSHR \\ O\text{-}O^- \end{array}\right] \rightarrow\rightarrow PhSSPh + RCHO \quad (5)$$

9

These observations suggest that the reaction proceeds through an initial formation of a dual or a ternary complex to activate α-methylene proton which may be abstracted by the superoxo-intermediate to give an α-carbanion

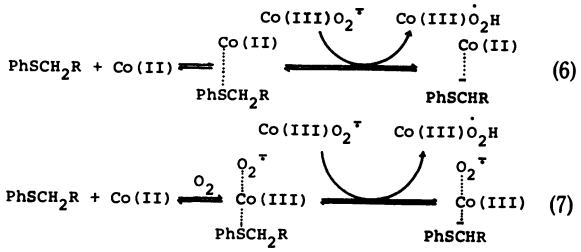

In the oxygenation of *t*-butyl-substituted phenols, Nishinaga *et al.* suggested the direct hydrogen abstraction by superoxo-Co(III) complex (Eq. 9) to be the rate-determining step, followed by subsequent fast electron transfer from the divalent Co(II) complex to the substrate radical (Eq. 10).[11,12,23]

$$Co(II) + O_2 \rightleftharpoons Co(III)O_2^{\cdot} \quad (8)$$

$$Co(III)O_2^{\cdot} + R\text{–}H \longrightarrow Co(III)^{-}O_2H + R\cdot \quad (9)$$

$$Co(II) + R\cdot \xrightarrow{fast} R^{-}Co(III) \quad (10)$$

$$R^{-}Co(III) + O_2 \longrightarrow ROO^{-}Co(III) \quad (11)$$

On the other hand, Jefford and Cadby[3] pointed out the cobalt–Schiff base complex to localize the π-anion charge into an orbital with more [sp^3] character; *i.e.*, cobalt–Schiff base complex catalyzes the reaction of carbanion with molecular oxygen to afford peroxy intermediate.

We cannot conclude which process is involved in the actual oxygenation pathway; *i.e.*, direct deprotonation or hydrogen abstraction and subsequent electron transfer to afford the carbanion, however, all these results would support the direct deprotonation mechanism as indicated in Eqs. 6 and 7.

Finally, the superoxo-Co(III)–carbanion complex is presumed to give peroxo-intermediate (**10**) and the products (Eq. 12).

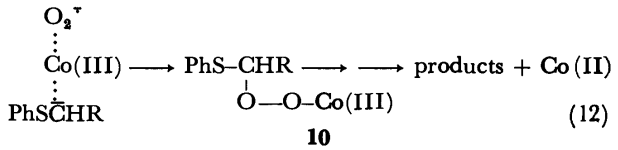

10 (12)

Although a few mechanisms are conceivable for the production of peroxy intermediate (**10**), Nishinaga *et al.* already isolated peroxy intermediates such as (**11**) and (**12**), which seem to support the formation of (**10**) in the oxygenation of sulfide with Co(II)(bzacen).[12,23]

After the oxygenation being carried out, a direct measurement of the ^{1}H NMR spectrum was attempted, however no clear signal was observed due to the presence of paramagnetic material which would be Co(II)(bzacen). Thus, Co(II)(bzacen) can catalyze the oxygenation reaction of sulfide. These results seem to support the mechanistic scheme shown in Eq. 12; *i.e.*, Co(II)(bzacen) is left after the reaction.

Incidentally, all these substrates (**1a—d**) are not susceptible to oxidation with superoxide with 18-crown-6 system.

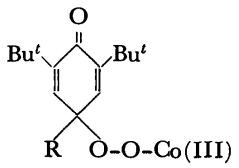

11

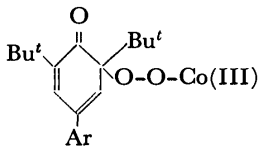

12

Experimental

Reagent. All reagents and solvents used in this study were of guaranteed grades and used without further purification. Methanol-d_1 (min. 99%) and deuterium oxide (min. 99.75%) were purchased from Merck.

General. Melting points were measured on a Yanaco instrument and uncorrected. The boiling points were observed on a Büchi K-R (Kugel Rohr). NMR spectra were recorded on a Hitachi Perkin Elmer R 20 spectrometer in $CDCl_3$ and CCl_4 using TMS as the internal standard. GLC analyses were taken with Hitachi 163 Gas Chromatography (10% SE 30, 2 m glass column). TLC and column chromatography were carried out with Kieselgel GF_{254} Type 60 and Kieselgel 60 (70—230 mesh) (Merck), respectively.

Preparation of Sulfides ***1*** *and* ***4****.* Preparation of unsubstituted sulfides (**1a—e**) were already reported in our recent paper.[15] *p*-Substituted **1b**'s (methyl and chloro) were obtained by treatment of *p*-substituted thiophenol with chloroacetonitrile in the presence of potassium hydroxide according to the ordinary procedure described previously,[24] and isolated through SiO_2 column chromatography (eluent; benzene). Mp and ^{1}H NMR (δ-value, ppm): *p*-$CH_3C_6H_4SCH_2CN$; 160 °C/2 mmHg** (lit, 120.5—127.5 °C/1.0 mmHg),[25] 2.31 (3H, s) 3.41 (2H, s) 7.00 (2H, d, J=8.3) 7.29 (2H, d, J=8.3). *p*-$ClC_6H_4SCH_2CN$; 88—99 °C (from hexane) (lit, 88—90 °C),[26] 3.48 (2H, s) 7.25 (2H, d, J=9.6) 7.33 (2H, d, J=9.6). α-Substituted β-keto sulfides (**4a—e**) were synthesized by treating benzenesulfenyl chloride with corresponding alkyl ketones in the presence of butyllithium or sodium hydride in tetrahydrofuran.

Benzenesulfenyl Chloride. Chlorine gas was bubbled into a dichloromethane solution of diphenyl disulfide at 0 °C for 20 min to give benzenesulfenyl chloride quantitatively.[27] The reaction mixture was condensed by evaporation of both solvent and excess chlorine *in vacuo* without warming. Benzenesulfenyl chloride was used without further purification.

*Preparation of 3-(Phenylthio)-*DL*-camphor (****4e****).* A solution of butyllithium (0.2 mol) in 10 mL of dry hexane was added to a solution of DL-camphor (4.5 g, 0.03 mol) in dry tetrahydrofuran (40 mL) at −72 °C and stirred for 10 min. After introduction of benzenesulfenyl chloride (2.8 g, 0.02 mol) into the reaction mixture at −72 °C, the solution was warmed to room temperature slowly for 1 h and stirred for 1 h additionally. The solution was evaporated under reduced pressure and the mixture was washed with water and extracted with chloroform. The chloroform layer was dried over anhydrous magnesium sulfate. The recovered DL-camphor was separated by distillation at 110 °C (bath temp)/2 mmHg. 3-(Phenylthio)-DL-camphor (**4e**) was isolated through SiO_2 column chromatography (2.9 g, 50% yield). From the ^{1}H NMR spectroscopic analysis, 90% of phenylthio group in **4e** was found to be substituted at *exo* position. When the reaction was carried out at −20 °C, the ratio of *exo* : *endo* was 65 : 35. Other sulfide (**4**) were also prepared similarly and their physical data were listed in Table 2.

Phenylglyoxal and Benzoylformic Acid. Phenylglyoxal and benzoylformic acid were synthesized according to the procedure described in Organic Synthesis.[28,29]

*Synthesis of Phenacyl Phenyl Ether (****5****).* A mixture of phenacyl chloride (6.0 g, 0.039 mmol) and phenol (4.0 g, 0.042 mol) in benzene (40 mL) was added to a solution of sodium hydroxide (1.6 g, 0.067 mol) and tetrabutylammonium chloride (140 mg, 0.5 mmol) in water (40 mL). The solution was refluxed for 10 h and acidified with 6 mol dm^{-3} HCl (pH 4). The solution was extracted with chloroform and the extract was washed with water and dried over anhydrous magnesium sulfate. After evaporation of solvent, the residue was chromatographed on SiO_2, using hexane–benzene (4 : 5) as eluent. The desired product was recrystallized from ethanol. Mp and ^{1}H NMR in $CDCl_3$; 73—74 °C (lit, 71—72 °C),[30] 4.93 (2H, s) 6.7—7.0 (3H, m) 7.0—7.5 (2H, m) 7.3 (5H, brs).

Preparation of Co(II)(bzacen). *Bzacen*; N,N′-*Bis(2-benzoyl-1-methylethylidene)ethylenediamine*: A solution of benzoylacetone (20 g, 0.2 mol) in abs. ethanol (25 ml) was refluxed for 5 min and ethylenediamine (6.0 g, 0.1 mol) in 6 mL of abs. ethanol was added dropwise slowly. After additional reflux for 15 min, the reaction mixture was cooled to room temperature to give a white precipitate in a quantitative yield. The product was recrystallized from ethanol (mp 182—184 °C; lit, 180.5 °C).[31]

Co(II)(bzacen): After refluxing a solution of bzacen (2.0 g, 5.7 mmol) in dry acetone for 2 h under argon atmosphere, anhydrous cobalt(II) chloride (0.75 g, 5.7 mmol) was added and the solution turned green at once. Then, sodium hydroxide (0.75 g, 5.7 mmol) was added to the reaction mixture which was refluxed until the precipitate turned red completely (about 7 h). The reaction mixture was cooled to 0 °C and filtrated. The precipitate was washed with cold water and decantation with methanol 3 times gave Co(II) bzacen) in 60% yield (mp 262—263 °C decomp; lit. 265 °C decomp).[31]

*Oxygenation Reaction of Phenacyl Phenyl Sulfide (****1a****) with Co(II)-(bzacen).* A solution of 105 mg of sulfide (**1a**) (0.46 mmol) in 16 mL of methanol was added to 44 mg of Co(II)-(bzacen) and the mixture was stirred, monitoring time to time the decrease of sulfide (**1a**) by TLC (benzene : hexane= 1 : 1). The reaction mixture was stirred for 30 min and poured into an ion exchange resin (Dowex-50W H^+ form, methanol suspension) and then stirred for 5 min. After filtration, the filtrate was evaporated. The residue was diluted

** 1 mmHg≈133.322 Pa.

with dichloromethane (8 mL) and products [phenylglyoxal (**2a**), methyl benzoate, and diphenyl disulfide (**3**)] were analyzed by GLC. Then the solution was cooled with ice bath and excess diazomethane (ether solution) was added to the solution which was then kept standing for 2 h at 0 °C. Then the reaction mixture was analyzed by GLC again (methyl benzoate and methyl benzoylformate) by comparison with those of authentic samples. PhSSPh (quant), $PhCOCHO$ (81%), $PhCOCO_2H$ (13%), $PhCO_2H$ (4.5%), and $PhCO_2Me$ (1.2%).

The other sulfides were oxygenated in the same procedure.

*The Reaction of Sulfide (**1**) with KO_2.* To a solution of sulfide (**1**) (0.1 mmol) in chloroform, 7 mg, of KO_2 (0.1 mmol) was added at room temperature under argon atmosphere and 26 mg of 18-crown-6 (0.1 mmol) in 4 mL of chloroform. The mixture was stirred for 26 h at room temperature. TLC and GLC measurements showed that sulfide (**1**) was inert to KO_2.

*The Autoxidation of Sulfides (**1a**) and (**1b**) in the Presence of Base. Oxygenation of Phenacyl Phenyl Sulfide (**1a**):* To a solution of **1a** (110 mg, 0.5 mmol) in 30 mL of dry tetrahydrofuran, sodium hydride (17 mg, 0.7 mmol) was added at −72 °C under argon atmosphere and the mixture was stirred for 30 min. Then the mixture was warmed to room temperature slowly and oxygen was bubbled for 20 min with stirring. After evaporation of solvent, the residue was extracted with chloroform. The extract was washed with 2 mol dm^{-3} HCl solution and dried over anhydrous magnesium sulfate. The products were determined by GLC [PhSSPh (10%), PhCOCHO (10%), and recovered (85%)].

*Oxygenation of Cyanomethyl Phenyl Sulfide (**1b**).* A solution of **1b** (149 mg, 1 mmol) and potassium *t*-butoxide (157 mg, 1.4 mmol) in 30 mL of dry dimethyl sulfoxide was stirred at −72 °C under argon atmosphere for 30 min and was warmed to room temperature. Oxygen was bubbled then into the reaction mixture for 30 min and the solution was evaporated. The products were analyzed by GLC. [PhSSPh (30%) and recovered (70%)].

*The H-D Exchange Reaction of Sulfides (**1b**) and (**4e**) with Co(II)(bzacen).* A mixture of sulfide (**1b**) (60 mg, 0.4 mmol) and Co(II)(bzacen) (162 mg, 0.4 mmol) in 2 mL of methanol-d_1 was incubated for 4 h at room temperature under oxygen atmosphere. Co(II)(bzacen) was removed by ion exchange resin and the supernatant was evaporated. The residue was extracted with chloroform and washed with water. The chloroform layer was dried over anhydrous magnesium sulfate and evaporated. The residue was subjected to SiO_2 column chromatography and eluted with hexane. The ^1H NMR spectrum of the recovered sulfide (**1b**) (*ca.* 50%) was determined to estimate the content of deuterium [$PhSCH_2(D_2)CN$; 69% deuterated]. A mixture of sulfide (**4e**) (110 mg, 0.42 mmol, *exo* : *endo*=9 : 1) and Co(II)(bzacen) (100 mg, 0.25 mmol) in 10 mL of methanol-d_1 was stirred for 19 h. After the usual work-up, the extent of the H-D exchange was also estimated by ^1H NMR (25% of *endo*-proton was deuterated).

*The H-D Exchange Reaction of Sulfide (**4e**) in the Presence of Pyridine.* A solution of sulfide (4e) (110 mg, 0.42 mmol *exo* : *endo*=9 : 1) and deuterium oxide (10 mmol) in pyridine, (20 mL) was stirred for 40 h under argon atmosphere at room temperature. The solution was acidified then to pH 4 by adding 4 mol dm^{-3} HCl into the solution at 0 °C which was extracted with chloroform. The chloroform layer was washed with 1 mol dm^{-3} HCl to remove a small amount of residual pyridine and dried over anhydrous magnesium sulfate. Chloroform was removed under reduced pressure and the deuterium content was determined by ^1H NMR (28% of *endo*-proton was deuterated).

References

1) "Molecular Mechanism of Oxygen Activation," ed by O. Hayaishi, Academic Press, New York (1974).
2) "Bioorganic Chemistry," ed by E. E. van Tamelen Academic Press, New York (1977, 1978).
3) "Progress in the Chemistry of Organic Natural Products," ed by W. Herz, H. Grisebach, and G. W. Kirby, Springer-Verlag, Wein (1981).
4) T. Matsuura, *Tetrahedron*, **33**, 2869 (1977).
5) J. T. Groves, "Metal Ion Activation of Dioxygen," ed by T. S. Spiro, John Wiley and Sons, New York (1980).
6) J. P. Collman, R. R. Gagne, H. B. Gray, and J. Hare, *J. Am. Chem. Soc.*, **96**, 6522 (1974).
7) J. P. Collman, R. R. Gagne, C. A. Reed, W. T. Robinson, and G. A. Rodley, *Proc. Natl. Acad. Sci. U. S. A.*, **71**, 1326 (1974).
8) J. P. Collman, R. R. Gagne, C. A. Reed, T. R. Halbert, G. Lang, and W. T. Robinson, *J. Am. Chem. Soc.*, **97**, 1427 (1975).
9) G. W. Everett, Jr., and R. H. Holm, *J. Am. Chem., Soc.*, **88**, 2442 (1966).
10) L. A. Crumbliss and F. Basolo, *J. Am. Chem. Soc.*, **92**, 55 (1970).
11) A. Nishinaga, *Chem. Lett.*, **1975** 273.
12) A. Nishinaga, H. Tomita, and T. Matsuura, *Tetrahedron Lett.*, **1979**, 2893.
13) Y. Watanabe, T. Iyanagi, and S. Oae, *Tetrahedron Lett.*, **21**, 3685 (1980).
14) Y. Watanabe, T. Numata, T. Iyanagi, and S. Oae, *Bull. Chem. Soc. Jpn.*, **54**, 1163 (1981).
15) R. E. White and M. J. Coon, *Ann. Rev. Biochem.*, **49**, 315 (1980).
16) G. A. Rodley and W. T. Robinson, *Nature*, **235**, 438 (1972).
17) E. Block, "Reactions of Organosulfur Compounds," Academic Press, New York (1978), p. 36.
18) T. H. Lowry and K. S. Richardson, "Mechanism and Theory in Organic Chemistry," Harper and Row Publisher, New York (1976), p. 124.
19) M. Mousseron and R. Jacquier, *C. R. Acad. Sci.*, **229**, 347 (1949); *Chem. Abstr.*, **45**, 2422c (1951).
20) W. E. Truce and F. E. Roberts, *J. Org. Chem.*, **28**, 961 (1963).
21) T. S. Murthy and B. D. Tilak, *J. Sci. Int. Res. (India)*, **19B**, 395 (1960); *Chem. Abstr.*, **55**, 11387i (1961).
22) T. Numata, Y. Watanabe, and S. Oae, *Tetrahedron Lett.*, **1978**, 4933.
23) A. Nishinaga, K. Nishizawa, H. Tomita, and T. Matsuura, *J. Am. Chem. Soc.*, **99**, 1287 (1977).
24) W. Tagaki, "Organic Chemistry of Sulfur," ed by S. Oae, Plenum Press, New York (1977), p. 231.
25) J. M. van der Zanden, J. Nieuwenhuis, and H. J. T. Bos, *Res. Trav. Chim.*, **76**, 669 (1967); *Chem. Abstr.*, **52**, 3026 (1958).
26) E. A. Falco, B. Roth, and G. H. Hitchings, *J. Org. Chem.*, **26**, 1143 (1961).
27) E. E. Reid, "Organic Chemistry of Bivalent Sulfur," Chemical Publisher, New York (1958), p. 262.
28) G. J. Mikol and G. A. Russell, *Org. Synth.*, Coll. Vol. IV, 937 (1973).
29) T. S. Oakwood and C. A. Weisgerber, *Org. Synth.*, Coll. Vol. III, 114 (1965).
30) C. O. Guss, *J. Am. Chem. Soc.*, **71**, 3460 (1949).
31) P. J. McCarthy, R. J. Hovey, K. Ueno, and A. E. Martell, *J. Am. Chem. Soc.*, **77**, 5820 (1955).

Addition Reaction of Carboxylic Anhydrides to the Carbon-Nitrogen Double Bond of Unsubstituted Cyclic Imidates

Shiro KOBAYASHI, Michihisa ISOBE, and Takeo SAEGUSA*
Department of Synthetic Chemistry, Faculty of Engineering, Kyoto University, Kyoto 606
(Received December 18, 1981)

Acyclic and cyclic (SAn and GAn) carboxylic anhydrides were added at room temperature to the C=N bond of unsubstituted cyclic imidates of 2-oxazoline (OZO) and 5,6-dihydro-4*H*-1,3-oxazine (OZI) to give addition products quantitatively. In contrast to these findings, the reactions of acetyl halides with OZO and OZI yielded ring-opened products and the reactions of carboxylic anhydrides with 2-benzyl-2-oxazoline (BzOZO) afforded also the ring-opened products. The bicyclic addition product of OZO with SAn is equilibrated with a mixture of starting materials. The stereochemistry of addition products having a six-membered ring system is discussed.

Reactions of substituted 2-oxazolines with carboxylic anhydrides have been reported in several papers.[1-4] In these reactions amide and imide derivatives were formed. For example, the reaction of 2-substituted 2-oxazoline (**1**) with succinic anhydride (**2**, SAn) gave a succinimide product (**4**), probably through an intermediate (**3**) which is an addition product of **2** onto the reactive C=N bond[5] of **1** and isomerized to **4**.[3] In the specific combination of 2-isopropyl-2-oxazolines and maleic anhydride, products **5** have been obtained,

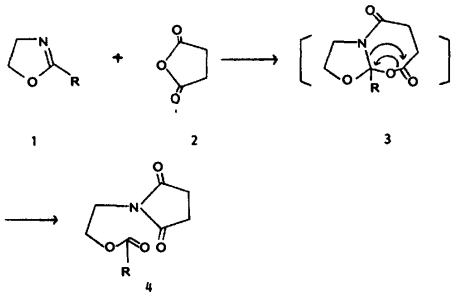

which has been claimed to correspond to the above intermediate **3**.[4]

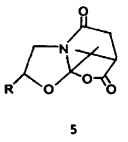

The present paper describes the addition reactions of carboxylic (acyclic and cyclic) anhydrides onto the C=N double bond of unsubstituted five- and six-membered cyclic imidates of 2-oxazoline (OZO) and 5,6-dihydro-4*H*-1,3-oxazine (OZI), respectively. Products exactly correspond to the intermediate **3** which has been assumed in the previous study.[3] It should be noted also that prior to the present work unsubstituted OZO and OZI had not been employed for the reaction with carboxylic anhydrides probably due to the difficulties of their preparation. In the polymerization chemistry, however, OZO and OZI have recently been used extensively as a monomer of cationic ring-opening polymerization to produce poly(*N*-formylaziridine) and poly(*N*-formylazetidine) respectively.[6]

Results and Discussion

Reactions of OZO and OZI with Acyclic Carboxylic Anhydrides. In $CHCl_3$ or CH_2Cl_2, OZO and OZI reacted with acyclic carboxylic anhydrides (**6**) at room temperature to give addition products (**7**). In all

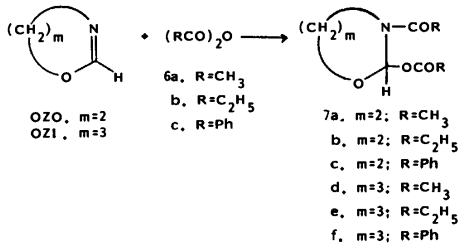

combinations, products **7a**—**f** were produced quantitatively. The structure of **7** was determined by IR and NMR spectroscopy, elemental analysis, as well as hydrolysis experiments of **7**.

Products **7** were readily hydrolyzed with an equimolar amount of water to give quantitatively formate derivatives (**8**) with elimination of one molecule of carboxylic acid. Products **8** were purified by distillation *in vacuo* and the structure was determined by IR and NMR spectroscopy and by elemental analysis. The production

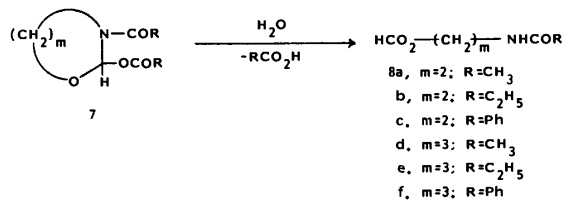

of **8a**, for example, is explained by the following course of reaction from **7a** and water through an intermediate **9**:

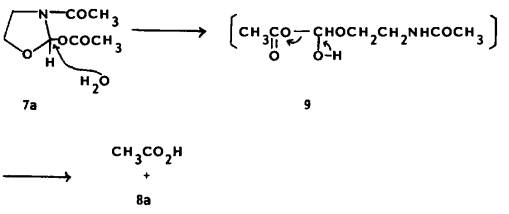

Results of hydrolysis experiments are taken to support the structure of the addition products **7**.

The addition reaction of **6** to the C=N bond of OZO or OZI proceeded much faster with OZI than with OZO, *i.e.*, the reactions of OZI with **6** finished within several minutes at room temperature whereas those of OZO with **6** took one day at the same temperature. This difference is due to the difference in nucleophilic reactivity of OZI and OZO in the formation of intermediate **10**, which is probably a rate-determining step.

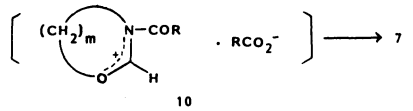

10

For example, our previous study has shown that the nucleophilic reaction of OZI with MeX (X=I and *p*-$CH_3C_6H_4SO_3$) producing *N*-methyl onium **11** proceeded about 12 times faster than that of OZO reflected by the second order rate constant (k_2).[7]

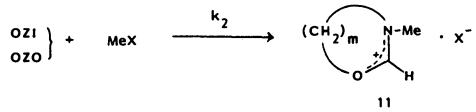

11

In the reaction of 2-substituted 2-oxazoline, *e.g.*, 2-benzyl-2-oxazoline (BzOZO), with acetic anhydride, the addition product corresponding to **7** was not produced but a new product (**12**) was obtained with liberation of an equimolar amount of acetic acid. This

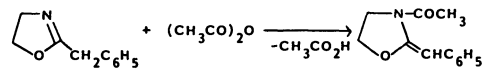

BzOZO **12**

phenomenon constitutes a sharp contrast with the result of OZO. Only unsubstituted OZO gave addition products.

In previous studies, various nucleophiles have been used in the reaction with 2-substituted 2-oxazolines, *e.g.*, alkyl halides, molecular chlorine, chloroformate esters, and acyl chlorides.[1,5,8] In these reactions all the products were ring-opened ones and no addition product at the C=N bond was formed. In order to examine the behavior of unsubstituted cyclic imidates, reactions of OZO and OZI with acetyl halides were carried out and found to give ring-opened products **13** but not an addition product corresponding to **7**. With

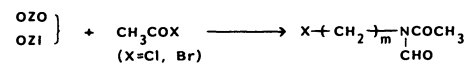

13a, m=2; X=Cl
b, m=2; X=Br
c, m=3; X=Cl
d, m=3; X=Br

an equimolar feed reactions of OZO–CH_3COCl, OZI–CH_3COCl, and OZI–CH_3COBr systems gave **13** quantitatively within a few minutes in CH_2Cl_2, which was confirmed by NMR of the reaction mixture. The reaction probably involves an onium intermediate **14**.

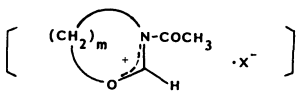

14

In the combination of OZO–CH_3COCl (1 : 1), on the other hand, it was found that the 2 : 1 reaction product (**15**) was first formed and then **15** was gradually converted to **13a** within one day at room temperature by reacting further with CH_3COCl. **15** was actually isolated

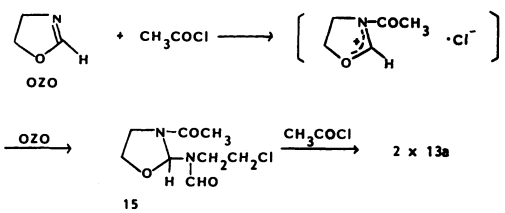

15

from the OZO–CH_3COCl (2.5 : 1) reaction system. **15** was formed *via* the intermediate **16** derived from **14a** and OZO. The reaction mechanism of **15** with CH_3COCl has not been fully understood.

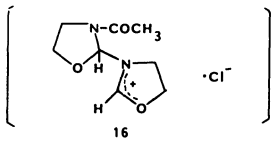

16

Thus, the reaction mode of acetyl halides with OZO and OZI is quite different from that of carboxylic anhydrides. The reaction mode of OZO and OZI toward acetyl halides, however, is analogous to that of 2-substituted 2-oxazolines toward acyl chlorides.[8]

Reactions of OZO and OZI with Cyclic Carboxylic Anhydrides. It was found by NMR study that the reaction of OZO with succinic anhydride (SAn) produced a bicyclic adduct 6,8-dioxa-1-azabicyclo-[5.3.0]decane-2,5-dione (**17a**), a product corresponding to **7** in the case of cyclic carboxylic anhydrides, and that **17a** is present in solution in equilibrium with starting materials of OZO and SAn. It has been unsuccessful

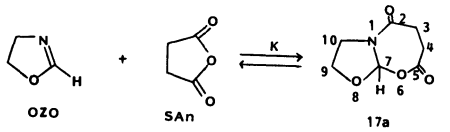

OZO SAn **17a**

so far to isolate **17a** in pure form. The NMR spectrum of the reaction system shows a new peak at δ 7.1 ascribed to the specific methine proton of **17a** beside a signal at δ 6.8 due to the methine proton of OZO. When the temperature was varied the intensities of these two signals changed. This change was reversible with the temperature variation. Therefore, the equilibrium constant (K, $1 \cdot mol^{-1}$) could be determined. Figure 1 shows the temperature dependency of K measured at −25, 35, 50, and 80 °C. From the observed plot of $\ln K$ *vs.* $1/T$, enthalpy (ΔH) and entropy (ΔS) values were calculated from the following equation:

$$-RT \ln K = \Delta H - T\Delta S$$

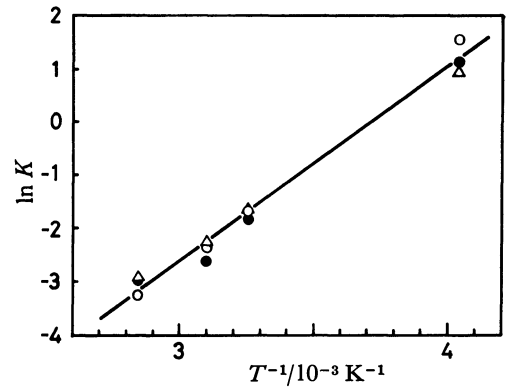

Fig. 1. Temperature dependency of the equilibrium constant $K(1\cdot mol^{-1})$: the total amount of OZO+SAn =2.0 mmol in 0.4 ml of CD_3CN: OZO/SAn ratio; ○, 2.0; △, 1.0; ●, 0.5.

as $\Delta H = -30$ kJ mol^{-1} and $\Delta S = -110$ J K^{-1} mol^{-1}.

To support the structure of **17a**, the IR spectrum of the reaction mixture of OZO–SAn in CH_2Cl_2 showed a new band at 1730 cm^{-1} ascribable to the ester group and no band around 1580 cm^{-1} assignable to a carboxylate anion was observed.

The reaction of OZO with glutaric anhydride (GAn) yielded a bicyclic addition product, 7,9-dioxa-1-azabicyclo[6.3.0]undecane-2,6-dione (**17b**) quantitatively, which was obtained as a white solid. It is considered that the reaction equilibrium goes far to the right in this system. **17b** is insoluble in most organic solvents and hence NMR spectrum of the compound has not been obtained.

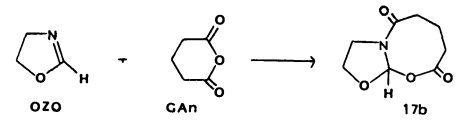

The hydrolysis of **17b** readily occured and gave a formic ester **18a**, which was taken to support the structure of **17b**.

$$\textbf{17b} \xrightarrow{H_2O} HCO_2CH_2CH_2NHCOCH_2CH_2CH_2CO_2H$$

18a

The reaction of OZI with GAn was exothermic, which was completed in a few minutes at room temperature to give a white solid of 7,9-dioxa-1-azabicyclo[6.4.0]-dodecane-2,6-dione (**17c**). The reaction equilibrium lies far to the side of product in this system, too.

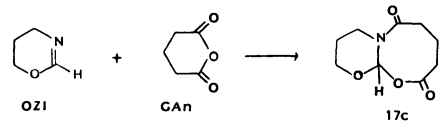

Similarly to **17b** the hydrolysis of **17c** gave **18b**, supporting the structure of **17c**.

$$\textbf{17c} \xrightarrow{H_2O} HCO_2CH_2CH_2CH_2NHCOCH_2CH_2CH_2CO_2H$$

18b

Formation of bicyclic addition products (**17**) is interestingly compared with that of bicyclic amide acetals (**19**) from 2-substituted 2-oxazolines and epoxides, where epoxides add to the C=N bond of the oxazolines.[9] In comparison with the results of unsubstituted cyclic imidates of OZO and OZI the reaction of BzOZO with GAn was examined. The reaction gave **20**, which is not a bicyclic addition product of GAn onto the C=N bond of BzOZO but corresponding to the product **12**. An intermediate **21** is probably involved.

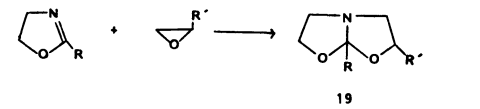

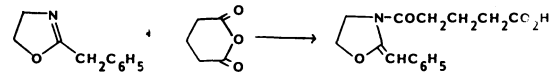

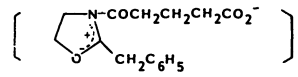

Stereochemistry of Cyclic Addition Products Having Six-membered Ring. Addition products of five-membered ring system, *e.g.*, **7a** and **17a**, showed a single peak of the methine proton at δ 7.1 in the NMR spectra ($CDCl_3$ solvent). In contrast, the methine proton of addition products derived from six-membered OZI, *e.g.*, **7d** and **17c**, appeared as two peaks. The peak of the higher field at δ 7.1 and that of the lower field at δ 7.5 are ascribed respectively to the axial and equatorial methine proton of a six-membered chair form,[10] *e.g.*,

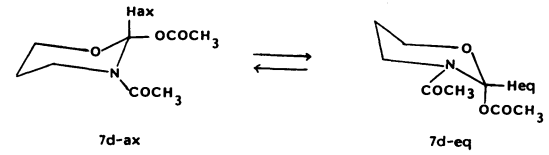

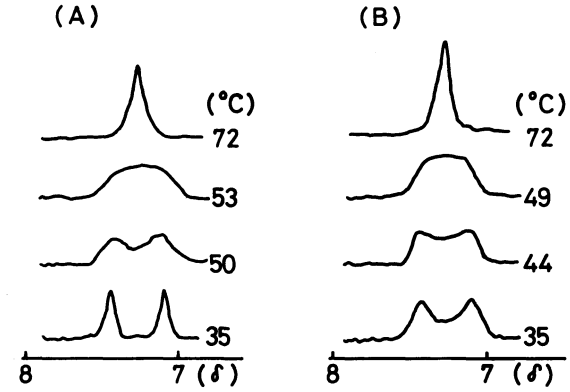

Fig. 2. Temperature-dependent NMR signals of the methine proton of **7d** (A) and **17c** (B) in CD_3CN.

With variation of temperature in CD_3CN, in which two methine signals at δ 7.1 and 7.5 appear as shown in Fig. 2, the coalescence time (T_c) was obtained as 53 °C for **7d** and 49 °C for **17c**, respectively. Then, the free-energy of activation ($\Delta F^{\neq}$) of the interconversion like **7d**-ax⇆**7d**-eq was calculated to be 69.4 kJ mol^{-1} for **7d** and 68.6 kJ mol^{-1} for **17c**, respectively.[11] These $\Delta F^{\neq}$ values are somewhat higher than those obtained for cyclohexane derivatives.[11a]

Experimental

Materials. Solvents of CH_2Cl_2, $CHCl_3$, $CDCl_3$, CH_3CN CD_3CN, and DMSO-d_6 were purified by distillation under nitrogen. 2-Oxazoline (OZO),[6a] 5,6-dihydro-4*H*-1,3-oxazine (OZI),[6b] and 2-benzyl-2-oxazoline (BzOZO)[12] were obtained according to the reported procedures. Acetic and propionic anhydrides were dried over $CaCl_2$ and distilled. Benzoic anhydride was purified by recrystallization from diethyl ether. Succinic (SAn) and glutaric (GAn) anhydrides were recrystallized from $CHCl_3$ and $CHCl_3$–diethyl ether, respectively. Acetyl chloride and bromide were purified by distillation under nitrogen after drying over $CaCl_2$.

Measurements. NMR spectra were recorded at 60 MHz on a Hitachi R-20B spectrometer. IR spectra were taken on a Hitachi EPI G31 spectrophotometer.

Reaction of OZO and OZI with Acyclic Carboxylic Anhydrides (6). A typical run was as follows. A mixture of OZO and acetic anhydride (**6a**) (10 mmol each) in 4 ml of $CHCl_3$ was allowed to react at room temperature for 24 h under nitrogen. At this point it was confirmed by NMR of the mixture that the reaction was completed to yield addition product (**7a**) quantitively. The product **7a** was isolated by distillation *in vacuo* using Kugelrohl to give **7a** (1.63 g, 94% yield). Likewise, **7b** (91%), **7d** (92%), and **7e** (89%) were obtained. The quantitative production of **7c** and **7f** was confirmed by NMR of the reaction system carried out in $CDCl_3$ but the isolation of **7c** and **7f** has not been succeeded.

Data for the structural determination of products **7** are as follows. **7a**: bp 95—96 °C/0.13 Torr (1 Torr=133.322 Pa); IR (neat): 1730 and 1660 cm^{-1}; NMR ($CDCl_3$): δ 2.05 (s, 6H), 3.64 (t-like, 2H), 4.23 (t-like, 2H), and 7.08 (s, 1H). Found: C, 48.25; H, 6.37; N, 8.15%. Calcd for $C_7H_{11}NO_4$: C, 48.55; H, 6.40; N, 8.09%. **7b**: bp 110—112 °C/0.15 Torr; IR (neat): 1735 and 1665 cm^{-1}; NMR ($CDCl_3$): δ 1.15 (t, 6H), 2.33 (q, 4H), 3.65 (t-like, 2H), 4.21 (t-like, 2H), and 7.10 (s, 1H). Found: C, 53.89; H, 7.41; N, 6.97%. Calcd for $C_9H_{15}NO_4$: C, 53.72; H, 7.51; N, 6.96%. **7c**: NMR($CDCl_3$): δ 3.84 (2H), 4.25 (2H), and 7.1—8.1 (11H). **7d**: bp 83—84 °C/0.09 Torr; IR (neat): 1720 and 1660 cm^{-1}; NMR ($CDCl_3$): δ 1.73 (2H), 2.08 (6H), 3.0—4.5 (4H), and 7.1+7.5 (1H). Found: C, 51.09; H, 7.25; N, 7.47%. Calcd for $C_8H_{13}NO_4$: C, 51.33; H, 7.00; N, 7.48%. **7e**: bp 109—111 °C/0.15 Torr; IR (neat): 1730 and 1660 cm^{-1}; NMR ($CDCl_3$): δ 1.15 (t, 6H), 1.75 (2H), 2.36 (q, 4H), 3.5—4.5 (4H), and 7.1+7.5 (1H). Found: C, 55.74; H, 7.96; N, 6.33%. Calcd for $C_{10}H_{17}NO_4$: C, 55.80; H, 7.96; N, 6.51%. **7f**: NMR ($CDCl_3$): δ 1.4—2.5 (2H), 3.1—4.6 (4H), and 7.0—8.2 (11H).

Hydrolysis of Addition Products (7). A typical example of hydrolysis of **7a** was carried out as follows. To 3.24 mmol of **7a** 5.6 mmol of water was added and stirred at room temperature. The hydrolysis took place exothermically. After 10 min the vacuum distillation with Kugelrohl gave 3.90 g (92% yield) of **8a**. Furthermore, 1.90 g (97% yield) of acetic acid was obtained in the trap cooled in a Dry-Ice bath during the distillation. Analogous procedures for **7b**—**f** gave respectively **8b** (96%), **8c** (85%), **8d** (90%), **8e** (87%), and **8f** (80%).

The structure of these six hydrolysis products was determined based on the following data. **8a**: bp 83—85 °C/0.1 Torr; IR (neat): 3280, 3070, 1725, 1660, 1545, and 1180 cm^{-1}; NMR ($CDCl_3$): δ 2.00 (s, 3H), 3.45 (2H), 4.20 (t, 2H), 7.05 (br s, 1H), and 7.98 (s, 1H). Found: C, 46.01; H, 7.01; N, 10.70%. Calcd for $C_5H_9NO_3$: C, 45.80; H, 6.92; N, 10.68%. **8b**: bp 116—118 °C/0.3 Torr; IR (neat): 3280, 3070, 1720, 1650, 1540, and 1180 cm^{-1}; NMR ($CDCl_3$): δ 1.13 (t, 3H), 2.17 (q, 2H), 3.48 (2H), 4.18 (t, 2H), 6.9 (br s, 1H), and 7.95 (s, 1H). Found: C, 49.76; H, 7.85; N, 9.73. Calcd for $C_6H_{11}NO_3$: C, 49.65; H, 7.64; N, 9.65%. **8c**: bp 158—162 °C/0.25 Torr; IR (neat): 3300, 3070, 1725, 1650, 1540, and 1180 cm^{-1}; NMR ($CDCl_3$): δ 3.65 (2H), 4.27 (t, 2H), 6.58 (br s, 1H), 7.4 (5H), and 7.94 (s, 1H). Found: C, 62.50; H, 5.89; N, 7.24%. Calcd for $C_{10}H_{11}NO_3$: C, 62.17; H, 5.74; N, 7.25%. **8d**: bp 105—108 °C/0.25 Torr; IR (neat): 3280, 3070, 1720, 1650, 1550, and 1180 cm^{-1}; NMR ($CDCl_3$): δ 1.86 (2H), 1.96 (s, 3H), 3.25 (2H), 4.15 (t, 2H), 6.3 (br s, 1H), and 7.95 (s, 1H). Found: C, 49.46; H, 7.74; N, 9.79%. Calcd for $C_6H_{11}NO_3$: C, 49.65; H, 7.64; N, 9,65%. **8e**: bp 117—119 °C/0.3 Torr; IR (neat): 3280, 3070, 1720, 1650, 1550, and 1180 cm^{-1}; NMR ($CDCl_3$): δ 1.14 (t, 3H), 1.86 (2H), 2.18 (q, 2H), 3.28 (2H); 4.15 (t, 2H), 5.9 (br s, 1H) and 7.96 (s, 1H). Found: C, 53.04; H, 8.46; N, 8.89%. Calcd for $C_7H_{13}NO_3$: C, 52.82; H, 8.23; N, 8.80%. **8f**: bp 170—175 °C/0.25 Torr; IR (neat): 3300, 3060, 1720, 1640, 1540, and 1180 cm^{-1}; NMR ($CDCl_3$): δ 1.95 (2H), 3.45 (2H), 4.18 (t, 2H), 6.74 (1H), 7.4 (5H), and 7.94 (s, 1H). Found: C, 63.99; H, 6.26; N, 6.55%. Calcd for $C_{11}H_{13}NO_3$: C, 63.76; H, 6.32; N, 6.76%.

Reaction of BzOZO with Acetic Anhydride. BzOZO and acetic anhydride (**6a**) (10 mmol) each were allowed to react in 4 ml of CH_2Cl_2 at room temperature for 30 min. Evaporation of the solvent gave a white solid of **12** which was purified by recrystallization from a $CHCl_3$/diethyl ether mixed solvent (1.40 g, 96% yield); mp 128—129 °C; IR (KBr): 1675 and 1640 cm^{-1}; NMR ($CDCl_3$): δ 2.10 (s, 3H), 3.65 (t-like, 2H), 4.10 (t-like, 2H), 6.07 (s, 1H), and 7.1 (5H). Found: C, 70.72; H, 6.40; N, 6.86%. Calcd for $C_{12}H_{13}NO_2$: C, 70.92; H, 6.45; N, 6.89%.

Reactions of OZO and OZI with Acetyl Chloride or Bromide. In 0.5 ml of $CDCl_3$, OZO, or OZI (1 mmol) and acetyl chloride or bromide (1 mmol) were mixed. By NMR the reaction was found to finish within several minutes except for the OZO–acetyl chloride system which took one day for the completion of the reaction. The product (**13**) was isolated by using Kugelrohl and data for the structure determination are given as follows. **13a**: bp 81—83 °C/0.25 Torr; IR (neat): 1725 and 1670 cm^{-1}; NMR ($CDCl_3$): δ 2.42 (s, 3H), 3.58 (t, 2H), 4.01 (t, 2H), and 9.08 (s, 1H). Found: C, 40.30; H, 5.60; N, 9.48%. Calcd for $C_5H_8NO_2Cl$: C, 40.15; H, 5.39; N, 9.36%. **13b**: bp 96—98 °C/0.20 Torr; IR (neat): 1725 and 1670 cm^{-1}; NMR ($CDCl_3$): δ 2.43 (s, 3H), 3.40 (t, 2H), 4.03 (t, 2H), and 9.08 (s, 1H). Found: C, 30.82; H, 4.12; N, 7.06%. Calcd for $C_5H_8NO_2Br$: C, 30.95; H, 4.16; N, 7.22%. **13c**: bp 85—87 °C/0.30 Torr; IR (neat): 1725 and 1665 cm^{-1}; NMR ($CDCl_3$): δ 1.98 (m, 2H), 2.40 (s, 3H), 3.50 (t, 2H), 3.77 (t, 2H), and 9.09 (s, 1H). Found: C, 44.33; H, 6.28; N, 8.65%. Calcd for $C_6H_{10}NO_2Cl$: C, 44.05; H, 6.16; N, 8.56%. **13d**: bp 104—107 °C/0.25 Torr; IR (neat); 1725 and 1670 cm^{-1}; NMR ($CDCl_3$): δ 2.05 (m, 2H), 2.43 (s, 3H), 3.35 (t, 2H), 3.78 (t, 2H), and 9.12 (s, 1H). Found: C, 34.92; H, 4.85; N, 6.82%. Calcd for $C_6H_{10}NO_2Br$: C, 34.64; H, 4.84; N, 6.73%.

A mixture of OZO (10 mmol) and acetyl chloride (4 mmol) was allowed to react in 3.2 ml of $CHCl_3$ at room temperature for 24 h. The evaporation of $CHCl_3$ and unreacted OZO

gave a 2 : 1 reaction product **15** (92% yield), which was further purified by silica-gel TLC (ethanol solvent). IR (neat): 1660, and 1100 cm^{-1}; NMR ($CDCl_3$): δ 2.95 (s, 3H), 3.5—4.4 (m, 8H), 6.18 (s, 1H), and 8.36 (s, 1H). Found: C, 43.38; H, 6.08; N, 12.65%. Calcd for $C_8H_{13}N_2O_3Cl$: C, 43.55; H, 5.94; N, 12.70%. An attempt to distill **15** with Kugelrohl *in vacuo* resulted in decomposition to give **13a**

Reaction of OZO with GAn. All operations were performed under nitrogen. In 4 ml of CH_3CN,OZO (10 mmol) and GAn (10 mmol) were mixed at 0 °C. A white solid precipitated after several minutes. Then, the solid product (**17b**) was separated using a sintered-glass filter and washed several times with CH_2Cl_2 (1.73 g, 93% yield): mp 87—88 °C; IR (KBr): 1735 and 1670 cm^{-1}. Found: C, 51.66; H, 6.01; N, 7.75%. Calcd for $C_8H_{11}NO_4$: C, 51.89; H, 5.99; N, 7.56%.

Reaction of OZI with GAn. All operations were carried out under nitrogen. A mixture of OZI (10 mmol) and GAn (10 mmol) was stirred at 0 °C in 4 ml of CH_2Cl_2. The reaction mixture immediately become viscous. After 30 minutes dry diethyl ether (5 ml) was added to the system, well shaken and kept at −25 °C for 2 h. Then, the system was separated into two layers. The lower layer was dissolved in 4 ml of CH_2Cl_2. This solution was added to a large amount of diethyl ether to separate a viscous liquid material. This reprecipitation procedure was repeated twice. The separated viscous liquid product (**17c**) became a white solid after drying *in vacuo* (1.75 g, 88% yield): mp 53—55 °C; IR (KBr): 1715, 1650, and 1090 cm^{-1}; NMR ($CDCl_3$): δ 1.4—2.7 (8H), 3.2—4.6 (4H), and 7.1+7.5 (1H). Found: C, 51.33; H, 7.04; N, 6.71%. Calcd for $C_9H_{13}NO_4(H_2O)_{0.6}$: C, 51.47; H, 6.82; N, 6.67%.

Hydrolysis of 17b and 17c. **17b** (or **17c**) (5 mmol) was reacted with 30 mmol of water. The hydrolysis finished immediately. The evaporation of excess water gave a viscous liquid. This liquid was dissolved in CH_3CN and poured into a large amount of diethyl ether to separate the liquid again. This procedure of purification was repeated three times to give an oily product **18a** (or **18b**) in almost quantitative yield. **18a**: IR (neat): 3280, 3070, 1720, 1640, 1550, and 1180 cm^{-1}; NMR (CD_3CN): δ 1.5—2.5 (m, 6H), 3.30 (q-like, 2H), 4.04 (t, 2H), 6.63 (br s, 1H), and 7.89 (s, 1H). Found: C, 47.35; H. 6.61; N, 7.01%. Calcd for $C_8H_{13}NO_5$: C, 47.29; H, 6.45; N, 6.89%. **18b**: IR (neat): 3280, 3070, 1725, 1640, 1560, and 1180 cm^{-1}; NMR (CD_3CN): δ 1.4—2.5 (m, 8H), 3.14 (q-like, 2H), 4.05 (t, 2H), 6.78 (br s, 1H), and 7.91 (s, 1H). Found: C, 48.96; H, 7.35; N, 6.47%. Calcd for $C_9H_{15}NO_5$: C, 49.76; H, 6.96; N, 6.45%.

Reaction of BzOZO with GAn. A mixture of BzOZO and GAn (5 mmol each) in CH_3CN (2 ml) was kept at room temperature for 20 h to give needle crystals **20**, which was separated and washed with CH_2Cl_2 (0.72 g, 52%): mp 63—64 °C (from DMSO); IR (KBr): 1690, 1630, and 1120 cm^{-1}; NMR (DMSO-d_6): δ 1.5—2.7 (m, 6H), 3.88 (t-like, 2H), 4.29 (t-like, 2H), 6.25 (s, 1H), and 6.7—7.4 (m, 5H). Found: C, 65.41; H, 6.31; N, 5.28%. Calcd for $C_{15}H_{17}NO_4$: C, 65.44; H, 6.22; N, 5.09%.

References

1) J. A. Frump, *Chem. Rev.*, **71**, 483 (1971).

2) P. F. Tryon, U. S. Patent, 2410318 (1946); *Chem. Abstr.*, **41**, 2076b (1947).

3) S. P. Rowland, U. S. Patent, 2547542, 2547494 (1951); *Chem. Abstr.*, **45**, 9567d (1951), **46**, 1050c (1952).

4) R. Nehring and W. Seeliger, *Justus Liebigs Ann. Chem.*, **82**, 448 (1970).

5) W. Seeliger, E. Aufderhaar, W. Diepers, R. Feinauer, R. Nehring, W. Thier, and H. Hellmann, *Angew. Chem.*, **78**, 913 (1966).

6) a) T. Saegusa, H. Ideda, and H. Fujii, *Polym. J.*, **3**, 35 (1972); b) T. Saegusa, Y. Nagura, and S. Kobayashi, *Macromolecules*, **6**, 495 (1973); c) T. Saegusa and S. Kobayashi, "International Review of Science, Physical Chemistry Series Two, Vol. 8, Macromolecular Science," Butterworth, London, (1975), Chap. 4; d) T. Saegusa and S. Kobayashi, "Encyclopedia of Polymer Science and Technology," John Wiley and Sons, Inc., New York (1976), Suppl. Vol. 1, pp. 220—237; e) S. Kobayashi, M. Isobe, and T. Saegusa, *Macromolecules*, in press.

7) T. Saegusa, S. Kobayashi, and Y. Nagura, *Macromolecules*, **7**, 265 (1974).

8) R. Nehring and W. Seeliger, *Justus Liebigs Ann. Chem.*, **709**, 113 (1967).

9) R. Feinaurer, *Synthesis*, **1971**, 16; R. Feinauer and W. Seeliger, *Justus Liebigs Ann. Chem.*, **698**, 174 (1966).

10) L. M. Jackman and S. Sternhell, "Nuclear Magnetic Resonance Spectroscopy in Organic Chemistry," 2nd ed, Pergamon, Oxford (1969), p. 238.

11) L. M. Jackman and F. A. Cotton, "Dynamic Nuclear Magnetic Resonance Spectroscopy," Academic Press, New York (1975), Chap. 14; L. W. Reeves, "Adv. Phys. Org. Chem.," Academic Press, New York (1965), Vol. 3, p. 187; M. Tabei, T. Tezuka, and M. Hirota, *Tetrahedron*, **27**, 301 (1971).

12) T. Kagiya, S. Narisawa, T. Maeda, and K. Fukui, *Kogyo Kagaku Zasshi*, **69**, 732 (1966); *Chem. Abstr.*, **65**, 15510d (1966).

Effects of Chelating Agents on the Preparation of Benzenediols by Oxidation of Phenol with Peracetic Acid

Tohru Tsuchiya,* Kazuhiro Ikehira, and Juichi Imamura

Catalyst Division, National Chemical Laboratory for Industry, Tsukuba Research Center, Yatabe, Tsukuba, Ibaraki, 305

(Received October 28, 1980)

The oxidation of phenol with peracetic acid has been investigated in connection with the industrial preparation of benzenediols. The effects of 25 additives, such as derivatives of monomeric and condensed phosphoric acid, chelating agents, and salts of polybasic carboxylic acids, were examined; derivatives of condensed phosphoric acid were found to be most effective. The oxidation of phenol (213 mmol) with peracetic acid (21 mmol) in the absence of the additives gave 1,2- and 1,4-benzenediols in only 5.8% and 7.6% yields, respectively. But in the presence of 2.0×10^{-7} mol of potassium diphosphate the yields of 1,2- and 1,4-benzenediol were 47% and 31%, respectively. The improvement in the yields by the additives is attributable to the masking of a trace of metals, especially iron and cobalt, present in the reaction mixture. These metals tend to catalyze the further oxidation of the benzenediols formed.

Benzenediols are important feedstocks in chemical industries and are extensively used as powerful reducing agents in the photography industry. 1,2-Benzenediol has been manufactured by means of alkali-fusion of 2-chlorophenol,[1] and 1,4-benzenediol by reduction of *p*-benzoquinone or by autooxidation of 1,4-bis(1-methylethyl)benzene.[2,3]

Preparation of benzenediols by oxidation of phenol with peroxides is important because it protects the enviroment from heavy metals or strong acid pollution. Many studies on this process have been described in patent applications.[4-9] On the other hand, the peroxy acid oxidation of phenol has been studied as a model reaction in the oxidative treatment of monomeric lignin[10] and in the metabolism of aromatic compounds *in vivo*.[11]

In cases of industrial preparation of benzenediols by oxidation of phenol with peracetic acid, it is recognized that the methods for the preparation of peracetic acid seriously affect the yields of benzenediols.[12] In order to suppress undesirable reactions such as the further oxidation of benzenediols, many additives have been tested:

1. Acids[6] (sulfuric acid, phosphoric acid, condensed phosphoric acids, hydrogen fluoride, and ion-exchanging resins of the sulfonic acid type);
2. Stabilizers for peroxides[12-14] (2,6-bis(hydroxymethyl)pyridine, 8-quinolinol, and dioctyl dihydrogendiphosphate);
3. Chelating agents[12-13] (iminodiacetate, nitrilo triacetate, ethylenediamine tetraacetate, citrate and tartarate); and
4. Vicinal benzenepolyols[9] (1,2-benzenediol and 1,2,3-benzenetriol).

This article describes the effects of both additives and metal ions.

Experimental

Materials. Peracetic acid was prepared by means of autooxidation of acetaldehyde in acetone by using 1,2,3,4-benzenetetracarboxlic acid as a catalyst.[15] After a stabilizer[14a] was added, acetaldehyde was evaporated and the residue was concentrated under a reduced pressure. After the addition of butyric acid, the solution was distilled under a reduced pressure (1.3 kPa) on a water bath of 30 °C. The distillate contained about 50 wt% of peracetic acid and acetic acid without water or hydrogen peroxide. This solution of peracetic acid can be stored in a refrigerator with no change for several months in the absence of stabilizers. This solution was diluted just before use with guaranteed grade acetic acid, and the concentration of peracetic acid was determined by iodometric titration.

Guaranteed grade phenol, glacial acetic acid, potassium diphosphate, and all other additives and metal salts except for octamethyldiphorphoric tetramide[16] were commercially supplied and used without purification.

General Reaction Procedure. Twenty grams (213 mmol) of phenol was stirred at 60 °C, under a nitrogen atmosphere, in a 100 ml two necked flask equipped with a dropping funnel and a thermometer. An acetic acid solution (11 ml) of peracetic acid (21 mmol) and an additive was added dropwise to the phenol through the dropping funnel within 10 min; the reaction mixture was kept at 60 °C for 2 h and then cooled in an ice water bath and analyzed by VPC. The conversion of phenol and the yields of benzenediols were all calculated based on the amount of peracetic acid used. Quinones and other further oxidized compounds were not analyzed.

Conditions of VPC Analysis. Phenol and 1,2- and 1,4-benzenediols were determined with a 1 m column packed with Tenax-GC at programmed temperatures from 150 °C to 200 °C (the rate of temperature increace; 6 °C min^{-1}); chlorobenzene was used as an internal standard and helium as a carrier gas (flow rate: 60 ml min^{-1}). The values of 1.0, 1.8, 6.6, and 8.5 min were observed as retention times of chlorobenzene, phenol, 1,2-benzenediol and 1,4-benzenediol, respectively.

Results and Discussion

The Oxidation in the Presence of Additives. Figure 1 illustrates a typical change in the conversion of phenol and in the yields of benzenediols as a function of the increasing amount of potassium diphosphate. As the amount of additive is increased, the total yield of benzenediols increased up to a constant value (Y_{max}), while the ratio of 1,2-benzenediol to the 1,4-isomer increased from 0.6 to 1.5. No improvement in the yields of benzenediols was observed with the addition of an amount larger than X_{max}, the amount of additive needed to get Y_{max}. From the industrial viewpoint, an additive with a greater Y_{max} and a smaller X_{max} is desirable. Figure 2 shows the effects of some additives on the total

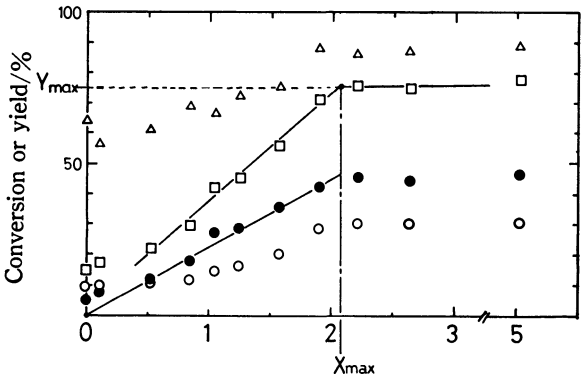

Fig. 1. Effects of potassium diphosphate on the conversion of phenol and the yields of 1,2- and 1,4-benzenediols.
△: Conversion of phenol, □: total yield of benzenediols, ●: yield of 1,2-benzenediol, ○: yield of 1,4-benzenediol. Phenol: 213 mmol, peracetic acid: 21 mmol, 60 °C, after 130 min.

yields of benzenediols.

Table 1 summarizes the X_{max}'s and Y_{max}'s of some additives tested. This table indicates the excellence of condensed phosphates as additives. For example, in the presence of 2.0×10^{-7} mol of potassium diphosphate, 9.6 mmol (47%) of 1,2-benzenediol and 6.6 mmol (31%) of 1,4-benzenediol were obtained, while in the absence of the additive, the yields of 1,2- and 1,4-benzenediol were only 1.2 mmol (5.8%) and 1.6 mmol (7.6%), respectively. Chelating agents, such as ethylenediamine tetraacetate and diethylenetriamine pentaacetate, were good additives. Derivatives of monomeric phosphoric acid and 1,2,3-benzenetriol were also good additives. The effects of diammonium hydrogenphosphate can be attributable to trace contaminants of

Table 1. Comparison of the effects of additives on the total yield of benzenediols[a)]

Additive	$X^{b)}_{max}$/mol	$Y^{c)}_{max}$/%
Sodium hexametaphosphate	9.1×10^{-8}	73
Sodium triphosphate	2.5×10^{-7}	73
Potassium diphosphate	1.85×10^{-7}	79
DTPA[d)]	3.9×10^{-7}	71
EDTA[e)]	1.4×10^{-6}	73
NTA[f)]	2.4×10^{-5}	73
Sodium imidobis(sulfate)	1.4×10^{-4}	50[g)]
1,2,3-Benzenetriol	5.2×10^{-4}	75
Diammonium hydrogenphosphate	1.1×10^{-6}	74
DMP–MMP[h)]	1.1×10^{-6}[i)]	74
Dimethyl phosphonate	1.1×10^{-3}	17[g)]
OMDPT[j)]	3.0×10^{-4}	64
Hexamethylphosphoric triamide	8.7×10^{-4}	29[g)]
Sodium malate	1.0×10^{-5}	34
Sodium citrate	8.2×10^{-5}	47
Sodium fumarate	9.4×10^{-5}	48
Sodium tartarate	1.7×10^{-5}	50
Acetylacetone	1.4×10^{-3}	52[g)]
8-Quinolinol	2.4×10^{-4}	43
Pyridine	3.1×10^{-4}	43
Sodium hydroxide	1.8×10^{-3}	34[g)]
Sodium borate	1.1×10^{-4}	26

a) Phenol: 213 mmol, peracetic acid 21 mmol, 60 °C, after 130 min. b) The smallest amount of additive needed for giving the maximum yields of benzenediols. c) The maximum total yield of benzenediols. d) Disodium trihydrogen diethylenetriamine pentaacetate. e) Disodium dihydrogen ethylenediamine tetraacetate. f) Sodium nitrilotriacetate. g) The maximum in the range tested. h) A 1 : 1 mixture of methyl dihydrogenphosphate and dimethyl hydrogenphosphate. i) Based on the average molecular weight. j) Octamethyldiphosphoric tetramide.

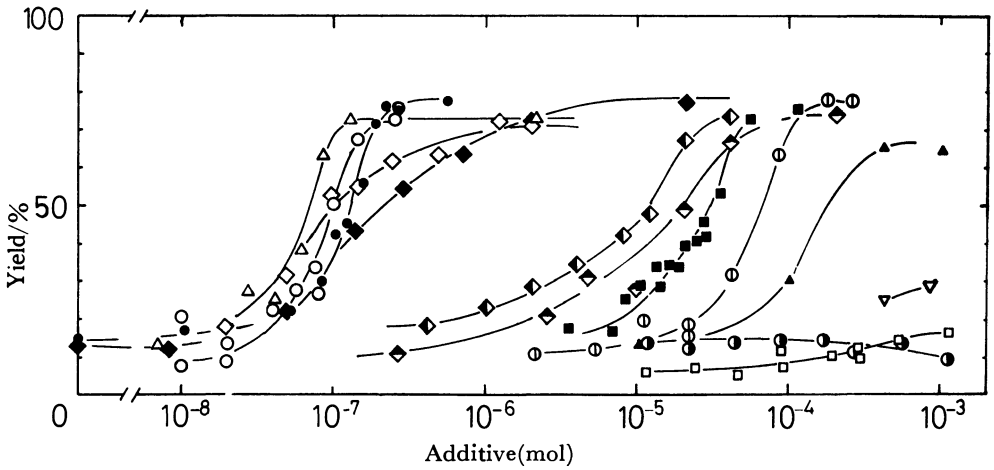

Fig. 2. Effects of some additives on the total yield of benzenediols.
△: Sodium hexametaphosphate, ○: sodium triphosphate, ●: potassium diphosphate, ■: diammonium hydrogen phosphate, ⓘ: 1 : 1 mixture of methyl and dimethyl phosphate, ▲: octamethyldiphosphoric tetramide, ▽: hexamethylphosphoric triamide, ◑: trimethyl phosphate, □: dimethyl phosphonate ◇: disodium trihydrogen diethylenetriamine pentaacetate, ◆: disodium dihydrogen ethylenediamine tetraacetate, ◐: sodium nitrilotriacetate, ◈: 1,2,3-benzenetriol. Phenol: 213 mmol, peracetic acid 21 mmol, 60 °C, after 130 min.

Table 2. Effects of the metals on the yields of benzenediols[a)]

Metal	Yields of benzenediols/%		
	1,2-	1,4-	Total
None	5.8	7.6	13.4
$Cr(OAc)_3 \cdot H_2O$	7.5	4.7	12.1
$Mn(OAc)_2 \cdot 4H_2O$	7.5	3.4	10.9
$Fe(NO_3)_3 \cdot 6H_2O$	0.2	4.4	4.6
$Co(OAc)_2 \cdot 4H_2O$	0.2	4.9	5.1
$Ni(OAc)_2 \cdot 4H_2O$	5.6	5.7	11.3
$Cu(OAc)_2 \cdot H_2O$	2.9	4.5	7.4
$Zn(OAc)_2 \cdot 2H_2O$	7.0	5.2	12.1
$K_3Fe(CN)_6$	3.2	5.1	8.3
$K_4P_2O_7$	45.8	30.6	76.4

a) Phenol: 213 mmol, peracetic acid: 21 mmol, 60 °C, after 130 min, in the presence of 2.4×10^{-7} mol of the salts.

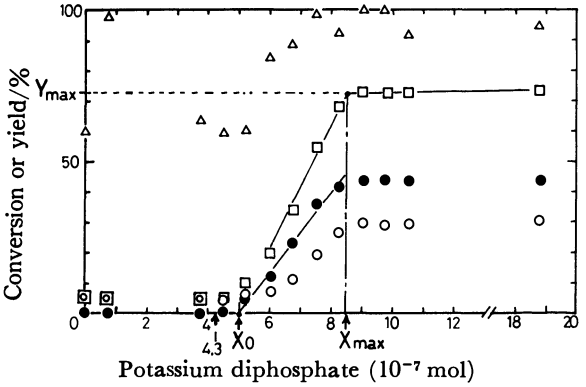

Fig. 3. Effects of potassium diphosphate on the conversion of phenol and the yields of 1,2- and 1,4-benzenediol in the presence of 4.3×10^{-7} mol of iron(III) nitrate. △: Conversion of phenol, □: total yield of benzenediols, ●: yield of 1,2-benzenediol, ○: yield of 1,4-benzenediol. Phenol: 213 mmol, peracetic acid: 21 mmol, 60 °C, after 130 min.

derivatives of condensed phosphoric acid. This same effect is seen for a mixture of methyl dihydrogenphosphate and dimethyl hydrogenphosphate. On the other hand, bases, salts of organic polybasic acids, and ligating reagents such as acetylacetone and 8-quinolinol showed little effect. Crown ethers (15-crown-5, dibenzo-18-crown-6 and perhydrodibenzo-24-crown-8) were also tested, but they did not improve the yields of benzenediols.

These facts show that additives mask the effects of trace metal ions in the system.[17] The indicated additives with higher Y_{max} and lower X_{max} values mask the metal ions better.

The Oxidation in the Presence of Transition-metal Salts. The effects of transition-metal salts on the oxidation were tested. Table 2 shows that the addition of iron(II) or cobalt(II) salts depressed the yield of 1,2-benzenediol and had little effect on the yield of 1,4-benzenediol. On the other hand, the table also shows that salts of chromium(III), manganese(II), nickel(II), and zinc had little effect on the yields of both benzenediols.

In the presence of peracetic acid, transition-metal ions are in their higher oxidation states[18] and the benzenediols to be oxidized form complexes with these transition metal ions.[19-24] Therefore, it is reasonable that metal ions accelerate the further oxidation of benzenediols formed in this reaction.[25-27]

The Oxidation in the Presence of Both Potassium Diphosphate and a Transition-metal Salt. In order to clarify the relation between additives and metal ions in this system, phenol was oxidized in the presence of both diphosphate and a transition-metal salt.

Figure 3 illustrates the effect of potassium diphosphate on the conversion of phenol and the yields of 1,2- and 1,4-benzenediols in the presence of iron(III) nitrate (4.3×10^{-7} mol). In these cases, even upon increasing the amounts of potassium diphosphate up to X_0 (5.0×10^{-7} mol) no 1,2-benzenediol was obtained, and almost no change was observed in the yield of 1,4-benzenediol. Here X_0 means the smallest amount of potassium

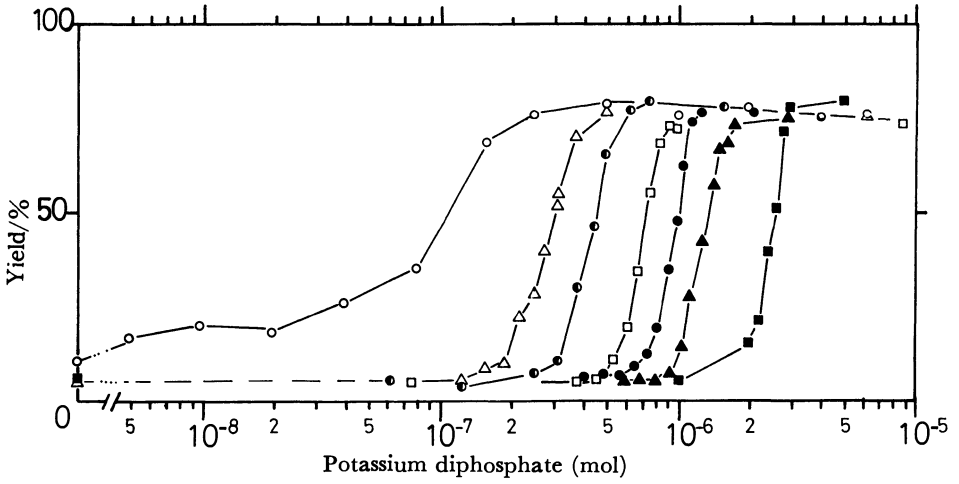

Fig. 4. Effect of potassium diphosphate in the presence of iron(III) nitrate on the total yield of benzenediols.
Iron(III) nitrate added: ○: nil, △: 1.1×10^{-7} mol, ◐: $21. \times 10^{-7}$ mol, □: 4.3×10^{-7} mol, ●: 6.4×10^{-7} mol, ▲: 8.5×10^{-7} mol, ■: 1.7×10^{-6} mol, phenol: 213 mmol, peracetic acid: 21 mmol, 60 °C, after 130 min.

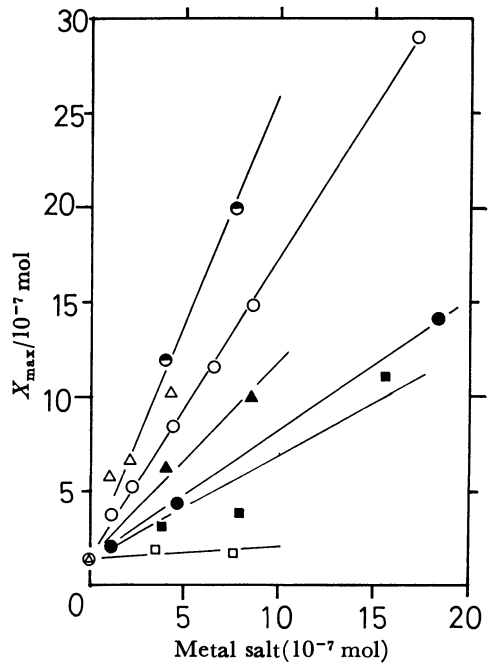

Fig. 5. Relation of X_{max} and the species and the amount of the metal salt added.
Metal salt: □: chromium(III) acetate, ▲: manganese-(II) acetate, ○: iron(III) nitrate, △: cobalt(II) acetate ■: nickel(II) acetate, ◓: copper(II) acetate, ●: zinc acetate. Phenol: 213 mmol, peracetic acid 21 mmol, 60 °C, after 130 min. X_{max}: the least amount of potassium diphosphate needed for giving the maximum yields of benzenediols.

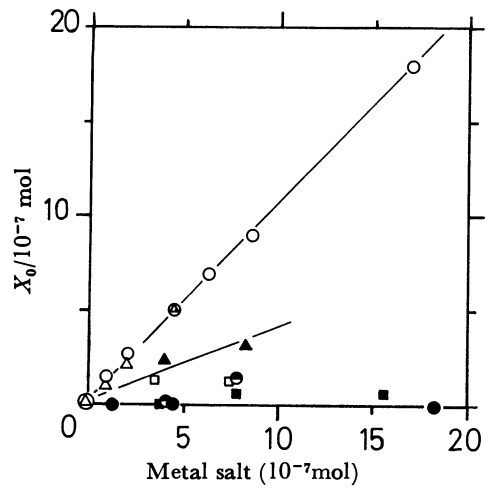

Fig. 6. Relation between X_0 and the metal salt added. X_0: The least amount of potassium diphosphate needed for giving 1,2-benzenediol (Notations and the conditions are the same as those in Fig. 5).

diphosphate needed for producing 1,2-benzenediol. The increase in the yields of benzenediols was observed with increasing amounts of diphosphate beyond X_0; the yields were saturated at the last stage.

Figure 4 shows the change in the total yield of benzenediols, in the presence of iron(III) nitrate (0—1.7×10^{-6} mol) and potassium diphosphate. The salts of cobalt and manganese exhibited the same kinds of feature, but the salts of chromium, nickel, copper, and zinc did not suppress the formation of 1,2-benzenediol. These findings are summarized in Figs. 5 and 6, which show that plots of X_{max}'s and X_0's against the amount of metal added are almost linear; their gradients are shown in Table 3.

Table 3. The gradients of the plots of X_{max}'s and X_0's against the amount of transition-metal salts added[a)]

Metal salts	$X^{b)}_{max}$/Metal	$X^{c)}_0$/Metal
Chromium(III)	0.1	0.13
Manganese(II)	1.01	0.35
Iron(III)	1.67	1.05
Cobalt(II)	2.05	1.16
Nickel(II)	0.63	0.04
Copper(II)	2.37	0.14
Zinc(II)	0.69	−0.18

a) Phenol: 213 mmol, peracetic acid: 21 mmol, 60 °C, after 130 min. b) The smallest amount of potassium diphosphate needed for giving the maximum yields of benzenediols. c) The smallest amount of potassium diphosphate needed for producing 1,2-benzenediol.

These findings support the explanation that these additives mask the metal ions contaminating the reaction mixture and that the presence of free metal ions, especially iron and cobalt, suppress the yields of benzenediols.

Quantitative Measurement of Metals Originally Present in the Reaction Mixture. After the reaction, X-ray flouresence was used to determine the concentration of iron in the reaction mixture; it was determined to be 180 mg m^{-3}. By flameless-atomic-absorption spectroscopy the concentrations of copper and cobalt were also determined to be 6.5 mg m^{-3} and less than 0.5 mg m^{-3}, respectively.

The intersections of the plots of X_{max}'s with the ordinate, in Fig. 5, correspond to the smallest quantitions of diphosphate needed for maximizing the yields of benzenediols when no metal was added. The amount of metal ions originally contained in the system can be estimated from this intersection and the gradients. This was calculated to be 173 mg m^{-3} if all of the metal contained was assumed to be iron; this value was in good agreement with that of 180 mg m^{-3} obtained from X-ray-fluorescence measurement.

On the basis of these findings, it is concluded that there was a trace of iron in the system, and that this catalyzed the further oxidation of benzenediols formed. The additives masking metal ions, consequently, improve the yields of benzenediols. From an industrial point of view, such a masking-reagent is useful for instant removal of these metal ions.

The authors wish to express their thanks to Mr. S. Nakamura and Mrs. N. Fudakawa for their X-ray-fluorescence and atomic-absorption analysis on metals.

References

1) Kirk-Othmer, "Encyclopedia of Chemical Technology," 2nd ed, John. Wiley, and Sons, New York (1976), Vol. 11, p. 466.
2) Ref. 1, p. 485.

3) Distillers, British Patent, 641250 (1950); Hercules, Fr. Patent, 979665 (1951), U. S. Patent, 2548435 (1951); Mitsui Petrochem. Ind., Jpn. Kokai, 48-72140 (1973).

4) Ube Ind., Jpn. Kokai, 50-130727, 50-142518 (1975), 51-6933 (1967); Baeyer A. G., Jpn. Kokai, 50-121235, 50-121236 (1975); Rhone-Poulenc A. S., Deutsch. Offen., 2064497 (1971), U. S. Patent, 3849502 (1974), Jpn. Kokai, 52-14733 (1977); J. Varagnat, *Ind. Eng. Chem., Prod. Res. Dev.*, **15**, 212 (1976).

5) Rhone-Poulenc S. A., Deutsch. Offen., 1593968 (1970); U. S. Patent, 3514490 (1970).

6) Y. Ogata and M. Mineno, *Kogyo Kagaku Zasshi*, **73**, 1849 (1970); T. Hamamoto, N. Kuroda, N. Takamitsu, and S. Umemura, *Nippon Kagaku Kaishi*, **1980**, 1137.

7) Ya. M. Paushkin, R. I. Fedorova, S. A. Nizova, B. V. Mitina, and N. M. Zahar'eva, *Zh. Prikl. Khim.*, **52**, 183 (1979); *J. Appl. Chem. USSR*, **52**, 161 (1979).

8) Mitsubishi Chem. Ind., Jpn. Patent, 47-34325 (1972), 51-11103, 51-11104 (1976); Ube Ind., Jpn. Kokai, 49-30330 (1974), 50-129527, 50-142518, 50-130727 (1975); S. N. Massle, U. S. Patent, 49-24056 (1974); The Calpis Food Ind., Jpn. Kokai, 48-103529 (1973); Polaroid, U. S. Patent, 3652597 (1972); Y. Ogata, I. Urasaki, K. Nagura, and N. Satomi, *Tetrahedron*, **30**, 3021 (1974).

9) Mitsui Petrochem. Ind., Jpn. Kokai, 54-84538 (1979).

10) H. H. Nimz and H. Schwind, *Cell. Chem. Technol.*, **13**, 35 (1979); J. C. Farrand and D. C. Johnson, *J. Org. Chem.*, **36**, 3606 (1971).

11) R. A. G. Marshall and R. Naylor, *J. Chem. Soc., Perkin Trans. 2*, **1974**, 1242.

12) M. Andoh and J. Imamura, Jpn. Patent, 52-10852, 52-10853 (1977), 51-11099 (1976); M. Andoh, J. Imamura, and K. Sasaki, Jpn. Patent, 52-18179 (1977); M. Andoh, J. Imamura, K. Sasaki, and I. Ito, Jpn. Patent, 52-12691, 52-38023 (1977).

13) T. Tsuchiya, M. Andoh, and J. Imamura, *Nippon Kagaku Kaishi*, **1979**, 370.

14) "Ullmans Encyclopaedie der Technischen Chemie," Ergaenzungsband, Urban & Schwarzenberg, Muenchen (1970), p. 182; Ref. 1, Vol. 14, p. 797. a) In this work $Na_5R_5(P_3O_{10})_2$ (R=2-ethylhexyl) was used; this was supplied by Victor Chemical Work as Victor Wet 35 B, in the form of 70 wt% mixture with water.

15) M. Andoh, T. Matsuzaki, M. Fukuda, and J. Imamura, *Nippon Kagaku Kaishi*, **1975**, 1383.

16) A. P. F. Toy and E. N. Walsh, *Inorg. Synth.*, **7**, 73.

17) D. D. Perrin, "Masking and Demasking of Chemical Reactions," Wiley-Interscience, New York (1970), pp. 41—44 and Chap. 12; see also the literature cited therein.

18) R. A. Sheldon and J. K. Kochi, "Advances in Catalysis," Academic Press, New York (1976), Vol. 25, p. 295.

19) E. Mentasti, E. Pelizetti, and G. Saini, *J. Chem. Soc., Dalton Trans.*, **1973**, 2605, 2909.

20) E. Pelizetti, E. Mentasti, and E. Pramauro, *J. Chem. Soc., Dalton Trans.*, **1976**, 23.

21) E. Mentasti, E. Pelizzetti, and G. Saini, *J. Chem. Soc., Dalton Trans.*, **1974**, 721; *Gazz. Chim. Ital.*, **104**, 1015 (1974).

22) J. H. Baxendale, H. R. Hardy, and L. H. Sutcriffe, *Trans. Faraday Soc.*, **47**, 963 (1951); **49**, 1140 (1953).

23) C. F. Wells and L. V. Kuritsyn, *J. Chem. Soc., A*, **1969**, 2575 and 2930.

24) G. Davis and K. Kustin, *Trans. Faraday Soc.*, **65**, 1630 (1969); C. F. Wells and L. V. Kuritsyn, *J. Chem. Soc., A*, **1970**, 676; J. C. Sullivan and J. E. French, *J. Am. Chem. Soc.*, **87**, 5380 (1965).

25) A. J. Pandell, *J. Org. Chem.*, **41**, 3992 (1976).

26) M. M. Taqui Kahn and A. E. Martell, "Homogeneous Catalysis by Metal Complexes," Academic Press, New York (1974), Vol. 1, p. 150.

27) G. A. Hamilton, "Molecular Mechanisms of Oxygen Activation," ed by O. Hayaishi, Academic Press, New York (1974), p. 425.

 © 1982 The Chemical Society of Japan Bull. Chem. Soc. Jpn., 55, 1931—1933 (1982)

Liquid-phase Oxidation of Anthracene in Acetic Acid by Use of Copper(II) Chlorocomplexes. II.[1] Kinetic Study

Jinya KOSHITANI,* Toshio KADO, Yoshio UENO, and Takatoshi YOSHIDA
Department of Industrial Chemistry, Nagoya Institute of Technology, Gokiso-cho, Showa-ku, Nagoya 466
(Received June 18, 1981)

A kinetic study was performed on the oxidation of anthracene by use of copper(II) chlorocomplexes, which were produced in reactions of copper(II) acetate with lithium chloride in acetic acid. When the pressure of oxygen was high enough that the rate of oxidation was not affected, the result was as follows:

$$-\frac{dO_2}{dt} \propto [RH]^1 [Cu_2(OAc)_4]_0^{1/2} [LiCl]_0^{1/2-0}.$$

A kinetic approximation to the experimental result was attempted.

It is known that metal ions[2-4] decompose hydrolithium chloride in acetic acid.

$$ROOH + M^{(n+1)+} \xrightarrow{k_1} ROO\cdot + H^+ + M^{n+} \quad (1)$$

$$ROOH + M^{n+} \xrightarrow{k_2} RO\cdot + OH^- + M^{(n+1)+} \quad (2)$$

peroxides and that metal ions[5,6] in their higher valency may oxidize substrates and generate free radicals. On the other hand, it is known that copper(II) chlorocomplexes[7-19] are formed in reactions of Cu^{2+} with Cl^- in molten salts, and in aqueous and nonaqueous solutions. We previously reported that liquid-phase oxidation[1] of anthracene was effected by these chlorocomplexes, producing mainly anthraquinone. It is interesting to learn the role of these chlorocomplexes at the initiation stage of the oxidation.

$$RH + M^{(n+1)} \xrightarrow{k_3} RH^+ + M^{n+} \quad (3)$$

$$RH^+ \xrightarrow{k_4} R\cdot + H^+ \quad (4)$$

The mechanism of autoxidation of anthracene is complex and not yet clearly explained in spite of great interest. In this paper, we report a kinetic study of the oxidation of anthracene by use of copper(II) chlorocomplexes formed by the reactions of copper(II) acetate with

Experimental

The experimental procedures were the same as those described in the previous paper,[1] with the following exceptions. Gas compositions of the mixtures of oxygen and nitrogen in the reaction vessels were determined on a Yanagimoto model GCG 550-TF gas chromatograph with TCD detector, using helium gas as a carrier. The reactions were performed according to the method of Morimoto and Ogata.[20] The reactions, except for the experiments on the effect of partial pressure of oxygen, were performed under 6.1×10^{-1} bar partial pressure of oxygen, at which pressure the rates of oxidations were not affected. Iodometry was performed in a nitrogen atmosphere.

Results and Discussion

Kinetics. How the initial rates of oxygen absorption depend on concentrations of anthracene, initially added copper(II) acetate, and initially added lithium chloride is shown in Table 1. The rate is expressed as

$$-\frac{dO_2}{dt} = k_{obsd}[RH]^1 [Cu_2(OAc)_4]_0^{1/2} [LiCl]_0^{1/2}$$

Table 1. Effect of concentrations of anthracene, copper(II) acetate, and lithium chloride on initial rate of oxygen absorption at 90 °C

$[RH]$ / mol dm^{-3}	$[Cu_2(OAc)_4]_0$ / mol dm^{-3}	$[LiCl]_0$ / mol dm^{-3}	$-\frac{dO_2}{dt}$ / mol dm^{-3} s^{-1}	k_{obsd} / dm^3 mol^{-1} s^{-1}	k'_{obsd} / dm$^{3/2}$ mol$^{-1/2}$ s^{-1}
0.008	0.0050	0.010	4.5×10^{-7}	7.9×10^{-3}	7.9×10^{-4}
0.010	0.0050	0.010	5.7×10^{-7}	8.1×10^{-3}	8.1×10^{-4}
0.020	0.0050	0.010	1.1×10^{-6}	7.7×10^{-3}	7.7×10^{-4}
0.030	0.0050	0.010	1.7×10^{-6}	7.9×10^{-3}	7.9×10^{-4}
0.040	0.0050	0.010	2.3×10^{-6}	8.0×10^{-3}	8.0×10^{-4}
0.050	0.0050	0.010	2.9×10^{-6}	8.2×10^{-3}	8.2×10^{-4}
0.050	0.0005	0.010	8.4×10^{-7}	7.5×10^{-3}	7.5×10^{-4}
0.050	0.0010	0.010	1.3×10^{-6}	7.9×10^{-3}	7.9×10^{-4}
0.050	0.0033	0.010	2.4×10^{-6}	8.4×10^{-3}	8.4×10^{-4}
0.050	0.0100	0.010	4.2×10^{-6}	8.4×10^{-3}	8.4×10^{-4}
0.050	0.0050	0.001	8.3×10^{-7}	7.4×10^{-3}	—
0.050	0.0050	0.002	1.2×10^{-6}	7.5×10^{-3}	—
0.050	0.0050	0.003	1.6×10^{-6}	8.1×10^{-3}	—
0.050	0.0050	0.005	2.1×10^{-6}	8.2×10^{-3}	—
0.050	0.0050	0.015	2.9×10^{-6}	—	8.2×10^{-4}
0.050	0.0050	0.020	2.9×10^{-6}	—	8.2×10^{-4}
0.050	0.0050	0.030	2.9×10^{-6}	—	8.2×10^{-4}

at $[LiCl]_0$ of 0.0001—0.01 mol dm^{-3}. The rate is

$$-\frac{dO_2}{dt} = k'_{obsd}[RH]^1 [Cu_2(OAc)_4]_0^{1/2}$$

at $[LiCl]_0$ of 0.01—0.03 mol dm^{-3}. The rate shows zeroth-order dependence with respect to $[LiCl]_0$ in a large excess of $[LiCl]_0$. The dependency of this rate on the partial pressure of oxygen is shown in Fig. 1. The rate was nearly proportional to the partial pressure of oxygen of 1.3×10^{-1}—4.8×10^{-1} bar, while the rate was zeroth-order with respect to the partial pressure of oxygen of 4.8×10^{-1}—6.1×10^{-1} bar.

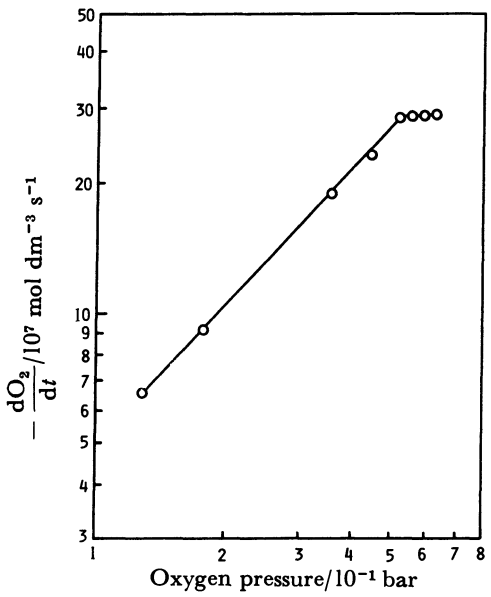

Fig. 1. Effect of oxygen pressure on initial rate of oxygen absorption at 90 °C.
[RH]: 0.05 mol dm^{-3}, $[Cu_2(OAc)_4]_0$: 0.005 mol dm^{-3}, $[LiCl]_0$: 0.01 mol dm^{-3}.

Reaction. No induction period was observed. The possibility of the accumulation of peroxide was investigated at [RH] of 0.05 mol dm^{-3} under the high pressure of oxygen. The amount of peroxide in the solution was determined to be very small on the basis of iodometry, taking the consumption of sodium thiosulfate by the initially added copper(II) acetate into account. Since the variation of the spectrum at the early stage of the reaction was small, there was presumably no prominent variation in kinds or amounts of species of copper(II) salts and copper(II) chlorocomplexes during this period. The amount of oxygen absorption was measured during the period, and the rate of oxygen absorption was calculated. After the period, the absorption near 685 nm was found to increase. This was because a portion of the copper(II) chlorocomplexes or of the monomer of copper(II) acetate changed to the dimer[21,22] of copper(II) acetate again.

Kinetic Approximation. On the basis of kinetics, a tentative mechanism was deduced. M^{2+} and M^+ represent copper(II) ion as active species and copper(I) ion as active species, respectively. Within the range of $[LiCl]_0$ of 0.001—0.01 mol dm^{-3}, the following is assumed:

$$[M^{2+}] \propto [Cu_2(OAc)_4]_0^{1/2}\,[LiCl]_0^{1/2}.$$

And within the range of $[LiCl]_0$ of 0.01—0.03 mol dm^{-3}, the following is assumed:

$$[M^{2+}] \propto [Cu_2(OAc)_4]_0^{1/2}.$$

As shown in Eqs. 3 and 4, RH may react with M^{2+} to give R·.[23,24] R· and oxygen molecule combine to give ROO·.

$$R\cdot + O_2 \underset{k_{-5}}{\overset{k_5}{\rightleftharpoons}} ROO\cdot \qquad (5)$$

ROO· reacts with RH to give ROOH and R·.

$$ROO\cdot + RH \xrightarrow{k_6} ROOH + R\cdot \qquad (6)$$

As shown in Eqs. 1 and 2, ROOH reacts with M^{2+} and M^+. RO· is generated from ROO· and then reacts with

$$2ROO\cdot \xrightarrow{k_7} 2RO\cdot + O_2 \qquad (7)$$

$$RO\cdot + RH \xrightarrow{k_8} ROH + R\cdot \qquad (8)$$

RH. Equation 9 has been reported for the keto-enol tautomerism between 9-anthrol and anthrone.[25-28]

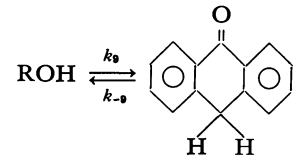

(9)

RO· resonates in the following way and may react with an oxygen molecule.[29-32] By reference to works,[32-34]

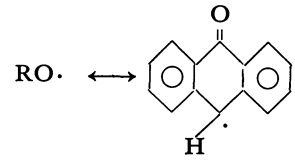

(10)

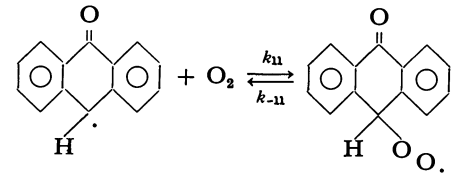

(11)

we thought that the peroxyl radical may react with M^+.

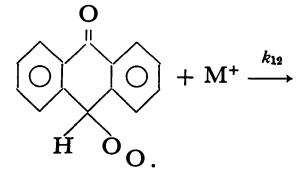

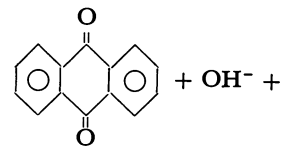

(12)

Steady-state treatment is applied in Eqs. 1—12. On the basis of the experimental results,

$$\frac{d[ROOH]}{dt} \approx 0,$$

$$-\frac{d[M^{2+}]}{dt} \approx 0.$$

Therefore,

$$-\frac{dO_2}{dt} \approx (k_1[ROOH][M^{2+}] + k_3[RH][M^{2+}]) \times \left(\frac{3}{2} + \frac{1+\frac{k_{-11}}{k_{12}[M^+]}}{2k_{11}[O_2]} \times k_8[RH]\right),$$

$$\frac{d[anthraquinone]}{dt} \approx k_1[ROOH][M^{2+}] + k_3[RH][M^{2+}],$$

$$\frac{d[anthrone]}{dt} \approx \frac{1+\frac{k_{-11}}{k_{12}[M^+]}}{k_{11}[O_2]} \times k_8(k_1[ROOH][M^{2+}] + k_3[RH][M^{2+}])[RH].$$

Since, on the basis of the experimental result, [ROOH] may be very small,

$$\frac{k_3[RH]}{[ROOH]} \gg k_1.$$

The relation between the rate of production of anthrone and the rate of production of anthraquinone is represented:

$$\frac{d[anthrone]}{dt} = G \times \frac{d[anthraquinone]}{dt},$$

where G is a function. Therefore,

$$\frac{-\frac{dO_2}{dt}}{\frac{d[anthraquinone]}{dt}} \approx \frac{1}{2}(3 + G).$$

Here, G may be determined experimentally. For example, G is nearly constant at the early stage of the oxidation shown in Fig. 1,[1)] with a value of around 1.4. Therefore, at the early stage of the oxidation,

$$-\frac{dO_2}{dt} \approx 2.2k_3[RH][M^{2+}],$$

$$\frac{d[anthraquinone]}{dt} \approx k_3[RH][M^{2+}],$$

$$\frac{d[anthrone]}{dt} \approx 1.4k_3[RH][M^{2+}],$$

$$\frac{-\frac{dO_2}{dt}}{\frac{d[anthraquinone]}{dt}} \approx 2.2.$$

The results of these calculations fit the experimental facts in Fig. 1.[1)]

Further, selective production of anthraquinone without production of anthrone could be explained in this mechanism without Eqs. 8 and 9; in this case no approximation is necessary.

Rerefences

1) Part I: J. Koshitani, M. Hiramatsu, Y. Ueno, and T. Yoshida, *Bull. Chem. Soc. Jpn.*, **51**, 3667 (1978).
2) F. Haber and J. Weiss, *Proc. R. Soc. London, Ser. A*, **147**, 332 (1934).
3) J. Weiss, *Trans. Faraday Soc.*, **31**, 1547 (1935).
4) Y. Kamiya, S. Beaton, F. Lafortune, and K. U. Ingold, *Can. J. Chem.*, **41**, 2034 (1963).
5) C. E. H. Bawn, *Discuss. Faraday Soc.*, **14**, 181 (1953).
6) E. I. Heiba, R. M. Dessau, and W. J. Koehl, Jr., *J. Am. Chem. Soc.*, **91**, 138 (1969).
7) E. Doehlemann and H. Tromhers, *Z. Phys. Chem. (Leipzig), A*, **171**, 371 (1934).
8) H. McConnell and N. Davidson, *J. Am. Chem. Soc.*, **72**, 3164 (1950).
9) D. W. Meek, D. K. Staub, and R. S. Drago, *J. Am. Chem. Soc.*, **82**, 6013 (1960).
10) M. Baaz, V. Gutmann, G. Hampel, and J. R. Masaguer, *Monatsh. Chem.*, **93**, 1416 (1962).
11) H. Hubacek, B. Stancic, and V. Gutmann, *Monatsh. Chem.*, **94**, 1118 (1963).
12) A. Ludi and W. Feitknecht, *Helv. Chim. Acta*, **46**, 2238 (1963).
13) R. D. Willett, *J. Chem. Phys.*, **41**, 2243 (1964).
14) W. E. Hatfield and T. S. Piper, *Inorg. Chem.*, **3**, 841 (1964).
15) M. Sharnoff, *J. Chem. Phys.*, **41**, 2203 (1964).
16) M. Sharnoff, *J. Chem. Phys.*, **42**, 3383 (1965).
17) R. A. Howald and D. P. Keeton, *Spectrochim. Acta*, **22**, 1211 (1966).
18) M. Sharnoff and C. W. Reimann, *J. Chem. Phys.*, **46**, 2634 (1967).
19) R. P. Eswein, E. S. Howald, R. A. Howald, and D. P. Keeton, *J. Inorg. Nucl. Chem.*, **29**, 437 (1967).
20) T. Morimoto and Y. Ogata, *J. Chem. Soc., B*, 62 (1967).
21) S. Imamura, M. Teramoto, T. Sumi, H. Aomi, H. Teranishi, and Y. Takegami, *Bull. Chem. Soc. Jpn.*, **49**, 1659 (1976).
22) J. Koshitani, K. Watanabe, Y. Ueno, and T. Yoshida, *Nippon Kagaku Kaishi*, **1981**, 265.
23) T. Aratani and M. J. S. Dewar, *J. Am. Chem. Soc.*, **88**, 5479 (1966).
24) E. I. Heiba, R. M. Dessau, and W. J. Koehl, Jr., *J. Am. Chem. Soc.*, **91**, 6830 (1969).
25) K. H. Meyer, *Justus Liebigs Ann. Chem.*, **379**, 37 (1911).
26) K. Nukada and Y. Bansho, *Bull. Chem. Soc. Jpn.*, **26**, 454 (1953).
27) Y. Bansho and K. Nukada, *Kogyo Kagaku Zasshi*, **63**, 620 (1960).
28) H. Baba and T. Takemura, *Nippon Kagaku Zasshi*, **89**, 629 (1968).
29) T. Yoshida, Y. Ueno, and S. Wakabayashi, *Kogyo Kagaku Zasshi*, **72**, 338 (1969).
30) C. Walling "Free Radicals in Solution," Wiley, New York (1963), p. 457.
31) Y. Ogata, Y. Kosugi, and K. Nate, *Tetrahedron*, **27**, 2705 (1971).
32) Y. Ogata, K. Nate, and M. Yamashita, *Bull. Chem. Soc. Jpn.*, **47**, 174 (1974).
33) E. C. Horswill and K. U.Ingold, *Can. J. Chem.*, **44**, 263 (1966).
34) E. C. Horswill and K. U. Ingold, *Can. J. Chem.*, **44**, 269 (1966).

Manufacture of High Pure Titanium(IV) Oxide by the Chloride Process. I. Kinetic Study on Leaching of Ilmenite Ore in Concentrated Hydrochloric Acid Solution

Hisashi Tsuchida,† Eiichi Narita,* Hitoshi Takeuchi, Masahiro Adachi, and Taijiro Okabe

Department of Applied Chemistry, Faculty of Engineering, Tohoku University, Aramaki, Sendai 980
†Mizusawa Factory, Mizusawa Industrial Chemicals, Ltd., Tsuruoka, Yamagata 999-75

(Received October 2, 1981)

Kinetic study of the leaching of powdered ilmenite ore was carried out in highly concentrated hydrochloric acid (11.3—11.6 mol dm^{-3}) at temperatures of 30 to 80 °C. The changes in shape and grain size of the ore particles with progress of the leaching was simultaneously observed with X-ray diffraction and electron microscope techniques. Titanium and iron were dissolved in a nearly stoichiometric ratio; the rate of the dissolution was significantly affected by the temperature of the acid solutions. From the analysis of the dissolution rates on the basis of the core-model, it was found that the dissolution rates at temperatures of 30 to 50 °C were well expressed by the rate equation based on the rate-determining step of the surface chemical reaction. The apparent activation energies were 81.2 kJ mol^{-1} for titanium and 73.2 kJ mol^{-1} for iron. The rate-determining step of the dissolution was changed at a temperature of about 50—60 °C; the dissolution rates at temperatures of 60 to 80 °C were limited by the diffusion of the dissolved metal ions through a residual layer of the ore. However, the rates after 2 or 3 h at high temperatures deviated from the rate equation because of the precipitation of hydrous titanium(IV) oxide on the surface of the ore by hydrolysis of the dissolved titanium(IV) ion.

Titanium(IV) oxide is used as a raw material of the white pigment which is utilized extensively in paints, paper, porcelain, and fibers. Some new uses based on being an n-type semiconductor, for example an electrode or a catalyst have recently been tried.

Titanium(IV) oxide is produced industrially by the sulfuric acid leaching of its minerals and the subsequent thermal hydrolysis of titanium(IV) sulfate solutions; this is commonly known as the sulfate process. It is also produced by the vapor phase oxidation of titanium(IV) tetrachloride.[1,2] Although the manufacture of titanium-(IV) oxide by this latter process is gradually increasing, the former is still the most widely used.[2] The sulfate process, however, has serious disadvantages because the treatments of crude iron(II) sulfate and of the waste acid solution are difficult.[3] On the other hand, hydrochloric acid, which is very useful for decomposition of natural ores, allows comparatively easier recovery of the useful free acid from its waste solution than does sulfuric acid. In practice, the recovery of free hydrochloric acid from the waste solutions of steel cleansing is now feasible.[4—8] Accordingly, if it becomes possible to leach ilmenite ore in hydrochloric acid, the closed system of the manufacturing process of titanium(IV) oxide will be achieved. The pressurized leaching of ilmenite ore in hydrochloric acid solutions is now carried out to upgrade the ore, in which a large portion of iron is dissolved.[9—11] Titanium can also be dissolved in concentrated hydrochloric acid solutions by keeping the leaching solution at temperatures below about 90 °C.[12—14] In addition, the recovery of a number of metal ions by liquid-liquid extraction from hydrochloric acid solutions is considerably easier than that from sulfuric acid solutions.[15,16] The authors, therefore, intended to develop a new manufacturing process of high pure titanium(IV) oxide, which would be based on the leaching of ilmenite ore in concentrated hydrochloric acid solutions and the selective solvent extraction of titanium(IV) from the leaching solution by neutral organophosphorus compounds.

In this study, we investigated the leaching kinetics of powdered ilmenite ore in concentrated hydrochloric acid. Static leaching studies of ilmenite ore in hydrochloric acid solutions were performed by earlier workers[12—14] in order to obtain optimum conditions, but only a few reports on the kinetic study (using diluted hydrochloric acid solutions of 3 mol dm^{-3}) have been presented[17] and there is still a lack of the essential information in the kinetics of the dissolution behavior of titanium and iron in concentrated hydrochloric acid with respect to the leaching mechanism.

Experimental

Unless otherwise stated, the ilmenite ore having a grain size range of 250 to 325 mesh was used in this study. The chemical composition after the sample was dried by heating at 110 °C is shown in Table 1. In one part of the experiments, the ilmenite ore having a grain size of 150—250 mesh, whose chemical composition was the same as that shown in Table 1 was also used. The leaching experiments of the powdered ilmenite ore were carried out in the highly concentrated HCl solutions of 11.3—11.6 mol dm^{-3} at temperatures of 30 to 80 °C. A 0.5 dm^3 three-necked flask equipped with a reflux condenser, a thermometer, and a stirrer was used as a reaction vessel. Five g of the ilmenite ore was suspended in 200 cm^3 of leaching solution, temperature-regulated at 30—80 °C; this

Table 1. Chemical composition of the ilmenite ore

Constituent	Content / wt%
TiO_2	52.0
Fe[a)]	27.2
MnO	3.07
Al_2O_3	2.30
MgO	0.41
Cr_2O_3	0.04

a) $FeO+Fe_2O_3$.

was stirred continuously with a mechanical stirrer. The dissolution rates of titanium and iron were determined by pipetting about 5 cm^3 of the suspension from the flask as regular time intervals, filtering out the insoluble residue, and chemically analyzing the supernatant solution. Titanium and iron were determined by colorimetric methods.[18] The X-ray diffraction patterns were obtained by using a Rigaku Denki Geigerflex 2013 with Ni filtered Cu *Kα* radiation, with 30 kV and 10 mA. The surface observation was performed by using a Hitachi-Akashi Scanning Electron Microscope MSM 4C-102.

Results and Discussion

Analysis of Dissolution Rate. The electron micrographs of the ilmenite ore and the insoluble residues obtained from the suspension after the leaching experiment at 60 °C are shown in Fig. 1. Although the surface of the residues became rather porous during the leaching, no prominent changes were observed in the grain size and shape of the ores after the leaching. In this experiment, about 85% of the titanium and 90% of the iron in the ore were dissolved after 5 h. With these major constituents, most of the manganese and magnesium also dissolved. But the chemical analysis of the residue indicated that large amounts of aluminum, chromium, and silicon were still in it. However, the amounts of these residual minor constituents are not enough to maintain the grain size and shape of the ore particles. Therefore, a small portion of the dissolved titanium ion seemed to precipitate continuously by the hydrolysis at the ilmenite surface and to maintain the grain size and shape of the ore particles with other residual minor constituents during the leaching reaction. This assumption was supported experimentally by the result that the dissolution rate of titanium was slightly smaller than that of iron, although titanium and iron were dissolved in a near stoichiometric ratio. As described later, the X-ray diffraction patterns of the insoluble residues indicated the presence of rutile, anatase, and Ti_2O_3. On the other hand, at lower temperatures, the grain size of the ore particles was changed and gradually became smaller with the progress of the leaching, because of the absence of any precipitation of titanium oxides.

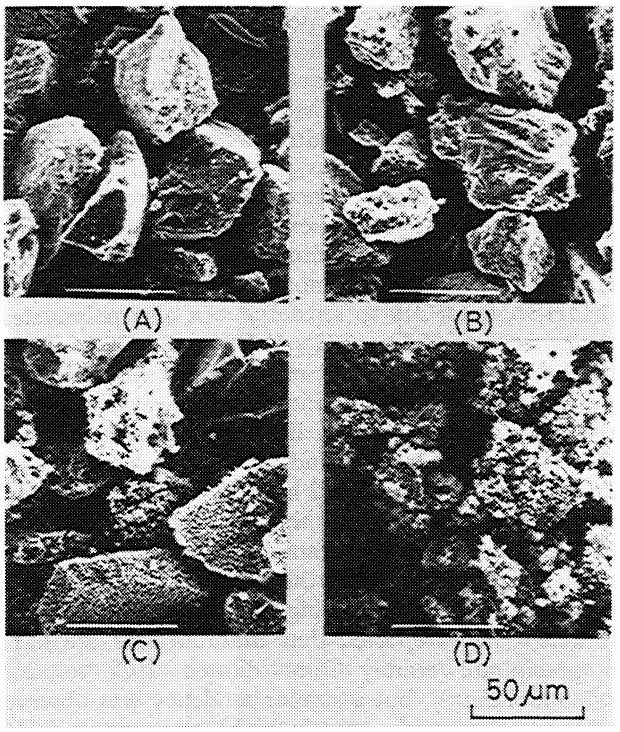

Fig. 1. Scanning electron micrographs of ilmenite ore and reaction residues.
HCl: 11.6 mol dm^{-3}, temperature: 60 °C, stirring speed: 400 min^{-1}. (A): ilmenite ore, (B): residue (0.5 h), (C): residue (2 h), (C): residue (5 h).

Accordingly, the dissolution rates of titanium and iron were analyzed on the basis of the extraction type core-model under the assumption that the ore is a homogeneous spherical solid phase.

The dissolution reaction of the ilmenite ore in hydrochloric acid solution is written as:

$$FeTiO_3 + 4HCl = TiOCl_2 + FeCl_2 + 2H_2O. \quad (1)$$

The reaction in Eq. 1 can be represented simply as Eq. 2:

$$A(l) + bB(s) = \nu P(l). \quad (2)$$

When the reaction percentage of component P was represented as x and the steady state of the reaction was assumed, the following Eq. 3 was obtained as the rate equation:

$$\frac{dx}{dt} = \frac{3\nu C_A}{\rho_P R} = \frac{1}{\frac{1}{k_L} + \frac{R}{D_e}\{(1-x)^{-1/3}-1\} + \frac{1}{k_C}(1-x)^{-2/3}}. \quad (3)$$

Three rate-determining steps were studied: the diffusion in liquid film, the diffusion in residual layer, and the surface chemical reaction.[19] However, the diffusion in liquid film should not be the rate-determining step because the dissolution rate of titanium and iron was apparently not zero-order and was not affected by the stirring speed, as described in the next paragraph. Therefore, the following two equations were obtained

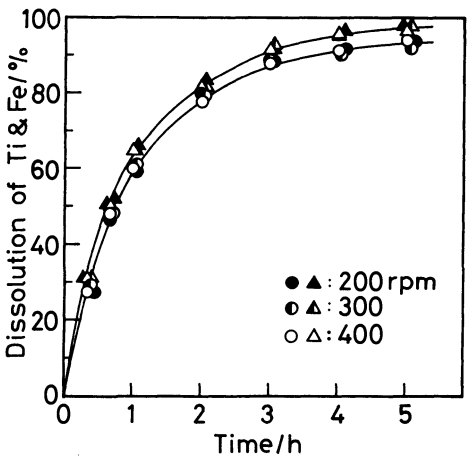

Fig. 2. Effect of stirring speed on the dissolution rates of Ti and Fe of ilmenite ore in concentrated HCl solution. HCl: 11.4 mol dm^{-3}, temperature: 70 °C. ○, ◐, ●: Ti, △, ◭, ▲: Fe.

for each rate-determining step by integration of Eq. 3.

i) For diffusion in residual layer (k_L, $k_C \gg D_e/R$)

$$1 + 2(1 - x) - 3(1 - x)^{2/3} = \frac{6\nu C_A k_C}{\rho_P R^2} t, \quad (4)$$

ii) for surface chemical reaction (k_L, $D_e/R \gg k_C$)

$$1 - (1 - x)^{1/3} = \frac{C_A k_C}{\rho_P R} t. \quad (5)$$

Effect of Stirring Speed. Figure 2 shows the effect of stirring speed on the dissolution rate of titanium and iron in 11.4 mol dm^{-3} HCl solution at 70 °C. The diffusion in liquid film was not the rate-determining step of the reaction in Eq. 1. The dissolution rate of iron was slightly faster than that of titanium, but both were in a nearly stoichiometric ratio. On the basis of the data, subsequent experiments were carried out at the stirring speed of 400 min^{-1}.

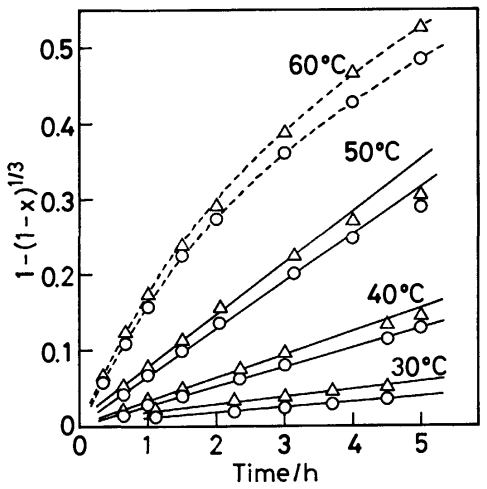

Fig. 3. Effect of temperature on the dissolution rates of Ti and Fe of ilmenite ore in concentrated HCl solution. $\{1-(1-x)^{1/3}\}$ *vs.* t.
HCl: 11.6 mol dm^{-3}, stirring speed: 400 min^{-1}. ○: Ti, △: Fe.

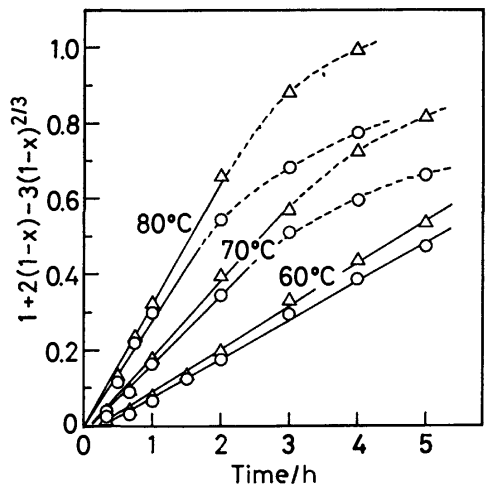

Fig. 4. Effect of temperature on the dissolution rates of Ti and Fe of ilmenite ore in concentrated HCl solution. $\{1+2(1-x)-3(1-x)^{2/3}\}$*vs.* t.
HCl: 11.6 mol dm^{-3}, stirring speed: 400 min^{-1}. ○: Ti, △: Fe.

Effect of Temperature. Figures 3 and 4 show the effect of temperature on the dissolution rates of titanium and iron in 11.6 mol dm^{-3} HCl solution at temperatures of 30 to 80 °C. The dissolution rates at 30—50 °C shown in Fig. 3 were well expressed by Eq. 5, which is based on the rate-determining step of the surface chemical reaction; namely, there was a good linear relationship between $\{1-(1-x)^{1/3}\}$ and t. However, the linear relationship was no longer observable in the dissolution rate at 60 °C. This result indicates that the leaching reaction at temperatures above 60 °C was not limited by the surface chemical reaction. The rate constants, k_C, for the leaching reactions were calculated from the slopes of the straight lines in Fig. 3 and are given in Table 2. The apparent activation energies calculated from the Arrhenius plots of k_C were 81.2 kJ mol^{-1} for titanium and 73.2 kJ mol^{-1} for iron.

Table 2. Kinetic parameters of the leaching of ilmenite ore in concentrated HCl solution at low temperature

Temp / °C	$k_C \times 10^6$/m h^{-1}	
	Ti	Fe
30	1.23	1.72
40	3.83	4.29
50	9.20	10.4
Activation energy/kJ mol^{-1}	81.2	73.2

On the other hand, the dissolution rates at 60—80 °C shown in Fig. 4 were also well expressed by Eq. 4, which is based on the rate-determining step of the diffusion in the residual solid layer. That is to say, the surface chemical reaction at temperatures above 60 °C became so fast that the dissolution rates were limited by the diffusion in the residual layer. In this case, the diffusion rate of H_3O^+ was presumed to be quite fast because we used highly concentrated hydrochloric acid solution in the leaching experiments. Accordingly, the diffusion of Ti^{4+} (titanium ions present in aqueous solutions were not only mononuclear species such as $Ti(OH)^{3+}$, $TiO(OH)^+$, $Ti(OH)_3^+$ but also polynuclear species such as $(TiO)_8(OH)_{12}^{4+}$ [20]) and Fe^{2+} produced by the surface chemical reaction of the unreacted core was the rate-determining step. However, as shown in Fig. 4, there was not a linear relationship between $\{1+2(1-x)-3(1-x)^{2/3}\}$ and t in the dissolution curves after 4 h at 70 °C or after 3 h at 80 °C. This deviation from the rate equation was thought to be dependent on the precipitation of the titanium(IV) oxide on the ore particles by hydrolysis of the titanium ion present in the leaching solution at high temperatures. Earlier workers[17] have reported that titanium ions are liable to precipitate readily from diluted HCl solutions ($<$0.3 mol dm^{-3}), but a similar tendency was observed to happen frequently even in highly concentrated HCl solutions.The X-ray diffraction patterns and the electron

$$TiOCl_2 + H_2O = TiO_2 + 2HCl$$

micrographs of the reaction residues obtained after the leaching experiment at 70 °C were shown in Figs. 5 and

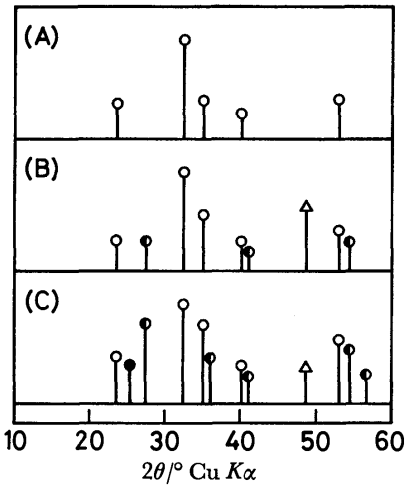

Fig. 5. X-Ray diffraction patterns of ilmenite ore and reaction residues.
HCl: 11.6 mol dm^{-3}, temperature: 70 °C, stirring speed: 400 min^{-1}. (A): ilmenite ore, (B): residue (2 h), (C): residue (4 h). ○: ilmenite, ◐: rutile, ●: anatase, △: Ti_2O_3.

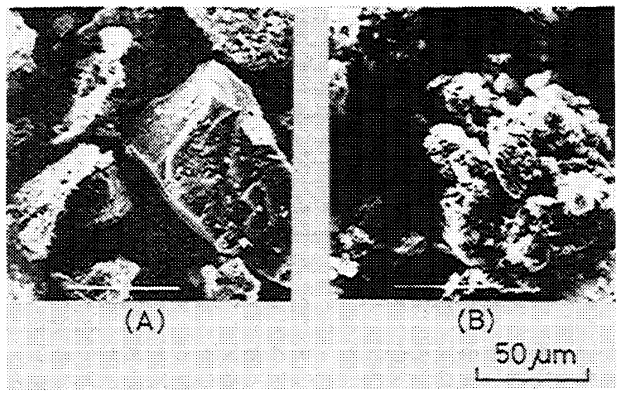

Fig. 6. Scanning electron micrographs of reaction residues.
HCl: 11.6 mol dm^{-3}, temperature: 70 °C, stirring speed: 400 min^{-1}. (A): residue (2 h), (B): residue (4 h).

6, respectively. The intensity of the diffraction peaks based on ilmenite decreased as the leaching continued, while the peaks of rutile gradually appeared. The peaks based on anatase and Ti_2O_3[21] were also observed in the X-ray diffraction patterns of the residues, though they were minor peaks. Ti_2O_3 was presumed to be produced by hydrolysis of Ti(III) ion formed by the reduction of Ti(IV) ion with chloride ion during the leaching. The times of formation of rutile as an insoluble matter were consistent with that of the deviation of titanium dissolution curves from the rate equation shown in Fig. 4. It can therefore be said that the hydrolysis of a part of dissolved titanium ion and the change in thickness of the residual layer have caused the deviation of the titanium dissolution curves. The deviation of the iron dissolution curves from the rate equation was also observed to follow that of titanium. This tendency was considered to depend upon the adsorption of dissolved iron ion and the change in thickness of the residual layer by the precipitation of titanium(IV) oxide. The

Table 3. Kinetic parameters of the leaching of ilmenite ore in concentrated HCl solution at high temperature

Temp °C	$D_e \times 10^{10}$/m^2 h^{-1}	
	Ti	Fe
60	1.84	2.03
70	3.14	3.51
80	4.98	6.09
Activation energy/kJ mol^{-1}	48.9	53.7

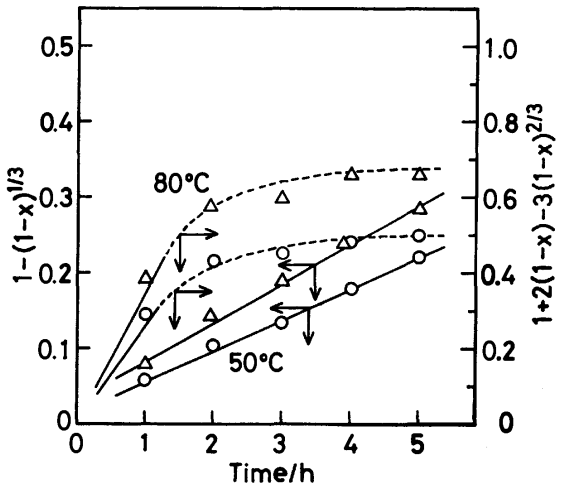

Fig. 7. Effect of ore grain size on the dissolution rates of Ti and Fe of ilmenite ore in concentrated HCl solution.
$\{1-(1-x)^{1/3}\}$ and $\{1+2(1-x)-3(1-x)^{2/3}\}$ *vs.* t.
HCl: 11.6 mol dm^{-3}, stirring speed: 400 min^{-1}, ore grain size: 150—250 mesh. ○: Ti, △: Fe.

effective diffusion coefficient, D_e, was calculated from the slopes of the straight lines in Fig. 4 and is given in Table 3. The apparent activation energies calculated from the Arrhenius plots of D_e were 48.9 kJ mol^{-1} for titanium and 53.7 kJ mol^{-1} for iron.

Effect of Ore Grain Size. Figure 7 shows the result obtained by using the powdered ilmenite ore of 150—250 mesh in 11.6 mol dm^{-3} HCl solution at 50 and 80 °C. The dissolution rate at 50 °C was well expressed by Eq. 5, while the initial dissolution rate at 80 °C was expressed by Eq. 4. On the basis of the data, the following reaction constant, k_C, and effective diffusion coefficient, D_e, for titanium were calculated: $k_C(50\ °C) = 9.38 \times 10^{-6}$ and $D_e(80\ °C) = 6.03 \times 10^{-10}$. These values agreed approximately with the results obtained by using the ilmenite ore of 250—325 mesh, as shown in Tables 2 and 3. It can therefore be said that the rate analysis used in this study was reasonable.

Nomenclature

b = Stoichiometrical coefficient (—).
C_A = Hydrochloric acid concentration in the solution (kg mol m^{-3}).
D_e = Effective diffusion coefficient in the residual layer of the particle (m^2 h^{-1}).

k_C=Rate constant for the reaction Eq. 2 (m h^{-1}).
k_L=Mass transfer coefficient (m h^{-1}).
R=Particle radius (m).
t=Time (h).
x=Reaction percentage (−).
ρ_P=Mole density (kg mol m^{-3}).
ν=Stoichiometrical coefficient (−).

References

1) Kirk-Othmer, "Encyclopedia of Chemical Technology," 2nd ed, John Wiley and Sons, Inc., New York,(1964), Vol. 14, p. 221.
2) N. Ohta, *Kagaku Keizai*, **28**, 49 (1981).
3) Research Committee Meeting of Waste Sulfuric Acids, *Ryusan To Kogyo*, **28**, 193 (1975).
4) H. Tsuruta and N. Wakamatsu, *Bunri Gijutsu*, **8**, 346 (1978).
5) H. Tsuruta and K. Murakami, *Kagaku Kojo*, **24**, 29 (1980).
6) G. H. Rupy and C. J. Jewell, *CIM Bulletin*, **68**, 89 (1975).
7) A. A. Schuldt, *CIM Bulletin*, **68**, 82 (1975).
8) A. Conners, *CIM Bulletin*, **68**, 75 (1975).
9) N. R. Iammartino, *Chem. Eng.*, **83**, 100 (1976).
10) J. W. Burtch, *CIM Bulletin*, **68**, 96 (1975).
11) J. J. Henn and J. A. Barclay, *Bureau of Mines*, Information Circular 8450 (1970).
12) D. A. Ellis, U. S. Patent 3104950 (1963).
13) T. Yamamura *et al.*, Japan Patent 49995 (1972).
14) "Gmelins Handbuch der Anorganischen Chemie," 8th ed, "Titan," Verlag Chemie, Weinheim (1951), No. 41, p. 88.
15) A. K. De, S. M. Khophar, and R. A. Chalmers, "Solvent Extraction of Metals," Van Nostrand Reinhold Co., London (1970).
16) M. Tanaka, "Chemistry of Solvent Extraction," Kyoritsu, Tokyo (1977).
17) M. Imahashi and N. Takamatsu, *Bull. Chem. Soc. Jpn.*, **49**, 1549 (1976).
18) E. B. Sandell, "Colorimetric Determination of Traces of Metals," 3rd ed, Interscience Publishers Inc., New York (1959), pp. 524, 870.
19) S. Yagi and D. Kunii, *Kagaku Kikai*, **16**, 283 (1952); *Kogyo Kagaku Zasshi*, **56**, 131 (1953).
20) H. Einaga, *J. Chem. Soc., Dalton Trans.*, **1979**, 1917.
21) X-Ray powder data file (ASTM card 10-63).

 © 1982 The Chemical Society of Japan Bull. Chem. Soc. Jpn., 55, 1939—1942 (1982)

Thermochemical Hydrogen Production by the Magnesium-Sulfur-Iodine Cycle

Susumu MIZUTA* and Toshiya KUMAGAI

Energy Chemistry Division, National Chemical Laboratory for Industry, Tsukuba Research Center, Yatabe, Ibaraki 305

(Received November 6, 1981)

A new thermochemical cycle, consisting of (i) redox reaction of sulfur dioxide and iodine with magnesium oxide in aqueous phase, (ii) hydrolysis of magnesium iodide, (iii) thermal decomposition of magnesium sulfate, and (iv) thermal dissociation of hydrogen iodide, is presented for hydrogen production. The key reactions (i) and (ii) are experimentally verified.

Among a number of thermochemical cycles so far proposed for hydrogen production, the sulfur-iodine cycle has been considered as one of the most promising. This cycle comprising (i) redox reaction of sulfur dioxide and iodine, (ii) thermal decomposition of sulfuric acid, and (iii) thermal dissociation of hydrogen iodide is expressed by the following sequence,

$$I_2(c) + SO_2(g) + 2H_2O(l) \longrightarrow H_2SO_4(aq) + 2HI(aq), \quad (1')$$

$$H_2SO_4(g) \longrightarrow H_2O(g) + SO_2(g) + (1/2)O_2(g), \quad (2')$$

$$2HI(g) \longrightarrow H_2(g) + I_2(g). \quad (3')$$

The key operation for the cycle consists in the separation process of the acid mixture (H_2SO_4–HI) formed by Reaction 1′ since simple distillation causes the reverse reaction resulting in evolution of I_2 and SO_2. Thus, several proposals have been made on the separation: addition of excess iodine to form polyiodides (HI_x),[1] use of nickel metal,[2] and electrolytic promotion[3] of Reaction 1′.

The present authors have examined an addition of a series of metal oxides (Fe_2O_3, CoO, NiO, CuO, ZnO, PbO, MgO *etc.*), whose sulfates decompose at relatively low temperatures (<1200 °C), to the acid mixture. As a result of preliminary experiments, following points were obtained:

(i) Metal oxides are easily dissolved into the acid mixture by heating, however, the reverse reaction takes place as the solution gets concentrated when the amount of metal oxide is less than the equivalent to the acids.

(ii) Neither HI vapor nor H_2 is observed to be evolved directly from the solution.

(iii) For complete prevention of the reverse reaction, the amount of metal oxide should be equivalent to that of the acids. In other words, the formation of metal sulfate and iodide is considered to be inevitable.

Since a separation of the metal sulfate and iodide solution is another troublesome operation for the cycle, effects of the addition of metal oxide seemed unfavorable. However, the present authors noticed that it would be unnecessary to separate the sulfate and iodide in the case of magnesium oxide, because the temperature required for the thermal decomposition of $MgSO_4$ (1100 °C) is far apart from that for the hydrolysis of MgI_2 (400 °C). Such a temperature difference between these reactions was considered to have a possibility of allowing HI and SO_3 to be evolved separately.

Thus, a new thermochemical cycle using magnesium, sulfur, and iodine was designed as follows:[4–6]

$$2MgO(c) + SO_2(aq) + I_2(c) \xrightarrow{70\,^\circ C} MgSO_4(aq) + MgI_2(aq), \quad (1)$$

$$MgSO_4(aq) + MgI_2(aq) \xrightarrow{400\,^\circ C} MgSO_4(c) + MgO(c) + 2HI(g) + nH_2O(g), \quad (2)$$

$$MgSO_4(c) \xrightarrow{1100\,^\circ C} MgO(c) + SO_2(g) + (1/2)O_2(g), \quad (3)$$

$$2HI(g) \xrightarrow{300\text{—}700\,^\circ C} H_2(g) + I_2(g). \quad (4)$$

Each of the reactions was studied in this work. Experimental verifications were particularly focused on the key reactions 1 and 2.

Reaction Characteristics and Experimental Verification

Reaction 1(Redox Reaction of SO_2 and I_2 with MgO in Aqueous Phase). Iodine powder 552 mg was added to 2 cm^3 of approximately 6.8 wt% SO_2 aqueous solution in a beaker and the mixture was agitated until a colorless solution was obtained. Then, 174 mg of MgO powder, prepared by the decomposition of $MgSO_4$, was added to the resulting mixed acid solution at 70 °C with stirring. The magnesium oxide was easily dissolved to make a transparent solution after several minutes.

This mixed solution was subjected to EDTA chelate analysis, sulfate gravimetry, and thiosulfate iodometric titration for concentrations of Mg^{2+}, SO_4^{2-}, and I^- ions, respectively. Molar ratio $[Mg^{2+}] : [SO_4^{2-}] : [I^-] = 2.0 : 1.0 : 2.0$ was obtained. Thus, 100% yield and high reaction rate were verified for this reaction.

Reaction 2(Hydrolysis of MgI_2 Hydrate). X-Ray Analysis: In order to grasp an outline of Reaction 2, an X-ray analysis was made on solid phases. A mixed solution of $MgSO_4$ and MgI_2 produced by Reaction 1, was heated in a quartz boat in an atmosphere of N_2 at 100, 200, 240, 300, 350, or 1100 °C. Each of the solid residues was examined by X-ray analysis. Results are shown in Fig. 1. Since magnesium iodide and magnesium hydroxyiodides are extremely hygroscopic or easily oxidized in air, samples were kept in an N_2 atmosphere during measurement.

Based on the results shown in Fig. 1, changes in solid phases in course of Reaction 2 is expressed by

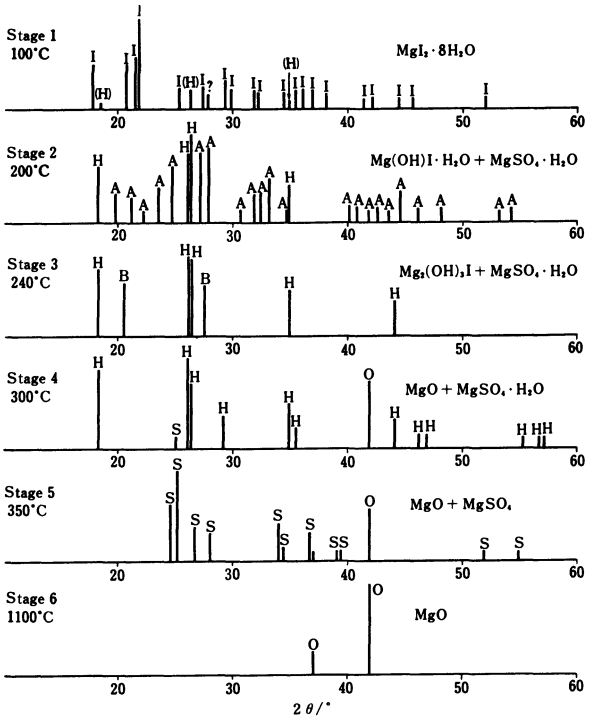

Fig. 1. Changes in X-ray diffraction patterns during heating of a mixed solution of MgI_2 and $MgSO_4$ (Cu $K\alpha$).
I: $MgI_2 \cdot 8H_2O$, H: $MgSO_4 \cdot H_2O$, A: $Mg(OH)I \cdot H_2O$
B: $Mg_2(OH)_3I$, S: $MgSO_4$, O: MgO.

$$MgSO_4(aq) + MgI_2(aq)$$
$$\longrightarrow MgSO_4 \cdot H_2O + MgI_2 \cdot 8H_2O$$
$$\longrightarrow MgSO_4 \cdot H_2O + Mg(OH)I \cdot H_2O$$
$$\longrightarrow MgSO_4 \cdot H_2O + (1/2)Mg_2(OH)_3I$$
$$\longrightarrow MgSO_4 \cdot H_2O + MgO$$
$$\longrightarrow MgSO_4 + MgO \longrightarrow 2MgO.$$

Thus, the hydrolysis of $MgI_2 \cdot 8H_2O$ and the dehydration or thermal decomposition of $MgSO_4 \cdot H_2O$ were found to separately proceed, as far as the result of X-ray analysis is concerned.

Thermal Analyses: A mixed solution of $MgSO_4 + MgI_2$ was also analyzed by TG and DTA from 25 to 1200 °C in a stream of argon at a heating rate of 200 °C/h. Results are shown in Fig. 2, where each arrow shows the theoretical weight calculated by using atomic weights for possible products. The plateaus observed at 130, 210, 260—300, and 350 °C correspond exactly to

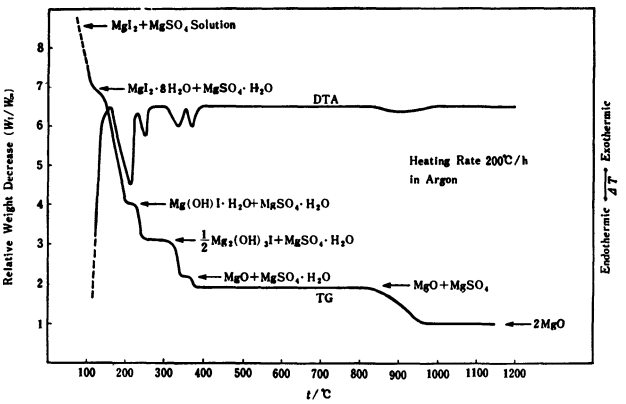

Fig. 2. TG and DTA curves for heating a mixed solution of MgI_2 and $MgSO_4$.

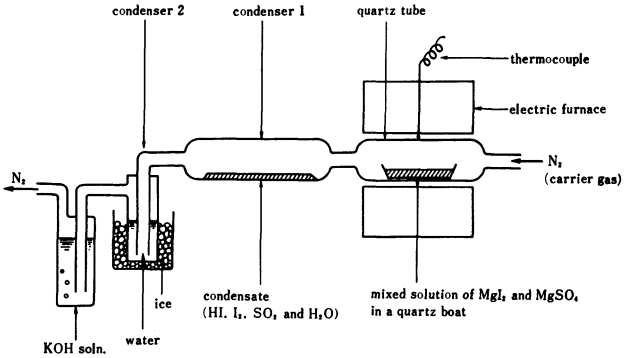

Fig. 3. Apparatus for hydrolysis of a mixed solution of MgI_2 and $MgSO_4$.

$MgSO_4 \cdot H_2O + MgI_2 \cdot 8H_2O$, $MgSO_4 \cdot H_2O + Mg(OH)I \cdot H_2O$, $MgSO_4 \cdot H_2O + (1/2)Mg_2(OH)_3I$, and $MgSO_4 \cdot H_2O + MgO$, respectively, while the one at 400—800 °C lies slightly lower than the calculated position for $MgSO_4 + MgO$, *i.e.*, the weight decrease observed for the reaction at 350—400 °C is slightly larger than the theoretical.

At any rate, general tendency of the results of thermal analyses may be considered to be in good agreement with those of X-ray analysis. To clarify the details of the reactions in the range 300—400 °C, a further study resorting to chemical analyses was performed as described below.

Chemical Analysis: Products of Reaction 2 were chemically analyzed. As shown in Fig. 3, a mixed solution of $MgSO_4$ and MgI_2 in a quartz boat was

TABLE 1. RESULTS OF CHEMICAL ANALYSIS FOR HYDROLYSIS OF A MIXED SOLUTION OF MgI_2 AND $MgSO_4$[a]

Heating mode	No. 1[b]			No. 2[c]			
Species determined	Distillate (25—430 °C)	Residue	Total	Distillate 1 (25—300 °C)	Distillate 2 (300—430 °C)	Residue	Total
I^-	1.85[d]	0.02[d]	1.99	1.62[d]	0.24[d]	0.02[d]	1.99
I_2	0.12	0		0.06	0.05	0	
SO_4^{2-}	0	1.91	2.01	0	0	1.92	2.01
SO_3^{2-}	0.04	0.06		0	0.06	0.03	
R[e]		$R=0.050$			$R=0.045$		

a) The figures give quantities in mmol. b) Direct heating (see text). c) Two-step heating (see text).
d) Calculated by I_2 ($I^-/2$). e) $R \equiv SO_3^{2-}/(SO_4^{2-}+SO_3^{2-})$.

heated in an N_2 atmosphere. Evolved vapors of I_2, HI, and SO_2 were collected in condensers while a solid residue in a quartz boat was dissolved in HCl.

The amounts of I_2, and I^- and the total amount of SO_3^{2-} and SO_4^{2-} for each reaction product were determined by thiosulfate iodometric titration and sulfate gravimetry. The amount of SO_3^{2-} was determined by back-titration of excess free iodine after adding a measured amount of I_2 to the sample.

Results for the cases of direct heating up to 430 °C (designated No. 1) and of heating in two steps of 25→300 and 300→430 °C (designated No. 2) are shown in Table 1. For the case of No. 2, evolution of SO_2 was undetected in the range of 25—300 °C whereas considerable amounts of I_2 and SO_2 were generated at 300—430 °C. A slight amount of I_2 formation would be attributable to the thermal dissociation of HI, though, this I_2 formation is only assumed to result from the reverse reaction of Reaction 1 since the total amount of I_2 evolved is almost equal to that of SO_3^{2-}. The contribution of the reverse reaction was calculated to be $R=0.050$ for No. 1 and $R=0.045$ for No. 2, where R (reverse reaction factor) is defined by

$$R \equiv \frac{SO_3^{2-}}{SO_3^{2-}+SO_4^{2-}}. \quad (5)$$

Thus, it is concluded that 95% of each of HI and H_2SO_4 was successfully separated by the addition of MgO.

Discussions on Reaction 2: As results of X-ray, thermal, and chemical analyses, total reactions are conclusively expressed as follows:

$$MgSO_4(aq) + MgI_2(aq) \xrightarrow{100\,^\circ C} MgSO_4\cdot H_2O(c) + MgI_2\cdot 8H_2O(c), \quad (2\text{-}1)$$

$$MgSO_4\cdot H_2O(c) + MgI_2\cdot 8H_2O(c) \xrightarrow{150\text{—}200\,^\circ C} MgSO_4\cdot H_2O(c) + Mg(OH)I\cdot H_2O(c) + HI(g) + 6H_2O(g), \quad (2\text{-}2)$$

$$MgSO_4\cdot H_2O(c) + Mg(OH)I\cdot H_2O(c) \xrightarrow{220\text{—}250\,^\circ C} MgSO_4\cdot H_2O(c) + (1/2)\,Mg_2(OH)_3I(c) + (1/2)\,HI(g) + (1/2)\,H_2O(g), \quad (2\text{-}3)$$

$$MgSO_4\cdot H_2O(c) + (1/2)\,Mg_2(OH)_3I(c) \xrightarrow{300\text{—}340\,^\circ C} MgSO_4\cdot H_2O(c) + MgO(c) + (1/2)\,HI(g) + (1/2)\,H_2O(g), \quad (2\text{-}4)$$

$$MgSO_4\cdot H_2O(c) + MgO(c) \xrightarrow{360\text{—}380\,^\circ C} MgSO_4(c) + MgO(c) + H_2O(g). \quad (2\text{-}5)$$

This reaction sequence is also supported excellently by the results of hydrolysis of pure $MgI_2\cdot 6H_2O$ previously reported by the present authors.[7]

The reverse reaction was observed to proceed at 300—430 °C within an extent of 5%; as least 95% of reactants was consumed in accordance with this sequence. A slight amount of some complex compound (Mg–I–SO_4) capable of causing the reverse reaction, though undetectable by X-ray analysis, might be present in the mixture of MgI_2 and $MgSO_4$ hydrates after drying the mixed solution.

Reaction 3 (Thermal Decomposition of $MgSO_4$). Thermal decomposition of $MgSO_4$ is reported[8] to take place as follows:

$$MgSO_4(c) \longrightarrow MgO(c) + SO_2(g) + (1/2)O_2(g). \quad (3)$$

The present experiments also confirmed the complete conversion of $MgSO_4$ into MgO at 1100 °C as shown in Figs. 1 and 2. Decomposition of SO_3 to SO_2 and O_2 is reported to proceed to almost 100% conversion at 1100 °C.[9]

Reaction 4 (Thermal Dissociation of HI). Thermal dissociation of HI is well known to occur according to

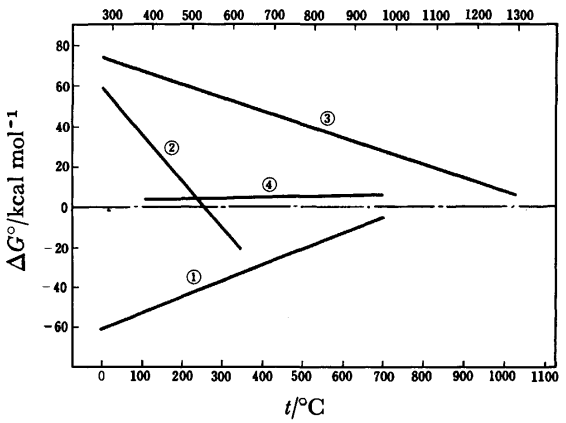

Fig. 4. Free energy change (ΔG°) *vs.* temperature plot for Reactions 1—4.
(1) $I_2(c)+SO_2(g)+2MgO(c)+6H_2O(l)\rightarrow MgI_2\cdot 6H_2O(c)+MgSO_4(c)$, (2) $MgI_2\cdot 6H_2O(c)\rightarrow MgO(c)+2HI(g)+5H_2O(g)$, (3) $MgSO_4(c)\rightarrow MgO(c)+SO_2(g)+(1/2)O_2(g)$, (4) $2HI(g)\rightarrow H_2(g)+I_2(g)$.

Table 2. Enthalpy, entropy, and freee nergy changes (ΔH°_{298}, ΔS°_{298}, and ΔG°) for Reactions 1—6[a]

Reaction	ΔH°_{298}/kcal mol^{-1} [b]	ΔS°_{298}/cal mol^{-1} K^{-1} [b]	ΔG°/kcal mol^{-1} [b]
1	−83.5	−81.1	−59.3 at 298 K
2	+123.4	+233.5	−33.7 at 673 K
3	+92.5	+68.3	+0.6 at 1400 K
4	+2.3	−5.3	+5.6 at 700 K
5	−14.9	−34.4	−4.7 at 298 K
6	−51.5	−142.0	−9.5 at 298 K
Total	+68.3	+39.0	

a) (1) $I_2(c)+SO_2(g)+2MgO(c)+6H_2O(l)\longrightarrow MgI_2\cdot 6H_2O(c)+MgSO_4(c)$, (2) $MgI_2\cdot 6H_2O(c)\longrightarrow MgO(c)+2HI(g)+5H_2O(g)$, (3) $MgSO_4(c)\longrightarrow MgO(c)+SO_2(g)+1/2O_2(g)$, (4) $2HI(g)\longrightarrow H_2(g)+I_2(g)$, (5) $I_2(g)\longrightarrow I_2(c)$, (6) $5H_2O(g)\longrightarrow 5H_2O(l)$. b) 1 cal=4.184 J.

$$2HI(g) \longrightarrow H_2(g) + I_2(g). \quad (4)$$

The extent of conversion is reportedly 18—29% at 600—1000 K according to Bodenstein.[10]

Thermodynamic Calculation

The enthalpy change (ΔH°_{298}), entropy change (ΔS°_{298}) and free energy change (ΔG°) for each of the processes involved in the present cycle were calculated based on the thermochemical data by Barin and Knacke[11] and estimated values for $MgI_2 \cdot 6H_2O$.[7] The results are shown in Fig. 4 and Table 2.

Conclusion

1) A new thermochemical cycle for hydrogen production (Magnesium-Sulfur-Iodine cycle) was successfully presented on the basis of a combination of MgO and a sulfur-iodine scheme.

2) The feasibility of the two key reactions, (i) redox reaction of SO_2 and I_2 with MgO in aqueous phase and (ii) hydrolysis of MgI_2 hydrate, were experimentally verified. Conversion was found to be 100% for reaction (i) at 70 °C and 95% for reaction (ii) at 400 °C, respectively. Sufficiently high reaction rates were observed for both the reactions.

3) For this cycle it is unnecessary to separate the mixed solution of $MgSO_4$ and MgI_2, that is, HI and SO_3 are separately evolved at different temperatures. Therefore, the material flow-sheet can be so simple, as shown in Fig. 5.

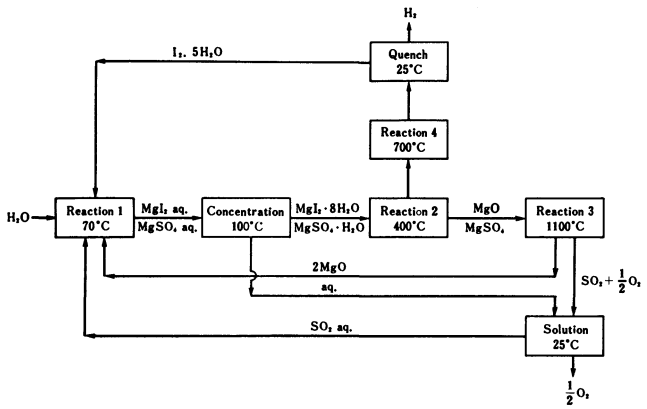

Fig. 5. Material flow in magnesium-sulfur-iodine cycle.

References

1) G. E. Besenbruch, K. H. McCorkle, J. H. Norman, D. R. O' Keefe, J. R. Schuster, and M. Yoshimoto, *Proc. 3rd World Hydrogen Energy Conference, Tokyo*, **1**, 243 (1980).

2) S. Sato, S.Shimizu, H. Nakajima, and Y. Ikezoe, *Proc. 3rd World Hydrogen Energy Conference, Tokyo*, **1**, 389 (1980).

3) M. Dokiya, K. Fukuda, T. Kameyama, Y. Kotera, and S. Asakura, *Denki Kagaku*, **45**, 139 (1977).

4) S. Mizuta, T. Kumagai, and T. Hakuta, Japan Patent 1067586 (1978).

5) S. Mizuta and T. Kumagai, Proc. 46th Annual Meeting of Electrochemical Soc. of Japan, Osaka ,May 1979 No. A-104, p. 4.

6) S. Mizuta and T. Kumagai, *Chem. Lett.* **1982**, 81.

7) S. Mizuta and T. Kumagai, *Denki Kagaku*, **47**, 100 (1979).

8) "Gmelins Handbuch der anorganischen Chemie," No. 27, Mg [B], p. 214.

9) "Gmelins Handbuch der anorganischen Chemie," No. 9, S [B], p. 353.

10) M. Bodenstein, *Z. Phys. Chem.* **13**, 56 (1894); **22**, 1 (1897); **29**, 295 (1899).

11) I. Barin and O. Knacke, "Thermochemical properties of inorganic substances," Springer-Verlag, Berlin, Heidelberg, New York (1973).

Application of Regular Solution Theory to Extraction of Salicylaldehyde Oxime Chelates

S. Narayanan and G. N. Rao*

Department of Chemistry, Indian Institute of Technology, Hauz Khas, New Delhi 110016, India

(Received August 6, 1981)

The distribution coefficients of salicylaldehyde oxime and its metal chelates, namely of Co(II), Cu(II), and Zn(II) were determined between aqueous acetate phase (μ=0.1) and eight 'inert' organic solvents at 25 °C. On the basis of regular solution theory, the correlation between the distribution coefficients of the ligand (P_{HA}) and that of the metal chelates (P_M) expressed by log $P_M = n$ log P_{HA} + const, was shown to be valid satisfactorily in most of the systems. Hexane and cyclohexane showed abnormal behaviour in extraction with Cu(II), while with Zn(II) extraction to the desired level was not possible with these two solvents. A good correlation was also observed between the distribution coefficient of salicylaldehyde oxime and the 'solubility parameter' of the solvents and the solutions are shown to be regular.

In the solvent extraction of metal complexes, studies have been made qualitatively in several systems. Also in many studies the solvents have been chosen semiempirically without understanding what physicochemical properties of the solvent govern the distribution of the species. The solvent plays an important role not only in the effective separation of the species from a mixture but also in synergistic studies, organic phase reactions, kinetics of extraction *etc.* Thus, role of solvent is quite important and a quantitative approach on the basis of regular solution theory[1] has been made. Studies have revealed that the distribution coefficient of a species can be correlated with the solubility parameter of the organic solvent. Also a correlation can exist between the distribution coefficients of the ligand and its metal chelate when the nature of their interaction with solvent molecules are same. Such correlations have been established by Suzuki, Akiba, and others in their studies with thenoyltrifluoroacetone with different metals and different solvents[2-7] and by Honjo *et al.* with thiothenoyl trifluoroacetone.[8] Similar relations for benzoyltrifluoroacetone and for 4-benzoyl-5-methyl-2-phenyl-4-pyrazolin-3-one (BMPP) have been recently established.[9] The present study on above lines has been described with salicylaldehyde oxime as the ligand. Salicylaldehyde oxime has been specifically selected due to its characteristic nature of being biprotonic, and having fair solubility in water, these two properties being absent in the ligands studied so far.

Experimental

Material. Salicylaldehyde oxime (Merck) was used as supplied without further purification.

Carbon tetrachloride, chlorobenzene, cyclohexane (all BDH), chloroform, dichloromethane, hexane (all Merck), benzene (IDPL), and toluene (Rechem) were purified whenever necessary and used.

Co(II), Cu(II), and Zn(II) solutions were prepared from cobalt acetate, copper(II) sulfate, and zinc sulfate respectively (all A. R. grade).

Procedure. Determination of Distribution Coefficient (P_{HA}) of Salicylaldehyde Oxime: Aqueous solution of salicylaldehyde oxime of suitable concentration was prepared at pH=1 and its absorbance measured at 258 nm in a spectrophotometer (SP-700A PYE UNICAM) and the molar absorptivity coefficient was determined (ε=8400). Solution of salicylaldehyde oxime of known concentration in the desired organic solvent was equilibrated with aqueous phase (pH=1) and the absorbance of suitable aliquot of aqueous phase was measured. Knowing ε=8400, and the concentration in the aqueous phase, by difference the concentration in organic phase was determined and hence the distribution coefficient. The values of P_{HA} with different solvents are presented in Table 1.

Determination of Distribution Ratio (K_d) of the Metal Salicylaldehyde Oxime Chelate: Ten milliliters of the aqueous phase containing the acetate buffer at appropriate pH and the metal ion at 10—20 ppm level was equilibrated with 10 ml of the desired organic solvent containing salicylaldehyde

Table 1. Distribution coefficients of salicylaldehyde oxime and extraction constants of metal salicylaldehyde oxime

No.	Solvent	δ[a]	ε[b]	log P_{HA}	log K_{ex}		
					Co(II)	Cu(II)	Zn(II)
1	Cyclohexane	8.2	2.0	−0.59	−7.32±0.02	2.62±0.04[c]	d)
2	Hexane	7.3	1.9	−0.53	−7.50±0.02	2.82±0.10[c]	d)
3	Carbon tetrachloride	8.6	2.2	0.104	−7.40±0.02	2.22±0.02	−11.85±0.04[e]
4	Toluene	8.9	2.4	0.58	−8.56±0.02	1.12±0.02	−11.10±0.04[f]
5	Benzene	9.15	2.3	0.98	−9.23±0.02	0.96±0.04	−12.18±0.02[e]
6	Chlorobenzene	9.5	5.6	0.68	−8.30±0.10	1.56±0.04	−12.20±0.10[e]
7	Chloroform	9.3	4.8	1.00	−9.68±0.04	0.86±0.08	−11.14±0.02[f]
8	Dichloromethane	9.7	9.1	1.18	−9.00±0.06	0.60±0.08	−11.30±0.10[f]

a) δ: Solubility parameter. b) Dielectric constant. c) Slope=3. d) No quantitative extraction possible. e) Extracted species contain one ligand molecule. f) Extracted species contain two ligand molecules.

oxime (10^{-2} M; 1 M=1 mol dm^{-3}) for 5 min. After equilibration, pH of aqueous phase was measured and the concentration of metal in the aqueous phase was determined by atomic absorption spectrophotometer (SP-191 PYE UNICAM) and then the distribution ratio was determined. Experiments were also done with varying ligand concentration (2×10^{-3} M to 10^{-2} M) in the organic phase while maintaining a fixed pH in the aqueous phase.

Results and Discussion

The extraction equilibria for the distribution of a bivalent metal (M) with a ligand (HA) can be written as:

$$HA_{aq} \rightleftharpoons HA_{org} : P_{HA}, \quad (1)$$

$$HA_{aq} \rightleftharpoons H^+_{aq} + A^-_{aq} : K_a, \quad (2)$$

$$M^{2+}_{aq} + nA^-_{aq} \rightleftharpoons MA^{(2-n)+}_{n,aq} : \beta_n, \quad (3)$$

$$MA_{2,aq} \rightleftharpoons MA_{2,org} : P_M, \quad (4)$$

where the subscripts org and aq represent the species in the organic and aqueous phase respectively. The symbol on the right side represents the equilibrium constant for that particular step.

Under the conditions when the concentration of the metal chelate is sufficiently low compared to that of the metal, M^{2+}, in the aqueous phase and if the metal species exist as MA_2 chelate in the organic phase then the distribution ratio, K_d, of the chelate can be given as:

$$K_d = P_M\beta_2(A^-)^2, \quad (5)$$

where A^- is the anion of the ligand and its concentration can be determined from the expression

$$[A^-] = \frac{[HA]_{org,ini}}{[P_{HA}+1][H^+]/K_a+1}. \quad (6)$$

The experimental extraction behaviour of metal complexes can be followed through theoretical plots and slope analysis. Plots of $\log K_d$ *vs.* pH and $\log K_d$ *vs.* log of ligand concentration indicate the number of hydrogen ions released and the number of ligand molecules involved respectively, during the complexation process. Further, plots of $\log K_d$ *vs.* pA (pA= $-\log [A^-]$) can be drawn at fixed pH or at fixed ligand concentration. These plots give negative slopes indicating the number of ligand molecules participating in the simple complexation process. The distribution coefficient (P_M) of the chelate, generally, cannot be measured experimentally and it is related to the measurable distribution ratio, K_d, as a function of pA. Mathematically,

$$K_d = P_M \cdot f[A^-] \quad (7)$$

Thus, if the value of distribution ratio could be known at a fixed pA, it is possible to relate the distribution coefficient of the chelate with the distribution coefficient of ligand and the relation

$$\log P_M = n \log P_{HA} + \text{const}, \quad (8)$$

could be validated as expected from regular solution theory.[12]

In the present work the correlation shown by Eq. 8 has been found to obey satisfactorily with the three metals studied.

Co(II)–Salicylaldehyde Oxime System. The extraction takes place in the pH range 5.6 to 6.6 in all the eight solvents. Slope analysis of plots, discussed already, gave values of two indicating release of two hydrogen ions and involvement of two molecules of salicylaldehyde oxime. It is thus obvious that one hydrogen ion is released from each ligand molecule. The mechanism can be written as:

$$Co^{2+}_{aq} + 2(H_2\cdot sal)_{org} \rightleftharpoons Co(H\cdot sal)_{2\,org} + 2H^+_{aq}, \quad (9)$$

where $(H_2\cdot sal)$ represents one salicylaldehyde oxime molecule.

The values of extraction constants, $\log K_{ex}$, for the above reaction for different solvents have been calculated from the relation

$$\log K_{ex} = \log K_d - 2\text{pH} - 2\log [H_2\cdot sal] \quad (10)$$

and are presented in Table 1.

Salicylaldehyde oxime has fair solubility in water. A correction is to be applied since the actual value of the ligand concentration will be less than that taken for equilibration in the organic phase. Utilising the P_{HA} values, the solubility correction has been incorporated while computing the values of K_{ex} presented in Table 1.

Plots of $\log K_d$ *vs.* pA also give negative slope of two for all solvents. Figure 1 indicates such plots for some solvents. From these plots, the values of $\log K_d$ at a fixed pA were plotted against $\log P_{HA}$, and it was found that there is a satisfactory regularity with most of the solvents.

Cu(II)–Salicylaldehyde Oxime System. The extraction takes place in acidic range *i.e.*, pH range 1 to 2 in all solvents. Slope analysis confirms the mechanism similar to the extraction in Co(II) system shown in Eq. 9, in all solvents except hexane and cyclohexane. These two solvents, however, show different behaviour and they give slope value of ≈ 3 in $\log K_d$ *vs.* pH and $\log K_d$ *vs.* $\log [H_2\cdot sal]$ plots. This indicates involve-

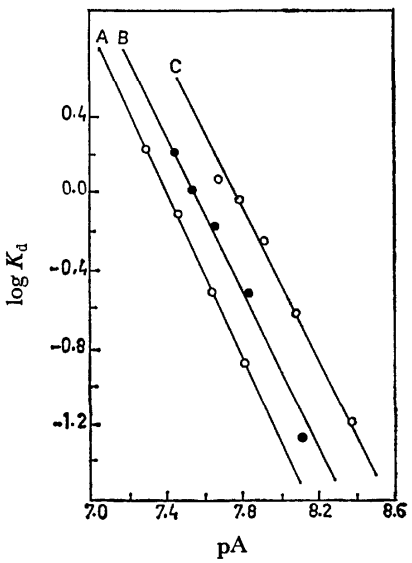

Fig. 1. Variation of distribution ratio of cobalt–salicylaldehyde oxime chelate as a function of pA.
A: Benzene; $(HA)_0=10^{-1}$ M, B: chlorobenzene; pH= 6.4, C: dichloromethane; pH=6.6.

ment of three molecules of ligand and release of three hydrogen ions and the complex will be anionic. Since extraction does take place into the organic phase, this anion perhaps forms an ion pair chelate, of the type $Cu(H\cdot sal)_3^-\cdot H^+$ where the H^+ probably coming from the aqueous phase. The mechanism is probably

$$Cu^{2+}_{aq} + 3(H_2\cdot sal)_{org} \rightleftharpoons 3H^+_{aq} + Cu(H\cdot sal)_{3,aq} \longrightarrow Cu(H\cdot sal)_3^-\cdot H^+_{org}. \quad (11)$$

The formation of higher complexes involving three ligand molecules may be due to nature of these two solvents. These two solvents, show more resemblance to aqueous phase so far as the distribution coefficient of salicylaldehyde oxime with these two solvents are concerned. The P_{HA} values are so low that the anion concentration of salicylaldehyde oxime can be expected to be high in the aqueous phase resulting in the formation of higher complexes. In the case of both solvents at higher pH (>2) the extraction declines and this can be attributed to low availability of H^+ to form ion pair. The values of log K_{ex} with different solvents are given in Table 1.

In the log K_d *vs.* log P_{HA} plot, shown in Fig. 2, there is satisfactory regularity. Hexane and cyclohexane show abnormal deviation and it is difficult to pinpoint the reason with the present information.

Zn(II)–Salicylaldehyde Oxime System. Dahl, in his studies[10] has emphasized the importance of reagent concentration in the extraction of Zn(II) with various solutions of salicylaldehyde oxime. The present studies also indicated requirement of different ligand concentration in different solvents, 5×10^{-2} M solution of salicylaldehyde oxime in benzene, toluene, chlorobenzene, and carbon tetrachloride and 10^{-1} M solution were needed in chloroform and dichloromethane for extraction which was in the pH range 6.4 to 7.6; in case of cyclohexane, however, it was noted that quantitative extraction could not be achieved with 10^{-1} M or even slightly higher concentration. Still higher concentration rendered the ligand insoluble in these two solvents and hence no satisfactory extraction could be done with hexane and cyclohexane.

Analysis of plots reveal interesting results. With toluene, chloroform, and dichloromethane the extraction mechanism was similar to those noted in Co(II) and Cu(II) system. But with carbon tetrachloride, benzene and chlorobenzene slope analysis indicated release of two hydrogen ions and involvement of only one ligand molecule in the complexation. This indicates the release of the two hydrogen ions from the same salicylaldehyde oxime molecule and the mechanism can be written as:

$$Zn^{2+}_{aq} + (H_2\cdot sal)_{org} \rightleftharpoons Zn(sal)_{org} + 2H^+_{aq}. \quad (12)$$

The extraction constant values are shown in Table 1.

In the plots of log K_d *vs.* log P_{HA}, slope of two was observed for toluene, chloroform, and dichloromethane while for carbon tetrachloride, benzene, and chlorobenzene slope of one was noted. This is in conformity with the predicted mechanism of involvement of only one molecule of ligand for the latter three solvents. It can be seen from Fig. 3 that there is good regularity with all solvents.

The molar volume of salicylaldehyde oxime was determined to be 100±5.0 through density measurement using petroleum ether as solvent. This experimental value was checked to be correct by the graphical method employed for β-diketones by Wakahayashi *et al.*[11,12] and later by Kojima *et al.*[13] Knowing the molar volume, the solubility parameter (δ) of salicylaldehyde oxime in different solvents, using hexane as standard, was calculated employing Siekierski-Olszer equation.[14] The solubility parameter value was found to be 13.0±0.8. A plot between the distribution coefficient of the ligand and the solubility parameter of the solvents gave a parabolic curve, as Fig. 4 shows, and this is in accordance with regular solution theory. The points in the figure for different solvents are on the same side since $\delta_{ligand} > \delta_{solvent}$ for all the solvents and since all points fall in the parabola with no deviation it can be concluded that the solutions of salicylaldehyde oxime in different solvents are regular.

The basis for regular solution theory is on the concept of solubility parameter. The importance of this in relation to other parameters like dielectric constant was also investigated, on the basis of Pearson's cor-

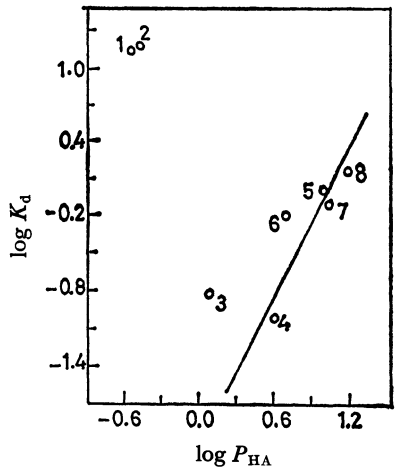

Fig. 2. Correlation between the distribution coefficient of salicylaldehyde oxime and that of its copper chelate. The numbers in the figure correspond to those in Table 1.

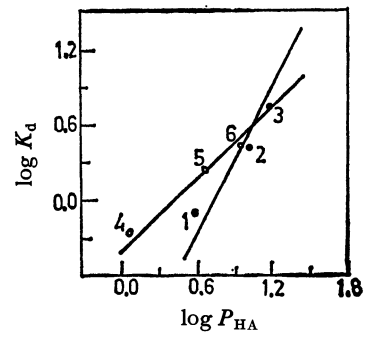

Fig. 3. Correlation between the distribution coefficient of salicylaldehyde oxime and that of its zinc chelate at a fixed pA.
1: Toluene, 2: chloroform, 3: dichloromethane (at pA=6.2), 4: carbon tetrachloride, 5: chlorobenzene, 6: benzene (at pA=15.0).

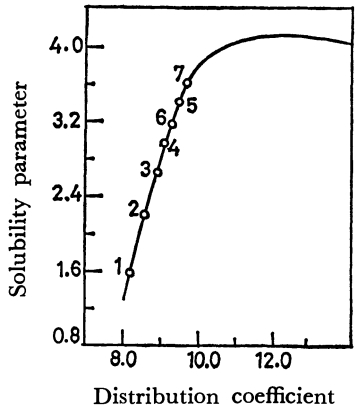

Fig. 4. Distribution of salicyladehyde oxime as a function of solubility parameter of organic solvents based on Siekierski-Olszer equation using Hexane as standard.
1: Cyclohexane, 2: carbon tetrachloride, 3: toluene, 4: benzene, 5: chlorobenzene, 6: chloroform, 7: dichloromethane.

relation coefficient. The correlation coefficient is used to measure the degree of linear correlation between two variables. Pearson's correlation coefficient is given by

$$\text{Correlation coefficient} = \frac{\sum \delta x . \delta y}{\sqrt{\sum(\delta x)^2 \times \sum(\delta y)^2}},$$

where δx is deviation from the mean of one of the first variable and δy is the deviation from the mean of the corresponding second variable. When the correlation coefficient is $+1$ there is a positive correlation between the two variables and all the points fall exactly on a line. If the points are completely random on the graph the correlation coefficient will be zero. In the present study, in the plot between $\log P_{HA}$ and δ, the solubility parameter, the correlation coefficient is obtained as $+0.88$ while in the plot of $\log P_{HA}$ *vs.* ε, the dielectric constant the value is $+0.58$. Thus, the values P_{HA} are much better correlated with solubility parameter than with dielectric constant.

In conclusion, it may be said that for a ligand like salicylaldehyde oxime, regular solution theory appears to be valid from the present studies and it is thus possible to make choice of appropriate solvent for extraction.

References

1) J. Hildebrand and R. L. Scott "Regular and related solutions," Van Nostrand Reinhold Co., N. Y. (1970).
2) N. Suzuki, K. Akiba, T. Kanno, T. Wakahayashi, and K. Takaizumi, *J. Inorg. Nucl. Chem.*, **30**, 3047 (1968).
3) N. Suzuki, K. Akiba, and T. Kanno, *Anal. Chim. Acta*, **43**, 311 (1968).
4) N. Suzuki, K. Akiba, and H. Asano, *Anal. Chim. Acta*, **52**, 115 (1970).
5) K. Akiba, N. Suzuki, H. Asano, and T. Kanno, *J. Radioanal. Chem.*, **7**, 203 (1971).
6) N. Suzuki and K. Akiba, *J. Inorg. Nucl. Chem.*, **33**, 1897 (1971).
7) K. Akiba, N. Suzuki, and T. Kanno, *Anal. Chim. Acta*, **58**, 379 (1972).
8) T. Honjo, R. Honda, and T. Kiba, *Anal. Chem.*, **49**, 2246 (1977).
9) S. Narayanan, Ph. D. Thesis, IIT Delhi (1980).
10) I. Dahl, *Anal. Chim. Acta*, **41**, 9 (1968).
11) T. Wakahayashi, S. Oki, T. Omori, and N. Suzuki, *J. Irong. Nucl. Chem.*, **26**, 2255 (1964).
12) T. Omori, T. Wakahayashi, S. Oki, and N. Suzuki, *J. Inorg. Nucl. Chem.*, **26**, 2265 (1964).
13) I. Kojima, M. Yoshida, and M. Tanaka, *J. Inorg. Nucl. Chem.*, **32**, 987 (1970).
14) S. Siekierski and R. Olszer, *J. Inorg. Nucl. Chem.*, **25**, 1351 (1963).

The Thermodynamics of Ion Exchange of Singly Charged Cobalt(III) Complex with Sodium Ions on Cation Exchange Resin

Katsumi KUROTAKI* and Shoichi KAWAMURA
Division of Chemistry, National Institute of Radiological Sciences, 4-9 Anagawa, Chiba 260

(Received April 25, 1981)

Synopsis. Thermodynamic values of the ion exchange of $[Co^{III}L_4B_2]^+$ (L=NH_3, ethylenediamine/2 (=en/2), or dimethylglyoximato(1−) anion/2 (=dmgH/2); B=NO_2^-, NCS^-, $CO_3^{2-}/2$, NH_3, or $C_2H_5NH_2$) with Na^+ on Dowex AG 50W-X2 resin were determined at 25 °C by measurements of selectivity coefficient and heat of exchange. Heats and entropies are negative for the uptake of $[Co(NH_3)_4(NO_2)_2]^+$ and $[Co(en)_2B_2]^+$, while they are positive for the uptake of $[Co(dmgH)_2(C_2H_5NH_2)_2]^+$.

In our previous paper,[1] we determined thermodynamic values of ion exchange of trivalent metal complex ions and pointed out that heats and entropies of ion exchange, which are related to the interaction of these ions with water, are functions of polarization charge densities at the surface of these ions. On the other hand, several investigators have reported affinities of some singly charged cobalt(III) complex ions against ion exchange resins.[2-4] However, the thermodynamics of these ion exchange reactions have not yet been studied. In this paper, thermodynamic values of ion exchange of singly charged cobalt(III) complex ions on Dowex AG 50W-X2 are determined and interactions of these ions with water are discussed.

Experimental

Materials. The poly(styrenesulfonic acid) cation exchange resin (Dowex AG 50W-X2, 50—100 mesh, Bio Labo.) was obtained in the sodium form after conditioning, and dried in air current. Cobalt(III) complex chlorides were prepared by the literature methods.[5,6]

Equilibrium Measurements. Batch method was employed to measure the selectivity coefficient; 0.2 g of sodium form resin was equilibrated with 40 cm^3 of 0.04 mol dm^{-3} mixed salt solution containing the complex and sodium chlorides of several compositions (ionic strength of equilibrium solution is 0.04). Equilibration was achieved within a few hours by agitating at 25±0.1 °C. Concentrations of complex and sodium ions in aqueous phase were determined from optical absorbance and from radioactivity of ^{22}Na, respectively.

Heat of Exchange. A twin type conduction calorimeter of a commercial model (Lesca Co., Tokyo, CM-204S) was employed to measure the heat of ion exchange; 0.2—1.0 g of sodium form resin was weighed into sample holding tubes of sample and reference calorimeters, and then added 5 cm^3 of water to eliminate the heat of swelling, while 40 cm^3 of 0.05 mol dm^{-3} salt solution and water were introduced into the sample and reference cells. After thermal equilibrium, the resins in sample holding tubes were mixed with the salt solution and water in the cells. The heat evolved was recorded as a differential electromotive force.

Results and Discussion

The selectivity coefficient of ion exchange, $X^+ + NaR = Na^+ + XR$, can be defined as

$$K_c' = N_X m_{Na} / N_{Na} m_X,$$

where N and m are the mole fraction in resin and the molality of solution of subscript ions, X^+ and Na^+, respectively. Selectivity coefficients plotted against the mole fraction of complex ion in resin (*i.e.*, Kielland plots) are shown in Fig. 1. All of the Kielland plots are nearly linear. The preferential uptake of $[Co(en)_2(NO_2)_2]^+$, $[Co(en)_2(NCS)_2]^+$, $[Co(NH_3)_4(NO_2)_2]^+$, and $[Co(dmgH)_2(NH_3)_2]^+$ increases with increasing mole fraction of these ions in resin, that is, the slope of Kielland plots of these ions is positive. This trend can be explained in terms of the cluster formation of these ions and resin matrix.[7,8]

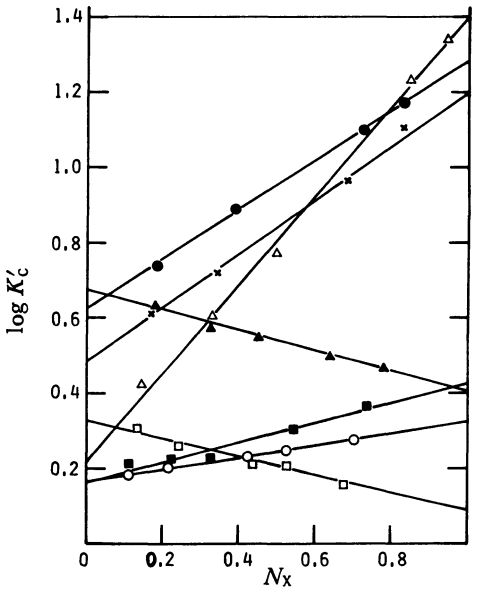

Fig. 1. Selectivity coefficients as functions of ionic compositions in resin.
●: *cis*-$[Co(en)_2(NO_2)_2]^+$, ○: *trans*-$[Co(en)_2(NO_2)_2]^+$, ▲: $[Co(en)_2CO_3]^+$, △: *cis*-$[Co(en)_2(NCS)_2]^+$, ×: *cis*-$[Co(NH_3)_4(NO_2)_2]^+$, ■: $[Co(dmgH)_2(NH_3)_2]^+$, □: $[Co(dmgH)_2(C_2H_5NH_2)_2]^+$.

The free energy $\Delta G°$ and entropy $\Delta S°$ of ion exchange are calculated by

$$\Delta G° = -RT\int_0^1 \ln K_c'[\gamma(Na^+)/\gamma(X^+)]dN_X$$

$$\Delta G° = \Delta H° - T\Delta S°.$$

Since the ionic strength of aqueous phase is sufficiently low (0.04), the values of $\gamma(Na^+)/\gamma(X^+)$ are approximated to 1. Standard heats of exchange $\Delta H°$ are approximated to heats of exchange ΔH, since the heat content terms are small. Thermodynamic values of ion exchange are

Table 1. Thermodynamic values of ion exchange for $A^+ + NaR = AR + Na^+$ on Dowex AG 50W-X2 at 25 °C (I=0.04)

Cation	$\Delta G°$	$\Delta H°$	$\Delta S°$
	kJ mol^{-1}	kJ mol^{-1}	J K^{-1} mol^{-1}
cis-$[Co(NH_3)_4(NO_2)_2]^+$	−4.81	−11.92	−23.8
cis-$[Co(en)_2(NO_2)_2]^+$	−5.52	−8.99	−11.7
trans-$[Co(en)_2(NO_2)_2]^+$	−1.38	−3.77	−8.0
trans-$[Co(en)_2(NCS)_2]^+$	−4.39	−8.74	−14.6
$[Co(en)_2CO_3]^+$	−3.05	−5.61	−8.4
$[Co(dmgH)_2(NH_3)_2]^+$	−1.67	−1.59	+0.4
$[Co(dmgH)_2(C_2H_5NH_2)_2]^+$	−1.17	+3.14	+14.6

presented in Table 1.

The exothermic heats cause the preferential uptake of $[Co(NH_3)_4(NO_2)_2]^+$ and $[Co(en)_2B_2]^+$ (Table 1). This trend can be explained in terms of strong interaction between these ions and resin matrix. *cis*-$[Co(en)_2(NO_2)_2]^+$ has a larger dipole moment than *trans*-$[Co(en)_2(NO_2)_2]^+$. This causes the more exothermic heat and stronger affinity of the former than those of the latter.

It was recognized that ions are classified into three groups on the basis of ion-water interaction: (a) Electrostrictive structure makers such as Na^+, (b) structure breakers such as Cs^+, and (c) hydrophobic structure makers.[9,10] Since the structure maker increases the structural order of water near itself, its removal from aqueous phase gives a positive entropy. Furthermore, as an ion of the same charge becomes more structure making, the water content of its form resin increases, that is, the extent of dehydration of ion by transfer from the aqueous to resin phase decreases.[1,11-13] These facts suggest that the sign and magnitude of the entropy of ion exchange gives a reliable indication of the structure altering property of an ion.

Table 1 shows that the values of $\Delta S°$ for $[Co(dmgH)_2B_2]^+$ are positive and they become more positive with alkyl chain. A similar behaviour was shown in ion exchanges of tetraalkylammonium ions.[13] The alkyl (hydrophobic) groups of the dmgH ligands are in contact with water. Furthermore, the dmgH ligands coordinated in plane are hydrogen bonded with one another and therefore, the anionic groups are not localized. These facts suggest that $[Co(dmgH)_2B_2]^+$ has a hydrophobic structure making property which causes its preferential uptake against the resin.

The values of $-\Delta S°$ of $[Co(en)_2B_2]^+$ and $[Co(NH_3)_4(NO_2)_2]^+$ are larger than that of Cs^+ with Na^+ on Dowex 50 (2% DVB).[12] This fact shows that $[Co(en)_2B_2]^+$ and $[Co(NH_3)_4(NO_2)_2]^+$ are structure breakers. Interestingly, it has been shown that $[Co(en)_3]^{3+}$ is a hydrophobic structure maker.[10] Water dipoles near an anion are oriented in the opposite direction to those near a cation. Therefore, the water structure near anion ligands of $[Co(en)_2B_2]^+$ should be disturbed in a wide range. Thus, $[Co(en)_2B_2]^+$ as well as $[Co(NH_3)_4(NO_2)_2]^+$ acts as a structure breaker. The order of structure breaking tendencies of $[Co(en)_2B_2]^+$ is $NCS^- > NO_2^- > CO_3^{2-}/2$. This order seems to accord with the structure breaking tendencies of these anions. *cis*-$[Co(NH_3)_4(NO_2)_2]^+$ is more structure breaking than *cis*-$[Co(en)_2(NO_2)_2]^+$, since $-\Delta S°$ of the former is larger than that of the latter. This trend accords with the relation between $[Co(NH_3)_6]^{3+}$ and $[Co(en)_3]^{3+}$.[1]

References

1) K. Kurotaki and S. Kawamura, *J. Chem. Soc., Faraday Trans. 1*, **75**, 925 (1979).

2) E. L. King and R. R. Walter, *J. Am. Chem. Soc.*, **74**, 4471 (1952).

3) M. Mori, M. Shibata, and J. Azami, *Nippon Kagaku Zasshi*, **76**, 1003 (1955).

4) M. Mori, M. Shibata, and M. Nanasawa, *Bull. Chem. Soc. Jpn.*, **29**, 947 (1956).

5) "Shin Jikken Kagaku Kohza," ed by the Chemical Society of Japan, Maruzen, Tokyo (1977), Vol. 8.

6) R. Tsuchida, H. Yoneda, and S. Kida, "Muki Busshitsu Seiho," Nikkan Kogyo Shinbun, Tokyo (1962).

7) F. Helfferich, "Ion Exchange," McGraw-Hill, New York (1962), p. 174.

8) H. P. Gregor, L. Belle, and R. A. Marcus, *J. Am. Chem. Soc.*, **77**, 2713 (1955).

9) H. S. Frank, *Z. Phys. Chem. (Leipzig)*, **228**, 365 (1965).

10) K. Kurotaki and S. Kawamura, *J. Chem. Soc., Faraday Trans. 1*, **77**, 217 (1981).

11) D. S. Flett and P. Meares, *Trans. Faraday Soc.*, **62**, 1469 (1966).

12) G. E. Boyd, F. Vaslow, and S. Lindenbaum, *J. Phys. Chem.*, **68**, 590 (1964).

13) G. E. Boyd and Q. V. Larson, *J. Am. Chem. Soc.*, **89**, 6038 (1967).

The Gibbs Free Energy of the Formation of the $Al(OH)_4^-$ Ion at Elevated Temperatures

Byong-Tae CHANG
Department of Chemistry, Faculty of Science, Korea University, Kodaira, Tokyo 187
(Received July 16, 1981)

Synopsis. The Gibbs free energy of the formation of the $Al(OH)_4^-$ ion, $\Delta G_f^\circ[Al(OH)_4^-]$, has been determined from the solubility data of alumina hydrates at temperatures up to 300 °C. According to the results of thermodynamical calculations, $\Delta G_f^\circ[Al(OH)_4^-]$ is -1305.3 kJ/mol at 25 °C, and it decreases almost linearly with an increase in the temperature. Its temperature dependence between 25 and 300 °C can be expressed as follows: $\Delta G_f^\circ[Al(OH)_4^-] = -1152.7 - 3.318T - 5.64\times10^{-4}T^2 + 1.202T\log T$.

The Gibbs free energy of the formation of the $Al(OH)_4^-$ ion, $\Delta G_f^\circ[Al(OH)_4^-]$, is very important in understanding thermodynamically the alumina production by the Bayer process, the aqueous geochemistry of aluminous minerals, and the corrosion of aluminum in alkaline solutions. Previously, various values for $\Delta G_f^\circ[Al(OH)_4^-]$ at 25 °C have been reported by many investigators.[1-6] Unfortunately, these values are very discrepant, ranging from -1297.2 to -1314.2 kJ/mol. Furthermore, $\Delta G_f^\circ[Al(OH)_4^-]$ at elevated temperatures has not yet been presented. The alumina extraction from bauxite and the formation of alumina minerals proceed usually at a high temperature. It is, therefore, important to know $\Delta G_f^\circ[Al(OH)_4^-]$ at high temperatures.

The present author previously determined the ionic solubility products, K_s, of gibbsite[7] and boehmite[8] in the alkaline pH range by applying an extending Debye-Hückel equation to their solubility data in NaOH solutions. The purpose of this paper is to determine $\Delta G_f^\circ[Al(OH)_4^-]$ at temperatures from 25 to 300 °C, based on K_s°.

The dissolution processes of alumina hydrates are given by the following equations:

a) For gibbsite,

$$Al(OH)_3(s) + H_2O(l) = Al(OH)_4^-(l) + H^+(l), \quad (1)$$

$$K_{s,1}^\circ = a_{Al}a_H/a_w, \quad (2)$$

$$\Delta G_1^\circ = -RT\ln K_{s,1}^\circ. \quad (3)$$

b) For boehmite,

$$AlOOH(s) + 2H_2O(l) = Al(OH)_4^-(l) + H^+(l), \quad (4)$$

$$K_{s,2}^\circ = a_{Al}a_H/a_w^2, \quad (5)$$

$$\Delta G_2^\circ = -RT\ln K_{s,2}^\circ, \quad (6)$$

where a_{Al}, a_H, and a_w are the activities of $Al(OH)_4^-$, H^+ ions, and water, and where ΔG_1° and ΔG_2° are the Gibbs free energy changes in Reaction 1 and 4 respectively.

The temperature dependences of log K_s° can be expressed throughout the temperature range as follows:

a) For gibbsite,

$$\log K_{s,1}^\circ = -22.11 - 3.368\times10^{-3}T - 5835.9/T + 6.390\ln T. \quad (7)$$
$$(313.2 \leq T \leq 443.2\ K)$$

b) For boehmite,

$$\log K_{s,2}^\circ = -29.64 - 8.149\times10^{-3}T - 2263.0/T + 4.3721\ln T. \quad (8)$$
$$(353.2 \leq T \leq 573.2\ K)$$

The above equations are the results of the least-square treatment of the data for K_s° obtained in Refs. 7 and 8.[9]

According to Eq. 1 or 4,

$$\Delta G_f^\circ[Al(OH)_4^-]_1 = \Delta G_1^\circ + \Delta G_f^\circ[Al(OH)_3] + \Delta G_f^\circ(H_2O) - \Delta G_f^\circ(H^+), \quad (9)$$

$$\Delta G_f^\circ[Al(OH)_4^-]_2 = \Delta G_2^\circ + \Delta G_f^\circ(AlOOH) + 2\Delta G_f^\circ(H_2O) - \Delta G_f^\circ(H^+). \quad (10)$$

The Gibbs free energy of the formation of a substance for which heat capacity data are available can be calculated by the usual thermodynamical method. For gibbsite, boehmite, and water, highly accurate heat capacity data have been presented in the literature.[10,11] It is most important and most difficult to evaluate $\Delta G_f^\circ(H^+)$ exactly at high temperatures. In this paper, the $\Delta G_f^\circ(H^+)$ values were calculated approximately by using the "correspondence principle" presented by Criss and Cobble.[12] They demonstrated that reliable estimates of "absolute" (*i.e.* "third law") ionic entropies and heat capacities can be made using their correspondence principle.

The thermodynamic data necessary to evaluate ΔG_f° are listed in Table 1. It should be noted that an ionic entropy of the hydrogen ion at 25 °C, which is usually defined as zero based on the conventional scale, was assigned to 20.92 J/K mol according to the correspondence principle.

TABLE 1. SELECTED STANDARD THERMODYNAMIC DATA FOR GIBBSITE, BOEHMITE, WATER, AND HYDROGEN IONS

Substance	$\Delta G_{f,298}^\circ$ / kJ mol^{-1}	S_{298}° / J K^{-1} mol^{-1}	c_p° / J K^{-1} mol^{-1}
$Al(OH)_3$	-1154.9 [a]	68.44 [a]	$81.57+0.101T-1.75\times10^6T^{-2}$ [c]
AlOOH	-915.0 [b]	48.45 [a]	$53.99+8.66\times10^{-2}T-1.26\times10^6T^{-2}$ [c]
$H_2O(l)$	-237.2	69.91	
$H^+(l)$	0	-20.92	

a) From Ref. 5. b) From Ref. 4. c) From Ref. 10.

Table 2. The Gibbs free energies of formation for gibbsite, boehmite, water, H^+, and $Al(OH)_4^-$ ions at elevated temperatures

	$\Delta G^\circ_{f,T}$/kJ mol^{-1}						
T/K	298.15	333.15	373.15	423.15	473.15	523.15	573.15
$Al(OH)_3$	−1154.9	−1157.6	−1160.9	−1165.8	—	—	—
AlOOH	−915.0	−916.8	−919.2	−922.7	−926.7	−931.1	−936.0
$H_2O(l)$	−237.2	−239.8	−243.1	−247.7	−252.7	−258.1	−263.9
$H^+(l)$	0	0.5	0.6	−0.3	−2.6	−6.0	−10.1
$Al(OH)_4^-$ a)	−1304.7	−1310.3	−1315.5	−1320.0	—	—	—
$Al(OH)_4^-$ b)	−1305.2	−1309.2	−1314.2	−1320.7	−1326.8	−1332.6	−1338.7

a) $\Delta G^\circ_f[Al(OH)_4^-]_1$ obtained from Eq. 9. b) $G^\circ_f[Al(OH)^\circ_4]_2$ obtained from Eq. 10.

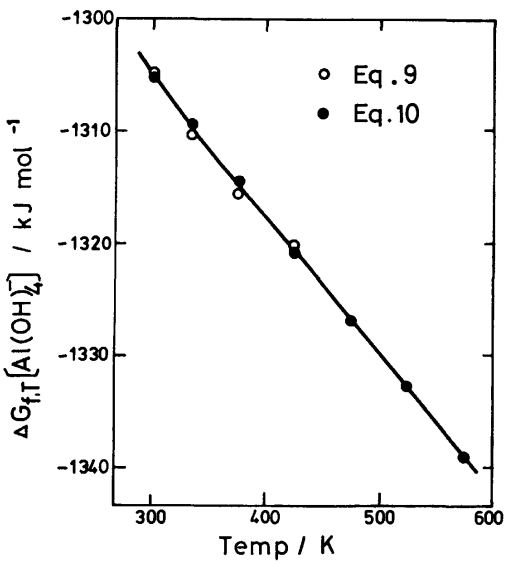

Fig. 1. Temperature dependence of the Gibbs free energy of formation for $Al(OH)_4^-$ ion at temperatures between 25 and 300 °C.

Table 2 gives the results of calculation of the free energies of formation at elevated temperatures for the species in Table 2. The $\Delta G^\circ_f(H_2O)$ values at high temperatures were obtained using the heat capacities of pure water[11] under its saturated vapor pressure at each temperature above 100 °C.

In the temperature range from 25 to 150 °C, $\Delta G^\circ_f[Al(OH)_4^-]_1$ and $\Delta G^\circ_f[Al(OH)_4^-]_2$ are consistent with each other within 1.3 kJ/mol. As is shown in Fig. 1, $\Delta G^\circ_f[Al(OH)_4^-]$ decreases almost linearly with the increase in the temperature; its temperature dependence between 25 and 300 °C can be expressed, after the least-square treatment, as follows:

$$\Delta G^\circ_f[Al(OH)_4^-] = -1152.7 - 3.318\,T - 5.64 \times 10^{-4}T^2 + 1.202\,T\log T. \quad (11)$$

The value of $\Delta G^\circ_f[Al(OH)_4^-]$ at 25 °C is −1305.3 kJ/mol, which agrees very well with the value of −1305 kJ/mol recently reported by Hemingway.[5]

References

1) M. Pourbaix, "Atlas of Electrochemical Equilibria," Pergamon, Oxford (1964).
2) J. A. Kittrick, *Proc. Soil Sci. Am.*, **30**, 595 (1966).
3) D. D. Wagman, W. H. Evans, V. B. Parker, I. Halow, S. M. Baily, and R. H. Schumm, *U. S. Natl. Bur. Stand. Tech. Note*, 270—273 (1968).
4) G. A. Parks, *Am. Mineral.*, **57**, 1163 (1972).
5) B. S. Hemingway, R. A. Robie, and J. A. Kittrick, *Geochem. Cosmochim. Acta*, **42**, 1553 (1978).
6) H. M. May, P. A. Helke, and M. L. Lackson, *Geochim. Cosmochim. Acta*, **43**, 861 (1979).
7) B.-T. Chang, *Bull. Chem. Soc. Jpn.*, **54**, 1960 (1981).
8) B.-T. Chang, *Bull. Chem. Soc. Jpn.*, **54**, 2579 (1981).
9) In Refs. 7 and 8, the temperature dependences of K°_s have been expressed, using a linear relationship between log K°_s and $1/T$, in the temperature ranges of 40—110 °C for gibbsite and 80—250 °C for boehmite. In order to improve their approximation over the whole temperature range, an equation form such as Eqs. 7 and 8 was used in this paper.
10) Y. Takahashi, K. Yamada, T. Fukunaga, and T. Mukaibo, *Denki Kagaku*, **41**, 287 (1973).
11) "Kagaku Binran," ed by the Chem. Soc. Jpn., Maruzen (1958), pp. 686—687.
12) C. M. Criss and J. W. Cobble, *J. Am. Chem. Soc.*, **86**, 5385, 5390 (1964).

Effect of Polymorphic Transition on Molecular Diffusion in Some Molecular Complexes, as Evidenced by Exchange Reaction Rate and by Electrical Resistivity

Tamotsu INABE and Yoshio MATSUNAGA*
Department of Chemistry, Faculty of Science, Hokkaido University, Sapporo 060
(Received October 29, 1981)

Synopsis. Marked increases in electron donor and acceptor-exchange reaction rates and also large differences in the temperature dependence of the electrical resistivity of polycrystalline compactions between the first and the second heating processes indicate the enhanced molecular diffusion near and above the polymorphic transition temperatures of some molecular complexes.

The appearance of isomorphous high-temperature forms upon polymorphic transitions in over twenty molecular complexes consisting of aromatic hydrocarbons and various electron acceptors has been ascribed to the onset of molecular rotation.[1] In this connection, these complexes bear some similarity to plastic crystals, which are composed of globularly shaped and orientationally disordered molecules. As plastic crystals are known to show diffusion coefficients approximately 10^4 times higher than normal crystals when compared at their melting points,[2] an appreciable increase of the translational mobility upon the transitions might be expected for the above-mentioned molecular complexes. Attempts were made to follow such changes in some selected complexes by measurements of electron donor and acceptor-exchange reaction rates covering the transition temperature and also by comparison of the electrical resistivity of polycrystalline compactions between the first and the second heating processes.

The following three 1 : 1 complexes seemed to suit the study of the exchange reactions because of their relatively low transition temperatures and large entropy changes: pyrene-2,4-dinitrotoluene (Py–DNT), 53.5 °C, 37 J mol^{-1} K^{-1}; pyrene-2,4,6-trinitrotoluene (Py–TNT), 59 °C, 36 J mol^{-1} K^{-1}; fluoranthene-2,4,6-trinitrochlorobenzene (Fl–TNC), 54 °C, 54 J mol^{-1} K^{-1}. The acceptors employed for the exchange reactions were 2,4,7-trinitrofluorenone (TNF) and 4,6-dinitrobenzofuroxan (DNBF). They are stronger as acceptors than any in the complexes and have melting points higher than those of the complexes. Because of the former condition, the complex formed by the exchange reaction gives a charge-transfer absorption band in a region separated from that of the original complex. The latter condition was expected to mean that the molecules in the added component compound would be less mobile than those in the complex. The donor-exchange reaction was examined with the combination of Fl–TNC and Py. Py is stronger as a donor than Fl and its melting

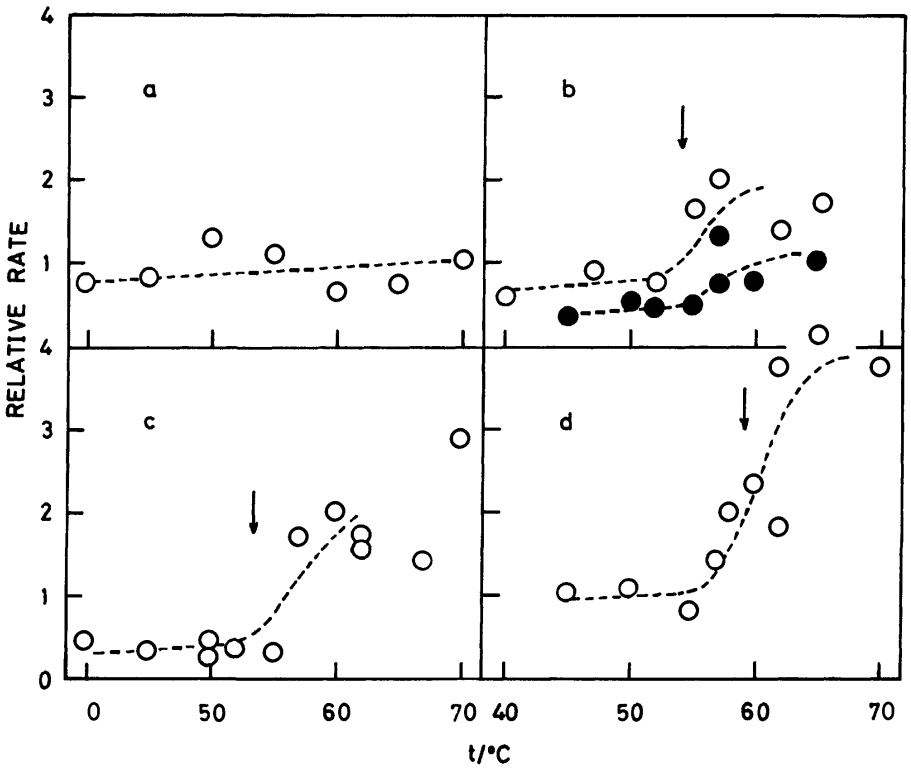

Fig. 1. Relative rates of the exchange reactions between (a) fluoranthene-3-nitrophthalic anhydride and 4,6-dinitrobenzofuroxan, (b) fluoranthene-2,4,6-trinitrochlorobenzene and 4,6-dinitrobenzofuroxan (○) or pyrene (●), (c) pyrene-2,4-dinitrotoluene and 2,4,7-trinitrofluorenone, and (d) pyrene-2,4,6-trinitrotoluene and 2,4,7-trinitrofluorenone.

point is higher than that of Fl–TNC.

The complex and the component compound to be added to the complex were separately ground, and then mixed in a weight ratio of 45 : 1 by grinding for short time. The mixed powdered sample, packed into a holder for reflectance measurements, was kept in a thermostat. The spectrum was recorded at intervals of 10 to 120 min by means of a Beckman DK 2A spectro-reflectometer. The intensity (I) of the new charge-transfer band estimated by the Kubelka-Munk function was considered to be proportional to the concentration of the complex formed by the exchange reaction. The ratio was chosen to make the final reflectance not less than 20%. The plot of $\ln I/(I_\infty - I)$ against the reaction time gave a straight line at each temperature. The slope naturally depends on the absorption coefficient of the charge-transfer band; therefore, it may be taken as a measure of the reaction rate only for each complex.

In order to check the reliability of the procedure, the reaction between Fl–3-nitrophthalic anhydride and DNBF was studied. This complex exhibits no polymorphic transition in the measured temperature range and has a melting point lower than that of DNBF (136 °C *vs.* 172 °C). The rate appears to increase slightly by raising the temperature (see Fig. 1a). The results obtained with Fl–TNC complex are presented in Fig. 1b. Although the measured rates are rather scattered, one can clearly see an increase near and above the transition temperature indicated by the vertical arrow. Similar and more pronounced changes were observed with the reactions between the Py complexes and TNF shown in Figs. 1c and 1d.

The increase of reactivity during polymorphic transition has been noted by Hedvall.[3] He reported many examples demonstrating that the transition temperature or the temperature range coincides with the maximum reactivity. The explanation given by him is the appearance of unstable and highly-reactive transitional states during the transition. No such maximum rate could be found in the present cases; however, the observed rate increase is undoubtedly indicative of enhanced molecular diffusion upon the transition of the complex.

The electrical resistivity of polycrystalline compactions of the five complexes in this group examined earlier showed an abrupt decrease in the transition temperature range.[4] This observation resembles that made for some plastic crystals by Swiatkiewicz and Pigon.[5] Now, we wish to report that the behavior in the first heating process can be quite different from that described before if the compaction is made of a thoroughly powdered sample. The best example was provided with the Fl–2,4,6-trinitrophenol complex, which is transformed into the isomorphous form at 93.5 °C with an entropy of 42 J mol^{-1} K^{-1}. As is shown in Fig. 2, an encrease of the resistivity by a factor of about five was found in the first run just below the transition temperature. On the other hand, the change in the second heating process is normal and reproducible. The decrease in the transition temperature range is as much as by a factor of twenty. The marked difference between the two

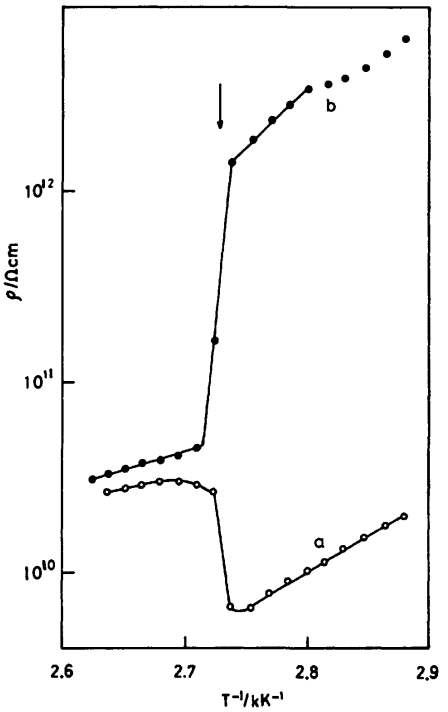

Fig. 2. Electrical resistivity changes of a polycrystalline compaction of fluoranthene-2,4,6-trinitrophenol during (a) the first heating process and (b) the second heating process.

runs can be explained if one assumes that the conduction in the compaction, which is not yet heated to the transition temperature, predominantly arises from surface current. Then, the resistivity increase near the transition temperature may be attributed to the decrease of the surface area by rapid recrystallization due to the enhanced molecular diffusion. The electrical behavior observed in the second run reflects the bulk property of the complex. Similar but less drastic changes have been recorded with the following complexes: Fl–TNC, Fl–TNT, and Fl–4-nitrophthalic anhydride. The anomalous change near the transition temperature has been reported in the work of Swiatkiewicz and Pigon on plastic crystals, and has been ascribed also to the recrystallization.

The present work was partly supported by a Grant-in-Aid for Scientific Research No. 543001 from the Ministry of Education, Science and Culture.

References

1) T. Inabe, Y. Matsunaga, and M. Nanba, *Bull. Chem. Soc. Jpn.*, **54**, 2557 (1981).

2) J. N. Sherwood, *Bull. Soc. Fr. Mineral. Cristallogr.*, **95**, 253 (1972).

3) J. A. Hedvall, "Solid State Chemistry," Elsevier Publ. Co., Amsterdam, London, New York (1966), pp. 28—34.

4) N. Inoue and Y. Matsunaga, *Bull. Chem. Soc. Jpn.*, **51**, 90 (1978).

5) J. Swiatkiewicz and K. Pigon, *Acta Phys. Pol. A*, **53**, 165 (1978).

Liquid Crystal Formation in Binary Systems. VI.[1] Smectic Liquid Crystals Induced in *N*-[4-(Diethylamino)benzylidene]-4-ethoxyaniline-*N*-(4-Nitrobenzylidene)-4-ethoxyaniline and Related Systems

Kotaro ARAYA, Noriko HOMURA, and Yoshio MATSUNAGA*
Department of Chemistry, Faculty of Science, Hokkaido University, Sapporo 060
(Received October 29, 1981)

Synopsis. The replacement of the dimethylamino group in the combinations of the 4-dimethylamino-4-alkoxy and 4-nitro-4-alkoxy derivatives of *N*-benzylideneaniline by a diethylamino group favors the induction of smectic phases in their mixtures.

In Part II of this series, we described the induction of nematic and smectic liquid crystals by mixing electron donors and acceptors of the type 4-X-C_6H_4-CH=N-C_6H_4-Y-4.[2] The donor molecules had a dimethylamino group as X or Y, while the acceptor molecules had a nitro group as X or Y. The substituents on the remaining ends were methoxyl, ethoxyl, or propoxyl groups. The stabilization of mesophases in these binary mixtures was ascribed to the parallel molecular arrangement achieved by an electron donor-acceptor interaction.

In order to obtain a better understanding of the relations between the induction of liquid crystals and molecular structure, systematic studies of the effects of substituents are obviously important. As the first step along this line, we wish to report on the liquid crystals induced by mixing the diethylamino and nitro derivatives of *N*-benzylideneaniline.

N-[4-(Diethylamino)benzylidene]-4-alkoxyanilines, hereafter abbreviated (Et_2N, RO), and *N*-(4-alkoxybenzylidene)-4-(diethylamino)anilines, (RO, Et_2N) were prepared by the condensation reaction between appropriate benzaldehyde and aniline, and had the following melting points: (Et_2N, MeO) 100 °C, (MeO, Et_2N) 89.5 °C, (Et_2N, EtO) 106 °C, (EtO, Et_2N) 107 °C, (Et_2N, PrO) 110 °C, and (PrO, Et_2N) 98.5 °C. The nitro derivatives were similarly prepared. The measurements were carried out as described in our earlier works.[1,2]

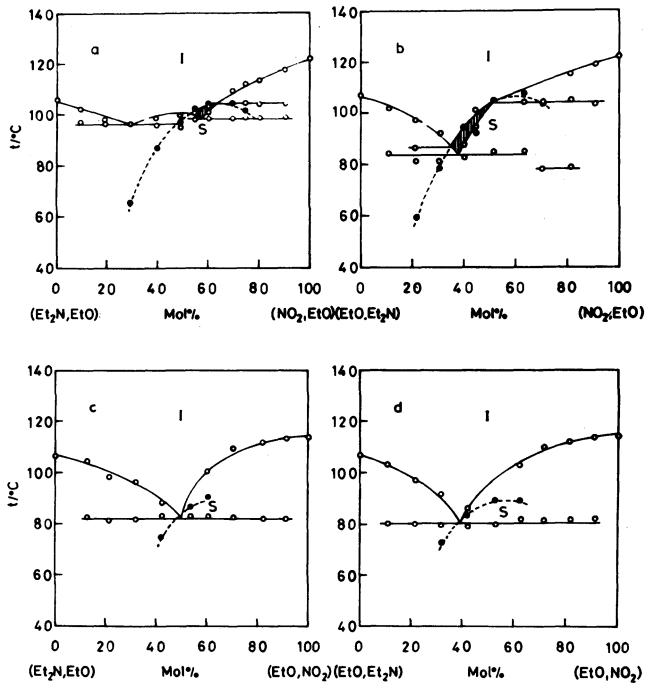

Fig. 1. Phase diagrams of (a) (Et_2N, EtO)-(NO_2, EtO), (b) (EtO, Et_2N)-(NO_2, EtO), (c) (Et_2N, EtO)-(EtO, NO_2), and (d) (EtO, Et_2N)-(EtO, NO_2) systems. The open and shaded circles are transitions recorded in the processes of heating and cooling respectively.

No liquid crystal could be found in the systems consisting of the methoxy derivatives. The results are in sharp contrast to the observation that the induction of nematic liquid crystals occurs with the corresponding dimethylamino compounds. As the diethylamino group is known to be less efficient in promoting nematic liquid crystals than the dimethylamino group,[3] the absence of nematic liquid crystals in the present systems may not be unexpected.

Figure 1 indicates that all the four combination of the ethoxy derivatives can induce smectic liquid crystals. The (Et_2N, EtO)-(NO_2, EtO) system produces a 1 : 1 solid complex which melts congruently at 100.5 °C. The induced mesophase is stable between 53 and 64 mol% of (NO_2, EtO) but it is observable as a metastable phase in a much wider range: from 20 to 75 mol%. The isotropic liquid-smectic liquid crystal (I-S) transition temperature at the former composition is as low as 65 °C. An incongruently melting complex, possibly of the 1 : 2 mole ratio, is found in the phase diagram of the (EtO, Et_2N)-(NO_2, EtO) system. The I-S transition curve meets the freezing point curve of the donor compound at 86.5 °C and 35 mol% of (NO_2, EtO) and that of the acceptor compound at a point which is not distinguishable from the peritectic point located at 104 °C and 51 mol%. The maximum lies at 106 °C and near 60 mol%.

The combination of (Et_2N, EtO) and (EtO, NO_2) gives a diagram of the eutectic type. The mesophase is observed in the range from 40 to 60 mol% and is metastable with the possible exception of a very small area near the eutectic point: 82 °C and 50 mol%. No solid complex is formed in the (EtO, Et_2N)-(EtO, NO_2) system. The induced smectic phase seems to be wholly metastable but covers a range wider than that in the (Et_2N, EtO)-(EtO, NO_2) system. The I-S transition curve passes through the eutectic point located at 81.5 °C and 39 mol% of (EtO, NO_2) and reaches the maximum at 89 °C and about 57 mol%.

We reported earlier the formation of congruently melting solid complexes in both the (Me_2N, EtO)- and (EtO, Me_2N)-(NO_2, EtO) systems and that of an

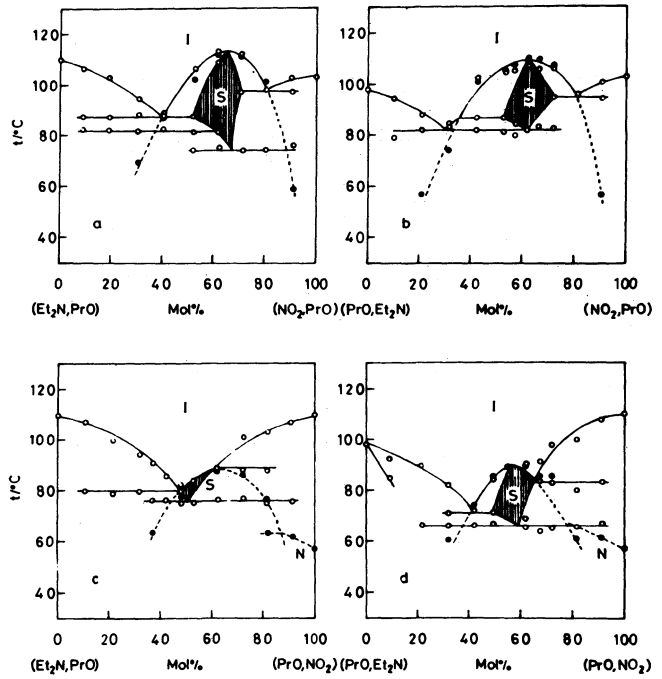

Fig. 2. Phase diagrams of (a) (Et_2N, PrO)–(NO_2, PrO), (b) (PrO, Et_2N)–(NO_2, PrO), (c) (Et_2N, PrO)–(PrO, NO_2), and (d) (PrO, Et_2N)–(PrO, NO_2) systems. As to the open and shaded circles, see the caption of Fig. 1.

incongruently melting one in the (EtO, Me_2N)–(EtO, NO_2) system and also the induction of nematic liquid crystals with all the combinations.[2] Thus, smectic mesophases appear to be markedly stabilized by the introduction of a diethylamino group instead of a dimethylamino group into the donor molecules, while nematic mesophases and solid complexes are destabilized.

As is shown in Fig. 2, the solid complex in the (Et_2N, PrO)–(NO_2, PrO) system has the composition of a 1 : 1 mole ratio and ceases to exist at 81.5 °C, giving a peritectic point at 62 mol% of (NO_2, PrO). A stable smectic liquid crystal appears in the composition range from 40 to 81 mol% and the maximum temperature of 114 °C is found at 65 mol%. The mesophase coexists with the isotropic melt except for the hatched area. The eutectic point is at 74 °C and 67 mol%. The diagram of the (PrO, Et_2N)–(NO_2, PrO) system is of the eutectic type. The I-S transition curve intersects the freezing point curve of (NO_2, PrO) at 86.5 °C and 36 mol% and at 95 °C and 81 mol%. The maximum is found at 109 °C and 62 mol%. The combination of (Et_2N, PrO) and (PrO, NO_2) also gives a diagram of the eutectic type. The maximum stabilization of the induced smectic phase is achieved at the intersection between the I-S transition curve and the freezing point curve of the acceptor compound: 89 °C and 62 mol% of (PrO, NO_2). As the melt of this acceptor compound can be supercooled to the latent I-N transition temperature (57.5 °C), the induction of the nematic liquid crystal is observable above 87 mol%. The (PrO, Et_2N)–(PrO, NO_2) system produces no solid complex. The I-S transition curve meets the freezing point curve of the donor compound at 71 °C and 41 mol% of (PrO, NO_2) and that of the acceptor compound at 83 °C and 66 mol%.

It must be emphasized that the tendencies noted with the ethoxy derivatives are more pronounced with the propoxy derivatives. First of all, the four systems of the corresponding dimethylamino compounds produce solid molecular complexes stable up to their own melting points, while only the (Et_2N, PrO)–(NO_2, PrO) system can form a solid complex with a limited stability. On the other hand, the induced smectic phases are stable in all the systems of the present compounds, contrary to those induced with the dimethylamino compounds, which are entirely metastable.

The present work was partly supported by a Grant-in-Aid for Scientific Research No. 543001 from the Ministry of Education, Science and Culture.

References

1) Part V: K. Araya and Y. Matsunaga, *Bull. Chem. Soc. Jpn.*, **55**, 1710 (1982).

2) K. Araya and Y. Matsunaga, *Bull. Chem. Soc. Jpn.*, **53**, 3079 (1980).

3) J. S. Dave and R. A. Vora, "Liquid Crystals and Plastic Crystals," ed by G. W. Gray and P. A. Winsor, E. Horwood, Chichester (1974), Vol. 1, p. 159.

The Determination of the Ratio of Two Kinds of Hydrogen in Metal Hydrides by Means of Pulsed NMR

Shigenobu HAYASHI,* Kikuko HAYAMIZU, and Osamu YAMAMOTO
National Chemical Laboratory for Industry, Tsukuba, Ibaraki 305

(Received November 19, 1981)

Synopsis. A method is proposed by which the composition of the two kinds of hydrogen with different diffusional behavior in metal hydrides can be determined accurately by means of ^{1}H NMR; using the method, it is found that the energy difference between the two sites occupied by the two kinds of hydrogen is 7.9 kJ/mol in $VH_{0.77}$.

Metal-hydrogen alloys have recently attracted much attention as hydrogen-storage materials because they can absorb and desorb large amounts of hydrogen reversibly; many studies have been performed by various methods.[1)]

A number of phases have been observed in the metal-hydrogen systems; they are called α-, β-, and γ-phases, and so on. There exist, in most of the hydrides, wide two phase regions, where at least two kinds of hydrogen are observed by means of ^{1}H NMR spectroscopy.[2)] Even if the metal lattice is in a single phase, the existence of several kinds of hydrogen is occasionally observed within a limited temperature range. It was observed by continuous-wave (cw) NMR spectroscopy that hydrogen in the hydrides of the Va group metals consists of two components in the β-phase at about 160 K;[3–5)] the same is true of hydrogen in $ZrH_{1.99}$ at about 440 K.[6)] The nature of each component is almost unknown, and, thus far, no quantitative investigations have been made of the concentration of each component. In metal-hydrogen alloys, the existence of several kinds of hydrogen is common, and it is very important to determine the composition accurately. However, in solids it is difficult to determine the true composition accurately because of instrumental limitations.

In this paper we propose a method for accurately determining the composition by means of pulsed NMR method, making use of the difference in the spin-spin relaxation times. Then, using the method, the concentrations of two kinds of hydrogen with different diffusional behavior which are observed in the β-phase of $VH_{0.77}$ are determined.

Experimental

Vanadium hydride, $VH_{0.77}$, was prepared by a reaction between vanadium metal and hydrogen gas in an autoclave. The synthesized sample was pulverized, passed through a 200-mesh screen, and sealed in a Pyrex glass ampoule.

The equipment used for the NMR measurements was a Bruker CXP-100 pulsed spectrometer whose 90° pulse width was about 1.5 μs. The measurements were performed at 55 MHz for the ^{1}H observation. The spectra were obtained by the Fourier-transformation of the free-induction decay (FID) after 90° -pulse, the solid-echo, and the spin-echo signals.

Results and Discussion

Figure 1 shows the ^{1}H Fourier-transformed (FT) NMR spectra of $VH_{0.77}$ at 133 K obtained by the spin-echo method. The spectra are assumed to be superpositions of two components with different linewidths. Similar superimposed spectra are also obtained by the FID and solid-echo methods. These superimposed spectra are observed at temperatures between 120 and 180 K. Above 180 K, motional narrowing occurs, after which the spectra appears to consist of only one component.

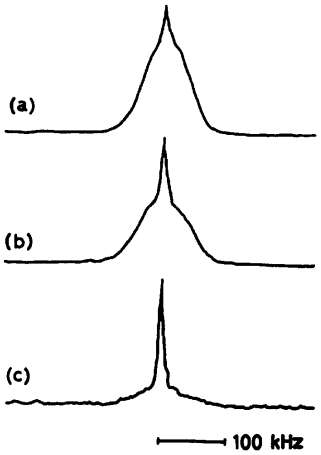

Fig. 1. FT-NMR spectra of ^{1}H in $VH_{0.77}$ at 133 K obtained by the spin-echo metod. The t_d values, which is twice the separation of the two pulses, are (a) 20 μs, (b) 30 μs, and (c) 50 μs, respectively.

The broader line is broadened mostly by the ^{1}H-^{51}V and ^{1}H-^{1}H dipole-dipole interaction, and then assumed to be Gaussian. The narrower line is assumed to be Lorentzian because it seems to be in the region of motional narrowing. The line separation is then carried out, assuming the above-mentioned line-shapes for each component. Thereafter, the ratio of the two components is obtained by integrating the area of each line. However, the ratio is not equal to the true ratio of the two kinds of hydrogen, for the line-shape of the spectra varies, depending on t_d, the time interval between the first 90°_x pulse and the beginning of the signal acquisition, as is shown in Fig. 1. The ratio of the narrower component (II) to the broader one (I) increases as t_d increases. The t_d dependence of the spectra can be explained by the well-known principles of pulsed NMR spectroscopy.[7)] The magnetization of the i-th component at the echo maximum, $M_i(t_d)$, is expressed as:

$$M_i(t_d) = M_i^\circ \exp(-t_d/T_{2i}), \quad (1)$$

where M_i° is the magnetization at $t_d=0$ and where T_{2i} is the spin-spin relaxation time of the i-th component. The observed magnetization is the sum of that of each component. Component I has a shorter T_2 than Component II, so $M_I(t_d)$ decreases faster than $M_{II}(t_d)$ as t_d increases. If we could make t_d equal to zero, the true ratio of the two kinds of hydrogen, M_{II}°/M_I°, could

be determined. This is generally impossible, however, because of instrumental limitations. The receiver cannot work for a short period, which is called "dead time," after a transmission of the radiofrequency pulse. For our equipment it is about 8 μs. The observed linewidth of the broader component in $VH_{0.77}$ is about 50 kHz, and the T_2 value is estimated to be 6 μs, which is comparable to the "dead time." However, $M_{II}^{\circ}/M_{I}^{\circ}$ can be determined by the extrapolation of $M_{II}(t_d)/M_{I}(t_d)$ to $t_d=0$, as is shown in Fig. 2. A very good linearity is obtained, and the slope is defined as a function of the two T_{2i} values.

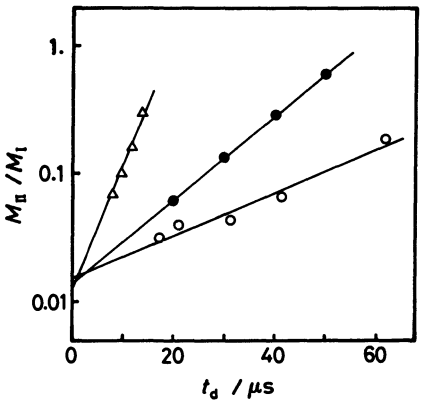

Fig. 2. The t_d dependence of the apparent ratio of the two components in $VH_{0.77}$ at 133 K.
○: Solid echo, ●: spin echo, and △: FID.

Similar t_d dependences of the line-shapes are observed by the other two methods, the solid-echo and the FID methods, as is shown in Fig. 2. The M_{II}/M_{I} values change exponentially with t_d, the slope being different in the three methods. In the solid-echo method, the magnetization of each component at the echo maximum decays with a time constant longer than T_2. The FID curve falls faster than the other two methods. If the line-shape of the FT spectra is of a Lorentzian type, the FID curve shows an exponential decay whose time constant is expressed as:

$$1/T_{2i}^{*} = 1/T_{2i} + \text{(magnetic inhomogeneity term)}. \quad (2)$$

While the broader component seems to be a Gaussian type in the present case of $VH_{0.77}$, it can be assumed to be approximately a Lorentzian type, as is shown in Fig. 2, for the linear extrapolation is possible and the extrapolated value, $M_{II}^{\circ}/M_{I}^{\circ}$, in this method is in excellent agreement with the values in the other two methods.

The agreement of the extrapolated values in the three methods, within the limits of experimental error, proves the validity of this extrapolation method for determining the ratios of each hydrogen. The first 90_x° pulse width should be taken into consideration if it is not negligible compared to t_d. It is about 1.5 μs for our equipment, though, and is negligible, considering the experimental error. The accuracy of the extrapolated

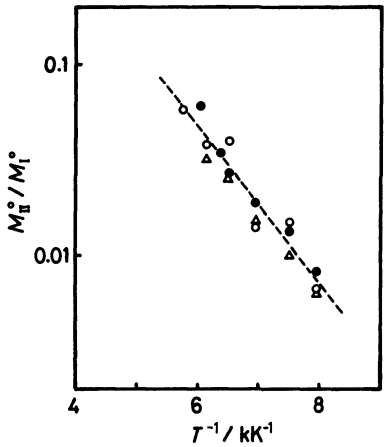

Fig. 3. The temperature dependence of the ratio of the two kinds hydrogen in $VH_{0.77}$.
○: Solid echo, ●: spin echo, and △: FID.

value becomes higher as the difference of T_{2i} decreases, due to the nature of the extrapolation method. However, a component with an extremely low concentration and a long spin-spin relaxation time will be observed by a good choice of t_d values, and then the approximate concentration of the component can be obtained by the extrapolation method described above.

Figure 3 shows the temperature dependence of the ratio of the two kinds of hydrogen in $VH_{0.77}$. The Arrhenius relation is satisfied in the temperature range from 120 to 170 K, and from its slope, the apparent energy difference of the two components is calculated to be 7.9 kJ/mol. Hydrogen atoms of Component I occupy more stable sites than those of Component II, and the exchange of hydrogen atoms between the two sites is slow. "Motional narrowing" has already occurred in Component II in the temperature range studied, but not in Component I; *i.e.*, hydrogen of Component II diffuses faster than that of Component I. Thus, we can determine the composition of different kinds of hydrogen with different diffusional behavior in metal hydrides by means of pulsed NMR spectroscopy.

References

1) "Hydrogen in Metals I, Metals II," ed by G. Alefeld and J. Völkl, Springer-Verlag, Berlin (1978).
2) For example, S. Kazama and Y. Fukai, *J. Less-Common Met.*, **53**, 25 (1977).
3) O. J. Żogał and B. Staliński, *Proc. XIVth Colloque Ampere*, North-Holland, Amsterdam (1967), p. 432.
4) D. Zamir and R. M. Cotts, *Phys. Rev. A*, **134**, 666 (1964).
5) B. Staliński and O. J. Żogał, *Bull. Acad. Pol. Sci., Ser. Sci. Chim.*, **14**, 143 (1966).
6) J. F. Hon, *J. Chem. Phys.*, **36**, 759 (1962).
7) E. L. Hahn, *Phys. Rev.*, **80**, 580 (1950).

Isotope Effect on Hydrogen Atom Abstraction Reaction by Recoil T Atoms in Solid n-$C_{10}D_{22}$–n-$C_{10}H_{22}$ Mixtures. Comparison of Recoil T Atoms with D Atoms in γ-Radiolysis

Yasuyuki ARATONO, Enzo TACHIKAWA, Tetsuo MIYAZAKI,*,† and Kenji FUEKI†

Division of Chemistry, Japan Atomic Energy Research Institute, Tokai-mura, Ibaraki 319-11

†*Department of Synthetic Chemistry, Faculty of Engineering, Nagoya University, Chikusa-ku, Nagoya 464*

(Received November 26, 1981)

Synopsis. An isotope effect on the hydrogen atom abstraction reaction by recoil T atoms in the n-$C_{10}D_{22}$–n-$C_{10}H_{22}$ mixtures in the solid phase is compared with the reaction by D atoms in the γ-radiolysis. A small isotope effect for the recoil T atoms is explained by a track model.

So far many studies have been undertaken on hot tritium reactions in the gas phase,[1] but only a few studies have been reported for solid organic compounds. It has been reported for solid neopentane that most of the recoil T atoms react in their own tracks and the thermal diffusion of the T atoms in the bulk matrix plays only a minor role.[2] Recently a large isotope effect on the hydrogen atom abstraction by D atoms produced by γ-radiolydis has been found in n-$C_{10}D_{22}$–n-$C_{10}H_{22}$ mixtures at 77 K.[3]

Here the isotope effect on the hydrogen atom abstraction reaction by recoil T atoms is examined in n-$C_{10}D_{22}$–n-$C_{10}H_{22}$ mixtures in the solid phase and compared with the results for D atoms produced by γ-radiolysis of decane.

Experimental

n-$C_{10}D_{22}$ and n-$C_{10}H_{22}$ were the same as used before.[3c] ^{6}Li enriched LiF, used as a target for ^{6}Li (n, α) T, has the ^{6}Li/(^{7}Li+^{6}Li) ratio of 0.95. The details of the neutron irradiations, performed in the KUR reactor of Kyoto University[4] and the JRR-4 reactor of the Japan Atomic Energy Research Institute, were described in the previous papers.[2] The irradiation times were 54 h at 20 K and 15 s at other temperatures. HT and DT were analyzed by radio-gas chromatography (5 m ferric oxide γ-alumina column at 77 K).

Results and Discussion

Though recoil T atoms cause abstraction, replacement, and fragmentation reactions with alkanes, the discussion in this paper will be confined only to the abstraction reaction which is one of the main processes in the T atom reactions and is closely related to the reaction by D atoms in the radiolysis. An apparent overall abstraction reaction in the n-$C_{10}D_{22}$–n-$C_{10}H_{22}$ system will be represented by the following scheme.

$$\underset{(D)}{T} + n\text{-}C_{10}D_{22} \xrightarrow{p_D} \underset{(D_2)}{DT} + C_{10}D_{21}, \quad (1)$$

$$\underset{(D)}{T} + n\text{-}C_{10}H_{22} \xrightarrow{p_H} \underset{(HD)}{HT} + C_{10}H_{21}, \quad (2)$$

where p is the relative probability of the reactions. The T and D atoms are produced by the ^{6}Li(n, α)T reaction and the radiolysis of n-$C_{10}D_{22}$, respectively. The ratios of the HT yields to the DT yields at 77 K are shown in Fig. 1 and compared with HD/D_2 ratios for D atoms.[3]

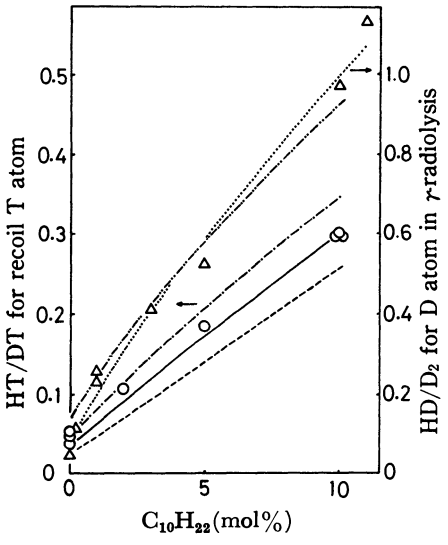

Fig. 1. Concentration dependence of HT/DT for recoil T atoms in the n-$C_{10}D_{22}$–n-$C_{10}H_{22}$ mixtures at 77 K.
○: Experimental value for recoil T atoms, △···△, experimental value for D atoms in the radiolysis,[3a-c] –·–·–: calculated value for x=0.1, –·–·: calculated value for x=0.05, ——: Calculated value for x=0.03, – – –: calculated value for x=0.01. x is a fraction of diffusive T atoms to total recoil T atoms.

HT/DT is much lower than HD/D_2. Since 38% of the D_2 yield is formed by molecular detachment from n-$C_{10}D_{22}$ in the γ-radiolysis,[3c] HD/D_2 by the hydrogen atom abstraction reactions should be higher than the values in Fig. 1, resulting in the large difference between HT/DT and HD/D_2.

Recent studies show that thermal H atoms easily abstract H or D atom from alkanes at low temperature by a quantum mechanical tunneling.[5] Thus, both hot and thermal T atoms can abstract a hydrogen atom in Reactions 1 and 2. The ratio of relative probabilities for Reactions 1 and 2 is approximated by the following equation:

$$P = \frac{p_H}{p_D} = \frac{[HT][C_{10}D_{22}]}{[DT][C_{10}H_{22}]}. \quad (3)$$

The temperature effect on p_H/p_D for recoil T atoms is shown in Fig. 2. p_H/p_D for D atoms in the γ-radiolysis is also shown in Fig. 2.[3b,3c] Though the $(p_H/p_D)_D$ depends remarkably upon temperature, the $(p_H/p_D)_T$ shows little temperature effect.

The remarkable difference between the recoil T atom reaction and the D atom reaction in the γ-radiolysis can be explained by the following track model. The recoil T atom produced by the ^{6}Li(n, α)T reaction has an initial energy of 2.7 MeV and produces a high LET

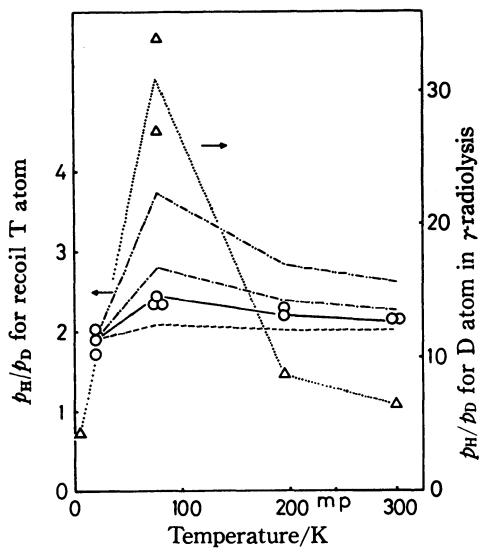

Fig. 2. Temperature dependence of p_H/p_D for recoil T atoms in the n-$C_{10}D_{22}$–n-$C_{10}H_{22}$ mixtures.
○: Experimental value for recoil T atoms, △···△: experimental value for D atoms in the radiolysis,[3a-c] ·-·-·: calculated value for $x=0.1$, ·-·-·: calculated value for $x=0.05$, ——: calculated value for $x=0.03$, ——: calculated value for $x=0.01$. x is a fraction of diffusive T atoms to total recoil T atoms. Mp denotes a melting point of decane.

track along its trajectory in the solid phase. Some of the energetic T atoms react with n-$C_{10}D_{22}$ in the track by a hot atom reaction. However, a certain fraction of them escape reaction and finally become thermalized T atoms in the track. A fraction of the thermalized T atoms react near the end of the track, while the rest of them diffuse into the bulk matrix and react in a similar manner to D atoms in the γ-radiolysis.[6] Therefore the reaction of the recoil T atoms in the solid phase consists of two types; one occurs in the track of the recoil T atom and the other in the bulk matrix by diffusive T atoms. Then, Reactions 1 and 2 take place both in the track and in the bulk matrix. $P^t(=p_H{}^t/p_D{}^t)$ and $P^b(=p_H{}^b/p_D{}^b)$ can be defined in the track and in the bulk matrix, respectively. If x is the fraction of the T atoms, which diffuse into the bulk matrix, to the total T atoms, [HT]/[DT] can be evaluated by the following equation.

$$\frac{[HT]}{[DT]}=\frac{\dfrac{0.42(1-x)P^tm}{1+P^tm}+\dfrac{xP^bm}{1+P^bm}}{\dfrac{0.42(1-x)}{1+P^tm}+\dfrac{x}{1+P^bm}}, \quad (4)$$

where m is $[C_{10}H_{22}]/[C_{10}D_{22}]$.

It has been reported in solid neopentane that almost all the recoil T atoms react in the track at 20 K without diffusion into the bulk matrix and that 42% of the total T atoms produce hydrogen.[2b] Thus, it is assumed here that 42% of the recoil T atoms in the track reaction also produce hydrogen in the decane mixture. Then, the first and second terms in the numerator of Eq. 4 represent HT yields in the track and in the bulk matrix, respectively. The denominator represents the DT yields. Since the thermal diffusion of T atoms is suppressed at 20 K, the ratio $P(=p_H/p_D)$, calculated from [HT]/[DT] at 20 K, represents the ratio in the track reaction (P^t). P^b for diffusive T atoms may be equal to that for diffusive D atoms produced by γ-radiolysis.[6]

Then, [HT]/[DT] can be estimated in the cases of $x=0.1$, 0.05, 0.03, and 0.01 by using Eq. 4 (*cf.* Fig. 1).[7] The experimental data fit the cuves for $x=0.03$ or 0.05, suggesting that the amount of the diffusive T atoms is only 3—5% of the total T atoms. p_H/p_D can also be estimated at each temperature (*cf.* Fig. 2). The experimental data fit the curve for $x=0.03$.

In conclusion most of the recoil T atoms react in their own track and only a few percent of them diffuse into the decane matrix.

The authors wish to thank Prof. Hiroyuki Yoshida and the staff of the low temperature irradiation laboratory of the Research Veactor Institute, Kyoto University, for their fruitful advice. Part of this work was carried out under the Visiting Researchers Program of Research Reactor Institute, Kyoto University. This work was partially supported by a Grant-in-Aid for Scientific Research from the Ministry of Education, Science and Culture.

References

1) R. Wolfgang, *Prog. React. Kinet.*, **3**, 97 (1965); F. S. Rowland, *MTP Int. Review of Science, Phys. Chem. Ser.*, **9**, 109 (1972).

2) a) Y. Aratono, E. Tachikawa, T. Miyazaki, M. Sakurai, and K. Fueki, *Bull. Chem. Soc. Jpn.*, **54**, 1627 (1981); b) Y. Aratono, E. Tachikawa, T. Miyazaki, Y. Kawai, and K. Fueki, *J. Phys. Chem.*, **86**, 284 (1982).

3) a) T. Miyazaki, *Radiat. Phys. Chem.*, **10**, 219 (1977); b) O. Claesson and A. Lund, *Chem. Phys. Lett.*, **47**, 155 (1977); c) T. Miyazaki, J. Kasugai, M. Wada, and K. Kinugawa, *Bull. Chem. Soc. Jpn.*, **51**, 1676 (1978); d) O. Claesson and A. Lund, *Radiat. Phys. Chem.*, **17**, 241 (1981).

4) T. Shibata, S. Iwata, H. Yoshida, M. Nakagawa, and M. Okada, *Ann. Repts. Res. Reactor Inst. Kyoto Univ.*, **2**, 89 (1969).

5) M. Iwasaki, K. Toriyama, H. Muto, and K. Nunome, *Chem. Phys. Lett.*, **56**, 464 (1978); H. Y. Wang and J. E. Willard, *J. Phys. Chem.*, **83**, 2585 (1979).

6) The selective hydrogen atom abstraction from a solute is effectively caused by both H and D atoms. There exists no definite isotope effect between them (*cf.* T. Miyazaki *et al.*, *Bull. Chem. Soc. Jpn.*, **53**, 1813 (1980)). Thus, the T atoms with energies similar to those of the atoms produced by the radiolysis should also cause the selective hydrogen atom abstraction.

7) n-$C_{10}D_{22}$ contains H atoms equivalent to 1% $C_{10}H_{22}$. Thus some HT formation is expected in the n-$C_{10}D_{22}$ sample used here.

On the Viscosity Correction of Line Width in ^{35}Cl NMR

Tadashi SUGAWARA, Masako YUDASAKA,† Katsuo TAKAHASHI,†† Reita TAMAMUSHI,††
Hiizu IWAMURA,* and Tsunetake FUJIYAMA**
Institute for Molecular Science, Myodaiji, Okazaki 444
†*Department of Applied Chemistry, Faculty of Engineering, Yokohama National University, Hodogaya-ku, Yokohama 240*
††*The Institute of Physical and Chemical Research, 2-1 Hirosawa, Wako, Saitama 351*

(Received November 2, 1981)

From the view point of the effect of viscosity, the ^{35}Cl NMR line widths and the electrical conductivities were compared for the aqueous solutions of sodium chloride in the presence of polyethylene glycol. A criterion was proposed on the validity of the viscosity correction treatment for the NMR line width.

The line width of ^{35}Cl NMR, $\Delta\nu_{1/2}$, is governed by quadrupolar relaxation, and it is proportional to the product of the square of the quadrupolar coupling constant, e^2Qq, and the correlation time, τ_c, for molecular reorientation,

$$\Delta\nu_{1/2} \propto (e^2Qq)^2\tau_c. \quad (1)$$

In order to obtain information about the change in the field gradient, q, around a ^{35}Cl nucleus and to utilize the line width as a probe for investigating the condition of the nearest neighbours around a ^{35}Cl ion, the effect of τ_c on the line width has been eliminated effectively by dividing the line width by the macroscopic viscosity using the Einstein-Stokes relation, $\tau_c=4\pi a^3\eta/3kT$, where a is an ion radius, η is viscosity, and $3kT$ is thermal energy.[1,2] The validity and limitation of this viscosity correction treatment, however, have to be examined carefully, because the viscosity η should be microscopic in nature instead of macroscopic. Here we wish to present an example to discuss this problem and show a criterion on the validity of this viscosity correction treatment for the line width.

As a measure for the microscopic viscosity, we focus our attention on the electrical conductivity, κ, because it is well known that this relationship holds between the electrical conductivity and viscosity.

$$\kappa\eta = \text{constant}, \quad (2)$$

so far as Stokes' law is satisfied for a slowly moving sphere in a liquid. It is also known that this simple relation is valid only when we use the microscopic viscosity for η.[3,4]

Aqueous solutions of sodium chloride (0.1 mol kg^{-1}) in the presence of polyethylene glycol (PEG) with various molecular weights were studied, since the electrical conductivity of aqueous sodium chloride was determined in these solutions, the macroscopic viscosities of which range from 0.9 to 138 cP (1 cP=10^{-3} Pa s).[5] The composition of the solution, macroscopic viscosity, electrical conductivity, Walden product, and ^{35}Cl line width are summarized in Table 1. The results were quite straightforward. It is noticeable that both $\Delta\nu_{1/2}$ and κ^{-1} do not correlate with the macroscopic viscosity, which is illustrated in Fig. 1. These results arise from the fact that Eqs. 1 and 2 can be satisfied only for microscopic viscosity. A reasonably good linear correlation was found, on the other hand, in the $\Delta\nu_{1/2}$ against κ^{-1} plot of Fig. 2. This result indicates that $\Delta\nu_{1/2}$ and κ^{-1} are governed by the same physical quantity, namely, microscopic viscosity, although they correspond to different dynamical motions, namely, rotational and translational ones, respectively. It is also noticeable in Fig. 1 that a linear correlation could be recognized between $\Delta\nu_{1/2}$ and κ, or between κ^{-1} and η, for the entries 1, 2, and 6. The Walden products of these three are close to 1.0.

Based upon the above results, we propose a criterion to judge whether macroscopic viscosity can be used for the correction of line width in place of the microscopic one. The Walden product for a certain concentration of aqueous sodium chloride is to be determined

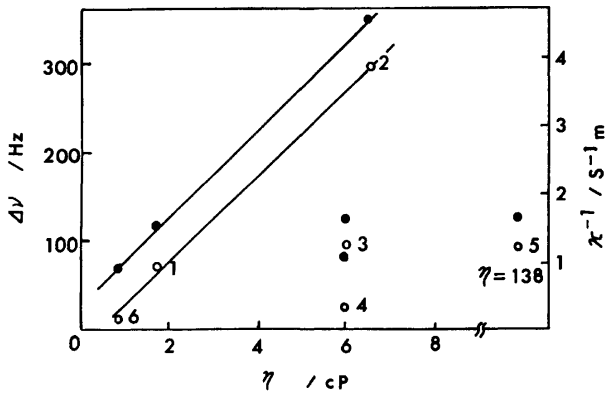

Fig. 1. Plots of the ^{35}Cl line width (○), and the inverse of electrical conductivity (●), *vs.* macroscopic viscosity η.

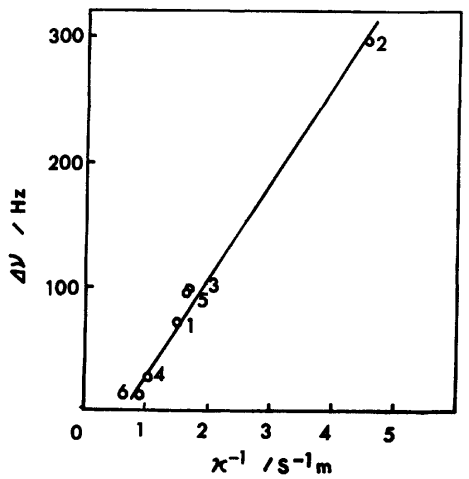

Fig. 2. The correlation between ^{35}Cl line width $\Delta\nu_{1/2}$ and the inverse of electrical conductivity κ^{-1}.

** Deceased November 18, 1981.

Table 1. The viscosity, electrical conductivity, reciprocal conductivity, and ^{35}Cl line width of sodium chloride in aqueous polyethylene glycol

Entry	Polymers	Concn of PEG/wt%	η/cP	κ/S m^{-1}	κ^{-1}/S^{-1} m	$\Delta\nu$/Hz	$\eta\kappa$
1	PEG 200	20	1.786	0.647	1.546	71	1.15
2	PEG 200	50	6.577	0.220	4.545	298	1.45
3	PEG 4000	20	6.058	0.608	1.645	96	3.68
4	PEG 20000	5	5.98	0.932	1.073	25	5.57
5	PEG 20000	20	138	0.605	1.653	95	83.5
6	none	0	0.890	1.066	0.938	12	0.949

a) Concentration of sodium chloride was 0.1 mol kg^{-1} at 25 °C.

from conductivity and viscosity measurements in the absence of additives. If the Walden product of aqueous sodium chloride in the presence of additives (PEG in the present case) is close to the former value, microscopic viscosity can be replaced with macroscopic one in this solution. The idea obtained here would be quite useful for analyzing NMR line width on ionic species of quadrupolar nuclei.

Experimental

Polyethylene glycol (PEG 200, 4000, 20000) were supplied by Wako Pure Chemical Industries Ltd.[3] Sodium chloride was purchased as a special grade and used without further purification.

^{35}Cl FT-NMR was recorded on Varian's FT 80A in the same condition as described elsewhere.[2] The temperature of the probe was kept at 25±0.5 °C by the temperature variation accessary.

References

1) H. A. Berman and T. R. Stengle, *J. Phys. Chem.*, **79**, 1001 (1975); H. A. Berman, H. J. C. Yeh, and T. R. Stengle, *ibid.*, **79**, 2551 (1975).

2) M. Yudasaka, T. Sugawara, H. Iwamura, and T. Fujiyama, *Bull. Chem. Soc. Jpn.*, **54**, 1933 (1981); M. Yudasaka, T. Sugawara, H. Iwamura, and T. Fujiyama, *ibid.*, **55**, 311 (1982).

3) R. A. Robinson and R. H. Stokes, "Electrolyte Solutions," revised ed, Butterworths, London (1965), pp. 302—313.

4) R. H. Stokes and R. Mills, "Viscosity of Electrolytes and Related Properties," Pergamon, Oxford (1965), Chap. 6.

5) T. Isono, K. Takahashi, and R. Tamamushi, *Bull. Chem. Soc. Jpn.*, **54**, 2183 (1981).

Zero-field Energy Levels in Near-doubly-degenerate Triplet States

Jiro Higuchi
Department of Chemistry, Faculty of Engineering, Yokohama National University, Hodogaya-ku, Yokohama 240

(Received November 14, 1981)

Synopsis. The zero-field energy levels in near-doubly-degenerate triplet states are discussed on molecules which are distorted so as to lose their trigonal symmetry axes. As an example, the second excited triplet states of a deformed benzene molecule are calculated from the electron spin-spin interactions.

In a previous paper,[1] the zero-field splitting (ZFS) parameters of the lowest and second excited triplet states of molecules with a trigonal symmetry axis were calculated from the electron spin-spin interactions:

$$\mathcal{H}_{ss} = \frac{\mu_0 g^2\beta^2}{4\pi}\left[\frac{(s_1\cdot s_2)}{r_{12}^3} - \frac{3(s_1\cdot r_{12})(s_2\cdot r_{12})}{r_{12}^5}\right]$$
$$= \frac{\mu_0 g^2\beta^2}{4\pi}\left[S_x^2\left(\frac{r_{12}^2-3x_{12}^2}{r_{12}^5}\right) + S_y^2\left(\frac{r_{12}^2-3y_{12}^2}{r_{12}^5}\right)\right.$$
$$+ S_z^2\left(\frac{r_{12}^2-3z_{12}^2}{r_{12}^5}\right) - (S_yS_z + S_zS_y)\frac{3y_{12}z_{12}}{r_{12}^5}$$
$$- (S_zS_x + S_xS_z)\frac{3z_{12}x_{12}}{r_{12}^5}$$
$$\left. - (S_xS_y + S_yS_z)\frac{3x_{12}y_{12}}{r_{12}^5}\right] \quad (1)$$

(μ_0: vacuum permeability; $S=s_1+s_2$: total spin) When such molecules are slightly distorted so as to lose their trigonal symmetry axes, the separations of ZFS in such near-degenerate states are not so simple, because of the interaction between these states. Although the ZFS parameters in the degenerate states were given in the previous paper,[1] the change in the zero-field (ZF) energy levels in such conformations was not discussed in detail. Also, no similar discussion has yet been carried out for aromatic molecules,[2] possibly because of a lack of experimental evidence. In the present work, therefore, the influence of such molecular deformation upon the ZF energy levels in near-doubly-degenerate triplet states is studied semi-quantitatively. In the course of this study, the ZFS's were simply evaluated by assuming them to originate from the electron spin-spin interactions, $\mathcal{H}_{ss}$.

In discussing near-doubly-degenerate states, a set of the corresponding near-degenerate real orbital functions is expressed as Ψ_X and Ψ_Y, which are orthogonal with each other and which are assumed to be symmetric with respect to the x and y axes respectively, and antisymmetric with respect to the y and x axes respectively [the x and y axes are perpendicular to the trigonal symmetry axis (z)]. It may be noted here that the ZF energy levels should not be calculated separately using each of these near-degenerate orbital parts because of the non-zero off-diagonal element of $\langle\Psi_X|-2x_{12}y_{12}/r_{12}^5|\Psi_Y\rangle$. Therefore, the basis set chosen consist of the following six functions:

$$|\Psi_X{}^3\Theta_X\rangle,\ |\Psi_X{}^3\Theta_Y\rangle,\ |\Psi_X{}^3\Theta_Z\rangle,$$
$$|\Psi_Y{}^3\Theta_X\rangle,\ |\Psi_Y{}^3\Theta_Y\rangle,\ \text{and}\ |\Psi_Y{}^3\Theta_Z\rangle. \quad (2)$$

Here,

$$^3\Theta_X = 2^{-1/2}[\beta(1)\beta(2) - \alpha(1)\alpha(2)]$$
$$^3\Theta_Y = 2^{-1/2}i[\beta(1)\beta(2) + \alpha(1)\alpha(2)] \quad (3)$$
$$^3\Theta_Z = 2^{-1/2}[\alpha(1)\beta(2) + \beta(1)\alpha(2)].$$

If the spin-free Hamiltonian is expressed as $\mathcal{H}_0$, the matrix of the Hamiltonian $\mathcal{H}=\mathcal{H}_0+\mathcal{H}_{ss}$ with the above six basis functions may be described as follows:

$$\begin{array}{c} \\ \langle\Psi_X{}^3\Theta_X| \\ \langle\Psi_X{}^3\Theta_Y| \\ \langle\Psi_X{}^3\Theta_Z| \\ \langle\Psi_Y{}^3\Theta_X| \\ \langle\Psi_Y{}^3\Theta_Y| \\ \langle\Psi_Y{}^3\Theta_Z| \end{array} \begin{array}{c} \begin{array}{cccccc} |\Psi_X{}^3\Theta_X\rangle & |\Psi_X{}^3\Theta_Y\rangle & |\Psi_X{}^3\Theta_Z\rangle & |\Psi_Y{}^3\Theta_X\rangle & |\Psi_Y{}^3\Theta_Y\rangle & |\Psi_Y{}^3\Theta_Z\rangle \end{array} \\ \begin{pmatrix} W_X+\frac{1}{3}D_X-E_X & 0 & 0 & 0 & -F_{XY} & 0 \\ 0 & W_X+\frac{1}{3}D_X+E_X & 0 & -F_{XY} & 0 & 0 \\ 0 & 0 & W_X-\frac{2}{3}D_X & 0 & 0 & 0 \\ 0 & -F_{XY} & 0 & W_Y+\frac{1}{3}D_Y-E_Y & 0 & 0 \\ -F_{XY} & 0 & 0 & 0 & W_Y+\frac{1}{3}D_Y+E_Y & 0 \\ 0 & 0 & 0 & 0 & 0 & W_Y-\frac{2}{3}D_Y \end{pmatrix} \end{array} \quad (4)$$

where:

$$W_i = \langle\Psi_i|\mathcal{H}_0|\Psi_i\rangle \qquad (i = X, Y) \quad (5)$$

$$D_i = \frac{3\mu_0 g^2\beta^2}{16\pi hc}\left\langle\Psi_i\left|\frac{r_{12}^2-3z_{12}^2}{r_{12}^5}\right|\Psi_i\right\rangle$$

$$E_i = \frac{3\mu_0 g^2\beta^2}{16\pi hc}\left\langle\Psi_i\left|\frac{y_{12}^2-x_{12}^2}{r_{12}^5}\right|\Psi_i\right\rangle \qquad (i = X, Y) \quad (6)$$

and

$$F_{XY} = \frac{3\mu_0 g^2\beta^2}{16\pi hc}\left\langle\Psi_X\left|\frac{-2x_{12}y_{12}}{r_{12}^5}\right|\Psi_Y\right\rangle.$$

When Ψ_X and Ψ_Y are perfectly degenerate, that is, $W_X=W_Y=W^\circ$, the following relations are obtained:

$$D_X = D_Y = D^\circ$$
$$\text{and} \qquad E_X = -E_Y = F_{XY} = E^\circ \quad (7)$$

As a result, the energies of the ZF levels obtained are two single and two doubly degenerate ones:

$$W = \frac{1}{3}D^\circ + 2E^\circ, \frac{1}{3}D^\circ, \frac{1}{3}D^\circ,$$
$$\frac{1}{3}D^\circ - 2E^\circ, -\frac{2}{3}D^\circ, \text{and} -\frac{2}{3}D^\circ, \quad (8)$$

relative to W°. Since the representation of the spin function $^3\Theta_i$ (i=X, Y, Z) is the same as that of the corresponding component of angular momentum (*e.g.*, E_{1g} and A_{2g} for the D_{6h} symmetry), the above numbers of single and doubly degenerate levels can be deduced from a consideration of the group theory. For example, in the case of the $^3E_{1u}$ state of benzene with the D_{6h} symmetry,

$$E_{1u} \times (A_{2g} + E_{1g}) = A_{1u} + A_{2u} + E_{1u} + E_{2u}. \quad (9)$$

The above conclusion should not be changed if the complex orbital parts of $2^{-1/2}[\Psi_X \pm i\Psi_Y]$ are used instead of the real functions of Ψ_X and Ψ_Y.

When the molecule is distorted very slightly so as to lose a trigonal symmetry axis and the electronic energy

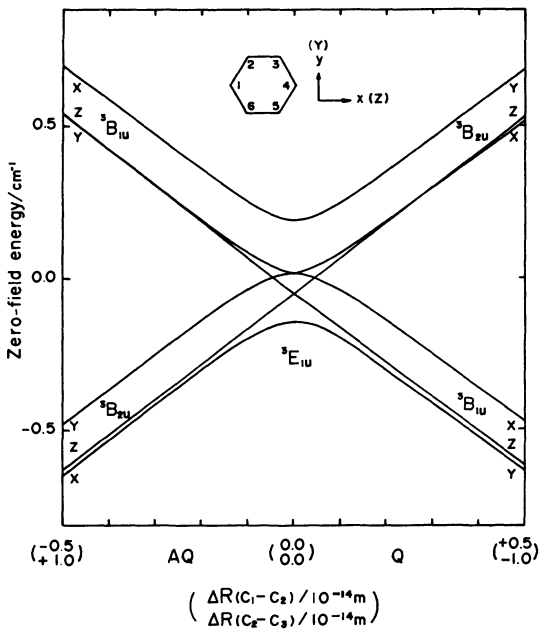

Fig. 1. Zero-field energy levels in the second excited triplet states of benzene with antiquinonoidal(AQ) and quinonoidal (Q) forms. The axis system for D_{2h} symmetry is indicated in parentheses.

separation between these near-degenerate states, $\Delta W = |W_X - W_Y|$, becomes the same order as $|F_{XY}|$, the ZF energy levels except for $|\Psi_X{}^3\Theta_Z\rangle$ and $|\Psi_Y{}^3\Theta_Z\rangle$ are somewhat complicated because of the considerable contribution of F_{XY}, as can be seen in Fig. 1. However, when the molecule is further distorted with an energy separation of $\Delta W \gg |F_{XY}|$, the energies of these states with ZFS may be approximately expressed as:

$$W = W_X - \frac{2}{3}D_X,$$

$$W_X + \frac{1}{3}D_X \pm E_X + F_{XY}{}^2/(W_X - W_Y),$$

$$W_Y - \frac{2}{3}D_Y, \text{ and}$$

$$W_Y + \frac{1}{3}D_Y \pm E_Y - F_{XY}{}^2/(W_X - W_Y). \quad (10)$$

As a result, the apparent D values observable in these states are:

$$D_X{}^\dagger = D_X + F_{XY}{}^2/(W_X - W_Y)$$

and (11)

$$D_Y{}^\dagger = D_Y - F_{XY}{}^2/(W_X - W_Y),$$

while the E values are not changed from E_X and E_Y respectively. As $D_X \approx D_Y$ in these near-degenerate states, the difference in the apparent D values may possibly be useful as a factor in estimating the molecular distortion. In the above cases, the principal magnetic x and y axes are not perfectly parallel to any symmetry axis of the molecule, for example, the x and y axes of the distorted benzene molecule shown in Fig. 1. On the other hand, when the magnetic field is applied not parallel to the trigonal symmetry axis (z), the energy levels are more complicated because of the mixing of more than two basis functions (2).

As a typical example, Fig. 1 shows the ZF energy levels of distorted benzene in the second excited triplet states with the D_{2h} symmetry. The coordinate system and the numbering of the constituent carbon atoms are taken as shown in Fig. 1. The conformation of the distorted molecule is assumed to be as follows: (i) All the bond angles are unchanged from those of the ground state with the D_{6h} symmetry;[3] and (ii) the bond lengths are changed as follows:

$$\Delta R(C_1\text{–}C_2) = \Delta R(C_3\text{–}C_4) = \Delta R(C_4\text{–}C_5)$$
$$= \Delta R(C_6\text{–}C_1) = -\Delta R(C_2\text{–}C_3)/2 = -\Delta R(C_5\text{–}C_6)/2.$$

The calculations carried out for the electronic energy and for the ZFS parameters were quite the same as those of Treatment (C) in the previous paper.[1] Further, the influence on the change of bond angels was examined on the assumptions that: (i) all the C–C bond lengths are unchanged from those of the ground state;[3] and (ii) the bond angles are changed as follows:

$$\Delta\angle C_6C_1C_2 = \Delta\angle C_3C_4C_5 = -2\Delta\angle C_1C_2C_3$$
$$= -2\Delta\angle C_2C_3C_4 = -2\Delta\angle C_4C_5C_6 = -2\Delta\angle C_5C_6C_1.$$

In this case, the trend of the ZF energy levels due to the changes in the bond angles is very close to that due to the changes in the bond lengths within the ranges shown in Fig. 1 if one reads $\Delta\angle C_6C_1C_2 \approx \pm(2.7\times10^{-2})°$ for $\Delta R(C_1\text{–}C_2) = \pm 0.1\times10^{-14}$ m, respectively.

In general, the excited molecules trapped in host glasses or crystals are more distorted than the distortion discussed here.[4] As a result, it may actually be impossible to observe transitions among ZF energy levels in degenerate triplet states, while there remains some possibility of detecting molecules with a very slight Jahn-Teller distortion in the gas phase. Although the experimental technique has not yet been improved for observing the magnetic resonance of the second excited triplet states of aromatic molecules, the present relation expected in near-degenerate triplet states may be of interest in discussing the molecular deformation due to environmental influence in orbitally degenerate phosphorescent triplet states of molecules such as aromatic ions, ESR experiments on which were made by de Groot *et al.*[5]

The author wishes to thank Professor Takashi Itoh, Ochanomizu University, for his helpful suggestion.

References

1) J. Higuchi, *Bull. Chem. Soc. Jpn.*, **54**, 2864 (1981).
2) For a review, see, for example, R. Englman, "The Jahn-Teller Effect in Molecules and Crystals," Wiley-Interscience, London (1972), p. 235.
3) A. Langseth and B. P. Stoicheff, *Can. J. Phys.*, **34**, 350 (1956).
4) For example, Ph. J. Vergragt and J. H. van der Waals, *Chem. Phys. Lett.*, **36**, 283 (1975); **42**, 193 (1976).
5) M. S. de Groot, I. A. M. Hesselmann, and J. H. van der Waals, *Mol. Phys.*, **10**, 241 (1966).

Selective Transport of Potassium Ions against Their Concentration Gradient by Pentaethylene Glycol Derivative Containing Both 8-Quinolyl and *o*-Carboxylphenyl Terminal Groups[1]

Kazuhisa HIRATANI

Industrial Products Research Institute, Higashi 1-chome, Yatabe-machi, Tsukuba-gun, Ibaraki 305

(Received June 8, 1981)

Synopsis. A pentaethylene glycol derivative containing both 8-quinolyl and *o*-carboxylphenyl terminal groups can transport potassium ions selectively against the concentration gradient in liquid membrane systems containing more than one alkali ion species in aqueous solution. Uptake of cations by this synthetic ionophore from the aqueous solution into the organic layer is confirmed to be important for exhibiting this excellent selectivity toward potassium ions.

Some of the noncyclic polyether compounds have been reported to be selective carriers of cations in the liquid membrane system.[2] The author and coworkers have recently reported that the oligoethylene glycol derivatives containing both basic quinolyl and acidic carboxyl terminal groups exhibit the selective uptake of an alkali ion into chloroform.[3] They also exhibit the transport of alkali ions against the concentration gradient in the presence of single cation species in the aqueous solution; the properties of complexation and transport are largely dependent on the length of the oxyethylene chain.[4] In this study the author wishes to report the selective transport of potassium ions in aqueous solutions containing some other alkali ion species through liquid membranes by a synthetic polyether (**1**).

Results and Discussion

The pentaethylene glycol derivative (**1**), in which the 4-*t*-butyl *o*-phenylene group is introduced among the oxyethylene chains, was prepared by the procedure described below. It is a glassy solid (pale yellow): $UV_{max}(CHCl_3)$ 286 nm (ε=8300); IR (neat) 3250 and 2550 (carboxyl OH), 1740—1680 (broad, carboxyl C=O), and 1160—1080 cm^{-1} (ether C–O–C); NMR ($CDCl_3$) δ=8.93 (1H, m, aromatic), 8.15 (1H, m, aromatic), 8.02 (1H, m, aromatic), 7.5—6.8 (10H, m, aromatic), *ca.* 7.5 (1H, broad, COOH), 4.5—3.7 (16H, m, O–CH_2–CH_2–O), and 1.28 (9H, s, C–CH_3). Found: C, 69.91; H, 6.23; N, 2.54%. Calcd for $C_{34}H_{39}N_1O_8$: C, 69.25; H, 6.67; N, 2.38%.

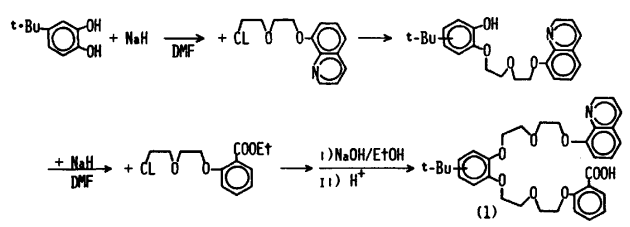

Transport of alkali ions across a chloroform liquid membrane by the synthetic ionophore (**1**) was carried out in a previously-described U-type cell[4] at 25±0.2 °C. The solution was stirred at 200 min^{-1}. The amounts of the metal ion transported from Phase I (an alkaline aqueous solution) to Phase II (an acidic aqueous solution) were determined by atomic absorption analysis for lithium, sodium, and potassium ions, and flame analysis for rubidium and caesium ions.

The experimental results are shown in Figs. 1 and 2. In the control experiment (without ionophore) the ion transport was confirmed to be negligible even after 2 d.[4] As indicated in Fig. 1,[5] in the ion transport experiment for the single alkali ion species, the difference of the transport capability of the ionophore (**1**) for each alkali ion seems to be small. Surprisingly, the transport phenomena for the three alkali ion species (Li, Na, and K) existing together, as shown in Fig. 2, are quite different from that in Fig. 1. Under these conditions, potassium ions were selectively transported by **1**, while little transport of lithium ions was detected in Phase II and the amount of sodium ions transported was less than 1/4 of the amount of potassium ions. The ionophore

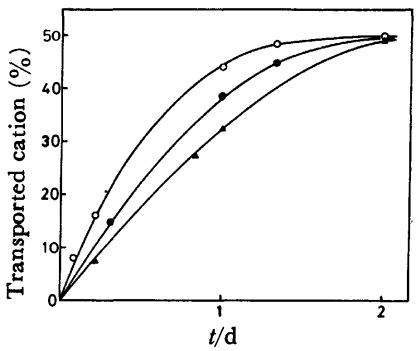

Fig. 1. Ion transport by **1** for single cation species.[5] Phase I: 15 ml of 0.1 M alkali hydroxide aqueous solution; Phase II: 15 ml of 0.1 M alkali chloride +0.1 M HCl aqueous solution; Phase III: 30 ml of chloroform containing 1.5×10^{-4} mol of **1**. —○—: K^+, —●—: Na^+, —▲—: Li^+.

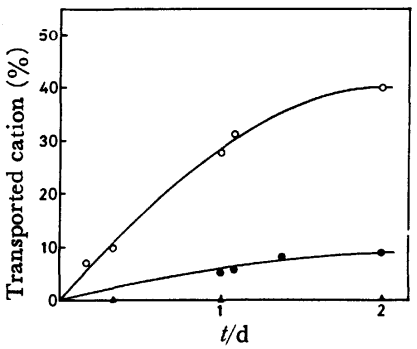

Fig. 2. Ion transport by **1** for lithium, sodium, and potassium ion species existing together. Conditions: see Table 1. —○—: K^+, —●—: Na^+, —▲—: Li^+.

Table 1. Ion transport by 1 through chloroform membrane

Coexistent cations	Transported cation after 2 d (%)[d] Li (1.32)	Na (1.90)	K (2.66)	Rb (2.98)	Cs (3.38)	Total	Selectivity for K^+
Li/Na/K (1 : 1 : 1)[a]	≈0	9	40	—	—	49	K/Li≫10 K/Na=4.4
Na/K/Ca (1 : 1 : 1)[b]	—	5	36	—	8	49	K/Na=7.2 K/Cs=4.5
K/Rb (1 : 1)[c]	—	—	33	17	—	50	K/Rb=1.9

a) Phase I: 15 ml of 0.1 M LiOH+0.1 M NaCl+0.1 M KCl aqueous solution; Phase II: 15 ml of 0.1 M LiCl+0.1 M NaCl+0.1 M KCl+0.1 M HCl aqueous solution; Phase III: 30 ml of chloroform containing 1.5×10^{-4} mol of **1**. b) Phase I: 15 ml of 0.1 M NaOH+0.1 M KCl+0.1 M CsCl aqueous solution; Phase II: 15 ml of 0.1 M NaCl+0.1 M KCl+0.1 M CsCl+0.1 M HCl aqueous solution; Phase III: 30 ml of chloroform containing 1.5×10^{-4} mol of **1**. c) Phase I: 15 ml of 0.1 M KOH+0.1 M RbCl aqueous solution; Phase II: 15 ml of 0.1 M KCl +0.1 M RbCl+0.1 M HCl aqueous solution; Phase III: 30 ml of chloroform containing 1.5×10^{-4} mol of **1**. d) The values in parentheses are the ionic diameters (Å) of each cation.

(**1**) also exhibits a large selectivity toward potassium ions both for sodium, potassium, and caesium ions existing together and for potassium and rubidium ions existing together; these latter have almost the same ionic diameter, 2.66 and 2.98 Å respectively (see Table 1).

From Table 1, the order of the cation selectivity of **1** is as follows: $K^+>Rb^+>Cs^+\approx Na^+>Li^+$. And in every case, the total amounts cations transported reach finally about 50% after two days. It is considered that hydrochloric acid not only is consumed to release the cation transported into Phase II from Phase III (an organic layer), but also reacts with alkali hydroxide in Phase I to give the alkali halide, because hydrochloric acid can be carried as the quinolinium salt of **1** in the reverse direction from Phase II to Phase I across Phase III.[4]

In Table 2 are shown the results of uptake of alkali ions into the organic layer from aqueous solution in the presence of the ionophore (**1**). These results correspond to those of the transport experiment (see Table 1). Thus, it is considered that the step of the uptake of the cation into the chloroform layer from Phase I is important for exhibiting the excellent selectivity with 9 toward potassium ions in these transport experiments. The detailed mechanism of the cation selectivity of **1** is now under investigation.

Experimental

General Procedure of Ion Transport. In the cell was placed 30 ml of chloroform containing 1.5×10^{-4} mol of **1**. The two kinds of aqueous solutions used for Phases I and II were subsequently poured into the appropriate side. The cell was placed in a water bath. The transport of alkali ions was initiated by the addition of the aqueous solutions. At each time point, 50-μl of solution was withdrawn from each phase, and the concentration of cation was adjusted by using a measuring flask and determined by atomic absorption or flame analysis.

Table 2. Extraction of alkali ions into chloroform layer

a) For single ion species.

Alkali ion species	Li	Na	K	Rb	Cs
Decrease of cation in aq solution (%)	39	43	43	41	41

Initial aqueous layer: 1.0 ml of 0.1 M alkali hydroxide; Organic layer: 0.05 mmol of **1** in 2.0 ml of $CHCl_3$.

b) For multiple ion species.

Alkali ion species	Li Na K	Na K Cs	K Rb
Decrease of cation in aq solution (%)	3 7 36	5 32 7	32 17
Composition of cation in 1.0 ml of initial aqueous layer	0.1 M LiOH +0.1 M NaCl +0.1 M KCl	0.1 M NaOH +0.1 M KCl +0.1 M CsCl	0.1 M KOH +0.1 M RbCl
Organic layer	0.05 mmol of **1** in 2.0 ml of $CHCl_3$		

Extraction of Alkali Ion with 1 into Chloroform. In a 5-ml microvial, which contained a small stirrer, was placed 2.0 ml of chloroform containing 0.5×10^{-4} mol of **1** and 1.0 ml of an aqueous solution containing one or more alkali ions, as described in Table 2. After the solution was stirred at room temperature for 1 d, the concentration of alkali ions in the upper aqueous solution was determined by atomic absorption or flame analysis.

References

1) Part III: "Synthesis and Properties of Noncyclic Polyether Compounds."

2) E. M. Choy, D. F. Evans, and E. L. Cussler, *J. Am. Chem. Soc.*, **96**, 7085 (1974); N. Yamazaki, S. Nakahama, A. Hirao, and S. Negi, *Tetrahedron Lett.*, **1978**, 2429; N. Yamazaki, A. Hirao, and S. Nakahama, *J. Macromol. Sci., Chem.*, **13**, 321 (1979); W. Wierenga, B. R. Evans, and J. A. Woltersom, *J. Am. Chem. Soc.*, **101**, 1334 (1979); J. K. Schneider, P. Hofstetter, E. Pretsch, D. Ammann, and W. Simon, *Helv. Chim. Acta*, **63**, 217 (1980).

3) K. Hiratani, S. Aiba, and T. Nakagawa, *Chem. Lett.*, **1980**, 477.

4) K. Hiratani, *Chem. Lett.*, **1981**, 21.

5) In Fig. 2, only the results in the cases of Li, Na, and K ions are depicted because the five curves for the five cations are too close together; the curves for Rb and Cs ions are located between those for K and for Na ions.

Extraction of Lead(II) in Aqueous Halide-Perchlorate Solutions with Trioctylphosphine Oxide in Hexane

Satoshi KUSAKABE and Tatsuya SEKINE*
Department of Chemistry, Science University of Tokyo, Kagurazaka, Shinjuku-ku, Tokyo 162
(Received April 23, 1981)

Synopsis. The stability and the extractability with trioctylphosphine oxide(L) in hexane of lead(II) halide complexes in 1 mol dm^{-3} Na(ClO_4) were studied. The complexes were stable and more extractable in the following order of the ligands: $Cl^- < Br^- < I^-$. The maximum numbers of the ligand (n) in the complexes PbX_n^{2-n} were 2(Cl^-), 3 (Br^-), and 4 (I^-). The chemical forms of the extracted species with L were in all cases $Pb(ClO_4)_2L_2$, $PbX(ClO_4)L_3$, and PbX_2L_2.

The solvent extractions of lead(II) in aqueous 1 mol dm^{-3} Na(X, ClO_4) ionic media (where X^- is Cl^-, Br^-, or I^-) with 2-thenoyltrifluoroacetone (TTA) in carbon tetrachloride and with trioctylphosphine oxide (TOPO) in hexane have been measured at 25 °C and the stability constants of the PbX_n^{2-n} species as well as their extraction constants with the latter extractant were calculated.

Experimental and Statistical

Experiments were made in the same way as described previously[1] except that sodium halides were used instead of sodium thiocyanate. The initial aqueous concentration of lead(II) was always 1×10^{-4} mol dm^{-3}. The distribution ratio of lead(II) is defined by:

$$D = [Pb(II)]_{org}/[Pb(II)] \quad (1)$$

$$= K_{TTA,O}[H^+]^{-2}[Htta]_{org}^2/(1 + \beta_1[X^-] + \beta_2[X^-]^2 + \cdots + \beta_n[X^-]^n) \quad (2)$$

$$D[H^+]^2[Htta]org^{-2}/K_{TTA,O} = D/D_0 = 1/(1 + \sum \beta_i[X^-]^i), \quad (3)$$

where D_0 is the distribution ratio in the absence of halide ions. The stability constants may be calculated from the decrease in the distribution ratio as a function of the ligand concentration.

The distribution ratio in the extraction with TOPO(L) from these solutions could be represented by:

$$D = \sum [PbX_n(ClO_4)_{2-n}L_m]_{org}/[Pb^{2+}](1 + \sum \beta_i[X^-]^i) = \sum K_{ex\ n,m}[X^-]^n[ClO_4^-]^{2-n}[L]_{org}^m/(1 + \sum \beta_i[X^-]^i), \quad (4)$$

where $n=0$ to 2, $m=4-n$, and the extraction constants are defined by:

$$K_{ex\ n,m} = \frac{[PbX_n(ClO_4)_{2-n}L_m]_{org}}{[Pb^{2+}][X^-]^n[ClO_4^-]^{2-n}[L]_{org}^m}. \quad (5)$$

The free TOPO concentration at equilibrium, $[L]_{org}$, can be related to its initial concentration, $[L]_{org,I}$, as:

$$[L]_{org,I} = [L]_{org} + \sum m[PbX_n(ClO_4)_{2-n}L_m]_{org} + 3[NaClO_4L_3]_{org} = [L]_{org} + \sum mK_{ex\ n,m}[X^-]^n[ClO_4^-]^{2-n}[L]_{org}^m + 3K_{ex\ Na}[ClO_4^-][L]_{org}^3. \quad (6)$$

The extraction constants of lead perchlorate, $K_{ex\ 0,4}$, and sodium perchlorate, $K_{ex\ Na}$ with TOPO in hexane have been reported to be $10^{6.92}$,[1] and $10^{1.01}$,[2] respectively. By using a least squares program including a successive approximation procedure of the free TOPO concentration on the basis of Eqs. 4 and 6, the stability constants and the extraction constants were calculated.

Results and Discussion

In the lead(II) extraction with TTA from aqueous solutions above 0.04 mol dm^{-3} of iodide, the recovery of the metal was not quantitative and dark-red precipitations were found on the interface. Thus the chelate extraction from the iodide solutions was made only in the concentration range lower than this. The extraction of lead(II) from the 1 mol dm^{-3} Na(X, ClO_4) solutions with TOPO in hexane as a function of the ligand concentration in the aqueous phase is shown in Figs. 1 and 2. Precipitations of iodide were not observed in the case of TOPO extraction, but loss of the metal from the two phases was found when TOPO concentration was 2×10^{-3} mol dm^{-3} and the iodide concentration was 0.1 to 0.2 mol dm^{-3}. For this reason, those data were not included in the data analysis.

In the chloride and bromide systems, a set of stability constants which could explain both the TTA and TOPO extraction data were obtained; these are listed in Table 1. In the iodide system, the TTA extraction could be carried out only in the lower ligand concentration range and thus only β_1 could be obtained. On the other hand, the TOPO extraction could cover the whole concentration range and the values β_1, β_2, β_3, and β_4

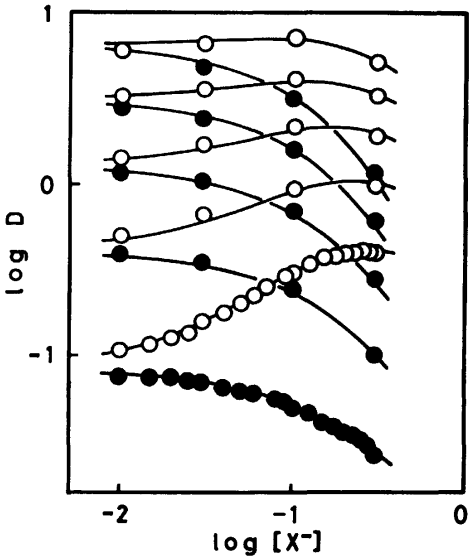

Fig. 1. Extraction of Pb(II) in 1 mol dm^{-3} Na(X, ClO_4) with TOPO in hexane, where $X^- = Cl^-$ (●) and Br^- (○). The initial concentration of TOPO in the organic phase was 0.03, 0.025, 0.02, 0.015, and 0.01 mol dm^{-3} from the top to bottom, respectively. The solid curves were calculated by Eqs. 4 and 6 using the constants in Table 1.

Table 1. Summary of the stability and extraction constants of lead(II) halide complexes

X^-	$\log \beta_1$	$\log \beta_2$	$\log \beta_3$	$\log \beta_4$	$\log K_{ex1,3}$	$\log K_{ex2,2}$
Cl^-	0.83±0.20	1.3	nil	nil	5.52±0.21	3.5
Br^-	0.93±0.21	1.6±0.3	2.0	nil	6.52±0.15	5.57±0.11
I^-	1.29±0.15	1.8	3.0	3.9	8.0	8.35±0.11

The possible error is 3σ. When the possible error is not given, it is larger than 0.3. The $K_{ex\ n,m}$ (Eq. 5) were calculated by means of Eq. 4, using the above stability constants and the value of $K_{ex\ 0,4}=10^{6.92}$.

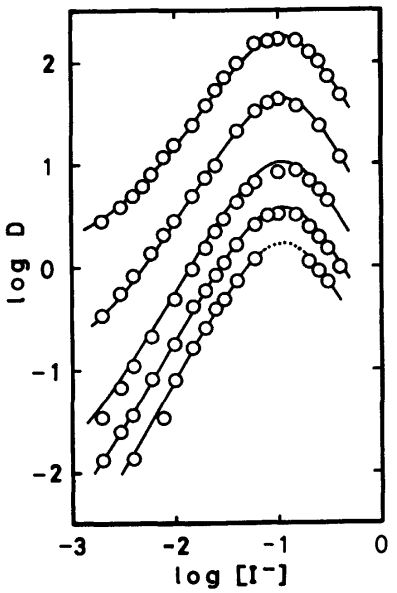

Fig. 2. Extraction of Pb(II) in 1 mol dm^{-3} Na(I, ClO_4) solutions with TOPO in hexane. The initial concentration of TOPO in the organic phase was 0.02, 0.01, 0.005, 0.003, and 0.002 mol dm^{-3} from the top to bottom, respectively. The solid curves were calculated by Eqs. 4 and 6 using the constants in Table 1.

were obtained. However, the possible errors of these constants are not small. The extraction constants with TOPO of the lead(II) species listed in Table 1 were also computed from these data.

The stability constants of lead(II) halide complexes in the present paper agreed well with the literature values obtained under the identical conditions by means of polarography.[3,4] The first complexes, PbX^+, are more stable than the thiocyanate complex ($\beta_1=10^{0.49}$).[1] The sum of the number of the ligand and TOPO molecules in the extracted species was always four, although that of the thiocyanate complexes was four or five.[1] Similar numbers were reported in the extraction of zinc(II) from perchlorate–halide[5] and –thiocyanate[6] systems. This suggests that the ligand ions and TOPO molecules are coordinated with the metal ion in the halides but some of the ligand ions are electrostatically attracted in the extracted thiocyanate species.

The extraction of lead(II) under the same concentration of TOPO and a certain given ligand ions was in the order of $I^->SCN^->Br^->Cl^-$, while the stabilities of the lead complexes in the aqueous phase was $I^->Br^->Cl^->SCN^-$. In the case of zinc(II),[5] the order of the stability in the aqueous solution was $SCN^->Cl^->Br^->I^-$ and that of the extraction was $SCN^->I^->Br^->Cl^-$. The orders found with zinc(II) were explained in the previous paper in terms of the size and the stability of the halide and thiocyanate complexes. The extractability of the unchanged complexes with TOPO is represented by:

$$MX_2 + 2L(org) \rightleftarrows MX_2L_2(org)$$

$$K^*_{ex\ 2,2} = [MX_2L_2]_{org}[MX_2]^{-1}[L]_{org}^{-2} = K_{ex\ 2,2}/\beta_2. \quad (7)$$

The following values of $K^*_{ex2,2}$ were obtained from the results in Table 1: $10^{2.2}$, $10^{4.0}$, and $10^{6.6}$ for $PbCl_2$, $PbBr_2$, and PbI_2, respectively. Dihalogenozinc(II) complexes are too unstable to be measured, but it should be reasonable to assume that the β_2 values are smaller than unity. Thus from Eq. 7, the $K^*_{ex2,2}$ values for dihalogenozinc(II) complexes should be larger than the $K_{ex2,2}$ values, ($10^{3.64}(ZnCl_2)$, $10^{4.51}(ZnBr_2)$, and $10^{6.12}(ZnI_2)$).[5] From the range of these $K^*_{ex2,2}$ values, the dihalogenolead(II) complexes are assumed to be less extractable with TOPO than the corresponding zinc(II) complexes, although they are thermodynamically more stable than the corresponding zinc(II) complexes.

The extractability of uncharged complexes with solvating extractants such as TOPO is affected by both of the partition coefficient of the unchanged complexes and by their tendency to solvate in the organic phase,[7] but since the values $[PbX_2]_{org}/[PbX_2]$ for hexane containing no TOPO were too small to be determined, no conclusion about this problem could be reached in this study.

References

1) S. Kusakabe and T. Sekine, *Bull. Chem. Soc. Jpn.*, **54**, 2533 (1981).

2) S. Kusakabe and T. Sekine, *Bull. Chem. Soc. Jpn.*, **53**, 1759 (1980).

3) V. E. Mironov, F. Ya. Kul'ba, V. A. Fedorov, and O. B. Tikhomirov, *Zh. Neorg. Khim.*, **8**, 2524, 2536 (1963).

4) P. Kivalo and A. Ekman, *Suomen Kemistil. B*, **29**, 139 (1956).

5) H. Moriya and T. Sekine, *Bull. Chem. Soc. Jpn.*, **45**, 1626 (1972).

6) H. Moriya and T. Sekine, *Bull. Chem. Soc. Jpn.*, **44**, 3347 (1971).

7) T. Sekine and T. Ishii, *Bull. Chem. Soc. Jpn.*, **43**, 2422 (1970).

Effect of Molecular Size on the Association of *p*-Quinone Anion and Lithium Ion in *N,N*-Dimethylformamide

Tsutomu NAGAOKA,* Satoshi OKAZAKI, and Taitiro FUJINAGA
Department of Chemistry, Faculty of Science, Kyoto University, Sakyo-ku, Kyoto 606
(Received September 29, 1981)

Synopsis. Ion pair formation effects of metal ions on the electro-reduction of *p*-quinones in *N,N*-dimethylformamide were studied systematically by polarography. The formation constants of 1 : 1 and 1 : 2 associates, as evaluated by the $1/F_0^2$-weighted least squares method, decrease with increase in the anion size.

In a previous paper,[1] the authors presented effects of the carbonyl group geometry on ion association of several types of carbonyl compound anions and metal cations. The degree of the half-wave potential shifts due to the ion pair formation was observed in the order of *p*-quinones<ketones<*o*-quinones with various uni- and bivalent metal cations. The interaction between the anion and cation can be considered to occur mainly near the carbonyl oxygen of the anion. Taking into consideration the probability of two ions to come into contact, stronger association is expected for the *p*-quinone ion pairs than for the ketone ones. However, the experimental results showed the contrary and, therefore, it was concluded that the factor affecting the ion pair formation of these compounds is not the number of carbonyl groups but their geometry (*i.e.*, charge localization).

In the present paper, we will discuss another factor affecting the association behavior of carbonyl compound anions, *i.e.*, their anion size, studied by polarography. *p*-Quinones were studied because their half-wave potential shifts due to ion pair formation are not large and, therefore, the above effect could be expected to be predominant compared to the geometry effect. In these systems, however, formation of 1 : 2 associates as well as 1 : 1 ones must be taken into consideration.

Experimental

Reagent grade *p*-quinones were used without further purification except for 9,10-anthraquinone which was recrystalized twice from ethanol. Reagent grade *N,N*-dimethylformamide (DMF, Nakarai Chemicals Co.) was distilled by the method described previously.[2] Polarographic measurements were made with a PAR model 173 and a Yanaco P-1000 at 25 °C. The potential scan rate used was 0.5 mV/s and the initial potential was measured to 0.1 mV with a Digital Multimeter TR-6854 (Takeda Riken Co.). The measured value of potential gave a precision of about 0.5 mV. Numerical calculation was carried out on a FACOM M-200 computer at the data processing center of Kyoto University with time sharing services.

Results and Discussion

All *p*-quinones studied underwent 2 one-electron reductions and generated stable mono- and dianions. In the presence of excess alkali metal ion, it is known from ESR studies in ether that 1 : 2 associates as well as 1 : 1 ones are formed.[3] In a previous study,[1] their presence was confirmed by polarography even in the dipolar solvent of DMF, provided the metal ion was present in large excess.

The polarographic half-wave potential shift, $\Delta E_{1/2}$, due to ion pair formation can be explained by the following mechanism: after the first one-electron reversible reduction, the following equiliblium formulas are possible:

$$Q^{-\cdot} + M^+ \rightleftharpoons Q^{-\cdot}M^+, \quad (1)$$

$$Q^{-\cdot}M^+ + M^+ \rightleftharpoons Q^{-\cdot}(M^+)_2, \quad (2)$$

where $Q^{-\cdot}$, M^+, $Q^{-\cdot}M^+$, and $Q^{-\cdot}(M^+)_2$ represent a *p*-quinone anion, a metal cation, 1 : 1 associates and 1 : 2 associates, respectively. Accordingly, 59 and 118 mV potential shifts should be observed at 25 °C for the quantitative formation of 1 : 1 and 1 : 2 associates with tenfold increase in the metal ion concentration, respectively. For the evaluation of association constants from the polarographic results, the $1/F_0^2$-weighted least squares method described by Momoki *et al.* was applied.[1,4] The variation in the junction potential between a reference electrode and the solution with the metal ion concentration was found to be negligible from the following experimental result: the half-wave potential due to the reduction of potassium or sodium perchlorate remained constant with various concentrations of lithium perchlorate where the ionic strength of the solution was adjusted to 0.3 M (1 M=1 mol dm^{-3}) with tetraethylammonium perchlorate. As seen from Fig. 1, $\Delta E_{1/2}$ was largest for 1,4-benzoquinone and

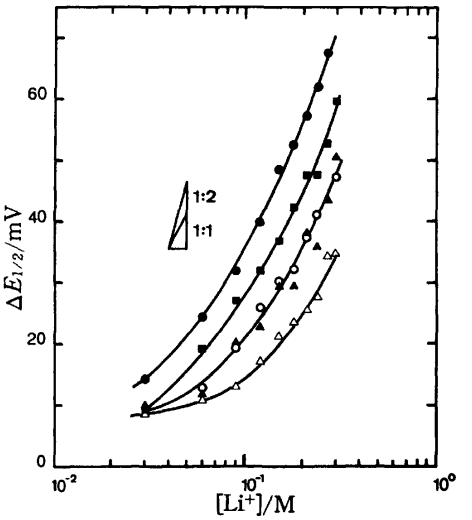

Fig. 1. Relationships between first half-wave potentials of *p*-quinons and lithium ion concentrations.
1,4-Benzoquinone (●), 1,4-naphtoquinone (■), 9,10-anthraquinone (○), 5,12-naphtacenequinone (▲), anthanthrone (△). Slopes for the quantitative formation of 1 : 1 and 1 : 2 associates are also shown in the figure.

Table 1. Association constants and contact distances of ion pairs of *p*-quinone aniones with lithium ions at 25 °C[a)]

Compound	K_1/M^{-1} [b)]	K_2/M^{-2} [b)]	$10^{10}a/m$
1,4-Benzoquinone	18.9±1.2	108.5±7.0	2.45
1,4-Naphtoquinone	15.6±1.4	41.4±6.5	2.61
9,10-Anthraquinone	11.5±0.8	18.4±3.5	2.95
5,12-Naphthacenequinone	8.1±1.5	20.4±6.0	3.6
Anthanthrone	7.3±1.3	9.8±4 0	4.0

a) Ionic strength was adjusted to 0.3 M with tetraethylammonium perchlorate. b) K_1 and K_2 represent formation constants of 1 : 1 and 1 : 2 associates, respectively.

decreased with increase in molecular size. The associates of 1 : 2 were also formed at higher lithium ion concentrations. Table 1 shows the results of the above calculation together with 95% confidence levels based on Student's T. From this table, it is obvious that the formation constants of both the 1 : 1 and 1 : 2 associates decrease with increase in anion size. Although the 1 : 1 associate has a zero net charge, the second cation can approach it because it constitues an electrostatic dipole.

For the association between two spherical univalent ions, the Fuoss equation can be applied[5)] and the formation constant, K_A (M^{-1}), is expressed by

$$K_A = (4\pi La^3 \times 10^{27}/3)\exp(e^2/4\pi\varepsilon_0\varepsilon_r akT), \quad (3)$$

where L, a, and ε_r represent the Avogadro constant, the contact distance between two ions (m), and the relative permittivity of the solvent, respectively, and the other symbols are used with usual meanings. In Table 1, the a-values for 1 : 1 associates calculated from the experimental results are also given. Applying the Fuoss equation, we ignored the solvent dielectric saturation effect, which often makes the ε_r-value decrease in the case of relatively small ions. This will cause relatively large increase in the contact distance a. Although it is also difficult to estimate a-values of actual ion pairs, reasonable correlations were obtained between the calculated a-values and the anion molecular sizes. From the formation constant 1.0×10^4 M^{-1} of Li+-9, 10-phenanthraquinone$^{-\cdot}$ ($PQ^{-\cdot}$) evaluated in our previous study,[1)] an a-value of 1.0×10^{-10} m was estimated. Since the van der Waals' radius of the oxygen atom is about 1.4×10^{-10} m, the lithium ion appears to interact solely with carbonyl oxygens of $PQ^{-\cdot}$. Therefore, it can be proposed that the association behavior of *o*-quinone anions is not influenced by their size. It was confirmed from the fact that the $\Delta E_{1/2}$'s of 1,2-naphtoquinone and PQ are 197 and 201 mV in the presence of 0.1 M lithium perchlorate in DMF, respectively.[1)] Consequently, for the anions having large formation constants (charge-localized anion), their association constants are determined only by the geometry of carbonyl groups of the anion. On the other hand, for the anions possessing small formation constants (charge-delocalized anion in aprotic polar solvents), the most important factor influencing the association constant can be said to be the molecular size. In the case of the latter, the carbonyl oxygen plays no important role in comparison with the former, and the latter can be considered as being almost spherical in shape. In conclusion, in the *p*-quinone anions their ring portions interact with the cation as well as the carbonyl oxygens, as suggested by the large a-values. This interaction becomes weak as their anion sizes increase, which, of course, cause their formation constants to be small.

References

1) T. Nagaoka, S. Okazaki, and T. Fujinaga, *J. Electroanal. Chem.*, **133**, 89 (1982).
2) T. Fujinaga, S. Okazaki, and T. Nagaoka, *Bull. Chem. Soc. Jpn.*, **53**, 2241 (1980).
3) T. E. Gough and P. R. Hindle, *Can. J. Chem.*, **47**, 3393 (1969).
4) K. Momoki, H. Sato, and H. Ogawa, *Anal. Chem.*, **39**, 1072 (1967).
5) R. M. Fuoss, *J. Am. Chem. Soc.*, **80**, 5059 (1958).

Comparison of Association Constants Derived from CD and UV Measurements. The Case of Λ-Tris(ethylenediamine)-cobalt(III) and Λ-Tris((1*R*, 2*R*)-1,2-cyclohexanediamine)cobalt(III) with Thiosulfate Ion

Hayami YONEDA,* Katsuhiko MIYOSHI, and Hitoshi MATSUKAWA
Department of Chemistry, Faculty of Science, Hiroshima University, Higashi-senda-machi, Naka-ku, Hiroshima 730
(Received October 9, 1981)

Synopsis. The association constant K_A determined by CD measurement is much smaller than that by UV measurement for the Λ-$[Co(en)_3]^{3+}$–$S_2O_3^{2-}$ system in water, whereas the two kinds of measurements yield almost the same K_A values for the Δ-$[Co(l\text{-chxn})_3]^{3+}$–$S_2O_3^{2-}$ system. These results are discussed in relation to possible interaction modes involved.

Absorption (AB) and circular dichroism (CD) spectra of metal-amine complex cations like $[Co(en)_3]^{3+}$ are changed in shape and/or magnitude upon addition of polarizable oxoanions such as PO_4^{3-}, $S_2O_3^{2-}$, SeO_3^{2-}, and SO_4^{2-}.[1,2] These changes have been utilized to investigate outer-sphere interactions of these complexes with added anions in solution.[3,4] Norden[5] was the first to demonstrate that CD change (in the visible region) gives an appreciably smaller association constant K_A than AB change (in the UV region) for the $[Co(en)_3]^{3+}$–(*R*,*R*)-tartrate^{2-} system in water. Taura[6] has recently presented the same trend in K_A values of $[Co(en)_3]^{3+}$ with (*R*,*S*)-tartrate^{2-} ion. The anomalous trend pointed out anew by Yamatera[7] remains still unsolved. In the present study, association constants of two chiral complexes, Λ-$[Co(en)_3]^{3+}$ and Δ-$[Co(l\text{-chxn})_3]^{3+}$ (*l*-chxn=(1*R*,2*R*)-1,2-cyclohexanediamine), with $S_2O_3^{2-}$ ion were determined by CD and AB measurements under identical conditions, and were compared with each other.

Experimental

Materials. Λ-$[Co(en)_3]^{3+}$ and Δ-$[Co(l\text{-chxn})_3]^{3+}$ prepared as chloride salts[8] were identified by their AB and CD spectra. Optically active $[Co(Hbg)_3]^{3+}$ and $[Co(tri)_2]^{3+}$ (Hbg=biguanide and tri=tribenzo[*b*,*f*,*i*][1,5,9]triazacyclododecine) were also prepared according to the procedures described in the literature.[9,10] All the other chemicals used were of reagent grade.

Measurements. AB and CD changes of aqueous solutions of the chiral complexes (2.0×10^{-3} mol/dm^3) were recorded at 25±0.1 °C on Shimadzu UV-200 and JASCO J-40CS spectrometers, as a function of the concentration of $Na_2S_2O_3$ (2.50×10^{-3} to 2.75×10^{-2} mol/dm^3). Ionic strength *I* was adjusted with NaCl and not with $NaClO_4$ because of low solubility of $[Co(l\text{-chxn})_3](ClO_4)_3$. Freshly prepared sample solutions were subjected to spectral measurements which were carried out at 460, 315, or 300 nm. No spectral changes with standing time over 1 h were detected, and interference due to Cl^- ion added was found negligible at each wavelength. A standard analysis[5,11] of the data thus obtained gave the association constant K_A.

Results and Discussion

Figure 1 shows AB and CD spectra of Δ-$[Co(l\text{-chxn})_3]^{3+}$ in aqueous solutions with and without $Na_2S_2O_3$. In addition to the usual changes in the AB (UV region) and CD (visible region) spectra, an appreciable CD change is observed in the UV region, which is also attributed to ion association with $S_2O_3^{2-}$ ion.[4] Essentially the same spectral changes are found in the Λ-$[Co(en)_3]^{3+}$ system. Thus, we attempted to determine the association constant K_A by utilizing these CD changes in the UV region as well as the usual spectral changes.

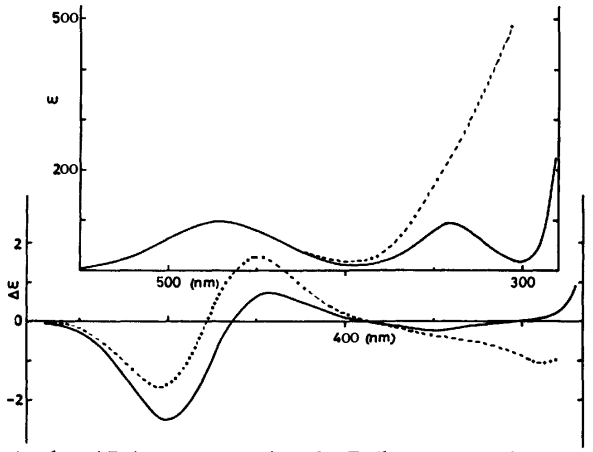

Fig. 1. AB (upper curves) and CD (lower curves) spectra of aqueous Δ-$[Co(l\text{-chxn})_3]^{3+}$ (2.0×10^{-3} mol/dm^3) in the absence (solid curves) and presence (dotted curves) of $Na_2S_2O_3$ (2.5×10^{-2} mol/dm^3).

Table 1. Association constants K_A with $S_2O_3^{2-}$ ion at I=0.1 (NaCl) in water at 25 °C

K_A	Λ-$[Co(en)_3]^{3+}$	(λ/nm)	Δ-$[Co(l\text{-chxn})_3]^{3+}$	(λ/nm)
K_{UV}	59.0±0.5	(300)	70.4±0.3	(315)
	59.6±0.7	(300)	70.0±0.5	(315)
$K_{CD(V)}$	43.7±0.4	(460)	69.0±0.4	(460)
	44.5±0.7	(460)	69.1±0.5	(460)
$K_{CD(UV)}$	51.5±0.4	(300)	61.6±0.5	(315)
	51.1±0.5	(300)	62.9±0.4	(315)

In Table 1 are given the K_A values obtained by the two independent measurements, where K_{UV}, $K_{CD(V)}$, and $K_{CD(UV)}$ refer to the association constants derived from the AB (UV region), CD (visible region), and CD (UV region) measurements, respectively. The most strinking finding in Table 1 is that $K_{CD(V)}$ is appreciably smaller than K_{UV} for the $[Co(en)_3]^{3+}$ system as already observed with (*R*,*R*)-tartrate^{2-} [5] and (*R*,*S*)-tartrate^{2-},[6] while the two values are the same within our experimental errors for the $[Co(l\text{-chxn})_3]^{3+}$ system.

In Table 2 are summarized the K_A values of Λ-

Table 2. Association constants K_A of Λ-$[Co(en)_3]^{3+}$ with some anions at $I=0.1$ ($NaClO_4$) in water at 25 °C

Anions	K_A		Ref.
(*R*,*R*)-Tartrate^{2-}	K_{UV}	26±2	5,14
		22.5±0.4	6
	$K_{CD(V)}$	16±3	5
		13.6±0.2	6,11b
(*R*,*S*)-Tartrate^{2-}	K_{UV}	60.7±0.7	6
	$K_{CD(V)}$	39.6±0.5	6,11b
SO_4^{2-}	K_{UV} [b]	49±2	14
	$K_{CD(V)}$	30.3±0.4	a)

a) H. Yoneda *et al.*, unpublished work. b) $K_{UV}=70\pm2$ for the Λ-$[Co(d\text{-pn})_3]^{3+}$–SO_4^{2-} system at $I=0.1$ (Ref. 14).

$[Co(en)_3]^{3+}$ with some anions reported by earlier workers. It seems a general observation that $K_{CD(V)}$ is smaller than K_{UV} as far as $[Co(en)_3]^{3+}$ is concerned. Here, we assume that the CD change in the visible region is due to the asymmetry around the coordinated N atoms, which is newly generated through the hydrogen-bonding of the N–H protons with added oxoanions along the C_3 axis of the complex.[1a,4b,12] This assumption is supported indirectly by the fact that $[Co(Hbg)_3]^{3+}$ and $[Co(tri)_2]^{3+}$, either having no N–H proton directed parallel to their C_3 axis, do not suffer any CD change in the visible region upon addition of some oxoanions.[9] If the above assumption is valid, it follows that the $K_{CD(V)}$ value reflects predominantly the magnitude of ion-pair formation with anions along the C_3 axis.

The K_{UV} value, on the other hand, contains all the contributions from the association modes which give rise to the interionic charge transfer (CT) band(s) in the UV region. Since the above-mentioned association mode along the C_3 axis contributes to the CT band,[13] the AB change (UV region) is expected to detect association modes not only along the C_3 axis but also along other directions, K_{UV} thus being greater than $K_{CD(V)}$ for the $[Co(en)_3]^{3+}$ system.

If the same interpretation is applied to the $[Co(l\text{-chxn})_3]^{3+}$ system, the K_A values given in Table 1 suggest that this complex interacts with $S_2O_3^{2-}$ ion along the C_3 axis only. In fact, the association modes other than that along the C_3 axis are sterically prohibited for this complex owing to the bulky chxn ligands. However, since $[Co(l\text{-chxn})_3]^{3+}$ adopts a rigid lel_3 conformation with three N–H protons oriented favorably for hydrogen-bonding along the C_3 axis, greater $K_{CD(V)}$ and K_{UV} values are expected for this complex than for conformationally less rigid $[Co(en)_3]^{3+}$. This expectation is actually fulfilled as seen in Table 1. Similarly, a greater K_{UV} value with SO_4^{2-} ion has been reported[14] for Λ-$[Co(d\text{-pn})_3]^{3+}$ with a lel_3 conformation than for Λ-$[Co(en)_3]^{3+}$. Finally, let us discuss the $K_{CD(UV)}$ values obtained for the first time in the present study. Mason *et al.*[4] proposed for some time that the CD change in the first d-d transition results from the electronic interaction with the interionic CT band, which exhibits an accompanying CD change upon addition of oxoanions (Fig. 1). If their proposal is valid, the CD change in the visible region should be proportional to that in the CT region. In other words, the $K_{CD(UV)}$ value is expected to be equal to the $K_{CD(V)}$ value. Contrary to this expectation, $K_{CD(UV)}$ is in the middle of K_{UV} and $K_{CD(V)}$ for the $[Co(en)_3]^{3+}$ system, whereas it is slightly smaller than K_{UV} or $K_{CD(V)}$ for the $[Co(l\text{-chxn})_3]^{3+}$ system. As a result, the significance of these $K_{CD(UV)}$ values is not clear at present. Wavelength dependence of the K_A values might give some insight into these problems.

References

1) a) S. F. Mason and B. J. Norman, *Proc. Chem. Soc.*, **1964**, 339; b) S. F. Mason and B. J. Norman, *J. Chem. Soc., Chem. Commun.*, **1965**, 73.

2) H. L. Smith and B. E. Douglas, *Inorg. Chem.*, **5**, 784 (1966).

3) For example, J. Bjerrum, *Adv. Chem. Ser.*, **62**, 178 (1967).

4) a) R. Larsson, S. F. Mason, and B. J. Norman, *J. Chem. Soc., A*, **1966**, 301; b) S. F. Mason and B. J. Norman, *ibid.*, **1966**, 307.

5) B. Norden, *Acta Chem. Scand.*, **26**, 111 (1972).

6) T. Taura, Ph. D. Thesis, Hiroshima University, 1979.

7) H. Yamatera, the 37th National Meeting of the Chemical Society of Japan, Tokyo, April 1978, Abstr. No. 4V2.

8) S. E. Harnung, B. S. Sørensen, I. Creaser, H. Maegaard, U. Pfenninger, and C. E. Schäffer, *Inorg. Chem.*, **15**, 2123 (1976).

9) T. Tada, Y. Kushi, and H. Yoneda, *Bull. Chem. Soc. Jpn.*, **54**, 1538 (1981) and references cited therein.

10) S. C. Cummings and D. H. Busch, *J. Am. Chem. Soc.*, **92**, 1924 (1970).

11) a) H. Yoneda, K. Miyoshi, S. Suzuki, and T. Taura, *Bull. Chem. Soc. Jpn.*, **47**, 1661 (1974); b) H. Yoneda and T. Taura, *Chem. Lett.*, **1977**, 63.

12) J. E. Sarneski and F. L. Urbach, *J. Am. Chem. Soc.*, **93**, 884 (1971).

13) J. K. Beattie, R. A. Binstead, and M. Broccardo, *Inorg. Chem.*, **17**, 1822 (1978).

14) K. Ogino, *Bull. Chem. Soc. Jpn.*, **42**, 447 (1969).

Preparation and Molecular Structure of *cis*-Diaqua[(7*S*, 14*S*)-5,5,7,12,12,14-hexamethyl-1,4,8,11-tetraazacyclotetradecane]nickel(II) Chloride

Haruko Ito,† Masako Sugimoto, and Tasuku Ito*
Division of Applied Molecular Science, Institute for Molecular Science, Okazaki National Research Institutes, Okazaki 444
(Received December 16, 1981)

Synopsis. A six-coordinate diaqua nickel(II) complex with the title macrocyclic ligand, $[Ni(H_2O)_2(S,S\text{-L})]Cl_2$, has been synthesized and its structure has been determined by the X-ray analysis. Coordination geometry about the Ni is of *cis*-NiO_2N_4 type with the macrocyclic ligand folded.

It is well known that a certain tetraazamacrocyclic nickel(II) complex exists as an equilibrated mixture of four-coordinate and diaquated six-coordinate species in an aqueous solution. However, in the case of a nickel(II) complex with 5,5,7,12,12,14-hexamethyl-1,4,8,11-tetraazacyclotetradecane, $[NiL]^{2+}$, neither the occurrence of such an equilibrium nor the existence of a diaqua six-coordinate complex had been reported until our previous study[1] on the complex having the optically active ligand. We found in the circular dichroism (CD) spectral study of $[Ni(S,S\text{-L})]^{2+}$ that a very small amount of six-coordinate diaqua complex exists in a dilute perchloric acid solution of *α*-$[Ni(S,S\text{-L})](ClO_4)_2$, where *S,S*-L denotes 7*S*,14*S*-form of the ligand L and a symbol "*α*" designates in this case that chiral secondary amine nitrogens adopt 1*R*,4*R*,8*R*,11*R*-configuration.[2] From the CD band positions, the structure about the Ni of the six-coordinate species was tentatively assigned to be of *cis*-NiO_2N_4 type.

In this study, we isolated successfully the diaqua six-coordinate complex, *cis*-$[Ni(H_2O)_2(S,S\text{-L})]Cl_2$. The blue diaqua complex is obtained from an acetonitrile solution of *cis*-$[NiCl_2(S,S\text{-L})]$, which contains an appropriate amount of water. When the acetonitrile contains an insufficient amount of water, green crystals of *cis*-$[NiCl_2(S,S\text{-L})]$ are recovered. When the water content is too much, a yellow compound (probably four-coordinate $[Ni(S,S\text{-L})]Cl_2$) is obtained. The diaqua complex was obtained only when secondary amine nitrogens are in the *α*-form.

Figure 1 shows a stereoscopic view of $[Ni(H_2O)_2(S,S\text{-L})]^{2+}$. Coordination geometry about the Ni is of *cis*-NiO_2N_4 type, two water molecules occupying the *cis* positions. The ligand L is folded about N(4)–Ni–N(11), as is in the crystals of $[Ni(OAc)(rac\text{-L})](ClO_4)$[3] and $[\{Ni(S,S\text{-L})\}_2(H_2O)(d\text{-tart})](ClO_4)_2\cdot 2H_2O$.[1] Each chelate ring adopts the most strain free conformation: all the six-membered rings take the chair form with the single methyl groups in equatorial positions; all the five-membered rings are in the gauche conformation. Table 1 lists bond lengths and angles about the Ni. Other structural parameters are deposited as supplementary data.[4] Chloride ions are hydrogen-bonded to coordinated water molecules, giving one dimensional chains along the c-axis.[4]

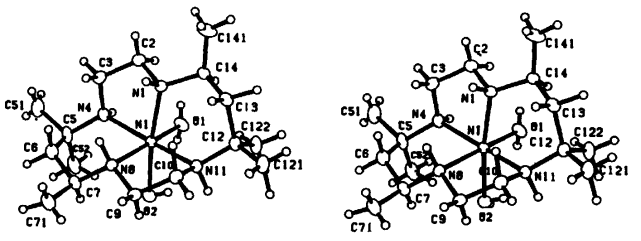

Fig. 1. A stereo view of the structure of *cis*-$[Ni(H_2O)_2(S,S\text{-L})]^{2+}$.

† Present address: Department of Chemistry, Aichi Kyoiku University, Kariya 448.

Table 1. Bond lengths (*l*/Å) and angles (*φ*/°) about the Ni, and their estimated standard deviations

NI	-O(1)	2.162(3)		NI	-O(2)	2.142(3)		
NI	-N(1)	2.095(3)		NI	-N(4)	2.163(4)		
NI	-N(8)	2.113(3)		NI	-N(11	2.164(4)		
O(1)	-NI	-O(2)	84.2(1)	O(1)	-NI	-N(1)	90.1(1)	
O(1)	-NI	-N(4)	85.3(1)	O(1)	-NI	-N(11)	103.5(1)	
O(2)	-NI	-N(4)	100.2(1)	O(2)	-NI	-N(8)	87.7(1)	
O(2)	-NI	-N(11)	87.3(1)	N(1)	-NI	-N(4)	84.8(1)	
N(1)	-NI	-N(8)	98.7(1)	N(1)	-NI	-N(11)	88.6(1)	
N(4)	-NI	-N(8)	88.3(1)	N(8)	-NI	-N(11)	84.0(1)	
O(1)	-NI	-N(8)	168.7(1)	O(2)	-NI	-N(1)	172.0(1)	
N(4)	-NI	-N(11)	169.1(1)					

Table 2. Fractional coordinates ($\times 10^5$) with B_{eq}[a]

Atom	*x*	*y*	*z*	B_{eq}/Å^2 [b]
NI	10671(3)	12643(3)	15170(6)	2.0
CL(1)	-13189(9)	27409(7)	14234(18)	4.6
CL(2)	-31806(9)	45145(7)	38718(13)	3.7
O(1)	24465(21)	11579(16)	4645(36)	3.3
O(2)	14669(21)	2721(15)	26854(33)	2.9
N(1)	8682(23)	22871(17)	4405(38)	2.4
N(4)	5211(23)	7944(18)	-5514(41)	2.5
N(8)	-3030(22)	11418(17)	24591(36)	2.1
N(11)	13686(22)	18594(17)	35802(41)	2.3
C(2)	7809(33)	21056(24)	-11813(50)	3.3
C(3)	1395(31)	14403(24)	-13625(50)	3.1
C(5)	-1344(32)	1350(25)	-5370(54)	3.2
C(6)	-9772(33)	2782(24)	5231(52)	3.2
C(7)	-8014(29)	4148(21)	21928(51)	2.6
C(9)	-2017(28)	13101(24)	40683(44)	2.6
C(10)	4315(31)	19857(24)	42690(49)	2.8
C(12)	19783(28)	25457(21)	35680(54)	2.7
C(13)	15961(34)	31029(23)	23912(52)	3.0
C(14)	15950(31)	28800(22)	7270(51)	2.8
C(51)	-5405(40)	-59(33)	-21256(61)	4.8
C(52)	4362(35)	-5476(25)	-745(66)	4.1
C(71)	-17562(33)	3694(26)	30124(61)	3.9
C(121)	19788(36)	29340(28)	51064(61)	4.1
C(122)	29940(31)	23028(27)	32009(59)	3.7
C(141)	13942(45)	35671(25)	-2191(61)	4.8

a) Estimated standard deviations are in parentheses.

Figure 2 shows nujol-mull solid state absorption (AB) spectra of *cis*-$[Ni(H_2O)_2(S,S\text{-L})]Cl_2$ ($\tilde{\nu}_{max}$/cm^{-1}: 10100, 17000, 27100) and *cis*-$[NiCl_2(S,S\text{-L})]$ ($\tilde{\nu}_{max}$/cm^{-1}: 8550, 15700, 25400). They are very similar to each other except that the AB maxima of *cis*-$[NiCl_2(S,S\text{-L})]$ are shifted to longer wavelengths. The green dichloro complex gives the same AB spectrum in the solid state

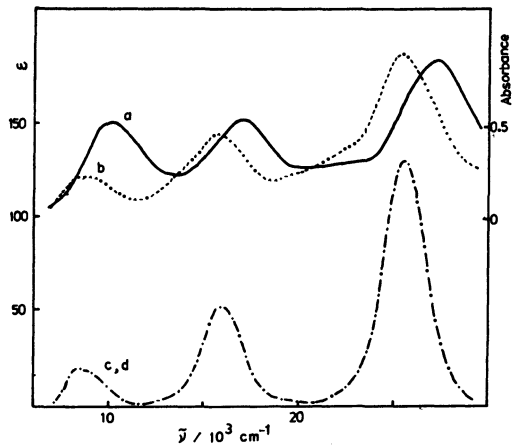

Fig. 2. Nujol-mull solid state absorption spectra of *cis*-$[Ni(H_2O)_2(S,S\text{-L})]Cl_2$ (a) and *cis*-$[NiCl_2(S,S\text{-L})]$ (b) [right-hand ordinate], and absorption spectra of *cis*-$[Ni(H_2O)_2(S,S\text{-L})]Cl_2$ (c) and *cis*-$[NiCl_2(S,S\text{-L})]$ (d) in acetonitrile [left-hand ordinate].

as in the acetonitrile solution [$\tilde{\nu}_{max}/cm^{-1}$ (ε): 8500(20.9), 15800(53.4), 25600(130)]. On the other hand, when the diaqua complex is dissolved in acetonitrile, nitromethane, or acetone, it gives green solution. The spectrum of the solution is exactly the same as that of *cis*-$[NiCl_2(S,S\text{-L})]$. The ionic diaqua complex turns the dichloro complex and exists as a chargeless complex in such organic solvents.

The positions of AB maxima of the solid state spectrum of *cis*-$[Ni(H_2O)_2(S,S\text{-L})]Cl_2$ are the same as those for the triplet species of α-$[Ni(S,S\text{-L})](ClO_4)_2$ in dilute perchloric acid.[2]

Experimental

Materials. cis-[*NiCl*$_2$(S,S-*L*)]: To an acetonitrile solution (50 cm^3) containing 0.5 g of α-$[Ni(S,S\text{-L})](ClO_4)_2$[1] was added an excess of tetrabutylammonium chloride (0.5 g). The solution was rotoevaporated to *ca.* 10 cm^3. Green precipitates were filtered and washed with a minimum amount of acetonitrile (yield, 0.4 g). Found: C, 45.73; H, 9.02; N, 13.51%. Calcd for $NiC_{16}H_{36}N_4Cl_2$: C, 46.41; H, 8.76; N, 13.53%.

cis-[*Ni*(H_2O)$_2$(S,S-*L*)]Cl_2: 0.4 g of *cis*-$[NiCl_2(S,S\text{-}L)]$ was dissolved in 30 cm^3 of acetonitrile containing two drops of water. Blue prismatic crystals of *cis*-$[Ni(H_2O)_2(S,S\text{-L})]Cl_2$ were obtained upon standing the solution in a refrigerator for a few days. (yield, 0.1 g). Found: C, 42.66; H, 8.87; N, 12.41%. Calcd for $NiC_{16}H_{40}N_4O_2Cl_2$: C, 42.69; H, 8.96; N, 12.45%. When an amount of water present in the solvent acetonitrile is insufficient or too much, the desired compound cannot be isolated.

X-Ray Analysis. The intensity measurement and the structure analysis were carried out in the same way as described previously.[1] A specimen with dimensions 0.28 mm×0.13 mm×0.10 mm was used for the X-ray work. Crystal data: orthorhombic, $P2_12_12_1$, a=14.070(3), b=18.022(3), c=8.876 (2) Å, U=2250.6(8) Å^3, Z=4, D_m=1.34, D_X=1.33 g cm^{-3}, μ(Mo $K\alpha$)=11.1 cm^{-1}. All the hydrogen atoms located by the difference synthesis were included in the final refinement with the isotropic temperature factors. The final R indices were R=0.033 and R_w=0.035. Table 2 lists the atomic coordinates.[5]

Measurements. Absorption spectra in solution were measured with a Hitachi 340 spectrophotometer. Solid state absorption spectra were taken as Nujol mulls on a Hitachi 323 spectrophotometer equipped with an attached integrating sphere.

References

1) H. Ito, J. Fujita, K. Toriumi, and T. Ito, *Bull. Chem. Soc. Jpn.*, **54**, 2988 (1981).

2) See Ref. 2 and references cited therein for the notation.

3) P. O. Whimp, M. F. Bailey, and N. F. Curtis, *J. Chem. Soc., A*, **1970**, 1956.

4) Tables of atomic parameters, structure factors, bond lengths and angles, and a stereoview of packing of complexes are kept in the Office of the Chemical Society of Japan (Document No. 8235).

5) $B_{eq}=(4/3)\sum_I\sum_J\beta_{IJ}(\boldsymbol{a}_I\cdot\boldsymbol{a}_J)$, where $\boldsymbol{a}_I$ is a unit cell edge in direct cell and β_{IJ} is an anisotropic temperature factor in the form of $\exp\{-(\beta_{11}h^2+\beta_{22}k^2+\beta_{33}l^2+2\beta_{12}hk+2\beta_{13}hl+2\beta_{23}kl)\}$.

Acylthiocyclopropenium Ions

Hiroshi YOSHIDA,* Mikito NAKAJIMA, Tsuyoshi OGATA, and Kiyoshi MATSUMOTO†
Department of Synthetic Chemistry, Faculty of Engineering, Shizuoka University, Hamamatsu 432
†College of Liberal Arts and Science, Kyoto University, Kyoto 606

(Received June 11, 1981)

Synopsis. On treatment with a mixture of thiocarboxylic acid and perchloric acid in acetic anhydride, cyclopropenone gave acylthiocyclopropenium perchlorate in a good yield. Bis(acylthio)cyclopropene also yielded the salt under similar reaction conditions. The salt was stable under nitrogen at low temperatures, but was easily hydrolyzed to yield the corresponding cyclopropenethione.

The chemistry of cyclopropenone and their derivatives has attracted considerable attention in the past two decades.[1] Cyclopropenium ions substituted with tris(alkylthio), triamino, or triaryl groups have been isolated as stable crystals.

In a previous paper[2] the present authors have shown the reaction of cyclopropenones, **1**, with thiocarboxylic acids in the presence of strong acids. The reaction in dichloromethane yields the corresponding cyclopropenethiones, **4**, in good yields, while the reaction in ethanol gives bis(acylthio)cyclopropenes, **2**. In this communication we will show two easy routes for the preparation of acylthiocyclopropenium ions, **3**, which are believed to be intermediates for the reaction of **1** with thiocarboxylic acid to yield **4**.

Although it has been reported that unsubstituted cyclopropenone yields a 1 : 2 addition product, **5**, by a reaction with thioacetic acid, no precise study has been made.[3]

No reaction was observed between **1a** and thioacetic acid without a strong acid. When a mixture of **1a**, thioacetic acid, and 70% perchloric acid in acetic anhydride was allowed to stand at room temperature, colorless needles appeared within a few minutes. One hour later crystals were collected. Similarly, the treatment of **1b** with a mixture of thiocarboxylic acids and perchloric acid in acetic anhydride yielded the crystalline products. The structure of the products was confirmed to be **3** on the basis of their ^{13}C- and ^{1}H-NMR and IR spectra, molecular-weight determination, and the subsequent acid hydrolysis.

The ^{13}C chemical shifts for some **3** ions, together with the cyclopropene derivatives, are given in Fig. 1. The assignments were made by considering the signal multiplicities from off-resonance decoupling experiments or from coupled spectra, line intensities, and chemical shifts in comparison with substituted cyclopropenium ions. The chemical shifts for ring carbons of trimethyl-, tris(*t*-butylthio)-, and triphenylcyclopropenium ions are observed at δ 179.3, 156.1, and 155.4 (154.0)[4] ppm respectively.[1] The ^{13}C chemical shifts for carbonium ions are interpreted in terms of the charge densities.[5] Figure 1 indicates that positive charges on the carbons of the cyclopropenium ions would be furnished in this order with respect to the substituents: Me>MeS>Acylthio≥Ph.

The reaction of **2** with perchloric acid in acetic anhydride also yielded **3**. The results are collected in Table 1.

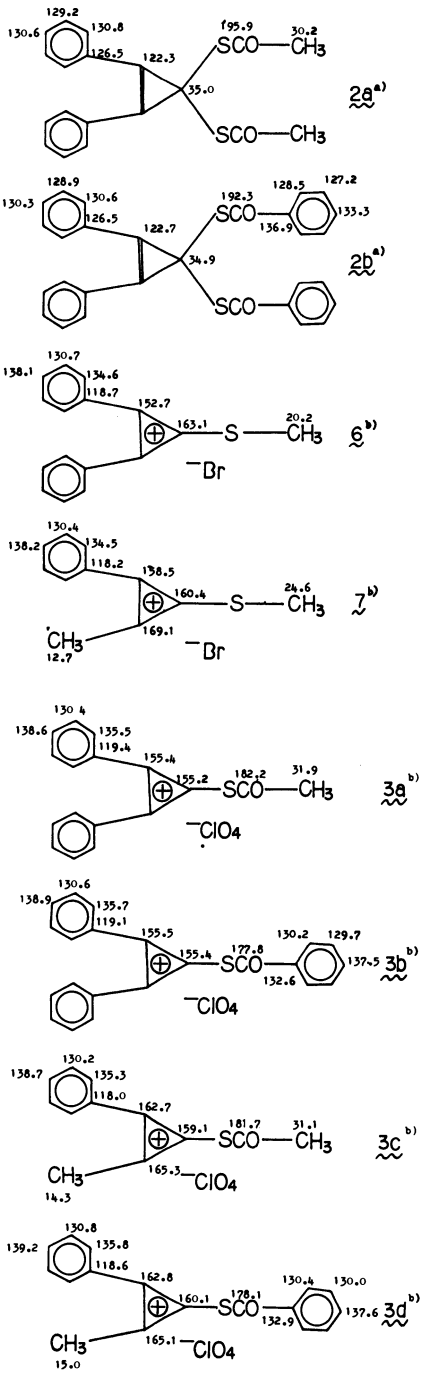

Fig. 1. Selected ^{13}C-NMR data.
a) Solvent: $CDCl_3$, b) solvent: $CDCl_3$–CF_3CO_2H (1 : 0.1—0.3 v/v).

Although the **3** salts were stable under nitrogen at low temperatures, the **3** were easily hydrolyzed under acidic

Table 1. Physical properties of 3

	R^1	R^2	Mp θ_m/°C	Yield/% (from)	NMR[a)]	IR ν/cm^{-1}(Nujol)
3a	Ph	Me	132—142	94(**1a**) 91(**2a**)	2.90(s,3H,Me), 7.8—8.5(m,10H,Ph)	1910,1650
3b	Ph	Ph	150—153.5	65(**1a**) 75(**2b**)	7.6—8.4(m,15H,Ph)	1720,1600
3c	Me	Me	84.5—85.5	62(**1b**)	2.81(s,3H,MeCO), 3.25(s,3H,MeC=C), 7.6—8.2(m,5H,Ph)	1790,1590
3d	Me	Ph	107—109	73(**1b**)	3.33(s,3H,MeC=C), 7.6—8.4(m,10H,Ph)	1750,1600
3e	Me	*p*-$MeOC_6H_4$	126—129.5	62(**2c**)	3.32(s,3H,MeC=C), 3.95(s,3H,MeO), 7.0—8.3(m,9H,Arom)	1720,1600

a) In $CDCl_3$–CF_3CO_2H (10 : 1 v/v).

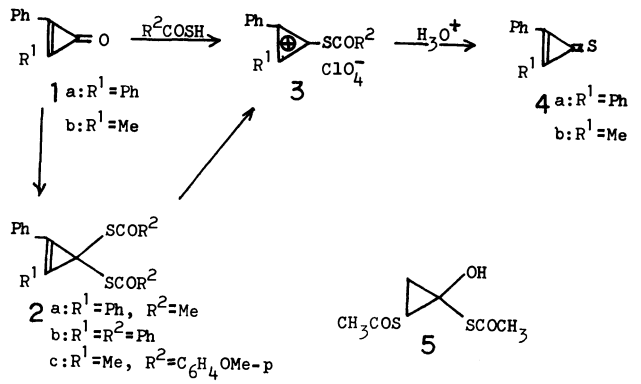

conditions at room temperature to yield the corresponding cyclopropenethione, **4**, in fairly good yields.

Experimental

General. The ^{13}C FT NMR spectra were recorded on a JEOL JNM FX-60 spectrometer (15.04 MHz), and ^1H-NMR spectra, on a Hitachi Perkin Elmer R-24 (60 MHz). The IR spectra were recorded on a JASCO A-3 spectrometer.

Preparation of 3 from 1. To a solution of perchloric acid (70%, 1.1 mmol) in acetic anhydride (3 cm^3), we added **1** (1 mmol) to give a clear solution. Thiocarboxylic acid (1.1 mmol) was then added to the mixture, and the stirring was continued at room temperature. The colorless needles which appeared in the reaction mixture within 5 min were collected after 1 h, washed with dry benzene, and dried *in vacuo*.

Preparation of 3 from 2. To a solution of perchloric acid (70%, 1.1 mmol) in acetic anhydride (3 mmol), we added **2** (1 mmol) at room temperature, and then we stirred the mixture well. The colorless needles which appeared were collected and treated as above.

Hydrolysis of 3. To a cold mixture of 2 mol dm^{-3} hydrochloric acid and dichloromethane (10 cm^3 each), we added **3** (1 mmol). The reaction mixture was stirred well for 30 min, and the organic layer was separated. The condensation of the solution and recrystallization gave **4** in good yields: **4a** from **3a** in a 96% yield and from **3b** in a 90% yield, and **4b** from **3c** in a 89% yield respectively. The structures of **4a** and **4b** were confirmed by a comparison of their mp's and ^1H-NMR spectra with those of authentic samples.[2)]

Molecular-weight Determination. The molecular weights of **3** were determined as follws: an exactly weighed amount of **3** (*ca.* 200 mg) was dissolved in dry ethanol (5 cm^3). To the solution under nitrogen we added an excess amount of potassium hydroxide in ethanol (5% solution). The resulting mixture was stirred well for 20 min. The precipitated potassium perchlorate (the solubility in ethanol: 0.008% at 21 °C) was collected in a glass-sintered filter, washed with dry ethanol and benzene under nitrogen, dried at 100 °C, and weighed. The observed (calcd) molecular weights for **3a—e** were **3a**: 360 (365), **3b**: 442 (427), **3c**: 316 (303), **3d**: 352 (365), and 373 (395). Studies of the elemental and mass spectroscopic analyses of **3a—e** were unsuccessful because of the decomposition of the samples.

References

1) K. Matsumoto, *J. Syn. Org. Chem. Jpn.*, **30**, 1035 (1972); K. T. Potts and J. S. Baum, *Chem. Rev.*, **74**, 189 (1974); Z. Yoshida and H. Konishi, "The Chemistry of New Aromatics, Kagaku Sosetsu No. 15," ed by the Chemical Society of Japan, Japan Scientific Societies Press, Tokyo (1977), p. 53.

2) H. Yoshida, M. Nakajima, and T. Ogata, *Synthesis*, **1981**, 36.

3) R. Breslow, M. Oda, and J. Pecosalo, *Tetrahedron Lett.*, **1972**, 4415.

4) E. V. Dehmlow, R. Zeisberg, and S. S. Dehmlow, *Org. Magn. Reson.*, **7**, 418 (1975).

5) G. C. Levy, R. L. Lichter, and G. L. Nelson, "Carbon-13 Nuclear Magnetic Resonance Spectroscopy," John Wiley and Sons, New York (1980), p. 171.

Application of the Water-gas Shift Reaction. III. Reduction of Oxidized Nitrogen Compounds with CO and H_2O Catalyzed by $[Ru(cod)py_4](BPh_4)_2$

Tamon OKANO,* Kensuke FUJIWARA, Hisatoshi KONISHI, and Jitsuo KIJI*
Department of Environmental Chemistry and Technology, Faculty of Engineering, Tottori University, Tottori 680

(Received August 29, 1981)

Synopsis. The ruthenium(II) complex, $[Ru(cod)py_4](BPh_4)_2$ (cod=1,5-cyclooctadiene, py=pyridine) has been shown to catalyze the reduction of oxidized nitrogen compounds with CO and H_2O. In this reaction, primary, secondary, and tertiary nitroalkanes are converted into amides, ketones, and amines, respectively. Nitrosobenzene and picoline *N*-oxides are also reduciable to amines in good yields.

Much attention has been devoted to the reduction of organic molecules with CO and H_2O without using molecular hydrogen. The reduction of nitrobenzenes with this system has been thoroughly investigated,[1-3] yet the reductions of other compounds have rarely been known.[4-5] We have previously reported that the ionic ruthenium(II) complex, $[Ru(cod)py_4](BPh_4)_2$ (**1**), is an efficient catalyst for the reduction of nitrobenzenes with CO and H_2O. In this paper, we describe the application of this catalytic system to the reduction of some compounds containing oxidized nitrogen.

Unlike the reduction of nitrobenzenes, 1-nitropropane reacted with CO and H_2O in the presence of **1** to give mainly propionamide. Small amounts of propionitrile and propylamine derivatives such as $CH_3CH_2CH_2$-$NHCOCH_2CH_3$ and $(CH_3CH_2CH_2)_2NCHO$ were formed as organic by-products, but propylamine was not detected. As an inorganic product a small quantity of ammonium hydrogencarbonate was found. For this reaction the presence of both CO and H_2O was essential. However, either the presence of a large excess of H_2O or the application of a high pressure of CO resulted in decrease in the yield of the amide but increase in the formation of ammonium hydrogencarbonate. The favorable reaction conditions were as follows: CO=15 atm, H_2O/RNO_2=2 mol/mol. 1-Nitrohexane was similarly reduced to the corresponding amide and nitrile.

Interestingly, the reaction of secondary nitroalkane, 2-nitropropane, gave acetone and acetone oxime. This oxime formation suggests that oximes may be one of the intermediates in the reaction of primary and secondary nitro compounds. In fact, under these conditions acetone oxime was hydrolyzed to acetone in 66% yield. Propionaldehyde oxime was also converted into a mixture of propionamide (63%) and propionitrile (4%). This is the Beckmann rearrangement of aldoxime, which has been known to be catalyzed by some transition metal complexes.[6] For this reaction, neither CO nor H_2O was needed, while the product ratio was affected; the yield of propionitrile was increased up to 47% in the absence of CO and H_2O, whereas propionamides was formed in 36% yield.

On the other hand, the reaction of 2-nitro-2-methylpropane gave *t*-butylamine exclusively. The difference between tertiary and secondary or primary nitroalkanes seems to be attributed to the hydrogens on the α-carbon atom. It may be deduced that at the first stage of the catalysis a nitroso compound is formed as an intermediate. Actually, nitrosobenzene was readily reduced to aniline in a high yield compared with the reduction of nitrobenzene (76%). The reaction scheme is illustrative as follows.

Table 1. Reduction of nitroalkanes with CO and H_2O catalyzed by $[Ru(cod)py_4](BPh_4)_2$[a]

Sub. (RNO_2) R–	CO (atm)	Products (Yield /%)[b]				
$CH_3CH_2CH_2$–	10	$CH_3CH_2CONH_2$ (47)	CH_3CH_2CN (1)	$CH_3CH_2CH_2NHCOCH_2CH_3$ (1)	$(CH_3CH_2CH_2)_2NCHO$ (1)	NH_4CO_3H (≈0)
$CH_3CH_2CH_2$–	15	$CH_3CH_2CONH_2$ (54)	CH_3CH_2CN (1)	$CH_3CH_2CH_2NHCOCH_2CH_3$ (2)	$(CH_3CH_2CH_2)_2NCHO$ (4)	NH_4CO_3H (≈0)
$CH_3CH_2CH_2$–	50	$CH_3CH_2CONH_2$ (32)	CH_3CH_2CN (1)	$CH_3CH_2CH_2NHCOCH_2CH_3$ (2)	$(CH_3CH_2CH_2)_2NCHO$ (3)	NH_4CO_3H (56)[c]
$CH_3CH_2CH_2$–	80	$CH_3CH_2CONH_2$ (11)	CH_3CH_2CN (1)	$CH_3CH_2CH_2NHCOCH_2CH_3$ (2)	$(CH_3CH_2CH_2)_2NCHO$ (2)	NH_4CO_3H (23)[c]
$CH_3CH_2CH_2$–[d]	15	$CH_3CH_2CONH_2$ (48)	CH_3CH_2CN (1)	$CH_3CH_2CH_2NHCOCH_2CH_3$ (2)	$(CH_3CH_2CH_2)_2NCHO$ (1)	NH_4CO_3H (2)[c]
$CH_3(CH_2)_5$–	15	$CH_3(CH_2)_4CONH_2$ (42)	$CH_3(CH_2)_4CN$ (8)	NH_4CO_3H (11)[c]		
$(CH_3)_2CH$–	15	CH_3COCH_3 (58)	$(CH_3)_2C{=}NOH$ (15)	NH_4CO_3H (34)[c]		
$(CH_3)_3C$–[e]	50	$(CH_3)_3CNH_2$ (63)	NH_4CO_3H (≈0)			

a) Reaction conditions: complex **1** (0.1 mmol), substrate (20 mmol), H_2O (40 mmol), THF (5 ml), 140 °C, 20 h. b) The yields were determined by GC using internal standards. c) Isolated yields. d) H_2O (100 mmol) was used. e) At 170 °C.

Table 2. Catalytic reduction of oxidized nitrogen compounds

Substrate	Condition[a]	Product	Yield/%[b]
Nitrosobenzene	A	Aniline	82
β-Picoline *N*-oxide	A[c]	β-Picoline	89
γ-Picoline *N*-oxide	A[c]	γ-Picoline	99
m-Nitrobenzonitrile	B	*m*-Aminobenzonitrile	93
m-Nitroacetophenone	B	*m*-Aminoacetophenone	81
m-Nitrobenzaldehyde	B	Poly(nitrilo-1,3-phenylenemethylidyne)	100[d]

a) Condition A: complex **1** (0.2 mmol), substrate (20 mmol), H_2O (40 mmol), THF (5 ml), CO (50 atm), 100 °C, 20 h; Condition B: complex **1** (0.05 mmol), substrate (10 mmol), H_2O (20 mmol), THF (5 ml), CO (50 atm), 150 °C, 20 h. b) GC yields. c) H_2O was not used. d) Isolated yield.

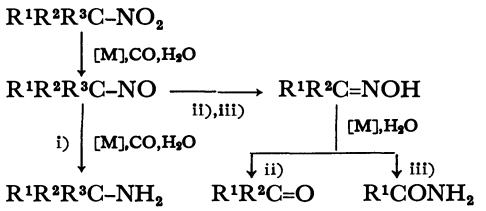

i) R^1,R^2,R^3 = alkyl. ii) R^1,R^2 = alkyl, R^3 = H.
iii) R^1 = alkyl, R^2,R^3 = H.

The applications of the catalyst **1** to the reductions or various organic compounds such as 1-hexane, methyl cinnamate, acetophenone, benzonitrile, *N*-benzylidenecyclohexylamine, triphenylphosphine oxide, and diphenyl sulfone were attempted, but these compounds were virtually inert under Condition A shown in Table 2. Picoline *N*-oxides were exceptionally reduciable to picolines, though the presence of H_2O is not required. These results indicate that the catalysis of **1** is selective to the reduction of compounds containing oxidized nitrogen. Consequently, it was possible to achieve the selective reduction of the nitro group of substituted nitrobenzenes containing cyano or carbonyl group.

Experimental

GC-MS spectra were recorded on a Hitachi M-52 spectrometer. ^{1}H-NMR spectra were recorded with a Varian T-60A spectrometer. All liquid compounds were distilled under an atmosphere of nitrogen before use.

General Procedure. All reactions were carried out in a stainless steel autoclave of 65 ml capacity, heated by an external rocking electric oven. A THF solution of $[Ru(cod)(py_4](BPh_4)_2$, substrate, and H_2O was placed in the autoclave, which was subsequently charged with CO. After heating for 20 h, the autoclave was cooled to room temperature. The reaction mixture was analyzed by the GC method using an internal standard. The identification of the products was accomplished by GC/MS, IR, and ^{1}H-NMR techniques, and by comparison with those of authentic samples. Some spectral data were as follows; $CH_3CH_2CH_2NHCOCH_2CH_3$: MS, 115 (M^+); IR (cm^{-1}), 3350 (ν_{NH}), 1640 (ν_{CO}); ^{1}H-NMR (CCl_4, δ), 0.9 (t, CH_3CCN), 1.5 (h, CH_2CN), 3.1 (q, CH_2N), 1.1 (t, CH_3CCO), 2.2 (q, CH_2CO), 7.6 (b, NH); $(CH_3CH_2CH_2)NCHO$: MS, 129 (M^+); IR (cm^{-1}), 1660 (ν_{CO}); ^{1}H-NMR (CCl_4, δ), 0.9 (t, CH_3), 1.5 (h, CH_2CN), 3.2 (t, CH_2N), 8.0 (s, CHO).

References

1) T. Cole, R. Ramage, K. Cann, and R. Pettit, *J. Am. Chem. Soc.*, **102**, 6182 (1980); Y. Watanabe, N. Suzuki, S. C. Shim, M. Yamamoto, T. Mitsudo, and Y. Takegami, *Chem. Lett.*, **1980**, 429. K. Cann, T. Cole, W. Slegeir, and R. Pettit, *J. Am. Chem. Soc.*, **100**, 3969 (1978); A. F. M. Iqbal, *Tetrahedron Lett.*, **1971**, 5833.

2) R. C. Ryan, G. M. Wilemon, M. P. Dalsanto, and C. U. Pittman, Jr., *J. Mol. Catal.*, **5**, 319 (1979).

3) T. Okano, K. Fujiwara, H. Konishi, and J. Kiji, *Chem. Lett.*, **1981**, 1083.

4) A few studies on the hydrogenation of olefins has been reported: T. Okano, T. Kobayashi, H. Konishi, and J. Kiji, *Bull. Chem. Soc. Jpn.*, **54**, 3799 (1981); K. Murata and A. Matsuda, *ibid.*, **54**, 1899(1981); T. Kitamura, T. Jor, and N. Hagihara, *Chem. Lett.*, **1975**, 203.

5) It has been reported that nitroalkanes are virtually inert in the presence of $Ph_6(CO)_{16}$–amine catalyst which is active for the reduction of nitrobenzenes with CO and H_2O: Ref. 3.

6) F. Falbe, *Angew. Chem., Int. Ed. Engl.*, **5**, 444 (1966); L. Field, P. B. Hughmark, S. H. Shumaker, and W. S. Marshall, *J. Am. Chem. Soc.*, **83**, 1983 (1961).

Synthesis and Lithiation of 2-Alkylthio- and 2-Arylthio-1,3-dithiolanes

Shigeo TANIMOTO,* Tatsuo OIDA, Hideyuki IKEHIRA, and Masaya OKANO
Institute for Chemical Research, Kyoto University, Uji, Kyoto 611

(Received September 24, 1981)

Synopsis. Several 2-alkylthio- and 2-arylthio-1,3-dithiolanes were synthesized by the reaction of 2-ethoxy-1,3-dithiolane with aliphatic and aromatic thiols in the presence of $ZnCl_2$. The lithiation of 2-alkylthio-1,3-dithiolanes with butyllithium in tetrahydrofuran followed by the addition of alkyl halides gave unsymmetrical dialkyl trithiocarbonates in moderately good yields.

Although the so-called six-membered cyclic trithioorthoformates (derivatives of 1,3-dithiane) have been studied[1] intensively, little is known about the five-membered analogues (derivatives of 1,3-dithiolane). To our knowledge, only a few compounds are reported in the literature. Nakayama[2] described the replacement of the butoxy-group of 2-(3-methylbutoxy)-1,3-benzodithiole by alkylthio- and arylthio-groups producing 2-alkylthio- and 2-arylthio-1,3-benzodithioles. The others are 2-phenylthio-1,3-dithiolane and 2,2′-[1,2-ethanediylbis(thio)]bis(1,3-dithilane); the former was synthesized in 1976 by Yoshida and his co-workers,[3] who obtained this compound by the thiolysis of the *N*-tosylsulfilimine derived from 1,3-dithiolane, and the latter is most easily available,[4] but it appears to be far from general. Recently, we described a process for the introduction of a formyl moiety to some phenols.[5] This procedure involved the reaction of the phenols with 2-ethoxy-1,3-dithiolane[4] in the presence of $BF_3 \cdot Et_2O$ and subsequent hydrolysis of the resulting 1,3-dithiolan-2-ylated phenols. We have now found that the reaction of aromatic thiols with 2-ethoxy-1,3-dithiolane proceeds smoothly by using $ZnCl_2$ as a catalyst to afford 2-arylthio-1,3-dithiolanes; in this case no nuclear substitution products are formed. This sulfur-for-oxygen interchange reaction proved to be quite general even when aliphatic thiols were used, although in the cases with low-boiling aliphatic thiols the reaction had to be performed with a large excess of the thiols. If the aliphatic thiols are not used in excess, the products are often isolated in an impure state. Thus an interchange reaction of 2-ethoxy-1,3-dithiolane with aliphatic and aromatic thiols was demonstrated; it was analogous to that observed previously in the case of 2-(3-methylbutoxy)-1,3-benzodithiole.[2] The results are summarized in Table 1.

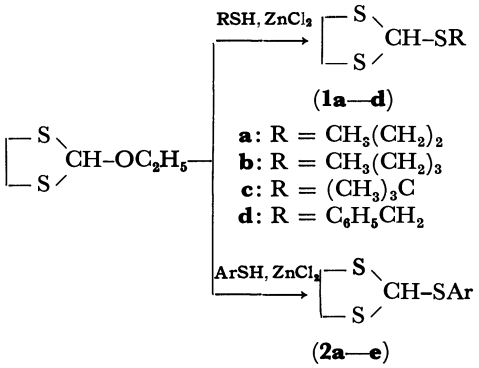

a: Ar = C_6H_5, **b**: Ar = *p*-ClC_6H_4, **c**: Ar = *p*-$CH_3C_6H_4$, **d**: Ar = *o*-$CH_3C_6H_4$, **e**: Ar = *m*-$CH_3C_6H_4$.

TABLE 1. REACTION OF 2-ETHOXY-1,3-DITHIOLANE WITH THIOLS

Run	RSH or ArSH	2-Alkylthio- or 2-arylthio-1,3-dithiolane: Abbr.	Yield[a] %	Bp θ_b/°C(Torr)	^{1}H-NMR (δ, in $CDCl_3$)
1	$CH_3(CH_2)_2SH$	**1a**[b]	75	153—158 (22.5)	5.60(s,1H),3.5—3.1(m,4H),2.66 (t,2H),1.9—1.3(m,2H),0.99(t,3H)
2	$CH_3(CH_2)_3SH$	**1b**[b]	76	167—173 (22.5)	5.58(s,1H),3.5—3.2(m,4H),2.66 (t,2H),1.9—1.2(m,4H),0.93(t,3H)
3	$(CH_3)_3CSH$	**1c**[b]	37	152—157 (22.5)	5.66(s,1H),3.5—3.1(m,4H),1.36 (s,9H)
4	$C_6H_5CH_2SH$	**1d**[c]	54	174—180 (4.5)	7.4—7.1(m,5H),5.31(s,1H), 3.79(s,2H),3.4—3.1(m,4H)
5	C_6H_5SH	**2a**[c]	72	156—159 (3.5) [lit,[3] 132—134(1)]	7.6—7.1(m,5H),5.73(s,1H), 3.4—3.1(m,4H)
6	*p*-ClC_6H_4SH	**2b**[c]	53	181—186 (4.5)	7.6—7.1(m,4H),5.73(s,1H), 3.5—3.1(m,4H)
7	*p*-$CH_3C_6H_4SH$	**2c**[c]	57	168—171 (5)	7.5—7.0(m,4H),5.71(s,1H), 3.4—3.1(m,4H),2.30(s,3H)
8	*o*-$CH_3C_6H_4SH$	**2d**[c]	63	162—166 (3.5)	7.6—7.0(m,4H),5.75(s,1H), 3.4—3.1(m,4H),2.43(s,3H)
9	*m*-$CH_3C_6H_4SH$	**2e**[c]	41	169—174 (4)	7.4—7.0(m,4H),5.77(s,1H), 3.4—3.1(m,4H),2.30(s,3H)

a) Yield of isolated product based on 2-ethoxy-1,3-dithiolane. b) Isolated by distillation under reduced pressure. c) Isolated by column chromatography on silica gel.

The removement of the trithioorthoformate proton of 2-alkylthio- and 2-arylthio-1,3-dithiolanes could be achieved by observing at −5——10 °C and by the addition of an easily available metalating agent such as butyllithium. In reaction with 2-alkylthio-1,3-dithiolanes, the initially formed anion is assumed to be **3**, which decomposes to ethylene and alkyl trithiocarbonate anion (**4**), and the latter is subsequently alkylated by alkyl halides to afford the unsymmetrical dialkyl trithiocarbonates (**5**).[6—8]

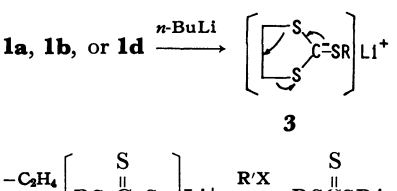

R = $CH_3(CH_2)_2$, $CH_3(CH_2)_3$, $C_6H_5CH_2$
R′X = CH_3I, C_2H_5I, $CH_3(CH_2)_2I$, $CH_3(CH_2)_3I$, $C_6H_5CH_2Br$

In cases where the experiments using 2-arylthio-1,3-dithiolanes were performed in the same way as that applied to 2-alkylthio-1,3-dithiolanes, the similarly formed aryl trithiocarbonate anion (**7**) undergoes further fragmentation to afford carbon disulfide and arenethiolate anion (**8**), presumably due to the electron-withdrawing effect of the benzene ring. The anion (**8**) would be then trapped by methyl iodide. In three cases where Ar=C_6H_5, *p*-$CH_3C_6H_4$, *m*-$CH_3C_6H_4$ in 2-arylthio-1,3-dithiolanes, none of the corresponding aryl methyl trithiocarbonates were recognized, but **9a**, **9c**, and **9e** were obtained in 75, 97 and 84% yield, respectively. It is also confirmed that **7** is unstable and decomposes similarly even at −78 °C. Thus an obvious difference in behavior between 2-alkylthio- and 2-arylthio-1,3-

Table 2. Lithiation of 2-alkylthio-1,3-dithiolanes

Run	2-Alkylthio-1,3-dithiolane	R′X	Unsymmetrical dialkyl trithiocarbonate (5)			
			R in 5	Yield[a] %	Bp θ_b/°C(Torr)	^{1}H-NMR (δ, in $CDCl_3$)
1[b]	**1a**	CH_3I	$CH_3(CH_2)_2$	99	66—71 (2) [lit,[7] 129—130 (21)]	3.34(t,2H),2.72(s,3H), 2.0—1.3(m,2H),1.00(t,3H)
2	**1a**	C_2H_5I	$CH_3(CH_2)_2$	94	89—94 (2.5)	3.34(q,2H),3.32(t,2H), 2.0—1.3(m,2H),1.32(t,3H), 1.01(t,3H)
3	**1a**	$C_6H_5CH_2Br$	$CH_3(CH_2)_2$	71	162—167 (3)	7.4—7.1(m,5H),4.54(s,2H), 3.28(t,2H),2.0—1.3(m,2H), 0.94(t,3H)
4	**1b**	CH_3I	$CH_3(CH_2)_3$	88	92—93 (3)	3.36(t,2H),2.72(s,3H), 1.9—1.1(m,4H),0.93(t,3H)
5	**1b**	C_2H_5I	$CH_3(CH_2)_3$	88	99—104 (2.5) [lit,[6] 80—82 (0.1)]	3.33(q,2H),3.32(t,2H), 1.8—1.1(m,4H),1.32(t,3H), 0.92(t,3H)
6	**1b**	$C_6H_5CH_2Br$	$CH_3(CH_2)_3$	87	167—170 (3)	7.4—7.2(m,5H),4.55(s,2H), 3.32(t,2H),1.8—1.1(m,4H), 0.91(t,3H)
7	**1d**	CH_3I	$C_6H_5CH_2$	78	140—144 (2.5) [lit,[7] 134—136 (1)]	7.4—7.1(m,5H),4.52(s,2H), 2.63(s,3H)
8	**1d**	$CH_3(CH_2)_2I$	$C_6H_5CH_2$	77	154—156 (2.2)	——[c]
9	**1d**	$CH_3(CH_2)_3I$	$C_6H_5CH_2$	81	165—167 (2.5)	——[d]

a) Yield of isolated product based on 2-alkylthio-1,3-dithiolane. b) The product in this case was isolated by column chromatography on silica gel, using 10% ether–hexane as the eluent. c) The product is identical with that obtained in the case of Run 3. d) The product is identical with that obtained in the case of Run 6.

dithiolanes has been noted.

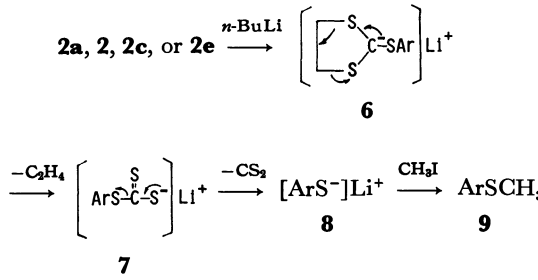

a: Ar = C_6H_5, **c**: Ar = *p*-$CH_3C_6H_4$, **e**: Ar = *m*-$CH_3C_6H_4$

Experimental

Reaction of 2-Ethoxy-1,3-dithiolane with a Thiol. The reaction was carried out by stirring a mixture of 2-ethoxy-1,3-dithiolane (5.0 g, 33.3 mmol), a thiol (33.6 mmol) (100 mmol was used in the cases of low-boiling aliphatic thiols, *i.e.*, in Runs 1, 2, and 3 in Table 1) and $ZnCl_2$ (4.6 g, 33.8 mmol) at room temperature for 24 h. The mixture was poured into a large quantity of dilute aqueous NaOH and extracted with several portions of ether. The combined ethereal extracts were washed repeatedly with dilute aqueous NaOH, dried, filtered, and concentrated *in vacuo* to give a residue. The product was isolated by distillation under reduced pressure or by column chromatography on silica gel, using 10% ether–hexane as the eluent.

Conversion of a 2-Alkylthio-1,3-dithiolane to an Unsymmetrical Dialkyl Trithiocarbonate (5). To a stirred solution of a 2-alkylthio-1,3-dithiolane (5.0 mmol) dissolved in tetrahydrofuran (20 ml), under nitrogen at −5—−10 °C, was added a 1.56 molar solution (3.8 ml, 5.9 mmol) of butyllthium in hexane; the stirring was continued for 20—30 min at that temperature. A solution of an alkyl halide (10 mmol) (6—7 mmol was used in the case of benzyl bromide) in tetrahydrofuran (2—3 ml) was added, and the mixture was stirred at −5—−10 °C for 1 h and further at room temperature for 4 h. Water (30 ml) and a saturated aqueous solution (30 ml) of ammonium chloride were added, and the mixture was extracted with several portions of ether. The combined ethereal extracts were dried, filtered, and concentrated *in vacuo* to give a residue, which was distilled under reduced pressure to afford an unsymmetrical dialkyl trithiocarbonate. Only in the case of Run 1 (Table 2) was the product isolated by column chromatography.

References

1) W. D. Woessner, *Chem. Lett.*, **1976**, 43; D. Seebach, *Angew. Chem., Int. Ed. Engl.*, **6**, 442 (1967); D. Seebach, K.-H. Geiss, A. K. Beck, B. Graf, and H. Daum, *Chem. Ber.*, **105**, 3280 (1972); R. M. Carlson and P. M. Helquist, *Tetrahedron Lett.*, **1969**, 173; K. Araki and M. Ōki, *Bull. Chem. Soc. Jpn.*, **49**, 553 (1976).

2) J. Nakayama, *Synthesis*, **1975**, 436.

3) H. Yoshida, M. Yoshikane, T. Ogata, and S. Inokawa, *Synthesis*, **1976**, 551.

4) S. Tanimoto, T. Miyake, and M. Okano, *Bull. Inst. Chem. Res., Kyoto Univ.*, **55**, 276 (1977).

5) S. Jo, S. Tanimoto, T. Sugimoto, and M. Okano, *Bull. Chem. Soc. Jpn.*, **54**, 2120 (1981).

6) W. D. Habicher and R. Mayer, Ger. (East) 67416; *Chem. Abstr.*, **72**, 12149e (1970).

7) H. Yoshida, *Nippon Kagaku Zasshi*, **89**, 883 (1968).

8) H. C. Godt, Jr., and R. E. Wann, *J. Org. Chem.*, **26**, 4047 (1961).

Stereoselective Micellar Catalysis. II. Kinetic Properties of Optically Active Micellar Catalysts for Cleavage of Amino Acid Ester Derivatives

Yasuji IHARA* and Reiko HOSAKO

Yamaguchi Women's University, 3-2-1 Sakurabatake, Yamaguchi 753

(Received June 29, 1981)

Synopsis. Stereoselective reactions of the enantiomers of *N*-acylamino acid *p*-nitrophenyl esters with *N*-decanoyl-(D or L)-histidine (DecHis) in an optically active surfactant (DMEBr) derived from (*l*)-ephedrine were studied at 25 °C and pH 7.30 in comparison with those of simple surfactant, hexadecyltrimethylammonium bromide (CTABr). The mixed micelles of DecHis and DMEBr are effective stereoselective catalysts and the catalytic effects are determined mainly by the nucleophilic reactivity of the optically active histidine residue of DecHis.

Surfactant micelles have been extensively investigated as favorable models for enzyme catalysis;[1] particularly, several esterolysis reactions have been performed with optically active micellar systems in order to gain further insight into stereoselective properties of enzymic reactions.[2]

In our previous papers,[3] we showed that functional mixed micelles of optically active catalysts containing a histidine residue and hexadecyltrimethylammonium bromide (CTABr) are very effective stereoselective catalysts for cleavage of enantiomeric substrates, and a mechanism was suggested for reaction in mixed micelles involving acylation of the optically active histidine residue.

In this paper, we describe kinetic results for cleavage of amino acid ester derivatives in a mixed micellar system formed from *N*-decanoly-(D or L)-histidine (DecHis) and an optically active cationic surfactant (DMEBr) having the hydroxyl function at the polar head, and results are compared with those observed in the mixed micelles with CTABr.

Catalyst

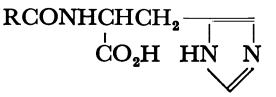

DecHis; $R=CH_3(CH_2)_8$
BzHis; $R=C_6H_5$

Substrate

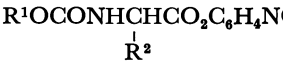

ZPheONp; $R^1=R^2=C_6H_5CH_2$
ZAlaONp; $R^1=C_6H_5CH_2$, $R^2=CH_3$
ZGlyONp; $R^1=C_6H_5CH_2$, $R^2=H$
MocPheONp; $R^1=CH_3$, $R^2=C_6H_5CH_2$

Surfactant

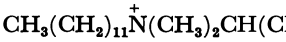

DMEBr

Experimental

Materials. Hexadecyltrimethylammonium bromide (CTABr) was purified by established methods.[4] *N*-Dodecyl-*N*-methyl-*l*-ephedrinium bromide (DMEBr) and *N*-decanoyl-(D or L)-histidine (DecHis) were prepared and purified by standard methods.[5] *N*-Benzoyl-L-histidine (BzHis) was obtained from Sigma Chemical Co. The substrates, *p*-nitrophenyl esters of *N*-benzyloxycarbonyl-D-alanine, and *N*-methoxycarbonyl-D and L-phenylalanine were synthesized by the dicyclohexylcarbodiimide method.[6] Other *p*-nitrophenyl esters of *N*-benzyloxycarbonyl amino acids were purchased from Sigma Chemical Co., and were used without further purification. The purity of these esters was confirmed by kinetic analysis.

Kinetic Measurements. The cleavage of *p*-nitrophenyl esters was performed at pH 7.30, 0.02 mol dm^{-3} of phosphate buffer, and 25 °C in 0.83% CH_3CN–H_2O, and the formation of the *p*-nitrophenolate anion was followed spectrophotometrically at 400 nm. The pseudo-first-order rate constants were obtained from plots of $\log(A^{\infty}-A^{t})$ *vs.* time (t) by use of the least-squares method. Correlation coefficients were >0.999.

Results and Discussion

Optically active DMEBr micelles showed considerably different catalytic efficiencies for the hydrolysis of enantiomeric *p*-nitrophenyl α-methoxyphenylacetate.[7] However, no appreciable stereoselectivity was observed for the above esters in the presence of a simple optically active surfactant, hexadecyldimethyl-(α-methylbenzyl)ammonium bromide.[8]

In this study, substrates, ZPheONp, ZAlaONp, and MocPheONp, were hydrolyzed in the presence of

Table 1. Hydrolysis of enantiomeric substrates in the presence of DMEBr[a]

Substrate	$10^3(k_\psi-k_0)/s^{-1}$		D/L
	D	L	
ZPheONp	4.46±0.11	3.99±0.15	1.12
ZAlaONp	2.23±0.08	2.06±0.05	1.08
MocPheONp	1.87±0.08	1.78±0.05	1.05

a) In 6.00×10^{-3} mol dm^{-3} DMEBr, at pH 7.30, 0.02 mol dm^{-3} of phosphate buffer, and 25 °C. [Substrate] $=1.0\times10^{-5}$ mol dm^{-3}. k_ψ and k_0 denote the pseudo-first-order rate constants in the presence and absence of DMEBr.

Table 2. Rate constants on variation of surfactant concentration[a]

10^3[DMEBr] / mol dm^{-3}	$10^3(k_\psi-k_{surfact})/s^{-1}$		
	L	D	L/D
3.00	214(5.86)	90.6(4.06)	2.36(1.44)
4.00	164(5.32)	65.6(3.96)	2.50(1.34)
5.00	(5.20)	(3.64)	(1.43)
6.00	104(4.70)	41.6(3.44)	2.50(1.37)
8.00	64.0	26.8	2.39

a) In 2.00×10^{-4} mol dm^{-3} L-DecHis at pH 7.30, 0.02 mol dm^{-3} of phosphate buffer, 25 °C, and [ZPheONp] $=1.0\times10^{-5}$ mol dm^{-3}. The values in parentheses are for L-BzHis.

Table 3. Apparent catalytic rate constants in optically active mixed micellar systems[a]

Substrate	Surfactant	k_c/mol^{-1} dm^3 s^{-1}		L/D (D/L)
		L-DecHis	D-DecHis	
PNPA[b]	DMEBr[b]	5.97	5.77	1.03
PNPH[b]	DMEBr[b]	15.4	15.2	1.01
ZGlyONp	DMEBr	121	116	1.04
	CTABr	162	161	1.01
L-ZAlaONp	DMEBr	139 (85.4)	85.5 (121)	1.63 (1.42)
	CTABr	280 (140)	141 (283)	1.99 (2.02)
L-ZPheONp	DMEBr	522 (208)	192 (462)	2.72 (2.22)
	CTABr	572 (231)	228 (569)	2.51 (2.46)
L-MocPheONp	DMEBr	229 (127)	114 (229)	2.01 (1.80)
	CTABr	314 (141)	145 (315)	2.17 (2.23)

a) In 6.00×10^{-3} mol dm^{-3} DMEBr or CTABr, at pH 7.30, 0.02 mol dm^{-3} of phosphate buffer, and 25 °C. [DecHis] = 0.40—5.33×10^{-4} mol dm^{-3} and [substrate] = 1.0×10^{-5} mol dm^{-3}, unless otherwise specified. Values in parentheses are for D-substrates. The k_c values are calculated by the least-squares method and generally have correlation coefficients of over 0.99. b) [PNPA or PNPH] = 1.0×10^{-4} mol dm^{-3} and [DMEBr] = 5.00×10^{-2} mol dm^{-3}.

6.00×10^{-3} mol dm^{-3} DMEBr at pH 7.30 and 25 °C (Table 1). DMEBr micelles show slightly different catalytic efficiencies in the hydrolysis of the enantiomeric substrates; D substrates are more reactive than L enantiomers. In CTABr micelles there was no difference between the rates of hydrolysis of the enantiomeric substrates within experimental error.[3]

The catalytic effects of L-DecHis and L-BzHis for ZPheONp hydrolysis were first examined by varing the DMEBr concentration at pH 7.30 and 25 °C (Table 2). At higher ratios the rates decrease but the stereoselective effect is almost unchanged when L-DecHis is diluted with DMEBr. A similar effect is observed in the mixed micelles of L-BzHis and DMEBr. Therefore, the stereoselective kinetic analysis was carried out at a fixed surfactant concentration (6.00×10^{-3} mol dm^{-3}). The catalytic second-order rate constants (k_c) were obtained from the linear slope of a plot of the observed pseudo-first order rate constants (k_ψ) against catalyst concentration under the condition: [surfactant] > [catalyst] > [substrate]. Table 3 summarizes results for the cleavage of the substrates by (D or L)-DecHis in the presence of DMEBr. For comparison, (D or L)-DecHis–CTABr catalyzed rates also are determined and listed in Table 3.

From Table 3, it is apparent that there is no rate difference between D- and L-DecHis for cleavage of nonspecific substrates, such as *p*-nitrophenyl acetate (PNPA) and hexanoate (PNPH), and optically inactive substrate (ZGlyONp). On the other hand, it is found that L-DecHis reacts more selectively than D-DecHis with L substrates, and D-DecHis with D substrates. The pattern of stereoselective effects for the optically active substrates in the mixed (D or L)-DecHis–DMEBr micelle is similar to that found in the mixed (D or L)-DecHis–CTABr. These results show that the stereoselectivity is determined mainly by the nucleophilic reactivity of the optically active histidyl residue of DecHis. It is well known that the imidazolyl and hydroxyl groups act as nucleophiles giving acylated products, and that the imidazolyl group is more reactive than the hydroxyl group under neutral conditions. Thus, reaction rates with the mixed DecHis–DMEBr micelle are two orders of magnitude higher than those with the DMEBr micelle alone at pH 7.30.

A comparison of the rate constants between mixed micelles with DMEBr and CTABr indicates that both the reactivity and stereoselectivity of ZPheONp are essentially the same, but that the rates of less hydrophobic substrates such as ZAlaONp bring about 2-fold decreases with the extent of stereoselectivity also decreasing from 2.0 to 1.4—1.6. Although the reactions with mixed D-DecHis–CTABr and L-DecHis–CTABr micelles produced the same differences between D and L substrates in the opposit direction within experimental error, the D-DecHis–DMEBr and L-DecHis–DMEBr micelles show slightly different catalytic efficiencies in the reactions with D and L enantiomers.

References

1) For example: J. H. Fendler and E. J. Fendler, "Catalysis in Micellar and Macromolecular Systems," Academic Press, New York (1975); C. A. Bunton, "Micellar Reactions," in "Application of Biochemical Systems in Organic Chemistry," ed by J. B. Jones, C. J. Sih, and D. Perlman, Wiley, New York (1976), Part 2.

2) For example: J. M. Brown and C. A. Bunton, *J. Chem. Soc., Chem. Commun.*, **1974**, 969; R. A. Moss, Y-S. Lee, and T. J. Lukas, *J. Am. Chem. Soc.*, **101**, 2499 (1979); R. A. Moss, Y-S. Lee, and K. W. Alwis, *ibid.*, **102**, 6646 (1980); K. Ohkubo, K. Sugahara, K. Yoshinaga, and R. Ueoka, *J. Chem. Soc., Chem. Commun.*, **1980**, 637; H. Ihara, S. Ono, H. Shosenji, and K. Yamada, *J. Org. Chem.*, **45**, 1623 (1980).

3) Y. Ihara, *J. Chem. Soc., Chem. Commun.*, **1978**, 984: *J. Chem. Soc., Perkin Trans. 2*, **1980**, 1483; Y. Ihara, N. Kunikiyo, T. Kunimasa, M. Nango, and N. Kuroki, *Chem. Lett.*, **1981**, 667.

4) E. F. J. Duynstee and E. Grunwald, *J. Am. Chem. Soc.*, **81**, 4540 (1959); C. A. Bunton and L. Robinson, *J. Org. Chem.*, **34**, 773 (1973).

5) C. A. Bunton, L. Robinson, and M. Stam, *J. Am. Chem. Soc.*, **92**, 7393 (1970); C. Gitler and A. Ocha-Solano, *ibid.*, **90**, 5004 (1968); T. Inoue, K. Nomura, and H. Kimizuka, *Bull. Chem. Soc. Jpn.*, **49**, 719 (1976).

6) M. Bodanszky and V. Du. Vigneaud, *J. Am. Chem. Soc.*, **81**, 5688 (1959); D. T. Elmore and J. J. Smyth. *Biochem. J.*, **94**, 563 (1965).

7) C. A. Bunton, L. Robinson, and M. F. Stam, *Tetrahedron Lett.*, **1971**, 121.

8) R. A. Moss and W. L. Sunshine, *J. Org. Chem.*, **39**, 1083 (1974).

Reaction of Electrochemically Generated Radical Anion of Thioketone with Alkylating Agents

Shinro YASUI, Kaoru NAKAMURA,† Atsuyoshi OHNO,*,† and Shinzaburo OKA†

Tezukayama Junior College, 3 Gakuen-Minami, Nara 631

†*Institute for Chemical Research, Kyoto University, Uji, Kyoto 611*

(Received December 17, 1981)

Synopsis. Electrochemically generated anion radicals of thioketones were allowed to react with alkyl halides (or tosylate). Electronic structure of the anion radical is discussed on the basis of the products.

It was reported that the polarization of thiocarbonyl group is largely affected by the substituent, and it is not uncommon that the dipole is oriented from positive sulfur to negative carbon.[1,2] It has also been proposed that the electronic structure of anion radical of thioketone reflects the electronic effect of the substituent; an anion radical from an aromatic thioketone being in carbanion-like structure, whereas that from an aliphatic thioketone being in thiolate-like structure.[3,4] However, the electronic structure of anion radical of thioketone is still ambiguous because the proposition bases on the behavior of transient reaction intermediate. Minoura and his co-worker reported the reactions of sodium thiobenzophenone thioketyl.[5] However, obviously the reaction does not represent the reaction of thiobenzophenone thioketyl since the anion radicals disproportionate easily into a dianion and a neutral molecule under the reaction conditions. At the same time, the anion radical from metal thioketyl is not free from large influence of the counter cation.[6] In order to understand intrinsic nature of anion radicals from thioketones, we generated them by cathodic reduction of thioketones, and studied their reactions with alkyl halides.

Results and Discussion

Appropriate amounts of thiobenzophenone (**1a**), 4,4'-dimethoxythiobenzophenone (**1b**), or thiopivalophenone (**2**) and an alkyl halide or tosylate were dissolved in acetonitrile and subjected to cathodic reduction

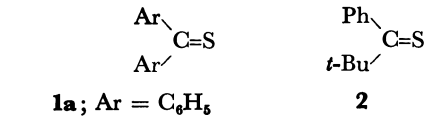

1a; Ar = C_6H_5
1b; Ar = *p*-$MeOC_6H_4$

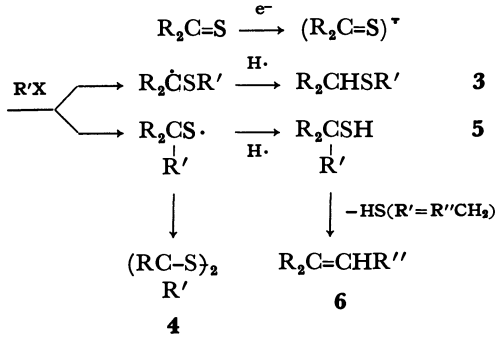

(−1.6 V *vs.* SCE) in the presence of tetraethylammonium perchlorate as supporting electrolyte. After the color of thioketone had disappeared completely, reaction products were analyzed. Results are summarized in Table 1. Since the reduction potentials of **1** (≈−1.0 V *vs.* SCE) and **2** (≈−1.3 V *vs.* SCE) are lower than those of alkyl halides,[7] the electrochemical reduction may reduce thioketone rather than the alkyl halide. Initial reduction of thioketone is also supported by the fact that the reaction with **1** affords *C*-alkylated product(s); diaryl or aryl alkyl thioketone is known to be a very efficient free-radical scavenger,[8] and if the alkyl halide were the species to be reduced initially, all products should be *S*-alkylated ones. However, it is plausible

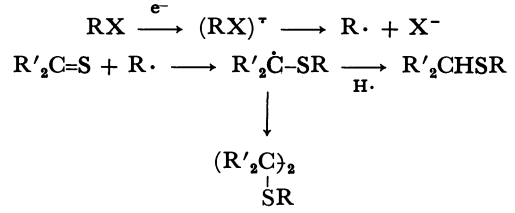

that the anion radical of thioketone transfers an electron to the alkyl halide within a solvent cage when they encounter each other, as proposed for the reaction of thiolate anion and alkyl halide.[9]

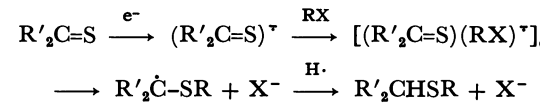

Although not major, the formation of *C*-alkylated product(s) from **1**, but not from **2**, suggests that the anion radical of diaryl thioketone has more carbanion-

Table 1. Isolated yields of products

Thioketone	Alkyl halide	Reaction time/min	Yield/% *S*-Alkylated product, **3**	*C*-Alkylated product **4**	**5**	**6**	Others
1a	MeI	50	20	6			18[a]
	MeOTs[b]	40	15	10			
	EtI	40	15	—[c]			
1b	MeI	50	26		3	12	
	MeOTs[b]	60	35		15	—[c]	35[a]
	EtI	30	24			14	
2[d]	MeI	—[e]	16				
	MeOTs[b]	—[e]	46				
	$PhCH_2Br$	—[e]	10				
	i-PrBr	—[e]	23				
	$BrCH_2$–CH_2CH_2Cl	—[e]	27[f]				

a) $Ar_2C=O$. b) Methyl *p*-toluenesulfonate. c) Trace amount. d) One mmol of **2** and 4 mmol of an alkyl halide were used. e) Overnight (≈20 h). f) ω-Chloro sulfide was obtained.

like character than alkyl aryl thioketone accordantly with the previous proposal.[2,3] Olefinic products are formed only when **1b** is subjected to the reaction, probably because electron-releasing effect of two *p*-methoxyl groups facilitates El-type elimination of hydrogen sulfide from the thiol resulted by *C*-alkylation.

It is interesting, in summary, to note that one can obtain *C*-alkylated product(s) when a neutral alkyl aryl or dialkyl thioketone is treated with a carbanion, whereas only *S*-alkylated product is obtained by the same reaction with diaryl thioketone.

Experimental

Materials. Thioketones were prepared according to the literature procedure.[10] Tetraethylammonium perchlorate, alkyl halides, and methyl tosylate were purchased from a commercial source (Nakarai Chem. Co.). Acetonitrile was distilled three times on phosphorus pentaoxide and once on potassium carbonate, then kept in a bottle filled with dry argon and capped by a silicon-rubber stopper.

Procedure. In both arms of a H-shaped electrolytic cell, each 5 cm^3 of acetonitrile containing 100 mg of tetraethylammonium perchlorate was placed. Then 0.25 mmol of a thioketone and 1 mmol of an alkyl halide (or tosylate) were dissolved in the cathode. Platinum electrodes were used. The reaction was run under a constant voltage of -1.6 V (*vs.* SCE) at room temperature. After the color of thioketone had disappeared, the solution in the cathode was taken out, quenched with water, and extracted three times with dichloromethane. The organic layer was washed once with saturated aqueous sodium chloride and dried over anhydrous sodium sulfate, then the solvent was removed *in vacuo*. The material thus obtained was chromatographed on a HPLC (silica gel) and product isolated were identified and quantitatively analyzed by NMR and mass spectroscopy.

References

1) F. Bernardi, I. G. Csizmnadia, H. B. Schlegel, and S. Wolfe, *Can. J. Chem.*, **53**, 1144 (1975).

2) T. Yamabe, S. Nagata, K. Akagi, R. Hashimoto, K. Yamashita, K. Fukui, A. Ohno, and K. Nakamura, *J. Chem. Soc., Perkin Trans. 2*, **1977**, 1516.

3) A. Ohno, K. Nakamura, M. Uohama, S. Oka, T. Yamabe, and S. Nagata, *Bull. Chem. Soc. Jpn.*, **48**, 3718 (1975).

4) A. Ohno, K. Nakamura, Y. Shizume, and S. Oka, *Bull. Chem. Soc. Jpn.*, **50**, 1003 (1977).

5) Y. Munoura and S. Tsuboi, *J. Org. Chem.*, **37**, 2064 (1972).

6) E. G. Janzan and C. M. Dubose, Jr., *J. Phys. Chem.*, **70**, 3372 (1960); *cf.* also H. C. Heller, *J. Am. Chem. Soc.*, **89**, 4288 (1967).

7) F. L. Lambert, *J. Org. Chem.*, **31**, 4184 (1966); M. von Stackleberg and W. Stracke, *Z. Electrochem.*, **53**, 118 (1949).

8) G. Tsuchihashi, M. Yamauchi, and A. Ohno, *Bull. Chem. Soc. Jpn.*, **43**, 968 (1970).

9) S. Bank and D. A. Boyd, *J. Am. Chem. Soc.*, **95**, 8203 (1973).

10) A. Ohno, K. Nakamura, Y. Nakazima, and S. Oka, *Bull. Chem. Soc. Jpn.*, **48**, 2403 (1975).

 © 1982 The Chemical Society of Japan Bull. Chem. Soc. Jpn., 55, 1983—1987 (1982)

Dynamic Structure of Pyrimidine-polyribonucleotides in Solution. ^{1}H NMR Studies[1)]

Atsuko YAMADA-NOSAKA,*,† Yoshio NOSAKA,*,† Kazuyuki AKASAKA, and Hiroyuki HATANO

Department of Chemistry, Faculty of Science, Kyoto University, Sakyo-ku, Kyoto 606

(Received June 25, 1981)

Temperature dependent conformations and molecular motions of pyrimidine polyribonucleotides, poly(C) and poly(U), have been studied in ^2H_2O solutions (pH 5.8±0.3, 5—72 °C) by measuring ^{1}H NMR intensities, chemical shifts, coupling constants, and spin-lattice relaxation times. Below 50 °C, poly(C) exists as a slowly exchanging mixture of double-stranded and single-stranded forms of which only the single-stranded form is observable by ^{1}H NMR. In this temperature range, the single-stranded poly(C) shows a strong base-stacking with dominated C_3'-*endo anti* conformation, whereas above 50 °C it takes partly C_2'-*endo* conformation with destabilization of the helical structure. Poly(U) exists as single strand within the whole temperature range studied, and the bases are nearly unstacked with 58% of C_2'-*endo* conformer. Poly(U) is more flexible than poly(C), which was characterized with rotational correlation times in the order of 10^{-9}—10^{-10} s.

Conformation of synthetic homopolynucleotides has been studied by many investigators as the first step toward the understanding of the structure of nucleic acids. In aqueous solution, each homopolynucleotide shows unique behaviour characteristic of its purine and pyrimidine bases.[2,3)] Nuclear magnetic relaxation measurements of ^{31}P showed different motions for different polynucleotides.[4)] However, their detailed structures in solution are still unknown although some of their structures in fiber states have been analyzed by X-ray diffraction.[5–7)]

At neutral pH, poly(C) takes single-stranded helix stabilized by base stacking, while at acidic pH (pH<5.0) it exists as a double-stranded helix in which the bases are held together by three hydrogen bonds, one of which can be formed only when a proton is added to N-3 for each pair of bases.[8–10)] In general, the ordered double helical form of high polymers does not give a high resolution NMR spectrum.[2)] Our previous ^{31}P NMR study[11)] exhibits that at acidic pH the signal is too broad to be observed presumably due to the double-stranded form, while at an intermediate pH between acidic and neutral the exchange between the double-stranded and single-stranded forms is slow in the NMR time scale, so that the single-stranded form and possibly partially double-stranded form can be observed.

In the present work, temperature dependence of ^{1}H chemical shifts, coupling constants and spin-lattice relaxation times of poly(C) and poly(U) were measured and the conformational features of single-stranded poly(C) are discussed together with those of poly(U) known to exist as a random coiled structure.

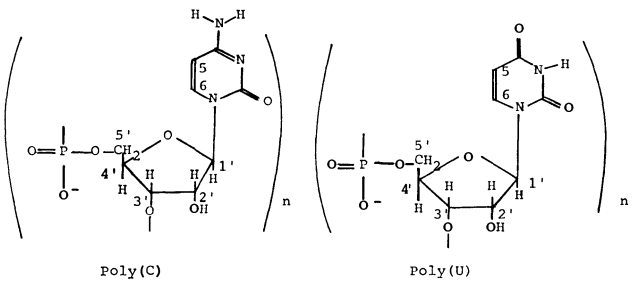

Poly(C) Poly(U)

† Present address: Department of Materials Science and Technology, The Technological University of Nagaoka, Nagaoka, Niigata 949-54.

Experimental

The potassium salts of poly(C) and poly(U) (molecular weight>10^5) were purchased from Sigma Chemical Company. The samples were dialysed against a large volume of 0.1 M (1 M=1 mol dm^{-3}) sodium chloride to remove low molecular species and paramagnetic metal ions. The solution was lyophilized and the residue was dissolved in ^2H_2O (99.7%). The lyophilization and addition of ^2H_2O were repeated three times to reduce ^1H_2O background. About 3 mM of EDTA was added to remove the effect of the remaining paramagnetic metal ions. No buffer was used. The final pH of the solution was 5.8±0.3 (direct pH meter reading). The samples were evacuated on a vacuum line and sealed in an NMR sample tube of 5 mm diameter. The final concentration of poly(U) and poly(C) were 92 mM and 53 mM in monomer unit, respectively, as determined from the optical absorption at 261 nm and 269 nm by using the molar extinction coefficients of 9600 and 6300 for poly(U) and poly(C), respectively.[12)]

Spin-lattice relaxation times (T_1) were measured at 100 MHz on a JEOL PFT Fourier transform NMR spectrometer using the inversion recovery pulse sequence (180°-t-90°). T_1 values were deduced with a non-linear least square fit method. Chemical shifts and coupling constants of poly(C) were measured at 360 MHz on a Bruker HX-360 spectrometer. Relative peak area was determined at 360 MHz by averaging the values obtained by three independent methods, *i.e.* measurement of peak height, integration of the peak area, and weighing the spectral sheet.

Results and Discussion

Poly(C). Figure 1(a) shows the peak area of the three protons (H_5, H_6, and H_1') of poly(C) at pH 5.8 as a function of temperature. It is noted that the peak area of each of the three protons shows an abrupt increase at about 45 °C. The loss of signal intensity below 45 °C seems to be best interpreted as due to the formation of the double-stranded form of poly(C) whose ^{1}H NMR signals are too broad to be observed. Moreover, the exchange between the single-stranded form and the double-stranded form of poly(C) must be slow in the NMR time scale,[11,13)] so that the observed signals correspond to the poly-

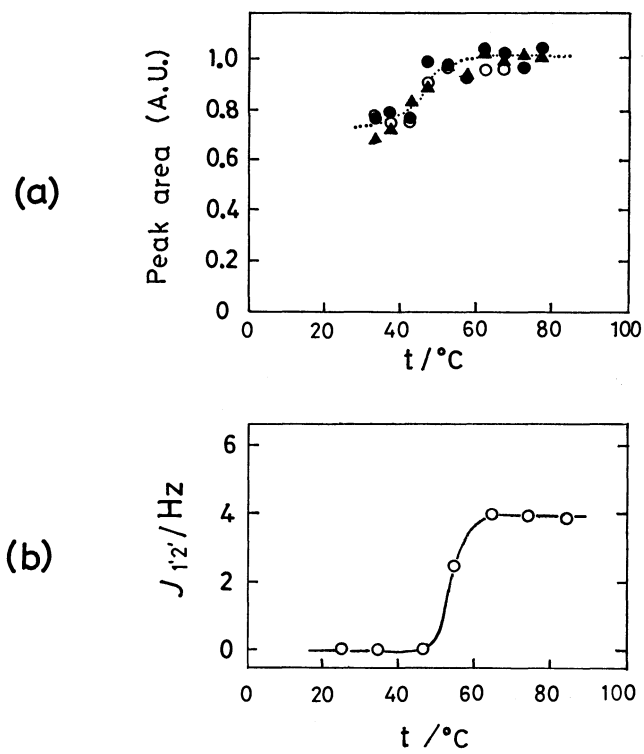

Fig. 1. Temperature dependence of ^{1}H NMR parameters of poly(C) measured at 360 MHz (53 mM in ^2H_2O, pH=5.8±0.3, [Na^+]=0.1).
(a): Peak area of H_5 (●), H_6 (▲), and $H_{1'}$ (○),
(b): coupling constant $J_{1'2'}$.

(C) in the single-stranded form and possibly in the partially double-stranded form. This interpretation is in accordance with the earlier observation that, in the acidic pH range, the signal intensity of ^{31}P resonance decreases upon protonation of poly(C) by the formation of a double strand.[11]

Figure 1(b) shows that the coupling constant between $H_{1'}$ and $H_{2'}$ ($J_{1'2'}$) is almost nil below 50 °C. From the Karplus relation, this result means that the dihedral angle ($\angle H_{2'}C_{2'}C_{1'}H_{1'}$) is close to 90°, *i.e.*, that the ribose ring of the single-stranded poly(C) takes exclusively $C_{3'}$-*endo* (N) conformation below 50 °C. $J_{1'2'}$ shows a sharp increase in the narrow temperature range of 50—65 °C, and above 65 °C becomes constant at 3.9 Hz. The increase in the coupling constant reflects the increase in the population of the $C_{2'}$-*endo* (S) conformer under the assumption of a rapid equilibrium between N and S conformers.[14] The population of the S conformer above 65 °C is then estimated to be 42% by using the equations given by Altona and Sundaralingam.[14]

In contrast, the chemical shifts of the three protons of poly(C) increase rather monotonically in the temperature range of 28—70 °C as shown in Fig. 2. This observation implies that at low temperature these protons receive strong deshielding effects from the ring currents of neighbouring bases, but that the effects are relieved at higher temperatures by gradual unstacking of bases, in agreement with the conclusion obtained from other methods.[13,15,16]

Lee and co-workers have suggested that the base

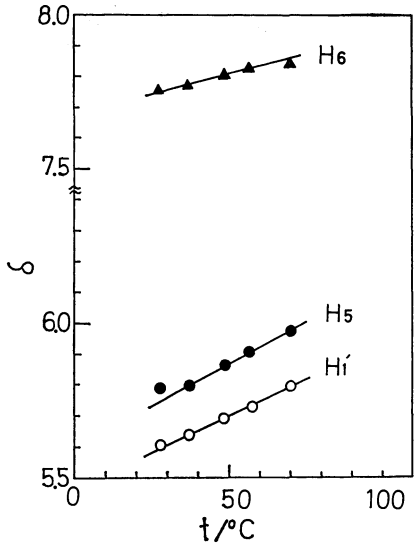

Fig. 2. Temperature dependence of chemical shifts of H_5, H_6, and $H_{1'}$ of poly(C) as measured from an internal standard of DSS (H_6 ▲, H_5 ●, $H_{1'}$, ○).

stacking arrangement prohibits the ribose ring to take the S-conformation, based on the fact that the ribose ring of dinucleotides has a large fraction of N-conformer corresponding to the increase in the fraction of base stacking.[17] The present results have shown that, similarly in poly(C), a single helical or partial double helical form with stacked bases and exclusive N ribose conformation is highly stabilized at low temperature, but that upon destacking of bases, poly(C) is allowed to take the S-conformation.

We may conclude that under the present experimental conditions, the conformational equilibria in poly(C) could be summarized in the following schemes:

$$\left.\begin{array}{ccc} \mathrm{Poly(C)_N^*} + \mathrm{H^+} & \overset{\text{rapid}}{\rightleftharpoons} & \mathrm{Poly(C)_N^*H^+} \\ \Big\| \text{rapid} & & \Big\| \text{rapid} \\ \mathrm{Poly(C)_S^*} + \mathrm{H^+} & \overset{\text{rapid}}{\rightleftharpoons} & \mathrm{Poly(C)_S^*H^+} \end{array}\right\} \quad (>65\,^\circ\mathrm{C}), \qquad (1)$$

$$\mathrm{Poly(C)_N^*} + \mathrm{H^+} \overset{\text{rapid}}{\rightleftharpoons} \mathrm{Poly(C)_N^*H^+} \quad (<50\,^\circ\mathrm{C}), \qquad (2)$$

$$\mathrm{Poly(C)_N^*} + \mathrm{Poly(C)_N^*H^+} \overset{\text{slow}}{\rightleftharpoons} \mathrm{Poly(C)_N^*H^+Poly(C)^*} \quad (<50\,^\circ\mathrm{C}), \qquad (3)$$

where Poly(C)* and Poly(C)*H$^+$Poly(C)* represent the single- and double-stranded forms of poly(C), respectively, and subscripts N and S represent N and S conformers of the ribose, respectively.

Figure 3 shows the temperature dependence of T_1's of H_5, H_6, and $H_{1'}$ of poly(C). In spite of the remarkable change of the coupling constant in the range of 50—60 °C, T_1 shows no abrupt change in the corresponding temperature range. Akasaka showed that the dynamic structure of a polynucleotide can be studied from the temperature dependence of T_1.[18] Namely, in an isotropic motional approach with a single τ_c, the T_1 minimum occurs at a rotational correlation time τ_c of 9.9×10^{-10} s at 100 MHz, and by using this τ_c and the minimum value of T_1, relevant interproton distances can be obtained. As shown in

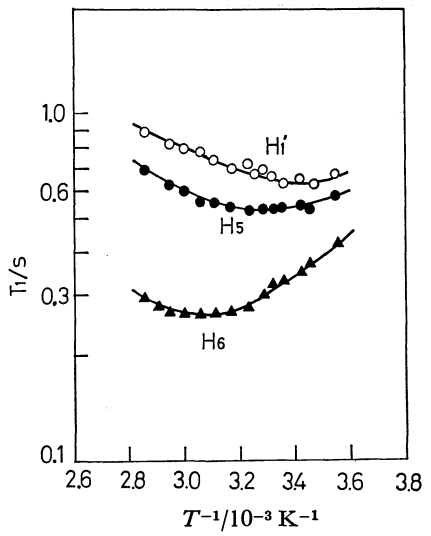

Fig. 3. Semilogarithmic plots of spin-lattice relaxation times (T_1) of poly(C) against reciplocal absolute temperature (H_6 ▲, H_5 ●, $H_{1'}$ ○).

Fig. 3, T_1's of all the three protons of poly(C) go through minima. However, they occur at different temperatures.

In principle, the occurence of different $T_{1\,min}$ temperatures indicates the possibility of differential motions of the three protons. The effect does not seem to arise from the cross-relaxation effect among protons,[19] since around $T_{1\,min}$, where $\omega\tau_c \approx 1$ holds, the cross-relaxation term is close to nil. By taking a simple approach of isotropic motion, the value of r_{iobsd} was obtained for each proton from the minimum values of T_1 (see Appendix), and the results are shown in Table 1.

The values of r_{iobsd} may be compared with r_{icalcd} calculated with atomic coordinates given for 5'-CMP,[20] by taking into account of dipolar interactions within the same nucleotide unit only. The r_{icalcd} values were computed for different torsional angles about the glycosidic bond (χ) varied at an interval of 10° and the dihedral angle ($\angle C_{3'}C_{4'}C_{5'}O_{5'}$) ($\phi$) at interval of 30°, respectively. The ribose conformation was fixed to $C_{3'}$-*endo*. The values of r_{icalcd} for H_6 was not calculated since T_1 for H_6 goes through minimum above 50 °C where the fraction of $C_{2'}$-*endo* conformer cannot be neglected.

On computation r_{icalcd} showed little dependence on ϕ. Therefore, the curves in Fig. 4 show r_{icalcd} as a function of χ for a fixed ϕ (=60°).[21] For H_5, r_{icalcd} and r_{iobsd} coincide in the whole region of χ within the experimental errors of T_1 (±5%), as is expected from the chemical structure of cytidine base

Table 1. r_{iobsd}'s deduced from minimum values of T_1 by using Eq. 3 in Appendix

	r_{iobsd}/Å		
	H_6	H_5	$H_{1'}$
Poly(C)	2.16±0.12	2.43±0.14	2.50±0.14
Poly(U)	2.15±0.12	2.48±0.15	2.48±0.15

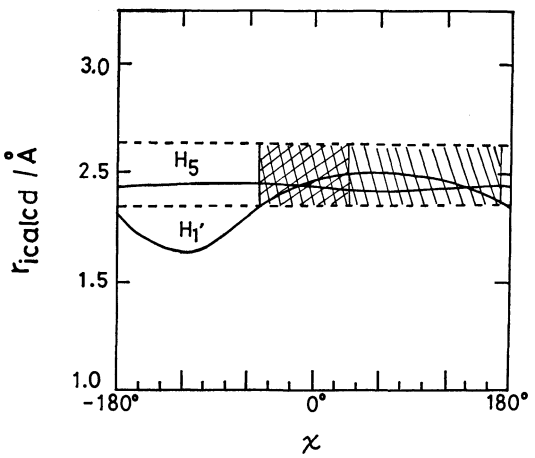

Fig. 4. r_{icalcd}'s $(\sum_j r_{ij}^{-6})^{-1/6}$ are plotted against torsional angle about glycosidic bond (χ).
Ribose ring and ϕ are fixed to $C_{3'}$-*endo* and 60°, respectively. The region where r_{icalcd} and r_{iobsd} coincide within experimental errors is shown by hatched line for $H_{1'}$. The cross-hatched area shows the allowed and plausible region obtained by taking account of the van der Waals exclusion.

where T_1 of H_5 is mainly determined by the dipolar interaction with H_6. The hatched region between the dotted lines in Fig. 4 shows where r_{icalcd} and r_{iobsd} of $H_{1'}$ coincide within experimental errors of T_1. The allowed region of χ for van der Waals contact was estimated to be −130°—40°, where the exclusive atomic radii for H and O were taken to be 0.95 and 1.1 Å, respectively. Therefore, the allowed and plausible region of χ for $H_{1'}$ is in the range of −50°—40° as is represented by the cross-hatched area in Fig. 4, showing that the orientation of the base is restricted to *anti*.

This result is consistent with the theoretical calculation in mononucleotides which predicts that the most probable value of χ for the pyrimidine base lies in the range of 0°—30° for the $C_{3'}$-*endo* sugars.[21] In solution, mononucleotides are shown to exist as equilibrium mixtures of *syn* and *anti* conformers with preference of *anti*. However, in CpC the angle decreases with increasing stacking of base.[17] Our conclusion that single-stranded poly(C) takes predominantly $C_{3'}$-*endo anti* orientation of the base at low temperatures is in accordance with these results. A consistent result has also been presented for single stranded poly(C) in the fiber state by X-ray analysis ($C_{3'}$-*endo anti*, χ=80°).[7] The fraction of *syn* conformers, however, might not be neglected above 50 °C, in view of the coexistence of a substantial fraction of $C_{2'}$-*endo* ribose conformers (42%).

Poly(U). In contrast with poly(C), no temperature dependence of peak area of protons was observed for poly(U). As shown in Fig. 5, neither the chemical shifts of H_5 nor H_6 of poly(U) show significant temperature dependence, indicating that the base-stacking is negligible in this polymer, in accordance with the reported random coil property of poly(U).[2,3]

Temperature dependence of coupling constant $J_{1'2'}$

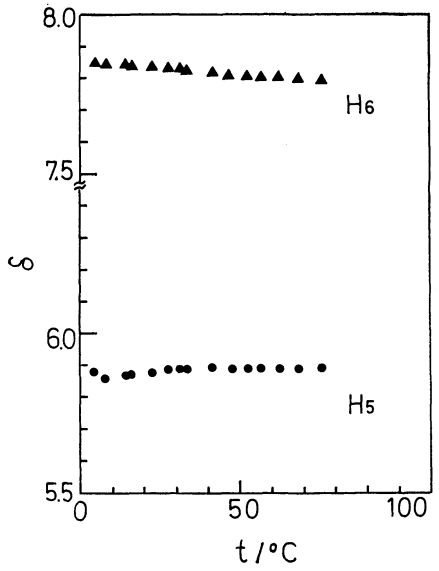

Fig. 5. Temperature dependence of chemical shifts of H_5 and H_6 of poly(U) as measured from an internal standard of DSS (H_5 ●, H_6 ▲).

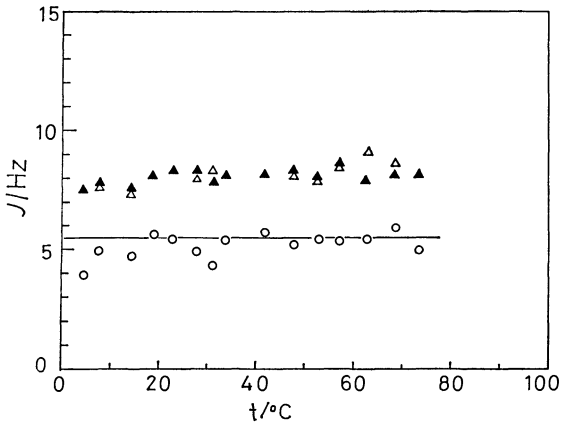

Fig. 6. Temperature dependence of coupling constants $J_{1'2'}$ and J_{56} of poly(U).
$J_{1'2'}$ ○, J_{56} (measured on H_5 signal) △ J_{56} (measured on H_6 signal) ▲.

of poly(U) is shown in Fig. 6 together with that of J_{56}. $J_{1'2'}$ is measured on the $H_{1'}$ signal under homo-decoupling H_6 proton, since the H_5 and $H_{1'}$ signals partially overlap in poly(U). Since J_{56} shows little temperature dependence, it appears safe to conclude that $J_{1'2'}$ is also invariant with temperature within the experimental accuracy of ±1.5 Hz. Based on the detailed analysis of coupling constants of ribose protons at 36 °C at 220 MHz by Kreishman and Chan,[22] Davies and Danyluk have estimated ring-conformer population of poly(U) to be 42% and 58% for N and S conformers, respectively.[23] The result of Fig. 6 shows that such conformation of the ribofranosyl ring of poly(U) does not change within the temperature range studied. Richards and co-workers[24] reported that poly(U) could undergo a co-operative transition to an order form below 15 °C. However, since their optical experiments were performed under high salt concentration, it could not be compared directly with the present results.

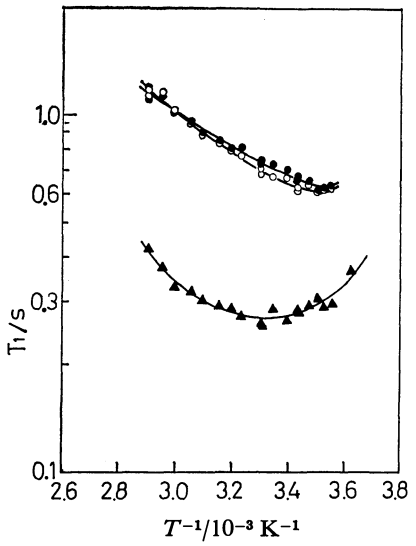

Fig. 7. Semilogarithmic plots of spin-lattice relaxation times (T_1) of poly(U) against reciprocal absolute temperature (H_5 ●, H_6 ▲, $H_{1'}$ ○).

Figure 7 shows the temperature dependence of T_1 for H_5, and H_6, and $H_{1'}$. T_1 of the three protons go through minima, but at different temperatures. Interproton distances, r_{lobsd} were obtained similarly as in poly(C) (Table 1). These distances must reflect local conformation of poly(U). The r_{lcalcd} values were computed for many conformers and compared with r_{lobsd} similarly as for poly(C). As the result, the base orientation of poly(U) is restricted to *anti* and *syn*.

The population of S conformer above 65 °C is 16% higher in poly(U) than in poly(C). This would arise from the fact that poly(U) is free from base stacking at all the temperatures studied, whereas poly(C) takes partial base stacking even above 65 °C as judged from Fig. 2, where N conformer is preferable to S conformer discussed for poly(C).

From the T_1 values, rotational correlation times τ_c were estimated to be in the order of 10^{-10}—10^{-9} s, corresponding to the local motions of polynucleotides.[4,18,25,26] The higher flexibility of poly(U) is implied from the fact that $T_{1\,\text{min}}$ of poly(U) protons appear at lower temperature than those of poly(C). The above observation is in accordance with the earlier conclusion from ^{31}P T_1 measurements.[4]

Appendix

When T_1 of a proton i is determined by dipolar interaction which is modulated by an isotropic rotation of the molecule with a characteristic time constant τ_c, the following equation is given for the interacting protons separated by a fixed distance r,[27]

$$\frac{1}{T_1} = \sum_j \frac{\gamma^4\hbar^2}{r_{ij}^6}\left(\frac{3}{10}\frac{1}{1+\omega^2\tau_c^2}+\frac{12}{10}\frac{1}{1+4\omega^2\tau_c^2}\right)\tau_c, \qquad (1)$$

where γ and ω are the gyromagnetic ratio and Larmor angular frequency of a proton, respectively, and suffix i and j represent the observed proton and the other proton interacting with proton i, respectively. Equation 1 predicts that T_1 goes through a minimum when $\omega\tau_c \simeq 0.62$ or $\tau_c =$

9.9×10^{-10} s. Therefore, for T_1 at the minimum, Eq. 1 could be rewritten as follows,

$$\frac{1}{T_{1\,\mathrm{min}}} = \sum_j \frac{\gamma^4\hbar^2}{r_{ij}^6}\times 6.81\times10^{-10}. \quad (2)$$

Accordingly, with the minimum value of T_1 we can evaluate interacting proton-proton distance in a form of

$$r_{\mathrm{lobsd}} = (T_{1\,\mathrm{min}}\gamma^4\hbar^2\times6.81\times10^{-10})^{1/6} \quad (\text{in Å}). \quad (3)$$

Chemical shifts and coupling constants of poly(C) were measured at 360 MHz at the Max-Planck Institut für Medizinische Forschung, Heidelberg, FRG. The authors are grateful to Professor K. H. Hausser for this opportunity.

References

1) Presented at 6th International Biophysics Congress, Kyoto, Japan, September 1978.
2) V. A. Bloomfield, D. M. Crothers, and I. Tinoco, "Physical Chemistry of Nucleic Acids," Harper and Row, New York (1974).
3) W. Guschlbauer, "Nucleic Acid Structure," Heidelberg Science Library, Springer-Verlag, New York (1976), Vol. 21.
4) K. Akasaka, A. Yamada, and H. Hatano, *Bull. Chem. Soc. Jpn.*, **50**, 2858 (1977).
5) A. Rich, D. R. Davies, F. H. C. Crick, and J. D. Watoson, *J. Mol. Biol.*, **3**, 71 (1961).
6) S. B. Zimmerman, G. H. Cohn, and D. J. Davies, *J. Mol. Biol.*, **92**, 181 (1975).
7) S. Arnott, R. Chandrasekaran, and A. G. W. Leslie, *J. Mol. Biol.*, **106**, 735 (1976).
8) K. A. Hartman, Jr., and A. Rich, *J. Am. Chem. Soc.*, **87**, 2033 (1965).
9) G. D. Fasman, C. Lindblow, and L. Grossman, *Biochemistry*, **3**, 1015 (1964).
10) W. Guschlbauer, *Nucleic Acid Res.*, **2**, 353 (1975).
11) K. Akasaka, A. Yamada, and H. Hatano, *FEBS Lett.*, **53**, 339 (1975).
12) R. C. Warner, *J. Biol. Chem.*, **229**, 771 (1957).
13) H. Klump, *Biochim. Biophys. Acta*, **383**, 1 (1975).
14) C. Altona and M. Sundaralingam, *J. Am. Chem. Soc.*, **95**, 2333 (1973).
15) A. Adler, L. Grossman, and G. D. Fasman, *Proc. Natl. Acad. Sci. U.S.A.*, **57**, 423 (1967).
16) R. Langridge and A. Rich, *Nature*, **198**, 725 (1963).
17) Che-Hung Lee, F. S. Eza, N. S. Kondo, R. H. Sarma, and S. S. Danyluk, *Biochemistry*, **15**, 3627 (1976).
18) K. Akasaka, *Biopolymers*, **13**, 2272 (1974).
19) M. S. Broid and D. R. Kearns, *J. Magn. Reson.*, **41**, 496 (1981).
20) A. V. Lakshiminarayanan and V. Sasisekharan, *Biochim. Biophys. Acta*, **204**, 49 (1970).
21) N. Yathindra and M. Sundaralingam, *Biopolymers*, **12**, 2261 (1973).
22) G. P. Kreishman and S. Chan, *Biopolymers*, **10**, 159 (1971).
23) D. B. Davies and S. S. Danyluk, *Biochemistry*, **13**, 4417 (1974).
24) E. G. Richards, C. P. Flessel, and J. R. Fresco, *Biopolymers*, **1**, 431 (1963); H. Simpkins and E. G. Richards, *J. Mol. Biol.*, **29**, 349 (1967).
25) A. Yamada, K. Akasaka, and H. Hatano, *Biopolymers*, **17**, 745 (1978).
26) P. H. Bolton and T. L. James, *J. Am. Chem. Soc.*, **102**, 25 (1980); *J. Phys. Chem.*, **83**, 3359 (1979).
27) A. Abragam, "Principles of Nuclear Magnetism," Oxford University Press, Oxford (1967), Chap. 8.

Studies on Molecular Motion in Lyotropic Mesophases of Hexaethylene Glycol Dodecyl Ether–D_2O System by ^{13}C Nuclear Magnetic Resonance

Shigeru MITA,* Shoichi KONDO, and Masatami TAKEDA

Department of Chemistry, Faculty of Science, Science University of Tokyo, Kagurazaka, Shinjuku-ku, Tokyo 162

(Received July 7, 1981)

The ^{13}C spin-lattice relaxation time(T_1) and the resonance line width corresponding to T_2* were measured for each of the carbons in hexaethylene glycol dodecyl ether–water(D_2O) system, which exists as two distinct lyotropic mesophases(neat and middle phase). The line width is very narrow in the isotropic state, such as in organic solvents and in a lower concentration aqueous solution, whereas in a mesophase and in a higher concentration aqueous solution, the line width of the alkyl chain was broadened. Here the line widths for glycol carbons were about an order of magnitude smaller than for an alkyl chain, demonstrating the difference of molecular motion. The chemical shifts of the alkyl chain in the middle phase were different from those in the isotropic state; this difference was clearly shown in the spectrum of the middle/isotropic coexistent phase. ^{13}C-T_1 was not sensitive enough to differentiate between the isotropic and the lyotropic phase at room temperature. It was found that T_1 did not equal T_2* for any of the methylene carbons, the difference being most marked for the terminal methyl carbon in the alkyl chain. The orientational order in the phases had an influence on the T_2* values.

One of the most fruitful techniques used to study lyotropic mesophases is magnetic resonance.[1] Proton nuclear magnetic resonance (^1H NMR) and relaxation measurements have been used to study the interaction of an ester with a polyethylene glycol alkyl ether as a nonionic surfactant.[2] It is difficult by ^1H NMR to measure separately the hydrophilic and hydrophobic parts of a mesophase because of the overlapping and the broadening of resonance lines.[2,3]

^{13}C Nuclear magnetic resonance (^{13}C NMR) has become an important tool in the investigation of the microstructure and molecular dynamics of liquid crystals.[3] The ^{13}C spin lattice relaxation time T_1 can readily be measured for all resolved resonances from partially-relaxed Fourier transform spectra. Ribeiro and Dennis measured ^{13}C NMR and T_1 values in isotropic states for octaethylene glycol dodecyl ether and suggested there were differences in mobility of the various groups in the surfactant.[3] The present study examines the ^{13}C-T_1 and the line width in an aqueous system of hexaethylene glycol dodecyl ether ($C_{12}EG_6$), as a function of aqueous concentration in D_2O and temperature in both the isotropic micellar solution and the mesophase. The $C_{12}EG_6$–water system is known to form two distinct lyotropic mesophases (neat and middle phase).[1,4] The results yield considerable information concerning the motional behavior of the hydrophilic and hydrophobic part of the miceller phases.

Experimental

Samples. Hexaethylene glycol dodecyl ether was obtained from Nikko Chemical Co., Ltd. and used without further purification. Purity of the sample is ≧99% by gas chromatography. NMR measurements were made for an undiluted liquid $C_{12}EG_6$; sample A comprised 90% $C_{12}EG_6$ and 10% D_2O (Merck, Uvasol 99.75%) by weight; sample B was a neat phase comprising 72% $C_{12}EG_6$ and 28% D_2O; sample C contained 65% $C_{12}EG_6$; sample D as a middle phase contained 50% $C_{12}EG_6$, and sample E, 10% $C_{12}EG_6$.[4] These samples were prepared according to the phase diagram established by Clunie *et al.*[4]

NMR Measurements. ^{13}C NMR spectra were measured at 25.03 MHz on a JEOL PFT-100 NMR spectrometer equipped with a PG-100 pulse programmer and a JEOL temperature controller. Samples were studied under conditions of complete proton noise decoupling or the gated decoupling, which minimize the rise of temperature in the sample by proton irradiation. The temperature of the sample in the probe was selected and maintained within ±1 K in accuracy in the range of 301 to 348 K.

Values of T_1 were measured using the inversion recovery method (T-180°-t-90°) over a 2 kHz band width with 8192 time domain data points. The 90° pulse length was calibrated prior to each set of experiments and varied between 20—25 μs. The delay time T was more than 5 times the longest T_1 value. For the relaxation time measurements, the sample was put into a spherical glass, and sealed after being degassed by freezed-thaw cycles. All such sample tubes were equilibrated for more than one weak at room temperature.[1]

Results and Discussion

Assignment of ^{13}C NMR Spectra. In Fig. 1, the ^{13}C NMR spectrum and tentative assignments are shown for the carbons in undiluted liquid $C_{12}EG_6$ at room temperature. The identification of the alkyl

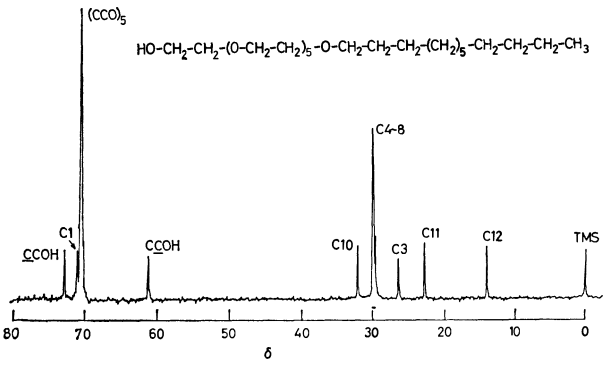

Fig. 1. ^{13}C NMR spectrum and assignment of undiluted liquid of $C_{12}EG_6$ at 301 K.

chain carbons in $C_{12}EG_6$ is based on assignments for $C_{10}OH$ and for other aliphatic compounds. Comparing the $C_{12}EG_6$ spectrum with that of $C_{12}OH$, we find no signal in the $C_{12}EG_6$ spectrum at the position of the C2 carbon of $C_{12}OH$. The C2 signal was shifted upfield and overlapped with the C4—9 signal by an increase of the electron density of C2 in $C_{12}EG_6$, owing to the oxyethylene group. Rebeiro and Dennis have assigned the C2 carbon to the signal which is assigned here to the C3 carbon.[3] The assignment for the carbons of the oxyethylene group has been made by ^{13}C NMR measurements of polyethylene glycol dodecyl ethers ($C_{12}EG_n$, n=1—8) and of compounds with several oxyethylenes and otherwise agreed with that of Ribeiro and Dennis.[3]

^{13}C NMR Spectra in the Mesophase. Sample B was measured by ^{1}H NMR at 100 MHz. At temperatures below the transition point of 343 K, there are two very much broadened peaks of alkyl chain and oxyethylene group in the ^{1}H NMR spectrum. It is difficult by ^{1}H NMR to separate the alkyl chain and the oxyethylene group.[4] In Fig. 2 are shown ^{13}C NMR spectra of a neat phase and of the isotropic phase for sample B. The upper spectrum, corresponding to the neat phase, and the lower spectrum in the isotropic phase at 348 K were obtained from the same solution. The lower spectrum was almost the same as the undiluted liquid spectrum in Fig. 1. In Fig. 3 are shown the ^{13}C NMR spectra of samples A, D, and E. The ^{13}C NMR spectrum in the middle phase for sample D is substantially the same as that in the neat phase in Fig. 2(1).

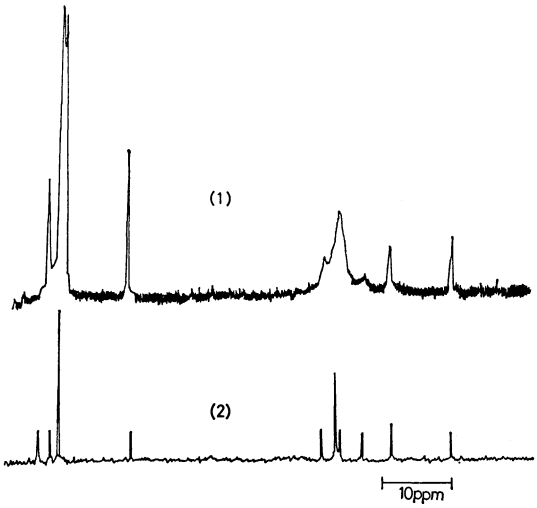

Fig. 2. ^{13}C NMR spectra for $C_{12}EG_6$ 75 w/w% in D_2O.
(1): Neat phase at 338 K, (2): isotropic phase at 348 K.

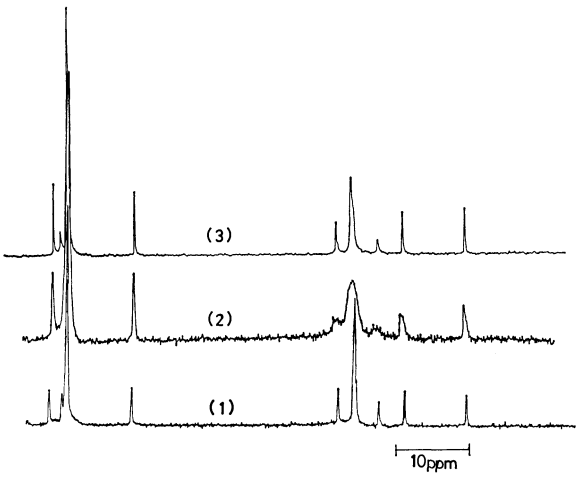

Fig. 3. ^{13}C NMR spectra of $C_{12}EG_6+D_2O$ system at 301 K.
(1): 90% $C_{12}EG_6+D_2O$, (2): 50% $C_{12}EG_6$, (3): 10% $C_{12}EG_6$.

In the neat and the middle phase spectra, the peaks arising from the carbons of the alkyl chain are much broader than those of the isotropic phase spectrum. The ^{13}C peaks of the oxyethylene group are slightly broadened. It is considered for mesophases that the alkyl chains overlap and that the paraffinic layer is rigid. The line width narrowing for the oxyethylene group is presumed to be due to a diffusional motion of this group, which is loosely restrained because of a hydration to the oxyethylene group. A low angle X-ray diffraction study on the $C_{12}EG_6$–H_2O system by Corkill et al. supported this assumption.[2] Samples A and E are both in the isotropic phase at room temperature. In the spectrum of sample E, the peaks of the alkyl chain are shown to be slightly broadened and the line shapes are different from those of the neat and middle phase. The spectrum of sample A is similar to that of the undiluted liquid $C_{12}EG_6$ and to that of the isotropic phase of sample B.

Chemical Shift. The data of chemical shifts for all samples are summarized in Table 1. Previously, it was shown that the peaks of the alkyl chain in the isotropic phase are displaced downfield by 0.5 ppm from those in the lyotropic neat and middle meso-

Table 1. The relative ^{13}C chemical shift in sample C

Phase	($\delta-\delta$(C*COH)) M[a]	M+I[b]	I[c]
Carbon number			
C-12		−46.53	−46.68
	−46.98	−46.92	
C-11		−37.79	−37.88
	−38.29	−38.74	
C-10		−28.46	−28.54
	−29.00	−29.54	
C-4-8		−30.53	−30.65
	−31.51	−31.52	
C-3		−34.14	−34.31
	−34.04	—	
C-1		10.53	10.54
	—	—	
(CCO)		9.50	9.44
	9.23	9.21	
CC*OH	11.47	11.47	11.53

a) M: Middle phase at 300 K. b) M+I: Middle/isotropic coexisting phase at 302 K. c) I: Isotropic phase at 305 K.

phases. On the other hand, ^{13}C chemical shifts of the oxyethylene group do not differ for the lyotropic and isotropic states. In Fig. 4, all oxyethylene group signals except that of terminal oxyethylene for sample C are coincident. But each alkyl carbon signal consists of two resonance lines, as shown in Fig. 4. The lower-field peaks in this region were assigned to the alkyl carbons in the isotropic phase and the upper field peaks to the middle phase, by comparing the chemical shifts in samples B, D, and C. Thus, this spectrum suggests that the state corresponds to a middle/isotropic coexistent phase denoted as an interpenetrated broad boundary in the phase diagram by Clunie *et al.*[4]

Spin-lattice Relaxation Times. In Table 2 are summarized the ^{13}C spin-lattice relaxation times, T_1s, of the undiluted liquid, and samples B and D at several temperatures. At room temperature, samples B and D form the neat and middle phase, respectively. Small differences in magnitude of T_1 values were observed among carbons in the middle phase, indicating that there are small differences in mobility in the molecule. We compared the T_1 values for the phases:

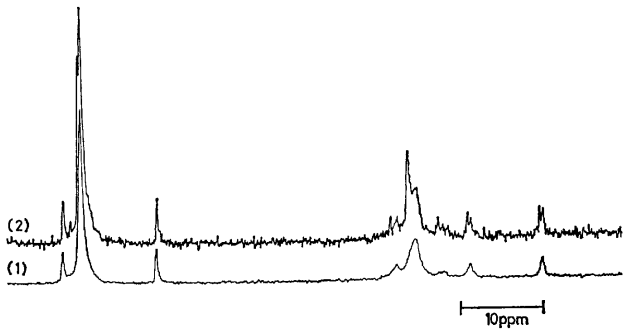

Fig. 4. ^{13}C NMR spectra of 65% $C_{12}EG_6+D_2O$ system (sample C).
(1): Middle phase at 296 K, (2): middle/isotropic coexistent phase at 298 K.

T_1(C12) of the neat phase is smaller than that of the isotropic and the middle phase. The T_1(C*COH) and T_1(CC*OH) values for the carbon (marked by the asterisk) of the middle phase are greater than that of the other phase. However, there is collectively no large difference in the T_1 values between phases. This result suggests that the mobility of a molecule in each phase is similar.

In 1-decanol or decylammonium trifluoroacetate, there is an increase in ^{13}C-T_1 on going from the carbons adjacent to an OH or NH_3 group to the terminal carbon in a molecule chain; this restriction is caused by intermolecular hydrogen bonding.[5,8] The alkyl chain has this tendency in our system. Ribeiro and Dennis had measured ^{13}C-T_1 of $C_{12}EG_8$ in micelles with D_2O as a good hydrogen bonding solvent.[3] They found that all T_1 values in aqueous solution are much smaller than those in the organic solvents.[2] There was little difference in ^{13}C-T_1 values of the corresponding carbons in the $C_{12}EG_6$ undiluted liquid, the neat phase, and the middle phase, as shown in Table 2.

Temperature dependences of T_1(C-11) and T_1-(C*COH) for the sample B and the undiluted liquid are shown in Fig. 5. T_1(C-11) plot for sample B has a minimum point at 308 K. The other curves show an inflection at about 301 K. It seems that this temperature is near to that of a minimum point of T_1. The plots of sample B show some scatter between 338 K and 343 K. This scatter agrees with the phase transition point from the neat to the isotropic phase.

Spin-Spin Relaxation Time. If a line shape is Lorentzian, a spin-spin relaxation time T_2^* is generally given by

$$T_2^* = 1/\pi \cdot \Delta\nu,$$

where $\Delta\nu$ is the half-height line width. T_2^* values calculated from this relationship are given in Table 3 T_2^* values of the undiluted liquid are longer than

Table 2. Temperature dependence of ^{13}C spin-lattice relaxation time (T_1)

Phase	T_1(U)/s[a]			T_1(B)/s[b]			T_1(D)/s[c]	
				N		I	M	I
T/K	301	313	348	301	318	348	301	318
Carbon number								
C-12	2.8	2.9	3.6	2.2	2.4	4.3	3.1	3.4
C-11	1.3	1.2	2.6	1.1	1.0	2.5	1.2	1.9
C-10	0.7	0.9	1.9	—	—	—	0.8	1.1
C-4-8	0.3	0.4	0.8	0.4	0.3	0.5	0.4	0.5
C-3	0.4	0.3	0.7	—	—	—	0.6	0.3
C-1	0.4	0.3	0.9	—	—	—	—	0.5
(CCO)	0.3	0.4	1.0	0.3	0.4	0.9	0.4	0.6
C*COH	0.4	0.6	1.7	0.6	0.8	1.8	0.9	1.6
CC*OH	0.5	0.5	1.7	0.6	0.8	1.8	0.9	1.6

N: Neat phase, M: middle phase, I: isotropic phase, U: undiluted liquid, B: sample B (72%$C_{12}EG_6+D_2O$), D: sample D (45%$C_{12}EG_6+D_2O$).
a) Estimated accuracy ±10%. b) Estimated accuracy ±20% in N, and ±10% in I. c) Estimated accuracy ±20% in M, and ±10% in I.

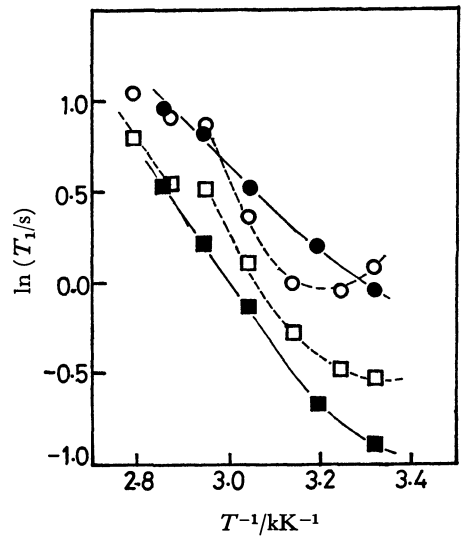

Fig. 5. Temperature dependence of ^{13}C[^{1}H] relaxation time T_1 at 25.03 MHz in $C_{12}EG_6$ (●: C-11, ■: C*COH, ——) and $C_{12}EG_6$ 72 w/w% in D_2O system (○: C-11, □: C*COH, ----).

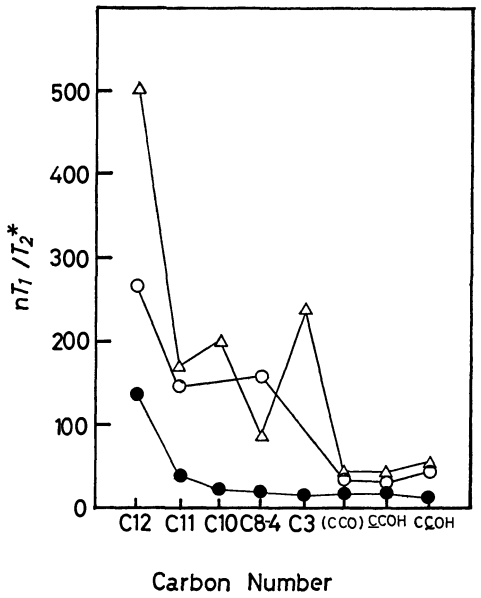

Fig. 6. Ratios of spin-lattice relaxation times (T_1) and spin-spin relaxation times (T_2*) estimated from line width.
●: Undiluted liquid, ○: neat phase, △: middle phase.

those of the other states, but T_2* values of each signal for the neat phase are similar to those for the middle phase. In the undiluted liquid, T_2* values for alkyl carbons were three to eight times greater than those in mesophase, but the values of T_2* for the oxyethylene group do not change between the undiluted liquid and the mesophase.

The Relationship between ^{13}C-T_1 *and* ^{13}C-T_2* *Values.* There is a disparity between the values of ^{13}C-T_1 and ^{13}C-T_2*. Figure 6 shows the nT_1/T_2* ratio for each carbon at 301 K which is close to the temperature of T_1 minimum for the carbons of oxyethylene

Table 3. The values of spin-spin relaxation times estimated from line width(T_2*), at 301 K

Carbon number	T_2*(U)/ms	T_2*(B)/ms	T_2*(D)/ms
C-12	61.0	25.0	18.0
C-11	69.0	15.0	14.0
C-10	57.0	7.0	8.0
C-4-8	30.0	5.0	9.0
C-3	46.0	7.0	5.0
(CCO)	31.0	17.0	18.0
C*COH	41.0	36.0	40.0
CC*OH	54·0	26.0	32.0

U: Undiluted liquid, B: sample B (73%$C_{12}EG_6$+D_2O), D: sample D (45%$C_{12}EG_6$+D_2O).

in the mesophases. In this case the relation of $T_1 > T_2$ should be held acoording to the classical work of Bloembergen *et al.*[9] On the other hand, when the temperature of T_1 minimum for alkyl carbons is higher than 301 K, the T_1 value can be expected to be much greater than the T_2* value. It is found that this expectation is actually valid, as shown in Fig. 6. The ratios of nT_1/T_2* for oxyethylene carbon are almost invariably less than fifty-six, while the ratios of alkyl carbons are more than a hundred.

In contrast to the mesophases, for the undiluted liquid the ratios of both oxyethylene carbons and alkyl carbons, except for terminal ethyl carbons, are almost constant (in the range of about 17 to 25), and less than the value for oxyethylene in mesophases. This result has been attributed to the fact that the undiluted liquid of low viscosity had narrow line widths for all carbons. It is interesting to note that the ratio of methyl carbon is higher than that of the other carbons.

The authors take this opportunity to express their thanks to Professor Roger S. Porter of University of Massachusetts for many helpful suggestions.

References

1) C. L. Khereapal, A. C. Kunwar, A. S. Tracy, and P. Diehl, "Nuclear Magnetic Resonance Studies in Lyotropic Liquid Crystals," in "NMR-Basic Principles and Progress," ed by P. Diehl, E. Fluck, and R. Kosfeld, Springer-Verlag, Berlin-Heidelberg-New York (1975), Vol. 9.

2) J. M. Corkill, J. F. Goodman, and J. Wyer, *Trans. Faraday Soc.*, **65**, 9 (1969).

3) A. A. Ribeiro and E. A. Dennis, *J. Phys. Chem.*, **81**, 957 (1977).

4) J. S. Clunie, J. F. Goodman, and P. C. Symons, *Trans. Faraday Soc.*, **65**, 287 (1969).

5) G. C. Levy, R. A. Komoroski, and J. A. Halstead, *J. Am. Chem. Soc.*, **96**, 5456 (1974).

6) J. M. Corkill and J. F. Goodman, *Adv. Colloid Interface Sci.*, **2**, 297 (1969).

7) J. S. Clunie, J. M. Corkill, and J. F. Goodman, *Proc. R. Soc. London, Ser. A*, **258**, 520 (1965).

8) D. Doddrel and A. Allerhand, *J. Am. Chem. Soc.*, **93**, 1558 (1971).

9) N. Bloembergen, E. M. Purell, and R. V. Pound, *Phys. Rev.*, **73**, 679 (1948).

Adsorption of Ethylene Oxide on Cab-O-Sil Silica, Reactive Silica, and Oxygen-treated Reactive Silica

Noriyuki SOTANI

College of Liberal Arts, Kobe University, Tsurukabuto, Nada-ku, Kobe 657

(Received July 16, 1981)

Ethylene oxide reacted with surface Si–OH of Cab-O-Sil silica to form Si–O–CH_2–CH_2–OH, while ethylene oxide was adsorbed on the silicon radicals of the reactive silica, and the oxygen radicals of the oxygen-treated reactive silica on which the adsorbed species polymerized to form $(-CH_2-O-CH_2-)_n$.

It is well known that ethylene oxide radicals are formed by pyrolysis[1] and photolysis,[2–4] and that these radicals can be easily polymerized without catalyst. The polymerization reaction of ethylene oxide occurs on various oxides, hydroxides and metal carbonates.[5–7] Furukawa *et al.*[5] have carried out a large number of experiments using solid catalysts. Ethylene oxide is easily polymerized under the influence of water and other substances containing labile hydrogen atoms such as amines and alcohols. The hydroxyl group appears to be the active centers in the polymerization reaction of ethylene oxide.[8] This polymerization occurs as an ionic type reaction.[9] On the other hand, a non-acid solid, for instance, silica gel with 5.6% of water bound on the surface is inactive in this polymerization.[9]

The polymerization product of ethylene oxide was studied by X-ray diffraction technique[10,11] and infrared spectroscopy,[12,13] and was confirmed to be a polyethylene glycol. In the presence of a strong acid or base catalyst the successive addition of ethylene oxide molecules yielded a polyethylene glycol. Aldehyde was presumably formed through oxyethylene biradicals.[14]

Reactive silica (RS) shows high reactivity in chemisorbing a variety of gases,[15–19] and it has been shown that acetylene, ethylene, several alkenes,[20,21] and ethylene oxide[22] are polymerized on its surface. Surface structure unlike those found on ordinary silica is formed. The high activity is thought to arise from the presence of unusual reaction center on the silica surface, *i.e.*, a pair of silicon radicals,[23] shown schematically in the following structure (I). Acetylene,

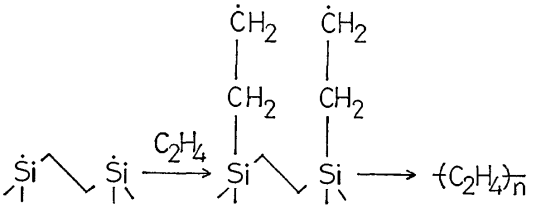

(I) (II)

ethylene, and several alkenes are adsorbed on silicon radicals of RS, and acetylene, ethylene and alkene radicals are formed as shown in structure (II). These radicals are easily polymerized[19–21] and these polymerization should be a radical type reaction.

Polymerization of ethylene oxide on RS can be expected to be a radical type reaction. Therefore, the present author studied the adsorption of ethylene oxide on Cab-O-Sil silica, RS and oxygen-treated reactive silica(ORS), and tried to find the difference in the reaction mechanisms on these silicas and the mechanism of the polymerization reaction.

Experimental

RS was prepared from Cab-O-Sil silica (obtained from G. Carbot Co., Boston, Mass.). It was methoxylated by using methoxy-containing compounds,[18] of which trimethoxymethane (trimethyl orthoformate, TMM) was the most efficient.[19] The methoxylated samples were pyrolyzed and then degassed at high temperature.[16,17] ORS was obtained from RS by exposing it to dry oxygen.[17] The samples were treated in the cell described elsewhere[17] and the conventional high vacuum technique was employed. Infrared spectra were recorded on Perkin Elmer Models 421 and 621 spectrometers.

Ethylene oxide (Eastman Kodak "pure grade") was degassed at liquid nitrogen temperature and distilled several times prior to the use.

Results

Cab-O-Sil Silica. Ethylene oxide was added to Cab-O-Sil silica, which was treated in about 100 Torr of wet oxygen at 650 °C for 1 h and was degassed at 700 °C for 1 h. When the silica was exposed to ethylene oxide, infrared absorption bands appeared immediately at 3350, 3085, 3066, 3007, 2970, 2929, 2870, 2720, 1736, 1468, and 1455 cm^{-1}, in addition to the band at 3747 cm^{-1} due to OH stretching vibration attached to surface Si atoms (Si–OH)[15–17] as shown in Fig. 1(A). Figure 2 shows the changes in intensities of the bands at 3747, 3350, and 2929 cm^{-1} when ethylene oxide was added to the silica. The band intensity was determined after 20 min. The intensity of the 3747 cm^{-1} band decreased with the increase of pressure of ethylene oxide. On the other hand, the intensities of the bands at 3350 and 2929 cm^{-1} increased with the increase of the pressure. This result shows that these three bands strongly correlate with each other. Namely, this means that the surface OH of Cab-O-Sil silica was reacted with added ethylene oxide and that a new adsorbed species showing the bands at 3350 and 2929 cm^{-1} was formed.

The sample adsorbed with ethylene oxide was degassed for 5 min at room temperature and at 105 °C. The bands at 3085, 3066, 3007, 2970, 2720, and 1736 cm^{-1} disappeared completely by degassing, but the bands at 3747, 3350, 2955, 2925, 2878, 1468, and 1451 cm^{-1} were maintained as shown in Figs. 1(B) and (C), and they still remained at 400 °C (Fig.

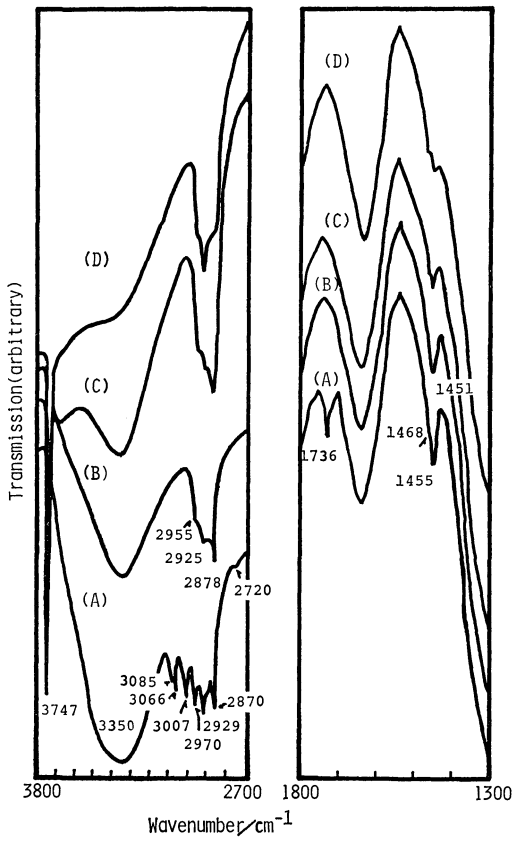

Fig. 1. IR spectra of ethylene oxide adsorbed on Cab-O-Sil silica.
A: 95 Torr† ethylene oxide at room temperature for 15 h, B: degassed at room temperature for 5 min, C: degassed at 105 °C for 5 min, D: degassed at 400 °C for 5 min.

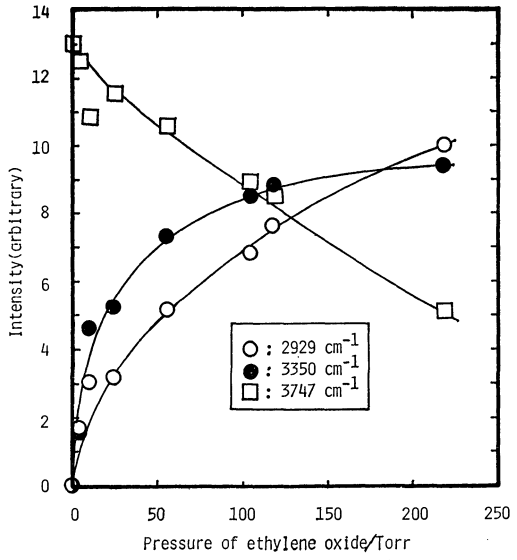

Fig. 2. Changes in intensities of the bands at 3747 (□), 3350(●), and 2929(○) cm^{-1} with pressure of ethylene oxide.

1(D)). The bands at 2720 and 1736 cm^{-1} are characteristic frequencies of aldehyde,[24] which is weakly adsorbed. The bands at 3085, 3066, 3007, and 2970 cm^{-1} are identified with typical bands of gaseous

† 1 Torr≈133.322 Pa.

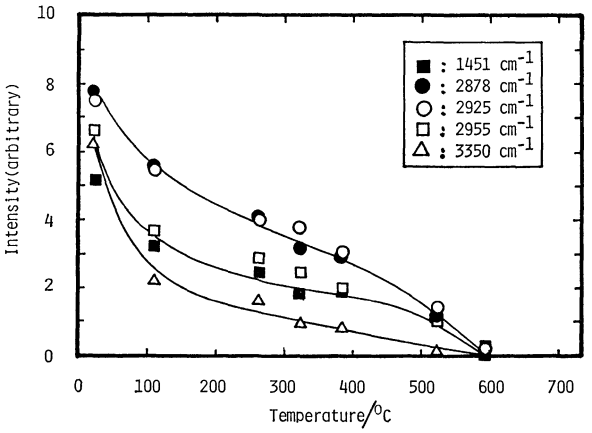

Fig. 3. Changes in intensities of the bands at 3350 (△), 2955(□), 2925(○), 2878(●), and 1451(■) cm^{-1} with evacuation temperature.

ethylene oxide reported by Potts,[25] which are CH_2 stretching vibration. The fact that the bands at 3085, 3066, 3007, and 2970 cm^{-1} disappeared easily by degassing at room temperature means that ethylene oxide kept its ring structure and was weakly adsorbed on Cab-O-Sil silica.

Figure 3 shows the change in band intensities by degassing at different temperatures. The band intensities at 3350, 2955, 2925, 2878, and 1451 cm^{-1} gradually decreased with elevation of degassing temperature. From Figs. 2 and 3, it is clear that the band at 3747 cm^{-1} correlates strongly with the bands at 3350, 2955, 2925, 2878, and 1451 cm^{-1}. Considering these results two types of adsorbed ethylene oxide are presumed, that is, one is the weakly adsorbed ethylene oxide molecules which keep a ring structure, and the other, the new adsorbed species reacts with surface OH which shows the band at 3350, 2955, 2925, 2878, and 1451 cm^{-1}.

RS (Reactive Silica). Sixty five Torr of ethylene oxide was added to RS. Figure 4(A) shows an infrared spectrum of ethylene oxide introduced on RS, which shows the bands at 3092, 3063, 3025, 3007, 2960, 2931, 2917, 2865, and 1450 cm^{-1}. Among these, the intensities of the bands at 3092, 3063, 3025, 3007, and 2917 cm^{-1} decreased as the time went on, on the other hand, the intensities of the bands at 2960, 2931, 2865, and 1450 cm^{-1} increased. Figure 5 shows the changes in intensities of the bands at 3063, 3007, 2931, 2865, and 1450 cm^{-1} by the same procedure. It is clear that the intensities of the bands at 2931, 2865, and 1450 cm^{-1} increased with the decrease of the band intensities at 3063 and 3007 cm^{-1}. The bands at 3063 and 3007 cm^{-1} are typical of ethylene oxide molecules.[25] Namely, Fig. 5 shows that the weakly adsorbed ethylene oxide molecules were converted into the new adsorbed species on RS.

The sample exposed to ethylene oxide vapor was degassed at room temperature for 5 min. The bands due to ethylene oxide disappeared completely, the bands at 2960, 2876, and 1455 cm^{-1} were maintained and a new band at 1465 cm^{-1} appeared as shown in Fig. 4(B). No further change was observed by degassing at room temperature for 1 h. The band at 2876

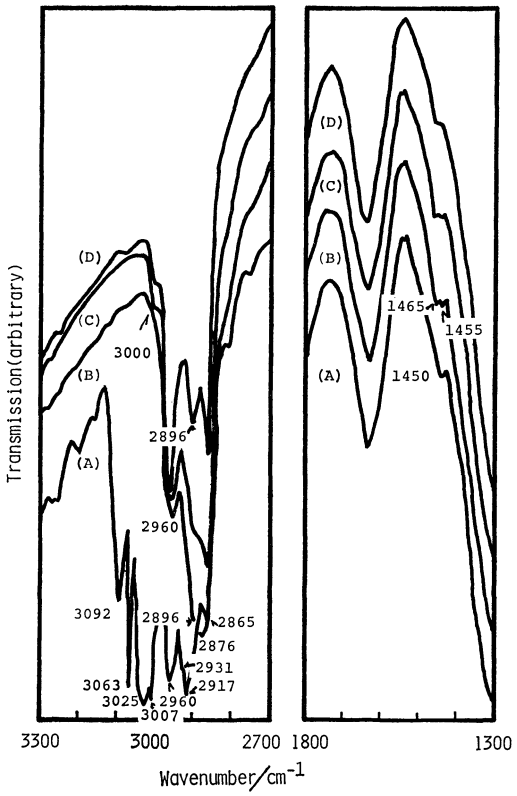

Fig. 4. IR spectra of ethylene oxide adsorbed on RS. A: 65 Torr ethylene oxide at room temperature, B: degassed at room temperature for 5 min, C: degassed at 200 °C for 5 min, D: degassed at 440 °C for 5 min.

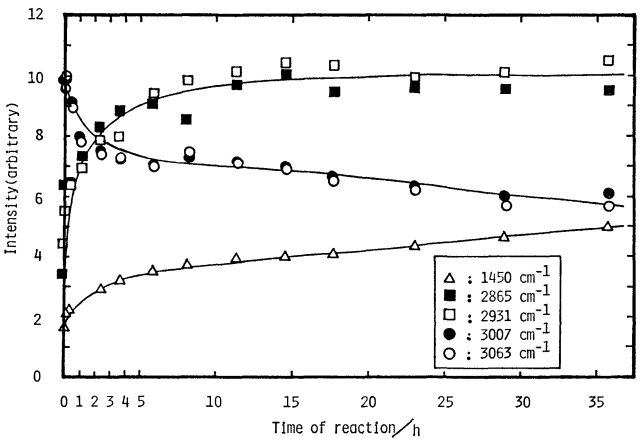

Fig. 5. Changes in intensities of the bands at 3063(○), 3007(●), 2931(□), 2865(■), and 1450(△) cm^{-1} with the time of reaction.

cm^{-1} split into two bands (2896 and 2865 cm^{-1}), and a new small band appeared at 3000 cm^{-1} by degassing at 200 °C and at higher temperatures even though the band intensities were changed as shown in Figs. 4(C) and (D).

As in the case of adsorption of ethylene oxide on Cab–O–Sil silica, the bands at 3092, 3063, 3025, 3007, and 2917 cm^{-1} disappeared easily and completely by degassing at room temperature. These bands due to gaseous ethylene oxide molecules having a ring structure as reported by Potts,[25] and by Lord and Nolin.[26]

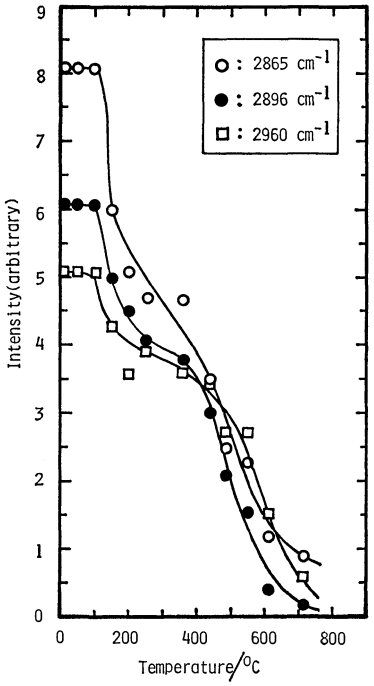

Fig. 6. Changes in intensities of the bands at 2960(□), 2896(●), and 2865(○) cm^{-1} with evacuation temperature.

This means that ethylene oxide is weakly adsorbed on RS.

Figure 5 shows the changes in intensities of the bands at 3063, 3007, 2931, 2865, and 1450 cm^{-1}. The intensities of the 3063 and 3007 cm^{-1} bands due to ethylene oxide molecules decreased at room temperature with the time of reaction. On the contrary, the intensities of the bands at 2931, 2865, and 1450 cm^{-1} increased. This result suggests that the weakly adsorbed ethylene oxide is converted into another new type of adsorbed species. While the intensities of both bands at 2931 and 2865 cm^{-1} increased similarly, but, as shown in Fig. 4, the band at 2931 cm^{-1} disappeared by degassing at room temperature, and the band at 2865 cm^{-1} was maintained even by degassing at 720 °C. Considering these results, there exist two different species showing the 2931 cm^{-1} band and the 2865 cm^{-1} band.

Figure 6 shows the changes in intensities of the bands (2960, 2896, and 2865 cm^{-1}) with evacuation temperature. No change was observed under 150 °C, but the intensities of three bands decreased above 150 °C. These bands were kept even at 720 °C. From Figs. 5 and 6, it is assumed that there are two kinds of adsorbed species on RS. One is the weakly adsorbed species, and the other, the strongly adsorbed one. Therefore, it is reasonable to consider that the weakly adsorbed species having the band at 2931 cm^{-1} was converted into another strongly adsorbed species having the bands at 2960, 2896, and 2865 cm^{-1}. Namely, the species having the band at 2931 cm^{-1} is assumed to be an intermediate on RS.

ORS (Oxygen-treated Reactive Silica). RS chemisorbs O_2 at room temperature, the reaction being complete within a few second. Oxygen-chemisorbed

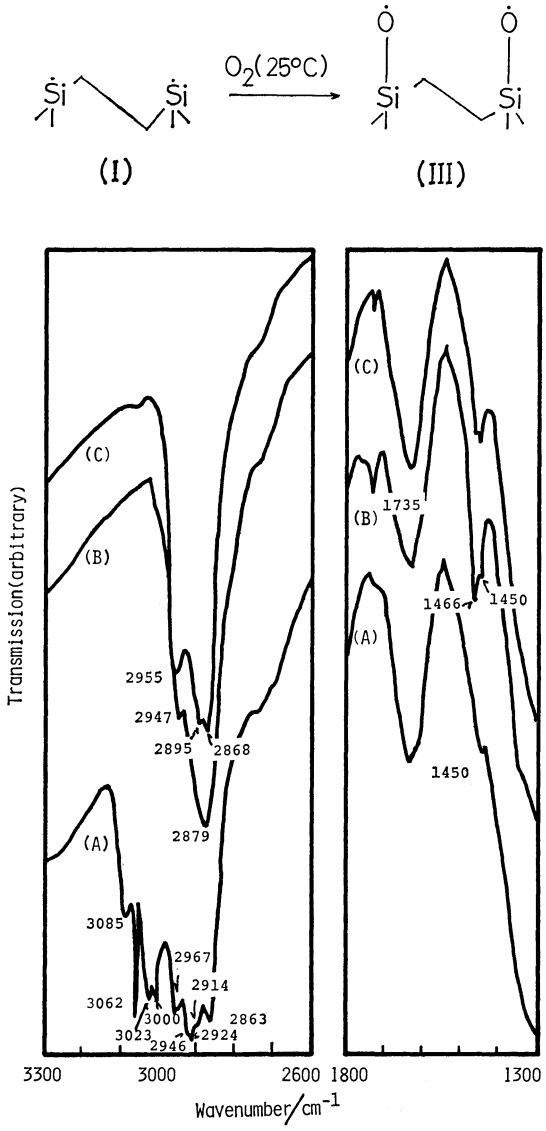

Fig. 7. IR spectra of ethylene oxide adsorbed on ORS. A: 71 Torr ethylene oxide at room temperature for 17 h, B: degassed at room temperature for 5 min, C: degassed at 460 °C for 5 min.

RS has a pair of oxygen radicals in structure (III).[17] It shows high activity and reacts with various gases as in the case of RS.[17]

Figure 7(A) shows the spectrum of ethylene oxide added to ORS at room temperature. The bands at 3085, 3062, 3023, 3000, 2967, 2924, 2914, 2863, 1735, and 1450 cm^{-1} were observed. Among these the bands at 3085, 3023, 3000, 2967, 2924, and 2914 cm^{-1} disappeared by degassing at room temperature, but the band intensity at 1735 cm^{-1} increased. The band at 1450 cm^{-1} split into two bands (1466 and 1456 cm^{-1}). By degassing at 460 °C, the band at 2947 cm^{-1} shifted to 2955 cm^{-1} and the band at 2879 cm^{-1} split into two bands (2895 and 2868 cm^{-1}) as shown in Fig. 7(C). These bands are similar to those in the case of RS except the one at 1735 cm^{-1}.

Discussion

Cab–O–Sil Silica. It is well known that the band at 3747 cm^{-1} is due to the surface OH(Si–OH).[15–17] The intensity of the 3747 cm^{-1} band decreased with the increase of those of the 3350 and 2929 cm^{-1} bands which were kept even by degassing at 600 °C as shown in Fig. 3. As mentioned above, this means that ethylene oxide reacts with surface OH. If the adsorbed species interacts with surface OH, the band due to OH shifts to lower frequencies by hydrogen bonding. In that case ethylene oxide should be adsorbed on the different site from surface OH, and this species was adsorbed weakly on Cab–O–Sil silica. This adsorbed species should be removed easily by degassing at room temperature. In the case of OH bonded to hydrocarbon such as alcohol (R–OH), the OH stretching vibration shifts to lower frequencies by hydrogen bonding and appears at near 3300 cm^{-1}.[8,27,28] The band at 3350 cm^{-1} just falls in this range and this may result from OH attached to the end of hydrocarbon. Therefore, it should be concluded that ethylene oxide reacted with the surface OH of Cab–O–Sil silica to form the new adsorbed species having the end OH group.

Considering that the ethylene oxide ring opens at C–O and fragment $-CH_2-CH_2-O-$ reacts with surface ≡Si–OH, the reaction product should have structure (IV). This is what is called an ionic type reaction. Structure(IV) is very similar to ethylene glycol except for the fact that one of the end OH groups is replaced with Si atom. Kanbayashi and Nukada[29] reported that the bands due to ethylene glycol appeared at 2947, 2924, 2881, and 1462 cm^{-1}. The bands at 2955, 2925, 2878, and 1451 cm^{-1} observed in this work (Fig. 1(B)) show little shift from those of ethylene glycol. These differences result from strong adsorption on Si atom of Cab–O–Sil silica like structure(IV). Indeed, Fig. 3 proved the presence of the strong adsorption species.

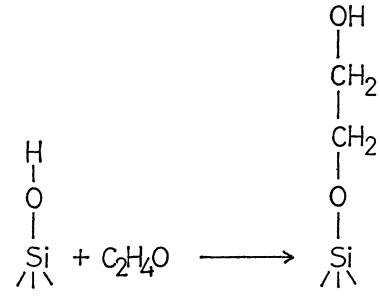

(IV)

The results and reasons mentioned above lead to the following conclusions; (i) Ethylene oxide is weakly adsorbed on Cab–O–Sil silica, forming a ring structure. That is, this is physical adsorption; (ii) Small amount of aldehyde is formed; (iii) Ethylene oxide reacts with the surface OH to form the adsorption species of structure (IV) which is similar to ethylene glycol. This is an ionic type reaction.

RS and ORS. As shown in Fig. 4, the bands at 3063 and 3007 cm^{-1} disappeared completely by degassing at room temperature, and at the same time the band at 2931 cm^{-1} also disappeared completely. The bands at 3063 and 3007 cm^{-1} are characteristic bands due to ethylene oxide having a ring structure, but the band at 2931 cm^{-1} is not. That is, the weakly adsorbed ethylene oxide molecule on RS is converted into the species having the band at 2931 cm^{-1}. On the other hand, the intensity of the band at 2931 cm^{-1} increases with the increase of the band intensities at 2865 and 1450 cm^{-1}, but the weakly adsorbed species having the band at 2931 cm^{-1} differs markedly from those having the bands at 2865 and 1450 cm^{-1} and also differs from the one resulted on Cab-O-Sil silica. Therefore, the author may safely predict that the species having the band at 2931 cm^{-1} is an intermediate of the reaction.

According to Markova,[30] adsorption species of ethylene oxide on $Mg(OH)_2$ showed three bands at 3055, 2925, and 2880 cm^{-1}. By degassing at room temperature the band at 3055 cm^{-1} disappeared completely and the band at 2925 cm^{-1} gradually disappeared by degassing at 180—200 °C. Only the band at 2880 cm^{-1} was kept. He proposed that the band at 3055 cm^{-1} was due to the characteristic of gaseous ethylene oxide which was physically adsorbed, and the bands at 2925 and 2880 cm^{-1} were due to valence vibration of CH_2 groups of the polymer molecule. Especially, he reported that the band at 2925 cm^{-1} was due to the band of the intermediate between ethylene oxide monomer and polymer.

The intensities of the bands at 2931 and 2865 cm^{-1} increased as shown in Fig. 5. The band at 2865 cm^{-1} was kept by degassing at room temperature and even at higher temperatures as shown in Fig. 6, while the band at 2931 cm^{-1} disappeared by degassing at room temperature. It is clear that the species having the band at 2865 cm^{-1} was formed when the species having the band at 2931 cm^{-1} existed. Namely, the species having the band at 2931 cm^{-1} plays an important role in inducing the species having the band at 2865 cm^{-1}. In addition to the results by Markova,[30] this result leads to the conclusion that the species having the 2931 cm^{-1} band is the intermediate. This result was recognized in the case of ORS.

As shown in Fig. 6, the intensities of the bands at 2960, 2896, and 2865 cm^{-1} were kept by degassing under 200 °C, but those decreased above 200 °C. On the other hand, a new band appeared at 3000 cm^{-1} and the shoulder at 2896 cm^{-1} appeared clearly. Namely, as shown in Figs. 4(C) and (D), three strong bands at 2960, 2896, and 2865 cm^{-1} appeared clearly. The intensities of these bands decreased similarly by degassing above 200 °C, and these bands were kept even by degassing at 720 °C. This result means that the species was strongly adsorbed on RS. In the case of ethylene oxide adsorption on ORS, the band appeared at 1735 cm^{-1} by degassing at room temperature and was kept at higher temperatures as shown in Fig. 7. But the other bands behaved similarly as those of RS except the band at 3000 cm^{-1}.

Ethylene oxide ring opens in two ways as $-CH_2-CH_2-O-$(V) and $-CH_2-O-CH_2-$(VI). Usually, ethylene oxide reacts with hydrogen atoms such as alcohols, amines, hydroxyl groups and strong acids by cleavage at the C-O linkage and forms $-CH_2-CH_2-OH$ structure (V'). That is, this proceeds as an ionic type reaction. Indeed, as described above, in the case of Cab-O-Sil silica, ethylene oxide reacts with surface OH and forms $Si-O-CH_2-CH_2-OH$. RS and ORS have no hydrogen or hydroxyl group, but they have silicon radicals(I) and oxygen radicals(III). Therefore, it is easy to predict that reaction of ethylene oxide on RS and ORS differs from that on Cab-O-Sil silica. Low reported[16,17] that silicon radicals of RS and oxygen radicals of ORS reacted with various gases in the same way. Especially, radicals were formed on RS and ORS such as ethylene radicals (structure (II)) and these radicals were polymerized on them. Low also reported[21] that ethylene reacted with oxygen radicals of ORS to form species (VII) and then species (VIII). If species (V) reacted with

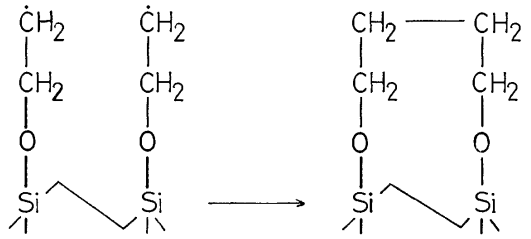

(VII) (VIII)

silicon radicals(I), species (VII) should be formed and then species (VIII). But there was no evidence, *i.e.*, there was no band for which Low[21] assigned species (VII) and species (VIII). On the other hand, if species (V) reacted with oxygen radicals of ORS, a peroxide having structure (IX) should be formed. If peroxide (IX) was formed, the band due to CH vibra-

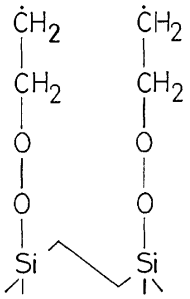

(IX)

tion was expected to shift to lower frequencies than that of ethoxide by effect of oxygen atom, but there was no evidence of the shift as shown in Fig. 7. Namely, the bands due to vibration of CH_2 group show no difference between the cases of RS and ORS. Therefore, there is little probability that species (IX) exists.

Generally, CH stretching vibration in CH_2 groups appears at 2940—2915 and 2870—2845 cm^{-1}.[24,31-34]

But the bands due to CH_2 in ether as the structure of R–O–CH_2– shift to higher frequencies at 2955—2922 and 2878—2835 cm^{-1}.[31,34] According to Miyazawa *et al.*[13] polyethylene glycol has the –CH_2–O–CH_2– repeating unit and shows the bands at 2950, 2890, 1470, and 1453 cm^{-1}. Naccache *et al.*[9] reported that the polymer of ethylene oxide showed the bands at 2943, 2887, 1467, and 1455 cm^{-1}. The bands observed in the present work (Fig. 4(B): 2960, 2876, 1465, and 1455 cm^{-1}, and Fig. 7(B): 2947, 2879, 1466, and 1456 cm^{-1}) are very similar to those by Miyazawa *et al.*[13] and Naccache *et al.*[9] The structure of –CH_2–O–CH_2– is, therefore, expected.

The band at 2876(ORS;2879) cm^{-1} splits into two bands at 2896(ORS;2895) and 2865(ORS;2865) cm^{-1} by degassing at high temperature and these band intensities decreased similarly as shown in Fig. 6. From the result mentioned above, it is speculated that polymerization of ethylene oxide proceeds at high temperature. At the same time, a new band appeared at 3000 cm^{-1} on RS and 1735 cm^{-1} on ORS. The former predicts the existence of CH_3 group, and the latter C=O group. These groups should be formed by depolymerization at higher temperature.

Considering the above results, it is concluded as follows; (i) Ethylene oxide is weakly adsorbed on RS and ORS, forming a ring structure. This is physical adsorption; (ii) The intermediate is formed on silicon and oxygen radicals as species (X) and (XI), which are adsorbed weakly; (iii) Species (X) and (XI) open its ring at C–C bond as a radical type reaction to form species (XII) and (XIII), and, then, they are polymerized as species (XIV) and (XV), (iv) One of species (XIV) and/or (XV) depolymerizes at higher temperatures to form species (XVI) and/or (XVII).

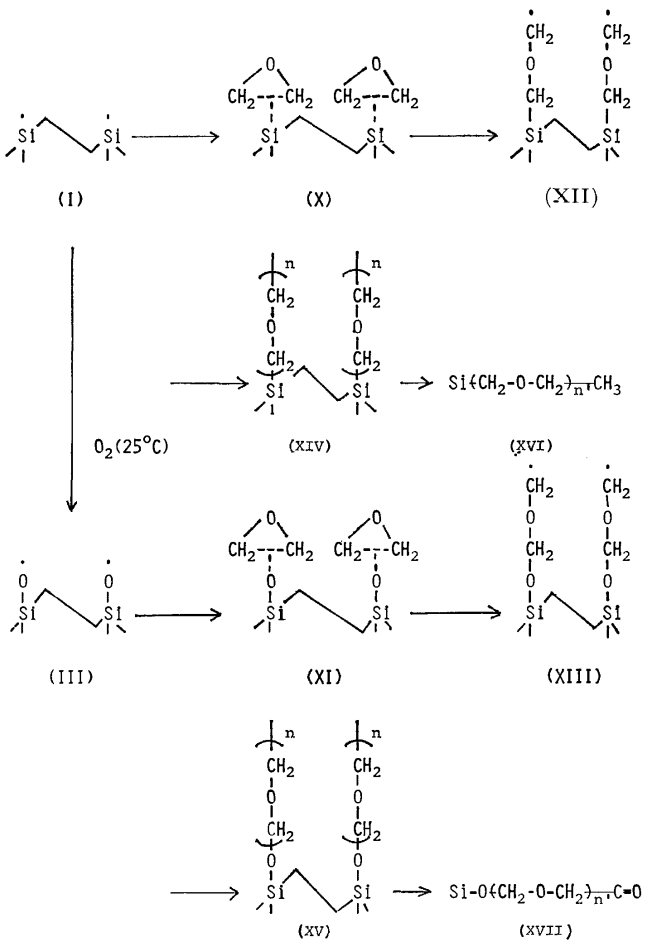

The author is very grateful to Professor Manfred J. D. Low of New York University for his giving the chance to study at his laboratory and for his obliging permission to present this paper. The author is also grateful to Mr. Koji Watanabe of Kobe University for his kind suggestions with respect to this manuscript.

References

1) K. H. Mueller and W. D. Walter, *J. Am. Chem. Soc.*, **73**, 1458 (1951); **76**, 330 (1954).
2) R. Gomer and W. A. Noyes, Jr., *J. Am. Chem. Soc.*, **72**, 101 (1950).
3) R. J. Cvetnovic, *Can. J. Chem.*, **33**, 1684 (1955); **36**, 623 (1958).
4) R. J. Cvetnovic, *J. Chem. Phys.*, **25**, 376 (1956); **30**, 19 (1959).
5) J. Furukawa, T. Saegusa, T. Tsuruta, and G. Kakogawa, *Makromol. Chem.*, **36**, 25 (1959).
6) F. N. Hill, F. E. Bailey, and J. T. Fitzpatrick, *Ind. Eng. Chem.*, **50**, 5 (1958).
7) O. V. Krylov and Y. E. Sinyak, *Vyskomol. Sojedin.*, **3**, 898 (1961).
8) P. J. Florys, *J. Am. Chem. Soc.*, **62**, 1561 (1940).
9) C. Naccache, J. Bandiera, G. Wicker, and B. Imelik, *Proc. 3rd International Congress and Catalysis*, I-37, Amsterdam (1964).
10) W. H. Barnes and S. Ross, *J. Am. Chem. Soc.*, **58**, 1129 (1936).
11) E. Santer, *Z. Phys. Chem.*, **B21**, 161 (1933).
12) W. H. T. Davison, *J. Chem. Soc.*, **1955**, 3270.
13) T. Miyazawa, K. Fukushima, and Y. Ideguchi, *J. Chem. Phys.*, **37**, 2764 (1962).
14) "The Chemistry of Heterocyclic Compounds," ed by A. Weissberger, John Wiley and Sons, N. Y. (1964), Part 1.
15) C. Mortera and M. J. D. Low, *Chem. Commun.*, **1968**, 203.
16) C. Mortera and M. J. D. Low, *J. Phys. Chem.*, **73**, 321, 327 (1969).
17) C. Mortera and M. J. D. Low, *Ann. N. Y. Acad. Sci.*, **220**, 133 (1973).
18) M. J. D. Low, Y. E. Rhodes, and P. D. Orphanos, *J. Catal.*, **40**, 236 (1975).
19) M. J. D. Low and H. Mark, *J. Catal.*, **44**, 300 (1976).
20) M. J. D. Low and H. Mark, *J. Res. Inst. Catal., Hokkaido Univ.*, **25**, 1 (1977).
21) M. J. D. Low and H. Mark, *J. Catal.*, **48**, 104 (1977), **50**, 373 (1977).
22) N. Sotani and M. J. D. Low, *React. Kinet. Catal. Lett.*, **13**, 339 (1980).
23) M. J. D. Low, *J. Catal.*, **32**, 103 (1974).
24) L. J. Bellamy, "The Infrared Spectra of Complex Molecules," John Wiley and Sons, N. Y. (1966).
25) W. J. Potts, *Spectrochim. Acta*, **21**, 511 (1965).
26) P. C. Lord and B. Nolin, *J. Chem. Phys.*, **24**, 656 (1956).
27) A. V. Stuart and G. B. B. M. Sutherland, *J. Chem. Phys.*, **24**, 559 (1956).

28) G. C. Pimentel and A. L. McClellan, "The Hydrogen Bond," Freeman, San Francisco, California (1960).
29) U. Kambayashi and K. Nukada, Symposium on Infrared and Raman Spectra, Tokyo, October 1961.
30) Markova, *Kinet. Katal.*, **3**, 366 (1962).
31) S. E. Wiberley, S. C. Bunce, and W. H. Bauer, *Anal. Chem.*, **32**, 217 (1960).
32) L. H. Little, "Infrared Spectra of Adsorbed Species," Academic Press, N. Y. (1966).
33) K. Nakanishi, "IR Adsorption Spectroscopy-Practical," Nankodo, Tokyo (1970).
34) N. B. Colthup, L. H. Daly, and S. E. Wiberley, "Introduction to Infrared and Raman Spectroscopy," 2nd ed, Academic Press, N. Y. (1975).

 © 1982 The Chemical Society of Japan Bull. Chem. Soc. Jpn., 55, 1999—2004 (1982)

Circular Dichroism of *N*-Acetyl-L-amino Acid Methylamides with Aromatic Side Groups

Hiroatsu MATSUURA,* Kodo HASEGAWA,†,†† and Tatsuo MIYAZAWA†,†††

Department of Chemistry, Faculty of Science, Hiroshima University, Higashisenda-machi, Naka-ku, Hiroshima 730

† *Institute for Protein Research, Osaka University, Yamadaoka, Suita, Osaka 565*

(Received August 21, 1981)

The circular dichroism (CD) and its temperature dependence were studied on *N*-acetyl-L-phenylalanine methylamide, *N*-acetyl-L-tyrosine methylamide, and *N*-acetyl-L-tryptophan methylamide, as model molecules of aromatic amino acid residues in proteins. The CD spectra indicated that the increase in temperature and the decrease in solvent polarity give a similar effect on the amide $\pi^* \leftarrow n$ transition. The CD behavior of the tryptophan derivative was different from that of the phenylalanine and tyrosine derivatives, suggesting that the bulkier indolyl side group interacts with the peptide backbone in a different way. The noticeable temperature dependence of the CD intensities in the 250—300 nm region observed for the phenylalanine and tryptophan derivatives suggested the coexistence of various conformers at higher temperatures.

Protein molecules contain chromophoric groups such as amides, disulfides, and aromatic groups. Although the amides and aromatic groups themselves possess planes of symmetry, they are made optically active by the asymmetric configuration of the amino acid residues and the asymmetric arrangement of these chromophoric groups. Accordingly, the optical activity depends on the conformation of the groups surrounding the chromophores. Studies on circular dichroism (CD) of model molecules of proteins, containing aromatic side groups are, therefore, important in understanding the relation between the conformation and the optical rotation of the amide and aromatic groups. The CD spectra of phenylalanine, tyrosine, tryptophan, and their derivatives of *N*-acetyl amino acid amides and *N*-acetyl amino acid ethyl esters have been studied by several investigators. However, since amino and carboxyl groups of amino acids are involved in forming the peptide bonds of protein main chains, the most appropriate model molecules of amino acid residues in proteins are *N*-acetyl amino acid methylamides ($CH_3CONHCHRCONHCH_3$). Accordingly, in the present study, the CD and ultraviolet absorption spectra of *N*-acetyl-L-phenylalanine methylamide (AcPheMA), *N*-acetyl-L-tyrosine methylamide (AcTyrMA), and *N*-acetyl-L-tryptophan methylamide (AcTrpMA) have been measured in a temperature range between −70 and 50 °C.

The CD spectra of *N*-acetyl-L-phenylalaninamide (AcPheA), *N*-acetyl-L-tyrosinamide (AcTyrA), and *N*-acetyl-L-tryptophanamide (AcTrpA), and their related compounds have previously been studied by Shiraki,[1] and Strickland *et al.*[2-7] Strickland *et al.* measured the CD spectra at 25 and −196 °C and analyzed the vibrational structure. They suggested that the observed temperature dependence of the spectra was related to the shift of equilibrium of various conformers. In the present study, temperature dependence of the CD spectra of AcPheMA, AcTyrMA, and AcTrpMA was studied in a wavelength region between 200 and 300 nm in aqueous, methanol, and 1,4-dioxane solutions, and a change in intensity of the CD bands assignable to the amide and aromatic chromophores was examined. The results were also compared with those obtained for the primary amides of AcPheA, AcTyrA, and AcTrpA.

Experimental

AcPheMA, AcTyrMA, and AcTrpMA were prepared from the corresponding *N*-acetyl amino acid ethyl esters by the following method. Each of the esters was dissolved in methanol. Vapor of methylamine was then blown into the methanol solution until concentration of methylamine was about 25%. After being kept for 2 or 3 d, the reacting solution of *N*-acetyl-L-phenylalanine ethyl ester with methylamine yielded white needle crystals of AcPheMA, which was then recrystallized from methanol. For the derivatives of L-tyrosine and L-tryptophan, methylamine and methanol were evaporated after the reaction to give pale yellow powders. Repeated recrystallization from a mixture of ethanol and hexane gave white powders of AcTyrMA or AcTrpMA. Elemental analyses gave the following results. AcPheMA. Found: C, 65.48; H, 7.51; N, 12.94%. Calcd for $C_{12}H_{16}N_2O_2$: C, 65.43; H, 7.32; N, 12.72%. AcTyrMA. Found: C, 61.01; H, 7.01; N, 12.01%. Calcd for $C_{12}H_{16}N_2O_3$: C, 61.00; H, 6.83; N, 11.86%. AcTrpMA. Found: C, 64.70; H, 6.80; N, 16.15%. Calcd for $C_{14}H_{17}N_3O_2$: C, 64.85; H, 6.61; N, 16.20%.

The CD spectra were measured with a JASCO J-20 spectropolarimeter and the ultraviolet absorption spectra with a Hitachi 124 spectrophotometer. Molar ellipticity $[\theta]$, in $10^{-2\circ}$ M^{-1} cm^{-1} $= {}^\circ$ cm^2 $dmol^{-1}$, was calculated by a relationship, $[\theta]=3300\ (\varepsilon_l-\varepsilon_r)$, where ε_l and ε_r are molar absorption coefficients for the left- and right-circularly polarized lights, respectively. The CD intensity was calibrated against the intensity ($\varepsilon_l-\varepsilon_r=2.20$ M^{-1} cm^{-1})** of the 290.5 nm band of an aqueous solution of (+)-10-camphorsulfonic acid. Sample cells of path lengths of 5 and 10 mm were used for a wavelength region of 230—300 nm, while cells of path lengths of 0.1 and 1 mm were used for a region of 200—250 nm to reduce absorptions of solvents. The path length of the 0.1 mm cell was corrected by the ultraviolet absorption of a standard aqueous solution of potassium chromate.

The temperature of the sample cells was controlled with two kinds of constant-temperature apparatus.[8] For the measurements at −70 °C, a low-temperature cell was used

†† Present address: Hokuriku Seiyaku Co., Ltd., Katsuyama, Fukui 911.

††† Present address: Department of Biophysics and Biochemistry, Faculty of Science, The University of Tokyo, Hongo, Bunkyo-ku, Tokyo 113.

** 1 M = 1 mol dm^{-3}.

with Dry Ice-acetone as coolant. Inside the low-temperature cell, a sealed sample cell was fixed to cooled copper block. The outer cell was kept vacuum to prevent the sample cell from condensation of water vapor. For temperatures higher than −10 °C, a brass-block cell holder was used. Through the brass block, externally temperature-controlled water or ethanol was circulated to keep the cell holder at constant temperature. Nitrogen gas was blown onto the sample-cell surface to avoid water-vapor condensation for temperatures below room temperature.

Results and Discussion

N-Acetyl-L-phenylalanine Methylamide (AcPheMA). The CD spectra of AcPheMA measured in methanol at various temperatures are shown in Figs. 1 and 2. The ultraviolet absorption spectrum measured in methanol at 22 °C is very similar to the absorption spectrum of AcPheA in methanol–glycerol at 25 °C (Fig. 1 of Ref. 2). The CD spectral pattern in the wavelength region longer than 250 nm are essentially the same for the temperature range from −7 to 57 °C; three negative CD bands assignable to the phenyl group were observed at 255, 261.5, and 267.5 nm. The intensities of the three CD bands increased as temperature was lowered. At −70 °C, these bands have intensities threefold stronger than those at 57 °C, and three positive CD bands appeared at 251.5, 257.5, and 264 nm. Also, two shoulders appeared at 260 and 266 nm in the CD spectrum measured at −70 °C, but no corresponding absorption bands were detected at 22 °C. These spectral features of AcPheMA resemble those of AcPheA measured by Strickland *et al.*[2] The difference in intensity of the CD vibronic bands observed at −70 °C and higher temperatures suggests the coexistence of various conformers at higher temperatures, as in the case of AcPheA.

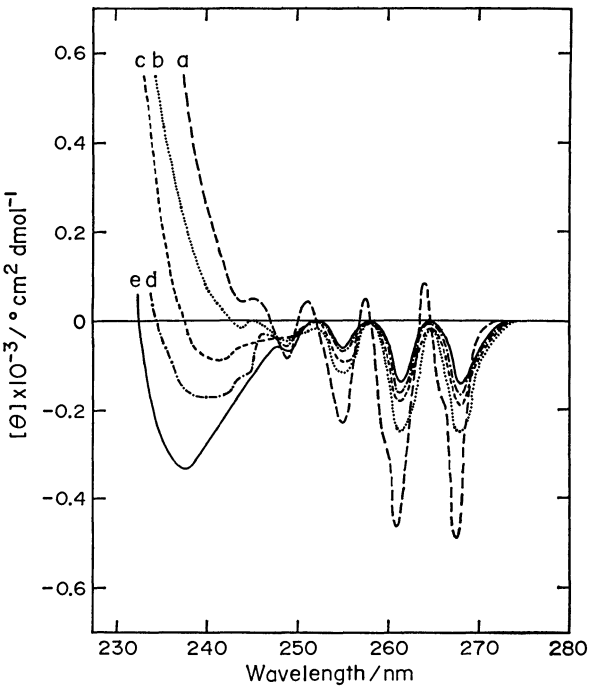

Fig. 1. CD spectra of *N*-acetyl-L-phenylalanine methylamide (AcPheMA) in methanol.
a: −70 °C, b: −7 °C, c: 22 °C, d: 40 °C, e: 57 °C.

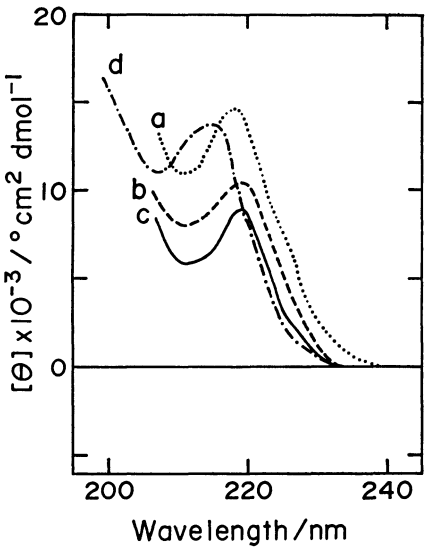

Fig. 2. CD spectra of *N*-acetyl-L-phenylalanine methylamide (AcPheMA) in methanol (a—c) and in water (d).
a: −5 °C, b: 22 °C, c: 40 °C, d: 22 °C in water.

The CD bands observed in the 240—270 nm region are assigned to the vibrational structure of the $^1B_2 \leftarrow {}^1A_1$ electronic transition of the phenyl group. The vibronic assignments of the absorption and CD bands of AcPheMA were attempted in the light of the analysis for AcPheA.[2] The observed bands and their possible assignments are summarized in Table 1. The 0-0 band and the bands associated with the 0+930 cm^{-1} mode have a negative CD sign, while the 0+520 cm^{-1} progression observed only at −70 °C has a positive sign. The shoulders at 260 and 266 nm belong to the 0+180 cm^{-1} progression. The 0+180 cm^{-1} transition may be assigned to the B_1 vibrational mode, since this vibrational transition is electronically forbidden (total wavefunction is A_2). The absorption bands of the 0+180 cm^{-1} progression were, in fact, observed for neither AcPheMA nor AcPheA. The CD bands in the 240—250 nm region are likely to be distorted by overlapping tails of the phenyl $^1A_1 \leftarrow {}^1A_1$ and amide $\pi^* \leftarrow$n bands with band centers around 220 nm. This effect will be discussed later in detail.

In the CD spectrum of the methanol solution, a negative extremum was observed at 235—250 nm (Fig. 1). As temperature was raised, the intensity of this extremum increased with a blue shift, contrary to the $^1B_2 \leftarrow {}^1A_1$ bands whose intensities decreased. Judging from the band shape and the wavelength, this band is not likely to be due to the phenyl $^1B_2 \leftarrow {}^1A_1$ vibronic transition. In fact, no absorption band was observed in this wavelength region. This band at 235—250 nm is probably an apparent extremum formed as a residual difference between the overlapping tails of the shorter-wavelength CD bands assignable to the phenyl $^1A_1 \leftarrow {}^1A_1$ and amide $\pi^* \leftarrow$n transitions with the CD signs different from each other. Accordingly, temperature dependence of the CD spectrum in the 200—240 nm region was examined (Fig. 2). The CD extremum at about 220 nm for the methanol

TABLE 1. VIBRONIC BANDS OF THE PHENYL $^1B_2 \leftarrow {}^1A_1$ TRANSITION FOR *N*-ACETYL-L-PHENYLALANINE METHYLAMIDE (AcPheMA)

Absorption (at 22 °C)		Circular dichroism (at −70 °C)			Vibronic wave number	Possible assignment[a,b]	Symmetry[b]
Wavelength nm	Intensity	Wavelength nm	Sign	Intensity	cm^{-1}	cm^{-1}	
267.5	Weak	267.5	Negative	Strong	0−0	0−0	A_1
		266		Shoulder	0+210	0+180	(B_1)
264	Medium	264	Positive	Weak	0+500	0+520	B_2
261	Shoulder	261	Negative	Strong	0+930	0+930	A_1
		260		Shoulder	0+1080	0+930+180	(B_1)
258	Strong	257.5	Positive	Weak	0+1450	0+930+520	B_2
		255	Negative	Medium	0+1835	0+2×930	A_1
252.5	Medium				0+2220	(0+2×930+180)	(B_1)
		251.5	Positive	Weak	0+2380	(0+2×930+520)	(B_2)
247.5	Weak	248	Negative	Weak	0+2940	(0+3×930)	(A_1)
		245	Positive	Weak	0+3435	(0+3×930+520)	(B_2)

a) Wave numbers given are those for *N*-acetyl-L-phenylalaninamide (Ref. 2). b) Assignment and symmetry in parentheses are tentative.

solution showed appreciable dependence on temperature; its intensity increased about 1.5 times as temperature was lowered from 40 to −5 °C. This band was also found to be sensitive to the solvent. The CD intensity in water is about 40% stronger than in methanol, as seen in Fig. 2. Similar spectral changes have been noted by Barel and Glazer[9] for AcPheA in water and ethylene glycol–water (9:1). These authors considered that this spectral change was due to the change in solvent polarity and that the intensity decrease of the 220 nm band and the intensity increase of the 240 nm band were related to the dependence of the amide $\pi^* \leftarrow$n optical rotation on the solvent polarity. Thus, the solvent-polarity dependence and the temperature dependence of the CD spectrum of AcPheMA is quite similar in the 200—250 nm region.

In order to examine temperature dependence of the amide $\pi^* \leftarrow$n CD band free from the overlap of other bands, the CD spectrum of *N*-acetyl-L-leucine methylamide (AcLeuMA), $CH_3CONHCH(CH_2CH(CH_3)_2)CONHCH_3$, was measured in methanol at 0, 22, and 40 °C (Fig. 3). The spectral change with the increase in temperature resembles the spectral change with the decrease in solvent polarity.[10] Similar observations have been reported of the temperature dependence of the CD spectrum for *N*-acetyl-L-alanine ethylamide[11] and of the solvent dependence for *N*-acetyl-L-alaninamide.[9] Accordingly, it may be concluded that the increase in temperature and the decrease in solvent polarity give a similar effect on the amide $\pi^* \leftarrow$n transition. In order to confirm the above conclusion, the CD spectra of AcPheMA in water and 1,4-dioxane, whose polarities are higher and lower, respectively, than methanol, have also been measured. The aqueous-solution spectrum did not show a remarkable change in the 240 nm region as temperature was raised. This quite small spectral change may be due to the 215 nm positive band whose intensity is strong enough to screen the intensity change of the amide $\pi^* \leftarrow$n band. In 1,4-dioxane, on the other hand, a very strong negative CD band was

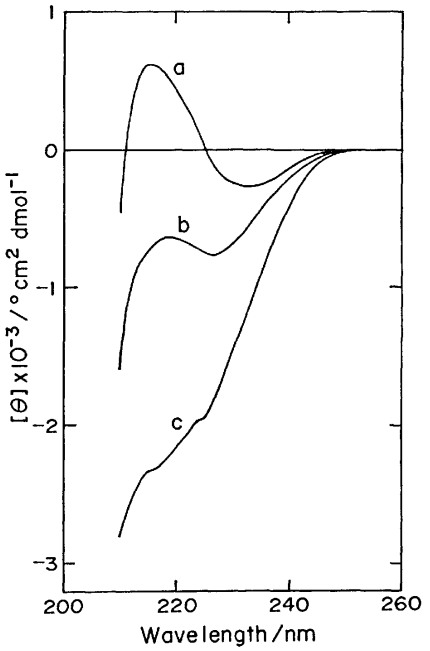

Fig. 3. CD spectra of *N*-acetyl-L-leucine methylamide (AcLeuMA) in methanol.
a: 0 °C, b: 22 °C, c: 40 °C.

observed at 233 nm (Fig. 4), which was blue-shifted with progressive intensity enhancement from 240 nm in methanol. These spectral observations indicate that the apparent negative CD extremum of AcPheMA around 240 nm is formed as a result of the overlap of the two CD bands with different signs. The CD spectra of AcPheA have been measured by Shiraki[1] in water, methanol, and 1,4-dioxane. The spectral changes with solvent are similar to those for AcPheMA studied in the present work, but the spectral patterns of AcPheA resemble the AcPheMA spectra measured at higher temperatures.

From the above considerations of the temperature and solvent dependence of the CD spectra, it is sug-

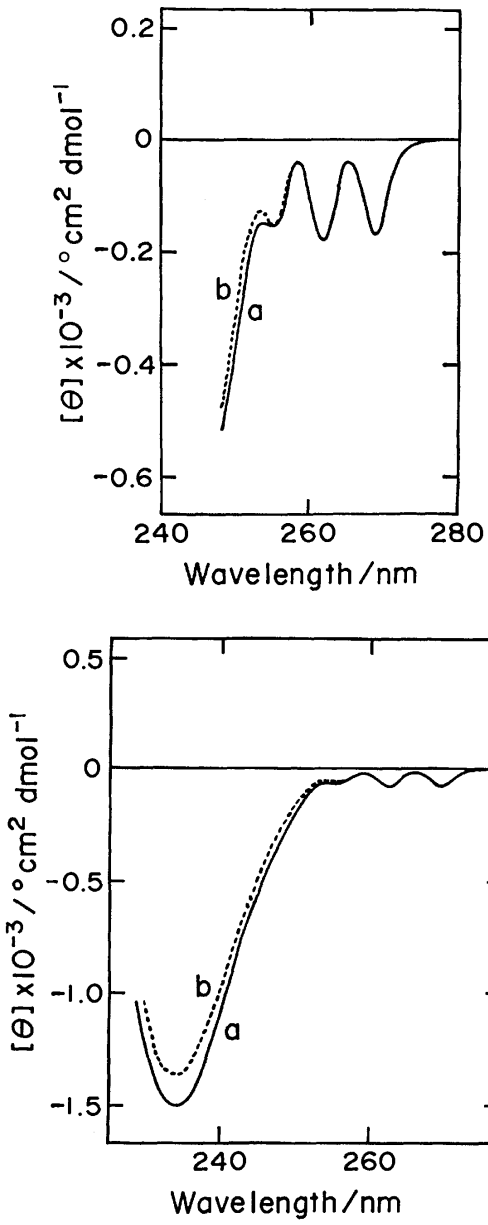

Fig. 4. CD spectra of *N*-acetyl-L-phenylalanine methylamide (AcPheMA) in 1,4-dioxane.
a: 20 °C, b: 40 °C.

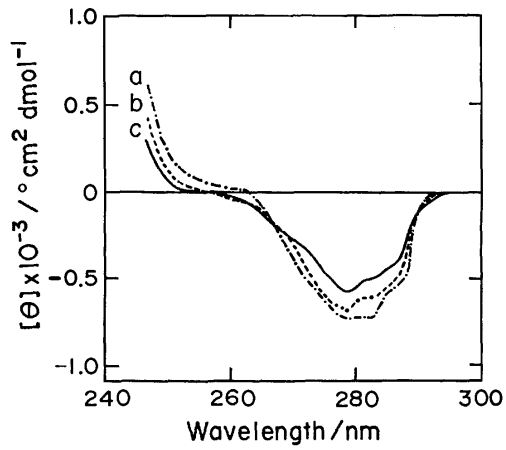

Fig. 5. CD spectra of *N*-acetyl-L-tyrosine methylamide (AcTyrMA) in methanol.
a: −70 °C, b: −7 °C, c: 22 °C.

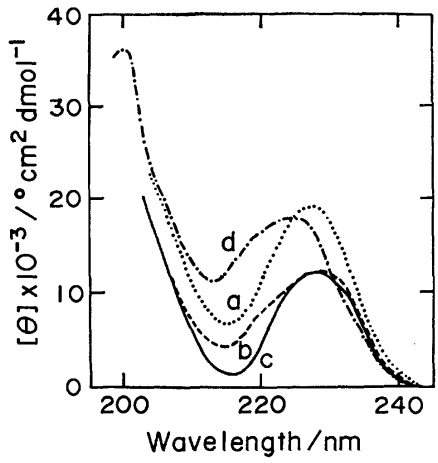

Fig. 6. CD spectra of *N*-acetyl-L-tyrosine methylamide (AcTyrMA) in methanol (a—c) and in water (d).
a: −7 °C, b: 22 °C, c: 40 °C, d: 22 °C in water.

gested that the hydrogen bonds between the amide group of AcPheMA and solvent molecules affect the amide $\pi^*\leftarrow$n transition. However, further studies are necessary to conclude whether the hydrogen bonding causes the conformational change or only the change of the electronic state of the amide group.

N-Acetyl-L-tyrosine Methylamide (AcTyrMA). The CD spectra of AcTyrMA measured in methanol at various temperatures are shown in Figs. 5 and 6. In the wavelength region of 260—290 nm, a negative extremum was observed at 278.5 nm with shoulders at 282.5 and 287 nm at room temperature. These bands are assigned to the vibrational structure of the phenolic $^1B_2\leftarrow{}^1A_1$ transition, similarly to the 240—270 nm bands of AcPheMA assigned to the phenyl $^1B_2\leftarrow{}^1A_1$ transition. The 278.5 and 282.5 nm CD bands of AcTyrMA correspond to the absorption bands at 277 and 283 nm observed with the same condition. The 287 nm CD shoulder, with no counterpart in the absorption spectrum, may be assigned to the 0-0 transition, with reference to the assignment of the 286 nm CD band of AcTyrA to the 0-0 transition.[3] As seen in Fig. 5, the shoulders at 282.5 and 287 nm became better resolved when temperature was lowered to −70 °C, and the peak intensity of the former was comparable to the intensity of the main peak at 278.5 nm. However, no remarkable spectral change with temperature was observed in this wavelength region. The CD spectrum at 40 °C was essentially the same as the spectrum at 22 °C. Thus, the temperature dependence of the spectral feature from −70 to 40 °C is much less than that for AcPheMA or AcTrpMA. The CD spectra in water and 1,4-dioxane were also similar to the spectrum of the methanol solution, with no appreciable spectral change with temperature. The resemblance of the CD and absorption spectra of AcTyrMA and other L-tyrosine derivatives in this wavelength region is accounted for by the reasoning that all of the vibronic bands have the same CD sign[3]

and that the rotational strength is nearly proportional to the dipole strength. In *N*-acetyl-L-tyrosine ethyl ester (AcTyrEE), the CD sign of this vibronic progression is different between the methanol and 1,4-dioxane solutions.[3] The fact that the very little variation of the CD spectra of AcTyrMA measured for various conditions suggests that the mobility of the *p*-hydroxyphenyl groups in AcTyrMA is more restricted than in AcTyrEE.

In the wavelength region shorter than 250 nm, a positive CD band appeared at 227.5 nm in methanol (Fig. 6), corresponding to the strong absorption band at 226 nm ($\varepsilon_{max}=12000\ M^{-1}\ cm^{-1}$). This band is probably due to the phenolic $^1A_1 \leftarrow {}^1A_1$ transition. The aqueous-solution CD spectrum exhibits a peak at 225 nm (blue-shifted by 2.5 nm) with an intensity about 50% stronger than in methanol. The intensity of this CD band in methanol increased as temperature was lowered, similarly to the temperature dependence of the 220 nm CD band of AcPheMA. This spectral change is ascribed to the dependence of the $\pi^* \leftarrow n$ transition on temperature. This is supported by the observation that in a 1,4-dioxane–methanol mixture (2:1, v/v) an apparent negative CD band appeared around 246 nm at 55 °C, but no distinct peak at 17 °C (Fig. 7). These observations of the spectral changes with temperature may be compared with the solvent effect on the CD spectra of AcTyrA observed in water, methanol, and 1,4-dioxane.[1] The effects of the increase in temperature and the decrease in solvent polarity resemble closely each other, as in AcPheMA.

N-Acetyl-L-tryptophan Methylamide (AcTrpMA). The CD spectra of AcTrpMA measured in methanol at various temperatures are shown in Figs. 8 and 9. It should be mentioned that in AcTrpMA the absorption strength relative to the rotational strength is much stronger than in AcPheMA or AcTyrMA. Accordingly, the solution concentration and the path length were limited in the measurements, giving very weak CD signals and consequently low signal-to-noise ratios. As temperature was lowered to −70 °C, the CD intensity in the longer-wavelength region increased progressively and the vibronic bands were well resolved (Fig. 8). The vibronic bands in this region are assigned to the $^1L_a \leftarrow {}^1A$ and $^1L_b \leftarrow {}^1A$ transitions of the indolyl side group. The low-temperature spectrum has

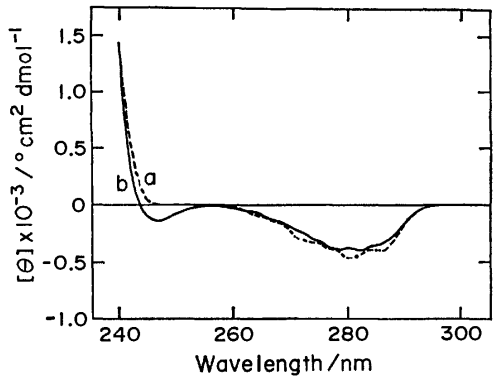

Fig. 7. CD spectra of *N*-acetyl-L-tyrosine methylamide (AcTyrMA) in 1,4-dioxane–methanol (2:1, v/v).
a: 17 °C, b: 55 °C.

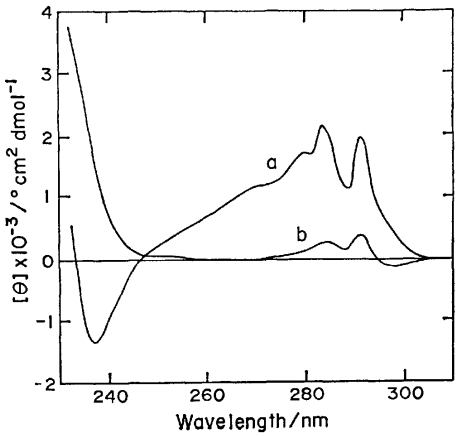

Fig. 8. CD spectra of *N*-acetyl-L-tryptophan methylamide (AcTrpMA) in methanol.
a: −70 °C, b: 22 °C.

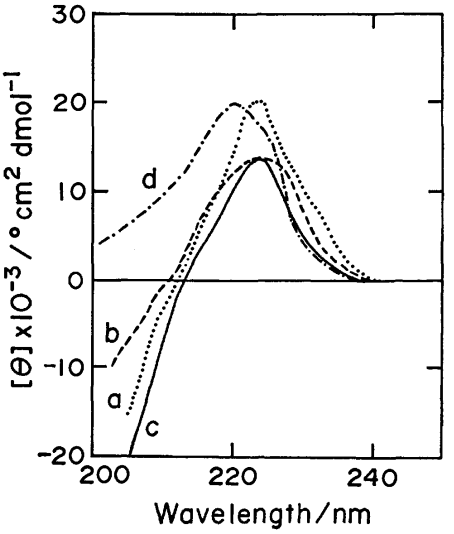

Fig. 9. CD spectra of *N*-acetyl-L-tryptophan methylamide (AcTrpMA) in methanol (a—c) and in water (d).
a: −5 °C, b: 22 °C, c: 40 °C, d: 22 °C in water.

two distinct positive peaks at 283.5 and 291 nm and a shoulder at 280 nm. An additional shoulder was observed around 270 nm at low temperature. These spectral features resemble those of the CD spectrum of AcTrpA.[5] The peaks of AcTrpMA at 283.5 and 291 nm are assigned to the 0+850 cm^{-1} $^1L_b \leftarrow {}^1A$ band and the 0—0 $^1L_b \leftarrow {}^1A$ band, respectively, with reference to the assignment of the corresponding CD bands of AcTrpA at 283 and 290 nm.[5] The noticeable difference in the CD spectra at room and lower temperatures suggests the coexistence of various conformers at higher temperatures, as in the case of AcPheMA. The CD spectrum of AcTrpMA in water in the 240—300 nm region resembles the aqueous-solution spectrum of L-tryptophan with unblocked amide and carboxyl groups;[12] three positive peaks with similar intensities were observed at 272, 281, and 291 nm.

In the spectral region of 200—240 nm, a positive CD band appeared at 223.5 nm in methanol and at 220 nm in water (Fig. 9), corresponding to the strong absorption band ($\varepsilon_{max}=45000\ M^{-1}\ cm^{-1}$) at 221.5 nm

in methanol. With the decrease in temperature, the intensity of this CD band increased but the peak position remained almost unshifted, indicating that this band of AcTrpMA is due largely to the transition of the indolyl side group ($^1L_b \leftarrow {}^1A$ transition). A noticeable spectral feature in Fig. 9 is that the CD curve of the methanol solution crosses over the base line at about 210 nm to the negative region. This observation shows the presence of a negative CD band in the shorter-wavelength region, in striking contrast to an anticipated positive band for AcPheMA (Fig. 2) or AcTyrMA (Fig. 6). Another spectral feature to remark for AcTrpMA is the appearance of a negative band at 237 nm at −70 °C. This spectral change appears to be opposite to the temperature effect on the apparent band of AcPheMA or AcTyrMA observed at 230—240 nm. However, the band at 237 nm is also ascribable to the overlap of two CD bands with different signs, as suggested by its wavelength. These peculiar spectral patterns for AcTrpMA lead to an inference that the CD behavior of the amide $\pi^* \leftarrow n$ and $\pi^* \leftarrow \pi$ transitions is different from that for AcPheMA or AcTyrMA. The difference is probably related to the bulkier indolyl group, which may interact with the peptide backbone in a way different from the phenyl or *p*-hydroxyphenyl group.

The authours wish to express their thanks to Dr. Toshio Takagi, Institute for Protein Research, Osaka University, for his valuable discussions and advices throughout the present work.

References

1) M. Shiraki, *Sci. Papers College of Gen. Education, Univ. of Tokyo*, **19**, 151 (1969).
2) J. Horwitz, E. H. Strickland, and C. Billups, *J. Am. Chem. Soc.*, **91**, 184 (1969).
3) J. Horwitz, E. H. Strickland, and C. Billups, *J. Am. Chem. Soc.*, **92**, 2119 (1970).
4) E. H. Strickland, M. Wilchek, J. Horwitz, and C. Billups, *J. Biol. Chem.*, **247**, 572 (1972).
5) E. H. Strickland, J. Horwitz, and C. Billups, *Biochemistry*, **8**, 3205 (1969).
6) E. H. Strickland, J. Horwitz, and C. Billups, *Biochemistry*, **9**, 4914 (1970).
7) E. H. Strickland, J. Horwitz, E. Kay, L. M. Shannon, M. Wilchek, and C. Billups, *Biochemistry*, **10**, 2631 (1971).
8) T. Takagi and N. Ito, *Biochim. Biophys. Acta*, **257**, 1 (1972).
9) A. O. Barel and A. N. Glazer, *Biopolymers*, **7**, 275 (1969).
10) H. Yoshioka and T. Miyazawa, unpublished.
11) T. Takagi, R. Okano, and T. Miyazawa, *Biochim. Biophys. Acta*, **310**, 11 (1973).
12) Y. P. Myer and L. H. MacDonald, *J. Am. Chem. Soc.*, **89**, 7142 (1967).

Synthesis and Alkali-cation Complexing Properties of 12-Crown-4 Derivatives†

Takeshi MIYAZAKI, Shozo YANAGIDA,* Akira ITOH, and Mitsuo OKAHARA

Department of Applied Chemistry, Faculty of Engineering, Osaka University, Yamadaoka, Suita, Osaka 565

(Received September 9, 1981)

Benzyloxymethyl-12-crown-4, a precursor of hydroxymethyl-12-crown-4, is prepared in an excellent yield by the reaction of 3-benzyloxy-1,2-propanediol with 1,8-dichloro-3,6-dioxaoctane in the heterogeneous *t*-BuOLi/*t*-BuOH/LiBr·$2H_2O$ reaction system. The hydrogenolysis in the presence of *p*-toluenesulfonic acid leads to a good yield of hydroxymethyl-12-crown-4. The sandwich-type 2:1 complexation with Na^+ of 12-crown-4 and hydroxymethyl-12-crown-4 derivatives was discussed on the basis of the stability constants and the solvent extraction in the CH_2Cl_2–water system.

Among a series of macrocyclic ethers, twelve-membered macrocycles, 12-crown-4 and its derivatives, long drew little attention because of their weak complexation due to their small cavity size and because of the difficulty in their preparation. Steiner and his group first reported that 12-crown-4 forms crystalline complexes with alkali and alkaline-earth metal salts and clarified some of their crystalline structure by means of X-ray crystallography.[1,2] We have been interested in their findings that the 2:1 sandwich-type complexes of 12-crown-4 are formed with NaCl and NaOH and have square-antiprismatic coordination structures. In our previous ^1H NMR studies of polyethers,[3] we found that, in methanol, 12-crown-4 showed an unusual downfield shift of protons in the presence of Na^+, and that the 2:1 complex with NaSCN including water of crystallization is formed in aqueous methanol and can be recrystallized in acetone. With these facts in view, the present work was undertaken in order to clarify the characteristic interaction of 12-crown-4 macrocycles with Na^+. Although we previously reported a method for the preparation of hydroxymethyl crown ethers,[4] this paper will describe another facile synthesis of hydroxymethyl-12-crown-4 and its derivatives from commercially available starting materials, and will discuss their complexation with alkali metal cations in comparison with those of 15-crown-5 derivatives.

Results and Discussion

Synthesis of Hydroxymethyl-12-crown-4(3). The cyclization reactions to 12-crown-4 were generally in low yields because of the side reactions producing cyclic or acyclic oligomers.[5] As a route to hydroxymethyl-12-crown-4(**3**), we investigated the reactions shown in Scheme 1, and tried to determine whether a high yield of cyclization to benzyloxymethyl-12-crown-4(**2**) could be achieved under the influence of high dilution and the template effect of Li^+.[6]

3-Benzyloxymethyl-1,2-propanediol(**1**) can be prepared by the benzylation of commercially available 2,2-dimethyl-4-hydroxymethyl-1,3-dioxolane, followed by the hydrolysis of the dioxolane ring. The diol(**1**) was allowed to react with triethylene glycol ditosylate

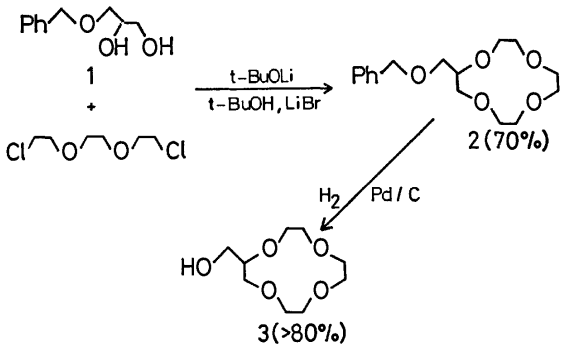

Scheme 1.

in a 1:1 molar ratio in the presence of lithium bases. As is shown in Table 1, the use of *t*-butyl alcohol as a solvent gave satisfactory results for the cyclization. Further, when commercially available 1,8-dichloro-3,6-dioxaoctane was employed instead of the ditosylate with an equimolar quantity of LiBr·H_2O, the cyclization occurred almost quantitatively, giving an excellent yield of the 12-crown-4(**2**), although a long reaction time was required (see Run Nos. 7 and 8). Without LiBr·H_2O, however, no cyclization was observed after a 9-day reaction, indicating that the halogen-exchange reaction to the bromide and its moderate reactivity are possibly favorable for the cyclization. The employment of lithium iodide, however, was accompanied by an unidentified by-product having a smaller retention volume in GLPC analysis, leading to a low yield (*ca.* 15% GLPC yield).

It is worth noting that a drop-by-drop addition of the diol(**1**) to a *t*-butyl alcohol solution of *t*-BuOLi immediately causes the turbidity of the finely dispersed lithium salt of the diol(**1**); thus, the reaction system is heterogeneous through the reaction. The heterogeneous intermolecular cyclization was extended to the synthesis of benzyloxymethyl-15-crown-5 from the diol(**1**) and 1,11-dichloro-3,6,9-trioxaundecane. An excellent yield(74%) was confirmed in the *t*-BuOLi/*t*-BuOH/LiBr·H_2O reaction system rather than in the *t*-BuONa/*t*-BuOH system(65%). Recently Czech[7] and Gokel *et al.*[8] have independently reported the same cyclization. Lower yields, 35% and 62%, were noted in the reaction systems with dichloride/NaOH/dioxane and with ditosylate or bis(methanesulfonate)/NaH/THF, respectively. Benzyloxymethyl-18-crown-6 could be isolated in a 46% yield according to the

† A preliminary report of this work was presented at the 19th Annual Meeting of the Japan Oil Chemists' Society, Hiroshima, October 1980.

Table 1. Synthesis of benzyloxymethyl-12-crown-4(**2**)

Run No.	XOOX	Reaction conditions[a]				Yield[b]
		Base	Solvent	Temp/°C	Time/d	%
1	X=OTs	LiH	Xylene	Reflux	1	14[c]
2	X=OTs	*t*-BuOLi	Xylene	Reflux	1	15[c]
3	X=OTs	*t*-BuOLi	Xylene	Reflux	3	17[c]
4	X=OTs	*t*-BuOLi	Xylene/*t*-BuOH(1:1)	85—95	2	58[c]
5	X=OTs	*t*-BuOLi	*t*-BuOH	Reflux	1	54(64)
6	X=Cl	*t*-BuOLi	*t*-BuOH	Reflux	9	0
7	X=Cl	*t*-BuOLi/LiBr·H_2O	*t*-BuOH	Reflux	10	70(92)
8	X=Cl	*t*-BuOLi/LiBr·H_2O	*t*-BuOH	Reflux	12	70(92)[d]

a) Under high dilution conditions: the diol (**1**) (2 g) and the dichloride (2 g) were allowed to react using 150 ml of the solvent. b) The values in parentheses are the GLPC yields. c) The product was extracted by hot hexane to remove the unreacted ditosylated and then distilled by means of a Kugelrohr apparatus. The formation of oligomers was confirmed by means of GLPC. d) Less diluted conditions (see the procedure in the Experimental section).

Table 2. Stability constants in methanol at 25 °C[a]

Macrocyclic polyethers	NaCl			KCl		
	log K_1'	log K_2'	K_2'/K_1'	log K_1'	log K_2'	K_2'/K_1'
12-Crown-4	1.41	2.20	6.15	1.58	0.15	0.08
Benzyloxymethyl-12-crown-4(**2**)	1.35	1.98	4.30	1.42	1.29	0.74
Hydroxymethyl-12-crown-4(**3**)	1.37	1.79	2.61	1.43	<0	0
Octyloxymethyl-12-crown-4	1.32	1.97	4.52	1.36	<0	0
15-Crown-5	3.30	1.44	0.01	3.34	2.21	0.07
Benzyloxymethyl-15-crown-5	3.07	1.94	0.07	3.16	1.27	0.01

a) K_1' and K_2' in L/mol; 99% confidence limits ±0.01.

present method, using 1,14-dichloro-3,6,9,12-tetraoxatetradecane.

The *t*-BuOLi/LiBr/*t*-BuOH reaction system was extended to the synthesis of unsubstituted 12-crown-4 from ethylene glycol and 1,8-dichloro-3,6-dioxaoctane. However, the quantitative cyclization was not confirmed by GLPC analysis; *i.e.*, the dichloride was left unreacted even after a 10-day reaction, and some by-products with a longer retention volume were formed with 12-crown-4. This was also true for the reaction of triethylene glycol and 1,8-dichloro-3,6-dioxaoctane under the same conditions. The yield of 18-crown-6(4 h, <10%) was quite inferior to those of such homogeneous reactions at *t*-BuOK/KBr/*t*-BuOH reactions system(20 h, 51%). In view of these facts, the quantitative cyclization to the benzyloxymethyl-12-crown-4 may be attributed to the heterogeneous reaction on the dispersed Li salt of the diol(**1**), in which the coupling by the attack of the primary alkoxide of the diol(**1**) and the subsequent intramolecular attack of the secondary alkoxide, must occur advantageously under the influence of the template effect of Li^+. A similar heterogeneous metal template synthesis has already been disclosed for the synthesis of 18-crown-6.[9,10]

The benzyl group of the benzyloxymethyl-12-crown-4 can be readily removed by hydrogenolysis on the Pd-carbon catalyst in the presence of a catalytic amount of *p*-toluenesulfonic acid, giving more than an 80% yield of hydroxymethyl-12-crown-4. The hydrogenolysis is very slow in the absence of *p*-toluenesulfonic acid. The co-catalysis of *p*-toluenesulfonic acid was discovered by the observation of the smooth debenzylation of the crude benzyloxymethyl-12-crown-4 obtained using the ditosylate. Matsui and Koga[11] previously reported the debenzylation of the 18-crown-6 derivatives by means of hydrogenolysis in acetic acid. It seems likely that protic acids catalyze the hydrogenolysis of benzyloxy macrocyclic ethers.

Hydroxymethyl-12-crown-4 can be alkylated in good yields by a reaction using alkyl bromide, potassium *t*-butoxide as the base, and *t*-butyl alcohol as the solvent.

Stability Constants of 12-Crown-4 Complexes with Na^+ and K^+ in Methanol. Employing potentiometry using ion-selective electrodes, the stability constants, *i.e.*, the equilibrium constants for complexation, of 12-crown-4 and its derivatives have been determined in methanol. According to the Frensdorff equations,[12] the stability constants, K_1' for 1:1 complexation and K_2' for 2:1 complexation, and K_2'/K_1' were precisely determined. For purposes of comparison, those of 15-crown-5 and benzyloxymethyl-15-crown-5 have also been determined (Table 2). The results show that, as for all Na^+ complexes with 12-crown-4 derivatives, the K_2' values are from 2 to 6 times larger than K_1', indicating the stronger tendency of the 2:1 complexation of 12-crown-4 in methanol as well as in the crystalline complexes with Na^+ salts. The proportions of 2:1 complexation have been calculated; they are

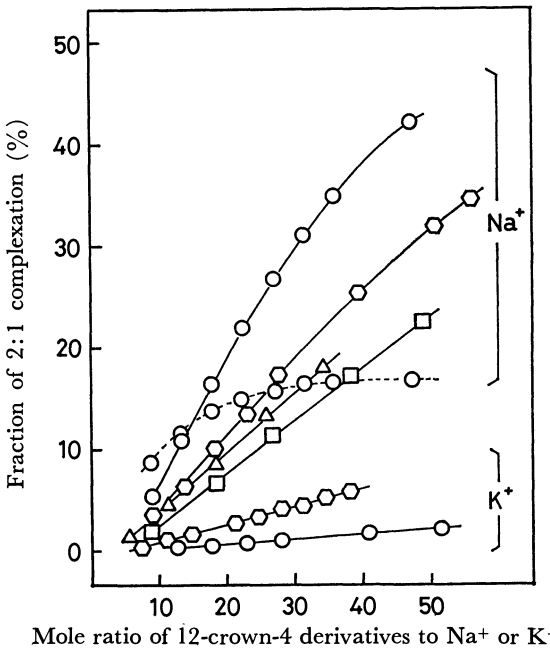

Fig. 1. Fraction of 2:1 complexation *vs.* mole ratio of 12-crown-4 derivatives to Na^+ or K^+.
—○—: 12-Crown-4, —◇—: benzyloxymethyl-12-crown-4, —□—: hydroxymethyl-12-crown-4, —△—: octyloxymethyl-12-crown-4, ···○···: fraction of the 1:1 complexation of 12-crown-4 with Na^+.

shown graphically in Fig. 1, along with that of the 1:1 complexation of 12-crown-4(see the dotted line in Fig. 1). The sandwich-type complexation increases with an increase in the ratio of the 12-crown-4 to Na^+. These findings, then, demonstrate that the sandwich-type complexation of 12-crown-4 derivatives gradually overcomes the solvation of methanol to Na^+, even if the large-side group causes steric interference in the 2:1 complexation.[13] Much the same, but a more remarkable, tendency has recently been observed for 12-crown-4 in propylene carbonate.[14]

In contrast, the stability constants for K^+ and the small or negligible proportion of the 2:1 complexation for K^+ (Fig. 1) suggest that 12-crown-4 derivatives are rather inclined to form 1:1 complexes with K^+ in methanol, contrary to the formation of the solid 2:1 complex of 12-crown-4 with KCl.[1] This is also true for the complexation of 15-crown-5 derivatives with Na^+ and K^+ in methanol. Thus, the characteristic complexation of 12-crown-4 with Na^+ is apparently due to the contribution of their sandwich-type complexation.

It is interesting to note that, although the log K_1' values of 15-crown-5 are almost the same for both Na^+ and K^+, the log K_2' value for K^+ is larger than that for Na^+. The selective complexation of 15-crown-5 with K^+ is also related to a sandwich-type complexation, just as in the case of 12-crown-4 for Na^+.

The effect of a benzyloxymethyl group on complexation with K^+ is worth noting. The stability constant, K_2', for K^+ of benzyloxymethyl-12-crown-4 is about ten times larger than that of 12-crown-4, while benzyloxymethyl-15-crown-5 has a smaller K_2' than 15-crown-5. In other words, the benzyloxymethyl group bound to 12-crown-4 strengthens the 2:1 complexing of K^+. The same effect of a benzyloxymethyl group has also been confirmed in the following solvent extraction.

Extraction of Alkali Picrates. The sandwich-type complexation of 12-crown-4 derivatives with Na^+ has also been derived from solvent extraction using dichloromethane as the solvent. 12-Crown-4 is lipophilic enough for it to be used as an extractant, because 95% of the crown in water can be removed by one extraction with chloroform(see Experimental section). However, because of the low stability constants, 12-crown-4 derivatives were used in a large excess against the picrates. The degree of extraction and the distribution ratio have been determined for alkai picrates; they are summarized in Table 3.

Compared with the extraction of 15-crown-5, 12-crown-4 derivatives all show weak extraction abilities, as expected. However, their selective extraction for Na^+ has now been confirmed. 12-Crown-4 and dodecyloxymethyl-12-crown-4 are the most selective. Benzyloxymethyl-12-crown-4(**2**) also extracts potassium picrate to a comparable extent, which is consistent with its large stability constant, K_2', for K^+ in methanol. It seems likely that the benzyloxymethyl group serves as a π donor for the 2:1 sandwich-type complexation especially with K^+.[15]

Extraction with 12-crown-4 was recently reported in a benzene–water system.[16] The stoichiometry of the extracted Na^+ species was determined to be 1:1. To ascertain the stoichiometry in the present extraction, the logarithm of the distribution ratios was plotted against the logarithm of the ratio of the 12-crown-4 to the picrate (Fig. 2). The coordination number of the crown in the extracted species can be determined from the slope of the line. A curved line is obtained, indicating that the coordination number changes ap-

Table 3. Solvent extration of alkali picrates with 12-crown-4 derivatives[a]

	12-Crown-4		Benzyloxymethyl-12-crown-4(**2**)		Dodecyloxymethyl-12-crown-4		15-Crown-5	
	EX(%)	D	EX(%)	D	EX(%)	D	EX(%)	D
Li^+	1.7	0.017	2.6	0.027	1.8	0.018	9.0	0.10
Na^+	19.9	0.249	15.2	0.179	15.4	0.181	33.2	0.50
K^+	5.3	0.056	14.1	0.164	4.2	0.044	93.2	13.75
Rb^+	3.5	0.036	13.0	0.149	3.1	0.032	85.4	5.85
Cs^+	2.6	0.027	12.6	0.144	2.6	0.027	43.4	0.76

a) EX(%): Degree of extraction, D: distribution ratio.

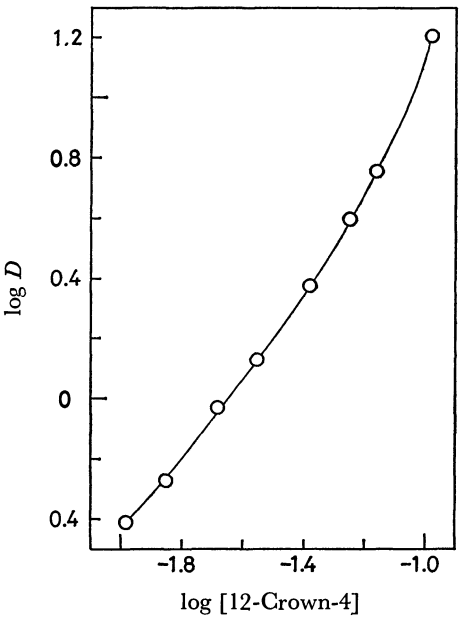

Fig. 2. Distribution ratio of sodium picrate *vs.* concentration of 12-crown-4.

proximately from 1 to 2 as the concentration of the crown increases. This is probably due to the increasing sandwich-type complexation.

The selective complexation of 12-crown-4 derivatives for Na^+ has now been confirmed due to the 2:1 sandwich-type complexation. The specific complexation for Na^+ might be related to the fulfillment of the Na^+ coordination geometry.[2]

In view of the facile synthesis and the sandwich-type interaction of 12-crown-4 macrocycle, hydroxymethyl-12-crown-4 may be utilized as a new functional substituent causing a Na^+-promoted bimolecular interaction.

Experimental

Materials. 3-Benzyloxymethyl-1,2-propanediol (**1**) was prepared according to Howe and Malkin.[17] The 1,11-dichloro-3,6,9-trioxaundecane, 1,14-dichloro-3,6,9,12-tetraoxatetradecane, and triethylene glycol ditosylate were prepared by the chlorination of tetraethylene glycol and pentaethylene glycol with $SOCl_2$, and by the reaction with tosyl chloride, respectively. The 12-crown-4 (Bokusui Brown Co., Ltd.) and 15-crown-5 (Nakarai Chemical Ltd.,) were purified by distillation. All the other reagents and solvent were obtained commercially and were used without further purification.

Measurement of Spectra. The ^1H NMR, IR, and mass spectra were obtained using JEOL LMN-PS-100, Hitachi 260-10, and Hitachi RMU-6E spectrometers respectively. GLPC analyses were carried out on a Shimadzu GC-4BPT apparatus using Silicone SE-30 on a Diasolid L (60—80 mesh) (4 mm × 1 m).

Preparation of Benzyloxymethyl-12-crown-4 (2). A 3—1 three-necked flask equipped with a reflux condenser, an addition funnel, and a magnetic stirrer was charged with *t*-butyl alcohol (1500 ml) and metal lithium (5.7 g, 0.82 mol). After an hour's reflux under stirring, 3-benzyloxy-1,2-propanediol (50 g, 0.27 mol) was added drop by drop, causing the solution to become cloudy because of the precipitation of the lithium salts of 3-benzyloxy-1,2-propanediol (**1**). To the above heterogeneous solution we added 1,8-dichloro-3,6-dioxaoctane (51.4 g, 0.27 mol) and $LiBr \cdot H_2O$ (28.8 g, 0.27 mol) successively. The heterogeneous reaction mixture was refluxed and stirred until the dichloride almost disappeared upon GLPC analysis (12 d). After the bulk of *t*-butyl alcohol had been evaporated under reduced pressure, a 100-ml portion of water was added to the residue. After neutralization, the product was extracted three times with a 100-ml portion of diethyl ether. The extract was dried and condensed under reduced pressure. The resulting liquid was distilled under reduced pressure, giving 56.9 g of benzyloxymethyl-12-crown-4 (**2**) (70% yield): bp 120—130 °C/0.03 Torr (1 Torr=133.322 Pa); IR (neat, NaCl plates), 3035 (w), 2930 (s), 2870 (s), 1500 (w), 1460 (m), 1135 (s), 1100 (s), 740 (m) cm^{-1}. ^1H NMR ($CDCl_3$), δ 3.48—3.90 (m, 17H), 4.55 (s, 2H), 7.25 (s, 5H); mass spectrum (*m/e* rel intensity) 296 (M^+), 205 (6), 175 (28), 146 (17) 133 (11), 91 (100), 87 (81), 73 (19), 59 (26), 45 (90). Found: C, 64.73; H, 8.16%. Calcd for $C_{16}H_{24}O_5$: C, 64.84; H, 8.16%. Under comparable conditions, benzyloxymethyl-15-crown-5 and 18-crown-6 were prepared by the reaction of 3-benzyloxymethyl-1,2-propanediol with 1,11-dichloro-3,6,9-trioxaundecane and 1,14-dichloro-3,6,9,12-tetraoxatetradecane respectively: Benzyloxymethyl-15-crown-5 (74% yield); bp 160—180 °C/0.01 Torr (Kugelrohr); IR (neat, NaCl plates) 3035 (w), 2870 (s), 1500 (w), 1460 (w), 1125 (s), 740 (m), 700 (m) cm^{-1}: ^1H NMR ($CDCl_3$) δ 3.48—3.90 (m, 21H), 4.55 (s, 2H), 7.25 (s, 5H); mass spectrum (*m/e*, rel intensity) 340 (M^+, 6), 249 (10), 219 (11), 177 (3), 146 (18), 133 (14), 91 (100), 87 (98), 73 (18). Found: C, 63.49; H, 8.55%. Calcd for $C_{18}H_{28}O_6$: C, 63.51; H, 8.21%. Benzyloxymethyl-18-crown-6 (46% yield), bp 190—195 °C/0.03 Torr (Kugelrohr); IR (neat, NaCl plates) 3040 (w), 2860 (s), 1455 (m), 1355 (m), 1300 (w), 1250 (m), 1105 (s), 955 (m), 840 (m), 740 (m), 700 (m). ^1H NMR ($CDCl_3$) δ 3.48—3.90 (m, 25H), 4.52 (s, 2H), 7.30 (s, 5H). Mass spectrum (*m/e*, rel intensity), 384 (M^+), 293 (13), 263 (7), 175 (10), 146 (10), 133 (20), 91 (94), 87 (100), 73 (28), 59 (28). Found: C, 62.20; H, 8.48%. Calcd for $C_{20}H_{32}O_7$: C, 62.47; H, 8.38%.

Preparation of Hydroxytmethyl-12-crown-4 (3). Benzyloxymethyl-12-crown-4 (**2**) (4.5 g, 0.022 mol) and 10 ml of 1,4-dioxane were placed in a 20-ml test tube equipped with a hydrogen inlet. To the solution we then added 0.1 g of Pd–carbon (5%) (Mitsuwa Pure Chemicals) and 50 mg of *p*-toluenesulfonic acid. Hydrogen gas was passed through the solution at 50 °C for 5 h. After the filtration and removal of 1,4-dioxane by means of a rotary evaporator, the residue was distilled under reduced pressure to yield 2.6 g of hydroxymethyl-12-crown-4 (81%): bp 112—113 °C/0.02 Torr [lit,[4] 115 °C/0.04 Torr] IR (neat, NaCl plates), 3250 (s), 2930 (s), 2870 (s), 1135 (s), 1100 (s) cm^{-1}: ^1H NMR ($CDCl_3$) δ 3.05 (s, 1H), 3.45—3.90 (m, 17H); mass spectrum (*m/e*, rel intesity), 206 (M^+), 188 (3), 175 (21), 133 (6), 103 (5), 87 (51), 45 (100). Found: C, 52.14; H, 9.09%. Calcd for $C_9H_{18}O_5$: C, 52.41; H, 8.80%.

Preparation of Dodecyloxymethyl-12-crown-4. Hydroxymethyl-12-crown-4 (1.0 g, 4.9 mmol) was allowed to react with dodecyl bromide (1.57 g, 6.4 mmol) at 70 °C for 10 h, using lithium *t*-butoxide (0.71 g, 6.3 mmol) as the base and *t*-butyl alcohol (15 ml) as the solvent. After the subsequent removal of the solvent, water was added and the mixture was neutralized and extracted with diethyl ether. After the usual work-up, dodecyloxymethyl-12-crown-4 (1.4 g, 78% yield) was obtained: bp 150 °C/0.03 Torr, ^1H NMR ($CDCl_3$) δ 0.88 (t, 3H), 1.27 (bs, 20H), 3.35—3.50 (m, 19H); mass

spectrum, 374 (M^+). Found: C, 67.15; H, 11.37%. Calcd for $C_{21}H_{42}O_5$: C, 67.34; H, 11.30%. Octyloxymethyl-12-crown-4 was similarly prepared (85% yield): bp 125 °C/0.04 Torr, ^1H NMR ($CDCl_3$) δ 0.88 (t, 3H), 1.27 (bs 12H), 3.33—3.90 (m, 19H); mass spectrum, 318 (M^+). Found: C, 64.26; H, 10.64%. Calcd for $C_{17}H_{34}O_5$: C, 64.12; H, 10.76%.

Measurement of Stability Constant. According to Frensdorff's method based on potentiometry with cation-selective electrodes, the stability constants for 1:1 and 2:1 complexes of the crown ethers were determined for Na^+ and K^+. The solvent was absolute methanol (less than 0.1% water) (Wako Pure Chemicals Industry, Ltd.) The following Tohkoh Chemical measuring electrodes were used after step-by-step conditioning: the sodium-ion electrode (Na1100) and a reference electrode (MR-501C) for Na^+, and the potassium-ion electrode (K1200) and a reference electrode (CR-501C) for K^+. The emf was measured with a Beckman 4500 digital pH meter. The R values[10] were computed by minimizing the deviation of average K_1' values within 1% using an NEC PC-8001 computer. Seven to 9 measurements were included in regression analysis.

Solvent Extraction. In a stoppered, 30-ml glass tube we placed 10 ml of a dichloromethane solution containing an extractant (1.05×10^{-2} M or more), 5 ml of an alkali hydroxide solution (0.02 M), and 5 ml of a picric acid solution (1.4×10^{-4} M). The solution was shaken for 10 min at 25 °C and then left standing in a thermostated water bath (at 25 °C±0.5) for 12 h. The picrate concentration in the water phase was determined at 354 nm by means of a Shimadzu UV 200 spectrophotometer ($\varepsilon=1.414\times10^4$ $cm^{-1}M^{-1}$).

Table 4. The extraction of sodium picrate by means of 12-crown-4

Concentration of 12-crown-4	Extraction (%)	Distribution ratio (D)
1.05×10^{-2}	28.2	0.3929
1.40×10^{-2}	35.2	0.5421
2.10×10^{-2}	48.2	0.9292
2.80×10^{-2}	57.4	1.3471
4.20×10^{-2}	70.5	2.3911
5.60×10^{-2}	79.8	3.9607
7.00×10^{-2}	85.1	5.7155
10.50×10^{-2}	94.2	16.3625

The extraction percentages and the distribution ratios were determined at different concentrations of 12-crown-4 (Table 4).

Determination of Lipophilicity of 12-Crown-4. 12-Crown-4 (0.055 g), dissolved in 0.552 g (*ca.* 0.5 ml) of D_2O, was extracted with 0.727 g (*ca.* 0.5 ml) of $CDCl_3$. The concentration of 12-crown-4 in the aqueous phase was determined by ^1H NMR, using nitromethane as the internal reference. Ninety-five percent of the 12-crown-4 was extracted by $CDCl_3$ just as in the case of 15-crown-5.

The authors wish to express their thanks to Mr. Masaie Fujino for his kind advice on computation by means of a PC-8001 computer.

References

1) E. C. Steiner, R. A. Newton, and F. Boer, U. S. Patent 4025523.
2) a) F. P. Van Remoortere and F. P. Boer, *Inorg. Chem.*, **13**, 2071 (1971); b) F. P. Boer, M. A. Neuman, F. P. Van Remoortere, and E. C. Steiner, *ibid.*, **13**, 2826 (1974).
3) S. Yanagida, K. Takahashi, and M. Okahara, *Bull. Chem. Soc. Jpn.*, **51**, 3111 (1978).
4) I. Ikeda, S. Yamamura, N. Nakatsuji, and M. Okahara, *J. Org. Chem.*, **45**, 5355 (1980).
5) F. L. Cook, T. C. Caruso, M. P. Byrne, C. W. Bowers, D. H. Speck, and C. L. Liotta, *Tetrahedron Lett.*, **1974**, 4029.
6) P-L. Kuo, N. Kawamura, M. Miki, and M. Okahara, *Bull. Chem. Soc. Jpn.*, **53**, 1689 (1980).
7) B. Czeck, *Tetrahedron Lett.*, **1980**, 533.
8) G. W. Gokel, D. M. Dishong, and C. J. Diamond, *J. Chem. Soc., Chem. Commun.*, **1980**, 1053.
9) P-L. Kuo, M. Miki, and M. Okahara, *J. Chem. Soc., Chem. Commun.*, **1978**, 504.
10) J. Yamawaki and T. Ando, *Chem. Lett.*, **1980**, 533.
11) T. Matsui and K. Koga, *Chem. Pharm, Bull.*, **27**, 2295 (1975).
12) H. K. Frensdorff, *J. Am. Chem. Soc.*, **93**, 600 (1971).
13) D. M. Dishong, C. J. Diamond, and G. W. Gokel, *Tetrahedron Lett.*, **1981**, 1663.
14) J. Massaux, J. F. Desreux, and G. Duyckaerts, *J. Chem. Soc., Dalton Trans.*, **1980**, 865.
15) N. Kawashima, T. Kawashima, T. Otsubo, and S. Misumi, *Tetrahedron Lett.*, **1978**, 5025.
16) Y. Takada, *Bull. Chem. Soc. Jpn.*, **53**, 2393 (1980).
17) R. J. Howe and T. Malkin, *J. Chem. Soc.*, **1951**, 2663.

Photoreduction of Silver Ion in a Titanium Dioxide Suspension

Hiroshi HADA,* Yoshiro YONEZAWA, and Masahiko SAIKAWA

Department of Industrial Chemistry, Faculty of Engineering, Kyoto University, Yoshida, Sakyo-ku, Kyoto 606

(Received September 19, 1981)

Quantum yields ranging from 0.084 to 0.191 were obtained for the reduction of Ag^+ by irradiation of light at 365 nm on a TiO_2 surface in aqueous solutions containing 1×10^{-4} to 1×10^{-2} mol dm^{-3} $AgClO_4$. Some features of the reduction were preliminarily examined with the aid of an electrochemical measurement of TiO_2 sinter. It is proposed that some conduction-band electrons, produced in the TiO_2 by irradiation, transfer to Ag^+ adsorbed on the TiO_2 surface and that positive holes react with water molecules. The photoreduction of Ag^+ is optically sensitized by addition of Uranine. The apparent quantum yield (the number of reacted ions/the number of photons incident to the suspension) of the dye-sensitized photoreduction of Ag^+ is 0.01.

Photodeposition of metals at semiconductor surface is interesting in that it is related to many applications including the solar energy conversion: the solid-state photogalvanic cell capable of storing light energy in the form of deposited metal and supplying electrical energy from it;[1] semiconductor photocatalysis and anticorrosion of semiconductors;[2-6] non-silver halide imaging materials of interesting use.[7,8] However, only a few reports have dealt with the mechanism of the photodeposition.[9] This may be first because even deposition of colloidal metal by either photolysis or radiolysis of aqueous solution of metal ions is rather a complex reaction as revealed by several investigators,[10,11] and second because deposited metal may considerably change semiconductor surface in its physical and chemical properties. For these reasons, investigations on photodeposition of metals are limited to SnO_2–, ZnO–, and TiO_2–Ag^+ systems,[9,12,13] TiO_2–Pd^{2+} system,[14] TiO_2–Pd^{2+} and –$PtCl_6^{2-}$ systems,[15] TiO_2– and WO_3–Cu^{2+} systems,[16] and TiO_2–$PtCl_6^{2-}$, –$PdCl_4^{2-}$, –Ag^+, and –Cu^{2+} systems.[17] As to dye-sensitized reduction of metal ions, only a few reports have been published which treat TiO_2–Ag^+–triphenylmethane dye[9] and ZnO–Ag^+–xanthene dye systems,[13] apart from a qualitative study for photographic application.[18]

We have been interested in photochemical reactions of the ZnO–Ag^+ system and carried out photochemical and electrochemical studies on photoreduction of Ag^+ both in ZnO suspension and at ZnO sinter surface.[13] We have found that the net photochemical reaction induced by irradiation of UV-light obeys the local-cell mechanism. In photochemical reactions at TiO_2 surface, positive holes produced by optical excitation of TiO_2 will not induce dissolution of the semiconductor itself, in contrast to the ZnO system, which suggests some different situation involved in this case. We thus investigated photoreduction of Ag^+ in a TiO_2 aqueous suspension by using 365 nm light, which is within the fundamental absorption band of TiO_2, and examined optical sensitization of this reaction by Uranine. Also, we carried out preliminary measurements of electrochemical properties of the TiO_2–aqueous solution interface. We have thus clarified several characteristics of the photoreduction of Ag^+ at TiO_2 surface.

Experimental

The experimental set-up and procedure were almost the same as those previously reported for the ZnO–Ag^+ aqueous suspension.[13] The TiO_2 used was a highly purified powder offered from Teikoku Kakou Co., Okayama. This material had a surface area of 7.3 m^2/g-TiO_2, an average particle size of 0.5 μm, and low-level impurities of Nb, Al, and P (below 0.01%). In an 50 ml aqueous solution containing 1×10^{-4} to 1×10^{-2} M† $AgClO_4$ and 0.5 M KNO_3 was suspended 0.5 g TiO_2 powder. For the study of dye-sensitized reduction, Uranine was added to the aqueous suspension. Before the reaction, dissolved oxygen was purged by introduction of high-purity nitrogen gas.

The same combination of the light source, monochrometer, and glass filter as in our previous work[13] was used to select either the 365 nm light (designated TiO_2-light) or 500 nm light (dye-light). The half-band width of the monochromator was about 20 nm. Irradiation was commenced after the adsorption equilibrium of Ag^+ at the TiO_2 surface had been established. After irradiation, the amount of photoreduced silver was determined by atomic absorption spectrometry with a Jarrel-Ash AA-780 spectrophotometer. The number of incident photons was 1.10×10^{15} cm^{-2} s^{-1} for TiO_2-light and 2.00×10^{15} cm^{-2} s^{-1} for dye-light.[19] The transmittance and reflectance for suspensions were measured with Shimadzu spectrophotometers, MPS-5000 and QV-50 equipped with an integrating sphere, respectively. The quantum yield of photoreduction of Ag^+ for the unsensitized system and the apparent quantum yield for the dye-sensitized system were evaluated by use of the equation:

$$\Phi_{Ag} = \frac{1}{Q}\frac{d[Ag]}{dt}, \quad (1)$$

where Φ_{Ag} is the quantum yield for the unsensitized system or the apparent quantum yield for the dye-sensitized system, d[Ag]/dt is the initial rate of formation of the reduced silver (atoms s^{-1}), and Q is either the number of the photons absorbed by the suspension (unsensitized system) or of those incident to the suspension (sensitized system) (photons s^{-1}). The amount of Ag^+ adsorbed at adsorption equilibrium was determined after TiO_2 powder had been immersed in a solution of 1×10^{-4} to 1×10^{-2} M $AgClO_4$ plus 0.5 M KNO_3 for 3 h under constant stirring.

Electrochemical measurements on a TiO_2 sinter electrode were carried out in the conventional manner.[20,21] A pellet from TiO_2 powder was placed on a disk 12 mm in diameter and 0.5 mm thick and then sintered at 1300 °C for 2 h in air. After cooling to room temperature, the pellet was reduced at 600 °C in a hydrogen atmosphere for 2 h. Indium was evaporated onto one face of the sinter to provide an ohmic contact, and a copper wire was soldered on it. Then, all surfaces, except the other face of the sinter to be exposed to the electrolyte solution (*ca.* 0.64 cm^2), were cov-

† 1 M = 1 mol dm^{-3}.

ered with epoxy resin. The electrode prepared in this manner was dipped into aq HNO_3 for 30 s and washed in water before use. The construction of the electrochemical cell and electrochemical measurements were carried out by employing the same procedures previously described.[13] The number of incident photons on the electrode (TiO_2-light) was 9.00×10^{14} cm^{-2} s^{-1}. The electrolyte solutions were composed of 0.5 M KNO_3 or a mixed solution of 0.5 M KNO_3 and 1×10^{-5} to 1×10^{-3} M $AgClO_4$. High purity nitrogen gas was bubbled through the solution in order to remove oxygen before the measurement.

Results

Photoreduction in the Unsensitized System. The dependence of the amount of reduced silver on the irradiation time of TiO_2-light for the TiO_2–Ag^+ aqueous suspension is given in Fig. 1. The reduced silver resulting from thermal reduction in the dark was about 0.15 μmol irrespective of either irradiation time or $AgClO_4$ concentration. This value was previously subtracted before constructing this figure. Quantum yields of the photoreduction of Ag^+ are 0.191 ± 0.014 ($AgClO_4$; 1×10^{-2} M), 0.159 ± 0.005 (2×10^{-3} M), 0.090 ± 0.003 (1×10^{-3} M), 0.090 ± 0.003 (5×10^{-4} M), and 0.084 ± 0.0 (1×10^{-4} M). The pH of the suspension was about 4.5. The quantum yields obtained here are in the same magnitude as those reported for TiO_2 thin film–Ag^+ system.[9] However, the dependence of Φ_{Ag} on the initial Ag^+ concentration, C_{Ag^+}, significantly deviates from the Stern-Volmer relation proposed by Fleischauer *et al.* (Fig. 2).

The adsorption of Ag^+ on the TiO_2 surface was measured at 20 °C, the adsorption isotherm being given in Fig. 3. The equilibrium concentration of Ag^+ in the aqueous phase, $C^{eq}_{Ag^+}$, and the equilibrium amount of Ag^+ adsorbed on the surface of 1.0 g TiO_2, N_{Ag^+}, satisfy Freundlich's adsorption formula at $AgClO_4$ concentrations less than 5×10^{-3} M:

$$N_{Ag^+} = A(C^{eq}_{Ag^+})^{1/n}, \quad (2a)$$

$$\log N_{Ag^+} = \log A + \frac{1}{n}\log C^{eq}_{Ag^+}, \quad (2b)$$

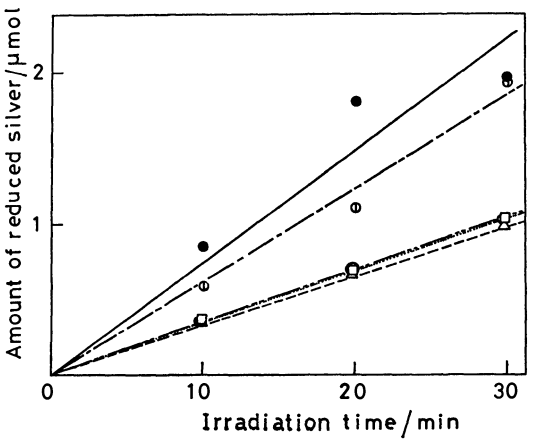

Fig. 1. Growth of the amount of reduced silver in TiO_2 suspension containing $AgClO_4$ and 0.5 M KNO_3 with irradiation time.
●: $[AgClO_4]=1\times10^{-2}$ M, ◑: 2×10^{-3} M, ○: 1×10^{-3} M, □: 5×10^{-4} M, and △: 1×10^{-4} M.

where A and n are constants. The adsorption index $1/n$ is 0.78. However, at higher concentrations, N_{Ag^+} began to increase more steeply than expected from Eq. 2. Substitution of N_{Ag^+} for C_{Ag^+} in Fig. 2 could scarcely improve the linear relation of Stern-Volmer plot (Fig. 2).

We tried to clarify the behavior of positive holes through detection of increase in the dissolved oxygen in the aqueous phase during the photoreaction. A 200 ml aqueous suspension composed of 2.0 g of TiO_2, 0.5 M KNO_3, and 1×10^{-3} M $AgClO_4$ was prepared.

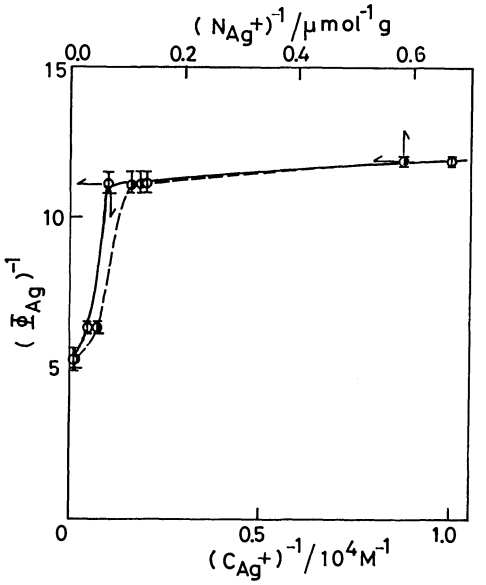

Fig. 2. Stern-Volmer plots for the reduction of Ag^+ on TiO_2.
◑: Reciprocal plot between the quantum yield Φ_{Ag} and C_{Ag^+}, ◑: reciprocal plot between Φ_{Ag} and N_{Ag^+}. C_{Ag^+} and N_{Ag^+} denote the initial concentration of $AgClO_4$ and the amount of adsorbed Ag^+ on TiO_2 surface.

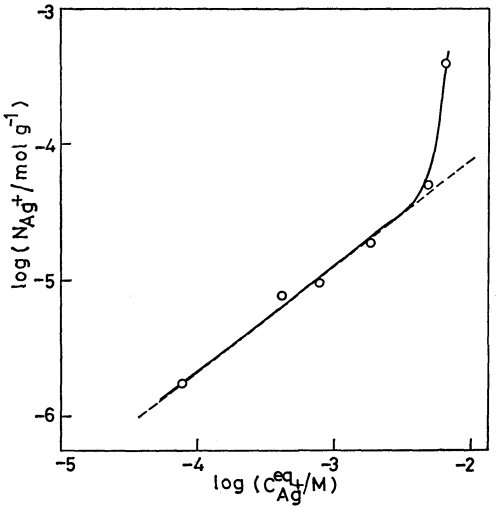

Fig. 3. Freundlich type plot for Ag^+ adsorption on TiO_2 surface.
N_{Ag^+} and $C^{eq}_{Ag^+}$ denote the amount of adsorbed Ag^+ on TiO_2 surface and the concentration of Ag^+ in aqueous phase.

After bubbling nitrogen, the suspension was irradiated by 365 nm light from a 500 W high-pressure mercury lamp (Ushio Denki Type USH-500D), and the increase in dissolved oxygen was recorded on an oxygen meter (Nisshin Rika Model OX-36). After 30 min irradiation, the increase of dissolved oxygen and the amount of reduced silver were registered as 8.2 μmol and 39.6 μmol, respectively. The observed O_2/Ag ratio is close to the theoretical value of 1/4. With suspensions containing no $AgClO_4$, on the contrary, dissolved oxygen after irradiation was at somewhat a lower level than that before irradiation. These facts lead to a conclusion that the positive hole produced by TiO_2-light can react with water and generate oxygen in the presence of Ag^+.[22-24]

Photoreduction in the Dye-sensitized System. The dependence of the amount of photoreduced silver on the irradiation time is given in Fig. 4. The concentrations of $AgClO_4$ and Uranine were 1×10^{-4} and 1×10^{-5} M, respectively. The apparent quantum yield of the photoreduction of Ag^+ is 0.01. The optical absorption spectrum of Uranine solution and the diffuse reflection spectrum of TiO_2 suspension were recorded on an MPS-5000 spectrophotometer (Fig. 5). The dependence of apparent quantum yield on the wavelength of incident light (photochemical action spectrum) was determined from the amount of photoreduced silver after 2 h irradiation. It has a maximum at *ca.* 500 nm (Fig. 5).

Discussion

Reaction Scheme for the Unsensitized System. In our previous paper,[13] we examined, with a help of electrochemical study, a simple reaction scheme proposed by Fleischauer *et al.*[9] and concluded that the scheme is capable of interpreting the general feature of Ag^+ reduction at ZnO surface. Such a simple scheme, as it is, is not applicable to the present TiO_2–Ag^+ system, as seen from the significant departure from linear plot shown in Fig. 2. Nevertheless, aside

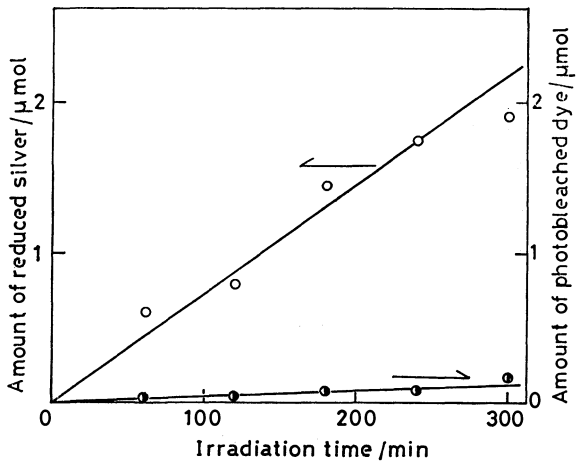

Fig. 4. Growth of the amount of reduced silver in TiO_2 suspension containing $AgClO_4$, KNO_3, and Uranine with irradiation of 500 nm light (○——○). Growth of the amount of photobleached dye is also given (◑——◑).

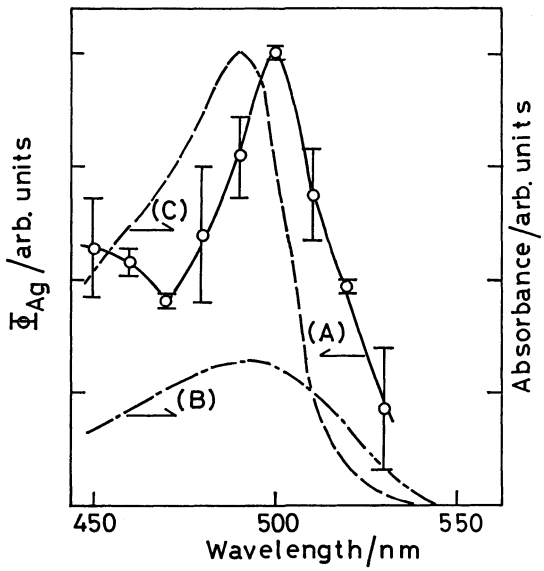

Fig. 5. Photochemical action spectrum for sensitized reduction of Ag^+ on TiO_2 (A) and absorption spectra of Uranine adsorbed on TiO_2 (B) and in aqueous solution (C).
Bulk solution contains 1×10^{-4} M $AgClO_4$, 1×10^{-5} M Uranine and 0.5 M KNO_3.

from the detailed mechanism, it is natural to assume, as the above scheme does, that the photoreduction at semiconductor surface will proceed under the local-cell condition, *i.e.*, that the rate of net cathodic reaction is equal to that of net anodic reaction in the photostationary state.

To examine this assumption, we carried out the present photoelectrochemical study on the TiO_2 sinter electrode. Figure 6 shows polarization curves of the TiO_2 electrode in 0.5 M KNO_3 solutions with and without 5×10^{-4} M $AgClO_4$. The curves indicate both the current measured in the dark and the partial anodic photocurrent as obtained by subtracting the current measured in the dark from the current measured under irradiation. The irradiation did not affect the cathodic current in our study, contrary to the finding of Sprünken *et al.*[25] Therefore, the partial anodic photocurrent indicates the real anodic element of the current under irradiation. From these curves, we have obtained both the zero-current-potential, E_{zcp}, at which the total current under irradiation is zero, and the cathodic current at this potential, i_{dzcp}. If all the cathodic current contributes to the reduction of Ag^+, we can estimate the rate of photoreduction of Ag^+ on this electrode from the value of this current. Indeed, the rate evaluated in this manner at 1×10^{-3} M $AgClO_4$ is in accord with the value obtained by the chemical-analysis method for the same electrode system, within the limit of experimental error. Therefore, almost all the cathodic current at the zero-current-potential can be said to contribute to the silver reduction.

Now, let us assume that the results on the TiO_2 suspension can be analyzed through electrochemical study of the TiO_2 sinter. On the local-cell model for the photoreduction at TiO_2 surface, the electrode

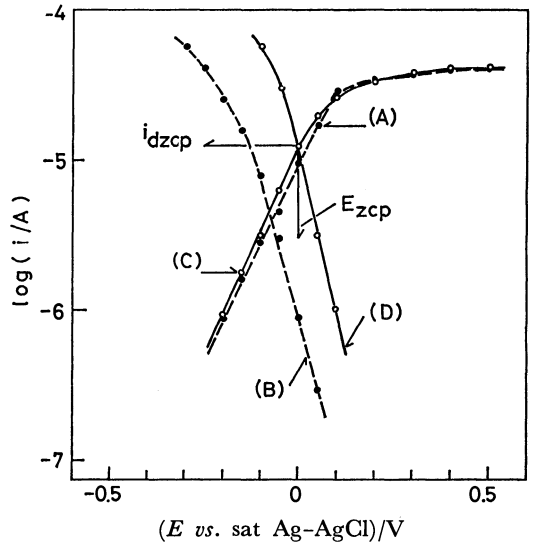

Fig. 6. Polarization curves of TiO_2 electrode in 0.5 M KNO_3 solution with and without 5×10^{-4} M $AgClO_4$.
(A) ●——●: Partial anodic photocurrent without $AgClO_4$, (B) ●——●: dark cathodic current without $AgClO_4$, (C) ○——○: partial anodic photocurrent with $AgClO_4$, (D) ○——○: dark cathodic current with $AgClO_4$. E_{zcp} and i_{dzcp} denote the zero-current-potential and the corresponding cathodic current in solution with $AgClO_4$.

potential (Fermi level) of the TiO_2 immersed in a solution under irradiation is equal to the E_{zcp}. According to Fig. 6, the upward band bending still exists in the space-charge layer of TiO_2, because the onset potential of the partial anodic photocurrent of the TiO_2 electrode is more negative than E_{zcp}. Furthermore, the photopotential measurement on this electrode showed that the electrode potential shifts to a more positive value when the TiO_2-light is cutoff. From these facts, the surface barrier of the TiO_2 in the $AgClO_4$ solution seems to be much smaller under irradiation of TiO_2-light. The photoelectrons in the conduction band can react with the adsorbed Ag^+ over the surface barrier, which is considerably smaller than that in the dark.

We have determined the quantum efficiency of the photocurrent at $E=E_{zcp}$, $\Phi_{h\nu}$, as

$$\Phi_{h\nu} = \frac{1}{eI} i_{dzcp}, \tag{3}$$

which corresponds to the quantum yield of the photoreduction of Ag^+ at the TiO_2 sinter surface. Here, I denotes the number of photons incident to the electrode surface and e the elementary electric charge. A linear relation is observed between the logarithms of $\Phi_{h\nu}$ and C_{Ag^+} (Fig. 7). We have next examined a similar relation between Φ_{Ag} and N_{Ag^+} for the TiO_2 suspension. The linearity shown in Fig. 7 seems to be better than that in Fig. 2. If we note a small amount of the Ag^+ adsorbed on the TiO_2 sinter surface, we may state that log (Φ_{Ag^+}) for both the TiO_2 suspension and sinter systems depends linearly on log (N_{Ag^+}). Such a relation seems to be characteristic

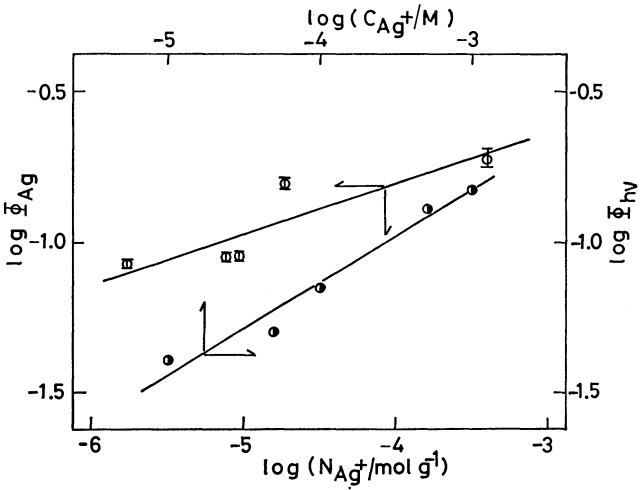

Fig. 7. Relation between the quantum yield and the concentration of $AgClO_4$.
◑——◑: Logarithmic plot between the quantum yield Φ_{Ag} and N_{Ag^+}, ◑——◑: logarithmic plot between the quantum efficiency of the photocurrent $\Phi_{h\nu}$ and C_{Ag^+}.

of the TiO_2–Ag^+ reaction systems studied here. It contrasts markedly with a Stern-Volmer relation previously reported for ZnO– and TiO_2–Ag^+ systems.[9,13] We have further found that E_{zcp} depends linearly on log(C_{Ag^+}) and that i_{dzcp} is proportional to $I^{0.64}$ irrespective of the Ag^+ concentration. These findings will offer a clue to the mechanism of photoreduction at the TiO_2–Ag^+ system. However, the details of actually operative reaction mechanisms will considerably change depending on physicochemical properties of semiconductor surfaces. It is, therefore, desirable to employ the same semiconductor sample for both photochemical and electrochemical studies; a research along this line is now in progress.

The Mechanism of Dye Sensitization. Though there have been many studies on the dye-sensitization of TiO_2 electrode,[26–29] little is known about the sensitized photoreaction at TiO_2 surface. We have shown in Fig. 4 that silver reduction proceeds by dye-light in the presence of both TiO_2 and Uranine. However, the amount of photoreduced silver after 4 h irradiation of dye-light was only 0.1 μmol in the absence of Uranine and it was still as small as about 0.15 μmol even when Uranine–$AgClO_4$ aqueous solution was irradiated by dye-light for 2 h. Such findings further support the role of both TiO_2 and Uranine in this reaction. The photochemical action spectrum in Fig. 5 may suffer the influence of the filter effect due to the optical absorption of dye molecules in the solution bulk. However, apart from the somewhat longer wavelength maximum in the photochemical action spectrum, the general features of these three spectra may be considered not to be so different from one another, if we note the relatively large half-width of the monochromator employed. The sensitized reaction at TiO_2 surface will be initiated by either electron transfer (the electron transfer mechanism) or energy transfer (the energy transfer mechanism) from excited dye molecules to TiO_2, which results in increase in the

concentration of conduction-band electrons. Then, conduction-band electrons are transferred to the Ag^+ adsorbed on the surface. In this way, TiO_2 serves to accept electrons and send them to Ag^+ in such a manner that the reverse electron transfer is prevented from proceeding.

It was observed that a photobleach of dye occurs in the course of silver reduction. The amount of photobleached dye in the suspension was determined by employing the same procedures previously described[13] and is given in Fig. 4. Apparent quantum yield of the photobleach is only 0.0005. However, a similar reaction proceeds to some extent even in the absence of Ag^+, because the photobleached dye in the TiO_2–Uranine system amounted to 0.12 μmol after 5 h irradiation of dye-light. It is remarkable that the amount of photoreduced silver after more than 2 h irradiation is larger than the amount of Uranine initially added to the suspension. To interpret the discrepancy between them, we may as well take into consideration complicated reactions of dye molecule following its sensitizing action, including its regeneration, at least in the case of the electron transfer mechanism for spectral sensitization. Similar phenomena have been reported for the ZnO–Ag^+–Uranine system by us.[13] The mechanism of the sensitized reduction of Ag^+ seems to be much more complicated than that of the unsensitized one and must be far beyond the simple local-cell consideration.

The authors wish to thank Teikoku Kakou Co., for kindly providing us with the TiO_2 powder. This work was carried out with a financial support from the Ministry of Education, Science and Culture of Japan (Grant-in-Aid No. 311607).

References

1) H. Hada and Y. Yonezawa, *Denki Kagaku*, **49**, 60 (1981); H. Hada, K. Takaoka, M. Saikawa, and Y. Yonezawa, *Bull. Chem. Soc. Jpn.*, **54**, 1640 (1981).

2) Y. Nakato, K. Abe, and H. Tsubomura, *Ber. Bunsenges. Phys. Chem.*, **80**, 1002 (1976); Y. Nakato, S. Tonomura, and H. Tsubomura, *ibid.*, **80**, 1289 (1976).

3) B. Kraeutler and A. J. Bard, *J. Am. Chem. Soc.*, **100**, 5985 (1978); H. Reiche and A. J. Bard, *ibid.*, **101**, 3127 (1979).

4) K. Kogo, H. Yoneyama, and H. Tamura, *J. Phys. Chem.*, **84**, 1705 (1980).

5) T. Kawai and T. Sakata, *J. Chem. Soc., Chem. Commun.*, **1980**, 694; *Nature*, **286**, 474 (1980); *Chem. Phys. Lett.*, **72**, 87 (1980).

6) M. Grätzel, *Ber. Bunsenges. Phys. Chem.*, **84**, 981 (1980); E. Borgarello, J. Kiwi, E. Pelizzetti, M. Visca, and M. Grätzel, *Nature*, **289**, 158 (1981).

7) H. Jonker, C. J. Dippel, H. J. Houtman, C. J. G. F. Janssen, and L. K. H. van Beek, *Photogr. Sci. Eng.*, **13**, 1 (1969); H. Jonker, L. K. H. van Beek, C. J. Dippel, C. J. G. F. Janssen, A. Molenaar, and E. J. Spiertz, *J. Photogr. Sci.*, **19**, 96 (1971).

8) G. L. McLeod, *Photogr. Sci. Eng.*, **13**, 93 (1969).

9) P. D. Fleischauer, H. K. Alan Kan, and J. R. Shepherd, *J. Am. Chem. Soc.*, **94**, 283 (1972); A. W. Adamson and P. D. Fleischauer, "Concepts of Inorganic Photochemistry," John Wiley & Sons, New York (1975), p. 400.

10) J. Pukies, W. Roebke, and A. Henglein, *Ber. Bunsenges. Phys. Chem.*, **72**, 842 (1968); M. Kelm, J. Lilie, A. Henglein, and E. Janata, *J. Phys. Chem.*, **78**, 882 (1974); M. Kelm, J. Lilie, and A. Henglein, *J. Chem. Soc., Faraday Trans. 1*, **71**, 1132 (1975); M. Breitenkamp, A. Henglein, and J. Lilie, *Ber. Bunsenges. Phys. Chem.*, **80**, 973 (1976); A. Henglein, *ibid.*, **81**, 556 (1977); R. Tausch-Treml, A. Henglein, and J. Lilie, *ibid.*, **82**, 1335 (1978); A. Henglein, *J. Phys. Chem.*, **83**, 2209 (1979).

11) H. Hada, Y. Yonezawa, A. Yoshida, and A. Kurakake, *J. Phys. Chem.*, **80**, 2728 (1976).

12) H. Lerner, *Photogr. Sci. Eng.*, **13**, 103 (1969).

13) H. Hada, H. Tanemura, and Y. Yonezawa, *Bull. Chem. Soc. Jpn.*, **51**, 3154 (1978).

14) F. Möllers, H. J. Tolle, and R. Memming, *J. Electrochem. Soc.*, **121**, 1160 (1974).

15) H. Yoneyama, N. Nishimura, and H. Tamura, *J. Phys. Chem.*, **85**, 268 (1981).

16) M. S. Wrighton, P. T. Wolczanski, and A. B. Ellis, *J. Solid State Chem.*, **22**, 17 (1977).

17) B. Kraeutler and A. J. Bard, *J. Am. Chem. Soc.*, **100**, 4317 (1978); H. Reiche, W. W. Bunn, and A. J. Bard, *J. Phys. Chem.*, **83**, 2248 (1979).

18) R. H. Sprague and J. H. Keller, *Photogr. Sci. Eng.*, **14**, 401 (1970).

19) C. A. Parker, *Proc. R. Soc. London, Ser. A*, **220**, 104 (1953).

20) D. M. Shub, A. A. Remnev, and V. I. Veselovskii, *Elektrokhimiya*, **9**, 676, 680, 1043 (1973).

21) M. Shiozawa, K. Narita, Y. Fujita, S. Kurita, and H. Yanagida, *Yogyo Kyokai Shi*, **83**, 471 (1975).

22) A. Fujishima and K. Honda, *Nature*, **238**, 37 (1972).

23) T. Ohnishi, Y. Nakato, and H. Tsubomura, *Ber. Bunsenges. Phys. Chem.*, **79**, 523 (1975).

24) P. Clechet, C. Martelet, J. R. Martin, and R. Olier, *Electrochim. Acta.*, **24**, 457 (1979).

25) H. R. Sprünken, R. Schumacher, and R. N. Schindler, *Ber. Bunsenges. Phys. Chem.*, **84**, 1040 (1980).

26) A. Fujishima, E. Hayashitani, and K. Honda, *Seisan Kenkyu*, **23**, 363 (1971); T. Watanabe, A. Fujishima, O. Tatsuoki, and K. Honda, *Bull. Chem. Soc. Jpn.*, **49**, 8 (1976).

27) M. T. Spitler and M. Calvin, *J. Chem. Phys.*, **66**, 4294 (1977).

28) A. Hamnett, M. P. Dare-Edwards, R. D. Wright, K. R. Seddon, and J. B. Goodenough, *J. Phys. Chem.*, **83**, 3280 (1979).

29) W. D. K. Clark and N. Sutin, *J. Am. Chem. Soc.*, **99**, 4676 (1977).

 © 1982 The Chemical Society of Japan Bull. Chem. Soc. Jpn., 55, 2015—2020 (1982)

The Synthesis and Electrical Resistivities of Complexes of Cation–TCNQ–Salts with Crown Ethers, Cryptands, and 1,13-Di(8-quinolyl)-1,4,7,10,13-pentaoxatridecane

Katsumi Matsuoka, Takashi Nogami,* Tsuruyoshi Matsumoto, Hidekazu Tanaka, and Hiroshi Mikawa

Department of Applied Chemistry, Faculty of Engineering, Osaka University, Yamada-oka, Suita, Osaka 565

(Received July 24, 1981)

Cation–TCNQ complexes with crown ethers, cryptands, and 1,13-di(8-quinolyl)-1,4,7,10,13-pentaoxatridecane were isolated. The cations include alkali-metal, and alkyl- and arylammonium ions. Nine types of complexes were isolated. These complexes are classified into two groups: complexes containing neutral TCNQ, and the complexes not containing neutral TCNQ. The electrical resistivities of the compaction samples were mainly measured at room temperature. The complexes containing neutral TCNQ were much more conductive than the other type of complexes; they exhibit resistivities of 8.2—10^3 Ω cm. The complexes of 1,13-di(8-quinolyl)-1,4,7,10,13-pentaoxatridecane contained methanol when we synthesized them from methanol solution.

We previously reported the synthesis and electrical resistivities of many alkali-metal and alkaline-earth-metal cation–TCNQ–crown ether complexes.[1-4] By using crown ether, we could isolate the complex salts, $[M^{n+}(TCNQ^-)_n]_m(TCNQ)_i(\text{crown ether})_j$, which contain neutral TCNQ, as well as simple salts, $[M^{n+}(TCNQ^-)_n]_m(\text{crown ether})_i$. A comparison of the electrical conductivities of the crown ether–TCNQ complexes with those of the original TCNQ salts, $M^{n+}(TCNQ^-)_n$, shows that simple salts are much less conductive than the original TCNQ salts.[1,2] On the other hand, complex salts including the alkali-metal cation are about 10 times more conductive than the corresponding original TCNQ salts, M^+TCNQ^-.[1,2] In the case of the complex salts including alkaline-earth-metal cations, however, most of them were much more conductive than the original TCNQ salts, $M^{2+}(TCNQ^-)_2$. The fact that the conductivities of the complex salts including alkaline-earth-metal cations were higher than those of the alkali-metal cations was explained by the closer distance between TCNQ molecules in the former complexes.[3]

1,13-Di(8-quinolyl)-1,4,7,10,13-pentaoxatridecane (usually called simply "Kryptofix-5") is an acylic polyether with two quinolyl groups at both ends of the molecule, and it has a property of coordinating metal cations by means of its five oxygens and two nitrogens.[5] The electrical conductivities of TCNQ–"Kryptofix-5" complexes are interesting in connection with famous good conductor, quinolinium–TCNQ complex.[6] We have now isolated several alkali-metal cation–TCNQ–"Kryptofix-5"-complexes.

Crown ethers are known to include ammonium ions.[7] We have previously reported several ammonium–TCNQ–crown ether complexes.[1,2] We have now synthesized alkyl- and arylammonium–TCNQ–crown ether complexes in order to see the effect of the substituent groups on the electrical conductivities.

We measured the electrical resistivities of the several types of new complexes mentioned above with the compaction samples, mainly at room temperature. We also measured the diffuse-reflection spectra of the new complexes in order to ascertain the electronic interaction between TCNQ molecules.

Experimental

Materials. The crown ethers, cryptands, and 1,13-di(8-quinolyl)-1,4,7,10,13-pentaoxatridecane were purchased from Tokyo Kasei Kogyo Co. Ltd.

Synthesis of the Complexes. The following four methods were employed for the synthesis of the complexes.

Method 1: Most of the complexes not containing neutral TCNQ (Types A, B, and H in Fig. 1) were obtained by the reactions of cation TCNQ salts with crown ethers. The details have been presented previously.[2]

Method 2: Most of the complexes containing neutral TCNQ (Types C and I in Fig. 1) were obtained by the reactions of cation-TCNQ salts, neutral TCNQ, and crown ether. The details have been presented previously.[2]

Method 3: The quinolinium-type "Kryptofix-5" complexes (Types D, E, and F in Fig. 1) were obtained by this method. This method is subdivided into four subtypes: (*3-1*) "Kryptofix-5" and 2,3,5,6-tetramethyl-1,4-benzenediol (1:2.1 molar ratio) were dissolved in acetonitrile. To this solution we then added an acetonitrile solution of TCNQ (3—4 molar ratio); this mixtures was then refluxed for 10 min, and the hot solution was filtered. After the solution had been kept at 0 °C for a few hours, the precipitate was filtered, washed with a small amount of acetonitrile and diethyl ether, and dried in a vacuum. (*3-2*) "Kryptofix-5" was dissolved in dioxane, and the solution was heated to 60 °C. To the solution we then added an equimolar amount of aqueous hydrogen iodide, and the "Kryptofix-5"-hydroiodide precipitated was collected quickly. (When the filtration was done too slowly, we obtained a reddish brown oil.) In this case, the solvent was distilled out completely, and then hexane was added to the oil which remained; we thus obtained the powder of "Kryptofix-5"-hydroiodide. The hydroiodide was then dissolved in a small amount of water, and an aqueous solution of Li^+TCNQ^- (2.1 molar ratio) was added through a filter paper. The precipitate was collected, washed with water, and dried in a vacuum. (*3-3*) To the acetonitrile solution of the complex obtained by Procedure (*3-1*) or Procedure (*3-2*), we added acetonitrile solutions of alkali metal TCNQ salt (equimolar amount) and TCNQ (1—3 molar ratio). The solution was heated for 10 min, and the hot solution was filtered. The filtrate was allowed to stand at room temperature and then kept 0 °C for several hours. The precipitate was collected, washed with a small amount of acetonitrile, and dried in a vacuum. (*3-4*) The complexes

obtained by Method 1 or Method 2 were dissolved in acetonitrile, and 2,3,5,6-tetramethyl-1,4-benzenediol (2.1 molar fraction) was added. The solution was heated to dissolve the reactants, and then an acetonitrile solution of TCNQ (3—4 molar ratio) was added. After the solution had been refluxed for 10 min, the hot solution was filtered. The filtrate was allowed to stand at room temperature and then kept at 0 °C for several hours. The precipitate was collected, washed with a small amount of acetonitrile, and dried in a vacuum.

Method 4: Ammonium–TCNQ–crown ether complexes (Type G in Fig. 1) were obtained by the same procedures as in Method 1. In this case, however, we obtained complexes containing neutral TCNQ. The solvents we used were methanol in the case of the methylammonium complex and 2-propanol in the cases of the other complexes.

Measurements of the Electrical Resistivities. The room-temperature resistivities of the complexes were measured by the procedures described before.[2] The temperature dependence of the resistivity was measured by means of a type-D cryomini refrigerator (Osaka Sanso Co., Ltd).

Measurements of Diffuse Reflection Spectra. The diffuse reflection spectra of the complexes were measured by means of a Hitachi 340 recording spectrophotometer, with an integrating sphere attached.

Differential Thermal Analysis and Thermogravimetry. Differential thermal analysis was done by the use of a Dainiseikosha SSC 560 apparatus, and thermogravimetry, by the use of a Rigaku Thermoflex.

Results and Discussion

Isolation of the Complexes. The following crown ethers, cryptands, acyclic polyether, and cation-TCNQ salts were used for the preparation of the complexes: 12-crown-4, 15-crown-5, 18-crown-6, dibenzo-18-crown-6, "dicyclohexyl-18-crown-6"[8], cryptand[2.2], cryptand[2.2.2], "Kryptofix-5"[9], Na^+TCNQ^-, K^+TCNQ^-, Rb^+TCNQ^-, Cs^+TCNQ^-, $CH_3NH_3^+TCNQ^-$, $n\text{-}C_4H_9NH_3^+TCNQ^-$, $n\text{-}C_8H_{17}NH_3^+TCNQ^-$, $n\text{-}C_{16}H_{33}NH_3^+TCNQ^-$, and *p*-phenylenediammonium TCNQ; their structures are shown below. In this figure, Cr, DB, DCH, Crypt, and Kry-5 indicate crown ether, dibenzo and perhydrodibenzo groups, crystand, and

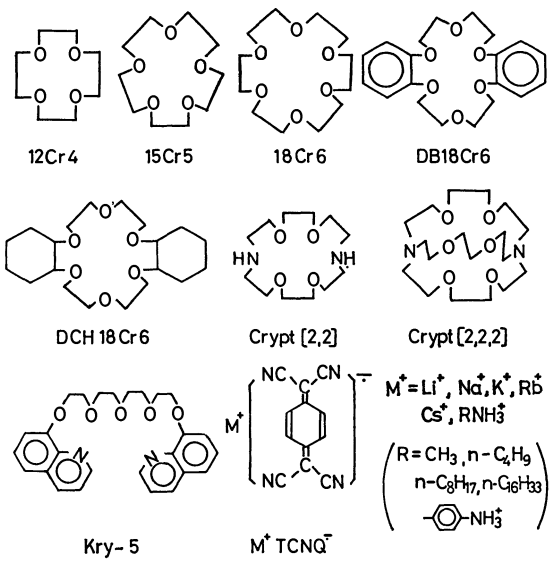

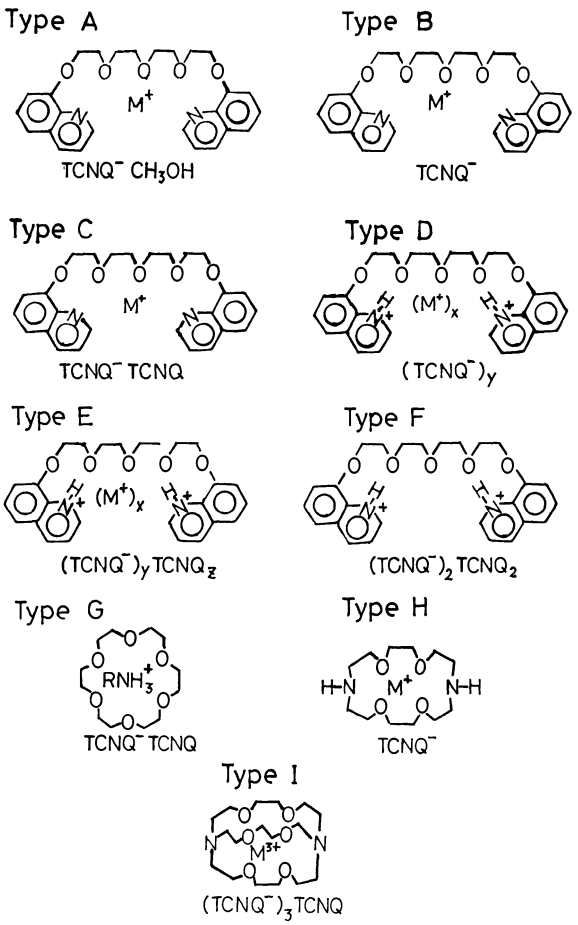

Fig. 1. Nine kinds of complexes isolated.

"Kryptofix-5" respectively. We have isolated nine kinds of complexes; they are designated as Types A, B, C, D, E, F, G, H, and I.[10] Figure 1 shows the structures of these complexes. All the complexes are stable and have a good solubility in many organic solvents; this may be useful for their practical application. Table 1 lists the complexes isolated and their yields, melting points, analytical data, synthetic methods, appearances, and resistivities.

Cation–TCNQ–"Kryptofix-5" Complexes: Types A, B, C, D, E, and F are included in these complexes. The complexes, of Types C, D, E, and F contain neutral TCNQ, while those of the Types A and B do not contain neutral TCNQ.

The complexes of Types A and B were isolated by means of procedures described before.[2] It is noteworthy that the complex of Type A contained one molecule of methanol when we crystallized it from a methanol solution. However, when we used other solvents, such as ethyl acetate or ethanol, we obtained solvent-free complexes (Type B). The colors of the complexes of Type A were yellow green. On the other hand, the colors of the complexes of Type B were purple. When the Type-A complexes were heated under vacuum, the corresponding complexes of Type B were obtained, hence giving rise to the color change. In order to see the conversion from Type A to Type B, we performed differential thermal analyses and thermogravimetries of Type-A complexes;

TABLE 1. CATION-TCNQ-CROWN ETHER COMPLEXES AND THEIR RESISTIVITIES

Complexes	Method	Yields/%	Mp θ_m/°C	Found(Calcd)(%) C	H	N	Appearances	Resistivities/Ω cm[a)]
Type A								
Kry-5 $Na^+TCNQ^-CH_3OH$	1	10	119—121	66.43 (66.19)	5.03 (5.12)	12.13 (11.87)	dark green microcrystal	
Kry-5 $K^+TCNQ^-CH_3OH$	1	10	113—114	64.90 (64.72)	4.81 (5.01)	11.69 (11.61)	yellow green microcrystal	1.1×10^8
Kry-5 $Rb^+TCNQ^-CH_3OH$	1	69	134—135	60.87 (60.82)	4.59 (4.71)	11.05 (10.91)	yellow green microcrystal	1.8×10^{10}
Kry-5 $Cs^+TCNQ^-CH_3OH$	1	70	102—104	57.46 (57.29)	4.30 (4.44)	10.36 (10.27)	yellow green microcrystal	1.7×10^8
Type B								
Kry-5 Na^+TCNQ^-	1	38	116—118	67.22 (67.55)	4.76 (4.77)	12.39 (12.44)	green cube	1.2×10^8
Kry-5 K^+TCNQ^-	1	10	138—139	66.18 (65.98)	4.86 (4.66)	12.19 (12.15)	purple hexahedral	1.5×10^{10}
Kry-5 Rb^+TCNQ^-	1	62	140—141	61.92 (61.82)	4.37 (4.37)	11.48 (11.39)	purple hexahedral	2.5×10^{10}
Kry-5 Cs^+TCNQ^-	1	28	108—110	58.35 (58.09)	4.32 (4.11)	10.75 (10.70)	purple hexahedral	6.0×10^9
Type C								
Kry-5 K^+TCNQ^-TCNQ	2	13	159—162	67.60 (67.03)	4.00 (4.05)	15.59 (15.63)	black powder	34
Kry-5 $(Rb^+TCNQ^-)_x(TCNQ)_y$[b)]	2	31	154—157				black powder	32
Kry-5 $(Cs^+TCNQ^-)_x(TCNQ)_y$[b)]	2	34	160—163				black powder	63
Type D								
Kry-5-2H$^+$ $Na^+(TCNQ^-)_3$	3-3, 3-4	64	147—148	68.65 (68.55)	3.85 (3.90)	17.89 (18.06)	black powder	
Type E								
Kry-5-2H$^+$ $K^+(TCNQ^-)_3TCNQ$	3-3, 3-4	53	152—154	68.18 (68.04)	3.89 (3.55)	19.23 (19.30)	black powder	10.0
Kry-5-2H$^+(Rb^+)_x(TCNQ^-)_yTCNQ_z$[b)]	3-3, 3-4	46	140—142				black powder	8.8
Kry-5-2H$^+(Cs^+)_x(TCNQ^-)_yTCNQ_z$[b)]	3-3, 3-4	57	145—147				black powder	8.2
Type F								
Kry-5-2H$^+$ $(TCNQ^-)_2(TCNQ)_2$	3-1, 3-2	44	167—171	69.59 (70.11)	3.73 (3.67)	19.40 (19.90)	black powder	22
Kry-5-H$^+$ $TCNQ^-TCNQ$	3-1, 3-2	24	155—157	69.41 (69.97)	4.40 (4.36)	16.99 (16.35)	black powder	27
Type G								
$(15Cr5)(CH_3NH_3^+)TCNQ^-TCNQ$	4	27	151	63.71 (63.63)	4.89 (5.19)	19.20 (19.09)	black plate	9.2×10^2
$(18Cr6)(CH_3NH_3^+)TCNQ^-TCNQ$	4	69	165	63.29 (63.06)	5.68 (5.43)	17.94 (17.89)	black plate	7.3×10^3
$(DB18Cr6)(CH_3NH_3^+)TCNQ^-TCNQ$	4	58	169—170	67.34 (67.49)	4.69 (4.78)	15.77 (15.74)	black plate	4.5×10^2
$(DCH18Cr6)(CH_3NH_3^+)TCNQ^-TCNQ$	4	19	152—153	66.76 (66.49)	6.22 (6.20)	15.94 (15.94)	black plate	1.5×10^2
$(18Cr6)(n\text{-}C_4H_9NH_3^+)TCNQ^-TCNQ$	4	32	130	64.78 (64.32)	5.70 (5.94)	17.56 (17.57)	black plate	46
$(18Cr6)(n\text{-}C_8H_{17}NH_3^+)TCNQ^-TCNQ$	4	15	127	65.97 (65.81)	6.71 (6.03)	15.68 (15.70)	black powder	1.1×10^7
$(18Cr6)(n\text{-}C_{16}H_{33}NH_3^+)TCNQ^-TCNQ$	4	7	127—133	66.84 (68.25)	7.62 (7.49)	13.60 (13.77)	black powder	
$(15Cr5)_2(^+H_3NC_6H_4NH_3^+)(TCNQ^-)_2TCNQ_2$	4	16	138	65.16 (65.00)	4.73 (4.87)	18.97 (18.44)	black microcrystal	
$(18Cr6)_2(^+H_3NC_6H_4NH_3^+)(TCNQ^-)_2TCNQ_2$	4	32	205	64.29 (64.36)	5.12 (5.12)	17.33 (17.32)	black microcrystal	7.2×10^2
$(DB18Cr6)_2(^+H_3NC_6H_4NH_3^+)(TCNQ^-)_2TCNQ_2$	4	31	165—170	68.68 (68.52)	4.15 (4.53)	16.55 (15.30)	black microcrystal	1.3×10^2

Table 1. (Continued)

Complexes	Method	Yields/%	Mp θ_m/°C	Found(Calcd)(%) C	H	N	Appearances	Resistivities/Ω cm[a)]
$(DCH18Cr6)_2(^+H_3NC_6H_4NH_3^+)$-$(TCNQ^-)_2TCNQ_2$	4	24	145	66.90 (67.53)	5.72 (5.91)	16.41 (15.08)	black microcrystal	3.9×10^2
Type H								
crypt[2.2]Na+TCNQ$^-$	1	7	170—171	58.87 (58.90)	6.27 (6.13)	17.06 (17.18)	dark blue hexagonal	
crypt[2.2]K+TCNQ$^-$	1	39	184—185	57.22 (57.02)	6.20 (5.94)	16.65 (16.63)	dark blue hexagonal	
crypt[2.2]Rb+TCNQ$^-$	1	3	145—146	52.20 (52.22)	5.47 (5.44)	15.34 (15.23)	dark blue needle	
Type G								
crypt[2.2.2]$Ce^{3+}(TCNQ^-)_3$-TCNQ[c)]	2	27	186—188	60.83 (59.45)	5.14 (3.93)	17.63 (18.91)	black powder	1.5×10^3
crypt[2.2.2]$Sm^{3+}(TCNQ^-)_3$-TCNQ[c)]	2	33	194—196	61.95 (59.01)	4.72 (3.90)	18.83 (18.76)	black powder	68

a) Pressed pellt sample. b) We could not obtain the complex with a stoichiometric composition. c) We could not obtain a good analytical agreement.

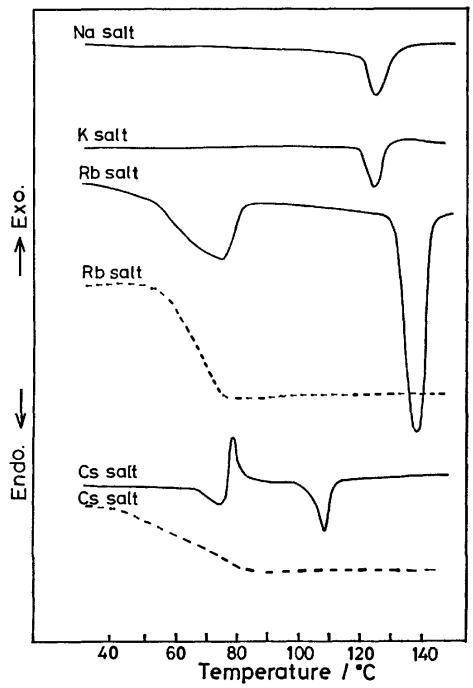

Fig. 2. Differential thermal analysis and thermogravimetry of the methanol-containing "Kryptofix-5" complexes.
——: Differential thermal analysis, ……: thermogravimetry.

the results are shown in Fig. 2. The sodium and potassium complexes in Type A showed only one endothermic signal at their melting points, and the weight losses were not observed. On the other hand, the rubidium and cesium complexes of Type A showed two endothermic signals. The lower-temperature signals were accompanied by weight losses. The higher-temperature signals correspond to the melting points. Thus, methanol is bound more tightly in the sodium and potassium complexes than in the rubidium and cesium complexes in Type A.

The Type-C complexes were isolated by means of procedures described before.[2)] Unfortunately, except for the potassium complex, they did not give the stoichiometric compositions.

The Type-D and Type-F complexes were obtained principally by two methods: by the reaction of "Kryptofix-5", 2,3,5,6-tetramethyl-1,4-benzenediol, and neutral TCNQ, and by the reaction of "Kryptofix-5"-dihydroiodide and Li+TCNQ$^-$. We obtained metal containing (Type D) and metal-free (Type F) complexes with quinolinium structures. The Type-F complexes and sodium and potassium complexes of Types D and E gave stoichiometric compositions. However, the rubidium and cesium complexes in Type D gave nonstoichiometric compositions. The complexes in Types C, D, and F were black.

Substituted Ammonium–TCNQ–Crown Ether Complexes: The complexes of Type G are included in these complexes. Several alkyl- and arylammonium–TCNQ salts were obtained by the reactions of the corresponding ammonium iodides with Li+TCNQ$^-$. Their reactions with crown ether in methanol gave Type-G complexes. To our surprise, all the complexes contained neutral TCNQ, whereas we did not add neutral TCNQ to the reaction system. The reason for this remains to be clarified.

Miscellaneous Complexes: The complexes of Types H and I were obtained by means of procedures described before.[2)] The Type-I complexes containing Ce^{3+} and Sm^{3+} did not give good analytical agreements.

Electrical Resistivities of the Complexes. We measured the electrical resistivities of the complexes isolated with the compaction samples, mainly at room temperature; the results are shown in Table 1.

Cation–TCNQ–"Kryptofix-5" Complexes: The complexes of Types A, B, and D, none of which contain neutral TCNQ, were poor conductors and exhibited resistivities of 10^8—10^{10} Ω cm. On the other hand, the complexes of Types C, E, and F, which contain neutral TCNQ, were much more conductive than the

former type of complexes and exhibited resistivities of the order of $10^1\,\Omega$ cm. The resistivities of the complexes of Types E and F were less than $10\,\Omega$ cm. The best conductor was found in the Type-E complexes possessing Cs ions, which exhibited $8.2\,\Omega$ cm. Unfortunately, we could not obtain these complexes as single crystals. The temperature dependence of the resistivities of Kry-5-2H$^+$(Rb$^+$)$_x$(TCNQ$^-$)$_y$(TCNQ)$_z$ and Kry-5-2H$^+$(Cs$^+$)$_x$(TCNQ$^-$)$_y$(TCNQ)$_z$ measured between 125 K and 250 K showed semiconducting properties; the activation energies were 0.05 eV and 0.06 eV respectively.[11]

Substituted Ammonium–TCNQ–Crown Ether Complexes: The resistivities of most of the substituted ammonium–TCNQ–crown ether complexes were 10^2—$10^3\,\Omega$ cm. However, (18-crown-6)$C_8H_{17}NH^+_3$TCNQ$^-$TCNQ showed a very low conductivity. When we see the effect of the alkyl groups on the electrical resistivities, we find that (18-crown-6)$C_4H_9NH_3^+$TCNQ$^-$TCNQ is more conductive than (18-crown-6)$CH_3NH_3^+$TCNQ$^-$-TCNQ and (18-crown-6)$C_8H_{17}NH_3^+$TCNQ$^-$TCNQ.

Miscellaneous Complexes: As has been described in the Introduction, multivalent cation–TCNQ–crown ether complexes can be expected to be highly conductive materials. In line with this, Sm^{3+}(TCNQ$^-$)$_3$-TCNQ crypt[2.2.2] was a relatively good conductor ($68\,\Omega$ cm); it was *ca.* 300 times more conductive than the original salts, Sm^{3+}(TCNQ$^-$)$_3$ ($2\times10^4\,\Omega$ cm).[6]

Electronic Diffuse Reflection Spectra of the Complexes. We measured the electronic diffuse reflection spectra of the complexes isolated in order to ascertain the electronic interaction between TCNQ molecules in the solid state.[12]

Type-A and Type-B Complexes: As has been discussed above, we obtained methanol-containing complexes (Type A) and methanol-free complexes (Type B). Figure 3 shows the diffuse reflection spectra of both types of complexes. (Kry-5)K$^+$TCNQ$^-$CH$_3$OH and (Kry-5)K$^+$TCNQ$^-$ were chosen as typical examples in this figure, together with the absorption spectrum of K$^+$TCNQ$^-$ in an acetonitrile solution. The reflection spectrum of the methanol-containing complex has a characteristic vibrational structure, which resembles the absorption spectrum of K$^+$TCNQ$^-$ in an acetonitrile solution. This fact suggests that TCNQ$^-$ is isolated in this complex. On the other hand, the methanol-free complex showed two broad absorption bands in the near-IR region. The lower-energy band may have mainly the charge-transfer character between TCNQ anion radicals, while the higher-energy band has mainly the local excitation character within TCNQ anion radicals, like many TCNQ salts.[13]

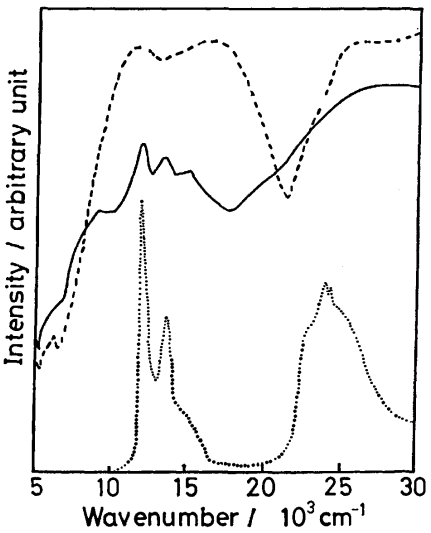

Fig. 3. Electronic diffuse reflection spectra and electronic absorption spectrum of the complexes.
----: Kry-5 K$^+$TCNQ$^-$, ——: Kry-5 K$^+$TCNQ$^-$-CH$_3$OH, ·····: K$^+$TCNQ$^-$ in acetonitrile solution.

Type-C, E, F, G, and I Complexes: All the complexes containing neutral TCNQ have absorption bands below 7×10^3 cm^{-1}; this may be ascribable to the charge-transfer transition from the TCNQ anion radical to neutral TCNQ.

Correspondence between the Electrical Resistivities of the Complexes and Their Electronic Reflection Spectra. As has been discussed above, the complexes containing neutral TCNQ (Types C, E, F, G, and I) are much more conductive than those not containing neutral TCNQ (Types A, B, D, and H). All the complexes of the first type have absorption bands below 7×10^3 cm^{-1}, originating from the charge-transfer transition from TCNQ$^-$ to TCNQ. This fact shows that TCNQ$^-$ and TCNQ are located close together in the complex. Since electrons flow through TCNQ molecules under an electric field, the reduced Coulomb repulsion force between mobile electrons[14] because of the existence of neutral TCNQ gives rise to relatively high conductivities for the former type of complex.

Many complexes of the latter type (Types B, D, and H) have two absorption bands at the near-infrared region (charge-transfer transition between TCNQ$^-$ molecules); this fact suggests the dimer structure of TCNQ$^-$ molecules. In this case, it is well known that a band-gap is formed;[14] this results in the poor conductivity, in line with the experimental observations.

The absorption spectra of the Type-A complexes showed that TCNQ$^-$ is isolated in the complexes; this fact gives rise to the poor conductivities of Type-A complexes.

Summary of the Electrical Resistivities of a Series of Cation–TCNQ–Crown Ether Complexes

Comparison of the Electrical Resistivities. We previously synthesized about 100 kinds of cation–TCNQ–crown ether complexes and measured their electrical resistivities, mainly with the compaction samples at room temperature.[1–4] The cations we used were alkali-metal ions, alkaline-earth-metal ions, alkyl- and arylammonium ions, and transition-metal ions. We classified the complexes into two groups: the complexes containing neutral TCNQ, and the complexes not containing neutral TCNQ. The former type of complexes were semiconductors and were much more conductive than the latter type of complexes; most of the latter type of complexes were insulators. We

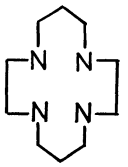

"Cyclam"

used not only crown ethers, cryptands, and "Kryptofix-5," but also 1,5,8,12-tetraazacyclotetradecane (usually called "cyclam"), since the latter compounds can include many transition-metal ions.[15]

As a summary of our work, we compared the electrical resistivities of the cation–TCNQ–crown ether complexes with the original TCNQ complexes; this is shown schematically in Fig. 4. The upper half of this figure shows the resistivity range of the cation–TCNQ–crown ether complexes, classified by the cations. We have shown only the resistivity ranges of the complexes containing neutral TCNQ, since they are relatively good conductors. The lower half of Fig. 4 shows the resistivity ranges of the original TCNQ complexes, also classified by the cations.

Roughly speaking, many of the alkali-metal–TCNQ–crown ether complexes are about 10 times more conductive than the original alkali-metal–TCNQ complexes. It is interesting to note that the alkali-metal–TCNQ–"Kryptofix-5" complexes are from about 1000 to about 10000 times more conductive than the alkali-metal–TCNQ complexes. All the alkaline earth metal–TCNQ–crown ether complexes are more conductive (up to 1000 times) than the alkaline earth metal–TCNQ complexes.[6] Many of the ammonium–TCNQ–crown ether complexes are about 10 to 100 times more conductive than the corresponding original TCNQ complexes.[6] Thus, most of the cation–TCNQ–crown ether complexes are more conductive than the corresponding original TCNQ complexes. However,

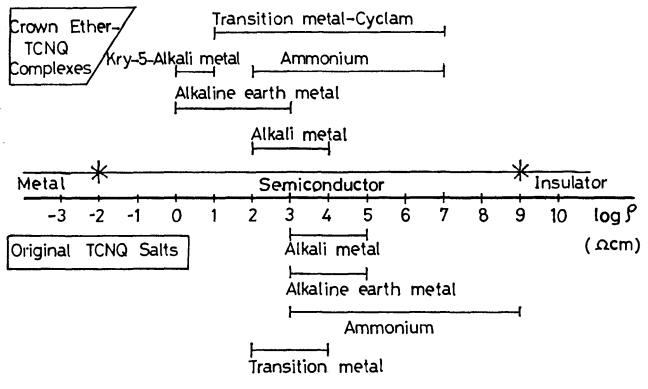

Fig. 4. Comparison of the electrical resistivities of cation–TCNQ–crown ether complexes with those of the corresponding cation–TCNQ complexes.

we could not find any significant improvement in the conductivities of transition metal–TCNQ–"cyclam" complexes[4] as compared with transition metal–TCNQ complexes.[6] The most striking difference in the chemical properties of the cation–TCNQ–crown ether complexes from the original TCNQ complexes is that the former complexes are very soluble to the organic solvents, whereas the solubilities of the latter complexes are very low. This fact may be useful for the practical application of the cation–TCNQ–crown ether complexes.

We are grateful to Miss Junko Maenaka, Mr. Kazuaki Muneishi, and Miss Yuriko Sako, Faculty of Engineering, Osaka University, for the elemental analysis.

References

1) M. Morinaga, T. Nogami, Y. Kanda, and H. Mikawa, *Chem. Lett.*, **1979**, 111.
2) M. Morinaga, T. Nogami, Y. Kanda, T. Matsumoto, K. Matsuoka, and H. Mikawa, *Bull. Chem. Soc. Jpn.*, **53**, 1221 (1980).
3) T. Matsumoto, T. Nogami, H. Tanaka, and H. Mikawa, *Bull. Chem. Soc. Jpn.*, **55**, 369 (1982).
4) K. Matsuoka, T. Nogami, and H. Mikawa, *Mol. Cryst. Liq. Cryst.*, in press.
5) F. Vogtle and E. Weber, *Angew. Chem., Int. Ed. Engl.*, **18**, 753 (1979).
6) L. R. Melby, R. J. Harder, W. R. Hertler, M. Mahler, R. E. Benson, and W. E. Mochell, *J. Am. Chem. Soc.*, **84**, 3374 (1962).
7) "Synthetic Multidentate Macrocyclic Compounds," ed by R. M. Izatt and J. J. Christensen, Academic Press, New York (1978).
8) Formal name: perhydrodibenzo[*b*,*k*][1,4,7,10,13,16]-hexaoxacyclooctadecin.
9) Formal name: 1,13-di(8-quinolyl)-1,4,7,10,13-pentaoxatridecane.
10) In Type-G complexes, we used not only 18-crown-6, as is shown in Fig. 1, but also 15-crown-5, dibenzo-18-crown-6, and "dicyclohexyl-18-crown-6".
11) Kry-5-2H$^+$ denotes the following diprotonated "Kryptofix-5".

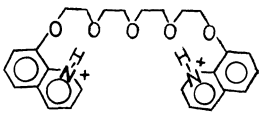

12) Uncorrected spectra.
13) J. Tanaka, M. Tanaka, T. Kawai, T. Takabe, and O. Maki, *Bull. Chem. Soc. Jpn.*, **49**, 2358 (1976).
14) J. B. Torrance, *Acc. Chem. Res.*, **12**, 79 (1979).
15) E. J. Bounsall and S. R. Koplich, *Can. J. Chem.*, **48**, 1432 (1970).

 © 1982 The Chemical Society of Japan Bull. Chem. Soc. Jpn., 55, 2021—2025 (1982)

Experimental and Calculated Magnetic Circular Dichroism Spectra of Iron(II) Low Spin Hemoglobin and Myoglobin with CO, NO, and O_2

Takao YAMAMOTO,† Tsunenori NOZAWA, Akira KAITO,†† and Masahiro HATANO*

Chemical Research Institute of Non-aqueous Solutions, Tohoku University, Katahira, Sendai 980

(Received October 5, 1981)

The ratios of the apparent Faraday A terms to the dipole strengths (A'/D) were obtained from the experimental magnetic circular dichroism (MCD) data for the iron(II) low spin derivatives of human hemoglobin and its α and β chains, and myoglobins (whale and bovine). The observed MCD peak height and trough depth exhibit the decreasing order of $CO > O_2 > NO$ in the Soret band and $O_2 > CO > NO$ for the Q band. The moment analysis also showed the decreasing order of the A'/D values of $CO > O_2 > NO$ in the Soret bands for all hemoglobin and myoglobin derivatives experimentally studied. The molecular orbital calculation of the porphyrin π electron system based on the PPP CI approximation method demonstrated that the calculated spectra for the pyrrole nitrogen core-charge of 1.5 showed characteristics for the CO complex of hemoglobin and myoglobin, and that the NO and O_2 complexes could be simulated by the calculations for the core charge values smaller than 1.5 (*i.e.* 1.4—1.3). These results suggest that the change in the porphyrin π electronic state which is caused by the electronic interaction between the diatomic molecule such as CO, NO, or O_2 and the heme iron can be explained by the change in the σ core charge in the pyrrole nitrogen possibly through changes in the electronic states of the heme iron.

All complexes of hemoglobin and myoglobin with CO, NO, and O_2 exhibit the Soret and Q electronic absorption spectra characterized as the iron(II) low spin complexes.[1] However, appreciable differences among the complexes have been detected by several techniques. The quadrupole splitting in Mössbauer spectra for the CO complexes ($\Delta E_Q = 0.36$ mm s^{-1}) is typical of the iron(II) low spin heme, while that for the O_2 complexes ($\Delta E_Q = -2.2$ mm s^{-1}) is rather similar to those for the iron(III) low spin complexes.[2,3] In resonance Raman spectra the CO, NO, and O_2 complexes of hemoglobin gave somehow different energies for the porphyrin vibration band.[4,5] Furthermore, the IR frequencies of ligand diatomic molecules, O_2, CO, and NO exhibited different relative change on binding with the heme iron.[6-8]

Since the magnetic circular dichroism (MCD) technique has been revealed to be a very powerful technique to explore the electronic structures of hemoproteins,[9,10] the technique has been applied to the hemoproteins complexes with the above diatomic molecules to get insight on the electronic structures of these heme complexes. Although many previous papers have presented MCD spectra on the CO, NO, and O_2 complexes of hemoglobin and myoglobin,[11-20] there has been no quantitative analysis among them. In this paper the magnitudes of the Faraday parameters for the Soret and Q bands were extracted from the experimental MCD spectra on various hemoglobin and myoglobin derivatives, and were compared with the theoretically calculated data to analyze the effect of the diatomic molecules as ligands on the heme electronic states.

Experimental

Whale myoglobin (type II) and human hemoglobin (type IV) were purchased from Sigma. Bovine myoglobin was generous gift of Dr. Y. Sugawara of Tohoku University. Each separated chain of human hemoglobin was prepared by the method of Bucci and Franticelli.[21]

Myoglobin and hemoglobin in phosphate buffer (0.01 mol dm^{-3}, pH 7.0) were reduced by a small amount of sodium dithionite and the excess reductant was removed by passing the solution through a Sephadex G-25 column (30 cm height and 3 cm ϕ). Myoglobin (Mb) and hemoglobin (Hb) became to MbO_2 and HbO_2 during this process. CO complexes were prepared by bubbling CO gas to MbO_2 and HbO_2 solutions for 3 min. MbNO and HbNO were made by adding sodium dithionite and sodium nitrite to MbO_2 and HbO_2 solutions.

The concentrations of hemoglobin and myoglobin were determined by the usual pyridine hemochromogen method by using $\varepsilon_{557} = 32000$.[1]

The MCD spectra were taken with a JASCO circular spectrodichrometer model J-20A equipped with a JASCO electromagnet which produces as high as 1.14 T magnetic field. MCD magnitude is expressed by the molar ellipticity per Tesla (T) ($[\theta]_M/10^4$ degree mol^{-1} dm^3 m^{-1} T^{-1} or 10 degree m^2 mol^{-1} T^{-1}).

The method of moments[22,23] was used to extract Faraday parameters.

The transition energies, oscillator strengths and Faraday parameters were calculated on the basis of PPP CI method, the details of which have been reported previously.[24,25]

Results and Discussion

Figure 1 demonstrates the absorption and MCD spectra for the CO, NO, and O_2 complexes of the β chain of human hemoglobin. The complexes of diatomic molecules with human hemoglobin and its α chain as well as myoglobins from bovine and whale also exhibit similar spectra (not shown). General features in the electronic absorption and MCD spectra of the CO, NO, O_2 complexes of hemoglobin and

† Present address: Kawamura Research Institute, 2-7-8, Kamikizaki, Urawa, Saitama 338.

†† Present address: Research Institute for Polymers and Textiles, 1-1-4, Yatabe-Higashi, Tsukuba, Ibaraki 305.

myoglobin are similar and bear characteristics of the iron(II) low spin hemoproteins in that the MCD spectra show apparent Faraday A terms for the Soret, Q_{0-0} and Q_{v-0} bands.[9,10] However, the magnitudes and relative intensities of the Soret to the Q_{0-0} were seen to be different significantly among them. The apparent MCD magnitudes (the peak height and the trough depth) show the decreasing order of CO>O_2>NO for the Soret bands and O_2>CO>NO for the Q_{0-0} bands. It is also noted that the Soret MCD's of the CO complexes are larger than those of the Q bands, while for the O_2 complex the MCD spectra in the Q region are larger than those in the Soret region, and that for the NO complex the Soret and Q MCD have similar magnitudes.

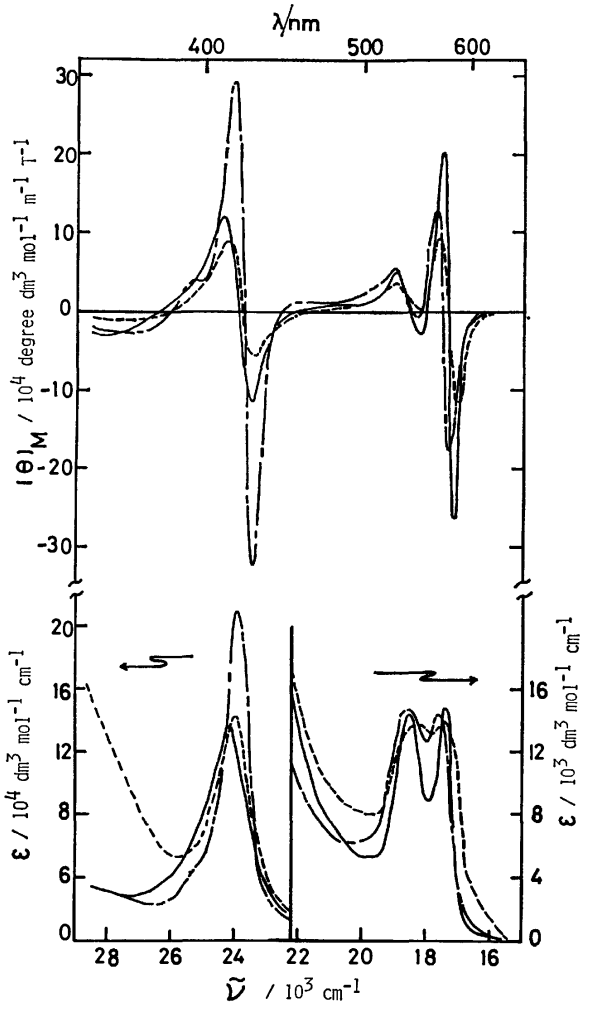

Fig. 1. The MCD and electronic absorption spectra of the CO (———), NO (– – –), and O_2 (——) complexes of the β chain of the human hemoglobin. Concentration: 4×10^{-6} mol dm^{-3} (for the Soret region) and 4×10^{-5} mol dm^{-3} (for the Q region), cell length: 1 cm, magnetic field: 1.14 T, temperature: 1 °C.

The quantitative magnitudes of the MCD spectra were evaluated by the quantities A'/D, where A' and D represent the magnitude of the apparent Faraday A term[26] and the dipole strength of the electronic transition in the electronic absorption spectra.[22-25] The experimental A'/D values obtained by use of the method of moment[22,23] are summarized in Tables 1 and 2. The A'/D values for the Soret band for all the hemoglobin and myoglobin studied here show the same decreasing order of CO>O_2>NO in each hemoprotein. On the contrary the orders of A'/D for the Q_{0-0} and Q_{v-0} bands are rather random. Since the random order of the A'/D values for the Q_{0-0} and Q_{v-0} seems to be due to the difficulty in resolving the superimposed bands, the comparison of the A'/D values in the Q band region could not be done.

Table 2 shows that CO, O_2 ,and NO complexes have the Soret A'/D values of (0.30—0.19)β,[27] (0.15—0.10)β, and (0.09—0.03)β, respectively, for all the hemoglobin and myoglobin studied. The A'/D values for the Soret band in Tables 1 and 2 reveal that the α chain of hemoglobin gave larger A'/D values for all the three complexes than the β chain, and that the β chain showed similar A'/D values to those for human hemoglobin, and bovine and whale myoglobin. For example the O_2 complexes for human hemoglobin, its β chain, bovine and whale myoglobin gave the similar Soret A'/D values which are smaller than that of the α chain of human hemoglobin by (0.07—0.12)β. The difference of this order is significant and may imply some peculiar electronic structure for the O_2 complex of the α chain of human hemoglobin as compared with those of human hemoglobin, its β chain, bovine and whale myoglobin. It is also interesting to note that the A'/D values for the O_2 complex of the α chain of human hemoglobin exhibit similar magnitude of that for the CO complexes of the β chain, bovine myoglobin and human hemoglobin.

Table 1. The experimental MCD data of the α and β chains of the human hemoglobin

	$Q_{0\leftarrow0}$			$Q_{v\leftarrow0}$			Soret		
	$\frac{\tilde{\nu}\times10^{-3}}{\text{cm}^{-1}}$	f[a]	$\frac{A'/D}{\beta}$[b,c]	$\frac{\tilde{\nu}\times10^{-3}}{\text{cm}^{-1}}$	f	A'/D	$\frac{\tilde{\nu}\times10^{-3}}{\text{cm}^{-1}}$	f	$\frac{A'/D}{\beta}$
Human Hb-α CO	17.51	0.017	0.98	18.55	0.095	0.36	24.18	1.204	0.27
Human Hb-α NO	17.52	0.022	1.88	18.57	0.119	0.59	24.33	1.402	0.13
Human Hb-α O_2	17.39	0.019	1.36	18.50	0.084	0.11	24.34	1.292	0.23
Human Hb-β CO	17.46	0.025	2.24	18.53	0.095	0.63	24.14	1.217	0.20
Human Hb-β NO	17.49	0.014	2.93	18.64	0.111	0.34	24.29	1.242	0.08
Human Hb-β O_2	17.26	0.021	2.18	18.61	0.093	0.16	24.31	1.177	0.16

a) f: Oscillator strength. b) β: Bohr magneton.[27] c) D: Dipole strength.

Table 2. The experimental MCD data of the bovine and whale myoglobin and hemoglobin (Soret band)

		$\tilde{\nu}\times10^{-3}$ / cm^{-1}	f[a]	$A'D$[c] / β[b]
Bovine	MbCO	24.06	1.18	0.19
	MbNO	24.18	1.22	0.08
	MbO_2	24.21	1.20	0.13
Human	HbCO	24.11	1.27	0.20
	HbNO	24.25	1.33	0.09
	HbO_2	24.35	1.22	0.14
Whale	MbCO	24.97	1.15	0.30
	MbNO	24.12	1.21	0.03
	MbO_2	24.25	1.14	0.11

a) f: Oscillator strength. b) β: Bohr magneton.[27] c) D: Dipole strength.

Our previous theoretical studies have succeeded in calculating the reasonable values of Faraday parameters of the iron(II) low spin type heme-chromophore for the Soret and Q transitions by use of the PPP CI MO method.[24] Although the calculation was rather simple one which neglects the orbitals of the iron and the axial ligands, it can predict the experimental apparent Faraday A terms for the π-π^* transitions. This is somewhat rationalized by the fact that the iron(II) low spin complex does not show the contribution from the Faraday C term. The Faraday parameters of the iron(II) low spin complexes on the Soret and Q bands were determined to be Faraday A and B terms which predominantly come from the porphyrin π electron system.

The present experimental results which show subtle but clear differences in the A'/D values in the Soret band region among CO, O_2, and NO complexes which will be better examined by the calculation including the orbitals of iron and axial ligands. However, since the Soret band for the iron(II) low spin complexes mainly depends on the π-electronic systems, a simple calculation which neglects these orbitals was used to examine the possible reasons for the axial ligand dependence on the A'/D values in the Soret MCD bands.

Within the framework of our π-electron approximation which neglects the iron and axial ligand orbitals, the effect of axial ligands can be included by changing the α-electron population on the pyrrole nitrogen atoms through the iron orbitals. Thus the core-charge of the nitrogen atom, *i.e.*, the α-electron density on the nitrogen atom will be altered by the effect of the axial ligands. For example the extent of the electron back-donation which depends on the π^* orbital level of the diatomic molecules will determine the strength of the α coordination of the axial ligand to the central iron, and further control the degree of the α coordination of the pyrrole nitrogen to the heme iron. Thus, the axial ligands (diatomic molecules) will vary the core-charge of the pyrrole nitrogen. Under these consideration the calculations of the A'/D values using the different nitrogen core-charges of 1.5, 1.4, 1.3, 1.2, 1.1, and 1.0 were examined. Only the core-charge values of 1.5, 1.4, and 1.3 gave reasonable A'/D values for the Soret and Q bands, and the calculated results are shown in Table 3. With these calculated A'/D values and the calculated energies of the splitting in the Soret and Q transitions, the expected MCD peak and trough magnitudes were calculated by assuming the gaussian band shape. The results are shown in Fig. 2 which shows that the calculated MCD's for the decreasing nitrogen core-charge values from 1.5 to 1.3 can reproduce at least the relative magnitudes of the Soret and Q MCD bands for the CO, NO, and O_2 complexes. Unfortunately the calculated energy difference between the Soret and Q bands as well as the calculated absolute magnitude and the splitting between plus and minus components in the Soret and Q bands did not correspond strictly to the experimental results, the reason for which may be partly due to the neglect of the iron(II) and ligand orbitals in the present stage of calculations.

Table 3. The calculated MCD data for the model protoheme with the pyrrole nitrogen core charge of 1.5, 1.4, and 1.3

Core charge of nitrogen		$Q_{0\leftarrow0}$ $\tilde{\nu}\times10^{-3}$ / cm^{-1}	f[a]	A'/D[c] / β[b]	Soret $\tilde{\nu}\times10^{-3}$ / cm^{-1}	f	A'/D / β
1.5	$\vec{\gamma}$[d]		0.01	2.08		2.752	0.040
		16.7			23.9		
	$\vec{\nabla}$[e]		0.004	2.08		0.908	0.040
1.4	$\vec{\gamma}$		0.005	1.93		2.479	0.023
		16.5			23.4		
	$\vec{\nabla}$		0.002	1.93		0.821	0.023
1.3	$\vec{\gamma}$		0.013	1.84		2.110	0.022
		16.1			22.9		
	$\vec{\nabla}$		0.0003	1.84		0.714	0.022

a) f: Oscillator strength. b) β: Bohr magneton.[27] c) D: Dipole strength. d) $\vec{\gamma}$: Dipole length operator. e) $\vec{\nabla}$: Dipole velocity operator.

Table 4 summarizes the π bond orders in the ground

Table 4. The calculated π bond orders of the model protoheme for several nitrogen core charge values

Core-charge	π Bond order[a] C_β-C_β	C_α-C_β	C_α-N	C_α-C_m
1.5	0.756—0.805	0.439—0.482	0.485—0.493	0.604—0.622
1.4	0.762—0.812	0.429—0.471	0.509—0.518	0.603—0.617
1.3	0.766—0.817	0.421—0.462	0.528—0.539	0.600—0.614

a) The symbols C_α, C_β, and C_m in the table denote the α cabon, β carbon of the pyrrole and the meso carbon of the porphyrin.

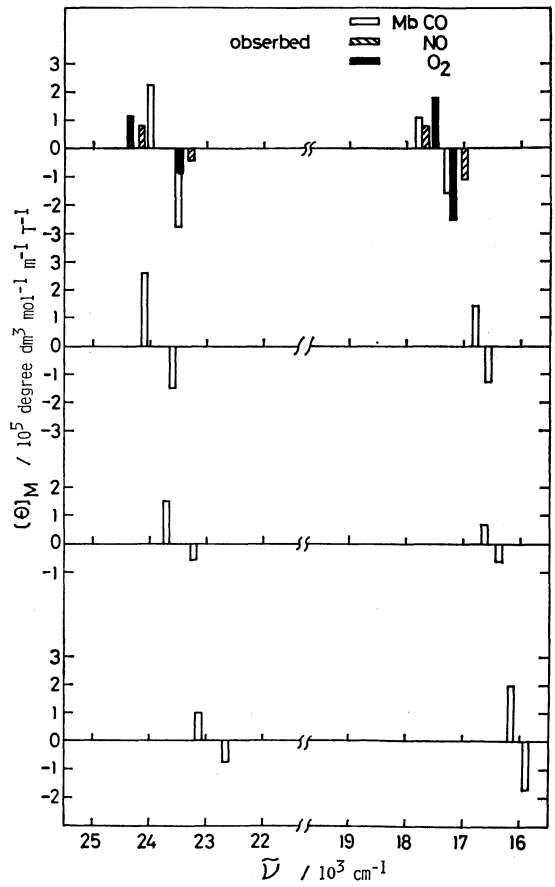

Fig. 2. The stick diagram of the experimental and calculated MCD spectra for the CO, NO, and O_2 complexes of hemoglobin and model protoheme. The calculated spectra were based on the A' values and the splitting energies from the PPP π electron calculation assuming the gaussian band shapes, and the experimental bandwidth. The top column is the experimental data, and from the second to the bottom colums are the calculated data for the pyrrole nitrogen core-charge of 1.5, 1.4, and 1.3, respectively.

states for the calculation with the varied nitrogen core-charge values. The larger changes in the π bond order in the pyrrole (0.010—0.012, −0.018——0.020, and 0.043—0.046 for C_β–C_β, C_α–C_β, and C_α–N, respectively) with varying the nitrogen core-charge from 1.5 to 1.3 were compared with the smaller changes in the C_α–C_m bond (0.004—0.008). Among all, the bond order change in the C_α–N is prominent and is two to three times as large as those in other pyrrole bonds. These calculated results can be compared with the resonance Raman spectral results as follows. The band IV in the heme resonance Raman spectral lines which is one of the spin and oxidation markers appears at 1372, 1375, and 1380 cm^{-1} for the CO, NO, and O_2 hemoglobin complexes, respectively.[4,5] Since the band IV was assigned to be dependent primarily on the C_α–N bond stretching, the above experimental frequencies indicate that the C_α–N bond order increases in the order of the CO, NO, and O_2 complexes. This order shows a similar trend with the calculated bond orders for the decreasing nitrogen core-charge values from 1.5 to 1.3. This means that some factors which induce the bond order changes of the porphyrin pyrrole C_α–N bond in the iron(II) low spin hemoprotein with diatomic molecules could be also explained by the PPP-CI calculations with the varied nitrogen core-charge values.

In conclusion the subtle but clear differences in the MCD's among the CO, NO, and O_2 complexes of the iron(II) low spin hemoproteins were found to be explained by considering the change in the core-charge of the pyrrole nitrogen which might be induced by axial ligands through the iron orbitals. The calculation also demonstrated the π bond order changes in the pyrrole C_α–N bond with the pyrrole nitrogen core charge variation, which seemed to refect on the heme resonance Raman spectral line IV.

The authors would like to express their thanks to Prof. Y. Yoneyama, Dr. S. Matsukawa, and Dr. K. Mawatari (Kanazawa University) for the kind guidances in preparing the α and β chains of human hemoglobin. The authors ackowledge support from Grant-in-Aid for Scientific Research of Japanese Government.

References

1) E. Antonini and M. Burunori, "Hemoglobin and Myoglobin in their Reactions with Ligands," North-Holland Publishing Co., Amsterdam (1971), p. 19.
2) G. Lang and W. Marshall, *Proc. Phys. Soc. (London)*, **87**, 3 (1966).
3) A. Trautwein, Y. Maeda, F. E. Harris, and H. Formanek, *Theoret. Chim. Acta*, **36**, 67 (1974).
4) T. Kitagawa, Y. Kyogoku, T. Iizuka, and M. I. Saito, *J. Am. Chem. Soc.*, **98**, 5169 (1976).
5) L. Rimai, I. Salmeen, and D. H. Petering, *Biochemistry*, **14**, 378 (1975).
6) C. H. Barlow, J. C. Maxwell, W. J. Wallace, and W. S. Caughey, *Biochem. Biophys. Res. Commun.*, **55**, 91 (1973).
7) J. O. Alben and W. S. Caughey, *Biochemistry*, **7**, 175 (1968).
8) J. C. Maxwell and W. S. Caughey, *Biochemistry*, **15**, 388 (1976).
9) L. Vickery, T. Nozawa, and K. Sauer, *J. Am. Chem. Soc.*, **98**, 343 (1976).
10) M. Hatano and T. Nozawa, "Advances in Biophys," ed by M. Kotani, S. Yomosa, and M. Hatano, Japan Scientific Soc. Press Tokyo, University Park Press Baltimore (1978), Vol. 11, p. 95.
11) C. Djerassi, E. Bunnenberg, and D. L. Elder, *Pure Appl. Chem.*, **25**, 57 (1971).
12) J. I. Treu and J. J. Hopfield, *J. Chem. Phys.*, **63**, 613 (1975).
13) D. A. Schooley, E. Bunnenberg, and C. Djerassi, *Proc. Natl. Acad. Sci. U.S.A.*, **53**, 579 (1965).
14) H. Kobayashi, M. Shimizu, and I. Fujita, *Bull. Chem. Soc. Jpn.*, **43**, 2335 (1970).
15) J. C. Sutherland, L. E. Vickery, and M. P. Klein, *Rev. Sci. Instrum.*, **45**, 1089 (1974).
16) J. Bolard and A. Garnier, *Biochim. Biophys. Acta*, **263**, 535 (1972).
17) J. Springall, M. J. Stillman, and A. J. Thomson, *Biochim. Biophys. Acta*, **453**, 494 (1976).
18) J. C. Cheng, G. A. Osborne, P. J. Stephens, and W. A. Eaton, *Nature*, **241**, 193 (1973).
19) T. Nozawa, T. Yamamoto, and M. Hatano, *Bio-*

chim. Biophys. Acta, **427**, 28 (1976).
20) J. H. Dawson and S. P. Cramer, *FEBS Lett.*, **88**, 127 (1978).
21) E. Bucci and C. Fronticelli, *J. Biol. Chem.*, **240**, 551 (1965).
22) P. N. Schatz and A. J. McCaffery, *Quart. Rev. Chem. Soc.*, **23**, 552 (1969).
23) A. D. Buckingham and P. J. Stephens, *Ann. Rev. Phys. Chem.*, **17**, 399 (1969).
24) A. Kaito, T. Nozawa, T. Yamamoto, M. Hatano, and Y. Orii, *Chem. Phys. Lett.*, **52**, 154 (1977).
25) T. Nozawa, Y. Orii, A. Kaito, T. Yamamoto, and M. Hatano "Development in Biochemistry," ed by T. E. King, Y. Orii, B. Chance, and K. Okunuki, Elsevier/North-Holland, Amsterdam (1979), Vol. 5, p. 117.
26) Since heme b in myoglobin has not true C_{4v} symmetry when all the substituents on the periphery of the porphyrin are taken into consideration, the porphyrin lowest unoccupied e orbitals (C_{4v}) slightly split into two closely positioned orbitals in the actual symmetry lower than C_{4v}. Hence there can not be expected true Faraday *A* term. However as the calculation indicated (A. Kaito, *et al.*, *Chem. Phys. Lett.*, **52**, 154 (1977)) the Faraday *B* terms predominantly mix among these split two orbitals gave an S-shaped MCD band which is a mimic Faraday *A* term. In this paper this apparent *A* term has been treated just like true Faraday *A* term.
27) 1 Bohr magneton (β)$=0.9273\times10^{-23}$ J T^{-1}.

Molecular Structure of [2](2,5)(7,7,8,8-Tetracyanoquinodimethano)-[2](1,4)naphthalenophane†

Takashi Mizuma,†† Kunio Miki, Yasushi Kai, Nobuo Tanaka,††† and Nobutami Kasai*

Department of Applied Chemistry, Faculty of Engineering, Osaka University, Yamadaoka, Suita, Osaka 565

(Received October 23, 1981)

Molecular structure of [2.2](1,4)naphthalenophane containing 7,7,8,8-tetracyanoquinodimethan moiety as an electron acceptor has been determined by means of X-ray diffraction. Crystals belong to monoclinic system, space group Cc with four molecules per unit-cell; $a=9.770(1)$, $b=15.176(2)$, $c=13.299(2)$ Å, $\beta=98.43(1)°$. The structure was established by the direct method and refined by the full-matrix least-squares to $R=0.035$ for 1217 non-zero reflections. The [2.2]paracyclophane skeleton has the usual structure; a half of the naphthalene moiety has a boat-form, the six-membered ring of the TCNQ moiety also has a boat-form, and two $C(CN)_2$ portions in the TCNQ moiety are bent out and slightly twisted from the six-membered ring. The other half of the naphthalene ring free from the bridging is planar and are slightly bent out from the [2.2]paracyclophane skeleton.

As a part of a series of structural studies on layered cyclophanes, molecular structures of [2.2]paracyclophanes containing 7,7,8,8-tetracyanoquinodimethan (TCNQ) moiety as an electron acceptor have been determined;[1] they are [2](2,5)(7,7,8,8-tetracyanoquinodimethano)[2]paracyclophane (TCNQ-X) and 14,17-dimethoxy[2](2,5)(7,7,8,8-tetracyanoquinodimethano)-[2]paracyclophane (TCNQ-X(OMe)$_2$). In relation with these structures, this paper will deal with the molecular structure of [2](2,5)(7,7,8,8-tetracyanoquinodimethano)[2](1,4)naphthalenophane (TCNQ-N^{1,4}), in which a TCNQ and a naphthalene moieties are contained as an electron acceptor and electron donor respectively.

Experimental

A dark violet, needle crystal of TCNQ-N^{1,4} with approximate dimensions of $0.08\times0.15\times0.25$ mm^3 was used. The unit-cell dimensions were determined by the least-squares fit of 2θ values of high order reflections. The systematic absence of reflections showed that the corresponding space group is either Cc or C2/c. The value of calculated density of the crystal [$D_c=1.309$ g cm^{-3}] for $Z=4$ exclude the possibility of the space group C2/c, which was later confirmed by the structure determined.

Crystal Data. $C_{26}H_{16}N_4$, *F.W.* 384.44, monoclinic, space group Cc, $a=9.770(1)$, $b=15.176(2)$, $c=13.299(2)$ Å, $\beta=98.43(1)°$, $V=1950.5(3)$ Å^3, $D_c=1.309$ g cm^{-3} for $Z=4$.

Integrated intensities were measured on a Rigaku automated, four-circle diffractometer with Ni-filtered Cu $K\alpha$ radiation. The $\theta-2\theta$ scan technique was applied at a scan rate of 4° min^{-1} in 2θ; scan width was $\Delta2\theta=(2+0.30\tan\theta)°$. Backgrounds were counted for 7.5 s at both ends of a scan. A total of 1232 (1217 non-zero) reflections was collected. Usual Lp corrections were made but absorption correction was ignored [μ(Cu $K\alpha$)$=6.35$ cm^{-1}].

Structure Solution and Refinement

The structure was solved by the direct method (*MULTAN* 74).[2] Twelve ring carbon atoms which consist of the [2.2]paracyclophane skeleton of the molecule could be located on the *E* map. The location of these atoms was confirmed to be consistent with the result of three-dimensional Patterson function. The Fourier synthesis revealed 28 carbon atoms out of 30, and the successive Fourier synthesis revealed the remaining carbon atoms.

The structure was refined isotropically by the block-diagonal least-squares method (*HBLS* V).[3] When the *R* value reduced to 0.14, anisotropic thermal parameters were introduced for all the non-hydrogen atoms. Ten strong reflections, of which intensities were considered largely affected by the counting loss of the scintillation counter and/or affected by the extinction, were excluded from the subsequent refinement. The refinement was continued by the full-matrix least-squares procedure.[4] At the later stage, all the hydrogen atoms located on a difference Fourier synthesis, were also included in the refinement, isotropic temperature factors being used. Finally, the *R* index converged to 0.035 ($R_w=0.045$) for 1217 non-zero reflections. The weighting schemes used at the final stage were $w=\{\sigma^2(F_o)+0.0523|F_o|+0.0025|F_o|^2\}^{-1}$ for $|F_o|>0$ and $w=2.2827$ for $|F_o|=0$. σ is the standard deviation obtained by the counting statistics of reflection intensities. Atomic scattering factors used for the C, N, and H atoms were taken from International Tables for X-Ray Crystallography, Vol. IV.[5] Computations were carried out on an ACOS 700S computer at the Crystallographic Research Center, Institute for Protein Research, Osaka University. Final atomic parameters are listed in Table 1.**

Results and Discussion

Molecular Structure. Perspective and side views of the present TCNQ-N^{1,4} molecule (*ORTEP* II)[7] and those of TCNQ-X for comparison are shown in Figs. 1 and 2. Selected bond distances and bond angles are given in Fig. 3.

The [2.2]paracyclophane skeleton in the TCNQ-N^{1,4} molecule has the similar structure as those in

† Structural Chemistry of Layered Cyclophanes. VIII.

†† Present address: Fuji-FACOM Corporation, 23-5 Nishishinbashi 3 chome, Minato-ku, Tokyo 105.

††† Present address: Institute for Protein Research, Osaka University, Yamadaoka, Suita, Osaka 565.

** Tables of observed and calculated structure factors and anisotropic thermal parameters are kept at the Chemical Society of Japan, Document No. 8236.

TCNQ-X and TCNQ-X$(OMe)_2$. Almost all of the bond distances and bond angles in the TCNQ-$N^{1,4}$ molecule are equal to the corresponding distances and angles in the TCNQ-X within the limits of errors. The better coincidence is observed between two molecules in the TCNQ portion than in the other portions. A few exceptions are observed: the C(4)–C(9) and C(9)–C(10) distances [1.427(4) and 1.426(4) Å] are longer than the corresponding ones in the TCNQ-X[1.386(6) and 1.385(6) Å].

The upper six-membered ring of the [2.2]paracyclophane skeleton, which is a half of the naphthalene moiety, takes a boat form: the planes defined by the C(3), C(4), and C(12) atoms and by the C(9), C(10), and C(11) form angles of 12.7 and 11.8° respectively with the mean plane made by the C(4), C(9), C(11), and C(12) atoms. The other half of the naphthalene moiety, formed by the C(4) to C(9) atoms, is planar within 0.007 Å, and slightly bent up by 4.2° from the

Table 1. Fractional atomic coordinates of TCNQ-$N^{1,4}$ with estimated standard deviations in parentheses

(a) C, N, and O atoms with equivalent temperature factors.[6]

Atom	x	y	z	B_{eq}/Å^2
C (1)	0.2792 (4)	0.6500 (2)	0.1740 (3)	3.56
C (2)	0.2176 (4)	0.6213 (3)	0.2714 (3)	3.93
C (3)	0.3171 (4)	0.5608 (2)	0.3377 (3)	3.19
C (4)	0.4507 (4)	0.5918 (2)	0.3812 (2)	3.17
C (5)	0.4805 (5)	0.6821 (3)	0.3970 (3)	4.41
C (6)	0.6110 (5)	0.7111 (3)	0.4331 (4)	5.39
C (7)	0.7180 (5)	0.6502 (3)	0.4538 (4)	5.30
C (8)	0.6951 (4)	0.5622 (3)	0.4391 (3)	4.15
C (9)	0.5605 (4)	0.5295 (2)	0.4024 (3)	3.12
C (10)	0.5348 (4)	0.4380 (2)	0.3837 (3)	3.36
C (11)	0.3983 (4)	0.4110 (2)	0.3654 (3)	3.65
C (12)	0.2907 (4)	0.4726 (2)	0.3396 (3)	3.40
C (13)	0.6472 (4)	0.3762 (3)	0.3587 (3)	4.11
C (14)	0.6308 (4)	0.3571 (2)	0.2422 (3)	3.35
C (15)	0.5575 (3)	0.4306 (2)	0.1799 (3)	2.67
C (16)	0.4230 (3)	0.4189 (2)	0.1395 (3)	2.84
C (17)	0.3269 (3)	0.4907 (2)	0.1123 (3)	2.73
C (18)	0.3738 (4)	0.5579 (2)	0.1432 (3)	2.76
C (19)	0.5125 (4)	0.5913 (2)	0.1635 (3)	2.90
C (20)	0.6112 (3)	0.5200 (2)	0.1749 (3)	2.60
C (21)	0.1954 (3)	0.4708 (2)	0.0642 (3)	3.16
C (22)	0.1539 (4)	0.3826 (3)	0.0382 (3)	4.15
C (23)	0.0893 (4)	0.5340 (3)	0.0305 (3)	4.01
C (24)	0.7506 (4)	0.5402 (2)	0.1884 (3)	3.20
C (25)	0.7995 (4)	0.6287 (3)	0.1897 (3)	4.32
C (26)	0.8598 (4)	0.4761 (3)	0.2014 (3)	3.96
N (1)	0.1154 (4)	0.3128 (3)	0.0156 (4)	6.54
N (2)	0.	0.5794 (3)	0.	5.71
N (3)	0.8430 (4)	0.6991 (3)	0.1941 (4)	7.20
N (4)	0.9511 (4)	0.4278 (3)	0.2102 (4)	5.99

(b) H atoms with isotropic temperature factors.

Atom	x	y	z	B/Å^2
H (1A)	0.335 (4)	0.714 (3)	0.183 (3)	4.2 (8)
H (1B)	0.208 (4)	0.673 (3)	0.117 (3)	4.6 (8)
H (2A)	0.188 (4)	0.676 (3)	0.306 (3)	5.4 (9)
H (2B)	0.127 (5)	0.588 (3)	0.257 (3)	4.9 (8)
H (5)	0.410 (4)	0.723 (3)	0.384 (3)	4.8 (8)
H (6)	0.624 (5)	0.783 (3)	0.446 (3)	5.6 (9)
H (7)	0.809 (5)	0.672 (3)	0.479 (4)	5.9 (9)
H (8)	0.779 (4)	0.520 (3)	0.457 (3)	4.6 (8)
H (11)	0.380 (4)	0.349 (3)	0.350 (3)	4.1 (7)
H (12)	0.203 (4)	0.450 (3)	0.309 (3)	4.7 (8)
H (13A)	0.744 (5)	0.410 (3)	0.383 (4)	5.7 (9)
H (13B)	0.650 (5)	0.331 (3)	0.398 (4)	6.1 (9)
H (14A)	0.577 (4)	0.303 (3)	0.224 (3)	4.7 (8)
H (14B)	0.722 (4)	0.345 (3)	0.218 (3)	5.0 (8)
H (16)	0.382 (4)	0.355 (2)	0.139 (3)	2.9 (6)
H (19)	0.553 (4)	0.650 (2)	0.178 (3)	3.5 (6)

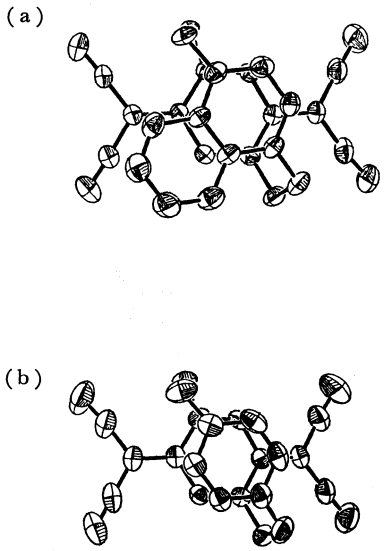

Fig. 1. A perspective view of the TCNQ-$N^{1,4}$ molecule (a) compared with that of TCNQ-X (b). Non-hydrogen atoms are expressed as thermal ellipsoids with 50% probability level. Hydrogen atoms are omitted for clarity.

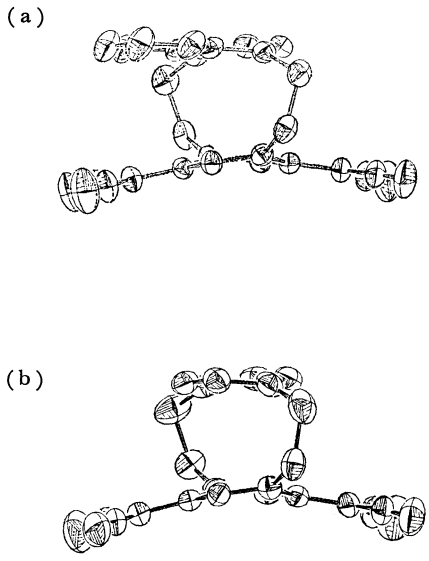

Fig. 2. A side view of the TCNQ-$N^{1,4}$ molecule (a) compared with that of TCNQ-X (b).

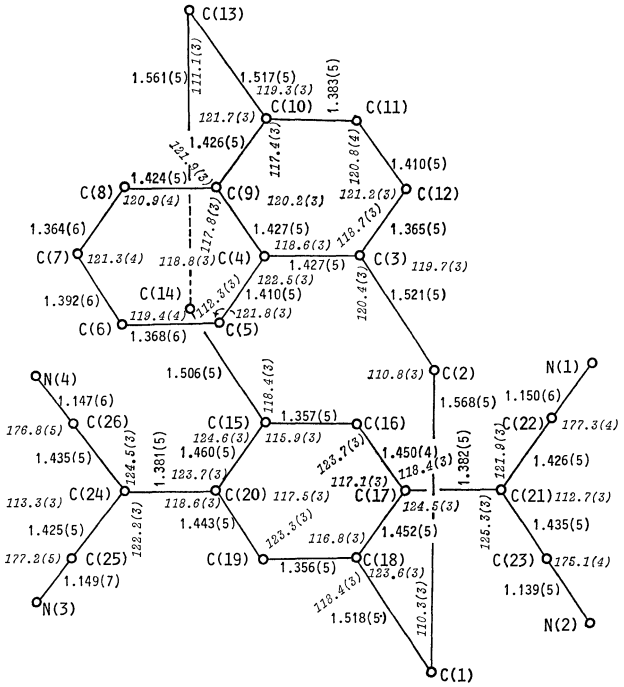

Fig. 3. Bond distances(l/Å) and bond angles(ϕ/°) in the TCNQ-N[1,4] molecule (Estimated standard deviations in parentheses).

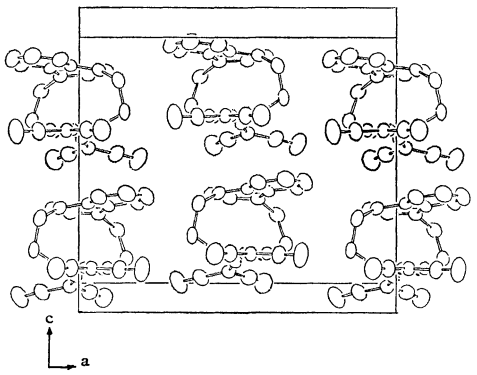

Fig. 4. A perspective view of the crystal structure of TCNQ-N[1,4].

Table 2. Short intermolecular atomic contacts (l/Å) less than 3.5 Å, with estimated standard deviations in parentheses

C (25) ··· N (2) [a]	3.495 (5)	C (21) ··· C (12) [c]	3.368 (4)
N (4) ··· C (21) [a]	3.355 (5)	C (3) ··· C (22) [c]	3.412 (5)
N (4) ··· C (22) [a]	3.311 (5)	C (4) ··· C (16) [c]	3.489 (4)
N (4) ··· C (23) [a]	3.328 (6)		
N (3) ··· N (1) [b]	3.465 (7)	Key: a, $1+x$, y, z;	
C (16) ··· C (4) [b]	3.489 (4)	b, x, $1-y$, $-0.5+z$;	
C (21) ··· C (3) [b]	3.430 (4)	c, x, $1-y$, $0.5+z$.	

plane made by the C(4), C(9), C(11), and C(12). The C(3)–C(2) and C(10)–C(13) bonds are further bent down by 11.0 and 12.6° from planes defined by the C(3), C(4), and C(12) atoms and by the C(9), C(10), and C(11), respectively.

The TCNQ moiety has a twisted structure. The central six-membered ring is in a boat form, the planes formed by the C(17), C(18), and C(19) atoms and by the C(15), C(16), and C(20) are bent up from the mean plane defined by the C(16), C(17), C(19), and C(20) by 15.8 and 14.4°, respectively. On the other hand, both of the two $C(CN)_2$ portions slightly bent down from the mean plane. The C(17)–C(21) and C(20)–C(24) vectors respectively make angles of 10.7 and 9.2° with the mean plane formed by the C(16), C(17), C(19), and C(20) atoms. Two $C(CN)_2$ planes have tilt angles of 12.4 and 9.4° to the mean planes mentioned above. The deviations of C(14)–C(15)–C(20), C(15)–C(20)–C(24), C(20)–C(24)–C(26), C(1)–C(18)–C(17), C(18)–C(17)–C(21), and C(17)–C(21)–C(23) angles[av. 124.4°] from 120° are observed, which are considered as due to the repulsions between $C(CN)_2$ portions and $-(CH_2)_2-$ bridges.

Two $-(CH_2)_2-$ bridges are twisted: the torsion angles about their central C–C bonds are 29.8 and 26.2°.

As described above, the electron donor and electron acceptor moieties in the present molecule are no more planar after they were linked by two $-(CH_2)_2-$ bridges: a half of the naphthalene moiety deformed into a boat form and the TCNQ moiety changed into a twisted structure. These deformations probably caused the electronic state in these moieties unfavorable to the charge-transfer interaction. In the similar manner little charge-transfer interaction between the benzene and TCNQ and *p*-methoxybenzene and TCNQ moieties respectively in the TCNQ-X and TCNQ-X-$(OMe)_2$ molecules can be explained well.

Crystal Structure. A perspective view[7] of the crystal structure is shown in Fig. 4. Short intermolecular atomic contacts less than 3.5 Å are given in Table 2. Most of them are involved between the neighboring TCNQ moieties.

The authors wish to express their deep thanks to Professor Soichi Misumi and his co-workers, Institute of Scientific and Industrial Research, Osaka University for the supply of crystals and their helpful discussions.

References

1) T. Mizuma, H. Matsu-ura, Y. Kai, N. Yasuoka, and N. Kasai, *Bull. Chem. Soc. Jpn.*, **55**, 979 (1982).

2) P. Main, M. M. Woolfson, L. Lessinger, G. Germain, and J. P. Declercq, *MULTAN* 74; "A System of Computer Programs for the Automatic Solution of Crystal Structures from X-Ray Diffraction Data," Univs. of York, England, and Louvain, Belgium (1974).

3) T. Ashida, *HBLS*-V, "The Universal Crystallographic Computing System-Osaka," The Computation Center, Osaka Univ. (1973), pp. 55—61.

4) W. R. Busing, K. O. Martin, and H. A. Levy, *ORFLS*, "A FORTRAN Crystallographic Least-squares Program," Report ORNL-TM-305, Oak Ridge National Laboratory, Tennessee (1962).

5) "International Tables for X-Ray Crystallography," Kynoch Press, Birmingham (1974), Vol. IV, p. 71.

6) W. C. Hamilton, *Acta Crystallogr.*, **12**, 609 (1959).

7) C. K. Johnson, *ORTEP*-II, Report ORNL-5138, Oak Ridge National Laboratory, Tennessee (1974).

 © 1982 The Chemical Society of Japan Bull. Chem. Soc. Jpn., 55, 2029—2033 (1982)

Surface Free Energies of Two Kinds of Graphite Fluorides, $(CF)_n$ and $(C_2F)_n$

Nobuatsu WATANABE, Tsuyoshi NAKAJIMA,* and Noboru OHSAWA†

Department of Industrial Chemistry, Faculty of Engineering, Kyoto University, Sakyo-ku, Kyoto 606

† *Sumitomo Aluminium Smelting Co. Ltd., Toyo Works, Hojo, Toyo, Ehime 799-13*

(Received October 29, 1981)

The surface free energies of two kinds of graphite fluorides, $(CF)_n$ and $(C_2F)_n$, were estimated from the contact angles of several liquids. The contact angles of water on flaky $(CF)_n$ and $(C_2F)_n$ were 117° and 116°, respectively, being slightly larger than that for poly(tetrafluoroethylene), while the values for tablets of powdery $(CF)_n$ and $(C_2F)_n$ were 143° and 141°, respectively, which indicates that powdery graphite fluoride is hardly wetted by water. From the contact angles obtained, the surface free energies were estimated to be *ca.* 18 mJ/m² for both flaky $(CF)_n$ and $(C_2F)_n$, *ca.* 2 mJ/m² for powdery $(CF)_n$ and *ca.* 3 mJ/m² for powdery $(C_2F)_n$. These differences depend on the surface conditions such as the packing of fluorine atoms, the roughness and porosity. From the contact angles for the tablets of $(CF)_n$–polyethylene mixtures, it is suggested that the anode effect in the fluorine or aluminium electrolysis takes place when the surface of carbon anode is partially covered by graphite fluoride.

During the electrolysis of molten KF·2HF or alumina in cryolite melt, it sometimes happens that the cell voltage suddenly increases with arc-discharging. This phenomenom is called the anode effect, on which a number of mechanisms have been reported by many investigators.[1,2]

Watanabe *et al.* proposed that the anode effect is attributed to the formation of graphite fluoride film on the surface of carbon electrode.[3–5] The formation of graphite fluoride on carbon anode surface extremely decreases the wettability of molten salt owing to its low surface free energy. On the basis of the mechanism, various experiments have been performed.[6–9] Graphite fluoride was detected on the surface of carbon anode after the anode effect from ESCA spectra.[10–11] Furthermore, during the studies on the relationship between composition and structure of graphite fluoride, it was found that a new compound, poly(dicarbon monofluoride), $(C_2F)_n$, is formed at a relatively low reaction temperature.[12] This compound might also be concerned with the anode effect besides $(CF)_n$.

The present study was carried out to clarify the roles of graphite fluorides on the anode effect. The extent of wetting between anode and electrolyte was evaluated physically from the surface free energies obtained from the contact angles of several liquids on two kinds of graphite fluorides at room temperature.

Experimental

Material. The following four samples of graphite fluorides were prepared. (1) Flaky poly(carbon monofluoride), $(CF)_n$ with F/C ratio of 1.0 was prepared by the direct fluorination of natural graphite (produced in Madagascar, purity: more than 99%) having a sieve size of 1.981—0.833 mm under F_2 pressure of 26664 Pa at 630 °C for 2 d. (2) Powdery $(CF)_n$ with F/C ratio of 1.1, prepared from petroleum coke of less than 37 μm, was supplied by Daikin Kogyo Co. Ltd. (3) Flaky poly(dicarbon monofluoride), $(C_2F)_n$ with F/C ratio of 0.65 was prepared by the fluorination of flaky natural graphite (1.981—0.833 mm) under F_2 pressure of 101325 Pa at 380 °C for 14 d. (4) Powdery $(C_2F)_n$ with F/C ratio of 0.65 was prepared by the fluorination of natural graphite of less than 37 μm under F_2 pressure of 101325 Pa at 380 °C for 3 d. All the samples were analyzed by X-ray diffractometry and their compositions were determined from elemental analysis of carbon and fluorine. For the purpose of comparison, flaky natural graphite with a sieve size of 1.981—0.833 mm, grafoil made by compressing exfoliated graphite from Union Carbide Corporation, poly(tetrafluoroethylene) (PTFE) supplied by Daikin Kogyo Co. Ltd. and polyethylene(PE) of E. Merck were used for the contact angle measurement.

Liquids used for the contact angle measurement were distilled water, reagent grade glycerol, formamide, 1,4-butanediol, hexadecane and 17% and 31% NaOH solutions.

Contact Angle Measurement. All the measurements were made at 30 °C using the CA-D type contact angle meter of Kyowa Kagaku Co. Ltd. For the flaky samples, the liquids were dropped onto them immediately after peeling off the thin layer with plastic adhesion tape. For the powdery samples, they were compressed and molded under a pressure of *ca.* 49 MPa to the tablets of 13 mm diameter and supplied for the contact angle measurement. The measurements for each sample were repeated 10 to 20 times and their average value was taken.

Results and Discussion

Surface Free Energy. Table 1 shows the contact angles of several liquids on each samples and water drops on the typical samples are shown in Fig. 1. It is of interest that water shows an extremely large contact angle on the tablet of graphite fluoride. The contact angles for PTFE and PE are in good agreement with the results measured by other investigators.[13–15] The data of water on natural graphite and grafoil are slightly larger than the values (60—86°) measured by others.[16–18] The difference of the data between natural graphite and grafoil would be attributed to the surface conditions such as the roughness and porosity. The large deviations in the data for flaky graphite fluorides might be due to the surface roughness and cracks made by fluorination, or/and the groups of $=CF_2$ and $-CF_3$ produced around the crack. Furthermore, the liquids with a surface tension lower than that of 1,4-butanediol penetrated into the flakes through the cracks. It was impossible to measure the contact angles of the liquids with a low surface tension such as hexadecane, since the powdery graphite fluorides were also too poor in cohesiveness

Table 1. Contact angles for graphite fluorides and other samples at 30 °C

Sample	Liquids						
	31%NaOH soln	17%NaOH soln	Water	Glycerol	Formamide	1,4-Butane-diol	Hexa-decane
$(CF)_n$, flake	121±6	116±8	117±11	100±12	96±8	penetrate	penetrate
$(C_2F)_n$, flake	—	—	116±10	102±10	95±10	penetrate	penetrate
$(CF)_n$, tablet	146±3	139±2	143±3	151±2	128±3	103±2	penetrate
$(C_2F)_n$, tablet	—	—	141±6	145±7	129±9	—	penetrate
Graphite, flake	108±4	96±7	96±4	77±4	75±4	56±4	spread
Grafoil	110±2	101±5	95±2	91±2	81±2	65±3	spread
PTFE, tablet	118±3	114±3	109±3	105±2	95±1	86±2	44±1
PE, tablet	115±3	109±2	98±2	89±3	83±2	70±2	spread

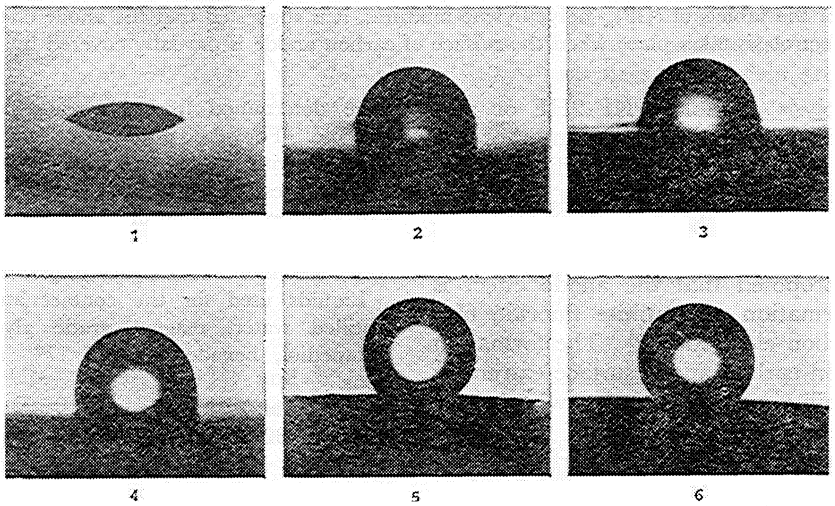

Fig. 1. Contact angles of water at 30 °C.
1. Glass, $\theta=27°$, 2. PE, $\theta=94°$, 3. Grafoil, $\theta=95°$, 4. PTFE, $\theta=109°$, 5. $(C_2F)_n$ tablet, $\theta=141°$, 6. $(CF)_n$ tablet, $\theta=143°$.

to make a tablet without pore.

It was attempted to estimate the critical surface tensions, γ_c, from the Zisman plots in Fig. 2 using the data in Table 1. In Fig. 2, the surface tensions of the liquids, γ_L, at 20 °C were adopted because the values at 30 °C were not available. The difference in the data between 20 °C and 30 °C would be negligibly small, being less than 2 mN/m.[19] The critical surface tension is determined from a point where the extrapolated line of Zisman plot intersects the abscissa of cos $\theta=1$, which is approximately equal to the surface free energy. As shown by the dashed lines in Fig. 2, the critical surface tensions of PTFE and PE are 18 and 31 mN/m, respectively.[20] It is also known that the Zisman plot consists of two lines for nonpolar and polar liquids. Although graphite fluorides could not be measured for the nonpolar liquids in this work, if the samples without crack and pore were prepared, their Zisman plots for the nonpolar liquids would give a line with a slope similar to the dashed line for PTFE. Accordingly, it is suggested that the critical surface tensions for flaky graphite fluorides, $(CF)_n$ and $(C_2F)_n$ are nearly equal to that of PTFE. As shown in Fig. 3, two kinds of graphite fluorides have different structures, however, the packings of fluorine atoms on the basal plane are

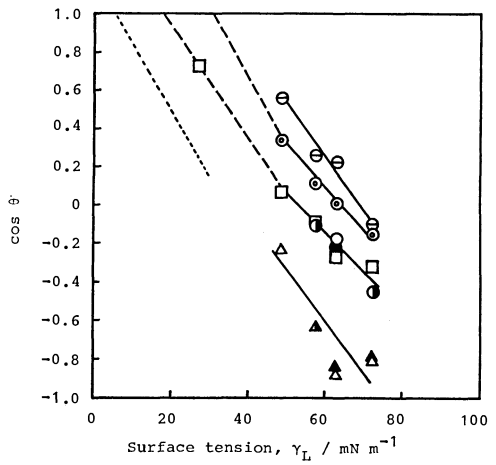

Fig. 2. Zisman plots for $(CF)_n$, $(C_2F)_n$, graphite, PTFE, and PE.
○ $(CF)_n$, flake, ●: $(C_2F)_n$, flake, △: $(CF)_n$, tablet, ▲: $(C_2F)_n$, tablet, ⊖: graphite, □: PTFE, ◎: PE, ……: perfluorolauric acid monolayer.

equal to each other, being *ca.* 1.9×10^{19} F/m^2 (The packing for PTFE is calculated to be *ca.* 3.2×10^{19} F/m^2 along the long chain and *ca.* 1.0×10^{19} F/m^2 at the chain edge.[21]). It is therefore reasonable that

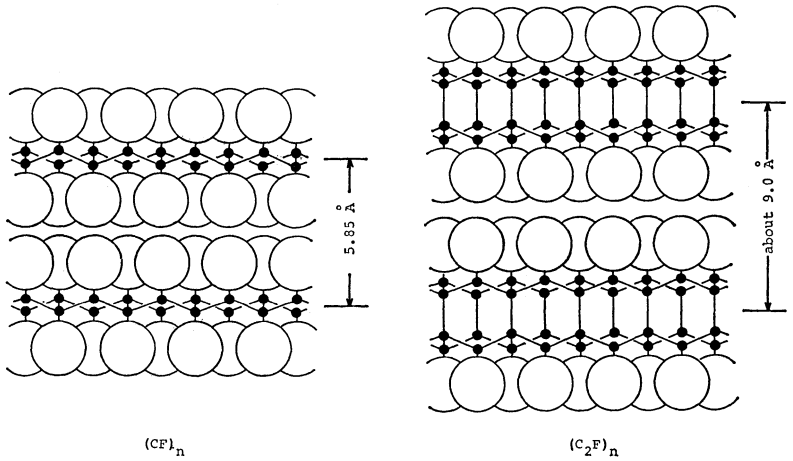

Fig. 3. Crystal structures of $(CF)_n$ and $(C_2F)_n$.
●: Carbon atom, ○: fluorine atom.

two kinds of flake samples have the same surface free energy.

The combination of Young's and Fowkes's equations for the interfacial tension[22,23] leads the relation between the contact angle and the surface free energy in the solid–liquid system depending only on the dispersion force.

$$\cos\theta = -1+2(\gamma_s^d\cdot\gamma_l^d)^{1/2}/\gamma_L,$$

where θ is contact angle, γ_s^d and δ_l^d are the surface free energies of solid and liquid, respectively, and γ_L is the surface tension of liquid. The calculations for water, glycerol and formamide gave the average surface free energies of *ca.* 18 mJ/m² for flaky $(CF)_n$, *ca.* 18 mJ/m² for flaky $(C_2F)_n$, *ca.* 2 mJ/m² for powdery $(CF)_n$, *ca.* 3 mJ/m² for powdery $(C_2F)_n$, *ca.* 20 mJ/m² for PTFE and *ca.* 33 mJ/m² for PE. (*cf.* published data: 19.5 mJ/m² for PTFE and 35.0 mJ/m² for PE.[23]) The surface free energies of two powdery graphite fluorides are much lower than those of the flakes, being nearly equal to that of perfluorolauric acid monolayer having the group of $-CF_3$ on the surface (γ_c=6 mN/m).[24] This might be attributable to the group of $-CF_3$ or $=CF_2$ on the edge plane of graphite fluoride crystallite as shown in Fig. 4. The surface free energy of graphite fluoride would depend on the ratio of the basal and edge planes on the surface of graphite fluoride particle.

Relation between Surface Free Energy and Anode Effect. Both of the basal and edge planes of graphite crystallite would be present at random on the surface of actual carbon electrode. Powdery graphite fluoride is preferred to investigate influence of surface covering by graphite fluoride on the anode effect or the contact angle. Since it was difficult to make a tablet from graphite and graphite fluoride because of their poor cohesiveness, PE having the surface free energy analogous to that of graphite was used as a binder on preparing a tablet.

The effect of the surface covering by graphite fluoride on the contact angles is shown in Fig. 5, together with the result of PTFE–PE system. In the latter, the contact angles increased linearly with increasing content of PTFE, which satisfied the following equation;[25]

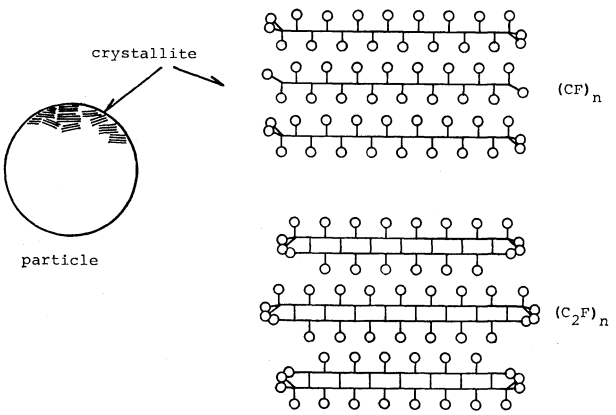

Fig. 4. Illustration of particle and crystallite of graphite fluoride.

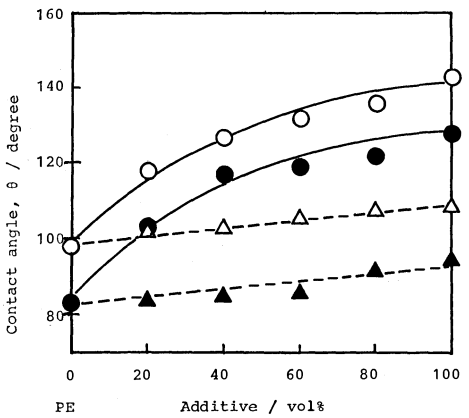

Fig. 5. Effect of additive content in the tablet on contact angle.
○: $(CF)_n$–water, ●: $(CF)_n$ formamide, △: PTFE–water, ▲: PTFE–formamide.

$$\cos\theta_{mix} = f_A\cdot\cos\theta_A + f_B\cdot\cos\theta_B,$$

where θ is contact angle, f is volume percentage of composite, A or B, and $f_A+f_B=1$. On the other hand, $(CF)_n$–PE mixture dosen't obey this relation, which would be due to the low surface free energy

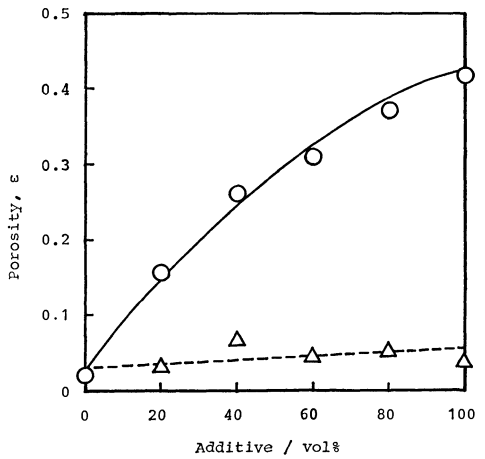

Fig. 6. Plots of porosity *vs.* additive content of $(CF)_n$–and PTFE–PE tablets pressed at *ca.* 49 MPa.
Additive: ○: $(CF)_n$, △: PTFE.

of graphite fluoride or the surface roughness or porosity of the tablet. Wenzel[26] found that when a true contact angle is larger than 90°, a larger contact angle than the true one is observed by the surface roughness, and Ito *et al.*[27] also reported the similar effect by the porosity. The porosity of $(CF)_n$–PE tablet calculated from the weight and size of tablet and the density of mixture increases with the content of $(CF)_n$ as shown in Fig. 6. In this case, the effect increasing a contact angle by porosity or roughness and another effect decreasing a contact angle by penetration of liquid through the pore would give some change to the contact angle. If a tablet having the smooth surface like that of PTFE–PE system is made, the true contact angle would be measured. In case of the tablet composed of only $(CF)_n$, no tablet with the porosity less than 0.4 could be made even under the pressure of *ca.* 490 MPa.

Although this problem still remains, it was attempted to discuss the effect of the surface covering by graphite fluoride on the anode effect on the basis of the data in Fig. 5 and the contact angles of 17 and 31% NaOH solutions with high surface tensions. The cosine of contact angle *vs.* surface tension of liquid is plotted in Fig. 7. The contact angle of molten cryolite having the surface tension of 134 mN/m at 1000 °C is reported to be in the range of *ca.* 130 to 140° on natural graphite.[1] It is likely that the contact angle increases with increasing surface tension of liquid as shown in the solid line for natural graphite in Fig. 7. In the range of $(CF)_n$ content of more than 60% for $(CF)_n$–PE system, the contact angles seem to reach constant in spite of increase in the surface tensions of liquids, which would be due to the limit of the experimental method used in this study. If a liquid behaves like a rigid sphere, its contact angle would be measured accurately up to 180°. In practice, it is known that the contact angle of mercury on PTFE is *ca.* 150° which is the critical value for wetting in contact angle measurement by sessile drop method. Thus, the contact angle for $(CF)_n$–PE tablet would vary with the surface tension of liquid as shown by the dotted lines in Fig. 7.

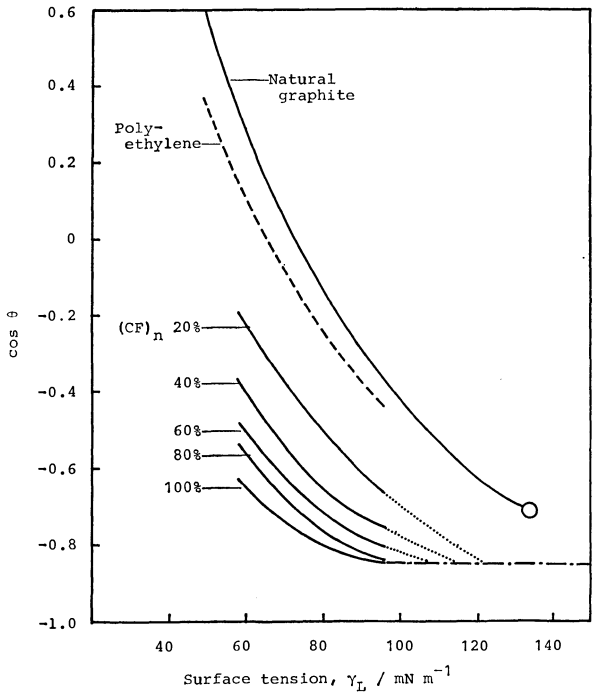

Fig. 7. Influence of $(CF)_n$ surface covering upon contact angle.
%: Vol% of $(CF)_n$ in $(CF)_n$–PE tablet. ○: contact angle of cryolite melt on natural graphite.

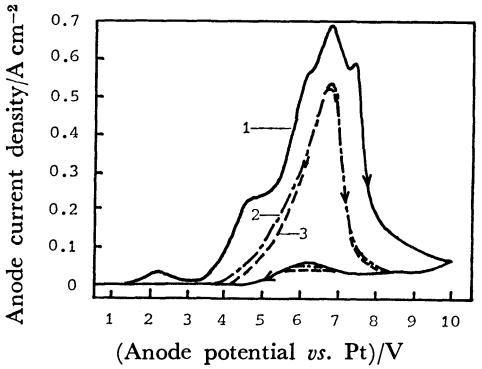

Fig. 8. Potential-sweep diagram for carbon anode in KF·2HF melt.
Sweep rate: 0.2V/s. 1: 1st sweep, 2: 2nd sweep, 3: 3rd sweep.

It is assumed that the anode effect occurs when the contact angle of molten salt on carbon anode reaches the critical value shown in Fig. 7. If the wettability of anode surface is determined by the relation between the surface tension of molten salt and the property of anode surface, the anode effect in the aluminium electrolysis is expected to occur at the surface covering of 10 to 20% by graphite fluoride on the basis of above surface tension of molten cryolite. Likewise, the anode effect in the fluorine electrolysis is expected to occur at the surface covering of 60 to 80% by graphite fluoride since the surface tension of molten KF·2HF is reported to be *ca.* 100 mN/m at 100 °C.[6]

Figure 8 shows the current-potential curves for carbon anode in molten KF·2HF.[5] In the first sweep,

OH^- ion is first discharged owing to its low discharge potential and through the discharge of F^- ion, the anode effect occurs when anode surface is covered by graphite fluoride to some extent. The second and third sweeps indicate that the anode surface partially covered by graphite fluoride remaining without decomposition is not wetted by the species including OH^- ion but wetted by the species including F^- ion, which means that the surface tension of the species including OH^- ion is higher than that of the species including F^- ion. If water exists as a molecule in molten $KF \cdot 2HF$, it should be easily adsorbed by carbon anode prior to molten $KF \cdot 2HF$ because of its low surface tension, *ca.* 60 mN/m at 100 °C. This is in conflict with the above experimental result. The wettability of anode surface under electrolysis would be dominated by other species different from the bulk species of molten $KF \cdot 2HF$ or water itself.

In order to estimate accurately the anode surface covering by graphite fluoride at the onset of anode effect, the surface tension of the dominant species present in the vicinity of anode surface must be evaluated, taking into account the other factors such as the roughness of anode surface, temperature, polarizing effect by electric current and composition of molten salt.

From the results obtained in this work, it is inferred that the partial covering of anode surface by graphite fluoride can easily cause the anode effect in the system having substantially poor wettability between carbon electrode and melt as in the case of aluminium electrolysis.

Financial support and experimental assistance from Sumitomo Aluminium Smelting Co. Ltd. are acknowledged. The authors thank Dr. Hidekazu Touhara and Dr. Akimasa Tasaka for their helpful discussions.

References

1) K. Grjotheim, C. Krohn, M. Malinovsky, K. Matiasovsky, and J. Thonstad, "Aluminium Electrolysis, The Chemistry of the Hall-Heroult Process," Aluminium-Verlag GmbH Düsseldorf (1977), pp. 237, 121, 125.
2) B. Mazza, P. Pedeferri, and G. Re, *Electrochim. Acta*, **23**, 87 (1978).
3) N. Watanabe and M. Ishii, *Denki Kagaku*, **29**, 364 (1961).
4) N. Watanabe, M. Inoue, and S. Yoshizawa, *Denki, Kagaku*, **31**, 693 (1963).
5) N. Watanabe and M. Nishimura, *Yoyuen*, **11**, 267 (1968).
6) N. Watanabe, M. Ishii, and S. Yoshizawa, *Denki Kagaku*, **29**, 492, 497 (1961).
7) N. Watanabe and T. Asaue, *Denki Kagaku*, **39**, 107, 123 (1971).
8) H. Imoto, S. Koyama, and N. Watanabe, *Denki Kagaku*, **46**, 680 (1978).
9) H. Imoto, K. Ueno, and N. Watanabe, *Bull. Chem. Soc. Jpn.*, **51**, 2822 (1978).
10) H. Imoto, T. Nakajima, and N. Watanabe, *Bull. Chem. Soc. Jpn.*, **48**, 1633 (1975).
11) N. Watanabe and O. Takagi, *Denki Kagaku*, **49**, 37 (1981).
12) Y. Kita, N. Watanabe, and Y. Fujii, *J. Am. Chem. Soc.*, **101**, 3832 (1979).
13) L. J. Hayes, *J. Fluorine Chem.*, **8**, 69 (1976).
14) A. H. Ellison and W. A. Zisman, *J. Phys. Chem.*, **58**, 503 (1954).
15) J. R. Dann, *J. Colloid Interface Sci.*, **32**, 302 (1970).
16) R. A. Erb, *J. Phys. Chem.*, **69**, 1306 (1965).
17) a) I. Morcos, *J. Colloid Interface Sci.*, **34**, 469 (1970); b) I. Morcos, *J. Chem. Phys.*, **57**, 1801 (1972).
18) A. W. Neumann, *J. Colloid Interface Sci.*, **34**, 1 (1970).
19) a) J. A. Riddick and W. B. Bunger, "Techniques of Chemistry, Organic solvents," 3rd ed, John Willey & Sons, Inc. (1970), Vol. II; b) "Handbook of Chemistry and Physics," 48th ed, Chemical Rubber Co. (1967—1968).
20) W. A. Zisman, *Ind. Eng. Chem.*, **55**, 19 (1963).
21) F. M. Fowkes, *J. Colloid Interface Sci.*, **28**, 493 (1968).
22) T. Young, *Trans. Roy. Soc.*, **95**, 65 (1805).
23) F. M. Fowkes, *Ind. Eng. Chem.*, **56**, 40 (1964).
24) E. F. Hare, E. G. Shafrin, and W. A. Zisman, *J. Phys. Chem.*, **58**, 236 (1954).
25) A. B. D. Cassie, *Discuss. Faraday Soc.*, **3**, 11 (1948).
26) R. W. Wenzel, *Ind. Eng. Chem.*, **28**, 988 (1936).
27) J. Kimura, T. Itoh, and M. Koishi, *Shikizai*, **50**, 432 (1977).

Photoelectrochemical Reduction of Carbon Dioxide at p-Type Gallium Phosphide Electrodes in the Presence of Crown Ether

Yasuhiko TANIGUCHI, Hiroshi YONEYAMA,* and Hideo TAMURA
Department of Applied Chemistry, Faculty of Engineering, Osaka University, 2-1 Yamada-oka, Suita, Osaka 565
(Received November 6, 1981)

Reduction of carbon dioxide at p-type GaP photocathodes was investigated in lithium carbonate electrolytes. The reduction occurs in competition with hydrogen evolution and its current efficiency is enhanced by dissolving crown ether such as 15-crown-5 in the electrolyte. It is proposed that a chemical reaction pathway is involved in which the reduction of carbon dioxide is initiated by cathodically deposited lithium with formation of the anion radical of carbon dioxide.

Electrochemical reduction of carbon dioxide in aqueous solutions has been investigated by using metal cathodes of high hydrogen-overvoltage such as mercury and lead. Since Teeter and Rysselberghe[1] observed a cathodic wave due to reduction of carbon dioxide in polarograms, many investigators[2-6] have assumed that the electrochemical reduction of carbon dioxide is initiated by accepting single electron to give the anion radical of carbon dioxide. This view was confirmed by reflectance spectroscopy[5] and by measurement of photoemmission current of mercury cathodes in the presence of carbon dioxide.[6] The reduction product at mercury cathodes is in general exclusively formic acid[7] and high current yields for the reduction can be achieved by appropriate choice of electrolysis conditions.[1,4] However, the problem in using metal cathodes is that a large applied voltage of *ca.* 3 V seems to be required, as deduced from reported electrode potentials of the cathode.

Recently, photoelectrochemical reduction of carbon dioxide has been reported by Halmann[8] who used a p-type GaP photocathode to cut down the electrical energy input to a large extent. The photo-assisted reduction of carbon dioxide can also occur, even in the absence of electrical energy input, if heterogeneous reaction systems using semiconductor photocatalysts are employed,[9,10] although the rate of reduction is quite low in this case.

The present study was carried out with a view of elucidating the mechanism of the photoelectrochemical reduction of carbon dioxide at p-type GaP cathodes in lithium carbonate electrolytes. As will be reported in a separate paper,[11] lithium deposits onto illuminated p-type GaP cathodes to give Li_xGaP. This phenomenon is noticeable especially in the presence of crown ethers such as 15-crown-5 in the electrolyte. In this paper, it will be shown that the deposited lithium contributes to the reduction of carbon dioxide by providing a chemical reaction pathway in the initial stage of reduction to give the anion radical of carbon dioxide. A chemical reaction mechanism similar to this was postulated for the electrochemical reduction at mercury under a high cathodic bias in the presence of sodium cation, in which carbon dioxide reacts with sodium amalgam,[12] but no confirmative data has been presented. Rather, according to detailed studies by Park *et al.*,[4] such a mechanism is believed to be unlikely in general cases at metal electrodes.

Experimental

Single crystal wafers of zinc-doped p-type GaP, donated by Sanyo Electric Co., were used as the electrode material. The acceptor concentration determined by the manufacturer was 4×10^{17} cm^{-3}, and the (111) face was chosen as the electrode surface. The preparation of the electrode was etched in aqua regia for 2 min, and then washed with deionized water for 15 min.

Current-potential curves were obtained by employing the potential sweep method, in which a potentiostat (Hokuto Denko Model FG-2) and an X-Y recorder (Yokogawa Electric Model 3077) were used. Photoelectrolysis was carried out under potentiostatic control with the charge being measured with an electronic coulometer (Hokuto Denko Model HF-201). Techniques of anodic stripping voltammetry were used for cathodically prepolarized electrodes at a sweep rate of 0.7 V s^{-1} by allowing the relay of the function generator to be excited whenever the cathodic polarization at a fixed potential was just enough to give a desired charge. An SCE served as the reference electrode.

Electrolysis experiments were usually carried out in a 3-compartment cell, and carbon dioxide was continuously bubbled into both the anode and cathode compartments after being saturated with water vapor. In order to collect reduction products, the effluent gas was passed through a trap which was cooled in a mixture of dry ice and acetone. In the case where the production of methane was to be investigated, a sealed 1-compartment cell was used under a carbon dioxide atmosphere.

Quantitative analysis of formic acid, formaldehyde and methanol was carried out for both the electrolyte and residues in the cooled trap. Methanol was analyzed by gas chromatography using a Porapak Q column and a FID detector. Formic acid and formaldehyde were determined by a colorimetric analysis using chromotropic acid.[14] For the analysis of formaldehyde in sample solutions containing either crown ether or CO_3^{2-} or both 4 cm^3 of HCl was added to 10 cm^3 of sample solution to make the solution acidic. In the case where the solution contained crown ether, it was then distilled to get rid of the crown ether.

Formic acid was indirectly determined by first reducing it to formaldehyde,[15] by which the formaldehyde in sample solutions was increased by the amount corresponding to that of formic acid, and then subtracting the original amount of formaldehyde from the total amount determined. For this purpose, 100 mg of Mg ribbons was dropped into 0.5 cm^3 of sample solution and then 0.05 cm^3 of HCl was added to the solution ten times at intervals of 1 min, to reduce formic acid to formaldehyde. Analysis of methane was carried out by gas chromatography using a Porapak Q column.

Current yields for the formation of the analyzed components were evaluated on the assumption that they are produced according to the following reduction schemes:

$$CO_2 + 2H^+ + 2e^- \longrightarrow HCOOH, \quad (1)$$

$$CO_2 + 4H^+ + 4e^- \longrightarrow HCHO + H_2O, \quad (2)$$

$$CO_2 + 6H^+ + 6e^- \longrightarrow CH_3OH + H_2O, \quad (3)$$

$$CO_2 + 8H^+ + 8e^- \longrightarrow CH_4 + 2H_2O. \quad (4)$$

Spectroscopic measurements for the chemical reaction of carbon dioxide with lithium were carried out by using a Shimadzu MPS-5000 spectrophotometer. The cell used had a glass capillary through which carbon dioxide was bubbled.

A 500 W super high-pressure mercury arc lamp (Ushio Electric Model UXL-500) served as the light source. Light was collimated, passed through a Toshiba UV-37 filter which cut off lights of wavelengths shorter than 370 nm, and then focused so as to illuminate just the electrode surface. The intensity of the light effective for the excitation of electrode, which covered from 370 to 550 nm, was 0.05 W, as measured with a laser power meter (Coherent Radiation Model 201).

All the chemicals used were of reagent grade and no further purification was made except for the propylene carbonate, which was subjected to distillation under reduced pressure twice before use.

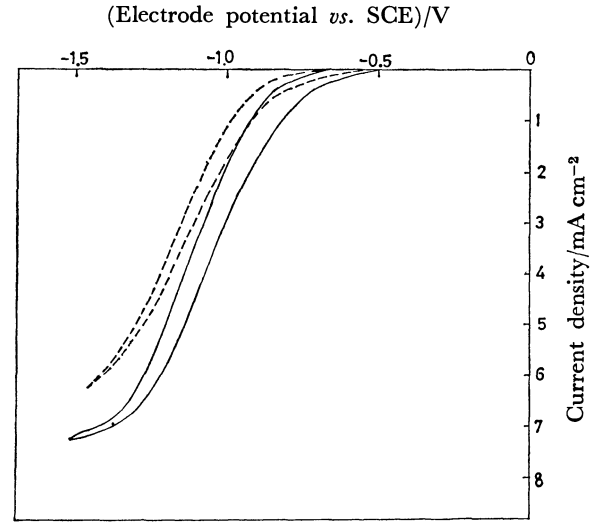

Fig. 1. Current-potential curves of an illuminated p-type GaP electrode under N_2 atmospheres in 0.1 mol dm^{-3} Li_2CO_3.
— —: In the presence of 0.1 mol dm^{-3} 15-crown-5,
——: in the absence of the crown ether. Sweep rate: 0.1 V s^{-1}.

Results and Discussion

Current Efficiency for the Formation of Reduction Products. Figure 1 shows current-potential curves for the illuminated p-type GaP electrode obtained under nitrogen atmospheres in 0.1 mol dm^{-3} 15-crown-5. The crown ether seems to suppress the saturated photocurrent a little, but not to have any other noticeable effects on current-potential curves. A replacement of nitrogen with carbon dioxide in the bubbling gas brought about no marked change in current-potential curves.

The current efficiency for the production of formic acid, formaldehyde, and methanol was obtained with the same electrolytes as those given in Fig. 1 at three different electrode potentials, where photocurrents were greatly different in magnitude from one another. The electrolysis time chosen was 22 h. The results are shown in Fig. 2, from which it is noticed that the efficiency is enhanced by the addition of crown ether to the lithium carbonate electrolyte for all the three kinds of products. No enhancement in the current efficiency is brought about by any decomposition reactions of crown ether, because when an electrolysis was carried out under the same conditions but that an electrolyte of 0.1 mol dm^{-3} LiOH containing 0.1 mol dm^{-3} 15-crown-5 was used under a nitrogen atmosphere, no production of formic acid, formaldehyde, or methanol occurred.

According to the results given in Fig. 2, the current efficiency for the production of every product de-

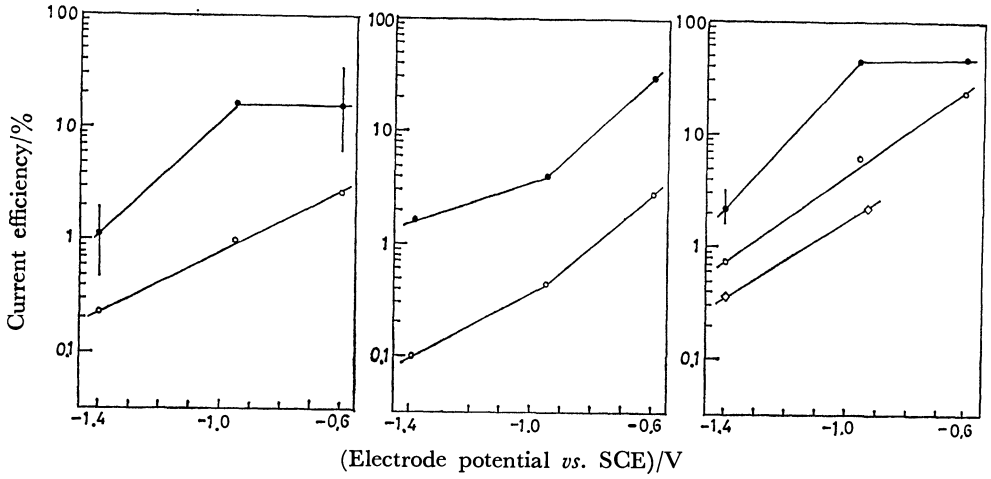

Fig. 2. The current efficiency for the production of formic acid (left), formaldehyde(middle), and methanol (right) as a function of electrode potentials.
—○—: 0.1 mol dm^{-3} Li_2CO_3 under bubbling CO_2, —●—: 0.1 mol dm^{-3} Li_2CO_3 containing 0.1 mol dm^{-3} 15-crown-5 under bubbling CO_2, —◇—: 0.1 mol dm^{-3} Li_2CO_3 containing 0.1 mol dm^{-3} 15-crown-5 under bubbling N_2.

creases with an increase in the cathodic polarization. A replacement of the bubbling gas from carbon dioxide to nitrogen caused a decrease in the current efficiency for the formation of methanol by approximately one order of magnitude, as shown in Fig. 2, which confirms the well estabilished view that major electroactive species is not CO_3^{2-} but CO_2.[16,17]

Besides the products given in Fig. 2, methane seems to be formed. Although no systematic investigation has been done, a current efficiency of *ca.* 5% was obtained for an electrolysis at −0.95 V *vs.* SCE in the presence of crown ether. It is characteristic of semiconductor photoelectrodes[8] and photocatalysts[9,10] that several reduction products are simultaneously formed.

Figure 3 shows effects of the concentration of 15-crown-5 on the production of formic acid, formaldehyde, and methanol. It is seen that the current efficiency for every product increases with an increase in the concentration of the crown ether. Since the crown ether affects the photodeposition of lithium in proportion to its concentration,[11] the results shown in this figure give an indication that the efficiency for the reduction of carbon dioxide is closely related to the feasibility of the lithium photodeposition.

Current Efficiency Obtained in the Presence of 18-Crown-6. Table 1 shows the current efficiency obtained in the presence of 18-crown-6, together with that obtained in the presence of 15-crown-5. It is seen that the current efficiency for the three kinds of products is higher in 15-crown-5 than in 18-crown-6. This difference seems to be caused by the feasibility of the lithium deposition which takes place in course of the cathodic polarization of electrode. As will be shown in detail in another paper,[11] the amount of deposited lithium increases with an increase in the cathodic charge and decreases with an increase in the molecular dimension of crown ethers. The kind of lithium salt electrolytes is not a problem for appearence of the phenomena. Typical examples of anodic stripping voltammetric waves of a cathodically prepolarized electrode in 0.2 mol dm^{-3} LiOH are given in Fig. 4 for the presence of 15-crown-5 and 18-crown-6. The anodic peak observed in the voltammogram is due to oxidation of the deposited lithium.

It is then speculated that there is a chemical reaction between carbon dioxide and deposited lithium to give the anion radical of carbon dioxide as the initial step of carbon dioxide reduction:

$$Li + CO_2 \longrightarrow Li^+ + CO_2^{\cdot-}. \quad (5)$$

In order to confirm this idea, the following experi-

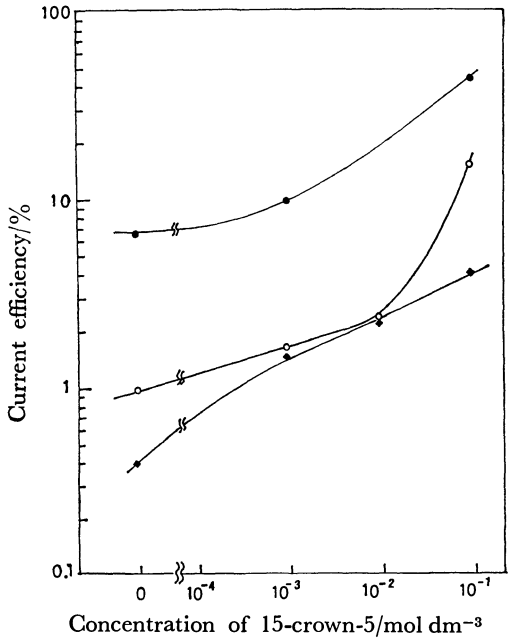

Fig. 3. Effects of the concentration of 15-crown-5 in 0.1 mol dm^{-3} Li_2CO_3 on the current efficiency for the production of formic acid (—○—), formaldehyde (—◆—), and methanol (—●—).

Table 1. Current efficiency for formation of formic acid, formaldehyde, and methanol[a]

Electrolyte	Current efficiency/%		
	Formic acid	Formaldehyde	Methanol
0.1 M[b] 15-Crown-5/ 0.1 M Li_2CO_3	15	4.0	44
0.1 M 18-Crown-6/ 0.1 M Li_2CO_3	4.8	u. d.[c]	6.5
0.1 M Li_2CO_3	1.0	0.5	6.5

a) The electrolysis was carried out at −0.95 V *vs.* SCE for 22 h. b) 1 M = 1 mol dm^{-3}. c) Undetermined.

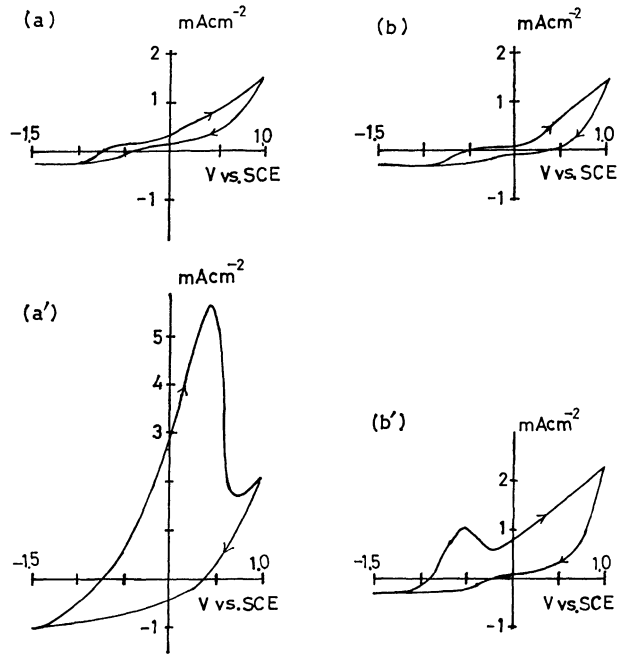

Fig. 4. Anodic stripping voltammograms of cathodically pre-polarized electrodes.
Electrolytes: (a) and (a') 0.2 mol dm^{-3} LiOH containing 0.1 mol dm^{-3} 15-crown-5. (b) and (b') 0.2 mol dm^{-3} LiOH. Cathodic pre-polarization charge: (a) and (b) zero (no prepolarization was made), (a') and (b') 5.5 C cm^{-2} at −1.5 V *vs.* SCE. Sweep rate: 0.7 V s^{-1}. The experiments were carried out under N_2 atmospheres.

ments were carried out.

Spectroscopic Studies on the Chemical Reaction of Carbon Dioxide with Lithium. If Reaction 5 occurs in aqueous electrolytes, the resulting anion radical will instantly react with water to give formate radical:[4,7]

$$CO_2^{\cdot-} + H_2O \longrightarrow HCO_2\cdot + OH^-. \quad (6)$$

The occurrence of Reaction 5 was then investigated in propylene carbonate solutions by taking absorption spectra characteristic of the anion radical.[5] Figure 5 shows the results obtained with a solution into which carbon dioxide was continuously bubbled. A CO_2-saturated propylene carbonate containing 0.1 mol dm^{-3} $LiClO_4$ shows no noticeable absorption in the UV region, but in the presence of lithium metal a strong absorption appeared at 265 nm which is due to $\sigma^* \leftarrow n^*$ transition of the anion radical,[5] confirming the occurrence of Reaction 5.

In order to obtain information on whether or not the deposited lithium can easily reduce formic acid to formaldehyde, similar experiments were carried out in propylene carbonate. Formic acid gave the absorption maxima at *ca.* 220 nm and formaldehyde at *ca.* 275 nm in a broad absorption band, as shown in Fig. 6. When a piece of lithium was dropped in propylene carbonate containing 64 mmol dm^{-3} formic acid and shaken vigorously under an air-tight condition for 10 min, the resulting solution gave an enhancement of the broad absorption due to formaldehyde. Simultaneously, the absorption due to formic acid was weakened. When the propylene carbonate solution initially contained a small amount of water (0.025 cm^3/10 cm^3 propylene carbonate), the absorption at 275 nm was much stronger.

Judging from these results, the reduction of formic acid to formaldehyde with lithium is likely to occur in the course of photoelectrochemical reduction of CO_2 at illuminated GaP cathodes:

$$HCOO^- + 2Li + 2H_2O \longrightarrow HCOOH + 2LiOH + OH^-. \quad (7)$$

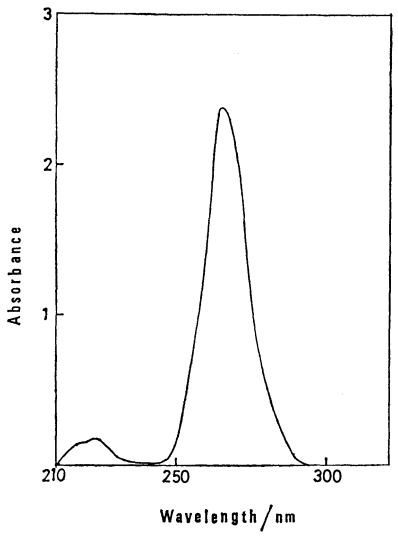

Fig. 5. An absorption spectrum showing the formation of $CO_2^{\cdot-}$ by chemical reaction of CO_2 with lithium in propylene carbonate.

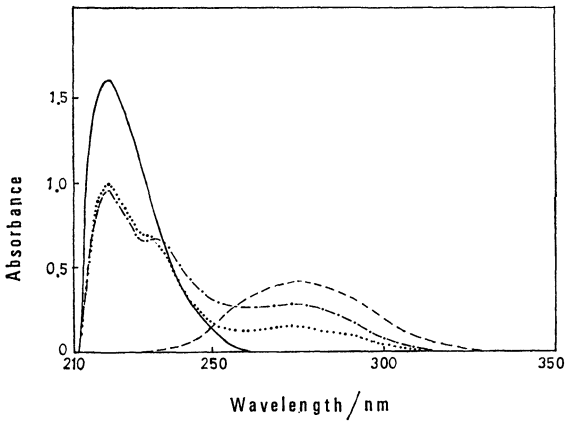

Fig. 6. Change in absorption spectra of formic acid in propylene carbonate by addition of a piece of lithium.
——: 64 mmol dm^{-3} HCOOH, ·····: after adding a piece of lithium to 64 mmol dm^{-3} HCOOH, – – –: after adding a piece of lithium and 0.025 μdm^3 of H_2O to 10 cm^3 of 64 mmol dm^{-3} HCOOH, — —: 30 mmol dm^{-3} HCHO.

In this section, we have discussed chemical reaction paths for the production of analytically determined species. However, it seems important to stress here that the reduction of carbon dioxide by purely electrochemical processes[7] is not excluded, at least in cases where no crown ether is dissolved in the electrolyte.

Energy Conversion Efficiency. The energy conversion efficiency for the photoproduction of carbon dioxide was estimated for the results given in Fig. 2 by using the following equations:

$$\eta_{ph} = \frac{[\Sigma n_i \Delta G_i^0 - VC]}{W_{ph} t} \times 100, \quad (8)$$

where n_i is the number of moles of produced species i, ΔG_i have been evaluated as

$$CO_2 + H_2O \longrightarrow HCOOH + 1/2O_2 \qquad \Delta G^0 = 270.1 \text{ kJ mol}^{-1}, \quad (9)$$

$$CO_2 + H_2O \longrightarrow HCHO + O_2 \qquad \Delta G^0 = 521.7 \text{ kJ mol}^{-1}, \quad (10)$$

$$CO_2 + 2H_2O \longrightarrow CH_3OH + 3/2O_2 \qquad \Delta G^0 = 702.5 \text{ kJ mol}^{-1}. \quad (11)$$

V is the applied voltage between the anode and cathode, C is the amount of charge consumed in the electrolysis for 22 h, W_{ph} is the optical energy input which was 0.05 W for incident photons effective for the excitation of electrode, and t the electrolysis time, 22 h. The experiments for Fig. 2 were carried out by controlling the photocathode potential but not the anode potential. In the present estimation of energy conversion efficiency, however, the anode potential needs to be evaluated, and this value was assumed here to be 0.52 V *vs.* SCE on the assumption of the oxygen overvoltage at the anode being 0.2 V, which will be achieved at the best anode (DSA) for the current density region chosen in the present study.

Table 2 gives calculated results for the total amount of formic acid, formaldehyde, and methanol produced.

TABLE 2. ENERGY CONVERSION EFFICIENCY FOR PHOTOELECTROCHEMICAL REDUCTION OF CARBON DIOXIDE IN A CELL USING A P-TYPE GALLIUM PHOSPHIDE CATHODE[a)]

Electrolyte	$E_{cathode}$ *vs.* SCE / V	q / C	Appl. V[b)] / V	VC / J	$\Sigma n_i \Delta G_i^0$ / J	W_{ph} / J	η_{ph} / %	η_t / %
0.1 M 15-Crown-5/ 0.1 M Li_2CO_3	−0.6	0.78	1.12	0.87	0.90	3960	9.1×10^{-4}	2.3×10^{-2}
	−0.95	1.7	1.47	2.5	1.40	3960	—	3.5×10^{-2}
	−1.40	37.4	1.92	71.6	3.20	3960	—	8.0×10^{-2}
0.1 M Li_2CO_3	−0.6	0.93	1.12	1.04	0.59	3960	—	1.4×10^{-2}
	−0.95	11.3	1.47	16.6	1.10	3960	—	2.8×10^{-2}
	−1.4	134	1.92	257.4	1.50	3960	—	3.5×10^{-2}

a) The efficiency was obtained for the production of formic acid, formaldehyde, and methanol. b) Applied voltage between the anode and cathode. An overpotential of 0.2 V was assumed for the oxygen evolution reaction at the anode.

The production of methane was neglected in this case, but this is not serious for the present purpose of estimating a rough order of conversion efficiency, because the methane production is believed to be minor. According to the obtained results which are given in Table 2, storage of optical energy was achieved only for one case where the electrolysis was carried out at −0.6 V *vs.* SCE in the presence of 15-crown-5. The estimated conversion efficiency in this case was as low as 9.1×10^{-4}%, which has no practical significance. In the other cases, the electrical energy input was found to exceed the sum of chemical energies produced.

Then, another measure for the total energy conversion efficiency was defined by Eq. 12, which gives the ratio of stored chemical energy to total energy input consumed for obtaining the chemicals in question:

$$\eta_t = \frac{\Sigma n_i \Delta G_i^0}{VC + W_{ph}t} \times 100. \quad (12)$$

Results obtained by applying this equation are also shown in Table 2, which indicates that the efficiency is still low even if estimated in this measure.

As indicated in Table 2, the principal cause responsible for such low conversion efficiencies is low utilization of optical energy in producing cathodic photocurrents. The low utilization is, of course, inevitable for the electrolysis at potentials where saturated photocurrents are not attained. Judging from the results shown in Fig. 1, the electrolysis at −0.6 V, for example, will give a relative utilization of optical energy of less than one twentieth that at −1.4 V. Furthermore, a gradual decrease in photocurrent, which occurs in the course of electrolysis, is very serious. If one estimates the average photocurrent in the electrolysis by dividing the amount of measured charges by the electrolysis time (22 h), the following values are obtained: 27.6 μA cm^{-2} at −0.6 V, 62.9 μA cm^{-2} at −0.95 V, and 1.38 mA cm^{-2} at −1.4 V *vs.* SCE. If these values are compared with those given in Fig. 1, it will be noticed that the degradation of electrode is serious. The major cause for bringing about such degradation is believed to be due to the incorporation of lithium which causes a noticeable decrease in quantum yield of photocurrent in the intrinsic absorption region.[11)] Similar degradation, though to a less extent, is in general caused to occur at p-type GaP photocathodes by impregnation of hydrogen.[13)] In order to achieve a high conversion efficiency of optical energy, such unstable behavior of photocathodes should be avoided.

Judging from the results given in Fig. 2, the sum of the current efficiencies for the production of formic acid, formaldehyde, and methanol is less than 100%, indicating that a hydrogen evolution took place competitively. Since hydrogen is a useful fuel which can store optical energy, η_t was again calculated for the whole cathodic reactions including the hydrogen evolution from the results shown in Table 2 on the assumption that 100% efficiency will be attained for the production of formic acid, formaldehyde, methanol, and hydrogen. The results obtained in the presence of the crown ether were 2.55×10^{-2}, 5.4×10^{-2}, and 1.1% for the cathodic potentials −0.6, −0.95, and −1.4 V, respectively, while in the absence of the crown ether η_t was 2.5×10^{-2}, 0.35, and 3.9% at −0.6, −0.95, and −1.4 V, respectively. The observed increase in η_t with an increase in the cathodic polarization in this case simply reflects the tendency that both the quantum yield of cathodic photocurrents and the current efficiency for the hydrogen evolution will increase with increasing cathodic polarization.

In the present study, unsatisfactory results were obtained in the point of energy conversion efficiency for the reduction of carbon dioxide. The results obtained, however, have revealed that carbon dioxide can be reduced at −0.6 V *vs.* SCE at p-type GaP photocathodes with current efficiency enhanced by addition of crown ether to lithium salt electrolyte. This implies that replacement of conventional metal cathodes by the present systems can save us more than 1 V of electrical energy input for the carbon dioxide reduction.

The present study was supported by Grant-in-Aid for Energy Research No. 5604011 from the Ministry of Education, Science and Culture.

References

1) T. E. Teeter and P. Van Rysselberghe, *J. Chem. Phys.*, **22**, 759 (1954).
2) J. Jordan and P. T. Smith, *Proc. Chem. Soc.*, **1960**, 246.
3) L. V. Hagnes and D. T. Sayer, *Anal. Chem.*, **39**, 332 (1967).

4) W. Park, T. N. Andersen, and H. Eyring, *Electrochim. Acta*, **14**, 1217 (1969).
5) A. W. B. Aylmer-Kel, A. Bewick, P. R. Cantrill, and A. M. Tuxford, *Faraday Discuss. Chem. Soc.*, **56**, 96 (1973).
6) D. J. Schiffrin, *Faraday Discuss. Chem. Soc.*, **56**, 75 (1973).
7) J-P. Randin, "Encyclopedia of Electrochemistry," ed by A. J. Bard, Dekker, New York (1976), Vol. VII, p. 172.
8) M. Halmann, *Nature*, **275**, 115 (1978).
9) T. Inoue, A. Fujishima, S. Konishi, and K. Honda, *Nature*, **272**, 637 (1979).
10) B. Aurian-Blajeni, M. Halmann, and J. Manassen, *Solar Energy*, **25**, 156 (1980).
11) Y. Taniguchi, H. Yoneyama, and H. Tamura, *J. Electroanal. Chem*, **134**, 335 (1982).
12) K. S. Udupa, G. S. Subramanian, and H. V. K. Udupa, *Electrochim. Acta*, **16**, 1593 (1971).
13) H. Uchida, H. Yoneyama, and H. Tamura, *J. Electrochem. Soc.*, **127**, 99 (1980).
14) "Colorimetric Analytical Methods," 9th ed, ed by L. C. Thomas and G. J. Chamberlin, The Tintometer Ltd., Salisbury (1980), p. 48.
15) W. M. Grant, *Anal. Chem.*, **20**, 267 (1948).
16) U. Kaiser and E. Heitz, *Ber. Bunsenges. Phys. Chem.*, **77**, 818 (1973).
17) J. Ryu, T. N. Andersen, and H. Eyring, *J. Phys. Chem.*, **76**, 3278 (1972).
18) W. O'Grady, C. Iwakura, J. Haung, and E. Yeager, "Electrocatalysis," ed by M. W. Breiter, The Electrochemical Society, Princeton, N. J. (1974), p. 286.

A Conductance Study of Alkali Metal Ion–Benzo-15-crown-5 Complexes in Propylene Carbonate

Yasuyuki TAKEDA

Department of Chemistry, Faculty of Science, Chiba University, Yayoi-chō, Chiba 260

(Received November 28, 1981)

The formation constants (K_{ML^+}) for 1:1 complexes of benzo-15-crown-5 (B15C5) with alkali metal ions at 25 °C, and the enthalpy (ΔH) and entropy changes (ΔS) of the K^+–B15C5 complex in propylene carbonate (PC) have been determined conductometrically. The K_{ML^+} series of B15C5 for the alkali metal ions are given in the order $Na^+ > Li^+ > K^+ > Rb^+ > Cs^+$. The selectivity tendency of B15C5 for the alkali metal ions is consistent with the size-fit concept, however, B15C5 shows poor selectivity. Both the ΔH and ΔS values for the complexation reaction of B15C5 with K^+ are negative. In the cases of Na^+, K^+, Rb^+, and Cs^+, the size of the moving entity in PC is larger for the B15C5 complex than for the corresponding alkali metal ion, while, in the case of Li^+, that is completely the reverse.

Benzo-15-crown-5 (B15C5) forms stoichiometric complexes with alkali metal ions. Most of them are 1:1 complexes, however, B15C5 also forms 2:1 complexes with K^+, Rb^+, and Cs^+ whose sizes are larger than the cavity size of the ligand.[1,2] In a water–methanol mixed solvent system,[1] B15C5 shows poor selectivity for alkali metal ions and the 1:1 complexes of B15C5 with alkali metal ions are not so much stable. In the present paper, the enthalpy and entropy changes of the K^+–B15C5 complex as well as the formation constants of the 1:1 complexes of B15C5 with alkali metal ions at 25 °C have been determined conductometrically in propylene carbonate (PC). The results have been compared with those of the corresponding 15-crown-5 (15C5) complexes with alkali metal ions in PC.

Experimental

Materials. Benzo-15-crown-5 (Merck Japan Ltd.) was dissolved in heptane, and filtered while hot. Then it was recrystallized from heptane three times and, prior to use, dried at 40 °C in a vacuum oven. Lithium, sodium, and potassium perchlorates were obtained commercially. The method of preparing rubidium and caesium perchlorates, as well as that of purifying alkali metal perchlorates were previously described.[3] Propylene carbonate was distilled twice under nitrogen atmosphere at 2.4 kPa. The water content of the finally purified PC determined by Karl Fischer titration was less than 0.02%. The conductivity of the final product was less than $4\times10^{-8}\ \Omega^{-1}\ cm^{-1}$.

Apparatus and Procedure. The apparatus and the experimental procedures were the same as those described in the previous paper.[3] For the K^+ system, the conductance measurements were performed at 5, 10, 15, 20, 25, 30, and 35±0.02 °C.

Results

The molar conductivity, Λ, *vs.* $[L]_t/[M]_t$ plots are given in Fig. 1, where $[L]_t$ and $[M]_t$ are the total concentrations of B15C5 and an alkali metal ion respectively. It is supposed that the association between a cation and perchlorate ion in PC is negligible under these highly dilute experimental conditions and that, in the present study, B15C5 forms 1:1 complexes with alkali metal ions in PC. Since the B15C5 concentration was kept below 3.0×10^{-3} M (1 M = 1 mol dm^{-3}) during these experiments, corrections for viscosity changes were neglected. The procedure for

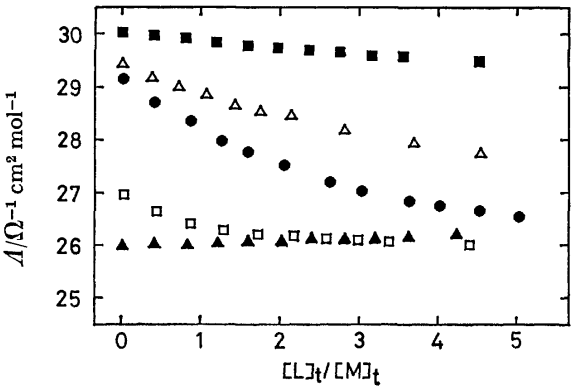

Fig. 1. Λ *vs.* $[L]_t/[M]_t$ curves for B15C5–alkali metal perchlorate systems in PC at 25 °C.
▲: Li^+, □: Na^+, ●: K^+, △: Rb^+, ■: Cs^+, $[M]_t = 5\times10^{-4}$ M.

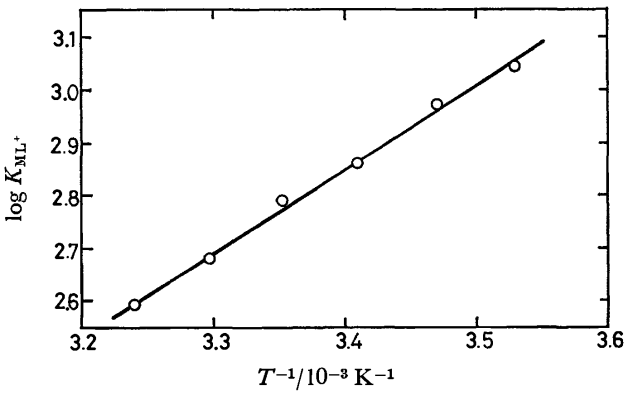

Fig. 2. log K_{ML^+} *vs.* T^{-1} plots for the K^+–B15C5 system in PC.

obtaining complex-formation constant, K_{ML^+}, of an alkali metal ion–B15C5 complex was just the same as that described in the previous paper,[3] where M^+ and L denote an alkali metal ion and B15C5, respectively. The log K_{ML^+} *vs.* T^{-1} plots for the K^+–B15C5 system in PC are given in Fig. 2. The log K_{ML^+} *vs.* T^{-1} plots show a linear relationship. The log K_{ML^+} values, and the values of enthalpy and entropy changes are listed in Tables 1 and 2, together with the literature values, respectively.

TABLE 1. $\log (K_{ML^+}/mol^{-1}\,dm^3)$ VALUES IN PC AT 25 °C

	15C5[4]	B15C5
Li^+	4.2_6	3.7_7
Na^+	3.7	4.3_5
K^+	3.4_1	2.7_8
Rb^+	3.0_4	2.3_8
Cs^+	2.6_9	2.0_3

TABLE 2. ΔH AND ΔS VALUES FOR THE COMPLEXATION OF THE POTASSIUM ION WITH CROWN ETHERS

Crown ether	Solvent	$\log K_{ML^+}$ (at 25 °C)	$-\Delta H$ / kJ mol^{-1}	$-\Delta S$ / J K^{-1} mol^{-1}
B15C5	PC	2.7_8	$26._4$	$35._4$
	H_2O[1]	0.38	9.75	26
DB24C8	PC[3]	3.7_3	$34._5$	$44._4$

Discussion

As can be seen from Table 1, the $\log K_{ML^+}$ series of B15C5 for alkali metal ions in PC are given in the order $Na^+ > Li^+ > K^+ > Rb^+ > Cs^+$. The selectivity tendency of B15C5 (cavity radius: 0.85—1.1 Å[5]) for the alkali metal ions is consistent with the size-fit concept, however, B15C5 shows poor selectivity. The B15C5 complex with the same alkali metal ion in PC is more unstable than the 15C5 complex except for the case of Na^+. This may be attributable to the fact that B15C5 has two aromatic ether oxygen atoms whose basicity is lower than that of the aliphatic ether oxygen atom. The value of enthalpy change (ΔH) of the 15C5 complex with Na^+ may be smaller than that of the B15C5 complex because of the two aromatic ether oxygen atoms. Thus, the reason why the 15C5 complex with Na^+ is more unstable than the B15C5 complex is presumably due to that the 15C5 complex may be much more entropy destabilized than the B15C5 complex.

Table 2 shows that the complexation reaction of B15C5 with K^+ in PC is exothermic and the ΔS value is negative. The smaller $-\Delta H$ and $-\Delta S$ (entropy change) values of B15C5 compared to dibenzo-24-crown-8 (DB24C8) may reflect the smaller number of donor oxygen atom and much more rigid structure of B15C5, respectively (Table 2). Very much greater $-\Delta H$ and slightly greater $-\Delta S$ values of B15C5 in PC result in the very much larger $\log K_{ML^+}$ value compared to water. The hydrogen bond between an ether oxygen atom of uncomplexed B15C5 and a water molecule may be the reason why the $-\Delta H$ value of PC is very much larger than that of water. In the previous paper,[6] it has been reported that, although the solvation power of water for the same alkali metal ion (Na^+, K^+, Rb^+, and Cs^+) is the third largest of all the solvents (acetonitrile, PC, water, methanol, DMF, and DMSO), the $\log K_{ML^+}$ value of water is the smallest for every alkali metal ion–crown ether (18-crown-6 and dibenzo-18-crown-6) system. This may also largely depend on the hydrogen bond between an ether oxygen atom of the uncomplexed crown ether and a water molecule. Since water is a three-dimensional structural solvent and PC is not, the $-\Delta S$ value of B15C5 in PC is expected to be smaller than that in water. On the contrary, Table 2 shows that $-\Delta S$ value of B15C5 in PC is larger than that in water. This fact seems to be related to that K^+ plays a net structure breaking role in water.

The Λ *vs.* $[L]_t/[M]_t$ plots in Fig. 1 show a decrease of Λ with an increase in the B15C5 concentration for Na^+, K^+, Rb^+, and Cs^+ systems, and on the contrary for the Li^+ system. This indicates that, in the cases of Na^+, K^+, Rb^+, and Cs^+, the size of the moving entity in PC is larger for the B15C5 complex than for the corresponding alkali metal ion, while, in the case of Li^+, that is completely the reverse. The Λ *vs.* $[L]_t/[M]_t$ plots for the 15C5 system in PC show the same tendency for the B15C5 system except for the case of Na^+.[4] The B15C5 complex with Na^+ is bulkier than the Na^+ ion in PC, and on the contrary for the case of 15C5.[4] Both B15C5 and 15C5 complexes with Na^+ may be scarcely solvated in a PC solution. It thus appears that the size of the moving entity of a Na^+ ion in PC is approximately equal to the size between that of the B15C5 complex with Na^+ and that of the 15C5 complex.

References

1) R. M. Izatt, R. E. Terry, D. P. Nelson, Y. Chan, D. J. Eatough, J. S. Bradshaw, L. D. Hansen, and J. J. Christensen, *J. Am. Chem. Soc.*, **98**, 7626 (1976).
2) Y. Takeda, Y. Wada, and S. Fujiwara, *Bull. Chem. Soc. Jpn.*, **54**, 3727 (1981).
3) Y. Takeda and H. Yano, *Bull. Chem. Soc. Jpn.*, **53**, 1720 (1980).
4) Y. Takeda, H. Yano, M. Ishibashi, and H. Isozumi, *Bull. Chem. Soc. Jpn.*, **53**, 72 (1980).
5) C. J. Pedersen and H. K. Frensdorff, *Angew. Chem., Int. Ed. Engl.*, **11**, 16 (1972).
6) Y. Takeda, *Bull. Chem. Soc. Jpn.*, **54**, 3133 (1981).

Distinct Activation Energies for Temporal and Spatial Oscillations in the Belousov-Zhabotinskii Reaction

Kenichi YOSHIKAWA
College of General Education, University of Tokushima, Minami-josanjima, Tokushima 770
(Received December 7, 1981)

Temperature dependence of the frequencies in temporal oscillations and of the moving-wave velocities of concentric waves in spatial oscillation in the Belousov-Zhabotinskii reaction was studied in detail using the same starting concentrations of the reactants. When cerium ions were used as catalyst, the activation energies were found to be 60—65 kJ/mol for the temporal oscillation and 46±4 kJ/mol for the spatial oscillation. The difference in the activation energies was well explained by the theoretical prediction based on kinetic-diffusion coupling. When $[Fe(phen)_3^{2+}]$ or $[Fe(bpy)_3^{2+}]$ was used as catalyst, the apparent activation energy in the temporal oscillation depends markedly on the concentration of the catalyst used.

During the last decade, sustained oscillations and traveling chemical waves in the Belousov-Zhabotinskii reaction[1,2] have received much attention as a typical cooperative phenomenon in thermal nonequilibrium. When this reaction is allowed to proceed in a well-stirred vessel, sustained oscillation of the concentrations of several chemical species occurs (referred to as the temporal oscillation). On the other hand, when the reaction is run in an unstirred shallow layer (*e.g.* in a petri dish), spatio-temporal structures of the concentrations of chemical species appear.[3] The dynamic structure that has been most commonly studied is the concentration waves with concentric symmetry (referred to as the spatial oscillation).

For the temporal oscillation, the period of the oscillation has been studied as a function of temperature by some workers,[4-8] who demonstrated an Arrhenius dependence of the frequency (inverse period) on temperature. It has also been reported[9] that the period of the oscillation varied with the catalyst used, but the reason for this has not been clarified yet. For the spatial oscillation, on the other hand, only a few experimental studies have been reported on the temperature dependence of the moving-wave velocities of the concentric chemical waves.[10-12]

The present work deals with studies of the temperature dependences of the oscillation periods in the temporal oscillation and of the velocities of the moving-waves in the spatial oscillation, using the same starting concentrations of the reagents. We demonstrated a marked difference in activation energies between the temporal and spatial oscillations. This difference is explained on the basis of the proposed chemical mechanisms.

Experimental

Materials. Reagent grade chemicals were used throughout. Iron phenanthroline (ferroin), $[Fe(phen)_3^{2+}]$, was prepared from 1,10-phenanthroline and iron(II) sulfate, and iron bipyridyl, $[Fe(bpy)_3^{2+}]$, was prepared from 2,2′-bipyridyl and iron(II) sulfate.

Measurement of Temporal Oscillations. The redox potential was measured by monitoring the e.m.f. generated by a platinum electrode and a calomel reference electrode with a Hitachi-Horiba F-7 pH/mV meter. A double junction reference electrode (Hitachi-Horiba 253A-05T) was used with the bridging solution of saturated potassium nitrate. The reacting mixture was prepared by successive additions of stock solutions of sodium bromate, malonic acid and metal-catalyst ($[Fe(phen)_3^{2+}]$ or $[Fe(bpy)_3^{2+}]$ or Ce^{3+} or Ce^{4+} or Mn^{2+}) to sulfuric acid in a 50-dm^3 beaker thermostated to a desired temperature between 10 and 45 °C. Throughout the measurement of redox potential, the reacting mixture was constantly stirred under appropriate conditions. The first oxidation peak observed was taken as the onset of the first period of oscillation. As the frequency changes slightly with time in accordance with the changes in the concentrations of the reactants, the average value for the ten periods between the 2nd and the 11th oscillations is taken as the frequency.

Measurement of Spatial Oscillations. The reaction was initiated by adding a metal-catalyst, cerium ion, to a thermostated beaker containing sulfuric acid, sodium bromate, and malonic acid. After being stirred for 5 min, the reaction mixture was poured into a thermostated petri dish with a diameter of 87 mm. The concentrations of the reactants were adjusted to the same concentrations as used for the temporal oscillation. Trigger (concentric) waves were generated by adding a small piece of poly(vinyl alcohol) (Nakarai Chemical, Av. Mol. Wt. 2200) as a pacemaker.[13] Other deformed moving-waves were considered as interferences and are therefore not discussed in this article. The oscillating reaction taking place in the petri dish was photographed at appropriate intervals, and the velocities were determined by measuring the distance from the center (the position of the pacemaker) of the concentric traveling band to the outer propagating bands. Photographs were taken using a Polaroid 600 SE camera with type 667 film under UV light.

Results

Activation Energies in Temporal Oscillations. Figure 1 exemplified the temporal oscillation of redox potential obtained when Ce^{3+} was used as catalyst. It is apparent that the period of oscillation was kept nearly constant. Therefore, the average value of the periods between the 2nd and the 11th oscillation was regarded as the "period" of a given oscillating system. The periods were measured at temperatures ranging from 10 to 45 °C. An Arrhenius plot for the oscillating frequency, F_{osc} (reciprocal of the period), is shown in Fig. 2. From the slope of the figure, 64.9± 2 kJ/mol is obtained as the activation energy, E_a, for the temporal oscillation catalyzed by cerium ion

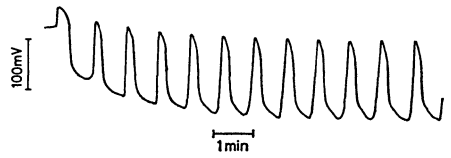

Fig. 1. Temporal oscillation of redox potenital. $[H_2SO_4]_0=0.4$ M, $[NaBrO_3]_0=0.35$ M, $[KBr]_0=0.06$ M, [Malonic Acid]$_0=0.12$ M, $[Ce(NH_4)_2(NO_3)_5]_0=0.002$ M. Temperature=25.1 °C. Volume, 20 dm^3.

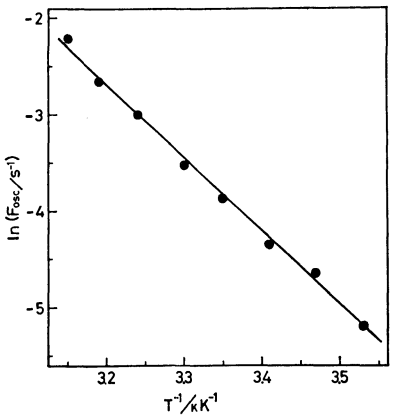

Fig. 2. Arrhenius dependence on temperature of oscillating frequency, F_{osc}, with Ce^{3+} as catalyst. The concentrations are the same as described in the legend to Fig. 1.

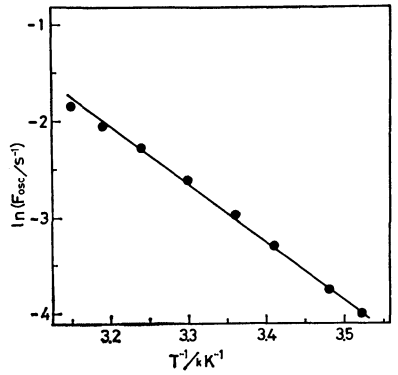

Fig. 3. Arrhenius dependence on temperature of oscillating frequency, F_{osc} with [Fe(phen)$_3^{2+}$] as catalyst (0.002 M). Other concentrations of the reagents are the same as described in the legend to Fig. 1.

($[Ce(NH_4)_2(NO_3)_5]=0.002$ M†).

We then carried out similar experiments with several different catalysts, such as [Fe(phen)$_3^{2+}$], Ce^{4+}, and Mn^{2+} at the concentration of 2 mM. An Arrhenius plot for the oscillation catalyzed by [Fe(phen)$_3^{2+}$] is shown in Fig. 3. Apparent activation energies for the temporal oscillation obtained with the different catalysts are listed in Table 1. The E_a values with Ce^{3+}, Ce^{4+}, and Mn^{2+} are essentially the same at the same concentration, 2 mM, of the catalyst, but greatly differ from the E_a value with [Fe(phen)$_3^{2+}$]. In order to study further the effects of the catalysts on the oscillation, E_a values were determined with different concentrations of the catalysts, [Fe(phen)$_3^{2+}$]

† 1 M=1 mol dm^{-3}.

Table 1. Apparent activation energies in temporal oscillations

Catalyst	Concentration / mM	Frequency[a] at 25 °C / Hz	E_a[b] / kJ mol^{-1}
[Fe(phen)$_3^{2+}$]	2	0.051	46.6
	1	0.055	44.9
	0.3	0.056	56.6[c]
	0.2	0.060	57.4[c]
	0.1	0.068	72.4[c]
[Fe(bpy)$_3^{2+}$]	0.3	0.071	71.6[c]
Ce^{3+}	2	0.021	62.4
Ce^{4+}	5	0.021	64.9
	2	0.021	64.9
	1	0.022	59.9
	0.3	0.023	59.9
	0.2	0.025	60.7
	0.1	0.025	60.7
Mn^{2+}	2	0.025	64.1

a) Estimated experimental errors are ±5%. b) Estimated experimental errors are ±2—3 kJ/mol, except for the E_a values marked c). c) Estimated experimental erros are ±5—7 kJ/mol.

and Ce^{4+} (Table 1). The E_a values with Ce^{4+} remain nearly constant at different concentrations, while those with [Fe(phen)$_3^{2+}$] change remarkably, from 46.6 to 72.4 kJ/mol, with decreasing concentration of the [Fe(phen)$_3^{2+}$]. A possible explanation for the dependence of the E_a value on the catalyst concentration is that [Fe(phen)$_3^{2+}$] does decompose gradually in the reaction medium and that this, in turn, affects the kinetics of the oscillating reaction. Thus, the rate of the decomposition of [Fe(phen)$_3^{2+}$] in 0.4 M sulfuric acid was measured by monitoring spectrometrically the decrease of the absorption maximum at 522 nm (data not shown). For comparison, the rate of the decomposition of [Fe(bpy)$_3^{2+}$] was also measured under similar conditions. The decreasing rate of the absorption showed that the kinetic constant, k, was 0.007 min^{-1} for [Fe(phen)$_3^{2+}$] and 0.097 min^{-1} for [Fe(bpy)$_3^{2+}$] at 26 °C and that the half-life periods of these iron-complexes at 26 °C are 90 and 7.1 min, respectively. The rate of the decomposition was enhanced at elevated temperatures. It seems that the decomposition of these iron-complexes cannot be ignored during the chemical oscillations, suggesting that these iron-complexes are not suitable as a catalyst for the kinetic study of the Belousov-Zhabotinskii reaction.

Activation Energies in Spatial Oscillations. Concentric trigger waves (spatial oscillation) were generated using cerium ion as catalyst. To compare the activation energy for temporal oscillation with that for spatial oscillation, the oscillating reactions were run with the same starting concentrations of the reagents. Figure 4 shows the time dependence of the distance of each wave from the center of the cylindrical bands. The slopes in Fig. 4 represent the moving-wave velocities, v. Similar experiments were carried out at several temperatures. The results obtained

are shown as an Arrhenius plot in Fig. 5. From this figure, the apparent activation energy of 46±4 kJ/mol is obtained for the propagation of the cylindrical waves with Ce^{4+} as catalyst.

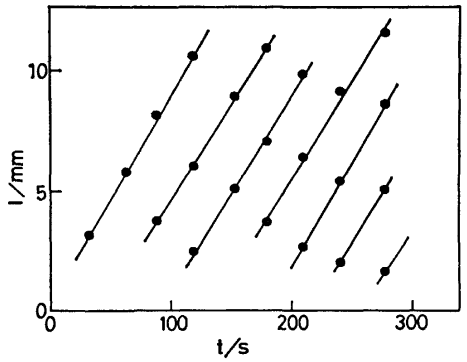

Fig. 4. Time dependence of the band position (distance from the center) in a spatial oscillating reaction with the cylindrical pattern.
The concentrations are the same as described in the legend to Fig. 1. Ce^{4+}-catalyst at 25 °C. Volume, 7 dm^3.

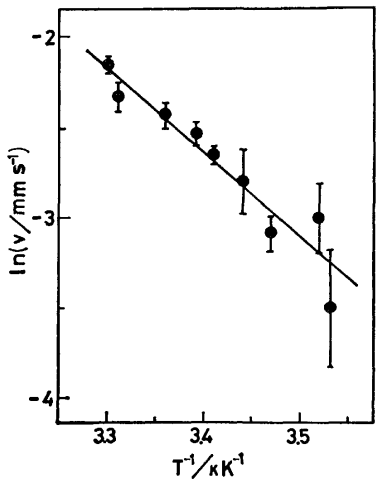

Fig. 5. Arrhenius dependence of moving-wave velocity, v.
Ce^{4+}-catalyst. The concentrations are the same as described in the legend to Fig. 1. The limits shown are estimated errors of the mean. Volume, 7 dm^3.

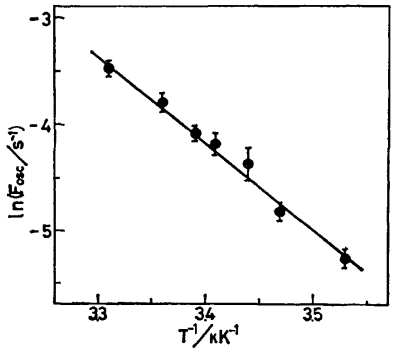

Fig. 6. Arrhenius dependence of oscillating frequency, F_{osc}, at a place 1 cm away from the center in spatial oscillation.
The data were taken from the same experiments as shown in Fig. 5. The limits shown are estimated errors of the mean.

From the photographs of the moving-wave, one can also obtain the frequencies of the chemical oscillation at a fixed position. The frequencies at the position 1 cm distant from the center were obtained and are depicted as an Arrhenius plot in Fig. 6. The activation energy was thus determined to be 69±4 kJ/mol, which is close to that for the temporal oscillation (64.9±2 kJ/mol) obtained at the same concentration of cerium ions (2 mM). The small difference in the activation energies of the frequencies between the temporal and spatial oscillations may have resulted from the different experimental conditions used, *i.e.*, continuous mixing for the former reaction and standing still for the latter.

Discussion

No attempt has been made to compare the kinetics of the temporal and spatial oscillations with the same starting concentrations of the reagents. We demonstrated that the activation energies for the two types of oscillating reactions are apparently different. We now wish to discuss these results in relation to the mechanism of the chemical oscillations.

Field and Noyes proposed[14,15] a mechanism of the spatial oscillation of the concentric wave, coupled with diffusion of the chemical species. Based on the assumption that the velocity of the band propagation is controlled by the concentration of bromide ion and bromous acid in the band front and that the traveling band of bromide ion does not affect the velocity of the band propagation, the following differential equations are obtained:[15,16]

$$\left(\frac{\partial C_A}{\partial t}\right)_x = D_A\left(\frac{\partial^2 C_A}{\partial x^2}\right)_t + k_3[H^+][BrO_3^-]C_B - k_2[H^+]C_AC_B + k_5[H^+][BrO_3^-]C_A - 2k_4C_A^2, \quad (1)$$

$$\left(\frac{\partial C_B}{\partial t}\right)_x = D_B\left(\frac{\partial^2 C_B}{\partial x^2}\right)_t - k_3[H^+][BrO_3^-]C_B - k_2[H^+]C_AC_B. \quad (2)$$

Here $C_A=[HBrO_2]$ and $C_B=[Br^-]$. The definitions of the other symbols in these equations are identical to those in Refs. 15 and 16. Experimentally, the propagating bands move with a constant velocity, as is shown in Fig. 4; then

$$v = \left(\frac{\partial x}{\partial t}\right)_{C_A, C_B}, \quad (3)$$

$$\left(\frac{\partial C_A}{\partial t}\right)_x = v\left(\frac{\partial C_A}{\partial x}\right)_t. \quad (4)$$

The autocatalytic reaction (5) with the rate constant, k_5, is rate-determining in the Belousov-Zhabotinskii reaction.[15,16]

$$BrO_3^- + HBrO_2 + H^+ \xrightarrow{k_5} 2BrO_2\cdot + H_2O. \quad (5)$$

Under the approximation that this autocatalytic term is much more important than others in the face of an advancing band, Eq. 1 can be simplified as follows:

$$D_A\frac{d^2C_A}{dx^2} - v\frac{dC_A}{dx} + k_5[H^+][HBrO_3^-]C_A = 0. \quad (6)$$

Under the condition of maximum sharpness,[15,16] an approximate solution of Eq. 6 is given as follows:

$$v = (4D_A k_5[H^+][BrO_3^-])^{1/2}. \quad (7)$$

As for the temporal oscillation, the diffusion term in Eqs. 1 and 2 can be neglected, and the autocatalytic reaction (5) is also most important for the rate of the oscillation.[17] Tyson *et al.*[18] have suggested that the period of the oscillation is determined by Reaction 5 and that the activation energy of the oscillation is nearly equal to that of Reaction 5. Quite recently, from the result of a mathematical analysis for the Belousov-Zhabotinskii reaction using "Oregonator" model, Edelson *et al.*[19] have concluded that the principal factor determining the period of the temporal oscillation is k_5 and that this reaction is almost an order of magnitude more significant than the others. Therefore, the frequency, F_{osc}, is approximately given by (8), using the rate equation of Reaction 5. In

$$F_{osc} \propto k_5[H^+][BrO_3^-]. \quad (8)$$

Eqs. 7 and 8, D_A and k_5 are temperature dependent and may be expressed as follows:

$$D_A = D_0 \exp(-E_D/RT), \quad (9)$$

$$k_5 = k_0 \exp(-E_k/RT). \quad (10)$$

E_D and E_K are the activation energies for the diffusion of A ($=HBrO_3$) and Reaction 5, respectively. The activation energy of self-diffusion of water has been experimentally reported to be 4.8 kcal/mol (20 kJ/mol).[20] Thus, it is probable that E_D is about 20 kJ/mol. In our experiment, E_K (the activation energy of F_{osc}) is about 69 kJ/mol in the spatial oscillation (Fig. 6) and about 65 kJ/mol in the temporal oscillation (Table 1) when $[Ce^{4+}]_0=2$ mM. The small difference between the activation energies may be due to the stirring effect[9] and/or to the oxygen effect.[21] From Eqs. 7, 9, and 10, the relationship between the activation energies becomes

$$E_v = \frac{1}{2}(E_D + E_k). \quad (11)$$

Here E_v is the activation energy of v in the spatial oscillation. E_v is thus calculated to be $(20+69)\div 2 = 44.5$ (kJ/mol) or $(20+65)\div 2 = 42.5$ (kJ/mol). These values agree well with the value of E_v, 46 kJ/mol, experimentally obtained in this study (Fig. 5).

It may be worthwhile to compare the activation energies obtained in this study with the previously reported values. From the measurement of the frequency of the temporal oscillation at three different temperatures (288, 298, 308 K), Körös[4] has derived an activation energy of 67.5 kJ/mol, which was the same for different catalysts: Ce^{3+}, Mn^{2+}, and $[Ru(bpy)_3^{2+}]$. Blandamer *et al.*[6] reported an activation energy of 70 kJ/mol for the frequency in the temporal oscillation, using the system of malonic acid–BrO_3^-–H_2SO_4–Ce^{3+}. Rastogi *et al.*[5] have also reported the dependence of the frequency on temperature. Though they did not report the activation energy, we can obtain an activation energy of 54 kJ/mol from the figure of the Arrhenius relation of the oscillation period given in their paper.[5] The large difference of the activation energies may be mainly due to the difference of the concentrations of the reactants and the catalyst. This may be not surprising, as the Belousov-Zhabotinskii reaction is a quite complicated system consisting of many elemental reactions. It is also to be noted that the difference of the experimental conditions causes a large difference of the frequencies of the oscillation, for example, the frequency at 25 °C is 0.05 s^{-1} in the experiment of Blandamer *et al.*[6] and 0.021—0.025 s^{-1} in our experiment. It is thus apparent that starting concentrations of the reagents should be the same if one wishes to compare the kinetics between the temporal and spatial oscillating reactions, as has been done in this study.

Thoenes[10] has reported an activation energy of 100 kJ/mol for the oscillation frequency in the spatial oscillation for the system of malonic acid–BrO_3^-–H_2SO_4–$[Fe(phen)_3^{2+}]$. As he has not shown the actual values of the frequencies at different temperatures in his paper, we can not discuss about the error or accuracy of his experiment. However, it should be pointed out again that ferroin ($[Fe(phen)_3^{2+}]$) is not suitable as the catalyst for the study of the reaction kinetics in the Belousov-Zhabotinskii reaction.

The author thanks Prof. Takeshi Waki for his encouragement and Miss Chikako Kawase for her assistance. The author is indebted to Dr. Akira Ohsaka and Mr. Toshimi Hayakawa for their helpful discussions.

References

1) B. P. Belousov, *Ref. Radiats. Med.*, **1958**, 145 (1959).
2) A. M. Zhabotinskii, *Dokl. Akad. Nauk SSSR*, **157**, 392 (1964).
3) A. N. Zaikin and A. M. Zhabotinskii, *Nature (London)*, **225**, 535 (1970).
4) E. Körös, *Nature (London)*, **251**, 703 (1974).
5) R. P. Rastogi, K. D. S. Yadava, and K. Prasad, *Indian J. Chem.*, **12**, 974 (1974).
6) M. J. Blandamer and S. H. Morris, *J. Chem. Soc., Faraday Trans. 1*, **71**, 2319 (1975).
7) V. J. Farage, P. Strrot, and D. Janjic, *Helv. Chim. Acta*, **60**, 231 (1977).
8) C. S. Swamy and K. S. G. Doss, *J. Chem. Educ.*, **56**, 321 (1979).
9) M-L. Smoes, *J. Chem. Phys.*, **71**, 4669 (1979).
10) D. Thoenes, *Nature Phys. Sci.*, **243**, 18 (1973).
11) M-L. Smoes, "Dynamics of Synergetic Systems," ed by H. Haken, Springer-Verlag, Berlin (1980), p. 80.
12) K. Yoshikawa, A. Takashima, T. Waki, and T. Hayakawa, *Kagaku Kyoiku*, **28**, 386 (1980).
13) T. Hayakawa, K. Yoshikawa, and T. Waki, *Kagaku Kyoiku*, **27**, 355 (1979).
14) R. J. Field and R. M. Noyes, *Nature (London)*, **237**, 390 (1972).
15) R. J. Field and R. M. Noyes, *J. Am. Chem. Soc.*, **96**, 2001 (1974).
16) J. Jorne, *J. Am. Chem. Soc.*, **102**, 6196 (1980).
17) R. J. Field, E. Körös, and R. M. Noyes, *J. Am. Chem. Soc.*, **94**, 8649 (1972).
18) J. J. Tyson and P. C. Fife, *J. Chem. Phys.*, **73**, 2224 (1980).
19) D. Edelson and V. M. Thomas, *J. Phys. Chem.*, **85**, 1555 (1981).
20) J. H. Wang, *J. Phys. Chem.*, **69**, 4412 (1965).
21) K. Bar-Eli and S. Haddad, *J. Phys. Chem.*, **83**, 2952 (1979).

Optical Studies on the Lowest Triplet State of Chromone

Yasuko YAMADA, Seigo YAMAUCHI,* and Noboru HIROTA*

Department of Chemistry, Faculty of Science, Kyoto University, Kitashirakawaoiwake-cho, Sakyo-ku, Kyoto 606

(Received January 18, 1982)

The lowest excited triplet state of chromone was investigated *via* high resolution phosphorescence spectra, phosphorescence excitation spectra and triplet lifetimes in the neat crystal, in the single crystals of durene and benzoic acid at liquid helium temperature. Including the cases in other solvents such as 3-methylpentane, methylcyclohexane and ethanol, the lowest triplet state was assigned to be $\pi\pi^*$ type contrary to the previous assignment. The triplet sublevel properties including the sublevel spectra were obtained in the benzoic acid host. T_y is radiative at the 0-0 band. T_z is radiative at the nontotally symmetric bands and is active in nonradiative transitions. These properties are discussed and compared with those of other carbonyl compounds. A brief comment on the photochemical reactions are given.

There have been some interests in the photochemical behavior of chromone (**1**) and several works have been reported in recent years.[1-4] It has been sug-

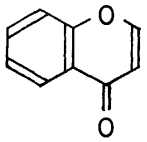

1

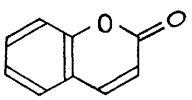

2

gested that the lowest excited triplet state T_1 is involved in the photochemical reactions and the orbital character ($n\pi^*$ or $\pi\pi^*$) of the T_1 state has been discussed from the photoproducts. $n\pi^*$ assignment was favored in these works.

The phosphorescence spectra and triplet lifetimes at 77 K have been reported by Hanifin and Cohen,[1] Gallivan,[5] and Brinen.[6] They assigned the lowest triplet state to be $\pi\pi^*$ type in ethanol, but $n\pi^*$ in 3-methylpentane and 2-methyltetrahydrofuran based on the spectra and the lifetimes of 15—38 ms. This assignment, however, is questionable for the following reasons. Firstly, the reported phosphorescence spectra are too complex to be assigned to $n\pi^*$ spectra.[7] Secondly, the lifetimes of 15—38 ms appear to be somewhat long as lifetimes of $^3n\pi^*$ states. Furthermore, the use of lifetimes as a criterion to decide the triplet character is sometimes ambiguous, because the lifetimes of the $\pi\pi^*$ carbonyls at 77 K may be markedly shortened by thermal mixing with higher vibronic states and second triplet ($^3n\pi^*$) states.[7]

In order to decide the character of the T_1 state unambiguously, we have taken high resolution phosphorescence emission and excitation spectra and measured the lifetimes in different host crystals at liquid helium temperature. Comparing the obtained spectra with those of typical $^3n\pi^*$ and $^3\pi\pi^*$ types, we discuss whether the T_1 state is $^3n\pi^*$ or $^3\pi\pi^*$ in nature. The lifetimes and excitation spectra are used to confirm the assignment. We also discuss a correlation between the phosphorescence properties and ΔE_{TT} (energy difference between T_1 and T_2).

In a previous work we have studied the properties of the T_1 state of coumarin (**2**) which is isomeric to chromone.[8] It was found that the decay properties of coumarin are very different from those of benzaldehyde type aromatic carbonyls. This difference was thought to arise from the large difference in ΔE_{TT}. It seemed interesting to examine the decay properties of chromone in this connection. Accordingly, we have made zero field optically detected magnetic resonance (ODMR) experiments in benzoic acid host to obtain the zero field splitting, the total decay rate constants from sublevels, the relative decay rate constants and sublevel spectra. We discuss the mechanisms of the radiative and non-radiative transitions and compare the properties with those of other carbonyls. Lastly we briefly comment on the implication of the present work on the photochemical behavior of chromone.

Experimental

Chromone, durene, and benzoic acid were purified by zone melting after recrystallization from ethanol. Single crystals were grown by the Bridgman method. The mole fractions of chromone were *ca.* 10^{-2} in the melts, but those of the samples used in the experiments were not measured.

The phosphorescence emission and excitation spectra were obtained at 4.2 K with an Osram 900 W Xe lamp, a Spex 1704 1 m monochromator and an EMI 9502 photomultiplier. The excitation spectra were observed by monitoring the total phosphorescence. The phosphorescence lifetimes were obtained at 1.4 K. The zero field ODMR and microwave induced delayed phosphorescence (MIDP) experiments were made using the mixed crystal of benzoic acid with the apparatus already described.[9] The individual triplet spin sublevel spectra were obtained by observing the time resolved spectra and MIDP spectra at 1160 ms after excitation cut-off, with a PAR 160 boxcar integrator.[10]

Results

The phosphorescence spectra of chromone obtained at 4.2 K in the neat crystal, in the single crystals of durene and of benzoic acid are shown in Fig. 1. The 0-0 band was observed at 379.29 nm, 383.08 nm, and 382.91 nm, respectively. Three sites were observed in benzoic acid as shown in the figure. The triplet lifetimes at 1.4 K are shown in Table 1. In the case of benzoic acid, the lifetime of site III is tabulated. Even at 1.4 K chromone in benzoic acid shows a single exponential decay except in the site I. The lifetime in the durene host at 77 K is 8 ms, which is markedly shorter than that at 1.4 K.

$\Delta E_{TT}(=E(T_2)-E(T_1))$ obtained from the phospho-

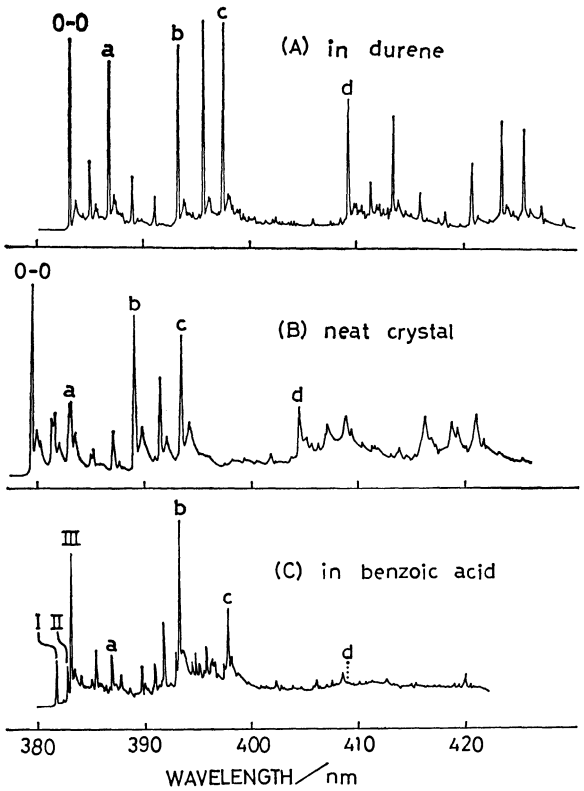

Fig. 1. Phosphorescence spectra of chromone at 4.2 K in durene(A), in a near crystal (B), and in benzoic acid(C).
I, II, and III denote the 0-0 bands of the three sites. a, b, c, and d represent 0-252 cm^{-1}, 0-682 cm^{-1}, 0-980 cm^{-1} bands (see Table 3.) and C=O stretching band respectively.

Table 1. Phosphorescence lifetimes and energy gaps between $T_1(\pi\pi^*)$ and $T_2(n\pi^*)$ states of chromone

Host	Lifetime/ms	$\Delta E_{TT}/cm^{-1}$
Durene	35	371
Neat	55	539
Benzoic acid	241	2356

rescence excitation spectra are also shown in Table 1. A typical excitation spectrum in a lower energy region is shown in Fig. 2. The 0-0 bands of the T_1 and T_2 states are assigned as shown in the figure. In the benzoic acid host, the $S_0 \rightarrow T_2$ ($n\pi^*$) absorption is buried under the $S_0 \rightarrow T_1$ absorption of the benzoic acid. In order to estimate an approximate value we used $\Delta E'_{ST}=1750\ cm^{-1}$ ($\Delta E'_{ST}=E(^1n\pi^*)-E(^3n\pi^*)$), obtained from the neat crystal. This value is known to be appropriate in a series of substituted benzaldehydes.[11]

Spin sublevel properties could be investigated only for the site I in benzoic acid, where the spin-lattice relaxation was suppressed. The zero field splitting constants, the total decay rate constants and the relative radiative decay rate constants at vibronic bands are given in Table 2. The T_z and T_y sublevel spectra are shown in Fig. 3.

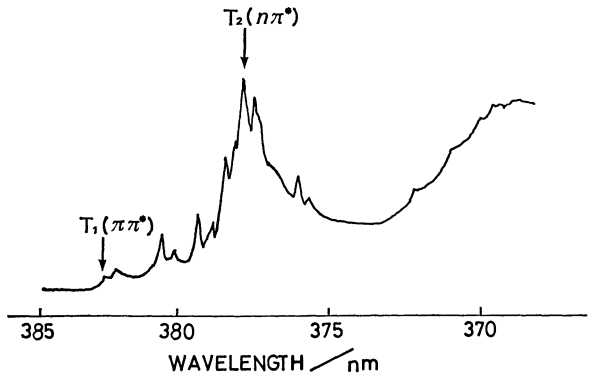

Fig. 2. Phosphorescence excitation spectrum of chromone in durene at 4.2 K.
The 0-0 bands of $T_1(\pi\pi^*)$ and $T_2(n\pi^*)$ are shown.

Table 2. Sublevel energies, total deday rate constants, and relative radiative decay rate constants of the lowest triplet state of chromone in benzoic acid

	ε_i[a]/GHz	k_i/s^{-1}	k_i^r(rel) 0-0	k_i^r(rel) 0-682 cm^{-1}
T_z	1.29	6.79	0.24	1.00
T_y	0.82	2.19	1.00	0.12
T_x	−2.11	0.21	0.11	0.03

a) $\varepsilon_z+\varepsilon_y+\varepsilon_x=0$.

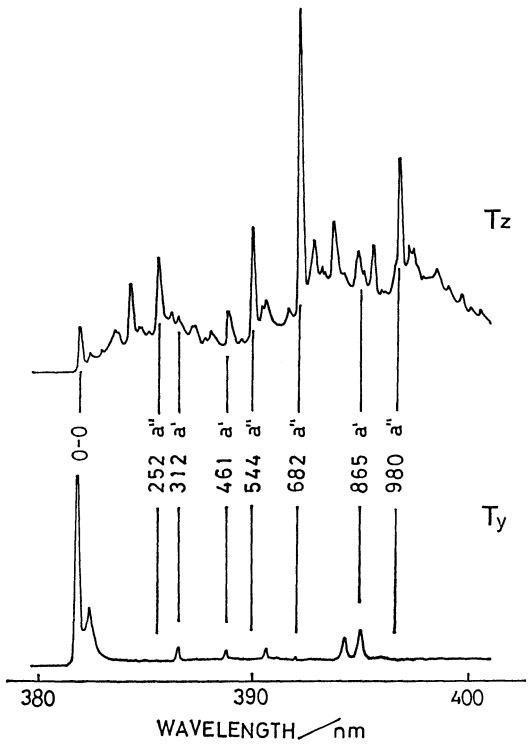

Fig. 3. T_z and T_y sublevel phosphorescence spectra of chromone in benzoic acid.
Vibrational analysis is summarized in Table 3.

Discussion

Assignment of the Lowest Triplet State. In many aromatic carbonyl compounds, phosphorescence spectra are quite different, depending on whether the lowest triplet states are $n\pi^*$ or $\pi\pi^*$ type.[7,12,13] If a phosphorescence state is of $n\pi^*$ character, its spectrum is very simple consisting mainly of a 0-0 band and vibronic bands involving C=O stretching vibration. Occasionally bands involving nontotally symmetric vibrations give rise to strong progressions due to molecular distortion.[14,15] On the other hand, a $\pi\pi^*$ triplet state gives a more complicated spectrum because of a $n\pi^*$—$\pi\pi^*$ vibronic coupling. Especially when a $^3n\pi^*$ triplet state is located near a $^3\pi\pi^*$ state, a spectrum is composed of many vibronic bands of comparable intensities.[13]

Keeping these facts in mind, we examine the spectra in Fig. 1. In all spectra, many strong bands appear in addition to the 0-0 band and the C=O stretching band. Any progression except the C=O stretching band is not observed. Obviously these are the characteristics of the $^3\pi\pi^*$ phosphorescence spectra. Almost all the strong bands in these spectra except the C=O band must be the bands involving nontotally symmetric vibrations. Detailed vibrational assignment is given in the later section.

The phosphorescence excitation spectra support this conclusion. The intensity of the 0-0 band of T_1 is much weaker than the vibronic bands and the 0-0 band of T_2 (Fig. 2). The phosphorescence lifetimes of 35—241 ms are also consistent with the $\pi\pi^*$ assignment. The lifetime of a $^3n\pi^*$ carbonyl is usually in the order of at most a few milliseconds.[12] Combined with all of these facts, the lowest triplet states of chromone in these hosts are definitely assigned to be of $\pi\pi^*$ character. Judging from the lifetimes and spectra, the T_1 states in 3-methylpentane and 2-methyltetrahydrofuran previously assigned to be $n\pi^*$ states are also assigned to be of the $\pi\pi^*$ type, though ΔE_{TT} is relatively small. In all other solvents we examined, hexane, methylcyclohexane, and ethanol, T_1 was found to be of $\pi\pi^*$ type.

Next we discuss a correlation between ΔE_{TT} and some properties of phosphorescence. ΔE_{TT} increases in the order, in durene, in neat crystal, in benzoic acid. The total decay rate constant and the relative intensity of the C=O band decrease in the same order. This correlation is interpreted in terms of a magnitude of the mixing between $T_1(\pi\pi^*)$ and $T_2(n\pi^*)$ states, that is, how much $^3n\pi^*$ state character is contaminated in T_1 state determines the properties of T_1 in durene and neat crystal.

Radiative and Non-radiative Mechanisms for the Triplet Spin Sublevels. With the MIDP technique, the relative radiative decay rate constants of the vibronic bands are obtained as $k_z^r(0\text{-}0):k_y^r(0\text{-}0):k_x^r(0\text{-}0)=0.24:1:0.11$ and $k_z^r(0\text{-}682\ cm^{-1}):k_y^r(0\text{-}682\ cm^{-1}):k_x^r(0\text{-}682\ cm^{-1})=1:0.12:0.03$. Together with these values, the spin sublevel spectra (Fig. 3) give the ratio of the total radiative decay rate constants as $k_y^r \gtrsim 0.3k_z^r$ ($k_i^r \equiv \sum_\nu k_i^r(\nu)$). If we use the equation $k_y \simeq 0.3k_z$ (Table 2) and the inequality $k_y^r \geq 0.3k_z^r$, we can obtain $k_y^{nr} \leq 0.3k_z^{nr}$. The spin sublevel spectra also show that the ratio of the radiative decay at the nontotally symmetric bands of strong intensities are nearly equal to that of the 0-682 cm^{-1} band. Therefore, T_y is radiative at the 0-0 band, whereas T_z is radiative at the nontotally symmetric bands and also active in the nonradiative transition. T_x is less active in both radiative and nonradiative transitions. The symmetry of the molecule is C_s and the lowest triplet state belongs to $A'(\pi\pi^*)$. If we assume that one center integral at the oxygen atom is dominant in the relevant spin orbit coupling matrix elements, the T_z and T_y sublevels couple with the $^1n\pi^*$ and $^1\sigma\pi^*$ states, respectively.

Radiative Mechanisms: The radiative mechanisms at the 0-0 band and the totally symmetric a' bands are summarized as follows,

$$T_z \xrightarrow{H_{so}(1)} {}^1n\pi^*(A'') \xrightarrow{er} S_0, \quad (1)$$

$$T_y \xrightarrow{H_{so}(1)} {}^1\sigma\pi^*(A'') \xrightarrow{er} S_0, \quad (2)$$

$$\xrightarrow{H_{so}(2)} {}^1n\pi^*(A'') \xrightarrow{er} S_0, \quad (3)$$

$$T_x \xrightarrow{H_{so}(3)} {}^1\pi\pi^*(A') \xrightarrow{er} S_0. \quad (4)$$

H_{so} and er denote a spin orbit coupling and a dipole transition, respectively. H_{so} (1), H_{so} (2), and H_{so} (3) represent matrix elements which involve one center, two center and three center atomic integrals. $\sigma\pi^*$ denotes botn $\sigma\pi^*$ and $\pi\sigma^*$ states. The contribution of the two center terms involving the $\sigma\pi^*$ states is neglected because of the weak coupling due to the large energy denominator. The magnitude of the spin orbit coupling is large in both T_z and T_y owing to one center terms. Although the energy denominator ($\Delta E_{ST}=E(S)-E(T_1)$) is favorable for T_z, the transition dipole moment for the $S_0 \rightarrow S_1$ ($n\pi^*$) transition is expected to be much smaller than those for the $S_0 \rightarrow S_1$ ($\sigma\pi^*$) transitions. Indeed, CNDO/S calculation on chromone predicts that the oscillator strengths for the $S_0 \rightarrow S_1$ ($\sigma\pi^*$) transitions are about two orders of magnitude larger than that for the $S_0 \rightarrow S_1$ ($n\pi^*$) transition. Considering these factors, we expect that T_y is more radiative than T_z at the 0-0 and a' bands. T_x will be only slightly active owing to three center terms. These expectations are born out by the observation, $k_z^r(0\text{-}0):k_y^r(0\text{-}0):r_x^r(0\text{-}0)=0.24:1:0.10$. As a result the mechanism (2) is the most important in the radiative decay at the 0-0 band.

For the nontotally symmetric bands, we must consider vibronic couplings. We will discuss the mechanisms paying attention to the result, $k_z^r(nt):k_y^r(nt)=1:0.12$ (nt denotes to nontotally symmetric vibronic bands.). The mechanisms similar to the mechanisms (1)—(4) are summarized as follows:

$$T_z \xrightarrow{a''} {}^3n\pi^*(A'') \xrightarrow{H_{so}(1)} {}^1\pi\pi^*(A') \xrightarrow{er} S_0, \quad (5)$$

$$\xrightarrow{H_{so}(1)} {}^1n\pi^*(A'') \xrightarrow{a''} {}^1\pi\pi^*(A') \xrightarrow{er} S_0, \quad (6)$$

$$T_y \xrightarrow{a''} {}^3\sigma\pi^*(A'') \xrightarrow{H_{so}(1)} {}^1\pi\pi^*(A') \xrightarrow{er} S_0, \quad (7)$$

$$\xrightarrow{a''} {}^3n\pi^*(A'') \xrightarrow{H_{so}(2)} {}^1\pi\pi^*(A') \xrightarrow{er} S_0, \quad (8)$$

$$\xrightarrow{H_{so}(1)} {}^1\sigma\pi^*(A'') \xrightarrow{a''} {}^1\pi\pi^*(A') \xrightarrow{er} S_0, \quad (9)$$

$$\xrightarrow{H_{so}(2)} {}^1n\pi^*(A'') \xrightarrow{a''} {}^1\pi\pi^*(A') \xrightarrow{er} S_0. \quad (10)$$

The difference between T_z and T_y is that T_z involves a spin orbit coupling with the $n\pi^*$ state *via* one center terms, while T_y involves spin orbit coupling with the $\sigma\pi^*$ states via one center terms and with the $n\pi^*$ state *via* two center terms. As the $\sigma\pi^*$ states are higher in energy and the two center terms are smaller, T_z is expected to be more active at the nontotally symmetric bands. This expectation was again realized by the observation, $k_z^r(nt):k_y^r(nt)=1:0.12$. Next we discuss the relative importance of $\sigma\pi^*$ and $n\pi^*$ states as the intermediate in the T_y mechanism. In the T_y radiative decay at the nontotally symmetric bands, the mechanism involving the $\sigma\pi^*$ states ((7), (9)) is likely to be more important than that involving the $n\pi^*$ state, because the magnitude of one center terms is expected to be more than 100 times of that of two center terms as found in the case of quinoxaline.[10] T_x sublevel is again less active because of the three center terms A detailed vibrational assignment is made by the sublevel spectra and fm-ODMR spectra and is shown in Table 3. In-plane (a′) and out-of-plane (a″) vibrations are distinguished.

Nonradiative Mechanisms: The mechanisms of the nonradiative transitions resemble to those of radiative transitions of vibronic bands (*cf.* mechanism (5)—(10)). The mechanisms are the following, based on the foregoing discussion.[16]

$$T_z \xrightarrow{a''} {}^3n\pi^*(A'') \xrightarrow{H_{so}(1)} S_0, \quad (11)$$

$$\xrightarrow{H_{so}(1)} {}^1n\pi^*(A'') \xrightarrow{a''} S_0, \quad (12)$$

$$T_y \xrightarrow{a''} {}^3\sigma\pi^*(A'') \xrightarrow{H_{so}(1)} S_0, \quad (13)$$

$$\xrightarrow{H_{so}(1)} {}^1\sigma\pi^*(A'') \xrightarrow{a''} S_0, \quad (14)$$

$$T_x \xrightarrow{H_{so}(3)} S_0. \quad (15)$$

As in the case of radiative transition at the nontotally symmetric bands, T_z involves the spin orbit coupling with the $n\pi^*$ states and T_y with the $\sigma\pi^*$ states, and the energy denominator favors the T_z mechanism. Similar results for $k_z^r(nt)/k_y^r(nt)$ and k_z^{nr}/k_y^{nr} are expected. As expected, T_z is most active in the nonradiative transition. Although T_x involves direct coupling with the ground state, T_x is not expected to be active, again due to three center atomic integrals.

Table 3. Vibrational analysis of the phosphorescence spectrum of chromone in benzoic acid

Wavelength/nm	Wave number/cm^{-1}	$\Delta\nu$/cm^{-1}	Assignment
381.62	26197	0	
384.01	26034	163	a″
385.32	25945	252	a″
386.22	25885	312	a′
388.45	25736	461	a′
388.54	25730	467	a″
389.71	25653	544	a″
390.39	25608	589	a′
391.82	25515	682	a″
393.45	25409	788	a″
393.89	25381	816	a′
394.52	25340	857	a″
394.65	25332	865	a′
395.22	25295	902	a″
396.44	25217	980	a″

Comparison with Other Carbonyl Compounds. We compare the dynamical properties of chromone in benzoic acid with those of coumarine (**2**) in durene,[8] anti-(CH_3,H)bimane(4,8-dimethyl-1,5-diazabicyclo-[3.3.0]octa-3,7-diene-2,6-dione) (**3**) in durene[17] and benzaldehyde (**4**) in benzoic acid.[18]

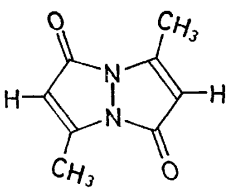

3

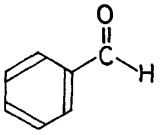

4

In all cases, the lowest triplet states are of $\pi\pi^*$ type with relatively large ΔE_{TT} (2300—6300 cm^{-1}). In coumarin ($k_z=9.7$ s^{-1}, $k_y=2.0$ s^{-1}, $k_x=0.32$ s^{-1}; $k_z^r(0\text{-}0):k_y^r(0\text{-}0):k_x^r(0\text{-}0)=0.25:1:0.03$) and anti-bimane ($k_z=1.83$ s^{-1}, $k_y=2.99$ s^{-1}, $k_x=0.14$ s^{-1}; $k_z^r(0\text{-}0):k_y^r(0\text{-}0):k_x^r(0\text{-}0)=0.04:1:0.02$) these properties are very similar to those of chromone, T_y is radiatively active at the 0-0 band, whereas T_z is active in the nontotally symmetric bands. On the other hand in benzaldehyde ($k_z=18$ s^{-1}, $k_y=0.44$ s^{-1}, $k_x=0.46$ s^{-1}; $k_z^r(0\text{-}0):k_y^r(0\text{-}0):k_x^r(0\text{-}0)=1:0.06:0.06$) and substituted benzaldehydes, k_y is not large and T_y is less radiative even at the 0-0 band. Possible reasons for the difference between the two types of molecules are the following.

(1) The oscillator strength for the $S_0\rightarrow S_1$ ($n\pi^*$) transition is larger in benzaldehyde type molecules. This has been found experimentally[19] and is also supported by the CNDO/S calculation.

(2) The energies of the $\sigma\pi^*$ states are lower in chromone than in benzaldehyde. The oscillator strengths for the $S_0\rightarrow S_i$ ($\sigma\pi^*$) transitions for the lower energy states may be larger for chromone and coumarin as indicated by the results of CNDO/S calculation.

Comment on the Photochemical Reactions. We have assigned T_1 of chromone as $\pi\pi^*$ states in all solvents and host crystals at low temperatures. This is somewhat contradictory to the conclusion derived from the photochemical studies. In the non-polar solvents ΔE_{TT} is in the same order of magnitude as measured in the durene crystal ($\Delta E_{TT}=371$ cm^{-1}). With this value of ΔE_{TT} the ratio between the population in the $^3n\pi^*$ and that in the T_1 state in Boltzmann distribution is 0.17 at 300 K. Therefore, it is quite probable that both $^3n\pi^*$ and $^3\pi\pi^*$ type photochemical reactions take place. Although the phosphorescence spectra and lifetimes indicate the mixed character of the T_1 state, the actual $n\pi^*$ character induced by the vibronic mixing is at most 3%. Thus the thermal population of the $^3n\pi^*$ state is likely to be responsible for the $^3n\pi^*$ type reaction.

The report that the $^3n\pi^*$ type reaction takes place in methanol[3] is puzzling. ΔE_{TT} in methanol is in the same order as that in benzoic acid and the ratio of the population of the $^3n\pi^*$ state is *ca.* 10^{-5} at 300 K. It is possible that chromone in solution at 300 K has a smaller ΔE_{TT} than that estimated in solid at 4.2 K or has a considerably different configuration. However, whether or not a $^3n\pi^*$ type reaction is really taking place still seems to be uncertain.

We wish to thank Dr. Tadamasa Shida for discussions on CNDO/S calculations, and Mr. Masaaki Baba for experiments.

References

1) J. W. Hanifin and E. Cohen, *J. Am. Chem. Soc.*, **91**, 4494 (1969).
2) R. Matsushima, T. Kishimoto, M. Suzuki, M. Morioka, and H. Mizuno, *Bull. Chem. Soc. Jpn.*, **53**, 2938 (1980).
3) Y. Yamamoto and E. Toyota, *Chem. Pharm. Bull.*, **26**, 2277 (1978).
4) K. Hamanoue, T. Nakayama, T. Miyake, and H. Teranishi, *Chem. Lett.*, **1981**, 39.
5) J. B. Gallivan, *Can. J. Chem.*, **48**, 3938 (1970).
6) J. B. Gallivan and J. S. Brinen, *Chem. Phys. Lett.*, **10**, 455 (1971).
7) L. Goodman and M. Koyanagi, *Mol. Photochem.*, **4**, 369 (1972).
8) E. T. Harrigan, A Chakrabarti, and N. Hirota, *J. Am. Chem. Soc.*, **98**, 3460 (1976).
9) T. H. Cheng and N. Hirota, *J. Chem. Phys.*, **56**, 5019 (1972); J. Schmidt, W. S. Veeman, and J. H. van der Waals, *Chem. Phys. Lett.*, **4**, 341 (1969); D. A. Antheunis, J. Schmidt, and J. H. van der Waals, *ibid.*, **6**, 255 (1970); *Mol. Phys.*, **22**, 1 (1971).
10) S. Yamauchi and T. Azumi, *J. Chem. Phys.*, **68**, 4138 (1978).
11) H. Hayashi and S. Nagakura, *Mol. Phys.*, **27**, 969 (1974).
12) E. T. Harrigan and N. Hirota, *Mol. Phys.*, **31**, 681 (1976).
13) A. Després, V. Lejeune, E. Migirdicyan, and W. Siebrand, *Chem. Phys.*, **36**, 41 (1979).
14) S. Yamauchi and D. W. Pratt, *Mol. Phys.*, **37**, 541 (1979).
15) M. Baba and N. Hirota, *Chem. Phys. Lett.*, **64**, 321 (1979).
16) F. Metz, S. Friedrich, and G. Hohlneicher, *Chem. Phys. Lett.*, **16**, 353, (1972).
17) M. Baba, N. Hirota, and E. M. Kosower, *J. Phys. Chem.*, **85**, 1469 (1981).
18) Y. Hirata and N. Hirota, *Mol. Phys.*, **39**, 129 (1980).
19) Y. Kanda, H. Kaseda, and T. Matsumura, *Spectrochim. Acta, Part A*, **20**, 1387 (1964).

 © 1982 The Chemical Society of Japan Bull. Chem. Soc. Jpn., 55, 2051—2055 (1982)

The Discrimination of the Oxidation States of Neptunium in Sodium Hydroxide Solutions by Means of Chromatography on Alumina

Yoshinobu SHIOKAWA*, Hajimu YAMANA, Akiko SATŌ, and Shin SUZUKI

The Research Institute for Iron, Steel and Other Metals, Tohoku University, Katahira, Sendai 980

(Received August 27, 1981)

A method of discriminating the oxidation states of Np in a NaOH solution by means of chromatography on alumina is proposed. In a NaOH solution of 0.5—1.7 M(1 M=1 mol dm^{-3}), the separation of Np(VI) from Np(VII) can be made effectively by means of chromatography on alumina. Only a little Np(VI) is adsorbed on alumina the Np(VII) adsorbed to some extent, and the Np(V), strongly, under the same conditions. By applying this chromatographic method, the method of preparing Np(VI) and Np(VII) of a tracer quantity in 1 M NaOH is established.

It has been found by polarography that the possible oxidation states of Np in a NaOH solution are the penta-, hexa-, and heptavalent states.[1] In a basic solution, the color of the Np(VII) is green, and its existence is easily confirmed by spectrophotometry because of its large extinction coefficient and high solubility.[2] On the other hand, since both Np(V) and Np(VI) have a small extinction coefficient and a low solubility,[2] the spectrophotometry cannot be used even for an ordinary concentration of Np. Therefore, a method other than spectrophotometry is required if we are to ascertain the distribution of the oxidation states of Np of a low concentration in a basic solution. However, no such method has yet been established, and the chemical behavior of Np(V), Np(VI), and Np(VII) in a basic solution is not sufficiently clarified.

In a previous paper,[3] we ourselves reported that, in a NaOH solution of 1—2 M, the Np(V) was almost completely adsorbed on zirconium(IV) hydroxide, while the Np(VI) and Np(VII) remained in the supernatant. The present study is an attempt to establish a method for discriminating, in a NaOH solution Np(VI) and Np(VII), which are indistinguishable by adsorption on zirconium(IV) hydroxide. For this purpose, column chromatography on alumina is found to be excellent. A method of preparing Np(VI) and Np(VII) of a tracer quantity in a NaOH solution is also proposed by the application of this method.

Experimental

The sodium hydroxide solution of Np was prepared from a 0.5 M nitric acid solution of Np by adding an adequate oxidant or reductant after the addition of NaOH. The NaOH stock solution was prepared by filtering its saturated solution through a Millipore Mitex filter with a pore size of 5 μm, the necessary experimental procedures were carried out in a polyethylene bag filled with nitrogen gas to avoid contamination with carbon dioxide.

Alumina (Merck aluminium oxide 60, active basic 70—230 mesh) was heated in a 2 M NaOH solution containing bromine at 80—100 °C for 1 h. After cooling, the alumina was transferred into a black glass tube with a carbon dioxide absorber of 0.6 cm in diameter and with its length adjusted to 10.0—10.2 cm. Then the alumina bed was rinsed with water and the eluent used in each run. NaOH solution of various oxidation states of Np of 1 cm^3 was carefully transferred to the top of the bed and allowed to flow through. After the tube had been washed, the eluent was allowed flow through at 0.2—0.3 cm/min.

The ^{237}Np was obtained from The Radiochemical Centre, Amersham, while the ^{239}Np tracer was prepared by milking from ^{243}Am through a cation exchanger. By measuring the ^{239}Np activity by means of a NaI scintillator or Ge detector, the neptunium was determined. The optical density was measured by means of a Hitachi 330 spectrophotometer.

Results and Discussion

Chromatographic Behavior of Np(VII) and Np(V). The chromatographic behavior of Np(VII), prepared by a conventional ozone oxidation,[4] is shown in Fig. 1 for its ordinary concentration of 4.3×10^{-4} M in 1.2 M NaOH. In this figure, the ordinate represents the ratio of the amounts of Np found in each fraction of the effluent to the total amount placed in the column. In the first peak of the chromatogram, the effluent was colorless, but in the second peak the color was the green characteristic of a heptavalent state. Moreover, the recovery of Np was 99%, which showed that almost all the Np loaded on the column was eluted. As is shown in Fig. 1, the Np(VII) of an

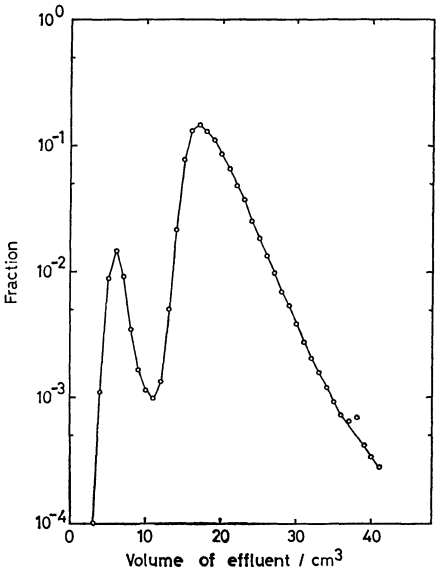

Fig. 1. Column chromatogram of Np(VII) on alumina.
Influent: 4.3×10^{-4} M Np(VII) in 1.2 M NaOH, eluent: 1.1 M NaOH, recovery: 99%.

ordinary concentration prepared by ozone oxidation is separated into two parts by means of alumina chromatography.

The chromatographic behavior of Np(V), prepared by the addition of hydrazine,[3] was investigated for an extremely low concentration of 5×10^{-12} M. However, no neptunium was eluted at all, even by the use of 60 ml of the eluent (1 M NaOH+10^{-3} M $N_2H_4\cdot2HCl$). Also, the adsorption of Np(V) on 100 mg of alumina was found to be above 98% by the agitation of 4 ml of Np(V) in a 1 M NaOH solution containing hydrazine. Thus, the Np(V) in a 1 M NaOH solution may be said to be strongly adsorbed on alumina.

Chromatographic Behavior of Np(VI). A basic Np(VI) solution of an ordinary concentration is usually prepared by alkalizing an acidic Np(VI) solution without any foreign oxidants,[5] by dissolving Np(VI) salt in a solvent of interest,[2] or by electrolyzing a basic Np(VII) solution.[6] However, there is some probability of a partial formation of a pentavalent state in the basic Np(VI) solution prepared by the above-mentioned method. Here we prepared not pure Np(VI), but various mixed solutions of Np(VI) and Np(VII) by adding hydrazine to Np(VII) solutions prepared by ozone oxidation, as is tabulated in Table 1. This table shows the fraction of Np(VII) as calculated from the optical densities at 618 nm before and after the addition of hydrazine. In these mixtures of Np(VII) and Np(VI), there is no probability of the existence of the pentavalent state at all, because the reaction of Np(V)+Np(VII)→2Np(VI) is rapid and complete.[2]

The chromatographic behavior of Np(VII) and Np(VI) can be examined without any consideration of Np(V). The elution chromatograms of the mixtures are shown in Fig. 2, in which the numbers correspond to the index numbers in the first column of Table 1. As the fraction of Np(VII) in a mixture decreases, the intensity of the first peak in Fig. 2 becomes larger, and that of the second peak, smaller. The fractions of the second peak, observed by means of chromatograms, are shown in the sixth column of Table 1. These values agree fairly well with the fractional values of Np(VII) in the mixtures obtained by spectrophotometry. From Table 1 and Fig. 2, it may be concluded that the first peak in the chromatogram is due to Np(VI), and the second peak, to Np(VII), and that the intensity ratio of the two peaks corresponds to the concentration ratio of Np(VI) and Np(VII).

The difference between the D_1/D_0 ratio and the second peak fraction may result either from the reduction of Np(VII) during chromatography or from an incomplete preparation of pure Np(VII) in 1 M NaOH, as shown by controlled potential coulometry.[6]

Preparation of Tracer-scale Np(VII) and Np(VI) in a 1 M NaOH Solution. As is shown in Table 1 and Fig. 2, Np(VII) and Np(VI) of an ordinary concentration can easily be discriminated by chromatography on alumina. Here, we are concerned with the preparation of Np(VII) and Np(VI) of a tracer quantity in a 1 M NaOH solution.

Neptunium solutions from 5×10^{-4} M to an extremely low concentration were oxidized by ozone in a 1 M NaOH solution containing bromine. The chro-

Table 1. The composition of a mixture of Np(VI) and Np(VII) in a 1.1 M NaOH solution and the results of the chromatography

No.	[Np]/M	D_0[a]	D_1[b]	Np(VII) fraction[c]/%	The 2nd peak fraction/%	Recovery of Np/%
1	4.78×10^{-4}	0.186	0.186	100	92	101
2	4.81×10^{-4}	0.183	0.137	75	71	103
3	4.74×10^{-4}	0.187	0.095	50	46	101
4	4.97×10^{-4}	0.187	0.042	22	18	99

a) D_0: The optical density at 618 nm for the solution of Np(VII) prepared by ozone oxidation. b) D_1: The optical density at 618 nm for the mixture of Np(VI) and Np(VII). c) D_1/D_0.

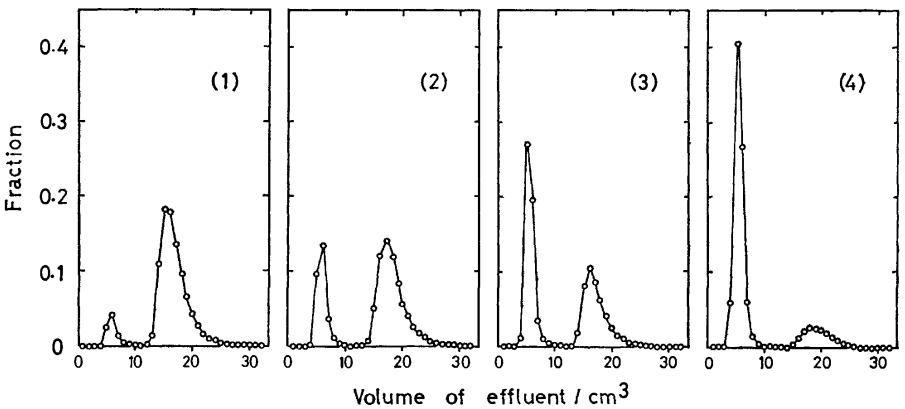

Fig. 2. Chromatogram of the mixture of Np(VI) and Np(VII).
Influent: see Table 1, eluent: 1.1 M NaOH.

matogram is shown in Fig. 3. A comparision of Fig. 3-(1) with Fig. 1, makes it obvious that Np(VII) of a higher purity is obtained by ozone oxidation in a NaOH solution containing bromine; the contamination of Np(VI) is estimated to be about 1% from the chromatogram of Fig. 3-(1). Figure 3 shows that the distribution coefficient of Np(VII) on alumina grows larger as its concentration decreases, though that of Np(VI) is apparently constant from an ordinary to an extremely low concentration. Also, Np(VII) of a tracer quantity in 1 M NaOH can be prepared by ozone oxidation in a 1 M NaOH solution containing bromine, as is shown in Fig. 3-(4).

Np(VI) in a 1 M NaOH solution may be obtained by the use of an oxidant with a formal electrode potential of about 0.45 V, because the potential in a 1 M NaOH solution is 0.59 V for a Np(VII)/Np(VI) couple[6] and 0.30 V for a Np(VI)/Np(V) couple.[7] However there are not any suitable oxidants in basic solutions. Therefore, we tried to prepare Np(VI) by oxidation with mixture of $K_3[Fe(CN)_6]$ and $K_4[Fe(CN)_6]$. For a $[Fe(CN)_6]^{3-}/[Fe(CN)_6]^{4-}$ couple, the standard electrode potential is 0.36 V and the formal electrode potential is 0.46 V at 0.01 M NaOH and 0.52 V at 5 M NaOH.[8] By oxidation with this mixture, Np(VI) must be obtained, because the potential of the mixture will vary with the concentration ratio, Q, where $Q=[[Fe(CN)_6]^{4-}]/[[Fe(CN)_6]^{3-}]$. The preliminary spectrophotometric experiments showed that the concentrations of $[Fe(CN)_6]^{3-}$ and $[Fe(CN)_6]^{4-}$

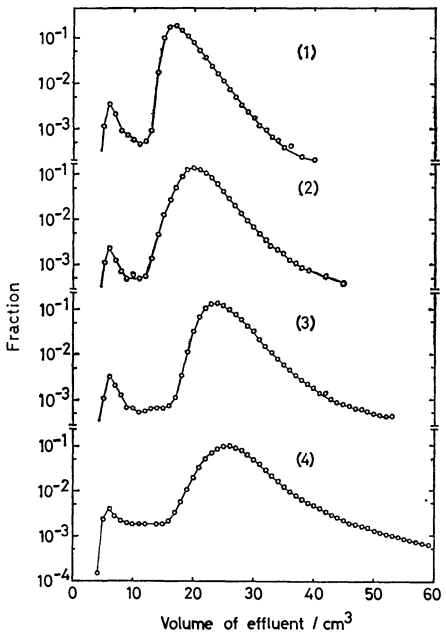

Fig. 3. Chromatogram of Np oxidized by ozone in 1.2 M NaOH+0.16 M Br_2.
Influent: (1) $[Np]=4.6\times10^{-4}$ M, (2) $[Np]=4.3\times10^{-5}$ M, (3) $[Np]=8.9\times10^{-6}$ M, (4) $[Np]=5\times10^{-12}$ M, eluent: 1.1 M NaOH+0.08 M Br_2.

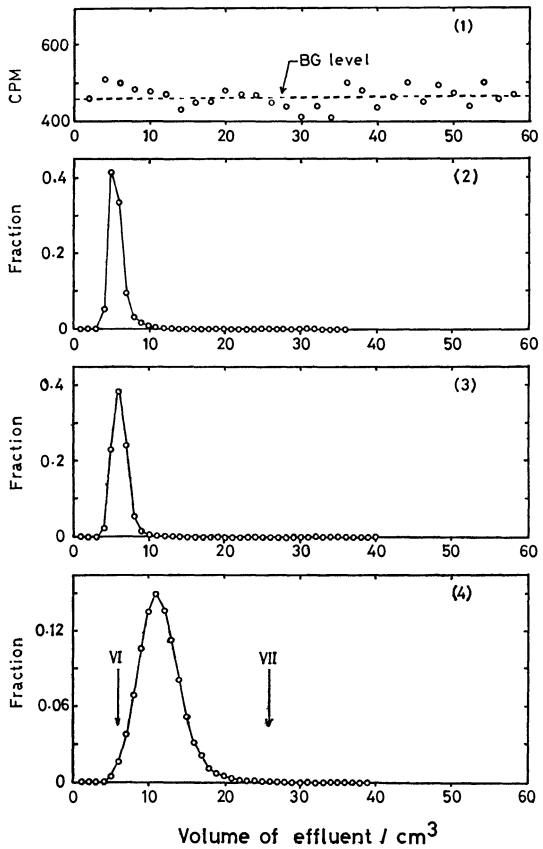

Fig. 4. Chromatogram of Np in the mixture of $K_4[Fe(CN)_6]$ and $K_3[Fe(CN)_6]$.
(1): 1.1 M NaOH+1.0×10^{-3} M $K_4[Fe(CN)_6]$, $R<0.1\%$. (2): 1.1 M NaOH+9.2×10^{-4} M $K_4[Fe(CN)_6]$ +1.0×10^{-4} M $K_3[Fe(CN)_6]$, $Q=9$, $R=99\%$. (3): 1.1 M NaOH+8.1×10^{-4} M $K_4[Fe(CN)_6]$+2.0×10^{-4} M $K_3[Fe(CN)_6]$, $Q=4$, $R=97\%$. (4): 1.1 M NaOH +1.0×10^{-3} M $K_3[Fe(CN)_6]$, $R=100\%$. Where, $Q=[[Fe(CN)_6]^{4-}]/[[Fe(CN)_6]^{3-}]$ and R is recovery of Np.

Table 2. Adsorption of Np in a mixture of $K_4[Fe(CN)_6]$ and $K_3[Fe(CN)_6]$ on zironium(IV) hydroxide

$[K_4[Fe(CN)_6]]$ / 10^3 M	$[K_3[Fe(CN)_6]]$ / 10^3 M	Q[a]	Adsorption[b]/% RT, 1 h[c]	50 °C, 2 h[c]	RT, 20 h[c]	Oxidation state
0.99	0		70	60		5, (6)
0.94	0.05	19	9	9		(5), 6
0.91	0.10	9	5		4	6, 7
0.81	0.20	4	5		4	6, 7
0.49	0.48	1	4	5		6, 7
0	1.0	0	4	6		6, 7

a) $Q=[K_4[Fe(CN)_6]]/[K_3[Fe(CN)_6]]$. b) [NaOH]=1.1 M, [Zr(IV)]=0.6 mg/ml. c) Time of standing.

in a mixture of them at 1 M NaOH remained almost constant over 2 d. This means that the potential of the mixture in 1 M NaOH is almost constant.

The distribution of the oxidation states of Np in the mixture was examined both by adsorption on zirconium(IV) hydroxide[3] and by chromatography on alumina. The results are shown in Table 2 and Fig. 4. As is shown in Table 2, the adsorption of Np is almost constant, independent of the standing time and the temperature, and the Np in the mixture with the concentration ratio of $Q<10$ is adsorbed a little, though much of the Np in the $[Fe(CN)_6]^{4-}$ solution is adsorbed. Since the oxidation into Np(VII) by $[Fe(CN)_6]^{3-}$ in a NaOH solution is incomplete,[9] the result of adsorption shows that the Np in a mixture with a ratio of $Q<10$ is a pure hexavalent state or a mixture of hexa- and heptavalent states. And also the results show that Np in $[Fe(CN)_6]^{4-}$ solution is a mixture of penta- and hexavalent state. The possible oxidation states of Np are shown in the seventh column of Table 2.

The chromatographic behavior of Np in $[Fe(CN)_6]^{4-}$ and $[Fe(CN)_6]^{3-}$ solutions are shown in Figs. 4-(1) and 4-(4) respectively. Though Np(VI) exists in both solutions, Np is not eluted at all in the $[Fe(CN)_6]^{4-}$ solution, as is shown in Fig. 4-(1), while it is eluted at an intermediate position between Np(VI) and Np(VII) in the $[Fe(CN)_6]^{3-}$ solution, as is shown in Fig. 4-(4). The curious behavior can be easily explained by the concept of repeated extractions for chromatography as follows. If there are two different oxidation states of Np which are produced by a reversible redox reaction, these two states of Np are not separated by chromatography, and the elution of Np is observed at the intermediate position between intrinsic positions for each oxidation state, because Np in the mobile and stationary phase is forced to become two different oxidation states by a reversible redox reaction, and it is partly and repeatedly adsorbed or desorbed on alumina between the two phases.

Figures 4-(2) and 4-(3) show the chromatograms of Np in mixtures with the concentrations ratio, Q, of 9 and 4 respectively. Almost all the Np was eluted at an intrinsic peak position for Np(VI). Therefore, in a 1 M NaOH solution Np(VI) in a tracer quantity can be prepared by oxidation with the mixture of $K_3[Fe(CN)_6]$ and $K_4[Fe(CN)_6]$ having concentration ratio, Q, from 4 to 9.

Effect of the Concentration of Na_2CO_3 and NaOH on the Chromatographic Behavior of Np(VII) and Np(VI). The effects of the concentration of Na_2CO_3 and NaOH on the chromatographic behavior of Np(VII) and Np(VI) were examined. The mixtures of Np(VII) and Np(VI) were prepared by the addition of bromine. Figure 5 shows the effect of the concentration of Na_2CO_3, where Np was been prepared by heating at 80—90 °C for an hour in a 1 M NaOH solution containing bromine, so that the fraction of Np(VII) was rich. As is shown in Fig. 5, the elution peak

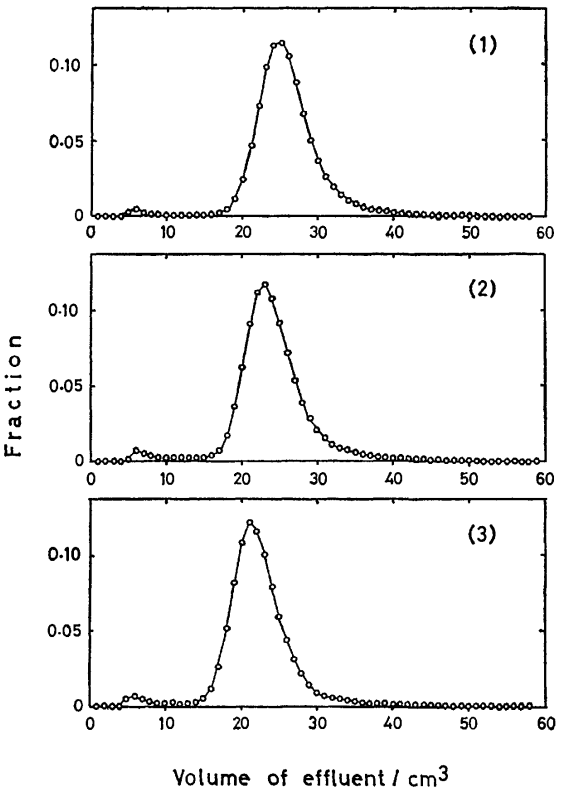

Fig. 5. Influence of the concentration of Na_2CO_3 on the chromatogram of Np(VI) and Np(VII).
(1): 1.1 M NaOH+0.08 M Br_2, (2): 1.1 M NaOH+0.08 M Br_2+0.02 M Na_2CO_3, (3): 1.1 M NaOH+0.08 M Br_2+0.05 M Na_2CO_3.

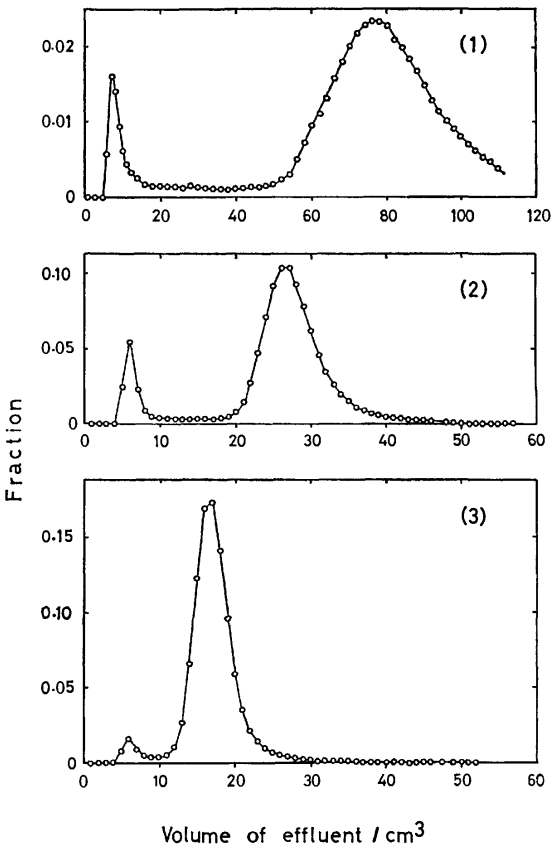

Fig. 6. Influence of the concentration of NaOH on the chromatogram of Np(VI) and Np(VII).
(1): 0.57 M NaOH+0.08 M Br_2, (2): 1.1 M NaOH +0.08 M Br_2, (3): 1.7 M NaOH+0.08 M Br_2.

position on Np(VII) is dependent on the concentration of CO_3^{2-}, but that of Np(VI) is independent of it. It is found that the discrimination between Np(VII) and Np(VI) can be made up to 0.05 M Na_2CO_3 in a 1 M NaOH solution.

Figure 6 shows the effect of the concentration of NaOH, where Np has been prepared by standing at room temperature in a 1 M NaOH solution containing bromine, so that the fraction of Np(VI) was larger. This figure shows that the discrimination can also be made in a NaOH solution of 0.5—1.7 M.

By combining the chromatography on alumina with the adsorption on zirconium(IV) hydroxide, it is possible to analyze the distribution of all the oxidation states of Np, Np(V), Np(VI), and Np(VII) in a 1 M NaOH solution.

The present work was partially supported by a Grant-in-Aid for the Encouragement of Young Scientists (No. 56740239) from the Ministry of Education, Science and Culture.

References

1) V. P. Peretrukhin and D. P. Alekseeva, *Radiokhimiya*, **16**, 836 (1974).
2) D. Cohen and S. Fried, *Inorg. Nucl. Chem. Lett.*, **5**, 653 (1969).
3) Y. Shiokawa, A. Sato, and S. Suzuki, *Bull. Chem. Soc. Jpn.*, **53**, 2861 (1980).
4) V. I. Spitsyn, A. D. Gelman, N. N. Krot, M. P. Mefordiyeva, F. A. Zkharova, Yu. A. Komokov, V. P. Shilov, and I. V. Smirnova, *J. Inorg. Nucl. Chem.*, **31**, 2733 (1969).
5) V. B. Nikolaevskii, V. P. Shilov, N. N. Krot, and V. F. Peretrukhin, *Radiokhimiya*, **17**, 426 (1975).
6) A. J. Zielen and D. Cohen, *J. Phys. Chem.*, **74**, 394 (1970).
7) G. A. Simakin, I. V. Matyashchuk, and N. A. Vladimirova, *Radiokhimiya*, **15**, 98 (1973).
8) G. Charlot, "Les Reactions Chimiques en Solution," Masson et Cie (1969).

Voltammetric Studies of the Use of the Rotated Oxide Electrode as an Indicator Electrode and as a View to the Determination of EDTA and Other Complexanes

Tadayosi YOSHIMURA

Department of Industrial Chemistry, Fukui Technical College, Sabae, Fukui 916

(Received September 7, 1981)

The accessible potential ranges of rotated lead dioxide (PbO_2) and manganese dioxide (MnO_2) electrodes were investigated in supporting electrolyte solutions of 0.1 mol/l (mol/dm^3) KNO_3 at various pH values, by measuring the base currents of these oxide electrodes. The anodic and cathodic ascending potentials of both the oxide electrodes are pH-independent in a neutral solution. In each neutral system of KNO_3, $KClO_4$, K_2SO_4, and KCl, the accessible potential range of the PbO_2 electrode was from +1.4 to +0.2 V *vs.* SCE, while that of the MnO_2 electrode was from +1.2 to +0.3 V, and the lower manganese oxide electrode from +0.3 to −0.9 V. Furthermore, the applications of these electrodes to the determination of EDTA and other complexanes were examined. Both the oxide electrodes gave a good calibration curve which could establish a linear relationship to the EDTA concentration, passing through the point of origin. The rotated PbO_2 and MnO_2 electrodes seem to be useful for determining depolarizers such as the EDTA-type complxanes.

The voltammetric fundamentals of the oxide electrodes have been reported by several investigators. With regard to the Pt electrode, Kolthoff and Tanaka[1] reported the residual current-voltage curves and dissolution patterns of rotated and stationary platinum wire electrodes in supporting electrolytes. When the curves are recorded from the evolution potential of oxygen in the negative direction, a small cathodic dissolution pattern is observed starting at a potential which approximately corresponds to the equilibrium value of the platinum-platinous hydroxide electrode. Sato *et al.*[2] reported the electrodeposition and reduction of the manganese dioxide (MnO_2) electrode; two cathodic waves were observed in an acidic solution in a cathodic sweeping. Similar results were reported by Reynaud,[3] Lee *et al.*,[4] and Yoshimura:[5]

$$MnO_2 + H^+ + e^- \longrightarrow MnOOH, \quad (1)$$

$$MnOOH + 3H^+ + e^- \longrightarrow Mn^{2+} + 2H_2O. \quad (2)$$

The lead dioxide (PbO_2) electrode was reviewed by Carr and Hampson.[6] Under acidic conditions and within the anodic potential range, the primary redox equilibrium is between lead dioxide and the lead(II) ion:

$$PbO_2 + 4H^+ + 2e^- \rightleftharpoons Pb^{2+} + 2H_2O. \quad (3)$$

The electrode reactions of ethylenediaminetetraacetic acid (EDTA), other polyamine *N*-polycarboxylic acids (complexanes),[7,8] chromium(III),[9] acetylacetone,[10] 8-quinolinol,[11] and ethanol[12] have previously been reported by using the stationary MnO_2 and PbO_2 electrodes as indicator electrodes. In the case of the MnO_2 electrode,[7] a characteristic cathodic peak due to the complex formation of EDTA was observed, and two further anodic peaks or the coalesced anodic peak were at last also observed in an acidic solution. In the case of the PbO_2 electrode,[8] an anodic peak and a cathodic peak due to the complex formation of EDTA were obtained in a 0.1 mol/l KNO_3 solution. Both the cathodic and anodic peaks of these oxide electrodes increase with the increase in the complexane concentration.

For the analytical use of the PbO_2 and MnO_2 electrodes, it seems to be most useful to investigate and clarify the voltammetric behavior of the rotated oxide electrodes. In this work, the accessible potential ranges of these oxide electrodes were investigated in the supporting electrolyte solutions of 0.1 mol/l KNO_3 at various pH values; this was done by measuring the base currents of the rotated PbO_2 and MnO_2 electrodes. Furthermore, the use of these oxide electrodes for the determination of EDTA and other complexanes was examined.

Experimental

Chemicals. The chemicals used were of an analytical reagent grade. The supporting electrolyte solution used mainly was a 0.1 mol/l concentration of potassium nitrate. Since the oxide electrodes were sensitive to the anion components of most buffer solutions,[5,8] the pH of the electrolyte solution was adjusted with 0.1 mol/l nitric acid and potassium hydroxide. The variation in pH value of the solution before and after the voltammetric measurements was ±0.0039 in the pH range from near 2 to 11.[10] The nitrilotriacetic acid (NTA), ethylenediaminetetraacetic acid (EDTA), and diethylenetriaminepentaacetic acid (DTPA) were used without further purification. Redistilled water was used throughout this investigation.

Preparation of the Oxide Electrodes. The rotated lead dioxide (PbO_2) electrode was prepared by the electrolytic oxidation of 1.0 mol/l lead nitrate[8] on a platinum disk microelectrode (0.046 cm^2) at 30±2 °C, rotated with a synchronous motor at a rate of 600 min^{-1}. Similarly, the rotated manganese dioxide (MnO_2) electrode was prepared by the electrolytic oxidation of 1.0 mol/l manganese sulfate[7] on a platinum disk microelectrode (0.046 cm^2) in a 0.5 mol/l sulfuric-acid solution at 90±3 °C. The stationary MnO_2 electrode was prepared by the electrolytic oxidation of the same solution without being rotated.[7] After the electrolytic oxidation of the electrode, these oxide electrodes were washed with redistilled water and used.

Apparatus and Procedures. A Yanagimoto polarograph Model P8-AP and a Princeton Applied Research Model 174A polarographic analyzer with a three-electrode system were used for the voltammetric measurements. A Corning pH-meter Model 125 was used for the pH measurements. During all the voltammetric measurements, the rotated oxide electrode was used at a rotation rate of 600 min^{-1} with a synchronous motor, Yanagimoto Model SM6S2, except for the

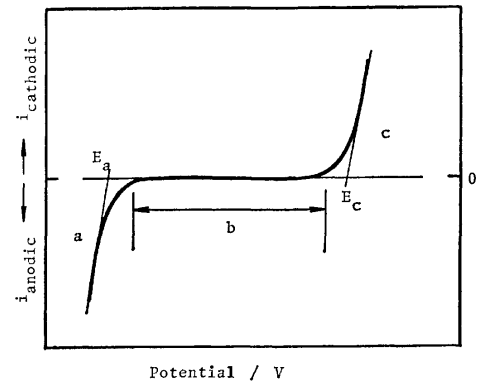

Fig. 1. Typical current-voltage curve of an indicator electrode.
a: Anodic ascending current [decomposition of medium], b: accessible potential range for an analytical application, c: cathodic ascending current [dissolution of electrode or evolution of hydrogen gas]. Ascending potential: E_a, anodic; E_c, cathodic.

investigation of the effect of the rotation rate on the redox wave. All the voltammetric measurements were carried out at a sweep rate of 5 mV/s in a thermostat of 25±0.2 °C without any deaeration of the solution. When current-voltage curves are measured at a more negative potential than zero **V** *vs.* SCE, the solution was deoxygenated by bubbling nitrogen gas. A saturated calomel reference electrode (SCE) and a platinum counter electrode were used.

Measurements of the Ascending Potential. Figure 1 shows a typical current-voltage curve of an indicator electrode; the anodic ascending current corresponds to a decomposition of the medium, while the cathodic one corresponds to a dissolution of the electrode or an evolution of hydrogen. The ascending potential was measured in the following way (see Fig. 1): the current-voltage curves of the rotated oxide electrode were recorded starting from +0.50 V both anodically and cathodically, and the ascending potential has defined as the potential of the point at which the tangent to the ascending curve of about 300 μA intersects with the tangent to the residual curve.

Results and Discussion

Accessible Potential Range. The accessible potential ranges have been studied for the assessments of the PbO_2 and MnO_2 indicator electrodes. The base currents of these rotated electrodes in 0.1 mol/l KNO_3 with various pH values are shown in Figs. 2 and 3 respectively.

The rotated PbO_2 electrode shows one cathodic wave at a pH value lower than 4 and one anodic wave at a pH value higher than 9, as is shown in Fig. 2. The anodic ascending current corresponds to oxygen evolution. The PbO_2 electrode may have the accessible potential range of +1.4 to +0.2 V in a 0.1 mol/l KNO_3 solution at pH values between 4 and 9.

On the other hand, the rotated MnO_2 electrode shows a small cathodic wave in its base current at the cathodic sweep, which corresponds to the reduction of MnO_2 to the lower manganese oxide, according to Eqs. 1 and 2. The anodic ascending current corresponds to oxygen evolution, while the cathodic

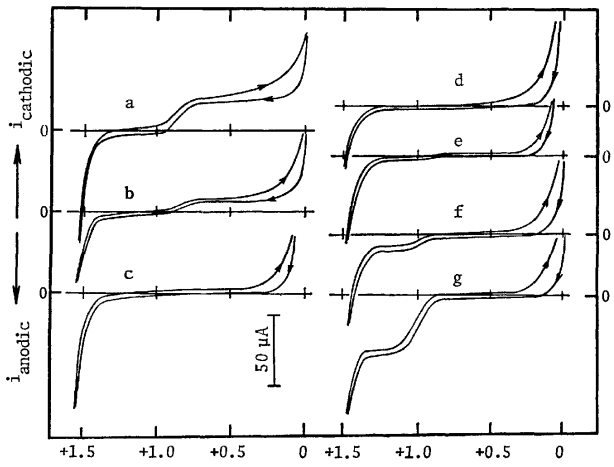

Fig. 2. Current-voltage curves of the PbO_2 electrode in 0.1 mol/l KNO_3 with various pH.
Sweep rate: 5 mV/s at a rotation rate of 600 min^{-1}.
The pH of solution: a, 3.06; b, 3.51; c, 4.18; d, 6.14; e, 9.09; f, 9.72; g, 10.46.

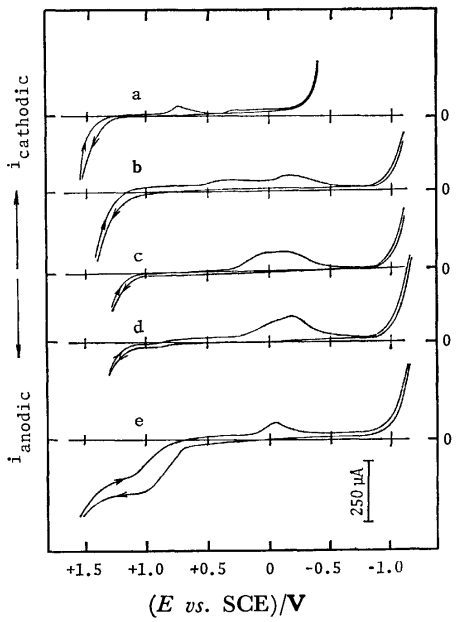

Fig. 3. Current-voltage curves of the MnO_2 electrode in 0.1 mol/l KNO_3 with various pH.
Sweep rate: 5 mV/s at a rotation rate of 600 min^{-1}.
The pH of solution: a, 1.05; b, 3.05; c, 5.74; d, 10.11; e, 11.79.

ascending current corresponds to hydrogen evolution. Thus, the accessible potential range of the MnO_2 electrode was +1.2 to +0.3 V in a 0.1 mol/l KNO_3 solution at pH values between 3 and 10.

Ascending Potentials and Self-reduction Waves of the Oxide Electrodes. In Fig. 4, the ascending potentials of the PbO_2 electrode and the half-wave potentials of the cathodic and anodic waves are plotted against the pH values. Curve a indicates the evolution potential of oxygen, while Curve b shows the ascending potential at which the PbO_2 is reduced and dissolved as Pb^{2+}, according to Eq. 3.[6] At pH values lower than 4, the cathodic wave appears and the height

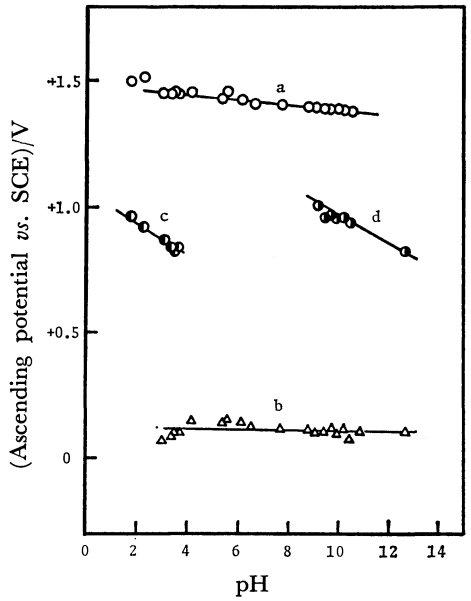

Fig. 4. Relationship between pH and wave potential of the PbO_2 electrode in 0.1 mol/l KNO_3 solution. Ascending potential: a(○), oxygen evolution; b(△), cathodic dissolution. Half-wave potential: c(◐), cathodic wave; d(◑), anodic wave.

increases with a decrease in the pH. The potential shift is −60 mV/pH (Curve c). Thus, the electrode process may be assumed to be as follows:[8]

$$PbO_2 + H^+ + e^- = PbOOH. \quad (4)$$

At pH values higher than 9, on the other hand, the anodic wave appears, and it increases with an increase in the pH values. Its potential is also shifted by −60 mV/pH, as is indicated by Curve d. Thus, the electrode process may be assumed to be as previously reported:[8]

$$PbO_2 + 2H_2O + 2e^- = Pb(OH)_2 + 2OH^-. \quad (5)$$

The ascending potential shown by Curve a is scarcely dependent on the pH of the solution. Therefore, the oxygen evolution may proceed *via* a rate-determining step, Eq. 6, as follows:

$$2PbO_2 \xrightarrow{\text{slow}} 2PbO^+ + O_2\uparrow + 2e^-, \quad (6)$$

$$PbO^+ + H_2O \xrightarrow{\text{fast}} PbO_2 + 2H^+ + e^-. \quad (7)$$

Curve b indicates that the cathodic dissolution of the PbO_2 may include a rate-determining step, Eq. 9, which is pH-independent, as follows:

$$PbO_2 + 2H^+ + e^- \xrightarrow{\text{fast}} PbO^+ + H_2O, \quad (8)$$

$$PbO^+ + e^- \xrightarrow{\text{slow}} PbO. \quad (9)$$

Similar plots are given in Fig. 5 for the rotated MnO_2 electrode. At pH values lower than 3, all the waves depend upon the pH. The ascending potential of the oxygen evolution shown by Curve a has a slope of −60 mV/pH. Thus, the following reaction may take place:

$$H_2O \longrightarrow \tfrac{1}{2}O_2\uparrow + 2H^+ + 2e^-. \quad (10)$$

The reduction potential of the MnO_2 (Curve c′) is shifted by −120 mV/pH at pH values lower than 3.

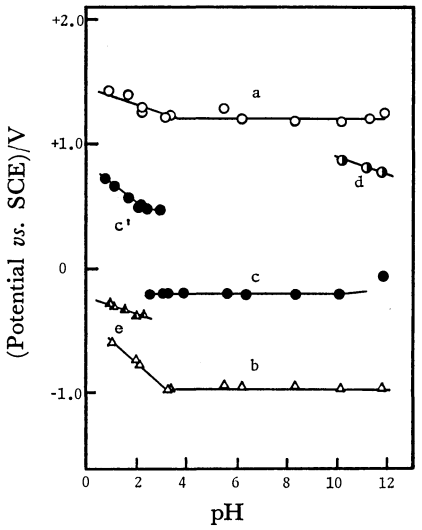

Fig. 5. Relationship between pH and wave potential of the MnO_2 electrode in 0.1 mol/l KNO_3 solution. Ascending potenital: a(○), oxygen evolution; b(△) and e(◭), hydrogen evolution. Wave potential: c and c′(●), reduction of MnO_2; d(◑), oxidation of $Mn(OH)_2$.

This result indicates that the MnO_2 on the electrode is reduced to the lower manganese state, as follows:[2]

$$MnO_2 + 4H^+ + 2e^- \longrightarrow Mn^{2+} + 2H_2O. \quad (11)$$

Curves e and b correspond to the evolution of hydrogen gas, and the simultaneous elution of the lower manganese state from the electrode, respectively. The wave height for Curve e decreased with an increase in the pH and disappeared at pH 3. The slopes of Curves b and e were −180 mV/pH and −60 mV/pH respectively. This phenomenon is too complicated to explain the reaction mechanism.

At pH values higher than 3, the potential of the oxygen evolution (Curve a) was pH-independent, indicating that the reaction scheme may be the same as that for the PbO_2 electrode:

$$2MnO_2 \xrightarrow{\text{slow}} 2MnO^+ + O_2\uparrow + 2e^-, \quad (12)$$

$$MnO^+ + H_2O \xrightarrow{\text{fast}} MnO_2 + 2H^+ + e^-. \quad (13)$$

The reduction wave of the MnO_2 appeared near −0.2 V and was pH-independent at pH values higher than 3. The same scheme as that for PbO_2 is assumed for this wave:

$$MnO_2 + 2H^+ + e^- \xrightarrow{\text{fast}} MnO^+ + H_2O, \quad (14)$$

$$MnO^+ + e^- \xrightarrow{\text{slow}} MnO. \quad (15)$$

The chemical species of MnO might not be eluted from the electrode, in contrast with the cathodic dissolution of the PbO_2 electrode. The evolution potential of hydrogen (Curve b) was also independent of the pH of the solution. This result indicates that the evolution may take place by means of the catalytic action of the oxide electrode and may include a rate-determining step, Eq. 17, as follows:

$$MnO + H_2O \xrightarrow{\text{fast}} Mn^+OH + OH^-, \quad (16)$$

$$Mn^{+}OH + H_2O + e^- \xrightarrow{slow} MnO_2 + \tfrac{2}{3}H_2\uparrow, \quad (17)$$

$$MnO_2 + 3H^+ + 2e^- \xrightarrow{fast} Mn^{+}OH + H_2O. \quad (18)$$

Tafel Slope. A useful electrode for the evolution of oxygen or hydrogen is generally estimated by means of a Tafel plot ($\eta = a + b \log [i/\mathrm{A\ m^{-2}}]$). In this investigation, the Tafel plot was examined for both the PbO_2 and MnO_2 electrodes from the ascending current-voltage curves of the evolution of oxygen and hydrogen. Figure 6 shows the relation between the pH and the *b* value of the Tafel slope of both the oxide electrodes. From Ref. 13, the Tafel slope (*b*) of oxygen evolution at the Pb/PbO_2 electrode is 0.12 V. In Fig. 6, Curve a indicates that the Tafel slope at the PbO_2 (Pt/PbO_2) electrode is constant, 0.08 V, against the pH of the solution. From Curve b of the MnO_2 (Pt/MnO_2) electrode, it was found that the *b* value of oxygen evolution is pH-dependent; this indicates that the electrode would be excellent in an acidic solution. Curve c displays the Tafel slope of hydrogen evolution at the MnO_2 electrode, on which the chemical species may be the lower manganese oxide. The *b* value is satisfactory for the electrode.

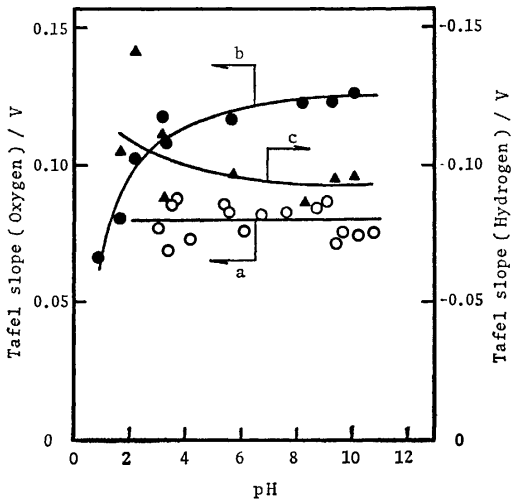

Fig. 6. Relationship between pH and Tafel slope of the evolutions of hydrogen and oxygen.
Curves: a(○), oxygen evolution at the PbO_2 electrode; b(●), oxygen evolution and c(▲), hydrogen one at the MnO_2 electrode.

Accessible Potential Ranges with Other Supporting Electrolytes. As to other systems of supporting electrolytes (constant concentration, 0.1 mol/l), each accessible potential range of both the oxide electrodes was investigated. Table 1 shows the relation between the accessible potential range at pH 5—6 and the supporting electrolyte. In each system—KNO_3, $KClO_4$, K_2SO_4, and KCl— at pH 5—6, the accessible potential range of the PbO_2 electrode was +1.4 to +0.2 V *vs.* SCE, and that of the MnO_2 electrode was +1.2 to +0.3 V, while the latter was +0.3 to −0.9 V at the lower-manganese-state electrode. The same potential ranges were obtained in the supporting electrolyte of the sodium salt instead of potassium salt.

In an acidic solution with a pH value lower than 1, the PbO_2 on the electrode was dissolved in a solution of HNO_3 and $HClO_4$, but produced insoluble films of $PbSO_4$ and $PbCl_2$ on the surface of the electrode in the solutions of H_2SO_4 and HCl respectively. This is also based upon the value of the stability constant, $\log k_1$.[14] As to the MnO_2 electrode, on the other hand, the accessible potential range was +1.4 to +0.9 V in the systems of HNO_3, $HClO_4$, and H_2SO_4, but not that of HCl (chlorine evolution).[5,7] In a basic solution, each oxide on the electrode might change to a hydroxide: $Pb(OH)_2$[8] or $Mn(OH)_2$.[5] Thus, these oxide electrodes cannot be used as dioxide electrodes, but they can be used as hydroxide electrodes.

When a buffer solution of an acetic system was used as the supporting electrolyte instead of an unbuffered solution such as KNO_3, both the oxide electrodes showed the redox waves, in spite of the small values of the stability constant,[14] as is tabulated in Table 1. Furthermore, other general buffer solutions (0.1 mol/l potassium dihydrogen phosphate, 0.1 mol/l potassium hydrogen phthalate, 0.1 mol/l potassium dihydrogen citrate, Gomori's buffer, *etc.*) were used. Similarly, both the oxide electrodes showed redox

Table 1. Accessible potential range of the rotated PbO_2 and MnO_2 electrodes in several supporting electrolyte solutions at pH 5—6

Supporting electrolyte	PbO_2 electrode		MnO_2 electrode	
	$\log k_1$[a]	Accessible potential/V[b]	$\log k_1$[a]	Accessible potential/V[b]
KNO_3	0.3	+1.4—+0.2[c]	0.46	+1.2—+0.3[d] ——0.9[e]
$KClO_4$	—	+1.4—+0.2	—	+1.2—+0.3 ——0.9
K_2SO_4	2.4	+1.4—+0.2	2.14	+1.2—+0.3 ——0.9
KCl	1.32	+1.4—+0.2	0.1	+1.2—+0.3 ——0.9
CH_3COOK	0.85	Redox wave	0.80	Redox wave

a) L. G. Sillén and A. E. Martell, "Stability Constants," The Chemical Society, London (1971); Combination of the anion ligand of supporting electrolyte with the metal(II) ion. b) V *vs.* SCE. c) Dissolution of PbO_2. d) Reduction of MnO_2. e) Evolution of hydrogen.

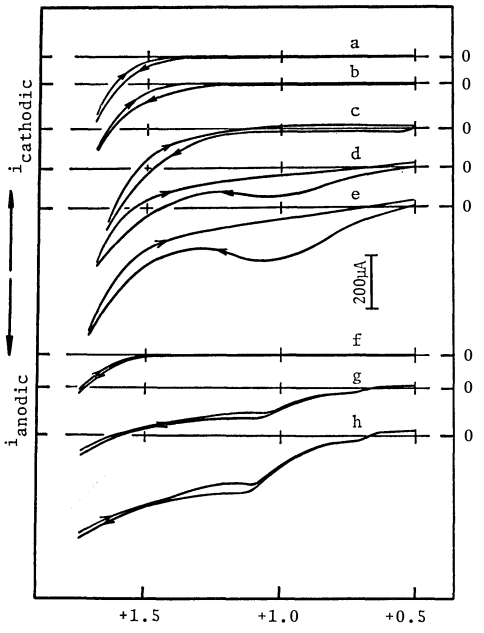

Fig. 7. Current-voltage curves of the Pt, MnO_2 and PbO_2 electrodes in 0.1 mol/l KNO_3 solution (pH 5.9) with (Curves b, d, e, g, and h) and without (Curves a, c, and f) EDTA.
Pt electrode: a and b; MnO_2 electrode: c, d, and e; PbO_2 electrode: f, g, and h. Concentration of EDTA (mmol/l), 0: a, c and f; 2.0: b, d and g; 4.0: e and h. Sweep rate: 5 mV/s at a rate of 600 min^{-1}.

waves in all these buffer solutions. Thus, these buffer solutions were not used as supporting electrolytes in this work.

Electrolytic Behavior of EDTA and the Concentration Dependence. The behavior of EDTA and other complexanes at the rotated MnO_2 and PbO_2 electrodes was also investigated. Figure 7 displays the current-voltage curves at the Pt, MnO_2, and PbO_2 electrodes in a 0.1 mol/l KNO_3 solution in the absence and in the presence of EDTA. The anodic ascending potential of the Pt electrode became a little negative only, and an anodic wave of EDTA was not observed[15] (Curve b). At the MnO_2 electrode, the anodic wave at +1.0 V appeared only in the anodic sweep. At the PbO_2 electrode, however, the pre-wave at +0.67 V and the main-wave at +0.97 V were observed in both the anodic and cathodic sweeps.

The author has previously reported on the discovery of the anodic pre-wave of EDTA at the stationary PbO_2 electrode.[8] The concentration dependence of the anodic waves of EDTA at the rotated PbO_2 electrode are shown in Fig. 8. The heights of the anodic pre-wave and main-wave were directly proportional to the EDTA concentration. The half-potential of each wave was constant. These data were reproducible within about ±3% on repeated runs. From the measurement of the anodic wave height with the PbO_2 electrode, it was possible to determine the EDTA of a concentration down to 1×10^{-5} mol/l. Figure 9 shows the relations between the wave heights and the angular velocity ω ($=2\pi N$, N: rotation rate) at the

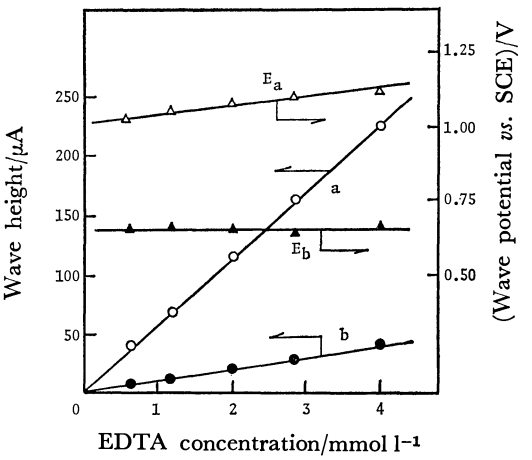

Fig. 8. Relationship between wave height, wave potential, and concentration of EDTA in 0.1 mol/l KNO_3 solution (pH 5.9).
Wave height: a(○), anodic main-wave; b(●), pre-wave. Wave potential: E_a(△), peak potential of main-wave, E_b(▲): half-wave potential of pre-wave. Electrode: PbO_2 electrode at a rate of 600 min^{-1}.

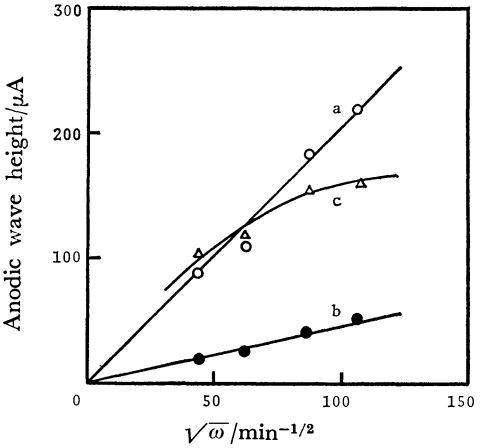

Fig. 9. Effect of angluar velocity on the anodic wave heights of 2.0 mmol/l EDTA in 0.1 mol/l KNO_3 solution (pH 6.1) with the PbO_2 (lines a and b) and MnO_2 (Curve c) electrodes.
Sweep rate: 5 mV/s. Lines a(○): PbO_2—anodic main-wave; b(●): PbO_2—pre-wave. Curve c(△): MnO_2—anodic wave.

PbO_2 and MnO_2 electrodes. A linear relationship between the wave heights and $\omega^{1/2}$ with the PbO_2 electrode was found, as is shown by Curves a and b in Fig. 9. According to Levich's opinion,[16] it follows that the limiting diffusion current, i, of the rotated disk electrode can be obtained by the use of the following equation:

$$i = \alpha\omega^{1/2}, \tag{19}$$

where α denotes the proportionality constant. It was found that the limiting currents of both the anodic waves are diffusion-controlled, because these currents were directly proportional to the $\omega^{1/2}$, Eq. 19. The anodic pre-wave is considered to be due to the adsorption of EDTA onto the electrode.[8] The anodic main-wave may be due to the complex formation of EDTA for the electrode.[8]

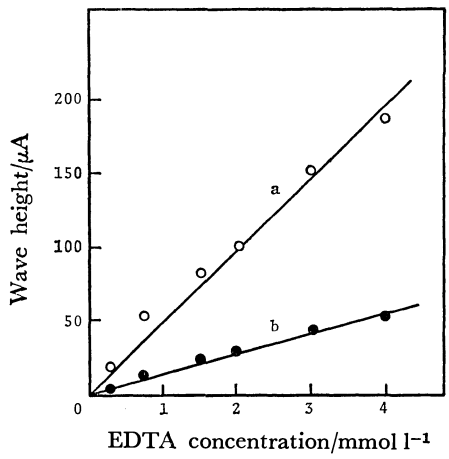

Fig.10. Relationship between wave height and concentration of EDTA in 0.1 mol/l KNO_3 solution (pH (5.9).
Lines a(○): anodic sweep; b(●): cathodic sweep.
Electrode: MnO_2 electrode at a rate of 600 min^{-1}.

For the anodic limiting current of EDTA at the rotated MnO_2 electrode, a linear concentration dependence was also found passing through the point of origin, as is shown in Fig. 10. The MnO_2 electrode showed a broader anodic wave in the anodic sweep than aid of the PbO_2 electrode. In the cathodic sweep, though no well-defined anodic wave was observed, a positive current was followed (Figs. 7-d and e). The heights of the anodic wave and the positive current in Fig. 10 were measured between the anodic current at the anodic wave potential of +1.0 V and that of the base current (Figs. 7-c, d, and e). These data obtained were reproducible within about ±5% on repeated runs. From the measurement of the anodic wave height with the MnO_2 electrode, it was possible to determine the EDTA of a concentration down to 1×10^{-5} mol/l. The effect of the rotation rate of the MnO_2 electrode on the anodic wave height was also examined. In this case, however, no linear relation was found, as is shown by Curve c in Fig. 9. This finding suggests the anodic limiting current is reaction-controlled.[16] The anodic wave is considered to be due to the complex formation of EDTA for the MnO_2 electrode.

The determination of NTA and DTPA as the EDTA-type complexanes was similar to that of EDTA with the rotated PbO_2 and MnO_2 electrodes.

Comparison with Other Methods. The techniques of the determination of complexane, such as absorption spectroscopy, chelate titrimetry, and the electroanalytical method, have been described by Ueno.[17] The determining precision of each technique is not very sharp at concentrations of a complexane lower than 1×10^{-3} mol/l. A conventional electroanalytical method, such as the polarographic method and electrometric titration, is well suited for the separation and determination of complexanes, but not for trace amounts of complexane. While the present method is an electroanalytical method, it consists of the use of an anodic limiting current dependent upon the concentration of complexane, and it is as simple as a polarographic method. This method is capable of greater precision than previously reported methods,[17] and it is well suited for small amounts, 1×10^{-5} mol/l, of complexane. The PbO_2 electrode seems to be useful for determining complexane.

Behavior of the MnO_2 Electrode in an Acidic Solution. In an acidic solution, it was found that the rotated PbO_2 electrode cannot be used as an indicator electrode, since the PbO_2 shows a self-redox wave.[8] The rotated MnO_2 electrode in the acidic solution (0.1 mol/l HNO_3) has an accessible potential range of +1.4 to +0.9 V *vs.* SCE as the rotated electrode.

The electrode reaction of complexanes on the stationary MnO_2 electrode has been reported previously;[7] a characteristic cathodic current peak of manganese dioxide which increases in the presence of complexane was observed. This is because the reduction of manganese dioxide is accelerated through the complex formation. The electrode reaction is extremely dependent on the pH of the electrolysis solution. Figure 11 shows the current-voltage curves of the rotated Pt and MnO_2 electrodes in 0.1 mol/l HNO_3 containing EDTA in anodic and cathodic sweeps. When the surface of the rotated electrode was observed during this experiment, the MnO_2 was eluted and removed at +0.85 V in the cathodic sweep (Curve d) and at +1.05 V in the anodic sweep (Curve e). At these potentials, the black color of the MnO_2 material disappeared, and the white color of the base material of platinum was observed. The MnO_2 material was removed completely from the electrode after this experiment. Thus, the rotated MnO_2 electrode is considered not to be necessary for the determination of

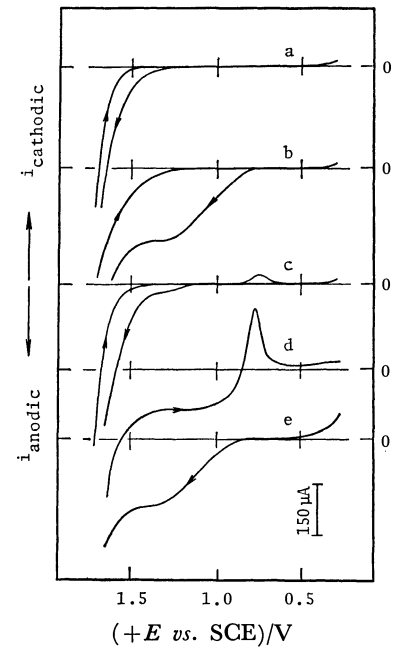

Fig.11. Current-voltage curves of the Pt and MnO_2 electrodes in 0.1 mol/l HNO_3 solution with (Curves b, d, and e) and without (Curves a and c) 1.0 mmol/l EDTA.
Pt electrode: a and b; MnO_2 electrode: c, d, and e. Surface area of both the electrodes: 0.098 cm^2. Sweep rate: 3.3 mV/s at a rate of 600 min^{-1}.

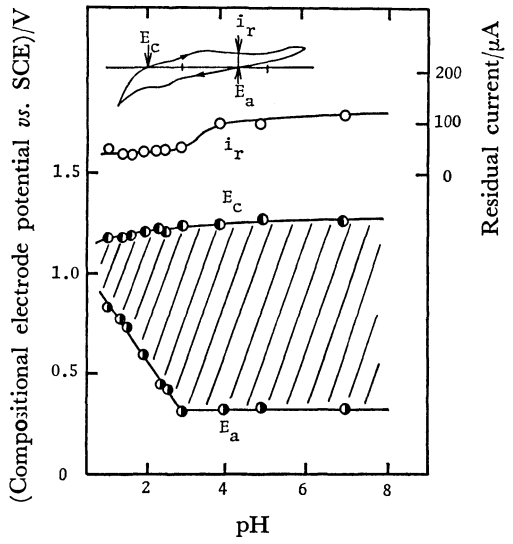

Fig.12. Effect of pH on the compositional electrode potential (zero-current level) and the residual current i_r(○) of stationary MnO_2 electrode in 0.1 mol/l KNO_3 solution with various pH.
The potential sweep range was +0.3 to +1.4 V *vs.* SCE at 30 mV/s. Compositional electrode potential: E_a(◑), anodic sweeping; E_c(◐): cathodic one. Shaded parts indicate the usable region of the stationary MnO_2 electrode as an indicator electrode.

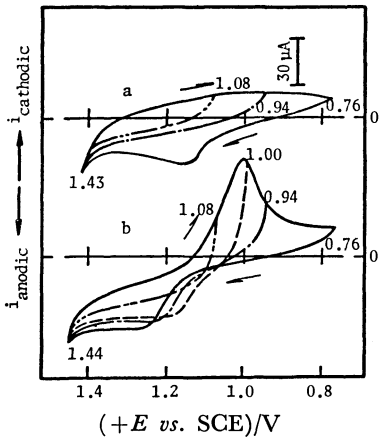

Fig.13. Cyclic current-voltage curves of stationary MnO_2 electrode with (Curve b) and without (Curve a) 1.0 mmol/l DTPA in 0.1 mol/l HNO_3 solution (pH 1.5) at a sweep rate of 3.3 mV/s.
Potentials returned in the reverse direction varied from +1.44 to +0.76 V *vs.* SCE as indicated.

complexane in an acidic solution.

According to a previous paper,[7] the stationary MnO_2 electrode is adequate as an indicator electrode for the determination of complexane in an acidic solution. The accessible potential range of the stationary MnO_2 electrode was also examined against the pH of the solution. Figure 12 shows the influence of the pH on the compositional electrode potential of the stationary MnO_2 electrode, which is defined as the potential of zero-current in the cyclic current-voltage curve (E_a and E_c). The shaded parts in Fig. 12 indicate the accessible potential range of the MnO_2

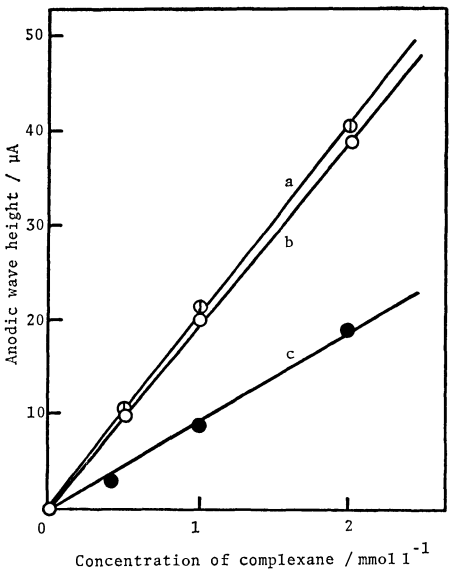

Fig.14. Relationship between concentration of complexanes and anodic wave heights in 0.1 mol/l HNO_3 solution (pH 1.5) at a sweep rate of 3.3 mV/s.
Electrode: MnO_2. Complexane: a(ⓓ), DTPA; b (○), EDTA; c(●), NTA. The potential at which the wave height was measured from the curve was +1.3 V *vs.* SCE.

electrode in the pH region of solution. As the residual current of the MnO_2 electrode became large and the electrode became voltammetrically inert at pH values higher than 3 (Fig. 12-i_r), the stationary MnO_2 electrode is considered to be suitable for use at pH values lower than 3. In the application of the stationary MnO_2 electrode, the base current and the redox wave of DTPA in the accessible potential range are shown in Fig. 13. When current-voltage curves are measured over the accessible potential range, the electrolytic process of the anodic wave is complicated. In order to study the concentration-dependence of each complexane (DTPA, EDTA, and NTA), the height of the anodic wave was measured at +1.3 from the abscissa of the zero-current level. Figure 14 shows the relation between the wave heights and the concentrations of DTPA, EDTA, and NTA in a 0.1 mol/l HNO_3 solution. Each height was directly proportional to the concentration of complexane. These data were reproducible within about ±5% on repeated runs. From the measurement of the anodic wave-height of complexane with the stationary MnO_2 electrode, it was possible to determine the quantities of complexane in concentrations down to 1×10^{-4} mol/l.

The author wishes to express his thanks to Professor Taitiro Fujinaga and Doctor Satoshi Okazaki of Kyoto University, and Professor Kazunori Takaoka of Fukui Technical College for their valuable advice and discussions throughout this work.

References

1) I. M. Kolthoff and N. Tanaka, *Anal. Chem.*, **26**, 632 (1954).

2) M. Sato, K. Matsuki, and Y. Sugawara, *Kogyo Kagaku Zasshi*, **71**, 484 (1968); **74**, 872 (1971).
3) J. Reynaud, *Bull. Soc. Chim. Fr.*, **1968**, 4769.
4) J. A. Lee, W. C. Maskell, and F. L. Tye, *J. Electroanal. Chem.*, **79**, 79 (1977).
5) T. Yoshimura, *Res. Rep. Fukui Tech. Coll., Natural Science*, **14**, 149 (1980).
6) J. P. Carr and N. A. Hampson, *Chem. Rev.*, **72**, 679 (1972).
7) T. Yoshimura, *Nippon Kagaku Kaishi*, **1981**, 240; T. Fujinaga and T. Yoshimura, *Chem. Lett.*, **1980**, 865.
8) T. Yoshimura, *Fresenius' Z. Anal. Chem.*, **307**, 197 (1981); T. Fujinaga and T. Yoshimura, *Chem. Lett.*, **1980**, 895.
9) T. Fujinaga and T. Yoshimura, *Fresenius' Z. Anal. Chem.*, **306**, 20 (1981).
10) T. Yoshimura, *Fresenius' Z. Anal. Chem.*, **308**, 445 (1981).
11) T. Yoshimura, *Fresenius' Z. Anal. Chem.*, **307**, 378 (1981).
12) T. Yoshimura, *Nippon Kagaku Kaishi*, **1981**, 307.
13) D. J. Pickett, "Electrochemical Reactor Design," Elsevier, Amsterdam (1977).
14) L. G. Sillén and A. E. Martell, "Stability Constants," The Chemical Society, London (1971).
15) K. Stulík and F. Vydra, *J. Electroanal. Chem.*, **16**, 385 (1968).
16) V. G. Levich, "Physicochemical Hydrodynamics," Prentice-Hall, N. J. (1962).
17) K. Ueno, "EDTA-Chemistry of Complexane," Nankodo, Tokyo (1977), p. 231.

The Crystal and Molecular Structure of $Cu(AlCl_4)_2$

Nobumasa KITAJIMA, Hirotaka SHIMANOUCHI,† Yoshio ONO,* and Yoshio SASADA†

Department of Chemical Engineering, Tokyo Institute of Technology, Ookayama, Meguro-ku, Tokyo 152

†*Laboratory of Chemistry for Natural Products, Tokyo Institute of Technology, Nagatsuta, Midori-ku, Yokohama 227*

(Received July 25, 1981)

The structure of copper(II) tetrachloroaluminum $Cu(AlCl_4)_2$ was determined by the single-crystal X-ray diffraction technique. The crystal is triclinic: $a=6.582(6)$, $b=7.362(5)$, and $c=12.265(5)$ Å; $\alpha=89.99(5)$, $\beta=85.97(6)$, and $\gamma=89.77°$; space group $P\bar{1}$ and $Z=2$. The structure was solved by the heavy-atom method and refined by applying the block-diagonal matrix least-squares technique on 2628 independent reflections up to a final R value of 0.110. The structure consists of closely-packed centrosymmetric $Cu(AlCl_4)_2$ molecules with copper atoms tetragonally coordinated. Structural difference between $Cu(AlCl_4)_2$ and $Co(AlCl_4)_2$ is described.

Aluminium halides form complexes with various halides in gas phase, and their structures and thermal properties have been extensively studied.[1-5] However, no attempt has been made to isolate crystals of such complexes and determine their crystal structures by single-crystal X-ray analysis, except for $Co(AlCl_4)_2$.[6]

We have reported that aluminium chloride and copper(II) chloride form a 2:1 complex, $2AlCl_3 \cdot CuCl_2$, when heated together.[7] The complex is a very active catalyst for isomerization of pentane at room temperature.[8,9] Studies on the structure of this complex by ESR and Raman spectroscopy have suggested that the complex contains $(AlCl_4)^-$ units and that the coordination environment of Cu(II) ions is of distorted octahedron, though the structure of $CuCl(Al_2Cl_7)$ was proposed for the complex in gas phase.[10,11]

Though the structure of $Co(AlCl_4)_2$ has been determined by Ibers,[6] the powder X-ray pattern of the present complex[8] is different from that of $Co(AlCl_4)_2$.

In the present work, the structure of $2AlCl_3 \cdot CuCl_2$ is determined in order to obtain the structural basis for the catalytic activity of this compound.

Experimental

Suitable crystals for diffraction measurements were prepared by the chemical transport method. A mixture of $AlCl_3$ and $CuCl_2$ (0.5 g each) was sealed under vacuum in a Pyrex glass tube of about 15 cm length with a diameter of 1.5 cm. Then, the tube was partitioned into three parts, which were heated in an electronic furnance at 170, 190, and 230 °C, respectively. Fine yellow prismatic crystals were deposited on the glass wall at the middle part. The density of the crystal was determined by flotation in a mixture of CCl_4 and CH_2Br_2. Since the compound is hygroscopic, a crystal of approximately $0.2\times0.3\times0.55$ mm³ was sealed in a thin-walled glass capillary filled with nitrogen. Cell constants were obtained from the least-squares treatment on angular settings of 25 high angle reflections. Data collection was carried out on a Rigaku computer-controlled four-circle diffractometer, using the graphite-monochromated Mo $K\alpha$ radiation. The crystal data and the details of experimental conditions are summarized in Table 1. Attenuators were automatically inserted to keep the counting rate below 8000 cps. Backgrounds were counted for 10 s at each end of scan range. Intensities were corrected for the Lorentz and polarization factors but not for the absorption. Four standard reflections measured after every 100 reflections indicated no significant intensity variation throughout the experiment.

Structure Determination

The structure was solved by the heavy-atom method and atomic parameters were refined by the block-diagonal least-squares technique. The quantity minimized was $\Sigma w(|F_o| - k|F_c|)^2$ with $w=1/\sigma^2(F_o)$. Zero reflections were included in the least-squares calculation by assuming $|F_o|=F_{lim}$ $(=1.86)$ where F_{lim} is the observed threshold value, but they were omitted when $|F_c|-F_{lim}$. The final R value was 0.110 for non-zero reflections. Final atomic parameters are listed in Table 2.[12] Atomic scattering factors were taken from the International Table for X-ray Crystallography.[13] Computations were done on a HITAC M-170 computer in Tokyo Institute of Technology by use of the program system XSEN.[14] The programs

Table 1. Crystal data and detail of experimental conditions

Formula	$CuAl_2Cl_8$
Formula weight	401.1
Crystal system	$P\bar{1}$
a/Å	6.582(6)
b/Å	7.362(5)
c/Å	12.265(5)
α	89.99(5)°
β	85.97(6)°
γ	89.77(6)°
V/Å³	592.8
Z	2
D_m/g cm^{-3}	2.25
D_x/g cm^{-3}	2.25
μ(for Mo $K\alpha$)/cm^{-1}	37.9
Crystal size/mm	$0.20\times0.30\times0.55$
Scan technique	ω-2θ scan
Scan range (ω)	$1.0°+0.35°\tan\theta$
Scan speed (ω)/min^{-1}	2°
Maximum 2θ	54°
No. of reflections measured	2628
No. of non-zero reflections ($\|F_o\|>3\sigma(F)$)	2594

Table 2. Final atomic coordinates and e.s.d.'s

Atom	10^4x	10^4y	10^4z	$10B_{eq}$/Å^2
Cu(1)	0	0	0	33
Cu(2)	0	5000	5000	32
Al(1)	−1915(7)	2752(5)	1812(3)	28
Al(2)	1910(7)	7654(5)	3192(3)	28
Cl(1)	1109(6)	2442(4)	941(3)	34
Cl(2)	−2993(6)	130(5)	1082(3)	36
Cl(3)	−1650(7)	2333(5)	3502(3)	42
Cl(4)	−3589(7)	4868(6)	1368(4)	49
Cl(5)	−1123(6)	7441(5)	4053(3)	33
Cl(6)	3003(6)	5141(5)	3916(3)	35
Cl(7)	1666(7)	7332(5)	1500(3)	41
Cl(8)	3555(7)	9871(6)	3637(3)	50

a) B_{eq} is the equivalent isotropic temperature factor, defined by $B_{eq}=8\pi^2(U_1+U_2+U_3)/3$ where U_1, U_2, and U_3 are the principal components of U matrix.

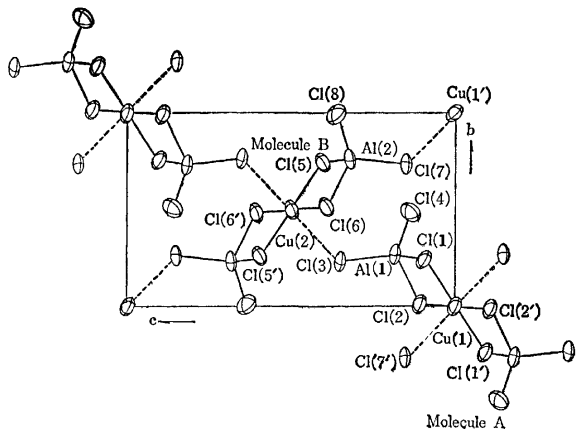

Fig. 1. Atomic numbering and thermal ellipsolids at the 50% probability level.

DCMS for plotting thermal ellipsolids[15] and DCMSGD for drawing crystal structures[16] were also used.

Results and Discussion

The crystal structure of the complex $2AlCl_3\cdot CuCl_2$ consists of two crystallographically independent molecules of $Cu(AlCl_4)_2$ as shown in Fig. 1. Each molecule has a crystallographic center of symmetry; molecule A is on the origin while molecule B resides at (0, 1/2, 1/2). Both molecules are approximately related by a twofold screw axis at $x=0$, $z=1/4$ or by a c glide plane at $y=1/4$, indicating a pseudo $P2_1/c$ symmetry, which was inferred from the systematically weak intensities of $0k0$ and $h0l$ reflections.

The interatomic distances and angles are listed in Table 3. There are no significant structural differences between the two molecules. Each copper atom is tetragonally coordinated by chlorine atoms with a mean Cu–Cl distance of 2.295 Å, slightly shorter than the sum of the tetrahedral covalent radii.[17] The next nearest neighboring chlorine atoms are located above and below the plane of this group at a distance of 2.951 Å as indicated with the broken lines in Fig. 1. This distance corresponds to a bond number of about 0.1,[18] implying very weak interaction. Similar situations are usually observed with many copper (II) complexes.[19] The Cu(1)→Cl(7') and Cu(2)→Cl(3) vectors make angles of 86.4° and 86.5° with the corresponding basal planes, respectively.

Table 3. Interatomic distances and angles

(a) Bond distances (l/Å)			
Cu(1)–Cl(1)	2.286(4)	Cu(2)–Cl(5)	2.288(4)
Cu(1)–Cl(2)	2.298(4)	Cu(2)–Cl(6)	2.306(4)
Cu(1)–Cl(7')	2.951(4)	Cu(2)–Cl(3)	2.951(4)
Cl(7')–Cl(1)	3.844(5)	Cl(3)–Cl(5)	3.842(5)
Cl(7')–Cl(2)	3.752(5)	Cl(3)–Cl(6)	3.766(5)
Cl(7')–Cl(1')	3.618(5)	Cl(3)–Cl(5')	3.624(5)
Cl(7')–Cl(2')	3.729(5)	Cl(3)–Cl(6')	3.725(5)
Cl(1)–Cl(2)	3.192(5)	Cl(5)–Cl(6)	3.189(5)
Cl(1)–Cl(2')	3.291(5)	Cl(5)–Cl(6')	3.307(5)
Al(1)–Cl(1)	2.197(5)	Al(2)–Cl(5)	2.198(5)
Al(1)–Cl(2)	2.203(5)	Al(2)–Cl(6)	2.193(5)
Al(1)–Cl(3)	2.105(6)	Al(2)–Cl(7)	2.106(6)
Al(1)–Cl(4)	2.060(6)	Al(2)–Cl(8)	2.057(6)
Cl(1)–Cl(3)	3.517(5)	Cl(5)–Cl(7)	3.517(5)
Cl(1)–Cl(4)	3.571(6)	Cl(5)–Cl(8)	3.573(6)
Cl(2)–Cl(3)	3.550(5)	Cl(6)–Cl(7)	3.538(5)
Cl(2)–Cl(4)	3.523(6)	Cl(6)–Cl(8)	3.517(6)
Cl(3)–Cl(4)	3.523(6)	Cl(7)–Cl(8)	3.520(6)
Al(1)–Cu(1)	3.150(4)	Al(2)–Cu(2)	3.153(4)
(b) Bond angles (ϕ/°)			
Cl(1)–Cu(1)–Cl(2)	88.3(1)	Cl(5)–Cu(2)–Cl(6)	87.9(1)
Cl(7')–Cu(1)–Cl(2)	90.4(1)	Cl(3)–Cu(2)–Cl(6)	90.7(1)
Cl(7')–Cu(1)–Cl(1)	93.6(1)	Cl(3)–Cu(2)–Cl(5)	93.5(1)
Cl(1)–Al(1)–Cl(2)	93.0(2)	Cl(5)–Al(2)–Cl(6)	93.2(2)
Cl(1)–Al(1)–Cl(3)	109.7(2)	Cl(5)–Al(2)–Cl(7)	109.6(2)
Cl(1)–Al(1)–Cl(4)	114.1(2)	Cl(5)–Al(2)–Cl(8)	114.2(2)
Cl(2)–Al(1)–Cl(3)	111.0(2)	Cl(6)–Al(2)–Cl(7)	110.7(2)
Cl(2)–Al(1)–Cl(4)	111.5(2)	Cl(6)–Al(2)–Cl(8)	111.7(2)
Cl(3)–Al(1)–Cl(4)	115.5(3)	Cl(7)–Al(2)–Cl(8)	115.4(3)
Cu(1)–Cl(2)–Al(1)	88.8(2)	Cu(2)–Cl(6)–Al(2)	89.0(2)
Cu(1)–Cl(1)–Al(1)	89.3(2)	Cu(2)–Cl(5)–Al(2)	89.3(2)
Cu(2)–Cl(3)–Al(1)	126.8(2)	Cu(1')–Cl(7)–Al(2)	126.6(2)

Each aluminium atom is tetrahedrally coordinated by chlorine atoms, and the more strongly the chlorine atom is coordinated to the copper atom, the longer the Al–Cl distance becomes as in the case of $Co(AlCl_4)_2$.[6] The uncoordinated chlorine atoms have the shortest Al–Cl distances of 2.057 and 2.060 Å. These values are smaller than those obtained for $Co(AlCl_4)_2$ (2.105 Å),[6] $C_6H_6CuAlCl_4$ (2.078 Å),[20] $(C_6H_6PdAlCl_4)_2$ (2.10 Å),[21] and $NaAlCl_4$ (2.11 Å),[22] indicating that the $AlCl_4$ tetrahedra in the present complex are the most distorted among these chloroaluminate complexes.

The interplanar angle between the Cu(1), Cl(1), Cl(2), and Cl(1), Cl(2), Al(1) planes and that between the Cu(2), Cl(5), Cl(6), and Cl(5), Cl(6), Al(2) planes are 8.3° and 8.7°, respectively. The Cu–Al distances are long and the bridging Cu–Cl–Al angles are not highly acute, implying that there is no direct metel-metel interaction.[23]

The networks composed of $AlCl_4$ tetrahedra and $CuCl_6$ distorted octahedra lie parallel to the bc plane

of the unit cell, forming a layer structure. The closest distance between the layers is about 3.60 Å for Cl(7) Cl(4) at $(1+x, y, z)$. It is equal to twice the van der Waals radius of chlorine (1.80 Å).

The crystal structures of $Co(AlCl_4)_2$[6] and $Cu(AlCl_4)_2$ are compared in Figs. 2(a) and 2(b). In both structures $AlCl_4$ groups play a dual role as monocoordinate as well as bicoordinate ligands. An important difference is the fact that the cobalt atom resides on the crystallographic two-fold axis and has *cis* configuration, 1, whereas the copper atom sits on the center of symmetry and possesses *trans* configuration, 2, as far as the monocoordinate ligands are concerned.

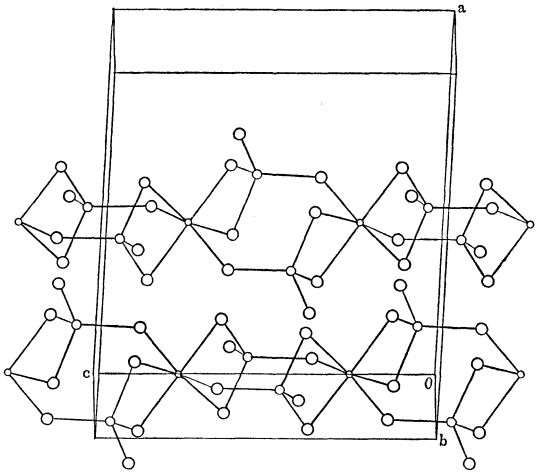

Fig. 2(a). Crystal structure of $Co(AlCl_4)_2$.

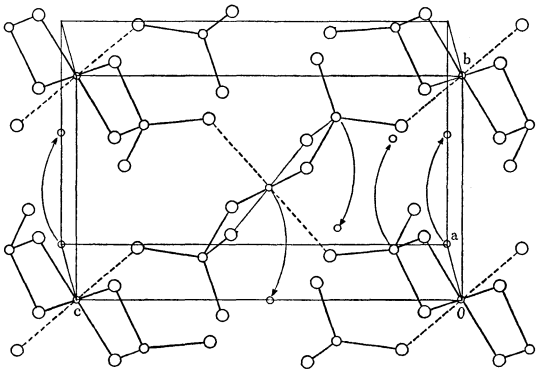

Fig. 2(b). Crystal structure of $Cu(AlCl_4)_2$.
If the copper and aluminum atoms would be transfered as indicated with arrows, the hypothetical structure could be derived as shown in Fig. 2(c).

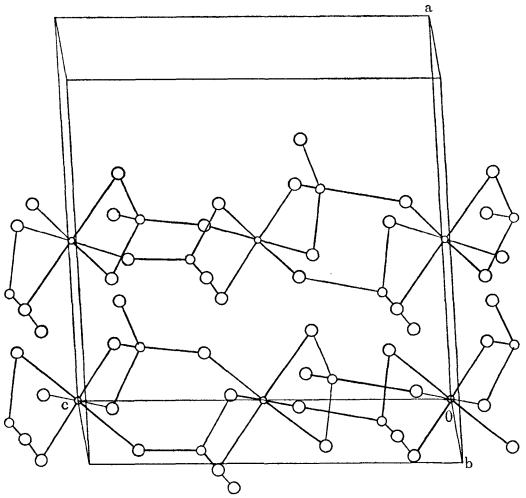

Fig. 2(c). Hypothetical crystal structure of $Cu(AlCl_4)_2$.

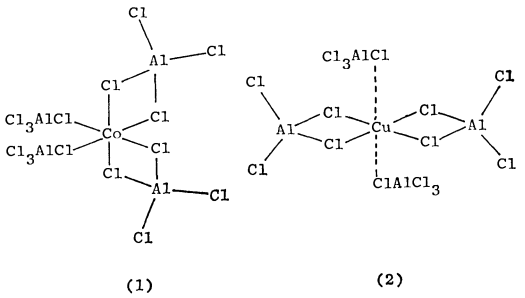

(1) (2)

The crystal structure of the present compound, like that of $Co(AlCl_4)_2$,[6] consists of layers parallel to the (001) plane, each containing atoms of one kind. The layers repeat in the sequence Cu–Cl–Al–Al–Cl. As shown in Fig. 3, the chlorine atoms are arranged in the unit cell in approximately hexagonal close-packed arrays like those observed with $Co(AlCl_4)_2$,[6] with copper and aluminium atoms occupying a part of the available octahedral and tetrahedral interstices, respectively. The volume per chlorine atom is 37.1 Å^3, which is slightly larger than the volume for $Co(AlCl_4)_2$,[6] 35 Å^3.

The essential difference between the two structures originates from the different intralayer arrangement of cobalt and copper atoms, and from the interlayer displacement of aluminium atoms in two successive layers. Thus, the hypothetical structure of $Co(AlCl_4)_2$ type could be generated from the observed structure of $Cu(AlCl_4)_2$ by simply translating metal atoms along the b axis in the way given in Fig. 2(b), though the obtained structure (Fig. 2(c)) as it is, has abnormalities in some of interatomic distances and bond angles. On the other hand, if cobalt atoms in $Co(AlCl_4)_2$ were replaced by copper atoms, these atoms would inevitably be in an octahedral geometry with nearly equal Cu–Cl distances. The structural difference between $Cu(AlCl_4)_2$ and $Co(AlCl_4)_2$[6] may result from the difference in preferred coordination geometries of the transition metals in this system.

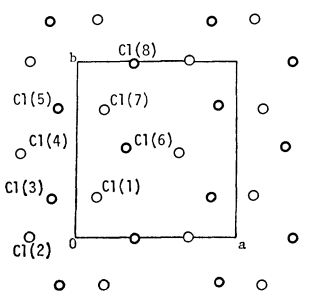

Fig. 3. Projection of chlorine layers.
The atoms drawn with thicker circles are nearer to the viewer.

The authors are grateful to Dr. Akio Takenaka for his advice in computer calculation and Professor Tominaga Keii for his helpful discussion.

References

1) A. Dell'Anna and F. P. Emmenegger, *Helv. Chim. Acta*, **58**, 1145 (1975).
2) A. Anundskas and H. A. Øye, *J. Inorg. Nucl. Chem.*, **37**, 1609 (1975).
3) W. C. Laughlln and N. W. Gregory, *J. Phys. Chem.*, **80**, 127 (1976).
4) G. N. Papatheodorou and G. H. Kucera, *Inorg. Chem.*, **16**, 1006 (1977).
5) H. Schafer, *Angew. Chem., Int. Ed. Engl.*, **15**, 713 (1976).
6) J. A. Ibers, *Acta Crystallogr.*, **15**, 967 (1962).
7) N. Kitajima and Y. Ono, *J. Mol. Catal.*, **10**, 121 (1981).
8) Y. Ono, N. Kitajima, T. Nakajima, and T. Keii, *Proc. 7th Int. Congr. Catal., Tokyo*, p. 1006 (1980).
9) Y. Ono, T. Tanabe, and N. Kitajima, *J. Catal.*, **56**, 47 (1979).
10) F. P. Emmenengger, C. Rohrbasser, and C. W. Schlapfer, *Inorg. Nucl. Chem. Lett.*, **12**, 127 (1976).
11) C. W. Schlapfer and C. Rohrbasser, *Inorg. Chem.*, **17**, 1623 (1978).
12) The anisotropic thermal parameters and the list of the observed and calculated structure factors are kept at the Chemical Society Japan as Document No. 8239.
13) "International Tables for X-Ray Crystallography," Kynoch Press, Birmingham (1974), Vol. IV, p. 71.
14) A. Takenaka, XSEN, The crystallographic Computing System, Laboratory of Chemistry for Natural Products, Tokyo Institute of Technology (1980).
15) A. Takenaka, Program DCMS, Schematic Drawing of Crystal and Molecular Structures Containing Atomic Thermal Motions, Laboratory of Chemistry for Natural Products, Tokyo Institute of Technology (1974).
16) K. Harata, Program DCMSGD, A Computer Program for Drawing Crystal and Molecular Structures on Graphic Display or X-Y Plotter, Research Institute for Polymers and Textiles, Yatabemachi Higashi, Tsukuba-gun, Ibaraki 305 (1978).
17) L. Pauling, "Nature of the Chemical Bond," 3rd ed, Cornell University Press, Ithaca, N. Y. (1960), p. 246.
18) L. Pauling, "Nature of the Chemical Bond," 3rd ed Cornell University Press, Ithaca, N. Y. (1960), p. 255.
19) B. J. Hathaway and D. E. Billing, *Coord. Chem. Rev.*, **5**, 143 (1970).
20) R. W. Turner and E. L. Amma, *J. Am. Chem. Soc.*, **88**, 1877 (1966).
21) G. Allegra, G. T. Casagrande, A. Immirzi, L. Porri, and G. Vitulli, *J. Am. Chem. Soc.*, **92**, 289 (1970).
22) N. C. Baenziger, *Acta Crystallogr.*, **4**, 216 (1951).
23) L. F. Dahl, E. R. de Gil, and R. D. Feltham, *J. Am. Chem. Soc.*, **91**, 1653 (1969).

Kinetic Studies of the Oxidation of L-Ascorbic Acid by the Peroxodisulfate Ion, and of Copper(II)-catalysis

Masaru KIMURA,* Akiko KOBAYASHI, and Keiko BOKU
Department of Chemistry, Faculty of Science, Nara Women's University, Nara 630
(Received October 5, 1981)

Kinetic studies of the oxidation reaction of L-ascorbic acid by the peroxodisulfate ion($S_2O_8^{2-}$) are carried out in an aqueous solution over the pH range of 3.4—4.6 at various ionic-strengths from 0.071 to 1.07 M (1 M= 1 mol dm^{-3}) with $NaClO_4$, and at four temperatures between 15 and 30 °C, at an ionic-strength of 1.07 M. The variations in the rate of the oxidation with the hydrogen-ion concentrations are consistent with the reaction schemes involving two pH-related species; ascorbic acid H_2A ($k_1=0.032$ M^{-1} s^{-1} at 25 °C, $\Delta H_1^{\ddagger}=17$ kJ mol^{-1}, $\Delta S_1^{\ddagger}=-220$ J deg^{-1} mol^{-1}) and the ascorbic anion HA^- ($k_2=0.43$ M^{-1} s^{-1} at 25 °C, $\Delta H_2^{\ddagger}=45$ kJ mol^{-1}, $\Delta S_2^{\ddagger}=-102$ J deg^{-1} mol^{-1}). A relationship of $\log k_2=-1.47+2.17\,I^{1/2}/(1+I^{1/2})$ is found with the ionic-strength (I) at 25 °C. The reaction rate is greatly catalyzed by the presence of trace amounts of the copper(II) ion; the mechanisms of the copper(II)-catalyzed reaction are discussed.

The peroxodisulfate ion is known as a powerful two-electron oxidizing agent, and its reactions with organic and inorganic substrates have been extensively studied by many researchers and reviewed by several authors.[1-4] Previously, we studied the kinetics of the oxidation reactions of oxalic acid,[5] formic acid,[6] the thallium ion,[7] and the silver(I) ion[8] by the peroxodisulfate ion in an aqueous solution. The present paper intends to propose a reaction mechanism and the kinetic parameters for the reaction between L-ascorbic acid and the peroxodisulfate ion in an acidic aqueous solution, and also to propose the kinetic properties of the copper(II) ion-catalyzed reaction for this reaction system.

Experimental

Reagents. Reagent-grade potassium peroxodisulfate was recrystallized twice from redistilled water and dried at 25 °C in a vacuum desiccator. L-ascorbic acid of a guaranteed-reagent grade of the Wako Pure Chemical Co., Ltd., was used without further purification. Solutions of peroxodisulfate and L-ascorbic acid were prepared just before each use. The sodium perchlorate used for adjusting the ionic-strength was purified by filtering the aqueous solution through filter-paper coated with activated carbon[9] and then recrystallized twice from redistilled water. The redistilled water was prepared from the deionized water by successive distillation of solutions with and without permanganate in a glass still. All the other chemicals used were guaranteed reagents of the Wako Pure Chemical Co., Ltd.

Reaction Solution. Preliminary experiments showed that (1) the rate of reaction decreased with a decrease in the pH in the reacting solution, and thus gradually became slow by the pH decrease, according to the progress of the reaction in an unbuffered solution for pH (refer to Table 1), and that (2) the rate of reaction was greatly catalyzed by a trace amount of the copper(II) ion (see Table 4 and Fig. 5); it seemed that the rate was slightly accelerated by the trace impurity of the copper(II) ion present in the reagents used (see line(2) in Fig. 3), and such a catalytic effect of the copper(II) ion was masked by the presence of ethylenediaminetetraacetate (EDTA) (see a closed mark (●) in Fig. 3 and also Table 4). Thus, we used pH buffer solutions of acetate-acetic acid involving 0.05 M in sodium acetate, and 0.005 M in disodium dihydrogen ethylenediaminetetraacetate (EDTA), as masking agents against the copper(II)-catalysis.

Kinetic Measurements. The reaction was started by mixing the peroxodisulfate solution with an L-ascorbic acid solution containing the pH buffer, EDTA, and sodium perchlorate. The pH value, ionic strength, and temperature of the reaction solution were kept constant at a given value. The reaction vessel was covered with black adhesive-plastic tape to ensure darkness and placed in a thermostat bath. Aliquot samples were withdrawn at appropriate times, and the concentration of the peroxodisulfate ion remaining was measured at 0.15 V *vs.* SCE (a saturated calomel electrode) by means of polarography in a solution of 0.05 M perchloric acid, 0.1 M sodium perchlorate, and 0.01% gelatin at 25 °C, essentially as has been described previously.[5-8] The gelatin was used as a maximum suppressor. Preliminary experiments showed that the rate of reaction between L-ascorbic acid and peroxodisulfate was so slow in a perchloric acid solution of 0.05 M that the loss of both the reactants during the period of about 5 min. needed for the measurement of the polarogram was, in practice, negligible. Since the reaction rate was not affected by the oxygen dissolved in a solution, the kinetic runs were carried out in solutions without removing the dissolved air, unless otherwise stated. The pH of the reacting solution was measured for the aliquot samples by the use of a Hitachi-Horiba M-5 pH meter. Sodium chloride was used instead of potassium chloride as the electrolyte in the reference electrode of the pH meter. The ionic strength was adjusted by the addition of sodium perchlorate. The activity coefficients f_i at varying ionic strengths (I) were obtained by using $\log f_i=-0.358\times Z_i^2\,I^{1/2}/(1+10^8\,a_i\times 0.2325\,I^{1/2})$ with $a_i=900$ pm and $Z_i=1$.[10] The activity coefficients used in this paper were 0.88 (0.071), 0.83 (0.2), 0.79 (0.47), and 0.77 (1.07), with the ionic strength in parentheses.

Results and Discussion

Stoichiometry. With concentration of 5.0×10^{-3} M for each reactant of peroxodisulfate and L-ascorbic acid, the concentrations of the reactants disappearing according to the reaction were determined at the reaction times. The results are shown in Table 1. The concentrations of peroxodisulfate and L-ascorbic acid were measured at 0.15 V *vs.* SCE and 0.375 V *vs.* SCE, respectively by means of polarography in a solution of 0.05 M perchloric acid, 0.1 M sodium perchlorate, and 0.01% gelatin at 25 °C. Under these conditions, only the reduction current of the peroxodisulfate ion was measured at 0.15 V, while the total

Table 1. Stoichiometry[a)]

Reaction time h	pH	$10^3[S_2O_8^{2-}]_{disapp.}$ M	$10^3[AA]_{disapp.}$ M	$[S_2O_8^{2-}]_{disapp.}/[AA]_{disapp.}$
0	4.06	—	—	—
1	3.36	1.30	1.32	0.98
2	3.10	1.63	1.65	0.99
3	2.99	1.75	1.78	0.98
4	2.88	1.91	1.96	0.97
5	2.81	2.07	2.09	0.99
				Av. 0.98

a) The initial concentrations are: $[S_2O_8^{2-}]_i=[AA]_i=5.0\times10^{-3}$ M. Unbuffered solutions at an ionic strength of 0.02 M at 25 °C and in the dark.

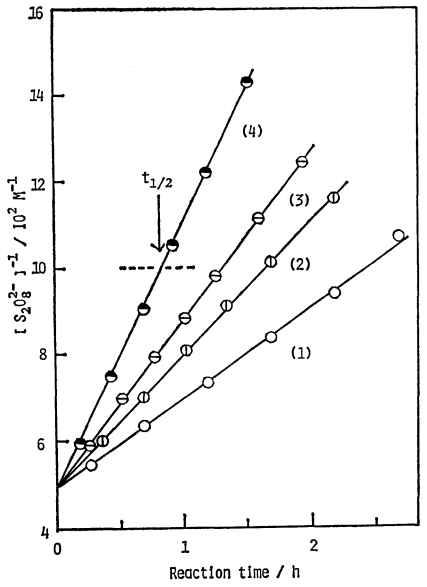

Fig. 1. Examples of plots of $[S_2O_8^{2-}]^{-1}$ *vs.* t (Eq. 1). The pH values are 3.50, 3.71, 3.90, and 4.40 for lines (1), (2), (3), and (4), respectively. Other conditions are the same as those of a) in Table 2 at an ionic strength of 0.47 M.

currents of reduction of the peroxodisulfate ion and of the oxidation of L-ascorbic acid were measured at 0.375 V. The results in Table 1 may indicate the stoichiometry to be 1:1. This stoichiometry was confirmed by kinetic experiments such as those illustrated in Fig. 1.

Kinetics of Reaction. The kinetic runs were carried out over the pH range from 3.3 to 4.6. In this pH range, the thermal decomposition of both peroxodisulfate and L-ascorbic acid was so slow that it could be neglected. When the reaction was started at the same concentrations for both reactants, the plots of $[S_2O_8^{2-}]^{-1}$ *vs.* t were rectilinear; some examples of the plots are given in Fig. 1. Thus, the empirical rate law may be written as follows:

$$-d[S_2O_8^{2-}]/dt = -d[AA]/dt = k_0[AA][S_2O_8^{2-}] \quad (1)$$

where k_0 is the observed second-order rate constant and where [AA] indicates the total concentration of all the forms of L-ascorbic acid and can be set as $[H_2A]+[HA^-]$ in the present pH range. The rate constants (k_0) were determined by treating plots of $[S_2O_8^{2-}]^{-1}$ *vs.* t with a least-squares method. The values of k_0 obtained are given in Table 2. The plots of k_0 *vs.* $K_1/(K_1+[H^+])$ showed a straight line with an intercept; some examples of the plots are given in Fig. 2. Thus, the relationship of the k_0 with $[H^+]$ is accounted for by Eq. 2, consistent with the reaction mechanisms (*v.i.*):

$$k_0 = k_1 + (k_2-k_1)\frac{K_1}{[H^+]+K_1}, \quad (2)$$

where K_1 is the first acid-dissociation constant of L-ascorbic acid of Eq. 3. The rate constants, k_1 and k_2, were determined by treating plots of k_0 *vs.* $K_1/([H^+]+K_1)$ with a least-squares method; they are listed in Table 3. The values of K_1 were necessary for making the plots such as in Fig. 2. Recently,[11] we determined the K_1 values by the pH titration of L-ascorbic acid under various conditions. The values of pK_1 used in this work are as follows: at an ionic strength of 1.07 M (with the temperature (°C) in parentheses): 4.04 (15), 4.00 (20), 3.95 (25), and 3.90 (30), and at 25 °C (with the ionic strength in parentheses): 4.09 (0.071), 4.00 (0.2), and 3.96 (0.47).

Mechanisms of Reaction. The following three schemes can be presented to account for the empirical results:

$$H_2A \overset{K_1}{\rightleftharpoons} HA^- + H^+ \quad (3)$$

Scheme 1:

$$H_2A + S_2O_8^{2-} \xrightarrow{k_1} 2SO_4^{2-} + A + 2H^+ \quad (4)$$

$$HA^- + S_2O_8^{2-} \xrightarrow{k_2} 2SO_4^{2-} + A + H^+ \quad (5)$$

Scheme 2:

$$H_2A + S_2O_8^{2-} \xrightarrow{k_1} (H_2A^+ + SO_4^{\cdot-} + SO_4^{2-}) \xrightarrow{\text{fast}} 2SO_4^{2-} + A + 2H^+ \quad (6)$$

$$HA^- + S_2O_8^{2-} \xrightarrow{k_2} (HA\cdot + SO_4^{\cdot-} + SO_4^{2-}) \xrightarrow{\text{fast}} 2SO_4^{2-} + A + H^+ \quad (7)$$

Scheme 3:

$$H_2A + S_2O_8^{2-} \xrightarrow{k_1} H_2A^+ + SO_4^{\cdot-} + SO_4^{2-} \quad (8)$$

$$H_2A + SO_4^{\cdot-} \longrightarrow H_2A^+ + SO_4^{2-} \quad (9)$$

$$S_2O_8^{2-} + H_2A^+ \longrightarrow SO_4^{\cdot-} + SO_4^{2-} + A + 2H^+ \quad (10)$$

TABLE 2. THE OBSERVED SECOND-ORDER RATE CONSTANTS, k_0, OF Eq. 1[a]

Ionic strength (I) / M	Temp / °C	pH	$10^2 k_0$ / $M^{-1} s^{-1}$	
1.07	15	3.72	7.59	
		3.73	7.72	
		3.93	9.90	
		4.12	12.4	
		4.21	13.3	
		4.39	14.8	
1.07	20	3.49	7.69	
		3.67	10.9	
		3.91	13.7	
		4.11	17.1	
		4.39	20.6	
1.07	25	3.45	10.7	
		3.69	15.5	
		3.88	19.8	
		4.08	23.6	
		4.13	24.7	
1.07	30	3.43	14.8	
		3.44	15.1	
		3.67	20.9	
		3.87	27.2	27.3
		4.07	33.0	
		4.08	33.5	
0.47	25	3.50	5.88	
		3.71	8.50	
		3.90	10.8	
		4.40	17.4	
0.20	25	3.58	3.68	
		3.80	5.48	
		4.00	7.07	
		4.01[b]	6.68[b]	
		4.22[b]	8.55[b]	
		4.47	11.1	
		4.51[b]	10.5[b]	
0.071	25	3.70	2.47	
		3.88	3.68	
		3.90[d),c)]	3.56[d)]	4.50[c)]
		4.10	4.76	
		4.15[c)]	5.95[c)]	
		4.31[c)]	6.88[c)]	
		4.40[c)]	7.37[c)]	
		4.60	7.14	

a) The initial concentrations are 2.0×10^{-3} M for potassium peroxodisulfate and L-ascorbic acid, 5×10^{-3} M in disodium dihydrogen ethylenediaminetetraacetate (EDTA), 0.05 M in sodium acetate, and the given concentrations of acetic acid and sodium perchlorate. b) In the presence of 1% acrylonitrile; the other conditions are the same as those in a). c) In the absence of EDTA; the other conditions are the same as those in a). d) In the presence of 1×10^{-6} M in copper(II) sulfate; the other conditions are the same as those in a).

$$H_2A^+ + SO_4^{\cdot-} \xrightarrow{\text{fast}} SO_4^{2-} + A + 2H^+ \quad (11)$$

$$HA^- + S_2O_8^{2-} \xrightarrow{k_2} HA\cdot + SO_4^{\cdot-} + SO_4^{2-} \quad (12)$$

$$HA^- + SO_4^{\cdot-} \longrightarrow HA\cdot + SO_4^{2-} \quad (13)$$

$$S_2O_8^{2-} + HA\cdot \longrightarrow SO_4^{\cdot-} + SO_4^{2-} + A + H^+ \quad (14)$$

$$HA\cdot + SO_4^{\cdot-} \xrightarrow{\text{fast}} SO_4^{2-} + A + H^+, \quad (15)$$

where A represents dehydroascorbic acid; dehydroascorbic acid is known as the final product in the oxidation of L-ascorbic acid by many oxidizing agents;[12] the presence of free radicals of H_2A^+ and HA· in the oxidation of L-ascorbic acid has been confirmed by ESR measurements and kinetic investigations by many researchers.[12] Every one of the above three schemes is consistent with the empirical rate law of Eqs. 1 and 2. For the purpose of examining whether or not the reaction occurs *via* a successive one-electron transfer involving the free radicals, as in schemes 2 and 3, the acrylonitrile of a radical scavenger was added to the reaction solution at the initiation of the reaction. The results are given in Table 2 and Fig. 3; the polyacrylonitriles were not

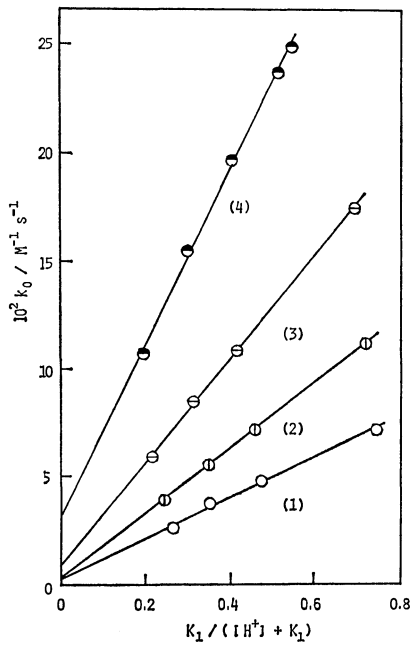

Fig. 2. Examples of plots of K_0 *vs.* $K_1/([H^+]+K_1)$ (Eq. 2).
Ionic strengths are 0.071, 0.20, 0.47, and 1.07 M for lines (1), (2), (3), and (4), respectively. Other conditions are the same as those of a) in Table 2 at 25 °C.

TABLE 3. THE SECOND-ORDER RATE CONSTANTS, k_1 AND k_2 IN Eq. 2, AND THE KINETIC PARAMETERS FOR EACH REACTION PATH[a]

Temp / °C	Ionic strength (I) / M	$10^2 k_1$ / $M^{-1} s^{-1}$	$10\,k_2$ / $M^{-1} s^{-1}$
15	1.07	2.2±0.4	2.3±0.1
20	1.07	2.8±0.6	3.1±0.2
25	1.07	3.2±0.7	4.3±0.2
30	1.07	3.3±0.4	6.0±0.1
25	0.07_1	0.2±0.3	1.0±0.1
25	0.20	0.0±0.1	1.57±0.04
25	0.47	0.9±0.3	2.5±0.08

$\Delta H_1^* = 17\pm5$ kJ mol^{-1} $\Delta S_1^* = -220\pm20$ J deg^{-1} mol^{-1}
$\Delta H_2^* = 45\pm1$ kJ mol^{-1} $\Delta S_2^* = -102\pm4$ J deg^{-1} mol^{-1}

a) The conditions are the same as those of a) in Table 2.

found in the reacting solution, and the reaction rate appeared to be a little slower than that in the absence of acrylonitrile. In most of the previous works on peroxodisulfate reactions,[5-8] the acrylonitrile was a strong retarder of the reaction rate, forming polyacrylonitrile as a white sediment. Thus, the acrylonitrile effect obtained in this work was extraordinarily different from most cases of peroxodisulfate reactions; this may indicate, at least apparently, a two-electron transfer reaction without forming radicals, *i.e.*, Scheme 1. Scheme 2 will be not very sensitive to the presence of a radical scavenger, while Scheme 3 is probably very sensitive to such a scavenger for radicals.

Temperature Dependence. The activation parameters corresponding to the specific rate constants are shown in Table 3. The values of both $\Delta H_1^{\ddagger}$ and $\Delta S_1^{\ddagger}$ are smaller than those of $\Delta H_2^{\ddagger}$ and $\Delta S_2^{\ddagger}$. Although the k_1 values were much smaller than the k_2 values over the temperature range of 15—30 °C, the k_1 should become larger than the k_2 at temperatures lower than −36 °C, which is obtained as the isokinetic temperature by using the kinetic parameters. In most of the oxidation reactions of L-ascorbic acid, the values of k_1 are much smaller than those of k_2. For example, the k_2/k_1 ratio at 25 °C (with the oxidizing agent in parentheses) is 13 (peroxodisulfate) at I=1.07 M in this work, 34 (tris(oxalato)cobaltate(III)),[11] 3.7×10^3 (tris(1,10-phenanthroline)iron(III),[11] 6×10^2 (thioureapentacyanoferrate(III)),[13] and 1.3×10^3 (hexacyanoferrate(III)).[14] The trend toward less negative $\Delta S^{\ddagger}$ values on going from H_2A to HA^- is similar to that ($\Delta S_1^{\ddagger}=-192$ J deg^{-1} mol^{-1}; $\Delta S_2^{\ddagger}=-134$ J deg^{-1} mol^{-1}) found in the reaction of L-ascorbic acid with thioureapentacyanoferrate(III).[13] The larger $\Delta H_2^{\ddagger}$ values than $\Delta H_1^{\ddagger}$ indicate the stronger hydration for HA^- than that for H_2A.

Ionic Strength Dependence. Although the ionic-strength values employed in this work lie outside the Debye-Hückel region, plots of $\log k_2$ *vs.* $I^{1/2}/(1+I^{1/2})$ showed a straight line, with a relationship of $\log k_2 = -(1.47\pm0.02) + (2.17\pm0.04)I^{1/2}/(1+I^{1/2})$. This dependence is as expected for the reaction between two ions of a like sign; the positive value of 2.17 is in good agreement with that of 2.04 which is obtained from the theoretical term of $1.02Z_aZ_b\times I^{1/2}/(1+I^{1/2})$ with $Z_a=-1$ for HA^- and $Z_b=-2$ for $S_2O_8^{2-}$.

Effect of the Copper(II) Ion. When the reaction solution did not contain EDTA, the k_0 values increased to some extent (see line(2) in Fig. 3). However, such an increase in k_0 was depressed by the presence of EDTA (see line(1) in Fig. 3) and thus, was thought to be due to the copper(II) ion present as an impurity in the reaction solution; most of the copper(II)-ion impurity may come from the acetate-buffer solutions used. Moreover, it was found that the rate of reaction between L-ascorbic acid and peroxodisulfate was greatly accelerated by the presence of trace amounts of the copper(II) ion, and that the copper(II)-catalyzed reaction rate was: (1) indifferent to the presence or absence of oxygen, (2) retarded completely by the

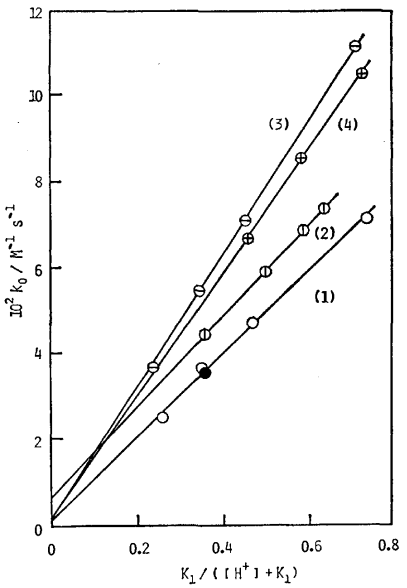

Fig. 3. Effects of acrylonitrile, EDTA, and copper(II) ion (as an impurity) on the rate constant k_0 in Eq.1 at an ionic strength 0.07 M and at 25 °C.
Line (1) indicates the results in the presence of 5×10^{-3} M in disodium dihydrogen ehthenediaminetetraacetate (EDTA); line (2) indicates the results in the absence of EDTA under the other conditions same as those in line (1); line (3) indicates the results at an ionic strength 0.2 M under the other conditions same as those in line (1); line (4) indicates the results in the presence of 1% acrylonitrile under the other conditions same as those in line (3); a plot ● in line (1) indicates a result in the presence of 1×10^{-6} M in copper(II) sulfate under the conditions same as those in line (1).

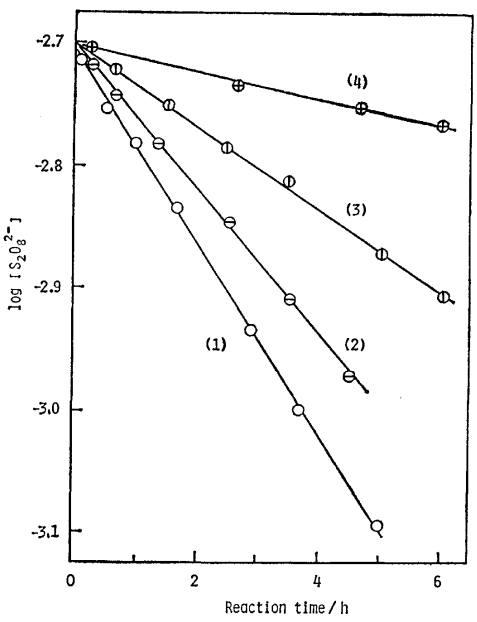

Fig. 4. Examples of plots of log $[S_2O_8^{2-}]$ *vs.* t (Eq. 16). Initial concentrations of L-ascorbic acid are 0.03, 0.02, 0.01, and 0.002 M for lines (1), (2), (3), and (4), respectively. The catalyser's concentration is 2×10^{-6} M in copper(II) sulfate. Other conditions are the same as those of a) in Table 5.

presence of EDTA, and (3) not retarded by the presence of acrylonitrile; nevertheless, polyacrylonitrile in the forms of a white sediment was obviously found in the reacting solution. These effects are shown in Table 4. When pseudo first-order conditions were satisfied, the plots of log $[S_2O_8^{2-}]$ *vs.* t were rectiliniear up to at least the half-time ($t_{1/2}$) of reaction. Some examples are given in Fig. 4. The rate constants, $k_{cat.}$, in Eq. 16 were obtained under various conditions. The results are given in Table 5. Plots of both $k_{cat.}$ *vs.* $[Cu(II)]_i$ and $k_{cat.}$ *vs.* $[AA]_i$ showed straight lines with intercepts. Some examples of plots of $k_{cat.}$ *vs.* $[Cu(II)]_i$ are given in Fig. 5. These relationships can be described by Eqs. 16 and 17:

$$-d[S_2O_8^{2-}]/dt = k_{cat.}[S_2O_8^{2-}] \quad (16)$$

$$k_{cat.} = k_a[Cu(II)]_i + (k_b + k_c[Cu(II)]_i)[AA]_i$$
$$= k_b[AA]_i + (k_a + k_c[AA]_i)[Cu(II)]_i, \quad (17)$$

where [ ]$_i$ indicates the concentration at the initial stage of reaction. The values of k_a ($M^{-1}s^{-1}$), k_b ($M^{-1}s^{-1}$), and k_c ($M^{-2}s^{-1}$) were determined at 25 °C to be: $k_a=2.0$, $k_b=5.5\times10^{-4}$, $k_c=5.6\times10^2$ at pH 2.1, and $k_a=1.5\times10^2$, $k_b=5.0\times10^{-2}$, $k_c=7.1\times10^5$ at

Table 4. Effects of oxygen, acrylonitrile (AN), and EDTA on the rate of the copper(II)-catalyzed reaction

t / min	$10^3[S_2O_8^{2-}]_{disapp.}$/M					
			Air-sat.[c]	N_2-sat.[c]	0.5% AN[d]	1% AN[d]
5	—	—	0.30	0.29	0.52	0.66
10	0.10[a]	—	—	0.56	1.01	0.92
15	0.15[a]	0.16[b]	0.84	0.83	1.28	1.07
20	0.20[a]	—	1.03	1.03	1.44	1.17
25	—	—	1.18	1.19	1.53	1.26
30	0.28[a]	0.24[b]	1.34	1.34	1.61	1.33
60	0.55[a]	0.42[b]	—	—	—	—
90	0.75[a]	0.60[b]	—	—	—	—
120	—	0.70[b]	—	—	—	—

a) The conditions are: 2.0×10^{-3} M for potassium peroxodisulfate and L-ascorbic acid; an ionic strength of 0.07 M; pH 3.9 (acetate buffer); 25 °C, and in solutions containing dissolved air. b) In the presence of 1×10^{-6} M in copper(II) sulfate and of 5×10^{-3} M in disodium dihydrogen ethylenediaminetetraacetate (EDTA); the other conditions are the same as those in a). c) In the presence of 1×10^{-6} M in copper(II) sulfate; air or nitrogen gas was bubbled through the reacting solution; the other conditions are the same as those in a). d) In the presence of 1×10^{-6} M in copper(II) sulfate, 0.5 or 1% acrylonitrile (AN); the other conditions are the same as those in a). The white sediments of polyacrylonitrile were found in the reacting solution; thus, the concentrations of peroxodisulfate were determined after the removal of the sediments.

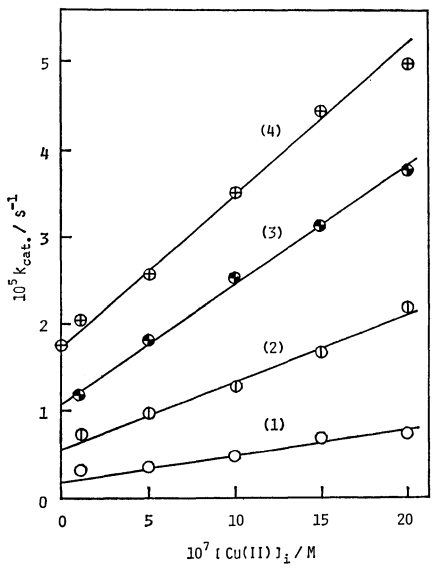

Fig. 5. Examples of plots of $k_{cat.}$ *vs.* $[Cu(I)]_i$ (Eq. 17).
All lines——indicate the calculated ones by using the rate constants k_a, k_b, and k_c obtained from the data at 0.01 M perchloric acid (pH 2.1) in Table 5. Initial concentrations of L-ascorbic acid are 0.002, 0.01, 0.02, and 0.03 M for lines (1), (2), (3), and (4), respectively.

Table 5. Rate constants, $k_{cat.}$, in Eq. 16 at varying concentrations of L-ascorbic acid and copper(II)[a]

$10^7[Cu(II)]_i$ / M	$10^5 k_{cat.}/s^{-1}$ $10^3[AA]_i$/M							
	1	2		3	4	10	20	30
0	7[b]	—	10[b]	14[b]	24[b]	—	—	1.67[b]
1	18[b]	0.30	31[b]	40[b]	62[b]	0.71	1.14	2.06
5	50[b]	0.37	98[b]	130[b]	169[b]	0.95	1.77	2.55
8	77[b]	—	147[b]	180[b]	241[b]	—	—	—
10	91[b]	0.47	180[b]	255[b]	444[b]	1.25	2.54	3.47
15	—	0.66	—	—	—	1.63	3.15 3.13[c]	4.44
20	—	0.73	—	—	—	2.17	3.75	4.95

a) The conditions are $[S_2O_8^{2-}]_i=2.0\times10^{-3}$ M, $[HClO_4]=0.01$ M (pH 2.1), and in solutions containing dissolved air at 25 °C (in the dark). b) The conditions are the same as those in a), but the pH value in 4.31 in the 0.05 M sodium acetate—0.1 M acetic acid solution, with no perchloric acid ($HClO_4$) added. The values of $k_{cat.}$ in this case were evaluated by using the initial slope of the plots of $[S_2O_8^{2-}]$ *vs.* t with a relationship of $-\Delta[S_2O_8^{2-}]_i/\Delta t = k_{cat.}[S_2O_8^{2-}]_i$. c) The conditions are the same as those in a), but in a solution saturated with pure nitrogen gas.

pH 4.31. The k_b corresponds to the rate constant for the uncatalyzed-reaction path, while the rate constants k_a and k_c are those for the catalyzed-reaction paths. The ratios of $k_b:k_a:k_c$ were $1:3600:1\times10^6$ at pH 2.1 and $1:3000:1.4\times10^7$ at pH 4.31. These values indicate that the copper(II) ion is very strong catalyst for the reaction between L-ascorbic acid and peroxodisulfate. It is obvious that the copper(II)-catalyzed reaction is complosed of a chain reaction of the redox cycle of Cu(I) and Cu(II), and that the origin of the reaction mechanism can be written as follows:

$$\left\{\begin{array}{c}H_2A\\ \uparrow\downarrow H^+\\ HA^-\end{array}\right\} + Cu^{2+} \rightleftharpoons Cu^+ + \text{Radicals} \qquad (18)$$

$$S_2O_8^{2-} + Cu^+ \longrightarrow Cu^{2+} + SO_4^{\cdot-} + SO_4^{2-}. \qquad (19)$$

The rate constant for Reaction 19 has been reported as $1.4\times10^3\ M^{-1}\ s^{-1}$ in 1 M potassium chloride at 25 °C,[15] about 100-fold that for Reaction 20:

$$O_2 + Cu^+ \longrightarrow Cu^{2+} + O_2^-. \qquad (20)$$

Recently, Ito *et al.*[16] reported that the rate of Reaction 18 was 5×10^5-fold faster than that of Reaction 20. Therefore, it can be said that Reaction 20 hardly ever occurs in a catalyzed reaction, even in an air-saturated solution. This is consistent with the fact that the catalyzed-reaction rate is utterly indifferent to the presence or absence of oxygen (see Table 4). The strong inhibition effect of EDTA on the catalyzed reaction is attributable to the retardation of Reaction 18 by the complex formation of EDTA with the copper (II) ion. Separate, preliminary experiments showed that Reaction 18 was retarded by either nitrilotriacetate (NTA) or oxalate as well as by EDTA. The acrylonitrile effect may be accounted for by the following reactions:

$$X + Cu^{2+} \rightleftharpoons Cu^+ + X^{\cdot+} \qquad (18)$$

$$S_2O_8^{2-} + Cu^+ \longrightarrow Cu^{2+} + SO_4^{\cdot-} + SO_4^{2-} \qquad (19)$$

$$Cu^+ + SO_4^{\cdot-} \longrightarrow Cu^{2+} + SO_4^{2-} \qquad (21)$$

$$Cu^{2+} + X^{\cdot+} \longrightarrow Cu^+ + \text{Products} \qquad (22)$$

$$X^{\cdot+} + SO_4^{\cdot-} \longrightarrow SO_4^{2-} + \text{Products}, \qquad (23)$$

where $X=H_2A+HA^-$ and $\text{Products}=A+H^+$. The backward reaction of (18) and Reaction 19 are competing with Reactions 20 and 21. Thus, when the acrylonitrile scavenged the radicals of $SO_4^{\cdot-}$ and/or $X^{\cdot+}$, the rate of the forward reactions of (18) and (19) might be accelerated. Actually, polyacrylonitrile was found in the reacting solutions upon the addition of acrylonitrile of the monomer, indicating the removal of the radicals, and the copper(II)-catalyzed reaction was a little accelerated by the presence of acrylonitrile (see Table 4). On the other hand, no clearly rational explanations could be made for the fact that the rate in the presence of 1% acrylonitrile is slightly slower than that in the 0.5% acrylonitrile; the propagating radical of an acrylonitrilepolymer may react with the copper(I) ion, competing with Reaction 19 or other competing reactions may occur.

References

1) D. A. House, *Chem. Rev.*, **62**, 185 (1962).
2) W. K. Wilmarth and A. Haim, "Peroxide Reaction Mechanisms," ed by J. O. Edwards, Interscience, New York (1962), p. 175.
3) I. R. Wilson, "Comprehensive Chemical Kinetics," ed by C. H. Bamford and C. F. H. Tipper, Elsevier, New York (1972), Vol. 6, p. 340.
4) G. J. Buist, "Comprehensive Chemical Kinetics," ed by C. H. Bamford and C. F. H. Tipper, Elsevier, New York (1972), Vol. 6, p. 456.
5) M. Kimura, *J. Phys. Chem.*, **77**, 1265 (1973).
6) M. Kimura, *Inorg. Chem.*, **13**, 841 (1974).
7) M. Kimura, T. Akazome, K. Takenaka, and A. Kobayashi, *Bull. Chem. Soc. Jpn.*, **53**, 1271 (1980).
8) M. Kimura, T. Kawajiri, and M. Tanida, *J. Chem. Soc., Dalton Trans.*, **1980**, 726.
9) M. Kimura and K. Kawanami, *Nippon Kagaku Kaishi*, **1981**, 1.
10) S. Toshima, "Kiso Denkikagaku," Asakusashoten, Tokyo (1965), p. 68; J. Kielland, *J. Am. Chem. Soc.*, **59**, 1675 (1937).
11) M. Kimura, M. Yamamoto, and S. Yamabe, *J. Chem. Soc., Dalton Trans.*, **1982**, 423.
12) E. Pelizzetti, E. Mentasti, and E. Pramauro, *Inorg. Chem.*, **17**, 1181 (1978), and the references cited therein.
13) D. H. Macartney and A. McAuley, *Can. J. Chem.*, **59**, 132 (1981).
14) U. S. Mehrotra, M. C. Agrawal, and S. P. Mushraw, *J. Phys. Chem.*, **73**, 1996 (1969).
15) I. M. Kolthoff and R. Wood, *J. Am. Chem. Soc.*, **88**, 1371 (1966).
16) S. Ito, T. Yamamoto, and Y. Tokushige, *Chem. Lett.* **1980**, 1411.

Structural Studies of Partially Oxidized One-dimensional Bis(oxalato)-platinate Salts Containing Bivalent Cations: $Ni_{0.84}[Pt(C_2O_4)_2]\cdot 6H_2O$

Akiko KOBAYASHI,* Hidetaka KONDO,** Yukiyoshi SASAKI, Hayao KOBAYASHI,†
Allan E. UNDERHILL,†† and David M. WATKINS††

Department of Chemistry, Faculty of Science, The University of Tokyo, Hongo, Bunkyo-ku, Tokyo 113
†*Department of Chemistry, Faculty of Science, Toho University, Funabashi, Chiba 274*
††*School of Physical and Molecular Sciences, University College of North Wales, Bangor, Gwynedd, LL57 2UW, U.K.*

(Received October 16, 1981)

Fundamental structure, k_F and $2k_F$ satellite reflections, and electrical properties of $Ni_{0.84}[Pt(C_2O_4)_2]\cdot 6H_2O$ (Ni–OP) were determined. Complex Ni–OP crystallizes in the orthorhombic space group Pccn with cell parameters of $a=14.296(2)$, $b=16.387(3)$, and $c=5.671(1)$ Å and $Z=4$. Ni–OP is essentially isostructural with Mg–OP ($Mg_{0.82}[Pt(C_2O_4)_2]\cdot 5.3H_2O$) and Co–OP ($Co_{0.83}[Pt(C_2O_4)_2]\cdot 6H_2O$). The space group of Mg–OP and Co–OP is Cccm. Owing to the change in the space group, there are two independent Pt chains in Ni–OP. X-Ray studies of M–OP (M=Co, Ni) show that there exist strong k_F satellite spots and weak $2k_F$ spots. One M^{2+} cation is vacant per period of the lattice modulation wave of the platinum chain, λ_{2k_F}. The periodic cation defect induces the k_F modulation waves. The $2k_F$ waves do not have a Peierls origin but are induced by the k_F modulation wave. A second order phase transition is observed at about 305 K above which the $2k_F$ spots disappear.

In recent years partially oxidized cyanoplatinates and bis(oxalato)platinate complexes have been attracting much interest because of their quasi-one-dimensional metallic behavior.

The prototype compound $K_2[Pt(CN)_4]Br_{0.3}\cdot 3.2H_2O$ (KCP(Br)) undergoes a gradual transition from a room temperature one-dimensional conductor state to a low temperature insulating state. Observations of a giant Kohn anomaly and a low temperature three-dimensional superlattice have been proposed as evidence for the Peierls transition with this compound. The nature of sinusoidal modulation of the one-dimensional platinum chain has been investigated by many workers through various neutron and X-ray diffuse scattering studies.[1–3]

One-dimensional metallic system is unstable at low temperature and exhibits lattice distortions with a wave number equal to twice the Fermi momentum ($2k_F$). The period of a Peierls distorted cell is determined by the degree of partial oxidation (DPO).[4]

Bis(oxalato)platinate salts have the formula $M_x[Pt(C_2O_4)_2]\cdot yH_2O$ (M–OP). For bivalent cations Mg^{2+}, Zn^{2+}, Mn^{2+}, Ni^{2+}, and Cu^{2+}, $0.81<x<0.84$ and $y\approx 6$.[5–8, 10,11] For monovalent cations NH_4^+, Rb^+, and K^+, $1.6<x<1.81$ and $y=1$—4.

In the present paper, fundamental structure, X-ray satellite reflections (k_F and $2k_F$), and diffuse scattering of Ni–OP are reported together with electrical conductivity measurements and 2nd-order phase transition.

Experimental

Ni–OP was prepared by the method previously reported.[6] A crystal of $0.43\times 0.36\times 0.01$ mm³ was used for data collection. Data were collected on a Rigaku automated diffractometer equipped with a graphite monochromator.

Crystal data:

$a=14.296(2)$, $b=16.387(3)$, and $c=5.671(1)$ Å,

$V=1328.54$ Å³, $Z=4$, $d_{calcd}=2.643$ g cm^{-3}, and $\mu=123.32$ cm^{-1} (Mo $K\alpha$ radiation, $\lambda=0.71069$ Å).

Intensity data were collected with monochromatized Mo $K\alpha$ radiation by the ω-2θ scan technique up to $2\theta=60°$. Corrections were made for the Lorentz and polarization factors. Data revealed systematic extinctions consistent with the orthorhombic space group Pccn. The space group of Mg–OP and Co–OP is Cccm.[5,8] Data were corrected for absorption. Initial locations of the Pt and Ni atoms were assumed from the structure of Co–OP. Positions of the oxalate ligand atoms and independent oxygen atoms coordinated to the Ni^{2+} ion were determined by the standard Fourier and least-squares refinement procedures. Site occupancies of the Ni atoms and four independent oxygen atoms of water molecules were determined by use of the full matrix least-squares program LINUS. Site occupancies are 0.415(6) for Ni, 0.90(4), 0.84(4), and 0.81(4) for the coordinated O atoms, and 1.05(4) for the uncoordinated O atoms. For the three coordinated oxygen atoms, site occupancies are almost equivalent and nearly equal to twice the Ni site occupancy. Discrepancy indexes are $R(|F_o|)=0.050$ and $Rw(|F_o|^2)=0.069$. The weighting scheme used was $w^{-1}=\sigma^2(|F_o|)+c|F_o|^2$, where the value of c is 0.02, as estimated from the fluctuation of intensities of the standard reflections. The atomic coordinates of Pt are (0.25, 0.25, 0.0177). The Z coordinate deviates ≈ 0.1 Å from the $Z=0$ point. This deviation causes the lattice change from C to P. Positional parameters determined from the final least-squares cycle are presented in Table 1. Atomic scattering factors were taken from International Tables for X-ray Crystallography.[12] Calculations were performed on the HITAC 8800/8700 computer at the Computer Centre of the University of Tokyo. $|F_o|-|F_c|$ tables and thermal parameters are kept at the Office of this Bulletin as Document No. 8227.

Results and Discussion

Fundamental Structure. The c axis and a axis projections of the structure of Ni–OP are shown in Fig. 1. Bond lengths and bond angles are almost the same as those of Co–OP within 3σ. Slight differences of bond lengths and angles are found in the hexahydrated cations. The main structural difference

**Present address: Systems Development Laboratory, Hitachi Ltd., Ohzenji, Tama-ku, Kawasaki, Kanagawa 215.

TABLE 1. FRACTIONAL COORDINATES AND ISOTROPIC THERMAL PARAMETERS ($\times 1000$ FOR HEAVY ATOMS, $\times 100$ FOR THE OTHERS, AND $\times 1000$ FOR U_{eq})

Atom	Site occupancy	x	y	z	U_{eq}/Å^2
Pt	1.0	2500	2500	177(1)	18(1)
Ni	0.415(6)	2533(12)	5901(3)	2516(9)	49(2)
O(1)	1.0	299(1)	364(1)	17(2)	25(3)
O(2)	1.0	435(1)	429(1)	19(2)	53(5)
O(3)	1.0	527(1)	280(1)	20(2)	30(3)
O(4)	1.0	385(1)	221(1)	19(2)	24(3)
C(1)	1.0	390(1)	367(1)	18(2)	27(4)
C(2)	1.0	440(1)	284(1)	20(2)	25(4)
$H_2O(1)$	0.90(4)	189(1)	503(1)	21(4)	83(10)
$H_2O(2)$	0.84(4)	184(1)	676(1)	−22(5)	108(13)
$H_2O(3)$	0.80(4)	359(1)	586(1)	−1(3)	59(7)
$H_2O(4)$	1.0	0	500	0	193(29)

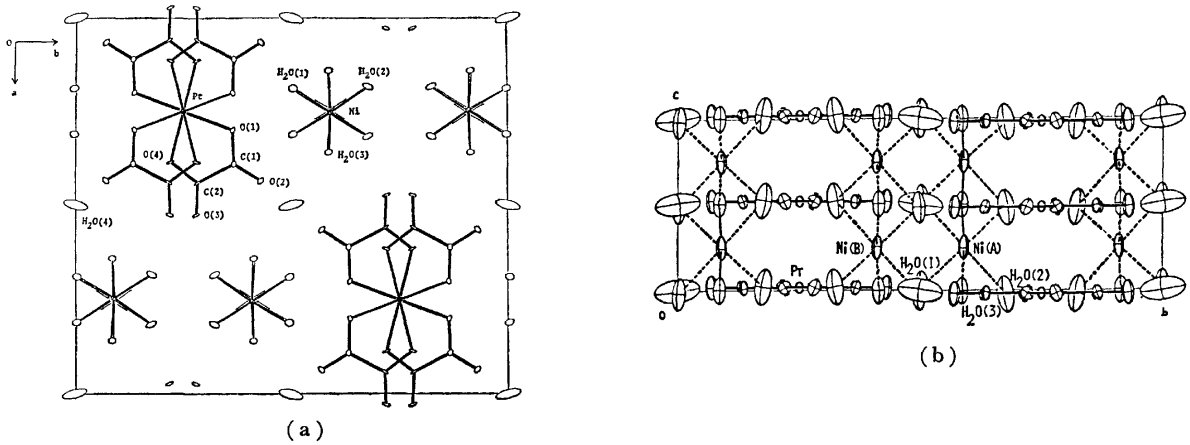

Fig. 1. The c axis(a) and the a axis(b) projection of the structure of Ni–OP. The disordered cation sites are shown as A and B.

TABLE 2. AVERAGED MOLECULAR STRUCTURES OF THE BIS(OXALATO)PLATINATE ANIONS

	a/Å	b/Å	c/Å	d/Å	α/°	β/°	γ/°	δ/°	ε/°
A[a]	2.00	1.28	1.55	1.22	82	115	115	126	120
B[a]	2.013(5)	1.26(1)	1.57(2)	1.23(1)	82.7(3)	113.1(4)	115.7(7)	124.5(7)	120.0(7)
C[a]	2.00	1.29	1.54	1.22	83	113	116	124	120
D[a]	2.00(1)	1.30(2)	1.55(2)	1.22(2)	83.6(4)	113.0(9)	115(1)	125(1)	120(1)

a) A: $Mg_{0.82}[Pt(C_2O_4)_2]\cdot 5.3H_2O$; B: $Co_{0.83}[Pt(C_2O_4)_2]\cdot 6H_2O$; C: $K_2[Pt(C_2O_4)_2]\cdot 2H_2O$; D: $Ni_{0.84}[Pt(C_2O_4)_2]\cdot 6H_2O$.

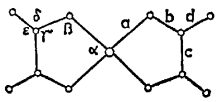

between Ni–OP and Co–OP (Mg–OP) is in the different space groups Pccn for Ni–OP and Cccm for Co–OP (Mg–OP). This fact indicates that there are two independent Pt chains in Ni–OP.

Within a platinum chain, oxalate ligands are staggered with respect to the ligands located directly above and below them. The staggered angles are approximately 55°. There are two platinum atoms per unit cell in the c-direction with spacing $c'=c/2=$ 2.836 Å. The Ni^{2+} ions are located between the planes containing $[Pt(C_2O_4)_2]^{x-}$ ions and are coordinated by six water molecules with slightly distorted octahedral symmetry. Table 2 shows averaged molecular structures of the anion. The Pt–O distance is 2.00(1) Å on the average. The O–Pt–O angles is 83.6(4)°, the C–O bond distance in the five-membered ring is 1.30(2) Å, and the C–C distance is on the average 1.55(2) Å. The molecular structure of partially oxidized bis(oxalato)platinate complexes with bivalent metal cations (Ni, Co, and Mg) is approximately equal to the molecular structure with $[Pt(C_2O_4)_2]^{2-}$ anion in $K_2[Pt(C_2O_4)_2]\cdot 2H_2O$.[5,8,13] In a cobalt bis(oxalato)platinate salt, a new water site which is not within the Co^{2+} coordination sphere was found. The Ni^{2+} salt also contains this additional water molecule, which was not found in the Mg^{2+} salt. The neighboring Pt chains are linked by hydrogen bonds involving the water molecules. Table 3 compares the bond lengths and angles around each cation in Ni–OP, Co–OP, and Mg–OP.

k_F, $2k_F$ Satellite Reflections. The structure was solved by using intensities of the main reflections. However, characteristic satellite reflections and diffuse scattering are observed on X-ray photographs indi-

TABLE 3. BOND LENGTHS AND ANGLES AROUND THE CATION OF M-OP (M=Ni, Co, Mg) AND BOND DISTANCES FOR THE HYDROGEN BONDING OF WATER MOLECULES

	Ni-OP	Co-OP	Mg-OP
M-H_2O(1)	2.13(2)	2.227(8)	2.23(5)
M-H_2O(2)	2.09(2)	2.138(7)	2.13(5)
M-H_2O(3)	2.32(2)	2.259(9)	2.23(5)
H_2O(1)-O(1)	2.78(3)	2.81(1)	
H_2O(2)-O(3)	2.73(2)	2.74(1)	2.75(8)
H_2O(2)-O(2)	2.79(2)	2.81(1)	2.89(8)
H_2O(3)-O(3)	2.82(3)	2.82(1)	2.85(8)
H_2O(4)-H_2O(1)	2.71(2)	2.70(1)	
H_2O(1)-M-H_2O(2)	79(1)	82.0(3)	81
H_2O(1)-M-H_2O(3)	82(1)	82.2(3)	82
H_2O(2)-M-H_2O(3)	88(1)	84.6(3)	83

cating that the lattice is periodically modulated. Extra reflections are located at $\boldsymbol{G}(hkl)+nk_F\boldsymbol{c}^*$ $(n=1,2,\cdots)$ and classified into three groups:

I) k_F Satellite Reflections: Intensities of the k_F satellite reflections are comparatively strong.

Satellites are located near the a* and a*±b* axes. Since some of these are accompanied by very weak 2nd order satellite reflections ($2k_F$ spots), these k_F satellites are considered to be associated with the sinusoidal modulation wave whose displacement vector is parallel to the a and a±b axes, perpendicular to the direction of wave propagation c*. The intensity of the n-th satellite spot of the sinusoidally modulated structure is proportional to the square of the Bessel function $J(2\pi(p\xi+g\eta+r\zeta))$, where (ξ,η,ζ) is the position in the reciprocal space $(\zeta=l+nk_F)$ and $p\boldsymbol{a}/a+q\boldsymbol{b}/b+r\boldsymbol{c}/c$ is the amplitude vector of the modulation wave (see Figs. 2, 3, and 4).†††

In addition to this, strong k_F satellite reflections are observed at low 2θ-values which appear not to originate from the sinusoidal modulation of lattice.

II) $2k_F$ Satellite Reflection: There are two kinds of $2k_F$ satellites.

(IIa) The 2nd order satellites originating from the transverse modulation wave with a wave vector k_F as shown in Fig. 2, which are observed around the a* and a*±b* axes.

(IIb) Satellite reflections which are weaker than k_F spots observed around the c* axis. This corresponds to a modulation satellite in Co-OP. Since these spots are observed around the c* axis, the amplitude vector of modulation may be nearly parallel to c*, which is parallel to the wave propagation vector. This is, therefore, a longitudinal modulation wave (see Figs. 2 and 4).

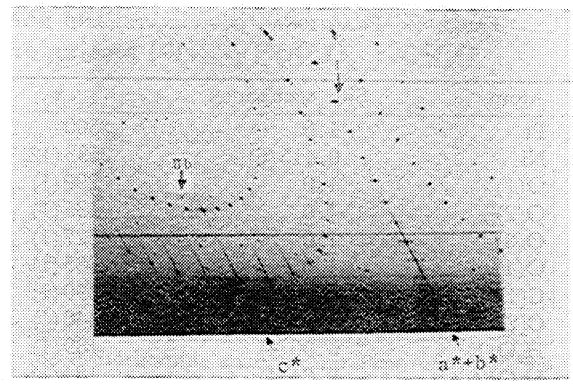

Fig. 2. Weissenberg photograph of the zero layer of the a-b axis of Ni-OP.
I and IIb satellite spots are shown.

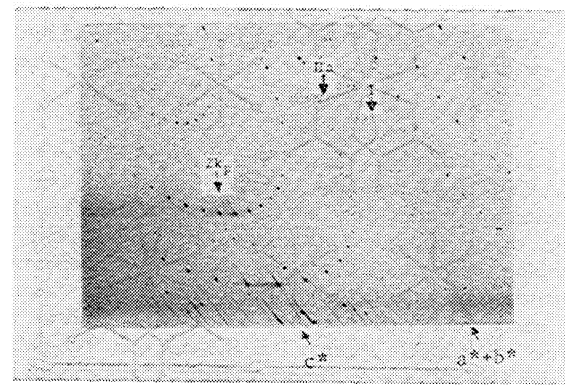

Fig. 3. Weissenberg photograph of the first layer of the a-b axis of Ni-OP showing I and IIa satellite spots and the $2k_F$- diffuse scattering (III).

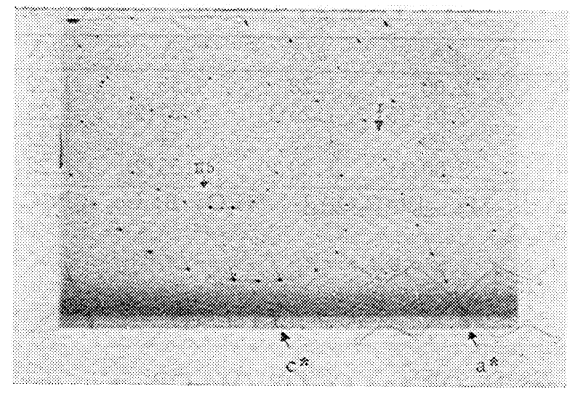

Fig. 4. Weissenberg photograph of an *h0l* reciprocal layer showing I and IIb satellite spots.

III) $2k_F$-Diffuse Scattering: This is the X-ray diffuse scattering distributing around the c* axis (see Fig. 3). As indicated by Braude *et al.*,[9-10] this scattering appears to be based on the low-frequency longitudinal lattice vibration with the Peierls origin. However, temperature dependence of the $2k_F$ diffuse scattering must be investigated in order to elucidate its origin.

The X-ray diffraction pattern described above suggests that the superstructure of Ni-OP is very complicated. The displacive periodic antiphase model of Bertinotti[14] suggests that the superstructure is formed by displacements of the oxalate ligands from the Pt

†††A. Bertinotti *et al.*[14] proposed a displacive periodic antiphase model for Co-OP. They found two kinds of satellite reflections. One appears for each $l=2n$ at h, k, $l\pm 1/2M$ where $h+k=2n+1$ and the value of M is 3.25, and the other appears at h, k, $l\pm 1/M$ where $h+k=2n$. The former corresponds to k_F spots and the latter to $2k_F$ spots. For Ni-OP, the extinction rule is more complicated and there are weak reflections which are not in accord with it.

atom in the transverse direction and that these displacements form the antiphase domain with the period $2M$.

The coexistence of $2k_F$ and k_F spots is a common feature of one-dimensional bis(oxalato)platinate complexes with bivalent cations. However, in general, the origin of $2k_F$ spots in bis(oxalato)platinate complexes with univalent cations will be a Peierls instability of the Pt chain.

Cation Distribution. In one-dimensional bis(oxalato)platinate complexes with bivalent cations, the relationship between the degree of partial oxidation (DPO) and the $2k_F$ value is as follows: DPO$=2(1-x)$, $k_F=\pi x/c$, and $2k_F'=2\pi/c-2k_F=(2\pi/c)(1-x)$. In the crystal lattice $2k_F'$ and $2k_F$ are equivalent. The wavelength of the $2k_F'$ (or $2k_F$) wave is $\lambda_{2k_F'}=c/(1-x)$. For example, when x is 0.84, $\lambda_{2k_F'}$ is $6.3c$ and $\lambda_{k_F'}$ is $12.6c$. The structure of bis(oxalato)platinate complex indicates that two cation sites exist within a tunnel. The arrangement of $[M(H_2O)_6]^{2+}$ is shown in Fig. 5. These cations cannot occupy both sites A and B (see Fig. 1b) due to a strong cation-cation Coulomb repulsion. If the cation sites are 50% occupied, each chain of $[M(H_2O)_6]^{2+}$ ions will be an ordered array of alternating vacant and occupied M sites. However, with 42% occupancy, one M^{2+} cation is vacant per one period of the $2k_F'$ wave of the platinum chain $\lambda_{2k_F'}$. Therefore, the cation site has a period of $\lambda_{k_F'}$.

This model satisfactorily explains the fact that k_F reflections are commonly observed with the bivalent bis(oxalato)platinate complexes but that they are not observed in the univalent complexes. The k_F spots are stronger than the usual $2k_F$ spots observed in the modulation structure. The presence of periodic cation defects will result in deformation of the surrounding structure. The neighboring cations and $[Pt(C_2O_4)_2]$ anions will move to fill up the vacancy and this produces modulation waves with a period of $\lambda_{k_F'}$. This may be the origin of k_F modulations.***

In one-dimensional systems, the origin of $2k_F$ waves and the lattice distortion are generally considered to have a relation to the Peierls instability. However, Braude *et al.*[10] from X-ray diffraction patterns proposed that $2k_F$ spots in Co–OP have a non-Peierls origin. In the bivalent bis(oxalato)platinate complexes, there exists a strong k_F lattice distortion, which has no direct relation to the Peierls instability.

Origin of the $2k_F$ Wave. In order to elucidate the origin of $2k_F$ satellite spots (IIb) and the relationship between $2k_F$ and k_F spots, we examined temperature dependence of X-ray diffraction spots. In Fig. 6 Weissenberg photographs at 295 K (6a) and 305 K (6b) are shown. The $2k_F$ spots disappear at 305 K, although the k_F spots are visible in this temperature range. In the bivalent complexes, the k_F spots are stronger than the $2k_F$ spots. Since periodic cation defects are the origin of k_F modulation, k_F spots can be thought to have no strong temperature dependence. From the X-ray diffraction experiments at high temperatures and the phase transition theory applied to K_2SeO_4 by Iizumi *et al.*,[15] the $2k_F$ wave may be considered to be induced by the primary k_F lattice distortion wave.†††

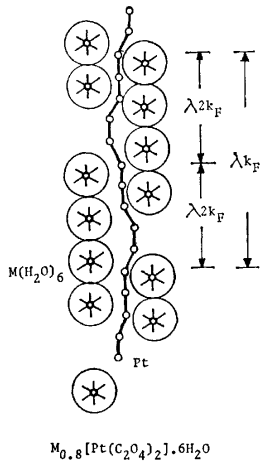

Fig. 5. The schematic arrangement of $[M(H_2O)_6]^{2+}$ is shown.
The cation is octahedrally surrounded by six water molecules. One M^{2+} cation is vacant per one period of the $2k_F$ wave of the platinum chain λ_{2k_F}. The cation site has a period of λ_{k_F}.

Electrical Resistivity Measurements. Results of the electrical resistivity study are shown in Fig. 7. DC resistivity was measured by use of the four probe method. Measurements were made on several specimens along the needle axis parallel to the Pt chains of crystal. Electrical contacts were made by four 0.025 mm gold wires attached with aquadag. The conductivity at room temperature is 5 $(\Omega\cdot cm)^{-1}$ and dI_NR/dT^{-1} diverges at about 305 K. This result agrees well with that of Watkins *et al.*[6] The anomaly at 305 K is in good agreement with the temperature at which the $2k_F$ spots begin to vanish. Therefore, this phase transition temperature corresponds to the temperature at which the secondary lattice distortion wave

***The k_F modulation is not simple since there are two types of k_F spots. However, the presence of transverse modulation spots suggests that k_F modulations contain a transverse sinusoidal component.

†††When there exists a lattice distortion wave with a wave vector $\boldsymbol{q}$ in the crystal, the atomic displacement is written as $\boldsymbol{u}=Q(\boldsymbol{q})\exp i\boldsymbol{q}.\boldsymbol{r}$. According to the phase transition theory applied to K_2SeO_4 by Iizumi,[15] the free energy of the modulated system is written as:

$$\mathbf{V}^{(1)}Q(\boldsymbol{q}_1)^2+\mathbf{V}^{(2)}Q(\boldsymbol{q}_2)^2+\cdots\mathbf{V}^{(n)}(\boldsymbol{q}_1,\boldsymbol{q}_2)Q(\boldsymbol{q}_1)^{n-1}Q(\boldsymbol{q}_2), \quad (1)$$

where $\mathbf{V}^{(n)}$ is the n-th energy factor, $Q(\boldsymbol{q}_1)$ is the amplitude of a primary lattice distortion which is characterized by the wave vector $\boldsymbol{q}_1$, and $Q(\boldsymbol{q}_2)$ is the amplitude of a secondary lattice distortion which is induced by the translational invariance, $(n-1)\boldsymbol{q}_1+\boldsymbol{q}_2=\boldsymbol{G}$, where $\boldsymbol{G}$ is a reciprocal-lattice vector or zero. Since the k_F spots in these bivalent bis(oxalato)platinate complexes are stronger than the usual $2k_F$ spots originating from the Peierls modulated lattice, the k_F wave can be regarded as the primary lattice distortion wave. Then the secondary lattice distortion wave is induced from the third energy term $(Q(\boldsymbol{k}_F)^2-Q(-2\boldsymbol{k}_F))$, whose wave number $\boldsymbol{q}_2$ is equal to $2\boldsymbol{k}_F$.

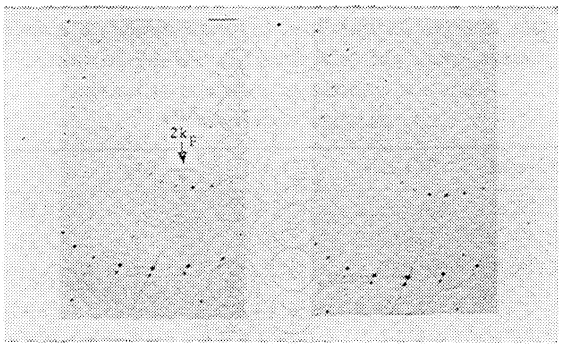

(a) (b)

Fig. 6 Weissenberg photograph of zero layer of diagonal axis a+b of Ni-OP at 295 K(6a) and 305 K(6b) are shown.
The exposure time of Cu $K\alpha$ radiation was 24 h. $2k_F$ spots (IIb) are visible at 295 K and vanish at 305 K.

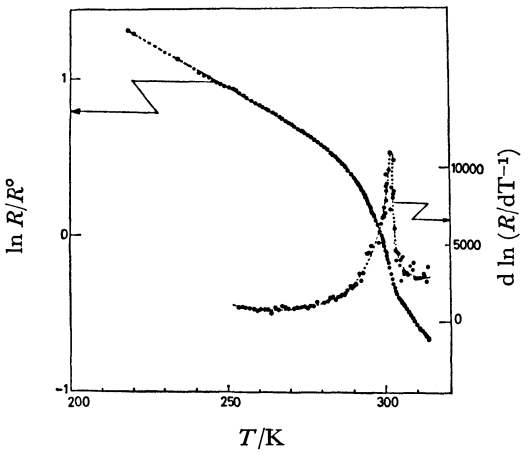

Fig. 7. The electrical resistivity measurements of Ni-OP is shown.
$dI_N R/dT^{-1}$ diverges at about 305 K. This anomaly corresponds to the temperature at which $2k_F$ spots are vanishing.

vanishes.

In order to understand lattice distortion waves of bis(oxalato)platinate complexes in crystal, precise structural studies and theoretical considerations on superstructures must be performed.

One of us (AEU) wishes to acknowledge the support of NATO (Grant No. 016-81).

References

1) R. Comès, M. Lambert, H. Launois, and H. R. Zeller, *Phys. Rev. B*, **8**, 571 (1973).
2) C. F. Eagan, S. A. Werner, and R. B. Saillant, *Phys. Rev. B*, **12**, 2036 (1975).
3) J. W. Lynn, M. Iizumi, and G. Shirane, *Phys. Rev. B*, **12**, 1154 (1975).
4) K. Krogmann, "One-Dimensional Conductors," ed by J. Ehlers, K. Hepp, and H. A. Weidenmüller, Springer-Verlag, Berlin (1975).
5) A. J. Schultz, A. E. Underhill, and J. M. Williams, *Inorg. Chem.*, **17**, 1313 (1978).
6) D. M. Watkins, A. E. Underhill, and C. S. Jacobsen, *J. Chem. Phys. Solids*, in press.
7) A. E. Underhill, D. M. Watkins, and C. S. Jacobsen, *Solid State Commun.*, **36**, 477 (1980).
8) K. Krogmann, *Z. Anorg. Allg. Chem.*, **358**, 97 (1968).
9) A. Braude, A. Lindegaard-Anderson, K. Carneiro, and A. S. Petersen, *Solid State Commun.*, **33**, 365 (1980).
10) A. Braude, A. Lindegaard-Andersen, K. Carneiro, and A. E. Underhill, *Synth. Metals*, **1**, 35 (1979/1980).
11) A. E. Underhill and D. M. Watkins, *Chem. Soc. Rev.*, **9**, 429 (1980).
12) "International Tables for X-Ray Crystallography," Kynoch Press, Birmingham (1974), Vol. VI.
13) R. Mattes, and K. Krogmann, *Z. Anorg. Allg. Chem.*, **332**, 247 (1964).
14) A. Bertinotti, C. Carcaillet, G. Jehanno, and R. Saint-James, *J. Phys. Lett. (Paris)*, **39**, L-37 (1978).
15) M. Iizumi, J. D. Axe, G. Shirane, and K. Shimaoka, *Phys. Rev. B*, **15**, 4392 (1977).

Spectrophotometric Determination of Iron(III) after Separation by Adsorption of Its 5-Chloro-7-iodo-8-quinolinol Complex on Microcrystalline Naphthalene

Masatada SATAKE,* Mool C. MEHRA,† and Taitiro FUJINAGA††

Faculty of Engineering, Fukui University, Fukui 910

†*Chemistry Department, Université de Moncton, Canada E1A 3E9*

††*Faculty of Science, Kyoto University, Kyoto 606*

(Received October 22, 1981)

A procedure is described for the spectrophotometric determination of iron(III) at ppm levels with 5-chloro-7-iodo-8-quinolinol. Iron(III) reacts with the reagent in an acidic solution to form a water-insoluble blue-black complex, which can be quantitatively adsorbed on the surface of freshly precipitated microcrystalline naphthalene at room temperature. The separated iron(III) complex is dissolved in *N,N*-dimethylformamide, together with the naphthalene, and the absorbance of the resulting solution is measured at 480 nm. Beer's law is obeyed over the range of 5—88 μg of iron in 10 ml of the solvent. The molar absorptivity of the complex was found to be 6.3×10^3 l mol^{-1} cm^{-1} at 480 nm. The effects of various factors, such as the pH, the amounts of the reagent and naphthalene, and diverse ions, were also examined. The proposed method was satisfactorily applied to the determination of iron in several selected samples, including standard reference materials, aluminum metal, and natural water.

5-Chloro-7-iodo-8-quinolinol, which is a derivative of 8-quinolinol, forms water-insoluble colored complexes with various metal ions, such as zinc, manganese, cobalt, nickel, cadmium, and iron(III). These complexes are easily extracted into chloroform or molten naphthalene under the optimum conditions. In this work, 5-chloro-7-iodo-8-quinolinol was chosen as a complexing reagent for the spectrophotometric determination of iron(III). This reagent reacts with iron (III) in the pH range of 1.8—4.5 to form a water-insoluble blue-black complex, which is quantitatively adsorbed on microcrystalline naphthalene at room temperature. The adsorbed naphthalene mixture is dissolved in *N,N*-dimethylformamide, and the absorbance of the solution is measured at 480 nm. The proposed method is characterized by the fact that the complex is easily adsorbed on micro crystalline naphthalene by vigorous shaking for a few seconds, even at room temperature, in contrast with the naphthalene-extraction method,[1-11] in which heating above 81 °C is required. In this paper, we describe a simple and convenient spectrophotometric method for the determination of iron(III) in the N.B.S. reference materials (alloys) and environmental samples.

Experimental

Reagents. Standard iron(III) solution, 100 ppm. Prepared by dissolving 0.8635 g of ammonium iron(III) sulfate in 100 ml of 0.5 M(1 M=1 mol dm^{-3}) H_2SO_4 and by diluting to 500 ml with water.

5-Chloro-7-iodo-8-quinolinol solution, 0.2%. Prepared by dissolving 0.2 g of this reagent in 100 ml of ethanol.

Naphthalene solution, 20%. Prepared by dissolving 20 g of naphthalene in acetone and by then diluting to 100 ml.

Buffer solutions were prepared by mixing 1 M acetic acid and 1 M ammonium acetate solution at pH 3—6, and 1 M aqueous ammonia and 1 M ammonium acetate solution at pH 8—11.

Apparatus. The absorption measurements were made with a Hitachi Model 200-20 spectrophotometer with 10-mm glass cells.

All the pH measurements were done with a Toa-Dempa Model HM-6A pH meter, equipped with a combination glass and calomel electrode assembly.

Naphthalene was dried with a Tabai Model K-2 drier (Tabai Mfg. Co., Japan).

Procedure. Transfer a sample solution containing 5—88 μg of iron(III) to a tightly stoppered Erlenmeyer flask, and dilute with water to about 45 ml. Add 4.0 ml of a 0.2% 5-chloro-7-iodo-8-quinolinol solution and adjust the pH of the solution to 3.5 with 2.0 ml of an acetate buffer solution. Mix the solution well and let stand for 10 min at room temperature. Add 2.0 ml of 20% naphthalene in acetone to this sample solution as fast as possible, using a small nozzled pipet attached to a rubber bulb, and shake the mixture vigorously for 1 min. Collect the colored naphthalene mixture on a filter paper placed flat on a Teflon filter plate in a funnel or a sintered glass filter (No. 2) by filteration. Wash it with water and dry at 50—60 °C. Then dissolve the mixture in *N,N*-dimethylformamide and dilute to exactly 10 ml. Measure the absorbance of the solution in a 10-mm glass cell against the reagent blank.

Results and Discussion

Absorption Spectra. Figure 1 shows the absorption spectra of the reagent and the iron(III) complex in a naphthalene-*N,N*-dimethylformamide solution. The iron(III) complex has two absorption peak, at 480 and 620 nm. The reagent blank shows strong absorption below 375 nm.

Effect of pH. The effect of the pH on the absorbance of the complex was investigated. The pH measurements were made at room temperature after the adsorption of the complex on naphthalene. Figure 2 shows that the maximum absorbance is obtained between pH 1.8 and 4.5.

Effect of Reagent Concentration. Varying amounts of a 0.2% 5-chloro-7-iodo-8-quinolinol solution were added to a sample solution containing 50 μg of iron (III) and 2.0 ml of the buffer solution (pH 3.5). The results are shown in Fig. 3. The absorbance increased with an increase in the amount of this reagent up to 1.2 ml of the 0.2% solution. It was reasonably

constant when 1.2—7.0 ml of this solution was used.

Effect of Buffer Solution and Digestion Time. The effect of the addition of buffer solution on the absorbance was also investigated. The absorbance was unaffected by the addition of up to 5 ml of the buffer solution. The effect of the digestion time on the absorbance was then investigated by digesting the iron(III) complex for 1—30 min. It was found that the absorbance was constant for this period of digestion.

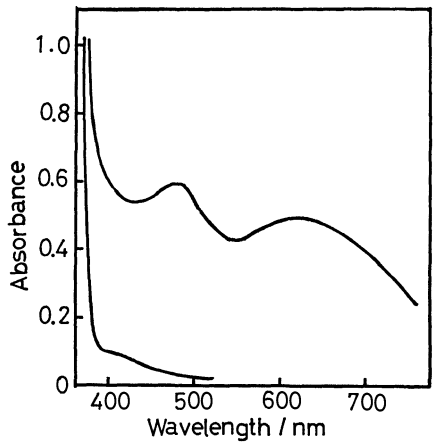

Fig. 1. Absorption spectra of reagent and iron(III)-complex in naphthalene–*N*,*N*-dimethylformamide solution.
Iron(III): 50 μg, 0.2% 5-chloro-7-iodo-8-quinolinol: 4.0 ml, pH: 3.5, 20% naphthalene–acetone: 2.0 ml, shaking time: 1 min, reference: water.

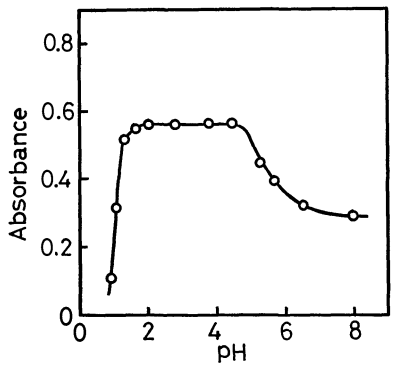

Fig. 2. Effect of pH.
Iron(III): 50 μg, 0.2% 5-chloro-7-iodo-8-quinolinol: 4.0 ml, wavelength: 480 nm, shaking time: 1 min, reference: reagent blank.

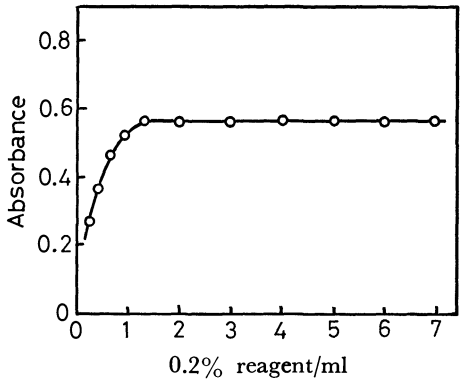

Fig. 3. Effect of reagent concentration.
Iron(III): 50 μg, wavelength: 480 nm, pH: 3.5, 20% naphthalene–acetone: 2.0 ml, standing time: 15 min, reference: reagent blank.

Effect of Naphthalene Concentration. 0.1—4.0 ml portions of 20% naphthalene in acetone were added to a sample solution containing the iron(III) complex. The results showed that the absorbance was independent of the amount of naphthalene.

Effect of Shaking and Standing Times. The effect of the shaking time on the absorbance of the complex was also examined. The rate of the adsorption of the complex on naphthalene was very fast, and no change in the degree of the adsorption was observed during the shaking period of 2—120 s. The adsorbed naphthalene mixture was dissolved in *N*,*N*-dimethylformamide. The color of the complex thus obtained is very stable, and the absorbance remained unchanged for a long time.

Calibration Curve. Based on the optimum conditions described above, a calibration curve for the iron(III) determination was prepared. A linear relationship was obtained between the concentration of iron(III) and the absorbance over the range of 5—88 μg of iron at 480 nm in 10 ml of *N*,*N*-dimethylformamide. The molar absorptivity was 6.3×10^3 l mol^{-1} cm^{-1} at 480 nm, the sensitivity being 0.009 μg/cm^2 for 0.001 absorbance. The relative standard deviation for ten replicate determinations was 0.72% for 50 μg of iron(III).

Choice of Solvent. Tests were made with various organic solvents to dissolve the adsorbed naphthalene mixture. This mixture is easily soluble in *N*,*N*-dimethylformamide, benzene, toluene, xylene, dioxane, chlorobenzene, chloroform, *o*-dichlorobenzene, acetonitrile, nitrobenzene, 1,2-dichloroethane, *etc.* at room temperature.

Effect of the Aqueous-phase Volume. Since the volume ratio of the organic to the aqueous phase is an important factor in the adsorption of the iron(III) complex on naphthalene, the effect of the volume of the aqueous phase on the absorbance was studied.

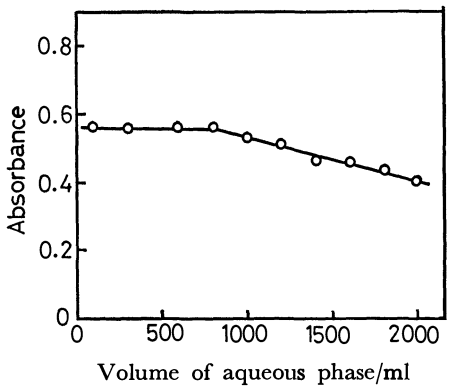

Fig. 4. Effect of volume of aqueous phase.
Iron(III): 50 μg, wavelength: 480 nm, pH: 3.5, 0.2% 5-chloro-7-iodo-8-quinolinol: 6.0 ml, 20% naphthalene–acetone: 4.0 ml, digestion time(30—35 °C): 20 min, reference: reagent blank.

Table 1. Determination of iron in standard reference materials(alloys) and environmental samples

Sample	Iron content (certified value) %	Number of determinations	Iron found	
			Present method (%)	1,10-phenanthroline method (%)
N.B.S. SRM-85b Al alloy	0.24	5	0.239±0.003	0.239±0.003
N.B.S. SRM-94c Zn alloy	0.018	5	0.017±0.001	0.017±0.001
N.B.S. SRM-158a Silicon-Bronze alloy	1.23	5	1.33 ±0.01	1.27 ±0.02
Metallic aluminum (powder)	—	5	0.135±0.001	0.139±0.002
Lake water (Kitagata, Fukui Pref.)	—	4	1.35 ±0.01 (ppm)	1.45 ±0.04 (ppm)

The results are shown in Fig. 4. Under the experimental conditions described, the absorbance remains almost constant up to about 800 ml of the aqueous phase. With further increases in the volume of the aqueous phase, however, the absorbance is gradually diminished.

Effect of Diverse Ions. The effect of diverse ions on the determination of 50 μg of iron(III) was studied. The following alkali metal salts and metal ions(present in the amounts given in parentheses) did not cause an error of more than ±5%: NaCl(8 g), Na_2SO_4 (8 g), NaI(8 g), NH_4Cl(8 g), KNO_3(7 g), sodium tartrate(5 g), sodium citrate(5 mg), sodium oxalate(3 mg), disodium EDTA(10 μg), Ca^{2+}(8 mg), Mg^{2+}(8 mg), Mn^{2+}(8 mg), Pb^{2+}(500 μg), Cr^{6+}(300 μg), Zn^{2+}(40 μg), Cd^{2+}(150 μg), Bi^{3+}(50 μg), Cu^{2+}(30 μg), Pd^{2+}(20 μg), Ni^{2+}(10 μg), Co^{2+}(5 μg). Most of the diverse metal ions gave a positive error, but the complexing reagents, such as sodium citrate, sodium oxalate, and disodium EDTA gave negative one.

Determination of Iron in Reference Materials and Environmental Samples. The proposed method was applied to the determination of iron in the reference materials, aluminum powder, and water samples. The results are in reasonably good agreement with those obtained by the standard spectrophotometric procedure employing 1,10-phenanthroline,[14] as is shown in Table 1. The analytical procedures were as follows: a 0.8279-g portion of standard aluminum alloy (N.B.S., SRM-85b) was gently dissolved in 40 ml of hydrochloric acid (1+1) and 2 ml of 30% hydrogen peroxide. The excess hydrogen peroxide was decomposed by gently heating the mixture on a boiling-water bath for a few minutes. After cooling, the volume of the sample was made up to 200 ml with water. A 5-ml aliquot was transferred to a 100-ml separatory funnel, and 50 ml of hydrochloric acid (1+3) was added. The iron(III) in this sample was extracted by vigorous shaking for 5 min with 20 ml of isobutyl methyl ketone (MIBK).[12] It was then back-extracted from the organic phase with 25 ml of water, and the proposed method was applied.

A 5.085-g portion of standard zinc alloy(N.B.S., SRM-94c) was dissolved in 60 ml of hydrochloric acid (1+1) and 1 ml of concentrated nitric acid. The excess of the acids was removed by evaporating the mixture on a boiling-water bath, and the volume of the sample made up to 200 ml with water. A suitable aliquot was transferred to a 100-ml separatory funnel, and 20 ml of hydrochloric acid (1+1) was added. The iron(III) in this sample was extracted by vigorous shaking for 3 min with 20 ml of an MIBK–isopentyl acetate(1+1) mixture.[13] The aqueous phase was drained off and discarded. The organic phase was washed first with 15 ml and then with 5 ml of hydrochloric acid(1+1). Then 20 ml of water was added to the organic phase, and the mixture was shaken for 3 min. After having been left standing for 5 min, the aqueous phase was drained off in a beaker. Again, 5 ml of water was added to the organic phase, followed by the same procedure. The combined aqueous solution was diluted to exactly 200 ml with water. To an aliquot of this sample solution, we then added 2.0 ml each of a 10% hydroxyammonium chloride solution and a 20% EDTA solution. The solution was then analyzed for iron by the proposed procedure and the 1,10-phenanthroline method.

A 108.6-mg portion of Silicon Bronze alloy(N.B.S., SRM-158a) was dissolved in 10 ml of hydrochloric acid(1+1), 1 ml of concentrated nitric acid, and 3 ml of concentrated sulfuric acid. The mixture was then gently heated on a boiling-water bath. The excess of the acids was evaporated, and then the volume of the sample was brought to 200 ml with water. This sample was used for the both methods.

Metallic aluminum powder was analyzed in the same way as in the case of the standard aluminum alloy.

Lake-water samples, adjusted to 0.1 M with hydrochloric acid immediately after collection, were filtered through a filter paper(No. 5C) to remove suspended particulates; the filtrates were analyzed for the total iron content using this method and the 1,10-phenanthroline method.[14]

References

1) T. Fujinaga, T. Kuwamoto, and E. Nakayama, *Talanta*, **16**, 1225 (1969).

2) T. Fujinaga, T. Kuwamoto, T. Yonekubo, and M. Satake, *Bunseki Kagaku*, **18**, 1113 (1969).
3) T. Fujinaga, M. Satake, and T. Yonekubo, *Bunseki Kagaku*, **19**, 216 (1970).
4) M. Satake, *Memoirs Fac. Engineering, Fukui Univ.*, **18**, 225 (1970).
5) T. Fujinaga, M. Satake, and T. Yonekubo, *Bunseki Kagaku*, **20**, 1255 (1971).
6) T. Fujinaga, M. Satake, and T. Yonekubo, *Talanta*, **19**, 689 (1972).
7) T. Fujinaga, M. Satake, and T. Yonekubo, *Bull. Chem. Soc. Jpn.*, **46**, 2090 (1973).
8) T. Fujinaga, M. Satake, and T. Yonekubo, *Bull. Chem. Soc. Jpn.*, **48**, 899 (1975).
9) T. Fujinaga, M. Satake, and M. Shimizu, *Bunseki Kagaku*, **25**, 313 (1976).
10) M. Satake and Y. Takagi, *Bunseki Kagaku*, **26**, 386 (1977).
11) M. Satake, *Anal. Chim. Acta*, **92**, 423 (1977).
12) JIS H1353 (1972).
13) JIS H1111 (1975).
14) JIS K0101 (1966).

 © 1982 The Chemical Society of Japan Bull. Chem. Soc. Jpn., 55, 2083—2088 (1982)

The Structure and Properties of (η-Cyclopentadienyl)(*O*-methyl dithiocarbonato)(triphenylphosphine)nickel(II)

Mamoru Shimoi,* Akira Ouchi, Shoichi Sato,† and Yoshihiko Saito†,††

Department of Chemistry, College of General Education, The University of Tokyo, Komaba 3-8-1, Meguro-ku, Tokyo 153

†*The Institute for Solid State Physics, The University of Tokyo, Roppongi-7, Minato-ku, Tokyo 106*

(Received October 17, 1981)

The title complex was synthesized, and the structure was determined by means of the X-ray diffraction technique. The crystal is triclinic; space group $P\bar{1}$, $a=9.944(1)$, $b=14.336(2)$, $c=9.759(1)$ Å, $\alpha=107.00(1)$, $\beta=117.35(1)$, $\gamma=76.55(1)°$, $Z=2$, $D_x=1.40$, $D_m=1.36(3)$ g cm^{-3}, μ(Mo $K\alpha$)$=1.08$ mm^{-1}. The *O*-methyl dithiocarbonato ion acts as a unidentate ligand, and it is coordinated with the metal through one sulfur atom. The coordination number of the metal is 3 if the cyclopentadienyl is regarded as a unidentate ligand. A series of [(η-cyclopentadienyl)(*O*-alkyl dithiocarbonato)(trialkyl- or triarylphosphine)nickel(II)], [Ni(C_5H_5)(S_2COR)(PR'_3)], where R=CH_3, C_2H_5, $CH_3(CH_2)_2$, $(CH_3)_2CH$, or $CH_3(CH_2)_3$; R'=C_6H_5, $C_6H_5CH_2$, or $CH_3(CH_2)_3$, were also obtained. The dissociation of the phosphine ligand of the complexes in solution was studied spectrophotometrically, and it was found that the more electron-donative the alkyl group of the *O*-alkyl dithiocarbonato ligand is, the weaker the phosphorus-nickel bond is.

The title complex is unique in that three different ligands are coordinated to the metal, also as will be shown in the later part of this paper, the *O*-alkyl dithiocarbonate ion acts as a unidentate in it. 1,1-Dithioacid ions, including *O*-alkyl dithiocarbonate ions, commonly act as bidentate ligands with their sulfur atoms; however, exceptionally, the ligand acts as a unidentate in the case of $[Sn(S_2COC_2H_5)_4]$,[1] $[Sn\{S_2CN(C_2H_5)_2\}_4]$,[2] $[Ru(NO)\{S_2CN(C_2H_5)_2\}_3]$,[3] $[As(C_6H_5)_4][Pt(S_2COC_2H_5)_3]$,[4] $[Sn(C_6H_5)_3\{S_2P(OC_2H_5)_2\}]$,[5] $[Sb(CH_3)_3\{S_2CN(CH_3)_2\}_2]$,[6] and $[(C_2H_5)_4N][Cd(S_2COC_2H_5)_3]$.[7]

Therefore, the present authors started to investigate this type of complex. In the course of the study, the crystal and molecular structure of the title complex was clarified by the X-ray diffraction technique; a part of the results have already been published.[8]

Recently, Tsipis and his collaborators have reported the crystal and molecular structure as well as the NMR results of the analoguous $[Ni(\eta\text{-}C_5H_5)(S_2COC_2H_5)\{P(C_6H_5)_3\}]$.[9] They gave a qualitative interpretation of the equilibrium between two non-equivalent conformations as well as the phosphine dissociation. Their work prompted us to investigate quantitatively the effect of the alkyl group in the *O*-alkyl dithiocarbonato ligand on the dissociation of phosphine in the complex. As a result, the dissociation constants, as well as some thermodynamic data of the equilibrium were obtained.

Experimental

Synthesis of (η-Cyclopentadienyl)(O-methyl dithiocarbonato)(triphenylphosphine)nickel(II). The chemicals used were all GR-grade reagents: they were purified further by distillation or recrystallization, if necessary. The starting materials, dicyclopentadienylnickel(II) and chlorobis(triaryl or trialkylphosphine)nickel(II), were synthesized by the methods of Cordes[10] and of Venanzi[11] respectivelly. The chloro(η-cyclopentadienyl)(triphenyl-, tribenzyl-, or tributylphosphine)nickel(II) (0.84 g, 2 mmol), obtained by the method of Yamazaki *et al.*,[12] was dissolved in 25 cm^3 of dichloromethane. To the solution, solid potassium *O*-methyl dithiocarbonate (0.29 g, 2 mmol) was then added, and the mixture was stirred at room temperature. The dithiocarbonate, initially insoluble, started to react, and the color of the solution changed from dark red to deep brown due to the product dissolved in it. The reaction was completed in several minutes. The precipitated potassium chloride was filtered off, and a 30 cm^3 portion of hexane was added to the filtrate. The solution was then concentrated to about 10 cm^3 using a rotary vacuum evaporator at room temperature, and finally was left standing. The precipitated crystals were filtered off and washed with hexane; yield, 0.69 g (70%). (Recrystallized from petroleum benzine.)

Synthesis of (η-Cyclopentadienyl)(O-alkyl dithiocarbonate)(triaryl- or trialkylphosphine)nickel(II), [Ni(C_5H_5)(S_2COR)(PR'_3)] (Where R=CH_3, C_2H_5, $CH_3(CH_2)_2$, $(CH_3)_2CH$, or $CH_3(CH_2)_3$; R'=C_6H_5, $C_6H_5CH_2$, or $CH_3(CH_2)_3$). These complexes were obtained by a technique similar to that used in the synthesis of $[Ni(C_5H_5)(S_2COCH_3)\{P(C_6H_5)_3\}]$ described above. Yield: 60—85%. Since the tribenzylphosphine derivatives are relatively sensitive to air-oxidation in solution, care had to be taken not to raise the temperature higher than 50 °C during the recrystallization.

The other alkyldithiocarbamato complexes, $[Ni(\eta\text{-}C_5H_5)(S_2CNHR)\{P(C_4H_9)_3\}]$ (where R=CH_3, C_2H_5, C_6H_5, $C_6H_5CH_2$), were also obtained by the same technique; however, no triphenylphosphine derivatives of this type were obtained.

The dialkyldithiocarbamato derivatives could not be synthesized. From the reaction between $[NiCl(\eta\text{-}C_5H_5)\{P(C_6H_5)_3\}]$ and dimethylammonium dimethyldithiocarbamate, $[Ni(\eta\text{-}C_5H_5)\{S_2CN(CH_3)_2\}]$ was obtained; it was stable only below 10 °C. An attempt was made to synthesize the complexes of this type by using a ligand containing an alkyl group longer than methyl, but no stable products were obtained.

Infrared, Visible, and NMR Spectra Measurements. The infrared spectra of samples were recorded by means of a JASCO infrared spectrophotometer (type 403G), using Nujol and hexachloro-1,3-butadiene mull.

The visible spectra of the samples in a benzene solution were measured by means of a Hitachi 124 spectrophotometer

†† Present address: Department of Chemistry, Faculty of Science and Technology, Keio University, 3-14-1, Kohoku-ku, Yokohama 223.

the temperature of the cell chamber kept at 15, 20, 25, or 30 °C by means of thermostatted circulating water.

The proton NMR spectra were obtained by the use of a JNM-MH-100 type NMR spectrometer, by using chloroform-*d* as the solvent and TMS as the internal standard.

X-Ray Measurement. The single crystals of $[Ni(C_5H_5)(S_2COCH_3)\{P(C_6H_5)_3\}]$ had grown in a dichloromethane-hexane solution kept in hexane vapor for several days at the ambient temperature. The crystal used was shaped into a sphere ($\phi=0.43$ mm). Crystallographic data: $C_{25}H_{23}NiOPS_2$, F.W.=493.25, triclinic, space group $P\bar{1}$, $a=9.944(1)$, $b=14.336(2)$, $c=9.759(1)$ Å, $\alpha=107.00(1)$, $\beta=117.35(1)$, $\gamma=76.55(1)°$, $Z=2$, $D_x=1.40$, $D_m=1.36(3)$ g cm^{-3}, $\mu=1.08$ mm^{-1} for Mo $K\alpha$(0.7107 Å). The reflections with 2θ less than 60° (Mo $K\alpha$ radiation) were collected on a Rigaku automated four-circle diffractometer, the θ-2θ scan technique being employed. The 5768 independent reflections with $|F_o|>3\sigma(|F_o|)$ were used for the structure refinement. The intensities were corrected for Lorentz and polarization factors, but no correction was made for absorption and extinction. The calculations were carried out mainly by means of the FACOM 230-48 computer at The Institute for Solid State Physics, The University of Tokyo, and partially by means of the HITAC 8700/8800 computer at The Computer Center of The University of Tokyo, using the local version of the UNICS program.[13] The atomic scattering factors were taken from Ref. 14.[14]

Structure Determination. The structure was solved by the heavy-atom method. The positions of the nickel, phosphorus, and sulfur atoms were deduced from a three-dimensional Patterson map; all the other non-hydrogen atoms successively located by means of Fourier syntheses. The positional and thermal parameters were refined by the use of the block-diagonal least-squares method. The positions of hydrogen atoms were obtained from a difference Fourier synthesis, and were also refined. In the final cycle of the refinement with anisotropic temperature factors for all the non-hydrogen atoms, all the parameter shifts were less than one-third of the corresponding standard deviations. The final R value was 0.030.[15]

Results and Discussion

The chemical formulae and the analytical data of the complexes, together with their melting points (or decomposition temperature), are shown in Table 1. The ir data are shown in Table 2. As the wave numbers of these peaks of the complexes are not very different from each other, the structure and the coordination mode of the ligands in them are also likely to be similar.

The final atomic parameters of [(η-cyclopentadienyl)(*O*-methyl dithiocarbonato)(triphenylphosphine)-nickel(II)] are listed in Table 3.[16] The interatomic distances and bond angles are tabulated in Table 4. A perspective drawing of the complex and the numbering scheme are shown in Fig. 1. Figure 2 gives a projection of the structure along c.

The crystal consists of discrete molecules. As may be seen from Fig. 1, the coordination number of the nickel atom is 3 if the cyclopentadienyl group is regarded as a unidentate. The dihedral angle between the cyclopentadienyl plane (the maximum deviation from the mean plane is 0.3 Å) and the plane formed by Ni, P, and S (coordinated) atoms is almost rectangluar (89.1°). The ∠P–Ni–S (coordinated) angle was close to a right angle (92.3°). All the non-hydrogen atoms of the *O*-methyl dithiocarbonato ligand and the central nickel atom are coplanar. The C(6) and O atoms of the ligand are likely to have sp^2 hybridization. The C(6)–O, C(6)–S (non coordinated), and to a lesser extent, C(6)–S (coordinated) bonds have

Table 1. Analyses and melting points of the $[Ni(\eta\text{-}C_5H_5)(S_2COR)(PR'_3)]$ complexes

R	R′	Ni(%) Found	Ni(%) Calcd	C(%) Found	C(%) Calcd	H(%) Found	H(%) Calcd	Mp θ_m/°C
Me	Ph[a]	11.62	(11.90)	60.61	(60.88)	4.85	(4.70)	98.0 (decomp)
Et	Ph[b]	11.56	(11.57)	61.53	(61.56)	4.93	(4.97)	90.0 (decomp)
Pr	Ph	11.11	(11.26)	62.36	(62.21)	5.30	(5.22)	93.5 (decomp)
i-Pr	Ph	11.16	(11.26)	62.44	(62.21)	5.33	(5.22)	92.0 (decomp)
Bu	Ph[c]	10.74	(10.97)	62.87	(62.82)	5.45	(5.46)	90.0 (decomp)
Me	Bu	13.39	(13.55)	52.84	(52.67)	8.18	(8.14)	87.0—88.0
Et	Bu	13.06	(13.12)	53.88	(53.70)	8.28	(8.34)	110.0—110.5
Pr	Bu	12.65	(12.72)	54.79	(54.67)	8.32	(8.52)	106.0—107.5
i-Pr	Bu	12.58	(12.72)	54.85	(54.67)	8.40	(8.52)	94.5— 95.0
Bu	Bu	12.26	(12.35)	55.63	(55.59)	8.69	(8.69)	84.0— 85.0
Me	Bz[d]	10.59	(10.96)	62.70	(62.82)	5.54	(5.46)	101.5—103.0
Et	Bz	10.46	(10.69)	63.07	(63.48)	5.69	(5.69)	103.0 (decomp)
Pr	Bz	10.34	(10.42)	64.56	(63.96)	6.18	(5.90)	117.0 (decomp)
i-Pr	Bz	10.09	(10.42)	63.74	(63.96)	5.93	(5.90)	118.0 (decomp)
Bu	Bz	9.89	(10.10)	64.65	(64.48)	6.17	(6.11)	114.0 (decomp)

Sulfur analyses: a), Found 12.74, Calcd 13.00; b), Found 12.46, Calcd 12.64; c), Found 11.71, Calcd 11.98; d), Found 11.26, Calcd 11.98%.

Analysis of $[Ni(C_5H_5)\{S_2CN(CH_3)_2\}]$: Found Ni, 23.76; C, 39.71; H, 4.40; S, 25.94; N, 5.55%. Calcd Ni, 24.06; C, 39.38; H, 4.54; S, 26.28; N, 5.74%.

Me=CH_3, Et=C_2H_5, Pr=$CH_3(CH_2)_2$, *i*-Pr=$(CH_3)_2CH$, Bu=$CH_3(CH_2)_3$, Ph=C_6H_5, Bz=$C_6H_5CH_2$, decomp=decomposed.

Table 2. Infrared spectra (cm^{-1}) of $[Ni(\eta\text{-}C_5H_5)(S_2COR)(PR'_3)]$ complexes (abbreviations in the table are the same as those in Table 1)

R	R′	ν(C⋯S)[b]			
Me	Ph	1198	1147	1050,	1038
Et	Ph	1179	1111	1029	
Pr	Ph	a)	1119	1034	
i-Pr	Ph	1203	1091	1026	
Bu	Ph	1178	1120	1037	
Me	Bu	1192	1145	1058,	1045
Et	Bu	1173	1109	1037	
Pr	Bu	1178	1123	1047	(broad)
i-Pr	Bu	1192	1095	1030	
Bu	Bu	1157	1126	1040	
Me	Bz	1192	1135, 1126	1056	
Et	Bz	1196	1110	1037	
Pr	Bz	1180 (broad)		1030	
i-Pr	Bz	1195	1088	1025	
Bu	Bz	1186	1121	1036	

a) Superimposed by the absorption of the phenyl group.
b) Some modes of vibrations caused by the C-O-C bond, such as ν(C-O), may be mixed.

a multiple-bond character.

The structural data indicate that the C–S (non coordinated) is shorter than the C–S (coordinated) in the case of unidentate 1,1-dithioacid ion. The steric conformations concerned with C–O are always E, except for $[M(S_2COC_2H_5)_3]$ (M=As or Sb), where the ligands are in an intermediate state between the

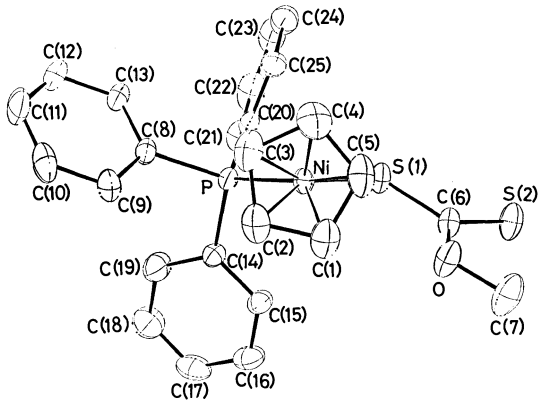

Fig. 1. A perspective drawing of the title complex with the numbering scheme of atoms.

Table 3. Final atomic coordinates ($\times 10^4$ for non-hydrogen atoms and $\times 10^3$ for hydrogen atoms) and isotropic temperature factors (B/Å^2) with estimated standard deviations in parentheses

Atom	x	y	z	B_{eq}/Å^2 a)	Atom	x	y	z	B_{eq}/Å^2 a)
Ni	3355.5(2)	1505.7(1)	2969.1(2)	3.16	C(11)	−3179(2)	2868(2)	1030(3)	7.50
S(1)	5392.0(4)	1864.7(3)	5168.4(5)	4.02	C(12)	−2479(2)	3036(2)	2641(4)	7.87
S(2)	8735.5(5)	1629.9(4)	6536.3(7)	5.55	C(13)	−906(2)	3052(2)	3430(3)	5.51
P	2039.5(4)	2853.3(3)	3580.0(4)	2.99	C(14)	2394(2)	3931(1)	3227(2)	3.63
O	6951(2)	1085(1)	3515(2)	5.70	C(15)	3744(2)	3943(1)	3161(2)	4.46
C(1)	3768(3)	710(2)	961(2)	5.78	C(16)	4026(3)	4770(2)	2922(3)	5.98
C(2)	2236(2)	1062(2)	492(2)	5.39	C(17)	2980(3)	5579(2)	2736(3)	6.35
C(3)	1636(2)	655(2)	1224(3)	5.80	C(18)	1639(3)	5573(2)	2796(4)	7.89
C(4)	2785(3)	15(2)	2108(3)	7.01	C(19)	1335(3)	4763(2)	3036(3)	7.03
C(5)	4120(2)	100(1)	2013(3)	5.83	C(20)	2407(2)	3131(1)	5658(2)	3.60
C(6)	7084(2)	1487(1)	4982(2)	4.09	C(21)	2535(2)	4068(2)	6604(2)	4.92
C(7)	8307(3)	658(2)	3253(3)	7.72	C(22)	2691(3)	4217(2)	8141(3)	6.76
C(8)	−42(2)	2895(1)	2587(2)	3.66	C(23)	2699(3)	3448(2)	8717(2)	7.31
C(9)	−776(2)	2750(2)	950(2)	4.97	C(24)	2062(3)	2529(2)	7806(3)	6.81
C(10)	−2341(2)	2725(2)	174(3)	6.10	C(25)	2467(2)	2357(2)	6277(2)	5.00
Atom	x	y	z	B_{iso}/Å^2	Atom	x	y	z	B_{iso}/Å^2
H(1)	456(3)	91(2)	67(3)	7.6(6)	H(13)	−42(2)	313(1)	456(2)	5.4(5)
H(2)	166(3)	148(2)	−30(3)	7.7(6)	H(15)	447(2)	339(1)	330(2)	5.1(5)
H(3)	71(3)	77(2)	120(3)	8.0(7)	H(16)	491(3)	471(2)	286(3)	6.7(6)
H(4)	277(3)	−28(2)	279(3)	7.8(6)	H(17)	323(3)	609(2)	256(3)	7.3(6)
H(5)	507(3)	−15(2)	259(3)	6.7(6)	H(18)	88(4)	607(2)	258(4)	10.7(9)
H(7-1)	804(3)	56(2)	218(3)	7.8(7)	H(19)	33(3)	480(2)	319(3)	8.3(7)
H(7-2)	860(3)	5(2)	364(3)	6.9(6)	H(21)	252(2)	457(1)	620(2)	5.1(5)
H(7-3)	911(3)	114(2)	386(3)	8.5(7)	H(22)	279(3)	484(2)	872(3)	7.3(6)
H(9)	−12(2)	269(2)	42(2)	5.9(5)	H(23)	280(3)	357(2)	978(3)	8.9(7)
H(10)	−284(3)	257(2)	−87(3)	8.1(7)	H(24)	269(3)	202(2)	831(3)	7.9(7)
H(11)	−427(4)	286(2)	52(4)	11.5(9)	H(25)	237(2)	177(1)	568(2)	5.0(4)
H(12)	−309(3)	324(2)	338(3)	9.7(8)					

a) The equivalent isotropic temperature factors for non-hydrogen atoms were computed using the following expression: $B_{eq}=4/3(B_{11}a^2+B_{22}b^2+B_{33}c^2+B_{12}ab\cos\gamma+B_{13}ac\cos\beta+B_{23}bc\cos\alpha)$. The B_{ij}'s are defined by: $\exp[-(h^2B_{11}+k^2B_{22}+l^2B_{33}+2klB_{23}+2hlB_{13}+2hkB_{12})]$.

Table 4. Interatomic distance and bond angles with their estimated standard deviations in parentheses

Interatomic distance (l/Å)			
Ni-S(1)	2.195(1)	C(8)-C(9)	1.390(3)
Ni-P	2.160(1)	C(9)-C(10)	1.388(3)
Ni-C(1)	2.126(2)	C(10)-C(11)	1.376(5)
Ni-C(2)	2.108(2)	C(11)-C(12)	1.365(4)
Ni-C(3)	2.096(2)	C(12)-C(13)	1.392(3)
Ni-C(4)	2.161(2)	C(13)-C(8)	1.384(3)
Ni-C(5)	2.085(2)	C(14)-C(15)	1.377(3)
S(1)-C(6)	1.719(2)	C(15)-C(16)	1.384(4)
S(2)-C(6)	1.651(1)	C(16)-C(17)	1.360(3)
C(6)-O	1.334(2)	C(17)-C(18)	1.362(5)
O-C(7)	1.449(3)	C(18)-C(19)	1.372(4)
C(1)-C(2)	1.386(3)	C(19)-C(14)	1.390(2)
C(2)-C(3)	1.416(4)	C(20)-C(21)	1.386(2)
C(3)-C(4)	1.400(3)	C(21)-C(22)	1.391(3)
C(4)-C(5)	1.407(4)	C(22)-C(23)	1.373(5)
C(5)-C(1)	1.412(4)	C(23)-C(24)	1.353(4)
P-C(8)	1.833(1)	C(24)-C(25)	1.385(3)
P-C(14)	1.818(2)	C(25)-C(20)	1.388(3)
P-C(20)	1.822(2)		
Bond angle (ϕ/°)			
S(1)-Ni-P	92.29(1)	C(11)-C(12)-C(13)	120.2(3)
C(5)-C(1)-C(2)	107.0(2)	C(12)-C(13)-C(8)	120.3(2)
C(1)-C(2)-C(3)	108.3(2)	C(19)-C(14)-C(15)	118.2(2)
C(2)-C(3)-C(4)	108.9(2)	C(14)-C(15)-C(16)	120.2(2)
C(3)-C(4)-C(5)	106.0(3)	C(15)-C(16)-C(17)	121.0(2)
C(4)-C(5)-C(1)	109.6(2)	C(16)-C(17)-C(18)	119.2(3)
S(1)-C(6)-S(2)	121.1(1)	C(17)-C(18)-C(19)	120.9(3)
S(1)-C(6)-O	115.3(1)	C(18)-C(19)-C(14)	120.5(3)
S(2)-C(6)-O	123.6(1)	C(25)-C(20)-C(21)	119.2(2)
C(6)-O-C(7)	119.5(2)	C(20)-C(21)-C(22)	119.4(2)
Ni-P-C(8)	117.35(5)	C(21)-C(22)-C(23)	120.6(3)
Ni-P-C(14)	114.47(7)	C(22)-C(23)-C(24)	120.2(3)
Ni-P-C(20)	111.56(6)	C(23)-C(24)-C(25)	120.5(3)
Ni-S(1)-C(6)	114.44(7)	C(24)-C(25)-C(20)	120.2(2)
C(8)-P-C(14)	103.35(8)	P-C(8)-C(9)	119.6(2)
C(14)-P-C(20)	106.46(8)	P-C(8)-C(13)	121.5(1)
C(20)-P-C(8)	102.36(7)	P-C(14)-C(15)	120.2(1)
C(13)-C(8)-C(9)	118.9(2)	P-C(14)-C(19)	121.6(2)
C(8)-C(9)-C(10)	120.4(2)	P-C(20)-C(21)	123.7(2)
C(9)-C(10)-C(11)	119.9(2)	P-C(20)-C(25)	117.0(1)
C(10)-C(11)-C(12)	120.4(2)		

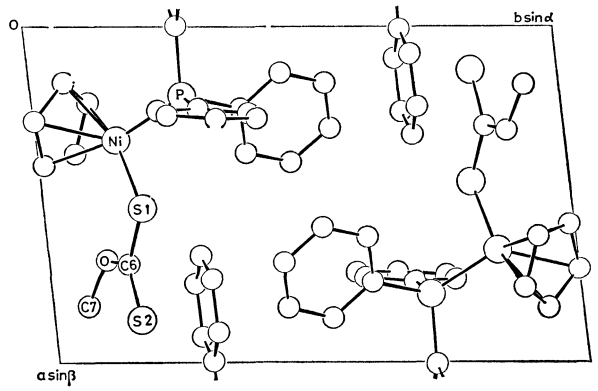

Fig. 2. Crystal packing diagram projected along **c**.

chelate and unidentate types of coordination.[17,18] The conformation of the ligand in the title complex is also E.

Of the present complexes, the bond distances between nickel and ligating sulfur atoms as well as between nickel and cyclopentadienyl are almost equal to the respective values of the *O*-ethyl dithiocarbonato complexes. On the other hand, the Ni–P distances of both the complexes are slightly, but significantly, different from each other (2,160(1) *vs.* 2.184(1) Å). This fact will be discussed later.

The visible spectra of the complex in benzene solution containing an excess of phosphine ligand are shown in Fig. 3. In the figure, two isosbestic points were found at 492 and 535 nm; they remained unchanged even when the concentration of the co-ex-

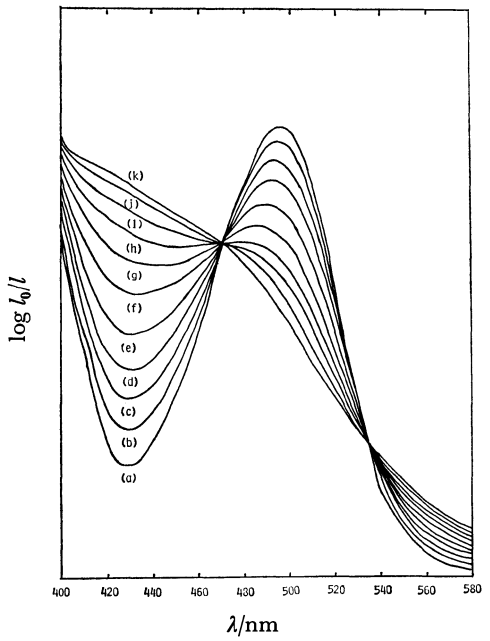

Fig. 3. Absorption spectra of the complex $[Ni(C_5H_5)(S_2COC_4H_9)\{P(C_6H_5)_3\}]$ in benzene solution containing excess of triphenylphosphine.
Concentration of Ni(II): 0.3285×10^{-3} mol dm^{-3}, total concentration of triphenylphosphine: a) 0.3285, b) 2.04, c) 4.33, d) 7.31, e) 11.8, f) 20.2, g) 32.3, h) 49.2, i) 76.8, j) 137.9, k) 197.5×10^{-3} mol dm^{-3}.

isting phosphine was varied from 1 to 600 times (mol/mol) to that of the original 1:1 complex adduct.

Tsipis proposed the following dissociation scheme of the phosphine from the complex in order to explain the temperature variation on the NMR spectra of the complex above 56 °C:[9] $[Ni(C_5H_5)(S_2COR)(PPh_3)] = PPh_3 + [Ni(C_5H_5)(S_2COR)]$ (where Ph=C_6H_5)

The equillibrium constant, K', of this reaction was obtained from the measured absorbance of the solutions at 430 nm containing the complex and the excess of the phosphine ligand at 15, 20, 25, and 30 °C. The procedure is as follows: The equilibrium constant, K', is given by $K'=[M][L]/[ML]$ (where M=$Ni(C_5H_5)(S_2COR)$, L=PPh_3, and ML=$Ni(C_5H_5)(S_2COR)(PPh_3)$.) The total amount of $PPh_3(l)$, and $Ni(m_o)$ are expressed by $l=[ML]+[L]$ and $m_o=[M]+[ML]$ respectively. The absorbance, $A_c=\varepsilon_2[ML]+\varepsilon_1[M]$, where ε_1 and ε_2 are the absorption coefficients of M and ML respectively. The equation becomes:

$$A_c = \varepsilon_2\frac{(m_o+l+K')-\sqrt{D}}{2} + \varepsilon_1\frac{(m_o-l-K')+\sqrt{D}}{2},$$

where $D=(m_o+l+K')^2-4m_ol$ by representing [ML] and [M] in terms of l,m_o, and K'. The values of ε_1, ε_2, and K' were obtained by using the least-squares method, which minimizes $\Sigma(A_o-A_c)^2$, where A_o is observed absorbance. The calculation was carried out on a HITAC M-200H computer at The Computer Center of The University of Tokyo, using the SALS program.[20]

The K''s were converted to the equilibrium constants in molar fraction units, K**. From the van't Hoff plots for each complex, the apparent standard enthalpy, entropy, and Gibb's free energy change of the reaction were obtained; the results are shown in Table 5. As is shown in the table, all of these dissociation reactions are endothermic, and their entropy changes are all positive. The relation between $\Delta H°$ or $\Delta S°$ and the aliphatic polar substituent constants, σ*,[21] of the alkyl groups of the *O*-alkyl dithiocarbonato ligand is shown in Fig. 4. The complex involving the more electron-donative alkyl group shows lower ΔH and ΔS values. At room temperature, the complexes having the higher electron-donative alkyl group of the ligand dissociate more easily. From the equilibrium constants, it is shown that, at the ambient temperature, the complex in the solution of about 10^{-4} mol dm^{-3} dissociates almost completely (more than 99%) in the absence of an excess of ligands. The Ni–P distance in the *O*-methyl dithiocarbonato complex, which is shorter than that of the *O*-ethyl dithio-

Table 5. Standard enthalpy $\Delta H°$, entropy $\Delta S°$, and Gibb's free energy $\Delta G°$ of the reaction $[Ni(C_5H_5)(S_2COR)\{P(C_6H_5)_3\}]=[Ni(C_5H_5)(S_2COR)]+P(C_6H_5)_3$ at 25 °C.

R	ΔH/kJ mol^{-1}	ΔS/J mol^{-1} K^{-1}	ΔG/kJ mol^{-1}
CH_3	42.1 (8)	82 (2)	18 (1)
CH_3CH_2	40.7 (16)	82 (5)	16 (3)
$CH_3(CH_2)_2$	39.5 (4)	80 (2)	16 (1)
$CH_3(CH_2)_3$	39.6 (14)	80 (5)	16 (3)
$(CH_3)_2CH$	38.4 (12)	79 (4)	15 (2)

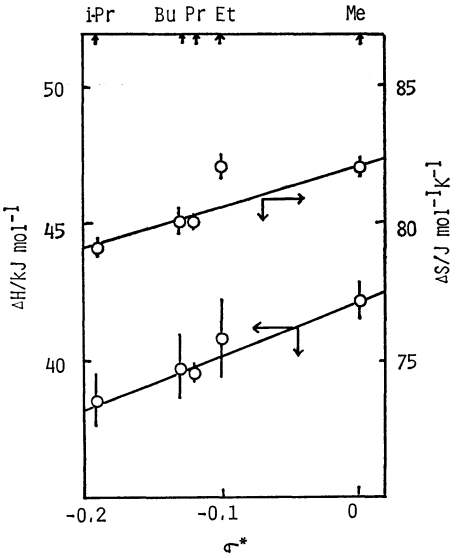

Fig. 4. Dependence of $\Delta H°$ and $\Delta S°$ of the reaction $[Ni(C_5H_5)(S_2COR)\{P(C_6H_5)_3\}]=[Ni(C_5H_5)(S_2COR)]+P(C_6H_5)_3$ on aliphatic polar substituent constants σ* of R.

** The temperature variation of the specific gravity of the solvent was also taken into consideration. The standard changes in enthalpy, *etc.*, obtained from the new K's stand for those in which all components of the equation are in the unit molar fraction.

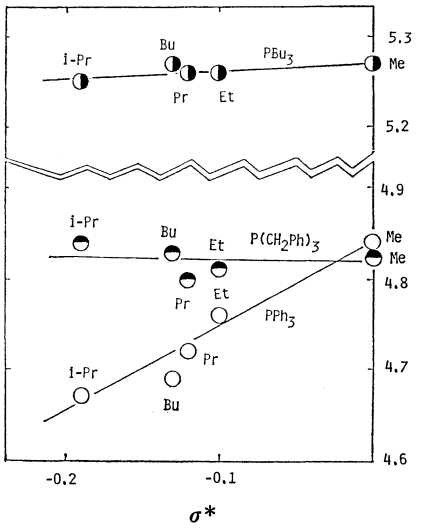

Fig. 5. Dependence of the chemical shifts of cyclopentadienyl protons on the aliphatic polar substitent constants σ^* of R in $[Ni(C_5H_5)(S_2COR)(PR'_3)]$. Abbreviations. For phosphines, Bu=$CH_3(CH_2)_3$, Ph=C_6H_5; for R of $(S_2COR)^-$, Me=CH_3, Et=CH_3CH_2, Pr=$CH_3(CH_2)_2$, *i*-Pr=$(CH_3)_2CH$, Bu=$CH_3(CH_2)_3$.

carbonato one, is explained by the fact that the methyl group is less electronegative than the ethyl group.

The relation between the chemical shifts of ^{1}H-NMR of the cyclopentadienyl proton of the complexes, and the aliphatic polar substituent constants, σ^*,[21] is shown in Fig. 5. The NMR study reveals that the dissociation of the complex in the solution is complete when the concentration of the solution is high (about 10^{-1} mol dm^{-3}), and that the cyclopentadienyl protons of complexes containing triphenylphosphine are more shielded when the alkyl group of the *O*-alkyl dithiocarbonato ligand is more electron-donative. However, this relation is not realized for the tributyl- and tribenzylphosphine complexes, as is shown in the figure. Therefore, in these cases some additional effects should be involved.

References

1) C. L. Raston, P. R. Tennant, A. H. White, and G. Winter, *Aust. J. Chem.*, **31**, 1493 (1978).
2) C. S. Harreld and E. O. Schlemper, *Acta Crystallogr., Sect. B*, **27**, 1964 (1971).
3) A. Domenicano, A. Vaciago, L. Zambonelli, P. L. Loader, and L. M. Venanzi, *Chem. Commun.*, **1966**, 476.
4) M. C. Cornock, R. O. Gould, C. L. Jones, J. D. Owen, D. F. Steele, and T. A. Stephenson, *J. Chem. Soc., Dalton Trans.*, **1977**, 496.
5) K. C. Molloy, M. B. Hossain, D. van der Helm, J. J. Zuckermann, and I. Haiduc, *Inorg. Chem.*, **18**, 3507 (1979).
6) J. A. Cras and J. Willemse, *Recl. Trav. Chim. Pays-Bas*, **97**, 28 (1978).
7) B. F. Hoskins and B. P. Kelly, *Inorg. Nucl. Chem. Lett.*, **8**, 875 (1972).
8) M. Shimoi and A. Ouchi, 36th National Meeting of the Chemical Society of Japan, Osaka, April 1977; 37th National Meeting of the Chemical Society of Japan, Tokyo, April 1978.
9) C. Tsipis, G. E. Manoussakis, D. P. Kessissoglou, J. C. Huffman, L. N. Lewis, M. A. Adams, and K. G. Caulton, *Inorg. Chem.*, **19**, 1458 (1980).
10) J. F. Cordes, *Chem. Ber.*, **95**, 3084 (1962).
11) L. M. Venanzi, *J. Chem. Soc.*, **1958**, 719.
12) H. Yamazaki, T. Nishido, Y. Matsumoto, S. Sumida, and N. Hagihara, *J. Organomet. Chem.*, **6**, 86 (1966).
13) "The Universal Crystallographic Computation Program System (UNICS)," ed by T. Sakurai, Crystallographic Society of Japan, Tokyo (1967).
14) "International Tables for X-Ray Crystallography," Kynoch Press, Birmingham, U. K. (1974), Vol. IV.
15) $R=\Sigma||F_o|-|F_c||/\Sigma|F_o|$.
16) The final thermal parameters and the final F_o-F_c table, are kept at the Chemical Society of Japan as Document No. 8228.
17) G. Carrai and G. Gottardi, *Z. Kristallogr.*, **113**, 373 (1960).
18) G. Gottardi, *Z. Kristallogr.*, **115**, 451 (1961).
20) Statistical Analysis with Least-squares Fitting (SALS), ed by T. Nakagawa and Y. Koyanagi, The Computer Center of The University of Tokyo, 2nd ed (1979).
21) J. E. Leffler and E. Grunward, "Rates and Equilibria of Organic Reactions," Wiley & Sons, New York, N. Y. (1963), p. 222.

 © 1982 The Chemical Society of Japan Bull. Chem. Soc. Jpn., 55, 2089—2093 (1982)

Syntheses and Structure of Bis(*O,O'*-diethyl dithiophosphato)bis-(hexamethylenetetramine)cadmium(II) and Related Adducts

Mamoru Shimoi,* Akira Ouchi, Masahiko Aikawa, Shoichi Sato,† and Yoshihiko Saito†,††

Department of Chemistry, College of General Education, The University of Tokyo, Komaba 3-8-1, Meguro-ku, Tokyo 153

† *The Institute for Solid State Physics, The University of Tokyo, Roppongi-7, Minato-ku, Tokyo 106*

(Received November 5, 1981)

The title complex was synthesized, and the crystal structure was determined by means of the X-ray diffraction technique. The crystal is monoclinic; space group $P2_1/n$, $a=16.310(3)$, $b=6.777(1)$, $c=14.576(3)$ Å, $\beta=96.13(1)°$, $Z=2$, $D_x=1.58$, $D_m=1.55(3)$ g cm^{-3}, μ(Mo $K\alpha$)$=1.12$ mm^{-1}. The molecule has a center of symmetry, and a distorted octahedron is formed around the central cadmium atom; two *O,O'*-diethyl dithiophosphato ions (dtp) act as bidentate ligands, and each ligand forms a four-membered chelate ring with its two sulfur atoms on the equatorial plane, while two hexamethylenetetramine molecules are coordinated to the metal atom by their nitrogen atoms from the axial direction. Related adducts, Cd(II)(dtp)$_2\cdot X_n$, where X is a donor and $n=1$ or 2, were also synthesized, and their structures were compared with those of the corresponding Co(II)(dtp)$_2\cdot X_n$-type complexes.

The present authors have reported in another paper[1] that the phosphine or amine adducts of bis(*O,O'*-diethyl dithiophosphato)cobalt(II) (hereafter, abbreviated as Co(II)(dtp)$_2$; the same types of abbreviations are used for related adducts) are very stable in air; however, the original Co(II)(dtp)$_2$ is easily oxidized. We have attempted to obtain similar types of adducts of other metals in order to compare them with the corresponding cobalt(II) complexes. As the electron paramagnetic resonance spectra, especially that of the single crystal, is expected to be effective in clarifying the stabilization mechanism, we have tried to synthesize adducts that are isostructural to the cobalt(II) analogues and contain a diamagnetic metal atom. Thus, the present authors have synthesized adducts containing cadmium(II) and compared their properties and structures with those of the corresponding cobalt(II) adducts. From their chemical compositions, the general features of their infrared spectra, and then X-ray powder diffraction patterns, the adducts of cobalt(II) and of cadmium(II) are found to resemble each other, and some of them are isostructural, as will be shown later. In the other paper,[1] we have suggested the octahedral structure for some adducts from the magnetic as well as the visible spectroscopic results; however, no structural analysis has been carried out. In this connection, the structure of Cd(II)(dtp)$_2$(hex)$_2$ (where hex=hexamethylenetetramine), which is expected to be octahedral, was determined by the X-ray diffraction technique. Another reason for the selection of the hex adduct in the present study was to examine the effect of such a bulky ligand on the coordination bond. In fact, the structure analysis of the metal complex involving this amine had been carried out only for Mn(II)Cl$_2$(hex)$_2$(H$_2$O)$_2$.[2] As cadmium(II) is a diamagnetic metal, the ^{1}H-NMR technique is easily applicable to the adducts. The results of the study revealed that the adducts are not completely dissociated, even in a solution.

†† Present address: Department of Chemistry, Faculty of Science and Technology, Keio University, Hiyoshi 3-14-1, Kohoku-ku, Yokohama, Kanagawa 223.

Experimental

Synthesis of Bis(O,O'-diethyl dithiophosphato)cadmium(II) Adducts, Cd(II)(dtp)$_2\cdot X_n$ (Where X is a Donor, and n=1 or 2). All the chemicals used were the GR- or EP-grade reagents of Wako Pure Chemicals Co., Ltd., and no further purification was necessary. Na(dtp) was obtained from phosphorus pentasulfide by the method of Livingstone.[3] The adducts were synthesized as follows:

Synthesis of Cd(II)(dtp)$_2$ (1): Into about 400 cm^3 of ethanol, 9.12 g (40 mmol) of hydrated cadmium(II) chloride ($CdCl_2\cdot 2.5\,H_2O$) and 16.6 g (80 mmol) of Na(dtp) were added, and the mixture was refluxed for 1 h. After cooling, the deposited crude complex was filtered off and recrystallized from ethanol. Yield: 18 g (93%).

Synthesis of Cd(II)(dtp)$_2$(hex) (2): Into about 35 cm^3 of benzene, 1.93 g (4 mmol) of **1**, and 0.56 g (4 mmol) of hex were dissolved. After filtration, the filtrate was left standing for a while and then filtered once more to remove the white turbid. To the filtrate, 5 cm^3 of benzene was added, and the mixture was left standing in a desiccator containing hexane for several days. A crystalline product came out. Yield: 0.6 g (25%). Found: Cd, 18.00; C, 27.20; H, 5.19; N, 9.07%. Calcd for $CdC_{14}H_{32}N_4O_4P_2S_4$: Cd, 18.04; C, 26.99; H, 5.18; N, 8.99%.

Synthesis of Cd(II)(dtp)$_2$(hex)$_2$ (3): Into 70 cm^3 of chloroform, 3.15 g (6.97 mmol) of **1** and 1.95 g (13.9 mmol) of hex were added, and the mixture was refluxed for 1 h. After cooling, it was filtered off, and the filtrate was left standing for several days in hexane vapor. Crystallines were thus precipitated. Yield: 2.9 g (55%). (It was also obtained from the evaporation residue of a mixed solution of the starting materials by repeated recrystallizations from diisopropyl ether.) Found: Cd, 14.76; C, 31.55; H, 5.80; N, 14.65%. Calcd for $CdC_{20}H_{44}N_8O_4P_2S_4$: Cd, 14.73; C, 31.48; H, 5.81; N, 14.68%.

Synthesis of Cd(II)(dtp)$_2$(PPh$_3$) (4) (Where PPh$_3$=Triphenylphosphine): Into 30 cm^3 of chloroform, 0.97 g, (2.0 mmol) of **1** and 1.05 g (4.0 mmol) of PPh$_3$ were added, and the mixture was refluxed for 30 min. The solvent was evaporated off, and from the residue the product was extracted by ligroine. The extracted solution was ice-cooled, and the crystals came out. The crude product was recrystallized from benzene containing PPh$_3$. Yield: 1.25 g (84%). Found: Cd, 15.07; C, 42.42; H, 4.73%. Calcd for CdC_{26}-

$H_{35}O_4P_3S_4$, Cd, 15.09; C, 41.49; H, 4.74%.

Synthesis of Cd(II)(dtp)$_2$(pip) (5) (Where pip=Piperazine): This complex was synthesized by the same procedure as that for **4**, 0.8 g (1.7 mmol) of **1** and 0.45 g (5.2 mmol) of pip being used. Toluene was employed in place of benzene for the extraction. Yield: 0.45 g (48%). Found: Cd, 19.66; C, 25.43; H, 5.28; N, 5.20%. Calcd for $CdC_{12}H_{30}N_2O_4P_2S_4$: Cd, 19.75; C, 25.33; H, 5.32; N, 4.92%.

Synthesis of Cd(II)(dtp)$_2$(pyr) (6) (Where pyr=Pyrazine): Into 30 cm^3 of chloroform, 0.8 g (1.7 mmol) of **1** and 0.4 g (5.0 mmol) of pyrazine were dissolved, after which the solution was evaporated using a rotary vacuum evaporator under 80 °C. The residue was recrystallized from 1,2-dichloroethane–ligroine (20/7=v/v). Yield: 0.35 g (38%). Found: Cd, 19.89; C, 25.62; H, 4.23; N, 4.71%. Calcd for $CdC_{12}H_{24}N_2O_4P_2S_4$: Cd, 19.97; C, 25.60; H, 4.30; N, 4.98%.

Synthesis of Cd(II)(dtp)$_2$(bzt)$_2$ (7) (Where bzt=Benzothiazole): The synthesis procedure for **6** was applied, starting from 0.8 g (1.7 mmol) of **1**, and 0.5 g (3.7 mmol) of bzt. The recrystallization solvent used was ligroine–toluene (1/1=v/v). Yield: 0.75 g (60%). Found: Cd, 14.97; C, 35.07; H, 4.00; N, 3.72%. Calcd for $CdC_{22}H_{30}N_2O_4P_2S_6$: Cd, 14.92; C, 35.08; H, 4.02; N, 3.72%.

Synthesis of Cd(II)(dtp)$_2$(bza)$_2$ (Where bza=Benzylamine): The crude product was synthesized by the same method as **6**, starting from 0.8 g (1.7 mmol) of **1** and 0.5 g (4.9 mmol) of bza. The product was extracted with ligroine and it was deposited by ice cooling. Yield: 0.69 g (52%). Found: Cd, 16.00; C, 37.71; H, 5.43; N, 4.13%. Calcd for $CdC_{22}H_{38}N_2O_4P_2S_4$: Cd, 16.17; C, 38.01; H, 5.22; N, 4.03%.

X-Ray Measurements. Powder X-Ray Diffraction Patterns: They were recorded on the diffractometer, Model DX-GO-F of GEOL, in the range from 6° to 30° in 2θ, Cu $K\alpha$ radiation being used.

Single-crystal X-Ray Analysis: The single-crystal specimen of **3** for the X-ray study was grown from a chloroform–hexane solution kept in hexane vapor for several days. The crystal was shaped into a sphere (ϕ=0.34 mm) and covered by cyanoacrylate resin to prevent decomposition by atmospheric moisture. The crystallographic data are: $CdC_{20}H_{44}N_8O_4P_2S_4$, F.W.=763.21, monoclinic, space group $P2_1/n$,** a=16.310(3), b=6.777(1), c=14.576(3) Å, β=96.13(1)°, Z=2, D_x=1.58, D_m=1.55(3) g cm^{-3}, μ(Mo $K\alpha$)=1.12 mm^{-1}. The reflections with 2θ less than 60° were collected on a Rigaku automated four-circle diffractometer with Mo $K\alpha$ radiation, θ-2θ scan technique being employed. Of 4670 reflections measured, 3654 independent reflections with $|F_o| > 3\sigma(|F_o|)$ were used for the structure refinement. The intensities were corrected for Lorentz and polarization factors, but no correction was made for absorption and extinction. The calculations were carried out mainly on the FACOM 230-48 computer at The Institute for Solid State Physics, The University of Tokyo, and partly on HITAC 8700/8800 computer at The Computer Center of The University of Tokyo, using the local version of UNICS program.[4] The atomic-scattering factors were taken from Ref. 5.[5]

Structure Determination: The structure was solved by the heavy-atom method. All the non-hydrogen atoms except for ethyl carbon atoms were deduced from a three-dimensional Patterson map, while the carbon atoms were located by successive Fourier syntheses. Their positional and thermal parameters were refined by the block-diagonal least-squares method. The positions of all the hexamethylenetetramine hydrogen atoms as well as of four ethyl hydrogen atoms were obtained from a difference Fourier synthesis; they were also refined. In the final cycle of the refinement with anisotropic temperature factors for all the non-hydrogen atoms, all the parameter shifts were less than one-third of the corresponding standard deviations. The final R value becomes 0.030.[6]

^{1}H-NMR Measurement. The ^{1}H-NMR spectra of their chloroform-*d* solutions were recorded on a JEOL JNM-MH-100 NMR spectrometer, using TMS as the internal standard.

Results and Discussion

The final atomic parameters for **3** are listed in Table 1,[7] while the interatomic distances, as well as the bond angles of the complex, are tabulated in Table 2. A perspective drawing of the adduct and the numbering scheme of the atoms are shown in Fig. 1, while Fig. 2 presents a projection of the structure along b.

The crystal consists of discrete molecules, and each

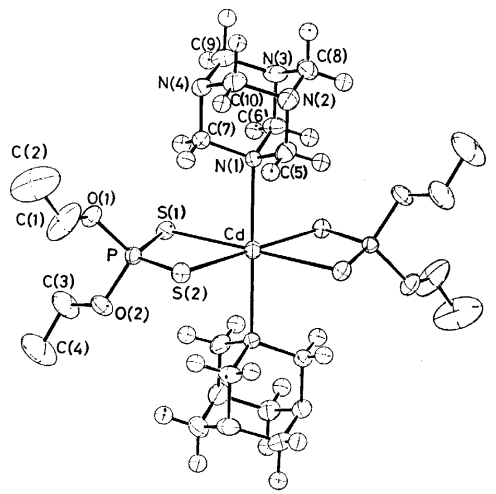

Fig. 1. A perspective drawing of the title compound with the numbering scheme of atoms.

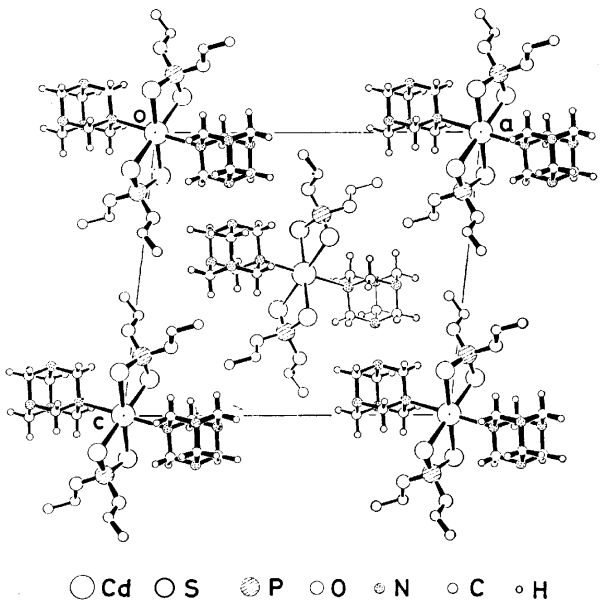

Fig. 2. Crystal packing diagram projected along b.

** Systematic absence of the reflections were $0k0$ for k=odd and $h0l$ for $h+l$=odd.

Table 1. Final atomic coordinates ($\times 10^4$ for non-hydrogen atoms, and $\times 10^3$ for hydrogen atoms) and isotropic temperature factors (B/Å^2), with estimated standard deviations in parentheses

Atom	x	y	z	B_{eq}/Å^2 a)	Atom	x	y	z	B_{eq}/Å^2 a)
Cd	0	0	0	3.19	C(1)	−116(3)	2152(8)	3536(3)	10.63
S(1)	282.6(4)	−2258.4(8)	1530.5(4)	3.35	C(2)	424(4)	2859(9)	4197(5)	14.60
S(2)	−665.1(4)	2134.5(8)	1281.7(4)	3.37	C(3)	−1175(2)	−2783(6)	2960(3)	7.90
P	−354.1(3)	−161.1(8)	2083.5(4)	3.00	C(4)	−1954(3)	−3268(8)	3178(4)	12.49
O(1)	175(1)	474(3)	3019(1)	4.44	C(5)	1444(2)	3709(4)	37(2)	4.13
O(2)	−1192(1)	−987(3)	2399(1)	4.67	C(6)	2087(2)	530(4)	170(2)	4.22
N(1)	1403(1)	1725(3)	470(1)	2.98	C(7)	1577(2)	2025(4)	1488(2)	3.91
N(2)	2242(2)	4681(3)	276(2)	4.76	C(8)	2881(2)	3381(5)	−20(2)	5.85
N(3)	2892(1)	1430(4)	414(2)	5.02	C(9)	3013(2)	1733(4)	1421(2)	4.91
N(4)	2373(1)	2968(3)	1748(1)	3.89	C(10)	2380(2)	4876(4)	1281(2)	4.70
Atom	x	y	z	B_{iso}/Å^2	Atom	x	y	z	B_{iso}/Å^2
H(3-1)	−85(3)	−253(7)	349(4)	12.0(17)	H(7-1)	156(2)	72(4)	178(2)	2.3(6)
H(3-2)	−99(3)	−392(8)	258(3)	11.3(16)	H(7-2)	110(2)	296(4)	166(2)	2.4(6)
H(4-1)	−187(3)	−449(6)	346(3)	7.1(11)	H(8-1)	343(2)	411(5)	14(2)	3.4(7)
H(4-2)	−232(4)	−348(9)	267(4)	14.3(19)	H(8-2)	277(2)	328(5)	−66(2)	4.4(8)
H(5-1)	130(1)	357(4)	−60(2)	1.8(5)	H(9-1)	354(2)	235(4)	163(2)	4.0(7)
H(5-2)	105(2)	448(4)	21(2)	1.6(5)	H(9-2)	294(2)	48(4)	175(2)	3.1(7)
H(6-1)	198(2)	39(4)	−43(2)	2.1(6)	H(10-1)	289(2)	545(4)	144(2)	3.4(7)
H(6-2)	206(2)	−76(4)	48(2)	2.5(6)	H(10-2)	196(2)	559(4)	152(2)	2.0(5)

a) The equivalent isotropic temperature factors for non-hydrogen atoms were computed using the following expression: $B_{eq}=4/3(B_{11}a^2+B_{22}b^2+B_{33}c^2+B_{13}ac\cos\beta)$. The B_{ij}'s are defined by: $\exp[-(h^2B_{11}+k^2B_{22}+l^2B_{33}+2klB_{23}+2hlB_{13}+2hkB_{12})]$.

cadmium atom is at the center of symmetry. A couple of dtp ligands are coordinated to the central metal atom by their two sulfur atoms, forming four-membered chelate rings on the equatorial plane. On the other hand, two hex molecules are coordinated to the central metal atom by their nitrogen atoms from the axial direction. Thus, the cadmium(II) atom takes a six-coordinate distorted octahedral configuration.

The Cd–S distances of the present adduct are 2.704(1) and 2.682(1) Å, slightly longer than those in Cd(II) (i-Pr_2dtp)$_2$ (where i-Pr_2dtp = O,O'-diisopropyl dithiophosphato group) (2.486(7)—2.590(8) Å.[8]) This is probably because of the fact that the former is in an octahedral configuration, while the latter is in tetrahedral configuration. In the present adduct, the two P–S distances in the ligand are about the same, *ca.* 1.98 Å, and intermediate between the single bond (2.09 Å) and the double bond (1.87 Å),[9] indicating that the double bond is delocalized. The four-membered ring formed by Cd, S(1), S(2), and P atoms is almost planar. In the present complex, the S(1)–Cd–S(2) bond angle is 77.09(2)°, smaller than those of common O,O'-dialkyl dithiophosphato complexes and of their adducts,[10–24] including the Co(Me_2dtp)$_2$(PPh_3) (where Me_2dtp = O,O'-dimethyl dithiophosphato group; PPh_3 = triphenylphosphine) reported in the other paper,[1] although there are some exceptions.[13,16]

The apparent C–C distances of the ethyl groups of the present adduct were found to be 1.323(8) and 1.382(7) Å, shorter than the common C–C single bond length (1.50 Å). This is probably a result of the fact that the carbon atoms are not fixed, but have large thermal parameters, as is shown in Table 2.

The Cd–N(1) distance is 2.595(2) Å, longer than the common Cd–N distances (about 2.3 Å) in cadmium(II) complexes.[25] Similar phenomenon has also been observed in Mn(II)Cl_2(hex)$_2$(H_2O)$_2$, where Mn–N is 2.40 Å.[2] In the present case, this is probably attributable to the repulsion between the hydrogen atoms of the hex and the sulfur atoms of the dtp ligand. As is shown in Table 2, H(7-1)···S(1), H(7-2)···S(2), H(5-1)···S(1′), and H(6-1)···S(2′) are all about 2.9 Å. They are shorter than the sum of the van der Waals radii of H and S atoms (3.05 Å), suggesting a strong repulsion. Thus, the long Cd–N distance of this adducts is probably attributable to the hindrance caused by the bulky ligand. As was shown in another paper, the Co–P distance of Co(II)(Me_2dtp)$_2$(PPh_3) is also large, because of the bulky ligand.[1] In the case of smaller ligands, the metal-nitrogen distances of the amine adducts, for example, the Ni–N distances of Ni(II)(dtp)$_2$·X_n-type adducts, are not unusually long (2.06—2.11 Å);[19–23] they are not much longer than the sum of the coordination radii (2.00 Å).

In the free hex molecule, all the C–N bonds are equivalent; their length is 1.476(2) Å. In contrast, the average distance between carbon and nitrogen atoms bonded to the metal atom in the present adduct is 1.488(5) Å, and the mean length of the other N–C bonds is 1.464(5) Å. This observation suggests that electrons flow from the ligand into the metal through the coordinated nitrogen atom. The same type of elongation of the C–N bond of hex has also been reported for its adducts of borane[27] and iodine.[28]

The powder X-ray diffraction pattern of **2** was compared with that of the same type of Co(II) adduct. The diffraction patterns are shown in Fig. 3a. The peak positions, as well as their intensities, correspond with each other, except for some weak peaks. Their infrared spectra in the 400—4000 cm^{-1} region are also similar. Thus, the cadmium(II) and cobalt(II) adducts are likely to be isostructural, exhibiting a five-coordinate trigonal bipyramidal configuration.

The powder X-ray diffraction patterns of **1**, **2**, **3**, and hex were compared with each other, but no coincidence between them were recognized. This fact indicates that **2** and **3** are not mixtures, but different kinds of compounds.

The adduct **5** and Co(II)(dtp)$_2$(pip), as well as **6** and Co(II)(dtp)$_2$(pyr), are found to be isostructural with one another, and the structure of **5** resembles that of **6**; the diffraction patterns of **5**, **6**, and Co(II)-

Table 2. Interatomic distance and bond angles, with estimated standard deviations in parentheses

Interatomic distance (l/Å)			
Cd-S(1)	2.704(1)	N(2)-C(5)	1.467(4)
Cd-S(2)	2.682(1)	N(2)-C(8)	1.464(4)
Cd-N(1)	2.595(2)	N(2)-C(10)	1.464(4)
P-S(1)	1.982(1)	N(3)-C(6)	1.457(3)
P-S(2)	1.979(1)	N(3)-C(8)	1.465(4)
P-O(1)	1.593(2)	N(3)-C(9)	1.474(4)
P-O(2)	1.590(2)	N(4)-C(7)	1.461(3)
O(1)-C(1)	1.471(5)	N(4)-C(9)	1.458(4)
C(1)-C(2)	1.323(8)	N(4)-C(10)	1.462(3)
O(2)-C(3)	1.465(4)		
C(3)-C(4)	1.382(7)	S(1)···H(7-1)	2.89(3)
N(1)-C(5)	1.490(3)	S(2)···H(7-2)	2.93(3)
N(1)-C(6)	1.482(3)	S(1')···H(5-1)	2.93(2)
N(1)-C(7)	1.493(3)	S(2')···H(6-1)	2.92(3)
Bond angle (ϕ/°)			
S(1)-Cd-S(2)	77.09(2)	C(5)-N(1)-C(6)	107.4(2)
S(1)-Cd-N(1)	88.24(4)	C(6)-N(1)-C(7)	107.4(2)
S(2)-Cd-N(1)	89.08(4)	C(7)-N(1)-C(5)	106.6(2)
Cd-S(1)-P	83.05(2)	C(5)-N(2)-C(8)	107.6(2)
Cd-S(2)-P	83.69(3)	C(8)-N(2)-C(10)	108.1(2)
S(1)-P-S(2)	115.85(4)	C(10)-N(2)-C(5)	108.4(2)
S(1)-P-O(1)	106.40(7)	C(6)-N(3)-C(8)	107.7(2)
S(1)-P-O(2)	111.66(8)	C(8)-N(3)-C(9)	107.4(2)
S(2)-P-O(1)	111.97(7)	C(9)-N(3)-C(6)	108.8(2)
S(2)-P-O(2)	105.87(7)	C(7)-N(4)-C(9)	108.2(2)
O(1)-P-O(2)	104.6(1)	C(9)-N(4)-C(10)	108.3(2)
P-O(1)-C(1)	118.2(2)	C(10)-N(4)-C(7)	108.5(2)
O(1)-C(1)-C(2)	115.3(5)	N(1)-C(5)-N(2)	112.6(2)
P-O(2)-C(3)	119.2(2)	N(1)-C(6)-N(3)	112.7(2)
O(2)-C(3)-C(4)	111.3(4)	N(1)-C(7)-N(4)	112.8(2)
Cd-N(1)-C(5)	111.9(1)	N(2)-C(8)-N(3)	113.0(3)
Cd-N(1)-C(6)	110.3(1)	N(3)-C(9)-N(4)	112.4(2)
Cd-N(1)-C(7)	113.1(1)	N(4)-C(10)-N(2)	112.2(2)

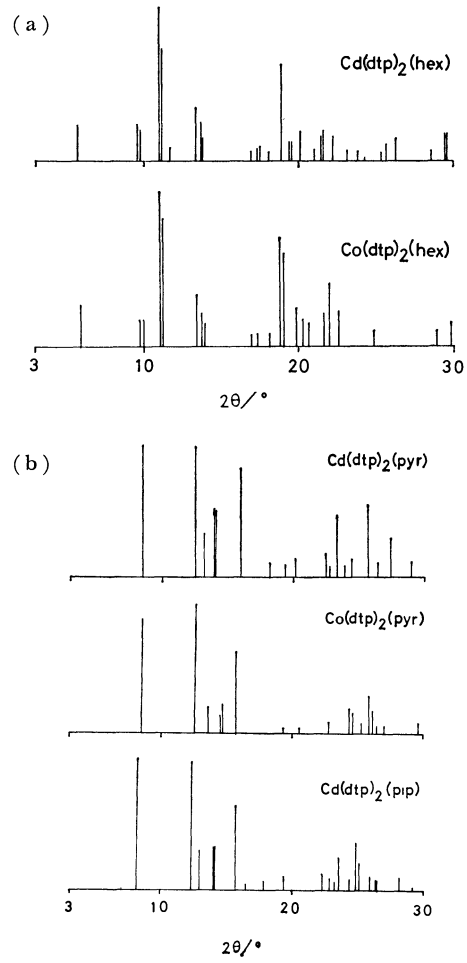

Fig. 3. Powder X-ray diffraction patterns of a) hexamethylenetetramine adducts, and b) pyrazine and piperazine adducts.

Table 3. ^{1}H-NMR data of Cd(II)(dtp)$_2\cdot X_n$-type adducts (in δ, solvent = chloroform-d)

	Ethyl protons of dtp		Ligand in Adducts		Free ligand	
[Cd(II)(dtp)$_2$]	4.30	1.42				
[Cd(II)(dtp)$_2$(hex)]	4.19	1.39	4.82		4.73	
Cd(II)(dtp)$_2$(PPh$_3$)]	4.15	1.36	7.44		7.17	7.14
[Cd(II)(dtp)$_2$(pip)]	4.20	1.42	3.11	1.96	2.83	2.00
[Cd(II)(dtp)$_2$(pyr)]	4.25	1.40	8.78	8.67	8.55	
[Cd(II)(dtp)$_2$(bzt)$_2$]	4.23	1.37	9.28	8.38	8.85	8.08
			7.99	7.51	7.88	7.41
[Cd(II)(dtp)$_2$(bza)$_2$]	4.18	1.37	7.37	4.08	7.30	3.84
			2.67		1.44	

dtp: *O,O'*-Diethyl dithiophosphato ligand; hex: hexamethylenetetramine; PPh$_3$: triphenylphosphine; pip: piperaziae; pyr: pyrazine; bzt: benzothiazole; bza: benzylamine.

$(dtp)_2(pyr)$ are shown in Fig. 3b. These cobalt(II) adducts are expected to have an octahedral configuration,[1] where two nitrogen atoms of the ligand act as donor atoms, and the ligand bridges two metal atoms. Therefore, the corresponding cadmium(II) adducts may have the same structure. The **4** and **7** adducts are not exactly isostructural to the corresponding $Co(II)(dtp)_2$ adducts, but each pair of adducts is likely to have structures resembling each other.

The chemical shifts of the ^{1}H-NMR of **1** and its adducts in a chloroform-*d* solution, together with those of the free ligands, are shown in Table 3. As expected, the signals of the dtp ethyl protons are shifted to a higher magnetic field by the formation of the adducts. On the other hand, the signals of the amine or phosphine protons of the adducts appear in a lower magnetic field than those of the corresponding ligands. This fact shows that the amine or phosphine molecules form bonds with the complex, even in a solution, or at least in equilibrium with the bonded form. Thus, the electrons appear to flow from the amine or phosphine to the dtp ligand through the central metal atom.

We gratefully acknowledged the assistance on the structure-analysis calculations by Mr. Yasuhiko Yukawa of the Faculty of Science and Technology, Sophia University.

References

1) M. Shimoi, A. Ouchi, T. Uehiro, Y. Yoshino, S. Sato, and Y. Saito, *Bull. Chem. Soc. Jpn.*, **55**, No. 8, in press.
2) Y. C. Tang and J. H. Sturdivant, *Acta Crystallogr.*, **5**, 74 (1952).
3) S. E. Livingstone and E. Mihkelson, *Inorg. Chem.*, **9**, 2545 (1970).
4) "The Universal Crystallographic Computation Program System (UNICS)," ed by T. Sakurai, Crystallographic Society of Japan, Tokyo (1967).
5) "International Tables for X-Ray Crystallography," Kynoch Press, Birmingham, U.K. (1974), Vol. IV.
6) $R=\Sigma||F_o|-|F_c||/\Sigma|F_o|$.
7) The final thermal parameters and the final F_o-F_c tables are deposited as Document No. 8229 at the Office of the Editor of the Bulletin of the Chemical Society of Japan.
8) S. L. Lawton and G. T. Kokotailo, *Inorg. Chem.*, **8**, 2410 (1969).
9) L. Pauling, "Nature of the Chemical Bond," 3rd ed, Cornell Univ. Press, N.Y. (1960), p. 246.
10) Q. Fernando and C. D. Green, *J. Inorg. Nucl. Chem.*, **29**, 647 (1967).
11) E. W. Hoffmann, W. Kuchen, W. Poll, and H. Winderlich, *Angew. Chem., Int. Ed. Engl.*, **18**, 415 (1978).
12) A. W. Edelblut, B. L. Haymore, and R. A. D. Wentworth, *J. Am. Chem. Soc.*, **100**, 2250 (1978).
13) B. W. Liebich and M. Tomassini, *Acta Crystallogr., Sect. B*, **34**, 944 (1978).
14) J. F. McConnell and A. Schwarz, *Acta Crystallogr., Sect. B*, **28**, 1546 (1972).
15) T. Ito, T. Igarashi, and H. Hagihara, *Acta Crystallogr., Sect. B*, **25**, 2303 (1969).
16) J. R. Knox and C. K. Prout, *Acta Crystallogr., Sect. B*, **25**, 2281 (1969).
17) V. Kastalsky and J. F. McConnell, *Acta Crystallogr., Sect. B*, **25**, 909 (1969).
18) J. F. McConnell and V. Kastalsky, *Acta Crystallogr.*, **22**, 853 (1967).
19) S. Ooi and Q. Fernando, *Inorg. Chem.*, **6**, 1558 (1967).
20) D. B. Sowerby and I. Haiduc, *Inorg. Chim. Acta*, **17**, L15 (1976).
21) P. S. Shetty and Q. Fernando, *J. Am. Chem. Soc.*, **92**, 3964 (1970).
22) S. K. Aurora, D. E. Carter, Q. Fernando, and K. Seff, *Acta Crystallogr., Sect. B*, **33**, 3230 (1977).
23) D. C. Craig, E. T. Pallister, and N. C. Stephenson, *Acta Crystallogr., Sect. B*, **27**, 1163 (1971).
24) L. Gastaldi, P. Porta, and A. A. G. Tomlinson, *J. Chem. Soc., Dalton Trans.*, **1974**, 1424.
25) From the XDC data base of The Computer Center of The University of Tokyo, which is the same as the "Crystallographic Data File" of the Crystallographic Data Center of Cambridge University.
26) L. N. Becka and D. W. J. Cruickshank, *Proc. R. Soc. London, Ser. A*, **273**, 435 (1963).
27) F. Hanic and V. Šubrtová, *Acta Crystallogr., Sect. B*, **25**, 405 (1969).
28) H. Pritzkow, *Acta Crystallogr., Sect. B*, **31**, 1589 (1975).

Studies on the High-pressure Reaction of Rare-earth Sesquioxides with Vanadium Dioxide

Tsutomu SHIN-IKE,* Gin-ya ADACHI,† Jiro SHIOKAWA,†
Masahiko SHIMADA,†† and Mitsue KOIZUMI††

Department of Chemistry, Osaka Dental University, Makino-honmachi, Hirakata, Osaka 573

† *Department of Applied Chemistry, Faculty of Engineering, Osaka University, Yamadaoka, Suita, Osaka 565*

†† *The Institute of Scientific and Industrial Research, Osaka University, Yamadaoka, Suita, Osaka 565*

(Received November 11, 1981)

The reaction of rare-earth sesquioxides (Ln_2O_3) with vanadium dioxide (VO_2) at 1400 °C and 50 kbar** and 30 kbar was studied. Quadrivalent vanadium ions were reduced to the trivalent state, rare-earth vanadates (III) ($LnVO_3$) being obtained. For $LnVO_3$ a typical transformation of the ABO_3-type compounds, one from the aragonite-type to the perovskite-type *via* the vaterite- or calcite-type structure was observed with a decrease in the ionic radius of the rare-earth ions. The magnetic properties of the vaterite-type $LnVO_3$ were studied.

We have previously studied the reaction of erbium sesquioxide (Er_2O_3) with vanadium dioxide (VO_2) at 1400 °C and 50 kbar and 30 kbar, and succeeded to obtain vaterite- and calcite-type $ErVO_3$.[1] Under these conditions quadrivalent vanadium ions are unstable and reduced to the trivalent state. $ErVO_3$ with the crystal structure other than the perovskite-type has been first obtained. In this paper, we report on the high-pressure reaction of the rare-earth sesquioxides (Ln_2O_3) with VO_2.

Experimental

The preparative and analytical methods were similar to those described previously.[1]

Results and Discussion

The Reaction Products of Ln_2O_3 with VO_2 at High Pressures. The Ln_2O_3–VO_2 mixtures in 1:2 were heated at 1400 °C and 50 kbar or 30 kbar. The atomic ratio of the rare-earth element to vanadium in the products was determined to be 1.0 by the fluorescent X-ray analysis. The valence states of vanadium in the products were estimated from the result of the oxygen analysis, which revealed that the quadrivalent vanadium ions in the products were reduced to the trivalent state and the formulae of the products were $LnVO_3$ in every case.

Crystal Structures of the Products. X-Ray diffraction data for aragonite-type $LaBO_3$[2] and the reaction product of the 1:2 mixture of La_2O_3 and VO_2 heated at 50 kbar for 30 min are given in Table 1. Similarity of the X-ray diffraction pattern of $LaVO_3$ to that of the aragonite-type compound suggests that the compound crystallizes in the orthorhombic system, $a=5.869$ Å, $b=8.261$ Å, and $c=5.103$ Å. The structural feature of $LaVO_3$ obtained at 30 kbar was equal to that of the product obtained at 50 kbar.

The crystal structures of $NdVO_3$ and $SmVO_3$ obtained by heating at 50 kbar and 30 kbar for 30 min belonged to the aragonite-type, same as that of $LaVO_3$. The cell parameters were $a=5.703$ Å, $b=8.032$ Å, and $c=5.011$ Å for the neodymium compound, and $a=$

** 1 bar$=10^5$ Pa.

Table 1. X-Ray diffraction results for aragonite-type $LaBO_3$ and $LaVO_3$

	$LaBO_3$[2] Orthorhombic $a=5.872$ Å $b=8.257$ Å $c=5.107$ Å		$LaVO_3$ $a=5.869$ Å $b=8.261$ Å $c=5.103$ Å		
hkl	*d*/Å	*I*	d_{obsd}/Å	d_{calcd}/Å	*I*
011	4.34	20	4.35	4.34	25
020	4.13	10	4.14	4.13	5
111	3.49	100	3.49	3.49	100
120	3.38	55	3.38	3.38	60
200	2.936	20	2.936	2.935	40
210	2.767	8	2.767	2.765	8
002	2.553	20	2.554	2.552	15
201	2.547	12	2.547	2.544	7
211	2.433	40	2.432	2.431	35
031	2.424	25	2.426	2.423	31
220	2.394	14	2.388	2.392	40
112	2.252	10	2.252	2.251	5
022	2.173	12	2.170	2.170	10
040	2.066	8	2.068	2.065	20
122	2.037	45	2.036	2.036	45
140	1.947	20	1.947	1.948	18
202	1.927	20	1.926	1.926	18
231	1.869	35	1.869	1.869	30
311	1.785	20	1.785	1.784	20
320	1.768	14	1.768	1.768	15
222	1.746	8	1.745	1.745	5
240	1.690	6	1.689	1.689	5
113 241	1.6039	14	1.603	1.603 1.603	12
142	1.5482	12	1.548	1.548	8
151	1.5176	10	1.519	1.518	7
213	1.4497	12	1.447	1.449	8
411	1.3906	8	1.389	1.390	6
233	1.2985	10	1.298	1.298	11
431			1.256	1.255	7
252			1.252	1.254	6
104			1.247	1.247	5
342			1.241	1.241	8
351			1.225	1.225	8

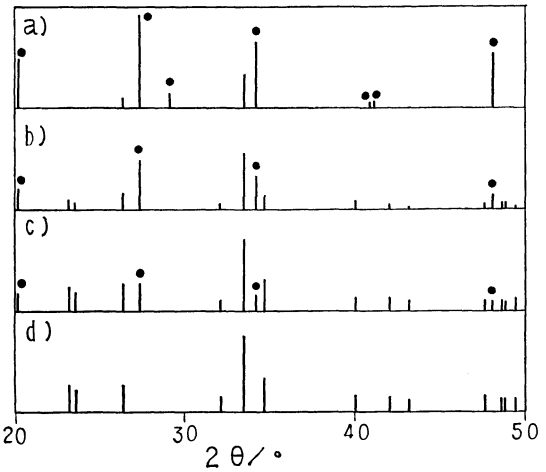

Fig. 1. X-Ray diffraction patterns for Y_2O_3–VO_2 1:2 mixtures at 1400 °C and 50 kbar.
Reaction period; a) 60 min, b) 30 min, c) 10 min, and d) perovskite-type YVO_3.

5.661 Å, b=7.992 Å, and c=5.028 Å for the samarium compound.

The crystal structure of $HoVO_3$ obtained by the reaction of the 1:2 mixture of Ho_2O_3 and VO_2 at 50 kbar for 30 min was isostructural with $HoBO_3$,[2] vaterite-type and belonged to the hexagonal system, while one obtained at 30 kbar was the calcite-type belonging to the rhombohedral (pseudo-hexagonal) system. These results are similar to those of the reaction of Er_2O_3 with VO_2.[1]

The X-ray diffraction patterns of the products obtained by the reaction of Y_2O_3–VO_2 (1:2 mixture) along with that of the perovskite type YVO_3 are shown in Fig. 1. The peaks marked by a dot can be assigned to the vaterite-type crystal. When the reaction was carried out at 1400 °C and 50 kbar for 10 min or 30 min, a mixture of perovskite- and vaterite-type YVO_3 was obtained. A prolonged reaction time (60 min) resulted in a decrease in the perovskite-type and an increase in the vaterite-type compounds.

The reaction product of Dy_2O_3–VO_2 (1:2 mixture) at 50 kbar for 30 min was the perovskite-type crystal including a trace amount of the vaterite-type compound, and those of Y_2O_3–VO_2 and Dy_2O_3–VO_2 (1:2 mixtures) at 30 kbar for 30 min were perovskite-type crystals along with a trace amount of the calcite-type compound. If the reaction time is longer for the Y_2O_3–VO_2 and Dy_2O_3–VO_2 systems, vaterite- or calcite-type crystals will be obtained.

For the reaction products of Eu_2O_3 or Gd_2O_3 with VO_2 their poor crystallinity prevented the determination of their crystal structures.

The reactions between Yb_2O_3, Tm_2O_3, and Lu_2O_3 with VO_2 at high pressures gave perovskite-type oxides.

The crystal structures of the high-pressure products as well as those of the rare-earth borates are summarized in Fig. 2. As is well known aragonite, vaterite and calcite are modifications of calcium carbonate (Fig. 3). The rare-earth borate transforms from the aragonite-type to the calcite-type structure *via* the vaterite-type structure with a decrease in ionic radius

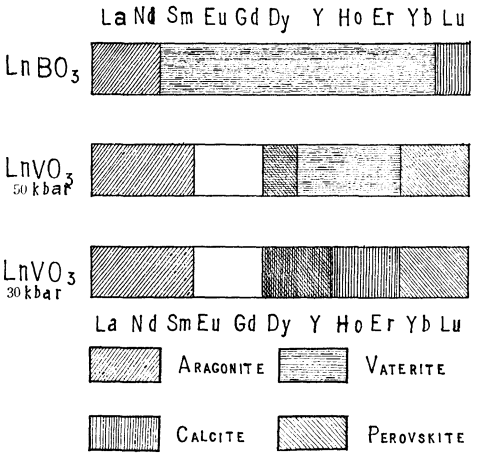

Fig. 2. Crystal structures for $LnVO_3$ and $LnBO_3$.[2]

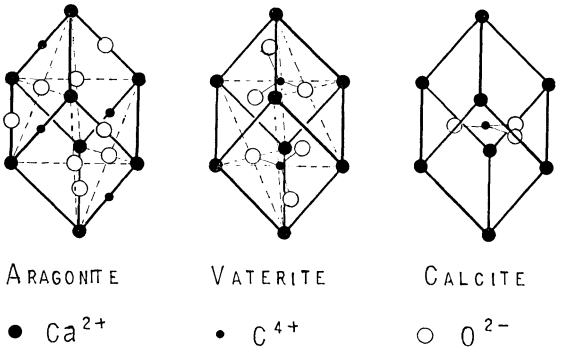

Fig. 3. Comparison of the idealized three structure types of calcium carbonate.

Table 2. Lattice constants and the specific gravity of $LnVO_3$

	Type	a/Å	b/Å	c/Å	S.G.
$LaVO_3$	Aragonite	5.869	8.261	5.103	6.41
	Perovskite	5.548		7.846	6.57
$NdVO_3$	Aragonite	5.703	8.032	5.011	7.07
	Perovskite	5.466	5.569	7.735	6.89
$SmVO_3$	Aragonite	5.661	7.992	5.028	7.31
	Perovskite	5.400	5.591	7.680	7.17
YVO_3	Vaterite	3.779		8.809	5.75
	Perovskite	5.274	5.590	7.579	5.61
$HoVO_3$	Vaterite	3.783		8.792	8.09
	Calcite	4.93		16.47	7.61
	Perovskite	5.281	5.591	7.582	7.86
$ErVO_3$	Vaterite	3.762		8.790	8.24
	Calcite	4.929		16.429	7.70
	Perovskite	5.263	5.585	7.557	7.99

of the rare-earth ions. For the rare-earth vanadates(III) a typical transformation observed for the ABO_3-type compounds,[3] one from the aragonite-type to the perovskite-type *via* the vaterite- or calcite-type structure was observed with a decrease in ionic radius of the rare-earth ions. That the crystal structure of the rare-earth vanadates(III) depends on the reaction pressure will be due to the difference in the compres-

Table 3. Magnetic properties of the vaterite-type $LnVO_3$

$LnVO_3$	Magnetic moment/μ_B				Transition temp	
	For $LnVO_3$		For Ln^{3+}	Per one vanadium ion at 4.5 K		
	$T>T_N$	$T_N>T>T_C$			T_N/K	T_C/K[a]
YVO_3	1.9	—	—	1.2	30	16
$HoVO_3$	9.8	10.5	10.5	1.7	35	13
$ErVO_3$	8.8	9.3	9.4	1.6	65	12

a) T_C were determined from the plots of σ^3 *vs.* T.

sibilities of the vanadium and rare-earth ions, and at high pressure, the vanadium ions are more compressible than the rare-earth ions.

The cell parameters and the density calculated from X-ray diffraction data of the high-pressure synthesized crystals are summarized in Table 2 along with those of the perovskite-type vanadates(III).[4] In general, the increase in pressure tends to stabilize the denser phase, and the most dense ABO_3 phase is considered to have the cubic-perovskite structure.[5] $LnVO_3$ with the perovskite-type structure are orthorhombically distorted from the ideal cubic perovskite structure, and the distortion increases with decrease in the ionic radius of the rare-earth ions.[4] Since packing of the ions in the perovskite-type crystals is insufficient because of the distortion, aragonite- and vaterite-type $LnVO_3$ crystals except $LaVO_3$ have a larger density than that of perovskite-type $LnVO_3$.

Magnetic Properties of the Vaterite-type $LnVO_3$. The magnetic susceptibility measurements were performed in the temperature range 4.5—300 K. The magnetic properties of the vaterite-type YVO_3, $HoVO_3$, and $ErVO_3$ are summarized in Table 3. As the observed values of the magnetic moment for these crystals are close to those for Ln^{3+}, V^{3+} ions order antiferromagnetically in the temperature range from T_N to T_C, and the observed transformations at high temperature are attributable to their antiferromagnetic ordering. All the compounds with the vaterite-type structure were paramagnetic, the magnetic susceptibility following the Curie-Weiss law above the Neel temperature, T_N. Below the temperature, T_C, they showed ferromagnetic behavior. The value of the magnetic moment at 4.5 K suggests that this transition is attributable to the rearrangement of the antiferromagnetically ordered V^{3+} ions to the ferromagnetic state.

References

1) T. Shin-ike, G. Adachi, J. Shiokawa, M. Shimada, and M. Koizumi, *Bull. Chem. Soc. Jpn.*, **53**, 3563 (1980).
2) E. M. Levin, R. S. Roth, and J. B. Martin, *Am. Mineral.*, **46**, 1030 (1960).
3) R. Kiriyama and H. Kiriyama, "Structural Inorganic Chemistry II," Kyoritsu, Tokyo (1970), p. 8.
4) T. Sakai, G. Adachi, J. Shiokawa, and T. Shin-ike, *Mater. Res. Bull.*, **11**, 1295 (1976).
5) J. B. Goodenough, J. A. Kafalas, and J. M. Longo, "High-Pressure Synthesis," Academic Press, Inc., New York (1972).

Fourier Transform Infrared Photoacoustic Spectroscopy of Polymers

Norio TERAMAE,* Masayuki HIROGUCHI, and Shigeyuki TANAKA
Department of Industrial Chemistry, Faculty of Engineering, The University of Tokyo, Hongo, Bunkyo-ku, Tokyo 113
(Received November 14, 1981)

Fourier transform infrared photoacoustic spectroscopy (FTIR-PAS) was applied to the structural elucidation of several kinds of organic polymers. By using a photoacoustic detection, infrared spectra of textile fabrics and rubbers containing carbon black could be measured without destructive and troublesome sample preparations. Curing process of resol type phenolic resins was examined by FTIR-PAS and conventional KBr disk method. FTIR-PAS was found to be sensitive to the structural change of the surface of the cured resins. Helmholtz resonance effect of the photoacoustic cell and the effect of the thermal properties of samples in FTIR-PAS were also discussed.

Photoacoustic spectroscopy (PAS) has been known to be a useful method for the analysis of bulk or rugged surface materials.[1] Most of the studies on PAS, however, are limited to the uv-visible spectral region, for which powerful excitation sources are readily available. On the other hand, high power sources tunable over a wide spectral range do not presently exist in the infrared spectral region. In recent years, there has been a growing interest in PAS using Fourier transform infrared spectroscopy (FTIR),[2-11] since a FTIR spectrometer has a greater throughput of radiation than the conventional dispersive infrared spectrometer.[12] However, few discussions on the characteristics of the Fourier transform infrared photoacoustic spectroscopy (FTIR-PAS) have been made. In this study, some discussions on the factors which affect the FTIR-PAS spectra are made, and some application of FTIR-PAS to the structural elucidation of organic polymers is presented.

Experimental

The PAS system was composed of a home-made PAS attachment and a Digilab FTS-15 FTIR spectrometer.

Figure 1 shows a schematic drawing of the PAS cell employed in this study. The PAS cell was made of brass and its internal volume was approximately 0.95 cm^3. A KBr plate (3 mm thick) was used as a cell window and a 1/2 inch Bruel Kjaer 4165 condenser microphone was used as a pressure transducer. These were mounted on the PAS cell body by O-rings to ensure an air tight seal. Although KBr is one of the most transparent materials in the infrared region, it is susceptible to humidity. It should be noted that both highly transparent and wet-proof windows can not be available in the infrared region, and that the Helmholtz resonance effect affects the FTIR-PAS spectra as will be mentioned later. Therefore, the cell was designed so that the windows could be replaced easily and also that the volume in front of the microphone diaphragm could be adjusted easily in order to obtain optimum efficiency.

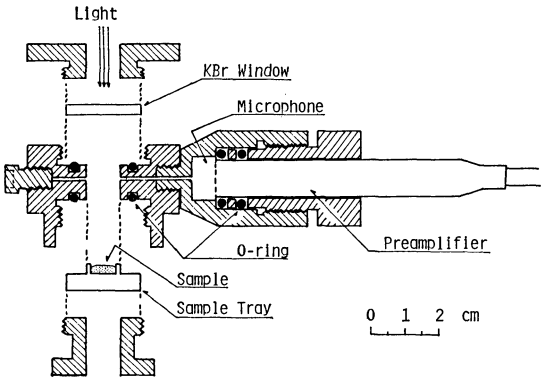

Fig. 1. Schematic drawing of photoacoustic cell.

The photoacoustic signals from the microphone attached to the PAS cell were amplified with a Brookdeal 9454 a.c. amplifier and were fed to the HgCdTe detector amplifier section of the FTIR spectrometer. All of the spectra were measured at 4 cm^{-1} resolution using 900 scans which took about 25 min.

Results and Discussion

Characteristics of FTIR-PAS. Figure 2 shows the photoacoustic spectrum of carbon black (benzene soot) and the source spectrum measured by a triglycine sulfate (TGS) detector. The carbon black PAS spectrum and the source spectrum measured by a pyroelectric detector such as TGS are known to be vir-

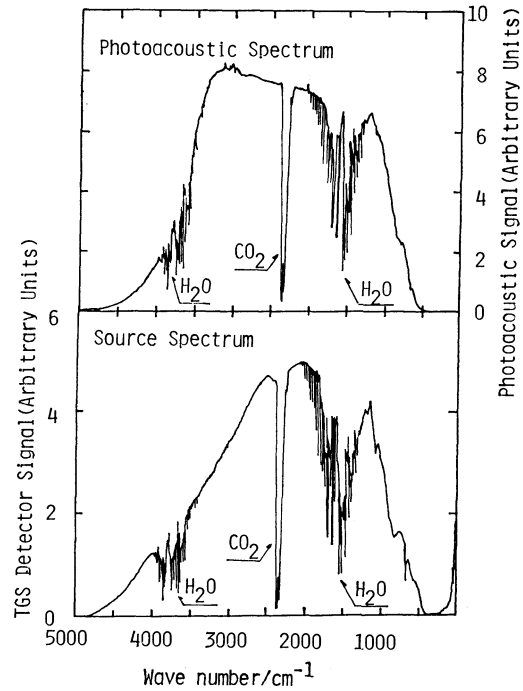

Fig. 2. Photoacoustic spectrum of carbon black (upper) and source spectrum measured by TGS detector (lower).

tually identical with each other in the dispersive PAS system with a fixed frequency light modulation.[13,14] As shown in Fig. 2, the above identity is not observed in the case of FTIR-PAS. This result can be considered to be attributed to the difference of the light modulation methods between the interferometry and the dispersive spectrometry. In the case of rapid scanning FTIR, the frequency of the radiation being emitted from the source, ν[cm^{-1}], corresponds to the modulation frequency, ω[s^{-1}], through the relationship, $\omega=2V\nu$, where V represents the velocity of the moving mirror in a Michelson interferometer.[12] Considering that the carbon black PAS signals are inversely proportional to the modulation frequencies,[15] carbon black PAS signals for FTIR-PAS must be larger in the lower wave number region. However, this expected tendency was not observed as shown in Fig. 2. Accordingly, another additional effect must be taken into consideration for the analysis of FTIR-PAS spectra. Since another type of PAS cell[2] showed a different spectral pattern of carbon black compared with the results shown in Fig. 2, the possibility of the influence of the Helmholtz resonance effect was examined by changing the volume in front of the microphone diaphragm.

The Helmholtz resonance frequency, ω_0, is given by[16]

$$\omega_0 = (v_0/2\pi)[\{(1/V_1)+(1/V_2)\}\sigma/\{L+(1/2)(\pi\sigma)^{1/2}\}]^{1/2},$$

where v_0 is the speed of sound, and V_1 and V_2 are the volume of the sample cavity and the volume in front of the microphone diaphragm, respectively. σ is the cross-sectional area of the tube of length L connecting the volume V_1 and V_2. Figure 3 shows the photoacoustic spectral changes due to the Helmholtz resonance effect when V_2 is changed from 90 to 750 mm^3. These curves were obtained by dividing the carbon black PAS spectra by the source spectrum presented in Fig. 2. As shown in Fig. 3, the peak which represents resonance frequency moves to lower wave numbers, as the volume V_2 becomes larger. The observed resonance frequencies were plotted against the $[(1/V_1)+(1/V_2)]^{1/2}$ values, and a good linear correlation was obtained as shown in Fig. 4. From the

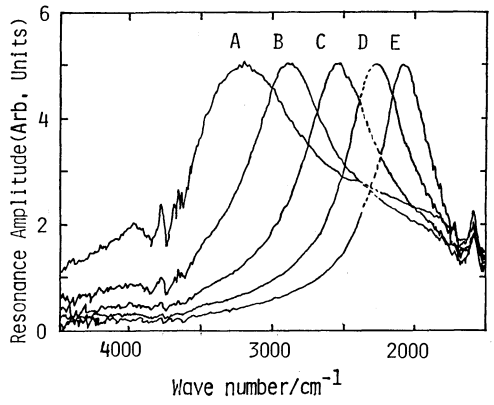

Fig. 3. Resonance effect obtained by changing the volume in front of the microphone diaphragm. The volumes, V_2, are 90(A), 150(B), 290(C), 420(D), and 750(E) in mm^3 units.

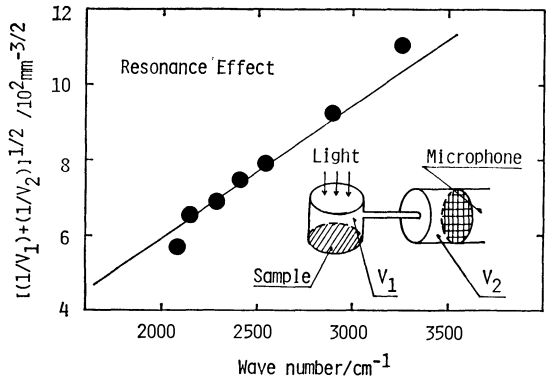

Fig. 4. Helmholtz resonance effect of the photoacoustic cell.

above-mentioned fact, the PAS signals in FTIR are considered to be influenced greatly by the Helmholtz resonance effect. Strictly speaking, the effect of the volume of sample must be taken into consideration for the normalization of FTIR-PAS spectra. However, the effect can be neglected if V_1 is sufficiently greater than V_2.

Although the above effect can be compensated when the normalization of the sample PAS spectra is carried out by using a carbon black PAS spectrum measured by the same PAS cell as a reference, the effect must be taken into account if the measurement of FTIR-PAS is carried out by the use of double beam measurement system which requires two PAS cells. Of cource, if a completely non-resonant type of PAS cell is used, the above-mentioned effect can be neglected. However, it is considered to be better to use a resonant type of PAS cell in order to improve the S/N ratio of PAS spectra, since the usual light source in the infrared spectral region is not powerful.

FTIR-PAS spectra of several kinds of polymers such as cloths, rubbers, cured resins *etc.* were measured. Although the features of these spectra were fairly similar to those of published spectra measured by a KBr method or an ATR method etc., photoacoustic signals were found to be larger in the lower wave number regions. This result can be attributed to the thermal properties of the samples, since the thermal diffusion length in the sample depends on the modulation frequency.[15] The samples investigated in this study are considered to be optically opaque and thermally thick solids, for which photoacoustic signals show $\omega^{-3/2}$ dependence, where ω is the modulation frequency. In this case, further normalization must be carried out by multiplying a factor of $\omega^{1/2}$, that is $(2V\nu)^{1/2}$, after simply dividing the raw PAS spectrum by a carbon black PAS spectrum, since carbon black PAS signals are inversely proportional to ω. The above mentioned normalizing procedures would be necessary if we wish to compare the PAS spectra with the standard spectral data such as IRDC cards.

FTIR-PAS Spectra of Polymers. Figure 5 shows the PAS spectra of nylon cloth and cotton cloth. The features of these spectra are fairly similar to those of the published spectra measured by a KBr method or a thermally pressed film method.[17] Using the

photoacoustic detection, infrared spectra of these textile fabrics can be obtained by simply putting a small piece of sample into the PAS cell. Thus, it can be said that FTIR-PAS could be a simple but still effective method for the identification of these compounds without troublesome and destructive sample preparations which are nescessary for conventional measurement techniques.

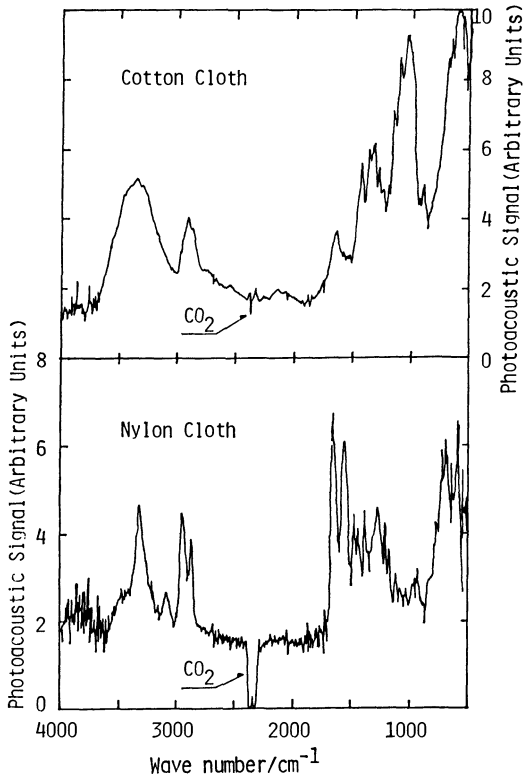

Fig. 5. Photoacoustic spectra of cotton (upper) and Nylon (lower) cloths.

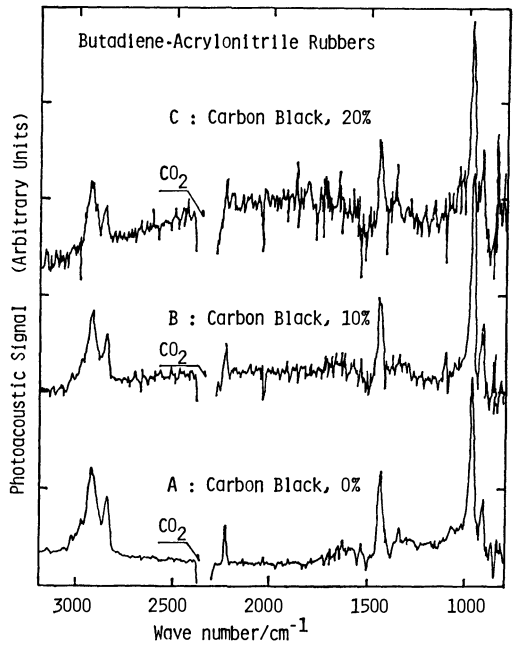

Fig. 6. Photoacoustic spectra of butadiene-acrylonitrile rubbers containing carbon black.
Carbon black content, A: 0%, B: 10%, C: 20%.

In Fig. 6, PAS spectra at the top, the middle and the bottom show butadiene–acrylonitrile rubbers containing carbon black, 20, 10, and 0%, respectively. Commercial rubbers usually contain carbon black or silica in order to enhance elasticity. The conventional measurement technique used to examine rubbers is an ATR method, which requires a specially designed apparatus,[18] capable of taking a large incident angle for obtaining spectra of the sample containing carbon black because of the high refractive indices of samples. As shown in Fig. 6, however, structural elucidation of rubbers can be made in the same manner regardless of the content of carbon black in the range of 0 to 20%. It can be seen that the S/N ratio of the PAS spectra decreases as the content of carbon black increases. This result is possibly due to the fact that the more carbon black a sample contains, the less light it receives. From the fact, FTIR-PAS would be more useful for the structural elucidation of rubbers which contain silica, since silica absorbs less light than carbon black does.

Figure 7 shows the spectral change by curing a resol type phenolic resin. These spectra were measured after heating the sample at 170 °C for 0, 15, 30, 60, and 120 min. The curing process of the resin was reported to be characterized as follows.[19] As the resin is heated, the intensity of the band due to C–O–C stretching vibrational mode at about 1050 cm^{-1} decreases, and a new band due to carbonyl stretching vibrational mode at about 1650 cm^{-1} appears. The new band is considered to be caused by the oxidation of the methylene group. The PAS spectral changes are well consistent with the above proposed curing process. In Fig. 8, spectra at the left and the right halves are the expanded spectra of the above-

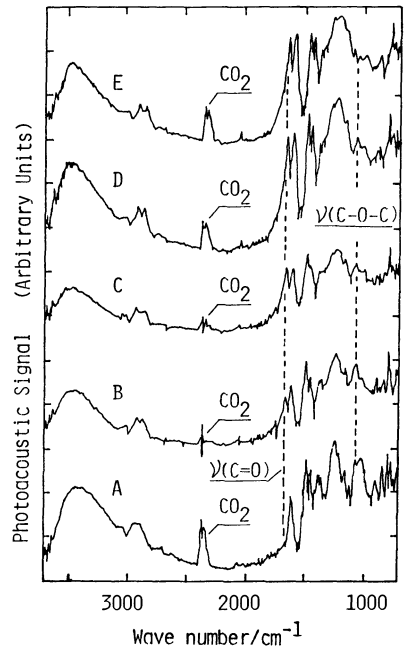

Fig. 7. Photoacoustic spectral change of resol type phenolic resin.
Heating temperature is 170 °C. Heating periods are 0(A), 15(B), 30(C), 60(D), and 120(E) min.

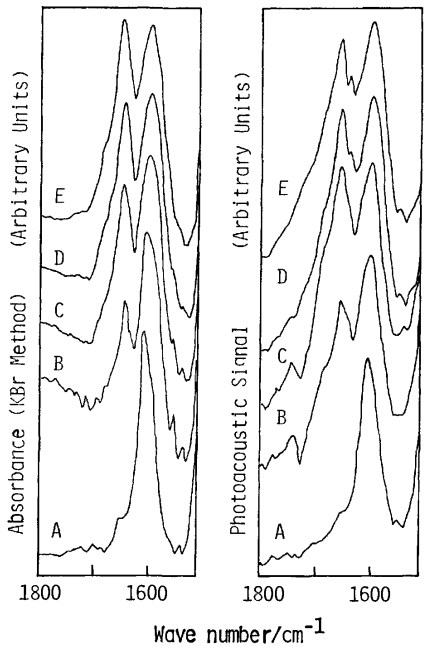

Fig. 8. Absorption spectra measured by a KBr method (left side) and photoacoustic spectra (right side) of cured resol type phenolic resins.
Heating periods are 0(A), 15(B), 30(C), 60(D), and 120(E) min.

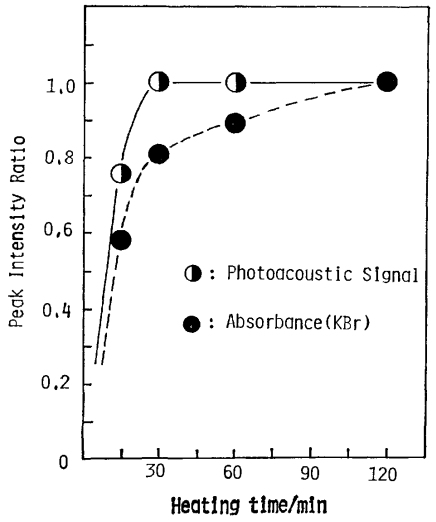

Fig. 9. Peak intensity ratio of the 1650 cm^{-1} band to the 1610 cm^{-1} band *vs.* heating time.

mentioned resins measured by absorption and photoacoustic techniques, respectively. The absorption spectra were obtained by a KBr method, in which the resins used for measuring FTIR-PAS were ground to fine powders. During the curing of resol type phenolic resins, the absorption intensity of the band at about 1610 cm^{-1} which is assigned to aromatic C=C stretching vibrational mode is said to be unchanged.[19] Therefore, in order to examine the degree of curing of the resin as well as to compare results which is obtained by the two measuring methods presented in Fig. 8, the ratio of the intensity of the carbonyl absorption band at 1650 cm^{-1} to that of the aromatic absorption band at 1610 cm^{-1} was plotted against the heating period by using absorption and photoacoustic spectra. The results are shown in Fig. 9. Comparing the two curves in Fig. 9, it is immediately seen that the ratio reaches to a constant value within 30 min by using the PAS spectral data. Whereas, as for the absorption spectral data, the ratio is gradually increases as the heating time increases. This result reflects that the PAS is sensitive to the structural change of the surface of cured resin, and that averaged information about the mixed species of cured and non-cured resins is obtained by the absorption method such as a KBr technique. If the constant value in the ratio shown in Fig. 9 is caused by the saturation effect of the photoacoustic signal,[15] the depth of the cured layer can be estimated. Assuming that the thermal diffusivity of the cured resin is 0.001 (cm^2/s), thermal diffusion length of 5.7 microns is obtained at 1650 cm^{-1} under the measuring conditions in our spectrometer.[3] Accordingly, the cured layer of several microns can be considered to be formed during the heating of 0 to 30 min. Thus, FTIR-PAS is useful for the surface characterization of cured resins. In some cases, cured resins are difficult to examine by conventional measurement techniques because of their mechanical hardness. For the analysis of such materials, FTIR-PAS is also effective, since FTIR-PAS requires minimal sample preparations.

The authors wish to express their thanks to Dr. Tsuguo Sawada and Professor Yohichi Goshi, The University of Tokyo, and Dr. Shohei Oda, Fuji Film Co., Ltd., for their helpful discussions. We also would like to thank Dr. Morio Tsuge, Sumitomo Bakelite Co., Ltd., for providing phenolic resins as samples.

References

1) A. Rosencwaig, *Anal. Chem.*, **47**, 592A (1975).
2) N. Teramae and S. Tanaka, *Spectrosc. Lett.*, **14**, 687 (1981).
3) N. Teramae, M. Hiroguchi, and S. Tanaka, *Chem. Lett.*, **1981**, 1091.
4) N. Teramae, T. Yamamoto, M. Hiroguchi, T. Matsui, and S. Tanaka, *Chem. Lett.*, **1982**, 37.
5) M. G. Rockley, *Chem. Phys. Lett.*, **68**, 455 (1979).
6) D. W. Vidrine, *Appl. Spectrosc.*, **34**, 314 (1980).
7) M. G. Rockley, D. M. Davis, and H. H. Richardson, *Science*, **210**, 918 (1980).
8) M. G. Rockley and J. P. Devlin, *Appl. Spectrosc.*, **34**, 407 (1980).
9) M. G. Rockley, *Appl. Spectrosc.*, **34**, 405 (1980).
10) G. Laufer, J. T. Huneke, B. S. H. Royce, and Y. C. Teng, *Appl. Phys. Lett.*, **37**, 517 (1980).
11) M. G. Rockley, *Chem. Phys. Lett.*, **75**, 370 (1980).
12) P. R. Griffiths, "Chemical Infrared Fourier Transform Spectroscopy," John Wiley & Sons, New York (1975).
13) W. R. Harshbarger and M. B. Robin, *Acc. Chem. Res.*, **6**, 329 (1973).
14) R. G. Gray, V. A. Fishman, and A. J. Bard, *Anal. Chem.*, **49**, 697 (1976).
15) A. Rosencwaig and A. Gersho, *J. Appl. Phys.*, **47**, 64 (1976).
16) N. C. Fernelius, *Appl. Opt.*, **18**, 1784 (1979).
17) D. O. Hummel, "Atlas der Kunstsoff-Analyse," Verlag Chemie (1968).
18) S. Tanaka and T. Matsui, *Bunseki Kagaku*, **20**, 1128 (1971).
19) M. Yamao, S. Nukui, and S. Tanaka, *Nippon Kagaku Kaishi*, **1972**, 914.

Circular Dichroism Spectra of *fac*(*D*)-[Co(a)(BC)(DDD)]$^{n+}$ Type Complexes with 1,4,7-Triazacyclononane, (2*R*)-2-Methyl-1,4,7-triazacyclononane, and 1,5,9-Triazacyclododecane

Shuhei Fujinami,* Yukio Matsunami, and Muraji Shibata
Department of Chemistry, Faculty of Science, Kanazawa University, Kanazawa 920
(Received November 16, 1981)

The complexes, [Co(L-val)(NH_3)(tacn)]$^{2+}$ (tacn=1,4,7-triazacyclononane), [Co(gly)(NH_3)(Me-tacn)]$^{2+}$ (Me-tacn=(2*R*)-2-methyl-1,4,7-triazacyclononane) have been prepared and separated into diastereomers by column chromatography. Six other complexes, [Co(a)(β-ala)(tacn)]$^{n+}$ (a=CN^-, NO_2^-, or NH_3) and [Co(a)(gly)(tacdd)]$^{n+}$ (a=NO_2^-, NCS^-, or H_2O; tacdd=1,5,9-triazacyclododecane) have also been prepared and resolved into enantiomers. By comparing the CD spectra of the L-valinato and the Me-tacn complexes with that of [Co(gly)(NH_3)(tacn)]$^{2+}$, the optical activities of [Co(a)(gly)(tacn)]$^+$ are considered to be mainly derived from chiral arrangements of four kinds of donor atoms. The change from five-membered chelate ring to a six-membered one has slight influence upon the CD spectral shapes in the β-alaninato complex, but a large influence in the tacdd complexes.

In recent studies on the CD spectra of a series of [Co(a)(gly)(tacn)]$^{n+}$ complexes (a=CN^-, NO_2^-, NH_3, NCS^-, H_2O, OH^-, N_3^-, or Cl^-; tacn=1,4,7-triazacyclononane), it has been concluded that, though two helical ring-pairs exist in the complexes, the optical activities of the complexes are mainly derived from a chiral arrangement of four kinds of donor atoms, each N donor in tacn and gly, O donor in gly, and the donor of a unidentate.[1] In this work, we aimed to confirm the above conclusion by extending the CD spectral studies to various *fac*(*D*)-[Co(a)(BC)(DDD)]$^{n+}$ complexes which contain tacn, Me-tacn(=(2*R*)-2-methyl-1,4,7-triazacyclononane) or tacdd (=1,5,9-triazacyclododecane) as DDD, and L-val or β-ala as BC. The Me-tacn complex has a preferable conformation due to the orientation of the methyl group. Therefore, the CD spectral comparison between the Me-tacn and tacn complexes will afford information about the conformational contribution to the optical activity in the latter complex. Since the L-valinate ion has a bulky isopropyl group, a large interaction between the substituent and the tacn molecule are anticipated in the [Co(a)(L-val)(tacn)]$^{n+}$ complex. Six-membered chelate rings exist in the β-alaninato and the tacdd complexes, and the CD spectra of these complexes are interesting to compare with those of [Co(a)(gly)(tacn)]$^{n+}$ which contains five-membered chelate rings.

Experimental

Ligand. 1,4,7-Triazacyclononane trihydrochloride (TACN·3HCl), (2*R*)-2-methyl-1,4,7-triazacyclononane trihydrobromide (Me-TACN·3HBr), and 1,5,9-triazacyclododecane trihydrochloride or trihydrobromide (TACDD·3HCl or TACDD·3HBr) were prepared according to the literatures.[2,3]

Preparation of Complexes. *1) (Ammine)(1,4,7-triazacyclononane)(L-valinato)cobalt(III) Chloride, [Co(L-val)(NH_3)(tacn)]Cl_2*: At first, a [Co(NCS)(L-val)(tacn)]$^+$ complex was prepared in the same way as a [Co(NCS)(gly)(tacn)]$^+$ complex,[1] by using of *mer*(*N*)-*trans*(NH_3)-[Co(CO_3)(L-val)(NH_3)$_2$][4] (3.5 g, 0.013 mol) and TACN·3HCl (3 g, 0.013 mol). At the second step, the isothiocyanato complex was oxidized with aqueous H_2O_2 (30%) at pH *ca.* 3.[1] The resulting solution was poured onto a column of SP-Sephadex C-25 in Na^+ form (3.5 cm×40 cm). The adsorbed band was eluted with a 0.05 mol/dm^3 Na_2SO_4 solution, and an orange band containing aimed bivalent cation was collected in a fraction. The effluent was concentrated at 40 °C and the eluting agent removed.

One fourth of the concentrate was dissolved in a large amount of water, and poured onto a column of SP-Sephadex C-25 in Na^+ form (2.5 cm×70 cm). By eluting with 0.075 mol/dm^3 K_2[Sb_2(*d*-tart)$_2$], the adsorbed band was separated into two components which were labelled E1 and E2 in the order of elution (these labels were also used to designate the isomers contained in each band). When the E1 band had descended to the neighborhood of the outlet of the column, the two bands were washed with water and then eluted with a 0.1 mol/dm^3 NaCl solution. The two bands were collected in each fraction. This procedure was repeated for the residual portion of the concentrate. The combined fractions were concentrated, and the eluting agent which precipitated was removed by repeated filtration. To the final filtrate was added a small amount of ethanol, and the whole was kept in a refrigerator. The crude products were recrystallized from warm water. The yield was *ca.* 0.05 g for E1, and 0.1 g for E2. Found for E1: C, 30.64; H, 7.36; N, 16.33%. Calcd for [Co(L-val)(NH_3)(tacn)]Cl_2·$2H_2O$=$C_{11}H_{32}N_5O_4Cl_2Co$: C, 30.85; H, 7.53; N, 16.35%. Found for E2: C, 31.83; H, 7.07; N, 17.16%. Calcd for [Co(L-val)(NH_3)(tacn)]Cl_2·H_2O=$C_{11}H_{30}N_5O_3Cl_2Co$: C, 32.21; H, 7.37; N, 17.07%.

2) (Ammine)(glycinato)[(2R)-2-methyl-1,4,7-triazacyclononane]cobalt(III) Perchlorate, [Co(gly)(NH_3)(Me-tacn)](ClO_4)$_2$: This complex was prepared in the same manner as a [Co(gly)(NH_3)(tacn)]$^{2+}$ complex,[1] except for the use of Me-TACN·3HCl in place of TACN·3HCl.

The reaction mixture was poured onto a column of Dowex 50W-X8 in H^+ form (5.5 cm×10 cm), and the adsorbed band was eluted by a 0.5 mol/dm^3 H_2SO_4 solution. The descended orange band was collected in a fraction, and the eluate was adjusted to pH 6 by $BaCO_3$. After filtration, the filtrate was concentrated, and small amount of ethanol was added to the concentrate. The whole system was kept in a refrigerator. The yield was about 0.1 g. Found: C, 26.31; H, 6.73; N, 17.28%. Calcd for [Co(gly)(NH_3)(Me-tacn)]SO_4·H_2O=$C_9H_{26}O_7N_5SCo$: C, 26.53; H, 6.45; N, 17.19%.

The orange crystals obtained were dissolved in water and the solution was subjected to a column chromatography on SP-Sephadex C-25 in Na^+ form (2.5 cm×110 cm). By elution with 0.05 mol/dm^3 K_2[Sb_2(*d*-tart)$_2$], the adsorbed

band was separated into three bands which were labelled B1, B2, and B3 in the order of elution (these labels were also used to designate the isomers contained in each band). When the B1 band had descended to the neighborhood of the outlet of the column, the band was washed with water and then eluted with a 0.1 mol/dm^3 NaCl solution. The absorption and CD spectra of the effluents were measured and the metal-concentrations were evaluated by atomic absorption spectrophotometry.

3) (β-Alaninato)(nitro)(1,4,7-triazacyclononane)cobalt(III) Chloride Dihydrate, [*Co(NO$_2$)(β-ala)(tacn)*]*Cl·2H$_2$O*: At the first step, a [Co(β-ala)(H$_2$O)(tacn)]$^{2+}$ complex was prepared similarly to a [Co(gly)(H$_2$O)(tacn)]$^{2+}$ complex.[1] The aqua complex could not be isolated because of the great solubility of the species in water. At the next step, a [Co(NO$_2$)(β-ala)(tacn)]$^+$ complex was derived from the aqua complex, according to the literature method.[1] Found: C, 27.41; H, 6.51; N, 17.48%. Calcd for [Co(NO$_2$)(β-ala)(tacn)]Cl·2H$_2$O=C$_9$H$_{25}$N$_5$O$_6$ClCo: C, 27.45; H, 6.41; N, 17.79%.

4) (β-Alaninato)(ammine)(1,4,7-triazacyclononane)cobalt(III) Perchlorate Monohydrate, [*Co(β-ala)(NH$_3$)(tacn)*](*ClO$_4$*)$_2$·*H$_2$O*: This complex was derived from the above [Co(β-ala)(H$_2$O)(tacn)]$^{2+}$ complex in the same manner as in the [Co(gly)(NH$_3$)(tacn)]$^{2+}$ complex.[1] Found: C, 21.13; H, 5.18; N, 13.63%. Calcd for [Co(β-ala)(NH$_3$)(tacn)](ClO$_4$)$_2$·H$_2$O=C$_9$H$_{26}$N$_5$O$_{11}$Cl$_2$Co: C, 21.18; H, 5.15; N, 13.73%.

5) (β-Alaninato)(cyano)(1,4,7-triazacyclononane)cobalt(III) Perchlorate, [*Co(CN)(β-ala)(tacn)*]*ClO$_4$*: This complex was also prepared similarly to the [Co(CN)(gly)(tacn)]$^+$ complex,[1] starting from the [Co(β-ala)(H$_2$O)(tacn)]$^{2+}$ by way of [Co(Cl)(β-ala)(tacn)](NO$_3$). The complex was isolated by column chromatography (SP-Sephadex C-25, 4.5 cm×25 cm, Na$^+$ form, by use of 0.05 mol/dm^3 NaClO$_4$ as eluent). Found: C, 29.62; H, 5.28; N, 17.56%. Calcd for [Co(CN)(β-ala)(tacn)]ClO$_4$=C$_{10}$H$_{21}$N$_5$O$_6$ClCo: C, 29.89; H, 5.28; N, 17.44%.

6) (Glycinato)(isothiocyanato)(1,5,9-triazacyclododecane)cobalt(III) Bromide 1,5-Hydrate, [*Co(NCS)(gly)(tacdd)*]*Br·1.5*H$_2$O: A [Co(gly)(H$_2$O)(tacdd)]$^{2+}$ complex was first prepared by use of *mer(N)-trnas(NH$_3$)*-[Co(CO$_3$)(gly)(NH$_3$)$_2$][5] (0.8 g, 0.0036 mol) and TACDD·3HCl (1 g, 0.0036 mol), by the method similar to that for the [Co(gly)(H$_2$O)(tacn)]$^{2+}$ complex.[1] Crystallization of the aqua complex was unsuccessful because of a great solubility of the complex species in water.

An isothiocyanato complex was then derived from the aqua complex in the same way as the [Co(NCS)(gly)(tacn)]$^+$ complex,[1] with slight modifications; an aqueous solution (20 cm^3) containing the aqua complex which had been prepared at 0.01 mol scale was adjusted to pH 2 with 20% HClO$_4$, after which KSCN (1.5 g, 0.015 mol) was added to the solution. The mixture was stirred at *ca.* 50 °C for 2 h. The resulting solution was poured onto a column of SP-Sephadex C-25 in Na$^+$ form (4.5 cm×30 cm). The adsorbed band was eluted with a 0.03 mol/dm^3 NaBr solution, and a red-violet band which descended was collected in a fraction. The eluate was concentrated by means of a rotary evaporator at 35 °C. After addition of ethanol, the solution was kept in a refrigerator. The crystal deposited was recrystallized from water. The yield was *ca.* 0.3 g. Found: C, 30.44; H, 6.06; N, 15.15%. Calcd for [Co(NCS)(gly)(tacdd)]Br·1.5H$_2$O=C$_{12}$H$_{28}$N$_5$O$_{3.5}$SBrCo: C, 30.71; H, 6.01; N, 14.92%.

7) (Glycinato)(nitro)(1,5,9-triazacyclododecane)cobalt(III) Bromide, [*Co(NO$_2$)(gly)(tacdd)*]*Br*: This complex was prepared by the same method as a [Co(NO$_2$)(gly)(tacn)]$^+$ complex,[1] except for the use of [Co(gly)(H$_2$O)(tacdd)]$^{2+}$ which had been prepared at 0.01 mol scale. The yield was *ca.* 0.3 g. Found: C, 30.48; H, 5.76; N, 16.00%. Calcd for [Co(NO$_2$)(gly)(tacdd)]Br=C$_{11}$H$_{25}$N$_5$O$_4$BrCo: C, 30.71; H, 5.76; N, 16.28%.

8) Trinitro(1,5,9-triazacyclododecane)cobalt(III), [*Co(NO$_2$)$_3$-(tacdd)*]: This complex was prepared by the same procedure as a [Co(NO$_2$)$_3$(tacn)] complex,[6] except for the use of TACDD·3HBr in place of TACN·3HBr. The crystals deposited in the course of the reaction were washed with a small amount of water. Starting from 0.1 mol TACDD·3HBr (2.96 g), the yield was *ca.* 0.1 g. Found: C, 29.26; H, 5.68; N, 22.79%. Calcd for [Co(NO$_2$)$_3$(tacdd)]=C$_9$H$_{21}$N$_6$O$_6$Co: C, 29.36; H, 5.75; N, 22.82%.

Optical Resolution. The three β-alaninato complexes, [Co(CN)(β-ala)(tacn)]$^+$, [Co(NO$_2$)(β-ala)(tacn)]$^+$, and [Co(β-ala)(NH$_3$)(tacn)]$^{2+}$, were resolved into each optical antipodes by means of a column chromatography of SP-Sephadex C-25 (2.5 cm×110 cm, Na$^+$ form), using 0.05 mol/dm^3 K$_2$[Sb$_2$(*d*-tart)$_2$] as eluent. Total resolution was attained for the ammine complex, and partial resolutions, for the cyano and nitro complexes.

All of the tacdd complexes were also resolved by means of a column chromatography of SP-Sephadex C-25 in Na$^+$ form (2.5 cm×110 cm, for the nitro and isothiocyanato complexes; 2.5 cm×130 cm, for the aqua complex). Total resolutions were attained for the nitro and isothiocyanato complexes, when the elutions were performed with 0.075 mol/dm^3 and 0.15 mol/dm^3 (saturated) K$_2$[Sb$_2$(*d*-tart)$_2$] solutions, respectively. As to the aqua complex, a 0.15 mol/dm^3 Na$_2$[Sb$_2$(*d*-tart)$_2$] solution was used as eluent. When each adsorbed band descended to four-fifths of the column height, the band was sufficiently washed with water and eluted with 0.1 mol/dm^3 NaCl or NaClO$_4$. The effluents were concentrated and submitted to the measurement of CD spectra, while the concentrations of the complex species were evaluated from the absorption spectral data.

Derivations from Optically Active Complex. $(+)^{CD}_{500}$[Co(NO$_2$)(gly)(tacdd)]$^+$ and $(+)^{CD}_{500}$[Co(NCS)(gly)(tacdd)]$^+$ could be derived from $(-)^{CD}_{500}$[Co(gly)(H$_2$O)(tacdd)]$^{2+}$ in the same way as described in *6)* and *7)*.

Measurements. The absorption spectra in aqueous solution were recorded with a Hitachi 323 recording spectrophotometer. The CD spectra were measured with a JASCO J-40C automatic recording spectropolarimeter equipped with a JASCO Model J-DPZ data processor for CD. As to [Co(gly)(H$_2$O)(tacdd)]$^{2+}$ and [Co(gly)(NH$_3$)(Me-tacn)]$^{2+}$, a Hitachi 170-50 Atomic Absorption Spectrophotometer was used in order to evaluate the metal-concentration.

Results and Discussion

1) The [*Co(L-val)(NH$_3$)(tacn)*]$^{2+}$ *Complex.* As described in Experimental, the [Co(L-val)(NH$_3$)(tacn)]$^{2+}$ complex was prepared by oxidation of a [Co(L-val)(NCS)(tacn)]$^+$ complex. When the reaction mixture of [Co(L-val)(H$_2$O)(tacn)]$^+$ and ammonia under the conditions of pH>10 and 60 °C was chromatographed on SP-Sephadex C-25 column, four bands of [Co(val)(NH$_3$)(tacn)]$^{2+}$ species appeared. The same situation was encountered by use of D-val. These facts showed that racemization of chelating L (or D)-valinate ion took place. On the other hand, aimed two diastereomers were obtained by the reaction of [Co(L-val)(NCS)(tacn)]$^+$ with H$_2$O$_2$ in an acidic solution.

The absorption and CD spectra of the diastereomers

are shown in Fig. 1, and numerical data are summarized in Table 1. The calculated vicinal and configurational contribution curves of the L-valinato complex are illustrated in Fig. 2. The vicinal contribution curve resembles that of $[Co(L\text{-val})(NH_3)_4]^{2+}$,[7] and the configurational contribution curve is similar to that of $(-)_{589}[Co(gly)(NH_3)(tacn)]^{2+}$.[1] This fact indicates that the earlier eluted isomer (E1) has the same absolute configurations as the $(-)_{589}[Co(gly)(NH_3)(tacn)]^{2+}$ isomer,[1,8] and that there is slight interaction between the isopropyl group of chelated L-val and the tacn rings. In other words, the orientation of the isopropyl group does not have much influence on the d-electron optical activity of the L-valinato complex. On this basis, it is considered that the interaction between the CH_2 group of glycinato ligand and the tacn chelate rings is small in the $(-)_{589}$-$[Co(gly)(NH_3)(tacn)]^{2+}$ complex.

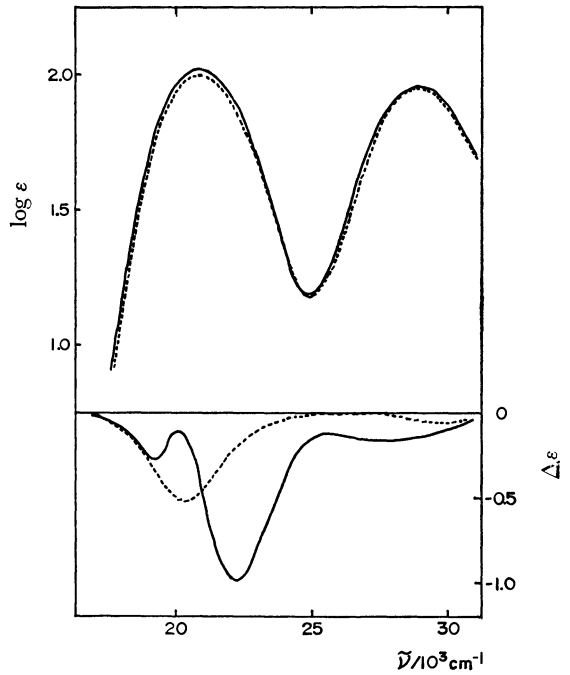

Fig. 1. Absorption and CD spectra of $[Co(L\text{-val})(NH_3)(tacn)]^{2+}$, E1 (——), E2 (·····).

2) The $[Co(gly)(NH_3)(Me\text{-}tacn)]^{2+}$ Complex. There are two coordination modes of Me-tacn, as shown in Fig. 3 (I). In the both modes, the C–CH_3

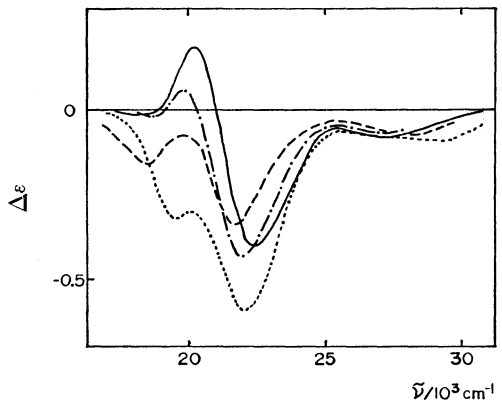

Fig. 2. Calculated configurational and vicinal contribution curves of $[Co(L\text{-val})(NH_3)(tacn)]^{2+}$, $[\Delta\varepsilon(E1)-\Delta\varepsilon(E2)]/2$; configurational contribution curve (——), $[\Delta\varepsilon(E1)+\Delta\varepsilon(E2)]/2$; vicinal contribution curve (·····), $(-)_{589}[Co(gly)(NH_3)(tacn)]^{2+}$ (·—·—), $[Co(L\text{-val})(NH_3)_4]^{2+}$ (- - -).

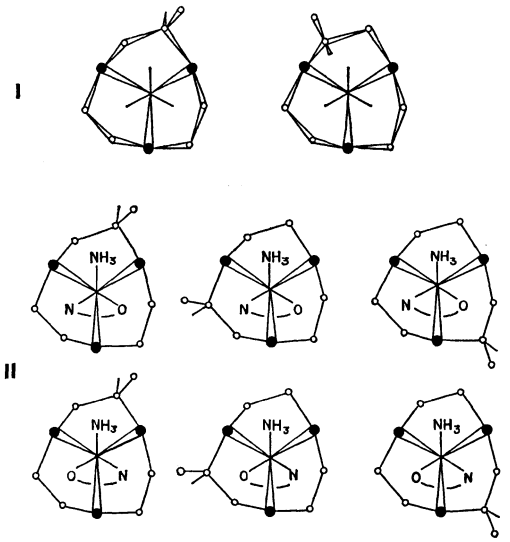

Fig. 3. Possible isomers of $[Co(gly)(NH_3)(Me\text{-}tacn)]^{2+}$.

Table 1. Absorption and CD spectral data of $[Co(L\text{-val})(NH_3)(tacn)]^{2+}$ and $[Co(gly)(NH_3)(Me\text{-}tacn)]^{2+}$ complexes

Complex	Absorption $\bar{\nu}/10^3$ cm^{-1} (log ε)	CD $\bar{\nu}/10^3$ cm^{-1} ($\Delta\varepsilon$)
$[Co(L\text{-val})(NH_3)(tacn)]^{2+}$ (E1)	20.8 (2.02)	19.2 (−0.26)
		22.2 (−0.98)
	29.0 (1.96)	27.8 (−0.17)
$[Co(L\text{-val})(NH_3)(tacn)]^{2+}$ (E2)	20.8 (1.99)	20.2 (−0.51)
	29.0 (1.95)	29.9 (−0.06)
$[Co(gly)(NH_3)(Me\text{-}tacn)]^{2+}$ (B1)	20.7 (1.95)	20.6 (1.28)
	29.0 (1.99)	27.0 (0.05)
		29.3 (−0.07)
$[Co(gly)(NH_3)(Me\text{-}tacn)]^{2+}$ (B2)	20.7 (1.95)	20.5 (1.29)
	29.0 (1.99)	27.0 (0.07)
		29.4 (−0.06)
$[Co(gly)(NH_3)(Me\text{-}tacn)]^{2+}$ (B3)	20.8 (1.97)	21.6 (1.15)
	29.0 (2.01)	27.0 (0.16)

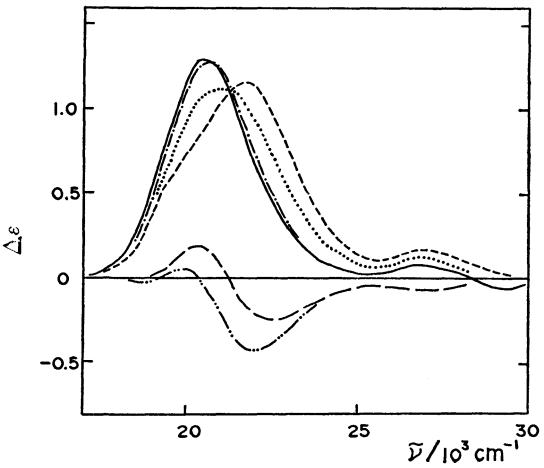

Fig. 4. CD spectra of $[Co(gly)(NH_3)(Me\text{-}tacn)]^{2+}$, B1 (·—·—), B2 (——), B3 (- - -), $[\Delta\varepsilon(B1)+\Delta\varepsilon(B3)]/2$ (·····), $[\Delta\varepsilon(B1)-\Delta\varepsilon(B3)]/2$ (— —), $(-)_{589}[Co(NH_3)(gly)(tacn)]^{2+}$ (··—··—).

bond in Me-tacn is directed to the equatorial position with respect to a mean plane of three chelate rings of Me-tacn and the chelate conformations are fixed to λ, but the configuration of the coordinated secondary nitrogen atoms in one mode is opposite to that in another mode. Since six diastereomers are possible for one mode (Fig. 3 (II)), twelve diastereomers may exist in the $[Co(gly)(NH_3)(Me\text{-}tacn)]^{2+}$ complex. The column chromatography separated three isomers of the complex, the distance between bands B1 and B2 being much smaller than that between bands B2 and B3.

The CD spectra of the diastereomers are shown in Fig. 4. The spectrum of B1 is similar to that of B2, but different from that of B3. It is assumed that the isomers with different configuration with respect to the arrangement of donor atoms are easily separable compared with those due to coordination modes or relative positions of the methyl group of Me-tacn. Therefore, the configuration of B1 is considered to be the same as that of B2 and opposite to that of B3. The conformational and vicinal contribution curve of $[Co(gly)(NH_3)(Me\text{-}tacn)]^{2+}$ was tentatively calculated from Eq. 1 and the configurational contribution curve, from Eq. 2.

$$[\Delta\varepsilon(B1 \text{ or } B2) + \Delta\varepsilon(B3)]/2 \quad (1)$$

$$[\Delta\varepsilon(B1 \text{ or } B2) - \Delta\varepsilon(B3)]/2 \quad (2)$$

As is seen in Fig. 4, the intensity of the resultant curve from Eq. 1 is higher than that of the resultant curve from Eq. 2. This corresponds to the large vicinal and conformational effects in the $[Co(Me\text{-}tacn)_2]^{3+}$ complex, the $\Delta\varepsilon$ values in the first absorption band region being *ca.* 5.[9] The calculated configurational contribution curve resembles the CD spectrum of $(-)_{589}[Co(gly)(NH_3)(tacn)]^{2+}$. However, the weak Cotton peak of the tacn complex observed at the lowest frequency in the first absorption band region disappeares at the calculated curve. From these observations, it is concluded that no fixed chiral conformation of chelated tacn exists in aqueous solution of $[Co(gly)(NH_3)(tacn)]^{2+}$, as described in the previous paper.[1]

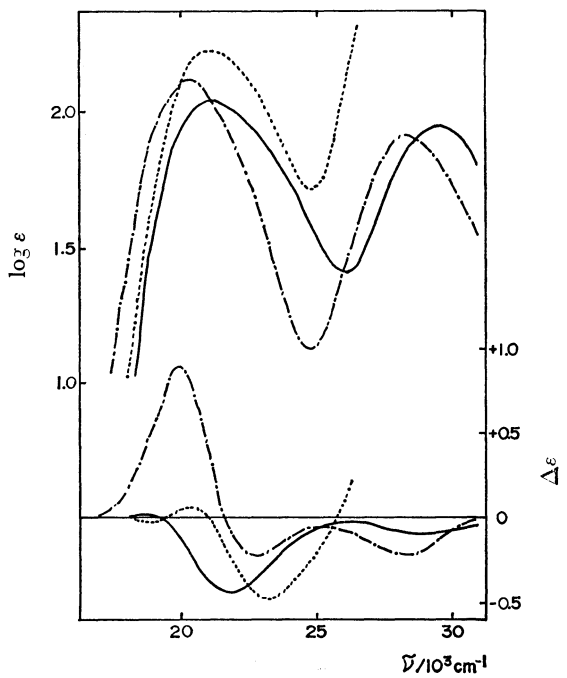

Fig. 5. Absorption and CD spectra of, $(-)^{CD}_{460}[Co(CN)(\beta\text{-ala})(tacn)]^+$ (——), $(-)^{CD}_{450}[Co(NO_2)(\beta\text{-ala})(tacn)]^+$ (·····), $(+)_{589}[Co(\beta\text{-ala})(NH_3)(tacn)]^{2+}$ (·—·—).

3) The $[Co(a)(\beta\text{-ala})(tacn)]^{n+}$ Complexes. The β-alaninato complexes were prepared similarly to the glycinato complexes. By chromatography on SP-Sephadex C-25, total resolution was achieved for the ammine complex, $[Co(\beta\text{-ala})(NH_3)(tacn)]^{2+}$, and partial resolution for the cyano and nitro complexes. The CD spectra of the earlier eluted isomers of these complexes are shown in Fig. 5, and numerical data are listed in Table 2. The $(+)_{589}[Co(\beta\text{-ala})(NH_3)(tacn)]^{2+}$ isomer exhibits two Cotton peaks with + and − signs from the lower frequency side in the first absorption band region, the positive peak being dominant. On the other hand, the corresponding $(-)_{589}[Co(gly)(NH_3)(tacn)]^{2+}$ isomer exhibits three Cotton peaks with −, +, and − signs from the lower frequency side, the negative peak at the highest frequency being dominant.[1] For the nitro complexes, both the $(-)_{589}$-glycinato and $(-)^{CD}_{450}$-β-alaninato complexes exhibit −, +, and − peaks in the first absorption band region. The CD spectrum of the $(-)_{589}$-$[Co(CN)(gly)(tacn)]^+$ complex shows a negative Cotton peak, and that of the $(-)^{CD}_{450}[Co(CN)(\beta\text{-ala})(tacn)]^+$ shows two peaks with opposite signs, the positive peak at the lower frequency being extremely weak. By comparison with the Cotton sign at the highest frequency, the absolute configurations of the earlier eluted isomers of $[Co(a)(\beta\text{-ala})(tacn)]^{n+}$ (a=NH_3, NO_2^-, or CN^-) are assumed to be the same as those of the corresponding $(-)_{589}[Co(a)(gly)(tacn)]^{n+}$ isomers.[1]

To confirm the above assumption, we attempted to determine the absolute configuration of $(-)_{589}[Co(\beta\text{-ala})(NH_3)(tacn)](ClO_4)_2\cdot HClO_4$, by an X-ray analysis. This was crystallized from the later eluted band. The absolute configuration found is shown in Fig. 6

Table 2. Absorption and CD spectral data of the earlier-eluted enantiomers

Complex	Absorption $\tilde{\nu}/10^3$ cm^{-1} (log ε)	CD $\tilde{\nu}/10^3$ cm^{-1} ($\Delta\varepsilon$)
$(-)_{460}^{CD}$[Co(NO_2)(β-ala)(tacn)]$^+$	21.0 (2.23)	18.6 (−0.01)
		20.3 (0.07)
		23.2 (−0.47)
	30.3 (3.19)	
$(+)_{589}$[Co(β-ala)(NH_3)(tacn)]$^{2+}$	20.3 (2.12)	20.0 (0.89)
		22.7 (−0.22)
	28.3 (1.91)	28.1 (−0.21)
$(-)_{460}^{CD}$[Co(CN)(β-ala)(tacn)]$^+$	21.1 (2.05)	18.7 (0.02)
		21.8 (−0.43)
	29.4 (1.94)	29.0 (−0.10)
$(-)_{500}^{CD}$[Co(NCS)(gly)(tacdd)]$^+$	19.1 (2.22)	19.4 (−0.65)
	31.0 (3.23 sh)	25.0 (0.08)
	41.6 (4.31)	
$(-)_{500}^{CD}$[Co(NO_2)(gly)(tacdd)]$^+$	20.1 (2.10)	19.5 (−0.30)
	29.4 (3.28)	22.0 (−0.17 sh)
	38.6 (4.35)	
$(-)_{500}^{CD}$[Co(gly)(H_2O)(tacdd)]$^{2+}$	19.2 (1.94)	17.6 (0.03)
		20.0 (−0.17)
	27.2 (1.93)	

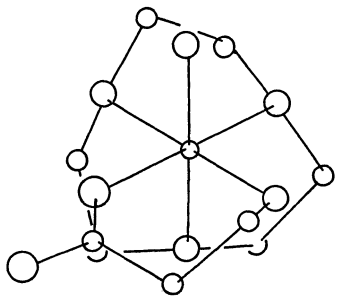

Fig. 6. Absolute configuration of $(-)_{589}$[Co(β-ala)(NH_3)(tacn)]$^{2+}$ complex.

(details will be published elsewhere). The structure of the complex closely resembles that of the corresponding glycinato complex.[7] However, the absolute configuration of the β-alaninato complex is opposite to that of the $(-)_{589}$-glycinato complex. In the previous work,[1] the absolute configuration of the [Co(a)(gly)(tacn)]$^{n+}$ complexes was determined on the basis of the Cotton sign of the dominant peak in the first absorption band region. In the present work, the absolute configuration of [Co(a)(amino acidato)(tacn)]$^{n+}$ can be determined not by the Cotton sign of dominant peak, but by the Cotton sign at the highest frequency.

A change from the five-membered glycinate chelate ring to the six-membered β-alaninate one causes the CD spectral shape to vary somewhat, especially, on the lower frequency side of the first absorption band region. It was previously assumed[1] that the optical source of the helical distributions of a NH_2–CH_2–COO^- chelate and –NH–CH_2–CH_2–NH– moieties of tacn had a small contribution to the optical activity of [Co(a)(gly)(tacn)]$^{n+}$, since the two helical ring-pairs canceled each other. The CD spectra of the β-alaninato complexes suggest that such cancellation is incomplete, but the spectra also indicate that the contribution of the helical ring-pairs is small. Thus, the main optical activities of the tacn complexes are

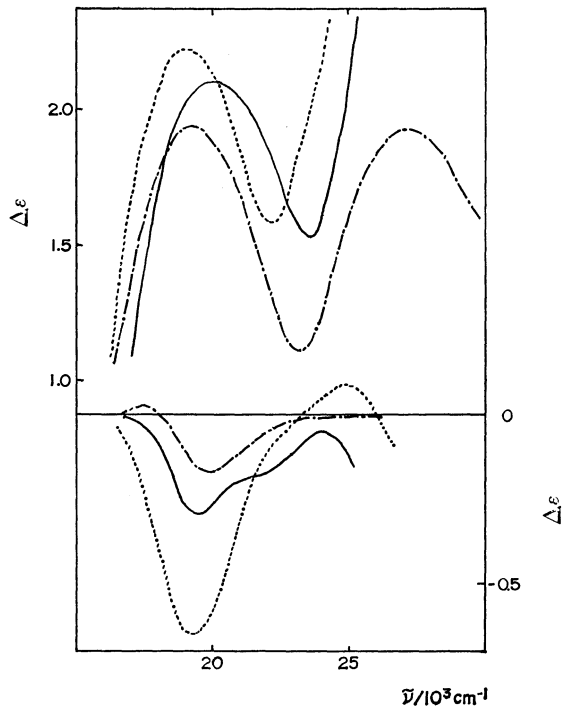

Fig. 7. Absorption and CD spectra of, $(-)_{500}^{CD}$[Co(NO_2)(gly)(tacdd)]$^+$ (——), $(-)_{500}^{CD}$[Co(NCS)(gly)(tacdd)]$^+$ (……), $(-)_{500}^{CD}$[Co(gly)(H_2O)(tacdd)]$^{2+}$ (·—·—).

considered to be derived from chiral arrangements of the donor atoms.

4) The [Co(a)(gly)(tacdd)]$^{n+}$ Complexes. Absorption and CD spectra of [Co(NO_2)(gly)(tacdd)]$^+$, [Co(NCS)(gly)(tacdd)]$^+$ and [Co(gly)(H_2O)(tacdd)]$^{2+}$ are shown in Fig. 7. At present, there are few complexes containing the tacdd ligand,[10,11] and the ligand field strength of this ligand has not been reported. The [Co(NO_2)(gly)(tacdd)]$^+$ complex exhibits the first absorption band at 20100 cm^{-1}, and the related [Co(NO_2)(gly)(tacn)]$^+$ and *fac(*NH_3*)*-[Co(NO_2)(gly)-

$(NH_3)_3]^+$,[12] at 21800 cm^{-1} and 20900 cm^{-1}, respectively. On this basis, it is found that the ligand field strengths decrease in the order, tacn>NH_3>tacdd. To obtain a ligand field parameter of tacdd (Δ(tacdd)=$3e_\sigma$), we prepared trinitro complex, $[Co(NO_2)_3(tacdd)]$, which exhibited an absorption maximum at 21300 cm^{-1} ($\log \varepsilon$=2.21). Since the absorption maximum of $[Co(NO_2)_3(tacn)]$ appears at 22700 cm^{-1}, the following relation of the ligand field parameters can be derived from an angular overlap model;[13]

$$\Delta(\text{tacdd}) = \Delta(\text{tacn}) - 2800\ (\text{cm}^{-1}).$$

The earlier eluted $(-)^{CD}_{500}[Co(NO_2)(gly)(tacdd)]^+$ complex exhibits a negative Cotton peak and a shoulder peak in the first absorption band region. The net rotatory strength of the tacdd complex is negative as well as that of the tacn complex, but the spectral shape is very different from that of the tacn complex. The CD spectra of the earlier eluted isomers, $(-)^{CD}_{500}$-$[Co(NCS)(gly)(tacdd)]^+$ and $(-)^{CD}_{500}[Co(gly)(H_2O)$-$(tacdd)]^{2+}$, show a single peak and two peaks, respectively, which resemble those of the corresponding isomers of the tacn complexes.

In the case of the tacn complexes, the earlier eluted isomers are all of the same absolute configuration.[1] This is not the case for the tacdd complexes, since the later eluted isomers, $(+)^{CD}_{500}[Co(NO_2)(gly)(tacdd)]^+$ and $(+)^{CD}_{500}[Co(NCS)(gly)(tacdd)]^+$, are derived from the earlier eluted $(-)^{CD}_{500}[Co(gly)(H_2O)(tacdd)]^{2+}$ isomer. Therefore, we were unable to determine the absolute configuration of the tacdd complexes, by CD comparison with the tacn complexes.

The reason why the CD spectra of the tacdd complexes are different from those of the corresponding acn complexes seems to be due to a large repulsive interaction between the bulky tacdd chelate and the glycinato chelate. The interaction may induce the presence of a chiral conformation of the tacdd chelate rings. It is interesting that the change from five-membered glycinate to six-membered β-alaninate chelate ring brings about only a slight variation of the CD spectral shapes, while the change from five-membered tacn to six-membered tacdd chelate ring causes a large variation. This suggests that non-ligating atoms of cyclic terdentate ligands somewhat influence the optical activity of the complexes.

References

1) S. Shimba, S. Fujinami, and M. Shibata, *Bull. Chem. Soc. Jpn.*, **53**, 2523 (1980).
2) J. E. Richman and T. J. Atkins, *J. Am. Chem. Soc.*, **96**, 2268 (1974).
3) S. F. Mason and R. D. Peacock, *Inorg. Chim. Acta*, **19**, 75 (1976).
4) K. Nakai, S. Kanazawa, and M. Shibata, *Bull. Chem. Soc. Jpn.*, **45**, 3544 (1972).
5) S. Kanazawa and M. Shibata, *Bull. Chem. Soc. Jpn.*, **48**, 2424 (1971).
6) M. S. Okamoto and E. K. Barefield, *Inorg. Chim. Acta*, **17**, 91 (1976).
7) T. Yasui, J. Hidaka, and Y. Shimura, *Bull. Chem. Soc. Jpn.*, **39**, 2417 (1966).
8) S. Sato, S. Ohba, S. Shimba, S. Fujinami, M. Shibata, and Y. Saito, *Acta Crystallogr., Sect. B*, **36**, 43 (1980).
9) M. Nonoyama, *Inorg. Chim. Acta*, **29**, 211 (1978).
10) M. Nonoyama, *Transition Met. Chem.*, **1**, 70 (1976).
11) H. Koyama and T. Yoshino, *Bull. Chem. Soc. Jpn.*, **45**, 481 (1972).
12) S. Fujinami and M. Shibata, *Chem. Lett.*, **1981**, 495.
13) C. E. Schäffer, *Struct. Bonding*, **5**, 68 (1968); *Pure Appl. Chem.*, **24**, 361 (1970).

A Kinetic Study of the Anation Reactions of Some Cobalt(III) Complexes Containing Macrocyclic Quadridentate Amine Ligands

Keiichi Tsukahara,* Hiroshi Oshita, Yasunobu Emoto, and Yasuo Yamamoto

Department of Chemistry, Faculty of Science, Shimane University, Nishikawatsu-cho, Matsue 690

(Received November 24, 1981)

The kinetics of the anation of *trans*-$[Co(OH)(N_4)(H_2O)]^{2+}$ by acetate ions (OAc^-) have been studied at 25 °C and at an ionic strength of 0.10 mol dm^{-3} ($LiClO_4$), and over the pH range from 3.62 to 5.17; N_4 represents a macrocyclic ligand. The reaction is considered to proceed through a dissociative mechanism. The rate constants of the loss of the coordinated water of $[Co(OH)(N_4)(H_2O)]^{2+}$ are estimated to be $(1.4\pm0.2)\times10^{-2}$ s^{-1}, $(8.9\pm1.6)\times10^{-2}$ s^{-1}, $(1.0\pm0.1)\times10^{-1}$ s^{-1}, and $(4.0\pm0.1)\times10^{-1}$ s^{-1} for [14]aneN$_4$,† Me$_6$[14]4,11-dieneN$_4$, *ms*-Me$_6$[14]aneN$_4$, and *rac*-Me$_6$[14]aneN$_4$ complexes respectively. These represent the steric acceleration by the methyl groups of the macrocyclic ligands. The anation of the [14]aneN$_4$ complex by chloride and bromide ions in acetate-buffer solutions has also been investigated. The relative effectiveness of entering groups for the coordination to the pentacoordinate intermediate follows the order: $H_2O<OAc^-<Cl^-<Br^-$. The substitution reaction of $[Co(OH)(N_4)(H_2O)]^{2+}$ is slower than the ascorbate reduction of this complex reported previously. It is concluded that the electron-transfer reaction does not proceed through an inner-sphere mechanism, but through an OH-bridged mechanism.

In a previous paper,[1] we reported that the ascorbate reduction of *trans*-diaqua cobalt(III) complexes containing macrocyclic quadridentate amine ligands (Fig. 1) proceeds through an outer-sphere mechanism; however, it has not yet been determined whether *trans*-aquahydroxo complexes are reduced through a substitution-limited inner-sphere mechanism or through an OH-bridged mechanism. The substitution reaction is an important factor in determining the electron-transfer mechanism.

Extensive investigations have been carried out on the kinetics of substitution reactions of cobalt(III) complexes of the type *trans*-$[CoX_2(N_4)]^{n+}$ (N_4=a macrocyclic quadridentate amine ligand and X=a replaceable group such as Cl^-, Br^-, or NO_2^-).[2] These reactions are considered to proceed through a dissociative mechanism; the increase of the steric crowding of methyl groups of the macrocyclic ligands accelerates the loss of the leaving group. The kinetics of the substitution reactions of the diaqua and aquahydroxo macrocyclic cobalt(III) complexes, however, have rarely been investigated except for porphyrin complexes.[3]

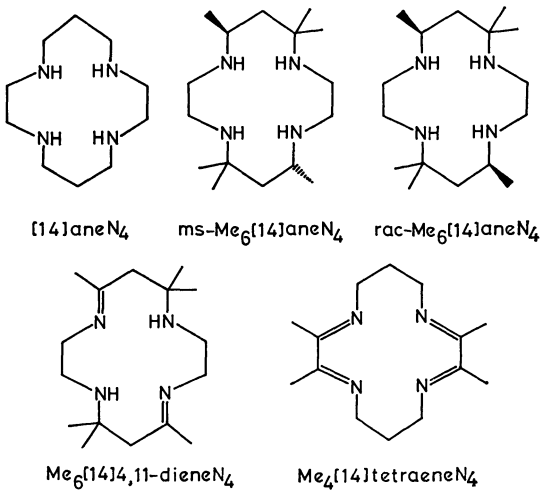

Fig. 1. Structures of tetraazamacrocycles (N_4).

In this paper we report the kinetics of the anation reaction of *trans*-$[Co(OH)(N_4)(H_2O)]^{2+}$ by an acetate ion (OAc^-), Cl^-, or Br^- and estimate the rate constants of the loss of the coordinated water of these complexes. The mechanism of the ascorbate reductions of the aquahydroxo complexes is discussed.

Experimental

Reagents. The *trans*-diaqua complexes $[Co([14]aneN_4)(H_2O)_2](ClO_4)_3$,[4] $[Co(ms\text{-}Me_6[14]aneN_4)(H_2O)_2](ClO_4)_3$,[5,6] $[Co(rac\text{-}Me_6[14]aneN_4)(H_2O)_2](ClO_4)_3$,[5,6] $[Co(Me_6[14]4,11\text{-}dieneN_4)(H_2O)_2](ClO_4)_3$,[6] and $[Co(Me_4[14]tetraeneN_4)(H_2O)_2](ClO_4)_3\cdot2.5H_2O$[7] were prepared as has been described elsewhere. The acetate-buffer solutions and the $LiClO_4\cdot3H_2O$ were obtained according to the procedure reported previously.[8] All the solutions used for the measurements were prepared from redistilled water. All the other reagents used were of guaranteed grade from Wako Pure Chemical Industries, Ltd.

Kinetic Measurements. Solutions containing a cobalt(III) complex and $LiClO_4$ were added to an optical cell, which was then sealed with a serum cap. After the solution had been purged with a nitrogen atmosphere for 15 min, the reaction was initiated by the injection of the acetate-buffer solution (or the solution containing the acetate buffer and lithium halide for the anation by halide ions). The change in the absorbance with the time was followed with either a Hitachi 200-20 or a Shimadzu UV 140-02 spectrophotometer. The wavelengths used for the measurements were 290 nm ($[Co(Me_4[14]tetraeneN_4)(H_2O)_2]^{3+}$), 310 nm ($[Co(rac\text{-}Me_6[14]aneN_4)(H_2O)_2]^{3+}$), 320 nm ($[Co([14]aneN_4)(H_2O)_2]^{3+}$ and $[Co(ms\text{-}Me_6[14]aneN_4)(H_2O)_2]^{3+}$), and 345 nm ($[Co(Me_6[14]4,11\text{-}dieneN_4)(H_2O)_2]^{3+}$). In order to ensure a pseudo-first-order condition, acetate or lithium halide was used in at least a 10^2 fold excess over the cobalt(III) complexes.

The temperature was controlled at 25.0±0.1 °C, and the ionic strength (I) was adjusted to 0.10 mol dm^{-3} with

† [14]aneN$_4$=1,4,8,11-Tetraazacyclotetradecane; *ms*- and *rac*-Me$_6$[14]aneN$_4$=*meso*- and *rac*-5,5,7,12,12,14-hexamethyl-1,4,8,11-tetraazacyclotetradecane; Me$_6$[14]4,11-dieneN$_4$=5,7,7,12,14,14-hexamethyl-1,4,8,11-tetraazacyclotetradeca-4,11-diene; Me$_4$[14]tetraeneN$_4$=2,3,9,10-tetramethyl-1,4,8,11-tetraazacyclotetradeca-1,3,8,10-tetraene.

lithium perchlorate. The pH of the solution was measured on a Hitachi-Horiba F-7 pH meter. The $[H^+]$ was computed from the pH, using a value of 0.83 for the activity coefficients of H^+.[9]

Acid-dissociation Constants. The acid-dissociation constants of the diaqua ligands of $[Co(ms\text{-}Me_6[14]aneN_4)(H_2O)_2]^{3+}$ and $[Co(rac\text{-}Me_6[14]aneN_4)(H_2O)_2]^{3+}$ were determined by pH titrations with a standard sodium hydroxide solution at 25 °C and $I=0.10$ mol dm^{-3} ($LiClO_4$) under a nitrogen atmosphere. The pK values thus obtained are listed in Table 1 along with those in the literature.

Results

Reactions of $[Co(OH)(N_4)(H_2O)]^{2+}$ with Acetate. The spectral changes observed during the reaction of $[Co(OH)([14]aneN_4)(H_2O)]^{2+}$ with acetate gave four isosbestic points over the range from 370 to 700 nm (Fig. 2). The absorption maxima of the spectra after the reaction was completed were 360 nm ($\varepsilon=79$ dm^3 mol^{-1} cm^{-1}), 443 nm ($\varepsilon=34$ dm^3 mol^{-1} cm^{-1}), and 565 nm ($\varepsilon=41$ dm^3 mol^{-1} cm^{-1}), which agreed with those of the species separated by the use of an SP-Sephadex C-25 column (H^+ form). This product, which has a 2+ charge in 0.1 mol dm^{-3} $HClO_4$, is considered to be $[Co(OAc)([14]aneN_4)(H_2O)]^{2+}$. In the case of the $Me_6[14]4,11\text{-}dieneN_4$ complex, two isosbestic points (at 549 nm and 630 nm) were observed at pH 4.17. The absorption maximum of the reaction product in this system was 567 nm ($\varepsilon=37$ dm^3 mol^{-1} cm^{-1}). The reaction product in the ms-$Me_6[14]aneN_4$ system, on the other hand, had the absorption maxima at 468 nm ($\varepsilon=40$ dm^3 mol^{-1} cm^{-1}) and 577 nm ($\varepsilon=42$ dm^3 mol^{-1} cm^{-1}). These results indicate that the reactions of these complexes with acetate can be represented as follows:

$$[Co(OH)(N_4)(H_2O)]^{2+} \text{ (or } [Co(N_4)(H_2O)_2]^{3+}) + OAc^- \longrightarrow [Co(OAc)(N_4)(H_2O)]^{2+} + H_2O. \quad (1)$$

The kinetics of the reactions were studied in various concentrations of acetate (0.020—0.25 mol dm^{-3}), cobalt(III) ($(1.00—2.40)\times10^{-4}$ mol dm^{-3}), and hydrogen ions ($(0.82—8.15)\times10^{-5}$ mol dm^{-3}). The plots of $-\ln(A_\infty-A_t)$ *vs.* the time were linear for at least 90% completion; here A_∞ and A_t represent the absorbance at infinity and time t respectively. The pseudo-first-order rate constant, k_{obsd}, increased with a decrease in the acidity when the total concentrations of acetate ($[OAc]_T$) were fixed. The acid dependency of the rate in the $[14]aneN_4$ system was analyzed as the occurrence of Reactions 2—7:

$$[Co(N_4)(H_2O)_2]^{3+} \overset{K_1}{\rightleftharpoons} [Co(OH)(N_4)(H_2O)]^{2+} + H^+, \quad (2)$$

$$HOAc \overset{K_a}{\rightleftharpoons} H^+ + OAc^- \ (pK_a=4.53^{12}), \quad (3)$$

$$[Co(N_4)(H_2O)_2]^{3+} + OAc^- \overset{k_1}{\longrightarrow} \text{products}, \quad (4)$$

$$[Co(N_4)(H_2O)_2]^{3+} + HOAc \overset{k_1^H}{\longrightarrow} \text{products}, \quad (5)$$

$$[Co(OH)(N_4)(H_2O)]^{2+} + OAc^- \overset{k_2}{\longrightarrow} \text{products}, \quad (6)$$

$$[Co(OH)(N_4)(H_2O)]^{2+} + HOAc \overset{k_2^H}{\longrightarrow} \text{products}. \quad (7)$$

Then, Eq. 8 can be derived for k_{obsd}:

$$k_{obsd}=\frac{k_1^H K_a^{-1}+(k_1+k_2^H K_1 K_2^{-1})[H^+]^{-1}+k_2 K_1[H^+]^{-2}}{(1+K_1[H^+]^{-1})(1+[H^+]K_a^{-1})[H^+]^{-1}}. \quad (8)$$

The plots of the values of $k_{obsd}(1+K_1[H^+]^{-1})(1+[H^+]K_a^{-1})[H^+]^{-1}$ *vs.* $[H^+]^{-1}$ gave a quadratic curve and the intercept was nearly zero. On the other hand, the plots of the values of $k_{obsd}(1+K_1[H^+]^{-1})\times(1+[H^+]K_a^{-1})$ *vs.* $[H^+]^{-1}$ gave a straight line (Fig. 3) and the intercept was very small. Therefore, both k_1 and k_2^H terms can be neglected under the present experimental conditions.[13] The pseudo-first-order rate constants showed nonlinear dependency on the total concentrations of acetate. The rate law was as follows:

$$-\frac{d[Co(III)]}{dt}=\frac{c[OAc]_T}{a+b[OAc]_T}[Co(III)], \quad (9)$$

where $k_{obsd}=c[OAc]_T/(a+b[OAc]_T)$. The plots of k_{obsd}^{-1} *vs.* $[OAc]_T^{-1}$ gave straight lines (Fig. 4). The values of a/c and of b/c are obtained from the slope

Table 1. pK values of *trans*-$[Co(N_4)(H_2O_2]^{3+}$ at 25 °C

$$[Co(N_4)(H_2O)_2]^{3+} \overset{K_1}{\rightleftharpoons} [Co(OH)(N_4)(H_2O)]^{2+} + H^+$$

$$[Co(OH)(N_4)(H_2O)]^{2+} \overset{K_2}{\rightleftharpoons} [Co(OH)_2(N_4)]^+ + H^+$$

N_4	pK_1	pK_2	Ref.
$[14]aneN_4$	2.9 ±0.1[a]	7.2±0.1[a]	10
ms-$Me_6[14]aneN_4$	2.7 ±0.05[b]	6.4±0.05[b]	11
	3.32±0.05[c]	6.6±0.1[c]	This work
rac-$Me_6[14]aneN_4$	3.46±0.05[c]	7.1±0.1[c]	This work
$Me_6[14]4,11\text{-}dieneN_4$	4.02±0.01[b]	8.2±0.1[b]	11
	3.93±0.02[c]	8.6±0.1[c]	1

a) $I=0.50$ mol dm^{-3} ($NaClO_4$). b) $I=1.0$ mol dm^{-3} ($NaClO_4$). c) $I=0.10$ mol dm^{-3} ($LiClO_4$).

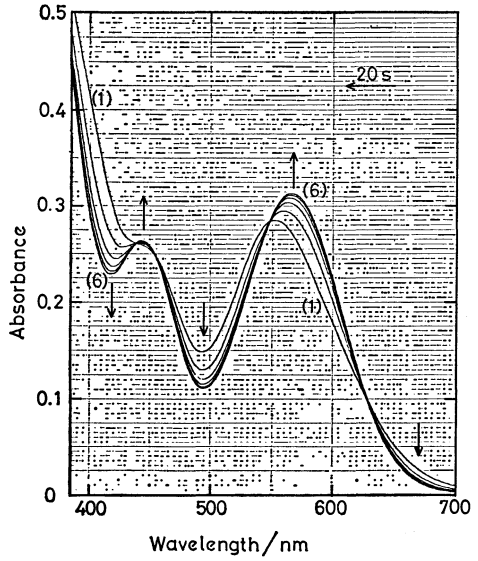

Fig. 2. Spectral changes during the reaction of $[Co([14]aneN_4)(H_2O)_2]^{3+}$ with acetate at $[Co(III)]_0=7.66\times10^{-3}$ mol dm^{-3}, $[OAc]_T=0.250$ mol dm^{-3}, pH=4.17, 25 °C, and $I=0.08$ mol dm^{-3}: (1) 45 s; (2) 4 min 25 s; (3) 8 min 25 s; (4) 12 min 25 s; (5) 17 min 25 s; (6) 25 min 25 s after the reaction. The time given are for the start of scan at 700 nm.

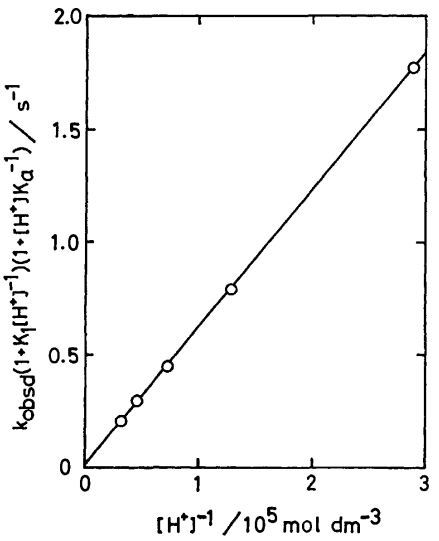

Fig. 3. Plots of $k_{obsd}(1+K_1[H^+]^{-1})(1+[H^+]K_a^{-1})$ *vs.* $[H^+]^{-1}$ for the $[Co([14]aneN_4)(H_2O)_2]^{3+}$–acetate system at $[Co(III)]_0=2.20\times10^{-4}$ mol dm^{-3}, $[OAc]_T=0.100$ mol dm^{-3}, 25 °C, and $I=0.10$ mol dm^{-3} ($LiClO_4$).

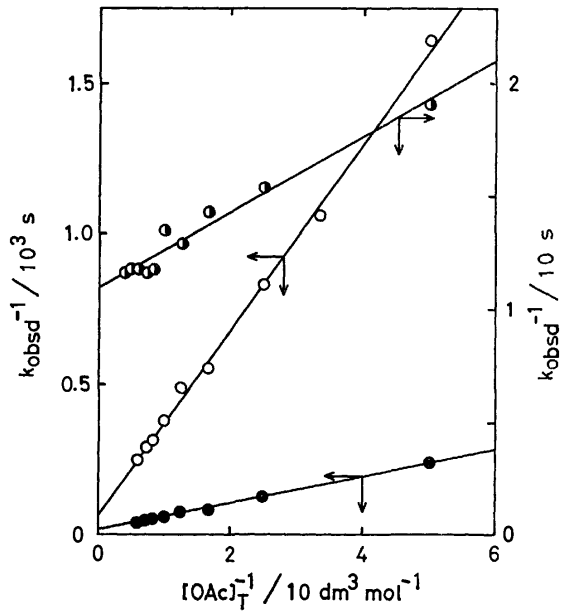

Fig. 4. Plots of k_{obsd}^{-1} *vs.* $[OAc]_T^{-1}$ for the $[Co(N_4)(H_2O)_2]^{3+}$–acetate system at $[Co(III)]_0=2.30\times10^{-4}$ mol dm^{-3}, 25 °C, and $I=0.10$ mol dm^{-3} ($LiClO_4$). ○: The $[14]aneN_4$ complex at pH 4.71, ●: the Me_6-$[14]4,11$-$dieneN_4$ complex at pH 4.71, ◑: the *ms*-$Me_6[14]aneN_4$ complex at pH 4.35.

and the intercept of this straight line respectively.

These are explained by either a dissociative mechanism (D-mechanism):

$$[Co(OH)(N_4)(H_2O)]^{2+} \underset{k^{H_2O}}{\overset{k_d}{\rightleftharpoons}} [Co(OH)(N_4)]^{2+} + H_2O, \quad (10)$$

$$[Co(OH)(N_4)]^{2+} + OAc^- \xrightarrow{k_1^{OAc}} [Co(OH)(OAc)(N_4)]^+, \quad (11)$$

$$[Co(OH)(OAc)(N_4)]^+ + H^+ \rightleftharpoons [Co(OAc)(N_4)(H_2O)]^{2+}, \quad (12)$$

or an interchange mechanism (I-mechanism):

$$[Co(OH)(N_4)(H_2O)]^{2+} + X^- \overset{Q^X}{\rightleftharpoons} \{[Co(OH)(N_4)(H_2O)]^{2+}\cdot X^-\} \xrightarrow{k_2^X} \text{products}. \quad (13)$$

These mechanisms lead to Eqs. 14a and 14b respectively (X=OAc):

$$\frac{1}{k_{obsd}} = \frac{1+[H^+]K_1^{-1}}{k_d} + \frac{k^{H_2O}(1+[H^+]K_1^{-1})(1+[H^+]K_a^{-1})}{k_d k_1^{OAc}} \times \frac{1}{[OAc]_T}, \quad (14a)$$

$$\frac{1}{k_{obsd}} = \frac{1}{k_2^{OAc}} + \frac{(1+[H^+]K_1^{-1})(1+[H^+]K_a^{-1})}{k_2^{OAc}Q^{OAc}} \times \frac{1}{[OAc]_T}, \quad (14b)$$

The values of k_d and k_1^{OAc}/k^{H_2O} or of k_2^{OAc} and Q^{OAc} obtained by means of the plots of k_{obsd}^{-1} *vs.* $[OAc]_T^{-1}$ are listed in Table 2.

The pseudo-first-order rate constants for the reactions of the $Me_4[14]tetraeneN_4$ complex with acetate and bromide ions are 1.2×10^{-6} s^{-1} at 0.10 mol dm^{-3} acetate and pH 5.17, and 6.3×10^{-7} s^{-1} at $[Br^-]=0.050$ mol dm^{-3}, $[OAc]_T=0.060$ mol dm^{-3}, and pH 5.17.

Reaction of $[Co(OH)([14]aneN_4)(H_2O)]^{2+}$ with Cl^-. The title reaction was examined in the presence of acetate. The plots of $-\ln(A_\infty-A_t)$ *vs.* the time were linear for at least 90% completion, when $[OAc]_T \gg [Cl^-]$.[14] Since the anation of $[CoCl([14]aneN_4)(H_2O)]^{2+}$ by Cl^- is very slow ($k=7.6\times10^{-7}$ dm^3 mol^{-1} s^{-1} at 25 °C),[15] the following parallel reactions are considered to occur:

$$[Co(OH)([14]aneN_4)(H_2O)]^{2+} + OAc^- \longrightarrow [Co(OH)(OAc)([14]aneN_4)]^+ + H_2O, \quad (15)$$

$$[Co(OH)([14]aneN_4)(H_2O)]^{2+} + Cl^- \longrightarrow [CoCl(OH)([14]aneN_4)]^+ + H_2O. \quad (16)$$

The pseudo-first-order rate constants show nonlinear dependency on the concentrations of Cl^- ions (Fig. 5). If the following reactions occur in addition to Reactions 10—12;

$$[Co(OH)(N_4)]^{2+} + Cl \xrightarrow{k_1^{Cl}} [CoCl(OH)(N_4)]^+, \quad (17)$$

$$[CoCl(OH)(N_4)]^+ + H^+ \rightleftharpoons [CoCl(N_4)(H_2O)]^{2+}, \quad (18)$$

Eq. 19 can be derived:

$$\frac{1}{k_{obsd}-k_{obsd}^{OAc}} = \frac{1}{k'-k_{obsd}^{OAc}} + \frac{k''}{k'-k_{obsd}^{OAc}} \times \frac{1}{[Cl^-]}. \quad (19)$$

Here k_{obsd}^{OAc} is the pseudo-first-order rate constant in the absence of Cl^-, $k'=k_d/(1+[H^+]K_1^{-1})$, and $k''=k_1^{OAc}/k_1^{Cl}+k_1^{OAc}[OAc]_T/k_1^{Cl}(1+[H^+]K_a^{-1})$. The plots of the left-hand side of Eq. 19 *vs.* $[Cl^-]^{-1}$ gave a linear relation (Fig. 5). The values of k_d and k_1^{OAc}/k_1^{Cl} were determined from the intercept and the slope of this straight line respectively. In the I-mechanism (Reaction 13), k' and k'' correspond to k_2^{Cl} and $(1+$

Table 2. Kinetic data of the substitution reactions of $[Co(OH)(N_4)(H_2O)]^{2+}$ at 25 °C and I=0.10 mol dm^{-3} ($LiClO_4$)

N_4	X	D-Mechanism		I-Mechanism	
		k_d / 10^{-2} s^{-1}	k_1^X/k^{H_2O} a)	k_2^X / 10^{-2} s^{-1}	Q^X / dm^3 mol^{-1}
[14]aneN$_4$	OAc$^-$	1.4±0.2	(2.5±0.5)×10^2	1.3±0.2	4.7±1.1
	Cl$^-$	2.1±0.2	(2.4±0.3)×10^3	2.0±0.2	(4.4±0.7)×10
	Br$^-$	4.2±2.3	(4.4±2.1)×10^3	4.2±2.3	(8.1±4.0)×10
ms-Me$_6$[14]aneN$_4$	OAc$^-$	10±1	(1.2±0.2)×10^4	9.0±0.3	(2.4±0.3)×10^2
rac-Me$_6$[14]aneN$_4$	OAc$^-$	40±2	(1.9±0.4)×10^3	27±5	(5.2±2.0)×10
Me$_6$[14]4,11-dieneN$_4$	OAc$^-$	8.9±1.6	(2.9±0.7)×10^2	7.7±1.9	6.2±1.7

a) These are multiplied by 55.5 to make a correction for the concentration of the water.

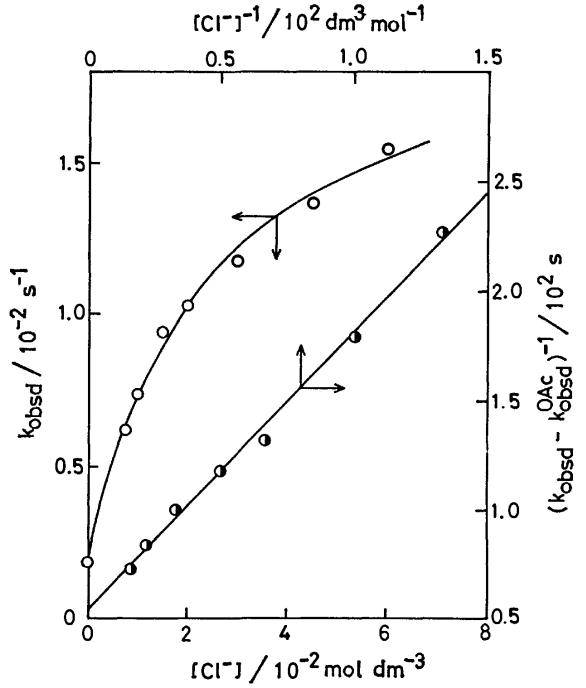

Fig. 5. Plots of k_{obsd} *vs.* [Cl$^-$] and of $(k_{obsd}-k_{obsd}^{OAc})^{-1}$ *vs.* [Cl$^-$]$^{-1}$ for the $[Co(N_4)(H_2O)_2]^{3+}$–Cl$^-$ system at $[OAc]_T$=0.060 mol dm^{-3}, pH 4.71, 25 °C, and I=0.10 mol dm^{-3} ($LiClO_4$).

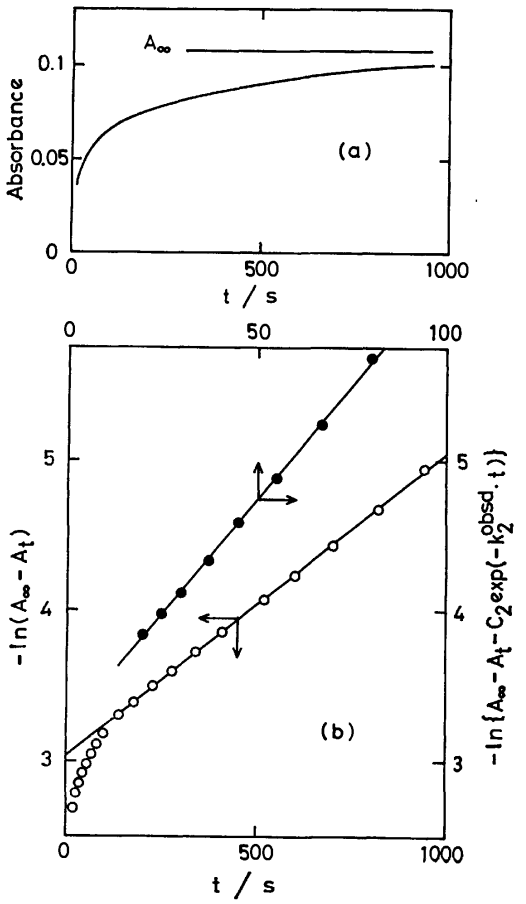

Fig. 6. Reactions of $[Co([14]aneN_4)(H_2O)_2]^{3+}$ with bromide ion at $[Co(III)]_0=7.98\times10^{-4}$ mol dm^{-3}, [Br$^-$]=0.060 mol dm^{-3}, $[OAc]_T$=0.060 mol dm^{-3}, pH, 4.71, 25 °C, and I=0.10 mol dm^{-3} ($LiClO_4$) followed at 320 nm: (a) absorbance-time profile; (b) resolution of the kinetic data into two component exponentials.

$[H^+]K_1^{-1})/Q^{Cl}+Q^{OAc}[OAc]_T/Q^{Cl}(1+[H^+]K_a^{-1})$ respectively. The data thus obtained are given in Table 2.

Reaction of $[Co(OH)([14]aneN_4)(H_2O)]^{2+}$ with Br$^-$. Figure 6 shows an example of the change in the absorbance at 320 nm against the time and of the consecutive reaction treatment[1] for the evaluation of the pseudo-first-order rate constants, k_1^{obsd} and k_2^{obsd}, for the first and second stages of the reaction. The second-stage rate constant, k_2^{obsd}, is given by the slope of the linear portion observed by means of a plot of $-\ln(A_\infty-A_t)$ *vs.* t:

$$-\ln(A_\infty-A_t) = k_2^{obsd}t - \ln C_2. \quad (20)$$

Using the values of k_2^{obsd} and C_2 thus obtained, a plot of the left-hand side of Eq. 21 against the time for the first-stage reaction gives k_1^{obsd} as a slope:

$$-\ln\{A_\infty-A_t-C_2\exp(-k_2^{obsd}t)\} = k_1^{obsd}t - \ln C_1, \quad (21)$$

where C_1 and C_2 are constant. The first-stage rate constant, k_1^{obsd}, depends on [Br$^-$], while k_2^{obsd} does not (Fig. 7). Therefore, the first-stage reaction is considered to be the simultaneous occurrence of Reactions 15 and 22:

$$[Co(OH)([14]aneN_4)(H_2O)]^{2+} + Br^- \longrightarrow [CoBr(OH)([14]aneN_4)]^+ + H_2O \quad (22)$$

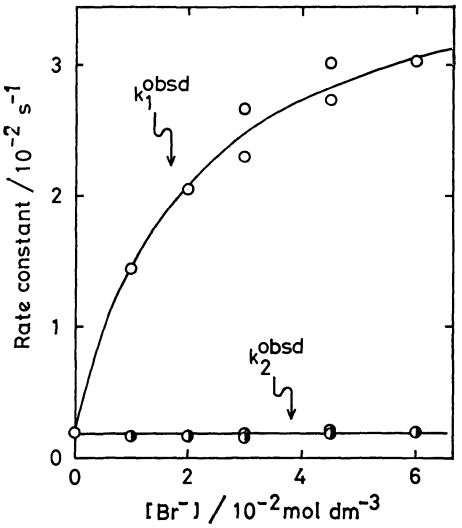

Fig. 7. Plots of k_1^{obsd} *vs.* [Br$^-$] and of k_2^{obsd} *vs.* [Br$^-$] for the [Co([14]aneN$_4$)(H$_2$O)$_2$]$^{3+}$–bromide system.

Discussion

Anation of trans-[*Co(OH)(N$_4$)(H$_2$O)*]$^{2+}$ *Ions.* There are two possible mechanisms for the anation of the [Co(OH)(N$_4$)(H$_2$O)]$^{2+}$ ions: (i) a dissociative mechanism (Eqs. 10—12) and (ii) an interchange mechanism (Eq. 13). The D-mechanism is more likely than the I-mechanism, because, if the reaction proceeds via the interchange mechanism, the large values of the ion-association constants cannot be explained (Q^{OAc} for the *ms*- and *rac*-Me$_6$[14]aneN$_4$ complexes or Q^{Cl} and Q^{Br} for the [14]aneN$_4$ complex); the expected value for a 2:1 electrolyte in water at 25 °C is about 2 dm^3 mol^{-1}. Poon[2] has demonstrated that the substitution reactions of [CoX$_2$([14]aneN$_4$)]$^+$ (X=a replaceable group such as Cl$^-$, Br$^-$, or NO$_2^-$) proceed through a dissociative mechanism.

The rate constants of the loss of the coordinated water of [Co(OH)(N$_4$)(H$_2$O)]$^{2+}$ range from 10^{-2} to 10^{-1} s^{-1} and increase in the following order: [14]aneN$_4$ < Me$_6$[14]4,11-dieneN$_4$ ≃ *ms*-Me$_6$[14]aneN$_4$ < *rac*-Me$_6$-[14]aneN$_4$. This order is similar to that of the hydrolysis of dichloro and dibromo complexes.[2] This similarity suggests that the methyl groups of the macrocyclic ligands accelerate the loss of the coordinated water. The increasing order of k_1^X/k^{H_2O} (X=OAc$^-$), [14]aneN$_4$ ≤ Me$_6$[14]4,11-dieneN$_4$ < *rac*-Me$_6$[14]aneN$_4$ < *ms*-Me$_6$[14]aneN$_4$, is coincident with the inference that [14]aneN$_4$ is more hydrophilic than the others and that its k^{H_2O} is larger. The relative effectiveness of the entering group for the coordination to the pentacoordinate intermediate follows the order: H$_2$O < OAc$^-$ < Cl$^-$ < Br$^-$.

The anation of the Me$_4$[14]tetraeneN$_4$ complex by OAc$^-$ and Br$^-$ is very slow. We have not found any reactions which signaled the rapid anation by means of a stopped-flow apparatus. However, it does not necessarily follow that the loss of the coordinated water of this complex is slow, because the Me$_4$[14]-tetraeneN$_4$ complex may have less affinity to OAc$^-$ and Br$^-$.

The substitution reaction of *trans*-[Co(OH)(N$_4$)-(H$_2$O)]$^{2+}$ obtained in this work is much faster than that of other cobalt(III) complexes;[2] this is explained by the "internal S_N1 conjugate-base mechanism" proposed by Mok and Poon.[16] As is shown in Fig. 8, the amido group, >N$^-$, can facilitate a dissociative reaction and may stabilize a tetragonal-pyramidal intermediate. The rate of the aquation of [CoCl(OH)-([14]aneN$_4$)]$^+$ is comparable with that of the loss of the coordinated water of [Co(OH)([14]aneN$_4$)(H$_2$O)]$^{2+}$ (2.1×10^{-2} s^{-1} at 25 °C);[15] therefore, the rate of the formation of the pentacoordinated intermediate may be independent of the nature of the leaving group. Interestingly, k_d of *trans*-[Co(OH)([14]aneN$_4$)(H$_2$O)]$^{2+}$ agrees with the rate constant of the N–H proton exchange of this complex (2×10^{-2} s^{-1} at 21 °C and I= 0.50 mol dm^{-3}).[10] These facts suggest that the N–H protons play a significant role in the substitution reactions of the macrocyclic cobalt(III) complexes.

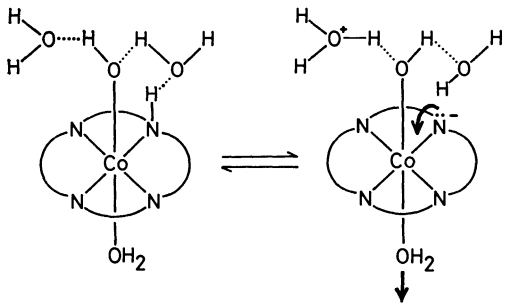

Fig. 8. Internal S_N1 conjugate-base mechanism.

Possible Structure of trans-[*Co(OH)(*rac-*M$_6$[14]aneN$_4$-(H$_2$O)*]$^{2+}$. Since the *trans*-[Co(*ms*-Me$_6$[14]aneN$_4$)-(H$_2$O)$_2$]$^{3+}$ complex has a center of symmetry with respect to the cobalt atom, there is only one possible structure for the aquahydroxo species (Fig. 9a). The *trans*-[Co(OH)(*rac*-Me$_6$[14]aneN$_4$)(H$_2$O)]$^{2+}$ complex, on the other hand, has two possible structures (Figs. 9b and 9c),[17] because *rac*-Me$_6$[14]aneN$_4$ has no axis of symmetry. We propose that the predominant structure of the *rac*-complex is (b) rather than (c). The *ms*- and *rac*-isomers are very similar in the first acid-dissiciation constants, pK_1 (Table 1). The pK_2 of the *ms*-isomer, however, is smaller than that of the

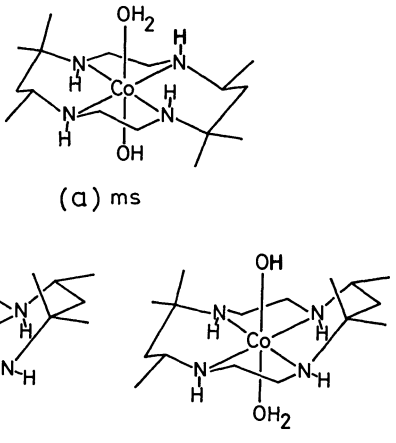

Fig. 9. Proposed structures of *trans*-[Co(OH)(Me$_6$[14]-aneN$_4$)(H$_2$O)]$^{2+}$.

rac-isomer; that is, the *ms*-dihydroxo species is more stable than the *rac*-dihydroxo species. The OH^- ligand, which faces the N–H proton, can make a chain of hydrogen bonds with the N–H proton through solvent water molecules (Fig. 8). In the *ms*-isomer two OH^- ligands are possible to make such a hydrogen bonding; in the *rac*-isomers, only one OH^- ligand is possible. Since the electronic effect of these ligands is identical, the difference in pK_2 can be ascribed to the stabilization by the hydrogen bonding. In the aquation of *trans*-$[CoCl_2(N_4)]^+$,[18] the loss of the coordinated chloride is accelerated by the increase of the steric crowding of methyl groups. The k_d of the *rac*-isomer is larger than that of the *ms*-isomer. This can be explained as the steric acceleration. The fact that k_1^{OAc}/k^{H_2O} of the *rac*-isomer is much smaller than that of the *ms*-isomer can also be explained as the steric hindrance.

Mechanism of Electron-transfer Reactions of trans-$[Co(OH)(N_4)(H_2O)]^{2+}$ *with Ascorbic Acid.* We have reported that the rate constants of the reactions of $[Co(OH)(N_4)(H_2O)]^{2+}$ with ascorbate (HA^-) range from 2.9×10 to 1.3×10^3 $dm^3\ mol^{-1}\ s^{-1}$.[1] If the reaction proceeds through an inner-sphere mechanism, the substitution reaction of $[Co(OH)(N_4)(H_2O)]^{2+}$ must be faster than the electron-transfer reaction. The kinetic data for the substitution reaction of the aqua-hydroxo complexes obtained in this work show that the ascorbate reduction of these complexes is faster than the substitution reaction. Therefore, an inner-sphere mechanism can be ruled out and the ascorbate reduction of *trans*-$[Co(OH)(N_4)(H_2O)]^{2+}$ is considered to proceed through an OH-bridged mechanism:

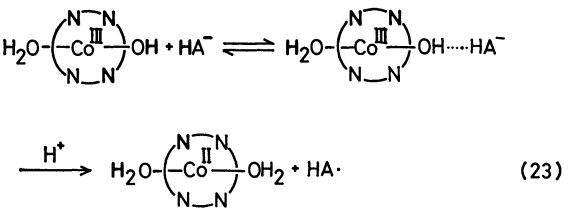

(23)

References

1) K. Tsukahara, T. Izumitani, and Y. Yamamoto, *Bull. Chem. Soc. Jpn.*, **55**, 130 (1982).
2) C. K. Poon, *Coord. Chem. Rev.*, **10**, 1 (1973).
3) R. F. Pasternack and G. R. Parr, *Inorg. Chem.*, **15**, 3087 (1976) and the references cited therein.
4) C. K. Poon and M. L. Tobe, *J. Chem. Soc., A*, **1968**, 1549.
5) P. O. Whimp and N. F. Curtis, *J. Chem. Soc., A*, **1966**, 867.
6) N. Sadasivan, J. A. Kernohan, and J. F. Endicott, *Inorg. Chem.*, **6**, 770 (1967).
7) D. P. Rillema, J. F. Endicott, and R. C. Patel, *J. Am. Chem. Soc.*, **94**, 394 (1972).
8) K. Tsukahara and Y. Yamamoto, *Bull. Chem. Soc. Jpn.*, **54**, 2642 (1981).
9) J. Kielland, *J. Am. Chem. Soc.*, **59**, 1675 (1937).
10) C. K. Poon and M. L. Tobe, *Inorg. Chem.*, **7**, 2398 (1968).
11) J. A. Kernohan and J. F. Endicott, *Inorg. Chem.*, **9**, 1504 (1970).
12) M. Yasuda, K. Yamasaki, and H. Ohtaki, *Bull. Chem. Soc. Jpn.*, **33**, 1067 (1960).
13) Since the $[Co(Me_6[14]4,11\text{-dieneN}_4)(H_2O)_2]^{3+}$ ion is less acidic than the $[Co([14]aneN_4)(H_2O)_2]^{3+}$ and the $[Co(ms\text{-}Me_6[14]aneN_4)(H_2O)_2]^{3+}$ ions, the contribution of the diaqua species cannot be ruled out.
14) When $[Cl^-]$ is larger than $[OAc]_T$, a subsequent reaction is found to occur; it is much slower than the first-stage reaction.
15) The rate constant was calculated by the use of the equilibrium constant and the rate constant of the aquation: C. K. Poon and M. L. Tobe, *J. Chem. Soc., A*, **1967**, 2069.
16) K. S. Mok and C. K. Poon, *Inorg. Chem.*, **10**, 225 (1971).
17) There are three isomers with respect to the configuration of *rac*-$Me_6[14]aneN_4$. For the Ni(II) complexes, the isomers shown in Figs. 9b and 9c are stable: P. O. Whimp, M. F. Bailey, and N. F. Curtis, *J. Chem. Soc., A*, **1970**, 1956; N. F. Curtis, D. A. Swann, and T. N. Waters, *J. Chem. Soc., Dalton Trans.*, **1973**, 1963.
18) W. K. Chau and C. K. Poon, *J. Chem. Soc., A*, **1971**, 3087.

 © 1982 The Chemical Society of Japan Bull. Chem. Soc. Jpn., 55, 2113—2117 (1982)

The Crystal Structure of $Na_2H_2[Co_4I_3O_{18}(OH_2)_6]$-$[Co_4I_3O_{16}(OH)_2(OH_2)_6]\cdot 22H_2O$

Hidetaka KONDO,† Akiko KOBAYASHI, and Yukiyoshi SASAKI*

Department of Chemistry and The Research Centre for Spectrochemistry, Faculty of Science, The University of Tokyo, Hongo, Bunkyo-ku, Tokyo 113

(Received December 4, 1981)

The title compound has the analytical formula of $Co_4H_{36}I_3NaO_{35}$ and is seemingly well formulated as $NaH_2[Co_4I_3O_{18}(OH_2)_6]\cdot 11H_2O$. But the structure determination revealed that the crystals contain non-protonated $[Co_4I_3O_{18}(OH_2)_6]^{3-}$ and doubly protonated $[Co_4I_3O_{16}(OH)_2(OH_2)_6]^-$. The anion itself has a new variation of the Anderson structure. The almost identical three pK's of the acid, $H_3[Co_4I_3O_{18}(OH_2)_6]$, explain the formation of the present crystals by co-precipitation of two forms of the anion with different degrees of protonation. Crystals are monoclinic, space group P2/c, with $a=15.172(2)$, $b=10.874(1)$, $c=19.436(3)$ Å, $\beta=116.58(1)°$, $U=2867.6(5)$ Å^3, and $Z=2$. The final R factor was 0.036 for 7010 independent reflections.

The periodate anion has been reported to form complex anions with various transition metal cations.[1,2] The Co^{III} and I^{VII} form a highly condensed anion, $[Co_4I_3O_{18}]^{3-}$, as reported by Malaprade.[3]

On the basis of spectroscopic and stereochemical data, Ama, Hidaka, and Shimura proposed the Anderson structure for this anion, consisting of seven octahedra condensed into a flat arrangement of D_{3d} symmetry by edge-sharing.[4] Two types of the Anderson structure are known: the first one has been found in $[TeMo_6O_{24}]^{6-}$,[5] and $[IMo_6O_{24}]^{5-}$,[6] which has no constitutional water, while the second one has been reported in the cases of $[CrMo_6O_{24}H_6]^{3-}$,[7] and $[CoMo_6O_{24}H_6]^{3-}$,[8] having six non-acidic protons per molecule. Our present study has confirmed that this (tetracobaltato)triperiodate anion belongs to a new type of the Anderson structure which has twelve non-acidic protons.

Experimental

At the beginning, our aim was to prepare the free acid form of the title compound from $Na_3[Co(CO_3)_3]\cdot 3H_2O$, $HClO_4$ and $NaIO_4$. The method reported by Williams and Nyman[9] was used, but crystals of the compound having the analytical formula of $Co_8H_{72}I_6Na_2O_{70}$ were obtained and used for the present study.

Data Collection. Preliminary Weissenberg photographs showed that the crystal system is monoclinic. A systematic absence $h0l$, $l=2n+1$, indicated the space group to be either Pc or P2/c; P2/c was assumed and confirmed by the successful structure analysis.

The intensities of the reflections were measured with a Rigaku automatic four-circle diffractometer (graphite monochromator, Mo $K\alpha$ radiation, ω-2θ scan mode) up to $2\theta=60°$. The crystal used here was a parallelepiped with dimensions $0.45\times 0.1\times 0.2$ mm^3. Independent 7010 reflections, $|F_o|\geq 3\sigma(|F_o|)$, were adopted for the structure determination. The crystal data are: $Co_8H_{72}I_6Na_2O_{70}$, FW=2471.88, monoclinic, space group P2/c, $a=15.172(2)$, $b=10.874(1)$, $c=19.436(3)$ Å, $\beta=116.58(1)°$, $U=2867.6(5)$ Å^3, $Z=2$, $D_x=2.864$ g cm^{-3}, μ for Mo $K\alpha$ ($\lambda=0.71069$ Å)$=57.85$ cm^{-1}.

Structure Determination and Refinement

The structure was solved by the heavy-atom method. All the non-hydrogen atoms were refined by the block-diagonal least-squares method using anisotropic temperature factors. Almost all of the hydrogens attached to anions 1 and 2 have been located on the difference Fourier maps and treated isotropically in the refinements. One hydrogen atom of an aqua ligand bound to a cobalt atom, the cationic proton, and all of the hydrogens of the water molecules were not found. The eleven waters of crystallization are in general positions and one of them, Aq(11), are distributed in two sites, Aq(11a) and Aq(11b), by the ratio of 0.45 and 0.55. This ratio was estimated from the peak heights in the difference Fourier maps and fixed in the structure refinements. The function minimized was $\Sigma w(|F_o|-|F_c|)^2$, where $w=1/[\sigma(|F_o|)^2+c^2|F_o|^2]$. The parameter c was estimatedto be 0.02 from the fluctuations of the intensities of the standard reflections during the data collection and $\sigma(|F_o|)$ was found from counting statistics. The final R values are $R=0.035$ and $R_w=0.036$, where $R=\Sigma||F_o|-|F_c||/\Sigma|F_o|$ and $R_w=\Sigma w||F_o|-|F_c||/\Sigma w|F_o|$. The atomic scattering factors and the corrections of anomalous dispersion were taken from International Tables for X-Ray Crystallography.[10] All the calculations were performed on a HITAC 8800/8700 computer at the Computer Centre of the University of Tokyo with a local version of UNICS.[11] The atomic fractional coordinates and the averaged bond distances and angles are listed in Tables 1 and 2. The F_o-F_c tables and anisotropic thermal parameters are kept at the office of this Bulletin as Document No. 8230.

Description of the Structure and Discussion

Structure of Polyanion. There are two forms of the anion, which are different not only crystallographically but also in the degree of the protonation. We describe the common features of the structures of both forms in this section.

The structure of the polyanion is shown in Fig. 1. The anion has principally the Anderson structure, as found in several heteropolymolybdates.[5-8] But in the present (tetracobaltato)triperiodate anion, the six peripheral sites are occupied by Co and I alternatively and there is a Co at the central heteroatom site. In general, the Anderson polyanion has three types of

† Present address: Systems Development Laboratory, Hitachi Ltd, Ohzenji, Tama-ku, Kawasaki, Kanagawa 215.

TABLE 1. FRACTIONAL COORDINATES
($\times 10^4$ for non-hydrogen atoms, $\times 10^3$ for hydrogen atoms)

Atom	x	y	z	Atom	x	y	z
Co*(a1)	0	2405(1)	2500	O_t(6b)	4407(3)	7049(3)	4002(2)
I(1)	0	5176(1)	2500	O_t(7a)	6126(3)	3053(3)	4882(2)
Co(2)	1647(1)	3715(1)	2545(1)	O_t(7b)	4332(3)	2066(3)	4046(2)
I(3)	1726(1)	1015(1)	2519(1)	O_t(8)	4186(3)	688(3)	2654(2)
Co(4)	0	−188(1)	2500	Na	1236(2)	2575(2)	5304(1)
Co*(a2)	5000	4500(1)	2500	Aq(1)	2236(3)	5747(5)	1016(3)
I(5)	5000	7264(1)	2500	Aq(2)	4951(4)	568(4)	5652(3)
Co(6)	5186(1)	5811(1)	3819(1)	Aq(3)	2379(4)	2759(4)	7659(3)
I(7)	5218(1)	3125(1)	3902(1)	Aq(4)	2408(4)	1183(5)	6093(3)
Co(8)	5000	1887(1)	2500	Aq(5)	2208(4)	2722(5)	4615(3)
O_c(12)	859(2)	3697(3)	3067(2)	Aq(6)	1991(4)	5949(6)	4792(4)
O_c(23)	804(2)	2424(3)	1972(2)	Aq(7)	590(5)	2483(5)	6179(4)
O_c(34)	853(2)	1101(3)	3064(2)	Aq(8)	−41(6)	4004(7)	431(4)
O_c(56)	4351(2)	5785(3)	2752(2)	Aq(9)	437(8)	775(10)	4634(4)
O_c(67)	5832(2)	4500(3)	3583(2)	Aq(10)	2941(6)	366(8)	4706(5)
O_c(78)	4343(2)	3180(3)	2741(2)	Aq(11)	1834(16)	1483(16)	220(11)
O_b(12)	765(3)	4948(3)	1967(2)	Aq(12)	1311(10)	2336(11)	540(9)
O_b(23)	2457(2)	2376(3)	3115(2)	H(2a)	295(8)	472(10)	332(7)
O_b(34)	729(3)	−104(3)	1926(2)	H(2a′)	233(8)	581(9)	286(7)
O_b(56)	5855(3)	7017(3)	3553(2)	H(2b)	238(10)	478(12)	175(8)
O_b(67)	4506(2)	4481(3)	4018(2)	H(2b′)	289(10)	328(12)	203(8)
O_b(78)	5825(2)	1942(3)	3571(2)	H(4)	84(9)	−216(10)	314(7)
O_t(1)	791(3)	6243(3)	3217(2)	H(6a)	655(8)	661(10)	507(7)
O_t(2a)	2523(3)	4946(3)	3229(2)	H(6a′)	599(8)	596(9)	530(6)
O_t(2b)	2311(3)	3767(3)	1892(2)	H(6b)	447(8)	761(9)	403(6)
O_t(3a)	2535(3)	−93(4)	3224(3)	H(6b′)	422(6)	693(8)	431(5)
O_t(3b)	2265(3)	998(4)	1859(3)	H(7b)	374(7)	217(8)	373(6)
O_t(4)	913(3)	−1399(3)	3184(3)	H(8)	347(10)	86(12)	228(8)
O_t(5)	4152(3)	8314(3)	2599(2)	H(8′)	416(10)	0(12)	261(8)
O_t(6a)	6171(3)	5825(3)	4886(2)				

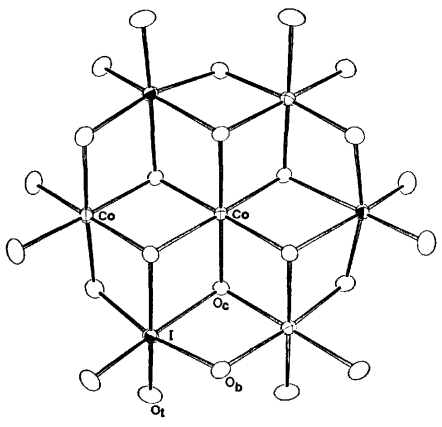

Fig. 1. Structure of $[Co_4I_3O_{18}(OH_2)_6]^{3-}$ "Anderson polyanion" (anion 1) viewed vertical to the hexagonal Co_4I_3 pseudo-plane.
The vibration ellipsoids are drawn at the 50% probability level (Johnson, 1965).[17] All the terminal oxygen atoms attached to Co are those of water molecules. The terminal oxygens attached to I are not protonated. In the anion 2 two of them are protonated.

oxygen atoms, denoted as O_t, O_b, and O_c. O_t represents the terminal oxygen bonding to one peripheral metal atom, O_b the one bridging between two peripheral metal atoms, and O_c the one coordinating to the central atom and two peripheral atoms. In this (tetracobaltato)triperiodate anion, however, there are two different O_t atoms. Half of them are the terminal oxygen atoms of Co, which are actually aqua ligands. Others are those of I which attract a proton in acidic media or form hydrogen bonds with the aqua ligands coordinated to Co atom.

The alternate arrangement of Co and I atoms at the peripheral metal sites causes the reduction of symmetry of the ion from $D_{3d}(\bar{3}m)$ of the Anderson structure to $D_3(32)$. The Co_3I_3 framework is not regularly hexagonal, while Mo_6 in $[IMo_6O_{24}]^{5-}$ is.[6]

It should be noted that there are only a few examples of structure determination of the Co^{III}–OH_2 distances. The only reliable example of Co^{III}–OH_2 distance is 1.954(1) Å, in $[Co(OH_2)(NH_3)_5]^{3+}$.[12] Our present study provides six crystallographically independent Co^{III}–OH_2 distances, 1.912—1.947(10) Å.

Crystal Structure. The crystal structure is shown in Fig. 2. The crystal contains two symmetrically independent Anderson polyanions. The first anion, referred to as anion 1, is not protonated and lies on the crystallographic two-fold axis at $x=0$, $z=1/4$ or 3/4 with the Co_4I_3 pseudo-plane almost parallel to

TABLE 2. AVERAGED BOND DISTANCES AND ANGLES IN $[Co_4I_3O_{18}(OH_2)_6]^{3-}$ (ANION 1) AND $[Co_4I_3O_{16}(OH)_2(OH_2)_6]^{1-}$ (ANION 2)
(Estimated standard deviation is given in parentheses)

a) Bond distances l/Å

Atoms	$[Co_4I_3O_{18}(OH_2)_6]^{3-}$		$[Co_4I_3O_{16}(OH)_2(OH_2)_6]^{1-}$	
	Averaged distance	Distribution	Averaged distance	Distribution
Co*-Co	2.835(1)	2.820—2.843	2.837(1)	2.834—2.834
Co*-I	3.011(1)	3.010—3.014	2.998(1)	2.995—3.005
Co-I	2.927(1)	2.913—2.940	2.921(1)	2.915—2.925
Co*-O_c	1.905(4)	1.897—1.916	1.909(4)	1.896—1.922
Co-O_c	1.887(4)	1.882—1.890	1.894(4)	1.883—1.900
I-O_c	2.038(4)	2.026—2.053	2.034(4)	2.002—2.056
Co-O_b	1.891(4)	1.873—1.908	1.890(4)	1.868—1.913
I-O_b	1.888(4)	1.880—1.900	1.882(4)	1.857—1.902
Co-O_t	1.942(5)	1.935—1.947	1.930(5)	1.912—1.944
I-O_t	1.808(5)	1.796—1.824	1.789(5)	1.783—1.794
I-OH	—	—	1.885(5)	1.885

b) Bond angles ϕ/° ("anti" means two O atoms transverse to Co_4I_3 plane; "syn" means two on the same side)

Atoms	$[Co_4I_3O_{18}(OH_2)_6]^{3-}$		$[Co_4I_3O_{16}(OH)_2(OH_2)_6]^{1-}$	
	Averaged angle	Distribution	Averaged angle	Distribution
Co-Co*-I	60.0(1)	59.9—60.2	60.0(1)	59.8—60.2
Co-I-Co	114.0(1)	113.9—114.3	114.5(1)	114.4—114.6
I-Co-I	126.0(1)	125.6—126.6	125.5(1)	125.1—125.6
O_c-Co*-O_c (anti)	83.2(2)	82.3—84.5	83.6(2)	83.0—85.1
O_c-Co*-O_c (syn)	96.8(2)	96.0—97.6	96.4(2)	95.8—97.0
O_c-Co-O_c (anti)	83.7(2)	83.4—84.1	83.9(2)	83.6—84.5
O_c-I-O_c (anti)	77.2(2)	76.8—77.3	77.9(2)	77.1—78.4
O_b-Co-O_b (anti)	175.1(2)	174.3—175.5	175.3(2)	174.7—176.3
O_b-I-O_b (anti)	165.2(2)	164.9—165.3	166.1(2)	163.7—167.2
O_t-Co-O_t (anti)	92.5(2)	91.6—94.3	92.6(2)	92.0—93.7
O_t-I-O_t (anti)	99.4(2)	99.2—99.6	100.9(2)	100.9
O_t-I-OH (anti)	—	—	94.5(2)	94.5

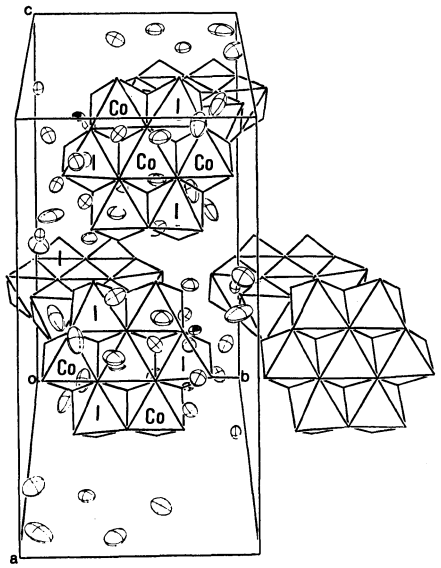

Fig. 2. Crystal structure viewed from the a*-axis. The shaded ellipsoids represent Na^+ ions and other ellipsoids are water molecules of crystallizations. Anions are shown with polyhedral models. The almost regular hexagonal shaped anions are the anion 1 and other are the anion 2.

the (001) plane. The second one, anion 2, contains two more protons and is on the diad axis at $x=1/2$, $z=1/4$ or 3/4 and almost parallel to the (100) plane. In Table 1, Co*(a1) and Co*(a2) mean the central Co atoms of anions 1 and 2 respectively and M(i), where M=Co or I, belongs to anion 1 for $1\leq i\leq 4$ and to anion 2 for $5\leq i\leq 8$.

Sodium Cation. The Na^+ ions do not interact with the polyanions directly. The Na^+ ion is coordinated by six water molecules of crystallization and forms an almost regular octahedral $[Na(OH_2)_6]^+$ ion, as is shown in Fig. 3. The distances of Na–O are 2.28—2.40(2) Å.

Anion-Anion Hydrogen Bond. As can be seen in Fig. 2, anion 1 is very close to its neighbour translated along the b-axis. Anion 2 is also in the same situation. This is because the O_t atoms of Co are aqua ligands, while those of I are oxygen atoms and inter-anionic hydrogen bonds are formed among them. As a result, 2 anions form a two-dimensional network (denoted 2D-net hereafter) parallel to the (100) plane shown in Fig. 4. These 2D-nets stack along the a-axis and the 1 anions link two 2D-nets with hydrogen bonds (Fig. 5). These inter-anionic hydrogen bonds are summarized in Table 3.

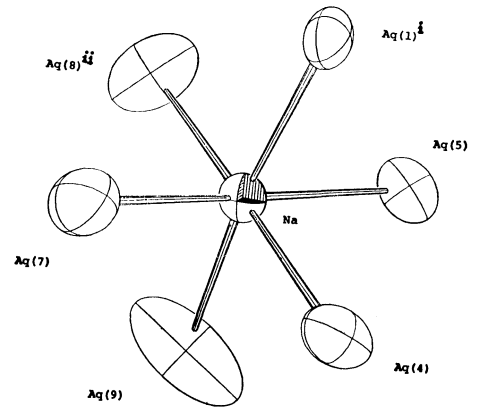

Fig. 3. The structure of the $[Na(OH_2)_6]^+$ cation.
Superscripts represent symmetry operations (i: $-x$, y, $1/2-z$; ii: x, $1-y$, $1/2+z$).

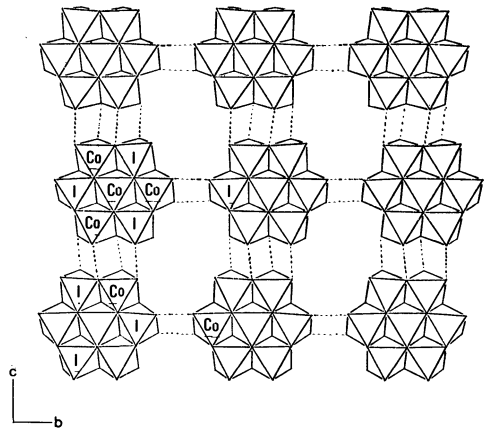

Fig. 4. The two-dimensional network (2D-net) of the anion 2 viewed from the a*-axis.
Dashed lines are inter-anionic hydrogen bonds.

TABLE 3. INTER-ANIONIC HYDROGEN BONDS

	H-donor	H-acceptor	Distance(l/Å)
Anion 1—Anion 1	O_t(4)	O_t(1)^i	2.548(7)
Anion 1—Anion 2	O_t(2a)	O_b(67)	2.709(6)
	O_t(2b)	O_c(78)	2.839(6)
	O_t(7b)	O_b(23)	2.610(6)
	O_t(8)	O_t(3b)	2.625(7)
Anion 2—Anion 2	O_t(6a)	O_b(67)^{ii}	2.758(6)
	O_t(6b)	O_t(7a)^{ii}	2.626(7)
	O_t(8)	O_t(5)^i	2.565(7)

i: x, $-1+y$, z
ii: $1-x$, $1-y$, $1-z$

Protonation of the Anions. One of the terminal oxygen atoms of I(7) in anion 2 is protonated. This oxygen, O_t(7b) is very close to O_b(23), a bridging oxygen atoms of the anion 1, with the distance of 2.61(1) Å. This short distance indicates that there is a strong hydrogen bond between O_t(7b) and O_b(23). Moreover, the I(7)–O_t(7b) distance is 1.885(5) Å, which agrees with the I–OH length, 1.89(2) Å, in H_5IO_6.[13] This value is significantly larger than the other I–O_t distances, 1.783—1.824(5) Å, in the anions

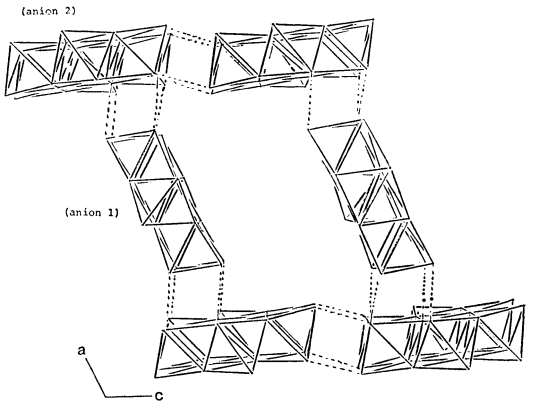

Fig. 5. Stacking scheme of the 2D-nets viewed from the b-axis.
The anion 1 acts as a girder between two 2D-nets.
Dashed lines represent inter-anionic hydrogen bonds.

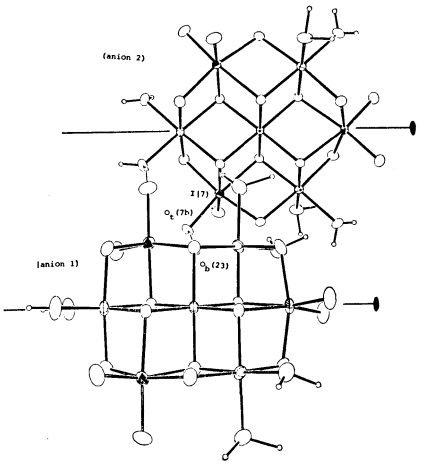

Fig. 6. Interaction of anions 1 and 2.
The protonated atom of anion 2 and the related atoms are shown. Small circles are hydrogen atoms included in the structure refinement. Fine lines are inter-anionic hydrogen bonds.

1 and 2. The minimum I–O_t length, 1.783(8) Å, is found in I(7)–O_t(7a), where O_t(7a) is the geminate O_t atom of O_t(7b). This short I(7)–O_t(7a) distance must be caused by the loose I(7)–O (7b) bond. In the difference Fourier maps, there is a peak with the height of ≈ 0.7 e/Å^3 at about 0.9 Å from O_t(7b) toward O_b(32). From these facts, we have concluded that O_t(7b) has a proton. There is no evidence for further protonation to the both polyanions. The anion 2 has a crystallographic 2-fold axis, so anion 2 is doubly protonated and should be formulated as $[Co_4I_3O_{16}(OH)_2(OH_2)_6]^{1-}$, while anion 1 is written as $[Co_4I_3O_{18}(OH_2)_6]^{3-}$. Figure 6 shows the interactions between anions 1 and 2. It has been reported that the acid is tri-basic, with virtually identical pK's (≈ 1.5).[14] Equilibrium calculations show that at the pH of 1.5, the concentrations of the four species: H_3X, H_2X^-, HX^{2-}, and X^{3-} ($X=Co_4I_3O_{18}(OH_2)_6^{3-}$) are equal in the solution.

The formation of the present crystals can be understood as the coprecipitation of H_2X^- and X^{3-}

anions; the one proton not found in this study must be present as an oxonium ion.

It is noteworthy that anion 2 is protonated at a terminal oxygen atom. There are several polyanions known to be protonated, but in most cases, the protonated sites are doubly or triply coordinated oxygen atoms, *e.g.* $[CrMo_6O_{24}H_6]^{3-}$.[7] The only exception is $[Mo_8O_{28}H_2]^{6-}$ anion, which has protonated terminal oxygen atoms.[15]

The bond distances and angles of the polyanions, except for the protonated sites, are the same as those of the Li salt determined by Lebioda, Ciechanowicz-Rutkowska, Baker, and Grochowski (1980).[16]

The authors thank Professor L. C. W. Baker for sending us his structure of the Li salt of the (tetracobaltato)triperiodate prior to the publication.

References

1) M. W. Lister, *Can. J. Chem.*, **39**, 2330 (1961).
2) Y. Yoshino, T. Takeuchi, and H. Kinoshita, *Nippon Kagaku Zasshi*, **86**, 978 (1965).
3) L. Malaprade, *Bull. Soc. Chim. Fr.*, **6**, 223 (1939).
4) T. Ama, J. Hidaka, and Y. Shimura, *Bull. Chem. Soc. Jpn.*, **46**, 2145 (1973).
5) H. T. Evans, Jr., *Acta Crystallogr., Sect. B*, **30**, 2095 (1974).
6) H. Kondo, A. Kobayashi, and Y. Sasaki, *Acta Crystallogr., Sect. B*, **36**, 661 (1980).
7) A. Perloff, *Inorg. Chem.*, **9**, 2228 (1970).
8) O. Nagano, Dissertation Thesis, The University of Tokyo, Tokyo, 1979.
9) J. M. Williams, and C. J. Nyman, *Inorg. Synth.*, **9**, 142 (1967).
10) "International Tables for X-Ray Crystallography," Kynoch Press, Birmingham (1974), Vol. IV.
11) T. Sakurai, UNICS, The Universal Crystallographic Program System (1967).
12) X. Solans, C. Miravittles, C. Germain, and J. P. Declercq, *Acta Crystallogr., Sect. B*, **35**, 2181 (1979).
13) Y. D. Feikema, *Acta Crystallogr.*, **20**, 765 (1966).
14) L. C. W. Baker, L. Lebioda, J. Grochowski, and H. G. Mukherjee, *J. Am. Chem. Soc.*, **102**, 3274 (1980).
15) M. Isobe, F. Marumo, T. Yamase, and T. Ikawa, *Acta Crystallogr., Sect. B*, **34**, 2728 (1978).
16) L. Lebioda, M. Ciechanowicz-Rutkowska, L. C. W. Baker, and J. Grochowski, *Acta Crystallogr., Sect. B*, **36**, 2530 (1980).
17) C. K. Johnson, ORTEP Report of ORNL-3794, Oak Ridge National Laboratory, Oak Ridge, Tennessee, 1965.

Ion-pair Extraction of Nickel(II) and Copper(II) Complexes of 8-Hydroxy-7-nitroso-5-quinolinesulfonic Acid with Zephiramine

Toyoko OZAKI

Department of Chemistry, Faculty of Science, Kyoto University, Sakyo-ku, Kyoto 606

(Received December 7, 1981)

The ion-pair extraction of nickel(II) and copper(II) complexes of 8-hydroxy-7-nitroso-5-quinolinesulfonic acid (H_2NQS) with zephiramine(benzyldimethyltetradecylammonium chloride) was studied. It was found that slope analysis can be used to determine the mechanism of these ion-pair extraction systems, as well as the continuous-variation method for three component systems or the mole-ratio method by choosing appropriate extraction conditions. As a result, the equation of these extraction equilibria can be represented as:

$$M^{2+} + 2HNQS^- + 2ZCl_{(o)} \rightleftharpoons M(NQS)_2Z_{2(o)} + 2H^+ + 2Cl^-$$

The extraction constants and the exchange constants were calculated.

As has previously been stated,[1] the author has applied 8-hydroxy-7-nitroso-5-quinolinesulfonic acid (H_2NQS) as a chelating reagent to the solvent extraction of the ternary complex, which is an ion-pair of water-soluble metal chelate with zephiramine (benzyldimethyltetradecylammonium chloride), in order to develop a sensitive colorimetric method for determining cobalt(II) and iron(II).

Since this reagent forms stable complexes with many other bivalent metal ions, in the present study it was applied to the solvent extraction of nickel(II) and copper(II). Subsequently, the compositions of extracted species were investigated. As a rule, the mechanism of ion-pair extraction is very complicated, as it includes a greater number of related chemical species than that of chelate extraction. For example, Kambara *et al.*[2,3] have presented a continuous-variation method for three components or a mole-ratio method to analyze the compositions of extracted species in the ion-pair extraction system. The compositions of ternary complexes of metal(Ni(II) and Cu(II)), 8-hydroxy-5-quinolinesulfonic acid (H_2QS) and zephiramine (ZCl) were reported by them to be $Ni(QS)_2(HQS)Z_3$ ($\lambda_{max}=400$ nm, $\varepsilon=1.35\times10^4$) and $Cu(QSZ)_3$ ($\lambda_{max}=410$ nm, $\varepsilon=9.45\times10^3$).

The present author has been attempted to apply a simple slope analysis, which is usually used in a chelate extraction system, to determine the compositions of extracted species in this extraction system. As a result, it could be seen that the slope analysis as well as the mole-ratio method can be successfully used for the ion-pair extraction system by choosing appropriate extraction conditions. The composition of the extracted species in this extraction system was confirmed to be 1:2:2 (M:H_2NQS:Z) for both the ternary complexes of nickel(II) and copper(II), differrent from the 1:1 complex synthesized in the auqeous phase by Aly *et al.*[4] In addition, the extraction constant of the complexes and the exchange constant between NQS and Cl^- were calculated from the distribution ratios in order to understand the extraction equilibria quantitatively.

Experimental

Reagents. Stock solutions of nickel(II) and Copper (II) (1000 ppm each) were prepared by dissolving weighed amounts of nickel sulfate and copper sulfate in water distilled and subsequentry standardized atomic absorptionmetrically, and diluted with distilled water as required.

The buffer solutions used were mixtures of a 0.2 M (1 M = 1 mol dm^{-3}) solution of sodium acetate and acetic acid for measurement at pH 3.9, and that of a 0.2 M solution of sodium borate and boric acid for measurement at pH 8.9. The ionic strength of the aqueous solutions used was kept at 0.1 with sodium sulfate and a small amount of buffer solutions, such as acetate and borate buffers. For low pH ranges, the ionic strength of the aqueous solutions was kept at 0.1 with mixtures of sodium sulfate, sulfuric acid, and sodium acetate.

All the other chemicals and apparatus used were essentially the same as those described earlier.[1]

Extraction Procedure. Ten ml of a buffered solution containing an appropriate amount of H_2NQS and nickel(II) or copper(II) was shaken with an equal volume of a chloroform solution of zephiramine. The pH value of the aqueous phase after extraction was taken as the equilibrium pH value. After a 3-min centrifugation(2000 min^{-1}), the phases were separated. The aqueous phase was immediately analyzed by atomic-absorption spectrophotometry, while the organic phase was analyzed after back-extraction into dilute hydrochloric acid.

Results and Discussion

Optimum Conditions for Extraction. The effect of the pH and the shaking time on the extraction percentage of Ni(II)–NQS and Cu(II)–NQS complexes with zephiramine were examined. Figure 1 shows that nickel and copper were quantitatively extracted in the pH ranges of 4.0—11.0 and 3.5—5.5 respectively.

A shaking time of 5 min was sufficient to establish equilibrium in all the systems.

Extraction Exchange Constant of H_2NQS Species. Since the values of the acid dissociation constants of H_2NQS are given as $pK_{a_1}<1$ and $pK_{a_2}=5.55$,[1] the dianion NQS^{2-} is the predominant H_2NQS species above pH 6.5, and the monoanion $HNQS^-$, below pH 4.5. These species are also extracted into the organic phase with zephiramine.

The equations of the extraction equilibria of H_2NQS with zephiramine can be represented as follows for both the cases:

at pH 3.9

$$HNQS^- + ZCl_{(o)} \rightleftharpoons HNQSZ_{(o)} + Cl^-, \quad (1)$$

at pH 8.9

$$NQS^{2-} + 2ZCl_{(o)} \rightleftharpoons NQSZ_{2(o)} + 2Cl^-. \quad (2)$$

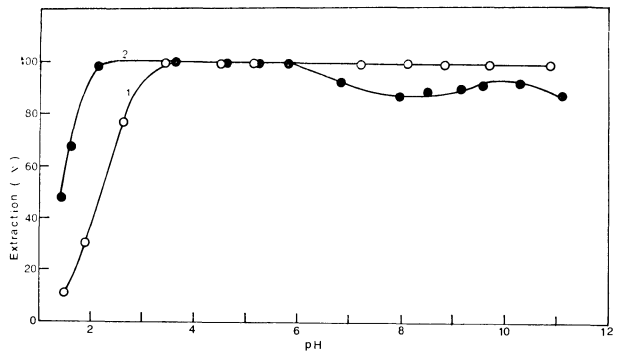

Fig. 1. The dependence of percentage extraction of nickel(II) and copper(II) complexes on the pH of the aqueous phase.
[NQS]=3.16×10^{-4} M, [ZCl]=10^{-3} M. 1: [Ni]=3.40×10^{-5} M, 2: [Cu]=3.15×10^{-5} M.

The extraction exchange constants of H_2NQS and Cl^- are given by:

$$K_{HNQS^-}^{Cl^-} = \frac{[HNQSZ]_o[Cl^-]}{[HNQS^-][ZCl]_o}, \quad (3)$$

$$K_{NQS^{2-}}^{Cl^-} = \frac{[NQSZ_2]_o[Cl^-]^2}{[NQS^{2-}][ZCl]_o^2}. \quad (4)$$

By taking logarithms of Eqs. 3 and 4, the following expression is derived:

$$\log\frac{[HNQSZ]_o}{[HNQS^-]} = \log K_{HNQS^-}^{Cl^-} - \log\frac{[Cl^-]}{[ZCl]_o}, \quad (5)$$

$$\log\frac{[NQSZ_2]_o}{[NQS^{2-}]} = \log K_{NQS^{2-}}^{Cl^-} - 2\log\frac{[Cl^-]}{[ZCl]_o}. \quad (6)$$

The total concentration of zephiramine is considered to be almost the same as that of $[ZCl]_o$ when the concentration of zephiramine far exceeds that of the reagent. The plots of $\log[HNQSZ]_o/[HNQS^-]$ *vs.* $\log[Cl^-]/[ZCl]_o$ at pH 3.9 and of $\log[NQSZ_2]_o/[NQS^{2-}]$ *vs.* $\log[Cl^-]/[ZCl]_o$ at pH 8.9 are shown in Fig. 2. The plots exhibited curves of slope −1 and slope −2 respectively, indicating that the theoretical extraction equilibria were actually established. The extraction exchange constants, as calculated from the ordinate intercept of plots in Fig. 2, are given in Table 1. Considering the values of the extraction exchange constants, it can be assumed that the reagent remains quantitatively in an aqueous phase when the concentrations of chloride are more than 10^3 and 10^2 times that of zephiramine at pH 3.9 and pH 8.9 respectively.

The Compositions of Ion-pairs of Metal–NQS Complexes with Zephiramine. The mole-ratio method and the continuous-variation method are generally used for determining the composition of an extracted ion-pair. However, it is not adequate to apply these methods to determining the ratio of zephiramine to metal when the formation constant of the ion-pair is significantly small, because they occasionally give results in which the apparent number of zephiramine related to metal is much greater than the actual one. Kambara *et al.* have presented a continuous-variation method for three-component systems with a trianglar coordinate to avoid the above-mentioned complication. The present auther has been attempted to apply a slope analysis, which is usually used in a chelate-extraction system, to settle the problem. At pH 3.9, the metal ion, M^{2+}, is extracted into chloroform by forming a water-soluble complex anion with n number of $HNQS^-$ and by subsequently aggregating with m number of zephiramine, which is necessary to maintain electrical neutrality in the organic phase.

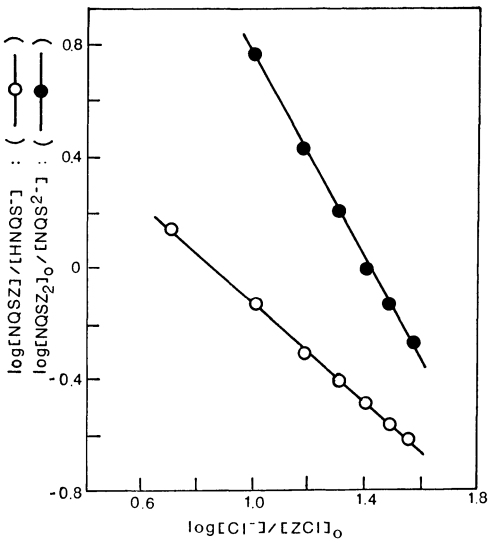

Fig. 2. Relationship between the distribution ratio of 8-hydroxy-7-nitroso-5-quinolinesulfonic acid and log $[Cl^-]/[ZCl]_o$.
[NQS]=7.9×10^{-5} M, [ZCl]=10^{-3} M.

For this extraction system, the equation can be written as:

$$M^{2+} + nHNQS^- + mZCl_{(o)} \rightleftharpoons M(NQS)_nZ_{m(o)} + mCl^- + nH^+, \quad (7)$$

where the extraction constant is given by:

$$K_{ex} = \frac{[M(NQS)_nZ_m]_o[Cl^-]^m[H^+]^n}{[M^{2+}][HNQS^-]^n[ZCl]_o^m}. \quad (8)$$

The total concentrations of NQS and zephiramine can be expressed as Eqs. 9 and 10:

$$[NQS]_{total} = [HNQS^-] + [HNQSZ]_o + n[M(NQS)_nZ_m]_o, \quad (9)$$

$$[Z]_{total} = [ZCl]_o + [HNQSZ]_o + m[M(NQS)_nZ_m]_o. \quad (10)$$

The distribution ratio of metal between the two phases is given as:

$$D = \frac{[M(NQS)_nZ_m]_o}{[M^{2+}]}. \quad (11)$$

By introducing Eq. 11 to Eq. 8, the following expression is derived:

$$\log D = \log K_{ex} + n\mathrm{pH} + m\log\frac{[ZCl]_o}{[Cl^-]} + n\log[HNQS^-]. \quad (12)$$

The ratio of metal to zephiramine is obtained as follows. When the concentration of both NQS and zephiramine are sufficiently excessive against that of the metal ion, the third term of Eqs. 9 and 10 can be omitted. When the amount of chloride ions present is more than 70 times that of zephiramine, the second terms of Eqs. 9 and 10 become negligible,

because $K^{Cl^-}_{HNQS^-}$ is given as 7.08 by Eq. 3. Under these conditions, $[HNQS^-]$ and $[ZCl]_0$ can be regarded as $[NQS]_{total}$ and $[Z]_{total}$ respectively.

Therefore, Eq. 12 can be rewritten as 13 when $[Cl^-]_{total} > [Z]_{total} \approx [NQS]_{total} \gg [M]_{total}$:

$$\log D = \log K_{ex} + n\mathrm{pH} + m\log\frac{[Z]_{total}}{[Cl^-]} + n\log[NQS]_{total}. \quad (13)$$

This equation represents the plot of $\log D$ *vs.* $\log[Z]_{total}/[Cl^-]$, with a slope corresponding to the ratio of metal to zephiramine under the conditions of a constant pH and a constant NQS concentration. The plots of $\log D$ *vs.* $\log[Z]_{total}/[Cl^-]$ for nickel(II) and copper(II) are shown in Fig. 3. As is evident from Fig. 3, the plots gave linear curves with a slope of 2 for nickel(II) and copper(II) in the anticipated ranges. This result indicates that the ratio of metal to zephiramine is 1:2 in each system.

Similarly, the ratio of metal to NQS is obtained as follows. By introducing Eq. 3 to Eq. 12, the following expression is derived:

$$\log D = \log K_{ex} - m\log K^{Cl^-}_{HNQS^-} + n\mathrm{pH} + m\log[HNQSZ]_0 + (m-n)\log[HNQS^-]. \quad (14)$$

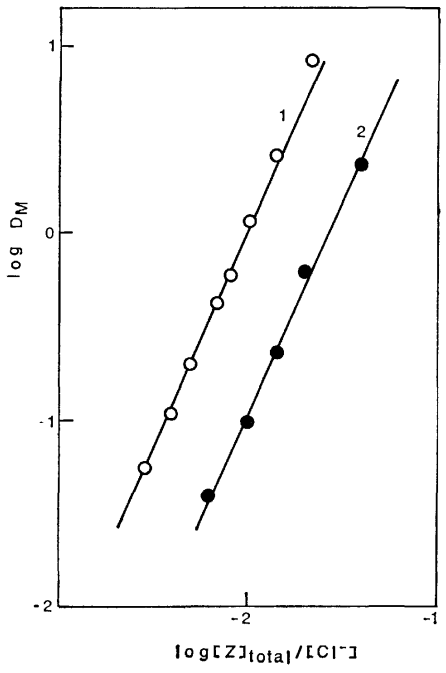

Fig. 3. Relationship between $\log D_M$ and $\log[Z]_{total}/[Cl^-]$.
$[NQS]=6.32\times10^{-4}$ M, $[ZCl]_{total}=10^{-3}$ M, pH=3.9.
1: $[Ni]=3.40\times10^{-5}$ M, 2: $[Cu]=3.15\times10^{-5}$ M.

As the terms of $[HNQS^-]$ and $[M(NQS)_nZ_m]_0$ in Eq. 9 can be neglected when the concentration of a ligand is sufficiently in excess against that of the metal ion and when moreover, the concentration of zephiramine exceeds that of the ligand, namely, $[Z]_{total} > [NQS]_{total} \gg [M]_{total}$, $[HNQSZ]_0$ can be regarded as $[NQS]_{total}$. Considering the electrical neutrality of the ion-pair, the numbers of zephiramine and ligand seem to coincide in this system.

Then, supposing $m=n$, Eq. 14 can be rewritten as follows:

$$\log D = \log K_{ex} - m\log K^{Cl^-}_{HNQS^-} + n\mathrm{pH} + m\log[NQS]_{total}. \quad (15)$$

This equation means that a plot of $\log D$ *vs.* pH gives a slope corresponding to the ratio of metal to the $HNQS^-$ of the extracted complex. The plots of $\log D$ *vs.* pH for nickel(II) and copper(II) at pH 3.9 are shown in Fig. 4. The fact that these plots give curves with a slope of 2 for both the metals indicates an M:NQS ratio of 1:2 in this extraction system. These results agree well with those obtained by the mole-ratio method, and in combination with the results presented above, they indicate that the composition of extracted complexes in the presence of zephiramine is M:NQS:Z=1:2:2. The composition of the precipitated complexes in the aqueous phase,

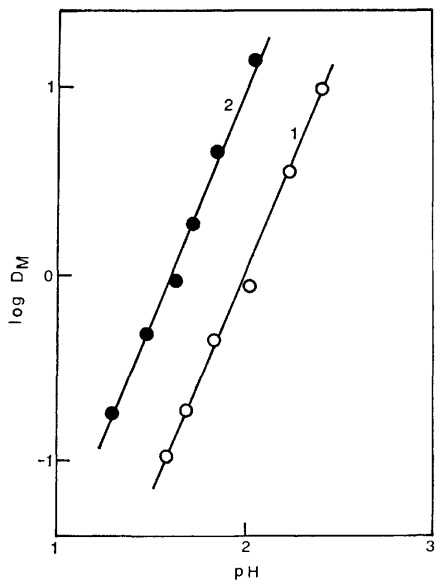

Fig. 4. Relationship between $\log D_M$ and pH.
$[NQS]=1.58\times10^{-3}$ M, $[ZCl]_{total}=10^{-2}$ M. 1: [Ni] $=3.40\times10^{-5}$ M, 2: $[Cu]=3.15\times10^{-5}$ M.

Table 1. Exchange-equilibrium constants and extraction constants for 8-hydroxy-7-nitroso-5-quinolinesulfonic acid(H_2NQS) and its metal complexes (Z; Zephiramine)

	λ_{max} / nm	Molar absorptivity / $1\,mol^{-1}\,cm^{-1}$	$\log K^{mCl^-}_{A^{m-}}$	$\log K_{ex}$
HNQS	390	2.9×10^3	0.85	—
$NQSZ_2$	440	5.3×10^3	1.42	—
$Ni(NQS)_2Z_2$	460	2.6×10^4	4.14	3.40
$Cu(NQS)_2Z_2$	455	2.5×10^4	3.16	4.10

however, was reported to be M:NQS=1:1 on the basis of the results of the IR spectra and elemental analysis, according to Aly *et al.*[4] Noriki *et al.*[5] have stated that zephiramine has the effect of changing a coordination-unsaturated chelate to an extractable coordination-saturated chelate by accelerating the replacement of water molecules with ligands in the case of magnesium oxinate. It can, therefore, be presumed that zephiramine has a similar effect in the case of NQS complexes.

The absorption maxima, the molar absorptivities, and the exchange-equilibrium constants of the extracted ion-pair complexes are listed in Table 1.

The author wishes to express her deep gratitude to Professor Taitiro Fujinaga, Assistant Professor Tooru Kuwamoto, Dr. Eiichiro Nakayama, and Dr. Etsu Yamada, all of Kyoto University, for their unfailing guidance through the course of this work. Almost all of this work has been done at the Instrumental Analysis Research Center, Kyoto University; the author is grateful to Professor Hiroyuki Hatano, the head of the Center, for his permission to use the facilities.

References

1) T. Ozaki, *Anal. Lett.*, submitted for publication.
2) T. Kambara, M. Sugawara, and K. Hasebe, *Bunseki Kagaku*, **19**, 1239 (1970).
3) T. Kambara, M. Maeyama, and K. Hasebe, *Bunseki Kagaku*, **20**, 1249 (1971).
4) M. M. Aly, M. Makhyoun, and S. El-Ezaby, *J. Inorg. Nucl. Chem.*, **35**, 2727 (1973).
5) S. Noriki and M. Nishimura, *Anal. Chim. Acta*, **76**, 215 (1975).

Binuclear Metal Complexes. XLV.[1] Synthesis and Magnetic, Spectral, and Electrochemical Studies of Strati-bis Copper(II) Complexes of Some Schiff Bases Derived from Primary Tetraamines and Salicylaldehydes

Tatsuo Izumitani, Masaaki Nakamura, Hisashi Ōkawa,* and Sigeo Kida
Department of Chemistry, Faculty of Science, Kyushu University 33, Hakozaki, Higashi-ku, Fukuoka 812

(Received December 8, 1981)

New Schiff base ligands, 1,2,3,4-tetrakis(R-salicylideneamino)-2,3-dimethylbutane (abbreviated as H_4(R-sata); R (substituent on the ring)=H, 5-Me, 5-Bu^t) and 1,2-bis(R-salicylideneamino)-1,2-bis(salicylideneaminomethyl)cyclohexane (H_4(R-sacta)), which are capable of forming "strati-bis" type binuclear copper(II) complexes, have been synthesized. Magnetic, spectral and electrochemical properties of the binuclear copper(II) complexes, Cu_2(R-sata) and Cu_2(R-sacta), were investigated in comparison with those of mononuclear copper (II) complexes Cu(R-salpn) and Cu(R-sacda), where H_2(R-salpn) is *N,N'*-bis(R-salicylidene)-1,2-propanediamine and H_2(R-sacda) 1-(R-salicylideneamino)-1-(R-salicylideneaminomethyl)cyclohexane. ESR spectra of Cu_2(sata), Cu_2(sacta) and Cu_2(5-Me-sacta) showed a seven-lined hyperfine structure whose hyperfine coupling constant ($A_\parallel \approx 85$ G, 1 G$=10^{-4}$ T) was about one half of that of the corresponding mononuclear copper(II) complex. Each electronic spectrum of these binuclear complexes showed the π-π^* transition originated from the azomethine group at a low frequency compared with that of the corresponding mononuclear complex. Cyclic voltammograms of these three complexes involved two redox couples. The first redox couple attributable to the Cu(II, II)/Cu(II,I) process is higher in potential than the Cu(II)/Cu(I) process of the corresponding mononuclear complex. These characteristics were discussed in terms of the electron-delocalization through the π-π interaction between the two [CuN_2O_2]-chromophores.

Recently, much attention has been devoted to electrochemical investigations of copper complexes in which two metal ions are bound in close proximity, in the hope to clarify the redox function of copper proteins.[2-6] Reduction of binuclear copper(II) complexes into the corresponding copper(I) complexes occurs *via* two monoelectronic steps[2,5] or one dielectronic step.[3,4,6] In most of these complexes two equatorial planes of the metal ions are linked so as to be coplanar with oxygen-bridges[2-5] and there are very few electrochemical investigations on binuclear copper(II) complexes whose coordination planes face to each other.

In the preliminary report[7] we have suggested that the binuclear copper(II) complex, Cu_2(sata) (H_4(sata) denotes 1,2,3,4-tetrakis(salicylideneamino)-2,3-dimethylbutane), takes a unique configuration in which two CuN_2O_2 planes are stacked in a face-to-face manner. In this study we have prepared the binuclear copper (II) complexes, Cu_2(R-sata) (R=5-Me, 5-Bu^t), which are the homologs of Cu_2(sata) containing methyl or *t*-butyl group at the 5-position of the aromatic ring. We have also prepared the copper(II) complexes, Cu_2(R-sacta), where H_4(R-sacta) denotes 1,2-bis(R-salicylideneamino)-1,2-bis(R-salicylideneaminomethyl)-cyclohexane. Magnetic, spectral and electrochemical properties of Cu_2(R-sata) and Cu_2(R-sacta) were investigated in comparison with those of the mononuclear copper(II) complexes, Cu(R-salpn) and Cu-(R-sacda) (H_2(R-salpn)=*N,N'*-bis(R-salicylidene)-1,2-propanediamine; H_2(R-sacda)=1-(R-salicylideneamino)-1-(R-salicylideneaminomethyl)cyclohexane), respectively, in the hope to elucidate the characteristics of the binuclear copper(II) complexes stacked in the face-to-face manner.

Experimental

Syntheses. 1-Aminomethyl-1-cyclohexanamine was prepared by the method in the literature.[8] Synthesis of Cu(R-salpn) (R=H, 5-Me, 5-Bu^t) was carried out by the method of Holm.[9]

2,3-Dicyano-2,3-butanediamine. A solution of 2,3-dicyano-2,3-butanediol[10] (40 g) in methanol (300 cm^3) was chilled by means of ice-water and to this was introduced a stream of dry ammonia. After the mixture was allowed to stand overnight, the solvent and ammonia were evaporated to give 2,3-dicyano-2,3-butanediamine as white crystals. They were recrystallized from ethanol as colorless needles melting at 138—141 °C. The yield was *ca.* 15 g.

Found: C, 52.25; H, 7.42; N, 40.23%. Calcd for $C_6H_{10}N_4$: C, 52.16; H, 7.30; N, 40.55%.

1,2-Dicyano-1,2-cyclohexanediamine. This was prepared by the reaction of 1,2-dicyano-1,2-cyclohexanediol[10] and ammonia in the same way as described above. It forms colorless needles melting at 169—171 °C. The yield was *ca.* 30%.

Found: C, 58.49; H, 7.42; N, 33.93%. Calcd for $C_8H_{12}N_4$: C, 58.52; H, 7.37; N, 34.12%.

2,3-Dimethyl-1,2,3,4-butanetetramine. A suspension of $LiAlH_4$ (25 g) in dry dioxane (500 cm^3) was stirred at 70 °C, and to this was added dropwise a solution of 2,3-dicyano-2,3-butanediamine (15 g) in dry dioxane (200 cm^3) and the mixture was refluxed for three hours. The reaction mixture was cooled by ice-water and decomposed by the addition of 50 cm^3 of water and then 50 cm^3 of a 15% sodium hydroxide solution. Inorganic substances that precipitated were filtered and washed with three 50 cm^3 portions of dioxane. The filtrate and the washings were combined and to this was added hydrobromic acid (60%, 20 cm^3). On evaporating the solvent there remained 2,3-dimethyl-1,2,3,4-butanetetramine tetrahydrobromide as a yellow mass. It was dissolved in water (10 cm^3) and to this solution was added potassium hydroxide (pellets 20 g). The free tetramine thus liberated was extracted with three 100 cm^3 portions of ether, and the combined ethereal solution was dried with KOH. Evaporation of the solvent left 2,3-dimethyl-1,2,3,4-butanetetramine as pale yellow, oily substance (3 g). It was used for preparation of complexes without further puri-

Table 1. Elemental analyses of Cu_2(R-sata), Cu_2(R-sacta), and Cu(R-sacda)

	Found(%)				Calcd(%)			
	C	H	N	Cu	C	H	N	Cu
Cu_2(sata)·$5/2H_2O$	55.70	4.61	7.54	17.52	55.88	4.83	7.67	17.39
Cu_2(5-Me-sata)·$1/2$EtOH	61.18	5.73	7.13	15.93	61.24	5.40	7.33	16.13
Cu_2(5-Bu^t-sata)·$2H_2O$	63.70	6.94	5.81	13.02	63.47	7.03	5.92	13.43
Cu_2(sacta)·H_2O	59.54	4.57	7.68	17.62	59.25	4.70	7.68	17.42
Cu_2(5-Me-sacta)·H_2O	61.43	5.31	7.19	16.34	61.13	5.31	7.19	16.17
Cu_2(5-Bu^t-sacta)·$3/2H_2O$	64.98	7.00	5.80	12.94	64.84	7.01	5.81	13.19
Cu(sacda)·$1/4H_2O$	62.69	5.52	6.89	16.08	62.67	5.57	6.96	15.80
Cu(5-Me-sacda)·$1/4H_2O$	64.17	6.17	6.41	15.98	64.16	6.15	6.51	16.13
Cu(5-Bu^t-sacda)·H_2O	66.27	7.86	4.99	13.02	65.94	7.63	5.30	13.43

fication.

1,2-Bis(aminomethyl)-1,2-cyclohexanediamine. This was prepared as yellow, oily substance by the reduction of 1,2-dicyano-1,2-cyclohexanediamine in a way similar to that described above.

Cu_2(R-sata) (R=H, 5-Me, 5-Bu^t). Synthetic methods for these complexes are practically the same. The methods were exemplified by that for Cu_2(sata) as follows. 2,3-Dimethyl-1,2,3,4-butanetetramine (0.5 g) and salicylaldehyde (1.7 g) were dissolved in ethanol (30 cm^3), and the mixture was heated at *ca.* 70 °C for 10 min. To this solution was added powdered copper(II) acetate monohydrate (1.4 g), and the mixture was stirred at 60 °C for 30 min and then allowed to stand in a refrigerator to give brown to dark green crystals. They were collected and recrystallized from a chloroform–ethanol mixture.

Cu_2(R-sacta) (R=H, 5-Me, 5-Bu^t). These complexes were obtained by a method similar to that of Cu_2(R-sata).

Cu(R-sacda) (R=H, 5-Me, 5-Bu^t). These complexes were prepared by the reaction of 1-aminomethyl-1-cyclohexanamine, salicylaldehyde, and copper(II) acetate monohydrate in a 1:2:1 mole ratio in ethanol.

Elemental analyses of Cu_2(R-sata), Cu_2(R-sacta), and Cu(R-sacda) are given in Table 1.

Measurements. Electronic spectra were measured in chloroform by a Shimadzu MPS-5000 spectrophotometer. Magnetic susceptibilities were measured by the Faraday method in the temperature range 80—300 K. The apparatus was calibrated by the use of $[Nien_3]S_2O_3$.[11] Effective magnetic moments were calculated by the equation, $\mu_{eff} = 2.828(\chi_A \times T)^{1/2}$, where χ_A is the magnetic susceptibility per copper atom corrected for the diamagnetism of the constituting atoms by the use of Pascal's constants.[12] ESR spectra were measured in chloroform at liquid nitrogen temperature (frozen solution) with a JES-FE3X ESR instrument. Cyclic voltammograms were recorded on a Yanagimoto P-1000 voltammetric analyzer in dichloromethane containing 0.1 M† tetrabutylammonium perchlorate as the supporting electrolyte. A three-electrode cell with a glassy carbon as the working electrode, a platinum coil as the auxiliary electrode, and a saturated calomel as the reference electrode was used for the measurements. All the potentials were corrected for liquid junction potential by the use of ferrocene as an internal standard.[13,14]

Results and Discussion

By the reaction of 2,3-dicyano-2,3-butanediol and ammonia two isomers of 2,3-dicyano-2,3-butanediamine were obtained; one is liquid and the other is solid.

† 1 M=1 mol dm^{-3}.

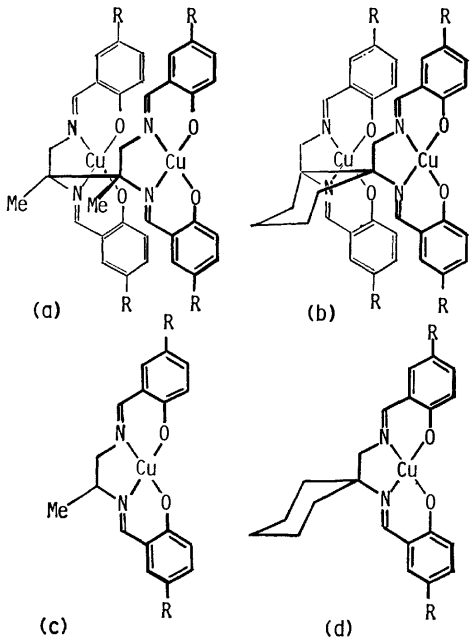

Fig. 1. Chemical structures of (a)Cu_2(R-sata), (b)Cu_2-(R-sacta), (c)Cu(R-salpn), and (d)Cu(R-sacda).

Similarly ammonolysis of 1,2-dicyano-1,2-cyclohexanediol gave two isomers (liquid and solid) of 1,2-dicyano-1,2-cyclohexanediamine. The presence of two isomers can be attributed to the fact that these diamino dinitriles are diastereomeric and exist as a mixture of *dl*- and *meso*-isomers. In this study, the solid diamino dinitriles were reduced to prepare 2,3-dimethyl-1,2,3,4-butanetetramine and 1,2-bis(aminomethyl)-1,2-cyclohexanediamine. However, we have not yet determined whether the tetramines are the *meso*- or the *dl*-isomer. In Fig. 1 the structures of Cu_2(R-sata) and Cu_2(R-sacta) of the *meso*-tetramines are shown.

The half of Cu_2(R-sata) corresponds to *N,N'*-bis(R-salicylidene)-1,2-propanediaminatocopper(II), Cu(R-salpn), which is hence adopted as the reference complex to Cu_2(R-sata). As the reference complex to Cu_2(R-sacta), we adopted the complexes Cu(R-sacda) of 1-(R-salicylideneamino)-1-(R-salicylideneaminomethyl)cyclohexane (H_2(R-sacda)), taking into account the steric characteristics of cyclohexane ring. The structures of Cu(R-salpn) and Cu(R-sacda) are also given in Fig. 1.

Table 2. Effective magnetic moments and Weiss constants of complexes

	μ_{eff}/BM(T/K)		θ/K
Cu_2(sata)	1.94(86.3)	1.87(295.6)	8
Cu_2(5-Me-sata)	1.90(87.4)	1.85(293.2)	3
Cu_2(5-Bu^t-sata)	1.86(86.9)	1.84(297.8)	≈0
Cu_2(sacta)	2.02(87.4)	1.87(296.1)	17
Cu_2(5-Me-sacta)	1.94(86.3)	1.84(295.4)	10
Cu_2(5-Bu^t-sacta)	1.88(88.5)	1.86(295.6)	≈0

Magnetic susceptibilities of Cu_2(R-sata) and Cu_2(R-sacta) were measured on solid samples in the temperature range from liquid nitrogen temperature to room temperature. The effective magnetic moments at room temperature and near liquid nitrogen temperature are given in Table 2. Magnetic moments of Cu_2(5-Bu^t-sata) and Cu_2(5-Bu^t-sacta) are almost independent of temperature. On the other hand, the moments of Cu_2(sata), Cu_2(5-Me-sata), Cu_2(sacta), and Cu_2(5-Me-sacta) increase with lowering of temperature. The χ_A *vs.* T^{-1} plotts for these complexes revealed that they obey the Curie-Weiss law, $\chi_A = C/(T-\theta)$. The Weiss constants thus determined are given in Table 2. Positive Weiss constants for Cu_2(R-sata) (R=H, 5-Me) and Cu_2(R-sacta) (R=H, 5-Me) imply the operation of an intramolecular, ferromagnetic spin-exchange interaction. This magnetic behavior resembles that of dimeric *N*,*N*′-disalicylideneethylenediaminatocopper(II), [Cu(salen)]$_2$.[15] Weiss constants for Cu_2(R-sacta) are larger than those of the corresponding Cu_2(R-sata). It is likely that two copper(II) ions are held in close distance in Cu_2(sacta) and Cu_2(5-Me-sacta) because of the steric requirement of cyclohexane ring, while two CuN_2O_2 planes of Cu_2(R-sata) can rotate about the C(2)–C(3) axis of the tetramine moiety. The temperature-independence of the magnetic moments of Cu_2(5-Bu^t-sata) and Cu_2(5-Bu^t-sacta) suggests that access of the copper(II) ions is sterically hindered by the bulky *t*-butyl group.

ESR spectra of Cu_2(R-sata) and Cu_2(R-sacta) were measured on frozen solutions in chloroform at liquid nitrogen temperature. The spectra of Cu_2(5-Me-sata), Cu_2(5-Bu^t-sata) and Cu_2(5-Bu^t-sacta) showed a tetragonal pattern with $A_\parallel \approx 190$G (1 G=1×10^{-4} T) and resemble the spectra of Cu(R-salpn) and Cu(R-sacda). This implies that metal-metal interaction is very weak in these complexes in chloroform solution. On the other hand, ESR spectra of Cu_2(sata), Cu_2(sacta), and Cu_2(5-Me-sacta) were characterized by a seven-lined hyperfine structure ($A_\parallel \approx 85$ G) centered around 3200 G. In Fig. 2 the ESR spectrum of Cu_2(sata) is shown as an example. It is evident that in these three complexes two copper(II) ions ferromagnetically couple to produce the $s=1$ ground state. The ESR spectral features of Cu_2(sata), Cu_2(sacta), and Cu_2(5-Me-sacta) resemble that of dimeric Cu(salen), which has been demonstrated to have a face-to-face structure[16] and displays a seven-lined hyperfine structure in ESR spectrum based on the $s=1$ ground state.[15]

Electronic spectra of Cu_2(R-sata) and Cu_2(R-sacta) were measured in chloroform. Electronic spectra of

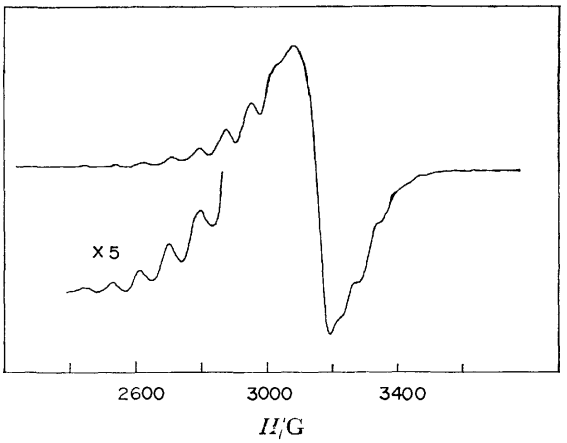

Fig. 2. ESR spectrum of Cu_2(sata) in chloroform at liquid nitrogen temperature.

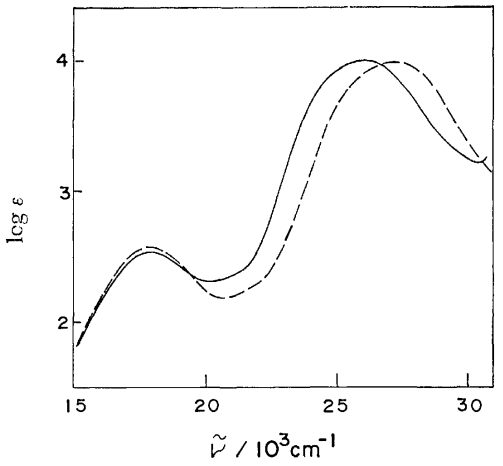

Fig. 3. Electronic spectra of (——) Cu_2(sata) and (– – –) Cu(salpn) in chloroform.

Cu_2(sata) and Cu(salpn) are given in Fig. 3. Absorption bands near 18×10^3 cm^{-1} is assigned to the d-d transition,[17–19] while the band around 26×10^3 cm^{-1} has been assigned to the π-π^* transition which involves the π-orbital functions of the azomethine group.[17,18] Table 3 includes the wavenumbers and the extinction coefficients of the d-d and the π-π^* transition bands of the binuclear complexes together with those of the mononuclear complexes as the reference. There is no substantial change in the frequency and the intensity of the d-d band between the binuclear and the corresponding mononuclear complexes. This clearly indicates that the configurations around the metal in Cu_2(R-sata) and Cu_2(R-sacta) are practically the same as those of Cu(R-salpn) and Cu(R-sacda), respectively. We presume that the configuration around the metal for Cu_2(R-sata) and Cu_2(R-sacta) is of planar, four-coordination as demonstrated for Cu(salen).[20]

The π-π^* transition frequencies of H_4(R-sata), H_4(R-sacta), H_2(R-salpn), and H_2(R-sacda) are almost the same and appear near 31×10^3 cm^{-1} (*e.g.*, 31.1×10^3 for H_4(sata), 31.0×10^3 for H_4(sacta), 31.3×10^3 for H_2(salpn), and 31.1×10^{3}cm^{-1} for H_2(sacda)). The π-π^* band shifts to lower wavenumber when the

Table 3. Absorption spectral data of complxes in chloroform ($\tilde{\nu}/10^3$ cm^{-1})

Binuclear complexes	d-d(log ε)	π-π*(log ε)	Mononuclear complexes	d-d(log ε)	π-π*(log ε)
Cu_2(sata)	17.92(358)	26.11(10400)	Cu(salpn)	17.89(389)	27.25(11100)
Cu_2(5-Me-sata)	17.61(380)	26.31(9470)	Cu(5-Me-salpn)	17.61(416)	26.18(10000)
Cu_2(5-Bu^t-sata)	17.99(305)	26.11(8970)	Cu(5-Bu^t-salpn)	17.54(421)	26.46(9520)
Cu_2(sacta)	17.73(321)	25.45(8730)	Cu(sacda)	17.67(358)	27.10(11700)
Cu_2(5-Me-sacta)	17.54(324)	25.19(8710)	Cu(5-Me-sacda)	17.79(372)	26.39(11200)
Cu_2(5-Bu^t-sacta)	17.86(288)	25.97(9120)	Cu(5-Bu^t-sacda)	17.86(389)	26.60(12000)

Table 4. Cyclic voltammetric data of complexes

Binuclear complexes	E_{pc}/V	E_{pa}/V	ΔE/mV	$E'_{1/2}$	Mononuclear complexes	E_{pc}/V	E_{pa}/V	ΔE/mV	$E'_{1/2}$
Cu_2(sata)	−1.28	−0.95	330	−1.12	Cu(salpn)	−1.36	−1.25	110	−1.31
	−1.42	−1.16	260	−1.29					
Cu_2(5-Me-sata)	−1.48	−1.36	120	−1.42	Cu(5-Me-salpn)	−1.44	−1.30	140	−1.37
Cu_2(5-Bu^t-sata)	−1.55	−1.35	200	−1.45	Cu(5-Bu^t-salpn)	−1.47	−1.35	120	−1.41
Cu_2(sacta)	−1.23	−0.94	290	−1.09	Cu(sacda)	−1.48	−1.34	140	−1.41
	−1.45	−1.34	110	−1.40					
Cu_2(5-Me-sacta)	−1.30	−0.97	290	−1.09	Cu(5-Me-sacda)	−1.49	−1.37	120	−1.43
	−1.51	−1.28	230	−1.40					
Cu_2(5-Bu^t-sacta)	−1.52	−1.28	240	−1.40	Cu(5-Bu^t-sacda)	−1.52	−1.38	160	−1.44

All potentials are corrected by the use of ferrocene as an internal standard and given in V (or mV) *vs.* NHE. Approximate redox potentials ($E'_{1/2}$) are given by the mean of E_{pc} and E_{pa}.

ligand coordinates to copper(II) ion. It is noteworthy that the band frequency for Cu_2(sata), Cu_2(sacta), and Cu_2(5-Me-sacta) are lower than those of Cu(salpn), Cu(sacda), and Cu(5-Me-sacda), respectively. The shift is more than 1,100 cm^{-1} (see Table 2). The red shift of the π-π* transition for these complexes suggests the stacking of the two CuN_2O_2 chromophores interacting through the π-bonding systems of the ligand. The π-π* transitions for Cu_2(5-Me-sata), Cu_2(5-Bu^t-sata), and Cu_2(5-Bu^t-sacta) are practically the same in wavenumber as that of the corresponding mononuclear complexes.

Electrochemical properties of Cu_2(R-sata), Cu_2(R-sacta), Cu(R-salpn), and Cu(R-sacda) were studied by means of cyclic voltammetry. Cathodic peak (E_{pc}), anodic peak (E_{pa}), peak separation (ΔE_p), and approximate redox potential ($E'_{1/2}$) given by the mean of the E_{pc} and E_{pa} are shown in Table 4. All waves observed are quasi-reversible or irreversible judging from the peak separations and the wave shapes. Each cyclic voltammogram of Cu_2(5-Me-sata), Cu_2(5-Bu^t-sata), and Cu_2(5-Bu^t-sacta) involves only one redox couple attributable to the process Cu(II,II)/Cu(I,I). Each redox potential is essentially the same as that of the corresponding mononuclear copper(II) complex. There is no interaction between the CuN_2O_2 chromophores of these complexes as demonstrated on the basis of ESR and visible spectra, and hence the two metal ions are reduced at an identical potential to copper(I) ion.

Cyclic voltammograms of Cu_2(sata), Cu_2(sacta), and Cu_2(5-Me-sacta) were characterized by two redox couples, a typical example being shown in Fig. 4. This separation is much larger than 0.036 V expected from the statistical effect.[21] The electrochemical behavior

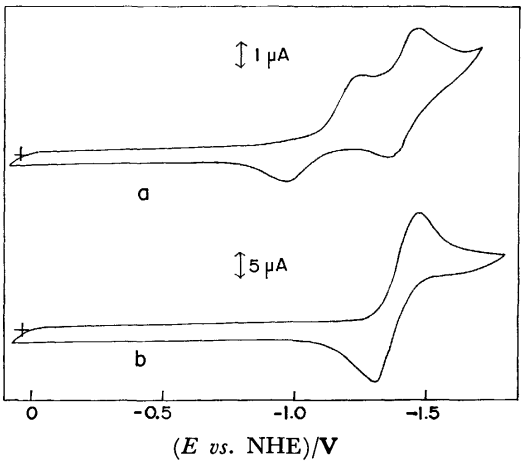

Fig. 4. Cyclic voltammograms of (a) Cu_2(sata) and (b) Cu(salpn) in dichloromethane (scan rate: 40 mV/s).

of this kind has usually been interpreted in terms of the stepwise redox-process, Cu(II,II)⇌Cu(II,I)⇌Cu(I,I).[2,5] Each of the first redox potentials for Cu_2(sata), Cu_2(sacta), and Cu_2(5-Me-sacta) is higher than that of the corresponding mononuclear complex. This may be ascribed to the stabilization of the Cu(II, I) state effected by the electron-delocalization over the molecule through the ligand π-system.

The second potential for these complexes well corresponds to the potential of the corresponding mononuclear complex. Thus, we tentatively assigned the second redox wave to the two-electron transfer from Cu(II,II) to Cu(I,I), although theoretical analysis[22] is impossible because of the irreversible process. Occurrence of the Cu(II,II)/Cu(I,I) and the Cu(II,II)/

Cu(II, I) processes is not clear at present. One plausible explanation is that an equilibrium exists between the stacked and the non-stacked forms at ambient temperature, and the latter form is reduced to the Cu(I, I) species at practically the same potential as that of the reference mononuclear complex.

The difference between the first and the second redox potentials, $E'_{1/2}$, is 0.17 V for Cu_2(sata), 0.31 V for Cu_2(sacta), and 0.26 V for Cu_2(5-Me-sacta). It is likely that the geometrical fixation of the CuN_2O_2 planes in the cases of Cu_2(sacta) and Cu_2(5-Me-sacta) owing to the cyclohexane ring brings about a considerable stabilization of the Cu(II,I) state compared with the case of Cu_2(sata), whose two chromophores can be remote from each other because of the free rotation around the C(2)–C(3) bond of the tetramine. Further, it seems that the stacking of the CuN_2O_2 planes may be sterically hindered by the substituent on the ring, since $E'_{1/2}$ decreases in the general trend R=H>5-Me>5-Bu^t and any indications of the stabilization of the Cu(II,I) state were not recognized in the cases of Cu_2(5-Bu^t-sata) and Cu_2(5-Bu^t-sacta).

The magnetic, spectral, and electrochemical characteristics found for the present complexes are particularily interesting in connection with the "dimeric bacteriochlorophyll", whose cation radical shows an ESR spectrum of a narrow line-width[23] and is reduced at a high potential compared with monomeric bacteriochlorophyll *in vitro*.[24]

References

1) Part XLIV: M. Mikuriya, H. Okawa, and S. Kida, *Bull. Chem. Soc. Jpn.*, **55**, 1086 (1982).
2) A. W. Addison, *Inorg. Nucl. Chem. Lett.*, **12**, 899 (1976).
3) D. E. Fenton, R. R. Schroeder, and R. L. Lintvedt, *J. Am. Chem. Soc.*, **100**, 1931 (1978).
4) D. E. Fenton and R. L. Lintvedt, *J. Am. Chem. Soc.*, **100**, 6367 (1978).
5) R. R. Gagne, C. A. Koval, and T. J. Smith, *J. Am. Chem. Soc.*, **99**, 8367 (1977).
6) J. P. Gisselbrecht, M. Gross, A. H. Alberts, and J. M. Lehn, *Inorg. Chem.*, **19**, 1386 (1980).
7) T. Izumitani, H. Okawa, and S. Kida, *Chem. Lett.*, **1981**, 483.
8) Fr. Hein and Schade, *Z. Anorg. Allg. Chem.*, **289**, 90 (1957).
9) R. H. Holm, *J. Am. Chem. Soc.*, **82**, 5632 (1960).
10) M. Marzadro, A. Farina, and G. Settimj, *Macrochim. Acta*, **1968**, 332.
11) N. F. Curtis, *J. Chem. Soc.*, **1961**, 3147.
12) P. W. Selwood, "Magnetochemistry," Interscience, New York(1956), pp. 78, 91.
13) R. R. Gagne, C. A. Koval, and G. C. Lisensky, *Inorg. Chem.*, **19**, 2855 (1980).
14) H. M. Koepp, H. Wendt, and H. Strehlow, *Z. Electrochem.*, **64**, 483 (1960).
15) G. O. Carlisle and W. E. Hatfield, *Inorg. Nucl. Chem. Lett.*, **6**, 633 (1970).
16) D. Hall and T. N. Waters, *J. Chem. Soc.*, **1960**, 2644.
17) R. S. Dowing and F. L. Urbach, *J. Am. Chem. Soc.*, **91**, 5977 (1969).
18) S. M. Crawford, *Spectrochim. Acta*, **19**, 255 (1963).
19) K. S. Patel and J. C. Bailar, Jr., *J. Inorg. Nucl. Chem.*, **33**, 1399 (1971).
20) E. N. Baker, D. Hall, and T. N. Waters, *J. Chem. Soc. A*, **1970**, 406.
21) F. Ammar and J. M. Saveant, *Electroanal. Chem. Interfac. Electrochem.*, **47**, 215 (1973).
22) D. S. Polcyn and I. Shain, *Anal. Chem.*, **38**, 370 (1966).
23) J. R. Norris, R. A. Uphans, H. L. Crespl, and J. J. Katz, *Proc. Natl. Acad. Sci. U.S.A.*, **68**, 625 (1971).
24) J. J. Katz and J. R. Norris, *Curr. Top. Bioenerget.*, **5**, 41 (1973).

 © 1982 The Chemical Society of Japan Bull. Chem. Soc. Jpn., 55, 2127—2130 (1982)

Pyrolytic Sulfurization Gas Chromatography. XI. An Improved Apparatus and Procedure for Practical Use

Tadashi HARA* and Fujio OKUI

Department of Chemical Engineering, Faculty of Engineering, Doshisha University, Karasuma Imadegawa, Kamigyo-ku, Kyoto 602

(Received December 10, 1981)

With the objectives of reducing the time necessary for an analysis and of improving the precision and accuracy of the analysis value, the isothermal gas-chromatographic optimum conditions were investigated and established. By the present method, the time necessary for an analysis is reduced to 25 min, from 35 min under the previous conditions, and both precision and accuracy are further improved together with an improvement of the calculation method of the calculation factors used in the calculation of the atomic ratio between C, H, O, and N. Thus many standard samples, including some liquid ones which are newly examined in this study, can be analyzed within an absolute error of about ±0.2%.

In order to establish a new elemental analysis method by which several elements can be simultaneously determined, pyrolytic sulfurization gas chromatography (PSGC) was originated[1] and has been investigated[2-9] fundamentally by the present authors to provide a simultaneous determination of the atomic ratio between C, H, O, and N in an organic compound. It has been successfully applied to an ordinaly organic compound,[1] a metal organic chelate compound,[3] a polymer,[5] and an organic halogen compound.[7,8]

The present study also intended to reduce the time necessary for an analysis and to improve both precision and accuracy of the analytical values. According to the PSGC, the reaction products from the pyrolytic sulfurization of a sample were restricted to nitrogen (N_2), carbon dioxide(CO_2), hydrogen sulfide(H_2S), calbonyl sulfide(COS), and carbon disulfide(CS_2). The additional products, water(H_2O) and sulfur dioxide (SO_2), were obtained only in the case of the atomic ratio C/O<1 in a sample. These products were separated and determined under the programmed gas-chromatographic conditions in the previous study.[2] According to this procedure, the next sample could not be applied until the column temperature went down at 85 °C and this led to an increase of the total analysis time. In the present study which aimed at the minimization of the total analysis time, the isothermal gas-chromatographic conditions were examined and optimum column conditions were obtained by combining a 150 cm Porapak QS column with a 50 cm Chromosorb 104 column in series and by interposing a six-way cock at a proper position of the column so as to reduce the retention time of CS_2. The present study reduced the net analysis time by gas chromatography to about 8 min, from about 18 min under the previous conditions. Thus the total time(including reaction time, standing time, and so on) necessary for an analysis is also reduced to about 25 min from about 35 min. Moreover, both precision and accuracy are also improved, together with the improvement of the calculation method of the calculation factors used in the calculation of the atomic ratio between C, H, O, and N. Thus many standard samples, including liquid ones which are newly examined in this study, can be analyzed within an absolute error of about ±0.2%.

Experimental

Reagents. All of the reagents used as the analytical samples were of reagent grade for elemental analysis except for cyanoguanidine, which was of reagent grade for melting point standard.

Apparatus. An analyzer used in the present study is shown in Fig. 1. It consists of a Shimadzu GC 4B gas chromatograph mounted with two six-way cocks in the column oven and a sampler similar to that in the previous work.[1] The gas chromatograph was operated under the following conditions: Columns a 45 cm stainless steel column C_1 packed with Porapak QS(80—100 mesh), a 105 cm stainless steel column C_2 with Porapak QS(80—100 mesh), and a 50 cm stainless steel column C_3 with Chromosorb 104 (80—100 mesh); the insides of the stainless steel columns were treated preliminarily by coating with water glass; column temperature 85 °C; flow rate of He as a carrier gas 50 cm³/min.

A high-frequency induction furnace was used for the pyrolytic sulfurization reaction under the same conditions as in the previous work.[9]

Procedure. The quartz ampule containing 0.3—0.5 mg of sample and 5 mg of S was prepared and treated for 1 min by the high-frequency induction furnace as in the previous study.[9] After standing for 3 min in the furnace, the ampule was inserted into the sampler. Replacing the inside of the sampler with He for 5 min, the sampler was connected with the gas chromatograph by operating the

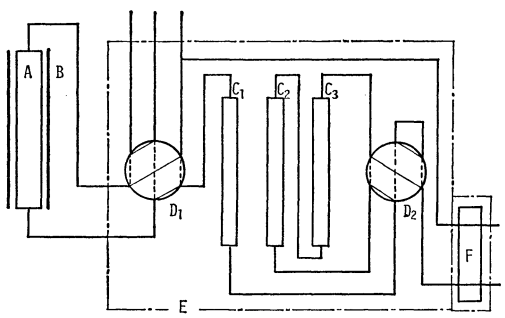

Fig. 1. Schematic flow diagram of the analyzer.
A: Gas sampler, B: vice, C_1: Porapak QS column (45 cm), C_2: Porapak QS column (105 cm), C_3: Chromosorb 104 column (50 cm), D_1, D_2: six-way cocks, E: column oven held at 85 °C, F: thermal conductivity detector.

six-way cock D_1. After 5 min, the time necessary for the stabilization of the base line in a gas chromatogram, the ampule was broken with a vice B and the evolved gases were subjected to gas-chromatographic analysis. After 4.5 min, the separation column was shortened to only a 45 cm Porapak QS column by operating the six-way cock D_2. On the basis of the data obtained by a digital integrator, the atomic ratio between C, H, O, and N in a sample was calculated by the use of calculation factors of the products.

Results and Discussion

Gas-chromatographic Separation of the Reaction Products under the Isothermal Conditions. According to the PSGC, the gaseous products of the pyrolytic sulfurization reaction were limited as follows: N_2, CO_2, H_2S, COS, H_2O, SO_2, and CS_2. Then, an investigation was undertaken to separate them under the isothermal gas-chromatographic conditions, instead of the programmed ones in the previous studies. Porapak Q, Porapak QS, Chromosorb 104, silica gel, Carbon molecular sieve B, and Molecular sieve 13X were chosen as representative gas-chromatographic packings to separate the above gaseous products. Each packing was investigated to determine the elution behavior of the products under the following standard conditions: Column length 100 cm, flow rate of He as a carrier gas 30 cm³/min, and column temperature 100 °C. All of the above-mentioned products were found to elute within 1 h when Porapak Q, Porapak QS, and Chromosorb 104, respectively, were used as a column packing. As can be seen from the retention time of each product in Table 1, H_2S cannot be separated from H_2O by Porapak Q or Porapak QS nor from COS by Chromosorb 104. It was suggested that the optimum column conditions to separate the seven kinds of products would be obtained by the combination of Porapak Q with Chromosorb 104(Q-104 type) or by that of Porapak QS with Chromosorb 104(QS-104 type) in series. Therefore, an examination was undertaken to separate the products by the above combination columns, and optimum conditions to separate them were obtained. Since two kinds of optimum conditions, however, indicated fairly large retention times for CS_2, the column was shortened by interposing the six-way cock at a proper position of the column so as to reduce the retention time of CS_2. Thus, the following optimum column conditions were obtained: (Q-104 type) first column a 50 cm Porapak Q(80—100 mesh) column, second column a 100 cm Porapak Q(80—100 mesh) column, third column a 45 cm Chromosorb 104(80—100 mesh) column, column temperature 90 °C, and flow rate of He 50 cm³/min. (QS-104 type) first column a 45 cm Porapak QS(80—100 mesh) column, second column a 105 cm Porapak QS (80—100 mesh) column, third column a 50 cm Chromosorb 104 (80—100 mesh) column, column temperature 85 °C, and flow rate of He 50 cm³/min. The six-way cock was interposed between the first column and the second column in each type. Typical chromatograms under the above-mentioned conditions are shown in Fig. 2. As can be seen from Fig. 2, the separation of the products is achieved

Table 1. The retention time of the products under the standard column conditions

Column packing	Retention time/min						
	N_2	CO_2	H_2S	COS	H_2O	SO_2	CS_2
Porapak Q	0.3	0.5	1.1	1.6	1.1	2.0	13.8
Porapak QS	0.3	0.5	1.0	1.3	1.0	1.8	12.5
Chromosorb 104	0.3	0.5	1.2	1.2	4.1	2.8	7.3

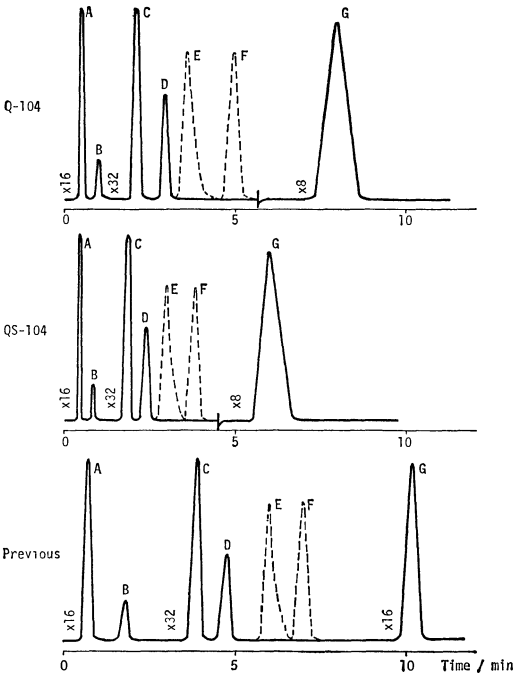

Fig. 2. Typical chromatograms of alanine as a standard sample.
A: N_2, B: CO_2, C: H_2S, D: COS, E: H_2O, F: SO_2, G: CS_2.

Table 2. Fluctuation of the ratio[a] of peak areas obtained by the previous and the present anaylytical conditions

	C. V. (%)[b] of peak area ratio				
	N_2	CO_2	H_2S	COS	CS_2
Q-104 type	1.81	2.44	1.34	1.48	1.89
QS-104 type	0.897	2.73	0.614	0.736	0.924
Previous	1.31	2.67	1.31	1.69	1.48

a) The ratio of each peak area of N_2, CO_2, H_2S, COS, and CS_2 to their sum was represented as a percentage. b) Calculated from 10 runs for alanine.

Table 3. Fluctuation of K(COS) and K(CO_2)

	C. V. (%)	
	K(COS)	K(CO_2)
Present	0.443[a]	0.778[b]
Previous	1.25[b]	1.18[b]

a) Calculated from 5 runs for 8-quinolinol. b) Calculated from 5 runs for sucrose.

Table 4. Analytical results of various organic compounds

Sample[a]	C (wt%)			H (wt%)			O (wt%)			N (wt%)		
	Calcd	Found	Error	Calcd	Found	Error	Calcd	Found	Error	Calcd	Found	Error
Acetanilide	71.09	71.03	−0.06	6.71	6.77	+0.06	11.84	11.95	+0.11	10.36	10.25	−0.11
Acetone 2,4-dinitrophenylhydrazone	45.38	45.41	+0.03	4.23	4.20	−0.03	26.87	27.04	+0.17	23.52	23.35	−0.17
DL-α-Alanine	40.44	40.27	−0.17	7.92	7.90	−0.02	35.92	36.09	+0.17	15.72	15.74	+0.02
Anthracene	94.34	94.43	+0.09	5.66	5.57	−0.09						
Antipyrine	70.19	70.06	−0.13	6.43	6.47	+0.04	8.50	8.66	+0.16	14.88	14.81	−0.07
Benzoic acid	68.85	68.68	−0.17	4.95	4.98	+0.03	26.20	26.34	+0.14			
Benzoin	79.22	79.20	−0.02	5.70	5.71	+0.01	15.08	15.09	+0.01			
Butyl *p*-hydroxybenzoate	68.02	68.01	−0.01	7.27	7.16	−0.11	24.71	24.83	+0.12			
Caffeine	49.48	49.51	+0.03	5.19	5.15	−0.04	16.48	16.56	+0.08	28.85	28.78	−0.07
Cholesterol	83.87	84.07	+0.20	11.99	11.93	−0.06	4.14	4.00	−0.14			
Cyclohexanone 2,4-dinitrophenylhydrazone	51.80	51.64	−0.16	5.07	5.05	−0.02	23.00	23.21	+0.21	20.13	20.10	−0.03
Cyclohexanone oxime	63.68	63.56	−0.12	9.80	9.85	+0.05	14.14	14.28	+0.14	12.38	12.31	−0.07
Cyclohexanone semicarbazone	54.17	54.05	−0.12	8.44	8.43	−0.01	10.31	10.26	−0.05	27.08	27.26	+0.18
m-Dinitrobenzene	42.87	42.80	−0.07	2.40	2.42	+0.02	38.07	38·08	+0.01	16.66	16.70	+0.04
N,N'-Diphenylthiourea	79.57	79.63	+0.06	6.16	6.12	−0.04				14.27	14.25	−0.02
Ethyl *p*-aminobenzoate	65.44	65.37	−0.07	6.71	6.80	+0.09	19.37	19.29	−0.08	8.48	8.54	+0.06
Guaiacol carbonate	65.68	65.69	+0.01	5.15	5.16	+0.01	29.17	29.15	−0.02			
Hippuric acid	60.33	60.24	−0.09	5.06	5.13	+0.07	26.79	26.66	−0.13	7.82	7.97	+0.15
Methyl α-D-glucoside	43.30	43.13	−0.17	7.27	7.28	+0.01	49.43	49.59	+0.16			
Naphthalene	93.71	93.58	−0.13	6.29	6.42	+0.13						
Nicotinic acid	58.54	58.42	−0.12	4.09	4.10	+0.01	25.99	25.96	−0.03	11.38	11.52	+0.14
p-Nitroaniline	52.17	52.20	+0.03	4.38	4.42	+0.04	23.17	23.28	+0.11	20.28	20.10	−0.18
Phenacetin	67.02	66.82	−0.20	7.31	4.41	+0.10	17.85	17.94	+0.09	7.82	7.83	+0.01
Stearic acid	75.99	75.90	−0.09	12.76	12.70	−0.06	11.25	11.40	+0.15			
Succinic acid	40.68	40.63	−0.05	5.12	5.10	−0.02	54.20	54.27	+0.07			
Sulfanilamide	51.43	51.29	−0.14	5.75	5.84	+0.09	22.83	22.78	−0.05	19.99	20.09	+0.10
Sulfathiazole	56.53	56.51	−0.02	4.75	4.86	+0.11	16.74	16.67	−0.07	21.98	21.96	−0.02
Thiourea	27.26	27.27	+0.01	9.15	9.15	0				63.59	63.58	−0.01
p-Toluenesulfonamide	60. ?	60.33	−0.09	6.52	6.53	+0.01	22.99	23.03	+0.04	10.07	10.11	+0.04
Triphenylphosphine	93.46	93.28	−0.18	6.54	6.72	+0.18						
Vanillin	63.15	63.29	+0.14	5.30	5.36	+0.06	31.55	31.35	−0.20			
Anthraquinone	80.76	80.71	−0.05	3.87	3.83	−0.04	15.37	15.46	+0.09			
2,2'-Bis(ethylsulfonyl)propane	51.21	51.25	+0.04	9.82	9.65	−0.17	38.97	39.10	+0.13			
Bis(2,4-pentanedionato)magnesium(II)	51.27	51.21	−0.06	7.75	7.85	+0.10	40.98	40.98	−0.04			
Tris(2,4-pentanedionato)iron(III)	60.59	60.58	−0.01	7.12	6.95	−0.17	32.29	32.47	+0.18			
Phenylmercury(II) acetate	70.58	70.55	−0.03	5.92	5.97	+0.05	23.50	23.48	−0.02			

a) Sulfur and metal atoms were neglected in the calculation of the compositions of samples, since they could not be determined.

TABLE 5. ANALYTICAL RESULTS OF LIQUID SAMPLES

Sample	C (wt%)			H (wt%)			O (wt%)			N (wt%)		
	Calcd	Found	Error	Calcd	Found	Error	Calcd	Found	Error	Calcd	Found	Error
Anisole	77.75	77.92	+0.17	7.46	7.32	−0.14	14.79	14.76	−0.03			
Nitrobenzene	58.54	58.53	−0.01	4.09	4.11	+0.02	25.99	25.80	−0.19	11.38	11.56	+0.18

under the isothermal gas-chromatographic conditions, and moreover the elution time of the products is reduced from 13 min under the previous conditions to 8 min under the present conditions.

Reproducibility of the Analytical Values. The reproducibility of the PSGC was examined using N_2, CO_2, H_2S, COS, and CS_2 obtained from alanine, since the atomic ratio of C/O in alanine was more than 1 and neither H_2O nor SO_2 was produced. The two sets of column conditions were compared with the previous column conditions by analyzing 10 samples of alanine and by estimating the coefficient of variation(C.V.) in the ratio of the individual peak area (Table 2). Table 2 shows that QS-104 type has the best reproducibility of the analytical values. Therefore, QS-104 type was employed in the present study.

Calculation Factor. In the PSGC, the atomic ratio between C, H, O, and N was calculated by using both the factors obtained by analyzing the standard compounds preliminarily and the peak areas of the individual product obtained from the sample. Judging from the meaning of the above factors, the term "calculation factor" is hereafter adopted instead of "correction factor" used in the previous papers.

The calculation factors of $N_2(K(N_2))$ and $CS_2(K(CS_2))$ were obtained by solving the following equations on the basis of the analytical data of cyanoguanidine:

$$\left(\frac{N}{H}\right)=\frac{2K(N_2)A(N_2)}{2K(H_2S)A(H_2S)}, \quad (1)$$

$$\left(\frac{C}{H}\right)=\frac{K(CS_2)A(CS_2)}{2K(H_2S)A(H_2S)}. \quad (2)$$

Here $A(X)$ is the peak area of X and $K(H_2S)$ is 1, as in the previous papers. The calculation actors of $CO_2(K(CO_2))$ and COS (K(COS)) were o tained by solving the following simultaneous equations on the basis of the analytical data of sucrose:

$$\left(\frac{O}{H}\right)=\frac{2K(CO_2)A(CO_2)+K(COS)A(COS)}{2K(H_2S)A(H_2S)}, \quad (3)$$

$$\left(\frac{C}{H}\right)=\frac{K(CO_2)A(CO_2)+K(COS)A(COS)+K(CS_2)A(CS_2)}{2K(H_2S)A(H_2S)}. \quad (4)$$

However, the values of $K(CO_2)$ and K(COS) obtained by Eqs. 3 and 4 were accompanied with the fluctuation of the value of $K(CS_2)$ in Eq. 4. Therefore an equation which is free from $K(CS_2)$ was necessary for an improvement of the values of $K(CO_2)$ and K(COS). In the present study, K(COS) was obtained from Eq. 5, which was obtained by neglecting $2K(CO_2)A(CO_2)$ in Eq. 3, by the use of the analytical data of 8-quinolinol in which the amount of CO_2 was negligibly small.

$$\left(\frac{O}{H}\right)=\frac{K(COS)A(COS)}{2K(H_2S)A(H_2S)} \quad (5)$$

Then $K(CO_2)$ was calculated by Eq. 3 by the use of the analytical data of sucrose. Table 3 shows the fluctuation of $K(CO_2)$ and K(COS) in the present and in the previous procedures. The values of C.V. in Table 3 indicate that the present procedure is superior to the previous one.

Analysis of Various Organic Compounds. Various organic compounds were analyzed by the present procedure (Table 4). Judging from the results in Table 4, both precision and accuracy were superior to those in the previous procedure.

Analysis of Liquid Samples. Liquid samples were newly analyzed in the following manner. A liquid sample was taken in a quartz capillary tube (0.5 mm i.d., 2 mm long) by the capillary action; 5 mg of S were inserted in the quartz tube which was closed at one end, and the inside of the quartz tube was replaced with He as in the previous study.[1] Ten minutes later, the stream of He was stopped, and the other end of the quartz tube was sealed. Each ampule thus obtained was analyzed by the present procedure. Analytical results of liquid samples are shown in Table 5. It shows that high boiling point liquid organic compounds can be analyzed with satisfactory results by the PSGC.

References

1) K. Tsuji, K. Fujinaga, and T. Hara, *Bull. Chem. Soc. Jpn.*, **50**, 2292 (1977).
2) T. Hara, K. Fujinaga, and K. Tsuji, *Bull. Chem. Soc. Jpn.*, **51**, 1110 (1978).
3) T. Hara, K. Fujinaga, and K. Tsuji, *Bull. Chem. Soc. Jpn.*, **51**, 2951 (1978).
4) T. Hara, K. Fujinaga, K. Tsuji, and F. Okui, *Bull. Chem. Soc. Jpn.*, **51**, 3079 (1978).
5) T. Hara, K. Fujinaga, F. Okui, and K. Nagayama, *Sci. Eng. Rev. Doshisha Univ.*, **21**, 241 (1981).
6) T. Hara, K. Fujinaga, and F. Okui, *Bull. Chem. Soc. Jpn.*, **53**, 951 (1980).
7) T. Hara, K. Fujinaga, and F. Okui, *Bull. Chem. Soc. Jpn.*, **53**, 1308 (1980).
8) T. Hara, K. Fujinaga, and F. Okui, *Bull. Chem. Soc. Jpn.*, **54**, 2956 (1981).
9) T. Hara and F. Okui, *Bull. Chem. Soc. Jpn.*, **55**, 329 (1982).

 © 1982 The Chemical Society of Japan Bull. Chem. Soc. Jpn., 55, 2131—2133 (1982)

A Potentiometric Study on Mixed Ligand Cadmium(II) Complexes with 2-Pyridinecarboxylic Acid and 2-Aminoalkanoic Acids

Haruo Matsui* and Hitoshi Ohtaki†

Government Industrial Research Institute, Nagoya, Hirate-cho, Kita-ku, Nagoya 462

† *Department of Electronic Chemistry, Tokyo Institute of Technology at Nagatsuta, Nagatsuta-cho, Midori-ku, Yokohama 227*

(Received December 21, 1981)

Formation constants of cadmium(II) complexes with 2-pyridinecarboxylic acid (Hpic) were determined in aqueous solutions containing 3 mol dm^{-3} $LiClO_4$ as a constant ionic medium at 25 °C by potentiometric titrations. On the basis of the formation constants of the complexes thus determined and those of the 2-aminoalkanoate complexes previously obtained, formation constants of mixed ligand cadmium(II) complexes CdL(pic) were determined, where L^- denotes a 2-aminoalkanoate ion such as glycinate (gly^-), α-alaninate (ala^-), 2-aminobutanoate (but^-), 2-aminopentanoate (pen^-), or 2-aminohexanoate (hex^-) ion. The formation constants $\log \beta_{111} = \log \{[CdL(pic)]/([Cd^{2+}][L^-][pic^-])\}$ of the 1:1:1 mixed ligand cadmium(II) complexes are: Cd(gly)(pic), 8.88; Cd(ala)(pic), 8.47; Cd(but)(pic), 8.42; Cd(pen)(pic), 8.73; and Cd(hex)(pic), 8.76. The equilibrium constant of the reaction between $Cd(gly)^+$ and pic^- was larger than that between $Cd(pic)^+$ and gly^-, and much larger than the equilibrium constants between CdL^+ and L'^- previously studied, where L^- and L'^- are 2-aminoalkanoate anions.

Formation equilibria of mixed ligand cadmium(II) complexes with various aliphatic 2-aminoalkanoic acids were studied in the previous work.[1] In the present investigation we examined the formation of mixed ligand cadmium(II) complexes containing aliphatic amino acids and 2-pyridinecarboxylic acid (Hpic) which can form five-membered chelate rings with the central cadmium(II) ion. 2-Quinolinecarboxylic acid (Hquin) was also used as another aromatic amino acid-like ligand, but the formation constant of neither $Cd(quin)_2$ nor CdL(quin) complex (L^-=2-aminoalkanoate ion) could be determined because of the formation of precipitates in solutions at an early stage of titrations.

Experimental

Reagents. 2-Pyridinecarboxylic acid was obtained from Wako Pure Chemicals Ind., Osaka, and used without further purification. Other reagents such as cadmium(II) perchlorate, lithium perchlorate, and lithium hydroxide were prepared and purified by the methods described in the previous paper.[1] Glycine (Hgly), α-alanine (Hala), 2-aminobutanoic acid (Hbut), 2-aminopentanoic acid (Hpen), and 2-aminohexanoic acid (Hhex) were used after analysis and purification by the previous method.[1]

Method of Measurements. Glass electrode, a pH meter and cells used were the same as those employed in the previous study.[1] Lithium perchlorate was used as an inert ionic medium (3 mol dm^{-3}).

The ratio of the total concentration of 2-pyridinecarboxylic acid (Hpic) to that of cadmium(II) ions (C^t_{pic}/C^t_{Cd}) was kept 5. When the mixed ligand systems were examined, the composition of the solution containing 2-pyridinecarboxylic acid, a 2-aminoalkanoic acid (HL), and cadmium(II) ion was kept 2.5:2.5:1, independent of the total concentrations of the species.

The method of emf measurements was essentially the same as that employed in the preceding work.[1] All the measurements were carried out at 25.00 °C±0.02 °C in a liquid paraffin bath under a nitrogen atmosphere.

Results and Discussion

The formation constants of the 1:1 and 1:2 complexes of cadmium(II) ion with 2-pyridinecarboxylic acid are given in Table 1, together with the acid dissociation constants (pK_1 and pK_2) of the ligand. The values were compared with those determined in other media.[2-4]

The formation constants of cadmium(II) complexes with 2-quinolinecarboxylic acid were determined under the same experimental conditions, but the formation constant (K_{12}) of the 1:2 complex was not determinable, because white precipitates were formed in solutions at an early stage of titrations. The acid dissociation constants of 2-quinolinecarboxylic acid were determined to be pK_1=2.17 and pK_2=5.58. The value

Table 1. Formation constants of cadmium(II) complex with 2-pyridinecarboxylic acid at 25 °C

Ligand	Medium (mol dm^{-3})	pK_1	pK_2	$\log K_{11}$	$\log K_{12}$	$\log \beta_2$	Ref.
2-Pyridinecarboxylic acid	3.0 $LiClO_4$	1.99	5.93	4.47	3.70	8.17	Present work[a]
	0.1 $NaNO_3$	1.60	5.54	4.36	3.18	7.54	2
	0	1.03	5.33	4.79	3.46	8.25	3
	0.5 $NaNO_3$	0.87	5.18	4.18	3.43	7.61	4

a) Standard deviations are ±0.02.

of $\log K_{11}$ for the 1:1 complex of cadmium(II) ion with 2-quinolinecarboxylic acid was 4.88, which was much larger than the literature value (4.12) at zero ionic concentration.[5]

Formation constants of mixed ligand cadmium(II) complexes with 2-pyridinecarboxylic acid were determined by the same procedure as described in the previous paper.[1] Typical titration curves are shown in Fig. 1, which were obtained in the Cd(II)–α-alanine–2-pyridinecarboxylic acid system. The solid lines in Fig. 1 were drawn by using calculated values of the degree of neutralization of the total ligands X (X_{calcd}) by the following equation:

$$X_{\text{calcd}} = \frac{C_{\text{L}}^{\text{t}} + K_{\text{i}}[\text{H}^+]^{-1} - [\text{H}^+] - \sum_p \sum_q \sum_r \sum_s q\beta_{pqrs}[\text{Cd}^{2+}]^p[\text{H}^+]^q[\text{L}^-]^r[\text{L}'^-]^s}{C_{\text{L}}^{\text{t}}}, \quad (1)$$

where K_{i} represents the autoprotolysis constant of water in the 3 mol dm^{-3} $LiClO_4$ aqueous solution at 25 °C ($10^{-13.87}$ mol^{2}dm^{-6} [6]). Since the only 1:1:1 type of mixed ligand complexes without protons has been found under the present experimental conditions (*i.e.*, $p=1$, $q=0$, and $r=s=1$), the formation constant of the mixed ligand complex will be denoted as β_{111}. The results obtained are summarized in Table 2 with values of F_{m}, F'_{m}, and b, which are indices of deviation of the formation constant of the mixed ligand complex from the statistical values defined by the following equations:

$$\left.\begin{aligned} &\text{CdL}_2 + \text{CdL}'_2 = 2\text{CdLL}' \\ &2\log\beta_{111} = \log\beta_{120} + \log\beta_{102} + \log F_{\text{m}} \end{aligned}\right\}, \quad (2)$$

$$\left.\begin{aligned} &\text{CdL}^+ + \text{CdL}'^+ = \text{CdLL}' + \text{Cd}^{2+} \\ &\log\beta_{111} = \log\beta_{110} + \log\beta_{101} + \log F'_{\text{m}} \end{aligned}\right\}, \quad (3)$$

$$\left.\begin{aligned} &\log F_{\text{m}} = 2\log F'_{\text{m}} + b \\ &b = \log\{(K_{110}\cdot K_{101})/(K_{120}\cdot K_{102})\} \end{aligned}\right\}. \quad (4)$$

It is well known that mixed ligand complexes which contain a ligand having a pyridine ring as one component are strongly stabilized.[7] The present results show the trend with the indication of large $\log F_{\text{m}}$ values compared with the statistical value of 0.6 and positive values of $\log F'_{\text{m}}$. The b values obtained in the present systems were much larger than those reported in the previous systems containing only 2-aminoalkanoate anions as ligands.[1]

The largest formation constant was obtained for the Cd(gly)(pic) complex. The degree of stabilization of mixed ligand 1:1:1 complex by coordination of the second ligand to the 1:1 complex can be indicated by the K_{12}^{m} value which is defined by the following equation:

$$\log K_{12}^{\text{m}} = \log\beta_{111} - \log K_{11}. \quad (5)$$

The $\log K_{12}^{\text{m}}$ values thus calculated are summarized in Table 3, together with those obtained for the mixed ligand cadmium(II) complexes with only 2-aminoalkanoate ions found in the previous work.[1] It is obvious that the coordination of a 2-pyridinecarboxylate anion to a 2-aminoalkanoatocadmium(II) complex remarkably stabilizes the 1:1:1 mixed ligand complex, because of a large coordination ability of the pyridine ring by electron-withdrawing from the central metal ion. However, it should be noted that the formation constant K_{12}^{m} between the 2-pyridinecarboxylatocadmium(II) complex and a 2-aminoalkanoate ion (*i.e.*, $\text{Cd(pic)}^+ + \text{L}^- = \text{CdL(pic)}$) was larger than that of the reaction between 2-aminoalkanoatocadmium(II) complex (CdL^+) and another 2-aminoalkanoate ion L'^- ($\text{L}^- \neq \text{L}'^-$) (see Table 3). The result indicates that the pyridine ring in the coordination sphere of the complex enhances the interaction between the central cadmium(II) ion and the entering 2-aminoalkanoate ion. It must be noted that the 2-pyridinecarboxylate anion coordinated to the central cadmium(II) ion does not significantly stabilize the interaction between the 2-pyridinecarboxyl-

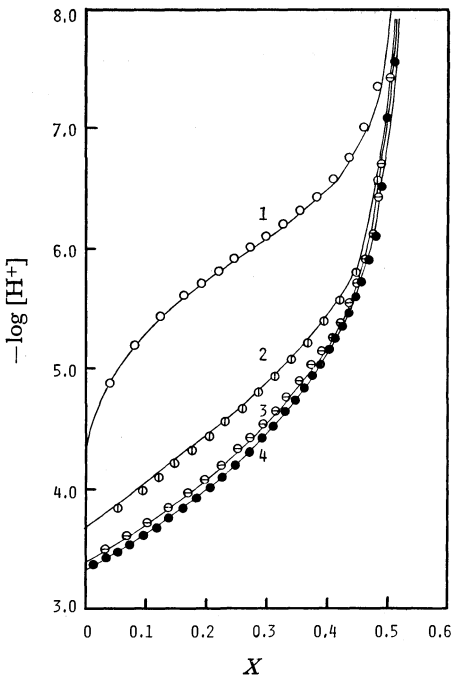

Fig. 1. Typical titration curves of cadmium(II)–α-alanine-2-pyridinecarboxylic acid mixed solutions. Curve 1 (○), C_{Cd}(mmol dm^{-3})=0, C_{ala}(mmol dm^{-3})=10.11, C_{pic}(mmol dm^{-3})=10.31; 2 (◑), 2.156, 5.409, 5.420; 3 (⊖), 6.565, 16.36, 16.39; 4 (●), 11.01, 27.44, 27.49. Solid lines represent calculated titration curves by using values listed in Tables 1 and 3 and Eq. 1.

TABLE 2. FORMATION CONSTANTS OF MIXED LIGAND COMPLEXES OF CADMIUM(II) ION AND F_{m}, F'_{m}, AND b VALUES IN 3 mol dm^{-3} $LiClO_4$ AT 25 °C

Complex[a]	$\log\beta_{111}$[b]	$\log F_{\text{m}}$	$\log F'_{\text{m}}$	b
Cd(gly)(pic)	8.88	2.10	0.40	1.30
Cd(ala)(pic)	8.47	1.84	0.31	1.22
Cd(but)(pic)	8.42	1.79	0.31	1.17
Cd(pen)(pic)	8.73	2.28	0.54	1.20
Cd(hex)(pic)	8.76	2.32	0.55	1.22

a) gly=Glycinate, ala=α-alaninate, but=2-aminobutanoate, pen=2-aminopentanoate, hex=2-aminohexanoate, pic=2-pyridinecarboxylate ions (α-picolinate ion). b) Standard deviations are ±0.02.

Table 3. The second stepwise formation constants ($\log K_{12}^{m}$) of the CdLL′ complexes in 3 mol dm^{-3} $LiClO_4$ at 25 °C[a]

CdL	L′					
	2-Pyridine carboxylate	Glycinate	Alaninate	2-Amino-butanoate	2-Amino-pentanoate	2-Amino-hexanoate
$Cd(pic)^+$	*3.70*	4.41	4.00	3.95	4.26	4.29
$Cd(gly)^+$	4.87	*3.48*[b]	3.46[b]	3.33[b]	3.40[b]	3.42[b]
$Cd(ala)^+$	4.78	3.78[b]	*3.24*	3.44	3.46	3.55
$Cd(but)^+$	4.78	3.70[b]	3.49	*3.24*	3.41	3.56
$Cd(pen)^+$	5.01	3.69[b]	3.43	3.33	*3.29*	3.59
$Cd(hex)^+$	5.02	3.69[b]	3.50	3.46	3.57	*3.29*

a) Values underlined are $\log K_{12}$ of the bis(2-pyridinecarboxylato)- and bis(2-aminoalkanoato)cadmium(II) complexes. b) Values obtained from Ref. 1.

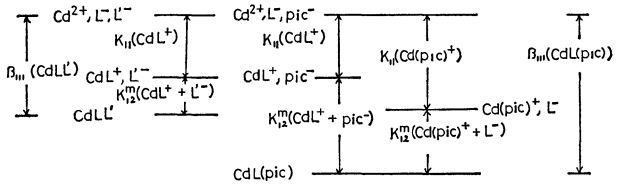

Fig. 2. A diagram showing relationships among the values of β_{111}, K_{11}, and K_{12}^{m}. Note that the magnitude of the K_{12}^{m} values are in the order $(CdL^+ + pic^-) > (Cd(pic)^+ + L^-) > (CdL^+ + L'^-)$.

atocadmium(II) complex and the second 2-pyridinecarboxylate ion (*i.e.*, $Cd(pic)^+ + pic^- = Cd(pic)_2$).

The values of K_{12}^{m} of the reaction, $CdL^+ + pic^- = CdL(pic)$, are larger than K_{12}^{m} value of the reaction, $Cd(pic)^+ + L^- = CdL(pic)$ (Fig. 2), the fact, no doubt, indicating a large affinity of pic^- compared with L^- to a cadmium(II) ion. The K_{12}^{m} values of the reaction, $Cd(pic)^+ + L^- = CdL(pic)$, are larger than those of the reaction, $CdL'^+ + L^- = CdLL'$. The result is explainable in terms of a large electron-withdrawing effect of the pyridine ring within pic^- which leads to a decrease in the electron density at the cadmium atom of the $Cd(pic)^+$ complex. The lowered electron density at the cadmium atom of the $Cd(pic)^+$ complex allows to transfer electron pairs from an entering second 2-aminoalkanoate ion. Therefore, a stronger electron donation from the second ligand of the 2-aminoalkanoate ion to the $Cd(pic)^+$ complex in comparison with the reaction between CdL^+ and L'^- can be done to form a strong σ-bonding between them. Thus, the K_{12}^{m} value of the CdL(pic) complex becomes larger than that of the CdLL′ complex.

References

1) H. Matsui and H. Ohtaki, *Bull. Chem. Soc. Jpn.*, **55**, 461 (1982).
2) K. Suzuki, M. Yasuda, and K. Yamasaki, *J. Phys. Chem.*, **61**, 229 (1957).
3) P. O. Lumme, *Suom. Kemistil. B*, **30**, 182 (1957).
4) J. P. Scharff, *Anal. Chim. Acta*, **87**, 499 (1976).
5) P. O. Lumme, *Ann. Acad. Sci. Fennicae*, **68A**, II, 7 (1955).
6) T. Kawai, S. Ishiguro, and H. Ohtaki, *Bull. Chem. Soc. Jpn.*, **53**, 2221 (1980).
7) H. Sigel, "Metal Ions in Biological System," Marcel Dekker Inc., New York (1973), Vol. 2, pp. 63—125.

C,O-Chelates of the Trifluoroacetylacetonate Dianion with Palladium(II). Molecular Structure of [Pd(tfac(2—)-*C,O*)(PPh_3)(2,6-Me_2-py)]

Seichi Okeya,* Yasuo Kawakita, Shinichi Matsumoto,† Yukio Nakamura,† Shinichi Kawaguchi,*,† Nobuko Kanehisa,†† Kunio Miki,†† and Nobutami Kasai*,††

Faculty of Education, Wakayama University, Masago-cho, Wakayama 640

† *Department of Chemistry, Faculty of Science, Osaka City University, Sumiyoshi-ku, Osaka 558*

†† *Department of Applied Chemistry, Faculty of Engineering, Osaka University, Suita, Osaka 565*

(Received December 28, 1981)

Reactions of bis(trifluoroacetylacetonato)palladium(II), [Pd(tfac)$_2$], with tertiary phosphines followed by pyridine or its derivatives afforded a series of the [Pd(tfac(2—)-*C,O*)LL']-type complexes which contain a C,O-chelating trifluoroacetylacetonate dianion and a couple of tertiary phosphine and/or heterocyclic nitrogen base ligands (L and L'). Their structures in solution were studied by ^{1}H, ^{13}C, ^{19}F, and ^{31}P NMR spectroscopy and the molecular structure in a crystal of [Pd(tfac(2—)-*C,O*)(PPh_3)(2,6-Me_2-py)]·C_6H_6 containing triphenylphosphine and 2,6-dimethylpyridine as L and L' was determined by means of X-ray diffraction.

β-Dicarbonyl compounds are very popular ligands[1] and widely used as chelating monoanions.[2] In recent years the reactions of bis(β-diketonato)palladium(II) and -platinum(II) with a variety of nitrogen bases[3] and tertiary phosphines[3a,4] have been extensively studied to demonstrate transformation of the chelating β-diketonate anion into the central-carbon-bonded[5] and other bonding states. The η-allylic complexes of monoanions of ethyl acetoacetate[6] and acetylacetone[7] were also shown to react with Lewis bases to afford the terminal-carbon-bonded complexes.[7,8]

In the course of these studies, four novel coordination modes of β-diketonate dianions have been found: η-allylic coordination of the acetylacetonate dianion to palladium(II)[9] and platinum(II)[10] and of the dianion of ethyl acetoacetate to palladium(II),[9] C,O-chelation of the trifluoroacetylacetonate dianion to platinum(II),[11] bridging of the acetylacetonate dianion between palladium(II) and another metal *via* the terminal carbon and two oxygen atoms,[12] and another type of bridging by dianions of acetylacetone and ethyl acetoacetate, η^3-bonding to palladium and O,O'-chelating another metal atom.[13]

This paper reports the preparation and NMR characterization of C,O-chelates of the trifluoroacetylacetonate dianion with palladium(II) and also the crystal and molecular structure of one complex containing triphenylphosphine and 2,6-dimethylpyridine as ancillary ligands.

Experimental

Preparation of Complexes. Bis(trifluoroacetylacetonato)-palladium(II), [Pd(tfac)$_2$] (**1**) was prepared by the method reported in a previous paper.[14] Tris(*o*-tolyl)phosphine, P(*o*-tolyl)$_3$, was recrystallized from ethanol. Triphenylphosphine, PPh_3, and nitrogen bases were used as supplied without further purification.

*Trifluoroacetylacetonato(2—)bis(triphenylphosphine)palladium(II)–Diethyl Ether (1/1), [Pd(tfac(2—)-C,O)(PPh_3)$_2$]·Et_2O (**2**):* A dichloromethane solution (0.5 cm^3) of 1,8-bis(dimethylamino)naphthalene (21 mg, 0.10 mmol) was added to a solution of **1** (41 mg, 0.099 mmol) and triphenylphosphine (52 mg, 0.20 mmol) in the same solvent and the mixture was left to stand at room temperature for one day. Diethyl ether (8 cm^3) and hexane (8 cm^3) were added to the solution and the mixture was kept in a refrigerator overnight to deposit yellow needles, which were filtered, washed with diethyl ether, and dried *in vacuo*. The yield was 58 mg (68%). Inclusion of one molecule of diethyl ether per palladium was confirmed by ^{1}H NMR spectroscopy.

*[Pd(tfac(2—)-C,O)(PPh_3)(py)] (**3**):* Pyridine (0.5 cm^3, 6 mmol) was added to a dichloromethane solution (5 cm^3) containing **1** (75 mg, 0.18 mmol) and triphenylphosphine (96 mg, 0.37 mmol) and the mixture was kept to stand at room temperature for one day. The solution was concentrated to 2 cm^3 by evaporation under reduced pressure and diethyl ether was added to the concentrate. Yellow plates deposited after standing for one day at room temperature were filtered, washed with diethyl ether, and dried *in vacuo*. On being washed with diethyl ether, yellow plates lost the solvent of crystallization (dichloromethane), turning opaque. The yield was 60 mg (56%).

*[Pd(tfac(2—)-C,O)(PPh_3)(4-Me_2N-py)]·1/2CH_2Cl_2 (**4**):* 4-(Dimethylamino)pyridine (31 mg, 0.25 mmol) was added to a solution of **1** (103 mg, 0.250 mmol) and triphenylphosphine (131 mg, 0.499 mmol) in benzene (5 cm^3) and the mixture was left to stand at room temperature overnight to precipitate yellow needles, which were filtered, washed with a mixture (1:2 by volume) of dichloromethane and hexane, and dried *in vacuo*. The yield was 91 mg (57%). Recrystallization from dichloromethane–hexane gave yellow needles which contain a half molecule of dichloromethane per palladium.

*[Pd(tfac(2—)-C,O)(PPh_3)(2,6-Me_2-py)] (**5**):* 2,6-Dimethylpyridine (3 cm^3, 26 mmol) was added to a solution of **1** (805 mg, 1.95 mmol) and triphenylphosphine (1045 mg, 3.98 mmol) in dichloromethane (25 cm^3) and the mixture was stirred for 3 h. The solution was concentrated to 5 cm^3 by evaporation under reduced pressure and diethyl ether was added to the concentrate to precipitate yellow crystals (1142 mg) in a 91% yield, which were recrystallized from dichloromethane–hexane or benzene. In the former case, yellow plates deposited lost the solvent of crystallization (probably dichloromethane) and turned opaque on being washed with diethyl ether. In the latter case the benzene solvate (**5'**) was obtained, which was submitted for X-ray analysis.

*[Pd(tfac(2—)-C,O){P(o-tolyl)$_3$}(2,6-Me_2-py)] (**6**):* 2,6-

Dimethylpyridine (2 cm³, 17 mmol) was added to a solution of [Pd(tfac)(tfac-*O*){P(*o*-tolyl)$_3$}][4b] (215 mg, 0.300 mmol) in dichloromethane (10 cm³) and the mixture was stirred for 5 h. Addition of diethyl ether to the solution precipitated yellow fuzzy crystals, which were filtered and dried *in vacuo*. The yield was 78 mg (39%).

[Pd(tfac(2−)-C,O){P(o-tolyl)$_3$}(4-Me$_2$N-py)] (7): Yellow crystals of **7** were prepared in a manner similar to **6**. The yield was as low as 5% because of formation of [Pd(4-Me$_2$N-py)$_4$](tfac)$_2$ as a by-product.

[Pd(tfac(2−)-C,O)(2,9-Me$_2$-phen)] (12): Complex **1** (823 mg, 1.99 mmol) was allowed to react with 2,9-dimethyl-1,10-phenanthroline–water (1/2) (416 mg, 1.91 mmol) in dichloromethane (30 cm³) at room temperature for 4 h. The solvent was removed under reduced pressure and the residue was dissolved in acetone (5 cm³). Diethyl ether (10 cm³) was added to the solution and the mixture was kept in a refrigerator overnight to deposit yellow cubes, which were filtered, washed with diethyl ether, and dried *in vacuo*. The yield was 600 mg (65%).

[Pd(tfac(2−)-C,O)(4-Me$_2$N-py)$_2$] (9): Complex **12** (234 mg, 0.501 mmol) and 4-(dimethylamino)pyridine (183 mg, 1.50 mmol) were dissolved in dichloromethane (5 cm³) and the mixture was left to stand for 1.5 h. On addition of hexane to the solution, yellow needles appeared immediately. After being kept in a refrigerator overnight, the crystals were filtered, washed with diethyl ether, and dried *in vacuo*. The yield was 210 mg (83%).

[Pd(tfac(2−)-C,O)(py)$_2$] (8): Yellow needles of **8** were obtained in a 50% yield in the same way as above. This complex dissolves in dichloromethane and acetone but a yellow precipitate deposits promptly, which has not been characterized.

[Pd(tfac(2−)-C,O)(bpy)] (10): When a dichloromethane solution (2 cm³) of 2,2′-bipyridine (156 mg, 1.00 mmol) was added to a solution of **1** (413 mg, 1.00 mmol) in the same solvent (10 cm³), an orange-red crystalline solid appeared, which was filtered, washed with diethyl ether, and dried *in vacuo*. The yield was 170 mg (41%). Recrystallization was performed from a mixture (1:1 by volume) of chloroform and methanol, the product containing one half molecule of chloroform per palladium. Alternatively, a suspension of [Pd(tfac)(bpy)](tfac)[3c] (100 mg, 0.176 mmol) in dichloromethane (5 cm³) was stirred at 40 °C for 40 min to result in a clear solution, which was cooled spontaneously to room temperature to deposit a yellow precipitate of **10** (27 mg) in a 37% yield.

[Pd(tfac(2−)-C,O)(phen)] (11): Compound **11** was obtained in a 30% yield by the reaction of **1** with 1,10-phenanthroline in a manner similar to **10**.

Measurements. IR spectra were recorded in Nujol mull on a Hitachi 295 infrared spectrophotometer. NMR spectra were measured with JEOL FX60Q (for ^{1}H, ^{13}C, and ^{31}P) and FX90Q (for ^{19}F) spectrometers. The molecular weight was determined by vapor pressure osmometry with an instrument manufactured by Knauer in West Berlin, West Germany.

X-Ray Diffraction: Crystal Data. [Pd(tfac(2−)-*C,O*)(PPh$_3$)(2,6-Me$_2$-py)]·(C$_6$H$_6$) (**5′**), C$_{30}$H$_{24}$O$_2$NF$_3$PPd·C$_6$H$_6$, F. W. 703.0, monoclinic, P2$_1$/c, a=10.035(2), b=17.941(6), c=18.903(5) Å, β=103.25(2)°, V=3312.6(16) Å^3, D_m=1.40 (flotation), D_c=1.41 g cm^{-3} for Z=4, μ(Mo $K\alpha$)=6.51 cm^{-1}.

The crystal was sealed in a thin-walled glass capillary tube, since it was rather unstable in air. The unit-cell parameters and reflection intensities of **5′** were measured on a Rigaku automated, four-circle diffractometer with graphite monochromatized Mo $K\alpha$ radiation (λ=0.71069 Å). Intensity data were collected by the θ-2θ scan technique. The scan rate was 4° min^{-1} and the scan width was $\Delta(2\theta)$=(2.0+0.7 tan θ)°. The background intensities were measured for 7.5 s at both ends of a scan. Four standard reflections (0, 10, 0, 500, 066, and 555) were measured at regular intervals to monitor crystal stability and orientation, and the intensities of these reflections remained constant throughout the data collection. Usual Lorentz and polarization corrections were made, but no absorption correction was carried out. A total of 6001 (5180 non-zero) reflections was measured (sin $\theta/\lambda \leqq 0.6$).

Solution and Refinement of the Crystal Structure of 5′. The structure was solved by the heavy atom method. Approximate coordinates of the palladium atom were obtained from a three-dimensional Patterson function. Subsequent Fourier synthesis revealed locations of all the non-hydrogen atoms. The existence of the solvated benzene molecule was also discovered. Including the carbon atoms of the crystalline benzene molecule, the structure was refined anisotropically by the block-diagonal least-squares procedure (*HBLS* **V**).[15] The function minimized was $\sum w(|F_o|-|F_c|)^2$. Hydrogen atoms except those of terminal methyl groups and solvated benzene molecule were located by the difference Fourier synthesis, and refined isotropically. The final R is 0.045 for non-zero (0.063 for all) reflections. The weighting schemes used at the final stage were $w=\{\sigma_{cs}^2(F_o)+0.0292|F_o|+0.0010|F_o|^2\}^{-1}$ for $|F_o|>0$ and $w=0.0504$ for $|F_o|=0$; σ_{cs} is the standard deviation obtained by the counting statics. The atomic scattering factors used for non-hydrogen atoms were taken from International Tables for X-Ray Crystallography[16] and those for hydrogen atoms from Stewart and co-workers.[17] Computations were done on an ACOS 700S computer at the Crystallographic Research Center, Institute for Protein Research, Osaka University. The final atomic coordinates with equivalent temperature factors[18] are given in Table 1.†††

Results and Discussion

Characterization of the Trifluoroacetylacetonate(2−) Complexes. The analytical data for the newly prepared complexes given in Table 2 conform to their proposed formulae, [Pd(tfac(2−)-*C,O*)LL′]. The molecular weight of complex **5** was determined in dichloromethane at 25 °C to be 616 in good agreement with the calculated value 627. In accord with the proposed structure, all complexes show the ν(C=O) bands in 1620—1600-cm^{-1} region, complex **5**, for instance, having a very strong band at 1615 cm^{-1}.

Table 3 presents the ^{1}H NMR spectra in CDCl$_3$. The spectrum of each complex is composed of signals assignable to CH$_2$, CH, L, and L′ protons. The methine proton of tfac dianion resonates in the 5.13—5.28-ppm region, the chemical shift being rather insensitive to natures of the ancillary ligands. On the other hand, the chemical shifts and multiplicities of the methylene signals clearly show dependence on natures of the neutral ligands L and L′, spanning a wider range of 2.54—3.14 ppm. Thus the signal for the methylene protons of **2** appears as a doublet of doublets due to couplings to both the trans and cis phosphorus atoms, ^3J(P-H) being 9.$_5$ and 5.$_9$ Hz,

††† Tables of anisotropic thermal parameters and observed and calculated structure factors are kept at the Chemical Society of Japan (Document No. 8234).

Table 1. Final atomic positional parameters with estimated standard deviations in parentheses

(a) Non-hydrogen atoms with equivalent temperature factors.[18]

Atom	x	y	z	B_{eq}/Å^2	Atom	x	y	z	B_{eq}/Å^2
Pd	0.30530(3)	0.17523(2)	0.01890(2)	2.78	C(24)	0.4348(6)	0.2900(4)	−0.2423(3)	5.0
P	0.2451(2)	0.28023(6)	−0.04268(6)	2.82	C(25)	0.4167(6)	0.5349(4)	−0.2068(3)	5.0
F(1)	0.5001(5)	−0.0597(2)	0.0982(3)	8.2	C(26)	0.3611(6)	0.3541(3)	−0.1465(3)	4.4
F(2)	0.6287(4)	−0.0193(3)	0.1946(3)	7.7	C(31)	0.2827(5)	0.3676(3)	0.0065(3)	3.6
F(3)	0.4146(4)	−0.0249(2)	0.1838(3)	7.4	C(32)	0.3849(6)	0.3713(3)	0.0704(3)	4.9
N	0.1000(4)	0.1346(2)	0.0134(2)	3.0	C(33)	0.4134(7)	0.4398(4)	0.1054(4)	6.8
O(1)	0.3693(3)	0.0773(2)	0.0749(2)	3.7	C(34)	0.3427(7)	0.5031(4)	0.0778(4)	6.9
O(2)	0.6671(4)	0.2424(2)	0.1292(2)	5.1	C(35)	0.2420(8)	0.4991(3)	0.0161(4)	6.4
C(1)	0.5055(5)	0.2033(3)	0.0244(3)	3.2	C(36)	0.2121(6)	0.4327(3)	−0.0190(3)	4.9
C(2)	0.5930(5)	0.1923(3)	0.0981(3)	3.4	C(41)	0.0310(5)	0.0971(3)	−0.0452(3)	3.9
C(3)	0.5947(4)	0.1190(3)	0.1316(3)	3.5	C(42)	−0.1030(6)	0.0724(4)	−0.0487(4)	5.5
C(4)	0.4903(4)	0.0690(3)	0.1149(3)	3.0	C(43)	−0.1643(5)	0.0863(4)	0.0084(4)	5.8
C(5)	0.5112(5)	−0.0080(3)	0.1480(3)	4.0	C(44)	−0.0902(5)	0.1222(4)	0.0681(4)	5.2
C(11)	0.0610(5)	0.2861(3)	−0.0805(3)	3.8	C(45)	0.0410(5)	0.1464(3)	0.0698(3)	4.0
C(12)	−0.0251(5)	0.2972(3)	−0.0323(4)	4.7	C(46)	0.1027(6)	0.0821(3)	−0.1066(3)	4.9
C(13)	−0.1644(6)	0.2960(4)	−0.0564(5)	6.8	C(47)	0.1238(6)	0.1856(4)	0.1353(3)	5.4
C(14)	−0.2212(7)	0.2823(5)	−0.1269(6)	8.9	C(B1)	0.0575(8)	0.4931(5)	0.1895(4)	8.5
C(15)	−0.1412(7)	0.2739(4)	−0.1775(4)	8.1	C(B2)	−0.0410(9)	0.5241(5)	0.2206(4)	7.8
C(16)	0.0023(6)	0.2746(3)	−0.1547(4)	5.5	C(B3)	−0.1518(8)	0.4809(5)	0.2238(5)	9.2
C(21)	0.3223(5)	0.2874(3)	−0.1210(3)	3.5	C(B4)	−0.1694(8)	0.4084(5)	0.1957(5)	9.0
C(22)	0.3449(6)	0.2222(3)	−0.1557(3)	4.5	C(B5)	−0.0751(9)	0.3794(6)	0.1668(6)	9.8
C(23)	0.4001(7)	0.2231(4)	−0.2169(3)	5.1	C(B6)	0.0420(9)	0.4197(6)	0.1635(5)	9.9

(b) Hydrogen atoms with isotropic temperature factors.

Atom	x	y	z	B/Å^2	Atom	x	y	z	B/Å^2
H(101)	0.518(4)	0.251(3)	0.009(3)	3(1)	H(25)	0.453(6)	0.391(3)	−0.220(3)	6(2)
H(102)	0.523(5)	0.167(3)	−0.007(3)	4(2)	H(26)	0.343(5)	0.395(3)	−0.123(3)	4(1)
H(301)	0.671(5)	0.107(3)	0.160(3)	4(1)	H(32)	0.435(5)	0.333(3)	0.085(3)	3(1)
H(12)	0.006(6)	0.294(3)	0.020(3)	6(2)	H(33)	0.497(6)	0.431(4)	0.155(4)	8(2)
H(13)	−0.218(6)	0.298(4)	−0.015(4)	7(2)	H(34)	0.343(6)	0.542(4)	0.100(4)	8(2)
H(14)	−0.319(7)	0.280(4)	−0.146(4)	8(2)	H(35)	0.194(5)	0.542(3)	−0.003(3)	5(2)
H(15)	−0.183(5)	0.262(3)	−0.226(3)	6(2)	H(36)	0.149(5)	0.431(3)	−0.062(3)	4(2)
H(16)	0.069(5)	0.266(3)	−0.189(3)	4(2)	H(42)	−0.145(6)	0.045(3)	−0.096(3)	7(2)
H(22)	0.315(6)	0.178(3)	−0.144(3)	5(2)	H(43)	−0.258(6)	0.069(3)	0.009(3)	5(2)
H(23)	0.411(6)	0.172(3)	−0.237(3)	6(2)	H(44)	−0.122(5)	0.132(3)	0.121(3)	6(2)
H(24)	0.472(5)	0.290(3)	−0.283(3)	4(1)					

Table 2. Analytical data for [Pd(tfac(2−)-*C*,*O*)LL′]

Compd	L	L′	Decomp temp °C	Found(Calcd) (%) C	H	N
2[a]	PPh_3	PPh_3	90—100	62.58(63.05)	4.83(5.06)	
3	PPh_3	py	208—210	55.95(56.06)	3.96(3.86)	2.36(2.34)
4[b]	PPh_3	4-Me_2N-py	163—166	54.93(54.70)	4.25(4.33)	4.27(4.22)
5	PPh_3	2,6-Me_2-py	200—203	57.68(57.38)	4.39(4.33)	2.31(2.23)
5′[c]	PPh_3	2,6-Me_2-py		60.44(61.29)	4.59(4.71)	1.86(1.98)
6	P(*o*-tolyl)$_3$	2,6-Me_2-py	*ca.* 200	59.19(59.16)	5.08(4.96)	2.05(2.09)
7	P(*o*-tolyl)$_3$	4-Me_2N-py	191—195	57.77(57.82)	4.53(4.85)	2.05(2.17)
8	py	py	190—200	43.37(43.24)	3.16(3.14)	6.79(6.72)
9	4-Me_2N-py	4-Me_2N-py	149—152	44.98(45.39)	4.65(4.61)	10.94(11.14)
10[d]	bpy		200—205	39.62(39.25)	2.51(2.44)	5.85(5.91)
11	phen		*ca.* 210	46.65(46.55)	2.56(2.53)	6.42(6.39)
12	2,9-Me_2-phen		*ca.* 150	49.02(48.89)	3.30(3.24)	6.04(6.00)

a) Containing one molecule of diethyl ether per Pd. b) Containing one half molecule of dichloromethane per Pd. c) Containing one molecule of benzene per Pd. d) Containing one half molecule of chloroform per Pd.

Table 3. ^{1}H NMR Data in $CDCl_3$[a)]

Compd	tfac(2−)		L and L′	
	CH_2	CH	CH_3	Other
2	2.76 dd [9.5, 5.9]	5.13		Ph: 7.3c
3	2.63 d [5.4]	5.32		py: $H^{2,6}$ 8.12 d(5) Ph and $H^{3,4,5}$ of py: 6.9—7.6c
4	2.54 d [5.4]	5.28	2.88	py: $H^{3,5}$ 6.08 d(6.6) Ph and $H^{2,6}$ of py: 7.3c
5	2.70 d [5.6]	5.27	2.81	py: $H^{3,5}$ 6.78 d(6.5) Ph and H^4 of py: 7.35, 7.27c
6	2.68 d [5.1]	5.25	2.83	py: $H^{3,5}$ 6.74 d(7.6) Ph and H^4 of py: 7.3c
9	2.68	5.23	3.04, 2.99	py: $H^{2,6}$ 8.02 d, 7.69 d; $H^{3,5}$ 6.44 d, 6.39 d (each 7)
10[b)]	2.85	5.24		bpy: 7.5—8.5c
12	3.14	5.27	2.17	phen: $H^{3,8}$ 8.26 d; $H^{4,7}$ 7.38 d (each 8.4); $H^{5,6}$ 7.78

a) Chemical shifts in ppm from internal Me_4Si. Signals are singlets except those marked with d(doublet), dd(doublet of doublets), and c(complex). Figures in parentheses and brackets give ^3J(CH–CH) and ^3J(P–H) in Hz, respectively. b) In a mixture (1:1 by volume) of $CDCl_3$ and CD_3OD at 50 °C.

respectively. The signal pattern closely resembles that of [Pt(tfac(2−)-*C,O*)(PPh_3)$_2$][11] except the ^{195}Pt satellites. The methylene protons of **4**, **5**, and **6** resonate as a doublet with smaller ^3J(P–H) values, indicating that the phosphine ligand lies on the position cis to the methylene in each of these complexes.

In the case of complexes containing the same kind of neutral ligands (L=L′), two sets of signals from L should be observed since the chelating tfac(2−) ligand is unsymmetric. In fact complex **9** shows two kinds of signals assignable to NMe_2 and pyridine-CH protons. However, complex **12** exhibits no splitting in signals from ring-CH and Me protons, suggesting some kind of fluxional motion (coordination-site exchange).

The ^{13}C NMR data are listed in Table 4. The methylene carbon of **2** resonates as a doublet owing to coupling to the trans ^{31}P, ^2J(P–C) being 70 Hz. Coupling to the cis ^{31}P is not detected contrary to the case of the corresponding platinum(II) complex in which couplings to both ^{31}P atoms were observed (72 and 4 Hz).[11] Complexes **4**, **5**, and **6** exhibit methylene doublets with ^2J(P–C) of 4—5 Hz in accordance with the proposed *cis*(CH_2, P) structure. The $\underline{C}F_3\underline{C}O$ carbons of these complexes also couple to ^{31}P, conforming with their positions trans to ^{31}P.

Complexes **2** and **9** exhibit two sets of signals attributable to PPh_3 and 4-Me_2N-py carbons, reflecting unsymmetry of the tfac(2−) chelate. In the case of **12** at room temperature, the methyl carbons of 2,9-Me_2-phen appear as two broad signals, while the ring carbons show one set of rather broad signals. The methyl signals merge at higher temperatures to a broad singlet at 52 °C and signals of the ring carbons are sharpened, indicating equivalence of two halves of the phen molecule. The tfac(2−) carbons are invariably sharp at these temperatures, suggesting that the coordination-site exchange occurs in an intramolecular fashion rapidly on the NMR time scale. Self catalysis by virtue of coordination of a neighboring molecule *via* the carbonyl oxygen of tfac(2−) as was observed for [Pd(acac)(6-chloro-3 or 4-pyridyl)(PPh_3)][19] is not a plausible mechanism for the present case, since a free ligand such as pyridine, triphenylphosphine, and tris(*o*-tolyl)phosphine added to a solution of **12** showed no promoting effect. No evidence to support mechanism *via* a three-coordinate[20] or a nonplanar four-coordinate[21] intermediate as proposed for some complexes has been obtained in the present case. The exact nature of the fluxional motion of **12** is not clear at the present stage of investigation.

The ^{19}F NMR spectrum of **5** shows a broad signal with the half-height width of 2.6 Hz at 72.60 ppm upfield from external $CFCl_3$. The broadness may be caused by coupling to the phosphorus atom situated at the trans position, since the ^{19}F signal from [Pt(tfac(2−)-*C,O*)(PPh_3)$_2$] appears as a doublet owing to coupling to ^{31}P with ^5J(P–F)=1.1 Hz.[11] Figure 1 shows the ^{31}P{^{1}H} NMR spectra of **2** and **5** in $CDCl_3$. Complex **5** exhibits a quartet at 37.2$_0$ ppm downfield from external H_3PO_4 with ^5J(P–F)=0.9 Hz in accord with the proposed trans arrangement. Complex **2** shows an AB quartet (^2J(P–P)=35.7 Hz), reflecting nonequivalence of the two phosphorus atoms. The broad signal at 38.5$_8$ ppm is assigned to P^2 trans to O, since the chemical shift is close to that observed for **5** and the broadening is thought to be caused by coupling to the ^{19}F atoms. The sharp doublet at 22.8$_4$ is thus assigned to P^1 trans to C. It may be worth noting that the relative positions of the P^1 and P^2 signals are reverse of those for [Pt(tfac(2−)-*C,O*)(PPh_3)$_2$].[11]

Formation of the Trifluoroacetylacetonato(2−) Complexes. In a previous paper[11] [Pt(tfac)$_2$] was reported to react with a Lewis base (L) such as triphenylphosphine, tris(*p*-chlorophenyl)phosphine, and triphenylarsine at room temperature to afford a C,O- chelate of the trifluoroacetylacetonate dianion, [Pt(tfac(2−)-

Table 4. ^{13}C NMR Data in $CDCl_3$[a]

Compd	tfac(2−) CH_2	tfac(2−) C=O	tfac(2−) CH	tfac(2−) CF_3C-O	tfac(2−) CF_3	L and L′
2	41.0 d [70]	203.7 d [3]	99.6	164.2 q {32}	b)	Ph: C^1 131—133c; C^2 134.1 d [13]; C^3 128.4 d [10], 128.2 d [9]; C^4 130.8 d [3], 129.9 d [3]
3	27.1 d [4]	204.5 d [2]	100.4 q {3}	165.2 dq {34} [2]	b)	Ph: C^1 b); C^2 134.0 d [12]; C^3 128.7 d [11]; C^4 131.0 d [3] py: C^2 150.1; C^3 124.3; C^4 137.2
4	27.2 d [5] (135)	205.2	100.2 q {2—3} (161)	165.2 dq {30} [8]	120.8 dq {282} [8]	Ph: C^1 b); C^2 134.2 d [12]; C^3 128.5 d [10]; C^4 130.8 d [3] Me_2N-py: Me 39.0; C^2 149.1; C^3 106.5; C^4 153.9
5	27.6 d [4] (137)	204.8	99.9 q {2} (160)	165.7 dq {31} [2]	120.6 dq {282} [9]	Ph: C^1 b); C^2 133.7 d [11]; C^3 128.6 d [11]; C^4 130.9 d [3] Me_2-py: Me 25.5; C^2 157.7; C^3 122.3; C^4 137.9
6	27.5 d [4] (137)	205.0	99.9 q {2} (163)	165.6 dq {31} [2]	b)	Tolyl: Me 27.5 d [2], ring-C[c]) Me_2-py: Me 25.5, 25.6; C^2 157.8; C^3 122.2; C^4 137.6
9	24.1 (135)	207.3	101.4 q {2} (161)	164.6 q {31}	120.2 q {281}	Me_2N-py: Me 39.1, 39.2; C^2 151.5, 147.8; C^3 107.9, 106.7; C^4 154.4, 154.1
10[d]	31.3	b)	b)	b)	b)	bpy: c)
12	22.4 (136)	206.0	101.6 q {2} (163)	164.8 q {32}	120.0 q {281}	Me_2-Phen[e]: Me 28.6 br, 23.2 br; $C^{1,1'}$ 127.4; $C^{2,2'}$ 126.5 br; $C^{3,3'}$ 137.4; $C^{4,4'}$ b); $C^{5,5'}$ 163.8 br; $C^{6,6'}$ 125.8 br

a) Chemical shifts in ppm from internal Me_4Si. Signals are singlet except those marked with d(doublet), dd(doublet of doublets), q(quartet), and dq(doublet of quartets). Figures in parentheses, brackets, and braces give ^1J(C-H), J(C-P), and J(C-F) in Hz, respectively. b) Indiscernible. c) Not be analyzed. d) In a mixture (1:1 by volume) of $CDCl_3$ and CD_3OD.

c)

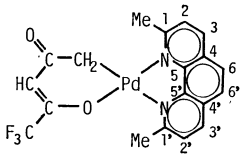

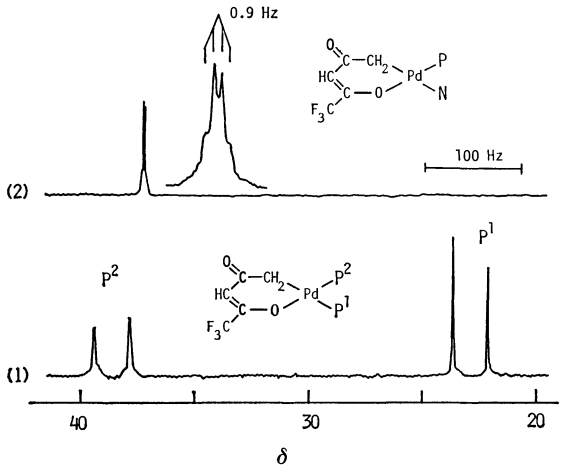

Fig. 1. $^{31}P\{^1H\}$ NMR spectra at 24.2 MHz of [Pd(tfac(2−)-*C,O*)$(PPh_3)_2$] (**2**) (curve 1) and [Pd(tfac-(2−)-*C,O*)(PPh_3)(2,6-Me_2-py)] (**5**) (curve 2) in $CDCl_3$ with H_3PO_4 as an external reference.

C,O)L_2]. The ^1H NMR monitoring revealed that when [Pt(tfac)$_2$] was mixed with a twice molar amount of triphenylphosphine in $CDCl_3$, [Pt(tfac)$(PPh_3)_2$](tfac) was produced at first, which was then converted gradually into [Pt(tfac(2−)-*C,O*)$(PPh_3)_2$].[4b] The tfac anion in the outer sphere of the salt-like compound was supposed to have abstracted a proton from the methyl group of the chelating tfac anion.

The reaction of [Pd(tfac)$_2$] with twice molar triphenylphosphine in $CDCl_3$ was also confirmed by ^1H NMR spectroscopy to form [Pd(tfac)$(PPh_3)_2$]-(tfac).[4b] Contrary to the platinum(II) case, however, the palladium(II) complex is stable and deprotonation of the chelating tfac does not occur spontaneously, although exchange of tfac anions in the inner and outer spheres is rapid on the NMR time scale.[4b] As was described in the Experimental section, addition of a powerful and noncoordinating base, 1,8-bis(dimethylamino)naphthalene ("proton sponge") to the solution of [Pd(tfac)$(PPh_3)_2$](tfac) in dichloromethane was effective for deprotonation of the chelating tfac to give rise to **2**. Employment of pyridine, 4-(dimethylamino)pyridine, and 2,6-dimethylpyridine as a base effected substitution of one phosphine molecule besides deprotonation of the chelating tfac to

result in **3**, **4**, and **5**, respectively. The reaction of $[Pd(tfac)_2]$ with tris(*o*-tolyl)phosphine produces [Pd(tfac)(tfac-*O*){P(*o*-tolyl)$_3$}] reversibly,[4b,22] which also reacts with pyridine derivative (L) to afford **6** and **7**. The latter reactions are also supposed to proceed *via* intermediates of the type [Pd(tfac){P(*o*-tolyl)$_3$}L](tfac).

$[Pd(tfac)_2]$ reacts readily with an equimolar amount of 2,2′-bipyridine in benzene at room temperature to afford [Pd(tfac)(bpy)](tfac).[3c] When the product is isolated and dissolved in hot dichloromethane, the salt-like complex is converted into **10**. Therefore the reactions of $[Pd(tfac)_2]$ with 2,2′-bipyridine, 1,10-phenanthroline, and 2,9-dimethyl-1,10-phenanthroline in dichloromethane to afford complexes **10**, **11**, and **12** are supposed to proceed *via* similar intermediary salt-like complexes. It is interesting that the bidentate base in **12** is easily displaced by pyridine and its derivatives to give **8** and **9**, for instance. These ligand substitution reactions are convenient for synthesis of **8** and related complexes, since the direct reactions between $[Pd(tfac)_2]$ and pyridines attain the following equilibria[3c] and do not give rise to **8** and the like.

$$[Pd(tfac)_2] \overset{py}{\rightleftharpoons} [Pd(tfac)(tfac\text{-}C^3)py] \overset{py}{\rightleftharpoons} [Pd(py)_4](tfac)_2$$

Deprotonation of the chelating tfac monoanion by a base (or tfac itself) might produce a dienediolate complex **13** as an intermediate. Such a dienediolate

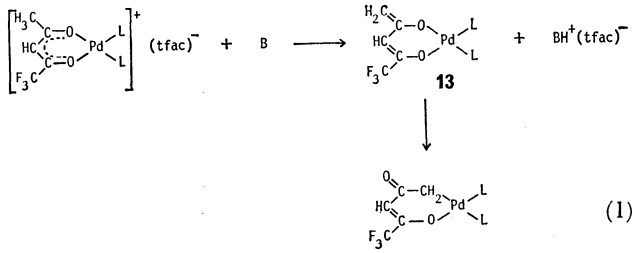

(1)

bonding of acetylacetonate dianion was found in $[(\eta\text{-}C_5H_5)(CO)_2Mn\{PPh(C_5H_6O_2)\}]$[23] and $[(CO)_5M\{PPh(C_5H_6O_2)\}]$ (M=Cr and W).[24] However, complex **13** seems to be unstable in the case of Pd(II) and Pt(II) compounds, transforming into the C,O-chelate. It should be recalled that deprotonation of $[PdCl(CH_2COCH_2COCH_3)(NN)]$ produced mainly the η^3 complex of acac dianion, [Pd(acac(2−)-*C*^{1}—*C*^{3})(NN)], accompanied by a 20—25% amount of [Pd(acac(2−)-*C*,*O*)(NN)] depending on the nature of NN (2,2′-bipyridine, 4,4′-dimethyl-2,2′-bipyridine, and 1,10-phenanthroline), whereas $[PdCl(CH_2COCH_2COOC_2H_5)(bpy)]$ gave solely the trihapto complex.[9] These results reflect the tendencies of the three β-dicarbonyl compounds in the keto-enol tautomerization equilibria. Ethyl acetoacetate, which prefers the keto tautomer,[25] forms the η^3-C^1—C^3 complex of its dianion. On the other hand, trifluoroacetylacetone exists almost totally as the enol tautomer[25] and its dianion forms C,O-chelates. Each of the tfac(2−)-C,O-chelates reported in this paper is not contaminated with the trihapto complex. Acetylacetone shows the intermediate behavior.

The fact must be added that $[Pd(tfac)(PPh_3)_2]ClO_4$[26] does not undergo the reaction with nitrogen bases to afford the tfac(2−) chelate. Some kind of cooperation of the tfac anion in the outer sphere might be necessary for deprotonation of the chelating tfac by a nitrogen base. On the other hand the reactions of $[Pd(tfac)(PCy_3)_2](tfac)$,[4b] where PCy_3 abbreviates tricyclohexylphosphine, with nitrogen bases did not afford the tfac(2−) chelate. Trials to prepare [Pd(tfac(2−)-*C*,*O*)$(PR_3)_2$] complexes by the reactions of $[Pd(tfac)_2]$ with trialkylphosphines such as PEt_3 were not successful either. Stronger basicities and/or larger steric demands of PCy_3 and PEt_3 than PPh_3 might be unfavorable for the deprotonation. Although the mechanism is not clear at present, it is worth noting that deprotonation of the chelating tfac anion (Eq. 1) occurs easily under very mild conditions, since dianions of β-dicarbonyl compounds are usually prepared under more severe conditions.[27]

To our knowledge, the first example of the reported β-dik(2−) C,O-chelates is bis(acetylacetonato(2−)-*C*,*O*)selenium(IV). This compound was claimed in patents to have been prepared by the reaction between selenium(IV) oxide and acetylacetone[28] and was used as a brightener in a copper plating bath.[29] The acac(2−) chelates of palladium(II) [Pd(acac(2−)-*C*,*O*)(NN)] could not be isolated either, but characterized only by ^{1}H NMR spectra in solution.[9] On the other hand, the corresponding tfac(2−)-C,O chelates of platinum(II) and palladium(II) were isolated as pure compounds to allow full characterization by NMR spectroscopy, and fortunately single crystals of **5′** suitable for X-ray analysis were obtained.

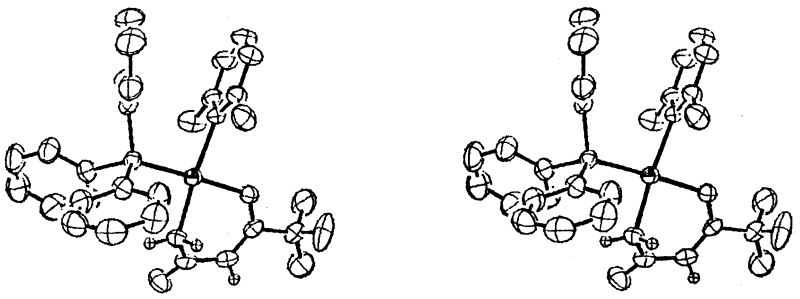

Fig. 2. A stereoscopic view of [Pd(tfac(2−)-*C*,*O*)(PPh_3)(2,6-Me_2-py)] (**5**) molecule. Non-hydrogen atoms are represented by thermal ellipsoids at 50% probability level. Hydrogen atoms attached only to the α- and γ-carbon atoms of the tfac(2−) dianion are drawn as spheres with the radius of 0.1 Å.

Table 5. Selected bond lengths and bond angles with estimated standard deviations in parentheses

(a) Bond length l/Å

Pd-C(1)	2.051(4)	C(1)-C(2)	1.481(6)
Pd-O(1)	2.075(3)	C(2)-C(3)	1.458(6)
Pd-P	2.224(1)	C(3)-C(4)	1.360(6)
Pd-N	2.165(3)	C(4)-C(5)	1.512(6)
P-C(11)	1.825(5)	C(4)-O(1)	1.283(5)
P-C(21)	1.827(5)	C(2)-O(2)	1.227(6)
P-C(31)	1.817(5)	C(5)-F(1)	1.307(7)
C(11)-C(12)	1.405(8)	C(5)-F(2)	1.316(6)
C(12)-C(13)	1.367(10)	C(5)-F(3)	1.339(6)
C(13)-C(14)	1.346(13)		
C(14)-C(15)	1.391(12)	N-C(41)	1.345(6)
C(15)-C(16)	1.406(9)	N-C(45)	1.349(6)
C(16)-C(11)	1.408(8)	C(41)-C(42)	1.403(8)
C(21)-C(22)	1.385(7)	C(42)-C(43)	1.382(9)
C(22)-C(23)	1.391(8)	C(43)-C(44)	1.362(9)
C(23)-C(24)	1.368(9)	C(44)-C(45)	1.380(8)
C(24)-C(25)	1.376(8)	C(41)-C(46)	1.524(7)
C(25)-C(26)	1.380(8)	C(45)-C(47)	1.501(8)
C(26)-C(21)	1.379(7)		
C(31)-C(32)	1.396(7)	C(B1)-C(B2)	1.377(12)
C(32)-C(33)	1.394(9)	C(B2)-C(B3)	1.368(12)
C(33)-C(34)	1.376(10)	C(B3)-C(B4)	1.401(13)
C(34)-C(35)	1.358(10)	C(B4)-C(B5)	1.304(13)
C(35)-C(36)	1.365(9)	C(B5)-C(B6)	1.394(14)
C(36)-C(31)	1.393(7)	C(B6)-C(B1)	1.402(13)

(b) Bond angle ϕ/°

P-Pd-C(1)	87.95(13)	Pd-C(1)-C(2)	112.2(3)
P-Pd-N	96.81(10)	C(1)-C(2)-C(3)	118.3(4)
N-Pd-O(1)	85.40(13)	C(1)-C(2)-O(2)	121.1(5)
O(1)-Pd-C(1)	89.82(15)	C(3)-C(2)-O(2)	120.5(5)
P-Pd-O(1)	177.54(9)	C(2)-C(3)-C(4)	124.2(5)
N-Pd-C(1)	174.54(15)	C(3)-C(4)-O(1)	129.4(4)
		C(3)-C(4)-C(5)	118.7(4)
		C(5)-C(4)-O(1)	111.9(4)
Pd-P-C(11)	112.50(16)	Pd-O(1)-C(4)	122.6(3)
Pd-P-C(21)	111.65(15)	C(4)-C(5)-F(1)	111.8(5)
Pd-P-C(31)	117.58(15)	C(4)-C(5)-F(2)	115.8(5)
C(11)-P-C(21)	105.0(3)	C(4)-C(5)-F(3)	111.6(4)
C(11)-P-C(31)	102.9(3)	F(1)-C(5)-F(2)	106.8(3)
C(21)-P-C(31)	106.1(3)	F(1)-C(5)-F(3)	104.6(4)
		F(2)-C(5)-F(3)	105.5(5)
C(11)-C(12)-C(13)	121.0(6)	Pd-N-C(41)	120.9(3)
C(12)-C(13)-C(14)	120.1(8)	Pd-N-C(45)	119.7(3)
C(13)-C(14)-C(15)	121.4(9)	C(41)-N-C(45)	119.5(4)
C(14)-C(15)-C(16)	120.0(7)	N-C(41)-C(42)	120.3(5)
C(15)-C(16)-C(11)	118.2(6)	N-C(41)-C(46)	118.2(5)
C(16)-C(11)-C(12)	119.2(5)	C(42)-C(41)-C(46)	121.6(5)
C(21)-C(22)-C(23)	121.6(5)	C(41)-C(42)-C(43)	120.0(4)
C(22)-C(23)-C(24)	118.9(6)	C(42)-C(43)-C(44)	118.4(7)
C(23)-C(24)-C(25)	120.0(6)	C(43)-C(44)-C(45)	120.3(6)
C(24)-C(25)-C(26)	121.0(6)	C(44)-C(45)-C(47)	120.8(5)
C(25)-C(26)-C(21)	119.9(5)	N-C(45)-C(44)	121.5(5)
C(26)-C(21)-C(22)	118.5(5)	N-C(45)-C(47)	117.7(5)
C(31)-C(32)-C(33)	118.9(6)	C(B1)-C(B2)-C(B3)	117.5(8)
C(32)-C(33)-C(34)	121.0(7)	C(B2)-C(B3)-C(B4)	122.8(9)
C(33)-C(34)-C(35)	120.0(7)	C(B3)-C(B4)-C(B5)	119.3(9)
C(34)-C(35)-C(36)	120.0(7)	C(B4)-C(B5)-C(B6)	120.7(10)
C(35)-C(36)-C(31)	121.7(6)	C(B5)-C(B6)-C(B1)	119.9(9)
C(36)-C(31)-C(32)	118.3(4)	C(B6)-C(B1)-C(B2)	119.7(8)

Molecular and Crystal Structure of [Pd(tfac(2−)-C,O)(PPh$_3$)(2,6-Me$_2$-py)]·C$_6$H$_6$ (5′). A stereoscopic drawing (*ORTEP* II)[30] of the **5** molecule is depicted in Fig. 2. Selected bond lengths and bond angles are listed in Table 5. Numbering scheme of atoms in **5** is given in Fig. 3.

The remarkable feature of the structure of **5** molecule is that the palladium atom is C,O-chelated by the tfac(2−) dianion as was expected from the spectroscopic studies (Figs. 2 and 3). The coordination around the palladium atom is essentially square-planar: the Pd atom shows the maximum deviation from the mean plane [0.034(2) Å]. The tfac(2−) dianion is not planar. Two locally planar parts are formed by the C(1), C(2), C(3), and O(2) atoms and by the C(3), C(4), C(5), and O(1) atoms. The dihedral angle between these planes is 29.3(2)°. The tfac(2−) dianion makes a distorted six-membered ring with a central palladium atom. The C(1) atom bonded to the palladium has a distorted sp^3 geometry, bond angles around the C(1) being 112.2(3), 114(3), 97(3), 109(3), 110(3), and 114(4)°. The Pd–C(1) bond length [2.051(4) Å] is consistent with the expected Pd(II)–C(sp^3) bond length and is equal to that (trans to N) in [PdCl(CH$_2$COCH$_2$COOCH$_2$Ph)(py)$_2$] [2.051(8) Å].[8b] The Pd–C(1) length is also equal to that in [(acac)PdCH$_2$COOH(PPh$_3$)][2.063(4) Å],[31] but shorter than those in [(PPh$_3$)$_2$Pd{(CH$_2$C=O)$_2$O}][2.124(11) and 2.141(13) Å].[32] The Pd–O(1) bond length [2.075(3) Å] seems to be equal to those in [(PPh$_3$)Pd(acac)-(acac-*C*^{3})][2.048(10) and 2.062(10) Å][5a] and that in a C,O-chelate, [Pd(C$_2$H$_2$O$_2$)(PPh$_3$)(py)][2.093(11) Å].[33] The Pd–N bond length [2.165(3) Å] is slightly longer than those in [PdCl(CH$_2$COCH$_2$COOCH$_2$Ph)-(py)$_2$][2.120(6) and 2.027(6) Å],[8b] and also longer than those in [{Pd(acac)(NHEt$_2$)$_2$}$^+$(acac)$^-$][both 2.044(3) Å],[34] whereas the Pd–N bond length in [Pd-(C$_2$H$_2$O$_2$)(PPh$_3$)(py)][2.144(12) Å] seems equal to that in the present complex **5′**. The 2,6-Me$_2$-py ring plane stands approximately normal to the coordination plane, the dihedral angle between these planes being 83.80(15)°.

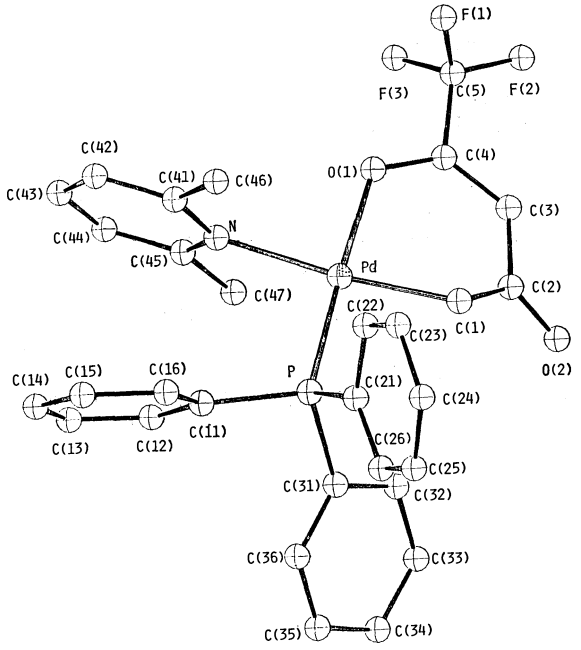

Fig. 3. The numbering scheme of non-hydrogen atoms of the **5** molecule.

Table 6. Intermolecular atomic constants[*l*/Å] less than 3.5 Å with estimated standard deviations in parentheses

F(1)···C(1)[a]	3.457(6)	
F(1)···C(22)[a]	3.365(7)	Key: a, 1−*x*, −*y*, −*z*,
C(24)···C(47)[b]	3.460(9)	b, *x*, 0.5−*y*, −0.5+*z*,
C(B3)···F(3)[c]	3.482(10)	c, −*x*, 0.5−*y*, 0.5−*z*,
C(B1)···F(2)[d]	3.406(9)	d, 1−*x*, 0.5+*y*, 0.5−*z*.

Complex **5′** forms the crystal structure shown in Fig. 4 (*ORTEP* II)[30] Intermolecular atomic contacts less than 3.5 Å are listed in Table 6. Close contacts are mainly involved between the fluorine atoms of the CF$_3$ group in one molecule and the carbon atoms in the neighboring molecules. The closest distance is F(1) (*x*, *y*, *z*)···C(22) (1−*x*, *y*, −*z*) [3.365(7) Å].

We wish to thank Mr. Junichi Gohda for elemental analyses and Mr. Tetsu Hinomoto of JEOL, Ltd. for ^{19}F NMR measurements. S. K. is grateful to the Ministry of Education, Science and Culture for Grant-in-Aid for Scientific Research, No. 243014.

References

1) R. C. Mehrotra, R. Bohra, and D. P. Gaur, "Metal β-Diketonates and Allied Derivatives," Academic Press, New York (1978).

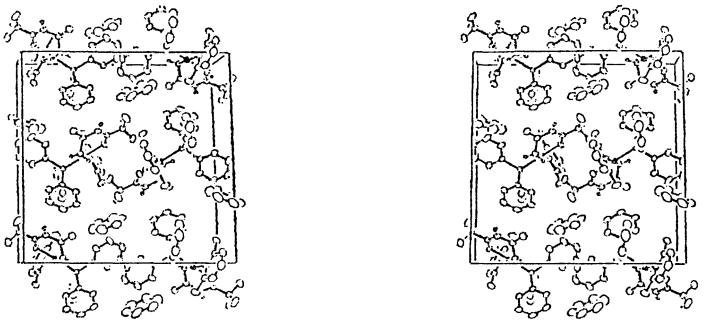

Fig. 4. A stereoscopic view of the crystal structure of [Pd(tfac(2−)-*C*,*O*)(PPh$_3$)-(2,6-Me$_2$py)]·C$_6$H$_6$ (**5′**).

2) J. P. Fackler, Jr., *Prog. Inorg. Chem.*, **7**, 361 (1966); K. C. Joshi and V. N. Pathak, *Coord. Chem. Rev.*, **22**, 37 (1977).
3) a) S. Baba, T. Ogura, and S. Kawaguchi, *Bull. Chem. Soc. Jpn.*, **47**, 665 (1974); b) T. Ito, T. Kiriyama, Y. Nakamura, and A. Yamamoto, *ibid.*, **49**, 3257 (1976); c) S. Okeya, H. Sazaki, M. Ogita, T. Takemoto, Y. Onuki, Y. Nakamura, B. K. Mohapatra, and S. Kawaguchi, *ibid.*, **54**, 1978 (1981) and references cited therein; d) S. Okeya, Y. Nakamura, and S. Kawaguchi, *ibid.*, in press.
4) a) T. Ito, T. Kiriyama, and A. Yamamoto, *Bull. Chem. Soc. Jpn.*, **49**, 3250 (1976); b) S. Okeya, Y. Nakamura, and S. Kawaguchi, *ibid.*, **54**, 3396 (1981) and references cited therein.
5) a) M. Horike, Y. Kai, N. Yasuoka, and N. Kasai, *J. Organomet. Chem.*, **72**, 441 (1974); b) S. Okeya, S. Kawaguchi, N. Yasuoka, Y. Kai, and N. Kasai, *Chem. Lett.*, **1976**, 53.
6) Y. Tezuka, T. Ogura, and S. Kawaguchi, *Bull. Chem. Soc. Jpn.*, **42**, 443 (1969); K. Oda, N. Yasuoka, T. Ueki, N. Kasai, and M. Kakudo, *ibid.*, **43**, 362 (1970).
7) Z. Kanda, Y. Nakamura, and S. Kawaguchi, *Inorg. Chem.*, **17**, 910 (1978).
8) a) S. Baba, T. Sobata, T. Ogura, and S. Kawaguchi, *Bull. Chem. Soc. Jpn.*, **47**, 2792 (1974); b) M. Horike, Y. Kai, N. Yasuoka, and N. Kasai, *J. Organomet. Chem.*, **86**, 269 (1975).
9) N. Yanase, Y. Nakamura, and S. Kawaguchi, *Inorg. Chem.*, **19**, 1575 (1980).
10) S. Okeya, Y. Nakamura, S. Kawaguchi, and T. Hinomoto, *Bull. Chem. Soc. Jpn.*, in press.
11) S. Okeya, Y. Nakamura, S. Kawaguchi, and T. Hinomoto, *Inorg. Chem.*, **20**, 1576 (1981).
12) N. Yanase, Y. Nakamura, and S. Kawaguchi, *Inorg. Chem.*, **17**, 2874 (1978).
13) Y. Otani, Y. Nakamura, S. Kawaguchi, S. Okeya, and T. Hinomoto, *Chem. Lett.*, **1981**, 11.
14) S. Okeya, S. Ooi, K. Matsumoto, Y. Nakamura, and S. Kawaguchi, *Bull. Chem. Soc. Jpn.*, **54**, 1085 (1981).
15) T. Ashida, *HBLS* V, "Universal Crystallographic Computing System-Osaka," Computation Center, Osaka Univ. (1973), p. 55.
16) International Tables for X-Ray Crystallography, The Kynoch Press, Birmingham (1974), Vol. IV, p. 71.
17) R. F. Stewart, E. R. Davidson, and W. T. Simpson, *J. Chem. Phys.*, **42**, 3175 (1965).
18) W. C. Hamilton, *Acta Crystallogr.*, **12**, 609 (1969).
19) H. Tanaka, K. Isobe, and S. Kawaguchi, *Chem. Lett.*, **1981**, 769.
20) R. Romeo, D. Minniti, and S. Lanza, *Inorg. Chem.*, **19**, 3663 (1980).
21) S. H. Strauss, S. E. Diamond, F. Mares, and D. F. Shriver, *Inorg. Chem.*, **17**, 3064 (1978); T. Yoshida, D. L. Thorn, T. Okano, S. Otsuka, and J. A. Ibers, *J. Am. Chem. Soc.*, **102**, 6451 (1980).
22) S. Matsumoto and S. Kawaguchi, *Bull. Chem. Soc. Jpn.*, **54**, 1704 (1981).
23) J. von Seyerl, D. Neugebauer, and G. Huttner, *Angew. Chem., Int. Ed. Engl.*, **16**, 858 (1977).
24) J. von Seyerl, D. Neugebauer, G. Huttner, C. Krüger, and Y.-H. Tsay, *Chem. Ber.*, **112**, 3637 (1979).
25) The enol contents of neat ethyl acetoacetate, acetylacetone, and trifluoroacetylacetone at 33 °C are 8, 81, and 97%, respectively [J. L. Burdett and M. T. Rogers, *J. Am. Chem. Soc.*, **86**, 2105 (1964)].
26) S. Okeya *et al.*, to be published.
27) T. H. Harris and C. M. Harris, *Org. React.*, **17**, 155 (1969); T.-H. Chan and P. Brownbridge, *J. Chem. Soc., Chem. Commun.*, **1979**, 578.
28) P. W. Moy, U. S. Patent 3497530; *Chem. Abstr.*, **72**, 96097x (1970).
29) P. W. Moy, U. S. Patent 3480524; *Chem. Abstr.*, **72**, 38310a (1970).
30) C. K. Johnson, *ORTEP* II, Report ORNL-5138, Oak Ridge National Laboratory, Tennessee (1976).
31) Y. Zenitani, K. Inoue, Y. Kai, N. Yasuoka, and N. Kasai, *Bull. Chem. Soc. Jpn.*, **49**, 1531 (1976).
32) Y. Zenitani, H. Tokunan, Y. Kai, N. Yasuoka, and N. Kasai, *Bull. Chem. Soc. Jpn.*, **51**, 1730 (1978).
33) Y. Kai, N. Yasuoka, and N. Kasai, *Bull. Chem. Soc. Jpn.*, **52**, 737 (1979).
34) S. Kotake, T. Sei, K. Miki, Y. Kai, N. Yasuoka, and N. Kasai, *Bull. Chem. Soc. Jpn.*, **53**, 10 (1980).

Solute-Solvent Interactions in Ion Pair Extraction of Tetraalkylammonium Iodides. II. The Effect of Hydration of Iodide in Organic Solvents on the Extraction Constant

Kazuaki Ito, Etsuro Iwamoto, and Yuroku Yamamoto*

Department of Chemistry, Faculty of Science, Hiroshima University, Naka-ku, Hiroshima 730

(Received January 21, 1982)

Solubilities of tetraalkylammonium iodides Et_4NI, Pr_4NI, and Bu_4NI in nitrobenzene, in water, and in their mutually saturated solvents, and of Pr_4NI in 1,1-dichloroethane and in its water saturated solvent were measured at 25 °C. Conductances of Et_4NI, Pr_4NI, and Bu_4NI in nitrobenzene and Bu_4NI in 1,1-dichloroethane, 1,2-dichloroethane, and dichloromethane have also been measured at 25 °C. A small amount of water in organic solvents increases the solubilities of the salts roughly twice those in pure solvents and decreases the association constants around 15% while a small amount of organic solvent in water gives a slight effect. Effects of mutual saturation of water and organic solvent on extraction equilibria of R_4NI were discussed in terms of the selective hydration of the iodide.

In the preceding paper,[1] we have investigated the extraction equilibria of tetraalkylammonium iodides (R_4NI) between water and eight organic solvents, and proposed a new treatment of "ionic" and "neutral" extraction constants. The results indicated that the influences of the solvents on the extractability of R_4NI can be interpreted in terms of the following properties; the dielectric constant for the ionic part, the solubility parameter for the neutral, and the hydrogen bonding for both.

The ion pair extraction is primarily concerned with the distribution of salts between water and an immiscible organic phase, but both water and organic solvent molecules are slightly soluble in each other. In addition, water is coextracted into the organic phase[2–6] with ion pairs, and organic solvent molecules are salted-in in the aqueous phase.[7,8] However, little is known concerning to what degree the mutual saturation of solvents contributes to the ion pair extraction equilibria.

The purpose of this paper is to investigate interactions between ion pairs and a minute quantity of water in an organic solvent or of organic solvent in aqueous phase by solubility and conductivity measurements and to clarify their effects on the process of ion pair extraction in connection with solvent effects on extractability of R_4NI.

Experimental

The purification of the solvents, {nitrobenzene (NB), 1,1-dichloroethane (1,1-DCE), 1,2-dichloroethane (1,2-DCE), and dichloromethane (DCM)} and of tetraalkylammonium iodides, R_4NI (R=Et, *n*-Pr, and *n*-Bu) and the distribution ratio measurements were the same as those reported previously.[1] The distribution ratio was calculated using the expression, D=[specific activity (cpm ml^{-1}) of radionuclide ^{131}I in organic phase]/[specific activity (cpm ml^{-1}) in aqueous phase].

The conductivity bridge and cell used have been described previously.[1] Anhydrous organic solutions were prepared in a dry box filled with dry nitrogen gas under slight pressure.

Solubility measurements were carried out as follows; (1) saturated solutions of the salts in pure water and organic solvents (*ca.* 40 ml) were prepared by vigorously agitating the solvents with an excess of the salts for at least 2 d in a thermostated water bath (25±0.05 °C). (2) Saturated solutions of the salts in organic solvents equilibrated with water (and vice versa) were prepared with an excess of both the salts and water (and of both the salts and organic solvents). An aliquot (*ca.* 1 ml) of the saturated aqueous solution was passed through a sintered-glass filter and weighed. Solubilities were determined by potentiometric titration of the iodide ion with silver nitrate. Salts in organic solvents were back-extracted into water for the titration; the salt-saturated organic solutions (*ca.* 1 ml) were shaken with water (*ca.* 50 ml) and the organic phase was separated from the aqueous phase by filtration (Toyo filter paper No. 5B). This procedure was repeated several times to back-extract the salt completely. The aqueous filtrates were combined, followed by titration. Measurements were usually continued for 1 week although the solubility equilibria were obtained in at least 2 d. Preliminary measurements confirmed that the back-extraction was completely carried out even in the nitrobenzene solution of Bu_4NI for which the solubility in water is very small compared with those of Pr_4NI and Et_4NI.

Water solubilities in organic solvents were determined coulometrically with a Hiranuma AQ-3 aquacounter. Nitrobenzene solubilities in water were determined by spectrophotometry at 252 nm after extraction into cyclohexane.[8a] Densities were obtained by an Anton Paar Model DMA O2D digital density meter at 25±0.01 °C.

Results

The solubilities of Et_4NI, Pr_4NI, and Bu_4NI at 25 °C are given in Table 1. A small amount of water in nitrobenzene increases the solubilities of R_4NI largely, while a small amount of nitrobenzene in water affects hardly. The increase in solubility of R_4NI in nitrobenzene corresponds to the salting-in of water by R_4NI. It was found that Pr_4NI (0.476 mol dm^{-3}) in nitrobenzene increases the solubility of water from 0.168 to 0.620 mol dm^{-3} and Pr_4NI (0.561 mol dm^{-3}) in water increases the solubility of nitrobenzene from 0.0156 to 0.0231 mol dm^{-3}. For the water–1,1-DCE system, a small amount of water increases also the solubility of Pr_4NI. Our value for Pr_4NI in dry 1,1-dichloroethane (1.96×10^{-2} mol dm^{-3}) agrees with the value (2.04×10^{-2} mol dm^{-3}) obtained by Abraham *et al.*[9] The solid phase in equilibrium with the saturated solution was checked by chemical analysis and differential thermal analysis, and no solvate was found.

Table 1. Solubilities in mol dm^{-3} of R_4NI at 25 °C

Salt	H_2O ($S_w°$)	H_2O equilibrated with NB (S_w)	$S_w/S_w°$	NB ($S_o°$)	NB equilibrated with H_2O (S_o)	$S_o/S_o°$
Et_4NI	1.416 a)			1.82×10^{-2}	3.33×10^{-2}	1.83
n-Pr_4NI	5.40×10^{-1}	5.61×10^{-1}	1.04	1.74×10^{-1}	4.76×10^{-1}	2.74
n-Bu_4NI	6.77×10^{-2}	6.84×10^{-2}	1.01	6.60×10^{-1}	1.27	1.92
Salt	H_2O ($S_w°$)	H_2O equilibrated with 1,1-DCE (S_w)	$S_w/S_w°$	1,1-DCE ($S_o°$)	1,1-DCE equilibrated with H_2O ($S_o°$)	$S_o/S_o°$
n-Pr_4NI	5.40×10^{-1}	5.68×10^{-1}	1.05	1.96×10^{-2}	4.94×10^{-2}	2.52

a) From Ref. 16, molal scale was converted to molar scale.

Table 2. Association constant, $K_a°$ and K_a at 25 °C

Solvent	Salt	Anhydrous solvent ($K_a°$)	Water-saturated solvent (K_a)	$K_a°/K_a$
NB	Et_4NI	38±1	35 a)	1.09
NB	*n*-Pr_4NI	35±1	33 a)	1.06
NB	*n*-Bu_4NI	38±1	33 a)	1.15
1,2-DCE	*n*-Bu_4NI	$(6.70\pm0.07)\times10^3$	5.83×10^3 a)	1.15
1,1-DCE	*n*-Bu_4NI	$(7.30\pm0.10)\times10^4$	6.54×10^4 a)	1.12
DCM	*n*-Bu_4NI	$(3.77\pm0.04)\times10^4$	3.26×10^4 a)	1.16

a) From Ref. 1.

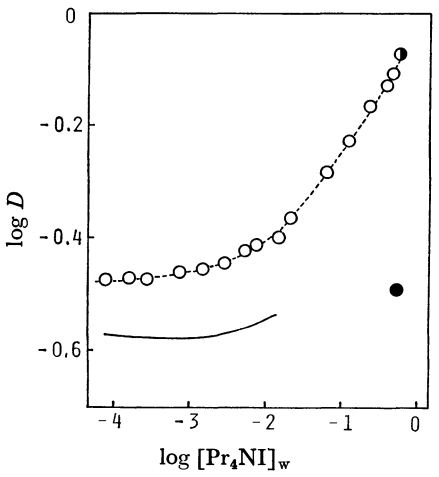

Fig. 1. Concentration dependence of distribution ratio for Pr_4NI in the water–nitrobenzene system at 25 °C. Solid line is the curve calculated from the extraction constants in Table 4. ◑: Solubility ratio for the mutually saturated solvent system, ●: solubility ratio for the pure solvent system.

Distribution ratios of Pr_4NI for the nitrobenzene–water extraction system were determined as a function of the salt concentration (Fig. 1). The distribution ratio increases with increasing the salt concentration and the solubility ratio (D=0.848) of Pr_4NI for mutually equilibrated solvents falls on the extended line. This also provides another evidence that no solvate is found.

The ionic association constant, K_a and the limiting conductance, Λ_0 of R_4NI were determined by the method of Shedlovsky.[10] The calculation was carried out using the conductances of the salts covering from 2×10^{-3} to 2×10^{-5} mol dm^{-3}. Shown in Table 2 are the ionic association constants of R_4NI in water-free and water-saturated organic solvents at 25 °C. The results indicated that the association constants in water-free solvents are larger by 10—15% than those in water-saturated solvents.

Discussion

Organic Phase. The quantity of water coextracted increases linearly with increasing salt concentration,[2-4] although the degree of dissociation of ion-pair changes markedly.[1] Pr_4NI,[3b] Bu_4NI,[4] $[Fe(phen)_3]I_2$,[2a] and $[Fe(bpy)_3]I_2$,[2a] coextract 0.98, 0.91, 1.1, and 1.1 mol of water per iodide ion into nitrobenzene, respectively, while Bu_4NBPh_4 does not coextract any water molecules. Similarly, in this study the values of 1.0, 0.95, and 1.1 mol of water per iodide ion were obtained in the saturated solutions of Et_4NI, Pr_4NI, and Bu_4NI, respectively. The value of 1.0 does not mean that the iodide anion in nitrobenzene carry exactly one water molecule, but more likely represents a distribution of the species involving hydrated and nonhydrated iodide anions and ion pairs.

The hydration of iodide anions (the ionic part) and ion pairs (the neutral part) is represented by the following equilibria,

$$I^-\cdot(m-1)H_2O + H_2O \rightleftharpoons I^-\cdot mH_2O$$

$$R_4NI\cdot(n-1)H_2O + H_2O \rightleftharpoons R_4NI\cdot nH_2O$$

with the corresponding formation constants,

$$K_m^- = [I^-\cdot mH_2O]/[I^-\cdot(m-1)H_2O]\,[H_2O], \quad (1)$$

$$K_n^p = [R_4NI\cdot nH_2O]/[R_4NI\cdot(n-1)H_2O]\,[H_2O]. \quad (2)$$

The hydration constants (K_1^-=3.45 mol dm^{-3}, K_2^-=2.60, and K_3^-=1.37) were determined from the dependence of the c.t.t.s. spectra between I^- and nitro-

benzene in the visible region on water contents in nitrobenzene solution of Pr_4NI.[11]

A small amount of protic solvent such as methanol significantly decreases the degree of ionic association for halide salts in low dielectric solvents.[12] The solubilities of water in the organic solvents used here are so small (below 0.02 mol fraction) that the water effects on dielectric constants are considered to be negligeble.[13] The change in the association constant by adding a small amount of water in organic solvents, thus, can be attributed to the hydration of the iodide anion.

The ionic association constant in organic solvents containing water is written by using Eqs. 1 and 2,

$$K_a = ([R_4NI]/[R_4N^+][I^-]f_\pm^2)(1+\sum^{n} K_1^p K_2^p \cdots K_n^p [H_2O]^n)/$$
$$(1+\sum^{m} K_1^- K_2^- \cdots K_m^- [H_2O]^m). \quad (3)$$

The first parenthesis on the right hand side in Eq. 3 is K_a°, the ionic association constant in pure organic solvent. The ratio of K_a° to K_a yields the relation,

$$(K_a^\circ/K_a) = (1+\sum^{m} K_1^- K_2^- \cdots K_m^- [H_2O]^m)/$$
$$(1+\sum^{n} K_1^p K_2^p \cdots K_n^p [H_2O]^n). \quad (4)$$

If the affinity of water for the iodide anion is greater than that for the iodide ion pair, the extent of ion pair association decreases in the presence of water. A small amount of water in nitrobenzene decreases the association constants of R_4NI by about 10% and the cation dependence is small (Table 2). This reveals that the hydration constants of the ion pairs are almost constant and are slightly less than that of the iodide anion. It has been reported that cation effects[14] were not observed in the formation phenol–halide anion complexes for a variety of quaternary ammonium salts in solvents of low dielectric constant such as dichloromethane in which salts are extensively ionic-associative. Ion pair formation between tetraalkylammonium cations and halide anions is almost electrostatic and has very modest geometrical requirements compared to mono-, di, and trialkylammonium salts which bear the sites for complex formation due to hydrogen bond.[14,15] So the hydration of the iodide ion pair is not so much different from that of the iodide anion. All the association constants of Bu_4NI in anhydrous NB, 1,2-DCE, 1,1-DCE, and DCM are about 15% greater than those in water-saturated solvents. The result that the value of K_a°/K_a is almost constant among the organic solvents would be partly because there is no specific interactions between the iodide and the solvents.

Aqueous Phase. The solubility of salts in water equilibrated with organic solvents is governed by the overall effect of mutual interactions among the three components (ion, water, and organic solvent) and can be examined from the view point of salting effects. Tetraalkylammonium salts increase the solubility of nitrobenzene in water although alkali metal halides such as NaBr do not.[8a] The salting-in by R_4N^+ is controlled mainly by the water structural effects through hydrophobic interactions which are decreased in the order, $Am_4N^+ > Bu_4N^+ > Pr_4N^+ > Et_4N^+$.[8a] Pr_4NI and Bu_4NI in the salt-saturated solutions increase solubilities of nitrobenzene with 48% and 9.6% in comparison with those in pure water, respectively (Table 3). The salting-in coefficient of Bu_4NI is reasonably larger (negative value) than that of Bu_4NBr (-0.513).[8a] Salting-in effects on benzene by aliphatic ions such as Bu_4N^+ were found to be weaker than those of aromatic ions such as Ph_4P^+ and BPh_4^- since van der Waals forces are less effective for aliphatic ions than for aromatic ions.[8b] Thus, the weaker interaction between R_4N^+ and nitrobenzene does not so much contribute to the solubility of R_4NI in aqueous phase.

Table 3. The salting-in of nitrobenzene by R_4NI in the salt-saturated aqueous solution at 25 °C

	Solubility		k_s[a]
	Nitrobenzene S/mol dm^{-3}	Salt C_s/mol dm^{-3}	
(Pure water)	0.0156[b]	—	—
n-Pr_4NI	0.0231	0.561	−0.304
n-Bu_4NI	0.0171	0.0684	−0.583

a) Salting effect coefficient $k_s = 1/C_s \times \log(S^\circ/S)$, where S° and S are the solubility of nitrobenzene in water and in a salt solution, respectively. b) From Ref. 8a.

Extraction Constant. In the extraction of tetraalkylammonium iodides the equilibrium is represented as

$$R_4N_w^+ + I_w^- + R_4NI_w \rightleftharpoons R_4N_o^+ + I_o^- + R_4NI_o,$$

where the subscripts w and o designate the aqueous and organic phases, respectively. The fraction of triple ions is so small that the triple ion term can be disregarded.[1] The extraction constant for the ionic species is

$$K_i = [R_4N^+]_o[I^-]_o f_{\pm o}^2/[R_4N^+]_w[I^-]_w f_{\pm w}^2 \quad (5)$$

for the associated species

$$K_n = [R_4NI]_o/[R_4NI]_w, \quad (6)$$

$$K_n' = [R_4NI]_o/[R_4N^+]_w[I^-]_w f_{\pm w}^2. \quad (7)$$

When the association constant of all the salts in water is taken as unity, we get the relation $K_n = K_n'$ since $[R_4NI]_w = [R_4N^+]_w[I^-]_w f_{\pm w}^2$ where $f_\pm$ is the mean ionic activity coefficient. The activity coefficient of ion pair is taken as unity. As mentioned above, since water and organic solvents are salted in by R_4NI for the solvent extraction system, the transfer free energy of R_4NI is different from that of the ion pair from one pure solvent to another pure solvent. The tetraalkylammonium cations are essentially non-hydrated in organic solvents and the solubilities of R_4NI in water equilibrated with organic solvents are almost the same as those in water, so Eqs. 5 and 6 can be rewritten upon introduction of Eqs. 1 and 2.

$$K_i'' = K_i \times (1+\sum^{m} K_1^- K_2^- \cdots K_m^- [H_2O]_o^m) \quad (8)$$

$$K_n'' = K_n \times (1+\sum^{n} K_1^p K_2^p \cdots K_n^p [H_2O]_o^n) \quad (9)$$

The extraction constants K_i'' and K_n'' for Pr_4NI in the water–nitrobenzene system were obtained at each concentration from the association constants (Table 2)

Table 4. Extraction constants of n-Pr_4NI for nitrobenzene–water system at 25 °C

From solubility ratio in pure solvents		From distribution ratio at $C_i^{a)} = 1.0 \times 10^{-3}$ mol dm^{-3}	
K_i	8.00×10^{-2}	K_i''	1.51×10^{-1} b)
K_n	2.81	K_n''	5.02 b)

a) C_i: The initial salt concentration in aqueous phase.
b) From Ref. 1.

and distribution ratios (Fig. 1). Activity coefficients of Pr_4NI in aqueous phase, which were reported by Lindenbaum and Boyd,[16] were converted to molarity scale from molality scale. Activity coefficients of ions in nitrobenzene were calculated by using the extended Debye-Hückel equation with a value for $\mathring{a}$ of 6 Å. The satisfactory constancy of extraction constants was also observed up to *ca.* 0.02 mol dm^{-3} in nitrobenzene phase as for Bu_4NI in the NB, 1,1-DCE, 1,2-DCE, and DCM systems,[1] showing that the parenthesis terms in Eqs. 8 and 9 are constant. The deviation from the constancy of extraction constants at higher concentration may be attributed to higher aggregates for the solvent extaction system and to the change in water activity in addition to the inadequate application of the Debye-Hückel equation to such concentrated nitrobenzene solutions. The extraction constants K_i and K_n for Pr_4NI in the pure solvent system, which were calculated in a similar way, are also given in Table 4. For this pure solvent system these extraction constants may be almost constant over a wider concentration range because no hydrates and triple ions are formed in nitrobenzene.[1] So imaginary distribution ratios of Pr_4NI in pure solvent system were calculated at any concentration to reproduce the extraction constants obtained and are shown in Fig. 1. This result shows that at an initial salt concentration of 1.0×10^{-3} mol dm^{-3} the hydration of the iodide in nitrobenzene increases the distribution ratio by 31% (from 0.263 for pure case to 0.345 for the mutual saturation case).

For nitrobenzene system the parenthesis terms in Eqs. 8 and 9 are 1.6 and 1.5, respectively, which were calculated using K_a°/K_a (=1.1) from Eq. 4, the hydration constants of the iodide ion, water solubility, and the self-association constant of water (1.054 mol^{-1} dm^3) in nitrobenzene.[17] These values and the extraction constants for the pure solvent system give $K_i''=1.3 \times 10^{-1}$ in Eq. 8 and $K_n''=4.2$ in Eq. 9 which are in good agreement with those obtained from the distribution ratio at the initial concentration 1.0×10^{-3} mol dm^{-3} (Table 4). The hydration for Pr_4NI in the nitrobenzene system thus decreases ΔG_i and ΔG_n by *ca.* 1.5 kJ mol^{-1} which is less than the methylene group contribution 2.6 kJ mol^{-1}.[1] Furthermore, as is seen from the hydration effects on the association constants (Table 2), the decrease in ΔG_i and ΔG_n by the hydration does not seem to depend so much on the organic solvents used.

Our conclusion is that the mutual saturation in both phases affects the extraction equilibria of tetraalkylammonium iodides. Especially the role of a small amount of water which is salted-in in organic solvents is marked but does not depend on the solvents.

This work was supported in part by a Grant-in-Aid for Scientific Research Nos. 443013 and 454183 from the Ministry of Education, Science and Culture.

References

1) E. Iwamoto, K. Ito, and Y. Yamamoto, *J. Phys. Chem.*, **85**, 894 (1981).
2) a) Y. Yamamoto, T. Tarumoto, and T. Tarui, *Bull. Chem. Soc. Jpn.*, **46**, 1466 (1973); b) T. Tarui, *J. Inorg. Nucl. Chem.*, **37**, 1213 (1975).
3) a) T. Kenjo and R. M. Diamond, *J. Phys. Chem.*, **76**, 2454 (1972); b) T. Kenjo and R. M. Diamond, *J. Inorg. Nucl. Chem.*, **36**, 183 (1974).
4) E. M. Arnett, B. Chawla, and N. J. Hornung, *J. Solution Chem.*, **6**, 781 (1977).
5) a) C. Klofutar, S. Paljk, and M. Ostanek, *J. Inorg. Nucl. Chem.*, **38**, 1045 (1976); b) C. Klofutar and Š. Paljk, *ibid.*, **40**, 515 (1978).
6) T. Iwachido, M. Minami, M. Kimura, A. Sadakane, M. Kawasaki, and K. Toei, *Bull. Chem. Soc. Jpn.*, **53**, 703 (1980).
7) F. A. Long and W. F. McDevit, *Chem. Rev.*, **51**, 119 (1952).
8) a) E. Iwamoto, Y. Hiyama, and Y. Yamamoto, *J. Solution Chem.*, **6**, 371 (1977); b) E. Iwamoto, Y. Tanaka, H. Kimura, and Y. Yamamoto, *ibid.*, **9**, 841 (1980).
9) M. H. Abraham and A. F. Danil De Namor, *J. Chem. Soc., Faraday Trans. 1*, **69**, 1375 (1976). The solubility value, 2.04×10^{-4} mol dm^{-3} of Pr_4NI in 1,1-DCE in this literature should read 2.04×10^{-2} mol dm^{-3}.
10) T. Shedlovsky, *J. Franklin Inst.*, **225**, 739 (1938).
11) K. Ito, E. Iwamoto, and Y. Yamamoto, unpublished result.
12) a) H. Sadek and R. M. Fuoss, *J. Am. Chem. Soc.*, **81**, 4507 (1959); b) J. B. Hyne, *ibid.*, **85**, 304 (1963); c) S. Petrucci and M. Battistini, *J. Phys. Chem.*, **71**, 1181 (1967).
13) M. Gerin and J. Fresco, *Anal. Chim. Acta*, **97**, 155, 165 (1978).
14) a) R. P. Taylor and I. D. Kuntz, Jr., *J. Phys. Chem.*, **74**, 4573 (1970); b) R. P. Taylor and I. D. Kuntz, Jr., *J. Am. Chem. Soc.*, **94**, 7963 (1972); c) I. D. Kuntz, Jr., and C. J. Cheng, *ibid.*, **97**, 4852 (1975).
15) a) M. Cl. Haulait and P. L. Huyskens, *J. Phys. Chem.*, **79**, 1812 (1975); b) P. L. Huyskens and Y. O. Lambeau, *ibid.*, **82**, 1886, 1892 (1978).
16) S. Lindenbaum and G. E. Boyd, *J. Phys. Chem.*, **68**, 911 (1968).
17) J. R. Johnson, S. D. Christian, and H. E. Affsprung, *J. Chem. Soc.*, **1967**, 1924.

Dehydrooligopeptides. III. Synthesis of (*Z,Z*)- and (*Z,E*)-Geometric Isomers of Dehydrodipeptides and Their Base-catalyzed Transformation to the Hydantoin Derivatives[1)]

Chung-gi SHIN,* Yasuchika YONEZAWA, Toyofumi YAMADA, and Juji YOSHIMURA†

Laboratory of Organic Chemistry, Faculty of Technology, Kanagawa University, Rokkakubashi, Kanagawa-ku, Yokohama 221

† *Laboratory of Chemistry for Natural Products, Faculty of Science, Tokyo Institute of Technology, Nagatsuta, Midori-ku, Yokohama 227*

(Received July 28, 1981)

N-Benzyloxycarbonyl (Cbz)-(*Z,E*)-dehydrodipeptides, comprised of both (*Z*)- and (*E*)-α-dehydroamino acid residues, were first synthesized by dehydrochlorination of Cbz-(*Z*)-dehydrodipeptides containing an erythro-3-chloro-2-aminobutanoate moiety. Base-catalyzed transformation of the individual Cbz-(*Z, Z*)- and (*Z, E*)-dehydrodipeptides was carried out to give the corresponding new hydantoin derivatives. The NMR spectroscopic differences between the geometric isomers of both dehydrodipeptides and their hydantoin derivatives were elucidated.

In the previous papers,[1-3)] we reported some useful synthetic methods for the currently interesting dehydropeptides which contain more than one α-dehydroamino acid (DHA) or ΔAA[4)] residue. The syntheses of the dehydrodipeptides (DHP), which consist of a (*Z*)-DHA and an α-amino acid (AA) or two (*Z*)-DHAs, were performed by the coupling of (*Z*)-DHA with AA, by the coupling between two (*Z*)-DHAs, or by the base-catalyzed β-elimination of (*Z*)-DHP including a serine (Ser) or a threonine (Thr) residue.

Although the preparation of (*E*)-geometric DHA has been reported,[5)] dehydropeptide containing (*E*)-DHA residue has not yet been synthesized and few studies on the reactivity of ordinary DHP have been undertaken. Here, we will report on the first synthesis of *N*-benzyloxycarbonyl (Cbz)-(*Z,E*)-DHP, composed of (*Z*)-ΔAA-(*E*)-ΔAA sequence, by dehydrochlorination of erythro-3-chloro-2-aminobutanoate [But(Cl)] moiety in (*Z*)-DHP and base-catalyzed transformations of both (*Z,Z*)- and (*Z,E*)-DHP to the corresponding new (*E*)- and (*Z*)-hydantoin derivatives. After the isomerization of the (*E*)-hydantoin derivative to the (*Z*)-isomer, the NMR spectroscopic differences between the (*E*)- and (*Z*)-isomers of both DHPs and the hydantoin derivatives were unambiguously characterized.

Results and Discussion

(Z,E)-Dehydrodipeptides. According to the method which we previously reported,[3)] Cbz-(*Z*)-ΔAA-(*Z*)-ΔAA-OMe [(*Z,Z*)-**6**: **b**, R=C_2H_5; **c**, R=*n*-C_3H_7; **e**, R=C_6H_5], except for **6a** (R=CH_3) and **6d** (R=*i*-C_3H_7),[1)] was prepared by the triethylamine-catalyzed elimination of Cbz-(*Z*)-ΔAA-Thr(Mes)-OMe, derived by the coupling of Cbz-(*Z*)-ΔAA-OH with Thr-OMe, followed by the mesylation of the dipeptide (**4**) obtained with methanesulfonyl (mesyl) chloride. On the other hand, Cbz-(*Z*)-ΔAA-(*E*)-ΔAA-OMe [(*Z,E*)-**7a—e**] was also obtained by the similar base-catalyzed β-elimination of Cbz-(*Z*)-ΔAA-But(Cl)-OMe (**5**) as follows. According to the dicyclohexylcarbodiimide (DCC) method,[1)] the coupling of Cbz-(*Z*)-DHA (**1**) with methyl erythro-3-chloro-2-aminobutanoate (**3**)[6)] as an amine component in CH_2Cl_2 at room temperature for 24 h gave the expected (*Z*)-dehydrodipeptide (**5**) as colorless needles in *ca.* a 64% yield. The subsequent β-elimination of **5** with triethylamine occurred stereoselectively to give the desired (*Z,E*)-isomer of DHP (**7**) in a fairly good yield.

In the IR spectral data of **6** and **7**, the characteristic differences between the (*Z,Z*)- and (*Z,E*)-isomers could not be recognized. In the spectrum of **6**, the absorption bands of NH (3375—3280 cm^{-1}), the ester carbonyl (1734—1718 cm^{-1}), the secondary amide (1700—1670 and 1648—1620 cm^{-1}), and the carbon-carbon double bond (1665—1638 cm^{-1} region) functions all appeared. On the other hand, from comparison with the IR spectrum of **6**, the appearances of a similar pattern of bands due to NH (3300—3250 cm^{-1}), the ester carbonyl (1725—1714 cm^{-1}), the secondary amide (1680—1663 and 1640—1623 cm^{-1}), and the C=C bond (1655—1623 cm^{-1} region) functions indicate clearly the formation of the dehydrodipeptide (**7**) structure.

As mentioned above, although the IR spectra of **6** and **7** are similar, in the NMR spectrum of **7**, the chemical shifts of *C*-terminus alone were found to be considerably different from those of **6**. Therefore, it is supposed that the two compounds **6** and **7** are geometrically isomeric.

From the NMR spectral data, the disappearance of the characteristic methine proton signals coupled as double-doublet in the δ 4.81—4.90 (J=4.0—4.2 and 8.2—8.5 Hz) region in the *C*-terminus of **5** (Table 1) and the appearance of olefinic proton signals in the δ 7.24—7.03 region of **7** (Table 2) indicate unambiguously the formation of a DHA moiety in the *C*-terminus of **7**. In particular, both the olefinic [at δ 6.80—7.24 (q, J=7.5 Hz)] and the methyl protons (at δ 2.04—2.08 region) in the *C*-terminus of **7** resonate at a lower magnetic field than those of **6** [at δ 1.72—1.77 (q, J=7.2 Hz) and 6.77—6.82 regions], whereas the γ-alkyl and β-olefinic protons of *N*-terminus of **6** and **7** resonate at almost the same magnetic fields, in the δ 1.73—2.80 and 6.30—7.24 regions respectively. Hence, it was found that the olefin moiety newly formed in **7** was consistent with an (*E*)-geometric structure.

From the above results, in the NMR spectrum of DHP, the chemical shifts of γ-alkyl and β-olefinic protons of (*Z*)-configurational DHA residue were found

TABLE 1. Cbz-(*Z*)-⊿AA-But(Cl)-OMe (**5**)

Compd No.	Yield %	Mp θ_m/°C[a]	Formula	Found (Calcd)(%) C	H	N	IR, ν/cm^{-1} in KBr NH	COOMe (C=C)	C=O	NMR, δ in $CDCl_3$ -CH= (J_{Hz})	-N-CH- (J_{Hz})	NH
5a	66	91— 92	$C_{17}H_{21}N_2O_5Cl$	55.30	5.80	7.65	3350	1740	1685	6.55 q	4.87 dd	6.88 bs
				(55.36	5.74	7.60)		(1655)	1686	(7.0)	(8.5, 4.2)	7.14 d
5b	62	87— 88	$C_{18}H_{23}N_2O_5Cl$	56.55	6.11	7.39	3235	1743	1680	6.34 t	4.89 dd	6.47 bs
				(56.47	6.06	7.32)		(1660)	1628	(7.2)	(8.2, 4.0)	6.92 d
5c	67	87— 88	$C_{19}H_{25}N_2O_5Cl$	57.54	6.30	7.10	3325	1745	1687	6.52 t	4.86 dd	6.48 bs
				(57.50	6.35	7.06)	3260	(1643)	1628	(7.5)	(8.5, 4.2)	7.00 d
5d	65	99—100	$C_{19}H_{25}N_2O_5Cl$	57.55	6.31	7.12	3300	1735	1696	6.34 d	4.90 dd	6.44 bs
				(57.50	6.35	7.06)	3200	(1655)	1620	(10.5)	(8.5, 4.2)	7.05 d
5e	70	100—101	$C_{22}H_{23}N_2O_5Cl$	59.98	5.40	6.51	3220	1740	1685	7.10 s	4.88 dd	6.66 bs
				(61.32	5.38	6.50)		(1657)	1625		(8.5, 4.2)	7.20— 7.52[b]

a) Colorless needles from diisopropyl ether. b) Overlapped on phenyl protons.

TABLE 2. Cbz-(*Z*)-⊿AA-(*Z*) AND -(*E*)-⊿But-OMe (**6** AND **7**)

Compd No.	Yield %	Mp θ_m/°C[a]	Formula	Found (Calcd)(%) C	H	N	NMR spectrum, δ in $CDCl_3$ R-C<u>H</u>=	R-CH= (J_{Hz})	Me-C<u>H</u>=	Me-CH= (J_{Hz})	-OCONH-	-CONH-
7a	78	syrup	$C_{17}H_{20}N_2O_5$	61.60	6.15	8.40	6.52 q	1.87 d	7.10 q	2.08 d	6.82	8.16
				(61.43	6.07	8.43)		(7.0)		(7.5)		
7b	79	syrup	$C_{18}H_{22}N_2O_5$	62.77	6.95	8.00	6.52 t	2.10 q[b]	7.03 q	2.04 d	7.20	8.30
				(62.41	6.40	8.09)		(7.0)		(7.5)		
6c	69	syrup	$C_{19}H_{24}N_2O_5$	63.38	6.88	7.59	6.52 t	2.11 m	6.80 q	1.72 d	6.76	7.73
				(63.32	6.71	7.77)		(7.2)		(7.2)		
7c	81	syrup	$C_{19}H_{24}N_2O_5$	63.48	6.89	7.61	6.52 t	2.80 q	7.04 q	2.04 d	7.24	8.36
				(63.32	6.71	7.77)		(7.0)		(7.5)		
7d	82	syrup	$C_{19}H_{24}N_2O_5$	63.50	6.79	7.62	6.32 d	2.60 m	7.10 q	2.10 d	6.82	8.22
				(63.32	6.71	7.77)		(10.0)		(7.5)		
6e	79	112—113	$C_{22}H_{22}N_2O_5$	66.97	5.78	7.23	7.24 s	2.58— 1.73	6.82 q	1.77 d	6.72	7.85
				(66.99	5.62	7.10)				(7.2)		
7e	80	75— 77	$C_{22}H_{22}N_2O_5$	67.05	5.65	7.17	7.20 s	2.80— 1.87	7.24 q	2.07 d	7.20	8.35
				(66.99	5.62	7.10)				(7.5)		

a) Colorless syrup and colorless needles from isopropyl ether. b) Quintet.

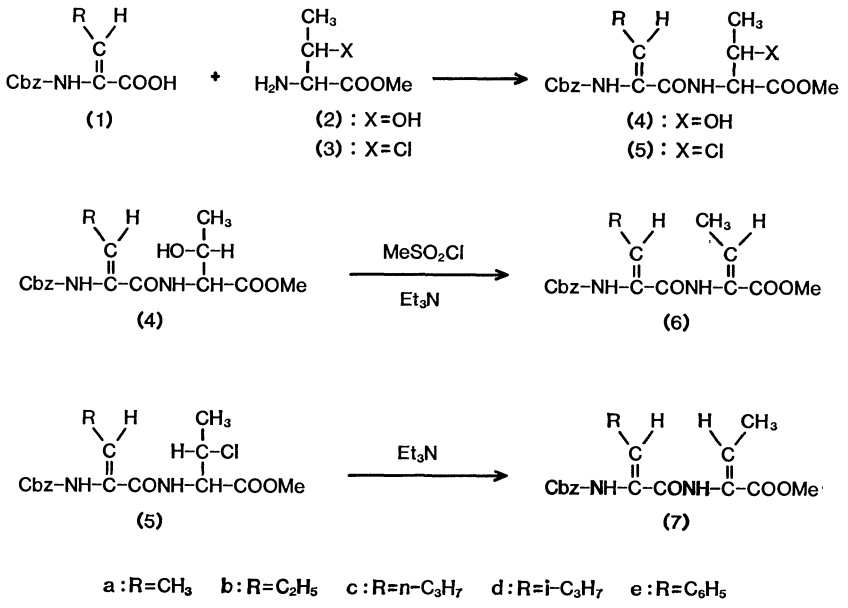

Scheme 1.

to resonate at higher magnetic fields than those of the (*E*)-DHA residue, as in the case of the differences between (*Z*)- and (*E*)-DHA derivatives.[7]

The melting points, physical constants, and spectral data of **5**, **6**, and **7** are summarized in Tables 1 and 2.

Hydantoin Derivatives. Recently, Srinivasan *et al.*[8] commented that, in the case of *N*,*N*-diacyl DHA, *e.g.*, alkyl 2-(phthalimido)crotonate, the protons of alkyl group in the γ-position of (*E*)-isomer shift to a lower magnetic field than that of (*Z*)-isomer, contrary to the *N*-free and *N*-monoacyl DHAs. They claimed that this is a reliable criterion for the confirmation of the geometric structure of DHA.

In order to further explain the differences of the chemical shifts of γ-alkyl protons between the *N*-monoacyl and *N*,*N*-diacyl DHAs and to study whether we can generalize the above criterion or not, compounds **6** and **7** were converted individually into the corresponding (*E*)- and (*Z*)-2-(hydantoin-3-yl)crotonate derivatives, which were the expected *N*,*N*-diacyl DHA structures. Instead of triethylamine,[9] sodium methoxide was used for the treatment of **6** to give colorless crystals. These were identified as methyl (*Z*)-2-[(*Z*)-5-alkylidenehydantoin-3-yl]crotonate (**8**) in *ca.* a 90% yield. In addition, instead of sodium methoxide, 1,8-diazabicyclo[5.4.0]undec-7-ene (DBU) and potassium *t*-butoxide as a stronger base was also used in this reaction to give **8** in a fairly good yield.

On the other hand, the treatment of **7** with the same base as used above was worked up similarly to give the (*E*)-isomer of **8**, methyl (*E*)-2-[(*Z*)-5-alkylidenehydantoin-3-yl]crotonate (**9**), as a colorless syrup or crystals in *ca.* a 76% yield.

Furthermore, it was found that the direct transformation of **4** and **5** with a strong base such as DBU to the hydantoin derivatives also occurred to give **8** and **9** in high yields respectively, *via* the β-elimination and then cyclization reactions. During the prolonged treatment of **7** with the base, **9** was initially

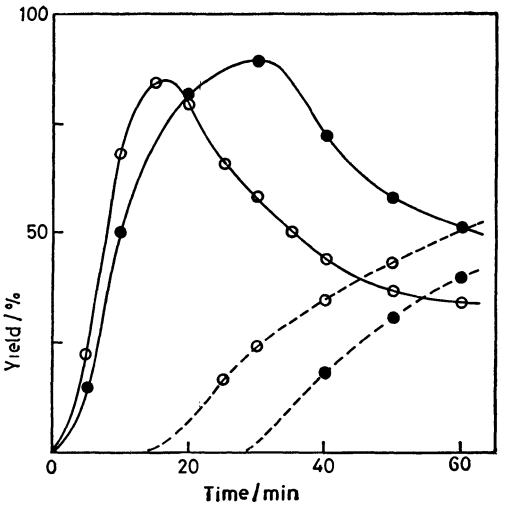

Fig. 1. Yields of **8e** and **9e** *vs.* reaction time and base concentration at room temperature.
8e (——), **9e** (- - -), 0.5 M-DBU (●), 1.0 M-DBU (○).

formed and then isomerization of only the (*E*)-crotonate moiety in **9** gradually occurred to give **8** almost quantitatively. For example, the successive conversion of **7e** to **9e** and **9e** to **8e** for various reaction times and base concentrations were examined in detail. The results are depicted by the curves in Fig. 1. The reaction of **7e** with 0.5 M-DBU (1 M=1 mol dm^{-3}) in $CHCl_3$ at room temperature gave the following results. The formation of **9e** first reached a maximum (*ca.* 90%) yield after 30 min. Then the quantity of **9e** decreased gradually with the isomerization of **9e** to **8e** and the yield of **8e** reached a maximum (*ca.* 80%) after 2 more h. Similarly, when 1.0 M-DBU was employed, the formation of **9e** attained rapidly to the maximum (*ca.* 80%) yield after 15 min; the yield of **8e** thus formed was found to reach its maximum (*ca.* 80%) within 2 h. These results suggested

Table 3. Methyl (*Z*)- and (*E*)-2-[(*Z*)-5-alkylidenehydantoin-3-yl]crotonates (**8** and **9**)

Compd No.	Yield %	Mp θ_m/°C[a]	Formula	Found (Calcd)(%)			NMR spectrum, δ in $CDCl_3$					
				C	H	N	R-C<u>H</u>=	<u>R</u>-CH= (J_{Hz})	Me-C<u>H</u>=	<u>Me</u>-CH= (J_{Hz})	NH[d]	-COO<u>Me</u>
8a	92	121—125	$C_{10}H_{12}N_2O_4$	53.65 (53.57	4.43 4.39	12.61 12.50)	6.05 q	1.88 d (7.8)	7.37 q	1.85 d (7.3)	9.48 s	3.82 s
9a	70	112—115	$C_{10}H_{12}N_2O_4$	53.59 (53.57	4.41 4.39	12.55 12.50)	6.10 q	2.25 d (8.0)	6.52 q	2.24 d (7.0)	9.38 s	3.78 s
8b	91	121—123	$C_{11}H_{14}N_2O_4$	55.49 (55.45	5.99 5.92	11.81 11.76)	6.00 t	2.25m (8.0)	7.40 q	1.86 d (7.0)	9.50 s	3.82 s
9b	73	128—129	$C_{11}H_{14}N_2O_4$	55.47 (55.45	5.97 5.92	11.80 11.76)	5.91 t	2.12m (7.5)	6.44 q	2.26 d (7.6)	9.10 s	3.80 s
8c	93	125—128	$C_{12}H_{16}N_2O_4$	57.18 (57.13	6.47 6.39	11.15 11.11)	6.02 t	2.24 dt (7.3)	7.37 q	1.86 d (7.3)	9.62 s	3.82 s
9c	71	syrup	$C_{12}H_{16}N_2O_4$	57.32 (57.13	6.51 6.39	11.23 11.11)	5.95 t	2.11 q (7.0)	6.48 q	2.23 d (7.7)	9.32 s	3.78 s
8d	90	54— 55	$C_{12}H_{16}N_2O_4$	57.22 (57.13	6.36 6.39	11.18 11.11)	5.82 d	2.64m (10.0)	7.45 q	1.87 d (7.5)	9.50 s	3.84 s
9d	72	syrup	$C_{12}H_{16}N_2O_4$	57.39 (57.13	6.45 6.39	11.34 11.11)	5.78 d	2.23 d (10.0)	6.44 q	2.24 d (7.7)	9.48 s	3.82 s
8e	85	166—167[b]	$C_{15}H_{14}N_2O_4$	63.08 (62.93	5.00 4.93	9.91 9.79)	6.84 s		7.34 q	1.84 d (7.0)	9.70 s	3.79 s
9e	92	212—213[c]	$C_{15}H_{14}N_2O_4$	62.90 (62.93	4.97 4.93	9.72 9.79)	6.74 s		6.50 q	2.28 d (7.5)	9.00 s	3.73 s

a) Colorless fibers from isopropyl alcohol. b) Colorless needles from CCl_4–isopropyl alcohol. c) Colorless needles from CCl_4–ethanol. d) Broad singlet.

to us that the higher the concentration of DBU or the other similar strong base was, the faster **7** transformed to **8** *via* **9**. In consequence, the expected (*Z*)- and (*E*)-2-(hydantoin-3-yl)crotonate [(*Z*,*Z*)-**8** and (*Z*,*E*)-**9**] were prepared readily as the *N*,*N*-diacyl DHA or enamine in high yields.

In the IR spectrum of **8** and **9**, the appearances of absorption bands of NH (3430—3230 cm^{-1}), ester carbonyl (1736—1715 cm^{-1}), carbon-carbon double bond (1660—1640 cm^{-1}), in particular, the characteristic hydantoin carbonyl bands (1778—1760 and 1720—1673 cm^{-1} regions) at higher wavenumber indicate the formation of the hydantoin ring and the presence of a crotonate moiety. Moreover, from the NMR spectral data of **8** and **9**, the disappearance of NH proton in peptide bonding at δ 6.72—7.20 and that of benzyl protons at about δ 7.20—7.34 (phenyl) and 5.06—5.14 (methylene) in **6** and **7** support the occurrence of a ring closure for hydantoin formation,[9] after the elimination of benzyl alcohol from **6** and **7**. In addition, we have compared the NMR spectrum of **8** with that of **9**. The olefinic proton of the crotonate moiety in (*Z*)-isomer (**8**) resonates at lower magnetic field (at δ 7.34—7.45) than that of (*E*)-isomer (**9**; at δ 6.44—6.52): $\Delta\delta$ *ca.* 0.9. But γ-methyl protons of (*Z*)-isomer shift at higher field (at δ 1.84—1.87) than that of (*E*)-isomer (at δ 2.23—2.28), $\Delta\delta$ *ca.* 0.4, whereas the chemical shifts of β- and γ-protons of the alkylidene group in the hydantoin rings of both **8** and **9** are similar (at δ 5.78—6.84 and δ 1.88—2.64 regions).

These facts are consistent with the Srinivasan comment. Consequently, the criterion became reliable for the confirmational assignment of the geometric structures for *N*-monoacyl and *N*,*N*-diacyl DHAs.

The yields, physical constants, and NMR spectral data of **8** and **9** are summarized in Table 3.

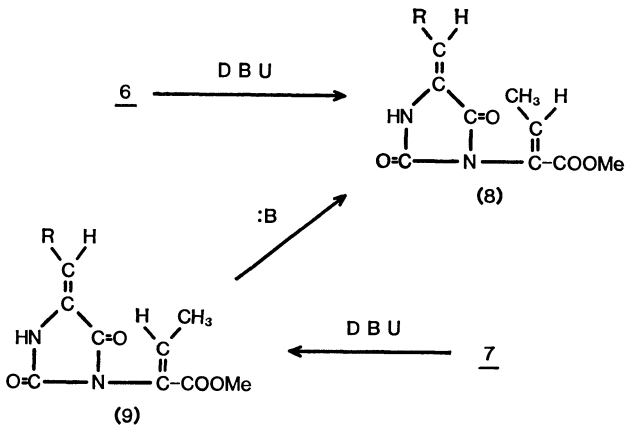

Scheme 2.

Experimental

All the melting points are uncorrected. The IR spectra were recorded with a Hitachi EPI-G3 Spectrometer. The NMR spectra were measured with a JNM-PS-100 Spectrometer (Japan Electron Optics Laboratory Co. Ltd.), using tetramethylsilane as the internal standard.

Materials. Compounds **3** and **4** were prepared according to the methods reported previously by Kinoshita and Umezawa[6] and by us.[7]

Preparation of **5**. First the hydrochloride of **3** (20 mmol) and triethylamine (20 mmol) in dry CH_2Cl_2 (20 ml) were stirred below 0 °C for 10 min. Into the resulting solution we stirred successively **1** (20 mmol) and DCC (20 mmol), portion by portion; stirring was continued at room temperature for 24 h and the *N*,*N*′-dicyclohexylurea which separated out was filtered off. Into the reaction solution was added CH_2Cl_2 (30 ml); the resulting solution was washed once with successive 1 M HCl, saturated aqueous $NaHCO_3$, and water and then dried over anhydrous Na_2SO_4. Removal of CH_2Cl_2 gave a syrupy residue, which was purified on a silica-gel column using a mixture of benzene and ethyl acetate (4:1 v/v) to give **5** as colorless crystals. See Table 1.

Preparation of **6**. According to the method reported previously,[1,10] compound **4** was subjected to the mesylation, followed by the elimination. Into a solution of **4** (4 mmol) and mesyl chloride (5 mmol) in dry CH_2Cl_2 (20 ml) we stirred triethylamine (12 mmol), drop by drop, at 0—2 °C for 1 h; stirring was continued at room temperature for 12 h. Into the reaction solution was added CH_2Cl_2 (20 ml); the resulting solution was worked up as above. The reaction solution thus obtained was concentrated under reduced pressure to give a crude syrupy substance: this was then purified on a silica-gel column using a mixture of benzene and ethyl acetate (3:1 v/v) as the eluent to give **6** as a colorless syrup or crystals. See Table 2.

Preparation of **7**. Into a solution of **5** (10 mmol) in dry CH_2Cl_2 (15 ml) we stirred triethylamine (30 mmol), drop by drop, under cooling for 2 h; stirring was continued at room temperature for 15 h. Dichloromethane (20 ml) was added to the reaction solution and the resulting solution was washed twice with 1 M HCl, once with saturated aqueous $NaHCO_3$, and three times with water, and finally dried over anhydrous Na_2SO_4. Evaporation of CH_2Cl_2 gave a syrupy residue; this was purified on a silica-gel column using a mixture of benzene and ethyl acetate (4:1 v/v) as the eluent to give **7** as a colorless syrup or crystals. See Table 2.

Preparation of **8**. Into a solution of **6** (10 mmol) in dry $CHCl_3$ (15 ml) we stirred DBU (10 ml) at room temperature for 3 h. To the reaction solution was added $CHCl_3$ (15 ml); this was then washed with 2 M HCl and three times with water and then dried over anhydrous Na_2SO_4. After removal of $CHCl_3$ and the small amount of benzyl alcohol formed as a by-product under reduced pressure, the residual syrup was purified on a silica-gel column using a mixture of benzene and ethyl acetate (4:1 v/v) as the eluent to give **8** as colorless crystals. See Table 3.

Preparation of **9**. Into a solution of **7** (10 mmol) in $CHCl_3$ (15 ml) we stirred some DBU (5 ml) at room temperature for half an hour. The reaction solution was acidified weakly with 1 M HCl. $CHCl_3$ (15 ml) was added and the resulting solution was worked up as the case of **8** mentioned above, to give **9** as a colorless syrup or crystals. See Table 3.

Isomerization of **9** *to* **8**. *From* **9**: A solution of **9** (10 mmol) in $CHCl_3$ (15 ml) in the presence of triethylamine (10 mmol) was stirred at room temperature for 3 d. The reaction solution was washed once with 2 M HCl and three times with water and then dried over anhydrous Na_2SO_4. Removal of $CHCl_3$ gave **8** quantitatively.

A similar isomerization of **9** to **8** was accomplished completely within only 10 h, by using DBU, sodium methoxide,

or potassium *t*-butoxide, instead of triethylamine.

From ***5*** via ***9***: Into a solution of **5** (20 mmol) in methanol (15 ml) we stirred sodium methoxide (12 mmol), drop by drop, below 0 °C; stirring was continued at room temperature for 6 h. After removal of methanol, the residual syrup thus obtained was dissolved in ethyl acetate (40 ml). The resulting solution was washed twice with 1 M HCl and three times with water and finally dried over anhydrous Na_2SO_4. Evaporation of the solvent under reduced pressure gave a residual substance, which was worked up as the case of **6** to give **8** in *ca.* an 85% yield.

References

1) Part II: C. Shin, Y. Yonezawa, M. Takahashi, and J. Yoshimura, *Bull. Chem. Soc. Jpn.*, **54**, 1132 (1981).
2) Y. Yonezawa, C. Shin, M. Kiyohara, and J. Yoshimura, *Tetrahedron Lett.*, **1979**, 3851.
3) Y. Yonezawa, C. Shin, Y. Ono, and J. Yoshimura, *Bull. Chem. Soc. Jpn.*, **53**, 2905 (1980).
4) In this paper, the symbol Δ indicates a double bond of the α-position in the DHA or DHA residue, while AA represents an α-amino acid or its residue.
5) A. Srinivasan, R. W. Stephenson, and R. K. Olsen, *J. Org. Chem.*, **42**, 2256 (1977).
6) M. Kinoshita and S. Umezawa, *Nippon Kagaku Zasshi*, **72**, 382 (1951).
7) C. Shin, M. Hayakawa, T. Suzuki, A. Ohtsuka, and J. Yoshimura, *Bull. Chem. Soc. Jpn.*, **51**, 550 (1978).
8) A. Srinivasan, K. D. Richards, and R. K. Olsen, *Tetrahedron Lett.*, **1976**, 891.
9) K. Nakajima, H. Kawai, M. Takai, and K. Okawa, *Bull. Chem. Soc. Jpn.*, **50**, 917 (1977).
10) C. Shin, Y. Yonezawa, K. Unoki, and J. Yoshimura, *Bull. Chem. Soc. Jpn.*, **52**, 1657 (1979).

Preferential Introduction of a Pyridylmethyl Group into Sulfonamides as an Approach to an Intramolecular Transimination[1)]

Masaaki IWATA* and Hiroyoshi KUZUHARA
The Institute of Physical and Chemical Research, Wako, Saitama 351

(Received September 21, 1981)

N,N'-Bis(*p*-tolylsulfonyl)-α,ω-alkanediamine disodium salts ($n=3$, 4, 5, 6, 7, 8, 9, 10) were subjected to monopyridylmethylation by the reaction with 5'-deoxy-5'-chloro- or 5'-deoxy-2'-chloro-3,4'-*O*-isopropylidenepyridoxine hydrochloride, accompanied by the corresponding bispyridylmethylation. Monopyridylmethylation became remarkable for longer methylene chains of the diamine. Thus, introduction of an amino group protected by a sulfonyl group at the end of either the C_2- or the C_5-side chains of pyridoxine derivatives was achieved.

Catalysis of coenzyme pyridoxal phosphate in the enzyme system has been belived to be initiated through transimination of the coenzyme originally bound to an ε-amino group of a lysine residue of the enzyme to the amino group of a substrate amino acid.[2)] The transimination of the coenzyme provides several orders faster rate acceleration of the coenzyme catalysis in the enzymic reaction, compared with the catalysis of the direct imine formation of the coenzyme with a substrate.[3)] The biologically inherent properties of the coenzyme process have become kinetically well understood[3)] and the essential part of the chemical process has been successfully applied to a solution of synthetic problem in several cases.[4)] The present work was started, expecting that if a suitable three-dimensional disposition of a primary amino group were introduced into pyridoxal molecule, then the catalytic potency would be remarkably increased through intramolecular transimination. In this context, Fisher and Metzler studied a cyclic imine derivative of pyridoxal,[5)] demonstrating that the imine is catalytically inactive, due to the formation of the stable six-membered ring; its electronic absorption spectrum is strikingly similar to those of pyridoxal phosphate-containing enzymes.

The development of a general method for the synthesis of diaza(2,5)pyridinophanes[6)] by the reaction of dichloropyridoxine derivative with *N,N'*-bis(*p*-tolylsulfonyl)-α,ω-alkanediamine disodium salts (**4**) encouraged us to examine systematically the possibility of the molecular construction of a "intramolecular transimination model" system by the use of 2'- or 5'-position of pyridoxal where the substituent is dispensable for catalysis in the nonenzymic system.[7)] The coupling method was expected to be equally applicable to the reaction of a monochloropyridoxine derivative with the alkanediamine disodium salt, even though the reaction will be accompanied by complete alkylation on two nucleophilic sites of the disodium salt. Therefore, the syntheses of 5'-deoxy-5'-chloro- and 5'-deoxy-2'-chloro-3,4'-*O*-isopropylidenepyridoxine, **1** and **2** respectively, were first examined; these were then subjected to a coupling reaction with **4**.

Results and Discussion

5'-Deoxy-5'-chloro-3,4'-*O*-isopropylidenepyridoxine hydrochloride (**1**) was synthesized by the known method[8)] from pyridoxine hydrochloride. For the synthesis of 5'-deoxy-2'-chloro-3,4'-*O*-isopropylidenepyridoxine hydrochloride (**2**), **1** was used as a starting material; neutralization of **1** followed by catalytic hydrogenation afforded 5'-deoxy-3,4'-*O*-isopropylidenepyridoxine (**5**) (92% yield). This was then oxidized to 5'-deoxy-3,4'-*O*-isopropylidenepyridoxine 1-oxide (**6**) with *m*-chloroperbenzoic acid (87% yield). The *N*-oxide was converted to 5'-deoxy-2'-acetoxy-3,4'-*O*-isopropylidenepyridoxine (**7**) in acetic anhydride–chloroform in 91% yield. Treatment of **7** with sodium methoxide afforded 5'-deoxy-2'-hydroxy-3,4'-*O*-isopropylidenepyridoxine (**8**) in 90% yield. This was subjected to chlorination with thionyl chloride to give **2** in 95% yield (Scheme 1).

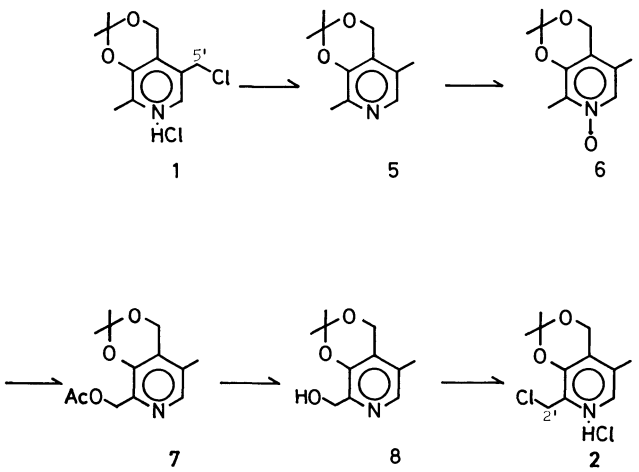

Scheme 1.

Utilizing a newly developed method,[6)] normalized reaction conditions were set up for the coupling reaction of monochloropyridoxine derivative hydrochloride with **4**, using *N,N'*-bis(*p*-tolylsulfonyl)-1,6-hexanediamine disodium salt (**4d**) as a representative counterpart; to a stirred suspension of **4d** in *N,N*-dimethylformaminde (DMF), which was prepared by the reaction of **3d** with sodium ethoxide, a solution of **1** or **2** in DMF[9)] was added dropwise (Scheme 2). Two products were detected on TLC; these were chromatographed to give *N*-[2,2,8-trimethyl-4*H*-[1,3]dioxino[4,5-*c*]pyridin-5-ylmethyl]-*N,N'*-bis(*p*-tolylsulfonyl)-1,6-hexanediamine (**9d**) and *N,N'*-bis[2,2,8-trimethyl-4*H*-[1,3]dioxino[4,5-*c*]pyridin-5-ylmethyl]-*N,N'*-bis(*p*-tolylsulfonyl)-1,6-hexanediamine (**10d**), when **1** was used. On the other hand, when **2** was used, detected and isolated products were *N*-[2,2,5-trimethyl-4*H*-[1,3]-dioxino[4,5-*c*]pyridin-8-ylmethyl]-*N,N'*-bis(*p*-tolylsul-

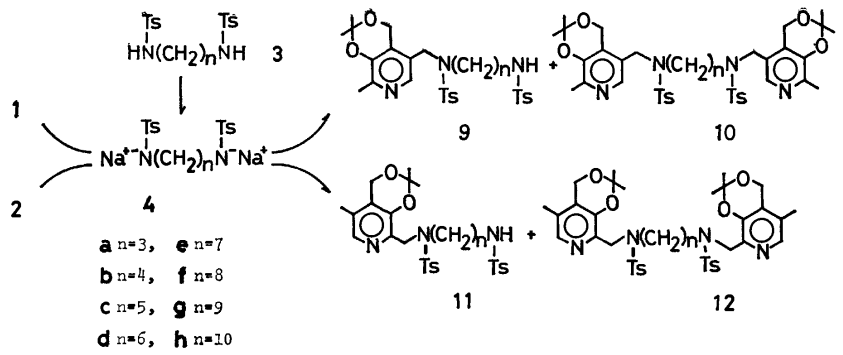

Scheme 2.

Table 1. Reaction of 5′-deoxy-5′-chloro-3,4′-*O*-isopropylidenepyridoxine hydrochloride (**1**) with *N*,*N*′-bis(*p*-tolylsulfonyl)-α,ω-alkanediamine disodium salt (**4**) in equivalent molar ratio

4	*n*	Product yield/%			Ratio **9**/**10**
		9	**10**	Total	
a	3	33	30	63	1.1
b	4	39	30	69	1.3
c	5	49	28	77	1.8
d	6	39	27	66	1.4
e	7	43	27	70	1.6
f	8	44	18	62	2.4
g	9	48	17	65	2.8
h	10	44	18	62	2.4

Table 2. Reaction of 5′-deoxy-2′-chloro-3,4′-*O*-isopropylidenepyridoxine hydrochloride (**2**) with *N*,*N*′-bis(*p*-tolylsulfonyl)-α,ω-alkanediamine disodium salt (**4**) in equivalent molar ratio

4	*n*	Product yield/%			Ratio **11**/**12**
		11	**12**	Total	
a	3	41	22	63	1.9
b	4	36	20	56	1.8
c	5	36	20	56	1.8
d	6	41	18	59	2.3
e	7	46	19	65	2.4
f	8	35	12	47	2.9
g	9	51	13	64	3.9
h	10	51	15	66	3.4

fonyl)-1,6-hexanediamine (**11d**) and *N*,*N*′-bis[2,2,5-trimethyl-4*H*-[1,3]dioxino[4,5-*c*]pyridin-8-ylmethyl]-*N*,*N*′-bis(*p*-tolylsulfonyl)-1,6-hexanediamine (**12d**). All other series of reactions were carried out as similarly as possible to those of **4d**. The results obtained are summarized in Tables 1 and 2. They demonstrate several features of the pyridylmethylation reaction; total yield of products lies in the range from 62 to 72% for **1**, and from 47 to 60% for **2**. It is quite interesting, however, to note that the ratio of the yield of **9** to that of **10** clearly increases as the methylene chain becomes longer (Table 1). A similar trend is obvious for the ratio of the yield of **11** to that of **12** as well (Table 2).

Table 3. ^{1}H NMR spectra of pyridoxine derivatives **6**, **7**, and **8**[a]

	R	X	$H^{2'}$	$H^{4'}$	$H^{5'}$	H^{6}	$C(\underline{CH_3})_2$
6	H	O	2.40	4.74	2.11	7.82	1.59
7	OAc	—	5.18	4.74	2.14	7.97	1.58
8	OH	—	4.71	4.79	2.18	7.97	1.60

a) Chemical shift in δ, in $CDCl_3$.

The ratio was not linearly correlated with the methylene chain length. The qualitative change in the ratios is interpreted as follows: in the shorter methylene chains ($n=3$—5), one pyridylmethyl group bound to one end of the diamine brings another pyridylmethyl group toward the other end of the diamine through an inductive effect such as stacking between the two aromatic rings. When the methylene chain becomes longer (more than seven), it is difficult for such an inductive effect to occur and, thus, the reaction favors monopyridylmethylation over bispyridylmethylation. Decreases in yields of **10** or **12** compared to increases in those of **9** or **11** without reduction in total yield as the chain length becomes longer, support the interpretation as well. Furthermore, a comparison of both ratios suggests that such a definite interactive distance between the aromatic rings will be longer in 5′-chloro derivatives (**1**) than in 2′-chloro derivatives (**2**) at the reactive points, probably due to spatial substituent interaction. In other words, monopyridylmethylation is more likely to occur in 2′-chloro derivatives (**2**) than in 5′-chloro derivatives (**1**).

^{1}H NMR spectral data are summarized in Table 3 for **6**, **7**, and **8**, Fig. 1 for **9** and **10**, and Fig. 2 for **11** and **12**, in which chemical shifts are correlated with the chain length. Although it is difficult to distinguish the effects of intermolecular and/or intramolecular interactions on the chemical shift changes, certain features are noteworthy. In general, it is seen that proton chemical shifts move to lower field as the methylene chain becomes longer. A linear correlation is apparent for C_6–H, pyr–$^{4'}C\underline{H_2}$–O, pyr–$^{5'}C\underline{H_2}$–N, and $C(C\underline{H_3})_2$ in **9**, and for pyr–$^{5'}C\underline{H_2}$–N, $C_6\underline{H}$, pyr–$^{4'}C\underline{H_2}$–O, ^{5}C–N–$C\underline{H_2}$–C, and $C(C\underline{H_3})_2$ in **10**

in the order of the slope magnitude, respectively, in contrast to nonlinear correlation of –NHTs, $^{5'}C$–N–CH_2–C (triplet), and HN–CH_2–C (quartet) in **9**, and the other –CH_2– in **9** and **10**. A constant chemical shift is shown for C_2–CH_3 and –$SO_2C_6H_4$–CH_3 in both **9** and **10**. As for **11** and **12**, no proton chemical shift in **11** is linearly correlated with the chain length except for the constant signals of C_5–CH_3 and –$SO_2C_6H_4$–CH_3, although pyr–$^{2'}CH_2$–N, C_6–H, $C(CH_3)_2$, and pyr–$^{4'}CH_2$–O in **12** have a linear correlation in the order of slope magnitude.

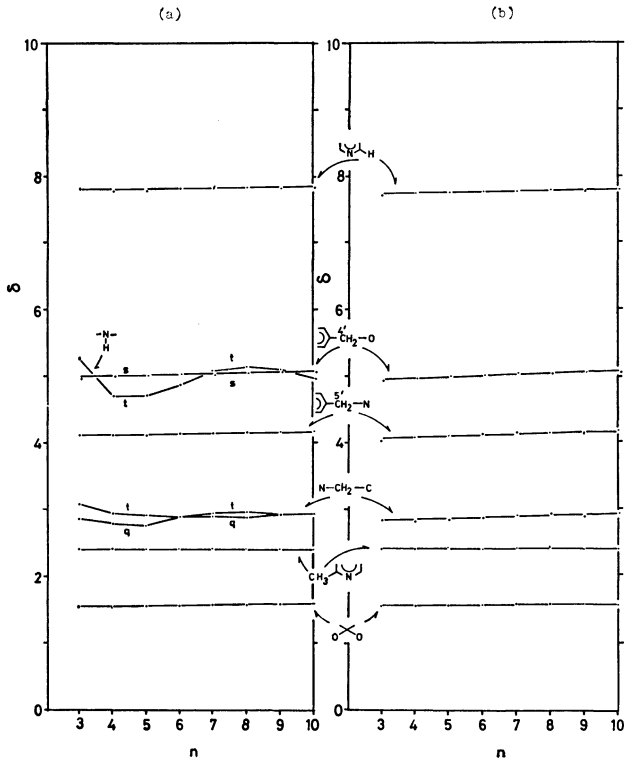

Fig. 1. Correlation of chemical shifts with the methylene chain length in ^1H NMR spectra of (a) **9** and (b) **10**, in $CDCl_3$.

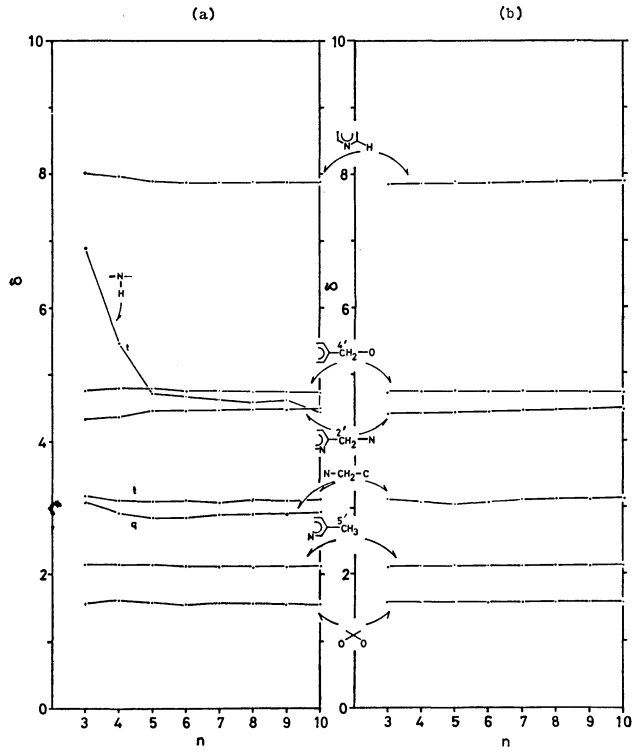

Fig. 2. Correlation of chemical shifts with the methylene chain length in ^1H NMR spectra of (a) **11** and (b) **12**, in $CDCl_3$.

The drastic chemical shift change for amino proton (triplet) and methylene protons (quartet) contiguous to the amino proton in both **9** and **11** suggests that intermolecular and/or intramolecular interaction is involved in the molecule through N–H···N or N–H···O hydrogen-bonding. It is very significant that the change becomes rather little when the methylene chain becomes longer than around six.

Experimental

The ^1H NMR spectra were recorded on a Varian HA-100D apparatus, with TMS as the internal standard in chloroform-*d*; the chemical shift and coupling constant are presented in ppm and Hz, respectively. Merck silica gel 60 (Art. 7734, 0.063—0.20 mm) was used for the column chromatography and Wakogel B-5 FM (Wako pure and Chem. Co., Ltd.) for the thin layer chromatography (TLC), in which products were visualized in an iodine-vapor bath. DMF was dried over molecular sieve (type-4A) and the supernatant was used directly for the reaction. The uncorrected mp were measured in a bilayered cover glass (18 m/m) with a micro melting point apparatus (Yanagimoto Seisakusho, serial No. 2647). For column chromatography and TLC analysis, benzene–ethyl acetate (3:2 v/v) (solvent A) was used as an eluent. 5′-Deoxy-5′-chloro-3,4′-*O*-isopropylidenepyridoxine hydrochloride (**1**) was prepared by a known method[8] from pyridoxine hydrochloride.

Preparation of 5′-Deoxy-3,4′-O-isopropylidenepyridoxine 1-Oxide (6). To 10.21 g (0.053 mol) of 5′-deoxy-3,4′-*O*-isopropylidenepyridoxine (**5**), which was prepared by the known method[8] from pyridoxine hydrochloride, in 150 ml of chloroform, 10.94 g (1.2 mol equiv. as 85% purity) of *m*-chloroperbenzoic acid was added at ambient temperature. After the mixture was stirred for *ca.* 3 h, it was neutralized with 2.55 g of sodium hydroxide and then extracted with chloroform. The extract was washed with water, dried over $MgSO_4$, and then evaporated to dryness to give a colorless powder; this was recryst. from acetone–diisopropyl ether to afford 9.67 g of **6** (87% yield); mp 157—158 °C. Found: C, 63.07; H, 7.27; N, 6.69%. Calcd for $C_{11}H_{15}O_3N$: C, 63.14, H, 7.23; N, 6.69%.

Preparation of 5′-Deoxy-2′-acetoxy-3,4′-O-isopropylidenepyridoxine (7). The mixture of 9.67 g of **6** in 20 ml of acetic anhydride and 30 ml of chloroform was refluxed for 2 h in an oil-bath. Solvents were evaporated under reduced pressure and the residue was chromatographed on a silica gel (250 g) column eluted with solvent A to give 10.58 g of **7** (91% yield) as a viscous liquid; R_f 0.43 (solvent A). Found: C, 61.97; H, 6.70; N, 5.50%. Calcd for $C_{13}H_{17}O_4N$: C, 62.14; H, 6.82; N, 5.57%.

Preparation of 5′-Deoxy-2′-hydroxy-3,4′-O-isopropylidenepyridoxine (8). To sodium methoxide in 200 ml of methanol, prepared by addition of 0.97 g of metal sodium, 10.08 g of **7** in 50 ml of methanol was added dropwise and the mixture was stirred for 1 h at ambient temperature; the reaction was completed instantly, monitored on TLC (R_f 0.3 (solvent

A)). The mixture was neutralized with the occasional addition of pieces of solid carbon dioxide, and then evaporated to dryness. The residue was triturated several times with chloroform and filtered through Celite (No. 545). The filtrate was evaporated to dryness and the residue was recrystallized from benzene (minor)–hexane (major) to give 7.51 g of **8** (89% yield), as colorless crystals; mp 125—126 °C. Found: C, 63.22; H, 7.16; N, 6.62%. Calcd for $C_{11}H_{15}O_3N$: C, 63.14; H, 7.23; N, 6.69%. IR (KBr disk): *v* 3180, 2990, 1600, 1570, 1450, 1405, 1387, 1377, 1350, 1292, 1280, 1270, 1252, 1196, 1140, 1050, 935, 855, 770, 732, 670, and 570 cm^{-1} as relatively strong characteristic bands.

Preparation of 5′-Deoxy-2′-chloro-3,4′-O-isopropylidenepyridoxine Hydrochloride (2). To a stirred suspension of 2 g of **8** in 40 ml of benzene, 0.7 ml (1 mol equiv.) of thionyl chloride in 10 ml of benzene was added dropwise at ambient temperature, resulting in an immediate clear solution and then in a precipitate. The precipitation was promoted by addition of 50 ml of dry diethyl ether. The colorless precipitate was collected by filtration, washed several times with dry diethyl ether, and then recryst. from acetone to give 2.39 g of **2** (95% yield) as colorless crystals; mp 140 °C (starts to become brown) and at 148 °C (darkening). Found: C, 50.13; H, 5.68; N, 5.36; Cl, 26.30%. Calcd for $C_{11}H_{15}O_2NCl_2$: C, 50.01; H, 5.72; N, 5.30; Cl, 26.85%. IR (KBr disk): *v* 3060, 3010, 2970, 2320, 2025, 1552, 1480, 1465, 1445, 1420, 1385, 1370, 1310, 1278, 1260, 1204, 1125, 1078, 1060, 867, 831, 770, 651, 582, and 560 cm^{-1} as relatively strong characteristic bands.

Preparation of N,N′-*Bis(*p-*tolylsulfonyl)-α,ω-alkanediamines (3) (n=3, 4, 5, 6, 7, 8, 9, 10).* To a α,ω-alkanediamine in pyridine, three molar equivalents of *p*-toluenesulfonyl chloride were added and the mixture was stirred at 80—90 °C for 0.5—1 h. The mixture was poured into water; after cooling, a precipitate resulted. This was collected by filtration and recryst. from ethanol. All the elemental analyses for C, H, N, and S (omitted) were coincident with those calculated. Mp 134—136 °C (**3a**), 125—126 °C (**3b**), 137—138 °C (**3c**), 155—156 °C (**3d**), 144.5—145.5 °C (**3e**), 151—152 °C (**3f**), 93.5—94 °C (**3g**), and 128—129 °C (**3h**).

Preparation of N,N′-*Bis(*p-*tolylsulfonyl)-α,ω-alkanediamine Disodium Salts (4) (n=3, 4, 5, 6, 7, 8, 9, 10) and Its Reaction with 1 and 2.* To a stirred sodium ethoxide solution, prepared by addition of three gram-atom equivalents of metal sodium to ethanol (*e.g.*, 30 ml), one molar equivalent of **3** (*e.g.*, 0.5 g) was added. The mixture was refluxed for 1 h, followed by complete evaporation of ethanol under reduced pressure. DMF (*e.g.*, 50 ml) was readded to the resulting powder (**4**); to this a solution[9] of one molar equivalent of **1** or **2** in DMF (*e.g.*, 15 ml) was added dropwise with stirring at around 90 °C over the period of 2—3 h. After cooling, the brown mixture was poured into water (*e.g.*, 700 ml). Precipitation was promoted by addition of sodium chloride (*e.g.*, 10 g) (salting out effect). The precipitate was collected by filtration. Thus, by silica gel chromatography of the precipitate eluted with solvent A, the following were isolated: *N*-[2,2,8-trimethyl-4*H*-[1,3]dioxino[4,5-*c*]pyridin-5-ylmethyl]-*N*,*N*′-bis(*p*-tolylsulfonyl)-α,ω-alkanediamine (**9**) and *N*,*N*′-bis[2,2,8-trimethyl-4*H*-[1,3]dioxino[4,5-*c*]pyridin-5-ylmethyl]-*N*,*N*′-bis(*p*-tolylsulfonyl)-α,ω-alkanediamine (**10**) prepared from **1**, or *N*-[2,2,5-trimethyl-4*H*-[1,3]dioxino[4,5-*c*]pyridin-8-ylmethyl]-*N*,*N*′-bis(*p*-tolylsulfonyl)-α,ω-alkanediamine (**11**) and *N*,*N*′-bis[2,2,5-trimethyl-4*H*-[1,3]dioxino[4,5-*c*]pyridin-8-ylmethyl]-*N*,*N*′-bis(*p*-tolylsulfonyl)-α,ω-alkanediamine (**12**) prepared from **2**.

All elemental analyses are tabulated in Table 4 for **9**, Table 5 for **10**, and Table 6 for **11** and **12**. ^1H NMR spec-

Table 4. Elemental analyses of **9**

	State	Calcd(%)				Found(%)			
		C	H	N	S	C	H	N	S
9a	am[a]	58.61	6.15	7.32	11.18	59.20	6.24	7.51	10.90
9b	liq[b]	59.26	6.35	7.15	10.91	59.27	6.45	6.96	10.85
9c	liq	59.87	6.53	6.98	10.66	59.81	6.45	6.91	10.51
9d	am	60.46	6.71	6.82	10.41	60.35	6.74	6.62	10.45
9e	am	61.02	6.88	6.67	10.18	60.98	6.92	6.62	10.10
9f	am	61.56	7.05	6.53	9.96	61.38	6.91	6.48	10.15
9g	am	62.07	7.20	6.39	9.75	62.23	7.27	6.29	9.74
9h	liq	62.56	7.35	6.25	9.54	62.36	7.13	6.19	9.65

a) Amorphous powder. b) Liquid.

Table 5. Elemental analyses of **10**

	State	Calcd(%)				Found(%)			
		C	H	N	S	C	H	N	S
10a	liq[a]	61.23	6.33	7.33	8.38	60.70	6.21	7.21	8.36
10b	am[b]	61.67	6.47	7.19	8.23	61.40	6.33	7.23	8.10
10c	c)	62.10	6.61	7.07	8.09	62.76	6.67	7.34	7.88
10d	d)	62.50	6.74	6.94	7·95	62.10	6.69	6.67	7.97
10e	am	62.90	6.88	6.82	7.81	62.75	6.94	6.90	7.70
10f	am	63.28	7.00	6.71	7.68	63.41	7.10	6.82	7.52
10g	am	63.65	7.12	6.60	7.55	63.41	7.25	6.41	7.60
10h	e)	64.01	7.24	6.49	7.43	64.09	7.30	6.15	7.50

a) Liquid. b) Amorphous powder. c) Mp 161—162 °C. d) Mp 217—218.5 °C. e) Mp 169—171 °C.

Table 6. Elemental analyses of **11** and **12**

	11a[a], Found (%)				**12**[b], Found (%)				
	State	C	H	N	S	State	C	H	N	S
a	c)	58.55	6.17	7.32	11.18	liq	60.93	6.38	7.10	8.23
b	liq[d]	58.93	6.39	6.97	10.95	liq	61.32	6.49	7.07	8.02
c	liq	59.77	6.60	6.74	10.70	am[e]	61.89	6.66	6.79	8.01
d	liq	60.05	6.72	6.56	10.28	liq	62.31	6.82	6.68	7.90
e	liq	61.03	6.95	6.55	10.20	liq	63.40	7.02	6.42	7.71
f	liq	61.46	7.10	6.40	9.78	liq	63.15	7.07	6.49	7.60
g	liq	62.07	7.23	6.32	9.72	liq	63.59	7.12	6.52	7.71
h	liq	62.30	7.33	6.10	9.58	liq	63.81	7.30	6.35	7.21

a) Calcd % values correspond to those for **9** in Table 4. b) Calcd % values correspond to those for **10** in Table 5. c) Mp 135—136 °C. d) Liquid. e) Amorphous powder.

tral data are illustrated in Figs. 1 and 2. IR, as common relatively strong bands through **9a** to **9h**, 3280, 2930, 1600, 1570, 1410, 1390, 1378, 1330, 1160, 1090, 1064, 860, 813, 655, and 548 cm^{-1}; as common relatively strong bands through **10a** to **10h**, 2930, 1600, 1570, 1450, 1407, 1385, 1372, 1340, 1159, 856, 653, 568, and 545 cm^{-1}; as common relatively strong bands through **11a** to **11h**, 3270, 2990, 2930, 2850, 1600, 1570, 1450, 1400, 1375, 1330, 1290, 1153, 858, 810, and 650 cm^{-1}; as common relatively strong bands through **12a** to **12h**, 2990, 2940, 2850, 1600, 1570, 1450, 1405, 1385, 1375, 1335, 1292, 1152, 1065, 855, 810, 710, 650, and 540 cm^{-1}.

The authors are grateful to Dr. Haruo Homma and his staff for performing elemental analyses, and to Dr. Jun Uzawa and Mrs. Tamiko Chijimatsu for ^1H NMR spectra measurements.

References

1) Partly reported at the 44th National Meeting of the Chemical Society of Japan, Okayama, October 1981, Abstr. No. 2H27.

2) E. E. Snell and W. T. Jenkins, *J. Cell. Comp. Physiol.*, **54**, *Suppl.*, **1**, 161 (1959); A. E. Braunstein, "The Enzymes," 3rd ed, ed by P. D. Boyer, Academic Press, New York and London (1973), Vol. 9, p. 379.

3) E. H. Cordes and W. P. Jencks, *J. Am. Chem. Soc.*, **84**, 826 (1962); *Biochemistry*, **1**, 773 (1962); T. C. Bruice and R. M. Topping, *J. Am. Chem. Soc.*, **85**, 1493 (1963); T. C. French, D. S. Auld, and T. C. Bruice, *Biochemistry*, **4**, 77 (1965).

4) G. E. P. Smith, Jr., and F. W. Bergstrom, *J. Am. Chem. Soc.*, **56**, 2095 (1934); T. I. Crowell and D. W. Peck, *ibid.*, **75**, 1075 (1953); C. Schroeder, S. Preis, and K. P. Link, *Tetrahedron Lett.*, **1960**, 23; M, Iwata, *Bull. Chem. Soc. Jpn.*, **54**, 2835 (1981).

5) T. L. Fisher and D. E. Metzler, *J. Am. Chem. Soc.*, **91**, 5323 (1969).

6) M. Iwata and H. Kuzuhara, *Chem. Lett.*, **1981**, 1749.

7) For example, dithia(2,5)pyridinophane models for pyridoxal revealed comparable catalytic potency to that of pyridoxal in a nonenzymic system; M. Iwata and H. Kuzuhara, *Chem. Lett.*, **1981**, 5.

8) W. Korytnyk and M. Ikawa, "Methods in Enzymology," ed by D. B. McCormick and L. D. Wright, Academic Press, New York and London (1970), Vol. 18A, p. 524.

9) **2** is more soluble into DMF than **1**.

The Reaction of 2,4,6-Triphenyl-1,3,5-thiadiazin-1-ium Salt with Active Methylene Compounds

Isao SHIBUYA

National Chemical Laboratory for Industry, Yatabe, Tsukuba-gun, Ibaraki 305

(Received September 28, 1981)

The reaction of 2,4,6-triphenyl-1,3,5-thiadiazin-1-ium tetrafluoroborate with several active methylene compounds was studied. Nitromethane and nitroethane gave 2*H*-1,3,5-thiadiazines. The compounds possessing a benzoyl group reacted with this salt to give 5-substituted 2,4,6-triphenylpyrimidines, while those possessing a carbamoyl group afforded 5-substituted 4-hydroxy-2,6-diphenylpyrimidines or 4(3*H*)-pyrimidinone. On the other hand, malononitrile and ethyl cyanoacetate gave 5-substituted 4-mercapto-2,6-diphenylpyrimidines, with the liberation of benzonitrile. It was thus found that 2,4,6-triphenyl-1,3,5-thiadiazin-1-ium tetrafluoroborate reacts with active methylene compounds in fashions similar to that of 2,4,6-triphenyl-1,3-thiazin-1-ium salt.

2,4,6-Triphenylpyrylium salt (**1**) and its *S*-analog (**2**) usually react with active methylenes in a similar way to give 1-substituted 2,4,6-triphenylbenzenes;[1,2] however, 2,4,6-triphenyl-1,3-oxazin-1-ium salt (**3**) and its *S*-analong (**4**) reacted with them in the different manners to afford various pyridines and other derivatives.[3,4] 2,4,6-Triphenyl-1,3,5-oxadiazin-1-ium salt (**5**) reacts with them in ways similar to **3** and produces several pyrimidines.[5,6] The *S*-analog of **5**, 2,4,6-triphenyl-1,3,5-thiadiazin-1-ium salt (**6**), has been synthesized recently,[7] but its behavior toward nucleophiles has not yet been checked. In this report, the reaction of **6** with active methylenes was investigated; the reactivity of these heteroaromatic cation compounds (**1**—**6**) with them was also discussed.

Results and Discussion

The starting material, 2,4,6-triphenyl-1,3,5-thiadiazin-1-ium tetrafluoroborate (**6**), was obtained by treating 4*H*-1,3,5-thiadiazine with triphenylcarbenium tetrafluoroborate.[7]

When **6** was treated with nitromethane and nitroethane under mild conditions, **7** and **8** were afforded in 62 and 53% yields respectively. The analytical data showed that both the products were adducts of the thiadiazin-1-ium cation and the carbanions given by each active methylene. Their IR spectra closely resembled each other and had no absorption assignable to N–H or S–H stretching. Moreover their UV spectra were almost the same (λ_{max}=252 nm, ε=34000). Therefore, for **7** and **8**, two probable structures, 2*H*- and 4*H*-1,3,5-thiadiazines, can be supposed. According to the MS data, the presence of the fragments at 135 *m/e* of **7** and 149 *m/e* of **8**, assigned to $PhCSCH_2^+$ and $[PhCSCHCH_3]^+$ respectively, strongly suggests that **7** and **8** are 2*H*-1,3,5-thiadiazine derivatives. It was thus confirmed that **7** and **8** are 2-nitromethyl- and 2-(1-nitroethyl)-2,4,6-triphenyl-2*H*-1,3,5-thiadiazine. This reaction mode is found in the reaction of **4** with nitromethane, nitroethane, and diethyl malonate; however, it is not found in that of the corresponding *O*-analogs, **3** and **5**.

Benzoylacetonitrile, ethyl benzoylacetate, and dibenzoylmethane were treated with **6** to give 5-cyano-, 5-ethoxycarbonyl-, and 5-benzoyl-2,4,6-triphenylpyrimidine (**9**, **10**, and **11**) in 85, 39, and 43% yields respectively. These reagents react also with **5** to give the respective common products; consequently, they appear to behave in the same fashion toward **5** and **6**. This reaction mode can also be found among the reactions of **1**—**6** with active methylenes; especially, the compounds possessing a benzoyl group are apt to obey this mode to afford 1-substituted 2,4,6-triphenylbenzenes, 3-substituted 2,4,6-triphenylpyridines, and 5-substituted 2,4,6-triphenylpyrimidines.[1-4,6]

Cyanoacetamide, benzoylacetamide, and benzoylacetanilide reacted with **6** to give 5-cyano- and 5-benzoyl-4-hydroxy-2,6-diphenylpyrimidines (**12**, **13**), and 5-benzoyl-2,3,6-triphenyl-4(3*H*)-pyrimidinone (**14**) in 73, 46, and 60% yields respectively. This reaction mode is commonly known in the reactions of **3**—**6** with the compounds possessing a carbamoyl group.

Malononitrile reacted with **6** to give a yellow powder,

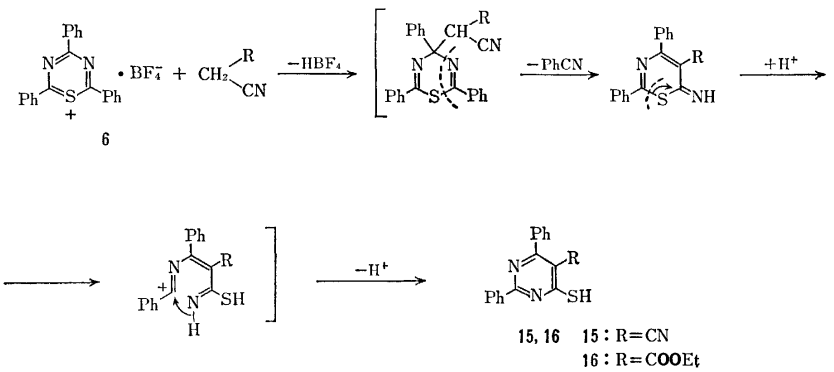

Scheme 1.

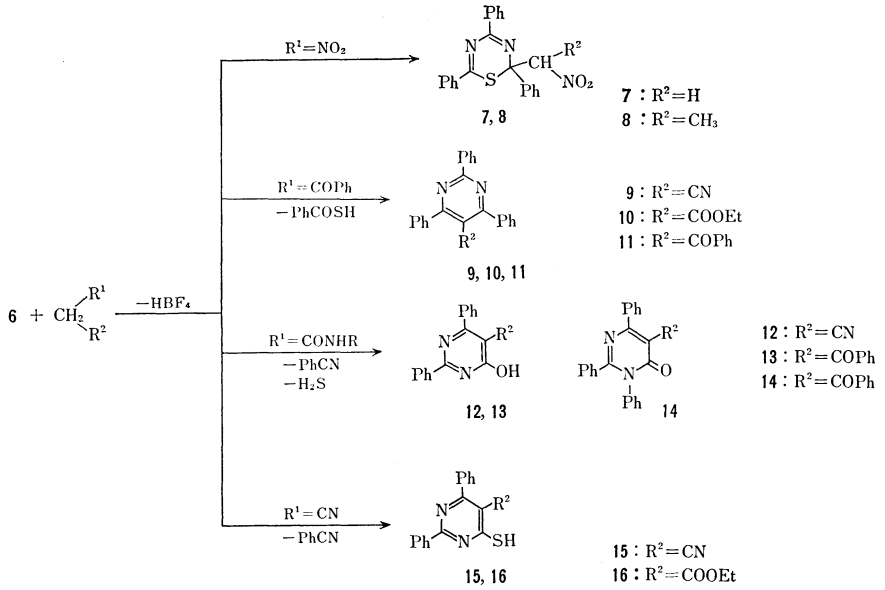

Scheme 2.

15, with the escape of benzonitrile, while ethyl cyanoacetate afforded yellow needles, **16**. Both **15** and **16** were weakly acidic. In their MS spectra the M^+ values were observed at 289 and 336 *m/e*, and a common peak at 264 *m/e*, assignable to $[M+1-CN]^+$ and $[M+1-COOC_2H_5]^+$ respectively, was present. Their UV spectra were similar to one another. Their IR spectra also resembled each other; that of **16** had absorptions assigned to an ester group (1728, 1257 cm^{-1}), but no absorption assigned to a cyano group. These facts suggested that they have the same skeletal structure, and that a cyano group of the reagents participates in this reaction. **15** was obtained by an alternative method as follows: 4-Chloro-5-cyano-2,6-diphenylpyrimidine was treated with hydrogen sulfide in triethylamine–benzene. It was thus concluded that **15** is 5-cyano-4-mercapto-2,6-diphenylpyrimidine; consequently, **16** is 5-ethoxycarbonyl-4-mercapto-2,6-diphenylpyrimidine. For the formation of **15** and **16**, a probable reaction course could be speculated about; it is shown in Scheme 1. This recyclization process into pyrimidine can be regarded as the same as the reaction of *N*-acyl imidoyl chloride with malononitrile.[8]

From all the results described above, the reaction of 2,4,6-triphenyl-1,3,5-thiadiazin-1-ium tetrafluoroborate with active methylenes could be deduced to be as is summarized in Scheme 2.

It is proved that the reaction manner of **6** toward active methylenes is more similar to that of **4** rather than to that of **5**; in addition, these heteroaromatic cations (**1**—**6**), treated with active methylenes, are useful materials for synthesizing benzenes, pyridines, pyrimidines, and other derivatives.

Experimental

2-Nitromethyl- or 2-(1-Nitroethyl)-2H-1,3,5-thiadiazine (7,8). Into a solution of nitromethane or nitroethane (1.5 mmol) and triethylamine (0.3 ml) in chloroform (3 ml), **6** (0.42 g, 1.0 mmol) was stirred at room temperature, after which the mixture was allowed to stand for 5 d. The solvent was distilled out under reduced pressure, and the residue was washed with dilute hydrochloric acid and recrystallized from acetonitrile to give **7** (0.24 g, 62%) or **8** (0.21 g, 53%). Their data are shown below.

7: Mp 166 °C; IR (KBr) 1645, 1555, 1448, 1372, 1224, and 917 cm^{-1}; UV_{max} (EtOH) 252 nm (ε 34000); ^{13}C NMR ($CDCl_3$), δ 82.69 (–C–), 86.02 ($-CH_2NO_2$), 127.21—132.69, 136.66, 137.89, 139.96, and 157.54; ^1H NMR ($CDCl_3$), δ 5.25 (s, $-CH_2NO_2$), 7.24—8.18 (m, arom H); MS, *m/e* (%), 327 (10.4, $[M-CH_2NO_2]^+$), 236 (18.5), 206 (14.6), 135 (36.2 $[PhCSCH_2]^+$), 121 (100, $PhCS^+$), and 103 (63.1, $PhCN^+$). Found: C, 68.41; H, 4.40; N, 10.88; S, 8.39%. Calcd for $C_{22}H_{17}N_3SO_2$; C, 68.20 H, 4.42 N, 10.84; S, 8.28%.

8: Mp 164 °C; IR (KBr), 1651, 1551, 1448, 1382, 1214, and 903 cm^{-1}; UV_{max} (EtOH), 252 nm (ε 34000); ^{13}C NMR ($CDCl_3$) δ 14.47 ($-CH_3$), 84.42 (–C–), 92.15 (>$CHNO_2$), 126.64—132.12, 136.16, 136.41, 139.35, and 156.71; ^1H NMR ($CDCl_3$) δ 1.71 (*d*, >CH–C$\underline{H}_3$), 5.54 (*q*, >C$\underline{H}$–CH_3), 7.24—8.18 (*m*, arom H); MS *m/e* (%), 355 (0.5, $[M-NO_2]^+$), 327 (13.7, $[M-CHNO_2CH_3]^+$), 149 (10.0, $[PhCSCHCH_3]^+$), 121 (100), and 103 (10.3). Found: C, 68.79; H, 4.75; N, 10.51; S, 8.04%. Calcd for $C_{25}H_{19}N_3SO_2$: C, 68.81; H, 4.77; N, 10.47; S, 7.98%.

5-Cyano-, 5-Ethoxycarbonyl-, or 5-Benzoyl-2,4,6-triphenylpyrimidine (9, 10, 11). Into a solution of benzoylacetonitrile, ethyl benzoylacetate, or dibenzoylmethane (1.5 mmol) in 1.0 mol dm^{-3} of MeOH–MeONa (3 ml), **6** (0.42 g, 1.0 mmol) was added; the mixture was stirred at room temperature for 10 min and then refluxed for 1 h. The reaction mixture was poured into dilute hydrochloric acid. The resulting precipitate was collected by filtration and recrystallized from acetonitrile or methanol to give **9** (0.28 g, 84%), **10** (0.15 g, 39%), or **11** (0.18 g, 43%). Their mp and IR spectra agreed with those of authentic samples.[6]

5-Cyano- or 5-Benzoyl-4-hydroxy-2,6-diphenylpyrimidine (12,13), and 5-Benzoyl-2,3,6-triphenyl-4(3H)-pyrimidinone (14). Cyanoacetamide, benzoylacetamide, and benzoylacetanilide (1.5 mmol) were treated with **6** (1.0 mmol), as in the preparation of **9**—**11**. The resulting precipitate was dissolved

in DMF and reprecipitated by the addition of ether to give **12** (0.20 g, 73%), **13** (0.16 g, 46%), and **14** (0.26 g, 60%) respectively. The IR spectra of **12** and **13** were completely superimposed on those of authentic samples.[6] The data of **14** are as below.

14: Mp 243 °C; IR, 1667, 1651, 1535, and 1492 cm^{-1}; UV_{max} (CH_2Cl_2) 252 nm (ε 30900), 315 (sh, ε 9500); ^1H NMR ($CDCl_3$) δ 7.27—8.00 (*m*, arom H); MS *m/e* (%), 428 (28.0, M^+), 400 (15.5, $[M-CO]^+$), 180 (87.6, $[PhC{\equiv}NPh]^+$), 105 (25.7, $PhCO^+$), and 77 (100, Ph^+). Found: C, 81.30; H, 4.67; N, 6.53%. Calcd for $C_{29}H_{20}N_2O_2$: C, 81.29; H, 4.70; N, 6.54%.

*5-Cyano- or 5-Ethoxycarbonyl-4-mercapto-2,6-diphenylpyrimidine (**15**, **16**).* Malononitrile or ethyl cyanoacetate (1.5 mmol) was treated with **6** (1.0 mmol), as in the preparation of **9**—**11**. The resulting precipitation was recrystallized from acetonitrile to give **15** (0.23 g, 80%) or **16** (0.18 g, 54%). Their data are shown below.

15: Mp 250 °C (decomp), IR (KBr), 3176, 3060, 2230, 1545, 1495, and 1240 cm^{-1}; ^1H NMR ($CDCl_3$) δ 7.45—8.16 (m, arom H), 8.51 (s, SH); UV_{max} (CH_2Cl_2), 283 (ε 26500), 307 (sh, ε 23000), 393 (ε 5000); MS *m/e* (%), 289 (55.6, M^+), 264 (22.8, $[M+1-CN]^+$), 186 (79.0), 153 (44.3), and 135 (100). Found: C, 70.32; H, 3.81; N, 14.47; S, 11.37%. Calcd for $C_{17}H_{11}N_3S$: C, 70.57; H, 3.83; N, 14.52; S, 11.08%.

16: Mp 182 °C; IR (KBr), 2963, 1728, 1546, 1491, 1257, and 1230 cm^{-1}; UV_{max} (CH_2Cl_2), 271 (ε 25200), 303 (sh, ε 17500), 388 (ε 7100); ^1H NMR ($CDCl_3$) δ 7.45—8.16 (m, arom H), 8.51 (s, SH); MS *m/e* (%), 336 (25.2, M^+), 307 (57.0, $[M-C_2H_5]^+$), 292 (20.5, $[M-CO_2]^+$), 290 (30.1, $[M-C_2H_5OH]^+$), 264 (43.3, $[M+1-COOC_2H_5]^+$), 158 (39.3), and 128 (100). Found: C, 67.64; H, 4.70; N, 8.19; S, 9.75%. Calcd for $C_{19}H_{16}N_2SO_2$: C, 67.84; H, 4.79; N, 8.32; S, 9.53%.

*Conversion of 4-Chloro-5-cyano-2,6-diphenylpyrimidine into **15**.* 4-Chloro-5-cyano-2,6-diphenylpyrimidine (0.20 g) was added to a solution saturated with hydrogen sulfide in benzene–triethylamine (2:1, 15 ml), after which the mixture was distilled under reduced pressure, the residue was washed with dilute hydrochloric acid and dissolved with 1 mol dm^{-3} of MeOH–MeONa (5 ml). The solution was filtered to separate an insoluble substance and acidified with hydrochloric acid to produce a yellow powder. The powder was recrystallized from acetonitrile to give **15** (0.15 g, 76%). The mp and the IR spectrum agreed with those of **15** obtained from **6**.

References

1) K. Dimroth, *Angew. Chem.*, **72**, 331 (1960).
2) Z. Yoshida, S. Yoneda, H. Sugimoto, and T. Sugimoto, *Tetrahedron*, **27**, 6087 (1971).
3) I. Shibuya and M. Kurabayashi, *Bull. Chem. Soc. Jpn.*, **48**, 73 (1975).
4) I. Shibuya, *Bull. Chem. Soc. Jpn.*, **52**, 3767 (1979).
5) I. Shibuya and M. Kurabayashi, *Bull. Chem. Soc. Jpn.*, **42**, 2382 (1969).
6) I. Shibuya and M. Kurabayashi, *Bull. Chem. Soc. Jpn.*, **46**, 3902 (1973).
7) I. Shibuya, *Bull. Chem. Soc. Jpn.*, **53**, 3369 (1980).
8) R. R. Schmidt, *Chem. Ber.*, **98**, 346 (1965).

Oxidizing Action of Hydroperoxides. Oxidation of Alkyl Aryl Ketones by Hydroperoxides

Kazuhiro MARUYAMA,*,† Hidetoshi IWAMOTO, Osamu SOGA, and Akio TAKUWA

† *Department of Chemistry, Faculty of Science, Kyoto University, Sakyo-ku, Kyoto 606*

Department of Chemistry, Faculty of Science, Shimane University, Nishikawatsu-cho, Matsue 690

(Received October 2, 1981)

The oxidation of alkyl aryl ketones by *t*-butyl hydroperoxide under basic conditions gave products which resulted from the fission of the carbon-carbon bond between carbonyl carbon and alkyl carbon. The reaction was investigated using chiral alkyl aryl ketones. On the basis of the results, a probable reaction mechanism is proposed.

Oxidation of alkyl aryl ketones by peracids under acidic conditions, *i.e.*, Baeyer-Villiger oxidation, is well documented.[1] On the contrary, oxidation of alkyl aryl ketones by hydroperoxides under basic conditions has not been so familiar to chemists, although it has some mechanistically attractive features in its reaction. Some of the reactions have been investigated by one of the present authors(K.M.) and a tentative reaction mechanism has been proposed, but detailed investigations remained to be done.[2] Oxidation of alkyl aryl ketones by *t*-butyl hydroperoxide under basic conditions gave carbon-carbon fission products between $C_{carbonyl}$–C_{alkyl}, but none of those resulted from fission between $C_{carbonyl}$–C_{aryl} without dependency on the structure of alkyl groups (see Eq. 1). In this

$$\text{Aryl–}\overset{\overset{O}{\|}}{C}\text{–Alkyl} + t\text{-BuOO}^- \longrightarrow \text{Aryl–}\overset{\overset{O}{\|}}{C}\text{–O}^- + \text{Oxidation Products of Alkyl Groups} + t\text{-BuO}^- \quad (1)$$

work we reinvestigated the reaction using chiral alkyl aryl ketones, and proposed the most probable reaction mechanism.

Results and Discussion

Oxidation of Chiral Alkyl Aryl Ketones. Chiral alkyl aryl ketones **1**, **4**, and **7** were subjected to the reaction, and the optical rotations of the alcohols resulting from the alkyl groups were examined. Addition of 18-crown-6 in a reacting mixture was a new device of our present oxidation conditions; this was done to make the reacting mixture homogeneous.[2]

Oxidation of (*S*)-(−)-2-ethyl-2,4-dimethyl-1-phenyl-1-pentanone (**1**) by *t*-butyl hydroperoxide anion afforded benzoic acid and (*S*)-(−)-3,5-dimethyl-3-hexanol (**2**) of 100% optical purity, $[\alpha]_{5805}^{25}$ −3.5°, and ester (**3**). The optical purity and the absolute configuration of the isolated 3,5-dimethyl-3-hexanol was confirmed by the literature.[3,4] Thus, alkyl aryl ketone reacted with retention of the configuration of the alkyl group.

An analogous result was obtained in the reaction with (*R*)-(−)-2-methyl-1,2-diphenyl-1-butanone (**4**). The specific optical rotation of 2-phenyl-2-butanol (**5**) isolated from the reacting mixture showed the value $[\alpha]_{5805}^{16}$ +18.9°, optical purity 93%. Correlation of the absolute configurations between (−)-**4** and (+)-**5** has been independently reported by D. J. Cram *et al.*[5] and S. Mitsui.[6] Thus, 2-phenyl-2-butanol (**5**) obtained in this reaction has an *R*-configuration, indicating unambiguously retention of its configuration in the alkyl group in the course of the reaction. Minor but distinctive amounts of 1-methyl-1-phenylpropyl benzoate (**6**) was also obtained in this reaction.

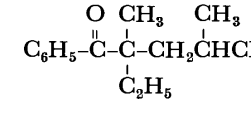

1 Bp 143—147 °C/15 mmHg**
$[\alpha]_{5805}^{25}$ −11.8°
(*c* 4.02, 99%-EtOH)

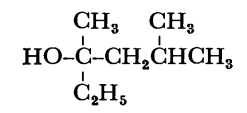

2 Bp 72—73 °C/50 mmHg
$[\alpha]_{5805}^{25}$ −3.5°
(*c* 5.36, 99%-EtOH)
Lit,[15] bp 152—153 °C
S-(−) $[\alpha]_{D}^{25}$ −3.5°
(*c* 8.5, 95%-EtOH)

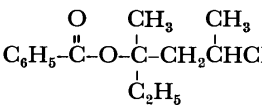

3 Bp 153 °C/28 mmHg
(slightly decomp)
Specific rotation was not determined.

Fig. 1.

From the results of the above two reactions we can conclude that the reaction of alkyl aryl ketone proceeds with retention of the configuration around the alkyl carbon adjacent to the carbonyl carbon. However, chiral alkyl aryl ketone, in which the alkyl group has enolizable hydrogen, lost its chirality in the course of the reaction. This is exemplified in the reaction of chiral 2-methyl-1-phenyl-1-octanone (**7**). The reaction of chiral **7** under similar conditions gave a mixture of benzoic acid, 2-octanone, *t*-butyl alcohol, and some recovered **7**. 2-Octanol was not detected in the reacting mixture, but its oxidation product, 2-octanone, was found in a reasonable yield (25%). Though diagnosis from 2-octanol was not achieved, the recovered **7** showed no optical rotation, indicating complete loss of the chirality in the course of the reaction, presumably *via* enolization.[7]

In conclusion, oxidation of alkyl aryl ketones by *t*-butyl hydroperoxide anion may be formulated best as shown in Eq. 2. Thus, the previously proposed reaction mechanism including an attack of *t*-butyl hy-

** 1 mmHg≈133.322 Pa.

droperoxide anion on carbonyl carbon and subsequent back-side attack of hydroxide anion on alkyl carbon[2] should be revised as described here. When one of R^1–R^3 was hydrogen, alkyl aryl ketone could be enolized to lose its chirality before attack by hydroperoxide anion. That the enolization of ketone occurred more quickly than the attack of hydroperoxide anion is suggested by the experimental results of the reaction of (−)-**7**.

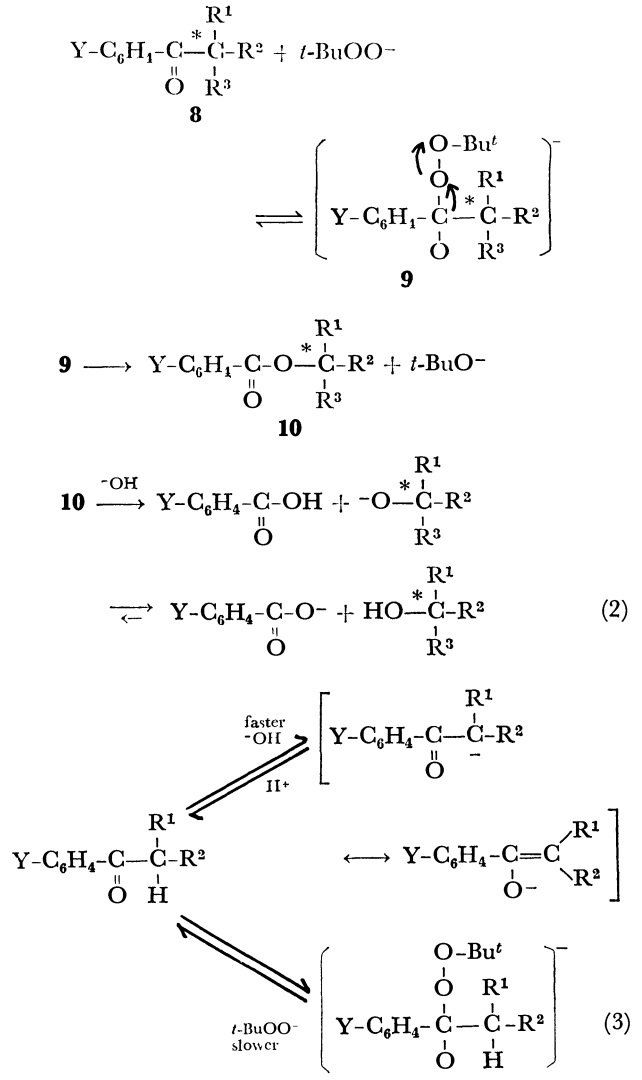

Comparison of our Reaction with the Baeyer-Villiger Reaction. The characteristics of our reaction and the Baeyer-Villiger reaction are illustrated in Table 1.

In the Baeyer-Villiger reaction, methyl and ethyl phenyl ketones (Rec. No. 1 and 2) gave preferentially carbon-carbon fission products between carbonyl carbon and phenyl carbon, whereas isopropyl and *t*-butyl phenyl ketones (Rec. No. 3 and 4) gave preferentially carbon-carbon fission products between carbonyl carbon and alkyl carbon. On the contrary, in our reaction all alkyl phenyl ketones gave carbon-carbon bond cleavage products between carbonyl carbon and alkyl carbon.

Thus, it is clear now that by choosing suitable reaction conditions of the peroxide oxidation one can attain a selective carbon-carbon bond cleavage of alkyl aryl ketones.

Experimental

All melting and boiling points are uncorrected. The infrared spectra were measured on a Hitachi 215 grating infrared spectrophotometer. ^{1}H NMR spectra were recorded on a JEOL JNM-MH 100 spectrometer. Gas chromatography was carried out with a Hitachi gas chromatograph, Model 163. The optical rotations were measured on a Union high sensitivity polarimeter PM-70. Elemental analyses were carried out at the Analytical Center of Kyoto University.

t-Butyl Hydroperoxide. This peroxide was prepared by the literature method:[8] bp 38—39 °C/19 mmHg; lit:[8] bp 33—34 °C/17 mmHg.

*Preparation of 2-Ethyl-2,4-dimethyl-1-phenyl-1-pentanone (**1**).* This procedure is a modification of that employed by D. J. Cram.[5] A mixture of 2-ethyl-2,4-dimethylpentanoic acid (**11**, 57 mmol) prepared from 2,4-dimethylpentanoic acid by the procedure of P. E. Pfeffer *et al.*[9] and thionyl chloride (75 mmol) was allowed to stand overnight at room temperature, the excess thionyl chloride being evaporated under vacuum. Two successive portions of anhydrous benzene

Table 1. Comparison of Baeyer-Villiger reaction with the present reaction

Reaction No.	Ketone	Baeyer-Villiger reaction[a]			Present reaction[b]	
		Ph-O-C(=O)-R (%)	Ph-C(=O)-O-R (%)	Recovered ketone (%)	Ph-C(=O)-OH (%)	Recovered ketone (%)
1	Ph-C(=O)-Me	85	0	15	45	55
2	Ph-C(=O)-Et	80	7	13	60	40
3	Ph-C(=O)-Pr^i	7	75	18	40	60
4	Ph-C(=O)-Bu^t	0	76	24	40	60

Reaction conditions: a) ketone: 2 mmol; *m*-chloroperbenzoic acid: 2.4 mmol; solvent: $CHCl_3$(12 ml); temp: 28 °C; reaction time: 7 d. b) Ketone: 2 mmol; *t*-BuOOH: 6 mmol; KOH: 7 mmol; 18-crown-6: 0.8 mmol; solvent: C_6H_6(20 ml); temp: 70 °C; reaction time: 1 h.

were added and evaporated under vacuum. The residual oil consisted of 2-ethyl-2,4-dimethylpentanoyl chloride was used for the next step without further purification. To a hot benzene solution of diphenylcadmium prepared in the usual way[10] was added the above residual oil. The reaction mixture was held at reflux for 30 min and worked up in the usual manner to give **1** (72%): bp 143—147 °C/15 mmHg; NMR (CCl_4) δ=7.70—7.50 (2H, m), 7.40—7.10 (3H, m), 2.10—1.30 (5H, m), 1.20 (3H, s), 1.00—0.65 (9H, m); IR (CCl_4) 1670 cm^{-1} (C=O).

Found: C, 82.68; H, 10.21%. Calcd for $C_{15}H_{22}O$: C, 82.51; H, 10.16%.

Optical resolution of **11** with the aid of burcine to the procedure of W. v. E. Doering and K. B. Wiberg[11] was unsuccessful, but we have accomplished this using quinine by the following procedures. A mixture of **11** (29 g) and quinine (50 g) was dissolved in 66%-ethanol by heating. The solution was allowed to stand in a refrigerator, and then filtered to give colorless crystals. These were recrystallized fifteen times from 66%-ethanol to give a quinine salt (9 g): mp 97.5—98.5 °C. The salt was suspended in dilute sulfuric acid and extracted with ether. The etherial extract was washed with dilute sulfuric acid, dried over sodium sulfate, and then the solvent was removed. The residual oil was purified by distillation to give (−)-**11** (2.5 g): bp 138—140 °C/20 mmHg; $[\alpha]_{5805}^{25}$ −22.7° (*c* 5.15, 99%-EtOH); lit[11] for (+)-**11**: bp 124—125 °C/12 mmHg; $[\alpha]_D^{25}$ +21.42° (*c* 10.3, 95%-EtOH).

The active (−)-**1** was prepared in 85% over-all yield from (−)-**11** by use of the above procedure: $[\alpha]_{5805}^{25}$ −11.8° (*c* 4.02, 99%-EtOH). The IR and NMR spectra of this ketone were identical with those of (±)-**1**.

Preparation of 2-Methyl-1,2-diphenyl-1-butanone (4). This ketone was prepared from 2-methyl-2-phenylbutanoic acid by the procedure given in the literature:[5,12] bp 139—140 °C/2 mmHg; lit:[5] bp 144—145 °C/2.5 mmHg.

Optically active (−)-**4** was prepared from (−)-2-methyl-2-phenylbutanoic acid: $[\alpha]_{5805}^{20}$ −32.1° (*c* 4.04, C_6H_6); mp 87—88 °C; lit:[12] $[\alpha]_D^{23}$ −30° (*c* 4.5, C_6H_6); mp 86—87 °C. After employing the above procedure to the synthesis of **4**, we obtained the active **4**: $[\alpha]_{5805}^{20}$ −69.7° (*c* 3.8, C_6H_6); lit:[5] $[\alpha]_D^{25}$ −63.7° (neat).

Preparation of 2-Methyl-1-phenyl-1-octanone (7). Ketone **7** was prepared in a yield of 84% by the Friedel-Crafts reaction of a mixture of 2-methyloctanoyl chloride (63 mmol), anhydrous aluminium chloride (75 mmol), and dry benzene: bp 130—131 °C/2 mmHg; lit:[13] bp 100 °C/0.01 mmHg.

Resolution of the 2-methyloctanoic acid was achieved in the following way. A mixture of 2-methyloctanoic acid (8.5 g) and cinchonidine (16 g) was dissolved in 95%-acetone by heating, and then allowed to stand in a refrigerator. The precipitated salts were collected by filtration and then repeatedly recrystallized using the same solvent until the optical rotation of the acid showed a very slight increase (twelve times). The salt was then decomposed in the usual manner to give (−)-2-methyloctanoic acid (745 mg): $[\alpha]_{5805}^{20}$ −20.0° (*c* 1.8, C_6H_6); lit[14] for (+)-isomer: $[M]_D^{20}$ +26° ($[\alpha]_D^{25}$ +16.45°).

Optically active (−)-**7** was prepared from (−)-2-methyloctanoic acid. After the above procedure similar to the synthesis of **7** was employed, we obtained the active **7**: $[\alpha]_{5805}^{20}$ −29.7° (*c* 2.9, C_6H_6); lit:[13] $[\alpha]_D$ −21.5° (*c* 5, Et_2O), $[\alpha]_D$ 24.5°.

General Procedure for Oxidation of the Ketone with t-Butyl Hydroperoxide. Powdered analytical grade potassium hydroxide (5 mmol) was suspended in benzene (10 ml). After the air in the reaction vessel was expelled completely with dry nitrogen gas and the temperature of the oil bath reached 80 °C, a benzene solution (5 ml) of ketone (2 mmol) was added to the reaction mixture; then a benzene solution (5 ml) of *t*-butyl hydroperoxide (4 mmol) and 18-crown-6 (5 mmol) was added sequentially with an injector. The reacting mixture was stirred at 80 °C for 3 h and cooled in an ice-water bath. Ether (10 ml) was added to the reacting mixture and the resulting carboxylic acid was extracted with water (10 ml) and twice with aqueous sodium hydrogencarbonate solution (10 ml). The combined aqueous layer was acidified with dilute sulfuric acid and then extracted twice with ether (10 ml). The amount of acid extracted was determined by gas chromatography after methylating with diazomethane. The unreacted ketone and the neutral products in the residual organic layer were determined by gas chromatography and then isolated by column chromatography on silica gel for analyses.

Oxidation of (±)-1. The resulting mixture consisted of benzoic acid (44%), recovered ketone (47%), 3,5-dimethyl-3-hexanol (**2**, 32%): bp 72—73 °C/50 mmHg; lit:[15] bp 152—153 °C, and 1-ethyl-1,3-dimethylbutyl benzoate (**3**, 9%): bp 153 °C/28 mmHg (slightly dec); NMR (CCl_4) δ=7.88 (2H, dd, J=8 and 2 Hz), 7.46—7.10 (3H, m), 2.10—1.64 (5H, m), 1.51 (3H, s), 1.04—0.80 (9H, m); IR (CCl_4) 1710 (ester C=O) and 1275 cm^{-1} (C–O–C).

Found: C, 76.84; H, 9.67%. Calcd for $C_{15}H_{22}O_2$: C, 76.88; H, 9.46%.

The specific rotation of **2** produced in the oxidation of (−)-**1** was as follows: $[\alpha]_{5805}^{25}$ −3.5° (*c* 5.36, 99%-EtOH); lit:[15] $[\alpha]_D^{25}$ −3.5° (*c* 8.5, 95%-EtOH).

Oxidation of (±)-4. Oxidation was done at 50 °C and the reaction products were analyzed as usual. The resulting mixture consisted of benzoic acid (65%), recovered ketone (20%), 2-phenyl-2-butanol (**5**, 13%): bp 111 °C/25 mmHg; lit:[16] bp 90—91 °C/14 mmHg, and 1-methyl-1-phenylpropyl benzoate (**6**, 9%): viscous oil; NMR (CCl_4) δ=7.98 (2H, dd, J=8 and 2 Hz), 7.50—7.10 (8H, m), 2.40—2.00 (2H, m), 1.92 (3H, s), 0.84 (3H, t, J=7 Hz); IR (CCl_4) 1720 (ester C=O) and 1270 cm^{-1} (C–O–C).

Found: C, 80.13; H, 7.21%. Calcd for $C_{17}H_{18}O_2$: C, 80.28; H, 7.13%.

The specific rotation of **5** produced from oxidation of (−)-**4** was as follows: $[\alpha]_{5805}^{16}$ +18.9° (*c* 2.16, C_6H_6); lit:[16] $[\alpha]_D^{22}$ +17.45° (neat).

Oxidation of (±)-7. The resulting mixture consisted of benzoic acid (41%), heptanoic acid (4%), hexanoic acid (4%), recovered ketone (57%), and 2-octanone (25%). 2-Octanol was not detected in the mixture.

References

1) C. H. Hassall, "Organic Reaction," ed by R. Adams, John Wiley and Sons, New York (1967), Vol. 9, Chap. 3, p. 73.

2) K. Maruyama, *Bull. Chem. Soc. Jpn.*, **33**, 1516 (1960); **34**, 102 and 105 (1961).

3) K. B. Wiberg, *Diss. Abstr.*, **13**, 18 (1953).

4) W. Kirmse, P. Feyen, W. Cruber, and W. Kapmeyer, *Chem. Ber.*, **108**, 1839 (1975).

5) D. J. Cram and J. Allinger, *J. Am. Chem. Soc.*, **76**, 4516 (1954).

6) S. Mitsui, S. Imaizumi, Y. Senda, and K. Konno, *Chem. Ind. (London)*, **1964**, 233.

7) Absence of 2-octanol in the reacting mixture is another challenging problem, which should be solved in future.

8) N. A. Milas and D. M. Surgenor, *J. Am. Chem. Soc.*, **68**, 205 (1946).

9) P. E. Pfeffer, L. S. Silbert, and J. M. Chirinki, Jr., *J. Org. Chem.*, **37**, 451 (1972).
10) J. Cason and H. Rapoport, "Laboratory Text in Organic Chemistry," Prentice-Hall, New York, N. Y. (1950), p. 325.
11) W. v. E. Doering and K. B. Wiberg, *J. Am. Chem. Soc.*, **72**, 2608 (1950).
12) D. J. Cram and J. D. Knight, *J. Am. Chem. Soc.*, **74**, 5835 (1952).
13) v. D. Seebach, D. Steinmuller, and F. Demuth, *Angew. Chem.*, **80**, 618 (1968).
14) A. Rothen and P. A. Levene, *J. Chem. Phy.*, **7**, 975 (1939).
15) W. v. E. Doering and H. H. Zeiss, *J. Am. Chem. Soc.*, **72**, 147 (1950).
16) H. H. Zeiss, *J. Am. Chem. Soc.*, **73**, 2391 (1951).

Rapid Peptide Synthesis in Liquid Phase. Preparation of Angiotensin II and Delta-sleep-inducing Peptide by the "Hold-in-Solution" Method[1,2]

Sukekatsu NOZAKI* and Ichiro MURAMATSU†

Department of Microbiology, Faculty of Pharmaceutical Sciences, Josai University, Sakado, Saitama 350-02

† *Department of Chemistry, College of Science, Rikkyo University, Nishi-Ikebukuro, Toshima-ku, Tokyo 171*

(Received October 3, 1981)

A new technique for rapid peptide synthesis has been demonstrated by the preparation of a protected angiotensin II, Z–Asp(OBzl)–Arg(NO_2)–Val–Tyr(Bzl)–Ile–His(Bzl)–Pro–Phe–OBzl (**1**), and a protected delta-sleep-inducing peptide, Z–Trp–Ala–Gly–Gly–Asp(OBzl)–Ala–Ser(Bzl)–Gly–Glu(OBzl)–OBzl (**2**). Elongation of the peptide chain was carried out in 1,2-dichloroethane by repeating the following series of operations: acylation of a benzyl ester of amino acid or peptide with Boc-amino acid by 1-ethyl-3-(3-dimethylaminopropyl)-carbodiimide hydrochloride and 1-hydroxybenzotriazole; washing of the organic layer; acidolysis of the α-amino protector; neutralization; and washing. Throughout the synthesis, the growing peptides were held in the organic layer without being isolated. The protected peptides, **1** and **2**, were obtained in overall yields of 78% and 53% based on their *C*-terminal amino acid esters, and were then hydrogenated to give angiotensin II and delta-sleep-inducing peptide, respectively, thus demonstrating the usefulness of this method for rapid peptide synthesis.

The liquid phase method for peptide synthesis is superior to the solid phase method especially with respect to variety of synthetic routes available and facility for purification of the intermediates. The former method, however, usually involves a considerable amount of time-consuming work; hence various attempts have been made to reduce the time required.[3] The present paper describes a new technique, tentatively named the "hold-in-solution" method, for rapid peptide synthesis in the liquid phase, in which a water-containing environment can be tolerated throughout the entire procedure for peptide elongation. Essentially, this method consists of a series of operations, the series being repeated in as many cycles as necessary to obtain the desired elongation (Fig. 1). The details of the operations, designated herein as (A), (B), (C), (D), and (E), are as follows: (A) Acylation of an amino acid benzyl ester with a Boc-amino acid by using 1-ethyl-3-(3-dimethylaminopropyl)-carbodiimide hydrochloride (WSCD·HCl)[4] and 1-hydroxybenzotriazole (HOBt)[5] as the coupling reagents in a water-immiscible organic solvent, 1,2-dichloroethane (DCE). The coupling reaction is carried out at room temperature. Completion of the acylation is easily detected by disappearance of the amine component on TLC. Excess amounts (usually 2 mol equivalents per mole of the amine component) of a Boc-amino acid, HOBt, and WSCD·HCl are used for the acylation. (B) Successive washing of the reaction mixture with 0.1 M (1 M = 1 mol dm^{-3}) HCl, water, 0.5 M Na_2CO_3, and water. Complete removal of the excess Boc-amino acid is sometimes difficult by the washing but is not necessary in this step. (C) Acidolysis of the α-amino protector by HCl in dioxane (concentration of HCl in the mixture; 1.7—2.2 M. 0 °C, 0.5 h). In this step the excess Boc-amino acid is converted to the free amino acid, which is easily removed from the organic layer in the following steps. (D) Neutralization of the mixture by 2 M Na_2CO_3 below 0 °C. (E) Removal of the aqueous layer and washing of the organic layer with water, 0.5 M Na_2CO_3, and water in that order. All the treatments are carried out in a single vessel. When a mixture emulsifies, the two layers are separated by centrifugation.

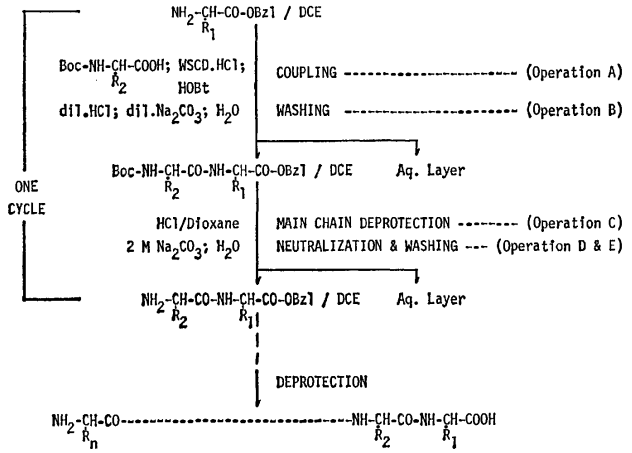

Fig. 1. Scheme of the synthesis of an oilgopeptide by the "hold-in-solution" method.

By repeating the series of operations through two or more cycles, a peptide chain can be elongated stepwise. During the preparation, the intermediate peptide is held in the organic layer without being isolated. It is desirable for best results that the *N*-terminal free peptide have low solubility in the aqueous layer.

Table 1 shows the effect of some additives on the preparation of a model peptide, Boc–Val–Ile–OBzl,

Table 1. Effect of additives on a one-hour coupling reaction of Boc–Val–OH and H–Ile–OBzl[a]

Additive	Yield of Boc–Val–Ile–OBzl (%) Solvent (ml)			
	DCE (12)	DCE/H_2O (10/2)	DMF (12)	DMF/H_2O (10/2)
None	58	30	16	12
HOBt	82	71	80	90
HOSu	21	33	9	20
HONb	27	35	11	23

a) See Experimental.

Table 2. Amino acid ratios in each cycle of acylation in the preparation of angiotensin II

Cycle No.	Pro	Phe	His[a]	Ile	Tyr[b]	Val	Arg	Asp
1	0.95	1.05						
2	0.98	1.02	—					
3	1.02	1.06	—	0.92				
4	1.02	1.06	—	0.92	0.82			
5	1.05	1.15	—	1.00	0.84	0.97		
6	1.03	1.01	—	0.99	0.37	0.99	0.88[c]	
Isolated **1** (crude)	1.03	1.02	—	0.78	0.35	1.03	1.33[c]	0.92
After hydrogenolysis (crude)	1.04	1.08	0.93	0.92	0.99	1.04	0.94	1.07

a) im-Benzyl group was not cleaved by the hydrolysis. b) Removal of the benzyl ether substituted on the phenyl group was incomplete. c) Sum of Arg and Orn.

Table 3. Amino acid ratios in each cycle of acylation in the preparation of DSIP

Cycle No.	Glu	Gly	Ser	Ala	Asp	Gly	Gly	Ala	Trp
1	1.00	1.00							
2	1.07	1.04	0.89						
3	1.08	1.05	0.92	0.95					
4	1.05	1.02	0.91	0.93	1.09				
5	1.06	0.96[a]	0.93	0.98	1.11	0.96[a]			
6	1.10	0.94[a]	0.95	1.04	1.10	0.94[a]	0.94[a]		
7	1.12	0.98[a]	0.93	0.94[b]	1.13	0.98[a]	0.98[a]	0.94[b]	
Isolated **2**	1.07	0.99[a]	0.93	0.97[b]	1.10	0.99[a]	0.99[a]	0.97[b]	—[c]

a) Average value for Gly. b) Average value for Ala. c) Destroyed by the hydrolysis.

by a one-hour coupling reaction of Boc–Val–OH and H–Ile–OBzl, both of which are rather less reactive because of the steric hindrance of their bulky side chains, in several solvent systems. Without the additives, the coupling yield was low even in the anhydrous solvents. The presence of water further lowered the yield. Addition of HOBt markedly improved the yield in the water-containing solvents as well as in the anhydrous media. It is interesting that the use of other additives, *N*-hydroxysuccinimide (HOSu)[6] and *N*-hydroxy-5-norbornene-2,3-dicarboximide (HONb),[7] rather lowered the yield in the anhydrous solvents. In the water-containing systems, they improved the yield but the effect was not as significant as that of HOBt. Thus, peptide elongation with sufficient yield is possible in water-containing media by addition of HOBt.

As a model peptide synthesis by this new method, preparation of a protected angiotensin II, Z–Asp(OBzl)–Arg(NO_2)–Val–Tyr(Bzl)–Ile–His(Bzl)–Pro–Phe–OBzl (**1**), and a protected delta-sleep-inducing peptide,[8] Z–Trp–Ala–Gly–Gly–Asp(OBzl)–Ala–Ser(Bzl)–Gly–Glu(OBzl)–OBzl (**2**), was carried out in DCE. Two equimolar amounts of the acylating reagents were used per mole of the amine components. Tables 2 and 3 show the amino acid ratios in the acid hydrolysates of the intermediate peptides held in the organic layer at the end of operation E of each cycle. Complete acylation was achieved in every coupling reaction This fact indicates that the acylation in this method proceeds more smoothly than that in the solid phase method employing the usual polystyrene resin as the support.[9] Centrifugation was required in operation E after introduction of valine at position 3 in the preparation of **1**, and of alanine at position 6 in the case of **2**. The protected peptides, **1** and **2**, were obtained in overall yields of 78% and 53%, respectively, based on their *C*-terminal esters. HPLC profiles of the products are shown in Fig. 2. After the catalytic hydrogenolysis of **1** and **2**, the free peptides were easily purified by partition chromatography on Sephadex[10] to give angiotensin II and DSIP, respectively. Homogeneities of the synthetic peptides were confirmed by HPLC analyses (Fig. 3).

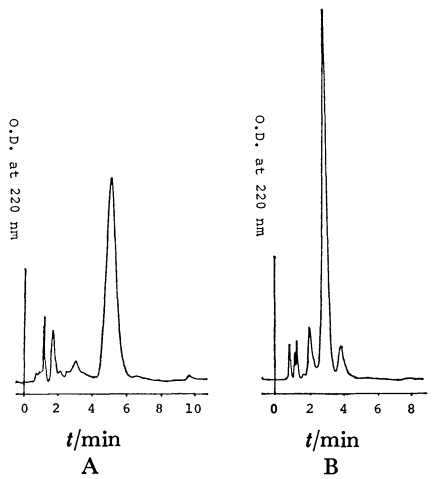

Fig. 2. HPLC profiles of (A) crude **1** ($MeOH/H_2O$, 8/1) and (B) crude **2** ($MeOH/H_2O$, 5/1).

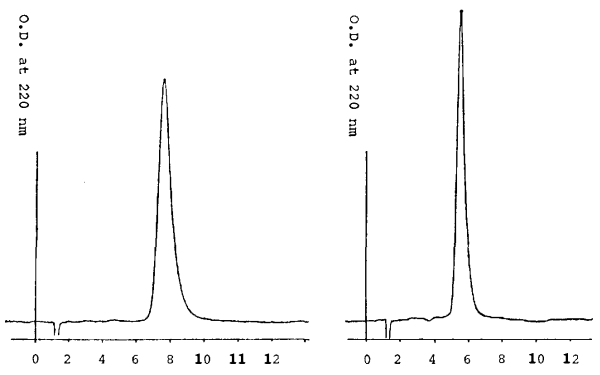

Fig. 3. HPLC profiles of (A) synthesized angiotensin II (MeOH/1% ammonium acetate, pH 6.90, 7/10) and (B) synthesized DSIP (MeOH/1% ammonium acetate, pH 6.90, 1/8).

Preparation of the octa- and nonapeptide demonstrated the utility of the new method for rapid synthesis of oligopeptides. The method has been applied successfully to the preparation of the fragment peptides which served as the building blocks in the construction of granuliberin R[11] and the active site of troponin I.[12]

Advantages of the "hold-in-solution" peptide synthesis are (1) that it is fast, (2) that it permits the intermediates to be characterized easily, and (3) that it does not require large excesses of the acylating reagents nor any special apparatus.

Experimental

The peptides were hydrolyzed in constantly boiling HCl (110 °C, 16 h) or in 3 M 2-mercaptoethanesulfonic acid (110 °C, 20 h). Amino acid analyses were carried out on a JLC-6AS automatic amino acid analyzer (JEOL). HPLC analyses were performed on a steel column (4 mm×250 mm) packed with LiChrosorb RP-18 (10 μm, Merck & Co.) and optical density at 220 nm was monitored at a flow rate of 1.83 ml/min. An authentic sample of angiotensin II was purchased from the Protein Research Foundation, Osaka, Japan.

Effect of Additives. Boc–Val–OH (0.5 mM, derived from the DCHA salt), H–Ile–OBzl tosylate (0.5 mM), triethylamine (0.5 mM), and an additive (0.5 mM) were dissolved in a solvent. To this solution, solid WSCD·HCl (0.5 mM) was added and the mixture was stirred for 1 h at room temperature. The solvent was removed *in vacuo*. The residue was dissolved in ethyl acetate (50 ml) and washed successively with 0.1 M HCl (10 ml×2), water (10 ml), 0.5 M Na_2CO_3 (20 ml), and water (10 ml×4). After removal of the solvent, the residue was dissolved in methanol/water (3/1) of a known volume (50—110 ml) and an aliquot of the solution (5—30 μl) was applied to HPLC (solvent: methanol/water, 3/1). The yield of the dipeptide was determined by use of the calibration curve of a standard solution of Boc–Val–Ile–OBzl (9.56 mg in 30 ml of methanol/water, 3/1).

Preparation of Angiotensin II. H–Phe–OBzl tosylate (222 mg, 0.5 mM), triethylamine (0.07 ml), Boc–Pro–OH (1.0 mM, 215 mg), and HOBt (135 mg, 1.0 mM) were dissolved in DCE (25 ml). WSCD·HCl (192 mg, 1.0 mM) in water (1 ml) was added to the solution and the mixture was stirred for 2 h at room temperature. The reaction mixture was washed successively with 0.1 M HCl (5 ml×3), water (5 ml), 0.5 M Na_2CO_3 (5 ml), and water (5 ml×4) below 10 °C. Each of the aqueous phases was removed by pipetting. To the organic layer, HCl in dioxane (7.2 M, 8 ml) was added at −10—0 °C and the mixture was stirred at 0 °C for 0.5 h, then chilled to −10 °C, and 2 M Na_2CO_3 (18 ml) was added to it. The aqueous layer was removed and the organic layer was washed successively with water (4 ml×2), 0.5 M Na_2CO_3 (4 ml), and water (4 ml×2). An aliquot (*ca.* 0.05 ml) of the organic layer was evaporated and the residue was hydrolyzed to determine the amino acid ratio (Table 2). In the second cycle, Boc–His(Bzl)–OH (345 mg, 1.0 mM) and HOBt (135 mg, 1.0 mM) were added to the organic layer followed by WSCD·HCl (192 mg, 1.0 mM) dissolved in water (1 ml). The mixture was stirred for 4.5 h, then otherwise subjected to the procedures described above for the first cycle. Further acylation was carried out successively by Boc–Ile–OH, Boc–Tyr(Bzl)–OH, Boc–Val–OH, Boc–Arg(NO_2)–OH, and Z–Asp(OBzl)–OH (1.0 mM each) using HOBt and WSCD·HCl (1.0 mM each) as the condensation reagents. The coupling reactions were carried out for 3 h to overnight. Oily Boc-amino acids, Boc–Ile–OH and Boc–Val–OH, were added as DCE solution (2 ml). Boc–Arg(NO_2)–OH was added as a DMF solution (2 ml). Centrifugation was required in operation E after addition of Boc–Val–OH. In the final acylation, the reaction mixture was diluted with DMF (10 ml) after addition of WSCD·HCl. After the acylation was completed, the mixture was further diluted with DCE (100 ml) and water (40 ml). The organic layer was separated and washed successively with 0.1 M HCl (10 ml×2), 0.5 M Na_2CO_3 (20 ml), and water (40 ml×2, 20 ml×3). The organic layer was concentrated to give an oil, which was then solidified by addition of ether. **1**: mp 169—178 °C decomp, 609 mg (78% based on H–Phe–OBzl tosylate). Calcd for $C_{86}H_{100}O_{16}N_{14}$: C, 65.14; H, 6.36; N, 12.37%. Found: C, 65.10; H, 6.43; N, 12.16%. R_f: 0.29 (Merck precoated silicagel plate, $CHCl_3$/MeOH, 95/5). A part of the product (200 mg) was hydrogenated in a mixture of DMF (30 ml), water (20 ml), and acetic acid (1 ml) for 42 h using Pd black. After removal of the catalyst and the solvent, a crude product was obtained. R_f: 0.54 (Avicel precoated cellulose plate, 1-butanol/pyridine/acetic acid/water, 16/10/3/12). Amino acid ratio in HCl–hydrolysate, Asp 1.07, Pro 1.04, Val 1.04, Ile, 0.92, Tyr 0.99, Phe 1.08, His 0.93, Arg 0.94. The product was purified by partition chromatography on a Sephadex G-25 column (1.6 cm×36 cm, 1-butanol/pyridine/acetic acid/water, 16/10/3/12). Fractions of 3 g each were collected and fractions 15—18 were combined and concentrated. The residue was applied to a Sephadex G-10 column (1.2 cm×24 cm) and eluted with 5% acetic acid. Fractions of 2 g each were collected and the desired peptide was recovered from fractions 5—9 by lyophilization: 94 mg; 63% from **1**. Amino acid ratio in HCl–hydrolysate (for 24 h): Asp 1.09, Pro 0.98, Val 1.02, Ile 0.91, Tyr 1.01, Phe 1.09, His 0.94, Arg 0.96. Calcd for $C_{50}H_{71}O_{12}N_{13}\cdot CH_3COOH\cdot 4H_2O$: C, 53.01; H, 7.10; N, 15.45%. Found: C, 53.24; H, 6.57; N, 15.14%. The biological activity (oxytocic activity on an isolated rat uterus) of the prepared peptide was the same as that of the authentic sample.

Preparation of DSIP. H–Glu(OBzl)–OBzl tosylate (250 mg, 0.5 mM) in DCE (25 ml) was acylated successively by Boc–Gly–OH, Boc–Ser(Bzl)–OH, Boc–Ala–OH, Boc–Asp(OBzl)–OH, Boc–Gly–OH, Boc–Gly–OH, Boc–Ala–OH, and Z–Trp–OH (1.0 mM each) using HOBt and WSCD·HCl

(1.0 mM each) as described above. The following reagents were used:

Operation B: 0.1 M HCl (5 ml×3), water (5 ml), 0.5 M Na_2CO_3 (5 ml), water (5 ml×4).

Operation C: 8.8 M HCl/dioxane (8 ml).

Operation D: 2 M Na_2CO_3 (18 ml).

Operation E: water (4 ml×2), 0.5 M Na_2CO_3 (4 ml), water (4 ml×4 to 6).

Centrifugation was required in operation E after introduction of Boc–Ala–OH at position 6 and in both operation B and E after introduction of Boc–Ala–OH at position 2. After the final acylation, the reaction mixture was washed with water (10 ml×3, the aqueous phases being separated by centrifugation). The organic layer was concentrated to give an oil, which was solidified in ether. The solid collected was dissolved in DMF, decolorized with charcoal, and reprecipitated by addition of ether. **2**: 284 mg. 53% based on H–Glu(OBzl)–OBzl tosylate. Mp 210—213 °C decomp. Calcd for $C_{71}H_{78}O_{17}N_{10}\cdot H_2O$: C, 62.26; H, 5.92; N, 10.29%. Found: C, 62.59; H, 5.88; N, 10.26%. Amino acid ratio in HCl–hydrolysate: Asp 1.10, Ser 0.93, Glu 1.07, Gly 2.96, Ala 1.94. In 2-mercaptoethanesulfonic acid–hydrolysate: Asp 1.12, Ser 0.96, Glu 1.10, Gly 2.90, Ala 1.92, Trp 0.73. A part of the product (166 mg) was hydrogenated for 7 h in DMF (60 ml) and water (20 ml) using Pd black. After the usual work-up, the crude product was applied to partition chromatography on a Sephadex G-25 column (1.6 cm×36 cm, 1-butanol/pyridine/acetic acid/water, 16/10/3/12). Fractions of 3 g each were collected and fractions 47—53 were combined, concentrated, and lyophilized from water (67 mg). The peptide was further applied to a Sephadex G-10 column (1.2 cm×26 cm), and eluted with water. Fractions of 1 g each were collected and fractions 12—19 were combined and lyophilized to give the desired peptide: 52 mg, 39% from **2**. R_f: 0.11 (silica gel, 1-butanol/acetic acid/water, 4/1/1). Calcd for $C_{35}H_{48}O_{15}N_{10}\cdot 4H_2O$: C, 45.65; H, 6.12; N, 15.20%. Found: C, 45.12; H, 5.58; N, 15.41%. Amino acid ratio in HCl-hydrolysate: Asp 1.01, Ser 0.92, Glu 1.09, Gly 2.96, Ala 2.01, Trp 0.85. In 2-mercaptoethanesulfonic acid–hydrolysate: Asp 0.91, Ser 0.97, Glu 1.08, Gly 2.99, Ala 2.06, Trp 0.98.

The authors are indebted to the Research Laboratory of Nihon Kayaku Co. Ltd. for the biological measurement and the Research Laboratory of Toyo Jozo Co. Ltd. for the elemental analyses. They also thank Dr. Yoshiaki Motoki for the amino acid analyses.

References

1) Preceding paper: S. Nozaki, A. Kimura, and I. Muramatsu, *Chem. Lett.*, **1977**, 1057. A part of this work has been preliminarily reported: I. Muramatsu, C. Hashimoto, A. Kimura, Y. Saika, and S. Nozaki, "Proceedings of the 15th Symposium on Peptide Chemistry," ed by T. Shiba, Protein Research Foundation, Osaka (1977), pp. 61—66.

2) Amino acids used are of L-configuration. The abbreviations for amino acids and peptides are in accordance with the rules of the IUPAC-IBU Commission of Biochemical Nomenclature. Other abbreviations are as follows: Boc= butoxycarbonyl, Z = benzyloxycarbonyl, Bzl = benzyl, NO_2=nitro.

3) For examples, J. C. Sheehan, J. Preston, and P. A. Cruickshank, *J. Am. Chem. Soc.*, **87**, 2492 (1965); C. H. Schneider and W. Wirz, *Helv. Chim. Acta*, **55**, 1062 (1972); M. Bodanszky, K. W. Funk, and M. L. Fink, *J. Org. Chem.*, **38**, 3565 (1973); R. Camble, R. Garner, and G. T. Young, *J. Chem. Soc., C*, **1969**, 1911; V. N. R. Pillai, M. Mutter, E. Bayer, and I. Gatfield, *J. Org. Chem.*, **45**, 5364 (1980).

4) J. C. Sheehan, P. A. Cruickshank, and G. L. Boshart, *J. Org. Chem.*, **26**, 2525 (1961).

5) W. König and R. Geiger, *Chem. Ber.*, **103**, 788 (1970).

6) F. Weygand, D. Hoffman, and E. Wünsch, *Z. Naturforsch., Teil B*, **21**, 426 (1966).

7) M. Fujino, S. Kobayashi, M. Obayashi, T. Fukuda, S. Shinagawa, and O. Nishimura, *Chem. Pharm. Bull.*, **22**, 1857 (1974).

8) G. A. Schoenenberger and M. Monnier, *Proc. Natl. Acad. Sci. U.S.A.*, **74**, 1282 (1977).

9) E. Antherton, D. L. J. Clive, and R. C. Sheppard, *J. Am. Chem. Soc.*, **97**, 6584 (1975).

10) D. Yamashiro, *Nature*, **201**, 76 (1964).

11) I. Muramatsu, A. Kimura, S. Nozaki, T. Nakajima, T. Yasuhara, and Y. Hirai, *Chem. Lett.*, **1977**, 1163.

12) S. Nozaki, K. Kobayashi, E. Katayama, and I. Muramatsu, *Chem. Lett.*, **1980**, 345.

The Synthesis of Highly Strained Buttaflanes with Aromatic Rings

Koji KIMURA,* Hideki OHNO, Kiyoshi MORIKAWA, Yasuhiro HIRAMATSU, and Yoshinobu ODAIRA

Department of Petroleum Chemistry, Faculty of Engineering, Osaka University, Suita, Osaka 565

(Received October 8, 1981)

Dibenzo[4.4.2.2]buttaflanes, *syn*-13,14:15,16-dibenzopentacyclo[6.4.2.2^{2,7}.0^{1,8}.0^{2,7}]hexadeca-13,15-diene, and *syn*-13,14:15,16-dibenzohexacyclo[6.4.2.2^{2,7}.0^{1,8}.0^{2,7}.0^{3,12}]hexadeca-13,15-diene, were synthesized by the intramolecular photocycloaddition of the dibenzo[*a,e*]cyclooctene derivatives, *syn*-13,14:15,16-dibenzotricyclo[6.4.2.2^{2,7}]hexadeca-1,7,13,15-tetraene and *syn*-13,14:15,16-dibenzotetracyclo[6.4.2.2^{2,7}.0^{3,12}]hexadeca-1,7,13,15-tetraene, which had themselves been derived by the catalytic hydrogenation of the biphenylene photodimer, *syn*-13,14:15,16-dibenzotricyclo[6.4.2.2^{2,7}]hexadeca-1,3,5,7,9,11,13,15-octaene, and the pentacyclic compound, *syn*-13,14:15,16-dibenzopentacyclo[6.4.2.2^{2,7}.0^{3,12}.0^{4,11}]hexadeca-1,5,7,9,13,15-hexaene, respectively.

The synthesis of strained compounds showing unusual chemical and physical properties has been of considerable interest.[1] As a part of our studies of the synthesis of a novel polycarbocyclic ring system, we ourselves have previously reported the synthesis of buttaflane (**1**),[2] wherein two propellane units share a cyclobutane ring.[3] The present [6.3.6.3]buttaflane (**1a**)

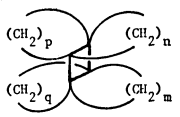

[m.n.p.q]Buttaflane

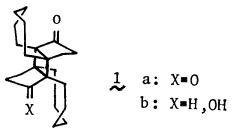

1 a: X=O
b: X=H,OH

[6.3.6.3]Buttaflane

had its long bonds in the planar cyclobutane ring,[4] and, concerning anomalous chemical behavior, a remarkably large rate constant was observed in the chromium trioxide oxidation of **1b**.[5] These noteworthy aspects are considered to be due to the nonbonded interaction of hydrogens between alicyclic rings facing each other. Therefore, when aromatic rings facing each other are incorporated into a buttaflane framework, it is very interesting to see if this buttaflane exhibits some π-π interaction,[6] as do cyclophanes[7] or janusenes,[8] in association with the closeness of the two facing benzene rings. However, what was, to the best of our knowledge, the first attempt to synthesize buttaflane with aromatic rings facing each other was unsuccessful.[9] That is, the direct or sensitized photolysis of 9,9',10,10'-tetradehydrobi(9,10-anthrylene) (**18**) provided no evidence for the formation of tetrabenzo[2.2.2.2]buttaflane. In this connection, we wish now to report the synthesis of new highly strained buttaflanes with aromatic rings facing each other, and the related compounds.

In this successful approach to the synthesis of buttaflanes, we make use of the ready photodimerization of biphenylene (**2a**). On the irradiation of biphenylene (**2a**)[10] in hexane through a Pyrex filter for 30 h, a *syn*-photodimer (**3**), with the dibenzo[*a,e*]cyclooctene structure, was obtained in a 60% yield, along with the pentacyclic compound (**4**, 10%). In this photoreaction, no *anti*-photodimer was detected at all. This *syn*-photodimer (**3**) might be formed from the excimer of biphenylene (**2a**), though the emission of the excimer fluorescence could not be observed. The quantum yield for the disappearance of biphenylene (**2a**) was 0.002.

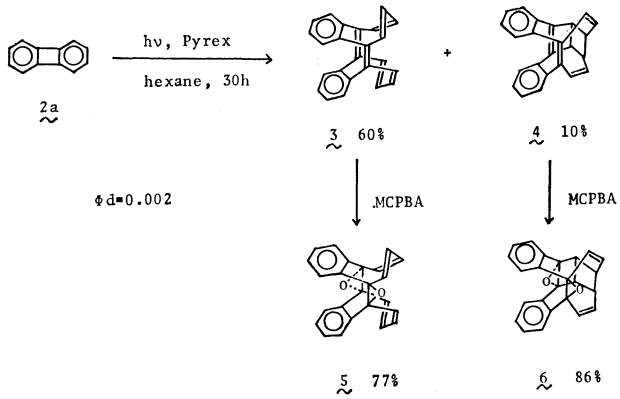

In 1968, Goldman *et al.* reported erroneously that the biphenylene photodimer was buttaflane (**7**) and also that the octahydrogenated biphenylene photodimer was buttaflane (**19**).[11] Afterward, as we were conducting our investigation, they corrected the structure of the octahydro dimer to correspond to ours (**9**) as a result of X-ray study,[12] and Nishida and Furusaki *et al.* reported independently, also as a result of X-ray analysis, that the biphenylene photodimer had the same structure as ours (**3**).[13] Significantly, in their photoreactions of biphenylene (**2a**), these two groups did not mention at all the formation of the pentacyclic compound (**4**), the intramolecular photocycloadduct of two peripheral double bonds of the biphenylene photodimer (**3**). In order to confirm the structures of **3** and **4**, epoxidation was examined. The epoxidation of **3** and **4** with *m*-chloroperbenzoic acid took place preferentially at two bridgehead double bonds to give the diepoxides, **5** and **6**, respectively.

Conceivably, the shortest way to the synthesis of buttaflanes is the intramolecular photocycloaddition of the respective two bridgehead double bonds of **3** and **4**. Unfortunately, the direct irradiation of **3** gave no buttaflane (**7**), but only biphenylene (**2a**) and the pentacyclic compound (**4**). The quantum yield for the disappearance of 3 was 0.01. A quenching experiment using 1,3-pentadiene and a sensitizing ex-

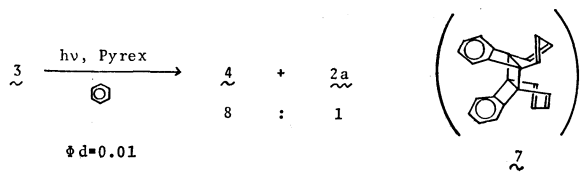

periment using acetone showed no effect on the formation of **4** and **2a**, indicating that this photoreaction proceeded *via* the singlet or unquenchable triplet state.

In the similar irradiation of **4**, cycloreversion took place to give **3** and **2a**, without any formation of buttaflane (**8**). The quantum yields for formation of **3** and **2a** were 0.009 and 0.007 respectively. These results obviously show that **2a**, **3**, and **4** are in a photostationary state. When **2a** was irradiated for 150 h, the ratio of **2a**, **3**, and **4** was 5:1:3. Moreover, the thermal cycloreversion of **4** to **3** also occurred above 180 °C.

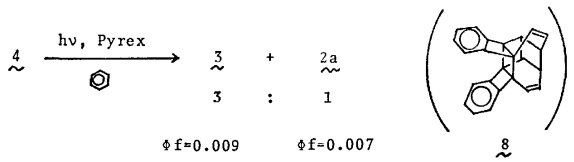

In the attempt at the one-step synthesis of buttaflanes (**7**) and (**8**) from **3** and **4**, some unfavorable reactions took place exclusively, as has been described above. Therefore, the selective hydrogenation of each peripheral double bond of **3** and **4** was attempted for the purpose of the photochemical synthesis of buttaflanes *via* **3** and **4**. The catalytic hydrogenation of **3** with Pd/C in ethyl acetate gave the desired octahydrogenated compound (**9**) retaining two bridgehead double bonds, along with a small amount of the decahydrogenated compound (**10**). In contrast, when Raney Ni was used as a catalyst, the decahydrogenated compound (**10**) was formed predominantly. The structure of dibutano-bridged dibenzo[*a*,*e*]cyclooctene (**9**) was confirmed by ozonolysis to give the diketone (**11**).[14] The epoxidation of **9** and **10** gave the corresponding diepoxide (**12**) and monoepoxide (**13**) quantitatively. On the other hand, the pentacyclic compound (**4**) was hydrogenated with Pd/C, Raney Ni, or PtO_2 to give the tetracyclic compound (**14**), accompanied by the reductive cleavage of one bond of the cyclobutane ring. In the case of the diimide reduction of **4** using potassium azodicarboxylate, the hexahydrogenated compound (**15**) was obtained in a 70% yield, together with a trace of a tetra-

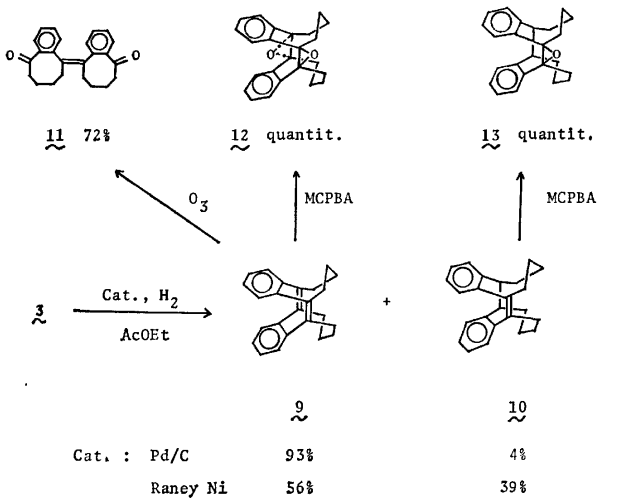

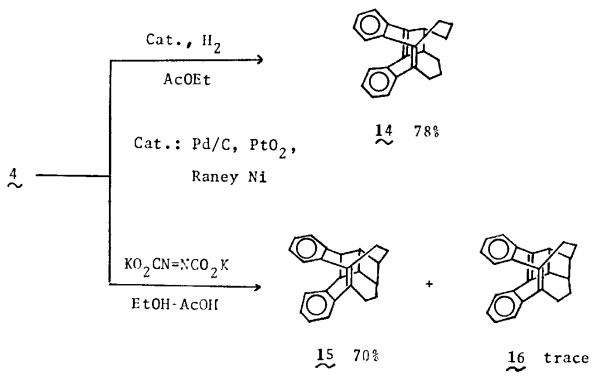

hydrogenated compound (**16**) retaining two bridgehead double bonds.

The photochemical behavior of dibenzo[*a*,*e*]cyclooctene derivatives (**9**) and (**14**), in which the central cyclooctatetraene ring takes a tub form and the two bridgehead double bonds are forced by their geometry to interact with each other, is of considerable interest in comparison with that of the fairly planar dibenzo[*a*,*e*]cyclooctene (**17**)[15] or similar tub-form compounds such as 9,9′,10,10′-tetradehydrobi(9,10-anthrylene) (**18**).[9]

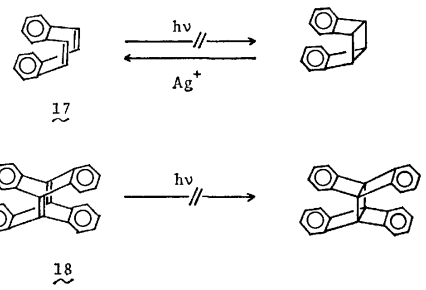

When the dibenzo[*a*,*e*]cyclooctene derivative (**9**) was irradiated in benzene, the expected buttaflane with aromatic rings facing each other, *syn*-13,14:15,16-dibenzopentacyclo[6.4.2.2^{2,7}.0^{1,8}.0^{2,7}]hexadeca-13,15-diene (**19**), could be synthesized quantitatively. The crystals were orthorhombic. The ^{13}C NMR spectrum of **19** with C_{2v} symmetry had six signals, especially, the signal at δ 138.8 ppm due to a quaternary olefinic carbon of **9** was replaced by the signal at δ 49.3 ppm, based on the newly formed cyclobutane ring carbon. Similarly, the more highly strained cage buttaflane, *syn*-13,14:15,16-dibenzohexacyclo[6.4.2.2^{2,7}.0^{1,8}.0^{2,7}.0^{3,12}]hexadeca-13,15-diene (**20**), was synthesized in an

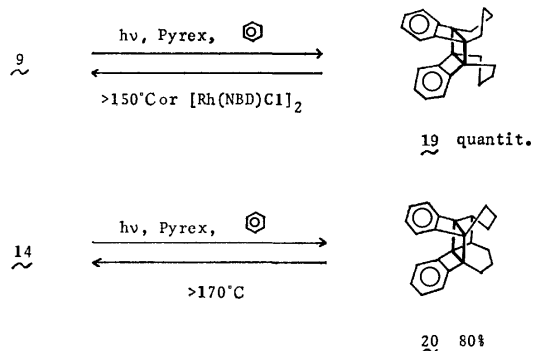

80% yield by the intramolecular photocycloaddition of **14**.

While it has been reported that the intramolecular [2+2]photocycloaddition of dibenzo[*a*,*e*]cyclooctene (**17**)[15] did not occur, the similar photocycloaddition of **9** and **14** to **19** and **20** took place excellently. This is probably because the two tetramethylene bridges between two bridgehead double bonds in **9** or **14** enforce the relatively small double-bond separations, as well as their parallel orientations,[13,16] which are preferable for photocycloaddition. On the other hand, the failure of the [2+2]photocycloaddition of the similar tub-form compound (**18**) may be attributed to the remarkable instability of the [2.2.2.2]buttaflane moiety of the supposed adduct.[17]

As expected, the tricyclo[4.2.0.0^{2,5}]octa-3,7-diene moiety in buttaflane (**19**) can be opened to **9** quantitatively by reaction with a catalytic amount of [Rh(NBD)Cl]$_2$(NBD=norbornadiene) or above 150 °C.[18] Similarly, the thermal cleavage of cage buttaflane (**20**) occurred to afford **14** almost quantitatively above 170 °C.

Attributable to the transannular π-π interaction, the aromatic ring protons of **19** and **20** in ^{1}H NMR appeared to show a somewhat high-field shift, and the electronic spectra of these compounds showed bathochromic and hyperchromic shifts. It is interesting that these interactions of **19**, **20**, and the cage compound (**21**)[19] successively decrease with an increase in the rigidity of the structure, as is shown by their UV spectra. An X-ray study of buttaflanes (**19**) and (**20**) will now be undertaken.

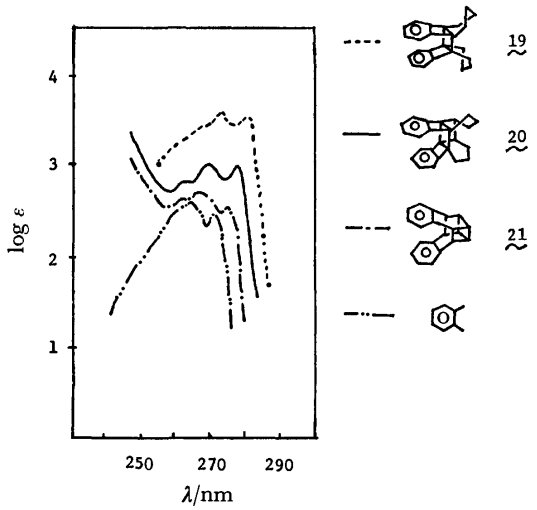

Fig. 1. UV spectra (in CH_3CN).

Experimental

The melting points are uncorrected. The infrared spectra were recorded on a JASCO IR-G spectrometer. The ^{1}H NMR and ^{13}C NMR spectra were obtained on JEOL JNM-PS-100 and JEOL JNM-FX60S spectrometers respectively, using $CDCl_3$ as the solvent and Me_4Si as the internal standard. The mass spectra were determined with a Hitachi RMU-6E spectrometer. The UV spectra were recorded on a Hitachi 356 spectrometer. Analytical GLC was carried out on a Hitachi 163 gas chromatograph, while preparative GLC separation was undertaken on a Varian Aerograph 90-P gas chromatograph.

Materials. The biphenylene (**2a**) was prepared according to the method of Friedman.[20] The 2-acetyl- (**2b**),[21] 2-methoxy- (**2c**),[22] and 2-cyanobiphenylenes (**2d**)[21] were prepared by a modification of the method of McOmie.

Photoreaction of Biphenylene (2a). A hexane solution of **2a** (0.04 mol dm^{-3}) was irradiated through a Pyrex filter at room temperature for 30 h using 500-W high-pressure mercury lamp. After the solvent had evaporated, the residue was chromatographed on silica gel with petroleum ether to elute biphenylene (**2a**), the pentacyclic compound (**4**, 10%), and the biphenylene photodimer (**3**, 60%), in this order (conv. 43%). When benzene, ether, or acetonitrile was used as the solvent, the yields of the biphenylene photodimer (**3**, 50—60%) and the pentacyclic compound (**4**, 8—15%) were somewhat similar to that of hexane (conv. 30—40%). Further irradiation gave rise to an increase in the formation of **4** and the decrease in that of **3**. After 150 h, the ratio of **2a**, **3**, and **4** was 5:1:3. In addition, when compounds **3** and **4** were allowed to stand for a long time on exposure to air, the diene moieties of **3** and **4** were easily oxidized. **3**; mp 247—252 °C decomp; Mass (*m/e*) 304 (M^+); UV (CH_3CN) λ 310 nm (ε, 1555); ^{1}H NMR ($CDCl_3$) δ 5.54—5.76 (m, 4H), 6.19—6.41 (m, 4H), 7.03 (s, 8H); ^{13}C NMR ($CDCl_3$) δ 124.0 (d), 125.0 (d), 127.1 (d), 134.6 (d), 140.4 (s), 141.2 (s); Found: C, 94.57; H, 5.27%. Calcd for $C_{24}H_{16}$: C, 94.70; H, 5.30%. **4**; mp 178—179 °C; Mass (*m/e*) 304 (M^+); UV (CH_3CN) λ 276 nm (ε, 1094), 267 (1600); ^{1}H NMR ($CDCl_3$) δ 3.32—3.52 (m, 2H), 3.68—3.80 (m, 2H), 5.20—5.54 (m, 2H), 6.45 (d, 2H), 6.92—7.20 (m, 8H); ^{13}C NMR ($CDCl_3$) δ 38.7 (d), 45.7 (d), 124.1 (d), 126.5 (d), 126.6 (d), 126.9 (d) 127.6 (d), 137.5 (s), 137.7 (s), 138.5 (d), 146.4 (s), 151.8 (s); Found: C, 94.83; H, 5.20%. Calcd for $C_{24}H_{16}$: C, 94.70; H, 5.30%.

Photoreaction of 2-Acetyl-(2b) or 2-Methoxybiphenylene (2c). A hexane solution (4.2×10^{-3} mol dm^{-3}) of 2-acetyl-(**2b**) or 2-methoxybiphenylene (**2c**) was irradiated under conditions similar to those used for biphenylene (**2a**). After the removal of the solvent, the residue was chromatographed to recover unreacted 2-acetyl- or 2-methoxybiphenylene almost quantitatively.

Photoreaction of 2-Cyanobiphenylene (2d). A hexane solution of 2-cyanobiphenylene (**2d**) (3.5×10^{-3} mol dm^{-3}) was irradiated for 50 h. After the removal of the solvent, the residue was chromatographed to give the photodimer (**3d**, 24%) and some polymeric compounds (conv. 35%). This photodimer (**3d**) was labile and readily reacted with atmospheric oxygen to give a new substance in a deuteriochloroform solution. This compound was found to have four oxygens, but the structure had not yet been determined. **3d**; mp 215—220 °C decomp; IR 2200 cm^{-1}; Mass (*m/e*) 354 (M^+); UV (CH_3CN) no maximum, but the end absorption is at 390 nm; ^{1}H NMR ($CDCl_3$) δ 5.64—5.84 (m, 4H), 6.22—6.56 (m, 4H), 7.02—7.45 (m, 6H); ^{13}C NMR ($CDCl_3$) δ 146.8, 147.6 (quaternary olefinic carbon).

Photoreaction of Biphenylene Dimer (3). A degassed benzene solution of the biphenylene dimer (**3**) (1.5×10^{-3} mol dm^{-3}) was irradiated in a sealed Pyrex tube at room temperature for 5 h. After the removal of the benzene, the residue was chromatographed on silica gel. Elution with petroleum ether afforded biphenylene (**2a**, 11%) and the pentacyclic compound (**4**, 88%) (conv. 91%).

Photoreaction of Pentacyclic Compound (4). The irradiation of a degassed benzene solution of **4** (1.5×10^{-3} mol dm^{-3}) in a sealed Pyrex tube for 3 h gave no buttaflane (**8**), but biphenylene (**2a**, 23%) and the biphenylene photodimer

(**3**, 69%) (conv. 36%).

Epoxidation of ***3***. To a dichloromethane solution (50 ml) of **3** (1 mmol) was added *m*-chloroperbenzoic acid (2.2 mmol) in dichloromethane (30 ml). The mixture was stirred at 20 °C for 48 h. The excess peracid was then destroyed by the addition of 10% sodium sulfite. The reaction mixture was washed with a 5% sodium hydrogencarbonate solution to extract the *m*-chlorobenzoic acid, followed by washing with water and finally with a saturated sodium chloride solution. The organic layer was dried and stripped of the solvent. The residue was chromatographed on silica gel with petroleum ether/ether (10/1) to give the diepoxide (**5**) in a 77% yield. **5**; mp 255—257 °C decomp; Mass (*m/e*) 336 (M^+); UV (CH_3CN) λ 275 nm (ε, 2447), 248 (4404); ^1H NMR ($CDCl_3$) δ 5.80 (s, 8H), 7.06—7.25 (m, 8H); ^{13}C NMR ($CDCl_3$) δ 68.3 (s), 124.4 (d), 125.0 (d), 128.3 (d), 134.1 (d), 134.3 (s); Found: C, 85.60; H, 4.56%. Calcd for $C_{24}H_{16}O_2$: C, 85.69; H, 4.79%.

Epoxidation of ***4***. The procedure described above was carried out to give the diepoxide (**6**) in an 86% yield. **6**; mp 234—236 °C decomp; Mass (*m/e*) 336 (M^+); UV (CH_3CN) λ 269 nm (ε, 315), 263 (396), 257 (360); ^1H NMR ($CDCl_3$) δ 3.36—3.52 (m, 2H), 3.76—3.96 (m, 2H), 5.24—5.42 (m, 2H), 6.32 (d, 2H), 7.04—7.44 (m, 8H); ^{13}C NMR ($CDCl_3$) δ 39.7 (d), 47.9 (d), 67.7 (s), 69.4 (s), 124.9 (d), 125.2 (d), 127.8 (d), 128.8 (d), 129.0 (d), 131.2 (d), 135.4 (s), 138.4 (s); Found: C, 85.62; H, 4.62%. Calcd for $C_{24}H_{16}O_2$: C, 85.69; H, 4.79%.

Catalytic Reduction of ***3***. A suspension of **3** (2 mmol) and Pd/C in ethyl acetate (30 ml) was reduced at room temperature during 3 d. After the removal of the catalyst and the solvent, the residue was chromatographed on silica gel. Elution with petroleum ether gave the octahydrogenated compound (**9**, 93%) and the decahydrogenated compound (**10**, 4%). In contrast, when Raney Ni (W7) was used as the catalyst, **10** was obtained in a 39% yield, along with **9** in a 56% yield. **9**; mp 182.5—183.5 °C; Mass (*m/e*) 312 (M^+); UV (CH_3CN) λ 276 nm (ε, 788), 268 (1089); ^1H NMR ($CDCl_3$) δ 1.30—1.92 (m, 8H), 1.95—2.41 (m, 4H), 2.55—2.87 (m, 4H), 6.68—6.95 (m, 8H); ^{13}C NMR ($CDCl_3$) δ 28.4 (t), 33.3 (t), 124.5 (d), 126.2 (d), 138.8 (s), 145.0 (s); Found: C, 92.10; H, 7.88%. Calcd for $C_{24}H_{24}$: C, 92.26; H, 7.74%. **10**; mp 182—183 °C; Mass(*m/e*) 314 (M^+); ^1H NMR ($CDCl_3$) δ 1.0—2.28 (m, 10H), 2.28—2.65 (m, 4H), 2.70—3.20 (m, 2H), 3.51—3.76 (m, 2H), 6.62—7.05 (m, 8H); ^{13}C NMR ($CDCl_3$) δ 25.6 (t), 26.6 (t), 32.2 (t), 32.6 (t), 48.7 (d), 125.8 (d), 126.1 (d), 126.2 (d), 126.5 (d), 129.4 (s), 137.4 (s), 144.4 (s); Found: C, 91.57; H, 8.15%. Calcd for $C_{24}H_{26}$: C, 91.67; H, 8.33%.

Epoxidation of ***9***. The procedure described above was carried out to give the diepoxide (**12**) quantitatively. **12**; mp 219—222 °C decomp; Mass (*m/e*) 344 (M^+); UV (CH_3CN) λ 276 nm (ε, 147), 266 (178), 263 (184); ^1H NMR ($CDCl_3$) δ 1.20—2.43 (m, 16H), 6.96—7.20 (m, 8H); ^{13}C NMR ($CDCl_3$) δ 24.1 (t), 35.4 (t), 69.6 (s), 125.5 (d), 127.7 (d), 138.2 (s); Found: C, 83.38; H, 6.97%. Calcd for $C_{24}H_{24}O_2$: C, 83.69; H, 7.02%.

Epoxidation of ***10***. A dichloromethane solution of *m*-chloroperbenzoic acid (1.2 mmol) was added to a dichloromethane solution of **10** (1 mmol). A monoepoxide (**13**) was thus obtained quantitatively. **13**; mp 180—181 °C; Mass (*m/e*) 330 (M^+); UV (CH_3CN) λ 274 nm (ε, 493), 266 (578), 261 (548); ^1H NMR ($CDCl_3$) δ 1.21—2.64 (m, 16H), 3.33—3.62 (m, 2H), 6.63—7.16 (m, 8H); ^{13}C NMR ($CDCl_3$) δ 22.9 (t), 25.6 (t), 32.0 (t), 32.3 (t), 49.6 (d), 72.6 (s), 126.0 (d), 126.3 (d), 127.0 (d), 129.7 (d), 140.5 (s), 141.5 (s); Found: C, 86.90; H, 7.93%. Calcd for $C_{24}H_{26}O$: C, 87.23; H, 7.93%.

Ozonolysis of ***9***. Ozone was passed through a solution of **9** (1 mmol) in ethyl acetate (30 ml) for 30 min at −78 °C. The ozonide residue was then reduced with Pd/C at room temperature for 24 h. After the subsequent removal of the catalyst and solvent, the residue was chromatographed on silica gel with petroleum ether/ether (7/3) to give the diketone (**11**) in a 72% yield. **11**; mp 171—172 °C; Mass (*m/e*) 344 (M^+); ^1H NMR ($CDCl_3$) δ 1.52—2.08 (m, 8H), 2.80 (t, 4H), 3.30 (t, 4H), 6.52—6.68 (m, 2H), 6.95—7.25 (m, 4H), 7.82—8.05 (m, 2H); Found: C, 83.69; H, 6.99%. Calcd for $C_{24}H_{24}O_2$: C, 83.69; H, 7.02%.

Catalytic Reduction of ***4***. Using Pd/C, Raney-Ni (W7), or PtO_2 as a catalyst, the tetracyclic compound (**14**) was obtained in a 78, 76, or 73% yield respectively. **14**; mp 162—166 °C decomp; Mass (*m/e*) 310 (M^+); UV (CH_3CN) λ 273 nm (ε, 679), 266 (931); ^1H NMR ($CDCl_3$) δ 1.85—2.47 (m, 6H), 2.55—3.15 (m, 6H), 3.63—3.78 (m, 2H), 6.75—7.10 (m, 8H); ^{13}C NMR ($CDCl_3$) δ 33.1 (t), 34.6 (t), 39.5 (t), 48.3 (d), 126.1 (d), 126.2 (d), 127.9 (d), 130.0 (d), 138.1 (s), 139.2 (s), 143.3 (s), 144.9 (s); Found: C, 92.73; H, 7.10%. Calcd for $C_{24}H_{22}$: C, 92.86; H, 7.14%.

Diimide Reduction of ***4***. A solution of **4** (0.35 mmol) in 30 ml of dry methanol containing potassium azodicarboxylate (4.7 mmol) was treated, drop by drop, under nitrogen at −78 °C with glacial acetic acid (1 ml). After the completion of the addition, the mixture was stirred for 2 h at −78 °C and for 24 h at room temperature. The mixture was then diluted with water and extracted with dichloromethane. The combined organic layers were washed with a 10% aqueous sodium hydrogencarbonate solution and water prior to drying and concentration. The subsequent chromatography of the residue on silica gel with petroleum ether afforded **15** in a 70% yield. **15**; mp 137—140 °C decomp; Mass (*m/e*) 310 (M^+); UV (CH_3CN) λ 275 nm (ε, 1010), 248 (3480); ^1H NMR ($CDCl_3$) δ 1.50—1.89 (m, 4H), 1.90—2.21 (m, 4H), 3.38—3.62 (m, 2H), 3.64—3.95 (m, 2H), 4.20—4.42 (m, 2H), 6.92—7.16 (m, 8H); ^{13}C NMR ($CDCl_3$) δ 24.0 (t), 24.5 (t), 41.8 (d), 44.5 (d), 52.2 (d), 126.2 (d), 126.2 (d), 126.9 (d), 131.8 (d), 138.9 (s), 142.3 (s), 147.4 (s); Found: C, 92.75; H, 7.12%. Calcd for $C_{24}H_{22}$: C, 92.86; H, 7.14%.

*Synthesis of Buttaflane (****19****).* A 90-ml degassed benzene solution of **9** (1 mmol) in a sealed Pyrex tube was irradiated at room temperature for 100 h using a 500-W high-pressure mercury lamp. After the removal of the solvent, the GLC of the residue revealed only one peak with the same retention time as that of **9** because the buttaflane (**19**) was cyclореversed thermally, but ^{13}C NMR showed a new signal at δ 49 ppm based on a cyclobutane ring carbon of buttaflane (**19**). A mixture of buttaflane (**19**) and unreacted **9** was chromatographed on silica gel or silver nitrate-impregnated silica gel, but the two components could not be completely separated. Therefore, the mixture in ethyl acetate was ozonized for 15 min at −78 °C. The workup was analogous to that of the ozonolysis of **9**. Elution with petroleum ether gave buttaflane (**19**, 66%), and elution with petroleum ether/ether (7/3) gave the diketone (**11**, 25%) as the ozonization product of the unreacted **9**. **19**; mp 179—183 °C decomp; Mass (*m/e*) 312 (M^+); UV (CH_3CN) λ 278 nm (ε, 3203), 271 (3503), 265 (2588); ^1H NMR ($CDCl_3$) δ 1.35—1.64 (m, 8H), 1.96—2.25 (m, 8H), 6.44—6.76 (m, 8H); ^{13}C NMR ($CDCl_3$) δ 22.2 (t), 25.0 (t), 49.3 (s), 121.2 (d), 126.5 (d), 150.1 (s); Found: C, 92.10; H, 7.69%. Calcd for $C_{24}H_{24}$: C, 92.26; H, 7.74%.

*Synthesis of Cage Buttaflane (****20****).* A 30-ml degassed benzene solution of **14** (0.5 mmol) in a sealed Pyrex tube

was irradiated for 50 h. After the removal of the solvent, the residue was chromatographed on silica gel. The subsequent elution of petroleum ether gave cage buttaflane (**20**) in an 80% yield. **20**; mp 204—208 °C decomp; Mass (*m/e*) 310 (M^+); UV (CH_3CN) λ 276 nm (ε, 1040), 268 (1095), 261 (889); ^1H NMR ($CDCl_3$) δ 1.24 (d, 2H), 1.84—3.40 (m, 10H), 3.44—3.56 (m, 2H), 6.52—6.96 (m, 8H); ^{13}C NMR ($CDCl_3$) δ 24.9 (t), 25.5 (t), 30.5 (t), 41.6 (s), 42.4 (d), 50.8 (s), 124.8 (d), 124.9 (d), 126.3 (d), 126.9 (d), 140.3 (s), 144.2 (s); Found: C, 92.72; H, 7.15%. Calcd for $C_{24}H_{22}$: C, 92.86; H, 7.14%.

Thermal Reaction of ***4***. The heating of a sealed Pyrex tube containing 10 mg of **4** at 180 °C for 20 min gave **3** quantitatively. In the case of 100 °C or 150 °C, no cycloreversion of **4** to **3** occurred.

*Thermal Reaction of Buttaflane (****19****)*. The heating of a sealed Pyrex tube containing 10 mg of **19** at 150 °C for 30 min gave **9** quantitatively.

*Thermal Reaction of Cage Buttaflane (****20****)*. The heating of a sealed Pyrex tube containing 10 mg of **20** at 170 °C for 2 h gave **14** almost quantitatively.

*Catalytic Reaction of Buttaflane (****19****) with [Rh(NBD)Cl]$_2$*. A catalytic amount of $[Rh(NBD)Cl]_2$ and **19** (20 mg) in 5 ml of $CDCl_3$ was allowed to stand at room temperature in a sealed Pyrex tube for 5 d. ^{13}C NMR showed clearly that the cycloreversion of **19** to **9** occurred quantitatively.

Quenching with 1,3-Pentadiene. Five samples were prepared each containing 10 ml of a degassed benzene solution of **3** (0.1 mmol). Four samples also contained 1,3-pentadiene (0.05, 0.10, 0.50, or 1.00 mol dm^{-3}). All the sealed samples were irradiated for 2 h. 1,3-Pentadiene exhibited no quenching effect on the formation of **4** and **2a** in any case.

Quantum Yield Measurement. The quantum yields were measured by the method using potassium ferrioxalate as the actinometer.[23]

References

1) J. F. Liebman and A. Greenberg, *Chem. Rev.*, **76**, 311 (1976).

2) Y. Tobe, K. Kimura, and Y. Odaira, *J. Org. Chem.*, **43**, 3776 (1978).

3) Compounds consisting of two propellanes that share a cyclobutane ring in the center were named "Buttaflane" by Greenberg and Liebman; *cf.* "Strained Organic Molecules," ed by A. Greenberg and J. F. Liebman, Academic Press, New York (1978).

4) H. Matsuura, S. Koshibe, Y. Kai, N. Yasuoka, and N. Kasai, *Acta Crystallogr., Sect. B*, **32**, 625 (1979).

5) Y. Tobe, K. Kimura, and Y. Odaira, *J. Org. Chem.*, **44**, 639 (1979).

6) There has been only one report on the synthesis of buttaflane with aromatic rings. Since the two benzene rings did not face each other, however, this dibenzo[3.3.3.3]buttaflane showed no π-π interaction; R. Greenhouse, W. T. Borden, K. Hirotsu, and J. Clardy, *J. Am. Chem. Soc.*, **99**, 1664 (1977).

7) For example, S. Misumi and T. Otsubo, *Acc. Chem. Res.*, **11**, 251 (1978); V. Boekelheide, *ibid.*, **13**, 65 (1980).

8) S. J. Cristol and B. B. Jarvis, *J. Am. Chem. Soc.*, **89**, 401 (1967); S. J. Cristol and D. C. Lewis, *ibid.*, **89**, 1476 (1967).

9) R. L. Viavattene, F. D. Greene, L. D. Cheung, R. Majeste, and L. M. Trefonas, *J. Am. Chem. Soc.*, **96**, 4342 (1974).

10) The irradiation of 2-acetyl- (**2b**) or 2-methoxybiphenylene (**2c**) under similar conditions gave no photodimer. In the case of 2-cyanobiphenylene (**2d**), on the contrary, a similar *syn*-photodimer (**3d**) was obtained in a 23% yield, though the position of the cyano substituents is not yet clear.

11) N. J. Goldman and R. A. Ruden, *Tetrahedron Lett.*, **1968**, 3951.

12) E. L. Passer, Ph. D. Thesis, Fordham University, New York, 1976.

13) A. Furusaki, N. Hashiba, T. Matsumoto, T. Aotsuka, and S. Nishida, *Bull. Chem. Soc. Jpn.*, **54**, 1617 (1981).

14) S. Nishida and T. Aotsuka, *Summer Symposium in the Hokkaido District*, **1978**, 51.

15) a) M. Avram, D. Dinu, G. Mateescu, and C. D. Nenitzescu, *Chem. Ber.*, **93**, 1789 (1960); b) W. Merk and R. Pettit, *J. Am. Chem. Soc.*, **89**, 4788 (1967); c) M. Stiles and U. Burdkhardt, *ibid.*, **86**, 3396 (1964).

16) E. Osawa, K. Aigami, and Y. Inamoto, *J. Org. Chem.*, **42**, 2621 (1977).

17) K. B. Wiberg, M. Matturro, and R. Adams, *J. Am. Chem. Soc.*, **103**, 1600 (1981).

18) R. Case, M. Dewar, S. Kirchner, R. Pettit, and W. Slegeir, *J. Am. Chem. Soc.*, **96**, 7581 (1974).

19) Y. Tobe, F. Hirata, K. Nishida, H. Fujita, K. Kimura, and Y. Odaira, *J. Chem. Soc., Chem. Commun.*, **1981**, 786.

20) F. Logullo, A. H. Seitz, and L. Friedman, *Org. Synth.*, Coll. Vol. V, 54 (1973).

21) W. Baker, J. W. Barton, and J. F. W. McOmie, *J. Chem. Soc.*, **1958**, 2666.

22) J. M. Blatchly, D. W. Gardner, and J. F. W. McOmie, *J. Chem. Soc., C*, **1967**, 272.

23) C. G. Hatchard and C. A. Paker, *Proc. R. Soc. London, Ser. A*, **235**, 518 (1956); **220**, 104 (1953).

Nucleophilic Reaction upon Electron-deficient Pyridone Derivatives. IV. Ring Transformation of 1-Substituted 3,5-Dinitro-2-pyridones with Ketones in the Presence of Amines

Eizo MATSUMURA,† Yasuo TOHDA,* and Masahiro ARIGA

Department of Chemistry, Osaka Kyoiku University, Minamikawahori-cho 4-88, Tennoji-ku, Osaka 543

(Received October 9, 1981)

Ring transformation of 1-substituted 3,5-dinitro-2-pyridones with 1,3-disubstituted acetones in the presence of secondary or primary amines gave *p*-nitroaniline derivatives and *N*-substituted 2-nitroacetamide. Two types of enamine intermediates, 2-azabicyclo[3.3.1]nonene derivatives and *N*-substituted 2-(5-amino-2-nitro-2,4-cyclohexadienyl)-2-nitroacetamides were isolated and characterized. The course of the base-catalyzed reaction is interpreted.

Recently we reported the ring transformation of 1-substituted 3,5-dinitro-2-pyridones (**1**) into *p*-nitrophenol derivatives (**2**) and 2-nitroacetamide derivatives (**3**) by treatment with monosodium salts of β-keto esters. In the case of the reaction of 3,5-dinitro-1-(2-pyridyl)-2-pyridone (**1b**), 2-oxo-2*H*-pyrido[1,2-*b*]-[1,2,4]triazine 4-oxide (**3b**) was isolated as the dehydration product of *N*-(2-pyridyl)-2-nitroacetamide (**3**, R=2-pyridyl). The course of these reactions was elucidated by the isolation of bicyclo intermediates (**4**) (Eq. 1).[1] The similar ring transformations of 1,3,5-

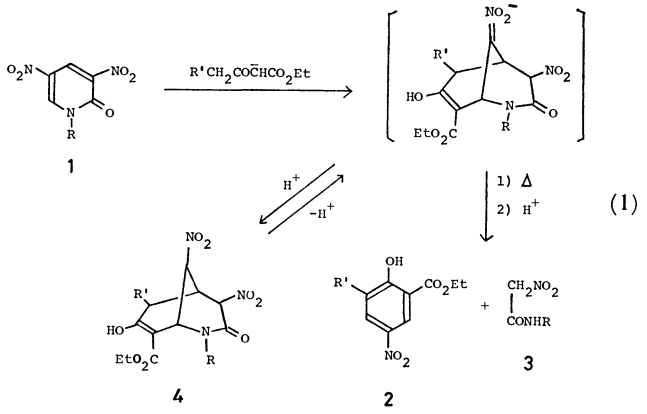

(1)

triazine[2,3] and 5-substituted uracils[4] into other six-membered aromatic systems have been studied by using sodium salts of β-keto esters or other 1,3-ambident nucleophiles. However these reactions were postulated to take place *via* open-chain intermediates rather than via such bicyclo intermediates. Another example of a similar ring transformation has been reported for 1,3,5-trinitrobenzene, which reacts with acetone and diethylamine to form *N*,*N*-diethyl-*p*-nitroaniline.[5] In this case, Strauss suggested the presence of a bicyclo[3.3.1]nonane derivative.[6] He also showed the generation of such meta-bridged compounds by the reaction of 1,3,5-trinitrobenzene with various 1,3-ambident nucleophiles.[7] In this paper, we wish to report on the reactions of 1-substituted 3,5-dinitro-2-pyridones (**1**) with 1,3-disubstituted acetones in the presence of secondary or primary amines.

Results and Discussion

Treatment of *N*-substituted 3,5-dinitro-2-pyridones (**1a**: R=Me, **1b**: R=2-pyridyl) with ketones, $R^1CH_2COCH_2R^2$ ($R^1=R^2=H$; $R^1=H$, $R^2=Me$; $R^1=R^2=Me$; $R^1=H$, $R^2=CO_2Et$; $R^1=R^2=CO_2Et$), in the presence of secondary or primary amines in pyridine at 80 °C for 5 h gave *p*-nitroaniline derivatives (**5a**—**h**) or *p*-nitrophenol derivatives (**2a**—**c**). The results are summarized in Eq. 2 and Table 1. Under

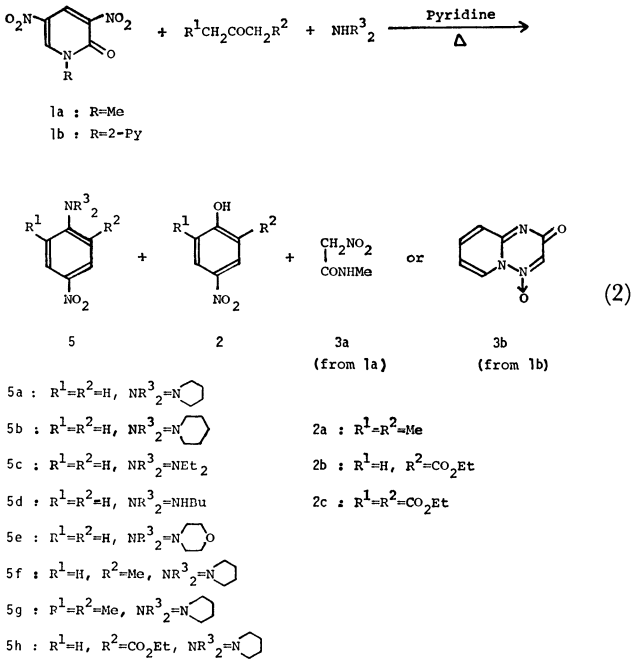

(2)

the reduced amount of pyrrolidine, *N*-methyl-2-nitroacetamide (**3a**) was obtained as the residual moiety of the substrate, **1a**, in poor yield (Table 1, run 6′). This fact suggests that excess of the amines in the reaction mixtures may decompose the acetamide produced (**3a**) under such conditions. In the case of the reaction of **1b**, 2-oxo-2*H*-pyrido[1,2-*b*][1,2,4]triazine 4-oxide (**3b**)[1] was isolated as the dehydration product of *N*-(2-pyridyl)-2-nitroacetamide (**3**, R=2-pyridyl).

In the presence of pyrrolidine, ketones such as acetone, 2-butanone, or 3-pentanone as well as ethyl acetoacetate (EAA) gave the corresponding *p*-nitroaniline derivatives (**5**) in good yields. The experimental data for a number of the ring transformations make it clear that the yields of **5** depend not only on the bulkiness of the ketones but also on the basicity

† Emeritus professor of Osaka Kyoiku University.

Table 1. Reaction of 1-substituted 3,5-dinitro-2-pyridones (**1**) with ketones and amines

Run	Substrate (mmol)	Ketone (mmol)	Amine (mmol)	Solvent (ml)	Temp °C	Time h	Products (Yields/%) **5**	**2**	**3**	
1	**1a**	Acetone	Pyrrolidine	Pyridine			**5a**			
	(1)	(10)	(3)	(10)	(80)	(5)	(95)	(0)	(0)	
1′	(1)	(1)	(1)	(10)	(80)	(5)	(69)	(0)	(0)	
2	**1a**	Acetone	Piperidine	Pyridine			**5b**			
	(1)	(10)	(3)	(10)	(80)	(5)	(97)	(0)	(0)	
3	**1a**	Acetone	Diethylamine	Pyridine			**5c**			
	(1)	(10)	(3)	(10)	(80)	(5)	(93)	(0)	(0)	
4	**1a**	Acetone	Butylamine	Pyridine			**5d**			
	(1)	(10)	(3)	(10)	(80)	(5)	(93)	(0)	(0)	
5	**1a**	Acetone	Morpholine	Pyridine			**5e**			
	(1)	(10)	(3)	(10)	(80)	(5)	(2)	(0)	(0)	
6	**1a**	2-Butanone	Pyrrolidine	Pyridine			**5f**		**3a**	**6a**
	(1)	(10)	(3)	(10)	(80)	(5)	(98)	(0)	(0)	(0)
6′	(1)	(1)	(1)	(10)	(80)	(5)	(53)	(0)	(8)	(19)
7	**1a**	2-Butanone	Diethylamine	Pyridine						
	(1)	(10)	(3)	(10)	(80)	(5)	(0)	(0)	(0)	
8	**1a**	3-Pentanone	Pyrrolidine	Pyridine			**5g**	**2a**		
	(1)	(10)	(3)	(10)	(80)	(5)	(58)	(11)	(0)	
8′	(1)	(1)	(1)	(10)	(80)	(5)	(2)	(4)	(0)	
9	**1a**	3-Pentanone	Diethylamine	Pyridine						
	(1)	(10)	(3)	(10)	(80)	(5)	(0)	(0)	(0)	
10	**1a**	EAA	Pyrrolidine	Pyridine			**5h**			
	(1)	(6)	(10)	(10)	(80)	(5)	(85)	(0)	(0)	
11	**1a**	EAA	Diethylamine	Pyridine				**2b**		
	(1)	(6)	(10)	(10)	(80)	(5)	(0)	(14)	(0)	
12	**1a**	DOPD	Pyrrolidine	Pyridine				**2c**		
	(1)	(6)	(10)	(10)	(80)	(5)	(0)	(98)	(0)	
13	**1b**	Acetone	Piperidine	Acetone			**5b**		**3b**	
	(2)	—	(6)	(20)	(60)	(5)	(85)	(0)	(25)	
14	**1b**	Acetone	Morpholine	Acetone			**5e**		**3b**	
	(2)	—	(6)	(20)	(60)	(5)	(53)	(0)	(20)	
15	**1b**	DOPD	Piperidine	Pyridine				**2c**	**3b**	
	(2)	(6)	(6)	(20)	(60)	(5)	(0)	(94)	(88)	

1a=1-Methyl-3,5-dinitro-2-pyridone, **1b**=3,5-dinitro-1-(2-pyridyl)-2-pyridone, **2a**=2,6-dimethyl-4-nitrophenol, **2b**=ethyl 5-nitrosalicylate, **2c**=diethyl 2-hydroxy-5-nitroisophthalate, **3a**=*N*-methyl-2-nitroacetamide, **3b**=2-oxo-2*H*-pyrido[1,2-*b*][1,2,4]triazine 4-oxide, **5a**=1-nitro-4-(1-pyrrolidinyl)benzene, **5b**=1-nitro-4-piperidinobenzene, **5c**=1-diethylamino-4-nitrobenzene, **5d**=1-butylamino-4-nitrobenezen, **5e**=1-morpholino-4-nitrobenzene, **5f**=2-methyl-4-nitro-1-(1-pyrrolidinyl)benzene, **5g**=1,3-dimethyl-5-nitro-2-(1-pyrrolidinyl)benzene, **5h**=ethyl 5-nitro-2-(1-pyrrolidinyl)benzoate, EAA=ethyl acetoacetate, DOPD=diethyl 3-oxopentanedioate.

of the amines. Thus easy formation of enamines can be postulated to take place in a series of reactions involving an initial nucleophilic attack of the amino group to the carbonyl carbon atom of the ketones. On the other hand, the treatment of **1a** or **1b** with highly acidic ketones such as diethyl 3-oxopentanedioate (DOPD) in the presence of the amines yields diethyl 2-hydroxy-5-nitroisophthalate (**2c**) quantitatively. The formation of the 4-nitrophenol suggests that the amines play a role of an acceptor of the proton of the acidic ketone to form the enolate ion. The reaction of the enolate ion with **1a** or **1b** follows essentially the identical course with that of diethyl 2-sodio-3-oxopentanedioate as shown in Eq. 1.[1] The reactivity of EAA was found to be intermediate between DOPD and the other dialkyl ketones. The treatment of **1a** with EAA in the presence of diethylamine only gave the phenol (**2b**) in 14% yield. The lower yield of the phenol can be attributed to the lower acidity of EAA, while the treatment of **1a** with EAA in the presence of pyrrolidine gave the *p*-nitroaniline derivative (**5h**) in 85% yield. This indicates that the basicity of the pyrrolidine is sufficient to bring about the formation of the enamine from EAA.

In order to isolate the intermediates, the reactions of **1a** or **1b** with ketones in the presence of secondary amines were carried out under somewhat milder conditions. When **1a** was treated with 2-butanone and pyrrolidine in pyridine at 70 °C for 1 h, **6a** was obtained as deep red crystals in 55% yield. The analytical data of **6a** were consistent with the formula, $C_{14}H_{20}N_4O_5$. The IR spectra had a carbonyl band at 1676 cm^{-1} and an N–H stretching band at 3270 cm^{-1}, which were attributable to a secondary amide group. The ^{1}H-NMR spectra also showed signals due to an *N*-methyl amide moiety at δ 2.44 (NCH_3, d, J=4 Hz) and 8.52 (N–H, m), and showed two doublets at δ 4.83 (J=8.5 Hz) and 7.71 (J=8.5 Hz), corresponding to two vicinal olefinic protons. The NMR spectra also showed a doublet of methyl protons at δ 1.16 (J=7 Hz). On the basis of these data, **6a** was assigned to be *N*-methyl-2-[6-methyl-2-nitro-5-

(1-pyrrolidinyl)-2,4-cyclohexadienyl]-2-nitroacetamide. The presence of a highly polarized 1-amino-4-nitro-1,3-butadiene system in the molecule was also suggested by very intense absorption at 497 nm (ε= 4.78×10^4) (Fig. 1). Similar cyclohexadiene intermediates (**6b** and **6c**) were also isolated by the reaction of **1a** or **1b** with 2-butanone and diethylamine (Eq. 3). Furthermore, reactions of **1a** or **1b** with 3-(pyrrolidinyl)-2-pentene gave similar enamine adducts, **6d** or **6e** (Eq. 4). The NMR, IR, and electronic spectra of **6** are summarized in Tables 2, 3, and Fig. 1.

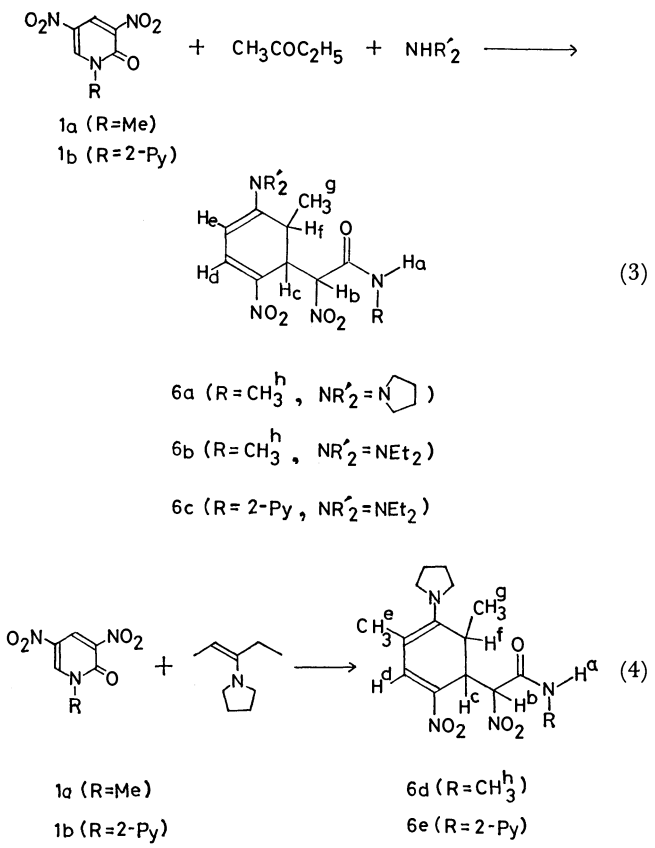

The intermediate, **6a**, on heating at 80 °C for 5 h in pyridine, afforded a mixture, which was separated by column chromatography on silica gel to give the final products, **5f** and **3a** in 78 and 47% yields, respectively. The intermediate, **6d**, was also converted into **5g** in 55% yield under the same reaction conditions (Eq. 5). Only by standing for 24 h in DMSO-d_6 at 35 °C, **6e** was completely converted into **5g**. These facts reveal that the cyclohexadiene derivatives (**6**) are one of the intermediates of the ring transformation.

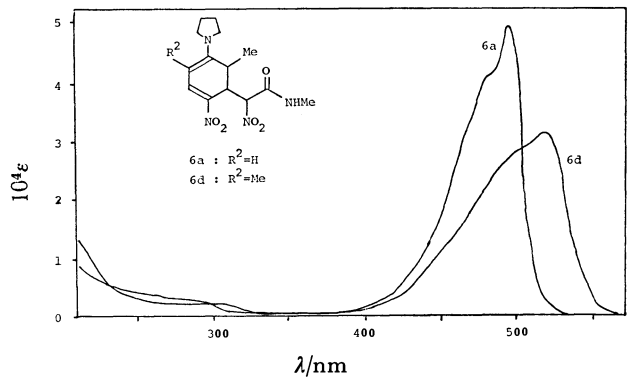

Fig. 1. Electronic spectra of the intermediate, **6a** and **6d**, in methanol.

TABLE 2. ^{1}H-NMR SPECTRA OF THE INTERMEDIATES, **6**[a,b]

Compound	Chemical shift (δ)							Coupling constant (Hz)			
	H_a	H_b	H_c	H_d	H_e	H_g	H_h	$J(H_d\text{-}H_e)$	$J(H_f\text{-}H_g)$	$J(H_b\text{-}H_c)$	$J(H_a\text{-}H_h)$
6a	8.52 (d-m)	5.20 (d)	3.83 (d-m)	7.71 (d)	4.83 (d)	1.16 (d)	2.44 (d)	8.5	7	2	4
6b	8.5 (d-m)	5.21 (d)	3.90 (d-m)	7.70 (d)	5.00 (d)	1.13 (d)	2.50 (d)	9	8	4	5
6c		5.69 (d)	4.02 (m)	7.68 (d)	4.80 (d)	1.15 (d)	—	8	7	3	—
6d	8.5 (m)	5.23 (d)	3.76 (m)	7.61 (s)	2.00 (d)	1.10 (d)	2.50 (d)	0	7	2	4
6e		5.67 (d)	3.90 (d)	7.64 (s)	1.65 (s)	1.10 (d)	—	0	7	8	—

a) In a DMSO-d_6 solution. b) Notations of the protons are shown in Eqs. 3 and 4.

TABLE 3. IR AND UV SPECTRA OF THE INTERMEDIATES, **6**

Compound	IR spectra (ν/cm^{-1})[a]				UV spectra[b]	
	ν(N-H)	ν(C=O)	ν(C_{vinyl}-H)	$\nu_{as}(NO_2)$	λ_{max}/nm(ε)	
6a	3262	1676	3090	1546, 1517	497 (4.78×10^4)	476 (sh)
6b	3270	1685	3085	1550, 1525	498 (5.00×10^4)	480 (sh)
6c	3240	1693	3110, 3070	1545, 1530	497 (2.52×10^4)	
6d	3245	1692	3070	1550, 1533	520 (2.98×10^4)	476 (sh)
6e	3210	1689	3085	1553, 1542	523 (2.97×10^4)	476 (sh)

a) In Nujol. b) In methanol.

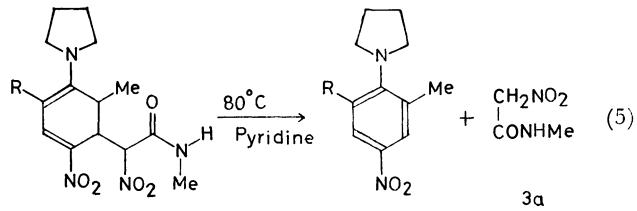

(5)

When **1a** was treated with diethylamine in acetone at room temperature, another type of intermediate, **7a**, was obtained in quantitative yield. The analytical data indicate that **7a** consists of **1a**, diethylamine, and an enamine derived from acetone and diethylamine in molar ratio 1:1:1. Similar treatment of **1a** with morpholine in acetone gave **7b** in quantitative yield. The analytical data of **7b** is composed of each one molecule of **1a**, morpholine, and an enamine derived from acetone and morpholine, and a half molecule of water. In a similar experiment using pyrrolidine as the amine component, the analogue of **7a** or **7b** was not afforded. However the final product, **5a**, was obtained from this reaction mixture.

When a methanol solution of **7a** was allowed to stand at room temperature, spontaneous decomposition occurred, **5c** and **3a** being obtained as the final products in 93 and 41% yields, respectively (Eq. 6). Under similar conditions, the contraction of **7b** did not occurred. However, on boiling with excess morpholine in methanol, **7b** afforded **5e** in quantitative yield (Eq. 7).

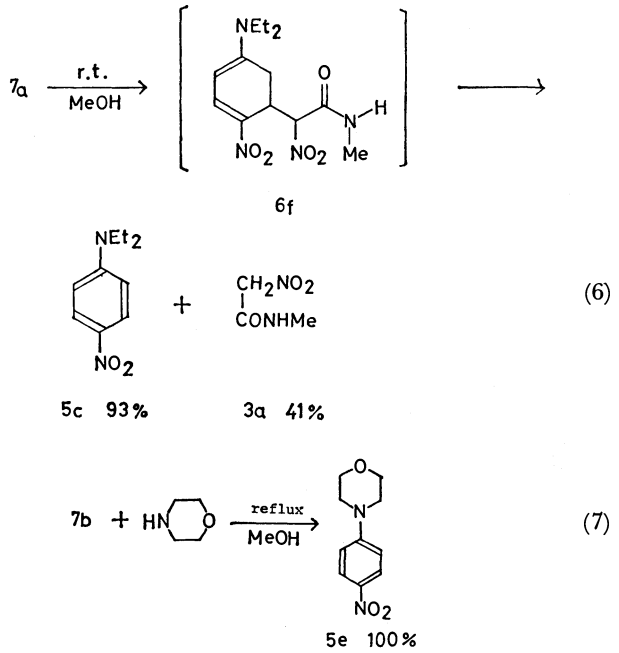

(6)

(7)

Figure 2 shows a change in the electronic spectrum of **7a** in methanol at room temperature. The intensity of the band at 310 nm decreases and that at 400 nm increases. It could be reasonably explained that the absorption at 300 nm corresponds to the diethylammonium salt of *N*-methyl-2-nitroacetamide (**3a**) and

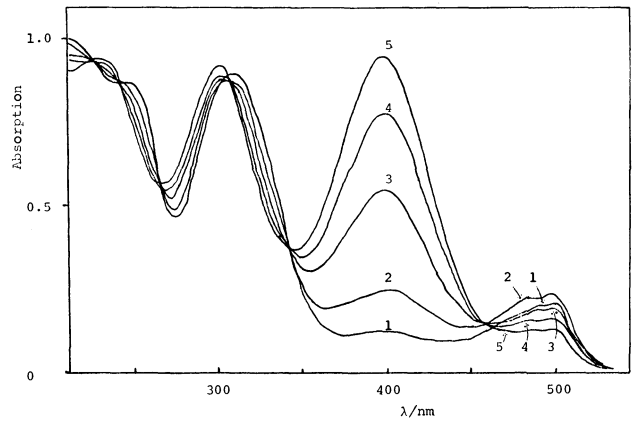

Fig. 2. Changes in electronic spectra of **7a** in methanol (8.34×10^{-5} mol/l) after (1) 3 min, (2) 18 min, (3) 52 min, (4) 82 min, and (5) 110 min at 20 °C.

that of 400 nm corresponds to 1-diethylamino-4-nitrobenzene (**5c**), because the authentic samples of **3a** and **5c** showed strong absorption maxima at 295 and 400 nm, respectively. An absorption band at about 500 nm indicates formation and subsequent decomposition of a transient species, which could be identified as the cyclohexadiene intermediate, 2-(5-diethylamino-2-nitro-2,4-cyclohexadienyl)-*N*-methyl-2-nitroacetamide (**6f**), by comparing the absorption band at 500 nm (Fig. 2) with that of the similar intermediates, **6a**—**c** (Fig. 1).

The ^{1}H-NMR spectra of **7a** showed an olefinic proton at δ 4.6 (a broad doublet, $J=3$ Hz). The IR spectra showed a C=C band at 1628 cm^{-1}, and the UV spectra showed an absorption at 248 nm ($\varepsilon=11400$). These data indicate the presence of an enamine moiety in **7a**. Broad absorptions at 2800—2300 cm^{-1} imply that **7a** is a diethylammonium salt. Since the diethylammonium salt of *N*-methyl-2-nitroacetamide absorbs UV light at 295 nm, the absorption of **7a** at 310 nm suggests the presence of a salt of the 2-nitroacetamide moiety. On the basis of these spectral data, as well as the elemental analysis and the chemical behavior shown in Eq. 6, the structure of diethylammonium 7-diethylamino-2-methyl-4,9-dinitro-3-oxo-2-azabicyclo[3.3.1]non-6(or 7)-en-4-ide was assigned to **7a** (Eq. 8).

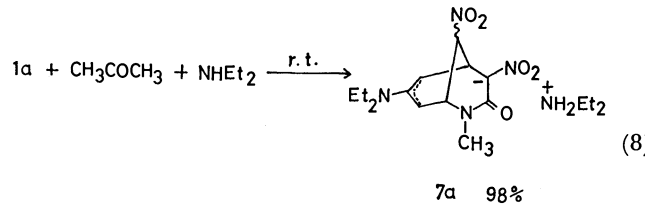

(8)

From these results, a possible process which occurs during the treatment of *N*-substituted 3,5-dinitro-2-pyridones (**1**) with the dialkyl ketones in the presence of the amines may start with the reaction of the ketones with the secondary amines to form an intermediate enamine. Usually the reaction of primary amines with aldehydes or ketones affords products which primarily contain imines (Schiff bases) rather than the enamine tautomers. Thus, in the initial reaction of

acetone and butylamine, the enamine may be a minor tautomer.

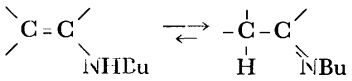

The amino olefinic component in the enamine as well as the enolate ion component in the β-keto ester anions has an electron-donating trend. Both the HOMO and the LUMO of these olefins are raised in energy relative to the HOMO and the LUMO of ethylene. The HOMO of enamine is the one which has the coefficient on the β-carbon atom larger than the α-carbon atom. On the other hand, the 1,3-dinitro-1,3-butadiene component of *N*-substituted 3,5-dinitro-2-pyridones has an electron-withdrawing trend, and the conjugation with the nitro group lowers both the energy of the HOMO and the LUMO relative to those of butadiene. The LUMO of the diene component is the one which has the largest coefficient on the C_6 atom of the 2-pyridone nucleus. By using the data given by Houk,[8] we can predict, as a favorable pathway, that the nucleophilic attack of the β-carbon of the enamine (HOMO) at the C_6 atom of the pyridone nucleus (LUMO of 1,3-dinitro-1,3-butadiene system) may lead to an adduct, **8**, as shown in Scheme 1. In this adduct, the intramolecular interaction between the β′-carbon of the enamine component and C_4 of the pyridone moiety would lead to the bicyclo adduct (**7**).

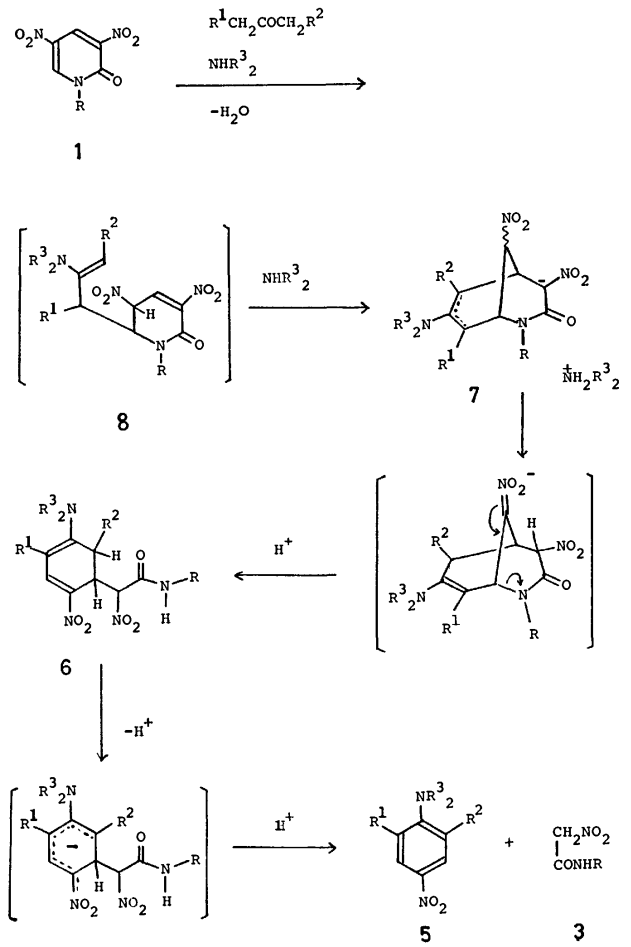

Scheme 1.

As described above, an excess amount of morpholine promotes the conversion of the intermediate, **7b**, to the final product, **5e** (Eq. 7). This suggests that the fission of the C_1–N_2 bond of the 2-azabicyclo[3.3.1]-nonene intermediate (**7**) is a base-catalyzed step. The transformation of **6** to **5** and **3** may also occur via base-catalyzed C–C bond fission. When the proton on C_6 of the intermediate, **6**, is removed by base, the heterolysis between C_6 and C_α in the deprotonated Meisenheimer-type species may lead to the final products. In the case of **6a—e**, the intermediates may be stabilized by the electron-donating character of the methyl group at C_6 and the deprotonation from this carbon atom may be more difficult than that in the case of **6f** which does not have any substituents at C_6.

From these results, it is concluded that the ring transformation of the 3,5-dinitro-2-pyridones to the *p*-nitroanilines is strongly promoted by the secondary or primary amines in each step.

Experimental

^{1}H-NMR spectra were measured using a Hitachi R-20 B spectrometer with TMS as an internal reference. UV spectra were recorded using a Hitachi EPS-3 spectrophotometer. Mass spectra were recorded with a JMS-D100 mass spectrophotometer. IR spectra were collected with a Hitachi 225 Grating IR spectrophotometer. All the melting points were uncorrected.

*Reaction of 1-Methyl-3,5-dinitro-2-pyridone (**1a**) with Dialkyl Ketones and Amines.* In a typical procedure, 0.21 g of pyrrolidine in 5 ml of pyridne was added slowly at 0 °C to a solution of 0.20 g of 1-methyl-3,5-dinitro-2-pyridone (**1a**) and 0.86 g of 3-pentanone in 5 ml of pyridine. Then the mixture was heated at 80 °C for 5 h. The solvent was removed under reduced pressure and the residual oil was column-chromatographed on silica gel (Wakogel C-300) and eluted with benzene. From the first elute, 0.13 g (58%) of 1,3-dimethyl-5-nitro-2-(1-pyrrolidinyl)benzene (**5g**) was obtained. The second elute gave 0.02 g (11%) of 2,6-dimethyl-4-nitrophenol (**2a**).

*1,3-Dimethyl-5-nitro-2-(1-pyrrolidinyl) benzene (**5g**)*: Yellow prisms (from hexane); mp 93—93.5 °C. NMR (CCl_4): δ 2.0 (4H, m), 2.28 (6H, s), 3.2 (4H, m), 7.73 (2H, s). Found: C, 65.83; H, 7.27; N, 12.70%. Calcd for $C_{12}H_{16}N_2O_2$: C, 65.43; 7.32; N, 12.70%.

*2,6-Dimethyl-4-nitrophenol (**2a**)*: Pale yellow needles (from hexane–benzene); mp 168—169 °C. NMR ($CDCl_3$): δ 2.28 (6H, s), 7.79 (2H, s). Found: C, 57.43; H, 5.28; N, 8.44%. Calcd for $C_8H_9NO_3$: C, 57.48; H, 5.43; N, 8.38%.

From the similar treatment of **1a** with other dialkyl ketones and amines, following compounds were obtained.

*1-Nitro-4-(1-pyrrolidinyl)benzene (**5a**)*: Yellow plates (from hexane); mp 167 °C. NMR ($CDCl_3$): δ 2.03 (4H, m), 3.34 (4H, m), 6.38 (2H, d, J=10 Hz), 8.00 (2H, d, J=10 Hz). Found: C, 62.77; H, 6.52; N, 14.58%. Calcd for $C_{10}H_{12}N_2O_2$: C, 62.48; H, 6.29; N, 14.58%.

*1-Nitro-4-piperidinobenzene (**5b**)*: Yellow plates (from hexane); mp 99.5—100 °C. NMR (CCl_4): δ 1.7 (6H, m), 3.3 (4H, m), 6.73 (2H, d, J=9.5 Hz), 8.01 (2H, d, J=9.5 Hz). Found: C, 64.36; H, 7.05; N, 13.72%. Calcd for $C_{11}H_{14}N_2O_2$: C, 64.06; H, 6.86; N, 13.58%.

*1-Diethylamino-4-nitrobenzene (**5c**)*: Yellow needles (from hexane); mp 73—74 °C. NMR (CCl_4): δ 1.19 (6H, t,

J=7 Hz), 3.41 (4H, q, J=7 Hz), 6.45 (2H, d, J=10 Hz), 7.90 (2H, d, J=10 Hz). Found: C, 61.61; H, 7.09; N, 14.20%. Calcd for $C_{10}H_{14}N_2O_2$: C, 61.83; H, 7.27; N, 14.42%.

*1-Butylamino-4-nitrobenzene (**5d**)*: Yellow needles (from hexane); mp 56 °C. NMR (CCl_4): δ 1.05 (3H, t, J=6 Hz), 1.5 (4H, m), 3.15 (2H, t, J=8 Hz), 4.65 (1H, m), 6.47 (2H, d, J=9 Hz), 7.99 (2H, d, J=9 Hz). Found: C, 62.01; H, 7.48; N, 14.59%. Calcd for $C_{10}H_{14}N_2O_2$: C, 61.83; H, 7.27; N, 14.42%.

*1-Morpholino-4-nitrobenzene (**5e**)*: Yellow needles (from hexane); mp 149.5—150 °C. NMR ($CDCl_3$): δ 3.33 (4H, m), 3.86 (4H, m), 6.79 (2H, d, J=10 Hz), 8.09 (2H, d, J=10 Hz). Found: C, 57.92; H, 6.06; N, 13.23%. Calcd for $C_{10}H_{12}N_2O_3$: C, 57.68; H, 5.81; N, 13.46%.

*2-Methyl-4-nitro-1-(1-pyrrolidinyl) benzene (**5f**)*: Yellow plates (from hexane); mp 100—100.5 °C. NMR (CCl_4): δ 1.96 (4H, m), 2.36 (3H, s), 3.40 (4H, m), 6.49 (1H, d, J=10 Hz), 7.7 (2H, m). Found: C, 63.90; H, 6.92; N, 13.64%. Calcd for $C_{11}H_{14}N_2O_2$: C, 64.06; H, 6.84; N, 13.58%.

*Reaction of 1-Methyl-3,5-dinitro-2-pyridone (**1a**) with Equimolar Amount of 2-Butanone and Pyrrolidine.* To a solution of 0.199 g of **1a** and 0.072 g of 2-butanone in 5 ml of pyridine 0.071 g of pyrrolidine in 5 ml of pyridine was added at 0 °C. The solution was heated at 80 °C for 5 h. The solvent was distilled off and the residual oil was dissolved in a minimum amount of tetrahydrofuran; then ether was added to the solution until it turned to cloudy. After 0.062 g (19%) of red precipitate (**6a**) was filtered off, the solvent was removed and the residue was column-chromatographed on silica gel. From a benzene elute, 0.109 g (53%) of 2-methyl-4-nitro-1-(1-pyrrolidinyl)benzene (**5f**) was obtained and 0.009 g (8%) of *N*-methyl-2-nitroacetamide (**3a**) was obtained from an ether elute; mp 75—75.5 °C; colorless needles (from i-Pr_2O).

*Reaction of 1-Methyl-3,5-dinitro-2-pyridone (**1a**) with Ethyl Acetoacetate and Diethylamine.* To a solution of 0.20 g of **1a** and 0.39 g of ethyl acetoacetate in 5 ml of pyridine, 0.38 g of diethylamine in 5 ml of pyridine was added slowly at 0°C. The mixture was heated at 80 °C for 5 h and the pyridine removed *in vacuo*. The residue was neutralized to pH 3—4 with dil. hydrochloric acid and extracted with chloroform. After the extract had been dried over anhydrous sodium sulfate, the chloroform was distilled off and the residue was column-chromatographed on silica gel. From a benzene elute, 0.060 g (14%) of ethyl 5-nitrosalicylate (**2b**) was obtained; mp 57.5—58.5 °C, colorless needles (from hexane).

The similar treatment of 0.40 g of **1a** with 1.21 g of DOPD and 0.43 g of pyrrolidine gave 0.54 g (98%) of diethyl 2-hydroxy-5-nitroisophthalate (**2c**); colorless needles (from hexane); mp 58—59 °C.

*Reaction of 1-Methyl-3,5-dinitro-2-pyridone (**1a**) with Ethyl Acetoacetate and Pyrrolidine.* To a solution of 0.40 g of **1a** and 0.78 g of ethyl acetoacetate in 10 ml of pyridine was added 0.71 g of pyrrolidine in 10 ml of pyridine at 0 °C. The mixture was heated at 80 °C for 5 h and the solvent was removed *in vacuo*. To the residue was added 20 ml of 10% sodium hydroxide and the mixture was extracted with chloroform. After the extract had been dried over anhydrous sodium sulfate, the chloroform was distilled off and the residual oil was column-chromatographed on silica gel. A benzene elute gave 0.45 g (85%) of ethyl 5-nitro-2-(1-pyrrolidinyl)benzoate (**5h**): yellow needles (from diisopropyl ether–diethyl ether); mp 128.5—129 °C. NMR ($CDCl_3$): δ 1.40 (3H, t, J=6.6 Hz), 2.0 (4H, m), 3.3 (4H, m), 4.36 (2H, q, J=6.6 Hz), 6.67 (1H, d, J=9 Hz), 8.07 (1H, dd, J=9 and 3 Hz), 8.42 (1H, d, J=3 Hz). Found: C, 59.08; H, 5.94; N, 10.70%. Calcd for $C_{13}H_{16}N_2O_4$: C, 59.08; H, 6.10; N, 10.60%. The water layer was acidified with 6 M (1 M=1 mol dm^{-3}) hydrochloric acid to pH 1—2 and then extracted with chloroform but the organic layer failed to give ethyl 5-nitrosalicylate (**2b**) or *N*-methyl-2-nitroacetamide (**3a**) after the usual work up.

*Reaction of 3,5-Dinitro-1-(2-pyridyl)-2-pyridone (**1b**) with Acetone and Piperidine.* To a solution of 0.54 g of **1b** in 20 ml of acetone was added 0.51 g of piperidine at 0 °C. After the mixture had been refluxed gently for 5 h, the acetone was removed under reduced pressure. The residual oil was washed with *ca.* 20 ml of chloroform. After insoluble solids had been filtered off, the organic layer was concentrated to a few milliliters and column-chromatographed on silica gel. A benzene elute gave 0.39 g (94%) of 1-nitro-4-piperidinobenzene (**5b**). A methanol elute and the chloroform-insoluble solids were combined together and recrystallized from water to give 0.08 g (25%) of 2-oxo-2*H*-pyrido-[1,2-*b*][1,2,4]triazine 4-oxide (**3b**); yellow needles; dec 210 °C.

*Reaction of 3,5-Dinitro-1-(2-pyridyl)-2-pyridone (**1b**) with DOPD and Piperidine.* To a solution of 0.54 g of **1b** and 1.21 g of DOPD in 15 ml of pyridine was added 0.51 g of piperidine in 5 ml of pyridine at 0 °C. The mixture was heated at 60 °C for 5 h and the pyridine was removed *in vacuo*. To this mixture 50 ml of chloroform and 20 ml of 1 M hydrochloric acid was added. Insoluble solids were filtered off and the organic layer was dried over anhydrous sodium sulfate. The organic layer was concentrated to a few milliliters and column-chromatographed on silica gel. A benzene elute gave 0.51 g (94%) of diethyl 2-hydroxy-5-nitroisophthalate (**2c**). A methanol elute and the chloroform-insoluble solids were combined and recrystallized from water to give 0.36 g (88%) of **3b**.

*Reaction of 1-Methyl-3,5-dinitro-2-pyridone (**1a**) with 3-(1-Pyrrolidinyl)-2-pentene.* To a solution of 0.20 g of **1a** in 5 ml of pyridine at 0 °C was added 0.42 g of 3-(1-pyrrolidinyl)-2-pentene in 5 ml of pyridine. The deep red solution was heated at 80 °C for 5 h. After the usual work up, 0.144 g (66%) of **5g** was obtained.

*Isolation of the Cyclohexadiene Intermediates (**6**).* *N*-Methyl-2-[6-methyl-2-nitro-5-(1-pyrrolidinyl)-2,4-cyclohexadienyl]-2-nitroacetamide (**6a**): To a mixture of 0.40 g of **1a** and 5 ml of 2-butanone in 10 ml of pyridine was added 0.43 g of pyrrolidine at 0 °C. The solution was heated at 70 °C for 1 h, and then the solvent was removed *in vacuo*. The residual oil was washed with water and crystallized from tetrahydrofuran–ether to give 0.37 g (55%) of **6a**; wine-red prisms; decomp 154—155 °C. Found: C, 51.95; H, 6.34; N, 17.44%. Calcd for $C_{14}H_{20}N_4O_5$: C, 51.84; H, 6.22; N, 17.28%.

*N-Methyl-2-(5-diethylamino-5-methyl-2-nitro-2,4-cyclohexadienyl)-2-nitroacetamide (**6b**)*: The treatment of 0.40 g of **1a** with 0.46 g of diethylamine and 5 ml of 2-butanone in 10 ml of pyridine at 70 °C for 2 h gave 0.30 g (43%) of **6b**; wine-red prisms (from methanol-ether); decomp 138—138.5 °C. Found: C, 51.49; H, 6.70; N, 17.18%. Calcd for $C_{14}H_{22}N_4O_5$: C, 51.52; H, 6.80; N, 17.17%.

*N-(2-Pyridyl)-2-(5-diethylamino-6-methyl-2-nitro-2,4-cyclohexadienyl)-2-nitroacetamide (**6c**)*: A treatment of 0.26 g of **1b** with 1.44 g of 2-butanone and 0.22 g of diethylamine in 10 ml of pyridine at 50 °C for 5 h gave 0.06 g (15%) of **6c**; wine-red prisms (from chloroform); decomp 135—136 °C. Found: C, 55.26; H, 6.23; N, 17.61%. Calcd for $C_{18}H_{23}N_5O_5$: C, 55.52; H, 5.95; N, 17.99%.

N-Methyl-2-[4,6-dimethyl-2-nitro-5-(1-pyrrolidinyl)-2,4-cyclo-

*hexadienyl]-2-nitroacetamide (**6d**)*: To a solution of 0.40 g of **1a** in 10 ml of pyridine was added 0.42 g of 3-(1-pyrrolidinyl)-2-pentene in 10 ml of pyridine at 0 °C. The solution immediately turned purple; it was heated at 70 °C for 1 h. After the pyridine was removed *in vacuo*, the residual oil was washed with ether and crystallized from tetrahydrofuran–ether to give 0.26 g (38%) of **6d**; purple prisms; decomp 156—157 °C. Found: C, 53.02; H, 6.67; N, 16.77%. Calcd for $C_{15}H_{22}N_4O_5$: C, 53.24; H, 6.55; N, 16.56%.

*N-(2-Pyridyl)-2-[4,6-dimethyl-2-nitro-5-(1-pyrrolidinyl)-2,4-cyclohexadienyl]-2-nitroacetamide (**6e**)*: Treatment of 0.26 g of **1b** with 0.21 g of 3-(1-pyrrolidinyl)-2-pentene in 10 ml of pyridine at 45 °C for 2 h gave 0.08 g (20%) of **6e**; purple prisms (from methanol–ether); decomp 156—157 °C. Found: C, 56.68; H, 5.62; N, 17.17%. Calcd for $C_{19}H_{23}N_5O_5$: C, 56.85; H, 5.78; N, 17.45%.

*Conversion of N-Methyl-2-[6-methyl-2-nitro-5-(1-pyrrolidinyl)-2,4-cyclohexadienyl]-2-nitroacetamide (**6a**) into 2-Methyl-4-nitro-1-(1-pyrrolidinyl)benzene (**5f**) and N-Methyl-2-nitroacetamide (**3a**)*. A solution of 0.324 g of **6a** and 0.71 g of pyrrolidine in 20 ml of pyridine was heated at 80 °C for 5 h. The solvent was removed *in vacuo*. When the residual solids were washed with a small portion of chloroform, 0.04 g of **6a** was recovered. The chloroform solution was concentrated and column-chromatographed on silica gel. A benzene elute gave 0.16 g (78%) of 2-methyl-4-nitro-1-(1-pyrrolidinyl)-benzene (**5f**) and an ether elute gave 0.055 g (47%) of *N*-methyl-2-nitroacetamide (**3a**).

*Isolation of the Bicyclo Intermediates (**7**)*. To a solution of 0.20 g of **1a** in 10 ml of acetone, 0.44 g of diethylamine was added slowly at 0 °C. After standing several hours at room temperature, yellow crystals began to precipitete. The crystals were collected by filtration and washed with acetone to give 0.76 g (98%) of **7a**; yellow prisms; decomp 122.5 °C. Found: C, 52.69; H, 8.38; N, 17.89%. Calcd for $C_{17}H_{31}N_5O_5$: C, 52.96, H, 8.11, N, 18.17%. IR (Nujol): 2740 cm^{-1} (ν_{N^+-H}), 1625 cm^{-1} ($\nu_{C=C}$ and $\nu_{C=O}$), 1540 cm^{-1} (ν_{NO_2}). NMR ($CDCl_3$): δ 0.97 ($NCH_2C\underline{H}_3$, 6H, t, J=7 Hz), 1.22 ($NC\underline{H}_2CH_3$, 6H, t, J=7 Hz), 2.2—3.3 ($\approx$11H, m), 2.90 (N–CH_3, 3H, s), 4.2—4.5 (2H, m), 4.6 (a broad doublet, J=3 Hz), 8.1—9.0 (N^+H_2, 2H, m). UV (MeOH): 250 nm (ε=9620), 309 nm (ε=9620).

Similarly **7b** was obtained in 96% yield; pale yellow prisms; decomp 139—140 °C. Found: C, 48.83; H, 6.48; N, 16.56%. Calcd for $C_{17}H_{28}N_5O_{7.5}$: C, 48.34; H, 6.68; N, 16.58%. IR: 2750, 2690, and 2530 cm^{-1} (ν_{N^+-H}), 1628 cm^{-1} ($\nu_{C=C}$ and $\nu_{C=O}$), 1548 cm^{-1} (ν_{NO_2}). NMR ($CDCl_3$): δ 2.3—3.3 (10H, m), 2.94 (N–CH_3, 3H, s), 3.5—4.0 (8H, m), 4.2—4.5 (2H, m), 4.5—4.9 (2H, m), 6.4—7.0 (N^+H_2, 2H, m). UV (MeOH): 314 nm (ε=12400).

*Conversion of **7a** into 1-Diethylamino-4-nitrobenzene (**5c**) and N-Methyl-2-nitroacetamide (**3a**)*. A solution of 0.39 g of **7a** in 50 ml of methanol was allowed to stand for 24 h at room temperature. The solvent was removed *in vacuo* and the residue was dissolved in 10 ml of chloroform and chromatographed on silica gel. A benzene elute gave 0.18 g (93%) of 1-diethylamino-4-nitrobenzene (**5c**). An ether elute gave 0.048 g (41%) of *N*-methyl-2-nitroacetamide (**3a**).

*Conversion of **7b** into 1-Morpholino-4-nitrobenzene (**5e**)*. When a solution of 0.42 g of **7b** in 50 ml of methanol was refluxed for 3 h, **7b** was recovered quantitatively. To the solution was added 0.87 g of morpholine and then refluxed for 3 h to give 1-morpholino-4-nitrobenzene (**5e**) quantitatively after the usual work up.

References

1) E. Matsumura, M. Ariga, and Y. Tohda, *Bull. Chem. Soc. Jpn.*, **52**, 2413 (1979); *Tetrahedron Lett.*, **1979**, 1393.
2) F. C. Schaefer, K. R. Hoffman, and G. A. Peter, *J. Org. Chem.*, **27**, 548 (1962); K. R. Hoffman, F. C. Schaefer, and G. A. Peter, *ibid.*, **27**, 551 (1962).
3) A. A. D. Kreutzberger, *Arch. Pharm. (Weinheim, Ger.)*, **303**, 715 (1970).
4) K. Hirota, K. A. Watanabe, and J. J. Fox, *J. Org. Chem.*, **43**, 1193 (1978); K. Hirota, Y. Kitade, S. Senda, M. J. Harat, K. A. Watanabe, and J. J. Fox, *J. Am. Chem. Soc.*, **101**, 4423 (1979).
5) a) T. Abe, *Bull. Chem. Soc. Jpn.*, **32**, 997 (1959); b) C. A. Allen, A. J. Brook, and E. F. Caldin, *J. Chem. Soc.*, **1961**, 2171; c) R. Foster and C. A. Fyfe, *Tetrahedron*, **22**, 1831 (1962).
6) M. J. Strauss and H. Schran, *J. Am. Chem. Soc.*, **91**, 3974 (1969).
7) M. J. Strauss, H. Schran, T. Jensen, and K. O'Conner, *J. Org. Chem.*, **35**, 383 (1970); H. Schran and M. J. Strauss, *ibid.*, **36**, 856 (1971).
8) K. N. Houk, *J. Am. Chem. Soc.*, **95**, 4092 (1973).

Synthesis and Cation-complexing Ability of Oxo Crown Ethers

Kenji MATSUSHIMA, Norio KAWAMURA,† Yohji NAKATSUJI,† and Mitsuo OKAHARA*,†

Department of Applied Chemistry, Faculty of Science and Technology, Kinki University, Kowakae, Higashi-osaka, Osaka 577

† *Department of Applied Chemistry, Faculty of Engineering, Osaka University, Yamadaoka 2-1, Suita, Osaka 565*

(Received October 9, 1981)

3-Substituted 2-oxo crown ethers and a novel dioxo crown ether with a point symmetry were synthesized by the cyclization of the corresponding substituted oligoethylene glycol monocarboxymethyl ethers using benzenesulfonyl chloride in the presence of alkali metal carbonates. The reaction mechanism was discussed. Their stability constants toward sodium and potassium cations were determined and the relation between their structures and complexing properties was discussed.

Since crown ethers were first synthesized by Pedersen, several thousand publications concerning these compounds and their derivatives have appeared.[1,2] Among them, attention has recently been denoted to the oxo crown compounds,[3,4] since some of these were shown to have a different complexing tendency towards cations than normal crown ethers. They may be considered as model compounds of natural macrocyclic antibiotics such as valinomycin and nonactin,[5,6] and those having the pyridine ring as mimics of enzymes such as NADH.[7,8]

A large number of oxo crown compounds have been synthesized and their properties investigated by Bradshaw,[9–17] Vögtle,[18–20] and Kellogg,[7,8,21,22] but most of these compounds were prepared through either the reaction between diacids and dihalides (ditosylates) of oligoethylene glycols, or the reaction between di(acid chloride)s and oligoethylene glycols; thus, the oxo crown compounds so far synthesized are mainly restricted to di- and tetraesters with limited kinds of substituents.

On the other hand, there are a few reports on the synthesis of monooxo crown ethers with rather special structure. Kellogg[23] prepared monooxo benzocrown ethers starting from salicylic acid, Cs_2CO_3 and oligoethylene glycol dibromides, while Newkome and coworkers[24,25] have synthesized pyridine macrocyclic lactones from 2-chloronicotinoyl chloride and oligoethylene glycol.

In the previous communications,[26,27] we have reported the synthesis of unsubstituted 2-oxo crown ethers *via* the intramolecular cyclization of monocarboxymethylated oligoethylene glycols. Here we describe the extension of this new method to the synthesis of monooxo crown ethers with substituents and a novel symmetrical dioxo crown ether. The characteristics of the complexing ability of monooxo crown ethers toward alkali metal cations were also examined in comparison with normal crown ethers and dioxo crown ethers.

Experimental

The ^{1}H NMR spectra were taken at 100 MHz on a JEOL-JNM-PS 100 spectrometer using tetramethylsilane as the internal standard. The infrared spectra were obtained on a Hitachi 260-10 spectrometer. The mass spectra were measured with a Hitachi RMU-6E mass spectrometer at an ionization potential of 70 eV. The GLC analyses were performed on a Shimadzu GC-3BF using a 2 m×3 mm column packed with 10% Silicone SE-30 on 60—80 mesh Celite 545. Stability constants were determined by potentiometry using an ion-selective electrode at 25 °C in methanol according to the literature.[28] Toko Na^+ 1100 and Toko K^+ 1200 were used as ion-selective electrodes for Na^+ and K^+ respectively. The emf was measured with a Beckmann 4500 digital pH meter.

General Procedure for Preparation of 2-Oxo Crown Ethers (4). In an appropriate oligoethylene glycol (**2**), one eighth molar amount of alkali metal was dissolved at 90—100 °C. To this solution, one eighth molar amount of alkali metal salt of a halo fatty acid (**1**) was added; the mixture was then stirred at 80—90 °C for 4—5 h. In some cases, where a halo acid was used in place of its salt, one quarter molar amount of alkali metal was used. The excess **2** was distilled off from the reaction mixture under reduced pressure, the residue was then dissolved in 2-propanol and the insoluble matter (alkali metal halide) was removed by filtration. The solvent was evaporated to give the intermediate **3**. One quarter molar amount of pulverized alkali metal carbonate was suspended together with **3** in dioxane. To this suspension, one eighth molar amount of benzenesulfonyl chloride in dioxane was added over a 2—3 h period at 65—70 °C, and the mixture was stirred for another 3 h. The insoluble salt was removed by filtration and the solvent was distilled off under reduced pressure. The residue was submitted to pyrolytic distillation using a Kugelrohr apparatus to give **4** as a distillate. Further purification of **4** was accomplished through redistillation or silicic acid column chromatography.

2-Oxo-15-crown-5 (4a). The sodium salt of tetraethylene glycol carboxymethyl ether (**3**, n=2, R^1, R^2=H), which was prepared according to the general procedure mentioned above from tetraethylene glycol (97.9 g, 0.504 mol), sodium metal (2.90 g, 0.126 mol), and bromoacetic acid (8.76 g, 0.063 mol), was treated with benzenesulfonyl chloride (11.1 g, 0.063 mol) and sodium carbonate (13.4 g, 0.126 mol) in dioxane (200 ml+50 ml) to give sodium cation complex of **4a**. The complex was destructively distilled and purified by redistillation to give a pale yellow oil. 2-Oxo-18-crown-6 (**4b**) was obtained according to a similar procedure. Spectral and analytical data have already been reported in the previous communication.[26]

2-Oxo-21-crown-7 (4c). A pale yellow oil; bp 134—137 °C/0.04 Torr (1 Torr=133.322 Pa) (Kugelrohr apparatus); n_D^{20} 1.4665; IR (neat) 2880(s), 1760—1740(s), 1455(m), 1350(m), 1290(m), 1250(m), 1200(m), 1135(s), 1040(w), 1000(w), 945(m), 850(w) cm^{-1}; ^{1}H NMR (CCl_4) δ 3.50—3.70 (m, 22H, OCH_2CH_2O), 4.12 (s, 2H, OCH_2COO), 4.16—4.28 (m, 2H, $COOCH_2CH_2O$); mass spectrum, *m/e* (relative intensity) 322 (M^+), 103(45), 102(23), 89(35),

87(34), 86(28), 73(28), 59(25), 58(27), 45(100), 44(29), 43(50), 42(21). Found: C, 51.82; H, 8.38%. Calcd for $C_{14}H_{26}O_8$: C, 52.16; H, 8.13%.

*3-Methyl-2-oxo-15-crown-5 (**4d**).* A pale yellow oil; IR (neat) 1730—1750 cm^{-1} ($\nu_{C=O}$); ^1H NMR (CCl_4) δ 1.30 (d, 3H), 3.52—3.72 (m, 14H), 3.88—4.40 (m, 3H); mass spectrum, *m/e* 248 (M^+). Found: C, 52.89; H, 8.31%. Calcd for $C_{11}H_{20}O_6$: C, 53.22; H, 8.12%.

*3,3-Dimethyl-2-oxo-15-crown-5 (**4e**).* A pale yellow oil; IR (neat) 1720—1740 cm^{-1} ($\nu_{C=O}$); ^1H NMR (CCl_4) δ 1.35 (s, 6H), 3.30—3.74 (m, 14H), 4.18 (t, 2H); mass spectrum, *m/e* 262 (M^+). Found: C, 54.66; H, 8.69%. Calcd for $C_{12}H_{22}O_6$; C, 54.95; H, 8.45%.

*3-Ethyl-2-oxo-15-crown-5 (**4f**).* A pale yellow oil; IR (neat) 1720—1740 cm^{-1} ($\nu_{C=O}$); ^1H NMR (CCl_4) δ 0.92 (t, 3H), 1.68 (m, 2H), 3.55—3.78 (m, 14H), 3.85 (t, 1H), 4.00—4.40 (m, 2H); mass spectrum, *m/e* 262 (M^+). Found: C, 54.69; H, 8.76%. Calcd for $C_{12}H_{22}O_6$: C, 54.95; H, 8.45%.

*3-Hexyl-2-oxo-15-crown-5 (**4g**).* A pale yellow oil; IR (neat) 1720—1750 cm^{-1} ($\nu_{C=O}$); ^1H NMR (CCl_4) δ 0.88 (t, 3H), 1.20—1.50 (m, 8H), 1.50—1.76 (m, 2H), 3.50—3.76 (m, 14H), 3.85 (t, 1H), 4.00—4.40 (m, 2H); mass spectrum, *m/e* 318 (M^+). Found: C, 60.20; H, 9.71%. Calcd for $C_{16}H_{30}O_6$: C, 60.35; H, 9.50%.

*3-Phenyl-2-oxo-15-crown-5 (**4h**).* A pale yellow oil; IR (neat) 1730—1750 ($\nu_{C=O}$), 730, 700 cm^{-1}; ^1H NMR (CCl_4) δ 3.50—3.78 (m, 14H), 3.92—4.40 (m, 2H), 4.98 (s, 1H), 7.15—7.45 (m, 5H); mass spectrum, *m/e* 310 (M^+). Found: C, 61.74; H, 7.29%. Calcd for $C_{16}H_{22}O_6$: C, 61.92; H, 7.15%.

*3-Methyl-2-oxo-18-crown-6 (**4i**).* A pale yellow oil; IR (neat) 1730—1745 cm^{-1} ($\nu_{C=O}$); ^1H NMR (CCl_4) δ 1.34 (d, 3H), 3.55—3.76 (m, 18H), 3.92—4.32 (m, 3H); mass spectrum, *m/e* 292 (M^+). Found: C, 53.20; H, 8.46%. Calcd for $C_{13}H_{24}O_7$: C, 53.41; H, 8.28%.

*3,3-Dimethyl-2-oxo-18-crown-6 (**4j**).* A pale yellow oil; IR (neat) 1730—1745 cm^{-1} ($\nu_{C=O}$); ^1H NMR (CCl_4) δ 1.36 (s, 6H), 3.36—3.80 (m, 18H), 4.20 (t, 2H); mass spectrum, *m/e* 306 (M^+). Found: C, 54.55; H, 8.80%. Calcd for $C_{14}H_{26}O_7$: C, 54.89; H, 8.55%.

*3-Ethyl-2-oxo-18-crown-6 (**4k**).* A pale yellow oil; IR (neat) 1720—1740 cm^{-1} ($\nu_{C=O}$); ^1H NMR (CCl_4) δ 0.92 (t, 3H), 1.68 (m, 2H), 3.55—3.80 (m, 18H), 3.90 (t, 1H), 4.15—4.35 (m, 2H); mass spectrum, *m/e* 306 (M^+). Found: C, 54.82; H, 8.81%. Calcd for $C_{14}H_{26}O_7$: C, 54.89; H, 8.55%.

*3-Hexyl-2-oxo-18-crown-6 (**4l**).* A pale yellow oil; IR (neat) 1730—1750 cm^{-1} ($\nu_{C=O}$); ^1H NMR (CCl_4) δ 0.88 (t, 3H), 1.20—1.48 (m, 8H), 1.50—1.76 (m, 2H), 3.50—3.76 (m, 18H), 3.88 (t, 1H), 4.10—4.28 (m, 2H); mass spectrum, *m/e* 362 (M^+). Found: C, 59.36; H, 9.71%. Calcd for $C_{18}H_{34}O_7$: C, 59.65; H, 9.45%.

*3-Phenyl-2-oxo-18-crown-6 (**4m**).* A pale yellow oil; IR (neat) 1740—1760 ($\nu_{C=O}$), 740, 700 cm^{-1}; ^1H NMR (CCl_4) δ 3.56—3.70 (m, 18H), 3.90—4.40 (m, 2H), 5.06 (s, 1H), 7.16—7.48 (m, 5H); mass spectrum, *m/e* 354 (M^+). Found: C, 60.70; H, 7.59%. Calcd for $C_{18}H_{26}O_7$: C, 61.00; H, 7.40%.

*3-Methyl-2-oxo-21-crown-7 (**4n**).* A pale yellow oil; IR (neat) 1730—1750 cm^{-1} ($\nu_{C=O}$); ^1H NMR (CCl_4) δ 1.32 (d, 3H), 3.55—3.75 (m, 22H), 4.05 (quartet, 1H), 4.24 (t, 2H); mass spectrum, *m/e* 336 (M^+). Found: C, 53.19; H, 8.50%. Calcd for $C_{15}H_{28}O_8$: C, 53.56; H, 8.39%.

*3,3-Dimethyl-2-oxo-21-crown-7 (**4o**).* A pale yellow oil; IR (neat) 1720—1740 cm^{-1} ($\nu_{C=O}$); ^1H NMR (CCl_4) δ 1.35 (s, 6H), 3.40—3.72 (m, 22H), 4.20 (t, 2H); mass spectrum, *m/e* 350 (M^+). Found: C, 54.77; H, 8.80%. Calcd for $C_{16}H_{30}O_8$: C, 54.84; H, 8.63%.

*3-Ethyl-2-oxo-21-crown-7 (**4p**).* A pale yellow oil; IR (neat) 1730—1750 cm^{-1} ($\nu_{C=O}$); ^1H NMR (CCl_4) δ 0.95 (t, 3H), 1.68 (m, 2H), 3.50—3.80 (m, 22H), 3.88 (t, 1H), 4.18—4.30 (m, 2H); mass spectrum, *m/e* 350 (M^+). Found: C, 55.00; H, 8.81%. Calcd for $C_{16}H_{30}O_8$: C, 54.84; H, 8.63%.

*3-Hexyl-2-oxo-21-crown-7 (**4q**).* A pale yellow oil; IR (neat) 1730—1760 cm^{-1} ($\nu_{C=O}$); ^1H NMR (CCl_4) δ 0.88 (t, 3H), 1.20—1.40 (m, 8H), 1.50—1.70 (m, 2H), 3.50—3.85 (m, 22H), 3.90 (t, 1H), 4.15—4.28 (m, 2H); mass spectrum, *m/e* 406 (M^+). Found: C, 58.72; H, 9.53%. Calcd for $C_{20}H_{38}O_8$: C, 59.09; H, 9.42%.

*3-Phenyl-2-oxo-21-crown-7 (**4r**).* A pale yellow oil; IR (neat) 1720—1760 ($\nu_{C=O}$), 730, 700 cm^{-1}; ^1H NMR (CCl_4) δ 3.50—3.72 (m, 22H), 4.10—4.28 (m, 2H), 5.00 (s 1H), 7.15—7.30 (m, 3H), 7.32—7.45 (m, 2H); mass spectrum, *m/e* 398 (M^+). Found: C, 59.93; H, 7.68%. Calcd for $C_{20}H_{30}O_8$: C, 60.29; H, 7.59%.

*2,11-Dioxo-18-crown-6 (**5**).* Metallic sodium (9.2 g, 0.4 mol) was dissolved in diethylene glycol (170 g, 1.60 mol) and bromoacetic acid (27.8 g, 0.2 mol) was added to the resultant solution at 90—100 °C; the mixture was then stirred at 95—100 °C for 5 h. The excess diethylene glycol was removed *in vacuo*. Methanol (200 ml) was added to the distillation residue and the sodium bromide was removed by filtration. On evaporation of the methanol from the filtrate, the sodium salt of diethylene glycol carboxymethyl ether (**3s**) was obtained. The intermediate was suspended in dioxane (250 ml) and sodium carbonate (31.8 g, 0.3 mol) and benzenesulfonyl chloride (35.3 g, 0.2 mol) in dioxane (60 ml) was added dropwise to the mixture at 65—70 °C for 4 h under stirring and the mixture was stirred for another 3 h. The resultant mixture was cooled to room temperature, and the insoluble matter was removed by filtration. The filtrate was evaporated under reduced pressure to give a brown solid. The crude product was pyrolized in a Kugelrohr apparatus under reduced pressure and recrystallized from acetone to give a white solid (10.5 g, 18%). Mp 115.0—116.0 °C; IR (KBr) 2930—2850(s), 1750 (s, $\nu_{C=O}$), 1450(m), 1405(m), 1350(m), 1215(s), 1125(s), 1030(m), 940(m), 860 cm^{-1} (m); ^1H NMR ($CDCl_3$) δ 3.65—3.88 (m, 12H), 4.28—4.45 (m, 8H); mass spectrum, *m/e* (relative intensity) 292 (M^+, 10), 249(7), 248(8), 147(29), 103(100), 102(65), 86(66), 73(25), 45(66). Found: C, 49.34; H, 6.90%. Calcd for $C_{12}H_{20}O_8$: C, 49.31; H, 6.93%.

Reaction of Tetraethylene Glycol with the Mixture of Acetic Acid and Benzenesulfonyl Chloride in the Presence of Sodium Carbonate. To a stirred suspension of 3.88 g (0.02 mol) of tetraethylene glycol and 8.48 g (0.08 mol) of sodium carbonate in 80 ml of dioxane, a mixture of 2.40 g (0.04 mol) of acetic acid and 10.71 g (0.06 mol) of benzenesulfonyl chloride in 20 ml of dioxane was added over a 1-h period at 60 °C. The reaction was followed by GLC and the peak corresponding to the desired ester was observed soon after the addition of the reagents. The mixture was then stirred at 60 °C for 30 h. The resultant mixture was cooled to room temperature and insoluble matter was removed by filtration. The solvent was evaporated under reduced pressure. Water (100 ml) was added to the residue and the mixture was extracted with dichloromethane (50 ml). The dichloromethane solution was concentrated to give 5.54 g of a slightly yellow liquid. The crude product was distilled under reduced pressure to give 3.42 g (61%) of tetraethylene glycol diacetate as a colorless liquid. Bp 163 °C/0.03 Torr (Kugelrohr apparatus); IR (neat) 2960(m), 2880(s), 1735(s), 1460(m), 1380(s), 1245(s), 1130(s), 1060(s), 960(m), 855(w)

cm^{-1}; ^1H NMR ($CDCl_3$) δ 2.05 (s, 6H), 3.52—3.80 (s+m, 12H), 4.20 (t, 4H).

Reaction of Tetraethylene Glycol Ditosylate with Acetic Acid in the Presence of Sodium Carbonate. A suspended mixture of 2.60 g (5.17×10^{-3} mol) of tetraethylene glycol ditosylate, 0.95 g (0.0158 mol) of acetic acid, and 1.65 g (0.0156 mol) of sodium carbonate in 25 ml of dioxane was stirred at 60 °C for 30 h. The required ester was not detected by GLC anlysis.

Results and Discussion

The alkali metal salts of oligoethylene glycol monocarboxymethyl ethers and their alkyl derivatives(**3**) were prepared from 2-halo carboxylic acids(**1**) and the appropriate oligoethylene glycols(**2**) through the Williamson ether synthesis, and successively cyclized to 2-oxo crown ethers (**4**) by the treatment with benzenesulfonyl chloride in dioxane in the presence of alkali metal carbonates (scheme 1). The results of synthesis of **4** are summarized in Tables 1 and 2.

The yields of unsubstituted 2-oxo crown ethers were not influenced significantly by the difference in the halogen atom (Table 1). However, the kind of alkali metal cation was observed to effect the yield considerably. Thus yields of both 2-oxo-15- and 2-oxo-18-crown ethers in the reactions with sodium carbonate were better than those with potassium carbonate, while for 2-oxo-21-crown-7 potassium carbonate gave good yields compared with sodium carbonate. A caesium base had been used to improve the yields in esterification and the related reactions instead of more common alkali metal bases,[29] and the effect of a change in the alkali metal cation on the yields in the synthesis of 2-oxo crown ethers was examined in this study. Although the general trend of the effect of the caesium cation was not clearly observed, the partial replacement of sodium carbonate by this cation gave somewhat improved yield in the case of **4a** as shown in Table 1.

In spite of the difference in the substituent group, the yields of 3-monosubstituted-2-oxo-15-, 18-, and 21-crown ethers were approximately 20, 40, and 25% respectively. In addition, it is noteworthy that the temperature used for pyrolytic distillation of the reaction products under reduced pressure in a Kugelrohr apparatus were almost constant for the crown ethers with the same ring size; the distillation conditions were as follows: 160 °C/0.03 Torr for 15-crown, 175 °C/0.02 Torr for 18-crown, and 190 °C/0.02 Torr for 21-crown ethers. This finding suggests that above-cited conditions correspond to the decomposition temperature of the complex with the alkali metal cation.

On the other hand, the sodium salt of diethylene glycol monocarboxymethyl ether(**3s**) was submitted

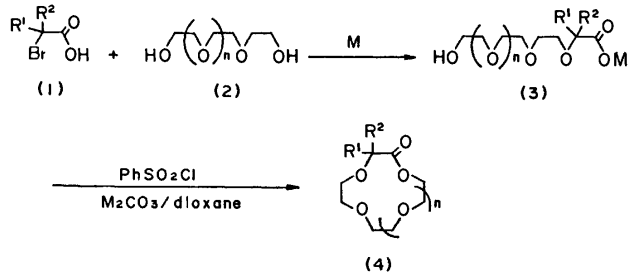

Scheme 1.

Table 1. Examination of reaction conditions in the synthesis of unsubstituted 2-oxo crown ethers(**4**)

Compd	n	R^1	R^2	X	M	Yield/%[a]
4a	2	H	H	Cl	Na	15
				Br	Na	16
				Br	K	11
				Br	Na:Cs (9:1)	16
				Br	Na:Cs (8:2)	24
4b	3	H	H	Cl	Na	42 (60)[b]
				Cl	K	— (30)[b]
				Br	Na	— (60)[b]
				Br	K	26 (30)[b]
				Br	Cs	37
4c	4	H	H	Cl	Na	10
				Cl	K	20
				Br	K	23

a) Isolated yield. b) Determined by GLC.

Table 2. Synthesis of 3-substituted 2-oxo crown ethers(**4**)

Compd	n	R^1	R^2	X	M	Yield/%
4d	2	CH_3	H	Br	Na	15
4e	2	CH_3	CH_3	Br	Na	10
4f	2	C_2H_5	H	Br	Na	21
4g	2	C_6H_{13}	H	Br	Na	17
4h	2	Ph	H	Br	Na	20
4i	3	CH_3	H	Br	Na	39
4j	3	CH_3	CH_3	Br	Na	32
4k	3	C_2H_5	H	Br	Na	41
4l	3	C_6H_{13}	H	Br	Na	37
4m	3	Ph	H	Br	Na	41
4n	4	CH_3	H	Br	Na, K[a]	18
4n	4	CH_3	H	Br	K	28
4o	4	CH_3	CH_3	Br	K	17
4p	4	C_2H_5	H	Br	K	24
4q	4	C_6H_{13}	H	Br	K	23
4r	4	Ph	H	Br	K	21

a) Metallic sodium and potassium carbonate were used at the first and the second steps respectively.

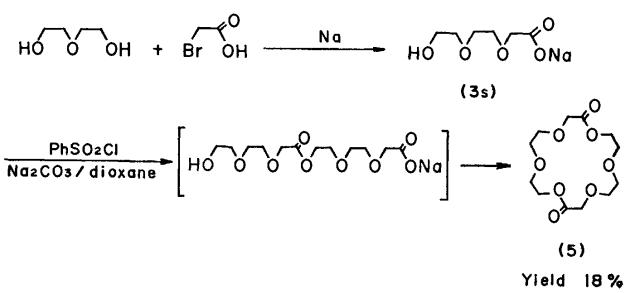

Scheme 2.

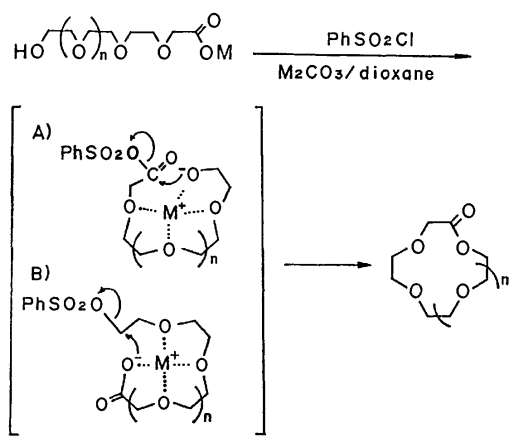

Scheme 3.

to the bimolecular esterification with each other followed by intramolecular cyclization in the presence of an effective template ion to give 2,11-dioxo-18-crown-6(**5**); this is a novel type of dioxo crown ethers possessing a point symmetry.

The postulated reaction mechanism of the cyclization to monooxo crown ethers was offered in Scheme 3. Two possible routes of cyclization (route **A** and **B**) can be conceived: differing in the first reaction site with the benzenesulfonyl chloride. Brewster *et al.* reported that the lactone formation reaction of *trans*-2-hydroxycyclohexaneacetic acid using *p*-toluenesulfonyl chloride in the presence of pyridine proceeded without losing its geometrical configuration.[30] This can be explained by assuming the first formation of a mixed acid anhydride. In addition, two model reactions under conditions similar to the case of 2-oxo crown ethers were carried out to clarify the mechanism. One was the reaction of oligoethylene glycol with acetic acid using benzenesulfonyl chloride in the presence of sodium carbonate in dioxane; the other was the reaction of oligoethylene glycol ditosylate with acetic acid in the presence of sodium carbonate in dioxane. Only the former reaction could give the required product, and from all these results route **A** seems to be probable in this case.

Finally, the complexing ability of the synthesized oxo crown ethers toward sodium and potassium cations was examined according to the method using ion selective electrode in methanol at 25 °C,[28] and compared with that of dioxo and normal crown ethers (Table 3).

The increase of the number of ester group was observed drastically to decrease the complexing ability toward alkali metal cations as expected from the decrease of the electron-donating ability of coordination sites. In general, monooxo crown ethers were concluded to be intermediate in properties between normal crown ethers and dioxo crown ethers.

As for the effect of the substituent, the introduction of alkyl substituent(s) on an oxo crown ring slightly reduced their complexing ability; a phenyl substituent does not affect the complexing ability as indicated by the fact that 3-phenyl-2-oxo-18-crown-6(**4m**) showed almost the comparable stability constant to that of unsubstituted 2-oxo-18-crown-6(**4b**).

On the other hand, the difference in the position of the ester groups of dioxo crown ethers does not seem to influence the complexing ability.

Table 3. Stability constant of oxo crown ethers

Compound	Na^+	K^+
15-Crown-5	(3.48)[a,b]	(3.77)[a,b]
2-Oxo-15-crown-5(**4a**)	1.98	2.12
3-Hexyl-2-oxo-15-crown-5(**4g**)	1.48	1.90
2,6-Dioxo-15-crown-5	(—)[a,b,d]	(—)[a,b,d]
18-Crown-6	4.30 (4.36)[a,c]	6.02 (6.06)[a,c]
2-Oxo-18-crown-6(**4b**)	3.27	4.18
3-Methyl-2-oxo-18-crown-6(**4i**)	3.07	4.05
3,3-Dimethyl-2-oxo-18-crown-6(**4j**)	2.93	3.99
3-Hexyl-2-oxo-18-crown-6(**4l**)	2.90	3.84
3-Phenyl-2-oxo-18-crown-6(**4m**)	3.23	4.23
2,6-Dioxo-18-crown-6	(2.5)[1,2]	(2.79)[a,b]
2,11-Dioxo-18-crown-6(**5**)	2.29	2.70
3-Hexyl-2-oxo-21-crown-7(**4q**)	2.40	3.39

a) Determined by a colorimetric titration procedure. b) Ref. 6. c) Ref. 31. d) Very small (unmeasurable).

References

1) M. Hiraoka, "Crown Compounds," Kodansha Scientific, Tokyo (1978).
2) R. M. Izatt and J. J. Christensen, "Syntheitic Multidentate Macrocyclic Compounds," Academic Press, New York and London (1978); "Progress in Macrocyclic Chemistry," Wiley, New York (1979), Vol. 1.
3) J. S. Bradshaw, G. E. Maas, R. M. Izatt, and J. J. Christensen, *Chem. Rev.*, **79**, 37 (1979).
4) J. S. Bradshaw, R. E. Asay, S. L. Baxter, P. E. Fore, S. T. Jolly, J. D. Lamb, G. E. Maas, M. D. Thompson, R. M. Izatt, and J. J. Christensen, *Ind. Eng. Chem., Prod. Res. Dev.*, **19**, 86 (1980).
5) R. M. Izatt, J. D. Lamb, G. E. Maas, R. E. Asay, J. S. Bradshaw, and J. J. Christensen, *J. Am. Chem. Soc.*, **99**, 2365 (1977).
6) J. D. Lamb, R. M. Izatt, C. S. Swain, J. S. Bradshaw, and J. J. Christensen, *J. Am. Chem. Soc.*, **102**, 479 (1980).
7) T. J. V. Bergen and R. M. Kellogg, *J. Chem. Soc., Chem. Commun.*, **1976**, 964.
8) T. J. V. Bergen and R. M. Kellogg, *J. Am. Chem. Soc.*, **99**, 3882 (1977).
9) G. E. Maas, J. S. Bradshaw, R. M. Izatt, and J. J. Christensen, *J. Org. Chem.*, **42**, 3937 (1977).
10) J. S. Bradshaw, C. T. Bishop, S. F. Nielsen, R. E. Asay, D. R. K. Masihdas, E. D. Flanders, L. D. Hansen, R. M. Izatt, and J. J. Christensen, *J. Chem. Soc., Perkin Trans. 1*, **1976**, 2505.
11) J. S. Bradshaw and S. T. Jolly, *J. Heterocycl. Chem.*, **16**, 1157 (1979).
12) M. D. Thompson, J. S. Bradshaw, S. F. Nielsen, C. T. Bishop, F. T. Cox, P. E. Fore, G. E. Maas, R. M. Izatt, and J. J. Christensen, *Tetrahedron Lett.*, **1977**, 3317.
13) J. S. Bradshaw, M. L. Campbell, L. A. Hassell, and J. K. Baxter, *J. Heterocycl. Chem.*, **16**, 721 (1979).
14) J. S. Bradshaw, L. D. Hansen, S. F. Nielsen, M. D. Thompson, R. A. Reeder, R. M. Izatt, and J. J. Christensen, *J. Chem. Soc., Chem. Commun.*, **1975**, 874.
15) J. S. Bradshaw and M. D. Thompson, *J. Org. Chem.*, **43**, 2456 (1978).

16) S. T. Jolly and J. S. Bradshaw, *J. Org. Chem.*, **45**, 3554 (1980).
17) J. S. Bradshaw, G. E. Maas, J. D. Lamb, R. M. Izatt, and J. J. Christensen, *J. Am. Chem. Soc.*, **102**, 467 (1980).
18) K. Frensch and F. Vögtle, *Tetrahedron Lett.*, **1977**, 2573.
19) K. Frensch, G. Oepen, and F. Vögtle, *Ann. Chem.*, **1979**, 858.
20) K. Frensch and F. Vögtle, *J. Org. Chem.*, **44**, 884 (1979).
21) O. Piepers and R. M. Kellogg, *J. Chem. Soc., Chem. Commun.*, **1978**, 383.
22) R. M. Kellogg, T. J. Bergen, H. Doren, D. Hedstrand, J. Kooi, W. H. Kruizinga, and C. B. Troostwijk, *J. Org. Chem.*, **45**, 2854 (1980).
23) B. J. V. Keulen, R. M. Kellogg, and O. Piepers, *J. Chem. Soc., Chem. Commun.*, **1979**, 285.
24) G. R. Newkome, T. Kawato, and W. H. Benton, *J. Org. Chem.*, **45**, 626 (1980).
25) G. R. Newkome, T. Kawato, F. R. Fronczek, and W. H. Benton, *J. Org. Chem.*, **45**, 5423 (1980).
26) K. Matsushima, N. Kawamura, and M. Okahara, *Tetrahedron Lett.*, **1979**, 3445.
27) Y. Nakatsuji, N. Kawamura, M. Okahara, and K. Matsushima, *Synthesis*, **1981**, 42.
28) H. K. Frensdorff, *J. Am. Chem. Soc.*, **93**, 600 (1971).
29) W. H. Kruizinga and R. M. Kellogg, *J. Chem. Soc., Chem. Commun.*, **1979**, 286.
30) J. H. Brewster and C. J. Ciotti, Jr., *J. Am. Chem. Soc.*, **77**, 6214 (1955).
31) J. D. Lamb, R. M. Izatt, C. S. Swain, and J. J. Christensen, *J. Am. Chem. Soc.*, **102**, 475 (1980).

The Preparation of Optically Pure 3-Hydroxyalkanoic Acid. The Enantioface-differentiating Hydrogenation of the C=O Double Bond with Modified Raney Nickel. XXXVII.

Masaaki NAKAHATA, Motomasa IMAIDA, Hiroshi OZAKI, Tadao HARADA, and Akira TAI*

Institute for Protein Research, Osaka University, Yamada-oka, Suita, Osaka 565

(Received November 28, 1981)

The enantioface-differentiating hydrogenation of methyl 3-oxoalkanoate ($CH_3(CH_2)_nCOCH_2COOCH_3$, n=0, 6, 8, 10, 12) over the (*R,R*)-tartaric acid–NaBr–modified Raney nickel catalyst ((*R,R*)-TA–NaBr–MRNi) gave methyl (*R*)-3-hydroxyalkanoate ($CH_3(CH_2)_nCH(OH)CH_2COOCH_3$, n=0, 6, 8, 10, 12) in an average optical yield of 85%. After the methyl ester had been converted to dicyclohexylammonium salt of 3-hydroxyalkanoic acid, the salt was recrystallized three times from acetonitrile and then treated with acid to give optically pure (*R*)-3-hydroxyalkanoic acid ($CH_3(CH_2)_nCH(OH)CH_2COOH$, n=0, 6, 8, 10, 12) in a reasonable yield. From the hydrogenation product with (*S,S*)-TA–NaBr–MRNi, optically pure (*S*)-3-hydroxyalkanoic acid was obtained by the same process as above.

Optically active 3-hydroxyalkanoic acids (**1**) and their derivatives exist widely in the biological system. For example, 3-hydroxydecanoic acid is a sprouting regulatory substance secreted by the leaf-cutting ant (*A sexdens*)[1] and is also a component of depsipeptide "Serataniolide,"[2] 3-hydroxytetradecanoic acid is a major fatty acid comprising "lipid-A in endotoxin,"[3] the choline ester of 3-acetoxyhexadecanoic acid is a fish toxin "pahutoxine,"[4] and 3-hydroxyoctadecanoic acid is a component of emposatilin, an antitumor reagent.[5]

Although various methods of synthesizing these important 3-hydroxyalkanoic acids have been proposed,[6–8] no practical ways for the preparation of these optically pure compounds have been reported. As has been briefly reported in a preliminary communication,[9] the present method consists of the enantioface-differentiating hydrogenation of the methyl 3-oxoalkanoate over an asymmetrically modified nickel and the preferential crystallization of an optically pure substance from the hydrogenation products. In this paper, the preparations of optically pure acids of carbon numbers from 10 to 16 in the practical scale will be reported.

Results and Discussion

The preparation of optically pure 3-hydroxyalkanoic acid (**1**) was carried out by the process outlined in Scheme 1.

Since the catalytic hydrogenation with the nickel catalyst is sensitive to the impurities of the substrate, one of the essential factors in the present process is the development of a suitable method to synthesize methyl 3-oxoalkanoate (**5**). Among the previously reported methods[10–13] here examined, a modification of the method of Oikawa and his co-workers[10] (Scheme 1) gave the best results with respect to the practical-scale preparation of chemically pure **5**. The isolation and purification of the intermediate (**4**) before the decarboxylation was necessary to obtain long-chain methyl 3-oxoalkanoate (**5**) in a high purity. The average yield of **4** was 70%, based on **3**.

The catalyst (TA–NaBr–MRNi) employed for the enantioface-differentiating hydrogenation of **5** to methyl 3-hydroxyalkanoate (**6**) was prepared by soaking the Raney nickel catalyst in an aqueous solution of tartaric acid (TA) and NaBr at 100 °C.[14]

Table 1. Enantioface-differentiating hydrogenation of methyl 3-oxoalkanoate over TA–NaBr–MRNi

No.	Substrate $CH_3(CH_2)_nCOCH_2COOCH_3$ (n)	Catalyst modifying reagent	Reaction products: $CH_3(CH_2)_nCHOHCH_2COOCH_3$ Configuration	e. e. (%)[a]	$CH_3(CH_2)_nCHOHCH_2COOH$ Isolated yield[b]
1	12 (**5a**)	(*R,R*)-TA	(*R*)	87.0	82.1
2		(*S,S*)-TA	(*S*)	84.4	81.2
3	10 (**5b**)	(*R,R*)-TA	(*R*)	85.5	79.7
4		(*S,S*)-TA	(*S*)	84.5	81.5
5	8 (**5c**)	(*R,R*)-TA	(*R*)	86.7	80.1
6		(*S,S*)-TA	(*S*)	84.8	79.8
7	6 (**5d**)	(*R,R*)-TA	(*R*)	83.3	79.0
8		(*S,S*)-TA	(*S*)	87.5	75.8
9	0	(*R,R*)-TA	(*R*)	83[c]	70
10		(*S,S*)-TA	(*S*)	83[c]	70

a) Determined by means of ^{1}H-NMR with a chiral shift reagent. b) Isolation yield based on **5**. c) Taken from our published data.

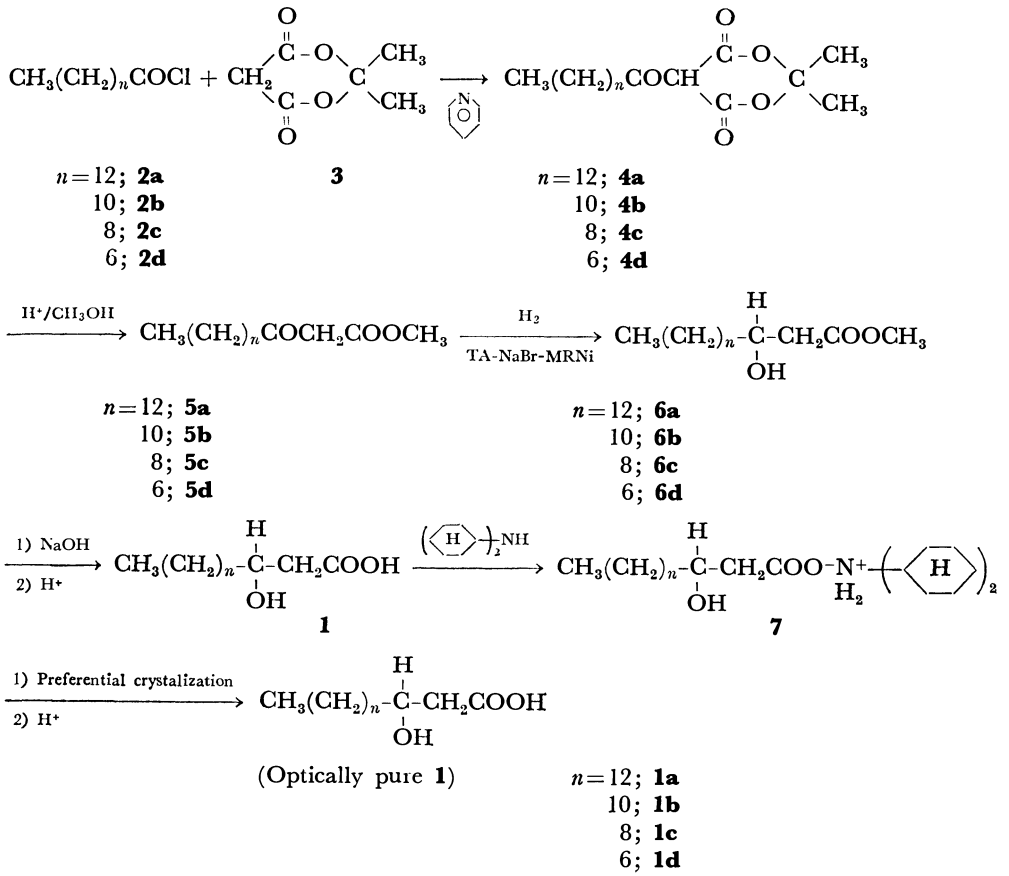

Scheme 1.

Table 2. The efficiencies of the preferential recrystallizations of various ammonium salts of 3-hydroxyhexadecanoic acid from acetonitrile[a)]

No.	Amine employed	Amount of solvent used for recrystallization per g salt (ml)	Recovery after three recrystallization (%)	Optical rotation of free acid recovered $[\alpha]_D^{20}$/°(c 1, $CHCl_3$)
1	Cyclohexylamine	73	36.8	−11.6
2	Benzylamine	45	76.1	−12.5
3	Aniline	7.7	58.5	−12.5
4	Dicyclohexylamine	27	90.7	−13.8 (e. e.>98%)
5	*n*-Hexylamine	>164[b)]	—	—

a) 3-Hydroxyhexadecanoic acid ($[\alpha]_D^{20}$ −10.7° (*c* 1, $CHCl_3$), 85% e. e.) was used as the starting material. b) The solubility of salt was too small for it to be used for recrystallization.

Table 3. Preferential recrystallization of dicyclohexylammonium salt of 3-hydroxyalkanoic acid from acetonitrile

No.	3-Hydroxyalkanoic acid $CH_3(CH_2)_nCH(OH)$-CH_2CO_2H (*n*)	Starting material: Configuration	Starting material: e. e. (%)	Amount of solvent used fore ach crystallization per g salt (ml)	Recovery after three recrystallization (%)	Product e. e. (%)
1	12(**1a**)	(*R*)	87	24.5	75.9	>98
		(*S*)	85		74.5	>97
2	10(**1b**)	(*R*)	85	19.0	72.1	100
		(*S*)	86		73.0	100
3	8(**1c**)	(*R*)	88	18.0	73.5	100
		(*S*)	85		72.5	100
4	6(**1d**)	(*R*)	87	11.5	50.5	>98
		(*S*)	85		51.5	>98
5	0(**1e**)	(*R*)	86	7.0	52[a)]	>98
		(*S*)	86		55[a)]	>98

a) Recovery after 6 recrystallizations.

The hydrogenations of **5** to **6** proceeded smoothly under an initial hydrogen pressure of 100 kg/cm² at 100 °C; they produced quantitative chemical yields and an optical yield of more than 83%. The saponification of **6** gave **1** in an averaged isolation yield of 95%, based on **5**. The results are listed in Table 1. In all cases, the use of (*R*,*R*)-TA–NaBr–MRNi gave (*R*)-**1** in excess. It is advantageous that the natural type of (*R*)-**1** can, incidentally, be obtained by the use of common (*R*,*R*)-TA as a modifying reagent.

The isolation of optically pure **1** from the reaction product (85% e.e.) was achieved by the preferential crystallization method.

To ascertain the most effective derivatives of **1** for the preferential crystallization, various ammonium salts of **1a** (C_{16} acid) were prepared and the efficiencies of resolution were examined. The results are listed in Table 2. Among the ammonium salts of **1** examined, the dicyclohexylammonium salt (**7**) gave the best result. An optically pure substance was obtained in a yield of 70% by three successive recrystallizations from acetonitrile.

The method was also effectively applicable to the resolution of **1b** to **1e** as is shown in Table 3.

The advantage of the present procedure is that optically pure 3-hydroxyalkanoic acid with various alkyl chain lengths is easily obtained by a simple unit process: catalytic hydrogenation and recrystallization. Furthermore, the preparation of TA–NaBr–MRNi is very simple, and the cost of the catalyst is negligible.

Experimental

The ^{1}H-NMR and IR spectra were taken with a JEOL FX-100 spectrometer and a Shimadzu IR 27G spectrometer respectively. The optical rotation was measured with a Perkin Elmer 241 Polarimeter. The GLC was carried out with a Shimadzu 6A-PF Gas Chromatography, using a 3 m-5 mm o.d. glass column packed with 2% Silicone OV-17 on Chromosorb W (OV-17).

All the chemicals except those described below were obtained from commercial sources and were used without further purification.

Substrate. Methyl 3-Oxohexadecanoate (5a): Tetradecanoyl chloride (**2a**) (217 g, 0.88 mol) was added, drop by drop, into a solution of 2,2-dimethyl-1,3-dioxane-4,6-dione (**3**) (115 g, 0.8 mol) and pyridine (128 g) in 1000 ml of CH_2Cl_2 at 5 °C. The reaction mixture was then stirred for 1 h at room temperature. The mixture was washed with three 200-ml portions of 10% HCl and a 200-ml portion of water successively, dried over anhydrous sodium sulfate, and concentrated under reduced pressure. The residue was dissolved in 200 ml of methanol and kept overnight at −20 °C. The crystalline intermediate, **4**, precipitated was collected by filtration and washed with a small portion of cold methanol. The resulting substance was dissolved in 1000 ml of methanol and subjected to decarboxylation under reflux for 5 h. After the evaporation of the solvent from the reaction product, the residue was crystallized from 100 ml of methanol at −20 °C. The separation of the crystals by filtration at −20 °C gave 170 g of **5a** in a yield of 75% based on **3**; mp 41 °C. Calcd for $C_{17}H_{32}O_3$: C, 71.78; H, 11.34%. Found C, 71.50; H, 11.57%. IR, (KBr disk) 2950, 1735, 1695 cm^{-1}. ^{1}H-NMR ($CDCl_3$); δ 0.89 (t, 3H, $-C\underline{H}_3$), 1.25 (m, 22H, $-(C\underline{H}_2)_n$), 2.55 (t, 2H, $-C\underline{H}_2-\overset{\overset{O}{\|}}{C}-$), 3.42 (s, 2H, $-CO-C\underline{H}_2-CO$), 3.72 (s, 3H, $-OC\underline{H}_3$).

Methyl 3-Oxotetradecanoate (5b) and Methyl 3-Oxododecanoate (5c): These substances were prepared by the same procedure as that used for **5a**, except for the use of dodecanoyl chloride (**2b**) and decanoyl chloride (**2c**) respectively, instead of tetradecanoyl chloride (**2a**), as starting materials.

From 193 g (0.88 mol) of **2b** and 115 g of **3** (0.8 mol), 147 g of **5b** were obtained. (Yield 72% based on **3**). Mp 30 °C. Calcd for $C_{15}H_{18}O_3$: C, 70.27; H, 11.01%. Found: C, 70.20; H, 11.21%.

From 167.6 g (0.88 mol) of **2c** and 115 g of **3**, 123 g of **5c** was obtained. The final purification was performed by vacuum distillation instead of crystallization. Bp 127 °C/3 mmHg.** Calcd for $C_{13}H_{24}O_3$: C, 68.38; H, 10.59%. Found: C, 67.80; H, 10.66%. The IR and ^{1}H-NMR spectra of these samples consisted of structures of **5b** and **5c**.

Methyl 3-Oxodecanoate (5d): Octanoyl chloride (**2d**) (162 g, 0.88 mol) and **3** (115 g, 0.8 mol) were subjected to the reaction under the same conditions as those described before. The resulting crude intermediate (**4**) in CH_2Cl_2 was washed three 200-ml portions of 10% HCl and three 200-ml portions of water, and then concentrated under reduced pressure. The residue was dissolved in 800 ml of methanol, and the mixture was refluxed for 5 h. After the evaporation of the methanol from the reaction mixture, the residue was dissolved in 400 ml of benzene, washed successively with two 100-ml portions of a 10% aqueous K_2CO_3 solution and two 100-ml portions of water, and dried over Na_2SO_4. The solvent was evaporated, and the residue was distilled under reduced pressure to give 83 g of **5d**. Bp 112 °C/3 mmHg, Calcd for $C_{11}H_{20}O_3$: C, 65.97; H, 10.07%. Found: C, 66.10; H, 10.07%. The ^{1}H-NMR and IR spectra of the sample consisted of the structure of **5d**.

Catalyst. (R,R)-TA–NaBr–MRNi: Into an alkaline solution (4.5 g of NaOH in 20 ml of H_2O) was added 1.9 g of the Raney nickel alloy (Ni:Al=42:58, Kawaken Fine Chemicals Co.) portion by portion. The resulting suspension was kept for 1 h at 100 °C, after which the supernatant was removed by decantation. The resulting Raney nickel catalyst (RNi) was washed 15 times with 30-ml portions of deionized water. (*R*,*R*)-TA (1 g) and NaBr (10 g) were dissolved in 100 ml of deionized water, and the pH of the solution was adjusted to 3.2 with 1 M NaOH solution. To the solution heated in a boiling-water bath was then added the Raney nickel previously prepared; the mixture was kept for 1 h with occasional stirring at 100 °C. After the removal of the supernatant by decantation, the residual catalyst was washed with a 10-ml portion of water, two 50-ml portions of methanol, and a 25-ml portion of methyl propionate, and then stored in 25-ml of methyl propionate. By the same process, (*S*,*S*)-TA–NaBr–MRNi was prepared by the use of (*S*,*S*)-TA.

3-Hydroxyalkanoic Acid 1a (or 1b, 1c, 1d). In an autoclave (100-ml capacity) were placed 10 g of **5a** (or **5b**, **5c**, **5d**), 30 ml of methyl propionate, 0.1 ml of acetic acid, and TA–NaBr–MRNi prepared from 1.9 g of the Raney alloy. Hydrogenation was carried out at an initial H_2-pressure of 100 kg/cm² at 100 °C until no more consumption of H_2 was observed. After the subsequent evacuation of H_2, the reaction product was dissolved in 50 ml of ether and filtered to separate the catalyst. The filtrate was washed with a 30-ml portion of 10% aqueous Na_2CO_3 and con-

** 1 mmHg≈133.322 Pa.

Table 4. Analytical data of optically pure 3-hydroxyalkanoic acid

Compound	$[\alpha]_D^{20}$/°(c 1, $CHCl_3$)	Mp θ_m/°C	Calcd(Found)(%)		
			$C_{16}H_{32}O_3$	C, 70.54;	H, 11.84
(*R*)-**1a**	−13.8	76.8		(70.90)	(12.06)
(*S*)-**1a**	13.9	77.0		(70.84)	(11.97)
			$C_{14}H_{28}O_3$	C, 68.81;	H, 11.55
(*R*)-**1b**	−16.2 lit,[9] −16	72.0		(68.55)	(11.88)
(*S*)-**1b**	16.1 (*c* 1, $CHCl_3$)	71.8		(68.61)	(11.89)
			$C_{12}H_{24}O_3$	C, 66.63;	H, 11.18
(*R*)-**1c**	−17.5	56.5		(66.43)	(11.42)
(*S*)-**1c**	17.4	56.8		(66.31)	(11.29)
			$C_{10}H_{20}O_3$	C, 63.79;	H, 10.71
(*R*)-**1d**	−20.6 lit,[10] −20.8	bp 129—131 °C		(63.48)	(10.80)
(*S*)-**1d**	19.8 (*c* 1, $CHCl_3$)	(1 mmHg)		(63.51)	(10.82)

centrated under reduced pressure to give crude **6a** (or **6b**, **6c**, **6d**). A 100-mg portion of crude **6a** (or **6b**, **6c**, **6d**) was purified on preparative TLC as the sample for NMR and IR analysis. The GLC (OV-17) of each purified sample showed a single peak. The retention times of the samples were 31.2 min (**6a**, 160 °C), 11.4 min (**6b**, 160 °C), 12.0 min (**6c**, 110 °C), and 4.2 min (**6d**, 100 °C). The IR and ^{1}H-NMR spectra of **6a** were as follows: IR (KBr disk), 3390, 2950, 1739, 1700; NMR ($CDCl_3$) δ 0.90 (t, 3H, $-C\underline{H}_3$), 1.30 (m, 24H, $-(C\underline{H}_2)_n-$), 2.50 (m, 2H, $-C\underline{H}(OH)-C\underline{H}_2-C(=O)-$), 3.72 (s, 3H, $-OC\underline{H}_3$), 4.00 (m, 1H, $-C\underline{H}(OH)-$). The spectra of **6b**, **6c**, **6d** were almost the same as those of **6a** and were consistent with their structures.

The optical purity of each sample as determined by ^{1}H-NMR in the presence of Eu(hfmc)$_3$, is listed in Table 1. The difference in the chemical shift for the methyl proton of $-C(=O)-OC\underline{H}_3$ (singlet) of (*S*)- and (*R*)-**6** was 6—10 Hz when the spectra were measured with a solution of **6** (10 mg) and Eu(hfmc)$_3$ (15 mg) in 400 μl of $CDCl_3$. The saponification of the major part of crude **6a** (or **6b**, **6c**, **6d**) with NaOH and subsequent acid treatment gave crude **1a** (or **1b**, **1c**, **1d**). The yields are listed in Table 1.

Preferential Crystallizations of Various Ammonium Salts of 1a. Cyclohexyl-, benzyl-, phenyl-, dicyclohexyl-, and hexylammonium salts of **1a** (85% e.e., $[\alpha]_D^{20}$ −10.7 (*c*=1, $CHCl_3$)) were prepared from 5.5 g of **1a** and a 1.1-mol equivalent of the amine. Each ammonium salt was dissolved in a minimum amount of boiling acetonitrile and crystallized at room temperature. The amounts of acetonitrile used are listed in Table 2. After three recrystallizations, the salt was acidified with 10% aqueous HCl and the liberated **1a** was extracted with ether. After drying over Na_2SO_4, the extract was concentrated to the crystals. The optical rotation of **1a** liberated from each recrystallized salt is listed in Table 2.

Optically Pure 3-Hydroxyalkanoic Acid 1a (or 1b, 1c, 1d). Crude **1a** (or **1b**, **1c**, **1d**) obtained by the hydrogenation was converted to dicyclohexylammonium salt. Three recrystallizations of the salt from a minimum amount of acetonitrile gave the optically pure salt of **1a** (or **1b**, **1c**, **1d**). The optical purity of the starting material, the amount of acetonitrile used for recrystallization, and the recovery of optically active salt as crystals are listed in Table 3.

Optically active **1a** (or **1b**, **1c**, **1d**) was obtained by the acid treatment of the salt as described above. The analytical data of the products are listed in Table 4.

A 100-mg portion of each acid was converted to the methyl ester with diazomethane and purified by preparative TLC. The optical purity of each purified sample as determined by ^{1}H-NMR, is listed in Table 3.

The authors are grateful to professors Yoshiharu Izumi, Tetsuo Shiba, and Shoichi Kusumoto, Osaka University for their helpful suggestions. This research was supported by a Scientific Research Grant-in-Aid from the Ministry of Education, Science, and Culture.

References

1) H. Schildknecht and K. Koob, *Angew. Chem., Int. Ed. Engl.*, **10**, 124 (1971).
2) D. G. Bishop and J. L. Still, *J. Lipid. Res.*, **4**, 81-6 (1963).
3) C. Galanos, O. Luderitz, E. T. Rietschel, and O. Westphal, "International Review of Biochemistry, Biochemistry of Lipids. II," University Park Press, Baltimore (1977), Vol. 14, p. 239.
4) D. V. Boylan and P. J. Sheuer, *Science*, **155**, 52 (1967).
5) W. Herz and R. P. Sharma, *J. Org. Chem.*, **41**, 1015 (1976).
6) K. Serck-Hanssen and E. Stenhagen, *Acta Chem. Scand.*, **9**, 866 (1955).
7) C. Mioskowskii and Guy Solladie, *J. Chem. Soc.*, **1962**, 1762.
8) M. Gutte and J. P. Gutte, *Tetrahedron Lett.*, **1969**, 3657.
9) A. Tai, M. Nakahata, T. Harada, Y. Izumi, S. Kusumoto, M. Inage, and T. Shiba, *Chem. Lett.*, **1980**, 1125.
10) Y. Oikawa, K. Sugano, and O. Yonemitsu, *J. Org. Chem.*, **43**, 2087 (1978).
11) R. Pellicciari, R. Fringuelli, P. Ceccherlli, and E. Sisani, *J. Chem. Soc., Chem. Commun.*, **1979**, 959.
12) W. Wieregna and H. I. Skulnick, *J. Org. Chem.*, **44**, 310 (1979).
13) S. N. Huckin and L. Weiler, *J. Am. Chem. Soc.*, **96**, 1082 (1974).
14) T. Harada, M. Yamamoto, S. Onaka, M. Imaida, H. Ozaki, A. Tai, and Y. Izumi, *Bull. Chem. Soc. Jpn.*, **54**, 2323 (1981).
15) M. Ikawa, J. B. Koepfli, S. G. Mudd, and C. Niemann, *J. Am. Chem. Soc.*, **75**, 1035 (1953).
16) M. M. Shemyakin, Yu. A. Cvchinnikov, V. K. Antonov, A. A. Kiryushkin, V. T. Ivanov, V. I. Shelokov, and A. M. Shkrob, *Tetrahedron Lett.*, **1964**, 47.

The Photocycloaddition of 6-Substituted Phenanthridines to Electron-rich Olefins

Shigeru FUTAMURA, Hiroyuki OHTA,* and Yoshio KAMIYA
Department of Reaction Chemistry, Faculty of Engineering, The University of Tokyo, Hongo, Bunkyo-ku, Tokyo 113
(Received December 1, 1981)

The photocycloaddition reaction of 6-substituted phenanthridines and electron-rich olefins, such as *trans*-anethole and phenyl vinyl ether, is described. This reaction proceeds from the $^1(\pi,\pi^*)$ states of 6-substituted phenanthridines *via* the exciplex to give azocine and/or azetidine derivatives in ethanol.

Photocycloaddition between multiple bonds seems to be common and many papers have been reported in this area.[1] However, the intermolecular photocycloaddition reactions of the carbon-nitrogen double bond are documented only for the cyclic imines, which are classified into two groups. One of them is the system where the carbon-nitrogen double bond is conjugated with the imino[2] or the carbonyl group,[3,4] while the other one is the system where a hetero atom, such as nitrogen,[4] oxygen,[5] and sulfur,[6] is attached to the imino linkage.

Our concern has been concentrated on the photochemical behavior of phenanthridine, and we have already reported its luminescence phenomena and photoesterification reaction.[7] Phenanthridine(**1**), which is isoelectronic to phenanthrene, can also be expected to undergo photocycloaddition reactions with olefins similar to phenanthrene derivatives.[8] We have probed the photochemical reactivity of **1** with olefins and wish now to present some novel photocycloaddition reactions of **1** with electron-rich olefins(**2a—c**).[9]

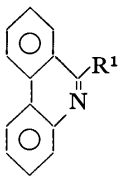

1a: $R^1=CH_3$
1b: $R^1=CN$

Experimental

Materials. **1a** and **1b** were synthesized according to the literature.[10,11] **1a**: mp 78.4—79.0 °C; NMR (δ) 7.46—8.51 (m, 8H), 2.94 (s, 3H); IR (cm^{-1}) 1615, 751, 720; UV (EtOH, nm) 254.5 (ε=36000), 329.6 (ε=3900), 344.5 (ε=3900). **1b**: mp 136—137 °C; NMR (δ) 7.57—8.82 (m, 8H); IR (cm^{-1}) 2220, 1608, 758, 722; UV (EtOH, nm) 257.0 (ε=28000), 351.2 (ε=2500), 367.9 (ε=2200).

Benzene was purified by the conventional method and was finally distilled. The following solvent and quenchers (reagent special grade) were used without further purification: ethanol, *N,N*-dimethylaniline, *trans*-anethole (**2a**), pyrrole, 1-methyl-pyrrole, triethylamine, β-methylstyrene, quinoline, 2,3-dimethyl-2-butene, furan, γ-picoline, *trans*-1,3-pentadiene, acrylonitrile, and pyridine.

The benzophenone and benzhydrol were recrystallized from hexane–benzene and ethanol respectively; benzophenone, mp 48.5—48.7 °C, benzhydrol, mp 68.9—69.2 °C.

cis-Anethole (**2b**) was prepared by Michler's ketone (10^{-2} M†)-sensitized isomerization of **2a** (10^{-1} M). The subsequent separation of **2b** from **2a** by column chromatography (silica gel, hexane) gave pure **2b** in a 50% yield. **2b**: colorless oil; NMR (δ) 1.86 (dd, 3H), 3.74 (s, 3H), 5.80 (m, 1H), 6.38 (dd, 1H), 6.82 (d, 2H), 7.25 (d, 2H); IR (cm^{-1}) 2870, 1609, 1510, 1250, 1178, 1038, 845.

Phenyl vinyl ether was synthesized according to the literature.[12] Its IR and NMR spectra were superimposable on those of an authentic sample.

Instrumental. The GC analyses were done on a Shimadzu GC-6A-FID apparatus equipped with a column of 5% OV 17 on chromosorb p. The products were analyzed on a Waters liquid chromatograph, Model 440, equipped with a column of μ-PORASIL. Photocycloadducts were also isolated by HPLC. The IR spectra were taken either on a JASCO Model IR-G Spectrophotometer or on a Shimadzu IR-420 Infrared Spectrophotometer. The NMR spectra were obtained either on a JEOL JNM-PMX (60 MHz) or on a Varian EM 360A NMR Spectrometer (60 MHz), using Me_4Si as the internal standard. The UV spectra were recorded on a JASCO NEW-UV-210A Digital Double-beam Spectrophotometer. The fluorescence and phosphorescence spectra were taken either on a Hitachi MPF 4A or on a Shimadzu RF-502A Fluorescence Spectrophotometer. The melting points were measured by means of a Yazawa Hot Plate and are uncorrected.

Irradiations. Irradiations on a preparative scale were carried out with Pyrex-filtered light from a 400-W high-pressure mercury lamp (Riko) under the continuous bubbling of nitrogen in an immersion apparatus at the temperature of running water. The samples for kinetic studies and the controlled experiments were irradiated using a merry-go-round mounted on an optical bench. The light source was a 200-W super-high-pressure mercury arc, and light at 366 nm was selected through a Shimadzu-Bausch-Lomb monochromator.

*Irradiations of **1** and **2**.* **1** (10^{-2} M) was irradiated in benzene or ethanol (200 ml) in the presence of **2** (10^{-1} M). The reaction mixtures were separated by means of column chromatography (Florisil, hexane–ether), and the products were purified by preparative HPLC. The products were identified by means of IR and NMR.

*Quenching of the Photocycloaddition Reaction of **1** to **2**.* A 10 ml ethanol solution of **1** (10^{-2} M) with **2** (10^{-1} M) was irradiated in the absence or presence of a quencher, such as acrylonitrile and *trans*-1,3-pentadiene (10^{-1} M). The reactions were then monitored by means of HPLC.

*Quantum Yield for the Formation of **3ba**.* Benzophenone-benzhydrol actinometry was used ($\lambda_{irrad.}$=366 nm).[13] The reactions were monitored by means of HPLC.

Results and Discussion

*Quenching of **1a** Fluorescence.* **1a** fluoresces only in hydroxyl solvents, such as ethanol and benzene–acetic acid.[7]

† 1 M=1 mol dm^{-3}.

Figure 1 shows that the **1a** fluorescence is attenuated by **2a** in ethanol, accompanied by the growing-in of a new emission at a longer wavelength. The **1a** fluorescence is also quenched by other electron-rich olefins and amines at almost the diffusion-controlled rate, and a new emission is observed similarly in the cases of triethylamine, pyrrole, 1-methylpyrrole, β-methylstyrene, and 2,3-dimethyl-2-butene. Figure 2 shows the correlation of the log k_q for **1a** with the ionization potential of the quencher(IP_Q).

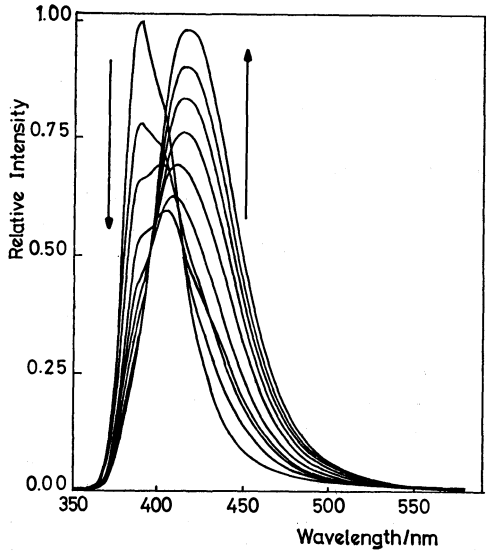

Fig. 1. Quenching of **1a** fluorescence by **2a** in ethanol at room temperature: concentration of **1a**=1.60×10^{-2} M, excitation wavelength=353.1 nm, K_{SV}=18.1 M^{-1}.

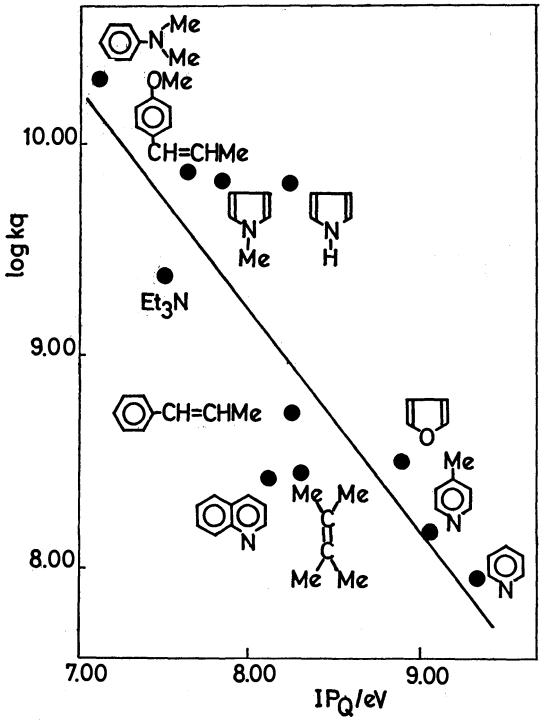

Fig. 2. Correlation of log k_q for **1a** with IP_Q; in EtOH under air, at room temperature.

The new emission is indicative of exciplex formation, and the good correlation of log k_q with IP_Q suggests that charge-transfer interaction is dominant in the above systems. Although it is generally accepted that exciplexes dissociate into radical ion pairs in a polar solvent and that exciplex emission is weak, in these cases a fairly strong exciplex emission is observed, even in a polar hydroxyl solvent.

*Photocycloaddition of **1a** with **2a** in Ethanol.* The azocine derivative **4aa** was afforded in a 56% yield, instead of the expected azetidine derivative, **3aa**. It is noteworthy that **5** was obtained in a 40% yield. **5** probably arises from the radical cation **2a**$^+$ *via* the *anti*-Markownikov addition of ethanol. This fact indirectly supports the exciplex formation, followed by its dissociation into radical ions.[14] In changing the solvent from ethanol to methanol or 2-propanol, the corresponding *anti*-Markownikov adducts were obtained. The yields were in the order of: methanol≅ethanol≧2-propanol. Although only 30% of the isomerization from **2a** to **2b** occurs on the direct irradiation of **2a**, 74% of the recovered anethole is *cis* in this reaction. It is known that exciplex formation often enhances intersystem crossing;[15] the observed fact suggests the presence of such a path for the collapse of the exciplex, which leads to the photoiso-

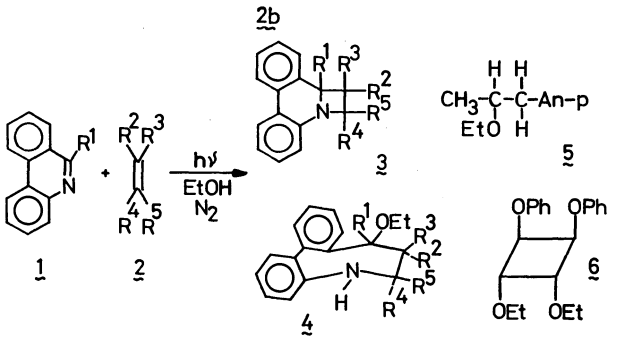

1a: R^1=CH$_3$ **2a**: R^2=*p*-Methoxyphenyl, R^3=R^4=H, R^5=CH$_3$
1b: R^1=CN **2b**: R^2=*p*-Methoxyphenyl, R^3=H, R^4=CH$_3$, R^5=H
2c: R^2=PhO, R^3=R^4=R^5=H

Scheme 1. Photochemical reactions of **1** with **2** in ethanol.

Table 1. Photocycloaddition reactions of **1** with **2** in ethanol

Substrate	Olefin	Irradiation time/h	Products (yield/%)
1a	**2a**	29	**2b** (37) **4aa** (56) **5** (40)
1a	**2b**	30	
1b	**2a**	5	**2b** (47) **3ba** (16) **4ba** (84)
1b	**2b**	6	
1b	**2c**	26	**4bc** (42) **6** (5)

merization from **2a** to **2b**.[16,17]

*Photocycloaddition of **1b** with **2a** in Ethanol.* **1b** reacted much faster than **1a** to give **3ba** and **4ba** in 16 and 84% yields respectively. The formation of both **3ba** and **4ba** greatly intrigued us as to the reaction course by which **4** is formed. In this reaction, 52% of the anethole was **2b**. However, no **5** was obtained.

*Photocycloaddition of **1** with **2b** in Ethanol.* As has been described above, no incorporation of **2b** into the photocycloadducts was observed, though a considerable amount of **2b** was accumulated after the photocycloaddition reaction of **1a** or **1b** with **2a**. Thus, **1a** or **1b** was irradiated in the presence of **2b**, but no photocycloadduct was obtained in either case. The unreactive nature of **2b** toward the excited state of **1** is ascribable to the following facts. (1) The non-emissive (**1**–**2b**) exciplex collapses to the ground states much faster than the (**1**–**2a**) exciplex, partly because of its instability caused by its less efficient resonance stabilization between the two molecules, and (2) the exciplex substitution might be occurring, as in the case of (9-cyanophenanthrene–**2b**) exciplex.[18] The quenching rate of S_1 of **1b** by **2b** ($k_q = 6.6 \times 10^9$ M^{-1} s^{-1}) is slower than the quenching by **2a** ($k_q = 1.7 \times 10^{10}$ M^{-1} s^{-1}), and the (**1b**–**2b**)* + **2a** → (**1b**–**2a**)* + **2b** reaction would be exothermic.

*Photocycloaddition of **1b** with **2c** in Ethanol.* **1b** was irradiated in the presence of **2c** to give **4bc** and **6** in 42 and 5% yields respectively. It has been reported that the radical cation of **2c** reacts with **2c** to give cyclobutane dimers,[19] but in our study no such compounds were obtained.

Table 2 summarizes the spectroscopic data of the products.

*Photocycloaddition of **1a** with **2a** in Benzene.* Even on the prolonged irradiation of **1a** and **2a** in benzene (99 h), no **3** was afforded, and **1** was recovered quantitatively, but a **2a** dimer[20] and **2b** were obtained in 49 and 32% yields respectively. These facts indicate that no photocycloaddition reaction between excited **1a** and **2a** proceeded.

*Photocycloaddition of **1b** with **2a** in Benzene.* A stereoisomeric mixture of **3** was obtained in a 52% yield on the irradiation of **1b** with **2a** in benzene for 1 h. The quantum yield for the formation of **3ba** was 0.04. This value is around a tenth as large as that for the formation of the cycloadduct between 9-cyanophenanthrene and **2a**.[18]

***3** as Precursor for **4**.* The irradiation of **3** in ethanol for 1 h gave **4** in a 50% yield, and its original stereochemistry was retained. This fact shows that **3** is the precursor for the formation of **4**.

Exciplex as Intermediate. Exciplexes have been postulated as intermediates in the photocycloaddition reactions of phenanthrene[21–23] or 9-cyanophenanthrene[18,24] by simultaneous observations of exciplex emission and photocycloadduct formation. Recently,

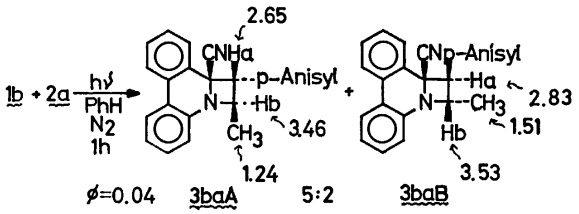

Scheme 3. Photocycloaddition reaction of **1b** with **2a** in benzene.

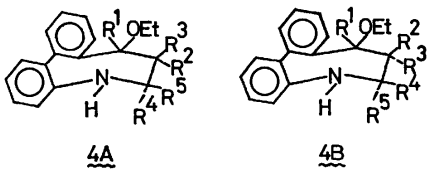

Scheme 2. Stereoisomers of **4**.

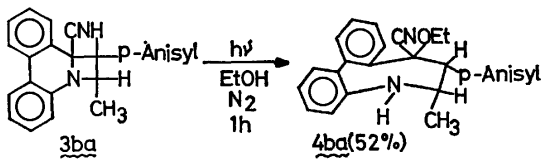

Scheme 4. Intermediacy of **3**.

TABLE 2. SPECTROSCOPIC DATA OF THE PRODUCTS

Compd	NMR δ								IR ν/cm⁻¹
	R^1	R^2	R^3	R^4	R^5	CH_3CH_2O	N–H	Aromatic H	
4aaA	1.29(s)	3.76(s) (CH_3O)	3.02(d)	2.02(dq)	1.21(d)	3.68(q) 1.28(t)	3.42(s)	6.50—8.57(m)	3350(N–H) 1176(C–O)
4baA		3.62(s) (CH_3O)	3.78(d)	3.37(dq)	1.21(d)	3.70(q) 1.05(t)	3.70(s)	7.10—8.59(m)	3340(N–H) 2250(C≡N)
4baB		3.62(s) (CH_3O)	3.81(d)	3.41(dq)	1.23(d)	3.70(q) 1.05(t)	3.70(s)	7.10—8.59(m)	3340(N–H) 2250(C≡N)
4bcA			5.12(dd)	4.47(d)	4.62(d)	3.36(q) 0.95(t)	3.39(s)	6.50—8.47(m)	3320(N–H) 2250(C≡N)
4bcB			5.24(dd)	4.17(d)	4.04(d)	3.36(q) 0.95(t)	3.39(s)	6.50—8.47(m)	3320(N–H) 2250(C≡N)
5	1.07(d, 3H), 1.08(t, 3H), 2.55(d, 1H), 2.67(d, 1H), 3.37(q, 2H), 3.39(dd, 1H), 3.69(s, 3H), 6.69(d, 2H), 7.00(d, 2H)								1175(C–O)
6	1.17(t, 6H), 3.50(q, 4H), 3.69(d, 2H), 3.97(d, 2H), 6.90—7.46(m, 10H)								1249(C–O) 1124(C–O)

Caldwell *et al.* have, by a kinetic study together with the spectroscopic evidence, established the exciplex as the intermediate in the photocycloaddition reaction of 9-cyanophenanthrene to **2a**.[18]

The (**1b**–**2a**) exciplex emission was quenched by acrylonitrile, which did not attenuate the **1b*** fluorescence. Acrylonitrile (10^{-1} M) also quenched the product formation in the photocycloaddition reaction of **1b** and **2a**, while the triplet quencher, *trans*-1,3-pentadiene did not suppress the formation of the photocycloadducts. These facts indicate that the singlet exciplex is the intermediate in this photocycloaddition reaction.

Stereochemistry of 3 and 4. LC analysis and NMR spectroscopy revealed that this photocycloaddition reaction proceeds regiospecifically, but that stereospecificity is low. **4b** was given as a mixture of the stereoisomers. The molar ratio of **A** to **B** is 4:3 in **4ba** and 8:5 in **4bc**. The less sterically hindered **A** predominated over **B**, and the above ratio reflects the ratio of **3**, which is the precursor of **4**. In fact, **3ba** was obtained as a mixture of the stereoisomers in a 5:2 (**3baA**: **3baB**) ratio in benzene. As Scheme 3 shows, the Hb proton of **3baA** appeared at a higher field than that of **3baB**. This is due to the diamagnetic anisotropy of the cyano group, which is *trans* to the Hb proton.[18b] The stereochemical assignment of **4** was based on the fact that the methyl protons(R^5) of the cycloadduct absorb at a magnetic field lower than 1 ppm.[25] This fact indicates that the methyl group (R^5) is *trans* to the aromatic ring.

The reason for the low stereospecificity even *via* the exciplex intermediate is not yet certain. We presume that the oriented structures of the exciplexes in these cases are not bound tightly; also the exciplexes may have two different structural orientations. The lack of any incorporation of **2b** into **3** or **4** suggests that the photodimerization from **2a** to **2b** competes with the photocycloaddition of **1** to **2a** and that the collapse of the exciplex to a biradical which gives a random stereoisomeric mixture of the adducts is unfavorable.

Solvent Effect. As Scheme 5 shows, a clear solvent effect is observed in this reaction. This may be ascribed to the different nature of the S_1 of **1** depending on the solvent. Table 3 clearly shows that the photocycloaddition reaction is governed by the nature of the S_1 of **1**. In ethanol, the emissive S_1 of **1** is of (π,π^*) and can undergo photocycloaddition with **2**. In benzene, the S_1 of **1a** is non-emissive, and its lifetime is considered to be shorter than in ethanol. The unreactive nature of **1a** in benzene may be ascribable to the (n,π^*) character of the S_1 of **1a**, whose short lifetime may be anticipated to be attributable to its non-emissiveness. That would be why **1a** is unreactive toward **2** in benzene. On the other hand, the S_1 of **1b** is of (π,π^*) even in benzene.[7] The simultaneous fluorescence emission and cycloadduct formation in this case support the above explanation.

Scheme 6 shows a plausible reaction scheme of the observed reaction.

In conclusion, we have found the novel photocycloaddition reaction of **1** with **2a** and **2c**. This reaction proceeds from the $^1(\pi,\pi^*)$ state of **1** to give **4** *via* **3**. The exciplex is considered to be the intermediate of **3**. The above reaction is affected by the solvent and by the structure of olefin.

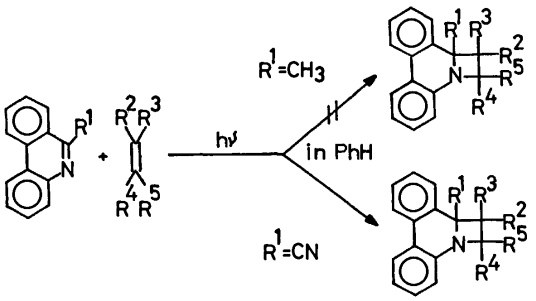

R^2=*p*-Methoxyphenyl, $R^3=R^4=H$, $R^5=CH_3$

Scheme 5. Solvent effect on photocycloaddition of **1** with **2a**.

Table 3. Solvent effect on the fluorescent state of **1**

	Fluorescence λ_{max}/nm	Excited state	Photocycloaddition
Benzene			
1a	Not observed	$^1(n,\pi^*)$	No
1b	401	$^1(\pi,\pi^*)$	Yes
Ethanol			
1a	388	$^1(\pi,\pi^*)$	Yes
1b	410	$^1(\pi,\pi^*)$	Yes

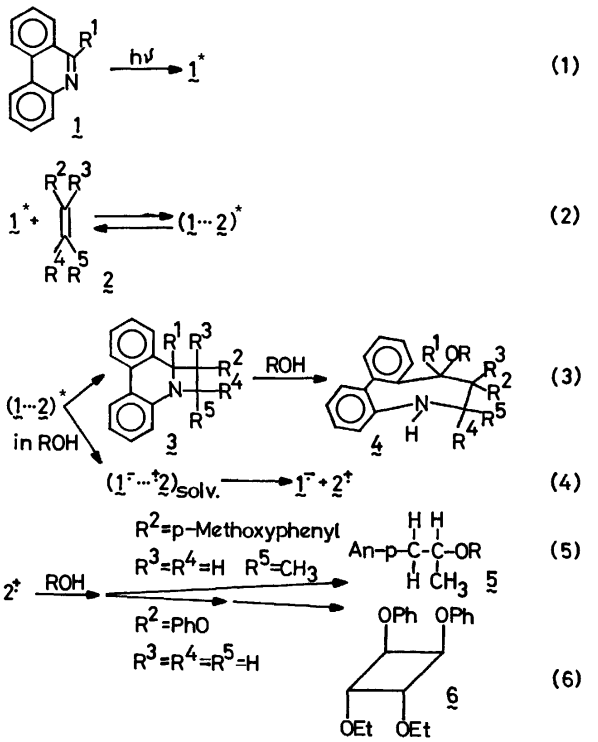

Scheme 6. Plausible reaction scheme.

References

1) N. J. Turro, "Modern Molecular Photochemistry," The Benjamin/Cummings Publishing Co., Menlo Park (1978), Chap. 11, pp. 414—472.

2) O. Tsuge, M. Tashiro, and K. Oe, *Tetrahedron Lett.*, **1968**, 3971; *Tetrahedron*, **29**, 41 (1973).

3) T. H. Koch and K. H. Howard, *Tetrahedron Lett.*, **1972**, 4035; D. R. Anderson, J. S. Keute, T. H. Koch, and R. H. Moseley, *J. Am. Chem. Soc.*, **99**, 6332 (1977).

4) J. A. Hyatt and J. S. Swenton, *J. Chem. Soc., Chem. Commun.*, **1972**, 1144; *J. Am. Chem. Soc.*, **96**, 4879 (1974).

5) Y. Kawamura, T. Kumagai, and T. Mukai, Symposium on Photochemistry, September 1981, Abstr., pp. 85—86.

6) M. S. -Kulyk and D. C. Neckers, *Tetrahedron Lett.*, **1981**, 2081.

7) S. Futamura, H. Ohta, and Y. Kamiya, *Tetrahedron Lett.*, **1979**, 4299.

8) R. A. Caldwell and D. Creed, *Acc. Chem. Res.*, **13**, 45 (1980), and the references cited therein.

9) Preliminary results have been published; see S. Futamura, H. Ohta, and Y. Kamiya, *Chem. Lett.*, **1980**, 655.

10) L. P. Walls, *J. Chem. Soc.*, **1945**, 294.

11) E. Hayashi and Y. Hotta, *Yakugaku Zasshi*, **80**, 834 (1960).

12) K. Mizuno, Y. Kimura, and Y. Otsuji, *Synthesis*, **1979**, 688.

13) S. L. Murov, "Handbook of Photochemistry," Marcel Dekker, New York (1973), pp. 125—126.

14) As to the *anti*-Markownikov addition of alcohol to olefin, see, for example R. A. Neunteufel and D. R. Arnold, *J. Am. Chem. Soc.*, **95**, 4080 (1973).

15) V. Breuninger and A. Weller, *Chem. Phys. Lett.*, **1973**, 40.

16) D. R. Arnold and D. C. Wong, *J. Am. Chem. Soc.*, **101**, 1894 (1979).

17) H. L. Roth and M. L. M. Schilling, *J. Am. Chem. Soc.*, **101**, 1898 (1979).

18) a) R. A. Caldwell and L. Smith, *J. Am. Chem. Soc.*, **96**, 2994 (1974); b) R. A. Caldwell, N. I. Ghali, C. -K. Chien, D. DeMarco, and L. Smith, *ibid.*, **100**, 2857 (1978).

19) K. Mizuno, J. Ogawa, M. Kamura, and Y. Otsuji, *Chem. Lett.*, **1979**, 731.

20) H. Nozaki, I. Otani, R. Noyori, and M. Kawanishi, *Tetrahedron*, **24**, 2183 (1968).

21) S. Farid, J. C. Doty, and J. L. R. Williams, *J. Chem. Soc., Chem. Commun.*, **1972**, 711; S. Farid, S. E. Hartman, J. C. Doty, and J. L. R. Williams, *J. Am. Chem. Soc.*, **97**, 3697 (1975).

22) R. A. Caldwell and D. Creed, *J. Am. Chem. Soc.*, **96**, 7369 (1974).

23) F. D. Lewis and C. E. Hoyle, *J. Am. Chem. Soc.*, **99**, 3779 (1977).

24) K. Mizuno, C. Pac, and H. Sakurai, *J. Am. Chem. Soc.*, **96**, 2993 (1974).

25) A. Gaudemer, "Stereochemistry," ed by H. B. Kagan, Georg Thieme Publishers, Stuttgart (1977), Vol. 1, pp. 83—89.

Applications of Homogeneous Water-gas Shift Reaction. IV. Hydrocarbonylation and Dimerization of Methyl Acrylate with CO and H_2O

Kazuhisa MURATA* and Akio MATSUDA

National Chemical Laboratory For Industry, Tsukuba Research Center, Yatabe, Tsukuba, Ibaraki 305

(Received December 2, 1981)

Hydrocarbonylation of methyl acrylate with CO and H_2O forms dimethyl 4-oxopimelate in 94% yield based on H_2O, the $Co_2(CO)_8$-1,2-bis(diphenylphosphino)ethane (diphos) catalyst system being used as in the case of ethylene or propylene. Increasing temperature tends to promote the dimerization and/or hydrodimerization of methyl acrylate to give 1,3-bis(methoxycarbonyl)-1-butene and/or dimethyl 2-methylglutarate. Effects of CO pressure and H_2O concentration on the hydrocarbonylation and dimerization were examined at 135 and 165 °C. Catalytically active intermediates for the hydrocarbonylation take part in the dimerization of methyl acrylate.

In connection with the synthesis of dialkyl 4-oxopimelate under oxo conditions using transition metal catalyst,[1] only one case is known, where a cobalt-catalyzed hydroesterification of methyl acrylate in the presence of pyridine produces the ketone as a minor product.[2]

Recently, we have described a homogeneous catalysis of hydrocarbonylation of ethylene or propylene with CO and H_2O where the $Co_2(CO)_8$–phosphine system is a catalyst precursor and symmetrical ketones are selectively produced.[3,4]

In the present paper, the applicability of this method to selective synthesis of dimethyl 4-oxopimelate from methyl acrylate is first tested, then an unexpected dimerization of the olefin under identical conditions is described, and finally a possible scheme effective for both hydrocarbonylation and dimerization is discussed in connection with catalytically active intermediates.

Experimental

Materials. Methyl acrylate, acrylonitrile, and H_2O were distilled before use. 1,2-Bis(diphenylphosphino)ethane (diphos) and the solvent were used without further purification. $Co_2(CO)_8$ was prepared by the conventional method.

Reaction Procedure. The hydrocarbonylation (dimerization) reaction was carried out in a 300 cm^3 stainless-steel autoclave. A reaction vessel containing $Co_2(CO)_8$, diphos, H_2O, substrate, and solvent was placed in the autoclave, and after sealing, CO was introduced. The vessel was kept heated with stirring at a reaction temperature for a certain period and then cooled down to room temperature. Liquid products formed were analyzed at 180 °C with a gas chromatograph equipped with an FID using a 4-m squalane column.

Results and Discussion

Typical Examples of Hydrocarbonylation with CO and H_2O. As shown in Table 1, dimethyl 4-oxopimelate[5] was formed in 94% yield based on H_2O when the reaction was carried out in dioxane with an initial CO pressure of 100 kg/cm^2 at 135 °C (Run 6). However, the yield drastically decreased as the methyl acrylate (MA): $Co_2(CO)_8$ ratio was decreased (Runs 4—6). The effectiveness of polar ether solvents for increasing the yield is in the order dioxane > 1,2-dimethoxyethane > THF (Runs 1—3). The use of H_2 as hydrogen donor resulted also in decrease in the yield and methyl 4-oxobutyrate was predominantly produced (Runs 7 and 8). These features of catalytic

$$2CH_2{=}CH\text{-}COOMe + 2CO + H_2O \longrightarrow CO(CH_2CH_2COOMe)_2 + CO_2 \quad (1)$$

behavior are similar to those observed for the hydrocarbonylation of ethylene[3] or propylene.[4] No detectable amounts of other isomers (n-to-iso or iso-to-iso ketone) were formed under these condition. Hydrogenation of MA to methyl propionate occurred (see Table 1, last column). Thus, the $Co_2(CO)_8$–diphos

$$CH_2{=}CH\text{-}COOMe + 2CO + H_2O \longrightarrow OHC\text{-}CH_2CH_2COOMe + CO_2 \quad (2)$$

complex, which is effective for the hydrocarbonylation of ethylene or propylene, was also found to be an active and selective catalyst for the reaction of MA with CO and H_2O to give dimethyl 4-oxopimelate.

$$CH_2{=}CH\text{-}COOMe + CO + H_2O \longrightarrow CH_3CH_2COOMe + CO_2 \quad (3)$$

It has been found that under the conditions employed, dimerization and/or hydrodimerization[6] of MA occur to give 1,3-bis(methoxycarbonyl)-1-butene (unsaturated head-to-tail dimer, UD) and dimethyl 2-methylglutarate (saturated dimer, SD) as identified by ^{13}C NMR and IR spectal analysis,[7] whereas no trace of dimethyl adipate (saturated head-to-head dimer) is formed; thus this is the first example of cobalt-catalyzed dimerization of MA with CO and H_2O.

$$2CH_2{=}CHCOOMe \longrightarrow CH_3CH(COOMe)CH{=}CHCOOMe \quad (4)$$

$$2CH_2{=}CHCOOMe + CO + H_2O \longrightarrow CH_3CH(COOMe)CH_2CH_2COOMe + CO_2 \quad (5)$$

Effect of Temperature. Effects of reaction parameters on product yields were examined by allowing the reaction of MA with $Co_2(CO)_8$ in a 100:2 molar ratio to proceed in dioxane for 4 h using the $Co_2(CO)_8$–diphos catalyst system.

Temperature dependence at 100 kg/cm^2 CO pressure is illustrated in Fig. 1. The yield of dimethyl 4-oxopimelate increased with an increase in tempera-

TABLE 1. HYDROCARBONYLATION OF METHYL ACRYLATE USING CO AND H_2O CATALYZED BY $Co_2(CO)_8$-DIPHOS SYSTEM

$Co_2(CO)_8$ 2 mmol, diphos 1.5 mmol, solvent 50 ml, temp 135 °C, time 10 h, and H_2O 35 mmol.

Run	MA (mmol)	Solvent	P_{CO}/kg cm^{-2}	Yield/mmol[a]				
				DP/%[b]	UD	SD	AD	MP
1	100	THF	70	22.6 (64.5)	1.44	0.1	0.15	—
2	100	1.2-Dimethoxy-ethane	70	24.9 (71.2)	1.71	0.12	0.23	—
3	100	Dioxane	70	29.6 (84.6)	1.1	0.16	0.08	<0.1
4	60	Dioxane	100	12.4 (35.4)	1.0	0.18	0.1	—
5	100	Dioxane	100	31.5 (90.0)	1.2	0.18	0.15	<0.1
6	150	Dioxane	100	32.7 (93.5)	1.3	0.20	0.20	0.15
7[c]	100	Dioxane	70	7.3 (20.8)	0.62	1.1	4.7	—
8[c]	100	Dioxane	70	7.7 (22.0)	—	0.9	10.6	—

a) Abbreviations DP, UD, SD, AD, and MP stand for dimethyl 4-oxopimelate, 1,3-bis(methoxycarbonyl)-1-butene, dimethyl 2-methylglutarate, methyl 4-oxobutyrate, and methyl propionate, respectively. b) Based on H_2O (35 mmol). c) H_2 35 mmol, time 4 h, temp 135 °C (Run 7), and 120 °C (Run 8).

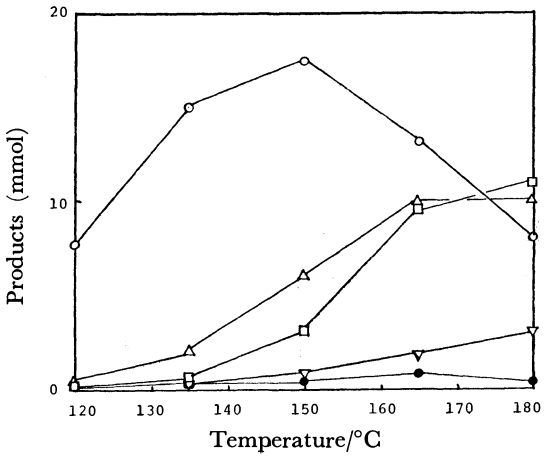

Fig. 1. Effect of temperature.
$Co_2(CO)_8$ 2 mmol, diphos 1.5 mmol, H_2O 35 mmol, dioxane 50 ml, CO 100 kg/cm² (initial), methyl acrylate 100 mmol, time 4 h. —○—: Dimethyl 4-oxopimelate, —△—: 1,3-bis(methoxycarbonyl)-1-butene, —▽—: methyl 2-methylglutarate, —□—: methyl propionate, —●—: methyl 4-oxobutyrate.

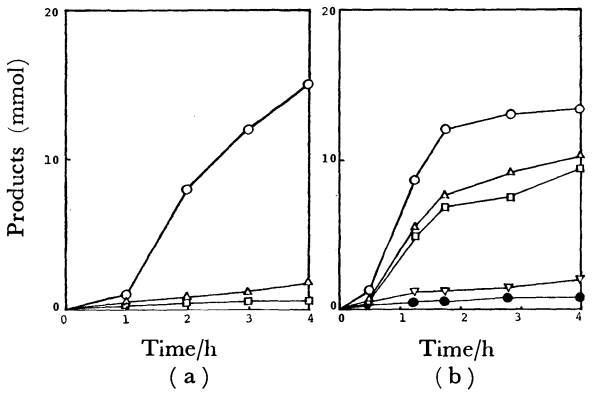

Fig. 2. Cobalt catalyzed hydrocarbonylation and dimerization as a function of time.
(a): 135 °C, (b): 165 °C. $Co_2(CO)_8$ 2 mmol, diphos 1.5 mmol, H_2O 35 mmol, dioxane 50 ml, CO 70 kg/cm², methyl acrylate 100 mmol. Marks (○, △, ▽, □, ●): See footnote of Fig. 1.

ture between 120 and 150 °C but decreased thereafter. Considerable amounts of dimers UD and SD as well as methyl propionate were formed at high reaction temperature. In order to examine catalytic properties of dimerization as well as hydrocarbonylation, two reaction temperatures 135 and 165 °C were adopted for varying parameters such as time course, P_{CO}, and P_{H_2O} in the experiments to be described below.

Time Course of Product Formation. As shown in Fig. 2, there was an induction period, similar in trend to those observed for the hydrocarbonylation of ethylene[3] and propylene.[4] Two dimers UD and SD were also formed with the same induction period with the ketone.

Effect of CO Pressure. As illustrated in Fig. 3a (135 °C), the yield of dimethyl 4-oxopimelate is slightyl dependent on CO pressure over the range from 50 to 130 kg/cm². Lowering the pressure reduces the yield because it induces partial decomposition of $Co_2(CO)_8$. At 165 °C, the yield incerased with the increase in CO pressure (Fig. 3b). On the contrary, yields of the two dimers UD and SD as well as methyl propionate decreased with the increase in CO pressure (Fig. 3b).

Effect of H_2O Concentration. The results are shown in Fig. 4a; the yield of the ketone increased with in-

creasing H_2O concentration in the range 30—180 mmol but leveled off thereafter. At 165 °C, the yield increased initially as the H_2O concentration increased from 10 to 60 mmol, but a further increase in H_2O concentration resulted in decrease in the yield (Fig. 4b). The formation of dimer UD showed a H_2O dependence similar to that of the ketone formation, while the formation of dimer SD was steadily accelerated with increase in H_2O concentration. The hydrogenation of MA to methyl propionate was favored at higher H_2O concentrations.

Catalytically Active Intermediates and a Possible Reaction Scheme. Since the hydrocarbonylation of MA with CO and H_2O selectively produces dimethyl 4-oxopimelate (Table 1), catalytically active intermediates responsible for this reaction may be $HCo(CO)_m(diphos)_n$, as in the case of ethylene[3] and propylene.[4] In fact, induction period was observed for the reaction (Fig. 2) and their catalytic characteristics are similar, especially at 135 °C (Figs. 1a, 3a, and 4a).

Dimerization and/or hydrodimerization, by which dimers UD and/or SD were produced from MA, occurred under the conditions described above (Table 1). It seems likely that the intermediates $HCo(CO)_m$-$(diphos)_n$ catalyze the hydrocarbonylation as well as the dimerization. In fact, there was an induction period for the formation of two dimers UD and SD (Fig. 2). Also, a support for the contention was furnished by an experiment in which a catalyst solution, consisting of $Co_2(CO)_8$, diphos, H_2O, and dioxane, and active in the water-gas shift reaction, was prepared at 165 °C[8] and, in the absence of gaseous CO, a stoichiometric reaction of the solution with MA occurred even at room temperature to give both dimethyl 4-oxopimelate and the two dimers UD and

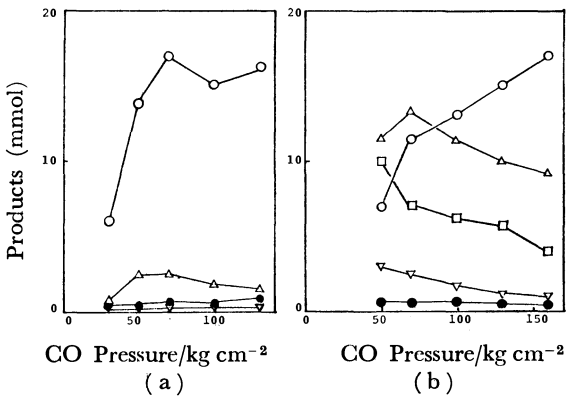

Fig. 3. Effect of CO pressure.
(a): 135 °C, (b): 165 °C. $Co_2(CO)_8$ 2 mmol, diphos 1.5 mmol, H_2O 35 mmol, dioxane 50 ml, methyl acrylate 100 mmol, time 4 h. Marks: See footnote of Fig. 1.

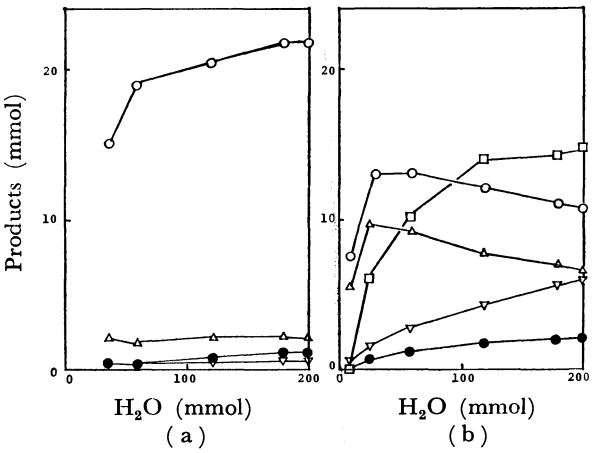

Fig. 4. Effect of H_2O concentration.
(a): 135 °C, (b): 165 °C. $Co_2(CO)_8$ 2 mmol, diphos 1.5 mmol, CO 70 kg/cm² (initial), dioxane 50 ml, methyl acrylate 100 mmol, time 4 h. Marks: See footnote of Fig. 1.

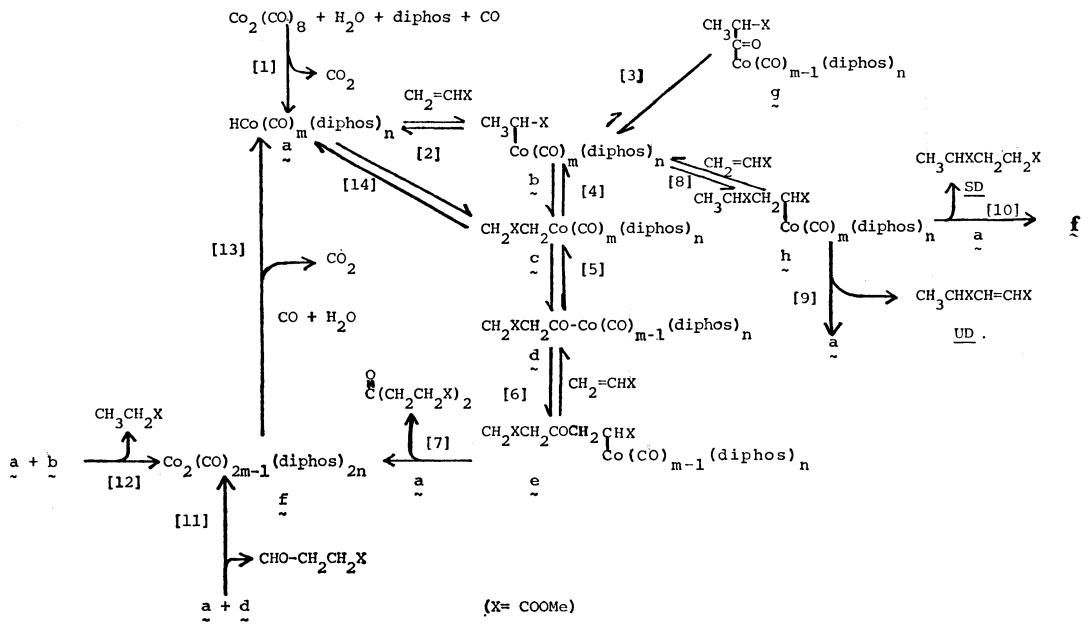

Scheme 1. A possible reaction scheme of the hydrocarbonylation and dimerization of methyl acrylate with CO and H_2O.

TABLE 2. HYDROCARBONYLATION OF ACRYLONITRILE BY $Co_2(CO)_8$-DIPHOS COMPLEX
$Co_2(CO)_8$ 2 mmol, diphos 1.5 mmol, CO 100 kg/cm²(initial), acrylonitrile 100 mmol, H_2O 35 mmol, and time 5 h.

Run	Temp °C	Ketone[a](mmol)			Propionitrile (mmol)	Aldehyde[b](mmol)	
		n-to-n	n-to-iso	iso-to-iso		n	iso
1	135	0.77	2.5	1.2	28.1	—	0.20
2	165	0.70	3.7	0.30	27.8	—	0.30

a) 4-Oxopimelonitrile (n-to-n), 2-methyl 3-oxoadiponitrile (n-to-iso), and 2,4-dimethyl 3-oxoglutaronitrile (iso-to-iso). b) 4-Oxobutyronitrile (n) and 2-methyl-3-oxopropionitrile (iso).

SD.[9,10]

Considering the scheme previously mentioned for the hydrocarbonylation of ethylene,[3] a possible scheme is proposed as Scheme 1, where [2- and 1-(methoxycarbonyl)ethyl]cobalt complexes **c** and **b**,[11] formed by the reaction of $HCo(CO)_m(diphos)_n$ with MA followed by hydride addition, are assumed to be other key imtermediates for the production of the ketone and two dimers; unlike the hydrocarbonylation of ethylene, CO insertion into **b** to yield [2-(methoxycarbonyl)-propionyl]cobalt complex, **g**, would occur very slightly because **g** is a β-dicarbonyl-type complex which is thermally unstable.[12] This is in agreement with the absence of n-to-iso or iso-to-iso ketone as well as methyl 2-methyl-3-oxopropionate (Table 1). At low reaction temperatures, a direct formation of **c** (step [14]) would predominantly occur because the higher selectivity for the ketone is achieved in 135 °C reactions (Table 1);[13] rapid CO insertion followed by MA addition to **d** gives complex **e** and the reaction of **a** with **e** forms dimethyl 4-oxopimelate (Table 1).[14]

Further addition of MA to [1-(methoxycarbonyl)-ethyl]cobalt complex **b** gives [1,3-bis(methoxycarbonyl)butyl]cobalt complex **h**, which undergoes β-elimination to yield 1,3-bis(methoxycarbonyl)-1-butene (dimer UD) and cobalt hydride complex **a**. The reaction of complex **h** with **a** affords dimethyl 2-methylglutarate (dimer SD) and dimeric cobalt complex **f**. Since there was no detectable amount of dimethyl adipate, CO insertion into [2-(methoxycarbonyl)ethyl]-cobalt complex **c** would be rapid and smooth.[15]

Steps [11] and [12] account for the formation of methyl 4-oxo butyrate and methyl propionate, respectively. The resulting complex **f** is converted into **a** by the water-gas shift reaction pathway [13] again, as described in the preceding paper.[3]

To obtain additional information about the catalytically active intermediate **b**, hydrocarbonylation of acrylonitrile was carried out under the same conditions with MA.

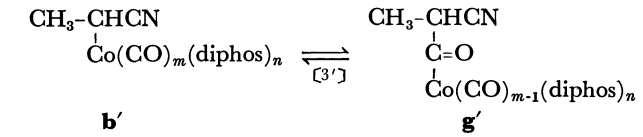

b' **g'**

In this case, we expect that CO insertion into (1-cyanoethyl)cobalt complex **b'** (step [3']) can occur to give (2-cyanopropionyl)cobalt complex **g'** and successively give n-to-iso and/or iso-to-iso ketones as well as n-to-n ketone. Satisfactory data are shown in Table 2, through a considerable amount of propionitrile was formed. It is worth noting that there were no detectable amounts of such dimers as 1,3-dicyano-1-butene and 2-methyl glutaronitrile.

Some attempts were tried in vain to isolate complexes **b** and **c** and identify them spectroscopically. Therefore, Scheme 1 needs to be considered as one of some probable schemes for the hydrocarbonylation and dimerization of methyl acrylate with CO and H_2O.

References

1) I. Wender and P. Pino, "Organic Synthesis *via* Metal Carbonyl," Wiley, New York (1977), Vol. 2; J. Falbe, "New Syntheses with Carbon Monoxide," Springer, New York (1980).

2) A. Matsuda, *Bull. Chem. Soc. Jpn.*, **42**, 571 (1969).

3) K. Murata and A. Matsuda, *Bull. Chem. Soc. Jpn.*, **54**, 2089 (1981).

4) K. Murata and A. Matsuda, *Bull. Chem. Soc. Jpn.*, **54**, 245 (1981); *Chem. Lett.*, **1980**, 11.

5) Satisfactory spectral data were obtained.

6) H. Kanai and K. Ishii, *Bull. Chem. Soc. Jpn.*, **54**, 1015 (1981).

7) Spectral data were as follows. UD: ^{13}C NMR (C_6D_6) δ=12.5, 33.8, 51.5, 51.6, 130.5, 133.4, 167.5, and 170.5; IR 1650 (C=C), 1715 and 1740 cm^{-1} (C=O); SD: ^{13}C NMR (C_6D_6) δ=16.8, 28.8, 31.6, 38.7, 51.1, 173, and 175.9; IR 1730 cm^{-1} (C=O).

8) The preparation was described in detail in the preceding paper.[3]

9) A trace amount of methyl 4-oxobutyrate was also detected.

10) No dimerization occurred in the presence of diphos without $Co_2(CO)_8$.

11) It has already been reported that a hydride $HCo(dmg)_2P(n\text{-}C_4H_9)_3$ (dmg=dimethylglyoximato) reacts with MA to yield [1-(methoxycarbonyl)ethyl]cobaloxime derivatives,[a] while the 2-(methoxycarbonyl)ethyl isomers are formed the protonation of the cobaloxime(I)–olefin π-complex.[b] a) G. N. Schrauzer and R. J. Holland, *J. Am. Chem. Soc.*, **93**, 1505 (1971); b) G. N. Schrauzer, *Angew. Chem.*, **88**, 465 (1976); G. N. Schrauzer, J. H. Weber, and T. M. Beckham, *J. Am. Chem. Soc.*, **92**, 7078 (1970):

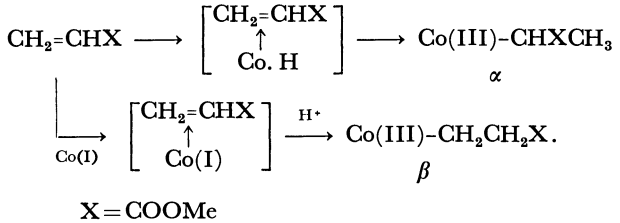

12) I. Ogata and T. Asakawa, *Kogyo Kagaku Zasshi*, **74**, 1640 (1971).

13) The isomerization of **c** to **b** ([4]) and the successive MA addition ([8]) would considerably occur as temperature rises; this may be responsible partially for the fact that higher temperatures favor the formation of two dimers UD and SD (Fig. 1).

14) There is an alternative route: acyl complex **d** reacts with alkyl complex **c** to yield the ketone and dimeric cobalt complex **f**.

15) MA addition to **c** to give [1,4-bis(methoxycarbonyl)-butyl]cobalt complex **h'** may not be ruled out:

$$\underset{\mathbf{c}}{CH_2XCH_2Co(CO)_m(diphos)_n} \underset{CH_2=CHX}{\rightleftharpoons} \underset{\mathbf{h'}}{CH_2XCH_2CH_2CHXCo(CO)_m(diphos)_n}.$$

However, this step would occur to a lesser extent, because no traces of 1,4-bis(methoxycarbonyl)-1-butene or dimethyl adipate were detected.

Kinetics and Mechanism of Decompositions of *N*-Methyl-*N'*-aryl-*N*-nitrosoureas and Related Compounds in Aqueous Buffer Solution

Kitaro YOSHIDA* and Kazuyuki YANO

Department of Chemistry, Saitama Medical School, 981 Kawakado, Moroyama, Iruma-gun, Saitama 350-04

(Received December 4, 1981)

The decomposition reactions of *N*-methyl-*N'*-aryl-*N*-nitrosoureas (**1**) and of *N,N'*-dimethyl-*N'*-aryl-*N*-nitrosoureas (**2**) were studied kinetically in phosphate buffer solution. All nitrosoureas **1** were easily hydrolyzed even under neutral conditions and the rates of hydrolysis were found to be proportional to the hydroxide ion concentration over pH range 5.4—7.6. General base catalysis by buffer components was negligible. The reaction was subjected to the elimination mechanism in which an abstraction of the ureido proton was involved as an initial step. On the other hand, nitrosoureas **2** had no significant reactivity under the same conditions.

N-alkyl-*N*-nitrosoureas are unstable and are readily hydrolyzed to produce alkanediazohydroxides, which are thought to be active alkylating agents toward genetic material in biological systems.[1] The simplest member of this class of compounds is *N*-methyl-*N*-nitrosourea (MNU). This is known to act as a powerful carcinogen and mutagen without need of enzymatic hydroxylation and its chemical and biological aspects have been well documented.[2]

In earlier work, we synthesized two families of substituted MNU, namely, *N*-methyl-*N'*-aryl-*N*-nitrosoureas (**1a—1c**, **1e**, **1g**) and *N,N'*-dimethyl-*N'*-aryl-*N*-nitrosoureas (**2**), and their mutagenic activities on *S. Typhimurium* TA 1535 were investigated.[3] All *N'*-monosubstituted derivatives (**1**) exhibited the higher mutagenisity than that of MNU, whereas no respectable activity was found for *N',N'*-disubstituted ones (**2**). The study showed that the presence of the proton on *N'* is significant to the mutagenic activity and also that this activity is influenced by the electronic effect of the para substituent X on the phenyl group. The structural and electrostatic natures of these nitrosoureas are thus important factors that govern their biological efficiency. However, the mode of decomposition as well as the intrinsic stability under physiological conditions have been left unclear. Therefore, we undertook a systematic degradation study of these nitrosoureas in neutral aqueous solution and elucidated their hydrolytic mechanism.

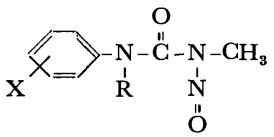

	X	R
1a:	*p*-OCH_3	H
1b:	*p*-CH_3	H
1c:	H	H
1d:	*m*-OCH_3	H
1e:	*p*-Cl	H
1f:	*m*-Cl	H
1g:	*p*-$COCH_3$	H
2a:	H	CH_3
2b:	*p*-NO_2	CH_3

Results and Discussion

The decomposition reactions of **1** and **2** were conducted in 0.1 M (1 M=1 mol dm^{-3}) phosphate buffer solution at constant ionic strength. The reaction was followed by monitoring the decrease of UV absorption of the substrate. The observed pseudo-first order rate constants (k) at pH 6.95 are summarized in Table 1.

Table 1 indicates the following features: (a) All *N'*-monosubstituted derivatives (**1**) that contain the labile proton on *N'* were rapidly decomposed even under neutral conditions ($t_{1/2}$=7—19 min at 36.8 °C). On the contrary, *N',N'*-disubstituted derivatives (**2**) in which the proton was replaced by methyl group were markedly stable up to pH 7.6 (see Experimental).

Table 1. The kinetic data of **1** and **2** at pH 6.95[a]

Nitrosourea[b]	Temp/°C	$10^4 \times k/s^{-1}$ [c]	ΔH^*/kcal mol^{-1}	ΔS^*/eu
1a	25.2	1.01±0.01		
	36.8	6.15±0.10	27.3±0.1	14.9±0.4
1b	25.2	1.05±0.02		
	36.8	6.76±0.04	29.5±0.3	22.0±0.7
1c	25.2	1.34±0.01		
	36.8	8.17±0.02	28.0±0.3	17.6±1.0
1d	25.2	1.51±0.07		
	36.8	9.55±0.08	28.6±0.2	19.8±0.5
1e	36.8	12.30±0.10		
1f	25.2	2.31±0.06		
	36.8	14.80±0.08	28.7±0.9	21.2±2.9
1g	25.2	2.63±0.11		
2a	36.8	Unreacted		
2b	36.8	Unreacted		

a) 0.1 M phosphate buffer, μ=0.222. b) (1.2—1.6)×10^{-4} M. c) Average of two runs.

Table 2. The pseudo-first order rate constants ($10^4 \times k/s^{-1}$) of **1** under various pH conditions (36.8 °C)

Nitrosourea[a]	pH[b]					
	5.40	5.82	6.29	6.72	7.20	7.60
1a	0.259	0.641	1.75	4.65	12.0	29.4
1b	0.263		1.83	4.91		30.4
1c	0.343	0.895	2.46	5.78	17.0	38.1
1d	0.410		2.85	7.13		47.0
1e	0.469	1.08	3.25	8.37		58.4
1f	0.583		3.73	10.2		73.0
1g	0.690			12.1	34.0	

a) $(1.2—1.6)\times 10^{-4}$ M. b) 0.1 M phosphate buffer, $\mu=0.5$.

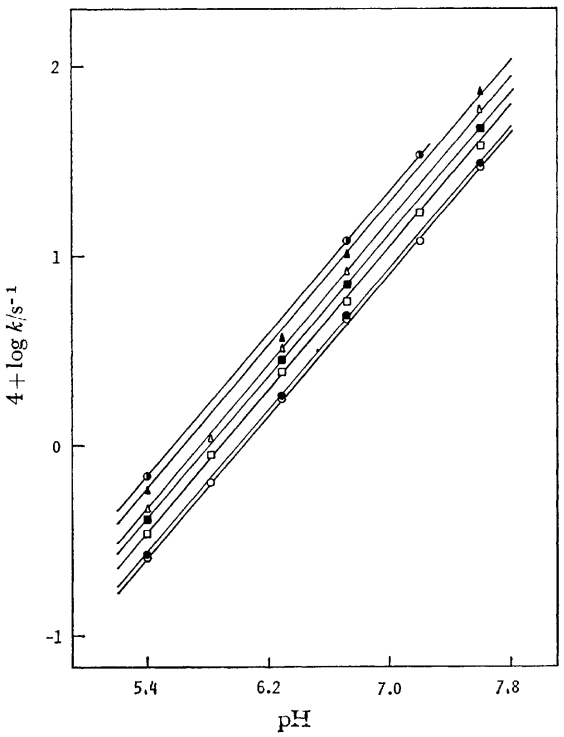

Fig. 1. pH-rate profiles for **1** at 36.8 °C (see Table 2).
○: **1a**, ●: **1b**, □: **1c**: ■: **1d**, △: **1e**, ▲: **1f**, ◑: **1g**.

This blocking effect by *N'*-methyl substituent under chemical hydrolytic conditions appears to be correlated with our previous finding in the mutagenic study.[3] (b) The decomposition rates within the series of **1** were in order of the substituent effect of X. Plot of log k against σ gave a positive slope ($\rho=0.65$, $r=0.991$,[4] 36.8 °C) which indicates that decreasing in the electron density at nitrogen atom (*N'*) results in increasing the decomposition rate of **1**.

It is clearly shown that the decomposition rate of every nitrosourea **1** depends on the hydroxide ion concentration (Table 2). The pH-rate profile exhibited positive slopes of exactly 0.94±0.02 over pH range 5.4—7.6 (Fig. 1). This indicates that the reaction can be described in a first order with respect to the hydroxide ion term.[5] Further, changing the buffer concentration at constant pH gave little effect on the observed rate (Table 3). Therefore, general base catalysis by hydrogenphosphate dianion is negligible in comparison with the specific base catalysis.[5]

Table 3. The effect of buffer concentration on the decomposition rate of **1c** at pH 6.72 (36.8 °C)[a]

$[HPO_4^{2-}]$/M	$10^4 \times k/s^{-1}$
0.003	5.25
0.015	5.45
0.031	5.60
0.061	5.78
0.122	6.79

a) **1c** $=1.64\times 10^{-4}$ M, $\mu=0.5$.

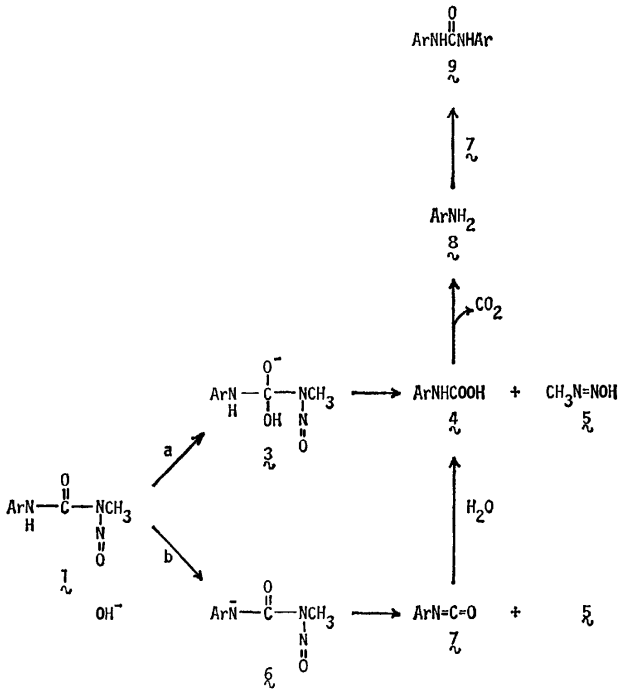

On the basis of these kinetic results, two possible mechanisms could be proposed to the aqueous decomposition of **1** as shown in the above scheme. One involves hydroxide ion attack on the carbonyl carbon of **1** to form tetrahedral intermediate **3** (or *via* direct S_N2 displacement), followed by the decomposition of **3** to give arylcarbamic acid **4** and methanediazohydroxide **5** ($B_{AC}2$ type mechanism, path a). The other involves an initial abstraction of the ureido proton by hydroxide ion to produce anion **6** which

releases aryl isocyanate **7** and **5** (E1cB type mechanism, path b). The aryl isocyanate is very reactive in water.[6] Accordingly, **4** may be formed again with this reaction mechanism. Thus, both types of mechanism can represent the same set of products.

The only different feature that distinguishes these two mechanisms is the presence of aryl isocyanate intermediate **7** along the reaction path b. Although **7** is not isolable from aqueous solution, this can be effectively trapped by aniline **8**[6a,7] which is formed from **4**. Degradation of **1c** in 0.1 M phosphate buffer under several pH conditions yielded *N,N'*-diphenylurea **9** as a major product. Undoubtedly, this is a striking evidence of the formation of the aryl isocyanate in the course of the reaction, indicating the occurrence of path b.

Generally, Arrhenius parameters are used to distinguish E1cB from $B_{AC}2$, where the former should show a considerably more positive entropy of activation than the latter.[8] The entropies of activation of **1** were 15—22 e.u. (see Table 1). There was no discernible difference in the kinetic behavior of each compound. Such a value is too large to be assigned to $B_{AC}2$ mechanism.[8b,8c] Consequently, the E1cB pathway is favored. Further, the effect of substituent X on the decomposition rate is relatively small ($\rho=0.65$), showing a close similarity to that reported for the ester hydrolysis involving an isocyanate intermediate ($XC_6H_4NHCOOC_6H_5$, $\rho=0.64$).[9]

Thus, the experimental results listed above are consistent with an interpretation that nitrosoureas **1** first react by the abstraction of the α proton to produce anion **6** and that the nucleophilic attack to the carbonyl group is excluded as possible mechanism. The presence of the isocyanate intermediate during the reaction of **1** may be of interest from the viewpoint of their carbamoylating abilities toward many nucleophiles in cellular environment.[10]

Snyder and Stock reported the aqueous decomposition of *N,N'*-dimethyl-*N*-nitrosourea (DMNU) in basic solution.[2d] This aliphatic nitrosourea represented evidence that the key reaction occurred with carbonyl group as a reaction site. In our neutral conditions, DMNU showed much lower reactivity ($k=6.40\times10^{-6}$ s^{-1}, pH 6.95, $\mu=0.222$, 36.8 °C) than those of **1**. The great increase of the decomposition rate from the aliphatic compound to the aromatic ones ($k_{1c}/k_{DMNU}=128$) can be interpreted in terms of the inductive effect of the aryl group of **1**.[11] The electron-withdrawing effect of the aryl substituent might more stabilize the negative charge on nitrogen (*N'*) and this facilitates the elimination process of **1**.

Our present observation provides the fact that, as in the cases of other reported alkylnitrosoureas,[1d,2d,5] the aqueous decomposition rate of **1** thoroughly depends on the hydroxide ion concentration around neutral pH. Owing to the absence of a labile proton on *N'*, disubstituted derivatives **2** are inert under neutral conditions. This stability of **2** in chemical process appears to limit their mutagenic potency.

Experimental

All melting points were uncorrected. IR spectra were recorded on a Shimadzu IR 400 spectrometer and UV spectra with a Shimadzu UV 200 spectrometer. NMR spectra were taken in acetone-d_6 solutions using a Hitachi R-24 (60 MHz) instrument and chemical shifts are given in δ with TMS as an internal standard. Microanalyses were performed in the microanalytical laboratory of the Institute of Physical and Chemical Research, Wako-shi, Saitama. pH was measured with a Toa-denpa HM-5A pH meter. Doubly distilled water was used for kinetics and buffer reagents were of commercial special grade.

N-Methyl-*N'*-arylureas were synthesized by the condensation reactions[12] of *p*- or *m*-substituted anilines with methyl isocyanate in quantitative yield. *N,N'*-Dimethyl-*N'*-arylureas were prepared from corresponding *N*-methylanilines. The ureas were purified by recrystallization from acetone and were used for subsequent nitrosation reactions. A typical procedure of the nitrosation was as follows.

*N-Methyl-N'-(p-methoxyphenyl)-N-nitrosourea (**1a**)*: To a stirred solution of *N*-methyl-*N'*-(*p*-methoxyphenyl)urea (900 mg, 5 mmol) in acetic acid (10 ml) and acetic anhydride (50 ml) was added sodium nitrite (518 mg, 7.5 mmol) in small portions at 0 °C. The resulting solution was allowed to stand in a refrigerator overnight. The mixture was poured onto ice and extracted with ether three times. The etheral solution was washed with cold 5% sodium hydrogencarbonate solution, dried ($MgSO_4$), and evaporated to give crude product, which was recrystallized from ether–hexane to yield **1a** (355 mg, 34%): mp 97.0—98.0 °C (decomp). IR (KBr): 3350 (NH), 1705 (C=O), 1470 (N=O) cm^{-1}. NMR: 3.21 (s, 3H, CH_3), 3.80 (s, 3H, OCH_3), 6.95 and 7.66 (2d, A_2B_2, $J=9$ Hz, 4H, C_6H_4), 9.59 (broad, 1H, NH). Found: C, 51.35; H, 5.27; N, 20.27%. Calcd for $C_9H_{11}O_3N_3$: C, 51.67; H, 5.30; N, 20.09%.

1b (44%): mp 102—103 °C (decomp). IR (KBr): 3310, 1720, 1460 cm^{-1}. NMR: 2.34 (s, 3H, CH_3), 3.19 (s, 3H, CH_3), 7.16 and 7.64 (2d, A_2B_2, $J=9$ Hz, 4H, C_6H_4), 9.67 (broad, 1H, NH). Found: C, 55.86; H, 5.74; N, 21.81%. Calcd for $C_9H_{11}O_2N_3$: C, 55.95; H, 5.74; N, 21.75%.

1c (52%): mp 83—84 °C (decomp) (lit,[13] 83—85 °C). IR (KBr): 3310, 1645, 1490 cm^{-1}. NMR: 3.19 (s, 3H, CH_3), 7.03—7.88 (m, 5H, C_6H_5), 9.69 (broad, 1H, NH). Found: C, 53.44; H, 5.07; N, 23.42%. Calcd for $C_8H_9O_2N_3$: C, 53.63; H, 5.06; N, 23.45%.

1d (55%): mp 98.0—98.5 °C (decomp). IR (KBr): 3330, 1730, 1460 cm^{-1}. NMR: 3.17 (s, 3H, CH_3), 3.75 (s, 3H, OCH_3), 6.56—7.74 (m, 4H, C_6H_4), 9.60 (broad, 1H, NH). Found: C, 51.52; H, 5.26; N, 20.22%. Calcd for $C_9H_{11}O_3N_3$: C, 51.67; H, 5.30; N, 20.09%.

1e (56%): mp 110—111 °C (decomp). IR (KBr): 3340, 1715, 1490 cm^{-1}. NMR: 3.16 (s, 3H, CH_3), 7.30 and 7.76 (2d, A_2B_2, $J=9$ Hz, 4H, C_6H_4), 9.85 (broad, 1H, NH). Found: C, 44.88; H, 3.81; N, 19.69%. Calcd for $C_8H_8O_2N_3Cl$: C, 44.98; H, 3.77; N, 19.67%.

1f (47%): mp 87—88 °C (decomp). IR (KBr): 3300, 1730, 1470 cm^{-1}. NMR: 3.20 (s, 3H, CH_3), 7.00—7.95 (m, 4H, C_6H_4), 9.87 (broad, 1H, NH). Found: C, 44.76; H, 3.73; N, 19.88%. Calcd for $C_8H_8O_2N_3Cl$: C, 44.98; H, 3.77; N, 19.67%.

1g (55%): mp 119—121 °C (decomp). IR (KBr): 3360, 1705, 1470 cm^{-1}. NMR: 2.57 (s, 3H, $COCH_3$), 3.22 (s, 3H, CH_3), 7.99 (s, 4H, C_6H_4), 10.06 (broad, 1H, NH). Found: C, 54.29; H, 5.05; N, 19.12%. Calcd for $C_{10}H_{11}O_3N_3$: C, 54.30; H, 5.01; N, 19.00%.

2a (59%): oil. IR (film): 1690, 1480 cm^{-1}. NMR: 2.40

(s, 3H, N'CH_3), 2.88 (s, 3H, CH_3), 6.70 (s, 5H, C_6H_5). Found: C, 55.56; H, 5.72; N, 21.65%. Calcd for $C_9H_{11}O_2N_3$: C, 55.95; H, 5.74; N, 21.75%.

2b (54%): mp 78—80 °C. IR (KBr): 1690, 1470 cm^{-1}. NMR: 2.48 (s, 3H, N'CH_3), 2.98 (s, 3H, CH_3), 6.95 and 7.60 (2d, A_2B_2, J=9 Hz, 4H, C_6H_4). Found: C, 45.32; H, 4.23; N, 23.59%. Calcd for $C_9H_{10}O_4N_4$: C, 45.38; H, 4.23; N, 23.52%.

Kinetics. The ionic strength of the buffer solution was adjusted with sodium chloride.[14] Thirty microliters of a stock solution of nitrosourea **1** (*ca.* 1.4×10^{-2} M in anhydrous methanol) was added by a microsyringe to 3 ml of the appropriate buffer solution in a thermostatted (±0.3 °C) UV cell. The final methanol concentration was 1% by volume. The disappearence of the characteristic absorption of the substrate (**1a**, 278; **1b**, 270; **1c**, 264; **1d**, 278; **1e**, 268; **1f**, 262; **1g**, 219 nm) was followed at intervals. The infinity reading was obtained after at least eight half lives had elapsed. For all the substrates, the kinetic plots showed good first order behavior up to 90% of the overall reaction. The stabilities of *N',N'*-disubstituted derivatives (**2**) were checked at pH 7.60 and at 36.8 °C. No spectral changes were observed for 52 h and 110 min for **2a** and **2b**, respectively.

Decomposition Products. Nitrosourea **1c** (50 mg) in 5 ml of ether was added to 300 ml of 0.1 M phosphate buffer solution (pH 7.20). The resulting suspension was allowed to stir for 140 min at 37 °C. The mixture was extracted with ether and evaporated to yield essentially pure *N,N'*-diphenylurea **9** [17 mg (57%), mp 238—239 °C, λ_{max} (H_2O) 252 nm]. Similar result was also obtained at pH 5.82 (37 °C, 43 h). An authentic sample of *N,N'*-diphenylurea (carbanilide) was prepared by the reaction of aniline with phenyl isocyanate [mp 238—240 °C,[15] λ_{max} (H_2O) 252 nm].

The authors wish to thank Professor K. Nagamatsu in this laboratory for his encouragement during this work.

References

1) Recent investigations; a) M. Colvin, J. W. Cowens, R. B. Brundrett, B. S. Kramer, and D. B. Ludlum, *Biochem. Biophys. Res. Commun.*, **60**, 515 (1974); b) J. W. Lawn, A. V. Joshua, and L. W. McLaughlin, *J. Med. Chem.*, **23**, 798 (1980); c) C. F. Hammer, R. A. Loranger, and P. S. Schein, *J. Org. Chem.*, **46**, 1521 (1981); d) D. E. G. Shuker, S. R. Tannenbaum, and J. S. Wishnok, *ibid.*, **46**, 2092 (1981); e) A. Chin, M. H. Hung, and L. M. Stock, *ibid.*, **46**, 2203 (1981).

2) a) P. D. Lawly, "Chemical Carcinogens," ed by C. E. Searle, American Chemical Society, Washington (1976), Chap. 4, and P. N. Magee, R. Montesano, and R. Preussmann, *ibid.*, Chap. 11; b) S. M. Hecht and J. W. Kozarich, *Tetrahedron Lett.*, **1972**, 5147; c) B. Singer, *J. Natl. Cancer Inst.*, **62**, 1329 (1979); d) J. K. Snyder and L. M. Stock, *J. Org. Chem.*, **45**, 1990 (1980).

3) K. Yano and M. Isobe, *Cancer Res.*, **39**, 5147 (1979).

4) The correlation coefficient was calculated without using the datum point of **1a**.

5) The same remark holds for the hydrolyses of MNU and other *N*-alkyl-*N*-nitrosoureas in phosphate buffer solution; E. R. Garrett, S. Goto, and J. F. Stubbins, *J. Pharm. Sci.*, **54**, 119 (1965); E. R. Garrett and S. Goto, *Chem. Pharm. Bull.*, **21**, 1811 (1973).

6) a) J. March, "Advanced Organic Chemistry," McGraw-Hill Inc., New York (1968), p. 658; b) R. S. Satchell and R. Nyman, *J. Chem. Soc., Perkin Trans. 2*, **1981**, 901.

7) A. F. Hegarty and L. N. Frost, *J. Chem. Soc., Chem. Commun.*, **1972**, 500; A. F. Hegarty, L. N. Frost, and J. H. Coy, *J. Org. Chem.*, **39**, 1089 (1974).

8) a) L. L. Schaleger and F. A. Long, *Adv. Phys. Org. Chem.*, **1**, 1 (1963); b) M. L. Bender and R. B. Homer, *J. Org. Chem.*, **30**, 3975 (1965); c) G. Sartore, M. Bergon, and J. P. Calmon, *J. Chem. Soc., Perkin Trans. 2*, **1977**, 650.

9) A. F. Hegarty and L. N. Frost, *J. Chem. Soc., Perkin Trans. 2*, **1973**, 1719. [The Hammett ρ constant reported for the $B_{AC}2$ hydrolysis of an anilide (XC_6H_4NHCOR) is close to unit: R=CH_3, ρ=1.00; M. L. Bender and R. J. Thomas, *J. Am. Chem. Soc.*, **83**, 4183 (1961), R=OCH_3, ρ=1.06; M. Bergon and J. P. Calmon, *Tetrahedron Lett.*, **22**, 937 (1981).]

10) B. B. Baril, E. F. Baril, J. Laszlo, and G. P. Wheeler, *Cancer Res.*, **35**, 1 (1975); P. S. Schein, L. C. Panasci, P. V. Woolley, and T. Anderson, *Cancer Treat. Rep.*, **60**, 801 (1976).

11) The mutagenic activity of **1c** was about 100 times as high as that of DMNU; Ref. 3, and M. Isobe and K. Yano, *Mutat. Res.*, **93**, 57 (1982).

12) S. R. Sandler and W. Karo, "Organic Functional Group Preparations," Academic Press, New York (1971), Vol. 2, p. 139.

13) J. K. Snyder and L. M. Stock, *J. Org. Chem.*, **45**, 886 (1980).

14) It has been reported that no salt effect by sodium chloride was observed in the aqueous decompositions of MNU and other related compounds: Ref. 2d.

15) "Merck Index," 9th ed, p. 1794.

Photosensitized *cis-trans* Isomerization of β-Alkylstyrenes

Tatsuo ARAI,* Hirochika SAKURAGI, and Katsumi TOKUMARU
Department of Chemistry, The University of Tsukuba, Sakura-mura, Ibaraki 305
(Received December 7, 1981)

Triplet sensitized isomerization of a series of β-alkylstyrenes has been investigated with the use of various sensitizers. Among the olefins employed β-*t*-butyl- and β-*t*-pentylstyrene were found to give remarkably high ratios of the *cis*-isomers (>80%) at the photostationary state. This fact is reasonably attributed to lower rate constants for energy transfer from the triplet sensitizers to the *cis*-isomers than to the *trans*-isomers.

The mechanism of triplet sensitized *cis-trans* isomerization of aromatic olefins has extensively been investigated.[1,2] However, the isomerization of β-alkylstyrenes has scarcely been learned.[3-8] This paper describes the triplet sensitized isomerization of a series of β-alkylstyrenes, that is, β-methyl- (**1**), β-ethyl- (**2**), β-isopropyl- (**3**), β-*t*-butyl- (**4**), and β-*t*-pentylstyrene (**5**)[9] with the use of triplet sensitizers with different triplet energies. Particularly, it was found that β-*t*-butyl- and β-*t*-pentylstyrenes exhibited remarkably high *cis*-isomer ratios at the photostationary state irrespective of the triplet energies of the sensitizers employed. This fact is reasonably attributed to inefficient energy transfer from the triplet sensitizers to the *cis*-isomers of these olefins as described below.[10]

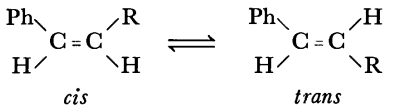

1: R=Me
2: R=Et
3: R=*i*-Pr
4: R=*t*-Bu
5: R=*t*-C_5H_{11}

Results and Discussion

Photostationary State Isomer Ratios. Isomeric β-alkylstyrenes, β-methyl-, β-ethyl-, β-isopropyl-, β-*t*-butyl- and β-*t*-pentylstyrene, were irradiated in the presence of sensitizers of various triplet energies in benzene at 26 °C for 2—24 h under degassed conditions with 366-nm light and the resulting photostationary ratios of the *cis*- and *trans*-isomers were accurately determined by GLPC. The pure *cis*- and *trans*-isomers were irradiated in the presence of the sensitizers of higher triplet energies. However, with the sensitizers of lower triplet energies like fluoranthene, benzil, and benz[*a*]anthracene, the irradiation was carried out for mixtures of the *cis*- and *trans*-isomers with compositions close to the photostationary state isomer ratios because of their lower efficiencies for the energy transfer to the olefins. The photostationary state isomer ratios extrapolated to infinite dilution with respect to sensitizer concentration are summarized in Table 1. Figure 1 shows the plots of the photostationary state compositions of these olefins against the triplet energies of the sensitizers employed. As this figure indicates, among the olefins examined, β-methyl-, β-ethyl-, and β-isopropylstyrene show quite similar profiles to that of stilbene[11,12] and confirm a strong similarity in mechanism of the photosensitized isomerization between these three alkylstyrenes and stilbene. On the other hand, β-*t*-butyl- and β-*t*-pentylstyrene exhibit

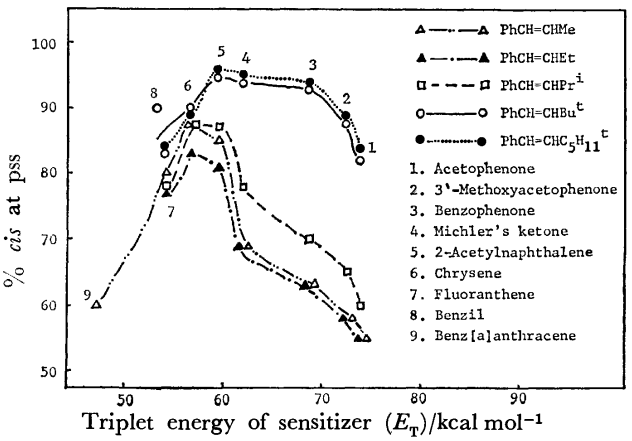

Fig. 1. Photostationary state compositions in triplet sensitized isomerization of β-alkylstyrenes.

TABLE 1. % *cis* AT PHOTOSTATIONARY STATE[a]

Sensitizer	E_T[b] / kcal mol^{-1}	R in PhCH=CHR				
		Me	Et	*i*-Pr	*t*-Bu	*t*-C_5H_{11}
Acetophenone	73.7	55	55	60	82	84
3'-Methoxyacetophenone	72.4	58	58	65	88	89
Benzophenone	68.6	63	63	70	93	94
Michler's ketone	62	69	69	78	94	95
2-Acetylnaphthalene	59.4	85	81	87	95	96
Chrysene	56.6	88	83	88	90	89
Fluoranthene	54.2	80	77	78	83	84
Benzil	53.4				90	
Benz[*a*]anthracene	47.2	60				

a) In benzene at 26 °C. b) Ref. 13.

quite different profiles from the above olefins; the *cis*-isomer ratios are remarkably high for all sensitizers employed. From the profiles in Fig. 1, the triplet excitation energies of the olefins can be estimated to be *ca.* 62 kcal mol^{-1} for the *cis*-isomers and *ca.* 56 kcal mol^{-1} for the *trans*-isomers of β-methyl-, β-ethyl-, and β-isopropylstyrene, and *ca.* 70 kcal mol^{-1} for the *cis*-isomers and *ca.* 60 kcal mol^{-1} for the *trans*-isomers of β-*t*-butyl- and β-*t*-pentylstyrene according to the well known method.[12]

The present photosensitized isomerization is assumed, by analogy with the isomerization of stilbene,[11] to proceed simply through the following processes,

$$S \xrightarrow{h\nu} {}^1S^* \xrightarrow{\Phi_{isc}} {}^3S^* \quad (1)$$

$${}^3S^* \longrightarrow S \quad (2)$$

$${}^3S^* + t \xrightarrow{k_{st}} S + {}^3t^* \quad (3)$$

$${}^3S^* + c \xrightarrow{k_{sc}} S + {}^3c^* \quad (4)$$

$${}^3c^* \longrightarrow {}^3p^* \quad (5)$$

$${}^3t^* \longrightarrow {}^3p^* \quad (6)$$

$${}^3p^* \xrightarrow{k_d} \alpha t + (1-\alpha)c, \quad (7)$$

where S stands for a sensitizer, t, c, and p mean transoid, cisoid, and twisted species, respectively, and α is the decay ratio from the twisted triplets to the *trans*-isomers of the olefins.

Based on the above scheme, the photostationary state composition, $([t]/[c])_{pss}$, is expressed by Eq. 8 and the quantum yields of *trans*-to-*cis* and *cis*-to-*trans* isomerization, $\Phi_{t\to c}$ and $\Phi_{c\to t}$, by Eqs. 9 and 10, respectively.

$$([t]/[c])_{pss} = \frac{k_{sc}}{k_{st}} \frac{\alpha}{1-\alpha} \quad (8)$$

$$\Phi_{t\to c} = \Phi_{isc}(1-\alpha) \quad (9)$$

$$\Phi_{c\to t} = \Phi_{isc}\alpha \quad (10)$$

Equation 8 suggests that the observed high ratios of the *cis*-isomers at the photostationary state of the β-*t*-alkylstyrenes might originate from the following possibilities: (1) The triplet state sensitizer, $^3S^*$, would undergo faster excitation transfer to the *trans*-isomers than to the *cis*-isomers ($k_{st}>k_{sc}$), and/or (2) the twisted triplet states, $^3p^*$, of the olefins would decay more efficiently to the *cis*-isomer than to the *trans*-isomer ($1-\alpha>\alpha$). In order to examine these possibilities attempts were made to determine the rate constants for the energy transfer and the quantum yields for the isomerization.

Rate Constants for Energy Transfer. Determination of the rate constants for triplet excitation transfer to the representative olefins, *cis*- and *trans*-β-methylstyrenes, and β-*t*-butylstyrenes, was undertaken for typical triplet sensitizers, benzophenone and chrysene, at ambient temperature. The rate constants for quenching of phosphorescence of benzophenone with these olefins were measured in carbon tetrachloride with the single photon counting technique, and quenching rate of the triplet-triplet absorption of chrysene with the olefins were determined in cyclohexane by the flash photolysis technique. The measured rate constants are summarized in Table 2.

Table 2. Rate constants for quenching of excited triplet sensitizers by β-alkylstyrenes in benzene[a]

Sensitizer	Olefin	k_{st}/l mol^{-1} s^{-1}	k_{sc}/l mol^{-1} s^{-1}
Chrysene	PhCH=CHMe	5.4×10^7	8.8×10^6
	PhCH=CHBu^t	1.1×10^7	6.2×10^5
Benzophenone	PhCH=CHMe	1.95×10^9	1.21×10^9
	PhCH=CHBu^t	1.21×10^9	1.25×10^8

a) At ambient temperature.

As Table 2 indicates, in the case of β-methylstyrenes, triplet benzophenone (E_T=68.6 kcal mol^{-1})[13] transfers excitation energy to both *cis*- and *trans*-isomers with nearly diffusion-controlled rate constants, but slightly less efficiently to the *cis*-isomer; however, the excitation transfer from triplet chrysene (E_T=56.6 kcal mol^{-1})[13] is much slower than the diffusion-controlled rate and the rate constant for the *cis*-isomer is six times smaller than to the *trans*-isomer. As for the excitation transfer to β-*t*-butylstyrenes, even when benzophenone was used as a sensitizer, the rate constant for the *cis*-isomer is about ten times lower than that for the *trans*-isomer. The magnitude of the rate constants is in good agreement with the aforementioned estimate of the triplet excitation energies of the olefins and suggests that the remarkably high composition of the *cis*-isomer of the β-*t*-alkylstyrenes at the photostationary state is mostly due to the smaller energy transfer rate constants from the triplet sensitizers to the *cis*-isomers.

Furthermore, the results in Table 2 indicate that the rate constants of the energy transfer are governed not only by the *exo*- and *endo*-thermicity of the processes but also by the steric effects exerted from the crowded olefins on approach to the triplet sensitizers. Thus, triplet benzophenone undergoes energy transfer to *cis*-β-methylstyrene about 1.6 times more slowly than to its *trans*-isomer. From the results of photoelectron spectroscopy, *cis*-β-methylstyrene is presumed to take a conformation where its benzene ring is twisted about 20° from the C=C molecular plane.[14] Therefore, the slower rate of energy transfer to the *cis*-isomer might be caused by the steric effect exerted by its twisted conformation to prevent the approach of the triplet sensitizer.[15] Also, the energy transfer rate from triplet benzophenone to *trans*-β-*t*-butylstyrene is about 1.6 times lower than to *trans*-β-methylstyrene. *trans*-β-*t*-Butylstyrene takes a planar conformation similar to that of *trans*-β-methylstyrene.[14] Accordingly, the triplet excitation energy of *trans*-β-*t*-butylstyrene will be close to that of *trans*-β-methylstyrene, 59.8 kcal mol^{-1} as reported by Lamola and Hammond[8] or less as suggested by the profile in Fig. 1. These results clearly indicate that in the energy transfer from triplet benzophenone the presence of the bulky *t*-butyl group in β-*t*-butylstyrene exerts steric hindrance to reduce the rate for accepting triplet energy as compared to the case of *trans*-β-methylstyrene. Herkstroeter, Jones, and Hammond showed the steric effect exerted in energy transfer from triplet states of sterically hindered benzophenones to stilbene.[16] The

Table 3. Quantum yield of isomerization of β-*t*-butylstyrene[a)]

Sensitizer	Sensitizer concn / mol l^{-1}	Olefin concn / mol l^{-1}	$\Phi_{t\to c}/\Phi_{isc}$	$\Phi_{c\to t}/\Phi_{isc}$
Benzophenone	0.1	0.02	0.53	0.23
	0.1	0.05	0.55	0.25
2-Acetyl-naphthalene	0.35	0.02	0.48	0.094
	0.35	0.05	0.49	0.15
		∞		0.24[b)]

a) In benzene at 26 °C. b) Quantum yield extrapolated to infinite olefin concentration.

present results provide an example of steric effects brought about by triplet energy acceptors on the energy transfer process.

The energy transfer rate from triplet benzophenone to *cis*-β-*t*-butylstyrene is about ten times lower than that to *trans*-β-*t*-butylstyrene. *cis*-β-*t*-Butylstyrene is presumed by PES to take a conformation where its benzene ring is twisted about 70° from the C=C molecular plane.[14] The highly twisted conformation will increase its triplet excitation energy to make the energy transfer from triplet benzophenone endothermic and will sterically hinder the approach of the triplet sensitizer.

Quantum Yields. Table 3 summarizes typical results of the quantum yields for the isomerization of β-*t*-butylstyrenes using benzophenone and 2-acetylnaphthalene as sensitizers. Both sensitizers give nearly the same value, 0.5±0.05, for $\Phi_{t\to c}/\Phi_{isc}$, which means that the energy transfer effectively takes place from the triplets of both sensitizers to the *trans*-isomer. The above value is in good agreement with the results of β-methylstyrene with various sensitizers reported by Caldwell.[3] The value for $\Phi_{c\to t}/\Phi_{isc}$ is nearly 0.25 in benzophenone sensitization almost irrespective of the olefin concentration. However, in 2-acetylnaphthalene sensitization, the value tends to increase with the olefin concentration, and leads to 0.24 by extrapolation to infinite olefin concentration, which agrees well with the above value for benzophenone sensitization. However, the value for $\Phi_{c\to t}/\Phi_{isc}$ thus obtained remains still nearly half of $\Phi_{t\to c}/\Phi_{isc}$.

This quantum inefficiency in the *cis*-to-*trans* process would result from formation of a *cis*-olefin-sensitizer exciplex followed by its decay to the *cis*-olefin as suggested by Caldwell[3,17] in the sensitized isomerization of β-methylstyrene with low energy sensitizers.

Effects of Sensitizer Concentration, Azulene, and Oxygen. Quenching of excited states with a number of species including ground-state sensitizers, azulene, and oxygen can serve to explore triplet energy surfaces of olefins as investigated on stilbene.[18,19]

These processes are expressed by Eqs. 11—14, where Az stands for azulene. The quenching of the *trans* triplet, $^3t^*$, by azulene might be an energy transfer process, and the quenching of $^3t^*$ by oxygen, if it takes place, should be energy transfer, but the quenching of the twisted triplet, $^3p^*$, by oxygen might be enhancement of the intersystem crossing from $^3p^*$ to a ground state with twisted geometry and this quenching cannot affect the photostationary state isomer ratios. Reactions 11, 12, and 14 were inferred to occur actually for stilbene.[18,19]

$$^3t^* + S \xrightarrow{k_{ts}} t + {}^3S^* \quad (11)$$

$$^3t^* + Az \xrightarrow{k_{az}} t + {}^3Az^* \quad (12)$$

$$^3t^* + O_2 \xrightarrow{k_{ot}} t + O_2 \quad (13)$$

$$^3p^* + O_2 \xrightarrow{k_{op}} \alpha t + (1-\alpha)c + O_2 \quad (14)$$

In the present investigation, attempts were done to examine the effects of azulene, oxygen, and sensitizer concentration on the photostationary isomer ratios in benzophenone-sensitized isomerization of β-methyl- and β-*t*-butylstyrene. However, no measurable effect was observed. This fact agrees with a previous result that azulene did not affect the photostationary isomer ratios in benzophenone-sensitized isomerization of β-methylstyrene.[20] The above results for the β-alkylstyrenes are in contrast with the results of stilbene, for which azulene and the sensitizer concentration are effective to change the photostationary isomer ratio.[18] Therefore, for β-alkylstyrenes, Reactions 11, 12, and 13 are unimportant, although Reaction 14 might be operative. The present results suggest that the *trans* as well as *cis* triplets of the β-alkylstyrenes are alive in too short lifetimes to be quenched by azulene, sensitizer, or oxygen, and undergo rapid relaxation into the twisted triplets which are incapable of being quenched by azulene. This mechanism is in contrast with the *trans* triplets of stilbene.[18]

Experimental

The NMR spectra and UV spectra were recorded on a JEOL JNM-MH-100 spectrometer and a Hitachi 200-20 spectrophotometer, respectively. Gas-liquid chromatographic analysis was performed on a Shimadzu GC-4CM-PF gas chromatograph equipped with an FID and a Hitachi K53 gas chromatograph equipped with a TCD was used for preparative purposes.

Materials. Isomeric β-methyl- (**1**), β-ethyl- (**2**), and β-*t*-butylstyrenes (**4**), were prepared as described previously.[13] A mixture of *cis*- and *trans*-β-isopropylstyrene (**3**) was prepared from 2-methylpropanal and benzyltriphenylphosphonium bromide according to literature.[21] Pure *cis*- and *trans*-**3** were separated by GLPC (polyethylene glycol 20 M (10%)). A mixture of *cis*- and *trans*-β-*t*-pentylstyrene (**5**) was similarly prepared. Pure *cis*- and *trans*-**5** were separated by column chromatography. Their structures were identified by NMR spectroscopy. The purity of all the samples was more than 99% as determined by GLPC (polyethylene glycol 20 M (5%)). These olefins were distilled under reduced pressure before use.

cis-**5**, bp 80—82 °C/12 Torr (1 Torr=133.322 Pa); NMR (CCl_4): δ 0.82 (t, J=6.0 Hz, 3H, C=C–C–C–CH_3), 0.88 (s, 6H, C=C–C(CH_3)$_2$–), 1.31 (q, J=6.0 Hz, 2H, C=C–C–CH_2–), 5.40 (d, J=12.6 Hz, 1H, Ph–C=CH–), 6.40 (d, J=12.6 Hz, 1H, PhCH=C–), 7.09 (m, 5H, aromatic H); Found: C, 89.73; H, 10.50%. Calcd for $C_{13}H_{18}$: C, 89.58; H, 10.41%.

trans-**5**, bp 84—86 °C/12 Torr; NMR (CCl_4): δ 0.85 (t, J=7.0 Hz, 3H, C=C–C–C–CH_3), 1.07 (s, 6H, C=C–C–(CH_3)$_2$–), 1.51 (q, J=7.0 Hz, 2H, C=C–C–CH_2–), 6.08 (d,

J=16.0 Hz, 1H, PhC=CH–), 6.23 (d, J=16.0 Hz, 1H, Ph–CH=C–), 7.25 (m, 5H, aromatic H). Found: C, 89.54; H, 10.49%. Calcd for $C_{13}H_{18}$: C, 89.58; H, 10.41%.

Benzene was purified by distillation. Aromatic hydrocarbons used as sensitizers were purified by column chromatography and recrystallization. Acetophenone and 3'-methoxyacetophenone were purified by distillation. Other aromatic ketones were purified by recrystallization.

Determination of the Photostationary State Isomer Ratios on Irradiation of 366-nm Light. Benzene solutions (3 ml) of a desired concentration of a sensitizer and *cis-* and *trans-β*-alkylstyrenes in Pyrex tubes were degassed using freeze-thaw cycles under about 10^{-5} Torr, and irradiated for 2—24 h by a 1 kW high pressure mercury lamp immersed in a Pyrex cooling well and further surrounded by Toshiba UV-D36B glass filters using a merry-go-round type Riko RH400-10W rotary photochemical reactor. The glass filters were used for isolation of the 366-nm line. The isomer ratios of *cis-* and *trans-β*-alkylstyrenes were determined by GLPC analysis. The following columns were used for quantitative analysis: polyethylene glycol 20 M (5%), Thermon 1000 (5%), and Silicone XF-1150 (5%).

Quantum Yield Measurements Using 366-nm Light. Benzene solutions of either a pure *cis* or *trans* substrate and a sensitizer in Pyrex tubes were degassed by freeze-thaw cycles and were irradiated in parallel with a 400 W high pressure mercury lamp surrounded by Toshiba UV-D36B glass filters using a merry-go-round type reactor. Light intensity was determined by benzophenone-benzhydrol actinometry using the method of Moore and Ketchum.[21] After being irradiated for 10 min the tubes containing the actinometry solutions were opened, and the contents were diluted with benzene and analyzed by UV spectroscopy. The total period of irradiation was adjusted so that usually 2—8% of an isomer was converted and the conversion was determined quantitatively by GLPC analysis.

Measurements of Photostationary State Isomer Ratios in the Presence of Azulene and/or Oxygen. Benzene solutions containing benzophenone (0.1 mol l^{-1}) and a *cis-* or *trans-β*-alkylstyrene and varying amounts of azulene (0.01—0.03 mol l^{-1}) in Pyrex tubes were degassed, aerated, or saturated with oxygen and irradiated for 2 h by a 1 kW high pressure mercury lamp surrounded by Toshiba UV-D36B glass filters using a merry-go-round type reactor. The isomer ratios of *cis-* and *trans-β*-alkylstyrenes were determined by GLPC analysis.

Rate Constants for Energy Transfer from Triplet Benzophenone to β-Alkylstyrenes. Phosphorescence lifetimes of benzophenone (1.1×10^{-3} mol l^{-1}) were measured in carbon tetrachloride at ambient temperature using a single photon counting apparatus, an Applied Photophysics SP-3X system, in the absence and in the presence of varying concentrations of *cis-* and *trans-β*-methyl- and *β-t*-butylstyrenes. The solutions were deaerated by bubbling with argon for more than 30 min. The phosphorescence lifetime of benzophenone monitored at 452 nm in this solvent in the absence of quenchers was 23 μs and the lifetime was diminished by addition of the quenchers. The energy transfer rate constants were calculated from these experiments.

Rate Constants for Energy Transfer from Triplet Chrysene to β-Alkylstyrenes. Rate constants for energy transfer from triplet chrysene to *cis-* and *trans-β*-methyl- and *β-t*-butylstyrenes were obtained by the measurements of lifetimes of the triplet-triplet absorption of chrysene monitored at 570 nm on a conventional flash photolysis apparatus (Applied Photophysics).

References

1) J. Saltiel, J. D'Agostino, E. D. Megarity, L. Metts, K. R. Neuberger, M. Wrighton, and O. C. Zafiriou, "Organic Photochemistry," ed by O. L. Chapman, Marcel Dekker, New York (1973), Vol. 3, p. 1.

2) J. Saltiel and J. L. Charlton, "Rearrangements in Ground and Excited States," ed by P. de Mayo, Academic Press, New York (1980), Vol. III, p. 25.

3) R. A. Caldwell, G. W. Sovocool, and R. J. Peresie, *J. Am. Chem. Soc.* **95**, 1496 (1973).

4) C. S. Nakagawa and P. Sigal, *J. Chem. Phys.*, **58**, 3529 (1973).

5) M. G. Rockley and K. Salisbury, *J. Chem. Soc., Perkin Trans. 2*, **1973**, 1582.

6) P. M. Crosby, J. M. Dyke, J. Metcalfe, A. J. Rest, K. Salisbury, and J. R. Sodeau, *J. Chem. Soc., Perkin Trans. 2*, **1977**, 182.

7) K. P. Ghibbino, K. Hara, G. R. Mant, D. Phillips, K. Salisbury, R. P. Steer, and M. D. Swords, *J. Chem. Soc., Perkin Trans. 2*, **1978**, 88.

8) A. A. Lamola and G. S. Hammond, *J. Chem. Phys.*, **43**, 2129 (1965).

9) In the present paper trivial names are used instead of systematic names, because the former is thought to help the readers in their better understanding of the contents. The systematic names are as follows: **1**, 1-phenyl-1-propene; **2**, 1-phenyl-1-butene; **3**, 3-methyl-1-phenyl-1-butene; **4**, 3,3-dimethyl-1-phenyl-1-butene; **5**, 3,3-dimethyl-1-phenyl-1-pentene.

10) Preliminary communication: T. Arai, H. Sakuragi, and K. Tokumaru, *Chem. Lett.*, **1980**, 261.

11) G. S. Hammond, J. Saltiel, A. A. Lamola, N. J. Turro, J. S. Bradshaw, D. O. Cowan, R. C. Counsell, V. Vogt, and C. Dalton, *J. Am. Chem. Soc.*, **86**, 3197 (1964).

12) W. G. Herkstroeter and G. S. Hammond, *J. Am. Chem. Soc.*, **88**, 4769 (1966).

13) S. L. Murov, "Handbook of Photochemistry," Marcel Dekker, New York, N. Y. (1973).

14) T. Kobayashi, T. Arai, H. Sakuragi, K. Tokumaru, and C. Utsunomiya, *Bull. Chem. Soc. Jpn.*, **54**, 1658 (1981).

15) One cannot rule out a possibility that the slower energy transfer to *cis*-**1** would be due to its much higher triplet energy, estimated as more than 70 kcal mol^{-1}, than that of *trans*-**1** as proposed by Caldwell,[3] although the triplet energy has not accurately determined by spectroscopy.

16) W. G. Herkstroeter, L. B. Jones, and G. S. Hammond, *J. Am. Chem. Soc.*, **88**, 4777 (1966).

17) R. A. Caldwell and R. P. Gajewski, *J. Am. Chem. Soc.*, **93**, 532 (1971).

18) J. Saltiel, D. W.-L. Chang, E. D. Megarity, A. D. Rouseau, P. T. Shannon, B. Thomas, and A. K. Uriarte, *Pure Appl. Chem.* **41**, 559 (1975).

19) H. Görner and D. Schulte-Frohlinde, *J. Phys. Chem.*, **85**, 1835 (1981).

20) R. E. Schwerzel and R. A. Caldwell, *J. Am. Chem. Soc.*, **95**, 1382 (1973).

21) K. Yasufuku, S. Hirose, S. Nozakura, and S. Murahashi, *Bull. Chem. Soc. Jpn.*, **42**, 2605 (1969).

21) W. M. Moore and M. Ketchum, *J. Am. Chem. Soc.*, **84**, 1368 (1962).

Bitter Diterpenoids from *Rabdosia shikokiana* (Makino) Hara

Masamitsu Ochi,* Mitsuyuki Okamura, Hiyoshizo Kotsuki,
Iwao Miura,† Isao Kubo,†† and Takashi Kubota†††

Faculty of Science, Kochi University, Akebono-cho, Kochi 780

† *Laboratories of Natural Products Chemistry, Otsuka Pharmaceutical Co. Ltd., Kawauchi-cho, Tokushima 771-01*

†† *Division of Entomology and Parasitology, College of Natural Resources, University of California, Berkeley, California 94720, U.S.A.*

††† *School of Medicine, Kinki University, Sayama-cho, Osaka 589*

(Received December 7, 1981)

Three new bitter diterpenoids, shikokianoic acid, shikokianal acetate, and 16,17-epoxyshikokianal acetate, have been isolated from the leaves of *Rabdosia shikokiana* (Makino) Hara. Their structures were established on the basis of spectral and chemical evidence.

In the previous paper,[1] we reported the structures of three *ent*-kaurenoids, rabdosianin A, B, and C, isolated from *Rabdosia shikokiana* (Makino) Hara. Our continuing search for bitter principles in this plant has now led to the isolation of three new diterpenoids, designated as shikokianoic acid, shikokianal, and 16,17-epoxyshikokianal, the last two as their acetates. The present paper deals with the structural elucidation of these new compounds.

Shikokianoic acid (**1**), $C_{24}H_{32}O_9$, mp 134—135 °C, $[\alpha]_D^{20}$ +3° (*c* 0.35, $CHCl_3$), was isolated as colorless flakes in 0.005% yield from the ether extract of the dried leaves by extensive column chromatography. It showed IR absorptions indicative of hydroxyl (3620, 3520) and carboxyl (3200—2500, and 1702 cm^{-1}) groups, and formed a triacetate (**2**), $C_{26}H_{34}O_{10}$, mp 144—145 °C, on acetylation with pyridine–acetic anhydride and a methyl ester (**3**), $C_{25}H_{34}O_9$, mp 224—226 °C, by treatment with diazomethane. The 400 MHz ^1H NMR spectrum showed signals due to two tertiary methyl groups at δ 1.00 and 1.22, two acetyl groups at δ 2.02 and 2.22, one methine proton on an oxygenated carbon atom at δ 3.94 (ddd, J=11.3, 9.2, and 8.4 Hz), one oxygenated methyl group at δ 4.62 and 5.00 (each d, J=12.7 Hz), two methine protons attached to carbon atoms bearing an acetoxyl group at δ 5.13 (dd, J=8.1 and 8.1 Hz) and 5.54 (dd, J=2.7 and 2.5 Hz), and one terminal methylene group at δ 5.00 (dd, J=2.5 and 0.8 Hz) and 5.21 (dd, J=2.7 and 0.8 Hz). In addition, extensive ^1H NMDR studies, summarized in Table 1, revealed the presence of the partial structures (**A**) and (**B**), the latter showing the following long-range couplings: $J_{H_{13},H_{17a}}=J_{H_{13},H_{17b}}=0.8$ Hz, $J_{H_{15},H_{17a}}=2.5$ Hz, and

Table 1. ^1H NMR spectra at 400 MHz of shikokianoic acid (**1**), shikokianal acetate (**8**), and 16,17-epoxyshikokianal acetate (**10**)[a]

	1	**8**	**10**
H_1	5.13 (dd, 8.1, 8.1)	4.73 (dd, 11.0, 4.3)	4.74 (dd, 11.0, 5.0)
$H_{2\alpha}$	*ca.* 1.90 (m)	1.88 (m)	*ca.* 1.85 (m)
$H_{2\beta}$	*ca.* 1.90 (m)	1.91 (m)	*ca.* 1.95 (m)
$H_{3\alpha}$	1.59 (m)	*ca.* 1.55 (m)	*ca.* 1.53 (m)
$H_{3\beta}$	1.52 (m)	1.49 (m)	*ca.* 1.53 (m)
H_5	3.67 (s)	3.19 (d, 2.7)	3.15 (d, 2.4)
H_6		9.99 (d, 2.7)	9.94 (d, 2.4)
H_9	2.49 (d, 11.3)	2.99 (d, 10.8)	3.05 (d, 10.3)
H_{11}	3.94 (ddd, 11.3, 9.2, 8.4)	4.95 (ddd, 10.8, 7.9, 7.9)	5.01 (ddd, 10.3, 10.3, 8.4)
$H_{12\alpha}$	2.63 (ddd, 12.9, 8.4, 8.4)	2.82 (ddd, 12.7, 8.7, 7.9)	2.58 (dd, 14.3, 10.3)
$H_{12\beta}$	1.34 (dd, 12.9, 9.2)	1.27 (ddd, 12.7, 7.9, 1.3)	1.34 (dd, 14.3, 8.4)
H_{13}	2.77 (dddd, 8.4, 5.4, 0.8, 0.8)	1.75 (dddd, 8.7, 4.9, 1.7, 1.4)	2.58 (m)
$H_{14\alpha}$	1.61 (d, 12.9)	1.60 (d, 11.9)	1.73 (d, 13.0)
$H_{14\beta}$	2.17 (dd, 12.9, 5.4)	2.28 (ddd, 11.9, 4.9, 1.3)	2.58 (m)
H_{15}	5.54 (dd, 2.7, 2.5)	5.60 (dd, 3.0, 2.7)	5.28 (s)
H_{17a}	5.00 (dd, 2.5, 0.8)	5.01 (dd, 2.7, 1.7)	2.77 (d, 4.6)
H_{17b}	5.21 (dd, 2.7, 0.8)	5.18 (dd, 3.0, 1.4)	2.93 (d, 4.6)
H_{20a}	4.62 (d, 12.7)	4.82 (d, 12.8)	4.70 (d, 12.7)
H_{20b}	5.00 (d, 12.7)	5.01 (d, 12.8)	4.86 (d, 12.7)
Me_{18}	1.00 (s)	1.09 (s)	1.06 (s)
Me_{19}	1.22 (s)	1.12 (s)	1.15 (s)
OAc	2.02, 2.22	2.01, 2.08, 2.30	2.03, 2.10, 2.29

a) The spectra were determined at 25 °C in $CDCl_3$ solutions with TMS as an internal standard. Multiplicity and J values (in Hz) are in parentheses.

Table 2. ^{13}C chemical shifts of shikokianoic acid (**1**), shikokianal acetate (**8**), and 16,17-epoxyshikokianal acetate (**10**)[a]

Carbon	1	8	10
1	75.7	75.5	75.4
2	24.2	24.3	24.2
3	39.5	40.0	40.2
4	34.3	35.0	34.8
5	57.6	61.8	61.9
6	173.9[b]	202.7	203.1
7	173.4[b]	172.3	172.1
8	51.2	51.3	52.3
9	44.3	40.9	40.6
10	42.5	43.8	43.4
11	65.7	68.2	68.0
12	44.3	40.4	40.6
13	35.6	35.4	35.8
14	31.0	32.3	32.8
15	82.2	82.2	81.9
16	153.6	152.7	70.5
17	111.3	111.3	48.8
18	23.6	24.1	24.0
19	33.6	33.7	33.7
20	66.9	66.3	66.1
$\underline{C}OCH_3$	170.5	169.9	169.9
	170.3	169.7	169.7
		168.8	169.0
$CO\underline{C}H_3$	21.4	21.3 (×2)	21.5
	20.9	20.8	21.4
			20.6

a) The spectra were measured at 100.61 MHz in $CDCl_3$ solutions and the shifts are given in ppm (δ) relative to the internal TMS. Assignments were made by off-resonance and selective proton-noise decoupling techniques. b) These assignments may be interchanged.

$J_{H_{15},H_{17b}}$=2.7 Hz. The ^{13}C NMR data (Table 2) showed the presence of one lactonic and one carboxylic carbon atoms (δ 173.4 and 173.9) along with four methylene groups, three methine groups, three oxygen-bearing methine groups, and three quaternary carbon atoms.

The spectral data and the analogy with the congeners isolated from *Rabdosia* species[1,2] suggested a B-seco-*ent*-kaurene type structure for shikokianoic acid, in which the partial structure (**A**) would form the A-ring and (**B**) the C- and D-rings. In the ^1H NMR spectrum of **3**, the chemical shifts of 18- and 19-methyl signals (δ 0.91 and 1.19) and the splitting pattern of the signal due to the methine proton on an oxygenated carbon atom in A-ring (dd, J=9.1 and 6.7 Hz) revealed that the location of the oxy linkage in A-ring is $C_{1\alpha}$ in analogy with isodonal (**4**).[2a,3] The β-configuration of the secondary hydroxyl group at C_{11} in **1** was evident from the coupling pattern and the large J values of H_{11} signal (ddd, $J_{H_9,H_{11}}$=11.3 Hz, $J_{H_{11},H_{12\alpha}}$=8.4 Hz, and $J_{H_{11},H_{12\beta}}$=9.2 Hz). The corresponding signal of shikodonin (**5**),[2b] in which the hydroxyl group at C_{11} is α-oriented, appeared as a doublet of doublets ($J_{H_9,H_{11}}$=6.0 Hz and $J_{H_{11},H_{12\alpha}}$=15.0 Hz).

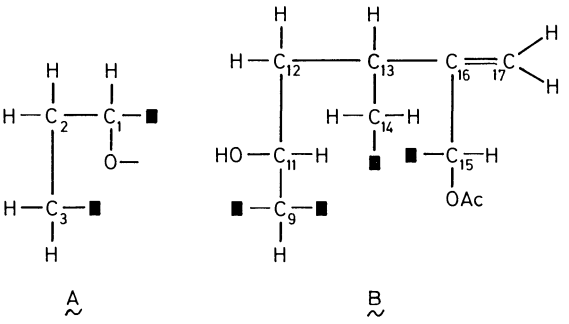

A B

The treatment of **2** with diazomethane gave a methyl ester (**6**), $C_{27}H_{36}O_{10}$, mp 216—218 °C. The catalytic hydrogenation of **6** yielded a dihydro compound (**7**), $C_{27}H_{38}O_{10}$, mp 245—248 °C, as the major product. It is well known that the hydrogenation of the C_{16} double bond in such a skeleton occurs from the less hindered α-side and, hence, the newly introduced secondary methyl group must be β-oriented.[4] The ^1H NMR spectrum of **7** showed a signal of H_{15} as a doublet at δ 5.08 (J=10.5 Hz), the large J value of which defined the configuration of the acetoxyl group at C_{15} as β.[4] Of the positions of the carboxyl group in **1**, C_6 and C_7, possible from biogenetic considerations, the latter is rejected by the IR spectrum of **1** which did not show the presence of a γ-lactone but of a δ-lactone (1738 cm^{-1}). If the carboxyl group was settled on C_7 position, a γ-lactone should be formed at C_6–C_1 or C_6–C_{20}.

The position of closure of the lactone ring remained to be assigned and this was done by the scrutiny of ^1H NMR data and the study of the nuclear Overhauser effect (NOE). The preceding discussion limited this to C_7–C_1 and C_7–C_{20}. The signals of H_1 and H_5 in **2** were shifted upfield, as compared with those of **1**, and the degree of the shift of both signals was identical [δ(**2**)−δ(**1**)=−0.47 ppm]. This fact suggested that the hydroxyl group in **1** is situated at equal distances from both H_1 and H_5. In addition, irradiation at the resonance of H_{11} under NOE condition did not lead to a significant change in signal intensity of H_5, while irradiation at the resonance of H_1 produced a clear and reproducible enhancement of the intensity of H_{11} (11%) and H_5 (4%) signals. This fact revealed that H_{11} is disposed across H_1 from H_5. These observations, combined with the examination of the model, can be satisfied only by the closure of the lactone ring at C_7–C_{20}. From the evidence outlined above, we proposed the structure **1** for shikokianoic acid.

Shikokianal acetate (**8**), $C_{26}H_{34}O_9$, mp 192—194 °C, $[\alpha]_D^{20}$ +89° (*c* 0.26, $CHCl_3$), was isolated in 0.021% as white needles by the acetylation of a crude fraction and exhibited spectral data quite similar to those of **1**, except for the following observations. The IR spectrum did not show the presence of the hydroxyl and carboxyl groups present in **1** and, instead, showed the presence of a formyl group at 2740 and 1718 cm^{-1}. The ^1H NMR spectrum contained the signals of three acetoxyl groups, one more than those of **1**, and a grouping $-\underset{|}{C}H-CHO$ [δ 3.19 and 9.99 (each d, J=

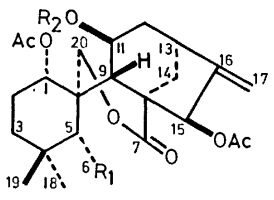

1 R_1 = COOH, R_2 = H
2 R_1 = COOH, R_2 = Ac
3 R_1 = COOMe, R_2 = H
6 R_1 = COOMe, R_2 = Ac
8 R_1 = CHO, R_2 = Ac

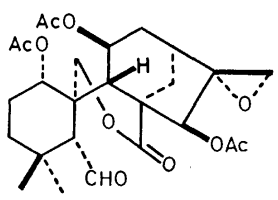

10

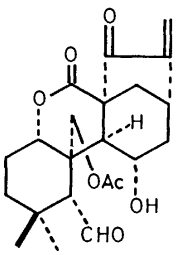

4

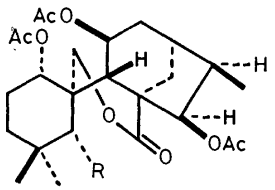

7 R = COOMe
9 R = CHO

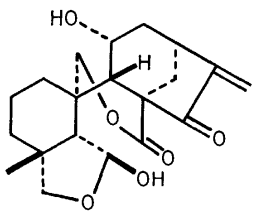

5

2.7 Hz)], the latter suggesting the location of the formyl group at C_6.[2a] These facts and the pertinent ^{13}C NMR data (Table 2) suggest that **8** has a structure close to that of **1**, in which the carboxyl and hydroxyl groups in **1** are displaced by the formyl and acetoxyl groups, respectively. This was confirmed by the chemical correlation of **8** with **1**. The catalytic hydrogenation of **8** gave a dihydro compound (**9**), $C_{26}H_{36}O_9$, mp 210—212 °C. The oxidation of **9** with Jones' reagent, followed by methylation with diazomethane, yielded a methyl ester (**7**), which was found to be identical with the compound derived from **1** as described above. Consequently, shikokianal acetate must be represented by structure **8**.

16,17-Epoxyshikokianal acetate (**10**), $C_{26}H_{34}O_{10}$, mp 205—206.5 °C, $[\alpha]_D^{20}$ +66° (*c* 0.32, $CHCl_3$), was isolated in 0.002% yield as colorless flakes by the acetylation of a crude fraction near shikokianal, the natural precursor of **8**. The spectral data suggested that the relationship of **8** to **10** was that of a olefin to the corresponding epoxide. In particular, the ^1H NMR spectrum of **10** contained signals due to a methylene group in an epoxide ring at δ 2.77 and 2.93 (each d, J=4.6 Hz) and lacked signals of an exocyclic methylene group, while the ^{13}C NMR spectrum contained two signals attributable to an epoxide moiety at δ 70.5 (s) and 48.8 (t). The structure of **10** was confirmed by its correlation with **8**. Thus, the treatment of **8** with *m*-chloroperbenzoic acid gave an epoxide, which was identical with **10** in all respects. This conversion also determines the configuration at C_{16} in **10**. Since the epoxidation of C_{16} double bond in such a compound is assumed to occur on the less hindered side of the molecule, the introduced oxygen atom must be α-oriented. Therefore, structure **10** is assigned to 16,17-epoxyshikokianal acetate. **10** is the first compound of *Rabdosia* diterpenoids which has an epoxide functionality at C_{16}–C_{17}.

Experimental

For general experimental details see Ref. 1.

Isolation. The ether extract (210 g)[1] of the dried leaves of *Rabdosia shikokiana* (Makino) Hara was subjected to chromatography over silicic acid (1.50 kg) eluting with $CHCl_3$–MeOH mixtures, with MeOH increasing from 0 to 10%. Elution with 5% MeOH in $CHCl_3$ gave a fraction (26.7 g) which was rechromatographed over silicic acid (900 g), using 50% ethyl acetate in petroleum ether, to yield a mixture of shikokianal and 16,17-epoxyshikokianal (7.10 g), and a fraction of shikokianoic acid (**1**) (718 mg). The former mixture was treated with acetic anhydride (30 ml) and pyridine (30 ml) at room temperature for 4 d and then worked up in the usual way. The resulting precipitates (3.10 g) were chromatographed over silicic acid (100 g), with ether as eluent, to give shikokianal acetate (**8**) (1.15 g) and 16,17-epoxyshikokianal acetate (**10**) (285 mg).

Shikokianoic Acid (1). The crude fraction was recrystallized from petroleum ether–ethyl acetate to give colorless flakes (262 mg), mp 134—135 °C, $[\alpha]_D^{20}$ +3° (*c* 0.35, $CHCl_3$); IR (nujol) 3620, 3520, 3200—2500, 1740, 1702, 1620, 1240, and 898 cm^{-1}; ^1H NMR (see Table 1); ^{13}C NMR (see Table 2); MS *m/e* 464 (M^+), 446 (M^+-H_2O), 422, 404 (M^+—AcOH), 386 (M^+-H_2O–AcOH), 362, and 344 (M^+—2AcOH). Found: C, 59.53; H, 6.99%. Calcd for $C_{24}H_{32}O_9\cdot H_2O$: C, 59.74; H, 7.10%.

Shikokianal Acetate (8). The crude material was recrystallized from EtOH to yield white needles (970 mg), mp 192—194 °C, $[\alpha]_D^{20}$ +89° (*c* 0.26, $CHCl_3$); IR (Nujol) 2740, 1760, 1740, 1718, 1660, 1240, and 915 cm^{-1}; ^1H NMR (see Table 1); ^{13}C NMR (see Table 2); MS *m/e* 490 (M^+), 448, 430 (M^+—AcOH), 388, 374, 370 (M^+—2AcOH), 360, 346, 328, 310 (M^+—3AcOH), and 300. Found: C, 63.33; H, 6.94%. Calcd for $C_{26}H_{34}O_9$: C, 63.66; H, 6.99%.

16,17-Epoxyshikokianal Acetate (10). The crude substance was recrystallized from ether-CH_2Cl_2 to afford colorless flakes (186 mg), mp 205—206.5 °C, $[\alpha]_D^{20}$ +66° (*c* 0.32, $CHCl_3$); IR (Nujol) 2755, 1745, 1730, 1720, 1230, and 908 cm^{-1}; ^1H NMR (see Table 1); ^{13}C NMR (see Table 2). Found: C, 61.46; H, 6.68%. Calcd for $C_{26}H_{34}O_{10}$: C, 61.65; H, 6.77%.

Acetylation of 1. A solution of **1** (30 mg) in acetic anhydride (1 ml) and pyridine (1 ml) was allowed to stand at room temperature for 2 d and then worked up in the usual way to give white precipitates (27 mg) which were subsequently recrystallized from ether–petroleum ether to yield a triacetate (**2**) as colorless needles (20 mg), mp 144—145 °C; IR (Nujol) 3200—2500, 1750, 1720, and 1220 cm^{-1}; ^1H NMR δ 1.03 and 1.16 (3H each, s, 18- and 19-Me), 2.04, 2.11, and 2.24 (3H each, s, 3Ac), 2.74 (1H, d, J=11.6 Hz, H_9), 3.20 (1H, s, H_5), 4.66 (1H, dd, J=11.0 and 4.3 Hz, H_1), 4.88 (1H, ddd, J=11.6, 8.5, and 8.5 Hz, H_{11}), 4.90 and 4.94 (1H each, d, J=12.8 Hz, H_{20}), 5.00 (1H, dd, J=2.4 and 1.2 Hz, H_{17a}), 5.21 (1H, dd, J=2.8 and 1.2 Hz, H_{17b}), and 5.58 (1H, dd, J=2.8 and 2.4 Hz, H_{15}). Found: C, 59.84; H, 6.81%. Calcd for $C_{26}H_{34}O_{10}\cdot 3/4H_2O$: C, 60.05; H, 6.88%.

Methylation of ***1***. A solution of **1** (60 mg) in ether (3 ml) was treated with ethereal diazomethane solution in the usual manner and the residue was recrystallized from ether–petroleum ether to give a methyl ester (**3**) as colorless plates (42 mg), mp 224—226 °C; IR ($CHCl_3$) 3580, 1735, 1220, and 902 cm^{-1}; ^1H NMR δ 0.91 and 1.19 (3H each, s, 18- and 19-Me), 2.02 and 2.27 (3H each, s, 2Ac), 2.22 (1H, dd, J=11.6 and 1.2 Hz, H_9), 3.72 (3H, s, OMe), 3.73 (1H, s, H_5), 3.84 (1H, ddd, J=11.6, 9.5, and 7.9 Hz, H_{11}), 4.69 (1H, dd, J=12.8 and 1.2 Hz, H_{20a}), 4.96 (1H, br s, H_{17a}), 4.98 (1H, d, J=12.8 Hz, H_{20b}), 5.14 (1H, dd, J=2.8 and 1.2 Hz, H_{17b}), 5.16 (1H, dd, J=9.1 and 6.7 Hz, H_1), and 5.54 (1H, dd, J=2.8 and 2.4 Hz, H_{15}). Found: C, 62.82; H, 7.19%. Calcd for $C_{25}H_{34}O_9$: C, 62.75; H, 7.16%.

Methylation of ***2***. A solution of **2** (35 mg) in ether (2 ml) was treated with ethereal diazomethane solution as described above and the product was recrystallized from ether–petroleum ether to yield a methyl ester (**6**) as colorless plates (34 mg), mp 216—218 °C; IR (Nujol) 1755, 1725, 1220, and 910 cm^{-1}. Found: C, 62.37; H, 6.82%. Calcd for $C_{27}H_{36}O_{10}$: C, 62.29; H, 6.97%.

Hydrogenation of ***6***. A mixture of **6** (34 mg) and 10% Pd–C (30 mg) in EtOH (3 ml) was stirred under a hydrogen atmosphere at room temperature for 12 h. The catalyst was removed by filtration and the filtrate was evaporated. The residue was recrystallized from ether–petroleum ether to give a dihydro compound (**7**) as white needles (26 mg), mp 245—248 °C; IR (Nujol) 1745, 1730, and 1225 cm^{-1}; ^1H NMR δ 0.83 (3H, d, J=7.6 Hz, 17-Me), 0.93 and 1.15 (3H each, s, 18- and 19-Me), 2.02, 2.13 ,and 2.25 (3H each, s, 3Ac), 2.60 (1H, d, J=11.9 Hz, H_9), 2.69 (1H, ddq, J= 10.5, 7.6, and 7.3 Hz, H_{16}), 3.19 (1H, s, H_5), 3.75 (3H, s, OMe), 4.64 (1H, dd, J=10.8 and 4.3 Hz, H_1), 4.82 (1H, ddd, J=11.9, 8.9, and 7.8 Hz, H_{11}), 4.93 and 5.01 (1H each, d, J=13.0 Hz, H_{20}), and 5.08 (1H, d, J=10.5 Hz, H_{15}). Found: C, 62.06; H, 7.40%. Calcd for $C_{27}H_{38}O_{10}$: C, 62.05; H, 7.33%.

Hydrogenation of ***8***. A mixture of **8** (52 mg) and 10% Pd–C (50 mg) in EtOH (5 ml) was treated under a hydrogen atmosphere as described above and the residue was recrystallized from EtOH to afford a dihydro compound (**9**) as colorless plates (35 mg), mp 210—212 °C; IR (Nujol) 1755, 1740, 1725, 1715, and 1225 cm^{-1}; ^1H NMR δ 0.83 (3H, d, J=7.5 Hz, 17-Me), 1.07 and 1.09 (3H each, s, 18- and 19-Me), 1.95, 2.07, and 2.21 (3H each, s, 3Ac), 5.07 (1H, d, J=10.2 Hz, H_{15}), and 9.93 (1H, d, J=2.2 Hz, H_6). Found: C, 63.32; H, 7.26%. Calcd for $C_{26}H_{36}O_9$: C, 63.40; H, 7.37%.

Conversion of ***9*** *into* ***7***. To a solution of **9** (30 mg) in acetone (2 ml) were added two drops of Jones' reagent with ice cooling. The mixture was stirred for 5 h at 0 °C, then worked up by dilution with water (20 ml), and extracted with ethyl acetate. The organic layer was washed with water, dried over Na_2SO_4, and evaporated to dryness. The amorphous residue was dissolved in ether (3 ml) and treated with ethereal diazomethane solution as described above. The product was recrystallized from ether–petroleum ether to give a methyl ester (18 mg) which was identified by mixed mp, IR, and ^1H NMR comparison with **7**.

Epoxidation of ***8***. A mixture of **8** (100 mg) and *m*-$ClC_6H_4CO_3H$ (40 mg) in dichloromethane (3 ml) was stirred at room temperature for 42 h under nitrogen atmosphere. The reaction mixture was worked up in the usual way and the product was chromatographed over silicic acid (8 g) with ether as eluent to yield an epoxide (46 mg) which was found to be identical with **10** in all respects.

We are grateful to Mr. Hideo Mori, Laboratories of Natural Products Chemistry, Otsuka Pharmaceutical Co. Ltd., for recording the mass spectra.

References

1) M. Ochi, M. Okamura, H. Kotsuki, I. Miura, I. Kubo, and T. Kubota, *Bull. Chem. Soc. Jpn.*, **54**, 2786 (1981).

2) For recent articles, see: a) I. Kubo, T. Kamikawa, and T. Kubota, *Tetrahedron*, **30**, 615 (1974); b) I. Kubo, M. J. Pettei, K. Hirotsu, H. Tsuji, and T. Kubota, *J. Am. Chem. Soc.*, **100**, 628 (1978); c) E. Fujita, N. Ito, I. Uchida, K. Fuji, T. Taga, and K. Osaki, *J. Chem. Soc., Chem. Commun.*, **1979**, 806; d) I. Kubo, T. Kamikawa, T. Isobe, and T. Kubota, *ibid.*, **1980**, 1206; e) T. Fujita, Y. Takeda, and T. Shingu, *Heterocycles*, **16**, 227 (1981); f) H. Sun, X. Sun, Z. Lin, Y. Xu, Y. Minami, T. Marunaka, and T. Fujita, *Chem. Lett.*, **1981**, 753.

3) The conformation of A-ring in **1** was proved to be identical with that of isodonal (**4**) on the basis of a NOE on H_5 (4%) upon irradiation of H_1.

4) T. Isobe, T. Kamikawa, I. Kubo, and T. Kubota, *Bull. Chem. Soc. Jpn.*, **46**, 583 (1973).

Bis(2,4-pentanedionato)phenylchromium(III). Preparation and Reactions with Organic Carbonyl Compounds and Alcohols

Takashi Ito,*,† Tsukasa Ono, Kazunori Maruyama, and Akio Yamamoto*

Research Laboratory of Resources Utilization, Tokyo Institute of Technology, Nagatsuta, Midori-ku, Yokohama 227

(Received December 21, 1981)

A phenylchromium complex $CrPh(acac)_2$ (**1**) (acac=2,4-pentanedionato ligand) was prepared from $Cr(acac)_3$ and $AlPh_3 \cdot Et_2O$. Complex **1** reacts with acetone to give benzene, 2-phenyl-2-propanol, and mesityl oxide and is converted into a hydroxo complex $[Cr(OH)(acac)_2]_2$. The mechanism involving the insertion of the carbonyl group of acetone into the Ph–Cr bond giving an alkoxo intermediate is proposed. Reactions of **1** with esters proceed similarly to give diphenylmethanol derivatives and alkoxochromium complexes. Complex **1** reacts with ROH to give benzene and alkoxo complexes $[Cr(OR)(acac)_2]_n$ (n=1 or 2) which were characterized by means of IR spectra, elemental analyses, molecular weight measurements, magnetic susceptibilities, and chemical reactions. The reactions of **1** with β-dicarbonyl compounds yield corresponding mixed chelate complexes $Cr(\beta\text{-dic})(acac)_2$, where β-dic=diethyl malonato and 1-ethoxy-1,3-butanedionato ligands.

A number of organochromium(III) complexes having σ-alkyl or aryl bond have been prepared by treatment of chromium(III) halides with alkyl(aryl)ating agents such as Grignard reagents, organolithium and aluminium compounds.[1] Most monoalkyl or monoaryl organochromium(III) complexes thus prepared such as $CrRCl_2(thf)_n$[2,3] and its phenyl analog, $CrPhCl_2(thf)_3$[4] (thf=tetrahydrofuran), contain halogen ligands. In the course of our studies on preparation of phenyl complexes of various transition metals using triphenylaluminium as arylating agents,[5–9] we found that a new, halogen-free, monophenylchromium complex $CrPh(acac)_2$ (**1**) was prepared from the system consisted of tris(2,4-pentanedionato)chromium(III), $Cr(acac)_3$ (acac stands for 2,4-pentanedionato ligand), $AlPh_3 \cdot Et_2O$, and tetrahydrofuran. Although extensive studies have been made on the systems consisted of alkyl- and arylaluminium compounds and $Cr(acac)_3$ with special reference to its catalytic behavior towards olefin and diene polymerization,[10] no characterizable compound has been isolated from the system. Sartori and Costa[11] suggested formation of an adduct between $Cr(acac)_3$ and $AlPh_3$ in a benzene solution through IR and ESR spectroscopic studies and conductivity measurements, but the characterization is not unequivocal. The only reasonably well established organochromium(III) complex so far isolated starting from $Cr(acac)_3$ is $CrBr(\eta\text{-}C_5H_5)(acac)$, which was prepared from $Cr(acac)_3$ and $Mg(C_5H_5)Br$.[12]

Although phenylchromium(III) complex of the type $CrPhCl_2(thf)_3$ has been known,[4] the study of its reactions is limited only to the oxidation with $HgCl_2$ and I_2.[1] In view of the importance of the species possessing carbon to transition metal σ-bond in a catalytic C–C bond formation reaction, we studied the reactions of the organic carbonyl compounds with phenylchromium complexes $CrPh(acac)_2$ (**1**) and $CrPhCl_2(thf)_3$. The reactions of **1** with some organic compounds having an active hydrogen such as alcohols and β-dicarbonyl compounds were also investigated to shed light on the mechanism of the reactions of the carbonyl compounds. A part of the present study has been communicated elsewhere.[13]

† Present address: Department of Materials Chemistry, Faculty of Engineering, Yokohama National University, Tokiwadai, Hodogaya-ku, Yokohama 240.

Results and Discussion

Preparation and Characterization of Bis(2,4-pentanedionato)phenylchromium(III). Kurras has reported that treatment of chromium(III) chloride with triphenylaluminium etherate in tetrahydrofuran at room temperature afforded yellow-green dichlorophenyltris(tetrahydrofuran)chromium(III).[4] In contrast, when tris(2,4-pentanedionato)chromium(III) was similarly treated with $AlPh_3 \cdot Et_2O$ in tetrahydrofuran, no apparent reaction occurred at room temperature. However, on heating the system at 80 °C, a wine red solution resulted, from which brilliant red crystals deposited on allowing it to stand at −78 °C for 1 d. The crystals which appear to be $CrPh(acac)_2(thf)$ as judged from the IR spectrum, easily released the solvated tetrahydrofuran molecule and turned into an orange powder of $CrPh(acac)_2$ (**1**) on drying *in vacuo* at room temperature for 1 h (Eq. 1).

$$Cr(acac)_3 + AlPh_3 \cdot Et_2O \xrightarrow[80°C]{\text{tetrahydrofuran}} \underset{\text{red crystals}}{CrPh(acac)_2(thf)} \xrightarrow{\text{drying } in\ vacuo} \underset{\text{orange powder}}{CrPh(acac)_2\ \mathbf{1}} \quad (1)$$

A triphenylaluminium adduct of $Cr(acac)_3$, in which $AlPh_3$ was assumed to be attached to one of two oxygen of the acac ligands, has been claimed to exist in the reaction mixture consisted of $Cr(acac)_3$ and $AlPh_3$ in benzene at room temperature.[11] The higher temperature employed in the present system might have transformed this unstable adduct to the more stable phenylchromium complex **1**. A qualitative test with the use of aluminon and alizarin indicated the absence of aluminium in the product. In contrast to the arylation of $CrCl_3$ with aryl Grignard reagents, which afforded triarylchromium as well as mono- and diaryl derivatives,[1] phenylation of $Cr(acac)_3$ with $AlPh_3 \cdot Et_2O$ yielded the monophenyl derivative exclusively, as in the case of analogous alkylation with aluminium alkyls.[2,3] Addition of an equimolar amount of triphenylphosphine or tricyclohexylphosphine to the system did not alter the reaction course and the phenyl complex **1** was isolated exlusively in

each case.

Complex **1** which is hardly soluble in diethyl ether and toluene can be recrystallized from tetrahydrofuran and is fairly inert to dry air in the solid state and even in solution. The magnetic moment of 3.52 BM, which is somewhat lower than the spin-only value of 3.88 BM for high spin Cr(III) complexes, was observed for complex **1**. Complex **1** decomposed *in vacuo* at 160—165 °C. The IR spectrum of **1** was very close to that of the parent $Cr(acac)_3$ except that there exist some additional bands due to the phenyl group at 3050 m (assignable to ν(C–H)), 675s, 695s, and 725s (π(C–H)), and 455 cm^{-1} (ν(Cr–C)). The characteristic absorptions of the acac ligand of **1** were observed as very strong bands at 1585, 1560, 1510, 1380, and 1345 cm^{-1}.

$CrPh(acac)_2$ (**1**) reacted with anhydrous HCl in diethyl ether to give benzene exclusively (91% of the calculated amount). The reaction of **1** with methyl iodide, allyl bromide, and acetyl chloride gave benzene (46—64%) and biphenyl. The yields of cross coupling products such as toluene, allylbenzene, or acetophenone, respectively, were very low (*ca.* 2%), indicating that the electrophilic attack of organic halogen compounds to the phenylchromium complex hardly occurred, unlike the similar reaction with phenylnickel(II) complex where certain amounts of cross coupled products have been obtained.[6] Although stable η^6-arene–chromium complexes such as $Cr(\eta^6\text{-}C_6H_6)_2$ are well known,[1,14] and formation of some η^6-arene–chromium complexes has been observed in the reaction of $CrCl_3$ with phenylmagnesium halides,[15] complex **1** is thought to have the phenyl-chromium σ-bond as is supported by the results of its reactions with organic carbonyl compounds (*vide infra*).

Reactions of $CrPh(acac)_2$ (1) with Organic Carbonyl Compounds. An orange-red heterogeneous mixture of phenylchromium complex **1** and rigorously dried acetone turned to a clear deep green solution on stirring at room temperature for 2 h. A GLC analysis of the resulting solution showed the formation of benzene, 2-phenyl-2-propanol, and 4-methyl-3-penten-2-one (mesityl oxide) in the yield listed in Table 1. Working up the system afforded a crystalline powder which was characterized as hydroxochromium complex $[Cr(OH)(acac)_2]_2$ **2** (0.84 mol/l) on the basis of IR spectrum, elemental analysis, and molecular weight measurement (*vide post*).

$$CrPh(acac)_2 + (CH_3)_2C{=}O \longrightarrow \underset{\mathbf{1}}{} PhH + Ph(Me)_2COH + Me_2C{=}CHCOMe + \underset{\mathbf{2}}{[Cr(OH)(acac)_2]_2} \quad (2)$$

The result indicates that two types of reactions, namely, protonation of the phenyl ligand and the insertion of the carbonyl group into the phenyl-chromium bond followed by protonation are taking place simultaneously in the present system. The result is in contrast to that of similar reactions of diphenylmanganese complex with acetone which afforded only benzene to give (2-oxopropyl)manganese complex indicating that protonation of the phenyl ligand with an active hydrogen of acetone was taking place exclusively.[8] On the other hand $Cr(acac)_3$ did not react with acetone upon heating under reflux for 2 h.

Formation of the hydroxochromium complex **2** and mesityl oxide indicates direct or indirect involvement of water in the reaction and it was suspected that the protonation was caused by water formed in the reaction giving mesityl oxide from 4-hydroxy-4-methyl-2-pentanone (diacetone alcohol), the dimerization product of acetone. However, kinetic examination of the reaction as represented by Fig. 1 excludes the water as the direct proton source for giving benzene and 2-phenyl-2-propanol. Figure 1 indicates that benzene and 2-phenyl-2-propanol are formed simultaneously without any induction period. If water produced by dehydration of the diacetone alcohol is acting as the proton source, the water would be produced concomitant with mesityl oxide. It is observed, however, that the sum of benzene and 2-phenyl-2-propanol far exceeds the amount of mesityl oxide at any moment in the reaction course supporting that the dehydration of diacetone alcohol yielding mesityl oxide does not provide a sufficient amount of water to liberate benzene and 2-phenyl-2-propanol. Furthermore, addition of 2 mol of water per mol of **1** to the system

Table 1. Reactions of $CrPh(acac)_2$ **1** with organic carbonyl compounds[a]

Compound	Reaction time (Solvent)	Products (mol/mol of **1**)			
		Alcohol	Dimer	Ketone	PhH
MeCOMe[b]	2 h (Neat)	$Me_2(Ph)COH$ (0.71)	$Me_2C{=}CHCOMe$ (0.36)		(0.27)
MeCOPh[b]	2 h (Et_2O)[f]	$Me(Ph)_2COH$ (0.75)	$Ph(Me)C{=}CHCOPh$ (0.91)		(0.26)
PhCOPh	1 d (Et_2O)	Ph_3COH (0.41)			(0)
MeCHO	2 h (Et_2O)[f]	Me(Ph)CHOH (0.81)	$MeCH{=}CHCHO$ (2.75)	PhCOMe (0.19)	(Trace)
EtCHO	1 d (Et_2O)	Et(Ph)CHOH (0.27)		PhCOEt (Trace)	(0.26)
PhCHO	1 d (Et_2O)		$PhCOOCH_2Ph$ (0.20)	PhCOPh (0.84)	(Trace)
MeCOOEt[c,d]	1 h (Neat)	$Me(Ph)_2COH$ (0.03)		PhCOMe (Trace)	(0.28)
MeCOOPh[d,e]	2 h (Neat)	$Me(Ph)_2COH$ (0.06)			(0.42)

a) Reactions were carried out under N_2 or *in vacuo* at room temperature unless otherwise stated. b) $[Cr(OH)(acac)_2]_2$ **2** was isolated from the reaction system (see text). c) $[Cr(OEt)(acac)_2]_2$ **4b** was isolated from the reaction system (see text). d) Reactions were carried out *in vacuo* at 80 °C. e) $Cr(OPh)(acac)_2$ **4i** was isolated from the reaction system (see text). f) The similar results were obtained when the reactions were carried out in the absence of solvent, diethyl ether.

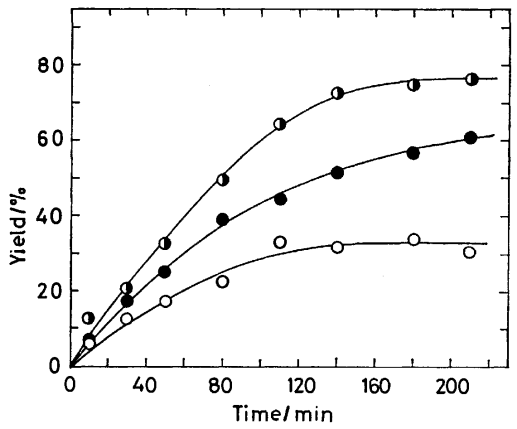

Fig. 1. Time dependence of the yields of benzene (○), mesityl oxide (●) and 2-phenyl-2-propanol (◑) in the reaction of $CrPh(acac)_2$ **1** with excess amount of acetone at 8 °C (Eq. 2).

did not affect the yields of benzene and the alcohol, but inhibited the formation of mesityl oxide. Figure 1 shows also that the yield of mesityl oxide still increased after *ca.* 150 min when more than 95% of the phenyl complex had been consumed as reflected by leveling off of the yields of benzene and 2-phenyl-2-propanol.

These results support that the phenyl complex **1** is more susceptible to acetone than to water. Benzene and 2-phenyl-2-propanol are considered to be formed by the following parallel reactions of **1** with acetone:

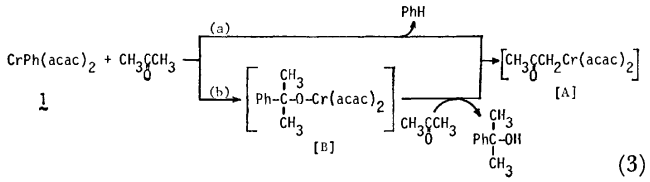

(3)

Since evidence supporting the formation of the 2-oxopropyl transition metal complex [**A**] was previously obtained for the diphenylmanganese complex on its treatment with acetone, it is likely that a similar complex may be produced in the present case by the reaction of **1** with acetone (route a). On the other hand, insertion of the carbonyl group of acetone into the Ph–Cr bond would produce the intermediate alkoxo complex [**B**] which may further react with acetone liberating 2-phenyl-2-propanol and [**A**].

The assumed intermediate [**A**], if present, must be quite susceptible to protonation to give mesityl oxide and the hydroxo complex **2**. The exact route to produce **2** and mesityl oxide remains unclarified. Mesityl oxide may be simply formed by an aldol condensation of acetone together with water, which further attacks the intermediate [**A**] to give **2**.

However, since the reaction to form mesityl oxide and **2** proceeds very readily at room temperature in the present system and the formation of mesityl oxide is inhibited by addition of water, it is certainly reasonable to assume the intervention of a chromium complex such as [**A**] which promotes the reaction to produce mesityl oxide and is susceptible to the attack of water. A possible route is given below where the second acetone insertion into the C–Cr bond of the intermediate [**A**] is assumed.

$$[CH_3\overset{\overset{O}{\|}}{C}CH_2Cr(acac)_2] + CH_3\overset{\overset{O}{\|}}{C}CH_3 \longrightarrow$$

[**A**]

$$[CH_3\overset{\overset{O}{\|}}{C}CH_2\overset{\overset{CH_3}{|}}{C}-O-Cr(acac)_2] \qquad (4)$$
$$\qquad\qquad\quad CH_3$$

[**C**]

The intermediate [**C**] may interact further with acetone to release diacetone alcohol with regeneration of [**A**].

$$[CH_3\overset{\overset{O}{\|}}{C}CH_2\overset{\overset{CH_3}{|}}{C}-O-Cr(acac)_2] + CH_3\overset{\overset{O}{\|}}{C}CH_3 \longrightarrow$$
$$\qquad\qquad\quad CH_3$$

[**C**]

$$[A] + CH_3\overset{\overset{O}{\|}}{C}CH_2\overset{\overset{CH_3}{|}}{C}CH_3 \qquad (5)$$
$$\qquad\qquad\quad OH$$

The diacetone alcohol thus produced may be dehydrated to liberate mesityl oxide and water which may readily attack [**A**] to produce the hydroxochromium complex **2**.

$$CH_3\overset{\overset{O}{\|}}{C}CH_2Cr(acac)_2 + H_2O \longrightarrow$$

[**A**]

$$\frac{1}{2}[Cr(OH)(acac)_2]_2 + CH_3\overset{\overset{O}{\|}}{C}CH_3 \qquad (6)$$

2

Acetophenone reacted with **1** in the essentially similar fashion as did acetone to give 1,1-diphenylethanol and 1,3-diphenyl-2-buten-1-one together with benzene and the hydroxochromium complex **2** (Table 1). The reaction paths can be accounted for similarly to the reaction of **1** with acetone. In contrast, benzophenone, bearing no hydrogen attached to the carbon atom α to the carbonyl group, did not yield benzene, but gave triphenylmethanol on reaction with **1** in diethyl ether. The proton source for producing triphenylmethanol was not clarified.

Acetaldehyde reacted with **1** affording mainly the insertion product of the aldehyde into the Ph–Cr bond accompanied by formation of only a trace amount of benzene (Table 1). The formation of 1-phenylethanol (81%) and acetophenone suggests the concurrent occurrence of protonation and β-hydrogen abstraction of the intermediate 1-phenylethoxochromium complex [**D**].

$$CrPh(acac)_2 + MeCHO \longrightarrow$$

1

$$\left[\begin{array}{l} CH_3 \\ PhC-O-Cr(acac)_2 \\ H \end{array}\right] \longrightarrow \begin{array}{l} \overset{\overset{CH_3}{|}}{Ph-C-OH} \\ \qquad H \end{array} \qquad (7)$$
$$\qquad\qquad\qquad\qquad\quad \longrightarrow PhC\overset{\overset{O}{\|}}{C}H_3$$

D

It is noted that crotonaldehyde was formed in greater than the stoichiometric amount. A chromium complex may be promoting the aldol condensation of acetaldehyde in a manner similar to that of acetone dimerization with repetition of processes expressed by Eqs. 4 and 5. A concomitant formation of polymeric products, possibly due to the aldol condensation reaction, prohibited the isolation of the chromium complex from the reaction system.

The reaction of propionaldehyde with **1** proceeded more slowly than that of acetaldehyde to give the products shown in Table 1. In addition to the products listed in Table 1, biphenyl (0.13 mol/mol of complex) was formed, but the mechanism of its formation is not clear.

Benzaldehyde carrying no acidic hydrogen α to the carbonyl group, did not give diphenylmethanol but yielded benzophenone almost exclusively as a result of the β-H abstraction from an alkoxo intermediate which can be produced by benzaldehyde insertion into the Cr–Ph bond of **1** (Table 1).

$$\underset{\mathbf{1}}{CrPh(acac)_2} + PhCHO \xrightarrow{\text{insertion}} [Ph\text{-}\underset{H}{\overset{Ph}{C}}\text{-}O\text{-}Cr(acac)_2]$$

$$\xrightarrow{\beta\text{-H abstraction}} PhC(Ph)=O + [HCr(acac)_2] \qquad (8)$$

This reaction system accompanied the formation of benzyl benzoate, the Tishtchenko type dimerization product. There are a few precedents of the Tishtchenko type reactions promoted by transition metal complexes.[8,16,17]

Ethyl and phenyl acetates reacted with $CrPh(acac)_2$ only at elevated temperatures accompanying a color change from orange-red to deep green (Table 1). Ethoxo- and phenoxochromium complexes, $[Cr(OEt)(acac)_2]_2$ and $Cr(OPh)(acac)_2$, were isolated from the reaction systems. They were characterized by comparison with the ethoxo and phenoxo complexes prepared by the independent reactions of **1** with ethanol and phenol, respectively. Isolation of the alkoxochromium complexes strongly supports that the reactions proceed by the insertion of the carbonyl group of the esters into the Cr–Ph bond followed by the alkoxo group elimination as generally assumed for the reactions of Grignard reagents with carboxylic esters. Higher yields of benzene than 1,1-diphenylethanol in these reactions suggest a facile protonation of the phenyl complex with esters or acetophenone as the proton source at the elevated temperature.

$$\underset{\mathbf{1}}{CrPh(acac)_2} + MeC(=O)OR \longrightarrow Ph\text{-}\underset{OR}{\overset{Me}{C}}\text{-}O\text{-}Cr(acac)_2$$

$$\longrightarrow Ph\text{-}\overset{Me}{C}=O + \frac{1}{2}[Cr(OR)(acac)_2]_2 \qquad (9)$$

For comparing the reactivity of the phenylchromium acetylacetonate with other phenylchromium complexes reactions of $CrPhCl_2(thf)_3$ (**3**) with some ketones and aldehydes were examined. The results are shown in Table 2. Although benzophenone and benzaldehyde afforded similar products to those of $CrPh(acac)_2$ (**1**), the reactions of acetone and acetaldehyde with **3** gave different results from those with **1**. Thus, the yields of aldol condensates such as mesityl oxide and crotonaldehyde which were formed in relatively high yields in the case of **1** decreased, whereas considerable amounts of olefins such as α-methylstyrene and styrene were produced. Since aldol condensation is known to be accelerated by the base and the dehydration of alcohol to give olefin is catalyzed by the acid, the present results seem to reflect a stronger acidic nature of complex **3** than **1**.

The formation of 2-phenyl-2-propanol in the reaction of acetone with **3** indicates the acetone insertion into the Ph–Cr bond in **3** giving $Ph(Me)_2C\text{-}O\text{-}Cr$ species which may be protonated by acetone to give the tertiary alcohol.

$$\underset{\mathbf{3}}{CrPhCl_2(thf)_3} + MeC(=O)Me \longrightarrow [Ph\text{-}\underset{Me}{\overset{Me}{C}}\text{-}O\text{-}CrCl_2]$$

$$\xrightarrow{H^+} Ph\text{-}\underset{Me}{\overset{Me}{C}}\text{-}OH \qquad (10)$$

Dehydration of the alcohol thus formed promoted

Table 2. Reactions of $CrPhCl_2(thf)_3$ **3** with organic carbonyl compounds[a]

Compound	Reaction time (Solvent)	Products (mol/mol of **3**)				
		Alcohol	Dimer	Ketone	Olefin	PhX
MeCOMe	1 d (Neat)	$Me_2(Ph)COH$ (0.54→0.02[c])	$Me_2C{=}CHCOMe$ (0.03→0.16[c])		$Ph(Me)C{=}CH_2$ (0.40→0.96[c])	PhH (0.06→0.17[c])
PhCOPh	0.5 h (Et_2O)	Ph_3COH (0.17)				
MeCHO	0.5 h (Et_2O)	Me(Ph)CHOH (0.20)	MeCH=CHCHO (Trace)	PhCOMe (Trace)	$PhCH{=}CH_2$ (0.21)	PhH (0.05)
PhCHO	1 d (Et_2O)		$PhCOOCH_2Ph$ (Trace)	PhCOPh (0.88)		PhPh (0.06)

a) Reactions were carried out under N_2 at room temperature. b) Three moles of tetrahydrofuran per mole of complex were found to be present in the reaction mixture. c) After the measurement of the yields of reaction products, phenol was added to the system. The figures placed after the arrows indicate the yields after treatment with phenol.

by acid gives α-methylstyrene. In the reaction of acetone with the phenylchromium chloride liberation of HCl is also likely. The acid thus formed may also act as the dehydration agent.

A quite similar reaction sequence as discussed above may be also operative in the reaction of **3** with acetaldehyde. The assumption that the alcohol is a precursor for the olefin formation in the system utilizing complex **3** was further confirmed by the following experiment. After the completion of the reaction between **3** and acetone, a weak acid such as phenol was introduced to the system, and the reaction mixture was stirred for 1 h at room temperature. This resulted in the appreciable increase in the yield of α-methylstyrene at the expense of the alcohol (see footnote c in Table 2).

*Reactions of CrPh(acac)$_2$ (**1**) with Alcohols.* In view of the possible intermediacy of alkoxochromium species in the reactions of phenyl complex **1** with organic carbonyl compounds, isolation of alkoxochromium complexes *via* direct reactions of alcohols with phenyl complex **1** was attempted.

Complex **1** readily reacted with an excess of various kinds of alcohols at room temperature to give a series of green alkoxochromium complexes **4** accompanied by release of quantitative amounts of benzene.

$$\underset{\mathbf{1}}{\mathrm{CrPh(acac)_2}} + \mathrm{ROH} \longrightarrow \frac{1}{n}\underset{\mathbf{4}}{[\mathrm{Cr(OR)(acac)_2}]_n} + \mathrm{PhH} \quad (n=1 \text{ and } 2) \qquad (11)$$

Although the homoleptic chromium alkoxides such as Cr(OR)$_n$ has been known,[18] complexes containing both the alkoxo- and β-diketonato ligands of the type [Cr(OR)(β-dik)$_2$]$_n$ have been prepared only recently by the reactions of alcohols with Cr(3-halo-2,4-pentanedione)$_2$[19,20] or of β-diketones with chromium trialkoxides under refluxing conditions.[21] The former method has a limitation that only such 2,4-pentanedionato derivatives that carries strong electronegative substituent can be replaced by alcohol, whilst the latter is inconvenient for getting complexes with an extensive series of alkoxo ligands. The present method shown in Eq. 11, albeit indirect, has an advantage that the reaction readily proceeds under mild conditions to give complexes with a variety of alkoxo ligands.

Table 3 lists analytical results of the alkoxo complexes thus obtained. Most alkoxo complexes are soluble in organic solvents such as hexane and toluene from which they were recrystallized to give green crystals. Molecular weight measurement by cryoscopy in benzene reveals that the alkoxo complexes are dimeric in solution in accordance with the observation by Mahendra *et al.*[21] and by Kasuga *et al.*[19] for [Cr(OR)(3-bromo-2,4-pentanedione)$_2$]$_2$. Alkoxo-bridged dimeric structure in the solid state has been demonstrated for the last complex by an X-ray crystal structure analysis.[20] By analogy, most alkoxo complexes prepared in the present study may have the structure as shown below:

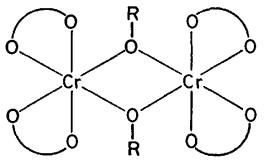

where O⌒O represents acac ligands. The phenoxo complex Cr(OPh)(acac)$_2$ was found to be monomeric in benzene. The presence of the phenoxo group may serve to make the phenoxo oxygen less basic for formation of the bridge structure. A steric reason may be also contributing here.

Assignment of their IR bands was performed by comparing them with those of the parent complex **1**, tris(2,4-pentanedionato)chromium(III), and some other related compounds.[19,22,23] For example, methoxo complex [Cr(OCH$_3$)(acac)$_2$]$_2$ (**4a**) showed, in addi-

Table 3. Alkoxochromium complexes formed by the reaction, nCrPh(acac)$_2$+nROH ⟶ [Cr(OR)(acac)$_2$]$_n$+nPhH[a]

	R	Yield %	Mol wt[b]	n	μ_{eff} BM	ν(C-O) cm^{-1}	Analysis[b] (%) C	H	Cr
4a	Me	100	541 (562)	2	3.52	1083	46.9 (47.0)	6.2 (6.1)	18.6 (18.5)
4b	Et	79	c)		3.63	1054, 1092	48.4 (48.8)	6.5 (6.5)	17.2 (17.6)
4c	*n*-Pr	99	c)		c)	1062	49.8 (50.5)	7.0 (6.8)	16.7 (16.8)
4d	*i*-Pr	87	575 (618)	2	3.41	1128	49.3 (50.5)	6.7 (6.8)	16.7 (16.8)
4e	*t*-Bu	43	c)		3.35	1178	51.5 (52.0)	7.3 (7.2)	16.2 (16.1)
4f	$PhCH_2$	99	c)		c)	1025, 1048, 1078	56.0 (57.1)	6.0 (5.9)	14.3 (14.6)
4g	Me(Ph)CH	23	c)		c)	1100	58.4 (58.2)	6.4 (6.2)	c)
4h	$(Me)_2PhC$	71	732 (770)	2	c)	1152	58.9 (59.2)	6.6 (6.5)	13.7 (13.5)
4i	Ph	63	398 (343)	1	3.53	1232	56.1 (56.0)	5.8 (5.6)	15.5 (15.1)
4j	*p*-MeO-C_6H_4	25	c)		c)	1210	53.6 (54.6)	6.0 (6.7)	c)
4k	$HOCH_2CH_2$	80	c)		c)	1063	46.4 (46.3)	6.4 (6.2)	15.8 (16.7)
2	H	99	528 (534)	2	3.78	3635[d]	45.4 (45.0)	5.8 (5.7)	c)

a) Reactions were carried out under N_2 at room temperature without solvent for **4a**—**d** and in Et_2O and tetrahydrofuran for **4e**—**4j**, and **4k** and **2**, respectively. b) Calcd values in parentheses. c) Not measured. d) Band assignable to ν(O-H) (see text).

tion to the bands due to the acac ligand, several bands assignable to the methoxo ligand: 2925m and 2820m (ν(C–H)), 1083s (ν(C–O)), 600s, 548s, and 453s cm^{-1} (bands due to Cr–O bond). In the case of the phenoxo complex, Cr(OPh)(acac)$_2$ (**4i**), the bands arising from the phenoxo group were 3050m (ν(C–H)), 1485s (ν(C–C)), 1232s (ν(C–O)), 767s (π(C–H)), 685s (δ(C–C)), and 600s and 480s cm^{-1} (bands due to Cr–O bond). The fairly distinctive C–O stretching bands of the alkoxo ligands are listed in Table 3.

In accordance with the observation by Mahendra *et al.*,[21] magnetic moments of the present alkoxo complexes were found to be in the region of 3.35 to 3.63 BM which are less than the value of 3.88 BM calculated for the spin only system of Cr(III), suggesting occurrence of the antiferromagnetism due to super exchange through bridging alkoxo ligands.[22]

The formation of the alkoxo complexes may be explained by considering nucleophilic attack of alcohol to a vacant site of the metal center of phenylchromium complex **1** followed by formation of Cr–O bond.

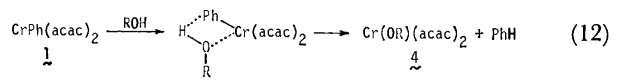

(12)

The necessity of a vacant site on the metal center was demonstrated by the following additional experiment. The orange phenylchromium complex **1**, on treatment with γ-picoline in tetrahydrofuran at room temperature, turned to a yellow adduct, CrPh(acac)$_2$(γ-picoline) (**5**), which was characterized on the basis of IR spectrum and elemental analysis. In contrast to the high reactivity of **1** toward alcohol as described above, coordinatively saturated complex **5** did not react with ethanol in tetrahydrofuran at room temperature, but reacted at 80 °C to give the alkoxo complex [Cr(OEt)(acac)$_2$]$_2$ liberating quantitative amounts of benzene and γ-picoline. This result implies that dissociation of γ-picoline ligand is a prerequisite for complex **5** to be attacked by alcohol according to Eq. 12.

The reaction of **1** with ethylene glycol in tetrahydrofuran at room temperature afforded a deep purple solution, from which a pale purple powder was obtained on working up. On treatment with hot toluene, the purple powder turned to a green powder **4k** which showed a strong IR band at 3490 cm^{-1} assignable to ν(OH). In view of the fact that the rest of the IR absorptions are quite similar to those of the other alkoxo complexes **4** and that the elemental analysis excludes the binuclear structure with a bridging $-OCH_2CH_2O-$ group, complex **4k** is tentatively formulated as a 2-hydroxyethoxo complex [Cr(OCH_2CH_2OH)(acac)$_2$]$_2$. The structure of the pale purple precursor which has no ν(OH) band is not certain.

Reactions of Alkoxochromium Complexes. Alkoxobis(2,4-pentanedionato)chromium(III) complexes **4a**, **4b**, **4d**, **4i**, and **4j** reacted with acetyl chloride to give quantitvatie amounts of corresponding esters. Since the reaction takes place readily at ambient conditions, it may be applicable to the rest of the alkoxo complexes listed in Table 3 which were not examined.

$$[Cr(OR)(acac)_2]_n + \text{excess MeCOCl} \xrightarrow{\mathbf{4}} n\ \text{MeCOOR} + \text{"complex"} \quad (13)$$

All the reaction products thus obtained showed the identical IR bands with those of the reaction products between **1** and HCl (*vide supra*), at 2790m, 1695s, 1170m, and 1050m cm^{-1} in addition to those of the acac ligand. The complex is tentatively assigned to $CrCl_n(acac)_m$. The reaction of acetyl chloride with the alkoxo complex, [Cr(OCH_2CH_2OH)(acac)$_2$]$_2$ (**4k**), derived from ethylene glycol afforded diester, ethylene glycol diacetate, the yield of which was one mol per Cr atom.

The alkoxo complexes **4** were found to be chemically inert to most reagents other than acetyl chloride. Thus, in contrast to trialkoxochromium(III) complexes, Cr(OR)$_3$, which reportedly react with isocyanate to give insertion product, $Cr(OR)_{3-n}\{N(Ph)COOR\}_n$,[24] complex **4b** did not react with excess phenyl isocyanate in toluene at room temperature. Methyl iodide and phenyl acetate did not react with **4b** even on heating at 80 °C. Only a trace amount of anisole was detected in the reaction of the phenoxo complex **4i** with methyl iodide at room temperature. When the ethoxo complex **4b** in toluene was stirred at room temperature in the presence of equimolar amount of phenol for 9 h, only 2% of ethanol per **4b** was formed, indicating that the alkoxo exchange reaction of **4** with more acidic alcohol proceeds very slowly. Neither CO_2 (4 atm, 80 °C) nor CO (1 atm, room temperature) reacted with **4b** in toluene solution or in ethanol suspension.

It is rather surprising that even the alkoxo complex **4h**, derived according to Eq. 12 from **1** and 2-phenyl-2-propanol, which was thought to be a possible reaction intermediate between **1** and acetone as shown in Eq. 3, was found to be inert to further reaction with acetone at room temperature. Heating **4h** in acetone under reflux yielded only a small amount of mesityl oxide and 2-phenyl-2-propanol. The result conflicts with the mechanism presented for the reaction between the phenyl complex **1** and acetone in which mesityl oxide was formed by room temperature *via* a postulated alkoxo intermediate **4h**. Tentatively, we elucidate this inconsistency by supposing a significant difference in the reactivity of **4h** toward acetone between monomeric and dimeric forms. As shown in the preceding section, most alkoxochromium complexes once isolated were found to be dimeric in solution, which are chemically inert. On the other hand, the pentacoordinated alkoxo intermediate [**B**] in Eq. 3 formed *in situ* by the reaction of phenyl complex **1** and excess acetone may exist as a monomer, since excess acetone, behaving as a Lewis base, may occupy the vacant coordination site of chromium which is necessary for the dimerization of alkoxide. The monomeric alkoxide may have a potential to react further with excess acetone. The formation of 2-phenyl-2-propanol and mesityl oxide by the reaction of **4h** with acetone at refluxing temperature suggests that the dissociation of dimeric alkoxide may take place at the elevated temperature in the presence of acetone.

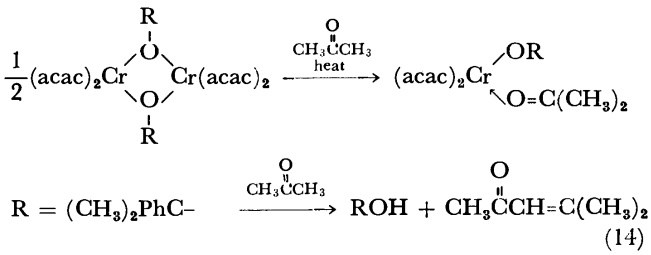

$$R = (CH_3)_2PhC- \xrightarrow{CH_3\overset{O}{\overset{\|}{C}}CH_3} ROH + CH_3\overset{O}{\overset{\|}{C}}CH{=}C(CH_3)_2 \quad (14)$$

Reaction of CrPh(acac)$_2$ (1) with Water. Complex **1** reacted slowly with an excess of water in the tetrahydrofuran solution at room temperature to afford benzene quantitatively and give purple crystals which were analyzed as dimeric hydroxo complex **2** on the basis of IR spectrum, elemental analysis, and magnetic susceptibility as well as molecular weight measurements. The analytical results are included in Table 3. IR spectrum of **2** showed a characteristically

$$\underset{\mathbf{1}}{2\,CrPh(acac)_2} + 2\,H_2O \xrightarrow[\text{room temp}]{\text{tetrahydrofuran}} 2\,PhH + \underset{\mathbf{2}}{[Cr(OH)(acac)_2]_2} \quad (15)$$

sharp ν(OH) band at 3635 cm^{-1} and bridging δ(OH) band at 820 cm^{-1}.[23] These bands shifted to 2665 (ν(OD)/ν(OH)=1.37) and 620 cm^{-1} (δ(CD)/δ(OH)=1.32), respectively in the deuterio analog [Cr(OD)(acac)$_2$]$_2$, which was similarly prepared from **1** according to Eq. 15 using D_2O in place of H_2O. The binuclear complexes bridged with the hydroxo group(s) have been reported for Cu,[25] Fe,[26] Co,[26] Ru,[27] and Pt,[28] as well as Cr(III) of the type [(L-L)$_2$Cr(OH)]$_2$X$_4$ (L-L=2,2'-bipyridine and 1,10-phenanthroline) and K$_4$[(C$_2$O$_4$)$_2$Cr(OH)]$_2$.[26]

Reactions of CrPh(acac)$_2$ (1) with β-Dicarbonyl Compounds. Phenyl complex **1** reacted with β-dicarbonyl compounds such as diethyl malonate (Hdem) and ethyl acetoacetate (Heac) at room temperature to give corresponding mixed chelate complexes **6** with accompanying release of quantitative amounts of benzene. Purple needles of **6a** had IR absorptions at

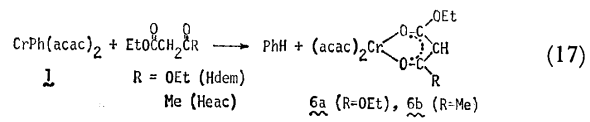

1620, 1143, and 1076 cm^{-1} assignable to the ester groups of dem ligand in addition to the bands due to acac ligands. Similarly, the IR bands due to the ester group in eac ligand in **6b** were observed at 1610, 1090, and 1058 cm^{-1}. Replacement of metal alkyls with nucleophiles such as β-dicarbonyl anion to give chelate complex has been reported for methylcopper and dimethylnickel complexes.[29] It has also been reported that Pt(acac){CH(COCH$_3$)$_2$}(PPh$_3$) reacted with dimethyl malonate (Hdmm) and Heac to replace central carbon bonded acac ligand {CH(COCH$_3$)$_2$} with dmm and eac which were also bonded to Pt through their central carbon atoms.[30] Absence of the ester carbonyl bands above 1700 cm^{-1} in the IR spectra of **6a** and **6b** indicates that dem and eac ligands are not attached unidentately through central carbon atom but chelated through two oxygens.

Experimental

Most reactions and manipulations were carried out either under dry, oxygen-free nitrogen or argon, or *in vacuo* using Schlenk-type flasks.

Solvents were dried, purified in the usual manner, and stored under an atmosphere of nitrogen. Commercial acetone was dried by Drierite, distilled under nitrogen, and stored with added molecular sieve 3A. Acetone thus purified was found to contain less than 1.5×10^{-3} M of water on the basis of GLC analysis. Acetaldehyde was dried over molecular sieve 3A, distilled under nitrogen, and stored in the presence of molecular sieve 3A. The other ketones, aldehydes, and esters were purified appropriately. Methanol was dried with Drierite, distilled under nitrogen, and distilled again over calcium hydride *in vacuo*. Commercial phenol, 2-phenyl-2-propanol, 1-phenylethanol, and *p*-methoxyphenol were used without further purification. Other alcohols were dried over anhydrous sodium sulfate. Acetyl chloride was distilled and stored under nitrogen in the presence of molecular sieve 3A. AlPh$_3$·Et$_2$O was prepared from PhMgBr and AlCl$_3$ according to the reported method.[31] Tris(2,4-pentanedionato)chromium(III) (Tokyo Kasei Industrial Co.) was used as purchased without further purification. CrPhCl$_2$(thf)$_3$ (**3**) was prepared by the literature method.[4]

Infrared spectra were recorded on a Hitachi model 295 spectrometer using KBr disks prepared under inert atmosphere. The magnetic susceptibility was measured by Gouy method using Shimadzu MB-100 apparatus at 23 °C and the diamagnetic corrections for the coordinated ligands were made on the basis of the Pascal's constants.[32] Molecular weight was measured cryoscopically in benzene solution. The organic products formed in the reactions were quantitatively analyzed by GLC using internal standard. GLC was recorded on a Shimadzu GC-3BT or GC-6A gas chromatography using SDC-550, SDC-410, and/or PEG-20M columns and helium as a carrier gas. Micro analyses (C and H) were carried out by Mr. T. Saito of our laboratory using Yanagimoto CHN Autocorder Type MT-2. Analysis of the chromium content was performed by a colorimetric method using diphenylcarbazide as a color-producing agent.[33]

Preparation of CrPh(acac)$_2$ (1). Tris(2,4-pentanedionato)-chromium(III) (2.8 g, 8.0 mmol) and AlPh$_3$·Et$_2$O (2.9 g, 8.4 mmol) in 20 cm^3 of tetrahydrofuran was heated under reflux for 8 h. The original deep purple solution changed to wine red in the initial 1 h. On allowing to stand the solution at −78 °C overnight, brilliant red crystals deposited, which were filtered, washed with tetrahydrofuran, and dried *in vacuo*. Orange powdery CrPh(acac)$_2$ thus obtained weighed 1.64 g (yield, 63% based on Cr(acac)$_3$ used) and was crystallized from hot tetrahydrofuran. Found: C, 58.4; H, 6.0%. Calcd for C$_{16}$H$_{19}$O$_4$Cr: C, 58.7, H, 5.9%.

Reaction of CrPh(acac)$_2$ (1) with Acetone. To a flask containing CrPh(acac)$_2$ (0.406 g, 1.24 mmol), 3 cm^3 of acetone was added by means of a trap-to-trap method. On stirring the mixture at room temperature for 2 h a dark green solution resulted, the GLC analysis of which using toluene as an internal reference showed the formation of benzene (0.335 mmol), 3-phenyl-2-propanol (0.880 mmol), 4-methyl-3-penten-2-one (mesityl oxide) (0.446 mmol), and 2,6-dimethyl-2,5-heptadien-4-one (0.062 mmol). Volatile liquid materials were evaporated from the solution to leave a dark colored solid. The resulting solid was successively washed at −10 °C with diethyl ether and hexane to give

a purple powder which was analyzed as $[Cr(OH)(acac)_2]_2$ (0.279 g, 84% based on **1** used).

The time-course of the yields of the organic products in the reaction of **1** and acetone (Fig. 1) was followed by submitting the aliquot of the reaction mixture maintained at 8 °C to GLC analysis at regular intervals.

The reactions of **1** with other ketones, aldehydes, and esters were carried out essentially in a similar fashion as described above, except that in some experiments diethyl ether was used as solvent and the reaction mixture was heated appropriately as shown in Table 1.

Reaction of $CrPhCl_2(thf)_3$ (3) with Acetone. Acetone (2 cm³) was condensed into a flask containing 0.114 g (0.273 mmol) of $CrPhCl_2(thf)_3$ by the trap-to-trap method. On stirring the mixture at room temperature for 10 min, a purple solution resulted. After being stirred overnight, the solution was analyzed by means of GLC to confirm the presence of benzene (0.016 mmol), styrene (0.109 mmol), 2-phenyl-2-propanol (0.147 mmol), mesityl oxide (0.007 mmol), and tetrahydrofuran (0.811 mmol). Addition of phenol to the solution changed the product distribution to benzene (0.046 mmol), styrene (0.261 mmol), 2-phenyl-2-propanol (0.005 mmol), and mesityl oxide (0.045 mmol) (Table 2).

The reactions of **3** and benzophenone, acetaldehyde, and benzaldehyde were carried out similarly except that diethyl ether was used as solvent.

Reaction of $CrPh(acac)_2$ (1) with Alcohols. Since the method is general the reaction of **1** with methanol is described as a representative example, and reaction conditions, yields, and analytical data are listed in Table 3.

To the flask containing 1.127 g (3.44 mmol) of **1** was added 5 cm³ of methanol by the trap-to-trap method. After being stirred at room temperature for 6 h, the volatile liquid was evaporated off *in vacuo* to leave 0.834 g (86%) of a green powder of $[Cr(OMe)(acac)_2]_2$ **4a**. The powder was crystallized from 8 cm³ of hot toluene.

In the reaction with less volatile alcohols, solvents such as diethyl ether and tetrahydrofuran were employed and freshly distilled alcohols were added to the mixture using a syringe (see Table 3).

Reactions of the Alkoxo Complexes (4) with Acetyl Chloride. To the flask containing 44.4 mg (0.079 mmol) of $[Cr(OMe)(acac)_2]_2$ (**4a**) and 2 cm³ of toluene, *ca.* 0.5 cm³ of acetyl chloride was added by means of the trap-to-trap method. After being stirred at room temperature for 30 min, the solution was analyzed by GLC using benzene as an internal reference to reveal the formation of 0.131 mmol (0.83 mol/Cr) of methyl acetate.

Similarly carried out were the reactions of acetyl chloride with $[Cr(OEt)(acac)_2]_2$ (**4b**) (the yield of ester was 0.99 mol/Cr), $[Cr(O\text{-}i\text{-}Pr)(acac)_2]_2$ (**4d**) (1.00 mol/Cr), $Cr(OPh)(acac)_2$ (**4i**) (0.97 mol/Cr), $[Cr(OC_6H_4\text{-}p\text{-}OMe)(acac)_2]_2$ (**4j**) (1.00 mol/Cr), and $[Cr(OCH_2CH_2OH)(acac)_2]_2$ (**4k**) (1.00 mol/Cr).

Reaction of $CrPh(acac)_2$ with Water. Stirring the mixture of 0.725 g (2.20 mmol) of $CrPh(acac)_2$ (**1**), 5 cm³ of tetrahydrofuran, and 0.2 cm³ (11.1 mmol) of water at room temperature for 2.5 h afforded a purple solution. Evaporating off the volatile liquid gave 0.529 g (90%) of a purple powder which was crystallized from hot toluene. The product was analyzed as $[Cr(OH)(acac)_2]_2$ (**2**) on the basis of IR spectrum, elemental analysis, and molecular weight measurement (Table 3). GLC analysis of the volatile liquid showed the formation of benzene in the yield of 1 mol per mol of complex.

Reaction of $CrPh(acac)_2$ (1) with Diethyl Malonate. To the flask containing 0.726 g (2.21 mmol) of $CrPh(acac)_2$ (**1**), 3 cm³ of diethyl malonate was condensed under high vacuum. The mixture was stirred at room temperature for 2 d and a reddish orange suspension turned to purple solution. GLC analysis of the resulting solution indicated the formation of 1.00 mol of benzene per mol of **1**. Evaporating off the volatile liquid from the system gave a purple solid of $Cr(dem)(acac)_2$ (**6b**) (0.448 g, yield 50% on the basis of **1**). The solid was recrystallized from toluene–hexane to give purple crystals. Found: C, 48.9; H, 5.9; Cr, 12.5%. Calcd for $C_{17}H_{25}O_8Cr$: C, 49.9; H, 6.2; Cr, 12.7%.

Reaction of **1** with ethyl acetoacetate to give $Cr(eac)(acac)_2$ (**6a**) was carried out similarly.

References

1) R. P. A. Sneeden, "Organochromium Compounds," Academic Press, New York (1975).
2) K. Nishimura, H. Kuribayashi, A. Yamamoto, and S. Ikeda, *J. Organomet. Chem.*, **37**, 317 (1972).
3) A. Yamamoto, Y. Kano, and T. Yamamoto, *J. Organomet. Chem.*, **102**, 57 (1975).
4) E. Kurras, *Naturwissenshaften.*, **46**, 171 (1959).
5) K. Maruyama, T. Ito, and A. Yamamoto, *J. Organomet. Chem.*, **90**, C28 (1975).
6) K. Maruyama, T. Ito, and A. Yamamoto, *J. Organomet. Chem.*, **155**, 359 (1978).
7) K. Maruyama, T. Ito, and A. Yamamoto, *J. Organomet. Chem.*, **157**, 463 (1978).
8) K. Maruyama, T. Ito, and A. Yamamoto, *Bull. Chem. Soc. Jpn.*, **52**, 849 (1979).
9) K. Maruyama, T. Ito, and A. Yamamoto, *Transition Met. Chem.*, **5**, 14 (1980).
10) See, for example, A. B. Deshpande, R. V. Subramanian, and S. L. Kapur, *J. Polym. Sci., Part A-1*, **4**, 1799 (1966).
11) G. Sartori and G. Costa, *Z. Elektrochem.*, **63**, 105 (1959).
12) J. C. Thomas, *Chem. Ind. (London)*, **1956**, 1388.
13) K. Maruyama, T. Ito, and A. Yamamoto, *Chem. Lett.*, **1978**, 479.
14) E. O. Fischer and W. Hafner, *Z. Naturforsch., Teil B*, **10**, 665 (1955).
15) M. Tsutsui and H. Zeiss, *J. Am. Chem. Soc.*, **81**, 1367 (1959).
16) H. Horino, T. Ito, and A. Yamamoto, *Chem. Lett.*, **1978**, 17; T. Ito, H. Horino, Y. Koshiro, and A. Yamamoto, *Bull. Chem. Soc. Jpn.*, **55**, 504 (1982).
17) S. Komiya, S. Tane-ichi, A. Yamamoto, and T. Yamamoto, *Bull. Chem. Soc. Jpn.*, **53**, 673 (1980).
18) N. Hagihara and H. Yamazaki, *J. Am. Chem. Soc.*, **81**, 3160 (1959); R. W. Adams, E. Bishop, R. L. Martin, and G. Winter, *Aust. J. Chem.*, **19**, 207 (1966); R. W. Adams, R. L. Martin, and G. Winter, *ibid.*, **20**, 773 (1967).
19) K. Kasuga, T. Itou, and Y. Yamamoto, *Bull. Chem. Soc. Jpn.*, **47**, 1026 (1974).
20) E. D. Estes, R. P. Scaringe, W. E. Hatfield, and D. J. Hodgson, *Inorg. Chem.*, **15**, 1179 (1976); **16**, 1605 (1977).
21) K. N. Mahendra, G. K. Parashar, and R. C. Mehrotra, *Synth. React. Inorg. Met.-Org. Chem.*, **9**, 213 (1979).
22) D. A. Brown, D. Cunningham, and W. K. Glass, *J. Chem. Soc., A*, **1968**, 1563.
23) K. Nakamoto, "Infrared and Raman Spectra of Inorganic and Coordination Compounds," 3rd ed, Wiley-Interscience, New York (1978).
24) K. N. Mahendra, P. C. Bharara, and R. C. Mehrotra, *Inorg. Chim. Acta*, **25**, L5 (1977).

25) J. R. Ferraro and W. R. Walker, *Inorg. Chem.*, **4**, 1382 (1965); W. R. McWhinnie, *J. Inorg. Nucl. Chem.*, **27**, 1063 (1965).
26) J. R. Ferraro, R. Driver, W. R. Walker, and W. Wozniak, *Inorg. Chem.*, **6**, 1586 (1967); G. Blyholder and N. Ford, *J. Phys. Chem.*, **68**, 1496 (1964).
27) T. V. Ashworth, M. J. Nolte, and E. Singleton, *J. Chem. Soc., Chem. Commun.*, **1977**, 936; D. R. Robertson and T. A. Stephenson, *J. Organomet. Chem.*, **157**, C47 (1978).
28) M. E. Fakley and A. Pidcock, *J. Chem. Soc., Dalton Trans.*, **1977**, 1444.
29) T. Yamamoto, M. Kubota, A. Miyashita, and A. Yamamoto, *Bull. Chem. Soc. Jpn.*, **51**, 1835 (1978); T. Yamamoto, T. Kohara, and A. Yamamoto, *ibid.*, **54**, 2010 (1981).
30) T. Ito and A. Yamamoto, *J. Organomet. Chem.*, **174**, 237 (1979).
31) T. Mole, *Aust. J. Chem.*, **16**, 794 (1963).
32) "Modern Coordination Chemistry," ed by J. Lewis and R. G. Wilkins, Interscience, New York (1960), Chap. 6.
33) E. B. Sandell, "Colorimetric Determination of Traces of Metals," 3rd ed, Interscience, New York (1959); "Shin-Jikken Kagaku Koza, Bunseki Kagaku-I," ed by the Chemical Society of Japan, Maruzen, Tokyo (1976), Vol. 9, p. 291.

Stereospecific Synthesis of (2*Z*,4*E*,6*E*)-3,7,11-Trimethyl-2,4,6,10-dodecatetraene [*trans*(C_{10})-Allofarnesene]

Norio Miyaura, Hiroshi Suginome,* and Akira Suzuki†

Organic Synthesis Division, Department of Chemical Process Engineering, Faculty of Engineering, Hokkaido University, Sapporo 060

† *Department of Applied Chemistry, Faculty of Engineering, Hokkaido University, Sapporo 060*

(Received December 24, 1981)

The stereospecific synthesis of the title acyclic sesquiterpene, isolated from *Perilla frutscens* f. viridis Makino (Japanese name, Aojiso) by the palladium-catalyzed cross-coupling of 2-(4,8-dimethyl-1,3,7-nonatrienyl)-1,3,2-benzodioxaborole with (*Z*)-2-bromo-2-butene, is described. The benzodioxaborole was prepared by the hydroboration of 4,8-dimethyl-3,7-nonadien-1-yne, newly prepared *via* three steps from geranial, with 1,3,2-benzodioxaborole.

Two isomers, **1** and **2** of α-farnesene were isolated from *Perilla frutscens* Makino (Japanese name, Aojiso) by Sakai and Hirose, who called them *trans*(C_{10})-allofarnesene and *cis*(C_{10})-allofarnesene and assigned the structures, (2*Z*,4*E*,6*E*)-3,7,11-trimethyl-2,4,6,10-dodecatetraene and its (2*E*,4*E*,6*E*)-isomer.[1]

In this paper, a stereospecific synthesis of (2*Z*,4*E*,6*E*)-3,7,11-trimethyl-2,4,6,10-dodecatetraene (**1**) corresponding to *trans*(C_{10})-allofarnesene by the palladium-catalyzed cross-coupling of 2-(4,8-dimethyl-1,3,7-nonatrienyl)-1,3,2-benzodioxaborole (**7**) with (*Z*)-2-bromo-2-butene[2] is described. The synthesis is based on the method developed by us and reported in previous papers.[3,4]

The alkenylborane, **7** required for the coupling reaction was prepared *via* three steps from geranial (**4**), itself previously prepared by the oxidation of geraniol (**3**) with active manganese dioxide.[5,6]

Thus, the reaction of geranial (**4**) with carbon tetrabromide and triphenylphosphine in dichloromethane in the presence of zinc, according to the method developed by Corey and Fuchs,[7] gave dibromide (**5**) in a 95% yield. Analysis by GC indicated that the geometry of geranial (**4**) was retained in dibromide, **5**, the ratio of (3*E*)- and (3*Z*)-isomer being 98:2. 4,8-Dimethyl-3,7-nonadien-1-yne (**6**) was prepared in a 90% yield by the reaction of dibromide, **5**, with butyllithium in hexane. The ratio of (3*E*)- and (3*Z*)-isomers in the product, **6**, was found by GC analysis to be 98:2.

The reaction of **6** with 1,3,2-benzodioxaborole[8] at 70 °C in an atmosphere of nitrogen gave 2-(4,8-dimethyl-1,3,7-nonatrienyl)-1,3,2-benzodioxaborole (**7**) as a viscous oil in a 72% yield. The ^{1}H NMR spectrum of borole, **7**, indicated that it was nearly a single isomer. It was found, however, that it gradually decomposed when exposed to air.

A mixture of borole **7** and (*Z*)-2-bromo-2-butene[2] in benzene containing $Pd(PPh_3)_4$[9] and sodium ethoxide was heated under reflux for 2 h in an atmosphere of nitrogen. The subsequent distillation of the product by Kugelrohr gave (2*Z*,4*E*,6*E*)-3,7,11-trimethyl-2,4,6,10-dodecatetraene (**1**) [*trans*(C_{10}) allofarnesene] in a 51% isolated yield. It was found that the use of THF as the solvent in this coupling considerably lowered the yield (29%) of **1** as well as the stereoselectivity of the coupling, the ratio of the (2*Z*,4*E*,6*E*) and (2*E*,4*E*,6*E*) isomers in the product being 32:68.[10]

The 200 MHz ^{1}H NMR spectrum of the synthetic *trans*(C_{10}) allofarnesene (**2**) thus obtained gave, for the

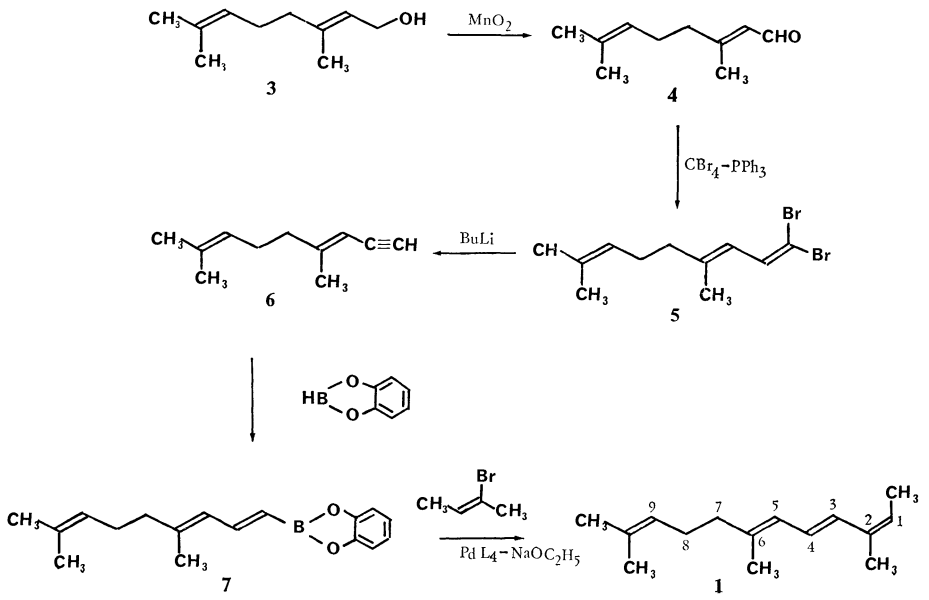

Scheme 1.

first time, well-resolved signals for all the olefinic protons and the methyl groups; their assignments are described in the Experimental section.

Experimental

The IR spectra were recorded on a Hitachi-Perkin Elmer Model 125 spectrometer. The ^{1}H-NMR spectra of all compounds with the exception of synthetic farnesene were determined with a Hitachi R-22 spectrometer (90 MHz) (solvent $CDCl_3$: TMS as the internal reference). The ^{1}H-NMR spectra of the synthetic farnesene was recorded with a JEOL JNM-FX-200 spectrometer (200 MHz). The mass spectra of **5** and **6** were determined with a JEOL JMS-D 300 spectrometer (70 eV) in the Faculty of Agriculture. Specimens for analysis were prepared by distillation with Kugelrohr (Shibata GTO-250 R). The bp shows the oven temperature of Kugelrohr. THF was distilled from benzophenone ketyl.

Geranial (4). This aldehyde was prepared by a procedure reported by Corey *et al.*[6] An analysis by VPC (10% Silicone OV-17 on Uniport B, 2m) indicated that this geranial contained 2% of neral (citral-b).

Preparation of (3E)-1,1-Dibromo-4,8-dimethyl-1,3,7-nonatriene (5). A mixture of PPh_3 (13.2 g, 50 mmol), CBr_4 (16.6 g, 50 mmol), and Zn powder (3.9 g, 60 mmol) in dry CH_2Cl_2 (250 ml) was stirred at room temperature for 48 h under an atmosphere of N_2. To this solution, we then added geranial (3.1 g, 20.5 mmol) in CH_2Cl_2 (10 ml) at 0 °C over a period of 15 min; the solution was stirred at that temperature for 1 h, after which the stirring was continued for another hour at room temperature. To the reaction mixture, we added hexane (500 ml) and colorless crystals and a viscous tarry material thus precipitated were removed by filtration. The removal of the solvent gave a mixture of products. This mixture was extracted with hexane (200 ml). The removal of the solid by filtration from the hexane solution and evaporation of the solvent gave a pale brown oil which was distilled with Kugelrohr to give dibromide, **5** (6.0 g, 95%); bp 80—85 °C(0.05 mmHg**). (Found: *m/z* 305.9643. Calcd for $C_{11}H_{16}Br_2$: M, 305.9621); MS *m/z* (rel intensity) 310 (M^++4, 0.2), 308 (M^++2, 0.4), 306 (M^+, 0.3), and 69 [$(CH_3)_2C{=}CH{-}CH_2^+$, 100]; n_D^{20}=1.5579; IR, (KBr disk), 1625, 1070, 845, and 775 cm^{-1}; ^{1}H NMR 1.60 (3H, s, 8-methyl), 1.68 (3H, s, 8-methyl), 1.74 (3H, s, 4-methyl), 2.08—2.12 (4H, m, 5 and 6-methylenes), 5.13 (1H, broad s, 7H), 5.90 (1H, broad d, J=10 Hz, 3-H), and 7.16 (1H, d, J=10 Hz, 2-H).

Preparation of 4,8-Dimethyl-3,7-nonadien-1-yne (6). To a solution of **5** (5.4 g, 17.5 mmol) in dry THF (30 ml) kept at −78 °C, was added dropwise BuLi in hexane (1.5 mol dm^{-3} solution, 28 ml, 42 mmol) over a period of 20 min; the solution was then stirred for 1 h at that temperature. The bath temperature was then gradually raised up to room temperature over the period of 1 h. After the solution had been further stirred for 1 h at room temperature, a saturated solution of NH_4Cl (5 ml) was added. The aqueous layer was separated and extracted with petroleum ether. The combined extracts were washed with saturated brine and with water and dried over anhydrous $MgSO_4$. The distillation of the product by Kugelrohr gave 4,8-dimethyl-3,7-nonadien-1-yne (**6**) (2.35 g, 90%); bp 75 °C (15 mmHg). (Found: *m/z* 148.1223. Calcd for $C_{11}H_{16}$: M, 148.1250); MS *m/z* (rel intensity) 148 (M^+, 0.4), 133 (M^+-CH_3, 8), and 69 [$(CH_3)_2C{=}CH{-}CH_2^+$, 100] n_D^{20}=1.4838; IR (film), 3296(C≡CH), 2104(C≡C), and 1632 cm^{-1}; ^{1}H NMR, 1.60 (3H, s, 8-methyl), 1.68 (3H, s, 8-methyl), 1.91 (3H, s, 4-methyl), 1.09—2.13 (4H, m, 5- and 6-methylene), 3.02 (1H, t, J=2 Hz, 1-H), 5.11 (1H, broad s, 7-H), and 5.32 (1H, broad s, 3-H).

2-(4,8-Dimethyl-1,3,7-nonatrienyl)-1,3,2-benzodioxaborole (7). A mixture of **7** (0.45 g, 3.0 mmol) and 1,3,2-benzodioxaborole (0.33 ml, 3.0 mmol) was heated at 70 °C for 3 h under an atmosphere of N_2: Distillation by using Kugelrohr gave trienylborane, **7**, as a viscous oil, bp 130 °C (0.05 mmHg) (0.58 g, 72%). A shorter reaction time (1 h) resulted in a lower yield (37%) of the borane. This borane was used immediately for the next step. This trienylborane has been found to decompose gradually when it is exposed to air, but it can be stored in an atmosphere of N_2 in a refrigerator. ^{1}H NMR, 1.63 and 1.70 (each 3H, s, *gem*-dimethyl), 1.94 (3H, s, 6-methyl), 2.15—2.20 (4H, m, 4- and 5-methylenes), 5.17 (1H, broad s, 3-H), 5.80 (1H, d, J=18 Hz, 9-H), 6.14 (1H, broad d, J=11 Hz, 7-H), 7.07—7.34 (4H, m, aromatic protons), and 7.73 (1H, dd, J=18 and 11 Hz).

(Z)-2-Bromo-2-butene. This bromide was prepared in an 80% yield according to the method reported by Bordwell and Landis.[2] It showed bp of 44 °C(160 mmHg) [lit,[2] bp 83.5—84.0 °C]. The isomeric purity of the product was found to be 99% by GC analysis (Hitachi K-53 instruments, SVS capillary column, 0.25 mm×45 m, Ucon Oil LB-550X). This bromide was immediately used for the next step, since it is gradually isomerized during storage in a refrigerator. After one-week storage, the isomeric purity went down to *Z*/*E* 91:9.

Synthesis of trans*(C$_{10}$)-Allofarnesene (1).* A mixture of $Pd(PPh_3)_4$ (0.033 g, 0.029 mmol), 2-(4,8-dimethyl-1,3,7-nonatrienyl)-1,3,2-benzodioxaborole (0.348 g, 1.43 mmol), and (*Z*)-2-bromo-2-butene (0.23 g, 1.7 mmol) in benzene (5 ml) containing 2 M-NaOEt†† in EtOH (2 ml) was heated under reflux for 2 h in an atmosphere of N_2. The unreacted borane was then removed by oxidizing with 3 M-NaOH (1 ml) and 30% H_2O_2 (0.3 ml) for 1 h at room temperature. The reaction mixture was extracted with 1:1 benzene–hexane, and the solution was washed with saturated brine and dried over anhydrous $MgSO_4$. Distillation of the product by Kugelrohr gave 0.15 g (51%) of *trans*(C$_{10}$)-allofarnesene (**1**); bp 70 °C(0.08 mmHg). It had n_D^{20}=1.5371. IR (KBr disk), 3040, 1640, and 955 cm^{-1}. ^{1}H NMR, (200 MHz), δ 1.61,††† 1.69,††† 1.80,††† and 1.85††† (each 3H, s, *gem*-dimethyl, 3-methyl, and 7-methyl groups), 1.74 (3H, d, J=7 Hz, protons on C_1), 2.10 (4H, broad s, C_8 and C_9 methylene protons), 5.11 (1H, broad s, 10-H), 5.41 (1H, q, J=7 Hz, 2-H), 5.97†† (1H, d, J=10 Hz, 6-H), 6.57 (1H, d, J=15 Hz, 4-H), 6.42 (1H, dd, J=10 and 15 Hz, 5-H). UV, λ_{max} (C_2H_5OH) 270 nm (inflection, ε 33700), 280 (ε 39500), and 291 (ε 33000); MS, *m/z* 204 (M^+). The yield of *trans*(C$_{10}$)-allofarnesene in this coupling, examined by GLC (Hitachi 163 instrument with a 2 m in 15% Ucon Oil HB-2000 on Uniport B column and with tetradecane as the internal standard), was 89% (1.27 mmol), accompanied by 6% (0.086 mmol) of *cis* (C$_{10}$)-allofarnesene.

References

1) T. Sakai and Y. Hirose, *Bull. Chem. Soc. Jpn.*, **42**, 3615 (1969).

2) F. C. Bordwell and P. S. Landis, *J. Am. Chem. Soc.*, **79**, 1593 (1957).

** 1 mmHg≈133.322 Pa.

†† 1 M=1 mol dm^{-3}.

††† A further small splitting (J=1 Hz) due to a long-range coupling is observed in this signal.

3) N. Miyaura, K. Yamada, and A. Suzuki, *Tetrahedron Lett.*, **1979**, 3437; N. Miyaura, H. Suginome, and A. Suzuki, *ibid.*, **22**, 127 (1981).

4) Subsequent to the preparation of this manuscript, the synthesis of the eight isomers of allofarnesene by the Wittig reaction was reported, H. J. Williams, M. R. Strand, and S. Vinson, *Tetrahedron*, **37**, 2763 (1981).

5) J. Attenburrow, A. F. B. Cameron, J. M. Chapmann, R. M. Evans, B. A. Hems, A. B. A. Jansen, and T. Walker, *J. Chem. Soc.*, **1952**, 1094.

6) E. J. Corey, N. W. Gilman, and B. E. Ganem, *J. Am. Chem. Soc.*, **90**, 5616 (1968).

7) E. J. Corey and P. L. Fuchs, *Tetrahedron Lett.*, **1972**, 3769.

8) H. C. Brown and S. K. Gupta, *J. Am. Chem. Soc.*, **93**, 1816 (1971).

9) D. R. Coulson, *Inorg. Synth.*, **13**, 121 (1972).

10) The observed lower stereoselectivity, when THF was used as the solvent, is probably due to the partial isomerization of (*Z*)-2-bromo-2-butene to its (*E*)-isomer before the coupling. The rate of the oxidative addition of the (*E*)-isomer to Pd(0) would probably be faster than that of the (*Z*)-isomer, since we observed that, in the cross-coupling reaction of a 1:1 mixture of (*E*) and (*Z*)-isomers of styryl bromide with (*E*)-1-hexenyl-1,3,2-benzodioxaborole catalyzed by $Pd(PPh_3)_4$, the rate of the disappearance of (*E*)-styryl bromide was some 10 times faster than that of the (*Z*)-isomer (unpublished results).

Methylation of a Benzene Ring as a Chemical Signal. Marked Changes in the Pattern of Temperature Dependence of the Selectivity in Oxidation of a Pair of Associating Thiols

Tadashi ENDO,* Akihiro OKUBO, Yuji KANEKO, Masatoshi UEHARA, Hidetoshi TASAI, Akiyoshi SATO, Kunio NIKKI,† Naoya NAKAGAWA,† and Shinichi KAMEI††

Department of Chemistry, College of Science and Engineering, Aoyama Gakuin University, Chitosedai, Setagaya-ku, Tokyo 157

† *The University of Electro-communications, Chofugaoka, Chofu, Tokyo 182*

†† *Kyowa Kagaku Co., Ltd., 3-4-5, Hongo, Bunkyo-ku, Tokyo 113*

(Received December 26, 1981)

Temperature dependence of the selectivity [the ratio of an unsymmetrical disulfide to symmetrical one] has been studied in oxidation of a pair of associating thiols, each with the recognition site [$C_6H_4N(CH_3)_2$ and R^1], with O_2 in 80% (v/v) acetonitrile–20% water in the range of −10 to 70 °C. The selectivity for $R^1=C_6H_4CH_3$ shows a minimum at 35 °C, whereas for $R^1=C_6H_5$ the selectivity exhibits a maximum at 35 °C; for $R^1=C_6H_4C_2H_5$ plots of the selectivity against temperature shows a sigmoid-like curve. The selectivity in oxidation of a pair of non-associating thiols, 2-(dimethylamino)ethanethiol and a para-substituted benzenethiol, remains practically unaltered with temperature in the same solvent. Though thiol-disulfide exchange reaction proceeds slowly below 35 °C, the selectivity in the exchange differs entirely from that in the oxidation. It has been found that changes in hydrophobicity with R^1 and temperature cannot explain dramatic alterations in the selectivity with R^1 and temperature.

Highly specific molecular recognition underlies living systems. Proteins such as restriction endonucleases[1] and modification methylases[1] can recognize the methyl group. The enzyme-catalyzed methylation of DNA,[2] proteins,[3] and phospholipids[4] is among the biological control mechanisms,[5] and has been investigated extensively: (1) methylation of nucleotide bases (5-methylcytosine and N^6-methyladenine) lying within the recognition sequence serves to protect the cell's own DNA from being degraded by its restriction endonucleases,[6] (2) methylation, for example, of cytosine is involved in gene regulation and differentiation,[7] (3) most eukaryotic, but not bacterial, messenger RNAs contain a methylated guanosine (7-methylguanosine) —— the "cap" —— at their 5′-ends,[8] and (4) methylation of protein-carboxyl groups (*e.g.*, γ-carboxyl group(s) of glutamic acid residue(s)) is associated with the control of chemotactic behavior and with signal transduction in both prokaryotes and eukaryotes.[9]

It is striking that biological systems make use of quite a "simple" chemical modification, *methylation*, in their control mechanisms as described above. In spite of biological significance, the problem of methylation has not so far been examined from a chemical point of view of, for example, what influence the methylation exercises on chemical events as well as of how noncovalent weak interactions are altered upon methylation. We report here that the methylation of a benzene ring remote from the reaction site radically alters the pattern of temperature dependence of the selectivity in oxidation of a pair of associating thiols.

In this study we used two reaction systems: the associating system (system A) and non-associating system (system N). These two systems are structurally related to each other except for the ability to associate. System A consists of a pair of thiols (**1** and **2**)[10] which can associate mainly through intermolecular hydrogen bonding.[11] Thiols **1** and **2** each have the three sites —— thereaction site (SH group) where model reaction takes place, the binding site (–CNHCNH–, acylurea bond) that can participate in intermolecular hydrogen bonding,[11] and the recognition site [$C_6H_4N(CH_3)_2$ or R^1] that can participate in the selective recognition. System A is further divided into system A_p (**1** and **2p**), system A_t (**1** and **2t**), system A_e (**1** and **2e**), and system A_a (**1** and **2a**). System N is made up of a pair of thiols, 2-(dimethylamino)ethanethiol (**3**) and a para-substituted benzenethiol (**4**); this system is also divided into system N_p (**3** and **4p**) and system N_t (**3** and **4t**).

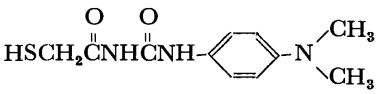

1

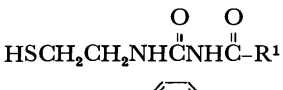

2p $R^1=$

2t $R^1=$ 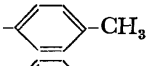

2e $R^1=$ 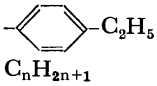

2a $R^1=C_nH_{2n+1}$

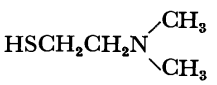

3

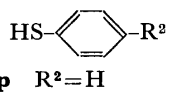

4p $R^2=H$
4t $R^2=CH_3$

As a model reaction, oxidation of system A or N with oxygen was chosen. Oxidation of system A gives three disulfides, two symmetrical disulfides (**5** and **7**) and an unsymmetrical disulfide (**6**) as shown in Eq.

1; similarly, oxidation of system N gives the corresponding three disulfides (**8**—**10**) (Eq. 1). The determination of the products in the case of oxidation of system A was made according to our method[12] which took advantage of separation by thin-layer chromatography (TLC) and UV absorption due to the moiety $-HNC_6H_4N(CH_3)_2$.[13] The selectivity (R) —— a measure of *molecular recognition* —— in this oxidation is represented by the ratio of the yield of **6** (or **9**) to that of **5** (or **8**) [R=**6**/**5** for system A or **9**/**8** for system N].[13,14]

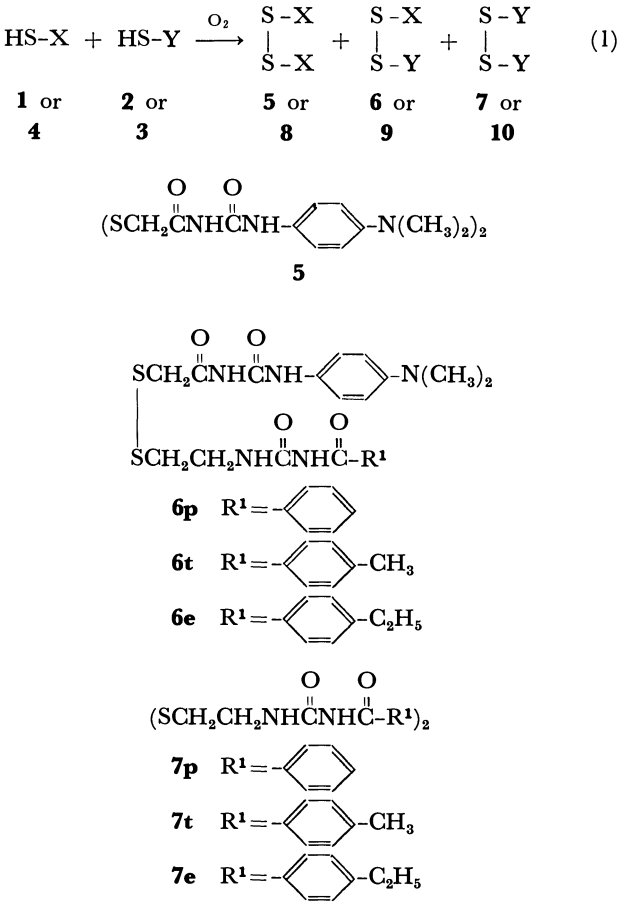

Results

Selectivity in Oxidation of a Pair of Thiols. The temperature dependence of the selectivity (R) in oxidation of system A was examined in 80% (v/v) acetonitrile–20% water within the temperature range from −10 to 70 °C. The results are shown in Table 1 and Fig. 1: (1) each of the three curves for systems A_p, A_t, and A_e shows considerable symmetry around 35 °C; (2) the selectivity for all the three systems increases in going from 0 to −10 °C; (3) even at 70 °C the R values do not approach 2 (the statistically expected value[15]) for this type of reaction) except in the case of system A_p, this result contrasting sharply with the fact[16] that for system A_a where R^1=*i*-C_5H_{11} and *n*-C_5H_{11} the R values at 70 °C were 2.9 and 2.3, respectively.

Control experiments were performed at 20, 35, and 70 °C using oxidation of system N. The R values were found to vary only slightly (*i.e.*, from 1.6 to 1.8) in both systems N_p and N_t within this temperature

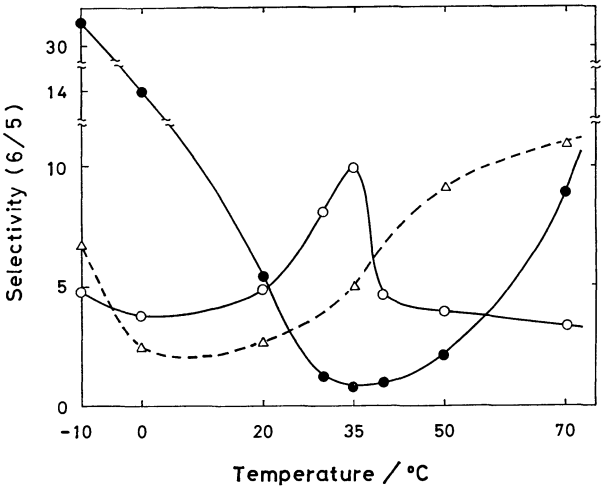

Fig. 1. Temperature dependence of the selectivity (**6**/**5**) in oxidation of system A with O_2 in 80% (v/v) CH_3CN–20% H_2O.
○: System A_p (**1**+**2p**), ●: system A_t (**1**+**2t**), △: system A_e (**1**+**2e**).

Table 1. Yields of disulfides (**5** and **6**) and the selectivity in oxidation[a] of system A with O_2

Temp/°C	System A_p (**1**+**2p**)			System A_t (**1**+**2t**)			System A_e (**1**+**2e**)		
	Yield[b]/%		Selectivity (**6**/**5**)	Yield[b]/%		Selectivity (**6**/**5**)	Yield[b]/%		Selectivity (**6**/**5**)
	5	**6**		**5**	**6**		**5**	**6**	
−10	14	67	4.8	2.9	89	31	11	75	6.8
0	16	61	3.8	5.9	84	14	22	54	2.5
20	14	68	4.9	13	70	5.4	21	56	2.7
30	9.5	77	8.1	30	38	1.3			
35	8.1	81	10	34	29	0.85	14	70	5.0
40	14	66	4.7	32	33	1.0			
50	16	64	4.0	22	46	2.1	8.6	79	9.2
70	18	61	3.4	9.0	80	8.9	7.5	81	11

a) The time required for the oxidation was 1.5 h for 70 °C, 3 h for 35 °C, and 50 to 70 h for 0 °C. b) Yields are calculated in such a way that (1) when **1** and **2** are converted exclusively to **5** and **7**, respectively, the yields of **5** and **7** are both 50% and (2) when **1** and **2** are converted exclusively to **6**, the yield of **6** is 100%.

range.

Selectivity in Thiol-Disulfide Exchange Reaction. We studied thiol-disulfide exchange reaction, known to take place generally as shown in Eqs. 2 and 3,[17] in order to elucidate whether or not the exchange affects the experimental results illustrated in Fig. 1. The exchange was carried out mainly between thiol **2** and disulfide **5** at 0, 35, and 70 °C for the same time as with the corresponding oxidation. Since resulting thiol **1** (Eqs. 2 and 3) could not be separated from disulfide **5** by TLC in the solvent required to separate the three disulfides **5**—**7** from one another, **1** was converted to the corresponding sulfide having the carbamoyl group (**11**), by treatment with iodoacetamide and Et_3N (Eq. 4),[18] so as to be determined by the method[12] described above.

$$\underset{\mathbf{2}}{\text{HS-Y}} + \underset{\mathbf{5}}{\text{XS-SX}} \rightleftharpoons \underset{\mathbf{6}}{\text{XS-SY}} + \underset{\mathbf{1}}{\text{HS-X}} \quad (2)$$

$$\underset{\mathbf{2}}{\text{HS-Y}} + \underset{\mathbf{6}}{\text{XS-SY}} \rightleftharpoons \underset{\mathbf{7}}{\text{YS-SY}} + \underset{\mathbf{1}}{\text{HS-X}} \quad (3)$$

$$\underset{\mathbf{1}}{\text{HS-X}} + \text{ICH}_2\overset{\overset{\text{O}}{\|}}{\text{C}}\text{NH}_2 \xrightarrow[-\text{Et}_3\text{N}\cdot\text{HI}]{\text{Et}_3\text{N}} \underset{\mathbf{11}}{\text{XSCH}_2\overset{\overset{\text{O}}{\|}}{\text{C}}\text{NH}_2} \quad (4)$$

In Table 2 are listed the experimental data: (1) at 0 °C the exchange reaction is slow in all cases; (2) at 35 °C the exchange proceeds to some extent except in the case of **2t** and **5**; (3) at 70 °C the reaction is fast; (4) the rate of the reaction increases progressively with increasing temperature as exemplified by the yield of **5**.

The exchange was also performed between thiol **1** and disulfide **7** for the same time as with the corresponding oxidation (Table 2). In view of the results with the exchange between **2** and **5**, the reaction temperature to be examined was limited to 35 and 70 °C, and disulfide **7** to **7p** and **7t**. As a result, 75 to 94% of **1** was found to remain unreacted in all cases. From the data shown in Tables 1 and 2, it has been demonstrated that the selectivity in the exchange differs entirely from the selectivity in the oxidation.

Further, we examined disulfide-disulfide exchange reaction between **5** and **7t** at 35.0 °C in the presence of Et_3N, but in the absence of a thiol, for 3 h (Eq. 5). The exchange proved not to occur practically, as

$$\underset{\mathbf{5}}{\text{XS-SX}} + \underset{\mathbf{7t}}{\text{YS-SY}} \rightleftharpoons 2\,\underset{\mathbf{6t}}{\text{XS-SY}} \quad (5)$$

indicated by the observation that recovery of **5** was 92% with the yield of **6t** being <1%; this agrees well with the generally accepted view.[17a]

Physicochemical Properties of the Associating Thiols. The degree to which molecules self-associate in solution can be represented, for example, by the "degree of association" (f): the f value for the solute is obtained by dividing the stoichiometric mole fraction of the solute by the effective mole fraction of the solute.[19] The data (in benzene at 36.0 °C) in Table 3 exhibit that thiols **1** and **2** are similar in f values to each other and that f values for **2** increase with increasing number of the carbon atoms introduced at the para position of its benzene ring.

The solubilities of **1** and **2** in aqueous acetonitrile, the same solvent as in the oxidation, in the range of 20 to 50 °C are illustrated in Fig. 2 and partly in Table 3 for comparison with the melting points of **1** and **2**. Figure 2 shows that (1) the solubility increases with increasing temperature for each thiol, (2) the solubility of **2** increases in the order **2t**<**2e**<**2p** at all temperatures studied, and (3) **1** is approximately equal in solubility to **2t** at all temperatures. There exists an empirical rule that solubilities decrease with increasing melting-points for a series of homologs.[20]

Table 2. Yields of **5**, **6**, and **11** and the selectivity in thiol-disulfide exchange reaction[a]

Temp/°C	Reactant	Yield[b]/%			Selectivity (**6**/**5**)
		5	**6**	**11**	
0	**2p**+**5**	42	≃0	9.5	≃0
0	**2t**+**5**	33	24	4.9	0.73
0	**2e**+**5**	33	25	5.7	0.76
35	**2p**+**5**	20	22	31	1.1
35	**2t**+**5**	9.0	43	33	4.8
35	**2e**+**5**	27	22	22	0.81
70	**2p**+**5**	≃0	10	87	≃∞
70	**2t**+**5**	3.7	21	65	5.7
70	**2e**+**5**	2.5	32	59	13
35	**1**+**7p**	4.5	13	75	2.9
35	**1**+**7t**	2.5	3.8	88	1.5
70	**1**+**7p**	≃0	11	87	≃∞
70	**1**+**7t**	0.6	1.0	94	1.7

a) The exchange reaction time was the same as with the oxidation; see footnote a in Table 1. b) The yields of **5** and **6** are calculated as in Table 1. The yield of **11** is calculated in such a way that when **5** is converted exclusively to **1**, the yield of **11** is 100%.

Table 3. Physicochemical properties of thiols **1** and **2**

Thiol	f[a]	Solubility[b] (35 °C)	Mp[c] θ_m/°C	Chemical shift[d] H^α (or H^γ)	Chemical shift[d] H^β (or H^δ)
1	1.31	3.06	173	9.50	10.17
2p	1.30	13.4	148	8.73	8.85
2t	1.33	3.15	187	8.58	9.02
2e	1.41	5.36	165	8.56	8.92

a) The values at 36.0 °C and 0.010 M (1 M = 1 mol dm^{-3}) in benzene. For the definition, see the text. b) Expressed in mmol per 100 g of 80% (v/v) CH_3CN-20% H_2O. c) Obtained from the DTA curves. d) The chemical shifts for the individual thiols in $CDCl_3$ at 34 °C and 0.020 M. The values are in ppm downfield from TMS. Greek letters (α, β, γ, and δ) indicate assignments as given in Fig. 4. When **1** and **2** were mixed together in equimolar amounts (0.010 M each) in $CDCl_3$ at 34 °C, the chemical shifts of the NH^α proton were 9.39, 9.36, and 9.38 ppm for systems A_p, A_t, and A_e, respectively, those of the NH^γ proton being 8.67, 8.58, and 8.58 ppm for systems A_p, A_t, and A_e, respectively.

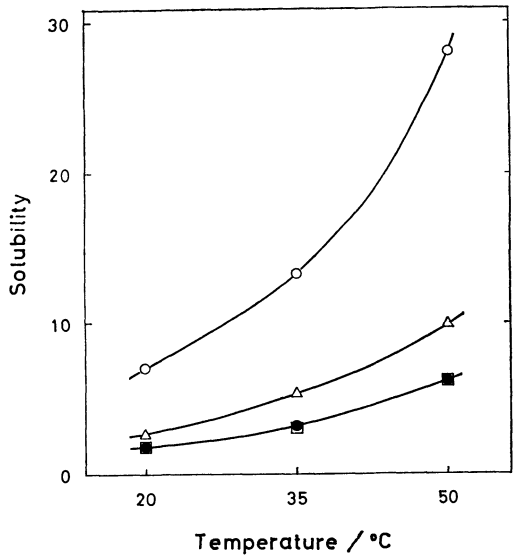

Fig. 2. Temperature dependence of the solubility for **1** and **2**. The solubilities are expressed in mmol/100 g of 80% (v/v) CH_3CN–20% H_2O.
□: **1**, ○: **2p**, ●: **2t**, △: **2e**.

The data in Table 3 show that this rule holds true for thiol **2**.

Using surface tension measurement, we have examined whether or not system A forms micelles in aqueous acetonitrile. As a result, it has been found that in 80% (v/v) acetonitrile–20% water surface tension for systems A_p, A_t, and A_e all remains constant (32.0±0.2 dyn/cm) over the concentration range of 1.3×10^{-6} to 1.0×10^{-2} M.[21]

Figure 3 provides the temperature dependence of the NH proton chemical shifts for system A in $CDCl_3$. The results shown in Fig. 3 reveal that the chemical shifts are more sensitive to temperature for the NH^{α} and NH^{γ} protons (Fig. 4), each participating in intermolecular hydrogen bond, than for the NH^{β} and NH^{δ} protons (Fig. 4), each participating in intramolecular hydrogen bond. Furthermore, chemical shift changes with the structure of R^1 proved to be larger for the NH^{γ} proton than for the NH^{α} proton.

Discussion

The most striking feature of the results reported above is the radical changes in temperature-selectivity profiles from one pattern to another around 35 °C —— from a maximum-having curve to minimum-having one (or to sigmoid-like one) —— on methylation (or ethylation) of the benzene ring in **2** at the para position.[22] This observation would imply that methylation of a benzene ring can function as a *chemical signal* (*or information*) in an associating system. In what follows, we would like to discuss some factors which have the possibility of affecting the temperature dependence of the selectivity on methylation and ethylation.

Intermolecular Association. Table 3 clarifies that **1** and **2** associate strongly with themselves in benzene. In Fig. 4 are given the association patterns[23] of three dimers, two homodimers (**12** and **14**) and a heterodimer (**13**), the association patterns being assigned mainly on the basis of the NMR results (Fig. 3) as in our previous work.[11] Moreover, our study

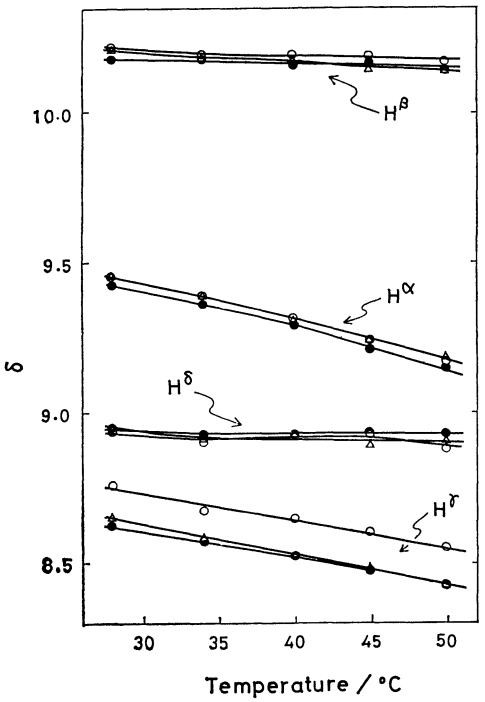

Fig. 3. Temperature dependence of the NH proton chemical shifts for a 1:1 mixture of **1** and **2** (0.010 M each) in $CDCl_3$ at 34 °C.
○: System A_p (**1**+**2p**), ●: system A_t (**1**+**2t**), △: system A_e (**1**+**2e**). For Greek letters, see Fig. 4.

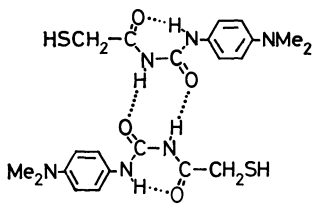

12

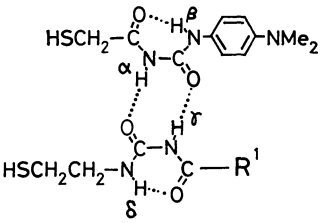

13

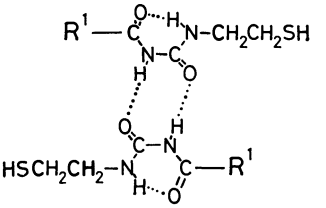

14

Fig. 4. Association patterns of three dimers **12**—**14**.

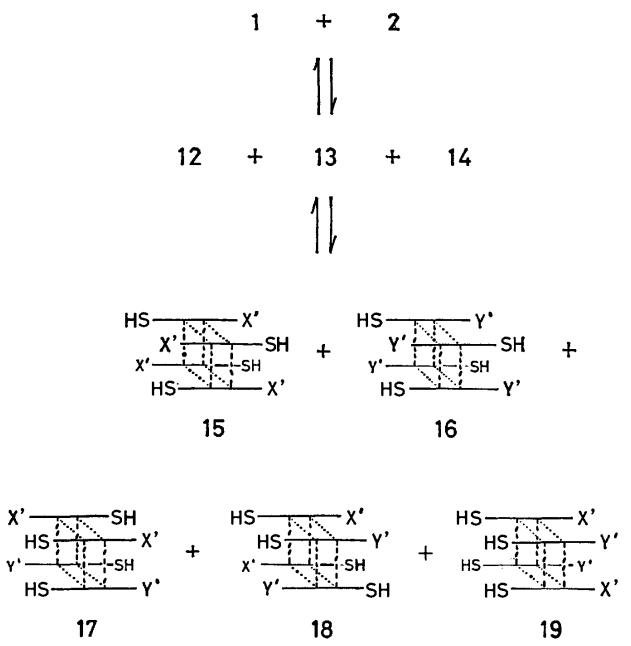

Fig. 5. Association schemes of tetramers **15**—**19** formed by dimerization of dimers **12**—**14**.
·····: Hydrogen bond responsible for stabilization of dimers, ----: noncovalent weak interactions responsible for stabilization of tetramers. The symbols X′ and Y′ represent $C_6H_4N(CH_3)_2$ and R^1, respectively.

has indicated that dimers **12**—**14** would dimerize to form tetramers (Fig. 5) —— two homotetramers (**15** and **16**) and three heterotetramers (**17**—**19**)[23,24] —— in equilibrium with dimers **12**—**14** and monomers (**1** and **2**) and that oxidation of system A_a proceeds through these tetramers **15**—**19**. Since the f value of 1.41 for **2a** ($R^1=i$-C_5H_{11}) is similar to those for **2p**, **2t**, and **2e** under the same conditions as in Table 3, it seems reasonable to assume that oxidation of systems A_p, A_t, and A_e proceeds also through tetramers **15**—**19**. There is substantial evidence for the presence of tetramers[25] and for their participation in biological reactions.[11]

Simple thiols are reported to be capable of forming very weak hydrogen bonds with themselves.[26] However, considering that f values even for the amide derivatives of **2** (**20**) which can form a single hydrogen bond are less than 1.05 in benzene at 36.0 °C and 0.010 M,[27] it is probably fair to say that thiols **3** and **4** are present mainly as monomers in dilute solutions.[26]

$$HSCH_2CH_2NHC(=O)-R^3$$

20

The selectivity remained approximately constant, when oxidation of system N was performed at 20, 35, and 70 °C. This finding together with the data in Fig. 1 demonstrates the importance of intermolecular association in molecular recognition, in agreement with our previous conclusion.[16]

Seeman *et al.* studied how the base pairs in double helical nucleic acids could be recognized by proteins, and concluded that using two hydrogen bonds, fidelity of base pair recognition might be achieved, whereas a single hydrogen bond was inadequate for uniquely identifying any particular base pair.[28]

Possibility of Micelle Formation in Aqueous Acetonitrile. It is recognized that when the concentration of a surfactant in an aqueous solution is increased, surface tension is initially reduced with its concentration, for example, to *ca.* 25 dyn/cm,[29] and then kept approximately constant beyond the critical micelle concentration (cmc).[30] In contrast, surface tension of system A in aqueous acetonitrile did not alter over the concentration range of 1.3×10^{-6} to 1.0×10^{-2} M, the latter corresponding to the concentration of a nearly saturated solution. This result clearly demonstrates that no micelle formation occurs for system A in the same solvent as in the oxidation.

Solubility Differences and Heterogeneity of Reactions. System A was homogeneous at higher temperatures in 80% (v/v) CH_3CN–20% H_2O under argon in the presence of a catalytic amount of Et_3N: system A_p was completely soluble above 40 °C, and systems A_t and A_e above 50 °C. Accordingly, differential solubilities of **1** and **2** at lower temperatures may influence the selectivity in oxidation of system A in such a way that the larger the solubility differences between **1** and **2** are, the smaller the R values become. Since solubility differences between **1** and **2** vary monotonously with temperature, the temperature dependence of solubility differences between **1** and **2** has no appreciable correlation with that of the selectivity for system A (Figs. 1 and 2).

Rys reported the mixing effects on the product distribution in competitive consecutive or parallel reactions.[31] This problem was not examined directly in the present case. However, if diffusion effects influence the selectivity, the temperature-selectivity profiles for systems A_p, A_t, and A_e all should become similar in pattern to one another as temperature increases. As is clear from Fig. 1, this does not hold true, suggesting that the selectivity would not be disguised by diffusion effects.

Exchange Reactions. It is generally accepted that thiol-disulfide exchange reaction occurs easily if a base is present and that the rate of the exchange increases with temperature.[17c] In contrast, in this study thiol-disulfide exchange has been found to take place to a small extent below 35 °C (Table 2), and no appreciable disulfide-disulfide exchange has occurred. It seems probable, therefore, that the exchange reactions have not so great influence on the selectivity in the oxidation of system A at least below 35 °C, judging from the fact that (1) there is a remarkable difference in the selectivity between the exchange and the oxidation (Tables 1 and 2) and (2) the amount of the thiols which can participate in thiol-disulfide exchange is reduced as the oxidation proceeds.

Hydrophobic Interaction.[32] The strength of hydrophobic interaction (hydrophobicity)[33] appears to increase with increasing surface area[34] of the nonpolar group removed from contact with water:[35] The $\Delta G°$ value for the transfer of solute from the pure liquid to aqueous solution increases in the order benzene (4.61 kcal/mol) < toluene (5.33 kcal/mol) < ethylben-

zene (6.07 kcal/mol).[36] Furthermore, hydrophobicity represented by ΔG° for the transfer is known to increase progressively with temperature.[36]

The temperature dependence of R described above was investigated in acetonitrile containing a given amount (20% (v/v)) of water. In addition, using acetonitrile with varying amounts (10 to 50% (v/v)) of water as solvents, oxidation of system A_p was performed similarly at 35.0 °C; R values were plotted against the volume percent of water. As a result, R values were found to show a maximum at 20% of water.[37] If hydrophobic interaction is responsible for the selectivity changes with temperature on methylation and ethylation, the R values for all of systems A_p, A_t, and A_e should vary progressively with volume percent of water and with temperature because of progressive increment of hydrophobicity with these two factors. This does not coincide with the experimental results. These arguments indicate that marked changes in the selectivity with temperature on methylation and ethylation (Fig. 1) cannot be interpreted at all in terms of hydrophobic interaction.

Evidence is now presented to force reexamination of the concept of hydrophobic interaction.[38-40] Lawaczeck and Wagner[38] pointed out that this interaction, though consistent with the behavior of proteins or nonpolar amino acids, failed to account for the thermodynamic data in the nucleic acid field —— the large positive entropy values obtained for nucleic acid melting and for transfer of nucleobases from organic solvents to water. Cramer III[39] showed that hydrophobic interaction was incompatible with relationships between the structures of various nonpolar solutes and their solvation energies by water and 1-octanol. Moreover, based on adhesion and surface free energy data to indicate that the forces between hydrocarbons and water in contact with each other are attractive and not repulsive, Hildebrand[40] has argued against the use of the word "hydrophobic" to describe the relative lack of attraction between water and nonpolar substances.

Three-dimensional Shape-specific Weak Interactions. We have recently suggested that weak interactions specific for three-dimensional shape of nonpolar groups are responsible for selective molecular recognition in oxidation of system A_a.[41] This type of interactions are assumed to possess the following features: (1) they have energies smaller than that for hydrogen bond, (2) they are made up of individual interactions between groups, between a group and an atom, or between atoms, and (3) they can reflect three-dimensional shape of nonpolar groups such as alkyl groups.[42]

The data in Fig. 3 indicate that there is inappreciable difference in the pattern of temperature dependence of the NH^α proton chemical shifts on methylation and ethylation. Hence it seems difficult to consider that specific weak interactions[43] are reflected in the NH^α proton resonance.

Abraham reported that the major contribution to the hydrophobic CH_2 free-energy increment ($\Delta G^\circ =$ 0.54 kcal/mol at 298 K) was an enthalpic effect ($\Delta H^\circ =$ 0.46 kcal/mol) and not an entropic effect ($-T\Delta S^\circ =$ 0.08 kcal/mol), by dissecting the gas→water CH_2 contribution into a favorable normal solvent effect and a true (unfavorable) hydrophobic effect.[44] Abraham's conclusion stimulates our view that the selectivity changes on methylation are better to understand by three-dimensional shape-specific weak interactions rather than by hydrophobic interaction.

Conclusion

The pattern of temperature dependence of the selectivity in oxidation of a pair of associating thiols varies radically from a maximum-having curve to a minimum-having one (or to a sigmoid-like one) upon methylation (or ethylation) of a benzene ring remote from the reaction site. This is not the case with the oxidation of a pair of non-associating thiols. These experimental results would mean that methylation of a benzene ring can function as a *chemical signal* in an associating system.

Further, any of the factors discussed in this work —— solubility differences, exchange reactions, hydrophobic interaction, and three-dimensional shape-specific weak interactions —— alone cannot, at present, satisfactorily explain the dramatic alterations in the selectivity with temperature on methylation and ethylation.

Experimental

Determination of Physicochemical Properties of Thiols and Disulfides. Melting points were obtained from the DTA (Differential Thermal Analysis) curves recorded with a Shimadzu DT-20B thermal analysis apparatus. The samples were finely powdered, diluted with fine-grained quarz wool in the specimen holder, and heated in a stream of nitrogen with a heating rate of 10 °C/min.

The effective mole fraction of the solute required to calculate the degree of association (f) was determined on a Hitachi Perkin-Elmer 115 molecular weight apparatus using a differential vapor pressure method at 36.0 °C and 0.010 M in benzene.

The solubility was measured gravimetrically by evaporating a saturated solution of **1** or **2** to dryness under reduced pressure. The saturated solution of **1** or **2** was prepared by vigorous stirring of the two-phase mixture for 8 h in a well-stirred water bath held at constant temperatures controlled to ±0.1 °C. Further stirring caused no increase in solubility. Separate experiments containing different ratios of residual solid solute to solvent yielded the same equilibrium solubility. The solubility recorded for a given temperature is the mean value of at least four measurements which did not deviated more than 4%.

Surface tension for three systems A_p, A_t, and A_e was measured on a Kyowa surface tensiometer CBVP-A3 using a counter balance and vertical plate method in 80% (v/v) CH_3CN–20% H_2O at 25 °C. The concentrations of each thiol employed for this measurement were 1.3×10^{-6}, 2.6×10^{-5}, 5.2×10^{-4}, and 1.0×10^{-2} M; the concentration of 0.010 M corresponds to that of a nearly saturated solution of system A. The uncertainty in surface tension is ±0.2 dyn/cm.

^1H NMR spectra were measured on a Hitachi R-20B spectrometer at 60 MHz. The chemical shifts for the NH protons shown in Fig. 3 were measured precisely by the sideband method with the aid of a frequency counter. The uncertainty in chemical shifts is ±0.01 ppm.

Materials. Acetonitrile was dried and purified by dis-

tillation from calcium hydride and phosphorus pentaoxide, and stored over molecular sieves. Water was distilled after deionization. Precoated TLC plates (silica gel 60 F_{254}) were purchased from Merck Darmstadt.

Thiol **1** was prepared as described before[45] and had the following properties (the melting point and NH proton chemical shifts are listed in Table 3): R_f 0.69 [silica, Et_2O-$EtCO_2H$-MeOH (30:3:1) and Et_2O-$EtCO_2H$-MeOH-AcOEt (60:6:1:1)]; NMR ($CDCl_3$) δ=2.10 (1H, t, J=9.0 Hz, SH), 2.94 (6H, s, $N(CH_3)_2$), 3.38 (2H, d, J=9.0 Hz, $HSCH_2$), 6.6—7.6 (4H, m, ArH). Found: C, 52.45; H, 6.10; N, 16.64; S, 12.69%; M^+, 253.

Thiol **3** was prepared by reaction of its hydrochloride (Tokyo Kasei Kogyo Co., Ltd.) with an excess of tetraethylenepentamine and purified by distillation (bp 57—58 °C (80 mmHg**)); satisfactory spectral data were used to support the assignment of **3**. Thiol **4** was obtained from Tokyo Kasei Kogyo Co., Ltd. and purified by distillation before use. Thiol **20** was synthesized as reported before.[27]

Preparation of Thiol 2. Freshly sublimated cysteamine (10 mmol) was dissolved in 35 ml of tetrahydrofuran (THF) under argon by heating. This solution was cooled to 0 °C. To the cold solution was added an acyl isocyanate (10.5 mmol) at 0 °C under argon with stirring. The reaction mixture was stirred for 2 h at room temperature under argon, evaporated to dryness, and recrystallized from benzene for **2p** and from acetonitrile for **2t** and **2e**. Thiol **2** had the following properties (the melting points and NH proton chemical shifts are listed in Table 3).

2p: NMR ($CDCl_3$) δ=1.44 (1H, t, J=7.6 Hz, SH), 2.72 (2H, m, $HNCH_2$), 3.54 (2H, m, CH_2SH), 7.2—8.3 (5H, m, ArH). Found: C, 53.78; H, 5.42; N, 12.44; S, 14.28%; M^+, 224. Calcd for $C_{10}H_{12}N_2O_2S$: C, 53.57; H, 5.39; N, 12.50; S, 14.27%; M, 224.

2t: NMR ($CDCl_3$) δ=1.44 (1H, t, J=8.6 Hz, SH), 2.44 (3H, s, $ArCH_3$), 2.74 (2H, m, $HNCH_2$), 3.56 (2H, m, CH_2SH), 7.2—8.1 (4H, m, ArH). Found: C, 55.28; H, 5.82; N, 11.82; S, 13.17%; M^+, 238. Calcd for $C_{11}H_{14}N_2O_2S$: C, 55.45; H, 5.92; N, 11.76; S, 13.43%; M, 238.

2e: NMR ($CDCl_3$) δ=1.26 (3H, t, J=7.5 Hz, CH_3), 1.45 (1H, t, J=8.0 Hz, SH), 2.5—2.9 (4H, m, CH_2NH and CH_2CH_3), 3.56 (2H, m, $HSCH_2$), 7.1—8.1 (4H, m, ArH). Found: C, 57.24; H, 6.42; N, 11.16; S, 12.72%; M^+, 252. Calcd for $C_{12}H_{16}N_2O_2S$: C, 57.13; H, 6.39; N, 11.11; S, 12.69%; M, 252.

Preparation of Disulfides. Symmetrical disulfides **5** and **8** were easily obtained by treatment with O_2 in the presence of Et_3N in CH_3CN at room temperature; disulfide **5** was recrystallized from CH_3CN-DMF. Satisfactory spectral data were used to support the assignment of disulfides **5**—**10**. Unsymmetrical disulfides **6** and **9** were prepared as described before,[46] recrystallized from CH_3CN for **6**, and had the following properties (NMR spectra of **5** and **6** were measured in Me_2SO-d_6 at 34 °C and 0.040 M).

5: Mp 210 °C; R_f 0.67 (silica, Et_2O-$EtCO_2H$-MeOH, 30:3:1) or 0.70 (silica, Et_2O-$EtCO_2H$-MeOH-AcOEt, 60:6:1:1); NMR δ=2.89 (12H, s, $N(CH_3)_2$), 3.81 (4H, s, SCH_2CO), 6.5—7.5 (8H, m, ArH), 10.02 (2H, s, NH^α), 10.65 (2H, s, NH^β). Found: C, 52.09; H, 5.58; N, 16.67; S, 12.95%. Calcd for $C_{22}H_{28}N_6O_4S_2$: C, 52.37; H, 5.59; N, 16.66; S, 12.69%.

6p: Mp 187 °C; R_f 0.83 (silica, Et_2O-$EtCO_2H$-MeOH-AcOEt, 60:6:1:1); NMR δ=2.7—3.8 (4H, m, SCH_2CH_2N), 2.84 (6H, s, $N(CH_3)_2$), 3.72 (2H, s, SCH_2CO), 6.5—8.3 (8H, m, ArH), 8.88 (1H, t, J=6 Hz, NH^δ), 10.03 (1H, s, NH^α), 10.68 (2H, s, NH^β and NH^γ). Found: C, 52.89; H, 5.33; N, 14.60; S, 13.54%. Calcd for $C_{21}H_{25}N_5O_4S_2$: C, 53.04; H, 5.31; N, 14.73; S, 13.48%.

6t: Mp 192 °C; R_f 0.84 (silica, Et_2O-$EtCO_2H$-MeOH, 30:3:1); NMR δ=2.37 (3H, s, $ArCH_3$), 2.83 (6H, s, $N(CH_3)_2$), 2.6—3.8 (4H, m, SCH_2CH_2N), 3.72 (2H, s, SCH_2CO), 6.5—8.1 (8H, m, ArH), 8.89 (1H, t, J=6 Hz, NH^δ), 10.04 (1H, s, NH^α), 10.60 (1H, s, NH^β), 10.67 (1H, s, NH^γ). Found: C, 54.15; H, 5.58; N, 14.47; S, 13.07%. Calcd for $C_{22}H_{27}N_5O_4S_2$: C, 53.97; H, 5.56; N, 14.30; S, 13.10%.

6e: Mp 195 °C; R_f 0.81 (silica, Et_2O-$EtCO_2H$-MeOH, 30:3:1); NMR δ=1.19 (3H, t, J=7.5 Hz, $ArCH_2CH_3$), 2.6—3.8 (6H, m, SCH_2CH_2N and $ArCH_2$), 2.82 (6H, s, $N(CH_3)_2$), 3.71 (2H, s, SCH_2CO), 6.5—8.1 (8H, m, ArH), 8.89 (1H, t, J=6 Hz, NH^δ), 10.03 (1H, s, NH^α), 10.60 (1H, s, NH^β), 10.64 (1H, s, NH^γ). Found: C, 54.68; H, 5.77; N, 13.83; S, 12.53%. Calcd for $C_{23}H_{29}N_5O_4S_2$: C, 54.86; H, 5.81; N, 13.91; S, 12.71%.

*2-(Dimethylamino)ethyl Phenyl Disulfide (**9p**)*: Oil; R_f 0.38 (silica, n-C_6H_{14}-EtOH, 17:2); NMR ($CDCl_3$) δ=2.20 (6H, s, $N(CH_3)_2$), 2.4—3.0 (4H, m, SCH_2CH_2N), 6.8—7.8 (5H, m, ArH); M^+, 213.

*2-(Dimethylamino)ethyl p-Tolyl Disulfide (**9t**)*: Oil; R_f 0.39 (silica, n-C_6H_{14}-EtOH, 17:2); NMR ($CDCl_3$) δ=2.18 (6H, s, $N(CH_3)_2$), 2.28 (3H, s, $ArCH_3$), 2.3—2.9 (4H, m, SCH_2CH_2N), 6.8—7.8 (4H, m, ArH); M^+, 227.

*Preparation of Sulfide (**11**).* To a mixture of iodoacetamide (10 mmol) and Et_3N (11 mmol) in 100 ml of CH_3CN was added **1** (10 mmol) with stirring at 0 °C under argon. Stirring was continued for 1 h at room temperature. The reaction mixture was evaporated to dryness, washed with water, dried under reduced pressure over phosphorus pentaoxide, recrystallized from CH_3CN to give a pale yellow crystal, and had the following properties (NMR spectra were measured in Me_2SO-d_6 at 34 °C and 0.040 M): mp 195 °C; R_f 0.40 (silica, Et_2O-$EtCO_2H$-MeOH, 30:3:1) or 0.37 (silica, Et_2O-$EtCO_2H$-MeOH-AcOEt, 60:6:1:1); NMR δ=2.84 (6H, s, $N(CH_3)_2$), 3.24 (2H, s, SCH_2CONH), 3.45 (2H, s, SCH_2CONH_2), 6.5—7.5 (6H, m, $CONH_2$ and ArH), 10.06 (1H, s, NH^α), 10.58 (1H, s, NH^β). Found: C, 50.41; H, 5.87; N, 18.31; S, 10.55%. Calcd for $C_{13}H_{18}N_4O_3S$: C, 50.31; H, 5.85; N, 18.06; S, 10.31%.

Oxidation of a Pair of Thiols. A mixture of **1** (0.50 mmol) and **2** (0.50 mmol) [or of **3** (0.50 mmol) and **4** (0.50 mmol)] in 12.5 ml of 80% (v/v) CH_3CN-20% H_2O was stirred vigorously under oxygen for 15 min in a well-stirred water bath (for 20 to 70 °C) or methanol bath (for −10 and 0 °C) which was thermostated to ±0.1 °C for 20 to 50 °C and to ±0.5 °C for −10, 0, and 70 °C. To this mixture was added Et_3N (0.05 mmol), and vigorous stirring was continued for the time required to complete the oxidation. When the oxidation was completed, the reaction mixture was evaporated to dryness. In the case of the oxidation of system A, the yields of **5** and **6** were determined by the use of their absorption at 310 nm (ε=20300 for **5**, 10300 for **6p**, 10500 for **6t**, and 10400 for **6e** in 90% (v/v) THF-10% H_2O) after separation by TLC [2 mm×1.2 cm×5 cm E. Merck precoated silica gel plates (60 F_{254}), Et_2O-$EtCO_2H$-MeOH (30:3:1) for systems A_t and A_e or Et_2O-$EtCO_2H$-MeOH-AcOEt (60:6:1:1) for system A_p] followed by elution with 90% (v/v) THF-10% H_2O.[12] The yield shown in Table 1 represents the mean value of four or more measurements, and was reproducible to <3% average deviation from the mean. With oxidation of system N, the yields of **8** and **9** were determined gravimetrically after

** 1 mmHg≈133.322 Pa.

separation by preparative TLC [1 mm×20 cm×20 cm silica gel plates (E. Merck 60 PF_{254}), n-C_6H_{14}–EtOH (17:2)] followed by elution with CH_2Cl_2 for **8** and with CH_3CN for **9**.

Thiol-Disulfide Exchange Reaction. A mixture of **2** (0.50 mmol) and **5** (0.25 mmol) was stirred in 12.5 ml of 80% (v/v) CH_3CN–20% H_2O vigorously under argon for 15 min in a well-stirred water bath or methanol bath which was thermostated as in the oxidation. To this mixture was added Et_3N (0.05 mmol), and vigorous stirring was continued for the same time as with the corresponding oxidation under argon. To this mixture were added iodoacetamide (0.55 mmol) and Et_3N (0.55 mmol). After vigorous stirring for 10 min at 35 and 70 °C or for 20 min at 0 °C, the resulting mixture was evaporated to dryness. The yields of **5**, **6**, and **11** (ε=10300 at 310 nm in 90% (v/v) THF–10% H_2O) were determined as described with the oxidation. The yield of the corresponding sulfide derived from **2** could not be determined by the method[12] because of its small molar extinction coefficient (ε=*ca.* 30 in 90% (v/v) THF–10% H_2O at 310 nm). Similarly, the exchange reaction between **1** and **7** was carried out. The yield shown in Table 2 represents the mean value of four or more measurements, and was reproducible to <3% average deviation from the mean.

Disulfide-Disulfide Exchange Reaction. A mixture of **5** (0.25 mmol) and **7t** (0.25 mmol) was stirred vigorously in 12.5 ml of 80% (v/v) CH_3CN–20% H_2O for 15 min in a well-stirred water bath held at 35.0 °C controlled to ±0.1 °C. To this mixture was added Et_3N (0.025 mmol), and vigorous stirring was continued for 3 h. The resulting reaction mixture was evaporated to dryness, and the yields of **5** and **6t** were determined as described above.

We thank Professor Yoshio Sasada, Dr. Motohiro Nishio, and Dr. Yuji Ohashi for their helpful discussions and reading the manuscript. We are grateful to Mrs. Yukiko Takeda, Mr. Tomoji Murata, Mr. Koji Kobinata, Mr. Shigeru Miyamoto, and Mr. Kazuhiro Furumoto for their valuable assistance.

References

1) H. O. Smith, *Science*, **205**, 455 (1979).
2) T. Lindahl, *Nature*, **290**, 363 (1981); M. Ehrlich and R. Y. -H. Wang, *Science*, **212**, 1350 (1981).
3) W. K. Paik and S. Kim, "Protein Methylation," Wiley, New York (1980).
4) F. Hirata and J. Axelrod, *Science*, **209**, 1082 (1980).
5) G. L. Cantoni, *Ann. Rev. Biochem.*, **44**, 435 (1975).
6) W. Arber, *Angew. Chem., Int. Ed. Engl.*, **17**, 73 (1978).
7) A. Razin and A. D. Riggs, *Science*, **210**, 604 (1980) and the references cited therein.
8) B. Griffin, *Nature*, **263**, 188 (1976); M. J. Clemens, *ibid.*, **279**, 673 (1979).
9) G. L. Hazelbauer, *Nature*, **279**, 18 (1979); M. S. Springer, M. F. Goy, and J. Adler, *ibid.*, **280**, 279 (1979); A. L. DeFranco and D. E. Koshland, Jr., *Proc. Natl. Acad. Sci. U.S.A.*, **77**, 2429 (1980).
10) The symbols p, t, and e represent the compounds or systems to have the phenyl, *p*-tolyl, and *p*-ethylphenyl groups, respectively, as R^1 or R^2.
11) T. Endo, Y. Takeda, T. Orii, Y. Kaneko, and M. Kondo, *Chem. Lett.*, **1979**, 1455.
12) This method improved the accuracy of quantitative analysis of substances of low solubility: T. Endo, A. Kuwahara, H. Tasai, and T. Ishigami, *J. Chromatogr.*, **140**, 263 (1977).
13) Disulfide **7** could not be determined by this method[12] because of its very small molar extinction coefficient (ε) at wavelengths longer than 260 nm in 90% (v/v) tetrahydrofuran–10% water: the ε value for **7** was *ca.* 30 at 310 nm.
14) In oxidation of system N, the symmetrical disulfide used for the calculation of R was **8** derived from **4**, but not **10** from **3**, because the spot of **10** on TLC plates could not be detected in UV light.
15) Oxidation of a mixture of methanethiol and ethanethiol yielded the three disulfides in a 1:2:1 ratio: D. T. McAllan, T. V. Cullum, R. A. Dean, and F. A. Fidler, *J. Am. Chem. Soc.*, **73**, 3627 (1951).
16) T. Endo, A. Kuwahara, H. Tasai, T. Murata, M. Hashimoto, and T. Ishigami, *Nature*, **268**, 74 (1977).
17) a) P. C. Jocelyn, "Biochemistry of the SH group," Academic, London (1972), Chap. 5; b) L. Eldjarn and A. Pihl, *J. Am. Chem. Soc.*, **79**, 4589 (1957); c) A. Fava, A. Iliceto, and E. Camera, *ibid.*, **79**, 833 (1957); d) R. P. Szajewski and G. M. Whitesides, *ibid.*, **102**, 2011 (1980).
18) This nucleophilic substitution (Eq. 4) is known to proceed very rapidly, and extensively used in protein chemistry: A. Fontana and C. Toniolo, "Detection and Determination of Thiols," in "The Chemistry of the Thiol Group," ed by S. Patai, Wiley, London (1974), Part 1, Chap. 5.
19) If a single multimer species in equilibrium with monomer is assumed to be dimer, f values range from 1.0 to 2.0: M. Davies and D. K. Thomas, *J. Phys. Chem.*, **60**, 763 (1956).
20) J. H. Hildebrand, E. T. Ellefson, and C. W. Beebe, *J. Am. Chem. Soc.*, **39**, 2301 (1917).
21) Surface tension is reported to be 71.97 for water (25 °C) and 29.3 for CH_3CN (20 °C): "Lange's Handbook of Chemistry," 11th ed, ed by J. A. Dean, McGraw-Hill, New York (1973), Section 10.
22) Similar, but less dramatic, variations in temperature-selectivity profiles were observed in oxidation of system A_a: a plot of R in 80% (v/v) CH_3CN–20% H_2O against temperature showed a peak of maximum selectivity (R=21) at 35 °C for R^1=i-C_5H_{11}, whereas for R^1=n-C_5H_{11} the R values altered progressively over a wide range (0.13 to 2.3).[16]
23) We have recently prepared a great variety of solid 1:1 complexes between a pair of acylurea bond-containing compounds (analogs of **1** and **2**) each with the *p*-(dimethylamino)phenyl or *p*-nitrophenyl group as one of the two substituents. X-Ray crystallographic studies of the two complexes and **1** have indicated that (1) they have the same pattern of hydrogen bonding as in Fig. 4 and (2) the packing modes of the four molecules in the unit cells of the complexes and of **1** are analogous to the association schemes of heterotetramer **18** and homotetramer **15**, respectively (Y. Ohashi, A. Uchida, and Y. Sasada, private communication). These observations encourage our view that there exist tetramers **15**—**19** in solution (Fig. 5).
24) Among many possibilities, five tetramers were chosen so that (1) the ratio of **1** to **2** in heterotetramers might be 1:1 and (2) the stabilization of tetramers might become strongest.[11]
25) Tetramer formation is shown for methanol in the gas (W. Weltner, Jr., and K. S. Pitzer, *J. Am. Chem. Soc.*, **73**, 2606 (1951)); the important multimer species of both methanethiol and ethanethiol in argon matrices at low concentrations at 20 K is the open chain dimer and cyclic tetramer, the latter being particularly stable for ethanethiol (A. J. Barnes, H. E. Hallam, and J. D. R. Howells, *J. Chem. Soc., Faraday Trans. 2*, **68**, 737 (1972)). For the other examples, see Ref. 11.
26) M. R. Crampton, "Acidity and Hydrogen-Bonding," in "The Chemistry of the Thiol Group," ed by S. Patai, Wiley, London (1974), Part 1, Chap. 8.

27) T. Endo, Y. Takeda, H. Kamada, S. Kayama, and H. Tasai, *Chem. Lett.*, **1980**, 417.
28) N. C. Seeman, J. M. Rosenberg, and A. Rich, *Proc. Natl. Acad. Sci. U.S.A.*, **73**, 804 (1976).
29) E. Hutchinson and K. Shinoda, "An Outline of the Solvent Properties of Surfactant Solutions," in "Solvent Properties of Surfactant Solutions," ed by K. Shinoda, Marcel Dekker, New York (1967), Chap. 1.
30) E. H. Cordes and C. Gitler, *Prog. Biorg. Chem.*, **2**, 1 (1973); J. H. Fendler and E. J. Fendler, "Catalysis in Micellar and Macromolecular Systems," Academic, New York (1975), Chap. 2.
31) P. Rys, *Angew. Chem., Int. Ed. Engl.*, **16**, 807 (1977).
32) W. P. Jencks, "Catalysis in Chemistry and Enzymology," McGraw-Hill, New York (1969), Chap. 8; C. Tanford, *Science*, **200**, 1012 (1978); H. A. Scheraga, *Acc. Chem. Res.*, **12**, 7 (1979); A. B. Naim, "Hydrophobic Interactions," Plenum, New York (1980).
33) The π value, an excellent parameter of hydrophobicity, increases in the order $CH_3 < C_2H_5 < i\text{-}C_3H_7 < n\text{-}C_3H_7 < i\text{-}C_4H_9 < n\text{-}C_4H_9 < n\text{-}C_5H_{11}$: C. Hansch, A. R. Steward, J. Iwasa, and E. W. Deutsch, *Mol. Pharmacol.*, **1**, 205 (1965).
34) A linear relationship is known to exist between "accessible surface area" (B. Lee and F. M. Richards, *J. Mol. Biol.*, **55**, 379 (1971)) for the amino acid side chains and hydrophobicity, represented by free energy change for the transfer of amino acid side chains from 100% organic solvents to water at 25 °C (C. Chothia, *Nature*, **248**, 338 (1974)). The "relative surface areas," estimated by covering CPK atomic models, were shown to be closely correlated with free energies of transfer of saturated hydrocarbon groupings from water to a nonpolar phase (S. M. J. Harris, T. Higuchi, and J. H. Rytting, *J. Phys. Chem.*, **77**, 2694 (1973)).
35) J. P. Guthrie, "Enzyme Models and Related Topics," in "Applications of Biochemical Systems in Organic Chemistry," ed by J. B. Jones, C. J. Sih, and D. Perlman, Wiley, New York (1976), Part II, Chap. III.
36) G. Némethy and H. A. Scheraga, *J. Chem. Phys.*, **36**, 3401 (1962); see also S. J. Gill and I. Wadsö, *Proc. Natl. Acad. Sci. U.S.A.*, **73**, 2955 (1976).
37) Similar phenomenon has been observed in the case of oxidation of system A_a ($R^1 = i\text{-}C_5H_{11}$).[16]
38) R. Lawaczeck and K. G. Wagner, *Biopolymers*, **13**, 2003 (1974).
39) R. D. Cramer III, *J. Am. Chem. Soc.*, **99**, 5408 (1977).
40) a) J. H. Hildebrand, *J. Phys. Chem.*, **72**, 1841 (1968); see response by G. Némethy, H. A. Scheraga, and W. Kauzmann, *ibid.*, **72**, 1842 (1968); b) J. H. Hildebrand, *Proc. Natl. Acad. Sci. U.S.A.*, **76**, 194 (1979); see response by C. Tanford, *ibid.*, **76**, 4175 (1979).
41) T. Endo, Y. Takeda, T. Orii, T. Murata, M. Sakai, N. Nakagawa, and K. Nikki, *Chem. Lett.*, **1980**, 1291.
42) Indeed, CH···N interaction between an alkyl group (R^1) in **2a** and the amino group [$N(CH_3)_2$] in **1** was observed to be specific for R^1, namely, to depend largely on whether R^1 was the isopentyl or pentyl group, through alterations in the NH proton chemical shifts.[41]
43) Specific weak interactions which would seem to operate between the recognition sites and between the recognition site and reaction site in **1** and **2** are CH···N interaction between the R^1 and $N(CH_3)_2$ groups, CH···CH interaction between the R^1 and methyl (and/or phenyl) groups and between the two R^1 groups, and CH···SH interaction between the R^1 and SH groups (Figs. 4 and 5).
44) M. H. Abraham, *J. Am. Chem. Soc.*, **102**, 5910 (1980). See also K. Shinoda and M. Fujihira, *Bull. Chem. Soc. Jpn.*, **41**, 2612 (1968) and K. Shinoda, *J. Phys. Chem.*, **81**, 1300 (1977).
45) T. Endo, K. Oda, and T. Mukaiyama, *Chem. Lett.*, **1974**, 443.
46) T. Endo, H. Tasai, and T. Ishigami, *Chem. Lett.*, **1975**, 813.

Syntheses of 2-Amino-3,4-dimethyl-3*H*-imidazo[4,5-*f*]quinoline and Its Related Compounds

Hiroshi KASAI* and Susumu NISHIMURA

Biology Division, National Cancer Center Research Institute, Tsukiji 5-1-1, Chuo-ku, Tokyo 104

(Received February 3, 1982)

The strongly mutagenic compound, 2-amino-3,4-dimethyl-3*H*-imidazo[4,5-*f*]quinoline (Me-IQ), isolated from broiled sardines was synthesized from 6-amino-7-methylquinoline. Several structurally related compounds were also synthesized to clarify the structure-activity relationship. Some of them also showed strong mutagenic activity towards *Salmonella typhimurium* TA98.

We previously isolated two new potent mutagens from broiled fish (sardine) and identified them as 2-amino-3-methyl-3*H*-imidazo[4,5-*f*]quinoline (IQ, compound **1**)[1-4] and 2-amino-3,4-dimethyl-3*H*-imidazo-[4,5-*f*]quinoline (Me-IQ, compound **2**).[5] They are strongly mutagenic, especially towards *Salmonella typhimurium* TA98.[2,5] For final structure assignment of Me-IQ and for studies on structure-activity relationship of 2-aminoimidazo[4,5-*f*]quinoline derivatives, we synthesized compound **2** and its related compounds from 6-aminoquinoline derivatives. In this paper, we describe detailed data on syntheses of these new imidazo[4,5-*f*]quinoline derivatives. A preliminary account of this work has been published.[2,5]

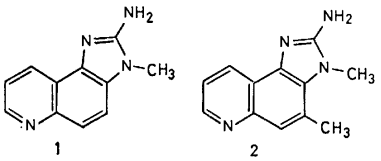

1 2

Results and Discussion

Compound **2** was synthesized from 6-amino-7-methylquinoline (**3**) as shown in Scheme 1. Compound **3** prepared by the method of Huisgen[6] was converted to the 6-acetamido derivative **4**. Nitration of compound **4** with KNO_3–H_2SO_4 mixture gave an *N*-nitro derivative **5**. Acid hydrolysis of compound **5** gave the 5-nitro derivative **6** with migration of the nitro group on nitrogen to the neighboring 5-C position of the quinoline nucleus. Compound **6** was treated with sodium hydride in *N*,*N*-dimethylformamide and methylated with methyl iodide to afford the *N*-methyl derivative **7**. Compound **7** was then reduced to the 6-methylamino-5-amino derivative with Fe/HCl mixture and the neutralized reaction mixture was treated with cyanogen bromide to afford compound **2**. Compound **2** was also prepared by methylation of compound **8**, which was obtained from compound **6**. In the latter reaction, the 1-methyl isomer, compound **9**, was also produced.

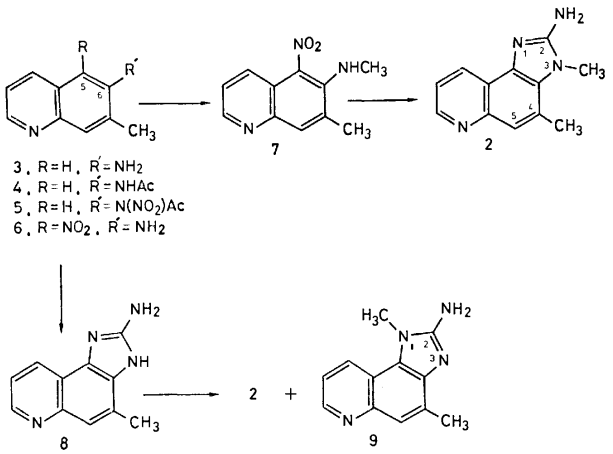

Scheme 1.

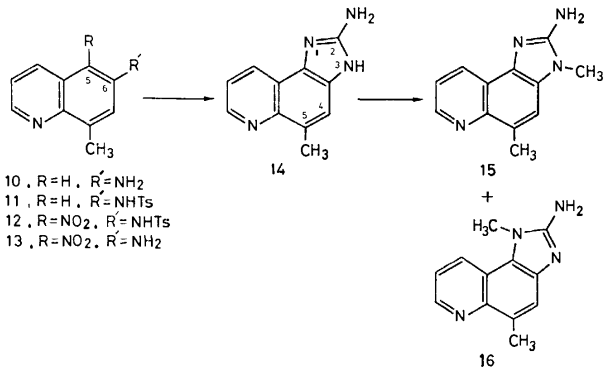

Scheme 2.

Compound **15** was synthesized from 6-amino-8-methylquinoline (**10**) as shown in Scheme 2. This method is practically the same as that reported for the synthesis of compound **1**.[2] Namely, the tosyl derivative **11**, prepared from compound **10**,[7] was converted to the nitro derivative **12** by treatment with 61% HNO_3. Compound **12** was then hydrolyzed with concentrated H_2SO_4, resulting in formation of 6-amino-5-nitro-8-methylquinoline (**13**). Compound **13** was converted to the diamine derivative by reduction with Fe/HCl mixture. The reaction mixture was neutralized, and then treated with cyanogen bromide to yield the cyclized derivative **14**. The 3-methyl derivative **15** was finally obtained as a major product by heating the tetramethylammonium salt of compound **14** in vacuum.[2,3,8] In this reaction 1-methyl derivative **16** was also obtained as a minor product.

The mass, UV, and ^{1}H-NMR spectra of compound **2**, isolated from broiled fish were exactly the same as those of the synthetic compound **2**, but different from those of compounds **9**, **15**, and **16**. Therefore, compound **2** was unambiguously identified as 2-amino-3,4-dimethyl-3*H*-imidazo[4,5-*f*]quinoline (**2**). Compounds **2**, **9**, **15**, and **16** showed strong mutagenic activity towards the *S. typhimurium* TA98 strain by

metabolic activation with microsomal enzymes. However compounds **8** and **14** showed almost no mutagenic activity.[9] Quantitative measurements of compounds **1** and **2** in various cooked foods by G.C.-mass spectrometry are in progress in this laboratory.

Experimental

Spectral Measurements. ^{1}H-NMR (270 MHz) spectra were recorded in a Bruker WH 270 spectrometer at 23 °C in $CDCl_3$ or CD_3OD. Chemical shifts were measured relative to the residual $CHCl_3$ signal (δ 7.25) or CHD_2OD signal (δ 3.40). Mass spectra were obtained by a Varian MAT-44 instrument. UV spectra were obtained using a Shimadzu UV-300 spectrophotometer.

6-Acetamido-7-methylquinoline (4). 6-Amino-7-methylquinoline (**3**)[6] (130 mg) was dissolved in acetic anhydride (1 ml) and the solution was allowed to stand at room temperature for 10 min. Then, cold water (6 ml) was added, and the solution was adjusted to pH 10 by adding NaOH solution. The product was extracted with ethyl acetate (3×10 ml) and crystallized from ethanol. Yield, 110 mg; mp 176—177 °C; MS: 200 (M^+), 158 (M^+−Ac).

6-(N-Nitroacetamido)-7-methylquinoline (5). Compound **4** (1.2 g) was dissolved in concentrated H_2SO_4 (5 ml), and KNO_3 (1.5 g) was added with vigorous stirring at 0 °C. Stirring was continued for 30 min at room temperature and then the reaction mixture was poured onto ice, neutralized with NaOH solution and extracted with ethyl acetate. The crude product was purified on a column of silica gel (3 cm×50 cm) with methanol–chloroform (3:97, v/v) as solvent. Compound **5** was crystallized from methanol. Yield, 500 mg; mp 240—242 °C; MS: 245 (M^+), 203 (M^+−Ac), 199 (M^+−NO_2): NMR ($CDCl_3$): δ=8.96 (1H, dd, J=4.2, 1.5 Hz, 2-H), 8.20 (1H, dd, J=8.6, 1.5 Hz, 4-H), 8.18 (1H, s, 8-H), 7.67 (1H, br s, 5-H), 7.51 (1H, dd, J=8.6, 4.2 Hz, 3-H), 2.52 (3H, s, 7-Me), 2.25 (3H, s, Ac).

6-Amino-7-methyl-5-nitroquinoline (6). Compound **5** (500 mg) was suspended in concentrated H_2SO_4 (2 ml) and heated at 70 °C for 30 min. The reaction mixture was poured onto ice and neutralized with NH_4OH. The precipitate was collected by filtration, washed with a small amount of water and dried. The crude product was crystallized from ethanol. Yield, 360 mg; mp 171—172 °C; MS: 203 (M^+), 157 (M^+−NO_2); NMR ($CDCl_3$): δ=8.98 (1H, ddd, J=8.8, 1.3, 1.0 Hz, 4-H), 8.68 (1H, dd, J=4.2, 1.3 Hz, 2-H), 7.95 (1H, dd, J=1.0, 0.8 Hz, 8-H), 7.46 (1H, dd, J=8.8, 4.2 Hz, 3-H), 6.72 (2H, br s, NH_2), 2.44 (3H, d, J=0.8 Hz, Me).

7-Methyl-6-methylamino-5-nitroquinoline (7). Compound **6** (27 mg) was dissolved in *N*,*N*-dimethylformamide (0.2 ml). Sodium hydride (7.8 mg, 50% oil suspension) was added and the reaction mixture was stirred for 30 min at room temperature. Then methyl iodide (10 μl) was added during 1 h and stirring was continued for 1 h at room temperature. After cold water (1 ml) was added, the reaction mixture was neutralized with NaOH solution and the product was extracted with ethyl acetate (3×1.5 ml). The crude product thus obtained was purified on a column of silica gel (1 cm×30 cm) with methanol–chloroform (5:95, v/v) as solvent. Yield, 4.3 mg; powder; MS: 217 (M^+), 170 (M^+−H−NO_2), 156 (M^+−NO_2−Me); NMR ($CDCl_3$): δ=8.69 (1H, dd, J=4.3, 1.5 Hz, 2-H), 8.18 (1H, ddd, J=8.6, 1.5, 0.7 Hz, 4-H), 7.86 (1H, dd, J=0.7, 0.7 Hz, 8-H), 7.40 (1H, dd, J=8.6, 4.3 Hz, 3-H), 5.17 (1H, d, J=5.5 Hz, NH), 3.00 (3H, d, J=5.5 Hz, N–Me), 2.47 (3H, d, J=0.7 Hz, 7-C–Me).

*2-Amino-3,4-dimethyl-3*H*-imidazo[4,5-f]quinoline (2).* Compound **7** (4 mg) was dissolved in concentrated HCl (0.1 ml) and reduced by adding Fe powder (10 mg). After 20 min, the reaction mixture was filtered and washed with water. The filtrate was neutralized with KOH solution, aqueous BrCN (12 mg, 0.2 ml) was added during 3 h with stirring, and stirring was coninued for 4 h. The reaction mixture was made alkaline with KOH solution and extracted with ethyl acetate (5×1 ml). The crude product thus obtained was purified by HPLC [Shimadzu LC-3A; μBondapak C_{18} (Waters); 30% methanol–0.04% formic acid]. Yield, 2.2 mg; mp 295—297 °C; MS: 212 (M^+), 197 (M^+−H−HCN); UV (MeOH): $\lambda(\varepsilon)$=219 (29000), 265 (48000), and 332 nm (4000); NMR ($CDCl_3$): δ=8.80 (1H, dd, J=4.2, 1.7 Hz, 7-H), 8.66 (1H, ddd, J=8.3, 1.7, 0.7 Hz 9-H), 7.53 (1H, dd, J=0.9, 0.7 Hz, 5-H), 7.36 (1H, dd, J=8.3, 4.2 Hz, 8-H), 4.51 (2H, br s, NH_2), 3.88 (3H, s, N–Me), 2.83 (3H, d, J=0.9 Hz, 4-C–Me), NOE (N–Me→4-C–Me) 3%±1%.

*2-Amino-4-methyl-3*H*-imidazo[4,5-f]quinoline (8).* Compound **6** (100 mg) was dissolved in concentrated HCl (1.5 ml) and reduced by adding Fe powder (200 mg). The reaction mixture was filtered and washed with water. The filtrate was neutralized with KOH solution, and aqueous BrCN (300 mg, 6 ml) was added during 1 h with stirring. Stirring was further continued for 2 h. Then the solution was made alkaline with KOH solution, and the crude product was extracted with ethyl acetate (5×100 ml). The ethyl acetate layer was evaporated to dryness, and the residue was fractionated on a column of silica gel (1.5 cm×30 cm) with methanol–chloroform (15:85, v/v) as solvent to isolate compound **8**. Yield, 36 mg; mp 280—290 °C (decomp): MS: 198 (M^+), 170 (M^+−H−HCN); NMR (CD_3OD): δ=8.81 (1H, dd, J=4.5, 1.6 Hz, 7-H), 8.73 (1H, ddd, J=8.4, 1.6, 0.8 Hz, 9-H), 7.67 (1H, dd, J=1.0, 0.8 Hz, 5-H), 7.60 (1H, dd, J=8.4, 4.5 Hz, 8-H), 2.74 (3H, d, J=1.0 Hz, Me).

*2-Amino-1,4-dimethyl-1*H*-imidazo[4,5-f]quinoline (9).* Compound **8** (16 mg) was dissolved in dimethyl sulfoxide (0.45 ml) and methylated with methyl iodide (20 μl) in the presence of K_2CO_3 (32 mg). The reaction was continued for 1 h at room temperature. In this reaction, compounds **2** and **9** were produced in approximately equal proportions. Compound **9** was separated from compound **2** by HPLC using the same conditions as those described above for purification of synthetic compound **2**. Yield, 3.5 mg; powder; MS: 212 (M^+), 197 (M^+−Me), 184 (M^+−H−HCN); NMR ($CDCl_3$): δ=8.81 (1H, d, J=4.0 Hz, 7-H), 8.54 (1H, d, J=8.5 Hz, 9-H), 7.76 (1H, s, 5-H), 7.39 (1H, dd, J=8.5, 4.0 Hz, 8-H), 5.98 (2H, br s, NH_2,), 4.02 (3H, s, N–Me), 2.72 (3H, s, 4-C–Me), NOE (N–Me→9-H)17%± 4%. UV (MeOH): $\lambda(\varepsilon)$=216 (26600), 276 (46500), and 344 nm (2400).

*8-Methyl-6-(*p*-tolylsulfonylamino) quinoline (11).* 6-Amino-8-methylquinoline (**10**)[7] (10 g), *p*-toluenesulfonyl chloride (12.1 g), and potassium acetate (6.2 g) were suspended in ethanol (200 ml) and refluxed for 2.5 h. The hot mixture was then filtered, and the filtrate was evaporated to dryness. The crude product was purified on a column of silica gel (5 cm×60 cm) with chloroform as solvent. Yield, 19 g; oil; MS: 312 (M^+), 248 (M^+−SO_2); NMR ($CDCl_3$): δ=8.84 (1H, dd, J=4.3, 1.7 Hz, 2-H), 8.01 (1H, dd, J=8.3, 1.7 Hz, 4-H), 7.73 (2H, d, J=8.1 Hz, tosyl-H_o), 7.42 (1H, d, J=2.4 Hz, 5-H), 7.35 (1H, dd, J=8.3, 4.3 Hz, 3-H), 7.29 (1H, dd, J=2.4, 0.9 Hz, 7-H), 7.18 (2H, d, J=8.1 Hz, tosyl-H_m), 2.67 (3H, d, J=0.9 Hz, 8-Me), 2.31 (3H, s, tosyl-Me).

8-Methyl-5-nitro-6-(p-tolylsulfonylamino) quinoline (12). Compound **11** (18.5 g) was nitrated with 61% HNO_3 (6.9 ml) at 70—80 °C for 1 h. The solution was poured onto ice, and the solid material formed was collected by filtration. The crude product was purified by crystallization from ethanol. Yield 16.6 g; mp 204—205 °C; MS: 357 (M^+), 246 ($M^+-SO_2-NO_2-H$); NMR ($CDCl_3$): δ=9.05 (1H, dd, J=4.4, 1.5 Hz, 2-H), 8.61 (1H, dd, J=8.9, 1.5 Hz, 4-H), 8.11 (1H, d, J=0.8 Hz, 7-H), 7.70 (2H, d, J=8.2 Hz, tosyl-H_o), 7.67 (1H, dd, J=8.9, 4.4 Hz, 3-H), 7.25 (2H, d, J=8.2 Hz, tosyl-H_m), 2.87 (3H, d, J=0.8 Hz, 8-Me), 2.37 (3H, s, tosyl-Me).

6-Amino-8-methyl-5-nitroquinoline (13). Compound **12** (16 g) was suspended in concentrated H_2SO_4 (20 ml) and heated for 1 h at 95 °C. The hydrolyzate was neutralized with NH_4OH. The precipitate was collected by filtration and dried. The crude product was purified by crystallization from toluene and then recrystallized from ethanol. Yield, 3 g; mp 161—162 °C; MS: 203 (M^+), 157 (M^+-NO_2); NMR ($CDCl_3$): δ=9.15 (1H, dd, J=8.8, 1.7 Hz, 4-H), 8.70 (1H, dd, J=4.2, 1.7 Hz, 2-H), 7.50 (1H, dd, J=8.8, 4.2 Hz, 3-H), 6.99 (1H, d, J=1.0 Hz, 7-H), 6.67 (2H, br s, NH_2), 2.71 (3H, d, J=1.0 Hz, Me).

2-Amino-5-methyl-3H-imidazo[4,5-f]quinoline (14). Compound **14** was synthesized and purified by the procedure used for preparation of compound **8**. Yield, 15%; mp 246—248 °C (decomp); MS: 198 (M^+), 170 ($M^+-H-HCN$); NMR ($CDCl_3$): δ=8.88 (1H, dd, J=4.1, 1.7 Hz, 7-H), 8.61 (1H, dd, J=8.4, 1.7 Hz, 9-H), 7.53 (1H, d, J=0.7 Hz, 4-H), 7.43 (1H, dd, J=8.4, 4.1 Hz, 8-H), 4.59 (2H, br s, NH_2), 2.84 (3H, d, J=0.7 Hz, Me).

2-Amino-3,5-dimethyl-3H-imidazo[4,5-f]quinoline (15) and 2-Amino-1,5-dimethyl-1H-imidazo[4,5-f]quinoline (16). An aqueous solution of compound **14** (135 mg) and tetramethylammonium hydroxide (62.3 mg) was lyophilized in a sublimation apparatus and heated slowly to 200 °C under vacuum pressure (3 mmHg†). At this temperature the sublimate began to collect on the condenser. The crude product thus obtained was purified on a column of silica gel (3 cm × 30 cm) with methanol–chloroform (10:90, v/v) as solvent. Compound **15** was crystallized from aqueous ethanol. Yield, 34 mg; mp >300 °C; MS: 212 (M^+), 184 (M^+), UV (MeOH): $\lambda(\varepsilon)$=213 (24900), 265 (45600), 354 nm (3600). NMR ($CDCl_3$): δ=8.91 (1H, d, J=4.0 Hz, 7-H), 8.67 (1H, d, J=8.2 Hz, 9-H), 7.48 (1H, dd, J=8.2, 4.0 Hz, 8-H), 7.44 (1H, s, 4-H), 6.07 (2H, br s, NH_2), 3.67 (3H, s, N–Me), 2.87 (3H, s, C–Me).

During purification by the silica gel column chromatography, compound **16** was also obtained as a minor component. Yield, 3 mg; powder; MS: 212 (M^+), 197 (M^+-Me), 184 ($M^+-H-HCN$); NMR ($CDCl_3$): δ=8.85 (1H, dd, J=4.2, 1.6 Hz, 7-H), 8.56 (1H, dd, J=8.6, 1.6 Hz, 9-H), 7.74 (1H, d, J=0.7 Hz, 4-H), 7.41 (1H, dd, J=8.6, 4.6 Hz, 8-H), 4.50 (2H, br s, NH_2), 4.00 (3H, s, N–Me), 2.84 (3H, d, J=0.7 Hz, C–Me).

† 1 mmHg≈133.322 Pa.

We wish to thank Dr. S. Yokoyama, the University of Tokyo, for measurements of NMR spectra and Dr. Yamaizumi of our institute for measurements of Mass spectra.

References

1) H. Kasai, Z. Yamaizumi, K. Wakabayashi, M. Nagao, T. Sugimura, S. Yokoyama, T. Miyazawa, N. E. Spingarn, J. H. Weisburger, and S. Nishimura, *Proc. Jpn. Acad.*, **56B**, 278 (1980).

2) H. Kasai, S. Nishimura, K. Wakabayashi, M. Nagao, and T. Sugimura, *Proc. Jpn. Acad.*, **56B**, 382 (1980).

3) H. Kasai, Z. Yamaizumi, S. Nishimura, K. Wakabayashi, M. Nagao, T. Sugimura, N. E. Spingarn, J. H. Weisburger, S. Yokoyama, and T. Miyazawa, *J. Chem. Soc., Perkin Trans. 1*, **1981**, 2290.

4) S. Yokoyama, T. Miyazawa, H. Kasai, S. Nishimura, T. Sugimura, and Y. Iitaka, *FEBS Lett.*, **122**, 261 (1980).

5) H. Kasai, Z. Yamaizumi, K. Wakabayashi, M. Nagao, T. Sugimura, S. Yokoyama, T. Miyazawa, and S. Nishimura, *Chem. Lett.*, **1980**, 1391.

6) R. Huisgen, *Ann.*, **559**, 101 (1948).

7) W. C. Hutchison and W. O. Kermack, *J. Chem. Soc.*, **1947**, 678.

8) T. C. Myers and L. Zeleznick, *J. Org. Chem.*, **28**, 2087 (1963).

9) M. Nagao, K. Wakabayashi, H. Kasai, S. Nishimura, and T. Sugimura, *Carcinogenesis*, **2** 1147 (1981).

The Crystal and Molecular Structure of 1-(2-Amino-4-pyrimidinyl)-β-carboline**

Yoshinobu YOKOMORI,* Kiyotane SEKIDO, Tian-Shung WU,†
Hsien-Jun TIEN,†† and Sakutaro HIROKAWA

Department of Chemistry, The National Defense Academy, Hashirimizu, Yokosuka 239
† *Chia-Nan Junior College of Pharmacy, Tainan, Taiwan, R.O.C.*
†† *Department of Chemistry, National Cheng Kung University, Tainan, Taiwan, R.O.C.*

(Received October 2, 1981)

An alkaloid extracted from a small evergreen tree, *Annona montata*, was identified as 1-(2-amino-4-pyrimidinyl)-β-carboline monohydrate by the X-ray method. The crystal data are; $a=20.699$, $b=4.453$, $c=15.720$ Å, and $\beta=112.16°$; space group, $P2_1/c$; $Z=4$. The structure was solved by the direct method and refined by the least-squares method to the final R value of 0.109 for 1451 independent reflections. The water molecule is connected to four nitrogen atoms by hydrogen bonds. Two of them are in different groups; one is in the five-membered ring of the β-carboline skelton, and the other is in the pyridine of the β-carboline skelton. The fifth hydrogen bond connects two nitrogen atoms, one of which is in the amino group, and the other, in the pyrimidine skelton.

As a part of studies of Formosan folk-medicines, the constituents of small evergreen tree, *Annona montana* Macf., have been investigated by several workers. Yang *et al.*[1] isolated seven species of alkaloids from this plant. The present report will describe the molecular and crystal structure of one of them, annomurine, which has thus been designated by us. This substance was identified as 1-(2-amino-4-pyrimidinyl)-β-carboline by this work.

Experimental

The EtOH extract of the stem bark was triturated with 3% AcOH, and the filtrate was shaken with $CHCl_3$ to separate a $CHCl_3$-soluble fraction and an aqueous fraction. Crystals were obtained from the $CHCl_3$-soluble fraction in the form of light yellow plates. They were recrystallized by slow evaporation from an aqueous solution of MeOH. The result of the structure analysis showed that they were monohydrates.

The cell dimensions were determined by the least-squares method using various sets of high-angle reflections on a diffractometer. The crystal data are given in Table 1. The crystal (0.31, 0.03, 1.86 mm) was mounted on a four-circle diffractometer (Rigaku AFC III), with Mo $K\alpha$ ($\lambda=0.7107$ Å) from a graphite monochromator. The intensities were collected for the independent 1759 reflections within $2\theta<60°$, using the ω-2θ scan technique with a scanning speed of 4° min^{-1} in 2θ, while 344 reflections with $|F_o|<3\sigma(F)$ were designated as unobserved. Corrections for the background and the Lorentz-polarization factor were made, but not for the absorption or the extinction.

Table 1. Crystallographic data for 1-(2-amino-4-pyrimidinyl)-β-carboline monohydrate

$C_{15}H_{11}N_5\cdot H_2O$, space group $P2_1/c$, $Mr=279.2$	
$a=20.699(7)$ Å	$D_m=1.396$ g cm^{-3} (flotation; $CHCl_3/CH_3C_6H_5$)
$b=4.453(2)$ Å	$D_x=1.439$ g cm^{-3} ($Z=4$)
$c=15.720(5)$ Å	μ (Mo $K\alpha$) $=0.856$ cm^{-1}
$\beta=112.16(2)°$	
$V=1341.8$ Å^3	

All the numerical calculations were carried out on a NEAC 2200 MODEL 575 computer at the Computing Center of the National Defense Academy with programs of the Universal Crystallographic Computing System.[2] The phase problem was solved without difficulty by the use of MULTAN.[3] The initial residual index was 0.44 for the trial structure. The structure was refined by a block-diagonal least-squares procedure. Five cycles of refinement reduced the R value to 0.201. Further refinements were made using anisotropic thermal parameters for the non-hydrogen atoms, together with isotropic B values of the hydrogen atoms, which were fixed assuming the angle of 120° for each carbon atom and a bond length of 1.09 Å for each C–H bond. The hydrogen positions of water were deduced from a difference Fourier synthesis. The R value at this stage was 0.109. The atomic scattering factors were taken from International Tables for X-Ray Crystallography.[4] The final atomic coordinates, together with B_{eq}, are given in Table 2.†††

Discussion

The R value did not decrease to less than 0.109, partly because attempts to obtain good-shaped single crystals suitable for X-ray analysis were not successful.

The mean standard deviations are 0.02 Å for the interatomic distance and 0.9° for the angle. These values may be sufficient to discuss the molecular geometry and the packing of the molecules in the unit cell, especially the role the hydrogen bonds play in the crystal.

Configuration of the Molecule. The numbering scheme of the nonhydrogen atoms and four molecular planes (A, B, C, D) is presented in Fig. 1.[5] The numbering scheme of the hydrogen atoms is shown in Table 2. The mean atomic deviations were ±0.007 Å for the A plane, ±0.005 Å for B, ±0.007 Å for C, and ±0.014 Å for D. The dihedral angle between A and B is 1.1°, while that between B and C is 1.0°. The value of the indole nucleus is 2.1°.[6] The two six-membered rings (A and C) make an angle of 1.9°.

** A preliminary report was presented at the 42nd National Meeting of the Chemical Society of Japan, Sendai, September 1980.

††† The complete tables of the anisotropic thermal parameters, the F_o-F_c data, and the torsion angles are deposited as Document No. 8226 at the Office of the Editor of the Bulletin, the Chemical Society of Japan.

Table 2. Final fractional atomic coordinates and their standard deviations (in parentheses)

Atom	x	y	z	B_{eq}/Å^2
C1	0.2692(4)	0.2985(18)	0.1557(5)	3.23
N2	0.2535(3)	0.4153(15)	0.0717(4)	3.45
C3	0.1919(4)	0.3438(20)	0.0042(4)	4.29
C4	0.1432(3)	0.1547(19)	0.0149(4)	3.69
C5	0.0560(4)	−0.3087(17)	0.1037(5)	3.56
C6	0.0377(4)	−0.4917(20)	0.1603(6)	4.19
C7	0.0819(4)	−0.5430(19)	0.2518(5)	3.69
C8	0.1467(4)	−0.4013(19)	0.2880(5)	3.51
N9	0.2264(3)	−0.0533(14)	0.2496(3)	3.32
C10	0.2233(3)	0.0991(16)	0.1725(4)	2.73
C11	0.1582(3)	0.0320(16)	0.1006(4)	2.70
C12	0.1660(3)	−0.2218(17)	0.2307(5)	3.23
C13	0.1224(3)	−0.1678(17)	0.1382(4)	3.10
C14	0.3360(3)	0.3878(18)	0.2291(5)	3.40
N15	0.3474(3)	0.2755(15)	0.3119(4)	3.94
C16	0.4059(4)	0.3670(19)	0.3802(5)	4.02
N17	0.4530(3)	0.5605(18)	0.3726(4)	4.76
C18	0.4395(4)	0.6637(23)	0.2885(5)	4.93
C19	0.3817(4)	0.5975(22)	0.2133(5)	4.35
N20	0.4154(3)	0.2643(19)	0.4654(4)	6.05
O21	0.3109(3)	−0.2111(16)	0.4583(4)	5.25
H1(C3)	0.180	0.443	−0.062	0.36
H2(C4)	0.095	0.106	−0.042	4.12
H3(C5)	0.021	−0.269	0.034	2.50
H4(C6)	−0.012	−0.602	0.134	1.25
H5(C7)	0.066	−0.694	0.294	4.45
H6(C8)	0.181	−0.429	0.359	4.27
H7(N9)	0.269	−0.046	0.315	2.95
H8(C18)	0.476	0.814	0.279	2.48
H9(C19)	0.372	0.678	0.146	3.71
H10(N20)	0.390	0.078	0.469	0.35
H11(N20)	0.452	0.267	0.509	8.23
H12(O21)	0.332	−0.386	0.471	5.57
H13(O21)	0.294	−0.170	0.513	5.90

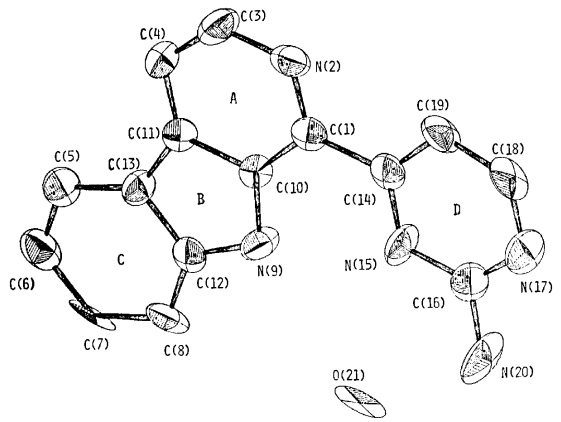

Fig. 1. Thermal ellipsoids representation of the molecule and water. The ellipsoids enclose 50 per cent probability.

The two benzene rings of carbazole make an angle of 1.6°.[7] The dihedral angle between A and D is 5.6°. The atomic deviations and dihedral angles are given in Table 3.

Table 3. Deviations(l/Å) of atoms from mean planes and dihedral angles(ϕ/°)

Plane A		Plane B		Plane C	
C(1)	0.011	N(9)	0.006	C(5)	0.009
N(2)	−0.003	C(10)	−0.003	C(6)	−0.002
C(3)	−0.002	C(11)	−0.002	C(7)	−0.009
C(4)	−0.002	C(12)	−0.007	C(8)	0.013
C(10)	−0.115	C(13)	0.006	C(12)	−0.006
C(11)	0.011			C(13)	−0.004

Plane D		Dihedral angles	
C(14)	0.009	A-B	1.12
N(15)	−0.012	A-C	1.88
C(16)	−0.025	B-C	1.00
N(17)	−0.009	A-D	5.62
C(18)	−0.001		
C(19)	0.014		
N(20)	0.026		

Table 4. Bond lengths and angles for non hydrogen atoms, with e.s.d.'s in parentheses

Bond length (l/Å)			
C(1)-N(2)	1.341(10)	C(1)-C(10)	1.395(10)
C(1)-C(14)	1.483(11)	N(2)-C(3)	1.355(11)
C(3)-C(4)	1.371(11)	C(4)-C(11)	1.377(10)
C(5)-C(13)	1.421(11)	C(5)-C(6)	1.362(11)
C(6)-C(7)	1.401(12)	C(7)-C(8)	1.394(12)
C(8)-C(12)	1.372(11)	N(9)-C(10)	1.370(9)
N(9)-C(12)	1.390(9)	C(10)-C(11)	1.426(10)
C(11)-C(13)	1.421(10)	C(12)-C(13)	1.412(10)
C(14)-N(15)	1.329(10)	C(14)-C(19)	1.387(11)
N(15)-C(16)	1.343(10)	C(16)-N(17)	1.339(10)
C(16)-N(20)	1.358(11)	N(17)-C(18)	1.325(11)
C(18)-C(19)	1.370(12)		

Bond angle (ϕ/°)			
N(2)-C(1)-C(10)	120.3(7)	N(2)-C(1)-C(14)	118.1(7)
C(10)-C(1)-C(14)	121.7(7)	C(1)-N(2)-C(3)	119.1(7)
N(2)-C(3)-C(4)	124.6(7)	C(3)-C(4)-C(11)	117.3(7)
C(6)-C(5)-C(13)	118.8(7)	C(5)-C(6)-C(7)	122.3(8)
C(6)-C(7)-C(18)	120.0(8)	C(7)-C(8)-C(12)	118.0(8)
C(10)-N(9)-C(12)	109.9(6)	C(1)-C(10)-N(9)	132.4(7)
C(1)-C(10)-C(11)	119.4(6)	N(9)-C(10)-C(11)	108.1(6)
C(4)-C(11)-C(10)	119.3(6)	C(4)-C(11)-C(13)	134.0(7)
C(10)-C(11)-C(13)	106.7(6)	C(8)-C(12)-N(9)	129.4(7)
C(8)-C(12)-C(13)	122.9(7)	N(9)-C(12)-C(13)	107.6(6)
C(5)-C(13)-C(11)	134.4(7)	C(5)-C(13)-C(12)	117.9(7)
C(11)-C(13)-C(12)	107.7(6)	C(1)-C(14)-N(15)	115.4(7)
C(1)-C(14)-C(19)	122.1(7)	N(15)-C(14)-C(19)	122.4(7)
C(14)-N(15)-C(16)	116.2(6)	N(15)-C(16)-N(17)	126.2(7)
N(15)-C(16)-N(20)	115.9(7)	N(17)-C(16)-N(20)	117.7(7)
C(16)-N(17)-C(18)	115.2(7)	N(17)-C(18)-C(19)	124.1(8)
C(18)-C(19)-C(14)	115.9(8)		

Bond Lengths and Bond Angles. The average C–C bond length in the benzene ring is 1.396 Å. The C(5)–C(6) bond (1.362 Å) is significantly shorter than the average value. These results compare well with those found in indole.[6] The C(11)–C(13) bond (1.421 Å) is longer than the standard aromatic C–C bond of 1.395 Å.[8] The mean C–N distance in the five-

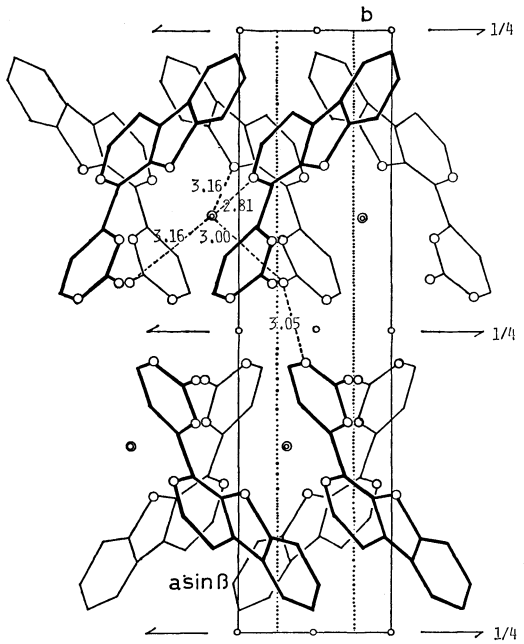

Fig. 2. Packing of the molecules viewed down c. Hydrogen bonds are shown by broken lines with their lengths in Å.

membered ring is 1.381 Å, and the C–C distance is 1.416 Å. The mean bond distances in the pyridine ring are 1.396 Å for C–C and 1.346 Å for C–N. As for the pyrimidine ring, the mean C–N distance is 1.335 Å. The angles at the nitrogen atoms are less than 120° by about 4°, in agreement with the values in similar heterocyclic systems. The angles at the carbon atoms are all greater than 120° [that at C(16) considerably so], with the exception of that at C(19), which is only 115.9°. These results compare well with those found in the structure of pyrimidine.[9]

Environment of the Molecule. Five types of hydrogen bonds can be seen in the structure. The first hydrogen bond connects N(20) with O(21) at a distance of 3.00 Å. The second (3.16 Å) connects N(9) with O(21). The third (2.81 Å) is the O(21)–N′(2) bond, in which N′(2) is equivalent to N(2). The fourth (3.16 Å) connects N″(20), which is equivalent to N(20), with O(21). The fifth hydrogen bond connects N(20) with N‴(17) at a distance of 3.05 Å.

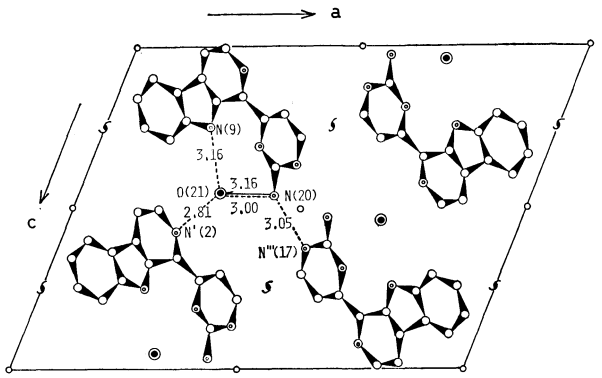

Fig. 3. The packing of the molecules in a unit cell seen along the b axis.

These hydrogen bonds are shown in Figs. 2 and 3.

We wish to thank Mr. Toshio Sato for giving us a chance to cooperate in this work; Professor Daihei Oda, Mr. Osamu Moriya, and Mr. Shigeru Hasegawa for their valuable suggestions, and Dr. Teruo Noguchi and Mr. Jun Ito for plotting the thermal ellipsoids. We also wish to thank Mr. Kazumasa Maruyama for help with the calculations.

References

1) T. H. Yang and M. Chen, *Proc. Natl. Sci. Counc. R. O. C.*, **3**, 63 (1979).
2) "The Universal Crystallographic Computing System," ed by T. Ashida, Library of Programs, Computing Center of Osaka University (1973).
3) G. Germain, P. Main, and M. M. Woolfson, *Acta Crystallogr., Sect. A*, **27**, 368 (1971).
4) "International Tables for X-Ray Crystallography," The Kynoch Press, Birmingham (1959), Vol. III, pp. 201—203.
5) C. K. Johnson, ORTEP, ORNL-3794, Oak Ridge National Laboratory, Tennessee (1965).
6) G. Falkenberg and D. Carlström, *Acta Crystallogr., Sect. B*, **27**, 411 (1971).
7) M. Kurahashi, M. Fukuyo, A. Shimada, A. Furusaki, and I. Nitta, *Bull. Chem. Soc. Jpn.*, **42**, 2174 (1969).
8) K. Chandrasekhal and V. Pattabhi, *Acta Crystallogr., Sect. B*, **36**, 1165 (1980).
9) M. M. Ripoll and H. P. Lorentz, *Acta Crystallogr., Sect. B*, **29**, 2260 (1973).

 © 1982 The Chemical Society of Japan Bull. Chem. Soc. Jpn., 55, 2239—2242 (1982)

The Effect of Quaternary Phosphonium Halides on the Temperature of the Maximum Density of Water

Katsuko TAKAIZUMI* and Toshiki WAKABAYASHI

The College of General Education, Tohoku University, Kawauchi, Sendai 980

(Received November 10, 1981)

The shifts in the temperature of the maximum density(tmd) of water produced by quaternary phosphonium halides, $(n\text{-Bu})_{4-n}Ph_nPX$($n$=0—4), were measured dilatometrically, and the Despretz constants, K_D, were determined. The K_D, which is positive when the tmd is lowered by a solute, increases nearly linearly with increasing n from 1.16 kK for $(n\text{-Bu})_3PhPCl$ to 1.57 kK for Ph_4PCl, while the K_D for Bu_4PCl, 0.933 kK, is considerably lower than that to be expected from those for other members. Since the standard partial molal volumes of the cations have been found to be nearly the same, the variation in K_D with n would originate from the difference in ion-water interaction between the cations. Some estimation was made for the contribution of the structural effect of the cations on the solvent water (K_{st}). The K_{st} is largely negative for the Bu_4P^+ ion, indicating that the cation is a structure maker. The K_{st} becomes less negative as n increases, indicating that the structure-making ability decreases with an increase in n.

The shifts in the temperature of the maximum density (tmd) of water produced by solutes contain information about the structural influence of the solutes on the solvent water. With nonelectrolytes as solutes, Franks and Watson[1] showed that the shifts (ΔT) are divided into two terms. One(ΔT_v) is dependent upon the size and expansibility of the solute in its pure liquid state, as derived by Wada and Umeda,[2] and it serves always to depress the tmd. The other(ΔT_{st}) is identified with the structural influence of the solute on the solvent water, positive for structure makers and negative for structure breakers. Some alcohols and amines[1,2] elevate the tmd at low concentrations.

On the other hand, the negative shifts alone have been found with electrolytes, including alkali metal halides and tetraalkylammonium halides. Darnell and Greyson[3] noticed, by comparing the tmd's of aqueous solutions of alkali metal halides with common ions, that the stronger the structure-breaking ability of the uncommon ions, the lower the tmd. They found, however, that tetraalkylammonium halides(R_4NX) depress the tmd; this effect becomes greater as the size of the alkyl group increases, contrary to our expectation that tmd would be raised as the size of the alkyl group increases because the structure-making ability of these groups increases with the alkyl-group size.[4] A similar trend was also found in D_2O as the solvent.[5] Darnell and Greyson interpreted their observation as showing that, at least in the neighborhood of the tmd, ion sizes play a more important role in influencing the water structure than the structure-making or structure-breaking properties of the ions which are observed at room temperature, and that, at low temperatures, R_4N^+ ions disrupt the water structure because of the incompatibility of the structure of the solvent.

However, this interpretation seems inconsistent with some facts which indicate that the lower the temperature, the greater is the structure-making ability of R_4N^+ ions, as found in the studies of the near-infrared spectra of Bu_4NBr and in the H_2O–D_2O mixture at 5 °C,[6] the NMR chemical shifts of the water proton in aqueous solution of R_4NX,[7] and the temperature dependence of the cationic partial molal heat capacities of R_4N^+ ions in water.[8] In order to discuss the influence of hydrophobic salts on the water structure, the extraction of ΔT_{st} from ΔT is essential. This is generally very difficult, however, because in this case we must be concerned with the volumetric properties of the salts in a hypothetical pure liquid state.

One way to approach the subject may be to examine the shifts produced by a series of salts which are nearly the same in their volumetric properties, but not in their interactions with water. Quaternary phosphonium salts, $(n\text{-Bu})_{4-n}Ph_nPX$($n$=0—4), satisfy this requirement comparatively well; their standard partial molal volumes[9] tend to approach one another as the temperature is lowered, and the structure-making ability decreases with n.

Experimental

Apparatus and Measurements. Measurements of the volume changes of aqueous solutions of $(n\text{-Bu})_{4-n}Ph_nPX$($n$=0—4) with the temperature were made in dilatometers of about 100-cm³ capacity, calibrated triply with conductivity-grade water, at 0.5 K intervals in the temperature range of 0.5—6 °C. The dilatometers were constructed of Pyrex tubing about 35 mm i.d. and capillary tubing about 0.5 mm i.d. with minimum graduations of 0.0005 cm³. The temperatures of the thermostat bath were controlled to within ±0.005 K. The temperatures of the bath were measured by a standard thermometer calibrated against a platinum-resistence thermometer (Leeds and Northrup).

The volume changes with the temperature were found to be approximately symmetrical near the tmd for all solutions. The tmd was obtained graphically from the temperature *vs.* volume curve, with a maximum error of ±0.05 K.

Materials. The tetraphenylphosphonium chloride was obtained from Merck. The other salts, $Bu_{4-n}Ph_nPCl$(n=0—3), were synthesized from the corresponding phosphines. The method of purifying the salts and their purity were similar to those reported previously[9]. The stock solutions were filtered through a Millipore-filter. The solutions for dilatometric measurement were prepared by the dilution of the stock solutions by weight, all weighings being vacuum-corrected.

Results and Discussion

The shifts, ΔT, in the tmd of water produced by

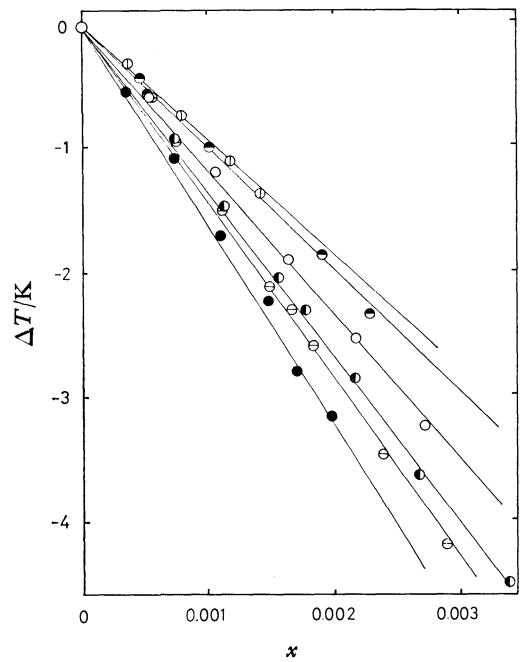

Fig. 1. Shifts(ΔT) in tmd produced by $Bu_{4-n}Ph_nPX$ as a function of salt mole fraction, x.
◓: Bu_4PBr, ⓘ: Bu_4PCl, ○: Bu_3PhPCl, ◐: Bu_2Ph_2PCl, ⊖: $BuPh_3PCl$, ●: Ph_4PCl.

Table 1. Despretz constants(K_D) for phosphonium halides

Salts	K_D / 10^3 K	σ[a] / 10^3
n-Bu_4PBr	0.982 (0.009)[b]	0.023
n-Bu_4PCl	0.933 (0.018)	0.032
n-Bu_3PhPCl	1.16 (0.019)	0.033
n-Bu_2Ph_2PCl	1.31 (0.02)	0.052
n-$BuPh_3PCl$	1.42 (0.029)	0.052
Ph_4PCl	1.57 (0.011)	0.016

a) Standard deviation. b) Uncertainty expected in K_D.

$Bu_{4-n}Ph_nPX$(n=0—4, X=Cl, Br) are shown in Fig. 1 as a function of the solute mole fraction, x. As may be seen from the figure, the ΔT for each salt seems to be nearly a linear function of x.

The Despretz constants, K_D, defined by:

$$\Delta T = -K_D x, \tag{1}$$

were determined by the least-squares method. The K_D values thus obtained are summarized in Table 1.

Table 2 lists the densities, d, of the solutions and the apparent molal volumes, ϕ_v, for $Bu_{4-n}Ph_nPCl$ at 5 °C in the concentration range of 0.02—0.2 mol kg^{-1}. The ϕ_v were calculated by means of the equation:

$$\phi_v = \frac{1}{m}\left(\frac{1000+mM}{d} - \frac{1000}{d_o}\right), \tag{2}$$

where m is the molality of salt; M, the formula weight of the salts, and d_o, the density of water at 5 °C, which was taken as 0.999965 g cm^{-3}.[10] The standard partial molal volumes, ϕ_v°, and the B_v coefficients for ϕ_v for the phosphonium halides were determined by fitting

Table 2. Densities and apparent molal volumes of $Bu_{4-n}Ph_nPX$ at 5 °C

m / mol kg^{-1}	d / g cm^{-3}	ϕ_v / cm^3 mol^{-1}
n-Bu_4PBr(n=0)		
0.02613	1.000722	310.11
0.05692	1.001661	309.00
0.10329	1.003073	308.28
0.12751	1.003874	307.47
0.20075	1.006089	306.95
n-Bu_3PhPCl(n=1)		
0.05956	1.000726	301.86
0.09170	1.001169	301.38
0.12130	1.001600	300.91
0.15123	1.002020	300.68
n-Bu_2Ph_2PCl(n=2)		
0.02930	1.000927	301.72
0.04245	1.001368	301.39
0.06283	1.002042	301.18
0.08685	1.002797	301.40
0.09832	1.003181	301.18
0.12020	1.003867	301.23
0.14859	1.004794	300.92
0.18875	1.006092	300.57
n-$BuPh_3PCl$(n=3)		
0.04120	1.002154	301.05
0.08237	1.004272	301.27
0.09234	1.004776	301.31
0.10126	1.005272	300.85
0.16062	1.008218	300.99
Ph_4PCl(n=4)		
0.06118	1.004330	302.18
0.08189	1.005795	301.89
0.09447	1.006648	302.09
0.10949	1.007675	302.09

Table 3. Standard partial molal volumes(ϕ_v°) and B_v coefficients for phosphonium halides at 5 °C

Salts	ϕ_v° / cm^3 mol^{-1}	B_v / cm^3 dm^3 mol^{-2}
n-Bu_4PBr	310.0 (0.37)[b]	−24.6 (3.2)[c]
n-Bu_4PCl	303.2[a]	
n-Bu_3PhPCl	302.4 (0.12)	−16.5 (1.1)
n-Bu_2Ph_2PCl	301.6 (0.12)	−8.7 (1.2)
n-$BuPh_3PCl$	301.0 (0.25)	−3.7 (2.5)
Ph_4PCl	301.9 (0.38)	−3.8 (4.5)

a) Estimated value from $\overline{V}^\circ(Br^-, 5°)$ and $\overline{V}^\circ(Cl^-, 5°)$; *cf.* Ref. 9. b) Uncertainty in ϕ_v°. c) Uncertainty in B_v.

the ϕ_v data to Eq. 3 by the method of least squares;

$$\phi_v - A_v c^{1/2} = \phi_v^\circ + B_v c, \tag{3}$$

where A_v is the Debye-Hückel limiting slope and where the value at 5 °C was taken as 1.529 cm^3 $dm^{3/2}$ $mol^{-3/2}$.[11] The results are summarized in Table 3.

The ΔT for liquid nonelectrolytes can be expressed as:

$$\Delta T = T - T^* = \frac{-\alpha_2 V_2^\circ x}{2\alpha_1(1-x)V_1^*} + \frac{-1}{2\alpha_1(1-x)V_1^*}\frac{\partial \Delta V_x^M}{\partial T}, \quad (4)$$

where the T and T^* are the temperature of the maximum density of a solution and of pure water(3.98 °C) respectively; x is the mole fraction of the solute; α_2 the thermal expansion coefficient of the solute, and α_1, a coefficient in a quadratic equation of T expressing the molal volume of pure water around T^*($\alpha_1 = 7.80\times10^{-6}$ K^{-2}),[2] V_1^* and V_2° are the molal volume of pure water at T^* and that of the solute in the pure liquid state at T, and ΔV_x^M is the excess volume of mixing referred to a mixture of the solute mole fraction, x. For dilute solutions, Eq. 4 is reduced to:

$$\Delta T = -\left(\frac{\alpha_2 V_2^\circ}{2\alpha_1 V_1^*} + \frac{1}{2\alpha_1 V_1^*}\frac{\partial b}{\partial T}\right)x = -(K_v + K_{st})x, \quad (5)$$

under the assumption that $\Delta V_x^M = bx(1-x)$,[12] where b is a constant with regard to the mole fraction. Thus, the Despretz constant can be divided into the volume-dependent term, K_v, and the structural term, K_{st}. With electrolytes containing large organic ions, as in the present case, the K_v would contribute largely to K_D.

As may be seen from Table 1 and Fig. 2, K_D increases with an increase in the number of phenyl groups on the cations. The K_D(Bu_4PBr) is larger by about 70 K than K_D(Bu_4PCl), indicating that the anionic contribution of Br^- to K_D is larger than that of the Cl^- ion. This difference is comparable to that, 50 K,[3] found for a set, K_D(Et_4NBr) and K_D(Et_4NCl). The contribution of the Br^- (and also of Cl^-) ion to K_D's would be comparatively small, say around 5×10^2 K for the Br^- ion, which is the mean value of K_D for HBr and KBr.[20] Thus, it appears that the cationic contribution to K_D increases with an increase in n, from 5×10^2 K for the Bu_4P^+ ion to 1.1×10^3 K for the Ph_4P^+ ion, assuming that the volumetric properties, V_+° and α_+, of the cations are nearly the same, as is suggested by the equality in their standard partial molal volumes(Table 2). This point is discussed below more elaborately.

The $\overline{V}_+^\circ$ may be written as the sum of the contributions of several factors: the intrinsic volume of the cation, $\overline{V}_{in}$; the structural volume change associated with the shift of the H-bond equilibria of the solvent water in the presence of the ion, $\overline{V}_{st}$, and the packing effect of the ion in the cavities in water structures, $\overline{V}_c$. The electrostriction effect can be neglected here because of the large cationic sizes. $\overline{V}_{in}$ will decrease with an increase in n, as is suggested by the molal volume of benzene and liquid butane at 25 °C, 89.4 and 100 cm^3 mol^{-1} (extrapolated values from higher homologs) respectively. $\overline{V}_+^\circ$(Bu_4P^+) in methanol was estimated as 267, and that of the Ph_4P^+ ion, as 264 cm^3 mol^{-1},[13] where the structural effects are much lower than in water. Thus, the $\overline{V}_+^\circ$ values of the present cations are expected to decrease as n increases. The expansion coefficients of the cations would also decrease with n because the polarizability of the butyl group is expected to be smaller than that of the phenyl group, and hence the dispersion force would increase with n.[14] Thus, the conclusion is obtained that K_v decreases somewhat with an increase in n and that, therefore, K_{st} increases with n. Since it has been confirmed that, with a nonelectrolyte as a solute, $\partial\Delta V_x^M/\partial T$ and so $\partial b/\partial T$ are negative for structure-makers and positive for structure-breakers,[2] the phenyl group may be either a structure-breaker or a weaker structure-maker than the butyl group. This conclusion is in agreement with the information obtained from the studies of the viscosity,[15] the molal volume,[9] the molal heat capacity,[13] and the differential near-infrared spectra[16] for Bu_4PBr or Bu_4NBr and Ph_4PCl solutions.

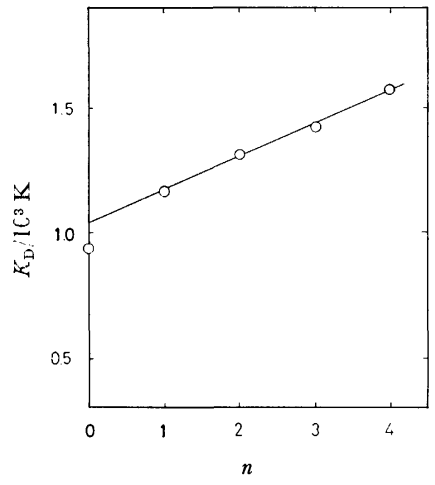

Fig. 2. Despretz constants(K_D) for $Bu_{4-n}Ph_nPCl$ as a function of n.

The estimation of K_{st} for the present cations is of interest and may be possible in the case of the Bu_4P^+ ion. Since Bu_4PBr is similar in molecular structure to Bu_4NBr, the K_{st} can be assumed to be nearly the same with these two salts, and we can obtain the following relation by subtracting K_D(Bu_4NBr) from K_D(Bu_4PBr):

$$K_D(Bu_4PBr) - K_D(Bu_4NBr) = \frac{\alpha_2}{2\alpha_1 V_1^*}(V_2^\circ(Bu_4PBr) - V_2^\circ(Bu_4NBr)), \quad (6)$$

where the thermal expansion coefficient, α_2, is assumed to be equal. From the equation, the value for α_2 is estimated by inserting the standard partial molal volumes, $\overline{V}_2^\circ$(5 °C), in place of V_2°. This approximation seems reasonable because $\overline{V}_{st}$ and $\overline{V}_c$ are expected to be equal for the two cations, and these contributions cancel each other out upon the subtraction. The value obtained for α_2 is 1.8×10^{-3} K^{-1}, with 310.0 and 295.15[8] cm^3 mol^{-1} at 5 °C for $\overline{V}_2^\circ$ of Bu_4PBr and Bu_4NBr respectively, and 888 K for K_D(Bu_4NBr).[5] The α_2 value is of the same order as those for C_5—C_9 alkanes,[14] and seems reasonable. From Eq. 5 with the α_2 value, we obtain 1.8 kK for K_v(Bu_4P^+), where $\overline{V}_+^\circ$(Bu_4P^+) is taken as 281.1 cm^3 mol^{-1}, which is obtained by subtracting $\overline{V}_-^\circ$(Br^-, 5°) 28.9 cm^3 mol^{-1},[9] from $\overline{V}_2^\circ$(Bu_4PBr, 5°). The estimation shows that K_{st} (Bu_4P^+) is largely negative, about −1.3 kK, indicating a strong structure-making ability of the cation, but overshadowed by the larger K_v(Bu_4P^+).

It is noticeable that the K_D for Bu_4PCl is considerably

smaller than that extrapolated from those for other members (Fig. 2). This would suggest the presence of a clathrate-like structure of Bu_4P^+ ion, which was proposed by Wen and Saito[17] for the hydration model for Bu_4N^+ and Pr_4N^+ ions. The cooperative nature in forming a hydrogen-bonded structure of water[18,19] may be responsible for the large increase in K_{st} value from the Bu_4P^+ to the Bu_3PhP^+ ion because of a different kind of water structure in the cosphere of the phenyl group. The aqueous-solution behavior of the Ph_4P^+ ion can, in comparison with that of the Bu_4P^+ ion, be characterized by the following: A low activation energy for viscous flow,[15,21] a low partial molal heat capacity,[13] a large molal expansibility with a negative temperature dependence,[9] a low negative value of B_v(Table 3) with a negative temperature dependence, in contrast with a positive dependence for Bu_4PBr,[9] *etc.* All these facts suggest that the water molecules in the phenyl-cosphere are less structured, and hence less hydrogen-bonded, than those in the butyl-group cospheres; in other words, the phenyl groups are hydrophilic rather than hydrophobic. This character of the phenyl groups would arise from delocalized charges on the phenyl groups[22] and the structure-breaking effect due to the poor fit of planar phenyl groups into the partly tetrahedral structure of water. The volumetric properties of the present salts, including a discussion of the B_v-coefficients, will be given in detail elsewhere.[23]

The approach attempted here seems promising for obtaining information, from the tmd data, about the structural influence of organic ions on the solvent water. The division of K_D for electrolytes into ionic contributions based on a sounder basis is required for a more comprehensive treatment of the tmd data. This will be one next subject.[24]

References

1) F. Franks and B. Watson, *Trans. Faraday Soc.*, **63**, 329 (1967).

2) G. Wada and S. Umeda, *Bull. Chem. Soc. Jpn.*, **35**, 646 (1962); **35**, 1797 (1962).

3) A. J. Darnell and J. Greyson, *J. Phys. Chem.*, **72**, 3021 (1968).

4) W. -Y. Wen, "Tetraalkylammonium Salt Solutions," in "Water and Aqueous Solutions," ed by R. A. Horne, Wiley-Interscience, London (1972), Chap. 15, pp. 613—661.

5) B. E. Conway and L. H. Laliberté, *Trans. Faraday Soc.*, **66**, 3032 (1970).

6) J. D. Worley and I. M. Klotz, *J. Chem. Phys.*, **45**, 2868 (1966).

7) M. -M. Marciaq-Rousselot, A. Trobriand, and M. Lucas, *J. Phys. Chem.*, **76**, 1455 (1972); G. P. Kreishman and L. Leifer, *J. Solution Chem.*, **7**, 239 (1978).

8) G. Perron, N. Desrosiers, and J. E. Desnoyers, *Can. J. Chem.*, **54**, 2163 (1976).

9) K. Takaizumi and T. Wakabayashi, *J. Solution Chem.*, **9**, 809 (1980).

10) G. S. Kell, *J. Chem. Eng. Data*, **12**, 66 (1967).

11) O. Redlich and D. M. Meyer, *Chem. Rev.*, **64**, 221 (1964).

12) J. H. Hildebrand and R. L. Scott, "The Solubility of Nonelectrolytes," 3rd ed, Dover Publications, New York (1964), Chap. 8.

13) C. Jolicoeur, P. R. Phillip, G. Perron, P. A. Leduc, and J. E. Desnoyers, *Can. J. Chem.*, **50**, 3167 (1972).

14) The thermal expansion coefficients of butane and benzene are 2.0×10^{-3} (extrapolated value from higher homologs, C_5–C_9) and 0.975×10^{-3} K^{-1} respectively, in the temperature range of 0—80 °C; *cf.* J. A. Riddick and W. B. Bunger, "Organic Solvents," 3rd ed, Wiley-Interscience, London (1970).

15) K. Takaizumi and T. Wakabayashi, *J. Solution Chem.*, **9**, 819 (1980).

16) C. Jolicoeur, N. D. The, and A. Cabana, *Can. J. Chem.*, **49**, 2008 (1971).

17) W. -Y. Wen and S. Saito, *J. Phys. Chem.*, **68**, 2639 (1964).

18) M. J. Mastroianni, M. J. Pikal, and S. Lindenbaum, *J. Phys. Chem.*, **76**, 3050 (1972).

19) W. J. M. Heuvelsland, M. Bloemendal, C. Visser, and G. Somsen, *J. Phys. Chem.*, **84**, 2391 (1980).

20) The K_D for HBr and KBr are 364 and 681 K, which were calculated from the data: "International Critical Tables," ed by E. W. Washburn, McGraw-Hill Book Co., New York (1933), Vol. 3, pp. 107—108.

21) K. Takaizumi and T. Wakabayashi, *Bull. Chem. Soc. Jpn.*, **49**, 2194 (1976).

22) S. O. Gim and W. McFarlane, *Can. J. Chem.*, **46**, 2071 (1968).

23) T. Wakabayashi and K. Takaizumi, submitted to *J. Solution Chem.*

24) T. Wakabayashi and K. Takaizumi, *Bull. Chem. Soc. Jpn.*, in press.

 © 1982 The Chemical Society of Japan Bull. Chem. Soc. Jpn., 55, 2243—2247 (1982)

Monolayers of Alkylammonium Alkanesulfonates

Osamu Shibata,* Shoji Kaneshina, Makoto Nakamura, and Ryohei Matuura†

College of General Education, Kyushu University-01, Ropponmatsu, Fukuoka 810

† *Department of Chemistry, Faculty of Science, Kyushu University-33, Higashi-ku, Fukuoka 812*

(Received January 26, 1982)

The surface pressure-area (π-A) curves for monolayers of cation-anion double long-chain salts, alkylammonium alkanesulfonates, were determined at the air-water interface by the Langmuir method. When the total chain length of cation and anion was constant, the transition pressure from the expanded to the condensed state in the monolayer was lowered as the chain length of cation elongated, and the lowest pressure at the transition point was observed in the case of the equal chain length of cation and anion. The lower the pressure at the transition point, the larger the value of the mean area per molecule at that point. The apparent molar entropy, enthalpy, and energy of transition from the expanded to the condensed phase were calculated from the temperature dependence of the transition pressure on the π-A curve. All the values calculated were negative. The magnitude in the changes of the apparent molar quantities was greatest when both a cationic and an anionic chain had the same length. These results were interpreted in terms of the orientation of double long-chain salt in the condensed state of monolayer. The increase in the chain length of cation and anion tends to increase the values of apparent molar quantity changes. The contributions of long-chain anion and cation to the phase transition of monolayer are not equivalent; the condensing effect of long-chain cation is larger than that of long-chain anion.

There are numerous studies on the adsorbed films from the mixture of cationic and anionic surfactant solutions at the air-water interfaces.[1-7] With respect to the mixed monolayers of cationic and anionic surfactants, a few studies have been reported.[8-12] Our previous investigation[13] has been made on the insoluble monolayers of double long-chain salts, which are composed of a long-chain cation and a long-chain anion, and has shown unique behavior with a series of alkyltrimethylammonium alkanesulfonates. The surface pressure-area curves of these salts exhibited the transition from an expanded to a condensed film, in such a manner as to depend upon the combination of the anion and cation chain-lengths. To elucidate this phenomenon in more detail, it is necessary to extend the study so as to include the double long-chain salts with a different polar group.

In the present study, alkylammonium alkanesulfonates were prepared, and the surface pressure of monolayers of these salts has been measured as a function of molecular area at various temperatures. The thermodynamic quantities on the phase transition from the expanded to the condensed state were determined.

Experimental

The double long-chain salts, that is, alkylammonium alkanesulfonates, were prepared by mixing equimolar solutions of alkylammonium chlorides and sodium alkanesulfonates (Tokyo Kasei Kogyo Co., Ltd.). The precipitates formed were purified by recrystallization from an acetone/ethanol mixture (3:1, v/v). In this study 16 salts of different hydrocarbon chain length shown in Table 1 were used. These salts are abbreviated as Cm–Cn, in which m is the number of carbon atoms in the cationic long chain and n is that in the anionic long chain. The purity of these salts was checked by elemental analyses, which gave correct results.

Table 1. Materials

Double long-chain salt		Abbreviation	
$C_mH_{2m+1}N^+H_3 \cdot C_nH_{2n+1}SO_3^-$		Cm–Cn	
m = 12, 14, 16, 18		(cationic long-chain)	
n = 12, 14, 16, 18		(anionic long-chain)	
Salt used for monolayers			
C12–C12	C12–C14	C12–C16	C12–C18
C14–C12	C14–C14	C14–C16	C14–C18
C16–C12	C16–C14	C16–C16	C16–C18
C18–C12	C18–C14	C18–C16	C18–C18

Each double long-chain salt was spread from a chloroform/methanol (4:1, v/v) mixture (both Merck, Uvasol) at the air-water interface. The substrate solution of 0.1 M (1 M = 1 mol dm^{-3}) sodium chloride was prepared by thrice-distilled water. Here the sodium chloride was roasted at 973 K to remove any surface active material.

The surface pressure was measured by an automatic Langmuir film balance, which was constructed in our laboratory, within an accuracy of ± 0.1 mN m^{-1}.[13] The temperature of the substrate was controlled within ± 0.1 K at the desired temperature by circulating thermostated water. The monolayer was compressed continuously with a constant velocity of 2.93×10^{-2} nm^2 molecule^{-1} min^{-1}.

Results and Discussion

The surface pressure-area (π-A) curve of C12–C12 was affected by the NaCl concentration of substrate, and showed a reasonable limiting area on the 4 M NaCl solution. Except for a C12–C12 system, the concentration of NaCl did not affect the π-A curves only if it is above 0.1 M; that is, the π-A curves coincide with each other. Considering this, the concentration of NaCl was held at 0.1 M except for the C12–C12 system.

The π-A curves of C12–C12, C14–C14, C16–C16, and C18–C18 salts, which have equal numbers of carbon atoms in the long-chain cation and anion, that is, m=n, are depicted in Fig. 1. The π-A curve of C12–C12 salt had a transition point from an expanded to a condensed state at 298.2 K under the high concentration of sodium chloride (4 M). The π-A curve of C14–C14 had also a transition point, while the curves of C16–C16 and C18–C18 exhibited only the condensed film. It is of interest to compare the monolayer of a double long-chain salt with that of the corresponding single long-chain salt, but the

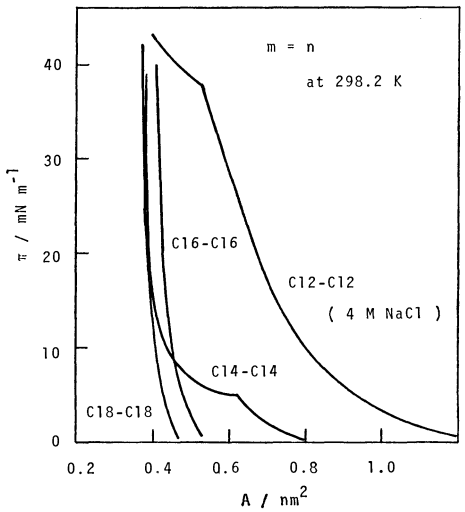

Fig. 1. The π-A curves of double long-chain salts on 0.1 M NaCl at 298.2 K. Except for C12–C12 on 4 M NaCl.

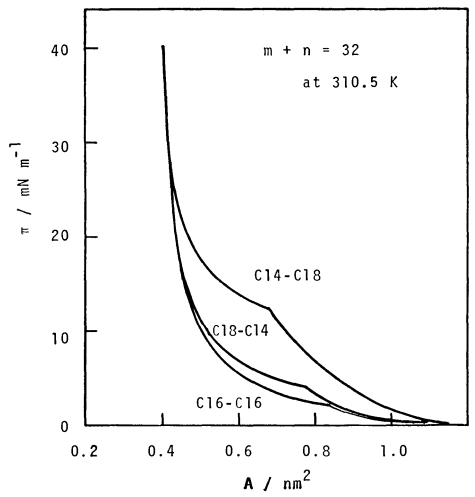

Fig. 2. The π-A curves in the case of total carbon number of long-chain cation and anion equal to 32. Substrate: 0.1 M NaCl at 310.5 K.

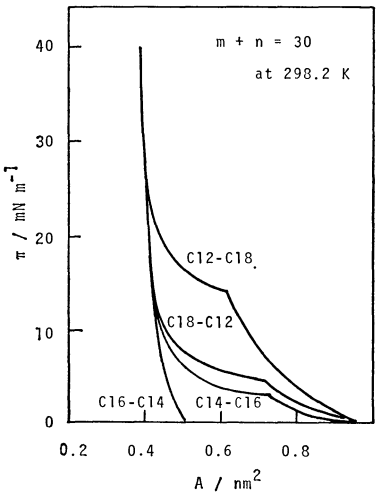

Fig. 3. The π-A curves in the case of total carbon number of long-chain cation and anion equal to 30. Substrate: 0.1 M NaCl at 298.2 K.

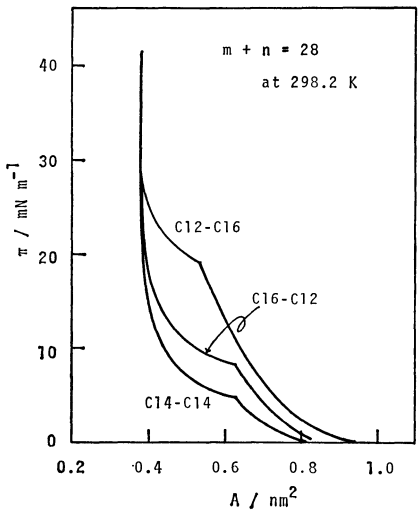

Fig. 4. The π-A curves in the case of total carbon number of long-chain cation and anion equal to 28. Substrate: 0.1 M NaCl at 298.2 K.

latter is soluble in water. So we compared the former with the monolayer of single long-chain fatty acid. For example, the π-A curve of tetradecanoic acid is of an expanded type, which has a transition from the expanded to the condensed state at 298.2 K. The π-A curve of C14–C14 in the present work has also a transition point under this condition. When the alkyl chain of double long-chain salt is longer, *i.e.*, m $(=n) \geq 16$, the monolayer shows only a condensed type film at 298.2 K. The same trend is shown for the monolayers of a single long-chain fatty acid. This result is different from the previous data of alkyltrimethylammonium alkanesulfonates.[13]

Figure 2 shows the π-A curves at 310.5 K for three double long-chain cation and anion when $m+n$ is equal to 32. At this temperature the C16–C16 salt shows phase transition and it has the lowest transition pressure among three compounds as seen in Fig. 2. It is noteworthy that in the case of the equal length of cation and anion, the condensing effect is most pronounced. This condensing effect seems to be due to the increase in the molecular interaction between the alkyl chains.

Figures 3—5 show the π-A curves for sets of double long-chain salts with the total carbon numbers of long-chain cation and anion, that is, $m+n$, equal to 30, 28, and 26, respectively. When the carbon number difference between a long-chain cation and anion is large as in the case of C12–C18 and C18–C12, the transition pressure is higher than that of C14–C16 and C16–C14. As is seen from Figs. 2—5, when the chain length of the cation is longer than that of the anion, the transition pressure is lower. The π-A curve of C16–C14, in this case, shows only a condensed type of film at 298.2 K. It can be concluded that when the chain length of the cation is longer than that of the anion, the monolayer is apt to be more condensed.

The π-A curves of alkylammonium alkanesulfonates studied in this paper, as shown in Figs. 1—5, show

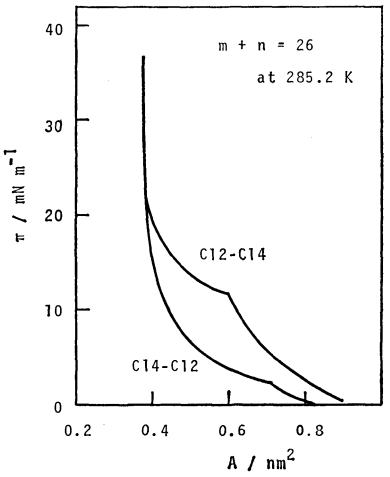

Fig. 5. The π-A curves in the case of total carbon number of long-chain cation and anion equal to 26. Substrate: 0.1 M NaCl at 285.2 K.

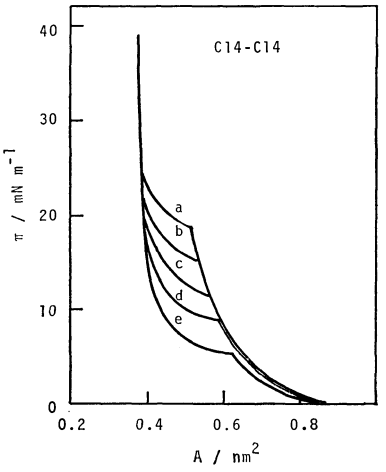

Fig. 6. Temperature dependence of π-A curves of C14–C14 salt. Substrate: 0.1 M NaCl. Temperature: (a) 308.4 K, (b) 306.4 K, (c) 303.2 K, (d) 300.9 K, (e) 298.2 K.

the same limiting area of about 0.4 nm². This value is in good agreement with twice area of corresponding single long-chain fatty acid.[17,19–21] The double long-chains of these salts are probably aligned perpendicular to the water surface when the film is fully compressed. We have reported previously the value of 0.6 nm² for alkyltrimethylammonium alkanesulfonate.[13] Corkill *et al.* reported also the value of 0.6 nm² for alkyltrimethylammonium alkyl sulfate.[8] The replacement of sulfate for sulfonate hardly causes the difference in the limiting area. It is evident, on the contrary, that the substitution of cationic ammonium group for trimethylammonium group leads to the appreciable increase in the limiting area. Compared with alkylammonium ion, the bulky head of alkyltrimethylammonium ion may be responsible for the larger limiting area in the π-A curve of the double long-chain salt containing alkyltrimethylammonium ion.

The studies of the temperature effect on the transition pressure in the monolayer are of much interest, since it provides us with thermodynamic information about the state of the monolayers. Figure 6 shows the π-A isotherms of C14–C14 at various temperatures. All the curves have break points, showing the phase transition from the expanded to the condensed state. As was expected, the transition pressure increased with an increase in the temperature. The π-A curves of other salts Cm–Cn with a transition pressure were also measured at various temperatures. In Fig. 7, the transition pressure (π^{eq}) is shown as a function of temperature for various double long-chain salts. The curves are almost linear. This figure includes the temperature effect of π^{eq} of tetradecanoic acid (C14 acid) in order to compare with that of double long-chain salts. The slopes of these lines were determined in order to calculate the apparent molar entropy change on the phase transition.

Exact thermodynamic equations for the multicomponent monolayers were recently derived by Motomura *et al.*[14–18] The thermodynamic quantities on the transition from the expanded to the condensed film can

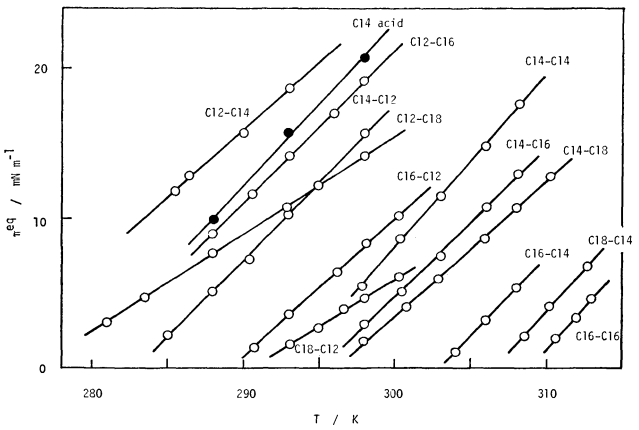

Fig. 7. Transition pressure (π^{eq}) as a function of temperature. Substrate: 0.1 M NaCl, C14 acid: tetradecanoic acid.

be determined by this thermodynamic treatment, which takes account of contribution of water in a monolayer. When a substance exists in the monolayer state, the apparent molar entropy change is evaluated by applying the relation

$$\Delta s^r = (a^c - a^e)\left[\left(\frac{\partial \pi^{eq}}{\partial T}\right)_p - \left(\frac{\partial \gamma^\circ}{\partial T}\right)_p\right], \quad (1)$$

which corresponds to Eq. 29 of Ref. 17. In this equation, Δs^r is the apparent molar entropy change, a^c and a^e are the molecular area (nm²) (superscripts c and e refer to the condensed and expanded state, respectively), π^{eq} is the transition pressure from the expanded to the condensed state, and γ° is the surface tension of pure water. a^c and a^e are estimated as follows. a^e is the area at the point where the film begins to change from the expanded to the condensed state. a^c is determined in the following way: when the point (π^{eq}, a^e) is shifted parallel to the area axis, it comes into contact with the elongated line of the π-A curve in the condensed state to the lower surface pressures. This point of intersection gives the a^c value. The right side of Eq. 1 is calculated numerically from

the results given in Figs. 6 and 7. Moreover, the apparent molar enthalpy change is calculated by the relation

$$\Delta h^r = T\Delta s^r. \quad (2)$$

Now the apparent molar energy change Δu^r is related to Δs^r by

$$\Delta u^r = -(\pi^{eq}-\gamma^\circ)(a^c-a^e) + T\Delta s^r, \quad (3)$$

which corresponds to Eq. 32 of Ref. 17. Thus we can determine Δu^r by use of the above experimental results.

The apparent molar quantity changes on the phase transition calculated by using these equations are given in Table 2. In Table 2, the column represents the cation chain length and the row represents the anion chain length. The element of any column or row shows the value of the apparent molar quantity change on the phase transition of the salt combined. It is seen from Table 2 that for the apparent molar enthalpy changes, all the values are negative as expected. That is, the transition from the expanded to the condensed state is exothermic. These values for the double long-chain salts may be expected to be close to twice the values for corresponding fatty acid. In the C14(+) system, however, the values were about four-fold that of tetradecanoic acid, ($\Delta h^r = -14$ kJ mol^{-1}),[17,19-21] Since the double long-chain salts of the type of alkylammonium alkanesulfonates are composed of a long-chain anion and a long-chain cation, the transition from the expanded to the condensed state causes the cohesion of alkyl chains as well as the formation of ionic pairs between ionic head groups. Therefore, the large exothermic change on the transition may be attributable to the combined effects of the cohesive interaction between the alkyl chains, and the electrostatic attraction between the charged head groups. Similar results are reflected upon the values of other apparent molar quantities, which are likely to be characteristic of the monolayers of these salts.

TABLE 2. THE APPARENT MOLAR QUANTITY CHANGES ON THE PHASE TRANSITION OF DOUBLE LONG-CHAIN SALTS $C_mH_{2m+1}N^+H_3 \cdot C_nH_{2n+1}SO_3^-$ AT 298.2 K

Cation	Anion			
	C12(−)	C14(−)	C16(−)	C18(−)
Entropy change ($-10^{-2}\Delta s^r$/J K^{-1} mol^{-1})				
C12(+)	—	0.6[a]	0.9	1.1
C14(+)	1.9[a]	1.8	2.2	2.3 1.8[c]
C16(+)	1.5	—	—	—
		2.7[b]	2.9[c]	—
C18(+)	1.5	—	—	—
		2.7[c]	—	—
Enthalpy change ($-\Delta h^r$/kJ mol^{-1})				
C12(+)	—	17[a]	28	31
C14(+)	55[a]	54	65	69 57[c]
C16(+)	44	—	—	—
		82[b]	89[c]	—
C18(+)	45	—	—	—
		85[c]	—	—
Energy change ($-\Delta u^r$/kJ mol^{-1})				
C12(+)	—	20[a]	32	39
C14(+)	66[a]	64	78	84 67[c]
C16(+)	53	—	—	—
		98[b]	106[c]	—
C18(+)	58	—	—	—
		99[c]	—	—

a) 285.5 K. b) 304.4 K. c) 310.4 K.
Thermodynamic quantities for tetradecanoic acid (C14 acid): $\Delta s^r = -0.47\times10^{-2}$ J K^{-1} mol^{-1}, $\Delta h^r = -14$ kJ mol^{-1}, $\Delta u^r = -17$ kJ mol^{-1}.

The longer the chain length of cation and anion, the larger the apparent molar entropy change (Δs^r) on the transition from the expanded to the condensed state. Holding the total carbon number of long-chain cation and anion constant, the salts with a small difference in the chain length or with the equal-chain-length cation and anion such as C14–C14, C16–C14, and C16–C16 tend to increase the value of the entropy change. The apparent molar enthalpy change (Δh^r) and the apparent molar energy change (Δu^r) follow similar trends.

In Fig. 8, the apparent molar entropy changes (Δs^r) are shown as a function of the carbon number of long-chain cation (m) or anion (n) when the total number ($m+n$) is equal to 28, 30, and 32 at a constant temperature. All the curves are convex upward. All the values of Δs^r are negative as mentioned before. In the case of total carbon number of long-chain cation and anion equal to 32 (the right side in Fig. 8), the magnitude of Δs^r for the C16–C16 salt is the greatest in three double long-chain salts. This means the C16–C16 salt has the most stable orientation in the condensed state of three salts. Similarly in the series of the salts with the total carbon number of long-chain cation and anion equal to 28, the magnitude of Δs^r is greatest for the C14–C14 salt. In the series of total carbon number of 30, the magnitude of Δs^r is the greatest for the C16–C14 salt. Con-

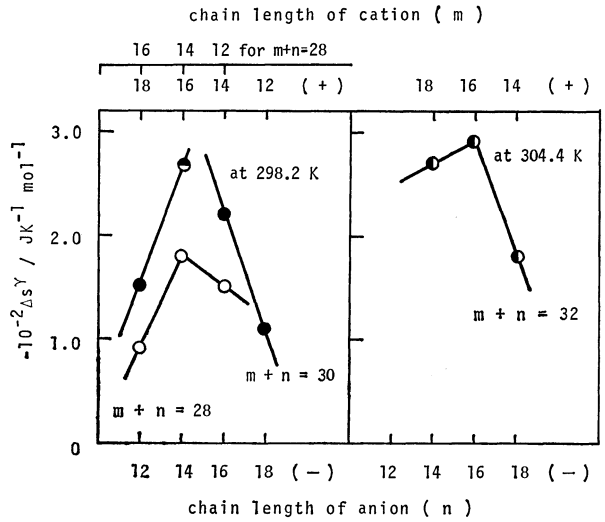

Fig. 8. The apparent molar entropy changes on the phase transition of double long-chain salts. m: cationic chain length, n: anionic chain length. ◓: C16–C14 salt at different temperature (304.4 K).

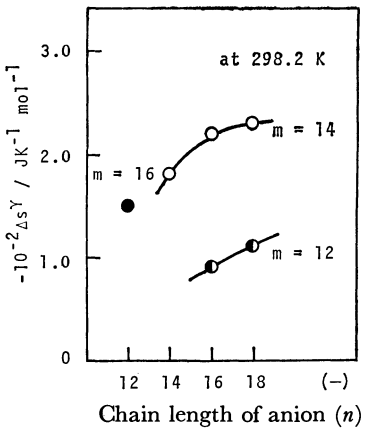

Fig. 9. Anionic chain length dependence of apparent molar entropy change at constant cationic chain length.

sidering above results, in the case of the total carbon number of long-chain cation and anion equal to 30, it is likely that the C15–C15 salt may have the most stable orientation in the condensed film. But the combination of odd carbon number was not treated in this study. This problem will be solved in the future. It is concluded from the above results that the change of apparent molar entropy on the transition tends to be greatest in its magnitude for the salts with the equal-chain-length cation and anion, and that the combination of the equal chain length of cation and anion makes the most stable arrangement in the monolayer of the condensed state.

Figure 9 shows the apparent molar entropy change as a function of the anion chain length at the constant length of the cationic chain. From Fig. 9, for the apparent molar entropy change (Δs^{γ}), it may be concluded that the contribution of long-chain cation and anion to the phase transition of monolayer is not equivalent, the contribution of long-chain cation being slightly larger than that of long-chain anion.

Corkill *et al.*[2] studied solution properties of double long-chain salts (alkyltrimethylammonium alkyl sulfates). They showed that C8–C12, C10–C10, and a mixture of C12 and C8 (all total carbon number 20) gave the same values of cmc or free energy of micelle formation, no difference being present between the contribution of long-chain cation and anion. It is evident that the results we obtained in the present study are characteristic of monolayer properties.

One of authors (O. S.) wants to express his deep gratitude to Dr. K. Motomura of the Department of Chemistry, Kyushu University, for many valuable and most stimulating discussions during this work and would like to thank Prof. I. Murase of College of General Education, Kyushu University for help with purification of starting materials.

This work has been financially supported in part by a Grant No. 574178 of the Ministry of Education, Science and Culture for Scientific Research of Japan.

References

1) J. M. Corkill, J. F. Goodman, C. P. Ogden, and J. R. Tate, *Proc. R. Soc. London, Ser. A*, **273**, 84 (1963).
2) J. M. Corkill, J. F. Goodman, S. P. Harrold, and J. R. Tate, *Trans. Faraday Soc.*, **62**, 994 (1966).
3) M. J. Schwuger, *Kolloid Z. Z. Polym.*, **243**, 129 (1971).
4) E. H. Lucassen-Reynders, *Kolloid Z. Z. Polym.*, **250**, 356 (1972).
5) E. H. Lucassen-Reynders, *J. Colloid Interface Sci.*, **81**, 150 (1981).
6) D. Góralczyk, *J. Colloid Interface Sci.*, **77**, 68 (1980).
7) D. Góralczyk and B. Waligora, *J. Colloid Interface Sci.*, **82**, 1 (1981).
8) J. M. Corkill, J. F. Goodman, S. P. Harrold, and J. R. Tate, *Trans. Faraday Soc.*, **63**, 247 (1967).
9) Y. Hendrix and L. Ter-Minassian-Saraga, "Advances in Chemistry Series. 144. Monolayers," ed by E. D. Goddard, Am. Chem. Soc., Washington, D. C. (1975), pp. 177—191.
10) M. A. McGregor and G. T. Barnes, *J. Colloid Interface Sci.*, **62**, 213 (1977).
11) Y. Hendrix, *J. Colloid Interface Sci.*, **69**, 493 (1979).
12) Y. Hendrix and D. Mari, *J. Colloid Interface Sci.*, **78**, 74 (1980).
13) O. Shibata, S. Kaneshina, M. Nakamura, and R. Matuura, *J. Colloid Interface Sci.*, **77**, 182 (1980).
14) K. Motomura, *J. Colloid Interface Sci.*, **23**, 313 (1967).
15) K. Motomura, *J. Colloid Interface Sci.*, **48**, 307 (1974).
16) K. Motomura, K. Sekita, and R. Matuura, *J. Colloid Interface Sci.*, **48**, 319 (1974).
17) K. Motomura, T. Yano, M. Ikematsu, H. Matuo, and R. Matuura, *J. Colloid Interface Sci.*, **69**, 209 (1979).
18) K. Motomura, *Adv. Colloid Interface Sci.*, **12**, 1 (1980).
19) K. Motomura, M. Ikematsu, Y. Hayami, H. Matuo, and R. Matuura, *Bull. Chem. Soc. Jpn.*, **53**, 2217 (1980).
20) N. Kuramoto, K. Sekita, K. Motomura, M. Nakamura, and R. Matuura, *Mem. Fac. Sci. Kyushu Univ. C*, **8**, 67 (1972).
21) K. Sekita, M. Nakamura, K. Motomura, and R. Matuura, *Mem. Fac. Sci. Kyushu Univ. C*, **10**, 51 (1976).

High Performance Liquid Chromatography Using Polymer Gels for Direct Analyses and Characterizations of Soluble Organic Pollutants in Water

Kohei URANO,* Hiroyuki FURUUNE, and Koji HAYASHI

Department of Safety and Environmental Engineering, Yokohama National University, 156 Tokiwadai, Hodogaya-ku, Yokohama 240

(Received October 9, 1981)

The optimum conditions in HPLC separations using columns packed with polymer gels were investigated for analyzing and characterizing directly various organic pollutants in water without complicated pretreatment. Experimental results showed that polystyrene gel column was unsuitable for direct analyses of water samples. Direct analyses of various organic compounds in water could be achieved on polyacrylester and polyhydroxystyrene columns by using 0.02 mol L^{-1} phosphoric acid and acetonitrile (85:15) as a mobile phase. At 40 °C, these systems of column and mobile phase gave values of height equivalent to a theoretical plate ranging from approximately 0.10 to 0.25 mm and retention times ranging from approximately 8 to 60 min for various compounds in water. Separation characteristics of these polymer column systems were discussed by taking into account solubilities, functional groups, aromaticities, or molecular weights of organic compounds in water. Furthermore, several wastewaters and their treated waters were directly analyzed for examples.

The conventionally used indices of organic pollution of water are biochemical oxygen demand (BOD), chemical oxygen demand (COD), and concentrations of several toxic pollutants. However, fractionations, characterizations, and analyses of soluble organic pollutants by chromatographic methods such as gel chromatography (Gel C), gas chromatography (GC), and high performance liquid chromatography (HPLC) have recently been used for evaluating organic pollutions and treatment processes of organic wastewater.[1] Since actual water samples contain miscellaneous compounds, there are many cases that the compounds in water need not necessarily to be separated and analyzed completely and need only to be classified and characterized by molecular weight, aromaticity, functional group, or solubility in water. Furthermore, it is expected especially that direct analytical methods without complicated pretreatments such as extraction and reaction are developed for evaluation of water qualities. Columns and operating conditions for direct analyses of water samples should be applicable in the analysis of a wide range of compounds. In other words, there is necessary to select the optimum columns and operating conditions so that analyses of water samples can be achieved within a short time by a very simple operation.

In previous papers, the authors reported about the characteristics of Gel C using Sephadex gel[2] and a specific GC using steam as carrier gas[3,4] for direct analyses and/or characterizations of organic pollutants in water. The characteristics of UV detector for Gel C and HPLC were also reported in another paper.[5] In this study, the optimum conditions together with applicability of HPLC using columns packed with typical polymer gels were investigated for analyses and characterizations of soluble organic pollutants in water without complicated pretreatment. By this series of studies about chromatographic methods for direct analyses and/or characterizations of organic pollutants in water, water pollution with organic matter and water treatment processes will be estimated more exactly than by the conventional indices only.

Materials and Methods

Aqueous solutions of 48 organic compounds whose properties are shown in Table 1, wastewaters from an oil refinery and a dye factory, and their treated waters by adsorption with activated carbon were used as samples in this study. The equipment used in this study consisted of Nipponbunko HPLC Model A-1, two ultraviolet (UV) absorption detectors, a refractive index (RI) detector, and a three pen recorder. Three kinds of commercial packed columns of synthetic polymer gels, whose properties are shown in Table 2, were tested for direct analyses of the water samples. The water samples of 5—50 μL were injected directly, and the organic compounds were separated on the polymer gels by using various mobile phases and were detected with the UV detectors at wavelengthes of 220 nm and 275 nm and the RI detector. Retention time (t_R) and time of peak width (W_t) were obtained for the aqueous solution of organic compound, and height equivalent to a theoretical plate (HETP) was calculated by the following equation:

$$\mathrm{HETP} = L\,W_t^2/16t_R^2.$$

Here, L is the length of packed column. Better resolutions can be achieved by using systems of column and mobile phase showing smaller values of HETP. In this study, the optimum conditions which can be used for a wide range of organic compounds without complicated operations will be selected, and applicability of the column systems for analyses and/or characterizations of various organic pollutants in actual water samples will be discussed.

Results and Discussion

Characteristics of Polystyrene Gel Column. Mobile Phase: The most important factor in the direct analyses of organic compounds in water is selection of the optimum system of column and mobile phase liquid. The column of polystyrene gel (Jascopack HP 01) can be used with mobile phases of organic

Table 1. Organic compounds used

Sample number	Compound name	Molecular weight	Solubility mol L^{-1}
1	Ethyl alcohol	46	∞
2	Propyl alcohol	60	∞
3	Hexyl alcohol	102	6.1×10^{-2}
4	Acetaldehyde	44	∞
5	Propionaldehyde	58	2.8
6	Butyraldehyde	72	5.0×10^{-1}
7	Valeraldehyde	86	3.8×10^{-1}
8	Formic acid	46	∞
9	Acetic acid	60	∞
10	Butyric acid	88	∞
11	Hexanoic acid	116	8.6×10^{-2}
12	Acetone	58	∞
13	Diethyl ketone	86	5.5×10^{-1}
14	Isobutyl methyl ketone	100	2.0×10^{-1}
15	Methyl acetate	74	4.4
16	Methylamine	31	—
17	Trimethylamine	59	6.9
18	2-Amino ethanol	61	∞
19	Malonic acid	104	5.8
20	Adipic acid	146	9.9×10^{-2}
21	Lactic acid	90	∞
22	Malic acid	134	4.2×10^{-1}
23	Sodium citrate	236	—
24	Glycine	75	3.0
25	Glycylglycine	132	—
26	Glutamic acid	147	—
27	D-Glucose	180	4.6
28	Lactose	342	4.2×10^{-1}
29	Raffinose	596	2.0×10^{-1}
30	Benzenesulfonic acid (B.S.)	158	v.s.[a]
31	Phenol	94	8.8×10^{-1}
32	Benzoic acid	122	2.4×10^{-2}
33	Benzaldehyde	106	2.8×10^{-2}
34	Aniline	93	3.9×10^{-1}
35	Benzonitrile	103	2.1×10^{-2}
36	Nitrobenzene	123	1.6×10^{-2}
37	Chlorobenzene	113	4.4×10^{-3}
38	Resorcinol	110	5.3
39	*m*-Cresol	108	2.1×10^{-1}
40	*p*-Cresol	108	1.8×10^{-1}
41	Salicylic acid	138	1.3×10^{-2}
42	*m*-Toluic acid	136	7.2×10^{-3}
43	*m*-Toluidine	107	3.0×10^{-2}
44	*d*-Phenyl alanine	166	7.9×10^{-2}
45	*p*-Ethyl B.S.	186	v.s.
46	*p*-Alkyl(C_{10}—C_{14}) B.S.[b]	—	v.s.
47	2-Naphthalenesulfonic acid	208	v.s.
48	2-Naphthol	144	5.1×10^{-3}

a) v.s.: Very soluble. b) Surfactant for detergent.

solvents or mixtures of polar organic solvents containing less than 10% water. Retention times and the values of HETP of several organic compounds were obtained at 40 °C with mixtures of methanol and water as mobile phases. The changes of t_R and HETP of several benzene substitutes with water contents of the mobile phases are shown in Fig. 1, representatively. With methanol only, the retention times were too short for separation of various compounds, and the values of HETP were slightly large. The mixtures of methanol and water were better than methanol only, but the variations of t_R among compounds was not large enough to separate various compounds. In the case of using mixtures of phosphoric acid solution and methanol or acetonitrile as the mobile phases, the values of HETP were improved, but the variation of t_R among compounds was also not large enough. Thus, it was concluded that direct analyses of various organic compounds in water could not be achieved by using the column packed with polystyrene gel, and other polymer columns were studied.

Table 2. Packed columns of polymer gels employed[a]

Polymer	Commercial name	Column size	Limit pressure
Polystyrene	Jascopack HP-01	$4.6\phi\times250$ L	50 kg cm^{-2}
Polyacrylester	Shodex OH pak M614	$6.0\phi\times250$ L	15 kg cm^{-2}
Polyhydroxy-styrene	Shodex Ion pak C811	$8.0\phi\times500$ L	30 kg cm^{-2}

a) These columns can be used at a temperature lower than 60 °C and a flow rate lower than 1.5 mL min^{-1}.

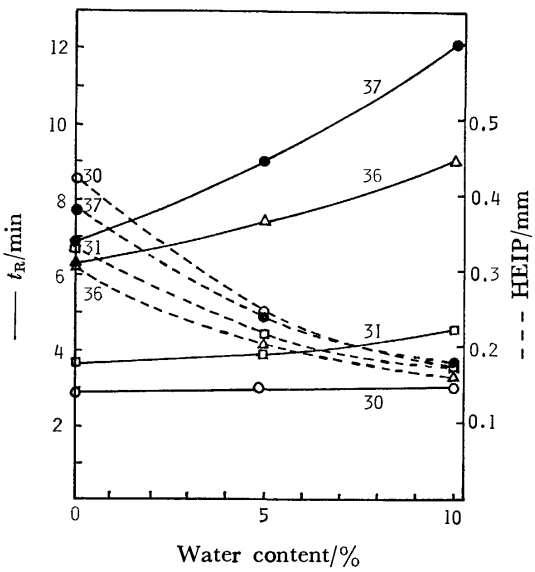

Fig. 1. Changes of retention time and HETP with water content in mobile phase for Jascopack HP 01.
1.0 mL min^{-1}, 40 °C.

Characteristics of Polyacrylester Gel Column. Mobile Phase: The column of polyacrylester gel (Shodex OH pak M614) can be used with the mobile phases of water or aqueous solutions containing less than 30% polar organic solvents. Retention times and the values of HETP for several typical organic compounds at 40 °C were obtained with various mobile phases of water, aqueous solution of phosphoric acid, or mixtures of aqueous solution of phosphoric acid and methanol or acetonitrile. The peaks showed tailing

or leading, and both values of t_R and HETP were large in the case of using water only. Though the values of HETP decreased by addition of phosphoric acid, t_R were still very long for several organic compounds. In the case of using mixture of aqueous solution of phosphoric acid and methanol, t_R was not satisfactorily decreased. The mixtures of 0.02 mol L^{-1} phosphoric acid with different contents of acetonitrile were tested as mobile phases at a flowrate of 0.57 mL min^{-1}. The changes of t_R for several benzene substitutes with the content of acetonitrile are shown in Fig. 2, representatively. From these results, the mixture of phosphoric acid solution and acetonitrile of 15% was thought to be better than the other mobile phases, because t_R was not too long, and variation of t_R among compounds was large enough to separate various compounds. Consequently, the mixture of 0.02 mol L^{-1} phosphoric acid and acetonitrile (85:15) was selected as a standard mobile phase of this column for the analyses of various organic compounds in water.

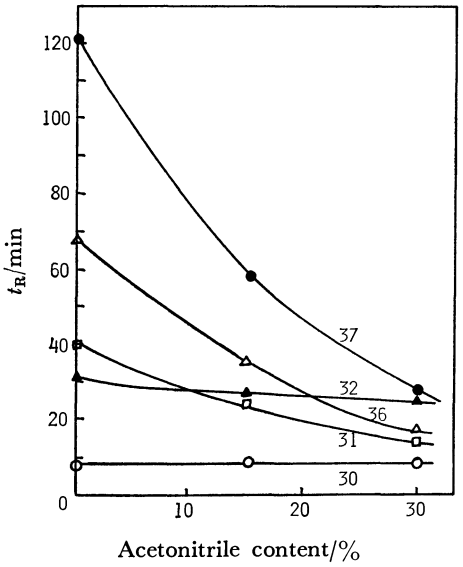

Fig. 2. Change of retention time with acetonitrile content in mobile phase for Shodex OH pak M614. 0.57 mL min^{-1}, 40 °C.

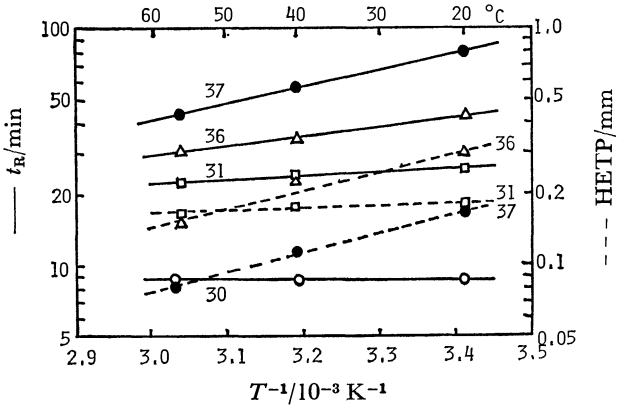

Fig. 3. Changes of retention time and HETP with temperature for Shodex OH pak M614. 0.02 mol L^{-1} H_3PO_4 and acetonitrile 15:85, 0.57 mL min^{-1}.

Influence of Column Temperature: Change of t_R and HETP with column temperature in the case of using the above standard mobile phase are representatively shown in Fig. 3 for several organic compounds. The values of HETP decreased with temperature, but the influence of temperature on the separation performance was small, because the apparent activation energies of separation were approximately 4 to 20 kJ mol^{-1}. Since the temperature higher than 40 °C made operation troublesome, 40 °C was chosen as a standard temperature in the following experiments.

Relation between Retention Times and Properties of Organic Compounds: Values of t_R and HETP for various organic compounds obtained using the standard mobile phase at a flowrate of 0.57 mL min^{-1} and 40 °C are shown in Table 3. The values of HETP for all the organic compounds were small ranging from approximately 0.13 mm to 0.25 mm.

The retention times of benzenesulfonate, ethylbenzenesulfonate, and naphthalenesulfonate were short, approximately 10 min, but those of alkylbenzenesulfonates in a synthetic detergent could be classified into 5 groups ranging from 20 to 60 min according to the number of alkyl carbons which ranged from 10 to 14 as shown in Fig. 4. The retention times of the aromatic compounds except the low molecular weight sulfonates exceeded 20 min. It was found that the retention times for hydrophobic aromatic compounds tend to be longer than those of hydrophilic compounds. The logarithmic relationships between the retention times and solubilities in water are shown in Fig. 5 for the aromatic compounds. These relationships could be shown by two lines for the two groups of the carboxylic acids and the others. The

Table 3. Values of t_R and HETP for various compounds with Shodex OH pak M614

Compound number	t_R min	HETP mm	Compound number	t_R min	HETP mm
4	13.0	0.25	30	8.7	0.20
5	18.3	0.22	31	23.9	0.18
6	15.8	0.25	32	27.6	0.19
8	9.7	0.14	33	24.1	0.18
9	13.3	0.13	34	26.0	0.22
10	14.5	0.17	35	25.3	0.24
12	11.8	0.20	36	36.0	0.21
14	16.1	0.17	37	58.0	0.12
16	13.3	0.18	38	20.0	0.16
17	13.8	0.17	39	28.5	0.20
18	13.8	0.17	40	28.7	0.20
19	10.3	0.16	41	32.7	0.18
20	12.8	0.19	42	35.9	0.16
22	10.9	0.24	43	31.8	0.20
23	13.0	0.16	44	23.1	0.22
24	13.5	0.18	45	9.1	0.25
25	15.7	0.18	47	9.9	0.24
26	11.7	0.15	48	84.0	0.13

Flow rate: 0.57 mL min^{-1}, mobile phase: 0.02 mol L^{-1} phosphoric acid and acetonitrile (85:15), temp: 40 °C.

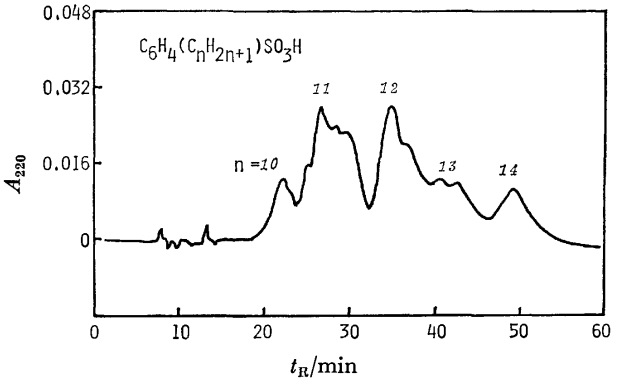

Fig. 4. Chromatogram of alkylbenzenesulfonates in synthetic detergent with Shodex OH pak M614. 0.02 mol L^{-1} H_3PO_4 and acetonitrile 15:85, 0.57 mL min^{-1}, 40 °C.

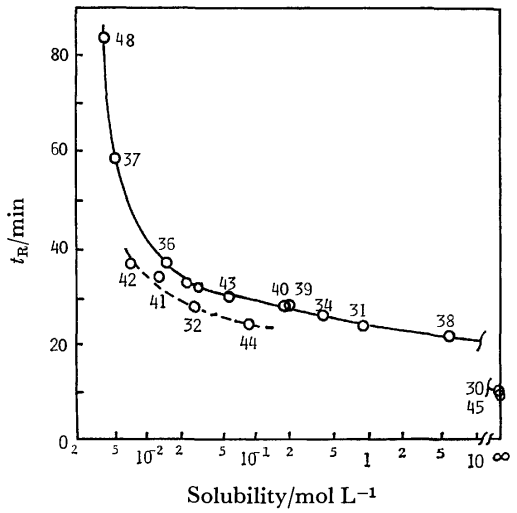

Fig. 5. Relationships between retention times and solubilities in water of aromatic compounds for Shodex OH pak M614.
Conditions are as in Fig. 4.

retention times for the carboxylic acids were slightly shorter than those of the other compounds, because they ionize partialy in the mobile phase. Consequently, the packed column of polyacrylester gel could be used for the direct analyses of various aromatic compounds in water. The retention time of an aromatic compound can, therefore, be predicted from its chemical structure and solubility, and conversely, the compound in an unknown sample can be characterized or identified from its retention time. Since the retention times of all the used aliphatic compounds, whose solubilities in water are larger than 10^{-1} mol L^{-1} were in the range from 10 to 18 min, separation was difficult when many kinds of aliphatic compounds coexist in water. However, the peaks for an unknown sample within 20 min could be characterized as the peaks of aliphatic compounds or the low molecular weight aromatic sulfonates.

Characteristics of Polyhydroxystyrene Gel Column.
Mobile Phase: Similar to the polyacrylester column, the column of poly(*p*-hydroxystyrene) gel (Shodex Ion pak C811) can be used with water or aqueous solutions

Table 4. Values of t_R and HETP for various compounds with Shodex Ion pak C-811

Compound number	t_R min	HETP mm	Compound number	t_R min	HETP mm
1	20.2	0.15	27	11.4	0.10
2	23.4	0.13	28	9.8	0.18
3	45.6	0.11	29	9.4	0.18
4	18.2	0.18	30	8.2	0.20
5	20.5	0.16	31	32.0	0.16
6	24.5	0.13	32	37.5	0.15
7	27.4	0.12	33	50.3	0.17
8	14.3	0.09	35	53.2	0.17
9	15.0	0.14	36	66.8	0.18
10	17.1	0.16	37	102.3	0.19
11	19.0	0.12	38	21.4	0.15
12	19.3	0.10	39	41.3	0.18
13	22.9	0.10	40	41.5	0.18
14	24.5	0.12	41	37.5	0.15
15	20.7	0.11	42	53.0	0.18
19	11.1	0.18	45	8.4	0.21
20	12.7	0.17	46	8.5	0.20
21	11.7	0.14	47	8.5	0.21
22	11.4	0.16			

Flow rate: 1.0 mL min^{-1}, mobile phase: 0.02 mol L^{-1} phosphoric acid and acetonitrile (85:15), temp: 40 °C.

containing less than 30% polar organic solvents. Further, the retention times with water or phosphoric acid as mobile phase were also very long for several hydrophobic compounds. Thus as with the case of the polyacrylester column, the mixture of 0.02 mol L^{-1} phosphoric acid and acetonitrile (85:15) was used for mobile phase, and the results are shown in Table 4. By this mobile phase, most organic compounds eluted within 60 min at a flow rate of 1.0 mL min^{-1}. The values of HETP were in the range from 0.10 mm to 0.21 mm for many organic compounds. This values were slightly better than those of the polyacrylester column. But amines and amino acids were not eluted within 120 min at a flow rate of 1.0 mL min^{-1}, because these cationic compounds combined strongly with the anionic group of the gel. Conversely, the retention times of all the sulfonates including alkylbenzenesulfonates in detergent were short and approximately 8.5 min, because they completely ionize to anions in mobile phase. Therefore, the anionic resin could not be used for separation of cationic compounds such as amines and amino acids and strong anionic compounds such as sulfonates.

Relation between Retention Times and Properties of Organic Compounds: The values of t_R of the aromatic compounds except sulfonates exceeded 20 min, and it was found that t_R tend to decrease with solubilities in water similar to the case of the polyacrylester column. Changes of t_R for the aromatic compounds with their solubilities are shown in Fig. 6. These relationships could be shown by two lines for carboxylic acids and the other compounds as in the case of the polyacrylester column. The retention times of the carboxylic acids were shorter than those of the other compounds for

a same solubility, because they ionize partialy to anions in mobile phase. On the other hand, there were no clear relationships between t_R and solubilities in water for aliphatic compounds. Variations of t_R with molecular weight are shown in Fig. 7 for each group of aliphatic compounds. The values of t_R for all the aliphatic compounds increased with their molecular weight in the similar series of compounds, and t_R increased in the following order for the compounds which have the same number of alkyl carbons: alcohols > aldehydes > ketones ≃ esters > monocarboxylic acids > dicarboxylic acids. However, the retention times of sugars decreased with molecular weight by gel permeation function as shown in also Fig. 7, and raffinose was eluted at a very short time. Consequently, this column could not be used for separation of nonaromatic compounds with molecular weights exceeding 600.

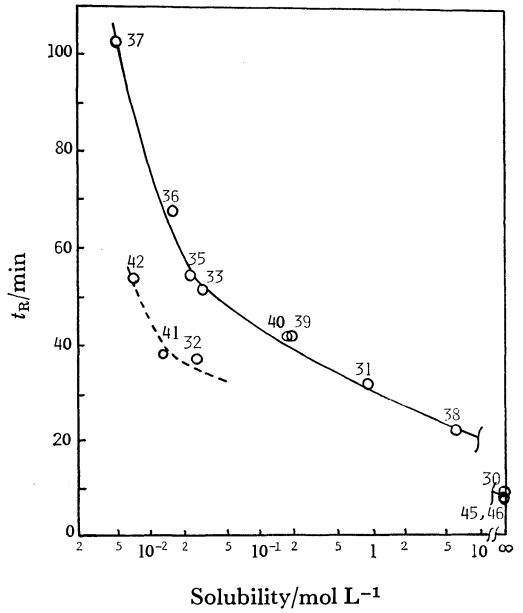

Fig. 6. Relationships between retention times and solubilities in water of aromatic compounds for Shodex Ion pak C811.
Flow rate; 1.0 mL min^{-1}, other conditions are as in Fig. 4.

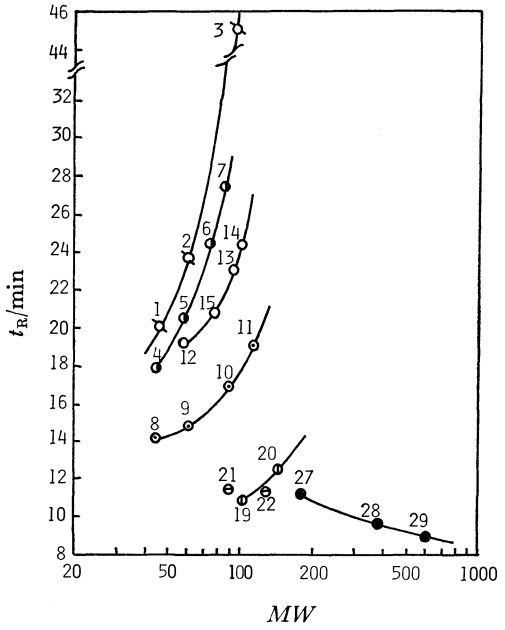

Fig. 7. Relationships between retention times and molecular weights of aliphatic compounds for Shodex Ion pak C811.
Conditions are as in Fig. 6.

From the foregoing results, the following conclusions were obtained:

(1) The column of polystyrene gel was unsuitable for direct analyses of water samples containing various organic compounds.

(2) The column of polyacrylester gel could be used for direct analyses of various organic compounds in water, but it was unsuitable for analyses of aliphatic compounds.

(3) The column of polyhydroxystyrene gel could be used for direct analyses of various aliphatic and aromatic compounds in water, but it could not be used for analyses of strong anionic compounds such as sulfonates, cationic compounds such as amines and amino acids, and nonaromatic compounds whose molecular weights exceed 600.

Application to Wastewater Analyses. For examples, raw and treated wastewaters from an oil refinery and a dye factory were directly analyzed after filtration with 0.45 μm membrane by the HPLC with Shodex OH pak M614 using the standard mobile phase at 40 °C. The chromatograms are representatively shown in Figs. 8 and 9. Eight peaks were found in the chromatogram of the raw wastewater from the oil refinery. The peaks 1—6 were characterized to be low molecular weight aliphatic compounds, and the peaks 7 and 8 were identified to be phenol, and *o*- and *m*-cresols respectively, the main pollutants in this wastewater, by their retention times, UV absorbances at two wave lengths,[5] and coloration with 4-aminoantipyrine. The chromatogram of its treated

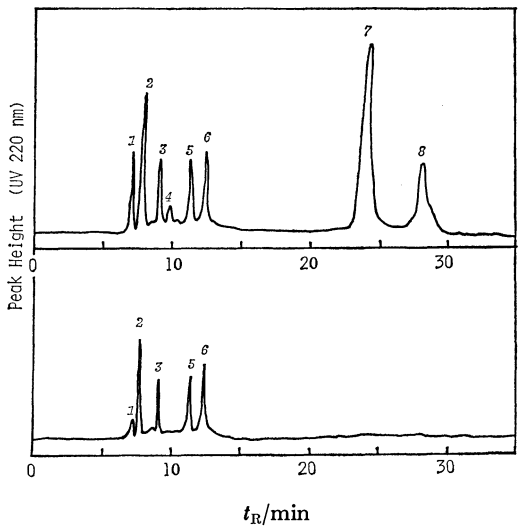

Fig. 8. Chromatograms of raw and treated wastewaters from an oil refinery by Shodex OH pak M614.
Conditions are as in Fig. 4.

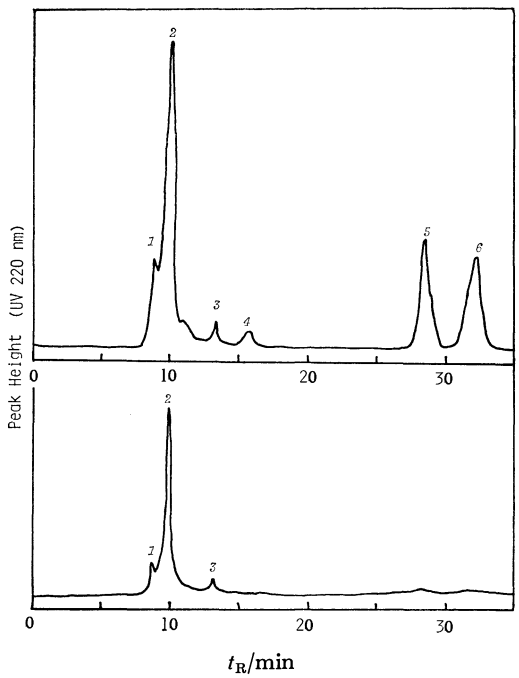

Fig. 9. Chromatograms of raw and treated wastewaters from a dye factory by Shodex OH pak M614. Conditions are as in Fig. 4.

water showed that phenol and cresols were completely removed by adsorption with activated carbon, but aliphatic compounds were only partially removed. On the other hand, six clear peaks were found in the chromatogram of the raw wastewater from the dye factory. The peaks 2—6 were identified to be naphthylaminedisulfonate, acetic acid, produced dye, cresols, and *m*-toluidine, respectively, and the peak 1 was assumed to be an aromatic sulfonate. The chromatogram of its treated water showed that dye, cresols, and toluidine were effectively removed by adsorption with activated carbon, but naphthylaminedisulfonate, acetic acid, and an unknown compound (peak 1) were only partially removed. As shown in these examples, the HPLC systems could be applied in direct analyses and characterizations of water containing various organic pollutants, and they are more superior than the conventional water quality tests in the evaluation of water quality and water treatment processes.

References

1) N. Tambo and T. Kamei, *Water Res.*, **12**, 931 (1978).
2) K. Urano, K. Katagiri, and K. Kawamoto, *Water Res.*, **14**, 741 (1979).
3) K. Urano, K. Ogura, and H. Wada, *Water Res.*, **15**, 225 (1980).
4) K. Urano, H. Maeda, K. Ogura, and H. Wada, *Water Res.*, **16**, 323 (1982).
5) K. Urano, K. Kawamoto, and K. Hayashi, *Jpn. J. Water Poll. Res.*, **4**, 43 (1981).

The Effect of the Vanadium Component on the Life of the WO_3–TiO_2 Catalyst Used for the Reduction of NO_x with NH_3

Shigeru Morikawa,* Kazumasa Takahashi, Junichi Mogi, and Satoru Kurita

Research Institute of Ishikawajima Harima Heavy Industries Co., Ltd., 3-15, Toyosu, Koto-ku, Tokyo 135-91

(Received November 6, 1981)

The 5000-h life test of the WO_3–TiO_2 catalyst for the reduction of NO_x with NH_3 has been investigated in real flue gases containing vanadium and SO_x on a pilot plant. When the present catalyst was used in a residual-oil-fired-boiler flue gas, steady activities over 90% of NO_x reduction were achieved for 5000 h at 400 °C (space velocity: 2700 h^{-1}). On the other hand, when the catalysts were taken out of the reactors at certain intervals and studied by means of a laboratory reactor, they were much more active than fresh catalyst at lower temperatures (250—350 °C). Also, the SO_2 oxidation efficiency increased with the reaction time. This activation was considered to be due to the vanadium component in the flue gas.

In many of the processes proposed hitherto, the selective reduction of NO_x with NH_3 on such catalyst systems as V_2O_5–TiO_2[1] and WO_3–TiO_2[2] has been considered to be the most promising process for removing NO_x from stationary sources. Furthermore, these catalysts are known to have an excellent activity and to be stable to SO_x; in particular, the WO_3–TiO_2 catalyst is thermally stable at 400 °C or higher temperatures and has a low oxidation activity from SO_2 to SO_3.

A mechanism for the reduction of NO_x with NH_3 in the presence of O_2 on the TiO_2–WO_3 catalyst was proposed by Imanari *et al.*[2] Kasaoka *et al.*,[3] reported the effect of the addition of WO_3 over V_2O_5 for activity on NO_x reduction with NH_3.

However, the life and effects of the vanadium component in real flue gas has not yet been reported with regard to the WO_3–TiO_2 catalyst. In this study, the life test for 5000 h as a pilot test has been investigated over WO_3–TiO_2 in connection with the reduction of NO with NH_3 using a Khafji residual-oil-fired-boiler flue gas. Also, catalysts were taken out of the reactor at certain intervals and their catalytic properties were examined by means of a X-ray photoelectron spectrometer.

Experimental

Catalyst Preparation. The 10 wt%WO_3–TiO_2 catalysts used in this study were prepared by impregnating TiO_2 (specific surface area: 70 m^2/g, mean pore radius: 320 Å, SO_4^{2-} content: 3.8%) in an aqueous solution of ammonium paratungstate ($5(NH_4)_2O12WO_3 \cdot 5H_2O$). After the impregnation, the catalysts were dried for 3 h at 120 °C and then calcined for 5 h at 550 °C in an air stream.

Activity Measurement. *Pilot-plant Test*: A life test was carried out with a pilot-plant test with an apparatus which consisted of a 150 mm-id reactor containing pellet catalysts (diam. 7 mmϕ). Activity measurements were carried out at 400 °C over the space velocity of 2700 h^{-1} using the combustion flue gas at a flow rate of 100 Nm^3/h from the Khafji residual-oil-fired-boiler (sulfur content: 5.2%, vanadium content: 220—230 ppm, NO_x: 95—105 ppm).

Laboratory scale Test: The reduction of NO with a model flue-exhaust gas consisting of NO, NH_3, H_2O, SO_2, and O_2 has also been studied over the WO_3–TiO_2 catalysts which were used in the pilot test. Activity measurements were carried out between 250 and 450 °C at a space velocity of 3500 h^{-1} using a conventional flow reactor made of a quartz tube reactor (length: 500 mm, dia.: 30 mm) under atmospheric pressure. A gas mixture consisting of 150 ppm of NO, 150 ppm of NH_3, 1000 ppm of SO_2, 5% of O_2, 8% of H_2O, and balance, N_2 was used as a standard feed. The analysis of NO and SO_2 was done with a chemiluminessence-type NO_x analyzer and a NDIR type SO_x analyzer respectively.

Measurements of Catalyst Property. The surface areas were measured by means of the BET method. An X-ray photoelectron spectrometer (Dupont-Shimadzu 650) was used to examine the surface properties of the catalysts. Mg $K\alpha$ (1253.6 eV) X-ray radiation was used as the excitation source. The measurements were conducted at room temperature under a vacuum of about 10^{-7} Torr (1 Torr≈ 133.322 Pa). The binding energies of the C (1 s) and Au ($4f_{7/2}$) electron peaks were used as the energy standards throughout the present work; they have taken to be 285.0 and 83.6 eV respectively.

Results and Discussion

Life Test of the WO_3–TiO_2 Catalyst for NO_x Removal. The life test of the 10% WO_3–TiO_2 catalyst on the reduction of NO with NH_3 was investigated in real flue gas containing 105 ppm of NO, 8% of H_2O, 4% of O_2, 10% of CO_2, 220—230 ppm of the vanadium component, and a 5.2% sulfur component at 400 °C over the space velocity, 2700 h^{-1}. The NH_3/NO inlet ratio was 1.0. Figure 1 shows the change in the conversion of NO with the reaction time. Steady activities over an NO_x reduction efficiency of 90% were achieved for 5000 h. Thus, the WO_3–TiO_2 catalyst was revealed to be highly resistant to the large amount of SO_x which was present in the residual oil and maintained a high activity for NO_x reduction. However, the color of the catalyst in a fresh catalyst changed from light yellow to green yellow over long periods of reaction time.

Figure 2 shows the results for the reduction of NO with NH_3 at 275—450 °C. In the pilot test, they were examined by means of a laboratory scale apparatus over the WO_3–TiO_2 catalysts used after 816 h, 1150 h, 2160 h, and 4800 h. Tests were conducted with simulated flue gas containing 8% of H_2O, 5% of O_2, 1000 ppm of SO_2, and 150 ppm of NO with 150 ppm of NH_3 (balance, N_2) over a space velocity

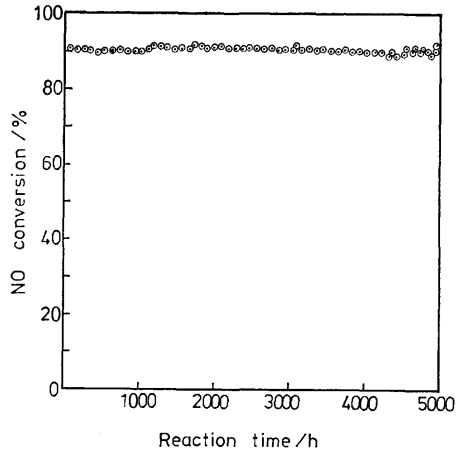

Fig. 1. Life test of WO_3–TiO_2 catalyst in real flue gas.
Reaction conditions: reaction temp; 400 °C, SV; 2700 h^{-1}. Composition of the flue gas: NO; 105 ppm, O_2; 4%, H_2O; 8%, CO_2; 10%, S component: 5.2%, vanadium component: 220—230 ppm

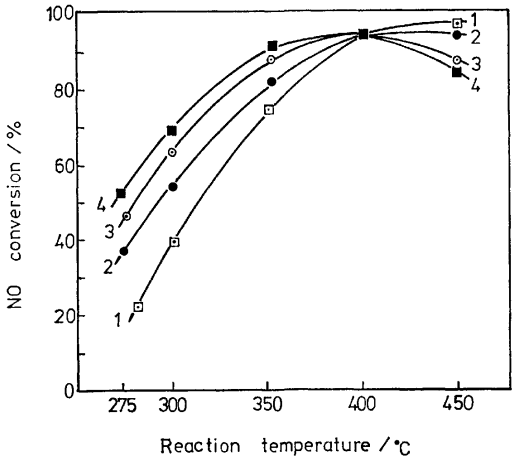

Fig. 2. Activity change in WO_3–TiO_2 catalyst with reaction time in simulated flue gas.
1: Fresh catalyst, 2: used for 1150 h, 3: used for 2160 h, 4: used for 4800 h. Reaction conditions: NO; 150 ppm, NH_3; 150 ppm, O_2; 5%, SO_2; 1000 ppm, H_2O; 8%, N_2; balance, SV; 3500 h^{-1}.

of 3500 h^{-1}. The conversion of NO was revealed to be 95% at the temperature of 400 °C, and the NO reduction efficiency did not change with the reaction time. This result fits well with that of the pilot test in Fig. 1. As shown in Fig. 2, however, the conversion of NO increased with the reaction time at 275—350 °C and decreased with the reaction time at 450 °C. In particular, the conversion of NO increased from 20 to 50% at 275 °C on a 4800-h catalyst. These observations suggest that catalysts were affected by the composition of real flue gas and changed in their surface properties. Although the present real flue gas contain a considerable amount of vanadium and sulfur components, as mentioned above, it may be supposed that such an increase in the NO reduction efficiency over a temperature range of 275—350 °C was due to the vanadium component accumulated on the catalyst, because the presence of the vanadium component is known to enhance the NO reduction efficiency at lower temperatures:[4] in contrast, SO_x is known to reduce the activities of the catalysts.[5]

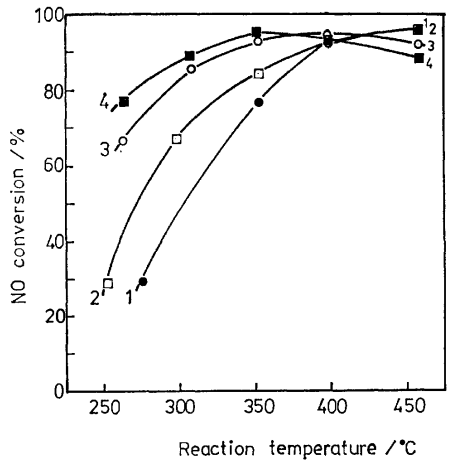

Fig. 3. Effect of amount of vanadium on activity for NO reduction.
Amounts of vanadium: 1; 0 wt%, 2; 0.5 wt%, 3; 1.5 wt% 4; 2.5 wt%. Reaction conditions are the same as for Fig. 2.

To clarify the effect of the vanadium component on NO_x reduction efficiency, we prepared the V_2O_5–WO_3–TiO_2 catalysts at various V_2O_5 concentrations and examined the activity, the conversion of NO *vs.* the reaction temperature. The results are shown in Fig. 3. The vanadium-loaded catalysts appear to be superior to the WO_3–TiO_2 catalyst in the NO reduction efficiency between 250 and 350 °C, and the increase in the amount of vanadium seems to be correlated with the activity, the 2.5 wt% V_2O_5–WO_3–TiO_2 catalyst in particular revealing the highest NO reduction efficiency. By contrast, at a high temperature (450 °C) the reduction efficiency decreased as the amount of vanadium loaded was increased. Similar behavior was seen on the V_2O_5–TiO_2 catalyst.[4] Furthermore, these results are in agreement with the experimental results obtained in Fig. 2. Thus, it was found that the conversion of NO in the reaction temperature range of 250—350 °C distinctly depends on the vanadium components.

Change in the Properties of the Catalyst. Next, surface analysis of the catalyst was conducted before and after use. Figure 4 shows the variations in the X-ray photoelectron spectra of the catalyst used in the NO reduction for V $2p_{3/2}$.

In Fig. 4, the V $2p_{3/2}$ peak was not observed on a fresh catalyst, but the intensity of the V $2p_{3/2}$ peak,[6] the binding energy being 517.2, increased with the reaction time, while the spectra of W $4f_{5/2}$, O_{1s}, and S_{2p} were almost unchanged with the reaction time, except for 4800 h. Each peak of the 4800-h catalyst was slightly shifted to the higher-binding-energy side.

Furthermore, to clarify the effect of catalytic properties, Table 1 shows the results of the analysis for dust components (K_2O, Na_2O), SO_4^{2-}, V_2O_5, WO_3, surface area (BET method), pore volume, surface

Table 1. Analytical results of WO_3–TiO_2 catalysts with the reaction time

Catalyst	$\frac{V\ 2p_{3/2}}{Au\ 4f_{7/2}}$	Surface area[1] / $m^2\ g^{-1}$ (Pore volume / $ml\ g^{-1}$)	Surface excess oxygen[2] / g equiv./g	Chemical analysis				
				V_2O_5(%)	WO_3(%)	SO_4^{2-}(%)	K_2O(%)	Na_2O(%)
Fresh	—	70 (0.29)	Trace	—	10.1	3.1	0.2	0.01
816 h	0.125	70 (0.29)	Trace	0.04	10.1	3.2	0.2	0.01
1150 h	0.185	71 (0.30)	2×10^{-6}	0.06	10.2	3.4	0.2	0.01
2160 h	0.250	71 (0.30)	4×10^{-6}	0.09	10.1	3.7	0.3	0.01
4800 h	0.256	71 (0.30)	7×10^{-6}	0.09	10.1	3.8	0.3	0.01

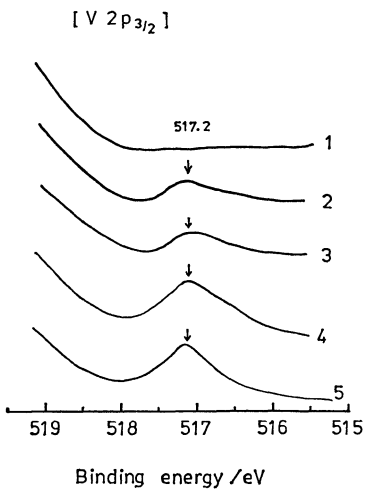

Fig. 4. Variation of photoelectron spectra for V $2p_{3/2}$.
1: Fresh catalyst, 2: used for 816 h, 3: used for 1150 h, 4: used for 2160 h, 5: used for 4800 h.
Binding energies were referenced to C 1s of contaminant carbon (285.0 eV).

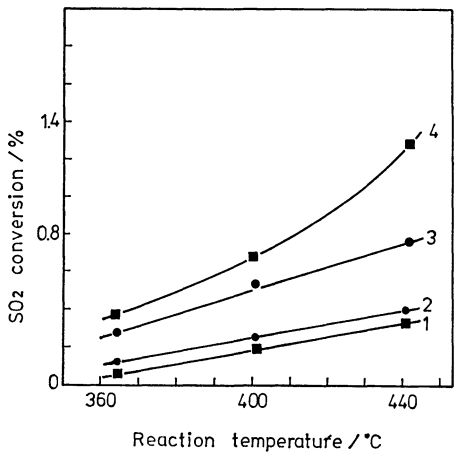

Fig. 5. Catalytic activity of WO_3–TiO_2 catalyst on SO_2 oxidation with reaction time in simulated flue gas.
1: Fresh catalyst, 2: used for 1150 h, 3: used for 2160 h, 4: used for 4800 h. Reaction conditions: NO; 150 ppm, $NO/NH_3=1$, H_2O; 8%, O_2; 5%, SO_2; 1000 ppm, SV; 3500 h^{-1}

excess oxygen by the KI method,[7] and the ratio of V $2p_{3/2}$/Au $4f_{7/2}$ over fresh, 816-h, 1150-h, 2160-h, and 4800-h catalysts. It may be seen that the surface area, pore volume, potassium and sodium as dust components, and WO_3 and SO_4^{2-} contents were almost unchanged with the reaction time. The activation of a catalyst at a lower temperature was not explained sufficiently only by the change in the surface area and the pore volume. However, the concentration of V_2O_5 and the ratio of intensities between V $2p_{3/2}$ and Au $4f_{5/2}$ (standard) in the 4800-h catalyst were two times than that of the 816-h catalyst. Similar behavior was seen in the amount of surface excess oxygen on the catalyst. Judging from the results shown in Table 1, no doubt the presence of vanadium influences this increase in NO reduction efficiency at lower temperatures.

On the other hand, a previous study[4] showed that the SO_2 oxidation was affected by the increase in vanadium concentration and enhanced by the amount of surface excess oxygen. Therefore, we examined the SO_2 oxidation over fresh and used catalysts at various temperatures. The results are shown in Fig. 5. The activity of the catalyst for SO_2 oxidation increased with an increase in the reaction time. At 365 °C, the SO_2 conversion in the 4800-h catalyst was four times that of the fresh catalyst. As is shown in Table 1, both the vanadium content and the surface excess oxygen increased with the reaction time, while the other dust components and the surface area were almost unchanged with the reaction time. Hence, it has been speculated that the increase in SO_2 conversion with the reaction time is mainly due to the vanadium accumulated on the catalyst and the amount of surface excess oxygen.

From our results, the following conclusions can be drawn. The NO reduction reached a constant value of 90%, and no change in efficiency was observed for 4500 h in real flue gases. Thus, the WO_3–TiO_2 catalyst performs well and maintains a high activity for NO reduction. However, when the WO_3–TiO_2 catalyst is used in flue gas containing a vanadium component such as Khafji residual oil, the NO reduction is not only increased at lower temperatures, but also the SO_2 oxidation is increased by accumulating vanadium on the surface of the catalyst. Therefore,

for practical purposes, if the WO_3–TiO_2 catalyst is used for NO_x reduction in a residual-oil-fired-boier flue gas, it may be necessary to retard the oxidation of SO_2 to SO_3 without affecting the high activity for NO_x reduction over WO_3–TiO_2 as well as over the V_2O_5–TiO_2 catalysts.[4)]

The details of the reaction mechanism of NO with NH_3 over the WO_3–TiO_2 catalyst will be reported later.

References

1) M. Inomata, A. Miyamoto, and Y. Murakami, *J. Catal.*, **62**, 140 (1980).

2) M. Imanari and Y. Watanabe, The Seventh International Congress on Catalysis Preprints, 1980, B-9.

3) N. Kasaoka, E. Sasaoka, and K. Senda, *Nenryo Kyokaishi*, **56**, 818 (1977).

4) S. Morikawa, H. Yoshida, K. Takahashi, and S. Kurita, *Chem. Lett.*, **1981**, 251.

5) N. Todo, M. Kurita, H. Hagiwara, A. Ueno, and T. Sato, The Japan-U.S.A. Seminar on Catalytic NO_x Reactions, Preprints, 1975, 4-L.

6) R. Larson, B. Folkesson, and G. Schon, *Chemica Scripta*, **3**, 88, (1973).

7) T. Uchijima, M. Takahashi, and Y. Yoneda, *J. Catal.*, **9**, 402 (1967).

Lanthanoid Shift Reagents. Synthesis and Spectral Studies†

Khalid IFTIKHAR,* Mohammad SAYEED, and Naseer AHMAD
Department of Chemistry, Aligarh Muslim University, Aligarh-202001, U.P., ndia

(Received May 21, 1981)

The seven coordinate adducts of [Ln(fod)$_3$]chelates are described. The NMR spectra of diamagnetic and paramagnetic adducts have been discussed. The europium, praseodymium and ytterbium adducts have been scanned as potential shift reagents and these seven coordinate adducts produce large dipolar shifts in the proton magnetic resonances of organic moieties. The dipolar shift produced by [Eu(fod)$_3$(pz)] in the spectrum of benzyl alcohol is different from that reported. Some interelectronic and spectral parameters ($\bar{\beta}$, $b^{1/2}$, and δ) have been calculated. Ligand field parameter (T_λ) and oscillator strengths have been computed and discussed.

NMR spectra may usually be obtained from the complexes of paramagnetic lanthanoid ions with organic ligands.[1,2] Such spectra commonly show paramagnetic shifts, mainly of dipolar (pseudo-contact) origin. This principle has been applied by Hinckley[3] to weak association between tris(dipivaloylmethanato)-europium(III) and cholesterol (the complex being used as its bis(pyridine)adduct). Further investigations have established that (1) [Eu(dpm)$_3$], dpm=2,2,6,6-tetramethyl-3,5-heptanedione, itself (*i.e.*, without the pyridine molecules appended) is even better than the pyridine adduct[4] (pyridine tends to block coordination of substrate) (2) the analogous praseodymium compound, [Pr(dpm)$_3$], induces NMR shifts of opposite sign[5] and also much larger than those reported for [Eu(dpm)$_3$]. Selbin *et al.*[6] reported a series of analogous lanthanoid complexes with the same bulky β-keto enolate and their mixed ligand complexes with uni and bidentate ligands. Ahmad *et al.*[7] studied the temperature dependant shifts. It has been pointed[8] out that the mixed ligand adducts [Eu(dpm)$_3$-(bpy)] and [Eu(dpm)$_3$(phen)] (bpy=2,2′-bipyridyl and phen=1,10-phenanthroline) are inefficient in producing shifts. We have also shown[9] that our eight coordinate adduct, [Pr(fod)$_3$(phen)] (fod=6,6,7,7,8,8,8-heptafluoro-2,2-dimethyl-3,5-octanedionato) does not produce dipolar shifts in the proton resonance of 1-butanol but it does not dissociate in solution as reported by Hinckley,[3] for eight coordinate complex. Recently[10–12] we have synthesized seven, eight and ten coordinate complexes of lanthanoid and studied their electronic spectra. During these investigations it has been found that as the coordination number increases the number of bands decrease and also the intensity of the hypersensitive bands increases.

The present paper deals with the synthesis and characterization of seven coordinate adducts of [Ln-(fod)$_3$] chelates with pyrazole (pz) and possible use of their europium, praseodymium, and ytterbium adducts as lanthanoid induced shift reagents. Covalency parameters[13–16] ($\bar{\beta}$ and δ), bonding parameter ($b^{1/2}$) have been calculated and discussed. Oscillator strength (P) have also been computed for some of the complexes[17–19]

Experimental

Rare earth oxides (Leico Chem., U.S.A.) were converted to corresponding chlorides. Hfod (Pierce Chem., U.S.A.), pyrazole, pz, (Fluka) and Xylenol Orange (BDH, England) were used in this study.

Synthesis. [Ln(fod)$_3$] chelates were synthesized by the method of Sievers *et al.*[20] with a slight modification. The adducts of all the lanthanoid with pyrazole were prepared as follows:

The pyrazole was refluxed in ethanol for 1 h; the solution of [Ln(fod)$_3$] chelates (in 1:1 ratio) was mixed with it. Finally the mixture was refluxed for 4 h on a water bath. The solvent of the resulting mixture was evaporated on a hot plate. The product thus, formed was crystallized from hexane by keeping it in the fridge for 30 d. Good crystals were obtained by recrystallization. Finally these were dried in vacuo over P_2O_5 for several days.

Methods. Carbon, hydrogen, and nitrogen contents of the complexes were estimated by microanalyses while the metals were estimated by complexometric titrations with edta using Xylenol Orange as the indicator. The IR spectra were recorded on a Perkin-Elmer model 621 spectrophotometer in the range 4000—200 cm^{-1}. A Beckman DU-2 spectrophotometer was used to obtain the optical spectra. The NMR spectra were recorded on a Varian A-60 NMR machine in carbon tetrachloride. The magnetic susceptibility was measured by Evans' NMR method[21] in methanol as well as in chloroform at the probe temperature. TGA and DTA studies were carried out at RRL Hyderabad, India.

Calculations

On complexation radial integrals of the valence orbital of the metal ion decrease. This phenomenon is known[13] as nephelauxetic effect and may be regarded as a measure of the covalency in a complex. Nephelauxetic ratio, $\bar{\beta}$, can be calculated from the relation

$$\bar{\beta} = \frac{1}{n}\sum_{n=1}^{n} \nu_{\mathrm{comp}}/\nu_{\mathrm{aq}}. \quad (1)$$

If the f orbitals are involved in covalent bond formation with the ligand the metal wave function can be expressed[14] as

$$<\phi_{4f}| = (1-b)^{1/2}<4f| - b^{1/2}<\phi_{\mathrm{ligand}}|, \quad (2)$$

where $b^{1/2}$ measures the amount of 4f-ligand mixing and is calculated from the relation[15]

$$b^{1/2} = \left[\frac{1}{2}(1-\bar{\beta})\right]^{1/2}. \quad (3)$$

The positive and negative values of $b^{1/2}$ for a complex, correspond to covalent and ionic characters respectively.

† Abstracted in part from the thesis submitted by K. Iftikhar to the Aligarh Muslim University for the degree of Doctor of Philosophy.

Sinha's covalency parameter, δ, is calculated from the relation[16]

$$\delta = \left[\frac{1-\bar{\beta}}{\bar{\beta}}\right]100. \quad (4)$$

The experimental values of the oscillator strength (P_{exptl}) of the absorption bands are calculated by performing Gaussian curve analyses of the curves and using the equation[19]

$$P_{\text{exptl}} = 4.31 \times 10^{-9}\left[\frac{9\eta}{(\eta^2+2)^2}\right]\int \varepsilon(\nu)\mathrm{d}\nu, \quad (5)$$

where η is the refractive index of the medium, ε is the molar extinction coefficient and ν is the energy of the transition in wave number.

The oscillator strengths (P_{calcd}) can be computed from an equation[17,18] derived from a theory in which the ligand field interaction with central ion causes a mixing of higher configuration of opposite parity into the $4f^n$ configuration giving rise to induced electric dipole transions.

$$P = \sum_{\lambda=2,4,6} T_\lambda \nu (f^n\psi_J||U^{(\lambda)}||f^n\psi'_{J'})^2(2J+1)^{-1}, \quad (6)$$

where ν is the energy of the transition, $\psi_J \rightarrow \psi'_{J'}$ and $U^{(\lambda)}$ is the unit tensor operator connecting the initial and final states *via* three phenomenological parameters $T_\lambda(\lambda=2, 4, \text{and } 6)$. The three T_λ parameters are related to the radial part of the $4f^n$ wave functions, the wave functions of the perturbing configurations, the refractive index of the medium and the ligand field parameters characterizing the environment of the ion. The three quantities, T_λ, can be treated as the parameters to be determined from the experimental oscillator strengths.

Results and Discussion

These adducts are well defined crystalline solids with sharp melting points. The melting points of pyrazole adducts are lower than those of imidazole adducts.[12] These are soluble in all organic solvents and are air stable. The molar conductances of these complexes in methanol (Table 1) showed their non-electrolytic behaviour.[22]

IR Spectra. The IR spectra of these adducts show the presence of coordinated pyrazole. The N–H frequency in pyrazole ligand appears as a broad band (2300—3500 cm^{-1}) because of intermolecular hydrogen bonding. It appears as a sharp band in the region 3000—2940 cm^{-1} in the adducts. The weak band found between 305 and 290 cm^{-1} in these adducts has been assigned to metal-nitrogen frequency. We have found the metal-nitrogen frequency in the same region (282—290 cm^{-1}) for imidazole adducts[12]

Table 1. Elemental analyses and some characterizing data

Complex	Found (Calcd) (%)				Mp θ_m/°C	Molar conductance $\Omega^{-1}cm^2$	μ_{eff} BM	Colour
	Metal	C	H	N				
[Y(fod)$_3$(pz)]	8.52	38.20	3.18	2.70	—	—	Diamag.	White
	(8.54)	(38.00)	(3.26)	(2.68)				
[La(fod)$_3$(pz)]	13.33	35.87	3.33	2.58	209	6.8	Diamag.	White
	(12.73)	(36.26)	(3.12)	(2.57)				
[Pr(fod)$_3$(pz)]	12.69	36.88	3.05	2.73	105	16.3	3.67	Green
	(12.89)	(36.20)	(3.11)	(2.56)				
[Nd(fod)$_3$(pz)]	12.82	36.90	3.32	2.35	118	9.9	3.81	Violet
	(13.13)	(36.10)	(3.10)	(2.55)				
[Sm(fod)$_3$(pz)]	13.60	35.83	3.10	2.58	112	19.0	2.45	White
	(13.63)	(35.90)	(3.08)	(2.54)				
[Eu(fod)$_3$(pz)]	13.73	36.10	2.97	2.51	—	6.3	3.62	Light yellow
	(13.76)	(35.84)	(3.08)	(2.53)				
[Gd(fod)$_3$(pz)]	14.30	35.52	3.18	2.39	108	6.0	7.96	Light yellow
	(14.16)	(36.68)	(3.06)	(2.52)				
[Tb(fod)$_3$(pz)]	14.33	35.83	3.26	2.51	—	—	9.87	Light yellow
	(14.30)	(35.61)	(3.06)	(2.52)				
[Dy(fod)$_3$(pz)]	15.18	34.98	3.18	2.47	139	—	10.70	Light yellow
	(14.56)	(35.50)	(3.04)	(2.51)				
[Ho(fod)$_3$(pz)]	14.53	36.25	3.08	2.55	109	10.0	10.55	Pink
	(14.76)	(35.42)	(3.04)	(2.50)				
[Er(fod)$_3$(pz)]	14.90	35.30	3.21	2.58	—	—	9.51	White
	(14.92)	(35.36)	(3.03)	(2.50)				
[Tm(fod)$_3$(pz)]	15.21	35.75	2.95	2.43	—	7.6	7.39	White
	(15.06)	(35.30)	(3.03)	(2.50)				
[Yb(fod)$_3$(pz)]	15.35	35.10	3.15	2.46	90	—	4.50	White
	(15.36)	(35.10)	(3.02)	(2.49)				
[Lu(fod)$_3$(pz)]	15.30	35.29	2.98	2.50	—	—	Diamag.	White
	(15.50)	(35.12)	(3.01)	(2.48)				

of $[Ln(fod)_3]$ chelates. The metal-oxygen frequency in $[Pr(fod)_3]$ and $[Sm(fod)_3]$ occurs at 390 cm^{-1}. These go up to 454 cm^{-1} and 450 cm^{-1} in the corresponding adducts. Thus the bands appearing between 445 and 460 cm^{-1} have been assigned to metal-oxygen frequency in these adducts. This is an observation in contrast to what is seen in imidazole[12] adducts.

The thermograms of the adducts of La, Eu, Gd, Tm, and Yb showed the same behaviour as reported for their respective chelates,[20] except in the temperature range of 200—220 °C in which pyrazole is eliminated. The total weight loss is consistent with the loss of pyrazole in this temperature range (Table 2). One sharp DTA peak is identified in all cases.

Thus, these adducts on the basis of their elemental analyses for carbon, hydrogen, nitrogen, and metals, molar conductance (Table 1), IR spectral and thermal studies have been assigned the general formula, $[Ln(fod)_3(pz)]$.

The magnetic moments (Table 1) of these adducts, when plotted against their increasing atomic number, showed the characteristic unequal double humped curve.

NMR Spectra. The NMR spectral data are summarized in Table 3. NMR signals of fod moiety of the adducts appear at 1.05—1.15 ppm for *t*-butyl protons and at 5.95—6.11 ppm for methine protons as sharp singlet (for diamagnetic adducts). It has been found that the signals due to *t*-butyl and methine protons have been shifted to higher fields as compared to their respective chelates.[20] Perhaps it is due to withdrawal of electron density from pyrazole, that the Ln^{3+} ions become more polarized and transfer some charge to diketonate ring, which can be very conveniently accommodated by the highly electronegative fluorine. Other signals can be assigned to those of the coordinated pyrazole.

Pyrazole is reported[23] to give two signals (one for H-4 and another for H-3 and H-5) with relative areas of 1 : 2. But we found all the three signals (for H-2, H-4, and H-3 and H-5) with relative areas of 1 : 1 : 2. The signals of the coordinated pyrazole are found to shift to the lower fields, except in the case of lanthanum in which the signals are slightly shifted to higher fields. This deshielding effect of pyrazole protons obviously suggests the coordination of pyrazole to metal ion.

Information concerning electron delocalization in lanthanoid complexes may be obtained from NMR studies of paramagnetic species, provided nuclear relaxation times are long enough to allow well-resolved spectra to be obtained. Paramagnetic lanthanoid complexes whose spectra have been recorded are few.[1,8] In the spectra of $[Pr(fod)_3(pz)]$ and $[Yb(fod)_3(pz)]$ the methine signal is not seen but the proton resonances of pyrazole show large chemical shifts as compared to their diamagnetic analogue. These shifts are due to pseudo-contact (dipolar) interaction as $\boldsymbol{g}$ tensor is anisotropic. If $\boldsymbol{g}$ is isotropic this interaction goes to zero. The dipolar shift is limited by the geometry of the complex species, as given by the expression[24]

$$\left(\frac{\Delta\nu}{\nu_0}\right) = -K_D f(\theta, r) f(g_\parallel, g_\perp),$$

or simply

$$\left(\frac{\Delta\nu}{\nu_0}\right) = -D\left(\frac{3\cos^2\theta - 1}{r^3}\right),$$

where all notations have their usual connotations.

One of the intents of this study was to examine praseodymium, europium and ytterbium adducts as potential shift reagents. $[Eu(fod)_3(pz)]$ added to a solution of 1-butanol show large chemical shifts (Fig. 1). The two methylene protons which resonate as a singlet get resolved into two individual signals. The substrate associates with the complex at the hydroxyl group and the induced shifts decrease rapidly with increasing distance of the protons from the hydroxyl group. When $[Pr(fod)_3(pz)]$ was used, it induced the 1-butanol spectrum to become first order and all peaks greatly shifted to high field (Fig. 3). On addition of $[Yb(fod)_3(pz)]$ the spectrum is amenable to a first order analysis and the magnitude of the induced shift is larger than the europium adduct, but with a little broadening and the coupling interactions of the nuclei having disappeared. This little broadening is due to long electron relaxation time of Yb(III) ion as compared to europium(III). In the above examples, the shifts of the hydroxyl protons are of course extremely large and have not been recorded, (See Tables 4—6).

In the normal ^1H NMR spectrum of benzyl alcohol

TABLE 2. TGA DATA FOR SOME OF THE COMPLEXES

Complex	Temperature °C	% Weight loss for pyrazole[a]
$[La(fod)_3(pz)]$	220	7.00 (6.22)
$[Eu(fod)_3(pz)]$	200	6.25 (6.15)
$[Gd(fod)_3(pz)]$	220	6.25 (6.12)
$[Tm(fod)_3(pz)]$	200	6.00 (6.06)
$[Yb(fod)_3(pz)]$	200	5.75 (6.04)

a) Theoretical weight loss is in parenthesis.

TABLE 3. NMR SPECTRAL DATA[a]

Complex	Signals due to pyrazole			Signals due to β-keto enolate	
	H-2	H-3 and H-5	H-4	CH	Bu^t
Pyrazole	13.73	7.57	6.26	—	—
$[Y(fod)_3(pz)]$	b)	7.61	6.36	6.11	1.13
$[La(fod)_3(pz)]$	b)	7.42	6.24	5.95	1.05
$[Lu(fod)_3(pz)]$	b)	7.73	6.45	6.08	1.15
$[Pr(fod)_3(pz)]$	b)	12.11	1.30	b)	−0.48[c]
$[Yb(fod)_3(pz)]$	b)	34.92	3.18	b)	3.72

a) Obtained in carbon tetrachloride at the probe temperature. chemical shift in ppm downfield from internal Me_4Si. b) Not observed. c) In ppm upfield w.r.t. Me_4Si.

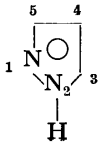

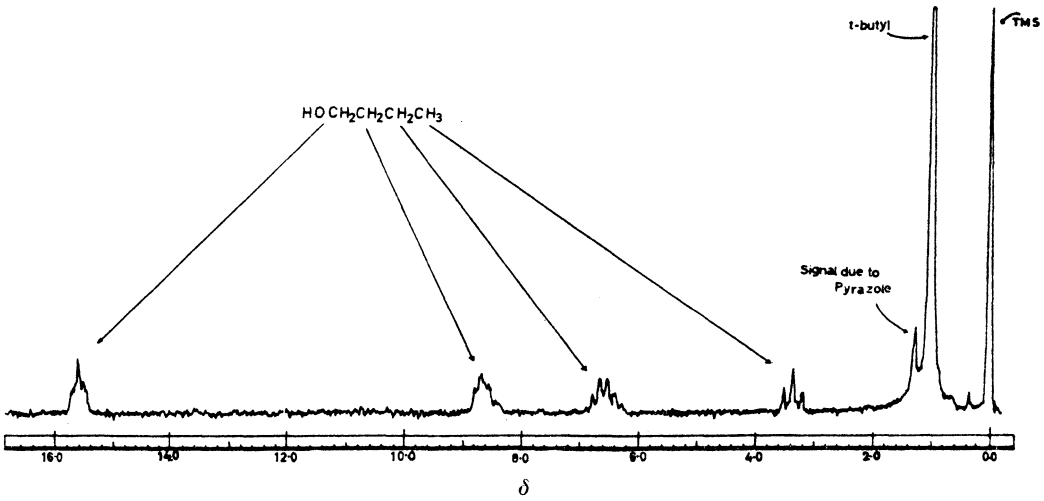

Fig. 1. 60 MHz ^{1}H NMR spectrum of 1-butanol (0.2 M, 1 M=1 mol dm^{-3}) and [Eu(fod)$_3$(pz)] (0.2 M) in CCl_4. Chemical shifts relative to internal Me_4Si.

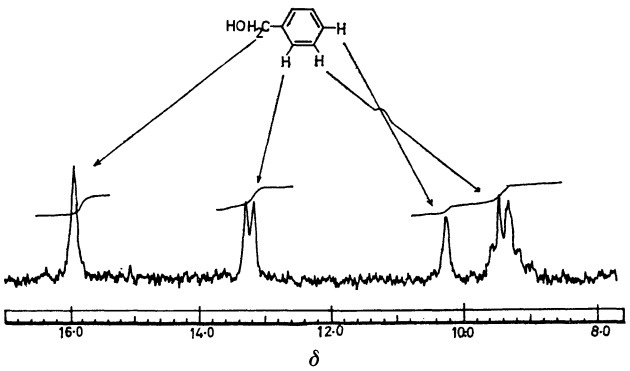

Fig. 2. 60 MHz ^{1}H NMR spectrum of benzyl alcohol (0.2 M) and [Eu(fod)$_3$(pz)] in CCl_4. Chemical shifts relative to internal Me_4Si.

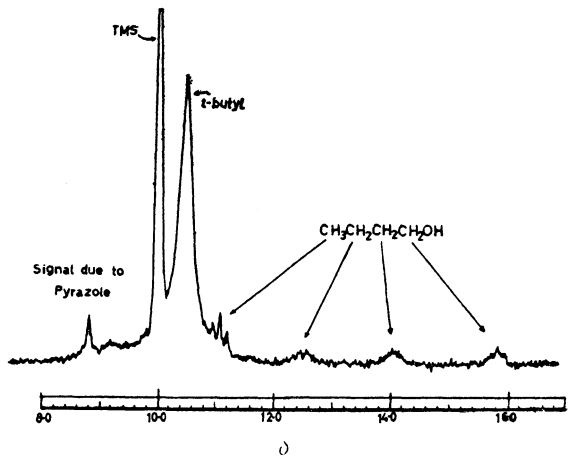

Fig. 3. 60 MHz ^{1}H NMR spectrum of 1-butanol (0.2 M) and [Pr(fod)$_3$(pz)] (0.2 M) in CCl_4. Chemical shifts relative to internal Me_4Si.

(CCl_4 solution) the aromatic protons resonate as a sharp singlet. Sanders and Williams[4] studied NMR spectrum of benzyl alcohol using [Eu(dpm)$_3$] and reported that the signals appear in order CH_2, *o*-protons, *m*-protons, and then *p*-proton (all lower field to TMS). Our studies gave a different result. [Eu-

Table 4. [Eu(fod)$_3$(pz)] shifts in ppm downfield

	H_α	H_β	H_γ	H_δ
1-Butanol	12.04	7.23	5.22	2.37
	CH_2	H_o	H_p	H_m
Benzyl alcohol	11.33	5.89	2.89	2.04

Table 5. [Pr(fod)$_3$(pz)] shifts in ppm

	H_α	H_β	H_γ	H_δ
1-Butanol	−9.40	−5.90	−3.90	−2.06
	CH_2	H_o	H_p	H_m
Benzyl alcohol	−6.77	3.14	1.09	0.78

Negative sign indicate shifts upfield w.r.t. Me_4Si and positive shifts are downfield w.r.t. Me_4Si.

Table 6. [Yb(fod)$_3$(pz)] shifts in ppm downfield

	H_α	H_β	H_γ	H_δ
1-Butanol	28.67	27.82	17.82	8.92

(fod)$_3$(pz)] when added to a CCl_4 solution of benzyl alcohol resolved all the ring protons (Fig. 2) but in a different manner as reported.[4] The CH_2 protons appear at the lowest field as a sharp singlet, the next resonance is due to *o*-protons after this appear signal for *p*-proton and the *m*-protons appear at the last (all lower field to TMS). When [Pr(fod)$_3$(pz)] is used only CH_2 signal appears at higher field to TMS the other signals lie within the TMS envelope. The CH_2 proton resonance shows that the angle between the principal axis and line joining the paramagnetic ion and the proton inquestion is greater than 54.7° or 125.3°.

The NMR spectra of these adducts show no resonance for free pyrazole. Even on keeping the solutions for several days no change in signal line width or position is seen. This shows that coordinated pyrazole does not dissociate in solution as suggested by Hinckley[3] for pyridine.

Electronic Spectra. The electronic spectra of the complexes are recorded in ethanol. The intraligand

Table 7. Covalency paramters

Complex	$\bar{\beta}$	$b^{1/2}$	δ
$[Pr(fod)_3(pz)]$	0.98284	0.09263	1.74596
$[Nd(fod)_3(pz)]$	0.99598	0.04483	0.40362
$[Er(fod)_3(pz)]$	0.99225	0.06225	0.78105

Table 8. T_λ parameters ($T_\lambda \times 10^8$)

Complex	T_2	T_4	T_6
$[Pr(fod)_3(pz)]$	23.53370	0.11519	1.31464
$[Nd(fod)_3(pz)]$	75.40279	−195.39910	280.95548
$[Er(fod)_3(pz)]$	2.01493	0.30832	0.03987

Table 9. Oscillator strength ($P \times 10^6$)

Complex	S'L'J'	P_{exptl}	P_{calcd}
$[Pr(fod)_3(pz)]$	$^1D_2$	4.57982	4.36339
	$^3P_0$	1.66622	3.90265
	$^3P_1$	2.20341	1.39446
	$^3P_2$	0.19348	8.19343
$[Nd(fod)_3(pz)]$	$^4F_{9/2}$	3.98525	16.10470
	$^2H_{11/2}$	32.38545	32.38533
	$[^4G_{5/2}\ ^2G_{7/2}]$	54.78670	54.78660
	$^2K_{13/2}\ ^4G_{7/2}\ ^4G_{9/2}$	9.34646	9.34695
$[Er(fod)_3(pz)]$	$^4F_{9/2}$	2.77998	2.78000
	$[^2H_{11/2}]$	24.86433	24.86433
	$^4F_{7/2}$	1.81117	1.81079

Hypersensitive transitions are enclosed in parentheses.

transitions occur in UV region and have not been discussed. The sharp line like f-f transitions originating within the $4f^n$ configuration of lanthanoid(III) ions are affected by the influence of the ligands on complexation. The shift of absorption bands to lower wave numbers (nephelauxetic effect) is usually of the order of a few percent[13] and is caused by a decrease in interelectronic repulsion parameter in the complexes.[25] A general red shift of the f-f transitions would be observed for these complexes as compared to the corresponding aqua ions. The $\bar{\beta}$ values for these complexes are presented in Table 7. The $\bar{\beta}$ values which are less than one show covalent nature of bonding between the metal and the ligand. The $\bar{\beta}$ value of Nd(III) complex is higher than the Pr-(III) complex but it is lower for Er(III) complex as compared to Nd(III) complex. This is in contrast to the general observation that the nephelauxetic effect is more pronounced in the beginning of the 4f group than in the later members. The bonding parameter, $b^{1/2}$ and Sinha's covalency parameter, δ are positive for these complexes indicating covalent bonding (Table 7). The greater the values of $b^{1/2}$ and δ the greater will be the degree of covalency. The $b^{1/2}$ and δ values of Nd(III) complex are less than those for Pr(III) complex showing decrease of covalency with increase of atomic number. The higher values of $b^{1/2}$ and δ for Er(III) complex than for Nd-(III) complex are surprising in view of the general observation and trend observed in case of $[Ln(fod)_3$-(im)] (im=imidazole) complexes.[12] The $[Ln(fod)_3$-(pz)] complexes are less covalent as compared to the corresponding $[Ln(fod)_3(im)]$[12] complexes since values of $b^{1/2}$ and δ are lower in the former case than in the later.

Another point of interest in these spectra are the intensities of the f-f transitions. Experimentally hypersensitivity refers to transitions having oscillator strengths which show a relatively large variability in oscillator strengths as the environment about the lanthanoid ion is changed. The large variability in oscillator strengths for the hypersensitive transitions is due to eigen perturbation.[26] Hypersensitivity can also be disccused from the theoretical point of view of Judd-Ofelt. According to this theory hypersensitivity is intimately associated with T_2 parameter of Eq. 6. Consequently only those transitions having relatively large values of $U^{(2)}$ matrix element should be called hypersensitive. Judd[27] has suggested that hypersensitivity may be due to symmetry of the crystal fields. Henrie[28] has shown that T_4 and T_6 appear to be primarily influenced by the symmetry of the complexes whereas T_2 seems to be correlated with the basicity of the ligand.

The oscillator strengths are listed in Table 9 and hypersensitive transitions classified by previous workers[28] are enclosed in parentheses. There is a good correlation between P_{exptl} and P_{calcd} showing that the intensity theory of Judd-Ofelt is applicable but poor correlation between P_{exptl} and P_{calcd} in case of Pr(III) complex strengthens the conclusion of the earlier workers[29,30] that this theory is not applicable to the complexes of Pr(III).

The transitions in Pr(III) and Er(III) complexes have values of $U^{(2)}$ which are significantly larger than either the $U^{(4)}$ or $U^{(6)}$ values and thus have oscillator strengths which are affected primarily by T_2 parameter.

In Nd(III) complex the magnitude of $U^{(2)}$ is not large enough to permic the effect of T_2 parameter to dominate instead T_4 and T_6 are more sensitive than T_2 and hence the observed oscillator strength is governed by these parameters. The oscillator strength of $^2H_{11/2}$ in Nd(III) complex shows a very large change as compared to the aqua ion. This change is larger than the change shown by hypersensitive transition (enclosed in parenthesis).

The oscillator strength of the hypersensitive transitions is related to the degree of covalency. As the covalency in the complex increases the oscillator strength of the hypersensitive transitions exhibits a corresponding increases. The oscillator strengths of the hypersensitive transitions of pyrazole complexes have lower values as compared to the corresponding imidazole complexes[12] since imidazole is more basic than pyrazole.

In the last we can say that pyrazole complexes, though less covalent, have superiority over imidazole complexes[12] since they can be used as potential shift reagents.

KI and MS thank the CSIR, New Delhi India, for the award of the research fellowships to them.

References

1) D. R. Eaton, *J. Am. Chem. Soc.*, **87**, 3097 (1965).
2) F. A. Hart, J. E. Newbery, and D. Shaw, *J. Chem. Soc., Chem. Commun.*, **1967**, 45; *J. Inorg. Nucl. Chem.*, **32**, 3585 (1970).
3) C. C. Hinckley, *J. Am. Chem. Soc.*, **91**, 5160 (1969); *J. Org. Chem.*, **35**, 2834 (1970).
4) J. K. M. Sanders and D. H. Williams, *J. Chem. Soc., Chem. Commun.*, **1970**, 422.
5) J. Briggs, G. H. Frost, F. A. Hart, G. P. Moss, and M. L. Staniforth, *J. Chem. Soc., Chem. Commun.*, **1970**, 749.
6) J. Selbin, N. Ahmad, and N. Bhacca, *Inorg. Chem.*, **10**, 1383 (1971).
7) N. Ahmad, N. S. Bhacca, J. Selbin, and J. D. Wander, *J. Am. Chem., Soc.*, **93**, 2564 (1971).
8) N. S. Bhacca, J. Selbin, and J. D. Wander, *J. Am. Chem. Soc.*, **94**, 8719 (1972).
9) K. Iftikhar, M. Sayeed, and N. Ahmad, *Inorg. Chem.*, **21**, 80 (1982).
10) M. Sayeed and N. Ahmad, *J. Inorg. Nucl. Chem.*, **43**, 3197 (1981).
11) K. Iftikhar, M. Sayeed, and N. Ahmad, *Indian J. Chem.*, **20A**, 1028 (1981).
12) K. Iftikhar and N. Ahmad, submitted for publication.
13) C. K. Jørgensen, *Prog. Inorg. Chem.*, **4**, 73 (1962).
14) S. P. Tandon and P. C. Mehta, *J. Chem. Phys.*, **52**, 4896, 5417 (1970).
15) D. E. Henrie and G. R. Choppin, *J. Chem. Phys.*, **49**, 477 (1968).
16) S. P. Sinha, *Spectrochim. Acta*, **22**, 57 (1966).
17) B. R. Judd, *Phys. Rev.*, **127**, 750 (1962).
18) G. S. Ofelt, *J. Chem. Phys.*, **37**, 511 (1962).
19) J. Hooschagen, *Physica*, **11**, 513 (1946).
20) C. S. Springer, D. W. Meek, and R. E. Sievers, *Inorg. Chem.*, **6**, 1105 (1967).
21) D. F. Evans, *J. Chem. Soc.*, **1959**, 2003.
22) W. J. Geary, *Coord. Chem. Rev.*, **7**, 81 (1971).
23) J. H. Ridd and R. F. M. White, *Biochem. J.*, **77**, 546 (1960).
24) H. M. McConnel and R. E. Robertson, *J. Chem. Phys.*, **29**, 1361 (1958).
25) S. P. Sinha and S. S. Schmidtke, *Mol. Phys.*, **10**, 7 (1965).
26) W. Pricke, *Z. Phys.*, **B 33**, 261 (1979).
27) B. R. Judd., *J. Chem. Phys.*, **44**, 839 (1966).
28) D. E. Henrie, R. L. Fellows, and G. R. Choopin, *Coord. Chem. Rev.*, **18**, 199 (1976).
29) W. T. Carnall, P. R. Fields, and B. G. Wybourne, *J. Chem. Phys.*, **42**, 3797 (1965).
30) W. T. Carnall, P. R. Fields, and K. Rajnak, *J. Chem. Phys.*, **49**, 4412 (1968).

Synthesis of Naturally Occurring Prenylated Benzophenones. Vismiaphenone A, Vismiaphenone B, and Isovismiaphenone B

Ved Prakash PATHAK and Rajinder Nath KHANNA*
Department of Chemistry, University of Delhi, Delhi-110007, India
(Received August 13, 1981)

2,4,6-Trihydroxybenzophenone on prenylation with 2-methyl-3-buten-2-ol in the presence of $(C_2H_5)_2O\cdot BF_3$ yielded 2,4,6-trihydroxy-3,5-diprenylbenzophenone (**3**), 2,6-dihydroxy-4-prenyloxybenzophenone, 2,6-dihydroxy-3-prenyl-4-prenyloxybenzophenone, a benzodipyran and 6-benzoyl-5,7-dihydroxy-2,2-dimethyl-3-prenylchroman. **3** on reaction with 2 moles of *p*-toluenesulfonyl chloride followed by methylation and detosylation gave a naturally occurring benzophenone, vismiaphenone A (**12**). Cyclodehydrogenation of 6-hydroxy-3,5-diprenyl-2,4-ditosyloxybenzophenone gave 8-benzoyl-2,2-dimethyl-6-prenyl-5,7-ditosyloxy-2*H*-1-benzopyran, which on detosylation gave another naturally occurring benzophenone, isovismiaphenone B, while cyclodehydrogenation of **3** gave vismiaphenone B, another naturally occurring benzophenone. 2,4-Dihydroxy-6-methoxybenzophenone on similar treatment with 2-methyl-3-buten-2-ol afforded **12** directly.

Monache *et al.*[1] recently reported the isolation of new prenylated benzophenones *viz.* vismiaphenone A (**12**), vismiaphenone B (**8**) and isovismiaphenone B (**9**) from the fruits of *Vismia decipiens*. The structures were assigned on the basis of spectroscopic and degradative studies. In order to confirm the proposed structures, we report the syntheses of these benzophenones starting from 2,4,6-trihydroxybenzophenone.

2,4,6-Trihydroxybenzophenone (**1**) (prepared by the condensation[2] of 1,3,5-trimethoxybenzene[3] with benzoyl chloride followed by demethylation) on reaction with 2-methyl-3-buten-2-ol in the presence of $(C_2H_5)_2O\cdot BF_3$ in dioxane at 25—30 °C furnished six products on TLC (benzene:hexane, 2:1), which were separated by column chromatography on silica gel and designated as compounds **A**, **B**, **C**, **D**, **E**, and **F**.

Compound **A** was obtained as yellow shining crystals, $C_{23}H_{26}O_4$, mp 94—95 °C. It exhibited positive iron(III) chloride reaction and negative Gibbs' reaction.[4] The infrared (IR) spectrum suggested the presence of hydroxyl groups (3350 and 3100 cm^{-1}) and carbonyl (1610 cm^{-1}) groups. Its ^1H NMR spectrum showed δ 7.33—7.65 (5H, m) due to the unsubstituted phenyl ring. It also indicated the presence of two prenyl groups [δ 1.77, 1.72 (6H, s each, $(CH_3)_2\times2$), 3.31 (4H, d, J=6.5 Hz, $-C\underline{H}_2-CH=\times2$), 5.2 (2H, t, J=6.5 Hz, $-CH_2-C\underline{H}=\times2$)] and three hydroxyl groups [δ 6.2 (1H), 8.85 (1H), 12.8 (1H) all exchangeable with deuterium]. Based on these data, compound **A** was assigned the structure 2,4,6-trihydroxy-3,5-diprenylbenzophenone (**3**), which was further confirmed by its acid cyclization to benzo[1,2-*b*:3,4-*b'*]dipyran (**6**). Compound **3** was also reported earlier by us[5] in poor yields by the reaction of **1** with prenyl bromide in the presence of sodium methoxide.

Compound **B** was obtained as light yellow needles, $C_{18}H_{18}O_4$, mp 121 °C. It exhibited positive Gibbs' reaction and indicated a hydroxyl (3250 cm^{-1}) and a carbonyl (1620 cm^{-1}) groups in IR spectrum. Its ^1H NMR spectrum showed a singlet at δ 6.08 integrating for two protons assigned to C_3–H and C_5–H and a multiplet at δ 7.4—7.78 assigned to unsubstituted phenyl ring. It also indicated the presence of a prenyloxyl group [δ 1.78, 1.84 (3H, s each $(CH_3)_2$), 4.57 (2H, d, J=7 Hz, $-C\underline{H}_2-CH=$), 5.5 (1H, t, J=7 Hz, $-CH_2-C\underline{H}=$)] and two hydroxyl groups [δ 8.98 (1H, s), 12.84 (1H, s), both exchangeable with deuterium]. On this basis compound **B** was assigned the structure as 2,6-dihydroxy-4-prenyloxybenzophenone (**4**).

Compound **C** was a brown oil, $C_{23}H_{26}O_4$, gave a positive iron(III) chloride reaction as well as Gibbs' reaction. ^1H NMR spectrum indicated the presence of one prenyloxyl group and one *C*-prenyl group [δ 4.18 (2H, d, J=6.5 Hz, $-C\underline{H}_2-CH=$), 3.38 (2H, d, J=7 Hz, $-C\underline{H}_2-CH=$), 5.3, 4.67 (1H, bt each, J=6.5 Hz, $-CH_2-C\underline{H}=\times2$), 1.74, 1.78, 1.64, 1.57 (3H, s each, $(CH_3)_2\times2$)]. It also showed the presence of an aromatic proton δ 5.95 (1H, s), an unsubstituted phenyl ring δ 7.36—7.71 (5H, m) and two hydroxyl groups at δ 10.8 (2H, s, C_2– and C_6–OH). It was assigned the structure as 2,6-dihydroxy-3-prenyl-4-prenyloxybenzophenone (**5**).

Compound **D** was obtained as white crystals, mp 176 °C, having molecular formula $C_{23}H_{26}O_4$. It exhibited positive iron(III) chloride reaction and the ^1H NMR spectrum revealed the presence of two 2,2-dimethylchroman units [δ 0.86, 0.38 (6H, s each, $(CH_3)_2\times2$), 1.27, 1.03 (2H, t each, J=7 Hz, $CH_2-C\underline{H}_2\times2$), 2.13, 1.93 (2H, t each, J=7 Hz, $C\underline{H}_2-CH_2\times2$)], unsubstituted phenyl ring δ 6.68—6.97 (5H, m) and a chelated hydroxyl δ 12.4 (1H, s). On the basis of these data, it was assigned 2,2,8,8-tetramethyl-2*H*,10*H*-benzo[1,2-*b*:3,4-*b'*] benzopyran structure (**6**), which was further confirmed by its methylation to give **7**, which corresponded to that derived from **12**.

Compound **E** was a light brown oil, $C_{23}H_{26}O_4$, exhibited positive iron(III) reaction. A positive Gibbs' test along with a singlet at δ 5.91 indicated that C_8–H *para* to C_5–OH is free and thus C_5 position of benzophenone must be linked to the $C_{10}H_{18}$ unit. It also showed in its ^1H NMR spectrum (i) two methyl groups attached to a saturated centre at δ 1.26, 1.44 (3H, s each), (ii) two methyl groups attached to an unsaturated centre, δ 1.63, 1.74 (3H, s each), (iii) a multiplet integrating for three protons at δ 2.0—2.41 assignable to two protons at C_d and one proton at C_3, (iv) C_4 protons at δ 2.79 (2H, dd, J=16 and 5 Hz) and a methine proton δ 5.11—5.36 (1H, m, H_c). Unsubstituted phenyl ring protons were indicated at their usual position at δ 7.36—7.77 (5H, m). Thus, on the above basis compound **E** was formulated as

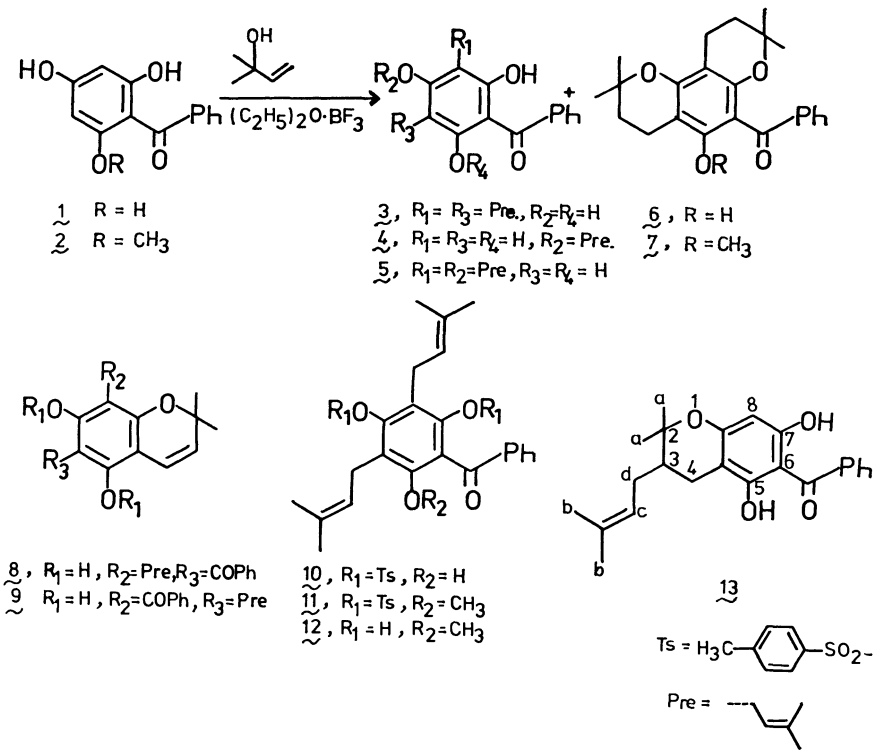

6-benzoyl-5,7-dihydroxy-2,2-dimethyl-3-prenylchroman (**13**). Compound **E** seems to arise by the attack of an isopentenyl carbonium ion, generated from 2-methyl-3-buten-2-ol, on the prenyl unit of 5-prenylbenzophenone.[6] Compound **F** was unreacted starting benzophenone **1**. Oxidative cyclodehydrogenation of **3** with DDQ afforded **8**, whose spectral data were in complete agreement with those reported for the natural sample of vismiaphenone B. Ditosylation of **3** with 2 mol of *p*-toluenesulfonyl chloride gave 6-hydroxy-3,5-diprenyl-2,4-ditosyloxybenzophenone (**10**) which on methylation followed by detosylation furnished **12**, identical in all respects with the reported data for vismiaphenone A. Compound **12** was also prepared by the reaction of 2,4-dihydroxy-6-methoxybenzophenone (**2**) (prepared by ditosylation of **1** followed by methylation and detosylation) with 2-methyl-3-buten-2-ol under similar reaction conditions as in **1**. This reaction showed the presence of two minor and two major products on TLC. The two major products were characterized to be **3** and **12**, while the minor products could not be identified.

Oxidative cyclodehydrogenation of **10**, followed by detosylation furnished **9**, identical with isovismiaphenone B in all respects.

Experimental

All melting points are uncorrected. IR and UV spectra were recorded on a Perkin-Elmer IR spectrophotometer Model-621 (ν_{max} in cm^{-1}) in KBr and on Perkin-Elmer UV spectrophotometer Model-554 (λ_{max} in nm) in methanol respectively. ^1H NMR spectra were measured on Perkin-Elmer R-32 (90 MHz) spectrometer in $CDCl_3$ or CCl_4 using tetramethylsilane as an internal standard (s, singlet; d, doublet; t, triplet; m, multiplet; br, broad).

Reaction of 2-Methyl-3-buten-2-ol with 2,4,6-Trihydroxybenzophenone. **1** (10 g, 27.3 mmol) was dissolved in dry dioxane (50 ml) and stirred vigorously at 25—30 °C. $(C_2H_5)_2O \cdot BF_3$ (3 ml in 15 ml of dioxane) was added to the stirring solution in 1 h. The solution was stirred for 1 h more. Then 2-methyl-3-buten-2-ol (4.5 ml, 52.3 mmol, in 10 ml of dioxane) was added in 10 min and the solution stirred for another 4 h. The reaction mixture was left overnight and diluted with water. It was extracted with ethyl acetate (2×250 ml) and the organic phase was washed with 5% aqueous sodium hydrogencarbonate (100 ml) and water. It was dried (Na_2SO_4) and solvent evaporated. The resulting brownish liquid (8.5 ml) was chromatographed on silica gel. On elution with light petroleum (boiling range 60—80 °C) with the increasing amount of ethyl acetate, following compounds were separated.

*Compound **A** (3).* Obtained as yellow shining crystals (950 mg), (Found: C, 75.35; H, 7.20%. Calcd for $C_{23}H_{26}O_4$: C, 75.46; H, 7.06%). UV(qualitative) 254 and 311. IR: 3350 (br), 3100 (br), 1610, 1552, 1390, 1320, 1252, 1155, 1095 and 940.

*Compound **B** (4).* Crystallized from chloroform as light yellow needles (80 mg), (Found: C, 72.46; H, 6.10%. Calcd for $C_{18}H_{18}O_4$: C, 72.48; H, 6.04%). UV (qualitative) 248 and 308, IR: 3250(br), 2900, 1620, 1459, 1375, 1150, 1082, and 820.

*Compound **C** (5).* Obtained as brown oil (60 mg), (Found: C, 75.38; H, 7.14%. Calcd for $C_{23}H_{26}O_4$: C, 75.46; H, 7.06%). UV (qualitative) 248 and 308; IR: 3360, 3120, 1620, 1510, 1385, 1290, 1165, 1060, and 935.

*Compound **D** (6).* Crystallised from light petroleum–benzene mixture as white crystals (50 mg), (Found: C, 75.41; H, 7.16%. Calcd for $C_{23}H_{26}O_4$: C, 75.46; H, 7.06%); UV: 210 and 312; IR: 3390, 2910, 1585, 1440, 1418, 1330, 1318, 1291, 1271, 1250, 1228, 1150, 1110, and 952.

*Compound **E** (13).* Obtained as light brown oil (740 mg), (Found: C, 75.40; H, 7.12%. Calcd for $C_{23}H_{26}O_4$: C, 75.46; H, 7.06%). UV: 253 and 310; IR: 3320, 2920,

1620, 1585, 1424, 1300, 1167, 1120, 1078, and 920.

Compound F. Obtained as light yellow crystals and was characterized to be the unreacted benzophenone **1** (500 mg).

2,4-Dihydroxy-6-methoxy-3,5-diprenylbenzophenone (12). A mixture of **3** (200 mg, 0.55 mmol) and *p*-toluenesulfonyl chloride (280 mg, 1.47 mmol) was dissolved in dry acetone (5 ml) and the solution was refluxed with ignited potassium carbonate (300 mg) for 6 h. Dimethyl sulfate (0.2 ml, 1.6 mmol) and potassium carbonate (100 mg) were added and the reaction mixture was further refluxed for 12 h. Inorganic salts filtered and acetone evaporated. The residue was treated with 10% ethanolic potassium hydroxide (20 ml) for 2 h at 50—55 °C. The solution was cooled, diluted with water (200 ml), acidified with HCl and extracted with ether. The ethereal layer was washed with 5% sodium hydrogen carbonate solution (45 ml) followed by water (100 ml) and dried (Na_2SO_4). The solvent was evaporated and the residue on purification by column chromatography afforded **12** as a light yellow oil (35 mg), (Found C, 75.81; H, 7.46%). UV: 255 and 310. IR: 3410, 1620, 1602, 1582, 1442, 1375, 1320, 1175, 1150, 1002. ^{1}H NMR(CCl_4): δ 11.8 (1H, s, O<u>H</u> at C-2), 7.75—7.31(5H, m, phenyl ring protons), 6.2(1H, br s, O<u>H</u> at C-4), 5.2(2H, br t, J=7 Hz, CH_2–C<u>H</u>=×2), 3.3—3.44(4H, m, C<u>H</u>$_2$–CH=×2), 3.21(3H, s, OCH_3), 1.75, 1.76(6H, s each, $(CH_3)_2$×2).

8-Benzoyl-5,7-dihydroxy-2,2-dimethyl-6-prenyl-2H-1-benzopyran (9). A mixture of **3** (250 mg, 0.68 mmol), *p*-toluenesulfonyl chloride (350 mg, 1.84 mmol) and potassium carbonate (360 mg) was refluxed in dry acetone (7 ml) for 8 h. The potassium salts were filtered off and washed with hot acetone (50 ml). The filtrate and washing were mixed and the solvent evaporated. The residue on purification with column chromatography on silica gel gave **10** as waxy solid (180 mg), mp 57 °C, ^{1}H NMR(CCl_4): δ 13.18 (1H, chelated OH), 7.81 (4H, d, J=7 Hz, tosyl protons at C-3′ and C-5′×2), 7.28—7.49 (5H, m, phenyl protons), 7.14 (4H, d, J=7 Hz, tosyl protons at C-2′ and C-6′×2), 4.94—5.14 (2H, m), 3.12—3.36 (4H, m), 2.48, 2.39 (3H, s each, methyl protons of tosyl×2), 1.68, 1.56 (6H, s each, $(CH_3)_2$×2).

Compound **10** (120 mg, 0.17 mmol) was dissolved in benzene (5 ml), DDQ (150 mg, 0.66 mmol) was added and refluxed for 16 h. The reaction mixture was filtered through a short column of silica gel. Solvent evaporated and the residue was treated with 10% ethanolic KOH (15 ml) at 55—60 °C for 2 h. Solvent evaporated, residue was diluted with water, acidified and extracted with ether (50 ml). The ethereal layer was washed with water, dried (Na_2SO_4) and the solvent evaporated. The residue on purification with column chromatography on silica gel afforded **9** as light yellow solid (25 mg), mp 117—118 °C (lit,[1] mp 118—120 °C), (Found: C, 75.85; H, 6.68%). UV: 295 and 305; IR: 3390, 3350, 1643, 1615, 1592, 1575, 1175, 1130, and 880; ^{1}H NMR ($CDCl_3$): δ 12.9 (1H, s, OH at C-2), 7.3—7.55 (5H, m, phenyl ring protons), 6.4 (1H, d, J=9 Hz, proton at C-4), 6.2 (1H, s, OH at C-7), 5.3 (1H, d, J=9 Hz, proton at C-3), 4.9—5.15(1H, m, –C<u>H</u>=CH$(CH_3)_2$), 3.3(2H, J=7 Hz, –C<u>H</u>$_2$–CH=), 1.75, 0.85 (12H, s each, $(CH_3)_2$×2).

6-Benzoyl-5,7-dihydroxy-2,2-dimethyl-8-prenyl-2H-1-benzopyran (8). **3** (50 mg, 0.14 mmol) was dissolved in dry benzene (5 ml) and refluxed with DDQ (30 mg, 0.13 mmol) for 3 h. The reaction mixture filtered through a small column of silica gel. On evaporation of solvent, **8** was left as light yellow oil (15 mg), (Found: C, 75.82; H, 6.62%). UV: 280 and 319; IR: 3390, 3340, 1642, 1615, 1590, 1570, 1175, 1160, 1128, 1120, and 880; ^{1}H NMR ($CDCl_3$): δ 12.6(1H, s, OH), 8.9(1H, s, OH), 7.3—7.6(5H, m), 6.45 (1H, d, J=8 Hz, proton at C-4), 5.45(1H, d, J=8 Hz, proton at C-3), 5.0—5.21(1H, t, J=7 Hz, –CH_2–C<u>H</u>=), 3.31(2H, d, J=7 Hz, –C<u>H</u>$_2$–CH=), 1.77, 1.25(6H, s each, $(CH_3)_2$×2).

Cyclization of 3. Compound **3** (50 mg, 0.14 mmol) was dissolved in chloroform (5 ml) and trifluoroacetic acid (0.5 ml) was added to it and left overnight. Solvent evaporated and the residue dissolved in benzene (25 ml) and filtered through a small column of silica gel. On evaporation of solvent, **6** was obtained as white crystals (30 mg).

Methylation of 6. The mixture of **6** (20 mg, 0.06 mmol), dimethyl sulfate (0.1 ml) and potassium carbonate (50 mg) was refluxed in acetone (5 ml) for 10 h. On working up in the usual manner, **7** was obtained as white solid which crystallized from hexane as white crystals (15 mg), mp 144 °C (lit,[1] mp 145—146 °C). ^{1}H NMR (CCl_4): δ 7.55—7.72 (2H, m, phenyl ring protons), 7.14—7.38 (3H, m, phenyl ring protons), 3.52(3H, s, OCH_3), 2.56, 2.42(2H, t each, J=7 Hz, C<u>H</u>$_2$–CH_2×2), 1.65, 1.56(2H, t each, J=7 Hz, –CH_2–C<u>H</u>$_2$×2), 1.26, 0.96(6H, s each, $(CH_3)_2$×2).

Reaction of 2 with 2-Methyl-3-buten-2-ol. Compound **2** (800 mg, 3.3 mmol) was treated with 2-methyl-3-buten-2-ol (0.5 ml) in the presence of $(C_2H_5)_2O\cdot BF_3$ (0.2 ml) as mentioned in case of **1**. On working up a brown oil (750 mg) was obtained, which was chromatographed on silica gel. On elution with light petroleum, two main fractions were separated and were characterized to be **12** and **3** respectively.

One of the authors (VPP) is grateful to the CSIR (New Delhi) for the award of Senior Research Fellowship.

References

1) G. D. Monache, J. G. Gonzalez, F. D. Monache, and G. B. M. Bettolo, *Phytochemistry*, **19**, 2025 (1980).
2) P. J. Cotterill and F. Scheinmann, *J. Chem. Soc., Perkin Trans. 1*, **1980**, 2353.
3) R. A. Eade and H. P. Pham, *Aust. J. Chem.*, **32**, 2483 (1979).
4) F. E. King, T. J. King, and L. C. Manning, *J. Chem. Soc.*, **1957**, 563.
5) V. P. Pathak and R. N. Khanna, *Indian J. Chem.*, under publication.
6) D. Roy and R. N. Khanna, *Indian J. Chem.*, **19B**, 583 (1980).

 © 1982 The Chemical Society of Japan Bull. Chem. Soc. Jpn., 55, 2267—2270 (1982)

Studies on 2-Methyl- and 2-Phenyl-4-arylmethylene-2-imidazolin-5-ones and Related Compounds

Mahmoud Zarif Badr, Hassan Ahmed Hassan El-Sherief,* and Magda Ebeid Tadros

Chemistry Department, Faculty of Science, Assiut University, Assiut, Egypt

(Received October 28, 1981)

Compounds 4-arylmethylene-2-methyl-2-oxazolin-5-ones and 4-arylmethylene-2-styryl-2-oxazolin-5-ones react with primary aromatic amines in the presence of anhydrous zinc chloride to give the corresponding 4-arylmethylene-2-methyl-2-imidazolin-5-ones and 4-arylmethylene-2-styryl-2-imidazolin-5-ones (**5**) respectively. Treatment of **5** with phosphorus pentasulfide gives the corresponding 2-imidazoline-5-thiones. Reaction of 4-arylmethylene-2-phenyl-2-oxazolin-5-ones with hydroxylamine hydrochloride gives the corresponding imidazolinones which was reacted with alkyl halides and acid chlorides to give the corresponding ethers and esters respectively. Structures of the resulting products have been characterized on the basis of elemental analysis, IR, and UV data.

It has been reported[1] that 4-benzylidene-2-methyl-2-oxazolin-5-one reacts with aniline to give 4-benzylidene-1-phenyl-2-methyl-2-imidazol-in-5-one. Recently,[2] under the influence of acetic acid and sodium acetate, 4-arylmethylene-2-phenyl-2-oxazolin-5-ones and primary amines have been reported to yield directly the corresponding imidazolin-5-ones.

The present investigation is mainly concerned with the study of the reaction of 4-arylmethylene-2-methyl-2-oxazlin-5-ones (**1**) and 4-arylmethylene-2-styryl-2-oxazolin-5-ones (**2**) with primary amines, under different conditions, and the study of their behavior with 4-arylmethylene-2-phenyl-2-oxazolin-5-ones (**7**).

1a and **1b** react with aniline in acetic acid and sodium acetate to give *N*-phenyl-2-acetamido-3-arylacrylamides (**3**), instead of the expected 2-imidazolin-5-ones. This can be explained by the fact that the stabilization of the imidazolinone ring by the 2-phenyl group is higher than by the 2-methyl group because the former has three double bonds in conjugation with the ring system than the later. However, when the reaction was carried out in the presence of anhydrous zinc chloride, the corresponding 4-arylmethylene-2-methyl-2-imidazolin-5-ones (**4a—h**) were obtained.

On the other hand, it was previously mentioned[3] that **2a** reacted with primary amines in a benzene solution to give the corresponding α-cinnamido-*N*-substituted cinnamamide. However, when the reaction was carried out in the presence of anhydrous zinc chloride or in acetic acid with sodium acetate gave the corresponding 4-arylmethylene-2-styryl-2-imidazolin-5-ones (**5a—n**). Also, **5a**, **5e**, **5f**, **5h**, **5l**, and **5n** were obtained either by refluxing a mixture of **1a** and **1b** with appropriate amine and aldehyde in acetic acid and sodium acetate or by heating a mixture of **4** and aldehyde in the presence of anhydrous zinc chloride.

Consequently, it can be suggested that transformation of **1** to **5** in acetic acid and sodium acetate must go through an intermediate (**2**) which simultaneously reacted with amines, under reaction condition used to the final products (**5**) according to Scheme 1.

The identity of the imidazolinones (**5**) obtained by any one of these methods was established by TLC (using a benzene–ethanol mixture in the ratio 19:1 respectively) and mixed melting-point determination.

The IR spectra of **2** showed a carbonyl frequency at 1800—1790 cm^{-1} and an unresolved band at 1640—1620 cm^{-1} (due to the C=N and CH=CH). The structural assignment for the products (**4** and **5**) was supported by the IR and UV spectra. The IR spectra of **4** and **5** showed a stretching frequency at 1715—1700 cm^{-1} characteristic of the C=O group and the other band at 1630—1620 cm^{-1} attributed to the C=N stretch in compound **4**, in addition to the unresolved band in compound **5** at 1650—1630 cm^{-1} (due to C=N and CH=CH).

The UV absorption spectra of **4** are characterized by a principal absorption band at 352—378 cm^{-1}, which assigned to n-π^* transition of the carbonyl group perturbed by intramolecular charge transfers from arylmethylene residue to the polarized carbonyl group. This was confirmed through the pronounced red shift to 378 nm observed in **4f** and **4h** which can be attributed to the donating character of the methoxyl group in the arylmethylene residue. The data obtained for **4** showed a hypsochromic shift of about 20—25 nm in comparison with 4-arylmethylene-2-phenyl-2-imidazolin-5-ones.[4]

The UV spectra of **5** were similar to those of **4** and exhibited a principal absorption band at 410—432 nm. The data obtained for **5** showed a bathochromic shift of about 55—60 nm and 30—40 nm when compared with that of **4** and 4-arylmethylene-2-phenyl-2-imidazolin-5-ones respectively.[4]

Treatment of **5a**, **5e**, **5h**, **5i**, and **5j** with phosphorus pentasulfide in dry pyridine produced the corresponding 4-arylmethylene-2-styryl-2-imidazoline-5-thione (**6a**, **6e**, **6h**, **6i**, and **6j**).

The IR spectra of **6** showed absorption bands within the range 1270—1258 cm^{-1} and 1660—1640 cm^{-1} which are characteristic for C=S and -C=N- groupings respectively. The UV spectra of **6a** and **6h** are characterized by two or three absorption bands. The far-UV band is located at longer wavelength than the corresponding one in **5**. This behavior is understandable in view of the higher energy level of the nonbounding electrons in sulfur as compared to the oxygen atom.[5]

Furthermore, the authors have also investigated the hitherto unknown reaction of 4-arylmethylene-2-phenyl-2-oxazolin-5-ones (**7a—c**) and hydroxylamine hydrochloride. Compounds **7a—c** react with hydroxyl-

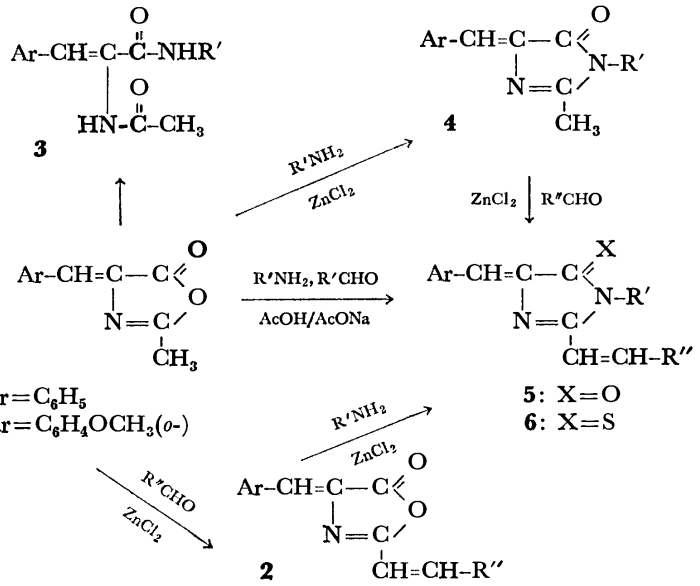

Ar = C_6H_5	R″
2a:	C_6H_5
b:	$C_6H_4N(CH_3)_2$-*p*
c:	C_6H_4Br-*p*
d:	$C_6H_4NO_2$-*p*

e: Ar = $C_6H_4OCH_3$-*o*, R″ = C_6H_5

3a: Ar = R′ = C_6H_5
b: Ar = $C_6H_4OCH_3$-*o*, R′ = C_6H_5

Ar = C_6H_5	R′	R″
5a:	C_6H_5	C_6H_5
b:	$C_6H_4CH_3$-*m*	C_6H_5
c:	$C_6H_4OCH_3$-*p*	C_6H_5
d:	C_6H_4OH-*p*	C_6H_5
e:	C_6H_5	$C_6H_4N(CH_3)_2$-*p*
f:	C_6H_5	$C_6H_4OCH_3$-*o*
g:	C_6H_5	$C_6H_4OCH_3$-*p*

Ar = C_6H_5	R′
4a:	C_6H_5
b:	$C_6H_4CH_3$-*o*
c:	$C_6H_4OCH_3$-*o*
d:	$C_6H_4OCH_3$-*p*

Ar = $C_6H_4OCH_3$-*o*	R′
4e:	$C_6H_4CH_3$-*o*
f:	$C_6H_4CH_3$-*p*
g:	$C_6H_4OCH_3$-*p*
h:	C_6H_4OH-*p*

Ar = $C_6H_4OCH_3$-*o*	R′	R″
5h:	C_6H_5	C_6H_5
i:	C_6H_4OH-*p*	C_6H_5
j:	$C_6H_4OCH_3$-*p*	C_6H_5
k:	$C_6H_4NO_2$-*o*	C_6H_5
l:	C_6H_5	$C_6H_4OCH_3$-*p*
m:	C_6H_5	C_6H_4OH-*p*
n:	C_6H_5	$C_6H_4OCH_3$-*o*

Scheme 1.

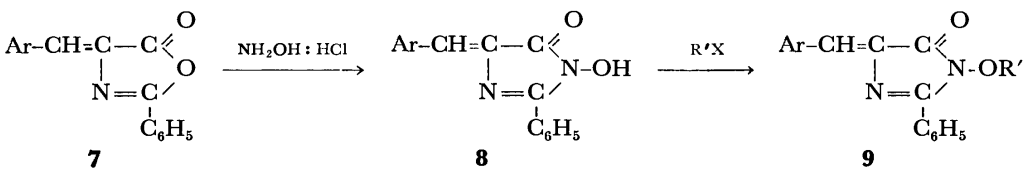

	Ar
7a:	C_6H_5
b:	$C_6H_4OCH_3$-*p*
c:	$C_6H_4OCH_3$-*o*

Ar = C_6H_5	R′
9a:	CH_3
b:	$CH_2C_6H_4NO_2$-*p*
c:	COC_6H_5
d:	$SO_2C_6H_4CH_3$-*p*

	Ar
8a:	C_6H_5
b:	$C_6H_4OCH_3$-*p*
c:	$C_6H_4OCH_3$-*o*

Ar = $C_6H_4OCH_3$-*p*	R′
9e:	CH_3
f:	C_2H_5
g:	$COCH_2C_6H_5$
h:	$SO_2C_6H_5$
i:	$SO_2C_6H_4CH_3$-*p*
j:	$COCH_3$

Ar = $C_6H_4OCH_3$-*o*	R′
9k:	CH_3
l:	C_2H_5
m:	$CH_2C_6H_5$
n:	$COCH_3$
o:	$SO_2C_6H_4CH_3$-*p*

Scheme 2.

amine hydrochloride in a methanol solution in the presence of sodium acetate to give 4-arylmethylene-2-phenyl-1-hydroxy-2-imidazolin-5-ones (**8a**—**c**) respectively.

The IR absorption spectra of the newly synthesized compounds showed absorption bands at 1710—1700 cm^{-1} and 3340—3330 cm^{-1}, which were assigned to the C=O and -OH stretching frequencies respectively, in addition to the -C=N- stretch appeared at 1640—1630 cm^{-1}. The ^1H NMR spectrum of **8c** in trifluoroacetic acid showed signals at 7.8 (S, 1H, -CH=C-), 7.4 (m, 5H, C=N-C_6H_5); 6.82 (m, 4H, C=C-C_6H_4) and 3.8 (S, 3H, -OCH_3) which are in good agreement with its structure.

Reaction of **8a**—**c** with alkyl halides, acid chlorides and sulfonyl chlorides in dry acetone in the presence of anhydrous potassium carbonate gave the corresponding ethers (**9a**, **9b**, **9e**, **9f**, **9m**, **9k**, and **9l**), esters (**9c**, **9g**, **9j**, and **9n**), and sulfonic esters (**9d**, **9h**, **9l**, and **9o**) respectively.

The IR spectra of compounds **9a**—**9o** showed an absorption band at 1715—1700 cm^{-1} attributed to the C-O group and another carbonyl, the ester group in compounds **9c**, **9g**, **9j**, and **9n** appeared at 1780—1770 cm^{-1}. The UV spectra of **8** and **9** were similar to those of 4-arylmethylene-2-phenyl-2-imidazolin-5-ones[4] and exhibited a principal absorption band at 385—406 nm.

The ^1H NMR spectrum of **9k** in trifluoroacetic acid showed signals at 7.8 (S, 1H, CH=C-), 7.44 (m, 5H, C=N-C_6H_5), 6.82 (m, 4H, C=C-C_6H_4) and 3.8 (S, 6H, C_6H_4-OCH_3 and N-OCH_3), which is in agreement with its structure.

Biological Screening Results. Compounds of the type **8a**—**c** and **9h**, **9k**, **9o** were tested *in vitro* for their biological activities on some microbes *viz. Bacillus megaterium* and *Staphylococcus albus* and fungi as *Aspergillus fumigatus* and *Penicillium nigricans*. The more active compounds against *Bacillus megaterium* was **9o**, against *Staphylococcus albus* were **8b** and **9o**; against *Aspergillus fumigatus* were **8a**, **9h**, **9k** and against *Penicillium nigricans* was **9k**.

4-Arylmethylene-2-styryl-2-oxazolin-5-ones (**2**)

Compd No.	Mp θ_m/°C	Formula	Calcd (Found) (%) C	H	N
2a	135[a]	$C_{18}H_{13}NO_2$	78.54 (78.08)	4.72 (4.39)	5.09 (5.00)
2b	210	$C_{20}H_{18}N_2O_2$	75.47 (75.38)	5.66 (5.42)	8.80 (8.68)
2c	130	$C_{18}H_{12}NO_2Br$	61.01 (60.80)	3.38 (3.19)	3.95 (3.72)
2d	230	$C_{18}H_{12}N_2O_4$	67.50 (67.27)	3.75 (3.40)	8.75 (8.38)
2e	140	$C_{19}H_{15}NO_3$	74.75 (74.63)	4.91 (4.68)	4.59 (4.26)

a) Lit, mp 135 °C[3]

N-Phenyl-2-acetamido-β-arylacrylamide (**3**)

Compd No.	Mp θ_m/°C	Formula	Calcd (Found) (%) C	H	N
3a	197	$C_{17}H_{16}N_2O_2$	72.85 (72.47)	5.71 (5.35)	10.00 (9.66)
3b	220	$C_{18}H_{18}N_2O_3$	69.67 (69.66)	5.80 (5.46)	9.03 (9.33)

4-Arylmethylene-2-methyl-2-imidazolin-5-ones (**4**)

Compd No.	Mp θ_m/°C	Formula	Calcd (Found) (%) C	H	N	R_f	λ_{max}/nm (ε_{max})
4a	143[a]	$C_{17}H_{14}N_2O$	77.86 (77.89)	5.34 (5.13)	10.68 (10.39)	0.25	358 (7800)
4b	135	$C_{18}H_{16}N_2O$	78.26 (78.18)	5.79 (5.48)	10.14 (10.02)	0.85	—
4c	160	$C_{18}H_{16}N_2O_2$	73.97 (73.62)	5.47 (5.23)	9.58 (9.36)	0.29	—
4d	150	$C_{18}H_{16}N_2O_2$	73.97 (73.72)	5.47 (5.28)	9.58 (9.32)	0.64	358 (8600)
4e	160	$C_{19}H_{18}N_2O_2$	74.50 (74.30)	5.88 (5.66)	9.15 (9.01)	0.80	—
4f	145	$C_{19}H_{18}N_2O_2$	74.50 (74.13)	5.88 (5.52)	9.50 (9.08)	0.81	378 (9200)
4g	182	$C_{19}H_{18}N_2O_3$	70.80 (70.61)	5.59 (5.30)	8.69 (8.31)	0.63	—
4h	220	$C_{18}H_{15}N_2O_3$	70.35 (70.06)	4.88 (4.76)	9.12 (9.10)	0.68	378 (8800)

a) Lit, mp 144 °C.[1]

Experimental

Melting points are uncorrected. IR spectra in KBr were recorded on a Perkin-Elmer infracord spectrophotometer. UV spectra were taken in ethanol on a Pye-Unicam SP 8000 spectrophotometer and ^1H NMR spectra were recorded on a Varian 60 MHz NMR instrument using TMS at the internal standard.

4-Arylmethylene-2-styryl-2-oxazolin-5-ones (2). A mixture of **1** (0.01 mol), appropriate aldehyde (0.012 mol) and anhydrous zinc chloride (0.001 mol) was fused together for 5 min. The cooled reaction mixture gave a yellow precipitate on adding ethanol, which recrystallized from the same solvent. The yield was about 80—85%.

N-Phenyl-2-acetamido-β-arylacrylamide (3). A mixture of **1** (0.01 mol), aniline (0.012 mol) and anhydrous sodium acetate (0.005 mol) in acetic acid (20 ml) was refluxed was refluxed for 3 h. The cooled reaction mixture was filtered off, then recrystallized from ethanol. The yield was about 85%.

4-Arylmethylene-2-methyl-2-imidazolin-5-ones (4). A mixture of **1** (0.01 mol), primary aromatic amine (0.012 mol) and anhydrous zinc chloride (0.001 mol) was fused together for 5 min. The yellow product was collected and crystallized from methanol. The yield was about 55—65%.

4-Arylmethylene-2-styryl-2-imidazolin-5-ones (5). A mixture of **1** (0.01 mol), appropriate aromatic amine (0.012 mol) and aromatic aldehyde (0.012 mol) in acetic acid (20 ml) containing freshly fused sodium acetate (0.005 mol) was refluxed for 3 h, the reaction mixture was cooled, then poured into water. The crude product was collected and crystallized from ethanol. The yield was about 70—75%.

The same products were obtained from **2** and the corresponding aromatic amine when the reaction was carried out either in the presence of anhydrous zinc chloride or in acetic acid solution containing freshly fused sodium acetate as describe above.

4-Arylmethylene-2-styryl-2-imidazoline-5-thiones (6). A mixture of **5a**, **5b**, **5h**, **5i**, and **5j** (0.003 mol) and phosphorus pentasulfide (0.0035 mol) was refluxed in anhydrous pyridine (25 ml) for 7 h. The solvent was evaporated under reduced pressure and the residue was treated with dilute acetic acid.

The product was filtered and crystallized from ethanol as reddish-brown crystals, yield about 55%.

4-Arylmethylene-2-styryl-2-imidazolin-5-ones (**5**)

Compd No.	Mp θ_m/°C	Formula	Calcd (Found) (%) C	H	N	R_f	λ_{max}/nm (ε_{max})
9a	105	$C_{17}H_{14}O_2N_2$	73.38 (73.16)	5.03 (4.86)	10.07 (10.02)	0.24	382 (14000)
9b	160	$C_{23}H_{17}O_4N_3$	69.17 (69.03)	4.26 (4.20)	10.52 (10.31)	0.82	—
9c	150	$C_{23}H_{16}O_3N_2$	75.00 (74.53)	4.34 (4.18)	7.60 (7.42)	0.93	—
9d	135	$C_{23}H_{18}O_4N_2S$	66.02 (65.79)	4.30 (4.02)	6.67 (6.42)	0.27	—
9e	130	$C_{18}H_{16}O_3N_2$	70.12 (69.93)	5.19 (5.03)	9.09 (9.06)	0.79	—
9f	136	$C_{19}H_{18}O_3N_2$	70.80 (70.63)	5.59 (5.32)	8.69 (8.43)	0.40	—
9g	145	$C_{25}H_{20}O_4N_2$	72.81 (72.60)	4.85 (4.65)	6.79 (6.69)	0.87	402 (15000)
9h	205	$C_{23}H_{18}O_5N_2S$	63.59 (63.38)	4.14 (4.02)	6.45 (6.13)	0.30	—
9i	150	$C_{24}H_{20}O_5N_2S$	64.28 (64.13)	4.46 (4.24)	6.25 (6.03)	0.25	—
9j	155	$C_{19}H_{16}O_4N_2$	67.85 (67.53)	4.76 (4.38)	8.33 (8.31)	0.96[a]	
9k	175	$C_{18}H_{16}O_3N_2$	70.12 (70.00)	5.19 (5.03)	9.09 (9.11)	0.83	—
9l	135	$C_{19}H_{18}O_3N_2$	70.80 (70.48)	5.59 (5.23)	8.69 (8.36)	0.50	406 (18000)
9m	145	$C_{24}H_{20}O_3N_2$	75.00 (74.81)	5.20 (5.04)	7.29 (7.08)	0.91	
9n	195	$C_{19}H_{16}O_4N_2$	67.85 (67.63)	4.76 (4.43)	8.33 (8.13)	0.63	—
9o	130	$C_{24}H_{20}O_5N_2S$	64.28 (64.20)	4.46 (4.12)	6.25 (6.13)	0.17	—

a) Using a benzene ethyl acetate mixture in the ratio 9 : 1 respectively.

4-Arylmethylene-2-styryl-2-imidazoline-5-thiones (**6**)

Compd No.	Mp θ_m/°C	Formula	Calcd (Found) (%) C	H	N	S	λ_{max}/nm (ε_{max})
6a	280	$C_{24}H_{18}N_2S$	78.68 (78.40)	4.91 (4.52)	7.65 (7.43)	8.74 (8.81)	442 (24000)
6e	260	$C_{26}H_{23}N_3S$	76.28 (76.07)	5.62 (5.31)	10.26 (10.13)	7.82 (7.46)	—
6h	240	$C_{25}H_{20}N_2OS$	75.75 (75.26)	5.05 (5.06)	7.07 (7.00)	8.08 (8.31)	463 (1500)
6i	210	$C_{25}H_{20}N_2O_2S$	72.81 (72.60)	4.85 (4.62)	6.79 (6.63)	7.76 (7.34)	—
6j	260—62	$C_{26}H_{22}N_2OS$	76.09 (76.30)	5.36 (5.12)	6.82 (6.75)	7.80 (7.63)	—

4-Arylmethylene-2-phenyl-1-hydroxy-2-imidazolin-5-ones (**8**)

Compd No.	Mp θ_m/°C	Formula	Calcd (Found) (%) C	H	N	R_f	λ_{max}/nm (ε_{max})
8a	235	$C_{16}H_{12}O_2N_2$	72.72 (72.38)	4.54 (4.32)	10.60 (10.38)	0.60	382 (12000)
8b	245	$C_{17}H_{14}O_3N_2$	69.38 (69.08)	4.76 (4.36)	9.52 (9.46)	0.70	406 (17800)
8c	220	$C_{17}H_{14}O_3N_2$	69.38 (69.32)	4.76 (4.39)	9.52 (9.32)	0.90	406 (18000)

4-Arylmethylene-2-phenyl-1-hydroxy-2-imidazolin-5-ones (8). A mixture of **7** (0.03 mol) and hydroxylamine hydrochloride (0.04 mol) in methanol (30 ml) containing sodium acetate (0.04 mol) was refluxed on a water bath for 6 h. The reaction mixture was cooled and the yellow precipitate was collected, washed with water and recrystallized from ethanol, yield 60%.

Reaction of 8 with Alkyl Halides and Acid Chlorides. A mixture of **8** (0.001 mol) and appropriate alkyl halide or acid chloride (0.0012 mol) in acetone (30 ml) in the presence of anhydrous potassium carbonate (0.01 mol) was refluxed for 2 h. The solvent was filtered and evaporated. The crude product obtained was crystallized from ethanol to give **9** yield about 70%.

Ethers and esters of 4-arylmethylene-2-phenyl-1-hydroxy-2-imidazolin-5-ones (**9**)

Compd No.	Mp θ_m/°C	Formula	Calcd (Found) (%) C	H	N	R_f	λ_{max}/nm (ε_{max})
5a	238	$C_{24}H_{18}N_2O$	82.28 (82.06)	5.14 (5.02)	8.00 (7.81)	0.93	410 (13000)
5b	205	$C_{25}H_{20}N_2O$	82.41 (82.92)	5.49 (5.32)	7.69 (7.52)	0.90	—
5c	190	$C_{25}H_{20}N_2O_2$	78.94 (78.61)	5.26 (5.00)	7.36 (7.12)	0.74	410 (13300)
5d	275	$C_{24}H_{18}N_2O_2$	78.68 (78.51)	4.91 (4.62)	7.65 (7.41)	0.27	—
5e	130	$C_{26}H_{23}N_3O$	79.38 (79.21)	5.85 (5.64)	10.68 (10.43)	0.92	—
5f	129	$C_{25}H_{20}N_2O_2$	78.94 (78.71)	5.26 (5.13)	7.36 (7.14)	0.80	—
5g	190	$C_{25}H_{20}N_2O_2$	78.94 (78.70)	5.26 (5.03)	7.36 (7.12)	0.87	—
5h	185	$C_{25}H_{20}N_2O_2$	78.94 (78.71)	5.26 (5.04)	7.36 (7.17)	0.86	432 (21000)
5i	240	$C_{25}H_{20}N_2O_3$	75.75 (75.41)	5.05 (5.00)	7.07 (7.01)	0.46	—
5j	136	$C_{26}H_{22}N_2O_3$	76.09 (76.01)	5.36 (5.24)	6.82 (6.61)	0.17	—
5k	215	$C_{25}H_{20}N_3O_4$	70.42 (70.31)	4.69 (4.31)	9.85 (9.51)	0.66	—
5l	180	$C_{26}H_{22}N_2O_3$	76.09 (76.01)	5.36 (5.07)	6.82 (6.59)	0.18	432 (14000)
5m	250	$C_{25}H_{20}N_2O_3$	75.75 (75.64)	5.05 (5.31)	7.07 (7.03)	0.67	—
5n	175	$C_{26}H_{22}N_2O_3$	76.09 (76.01)	5.36 (5.23)	6.82 (6.68)	0.79	432 (24000)

References

1) R. Pfleger and G. Market, *Chem. Ber.*, **90**, 1494 (1957); *Chem. Abstr.*, **54**, 8788 (1960).

2) A. M. Islam, A. M. Khalil, and I. I. Abd El-Gawad, *Aust. J. Chem.*, **26**, 827 (1973).

3) A. F. Fahmy and M. O. Orabi, *Indian J. Chem.*, **10**, 961 (1972).

4) M. Z. Badr, H. A. H. El-Sherief, and M. E. Tadros, *Indian J. Chem.*, **18B**, 240 (1979).

5) R. M. Silverstein and C. C. Bassler, "Spectrometric Identification of Organic Compounds," 2nd ed, Wiley, New York (1967).

© 1982 The Chemical Society of Japan

NOTES

Bull. Chem. Soc. Jpn., 55, 2271—2272 (1982)

Translational Energy Distribution of the Excited Hydrogen Atom (n=3) Obtained by Controlled Electron Impact on CH_4

Teiichiro OGAWA* and Junichi KURAWAKI

Department of Molecular Science and Technology, Kyushu University, Kasuga, Fukuoka 816

(Received November 5, 1981)

Synopsis. Dissociative excitation of CH_4 has been investigated through the analysis of the high resolution spectra of the Balmer-α line. Translational energy distribution of H*(n=3) obtained in e-CH_4 collisions has three distinct components and another indefinite component; their peaks lie at 3, 0—1 and 4, and 8—12 eV, respectively.

Translational energy distribution of a fragment produced in a collision process gives valuable information for the detailed analysis of the mechanism of dissociative excitation of the molecule. Translational energy distributions of ionic and metastable fragments have been obtained by mass-spectroscopic or time-of-flight techniques, whereas those of excited short-lived fragments have recently become possible by an analysis of the Doppler profiles of their emission spectra.[1]

We have recently reported the translational energy distribution of H*(n=4) from methane obtained in e-CH_4 collisions and their assignments together with discussion on the mechanism of dissociative excitation of methane.[2] The results on H*(n=3) will be described in this note.

Experimental

The apparatus consists of an electron-molecule collision chamber, a Fabry-Perot interferometer and a data acquisition system. The details were reported previously.[3]

Results and Discussion

Since the line shape of the Balmer line obtained in an electron-molecule collision process is determined by the Doppler effect, analysis of the line shape should clarify the kinetic behavior of the excited hydrogen atom produced. The high resolution spectra of the Balmer-α lines have been taken with the use of an interferometer. Typical results of H*(n=3) from CH_4 are shown in Fig. 1.

For a successful analysis of the line shape, it has to be determined without distortion due to such as insufficient resolution of the optical system or the effect of anisotropy.[3] The optical resolution used here was 0.029—0.032 Å, and distortion from this source should be negligible. The line shapes were measured from 55° and 90° with respect to the electron-beam. Since the line shapes show no obvious difference for the two angles (Fig. 1), the effect of anisotropy should be smaller than the experimental uncertainty. Thus, we assume that the effect of anisotropy is negligibly small for the analysis of the translational energy distribution.

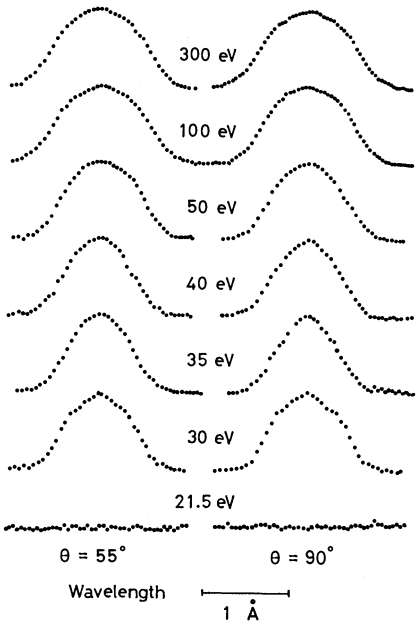

Fig. 1. High resolution spectra of Balmer-α line produced by controlled electron impact on CH_4. Electron energy: 21.5—300 eV, electron energy resolution: 1—2 eV, spectral resolution: 0.029—0.032 Å.

Ito *et al.* measured the Doppler profiles of the Balmer-α emission from methane with an etalon grating monochromator.[4] The observed linewidths of their measurement and of ours agree well within experimental uncertainties. They obtained the average translational energy from the halfwidth; however, the translational energy distribution calculated in this note contains more abundant and detailed information for the excitation process.

The differentiation of the line shape gives the translational energy distribution of the excited hydrogen atom;[3] the results are shown in Fig. 2. At an electron energy of 30 eV, the distribution has a peak at about 3 eV. As the electron energy increases, there appears a component with a peak at 0—1 eV. At higher electron energies, there is an intense peak at about 4 eV, and there seems to be another component in the 8—12 eV region. Thus, the translational energy distribution of H*(n=3) from methane has three distinct components and one indefinite component.

The translational energy distribution of H*(n=3) looks similar with those of H*(n=4),[2] H(HR),[5,6] and H^+.[7,8] Thus, the dissociative excitation of the short-lived and long-lived excited atoms and dissociative ionization proceed in similar processes. This finding is consistent with the core-ion model,[6] and justifies an

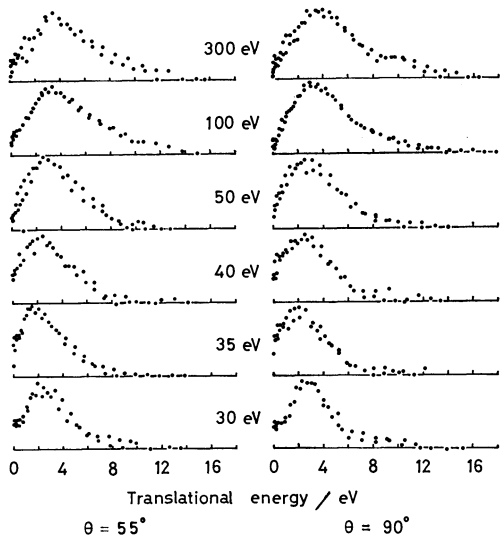

Fig. 2. Translational energy distribution of H*(n=3) produced by controlled electron impact on CH_4. Electron energy: 21.5—300 eV.

extension of this model to the formation of a low Rydberg atom.[2,4] Accordingly, we can conclude that the dissociative excitation of H*(n=3) proceeds through potential energy surfaces almost parallel to and reasonably close to that of the excited molecular ion core.

The component with the peak at 3 eV corresponds to component 1 of H*(n=4),[2] and the threshold of this component will be at about 21 eV. Thus, we can conclude that the formation of this component proceeds through excitation to Rydberg states converging to the $\tilde{A}^2A_1$ state of CH_4. The other components may be produced in a dissociative excitation through doubly excited Rydberg states converging to some excited ionic states or to some doubly ionized states.

The electron impact method has an distinct advantage for the investigation of molecular dissociation process, since optically-forbidden doubly excited states play important roles.

The authors thank Morihide Higo for discussion and Professor Nobuhiko Ishibashi for encouragement. The present study was partially supported by a Grant-in-Aid for Special Project Research from the Ministry of Education, Science and Culture.

References

1) T. Ogawa and M. Higo, *Chem. Phys. Lett.*, **65**, 610 (1979).
2) T. Ogawa, J. Kurawaki, and M. Higo, *Chem. Phys.*, **61**, 181 (1981).
3) T. Ogawa and M. Higo, *Chem. Phys.*, **52**, 55 (1980).
4) K. Ito, N. Oda, Y. Hatano, and T. Tsuboi, *Chem. Phys.*, **21**, 203 (1977).
5) T. G. Finn, B. L. Carnahan, W. C. Wells, and E. C. Zipf, *J. Chem. Phys.*, **63**, 1596 (1975).
6) J. A. Schiavone, D. E. Donohue, and R. S. Freund, *J. Chem. Phys.*, **67**, 759 (1977).
7) J. Appell and C. Kubach, *Chem. Phys. Lett.*, **11**, 486 (1971).
8) R. Locht, J. L. Olivier, and J. Momigny, *Chem. Phys.*, **43**, 425 (1979); **49**, 173 (1980).

Efficiency of Noble Metal Electrodes for Zirconia Oxygen Sensors in Detecting Oxygen at Lower Temperatures

Tsuyoshi ARAKAWA,* Akira SAITO, and Jiro SHIOKAWA
Department of Applied Chemistry, Faculty of Engineering, Osaka University, Yamadakami, Suita, Osaka 565
(Received July 16, 1981)

Synopsis. Metal Au, Ag, or Pt was deposited as electrode on the closed end of a stabilized electrolyte tube in the ZrO_2 oxygen sensor, and emf of the cell, $O_2|m|ZrO_2$–$Y_2O_3|m|O_2'$ (m=Au, Ag, Pt) with P_{O_2}=8.8 and $P_{O_2'}$= 159 Torr (1 Torr=133.322 Pa), was measured as a function of temperature between 150 and 950 °C. For cells with Ag electrodes, a good agreement is found between theoretical and measured emf's at lower temperatures (*ca.* 340 °C).

Solid oxide electrolytes are in use for construction of oxygen sensors, high temperature fuel cells, and oxygen pumps.[1-3] However, for their practical use, for example, electrodes in the system of $O_2|$stabilized zirconia$|O_2'$ play an important part. In this connection, a number of studies have been made of the use of Pt electrodes on stabilized electrolyte,[4] but no reports have been published of the other noble metal electrodes. The object of the present work is to investigate the efficiency of noble metal electrodes for stabilized zirconia oxygen sensors in detecting oxygen at lower temperatures.

Experimental

The solid electrolytes used were impervious ZrO_2–Y_2O_3 (8 mol%), ZrO_2–CaO(11 mol%), and ZrO_2–MgO(15 mol%) tubes closed at one end. The electrolyte tube had an i.d. of 11 mm, an o.d. of 15 mm, and a length of 300 mm. Each noble metal was first deposited on both the inside and outside surfaces near the closed end of the electrolyte tube. One Pt electrode was prepared by applying a nonfluxed platinum paste consisting of submicron platinum powder suspended in a 5:1 mixture of ethanol and surface active agent. This was heated to 800 °C for 30 min in air and then 1200 °C for 1 h in an atmosphere of hydrogen. One Au electrode was prepared by brushing a nonfluxed gold paste onto the surface of the electrolyte, and then firing at 600 °C for 2 h in an atmosphere of hydrogen. Three Ag electrodes were prepared in three ways: (i) Silver paste was applied on the surface of the electrolyte and fired at 600 °C for 2 h in a stream of hydrogen. (ii) When a formaldehyde solution was added dropwise to a 20% silver nitrate solution to which an excess ammonia solution had been added, silver was deposited on the faces of stabilized zirconia. This procedure was repeated twice or three times. The faces were washed with distilled water, dried at 100 °C and then heated at 600 °C for 2 h in a stream of hydrogen. (iii) A thin film on the surface of electrolyte was prepared by evaporation of silver metal and then heated at 600 °C for 2 h in an atmosphere of hydrogen. As illustrated in Fig. 1, the electrolyte tube was placed inside a quartz tube closed at one end. The electrolyte tube and the quartz tube were connected to the brass heads and the assembly was tightly closed by o-ring. Each of the inner and outer electrodes was linked by a Pt wire to the output terminal. A Pt *vs.* Pt/13% Rh thermocouple was used to measure temperatures. The outside of the electrolyte tube was kept in 159 Torr O_2 and the inside was allowed to contain 8.8

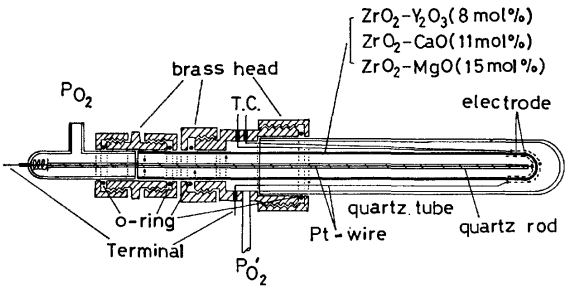

Fig. 1. Experimental cell assembly for evaluating the performance of the oxygen sensor.

Torr O_2. The effectiveness of these noble metal electrodes was determined by measuring the emf of the cell $O_2|m|Zr|m|O_2'$, where m is the metal electrode and Zr is the electrolyte as follows:

Cell number	Electrolyte (Zr)	Electrode (m)
1	ZrO_2–Y_2O_3	Pt
2	ZrO_2–Y_2O_3	Au
3	ZrO_2–Y_2O_3	Ag
4	ZrO_2–CaO	Ag
5	ZrO_2–MgO	Ag

In addition, the emf vs. relative oxygen-pressure ratio was determined by stepwise change of the inside oxygen partial pressure from 130 to 1 Torr, with the outside pressure kept 159 Torr. The emf was measured with a Takeda Riken electrometer. Measurements were carried out at 400—950 °C (Pt electrode) and 150—950 °C (Ag and Au electrodes).

Results and Discussion

In order to compare the abilities of the noble metal electrodes, each electrode prepared by applying the nonfluxed metal paste was tested, typical results being shown in Fig. 2. The solid line represents the theoretical emf as obtained from

$$E = \bar{t}_i \frac{RT}{4F} \ln \frac{P_{O_2'}}{P_{O_2}}, \quad (1)$$

where $\bar{t}_i$=1. All the noble metal electrodes, except the Au electrode (cell 2), were reversible in the measured temperature range, but the Ag electrode was deteriorated at temperatures over *ca.* 960 °C. With the cell $m|ZrO_2$–$Y_2O_3|m$, measurement of emf for the Ag electrode (cell 3) was possible from about 250 °C and a good agreement began around 340 °C to be found between the theoretical and measured emf's. Since the activity is in parallel with the temperature (T_g) at which the agreement between the theoretical and measured emf's begins, the sequence of activities for the noble metal electrodes is Ag>Au>Pt. Further, the emf-temperature curves for the other Ag electrodes

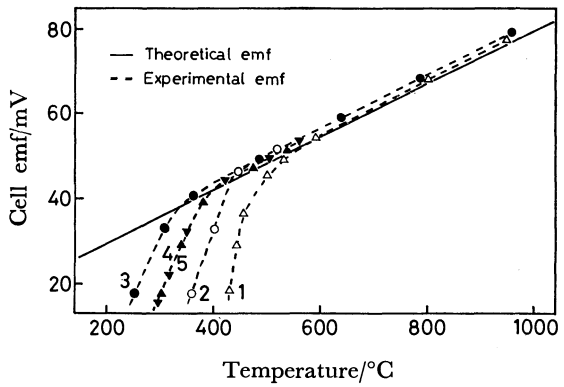

Fig. 2. Theoretical and experimental emf *vs.* temperature for the cell, where $P_{O_2}=8.8$ Torr and $P_{O_2'}=159$ Torr. The figures are cell number (see text).

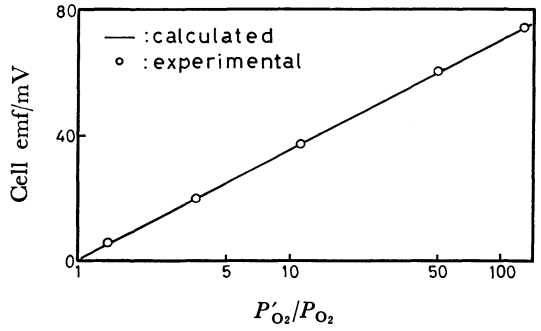

P'_{O_2}/P_{O_2}

Fig. 3. Dependence of emf on $P_{O_2}/P_{O_2'}$ for cell 4, $P_{O_2}|Ag|ZrO_2$–$Y_2O_3|Ag|P_{O_2'}$, where $P_{O_2'}=159$ Torr.

are similar to that for the Ag paste electrode, whereas for the other cells using Ag electrodes both cells 4 and 5 have T_g values slightly higher than that of cell 3. Thus it is concluded that electrodes greatly affect the detection of oxygen at lower temperatures and that the cells with Ag electrodes are better than those with the other electrodes.

In order to test the dependence of emf on $P_{O_2'}/P_{O_2}$, the emf of cell 3 was measured at 350 °C with P_{O_2} changed from 130 to 1 Torr. As shown in Fig. 3, the emf is proportional to $\ln P_{O_2'}/P_{O_2}$ and the slope is in good agreement with that calculated by using Eq. 1. Consequently, the cells with Ag electrodes may have the capability of detecting oxygen at lower temperatures, as described above.

Further, it is noted that for the cells with Ag or Pt (except Au) electrodes, T_g is close to the decomposition temperature, 300 or 560 °C, of the corresponding metal oxide Ag_2O or PtO, respectively.[5] In a potentiostatic experiment, Rickert and Steiner[6] found that for a cell $Fe(FeO)|electrolyte|Ag,O_2$ the oxygen moves from the silver electrode through the electrolyte to the opposite electrode, no product in the silver electrode being identified, whereas Belford and Alcock,[7] on the basis of findings obtained by using the galvanostatic technique, reported that, with respect to the diffusivity of oxygen through liquid tin, some evidence for limiting potential had been obtained at oxygen activities corresponding to those expected for unstable solid SnO. Thus it is concluded that cleavage of the metal-oxygen bond, which has been formed between the metal atom and the oxygen dissolved in the electrode, is an important process for the detection of oxygen at lower temperatures. Further physicochemical evidence shold be collected to support this result.

We thank the Ministry of Education of Japan for support of this work through a Grant-in-Aid for Scientific Research.

References

1) H. Yanagida, R. J. Brook, and F. A. Kröger, *J. Electrochem. Soc.*, **117**, 593 (1970).

2) T. H. Etsell and S. N. Flengas, *J. Electrochem. Soc.*, **118**, 1890 (1971).

3) D. Yuan and F. A. Kröger, *J. Electrochem. Soc.*, **116**, 594 (1969).

4) R. J. Brook, W. L. Pelzman, and F. A. Kröger, *J. Electrochem. Soc.*, **118**, 185 (1971).

5) "Selected Values of Chemical Thermodynamic Properties," Natl. Bur. Standards, Technical Note 270-4, U.S. Government Printing Office (1969).

6) H. Rickert and R. Steiner, *Z. Phys. Chem.*, **49**, 127 (1966).

7) T. N. Belford and C. B. Alcock, *Trans. Faraday Soc.*, **61**, 443 (1965).

Concentration Dependence of Ketone Hydrogenation Catalyzed by Ru, Pd, and Pt. Evidence for Weak Ketone Adsorption on Pd Surface

Choi Sungbom† and Kazunori Tanaka*

The Institute of Physical and Chemical Research, Wako, Saitama 351

(Received October 13, 1981)

Synopsis. As the ketone (cyclohexanone, 4-heptanone) concentration in cyclohexane was increased, the hydrogenation rate saturated even below 0.05 mol dm^{-3} on Ru and Pt, but at a much higher concentration of around 0.5 mol dm^{-3} on Pd. This result suggests that ketone adsorption on Pd is weak in comparison with other platinum group metals.

Although palladium is an excellent catalyst for olefin hydrogenation, its activity for ketone (aliphatic and alicyclic) hydrogenation is notoriously low.[1] Breither *et al.*[2] regarded this poor activity as due to the unusual strength of ketone adsorption on Pd. On the contrary, Nishimura *et al.*[3] suggested that the attractive interaction of carbonyl with Pd surface is rather weak compared with other platinum group metals. Preliminary experiments in our laboratory[4] support Nishimura's view. To obtain further evidence for this view, we have carefully studied the concentration dependencies of ketone hydrogenation on Pd, and also on Pt and Ru for comparison. The substrate ketones chosen were cyclohexanone and 4-heptanone.

Experimental

Apparatus. The gas chromatograph was a Shimadzu GC-3BT instrument equipped with a thermocouple detector and a 10%-diglycerol column (3 mm i.d. × 3 m, 60—80 mesh supported on C-22 SK). The stainless steel autoclave used for catalyst pretreatment had a capacity of 100 ml. The glass reaction vessel used for kinetic studies has been described before.[5]

Materials. All chemicals were obtained commercially, and used without further purification: cyclohexane (Wako, guaranteed, stated purity 99.99%), cyclohexanone (Wako, guaranteed, 99.93%), 4-heptanone (Tokyo Kasei, extra pure, 99.83%). H_2 (in cylinder). Catalysts (Ru/SiO_2, Pd/Al_2O_3, Pd/SiO_2, Pt/Al_2O_3, Pt/SiO_2) were in the form of cylindrical pellets (Nippon Engelhard, 0.5-wt% metal loaded, 3.9 mmϕ × 4.0 mm long for the SiO_2-supported, 3.2 mmϕ × 3.7 mm long for the Al_2O_3-supported).

Kinetic Procedure. All catalyst samples were subjected immediately before use to a standard hydrogen-pretreatment procedure as follows. A small glass test tube, after being loaded with an appropriate number (1—10) of catalyst pellets and 10 ml of cyclohexane, was placed in the autoclave. The autoclave was charged with hydrogen, heated to 80 °C, and kept at that temperature for 30 min without stirring. During this 30-min pretreatment no significant decrease in hydrogen pressure (*ca.* 80 atm, 1 atm = 101.325 kPa) was observed.

Immediately after pretreatment, while still hot, the catalyst pellets were taken out of the autoclave and transferred to the glass reaction vessel pre-charged with the 5-ml cyclohexane solution of cyclohexanone or 4-heptanone that had already been flushed with hydrogen. Care was taken to minimize the air exposure time for the catalyst. The reaction vessel was connected to a hydrogen reservoir, and flushed with hydrogen one more time. The hydrogenation was started by shaking the reaction vessel vigorously at 30 °C in hydrogen at atmospheric pressure. During reaction the reaction mixture was sampled (usually 5 μl) at intervals, and analyzed by gas chromatography using helium as the carrier gas. The column temperature was set to 115 °C for the cyclohexanone systems and to 80 °C for the 4-heptanone systems.

† On leave from Jilin University, Changchun, People's Republic of China.

Results

Preliminary. The hydrogenation rate (V) increased in proportion to the catalyst weight, suggesting that it is not controlled by hydrogen dissolution into the bulk solution. The observed V values were reproducible to within 5%.

In the hydrogenation of 4-heptanone, no product peaks other than the corresponding alcohol were observed by gas chromatography. Also for the cyclohexanone system, hydrogenation to the corresponding alcohol was clean on all of the catalysts but Pd/Al_2O_3. On Pd/Al_2O_3 an unidentified side-product peak (retention time 23.5 min against 6.5 min for cyclohexanol) was detected, but its amount was always 0.1% or less in comparison with cyclohexanol.

Concentration Dependence. Figure 1 shows typical reaction profiles observed in Pd- and Pt-catalyzed hydrogenation. At the initial period of reaction, the ketone concentration (C_K) decreases linearly with time on Pt although on Pd a brief induction period precedes the linear region. The higher the initial C_K, the shorter was this induction period, with its complete disappearance for the 1 mol/dm^3 C_K. The reaction profile for Ru resembled that for Pt, with no induction period.

The values for V at various C_K levels were estimated from the initial linear region of the appropriate reaction profile, and are shown in Fig. 2. Most of the data points are the averages of duplicate experiments. Evidently, Pd-catalysis is distinguished from Pt- and

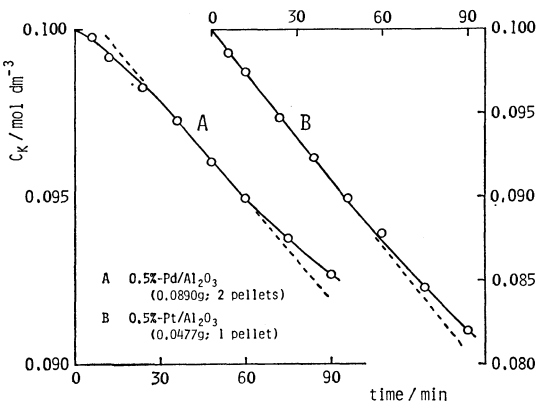

Fig. 1. Typical reaction profiles on Pd and Pt: plot of cyclohexanone concentration *vs.* time.

Table 1. Strength of ketone adsorption

Ketone	Catalyst	K_K / dm³ mol⁻¹	$\Delta G_K^\ddagger$ / kcal mol⁻¹	$\Delta G_K^\ddagger(M)^{a)} - \Delta G_K^\ddagger(Pd)$ / kcal mol⁻¹
4-Heptanone				
	Pt/Al_2O_3	66.9	−2.5	−1.3
	Pd/Al_2O_3	7.2	−1.2	
Cyclohexanone				
	Pt/Al_2O_3	50.5	−2.4	−0.4
	Pd/Al_2O_3	26.1	−2.0	
	Ru/SiO_2	186	−3.1	−1.6
	Pt/SiO_2	73.9	−2.6	−1.1
	Pd/SiO_2	12.2	−1.5	

a) Symbol (M) stands for a metal other than Pd.

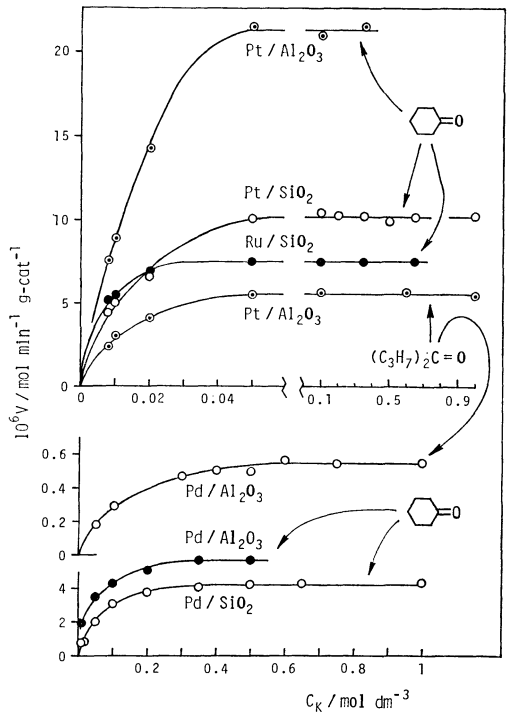

Fig. 2. Concentration dependence of ketone hydrogenation rate.

Ru-catalysis by the much slower increase in V with increasing C_K. This tendency is seen irrespective of the kind of catalyst support and reactant ketone, and therefore might be interpreted as due to the difference in ketone adsorption strength between Pd and the other metals.

Ketone Adsorption. All the plots in Fig. 2 have a long horizontal region, and there is no sign of rate decrease with increasing C_K at the higher C_K region. Rate V is thus given fairly well as a function of C_K:

$$V = kK_KC_K/(1+K_KC_K), \quad (1)$$

where k is the hydrogen pressure-dependent rate constant and K_K is the adsorption equilibrium constant of the substrate ketone. Rate expression (1) can be derived by assuming (a) the Langmuir isotherm for substrate ketone, (b) the neglect of alcohol adsorption, and (c) either the adsorption of hydrogen and ketone without mutual displacement or the hydrogenation of adsorbed ketone by a hydrogen source other than chemisorbed hydrogen. Item (b) is justified as far as the initial stage of reaction is concerned. Among examples of non-displacing hydrogen adsorption, in connection with item (c), might be hydrogen adsorption beneath the hydrocarbon ring or chain of the adsorbed ketone molecule. A small hydrogen atom or molecule might have access to this "shadow of ketone," but not another ketone molecule.

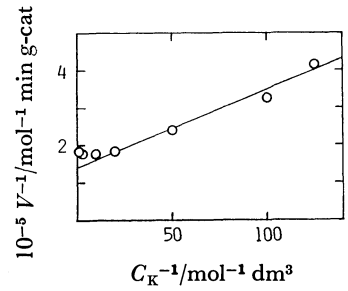

Fig. 3. Typical linear relationship due to Langmuir isotherm. 4-Heptanone on Pt/Al_2O_3.

Taking the reciprocal of both sides of Eq. (1), we have

$$\frac{1}{V} = \frac{1}{k} + \frac{1}{kK_KC_K}. \quad (2)$$

A typical linear relationship between $1/V$ and $1/C_K$ is shown in Fig. 3. The values of K_K were estimated from the slope and the intercept, and are listed in Table 1. Also included in Table 1 are the values for the standard free energy of ketone adsorption ($\Delta G_K^\ddagger$), which is calculated using the K_K values from

$$\Delta G_K^\ddagger = -RT\ln(K_KC^\ddagger) \quad (3)$$

where $C^\ddagger$ is a standard concentration. For the calculation of $\Delta G_K^\ddagger$, $C^\ddagger$ was set equal to 1 mol dm^{-3}, and T to 303 K. The $\Delta G_K^\ddagger$ data clearly indicate that ketone adsorption on Pd is weaker than on the other metals, as predicted in the Introduction.

There is a general rule proposed by Tanaka and Tamaru of Yokohama National University[6] for chemisorption of gases on metals. For many gases, according to this rule, the initial heat of chemisorption on various metals increases as the heat of formation of the highest oxide of the metal per metal atom ($-\Delta H_o^\ddagger$) is increased. Interestingly, in Table 1 the K_K values for cyclohexanone adsorption on the SiO_2-supported metals are in the sequence, Pd<Pt<Ru, which is parallel to the $-\Delta H_o^\ddagger$ sequence.

We thank Dr. Y. Takagi, Dr. S. Teratani, Dr. M. Kawai, and Mr. T. Chihara for a critical reading of the manuscript and their helpful comments.

References

1) P. N. Rylander, "Catalytic Hydrogenation over Platinum Metals," Academic Press, New York (1967), p. 258.
2) E. Breither, E. Roginski, and P. N. Rylander, *J. Org. Chem.*, **24**, 1855 (1959).
3) S. Nishimura, M. Murai, and M. Shiota, *Chem. Lett.*, **1980**, 1239.
4) T. Chihara, unpublished data.
5) K. Tanaka, Y. Takagi, O. Nomura, and I. Kobayashi, *J. Catal.*, **35**, 24 (1974).
6) K. Tanaka and K. Tamaru, *J. Catal.*, **2**, 366 (1963).

The Formation of Anion Radicals in Glassy *N*-Propyl and *N*-Benzyldimethacryloylamines γ-Irradiated at 77 K

Toshiyuki KODAIRA,* Makoto TANIGUCHI, Hiroaki HASE, and Tomochika MATSUYAMA†

Department of Industrial Chemistry, Faculty of Engineering, Fukui University, Bunkyo, Fukui 910

† *Research Reactor Institute, Kyoto University, Kumatori-cho, Sennan-gun, Osaka 590-04*

(Received January 8, 1982)

Synopsis. *N*-Propyl- and *N*-benzyldimethacryloylamines irradiated by γ-rays from ^{60}Co in their glassy state at 77 K yield anion radicals of their methacryloyl groups. These anion radicals afford a triplet with a coupling constant of 1.1 mT on measurement of the ESR and are bleached by a high-pressure mercury lamp at 77 K.

The primary effect of high-energy radiation is the excitation of the molecule, and ionization occurs subsequently. Electrons expelled are sometimes observed as trapped electrons in organic glasses, such as 2-methyltetrahydrofuran (MTHF)[1] and 3-methylpentane.[2] When electron-acceptors, for example, naphthalene or biphenyl, are added to organic glasses, the yield of the trapped electrons decreases and anion radicals of the solute electron-acceptors are formed through the reaction between the solute molecules and the electrons expelled from the solvent molecules.[3]

During the course of the studies of the solid-state cyclopolymerization of *N*-substituted dimethacryloylamines, *N*-propyl (DPA) and *N*-benzyl (DBA) derivatives were found to form a glassy state when they are quenched rapidly to the temperature of liquid nitrogen from above their melting points.[4] These results led us to ESR studies of these monomers in the glassy state, because the esters and amides of methacrylic acid trap electrons to form the anion radical of the methacryloyl group when they are exposed to ionizing radiation in such organic glasses as MTHF and 3-methylpentane.[5,6]

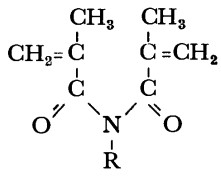

R=C_3H_7(DPA) or $CH_2C_6H_5$(DBA)

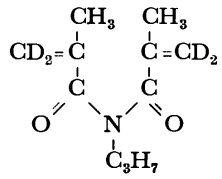

DPA-d_4

Experimental

DPA and DBA were synthesized as has been reported previously.[7,8] DPA deuterated at four methylene protons of methacryloyl groups(DPA-d_4) was prepared according to the procedure previously reported.[9] These monomers were dried over Drierite and distilled. The samples for ESR measurements were prepared in Suprasil tubes. The ESR spectra were recorded by means of a JEOL JES FE-1X X-Band spectrometer at a microwave power of 0.01 mW. The photobleach of the samples was carried out with a 100-watt high-pressure mercury lamp (Rikoh Scientific Industry Co., Ltd.) at a distance of 10 cm for 40 min at 77 K.

Results and Discussion

DPA and DBA subjected to γ-ray irradiation with a ^{60}Co source at 77 K in the dark afford the ESR spectra illustrated in Figs. 1a and 1d. After photobleaching, they changed to the spectral patterns depicted in Figs. 1c and 1f respectively. The 3-line spectra with a coupling constant of 1.1 mT were obtained by taking the difference between before and after the photobleaching of DPA and DBA irradiated at 77 K, as is shown in Figs. 1b and 1e. The spectra remaining after photobleaching at 77 K are mainly due to the 5-membered cyclic radical.[9] These results indicate that the active species which afford the 3-line spectra

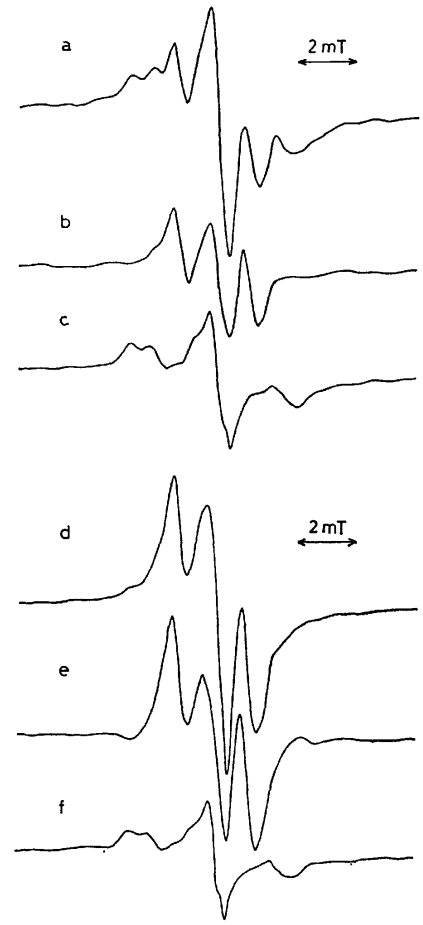

Fig. 1. ESR spectra of glassy DPA (a—c) and DBA (d—f) irradiated at 77 K for 2 h with a dose rate of 2.67×10^4 J/kg/h: (a,d) recorded at 77 K; (b,e) obtained by subtracting c from a and f from d, respectively; (c,f) measured at 77 K after photobleach.

with a coupling constant of 1.1 mT are formed on the γ-irradiation of glassy DPA and DBA at 77 K. The 3-line spectra with a separation of 1.1 mT observed on the ESR measurement of irradiated methacrylic acid derivatives in organic glasses have been ascribed to the anion radical of the methacryloyl groups.[5,6] The splitting was considered to be due to the methylene protons of the methacryloyl group, and the hyperfine splitting constant agreed well with the value obtained from theoretical calculations.[5] Accordingly, the triplets which disappeared during the photo-irradiation are attributable to the anion radicals of the methacryloyl groups of DPA and DBA.

To confirm the above identification, the ESR spectra of DPA-d_4 were measured. The spectrum illustrated by solid line in Fig. 2a was obtained when DPA-d_4 was γ-irradiated at 77 K. After photobleaching, it changed to the dotted spectrum depicted in Fig. 2a. The spectrum shown in Fig. 2b was obtained by subtracting the dotted line from the solid one. The large difference between the two spectra in Fig. 1b and Fig. 2b indicates that the methylene protons of the methacryloyl groups of DPA are responsible for the active species which yield the triplet with the coupling constant of 1.1 mT. In the case of DPA-d_4, a 5-line spectrum with an intensity ratio of 1:2:3:2:1 and with a coupling constant of about 0.17 mT should be observed if the photobleached spectrum is due to the anion radical of the methacryloyl group. The obtained spectrum (Fig. 2b) has a reasonable linewidth when we assume that it is a result of the line-broadening of the quintet. The 3-line spectra could not be detected when 14 mol% of CCl_4 known as a good electron-scavenger was added to the glasses of DPA and DBA. These results support the above conclusion that the triplets of 1.1 mT are due to the anion radicals of methacryloyl groups of DPA and DBA.

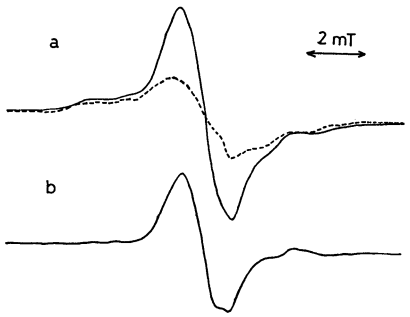

Fig. 2. ESR spectra of glassy DPA-d_4 irradiated at 77 K for 2 h with a dose rate of 2.67×10^4 J/kg/h: (a) solid line, recorded at 77 K; dotted line, measured at 77 K after photobleach; (b) obtained by subtracting dotted line from solid line in a.

When crystalline DPA and DBA were irradiated at 77 K, the anion radicals were not formed, and the main product was the 5-membered cyclic radical.[9]

A part of this work was done under the Visiting Researchers' Program of the Kyoto University Research Reactor Institute.

References

1) D. R. Smith and J. J. Pieroni, *Can. J. Chem.*, **43**, 876, 2141 (1965).
2) K. Tsuzi, H. Yoshida, and K. Hayashi, *J. Chem. Phys.*, **46**, 810 (1967).
3) M. R. Ronayne, J. P. Guarino, and W. H. Hamill, *J. Am. Chem. Soc.*, **84**, 4230 (1962).
4) T. Kodaira, M. Niimoto, F. Aoyama, and H. Yamaoka, *Makromol. Chem.*, **179**, 1791 (1978).
5) T. Gillbro, H. Yamaoka, and S. Okamura, *J. Phys. Chem.*, **77**, 1163 (1973).
6) T. Gillbro, *J. Polym. Sci., Polym. Lett. Ed.*, **11**, 309 (1973).
7) G. D. Rudkovskaya and T. A. Sokolova, *Zh. Org. Khim.*, **2**, 1220 (1966).
8) T. Kodaira, F. Aoyama, K. Morishita, M. Tsuchida, and S. Nogi, *Kobunshi Ronbunshu*, **31**, 682 (1974).
9) T. Kodaira, M. Taniguchi, and M. Sakai, *Polym. Prepr.*, **22**, 9 (1981).

The MoO_3–SnO_2 Catalysts. Acid-Base Properties and Catalytic Activities for 2-Butanol Decomposition and 1-Butene Isomerization

Tuo JIN, Hideshi HATTORI, and Kozo TANABE*
Department of Chemistry, Faculty of Science, Hokkaido University, Sapporo 060
(Received February 10, 1982)

Synopsis. Acidic and basic properties of MoO_3–SnO_2 catalysts with different compositions of MoO_3 were measured by adsorption of NH_3, CO_2, and acid-base indicators. Acidic property prevailed over basic property for all catalysts. Catalytic activities for 2-butanol dehydration and 1-butene isomerization correlated with the acidities measured under the reaction conditions.

A binary oxide of MoO_3–SnO_2 is known as a catalyst that promotes oxidation of propylene and of methanol.[1-3] Besides oxidation reactions, MoO_3–SnO_2 catalyzed acid-catalyzed reactions such as 1-butene isomerization.[4] Recently, MoO_3–SnO_2 was found to show a high activity for coal liquefaction.[5] Thus, the characterization of the surface property has become necessary.

Okamoto *et al.* studied the relationship between the structure of MoO_3–SnO_2 by XPS and the catalytic activity for 2-butanol decomposition.[6] They carried out the reaction in the presence of oxygen and proposed that the reaction proceeds by a Redox mechanism. Ai measured the acidity and found the correlation between the acidity and the catalytic activity for 1-butene isomerization, which was carried out in the presence of oxygen.[4]

In the present work, the acidic and basic properties of MoO_3–SnO_2 as well as the catalytic activities for 1-butene isomerization and 2-butanol decomposition in the absence of oxygen were studied, and the relationship between the properties and the activities is discussed.

Experimental

The MoO_3–SnO_2 was prepared by hydrolysis of mixed solution of ammonium molybdate ($(NH_4)_6Mo_7O_{24}\cdot 4H_2O$) and tin tetrachloride with ammonia water, the final pH being 8. The precipitate was aged over a water bath for 2 h, then washed with deionized water, dried at 120 °C for 24 h, and finally calcined at 500 °C for 2—3 h in air. The catalysts with different molar ratios of MoO_3 to SnO_2 were prepared from the different mixed solutions. The molar ratios were determined by fluorescence X-ray spectrometry. The MoO_3 was prepared from an aqueous solution of $(NH_4)_6Mo_7O_{24}\cdot 4H_2O$ by precipitation with hydrochloric acid. The SnO_2 was prepared from an aqueous solution of $SnCl_4$ by precipitation with ammonia water. The precipitates were aged, washed, dried, and calcined as above. Acidic and basic strengths of the catalysts were qualitatively determined by use of indicators. A series of Hammett indicators were used for measurement of acidic strength. Bromothymol Blue ($pK_a=7.1$) and phenolphtalein ($pK_a=9$) were used for measurement of basic strength. The amounts of irreversible adsorption of NH_3 at 150 °C were measured by a pulse technique.[7,8] Prior to the measurement, a catalyst was pretreated under a He stream at 500 °C for 2 h or subsequently treated with 2-butanol in a He stream at 200 °C. The adsorption of CO_2 was measured volumetrically at 0 °C. The amount of irreversible adsorption of CO_2 was calculated as the difference in the amount between the first run and the second run which was carried out after outgassing at 0 °C for 30 min.

Reaction Procedures. A recirculation reactor (volume 280 ml) was employed with 0.5 g catalyst for carrying out the isomerization of 1-butene at 100 °C. Prior to the reaction, a catalyst was outgassed at 500 °C for 2 h. For the decomposition of 2-butanol, a microcatalytic pulse reactor was employed at 200 °C. A 10 μl of the reactant was injected in a He stream which flowed at a rate of 85 ml/min over 0.1 g catalyst.

Results and Discussion

The MoO_3–SnO_2 catalysts containing 10, 25, and 40% MoO_3 showed a fairly high acid strength of $H_0=-3.0$——5.6, and the catalysts containing 50, 70, and 90% MoO_3, the SnO_2 catalyst and the MoO_3 catalyst showed $H_0=+1.5$——3.0. As the content of MoO_3 in the binary oxide catalysts decreased, the acid sites became strong. The amounts of irreversible adsorption of NH_3 per unit surface area are plotted against the composition of catalyst in Fig. 1. For the catalysts which were pretreated only with a He stream at 500 °C, the amount of NH_3 adsorption exhibited a maximum at 50% of the MoO_3 content, though the amount was less than that for the MoO_3 catalyst. On subsequent treatment with 2-butanol at 200 °C, the amount of NH_3 adsorption decreased for the catalysts containing 25 and 50% MoO_3, and the plot of the amount *vs.* the MoO_3 content showed a monotonous increase with the increase in the MoO_3 content.

Okamoto *et al.* reported on the basis of XPS observation of the MoO_3–SnO_2 catalyst that Mo^{6+} ions in the catalyst containing a small amount of MoO_3 were easily reduced to Mo^{5+} ions which were stable toward further reduction. On the contrary, Mo^{6+} ions in the catalyst containing a large amount of MoO_3 were hardly reduced to Mo^{5+} ions under mild reduction conditions. However, once the Mo^{5+} ions were formed, the Mo^{5+} ions underwent further reduction

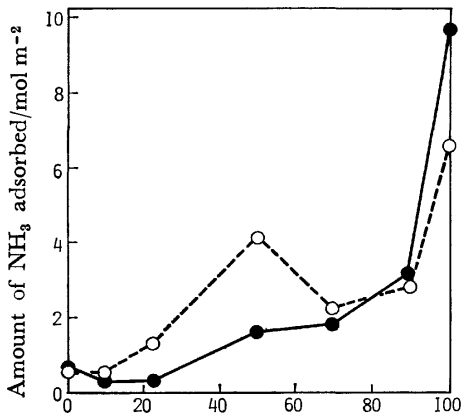

Fig. 1. Variation of the amount of NH_3 irreversibly adsorbed at 150 °C as a function of content of MoO_3 in catalyst.
--○--: Pretreated with a He stream at 500 °C,
—●—: subsequently pretreated with a 2-butanol at 200 °C.

to Mo^{4+} ions. This difference in reducibility with MoO_3 content seems to hold in the present case. It is assumed that the decrease in the amount of NH_3 adsorption on pretreatment with 2-butanol is caused by reduction of Mo^{6+} ions to Mo^{5+} ions for the catalysts containing small amounts of MoO_3. For the catalysts containing large amounts of MoO_3, Mo^{6+} ions persisted their oxidation states toward treatment with 2-butanol, and the amount of NH_3 adsorption did not change much.

Existence of weak basic sites ($H_-=7.1$—9) was observed for all the MoO_3–SnO_2 catalysts, but no basic sites were detected for the MoO_3 catalyst and the SnO_2 catalyst. The amounts of irreversible adsorption of CO_2 at 0 °C were 1.1—7.4 μmol/m², but all the adsorbed CO_2 were easily removed by evacuation at room temperature. This also indicates that basic sites on the catalysts are weak.

The rate of conversion of 1-butene to 2-butenes on unit surface area basis is plotted against the content of MoO_3 in Fig. 2. The catalysts containing 50 and 90% MoO_3 showed maximum activities. The variation of the activity for the isomerization with MoO_3 content correlated roughly with that of the amount of NH_3 adsorption on the catalysts pretreated with He except for MoO_3. This suggests that the active sites for the isomerization are acidic sites present on the MoO_3–SnO_2 catalysts. The higher activity of the catalysts containing 10 and 25% MoO_3 compared with SnO_2 catalyst is considered due to the higher acid strength. On the other hand, the higher activity of the catalyst containing 90% MoO_3 compared with the catalyst containing 50% MoO_3 is supposed to be due to a little cooperation of basic sites, since the acid strength of the former is lower than that of the latter. Since acid-catalyzed isomerization of 1-butene gives the cis/trans ratio in 2-butenes about 1 in most cases, the observed cis/trans ratios 0.9—1.5 also support that the acidic sites on the catalyst are acting mainly for the isomerization.

Degradation of activity for the reaction of 2-butanol with the pulse number was prominent for the catalyst

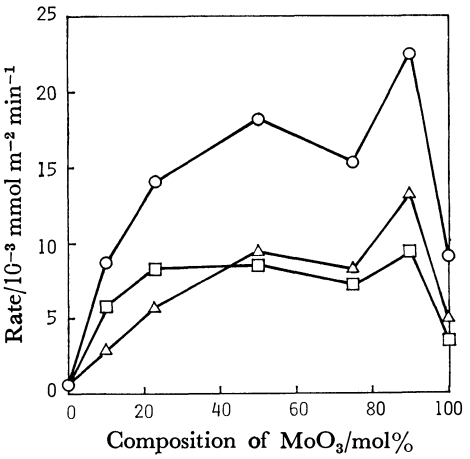

Fig. 2. Variation of the activity for 1-butene isomerization as a function of content of MoO_3 in catalyst.
—○—: Rate of 1-butene conversion, —△—: rate of *cis*-2-butene formation, —□—: rate of *trans*-2-butene formation.

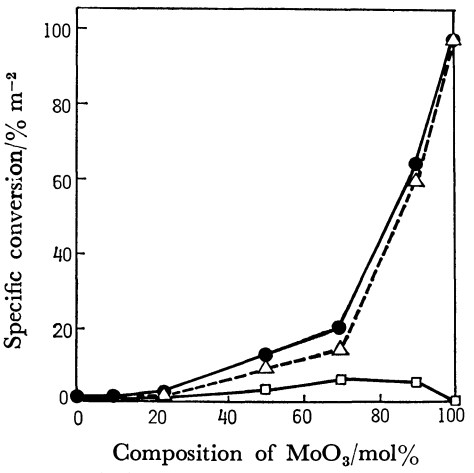

Fig. 3. Variation of the activity for 2-butanol decomposition as a function of content of MoO_3 in catalyst.
—●—: Total conversion, —△—: conversion to butenes, —□—: conversion to methyl ethyl ketone.

containing 10 and 50% MoO_3, while the activity did not decrease so much for the catalyst containing 90% MoO_3 and the MoO_3 catalyst. The variations of the conversions of 2-butanol to butenes and ethyl methyl ketone at the 5th pulse as a function of the composition of the catalysts are shown in Fig. 3. The conversion to butenes increased monotonously as the content of MoO_3 increased, and attained a maximum at the MoO_3 catalyst. Dehydrogenation to produce ethyl methyl ketone was minor reaction for all the catalysts. Only dehydration was observed on the MoO_3 catalyst. The variation of the conversion to butene with the composition of the catalyst correlated well with that of the amount of NH_3 adsorption on the catalyst pretreated with 2-butanol. During the reaction, a part of Mo^{6+} ions in the catalysts containing small amounts of MoO_3 may be reduced to Mo^{5+} ions. Prominent degradation of activity with increasing pulse number for the catalyst containing 10% and 50% MoO_3 supports the possibility of the reduction of Mo^{6+} ions and elimination of a part of the acidic sites.

Ai reported that the activities of MoO_3–SnO_2 for 1-butene isomerization and dehydration of isopropyl alcohol exhibited maxima at 30—60% of the MoO_3 content and that the activities correlated with the acidity. Taking into account that Ai carried out the reactions in the presence of oxygen, the present results are in accord with his results except for the MoO_3 catalyst. The reason for the discrepancy with MoO_3 is not certain.

References

1) J. Buiten, *J. Catal.*, **10**, 188 (1968).
2) S. Tan, Y. Morooka, and A. Ozaki, *J. Catal.*, **17**, 132 (1970).
3) M. Niwa, M. Mizutani, and Y. Murakami, *Chem. Lett.*, **1975**, 1295.
4) M. Ai, *J. Catal.*, **40**, 327 (1975).
5) T. Yamaguchi, M. Yamaguchi, and K. Tanabe, *Proc. Intern. Conf. Coal Science, Düsseldorf*, **1981**, 362.
6) Y. Okamoto, K. Oohiraki, E. Matsunaga, T. Imanaka, and S. Teranishi, *Shokubai*, **22**, 31 (1980).
7) H. L. Gruber, *Anal. Chem.*, **34**, 1828 (1962).
8) M. Ai, *J. Catal.*, **40**, 318 (1975).

Electrophoretic Behavior of Adenine, Adenosine, and Adenosine Nucleotides in Ion Exchange Cellulose Paper as a Support

Yoshinori KITAOKA

Research Reactor Institute, Kyoto University, Kumatori-cho, Sennan-gun, Osaka 590-04

(Received May 16, 1981)

Synopsis. Studies have been carried out on the effects of cationizable and anionizable groups of ion exchange cellulose papers on an electroosmotic flow over a range of pH=5—10 and on the electrophoretic migrations of adenine, adenosine, and adenosine nucleotides. The ionizable groups strongly affected the mobilities of adenosines.

An electrophoretic migration using a support is affected by many factors,[1,2] one of which is the chemical nature of the support. To improve the separability of the electrophoresis, many kinds of substances have been tried as a support. A filter paper having ionizable groups is one of them.

In this paper, we would like to report the electrophoretic behavior of adenine, adenosine, and adenosine 5′-mono, 5′-di-, 5′-tri-, and cyclic 3′,5′-monophosphates (AMP, ADP, ATP, and cAMP, respectively) in ion exchange cellulose papers at different pH-values. An electroosmotic flow is closely related to the ionic groups of a paper and affects the migration of a migrant. Thus, the flows in the papers were measured by movement of carbohydrates.

Reagents and Methods

Adenine and adenosine were purchased from Wako (Osaka, Japan), and the sodium salts of the nucleotides from Sigma (St. Louis, Mo., U.S.A.). Carbohydrates of guaranteed grade were used without further purification. Three different kinds of papers were used as a support: Toyoroshi No. 51A (=51A, pure cellulose paper), Whatman DEAE cellulose paper (=DE81, anion exchange cellulose paper), Whatman phosphate paper (=P81, cation exchange cellulose paper). Four kinds of supporting solutions were prepared; 0.1 M (1 M=1 mol dm^{-3}) NaCl solution (pH≈7.0, buffering capacity (β)=4.6×10^{-7}), citrate solution (pH=5.0, β=0.031, 0.1 M citric acid +0.2 M NaOH), phosphate solution (pH=7.0, β=0.027, 0.025 M Na_2HPO_4+0.025 M NaH_2PO_4) and glycine solution (pH=10, β=0.028, 0.06 M glycine+0.06 M NaCl+0.04 NaOH). The procedures and apparatus used were similar to those described previously.[3] A 5 μl volume of sample solution (5×10^{-2} M) was spotted at the position (see a footnote of Fig. 1) of a strip (1×40 cm) wetted with a supporting solution. It was then dipped in hexane in the migration chamber which was kept at constant temperature (*ca.* 25 °C). A d.c. voltage (1000 V per 30 cm) was applied for 30 min. The paper after migration was then dried and the position of adenines on the paper was detected under the irradiation of ultraviolet light (253 nm). The position of carbohydrates on the paper was detected an *o*-aminophenol solution.[4]

Results and Discussion

The movements of glucose, maltose, and maltotriose in three kinds of papers are shown in Fig. 1. The observed migrations are affected by capillary action, electroosmotic flow, and other physicochemical interactions in the system.[1,2] The differences of migration among spotting positions in a given paper are due to a capillary action, which is towards the center of a paper from both sides.[2,5] The movement due to the capillary action increases with increasing distances of the spotting position from the center of a paper.[1,2] The movement of carbohydrate spotted at the center is thought to be mainly due to an electroosmotic flow because the movement due to the capillary action is zero at the center. Three different carbohydrates showed similar movements in a given paper within experimental errors, showing that the effect of molecular weight on the capillary action and on the electroosmotic flow is small in this experimental range of molecular weight (mol wt: 180—504).

The movements of glucose spotted at the center of a paper dipped in four kinds of supporting solutions are shown in Fig. 2. The differences of migration among the pH-values in a given paper were small, while those among papers were large. The fact that the movement of glucose along with the supporting solution in DE81 paper was found in the anodic side of the paper indicates that the electroosmotic flow was towards the anode by the cationizable (diethylaminoethyl-) groups of the paper. The negative movements in 51A and P81 papers are due to an electroosmotic flow towards the cathode by the anionizable (–COOH and $-OPO_3H_2$, respectively) groups of the papers.

The observed migrations of adenine, adenosine, and adenosine nucleotides in three different papers are shown in Fig. 3. The largest migration of the nucleotides was seen in 51A paper, the next in DE81, and the smallest in P81.

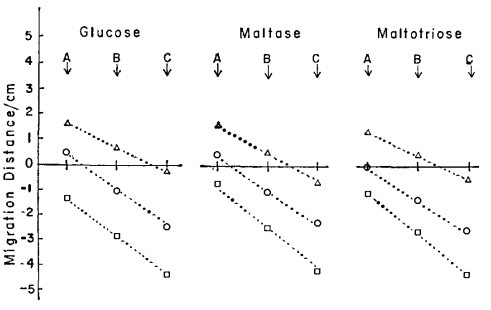

Fig. 1. Movements of carbohydrates at different spotting positions. Conditions: voltage gradient, 1000 V per 30 cm; migration time, 30 min; migration temperature, *ca.* 25 °C; supporting solution, 0.1 M NaCl. Spotting positions: A, 5 cm to the cathodic side from the center of the paper; B, the center of the paper; C, 5 cm to the anodic side from the center. Positive movement is towards the anode, negative movement towards the cathode. Supporting paper: △, DE81; ○, 51A; □, P81.

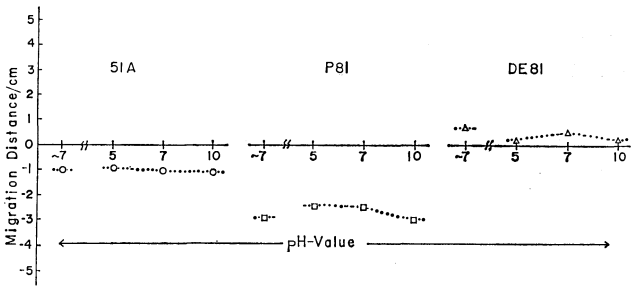

Fig. 2. Movements of glucose by different kinds of supporting solutions. Conditions: 1000 V per 30 cm; 30 min; *ca.* 25 °C. Supporting solutions: pH≈7.0, 0.1 M NaCl; pH=5.0, citrate solution; pH=7.0, phosphate solution; pH=10, glycine solution. Supporting papers: △, DE81; ○, 51A; □, P81.

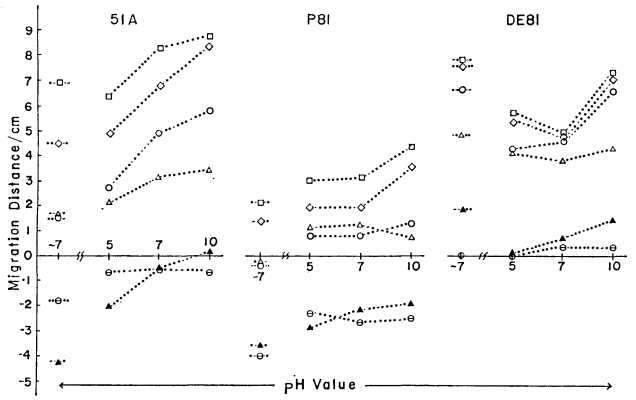

Fig. 3. Observed migrations of adenine, adenosine and adenosine nucleotides. Sample solutions: □, ATP; ◇, ADP; ○, AMP; △, cAMP; ⊖, adenosine; ▲, adenine. Conditions: 1000 V per 30 cm; 30 min; *ca.* 25 °C. Supporting solutions as in Fig. 2.

The migrations corrected for the electroosmotic flow shown in Fig. 2 are shown in Fig. 4. The migration of a weak acid or a weak base is very sensitive to the pH-value of a supporting solution.[6] When we dip a paper into a supporting solution, some ionizable groups in the paper will ionize. Thus, the pH-value of the supporting solution in the ion exchange paper becomes different from the initial pH-value. The pH change in the paper depends on the buffering capacity[7] of the supporting solution and the ion exchange capacity of the paper. The pH-value of the supporting solution in 51A paper will be not so different from the initial value because the number of ionizable (probably -COOH) groups in 51A is not sufficient to change

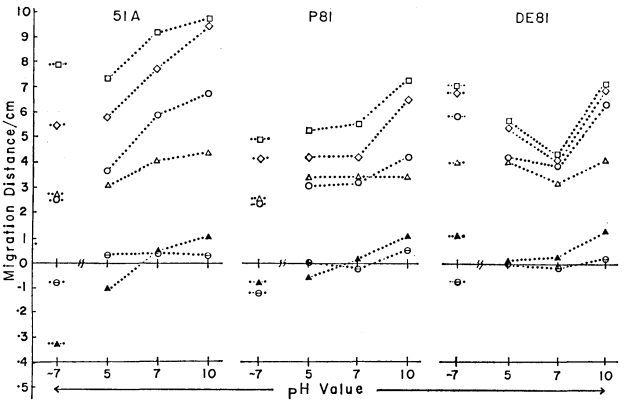

Fig. 4. Migrations corrected for electroosmotic flows. Electrophoretic conditions and symbols used are same as in Fig. 3.

the pH-value of the high buffering solution (approximately one carboxyl group per 500 glucose residues[1]). The increase[8] of the migrations due to the dissociation of the secondary-hydrogen of the phosphate group in the nucleotides is clearly observed at pH=7.0 in 51A (see Fig. 4). The migrations of the nucleotides on P81 or DE81 are strongly affected by ionizable groups of P81 or DE81 and the increase of migrations is not observed at pH=7.0. The migrations corrected for the electroosmotic flow on 51A are not identical with those on P81 or DE81. These results show that unestimated physicochemical interactions (mainly electrostatic forces) between the migrant and ionizable groups of the supporting paper are much involved in the migration of adenine, adenosine, and adenosine nucleotides, as well as an electroosmotic flow and/or a capillary action.

References

1) J. R. Whitaker, "Paper Chromatography and Electrophoresis," Academic Press, New York and London (1967), Vol. 1.
2) H. Waldmann-Meyer, *Chromatogr. Rev.*, **5**, 1 (1963).
3) Y. Kitaoka, *J. Chromatogr.*, **168**, 241 (1979).
4) V. B. Kupressova, *Izv. Sibirsk. Otd. Akad. Nauk SSSR, Ser. Biol. Med. Nauk*, **1965**, 141.
5) Y. Kitaoka, I. Yamase, T. Fukumura, and T. Kitao, *J. Chromatogr.*, **132**, 175 (1977).
6) Y. Kiso, M. Kobayashi, Y. Kitaoka, K. Kawamoto, and J. Takada, *J. Chromatogr.*, **36**, 215 (1968).
7) Y. Kitaoka, *Bull. Chem. Soc. Jpn.*, **54**, 757 (1981).
8) Y. Kitaoka, *J. Chromatogr.*, **111**, 206 (1975).

Studies of Lead-complex Formation in Sea Water by Anodic Stripping Methods

Ryuji NAKATA,*,† Satoshi OKAZAKI, and Taitiro FUJINAGA

Department of Chemistry, Faculty of Science, Kyoto University, Sakyo-ku, Kyoto 606

† *Department of Chemistry, Faculty of Education, Fukui University, Bunkyo, Fukui 910*

(Received November 30, 1981)

Synopsis. For the purpose of the determination and chemical speciation of trace lead in sea water by the use of an electrolytic concentration technique, the effects of the pH on the reduction potential of lead ions in the presence of various organic and inorganic ligands were investigated. In the pH range below *ca.* 5, the lead–chloro complex is dominant in sea water. Even in the presence of organic model ligands such as nitrilotriacetic acid (NTA), the electroactive species of lead was also its chloro complex when the sample solution was acidified enough below pH 2.

From the viewpoint of the electroanalytical studies of trace metals in natural waters, much attention has been paid not only to the total metal concentration, but also to the chemical speciation of the respective metals.[1] Particularly, for the direct identification of the metal complex in a very dilute solution *via* estimations of the ligand number and the complex stability constant, so-called "pseudo-polarography"[2,3] is one of the most promising methods; that is, the anodic stripping peak currents plotted as functions of the cathodic deposition potentials. The complexation of trace metals with organic ligands in natural waters has come to be of great interest in recent years.

We have developed an automatic coulopotentiographic analyzer system by utilizing several flow-electrolysis cells, and applied it to the analysis of trace lead and copper in sea water.[4] It was confirmed, by this method, that these metals at sub-ppb levels in sea water could be determined without any standards, and that the amounts of these metals determined depended remarkably upon the pH of the acidification of the sample sea water. This effect of pH seemed to be attributable to the distribution of the chemical species of these metals.

In this paper, we studied the relationships between the half-wave potential ($E^*_{1/2}$) of the pseudo-polarogram of lead and the pH of the solution in the presence of various organic and inorganic ligands in order to confirm the analytical conditions for the stripping coulopotentiographic determination of total lead and in order to clarify the distribution of chemical species of lead in sea water.

Experimental

Apparatus. The stripping voltammograms were recorded with a Yanagimoto voltammetric analyzer, model P-1000, and a National Pen-Recorder, model VP-654A. A three-electrode system was used; the working electrode was a hanging mercury drop electrode (Princeton Applied Research HMDE), and the potentials were controlled against an Ag/AgCl (saturated NaCl) reference electrode, with a platinum wire as an auxiliary electrode. During the pre-electrolysis stage, the sample solution was stirred for 5 min with a Yanagimoto magnetic stirrer, model MS-60, with a Teflon-covered stirring bar.

Reagents. The sodium perchlorate and humic acid were purified by the use of chelate or ion-exchange resins respectively. All the other chemicals used were of an analytical-reagent grade. Deionized water, after having been distilled from an all-quartz distillation apparatus, was used throughout for all the reagents. The sea-water sample was taken from the surface region of the Pacific Ocean off Wakayama and was filtered with conditioned 0.4 μm Nuclepore membrane filters.

Procedures. The pseudo-polarographic measurement consisted of the following stages, as usual: (1) to a 20 cm^3 base solution with adjusted pH in the electrolysis cell, we added 0.01 cm^3 of 1×10^{-4} mol dm^{-3} lead standard solution; (2) we passed nitrogen gas into the solution for 10 min (30 s for each subsequent run); (3) after renewing a mercury drop and setting the deposition potential, we pre-electrolyzed the solution for 5 min; (4) after stopping the stirrer and letting the solution equilibrate for 10 s, we recorded the anodic stripping voltammogram of lead ions at the scan-rate of 5 mV s^{-1}; (5) after changing the deposition potential, we repeated the procedures from Stage (2). Finally, each stripping current was plotted as a function of the corresponding deposition potential; that is, a pseudo-polarogram of lead was obtained. This pseudo-polarogram was then analyzed analogously to the classical d.c. polarogram, and its half-wave potential ($E^*_{1/2}$) was estimated.

Results and Discussion

In order to investigate the effects of the anions of the supporting electrolyte on the reduction potential of lead, the pseudo-polarogram of lead was measured in model solutions containing different supporting electrolytes at the ionic strength of 0.7, such as sodium perchlorate (ClO_4^- system), sodium chloride (Cl^- system), and sodium acetate plus acetic acid (CH_3COO^- system). Figure 1 shows the shift in $E^*_{1/2}$ with the pH of a lead solution containing a different supporting electrolyte. In the ClO_4^- system, the free lead ion is a dominant species in the pH range up to *ca.* 4. The negative shift of the half-wave potential with an increase in the pH is attributable to the formation of lead-hydroxy complexes. In the case of the Cl^- system, the lead ion preferentially forms chloro complexes ($K_1=10^{1.6}$, $K_2=10^{0.8}$) up to pH *ca.* 5, and then the half-wave potential shifts remarkably toward the negative side. The lead ion also forms weak complexes with the acetate anion in the pH range between 4 and 8 ($K_1=10^{2.4}$, $K_2=10^{1.5}$). The difference in the half-wave potentials between the Cl^- system and the CH_3COO^- system, −46 mV, was in good accordance with that calculated, *ca.* −44 mV, from the difference in the stability constants between the two complexes.

Figure 2 shows the shift in $E^*_{1/2}$ as a function of

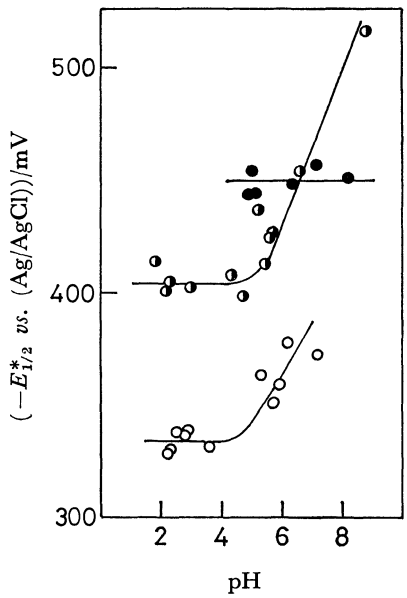

Fig. 1. Effect of pH on the $E^*_{1/2}$ values for the lead stripping peaks in model solutions (ionic strength= 0.7).
○: Sodium perchlorate, ◑: sodium chloride, ●: acetic acid+sodium acetate.

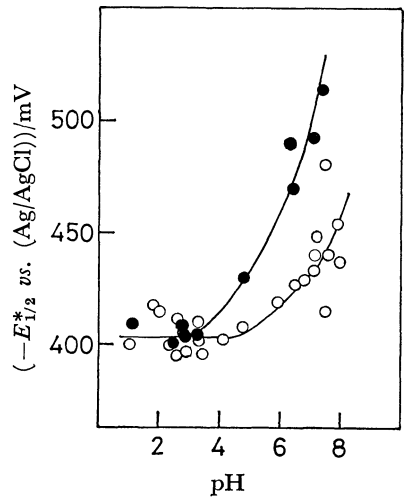

Fig. 2. Effect of pH on the $E^*_{1/2}$ values for the lead stripping peaks in sea water.
○: Sea water, ●: sea water with 5×10^{-5} mol dm^{-3} NTA.

the pH of sea water with or without the co-presence of the organic model ligand. The half-wave potential of lead in sea water was close to that in the Cl^- model system. However, the negative shift of the former was not so much as the latter at pH values greater than about 5. When the sea-water sample was pretreated with acetic acid, no notable shift of the half-wave potential was observed, not even in the presence of 0.1 mol dm^{-3} of acetic acid. For a detailed discussion of these phenomena, a more complicated metal complexation equilibrium should be taken into consideration for that complicated multicomponent system, sea water.

The complex-formation effects with organic ligands on the half-wave potential of lead were investigated in the same way using model ligands, such as NTA, cysteine, ethylenediaminetetraacetic acid (EDTA), and humic acid. As is shown in Fig. 2, in the co-presence of NTA, the electroactive species of lead also consisted of lead–chloro complexes when the pH of the sea-water sample was adjusted to below *ca.* 3. Cysteine behaves in a manner similar to NTA, while in the presence of EDTA, no definite stripping peak of lead was observed, not even by acidification to pH 3. Because of the stability constant of lead–EDTA ($K_1=10^{17.0}$), larger than those of lead–NTA ($K_1=10^{10.6}$) and lead–cysteine ($K_1=10^{13.2}$), this method is inapplicable to the study of lead–EDTA complexes.[5] However, the quantitative electrolysis of lead–EDTA can be performed by acidification with hydrochloric acid to pH 1.0. Concerning humic acid, the half-wave potential of lead was similar to that with NTA in a pH range up to *ca.* 3. In the higher pH range, however, no well-defined pseudo-polarogram of lead was obtained, though the stripping peaks were observed. The electrode process of lead reduction in the presence of humic acid seems to become rather complicated, as a result of the adsorption effect of humic acid on the electrode surface, *etc.*[6]

In conclusion, various chemical species of lead are distributed in sea water, and most of the organic and inorganic ligands of lead complexes can be replaced by chloride anions by acidification to pH 1.0. As a result, the pretreatment of the sea-water sample by acidification with hydrochloric acid to pH 1.0 is effective for the electrochemical determination of the total lead concentration in sea water at sub-ppb levels. For a quantitative discussion about metal complexation, it will be necessary also to take into account such effects as the reversibility of the electrode reaction and adsorption phenomena.

The present work was supported by the Nissan Science Foundation.

References

1) D. R. Turner and M. Whitfield, *J. Electroanal. Chem.*, **103**, 43 (1979).
2) S. D. Brown and B. R. Kowalski, *Anal. Chem.*, **51**, 2133 (1979).
3) S. P. Kounaves and A. Zirino, *Anal. Chim. Acta*, **109**, 327 (1979).
4) R. Nakata, S. Okazaki, and T. Fujinaga, *Nippon Kagaku Kaishi*, **1980**, 1615.
5) B. Raspor, H. W. Nurnberg, P. Valenta, and M. Branica, *J. Electroanal. Chem.*, **115**, 293 (1980).
6) S. A. Wilson, *Anal. Chem.*, **52**, 1515 (1980).

Salt Effects on the Intramolecular Cannizzaro Reaction of Phenylglyoxal. Specific Acceleration by Calcium Ion

Tadashi Okuyama,* Kazumasa Kimura, and Takayuki Fueno
Faculty of Engineering Science, Osaka University, Toyonaka, Osaka 560

(Received June 30, 1981)

Synopsis. Effects of added salts on the rate of alkaline rearrangement of phenylglyoxal to mandelic acid were examined in aqueous solution at 30 °C. The reaction showed positive salt effects. Specific acceleration was found with some metal ions, the efficiency decreasing in the order $Ca^{2+}>Tl^{+}>Sr^{2+}>Ba^{2+}$.

The intramolecular Cannizzaro reaction of α-keto aldehydes in alkaline solutions to give α-hydroxy carboxylate ions has long been known and established to proceed through a 1,2-hydride shift.[1-4] The reaction has recently attracted renewed interest in relation to a formally similar reaction catalyzed by the glyoxalase system,[5-9] which involves zinc ion as a constituent essential for the enzymatic activity.[10] Enzyme-model reactions were found to be affected only very slightly by added magnesium ion in aqueous solutions.[7,8b] In the course of the studies on some model reactions of glyoxalase I involving metal ion catalysis,[11,12] we have found that Ca^{2+} and some other metal ions effectively accelerate the alkaline rearrangement of phenylglyoxal to mandelic acid (an intramolecular Cannizzaro reaction). The present communication describes results of the studies on such metal ion catalyses.

Experimental

Phenylglyoxal hydrate was prepared according to the literature.[11,13] Inorganic salts of reagent grade were used without further purification. Glass-distilled water was used throughout the work.

The Cannizzaro reaction was initiated by addition of 0.03 cm^3 of an aqueous stock solution of phenylglyoxal (typically 7×10^{-3} M (1 M=1 mol dm^{-3})) into 3 cm^3 of an alkaline solution which had been equilibrated at 30±0.1 °C in a stoppered quartz cuvette. Reactions were monitored by following the decrease in UV absorption of phenylglyoxal at 250 nm on a Shimadzu UV 200 spectrophotometer. Pseudo-first-order plots were linear over 3 lifetimes for all the runs.

Results and Discussion

At a constant ionic strength of 0.10 maintained with added KCl, the rates are dependent on [NaOH] in accord with Scheme I as reported previously:[5] $k_1=1.5\times10^{-4}$ s^{-1} and $k_2K_2=5.7\times10^{-2}$ M^{-1} s^{-1} using an assumed value of $K_1=250$ M^{-1}.[5]

With the alkaline concentration and ionic strength maintained at [NaOH]=0.01 M and μ=0.10, respectively, the effects of different salts on the rate were examined. The results are summarized in Table 1. While the alkali metal ions and anions show virtually no specific effect, Ca^{2+}, Tl^{+}, Sr^{2+}, and Ba^{2+} accelerate the reaction significantly. Of the various cations examined, Ca^{2+} is the most effective, showing a 13-fold acceleration at its concentration of 0.01 M.

Table 1. Effects of added salts on the rate of rearrangement of phenylglyoxal[a]

Salt	$10^4 k_{obsd}/s^{-1}$
KCl	6.10
KNO_3	6.20
NaCl	6.15
$KCl+CaCl_2$[b]	81.3
$KCl+SrCl_2$[b]	16.4
$KCl+BaCl_2$[b]	11.1
KNO_3+TlNO_3[b]	21.4

a) [NaOH]=0.01 M, μ=0.10, 30 °C. b) The concentration of a second salt was 0.01 M.

When [NaOH] was kept constant at 0.01 M, the rate increased linearly with [$CaCl_2$] as is shown in Fig. 1. The slope is greater at lower ionic strength: 0.71 M^{-1} s^{-1} at μ=0.10 and 0.44 M^{-1} s^{-1} at μ=0.50. The effect of Ca^{2+} is thus largely dependent on the ionic strength. Figure 2 illustrates some details of such a dependence of the Ca^{2+} catalysis on μ. As is apparent from Fig. 2, the salt effect is positive in the absence of Ca^{2+} but is negative in the presence of Ca^{2+} ([$CaCl_2$]=0.001 M). In effect, the apparent catalytic efficiency of Ca^{2+} is the greater, the smaller the ionic strength. Addition of Ca^{2+} at a concentration as low as 10^{-3} M accelerates the reaction nearly 5-fold at the extrapolated zero ionic strength while it enhances the rate only by a factor less than 1.2 at ionic strengths greater than 0.5.

The marked catalytic effects of non-transition metal ions like Ca^{2+} found here may closely be related to the earlier observations of Pfeil *et al.*[14] They found that TlOH, $Ba(OH)_2$, and $Sr(OH)_2$ are much better catalysts for the benzilic acid rearrangement than alkali metal hydroxides in aqueous dioxane. They have not examined effects of $Ca(OH)_2$.[15] A univalent ion Tl^{+} also significantly accelerates the present reaction. Since the benzilic acid rearrangement takes place essentially in the same way as does the present

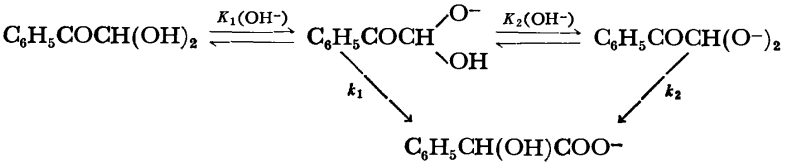

Scheme 1.

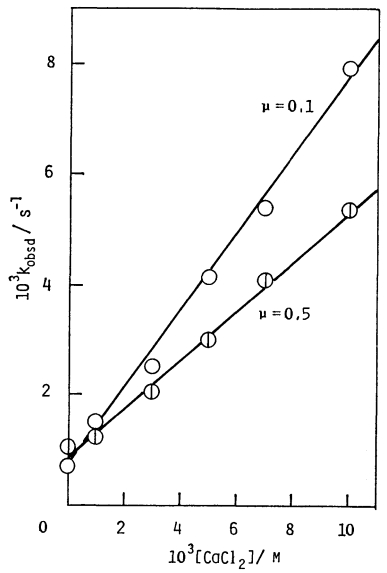

Fig. 1. Effects of $[CaCl_2]$ on the rate of rearrangement of phenylglyoxal in alkaline solution ([NaOH]=0.01 M) at μ=0.10 (○) and μ=0.50 (◐). Ionic strength was adjusted with KCl.

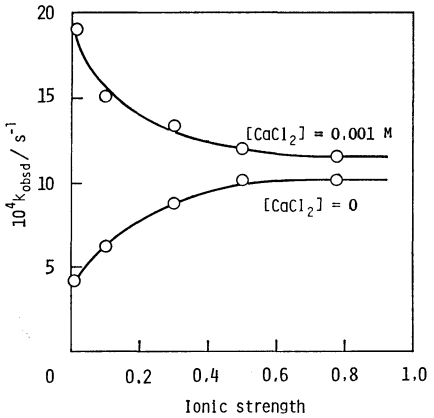

Fig. 2. Effects of ionic strength on the rate of rearrangement of phenylglyoxal in alkaline solution ([NaOH]=0.01 M) in the absence and in the presence of Ca^{2+} ($[CaCl_2]$=0.001 M) at 30 °C. Ionic strength was increased by the addition of KCl.

reaction,[17] the mechanisms of these catalytic actions of metal ions must be similar to each other.

The observed positive salt effect on the rearrangement of phenylglyoxal is not unexpected for a reaction of charged species.[4] The specific effects of Ca^{2+} may be accounted for by its influence either on the equilibrium constants, K_1 and/or K_2, or on the rate constants, k_1 and/or k_2. In any case, the transition state

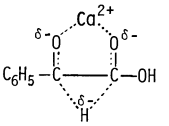

for the hydride shift must be stabilized by the formation of a Ca^{2+} chelate. Added potassium ion may compete with Ca^{2+} to interact with the ionized phenylglyoxal hydrate, thus greatly interfering with the transition-state chelation of Ca^{2+}. This would be a possible reason for the negative salt effects on the Ca^{2+} ion-catalyzed rearrangement. Stability constants for some metal chelations are also known to depend strongly on the ionic strength.[18]

References

1) H. Fredenhagen and K. F. Bonhoeffer, *Z. Phys. Chem. Abt. A*, **181**, 379 (1938).
2) E. R. Alexander, *J. Am. Chem. Soc.*, **69**, 289 (1947).
3) W. v. E. Doering, T. I. Taylor, and E. F. Schoenewaldt, *J. Am. Chem. Soc.*, **70**, 455 (1948).
4) P. Salomaa, *Acta Chem. Scand.*, **10**, 311 (1956).
5) J. Hine and G. F. Koser, *J. Org. Chem.*, **36**, 3591 (1971).
6) D. L. Vander Jagt, L.-P. B. Han, and C. H. Lehman, *J. Org. Chem.*, **37**, 4100 (1972).
7) J. Hine and C. D. Fischer, Jr., *J. Am. Chem. Soc.*, **97**, 6513 (1975).
8) a) S. S. Hall, A. M. Doweyko, and F. Jordan, *J. Am. Chem. Soc.*, **98**, 7460 (1976); b) S. S. Hall, A. M. Doweyko, and F. Jordan, *ibid.*, **100**, 5934 (1978).
9) S. Shinkai, T. Yamashita, Y. Kusano, and O. Manabe, *Chem. Lett.*, **1979**, 1323.
10) A.-C. Aronsson, E. Marmstål, and B. Mannervik, *Biochem. Biophys. Res. Commun.*, **81**, 1235 (1978).
11) T. Okuyama, K. Kimura, and T. Fueno, *Bull. Chem. Soc. Jpn.*, **55**, 1493 (1982).
12) T. Okuyama, S. Komoguchi, and T. Fueno, *J. Am. Chem. Soc.*, **104**, 2582 (1982).
13) H. A. Riley and A. R. Gray, *Org. Synth.*, Coll. Vol. II, 509 (1953).
14) E. Pfeil, G. Geissler, W. Jacquemin, and F. Lömker, *Chem. Ber.*, **89**, 1210 (1956).
15) Pfeil[16] studied also on the catalytic efficiencies of various metal hydroxides in the Cannizzaro reaction of formaldehyde. Although the differences were found to be small (less than 2-fold), $Ca(OH)_2$ was a slightly better catalyst than NaOH.
16) E. Pfeil, *Chem. Ber.*, **84**, 229 (1951).
17) S. Selman and J. F. Eastham, *Quart. Rev.*, **14**, 221 (1960).
18) R. J. Angelici, "Inorganic Biochemistry," ed by G. L. Eichhorn, Elsevier, Amsterdam (1973), Vol. 1, Chap. 2.

The Synthesis and Reactions of 2,6-Dimethyl-4-silaspiro[3.4]oct-6-ene

Daiyo Terunuma,* Noriyuki Shibuya, and Hiroyuki Nohira
Department of Applied Chemistry, Faculty of Engineering, Saitama University, Urawa, Saitama 338

(Received September 9, 1981)

Synopsis. A new silaspiro compound, *i.e.*, 2,6-dimethyl-4-silaspiro[3.4]oct-6-ene, was synthesized by treating 1,1-dichloro-3-methyl-1-silacyclobutane with isoprene in the presence of magnesium in tetrahydrofuran. The reactions of the silaspiro compound with $LiAlH_4$, H_2PtCl_6, dimethyl acetylenedicarboxylate in the presence of $PdCl_2(PPh_3)_2$, and the Simmons-Smith agent were investigated.

A number of reports on the preparations and the reactions of silacyclobutanes have appeared.[1] However, a little work has been done on the synthesis of four-membered spiro compound which contains silicon atom in the ring.[2]

In the course of our studies of the synthesis and reactions of silacyclic compounds,[3b] a new silaspiro compound, *i.e.*, 2,6-dimethyl-4-silaspiro[3.4]oct-6-ene (**1**), was obtained. Being interested in the point that **1** contains two kinds of functional groups, double bond and silicon containing four-membered ring, in the molecule, we carried out some investigations concerning the reactivity of **1**.

Results and Discussion

2,6-Dimethyl-4-silaspiro[3.4]oct-6-ene (**1**) was obtained in 59% yield by treating 1,1-dichloro-3-methyl-1-silacyclobutane (**2**) with an equimolar amount of isoprene in the presence of Mg in THF[3a] (Scheme 1).

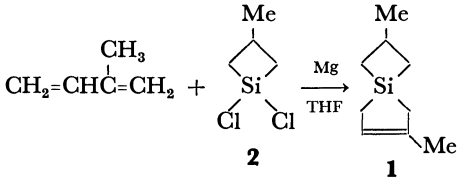

Scheme 1.

The reaction of **1** with $LiAlH_4$ gave the four-membered ring opening product, *i.e.*, 1-isobutyl-3-methyl-1-silacyclopent-3-ene (**3**), in 24% yield (Scheme 2).

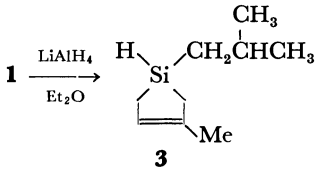

Scheme 2.

Polymerization of **1** was carried out in the presence of a small amount of H_2PtCl_6 in benzene. A solid polymer (**4**) ([η]=0.26 in benzene at 25 °C) was obtained in 74% yield. It was found that only the four-membered ring opening polymerization occurred and the five membered ring remained intact in the polymer, by comparing the IR and NMR spectra of **4** with those of **3**, and with those of the polymer obtained from 1,1,3-trimethyl-1-silacyclobutane (Scheme 3).

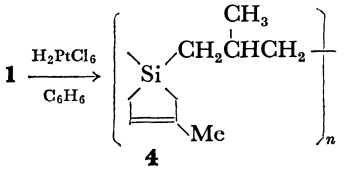

Scheme 3.

In the presence of a catalytic amount of $PdCl_2(PPh_3)_2$, the reaction of **1** with dimethyl acetylenedicarboxylate in benzene was carried out.[4] Another spiro compound, *i.e.*, 2,9-dimethyl-6,7-bis(methoxycarbonyl)-5-silaspiro[4.5]deca-2,6-diene (**5**), was obtained in 85% yield (Scheme 4).

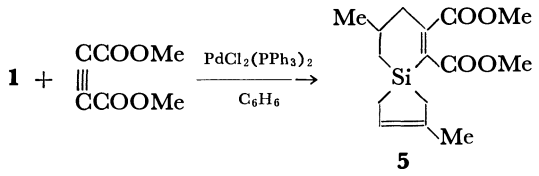

Scheme 4.

The reaction of **1** with the Simmons-Smith reagent in ether gave 1,3′-dimethylspiro[3-silabicyclo[3.1.0]hexane-3,1′-silacyclobutane] (**6**) in 47% yield. No methylene insertion product to the silicon-carbon or carbon-hydrogen bond of the four-membered ring was found in the reaction mixture (Scheme 5).

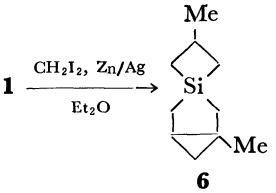

Scheme 5.

It is interesting that the silylene type fragment appears as the base peak in the case of 5-silaspiro[4.4]nona-2,7-diene,[5] whereas the silaethylene type fragment (*m/e* 110) is the base peak in the mass spectrum of **1**. Another silaethylene type fragment (*m/e* 95, relative intensity 71%) is also found in the spectrum of **1** (Scheme 6).

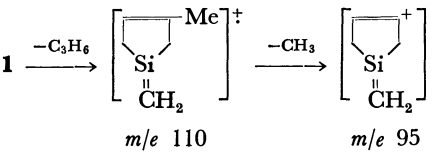

Scheme 6.

Experimental

The IR spectra were determined with a JASCO IR-A2 spectrometer. The NMR spectra were determined at 60

MHz with a Varian A-60D spectrometer in CCl_4 using TMS as the internal standard. Mass spectra were recorded on a JEOL-01SG instrument. The analytical GLC was carried out with a Shimadzu GC-5A chromatograph[1.5 m, 5% OV-1 on Chromosorb W(80—100 mesh)].

Preparation of 2,6-Dimethyl-4-silaspiro[3.4]oct-6-ene (1). In a flask Mg(5.5 g, 0.26 mol) was placed. A solution of isoprene (14.4 g, 0.21 mol) and **2**(29.5 g, 0.19 mol) in THF(85 ml) was added to the flask. The mixture was refluxed for 27 h with stirring. Water(150 ml) was added to the reaction mixture at 0 °C. The organic layer was washed three times with water, dried with Na_2SO_4. Subsequent evaporation and distillation gave **1** in 59%(17.1 g) yield. Bp 91—92 °C/38 Torr(1 Torr=133.322 Pa). n_D^{20} 1.5011. IR(neat) 1640, 1150, 1130, 950 cm^{-1}. NMR (δ) 0.6—1.2(m, 4, Si–CH_2), 1.16(d, 3, CH_3), 1.3—1.65(m, 4, Si–CH_2–C=), 1.75(broad s, 3, =C–CH_3), 2.1—2.8(m, 1, CH), 5.5(broad s, 1, =CH). Mass(*m/e*) 152(M^+), 124, 111, 110(base peak), 109, 96, 95, 83, 82, 81, 74, 69, 68, 67, 59, 55, 53, 31, 29. Found: C, 70.59; H, 10.61%. Calcd for $C_9H_{16}Si$: C, 70.97; H, 10.59%.

Reaction of 1 with $LiAlH_4$. A solution of **1**(1.0 g, 6.6 mmol) in ether(5 ml) was added to a suspension of $LiAlH_4$ (1.0 g, 0.026 mol) in ether(7 ml) with stirring. The reaction mixture was refluxed for 4 h. Saturated aqueous Na_2SO_4(about 20 ml) was added to the mixture with external cooling. Usual workup of the solution gave **3** in 24% (0.24 g) yield. Bp 90—92 °C/25 Torr. IR(neat) 2100, 1640 cm^{-1}. NMR(δ) 0.52(m, 2, Si–CH_2), 0.97(d, 6, C–CH_3), 1.3—1.6(m, 4, Si–CH_2–C=), 1.6—1.8(m, 3, CH_3), 2.1—2.3 (m, 1, CH), 4.2(m, 1, Si–H), 5.46(m, 1, =CH). Mass(*m/e*) 154(M^+), 149, 126, 112, 98, 97(base peak), 83, 71, 70, 69, 67, 59, 55, 45, 43, 31. Found: C, 69.70; H, 11.55%. Calcd for $C_9H_{18}Si$: C, 70.05; H, 11.76%.

Polymerization of 1. A solution of **1**(0.50 g, 3.3 mmol) in benzene(10 ml) was refluxed for 3 h in the presence of a small amount of H_2PtCl_6. The mixture was poured into methanol(250 ml). The polymer precipitated was collected, dried in a desiccator. Thus, **4** was obtained in 74%(0.37 g) yield. IR(KBr) 1640 cm^{-1}. NMR(δ) 0.5—0.7(m, 4, Si–CH_2), 0.97(d, 3, CH_3), 1.3—1.6(m, 4, Si–CH_2–C=), 1.6—1.8(m, 3, CH_3), 2.0—2.9(m, 1, CH), 5.5(m, 1, =CH).

Reaction of 1 with Dimethyl Acetylenedicarboxylate in the Presence of $PdCl_2(PPh_3)_2$. A solution of **1** (1.0 g, 6.6 mmol), $PdCl_2(PPh_3)_2$ (0.063 g, 0.065 mmol), and dimethyl acetylenedicarboxylate (1.0 g, 7.0 mmol) in benzene(16 ml) was refluxed for 2 h with stirring. Water was added to the reaction mixture. Usual workup of the organic layer gave **5** in 83%(1.6 g) yield. Bp 144—147 °C/3 Torr. n_D^{20} 1.5153. IR(neat) 1720, 1640, 1600 cm^{-1}. NMR(δ) 0.8—1.2(m, 2, Si–CH_2), 1.1(d, 3, CH_3), 1.25—1.6(m, 4, Si–CH_2–C=), 1.75 (m, 3, =C–CH_3), 1.9—2.2(m, 2, CH_2), 2.3—2.5(m, 1, CH), 3.62, 3.70(two singlets, 6, $COOCH_3$), 5.45(broad s, 1, =CH). Mass(*m/e*) 294(M^+), 279, 263, 262(base peak), 245, 228, 219, 218, 204, 190, 182, 162, 152, 126, 125, 57. Found: C, 61.06; H, 7.99%. Calcd for $C_{15}H_{22}O_4Si$: C, 61.20; H, 7.53%.

Reaction of 1 with the Simmons-Smith Reagent. Diiodomethane (4.0 g, 0.015 mol) was added slowly to the suspension of Zn–Ag couple(0.98 g, 0.015 mol) in dry ether (9 ml) at room temperature. The mixture was stirred for 1 h, and then **1**(1.0 g, 6.6 mmol) was added to the mixture. After the mixture was refluxed for 20 h with stirring, dil HCl was added to the mixture with cooling. Usual workup of the organic solution, gave **6** in 47%(0.52 g) yield. Bp 98—100 °C/20 Torr. IR(neat) 1130, 950 cm^{-1}. NMR(δ) −0.23(t, 1, C–H in cyclopropane ring), 0.2—0.45(m, 1, C–H in cyclopropane ring), 0.5—1.25(m, 8, Si–CH_2), 1.12 (d, 3, CH_3), 1.18(s, 3, CH_3), 1.2—1.4(m, 1, CH), 2.0—2.8 (m, 1, C–H in cyclobutane). Mass(*m/e*) 166(M^+), 138, 124, 109, 96(base peak), 83, 69, 55, 43. Found: C, 72.01; H, 10.80%. Calcd for $C_{10}H_{18}Si$: C, 72.21; H, 10.91%.

References

1) a) L. H. Sommer and G. A. Baum, *J. Am. Chem. Soc.*, **76**, 5002 (1954); b) H. Gilman and W. H. Atwell, *ibid.*, **86**, 5589 (1964); c) J. Laane, *ibid.*, **89**, 1144 (1967); d) V. M. Vdovin, N. S. Nametkin, and P. L. Grinberg, *Dokl. Akad. Nauk SSSR*, **150**, 799 (1963); e) D. Seyferth, R. Damrauer, S. B. Andrews, and S. S. Washburne, *J. Am. Chem. Soc.*, **93**, 3209 (1971).

2) a) N. S. Nametkin, N. A. Lepetukhina, O. V. Kuzumin, F. D. Babich, T. I. Chernyshewa, and V. M. Vdovin, *Dokl. Akad. Nauk SSSR*, **198**, 112 (1971); b) R. Damrauer, R. A. Davis, M. T. Buruke, R. A. Karn, and G. T. Goodman, *J. Organomet. Chem.*, **43**, 122 (1972); c) E. Block and L. K. Renelle, *J. Am. Chem. Soc.*, **100**, 1630 (1978).

3) a) G. Manuel, P. Mazerolles, and G. Cauquy, *Syn. React. Inorg. Metalorg. Chem.*, **4**(2), 133 (1972); b) D. Terunuma, S. Hatta, T. Araki, T. Ueki, T. Okazaki, and Y. Suzuki, *Bull. Chem. Soc. Jpn.*, **50**, 1545 (1977).

4) H. Sakurai and T. Imai, *Chem. Lett.*, **1975** 891.

5) R. G. Solomon, *J. Org. Chem.*, **39**, 3602 (1974).

A Convenient Synthesis of 2-Deuterio-1,3-benzodithiolylium Salts. Useful Synthon for the Preparation of One-carbon Homologated 1-Deuterio Aldehydes

Juzo NAKAYAMA

Department of Chemistry, Faculty of Science, Saitama University, Urawa, Saitama 338

(Received October 8, 1981)

Synopsis. 2-Deuterio-1,3-benzodithiolylium salt, a useful synthon for preparation of one-carbon homologated 1-deuterio aldehydes, can be prepared in excellent overall yield in three steps starting from easily accessible 2-isopentoxy-1,3-benzodithiole.

Very recently Degani *et al.*[1] have shown that 2-deuterio-1,3-benzodithiolylium perchlorate (**1a**) is a useful synthon for preparation of one-carbon homologated 1-deuterio aldehydes; it reacts with Grignard reagents yielding 2-alkyl- or 2-aryl-2-deuterio-1,3-benzodithioles, which in turn can be hydrolyzed to the corresponding 1-deuterio aldehydes. However, the reported method for the preparation of **1a** is not so favorable since it requires even four steps, though starting from easily accessible 2-isopentyloxy-1,3-benzodithiole (**2**),[2,3] and expensive CD_2Cl_2 (Scheme 1).

We wish to report a simple three-step synthesis of 2-deuterio-1,3-benzodithiolylium salts (**1**) from **2**. In the new method, 2-ethylthio-1,3-benzodithiole (**3**), readily obtainable from **2** and ethanethiol,[4] is deuterated[5] and the resulting 2-deuterio-2-ethylthio-1,3-benzodithiole (**4**) is converted to 2-deuterio-1,3-benzodithiolylium tetrafluoroborate (**1b**) by treatment with tetrafluoroboric acid in 79% overall yield.[6] The isotopic purity of **1b** is over 98%; the small loss of isotopic purity observed may result from a deuterium-hydrogen exchange reaction of the 1,3-benzodithiolylium ion.[7]

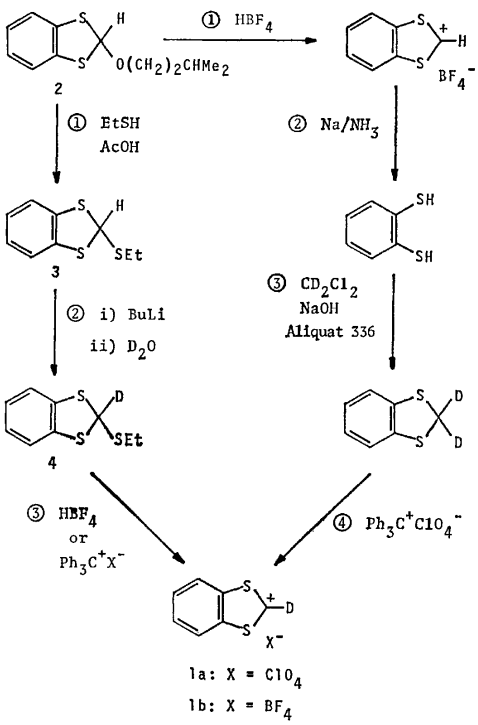

Scheme 1.

More isotopically pure **1** can be obtained by treatment of **4** with a trityl salt in aprotic medium, where no deuterium-hydrogen exchange reaction occurs. Thus treatment of **4** with trityl perchlorate in acetonitrile gives isotopically pure **1a** and ethyl trityl sulfide in excellent yield. In a similar way, isotopically pure **1b** can be prepared from **4** and trityl tetrafluoroborate in good yield.[8]

Accordingly, the procedure developed here, which requires neither the laborious ring-cleavage step on the dithiole skeleton (Birch reduction) nor any expensive reagents, is far more convenient than that reported by Degani *et al.*[1]

Experimental

Caution. 1,3-Benzodithiolylium perchlorate explodes violently at its melting point; see *Tetrahedron Lett.*, **22**, pp. i—ii, 1981. The fluoroborate salt is nonexplosive and chemically behaves similarly to the perchlorate salt, and therefore the use of **1b** instead of **1a** should highly be recommended.

2-Ethylthio-1,3-benzodithiole (3). A mixture of **2**[3] (24.0 g; 0.1 mol) and ethanethiol (25 ml; 0.34 mol) in acetic acid (300 ml) was allowed to stand at room temperature overnight and then diluted with ice–water (1000 ml). The resulting crystalline white solid was collected and washed with 40% aqueous methanol (150 ml). The material was thoroughly dried to give **3** of sufficient purity (20.6 g, 96%): mp 45—46 °C (lit,[4] mp 50—51 °C).

2-Deuterio-2-ethylthio-1,3-benzodithiole (4). To a stirred solution of **3** (20.5 g; 95 mmol) in dry tetrahydrofuran (420 ml) was added dropwise a 15% solution of butyllithium in hexane (90 ml; 120 mmol) at −73 °C under nitrogen. The mixture was stirred for 2 h and then 6 ml of deuterium oxide (E. Merck, D content>99.75%) dissolved in dry tetrahydrofuran (40 ml) was added at −73 °C. After being stirred for 1 h at −73 °C, the mixture was gradually warmed to room temperature and evaporated. The residue was partitioned between ether (300 ml) and water (200 ml). The ether layer was washed with water and dried. The ether was removed to leave 20.1 g (97%) of **4** which is sufficiently pure for the preparation of **1** and used without further purification (no absorption due to the proton at C-2 could be detected by ^{1}H NMR analysis).

2-Deuterio-1,3-benzodithiolylium Tetrafluoroborate (1b). To a stirred and ice-cooled solution of **4** (20.1 g; 93 mmol) in acetic anhydride (250 ml) was added dropwise 42% tetrafluoroboric acid (40 g; 0.19 mol) over a period of 0.6 h. After completion of the addition, ether (300 ml) was added to the mixture to precipitate the product completely. The precipitate was collected by filtration and washed with ether to give 19.0 g (85%) of **1b**, mp 148—149 °C [lit,[6] mp of the unlabeled compound, mp 150—150.5 °C (decomp)]: IR (KBr) 2300 and 2250 (C-D) and 1000—1100 cm^{-1} (BF_4^-); ^{1}H NMR (CF_3CO_2D) δ=8.0—8.4 and 8.6—9.0 (4H, AA'BB') (the content of the unlabeled compound was estimated to be less than 2% from the very weak

absorption due to the proton at C-2 of the unlabeled compound which appears at $\delta=11.53$).[9]

2-Deuterio-1,3-benzodithiolylium Salts (1) from 4 and Trityl Salts. **4** (2.15 g; 10 mmol) was added to a stirred suspension of trityl perchlorate (3.60 g; 10.5 mmol) in dry acetonitrile (20 ml) cooled at −10 °C. The mixture was gradually warmed to room temperature, stirred for 0.5 h, and diluted with dry ether (50 ml). The solid prepcipitate was collected and washed with ether to give 2.28 g (90%) of isotopically pure **1a** in white crystal, which will explode at 185 °C (lit,[1] explosion point 182 °C). From the filtrate, 2.80 g (92%) of ethyl trityl sulfide, mp 117—118 °C, was obtained.

A similar treatment of **4** (10 mmol) with trityl tetrafluoroborate (10.5 mmol) in acetonitrile gave **1b** in 80% yield.

References

1) I. Degani, R. Fochi, and V. Regondi, *Tetrahedron Lett.*, **1981**, 1821.
2) I. Degani and R. Fochi, *Synthesis*, **1976**, 471.
3) J. Nakayama, *Synthesis*, **1975**, 38.
4) J. Nakayama, *Synthesis*, **1975**, 436.
5) Deuteration of **2** cannot be attained since butyllithium reacts with **2** to give 2-butyl-1,3-benzodithiole in a good yield; S. Ncube, A. Pelter, and K. Smith, *Tetrahedron Lett.*, **1977**, 255.
6) J. Nakayama, K. Fujiwara, and M. Hoshino, *Bull. Chem. Soc. Jpn.*, **49**, 3567 (1976).
7) For the hydrogen-deuterium exchange reaction of 1,3-dithiolylium ions, see H. Prinzbach and E. Futterer, *Adv. Heterocycl. Chem.*, **7**, 39 (1966).
8) J. Nakayama, K. Fujiwara, M. Imura, and M. Hoshino, *Chem. Lett.*, **1977**, 177.
9) For ^{1}H NMR spectrum of the unlabeled compound, see K. Sakamoto, N. Nakamura, M. Ōki, J. Nakayama, and M. Hoshino, *Chem. Lett.*, **1977**, 1133.

The Stereoselective Diels-Alder Reaction of Bicyclo[3.2.0]nona-3,6-dien-2-one with Several Dienes

Hitoshi TAKESHITA,* Toshihide HATSUI, Isao SHIMOODA, and Hiroaki MAMETSUKA

Research Institute of Industrial Science, Kyushu University, Sakamoto, Kasuga, Fukuoka 816

(Received November 7, 1981)

Synopsis. The *endo-cis* adducts were selectively obtained by the Diels-Alder reaction of several dienes with bicyclo[3.2.2]nona-3,6-dien-2-one, prepared from tropone and ethylene. This selective formation from the bicyclic dienophile, the isolated C=C and ethano C–C bonds of which are situated in similar sterical environments within the molecule, was supported by an Extended Hückel calculation.

Recently, we have prepared a series of Diels-Alder adducts (**A**) of tropones with spiro[2.4]hepta-4,6-diene (**1**)[1] in connection with studying the cyclopropane effect on the singlet-oxygen oxidation of dispiro[cyclopropane-1,3′-tricyclo[5.2.1.0^{2,6}]deca-4′,8′-diene-10′,1″-cyclopropane],[2] a Diels-Alder dimer of **1**. During the studies, we have noticed the formation of 1:2 adducts (**B** and **C**), in which the geometry of the adducts was always *endo-cis* form with respects to the isolated double bond of the intermediate 1:1 adducts. Although Alder's classical rule for the stereochemistry of the adducts predicts the *endo-cis* adduct formation due to a maximal overlapping of the π-electron systems of the reacting molecules,[3] the previous discussions were restricted to the conjugated system, and only a few examples of stereoselective Diels-Alder addition controlled by an unconjugated π-electron system have been known.[4,5] It is known that the two π-electron systems of **A** show a transannular conjugation effect in the UV spectroscopy,[6] and this delocalization in the **A** may be reflected in the HOMO–LUMO interaction to favor the observed selective reaction. Thus, we thought it might be worthwhile to evaluate the role of this delocalized π-system in the selective 1:2 adduct formation on the sterically unhindered dienophile. With this in mind, we have made a study with bicyclo[3.2.2]nona-3,6-dien-2-one (**2**), the Diels-Alder adduct of tropone (**3**) with ethylene (**4**).[7] The isolated C=C and the ethano C–C of 2 are located in the same geometrical position with found to the α,β-unsaturated keto group of the reaction site.

When a mixture of **2** and **1** was heated in a sealed tube at 130 °C for 180 h, only one adduct (**5**) was obtained after the silica-gel chromatography of the reaction mixture. The NMR spectrum[8] of **5** clearly indicated the stereochemistry of the adduct, *endo-cis*, on the basis of the high-field shift for particular proton signals on the isolated double bond in an order of 1 ppm upon suffering a strong anisotropic effect of the other double bond. Similarly, the reaction of **2** with cyclopentadiene (**6**) also gave a sole 1:1 product (**7**), a colorless oil, which revealed an NMR spectrum very similar with that of **5**, suggesting the same stereochemistry. In this case, a small amount of 1:2 adduct (**8**) was obtained. In addition, cyclohexadiene (**9**) also gave a single product (**10**) by the reaction with **2**. The NMR features of **10** confirmed it to be an analogue of the other adducts in this series.

Parallel with the other experiments, we have carried out Extended Hückel MO calculations of the electronic structure of the ground-state geometry of **2**, which was figured out by inspecting the Dreiding Stereomodel; the stabilization energies of the HOMO level of **6**, as a representative diene, and the LUMO level of **2** for both *cis-cisoid* and *cis-transoid* geometries were calculated by the method of Herndon and Hall,[9] but the figures, $\Delta E_{cis}=7.7$ kJ/mol, and $\Delta E_{trans}=4.6$ kJ/mol, are too small for any definite conclusion to be drawn therefrom. The index for each carbon was also small, as is depicted in Fig. 1, but the signs are in accord with the adducts actually isolated.

As a whole, the Diels-Alder reaction of **2** with dienes proceeded with complete stereospecificity, and there is no isomer in any detectable quantity. It is clear now that the norbornene-type C=C of **2**, which prohibits,

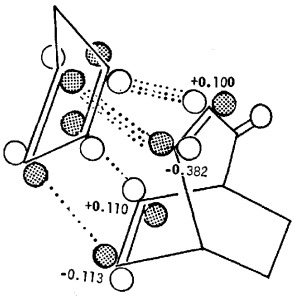

Fig. 1.

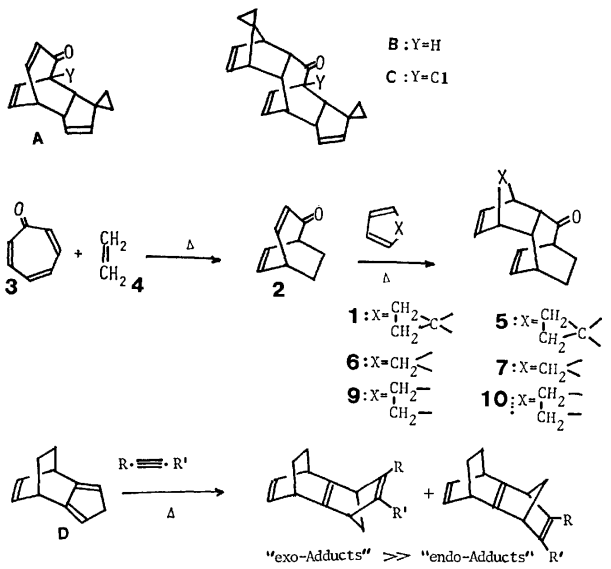

Scheme 1.

on structural grounds, full overlapping with the approaching diene, has determined the course of the product formation. On the contrary, a recent paper of Paquette *et al.*[4] described a somewhat inferior stereoselective adduct formation between a diene (**D**), with structural properties similar to those of **2**, and several acetylenic dienophiles. This seems to be attributable to the difference in the geometry of one component of the addends; linear acetylenic dienophiles can hardly interact with the isolated C=C of **D**.

Experimental

*Diels-Alder Reaction of **3** with **4**.* *Preparation of **2**:*[7] A toluene solution (100 cm³) of **3** (3 g) was placed in an autoclave, gaseous ethylene was introduced under *ca.* 30 atm, and the mixture was heated for 1.5 h at 225 °C. Then, the mixture was worked up in an ordinary manner. The product, purified on a silica-gel column, was **2** (2.93 g, 77%), which showed NMR spectral data identical with those previously reported.

*Diels-Alder Reaction of **2** with **1**.* A mixture of benzene (1 cm³), **2** (150 mg), **1** (1 cm³), and hydroquinone (20 mg) was heated in a sealed tube for 180 h at 130 °C. The mixture was then purified on a silica-gel column with hexane–ethyl acetate (9:1) to give a colorless oil, **5** (45 mg, 58%) [Found: *m/e*, 226.1354 (M^+). Calcd for $C_{16}H_{18}O$: 226.1358. δ: 0.15—0.60 (4H, m), 1.35—2.75 (8H, m), 3.13 (2H, m), 5.32 (1H, t, J=8 Hz), 5.88 (1H, dd, J=6, 3 Hz), 6.09 (1H, dd, J=6, 3 Hz), and 6.12 (1H, t, J=8 Hz). $\nu_{C=O}$: 1685 cm^{-1}], together with the recovered **2** (102 mg, 68%).

*Addition Reaction of **2** with **6**.* A mixture of benzene (1 cm³), **2** (150 mg), **6** (1 cm³), and hydroquinone (50 mg) was heated similarly in a sealed tube at 180 °C for 20 h. The mixture was then purified on a silica-gel column and then further by high pressure liquid chromatography to give **7** (31 mg, 20%) as colorless needles (mp 64—66 °C) [Found: *m/e*, 200.1210 (M^+). Calcd for $C_{14}H_{16}O$: 200.1201. δ: 1.20 (1H, dm, J=9 Hz), 1.34 (1H, dm, J=9 Hz), 1.4—2.0 (4H, m), 2.45 (1H, dt, J=9.5, 3 Hz), 2.57 (1H, m), 2.72 (1H, m), 3.01 (1H, dd, J=9.5, 4 Hz), 3.11 (1H, ddm, J=7.5, 4 Hz), 3.33 (1H, m), 5.31 (1H, ddm, J=8.5, 7.5 Hz), 5.85 (1H, dd, J=6, 3 Hz), 5.95 (1H, dd, J=6, 3 Hz), and 6.08 (1H, ddm, J=8.5, 8 Hz). $\nu_{C=O}$: 1690 cm^{-1}], recovered **2** (46 mg, 31%), and a colorless oil (**8**) [Found: *m/e*, 266.1680 (M^+). Calcd for $C_{19}H_{22}O$: 266.1671. $\nu_{C=O}$: 1685 cm^{-1}], 29 mg (16%).

*Addition Reaction of **2** with **9**.* A mixture of benzene (2 cm³), **2** (550 mg), **9** (2.2 g), and hydroquinone (5 mg) was heated in a sealed tube at 150 °C for 86 h. The mixture was then chromatographed on a silica-gel column with hexane–ethyl acetate (9:1) to give **10** (295 mg, 86%), colorless needles (mp 111—112 °C from benzene) [Found: C, 83.20; H, 8.62%. Calcd for $C_{15}H_{18}O$: C, 83.12; H, 8.97%. δ: 1.1—2.0 (8H, m), 2.24 (1H, dd, J=9.5, 3 Hz), 2.2—2.5 (2H, m), 2.79 (1H, dd, J=9.5, 3 Hz), 3.0—3.3 (2H, m), 5.49 (1H, ddd, J=8, 6, 1.5 Hz), 6.15 (1H, m), and 6.20 (1H, t, J=8 Hz). $\nu_{C=O}$: 1670 cm^{-1}].

References

1) H. Takeshita, T. Hatsui, R. Iwabuchi, and S. Itoh, *Bull. Chem. Soc. Jpn.*, **51**, 1257 (1978).

2) H. Takeshita, T. Hatsui, and H. Mametsuka, *Heterocycles*, **11**, 323 (1978).

3) a) K. Alder and G. Stein, *Angew. Chem.*, **50**, 510 (1937). For modern accounts, see: b) J. Sauer, *Angew. Chem.*, **79**, 76 (1967); c) R. B. Woodward and R. Hoffmann, "The Conservation of Orbital Symmetry," Academic Press, New York (1970), p. 145.

4) M. C. Bohm, R. C. V. Carr, R. Gleiter, and L. L. Paquette, *J. Am. Chem. Soc.*, **102**, 7218 (1980).

5) K. B. Astin and K. Mackenzie, *J. Chem. Soc., Perkin Trans. 2*, **1975**, 1004, and the references cited therein.

6) S. Itô, H. Takeshita, Y. Shoji, Y. Toyooka, and T. Nozoe, *Tetrahedron Lett.*, **1969**, 443.

7) The reaction conditions were slightly modified from those originally reported; T. Uehara and Y. Kitahara, *Chem. Ind. (London)*, **1971**, 354.

8) The NMR spectra were measured in $CDCl_3$ solutions using an FX-100 Model spectrometer, JEOL Co. The chemical shifts were expressed in δ units from the internal standard, Me_4Si.

9) W. C. Herndon and L. H. Hall, *Theor. Chim. Acta*, **7**, 4 (1967).

The Condensation of Isatin with *o*-Phenylenediamine

Kazuma NIUME,* Shigeru KUROSAWA, Fujio TODA,
Masaki HASEGAWA, and Yoshio IWAKURA†
Department of Synthetic Chemistry, Faculty of Engineering, The University of Tokyo, Hongo, Bunkyo-ku, Tokyo 113
(Received September 11, 1981)

Synopsis. The condensation of isatin with *o*-phenylenediamine has been studied in various kinds of solvents. The reaction gave pure indolo[2,3-*b*]quinoxaline (**1**) in acidic solvents, while it gave a mixture containing at least two out three compounds, **1**, an anil and a spiro compound, in neutral or basic organic solvents. The anil and spiro compounds were converted to **1** in the presence of acid or by heating them above their melting points. The mechanism of the formation of these compounds and the conversion could be explained by the presence of the intermediate of the adduct formed between the amino groups of *o*-phenylenediamine and the β-carbonyl of isatin.

o-Phenylenediamine reacts with both carbonyl groups of isatin to form indolo[2,3-*b*]quinoxaline (**1**) in acetic acid.[1,2] It has been reported that spiro compounds were obtained by the reaction of a variety of isatin with aromatic *o*-diamines.[3,4] However, the formation of an anil compound has not been reported. In the present study, it was found that reaction of isatin with *o*-phenylenediamine gave **1**, anil **2**, and spiro **3** compounds, depending upon the reaction conditions. The present paper is also concerned with the conversion of the anil and spiro compounds to **1**.

Results and Discussion

o-Phenylenediamine was allowed to react with isatin in various kinds of solvents (Scheme 1).

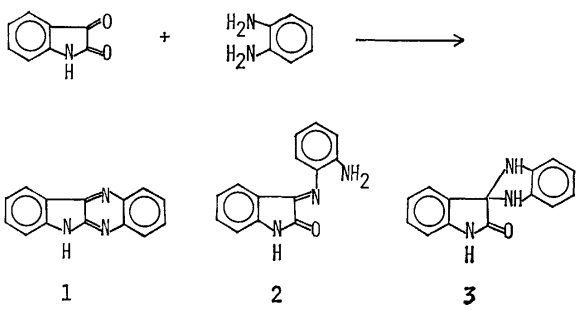

Scheme 1.

When the reaction was carried out in acidic solvents, **1** was obtained exclusively. When polar amide solvents, such as *N*,*N*-dimethylacetamide (DMA) and *N*-methyl-2-pyrrolidone (NMP), were used, the spiro compound (**3**) was obtained in a high yield. The anil compound (**2**) was prepared at a low reaction temperature. The reaction conditions and the yields of the products are summarized in Table 1.

The IR spectra of **3** show characteristic absorptions around 1710 cm^{-1}, they are in good agreement with those observed in the similar spiro compounds prepared by Popp.[3] The carbonyl absorption of **2** was found at 1670 cm^{-1}. Figure 1 shows the infrared spectra of these compounds.

Table 1. The reaction of isatin with *o*-phenylenediamine

Reaction conditions			Yields/%[a]		
Solvents	Temp/°C	Time/h	**1**	**2**	**3**
THF	60	24	—	78	Tr
Benzene	80	7	Tr	76	Tr
Methanol	65	3	39	30	Tr
Pyridine	115	4	41	35	—
DMA	135	3	23	38	27
HMP	180	3	Tr	Tr	89
HMP	200	5	Tr	—	96
Water (HCl)	90	2	79	—	—
Acetic acid	118	3	85	—	—
PPA	140	5	91	—	—

a) Tr: The infrared spectrum of the crude products indicated a trace of the products.

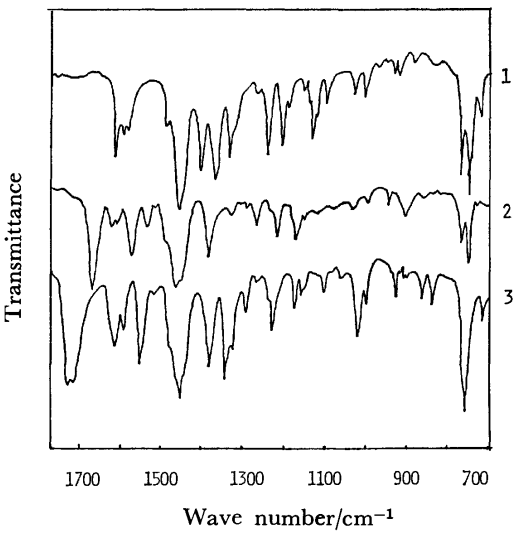

Fig. 1. Infrared spectra of **1**, **2**, and **3**.

As may be seen in Table 1, the reaction gave a mixture containing at least two products out of **1**, **2**, and **3** in neutral or basic organic solvents, while that gave **1** exclusively in acidic solvents. It is well known that ammonia reacts with the β-carbonyl of isatin at a low temperature to give the adduct **4**.[5] The analogous intermediate, **5**, would offer a reasonable explanation of the formation of **1**, **2**, and **3** in the organic solvents. The initial reaction of the amino group with the α-carbonyl of the intermediate, **5**, followed by the removal of two molecules of water would give **1**. The

† Present address: Department of Inductrial Chemistry, Faculty of Engineering, Seikei University, Kichijyoji-kita, Musashino Tokyo 180.

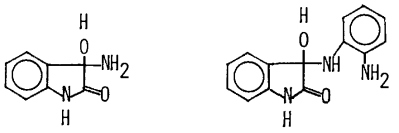

4 5

removal of one molecule of water from **5** appears to give **2**. The nucleophilic attack of the amino group on the β-carbon would lead to the formation of **3**.

Under acidic conditions, the reaction gave **1** exclusively, as has been mentioned previously, and **2** was easily converted to **1** by heating it in acetic acid, acetic anhydride, and polyphosphoric acid (PPA). The facile conversion in the presence of acid is accounted for by the *syn-anti* isomerism of the Schiff base. Apparently, **2** takes the *anti* form preferably, but it would be required to isomerize to the *syn* form, which provides the geometry necessary for the cyclodehydration. Under acidic conditions, the C–N double bond is protonated and the *anti-syn* interconversion is facilitated *via* the conjugated acid of the Schiff base.

In contrast to **2**, **3** was recovered unchanged after heating in acetic anhydride, formic acid, and PPA. However, it was easily converted to **1** by heating it in dilute hydrochloric acid. These results show that the conversion of **3** to **1** also proceeded *via* the intermediate, **5**, which was formed by the hydrolysis of the midazoline ring.

The formation of **1**, **2**, and **3**, and the rearrangements are summarized in Scheme 2.

It was also found out that **2** and **3** were rearranged into **1** by heating. The conversion of **2** proceeded very

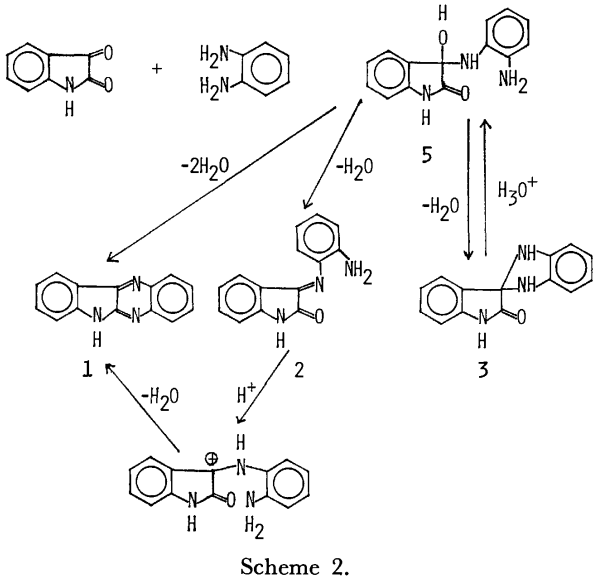

Scheme 2.

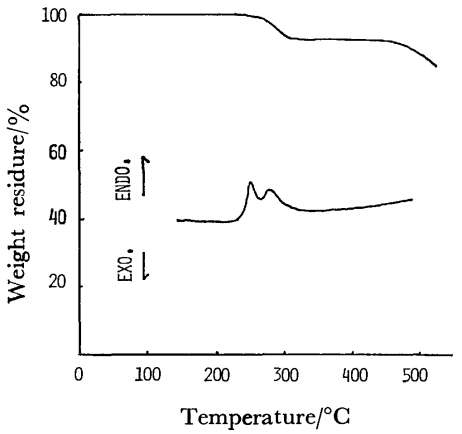

Fig. 2. TG-DSC for the conversion of **2** under nitrogen.

rapidly above its melting point. Figure 2 shows the TG-DSC curves for **2**. The conversion of **3** is a dehydration reaction involving the C–N bond cleavage, and the reaction proceeds slowly upon heating at a higher temperature than 280 °C.

Experimental

3-(o-Aminophenylimino)indolin-2-one (2). A 1.47 g (0.01 mol) of isatin and 1.08 g (0.01 mole) of *o*-phenylenediamine were dissolved in 70 ml of benzene. The solution was refluxed for 7 h and then allowed to stand at room temperature overnight to give orange needles, which were subsequently collected by filtration and washed with water. The spectrum of the crude product indicated the presence of small quantity of **1**. Recrystallization from methanol gave 1.85 g (78%) of **2** as orange needles; mp 249.5—250 °C. Found: C, 70.15; H, 4.87; N, 17.61%. Calcd for $C_{14}H_{11}N_{13}$-O: C, 70.87; H, 4.67; N, 17.71%.

1,3-Dihydrospiro[benzimidazole-2(3H),3'-indolin]-2'-one (3). A solution of a 1.47 g (0.01 mol) of isatin and 1.08 g (0.01 mol) of *o*-phenylenediamine in 40 ml of NMP was heated at 200 °C for 5 h. After cooling, the solution was poured into 500 ml of water to give a yellow precipitate, which was collected by filtration, washed with water, and dried. The IR spectrum of the crude product indicated the presence of a trace of **1**. Recrystallization from methanol gave 2.3 g (96%) of **3** as yellow crystals; mp 285—287 °C. Found: C, 70.87; H, 4.71; N, 17.62%. Calcd for $C_{14}H_{11}$-N_3O: C, 70.87; H, 4.67; N, 17.71%.

References

1) E. Schunck and L. Marchlewski, *Ber.*, **28**, 2528 (1895).
2) I. Schopov and N. Popov, *J. Polym. Sci., A-1*, **7**, 1803 (1969).
3) F. D. Popp, *J. Heterocycl. Chem.*, **6**, 125 (1969).
4) G. Henske and W. Lemke, *Chem. Ber.*, **91**, 101 (1958).
5) A. Reissert and H. Hoppmann, *Ber.*, **57B**, 972 (1924).

Synthesis of a 6-Methylpyridoxine Hydrochloride Derivative as an Electrophilic Precursor for Pyridoxal-like Functionalization

Masaaki IWATA* and Hiroyoshi KUZUHARA

The Institute of Physical and Chemical Research, Wako, Saitama 351

(Received November 11, 1981)

Synopsis. Through a key step of regioselective rearrangement of 5′-*O*-acetyl-3,4′-*O*-isopropylidene-6-methylpyridoxine 1-oxide, stable 5′-deoxy-2′,5′-dichloro-3,4′-*O*-isopropylidene-6-methylpyridoxine hydrochloride, which is expected to be a strong electrophile in an HCl free form, was synthesized from DL-alanine in good yield.

In relation to our systematic studies on the utilization of 2′- and/or 5′-chloropyridoxine derivatives as the electrophilic precursors for pyridoxal-like functionalization, the synthesis and electrophilic reactivity to thiols and sulfonamides have been successfully exemplified in the cases of 5′-deoxy-5′-chloro-3,4′-*O*-isopropylidenepyridoxine hydrochloride (**1**),[1] 5′-deoxy-2′-chloro-3,4′-*O*-isopropylidenepyridoxine hydrochloride (**2**),[1] and 5′-deoxy-2′,5′-dichloro-3,4′-*O*-isopropylidenepyridoxine hydrochloride (**3**).[2] Here we describe a synthetic method of 5′-deoxy-2′,5′-dichloro-3,4′-*O*-isopropylidene-6-methylpyridoxine hydrochloride (**4**) as an alternative precursor, required for completion of our present project. This method was characterized by novel regioselective isopropylidenation of **5** and regioselective rearrangement of an intermediate *N*-oxide (**8**).

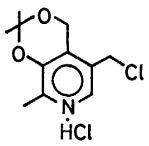
1

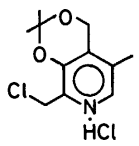
2

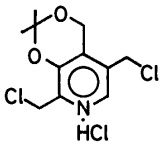
3

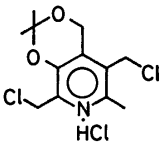
4

Synthesis began with 6-methylpyridoxine (**5**), which was prepared in good yield by the method previously reported.[3] Treatment of **5** with acetone saturated with hydrogen chloride gave 3,4′-*O*-isopropylidene-6-methylpyridoxine hydrochloride regioselectively, which was neutralized to yield the corresponding HCl free form (**6**). The usual acetylation of **6** with acetic anhydride and pyridine afforded 5′-*O*-acetyl-3,4′-*O*-isopropylidene-6-methylpyridoxine (**7**), which was, then,

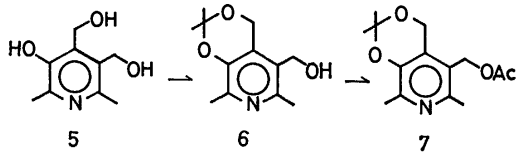
5 6 7

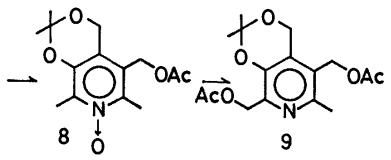
8 9

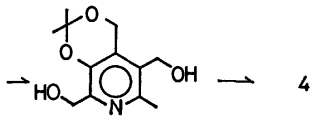
10 4

oxidized with *m*-chloroperbenzoic acid to give 5′-*O*-acetyl-3,4′-*O*-isopropylidene-6-methylpyridoxine 1-oxide (**8**). Rearrangement of **8** with acetic anhydride in chloroform regioselectively gave 2′-acetoxy-5′-*O*-acetyl-3,4′-*O*-isopropylidene-6-methylpyridoxine (**9**). Compound **9** was successfully deacetylated by treatment with sodium methoxide in methanol followed by neutralization with solid carbon dioxide and extraction with ethyl acetate to afford 2′-hydroxy-3,4′-*O*-isopropylidene-6-methylpyridoxine (**10**). This was successfully chlorinated with thionyl chloride in benzene to yield **4**.

The regioselectivity in isopropylidenation of **5** is due probably to the concentration of hydrogen chloride as was established in the previous report.[4] As reported by Traynelis and Pacini[5a] and others,[5b,c] the rearrangement of pyridine 1-oxide with acetic anhydride occurs intramolecularly through a rate-controlling conversion of 1-acetoxy-2-methylpyridinium ion to an anhydrobase by proton abstraction. Therefore, facility of proton release from either methyl group at C_2 or C_6 in **8** determines the product. Since C_6-methyl protons always appear at lower field in ^{1}H NMR spectra (Table 1) than C_2-methyl protons and are interacting with a neighboring acetyl carbonyl group at C_5, release of a proton from C_6-methyl group seems less favorable than that from a C_2-methyl group.

TABLE 1. ^{1}H NMR SPECTRAL DATA OF 6-METHYLPYRIDOXINE DERIVATIVES
(δ ppm, IN $CDCl_3$ AT AMBIENT TEMPERATURE)

Compound	$C(CH_3)_2$	$-COCH_3$	C_2-CH_3	C_6-CH_3	$5'CH_2-O$	$4'CH_2-O$	$2'CH_2-O$
6	1.53	—	2.36	2.44	4.58	4.59	—
7	1.54	2.06	2.39	2.51	5.00	4.91	—
8	1.57	2.07	2.45	2.56	5.00	4.95	—
9	1.54	a)	—	2.55	5.01	4.95	5.18
10	1.53	—	—	2.55	4.63	4.99	4.63

a) $5'C-O-COCH_3$ at 2.07 and $2'C-O-COCH_3$ at 2.12 ppm.

Utilization of **4** as a precursor for an electrophilic construction unit will be reported elsewhere.

Experimental

The ^{1}H NMR spectra were recorded on a Japan Electron Optics Laboratory JEOL FX-400 apparatus with TMS as the internal standard in chloroform-*d* and the chemical shift was represented by δ. IR spectra were recorded on a Shimadzu IR-27 instrument. Merck silica gel 60 (Art. 7734, 0.063—0.20 mm) was used for the column chromatography and Wakogel B-5 FM (Wako Pure Chem. Co., Ltd.) for the thin layer chromatography (TLC), in which product spots were visualized in an iodine-vapor bath. The mp are uncorrected, measured in a bilayered cover glass (18 m/m) with micro melting point apparatus (Yanagimoto Seisakusho, serial No. 2647). Solvent system:benzene:ethyl acetate, 3:2 v/v (solvent A) and 9:1 v/v (solvent B). 6-Methylpyridoxine (**5**) was prepared by the method described in Ref. 3, in good yield from DL-alanine and dimethyl maleate.

Preparation of 3,4'-O-Isopropylidene-6-methylpyridoxine (6). A suspended mixture of 10.34 g of **5** in 200 ml of dry acetone was saturated with hydrogen chloride while being stirred and cooled in an ice-bath. Then, the flask was allowed to stand in a refrigerator overnight. After 500 ml of diethyl ether was mixed and stirred into the flask, the resulting colorless precipitate (hydrochloride) was collected by filtration. The hydrochloride of **6** dissolved in a minimum amount of water was neutralized by portional addition of sodium hydrogencarbonate saturated in water followed by extraction with chloroform to give 10 g of **6** as a colorless liquid, which spontaneously crystalized; mp 141.5—143 °C. Found: C, 64.09; H, 7.63; N, 5.93%. Calcd for $C_{12}H_{17}O_3N$: C, 64.55; H, 7.68; N, 6.27%. ^{1}H NMR data are listed in Table 1. IR (KBr disk) ν 3180, 3000, 2940, 1601, 1440, 1386, 1375, 1280, 1245, 1200, 1146, 1104, 1069, 1040, 1024, 996, 983, 875, 867, 795, 703, 676, 564, 530, and 497 cm^{-1} as characteristic bands.

Preparation of 5'-O-Acetyl-3,4'-O-isopropylidene-6-methylpyridoxine (7). To a solution of 3.077 g of **6** in 15 ml of pyridine, 15 ml of acetic anhydride was added all at once while being stirred. After subsequent stirring at the ambient temperature for 1 h, the mixture was poured into water (*ca.* 200 ml) and, then, extracted with chloroform, which was dried over $MgSO_4$ and filtered through Celite (No. 545). The solvent was removed under reduced pressure and the residue was chromatographed on a silica gel (200 g) column, eluted with solvent A, to give 3.29 g of **7** (90% yield); colorless liquid, R_f 0.7 (solvent A). Found: C, 63.61; H, 7.10; N, 5.18%. Calcd for $C_{14}H_{19}O_4N$: C, 63.38; H, 7.22; N, 5.28%. ^{1}H NMR data are listed in Table 1. IR (KRS neat) $\nu_{C=O}$ 1738 cm^{-1}.

Preparation of 5'-O-Acetyl-3,4'-O-isopropylidene-6-methylpyridoxine 1-Oxide (8). To 0.37 g of **7** in 10 ml of chloroform, 0.283 g of 85% pure *m*-chloroperbenzoic acid was added portion by portion at the ambient temperature. The reaction was monitored by TLC until **7** disappeared. The reaction mixture was neutralized by addition of sodium acetate after addition of 10 ml of water. After the usual work-up, 0.34 g (87% yield) of **8** was obtained by chromatography (solvent A) as a colorless liquid; R_f 0.2 (solvent A). ^{1}H NMR data are listed in Table 1. IR (KRS neat) $\nu_{C=O}$ 1740; ν 1560, 1490, 1375, 1300, 1220, 1130, 1070, 1025, 878, 828, and 581 cm^{-1} as characteristic bands. Found: C, 59.24; H, 6.64; N, 4.64%. Calcd for $C_{14}H_{19}O_5N$: C, 59.77; H, 6.81; N, 4.98%.

Preparation of 2'-Acetoxy-5'-O-acetyl-3,4'-O-isopropylidene-6-methylpyridoxine (9). A solution of 0.3 g of **8** in 2 ml of acetic anhydride and 5 ml of chloroform was heated at 50 °C for 20 min. After removal of solvents under reduced pressure, the residue was chromatographed on a silica gel (20 g) column, eluted with solvent A, to afford 0.304 g (88% yield) of **9** as colorless liquid; R_f 0.7 (solvent A). Found: C, 59.43; H, 6.48; N, 4.14%. Calcd for $C_{16}H_{21}O_6N$: C, 59.43; H, 6.55; N, 4.33%. ^{1}H NMR data are summarized in Table 1. IR (KRS neat) ν 1740, 1440, 1378, 1282, 1220, 1145, 1112, 1025, 965, 870, 792, and 605 cm^{-1} as characteristic bands.

Preparation of 2'-Hydroxy-3,4'-O-isopropylidene-6-methylpyridoxine (10). To a sodium methoxide solution, which was prepared by addition of 0.05 g of metal sodium to 10 ml of methanol, 0.266 g of **9** in 5 ml of methanol was added dropwise. The reaction was completed immediately. The mixture was neutralized by portional addition of pieces of solid carbon dioxide. After removal of the solvent, the residue was triturated with ethyl acetate followed by filtration through Celite (No. 545). The filtrate was evaporated under reduced pressure followed by recrystallization from ethanol to give 0.15 g (76% yield) of **10**; colorless plates, mp 168.5—170 °C. Found: C, 60.30; H, 7.25; N, 5.76%. Calcd for $C_{12}H_{17}O_4N$: C, 60.24; H, 7.16; N, 5.85%. ^{1}H NMR data are listed in Table 1. IR (KBr disk) ν 3320, 3050, 2990, 2940, 2880, 2760, 1595, 1570, 1430, 1382, 1370, 1280, 1265, 1202, 1140, 1105, 1040, 1015, 1002, 990, 958, 940, 872, 800, 743, 676, 655, 635, 597, 535, and 490 cm^{-1} as characteristic bands. R_f 0.5 ($CHCl_3$: methanol 9:1 v/v).

Preparation of 5'-Deoxy-2',5'-dichloro-3,4'-O-isopropylidene-6-methylpyridoxine Hydrochloride (4). To a suspended mixture of 2.33 g of **10** in 40 ml of benzene, 1.41 ml of thionyl chloride in 10 ml of benzene was added dropwise, resulting in coagulation and, then, a transparent solution without color change. After stirred for 30 min at ambient temperature, 50 ml of diethyl ether was added for precipitation. The precipitate was collected by filtration and washed several times with diethyl ether to give 2.643 g (87% yield) of **4.** A part of the product was recrystallized from acetone for analytical use; colorless crystals, mp 143 °C (browning with melt) —150 °C (decomposed with evolving gas) and —162 °C (complete melt and decomposition with browning and resulting in viscous liquid). Found: C, 46.29; H, 5.22; N, 4.48; Cl, 34.02%. Calcd for $C_{12}H_{16}O_2NCl_3$: C, 46.10; H, 5.16; N, 4.48; Cl, 34.02%. IR (KBr disk) ν 3020, 2960, 2350, 1960, 1632, 1540, 1470, 1430, 1417, 1377, 1365, 1312, 1285, 1253, 1204, 1135, 1110, 1075, 1050, 1010, 990, 980, 967, 943, 925, 912, 850, 838, 736, 721, 649, 618, 552, 492, and 425 cm^{-1} as characteristic bands.

The authors are grateful to Dr. Haruo Homma and his staff in this Institute for elemental analyses.

References

1) M. Iwata and H. Kuzuhara, *Bull. Chem. Soc. Jpn.*, **55**, 2153 (1982).

2) M. Iwata, H. Kuzuhara, and S. Emoto, *Chem. Lett.*, **1976**, 983; H. Kuzuhara, M. Iwata, and S. Emoto, *J. Am. Chem. Soc.*, **99**, 4173 (1977); M. Iwata and H. Kuzuhara, *Chem. Lett.*, **1981**, 1749.

3) N. D. Doktrova, L. V. Ionova, M. Ya. Karpeisky, N. Sh. Padyukova, K. F. Turchin, and V. L. Florentiev, *Tetrahedron*, **25**, 3527 (1969).

4) W. Korytnyk, *J. Org. Chem.*, **27**, 3724 (1962); W. Korytnyk and W. Wiedeman, *J. Chem. Soc.*, **1962**, 2531.

5) a) V. J. Traynelis and P. L. Pacini, *J. Am. Chem. Soc.*, **86**, 4917 (1964); b) J. H. Margraf, H. B. Brown, Jr., S. C. Mohr, and R. G. Peterson, *ibid.*, **85**, 958 (1963); c) S. Oae, T. Kitao, and Y. Kitaoka, *ibid.*, **84**, 3359 (1962).

The Disproportionation of *cis*-Bicyclo[4.3.0]nona-3,7-diene Catalyzed by $Fe(CO)_5$ and $Cp_2Fe_2(CO)_4$

Takashi KAGAYAMA, Shinji OKABAYASHI, Yoichi AMAIKE, Yasuo MATSUKAWA, Yasutaka ISHII, and Masaya OGAWA*

Department of Applied Chemistry, Faculty of Engineering, Kansai University, Senriyama, Suita, Osaka 564

(Received November 12, 1981)

Synopsis. *cis*-Bicyclo[4.3.0]nona-3,7-diene (**1**) was catalytically disproportionated by the use of $Fe(CO)_5$ and $Cp_2Fe_2(CO)_4$ to bicyclo[4.3.0]non-1(6)-ene (**3**) and indan (**4**). However, the same reaction catalyzed by the use of other metal carbonyls gave merely small amounts of **3** and **4**, while those using Pd– and Rh–carbons yielded only **4** and the starting material, **1**, respectively.

A variety of double-bond migration reactions of olefins and dienes catalyzed by transition-metal complexes are well known.[1] Nonconjugated dienes are usually converted into conjugated dienes with $Fe(CO)_5$, and the resulting 1,3-dienes form metal carbonyl complexes.[2] Recently, Tureček has reported a titanocene-catalyzed isomerization of *cis*-bicyclo[4.3.0]nona-3,7-diene (**1**) to bicyclo[4.3.0]nona-2,9-diene (**2**) (Eq. 1).[3]

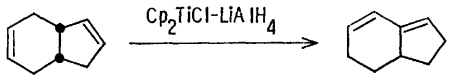

(1)

1 **2**

However, the reaction of **1** catalyzed by $Fe(CO)_5$ gave bicyclo[4.3.0]non-1(6)-ene (**3**) and indan (**4**) (Eq. 2). In this communication, we wish to report the disproportionation reaction of **1** catalyzed by several iron complexes.

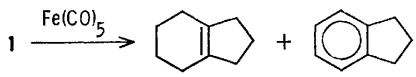

(2)

3 **4**

The reaction of **1** with a catalytic amount of $Fe(CO)_5$ at 230 °C for 4 h gave approximately equal amounts of **3** (40%) and **4** (39%), as well as, an oligomer (7%) containing a small amount of tetracarbonylbis(η^5-4,5,6,7-tetrahydroindenyl)diiron (**5**) (3%).[4]

Figure 1 shows some typical plots of the time conversion curves of **1**, **3**, and **4**. Since about the same amounts of **3** and **4** were obtained in all stages of the reaction, **1** should be disproportionally converted to **3** and **4**. The complex **5** was formed in much larger quantities in the early stage of the reactions. The stoichiometric reaction of **1** and $Fe(CO)_5$ gave **5**, in a yield of 35—40%, in addition to **3** and **4**.[5]

It is interesting to clarify whether the **5** complex is one of the products or a precursor of the disproportionation products. Thus, the reaction of **1** with **5** or tetracarbonylbis(η^5-cyclopentadienyl)diiron (**6**), which is structurally analogous to **5**, as a catalyst, was studied under similar conditions. The results are summarized in Table 1.

The reaction catalyzed by **5** gave **3** and **4** in a fashion similar to that found in the case of $Fe(CO)_5$, although the reaction rate was only about half as great. However, **5** was not recovered after the reaction because of the decomposition. Similarly, the **6** complex also promoted the disproportionation of **1** to give **3** and **4**. The reaction rate was slightly faster than that by $Fe(CO)_5$, and almost all of the **6** was recovered unchanged. Thus, **6** was found to be an excellent catalyst for the disproportionation of **1**.

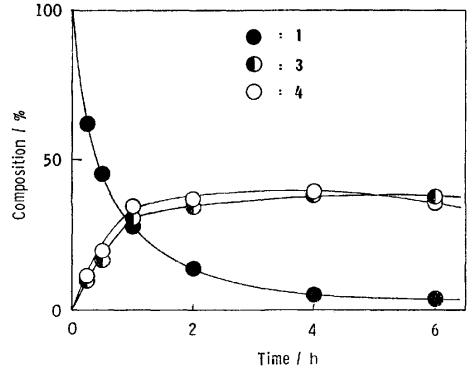

Fig. 1. Disproportionation of 1 catalyzed by $Fe(CO)_5$. **1**/$Fe(CO)_5$=10/1 (molar ratio), 230 °C

TABLE 1. DISPROPORTIONATION OF **1** BY VARIOUS IRON COMPLEXES[a]

Catalyst	Composition/%[b]			
	1	**3**	**4**	Oligomers
$Fe(CO)_5$	11.2	39.8	38.5	10.5[c]
5	44.5	23.6	22.8	9.1
6	6.2	44.2	42.8	6.8

a) The reactions were carried out on 100-mmol scale with **1**/catalyst (molar ratio **1**/$Fe(CO)_5$=10/1, **1**/**5**=20/1, **1**/**6**=20/1) at 230 °C for 4 h in an autoclave. b) Estimated on the basis of the **1** used. c) A small amount of **5** was present.

Sufficient evidence has not been provided to establish a detailed reaction pathway for the disproportionation of **1**. However, it may be noted that the first step in the disproportionation is the hydrogen-migration reaction of **1** to a conjugated diene, followed by a reaction with $Fe(CO)_5$ to give diene iron tricarbonyl complexes, such as **7**, **8**, or **9**, which are not isolated. Then, the iron atom abstracts an allylic hydrogen, yielding a π-allyl-hydro-iron complex (**10**),[6] which seems to be an essential intermediate for the disproportionation of **1**, followed by intra- or intermolecular hydrogen transfer with other organic or iron species to produce **3** and **4**.

The disproportionation of **1** catalyzed by **5** and **6** is probably initiated by the homolytic cleavage of **5**

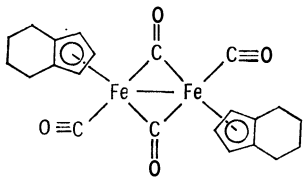

5

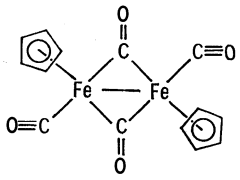

6

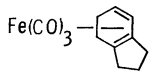

7

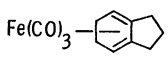

8

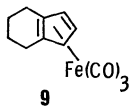

9

π-C_9H_{11}-$FeH(CO)_3$

10

and **6** to dicarbonyl(η^5-3,4,5,6-tetrahydroindenyl)iron (Fpi), and dicarbonyl(η^5-cyclopentadienyl)iron (Fp) fragments,[7] which then react with **1** to yield a diene iron complex. Subsequently, the reaction proceeds through a path analogous to that followed by $Fe(CO)_5$ to produce **3** and **4**. The outline of the disproportionation catalyzed by iron complexes is presented in Scheme 1.

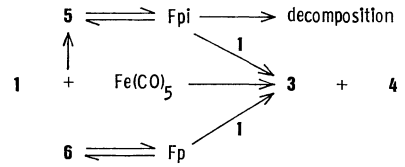

Scheme 1. Outline of Disproportionation of **1** Catalyzed by **5** and **6**.

The difference in catalytic activity between **5** and **6** may be due to the ease of their homolytic cleavage and the stability of the resulting Fpi and Fp moieties in the course of the reaction.

The same reaction catalyzed by several metal carbonyls, such as Cr, Mn, Mo, and $Cp_2Mo_2(CO)_6$, gave only small amounts of **3** and **4**. No disproportionation product was obtained by the reaction of **1** catalyzed by Pd- and Rh-carbons, which are typical hydrogenation catalysts; *i.e.*, the dehydrogenated product, **4**, was exclusively produced by Pd, and the starting material, **1**, was recovered only by the use of Rh-carbon.

Experimental

The melting points are uncorrected. The IR spectra were taken with a JASCO-A202 spectrometer. The ^{1}H-NMR and ^{13}C-NMR spectra were recorded with a JEOL PMX-60 and a JNM-PS-100 FT-NMR spectrometer respectively. The mass spectra were measured with a JEOL-01SG apparatus. The GLC analyses were carried out on a Yanagimoto G1800 apparatus.

Materials. *cis*-Bicyclo[4.3.0]nona-3,7-diene (**1**) was prepared by a procedure reported previously.[8]

Tetracarbonylbis(η^5-cyclopentadienyl)diiron (**6**) was prepared accordingly to the King method.[9]

Tetracarbonylbis(η^5-4,5,6,7-tetrahydroindenyl)diiron (**5**) was prepared as follows: *cis*-Bicyclo[4.3.0]nona-3,7-diene **1** (12.0 g, 100 mmol) was allowed to react with $Fe(CO)_5$ (19.6 g, 100 mmol) in an autoclave at 230 °C for 4 h. After the filtration of the reaction mixture, the filtrate was dissolved in dichloromethane (200 dm^3). The crystals which separated out were collected and recrystallized from a solution of dichloromethane and hexane (1:9); ^{13}C-NMR ($CDCl_3$) δ 22.1(t), 22.6(t), 83.4(d), 89.2(d), 104.1(s), 214.0(s), 217.2(s); IR (KBr) 634, 831, 1432, 1754, 1951, 2920 cm^{-1}; MS *m/e* 462 (M^+), 175, 171 (base peak), 115, 91; Found: C, 57.11; H, 4.79%. Calcd for $C_{22}H_{22}O_4Fe_2$: C, 57.18; H, 4.80%.

Disproportionation Catalyzed by $Fe(CO)_5$. A mixture of **1** (12.0 g, 100 mmol) and a catalytic amount of $Fe(CO)_5$ (1.96 g, 10 mmol) was heated in an autoclave under a nitrogen atmosphere at 230 °C for 1—6 h. The reaction mixture was then poured into hexane to separate the **5**. After the removal of **5** and the solvent, bicyclo[4.3.0]non-1(6)-ene, **3** and **4**, were isolated; **3**, ^{1}H-NMR (CCl_4) δ 1.66 (m, 4H), 1.76 (m, 2H), 1.92 (m, 4H), 2.13—2.16 (m, 4H); ^{13}C-NMR ($CDCl_3$) δ 21.9(t), 23.4(t), 26.6(t), 36.3(t), 134.1(s); **4**, ^{1}H-NMR (CCl_4) δ 1.82 (q, 2H), 2.54 (t, 4H), 6.34 (s, 4H); ^{13}C-NMR ($CDCl_3$) δ 25.3(t), 32.8(t), 124.2(d), 125.9-(d), 143.9(s).

Compound **3** was hydrogenated on Pd-carbon to *cis*-perhydroindene, which was also formed by the hydrogenation of **1**.

*Disproportionation Catalyzed by **5** and **6**.* The reaction was performed by the above procedure.

References

1) H. Alper, "Transition Metal Organometallics in Organic Synthesis," Academic Press, New York (1976), Vol. 1, p. 49.

2) J. E. Arnet and R. Pettit, *J. Am. Chem. Soc.*, **83**, 2954 (1961).

3) F. Tureček, H. Autropiusová, K. Mach, V. Hanuš, and P. Sedmera, *Tetrahedron Lett.*, **1980**, 637.

4) Complex **5** is derived from spirononadiene by the use of $Fe(CO)_5$: B. F. Hallam and P. L. Pauson, *J. Chem. Soc.*, **1958**, 646.

5) The yield is comparable to that obtained by Hallam method.[4]

6) π-Allyl-hydro-iron complex is proposed by Pettit in the isomerization of *cis*-1,3-pentadiene to *trans*-1,3-pentadiene: R. Pettit, G. Emerson, and J. Mahler, *J. Chem. Educ.*, **40**, 175 (1963).

7) M. Rosenblum, *Acc. Chem. Res.*, **7**, 122 (1974).

8) S. Tsuchida, T. Sasaki, and M. Ogawa, *J. Jpn. Petro. Inst.*, **15**, 294 (1972).

9) R. B. King and F. G. A. Stone, *Inorg. Synth.*, **7**, 110 (1963).

Optical Resolution of 2-(Anilinomethyl)pyrrolidine

Kazuhiko SAIGO,*,† Jun TANAKA, and Hiroyuki NOHIRA
Department of Applied Chemistry, Faculty of Engineering Saitama University, 255 Shimo-ohkubo, Urawa 338
(Received February 3, 1982)

Synopsis. (±)-2-(Anilinomethyl)pyrrolidine, prepared from (±)-5-oxopyrrolidine-2-carboxylic acid, was effectively resolved into a pair of the enantiomers by fractional crystallization of its mandelic acid salt. Moreover, the preferential crystallization of its *p*-hydroxybenzoic acid salt was found to give both enantiomers in high optical purities by alternate seeding.

Optically active 2-(anilinomethyl)pyrrolidine is widely used as an effective chiral source for asymmetric inductions.[1] The diamine has been prepared from optically active proline[1a] or glutamic acid[2] maintaining the asymmetric center. The methods have a problem in total yield, chemical purity and/or optical purity, especially in the case of the preparation in a large scale, since they involve multiple reaction steps or drastic reaction conditions. In this paper, we wish to report a convenient and practical method for the preparation of a pair of the enantiomers of 2-(anilinomethyl)pyrrolidine.

(±)-(Anilinomethyl)pyrrolidine ((±)-**1**) was easily prepared by the reaction of commercially available (±)-5-oxopyrrolidine-2-carboxylic acid and aniline according to the procedure in the literature, followed by the reduction with $LiAlH_4$. After several examinations of a suitable resolving agent for the resolution of (±)-**1**, it was found that the effective fractional crystallization was achieved by utilizing optically active mandelic acid (**2**) to give almost optically pure (+)- and (−)-**1** over 65% yields without recrystallization. Moreover, the efficiency of the resolution was found to unchange by reducing the amount of **2** to 0.8 equimolar amount because there is great difference in the solubilities of the diastereomeric pair and **1** is very soluble in the solvent used.

Next, to find out the derivative of **1** resolvable by preferential crystallization which gives more conveniently both enantiomers, salts of **1** with achiral carboxylic acids such as acetic, cinnamic, phthalic, *cis*-cyclohexanedicarboxylic, benzoic, *p*-nitrobenzoic, *p*-chlorobenzoic, and *p*-hydroxybenzoic acids were prepared. Among these salts, *p*-hydroxybenzoic acid salt (**3**) was found to be deposited as conglomerate, which can be resolved by preferential crystallization.

Actually, 1.73 g of (+)-**3** was obtained in 94% optical purity by seeding of optically pure (+)-**3** to the supersaturated solution of (±)-**3** and (±)-**1**·(±)-lactic acid salt, which is readily soluble in the solvent employed and plays as a kind of buffer to decrease the concentration change of 2-(anilinomethyl)pyrrolidinium ion during the crystallization. Alternate seeding of (−)- or (+)-**3** to the supersaturated solution in a similar magnitude gave (−)- or (+)-**3** in 93—98% optical purity. The initial part of the preferential crystallization is shown in Table 1.

Experimental

Melting points were determined on a Laboratory Devices Mel-Temp apparatus and are uncorrected. The values of specific rotation were measured on a JASCO DIP-181 digital polarimeter.

Materials. 5-Oxopyrrolidine-2-carboxanilide was prepared in 82% yield from 0.5 ml of (±)-5-oxopyrrolidine-2-carboxylic acid and 320 ml of aniline according to the method described in the literature,[3] and half the amount of aniline used was able to be recovered after the reaction period. The reaction of 0.36 mol of the anilide with 2.5 molar amounts of $LiAlH_4$ in THF gave (±)-**1** in 89% yield.

The optically pure diastereomeric salts ((+)-**1**·(+)-**2** and (−)-**1**·(−)-**2**) for seeds were prepared by the method described below in one-fourth scale without seeding, followed by recrystallizations from 99% methanol for three times: mp 172—173 °C; $[\alpha]_{435}^{18}$ + and −185.0° (*c* 1.00, 99% MeOH).

Table 1. Preferential crystallization of (±)-3

Run	(±)-3 Added / g	Seed	Cooling		Yield / g	$[\alpha]_{435}$[a]/°	Optical purity/%[b]
			Temp/°C	Time/min			
1	—	(+)	6	120	1.73	+76.9	94
2	2.50	(−)	6	120	3.50	−76.4	93
3	4.00	(+)	6	60	4.50	+78.2	95
4	4.50	(−)	15	50	4.76	−77.8	95
5	4.50	(+)	15	50	4.38	+79.0	96
6	4.50	(−)	15	40	4.23	−79.4	97
.	.	.	.	.	.	.	.
.	.	.	.	.	.	.	.
.	.	.	.	.	.	.	.

a) *c* 1.00, 99% MeOH. b) Based on $[\alpha]_{435}$ + or −82.0°.

† Present address: Department of Synthetic Chemistry, Faculty of Engineering, The University of Tokyo, Hongo, Bunkyo-ku, Tokyo 113.

Found: N, 8.64%; 8.53%. Calcd for $C_{19}H_{24}N_2O_3$: N, 8.53%.

Racemic and optically active **3** were obtained in 83—88% yields from equimolar amounts of *p*-hydroxybenzoic acid and (±)-, (+)-, and (−)-**1**, respectively, followed by recrystallization from 95% ethanol.

Racemic form: mp 160—162 °C.

Found: N, 8.96%. Calcd for $C_{18}H_{22}N_2O_3$: N, 8.91%.

Optically active forms: mp 176—177 °C, $[\alpha]_{435}^{18.5}$ + and −82.0° (*c* 1.00, 99% MeOH).

Found: N, 9.00%, 8.82%. Calcd for $C_{18}H_{22}N_2O_3$: N, 8.91%.

Fractional Crystallization of ***1*****·****2*** *Salt.* To a gently refluxing solution of (±)-**1** (35.25 g, 0.200 mol) in 99% methanol (300 ml) was added a solution of (+)-**2** (24.32 g, 0.160 mol) in 99% methanol (100 ml) in a period of 15 min. The solution was seeded with crystals of (+)-**1**·(+)-**2** salt (50 mg), stood for 40 min at room temperature, and cooled with an ice bath for 2.5 h. The precipitates appeared were collected by filtration, washed with a small amount of 99% methanol, and dried over P_2O_5 to yield 23.74 g (72%) of (+)-**1**·(+)-**2** salt: mp 172.5—173.5 °C; $[\alpha]_{435}^{14.5}$ +184.5° (*c* 0.99, 99% MeOH). The suspension of the salt in benzene (170 ml) was treated with 1 M NaOH solution (110 ml) to decompose the salt. After separation of the organic layer, the aq. solution was extracted with benzene (2×100 ml). The organic layer and the extracts were combined, dried with K_2CO_3, and concentrated under reduced pressure. Distillation of the oil remained gave 11.89 g (67% total yield) of (+)-**1**: bp 134—135 °C/80 Pa; $[\alpha]_{589}^{20}$ +19.3° (*c* 0.98, abs. EtOH).

The minus enriched diamine recovered from the mother liquor (21.70 g, 0.123 mol) in 99% methanol (200 ml) was similarly reacted with (−)-**2** (18.70 g, 0.123 mol) in 99% methanol (100 ml), and the solution was seeded with (−)-**1**·(−)-**2** salt (50 mg) to give 25.54 g (78%) of (−)-**1**·(−)-**2** salt: mp 172—173 °C; $[\alpha]_{435}^{15}$ −184.0° (*c* 0.96, 99% MeOH). The similar treatment of the salt with 1 M NaOH solution gave 12.66 g (72% total yield) of (−)-**1**: bp 133—134 °C/80 Pa; $[\alpha]_{589}^{18}$ −19.2° (*c* 1.07, abs. EtOH).

GLC analysis of the products, (+)- and (−)-**1**, gave no peak other than one arising from **1**. No rise of the specific rotations of (+)-**1**·(+)-**2** and (−)-**1**·(−)-**2** salts ($[\alpha]_{435}$ + and −185.0°) used as seeds was observed by recrystallizations for more three times, and the specific rotations at 589 nm in abs. ethanol of (+)- and (−)-**1** liberated from the salts were + and −19.3°, respectively, which were considered to be maximal values of the specific rotations. Based on the data, the chemical and optical purities of (+)- and (−)-**1** obtained here were considered to be over 99%.

The resolving agents used, (+)- and (−)-**2**, were satisfactorily recovered over 93% yield without racemization from the corresponding aq. solution by acidification with aq. HCl solution, followed by extraction with ether.

Preferential Crystallization of ***3****.* A refluxed clear solution of (±)-**3** (11.62 g) and (±)-**1**·(±)-lactic acid (12.78 g) in 95% ethanol (60 ml) was allowed to cool at about 40 °C, seeded with (+)-**3** (20 mg), and stood for 2 h at around 6 °C. The precipitates appeared were collected by filtration, washed with a small amount of 95% ethanol, and dried over P_2O_5 to give 1.73 g of (+)-**3** (94% optical purity). Successively, (±)-**3** (2.50 g) was added to the filtrate and dissolved at an elevated temperature. The solution was similarly cooled, seeded with (−)-**3** (20 mg), and stood at 6 °C for 2 h to yield 3.50 g of (−)-**3** (93% optical purity). The process was repeated in a similar manner supplying 4.50 g of (±)-**3** in each run to give 4.0—4.8 g of optically active **3** in 93—98% optical purity. The initial six runs is shown in Table 1. The crystals having the same sign of optical rotation were combined and recrystallized from 95% ethanol, giving almost optical pure (+)- or (−)-**3** in 86—90% yield. For examples, recrystallization of 10.30 g of (+)-**3** (95% optical purity on the average) from 95% ethanol (85 ml) gave almost optically pure (+)-**3**: 9.02 g (88%); $[\alpha]_{435}^{15}$ +81.7° (*c* 1.01, 99% MeOH); >99% optical purity. Suspension of the salt in benzene (60 ml) was treated with 3 M NaOH solution (120 ml). After separation of the organic layer, the aq solution was extracted with benzene (2×50 ml). The organic layer and the extracts were combined, dried with K_2CO_3, and concentrated under reduced pressure. Bulb to bulb distillation of the crude product gave 4.21 g (94%) of (+)-**1**: bp 150 °C (bath temperature)/106 Pa; $[\alpha]_{589}^{19}$ +19.2° (*c* 1.45, abs. EtOH); >99% chemical and optical purities.

Similarly, recrystallization of 12.19 g of (−)-**3** (95% optical purity on the average) gave almost optically pure (−)-**3**: 10.56 g (87%); $[\alpha]_{435}^{18.5}$ −81.8° (*c* 1.02, 99% MeOH). Decomposition of the salt, followed by distillation gave 5.01 g (93%) of (−)-**1**: $[\alpha]_{589}^{19}$ −19.3° (*c* 1.39, abs. EtOH); >99% chemical and optical purities.

The authors thank Yamakawa Chemical Industrial Co. Ltd. for a gift of optically active mandelic acid.

References

1) For examples: a) M. Asami, H. Ohno, S. Kobayashi, and T. Mukaiyama, *Bull. Chem. Soc. Jpn.*, **51**, 1869 (1978); b) T. Mukaiyama, Y. Sakito, and M. Asami, *Chem. Lett.*, **1978**, 1253; c) M. Asami and T. Mukaiyama, *ibid.*, **1979**, 569; d) T. Mukaiyama, Y. Sakito, and M. Asami, *ibid.*, **1979**, 705; e) M. Asami and T. Mukaiyama, *ibid.*, **1980**, 17.

2) S. Iriuchijima, *Synthesis*, **1978**, 684.

3) W. H. Gray, *J. Chem. Soc.*, **1928**, 1264.

A Cyclization of Humulene by Means of a Mercuric Salt in Aceto- and Benzonitrile

Kiyoharu HAYANO, Haruhisa SHIRAHAMA,* and Takeshi MATSUMOTO*
Department of Chemistry, Faculty of Science, Hokkaido University, Sapporo 060
(Received January 12, 1982)

Synopsis. Humulene was converted to 3,6-secoprotoilludane derivatives by treatment with mercury(II) trifluoroacetate in aceto- and benzonitrile.

For the purpose of accomplishing a biogenetically patterned chemical cyclization of humulene (**1**)[1] to illudoids and hirsutanoids,[2] mercury(II) salt induced cyclization of humulene had been examined. The key reaction, C(2)–C(9) bond formation, was previously achieved[1b,c] by using mercury(II) acetate in aqueous acetic acid or mercury(II) nitrate in aqueous tetrahydrofuran to give ethereal 3,6-secoprotoilludane derivatives **2**, **3**, and **4** (Fig. 1). The cyclization did not, however, proceed further to form the protoilludane or a hirsutane skeleton. Clearly, the formation of the ethereal products became favourable because of the presence of the cosolvent water. If the reaction was performed in a neat, polar aprotic solvent, further cyclized, tricyclic skeletons could be obtained. We report here the results of mercury induced cyclization of humulene in anhydrous nitriles.

Humulene was treated with more than 2 equivalents of mercury(II) trifluoroacetate in dry acetonitrile at room temperature and a product was demercurated with sodium borohydride and subsequently acetylated. Chromatographic purification gave a crystalline compound **5** in 60% yield. The mercuration-demercuration in benzonitrile was also carried out in the same manner without subsequent acetylation, and a crystalline mass **6** was obtained in 66% yield.

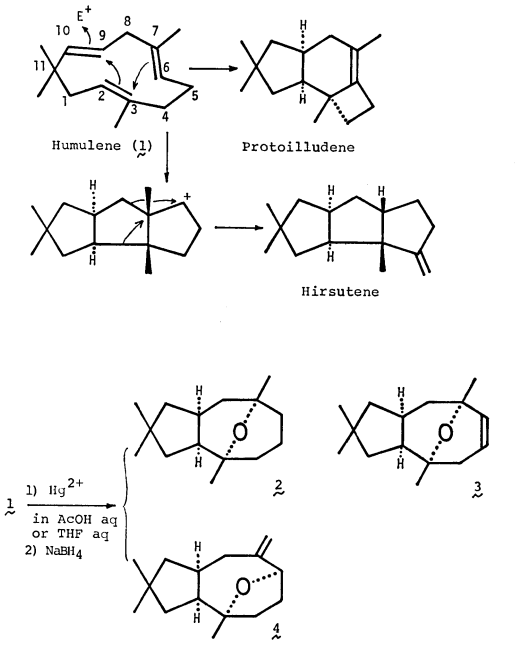

Fig. 1. Biosynthetic and chemical conversions of humulene.

The high resolution mass sepctra of the products showed that a solvent molecule had been added to a molecule of each substrate and in the case of **5** 1 mol of hydrogen was further incorporated in the product. ^{1}H NMR studies on the product **5** including extensive decoupling experiments in the presence of a shift reagent revealed the existence of partial structures depicted in Fig. 2. Taking into consideration the possible combination of these fragments, together with probable reaction courses, we deduced 3,6-secoprotoilludane structure **5** for the product. LIS-values[3] [11(CH_3CO), 11(2-H), 9.9(14-CH_3), 9(10-H), 7(6-H), 5.8(18-CH_3), 1.6(CH_2=)] supported the proposed structure and moreover indicated that 2-H, 6-H, 10-H are placed near the *N*-acetyl group. The conclusive reaction course[4] and stereostructure **7** were shown in Fig. 3.

^{13}C NMR spectrum of the product in benzonitrile was reminiscent of that of a previously obtained 3,6-secoprotoilludane derivative **4**,[1c] except for the peaks due to the phenyl group, in multiplicities and in part in chemical shifts. ^{1}H NMR spectral data were in conformity with the formula **6**. In contrast to the case of acetonitrile, compound **6** was not reduced by $NaBH_4$, probably because of the resonance and steric effects in the conjugated C=N double bond.

In conclusion, it was shown that the reaction of mercuric salt with humulene in anhydrous nitriles is

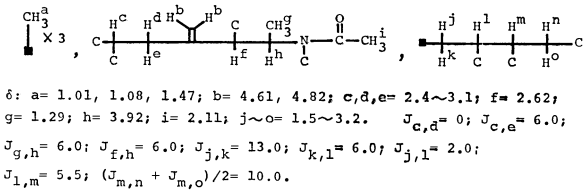

δ: a= 1.01, 1.08, 1.47; b= 4.61, 4.82; c,d,e= 2.4~3.1; f= 2.62; g= 1.29; h= 3.92; i= 2.11; j~o= 1.5~3.2. $J_{c,d}$= 0; $J_{c,e}$= 6.0; $J_{g,h}$= 6.0; $J_{f,h}$= 6.0; $J_{j,k}$= 13.0; $J_{k,l}$= 6.0; $J_{j,l}$= 2.0; $J_{l,m}$= 5.5; $(J_{m,n} + J_{m,o})/2$= 10.0.

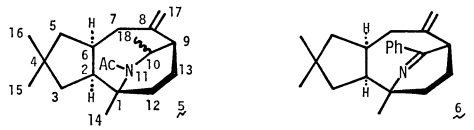

Fig. 2. Partial structures deduced from NMR studies. Chemical shifts (δ) and coupling constants (Hz) were shown.

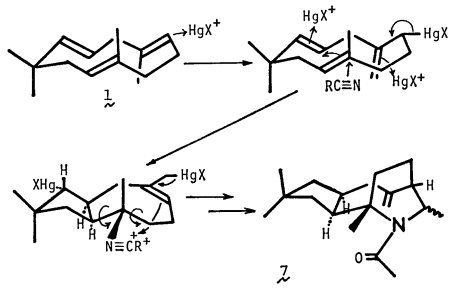

Fig. 3. Reaction course[4,5] in nitriles.

quite similar to that in the aqueous solvents, but the two reactions are different in that in the former solvents a new C–C bond is formed at C-6, and a C–N bond rather than a C–O bond is formed at C-3.

Experimental

All melting points were uncorrected. ^{1}H NMR and ^{13}C NMR spectra were recorded on a HITACHI R20B (60 MHz) and a JEOL JNM FX-100 (25 MHz) instrument using TMS as an internal standard respectively. High resolution mass spectra were measured on a JEOL JMS D-300 mass spectrometer.

11-Acetyl-1,4,4,10-tetramethyl-8-methylene-11-azatricyclo[7.2.2.0^{2,6}]tridecane (5). To a stirred solution of $Hg(OCOCF_3)_2$ (1.88 g, 4.4 mmol) in CH_3CN(15 ml) was added 300 mg (1.47 mmol) of humulene at room temperature under argon and the mixture was stirred for 2 h. The solvent was removed *in vacuo* and the residue was dissolved in 10 ml of THF–H_2O (1:1). The solution was made alkaline (3 mol dm^{-3} NaOH) and $NaBH_4$ (300 mg, 7.89 mmol) was added by portions at 0 °C and the mixture was stirred for 3 h at room temperature. After evaporation of the THF *in vacuo*, the solution was extracted with ether three times. The combined extracts were washed with water, dried and concentrated to give a pasty mass which was subjected to acetylation (Ac_2O–pyridine, 20 °C, 12 h). Usual workup followed by chromatographic purification (silica-gel column, 10% AcOEt–C_6H_6) afforded a crystalline product **5** (254 mg, 60%): mp 102—103 °C; ^{1}H NMR ($CDCl_3$) δ=1.01, 1.08 (each 3H, s), 1.29 (3H, d, J=6), 1.47, 2.11 (each 3H, s), 3.92 (1H, quintet, J=6), 4.61, 4.82 (each 1H, t, J=1.5). Found: m/z 289.2408. Calcd for $C_{19}H_{31}NO$: M, 289.2407.

1,4,4-Trimethyl-8-methylene-10-phenyl-11-azatricyclo[7.2.2.0^{2,6}]-tridec-10-ene (6). Humulene (100 mg, 0.44 mmol) was treated with $Hg(OCOCF_3)_2$ (427 mg, 1 mmol) and PhCN (5 ml) in the same manner as above. After evaporation of the polar solvent the residue was dissolved in 3 ml of a mixture of volatile solvent (THF, MeOH, H_2O/1:1:1). The solution was made alkaline (3 mol dm^{-3} NaOH) and $NaBH_4$ (150 mg, 3.9 mmol) was added by portions at 0 °C and the whole was stirred for 2 h at room temperature. The organic solvent was removed *in vacuo* and the residue was extracted with $CHCl_3$ three times. The combined extracts were washed with water, dried and concentrated to give a pasty mass which was throughly made free from PhCN under reduced pressure. The solid obtained was crystallized from hexane to give a pure product **6** (230 mg, 66%): mp 83—85 °C; ^{1}H NMR ($CDCl_3$) δ=1.01, 1.09, 1.39 (each 3H, s), 3.72 (1H, t, J=4), 4.7 (2H, bs), 7.0—8.0 (5H, m); ^{13}C NMR ($CDCl_3$) δ=24.2(t), 24.4(t), 31.7(q), 32.4(q), 35.1-(q), 36.8(s), 40.2(t), 40.7(d), 41.3(t), 42.4(d), 50.5(t), 53.6 (d), 58.1(s), 113.8(t), 126.6(d×2), 128.1(d×2), 129.0(d), 140.6(s), 144.5(s), 168.2(s). Found: m/z 307.2300. Calcd for $C_{22}H_{29}N$: M, 307.2302.

References

1) Recent studies on the biosynthetic like cyclization of humulene: a) H. Shirahama, K. Hayano, Y. Kanemoto, S. Misumi, T. Ohtsuka, H. Hashiba, A. Furusaki, S. Murata, R. Noyori, and T. Matsumoto, *Tetrahedron Lett.*, **21**, 4835 (1980); b) S. Misumi, T. Ohtsuka, Y. Ohfune, K. Sugita, H. Shirahama, and T. Matsumoto, *ibid.*, **1979**, 31; S. Misumi, Y. Ohfune, A. Furusaki, H. Shirahama, and T. Matsumoto, *ibid.*, **1979**, 3865; c) S. Misumi, T. Ohtsuka, H. Hashimoto, Y. Ohfune, H. Shirahama, and T. Matsumoto, *ibid.*, **1979**, 35; d) J. A. Mlotkiewicz, J. Murray-Rust, P. Murray-Rust, W. Parker, F. G. Riddell, J. S. Roberts, and A. Sattar, *ibid.*, **1979**, 3887; I. Bryson, J. S. Roberts, and A. Sattar, *ibid.*, **21**, 201 (1980).

2) Biogenetic like synthesis of illudoid and hirsutanoid sesquiterpene (a review): H. Shirahama, Y. Ohfune, S. Misumi, and T. Matsumoto, *J. Synth. Org. Chem. Jpn.*, **36**, 569 (1978).

3) LIS value=$\Delta\delta$/molar ratio of the shift reagent to the substrate.

4) It was figured referring the previous cyclization of humulene to ethers using mercury(II) salts. See Refs. 1b and c. For acylamination of olefins by means of Hg(II) in nitrile, see, for example, H. C. Brown and J. T. Kurek, *J. Am. Chem. Soc.*, **91**, 5647 (1969).

5) About humulene conformations, see H. Shirahama, E. Osawa, and T. Matsumoto, *J. Am. Chem. Soc.*, **102**, 3208 (1980).

A Convenient Method for the Preparation of *S*-Esters of Thio Analogs of Malonic Acid

Tsuneo IMAMOTO,* Masahito KODERA, and Masataka YOKOYAMA
Department of Chemistry, Faculty of Science, Chiba University, Yayoi-cho, Chiba 260

(Received February 12, 1982)

Synopsis. 2-Carboxyethanethioic *S*-esters ($RSCOCH_2COOH$) and propanebis(thioic) *S,S'*-diesters ($RSCOCH_2COSR$) were easily prepared in high yields by the direct condensation of malonic acid with thiols in the presence of ethyl polyphosphate (PPE).

In the previous paper[1] we reported that various thiocarboxylic *S*-esters were easily prepared by the direct condensation of carboxylic acids with thiols in the presence of ethyl polyphosphate (PPE).[2] The method compares favorably with others reported hitherto, in terms of simplicity, efficiency, generality, and in particular, the applicability to acid and/or base sensitive compounds such as penicillin G.

On the other hand, 2-carboxyethanethioic *S*-esters and propanebis(thioic) *S,S'*-diesters have been noticed as the useful intermediates for organic synthesis. The former esters are closely related to malonyl *S*-CoA and, in fact, undergo decarboxylative *C*-acylation under virtually natural conditions.[3,4] The latter ones are used for the synthesis of ethanol derivatives[5] and heterocycles.[6] We report herein a facile method for the preparation of these compounds from malonic acid and thiols using PPE as the condensation reagent.

When a thiol was treated with large excess of malonic acid[7] in PPE containing chloroform and tetrahydrofuran (THF), the condensation proceeded smoothly at room temperature without decarboxylation, and the corresponding 2-carboxyethanethioic *S*-esters (**1a—h**)

$$CH_2(COOH)_2 + RSH \xrightarrow[\text{in } CHCl_3\text{-THF}]{\text{PPE}} RSCOCH_2COOH \quad \mathbf{1a—h}$$

were produced in high yields. The results are summarized in Table 1. Since malonic acid is inexpensive, its use in excess detracts little from the utility of this process.

Next, we tried to prepare propanebis(thioic) *S,S'*-diesters. This was easily achieved by the treatment of malonic acid with two equivalents of thiols in PPE at room temperature. All the cases examined afforded

$$CH_2(COOH)_2 + 2\,RSH \xrightarrow{\text{PPE}} CH_2(COSR)_2 \quad \mathbf{2a—g}$$

the expected *S,S'*-diesters (**2a—g**) in excellent yields. The results are listed in Table 2. It is noted that sterically crowded *S,S'*-bis(2,4,6-trimethylphenyl) propanebis(thioate) (**2d**) was also prepared in a satisfactory yield.

We believe the present method has the superior attributes of high yields, ease of operation, and attractive economics.[8,9]

Experimental

Spectra. Proton NMR spectra were measured on a JEOL C-60HL spectrometer. The chemical shifts are given in ppm with TMS as an internal standard. Infrared spec-

TABLE 1. 2-CARBOXYETHANETHIOIC *S*-ESTERS ($RSCOCH_2COOH$)

R	Product	Yield %	Mp θ_m/°C	IR $\nu_{C=O}$/cm^{-1}	^{1}H-NMR δ	Found(Calcd)(%) C	H
C_6H_5	**1a**	88	74.0—75.5 (C_6H_6-C_6H_{14}) Lit,[a] 72—73	1690, 1710	3.62(s, 2H), 7.40(br s, 5H) 10.66(br s, 1H)	55.17 (55.09	4.17 4.11)
$C_6H_5CH_2$	**1b**	90	62—63 (C_6H_6-C_6H_{14})	1680, 1730	3.70(s, 2H), 4.26(s, 2H), 7.41(s, 5H), 9.5—9.9(br s, 1H)	57.29 (57.13	4.82 4.79)
o-$CH_3OC_6H_4$	**1c**	65	90—91 (C_6H_6)	1700, 1730	3.78(s, 2H), 3.92(s, 3H), 6.94—7.76 (m, 4H), 11.03(s, 1H)	53.25 (53.09	4.45 4.45)
2,4,6-$(CH_3)_3C_6H_2$	**1d**	88	112.0—113.5 (C_6H_6-C_6H_{14})	1680, 1730	2.33(br s, 9H), 3.66(s, 2H), 6.97(s, 2H), 11.05(s, 1H)	60.50 (60.48	5.93 5.92)
$C_2H_5OOCCH_2$	**1e**	73	Oil	1690(sh), 1730	1.29(t, J=7.5 Hz, 3H), 3.66(s, 2H), 3.72(s, 2H), 4.20(q, J=7.5 Hz, 2H), 11.08(s, 1H)	40.37 (40.77	5.09 4.89)
C_2H_5	**1f**	90	30—31 (C_6H_6-C_6H_{14})	1680, 1720	1.30(t, J=7.5 Hz, 3H), 2.97(q, J=7.5 Hz, 2H), 3.57(s, 2H), 10.86(s, 1H)	40.06 (40.53	5.48 5.44)
n-C_4H_9	**1g**	80	Oil Lit[b], Oil	1685, 1720	0.70—1.90(m, 7H), 2.97(t, J=7.0 Hz, 2H), 3.61(s, 2H), 10.98(s, 1H)	47.45 (47.71	6.99 6.86)
t-C_4H_9	**1h**	78	44—45 (C_6H_{14})	1680, 1720	1.49(s, 9H), 3.48(s, 2H), 10.86 (br s, 1H)	47.81 (47.71	6.80 6.86)

a) Ref. 8b. b) Ref. 4.

Table 2. Propanebis(thioic) *S,S'*-diesters [$CH_2(COSR)_2$]

R	Product	Yield %	Mp θ_m/°C [Bp θ_b/°C (Torr)†]	IR $\nu_{C=O}$/cm^{-1}	^{1}H-NMR δ	Found(Calcd)(%) C	H
C_6H_5	**2a**	94	94—95 (C_6H_6–C_6H_{14}) Lit,[a] 94	1695, 1720	3.93(s, 2H), 7.47(br s, 10H)	62.60 (62.48	4.26 4.19)
$C_6H_5CH_2$	**2b**	98	39—40 (C_6H_6–C_6H_{14})	1670, 1695(sh)	3.63(s, 2H), 4.08(s, 4H), 7.22(br s, 10H)	64.81 (64.53	5.16 5.10)
o-$CH_3OC_6H_4$	**2c**	88	70.0—71.5 (CH_3OH)	1690, 1710(sh)	3.75(s, 6H), 3.84(s, 2H), 6.75—7.65(m, 8H)	58.68 (58.60	4.65 4.63)
2,4,6-$(CH_3)_3C_6H_2$	**2d**	98	77—78 (C_6H_6–C_6H_{14})	1670, 1710	2.33(s, 18H), 3.84(s, 2H), 6.97(s, 4H)	68.01 (67.71	6.54 6.49)
$C_2H_5OOCCH_2$	**2e**	85	Oil	1680, 1705, 1735	1.27(t, J=7.5 Hz, 6H), 3.68(s, 4H) 3.83(s, 2H), 4.15(q, J=7.5 Hz, 4H)	42.77 (42.85	5.19 5.23)
C_2H_5	**2f**	95	[100[b](0.5)] [Lit,[c] 109(2.5)]	1675, 1695(sh)	1.30(t, J=7.5 Hz, 6H), 2.93(q, J= 7.5 Hz, 4H), 3.68(s, 2H)	43.65 (43.72	6.21 6.29)
n-C_4H_9	**2g**.	94	[150[b](0.4)]	1670, 1690(sh)	0.73—1.90(m, 14H), 2.91(t, J=7.0 Hz, 4H), 3.67(s, 2H)	53.29 (53.19	8.04 8.12)

a) Ref. 9d. b) Bath temperature. c) Ref. 9c. † 1 Torr≈133.322 Pa.

tra were recorded on a Hitachi 215 spectrophotometer. Products were identified by NMR and IR spectra together with elemental analyses.

Materials. PPE was prepared according to the method described in the Ref. 2. *o*-Methoxybenzenethiol[10] and 2,4,6-trimethylbenzenethiol[11] were synthesized by the methods described in the literatures. Other thiols were purchased from Tokyo Kasei Kogyo, Co., Ltd. and used without further purification.

*General Procedure for the Preparation of 2-Carboxyethanethioic S-Esters (**1a—h**).* A thiol (0.025 mol) was added to a stirred mixture of finely powdered malonic acid (10.4 g, 0.10 mol), PPE (15 g), purified chloroform (60 ml), and THF (10 ml).[12] After stirring for 30 h at room temperature, the reaction mixture was diluted with ether (200 ml) and treated successively with saturated aqueous $NaHCO_3$ solution (150 ml, 100 ml, and 50 ml). The combined aqueous extracts were acidified to pH 1—2 with 10% hydrochloric acid and extracted with chloroform (100 ml×2). The extracts were dried over Na_2SO_4 and concentrated by a rotary evaporator. The residue was purified by filtration through a column packed with silica gel (*ca.* 70 g) with benzene–ethyl acetate (1:1) as the eluent. Crystalline products were further purified by recrystallization.

*General Procedure for the Preparation of Propanebis(thioic) S,S'-Diesters (**2a—g**).* A mixture of malonic acid (10.4 g, 0.10 mol) and a thiol (0.20 mol) was stirred with PPE (30 g) at room temperature for 20 h. The reaction mixture was treated with saturated aqueous $NaHCO_3$ solution (600 ml) and the product was extracted into ether (150 ml×2). The combined extracts were washed with aqueous $NaHCO_3$ solution and dried (Na_2SO_4). The solvent was evaporated and the residue was filtered through a column packed with silica gel (*ca.* 70 g) with benzene. Evaporation of the solvent *in vacuo* afforded practically pure product, which was further purified by recrystallization or distillation under reduced pressure (Kugelrohr apparatus).

References

1) T. Imamoto, M. Kodera, and M. Yokoyama, *Synthesis*, **1982**, 134.

2) W. Pollmann and G. Schramm, *Biochem. Biophys. Acta*, **80**, 1 (1964).

3) D. W. Brooks, L. D. -L. Lu, and S. Masamune, *Angew. Chem., Int. Ed. Engl.*, **18**, 72 (1979).

4) Y. Kobuke and J. Yoshida, *Tetrahedron Lett.*, **1978**, 367.

5) H. -J. Liu and H. K. Lai, *Can. J. Chem.*, **57**, 2522 (1979).

6) W. Ried and G. Sell, *Chem. Ber.*, **113**, 2314 (1980).

7) The use of one equivalent of malonic acid to a thiol resulted in lower yield of the 2-carboxyethanethioic *S*-ester. For example, the treatment of malonic acid with one molar equivalent of benzenethiol afforded **1a** and **2a** in 40% and 36% yields, respectively.

8) Other methods for the preparation of 2-carboxyethanethioic *S*-esters were reported; a) Ref. 4; b) J. C. Howard, M. C. Lin, P. Matthews, and S. A. Singal, *J. Med. Chem.*, **8**, 888 (1965); c) S. Ohta and M. Okamoto, *Tetrahedron Lett.*, **1981**, 3245.

9) For the other methods for the preparation of propanebis(thioic) *S,S'*-diesters, see a) Ref. 5; b) Ref. 6; c) S. Scheithauer and R. Mayer, *Chem. Ber.*, **100**, 1413 (1967); d) E. Ziegler and H. Junck, *Monatsh. Chem.*, **86**, 29 (1955); e) K. Miyaki and S. Yamagishi, *J. Pharm. Soc. Jpn.*, **76**, 1196 (1956).

10) "Beilstein Handbuch der Organishen Chemie," Zweites Ergänzungeswerk, Band 6 (1944), p. 796.

11) W. E. Truce, H. G. Klein, and R. B. Kruse, *J. Am. Chem. Soc.*, **83**, 4636 (1961).

12) THF was necessary to achieve high yield.

X-Ray Microanalysis of Uranium on Fibrous Amidoxime-type Adsorbent

Takao KITAMURA,* Koji SAKANE, and Shunsaku KATOH
Government Industrial Research Institute, Shikoku 2-3-3 Hananomiyacho, Takamatsu 761
(Received July 29, 1981)

Synopsis. The adsorption process for uranium from sea water was studied by X-ray microanalysis on polyacrylamidoxime fiber, whose functional group was found to distribute uniformly. Uniform distribution of uranium was observed on cross sections of the adsorbents, which had contacted with sea water for 14 and 55 d. It was deduced that intrafiber diffusion of uranium is not the rate determining step in adsorption.

Recently much higher interest is around on the organic polymer adsorbents because of their high adsorption rate and versatile possibilities in organic synthesis.[1-4] Among these adsorbents the ones with amidoxime functional groups have the highest adsorption rate for uranium from sea water.

Improvement of adsorptive properties for practical application necessitates knowledges about uranium adsorption process from sea water, which hitherto were not obtained from direct analysis of distribution of adsorbed uranium. In this note, distributions of functional groups and uranium were measured by X-ray microanalysis of copper(II) and uranium, respectively, and the uranium adsorption process is briefly discussed.

Experimental

Adsorbent. Adsorbent was obtained by reacting commercially available acrylic fiber of *ca.* 15 μm diam. with hydroxylamine by the usual method to form amidoxime functional groups.[5] Then the fiber was treated for 24 h with a 1 M (1 M=1 mol dm^{-3}) NaOH solution for conditioning. The amount of the functional group in the adsorbent was determined from copper(II) ion adsorption capacity.[6] Adsorption of copper(II) ion was carried out by shaking 0.1 g of the adsorbent for 3 d at 25 °C in a solution of 0.05 M $CuCl_2$ (25 cm^3), which is buffered to pH 4.5 with CH_3COOH–CH_3COONa.

Uranium Adsorption. Uranium was adsorbed from filtered natural sea water in columns of 2.5 cm inner diam. and 20 cm length at linear flow rate of 20 cm min^{-1} for 55 d. The uranium content in the adsorbent was determined by fluorometry on an Aloka fluorimeter FMT-3B after desorption with diluted HCl solution.[6]

X-Ray Microanalysis. Apparatus used was JEOL JXM-50A scanning electron microscope-X-ray microanalyser. Crystals used for resolution of spectra were pentaerithritol for U $M\alpha$, and lithium fluoride for Cu $K\alpha$. Standard samples for Cu and U analyses were the cross sections of wires supplied by JEOL.

Sample Preparation for X-Ray Microanalysis. Fibrous adsorbent was buried in an acrylic resin. After hardening the cylindrical resin of 5 mm diam. was cut to 5 mm height. Electrical contact of the specimen was attained by coating vacuum-evaporated aluminum, which was found to serve more satisfactorily than gold and platinum in minimizing X-ray absorption and preventing charging of the specimen. In some cases one end of the fiber was buried in a resorcinol resin, the other end being razored and coated with aluminum.

Results and Discussion

Characterization of Adsorbent. Secondary electron image of the adsorbent in Fig. 1 shows a smooth surface and existence of a notch in the direction of axis. This notch gave a typical shape of the cross section for most of the fibers as in Figs. 2—4. Amount of the functional group of the fiber was determined to be 2.6 mmol g^{-1}. Distribution of the functional group was measured on a cross section of the adsorbent by measuring Cu $K\alpha$ radiation of adsorbed copper(II). Figure 2 shows the secondary electron image and Cu $K\alpha$ micrography across a section. The image was observed under the same electron beam conditions with that for X-ray measurement, *i.e.*, at high electron beam intensity of 2×10^{-8} A and accelerating voltage of 25 kV, which were necessary to measure characteristic X-rays of elements at rather low concentration. This resulted in low resolution of the secondary electron image, which in turn reflects approximately the resolution of the line profile. Constant counting rate of Cu $K\alpha$

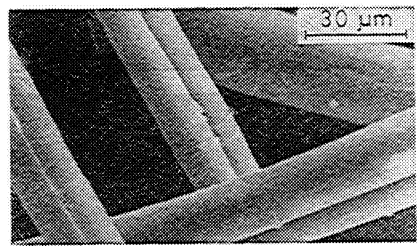

Fig. 1. Secondary electron image of the fibrous adsorbent.

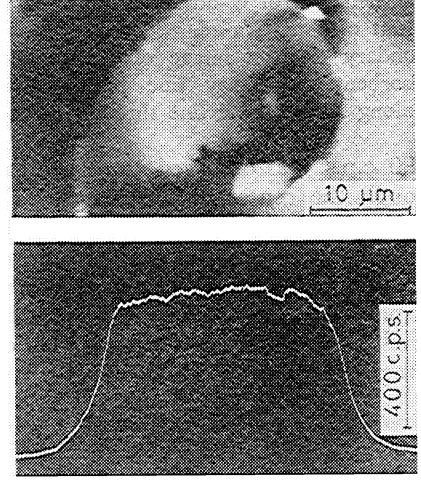

Fig. 2. Distribution of Cu(II) adsorbed from a buffered solution.
a: Secondary electron image of a cross section of the adsorbent, b: X-ray line profile analysis of Cu $K\alpha$ along a horizontal line through the center.

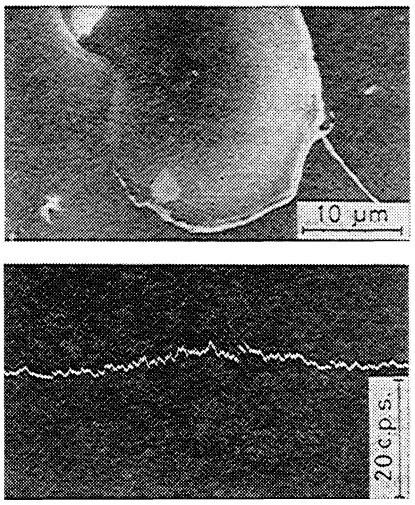

Fig. 3. Distribution of U adsorbed from sea water to an amount of 2 mg-U/g-ad.
a: Secondary electron image of a cross section of the adsorbent, b: X-ray line profile analysis of U *Mα* along a horizontal line through the center.

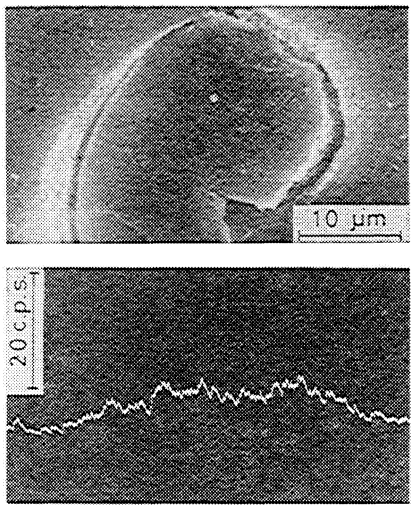

Fig. 4. Distribution of U adsorbed from sea water to an amount of 5 mg-U/g-ad.
a: Secondary electron image of a cross section of the adsorbent, b: X-ray line profile analysis of U *Mα* along a horizontal line through the center.

of about 490 c.p.s. was observed along the line, which passed through the center of the image. This result shows a uniform distribution of copper(II), hence the uniform formation of functional group in the adsorbent. The counting rate of Cu *Kα* of the standard sample was 7500 c.p.s. under the same conditions. The concentration of Cu(II) in the adsorbent was calculated to be 165 mg g^{-1}, giving correction factor[7] G of 2.5. This rather large G value can be attributed to the effect of absorption of electron and X-ray by coating materials.

Microanalysis of Uranium. The adsorbents at two different durations of uranium adsorption *i.e.* 14 and 55 d were examined. The former contained 2 mg g^{-1} and the latter 5 mg g^{-1} of uranium. Figure 3 shows a secondary electron image and U *Mα* X-ray line analysis of a cross section of the adsorbent after 55 d adsorption. Although the observed line is a little scattered, the counting rate around the center is nearly as high as that around the edge of the section. From the results observed above, it is found that the distribution of uranium in the fiber is approximately uniform. A similar observation with lower counting rate was made with adsorbents after 14 d adsorption as in Fig. 4. The above results of apparently uniform distribution of uranium for the two adsorbents at different durations of adsorption suggest that a boundary layer of adsorbed uranium does not exist, and intrafiber diffusion of uranium is not the rate determining step in adsorption from sea water.

For 0.3 mm diam. particle of hydrous titanium oxide adsorbent,[8] uranium-adsorbed layer of 0.03 mm thickness was calculated from the curve of adsorption rate, whereas the layer was not detected with the fibrous adsorbent, that is, the whole volume of the adsorbent was effective for uranium adsorption. The rate of uranium adsorption was 2 mg g^{-1} in 14 d with the fibrous adsorbent, whereas the rate with the hydrous titanium oxide adsorbent was 0.18 mg g^{-1} in 20 d.[8] These two characteristics of high adsorption rate and high effectivity can be denoted as the advantages of the fibrous amidoxime-type adsorbent for adsorption of uranium from sea water.

References

1) K. Schwochau, *Nachr. Chem. Tech. Lab.*, **27**, 563 (1979).
2) H. Egawa, H. Harada, and T. Shuto, *Nippon Kagaku Kaishi* **1980**, 1773.
3) E. G. Witte, L. Astheimer, H-J. Schenk, and K. Schwochau, *Ber. Bunsenges. Phys. Chem.*, **83**, 1121 (1979).
4) I. Tabushi, Y. Kobuke, and T. Nishiya, *Nature*, **280**, 665 (1979).
5) S. Katoh, K. Sakane, and K. Sugasaka, *Nippon Kagaku Kaishi*, in print.
6) K. Sugasaka, S. Katoh, N. Takai, H. Takahashi, Y. Umezawa, and K. Itagaki, Symposium on Separation Science and Technology for Energy Applications, Gatlinburg, Tennessee, May 5—8, 1981.
7) I. Uchiyama, A. Watanabe, and S. Kimoto, "X-Ray Micro-analyser," Nikkan Kogyo Shinbun Sha, Tokyo (1972), pp. 181—184.
8) R. V. Davies, J. Kennedy, R. W. Mcilroy, and R. Spence, *Nature*, **203**, 1110 (1964).

In-vitro Clot Forming Properties of Polyelectrolyte Complexes of [2-(Diethylamino)ethyl]dextran Hydrochloride with Poly(sodium-L-glutamate) and of Sodium Carboxymethyldextran with Chitosan

Yasuo KIKUCHI* and Tsutomu TAKEBAYASHI
Faculty of Engineering, Oita University, 700-Dannoharu, Oita 870

(Received August 31, 1981)

Synopsis. Polyelectrolyte complexes prepared at higher hydrogen ion concentrations may form clots in higher quantities than those prepared at lower hydrogen ion concentrations, irrespective of the content of anticoagulant reagents. This difference is attributable to the difference in molecular structure of polyelectrolyte complexes, especially to the presence of carboxyl groups.

We have reported[1,2] on novel chemical reactions, structures and properties of polyelectrolyte complexes (PEC) and their *in-vitro* clot formation and we have also reported[3] that different characters of blood coagulation are attributable to the difference in molecular structure among PECs, with an emphasis on the fact that formation of sulfo or carboxyl groups in PECs plays an important role in increasing the quantity of clot. This note deals mainly with attractive results of clot formation *in-vitro* by PECs of [2-(diethylamino)-ethyl]dextran hydrochloride with poly(sodium-L-glutamate),[4] and by carboxyl-containning PECs of sodium carboxymethyldextran of low molecular weight (about 5000) with chitosan.

Experimental

Chitosan (Tokyo Kasei Co., nitrogen content 7.89%, intrinsic viscosity 1.50 dl/g in 1 M (1 M=1 mol dm^{-3}) NaCl of pH 3.0 at 30 °C), sodium carboxymethyldextran (CMD) (Meito Sangyo Co., degree of substitution 1.38 mol/A.G.U., molecular weight about 5000), poly(sodium-L-glutamate) (PSLG), and [2-(diethylamino)ethyl]dextran hydrochloride (EA) were used. Properties of PSLG and EA are given in a previous paper.[4] When the pH of solution is below 4.0 or 3.0, no precipitate is formed by mixing PSLG with EA (system A) or chitosan with CMD solution (system B), respectively, and when the pH of chitosan solution is higher than 6.0, chitosan remains undissolved. Thus, reactions were carried out at pH 5.0, 6.0, and 8.0 (system A) and pH 3.5, and 5.5 (system B). General conditions, the apparatus and chemical analyses, and the blood clotting test used are the same as those described in previous papers.[1-4]

ACD bloods of types O and A (Red Cross Hospital Blood Center) were kept in a thermostat at 4—6 °C for 2—6 d.

Conditions, yields and results of elemental analyses for PECs prepared in such a way that a PSLG or CMD solution was added to EA or chitosan and *vise versa*, are given in the previous paper[4] and in Table 1.

In system B, all the PECs prepared at pH 5.5 have higher nitrogen contents, which represent the molar ratio CMD/chitosan, than the PEC prepared at pH 3.5 because of the higher dissociation of chitosan at pH 3.5 and similarly, in system A, all the PECs prepared at pH 5.0 have lower PSLG/EA molar ratios than the PECs prepared at pH 6.0 and 8.0 and those prepared by reagent addition in the reverse order have higher ratios as shown in the previous paper.[4]

IR spectra of PECs are similar to those of their corresponding mixtures of PSLG and EA or of CMD and chitosan.

Table 1. Experimental conditions[a], polymer yield, and elemental analyses of polyelectrolyte complexes[b] of chitosan[c] with CMD[d]

Sample code[e]	V_{CMD}[f] / cm^3	R[g]	Y[h] / g	N[i] / %
A-1	442	4.0	0.96	3.3
A-2[j]	298	2.7	0.96	3.3
A-3[k]	274	2.5	0.93	3.6
A-4	221	2.0	0.74	3.8
B-1	442	4.0	0.71	4.5
B-2[j]	88	0.8	0.69	4.8
B-3[k]	76	0.7	0.67	4.8
B-4	55	0.5	0.44	4.9
C-1	442	4.0	0.98	3.5
C-2	298	2.7	0.97	3.8
C-3	274	2.5	0.93	3.6
C-4	221	2.0	0.76	3.4
D-1	442	4.0	0.75	4.6
D-2	88	0.8	0.67	4.4
D-3	76	0.7	0.60	4.2
D-4	55	0.5	0.42	4.9

a) Concentrations of chitosan and sodium carboxymethyldextran (CMD), 2 and 4 g/L. b) Nitrogen analyses carried out according to the Kjeldahl method. c) Chitosan: Nitrogen content, 7.89%; intrinsic viscosity, 1.50 dl/g in 1 M NaCl of pH 3.0 at 30 °C. d) CMD: Degree of substitution, 1.38 mol/A.G.U.; molecular weight, about 5000. e) A, B series: CMD solution was added dropwise to chitosan solution; C, D series: Chitosan solution was added dropwise to CMD solution; A, C series: Both chitosan and CMD solutions were adjusted to pH 3.5; B, D series: Both chitosan and CMD solutions were adjusted to pH 5.5 (see text). f) V_{CMD} is one amount of CMD solution in ml/200 ml chitosan. g) R is the molar ratio of Na(CMD)/N(chitosan) for solution. h) Y is the yield of polymer. i) N is the nitrogen content. j) End of coagulation range. k) Beginning of coagulation range.

However, the PEC prepared at pH 5.0 (system A) or pH 3.5 (system B) has an absorption band around 1740 cm^{-1} which appears neither in the PEC prepared at pH 8.0 (system A) or pH 5.5 (system B) nor in the mixture of PSLG and EA or of chitosan and CMD; the PEC prepared at pH 6.0 (system A) has weaker absorption bands than the one prepared at pH 5.0. These absorption bands have been assigned to carboxyl groups.[5] Furthermore, the absorption band around 3500 cm^{-1} (assigned to the hydroxyl group) of the PEC prepared at pH 5.0 (system A) or pH 3.5 (system B) is caused to shift to lower wave numbers in both systems. In view of the formation of hydrogen bond between the hydroxyl and other functional groups, it is reasonable to expect such a shift in frequency.

The PECs differ appreciably from one another in such

properties as the degree of swelling, color reaction with Toluidine Blue, and solubility depending on experimental conditions of hydrogen ion concentration and molar mixing ratio of constituents, although they have common constituents. It appears that the degree of dissociation and the conformation of PSLG, EA, chitosan, and CMD change with hydrogen ion concentration.

The PECs of the same nitrogen content, representing the CMD content in PEC, is similar to one another, in such properties as IR spectra, solubility, swelling, and color reaction with Toluidine Blue, under the same conditions. Consequently, blood clotting tests were performed on PEC tables 1-B, 2-B, 3-B, 1-b, 2-b, and 3-b as reported in the previous paper,[4] and on PEC tablets A-1 A-2, B-1, B-2, C-1, D-3, and D-4 as given in Table 1, which were selected arbitrarily from within the nitrogen content range 3.3—4.9 according to the gravimetric procedure of Imai and Nose.[6] No change in IR absorption intensity for one carboxyl group was detected for the PECs which had long been kept dipped at pH 7.3. No firm clot was formed even after 10 min dipping with PEC tablets. Percentage formation of thrombus for the PECs (system A: 1-B, 2-B, and 3-B; system B: A-2, C-1, and D-3) is given in Figs. 1 and 2. For the PECs (system A: 1-b, 2-b, and 3-b; system B: A-1, B-1, B-2, and D-4) were obtained similar reactions between the percentage of thrombus formed and the molecular structure as well as results of observation similar to the above-mentioned. All the PEC tablets suppress the coagulation of blood. Moreover, quantities of clots for the PEC tablets prepared at pH 5.0, 6.0 (system A) and 3.5 (system B) are more than those for the PEC tablets prepared at pH 6.0 and 8.0, 8.0, and 5.5, respectively, although the content of PSLG or CMD (suppression of coagulation) in the PEC tablets prepared at pH 5.0 and 6.0 and 3.5 are higher than that in those prepared at pH 8.0 and 5.5, respectively. We have reported an experimental work on clot formation of PEC consisting of EA, CMD, and sodium dextran sulfate, pointing out a definite correlation between the character of blood coagulation and the molecular structure and the significance of formation of carboxyl or sulfo groups in PECs. Thus, the present experimental results have confirmed that the difference in the characters of blood coagulation is attributable to the difference in molecular structures of the PECs prepared; especially, the formation of carboxyl group in PECs has a great contribution to the increase in the quantity of clots as well as the above-mentioned experimental results.[3]

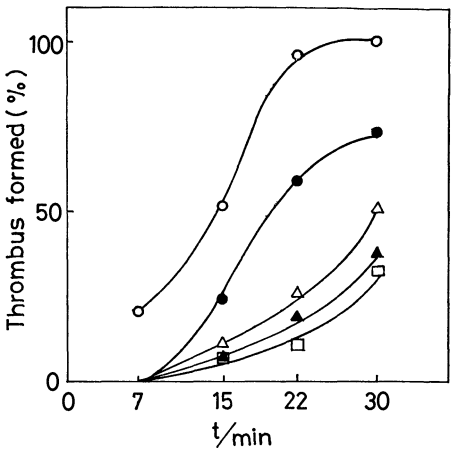

Fig. 1. Percentage of thrombus formed on polyelectrolyte complexes (PSLG→EA) compared with that on glass.
Storage time of A type blood: 6 d, ○: glass, ●: poly(vinyl chloride), △: 1-B, ▲: 2-B, □: 3-B. Sample codes 1-B, 2-B, and 3-B correspond to those in Table 1 in the previous paper.

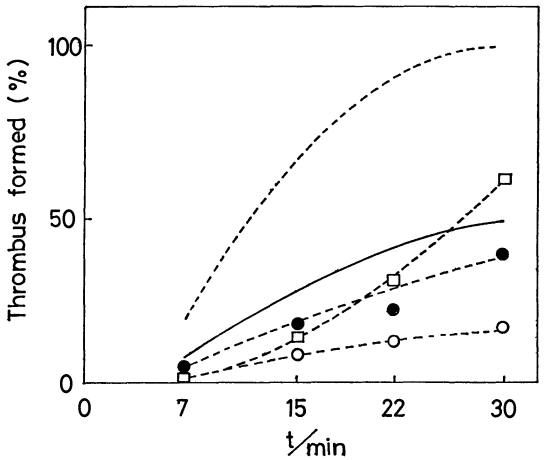

Fig. 2. Percentage of thrombus formed on polyelectrolyte complexes (EA–CMD) compared with that on glass.
Storage time of A type blood: 3 d, ----: glass, ——: poly(vinyl chloride), □: A-2, ●: C-1, ○: D-3. Sample codes A-2, C-1, and D-3 correspond to those in Table 1.

The mechanism of increasing the quantity of clots makes it likely that facters effective for blood coagulation are activated delicately by interaction of carboxyl groups in PEC with blood. On the other hand, the mechanism for the suppression of coagulation suggests the possibility that negative charges such as the carboxylate group may exist active on the surface of PEC.[7]

References

1) Y. Kikuchi and T. Koda, *Bull. Chem. Soc. Jpn.*, **52**, 880 (1979).
2) Y. Kikuchi and M. Okamura, *Makromol. Chem., Rapid Commun.*, **1**, 253 (1980).
3) Y. Kikuchi and K. Simizu, *Bull. Chem. Soc. Jpn.*, **54**, 2549 (1981).
4) Y. Kikuchi and K. Hori, *Nippon Kagaku Kaishi*, **1982**, 847.
5) K. Nakanishi, "IR Absorption Spectroscopy," Nankodo, Tokyo (1965), p. 56.
6) Y. Imai and Y. Nose, *J. Biomed. Mater. Res.*, **6**, 165 (1972).
7) M. K. Vogel, R. A. Cross, H. J. Bixer, and R. J. Guzman, *J. Macromol. Sci-Chem*, **A4(3)**, 675 (1970).

Conformation en Solution des Benzile-monoximes et des Dichloro-4,4′ benzile-monoximes *E* et *Z*

Jean BERNADOU,* Jean Pierre FAYET,† Monique BONNAFOUS, et Pierre MAURET†

Laboratoire de Pharmacie chimique Université Paul Sabatier, 31077 Toulouse Cedex, France

† *Laboratoire de Chimie Organique Structurale, Universite Paul Sabatier, 31077 Toulouse Cedex, France*

(Reçu Novembre 10, 1981)

Synopsis. Les auteurs ont synthétisé deux benzile-monoximes et deux dichloro-4,4′ benzile-monoximes. L' introduction de deux atomes de chlore en para sur les cycles permet, par comparaison des moments dipolaires expérimentaux et calculés, de confirmer les configurations et de préciser les conformations de chaque isomère.

Les configurations attribuées par Meisenheimer[1] aux benzile-monoximes *E* (composé **1**) et *Z* (composé **2**) ont été confirmées dans la suite par voie chimique[2,3] et par des études de radiocristallographie,[4] de spectroscopie IR[5,6] et RMN.[7,8]

Les conformations peuvent être influencées par l'état physique:

a) A l'état cristallin les dérivés *O-p* bromobenzoylés des benzile-monoximes *E* ou *Z* ont des conformations *s-trans* d'après l'étude de leurs spectres de rayons X.[4]

b) A l'état dissous: Sadler[9] par l'étude des spectres infrarouge en solution chloroformique et Armand[10] par l'étude du pK_a du groupe oxime attribuent à **2** la conformation *s-cis*. Cherry[6] en se basant sur les données de la RMN dans le chloroforme deutérié et de la spectrographie infrarouge dans le tetrachlorure de carbone suppose pour **1** et **2** la conformation *s-trans*. Lumbroso[11] à la suite d'une étude dipolemétrique en solution dans le dioxanne a émis la même hypothèse.

Nous avons déterminé en solution dioxannique les moments dipolaires de **1** et **2** ainsi que ceux de leurs dérivés dichlorés en para sur les cycles (**3** et **4**). Par comparaison avec les moments dipolaires calculés, l'introduction des substituants chlorés permet, si l'on admet la conjugaison du groupe O=C–C=N–OH, de confirmer les configurations *E* et *Z* de ces composés et surtout de lever l'indétermination sur leur conformation *s-cis* ou *s-trans* dans ce solvant. La polarité du chloroforme et le trop faible pouvoir dissolvant du tetrachlorure de carbone[12] ne permettent pas une étude dipolemétrique analogue.

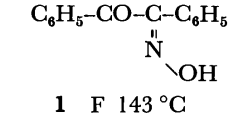

1 F 143 °C
(isomère *E*)

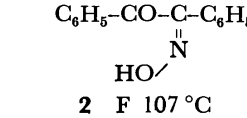

2 F 107 °C
(isomère *Z*)

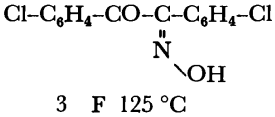

3 F 125 °C
(isomère *E*)

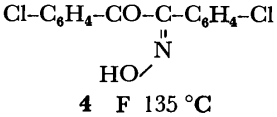

4 F 135 °C
(isomère *Z*)

Partie expérimentale

Synthèse. Les composés **1** et **2** ont été préparés selon la méthode de Taylor[13] reprise par Cherry[6] à partir du benzile par réaction avec l'hydroxylamine.

Les composés **3** et **4** ont été préparés selon la même méthode à partir du dichloro-4,4′ benzile; celui-ci est obtenu par condensation du chloro-4 benzaldéhyde en dichloro-4,4′ benzoine[14] puis oxydation.[15]

L'identification a été effectuée par IR et RMN, la pureté vérifiée par chromatographie; les configurations ont été confirmées par l'essai à l'acétate de cuivre[16] (**1** et **3** donnent un complexe vert, **2** et **4** ne donnent pas de complexes) et par RMN en solution dans le DMSO hexadeutéré en concentration inférieure à 5%: δ_{OH} en ppm=**1** 12,50, **2** 11,80 (8), **3** 12,82, **4** 12,05 (ce travail).

Moments Dipolaires. Moments Calculés (μ_{calc}): Par analogie avec la diméthylglyoxime[17] nous supposerons plan le motif conjugué O=C–C=N–OH. Nous avons obtenu les moments par additivité d'incréments de liaison suivant deux modes de calcul:

1°—avec les angles CCO, ONC, NCC, HON égaux à 120°,

2°—avec CCO=120°, ONC=111°, NCC=126°, HON=103°,

valeurs déduites des molécules de formaldoxime[18] et de diméthylglyoxime.[17]

Les incréments utilisés sont: μ(C=N)=1,8 D; μ(C=O)=3,0 D; μ(H–O)=1,5 D; μ(C_{Ar}–Cl)=1,5 D; μ(N–O)=0,3 D (19,20).

Moments Expérimentaux (μ_{exp}): Les moments μ_{exp} ont été mesurés dans le dioxanne à 25 °C, avec des fractions massiques comprises entre 0,0005 et 0,010; la formule de Debye a été utilisée ainsi que la méthode d'extrapolation mathématique d'Halverstadt et Kumler[21] pour le calcul de la polarisation totale. Les résultats figurent dans les tableaux:

	∞	β	RM_D	$P_{2\infty}$	μ_D
1	6, 05	−0, 27	66, 00	269, 96	3, 16
2	5, 85	−0, 20	66, 00	266, 95	3, 13
3	4, 90	−0, 26	75, 67	297, 80	3, 29
4	3, 33	−0, 28	75, 67	219, 99	2, 67

Discussion

La valeur expérimentale obtenue pour **1** n'est compatible qu'avec les structures **a** et **e**; pour **3**, le moment mesuré ne peut correspondre qu'aux structures **b** ou **e**. L'introduction d'un atome de chlore en para sur les cycles benzéniques ne peut avoir d'influence sur la conformation, l'halogène étant très éloigné du motif O=C–C=N–OH.[22,23] On doit alors attribuer à ces composés **1** et **3** la structure **e**.

De même, les valeurs expérimentales obtenues pour **2** et **4** sont compatibles respectivement avec les for-

TABLEAU 1.

Conformation	R	Configuration *E*		Configuration *Z*	
s-cis		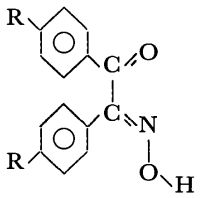 **a**	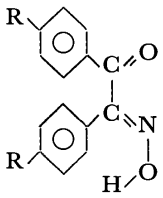 **b**	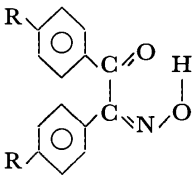 **c**	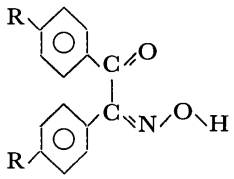 **d**
μ_{calc}	H	3, 04 (2, 79)	5, 56 (5, 48)	4, 48 (4, 85)	3, 46 (3, 62)
	Cl	1, 08 (0, 93)	3, 05 (2, 85)	1, 96 (2, 30)	1, 59 (1, 82)
s-trans		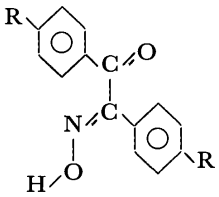 **e**	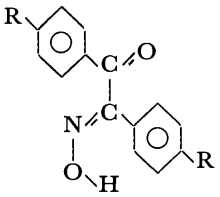 **f**	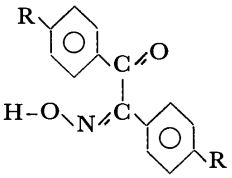 **g**	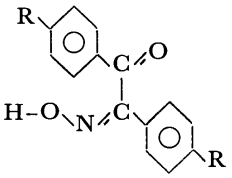 **h**
μ_{calc}	H	2, 56 (2, 68)	1, 08 (0, 30)	1, 08 (0, 89)	2, 56 (2, 57)
	Cl	2, 56 (2, 74)	1, 08 (0, 30)	1, 08 (0, 84)	2, 56 (2, 64)
μ_{exp}	H	3, 16[a]		3, 13[a]	
	Cl	3, 29		2, 67	

( ): Valeurs fournies par le deuxième mode de calcul. a) 3, 20 (11).

mules **d** ou **h**, et **c** ou **h** et nous permettent de leur attribuer la conformation **h**.

Ces déterminations viennent donc confirmer que les isomères *Z* et *E* de la benzile-monoxime et leurs dérivés *p*-chlorés se présentent en solution dioxannique sous la conformation *s-trans* (**e** pour *E*, **h** pour *Z*).

Références

1) J. Meisenheimer, *Ber.*, **54**, 3204 (1921), J. Meisenheimer et W. Theilacker, *Annalen*, **493**, 33 (1932).
2) J. C. Danilewicz, *J. Chem. Soc., C*, **1970**, 1049.
3) A. H. Blatt et A. H. Barnes, *J. Am. Chem. Soc.*, **56**, 1148 (1934).
4) K. A. Kerr, J. M. Robertson, G. A. Sim, et M. S. Newman, *Chem. Commun.*, **1967**, 170.
5) A. Palm et H. Werbin, *Can. J. Chem.*, **31**, 1004 (1953).
6) P. C. Cherry, W. R. T. Cottrell, G. D. Meakins, et E. E. Richards, *J. Chem. Soc.*, **1968**, 459.
7) G. G. Kleinspehn, J. A. Jung, et S. A. Studnarz, *J. Org. Chem.*, **32**, 461 (1967).
8) J. P. Guette, J. Armand, et L. Lacombe, *C. R. Acad. Sci. Paris, Ser. C*, **264**, 1509 (1967).
9) P. W. Sadler, *J. Chem. Soc.*, **1961**, 2162.
10) J. Armand et J. P. Guette, *Bull. Soc. Chim. Fr.*, **8**, 2894 (1969).
11) C. Pigenet, J. Armand, et H. Lumbroso, *Bull. Soc. Chim. Fr.*, **6**, 2124 (1970).
12) J. Bernadou, J. P. Fayet, M. Bonnafous, et P. Mauret, Communication aux Journées de Chimie Organique d'Orsay (1977).
13) T. W. J. Taylor et M. S. Marks, *J. Chem. Soc.*, **1930**, 2302.
14) R. Adams et C. S. Marvel, *Org. Synth.*, Coll. Vol. **I**, 94 (1956).
15) H. T. Clarke et E. E. Dreger, *Org. Synth.*, Coll. Vol. I, 87 (1956).
16) Tshugaev, *J. Prakt. Chem.*, **76**, 88 (1907).
17) W. C. Hamilton, *Acta Crystallogr.*, **14**, 95 (1961).
18) I. N. Levine, *J. Mol. Spectrosc.*, **8**, 279 (1962); *J. Chem. Phys.*, **38**, 2326 (1963).
19) Del. Re, *J. Chem. Soc.*, **1958**, 4031.
20) C. P. Smyth, "Dielectric Behavior and Structure," McGraw-Hill, N. Y. (1955).
21) I. F. Halverstadt et W. D. Kumler, *J. Am. Chem. Soc.*, **64**, 2988 (1942).
22) J. Sotiropoulos, P. Bedos, D. Mermillod-Blardet, et P. Mauret, *C. R. Acad. Sci. Paris, Ser. C*, **265**, 5 (1967).
23) M. Bordeau, J. Dedier, E. Frainnet, J. P. Fayet, et P. Mauret, *J. Organomet. Chem.*, **59**, 125 (1973).

 © 1982 The Chemical Society of Japan Bull. Chem. Soc. Jpn., 55, 2311—2312 (1982)

COMMENTS

Hydrogenolysis and Hydrogenation of Ethylene on $LaCoO_3$

Maria Alicia ULLA and Eduardo Agustin LOMBARDO*

Instituto de Investigaciones en Catálisis y Petroquímica (INCAPE), Facultad de Ingeniería Química, Santiago del Estero 2829, 3000 Santa Fe, Argentina

(Received May 25, 1981)

Synopsis. The hydrogenation and hydrogenolitic activity of $LaCoO_3$ reported by Ichimura *et al.*[1] can be rationalized in terms of the current literature by a model in which Co°, produced under reaction conditions, is the locus of catalytic activity. This interpretation disagrees with the model supported by the authors.

Recently, Ichimura *et al.*[1] reported the results of a study of the hydrogenolysis of ethylene and ethane on $LaCoO_3$. Regarding the nature of the possible active sites they advanced a model that, we understand, does not take into account and to a certain extent contradicts the existing body of knowledge in the field. They concluded that the pairs of lanthanum and oxygen ions are mainly responsible for the hydrogenation activity while the Co^{3+} ions play a role in the rupture of the carbon-carbon bond. Opossing this view we have reasons to believe that the loci of both hydrogenation and hydrogenolytic activities are Co° atoms that appear on the surface as a consequence of the reduction of Co^{3+} by hydrogen at the reaction temperature. We will now review the pertinent literature that support our point of view.

Sis *et al.*[2] have carefully studied the reduction of $LaCoO_3$ using various techniques. They were able to reduce the mixed oxide up to a mixture of La_2O_3 + Co° when the temperature reached 650 °C. However, they detected the appearance of Co° at temperatures as low as 300 °C. Similar results were reported by Petunchi *et al.*[3] and Crespin *et al.*[4] Furthermore, we have observed that at 80 °C $LaCoO_3$ could be rapidly reduced, under 170 Torr† of hydrogen pressure in a recirculating system, to $LaCoO_{2.9}$. Therefore, under the conditions Ichimura *et al.*[1] did the experiments, $H_2/C_2H_4 = 10$ and temperatures between 80 °C and 300 °C, it is very likely they had a partially reduced perovskite.

Another important clue to ascribe a metallic behavior to their system was found within the data reported by Ichimura *et al.*[1] The reaction between C_2H_4 and D_2 is a diagnostic tool to distinguish between metallic and metal oxide behavior. In the case of group VIII metals multiple exchanged ethylene and ethane are produced during the reaction.[5–8] Oxides on the other hand, produce $C_2H_4D_2$ almost exclusively while the unreacted ethylene shows none or very little deuterium exchanged.[9–12] This general trend also holds true for higher reaction temperatures (250—450 °C) in the case of a relatively inactive catalyst such as TiO_2.[12] In the table it is shown for comparisson the data obtained by Ichimura *et al.*[1] at 80 °C, our own data and a sample experiment reported by Tanaka *et al.*[9] on Co_3O_4. In both cases in which $LaCoO_3$ was the catalyst either pre-reduced or not, the product hydrocarbons show similar exchange patterns, *e.g.* the calculated binomial distributions closely duplicate the experimental values. The typical Co_3O_4 data shows the selective addition of deuterium to the double bond while the ethylene remains virtually free of deuterium.

Ichimura *et al.*[1] also reported tracer data obtained at 300 °C at which temperature there is no doubt Co° is already present in the solid.[2,13] Both ethane and ethylene were multiple exchanged but the data show some deviation from binomial distribution. The deuterium distribution in methane formed by hydrogenolisis does not seem to fit in line with those reported for both ethylene and ethane. Additional data would

TABLE 1. DEUTERATED PRODUCTS FROM $C_2H_4 + D_2$ REACTION OVER $LaCoO_3$ AND Co_3O_4

Catalyst	$LaCoO_{2.75}$[a]				$LaCoO_3$[b]				Co_3O_4[c]	
Reaction temp	50 °C				80 °C				23 °C	
Conversion	54%				42%				50%	
Products	Ethane		Ethylene		Ethane		Ethylene		Ethane	Ethylene
	Exptl	Calcd[d]	Exptl	Calcd[d]	Exptl	Calcd	Exptl	Calcd	Exptl	Exptl
d_0	23.5	17.5	40.6	34.7	11	9.5	19.5	21.4	2.6	97.7
d_1	29.7	35.4	35.9	42.0	25	27	42.8	40.3	3.6	2.4
d_2	27.5	29.8	16.0	19.1	32	32.9	28.8	28.4	92.2	0.2
d_3	12.1	13.4	4.9	3.9	22	21.1	8.1	8.9	1.6	0
d_4	5.6	3.4	2.6	0.3	9	8	0.8	1.0	0	0
d_5	1.6	0.5			2	1.5			0	
d_6	0	0			0	0				

a) $LaCoO_3$ pre-reduced at 300 °C in hydrogen, Ref. 14. b) Ref. 1. c) Ref. 9. d) Calculated assuming a binomial distribution.

† 1 Torr ≈ 133.322 Pa.

be needed to interpret the methane tracer results.

Ichimura *et al.*[1] argued that catalyst deactivation was due to the reduction of Co^{3+} to lower oxidation states. This is at variance with our finding[13] that the oxidized catalyst is inactive and its activity increases sharply going through a maximum with the extent of reduction of the oxide. Our experiments were conducted on two different aliquots of the catalyst that before each run received a standard re-oxidation and reduction pretreatment. The reaction temperature was 253 K. However, extrapolation of their results at this temperature fall within the activity range of our slightly reduced catalyst, *e.g.* $LaCoO_{3-x}$ ($x<0.2$). An alternative explanation for the deactivation process comes from the fact that most hydrocarbon reactions leave "residues" or "coke" on the surface which poison the catalyst. This system is no exception in this regard for we have measured the amount of strongly adsorbed molecules that remains on the surface after evacuation at reaction temperature, $2.2\pm1.0\times10^{14}$ atoms of C/cm^2.[14] This value is of the same order of magnitude as the maximum number of active sites estimated to exist on our catalyst by CO poisoning technique.[14]

In summary, the very likely reduction of even small amounts of Co^{3+} to Co° under reaction conditions and the tracer data that resemble those obtained over group VIII metals support a model in which finelly dispersed Co° on the matrix oxide is the responsible for both the hydrogenation and hydrogenolitic activity of $LaCoO_3$.

References

1) K. Ichimura, Y. Inoue, and I. Yasumori, *Bull. Chem. Soc. Jpn.*, **53**, 3044 (1980).
2) L. B. Sis, G. P. Wirtz, and S. C. Sorenson, *J. Appl. Phys.*, **44**, 5553 (1973).
3) J. O. Petunchi, M. A. Ulla, J. L. Nicastro, and E. A. Lombardo, *Proc. of 7th Iberoamerican Symposium on Catalysis*, 108 (1980).
4) M. Crespin and W. K. Hall, *J. Catal.*, **69**, 359 (1981).
5) J. Turkevich, F. Bonner, D. O. Schissler, and A. P. Irsa, *Discuss. Faraday Soc.*, **8**, 352 (1950).
6) J. N. Wilson, J. W. Otvos, D. P. Stevenson, and C. D. Wagner, *Ind. Eng. Chem.*, **45**, 1480 (1956).
7) C. Kemball, *J. Chem. Soc.*, **1956**, 735.
8) G. C. Bond and P. B. Wells, "Advances in Catalysis," Academic Press, New York (1964), Vol. XV, p. 92.
9) K. Tanaka, H. Nihira, and A. Osaki, *J. Phys. Chem.*, **74**, 4510 (1970).
10) P. L. Burwell, Jr., A. B. Littlewood, M. Cardew, C. Pass, and C. T. H. Stoddart, *J. Am. Chem. Soc.*, **82**, 6287 (1960).
11) W. C. Conner, Jr., and R. J. Kokes, *J. Phys. Chem.*, **73**, 2436 (1969).
12) I. J. S. Lake and C. Kemball, *Trans. Faraday Soc.*, **63**, 2535 (1967).
13) J. O. Petunchi, J. L. Nicastro, and E. A. Lombardo, *J. Chem. Soc., Chem. Commun.*, **1980**, 467.
14) J. O. Petunchi, M. A. Ulla, J. A. Marcos, and E. A. Lombardo, *J. Catal.*, **70**, 356 (1981).

Active State of the $LaCoO_3$ Catalyst. A Reply to the Comment, "Hydrogenolysis and Hydrogenation of Ethylene on $LaCoO_3$"

Kenji Ichimura, Yasunobu Inoue, and Iwao Yasumori*

Department of Chemistry, Tokyo Institute of Technology, Ookayama, Meguro-ku, Tokyo 152

(Received December 23, 1981)

The catalytic activities of mixed oxide perovskite, $LaCoO_3$, for oxidation as well as hydrogenation have been subjects of many researches because of this substance's peculiar valence-band structure, similar to those of transition metals. We have investigated this unique activity for ethylene hydrogenation and ethane hydrogenolysis,[1] and the hydrogenolysis of C_3–C_5 alkanes,[2] and have performed a comparative study of $LaCoO_3$, $LaAlO_3$, and $LaFeO_3$, in which the latter two perovskites showed only hydrogenation activity.[3] In our study, the activity of $LaCoO_3$ was stabilized by evacuation at 300 °C for 1 h prior to each kinetic run, and the catalyst exhibited a good reproducible activity for runs repeated several tens of times. After more than one hundred times, the catalyst was deactivated and an XPS analysis of the surface indicated that the Co^{3+} ions in the surface layer were reduced to Co^{2+} ions, which were characterized by the shake-up satellite peaks in the spectrum.[1]

Recently, Crespin and Hall have studied in detail the surface states of perovskite compounds, $BaTiO_3$, $SrTiO_3$, and $LaCoO_3$, and their changes during reduction.[4] They found that the Co^{3+} ions in their $LaCoO_3$ sample were easily reduced to the Co^{2+} by heating in hydrogen at 400 °C and that the compound was then decomposed to Co^0 and La_2O_3 by reduction at 500 °C. This reduced mixture was found to recover its original perovskite structure by reoxidation at as low a temperature 400 °C. By the use of $LaCoO_3$ prepared by the same procedure, Petunch *et al.* examined the change in activity for ethylene hydrogenation with an increase in the degree of reduction and proposed that the active state of $LaCoO_3$ was finely dispersed zerovalent Co particles on the La_2O_3 surface; a maximum activity for ethylene hydrogenation at −20 °C was observed on the $LaCoO_{3-x}$ catalyst at the $x=0.7$ composition for the first oxidation-reduction cycle and at $x=1.2$ for the second cycle.[5]

These results are quite different from ours, especially with regard to the stability of the catalyst in a reducing atmosphere; this difference may be attributed to the variation in the catalyst preparation and to the structure of the perovskite particles thus formed. The calcination of mixed hydroxides precipitates in the preparation of our catalyst was carried out by heating them at 900 °C for 3 h and then at 1100 °C for 12 h; a well-developed crystal of $LaCoO_3$ with a surface area of 0.33 m^2/g was thus obtained. The calcination temperature in their preparation was, however, lower than 800 °C, and the obtained compound had a large surface area of 16 m^2/g, about 50 times as large as that of ours, predicting that the difference in the average particle size between the two catalysts will be of the same order of magnitude.

This high reducibility of their compound and the recovery of the original structure by reoxidation at an extremely low temperature are surprising, as Crespin and Hall stated in their report; they ascribed those phenomena to the structure containing vacancies in the perovskite lattice and to the resultant high mobility of ions.[6] The fact that the surface area decreased from 16 to 13 m^2/g after the reoxidation, whereas the crystallite size decreased to some extent, supports this view. Such lattice imperfections may be exposed on the surface with a high concentration, so that some fraction of Co occupies "coordinatively unsaturated sites." The reported instability of hydrogenation activity which is seen from the drastic decrease in activity with an increased degree of reduction and the shift of activity maximum may reflect the labile nature of their catalyst. Moreover, it is amazing that the catalyst prepared by them is more reducible than that studied by Crespin and Hall, since their catalyst was reduced to some extent at 80 °C.[7]

It is not possible to compare the behavior of their catalyst for ethane hydrogenolysis with ours, since they examined the hydrogenation of ethylene only at temperatures up to 50 °C. As for the hydrogenolysis of ethane over our catalyst, the reaction orders with respect to ethane and hydrogen are 1.0 and −0.5 respectively, and the activation energy was estimated at 35 kJ/mol in the temperature range of 200—300 °C. These values of kinetic parameters are quite different from those for the reaction on metallic Co dispersed on carriers; the ethane and hydrogen orders are 1.0 and −0.8 respectively, the value of activation energy is 125 kJ/mol for Co/SiO_2.[8] The hydrogen order of −1.3 and the activation energy of 134 kJ/mol for Co/MgO were reported.[9] These results evidently show that the active state of our catalyst is far from that of metallic Co. By comparing the observed deuterium distributions of the reactant and the product molecules in the reaction of ethylene with D_2, Ulla and Lombardo insisted that our results were close to theirs and those obtained from the catalysis by "metal," and deviated from those observed in the reaction on "oxide," by illustrating the results of a reaction over Co_3O_4 at 23 °C.[10] It is, however, not reasonable to compare directly the properties of reactions which proceed in different temperature ranges and to classify the active state as simply "metal" or "oxide" without considering the variation in the character of oxides; in the cases of typical oxides, such as CaO[11] and MgO,[12] the most abundant species in the deuterium distribution of ethane, ethane-d_2, decreased its fraction with an increase in the reaction temperature and the distribution became broader. Even a comparison of our results (80 °C) with theirs (50 °C) shows that our distribution has a distinct maximum at ethane-d_2 and so is different from theirs.

It should also be noted that there is a limit to the amount of surface atoms detectable by means of XPS, a small percentage of the fraction of surface coverage, and that it is difficult to determine the oxidation state of a surface species when its amount is below this limit. Accordingly, a more sensitive method of surface analysis is needed to obtain a definite solution of this problem.

In conclusion, this reply does not detract from the results obtained by the use of their own catalyst, but we wish to point out that it is premature to generalize their view immediately on the basis of the conclusion deduced from a study using only a catalyst in a highly reducible state.

References

1) K. Ichimura, Y. Inoue, and I. Yasumori, *Bull. Chem. Soc. Jpn.*, **53**, 3044 (1980).
2) K. Ichimura, Y. Inoue, and I. Yasumori, *Bull. Chem. Soc. Jpn.*, **54**, 1787 (1981).
3) K. Ichimura, Y. Inoue, I. Kojima, E. Miyazaki, and I. Yasumori, *Proc. 7th Intern. Congr. Catal.*, 1980, **B**, 1281 (1981).
4) M. Crespin and W. K. Hall, *J. Catal.*, **69**, 359 (1981).
5) J. O. Petunch, M. A. Ulla, J. A. Marcos, and E. A. Lombardo, *J. Catal.*, **70**, 356 (1981).
6) Ref. 4, p. 363.
7) M. A. Ulla and E. A. Lombardo, *Bull. Chem. Soc. Jpn.*, **55**, 2311 (1982).
8) J. H. Sinfelt, *Adv. Catal.*, **23**, 91 (1973).
9) G. C. Bond, "Catalysis by Metals," Academic Press, London and N. Y. (1962), p. 396.
10) K. Tanaka, H. Nihira, and A. Ozaki, *J. Phys. Chem.*, **74**, 4510 (1970).
11) K. Kasama, Y. Inoue, and I. Yasumori, *Bull. Chem. Soc. Jpn.*, **53**, 1842 (1980).
12) M. Tezuka, Y. Inoue, and I. Yasumori, *Bull. Chem. Soc. Jpn.*, **54**, 2515 (1981).
13) Ref. 7, Table 1.

The Structure of the Cyclodextrin Complex. XIII. Crystal Structure of β-Cyclodextrin-1,4-Diazabicyclo[2.2.2]octane Complex Tridecahydrate

Kazuaki HARATA

Research Institute for Polymers and Textiles, 1-1-4, Yatabe-Higashi, Tsukuba, Ibaraki 305

(Received September 26, 1981)

The crystal structure of β-cyclodextrin–1,4-diazabicyclo[2.2.2]octane complex tridecahydrate was determined by the X-ray method. The crystal is monoclinic with the space group $P2_1$, $Z=2$, $a=15.395(2)$, $b=16.598(1)$, $c=15.441(2)$ Å, and $\beta=117.35(1)°$. The structure was solved by inspection of a Patterson map and a trial-and-error method combined with the rigid-body least-squares technique and refined by the block-diagonal least-squares method to the final R-value of 0.048 for 5649 reflections ($\sin\theta/\lambda<0.61$). The β-cyclodextrin molecule is in the shape of a distorted and truncated heptagonal pyramid. Two of seven primary hydroxyl groups are in a *gauche-trans* conformation, the others being in a *gauche-gauche* conformation. Secondary hydroxyl groups form intramolecular hydrogen bonds between adjacent glucose residues. The guest 1,4-diazabicyclo[2.2.2]octane is almost fully included in the cavity of β-cyclodextrin. Its methylene groups are in van der Waals contact with the methine groups and the glycosidic oxygen atoms at the interior surface of β-cyclodextrin, while two nitrogen atoms form hydrogen bonds with a water molecule and a secondary hydroxyl group of the neighboring β-cyclodextrin. β-Cyclodextrin molecules are arranged nearly parallel to the crystallographic ac plane to form a corrugated sheet of molecular layer. All of the thirteen water molecules fill vacant spaces between the molecular layers, forming a hydrogen-bond network in the crystal.

β-Cyclodextrin forms many crystalline inclusion complexes with a variety of guest molecules. Crystals of uncomplexed β-cyclodextrin[1] and its ethanol complex[2] have a cage-type structure in which β-cyclodextrin molecules are arranged in a zigzag mode. Crystal structures of the complexes with 1-propanol[3] and some benzene derivatives[4] consist of a dimer unit formed by two β-cyclodextrin molecules with their secondary hydroxyl sides facing each other. In this paper, we present a crystal structure of the β-cyclodextrin-1,4-diazabicyclo[2.2.2]octane (1,4-DO) complex; its molecular packing is different from those found previously. The host-guest geometry of the complex is interesting in relation to the 1,4-DO catalyzed hydrolysis of acyl-β-cyclodextrin.

Experimental

β-Cyclodextrin and 1,4-DO in a 1 : 1 molar ratio were dissolved in a hot aqueous solution, and the solution was allowed to stand at room temperature. Colorless and prismatic crystals were obtained. Lattice parameters and reflection intensities were measured on a Nicolet P3/F diffractometer with graphite-monochromated Cu $K\alpha$ radiation. The crystal was sealed in a quartz capillary with a drop of mother liquor since it breaks up in air. 5649 independent reflections with $|F_o|\geqq 3\sigma(F)$ were collected up to 140° in 2θ by using θ-2θ scan mode. No corrections were made for absorption or extinction effect.

Crystal Data: $C_{42}H_{70}O_{35}\cdot C_6H_{12}N_2\cdot 13H_2O$, $F.W.=1481.4$ monoclinic, space group $P2_1$, $Z=2$, $a=15.395(2)$, $b=16.598(1)$, $c=15.441(2)$ Å, $\beta=117.35(1)°$, $V=3504.7(7)$ Å^3, $D_x=1.404$, $D_m=1.40$ g cm^{-3}.

Determination and Refinement of the Structure

A Patterson map showed that the *pseudo* heptagonal axis of β-cyclodextrin makes an angle of *ca.* 10° against the crystallographic b axis. The rotation around the molecular axis and the translational parameters along the a and c axes were determined by a trial-and-error method. After the correction of the position and orientation of each glucose residue by the rigid-body least-squares technique, atomic parameters were refined by the block-diagonal least-squares method. Successive Fourier and difference-Fourier syntheses revealed the positions of 1,4-DO and hydrated water molecules. An occupancy factor of disordered water molecules (W10A and W10B) was estimated from an electron-density map, but it was not refined. Hydrogen atoms were found on a difference-Fourier map. Further refinement of the structure by the block-diagonal least-squares method converged the R-value to 0.048. The quantity minimized was $\sum w(|F_o|-|F_c|)^2$ with $w=1.0$ for all the reflections. Atomic scattering factors were taken from the "International Tables for X-Ray Crystallography."[6] Final atomic coordinates and B_{eq} of non-hydrogen atoms are given in Table 1. Tables of the observed and calculated structure factors, anisotropic temperature factors, atomic parameters of hydrogen atoms, bond distances, angles, and conformation angles of β-cyclodextrin are kept at The Chemical Society of Japan (Document No. 8232). The computation was carried out on a FACOM M-200 computer at the RIPS Center, Tsukuba.

Description and Discussion of the Structure

Outline of the Structure. A numbering scheme of the β-cyclodextrin–1,4-DO complex is shown in Fig. 1. β-Cyclodextrin is in the shape of a distorted and truncated heptagonal pyramid with the wide aperture at the secondary hydroxyl side and the smaller aperture at the primary hydroxyl side. The guest 1,4-DO molecule is situated in the β-cyclodextrin cavity at the secondary hydroxyl side (Fig. 2). β-Cyclodextrin molecules are arranged nearly parallel to the ac plane and form a corrugated sheet of molecular layers (Fig. 3). All the water molecules are located outside the β-cyclodextrin

TABLE 1. FINAL ATOMIC COORDINATES ($\times 10^4$) AND B_{eq} (B/Å^2) OF NON-HYDROGEN ATOMS[a,b]

	x	y	z	B_{eq}/Å^2
C(1,G1)	3272(4)	2895(4)	-187(4)	2.79
C(2,G1)	2705(4)	3679(4)	-383(4)	3.15
C(3,G1)	1909(4)	3621(3)	-65(4)	3.05
C(4,G1)	1262(4)	2893(3)	-532(4)	2.75
C(5,G1)	1885(4)	2133(3)	-334(4)	2.80
C(6,G1)	1302(4)	1395(3)	-877(5)	3.78
O(2,G1)	3367(3)	4313(3)	146(3)	3.69
O(3,G1)	1313(3)	4334(2)	-356(3)	3.65
O(4,G1)	645(2)	2823(3)	-77(2)	2.92
O(5,G1)	2614(2)	2256(2)	-668(3)	2.89
O(6,G1)	762(3)	1517(3)	-1895(3)	3.99
C(1,G2)	6500(4)	2208(3)	3062(4)	2.66
C(2,G2)	6351(4)	3058(3)	2630(4)	2.55
C(3,G2)	5267(4)	3238(3)	2075(4)	2.51
C(4,G2)	4783(3)	2600(3)	1282(4)	2.26
C(5,G2)	4974(3)	1763(3)	1742(3)	2.40
C(6,G2)	4590(4)	1088(3)	1008(4)	3.04
O(2,G2)	6849(3)	3634(2)	3384(3)	3.11
O(3,G2)	5135(3)	4021(2)	1654(3)	3.08
O(4,G2)	3749(2)	2761(2)	838(2)	2.51
O(5,G2)	6013(3)	1637(2)	2302(2)	2.52
O(6,G2)	4961(3)	1150(3)	317(3)	3.60
C(1,G3)	6940(4)	1437(4)	6586(4)	3.43
C(2,G3)	7575(4)	2094(4)	6456(4)	3.71
C(3,G3)	7053(4)	2470(4)	5449(4)	3.17
C(4,G3)	6736(4)	1807(4)	4666(4)	2.84
C(5,G3)	6132(4)	1169(4)	4868(4)	3.10
C(6,G3)	5922(5)	447(4)	4191(5)	4.51
O(2,G3)	7814(3)	2689(3)	7194(3)	4.43
O(3,G3)	7726(3)	3004(3)	5325(3)	4.15
O(4,G3)	6128(2)	2179(2)	3748(2)	2.63
O(5,G3)	6684(3)	852(2)	5838(3)	3.39
O(6,G3)	5295(3)	-117(3)	4327(3)	4.33
C(1,G4)	4370(4)	1782(3)	7958(4)	2.89
C(2,G4)	5249(4)	2345(4)	8371(4)	2.91
C(3,G4)	5623(4)	2464(4)	7630(4)	2.98
C(4,G4)	5843(4)	1652(4)	7326(4)	3.04
C(5,G4)	4947(4)	1110(3)	6952(4)	3.17
C(6,G4)	5161(5)	255(4)	6763(5)	4.48
O(2,G4)	4973(3)	3096(3)	8640(3)	3.76
O(3,G4)	6517(3)	2932(3)	8047(3)	3.70
O(4,G4)	6090(3)	1806(2)	6539(2)	2.96
O(5,G4)	4631(3)	1046(2)	7704(3)	3.17
O(6,G4)	4268(4)	-204(3)	6289(4)	5.50
C(1,G5)	623(4)	2569(3)	5944(4)	2.64
C(2,G5)	1298(4)	3193(3)	6677(4)	2.78
C(3,G5)	2336(4)	3096(3)	6811(4)	2.55
C(4,G5)	2673(4)	2235(3)	7116(4)	2.36
C(5,G5)	1955(4)	1641(3)	6360(4)	2.49
C(6,G5)	2177(4)	760(3)	6662(4)	2.95
O(2,G5)	952(3)	3987(2)	6325(3)	3.38
O(3,G5)	2993(3)	3615(2)	7568(3)	3.01
O(4,G5)	3606(2)	2160(2)	7124(2)	2.44
O(5,G5)	983(2)	1787(2)	6262(3)	2.58
O(6,G5)	2158(3)	631(2)	7571(3)	3.03
C(1,G6)	-1416(4)	2984(3)	2116(4)	2.59
C(2,G6)	-1223(4)	3727(3)	2761(4)	2.60
C(3,G6)	-290(4)	3604(3)	3720(4)	2.70
C(4,G6)	-340(4)	2820(3)	4194(4)	2.35
C(5,G6)	-492(4)	2128(3)	3479(4)	2.46
C(6,G6)	-538(4)	1301(3)	3868(4)	3.21
O(2,G6)	-1128(3)	4409(2)	2251(3)	3.06
O(3,G6)	-211(3)	4281(2)	4343(3)	3.21
O(4,G6)	604(2)	2730(2)	5028(2)	2.28
O(5,G6)	-1420(2)	2270(2)	2621(2)	2.50
O(6,G6)	-1302(3)	1245(3)	4146(3)	3.93
C(1,G7)	-372(4)	2645(4)	-682(4)	2.85
C(2,G7)	-980(4)	3380(4)	-683(4)	3.10
C(3,G7)	-801(4)	3544(3)	347(4)	2.73
C(4,G7)	-1008(4)	2795(3)	774(4)	2.55
C(5,G7)	-445(4)	2063(3)	699(4)	3.22
C(6,G7)	-775(6)	1282(4)	963(5)	5.37
O(2,G7)	-740(3)	4057(3)	-1108(3)	4.01
O(3,G7)	-1443(3)	4188(2)	316(3)	3.53
O(4,G7)	-690(2)	2645(2)	1794(2)	2.52
O(5,G7)	-624(3)	1972(2)	-305(3)	3.14
O(6,G7)	-1851(5)	1196(4)	255(5)	8.40
N(1,DO)	2623(4)	2495(4)	3387(4)	5.11
C(2,DO)	3623(8)	2447(7)	3568(12)	13.85
C(3,DO)	4228(7)	3170(7)	4232(10)	11.82
N(4,DO)	3591(4)	3738(3)	4336(4)	3.99
C(5,DO)	3127(9)	3373(8)	4855(8)	11.37
C(6,DO)	2607(8)	2572(7)	4336(7)	9.25
C(7,DO)	2175(9)	3235(6)	2825(8)	8.87
C(8,DO)	2839(9)	3967(6)	3386(8)	9.16
O(W1)	-2759(3)	251(3)	2793(4)	4.78
O(W2)	-708(5)	179(7)	7692(5)	11.02
O(W3)	-3126(4)	682(4)	880(4)	6.12
O(W4)	-3426(4)	3894(4)	49(4)	6.14
O(W5)	-1645(5)	4293(4)	6761(5)	8.61
O(W6)	6034(6)	4465(4)	7630(5)	8.86
O(W7)	3448(6)	154(6)	4376(5)	10.13
O(W8)	1652(6)	1073(4)	2499(6)	10.03
O(W9)	1825(6)	5294(4)	1266(4)	7.92
O(W10A)	619(5)	5685(4)	3996(5)	4.95
O(W10B)	-1246(12)	311(11)	5556(12)	5.83
O(W11)	390(5)	4638(4)	7541(4)	8.86
O(W12)	3825(3)	39(3)	8941(3)	3.42
O(W13)	2395(5)	394(4)	1303(5)	7.07

a) Occupancy factors of O(W10A) and O(W10B) are 0.7 and 0.3, respectively. b) $B_{eq} = 8\pi^2(u_1^2+u_2^2+u_3^2)/3$, where u_i is the root-mean-square deviation in the i-th principal axis of the thermal ellipsoid.

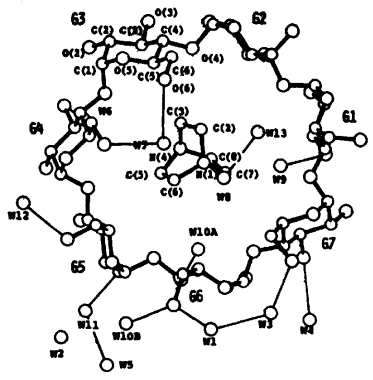

Fig. 1. A numbering scheme of β-cyclodextrin-1,4-DO complex tridecahydrate.

cavity. They fill the intermolecular space and form the hydrogen-bond network in the crystal.

Conformation of β-Cyclodextrin. β-Cyclodextrin consists of seven α-1,4-linked D-glucose residues of the $^4C_1$ chair conformation. Except for the orientation of the C(6)–O(6) bonds, the conformations of seven glucose residues are nearly identical with each other. The primary hydroxyl groups show two different types of conformations (Fig. 1). In G3 and G4 residues, they are inclined toward the β-cyclodextrin axis, having a *gauche-trans* conformation. This conformation is held by the hydrogen-bonds linking these hydroxyl groups through the W7 water molecule. The other primary hydroxyl groups in a *gauche-gauche* conformation turn away from the center of the β-cyclodextrin ring.

Average bond distances and angles for seven glucose residues are shown in Fig. 4. Characteristics similar to those found in α-cyclodextrin complexes[7] are also observed in them; the C(2)–C(3) and C(3)–C(4) bonds are slightly shorter than the C(1)–C(2) and C(4)–C(5) bonds, and the C(3)–C(4)–O(4) angle is smaller than the ideal tetrahedral angle. This indicates that the glucose conformation is only slightly affected by the size of the macrocyclic ring. A significant difference is observed in the glycosidic oxygen angle between α- and β-cyclodextrin. The average value of 117.4° is smaller than the corresponding angle of α-cyclodextrin (118—119°), but it is in good agreement with the angle of

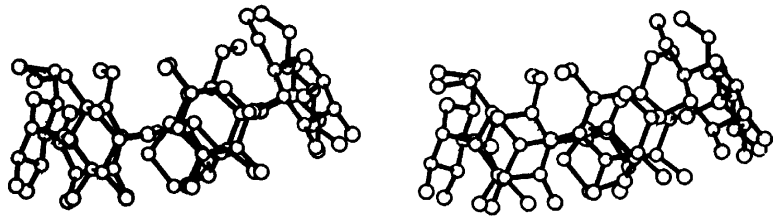

Fig. 2. A stereo-drawing of a side-view of the complex.

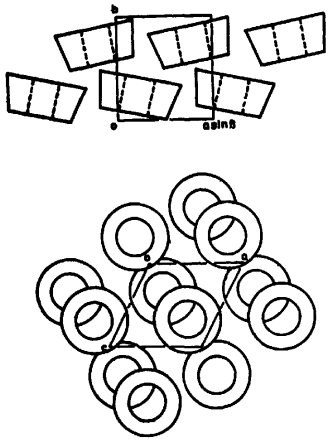

Fig. 3. An illustration of the packing feature of β-cyclodextrin in the crystal.

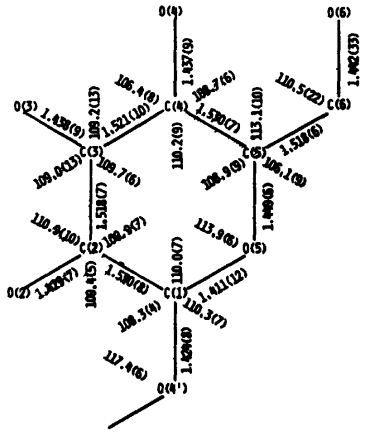

Fig. 4. Average bond distances and angles over seven glucose residues.
Standard deviations in parentheses were estimated according to the equation: $\sigma=[\sum_{i=1}^{7}(x_i-\bar{x})^2/6]^{1/2}$, where x_i referes to the bond distance or angle in the i-th glucose residue, and $\bar{x}$ is the average value.

disaccharides.[8–10] Distances between glycosidic oxygen atoms of adjacent glucose residues are in the range 4.25—4.46 Å. The average value of 4.36 Å is larger than that of the α-cyclodextrin complexes (4.23—4.25 Å). The torsion-angle indices[11] (Table 2) vary from 111.0° to 126.6°. A linear correlation between these values and O(4)···O(4) distances is shown in Fig. 5. Although the torsion-angle index and O(4)···O(4) distances are limited to a rather small region, the correlation is stronger than that found in the α-cyclodextrin complexes.

Seven glycosidic oxygen atoms form a distorted heptagon. The distances between the center of gravity of the seven O(4) atoms and each individual O(4) atom are in the range 4.91—5.10 Å with an average value of 5.02 Å. These O(4) atoms are roughly coplanar with a maximum deviation of 0.26 Å from their least-squares plane (Table 3). This deviation is larger than that observed in the β-cyclodextrin complexes which have a head-to-head dimer-type arrangement. The tilt-angles[12] of glucose residues were measured as the angle made by the O(4) plane and the plane through C(1), C(4), O(4), and O(4′) of each residue. Since the β-cyclodextrin ring is distored from the regular heptagon, the tilt-angles are not the same but vary within the

Table 2. Geometrical data for β-cyclodextrin

I. Radius of the O(4) heptagon.
The radius is measured from the center of gravity of seven O(4) atoms to each O(4) atom.

Residue	Radius l/Å	Residue	Radius l/Å
G1	5.10	G5	5.10
G2	5.00	G6	4.97
G3	4.91	G7	4.94
G4	5.09	Average	5.02

II. O(4)···O(4) distance between adjacent glucose residues.

	Distance l/Å		Distance l/Å
O(4,G1)···O(4,G2)	4.32	O(4,G5)···O(4,G6)	4.36
O(4,G2)···O(4,G3)	4.41	O(4,G6)···O(4,G7)	4.46
O(4,G3)···O(4,G4)	4.38	O(4,G7)···O(4,G1)	4.25
O(4,G4)···O(4,G5)	4.35	Average	4.36

III. Tilt-angle and torsion-angle index.[a,b]

Residue	Tilt-angle ϕ/°	Torsion-angle index ϕ/°
G1	7.5	125.0
G2	2.8	119.3
G3	21.1	122.0
G4	15.8	124.3
G5	5.7	120.8
G6	3.9	111.0
G7	23.1	126.6
Average	11.4	121.3

a) The tilt-angle is defined as an angle between the O(4) plane and the plane through C(1), C(4), O(4), and O(4′) of each glucose residue (see Ref. 12). b) The torsion-angle index is defined as: $|\phi(C(1)-C(2))|+|\phi(C(2)-C(3))|-|\phi(C(3)-C(4))|-|\phi(C(4)-C(5))|+|\phi(C(5)-O(5))|+|\phi(O(5)-C(1))|$, where $\phi(C(1)-C(2))$ is the conformation angle of O(5)-C(1)-C(2)-C (3) (see Ref. 11).

TABLE 3. LEAST-SQUARES PLANE THROUGH SEVEN O(4) ATOMS

The plane equation is of the $AX+BY+CZ=D$ form, where X, Y, and Z are the coordinates in Å units along the a, b, and c* axes, respectively.

$0.107X+0.984Y+0.144Z=4.966$

Atomic deviations

Residue	Distance l/Å	Residue	Distance l/Å
G1	−0.26	G5	0.02
G2	0.26	G6	0.20
G3	0.06	G7	−0.05
G4	−0.22		

TABLE 4. BOND DISTANCES AND ANGLES IN 1,4-DO

I. Bond distances

Distance l/Å		Distance l/Å	
N(1,DO)–C(2,DO)	1.44(3)	N(4,DO)–C(8,DO)	1.44(2)
N(1,DO)–C(6,DO)	1.48(2)	C(2,DO)–C(3,DO)	1.57(3)
N(1,DO)–C(7,DO)	1.48(2)	C(5,DO)–C(6,DO)	1.57(3)
N(4,DO)–C(3,DO)	1.42(2)	C(7,DO)–C(8,DO)	1.57(3)
N(4,DO)–C(5,DO)	1.43(3)		

II. Bond angles

	Angle ϕ/°
C(2,DO)–N(1,DO)–C(6,DO)	108(1)
C(2,DO)–N(1,DO)–C(7,DO)	109(1)
C(6,DO)–N(1,DO)–C(7,DO)	107(1)
C(3,DO)–N(4,DO)–C(5,DO)	109(1)
C(3,DO)–N(4,DO)–C(8,DO)	109(1)
C(5,DO)–N(4,DO)–C(8,DO)	108(1)
C(3,DO)–C(2,DO)–N(1,DO)	110(2)
C(2,DO)–C(3,DO)–N(4,DO)	110(2)
C(5,DO)–C(6,DO)–N(1,DO)	110(2)
C(6,DO)–C(5,DO)–N(4,DO)	110(2)
C(8,DO)–C(7,DO)–N(1,DO)	108(2)
C(7,DO)–C(8,DO)–N(4,DO)	112(2)

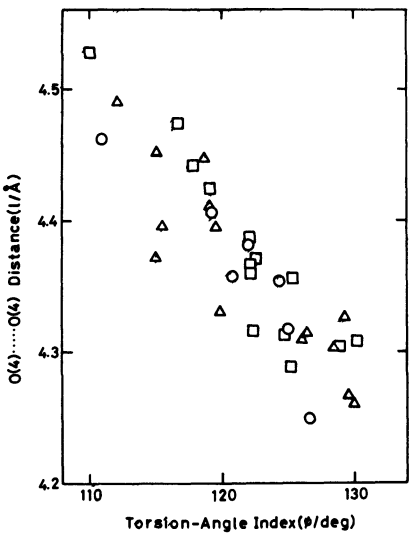

Fig. 5. Plot of the O(4)···O(4) distance against the torsion-angle index in β-cyclodextrin complexes with 1,4-DO (○) and 1-propanol (stable form △, unstable form □, see Ref. 13).

range 2.8—23.1°. The G2 and G6 residues are roughly perpendicular to the O(4) plane, while the G3 and G7 residues are inclined by angles of 21.2° and 23.1°, respectively, with the primary hydroxyl side nearer to the molecular axis.

β-Cyclodextrin-Guest Interaction. The guest 1,4-DO is situated near the secondary hydroxyl side in the β-cyclodextrin cavity, as shown in Figs. 1 and 2. The N(1) atom is located near the center of the cavity, while the N(4) atom located at the open end of the cavity is in contact with the neighboring β-cyclodextrin. The molecular axis through N(1) and N(4) does not coincide with the β-cyclodextrin axis, but inclines with the N(4) atom toward the G3 residue. The open space at the primary hydroxyl side is filled with three water molecules (W7, W8, and W13).

Bond distances and angles in 1,4-DO are shown in Table 4. The lengths of the chemically equivalent six C–N bonds vary from 1.40 Å to 1.48 Å with an average value of 1.45 Å, and the three C–C bonds are 1.57 Å. The C–N–C and C–C–N angles are in the range of 107—109° and 108—112°, respectively, and the corresponding average values are 108° and 110°. Figures 1 and 2 show that the hydrophobic methylene groups of 1,4-DO are in contact mainly with the hydrophobic surface in the host cavity. Most of these methylene

TABLE 5. HYDROGEN BOND DISTANCES (l/Å) AND ANGLES (ϕ/°) AND INTERMOLECULAR DISTANCES LESS THAN 3.0 Å

O	H	O		Distance O-H	Distance H···O	Distance O···O	Angle O-H···O
O(2,G1)	-H(O2,G1)	O(3,G2)		1.00	1.72	2.691	163
O(3,G1)	-H(O3,G1)	O(W9)		1.05	1.76	2.760	158
O(6,G1)	-H(O6,G1)	O(6,G5)	(d)	1.15	1.97	3.015	160
O(2,G2)	-H(O2,G2)	O(6,G4)	(h)	1.02	2.14	2.780	119
O(6,G2)	-H(O6,G2)	O(W12)	(d)	1.17	1.61	2.750	163
O(2,G3)	-H(O2,G3)	O(3,G4)		0.81	2.10	2.882	162
O(3,G3)	-H(O3,G3)	O(2,G2)		0.82	2.10	2.861	154
O(6,G3)	-H(O6,G3)	N(4,DO)	(k)	0.91	1.95	2.750	146
O(2,G4)	-H(O2,G4)	O(3,G5)		0.89	1.96	2.853	180
O(3,G4)	-H(O3,G4)	O(W6)		0.67	2.04	2.647	161
O(6,G4)	-H(O6,G4)	O(W7)		0.88	1.82	2.693	153
O(2,G5)	-H(O2,G5)	O(W11)		0.89	1.76	2.633	166
O(3,G5)	-H(O3,G5)	O(W1)	(g)	0.90	1.92	2.763	155
O(6,G5)	-H(O6,G5)	O(W12)		0.84	1.82	2.654	172
O(3,G6)	-H(O3,G6)	O(2,G5)		0.92	1.95	2.789	151
O(6,G6)	-H(O6,G6)	O(W10A)	(k)	0.88	1.90	2.726	156
O(6,G6)	-H(O6,G6)	O(W10B)		0.88	1.80	2.642	159
O(2,G7)	-H(O2,G7)	O(3,G1)		0.98	1.93	2.861	158
O(3,G7)	-H(O3,G7)	O(2,G6)		0.91	1.92	2.822	171
O(6,G7)	-H(O6,G7)	O(W9)	(i)	1.21	1.69	2.800	149
O(W1)	-H(1,W1)	O(6,G6)		0.93	1.89	2.749	163
O(W1)	-H(2,W1)	O(5,G2)	(b)	1.05	1.90	2.851	149
O(W3)	-H(1,W3)	O(W1)		1.15	1.88	2.833	137
O(W3)	-H(2,W3)	O(6,G7)		0.74	2.17	2.692	128
O(W4)	-H(1,W4)	O(3,G7)		0.63	2.49	2.928	129
O(W4)	-H(2,W4)	O(2,G4)	(e)	0.60	2.19	2.763	161
O(W5)	-H(1,W5)	O(2,G3)	(b)	1.02	2.27	2.957	123
O(W5)	-H(2,W5)	O(W11)		1.35	2.03	2.850	113
O(W6)	-H(2,W6)	O(W13)	(h)	0.99	1.95	2.698	130
O(W7)	-H(1,W7)	O(W5)	(j)	1.20	1.79	2.889	150
O(W7)	-H(2,W7)	O(6,G3)		1.19	1.91	2.914	139
O(W8)	-H(1,W8)	N(1,DO)		0.98	1.85	2.792	160
O(W9)	-H(1,W9)	O(W2)	(g)	1.14	2.16	2.850	116
O(W10A)	-H(1,W10A)	O(3,G6)		0.74	2.11	2.825	163
O(W10A)	-H(2,W10A)	O(W2)	(g)	1.10	2.02	2.801	125
O(W11)	-H(1,W11)	O(3,G1)	(c)	1.11	1.90	2.928	153
O(W12)	-H(1,W12)	O(3,G2)	(k)	0.68	2.10	2.759	164
O(W12)	-H(2,W12)	O(W4)	(j)	0.83	1.88	2.703	171
O(W13)	-H(1,W13)	O(W8)		1.25	1.95	2.817	122
O(2,G1)		O(W3)	(f)			2.696	
O(5,G5)		O(W10A)	(k)			2.947	
O(6,G5)		O(2,G6)	(k)			2.665	
O(3,G6)		O(W10B)	(g)			2.767	
O(2,G7)		O(W5)	(d)			2.952	
O(3,G3)		O(W5)	(a)			2.909	

Symmetry code

None	x,	y,	z	f	$-x$, $1/2+y$,	$-z$
a	$1+x$,	y,	z	g	$-x$, $1/2+y$,	$1-z$
b	$-1+x$,	y,	z	h	$1-x$, $1/2+y$,	$1-z$
c	x,	y,	$1+z$	i	$-x$, $-1/2+y$,	$-z$
d	x,	y,	$-1+z$	j	$-x$, $-1/2+y$,	$1-z$
e	$-1+x$,	y,	$-1+z$	k	$1-x$, $-1/2+y$,	$1-z$

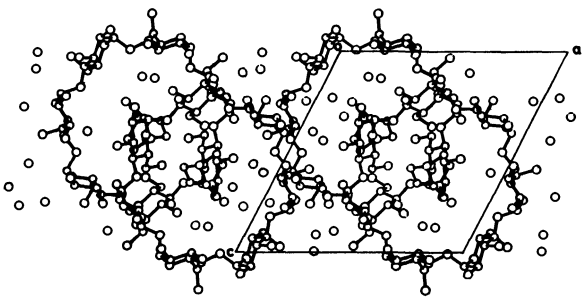

Fig. 6. The crystal structure viewed down along the b axis.

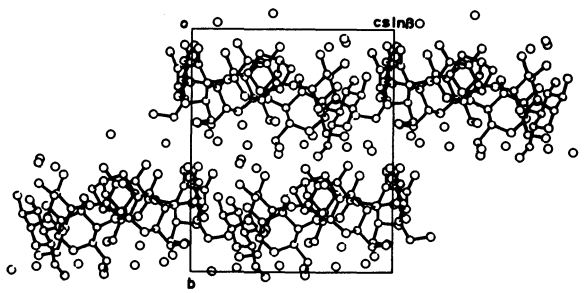

Fig. 7. The crystal structure viewed down along the a axis.

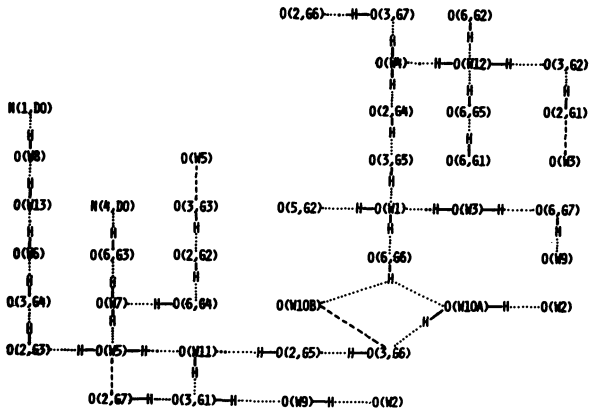

Fig. 8. A schematic representation of the hydrogen-bond network in the crystal. Dashed lines denote intermolecular contacts less than 3.0 Å.

groups are in van der Waals contact with the C(3) and C(5) methine groups and the O(4) atoms of β-cyclodextrin, although the C(8) methylene group located near the open end of the cavity is in contact with the neighboring β-cyclodextrin. The hydrophilic nitrogen atoms are not in contact with the host molecule, but instead are hydrogen-bonded to water or to a hydroxyl group lying outside the cavity.

Molecular Packing and Hydrogen Bonds. β-Cyclodextrin is located with its molecular axis making an angle of 10.3° with the b axis. The molecules arranged parallel to the ac plane form the corrugated molecular layers, of which the crystal is constructed. The intermolecular spaces between these layers are filled by water molecules which link these layers by hydrogen-bond bridges. A similar molecular packing has been observed in the α-cyclodextrin complexes with *para*-disubstituted benzenes,[7] but this is the first one found in the β-cyclodextrin complex. Other β-cyclodextrin complexes whose structures have been determined have a channel-type structure with head-to-head dimer-type packing or a cage-type structure in which the molecules are arranged in a zigzag mode. The crystal structure of the present β-cyclodextrin complex may belong to a modified cage-type structure. But unlike the typical cage-type structure, both ends of the β-cyclodextrin cavity are not completely blocked by neighboring β-cyclodextrin molecules, as shown in Fig. 3. Although the guest 1,4-DO is almost fully inserted into the host cavity, the C(8)–H bonds protrude outside the cavity. This may prevent the close contact between β-cyclodextrin molecules, and causes β-cyclodextrin to be packed more loosely, as indicated by the comparison of cell volumes between uncomplexed β-cyclodextrin (3070.3 Å^3) and the present complex (3504.7 Å^3).

Figure 8 shows the hydrogen-bond network in the crystal. Hydrogen-bond distances and angles are given in Table 5. Adjacent glucose residues in β-cyclodextrin are linked by O(2)–H···O(3) or O(3)–H···O(2) hydrogen bonds. Both the O(2) and the O(3) hydroxyl groups of the G3 and G7 residues donate hydrogen atoms to the hydroxyl groups of the adjacent residues, while those of the G2 and G5 residues only act as hydrogen acceptors.

Neighboring β-cyclodextrin molecules are linked by hydrogen bonds directly or through water molecules. N(1) and N(4) atoms of 1,4-DO act as hydrogen acceptors; thus, they are the terminal points of the hydrogen-bond chains. Of thirteen water molecules, the W10 water molecule is disordered, having a major position W10A of occupancy 0.7 and a minor position W10B of occupancy 0.3. There are two pairs and three trios of water molecules, in which individual water molecules are linked to each other by hydrogen bonds: O(W1)···H–O(W3), O(W9)–H···O(W2)···H–O(W10A), O(W4)···H–O(W12), O(W7)–H···O(W5)–H···O(W11), and O(W6)–H···O(W13)–H···O(W8). An infinite hydrogen-bond chain consists of a repetition unit comprising five hydroxyl groups and five water molecules: [···H–O(6,G7)···H–O(W3)–H···O(W1)–H···O(6,G6)–H···O(W10A)–H···O(3,G6)–H···O(2,G5)–H···O(W11)–H···O(3,G1)–H···O(W9)···]. W2 links this chain and that related by the translation along the z direction (x, y, 1+z) by the O(W10A)–H···O(W2)···H–O(W9) bridge.

References

1) K. Linder and W. Saenger, *Angew. Chem.*, **90**, 738 (1978).
2) R. Tokuoka, M. Abe, T. Fujiwara, K. Tomita, and W. Saenger, *Chem. Lett.*, **1980**, 491.
3) K. H. Jogun and J. J. Stezowski, *Nature*, **278**, 667 (1979).
4) M. M. Harding, J. M. MacLennan, and R. M. Paton, *Nature*, **274**, 621 (1978); J. J. Stezowski, K. H. Jogun, E. Eckel, and K. Bartels, *ibid*, **274**, 617 (1978); J. A. Hamilton, M. N. Sabesan, and L. K. Steinrauf, *Carbohydr. Res.*, **89**, 33 (1981).
5) M. Komiyama and M. L. Bender, *Proc. Natl. Acad. Sci. U. S. A.*, **73**, 2969 (1976).

6) "International Tables for X-Ray Crystallography," Kynoch Press, Birmingham (1974), Vol. IV, pp. 72—75.
7) K. Harata, *Bull. Chem. Soc. Jpn.*, **50**, 1416 (1977); K. Harata, K. Uekama, M. Otagiri, and H. Ogino, *ibid.*, **54**, 1954 (1981); B. Hingerty and W. Saenger, *J. Am. Chem. Soc.*, **98**, 3357 (1976).
8) G. J. Quigley, A. Sarko, and R. H. Marchessault, *J. Am. Chem. Soc.*, **92**, 5834 (1970).
9) S. S. C. Chu and G. A Jeffrey, *Acta Crystallogr., Sect. B*, **23**, 1028 (1967).
10) C. J. Brown, *J. Chem. Soc., A*, **1966**, 927.
11) A. D. French and V. G. Murphy, *Carbohydr. Res.*, **27**, 391 (1973).
12) K. Harata, *Bull. Chem. Soc. Jpn.*, **52**, 2451 (1979).
13) K. H. Jogun, Doctoral thesis, Universität, Stuttgart, 1979.

 © 1982 The Chemical Society of Japan Bull. Chem. Soc. Jpn., 55, 2321—2326 (1982)

New Potent Neuroleptic Drugs of Benzamide Derivatives. I. Crystal and Molecular Structure of *N*-[(2*RS*, 3*RS*)-1-Benzyl-2-methyl-3-pyrrolidinyl]-5-chloro-2-methoxy-4-methylaminobenzamide

Toshio Furuya,* Sumio Iwanami,† Akio Takenaka,†† and Yoshio Sasada††

Product Development Laboratories, Yamanouchi Pharmaceutical Co., Ltd., 1-1-8, Azusawa, Itabashi-ku, Tokyo 174

†*Central Reserach Laboratories, Yamanouchi Pharmeceutical Co., Ltd., 1-1-8, Azusawa, Itabashi-ku, Tokyo 174*

††*Laboratory of Chemistry for Natural Products, Tokyo Institute of Technology, Nagatsuta, Midori-ku, Yokohama 227*

(Received December 26, 1981)

The crystal and molecular structure of the title compound has been determined by the X-ray diffraction method. The crystal is monoclinic, space group $P2_1/c$, $a=11.694(1)$ Å, $b=12.117(1)$ Å, $c=14.482(1)$ Å, $\beta=100.01(1)°$, and $Z=4$. The structure was solved by the direct method and refined by a block-diagonal least-squares procedure to a final R value of 0.082. An intramolecular hydrogen bond between the amide nitrogen and the methoxyl oxygen atoms forms a new six-membered ring fused with the benzene ring. Structural features are discussed in relation to neuroleptic activity.

Typical neuroleptic drugs are classified into five major types by their parent molecules, benzamide, butyrophenone, phenothiazine, benzo[6,7]cyclohepta[1,2,3-*de*]pyrido[2,1-*a*]isoquinoline and pyrido[4,3-*b*]indole. These are antagonists to dopamine receptors located on synaptic membranes.[1] The molecular mechanisms for dopamine antagonists have not been completely established yet, though many studies on the structure-activity relationships and conformational requirements for neuroleptic drugs have been reported.[2–11]

The title compound, *N*-[(2*RS*,3*RS*)-1-benzyl-2-methyl-3-pyrrolidinyl]-5-chloro-2-methoxy-4-methylaminobenzamide (YM-09151-2), is a potent dopamine antagonist** (Fig. 1), and in the present paper we described its three-dimensional crystal structure and discuss on its structural features in relation to neuroleptic activity.

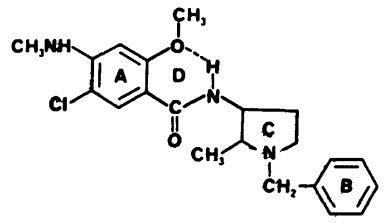

Fig. 1. Schematic structure of *N*-[(2*RS*, 3*RS*)-1-benzyl-2-methyl-3-pyrrolidinyl]-5-chloro-2-methoxy-4-methylaminobenzamide and the notation of each ring.

Experimental and Structure Determination

The title compound was prepared by the reaction of 5-chloro-2-methoxy-4-methylaminobenzoic acid with (2*RS*,3*RS*)-3-amino-1-benzyl-2-methylpyrrolidine as described in the previous paper.[13] It was recrystallized from acetone solution to give colorless plate crystals.

Preliminary Weissenberg photographs indicated a monoclinic space group $P2_1/c$. A crystal, $0.6\times0.3\times0.4$ mm in size, was used for data collection on a Rigaku automated four-circle diffractometer with graphite-monochromated Mo $K\alpha$ radiation ($\lambda=0.71073$ Å). Accurate unit-cell constants were determined using 40 high angle reflections of the angular range of $20°<2\theta<30°$. Density was measured by flotation in a mixture of benzene and carbon tetrachloride. The crystal data were summarized in Table 1.

Table 1. Crystal data

N-[(2*RS*,3*RS*)-1-Benzyl-2-methyl-3-pyrrolidinyl]-5-chloro-2-methoxy-4-methylaminobenzamide

$C_{21}H_{26}ClN_3O_2$

M.W. = 387.91

Crystal system ; Monoclinic

Spase group : $P2_1/c$

a/Å = 11.694(1)	U/Å^3 = 2020.8(4)
b/Å = 12.117(1)	Z = 4
c/Å = 14.482(1)	D_x/g cm^{-3} = 1.275
β/° = 100.01(1)	D_m/g cm^{-3} = 1.27

A complete set of independent reflections was collected within the angular range of $2°\leqq2\theta\leqq50°$ in the θ-2θ scan mode at scanning rate of 4° (2θ) min^{-1}. Stationary background counts were accumulated for 10 s before and after each scan. Five reference reflections showed no significant intensity deterioration throughout the data collection. A total of 3548 independent reflections were measured, of which 796 weak reflections below background were considered zero-reflections; the observational threshold value, F_{1lm}, was 2.12. The intensities were corrected for Lorentz and polarization factors, but not for absorption and secondary extinction. The standard deviations were estimated by the equation of $\sigma^2(F_o)=\sigma_P^2\times(F_o)+qF_o^2$, where $\sigma_P(F_o)$ was evaluated by counting statisitcs and $q(3.64\times10^{-5})$ was derived from the variations of monitored reflections.[14]

The structure was solved by the direct method. The refinement of the structure was carried out by block-diagonal least-squares calculations. All the hydrogen atoms found on a difference map were included. The quantity minimized was

** The affinity for the present molecule, as determined by [^3H]spiperone binding to the synaptic membrane obtained from canine caudate nucleus, exceeds apparently that for haloperidol by a factor of about 3 and that for chloropromazine by a factor of about 30.[12]

TABLE 2. FRACTIONAL COORDINATES AND ISOTROPIC TEMPERATURE FACTORS

The B values accompanied with 〈 〉 are the equivalent isotropic temperature factors calculated from anisotropic thermal parameters using the equation $B=8\pi^2(U_1+U_2+U_3)/3$, where U_1, U_2, and U_3 are principal components of the mean square displacement matrix $\boldsymbol{U}$. Values in 〈 〉 are anisotropicity defined by $(\sum(B-8\pi^2U_i)^2/3)^{1/2}$. The e.s.d.'s in ( ) refer to last decimal places.

Atom	x	y	z	B/Å^2
Cl	−0.11376(7)	0.16625(8)	0.27342(6)	6.21〈302〉
O(1)	0.2810(2)	0.3404(2)	0.1185(1)	4.32〈171〉
O(2)	0.2259(2)	0.4314(2)	0.3858(1)	4.8〈16〉
N(1)	−0.0712(2)	0.1259(2)	0.0813(1)	5.2〈24〉
N(2)	0.3390(2)	0.4577(2)	0.2766(2)	5.2〈28〉
N(3)	0.5796(2)	0.4913(2)	0.2690(1)	3.9〈3〉
C(1)	0.0097(2)	0.1916(2)	0.1331(2)	3.8〈7〉
C(2)	0.0016(2)	0.2190(2)	0.2256(2)	4.0〈9〉
C(3)	0.0803(2)	0.2870(2)	0.2774(2)	3.9〈11〉
C(4)	0.1745(2)	0.3325(2)	0.2436(2)	3.3〈4〉
C(5)	0.1856(2)	0.3021(2)	0.1520(2)	3.4〈4〉
C(6)	0.1048(2)	0.2349(2)	0.0986(2)	3.7〈9〉
C(7)	−0.0836(3)	0.1143(3)	−0.0192(2)	6.1〈23〉
C(8)	0.2990(3)	0.3060(3)	0.0271(2)	5.1〈19〉
C(9)	0.2492(2)	0.4095(2)	0.3077(2)	4.0〈6〉
C(10)	0.4190(3)	0.5374(3)	0.3301(2)	5.5〈20〉
C(11)	0.5370(3)	0.4871(3)	0.3574(2)	5.1〈19〉
C)12)	0.5395(3)	0.3720(3)	0.3998(2)	5.6〈15〉
C(13)	0.5559(3)	0.6042(3)	0.2343(2)	6.1〈10〉
C(14)	0.4399(3)	0.6365(3)	0.2686(2)	5.7〈17〉
C(15)	0,7018(3)	0.4599(3)	0.2734(2)	5.7〈19〉
C(16)	0.7337(2)	0.4512(3)	0.1765(2)	5.0〈9〉
C(17)	0.6555(3)	0.4143(3)	0.1011(2)	6.3〈20〉
C(18)	0.6909(4)	0.3965(3)	0.0164(2)	8.1〈34〉
C(19)	0.8040(4)	0.4155(3)	0.0078(3)	9.5〈54〉
C(20)	0.8805(3)	0.4539(4)	0.0827(3)	8.6〈39〉
C(21)	0.8457(3)	0.4734(3)	0.1669(2)	6.3〈14〉
H(1)	0.075(2)	0.308(2)	0.338(1)	0.9(5)
H(2)	0.116(2)	0.215(2)	0.040(1)	1.0(5)
H(3)	−0.125(2)	0.096(2)	0.109(2)	2.5(7)
H(4)	−0.106(2)	0.189(3)	−0.051(2)	4.3(9)
H(5)	−0.147(3)	0.064(3)	−0.041(2)	4.3(10)
H(6)	−0.016(3)	0.090(3)	−0.041(2)	3.6(9)
H(7)	0.377(2)	0.338(3)	0.024(2)	3.7(9)
H(8)	0.238(2)	0.334(2)	−0.022(2)	2.8(7)
H(9)	0.302(2)	0.223(2)	0.026(1)	2.7(6)
H(10)	0.359(2)	0.429(3)	0.225(2)	3.8(9)
H(11)	0.379(2)	0.556(3)	0.388(2)	3.9(9)
H(12)	0.583(2)	0.543(3)	0.407(2)	1.7(9)
H(13)	0.617(2)	0.355(3)	0.425(2)	7.4(9)
H(14)	0.499(3)	0.324(3)	0.355(2)	3.4(10)
H(15)	0.491(2)	0.378(2)	0.447(2)	6.7(8)
H(16)	0.558(2)	0.606(2)	0.161(2)	6.4(6)
H(17)	0.636(2)	0.650(2)	0.257(2)	6.4(7)
H(18)	0.451(2)	0.704(2)	0.308(2)	6.2(7)
H(19)	0.373(2)	0.643(2)	0.214(2)	6.7(6)
H(20)	0.751(2)	0.521(2)	0.314(2)	4.2(6)
H(21)	0.682(2)	0.388(2)	0.325(2)	7.4(7)
H(22)	0.576(2)	0.402(2)	0.110(2)	3.1(7)
H(23)	0.633(2)	0.368(2)	−0.033(2)	6.9(7)
H(24)	0.829(2)	0.412(3)	−0.053(2)	8.3(10)
H(25)	0.962(2)	0.473(2)	0.079(2)	6.9(7)
H(26)	0.903(2)	0.495(3)	0.220(2)	5.8(9)

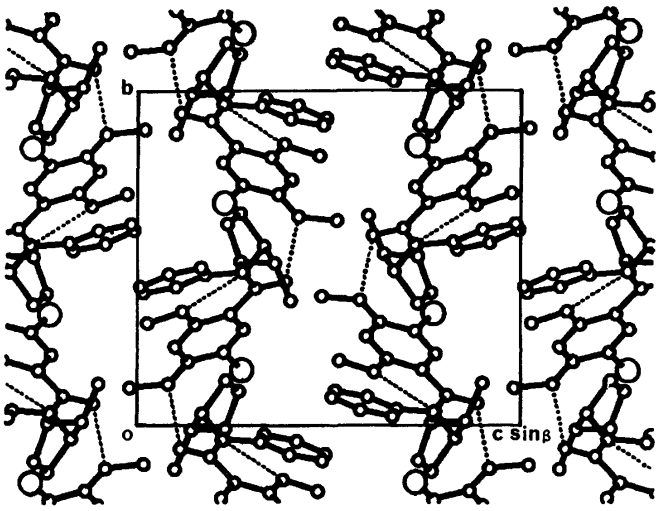

Fig. 2. Crystal structure of *N*-[(2*RS*, 3*RS*)-1-Benzyl-2-methyl-3-pyrrolidinyl]-5-chloro-2-methoxy-4-methylaminobenzamide projected along the a axis, and drawn by TSD:XTAL.[24]

$\sum w(|F_o|-|F_c|)^2$, with $w=1/\sigma^2(F_o)$. In the refinemetn procedure, the zero-reflections were assumed to be $F_o=F_{lim}$, but those for which $|F_c|<F_{lim}$ were omitted. The final R was 0.082; the maximum shifts of parameters in the last cycle were 0.3 σ for C, 0.2 σ for N, 0.07 σ for O, 0.01 σ for Cl and 0.9 σ for H atoms. Atomic scattering factors used were taken from "International Tables for X-Ray Crystallography."[15] Atomic parameters are listed in Table 2.[16]

Results and Discussion

Crystal Structure. The crystal structure is shown in Fig. 2. An intermolecular hydrogen bond is observed between the amino nitrogen N(1) and the carbonyl oxygen O(2) in the molecule related by screw, the N(1)–O(2) distance being 3.059 Å. The other intermolecular contacts are all larger than the sum of the van der Waals radii. The molecules are arranged to form columns along the screw axis by mediating the intermolecular hydrogen bond system. Benzamide moieties are inner part of the column, whereas pyrrolidine rings and benzyl groups are protruded from it and dove-tailed with those of adjacent one. Thus the molecules have some mobility in the latter two parts, as indicated by rather large temperature factors.

Molecular Structure. The stereoscopic view of the molecule is shown in Fig. 3. The bond lengths and bond angles are shown in Fig. 4 together with numbering system. The lengths C(2)–C(3) and C(5)–C(6) are short in comparison with the other lengths in the ring, whereas angles C(2)–C(1)–C(6) and C(3)–C(4)–C(5) are somewhat small. Moreover, the lengths C(1)–N(1) and C(4)–C(9) are short. These results indicate that the molecule has the contribution of the quinonoidal form shown in Fig. 5. This should be related to the hydrogen bond between N(1) and O(2) as mentioned above. The benzene ring A is almost planar with maximum atomic deviation of 0.013 Å.[16] The *N*-methylamino, methoxyl, and carbamoyl groups attached to this ring also lie on the plane. Torsion angles in

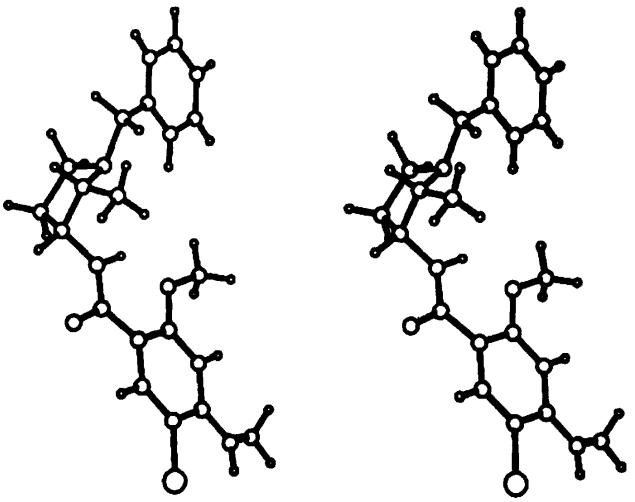

Fig. 3. Stereoscopic view of *N*-[(2*RS*, 3*RS*)-1-benzyl-2-methyl-3-pyrrolidinyl]-5-chloro-2-methoxy-4-methylaminobenzamide, drawn by TSD: XTAL.[24]

benzamide moiety are listed in Table 3.

An intramolecular hydrogen bond between the amide N(2) and the methoxyl O(1) (Fig. 6) forms a new six-membered ring (hereafter called as ring D) fused with the benzene ring A. This type of hydrogen bond is also observed in the benzamide neuroleptics such as metoclopramide[17] and sulpiride.[18] The N(2)–O(1) distance, 2.680 Å, is almost the same as that of metoclopramide, 2.683 Å.[17] The rings A and D are almost coplanar (the dihedral angle between them being 3.8°), and constitute a rigid part of this molecule.

The bond lengths and angles of the pyrrolidine ring do not differ significantly from those reported for the other related compound.[19] This ring has an intermediate conformation between the envelope and half-chair forms (deviations from the mean plane are −0.224, 0.326, −0.159, 0.177, and 0.039 Å for C(10), C(11), N(3), C(13), and C(14) atoms, respectively); the value of pseudorotation phase angle P is −9.85° (for the

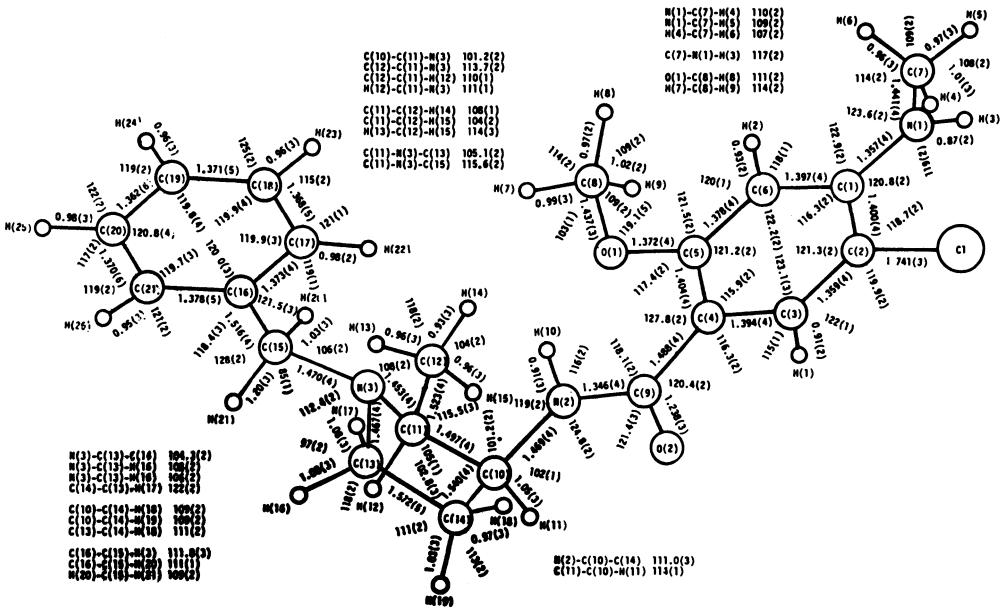

Fig. 4. Atomic numbering of *N*-[(2*RS*, 3*RS*)-1-benzyl-2-methyl-3pyrrolidinyl]-5-chloro-2-methoxy-4-methylaminobenzamide with bond lengths (l/Å) and angles (ϕ/°). Standard deviations are in parentheses.

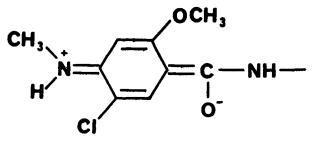

Fig. 5. Quinonoidal form of the benzamide moiety.

envelope conformation P is 18° or −18°, while for a half-chair P=0°).[20] Torsion angles of this ring are also given in Table 3. The methyl group and the acylamino group attached to this ring are in the same side about the least-squares plane of the ring, the internal rotation angle of these two groups around the C(10)–C(11) bond being 47.4° as shown in Fig. 7. On the other hand, the relative orientation of the methyl group and benzyl group is *trans*, to relax their steric repulsions. As a result, the molecule takes a rather folded conformation; the nitrogen lone pair lobe is buried by the methyl, methoxyl, and benzyl groups.

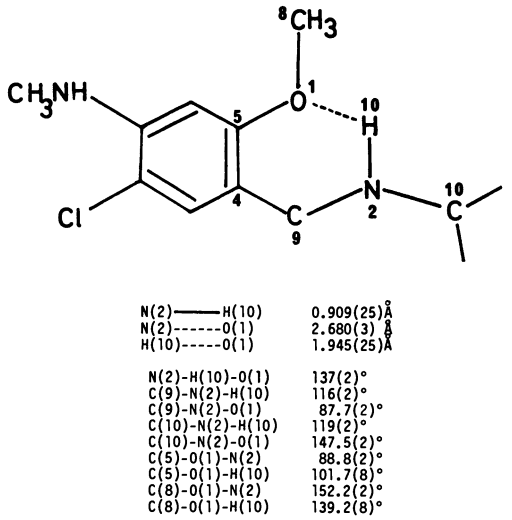

Fig. 6. Intramolecular hydrogen bond.

Table 3. Torsion angles ϕ/°

C(8)–O(1)–C(5)–C(4)	176.4(2)	C(10)–C(14)–C(13)–N(3)	6.0(3)
C(8)–O(1)–C(5)–C(6)	357.5(4)	N(2)–C(10)–C(11)–C(12)	312.5(3)
C(7)–N(1)–C(1)–C(2)	345.3(3)	C(14)–C(10)–C(11)–C(12)	193.8(3)
C(7)–N(1)–C(1)–C(6)	165.7(4)	C(13)–N(3)–C(11)–C(12)	172.7(3)
C(3)–C(4)–C(9)–N(2)	181.9(2)	C(11)–N(3)–C(13)–C(14)	326.5(3)
C(5)–C(4)–C(9)–N(2)	0.2(4)	C(13)–C(14)–C(10)–C(11)	22.3(3)
C(4)–C(9)–N(2)–C(10)	174.8(4)	C(14)–C(10)–C(11)–N(3)	317.0(3)
C(9)–N(2)–C(10)–C(11)	111.1(3)	C(14)–C(13)–N(3)–C(15)	200.0(2)
C(9)–N(2)–C(10)–C(14)	225.3(3)	C(15)–N(3)–C(11)–C(12)	297.1(3)
N(2)–C(10)–C(11)–N(3)	75.7(3)	C(11)–N(3)–C(15)–C(16)	172.0(2)
N(2)–C(10)–C(14)–C(13)	264.1(3)	C(13)–N(3)–C)15)–C(16)	292.7(3)
C(10)–C(11)–N(3)–C(13)	48.3(3)	N(3)–C(15)–C(16)–C(17)	325.6(4)
C(10)–C(11)–N(3)–C(15)	172.7(2)	N(3)–C(15)–C(16)–C(21)	150.3(3)

The torsion angle A–X–Y–B is the dihedral angle between planes AXY and XYB, measured clockwise when viewed down the bond X–Y.

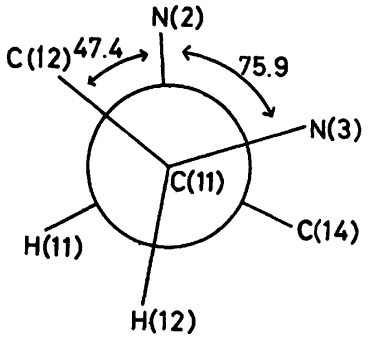

Fig. 7. Internal rotation angle along the C(10)–C(11) bond.

Bond angles in the benzene ring B are all close to 120°, but bond lengths are relatively shorter than 1.395 Å, probably due to the large thermal motions. This ring is almost planar with maximum atomic deviation of 0.014 Å.[16] The dihedral angle between this ring and the benzene ring A is 19.5°, so that these are nearly parallel. Relevant torsion angles are listed in Table 3.

Structure-activity Relationships. Every active neuroleptics ever known has at least a tertiary amino nitrogen atom and benzene or isosteric aromatic ring, and belong to one of the nine general structures classified by Janssen.[21] The present compound belongs to the class of the benzamide neuroleptic molecules with a common partial structure of the type A–C–N–C–C–N– (A= benzene or isosteric aromatic ring). Moreover, the present study reveals that this compound can also belong to another class with the type AA′–C–C–N– (AA′= indole or an isosteric aromatic fused ring structure), if the rings A and D are assumed to form an isosteric aromatic fused ring structure.

Geometrical parameters to express the relative arrangement of the benzene ring and the tertiary amino nitrogen atom have been used in the study of structure of neuroleptic drugs; the first is the distance, *l*, between the nitrogen atom and the center of the benzene ring, and the second is the deviation, *d*, of the nitrogen atom from the mean plane of the benzene ring.[8] Table 4 lists these parameters for the present molecule together with other typical neuroleptics. The distance, *l*, of the present molecule is almost the same as that of metoclopramide[17] and also compatible of those of the other classes of the neuroleptics. Moreover, the deviation, *d*, of the present molecule agrees with the values of the other neuroleptics except for chlorpromazine hydrochloride (for the active conformer of (+)-butaclamol,[8] see a foot-note of Table 4).

In addition to these two parameters, however, one more structural aspect should be taken into account. The tertiary amino nitrogen atom, common to all neuroleptic molecules should play an important role to be recognized by and interact with receptors. Since the nitrogen atom of the present molecule seemed to be buried, we calculated the accessible surface area of it.[23] The calculated area is zero. It suggests that the nitrogen lone pair lobe is unfavorable to interact with them and the present conformation may be different from that under the binding condition. A probable active conformer could be obtained by changing the pyrrolidine ring conformation so as to expose the nitrogen atom with retaining the two geometrical parameters.

Table 4. Geometrical parameters for typical dopamine antagonists

Compound	Type	Distance *l*/Å	Deviation *d*/Å	Reference
1. YM-09151-2	Benzamide	6.26	0.9	This work
2. Metoclopramide	Benzamide	6.3	1.6	Ref. 16
3. Haloperidol	Butyrophenone	7.3	1.4	Ref. 7
4. Chlorpromazine	Phenothiazine			
Base		5.12	1.5	Ref. 4
HCl		6.70	3.7	Ref. 4
5. (+)-Butaclamol	Benzo[6,7]cyclohepta[1,2,3-*de*]pyrido-[2,1-*a*]isoquinoline	5.1	0.19 (0.9)[a]	Ref. 8
6. Flutroline	Pyrido[4,3-*b*]indole	5.12	0.6	Ref. 22

a) By model building, the authors obtained an active conformer, in which the *d*-value was 0.9 Å.

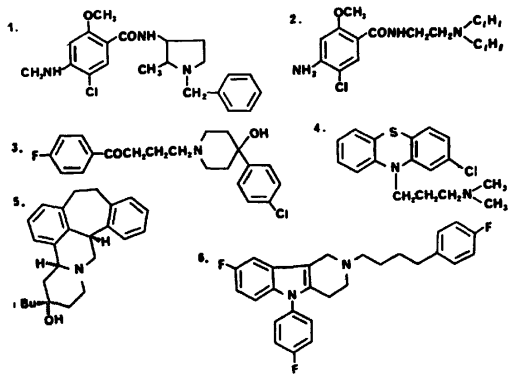

References

1) A. Carlsson and M. Lindquist, *Acta Pharmacol. Toxicol.*, **20**, 140 (1963).
2) A. S. Horn and S. H. Snyder, *Proc. Natl. Acad. Sci. U. S. A.*, **68**, 2325 (1971).
3) A. P. Feinberg and S. H. Snyder, *Proc. Natl. Acad. Sci. U. S. A.*, **72**, 1899 (1975).
4) A. S. Horn, M. L. Post, and O. Kennard, *J. Pharm. Pharmac.*, **27**, 553 (1975).
5) A. R. Martin, S. H. Kim, H. I. Yamamura, and A. S. Horn, *J. Med. Chem.*, **23**, 938 (1980).
6) M. H. J. Koch, *Mol. Pharmacol.*, **10**, 425 (1974).
7) J. P. Tollenaere, H. Moereels, and M.H. J. Koch, *Eur. J. Med. Chem.*, **12**, 199 (1977).
8) L. G. Humber, F. T. Brederlein, and K. Voith, *Mol. Pharmacol.*, **11**, 833 (1975).
9) L. G. Humber, F. T. Bruderlein, A. H. Philipp, M. Gotz, and K. Voith, *J. Med. Chem.*, **22**, 761 (1979).
10) A. H. Philipp, L. G. Humber, and K. Voith, *J. Med. Chem.*, **22**, 768 (1979).
11) C. A. Harbert, J. J. Plattner, W. M. Welch, A. Weissman, and B. K. Koe, *Mol. Pharmacol.*, **17**, 38 (1980).
12) H. Maeno, private communication.
13) S. Iwanami, M. Takashima, Y. Hirata, O. Hasegawa, and S. Usuda, *J. Med. Chem.*, **24**, 1224 (1981).
14) L. E. McCandlish and G. H. Staut, *Acta Crystallogr., Sect. A*, **31**, 245 (1975).
15) "International Tables for X-Ray Crystallography," Kynoch Press, Birmingham (1974), Vol. IV, p. 71.
16) Lists of structure factors, anisotropic thermal parameters, and least-squares plane equations and deviations of atoms from these planes have been deposited as Document No. 8244, at the Office of the Chemical Society of Japan.
17) M. Cesario, C. Pascard, M. E. Moukhtari, and L. Jung, *Eur. J. Med. Chem.*, **16**, 13 (1981).
18) P. C. Houttemane, J. C. Boivin, G. Nowogrocki, and D. J. Thomas, *Acta Crystallogr., Sect. B*, **37**, 981 (1981).
19) G. Gafner and L. J. Admiraal, *Acta Crystallogr., Sect. B*, **27**, 565 (1971).
20) C. Altona, H. J. Geise, and C. Romers, *Tetrahedron*, **24**, 13 (1968).
21) P. A. J. Janssen, *Int. Encyl. Pharmacol. Ther.*, **1**, 37 (1973).
22) W. M. Welch, F. E. Ewing, C. A. Harbert, A. Weissman, and B. K. Koe, *J. Med. Chem.*, **23**, 949 (1980).
23) B. Lee and F. M. Richard, *J. Mol. Biol.*, **55**, 379 (1971).
24) A. Takenaka and Y. Sasada, *J. Cryst. Soc. Jpn.*, **22**, 2141 (1980).

Crystal Structure of Mixed-valence Compound 1′,1‴-Dipropylbiferrocenium Triiodide with Averaged-valence Type Irons at 298 K and with Trapped-valence Type Irons at 110 K and Thermal Electron Transfer Process of Mono-oxidized Binuclear Ferrocene Derivatives

Michiko KONNO,* Shi-aki HYODO,† and Sei-ichiro IIJIMA†,††

The Institute for Solid State Physics, The University of Tokyo, Roppongi, Minato-ku, Tokyo 106

†*Department of Chemistry, Faculty of Science, Tokyo Metropolitan University, Fukasawa, Setagaya-ku, Tokyo 158*

(Received December 28, 1981)

The crystal structure of 1′,1‴-dipropylbiferrocenium $(PrFcFcPr)^+I_3^-$, which shows averaged-valence irons at 298 K and trapped-valence irons at 110 K, was determined by X-ray diffraction. The crystal at 298 K is triclinic, space group $P\bar{1}$, $a=8.5148(8)$, $b=8.5482(5)$, and $c=10.9032(13)$ Å, $\alpha=89.546(9)$, $\beta=115.582(9)$, and $\gamma=108.488(7)°$, $U=671.10(9)$ Å^3, and $Z=1$. The crystal at 110 K is triclinic, space group P1, $a=8.431(2)$, $b=8.478(2)$, and $c=10.816(3)$ Å, $\alpha=88.58(3)$, $\beta=117.39(2)$, and $\gamma=108.65(2)°$, $U=643.4(3)$ Å^3, and $Z=1$. Structures were refined to $R=0.042$ at 298 K and $R=0.050$ at 110 K. At 298 K cation $(PrFcFcPr)^+$ sits on the symmetry center and the two Fc units are crystallographically equivalent, whereas at 110 K the symmetry center is lost and ferrocene-like and ferrocenium-like Fc units are distinguished. A three-dimensional hydrogen-bond network is clearly found between the cation and iodine atoms at 110 K, in contrast to the result at 298 K. Infrared spectra of 1′,1‴-diethyl- and 1′,1‴-dipropylbiferrocenium$^+I_3^-$a nd μ-(as-indacenyl)-bis(cyclopentadienyliron)$^+I_3^-0.5I_2$ salts measured at 294 and 78 K indicate that a remarkable change in peak intensity is observed at 680 and 1525 cm^{-1} in the dialkyl salts, whereas no change is found in the remainder.

A number of mono-oxidized salts of binuclear ferrocene derivatives have been investigated to clarify the electronic interaction between two metal sites and the electron transfer process,[1] especially in connection with Mössbauer spectroscopic behavior, electronic configuration, and magnetic and optical properties of these compounds. The compounds are classified roughly into two types: one is the mixed-valence or trapped-valence type which contains ferrocene-like bivalent and ferrocenium-like tervalent iron atoms, including biferrocenium$^+$,[2,3] diferrocenylacetylenium$^+$,[4] and diferrocenylselenium$^+$ [5] cations; the other is the averaged-valence type which contains equivalent iron atoms, including 1′,1‴-diiodobiferrocenium$^+$,[6] [2.2]ferrocenophane-1,13-diyne$^+$,[4] and biferrocenylenium$^+$ [7,8] cations.

Recently, it was reported that 1′,1‴-diethyl- and 1′,1‴-dipropylbiferrocenium$(PrFcFcPr)^+I_3^-$ salts and μ-[1-3a(8b)-η : 6-8a(5a)-η-as-indacenyl]-bis(η-cyclopentadienyliron)$^+I_3^-0.5I_2$ salt give rise to a transition from the averaged-valence state of iron atoms to the trapped-valence state as temperature is lowered.[9–11] In addition, in the latter salt the line-broadening of Mössbauer spectrum was observed at higher temperatures.

We determined the crystallographic change in $(PrFcFcPr)^+I_3^-$ at 298 and 110 K, in order to clarify whether or not the transition in cation $(PrFcFcPr)^+$ from the averaged-valence to the trapped-valence state is accompanied with structural changes and how anion I_3^- affects this transition. It has been known that unsubstituted cation biferrocenium$^+$ shows a temperature-independent trapped-valence state, whereas cation 1‴,1′-diiodobiferrocenium$^+$ shows a temperature-independent averaged-valence state. The present paper also provides information concerning the effect of the propyl group on the electronic state of the cation.

Although Mössbauer spectroscopy can distinguish whether or not the rate of the thermal electron transfer between two iron atoms in these salts is higher than *ca.* 10^7 s^{-1}, infrared spectroscopy involves a different time scale of *ca.* 10^{13} s^{-1}. By comparing infrared spectra of 1′,1‴-diethyl and 1′,1‴-dipropylbiferrocenium$^+I_3^-$ salts and μ-(as-indacenyl)-bis(cyclopentadienyliron)$^+I_3^-0.5I_2$ salt at 294 and 78 K with Mössbauer spectra, the difference in electronic state between these salts is discussed.

Experimental

X-Ray Measurements. Crystals in dark-red thin plate were sealed into Lindemann-glass capillaries filled with Ar gas, since they will break down when exposed to air. Preliminary oscillation and Weissenberg photographs were taken at room temperature by using Cu *Kα* radiation. The crystal was determined to be triclinic. The space group was later confirmed to be $P\bar{1}$ at 298 K and P1 at 110 K by structure refinements. The final unit cell dimensions are refined by the least-squares method based on θ values of 27 reflections at 298 K and of 18 reflections at 110 K.

The cooling equipment was constructed of stainless steel according to the description by Bolhuis.[12] Crystal specimens were cooled by a stream of cold N_2 gas which was surrounded by warmer N_2 gas. Temperature was maintained at 110 ± 1 K electrically by monitoring with a chromel-almel thermocouple throughout the experiment.

Intensities were collected on an automated four-circle diffractometer with Ag *Kα* radiation monochromated by graphite. The absorption coefficient of elements for Ag *Kα* radiation is about half as large as that for Mo *Kα* radiation. Three standard reflections were observed every fifty reflections. Correction was made for Lorentz and polarization effects and for absorption. Crystal data and experimental conditions are summarized in Table 1.

Infrared Measurements. Infrared spectra were recorded

†† Present address: Research Institute for Polymers and Textiles, Yatabe-Higashi, Tsukuba, Ibaraki 305.

TABLE 1. CRYSTAL DATA

$(Fe_2C_{26}H_{30})^+I_3^-$, M.W. 834.92		
Temperature/K	298	110
	Triclinic	Triclinic
Space group	$P\bar{1}$	P1
a/Å	8.5148(8)	8.431(2)
b/Å	8.5482(5)	8.478(2)
c/Å	10.9032(13)	10.816(3)
α/°	89.546(9)	88.58(3)
β/°	115.582(9)	117.39(2)
γ/°	108.488(7)	108.65(2)
U/Å^3	671.10(9)	643.4(3)
Z	1	1
D_x/g cm^{-3}	2.066	2.155
μ(Ag $K\alpha$)/mm^{-1}	2.23	2.33
Crystal size/mm	0.016×0.36×0.37	0.03×0.29×0.30
Scan method	ω-2θ	ω
$\sin\theta/\lambda_{max}$	0.682	0.682
Independent reflections ($\|F\| > 3\sigma$)	1928	2061
Maximum repeating number	3	1
$R=\sum\|\|F_o\|-\|F_c\|\|/\sum\|F_o\|$	0.042	0.050
$R_2=\{\sum(\|F_o\|-\|F_c\|)^2/\sum\|F_o\|^2\}^{1/2}$	0.043	0.075

on a Fourier-transform spectrometer (NICOLET 7199). All samples were prepared as KBr pellets 13 mm in diameter. For low temperature measurements, the sample mounted in a holder was cooled by a copper plate linked to liquid nitrogen in a Dewar with KRS-5 windows.

Structure Determination

High-temperature Phase (298 K). The structure was solved by the conventional heavy-atom method. The positions of Fe and I atoms were deduced from sharpened Patterson maps. Successive three-dimensional Fourier syntheses phased by these atoms yielded the positions of all C atoms. Difference Fourier maps clarified not only the positions of H atoms but also the existence of rotational disorder of propylcyclopentadienyl ring. Several cycles of full-matrix least-squares refinements were carried out by using the RADIEL program.[13] The population of disordered propylcyclopentadienyl was also refined so as to converge to the ratio 75 : 25. Anisotropic thermal parameters were used for non-hydrogen atoms and isotropic thermal parameters for hydrogen and carbon atoms of disordered propylcyclopentadienyl with low population. Atomic scattering factors for non-hydrogen atoms were taken from International Tables for X-Ray Crystallography,[14] and those for H atoms from Stewart *et al.*[15] Unit weights were adopted for all reflections. Refinements led to a convergence of $R=0.042$. Final atomic parameters are given in Table 2.†††

Low-temperature Phase (110 K). The starting coordinates of the low-temperature phase could readily be deduced from the atomic coordinates of the high-temperature phase. Several cycles of full-matrix least-squares refinements reduced the R value to 0.064 for the structure with space group $P\bar{1}$ without disorder. At this stage, difference Fourier syntheses showed not only rotational disorder of propylcyclopentadienyl but also positional disorder of triiodide. Refinements with these disorders considered gave $R=0.055$. The space group was assumed to be P1 with no symmetry center. The structure was assumed to consist of a ferrocene-like divalent unit and ferrocenium-like tervalent unit for cation $(PrFcFcPr)^+$. Anisotropic thermal parameters were used for the I, Fe, and C atoms of fulvalene moiety and isotropic thermal parameters for the C atoms of disordered propylcyclopentadienyls and H atoms. The populations of two types of disorders were also refined and R was converged to 0.050. The final difference Fourier maps showed peaks of about 1.0 eÅ^{-3} near anion I_3^-. The final atomic parameters are tabulated in Table 3.†††

Results and Discussion

Description of Crystal Structure. High-temperature Phase: Packing: Projections of the structure in the high-temperature phase along the a and c axes are shown in Figs. 1 and 2. $(PrFcFcPr)^+$ cations are stacked along the c axis in a plane-to-plane manner to form a column. The structure is dominated by segregated columns of cation $(PrFcFcPr)^+$ and anion I_3^-. The column of anion I_3^- is surrounded by four columns of the cations. The cation and anion are interacted by van der Waals' force between hydrogen atoms of the cation and iodine atoms as shown in Table 4. Figures 3(a) and (b) show packing views in the high- and low-temperature phases, respectively. Five-membered rings of propylcyclopentadienyls between neighboring $(PrFcFcPr)^+$ cations overlap as shown in Fig. 4(b). Their interplanar distance is 3.47(2) Å and an intermolecular interaction is expected

††† Lists of structure factors and anisotropic thermal parameters in the high- and low-temperature phases and atomic parameters of hydrogen atoms in the low-temperature phase are kept in the Chemical Society of Japan as Document No. 8238.

TABLE 2. POSITIONAL PARAMETERS WITH e.s.d.'s IN PARENTHESES FOR THE HIGH-TEMPERATURE PHASE (298 K)

a) I, Fe atoms ($\times 10^5$), and C atoms ($\times 10^4$)

Atom	x	y	z	10^3U_{eq}/Å^2	Population
I(1)	0	50000	0	55(0)	1.0
I(2)	10015(10)	43861(9)	28387(8)	68(0)	1.0
Fe	41961(17)	10776(15)	17719(13)	40(1)	1.0
C(1)	2614(11)	33(10)	−250(8)	38(4)	1.0
C(2)	2247(13)	1469(11)	9(10)	48(5)	1.0
C(3)	3899(14)	2845(12)	519(10)	49(5)	1.0
C(4)	5302(12)	2271(10)	547(9)	43(4)	1.0
C(5)	4519(11)	547(10)	51(8)	37(4)	1.0
C(6)	3910(35)	−556(19)	3126(17)	56(10)	0.75(2)
C(7)	3025(23)	662(24)	3085(16)	52(8)	0.75
C(8)	4578(35)	2129(31)	3596(24)	56(11)	0.75
C(9)	6327(26)	1907(26)	3798(15)	62(8)	0.75
C(10)	5819(25)	182(25)	3511(15)	50(8)	0.75
C(11)	7189(24)	−664(20)	3616(17)	65(9)	0.75
C(12)	6383(27)	−2491(23)	3164(18)	74(10)	0.75
C(13)	7875(36)	−3199(32)	3294(28)	68(13)	0.75

b) H and C atoms of propylcyclopentadienyl with the low population ($\times 10^3$)

Atom	x	y	z	10^3U/Å^2	Population
C(6*)	301(7)	−76(7)	273(5)	38(11)	0.25
C(7*)	364(8)	108(7)	340(5)	33(11)	0.25
C(8*)	515(8)	240(8)	371(7)	35(15)	0.25
C(9*)	592(6)	118(7)	368(5)	36(10)	0.25
C(10*)	491(6)	−58(5)	314(4)	24(7)	0.25
C(11*)	560(5)	−193(4)	316(3)	35(9)	0.25
C(12*)	775(5)	−129(5)	362(4)	45(10)	0.25
C(13*a)	873(7)	−250(6)	329(6)	32(10)	0.19
C(13*b)	935(14)	−222(12)	411(11)	14(18)	0.06
H(C1)	170(11)	−103(9)	−62(8)	33(21)	1.0
H(C2)	109(12)	158(10)	−1(8)	48(24)	1.0
H(C3)	408(13)	393(12)	74(10)	61(29)	1.0
H(C4)	648(11)	294(9)	89(8)	32(21)	1.0
H(C6)	287(27)	−151(21)	279(18)	97(68)	0.75
H(C7)	203(10)	56(8)	278(7)	14(16)	0.75
H(C8)	476(16)	329(14)	365(11)	41(32)	0.75
H(C9)	742(18)	274(16)	407(13)	56(38)	0.75
H(C11a)	786(16)	−27(14)	297(12)	47(32)	0.75
H(C11b)	809(18)	−61(15)	459(14)	61(39)	0.75
H(C12a)	519(16)	−255(14)	224(12)	41(31)	0.75
H(C12b)	571(18)	−293(16)	364(13)	54(40)	0.75
H(C13a)	833(18)	−314(17)	385(12)	14(43)	0.75
H(C13b)	741(19)	−439(18)	314(14)	69(45)	0.75
H(C13c)	815(19)	−309(17)	270(13)	37(35)	0.75

to exist between the neighboring cations.

Structure of Cation (PrFcFcPr)$^+$: Each iron atom in a cation (PrFcFcPr)$^+$ is sandwiched by five-membered rings in *trans*-configuration. The cation sits on a symmetry center and the two Fc units are crystallographically equivalent. Therefore, electronic states of the two iron atoms are expected to be in an averaged-valence (+2.5) state. The interplanar distance between the two five-membered rings in a Fc unit is 3.33(2) Å and their dihedral angle is 6.6°. This ring-ring distance in the ferrocene-like unit was found to be 3.32 Å in the unoxidized compound biferrocene[16] and 3.277(19) Å in the trapped-valence salt diferrocenylselenium$^+$ iodine triiodide$^-$ hemi(dichloromethane),[5] whereas that for ferrocenium-like unit 3.40 Å in ferrocenium$^+$ tetrachlorobismuthate$^-$ [17] and 3.397(22) Å in cation diferrocenylselenium$^+$. Distances of the iron atom from the least-squares planes of two five-membered rings are found to be 1.656(5) Å for the fulvalene moiety and 1.678(13) Å for the propylcyclopentadienyl ring. Bond distances and bond angles are given in Table 5. Mean bond distances between the iron atom and five carbon atoms are 2.047(9) and 2.072(16) Å for the inner and outer rings, respectively. The mean distance between them is 2.059 Å, which lies midway between 2.045 Å for molecule ferrocene[18] and 2.075 Å for cation ferrocenium$^+$.[17]

The propylcyclopentadienyl ring is found to be

Table 3. Positional parameters with e.s.d.'s in parentheses for the low-temperature phase (110 K)

a) I, Fe, and C atoms of fulvalene moiety ($\times 10^4$)

Atom	x	y	z	10^3U_{eq}/Å^2	Population
I(1)	0(0)	5000(0)	0(0)	13(1)	0.90(1)
I(2)	1085(9)	4347(8)	2919(7)	24(2)	0.90
I(3)	−898(8)	5520(7)	−2876(7)	17(1)	0.90
Fe(1)	4279(14)	1076(13)	1803(10)	22(3)	1.0
Fe(2)	5902(12)	−1156(10)	−1716(10)	13(3)	1.0
C(1)	2585(55)	−43(59)	−390(50)	30(18)	1.0
C(2)	2204(55)	1362(58)	−118(46)	43(19)	1.0
C(3)	3773(45)	2778(32)	280(34)	10(10)	1.0
C(4)	5389(40)	2290(40)	549(28)	10(12)	1.0
C(5)	4582(71)	427(63)	110(49)	41(22)	1.0
C(14)	7585(47)	−51(39)	288(40)	16(11)	1.0
C(15)	7987(40)	−1414(33)	76(30)	14(10)	1.0
C(16)	6213(45)	−2952(49)	−525(36)	24(13)	1.0
C(17)	4781(49)	−2307(45)	−420(38)	32(15)	1.0
C(18)	5545(41)	−613(39)	22(34)	5(9)	1.0
I(1*)	1176(36)	4683(76)	2914(41)	144(31)	0.10
I(2*)	451(43)	5282(83)	254(36)	141(30)	0.10
I(3*)	−479(119)	6289(113)	−2849(49)	194(53)	0.10

b) C atoms of disordered propylcyclopentadienyls ($\times 10^3$)

Atom	x	y	z	10^3U/Å^2	Population
C(6)	387(6)	−68(6)	318(5)	13(9)	0.82(4)
C(7)	313(6)	48(6)	313(5)	26(10)	0.82
C(8)	483(11)	216(9)	373(8)	44(18)	0.82
C(9)	642(6)	195(6)	390(5)	9(9)	0.82
C(10)	572(9)	17(8)	347(6)	35(14)	0.82
C(11)	720(4)	−74(4)	369(4)	4(7)	0.82
C(12)	639(4)	−271(3)	326(3)	5(5)	0.82
C(13)	779(8)	−343(7)	338(6)	39(14)	0.82
C(19)	625(8)	61(7)	−299(5)	32(12)	0.89(4)
C(20)	691(4)	−90(5)	−315(3)	5(6)	0.89
C(21)	537(6)	−229(5)	−357(4)	6(7)	0.89
C(22)	372(7)	−199(6)	−374(5)	20(11)	0.89
C(23)	420(5)	−20(5)	−358(4)	3(7)	0.89
C(24)	278(6)	53(6)	−357(5)	31(10)	0.89
C(25)	373(5)	234(5)	−309(4)	28(9)	0.89
C(26)	227(5)	330(5)	−320(4)	10(7)	0.89
C(6*)	353(27)	−56(23)	333(17)	13	0.18
C(7*)	370(23)	104(21)	350(16)	13	0.18
C(8*)	521(24)	258(20)	381(18)	13	0.18
C(9*)	620(20)	126(22)	368(15)	13	0.18
C(10*)	492(24)	−26(17)	337(14)	13	0.18
C(11*)	511(17)	−197(14)	310(11)	13	0.18
C(12*)	745(21)	−146(20)	366(15)	13	0.18
C(13*)	840(19)	−277(17)	352(16)	13	0.18
C(19*)	678(39)	50(36)	−293(29)	13	0.11
C(20*)	630(39)	−155(35)	−323(26)	13	0.11
C(21*)	494(34)	−254(30)	−330(26)	13	0.11
C(22*)	387(32)	−139(33)	−399(25)	13	0.11
C(23*)	425(47)	17(37)	−366(32)	13	0.11
C(24*)	414(32)	164(25)	−321(20)	13	0.11
C(25*)	269(39)	117(37)	−354(27)	13	0.11
C(26*)	135(29)	233(26)	−342(23)	13	0.11

rotationally disordered, with two sites in population ratio 75 : 25, as shown in Fig. 4(a). The two sites are related to each other by a pseudo-mirror plane normal to the fulvalene moiety and passing through the C(5)–C(5′) bond. The outer ring with the high population and the five-membered ring of the fulvalene moiety are mutually displaced by about 0.5 Å in their gravity centers, are mutually rotated away from the eclipsed

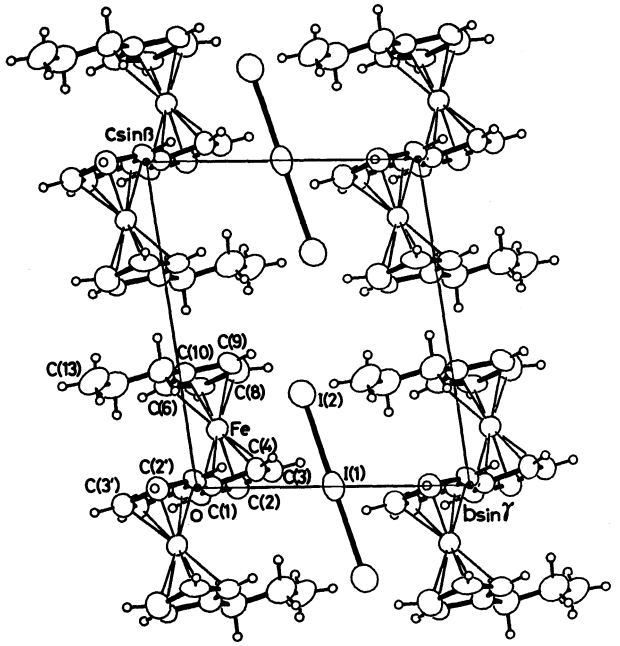

Fig. 1. The projection of the structure for the high-temperature phase (298 K) along the a axis.

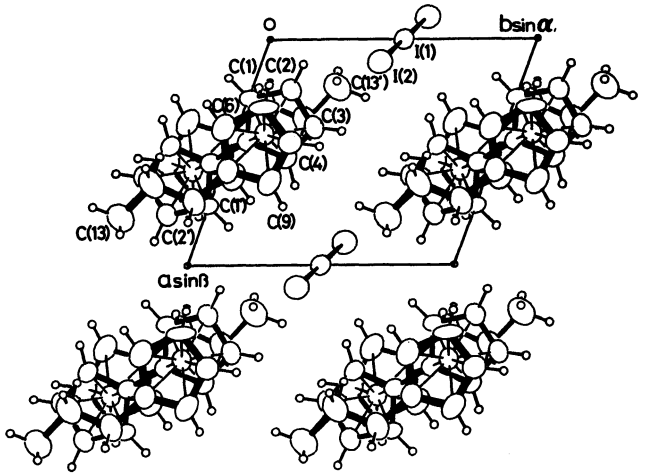

Fig. 2. The projection of the structure for the high-temperature phase (298 K) along the c axis.

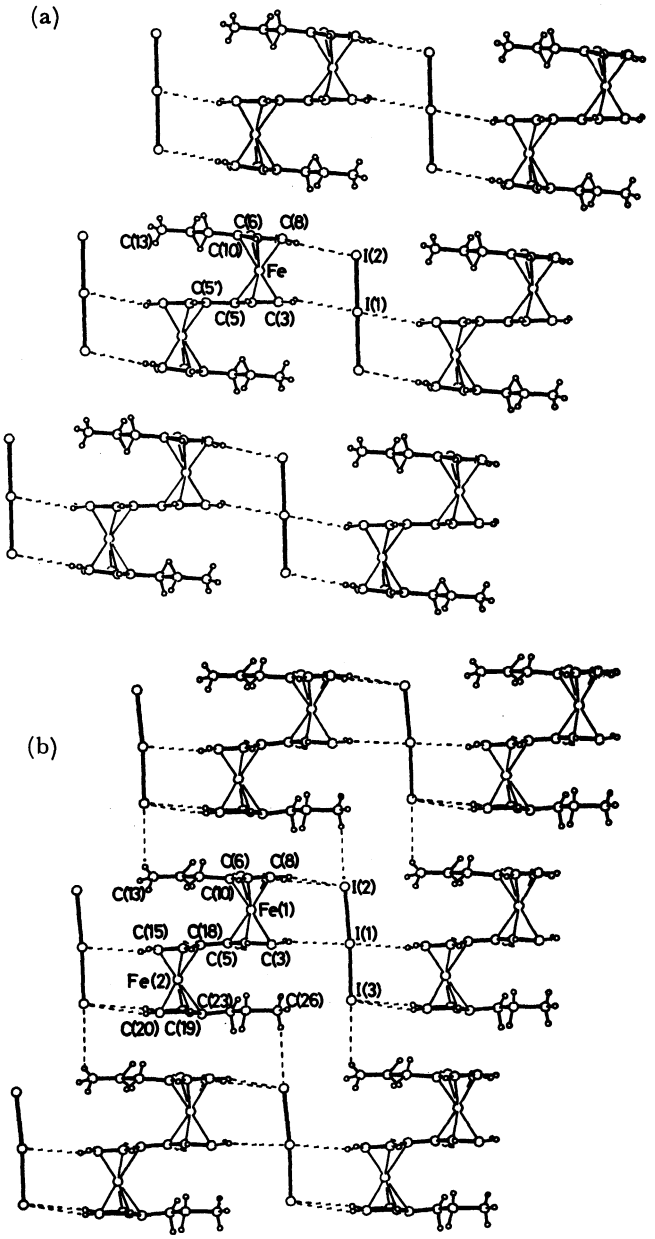

Fig. 3. Packing views in the (110) plane (a) for the high-temperature phase (298 K) and (b) for the low-temperature phase (110 K). Broken lines show short contacts between hydrogen and iodine atoms.

conformation by 10° in the mean value, and remain in a nearly eclipsed conformation. On the other hand, for the site with the low population the Fc unit is rotated in the opposite direction by about 15° and is about midway between eclipsed (0°) and staggered (36°) positions. Molecule ferrocene is known to take a nearly eclipsed conformation with a rotational angle of 9° in the disordered high-temperature phase and in the ordered low-temperature phase.[18,19] Rotational angles were observed to be 17, 3.6, 5.2, and 4.1° for biferrocene, 1′,1‴-diethylbiferrocene, 1′,1‴-dichlorobiferrocene, and 1′,1‴-diacetylbiferrocene,[16,20-22] respectively.

Data of some least-squares planes and deviations of atoms from their planes are given in Table 6. The dihedral angle between the planes of five-membered ring and propyl group within propylcyclopentadienyl is 3.5° and they sit essentially coplanar. The propyl group is also parallel to the fulvalene plane and sits at the position above the ring of the other sandwich of the fulvalene moiety deviating from the ideal position overlapped between their C–C bonds. This is in contrast to the unoxidized compound 1′,1‴-diethylbiferrocene, in which the ethyl group is not parallel to the fulvalene moiety and stands away from it.[20] Hydrogen atoms H(11a) and H(12a) in the propyl group are situated at 2.77(12) and 2.86(12) Å from the least-squares plane of the fulvalene moiety. There seems to exist a strong interaction within the cation between the propyl group

Table 4. Intermolecular distances (l/Å) shorter than 3.4 Å between hydrogen atoms of $(PrFcFcPr)^+$ cation and iodine atoms

Symmetry code							
None	x,	y,	z	(iv)	$-1+x$,	$1+y$,	z
(i)	$-x$,	$-y$,	$-z$	(v)	$-1+x$,	$1+y$,	$-1+z$
(ii)	$-1+x$,	y,	z	(vi)	x,	$1+y$,	z
(iii)	x,	y,	$1+z$				
a) High-temperature phase (298 K)							
I(1)–H(C2)	3.34(10)			I(2)–H($C2^{i}$)	3.24(7)		
I(2)–H(C8)	3.37(14)			I(2)–H($C4^{ii}$)	3.29(7)		
b) Low-temperature phase (110 K)							
I(1)–H(C3)	3.40(30)			I(1)–H($C14^{ii}$)	3.26(24)		
I(2)–H(C7)	3.39(33)			I(2)–H($C14^{ii}$)	3.18(21)		
I(2)–H(C8)	3.16(35)			I(3)–H($C19^{ii}$)	3.38(28)		
I(2)–H($C26a^{iii}$)	3.16(34)			I(1)–H($C1^{vi}$)	3.28(25)		
I(1)–H($C16^{iv}$)	3.31(30)			I(1)–H($C17^{vi}$)	3.29(28)		
I(3)–H($C20^{iv}$)	3.40(43)			I(2)–H($C6^{vi}$)	3.29(30)		
I(3)–H($C21^{iv}$)	3.35(37)			I(3)–H($C17^{vi}$)	3.10(20)		
I(3)–H($C13a^{v}$)	3.33(34)						

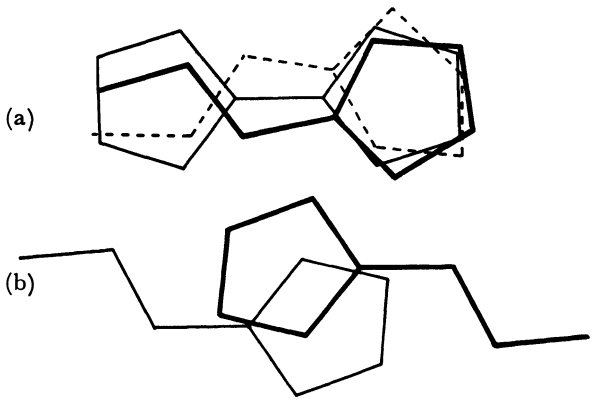

Fig. 4. Overlap between rings for the high-temperature phase.
(a) The projection of a disordered propylcyclopentadienyl along the normal to the plane of a fulvalene moiety (—— for the site with the high population and ------ for the site with the low population). (b) The projection of a propylcyclopentadienyl of a neighbouring $(PrFcFcPr)^+$ cation along the normal to the plane of a propylcyclopentadienyl.

and the fulvalene moiety in the high-temperature phase.

The mean C–C bond distances in the inner and outer five-membered rings are 1.413(4) and 1.428(18) Å, respectively, and the outer ring shows larger thermal vibrations. This distance agrees with 1.425 Å observed in compound ferrocene at 169 K.[18] The C(5)–C(5′) bond distance in the fulvalene moiety is 1.46(2) Å.

Anion I_3^-: The triiodide anion is at the symmetry center, showing a symmetric structure. The I(1)–I(2) bond distance is 2.926(1) Å corresponding to 2.920 Å in free I_3^- ion.[23]

Low-temperature Phase (110 K): *Packing*: Figure 3(b) shows a packing view at 110 K. The structure is constructed by segregated columns of cation $(PrFcFcPr)^+$ and anion I_3^- similarly to that in the high-temperature phase. A three-dimensional hydrogen bond network is clearly found between the hydrogen atoms of a cation and the iodine atoms, in contrast to that at 298 K. Short contacts are found in the data given in Table 4. The interplanar distance of five-membered rings between neighboring cations is 3.40(4) Å, which is shorter by 0.07 Å than that at 298 K.

Structure of Cation $(PrFcFcPr)^+$: The symmetry center is lost and ferrocene- and ferrocenium-like units are crystallographically discernible in the cation. Their ring-ring distances are 3.28(4) and 3.41(5) Å for ferrocene- and ferrocenium-like units, respectively. These values are in agreement with 3.277(19) Å for the ferrocene-like unit and 3.397(22) Å for the ferrocenium-like unit in the trapped-valence cation diferrocenylselenium$^+$ [5] and 3.291—3.320 Å for three ferrocene-like units and 3.428 Å for a ferrocenium-like unit reported for ferricenyl(III) tris(ferrocenyl(II))borate.[24] The mean bond distances of Fe(2)–C and Fe(1)–C are 2.04(3) and 2.11(2) Å for the ferrocene- and ferrocenium-like units, respectively.

The rotational disorder of the propylcyclopentadienyl rings remains at 110 K but the population increases from 0.75(2) to 0.90(4) and 0.82(4) in the sites having the high population in the ferrocene- and ferrocenium-like units, respectively.

Anion I_3^-: The triiodide anion sits at the regular position at 298 K, whereas it exhibits a positional disorder with population ratio 0.90 : 0.10 at 110 K. When the propylcyclopentadienyl ring changes its position from the site with the low population to that with the high population, the propyl group ought to rotate around the C(10)–C(11) bond. As this rotation gives rise to a short contact between the propyl group and iodine atoms, the I_3^- anion seems to move away from the propyl group, and the I_3^- anion causes a positional disorder with population ratio 0.90 : 0.10. Bond distances of I(1)–I(2) and I(1)–I(3) are found to be 2.948(8) and 2.902(7) Å, respectively.

Infrared Spectroscopy. Infrared spectral data obtained at 294 and 78 K are shown in Table 7. No

TABLE 5. BOND DISTANCES AND BOND ANGLES WITH e.s.d.'s IN PARENTHESES FOR THE HIGH-TEMPERATURE PHASE (298 K)

(a) Bond distance	l/Å		l/Å
Fe–C(1)	2.043(7)	Fe–C(6)	2.062(19)
Fe–C(2)	2.037(9)	Fe–C(7)	2.042(22)
Fe–C(3)	2.030(11)	Fe–C(8)	2.038(28)
Fe–C(4)	2.041(11)	Fe–C(9)	2.103(13)
Fe–C(5)	2.083(10)	Fe–C(10)	2.116(17)
C(1)–C(2)	1.417(15)	C(6)–C(7)	1.457(35)
C(2)–C(3)	1.398(12)	C(7)–C(8)	1.398(27)
C(3)–C(4)	1.417(18)	C(8)–C(9)	1.483(41)
C(4)–C(5)	1.409(11)	C(9)–C(10)	1.395(30)
C(1)–C(5)	1.422(13)	C(6)–C(10)	1.408(33)
		C(10)–C(11)	1.522(33)
C(5)–C(5′)	1.458(21)	C(11)–C(12)	1.481(24)
		C(12)–C(13)	1.527(43)
(b) Bond angles	ϕ/°		ϕ/°
C(2)–C(1)–C(5)	107.7(8)	C(7)–C(6)–C(10)	113.0(16)
C(1)–C(2)–C(3)	108.9(10)	C(6)–C(7)–C(8)	100.2(18)
C(2)–C(3)–C(4)	107.2(9)	C(7)–C(8)–C(9)	114.5(23)
C(3)–C(4)–C(5)	109.1(8)	C(8)–C(9)–C(10)	103.3(19)
C(1)–C(5)–C(4)	107.1(8)	C(6)–C(10)–C(9)	108.6(22)
C(1)–C(5)–C(5′)	125.7(7)	C(6)–C(10)–C(11)	128.5(20)
C(4)–C(5)–C(5′)	127.2(8)	C(9)–C(10)–C(11)	122.9(18)
		C(10)–C(11)–C(12)	115.7(16)
		C(11)–C(12)–C(13)	111.1(19)

TABLE 6. SOME LEAST-SQUARES PLANES AND DEVIATIONS (d/Å) OF ATOMS FROM THEIR PLANES IN THE HIGH-TEMPERATURE PHASE (298 K)

Equations of the least-squares planes refer to the orthogonal coordinate system defined by X along a Y in the ab plane, and Z along c^*. The atoms with asterisks were included in the calculations of the least-squares planes.

Plane(I) Fulvalene moiety
$(0.1360X+0.3284Y-0.9347Z=0.5793)$

C(1)*	0.013(9)	C(4)*	0.003(10)
C(2)*	−0.009(10)	C(5)*	−0.017(10)
C(3)*	0.006(10)	Fe	1.656(4)

Plane(II) Five-membered ring of propylcyclopentadienyl
$(-0.2012X-0.2358Y+0.9507Z=2.6798)$

C(6)*	0.021(22)	C(11)	−0.010(21)
C(7)*	−0.037(21)	C(12)	−0.098(23)
C(8)*	0.036(27)	C(13)	−0.120(31)
C(9)*	−0.021(20)	Fe	1.678(13)
C(10)*	−0.001(20)		

Plane(III) Four carbon atoms of propyl group
$(-0.2146X-0.2921Y+0.9320Z=2.5975)$

C(10)*	0.005(16)	C(12)*	−0.004(19)
C(11)*	−0.006(17)	C(13)*	0.005(28)

Dihedral angles (ϕ/°)

Plane(I)–Plane(II)	6.6
Plane(I)–Plane(III)	5.0
Plane(II)–Plane(III)	3.5

difference is found in the infrared spectral shapes for the two unoxidized compounds between 294 and 78 K, except for the narrowing of band width found at 78 K.

μ-(as-Indacenediyl)-bis(cyclopentadienyliron) System: Infrared spectra of the unoxidized molecule and mono-oxidized salt are illustrated in Fig. 5. The spectra of the mono-oxidized salt as well as the unoxidized molecule show no change at 294 and 78 K. A discernible difference between the infrared spectra of the unoxidized and mono-oxidized species is found in the band region from 400 to 500 cm^{-1} and in the bands in the vicinity of 800 cm^{-1}. By analogy with ferrocene,[25] the 470 cm^{-1} band of the unoxidized molecule may be assigned to the asymmetric ring-metal-ring strech and the 485 cm^{-1} band to the asymmetric ring-metal-ring tilt. These bands are reduced in intensity in the mono-oxidized salt as compared with the unoxidized molecule. A similar tendency was also observed in the ferrocene system.[26] The bands in the vicinity of 800 cm^{-1} can be assigned to the perpendicular CH bend. Although it was observed by means of Mössbauer spectroscopy that the mono-oxidized salt gradually undergoes a transition from an averaged-valence state of iron atoms to a trapped-valence state as temperature was lowered, infrared spectra of this salt is found to be temperature-independent. Supposing that the rate of electron transfer between two iron atoms is higher than the time scale of Mössbauer spectroscopy (*ca.* 10^7 s^{-1}), is lower than that of infrared spectroscopy (*ca.* 10^{13} s^{-1}) at room temperature, and becomes lower than 10^7 s^{-1} at 78 K, the results may be considered not to be in contradiction to the observation of line broadening at higher temperatures found in Mössbauer spectroscopy.[9,10]

1′1‴-Diethyl- and 1′,1‴-Dipropylbiferrocene System: Infrared spectra of the mono-oxidized salts of diethyl- and dipropylbiferrocene are similar except for the band at 736 cm^{-1}, which appears in cation dipropylbiferroce-

Table 7. Comparison between infrared spectral data and Mössbauer spectral data

Compound	Tmperature/K	Infrared spectra	Mössbauer spectra[9-11]
μ-(as-Indacenediyl)-bis-(cyclopentadienyliron)	294 78	No change	
1′,1‴-Diethylbiferrocene	294 78	No change	
μ-(as-Indacenyl)-bis(cyclopentadienyliron)$^+I_3^-$ 0.5 I_2	294 78	No change	Averaged-valence Trapped-valence
1′,1‴-Diethylbiferrocenium$^+I_3^-$	294 78	Remarkable change in intensity of bands at 680 and 1525 cm^{-1}	Averaged-valence Trapped-valence
1′,1‴-Dipropylbiferocenium$^+I_3^-$ (PrFcFcPr)$^+I_3^-$	294 78	Remarkable change in intensity of bands at 680 and 1525 cm^{-1}	Averaged-valence Trapped-valence

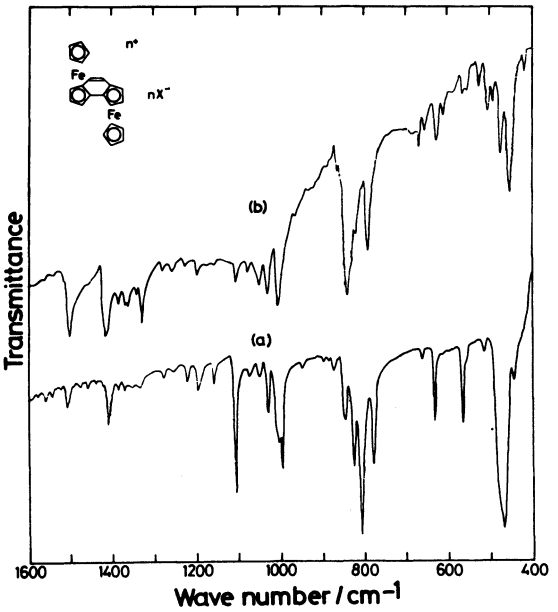

Fig. 5. Infrared spectra of KBr pellets of (a) μ-(as-indacenediyl)-bis(cyclopentadienyliron) at 294 K (n=0, X= none) and (b) μ-(as-indacenyl)-bis(cyclopentadienyliron)$^+I_3^-$ 0.5I_2 at 78 K (n=1, X=I_3-0.5I_2).

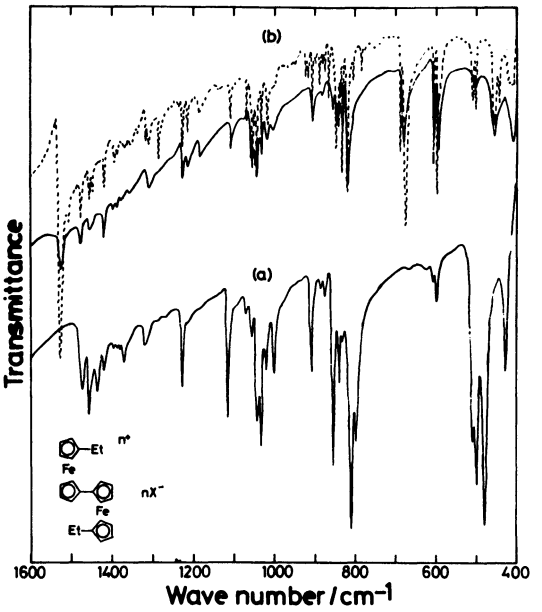

Fig. 6. Infrared spectra of KBr pellets of (a) 1′,1‴-diethylbiferrocene at 294 K (n=0, X=none) and (b) 1′,1‴-diethylbiferrocenium$^+I_3^-$ at 294 K (——) and 78 K (------) (n=1, X=I_3^-).

nium$^+$, attributable to the propyl group. Figure 6 shows spectra of diethylbiferrocene and its mono-oxidized salt. A discernible difference between these two species is observed in the band region from 400 to 500 cm^{-1} and in the bands around 800 cm^{-1}, similarly to the case of μ-(as-indacenediyl)-bis(cyclopentadienyliron) and its mono-oxidized cation. However, these bands change in the mono-oxidized salt, depending on temperature. It should be noted that new intense bands appear at 680 and 1525 cm^{-1} on going from the unoxidized molecule to the mono-oxidized salt. These bands are remarkably larger at 78 K than at 294 K. The band at 680 cm^{-1} seems to be assigned to the fulvalene moiety, because it is observed that a new band appears at 674 cm^{-1} in the biferricenylenium$^+PF^-_6$ salt with two fulvalene moieties.[6]

Conclusion

According to the results of infrared spectra and Mössbauer spectra,[11] the electrons in the (PrFcFcPr)$^+I_3^-$ salt are fully delocalized above the transition point (240 K), whereas below the transition temperature the salt has its electrons localized more in one Fc moiety than in the other. At 78 K, the electrons are almost localized and the ferrocene- and ferrocenium-like conformations become observable. The result of crystal structure suggests that a strong interaction within the cation is found between the propyl group and fulvalene moiety and the electrons get delocalized easily through the fulvalene moiety in consonance with this interaction, whereas at 110 K a three-dimensional hydrogen bond network is formed between the cation and iodine stoms, causing the interaction between the propyl group and fulvalene moiety to get weaker and the electrons to get localized. It was reported that the transition temperatures of 1′,1‴-diethylbiferrocenium$^+$-I_3^- and (PrFcFcPr)$^+I_3^-$ are 270 and 240 K, respectively. If the interaction between the substituent and fulvalene moiety brings about easier delocalization of electrons between the two iron atoms, the propyl group is expected to cause a stronger interaction than the ethyl group, and accordingly, to make the transition point from the averaged-valence state to the trapped-valence state lower in dipropyl- than in diethylbiferrocenium$^+$ cation.

The reason why the unsubstituted biferrocenium$^+$ cation is in a temperature-independent trapped-valence state, is also interpreted similarly by assuming an absence of this kind of interaction with the fulvalene ring. It should be mentioned that the interaction between the cation and the anion also has much to do with the electronic state of the cation.

In cation μ-(as-indacenyl)-bis(cyclopentadienyliron)$^+$, the electrons hop faster between the two iron atoms as temperature is raised. This indicates that the resonance energy is not large enough to delocalize the electrons between the two iron atoms.

We thank Professor Hirotoshi Sano of Tokyo Metropolitan University for his helpful suggestions and discussions. We also thank the late Professor Tsunetake Fujiyama of the Institute for Molecular Science for his valuable advice, discussions, and kind permission to use the infrared instruments. This work was partially supported by the Joint Studies Program (1981) of the Institute for Molecular Science.

References

1) G. C. Allen and N. S. Hush, *Prog. Inorg. Chem.*, **8**, 391 (1967).
2) F. Kaufman and D. O. Cowan, *J. Am. Chem. Soc.*, **92**, 6198 (1970).
3) D. O. Cowan, R. L. Collins, and F. Kaufman, *J. Phys. Chem.*, **75**, 2025 (1971).
4) I. Motoyama, M. Watanabe, and H. Sano, *Chem. Lett.*, **1978**, 513.
5) J. A. Kramer, F. H. Herbstein, and D. N. Hendrickson, *J. Am. Chem. Soc.*, **102**, 2293 (1980).
6) W. H. Morrison, Jr., and D. N. Hendrickson, *Inorg. Chem.*, **14**, 2331 (1975).
7) W. H. Morrison, Jr., and D. N. Hendrickson, *J. Chem. Phys.*, **59**, 380 (1973).
8) C. Le Vanda, K. Bechgaard, D. O. Cowan, U. T. Mueller-Westerhoff, P. Eilbracht, G. A. Candela, and R. L. Collins, *J. Am. Chem. Soc.*, **98**, 3181 (1976).
9) S. Iijima, I. Motoyama, and H. Sano, *Chem. Lett.*, **1979**, 1349.
10) S. Iijima, I. Motoyama, and H. Sano, *Bull. Chem. Soc. Jpn.*, **53**, 3184 (1980).
11) S. Iijima, R. Saida, I. Motoyama, and H. Sano, *Bull. Chem. Soc. Jpn.*, **54**, 1375 (1981).
12) F. V. Bolhuis, *J. Appl. Crystallogr.*, **4**, 263 (1971).
13) P. Coppens, T. N. Guru-Row, P. Leung, E. D. Stevens, P. J. Becker, and Y. W. Yang, *Acta Crystallogr., Sect. A*, **35**, 63 (1979).
14) "Internatinal Tables for X-Ray Crystallography," Kynoch Press, Birmingham (1974), Vol. IV, pp. 73—86.
15) R. F. Stewart, E. R. Davidson, and W. T. Simpson, *J. Chem. Phys.*, **42**, 3175 (1965).
16) A. C. Macdonald and J. Trotter, *Acta Crystallogr.*, **17**, 872 (1964).
17) N. J. Mammano, A. Zalkin, A. Landers, and A. L. Rheingold, *Inorg. Chem.*, **16**, 297 (1977).
18) P. Seiler and J. D. Dunitz, *Acta Crystallogr., Sect. B*, **35**, 1068 (1979).
19) F. Takusagawa and T. F. Koetzle, *Acta Crystallogr., Sect. B*, **35**, 1074 (1979).
20) Z. Kałuski, *Bull. Acad. Pol. Sci., Ser. Sci. Chim.*, **13**, 355 (1965).
21) Z. Kałuski and Y. T. Strushkov, *Bull. Acad. Pol. Sci., Ser. Sci. Chim.*, **14**, 719 (1966).
22) Z. Kałuski, A. I. Gusiev, and Y. T. Strutshkov, *Bull. Acad. Pol. Sci., Ser. Sci. Chim.*, **22**, 739 (1974).
23) J. Runsink, S. Swen-Walstra, and T. Migchelsen, *Acta Crystallogr., Sect. B*, **28**, 1331 (1972).
24) D. O. Cowan, P. Shu, F. L. Hedberg, M. Rossi, and T. J. Kistenmacher, *J. Am. Chem. Soc.*, **101**, 1304 (1979).
25) E. R. Lippincott and R. D. Nelson, *Spectrochim. Acta*, **10**, 307 (1958).
26) D. M. Duggan and D. N. Hendrickson, *Inorg. Chem.*, **14**, 955 (1975).

Phase Transition in Concentrated Latices and the Electrical Double Layer on Their Surfaces

Kunio FURUSAWA* and Satoshi YAMASHITA
Department of Chemistry, The University of Tsukuba, Sakura-Mura, Ibaraki 305
(Received January 21, 1982)

The phase diagrams of monodisperse latices were constructed under the various conditions. The variable of the phase diagrams, the particle size, the surface charge densities of the latices, the counter-ion valences, and the medium temperature were taken up. The results, especially, the coexistent/ordered boundary curves were analysed in terms of the closed packing of the effective particle volumes which consisted of the latex particles which were surrounded by the electrical double layer. The value of 1.5 kT ergs† of electrical repulsion, when used as a criterion in the DLVO potential to back-calculate the weight fraction of solid contents as a function of KCl concentration, yields a curve that is very similar to the experimental boundary curve. The same agreement was found in the curves mapped out for the other latices with a different particle size and a different surface charge density using KCl as an electrolyte. In the boundary curve constructed using $MgCl_2$, however, the agreement with the analyses was not enough where the divalent cation would be adsorbed preferentially on their surfaces as a Stern layer charge. The temperature effect could be reasonably explained by the same procedure.

Monodisperse polymer latices which usually appear milky white, exhibit beautiful irridescent colours under a certain condition. This irridescence is due to the Bragg reflection of visible light by the orderly arrays of the uniform spherical particles of latices.[1]

To date, several attempts have been made to give a reasonable explanation as to their order-disorder phase transitions. One explanation is based on the double layer interactions between the particles:[2,3] The latex particle in an aqueous system may be regarded as an effective particle volume whose size is determined by the thickness of an electrical double layer on its surface and the boundary curve between the ordered and coexistent states corresponds to the closed packing of the effective particle volumes with a critical thickness of an electrical double layer.

Another approach is based on the concept of the Kirkwood-Alder transition[4] which is expected only from the pure computer calculations. Their approach accounts for the presence of reasonable coexistent states of ordered and disordered structures.[5]

The problem is that these analytical works have been performed using very limited experimental data and only a few authors have mapped out the phase diagrams by themselves. In this work, the conditions for the occurrence of ordered and disordered structures were studied systematically under the various conditions. As the parameters of the phase diagram, the particle size and the surface charge densities of latices, the valency of added counter ions, and the medium temperature were taken up. Thereafter, the resulted phase diagrams, especially, the coexistent/ordered boundary curves were analysed according to the concept of closed packing of the effective particle volumes using the DLVO theory.[6]

Experimental

Latex Samples. In this work, three kinds of polystyrene latices were employed. Sample-A was prepared by an emulsion polymerization using sodium dodecyl sulfate as an emulsifier and $K_2S_2O_8$ as a polymerization initiator. Sample-B and -C were polymerized in the absolute absence of conventional emulsifiers.[7] Table 1 shows their preparation conditions and the characteristic results. The particle diameters were determined by measuring the diameters on an electron micrograph which was equipped with a projection scope. The diameters for Sample-A and -C are almost the same, and the diameter for Sample-B is about threefold more than either of the other two. Size distribution of these samples is kept very narrow, with $D_w/D_n < 1.01$.

The surface charge densities of these latices were determined by potentiometric and conductometric titrations according to the method described by Van den Hul and Vanderhoff.[8] The charge densities for Sample-A and -B are not so different, but the density is extremely high for Sample-C which is prepared by incorporating a small amount of ionic comonomer (sodium *p*-vinylphenylsulfonate) into the polystyrene chains.[9]

All samples were dialysed fully against pure water, and deionized by the ion-exchange resins to remove the ionic impurities, and then they were condensed by ultrafiltration using a Visking tube up to 30% of solid contents by the volume

TABLE 1. PREPARATION AND CHARACTERIZATION OF POLYSTYRENE LATICES

Sample	Polymerization conditions			Characterization		
	Styrene (g dm^{-3})	Svps[a] (g dm^{-3})	$K_2S_2O_8$ (g dm^{-3})	Diameter $2a$ / Å	Surface charge σ_0 / μC cm^{-2}	ζ-Potential / mV (25 °C, 10^{-3} mol KCl)
A	1.5×10^2	—	0.5	1960	0.9	−42
B	1.3×10^2	—	0.8	5720	0.7	−33
C	1.0×10^2	0.5	0.5	1650	7.0	−60

a) Sodium *p*-vinylphenylsulfonate.

† 1 erg = 10^{-7} J.

fraction.

Electrophoresis. The electrophoretic measurements of the latex samples were performed in a Rank Brothers micro-electrophoresis apparatus, using a rectangular cell. A complete parabolic curve for the velocity as a function of cell depths was measured on each sample and electrophoretic mobility(particle velocity at the level of zero liquid flow) was given at the reproducibility in samll percentages. The mobility of the particle was measured in various concentrations of KCl and $MgCl_2$. Also, the measurements were conducted under the different medium temperatures. Zeta-potential for the particle in each condition was calculated from the electrophoretic mobility with an allowance of Henry correction (if possible, Wiersema correction[10] was applied). The typical results obtained at 40 °C are shown in Fig. 1, in the form of a curve of zeta-potential against the molar concentration of each electrolyte.

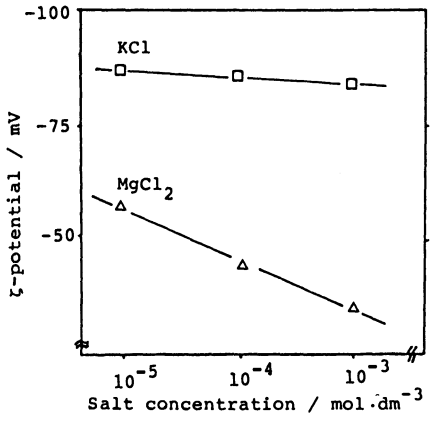

Fig. 1. Curves of zeta-potential of polystyrene latex (Sample-C) against molar concentration of salts at 40 °C.

Phase Diagrams. The conditions for the occurrence of ordered and disordered structures were measured using a slight modification of the method described by Hachisu *et al.*[5] The modification is related to the equilibration time of sample and the short equilibration took in this work brought about a reasonable removal from gravitational effect of the latex samples. The concentrated latices were diluted in Pyrex-stoppered vials of 10 cm^3 to desired solid content levels with some salt solutions of several concentrations, and left in the thermostat which was kept at various temperatures. After 3 d (Hachisu's work took the equilibration of 2 weeks), the conditions for the occurrence of ordered and disordered structures were studied making use of the irridescence exhibited by the ordered structures as an indicator.

In relation to the electrical double layer effects, phase diagrams were constructed with the volume fractions of solid content as the ordinate and log molar concentrations of electrolyte in the medium as the abscissa.

Results and Discussion

The phase changes in the monodisperse latices are depicted schematically in Fig. 2. Under a constant volume of solid, at high electrolyte concentrations, the electrical double layer around each particle is thin, the particles do not interact with each other and are distributed randomly (Fig. 2a). Decrease in electrolyte concentration leads to an increasing effective radius of the particle, and at a definite point, the interaction between the paticles becomes more favourable energetically to accommodate some of these particles in an ordered state which corresponds to the disordered/coexistent boundary state as shown in Fig. 2b. The existence of this state would be based on thermodynamic reasons where the entropy of the system is minimized by creating coexistent regions rather than going directly to an ordered state.[3] As the electrolyte concentration is further reduced, the system steadily increases the fraction of the ordered state (Fig. 2c), and finally the effective particle volumes are all in the closed-packed ordered arrangement as shown in Fig. 2d which is called a coexistent/ordered boundary state. In the present experiment, this coexistent/ordered boundary is thought as an important criterion and analysed in the terms of closed packing of effective particle volumes of the latex particles using the DLVO theory. Also, a further decrease in the electrolyte concentration leads to an overlap of the effective particle volumes (Fig. 2e), and then strong repulsive potentials will build up.

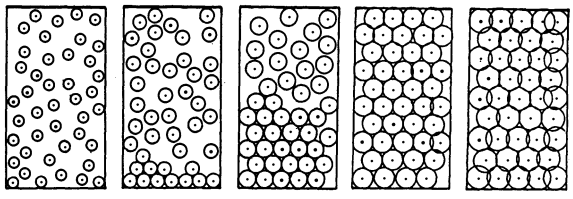

Fig. 2. Schematic representation of the phase changes in a monodisperse latex.
b: Disordered/coexistent boundary, d: coexistent/ordered boundary.

The size of the effective volumes at the coexistent/ordered phase boundary will be related to the particle separation at which some critical electrostatic repulsions are operating; the separation distances, (H), are calculated using the following relation in assuming that the particles in ordered phase are arranged in a hexagonal array.[3]

$$H = 2a[V_f(1 + \rho_p/\rho_s(1/\phi - 1))^{1/3} - 1], \quad (1)$$

where a is the radius of the particles, ρ_p and ρ_s the densities of the particles (1.05 g/ml for polystyrene) and the suspending fluid (1.00 g/ml for water), and ϕ the critical volume fraction at the coexistent/ordered phase boundary, and V_f is the packing density for a closed-packed arrangement, thus the value of 0.74 was chosen for regularly closed-packed spheres.

Furthermore, the interparticle distances at the critical boundary state can be estimated using the DLVO theory by assuming that at such a condition some definite repulsive energies which may be comparable to the thermal energies, are operating to maintain the ordered structures. As the formula to estimate the double layer potential, a following relation derived by Overbeek was employed.[6]

$$V_R = 3.469 \times 10^{19}\varepsilon(kT)^2(a\gamma^2/z^2)\exp(-\kappa aH)$$
$$\kappa = (8\pi nz^2e^2/\varepsilon kT)^{1/2} \quad (2)$$
$$\gamma = [\exp(ze\psi_o/2kT) - 1]/[\exp(ze\psi_o/2kT) + 1]$$

in the above equation, ε is the dielectric constant of the

medium, k the Boltzmann constant, T the absolute temperature, z the valency of the counter ion, n the counter ion density, e the elementary charge and ψ_0 the surface potential of the particles. If we assume the values of critical potential to maintain the ordered structure, the interparticle distances(H) can be calculated from Eq. 2, and, by introducing the H-values into Eq. 1, we can back-calculated the weight fraction of the solid(ϕ) as a function of electrolyte concentration-(n) through Eq. 2. Hereafter, the boundary curve calculated following the above process would be called an analytical boundary curve. In Fig. 3 the analytical

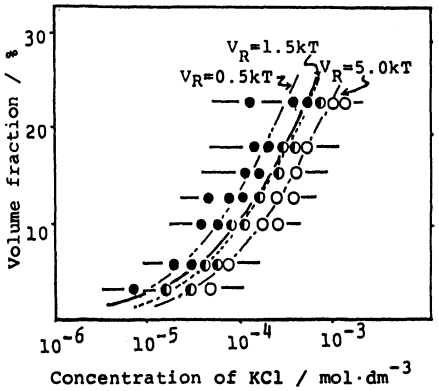

Fig. 3. Phase diagram of Sample-A ($2a$=1960 Å, σ_0= 0.9 μC cm^{-2}) constructed using KCl at 25 °C.
●: Ordered state, ○: disordered state, ◐: coexistent state. Each curve shows the experimental (——) and the analytical coexistent/ordered boundary curve assuming the various critical potentials; (-·-·-): V_R= 0.5 kT, (------): V_R=1.5 kT, (-···-···-): V_R=5.0 kT.

boundary curves with the experimental phase diagram of Sample-A, using KCl as the electrolyte, are compared. Each analytical line shows the calculated phase boundary for respective critical V_R which is illustrated on the figure. In this calculation, ζ-potential measured at the respective salt concentration was employed in place of ψ_0 in Eq. 2. As can be seen from Fig. 3, 1.5 kT ergs as a criterion of V_R yields a curve that closely fits the experimental coexistent/ordered boundary curve and the accordance attains the whole electrolyte levels examined. According to the computer analyses for the nature of the potential well in ordered state, revealed that with only 0.5 kT of interaction between the individual particles, it would require more than 8 kT to escape from the twelve nearest neighbours.[3] Under such an analysis, the value of 1.5 kT ergs estimated by the present calculation is a significant barrier as a criterion for the phase transition.

This critical value of 1.5 kT ergs is also confirmed by the direct observation study on the interparticle distances in the ordered state near the phase boundary.[11]

This analytical procedure may be used to predict the effect of the particle size, the surface potential, the valency of counter ion and the temperature of the medium on the phase boundary curves, since the interparticle potential between the particles varies also by these variables. To see the effects of the particle size, Fig. 4 shows a comparison of the experimental and

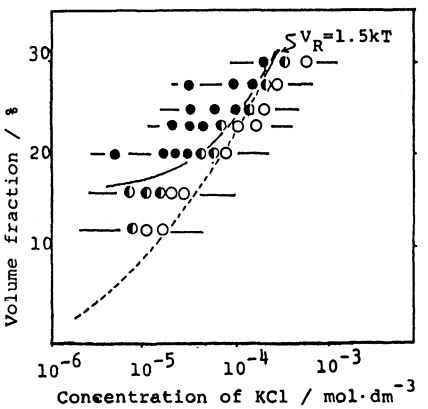

Fig. 4. Phase diagram of Sample-B($2a$=5720 Å, σ_0=0.7 μC cm^{-2}) constructed using KCl at 25 °C.
●: Ordered state, ○: disordered state, ◐: coexistent state. Each curve shows the experimental (——) and the analytical coexistent/ordered boundary curve assuming the critical potential of V_R=1.5 kT (------).

an analytical boundary curve for the Sample-B ($2a$= 5720 Å) using KCl. In these analyses, 1.5 kT ergs was used as a criterion of phase transition potential. Increasing the particle size, favours the disordered state as expected from the double layer theory. But the agreement between the experimental and the analytical boundary curves is very limited at the high electrolyte region and there are definite discrepancies in the low electrolyte level. These would be based on the gravitational settling of the large particles, where the particles form a sediment rather quickly to their own gravity of the large mass and the soft repulsive potential at the low electrolyte level.

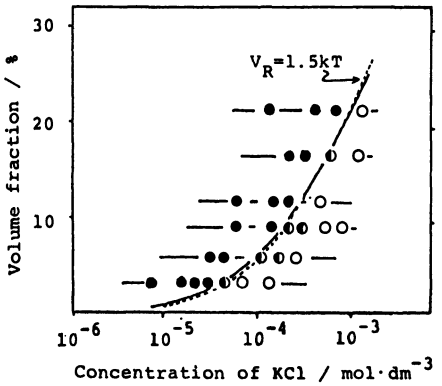

Fig. 5. Phase diagram of Sample-C ($2a$=1650 Å, σ_0= 7.0 μC cm^{-2}) constructed using KCl at 25 °C.
●: Ordered state, ○: disordered state, ◐: coexistent state. Each curve shows the experimental (——) and the analytical coexistent/ordered boundary curve assuming the critical potential of V_R=1.5 kT (------).

Figure 5 represents the effect of the surface potential on the phase transition curve. The Sample-C used here has the surface charge density of 7 μC cm^{-2}. As can be seen in Fig. 5, the ordered state becomes much more favourable and the analytical boundary curve which can calculated using the value of ζ-potential for the ψ_0 in Eq. 2 and the critical V_R of 1.5 kT ergs, agreed

exactly with the whole range of electrolyte concentration in the experimental. From such an accordance with the analytical curve, it is apparent that ζ-potential is a good measure for the electrostatic repulsion of colloid particle and is allowed analytically to use ζ-potential instead of the Stern layer potential.

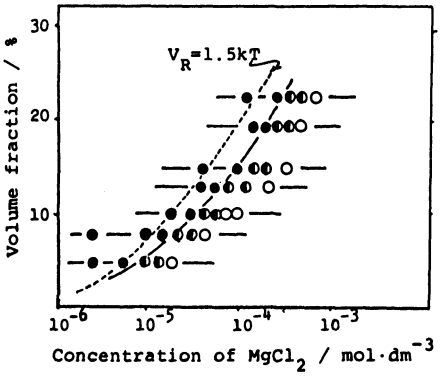

Fig. 6. Phase diagram of Sample-A ($2a$=1960 Å, σ_0= 0.9 μC cm^{-2}) constructed using $MgCl_2$ at 25 °C.
●: Ordered state, ○: disordered state, ◐: coexistent state. Each curve shows the experimental (——) and the analytical coexistent/ordered boundary curve assuming the critical potential of V_R=1.5 kT (------).

Figure 6 shows the phase diagram that was constructed using the electrolyte containing the divalent cation. In this coexistent/ordered boundary curve, there is some discrepancy on the whole electrolyte levels. It is probable that the divalent cation will be adsorbed preferentially on the latex surface as a Stern layer charge and the effective diffuse layer charge for the double layer repulsion would become much lower than the added electrolyte concentrations. According to Vanderhoff *et al.*,[12] Ba^{2+} ions adsorb extensively on the surface sulfonate groups of the latex particles and show an inflection point on the conductometric titration curve based on the strong fixation of Ba^{2+} ions. So, we can assume that the degree of deviation from the analytical curve reflects the extent of adsorbability of each counter ion in the Stern layer.

As a final parameter, the influence of temperature was studied. As can be seen in Fig. 7, over the whole electrolyte levels the ordered state becomes unfavorable at the high temperatures. It is because of this reason that the high temperature makes the double layer more diffusive. The precise analyses of temperature effects were carried out by taking into account the effects of medium dielectricity, ζ-potential and temperature itself. The results are compared to the experimental values on the two special salt concentrations. As can be seen in Fig. 8, the trends are the expected ones and qualitatively agree with the experimentals except for the results at the high temperatures of more than 40 °C, where the structural effects on desorption of the Stern layer ions exist, the desorbed ions would make unfavourable the ordered state and increase the volume fraction of the boundary.

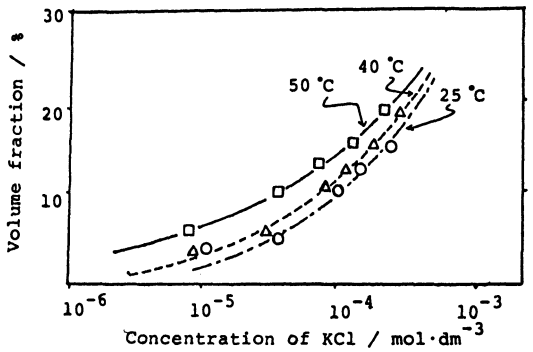

Fig. 7. Temperature dependence of the ordered/coexistent boundary curves of Sample-A constructed using KCl.
—○—: 25 °C, —△—: 40 °C, —□—: 50 °C.

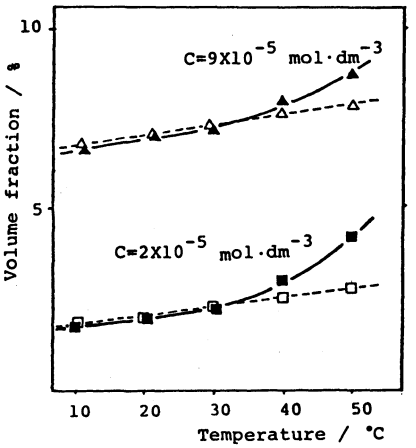

Fig. 8. Comparison of the temperature effect of phase boundary with the analytical one on the two KCl concentrations.
——: Experimental, ------: analytical.

At any rate, it can be concluded from the present work that the disordered/ordered phase transition in the concentrated latices is controlled largely by the electrostatic repulsion between the particles and the critical boundary condition of the coexistent/ordered state is reasonably explained by the DLVO electrostatic potential. Also, it is realized that the phase boundary analyses provides useful information on the nature of the electrical double layer and contributes as a new technique in the study of the electrical double layer.

The authors thank Prof. S. Hachisu, The University of Tsukuba, Japan, for his advice and cooperation.

References

1) W. Luck, M. Klier, and H. Wesslau, *Ber. Bunsenges. Phys. Chem.*, **67**, 75, 84 (1963).
2) C. J. Barnes, D. Y. C. Chan, D. H. Everett, and D. Yates, *J. Chem. Soc., Faraday Trans. I*, **74**, 136 (1978).
3) P. R. Krumrine and J. W. Vanderhoff, "Polymer Colloids 11," ed by R. M. Fitch, Plenum Press, New York (1980), p. 289.
4) B. J. Alder, W. G. Hoover, and D. A. Young, *J. Chem. Phys.*, **49**, 3688 (1968).
5) S. Hachisu, Y. Kobayashi, and A. Kose, *J. Colloid*

Interface Sci., **42**, 342 (1973).
6) E. J. W. Verwey and J. Th G. Overbeek, "Theory of the Stability of Lyophobic Colloids," Elsevier, Amsterdam (1948), p. 143.
7) A. Kotera, K. Furusawa, and Y. Takeda, *Kolloid Z. Z. Polym.*, **237**, 677 (1970).
8) H. J. Van den Hull and J. W. Vanderhoff, *J. Colloid Interface Sci.*, **28**, 336 (1968).
9) M. S. Juang and I. M. Krieger, *J. Polym. Sci.*, **14**, 2089 (1976).
10) P. H. Wiersema, A. L. Loeb, and J. T. G. Overbeek, *J. Colloid Interface Sci.*, **22**, 78 (1966).
11) K. Furusawa and N. Tomothu, *J. Colloid Interface Sci.*, in press.
12) J. W. Vanderhoff, H. J. Van den Hul, R. J. M. Tausk, and J. Th. G. Overbeek, "Clean Surface," ed by G. Goldfinger, Marcel Dekker, New York (1970), p. 15.

 © 1982 The Chemical Society of Japan Bull. Chem. Soc. Jpn., 55, 2341—2346 (1982)

Transient Species in Picosecond Pulse Radiolysis of Liquid Carbon Tetrachloride

Takashi SUMIYOSHI, Sadashi SAWAMURA, Yoshio KOSHIKAWA, and Meiseki KATAYAMA*

Department of Atomic Science and Nuclear Engineering, Hokkaido University, Sapporo 060

(Received January 5, 1982)

Formation and decay of transient species produced in pure liquid carbon tetrachloride by ionizing radiation were studied by using a stroboscopic pulse radiolysis technique in the time region 35—350 ps. Optical absorption spectra show two principal bands. One narrow band centered at 325 nm, which is formed during each fine structure electron pulse and decayed after pulse with $t_{1/2}=6.5$ ns, is attributed to CCl_4^+ cation. The other broad band centered at 470 nm built up after electron pulse is assigned to ($CCl_4^+ \cdot Cl^-$). A consideration on effects of cation scavengers on these bands furnishes a support for the above assignment.

Radiolysis of carbon tetrachloride in the condensed phase has been studied extensively over the past fifteen years. This is mainly because the comparatively high ionization potential of carbon tetrachloride ($I_p(CCl_4)=11.47$ eV) makes the carbon tetrachloride cation (CCl_4^+) quite suitable for transfer of a positive charge to a solute molecule. Optical spectra of a wide variety of solute cations have been obtained by the matrix isolation[1,2] and pulse radiolysis methods.[3,4] In pure CCl_4 and solutions of CCl_4 in alkane and argon matrices, many attempts have been made to establish the nature of primary species involved by means of low-temperature matrix isolation[1,5,6] and pulse radiolysis.[7-9] Both experiments revealed characteristic absorption bands with maxima located in two wavelength regions around 320—370 and 400—500 nm. However, the assignment of these absorption bands is not satisfactory as described below. Both the 367 nm band[5] observed in γ-radiolysis studies of CCl_4 in alkane hydrocarbons at 77 K and the 340 nm band[8] observed by pulse radiolysis on pure CCl_4 at 20 °C were assumed to be due to CCl_4^+. On the other hand, the band centered at 330 nm was assigned to dichlorocarbene radical (CCl_2) on the basis of an *ab initio* SCF CI study.[10] An earlier γ-radiolysis work with polycrystalline CCl_4 at 77 K revealed an absorption at 400 nm, which was assigned to positive hole.[1] Also, a spectrum of CCl_4, observed in an argon matrix at 25 K after argon discharge photoionization, exhibited a broad absorption at 425 nm,[6] which was assigned to CCl_4^+ cation since cation infrared absorptions in similar experiments exhibited the same photolysis behavior. On the contrary, both the broad absorption band centered around 470 nm,[5] observed in a γ-irradiated sample of CCl_4 in alkane hydrocarbons at 77 K, and the short-lived absorption band, observed at 480 nm[8] in an ns pulse radiolysis of CCl_4 at 20 °C, were assigned to a complex ($CCl_4^+ \cdot Cl^-$). A 500 nm band observed in a pulse irradiated liquid CCl_4 at −22 °C was assigned to another type of complex ($CCl_3^+ \cdot Cl^-$) on the basis of cation scavenger studies;[7,11] however, an *ab initio* configuration calculation[12] predicted no stability for any isolated contact ion-pairs between CCl_3^+ and Cl^-. We have constructed a stroboscopic pulse radiolysis instrument with time resolution of picoseconds and applied it to studying transient absorptions obtained in the pulse radiolysis of liquid CCl_4. By means of this instrument, it is possible to observe the formation and decay kinetics in the time region of 35—350 ps from the beginning of pulse.

The stroboscopic pulse radiolysis system was first designed and built by Bronskill *et al.*[13] Using 35 ns pulses from an S-band linear accelerator (LINAC) and a conventional photomultiplier optical detection system, they were able to study reactions of solvated electrons,[14] dry electrons,[15] and solvation of electrons in alcohols[16] in the time region of 20—350 ps. Jonah[17] applied this technique to a single picosecond pulse from an L-band LINAC[18] and was able to study similar aqueous systems in the time range 100 ps to as long as 3.5 ns after irradiation.[19,20] A distinct contribution of his method is that it has removed the upper limit on observation time (350 ps for an S-band LINAC and 770 ps for an L-band LINAC), which has inevitably accompanied experimental works using a train of fine structure pulses.

The present experiments were carried out with a 45 MeV S-band LINAC with no subharmonic prebuncher. Although the stroboscopic method using a train of electron pulses is essentially accompanied by a long time limit as mentioned above, it is capable of providing a good time resolution (≈20 ps) even with a conventional photomultiplier detection system.[13]

Experimental

Stroboscopic Pulse Radiolysis System. The stroboscopic pulse radiolysis system is shown in Fig. 1. The radiation source is 11 ns, 45 MeV electron pulse from the S-band LINAC installed in Hokkaido University. This 11 ns electron pulse consists actually of a train of fine structure pulses with time intervals of 350 ps. Simultaneous flashes of Čerenkov light are produced by these fine structure electron pulses in a 10 cm air path between the LINAC and a thin mirror. These light flashes are delayed 0.87 to 1.80 ns by a system of mirrors and are used as analyzing light flashes to observe absorption signals in irradiated samples. Čerenkov light has a continuous spectrum and is radiated outward from the path of 45 MeV electrons with an angle of 1.2°. A conical-shaped (axicon) lens was used to refract this conical beam of Čerenkov light into a pseudo-parallel beam.

In the stroboscopic pulse radiolysis system, three types of signals are required to obtain the absorption signal (S).[13] The electron beam and analyzing light are mechanically chopped to produce the three types of signals A, B, and C as illustrated in Fig. 2. Signal A is the sum of the analyzing light decreased in intensity by the absorption in the cell and the background Čerenkov light. Signal B consists of only the Čerenkov

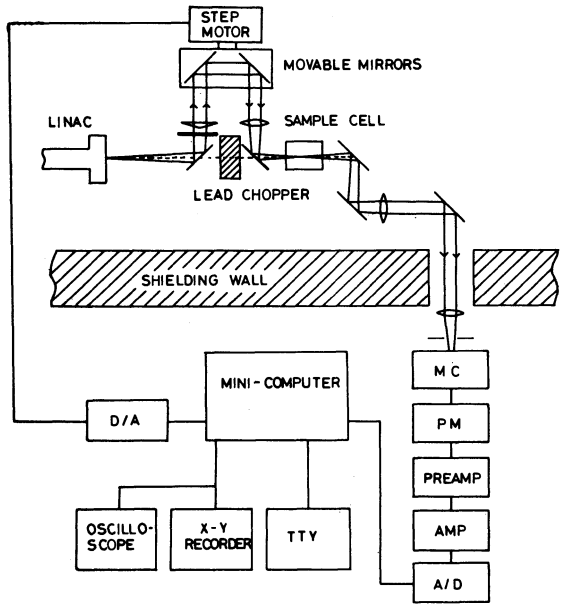

Fig. 1. Stroboscopic picosecond pulse radiolysis system. MC: Monochromator, PM: photomultiplier.

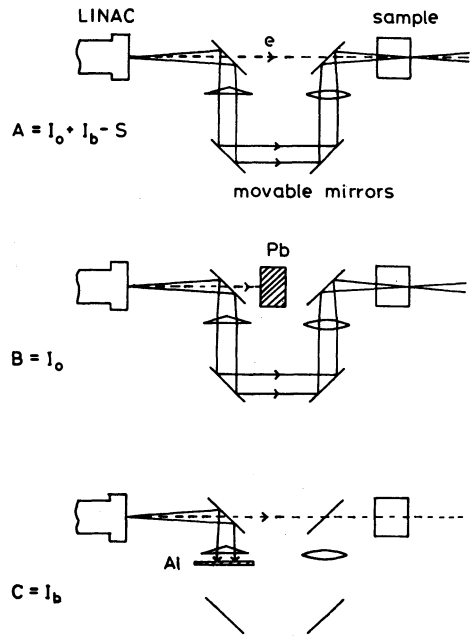

Fig. 2. Three types of Čerenkov light signals obtained by rotating the aluminum light chopper and the lead beam chopper.

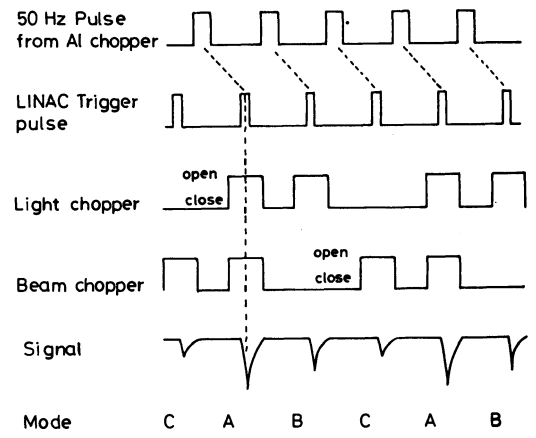

Fig. 3. Pulse timing sequence of the stroboscopic pulse radiolysis system.

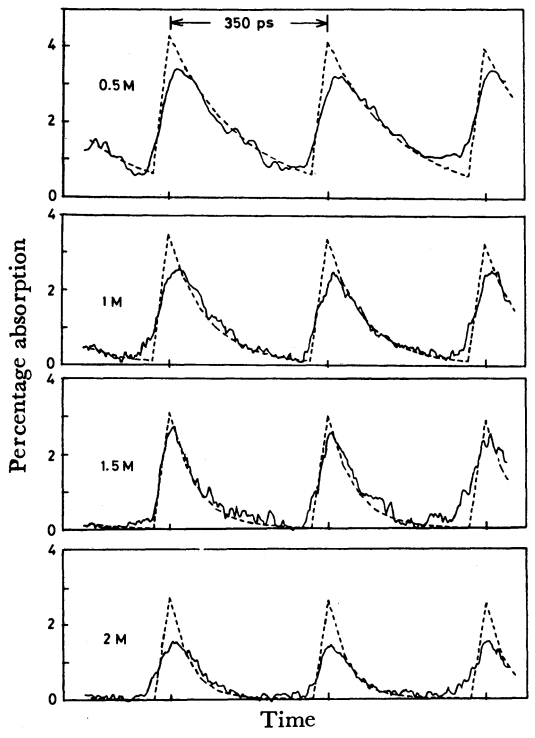

Fig. 4. Formation and decary of e^-_{aq} in 0.5—2 M $HClO_4$ (1 M = 1 mol dm^{-3}) solutions as observed at 633 nm. The dashed lines are simulated traces.

analyzing light, and signal C consists of the background Čerenkov lights produced in and near the sample cell. The absorption signal can be obtained by addition and subtraction of these signals, *i.e.*,

$$S = B + C - A,$$

and the percent absorption is calculated as

$$(S/B) \times 100\ \%.$$

These three signals are produced sequentially at the rate of 50 Hz with line-locking to minimize 50 Hz ripple effects in the LINAC and detection system.

Detection System. The three types of light pulses are detected by a system which consists of a monochromator (Bausch & Lomb), a photomultiplier (Hamamatsu TV Co., R446UR), a preamplifier, an amplifier (ORTEC 451), and an A/D converter (NAIG D-161). The photomultiplier was used in a five-stage configuration that had a linear response of up to 4 mA with a rise time of less than 3 ns. The linearity of the detection system was carefully checked by using pulses from a pulse generator and actual, well-known absorption signals, as will be described in the following section. The output signal from the A/D converter is fed into an on-line minicomputer (TACC 1200M) and stored before arrival of the next signal. Both the averaging of signals and the operation of the movable mirrors in the optical delay system are performed by a minicomputer. The timing sequence for synchronization of pulses and choppers is shown in Fig. 3.

Linearity and Time Resolution. Observation on the formation and decay of e^-_{aq} and Br_2^- was carried out as a critical check on the performance of the stroboscopic pulse radiolysis system. Linearity was tested by use of the baseline and the first-order decay of e^-_{aq} in concentrated $HClO_4$ solutions. Results obtained at 633 nm in solutions of 0.5—2 M $HClO_4$ are shown in Fig. 4. The baseline approaches a near-zero level with increasing concentration of H^+_{aq} as expected. The dashed lines in Fig. 4 are results from a computer simulation for the first order decay of e^-_{aq}. In these calculations it is assumed that a value of ε_{633nm} is 1.44×10^4 M^{-1} cm^{-1} for e^-_{aq},[21] and the decay of e^-_{aq} during the electron pulse is taken into account. Agreement on the decay traces is quite satisfactory. The rate constant was calculated to be $(1.2\pm0.06)\times10^{10}$ M^{-1} s^{-1}, which is in good agreement with the reported value of $(1.2\pm0.2)\times10^{10}$ M^{-1} s^{-1} over the range of 0.5—5 M H^+_{aq} by Bronskill *et al.*[22] A further test on the linearity of the detection system was carried out in the ultraviolet region. Figure 5 shows kinetic traces for the formation of Br_2^- at 360 nm in 0.5—2 M NaBr aqueous solutions. Both a fast and a slow component are shown, along with the contribution of the fast component, to increase with increasing NaBr concentration. These results are quite similar to those reported by Hunt *et al.*,[23] who suggested that the fast component is due to reactions of dry hole (H_2O^+) and Br^-:

$$H_2O^+ + Br^- \longrightarrow Br + H_2O,$$

followed by reaction

$$Br + Br^- \longrightarrow Br_2^-.$$

The observed rise time (10—90%) for the formation of hydrated electron in Fig. 4 is about 35 ps. Since the formation time of e^-_{aq} has been estimated to be less than 10 ps,[22] this rise time is attributed mainly to the following two factors: One is the width of fine structure electron pulses. The width of the fine structure pulse observed with a streak camera system (Hamamatsu TV Co., HTV-C979X) having a rise time of 10 ps is approximately 39 ps (FWHM), which is longer than the observed rise time of e^-_{aq}. It is thus thought that the real pulse width is less than 30 ps. The other factor is the desynchronization of pulses, which is due to different velocities of the high energy electrons and analyzing light in water. The 45 MeV electron pulse moves with a velocity close to that of light *in vacuo*, while the analyzing light moves more slowly with a velocity of c/n, where n is the index of refraction of light in solution and c is the velocity of light *in vacuo*. The desynchronization of pulses is given by

$$\Delta t = (n-1)l/c,$$

where l is the length of cell. The time difference of a 2 cm path in water is 21 ps. A shorter optical path is desirable for faster detection, though it will possibly decrease the absorption signal.

Chemicals and Flow System. The chemicals used were NaBr, 60% $HClO_4$, cyclohexane, and CCl_4 (Wako Junyaku), and all were used without further purification since on the experimental time scale, any small amounts of impurities would have a negligible effect. Aqueous solutions were prepared with triply distilled water.

Experiments were carried out in a 2 cm sample cell which connects to a 1 dm^3 sample reservoir and a pump. To prevent buildup of heat and radiolytic products, the sample was circulated at 160 ml/min. No attempt was made to degas the sample solution since on the experimental time scale, O_2 is known to have no effect on experiment results in aqueous solutions[22] or in pure CCl_4.[8] All experiments were carried out at room temperature 15—20 °C.

Results

Kinetic Traces. Figure 6 shows typical kinetic absorption traces in pure CCl_4 at 320, 350, and 480 nm. These traces were obtained by averaging more than 30 runs including those conducted on different days and by applying correction for variation in irradiation doses. There appear to be at least two different main formation processes of transient species. The absorption at 320 nm grows only during the irradiation of fine structure electron pulses and decays after the pulse, while the absorption at 480 nm grows after the pulse. The trace at 350 nm shows a rather fast buildup and a slow one, and sould consist of a set of contributions from the two

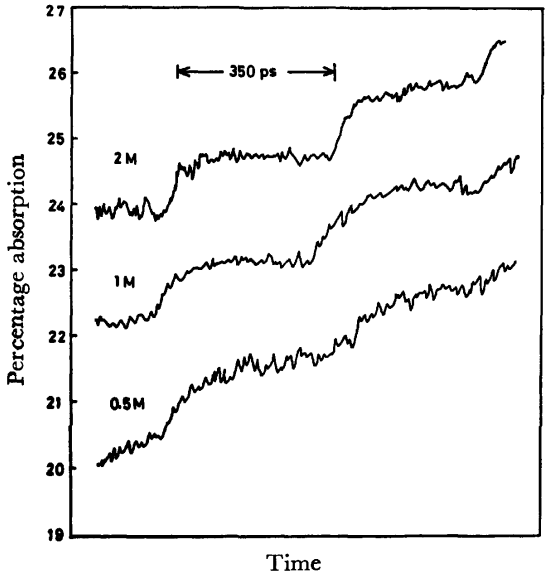

Fig. 5. Formation of the absorption signal of Br_2^- in 0.5—2 M NaBr at 360 nm.

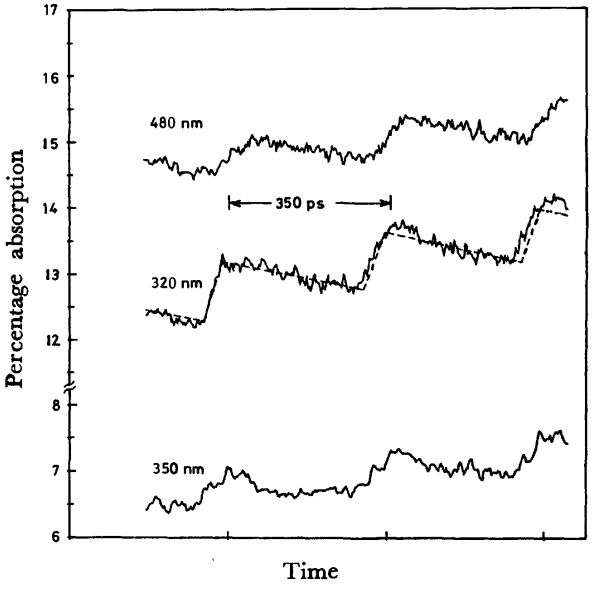

Fig. 6. Kinetic traces of the formation of the transient species observed at 320, 350, and 480 nm in CCl_4. The dashed line is a simulated trace with $t_{1/2}$=6.5 ns.

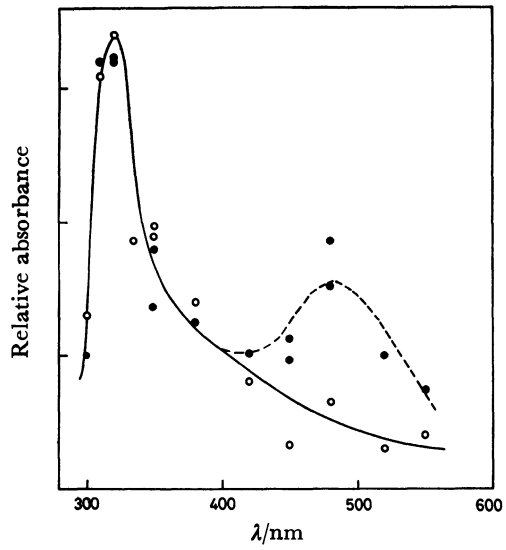

Fig. 7. Spectra of transient species in CCl_4.
○: Immediately after pulse, ●: 100 ps after pulse.

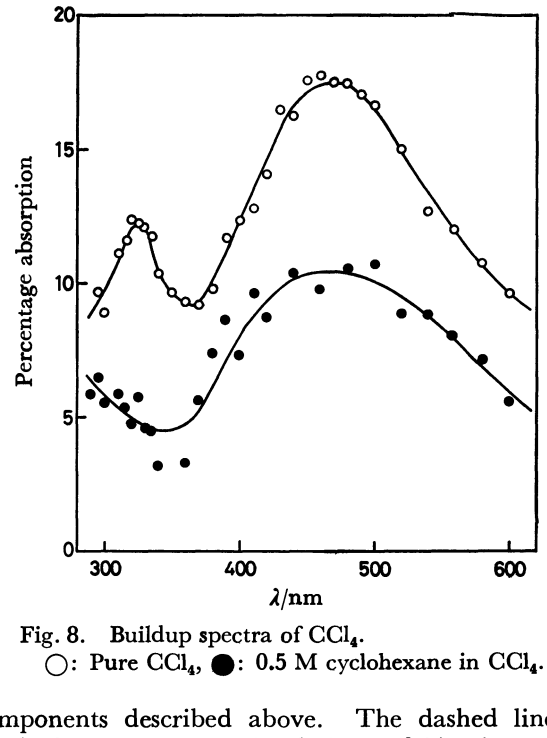

Fig. 8. Buildup spectra of CCl_4.
○: Pure CCl_4, ●: 0.5 M cyclohexane in CCl_4.

components described above. The dashed line is a result from computer simulations of kinetic traces at 320 nm. The simulations were done assuming a first-order decay and a contribution from only one transient species. The best fitted curve was obtained when the half-life time and $G\times\varepsilon$ were assumed to be 6.5 ns and 25500 M^{-1} cm^{-1}, respectively.

Spectra. Figure 7 shows absorption spectra obtained immediately after pulse (17 ps from the middle of pulse) and 100 ps after the pulse. Only the narrow band centered around 320 nm was observed immediately after pulse. In addition, at 100 ps a broad band was observed around 480 nm. Since none of the transient species observed decays considerably within 350 ps, the absorption signal produced by the fine structure electron pulse is superimposed by the background absorption

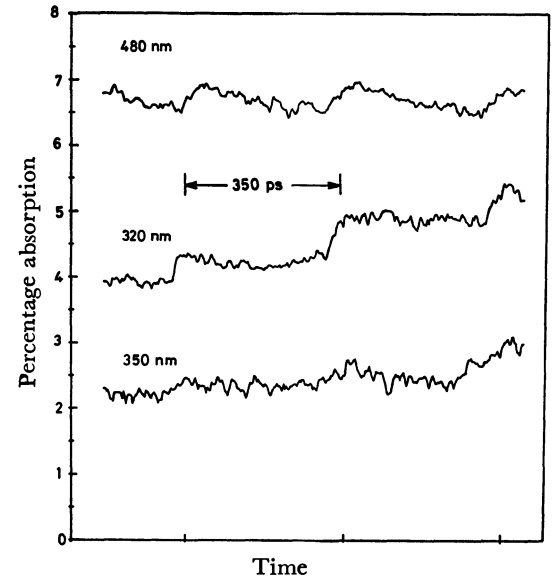

Fig. 9. Kinetic traces of the formation of the transient species observed at 320, 350, and 480 nm in 0.5 M cyclohexane in CCl_4.

shown in Fig. 6. The background absorption spectrum obtained by fixing the movable mirrors at the position nearest to the beam is shown in Fig. 8. In this spectrum two absorption bands are clearly shown and the broad band centered at 470 nm is more intense than that at 325 nm, in contrast to the spectrum at 100 ps after pulse in Fig. 7. Since in the stroboscopic method it is essential that the analyzing light is absorbed by transient species of different ages, the slower decaying species will contribute more to the background absorption. The difference between the spectra in Figs. 7 and 8 is that the former shows absorption by a fine structure pulse and that the latter shows contributions of both absorption intensity and decay rate.

Effect of Cation Scavenger. Since cyclohexane has a lower ionization potential (9.88 eV) than CCl_4, it was used as a cation scavenger.[7,8] Figure 9 shows kinetic absorption traces observed at 320, 350, and 480 nm in 0.5 M cyclohexane. Both the step height of absorption signals (the maximum absorption signal by a fine structure pulse) and the buildup absorption signal decrease to less than half of those in pure CCl_4 in Fig. 6. The buildup absorption spectrum is compared with that of pure CCl_4 in Fig. 7. The band centered at 320 nm observed in pure CCl_4 could not be observed any more, and instead the band peaked at $<$290 nm began to be observed. The latter species does not show fast decay as clearly seen in Fig. 9. From these results it is apparent that the species, having given the band at 325 nm, was scavenged more effectively than the one for 470 nm.

Discussion

Identification of the 325 nm Band. In th epresent study, observations showed that radiolysis of liquid CCl_4 initially produces a sharp band centered at 325 nm as seen in Fig. 7. This band is reduced to almost zero by addition of 0.5 M cyclohexane, which is known as a

scavenger for cationic species. The residual species which peaks below 290 nm does not show any decay. It was not clear whether this species originated from CCl_4 or from cyclohexane in this experiment. The 325 nm band can be assigned to a primary cation formed in the initial act of ionization for CCl_4. This assignment is consistent with previous works in which ns pulse radiolysis and low temperature matrix were used. Mehnert *et al.*[8] observed a transient absorption which peaked at 340 nm in pure liquid CCl_4 by ns pulse radiolysis and assigned it to CCl_4^+ cation. They determined rate constants of charge transfer reaction for 17 solutes from observations on the decay of cation. Ha *et al.*[10] carried out *ab initio* configuration calculations on electronic states of the CCl_2 radical and assigned a 330 nm band obtained by a pulse radiolysis experiment to it. Their assignment is based on a kinetic behavior which indicates that the band can be due to neither a transient ion nor any of the simple radicals of Cl and CCl_3; their experimental data have not yet been published. Also, in low temperature matrix studies, the CCl_4^+ cation was observed at 400 nm in a γ-irradiated polycrystalline CCl_4 at 77 K,[1] at 367 nm in a γ-irradiated CCl_4 in alkane hydrocarbons at 77 K,[5] and at 425 nm in an argon discharge photoionization during condensation at 25 K.[6] This variation in band peaks of CCl_4^+ cation seems to depend on the nature of matrix. For example, glassy solutions of CCl_4 in alkane hydrocarbons give a band maximum similar to that obtained in pulse radiolysis experiments. It should be pointed out that in an argon matrix, CCl_4^+ has been attributed to assymmetric $Cl_2CCl_2^+$ species by Prochaska and Andrews[24] through infrared studies. They suggested that one set of two carbon-chlorine bonds involves normal electron pair bonding, whereas the other set involves electron-deficient bonding with presumably delocalized electrons around the cation center.

Identification of the 470 nm Band. The present experiments revealed that the broad absorption band at 470 nm builds up after the electron pulse and is less sensitive to the cation scavenger than the species which peaked at 325 nm. These results suggest that the corresponding species should be an electrically neutral intermediate produced by reaction of primary radiation products, though more detailed investigations are needed before a precise conclusion is reached.

Mehnert *et al.*[8] observed a similar broad band centered at 480 nm by ns pulse radiolysis at 22 °C and assigned it to a complex ($CCl_4^+ \cdot Cl^-$). Also Bühler and Hurni[7] observed by ns pulse radiolysis a transient spectrum which peaked at 500 nm in CCl_4 at -22 °C and decayed with a half-life time of 33 ns. They studied effects of cation scavengers on this band and found that, though reducing the pulse end absorbance of the 500 nm band, they have no effect on the life time. They concluded that the CCl_4^+ cation must be a precursor to the 500 nm species and that the 500 nm species behaves like both cation and neutral species. They assigned the 500 nm band to another type of complex ($CCl_3^+ \cdot Cl^-$) on the assumption of a very short life time of CCl_4^+ cation. Since no mass spectrum of CCl_4^+ has been observed,[25] CCl_4^+ is considered to eliminate Cl atom readily in the gas phase. In liquid phases, however, stabilization of CCl_4^+ by surrounding molecules can be expected.[5,6] Considering the life time of 6.5 ns for CCl_4^+ observed in this work, it is strongly suggested that the 470 nm band is due to rather a neutral complex ($CCl_4^+ \cdot Cl^-$).

Louwrier and Hamill[5] observed an isothermal decay of 367 nm absorption and a growth of 470 nm absorption in γ-irradiation studies on solutions of CCl_4 in alkane hydrocarbons at 77 K and attributed these bands to CCl_4^+ and $CCl_4^+ \cdot Cl^-$), respectively. Their observations are in good agreement with the present work.

In conclusion, the present picosecond pulse radiolysis studies have provided direct observations on the initial process in irradiated CCl_4 as follows, provided that the absorption at 325 nm can be assigned to CCl_4^+:

$$CCl_4 \rightsquigarrow CCl_4^+(325\text{ nm}) + e^-, \quad (1)$$

and subsequent fomation of ion pairs

$$CCl_4 + e^- \longrightarrow CCl_3 + Cl^-, \quad (2)$$

$$CCl_4^+ + Cl^- \longrightarrow [CCl_4^+ \cdot Cl^-]\ (470\text{ nm}). \quad (3)$$

The authors wish to acknowledge Dr. John W. Hunt for his helpful discussions on the construction of the stroboscopic pulse radiolysis system. The authors also wish to acknowledge Dr. Takeaki Enoto and Messrs. Hiroaki Tanida and Koichi Sato for their help in stabilizing and operating the LINAC. Thanks are due to Messrs. Kaichi Takahashi and Keiji Kuriyama and Dr. Yoshikazu Kondo for their experimental assistance and to Dr. Masako Tanaka for her helpful advices in the early stage of the present investigation. The cooperation through designing and manufacturing the instrument by Shimadzu Seisakusho, Ltd., especially by Engineer Mr. Tadashi Kōtani, and the financial support by the Mitsubishi Foundation are gratefully acknowledged by one of the present authors (M. K.).

References

1) T. Shida and W. H. Hamill, *J. Chem. Phys.*, **44**, 2369 (1966).
2) T. Shida and W. H. Hamill, *J. Chem. Phys.*, **44**, 2375 (1966).
3) H. D. Burrows, D. Greatorex, and T. J. Kemp, *J. Phys. Chem.*, **76**, 20 (1972).
4) C. Capellos and A. O. Allen, *J. Phys. Chem.*, **73**, 3264 (1969).
5) P. W. F. Louwrier and W. H. Hamill, *J. Phys. Chem.*, **73**, 1702 (1969).
6) L. Andrews and F. T. Prochaska, *J. Phys. Chem.*, **83**, 368 (1979).
7) R. E. Bühler and B. Hurni, *Helv. Chim. Acta*, **61**, 90 (1978).
8) R. Mehnert, O. Brede, J. Bös, and W. Naumann, *Ber. Bunsenges. Phys. Chem.*, **83**, 992 (1979).
9) J. P. Suwalski, *Radiat. Phys. Chem.*, **17**, 393 (1981).
10) T. K. Ha, H.-U. Gremlich, and R. E. Bühler, *Chem. Phys. Lett.*, **65**, 16 (1979).
11) B. Hurni and R. E. Bühler, *Radiat. Phys. Chem.*, **15**, 231 (1980).
12) H.-U. Gremlich, T. K. Ha, G. Zumofen, and R. E. Bühler, *J. Phys. Chem.*, **85**, 1336 (1981).
13) M. J. Bronskill, W. B. Taylor, R. K. Wolff, and J. W.

Hunt, *Rev. Sci. Instrum.*, **41**, 333 (1970).
14) R. K. Wolff, M. J. Bronskill, and J. W. Hunt, *J. Chem. Phys.*, **53**, 4211 (1970).
15) K. Y. Lam and J. W. Hunt, *Int. J. Radiat. Phys. Chem.*, **7**, 317 (1975).
16) W. J. Chase and J. W. Hunt, *J. Phys. Chem.*, **79**, 2835 (1975).
17) C. D. Jonah, *Rev. Sci. Instrum.*, **46**, 62 (1975).
18) J. W. Hunt, R. K. Wolff, M. J. Bronskill, C. D. Jonah, E. J. Hart, and M. S. Matheson, *J. Phys. Chem.*, **77**, 425 (1975).
19) C. F. Jonah, M. S. Matheson, J. R. Miller, and E. J. Hart, *J. Phys. Chem.*, **80**, 1267 (1976).
20) C. D. Jonah, J. R. Miller, and M. S. Matheson, *J. Phys. Chem.*, **81**, 1618 (1977).
21) E. M. Fielden and E. J. Hart, *Radiat. Res.*, **32**, 564 (1967).
22) M. J. Bronskill, R. K. Wolff, and J. W. Hunt, *J. Chem. Phys.*, **53**, 4201 (1970).
23) J. W. Hunt, R. K. Wolff, and S. G. Chenery, "Fast Processes in Radiation Chemistry and Biology," ed by G. E. Adams, E.M. Fielden, and B. D. Michael, Wiley and Institute of Physics, London (1975), p. 109.
24) F. T. Prochaska and L. Andrews, *J. Chem. Phys.*, **67**, 1091 (1977).
25) A. S. Werner, N. P. Tsai, and T. Baer, *J. Chem. Phys.*, **60**, 3650 (1974).

 © 1982 The Chemical Society of Japan Bull. Chem. Soc. Jpn., 55, 2347—2351 (1982)

Pulse Radiolysis Studies on Methyl Methylthiomethyl Sulfoxide in Aqueous Solutions

Takashi SUMIYOSHI, Nobuyuki MIURA, Masayuki AIKAWA,† and Meiseki KATAYAMA*

Department of Atomic Science and Nuclear Engineering, Hokkaido University, Sapporo 060

†*College of General Education, Hokkai Gakuen University, Asahimachi Toyohiraku, Sapporo 062*

(Received January 25, 1982)

Reaction mechanisms between methyl methylthiomethyl sulfoxide (MTMSO) and hydrated electron (e^-_{aq}) or hydroxyl radical (OH· radical) have been studied in aqueous solutions with various pH values by means of pulse radiolysis technique. The acid and basic components of equilibrium

$$CH_3SCH_2\overset{\overset{OH}{|}}{S}CH_3 \rightleftharpoons CH_3SCH_2\overset{\overset{O}{|}}{S}CH_3 + H^+$$
$$(-)$$
$$(I)$$

and

$$CH_3\overset{\overset{OH}{|}}{S}CH_2\overset{\overset{O}{\downarrow}}{S}CH_3 \rightleftharpoons CH_3\overset{\overset{O}{|}}{S}CH_2\overset{\overset{O}{\downarrow}}{S}CH_3 + H^+$$
$$(-) \quad (II)$$

are formed for the reaction of $e^-_{aq} + CH_3SCH_2SOCH_3$ and OH· + $CH_3SCH_2SOCH_3$, respectively. The pK_a values of the respective equilibrium are 10 and 9. The anion (I) and (II) have absorption maxima at 375 nm and 360 nm, respectively. The sulfinic acid $CH_3SCH_2SO_2^-$ is also formed in the reaction of $CH_3SCH_2SOCH_3$+OH·. The rate constants have been determined to be $k(e^-_{aq} + \text{MTMSO}) = 1.3 \times 10^8$ M^{-1} s^{-1} and k (OH· + MTMSO) = 3.1×10^9 M^{-1} s^{-1} (1 M = 1 mol dm^{-3}). Relative reactivities of OH· radical with thio-methyl bond and sulfinyl group are also discussed.

Two organic bonds involving sulfur atoms, thiomethyl bond (sulfide S–C bond) and sulfinyl-methyl bond (sulfoxide S–C bond), are known to change reactivities with pH of the solutions. Pulse radiolysis method has provided one of the most successful approaches to investigate dynamics of the compounds. Meissner, Henglein and Beck have reported the study on the primary processes for the irradiated aqueous solutions of dimethyl sulfide and dimethyl sulfoxide.[1] They suggested that the formation of the radical anion $CH_3SOCH_3^-$· and the radical cation complex $(CH_3SCH_3)_2^+$· for the reaction of the OH· radical with CH_3SCH_3, and that the formation of the radical anion $CH_3SOCH_3^-$· in the reaction of the hydrated electron with CH_3SOCH_3. The formation of sulfinic acid RSO_2^- for the reaction of the OH· radical with sulfoxide (R_2SO) have been found by Veltwisch, Janata and Asmus from a pulse radiolysis study with the conductivity detection method.[2] Although primary processes of the individual compounds have been fairly well studied, relative reactivities of the sulfide S–C bond and sulfinyl group with OH· radical are not known.

Methyl methylthiomethyl sulfoxide ($CH_3SOCH_2SCH_3$; MTMSO) possessing the sulfide S–C bond and the sulfinyl group within one molecule is expected to show interesting reactivities. In the present study we propose the primary processes for the reaction of e^-_{aq}+MTMSO and OH·+MTMSO in aqueous solution in comparison with the dimethyl sulfide and the dimethyl sulfoxide. Spectral analysis of the transient absorption in the UV-Vis regions and an electrical conductivity analysis after pulse irradiation were two techniques to identify the transient species produced. Experimental results of reaction yields and reaction rate constants give information on the relative reactivities between the sulfide S–C bond and the sulfinyl group with OH· radical.

Experimental

MTMSO was purchased from Nisso LTD. and used without further purification. Solutions were prepared by dissolving *t*-BuOH, $HClO_4$, NaOH, and $NaClO_4$ in triply distilled water, and the pH values of the solutions were adjusted by adding perchloric acid or sodium hydroxide. For studies on the reaction of MTMSO with e^-_{aq}, solutions were bubbled with argon to remove oxygen. On the other hand, solutions for studies on the reaction with OH· radical were bubbled with dinitrogen monoxide in order to convert the e^-_{aq} into OH· radicals *via* the following reaction:

$$N_2O + e^-_{aq} \longrightarrow OH\cdot + OH^- + N_2. \quad (1)$$

Pulse radiolysis measurements were performed with electron pulses (45 MeV) from a S-band linear accelerator (Mitsubishi) installed at Hokkaido University.[3] The half-width of the electron pulse used was 20 ns and dose per pulse was up to 14 krad. The optical detection system was basically the same as that designed by Hunt and Thomas.[4] Analyzing light from Xe arc lamp (1 kW, Wako Denki) was chopped by a rotating disk at 25 Hz and sent to a sample cell. The absorption signal, after passing through the monochromator (Shimadzu-Bausch and Lomb, 200 mm, f/3.5), was detected by a photomultiplier (Hamamatsu T. V. R446UR) system. The output signal was displayed on to an oscilloscope (National VP5405A).

The sample cell for the D–C conductivity analysis has two rectangular electrodes (3×5 mm^2), which were set 5 mm apart. By the conductivity method, charged species being produced after pulse irradiation are monitored *via* a variation of the signal voltage. The relation between the change in the concentration of i-th charged species ΔC_i and a signal voltage on the oscilloscope ΔV_s as a result of the formation or

disappearance of the species in a solution is given by the following equation:[5]

$$\Delta V_s = \frac{VR}{k\,10^3} \sum \Delta C_i |Z_i| \Lambda_i, \qquad (2)$$

where V, R, and k indicate a voltage between two electrodes in the irradiation cell, a resistance and a cell constant (in cm^{-1}), respectively. $|Z_i|$ and Λ_i represent the number of charges (1 for one electron oxidation) and the corresponding conductivities (in $\Omega^{-1}\,cm^2$) for i-th charged species, respectively.

If only one acid species (XH) is produced by irradiation and G value of the species is given by G_{XH} which is directly proportional to ΔC_{XH}, then Eq. 2 is rewritten as

$$\Delta V_s \times K = G_{XH} \times (\Lambda_{X^-} + \Lambda_{H^+}), \qquad (3)$$

here K denotes certain constant determined experimentally.

Results and Discussion

Reaction of e^-_{aq} with MTMSO; Formation of Radical Anion. MTMSO aqueous solutions containing 1 M *t*-BuOH as a hydroxyl radical scavenger were irradiated to investigate the reaction mechanism of e^-_{aq} with MTMSO.

Figure 1 shows a representative decay curve for the transient absorption of e^-_{aq} which are produced after the pulse irradiation of the MTMSO aqueous solution. The decay curve fit a simple first-order kinetics as is shown in the figure. The pseudo-first-order rate for the absorption of the hydrated electron was plotted as a function of MTMSO concentration and the rate constant for the reaction e^-_{aq}+MTMSO was determined from

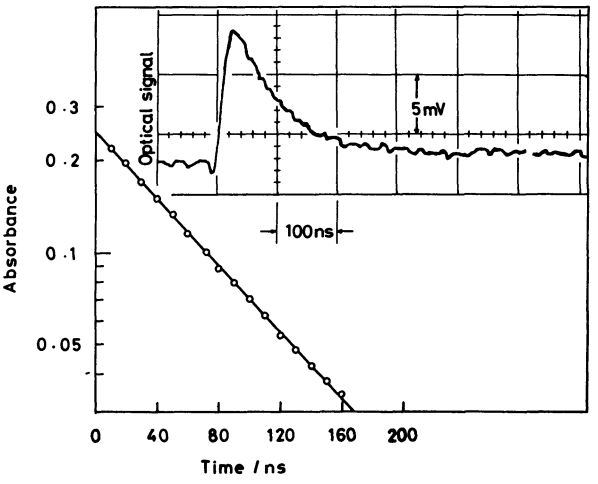

Fig. 1. First-order kinetic plot of log Abs. (e^-_{aq}) against time after the pulse irradiation of MTMSO aqueous solution ([MTMSO]=0.1 M, pH 7.1, monitoring wavelength; 600 nm). The solution was saturated with argon gas prior to the irradiation. Inset: an oscillogram trace of the decay curve for the absorption of e^-_{aq}. A change of 5 mV in the vertical axis corresponds to 22% transmittance.

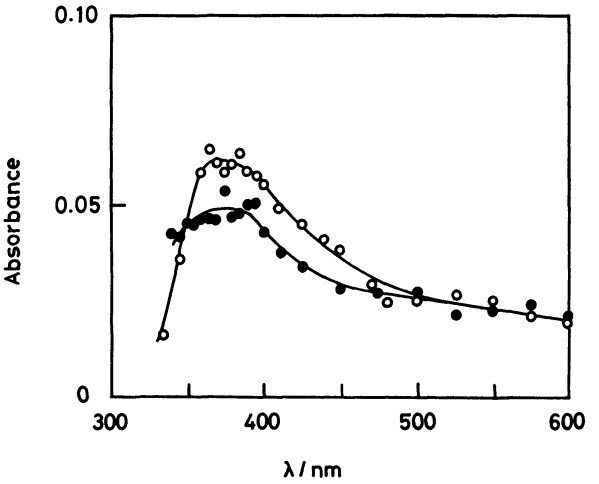

Fig. 2. Transient absorption spectra 2 μs after the pulse irradiation of MTMSO aqueous solutions ([MTMSO] =0.05 M, [*t*-BuOH]=1 M). Solutions were saturated with argon gas prior to the irradiation. ●: pH 6, ○: pH 10.

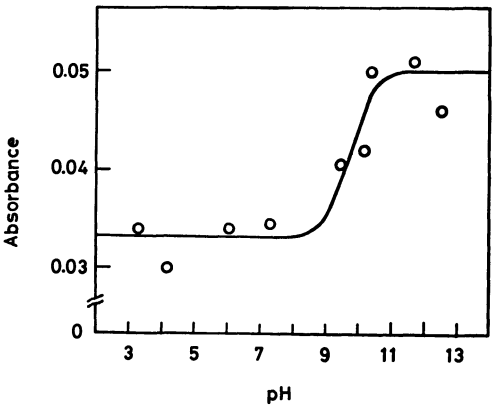

Fig. 3. Optical densities at 375 nm as a function of pH, 2 μs after the pulse. MTMSO aqueous solutions ([MTMSO]=0.05 M, [*t*-BuOH]=1 M) were saturated with argon gas prior to the irradiation.

the slope of the linear plot to be $(1.30\pm0.08)\times10^8\ M^{-1}\ s^{-1}$. The rate constant values thus obtained are summarized in Table 1 as a function of pH values. The values were constant with respect to the pH (from pH 6 to 11) of the solutions.

Figure 2 shows the transient absorption spectra observed for aqueous solutions containing MTMSO (0.05 M, pH 6 and 10) at 2 μs after the pulse where the absorption of e^-_{aq} is sufficiently diminished. The transient absorption spectrum thus obtained has a broad band with a λ_{max}=375 nm.

Figure 3 shows the change in the absorbance of the transients at λ=375 nm with changing pH values of MTMSO solutions. The intensity of the transient absorption increases sharply at pH 10. It has been

Table 1. Reaction rate constants of hydrated electron with MTMSO in aqueous solutions as a function of pH

pH	6.1	7.1	9.0	10.4	11.0
$k(e^-_{aq}+MTMSO)/M^{-1}\,s^{-1}$	1.30×10^8	1.38×10^8	1.28×10^8	1.30×10^8	1.23×10^8

reported for the reaction of $e^-_{aq}+CH_3SOCH_3$ that the following equilibrium between both species of acid and its conjugated basic form should be taken into consideration:[1]

$$CH_3SCH_3 + e^-_{aq} \longrightarrow CH_3\overset{\cdot}{S}CH_3 \underset{pK_a = 10.2}{\overset{+H^+}{\rightleftharpoons}} CH_3\overset{\cdot}{S}CH_3. \quad (4)$$
(O; O (−); OH)

The pK_a value of the equilibrium (4) is 10.2. From our observation of the pH dependence for the transients and by analogy with the reaction scheme (4), we may reasonably assign the transients formed in the reaction $e^-_{aq}+MTMSO$ to the radical anion which is in the following equilibrium:

$$CH_3SCH_2SCH_3 + e^-_{aq} \longrightarrow CH_3\overset{\cdot}{S}CH_2SCH_3$$
(O; O (−))

$$\underset{pK_a = 10}{\overset{+H^+}{\rightleftharpoons}} CH_3\overset{\cdot}{S}CH_2SCH_3. \quad (5)$$
(OH)

Thus, from Fig. 3 the pK_a value of the equilibrium (5) is determined to be 10.

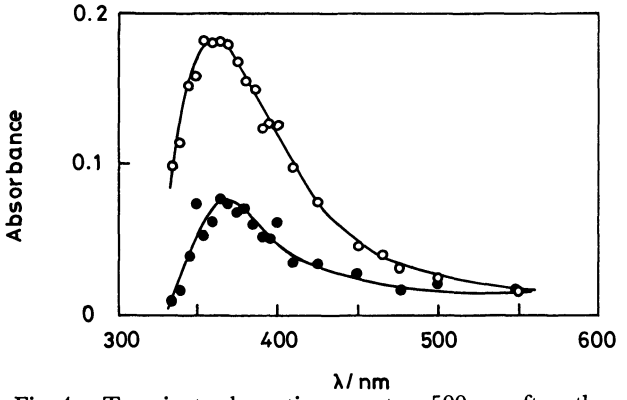

Fig. 4. Transient absorption spectra 500 ns after the pulse irradiation of MTMSO aqueous solutions ([MTMSO]=0.05 M). Solutions were saturated with N_2O gas prior to the irradiation. ●: pH 6, ○: pH 10.

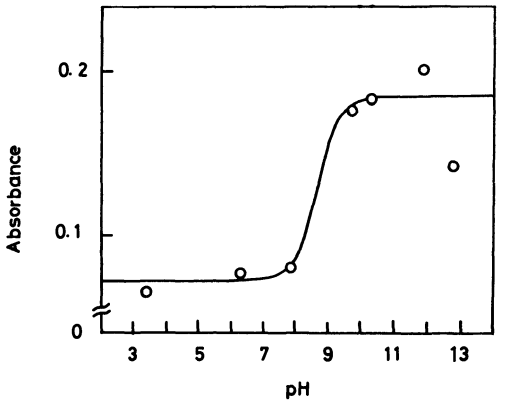

Fig. 5. Optical densities at 360 nm as a function of pH, 500 ns after the pulse. MTMSO aqueous solutions ([MTMSO]=0.05 M) were saturated with N_2O gas prior to the irradiation.

Reaction of OH· Radical with MTMSO. *a) Sulfide and OH· Radical*: Pulse radiolysis experiments of N_2O saturated MTMSO solutions (0.05 M, pH 6 to 10) were carried out in order to test the reaction mechanism of MTMSO with OH· radical. For N_2O saturated MTMSO solutions, no transient absorption being assignable to hydrated electron was observed. Figure 4 shows the transient absorption spectra observed at 500 ns after the pulse. Figure 5 shows the pH dependence of MTMSO aqueous solutions on the intensity of the transient absorption at 360 nm. The absorption intensity increases sharply at pH 9. The pH dependence indicates that the transients is in an acid-base equilibrium whose pK_a value is equal to 9. It has been reported that a radical anion $CH_3SOCH_3^-\cdot$ is formed in the reaction of the OH· radical with dimethyl sulfide, and that the radical anion is in an acid-base equilibrium:[1]

$$CH_3SCH_3 + OH\cdot \longrightarrow CH_3\overset{\cdot}{S}CH_3 \underset{pK_a = 10.2}{\overset{-H^+}{\rightleftharpoons}} CH_3\overset{\cdot}{S}CH_3. \quad (6)$$
(OH; O (−) 350 nm)

It is also known that the radical anion ($CH_3SOCH_3^-\cdot$) has the absorption with $\lambda_{max}=350$ nm.[1]

These facts suggest that the transient absorption spectrum observed here originates from the radical anion ($CH_3SOCH_2SOCH_3^-\cdot$) which is formed in the reaction between the OH· radical and sulfur atom of the thiomethyl bond of MTMSO. The radical anion is in an acid-base equilibrium with the $pK_a=9$:

$$CH_3SCH_2SCH_3 + OH\cdot \longrightarrow CH_3SCH_2\overset{\cdot}{S}CH_3$$
(O; O OH)

$$\underset{pK_a = 9}{\overset{-H^+}{\rightleftharpoons}} CH_3SCH_2\overset{\cdot}{S}CH_3. \quad (7)$$
(O O (−) 360 nm)

b) Sulfoxide and OH· Radical: It is probable that the OH· radical attacks not only the sulfide S–C bond but also the sulfoxide S–C bond of MTMSO. The following route has been also suggested for the reaction between OH· radical and R_2SO:[2]

$$RSR + OH\cdot \longrightarrow R\cdot + RSO_2^-/H^+. \quad (8)$$
(O)

By the analogy with Reaction 8, the sulfinic acid ($CH_3SCH_2SO_2^-$) is expected to be formed for the case of MTMSO, when the OH· radical attacks the sulfoxide S–C bond of MTMSO:

$$CH_3SCH_2SCH_3 + OH\cdot$$
(O)

$$\longrightarrow CH_3\cdot + CH_3SCH_2SO_2^-/H^+. \quad (9)$$

Detection of ionic species for the acidic solution of MTMSO will give a proof for the formation of the sulfinic acid. The conductivity detection method combined with the pulse radiolysis experiment was adopted for the acidic MTMSO (10^{-3} M) solution saturated by N_2O gas.

For the acid solution (pH 5.6), an increment in

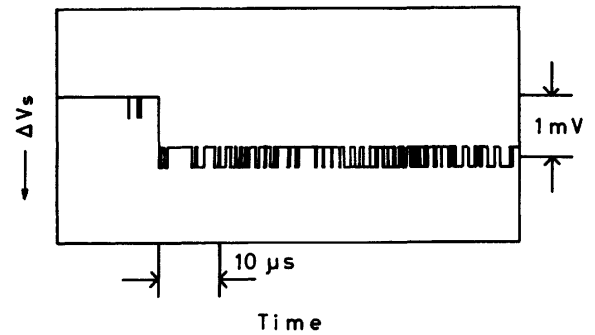

Fig. 6. Conductivity-time curve of pulse-irradiated aqueous N_2O saturated solutions of 10^{-3} M MTMSO at pH 5.6.

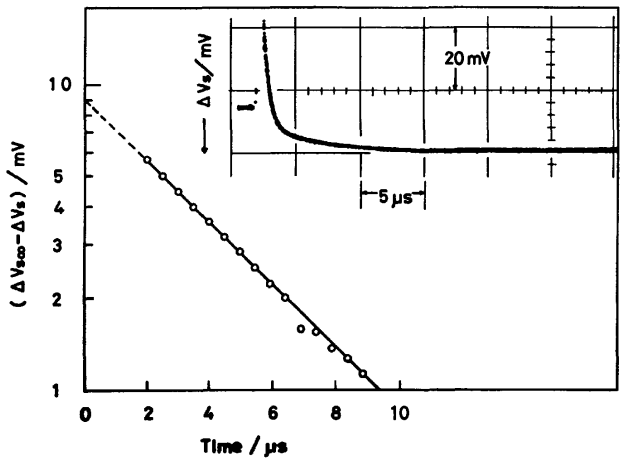

Fig. 7. First-order kinetic plot of $\log(\Delta V_{s\infty}-\Delta V)$ against time after the pulse irradiation of MTMSO aqueous solution ([MTMSO]$=5\times10^{-5}$ M, pH 4.9, $V=-30$ V, $R=50\ \Omega$). The solution were saturated with N_2O gas prior to the irradiation. Inset: An oscillogram trace of the conductivity change as a result of the formation of sulfinic acid $CH_3SCH_2SO_2^-$.

conductivity was observed. The signal of the conductivity after the pulse was a step function since the $CH_3SCH_2SO_2^-/H^+$ ion pair is stable over the detection period (Fig. 6). From the signal in Fig. 6, the yield of sulfinic acid can be determined as:

$$0.99\times K = G_{CH_3SCH_2SO_2^-/H^+}\times[\Lambda_{CH_3SCH_2SO_2^-}+\Lambda_{H^+}]. \quad (10)$$

Here the value of Λ_{H^+} is known to be 315 Ω^{-1} cm^2 and $K=9.74\times10^2$ which is determined experimentally. Using these values and assuming that $\Lambda_{CH_3SCH_2SO_2^-}$ is equal to $\Lambda_{CH_3SO_2^-}=42\ \Omega^{-1}$ cm^2 which is determined by Veltwisch *et al.*,[2] the yield of $CH_3SCH_2SO_2^-$ anion is calculated to be $G_{CH_3SCH_2SO_2^-}=2.7$. The value of the yield is 45% of the total yield of the OH· radicals ($G_{OH\cdot}=6.0$).[6] This fact indicates that 45% of the OH· radicals produced after the pulse irradiation attack the sulfinyl group of MTMSO, and that the residual 55% attack the sulfide S–C bond. Thus, in this case if we can ignore other reaction routes of OH· radical, it has the same reactivity for both the sulfoxide S–C bond and the sulfide S–C bond of MTMSO.

c) Kinetics for the Reaction between OH· Radical and MTMSO: Two methods were adopted for the determination of the rate constant for the reaction of OH·+ MTMSO. One is the conductivity method and the other is the KSCN method.

By the conductivity method, the rate constant was evaluated from a rise portion of build-up curve of the conductivity change after the pulse irradiation. Figure 7 shows a representative build-up curve in which the conductivity signal ΔV_S grows at short time and reaches a constant value $\Delta V_{S\infty}$. A plot of log $(\Delta V_{S\infty}-\Delta S_S)$ against time t gives a straight line, and the rate constant for the OH· radical with MTMSO was determined from the slope of the line to be 4.8×10^9 M^{-1} s^{-1}. The rate constant obtained from the conductivity method may correspond to the rate constant for the reaction of OH· radical with MTMSO.

By the KSCN method, the rate constant was determined utilizing the following competitive reaction of OH· radical with MTMSO.

$$\text{MTMSO} + \text{OH}\cdot \longrightarrow \text{Products} \quad (11)$$

$$CNS^- + OH\cdot \longrightarrow CNS\cdot + OH^- \quad (12)$$

$$CNS^- + CNS\cdot \longrightarrow (CNS)_2^{-}\cdot. \quad (13)$$

From the above reaction scheme, the concentration of $(CNS)_2^{-}\cdot$ after the pulse is obtained as follows:

$$[(CNS)_2^{-}\cdot] = \frac{k_C[CNS^-][OH\cdot]_0}{k_C[CNS^-]+k_F[MTMSO]}$$
$$[1-\exp\{-(k_F[MTMSO]+k_C[CNS^-])t\}], \quad (14)$$

where k_C and k_F denote the rate constants for Reactions 12 and 11, respectively, and $[OH\cdot]_0$ represents initial concentration of OH· radical after the pulse. From Eq. 14, one can evaluate the rate constant values k_C and k_F by monitoring the growth for the absorption intensity of $(CNS)_2^{-}\cdot$ which has an absorption maximum at 475 nm. Figure 8 shows some representative rise-curve of $(CNS)_2^{-}\cdot$ absorption in the absence and the presence of MTMSO. Absorption intensities of $(CNS)_2^{-}\cdot$ increase

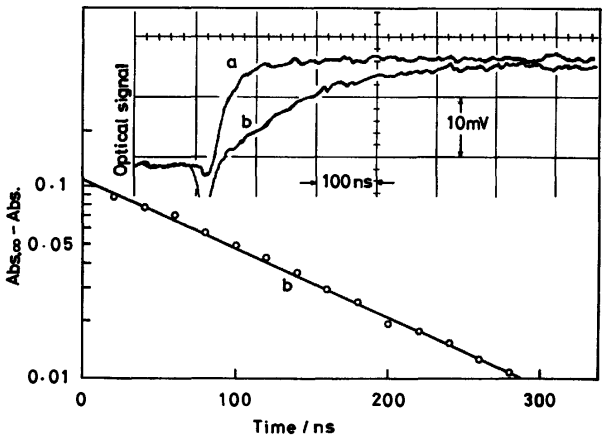

Fig. 8. First-order kinetic plot of $\log(Abs._\infty-Abs.)$ against time after the pulse irradiation of MTMSO aqueous solution. Solutions were saturated with N_2O gas prior to the irradiation. Inset: a) an oscillogram trace for the absorption of $(CNS)_2^-$. after the pulse irradiation of KSCN (10^{-2} M) solution in the absence of MTMSO solution. b) An oscillogram trace for the absorption of KSCN (10^{-3} M) solution in the presence of MTMSO (10^{-3} M). A change of 10 mV in the vertical axis corresponds to 16% transmittance. The monitoring wavelength for all the solution is 475 nm.

Table 2. Reaction rate cosntants of OH· radical with MTMSO obtained from KSCN method

[MTMSO]/M	τ/ns[a]	k_F/M^{-1} s^{-1}
0	199	5.02×10^{6} [b]
0.5×10^{-3}	157	2.68×10^{9}
1×10^{-3}	118	3.43×10^{9}
3×10^{-3}	85	2.25×10^{9}
6×10^{-3}	33[c]	4.19×10^{9}

a) The lifetime τ is the reciprocal value of (k_c[CNS^-]+k_F[MTMSO]). b) The value represent that for k_c[CNS^-]. c) The value may not be very accurate since the pulse width used is $\approx$20 ns.

within a short period of time, reach maxima and decay slowly. As is shown in the figure, a plot of log (Abs.$_\infty$ − Abs.) against t gives a straight line, where Abs.$_\infty$ and Abs. represent a maximum value and a value at t of the absorbances of $(CNS)_2^-\cdot$, respectively. The rate constants k_C[CNS^-] and (k_C[CNS^-]+k_F[MTMSO]) are determined from a slope of the linear plots for KSCN aqueous solutions in the absence and the presence of MTMSO. k_F is then evaluated by the use of k_C[CNS^-] and [MTMSO]. Table 2 summarizes k_F values obtained as a function of MTMSO concentration. Thus, the observation of the rise-curve of $(CNS)_2^-\cdot$ absorption after the pulse irradiation of the KSCN (1×10^{-3} M) with the different concentration of MTMSO (0 to 6×10^{-3} M), gives the k_F value to be 3.1×10^{9} M^{-1} s^{-1}. The rate constant value represents the rate constant for all kinds of reaction between OH· radical and MTMSO.

As well as the results of the yield values for the transients which is discussed in the previous section, information on the rate constants which are obtained independently from two methods leads to the conclusion that the OH· radical has almost the same reactivities with both the sulfoxide S–C bond and the sulfide S–C bond of MTMSO.

The authors wish to acknowledge Dr. Takeaki Enoto and Messrs. Hiroaki Tanida and Koichi Sato for their help in stabilizing and operating the LINAC.

References

1) G. Meissner, A. Henglein, and G. Beck, *Z. Naturforsh., Teil B*, **22**, 13 (1967).
2) D. Veltwisch, E. Janata, and K.-D. Asmus., *J. Chem. Soc., Perkin Trans. 2*, **1980**, 146.
3) Y. Kondo, M. Aikawa, T. Sumiyoshi, M. Katayama and J. Kroh, *J. Phys. Chem.*, **84**, 2544 (1980).
4) J. W. Hunt and J. K. Thomas, *Radiat. Res.*, **32**, 149 (1967).
5) K.-D. Asmus, *Int. J. Radiat. Phys.Chem.*, **4**, 417 (1972).
6) R. H. Schuler, L. K. Patterson, and E. Janata, *J. Phys. Chem.*, **84**, 2088 (1980).

Dynamic Studies on Electron Transport Across Micellar Phase. Intermicellar Migration of Hydrated Electrons

Masayuki AIKAWA,* Takashi SUMIYOSHI,† Nobuyuki MIURA,† and Meiseki KATAYAMA†

College of General Education, Hokkai Gakuen University, Asahimachi Toyohiraku, Sapporo 062

†*Department of Atomic Science and Nuclear Engineering, Hokkaido University, Sapporo 060*

(Received February 20, 1982)

The dynamics of hydrated electrons generated by pulsed electron beams was studied for micellar systems with a series of halogenated naphthalenes as substrates exclusively dissolved in micellar phase. Time behavior of absorption for hydrated electrons, displayed as a curve consisting of two exponential decays, affords evidence that two different routes exist in advance of dissociative electron attachement: 1) direct penetration of electrons through micellar phase with substrates, and 2) migration of hydrated electrons between micells in the absence and presence of substrates, prior to the penetration of electrons into the reactive center in the micelle. Electrostatic interaction of hydrated electrons with positively charged surface of micelles is also discussed.

Knowledge of electron transfer mechanisms with donor–acceptor systems, separated from each other by hydrophobic compartments in aqueous micellar solution, is essential for constructing artificial photosynthetic devices.[1-3] Ionic micelles, like charged colloids and ion-exchange resins, have the property of being able to bind with oppositely charged ions.[4] This aspect of micelles has been used to study a variety of reactions in conjunction with their ability to solubilize hydrophobic molecules in aqueous solutions. In previous works, it has been reported that adsorbed metal ions on anionic micelles can act as efficient electron acceptors from excited micelle solubilized species,[5] and that they can promote the rate of phosphorescence in some aromatic hydrocarbons.[6] Recently, kinetic studies on the movement of metal ions in aqueous micellar solutions have also been reported.[4,7,8] The use of hydrated electrons, generated in bulk aqueous phase, as a source of electrons for redox reactions seems to provide information on the reactivity of electrons with micelle-bound substrate. Few kinetic studies, however, have been directed at studying the movement of hydrated electrons in aqueous micellar solutions.[6,9] Hydrated electrons in aqueous cationic micellar solutions are expected to act in the same manner as metal ions which accelerate or inhibit reactions with oppositely or commonly charged surface of micelles.[4,10] We report here results of dynamic studies on the movement of hydrated electrons in an aqueous cationic micellar solution. The reaction of dissociative electron attachment was utilized to determine the rate of electron transfer from the surface to core of micelles.

Experimental

1-Chloronaphthalene (CN) and 1-bromonaphthalene (BN), purchased from Nakarai Chemicals, were purified by repeated vacuum distillation. 1,4-Dibromonaphthalene (DBN, Wako) was purified by vacuum sublimation. Hexadecyltrimethylammonium bromide (HDTBr, Sigma Chemicals) was used as supplied. For solubilization of halonaphthalenes as substrates, HDTBr detergent in triply distilled water was shaken with the substrate overnight. Concentrations of the substrates in micellar solutions were determined by their absorbances.

Halogenated naphthalenes (XN) are frequently used as effective electron scavengers in radiolyses of various chemical substances. This is based on the fact that XNs are highly reactive toward electrons, and that when an electron attaches to XN, it will dissociate into a neutral radical and a halide ion:[11]

$$XN + e^- \longrightarrow X^-N \longrightarrow X^- + N\cdot. \quad (1)$$

Reaction 1 is a so-called dissociative attachement. Since, however, kinetics between hydrated electrons (e^-_{aq}) and halogenated naphthalenes are not well known because of their low solubilities in water, the reactivity of reaction $e^-_{aq}+XN$ should be tested by monitoring the decay of hydrated electrons prior to running experiments on micellar systems. The decay curve for hydrated electron in an aqueous solution with EtOH (1.0 M) (1 M=1 mol dm^{-3}) consisted of a single exponential component over the range of halonaphthalene concentrations examined (5×10^{-5}—5×10^{-6} M). From observed decay rates of hydrated electrons as a function of XN concentration, rate constants of the reactions of e^-_{aq} with DBN, BN, and CN were determined to be 3.0×10^{10}, 1.8×10^{10}, and 1.4×10^{10} M^{-1} s^{-1}, respectively. These values should represent the rate constant for the following reaction:

$$XN + e^-_{aq} \longrightarrow N\cdot + X^- + H_2O. \quad (2)$$

By monitoring the decay rate for the absorption of hydrated electron after pulse irradiation, reaction kinetics of the electron transport from bulk aqueous phase to micellar phase could be examined if the rate changes with change in the concentration of substrates and/or micelles. Two series of micellar solutions were prepared by 1) changing the concentration of substrates (from 0 to 3×10^{-4} M) at a fixed HDTBr detergent concentration (0.05 M), and 2) changing both the concentrations of substrates [XN] and detergent [Det] at a fixed mean occupancy number ⟨XN⟩, which is the number of substrates bound per micelle. The substrates used are known to be exclusively micellized under the experimental conditions studied, since the binding constants between HDTBr micelle and halogenated naphthalenes are known to be 1.7×10^6 and 3.7×10^6 M^{-1} for BN and CN, respectively.[12,13]

Micellar solutions were deaerated by bubbling purified argon for 10 min through them.

Pulse radiolysis measurements were performed with electron pulses (45 MeV) from a linear accelerator (Mitsubishi) installed in Hokkaido University. The half-width of the electron pulse used was 20 ns. The dose per pulse was in a range of 9—12 krad. The design and performance of the optical detection system combined with the LINAC have been described in a previous paper.[14] The output signal from the detection system was displayed on a transient digitizer (IWATSU) with the shortest resolvable time of 10 ns.

Results and Discussion

Transient adsorption after pulse irradiation on micellar solution without substrate shows a broad spectrum around 400—750 nm, which is exclusively assigned to hydrated electron. With increase in detergent concentration, a little change in absorption decay of e^-_{aq} was observed. From the change in the decay rate of e^-_{aq}, rate constant for the reaction of e^-_{aq} with HDTBr micelle is approximately estimated to be less than 3×10^8 M^{-1} s^{-1}. Since the reaction of hydrated electrons with positively charged micelle does not occur,[6] though the attractive force of micelle for e^-_{aq} sometimes catalyzes reactions, the rate constant obtained in our experiment might be related partly to reactions of e^-_{aq} with some impurities contained in the micelle.

Variation in Absorption Decays of e^-_{aq} as a Function of Micelle and Substrate Concentrations at Fixed Mean Occupancy Number. The mean occupancy number of substrate in a micelle ⟨XN⟩ is defined as

$$\langle XN\rangle = \frac{[XN]}{[M]} = \frac{n}{[Det]-cmc}[XN], \qquad (3)$$

where [XN], [M], and [Det] are bulk concentrations of XN, micelle, and detergent, respectively, and n is the aggregation number of the detergent. Thus, [XN] may be changed by varying ⟨XN⟩, [Det], or n. All experiments were performed in concentration ranges of detergent for which n is not subject to significant variation.

Above the critical micelle concentration (*cmc*), dilution of a micellar solution with water does not significantly alter the value of ⟨XN⟩, *i.e.*, since the ratio [XN]/[Det] and n remain constant with aqueous dilution, ⟨XN⟩ also remains constant. Figure 1 shows the effect of aqueous dilution on absorption decays of e^-_{aq}, where a stock micellar solution with CN ([CN] $=1.4\times10^{-4}$ M; [Det] = [HDTBr] $=5\times10^{-2}$ M) was diluted with water by half, one fourth, and so on. From the literature values of $n=72$ and $cmc=8.5\times10^{-4}$ M,[15] we obtained by calculation that ⟨XN⟩ will vary from 0.21 to 0.25 in our experimental conditions. The increase in total decay rate with increasing concentration of micelle-bound substrate implies that the hydrated electron will react effectively with halogenated naphthalenes *via* Reaction 2.

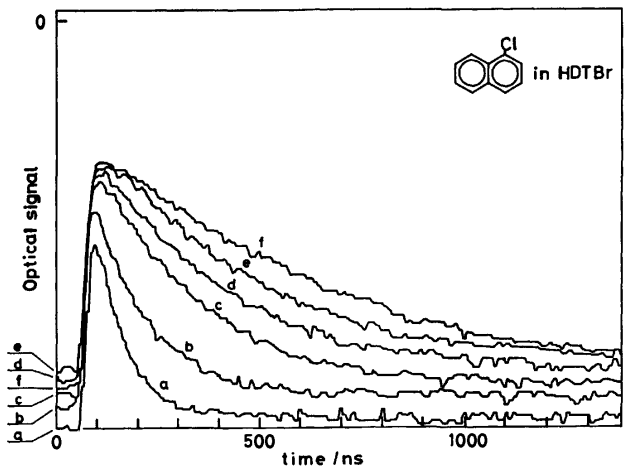

Fig. 1. The decay curves of e^-_{aq} after the pulse irradiation for the aqueous micellar solutions. The concentrations are a) [CN] $=1.4\times10^{-4}$ M, [HDTBr] $=5\times10^{-2}$ M, b) [CN] $=7\times10^{-5}$ M, [HDTBr] $=2.5\times10^{-2}$ M, c) [CN] $=3.5\times10^{-5}$ M, [HDTBr] $=1.25\times10^{-2}$ M, d) [CN] $=1.8\times10^{-5}$ M, [HDTBr] $=6.3\times10^{-3}$ M, and e) [CN] $=1.2\times10^{-5}$ M, [HDTBr] $=4.2\times10^{-3}$ M, respectively. The decay curve (f) is obtained for triply distilled water. The monitoring wavelength and the dose per pulse are 650 nm and 9 krad, respectively.

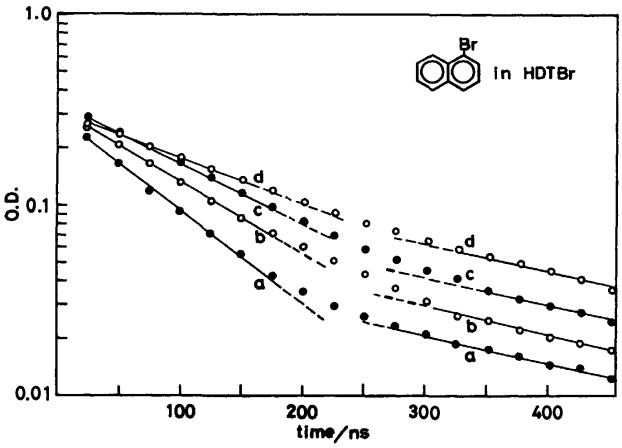

Fig. 2. First-order decay curves of the absorption of e^-_{aq} *vs.* time in aqueous solutions at different [BN] and [HDTBr]. The concentrations are a) [BN] $=2.9\times10^{-4}$ M, [HDTBr] $=5\times10^{-2}$ M, b) [BN] $=1.5\times10^{-4}$ M, [HDTBr] $=2.5\times10^{-2}$ M, c) [BN] $=7.3\times10^{-5}$ M, [HDTBr] $=1.3\times10^{-2}$ M, and d) [BN] $=3.7\times10^{-5}$ M, [HDTBr] $=6.3\times10^{-3}$ M, respectively. The monitoring wavelength and the dose per pulse are 650 nm and 9 krad, respectively.

The decay curves for the absorption of e^-_{aq}, however, do not fit a simple first-order decay, but consist of fast- and slow-decaying components. Figure 2 shows plots of log *O.D.* (e^-_{aq}) against time t as a function of [BN] and/or [M]. With increasing concentration of substrate, the fast-decaying component increases in decay rate, whereas the slow-decaying component remains constant, as shown in the figure. The plot of log *O.D.*(e^-_{aq}) *vs.* t for the time range far away from the time of pulse irradiation gives the first-order decay rate τ_s^{-1}, corresponding to the decay rate for the slow-decaying component. The decay rate for the fast-decaying component, τ_f^{-1}, can be obtained from the difference between the total decay curve and the first-order decay curve extrapolated toward shorter times by use of τ_s^{-1}. Apparent rate constants for the reaction of e^-_{aq} with XN in micelles were then obtained from the slope of the linear plots of τ_f^{-1} *vs.* [XN]. Rate constants thus obtained are summarized in Table 1.

The constancy of rate for the slow-decaying component with the change in micelle concentration at constant ⟨XN⟩ may arise from a constant ratio in number of the micelles possessing one substrate M_{XN} to those possessing zero substrate M_0. Since multiple occupancy of the substrate per micelle is neglected from

TABLE 1. RATE CONSTANTS/$M^{-1}s^{-1}$ OF REACTION OF HYDRATED ELECTRON WITH HALOGENATED NAPHTHALENES

	DBN	BN	CN
Aqueous solution (+1 M EtOH)	3.0×10^{10}	1.8×10^{10}	1.4×10^{10}
HDTBr micellar solution[a)]	2.9×10^{10}	2.0×10^{10}	2.2×10^{10}

a) Evaluated from fast-decaying components.

the Poisson statistics, hydrated electrons can encounter only those micelles with one or zero substrate.

It should be noted here that the initial intensity of absorption decay of e^-_{aq} after the pulse does not change with varying [XN] and/or [M], implying that only the reactions after the formation of hydrated electrons with micelles or substrates are observed.

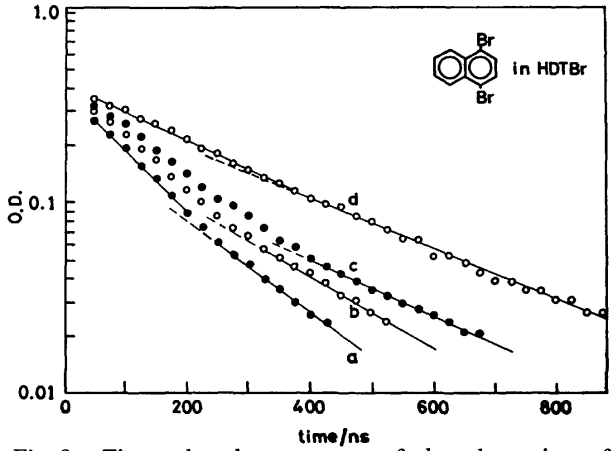

Fig. 3. First-order decay curves of the absorption of e^-_{aq} *vs.* time in 5×10^{-2} M HDTBr solutions at different [DBN]. The concentrations of DBN are a) 3.3×10^{-4} M, b) 9.8×10^{-5} M, c) 6.5×10^{-5} M, and d) 3.3×10^{-5} M, respectively. The monitoring wavelength and the dose per pulse are 650 nm and 9 krad, respectively.

Variation in Absorption Decays of e^-_{aq} as a Function of Substrate Concentration at Fixed Micelle Concentration.

In a series of experiments with [HDTBr] fixed at $=5\times10^{-2}$ M, the concentration of [XN] was varied from 3.3×10^{-5} to 3.3×10^{-4} M. Figure 3 shows semi-logarithmic plots of e^-_{aq} absorption against time as a function of [DBN] at fixed detergent concentration. The decay curves for the absorption of e^-_{aq} also consist of fast- and slow-decaying components. In this case, however, unlike the case of aqueous dilution experiments, both the fast- and slow-decaying components increase in decay rate with increasing concentration of substrate. Apparent rate constants for the reaction of e^-_{aq} with micelle-bound substrates were obtained from the slope of the plots of τ_f^{-1} *vs.* [XN] as in the case of aqueous dilution experiments. The rate constant values obtained are comparable with that obtained in the aqueous dilution experiment.

The rate of encounter between M_{XN} and M_0 is given by

$$k_e[M_{XN}][M_0] = k_e\cdot P_{XN}\cdot P_0[M]^2, \qquad (4)$$

where k_e is the rate constant for encounter between M_{XN} and M_0. P_{XN} and P_0 represent respective probability distributions of M_{XN} and M_0, which are based on the Poisson statistics. With increasing $\langle XN\rangle$ value from 0.05 to 0.5 at constant [M] (6.8×10^{-4} M), the value for $P_{XN}\times P_0$ increases from 0.048 to 0.23. The increase in the slow reaction rate τ_S^{-1} with increasing rate of encounter between M_{XN} and M_0 (in consequence of increasing $\langle XN\rangle$) suggests that, in the absence of substrates, micelles play a mechanistic role in electron transport from hydrated electrons to micelle-bound substrates.

Mechanisms for Electron Transport in Micellar Systems. The large positive charge on micelle surface forms a Gouy-Chapman double layer which is spread over several hundred Å from the surface of micelle.[16,17] Along the electrostatic field which is produced by the double layer, hydreted electrons move toward the surface. The electrostatic interaction between hydrated electrons and positive charges on the surface, then may lead to formation of a complex ($M_0\cdots e^-_{aq}$) or ($M_{XN}\cdots e^-_{aq}$). Electron transfer reaction (*viz.*, ($M_{XN}\cdots e^-_{aq}$)$\rightarrow$ $M_{X^-N}+H_2O$) will take place quickly for micelles in the presence of substrates. On the other hand, hydrated electrons may survive to form a complex ($M_0\cdots e^-_{aq}$), since the lifetime of hydrated electrons is practically unchanged by the addition of cationic detergent to aqueous solution. The following scheme represents the electron transport reaction relevant to our experimental data:

$$\begin{array}{ccc} & & M_{X^-N} \\ & & \uparrow \\ (M_0\cdots e^-_{aq}) + M_{XN} & \rightleftharpoons & M_0 + (M_{XN}\cdots e^-_{aq}). \\ \downarrow\uparrow & & \uparrow \\ M_0 + e^-_{aq} & & M_{XN} + e^-_{aq} \end{array} \qquad (5)$$

If a sizable percent of complex ($M_0\cdots e^-_{aq}$) is formed, migration of hydrated electrons from ($M_0\cdots e^-_{aq}$) to M_{XN} will occur on micelle surface before an electron penetrates the reactive center in micelle M_{XN}. This migration behavior of hydrated electron is similar to that of micelle-bound metal ion which moves through micelle-micelle collision, at which overlap of ionic charge clouds of micelles allows the ion to migrate from one micelle to another.[4,8] The migration of surface-bound hydrated electrons leads eventually to an electron transfer reaction from the surface to reactive halonaphthalenes. Qualitatively, this migration mechanism interprets the "slow" electron transport reaction which controls the slow-decaying component. Direct encounter between M_{XN} and e^-_{aq} leads to the "fast" electron transport reaction which controls the fast-decaying component. Collectively, the experimental results relating to the decay curves for e^-_{aq} absorption consisting of the slow- and fast-decaying components are consistent with Reaction Scheme 5 which would be expected from an electrostatic consideration.

A further kinetic and spectroscopic study was designed to investigate these systems and to evaluate exactly rate constants for the reaction scheme. Details of the kinetic analysis will appear in the successive paper.

Conclusion

This paper has described electron transport reactions between hydrated electrons and micelle-bound electron acceptors. Preliminary kinetic measurements indicate that, together with direct encounter between e^-_{aq} and M_{XN}, micelle plays a significant role in the reaction of electron transport from hydrated electron to micelle-bound substrate.

The authors wish to acknowledge Dr. Takeaki Enoto and Messrs. Hiroaki Tanida and Koichi Sato for their help in stabilizing and operating the LINAC.

References

1) M. S. Tunuli and J. H. Fendler, *J. Am. Chem. Soc.*, **103**, 2507 (1981).
2) W. E. Ford, J. W. Otvos, and M. Calvin, *Proc. Natl. Acad. Sci. U. S. A.*, **76**, 3590 (1979).
3) T. Matsuo, K. Takuma, Y. Tsutui, and J. Nishijima, *J. Coord. Chem.*, **10**, 187 (1980).
4) A. Henglein and Th. Proske, *Ber. Bunsenges. Phys. Chem.*, **82**, 471 (1978).
5) R. Scheerer and M. Grätzel, *J. Am. Chem. Soc.*, **99**, 865 (1977).
6) K. Kalyanasundaram, F. Grieser, and J. K. Thomas, *Chem. Phys. Lett.*, **51**, 101 (1977); J. K. Thomas, *Acc. Chem. Res.*, **10**, 133 (1977).
7) J. C. Dederen, M. Vander Auweraer, and F. C. Deschryver, *Chem. Phys. Lett.*, **68**, 451 (1979).
8) F. Grieser and R. T-Treml, *J. Am. Chem. Soc.*, **102**, 7258 (1980).
9) D. Meisel, M. S. Matheson, and J. Rabani, *J. Am. Chem. Soc.*, **100**, 117 (1978).
10) M. Grätzel and J. K. Thomas, *J. Phys. Chem.*, **78**, 2248 (1974).
11) A. Namiki, *J. Chem. Phys.*, **62**, 990 (1975); S. Arai, S. Tagawa, and M. Imamura, *J. Phys. Chem.*, **78**, 519 (1974).
12) M. Almgren, F. Grieser, and J. K. Thomas, *J. Am. Chem. Soc.*, **101**, 279 (1979).
13) N. J. Turro and M. Aikawa, *J. Am. Chem. Soc.*, **102**, 4866 (1980).
14) Y. Kondo, M. Aikawa, T. Sumiyoshi, M. Katayama, and J. Kroh, *J. Phys. Chem.*, **84**, 2544 (1980).
15) R. C. Dorrance and T. R. Hunter, *J. Chem. Soc., Faraday Trans. 1*, **68**, 1312 (1972); **70**, 1572 (1974).
16) J. H. Fendler and E. J. Fendler, "Catalysis in Micellar and Macromolecular Systems," Academic Press, New York (1975).
17) C. Wolff and M. Grätzel, *Chem. Phys. Lett.*, **52**, 542 (1977).

Preparations and Characterization of Some Carbonyl-(1-cyanoethyl)ruthenium(II) Complexes

Katsuma HIRAKI,* Naoyuki OCHI, Tsuneyuki KITAMURA, Yoko SASADA, and Sumio SHINODA†

Department of Industrial Chemistry, Faculty of Engineering, Nagasaki University, Bunkyo-machi, Nagasaki 852

†*Institute of Industrial Science, The University of Tokyo, Roppongi-7, Minato-ku, Tokyo 106*

(Received July 31, 1981)

A hydridoruthenium(II) complex [RuClH(CO)(PPh_3)$_3$] reacted easily with acrylonitrile and fumaronitrile to give chloro-bridged binuclear (1-cyanoethyl)ruthenium(II) complexes, [{Ru(MeCHCN)Cl(CO)(PPh_3)$_2$}$_2$] (**2**) and [{Ru(NCCH$_2$CHCN)Cl(CO)(PPh_3)$_2$}$_2$], respectively. Complex **2** reacted with 4-picoline (pic), Na[$BHPz_3$] (Pz=1-pyrazolyl), Na[BPz_4], and Na[Et_2NCS_2]·3H$_2$O to afford the corresponding (1-cyanoethyl)ruthenium(II) complexes, [{Ru(MeCHCN)Cl(CO)(pic)(PPh_3)}$_2$] (**3**), [Ru(MeCHCN)($BHPz_3$)(CO)(PPh_3)] (accompanied by a small amount of [Ru$_2$(MeCHCN)$_2$Cl($BHPz_3$)(CO)$_2$(PPh_3)$_4$]), [Ru$_2$(MeCHCN)$_2$Cl(BPz_4)(CO)$_2$(PPh_3)$_2$], and Na[Ru(MeCHCN)Cl(Et_2NCS_2)(CO)(PPh_3)], respectively. Complex **3** reacted with thallium(I) acetylacetonate [Tl(acac)], resulting in the formation of [{Ru(MeCHCN)(acac)(CO)(PPh_3)}$_2$] and [Ru(MeCHCN)(acac)(CO)-(pic)(PPh_3)]. These new complexes were characterized by means of elemental analysis and spectroscopic data. The diastereoisomerism was also discussed as regards these (1-cyanoethyl)ruthenium(II) complexes.

It is interesting to investigate the coordination behavior of (1- and 2-cyanoalkyl)ruthenium(II) complexes, in connection with catalytic hydrodimerization[1–3] and polymerization[4] of acrylonitrile with ruthenium complexes. However, little has been known about the (cyanoalkyl)ruthenium(II) complexes,[5] whereas only a few papers have been reported concerning the coordination behavior of octahedral alkylruthenium-(II) complexes.[6–9]

It has been recently reported from our laboratory that some substituted olefins insert into the hydridoruthenium (H–Ru) bond of (carbonyl)chlorohydridotris-(triphenylphosphine)ruthenium(II) (**1**) to give stable organoruthenium(II) complexes.[5] Since [{Ru-(MeCHCN)Cl(CO)(PPh_3)$_2$}$_2$] (**2**), prepared from the reaction of **1** with acrylonitrile, was insoluble in usual organic solvents, its 4-picoline (pic) derivative [{Ru-(MeCHCN)Cl(CO)(pic)(PPh_3)}$_2$] (**3**) was prepared. Complex **3** had also a binuclear structure and was assumed to consist of a few diastereoisomers.[5] In this paper, reactions of **2** and **3** with several anionic chelating ligands were carried out, in order to prepare mononuclear (1-cyanoethyl)ruthenium(II) complexes and to confirm whether the isomers in **3** were caused by asymmetric 1-carbon and ruthenium atoms or not. In addition, the resulting complexes were isolated and characterized on the basis of elemental analysis and spectroscopic data.

Experimental

General Procedures and Materials. Melting points, IR spectra, and ^{1}H and ^{31}P-NMR spectra were obtained according to the previous paper.[10] The molecular weight of a complex was determined in benzene using a Corona model 114 vapour pressure osmometer.

Solvents were dried and distilled by the usual methods, and all preparative operations were performed in an atmosphere of dry nitrogen. Complex **1**,[11] sodium poly(1-pyrazolyl)borates Na[BPz_3H] (Pz=1-pyrazolyl) and Na[BPz_4],[12] and thallium-(I) acetylacetonate[13] were prepared according to the literature methods. The other reagents were commercial samples, and were used without further purification.

Reaction of 1 with Acrylonitrile. A THF suspension (60 ml) containing **1** (1 mmol) and acrylonitrile (7.5 mmol) was stirred at room temperature for 23 h to give a pale yellowish green precipitate. The precipitate was collected and washed with hexane and diethyl ether to yield a greenish gray solid [{Ru(MeCHCN)Cl(CO)(PPh_3)$_2$}$_2$] (**2**).

Reaction of 2 with 4-Picoline. A THF suspension (35 ml) involving **2** (0.24 mmol) and 4-picoline (1.4 mmol) was stirred at room temperature for 20 h to yield a yellow solution. After concentration, the yellow solution was diluted with diethyl ether to give a pale green powder, [{Ru(MeCHCN)Cl(CO)-(pic)(PPh_3)}$_2$] (**3**).

Reaction of 1 with Fumaronitrile. A THF suspension (30 ml) containing **1** (1 mmol) and fumaronitrile (3.75 mmol) was stirred at room temperature for 20 h to result in an orange-brown solution. After concentration under a reduced pressure, the orange-brown solution was diluted with 80 ml of hexane to yield an orange-brown powder. The powder was collected and washed with diethyl ether to give a yellow-brown powder, [{Ru(NCCH$_2$CHCN)Cl(CO)(PPh_3)$_2$}$_2$] (**4**).

Reaction of 2 with Na[$BHPz_3$]. A THF suspension (20 ml) involving **2** (0.27 mmol) and Na[$BHPz_3$] (0.55 mmol) was stirred at 40 °C for 4 h. After filtration, the resulting filtrate was evacuated under a reduced pressure, and chromatographed over silica-gel column (Wako gel, 200 mesh, 150×12ϕ mm). A yellow fraction was eluted with benzene, and concentration of this afforded yellow solids, [Ru(MeCHCN)($BHPz_3$)(CO)-(PPh_3)] (**5**). Moreover, a pale yellow fraction was eluted with acetone, and evaporation of this gave a small amount of pale yellow solids, [Ru$_2$(MeCHCN)$_2$Cl($BHPz_3$)(CO)$_2$(PPh_3)$_4$] (**6**).

Reaction of 2 with Na[BPz_4]. A benzene suspension (40 ml) containing **2** (0.25 mmol) and Na[BPz_4] (0.55 mmol) was refluxed for 9 h. After filtration, the filtrate was concentrated and diluted with hexane to yield cream-yellow precipitates. The precipitates were recrystallized from dichloromethane-hexane to give a cream-yellow powder, [Ru$_2$(MeCHCN)$_2$Cl-(BPz_4)(CO)$_2$(PPh_3)$_2$] (**7**).

Reaction of 2 with Na[Et_2NCS_2]·3H$_2$O. A THF suspension (60 ml) of **2** (0.2 mmol) and Na[Et_2NCS_2]·3H$_2$O (0.48 mmol) was stirred at room temperature for 91 h to yield greenish white precipitates. The precipitates were washed with diethyl ether and hexane, successively, to afford greenish white solids, Na[Ru(MeCHCN)Cl(Et_2NCS_2)(CO)(PPh_3)] (**8**).

Reaction of 3 with Thallium(I) Acetylacetonate. A dichloromethane suspension (30 ml) containing **3** (0.52 mmol) and Tl(acac) (1.05 mmol) was stirred at room temperature for 72 h.

After filtration, the resulting solution was chromatographed upon the silica-gel column. A yellow fraction was eluted with benzene, concentrated under a reduced pressure, and diluted with hexane to give a light yellow powder, [{Ru(MeCHCN)(acac)(CO)(PPh_3)}$_2$] (**9**). The second yellow fraction was eluted with dichloromethane, and evacuated to dryness *in vacuo*. The resulting residue was washed with hexane to afford a pale yellow powder, [Ru(MeCHCN)(acac)(CO)(pic)(PPh_3)] (**10**).

Results and Discussion

Preparation. The hidridoruthenium(II) complex **1** reacted smoothly with acrylonitrile and fumaronitrile in THF at room temperature to give sparingly soluble binuclear complexes [{Ru(MeCHCN)Cl(CO)(PPh_3)$_2$}$_2$] (**2**)[5] and [{Ru(NCCH$_2$CHCN)Cl(CO)(PPh_3)$_2$}$_2$] (**4**), respectively. Complex **2** was treated with 4-picoline (in THF at room temperature), with Na[BPz_4] (in refluxing benzene), and with Na[Et_2NCS_2]·3H$_2$O (in THF at room temperature) to yield [{Ru(MeCHCN)Cl(CO)(pic)(PPh_3)}$_2$] (**3**), [Ru_2(MeCHCN)$_2$Cl(BPz_4)(CO)$_2$(PPh_3)$_2$] (**7**), and Na[Ru(MeCHCN)Cl(Et_2NCS_2)(CO)(PPh_3)] (**8**), respectively. Complexes **3** and **7** have also binuclear structures, whereas **8** has an ionic structure and is actually insoluble in usual organic solvents.

In order to obtain neutral mononuclear-type complexes, reactions between **2** and Na[$BHPz_3$] and between **3** and Tl(acac) were examined. The former reaction produced two complexes, which were separated by column chromatography and formulated as [Ru(MeCHCN)($BHPz_3$)(CO)(PPh_3)] (**5**) and [Ru_2(MeCHCN)$_2$Cl($BHPz_3$)(CO)$_2$(PPh_3)$_4$] (**6**). From the latter reaction, two complexes were formed, separated similarly, and formulated as [{Ru(MeCHCN)(acac)(CO)(PPh_3)}$_2$] (**9**) and [Ru(MeCHCN)(acac)(CO)(pic)(PPh_3)] (**10**). The yields and elemental analyses of **2**—**10** are summarized in Table 1.

General Properties. The IR spectra of **2**—**10** lacked a ν(Ru–H) band near 2000 cm^{-1}, which had been observed in the starting complex, **1**, and showed one strong band in the range of 1905—1945 cm^{-1}, assignable to a terminal carbonyl group, whereas **4**, **5**, and **7** exhibited one or two additional shoulders near 1910 and 1950 cm^{-1} (Table 2). Furthermore, **2**, **3**, **5**—**8**, and **10** exhibited a medium band near 2200 cm^{-1}, characteristic of an uncoordinated cyano group. The ^{1}H-NMR spectra of **3**, **5**—**7**, and **10** each exhibited two, three or four doublets in the region of δ 0.2—1.4, ascribable to methyl group adjacent to methine group. On the basis of these data and the elemental analyses, **2**, **3**, **5**—**8**, and **10** were attributed to carbonyl(1-cyanoethyl)ruthenium(II) complexes. Complex **4** showed two ν(C≡N) bands at 2205 and 2230 cm^{-1}, implying that **4** contained a 1,2-dicyanoethyl group.

Complexes **2**—**10** are stable in a solid state in the air and considerably stable in solution under a nitrogen stream. Their stability is possibly associated with electron-delocalization effect due both to the coordination of appropriately σ-donating and π-accepting carbonyl group and PPh_3 ligand and to the electron-accepting cyano group adjacent to the 1-carbon.

Table 1. Yields and elemental analyses of the ruthenium complexes

Complex		Yield/%	Mp θ_m/°C	Found(Calcd)(%) C	H	N
[{Ru(MeCHCN)Cl(CO)(PPh_3)$_2$}$_2$]	**2**	83	151—157	64.99(64.65)	4.85(4.61)	1.58(1.88)
[{Ru(MeCHCN)Cl(CO)(pic)(PPh_3)}$_2$]	**3**	58	165—171	59.23(58.59)	4.51(4.57)	4.66(4.88)
[{Ru(NCCH$_2$CHCN)Cl(CO)(PPh_3)$_2$}$_2$]	**4**	75	165—175	64.62(64.11)	4.42(4.33)	3.46(3.65)
[Ru(MeCHCN)($BHPz_3$)(CO)(PPh_3)]	**5**	31	158—160	56.60(56.55)	4.60(4.44)	14.50(14.89)
[Ru_2(MeCHCN)$_2$Cl($BHPz_3$)(CO)$_2$(PPh_3)$_4$]	**6**	9	130—131	65.52(64.24)	5.06(4.72)	5.73(6.73)
[Ru_2(MeCHCN)$_2$Cl(BPz_4)(CO)$_2$(PPh_3)$_2$]	**7**	41	224	55.88(55.73)	4.24(4.18)	10 83(11.61)
Na[Ru(MeCHCN)Cl(Et_2NCS_2)(CO)(PPh_3)]	**8**	38	210	49.12(49.73)	4.65(4.48)	4.18(4.30)
[{Ru(MeCHCN)(acac)(CO)(PPh_3)}$_2$]	**9**	26	162—168	59.88(59.55)	5.06(4.18)	2.41(2.57)
[Ru(MeCHCN)(acac)(CO)(pic)(PPh_3)]	**10**	29	174—175	62.31(62.16)	5.29(5.22)	3.99(4.39)

Table 2. Characteristic IR bands of the complexes[a]

Complex	ν_{CO}/cm^{-1}	$\nu_{C\equiv N}$/cm^{-1}	Others
2	1925 s	2215 m	
3	1930 s	2200 m	1620 m, 1502 w[(C=N)+(C=C)]
4	1910 sh, 1932 s 1960 sh	2230 m, 2205 w	
5	1943 s, 1950 sh	2200 m	2487 m[ν(BH)]
6	1943 s,	2200 m, 2238 w	2488 m[ν(BH)]
7	1919 s, 1942 sh	2182 m, 2217 sh	
8	1907 s	2195 m	1482 s[ν(C⋯N)], 1262 s[(C=S)]
9	1932 s	2200 sh, 2240 m	1591 s, 1520 s[ν(C=O)+ν(C=C)]
10	1924 s	2200 m	1589 s, 1520 s[ν(C=O)+ν(C=C)] 1622 m[ν(C=N)]

a) Measured in KBr disk, values in cm^{-1}.

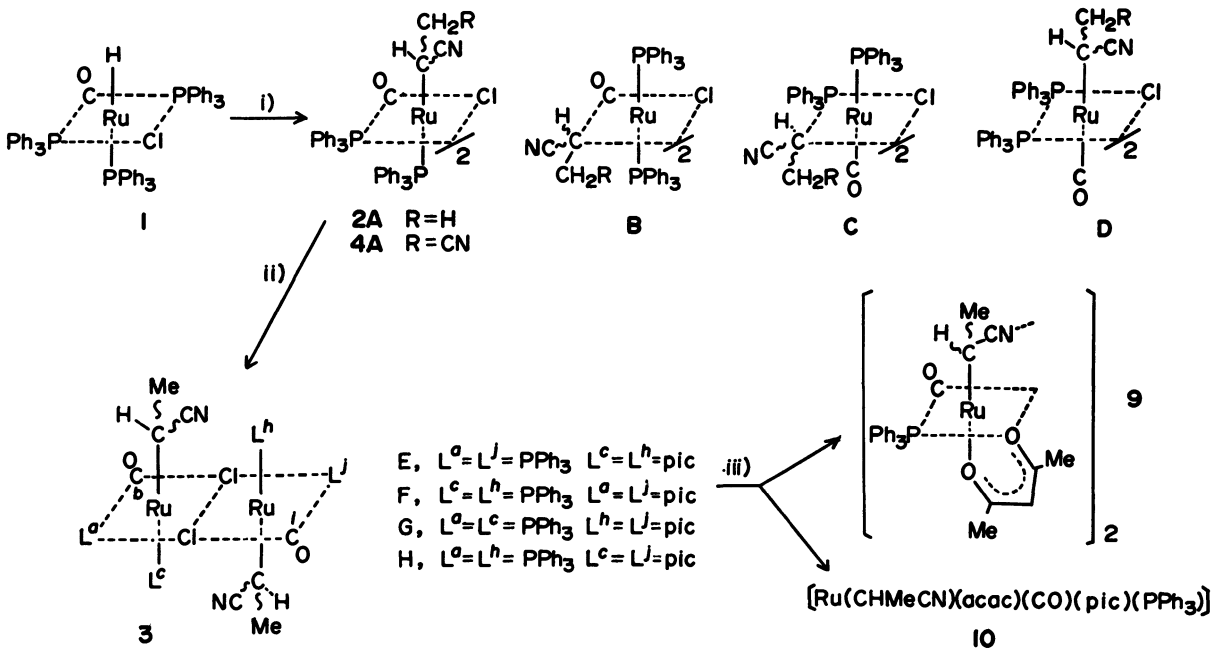

Scheme 1. i) Acrylonitrile (for **2**) or fumaronitrile (for **4**). ii) 4-Picoline (pic) with **2**. iii) Tl (acac). See Fig. 2 as regards the diasteroisomers of **3** and **4** and Fig. 4 as regards those of **9** and **10**.

Chloro-bridged Binuclear Complexes **2**—**4**. The elemental analyses of **2**—**4** imply that each of these three complexes has one chlorine atom and four other coordination sites per ruthenium atom, indicating a chloro-bridged binuclear structure (Scheme 1).[10] Indeed, chlorine atoms have been reported to serve as bridge-forming ligands in many chlororuthenium(II) complexes.[10,14,15] It is noteworthy that **2** and **3** showed the single intensive ν(C≡O) band, although they have the binuclear structures and consist of a few diastereoisomers (*vide infra*).[5] This indicates that the diastereoisomerism for **2** and **3** has actually little influence on the ν(C≡O) band and that the two carbonyl groups in the binuclear structure are coordinated in an inversion symmetry (a *b,i*-CO type in Scheme 1) rather than in a C_2 rotational one around the Cl-Cl axis (a *b,j*-CO type) and in a C_1 one (a *b,g*- or a *b,h*-CO type). A binuclear dicarbonyl complex in the C_2 or the C_1 symmetry would show two ν(C≡O) bands, according to group theory. As concerns mononuclear moiety in **2** or **4**, four types A-D are possible, as shown in Scheme 1. However, types C and D are ruled out, because relatively bulky ligands, two PPh_3 ones and one 1-cyanoethyl group are located at facial positions in these types, and because both carbonyl ligand and chloro one in **1** must remain unmoved at trans positions to each other in the mild reaction conditions from **1** to **2** and **4**, as elucidated in the cases of the reactions of **1** with carbon disulfide[16] and with 2-formylpyridine.[17]

The mononuclear moiety in **2** and **4** is diastereomeric, owing to both asymmetric 1-carbon and ruthenium atoms (Fig. 1). Accordingly, **4**, which consists of two $\{Ru(NCCH_2CHCN)Cl(CO)(PPh_3)_2\}$ moieties, has two, three, or four diastereoisomers. Indeed, the $^{31}P\{^1H\}$-NMR spectrum of **4** in CH_2Cl_2[18] showed six fairly sharp signals at 20.5, 28.1, 35.1, 45.9, 47.0, and 47.9 ppm to the lower field from 85% H_3PO_4 as an external

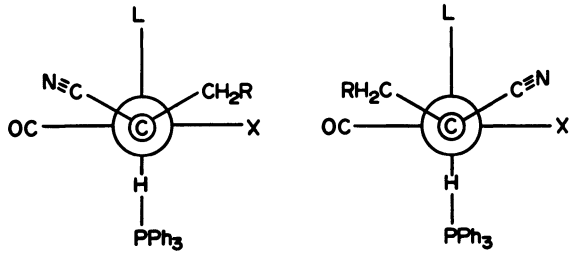

Fig. 1. Diastereoisomerism of $\{Ru(RCH_2CHCN)X(CO)L(PPh_3)\}$ moiety. The ruthenium atom is represented as an outer circle.

reference (virtually equal intensity, each *ca.* 0.45P; without clearly detectable coupling), two fairly broad ones at 23.0 and 30.1 ppm (each intensity, *ca.* 0.25P), and complicated ones in the range of 37.3—43.7 ppm (total intensity, *ca.* 0.8P).[19] Furthermore, it is clearly demonstrated by **10** that each of the $^{31}P\{^1H\}$-NMR signals corresponds to coordinated PPh_3 ligand in each diastereoisomer, unless the signals overlap with each other (*vide infra*). Therefore, the eight signals of **4**, *i.e.*, the six fairly sharp ones and the two fairly broad ones correspond to eight kinds of coordinated PPh_3 ligands due to three diastereoisomers of **4** (Fig. 2)[20] and are inconsistent with types B and D as regards the major components of **4**, since each of these two types would produce two diastereoisomers, and show only four ^{31}P-NMR signals. Accordingly, type A, where two PPh_3 ligands are situated at *cis* positions to each other, is most probable as the mononuclear moiety of the major components of **4** and possibly as that of **2**.[21] This conclusion is strongly supported both by the fact that $[\{Ru(MeCHCN)Cl(CO)(PPh_3)[P(OMe)_3]\}_2]$, derived from **2** and $P(OMe)_3$ at room temperature, exhibited relatively small ^2J(PP) values (26—32 Hz), which were

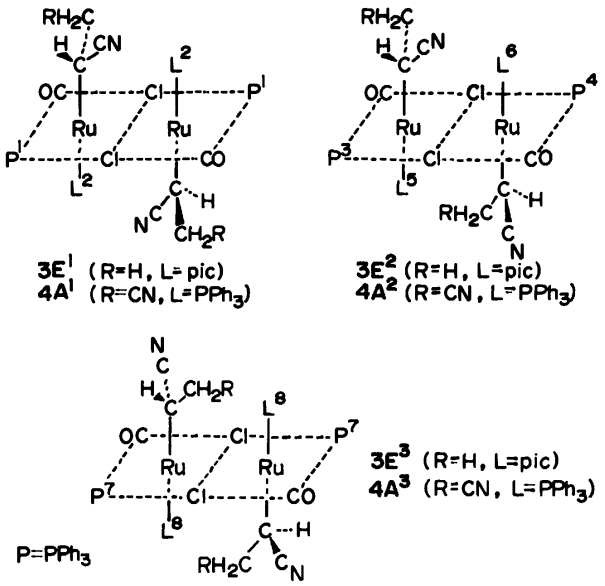

Fig. 2. Proposed structures for the diastereoisomers of **3** or **4**. See Ref. 19 as regards the minor components of **4**.

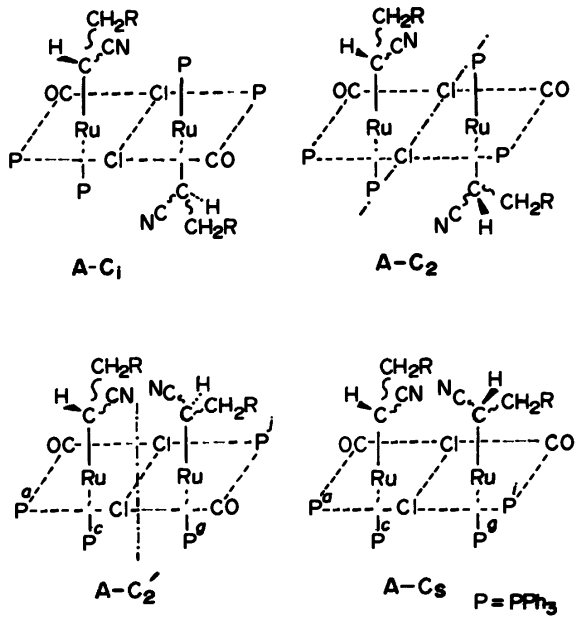

Fig. 3. Possible binuclear structures for **2A** and **4A**. See Ref. 23.

ascribable to *cis*-couplings between two nonequivalent phosphorus nuclei,[22] and by the *cis*-coordination of the two PPh_3 ligands confirmed for the analogous insertion products obtained from **1** and CS_2[16] or 2-formylpyridine[17] at mild conditions.

As for the binuclear structure of **2** or **4**, which consists of two A-typed $\{Ru(RCH_2CHCN)Cl(CO)(PPh_3)_2\}$ moieties, four structures A-C_1, -C_2, -C_2', and -C_s are possible in consideration of their symmetry groups,[23] as shown in Fig. 3. However, structures A-C_2' and -C_s

Table 3. ^{1}H-NMR data of the ruthenium(II) complexes[a]

Complex	1-Cyanoethyl Me[b]	1-Cyanoethyl CH[c]	Other ligand[d]		
3[e]	0.23(3H)	—[f]	2.26(3H,s,Me)[g]		
	0.36(3H)	—[f]	2.37(3H,s,Me)[g]		
5	0.52(1.8H)[h]	1.77(0.6H,q)[h]	6.06(0.6H,t,4-H)[h,i]	6.73(0.6H,d,3-H)[h,i]	8.00(0.6H,b,5-H)[h]
			6.16(0.6H,b,4-H)[h]	6.96(0.6H,d,3-H)[h,i]	
			5.84(1H,t,4-H)[j]	7.64(1.6H,b,3- and 5-H's)	7.80(1H,d,5-H)[i]
	1.36(1.2H)[h]	2.05(0.4H,q)[h]	6.03(0.4H,t,4-H)[h,i]	6.69(0.4H,d,3-H)[h,i]	7.77(0.4H,d,5-H)[h,i]
			6.25(0.4H,t,4-H)[h,i]	7.07(0.4H,d,3-H)[h,i]	7.88(0.4H,b,5-H)[h]
6	1.36(3.6H)	1.64(1.2H,b)	5.92(1H,t,4-H)[i]	6.69(1H,b,3-H)	7.86(0.6H,b,5-H)[j]
	1.24(1.2H)	—[f]	6.03(1H,b,4-H)	6.96(0.6H,b,3-H)	2.60(1H,b,BH)
	0.94(1.2H)	—[f]	6.23(1H,b,4-H)	7.11(0.6H,b,3-H)[j]	
7	0.84(3H)[k]	1.1—1.4(2H,c)	6.00—6.4(4H,c,4-H)[i]		
	0.92(3H)[k]				
9	0.95(4.2H)[k]	—[f]	1.68(4.2H,s,Me)	1.71(4.2H,s,Me)	4.74(1.2H,s,CH)
					4.70(0.2H,s,CH)
	0.93(1.8H)[k]	—[f]	1.62(1.8H,s,Me)	1.64(1.8H,s,Me)	4.76(0.4H,s,CH)
					4.80(0.2H,s,CH)
10	1.00(1.5H)	—[f]	2.34(2.1H,s,Me)[g]	1.56(3H,s,Me)	4.73(0.4H,s,CH)
	0.77(0.6H)	—[f]	2.05(0.6H,s,Me)[g]	1.63(0.6H,s,Me) 1.83(0.6H,s,Me)	5.07(0.2H,s,CH)
	1.16(0.6H)	—[f]		1.68(0.6H,s,Me) 1.89(0.6H,s,Me)	5.13(0.2H,s,CH)
	0.98(0.3H)	—[f]	2.31(0.3H,s,Me)[g]	1.94(0.3H,s,Me) 2.01(0.3H,s,Me)	4.64(0.1H,s,CH)
					5.31(0.05H,s,CH)
					5.52(0.05H,s,CH)

a) Value (ppm). In $CDCl_3$, except **3**. Proton number is given in parentheses. Phenyl protons and pyridine-ring protons are omitted. b) Doublet with $^3J(HH)$=*ca.* 8 Hz, unless noted elsewhere. c) Signal shape is also given in parentheses. d) Signal shape and assignment are also given in parentheses. 3-, 4-, and 5-H's belong to the 1-pyrazolyl groups. e) In CD_2Cl_2. f) Methine proton resonance was obscured by the other signals. g) Methyl group of 4-picoline. h) Resonances in two neighboring lines correspond to one isomer. i) $^3J(HH)$=2—2.3 Hz. j) The other signal was obscured by the phenyl protons. k) Doublet with $^3J(HH)$=*ca.* 7 Hz.

are unfavorable, because these two structures would give rise to considerable steric repulsion between four relatively bulky PPh_3 ligands coordinated together at near positions, *i.e.*, at *a*, *c*, *g*, and *i* or *j* sites. Both structures A-C_2 and -C_8 seem unlikely in consideration of the single ν(C≡O) band (*vide ante*).[24] On the basis of these discussions, both **2** and the major components of **4** are attributable to structure A-C_1.

It is noteworthy that 4-picoline gave rise to the replacement of two PPh_3 ligands in **2** instead of the splitting of the chloro-bridge,[10] to afford **3** with **E**-, **F**-, **G**-, and/or **H**-type structures due to geometrical isomerism and coordination position one (Scheme 1).[25] This replacement was facilitated both by strong trans influence of the 1-cyanoethyl groups located at *trans* positions to the leaving PPh_3 ligands and somewhat by steric interaction between the two *cis*-located PPh_3 ligands in **2**.[16,17] In addition, types **G** and **H** are unfavorable, since each of them is composed of two nonequivalent {Ru(MeCHCN)Cl(CO)LL'} moieties (where L and L' are PPh_3 and/or pic) which would show two ν(C≡O) bands (*vide ante*). Moreover, type **G** is also inadequate, because the second PPh_3 ligand coordinated to the ruthenium atom is insusceptible to the replacement by 4-picoline, owing to the considerably strong *trans* influence of PPh_3. On the basis of these considerations, **3** was assignable to type **E**.

The ^{1}H-NMR spectrum of **3** exhibited both two picoline-methyl resonances at δ 2.26 (3H) and 2.37 (3H) and two doublets at δ 0.23 (3H) and 0.36 (3H), assignable to the methyl protons of the 1-cyanoethyl moieties (Table 3). These data indicate that **3**, which consists of two {Ru(MeCHCN)Cl(CO)(pic)(PPh_3)} moieties, has three diastereoisomers, **3E**^{1}, **3E**^{2}, and **3E**^{3} similar to the cases of **4** (Fig. 2). Indeed, the ^{31}P-{^{1}H}-NMR spectrum in CH_2Cl_2 showed four singlets of a virtually equal intensity at 89.13, 89.25, 95.82, and 95.91 ppm from trimethyl phosphite as an external reference,[5] corresponding to four kinds of PPh_3 ligand in **3E**^{1}, **3E**^{2}, and **3E**^{3}. The population ratio of **3E**^{1}, **3E**^{2}, and **3E**^{3} is virtually 1 : 2 : 1 on the basis of the ^{31}P nuclear resonances, indicating an actually statistical isomer ratio. This implies that acrylonitrile was inserted into the H-Ru bond in **1** in a non-stereoselective fashion.

$BHPz_3$ and BPz_4 Complexes ***5*****—*****7***. The ^{1}H-NMR spectrum of the mononuclear $BHPz_3$ complex **5** exhibited both two sets of doublets at δ 0.52 (1.8H, Me) and 1.36 (1.2H, Me) and two sets of quartets at δ 1.77 (0.6H, CH) and 2.05 (0.4H, CH) (Table 3). These data indicate that **5** consists of two diastereoisomers, with a population ratio of about 6 : 4. Furthermore, **5** showed four triplets in the range of δ 5.8—6.3 and a broad signal at δ 6.16, assignable to 4-H's of the 1-pyrazolyl groups, supporting the existence of the two diastereoisomers.

Thus, the two diastereoisomers were detected for the mononuclear complex, **5**, which contains the C_3-symmetric $BHPz_3$ ligand. This is quite consistent with the three diastereoisomers, proposed for **3**. The two diastereoisomers of **5** could not be separated by the silica gel column chromatography. Similar [hydrotris(1-pyrazolyl)borato]ruthenium(II) complexes, [Ru(C_6H_4–N=NPh-*o*)($BHPz_3$)(CO)$_2$] and [Ru(C_6H_4–N=NPh-*o*,1-*C*,*N*')($BHPz_3$)(CO)] have been reported by Bruce *et al.*[15]

The reaction of **2** with Na[$BHPz_3$] produced a small amount of the binuclear complex, **6**, in which one tridentate [$BHPz_3$] group possibly serves as a bridging ligand. Since **6** contains two PPh_3 ligands per ruthenium atom, similarly to **2**, the relative positions of the two PPh_3 ligands are assumed to remain unchanged during the reaction. Two 1-pyrazolyl groups in the $BHPz_3$ ligand form a six-membered boat-typed ring[26–28] with one of the two ruthenium atoms. The third 1-pyrazolyl group is coordinated to the other ruthenium atom at the *cis* or *trans* position to the 1-carbonyl group. Accordingly, two {Ru(MeCHCN)(CO)(PPh_3)$_2$} moieties in **6** are nonequivalent. It looks unlikely that the third 1-pyrazolyl group is located at the axial site of the six-membered boat-formed Ru-(N-N)$_2$-B ring, because this configuration would give rise to a serious steric interaction between the Pz-Ru(MeCHCN)Cl(CO)(PPh_3)$_2$ moiety and the PPh_3 ligand coordinated

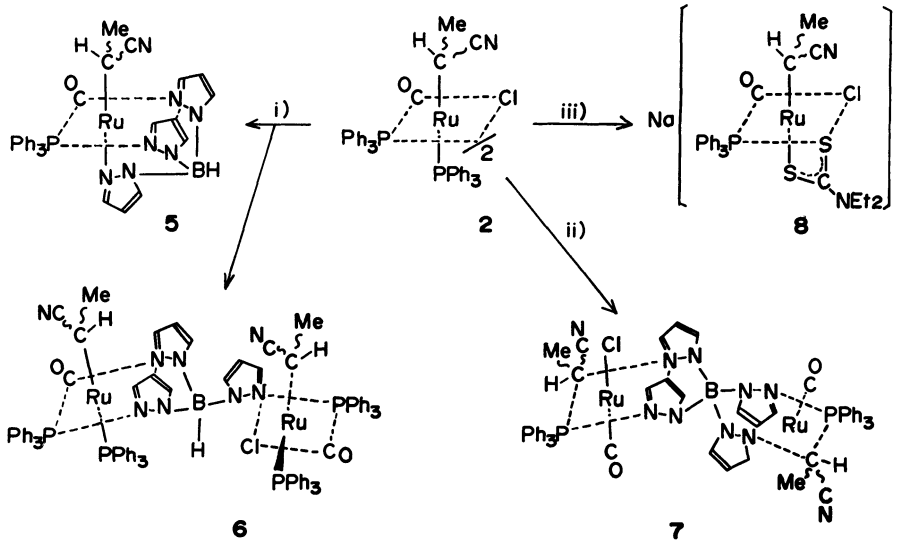

Scheme 2. i) Na[$BHPz_3$] at 40 °C. ii) Na[BPz_4] in refluxing benzene. iii) Na[Et_2NCS_2]·$3H_2O$.

to the first ruthenium atom. Since **6** is associated both with two kinds of diastereoisomerism due to the two nonequivalent [Ru(MeCHCN)(CO)(PPh_3)$_2$] moieties and with one *cis-trans* geometrical isomerism, there are at least eight possible isomers for **6**. However, **6** showed only three doublets at δ 1.36, 1.24, and 0.94 attributable to the methyl protons of the 1-cyanoethyl groups with about 3 : 1 : 1 of intensity ratio. While it is difficult to assign the three doublets to the isomers of **6**, probable configurations for **6** are tentatively shown in Scheme 2.[29] Complex **6** might be an intermediate in the reaction from **2** to **5**.

The binuclear complex, **7** involves one PPh_3 ligand per ruthenium atom in sharp contrast with **6**, and has one quadridentate $[BPz_4]^-$ ligand, which acts as two sets of bidentate chelates, bridging both a {Ru(MeCHCN)-Cl(CO)(PPh_3)} moiety and a {Ru(MeCHCN)(CO)-(PPh_3)} one. Trofimenko[30] has reported on similar bridging $[BPz_4]$-typed complexes, $[(\eta^3\text{-}CH_2CRCH_2)$-$Pd(Pz_2BPz_2)Pd(\eta^3\text{-}CH_2CRCH_2)]^+$.
Then, the two ruthenium atoms in **7** are six- and five coordinate, and nonequivalent. The latter five coordination of the ruthenium(II) complexes is unusual and probably associated with a steric interaction between fairly bulky PPh_3 ligand and BPz_4 one. Analogous five-coordinate ruthenium(II) complex has been reported as regards [Ru(dtim)Cl(PPh_3)$_2$] (dtim=1,3-di-*p*-tolyl-2-imidazolidinylidenato-2-*C*,2'-*C*).[31] On the basis of these discussions, there are many possible isomers for **7**. However, **7** exhibited only two doublets at δ 0.84 and 0.93 for the methyl protons of the 1-cyanoethyl moieties with a vertually equal intensity. Probable configurations for **7** are tentatively shown in Scheme 2,[32] like the case of **6**.

Acac Complexes **9** *and* **10**. The binuclear acac-type complex **9** was obtained together with the mononuclear complex, **10**. These two complexes showed two bands near 1590 and 1510 cm^{-1}, characteristic of the *O,O'*-chelating acac ligand. Complex **9** exhibited a ν(C≡N) band at 2240 cm^{-1}, which is about 20—40 cm^{-1} higher than those of the other (1-cyanoethyl)ruthenium-(II) complexes. The molecular weight of **9** was 1091; Calcd for [{Ru(MeCHCN)(acac)(CO)(PPh_3)}$_2$], 1089. These data indicate that **9** has a binuclear structure, and that two 1-cyanoethyl groups bridge two ruthenium atoms. A bridge structure with the acac-oxygen atoms is unfavorable in **9**. In a non-bridging state, bond angles Ru–C–C(≡N) and C–Ru←N(≡C) in a *cis*-form are expected to be approximately 109°28' and 90°, respectively, and a bonding chain, C–C≡N→Ru is virtually straight. Then, the bridging {Ru–CHMe–C≡N→}$_2$ moiety forms a rhombus or an octagon, and presumably holds more or less strain.

The ^{1}H-NMR spectrum of **9** exhibited four acac-methine proton resonances in an intensity ratio of nearly 6 : 2 : 1 : 1, whereas only two doublets (MeCHCN–) and four acac-methyl proton resonances were distinguished (Table 3). The ^{31}P-{H}-NMR spectrum in CH_2Cl_2 also showed four singlets at 34.6, 54.6, 31.6, and 53.0 ppm to the lower field from 85% H_3PO_4 in the similar intensity ratio to the acac-methine protons. It is noteworthy that the four ^{31}P-NMR signals appeared in unequal intensities as well as the four methine-proton ones did. Furthermore, the Ru–Ru

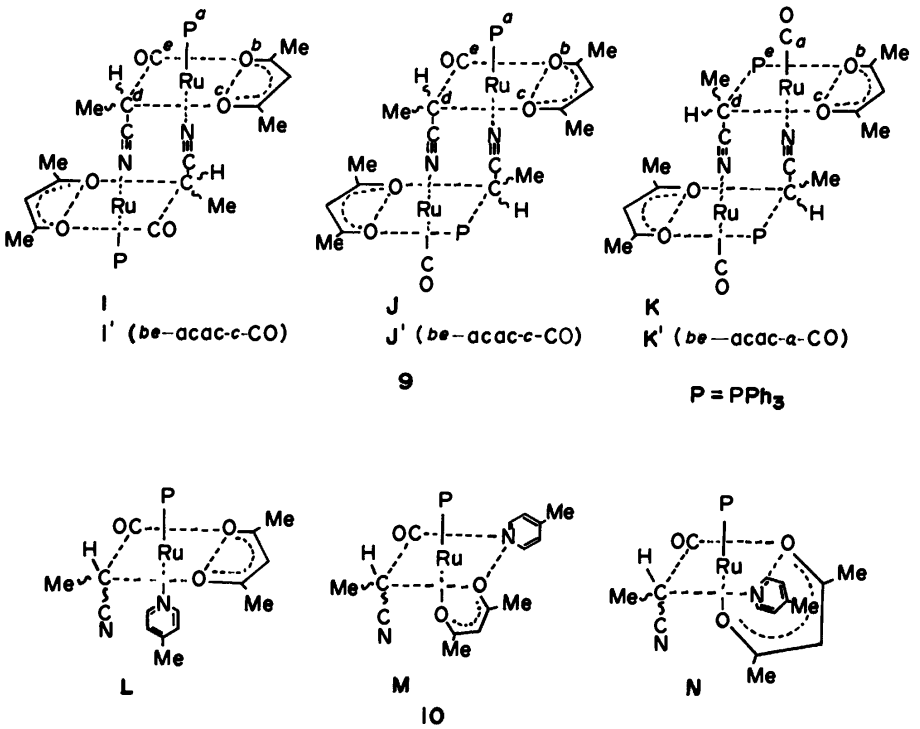

Fig. 4. Proposed structures for the isomers of **9** and **10**. The visual angles for **9** are changed from that in Scheme 1. See Ref. 33 as regards I', J', and K', the geometrical isomers of I, J, and K, respectively.

distance in **9** is so long that the two {Ru(MeCHCN)(acac)(CO)(PPh_3)} moieties have little influence on each other except the bridge formation through the two cyano groups. These facts indicate that the four ^{31}P-NMR signals are not caused by the diastereoisomerism of the binuclear structure of **9**, in contrast with the chloro-bridged binuclear complexes, **3** and **4**, but correspond to four kinds of PPh_3 ligand in the mononuclear {Ru(MeCHCN)(acac)(CO)(PPh_3)} moiety. It is certain that **9** retains PPh_3 and carbonyl and 1-cyanoethyl groups at facial positions together as well as **3** does, since these three ligands show the comparatively strong *trans* influence. Accordingly, the four kinds of PPh_3 ligand are assignable both to the diastereoisomerism due to the asymmetric 1-carbon and ruthenium atoms and to geometrical isomerism exemplified by PPh_3 ligand at *a*- or *e*-site, as shown in Fig. 4. Since the two {Ru(MeCHCN)(acac)(CO)(PPh_3)} moieties are combined in the binuclear structure with fairly free fashion, another geometrical isomerism in the binuclear structure probably takes place to produce new pairs, *e.g.*, I and I'.[33] Thus, **9** was associated with many isomers, as shown in Fig. 4.

Complex **10** contains 4-picoline ligand and is monomeric. Its ^{1}H-NMR spectrum showed six acac-methine proton resonances in an intensity ratio of approximately 4 : 2 : 2 : 1 : 0.5 : 0.5, together with four doublets (MeCHCN–), seven singlets for acac methyl protons and three singlets for picoline-methyl protons (Table 3). The ^{31}P-{^{1}H}-NMR spectrum in CH_2Cl_2 exhibited six singlets, overlapping with each other, at 52.6, 53.8, 54.6, 57.1, 58.2, and 58.9 ppm to the lower field from 85% H_3PO_4. These facts indicate that **10** consists of three geometrical isomers, L, M, and N, each of which contains two diastereoisomers with respect to {Ru(MeCHCN)(CO)(pic)(PPh_3)} moiety. The three ligands, PPh_3 and carbonyl and 1-cyanoethyl groups, which had been coordinated at facial positions in **3**, remain unmoved after the reaction with Tl(acac), by the same reason as the case of **9**. Then, it is certain that no other geometrical isomers than L, M, and N were formed. It is noted that the six isomers for **10** correspond to the ^{31}P-NMR signals very well as well as to the acac-methine proton ones (*vide ante*). Replacement of 4-picoline must take place during the reaction from **3** to two isomers, L and N.

Attempts to separate these isomers were unsuccessful, because chromatographic treatment of **10** yielded a mixture of **9** and **10**. The former complex was produced by liberating 4-picoline from **10** on the silica gel column with adsorbing ability.

Concluding Remarks. The binuclear 1-cyanoethyl complex **2** reacted fairly easily with 4-picoline and some uni-negative chelating ligands to give **3** and **5**—**8**. It is noteworthy that one of the two PPh_3 ligands per ruthenium atom in **2** is easily replaced, except for **6** produced in a low yield. The reaction of **3** with Tl(acac) gave rise both to the detachment of 4-picoline yielding **9** and to the rearrangement of 4-picoline yielding **10**-L and -N, in addition to the normal bridge-cleavage yielding **10**-M. The strong *trans* influence of the 1-cyanoethyl group is responsible for the substitution of the ligand located *trans* to the 1-cyanoethyl group.

The {Ru(RCH_2CHCN)(CO)(PPh_4)} moiety in **3**—**10** contains the asymmetric 1-carbon and ruthenium atoms, and gives rise to the diastereoisomerism. Accordingly, the mononuclear complex **5** involving the C_3-symmetric $BHPz_3$ ligand consists of two isomers, whereas the binuclear complex **3** is composed of three isomers. On the other hand, **6**, **7**, **9**, and **10** consist of several isomers, owing to the nonequivalent {Ru(MeCHCN)(CO)(PPh_3)$_n$} moieties and/or the geometrical isomerism, in addition to the diastereoisomerism.

The authors are grateful to Professor Yasukazu Saito, University of Tokyo, for the valuable discussions of the ^{31}P-NMR spectra and are thankful to Miss Yumi Kojima, Nagasaki University, for her technical assistance.

References

1) A. Misono, Y. Uchida, M. Hidai, and H. Kanai, *J. Chem. Soc., Chem. Commun.*, **1967**, 357.
2) J. D. McClure, R. Owyang, and L. H. Slaugh, *J. Organomet. Chem.*, **12**, 8 (1968).
3) A. Misono, Y. Uchida, M. Hidai, I. Inomata, Y. Watanabe, and M. Takeda, *Kogyo Kagaku Zasshi*, **72**, 1801 (1969).
4) S. Komiya, A. Yamamoto, and S. Ikeda, *Bull. Chem. Soc. Jpn.*, **48**, 101 (1975).
5) K. Hiraki, Y. Sasada, and T. Kitamura, *Chem. Lett.*, **1980**, 449.
6) J. Chatt and R. G. Hayer, *J. Chem. Soc.*, **1963**, 6017.
7) G. Sbrana, G. Braca, and E. Benedetti, *J. Chem. Soc., Dalton Trans.*, **1975**, 754.
8) C. F. J. Barnard, J. A. Daniels, and R.J . Mawby, *J. Chem. Soc., Dalton Trans.*, **1976**, 962; **1979**, 1331.
9) D. J. Cole-Hamilton and G. Wilkinson, *J. Chem. Soc., Dalton Trans.*, **1977**, 797.
10) K. Hiraki, Y. Obayashi, and Y. Oki, *Bull. Chem. Soc. Jpn.*, **52**, 1372 (1979).
11) J. J. Levison and S. D. Robinson, *J. Chem. Soc., A*, **1970**, 2948.
12) S. Trofimenko, *J. Am. Chem. Soc.*, **89**, 3170 (1967).
13) W. H. Nelson, W. J. Randall, and D. F. Martin, *Inorg. Synth.*, IX, 53 (1971).
14) M. I. Bruce and F. G. A. Stone, *J. Chem. Soc., A*, **1967**, 1238.
15) M. I. Bruce, M. Z. Iqbal, and F. G. A. Stone, *J. Chem. Soc., A*, **1971**, 2820.
16) S. D. Robinson and A. Sahajpal, *Inorg. Chem.*, **16**, 2718 (1977).
17) K. Hiraki, R. Katayama, K. Yamaguchi, and S. Honda, *Inorg. Chim. Acta.*, **59**, 11 (1982).
18) Owing to the poor solubility of **4**, its ^{31}P-{^{1}H}-NMR spectrum in CH_2Cl_2 was recorded after 17300 pulses for 14.4 h by the FT-NMR spectrometer.
19) The complicated signals were associated with a few minor components. However, these signals could not be analyzed clearly owing to overlapping with noise.
20) See the next section, with respect to the binuclear structure. The two smaller signals at 23.0 and 30.1 ppm may be attributable to a diastereoisomer with a small population ratio, presumably owing to stereochemical requirement.
21) It was erroneous that [{Ru(MeCHCN)Cl(CO)(PPh_3)$_2$}$_2$] had two sets of two *trans*-located PPh_3 ligands in Ref. 5.

22) K. Hiraki and N. Ochi, Unpublished data.
23) Both substituents upon the 1-carbon atom of the 1-cyanoethyl groups and those upon phosphorus atoms are ignored as for the symmetry.
24) Hypotetical structures for the diastereoisomers of **2** belonging to the C_2 or the C_s symmetry group and for their 4-picoline-substitution products are able to be drawn in similar manners as described for **4A** and **3E**, respectively (Fig. 2).
25) It was erroneous that the 4-picoline ligands in [{Ru(MeCHCN)Cl(CO)(pic)(PPh_3)}$_2$] were situated at *trans* positions to the remaining PPh_3 ligands in Ref. 5.
26) J. L. Calderon, F. A. Cotton, and A. Shaver, *J. Organometal. Chem.*, **38**, 105 (1972).
27) M. Onishi, K. Sugimura, and K. Hiraki, *Bull. Chem. Soc. Jpn.*, **51**, 3209 (1978).
28) M. Onishi, K. Hiraki, M. Shironita, Y. Yamaguchi, and S. Nakagawa, *Bull. Chem. Soc. Jpn.*, **53**, 961 (1980).
29) There are also the other possible configurations for **6**.
30) S. Trofimenko, *J. Coord. Chem.*, **2**, 75 (1972).
31) P. B. Hitchock, M. F. Lappert, P. L. Pye, and S. Thomas, *J. Chem. Soc., Dalton Trans.*, **1979**, 1929.
32) There are also the other possible configurations for **7**.
33) As for I′, J′, and K′, the geometrical isomers of I, J, and K, respectively, the coordination sites only for the acac ligand and carbonyl group are given in parentheses in Fig. 4 for simplification.

Structures of Cys-containing Peptide Complexes of Pd(II) in Organic Solvents

Norikazu UEYAMA, Kazuko SASAKI, Michio NAKATA, and Akira NAKAMURA*
Department of Macromolecular Science, Faculty of Science, Osaka University, Toyonaka, Osaka 560
(Received September 16, 1981)

Cysteine-containing peptide (pep) complexes of Pd(II) have been synthesized and their structures in organic solvents such as dimethyl sulfoxide (Me_2SO) and *N,N*-dimethylformamide (DMF) were examined by use of ^1H-, ^{13}C-NMR, visible, and CD spectroscopies. In all cases of the Pd(II) complexes, only the thiolato group of the peptides coordinates to the metal. Upon mixing $[PdCl_4]^{2-}$ and the peptide, a *trans*(*S*) isomer $[PdCl_2(pep)_2]^{2-}$ immediately forms, which gradually isomerizes to the *cis*(*S*) isomer at 20 °C in DMF. The reactivity of Pd(II)–S bonds in these complexes was examined by addition of 2,2′-bipyridyl, 2-mercaptoethanol, or 3,4-toluenedithiol.

Transition metal complexes of amino acids, and oligo- and polypeptides have been investigated on the basis of their importan e for providing fundamental chemical information about the coordination environment of metal ions in metalloenzymes and metalloproteins. The thiolato group of cysteine has been found to coordinate to bioactive metal ions such as Fe, Cu, Mo, Zn *etc.*, for example, in ferredoxin,[1] molybdoenzymes,[2] and blue copper proteins.[3] Recently, Ni(II)–cysteine thiolato bonding has been verified in urease.[4]

We have focussed our research efforts upon establishing the coordination behavior of a variety of cysteine-containing oligopeptides to d-block transition metal ions. Cysteine-containing peptides are generally air sensitive and are not easily prepared or purified because of the reactive thiol groups. The heavy metal ions usually form polynuclear complexes with alkanethiols through thiolato bridges (μ-thiolato groups),[5] and these complexes defy attempts to elucidate their structures by conventional chemical techniques.

We have chosen Pd(II) as the metal ion for the present investigation because a) it forms complexes which are usually square planar and diamagnetic, b) it possesses a high affinity for thiolato ligands and suitable rates in ligand exchange reactions, c) fairly intense electronic absorptions in the visible region are expected, and d) it resists electron-transfer reduction by the thiolato ligand, which helps the characterization process.

The general importance of aqueous media in the study of peptide/metal ion systems has provided an impetus for investigation of structures in aqueous solutions.[6,7] However, the active sites of many metalloenzymes or metalloproteins are found to be in hydrophobic parts of the proteins. These findings prompted us to study aprotic solutions of metal/peptide systems. The behaviour and structures of metal peptide complexes in such solutions were found to be totally different in some cases.

In this paper, Pd(II) complexes of Cys-containing peptides such as *N*-acetyl-L-cysteine(Ac-Cys), *N*-benzyloxycarbonyl-L-alanyl-L-cysteine methyl ester (Z-Ala-Cys-OMe) and *N*-benzyloxycarbonyl-L-prolyl-L-cysteine methyl ester (Z-Pro-Cys-OMe) were investigated in aprotic solvents such as *N,N*-dimethylformamide (DMF) and dimethyl sulfoxide (Me_2SO). For comparison, $Na_2[PdCl_2(Z\text{-}Ala\text{-}cys\text{-}OMe)_2]$ and $Na_2[PdCl_2(Z\text{-}Pro\text{-}cys\text{-}OMe)_2]$ were synthesized by the direct reactions of Na_2PdCl_4 with the corresponding Cys(Acm)-peptides (Acm=acetamidomethyl). In order to help to identify the part of amino acid residues coordinating to a metal, we used lower case symbols, *e.g.* cys, in the chemical formulas.

Experimental

Starting Materials. All solvents were distilled by standard procedures and stored under nitrogen. 2,2′-Bipyridyl, 3,4-toluenedithiol, and 2-mercaptoethanol used were of reagent grade quality. Ac-Cys was gifted by Sun-Orient Chemical Co. The preparations of Z-Ala-Cys(Acm)-OMe and Z-Pro-Cys(Acm)-OMe and the deprotections of their Cys(Acm) residue will be metioned elsewhere.[8]

Preparations. *1)* $Na_2[PdCl_2(Ac\text{-}cys)_2]\cdot 1/2(DMF)$: To a solution of Ac-Cys (0.4 g, 2.5×10^{-3} mol) in DMF (5 cm^3), 7 cm^3 of a Na_2PdCl_4 (0.36 g, 1.25×10^{-3} mol) solution in DMF was added, followed by the addition of ethyl acetate (50 cm^3). An orange powder precipitated immediately, which was collected, washed with ethyl acetate, and dried over silica gel. Found: C, 23.86; H, 3.81; N, 5.62%. Calcd for $C_{11.5}H_{19.5}N_{2.5}O_{6.5}S_2Cl_2PdNa_2$: C, 23.64; H, 3.36; N, 5.99%. ^1H NMR signals were observed at 2.9, 3.0, and 8.0 ppm assignable to DMF.

2) $Na_2[PdCl_2(Z\text{-}Ala\text{-}cys\text{-}OMe)_2]$[8b]: To a solution of Z-Ala-Cys(Acm)-OMe (0.2 g, 5.9×10^{-4} mol) in DMF (3 cm^3), 7 cm^3 of a Na_2PdCl_4 (0.09 g, 3.0×10^{-4} mol) solution in DMF was added, and stirred overnight. Water (50 cm^3) saturated with NaCl was added, and the powder precipitated was collected, washed with water, and dried. Found: C, 38.92; H, 4.35; N, 6.34%. Calcd for $C_{30}H_{38}N_4O_{10}S_2Cl_2PdNa_2$: C, 39.94; H, 4.25; N, 6.21%. Molar conductivity of the complex in DMF was 19.7 S cm^2 $equiv.^{-1}$ (5 mmol/dm^3, 20 °C).

3) $Na_2[PdCl_2(Z\text{-}Pro\text{-}cys\text{-}OMe)_2]$: This complex was prepared by the same procedure used for the synthesis of *1*). Found: C, 43.95; H, 4.85; N, 6.61%.† Calcd for $C_{34}H_{42}N_4O_{10}S_2Cl_2PdNa_2$: C, 42.79; H, 4.44; N, 5.90%. The molar conductivity was 14 S cm^2 $equiv.^{-1}$ in DMF (7.8 mmol/dm^3, 20 °C).

Spectral Measurement. To a DMF solution of an oligopeptide (concentration: approximately 2×10^{-3} mol/dm^3), a solution of Na_2PdCl_4 in DMF was added in appropriate molar ratios at room temperature. A Varian XL-100 was used to obtain ^1H- and ^{13}C-NMR spectra. CD spectra were recorded on a JASCO J-40 spectropolarimeter. Visible spectra and IR spectra were obtained on JASCO UVIDEC 5A and Hitachi

† The Cl ligand of the Pd(II) complexes was found gradually substituted with water. Drying *in vacuo* results in slight change in the values of elemental analysis.

Table 1. Circular dichroism spectra of Pd(II)–oligopeptide complexes in DMF at room temperature

Complex	Molar ratio (metal : ligand)	λ/nm[a] (Δε)					
Pd/Ac-Cys	(1 : 1)	540 (+0.04)	442 (+0.13)		376 (+0.17)	340 (+0.07)	312 (−0.97)
Pd/Ac-Cys	(1 : 2)	510 (−0.02)	470 (−0.34)		404 (−0.70)	351 (−0.60)	319 (−0.78)
Pd/Z-Ala-Cys-OMe	(1 : 1)		430 (+0.09)	399 (−0.06)	375 (+0.15)		309 (−0.88)
Pd/Z-Ala-Cys-OMe	(1 : 2)		485 (−0.28)	436 (+0.16)	396 (−0.57)	350 (+1.05)	318 (−0.76)
Pd/Z-Pro-Cys-OMe	(1 : 1)		428 (+0.18)	390 (−0.08)	360 (+0.03)		314 (−0.06)
Pd/Z-Pro-Cys-OMe	(1 : 2)		493 (−0.23)	438 (+0.17)	382 (−0.50)	343 (+0.16)	

a) These spectra were obtained after 24 h, and the Δε values were calculated on the basis of the concentration of Pd(II) ion.

FIR-3. CD spectra of the complexes on ligand substitution were also recorded after addition of 2,2′-bipyridyl, 3,4-toluenedithiol, and 2-mercaptoethanol to the DMF solution of these complexes with the corresponding molar ratios.

Results and Discussion

Stoichiometry of Interaction of Pd(II) with Cys-containing Peptides. Reactions between Pd(II) and Cys-containing oligopeptides were investigated stoichiometrically. CD and visible spectra of the reaction products in DMF solutions were obtained with various molar ratios of Pd(II) to peptide. When a molar ratio of 1 : 2 was taken, a Pd(II)/peptide (1 : 2) complex was formed immediately. CD and visible spectra of the solution changed slowly on standing. After 24 h, a (1 : 1) and another isomeric (1 : 2) complex were found to be formed, as indicated by the CD spectra. The transitions and absorptions of the CD and visible spectra thus obtained are listed in Tables 1 and 2. The similarities among the CD spectra of the Pd(II) complexes of Ac-Cys, Z-Ala-Cys-OMe, and Z-Pro-Cys-OMe suggest coordination of the same portion of the peptide to the metal atom in each case.

Functional Groups Coordinating to Pd(II). Pd(II)/Ac-Cys Complexes: As the simplest member of Cys-containing peptides, complexes of Ac-Cys were examined. Ac-Cys has i) a thiolato group, ii) a nitrogen atom in the amide bond, iii) an oxygen atom in the amide bond, and iv) an oxygen atom in the carboxylic acid part as possible donor sites. The ^{1}H- and ^{13}C-NMR spectra of Pd(II)/Ac-Cys (1 : 1) and (1 : 2) complexes

Table 2. Visible spectra of Pd(II)–oligopeptide complexes in DMF at room temperature

Complex	Molar ratio (metal : ligand)	λ/nm[a] (ε×10^{-3})		
Pd/Ac-Cys	(1 : 1)	390 (1.6)		310 (5.5)
Pd/Ac-Cys	(1 : 2)	405 (2.8)	370 (3.6)	310 (6.8)
Pd/Z-Ala-Cys-OMe	(1 : 1)	386 (1.4)		305 (5.2)
Pd/Z-Ala-Cys-OMe	(1 : 2)	380 (2.2)		310 (6.6)
Pd/Z-Pro-Cys-OMe	(1 : 1)	386 (1.3)		307 (5.0)
Pd/Z-Pro-Cys-OMe	(1 : 2)	382 (1.8)		309 (5.7)

a) ε was calculated on the basis of the concentration of Pd(II) ion.

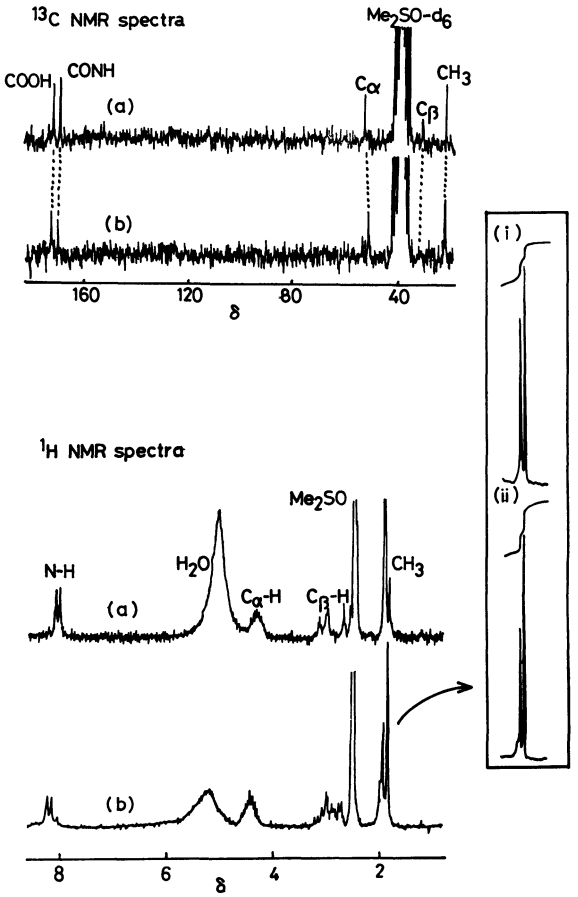

Fig. 1. ^{1}H- and ^{13}C-NMR spectra of Pd(II)/Ac-Cys in Me_2SO-d_6 at room temperature with a) the molar ratio of Pd(II)/Ac-Cys=1/1 and b)=1/2. The inset spectra show the time dependence of methyl signals in ^{1}H NMR spectra in Me_2SO-d_6 at 70 °C (Pd(II)/Ac-Cys=1/1). The spectra were taken i) after 1 h and ii) after 21.5 h.

in Me_2SO-d_6 are shown in Fig. 1. There were negligible differences between the spectra obtained in Me_2SO-d_6 and DMF, and similar spectra were obtained in each solvent. In the ^{13}C-NMR spectra, the resonance due to C_β of the cysteine residue was shifted downfield on complexation. The C_β of the (1 : 2) complex was observed with broadening at 33.73 ppm. A larger shift of Cys C_β (8.31 ppm from the C_β of the SH-free cysteine residue) for the (1 : 2) complex compared with that of the (1 : 1) complex (5.84 ppm from the Cys C_β of the SH-free cysteine) indicates the formation of the (1 : 2) complex with a stronger Pd(II)–S bond.

Possibility of the coordination of the other donor groups occurring in organic solvents was examined by recording the ^1H- and ^{13}C-NMR spectra. Especially, a deprotonated nitrogen atom in the amide bond is a potential candidate as a ligand group. For example, most of the known metal-peptide complexes have a metal-nitrogen bond formed by the deprotonated amide group[6,7] and a metal-oxygen bond with the carboxyl group[9] in aqueous solution.

Two carbon peaks around 170 ppm are assignable to the carbons of the amide and carboxylic acid groups. The shift of the signal of either the (1 : 1) or (1 : 2) complex from that of free Ac-Cys was observed to be less than 0.3 ppm. This fact suggests that only the thiolato group of Ac-Cys coordinates to the metal in Me_2SO-d_6 as illustrated in the following scheme. The H^+ released on the thiol of Ac-Cys should protonate the solvent such as DMF since the CD spectrum of the Pd(II)/Ac-Cys (1 : 2) complex with addition of the equimolar triethylamine remained the same. Fuhr and

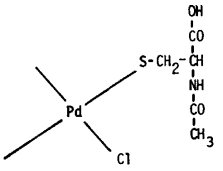

Rabenstein reported that Zn(II)/glutathione mixtures in aqueous solution provided a carbon signal due to Glu–CONH with a shift of 0.2 ppm from free glutathione.[10] Ionization of the peptide protons at pD 10.5 is followed by bonding of Zn(II) to the anionic N atom. Shifts of 0.8—1.0 ppm of the amide carbon and 1.0—3.0 ppm for the carboxyl carbon are observed, presumably due to their coordination to the Zn atom. The absence of deprotonation in the Pd(II)–peptide complex was also supported by the ^1H NMR spectra shown in Fig. 1. One NH proton was observed at 8.19 ppm for the (1 : 1) complex, and at 8.31 ppm for the (1 : 2) complex. The chemical shift values clearly show the absence of amide group coordination. Even if the amide NH is involved in coordination, a broad NH peak will be observed. As proton peak from contaminating water observed at 5.1—8.0 ppm (see Fig. 1) reveals that proton exchange between water and carboxylic acid occurs in Me_2SO-d_6. Usually, a peak assignable to water contaminated in the commercial Me_2SO-d_6 was observed at about 3 ppm, shifting to 5.1 ppm with an increase in the amount of water. The presence of the exchangeable proton assignable to the carboxyl group clearly indicates that the carboxylic acid part of the AcCys ligand does not coordinate to the metal.

TABLE 3. ^1H-NMR SPECTRA OF Cys-CONTAINING OLIGOPEPTIDES AND THE CORRESPONDING Pd(II) COMPLEXES IN Me_2SO-d_6 AT ROOM TEMPERATURE[11]

Compound	N–H region ppm	C_α–H region ppm
Ac-Cys	8.33	4.33
$Na_2[PdCl_2(Ac\text{-}cys)_2]$	8.31	4.43
Z-Ala-Cys-OMe	8.38(Cys)	4.50(Cys)
	7.3(Ala)	4.12(Ala)
$Na_2[PdCl_2(Z\text{-}Ala\text{-}cys\text{-}OMe)_2]$	8.32(cys)	4.70(cys)
	7.3(Ala)	4.14(Ala)
Z-Pro-Cys-OMe	8.38(Cys)	4.52(Cys)
		4.30(Pro)
$Na_2[PdCl_2(Z\text{-}Pro\text{-}cys\text{-}OMe)_2]$	8.24(cys)	4.70(cys)
		4.26(Pro)

Pd(II) Complexes of Dipeptides. The Pd(II) complexes of Z-Ala-Cys-OMe and Z-Pro-Cys-OMe, of which the amino- and carboxylic acid-ends are protected, were examined by CD and visible spectra. The

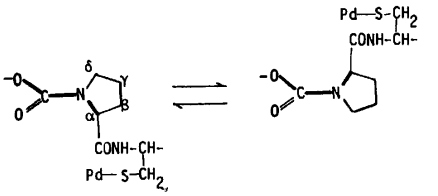

trans conformer *cis* conformer

same type of (1 : 2) complexes derived from the corresponding S-blocked peptides and Na_2PdCl_4 were isolated, which are air-stable and soluble in DMF, Me_2SO, methanol, or acetonitrile. The spectra of the isolated Pd(II) complexes were essentially the same as those of the reaction mixtures of $[PdCl_4]^{2-}$ and the SH peptides.

Table 3 shows the chemical shifts of the N–H and C_α–H protons for the isolated Pd(II) complexes. The urethane N–H signal of $[PdCl_2(Z\text{-}Ala\text{-}cys\text{-}OMe)_2]^{2-}$, which was overlapped with that of the benzyl protons, was made observable by the upfield shift of the peak resulting from the addition of chloroform. This observation indicates that even the more basic urethane group than the amide group was not involved in coordination.

The simple monodentate coordination through the thiolato group was supported by the ^{13}C-NMR spectra. The *cis* and *trans* conformers resulting from the planarity of the urethane bond in the above equilibrium were detectable by using the ^{13}C-NMR spectra of $[PdCl_2(Z\text{-}Pro\text{-}cys\text{-}OMe)_2]^{2-}$ in Me_2SO-d_6. The *cis* and *trans* signals of Pro C_β and C_γ which present in the equilibrium were clearly observed at 30.5 and 23.5 ppm, respectively. Assignments of the *cis* and *trans* signals of Pro C_β or C_γ were carried out according to the chemical shifts of a number of Pro-containing peptides in Me_2SO-d_6 assigned by Dorman and Bovey.[12] The same probabilities of the *cis* and *trans* conformers as those of the S-blocked peptide as shown in Fig. 3 imply that only the thiolato group is involved in the coordination. If

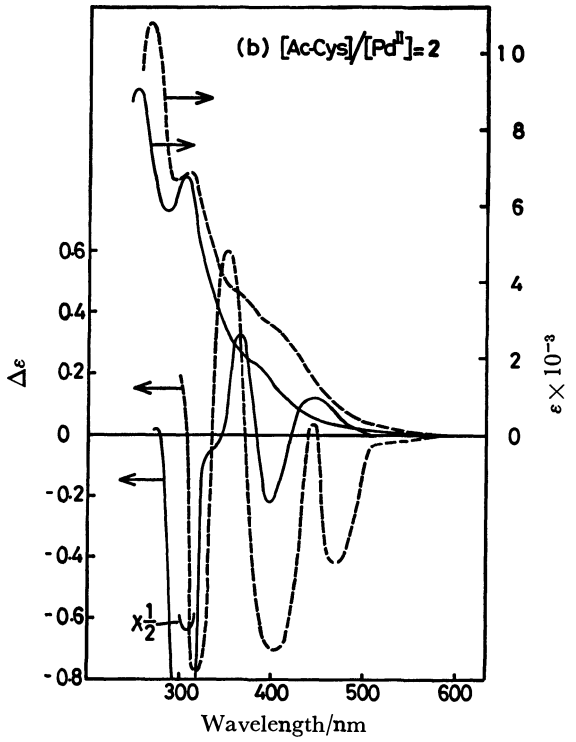

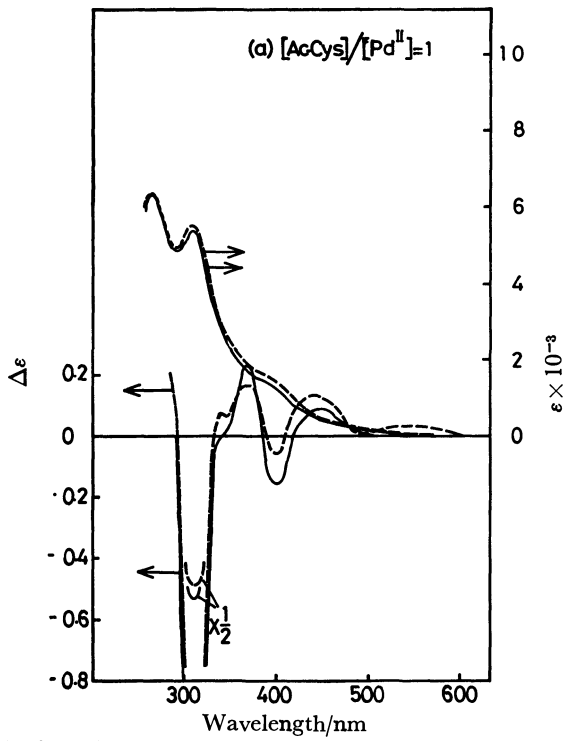

Fig. 2. Time dependence of the CD and visible spectra of Pd(II)/Ac-Cys= a) 1/1 and b) 1/2 in DMF at room temperature. The spectra after 10 min are represented by (——) and after 38 h by (------).

the N atom of the Pro residue coordinates to the metal, the probability of the *cis* or *trans* conformers will change with the coordination in the above equilibrium.

The presence of chloride ligands on the Pd(II) may not favor coordination of the amide nitrogen atoms of

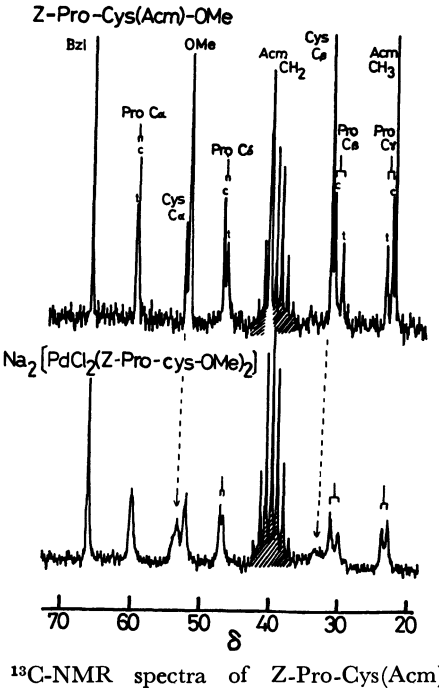

Fig. 3. ^{13}C-NMR spectra of Z-Pro-Cys(Acm)-OMe (Acm=acetamidomethyl) and $Na_2[PdCl_2(Z\text{-Pro-cys-OMe})_2]$ in Me_2SO-d_6 at room temperature.

the peptides used in this study. Therefore $Pd(NO_3)_2$ was used to further examine Pd(II)/peptide interactions in DMF. The CD spectrum of $Pd(NO_3)_2$/Z-Ala-Cys-OMe indicated the presence of the same type of the (1 : 2) complex as that of $PdCl_4^{2-}$/Z-Ala-Cys-OMe. The solvent seems to occupy the remaining coordination sites on Pd(II) in the case of $Pd(NO_3)_2$. Addition of NR_4Cl to the solution gave the same $[PdCl_2(Z\text{-Ala-cys-OMe})_2]^{2-}$ anion as prepared from $PdCl_4^{2-}$. Thus, absence of the amide coordination is one of the consequences of solvent effect coupled with the influence of thiolato coordination on the metal.

Infrared absorptions of these complexes are listed in Table 4 in comparison with those of the peptides themselves. The ν(S–H) band in all the peptides examined at 2500—2600 cm^{-1} disappeared in the Pd(II) complexes because of the coordination of the thiolato group to the metal. No shift of the ν(C=O) band of the Pd/Ac-Cys complex from the band of the free carboxylic acid was observed. The coordination of carboxylate usually results in thift to the lower wave number (1600—1650 cm^{-1}).[6] The bands of ν(N–H) and ν(C–O) of the amide group for all complexes remained unchanged. Observation of the bands due to Pd(II)–S and Pd(II)–Cl in the far infrared region indicates that the complexes possess a $PdCl_2S_2$ core.

Therefore the visible absorption and CD transitions mentioned above (Tables 1 and 2) should be due to the chromophore of the $PdCl_2S_2$ core. A visible absorption at 370—405 nm in Table 2 corresponds mainly to the overlapped bands of the d-d transitions of the Pd(II) ion.[13,14] On the other hand, an absorption around 310 nm is assignable to a charge transfer band (Pd(II)–S).[13,14] These bands are similar to the charge transfer band of $Pd(cys\text{-}OEt)_2$ at 312 nm,[15] and a d-d transition

TABLE 4. SELECTED IR FREQUENCIES OF Cys-CONTAINING OLIGOPEPTIDES AND THE CORRESPONDINGPd(II) COMPLEXES IN SOLID STATE

Compound	IR (ν/cm^{-1})				
	ν(N–H)	ν(S–H)	ν(C=O)	ν(Pd–S)	(Pd–Cl)
Ac-Cys	3360	2450	1710[a)] 1640[b)]		
$Na_2[PdCl_2(Ac\text{-}cys)_2]$	3250br	—	1730[a)] 1645[b)]	388	330
Z-Ala-Cys-OMe	3320	2570	1725[a)] 1680 1640[b)]		
$Na_2[PdCl_2(Z\text{-}Ala\text{-}cys\text{-}OMe)_2]$	3300br	—	1725[c)] 1660br[d)]	360	320
Z-Pro-Cys-OMe	3310	2590	1740[c)] 1690 1665[b)]		
$Na_2[PdCl_2(Z\text{-}Pro\text{-}cys\text{-}OMe)_2]$	3300	—	1740[c)] 1670br	362	310

a) Assignable to carbonyl group of free carboxylic acid. b) Carbonyl group of amide. c) Carbonyl group of ester. d) br refers to a broad band.

at 423 nm and a charge transfer band at 319 nm of $Pd(cys)_2$.[16] In the d-d transitions, the transitions of d_{xy}-$d_{x^2-y^2}$ and d_{xy},d_{yx}-$d_{x^2y^2}$ are magnetic dipole-allowed, while the transition of d_{xy}-$d_{x^2-y^2}$ is magnetic dipole-forbidden. The CD peak of the former transitions should be strongest and that of the latter transition should be weakest. In the CD spectra of the isolated (1 : 2) complexes in Table 1, the bands at about 480 nm are therefore assignable to d_{xy}-$d_{x^2-y^2}$ transition, and the positive peaks about 435 nm and the negative peaks about 390 nm to the d_{xy},d_{xy}-$d_{x^2-y^2}$ transitions. The strong peaks around 350 and 320 nm correspond to charge transfer bands (Pd(II)–S).

Coordination Geometry of Pd(II)/Peptide Complexes. Two acetyl peaks in the ^{1}H-NMR spectrum of the 1 : 2 complex, as shown in Fig. 1, were observed at 1.94 and 1.86 ppm. The latter peak grew up gradually at 70 °C, as shown in the inset of Fig. 1. In addition, the peaks due to NH and contaminating water were observed intact even after the solution was kept overnight. The water peak at 5.4 ppm indicates the existence of a proton exchange between water and –COOH because a peak of usual water in Me_2SO-d_6 should be observed between 2.5 and 5.1 ppm. The results indicate the interchange between *trans*(*S*) and *cis*(*S*) isomers of the $[PdCl_2(Ac\text{-}cys)_2]^{2-}$ complex. This interconversion was also observed in the CD and visible spectra. The *cis*(*S*) (1 : 2) complex could be isolated from a mixture of DMF and ethyl acetate, and the *cis*(*S*) isomer is thus thermodynamically more stable. Pneumatikakis and Hadjiliadis[6] concluded that a medium intensity band at 330 cm^{-1} for $PdCl_2(cys\text{-}OMe)_2$ which was immediately isolated after mixing $PdCl_4^{2-}$ and Cys-OMe is due to ν(Pd–Cl) stretching of a *trans*(*S*) isomer. Similarly the $Na_2[PdCl_2(Ac\text{-}cys)_2]$ isolated immediately showed a band at 330 cm^{-1} due to ν(Pd–Cl) of a *trans*(*S*) isomer. The same (1 : 2) complex obtained after aging overnight in DMF at 70 °C showed a few broad bands at 320—340 cm^{-1} due to ν(Pd–Cl) of a *cis*(*S*) isomer.

Figure 2 shows the CD and visible spectra of the DMF solution of Pd(II)/Ac-Cys (1 : 1) and (1 : 2) after 10 min or after one day from complex formation. The CD patterns of the both complexes are similar immediately after reaction, indicating formation of a (1 : 2) complex. The spectrum of the (1 : 1) solution does not change with time significantly, but that of the (1 : 2) solution clearly changes at 470 and 404 nm in DMF. The same trend was observed in the visible spectra. The absorption coefficient of the (1 : 2) solution after 1 d was 1.7 times larger than that after 10 min. This slow interchange between the *trans*(*S*) and *cis*(*S*) isomers with time is illustrated in the following scheme. A kinetically-controlled formation of the

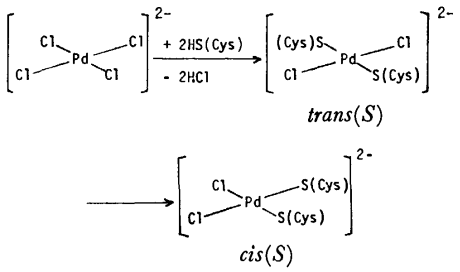

trans(*S*)

cis(*S*)

trans(*S*) isomer occurs immediately when $[PdCl_4]^{2-}$ and Ac-Cys are mixed. Then the complex isomerizes to a thermo-dynamically stabilized *cis*(*S*) form. A visible absorption of the *cis*(*S*) isomer (local C_{2v} symmetry) is known to be stronger than that for the *trans*(*S*) isomer (local D_{2h} symmetry).[9,17] Also, the stronger CD peak should be expected for the *cis*(*S*) isomer compared to that for the *trans*(*S*) isomer, in which the dipole moment is negligible. Figure 2(b) shows the peaks of d-d transitions at 472 nm in the CD spectra shifting to a longer wavelength. These results indicate that d electrons are delocalized over the PdS_2 core and the Pd(II)–S bond is stabilized in the *cis*(*S*) complexes.

In the case of the (1 : 1) solution, the *trans*(*S*) (1 : 2) isomer may form as an intermediate and is converted to polynuclear complexes. Similar complexes were formed by the corresponding dipeptides.

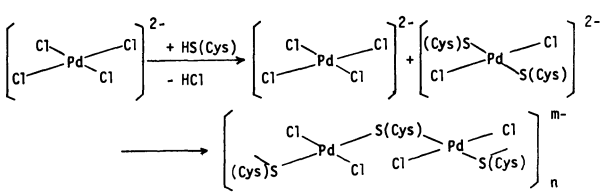

Reactivity of the Pd(II)–Dipeptide Complexes. The strength of the Pd(II)–thiolate bond was examined as follows. Addition of 3,4-toluenedithiol, 2-mercaptoethanol, or 2,2′-bipyridyl results in cleavage of the weaker bonds among the Pd(II)–S or Pd(II)–Cl bonds of the $PdCl_2S_2$ core. Figure 4 shows the spectral changes

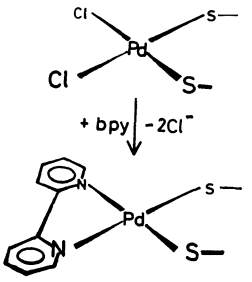

that occurred on addition of the above ligands to $Na_2[PdCl_2(Z\text{-Ala-cys-OMe})_2]$. Addition of 3,4-toluenedithiol first diminished the $\Delta\varepsilon$ values of the CD peaks. Addition of two molar equivalents of 3,4-toluenedithiol then results in complete disappearance of the CD peaks, while in the visible spectra, a d-d band at 860 nm and a charge transfer band at 360 nm were observed due to the formation of $[Pd(dithiolato)_2]^{2-}$. The results indicate that the 3,4-toluenedithiol easily breaks Pd(II)–Cl and Pd(II)–S(Cys) bonds because of its *cis*(*S*) chelating effect and the formation of an electron-delocalized complex having strong Pd(II)–S(–Ph–) bonds.

On the other hand, addition of 2-mercaptoethanol, which is a primary thiol, as is the cysteine residue, induced the formation of a different complex with two moles of the thiol to one mol of the Pd(II). Addition

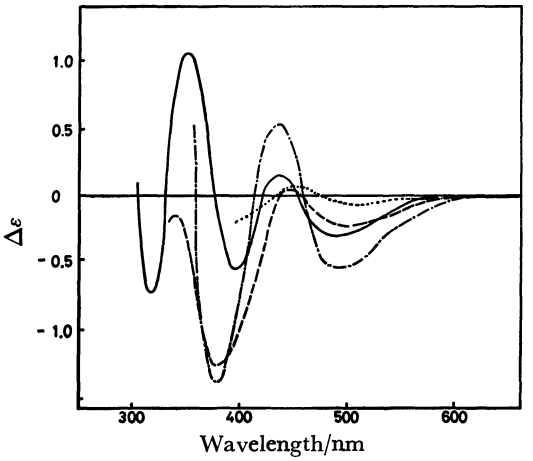

Fig. 4. CD-spectral change of $Na_2[PdCl_2(Z\text{-Ala-cys-OMe})_2]$ (——) in DMF upon addition of 2,2′-bipyridyl (– – –), 2-mercaptoethanol (–·–·–), and 3,4-toluenedithiol (------), the ratio, Pd(II)/additive, is 1/2.

of larger amounts of the thiol over the (1 : 2) molar ratio does not change the spectrum. These results clearly indicate the formation of $[Pd(SCH_2CH_2OH)_2(Z\text{-Ala-cys-OMe})_2]^{2-}$ which contains a PdS_4 core. 2-Mercaptoethanol cleaves the Pd(II)–Cl bonds, but does not affect the original Pd(II)–S bonds. Although simple thiols such as CH_3SH, PhSH, *etc.*, usually give polynuclear complexes $[Pd(SR)_2]_n$, the Pd(II)/peptide complex system containing a cysteine residue does not form a $[Pd(S(cys))_4]^{2-}$ or polynuclear species because of the steric hindrance around the cysteine thiolato group.

The CD spectrum obtained by addition of 2,2′-bipyridyl at a (1 : 1) molar ratio does not change with further addition of 2,2′-bipyridyl. Two chloride ligands of the complex are easily replaced by one 2,2′-bipyridyl. However, the Pd(II)–S bonds are resistant to such a substitution with 2,2′-bipyridyl.

It is plausible that the entering ligand such as 2,2′-bipyridyl or 3,4-toluenedithiol would give a transient five-coordinate intermediate with a trigonal bipyramidal configuration. Then each of the *cis*(*S*) or *trans*(*S*) complex provides the same *cis*(*S*) complex having the chelating ligand. However, further information is necessary for discussing the mechanism of such ligand substitution reaction.

Conclusion. Cys-containing peptides coordinate to Pd(II) ions through only the thiolato group in organic solvents, giving (1 : 1) and (1 : 2) Pd(II)–peptide complexes. A (1 : 2) molar ratio of reagents gives the kinetically controlled *trans*(*S*) isomers immediately, which are subsequently converted to the *cis*(*S*)-isomers. The Pd(II)–S bonds of the *cis*(*S*) complexes are not cleavable even with the strong donor ligand such as 2,2′-bipyridyl.

References

1) W. H. Orme-Johnson, *Annu. Rev. Biochem.*, **42**, 159 (1973).

2) S. P. Cramer, H. B. Gray, and K. V. Rajagopalan, *J. Am. Chem. Soc.*, **101**, 2772 (1979).

3) E. I. Solomon, J. W. Hare, D. M. Dooley, J.H. Dawsow, P. J. Stephens, and H. B. Gray, *J. Am. Chem. Soc.*, **102**, 168 (1980).

4) N. E. Dixon, C. Gazzola, R. L. Blakeley, and B. Zerner, *J. Am. Chem. Soc.*, **97**, 4131 (1975); N. E. Dioxon, R. L. Blakely, and B. Zerner, *Science*, **191**, 1144 (1976).

5) J. Boschi, B. Crociani, L. Toniolo, and U. Belluco, *Inorg. Chem.*, **9**, 532 (1970).

6) G. Pneumatikakis and N. Hadjilidas, *J. Inorg. Nucl. Chem.*, **41**, 429 (1979).

7) B. J. Trzebiatowska G. F. Kozlowska, and H. Kozlowski, *Bull. Acad. Pol. Sci., Ser. Sci. Chim.*, **26**, 561 (1978).

8) a) The experimentals for syntheses of Z-Ala-Cys-OMe and Z-Pro-Cys-OMe will be described elsewhere by N. Ueyama, M. Nakata, and A. Nakamura; b) The direct synthesis of Pd(II) complexes from $PdCl_4^{2-}$ and Cys(Acm)-containing peptides will be mentioned in detail elsewhere.

9) For example; E. A. Sullivan, *Can. J. Chem.* **57**, 62 (1979); Y. Wu and D. H. Busch, *J. Am. Chem. Soc.*, **94**, 4115 (1972).

10) B. J. Fuhr and D. L. Rabenstein, *J. Am. Chem. Soc.*, **95**, 6944 (1973).

11) All of the ^{1}H-NMR spectral data of these oligopeptides will be described elsewhere.
12) D. E. Dorman and F. A. Bovey, *J. Org. Chem.*, **38**, 2379 (1973).
13) T. Tarantelli and C. Furlani, *J. Chem. Soc., A*, **1971**, 1213.
14) H. Ito, J. Fujita, and K. Saito, *Bull. Chem. Soc. Jpn.*, **40**, 2584 (1967).
15) M. Chandrasekharan, M. R. Udupa, and G. Aravamudan, *J. Inorg. Nucl. Chem.*, **36**, 1417 (1974).
16) M. Chandrankharan, M. R. Udupa, and G. Aravamudan, *Inorg. Chim. Acta*, **7**, 88 (1973).
17) J. S. Coe and J. R. Lyons, *J. Chem. Soc., A*, **1971**, 829.

 © 1982 The Chemical Society of Japan Bull. Chem. Soc. Jpn., 55, 2371—2377 (1982)

Syntheses, Structure, and Properties of Several Bis(*O,O'*-dialkyl dithiophosphato)cobalt(II)Adducts[1)]

Mamoru Shimoi,* Akira Ouchi, Takashi Uehiro, Yukichi Yoshino,††
Shoichi Sato,† and Yoshihiko Saito†,†††

Department of Chemistry, College of General Education, The University of Tokyo, Komaba 3-8-1, Meguro-ku, Tokyo 153

†*The Institute for Solid State Physics, The University of Tokyo, Roppongi-7, Minato-ku, Tokyo 106*

(Received November 5, 1981)

Several amine or phosphine adducts of bis (*O,O'*-dialkyl dithiophosphato)cobalt(II), which were hardly oxidized in air at room temperature, were obtained as crystalline solids. The crystal and molecular structure of one adduct, $Co(Me_2dtp)_2$(triphenylphosphine) (Me_2dtp=*O,O'*-dimethyl dithiophosphato group), was determined by means of the X-ray diffraction method. The crystal is monoclinic: space group $P2_1/n$, a=26.712(4), b=9.495(1), c=11.180(5) Å, β=95.43(3)°, Z=4, D_x=1.495, D_m=1.45 g cm^{-3}, μ(Mo $K\alpha$)=1.17 mm^{-1}, and the final R value obtained is 0.062 for 4466 observed reflections. The coordinated atoms around the cobalt atom are in a trigonal bipyramidal configuration. The approximate first formation constants of the adducts, K=[Co(II)$(R_2dtp)_2$·X]/{[Co(II)$(R_2dtp)_2$][X]} (R=alkyl group, and X=donor) in solution, were obtained by means of the spectrophotometric as well as the NMR technique.

Dithioacid ions, such as *N,N*-dialkyl dithiocarbamate, *O*-alkyl dithiocarbonate, and *O,O'*-dialkyl dithiophosphate ions, are able to make four-membered chelates with 3d transition metals. Among them, the *O,O'*-dialkyl dithiophosphato chelates have various properties different from those of common Werner-type complexes. For example, bis(*O,O'*-diethyl dithiophosphato)nickel(II) (abbreviated as Ni(II)$(Et_2dtp)_2$ hereafter; the related complexes are also shown by the same type of abbreviation) is typical, and many studies have already been published about the complex itself as well as its adducts.[2-5)] On the other hand, only a few publications are to be found about Co(II)$(Et_2dtp)_2$, although Cavell and others[6)] have reported the isolation of Co(II)-$(Et_2dtp)_2$, and Jørgensen[7,8)] claimed the formation of its ethanol adducts in solution. This is probably because of the low stability of the complex. By way of studying sulfur-coordinated metal complexes, we found that, contrary to Co(II)$(R_2dtp)_2$ (R=alkyl group), some amine or phosphine adducts of them were very stable when once obtained in their solid state; they could be kept in air at room temperature for many months without any decomposition or air-oxidation.

As Co(II)$(Et_2dtp)_2$ is in a tetrahedral configuration, the geometry of the originally bonded Et_2dtp must be seriously affected by the formation of its adducts, while in the case of Ni(II)$(Et_2dtp)_2$, which is originally in a square planar form, the positions of the ligands are not much moved by the coordination of additional ligands. The adduct of the Co(II)$(R_2dtp)_2$·X_n type (where X=donor) will exhibit either a trigonal bipyramidal or a square pyramidal coordination around the central metal atom. In order to elucidate the geometry of the adduct, we have determined the crystal and molecular structure by means of the X-ray diffraction method.

Although the Co(II)$(R_2dtp)_2$·X_n adducts (n=1 or 2) are very stable in their solid states, they are easily hydrolyzed with water and are turned into hexaaquacobalt(II) ions in a dilute aqueous solution. The R_2dtp ligands are bonded strongly to the cobalt(II) atom in the complexes in a non-polar organic solvent, although a rapid broadening of the R_2dtp alkyl proton peak due to the ligand-exchange reaction between the two chelates is observed in their NMR spectra when the cobalt(II) complexes or their adducts in solution are added to a solution of the R_2dtp complexes of other diamagnetic metal ions, such as zinc(II) or cadmium(II).

On the other hand, the donor, X, of the Co(II)-$(R_2dtp)_2$·X adduct is shown to be labile in an organic solvent, and the equilibrium,

$$Co(II)(R_2dtp)_2 + X = Co(II)(R_2dtp)_2\cdot X$$

is attained soon after they are dissolved. Therefore, when more of the donor is added to a solution of the adduct, it shows more resistivity to air-oxidation. A quantitative study of the equilibrium will be presented in the later part of this paper.

Experimental

Synthesis of Adducts. All the chemicals used were GR-grade from Wako Pure Chemicals Co., Ltd., and were used without any further purification. The Co(II)$(R_2dtp)_2$·X_n (n=1 or 2) were synthesized as follows.

Synthesis of Co(II)$(Et_2dtp)_2$(hexamethylenetetramine). The benzene solution of cobalt(II)$(Et_2dtp)_2$ was obtained by extracting it from a mixture of cobalt(II) chloride hexahydrate (0.7 g, 3 mmol) and Na(Et_2dtp) (1.2 g, 6 mmol) in a concentrated aqueous solution with benzene. After the addition of an excess of hexamethyleneteramine (0.9 g, 6.4 mmol), the obtained mixture was stirred for several min, after which the supernatant fluid was separated and evaporated by the use of a vacuum rotary evaporator. From the residue, the adduct was extracted with a hot mixture of benzene and ligroine (1/1=v/v); crystals came out when it was cooled. Found: Co, 10.27; C, 29.74; H, 5.69; N, 10.01%. Calcd for $CoC_{14}H_{32}O_4P_2S_4$: Co, 10.35; C, 29.52; H, 5.66; N, 9.84%. Yield, 1.3 g (77%).

Synthesis of Co(II)$(Et_2dtp)_2$(triphenylphosphine). Six tenth of a gram (2.5 mmol) of cobalt(II) chloride hexahydrate, 1.1 g

†† Present address: Department of Chemistry, Faculty of Science, Toho University, Miyama, Funabashi, Chiba 274.

††† Present address: Department of Chemistry, Faculty of Science and Technology, Keio University, Hiyoshi 3-14-1, Kohoku-ku, Yokohama, Kanagawa 223.

(5.4 mmol) of $Na(Et_2dtp)$, about 20 cm^3 of a benzene solution containing 1.5 g (5.7 mmol) of triphenylphosphine, and 1 cm^3 of water were mixed and stirred for several min, after which benzene layer was separated and dried with anhydrous sodium sulfate. The solution was evaporated, and the residue was recrystallized from ligroine. Found: Co, 8.52; C, 45.24; H, 5.10%. Calcd for $CoC_{26}H_{35}O_4P_3S_3$: Co, 8.52; C, 45.15; H, 5.10%. Yield, 1.1 g (64%).

Synthesis of Co(II)(Me_2dtp)$_2$(triphenylphosphine) (Where Me=CH_3). This complex was synthesized in almost the same way as the Co(II)(Et_2dtp)$_2$(triphenylphosphine) described above by using 0.6 g (2.5 mmol) of cobalt(II) chloride hexahydrate and 0.9 g (3.0 mmol) of $Na(Me_2dtp)$. As the complex is more sensitive to air oxidation than Et_2dtp derivative, it was recrystallized from benzene–hexane (1/1=v/v) mixed solvent under a nitrogen atmosphere. Found: Co, 9.20; C, 41.16; H, 4.27%. Calcd for $CoC_{22}H_{27}O_4P_3S_3$: Co, 9.27; C, 41.58; H, 4.29%. Yield 0.8 g (50%).

Synthesis of Cobalt(II)(Et_2dtp)$_2$(benzothiazole)$_2$. This adduct was synthesized in the same way as was used for the triphenylphosphine adduct of Co(II)(Et_2dtp)$_2$, starting from 0.47 g (2 mmol) of cobalt(II) chloride hexahydrate, 0.83 g (4 mmol) of $Na(Et_2dtp)$, and 0.81 g (6 mmol) of benzothiazole. Recrystallized from ligroine. Found: Co, 8.41; C, 37,82; H, 4.33; N, 3.96%. Calcd for $CoC_{22}H_{30}O_4N_2P_2S_6$: Co, 8.42; C, 37.76; H, 4.32; N, 4.00%. Yield, 0.75 g (54%).

Synthesis of Co(II)(Et_2dtp)$_2$(benzothiazole). This adduct was obtained by the same method as was the bis adduct described above, except that a lower molar ratio of benzothiazole to cobalt(II) chloride was employed. For example, from 0.7 g (3 mmol) of cobalt(II) chloride hexahydrate, 1.25 g (6 mmol) of $Na(Et_2dtp)$, and 0.81 g (6 mmol) of benzothiazole, the mono-adduct was obtained as a blue green solid in a low yield. From the mother liquor, the bis-adduct was obtained, too. Found: Co, 10.34; C, 32.03; H, 4.47; N, 2.48%. Calcd for $CoC_{15}H_{25}NP_4S_5$: Co, 10.44; C, 31.91; H, 4.46; N, 2.48%. Yield, 0.4 g (24%).

Synthesis of Co(II)(Et_2dtp)$_2$(benzimidazole). The crude product was obtained by mixing and stirring 0.95 g (4 mmol) of cobalt(II) chloride hexahydrate, 1.7 g (8 mmol) of $Na(Et_2dtp)$, about 10 cm^3 of an acetone solution containing 0.9 g (8 mmol) of benzimidazole, 20 cm^3 of benzene, and 1 cm^3 of water, and by then evaporating the fluid. The residue containing the crude adduct was recrystallized from benzene. Found: Co, 8.64; C, 39.86; H, 4.85; N, 8.44%. Calcd for $CoC_{22}O_4N_4P_2S_4$: Co, 8.85; C, 39.70; H, 4.85; N, 8.42%. Yield, 1.6 g (73%).

Synthesis of Co(II)(Et_2dtp)$_2$(piperazine). This adduct was synthesized, using 2-propanol in place of benzene as the solvent, by means of the method used for the benzimidazole adduct mentioned above. We started with 0.71 g (3 mmol) of cobalt(II)chloride hexahydrate, 1.25 g (6 mmol) of Na(Et_2dtp), and 0.5 g (6 mmol) of piperazine. Recrystallized from ligroine. Found: Co, 11.57; C, 27.85; H, 5.76; N, 5.43%. Calcd for $CoC_{12}H_{30}O_4N_2P_2S_4$: Co, 11.43; C, 27.96; H, 5.87; N, 5.43%. Yield, 0.95 g (62%).

Synthesis of Co(II)(Et_2dtp)$_2$(pyrazine). To about 20 cm^3 of a benzene solution containing 0.16 g (2 mmol) of pyrazine, 1 cm^3 of water, 0.4 g (2 mmol) of $Na(Et_2dtp)$, and 0.24 g (1 mmol) of cobalt(II) chloride hexahydrate were added, after which the mixture was stirred for several min. The adduct was then precipitated, filtered, and washed with water. Recrystallized from the benzene–ligroine mixture (1/1=v/v). Found: Co, 11.50; C, 28.30; H, 4.73; N, 5.49%. Calcd for $CoC_{12}H_{24}O_4N_2P_2S_4$: Co, 11.57; C, 28.29; H, 4.75; N, 5.50%. Yield, 0.7 g (69%).

Attempt to Synthesize the 4,4'-Bipyridine Adduct of Co(II)(Et_2dtp)$_2$. Although many kinds of synthetic techinques have been applied to obtain the adduct, they have not been successful. It was found that the addition of 4,4'-bipyridine to a solution of Co(II)(Et_2dtp)$_2$ rather accelerated the air oxidation of the complex.

X-Ray Measurement. The single crystal of bis(*O,O'*-dimethyl dithiophosphato)(triphenylphosphine)cobalt(II) used for the X-ray measurement was a parallelepiped 0.28×0.35×0.39 mm^3 in size. All the edges of the crystal were ground off beforehand. The crystallographic data are: $CoC_{22}H_{27}O_4P_3S_4$, F. W.=635.55, monoclinic, space group $P2_1/n$,** a=26.712(4), b=9.495(1), c=11.180(5) Å, β=95.43(3)°, Z=4, D_x=1.495, D_m=1.45 g cm^{-3}, μ(Mo $K\alpha$)=1.17 mm^{-1}. The reflections within the range of $2\theta<55°$ were collected on a Rigaku automated four-circle diffractometer, with Mo $K\alpha$ radiation (0.7107 Å), the ω scan technique being employed. In total, 4466 independent reflections with $|F_o|>3\sigma(|F_o|)$ among the 6819 measured ones were used for the structure refinement. The intensities were corrected for Lorentz and polarization factors, but no correction was made for absorption and extinction. No decrease in the intensities attributable to the decomposition of the sample was recognized during the intensity measurement.

The calculations were mainly carried out on the FACOM 230-48 computer at The Institute for Solid State Physics, The University of Tokyo, but a part of them were done on the HITAC 8800/8700 computer at The Computer Center of The University of Tokyo, using the local version of the UNICS program.[9] The atomic-scattering factors were taken from the tables.[10]

Structure Determination. The structure was solved by the heavy-atom method. The positions of the Co, P, and S atoms were deduced from three-dimensional Patterson maps, while all the other non-hydrogen atoms were located by successive Fourier syntheses. Their positional and thermal parameters were refined by the block-diagonal least-squares method. Then the positions of all the hydrogen atoms, except one, were obtained from a difference Fourier synthesis, they were also refined. The coordinates of the H atom, H(1-2), that could not be located by the difference synthesis, was supplied by calculation. The isotropic temperature factor of 10.0 $Å^2$ was assumed for it. Anisotropic temperature factors were assumed for all non-hydrogen atoms. In the last cycle of the refinement, all the parameter shifts were less than one-third of the corresponding standard deviations. The final R value was 0.062 for 4466 reflections.[11]

Other Measurements. The megnetic monents of the solid products were measured using a Gouy balance at room temtemperature (20—15 °C).

The infrared absorption spectra were obtained by a Nujol and hexachloro-1,3-butadiene mull procedure using a 403G-type infrared spectrophotometer of JASCO, Ltd.

The visible spectra were recorded on Hitachi EPS-3- and Hitachi 124-type spectrophotometers. The reflectance spectra of the solid adducts were measured by a Hitachi 124-type spectrophotometer using an attachment. The temperatures of the sample solution and of the cell chamber were kept constant by circulating thermostated water through using a Haake F 4391 thermostat.

The ^1H-NMR spectra were obtained using a JEOL JNM-MH-100 (100 MHz) NMR spectrometer (TMS as the internal standard).

** The systematic absence of the reflections were those of $0k0$ (where k=odd) and those of $h0l$ (where $h+l$=odd).

TABLE 1. FINAL ATOMIC COORDINATES ($\times 10^4$ FOR NON-HYDROGEN ATOMS, AND $\times 10^3$ FOR HYDROGEN ATOMS) AND ISOTROPIC TEMPERATURE FACTORS (B/Å^2), WITH ESTIMATED STANDARD DEVIATIONS IN PARENTHESES

Atom	x	y	z	B_{eq}/Å^2 a)
Co	1455.9(3)	2253.9(7)	4684.1(7)	3.99
S(1)	1766.1(6)	118(2)	5453(2)	5.82
S(2)	648.0(6)	1361(2)	5507(2)	5.15
S(3)	1447.4(5)	4320(1)	5810(1)	3.85
S(4)	2363.7(6)	3218(2)	4301(2)	5.15
P(1)	1103.5(7)	−107(2)	6146(1)	4.85
P(2)	2085.1(5)	4827(1)	5115(1)	3.20
P(3)	996.4(5)	2285(1)	2577(1)	3.28
O(1)	1132(2)	−16(5)	7568(4)	7.12
O(2)	901(2)	−1655(4)	5973(4)	5.58
O(3)	1945(1)	6117(4)	4256(3)	3.76
O(4)	2495(1)	5419(4)	6102(3)	4.33
C(1)	1360(3)	−1063(8)	8312(5)	6.63
C(2)	781(3)	−2232(6)	4801(6)	5.24
C(3)	2327(3)	6773(8)	3622(6)	5.79
C(4)	2375(2)	6607(7)	6842(5)	5.16
C(5)	1297(2)	2958(5)	1287(4)	3.05
C(6)	1569(2)	4194(5)	1447(5)	3.88
C(7)	1785(2)	4797(6)	486(5)	4.64
C(8)	1735(2)	4167(6)	−622(5)	4.40
C(9)	1467(2)	2949(6)	−786(5)	4.25
C(10)	1249(2)	2332(6)	168(5)	3.87
C(11)	815(2)	495(5)	2152(4)	3.25
C(12)	1194(2)	−441(6)	1913(5)	4.31
C(13)	1075(3)	−1834(6)	1636(5)	5.06
C(14)	595(3)	−2315(6)	1629(5)	5.23
C(15)	223(2)	−1413(7)	1886(5)	5.08
C(16)	326(2)	−8(6)	2143(5)	4.25
C(17)	414(2)	3313(5)	2442(4)	3.05
C(18)	90(2)	3335(7)	1410(5)	4.54
C(19)	−338(2)	4168(8)	1339(5)	5.13
C(20)	−431(2)	5012(6)	2280(6)	4.26
C(21)	−110(2)	5013(6)	3295(4)	4.27
C(22)	314(2)	4178(5)	3392(4)	3.69

Atom	x	y	z	B_{iso}/Å^2
H(1-1)	137(3)	−81(10)	916(8)	12.5(27)
H(1-2)	169	−107	804	10.0
H(1-3)	127(3)	−198(8)	819(6)	8.4(19)
H(2-1)	75(2)	−313(7)	488(5)	6.3(15)
H(2-2)	110(4)	−196(10)	446(9)	14.0(31)
H(2-3)	55(2)	−178(6)	440(5)	5.8(14)
H(3-1)	258(2)	699(7)	409(6)	7.1(17)
H(3-2)	248(2)	598(8)	312(5)	8.0(18)
H(3-3)	220(3)	724(9)	319(7)	11.2(25)
H(4-1)	213(2)	646(7)	708(5)	6.7(16)
H(4-2)	266(3)	657(9)	754(7)	11.5(25)
H(4-3)	239(3)	749(7)	630(6)	7.6(18)
H(6)	163(2)	461(5)	214(4)	3.8(11)
H(7)	201(2)	548(7)	68(5)	6.8(16)
H(8)	191(2)	448(6)	−123(5)	5.1(13)
H(9)	149(2)	259(5)	−142(4)	3.6(11)
H(10)	106(2)	150(7)	−6(5)	6.5(15)
H(12)	157(2)	−5(6)	192(5)	6.1(15)
H(13)	134(2)	−233(5)	152(4)	3.9(11)
H(14)	52(2)	−326(5)	151(4)	3.8(11)
H(15)	−15(2)	−169(6)	199(5)	5.6(14)
H(16)	7(2)	62(6)	239(4)	4.7(12)
H(18)	15(2)	288(7)	77(6)	7.4(17)
H(19)	−51(2)	430(7)	64(6)	7.1(16)
H(20)	−70(2)	557(5)	223(4)	4.2(12)
H(21)	−18(2)	555(6)	388(5)	5.1(13)
H(22)	55(2)	416(6)	405(5)	5.3(13)

a) The equivalent isotropic temperature factors for non-hydrogen atoms were computed using the following expression: $B_{eq}=(4/3)(B_{11}a^2+B_{22}b^2+B_{33}c^2+B_{13}ac\cos\beta)$. The B_{ij}'s are defined by: $\exp[-(h^2B_{11}+k^2B_{22}+l^2B_{33}+2klB_{23}+2hlB_{13}+2hkB_{12})]$.

Results and Discussion

The crystal structure of bis(*O*,*O*′-dimethyl dithiophosphato)(triphenylphosphine)cobalt(II) will now be summarized. The final atomic parameters are listed in Table 1,[12] while the interatomic distances as well as bond angles are given in Table 2. A perspective drawing of the complex and a partial numbering scheme of the atoms are shown in Fig. 1. The remaining

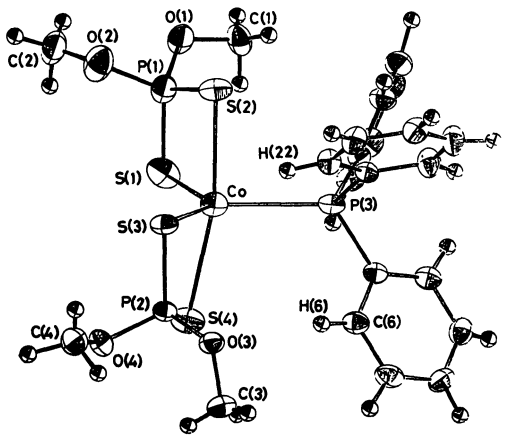

Fig. 1. A perspective drawing of [Co(II){$S_2P(OCH_3)_2$}$_2$-{$P(C_6H_5)_3$}], with their numbering scheme of atoms. (A part of the numbering scheme is shown; see text.)

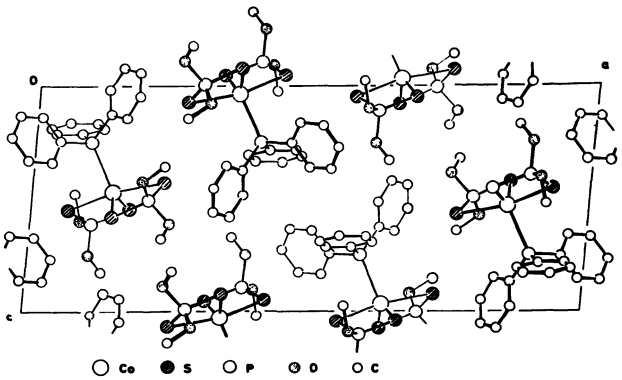

Fig. 2. Crystal packing diagram projected along b.

Table 2. Interatomic distances and bond angles, with estimated standard deviations in parentheses

Interatomic distance l/Å			
Co–S(1)	2.325(2)	C(6)–C(7)	1.390(8)
Co–S(2)	2.569(2)	C(7)–C(8)	1.370(8)
Co–S(3)	2.333(2)	C(8)–C(9)	1.363(8)
Co–S(4)	2.664(2)	C(9)–C(10)	1.391(8)
Co–P(3)	2.551(2)	C(10)–C(5)	1.380(7)
S(1)–P(1)	2.010(3)	C(11)–C(12)	1.392(8)
S(2)–P(1)	1.941(2)	C(12)–C(13)	1.388(8)
P(1)–O(1)	1.586(5)	C(13)–C(14)	1.362(10)
P(1)–O(2)	1.572(4)	C(14)–C(15)	1.363(9)
O(1)–C(1)	1.399(9)	C(15)–C(16)	1.386(8)
O(2)–C(2)	1.429(7)	C(16)–C(11)	1.390(7)
S(3)–P(2)	1.997(2)	C(17)–C(18)	1.376(7)
S(4)–P(2)	1.960(2)	C(18)–C(19)	1.385(9)
P(2)–O(3)	1.580(4)	C(19)–C(20)	1.363(8)
P(2)–O(4)	1.582(4)	C(20)–C(21)	1.356(7)
O(3)–C(3)	1.438(8)	C(21)–C(22)	1.379(8)
O(4)–C(4)	1.452(7)	C(22)–C(17)	1.389(7)
P(3)–C(5)	1.831(5)	S(3)···H(22)	2.95(5)
P(3)–C(11)	1.818(5)	S(2)···H(22)	3.11(6)
P(3)–C(17)	1.830(5)	S(4)···H(6)	3.24(5)
C(5)–C(6)	1.383(7)	S(4)···C(6)	3.776(6)
Bond angle ϕ/°			
S(1)–Co–S(3)	123.75(6)	Co–P(3)–C(11)	108.9(2)
S(1)–Co–P(3)	118.36(6)	Co–P(3)–C(17)	114.4(2)
S(3)–Co–P(3)	117.40(5)	C(5)–P(3)–C(11)	104.2(2)
S(1)–Co–S(2)	82.05(6)	C(11)–P(3)–C(17)	105.9(2)
S(3)–Co–S(4)	81.55(5)	C(17)–P(3)–C(5)	100.4(2)
S(2)–Co–S(4)	168.32(6)	P(3)–C(5)–C(6)	117.3(4)
S(2)–Co–P(3)	89.28(5)	P(3)–C(5)–C(10)	123.7(4)
S(4)–Co–P(3)	102.31(5)	C(10)–C(5)–C(6)	119.0(5)
S(1)–P(1)–S(2)	109.04(10)	C(5)–C(6)–C(7)	120.0(5)
S(1)–P(1)–O(1)	114.9(2)	C(6)–C(7)–C(8)	120.5(5)
S(1)–P(1)–O(2)	110.9(2)	C(7)–C(8)–C(9)	119.8(5)
S(2)–P(1)–O(1)	107.4(2)	C(8)–C(9)–C(10)	120.4(5)
S(2)–P(1)–O(2)	115.5(2)	C(9)–C(10)–C(5)	120.3(5)
O(1)–P(1)–O(2)	99.1(2)	P(3)–C(11)–C(12)	117.8(4)
P(1)–O(1)–C(1)	122.3(5)	P(3)–C(11)–C(16)	123.4(4)
P(1)–O(2)–C(2)	121.1(4)	C(16)–C(11)–C(12)	118.6(5)
S(3)–P(2)–S(4)	111.61(9)	C(11)–C(12)–C(13)	119.8(5)
S(3)–P(2)–O(3)	105.2(2)	C(12)–C(13)–C(14)	121.0(6)
S(3)–P(2)–O(4)	111.9(2)	C(13)–C(14)–C(15)	119.6(6)
S(4)–P(2)–O(3)	113.6(2)	C(14)–C(15)–C(16)	120.9(6)
S(4)–P(2)–O(4)	109.4(2)	C(15)–C(16)–C(11)	120.0(5)
O(3)–P(2)–O(4)	104.9(2)	P(3)–C(17)–C(18)	122.7(4)
P(2)–O(3)–C(3)	119.8(4)	P(3)–C(17)–C(22)	118.4(4)
P(2)–O(4)–C(4)	119.9(3)	C(22)–C(17)–C(18)	118.7(4)
Co–S(1)–P(1)	86.50(8)	C(17)–C(18)–C(19)	120.5(5)
Co–S(2)–P(1)	81.39(8)	C(18)–C(19)–C(20)	120.1(5)
Co–S(3)–P(2)	86.58(7)	C(19)–C(20)–C(21)	120.0(5)
Co–S(4)–P(2)	78.57(7)	C(20)–C(21)–C(22)	121.0(5)
Co–P(3)–C(5)	121.6(2)	C(21)–C(22)–C(17)	119.8(5)

numberings are: the phenyl carbons of the triphenylphosphine ligand are C(5)–C(10), C(11)–C(16), and C(17)–C(22) for those of the I, II, and III phenyl groups respectively, where C(5), C(11), and C(17) are bonded to P(3). The numbering of each hydrogen atom is the same as that of the phenyl carbon atom to which it is bonded. The hydrogen atoms of the methyl groups of Me_2dtp ligands are numbered H(n-1—3), where n is the number of the bonded methyl carbon atom. The arrangement of the molecules in a unit cell is shown in Fig. 2 (projection along the b axis).

The crystal consists of discrete molecules of [Co(II)-

TABLE 3. SPECTRAL AND MAGNETIC PROPERTIES OF THE ADDUCTS, $[Co(II)(Et_2dtp)_2L_n]$ (Et_2dtp=DIETHYL DITHIOPHOSPHATO LIGAND), IN THEIR SOLID STATE

n	L	Color		Reflectance spectra $\nu/10^3$ cm^{-1}				Magnetic moment $\frac{\mu}{BM^{a)}}$
		Solid	Benzene solution					
1	PPh_3	Green	Greenish blue	15.6	16.9			4.5
1	hex	Blue	Blue	15.6	17.7			4.5
1	bzt	Greenish blue	Green	16.0	17.2			4.5
1	pip	Red violet	Blue	15.7	17.0	18.5	19.6	5.1
1	pyr	Yellow	Green	16.3	17.4	18.3	19.3	5.0
2	bzt	Yellow brown	Green	16.1	17.9	18.6	20.0	5.0
2	bzi	Red violet	Blue	16.1	17.0	18.9	20.5	5.0

PPh_3=Triphenylphosphine, hex=hexamethylenetetramine, bzt=benzothiazole, pip=piperazine, pyr=pyrazine, bzi=benzimidazole. a) 1 BM=9.274078(36)$\times 10^{-24}$ J T^{-1}.

$\{S_2P(OCH_3)_2\}_2(PPh_3)]$, where PPh_3 means $P(C_6H_5)_3$, and no intermolecular interactions were observed except for van der Waals interaction. The central metal atom in this complex has a trigonal bipyramidal environment; two sulfur atoms of each Me_2dtp ligand are coordinated to the central metal from both the axial and equatorial directions. The phosphorus atom of the PPh_3 ligand is coordinated in the equatorial plane. As is shown in Fig. 1, Co, S(1), S(3), and P(3) atoms are almost on a plane, although the Co atom is deviated to the S(4) direction by about 0.097 Å from the S(1)–S(3)–P(3) plane. The bond angles around the Co atom on the equatorial plane (1 ∠S–Co–S and 2 ∠S–Co–P) are all about 120°. Although the ∠S(2)–Co–P(3) is almost rectangular, the ∠S(4)–Co–P(3) angle is 102.31(5)°. The Co–S(1) and Co–S(3) are about 2.33 Å, while Co–S(2) and Co–S(4) are about 2.6 Å; the latter are longer than the former. The two P–S bond distances in each Me_2dtp ligand also differ from each other; that for S(2) or S(4) atom, which coordinates to the Co atom from the axial direction, is shorter than the other. As the common P=S bond distance is about 1.92 Å, while that of P–S about 2.10 Å,[13] the double-bond character of the $-PS_2-$ moiety of the Me_2dtp ligand is localized rather to the P–S(axial) bond. The Co–P(3) bond distance is 2.551(2) Å; this is probably the longest Co–P distance of metal complexes ever reported. This may be due to the steric hindrance between the bulky ligands.

As will be described below, the magnetic as well as the spectral properties suggest that $Co(II)(Et_2dtp)_2(PPh_3)$, $Co(II)(Et_2dtp)_2$(hexamethylenetetramine), and $Co(II)(Et_2dtp)_2$(benzothiazole) have structures similar to that of $Co(II)(Me_2dtp)_2(PPh_3)$, whose crystal structure has been determined. Elemental analyses show that they are all 1 : 1 adducts with the general formula of $Co(II)(R_2dtp)_2\cdot X$. As may be seen from Table 3, their magnetic moments at room temperature range from 4.3 to 4.5 BM. The reflectance spectra of their solids give two peaks which can assigned to the $^4A'_2(P)\leftarrow{}^4A'_2(F)$ (higher wave number peak) and $^4E''(P)\leftarrow{}^4A'_2(F)$ of the pentacoordinated trigonal bipyramidal cobalt(II) complexes.[14,15]

Another group of adducts are the 1 : 1 adducts of piperazine and pyrazine, as well as the 2 : 1 adducts of benzothiazole and benzimidazole. As is shown in Table 3, their magnetic moments are 5.0—5.1 BM, and two peaks (one of them splits into three peaks) are observed in their reflectance spectra. They can be identified as $^4A_{2g}(F)\leftarrow{}^4T_{1g}(F)$ and $^4T_{1g}(P)\leftarrow{}^4T_{1g}(F)$ respectively of the octahedral cobalt(II) complexes.[16,17] In the 1 : 1 adducts of piperazine and pyrazine, these amines are likely to function as bidentate ligands with their two nitrogen atoms; consequently, the complexes may be polymeric. The splitting of the spectral peaks may be attributable to some deviation from an exact octahedral coordination.

The infrared spectra of all of these adducts show some characteristic bands; for example, ν(P–S) and a mixture of ν(P–S) and ν(P–O) appeared at about 800, 680, and 570 cm^{-1}, and ν(Co–S), at about 275 cm^{-1}.[18] The ν(Co–N) bands of amine adducts are rather ambiguous, although some peaks are found in the near-360 cm^{-1} region in their far-infrared spectra.

The visible absorption spectra of the benzene solution of $Co(II)(Et_2dtp)_2$(hexamethylenetetramine), which is the most stable in the series of adducts, gives five peaks in the region of 7100—28000 cm^{-1}. The absorption maxima given by the wave numbers with the log ε values in parentheses, are 9090(0.91), 12100(1.09), 15900(1.80), and 17200(1.76) for a 0.01 mol dm^{-3} solution, and 26100(3.17) for 0.0002 mol dm^{-3} one. The spectral pattern resembles that of pentacoordinated trigonal bipyramidal cobalt(II) complexes.[14] However, the absorption coefficients of the bands in the visible region do not obey Beer's law for they increase when the solution is diluted; moreover, the peak at 15900 cm^{-1} is broadened, and the maximum shifts to about 15000 cm^{-1}, which corresponds to the peak of the free $Co(II)(Et_2dtp)_2$.[6] This observation indicates that $Co(II)(Et_2dtp)_2$ and the pentacoordinated adduct are in equilibrium in the solution. The solutions of other adducts also show almost the same pattern as that of the hexamethylenetetramine adduct. Even the hexacoordinated adducts in their solid states also give a spectral pattern similar to that of pentacoordinated cobalt(II) in their solution; this is a result of partial dissociation. Therefore, the equilibrium studies described below take into account only the 1 : 1 adduct formation process; the second-step association is assumed to be negligible

Table 4. Formation constants of 1 : 1 adducts, $[Co(II)(R_2dtp)_2 \cdot X]$

R	X	Solvent	T/°C	From spectra		From ^{1}H-NMR		
				ε_1	log K	δ_A	δ_B	log K
C_2H_5	PPh_3	CCl_4	30	103	1.6_1	12.8	7.2_5	1.5_7
CH_3	PPh_3	C_6H_6	25	94	1.9			
C_2H_5	bzt	CCl_4	30	73	2.2_1	97.7	8.8_4	2.2_2
C_2H_5	hex	$CHCl_3$	30	56	3.4	26.5	4.7_6	a)
C_2H_5	pyr	$CHCl_3$	30			88.5	8.5_7	2.2_5

PPh_3=Triphenylphosphine, bzt=benzothiazole, hex=hexamethylenetetramine, pyr=pyrazine. a) The formation constant is too high to obtain by this method.

compared to the first one.

Although the $Co(II)(Et_2dtp)_2$ or $Co(II)(Me_2dtp)_2$ in carbon tetrachloride or in a benzene solution is gradually air-oxidized, the solutions were spectrophotometrically stable for 2 h after dissolution when the concentration was of the order of 3×10^{-3} mol dm^{-3}. Thus, practically, the absorbance of the solution did not change during the period of the measurement. After mixing a solution of $Co(II)(R_2dtp)_2$, or $Co(II)(R_2dtp)_2(PPh_3)$ with PPh_3, the equilibrium was attained in several min. All the other adducts also behaved in the same way. Therefore, the absorbance measurement of the mixture could be started about 7 min after mixing and could be finished in about 1 h. A series of the spectra of the mixture of $Co(II)(Me_2dtp)_2(PPh_3)$ and PPh_3 are shown in Fig. 3. Two isosbestic points are found, and the wavelengths of the absorption maxima of these spectra are kept at about 662 nm in the mixing-ratio region.

The same type of spectra posessing two isosbestic points were observed in the $Co(II)(Et_2dtp)_2$–PPh_3, and $Co(II)(Et_2dtp)_2$–benzothiazole systems. In the case of the $Co(II)(Et_2dtp)_2$–hexamethylenetetramine system, the hexamethylenetetramine adduct itself could not be used as the starting material because the formation constant of the adduct is too high. In this case, the PPh_3 adduct rather than the free complex was used as the starting material. Since the formation constant of the hexamethylenetetramine adduct is about 200 times that of PPh_3, the co-existence of the phosphine due to the use of its adduct was expected to be outside the range of experimental error. The isosbestic points were found in this system when $[Co(II)(Et_2dtp)_2]=3.0\times10^{-3}$ mol dm^{-3}, and [hexamethylenetetramine]$=0$—6.0×10^{-3} mol dm^{-3}.

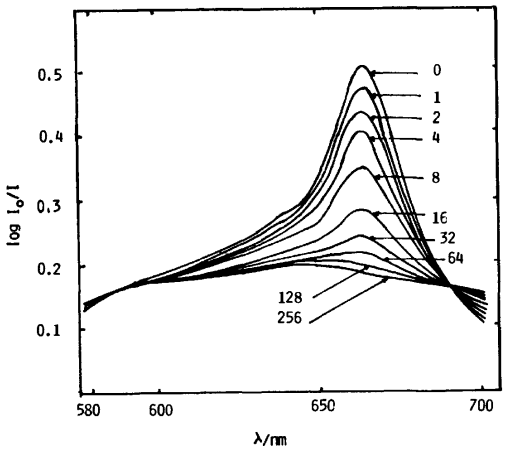

Fig. 3. Absorption spectra of the mixture of $[Co(II)(Me_2dtp)_2(PPh_3)]$ and PPh_3 (where Me_2dtp=*O,O'*-dimethyl dithiophosphato ligand, PPh_3=triphenylphosphine) in benzene, at 25 °C. $[Co(II)(Me_2dtp)_2(PPh_3)]$ added was always 2.00×10^{-3} mol dm^{-3}, and the concentration ratio of $[PPh_3]/[Co(II)(Me_2dtp)_2(PPh_3)]$ (originally added, mol/mol) are shown by numbers in the figure.

The apparent formation constants of the adducts, $K=[Co(II)(R_2dtp)_2\cdot X]/\{[Co(II)(R_2dtp)_2][X]\}$, where R=$CH_3$ or C_2H_5, X=PPh_3, benzothiazole, or hexamethylenetetramine are listed in Table 4. That of the pyrazine adduct was not obtained because of its low solubility.

The formation constant, K, was calculated as follows. Let the total concentration of Co(II) be m_o, and let that of the donor X be d, while x is the concentration of the $Co(II)(R_2dtp)_2\cdot X$ adduct.*** Then, $[Co(II)(R_2dtp)_2]$ and [X] in the solution are given by m_o-x and $d-x$ respectively. As the wavelength of the maximum absorption does not change in the concentration region, while the isosbestic points are retained, the absorbance can be written as $A=\varepsilon_1 x+\varepsilon_2(m_o-x)$, where ε_1 stands for the absorption coefficient of the $Co(II)(R_2dtp)_2\cdot X$ adduct, and ε_2, that of the free complex, $Co(II)(R_2dtp)_2$. From these relations, the following equation can be derived:

$$\frac{1}{m_oK[X](\varepsilon_1-\varepsilon_2)}+\frac{1}{m_o(\varepsilon_1-\varepsilon_2)}=\frac{1}{A-\varepsilon_2 m_o}.$$

Therefore, when $d\gg x$; *i.e.* $[X]\fallingdotseq d$, a linear relationship exists between $1/d$ and $1/(A-\varepsilon_2 m_o)$. From the gradient of the line and the intercept, the values of $1/\{m_oK(\varepsilon_1-\varepsilon_2)\}$ and $1/\{m_o(\varepsilon_1-\varepsilon_2)\}$ respectively can be known. Then, the ε_1 and K of each adduct can be calculated. The ε_2 of $Co(II)(Et_2dtp)_2$ was determined from the absorbance of the complex, extracted by the organic solvent from a mixture of cobalt(II) chloride and $Na(Et_2dtp)$ in aqueous solution; the concentration of Co(II) was estimated by titration after decomposing the ligand. The ε_2 of $Co(II)(Et_2dtp)_2$ and that of $Co(II)(Me_2dtp)_2$ were almost the same; *i.e.*, 315 mol^{-1} dm^3. This is slightly smaller than that reported by Jørgensen,[8b] although he stated that his result might be a little too high.

These apparent first-order adduct formation constants were also obtained from the ^{1}H-NMR paramagnetic

*** m_o, d, and x are in mol dm^{-3} units, accordingly, K is in mol^{-1} dm^3 units.

shifts of the donor protons caused by the addition of the $Co(II)(R_2dtp)_2 \cdot X$ adduct to the solution of a donor. The broadening of the peak by the addition of the adduct was not much, indicating that the exchange rate of the donors between the free state and that in the adduct is high. The paramagnetic shifts of the proton peak of the donor protons can thus be expected to be given by the weighed average of the chemical shifts of the proton of the donor in the free and bonded states. The most probable species existing in the solution is the 1 : 1 adduct, and the fraction of the 2 : 1 adduct or the higher ones can be expected to be low, even in such relatively concentrated solution of a donor.

Therefore, in this case, too, only the first step was considered, and the adduct formation constant was obtained by the use of the equation: $K=[Co(II)(R_2dtp)_2 \cdot X]/\{[Co(II)(R_2dtp)_2] \cdot [X]\}$. The calculations were as follows. The chemical shift of a proton of a donor, X, in a free state is denoted by δ_B; that in an adduct, by δ_A, and that of the observed, by δ_o. As in the case of the spectrophotometric method, m_o, d, and x are defined as the total concentration of Co(II), the total concentration of the donor, and the concentration of the existing adduct, respectively. Since d is enough larger than m_o and x in the NMR measurement, too, we use the approximation of $[X] \fallingdotseq d$. Therefore, we have $K=x/\{(m_o-x)d\}$. On the other hand, $\delta_o=\delta_B+x(\delta_A-\delta_B)/d$. From these relations, we obtain:

$$d = (\delta_A-\delta_B)\{m_o/(\delta_o-\delta_B)\} - (1/K).$$

From this linear relation between d and $m_o/(\delta_o-\delta_B)$, δ_A was obtained from its gradient. Next, the δ_o's of a series of samples with different d values, but with the same $m_o/d(\equiv a)$, were measured. The equation can be rewritten as: $1/\Delta=[1/\{a(\delta_A-\delta_B)\}][1+(1/K)(1/d)]$, where $\Delta=\delta_o-\delta_B$. When a is kept constant, there is a linear relationship between $1/\Delta$ and the formation constant, K, which was obtained from the gradient. The proton peaks used for the calculations were those of the phenyl ortho protons for the PPh_3 adduct, and the methine proton at the 2-position for the benzothiazole adduct. In the case of hexamethylenetetramine or the pyrazine adduct, a single peak in the ^1H-NMR was used. The obtained results, the δ_A, δ_B, and log K values, are listed in Table 4, also; they agreed well with those obtained from spectrophotometry.

The authors wish to express their appreciation to Mr. Yukio Yamada for his assistance about the experimental operations. We are also indebted to Professor Toschitake Iwamoto for his helpful discussions concerning the thesis. The cooperation in the calculations for the structure analysis by Dr. Fujio Ebina is also greatly appreciated.

References

1) A part of the content of this paper was published as Y. Yamada, M. Shimoi, and A. Ouchi, *Chem. Lett.*, **1978**, 867, and M. Shimoi, A. Ouchi, S. Sato, and Y. Saito, *ibid.*, **1979**, 319.

2) R. L. Carlin and D. B. Losee, *Inorg. Chem.*, **9**, 2087 (1970).

3) S. E. Livingstone and A. E. Mihkelson, *Inorg. Chem.*, **9**, 2545 (1970).

4) A. Furuhashi, T. Nomura, and M. Sugimoto, *J. Inorg. Nucl. Chem.*, **36**, 1415 (1974).

5) N. Yoon, M. J. Incorvia, and J. I. Zink, *J. Chem. Soc., Chem. Commun.*, **1972**, 499.

6) R. G. Cavell, E. D. Day, W. Byers, and P. M. Watkins, *Inorg. Chem.*, **11**, 1759 (1972).

7) C. K. Jørgensen, *J. Inorg. Nucl. Chem.*, **24**, 1571 (1962).

8) a) C. K. Jørgensen, *Acta Chem. Scand.*, **17**, 533 (1963); b) C. K. Jørgensen, *ibid.*, **16**, 2017 (1962).

9) "The Universal Crystallographic Computation Program System (UNICS)," ed by T. Sakurai, Crystallographic Society of Japan, Tokyo (1967).

10) "International Tables for X-Ray Crystallography," Kynoch Press, Birmingham, U. K. (1974), Vol. IV.

11) $R=\sum||F_o|-|F_c||/\sum|F_o|$

12) The final thermal parmaters and the final F_o-F_c, table are kept at the Office of the Editor of the *Bull. Chem. Soc. Jpn.* as Document No. 8233.

13) A. F. Wells, "Structural Inorganic Chemistry," 4th ed, Clarendon Press, Oxford, U. K. (1975), p. 695.

14) I. Bertini, D. Gatteschi, and A. Scozzafova, *Inorg. Chem.*, **14**, 812 (1975).

15) R. N. Mukherjee, M. S. Venkateshan, and M. D. Zingde, *J. Inorg. Nucl. Chem.*, **36**, 547 (1974).

16) D. W. Meek, R. S. Drago, and T. S. Piper, *Inorg. Chem.*, **1**, 285 (1962).

17) B. N. Figgis, "Introduction to Ligand Field," Interscience, London, U. K. (1966), p. 223.

18) W. Rudzinski, G. T. Behenke, and Q. Fernando, *Inorg. Chem.*, **16**, 1206 (1977).

The Extractability of Potassium as Picrates (KPic and K(L)Pic, L: 18-Crown-6) and Its Relationship to the Properties of the Solvents

Tadashi IWACHIDO,* Masayoshi MINAMI,† Hirohiko NAITO,† and Kyoji TÔEI†

College of Liberal Arts, Okayama University, 2-1-1, Tsushima-naka, Okayama 700

†*Department of Chemistry, Faculty of Science, Okayama University, 3-1-1, Tsushima-naka, Okayama 700*

(Received November 19, 1981)

The distribution ratios, D, of potassium between an aqueous KCl solution and 57 organic solvents (8 alcohols, 12 ketones, 6 esters, 3 ethers, and 28 hydrocarbons (24 halo- and 2 nitro-substituted and 2 unsubstituted)) were determined in the presence or in the absence of L. The presence of L markedly enhances the extractability of potassium when the halogenated hydrocarbon solvents are used, but only a slight enhancement can be observed for the oxygen-containing solvents. Among the properties showing good correlations with D, Hansen's three-dimensional solubility parameters and Dimroth's E_T values are most satisfactory for their applicability to a wide variety of solvents.

Potassium picrate in an aqueous solution can be extracted only when a highly polar substance is used as a solvent. Most such solvents are miscible with water; hence, only a limited number of water-immiscible solvents can be used.

L is a well-known ligand of the endopolarophilic type, with the polar binding sites turned inside towards the cation and the lipophilic methylene groups turned outside. A wider variety of solvents, therefore, are made subjects of the extraction study of K(L)Pic because of its increased lipophilicity.

Although the knowledge of the polarity of a solvent is important in solvent-extraction chemistry, there are only a few reports which describe a quantitative relation between the extractability of the ion-pair and the polarity of the solvent.[1,2] In chelate-extraction systems, however, the solubility parameter of the solvent is known to have a close relationship with the extractability of the chelate.

This paper will describe how, besides the solubility parameter, the transition energy for a solvatochromic indicator can serve as a numerical polarity scale for the present extractions.

Experimental

Materials. Reagent-grade solvents (Tokyo Kasei Co., Ltd.) were washed with an aqueous sodium carbonate solution and then with water several times. The K(L)Pic was prepared by adding an equimolar amount of commercially available L (Nisso Co., Ltd.) to an aqueous KPic solution and was then recrystallized repeatedly from methanol.

Distribution Ratios. Aqueous picrate solutions (10^{-4} mol dm^{-3}) were prepared by dissolving each picrate in a solvent-saturated potassium hydrogencarbonate solution, the total potassium concentration being 10^{-2} mol dm^{-3}. Twenty milliliters of the aqueous solution and an equal volume of a water-saturated solvent were transferred to a 50-cm^3 centrifuge tube. After being shielded tightly, the vessel was immersed in a water bath thermostated at (25±0.01) °C and gently shaken for 1 h. The value of D was calculated from the aqueous picrate concentration, as determined by the use of a Hitachi 124 spectrophotometer.

Water Miscibilities. The water content of the organic phase was determined in each distribution run by the use of a Mitsubishi Kasei CA-01 Karl-Fischer titrator.

Solubilities. The solubilities of the picrates in the water-saturated solvents at 25 °C were determined by means of HPLC (Shimadzu liquid chromatograph; column: 250 mm × 4 mm Zorbax PCH, mobile phase: methanol, detector: SPD-1 spectrophotometer).

Results and Discussion

D Values and Structures. The D values for oxygen-containing solvents are listed in Table 1, together with some other data.

Table 1 shows that the D value for benzyl alcohol is greater than that for 1-heptanol, though both have the same number of carbon atoms. Such a phenyl-substitution effect can also be seen with acetophenone, benzyl acetate, and probably anisole. The presence of double bonds also enhances the extractabilities of the picrates, as can be seen for mesityl oxide. Such is the case with allyl chloride, as will be seen later. The presentation of the D values on a logarithmic scale produces relatively simple relations with the number of carbon atoms, N, of the solvent molecule, as is shown in Fig. 1. It must

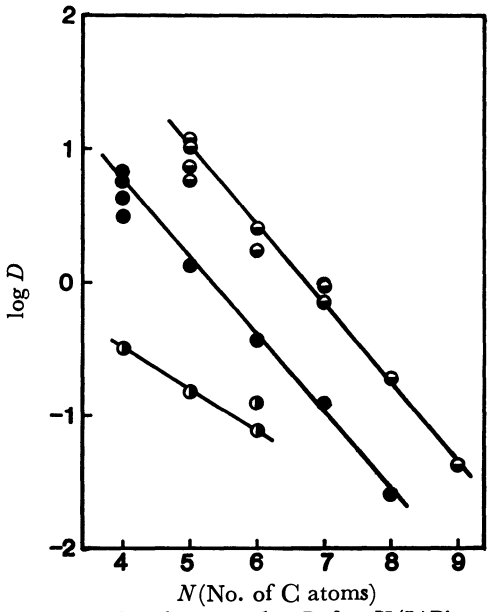

Fig. 1. Relation between log D for K(L)Pic and the number of carbon atoms of the solvent.
○: (Halogenated) hydrocarbons, ●: alcohols, ◒: ketones, ◑: esters, ◐: ethers.

TABLE 1. DISTRIBUTION RATIOS OF THE PICRATES AND SOME PROPERTIES OF OXYGEN-CONTAINING SOLVENTS

	Solvent	D		$10^4 s$ / mol dm^{-3}		$n(H_2O)$	δ[b]	δ_o[b]	δ_d[b]	δ_p[b]	δ_h[b]	V[c]	E_T[d]
		K(L)Pic	KPic	K(L)Pic	KPic		cal$^{1/2}$ cm$^{-3/2}$					cm^3 mol^{-1}	kcal mol^{-1}
1	*n*-BuOH	6.7	6.79	67	105	0.507	11.4	11.3	7.8	2.8	7.7	91.5	50.2
2	*i*-BuOH	3.0	2.9	32	55	0.470	11.19					92.3	
3	*s*-BuOH	4.3	4.0	132	312	0.724	11.05	10.8	7.7	2.8	7.1	92	
4	*n*-$C_5H_{11}OH$	1.3	1.2	29.1	25.8	0.380	10.95	10.61	7.81	2.2	6.8	108.7	
5	*n*-$C_6H_{13}OH$	0.37	0.25	10	9.1	0.309	10.65					125.5	
6	*n*-$C_7H_{15}OH$	0.12	0.05	4.0	3.4	0.249	10.5					141.4	
7	*n*-$C_8H_{17}OH$	0.03	0.01	3.6	4.0	0.255	10.24	10.3	8.3	1.6	5.8	157.7	
8	$PhCH_2OH$	5.7	2.9	2130	78.0	0.384	12.05	11.6	9.0	3.1	6.7	103.6	50.8
9	*n*-PrCOMe	7.3	4.9	321	168	0.155	8.7					106.1	
10	Et_2CO	5.7	2.9	311	104	0.107	8.8	8.9	7.7	3.7	2.3	106.4	
11	*n*-BuCOMe	2.5	1.3	130	50	0.101						123.3	
12	*i*-BuCOMe	1.7	0.85	100	48.8	0.097	8.3	8.3	7.5	3.0	2.0	125.8	
13	Mesityl oxide[a]	10	6.1	390	215	0.155	9.2	9.2	8.0	3.5	3.0	115.6	
14	*n*-$C_5H_{11}COMe$	0.96	0.47	78	32.2	0.084	8.4					139.3	
15	*i*-$C_5H_{11}COMe$	0.92	0.47	69	31.9	0.083	8.4	8.5	7.8	2.8	2.0	142.8	
16	*n*-BuCOEt	0.69	0.27	59	15.5	0.057	8.3					139.6	
17	$(i\text{-Pr})_2CO$	0.96	0.25	63	13.4	0.052	8.2					141.6	
18	*n*-$C_6H_{13}COMe$	0.19	0.11	41	18.2	0.068						156.6	
19	PhCOMe	11	4.9	1160	268	0.103	9.7	9.68	8.55	4.2	1.8	117.4	41.3
20	$(i\text{-Bu})_2CO$	0.04	<0.001	8	2.2	0.033	8.4					167.9	
21	CH_3COOR,R=Et	0.32	0.27	52	70.2	0.132	8.6	9.1	7.44	2.6	4.5	98.5	38.1
22	CH_3COOR, *n*-Pr	0.15	0.11	32.4	29.9	0.097	8.4					115	
23	CH_3COOR, *n*-Bu	0.08	0.05	17	19.1	0.070	8.3	8.5	7.7	1.8	3.1	132.5	
24	CH_3COOR,$PhCH_2$	0.12	0.04	84	10.2	0.070	9.5					144.4	
25	PC[a]	99	99	1500	1220	0.318	13.3	13.3	9.8	8.8	2.0	85	46.6
26	TBP[a]	15.7	13.3	52	1200	0.534	7.7					272	33.9
27	Et_2O	0.01	<0.001	3.1	0	0.052	7.4	7.7	7.1	1.4	2.5	104.8	34.6
28	$(n\text{-Bu})_2CO$	<0.001	<0.001	0.3	0	0.012	7.76					170.5	33.4
29	PhOMe	0.09	<0.001	177	0	0.012	9.9					108.7	37.2

a) PC=Propylene carbonate, TBP=tributyl phosphate, Mesityl oxide=4-methyl-3-pentene-2-one. b) Ref. 4.
c) V=mol wt/density (density: Ref. 5). d) Ref. 6.

be noted that, in Fig. 1, modified N values are used for the phenyl-substituted ($N-3$) and double-bond-containing solvents ($N-1$), so that the best fit can be obtained. Among the solvents with the same number of carbon atoms, the extractabilities of K(L)Pic decrease in the following sequence: ketones>alcohols>esters>ethers. A quite similar plot is obtained for the extraction of KPic.

The D values for hydrocarbon solvents are listed in Table 2. No hydrocarbon solvents can extract KPic. Nitro-substituted ones show exceptionally high extractabilities both for KPic and K(L)Pic. It is obvious that the D values decrease with an increase in the number of the CH_2 units of the solvent: C_3H_7Cl, C_4H_9Cl>$C_5H_{11}Cl$ >$C_6H_{13}Cl$. The double-bond containing solvents likewise show higher extractabilities than the corresponding saturated ones: allyl chloride>propyl chloride.

The extractability of K(L)Pic tends to decrease with an increase in the number of halogen atoms (CH_2Cl_2> $CHCl_3$>CCl_4, *o*-dichlorobenzene>chlorobenzene), and completely halogenated solvents, such as CCl_4 and $CBrCl_3$, do not show any appreciable extractabilities. The position of halogen atoms also has a significant influence, as can be seen for 1,1- and 1,2-dichloroethane, for example. It is noticeable that the extractability is greatly affected by the *cis-trans* isomerism (*cf.* 1,2-dichloroethylene).

The chlorinated solvents always show the highest extractability among the halogenated solvents, as is best shown in monohalogen derivatives of benzene.

Dielectric Constant, ε, and Dipole Moment, μ. The log D values tend to increase with ε, in accordance with Irving and Lewis' observation of the partition of indium chloride,[1] though the correlation is far from satisfactory. Freiser also pointed out, for the distribution of tridodecylammonium perrhenate, that there isverylittle correlation between the logarithmic distribution constants and the ε values.[2] The log D values also increase with μ, though the degree of correlation is much lower than that observed between log D and ε. It should, however, be noted that, among the solvent parameters investigated, only ε and μ show the expected low extractabilities of K(L)Pic into CCl_4 and *trans*-1,2-dichloroethylene.

Solubilities of the Picrates, s. The solubilities of the picrates in water-saturated solutions are shown in Tables 1 and 2. A log D *vs.* log s plot for K(L)Pic in the oxygen-containing solvents yields a straight line for

Table 2. Distribution ratios of the picrates and some properties of hydroca rbon solvents

	Solvent	D K(L)Pic	D KPic	$10^4\,s$ / mol dm^{-3} K(L)Pic	$10^4\,s$ / mol dm^{-3} KPic	$10^3\,n(H_2O)$	δ	δ_o	δ_d	δ_p	δ_h	V	E_T
							cal$^{1/2}$ cm$^{-3/2}$					cm^3 mol^{-1}	kcal mol^{-1}
30	CH_2Cl_2	1.13	<0.001	7240	0	7.8	9.7	9.9	8.9	3.1	3.0	63.9	41.1
31	$CHCl_3$	0.53	0	5270	0	5.7	9.3	9.3	8.7	1.5	2.8	80.7	39.1
32	CCl_4	<0.001	<0.001	490	0	0.9	8.6	8.7	8.7	0	0.3	97.1	32.5
33	CH_2Br_2	0.79	0.02			6.0						69.5	
34	$CHBr_3$	0.43	0.01			4.4	10.5					88	
35	CH_2BrCl	0.92	0.01			7.6						67.3	
36	$CHBrCl_2$	0.45	0.01			4.3						82.7	
37	$CBrCl_3$	<0.001	<0.001			1.1							
38	CH_2ClCH_2Cl	1.17	<0.001	1490	0	8.2	9.8	9.76	9.2	2.6	2.0	79.4	41.9
39	CH_3CHCl_2	0.23	<0.001			4.2	9.1	9.2	8.3	3.3	2.2	85	
40	CH_3CCl_3	0.05	<0.001			2.5	8.5					100	
41	ClCH=CHCl,*cis*-	0.67	0.03			5.8	9.7	8.7	7.8	3.8	1.0	76	
42	ClCH=CHCl,*trans*-	<0.001	<0.001			2.8	9					78	
43	*n*-PrCl	0.04	<0.001			2.7	8.5					88.3	
44	*i*-PrCl	0.05	<0.001			3.1						88	
45	CH_2=$CHCH_2Cl$	0.11	<0.001			6.2						81.5	
46	$CH_3CHClCH_2Cl$	0.16	<0.001			5.0						97.8	
47	*n*-BuCl	0.04	<0.001			2.3						104	
48	*n*-$C_5H_{11}Cl$	0.02	<0.001			2.1						121	
49	PhX, X=H	0.02	<0.001	33.9	0	2.84	9.2	9.1	9.0	0	1.0	89.4	34.5
50	PhX, X=F	0.09	<0.001			2.6						93.6	38.1
51	PhX, X=Cl	0.14	<0.001	113	0	2.7	9.5	9.6	9.3	2.1	1.0	102.1	37.5
52	PhX, X=Br	0.04	<0.001			2.1	9.87	10.6	10	2.7	2.0	105	37.5
53	PhX, X=I	0.03	<0.001			3.6						111	37.9
54	*o*-$PhCl_2$	0.27	<0.001	232	0	2.5	10	10	9.4	3.1	1.6	112.8	
55	$PhNO_2$	13.3	0.18	1130	3.64	14.9	11.1	10.9	9.8	4.2	2.0	102.7	42.0
56	$PhCH_3$	0.01	<0.001	13.4	0	2.68	8.93	8.9	8.8	0.7	1.0	106.8	33.9
57	*o*-$NO_2C_6H_4CH_3$	6.1	0.11	714	2.1	15.0						117.9	

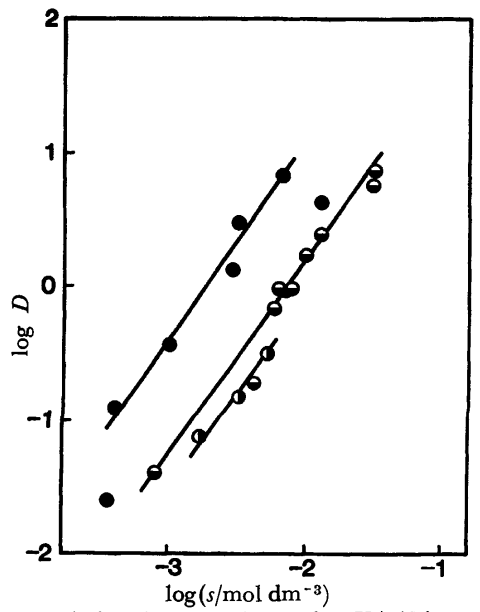

Fig. 2. Relation between log D for K(L)Pic and the solubility of the picrate in the solvent.
Symbols: see Fig. 1.

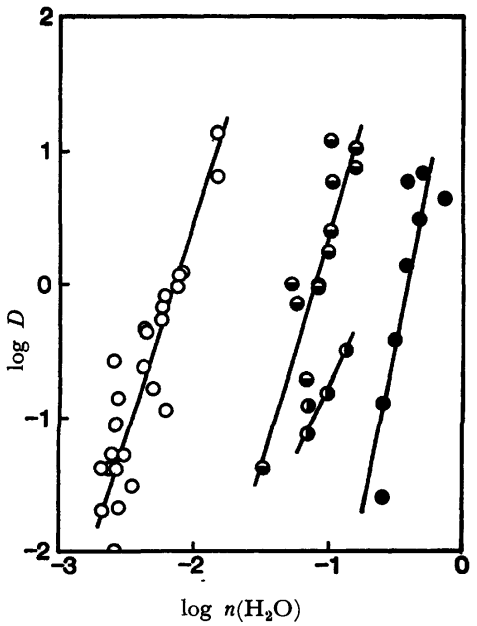

Fig. 3. Relation between log D for K(L)Pic and the water content of the solvent.
Symbols: see Fig. 1.

each solvent group, as is shown in Fig. 2. Such a linear relation holds for the extraction of KPic as well. The data points for the double-bond-containing and phenyl-substituted solvents show remarkable deviations; hence, these points are omitted from Fig. 2 so that the linear relationships for each solvent group can easily be seen.

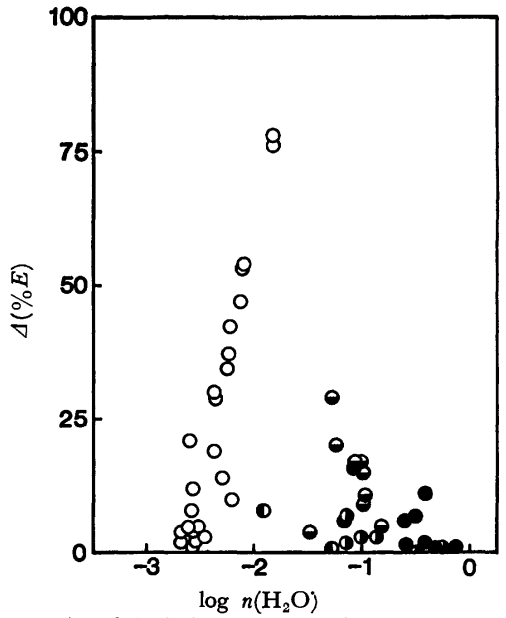

Fig. 4. Plot of $\Delta(\%E)$ *vs.* log $n(H_2O)$.
$\%E$=(picrate extracted/total picrate)×100. Symbols: see Fig. 1.

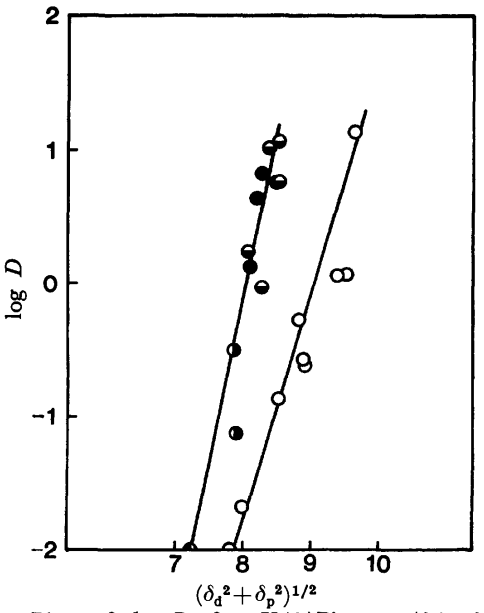

Fig. 6. Plot of log D for K(L)Pic *vs.* $(\delta_d^2+\delta_p^2)^{1/2}$.
Symbols: see Fig. 1.

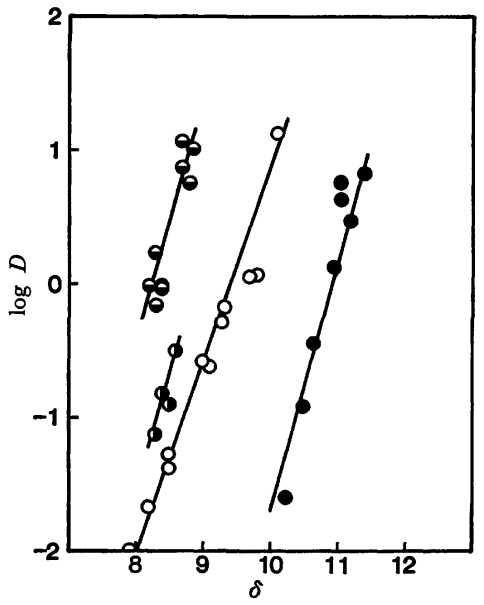

Fig. 5. Relation between log D for K(L)Pic and the solubility parameter of the solvent.
Symbols: see Fig. 1.

For the hydrocarbon solvents, the log D values for K(L)Pic also increase linearly with log s, though the fit is not so good as that which can be seen for the oxygen-containing solvents.

Water Miscibilities. Figure 3 shows that the log D values bear a linear relation to the logarithm of $n(H_2O)$, the mole fraction of water in the organic phase.

In order to investigate the effect of the complexation, percentage extraction increments, $\Delta(\%E)=\%E_{K(L)Pic}-\%E_{KPic}$, are plotted against log $n(H_2O)$ (Fig. 4). The extractability enhancement is maximal at $n(H_2O)=0.015$, indicating that the solvents which can dissolve water to a moderate extent are the best. The oxygen-containing solvents, contrary to the halogenated ones, exhibit a very slight enhancement. Taking into account the fact that crown-ether complexes are less stable in aqueous solutions than in alcohol solutions,[3] the reason for this is that the picrate complex is destabilized by the hydration of the potassium cations.

Solubility Parameters, δ. The regular solution theory has become increasingly important in chelate-extraction studies. However, little is known of its application to ion-pair extraction studies.

The dependence of the log D value for K(L)Pic on δ is illustrated in Fig. 5. The log D values increase linearly with δ. The slopes are identical for each solvent group except the halogenated one. It must be noted that modified δ values (*i.e.*, $\delta-1$ and $\delta-0.33$ for the phenyl-substituted and double-bond-containing solvents respectively) are used for the plot.

A solubility parameter can be divided into three components; thus, $\delta_o^2=\delta_d^2+\delta_p^2+\delta_h^2$, where δ_d, δ_p, and δ_h refer to the dispersion (London), polar (dipole-dipole), and hydrogen-bonding components of the solubility parameter respectively. A log D *vs.* $(\delta_d^2+\delta_p^2)^{1/2}$ plot yields a straight line for the oxygen-containing solvents, including strongly hydrogen-bonded solvents, such as alcohols, as is shown in Fig. 6; this finding indicates that the hydrogen-bonding components contribute much to the increase in δ_o values, but little to the enhancement of the extractabilities. It must noted that data points for the hydrocarbon solvents fall of another regression line, though the reason for this is not clear.

Molar Volume, V. A linear relation is also found between log D and V, as is shown in Fig. 7. The molar volume looks promising as a measure of the extractability in the following respects: V bears a closer relation with log D, especially for the hydrocarbon solvents, and there is no need to use modified V values, not even for the

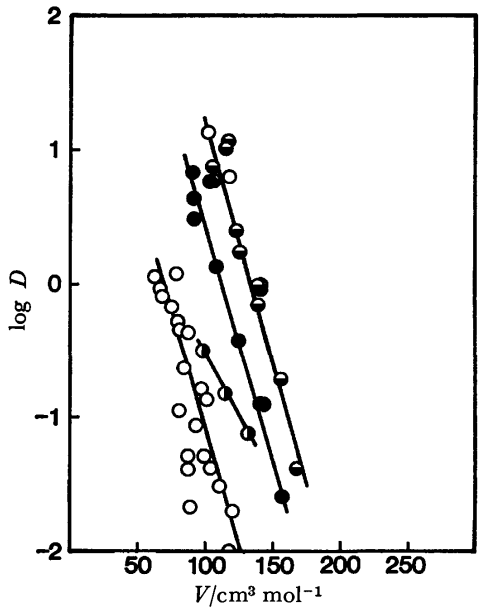

Fig. 7. Relation between log D for K(L)Pic and the molar volume of the solvent.
Symbols: see Fig. 1.

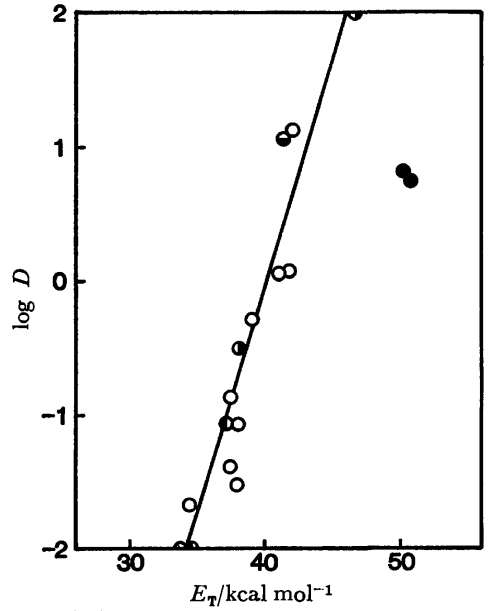

Fig. 8. Relation between log D for K(L) Pic and the E_T value of the solvent.
Symbols: see Fig. 1.

phenyl-substituted and double-bond-containing solvents. The data points for the chloro-substituted solvents (*i.e.*, CCl_4, $CBrCl_3$, *trans*-1,2-dichloroethylene, and 1,2-dichloroethane) and the nitro-substituted solvents show remarkable deviations from the regression line.

E_T Values. Several numerical scales for solvent polarity have been proposed based on the solvatochromism of indicators. The E_T values for 4-(2,4,6-triphenyl-1-pyridinio)-2,6-diphenylphenolate are known for as many as 70 solvents.[6] The dependence of log D on E_T is shown in Fig. 8. It is worth noting that the data points for all solvents except the alcohols fall on a linear line. A similar correlation is found to hold between log D and the spectral shift of 1-ethyl-4-(methoxycarbonyl)pyridinium iodide, which is known as Kosower's Z value,[7,8] though only 8 values are available. The data point for 1-butanol is significantly displaced from the regression line. The E_T values for Phenol Blue (N-[4-(dimethylamino)phenyl]-p-benzoquinone monoimine)[9] are found to correlate with log D, though the fit is not wholly satisfactory.

Miscellaneous. Kovats and Weisz have reported gas-chromatographic retention index values for 38 substances.[10] Although only 7 of them are available for the present purpose, they all fall on a line when plotted against log D.

On the other hand, no satisfactory correlation was observed between log D and Brownstein's S values.[11]

It can be concluded that, among the properties described here, the solubility parameters and Dimroth's E_T values are the most promising numerical scales for the extraction of the picrate.

References

1) H. Irving and D. C. Lewis, *Proc. Chem. Soc.*, **1960**, 222.
2) H. Freiser, *Anal. Chem.*, **41**, 1354 (1969).
3) For example, J. M. Lehn, "Structure and Bonding," Springer, Berlin (1973), Vol. 16, p. 1; R. M. Izatt, D. E. Terry, D. P. Nelson, Y. Chan, D. J. Eatough, J. S. Bradshaw, L. D. Hansen, and J. J. Christensen, *J. Am. Chem. Soc.*, **98**, 7626 (1976).
4) J. H. Hildebrand, J. M. Prausnitz, and R. L. Scott, "Regular and Related Solutions," Van Nostrand Reinhold, New York (1970); A. F. M. Barton, *Chem. Rev.*, **75**, 731 (1975); T. Takamatsu, *Bull. Chem. Soc. Jpn.*, **47**, 2647 (1974); C. M. Hansen and K. Skaarup, *J. Paint Technol.*, **39**, 511 (1963); K. L. Hoy, "Tables of Solubility Parameters," Union Carbide Co., 5-31-67.
5) "Handbook of Chemistry and Physics," ed by R. C. Weast, CRC Press, Ohio (1972—1973), p. C-75.
6) C. Reichard and K. Dimroth, *Fortschr. Chem. Forsch.* **11**, 1 (1968).
7) E. M. Kosower, *J. Am. Chem. Soc.*, **80**, 3523, 3261, 3267 (1958).
8) C. Walling and P. J. Wagner, *J. Am. Chem. Soc.*, **86**, 3368 (1964).
9) O. W. Kolling, *Anal. Chem.*, **53**, 54 (1981).
10) E. sz. Kovats and P. B. Weisz, *Z. Elektrochem.*, **69**, 812 (1965).
11) S. Brownstein, *Can. J. Chem.*, **38**, 1590 (1960).

Theoretical Prediction of Cotton Signs in CD Spectra of Λ-$[Co(N)_2(O)_4]^-$- and Λ-$[Co(N)_4(O)_2]^+$-type Complexes

Shuhei Fujinami,* Kenshi Tsuji, and Muraji Shibata
Department of Chemistry, Faculty of Science, Kanazawa University, Kanazawa 920
(Recieved December 11, 1981)

The crystal field model of d-d optical activity has been applied to complexes with *cis*(*N*)-$[Co(N)_2(O)_4]^-$ and *cis*(*O*)-$[Co(N)_4(O)_2]^+$ chromophores, and the Cotton signs of these complexes have been predicted. The model has shown that the Cotton signs in CD spectra of the complexes depend upon: 1) the energy difference between E_g^a and A_{2g} states, 2) the coordination angle in a bidentate chelate, and 3) the effective charge of the ligating atoms. The CD spectral difference between an optically active carbonato complex and the corresponding diaqua complex derived from the carbonato complex has been understood in terms of the effective charge of the ligating O atoms.

In our laboratory, we have been investigating CD spectra in the ligand-field transition region of complexes with *cis*(*N*)-$[Co(N)_2(O)_4]$ and *cis*(*O*)-$[Co(N)_4(O)_2]$ chromophores.[1-3] A method of assigning a transition component of a given Cotton peak was proposed on the basis of a regular CD spectral change due to a change of chelate ring size of bidentate OO ligand.[1] The CD spectrum of a diaqua complex, which had been derived from an optically active carbonato complex by an acid-hydrolysis, was found to be remarkably different from that of the parent carbonato complex.[1,3] For examples, $(-)_{589}[Co(CO_3)(ox)(en)]^-$ exhibits a single positive Cotton peak in the first absorption band region, which is assignable to the $A_{1g}\rightarrow E_g^a(D_{4h})$ transition component. On the other hand, $(+)_{589}[Co(ox)(en)(H_2O)_2]^+$ complex derived from the $(-)_{589}$ carbonato complex exhibits negative and positive Cotton peaks from the lower-frequency side in the region, the negative peak being assigned to the same transition component. That is to say, the Cotton sign in the diaqua complex is opposite to that in the parent carbonato complex.

The optical activity associated with the d-d transition of *cis*-$[Co(a)_2(en)_2]^{n+}$ (a represents unidentate ligands such as H_2O, Cl^-, *etc.*) has been discussed by McCaffery *et al.*[4] They attempted to relate the Cotton signs in the bis(ethylenediamine) complexes with those in the tris(ethylenediamine)cobalt(III) complex with D_3 symmetry, and found a rule that the Cotton peak of the $A_{1g}\rightarrow E_g$ transition component in the Λ-$[Co(a)_2(en)_2]^{n+}$ complexes has a positive sign, as does that in the Λ-$[Co(en)_3]^{3+}$ complex. However, an exception to the rule was reported, that is, the Cotton peak assignable to $A_{1g}\rightarrow E_g$ transition in Λ-$[Co(N_3)_2(en)_2]^+$ has a negative sign.[5] The rule is not useful for an understanding of the CD spectrum of $(+)_{589}[Co(ox)(en)(H_2O)_2]^+$.

There are two types of theoretical treatments of optical activity; one is called a crystal field model (or static coupling model), developed by Piper *et al.*,[6] and the other is called a dynamic coupling model, developed by Mason *et al.*[7] The former is based upon the crystal field theory, and optical activity of a metal complex is explained by anadmixture of d-orbitals with p- or f-orbitals in a central metal ion. In the latter, the optical activity is explained by an interaction of the hexadecapole moment at a central metal ion with transient electric dipole moments at ligands. However, the application of these models is mostly limited to the tris(diamine) complex with D_3 symmetry.

In this paper, a crystal field model for mixed complexes with lower symmetry than D_3 is proposed, in which the signs of rotatory strength of $A_{1g}\rightarrow A_{2g}(D_{4h})$ transition component are predicted in Λ-$[Co(NN)(OO)_2]^{n-}$ and Λ-$[Co(NN)_2(OO)]^{n+}$ complexes (OO=CO_3^{2-}, ox^{2-}, mal^{2-}, or $2H_2O$; NN=en or tn). The proposed model is useful for the understanding of the CD spectrum of the appropriate diaqua complex.

General Theory

The Hamiltonian for the octahedral coordination system may be written as

$$\boldsymbol{H} = \boldsymbol{H}_o + \boldsymbol{V}_g + \boldsymbol{V}_u \quad (1)$$

where $\boldsymbol{H}_o$ represents the unperturbed Hamiltonian in the regular octahedron, and $\boldsymbol{V}_g$ and $\boldsymbol{V}_u$ represent the potentials with even and odd parity, respectively. The eigenstates of $\boldsymbol{H}_o$ in cobalt(III) complexes are classified as

$|A_{1g}\rangle$ =nondegenerate ground state with even parity,
$|T_{1g}i\rangle$ =octahedral components (i=a, β, γ) of the first excited state with even parity,
$|T_{2g}j\rangle$ =octahedral components (j=ξ, η, ζ) of the second excited state with even parity,
$|M_uk\rangle$=octahedral components of higher excited states with odd parity.

The first-order perturbed wavefunctions for the ligand field excited states can be written in terms of the perturbation theory as follows:

$$\begin{aligned}|A_{1g}) = |A_{1g}\rangle &+ \sum_k |M_uk\rangle\langle M_uk|\boldsymbol{V}_u|A_{1g}\rangle\{E(M_uk) - E(A_{1g})\}^{-1} \\ &+ \sum_i |T_{1g}i\rangle\langle T_{1g}i|\boldsymbol{V}_g|A_{1g}\rangle\{E(T_{1g}i) - E(A_{1g})\}^{-1} \\ &+ \sum_j |T_{2g}j\rangle\langle T_{2g}j|\boldsymbol{V}_g|A_{1g}\rangle\{E(T_{2g}j) - E(A_{1g})\}^{-1} \quad (2)\end{aligned}$$

$$\begin{aligned}|T_{1g}i) = |T_{1g}i\rangle &+ \sum_k |M_uk\rangle\langle M_uk|\boldsymbol{V}_u|T_{1g}i\rangle\{E(M_uk) - E(T_{1g}i)\}^{-1} \\ &+ \sum_{i'\neq i} |T_{1g}i'\rangle\langle T_{1g}i'|\boldsymbol{V}_g|T_{1g}i\rangle\{E(T_{1g}i') - E(T_{1g}i)\}^{-1} \quad (3) \\ &+ \sum_j |T_{2g}j\rangle\langle T_{2g}j|\boldsymbol{V}_g|T_{2g}j\rangle\{E(T_{2g}j) - E(T_{1g}i)\}^{-1},\end{aligned}$$

where $E(M_uk)$, *etc.* denote the energy of the unperturbed states.

The rotatory strength associated with a $A_{1g}\rightarrow T_{1g}i$ transition, $R(T_{1g}i)$, is expressed by

$$R(T_{1g}i) = \mathrm{Im}\{(A_{1g}|\boldsymbol{P}|T_{1g}i)\cdot(T_{1g}i|\boldsymbol{M}|A_{1g})\}, \quad (4)$$

where $\boldsymbol{P}$ and $\boldsymbol{M}$ are the electric and magnetic dipole operators, respectively. If we neglect higher terms of the energy differences, the rotatory strength $R(T_{1g}i)$ can be expressed by using the first-order wavefunctions given in Eqs. 2 and 3.

A Crystal Field Model for Mixed Complexes

We deal with cobalt(III) complexes with *cis*(*N*)-$[Co(N)_2(O)_4]$ or *cis*(*O*)-$[Co(N)_4(O)_2]$ chromophore. Since the holohedrized symmetry[8] of those complexes is D_{4h}, the electronic states can be approximated by a treatment in D_{4h} symmetry. Therefore, we use tetragonal basis sets of 3d and 4p orbitals as zero-order wavefunctions. The wavefunction of the ground state is written in determinant form as follows:

$$|A_{1g}) = |\overset{+}{(yz)}\overset{-}{(yz)}\overset{+}{(zx)}\overset{-}{(zx)}\overset{+}{(xy)}\overset{-}{(xy)}|.$$

As for the excited states, T_{1g} state in octahedral symmetry splits into A_{2g} and E_g^a states in tetragonal symmetry, while T_{2g} state splits into B_{2g} and E_g^b states. The wavefunctions of the excited states are listed in Table 1, in which the wavefunctions are represented by a d- or p-orbital component of the occupied orbital and a d-orbital component of the hole orbital. Thus, the wavefunction for $|A_{2g})$ is:

$$|(xy)(x^2-y^2)| = \{|\cdots\overset{+}{(yz)}\overset{-}{(yz)}\overset{+}{(zx)}\overset{-}{(zx)}\overset{+}{(xy)}(x^2-\overset{-}{y^2})| + |\cdots(\overset{+}{x^2-y^2})\overset{-}{(xy)}|\}/\sqrt{2}.$$

Non-vanishing matrix elements of $\boldsymbol{P}$ and $\boldsymbol{M}$ are gathered in Tables 2 and 3. Using the wavefunctions in Table 1, the rotatory strength of $R(A_{2g})$, which arises from d-p and d-d mixings, can be expressed as follows:

$$\begin{aligned}
R(A_{2g}) = {} & (\sqrt{3}/4)[\langle x|\boldsymbol{V}_u|x^2-y^2\rangle\Delta E_{u2}^{-1} \\
& - \langle y|\boldsymbol{V}_u|xy\rangle\Delta E_{u1}^{-1}] \\
& \times [\{\langle x^2-y^2|\boldsymbol{V}_g|zx\rangle - \sqrt{3}\langle z^2|\boldsymbol{V}_g|zx\rangle\}\Delta E_1^{-1} \\
& - 2\langle xy|\boldsymbol{V}_g|yz\rangle\Delta E_2^{-1} \\
& - (3\sqrt{2}/2)\{\langle x^2-y^2|\boldsymbol{V}_g|zx\rangle \\
& + \sqrt{3}\langle z^2|\boldsymbol{V}_g|zx\rangle\}\Delta E_3^{-1} \\
& + 3\sqrt{2}\langle xy|\boldsymbol{V}_g|yz\rangle\Delta E_4^{-1}] \quad (5) \\
& - (\sqrt{3}/4)[\langle y|\boldsymbol{V}_u|x^2-y^2\rangle\Delta E_{u2}^{-1} \\
& + \langle x|\boldsymbol{V}_u|xy\rangle\Delta E_{u1}^{-1}] \\
& \times [\{\langle x^2-y^2|\boldsymbol{V}_g|yz\rangle \\
& + \sqrt{3}\langle z^2|\boldsymbol{V}_g|yz\rangle\}\Delta E_1^{-1} \\
& + 2\langle xy|\boldsymbol{V}_g|zx\rangle\Delta E_2^{-1} \\
& - (3\sqrt{2}/2)\{\langle x^2-y^2|\boldsymbol{V}_g|yz\rangle \\
& - \sqrt{3}\langle z^2|\boldsymbol{V}_g|yz\rangle\Delta E_3^{-1} \\
& - 3\sqrt{2}\langle xy|\boldsymbol{V}_g|zx\rangle\Delta E_4^{-1}].
\end{aligned}$$

Here,

$$\begin{aligned}
& \Delta E_{u1} = E(M_u) - E(A_{1g}),\ \Delta E_2 = E(E_g^a) - E(A_{2g}) \\
& \Delta E_{u2} = E(M_u) - E(A_{2g}),\ \Delta E_3 = E(E_g^b) - E(A_{1g}) \\
& \Delta E_1 = E(E_g^a) - E(A_{1g}),\ \Delta E_4 = E(E_g^b) - E(A_{2g}). \quad (6)
\end{aligned}$$

We use an average energy $E(M_u)$ instead of the individual energy levels of odd parity states.

We are interested in the Cotton sign of $A_{1g}\rightarrow A_{2g}(D_{4h})$ transition for the CD spectra of Λ-$[Co(NN)_2(OO)]^{n+}$ and Λ-$[Co(NN)(OO)_2]^{n-}$ complexes ($OO=CO_3^{2-}$, ox^{2-}, mal^{2-}, or $2H_2O$; NN=en or tn). To predict the Cotton sign, it is necessary to define the spherical coordinate (R_i, θ_i, ϕ_i) of the ligating atom L_i (i=1,2,⋯6). The adopted spherical and Cartesian coordinate systems are drawn in Fig. 1. In this model, we

Table 1. The wavefunctions of excited states

$\|A_{2g}\rangle = \|(xy)(x^2-y^2)\|$
$\|E_g^a1\rangle = \|(yz)(y^2-z^2)\|$
$\|E_g^a2\rangle = \|(zx)(z^2-x^2)\|$
$\|E_g^b1\rangle = \|(yz)(x^2)\|$
$\|E_g^b2\rangle = \|(zx)(y^2)\|$
$\|B_{2g}\rangle = \|(xy)(z^2)\|$
$\|B_{1u}^a\rangle = -\{\|(yz)(x)\|+\|(zx)(y)\|+\|(xy)(z)\|\}/\sqrt{3}$
$\|B_{1u}^b\rangle = -\{\|(yz)(x)\|+\|(zx)(y)\|-2\|(xy)(z)\|\}/\sqrt{6}$
$\|A_{1u}\rangle = -\{\|(yz)(x)\|-\|(zx)(y)\|\}/\sqrt{2}$
$\|A_{2u}\rangle = \{\|(zx)(x)\|+\|(yz)(y)\|\}/\sqrt{2}$
$\|B_{2u}\rangle = -\{\|(zx)(x)\|-\|(yz)(y)\|\}/\sqrt{2}$
$\|E_u^a1\rangle = \{\|(xy)(y)\|+\|(zx)(z)\|\}/\sqrt{2}$
$\|E_u^a2\rangle = \{\|(xy)(x)\|+\|(yz)(z)\|\}/\sqrt{2}$
$\|E_u^b1\rangle = -\{\|(xy)(y)\|-\|(zx)(z)\|\}/\sqrt{2}$
$\|E_u^b2\rangle = -\{\|(yz)(z)\|-\|(xy)(x)\|\}/\sqrt{2}$

Table 2. Zeroth-order d-p electric dipole transition matrix[a]

$\boldsymbol{P}$	z^2	x^2-y^2	xy	zx	yz
z	$2\boldsymbol{k}$	0	0	$\sqrt{3}\boldsymbol{i}$	$\sqrt{3}\boldsymbol{j}$
x	$-\boldsymbol{i}$	$\sqrt{3}\boldsymbol{i}$	$\sqrt{3}\boldsymbol{j}$	$\sqrt{3}\boldsymbol{k}$	0
y	$-\boldsymbol{j}$	$-\sqrt{3}\boldsymbol{j}$	$\sqrt{3}\boldsymbol{i}$	0	$\sqrt{3}\boldsymbol{k}$

$\boldsymbol{i}$, $\boldsymbol{j}$, and $\boldsymbol{k}$ are unit vectors in the x, y, and z directions. a) In units of $e\langle R_p|r|R_d\rangle/\sqrt{15}$.

Table 3. Zeroth-order d-d magnetic dipole transition matrix[a]

$\boldsymbol{M}$	z^2	x^2-y^2	xy	zx	yz
z^2	0	0	0	$-\sqrt{3}i\boldsymbol{j}$	$\sqrt{3}i\boldsymbol{i}$
x^2-y^2	0	0	$-\sqrt{2}i\boldsymbol{k}$	$i\boldsymbol{j}$	$i\boldsymbol{i}$
xy	0	$\sqrt{2}i\boldsymbol{k}$	0	$-i\boldsymbol{i}$	$i\boldsymbol{j}$
zx	0	$-i\boldsymbol{j}$	$i\boldsymbol{i}$	0	0
yz	0	$-i\boldsymbol{i}$	$-i\boldsymbol{j}$	0	0

$\boldsymbol{i}$, $\boldsymbol{j}$, and $\boldsymbol{k}$ are unit vectors in x, y, and z directions. a) In units of $\sqrt{2}\,he/(4mc)$.

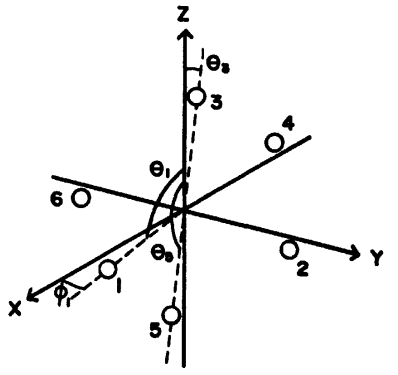

Fig. 1. The spherical and Cartesian coordinate systems.

consider a simplified arrangement of the ligating atoms, and ignore the existence of non-ligating atoms. The coordinate (R_i, θ_i, ϕ_i) of the ligating atom L_i (i=1,3,5) is converted into (R_{i+1}, θ_{i+1}, ϕ_{i+1}) by a C_2 axis intersecting the bidentate ligand L_iL_{i+1}. These three C_2 axes are supposed to deviate from the x, y, or z axis by 45°. The R_{i+1} coordinate is assumed to be equal to the R_i (i=1,3,5). On these assumptions, the V_u and V_g potentials at the non-vanishing matrix elements in Eq. 5 can be expressed as

$$\begin{aligned} V_u &= er^3\{A_{33}Y_3^3 + A_{3-3}Y_3^{-3}\} \\ V_g &= er^2(A_{21}Y_2^1 + A_{2-1}Y_2^{-1}) \\ &\quad + er^4(A_{41}Y_4^1 + A_{4-1}Y_4^{-1}) \\ &\quad + er^4(A_{43}Y_4^3 + A_{4-3}Y_4^{-3}), \end{aligned} \tag{7}$$

where r denotes the electron radical coordinate and e is the charge of an electron. The functions Y_l^m are spherical harmonics normalized to unity. The factors A_{lm} are defined as

$$\begin{aligned} A_{3\pm3} &= \mp(3\sqrt{5}/4)\sum_{k=1}^{6} q_k R_k^{-4}\sin^3\theta_k \exp(\mp 3\phi_k i) \\ A_{2\pm1} &= \pm\sqrt{6}\sum_{k=1}^{6} q_k R_k^{-3}\sin 2\theta_k \exp(\mp\phi_k i) \\ A_{4\pm1} &= \pm(\sqrt{5}/2)\sum_{k=1}^{6} q_k R_k^{-5}\sin 2\theta_k(7\cos^2\phi_k - 1)\exp(\mp\phi_k i) \\ A_{4\pm3} &= \pm(3\sqrt{5}/2)\sum_{k=1}^{6} q_k R_k^{-5}\sin 2\theta_k \sin^2\theta_k \exp(\mp 3\phi_k i), \end{aligned} \tag{8}$$

where q_k expresses the effective charge associated with the ligating atom L_k.

Idealized Model. We first consider the Cotton sign of $R(A_{2g})$ in Λ-$[Co(NN)_2(OO)]^{n+}$ and Λ-$[Co(NN)_2(OO)_2]^{n-}$ by an idealized model in which all ligating atoms are located on the xy, yz, and zx planes. The complexes can be classified into three groups.

Group 1) L_1CoL_2, L_3CoL_4, and L_5CoL_6<90°

Group 2) L_1CoL_2<90°, L_3CoL_4 and L_5CoL_6>90°

Group 3) L_1CoL_2>90°, L_3CoL_4 and L_5CoL_6<90°

The coordination angles of concerned complexes are cited in Table 4. The complexes Λ-$[Co(CO_3)(en)_2]^+$, Λ-$[Co(ox)(en)_2]^+$, Λ-$[Co(CO_3)(ox)(en)]^-$, and Λ-$[Co(ox)_2(en)]^-$ belong to Group 1), Λ-$[Co(ox)(tn)_2]^+$ and Λ-$[Co(mal)_2(en)]^-$ complexes to Group 2), and Λ-$[Co(mal)(en)_2]^+$, Λ-$[Co(CO_3)(mal)(en)]^-$, and Λ-$[Co(ox)(mal)(en)]^-$ complexes to Group 3).

The expressions for the rotatory strength of $R(A_{2g})$ in these groups are given in Table 5. Since the values of $\langle r^3\rangle$ and ΔE_{u2} are positive, the constant, K, becomes positive. In order to predict the sign of $R(A_{2g})$, the

Table 4. Data of coordination angles and bond lengths

	Coordination angle of the ligand θ/°	Bond length between central metal ion and the ligand l/Å	Reference
CO_3^{2-}	70	1.93	a)
ox^{2-}	85	1.94	13
mal^{2-}	96	1.90	11
en	86	1.98	11,13
tn	96	1.99	b)

a) M. R. Snow, *Aust. J. Chem.*, **25**, 1307 (1972). b) T. Nomura, F. Marumo, and Y. Saito, *Bull. Chem. Soc. Jpn.*, **42**, 1016 (1969); R. Nagao, F. Marumo, and Y. Saito, *Acta Crystallogr., Sect. B*, **29** 2438 (1973); H.V.F. Schousboe-Jensen, *Acta Chem. Scand.*, **26**, 3413 (1972).

Table 5. Rotatory strength of $R(A_{2g})$

Coordinates	Rotatory strength
Group 1) L_1 : (R_1, 90°, ϕ_1) L_2 : (R_1, 90°, 90°$-\phi_1$) L_3 : (R_3, θ_3, 180°) L_4 : (R_3, 90° $-\theta_3$, 180°) L_5 : (R_5, θ_5, 270°) L_6 : (R_5, 270° $-\theta_5$, 270°)	$R(A_{2g}) = -K\{(\cos 3\phi_1 - \sin 3\phi_1)q_1R_1^{-4} - \gamma(\sin^3\theta_3 + \cos^3\theta_3)q_3R_3^{-4}\} \times K_1 \sin 2\theta_5$ $- K\{(\cos 3\phi_1 - \sin 3\phi_1)\, q_1R_1^{-4} - \gamma(\sin^3\theta_5 - \cos^3\theta_5)q_5R_5^{-4}\} \times K_2 \sin 2\theta_3$
Group 2) L_1 : (R_1, 90°, ϕ_1) L_2 : (R_1, 90°, 90° $-\phi_1$) L_3 : (R_3, θ_3, 0) L_4 : (R_3, 90° + θ_3, 180°) L_5 : (R_5, θ_5, 90°) L_6 : (R_5, $-$90° + θ_5, 270°)	$R(A_{2g}) = K\{(\cos 3\phi_1 - \sin 3\phi_1)q_1R_1^{-4} + \gamma(\sin^3\theta_3 - \cos^3\theta_3)q_3R_3^{-4}\} \times K_1 \sin 2\theta_5$ $+ K\{(\cos 3\phi_1 - \sin 3\phi_1)q_1R_1^{-4} + \gamma(\sin^3\theta_5 + \cos^3{}_5)q_5R_5^{-4}\} \times K_2 \sin 2\theta_3$
Group 3) L_1 : (R_1, 90°, $-\phi_1$) L_2 : (R_1, 90°, 90° $+\phi_1$) L_3 : (R_3, θ_3, 180°) L_4 : (R_3, 90° $-\theta_3$, 180°) L_5 : (R_5, θ_5, 270°) L_6 : (R_5, 270° $-\theta_5$, 270°)	$R(A_{2g}) = -K\{(\cos 3\phi_1 + \sin 3\phi_1)q_1R_1^{-4} - \gamma(\sin^3\theta_3 + \cos^3\theta_3)q_3R_3^{-4}\} \times K_1 \sin 2\theta_5$ $- K\{(\cos 3\phi_1 + \sin 3\phi_1)q_1R_1^{-4} - \gamma(\sin^3\theta_5 - \cos^3\theta_5)q_5R_5^{-4}\} \times K_2 \sin 2\theta_3$

$K=(35/28)\langle r^3\rangle\Delta E_{u2}^{-1}$

$K_1=(3/28)R_5^{-3}\langle r^2\rangle(2\Delta E_2^{-1}-3\sqrt{2}\Delta E_4^{-1}+2\Delta E_1^{-1})q_5-(5/336)R_5^{-5}\langle r_4\rangle(16\Delta E_2^{-1}-24\sqrt{2}\Delta E_4^{-1}-12\Delta E_1^{-1})q_5$

$K_2=(3/28)R_3^{-3}\langle r^2\rangle(2\Delta E_2^{-1}-3\sqrt{2}\Delta E_4^{-1})q_3-(5/336)R_3^{-5}\langle r^4\rangle(16\Delta E_2^{-1}-24\sqrt{2}\Delta E_4^{-1}-12\Delta E_1^{-1})q_3$

$\langle r^2\rangle=\langle d|r^2|d\rangle$

$\langle r^3\rangle=\langle d|r^3|d\rangle$

$\langle r^4\rangle=\langle d|r^4|d\rangle$

$\gamma=\Delta E_{u2}/\Delta E_{u1}$

Table 6. Energy differences ($\tilde{\nu}$ in 10^3 cm^{-1})

Complex	ΔE_1	ΔE_2	ΔE_4
$[Co(CO_3)_2(en)]^-$	17.0	−1.45	8.10
$[Co(CO_3)(ox)(en)]^-$	17.4	−1.31	7.50
$[Co(ox)_2(en)]^-$	17.8	−1.18	7.50
$[Co(CO_3)(mal)(en)]^-$	17.4	−1.31	7.53
$[Co(ox)(mal)(en)]^-$	17.7	−1.19	7.50
$[Co(mal)_2(en)]^-$	17.7	−1.21	7.40
$[Co(CO_3)(en)_2]^+$	19.9	1.01	8.26
$[Co(ox)(en)_2]^+$	20.1	1.18	8.10
$[Co(mal)(en)_2]^+$	20.1	1.21	7.85
$[Co(ox)(tn)_2]^+$	19.5	0.97	8.33
$[Co(ox)(H_2O)_2(en)]^+$	17.8	−1.18	7.50
$[Co(mal)(H_2O)_2(en)]^+$	17.7	−1.19	7.59
$[Co(H_2O)_2(en)_2]^{3+}$	20.1	1.18	7.50

following variables have to be estimated:

1) radial integrals $\langle r^2\rangle$ and $\langle r^4\rangle$,
2) coordinates of the ligating atom L_i, (R_i, θ_i, ϕ_i),
3) energy differences, ΔE_1, ΔE_2, and ΔE_4,
4) effective charges of ligating atoms, q_i.

The radial integrals can be evaluated by Watoson's Hartree-Fock wavefunction,[9] that is, $\langle r^2\rangle$=0.293 Å and $\langle r^4\rangle$=0.184 Å. The coordinates of the ligating atoms can be estimated from the X-ray analytical data listed in Table 4. As for the energy differences, the ΔE_1 and ΔE_2 values can be evaluated in terms of an angular overlap model,[10] and the ΔE_4 value is approximated by the energy difference between the absorption maximum of the first absorption band and that of the second absorption band, the values being listed in Table 6. It is difficult to estimate accurately the effective charges of the ligating atoms. Since this model ignores the existence of the non-ligating atoms, it is better to treat the effective charge of a ligating atom as an empirical parameter. The effect of the non-ligating atom upon the rotatory strength may be included into the parameter. We adopt a crude assumption that the effective charge on an anionic ligand of OO type is minus and that on a neutral ligand is plus.

The Cotton sign of $R(A_{2g})$ of the Λ-$[Co(en)(ox)(ox)]^-$ ($=\Lambda$-$[Co(L_1L_2)(L_3L_4)(L_5L_6)]^-$) complex is predicted as follows. From the data of the bond distances and the coordination angles, the coordinates of the ligating atoms in the complex are written as

$$\begin{aligned}(R_1, \theta_1, \phi_1) &= (1.98, 90°, 2°)\\ (R_3, \theta_3, \phi_3) &= (1.94, 2.5°, 180°)\\ (R_5, \theta_5, \phi_5) &= (1.94, 177.5°, 270°).\end{aligned} \quad (9)$$

Using these coordinates and the values of the radial integrals, $R(A_{2g})$ of Λ-$[Co(ox)_2(en)]^-$ is expressed as the product of an effective charge term and an energy difference term:

$$R(A_{2g}) = -C \times q_{ox}(5.8q_{en} - 7.0\gamma q_{ox}) \times (8\ 5\,\Delta E_1^{-1} + 6.1\,\Delta E_2^{-1} - 13\,\Delta E_4^{-1}), \quad (10)$$

where q_{en} and q_{ox} denote the effective charge of the ligating atoms of en and ox, respectively, and C is a positive constant. Since the ΔE_1, ΔE_2, and ΔE_4 values are evaluated as 17800, −1180, and 7500 cm^{-1} respectively (Table 6), the sign of the energy difference term in Eq. 10 becomes minus, on account of a small minus value of ΔE_2. It may be noted that the energy difference term becomes minus in all $cis(N)$-$[Co(N)_2(O)_4]$ complexes. The q_{en} value is evaluated to be plus and the q_{ox} value to be minus. Since the value of $\gamma=\Delta E_{u2}/\Delta E_{u1}$ becomes plus, $R(A_{2g})$ is considered to be negative in the Λ-$[Co(ox)_2(en)]^-$ complex. Similar procedures in calculation lead to the same result in the Λ-$[Co(CO_3)(ox)(en)]^-$ and Λ-$[Co(CO_3)_2(en)]^-$ complexes.

As to the Λ-$[Co(ox)(en)_2]^+$ complex, which also belongs to Group 1), the following equation of $R(A_{2g})$ is obtained by a similar calculation:

$$R(A_{2g}) = -C \times q_{en}(6.1\,q_{ox} - 6.5\,\gamma q_{en}) \times (4.6\,\Delta E_2^{-1} - 0.8\,\Delta E_4^{-1} + 6.4\,\Delta E_1^{-1}). \quad (11)$$

In this complex, the energy difference term in Eq. 11 becomes plus, on account of the small plus value of ΔE_2. It is worth noting that the energy difference term is always plus in $cis(O)$-$[Co(N)_4(O)_2]$ complexes. If $q_{en}>0$ and $q_{ox}<0$, the resultant sign of $R(A_{2g})$ in Λ-$[Co(ox)(en)_2]^+$ becomes positive. Similarly, $R(A_{2g})$ in Λ-$[Co(CO_3)(en)_2]^+$ is predicted to have a positive sign.

Since the coordination angle of mal^{2-} in Λ-$[Co(mal)_2(en)]^-$ is reported to be 96°,[11] this complex belongs to Group 2). Using the equation in Table 5, $R(A_{2g})$ of the complex can be written as

$$R(A_{2g}) = Cq_{mal}(5.8\,q_{en} - 7.6\,\gamma q_{mal}) \times (7.7\,\Delta E_2^{-1} - 16\,\Delta E_4^{-1} + 11\,\Delta E_1^{-1}), \quad (12)$$

where q_{mal} denotes the effective charge on the malonato ligand. Since the chromophore is $cis(N)$-$[Co(N)_2(O)_4]^-$, the energy difference term becomes minus on account of the minus value of ΔE_2. The malonato ligand is anionic, and q_{mal} is also regarded to be minus. Therefore, $R(A_{2g})$ in Λ-$[Co(mal)_2(en)]^-$ is predicted to have a positive sign.

The Λ-$[Co(ox)(tn)_2]^+$ complex is also of Group 2), and its $R(A_{2g})$ is written as

$$R(A_{2g}) = Cq_{tn}(6.1\,q_{ox} - 6.3\,\gamma q_{tn}) \times (6.9\,\Delta E_2^{-1} - 15\,\Delta E_4^{-1} + 9.4\,\Delta E_1^{-1}). \quad (13)$$

The energy difference term is estimated to be plus, and if $q_{tn}>o$, the effective charge term becomes minus. Consequently, the sign of $R(A_{2g})$ in the complex is regarded as negative.

For complexes of Group 3), when the angle ϕ_1 is measured to have a minus value, the equation for group 1) can be utilized. For example, the coordinates of Λ-$[Co(mal)(en)_2]^+$ are,

$$\begin{aligned}(R_1, \theta_1, \phi_1) &= (1.90, 90°, -3°)\\ (R_3, \theta_3, \phi_3) &= (1.98, 2°, 180°)\\ (R_5, \theta_5, \phi_5) &= (1.98, 178°, 270°).\end{aligned} \quad (14)$$

The sign of $R(A_{2g})$ is plus, which is the same as in the case of Λ-$[Co(ox)(en)_2]^+$.

If it is postulated that H_2O molecules are linked on the coordinate axes, the Λ-$[Co(en)_2(H_2O)_2]^{3+}$ and Λ-$[Co(ox)(en)(H_2O)_2]^+$ complexes may be classified into Group 1). The rotatory strength for the former complex is given by

$$R(A_{2g}) = -C \times q_{en}(7.1\,q_{H_2O} - 6.5\,\gamma q_{en}) \times (6.4\,\Delta E_1^{-1} + 4.6\,\Delta E_2^{-1} - 9.8\,\Delta E_4^{-1}) \quad (15)$$

and, for the latter complex, by

$$R(A_{2g}) = -C \times q_{ox}(5.8\, q_{en} - 7.1\, \gamma q_{H_2O}) \times (8.5\, \Delta E_1^{-1} + 6.1\, \Delta E_2^{-1} - 13\, \Delta E_4^{-1}), \quad (16)$$

where q_{H_2O} denotes the effective charge of the ligating atom in H_2O. The energy difference term in the former complex is estimated to be plus, and that in the latter complex to be minus. According to the estimation of the q_{H_2O} value, the $R(A_{2g})$ in Eqs. 15 and 16 change their signs; if q_{H_2O} has a minus or slightly plus value, the $R(A_{2g})$ of the former complex exhibits positive sign and that of the latter complex a negative one. On the other hand, if q_{H_2O} has a considerable plus value compared with q_{en}, the $R(A_{2g})$ of the former shows a negative sign and that of the latter a positive one.

Deviated Ligand Model. In this model, the influence of the deviation of ligating atoms from xy, yz, and zx planes is studied. For example, the coordinates of a complex in Group 1) are given by

$$\begin{aligned}
(R_1, \theta_1, \phi_1) &= (R_1, 90° + \Delta\theta, \phi_1)\\
(R_2, \theta_2, \phi_2) &= (R_1, 90° - \Delta\theta, 90° - \phi_1)\\
(R_3, \theta_3, \phi_3) &= (R_3, \theta_3, 180° + \Delta\phi)\\
(R_4, \theta_4, \phi_4) &= (R_3, 90° - \theta_3, 180° - \Delta\phi)\\
(R_5, \theta_5, \phi_5) &= (R_5, \theta_5, 270° - \Delta\phi)\\
(R_6, \theta_6, \phi_6) &= (R_5, 270° - \theta_5, 270° + \Delta\phi)
\end{aligned} \quad (17)$$

When the angles $\Delta\theta$ and $\Delta\phi$ were varied from 1° to 3° in the calculation, the predicted sign of $R(A_{2g})$ was essentially coincident with that obtained by the idealized model.

Results and Discussion

1) CD Sign. For the *A*-$[Co(CO_3)_2(en)]^-$, *A*-$[Co(CO_3)(ox)(en)]^-$, and *A*-$[Co(ox)_2(en)]^-$ complexes with *cis*(*N*)-$[Co(N)_2(O)_4]$ chromophore, which are classified into Group 1),the signs of $R(A_{2g})$ are predicted to be negative. On the other hand, for the *A*-$[Co(CO_3)(en)_2]^+$ and *A*-$[Co(ox)(en)_2]^+$ complexes with *cis*(*O*)-$[Co(N)_4(O)_2]$ chromophore, which are also classified into Group 1), the predicted sign of $R(A_{2g})$ is positive. For the *A*-$[Co(mal)_2(en)]^-$ and *A*-$[Co(ox)(tn)_2]^+$ complexes of Group 2), the sign of $R(A_{2g})$ in the former is predicted to be positive, and that in the latter to be negative. Therefore, we can say that the sign of $R(A_{2g})$ in a *A*-$[Co(N)_2(O)_4]^-$ complex is reverse to that in a *A*-$[Co(N)_4(O)_2]^+$ complex, provided that the two complexes belong to the same group. This is because the equation of $R(A_{2g})$ is expressed as a product of two terms, one of which is an effective charge term and the other is an energy difference term, which is a function of inverted ΔE_1, ΔE_2, and ΔE_4. In both the *A*-$[Co(N)_2(O)_4]^-$ and the *A*-$[Co(N)_4(O)_2]^+$ complexes, the effective charge terms become minus. Since $|E_2|$ is much smaller than ΔE_1 and ΔE_4, the sign of the energy difference term depends upon the sign of ΔE_2, which is a energy difference between E_g^a and A_{2g} states. The ΔE_2 value becomes minus and plus in the *A*-$[Co(N)_2(O)_4]^-$ complexes and in the *A*-$[Co(N)_4(O)_2]^+$ complexes, respectively. Accordingly, the energy difference term becomes minus in the former complexes, and plus in the latter complexes.

With complexes with the same chromophore, the $R(A_{2g})$ in a complex of Group 1) is predicted to have the reverse sign to that in a complex of Group 2). This is because, for both the complexes, the products of the effective charge term and the energy difference term have the same sign, provided that the complexes have the same chromophore. However, the product has a minus coefficient in a complex of Group 1) and a plus one in a complex of Group 2), so these coefficients depend upon the coordinates of the ligating atoms. When the coordination angle of a bidentate ligand is smaller than 90°, the coefficient has a minus sign, whereas when the angle is larger than 90°, the coefficient has a plus sign.

Piper and Karipides[6] have predicted that the Cotton sign for $E^a(D_3)$ component in *A*-$[Co(tn)_3]^{3+}$ would be opposite to that in *A*-$[Co(en)_3]^{3+}$. The coordination angle in the trimethylenediamine complex is larger than 90° and that in the ethylenediamine complex is smaller than 90°. By the measurement of a single crystal CD spectrum in *A*-$(+)_{589}[Co(tn)_3]^{3+}$, Judkins and Royer[12] have concluded that a Cotton sign of a given transition should change when the coordination angle of the bidentate chelate ring changes from less than 90° to more than 90°. Our predictions in the mixed-complexes with lower symmetry corresponds well to these conclusions.

2) Absolute Configuration. It has been reported[1] that the $(-)_{589}[Co(CO_3)_2(en)]^-$, $(-)_{589}[Co(CO_3)(ox)(en)]^-$ and $(-)_{589}[Co(ox)_2(en)]^-$ complexes have *A* configurations, and the CD spectra of these complexes exhibit a single positive Cotton peak in the first absorption band region. In our previous paper,[2] these positive Cotton peaks were assigned to a component of $A_{1g} \rightarrow E_g(D_{4h})$. On the other hand, a component of $A_{1g} \rightarrow A_{2g}(D_{4h})$ was regarded as having a negative Cotton sign. Since these complexes have a *cis*(*N*)-$[Co(N)_2(O)_4]$ chromophore and belong to Group 1), the assignments agree well with our calculation results.

The CD spectra of $(+)_{589}[Co(CO_3)(en)_2]^+$, $(+)_{589}$-$[Co(ox)(en)_2]^+$, and $(+)_{589}[Co(mal)(en)_2]^+$ show a single positive Cotton peak in the first absorption band region. The first two complexes belong to Group 1), and the third to Group 3). Previously, the positive Cotton peaks in these complexes were assigned to the $A_{1g} \rightarrow A_{2g}(D_{4h})$ transition component.[2] The absolute configuration of $(+)_{589}[Co(ox)(en)_2]^+$ was determined to be *A* by an X-ray analysis.[13] Since the $(+)_{589}$-isomers of $[Co(ox)(en)_2]^+$ and $[Co(mal)(en)_2]^+$ can be derived from the $(+)_{589}$-isomer of $[Co(CO_3)(en)_2]^+$ by the reaction with oxalic and malonic acids, respectively, the absolute configurations of the carbonato and malonato complexes are also regarded to be *A*. Our calculation for $R(A_{2g})$of these three complexes predicts positive signs, which agrees with the previous experimental results.

The $(-)_{589}[Co(mal)_2(en)]^-$ complex that belongs to Group 2) exhibits three Cotton peaks with (+), (−), and (+) signs from the lower-frequency side in the first absorption band region.[14] The absolute configuration of the complex has been determined to *A*,[11] and the

component with the (−) sign has been assigned to the $A_{1g}\rightarrow A_{2g}(D_{4h})$ component.[1] However, our calculation for $R(A_{2g})$ of this complex predicts a positive sign. This discrepancy seems to arise from the neglect of non-ligating atoms in our model. It is known that non-ligating atoms have an important role in the optical activities of tris(diamine) cobalt(III) complexes.[7] The degenerate $E_g^a(D_{4h})$ state may split into two non-degenerate states by an action of the non-ligating atoms.

The $(+)_{589}[Co(ox)(tn)_2]^+$ complex that also belongs to Group 2) exhibits a single (+) Cotton peak in the first absorption band region. Although the absolute configuration of the complex has not yet been determined, if the positive peak is assignable to the $A_{1g}\rightarrow A_{2g}(D_{4h})$ component, as in the case of the $(+)_{589}[Co(ox)(en)_2]^+$ complex, our calculation predicts a *Δ* configuration.

3) The CD Spectra of Diaqua Complexes. As mentioned in the Introduction, when an optically active diaqua complex is derived from an optically active carbonato complex by an acid-hydrolysis, the CD spectrum of the diaqua complex is quite different from that of the parent carbonato complex. For example, Λ-$(-)_{589}[Co(CO_3)(ox)(en)]^-$ exhibits a Cotton peak with a positive sign in the first absorption band region. The Λ-$[Co(ox)(en)(H_2O)_2]^+$ complex which is derived from the Λ-$(-)_{589}[Co(CO_3)(ox)(en)]^-$ complex exhibits (−) and (+) Cotton peaks from the lower-frequency side in the region.

This phenomenon can be understood in terms of the effective charge of the ligating O atom of the water molecule; the rotatory strength $R(A_{2g})$ is expressed as a product of the effective charge term and the energy difference term, and the energy difference terms have a negative sign in the above two complexes. If q_{CO_3} is evaluated to be minus, the effective charge term in the $[Co(CO_3)(ox)(en)]^-$ complex becomes minus, the resultant sign of $R(A_{2g})$ being negative. In the previous section, it is pointed out that, if q_{H_2O} has a large, plus value, the effective charge term attains a plus value, resulting in a positive sign of $R(A_{2g})$. In order to understand the CD spectrum of the diaqua complex, it is better to regard the empirical q_{H_2O} parameter as plus. Since the aqua ligand is a neutral molecule and the diaqua complex is a cation, it is probable that the donor atom of the aqua ligand has a plus effective charge.

The CD spectrum of Λ-$[Co(CO_3)(en)_2]^+$ exhibits a positive Cotton peak which is assignable to $A_{1g}\rightarrow A_{2g}$ component.[2] Two Cotton peaks with opposite signs are observed in the CD spectrum of Λ-$[Co(en)_2(H_2O)_2]^{3+}$, and the negative peak is assigned to the $A_{1g}\rightarrow A_{2g}$ component. The significant difference of CD spectral shapes between the carbonato and the diaqua complex can also be understood by the difference between the effective charge of the donor atoms in the aqua molecules and that in the carbonato ligand. Our model is useful to explain the CD spectral behavior of the diaqua complexes.

4) CT States in the Crystal Field Model. Since a d-d transition is electronically forbidden, d-orbitals need to admix with an odd parity state. Piper and Karipides[6] have considered the admixture of p-orbitals of a central metal ion in their crystal field model of the optical activities. Our model is also constructed by considering the admixture of p-orbitals of a central metal ion. However, it is possible to consider the admixture of p-orbitals of a ligand, (*i.e.* CT states). Since the wavefunctions of the metal to ligand CT states have the same forms as those listed in Table 1,[15] the formula of rotatory strength expressed in Table 5 is obtained for the d-CT mixing model. The differen point between the d-p mixing model and the d-CT mixing model appears at the evaluation of the $\gamma=E_{u2}/E_{u1}$ value. However, the evaluation of the γ value has no influence upon predicting the sign of $R(A_{2g})$, since the γ value is always plus. Therefore, it is concluded that the d-CT mixing model gives the same results as the d-p mixing model, for the prediction of Cotton signs of a given transition.

Experimental

Derivation of the Malonato Complex. To an aqueous solution of $(+)_{546}[Co(CO_3)(en)_2]Cl$[16] (10 mg, 0.04 mmol in 10 cm^3 H_2O), potassium malonate (1 g, 5 mmol) and malonic acid (0.5 g, 5 mmol) were added, and the mixed solution was stirred at 40 °C for 3 h. The resulting solution was kept in a refrigerator for 2 d, and then filtered. The filtrate was diluted by water (250 cm^3), and charged onto a column of Dowex 50W-X8 resin in Na^+ form (100—200 mesh, 1 cm×5 cm). By elution with a 0.1 mol/dm^3 NaCl solution, one red band was discharged. The absorption and CD spectral data of the effluent were identical with those of $(+)_{546}[Co(mal)(en)_2]^+$.[17]

References

1) S. Muramoto, K. Kawase, and M. Shibata, *Bull. Chem. Soc. Jpn.*, **51**, 3505 (1978).
2) K. Tsuji, S. Fujinami, and M. Shibata, *Bull. Chem. Soc. Jpn.*, **54**, 1531 (1981).
3) Y. Enomoto, T. Ito, and M. Shibata, *Chem. Lett.*, **1974**, 423.
4) A. J. McCaffery, S. F. Mason, and B. J. Norman, *J. Chem. Soc.*, **1965**, 5094.
5) I. J. Kindred and D. A. House, *J. Inorg. Nucl. Chem.*, **37**, 1359 (1975); Y. Wada, K. Miyoshi, and H. Yoneda, *Chem. Lett.*, **1978**, 763; S. Yamazaki and H. Yoneda, *J. Chromatogr.*, **177**, 227 (1979).
6) T. S. Piper and A. Karipides, *Mol. Phys.*, **5**, 475 (1962); F. S. Richardson, *J. Phys. Chem.*, **75**, 692 (1971); G. Hilmes and F. S. Richardson, *Inorg. Chem.*, **15**, 2582 (1976).
7) S. F. Mason, *J. Chem. Soc., A*, **1971**, 667; S. F. Mason and R. H. Seal, *Mol. Phys.*, **31**, 755 (1976); J. A. Hearson, S. F. Mason, and R. H. Seal, *J. Chem. Soc., Dalton Trans.*, **1977**, 1026; R. W. Strickland and F. S. Richardson, *J. Phys. Chem.*, **80**, 164 (1976).
8) C. K. Jørgensen, "Modern Aspects of Ligand Field Theory," North-Holland Pub. Co., Amsterdam (1971).
9) M. Shinada, *J. Phys. Soc. Jpn.*, **19**, 1607 (1964).
10) H. Yamatera, *Bull. Chem. Soc. Jpn.*, **31**, 95 (1958); C. E. Schäffer and C. K. Jørgensen, *Mol. Phys.*, **9**, 401 (1965); C. E. Schäffer, *Pure Appl. Chem.*, **24**, 361 (1970); *Struct. Bonding*, **14**, 69 (1973).
11) K. Matsumoto and H. Kuroya, *Bull. Chem. Soc. Jpn.*, **45**, 1755 (1972).

12) R. R. Judkins and D. J. Royer, *Inorg. Nucl. Chem. Lett.*, **6**, 305 (1970).
13) T. Aoki, K. Matsumoto, S. Ooi, and H. Kuroya, *Bull. Chem. Soc. Jpn.*, **46**, 159 (1973).
14) B. E. Douglas, R. A. Haines, and J. G. Brushmiller, *Inorg. Chem.*, **2**, 1194 (1963).
15) S. Fujinami, M. Shibata, and H. Yamatera, *Bull. Chem. Soc. Jpn.*, **51**, 1391 (1978).
16) F. P. Dwyer, I. K. Reid, and F. L. Garvan, *J. Am. Chem. Soc.*, **83**, 1285 (1961).
17) W. T. Jordan, B. J. Brennan, L. R. Froebe, and B. E. Douglas, *Inorg. Chem.*, **12**, 1827 (1973).

Cobalt(III) Complexes with Tripodlike Quadridentate Ligands. III.[1,2] Absorption and Circular Dichroism Spectra of Cobalt(III) Complexes Containing *N*-(2-Aminoethyl)iminodiacetate and Amino Carboxylate or 1,2-Diamine

Keiji Akamatsu,* Takashi Komorita, and Yoichi Shimura
Department of Chemistry, Faculty of Science, Osaka University, Toyonaka, Osaka 560
(Received January 5, 1982)

Glycinato, L-alaninato, ethylenediamine, *N,N*-dimethylethylenediamine, (*R*)-propylenediamine, (*R,R*)-1,2-cyclohexanediamine and meso-2,3-butanediamine cobalt(III) complexes of a tripodlike ligand, *N*-(2-aminoethyl)-iminodiacetate have been prepared. The geometrical configurations are assigned on the basis of their absorption, circular dichroism, and ^{1}H-NMR spectra. The *trans*(*O*) isomer of *meso*-2,3-butanediamine complex is optically resolved and the relationship between the absolute configurations of the chiral 1,2-diamine complexes and their circular dichroism is discussed.

The aeida[3] ligand is a tripodlike quadridentate ligand with two nitrogen and two oxygen atoms as donors and, as well as *i*-dtma, can take two different configurations in the six-coordinate metal complex (s-type and u-type in Fig. 1). The s-type configuration with a plane of symmetry is achiral, while the u-type, for lack of it, chiral. The isomerism of the u-type [Co(tripod)-(bidentate)] complexes was mainly argued in the previous paper[2] concerning the *i*-dtma complexes.

Two different kinds of isomerism occur in the s-type [Co(tripod)(bidentate)] complexes: the geometrical isomerism in the glycinato complexes and the optical isomerism in the *meso*-2,3-butanediamine complexes, where both bidentate ligands, gly and *meso*-2,3-bn, are achiral (Fig. 2). When bidentate ligands are chiral (such as L-ala and (*R*)-pn), the two kinds of isomerism

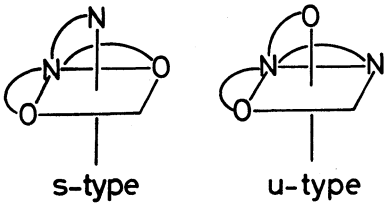

Fig. 1. Two different coordination modes of aeida ligand.

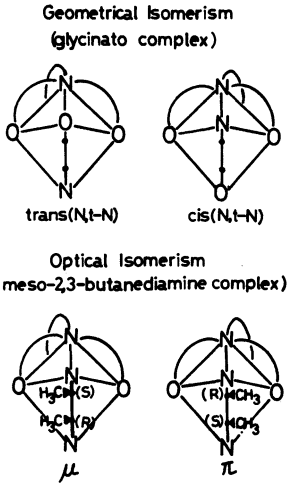

Fig. 2. Two different kinds of the s-type isomerism.

(geometrical and optical) arise at the same time.[1]

In the present paper the u- and s-types of isomersim in the aeida cobalt(III) complexes with an amino carboxylate or 1,2-diamine are reported.

Experimental

Preparations. *1)* [*Co(gly)(aeida)*]: One gram of Na-[Co(NO_2)$_2$(aeida)]·2H_2O[4] was treated with 10 cm^3 of acetic acid and 2 cm^3 of water on a steam bath for 1 h. The resulting red-violet solution was concentrated almost to dryness and to the residue was added 30 cm^3 of acetone to precipitate a pale violet powder, which contained the complex anion, [Co(CH_3CO_2)$_2$(aeida)]$^-$. The powder was filtered with suction and washed with a small amount of acetone several times and then with ether and dried in a desiccator. The dry powder was dissolved in 10 cm^3 of water and to this red-violet solution was added a solution of glycine (0.5 g) neutralized with an equimolar amount of NaOH. The solution was mechanically stirred for 2 h at 60 °C. The resulting deep red solution was poured into a cation-exchanger column (Dowex 50w-x2, H^+ form, 200—400 mesh) and the product was eluted with water. The adsorbed band separated into seven bands. The first and second bands were found to contain complex anions and the seventh band seemed to contain [Co(aeida)(H_2O)$_2$]$^+$ because it was not eluted with water. Fractions from the third to the sixth band contained neutral complexes. The fourth and the sixth turned out to contain *mer*- and *fac*-[Co-(gly)$_3$], respectively, from their absorption spectra and elemental analyses. The third (red; G-3) and the fifth (purple; G-5) contained the desired complexes. Each of them was evaporated almost to dryness and a small amount of methanol was added to the residue to precipitate the complex as a powder, which was recrystallized from warm water, washed with methanol and ether and dried in air. Found for G-3: C, 28.00; H, 5.27; N, 12.26%. Calcd for [Co(gly)(aeida)]·2H_2O: C, 27.99; H, 5.30; N, 12.25%. Found for G-5: C, 31.06; H, 4.65; N, 13.57%. Calcd for [Co(gly)(aeida)]: C, 31.28; H, 4.60; N, 13.68%.

2) [*Co(L-ala)(aeida)*]: This complex was prepared in the same way as that for the glycinato complex in *1)* using L-alanine instead of glycine. Sparingly soluble isomers of [Co-(L-ala)$_3$] deposited during the substitution reaction were filtered off and the filtrate was loaded on a cation-exchanger column. On elution with water, seven bands appeared, the desired bands being A-3 (red) and A-5 (purple). The other fractions turned out to be complex anions (A-1 and -2) and *mer*- and *fac*-[Co(L-ala)$_3$] (A-4 and -6) from their absorption

and circular dichroism spectra. Found for A-3: C, 29.86; H, 5.66; N, 11.65%. Calcd for [Co(L-ala)(aeida)]·$2H_2O$: C, 30.26; H, 5.65; N, 11.76%. Found for A-5: C, 30.85; H, 5.37; N, 11.76%. Calcd for [Co(L-ala)(aeida)]·$1.5H_2O$: C, 31.04; H, 5.51; N, 12.07%.

3) [Co(aeida)(en)]ClO_4: A reaction mixture containing this complex was prepared by the same method as described in the literature.[4] Two isomers, called E-1 and E-2 in the elution order, were obtained by a column chromatographic method, using a Sephadex C-25 column and 0.05 M $NaClO_4$ as an eluting solvent (1 M=1 mol dm^{-3}). Found for E-1: C, 24.50; H, 4.66; N, 14.39%. E-2: C, 24.33; H, 4.62; N, 14.15%. Calcd for [Co(aeida)(en)]ClO_4: C, 24.47; H, 4.63; N, 14.27%.

4) Other 1,2-Diamine Complexes with Aeida: (*R*)-Propylenediamine, (*R,R*)-1,2-cyclohexanediamine and *N,N*-dimethylethylenediamine complexes were prepared in the same way as that for the ethylenediamine complex using the relevant 1,2-diamine instead of en. Two isomers (M-1, blue-violet, and M-2, red-violet, in the elution order) were isolated for *N,N*-Me_2-en and only one isomer (*trans(O)*) for (*R*)-pn and (*R,R*)-chxn. Found for the (*R*)-pn complex: C, 26.46; H, 5.07; N, 13.88%. Calcd for [Co(aeida){(*R*)-pn}]ClO_4: C, 26.58; H, 4.97; N, 13.78%. Found for the (*R,R*)-chxn complex: C, 30.15; H, 5.90; N, 11.74%. Calcd for [Co(aeida){(*R,R*)-chxn}]ClO_4·$2H_2O$: C, 29.85; H, 5.89; N, 11.61%. Found for M-1: C, 27.96; H, 5.22; N, 13.07%. Calcd for [Co(aeida)(*N,N*-Me_2-en)]ClO_4·$0.5H_2O$: C, 27.95; H, 5.41; N, 13.04%. Found for M-2: C, 28.40; H, 5.32; N, 13.13%. Calcd for [Co(aeida)(*N,N*-Me_2-en)]ClO_4: C, 28.54; H, 5.28; N, 13.32%.

*5) Preparation and Optical Resolution of [Co(aeida)(*meso*-2,3-bn)]Cl·H_2O*: A red-violet solution prepared from Na[Co$(NO_2)_2$(aeida)]·$2H_2O$ (1 g), acetic acid (10 cm^3) and water (2 cm^3) was evaporated to about one tenth of the initial volume. To the syrupy material was added a small amount of water and the solution was evaporated again on a steam bath. To the residue were added 5 cm^3 of water and a solution (3 cm^3) of *meso*-2,3-butanediamine dihydrochloride[5] (0.8 g) neutralized with an equimolar amount of NaOH. The mixture was heated on a steam bath for 30 min. The resulting deep red solution was poured into a Sephadex C-25 column (Na^+ form) as is described in *1)* and the adsorbed band was eluted with a 0.05 M NaCl aqueous solution. Two bands appeared; the first band was overwhelmingly larger than the second. The first eluted band (B-1) was evaporated on a rotary evaporator almost to dryness below 40 °C and to the residue was added 50 cm^3 of methanol to extract the complex. The extract containing the desired chloride was evaporated and the red-violet powder deposited was collected on a glass filter and recrystallized from a small amount of warm water by adding methanol. The second band (B-2) was also treated with the same method as that for B-1 and pale pink powder was isolated. Found for B-1: C, 32.21; H, 6.34; N, 15.00%. For B-2: C, 32.00; H, 6.27; N, 14.84%. Calcd for [Co(aeida)(*meso*-2,3-bn)]Cl·H_2O: C, 32.05; H, 6.47; N, 14.95%.

The racemate, B-1, [Co(aeida)(*meso*-2,3-bn)]Cl·H_2O, (0.68 g; 1.8×10^{-3} mol) was dissolved in 10 cm^3 of water and to the solution was added a solution of $(+)_{546}$-Ag[Co(edta)][6] (0.87 g; 1.9×10^{-3} mol) in 10 cm^3 of water and the mixture was mechanically stirred for 10 min at 40 °C. Silver chroide deposited was filtered off, 20 cm^3 of methanol was added to the filtrate, and the solution was kept standing overnight in a refrigerator. Pale red-violet crystals deposited were collected with suction and recrystallized from a small amount of water by adding methanol. Found: C, 32.29; H, 5.45; N, 11.28%. Calcd for [Co(aeida)(*meso*-2,3-bn)][Co(edta)]·$4H_2O$: C, 32.44; H, 5.73; N, 11.35%.

The less-soluble diastereomer was dissolved in a small amount of water and converted into $(+)_{589}$-chloride by passing through an anion-exchanger column (Cl^- form) and evaporating the eluate on a rotary evaporator. Found: C, 32.70; H, 6.36; N, 15.13%. Calcd for $(+)_{589}$-[Co(aeida)(*meso*-2,3-bn)]Cl·$0.5H_2O$: C, 32.84; H, 6.35; N, 15.32%.

Measurements. The visible and ultraviolet absorption spectra were measured by a Shimadzu UV-200 spectrophotometer in aqueous solutions. The CD spectra were recorded on a Jasco MOE-1 spectropolarimeter in aqueous solutions and the ^{1}H-NMR spectra were obtained in deuterium oxide (D_2O) on a Varian XL-100-15 spectrometer using DSS (sodium 2,2-dimethyl-2-silapentane-5-sulfonate) as an internal standard.

Results and Discussion

a) Aeida Complexes with Amino Carboxylates. As an aeida ligand can take both s- and u-type configurations, four geometrical isomers are possible for the (amino carboxylato) complex (Fig. 3). In Fig. 3 the upper two are s-type and the lower two u-type with respect to the tripodlike ligand, and only one isomer, u-β, of the four is a *fac(O)*-isomer and the others (s-α and -β, and u-α) are *mer(O)*-isomers. Two isomers were isolated for each of the glycinato and the L-alaninato complexes: G-3 and -5 for gly; A-3 and -5 for L-ala. The fact that G-3 and A-3 show splitting of the first d-d absorption band (see Fig. 5) implies that A-3 and G-3 are *mer*-isomers, of structure s-α, s-β, or u-α. The absorption spectrum of A-5 corresponds well to that of G-5 showing a *fac* pattern, while the splitting of the first d-d band for A-3 is quite different from that for G-3. Thus G-3 and A-3 should have different geometrical structures in spite of their resemblance both in the column chromatographic behavior and in their formation ratio to the corresponding *fac*-isomer (G-5 or A-5).

^{1}H-NMR spectra lead one to more explicit distinction between the isomers. Figure 4 shows the ^{1}H-NMR spectra of four isomers obtained for the glycinato and L-alaninato complexes. For the gly complex, G-3 and -5 show an AB quartet pattern (4.42, 4.27, 4.08, and 3.94 ppm for G-3; 4.22, 4.06, 3.88, and 3.72 ppm for G-5) and a singlet peak due to the acetate methylene protons of aeida (G-3, 4.08; G-5, 3.92 ppm). Thus they are suggested to have the u-type structure (u-α or -β). Because G-5 is assigned to have the structure *mer*(u-β)

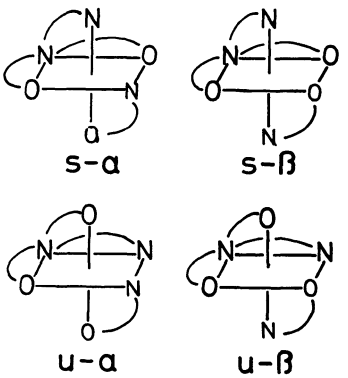

Fig. 3. Four geometrical isomers of [Co(am)(aeida)]-type complex (am=amino carboxylate).

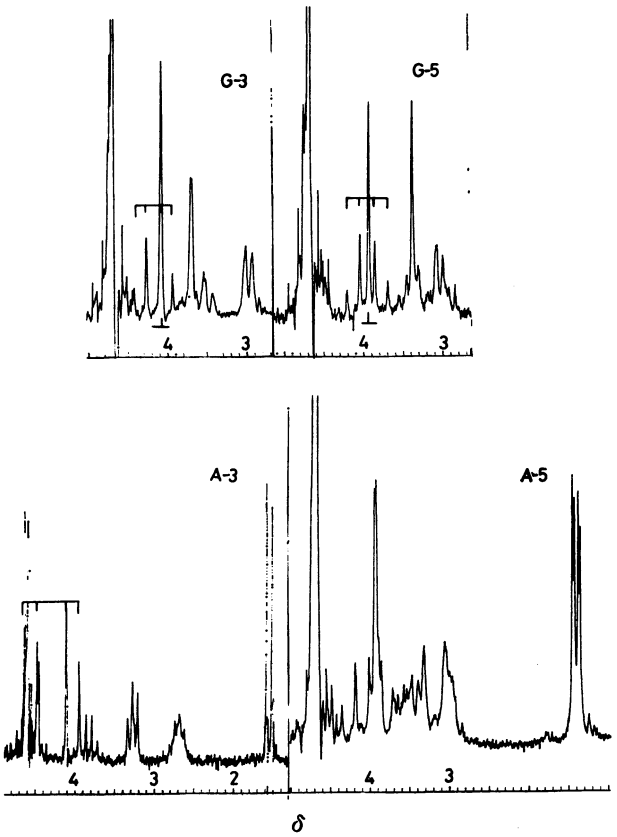

Fig. 4. ^{1}H-NMR spectra of isomers of [Co(am)(aeida)] (am=gly or L-ala).

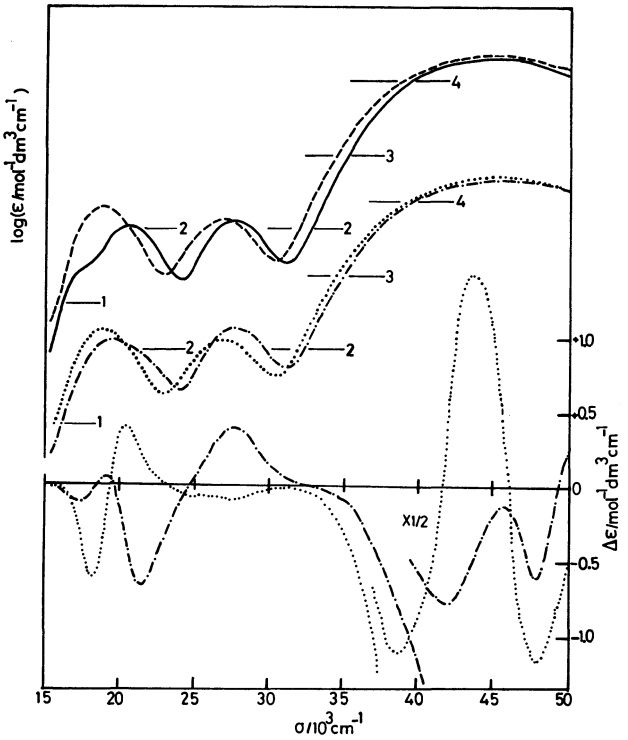

Fig. 5. Absorption and CD curves of [Co(am)(aeida)] (am=gly or L-ala): G-3 (——), G-5 (------), A-3 (-·-·-), and A-5 (·····).

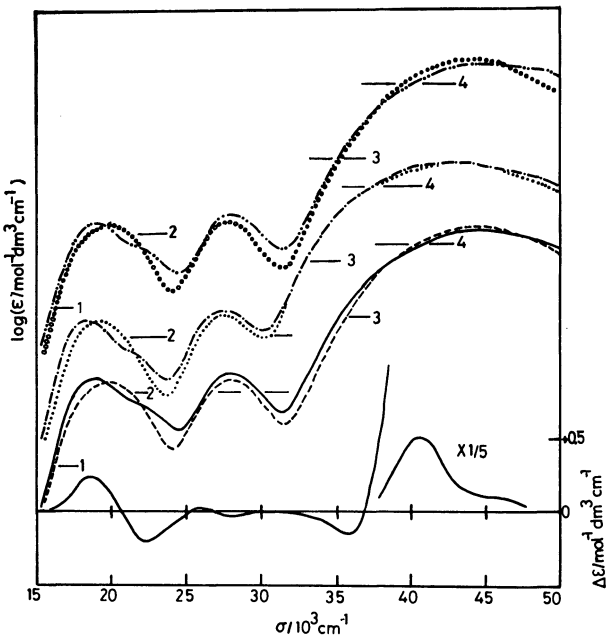

Fig. 6. Absorption and CD curves of [Co(aeida)(da)]$^+$ (da=en, *N*,*N*-Me$_2$-en, and *meso*-2,3-bn): E-1 (-·····-), E-2 (••••••), M-1 (-·-·-), M-2 (·····), B-1 (——), and B-2 (------).

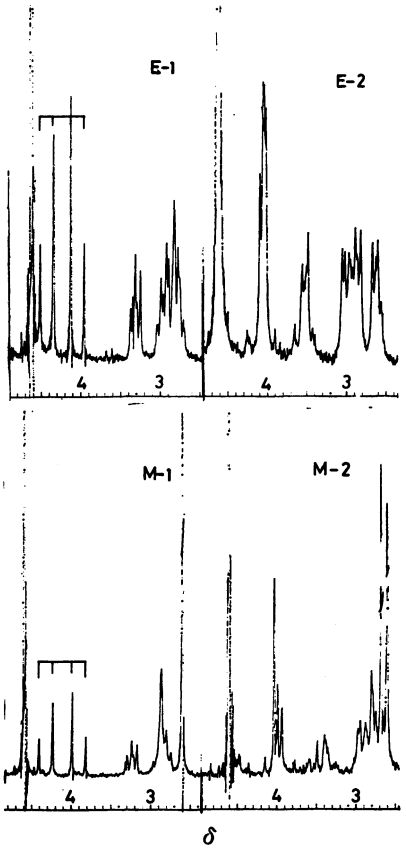

Fig. 7. ^{1}H-NMR spectra of isomers of [Co(aeida)(da)]$^+$ (da=en and *N*,*N*-Me$_2$-en).

from the absorption spectrum, G-3 should be of the structure u-*a*. The L-ala complex A-3 exhibiting an AB quartet (4.64, 4.48, 4.11, and 3.95 ppm) due to the aeida methylene protons and a methyl doublet (1.58 and

Table 1. Absorption data of [Co(A-B)(aeida)]-type complexes (A-B=gly, L-ala,en,*N*,*N*-Me_2-en, *meso*-2,3-bn, (*R*)-pn, and (*R*,*R*)-chxn)
Wave numbers and log ε values (in parentheses) are given in 10^3 cm^{-1} and mol^{-1} dm^3 cm^{-1}, respectively.

Complex	d-d transition band		UV band
	1st	2nd	
(G-3)-[Co(gly)(aeida)]	≈18.5 (sh 1.5) 20.55 (2.04)	27.66 (2.12)	45.15 (4.29)
(G-5)-[Co(gly)(aeida)]	18.87 (2.30)	26.88 (2.14)	44.84 (4.34)
(A-3)-[Co(L-ala)(aeida)]	19.47 (2.14) ≈22 (sh 1.8)	27.70 (2.29)	45.46 (4.28)
(A-5)-[Co(L-ala)(aeida)]	18.87 (2.27)	26.92 (2.13)	45.05 (4.33)
(E-1)-[Co(aeida)(en)]$^+$	19.05 (2.16) ≈22 (sh 1.8)	28.25 (2.26)	44.84 (4.26)
(E-2)-[Co(aeida)(en)]$^+$	20.06 (2.12)	27.93 (2.16)	44.15 (4.30)
(M-1)-[Co(aeida)(*N*,*N*-Me_2-en)]$^+$	18.47 (2.20) ≈21.5 (sh 1.8)	27.55 (2.33)	≈37 (sh) 43.01 (4.31) ≈48 (sh)
(M-2)-[Co(aeida)(*N*,*N*-Me_2-en)]$^+$	19.18 (2.20)	27.66 (2.28)	≈37 (sh) 43.10 (4.30) ≈48 (sh)
(B-1)-[Co(aeida)(*meso*-2,3-bn)]$^+$	18.94 (2.18) ≈22 (sh 1.8)	28.13 (2.26)	44.64 (4.25)
(B-2)-[Co(aeida)(*meso*-2,3-bn)]$^+$	19.96 (2.13)	28.03 (2.17)	44.44 (4.30)
[Co(aeida){(*R*)-pn}]$^+$	19.01 (2.18) ≈22 (sh 1.8)	28.13 (2.26)	44.94 (4.31)
[Co(aeida){(*R*,*R*)-chxn}]$^+$	18.94 (2.18) ≈22 (sh 1.8)	28.05 (2.33)	44.44 (4.33)

1.51 ppm) due to L-alaninate was assigned to have the s-type structure (s-*α* or s-*β*), while A-5 isomer which was assigned to the *fac*-isomer exhibits two methyl doublets (1.45 and 1.38; 1.43 and 1.36 ppm) with about the same intensity, and thus was assigned to a mixture of two diastereomers of the structure u-*β*.

Figure 5 shows the absorption and CD spectra of the gly and the L-ala complexes. The first absorption band of G-3 shows a large splitting: $\tilde{\nu}_{max}/10^3$ cm^{-1} (log (ε_{max}/cm^{-1} mol^{-1} dm^3)), ≈18.5 (sh 1.5), 20.55 (2.04); while G-5 a narrow and simple peak 18.87 (2.30). For the L-ala complex, A-3 shows a broad peak 19.47 (2.14) with an ambiguous shoulder at higher energy $\approx 22 \times 10^3$ cm^{-1}, while A-5 a simple peak. The CD pattern of A-3 resembles that of *trans*(*N*)-[Co(ata)(L-ala)]$^-$ complex;[1] three (−, + and −) for the first and one (+) component for the second d-d band. This suggests that A-3 has the structure s-*α*. The CD of A-5 (about 1 : 1 mixture of the diastereomers of the structure u-*β*) shows a pattern similar to those of the [Co(ata)(L-ala)]$^-$ and [Co(tren)(L-ala)]$^{2+}$ complexes of *cis*(*N*,*t*-*N*)-structure;[1] two (− and +) for the first and two (− and −) components for the second d-d band. These observations suggest that the relationship between the CD patterns in the d-d absorption band region and the coordination geometry of L-amino carboxylato complexes found for the ata and tren complexes also holds for the aeida complex, because structures s-*α* and s-*β* correspond to the structure *trans*(*N*,*t*-*N*) and *cis*(*N*,*t*-*N*), respectively. An equimolar mixing of the diastereomers of the structure u-*β* will cancel the chiralities of u-type aeida and leave only those of L-amino carboxylates to give a CD pattern corresponding to the structure *cis*(*N*,*t*-*N*).

Though four isomers are possible (Fig. 3) for each of the glycinato and the L-alaninato complexes, only two were isolated. It is difficult to explain why the main products isolated have different structures (s-*α* for the L-ala complex; u-*α* for the gly complex).

b) Aeida Complexes with 1,2-Diamines. Two isomers are possible for the en complex; *trans*(*O*) s-type and *cis*(*O*) u-type, and they can be distinguished by means of their absorption and ^{1}H-NMR spectra.[7] Though the *N*,*N*-Me_2-en complex has four possible isomers (two s-type and two u-type isomers similar to those in Fig. 3), only two were isolated. They can also be assigned to *trans*(*O*) and *cis*(*O*) by the same method as used for the en complex. Both E-1 and M-1 show a large splitting of the first d-d band: 19.05 (2.16), ≈22 (sh) for E-1; 18.47 (2.20), ≈21.5 (sh) for M-1), while E-2 and M-2 only a simple broad peak (Fig. 6 and Table 1). E-1 and M-1 show an AB quartet pattern (4.49, 4.32, 4.09, and 3.93 ppm for E-1; 4.41, 4.24, 3.99, and 3.82 ppm for M-1) due to the acetate methylene protons of aeida (Fig. 7). Though E-2 and M-2 show complicated acetate signals, two AB quartets are observed for E-2 (4.26, 4.10, 4.06, and 3.90; 4.23, 4.04, 4.02; and 3.84 ppm). The *N*-methyl signals (two singlets at 2.66 and 2.59 ppm) are more useful in the structural assignment than AB quartets for M-2. These results imply that E-1 and M-1 have s-type and E-2 and M-2 u-type structures, respectively, though the optical resolution of the u-type isomers was not successful. It is found that the two more-stable isomers the for the *N*,*N*-Me_2-en complex should have such structures that the two tertiary amine groups occupy *trans* positions each other by examining molecular models. The absorption spectra of the *N*,*N*-Me_2-en complex showed an absorp-

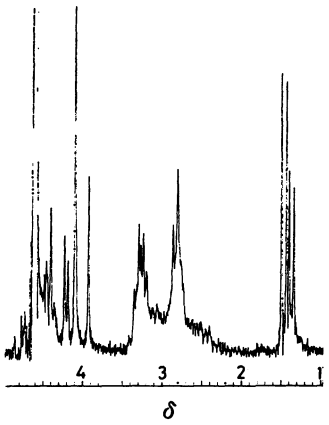

Fig. 8. ^{1}H-NMR spectrum of [Co(aeida){(*R*)-pn}]$^+$.

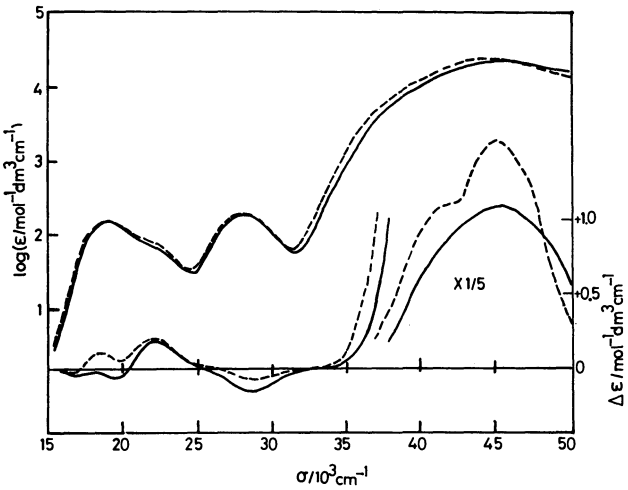

Fig. 9. Absorption and CD spectra of [Co(aeida){(*R*)-pn}]$^+$ (——) and [Co(aeida){(*R*,*R*)-chxn}]$^+$ (------).

tion shoulder at *ca.* 37×10^3 cm^{-1} characteristic of the complexes containing *N*,*N*-Me$_2$-en ligand.[8]

Six diastereomeric isomers (two s-type and four u-type), three diastereomeric isomers (one s-type and two u-type) and three pairs of the enantiomeric isomers (one s-type pair and two u-type pairs) are possible for the (*R*)-pn, (*R*,*R*)-chxn, and *meso*-2,3-bn complexes, respectively. Only one complex isolated for the (*R*)-pn or (*R*,*R*)-chxn was assigned to *trans*(*O*) s-type structure and two complexes B-1 and -2 of *meso*-2,3-bn to *trans*(*O*) and *cis*(*O*), respectively, from their absorption spectra (Table 1). The ^{1}H-NMR spectrum of the (*R*)-pn complex (Fig. 8) showed two methyl doublets (1.40 and 1.34; 1.30 and 1.24 ppm), indicating that the complex is composed of about 3 : 2 mixture of the two s-type isomers.

All possible two isomers of the s-type complexes with a chiral amino carboxylate have been isolated for the ata, tren and *i*-dtma, except for the aeida. The CD intensities in the d-d transition band region have been explained by assuming two contributions from the "intrinsic vicinal effect" of the asymmetric carbons and from the "quasi-enantiomeric effect" of the substituents. Meanwhile, the separation of the s-type isomers of the (*R*)-pn complexes for ata,[1] *i*-dtma[2] and aeida was unsuccessful and the only one isomer of the two for the tren complex was isolated.[1]

The (*R*)-pn complex has two sources of the optical activity, similar to those of the L-ala complex, one is the "intrinsic vicinal effect," and the other is the "quasi-enantiomeric effect," while the (*R*,*R*)-chxn complex has only one source of the optical activity from the "intrinsic vicinal effect" because the coordination of (*R*,*R*)-chxn produces no quasi-enantiomeric isomerism. The CD spectrum of the (*R*)-pn complex (a mixture of two diastereomers) exhibited three (−, −, and +), one (−) and one (+) component, while that of the (*R*,*R*)-chxn three (−, + and +), one (−) and one (+) component in the first, second d-d, and charge-transfer band region, respectively (Fig. 9 and Table 2). Their CD intensities and patterns in the d-d transition band region are similar to those of the complexes which have no "quasi-enantiomeric effect."

In the previous paper[1] it was pointed out that the (*R*)-pn complex with tren, which contains only one isomer, showed larger CD than the other (*R*)-pn complexes with ata and *i*-dtma, which contain two isomers. The large CD intensity of the (*R*)-pn tren complex is due to the "quasi-enantiomeric effect."

Table 2. CD Data of [Co(A-B)(aeida)]-type complexes (A-B=L-ala,(*R*)-pn, (*R*,*R*)-chxn, and *meso*-2,3-bn)
Wave numbers and Δε values (in parentheses) are given in 10^3 cm^{-1} and mol^{-1} dm^3 cm^{-1}, respectively.

Complex	d-d transition band		UV band
	1st	2nd	
(A-3)-[Co(L-ala)(aeida)]	17.24(−0.116) 19.14(+0.057) 21.53(−0.685)	27.55(+0.375)	42.02(−1.59) 47.85(−1.24)
(A-5)-[Co(L-ala)(aeida)]	18.25(−0.632) 20.35(+0.389)	≈25(−0.08) 27.40(−0.094)	38.76(−2.23) 43.86(+3.06) 47.85(−2.35)
[Co(aeida){(*R*)-pn}]$^+$	16.95(−0.045) 19.35(−0.064) 22.12(+0.190)	28.53(−0.150)	45.46(+5.48)
[Co(aeida)(*R*,*R*)-chxn]$^+$	16.53(−0.020) 18.52(+0.111) 21.98(+0.208)	28.99(−0.071)	≈41.5(sh+5.6) 44.84(+7.75)
(+)$_{589}$-[Co(aeida)(*meso*-2,3-bn)]$^+$ (B-1)	18.66(+0.232) 22.32(−0.208)	26.11(+0.009) 28.09(−0.035)	35.71(−0.17) 40.65(+2.53)

The *trans*(*O*) isomer of the *meso*-2,3-bn complex has the optical isomers which is "enantiomeric," and the CD pattern will be a measure of the "quasi-enantiomeric effect" for the (*R*)-pn complexes. The CD pattern of the $(+)_{589}$-[Co(aeida)(*meso*-2,3-bn)]$^+$ (**B-1**) showed two (+ and −), two (+ and −) and two (− and +) components in the first, second d-d transition and charge-transfer band region, respectively (Fig. 6 and Table 2) and the intensity in the d-d transition band region was similar to those of the "intrinsic vicinal effect" for the (*R*)-pn complexes with ata, *i*-dtma and aeida. The absolute configuration of the $(+)_{589}$-[Co(aeida)(*meso*-2,3-bn)]$^+$ complex can be assigned to π structure in Fig. 2 from the CD pattern in the d-d transition band region, if the relationship between the CD patterns of the "quasi-enantiomeric effect" and the absolute configurations for the [Co(tripod)(L-ala)] complexes is supposed to be applied to the *meso*-2,3-bn complex; The s-type *trans*(*N*,*t*-*N*) isomers of the L-ala complexes with ata, tren[1] and *i*-dtma,[2] which have π structure with regard to the methyl substituents, show two (+ and −) and one (+) component in the first and second d-d band region, respectively.

References

1) Part I of this series: K. Akamatsu, T. Komorita, and Y. Shimura, *Bull. Chem. Soc. Jpn.*, **54**, 3000 (1981).

2) Part II of this series: K. Akamatsu, T. Komorita, and Y. Shimura, *Bull. Chem. Soc. Jpn.*, **55**, 140 (1982).

3) Abbreviations of ligands: aeida=*N*-(2-aminoethyl)-iminodiacetate, L-ala=L-alaninate, ata=nitrilotriacetate, *meso*-2,3-bn=*meso*-2,3-butanediamine, (*R*,*R*)-chxn=(*R*,*R*)-1,2-cyclohexanediamine, en=ethylenediamine, gly=glycinate, *i*-dtma=*N*,*N*-bis(2-aminoethyl)glycinate, *N*,*N*-Me_2-en=*N*,*N*-dimethylethylenediamine, (*R*)-pn=(*R*)-propylenediamine, and tren=tris(2-aminoethyl)amine.

4) K. Kuroda, S. Ohtsuka, and N. Matsumoto, *Bull. Chem. Soc. Jpn.*, **48**, 1055 (1975).

5) F. H. Dickey, W. Fickett, and H. J. Lucas, *J. Am. Chem. Soc.*, **81**, 4185 (1959).

6) C. W. Maricondi and B. E. Douglas, *Inorg. Chem.*, **11**, 688 (1972).

7) M. W. S. Chu, D. W. Cooke, and C. F. Liu, *Inorg. Chem.*, **7**, 2435 (1968).

8) K. Akamatsu and Y. Shimura, *Bull. Chem. Soc. Jpn.*, **51**, 2586 (1978).

Rapid Differential Determination of Mixtures of Hydrazine and Hydroxylamine by Potentiometric Titration with an Iodide Ion-selective Electrode**

Junko MOTONAKA,* Sanae IKEDA,† and Nobuyuki TANAKA††
Technical College of Tokushima University, Minamijosanjima, Tokushima 770
†*Faculty of Engineering, Tokushima University, Minamijosanjima, Tokushima 770*
††*Faculty of Science, Tohoku University, Sendai 980*

(Received January 8, 1982)

A rapid method has been established for determination of mixtures of hydrazine and hydroxylamine by potentiometric titration using an iodide ion-selective electrode. Accurate values are obtainable when nitric acid is added to the sample solution. A recommended procedure is proposed in which the sum of hydrazine and hydroxylamine is titrated with an aliquot of sample solution and another aliquot is titrated to the end point for hydrazine after hydroxylamine has been decomposed with nitric acid. Hydrazine and hydroxylamine in mixture can be determined in the concentration range of 0.01—0.5 mmol/dm³. The best result, with relative error and relative standard deviation both of less than 0.7%, may be obtained on 0.5 mmol/dm³ hydrazine and hydroxylamine.

Hydrazine and hydroxylamine are widely used in chemical analysis as reducing agents. These two toxic substances have very similar chemical properties and therefore, it is very difficult to determine their respective concentrations in their mixtures.

Rapid methods for determination of each of hydrazine and hydroxylamine were previously reported.[1] The present paper describes a continuation of that work, in which concentrations of hydrazine and hydroxylamine in mixtures were measured.

Experimental

Apparatus. An automatic potentiometric titrator equipped with an iodide ion-selective indicator electrode and a pH meter were used; they were the same apparatus as described in the previous paper.[1]

Reagents. All reagents were of analytical-reagent grade (Wako Pure Chemical Industries, Ltd.). Redistilled water was used. For experimental runs, the following stock solutions were diluted as needed: 10 mmol/dm³ hydrazine sulfate (standardized by the JIS method[2]); 10 mmol/dm³ hydroxylamine sulfate (standardized by the JIS method[3]); 50 mmol/dm³ iodine–methanol solution (prepared by dissolving *ca.* 12.7 g of pure iodine in 1000 cm³ of pure methanol, stored in an amber bottle, and standardized by the indicator titration method); 100 mmol/dm³ silver nitrate solution (standardized by the amperometric titration[4]).

Recommended Procedure. Into one of two titration cells is measured exactly 5 cm³ of each of 0.2—10 mmol/dm³ hydrazine sulfate and hydroxylamine sulfate, and added 15 cm³ of 50 mmol/dm³ iodine–methanol solution. The volume is adjusted to 100 cm³ with redistilled water. The resulting solution is titrated potentiometrically with 10—100 mmol/dm³ standard silver nitrate solution.

Into the other cell is measured exactly 5 cm³ of each of 0.2—10 mmol/dm³ hydrazine sulfate and hydroxylamine sulfate, added 20 cm³ of 16 mol/dm³ nitric acid which will decompose hydroxylamine and 10 cm³ of 50 mmol/dm³ iodine–methanol solution, and finally added redistilled water to 100 cm³. The resulting solution is titrated in the same way as above.

Results and Discussion

Potentiometric Titration Curves. Potentiometric titration curves are shown in Fig. 1. The end point of curve (A) corresponds to the equivalence point for hydrazine, and that of curve (B) corresponds to the cquivalence point for the sum of hydrazine and hydroxylamine. The amount of hydroxylamine in the mixture is determined from the difference between these two end points. The procedure requires about 5 min for curve (A) and 15 min for curve (B).

Effect of the Amount of Nitric Acid. When the nitric acid is added, hydroxylamine tends to decompose immediately. Therefore, stabilities of hydrazine and hydroxylamine in nitric acid were examined. As shown in Fig. 2, measurement of hydrazine is not affected by the addition of 16 mol/dm³ nitric acid (0—30 cm³), but analytical values for hydroxylamine decrease with increase in the volume of nitric acid added, reaching zero at 15 cm³ of 16 mol/dm³ nitric acid. Similar results were obtained with a mixture of hydrazine and

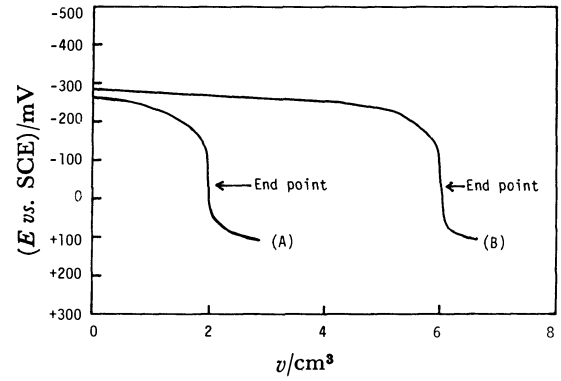

Fig. 1. Potentiometric titration curves for hydrazine and hydroxylamine mixtures.
v=Volume of 100 mmol dm^{-3} $AgNO_3$ solution added.
(A): Solution: 100 cm³, containing hydrazine sulfate (10 mmol dm^{-3}, 5 cm³), hydroxylamine sulfate (10 mmol dm^{-3}, 5 cm³), nitric acid (16 mol dm^{-3}, 20 cm³) and iodine–methanol (50 mmol dm^{-3}, 10 cm³), (B): Solution: 100 cm³, containing hydrazine sulfate (10 mmol cm^{-3}, 5 cm³), hydroxylamine sulfate (10 mmol dm^{-3}) and iodine–methanol (50 mmol dm^{-3}, 15 cm³).

** Part of a thesis submitted by one of the authors (J. M.) to Tohoku University of partial fulfillment of the requirement for the degree of Doctor of Science.

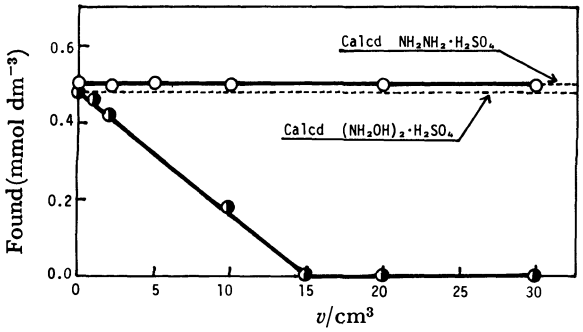

Fig. 2. Effect of nitric acid on determinations of hydrazine and hydroxylamine.
v=Volume of 16 mol dm^{-3} HNO_3 solution added. —○—: Solution: 100 cm^3, containing hydrazine sulfate (10 mmol dm^{-3}, 5 cm^3), nitric acid and iodine–methanol (50 mmol dm^{-3}, 5 cm^3), —◑—: solution: 100 cm^3, containing hydroxylamine sulfate (10 mmol dm^{-3}, 5 cm^3), nitric acid and iodine–methanol (50 mmol dm^{-3}, 10 cm^3).

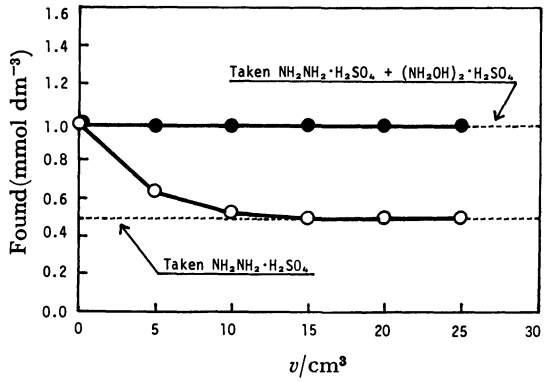

Fig. 3. Effect of nitric acid on the determinations of hydrazine and hydroxylamine in mixtures.
v=Volume of 16 mol dm^{-3} HNO_3 solution added. —○—: Solution: 100 cm^3, containing hydrazine sulfate (10 mmol dm^{-3}, 5 cm^3), hydroxylamine sulfate (10 mmol dm^{-3}, 5 cm^3), nitric acid and iodine–methanol (50 mmol dm^{-3}, 10 cm^3), —●—: solution: 100 cm^3, contining hydrazine sulfate (10 mmol dm^{-3}, 5 cm^3), hydroxylamine sulfate (10 mmol dm^{-3}, 5 cm^3), nitric acid and iodine–methanol (50 mmol dm^{-3}, 10 cm^3).

hydroxylamine (Fig. 3). All subsequent titrations of hydrazine were carried out in the presence of 20 cm^3 of 16 mol/dm^3 nitric acid.

Effect of the Amount of Iodine–Methanol. A mixture of hydrazine and hydroxylamine was titrated in the presence of various amounts of iodine–methanol (Fig. 4). Analytical values for hydrazine are in good agreement with those obtained by the JIS method provided that iodine is added in excess. Values for hydroxylamine are also in good agreement with those obtained by the JIS method provided that iodine is added in more than 1.7 times the equivalent amount.

In this experiment, in the presence of nitric acid iodine (50 mmol/dm^3, 10 cm^3) was added in 2.5 times the equivalent amount.

Effect of Temperature. Titration of hydrazine and

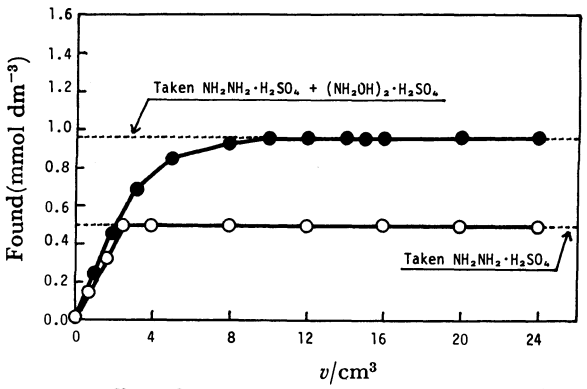

Fig. 4. Effect of the amount of iodine–methanol solution on the determination of hydrazine and hydroxylamine in mixtures.
v=Volume of 0.05 mol dm^{-3} I_2-CH_3OH solution added. —○—: Solution: 100 cm^3, of hydrazine sulfate (10 mmol dm^{-3}, 5 cm^3), hydroxylamine sulfate (10 mmol dm^{-3}, 5 cm^3), nitric acid (16 mol dm^{-3}, 20 cm^3) and iodine–methanol, —●—: solution: 100 cm^3, of hydrazine sulfate (10 mmol dm^{-3}, 5 cm^3), hydroxylamine sulfate (10 mmol dm^{-3}, 5 cm^3) and iodine–methanol.

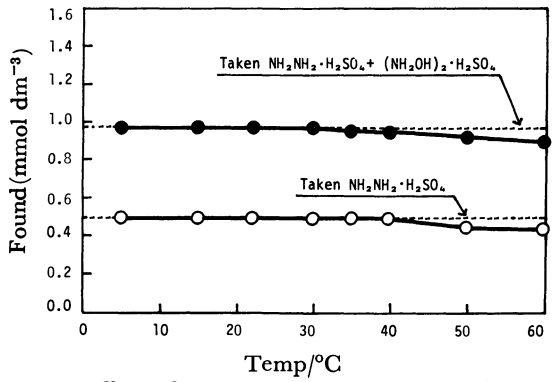

Fig. 5. Effect of temperature on the determination of hydrazine and hydroxylamine in mixtures.
—○—: Solution: 100 cm^3, of hydrazine sulfate (10 mmol dm^{-3}, 5 cm^3), hydroxylamine sulfate (10 mmol dm^{-3}, 5 cm^3), nitric acid (16 mol dm^{-3}, 20 cm^3), and iodine–methanol (0.05 mol dm^{-3}, 10 cm^3), —●—: solution: 100 cm^3, of hydrazine sulfate (10 mmol dm^{-3}, 5 cm^3), hydroxylamine sulfate (10 mmol dm^{-3}, 5 cm^3), and iodine–methanol (50 mmol dm^{-3}, 15 cm^3).

hydroxylamine mixtures is affected by temperature neither in the range of 5—30 °C when no nitric acid is added, in nor the range of 5—40 °C when nitric acid was added (Fig. 5). Hydroxylamine decomposes above 30 °C and hydrazine decomposes above 40 °C.

For convenience all subsequent measurements were conducted at room temperature (20 °C).

Effect of Concomitant Compounds. Mixtures of hydrazine and hydroxylamine were titrated in the presence of each of 15 compounds, the results being shown in Table 1.

The following compounds have little or no effect: sodium or magnesium nitrate in a molar ratio to hydrazine sulfate or hydroxylamine sulfate of 100 : 1,

TABLE 1. EFFECTS OF CONCOMITANT COMPOUNDS ON DETERMINATION OF HYDRAZINE AND HYDROXYLAMINE IN MIXTURE[a)]

Concomitant compound added	Molar ratio (Sample : Compound)	Relative error/% $NH_2NH_2 \cdot H_2SO_4$	Relative error/% $(NH_2OH)_2 \cdot H_2SO_4$
$NaNO_3$	1 : 100	+0.6	+0.1
$Mg(NO_3)_2$	1 : 100	+0.7	+0.2
$(NH_4)_2SO_4$	1 : 50	+0.9	−0.1
$Ni(NO_3)_2$	1 : 20	+0.1	−0.9
$Cd(NO_3)_2$	1 : 1	+1.0	−0.3
NH_4Cl[b)]	1 : 1	+0.1	+1.3
KCl[b)]	1 : 1	+1.4	-0.0_2
KBr[b)]	1 : 1	−2.9	+0.9
NaF	1 : 1	+0.4	−1.6
$Pb(NO_3)_2$	1 : 1	+1.7	−2.1
$(NH_4)_2CO_3$	1 : 1	+1.3	−1.9
K_2CO_3	1 : 1	+0.2	−2.9
$FeSO_4(NH_4)_2SO_4 \cdot 6H_2O$	1 : 1	+0.2	−15
$Fe_2(SO_4)_2(NH_4)_2SO_4 \cdot 24H_2O$	1 : 1	+0.7	−47
$NaNO_2$	1 : 1	−97	+19

a) Solution: 100 cm^3, containing 5 cm^3 of 10 mmol dm^{-3} hydrazine sulfate, 5 cm^3 of 10 mmol dm^{-3} hydroxylamine sulfate, a concomitant compound, and 10 cm^3 of 50 mmol dm^{-3} iodine–methanol with or without 20 cm^3 of 16 mol dm^{-3} nitric acid. b) With 10 cm^3 of 10 mmol dm^{-3} aluminium nitrate.[5)]

ammonium sulfate in a molar ratio of 50 : 1, nickel nitrate in a molar ratio of 20 : 1, and cadmium nitrate in a molar ratio of 1 : 1. Hydrazine and hydroxylamine can be determined with an error of about ±1% in the presence of any one of these compounds. However, lead nitrate, ammonium carbonate, and nitrous acid cause an interference. Ammonium chloride, sodium fluoride, potassium carbonate, ammonium iron(II) sulfate, and ammonium iron(III) sulfate do not affect the titration of hydrazine, and potassium chloride and potassium bromide do not affect the titration of hydroxylamine when aluminium nitrate is added.[5)]

Effect of the Ratio of Hydrazine to Hydroxylamine. Mixtures of hydrazine and hydroxylamine in various ratios were titrated (Table 2). Mixtures of hydrazine sulfate and hydroxylamine sulfate in ratios of 1 : 1, 5 : 2, and 5 : 1 can be determined with an error of less than ±1% and a relative standard deviation of less than 0.4%. However, with a mixture of hydrazine sulfate and hydroxylamine sulfate in a ratio of 1 : 5, the error is of the order of several percent.

Therefore, the amount of hydroxylamine should not be more than that of hydrazine.

Accuracy and Precision of the Method. Table 3 shows results obtained by the recommended procedure from four repeated titrations on mixtures of hydrazine and hydroxylamine of various concentrations.

Hydrazine and hydroxylamine in mixture can be determined in the concentration range of 0.01—0.5 mmol/dm^3. The best result, with relative error of less than ±0.7% and relative standard deviation of less than 0.4%, is obtained with the concentration of 0.5 mmol/cm.

Conclusion. Rapid and accurate differential determination is possible of hydrazine and hydroxylamine in mixture by potentiometric titration with silver nitrate solution and an iodide ion-selective electrode, if nitric acid is added to the sample solution. When 15 cm^3 or more of 16 mol/dm^3 nitric acid is added to a sample solution, analytical results for 0.05—0.5 mmol/dm^3 hydrazine sulfate in the presence of hydroxylamine sulfate are in good agreement with those obtained by the JIS method. The best result, with relative error and relative standard deviation both of less than 0.7%, is obtained with 0.5 mmol/dm^3 hydrazine sulfate and hydroxylamine sulfate.

By this method both hydrazine and hydroxylamine can be determined accurately at 5—30 °C.

TABLE 2. DETERMINATION OF HYDRAZINE AND HYDROXYLAMINE IN MIXTURE

Sample concentration/mmol dm^{-3} [a)] $NH_2NH_2 \cdot H_2SO_4$	Sample concentration/mmol dm^{-3} [a)] $(NH_2OH)_2 \cdot H_2SO_4$	Relative error/%[b)] $NH_2NH_2 \cdot H_2SO_4$	Relative error/%[b)] $(NH_2OH)_2 \cdot H_2SO_4$	Sr/%[c)] $NH_2NH_2 \cdot H_2SO_4$	Sr/%[c)] $(NH_2OH)_2 \cdot H_2SO_4$
0.5	0.5	−0.2	+0.7	0.2	0.4
0.5	0.2	−0.5	+1.0	0.2	0.2
0.5	0.1	+1.0	+1.0	0.1	0.2
0.1	0.5	+6.0	−2.7	1.1	0.1

a) Solution: 100 cm^3, containing hydrazine sulfate, hydroxylamine sulfate, and 10 cm^3 of 50 mmol dm^{-3} iodine–methanol with or without 20 cm^3 of 16 mol dm^{-3} nitric acid. b) Average of 4 titrations. c) Relative standard deviation.

TABLE 3. ACCURACY AND PRECISION DATA

Sample concentration/mmol dm^{-3} [a)] $NH_2NH_2 \cdot H_2SO_4$	Sample concentration/mmol dm^{-3} [a)] $(NH_2OH)_2 \cdot H_2SO_4$	Relative error/%[b)] $NH_2NH_2 \cdot H_2SO_4$	Relative error/%[b)] $(NH_2OH)_2 \cdot H_2SO_4$	Sr/%[c)] $NH_2NH_2 \cdot H_2SO_4$	Sr/%[c)] $(NH_2OH)_2 \cdot H_2SO_4$
0.5	0.5	−0.2	+0.7	0.2	0.4
0.1	0.1	+0.9	+0.6	0.2	0.2
0.05	0.05	+1.4	+1.0	0.2	0.6
0.01	0.01	+6.6	+0.7	1.1	1.6

a) Solution: 100 cm^3, containing hydrazine sulfate, hydroxylamine sulfate, and iodine–methanol with or without nitric acid. b) Average of 4 titrations. c) Relative standard deviation.

The determination is not affected by the presence of sodium nitrate, magnesium nitrate, ammonium sulfate, nickel nitrate, or cadmium nitrate, but is affected by lead nitrate, ammonium carbonate, and nitrous acid.

References

1) S. Ikeda and J. Motonaka, *Anal. Chim. Acta*, **90**, 257 (1977).
2) JIS K8992-1961.
3) JIS K8993-1961.
4) I. M. Kolthoff and P. K. Kuroda, *Anal. Chem.*, **23**, 1306 (1951).
5) J. Motonaka, S. Ikeda, and N. Tanaka, *Anal. Chim. Acta*, **105**, 417 (1979).

Non-covalent Interactions in Metal Complexes. V.[1] Stereoselectivity in Cobalt(III) Mixed-chelates with a Salen-like Schiff Base and 1-*l*-Menthyloxy-3-benzoylacetone

Michio NAKAMURA, Hisashi ŌKAWA,* Takahiko INAZU, and Sigeo KIDA
Department of Chemistry, Faculty of Science, Kyushu University 33, Hakozaki, Higashi-ku, Fukuoka 812
(Received February 1, 1982)

Cobalt(III) mixed-chelates, Co(SB)(*l*-moba), containing a salen-type Schiff base (SB) and 1-*l*-menthyloxy-3-benzoylacetone (H(*l*-moba)) have been synthesized, where H_2salen stands for *N,N'*-disalicylideneethylenediamine. These complexes were shown to have a *cis*-β-octahedral structure, based on electronic and infrared spectra. They showed circular dichroism in the visible region, demonstrating an induction of an asymmetry around the metal ion. On the basis of NMR and CD spectra and in comparison with the CD spectrum of Λ-Co(sal-(*S, S*)-ch)(bazc), it was shown that the Co(SB)(*l*-moba) complexes prefer the Λ-*cis*-β_1-configuration. The reaction of racemic *N,N'*-disalicylidene-*trans*-1,2-cyclohexanediaminatocobalt(II) (Co(salch)) and racemic *N,N'*-disalicylidene-1,2-propanediaminatocobalt(II) (Co(salpn)) with H(*l*-moba) in a 2 : 1 mole ratio yielded Λ-*cis*-β_1-Co(sal-(*S, S*)-ch)(*l*-moba) and Λ-*cis*-β_1-Co(sal-(*R*)-pn)(*l*-moba), respectively, as a main species. The stereoselectivity in the present complexes has been discussed in terms of the inter-ligand, hydrophobic CH/π-interaction which may occur between the *l*-menthyl group and an aromatic ring of the Schiff bases.

Recently, there has been an increasing interest in inter-ligand, hydrophobic interactions which bring about stereoselectivity and stereospecificity in metal complexes.[1-3] In the preceding paper of this series,[2] we have shown that tris(1-*l*-menthyloxy-3-benzoylacetonato)M(III), [M(*l*-moba)$_3$] (M=Co, Cr, Mn), prefers the *cis*-Δ-configuration. This stereoselectivity was attributed to the inter-ligand, hydrophobic CH/π-interaction[4] operating between an *l*-mentyl group of one ligand and the phenyl group of the adjacent ligand in the complex. In this study, we have prepared the cobalt(III) mixed-chelates, Co(SB)(*l*-moba), containing a salen-like Schiff base (SB) and *l*-moba$^-$, where H_2salen denotes *N,N'*-disalicylideneethylenediamine, and examined their configuration on the basis of ^{1}H-NMR and circular dichroism (CD) spectra. The purpose of this study is to investigate the stereoselectivity in Co(SB)(*l*-moba) in terms of the hydrophobic CH/π-interaction, which may occur between an aromatic ring of the Schiff base and the *l*-methyl group of *l*-moba$^-$. Schiff bases used in this study are *N,N'*-disalicylideneethylenediamine (H_2salen), its ring-substituted homologs (H_2(R-salen); R=3-MeO, 4-OH, 5-Me, 5-Br), (1*S*,2*S*)-*N,N'*-disalicylidene-1,2-cyclohexanediamine (H_2sal-(*S,S*)-ch), and (*R*)-*N,N'*-disalicylidene-1,2-propanediamine (H_2sal-(*R*)-pn). Further, in order to examine if *l*-moba$^-$ selectively reacts with one of the optical isomers of the racemic cobalt(II) complexes, cobalt(III) mixed-chelates, Co(salch)(*l*-moba), and Co(salpn)(*l*-moba), were prepared by reacting racemic *N,N'*-disalicylidene-*trans*-1,2-cyclohexanediaminatocobalt(II) (Co(salch)) and racemic *N,N'*-disalicylidene-1,2-propylenediaminatocobalt(II) (Co(salpn)) with H(*l*-moba) in a 2 : 1 mole ratio, respectively, and their configurations were studied.

Experimental

Syntheses. Synthetic method of H(*l*-moba) is described in the previous paper.[2] Syntheses of Co(salen) and its homologs were carried out by the usual method in the literatures.[5,6] (*R*)-1,2-Propanediamine[7] and (1*S*,2*S*)-1,2-cyclohexanediamine[8] were obtained by resolving racemic diamines.

Co(SB)(l-moba). Cobalt(III) mixed-chelates were obtained in nearly the same way. Synthesis of Co(salen)-(*l*-moba) is exemplified. A mixture of Co(salen) (0.2 g) and H(*l*-moba) (0.2 g) in methanol (30 cm^3) were refluxed for 3 h in an open atmosphere. Color of the solution turned from red to green. The reaction mixture was concentrated to 5 cm^3 and to this was added peroleum ether to give a green precipitate. It was dissolved in a benzene–ethanol mixture (5 : 3 in volume) and the solution was passed through an alumina column (1.5 cm × 20 cm). The eluent was concentrated to *ca.* 10 cm^3 and allowed to stand overnight in a refrigerator to give Co(salen)(*l*-moba) as green crystals.

Co(sal-(*S,S*)-ch)(bzac) was also prepared by the reaction of Co(sal-(*S,S*)-ch) and benzoylacetone (Hbzac).

Table 1. Elemental analyses of cobalt(III) mixed-chelates

Complex	Found(%)			Calcd(%)		
	C	H	N	C	H	N
Co(salen)(*l*-moba)	67.39	6.30	4.40	67.49	6.45	4.37
Co(5-Me-salen)(*l*-moba)	68.02	6.89	4.19	68.25	6.78	4.19
Co(5-Br-salen)(*l*-moba)	53.92	5.08	3.48	54.15	4.92	3.51
Co(4-OH-salen)(*l*-moba)	64.19	6.52	4.18	64.28	6.14	4.16
Co(3-MeO-salen)(*l*-moba)	63.98	6.40	4.31	64.13	6.47	4.00
Co(sal-(*S,S*)-ch)(*l*-moba)	68.80	6.81	4.02	69.15	6.82	4.03
Co(sal-(*S,S*)-ch(bzac)	66.49	5.54	5.25	66.66	5.41	5.18
Co(sal-(*R*)-pn)(*l*-moba)	68.40	6.66	4.32	68.09	6.33	4.29

Elemental analyses of the cobalt(III) mixed-chelates are given in Table 1.

Measurements. Electronic spectra were recorded on a Shimadzu MPS-5000 spectrophotometer in methanol. NMR spectra were recorded on JEOL Fourier Transform NMR Spectrometer Model FX90Q in $CDCl_3$, tetramethylsilane being used as an internal standard. CD spectra were recorded on a JASCO ORD/SP spectrometer in methanol.

Results and Discussion

It is known that cobalt(III) mixed-chelates of the Co(salen)(ab) type are obtainable by the reaction of Co(salen) and a bidentate ligand (ab) in the presence of molecular oxygen.[9-11] X-Ray analyses of Co(salen)-(acac) (acac$^-$=2,4-pentanedionate anion)[12] and Co-(salen)(bzac)[13] have revealed that salen^{2-} coordinates to the metal to form a *cis*-β-octahedral structure and the diketonate ion (acac$^-$ and bzac$^-$) coordinates to the metal with the oxygen atoms. The present complexes Co(SB)(*l*-moba) bear a marked similarity in infrared spectrum to Co(salen)(acac) and show the bands at 1590—1550 and 1540—1520 cm^{-1} characteristic of chelated 1,3-diketonate ion.[14,15] Electronic spectra of the complexes also resemble the spectra of Co(salen)-(acac)[10] and Co(salen)(bzac),[9] showing the bands around 16×10^3 (log $\varepsilon\approx2.5$) and 26×10^3 cm^{-1} (log $\varepsilon\approx3.9$) (Table 2). This spectral feature is quite comparable with those of pseudo-octahedral cobalt(III) complexes with a N_2O_4-donor set.[16,17] Based on these facts, we may conclude that the Co(SB)(*l*-moba) complexes possess a *cis*-β-octahedral structure.

There are two possible geometrical isomers for Co-(SB)(*l*-moba) due to the coordination attitude of *l*-moba$^-$. With respect to the imino nitrogens of the Schiff base and the carbonyl oxygen at the 2-position of *l*-moba$^-$, the geometrical isomers are described as *mer*(N,N,O) and *fac*(N,N,O). Hereafter, these isomers will be represented by *cis*-β_1 and *cis*-β_2, respectively. Each of these isomers is asymmetric about the central metal ion. Hence, four isomers are considered for Co(SB)(*l*-moba). They are exemplified by the isomers of Co(salen)(*l*-moba) in Fig. 1.

In order to determine the geometrical structure for Co(SB)(*l*-moba), ^{1}H-NMR spectra were measured in $CDCl_3$. The spectrum of Co(salen)(*l*-moba) is shown in Fig. 2 as an example. The signal of relatively high intensity in the region 0.65—0.94 ppm can be assigned to the menthyl protons. The signal at 3.77 ppm is ascribed to the methylene proton adjacent to the *l*-menthyloxyl group. This is obscured by the signals attributable to the ethylene signals of the Schiff base. However, assignment of the methylene signal of *l*-moba$^-$ can be unambiguously performed by comparing the spectrum with those of Co(salen)(acac) and Co(salen)-(bzac). The signal due to the methine proton of *l*-moba$^-$ should exist around 6.6 ppm, but this is concealed or superposed by the complicated signals of the aromatic protons. The most characteristic feature in the NMR spectrum is the singlets at 7.57 and 7.82 ppm, which can be attributed to the azomethine protons. Unequivalence of the azomethine signals is consistent with the *cis*-β-configuration of the salen^{2-} moiety. More careful examination of the NMR spectrum revealed that there are another pair of singlets at 7.47 and 7.84 ppm of weaker intensity. They are also assigned to the azomethine protons. Appearance of two pairs of azomethine signals implies that the two geometrical isomers, *cis*-β_1

Table 2. Electronic spectral data for cobalt(III) mixed-chelates in methanol

Complex	$\tilde{\nu}/10^3 cm^{-1}$(log ε)	
Co(salen)(*l*-moba)	16.3(2.54)	26.6(3.90)
Co(5-Me-salen)(*l*-moba)	16.0(2.59)	26.0(3.88)
Co(5-Br-salen)(*l*-moba)	16.3(2.63)	25.6(3.85)
Co(4-OH-salen)(*l*-moba)	16.7(2.77)	27.4(4.03)
Co(3-MeO-salen)(*l*-moba)	16.1(2.62)	26.3(3.87)
Co(sal-(*S,S*)-ch)(*l*-moba)	16.3(2.48)	26.0(3.89)
Co(sal-(*R*)-pn)(*l*-moba)	16.2(2.52)	26.6(3.91)

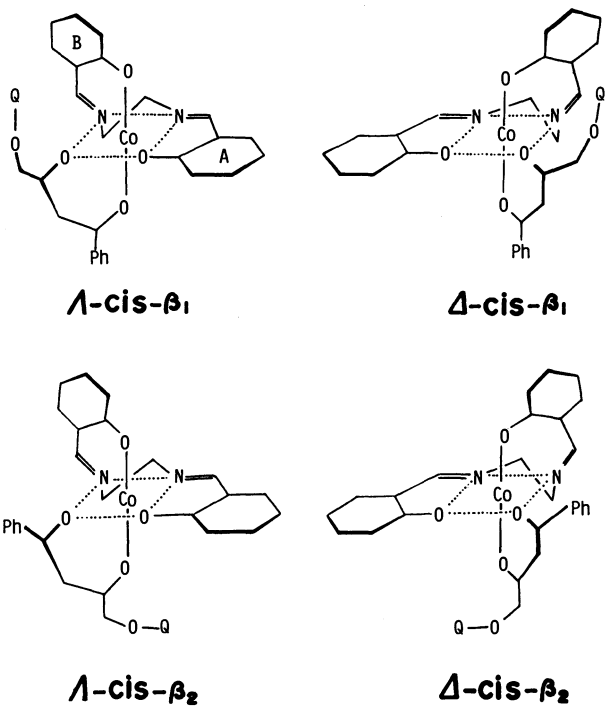

Fig. 1. Four isomeric structures of Co(salen)(*l*-moba) (Q=*l*-menthyl).

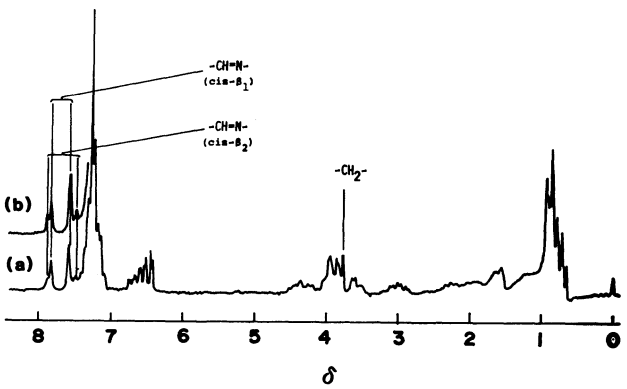

Fig. 2. NMR spectra of Co(salen)(*l*-moba) in $CDCl_3$. (a) Soon after dissolution and (b) at equilibrium.

Table 3. Selected ^{1}H-NMR spectral data of complexes (ppm)

Complex	CH_2[a]	Menthyl	Azomethine			
			cis-β_1		*cis*-β_2	
H(*l*-moba)	4.05	0.77—1.03				
Co(salen)(*l*-moba)	3.77	0.65—0.94	7.57	7.82	7.47	7.84
Co(5-Me-salen)(*l*-moba)	3.78	0.66—0.94	7.50	7.74		7.78
Co(5-Br-salen(*l*-moba)	3.76	0.65—0.94	7.50	7.75	7.45	7.82
Co(3-MeO-salen)(*l*-moba)	3.8	0.76—0.93	7.49	7.81		7.88
Co(sal-(*S*,*S*-ch)(*l*-moba)	3.8	0.64—0.96	7.44	7.80		7.90
Co(sal-(*R*)-pn)(*l*-moba)	3.75	0.65—0.95	7.55	7.80		7.85

a) Methylene adjacent to *l*-methyloxyl group.

Table 4. CD spectral data of Co(SB) (*l*-moba) and related complex in methanol

Complex	$\tilde{\nu}/10^3$cm^{-1} ($\Delta\varepsilon$)		
Co(salen)(*l*-moba)	15.9(0.32)	19.5(0.10)	23.0(−0.31)
Co(5-Me-salen)(*l*-moba)	16.3(0.85)	18.8(0.25)	22.2(−1.18)
Co(5-Br-salen)(*l*-moba)	16.4(0.88)	19.0(0.23)	22.6(−1.10)
Co(3-MeO-salen)(*l*-moba)	15.8(0.61)	18.2(0.23)	21.9(−0.61)
Co(4-OH-salen)(*l*-moba)	16.2(0.70)	19.4(0.26)	22.6(−0.67)
Co(sal-(*S*,*S*)-ch)(*l*-moba)	16.0(9.80)	19.5(2.00)	22.8(−15.80)
Co(sal-(*S*,*S*)-ch)(bzac)	16.0(10.00)	19.0(2.60)	22.7(−16.20)
Co(sal-(*R*)-pn)(*l*-moba)	16.1(1.60)	19.6(0.52)	
Co(salch)(*l*-moba)[a]	16.6(0.20)	19.4(0.08)	
Co(salpn)(*l*-moba)[b]	16.0(0.58)	19.4(0.16)	22.7(−0.84)

a) Complex obtained by the reaction of racemic Co(salch) and *l*-moba. b) Obtained by the reaction of racemic Co(salpn) and *l*-moba.

and *cis*-β_2, are present in solution.

The intensities of two pairs of the azomethine signals were shown to be time-dependent. The major pair decreased their intensity slightly with time, while the minor pair increased their intensity. This suggests that the *cis*-β_1- and *cis*-β_2-isomers are in equilibrium in solution. The equilibrium was attained within 2 d. A part of the NMR spectrum of Co(salen)(*l*-moba) at equilibrium is shown in Fig. 2. Judging from the intensities of the azomethine singlets at equilibrium, two geometrical isomers are assumed to exist in a *ca.* 1 : 5 mole ratio in the case of Co(salen)(*l*-moba). The ratio of two geometrical isomers for the other Co(SB)(*l*-moba) complexes is also estimated at 1 : 3—1 : 6. Some selected ^{1}H-NMR spectral data for Co(SB)(*l*-moba) at equilibrium are given in Table 3. Table 3 also includes the NMR spectral data for free H(*l*-moba).

When the NMR spectrum of Co(SB)(*l*-moba) is compared with that of H(*l*-moba), it is noted that the signal due to the methylene protons of *l*-moba$^-$ shifts upfield by complex formation. In the case of [Co(*l*-moba)$_3$], the methylene signal shifts downfield (4.31 ppm).[2] The downfield shift of the methylene signal relative to that of H(*l*-moba) is also observed for Pd(*l*-moba)$_2$ (4.20 ppm) and for [Pd(bipy)(*l*-moba)]ClO_4 (4.20 ppm).[18] These facts suggest that the methylene group adjacent to the *l*-methyloxyl group is shielded by a ring current in a predominant species of Co(SB)(*l*-moba). NMR spectrum of Co(salen)(acac) shows two methyl signals at 1.94 and 1.76 ppm. The latter has been assigned to the methyl group which is in a close proximity above the benzene ring (B benzene ring) (see Fig. 1).[12,19] Thus, upfield shift of the methylene signal in Co(SB) (*l*-moba) relative to that of H(*l*-moba) leads us to a conclusion that the *cis*-β_1-isomer is predominantly formed at the equilibrium.

Each Co(SB)(*l*-moba) complex showed CD bands around 16×10^3 (positive), 19×10^3 (positive shoulder), and 23×10^3 cm^{-1} (negative). This is a good indication for the occurence of an inter-ligand, hydrophobic CH/π-interaction between the B benzene ring of the Schiff base and the *l*-menthyl group of *l*-moba$^-$. Typical CD spectra are shown in Fig. 3, and the numerical data are given in Table 4.

In order to determine the absolute configuration of the present complexes, Co(sal-(*S*,*S*)-ch)(*l*-moba) and Co(sal-(*S*,*S*)-ch)(bzac) were prepared and their CD spectra were recorded (Fig. 3 and Table 4). CD spectra of these complexes bear a marked resemblance both in sign and in intensity. It is likely that the stereoselectivity in these complexes is mostly due to the steric requirement of the sal-(*S*,*S*)-ch^{2-} moiety and the weak hydrophobic CH/π-interaction is practically supressed in Co(sal-(*S*,*S*-ch)(*l*-moba). Fujii *et al.* have demonstrated that Co(sal-(*S*,*S*)-ch)(ab) preferentially takes the *A*-configuration because of the steric control of the (1*S*,2*S*)-1,2-cyclohexanediamine moiety.[20,21] Despite the low intensity of the CD bands, the similarity of the CD spectra of Co(SB)(*l*-moba) to those of Co(sal-(*S*,*S*)-ch)(*l*-moba) and Co(sal-(*S*,*S*)-ch)(bzac) leads us to the conclusion that the *A*-*cis*-β_1-isomer is predominantly formed in the present complexes. CD spectral pattern of Co(sal-(*R*)-pn)(*l*-moba) is also the same as those of Co(SB)(*l*-moba). This implies that the stereo-

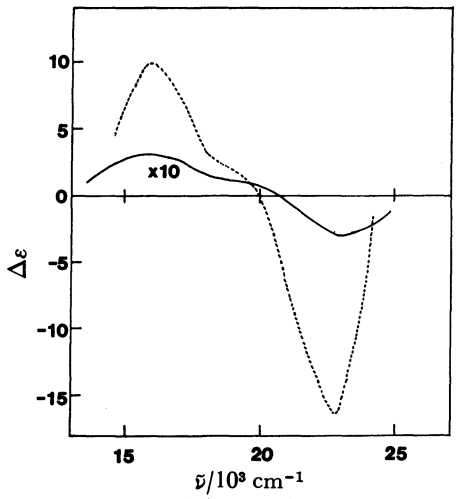

Fig. 3. CD spectra of (——) Co(salen)(*l*-moba) and (------) Co(sal-(*S,S*)-ch)(bzac).

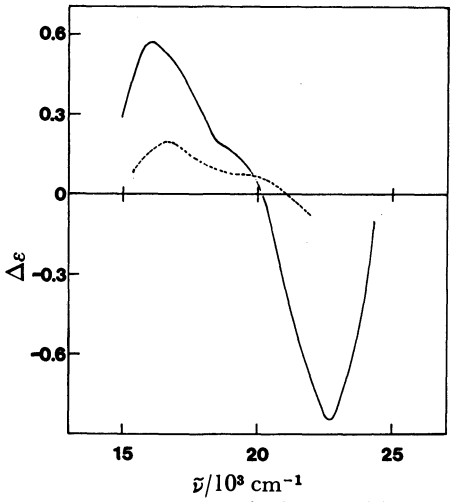

Fig. 4. CD spectra of (——) Co(salpn)(*l*-moba) and (------)Co(salch)(*l*-moba).

selectivity of sal-(*R*)-pn^{2-} is identical with that of sal-(*S,S*)-ch^{2-}.

In order to further demonstrate the potential contribution of the inter-ligand, hydrophobic CH/π-interaction to geometrical and optical selectivities in Co(SB)(*l*-moba), we have prepared Co(salch)(*l*-moba) and Co(salpn)(*l*-moba) by the reaction of racemic Co(salch-and racemic Co(salpn) with H(*l*-moba) in a 2 : 1 mole ratio, respectively. These complexes showed circular dichroism in the visible region (Fig. 4). For Co(salch)-(*l*-moba) eight isomers are considered: *Δ-cis-*β_1-Co(sal-(*S,S*)-ch)(*l*-moba), *Λ-cis-*β_1-Co(sal-(*S,S*)-ch)(*l*-moba), *Δ-cis-*β_1-Co(sal-(*R,R*)-ch)(*l*-moba), *Λ-cis-*β_1-Co(sal-(*R,R*)-ch)(*l*-moba), *Δ-cis-*β_2-Co(sal-(*S,S*)-ch)(*l*-moba), *Λ-cis-*β_2-Co(sal-(*S,S*)-ch)(*l*-moba), *Δ-cis-*β_2-Co(sal-(*R,R*)-ch)(*l*-moba), and *Λ-cis-*β_2-Co(sal-(*R,R*)-ch)(*l*-moba). Similarly eight isomers are considered for Co(salpn)-(*l*-moba). Although no informations are available at present on proportions of the isomers and on the sign and the intensity of circular dichroism of each isomer, a marked resemblance of the CD spectra of Co(salch)(*l*-moba) and Co(salpn)(*l*-moba) to those of Co(SB)(*l*-moba) suggests that *l*-moba$^-$ reacts selectively with one of the optical isomers, Co(sal-(*S,S*)-ch) and Co(sal-(*R*)-pn), respectively. This stereoselectivity may be interpreted in terms of the inter-ligand, hydrophobic CH/π-interaction between the *l*-menthyl group and the B benzene ring. Notably the CD intensity of Co(salch)(*l*-moba) is lower than that of Co(salpn)(*l*-moba) and the lowest among the complexes obtained in this study, although the CD intensity for Co(sal-(*S,S*)-ch)(*l*-moba) much exceeds that of Co(sal-(*R*)-pn)(*l*-moba). A strong stereoselectivity originated from the (1*S*,2*S*)-1,2-cyclohexanediamine moiety must diminish the contribution from the hydrophobic CH/π-interaction. It is likely that the stereoselectivity and the discrimination in metal complexes owing to the hydrophobic interactions are induced when a hydrophobic side chain attached to the ligand is flexible.

References

1) M. Nakamura, H. Ōkawa, and S. Kida, *Chem. Lett.*, **1981**, 547.
2) H. Ōkawa, K. Ueda, and S. Kida, *Inorg. Chem.*, **21**, 1594 (1982).
3) B. E. Fischer and H. Sigel, *J. Am. Chem. Soc.*, **102**, 2998 (1980), and references therein.
4) M. Nishio, *Kagaku No Ryoiki*, **31**, 16, 92 (1977).
5) R. H. Bailes and M. Calvin, *J. Am. Chem. Soc.*, **69**, 1886 (1949).
6) H. Aoi, M. Ishimori, S. Yoshikawa, and T. Tsuruta, *J. Organomet. Chem.*, **85**, 241 (1975).
7) R. G. Asperger and C. F. Lin, *Inorg. Chem.*, **4**, 1492 (1965).
8) F. P. Dwyer and E. F. Gyarfas, *J. Am. Chem. Soc.*, **81**, 290 (1959).
9) S. N. Podder and D. K. Biswas, *J. Inorg. Nucl. Chem.*, **31**, 565 (1969).
10) K. Day and R. L. De, *Z. Anorg. Allg. Chem.*, **402**, 120 (1973).
11) Y. Fujii, T. Isago, M. Sano, N. Yanagibashi, S. Hirasawa, and S. Takahashi, *Bull. Chem. Soc. Jpn.*, **49**, 3059 (1976).
12) M. Calligaris, G. Nardin, and L. Randaccio, *J. Chem. Soc., Chem. Commun.*, **1969**, 1248.
13) N. A. Bailey, B. M. Higson, and E. D. McKenzie, *J. Chem. Soc., Dalton Trans.*, **1972**, 502.
14) R. J. York, W. D. Bonds, Jr., B. P. Cotsoradis, and R. D. Archer, *Inorg. Chem.*, **8**, 789 (1969).
15) L. J. Boucher and D. R. Herington, *J. Inorg. Nucl. Chem.*, **33**, 4349 (1971).
16) R. A. D. Wentworth and T. S. Piper, *Inorg. Chem.*, **4**, 202 (1965).
17) L. J. Boucher, *Inorg. Chim. Acta*, **6**, 29 (1972).
18) The present authors, to be published.
19) S. Kinoshita, K. Ohta, H. Wakita, and I. Masuda, 40th National Meeting of the Chemical Society of Japan, Fukuoka, September 1979.
20) Y. Fujii, M. Sano, and Y. Nakano, *Bull. Chem. Soc. Jpn.*, **50**, 2609 (1977).
21) Y. Fujii, M. Matsufuru, A. Saito, and S. Tsuchiya, *Bull. Chem. Soc. Jpn.*, **54**, 2029 (1981).

Synthesis and Characterization of Copper(II) and Nikel(II) Complexes of 1,5-Diamino-3-pentanol and Its Derivatives

Ichiro MURASE,* Masao HATANO,† Masahiko TANAKA,† Shigehiro UENO,† Hisashi ŌKAWA,† and Sigeo KIDA†

Laboratory of Chemistry, College of General Education, Kyushu University 01, Ropponmatsu, Chuo-ku, Fukuoka 810

†*Department of Chemistry, Faculty of Science, Kyushu University 33, Hakozaki, Higashi-ku, Fukuoka 812*

(Received March 12, 1982)

Dihydrochloride of a binucleating ligand, 1,5-diamino-3-pentanol (Hdpl·2HCl) has been synthesized by a new method in a high yield (>70%). This ligand forms 1 : 1 complexes with copper(II), Cu(dpl)X(X=BF_4, ClO_4, NO_3, and Cl(H_2O)). The cryomagnetic study of the copper complexes has shown that they are binuclear, and a strong antiferromagnetic interaction is operating between two copper ions. The binuclear structure seems to be quite stable even in aqueous solution. The 1 : 1 complex with nickel(II) was also isolated as tetraphenylborate, which was essentially diamagnetic. A planar binuclear structure similar to the copper complexes was assumed for this complex. Its absorption band at 29.8×10^3 cm^{-1} ($\varepsilon=160$) was attributed to the charge transfer transition from the bridging oxygen to the nickel similarly to the bands in the 25—29×10^3 cm^{-1} region usually observed for alkoxo-oxygen bridged binuclear copper(II) complexes. Some 2 : 1 copper(II)–dpl complexes have also been synthesized and characterized as binuclear complexes. 1,5-Bis(dimethylamino)-3-pentanol has been synthesized, and its 2 : 1 copper(II) complexes have been isolated.

It is well known that linear aliphatic amino alcohols such as $R_2N(CH_2)_nOH$ and $R_2N(CH_2)_mNH(CH_2)_nOH$ (R=alkyl; m and n=2 or 3) form bi-, tri-, and tetranuclear complexes with copper(II).[1-7] The complexes have been extensively studied for their magnetisms, spectra,[3-7] and structures.[8-16] Since they are limited to those bridged with terminal alkoxo-oxygen atoms, they are readily hydrolyzed in water forming mononuclear species. In connection with the increasing attention to binuclear copper complexes in view of the elucidation of the function of copper protein, it has been desired to prepare binuclear copper complexes which are soluble and stable in water. The purpose of this study is to prepare such complexes with a saturated aliphatic amino alcohol. One of the reasons to adopt the saturated amino alcohol as a ligand is that it is transparent throughout the region of conventional electronic spectral measurements; this would facilitate the spectroscopic study of the complex with this ligand.

The molecular model investigation has revealed that the most suitable ligand for our purpose is 1,5-diamino-3-pentanol (abbreviated as Hdpl), which is capable of forming 6·6-membered fused chelate rings involving two metal ions bridged by an alkoxo-oxygen atom (*cf.*, Fig. 1-a). In this study we have succeeded in preparing the 1 : 1 binuclear copper(II) complexes with dpl which are stable even in aqueous solution. This ligand also enabled us to prepare the 1 : 1 binuclear nickel(II) complex similar to the copper complexes.

Alkoxo-oxygen bridged binuclear copper(II) complexes generally show an absorption band in the 23—28×10^3 cm^{-1} region which is attributed to a charge transfer transition from bridging oxygen to copper.[2] Such a band is naturally expected for the binuclear copper(II) complexes with dpl. It is interesting to see if a similar band is observed for the nickel complex, since planar binuclear nickel(II) complexes bridged by alkoxy-oxygen atoms have not been reported so far.

The ligand Hdpl was already prepared as a picrate by Taniyama *et al.*,[17] but the yield was so poor that it was difficult to prepare enough sample for the synthesis of metal complexes. Hence, in this study we have exploited a new synthetic route to this ligand with a high yield (>70%). This enabled us to prepare the new complexes as reported in this paper.

Experimental

Syntheses. *1,5-Diamino-3-pentanone Dihydrochloride*: To a suspension of potassium phthalimide (370 g, 2 mol) in 1.3 dm^3 of dry *N,N*-dimethylformamide (DMF), crude 1,5-dichloro-3-pentanone[18] (240 g, 1.3 mol) was added dropwise in 1 h with vigorous stirring. The temperature spontaneously rose from 15 °C to 65 °C during the addition, and the mixture was further heated at 80—85 °C for 6 h and allowed to stand overnight at room temperature. The resulting 1,5-diphthalimido-3-pentanone was collected by filtration and washed succesively with chloroform, water, and acetone. Curde yield 280 g (76%).

While the phthalide (280 g) was boiled with a mixture of 700 cm^3 of acetic acid and 450 cm^3 concd hydrochloric acid for 3 d, each 50 cm^3 of concd hydrochloric acid was added to this solution at 10 h intervals (total 250 cm^3). Phthalic acid deposited on cooling was filtered off and washed with water. The combined filtrate and washings were evaporated to near dryness under reduced pressure and the residue was treated with water to remove undissolved materials. The aqueous solution was again concentrated and a large amount of ethanol was added. The resulting precipitates were collected by filtration. Crude yield 135 g (96%).

The pure sample was obtained by repeated crystallization from dilute ethanol; mp 190—192 °C. IR: ν_{CO} 1720 cm^{-1}. Found: C, 31.52; H, 7.32; N, 14.79%. Calcd for $C_5H_{12}N_2O$·2HCl: C, 31.75; H, 7.46; N, 14.82%.

1,5-Diamino-3-pentanol dihydrochloride(Hdpl·2HCl): Crude 1,5-diamino-3-pentanone dihydrochloride (40 g, 0.21 mol) was added portionwise keeping the temperature below 20 °C to a solution containing sodium hydroxide (17 g, 0.4 mol) and sodium borohydride (8 g, 0.2 mol) in 300 cm^3 water. The mixture was stirred at room temperature for 48 h. Dilute hydrochloric acid was carefully added to the cold solution and a pH was brought to ≈1. The solution was evaporated to dryness under reduced pressure, and methanol was added

to the residue and evaporated. Addition of methanol and evaporation under reduced pressure was repeated several times to remove resulting boric acid as a methyl ester. The final residue was boiled with 100 cm³ of methanol, undissolved sodium chloride was filtered off, and the filtrate was concentrated to a small volume. A large amount of ether was added to the residual solution and the mixture was kept in a refrigerator overnight. The resulting crystals were collected and washed with ether. Crude yield 32 g (80%). They were recrystallized from methanol–ether mixture; mp 158—160 °C. Found: C, 31.35; H, 8.65; N, 14.57%. Calcd for $C_5H_{14}N_2O\cdot 2HCl$: C, 31.43; H, 8.45; N, 14.66%.

1,5-Bis(dimethylamino)-3-pentanol (Hmdpl):[19] A mixture of 1,5-bis(dimethylamino)-3-pentanone (30 g, 0.17 mol)[20] and sodium borohydride (5 g, 0.13 mol) in 130 cm³ of methanol was heated at 60 °C for 1 h. It was poured on ice, acidified to pH 2—3 with concd hydrochloric acid, and the solution was evaporated to near dryness under reduced pressure. The residue was dissolved in a small amount of water, saturated with potassium hydroxide, and extracted with 300 cm³ of ether. The ether extracts were dried over potassium carbonate and the ether was evaporated. The oily residue was distilled and the fraction bp 115—116 °C (1800 Pa) was collected. Yield 20 g (70%). Found: C, 61.58; H, 12.71; N, 15.97%. Calcd for $C_9H_{22}N_2O$: C, 62.02; H, 12.72; N, 16.07%.

$Cu_2(dpl)_2Cl_2\cdot H_2O$: To a solution of Hdpl·2HCl (1.9 g, 10 mmol) in 40 cm³ of methanol was added triethylamine until the solution became alkaline, and to this solution was added an equimolar amount of anhydrous copper(II) chloride in methanol. The resulting deep blue solution was heated on a water bath for a few minutes. On cooling to room temperature bluish violet crystals were separated and were recrystallized from a dilute methanol–water (1 : 1) mixture. Found: C, 26.58; H, 6.27; N, 12.23; Cu, 28.00%. Calcd for $C_{10}H_{28}N_4O_3Cl_2Cu$: C, 26.67; H, 6.27; N, 12.44; Cu, 28.22%.

The bromide, perchlorate, tetrafluoroborate, and nitrate were also prepared in similar manners using corresponding copper(II) salts and recrystallized from water containing soudim salt of the corresponding anion.

$Cu_2(dpl)_2Br_2\cdot H_2O$: Found: C, 22.14; H, 5.28; N, 10.31 %. Calcd for $C_{10}H_{28}N_4O_3Br_2Cu_2$: C, 22.27; H, 5.23; N, 10.39%.

$Cu_2(dpl)_2(ClO_4)_2$: Found: C, 21.48; H, 4.68; N, 9.80; Cu, 22.49%. Calcd for $C_5H_{13}N_2O_5CuCl$: C, 21.44; H, 4.68; N, 10.00; Cu, 22.68%.

$Cu_2(dpl)_2(BF_4)_2$: Found: C, 22.58; H, 4.95; N, 10.23; Cu, 23.52%. Calcd for $C_5H_{13}N_2OCuBF_4$: C, 22.45; H, 4.90; N, 10.45; Cu, 23.75%.

$Cu_2(dpl)_2(NO_3)_2$: Found: C, 24.75; H, 5.44: N, 17.23%. Calcd for $C_5H_{13}N_3O_4Cu$: C, 24.74; H, 5.40; N, 17.31%.

$Cu_2Cl_2(OCH_3)(dpl)\cdot CH_3OH$: To a warm methanol solution (20 cm³) of Hdpl·2HCl (0.4 g, 2 mmol) was added trimethylamine to make the solution alakline. Anhydrous copper(II) chloride (0.5 g, 4 mmol) dissolved in methanol was added to this solution and the mixture was heated on a water bath. Deep green crystals were soon separated out. They were collected by filtration, washed with methanol, and dried at room temperature under vacuum. The yield was almost quantitative. The complex is sparingly soluble in ordinary organic solvents and no further purification was carried out. Found; C, 22.44; H, 4.99: N, 7.51; Cu, 33.60; Cl, 18.48%. Calcd for $C_7H_{20}N_2O_3Cl_2Cu_2$: C, 22.23; H, 5.33; N, 7.41; Cu, 33.60; Cl, 18.75%.

$Cu_2Br_3(dpl)\cdot 2CH_3OH$: The procedure was the same as the above except for the use of anhydrous copper(II) bromide in place of the chloride. Olive green crystals, only slightly soluble in ordinary organic solvents. Found: C, 15.92: H, 3.68; N, 5.28%. Calcd for $C_7H_{21}N_2O_3Br_3Cu_2$: C, 15.34; H, 3.86; N, 5.11%.

$Cu_2Cl_2(mdpl)OH$: A solution of Hmdpl (0.4 g, 2.5 mmol) in 20 cm³ of methanol was mixed with anhydrous copper(II) chloride (0.7 g, 5 mmol) in methanol and the solution was made alkaline by the addition of excess trimethylamine. Green crystals were soon deposited on warming. They were collected by filtration and recrystallized from 1-butanol. Yield 0.8 g (90%). Found: C, 28.33; H, 5.55; N, 7.19; Cu, 33.23; Cl, 18.20%. Calcd for $C_9H_{22}N_2O_2Cu_2Cl_2$: C, 27.84; N, 5.71; N, 7.22; Cu, 33.73; Cl, 18.26%.

$Cu_2Br_2(mdpl)OH$: The synthetic procedure was the same as the above. Dark green fine needles were obtained by recrystallization from 1-butanol. Found: C, 22.27; H, 4.38; N, 5.67; Cu, 26.78; Br, 33.79%. Calcd for: $C_9H_{22}N_2O_2Cu_2Br_2$: C, 22.65; H, 4.65; N, 5.87; Cu, 26.63; Br, 33.49%.

$Ni_2(dpl)_2(Bph_4)_2(CH_3OH)_2$: Nickel perchlorate hexahydrate (0.76 g, 2 mmol) and Hdpl·2HCl (0.4 g, 2 mmol) were dissolved in 15 cm³ of methanol. To this solution was added solid sodium hydroxide (0.25 g, 6 mmol). The green solution gradually changed into dark red yielding a white preicpitate as the sodium hydroxide dissolved in the solution. The precipitate was filtered off, and to the filtrate was added an excess of sodium tetraphenylborate (about 1 g). Fine pink-red crystals were formed in the solution. These were filtered and washed with methanol. The crystals thus obtained were recrystallized from a methanol–DMF (10 : 1) solution by adding a methanol solution saturated with sodium tetraphenylborate (1 g). This compound is readily soluble in DMF, slightly soluble in methanol, and practically insoluble in water. Found: C, 68.21; H, 7.10; N, 5.45%. Calcd for $C_{30}H_{37}N_2O_2BNi$: C, 68.36; H, 7.07; N, 5.31%.

Measurements. The electric conductivities of solutions were measured with a Yanagimoto Conductivity Outfit Model MY 7. Infrared and electronic spectra were recorded on a Hitachi 295 Infrared spectrophotometer and a Shimadzu MPS-5000 Spectrophotometer, respectively. Magnetic susceptibilities were measured by the Faraday method. The apparatus was calibrated by the use of $[Ni(en)_3]S_2O_3$.[21] The susceptibilities were corrected for the diamagnetism of the constituting atoms by the use of Pascal's constants.[22] The effective magnetic moments μ_{eff} was calculated based on the equation $\mu_{eff}=2.828\sqrt{(\chi_A-60\times10^{-6})T}$.

Results and Discussion

1 : 1 Copper(II)–dpl Complexes. $Cu_2(dpl)_2X_2H_2O$ (X= Cl, Br), $Cu_2(dpl)_2Y_2$ ($Y=ClO_4$, BF_4, NO_3): These complexes show subnormal magnetic moments at room temperature (Table 1). The temperature dependence of magnetic susceptibility was measured for the chloride, tetrafluoroborate and perchlorate, and the results were well simulated by the Bleaney-Bowers equation[23] based on the assumption of binuclear structure with parameters, $2J=-640$ cm^{-1}, $Na=40\times10^{-6}$ cgs emu, $g=2.1$ for the chloride and $2J=-965$ cm^{-1}, $Na=46\times10^{-6}$ cgs emu, $g=2.1$ for the tetrafluoroborate, where J, Na, and g denote the general meanings. The perchlorate was practically diamagnetic in this temperature range. The binuclear structure was verified by the single-crystal X-ray structural analysis for $Cu_2(dpl)_2Cl_2(H_2O)_3$ which was obtained by recrystallization of $Cu_2(dpl)_2Cl_2H_2O$ from an aqueous solution. This compound consists of discrete binuclear units, where two dpl molecules and two copper atoms are roughly on a plane and a chloride ion and a water molecule weakly coor-

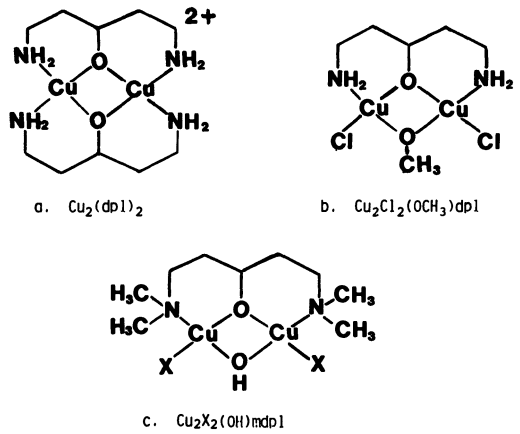

Fig. 1. Chemical structures of complexes.

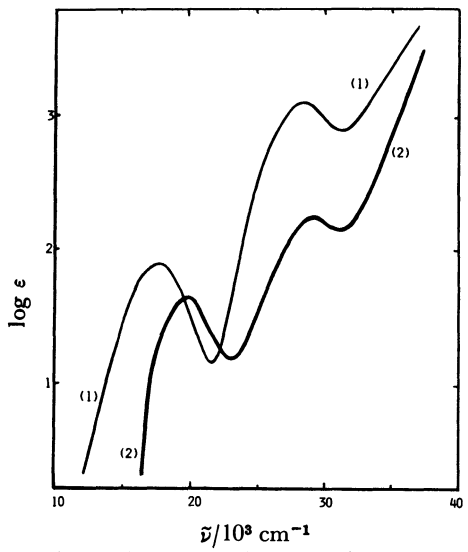

Fig. 2. Electronic spectra of (1) $Cu_2(dpl)_2(BF_4)_2$ in water (2) $Ni_2(dpl)_2(Bph_4)_2 \cdot 2CH_3OH$ in methanol.

dinate to the copper ions from the same side of the coordination plane. The details of the structural data were reported in a separate paper.[24]

The measurements of molar conductivities (Table 1) revealed that the perchlorate and tetrafluoroborate are 1 : 2 electrolytes in methanol solution (10^{-3} mol dm^{-3}), whereas in the case of the chloride partial coordination of Cl^- is occuring in the methanol solution, since its conductivity is considerably lower than those of the former ones.

Aqueous solutions of these complexes gave the same spectra (Fig. 2) irrespective of the counter anion, showing a d-d band at 17.7×10^3 cm^{-1} ($\varepsilon=76.6$) and a CT band at 28.4×10^3 cm^{-1} ($\varepsilon=1300$) which is characteristic of alkoxo-bridged copper(II) complexes. Since Beer's law is held for the aqueous solution, the complex ion, probably $[Cu_2(dpl)_2(H_2O)_4]^{2+}$, should be quite stable in aqueous solution. This is an important result, since no binuclear copper(II) complexes with alkoxide bridges which are stable in aqueous solution have been known so far.

2 : 1 Copper(II)–dpl Complexes. $Cu_2Cl_2(dpl)(OCH_3)CH_3OH$: This compound shows subnormal magnetic moments at room temperature (0.89 BM) and the temperature dependence of magnetic susceptibility can be simulated by the Bleaney-Bowers equation[23] with the parameters $-2J=595$ cm^{-1}, $g=215$, $N\alpha=60\times10^{-6}$ cgs emu in the range 130—300 K. The deviation from the theoretical curve in the low-temperature range (80—130 K) may be attributed to paramagnetic impurity, since recrystallization was not carried out due to the low solubility in any available solvents. From the above results we assume the binuclear structure as depicted in Fig. 1.

The Nujol mull spectrum shows two bands at 16.5 and 27.0×10^3 cm^{-1}. The former is assigned to the d-d transition and the latter to the CT (O→Cu) transition similarly to the case of the 1 : 1 complexes. The d-d band shifts to the lower energy side by 2.5×10^3 cm^{-1} relative to that of the $[Cu_2(dpl)_2]X_2$ (X=ClO_4 and BF_4) as shown in Table 1. This is compatible with the proposed structure in Fig. 1, where chloride ions are substituted for amino groups as compared with the structure in Fig. 1-a.

This compound decomposes in water forming a blue solution with pale blue amorphous precipitates. When

TABLE 1. MOLAR CONDUCTIVITIES $\Lambda(\Omega^{-1}$ cm^2 mol^{-1} AT 25 °C, 10^{-3} mol dm^{-3}) AND EFFECTIVE MAGNETIC MOMENTS AT ROOM TEMPERATURE

Complex	Λ	(Solvent)	$\frac{\mu_{eff}}{BM}$
$Cu_2(dpl)_2Cl_2H_2O$	138	(Methanol)	0.72
$Cu_2(dpl)_2(BF_4)_2$	184	(Methanol)	0.37
$Cu_2(dpl)_2(ClO_4)_2$	172	(Methanol)	0.22
$Cu_2Cl_2(mdpl)OH$	7.7	(DMF)	1.19
$Cu_2Br_2(mdpl)OH$	7.3	(DMF)	1.55
$Cu_2Cl_2(OCH_3)(dpl)\cdot CH_3OH$			0.89
$Ni_2(dpl)_2(Bph_4)_2\cdot 2CH_3OH$	149	(Methanol)	0.72

TABLE 2. ELECTRONIC SPECTRAL DATA (cm^{-1}, ε IN PARENTHESIS)

Complex	Solution		(Solvent)[a]	Nujol mull	
$Cu_2(dpl)_2Cl_2H_2O$	17.7(76.6)	28.4(1300)	w	16.5(sh), 17.5	27
	18.0(59.0)	28.5(1400)	m		
$Cu_2(dpl)_2(BF_4)_2$	18.0(57.0)	28.6(1520)	m	19.0	27
$Cu_2(dpl)_2(ClO_4)_2$	18.0(56.5)	28.6(1610)	m	19.0	27
$Cu_2Cl_2(dpl)OCH_3\cdot CH_3OH$				16.5	27
$Cu_2Cl_2(mdpl)OH$	14.1(175)	b)	DMF	15.0	26.0[c]
$Cu_2Br_2(mdpl)OH$	13.9(273)	b)	DMF	14.0	23[c]
$Ni_2(dpl)_2(Bph_4)_2\cdot 2CH_3OH$	19.8(46)	29.8(160)	m	20.1	31[c]

a) w: Water, m: methanol. b) Obscure due to the overlapping of bands. c) Shoulder.

the solution was filtered and evaporated, well formed blue crystals of $Cu_2(dpl)_2Cl_2 \cdot 3H_2O$ separated out. Thus, the reaction that had taken place can be described as

$$2Cu_2(dpl)Cl_2(OCH_3)CH_3OH + 2H_2O \longrightarrow [Cu_2(dpl)_2]^{2+} + Cu(OH)_2 + Cu_{aq}^{2+} + 4Cl^- + 4CH_3OH.$$

Copper(II) Complexes with mdpl. $Cu_2X_2(mdpl)OH$ (X=Cl, Br): All attempts to prepare the 1 : 1 complexes with mdpl similar to the dpl complexes were unsuccessful. This is most probably due to the steric repulsion between the methyl groups on the amine nitrogens. In contrast, the 2 : 1 complexes Cu_2X_2-(mdpl)OH (X=Cl, Br) were readily obtained. The electric conductivities showed that both compounds are nonelectrolytes in DMF (*cf.* Table 1). This is consistent with the structure in Fig. 1.

Magnetic moments of these complexes at room temperature are both subnormal, *i.e.*, 1.19 BM (X=Cl) and 1.55 BM (X=Br) for one copper atom, but their magnetic behaviors over the temperature range 80—300 K are quite different from each other. As seen in Fig. 3 the χ_A-T curve of the chloro complex can be well simulated by the Bleanery-Bowers equation[23] with $-2J=375$ cm^{-1}, $g=2.1$, and $Na=60\times10^{-6}$ cgs emu. Thus, the binuclear structure as illustrated in Fig. 1 is assigned to the chloro complex. On the other hand, the χ_A-T curve of the bromo complex cannot be interpreted by the Bleaney-Bowers equation,[23] but the χ_A^{-1}-T plots make a straight line in the range 110—300 K, giving a large Weiss constant -100 K (*cf.* Fig. 3). Such a magnetic behavior just corresponds to that of the group C-a according to the classification of Nishida and Kida.[7]

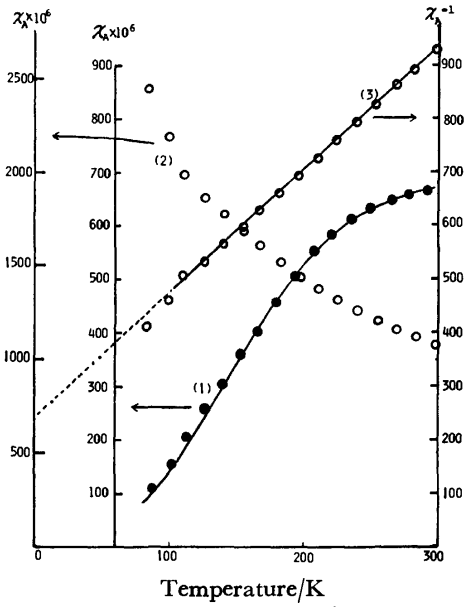

Fig. 3. Temperature dependence of magnetic susceptibilities, χ_A(cgs emu). (1) $CuCl_2$(mdpl)OH; The second left side scale. The solid line is the theoretical curve based on the Bleaney-Bowers equation[23] with the parameters, $2J=-375$ cm^{-1}, $g=2.1$, and $Na=60\times10^{-6}$ cgs emu. (2) $CuBr_2$(mdpl)OH: The first left side scale. (3) $CuBr_2$(mdpl)OH: The right side scale (χ^{-1}—T plots).

1 : 1 Nickel(II) Complex with dpl. $Ni_2(dpl)_2(Bph_4)_2 \cdot 2CH_3OH$: The magnetic susceptibility of this compound is very low ($\chi_A=223\times10^{-6}$ cgs emu at 294 K) and nearly constant in the range 80—300 K (234×10^{-6} cgs emu at 80 K). This indicates that the compound is a spin-paired planar complex similar to the structure of Fig. 1-a, and the observed paramagnetism is due to the second-order Zeeman term.

The absorption spectrum in methanol is shown in Fig. 2. In the ultraviolet and visible region a single absorption band is observed at 19.8×10^3 cm^{-1} ($\varepsilon=46$), which is undoubtedly attributed to the d-d transitions. Such a spectral feature is consistent with the planar coordination of nickel(II) with an N_2O_2 donor set. The band at 28.9×10^3 cm^{-1} ($\varepsilon=160$), however, is not likely to be of a d-d origin, though the intensity is a reasonable one for a d-d band. Because, the red nickel(II) complex with a planar N_2O_2 donor set, such as bis(*N*,*N*-dimethylethylenediamine *N*-oxide)nickel(II) perchlorate, has only a single broad absorption band at 19.34×10^3 cm^{-1} in the region of wavenumber lower than 30×10^3 cm^{-1};[25] furthermore, no d-d band has ever been reported for planar nickel(II) complexes in the region of wavenumber higher than 23×10^3 cm^{-1}.[26] Therefore, this band is attributable to the charge transfer transition from the bridging oxygen to nickel, similarly to the bands at 28.6×10^3 cm^{-1} observed for $[Cu_2(dpl)_2]^{2+}$.

It is to be noted that a stable alkoxo-oxygen bridged planar nickel(II) complex has been first reported and characterized in this study, and it shows a band in the near-ultraviolet region whose origin seems to be similar to that of the bands characteristic of alkoxo-oxygen bridged copper(II) complexes.

No trials have been so far succesful to isolate pure crystals of the complexes other than tetraphenylborate.

References

1) E. Uhlig and H. Schon, *Z. Anorg. Allg. Chem.*, **316**, 25 (1962).
2) E. Uhlig and K. Staiger, *Z. Anorg. Allg. Chem.*, **346**, 21 (1966).
3) Y. Ishimura, Y. Nonaka, Y. Nishida and S. Kida, *Bull. Chem. Soc. Jpn.*, **46**, 3728 (1973).
4) S. Kida, Y. Nishida and M. Sakamoto, *Bull. Chem. Soc. Jpn.*, **46**, 2428 (1973).
5) Y. Nishida and S. Kida, *Chem. Lett.*, **1974**, 339.
6) Y. Nishida, F. Numata, and S. Kida, *Inorg. Chim. Acta*, **11**, 189 (1974).
7) Y. Nishida and S. Kida, *J. Inorg. Nucl. Chem.*, **38**, 451 (1976).
8) R. Mergehenn and W. Haase, *Z. Naturforsch., Teil B*, **30**, 155 (1975).
9) N. Matsumoto, Y. Nishida, S. Kida, and I. Ueda, *Bull. Chem. Soc. Jpn.*, **49**, 177 (1976).
10) N. Matsumoto, Y. Nishida, I. Ueda, and S. Kida, *Bull. Chem. Soc. Jpn.*, **49**, 1308 (1976).
11) E. D. Este and D. J. Hodgson, *Inorg. Chem.*, **14**, 334 (1975).
12) W. Haase, *Chem. Ber.*, **106**, 3132 (1973).
13) R. Mergehenn, W. Haase, and R. Allmann, *Acta Crystallogr., Sect. B*, **31**, 1847 (1975).
14) N. Matsumoto, S. Kida, and I. Ueda, *J. Coord. Chem.*,

9, 133 (1979).
15) R. Mergehenn, L. Merz, and W. Haase, *J. Chem. Soc., Dalton Trans.*, **1980**, 1703.
16) L. Merz and W. Haase, *J. Chem. Soc., Dalton Trans.*, **1980**, 875.
17) H. Taniyama and B. Yasui, *Yakugaku Zasshi*, **81**, 1497 (1961).
18) G. R. Owen and C. B. Reese, *J. Chem. Soc., C*, **1970**, 2401.
19) J. H. Biel, U. S. Patent 2937185; *Chem. Abstr.*, **54**, 18362 (1960).
20) N. Whittaker, *J. Chem. Soc.*, **1969**, 85.
21) N. F. Curtis, *J. Chem. Soc.*, **1961**, 3147.
22) P. W. Selwood, "Magnetochemistry," Interscience, New York (1956).
23) B. Bleaney and K. D. Bowers, *Proc. R. Soc. London, Ser. A*, **214**, 451 (1952).
24) Y. Nishida and S. Kida, *Mem. Fac. Sci. Kyushu Univ., Ser. C*, **13**(**1**), 35 (1981).
25) S. Kida and T. Oniki, *Bull. Chem. Soc. Jpn.*, **45**, 1078 (1972).
26) Y. Nishida and S. Kida, *Coord. Chem. Rev.*, **27**, 275 (1979).

The Enhancement of Formose Formation with 2-Hydroxyacetophenone. A Mechanism Involving Aldol and Retro-aldol Reactions

Tomoya SAKAI,* Masahiko ISHIZAKI, and Masafumi GOTO

Department of Chemical Reaction Engineering, Faculty of Pharmaceutical Sciences, Nagoya City University, Tanabe-dori, Mizuho-ku, Nagoya 467

(Received March 12, 1981)

The rapid aldol addition of formaldehyde to 2-hydroxyacetophenone (HAP), an efficient accelerator for formose formation, took place to yield addition products of HAP with one and two molecules of formaldehyde at 35 °C in an aqueous 40% methanol mixture of formaldehyde, HAP, and $Ca(OH)_2$. No further addition product with more than two molecules of formaldehyde attached to HAP was detected throughout the reaction. On the contrary, benzaldehyde and benzoic acid were formed, accompanied by formose sugars. The initial molar amount of HAP corresponded to the sum of the compounds substituted with the phenyl group including benzaldehyde and benzoic acid. The retro-aldol reaction of the HAP derivatives is likely to be involved in the overall reaction to yield glycolaldehyde or trioses, which are good accelerators for formose formation.

Formose formation in an aqueous mixture of formaldehyde(C_{1A}) and $Ca(OH)_2$ at 50—60 °C reveals an autocatalytic feature: an S-shaped profile of the C_{1A} conversion *vs.* the reaction time. This characteristic feature arises from the slow dimerization of C_{1A} to form glycolaldehyde(C_{2A}) and a successive rapid aldol addition of C_{1A} to C_{2A}.

It is well known[1] that the introduction of compounds which have the structure of R–CO–CH_2OH or R–CH(OH)–CHO to the above reaction mixture enhances the formose formation by shortening the induction period and accelerating the successive consumption of C_{1A}. The initial step has been reported to be the addition of C_{1A} to the accelerator.[2] The order of efficiencies of accelerators has been evaluated by Langenbeck as follows : 2-hydroxyacetophenone (HAP)>2-hydroxy-2′-acetonaphthone> 1-hydroxy-2-propanone> 1,3-dihydroxyacetone (C_{3K}) > C_{2A} > 5-hydroxyacetylacenaphthene>D-fructose>D-glucose.[3] HAP is a unique accelerator because of its high efficiency and its structure containing a phenyl group. HAP seems to be a good candidate for analyzing the action of the accelerators because it is easy, with the accelerator, to distinguish the addition products of C_{1A} from the usual formose sugars by tracing the phenyl group among the products.

In this paper we describe the identification of addition products of C_{1A} with HAP and the change in the amounts of the products originated from HAP with the reaction time. No product with more than two molecules of C_{1A} attached to HAP was detected. On the contrary, degraded products, such as benzaldehyde and benzoic acid, were formed, accompanied by low-molecular-weight formose sugars. These observations suggest that the C–C bond dissociation of HAP derivatives through retro-aldol reaction is essential for the acceleration.

Experimental

Materials. The reagents, formaldehyde (C_{1A}), 1,3-dihydroxyacetone (C_{3K}), HAP, and $Ca(OH)_2$, were the same as those described previously.[4] Guaranteed-grade NaOH, $CaCl_2$, $NaBH_4$, $Si(CH_3)_3Cl$, D-fructose, and hexamethyldisilazane were used as received from Wako. The pyridine (Wako) was dried with molecular sieve 4A.

The 2,3-dihydroxypropiophenone (DHPP) was prepared according to the method of Cahnmann;[5] mp 78 °C (lit, 81.5 °C; softening point 78 °C).[5]

Formose-formation Procedure. The reaction was conducted following the "normal procedure" described previously.[4] An aliquot of the reaction mixture was periodically withdrawn from the flask and was neutralized with a dilute hydrochloric acid to quench the reaction.

Product Analyses. The C_{1A} and formic acid were determined by the use of a high-performance liquid (HPL) chromatograph, as has been described previously.[4] The benzoic acid and benzaldehyde were analyzed with an Ohkura 701 gas liquid chromatograph (GLC) equipped with a FID detector and a Silicone Grease (SE-30) column at 130 °C. Biphenyl was used as the internal standard. The other products were determined as trimethylsilyl derivatives after the reduction of the reaction mixture with $NaBH_4$[6] using the same GLC by increasing the temperature from 100 to 250 °C at the rate of 2 °C min^{-1}. Phenethyl alcohol was added as an internal standard prior to the trimethylsilylation. Several peaks detected in the GL chromatogram were identified by means of GLC-mass spectrometry employing a Hitachi M-52 mass spectrometer. The area of the GL chromatogram of each equimolar amount of C_{3K}, DL-glyceraldehyde (C_{3A}), glucose, HAP, and DHPP after the trimethylsilylation was confirmed to be proportional to the molecular weight; accordingly, the amounts of the product appearing in the GL chromatogram were determined on the basis of this proportionality. The amount of C_{2A} might be estimated too low, however, because of a partial loss during the evaporation of the reaction mixture.

The conversion of C_{1A} to formose (%) is defined by means of Eq. 1;

$$C_{1A}\text{ conversion to formose (\%)} = \left(1 - \frac{[C_{1A}]_{remained} - [HCOOH]}{[C_{1A}]_{initial}}\right) \times 100. \quad (1)$$

The recovery of C_{1A} (%) is defined by Eq. 2:

$$\text{Recovery of } C_{1A}(\%) = \{([C_{1A}]_{remained} + [HAPC_1] + 2[HAPC_2] + \sum_{n=2}^{7} n[C_n] - 6[Fru]_{initial} + [HCOOH])/[C_1]_{initial}\} \times 100, \quad (2)$$

where $HAPC_1$ and $HAPC_2$ represent the addition products of one and two molecules of C_{1A} respectively with HAP, where C_n represents the carbohydrates of n carbon atoms, and where Fru represents D-fructose.

Results and Discussion

A typical GL chromatogram of the reaction mixture after reduction and trimethylsilylation is shown in Fig. 1. The four peaks indicated by arrows appeared exclusively in the presence of HAP. The other peaks are those found in the usual $Ca(OH)_2$-catalyzed formose formation. The peaks are resolved for trimethylsilylated sugar alcohols according to the differences in carbon numbers and in either a straight (s) or branched (b) carbon skeleton of sugar alcohols. Therefore, the peaks are denoted as C_{4s} and so on, where C_{4s} represents tetroses with a straight carbon chain.

The four peaks originating from HAP were identified by means of GLC-mass spectrometry. Characteristic mass fragments measured for the peaks indicated as $HAPC_1$, $HAPC_2$(s), and $HAPC_2$(b) in the GLC are tabulated in Table 1. The presence of strong fragments of m/e=103, 205, and 307 has been reported to indicate -CH_2OTMS, -CH(OTMS)-CH_2OTMS, and -C(OTMS)(-$CH_2OTMS)_2$ respectively, where OTMS stands for $OSi(CH_3)_3$.[7] The peak denoted as $HAPC_1$ was identical to the sample derived from DHPP. The characteristic main fragments of m/e=281, 205, 179, and 103 are in accordance with the bond scissions shown below, as well as the fragment of m/e=295 (M−OTMS).

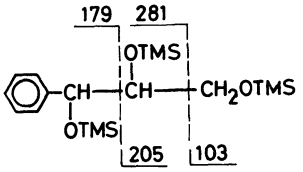

The peaks denoted as $HAPC_2$(s) and $HAPC_2$(b) showed a mass fragment of m/e=383(M−CH_2OTMS). The former has mass fragments of 281 and 205, similar to those of the $HAPC_1$ peak. On the contrary, the latter is characterized by the main fragments of 307 and 179, together with a strong fragment of 218(307−OTMS). These fragmentations are in accordance with the respective bond scissions of the straight and branched structures, as is shown below:

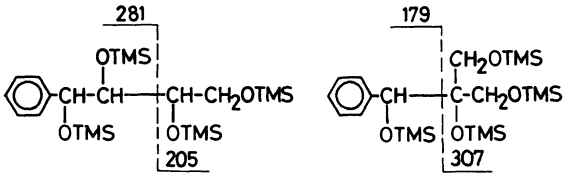

$HAPC_2$(s) Peak $HAPC_2$(b) Peak

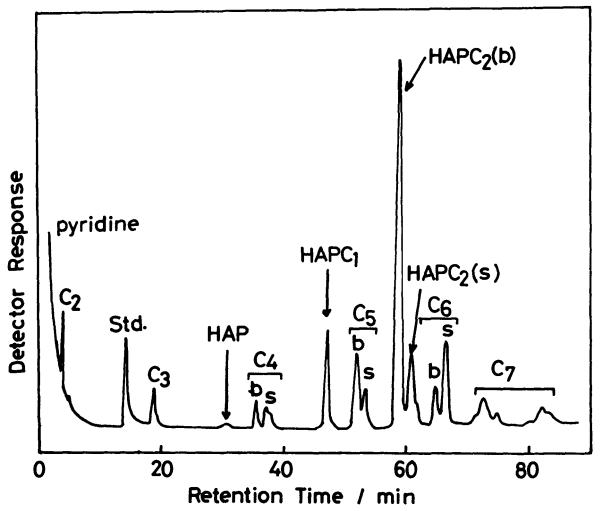

Fig. 1. A typical GL chromatogram of the products at the reaction time of 10 min after reduction with $NaBH_4$ and trimethylsilylation. 35 °C, 40 vol % CH_3OH–H_2O, $Ca(OH)_2$; 0.10 mmol cm^{-3}, C_{1A}; 1.0 mmol cm^{-3}, HAP; 0.20 mmol cm^{-3}.

Table 1. Mass fragments of reduced and trimethylsilylated DHPP, $HAPC_1$, $HAPC_2$(s), and $HAPC_2$(b)

Mass fragment in m/e					
$HAPC_1$, DHPP		$HAPC_2$(s)		$HAPC_2$(b)	
—		383	(w)	383	(w)
—		382	(w)	382	(w)
—		308	(w)	308	(w)
—		—		307	(st)
295	(st)	295	(w)	—	
281	(m)	281	(st)	—	
—		—		280	(m)
—		—		218	(st)
205	(st)	205	(m)	—	
—		—		204	(m)
179	(st)	179	(m)	179	(st)
149	(m)	149	(m)	149	(m)
116	(m)	116	(m)	—	
—		—		115	(m)
103	(m)	103	(w)	103	(st)
90	(w)	90	(m)	—	
73	(m)	73	(m)	73	(m)

st: Strong, m: medium, w: weak.

These characteristic fragmentations lead to the identifications of the $HAPC_2$(b) peak and $HAPC_2$(s) peak with tetrakis-*O*-trimethylsilyl-1-phenylerythritol and tetrakis-*O*-trimethylsilyl-1-phenyl-2-(hydroxymethyl)glycerol respectively. These results show that the addition products of C_{1A} with HAP belong to three classes of compounds which give 1-phenylglycerol, 2-(1-hydroxybenzyl)glycerol, and 1-phenyl-erythritol by reduction with $NaBH_4$. $HAPC_1$, $HAPC_2$(s), and $HAPC_2$(b) are, therefore, mixtures of phenyl-substituted sugars with the straight or branched carbon skeleton mentioned above.

The absence of compounds having a branched carbon skeleton for $HAPC_1$ in the product is worth notice.

The change in the amounts of HAP and its derivatives during the reaction is shown in Fig. 2. The rapid formation of $HAPC_1$ is the initial step of the reaction, followed by the formation of $HAPC_2$(b), presumably through a successive addition of C_{1A} to $HAPC_1$. Both $HAPC_1$ and $HAPC_2$(b) reach their maxima within

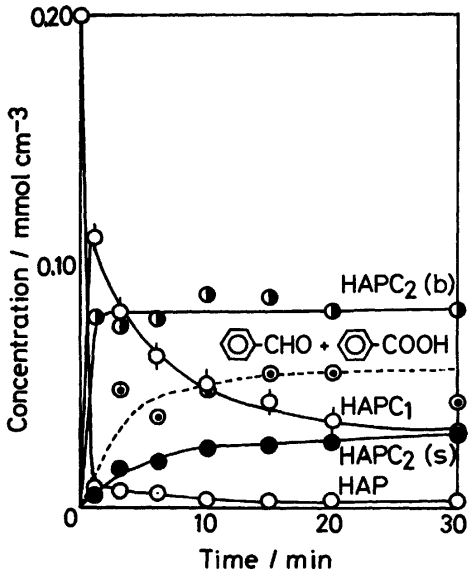

Fig. 2. Consumption of HAP and formations of $HAPC_1$, $HAPC_2$ (b), and $HAPC_2$ (s), and benzaldehyde+ benzoic acid. 35 °C, 40 vol % CH_3OH–H_2O, $Ca(OH)_2$; 0.10 mmol cm^{-3}, C_{1A}; 2.45 mmol cm^{-3}, HAP; 0.20 mmol cm^{-3}.

1 min after the addition of HAP to the mixture of $Ca(OH)_2$ and C_{1A}. The amount of $HAPC_1$ gradually decreases thereafter, but that of $HAPC_2$(b) is kept at *ca.* 0.8 mmol cm^{-3}. The formation of $HAPC_2$(s) appears to be slow, but its amount continues to increase as the reaction proceeds. As $HAPC_1$ decreases and $HAPC_2$(s) increases, benzaldehyde, benzoic acid, and low-molecular-weight formose sugars are formed in the reaction mixture. The summation over the molar amounts of HAP, $HAPC_1$, $HAPC_2$(s), $HAPC_2$(b), benzaldehyde, and benzoic acid was in agreement with the molar amount of HAP initially introduced.

The above observations suggest successive C_{1A} additions to HAP to form phenyl-substituted carbohydrates. However, no HAP derivative with more than two molecules of C_{1A} added to HAP was detected throughout the reaction. The occurrence of benzaldehyde and benzoic acid, accompanied by the simultaneous production of low-molecular-weight formose sugars, suggests the important role of the retro-aldol reaction of the phenyl-substituted carbohydrates. Benzaldehyde is expected to change to benzoic acid under the present reaction conditions, as will be discussed later.

A reaction scheme is drawn in Fig. 3 based on the aldol addition, retro-aldol reaction, and Lobry de Bruyn-Alberda van Ekenstein (LA) transformation, to which HAP and its derivatives are susceptible under basic conditions. In this scheme, $HAPC_1$ corresponds to either DHPP, **2**, and/or **3** : $HAPC_2$(s) corresponds to either **5**, **6**, **7**, and/or **8**, and $HAPC_2$(b) corresponds to either **4** and/or **9**.

HAP can undergo LA transformation, yielding 2-phenylglycolaldehyde (**1**) as has been reported previously,[4] and can undergo aldol addition, yielding DHPP. The results of GLC-mass spectrometry exclude the aldol addition of C_{1A} to **1** to form products possessing a

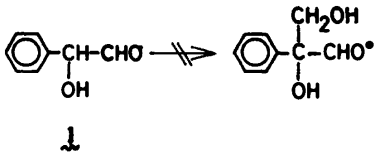

(3)

1

branched carbon skeleton, as is shown above. $HAPC_1$ and DHPP coincided exactly in the results of GLC and mass fragmentation data on reduction and trimethylsilylation. DHPP will isomerize to two isomers, 1-phenyl-1,3-dihydroxyacetone (**2**) and 3-phenylglyceraldehyde (**3**), through LA transformation and will undergo aldol addition with C_{1A} to yield 2-benzoylglycerol (**4**). The last compound can not add further C_{1A} because no hydrogen is available at the α-carbon atom to the carbonyl group. The retro-aldol reaction of DHPP can not be disregarded because a small amount of HAP remained throughout the reaction, as is shown in Fig. 2.

One of the tautomers of DHPP, **2**, which does not undergo retro-aldol reaction, adds C_{1A}, leading to 1-phenyl-2-ketotetrose (**6**). The product, **6**, can isomerize to three isomers; 1-benzoylglycerol (**5**), 4-phenyl-2-ketotetrose (**7**), and 4-phenylaldotetrose (**8**) and can undergo the retro-aldol reaction to yield C_{1A} and **2**. Compounds **5**, **7**, and **8** can degrade to C_{2A} and HAP, C_{3K} and benzaldehyde, C_{2A} and **1**, respectively, through retro-aldol reactions. The aldol addition of C_{1A} at the carbon atom adjacent to a phenyl group can be excluded in line with the fact that Eq. 3 scarcely proceeds.

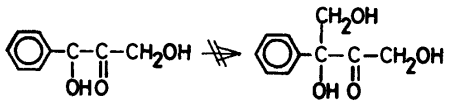

(4)

2

The last tautomer of DHPP, **3**, decomposes to yield C_{2A} and benzaldehyde through retro-aldol reaction and undergoes aldol addition with C_{1A}, yielding a product, **9**, which can not be distinguished from **4** on reduction and trimethylsilylation. Compounds **9** decomposes to C_{3A} and benzaldehyde through the retro-aldol reaction.

The rapid formation of $HAPC_1$ and $HAPC_2$(b) suggests that the entities of $HAPC_1$ and $HAPC_2$(b) in the early stage of the reaction (less than 1 min) are DHPP and 2-benzoylglycerol (**4**) respectively. The aldol addition of C_{1A} to the carbon atom next to the carbonyl group seems to proceed quickly. The compound, **4**, is a terminal product in respect to the aldol addition, and its amount can be equilibrated by means of a retro-aldol reaction. The slow decrease in [$HAPC_1$] is accounted for by the loss of the tautomers of DHPP, **2** and **3**, due to the aldol additions and the retro-aldol reaction.

It is uncertain at present which is the main path for the production of benzaldehyde among retro-aldol reactions of **3**, **7**, and **9**. Benzaldehyde will be oxidized to benzoic acid under the present reaction conditions. The ratio of [benzaldehyde] to [benzoic acid] decreased from 1 : 9 in the early stage to 0.5 : 9.5 in the later stage. The absence of benzyl alcohol indicates that

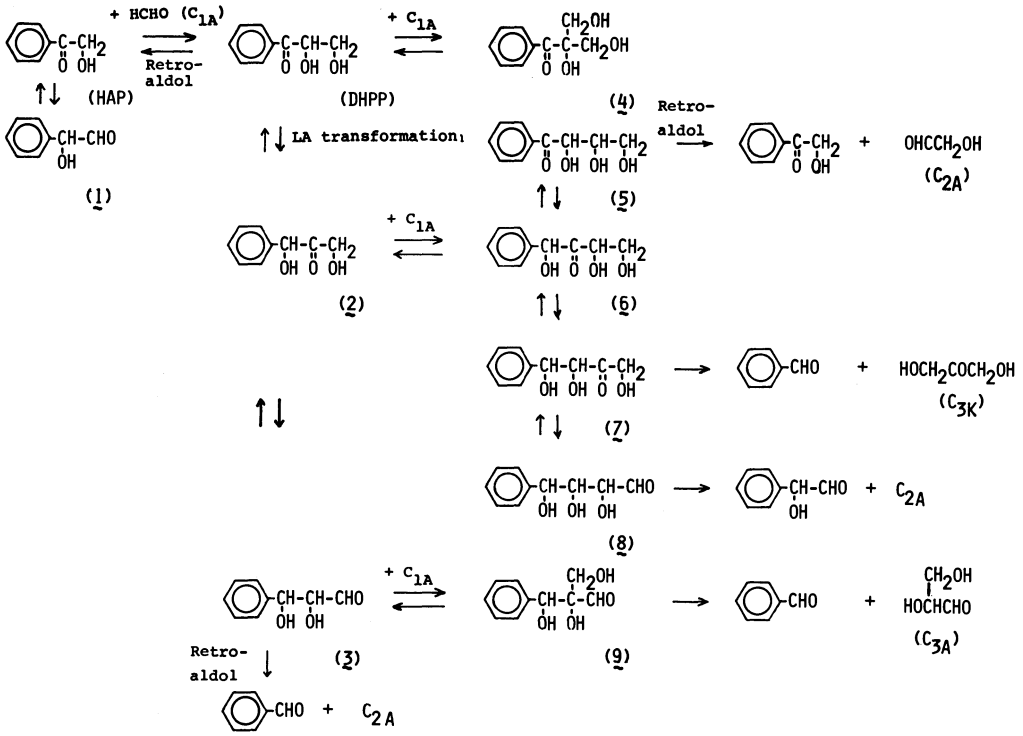

Fig. 3. A reaction scheme based on aldol addition, retro-aldol reaction and LA transformation.

benzoic acid is produced from benzaldehyde through cross-Cannizzaro reaction with aldoses and ketoses, as well as with C_{1A}.

The C_{1A} conversion to formose is plotted in Fig. 4 against the time in order to compare the reaction accelerated by HAP with that by C_{3K}, both in equimolar amounts. The initial rate in the presence of HAP exceeds that of C_{3K}, but the rate after *ca.* 1.5 min for the former is comparable to the initial rate for the latter. The amounts of C_{1A} consumed are 0.64 and 1.23 mmol cm^{-3} at 1 and 3 min respectively for an HAP-accelerated reaction, while the amounts of C_{1A} added to HAP are estimated to be 0.28 and 0.26 mmol cm^{-3} at 1 and 3 min respectively (Fig. 2). The remaining amounts of C_{1A}, 0.36 and 0.97 mmol cm^{-3} at 1 and 3 min respectively should have been converted to formose sugars which do not contain the phenyl group.

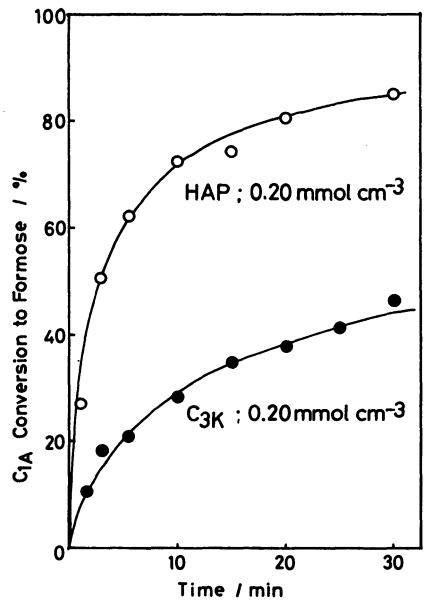

Fig. 4. Profiles of C_{1A} conversion to formose with HAP and C_{3K} as accelerators. 35 °C, 40 vol% CH_3OH–H_2O, $Ca(OH)_2$; 0.10 mmol cm^{-3}, C_{1A}; 2.45 mmol cm^{-3}, HAP or C_{3K}; 0.20 mmol cm^{-3}.

The sum of the amounts of benzaldehyde and benzoic acid in Fig. 4 is smaller than the amounts of glyceraldehyde and trioses estimated from the amount of C_{1A} converted to formose at 1 and 3 min. On the other hand, the dimerization of these low-molecular-weight sugars is expected to proceed more slowly than the C_{1A} addition to these sugars due to a high concentration of C_{1A} in the reaction mixture. Therefore, the efficient catalytic cycle of HAP *via* an intermediate, **5** or **8** (Fig. 3), can not be discarded at present.

The large initial consumption rate of C_{1A} in the presence of HAP is caused by the rapid aldol addition of C_{1A} to HAP; *i.e.*, HAP acts as a substrate. However the C_{1A} addition products of HAP are susceptible to a retro-aldol reaction to yield C_2 and C_3 compounds, which are accelerators in themselves for formose formation. The results shown above indicate that the high efficiency of HAP is a consequence of the pronounced production of glycolaldehyde, C_{3A}, and C_{3K}.

The efficiency of D-fructose in formose formation is lower than that of HAP.[3] The product distributions for the reaction accelerated by HAP and D-fructose are expected to be different in the production of lower carbohydrates. The product distributions for the HAP-accelerated reaction are illustrated in Fig. 5, while

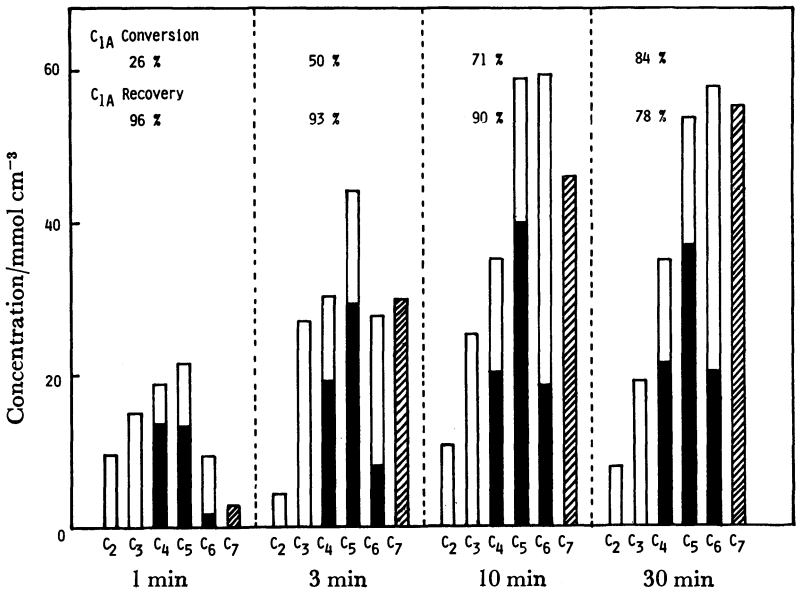

Fig. 5. C-number distributions in amounts of formose sugars and sugar alcohols obtained in the reaction accelerated by HAP. Reaction conditions; same as indicated in Fig. 2. C_n represents formose sugars and sugar alcohols having n carbon atoms. ■ or □ denotes branched chain or straight chain carbon skeleton, respectively.

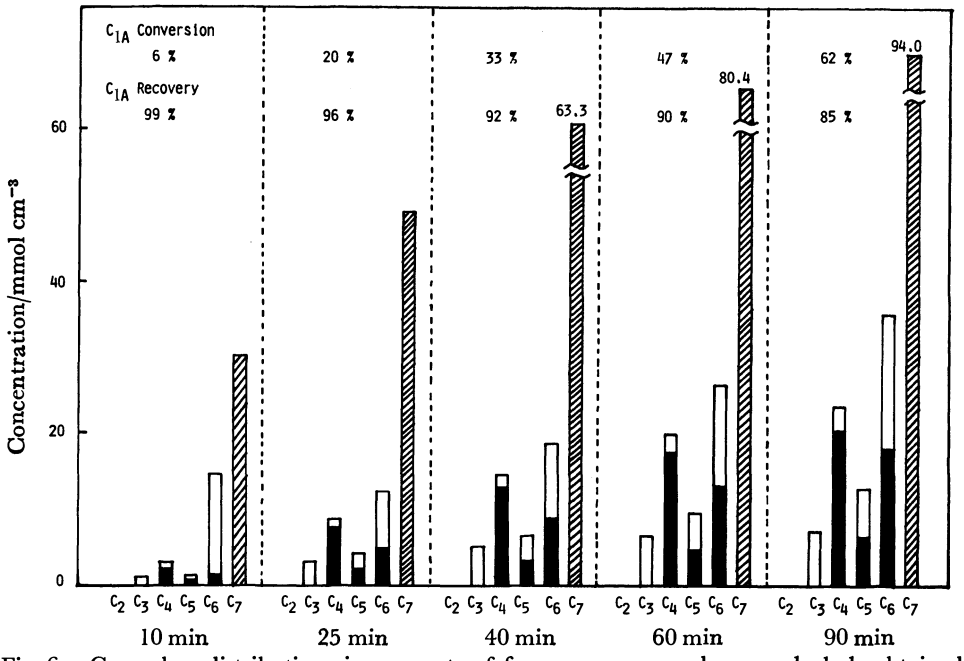

Fig. 6. C-number distributions in amounts of formose sugars and sugar alcohols obtained in the reaction accelerated by D-fructose. 45 °C, water, NaOH; 0.20 mol cm^{-3}, $CaCl_2$; 0.10 mmol cm^{-3}, C_{1A}; 2.0 mmol cm^{-3}, D-fructose; 0.05 mmol cm^{-3}.

analogous distributions for the fructose-accelerated reaction are illustrated in Fig. 6. These are determined from the GL chromatograms; therefore, the amount of C_{2A} is likely to have been evaluated too low as a result of evaporation loss during pretreatment. The amounts of C_2 and C_3 carbohydrates for the HAP-accelerated reaction are larger than those for the fructose-accelerated reaction. Moreover, the predominant carbohydrates for the fructose-accelerated reaction are aldo- and keto-heptuloses, which were presumably produced by the aldol addition of C_{1A} to D-fructose. The low efficiency of D-fructose is attributable to the low reactivity of D-fructose and/or heptuloses toward retro-aldol reactions.

References

1) T. Mizuno and A. H. Weiss, *Adv. Carbohydr. Chem. Biochem.*, **29**, 173 (1974).
2) H. Ruckert, E. Pfeil, and G. Scharf, *Chem. Ber.*, **98**, 2558 (1965).
3) W. Langenbeck, *Angew. Chem.*, **61**, 186 (1949).
4) T. Sakai, M. Ishizaki, K. Kobayashi, and M. Goto, *Bull. Chem. Soc. Jpn.*, **54**, 2083 (1981).
5) H. Cahnmann, *Bull. Soc. Chim. Fr., Ser. 5*, **4**, 226 (1937); *Chem. Abstr.*, **31**, 3893 (1937).
6) C. C. Sweely, R. Bentley, M. Makita, and W. W. Wells, *J. Am. Chem. Soc.*, **85**, 2497 (1963).
7) R. D. Partridge, A. H. Weiss, and D. Todd, *Carbohydr. Res.*, **24**, 29 (1972).

Synthesis of Dihydrobenzofuran Derivatives from Substituted *p*-Benzoquinones

Tadashi KOZUKA

Department of Chemistry, Faculty of Science, Kyoto University, Sakyo-ku, Kyoto 606

(Received October 30, 1981)

A series of *p*-benzoquinones having an ester functional group in the α position of alkyl side chains was prepared. Irradiation of these quinones, except for methyl 3-methyl-2-(4-methyl-3,6-dioxo-1,4-cyclohexadienyl)-butyrate (**3e**), rapidly gave methyl 3-substituted 2,3-dihydro-5-hydroxybenzofuran-2-carboxylate in fairly good yields, and it was found that rearrangement of the side chain occurred concomitantly. Photolysis of quinone **3e** afforded methyl 2-(2,5-dihydroxy-4-methylphenyl)-3-methyl-3-butenoate as the major product. An intermediate was postulated to account for the isolated photoproduct.

2,3-Dihydrobenzofurans are of interest as a potential synthetic intermediate of a variety of medicinally important natural products[1] in addition to their own pharmacological activity.

In this report, syntheses of a variety of methyl 2,3-dihydro-5-hydroxybenzofuran-2-carboxylate derivatives by way of photochemical reactions are described. One of the possible approaches to the synthesis of this system is photocyclization of substituted *p*-quinones.[2,3] The present author has developed a simple general route to the dihydrobenzofuran derivatives starting from alkyl substituted *p*-benzoquinones. The alkyl group has a methoxycarbonyl grouping in its α position.[4] It is anticipated that the β-hydrogen atom of the alkyl side chain will occupy a favorable position for the γ-hydrogen abstraction by a photoexcited quinonoid carbonyl group, because of the dipole-dipole repulsion between quinonoid carbonyl and methoxycarbonyl groups. The most interesting aspect of the present results is that the photochemical reaction of these quinones occurs with rearrangement to give methyl 3-substituted, 2,3-dihydro-5-hydroxybenzofuran-2-carboxylates.

Results and Discussion

Preparation of Quinones. All quinones **3a**—**n** were prepared in excellent yields by the synthetic route shown in Scheme 1. That is, oxythallation of the ketone **1** with thallium(III) nitrate (TTN)[5] and trimethyl orthoformate (TMOF) in methanol followed by oxidation of the ester **2** with ceric ammonium nitrate (CAN)[6a] in 70% aqueous acetonitrile to give the quinone **3**.

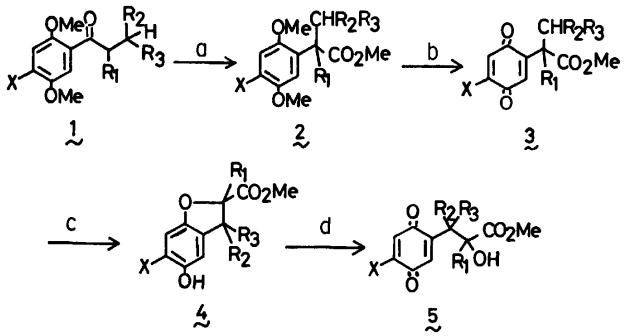

(a) $Tl(NO_3)_3 \cdot 3H_2O$, $CH(OCH_3)_3$, MeOH; (b) CAN/aq CH_3CN; (c) hν, benzene; (d) CAN/aq CH_3CN
R_1=H, Me
R_2=H, Me, Et, *n*-Pr, CO_2Me, $(CH_2)_2CO_2Me$, $(CH_2)_3$-NPht,* $(CH_2)_3NHCOCF_3$, $CH_2OCO_2C_6H_5$
R_3=H, Me
X=H, Me, Br, OMe
* NPht=phthalimido

Scheme 1.

Irradiation of Quinones. On irradiation of a solution of the quinone **3** (2 mmol) in dry benzene with a high pressure Hg lamp (300 W) after bubbling nitrogen, the quinone solution rapidly turned from yellow to colorless. The photochemical reaction was complete within several hours (0.5—5 h) at 0—10 °C and gave methyl 3-substituted 2,3-dihydro-5-hydroxybenzofuran-2-carboxylate **4** in relatively good yields after purification by column chromatography. The results of photolyses of the quinones **3a**—**n** are summarized in Table 1.

The structures of the irradiation products **4a**—**n** were established by their IR, ^1H NMR data, and chemical reactions. In particular, the structure of **4a** was confirmed as follows. The ^1H NMR spectrum of **4a** consisted of a characteristic AB pattern due to geminal protons at C-3 (J_{AB}=15 Hz),[7] indicating the presence of a C-2 methoxycarbonyl-substituted 2,3-dihydrobenzofuran ring (C-2 methoxycarbonyl, IR: 1740 cm^{-1}, CO). Such an ABX pattern of C-2 substituted 2,3-dihydrobenzofuran was similar to that of ethyl 2,3-

Table 1. Formation of photorearranged dihydrobenzofuran **4** from quinone **3**

Quinone	X	R_1	R_2	R_3	Product	Yield/%[a]
3a	Me	H	H	H	**4a**	41
3b	Me	H	Me	H	**4b**	65
3c	Me	Me	H	H	**4c**	45
3d	Me	H	Et	H	**4d**	68
3e	Me	H	Me	Me	**4e**[b]	40
3f	Me	H	*n*-Pr	H	**4f**	60
3g	Me	H	CO_2Me	H	**4g**	56
3h	Me	H	$(CH_2)_2CO_2Me$	H	**4h**	51
3i	Me	H	$(CH_2)_3NPht$	H	**4i**	75
3j	Me	H	$(CH_2)_3NHCOCF_3$	H	**4j**	69
3k	Me	H	$CH_2OCO_2C_6H_5$	H	**4k**	39
3l	H	H	Me	H	**4l**	60
3m	Br	H	Me	H	**4m**	31
3n	OMe	H	Me	H	**4n**	42

a) Reported yield are for isolated, purified products. b) No dihydrobenzofuran deriv was isolated. Product was methyl 2-(2,5-dihydroxy-4-methylphenyl)-3-methyl-3-butenoate.

dihydro-5-hydroxybenzofuran-2-carboxylate.[8]

For the photoproduct **4c**, the ^{1}H NMR spectrum showed a coupling (J_{AB}=15 Hz),[7] which suggested that the substitution pattern was similar to that of **4a**. Furthermore, the structures of **4a** and **4c** were also supported by oxidation with ceric ammonium nitrate[6b] to the corresponding quinones **5a** and **5c**. ^{1}H NMR spectra of **5a** and **5c** showed the presence of methylene protons directly attaching to the quinone ring. The methylene protons were long-range coupled with the quinone ring proton (J=1.2 Hz).[9]

The photoproduct **4g** was compatible with the structure of dimethyl 2,3-dihydro-5-hydroxy-6-methylbenzofuran-2,3-dicarboxylate on the basis of the spectral data outlined below. Its IR spectrum showed three characteristic bands at 3340 (phenolic OH), 1735 (ester CO), and 1695 cm^{-1} (ester CO). Its ^{1}H NMR spectrum showed two doublets at δ 4.41 (J=6 Hz) and δ 5.56 (J=6 Hz) due to the protons C_3–H and C_2–H, respectively, and a broad singlet at δ 5.32 due to the phenolic hydroxyl proton.

Irradiation of the quinones **3b**, **3d**, **3f**, **3l**, **3m**, and **3n** afforded predominantly the corresponding dihydrobenzofurans **4b**, **4d**, **4f**, **4l**, **4m**, and **4n**, respectively, and a small amount of isomers. The major photoproducts in the reactions wer eisolated by chromatoggraphy and/or fractional crystallization. The minor products were detected by ^{1}H NMR and GC, but not isolated. The ^{1}H NMR spectra of the above six major products showed similar chemical shifts and coupling constants for the proton signals at C-3 and C-2 on the dihydrobenzofuran ring as shown in Table 2. The regiochemistry for the substituents around C-2 and C-3 of these photoproducts cannot be determined directly by comparison with the chemical shifts of C-2 and C-3 protons of other products, *i.e.*, **4a**, **4c**, and **4g** as was already described. In general, chemical shifts of C-2 and C-3 protons on 2,3-disubstituted 2,3-dihydrobenzofurans are variable according to the substituent groups and stereospecific environment.[10] Therefore, **4b**, **4d**, and **4f** were converted by oxidation with CAN to quinones **5b**, **5d**, and **5f**, respectively. The structures of these three quinones were assigned on the basis of the spectroscopic data. For example, quinone **5f** showed three characteristic bands at 3470 (OH), 1720 (ester CO), and 1650 cm^{-1} (quinone CO) in its IR spectrum. Its ^{1}H NMR spectrum consisted of the signals at δ 1.64 (m, 4H), at δ 2.87 (d, J=7 Hz, 1H), at δ 3.31 (m, 1H), and at δ 4.31 (dd, J=3.5 Hz, and 7 Hz, 1H). On adding D_2O the signal at δ 2.87 disappeared and the double doublets signal at δ 4.31 was simplified to a doublet (J=3.5 Hz). Irradiation of the methylene proton at δ 1.64 changed the signal at δ 3.31 to a sharp doublet (J=3.5 Hz), and the signal at δ 4.31 coupled with the methine proton (δ 3.31) to a triplet (J=7 Hz) and the hydroxyl proton signal at δ 2.87 to a singlet. These results suggested that the quinone **5f** included the partial structure $-CH_2\overset{1}{C}HCH(OH)CO-$ in the side chains. Further support for the structure **5f** was provided by the reduction of the quinone **5f** with sodium dithionite followed by acetylation of the obtained hydroquinone with acetic anhydride–pyridine to the corresponding triacetate **7**. However, the methine proton signal adjacent to the acetoxyl group showed a downfield shift at δ 5.18 (d, J=5 Hz) due to a deshielding effect of the acetoxyl carbonyl. The above results indicated that these original photoproducts **4b**, **4d**, **4f**, **4l**, **4m**, and **4n** contain an ester group at C-2 position and other substituent group (R_2 and R_3) at C-3 position, respectively.

Irradiation of other substituted quinones **3h**, **3i**, **3j**, and **3k** also gave corresponding photocyclization products **4h**, **4i**, **4j**, and **4k**.

The ^{1}H NMR spectrum of photoproduct **4k** showed the presence of a methine proton signal at δ 5.02 (d, J=5.1 Hz), probably at C-2 position. This lower field shift can be explained in terms of the deshielding effect of the carbonate carbonyl group.

The structures of the major and the minor components were correlated with each other by their chemical reactions and by comparing their ^{1}H NMR spectra. Acetylation of crude photoproducts **4b**, **4d**, **4f**, and

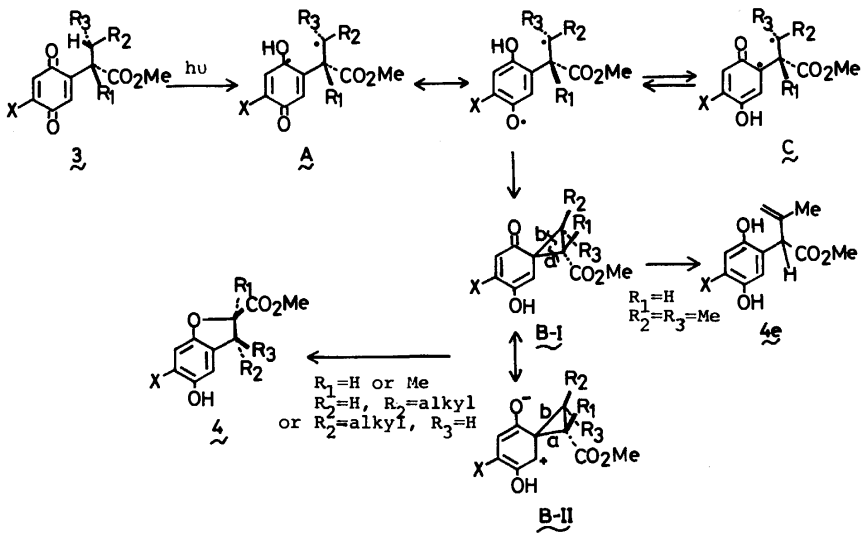

Scheme 2.

TABLE 2. ^{1}H NMR SPECTRA OF DIHYDROBENZOFURANS **4** AND QUINONES **5**

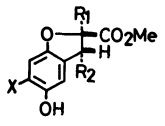
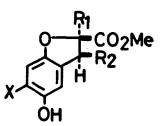
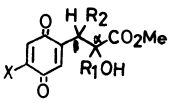

	X	R_1	R_2	Dihydrobenzofuran **4**					Quinone **5**		
				trans-Isomer			*cis*-Isomer				
				C_2–H	C_3–H	R_2=Me	C_2–H	R_2=Me	C_α–H	C_β–H	OH
a	Me	H	H	5.12(dd) J=7 Hz J=10 Hz	3.14 } (m) 3.62 A	—	—	—	4.13(dd) J=5 Hz J=8.5 Hz	D	B
b	Me	H	Me	4.63(d) J=7 Hz	3.40 } (m) 3.68	1.40(d) J=7 Hz	5.15(d) J=9 Hz	1.16(d)	4.30(bm)	3.46(dq) J=4 Hz J=7 Hz	3.00(bs)
c	Me	Me	H	—	3.00(d) J=15 Hz 3.50 J=15 Hz	—	—	—	—	2.70(d) J=13.5 Hz 2.97(d) J=13.5 Hz	3.34(s)
d	Me	H	Et	4.74(d) J=5 Hz	3.42(m)	—	5.14(d) J=8.5 Hz	—	4.36 J=3.5 Hz J=7.6 Hz	3.23(dt) J=3.5 Hz J=7 Hz	2.98(d) J=7.6 Hz
f	Me	H	*n*-Pr	4.76(d) J=5 Hz	3.46(m)	—	5.12(d) J=8.5 Hz	—	4.31(dd) J=3.5 Hz J=7 Hz	3.31(m) J=3.5 Hz J=7 Hz	2.87(d) J=7 Hz
g	Me	H	CO_2Me	5.56(d) J=6 Hz	4.41(d) J=6 Hz	—	C	—	4.86(d) J=4.2 Hz	4.32(d) J=4.2 Hz	3.75(bs)
h	Me	H	$(CH_2)_2CO_2Me$	4.77(d) J=6 Hz	3.44–	—	C	—	4.35(bs)	3.38(m)	3.07(bd) J=8 Hz
i	Me	H	$(CH_2)_3NPht$	4.76(d) J=5 Hz	B	—	C	—			
j	Me	H	$(CH_2)_3NHCOCF_3$	4.71(d) J=5 Hz	B	—	5.15(d) J=9 Hz	—			
k	Me	H	$CH_2OCO_2C_6H_5$	5.02(d) J=5.1 Hz	3.90(m)	—	C	—			
l	H	H	Me	4.64(d) J=7 Hz	3.53(m)	1.38(d) J=7 Hz	5.16(d) J=9 Hz	1.13(d) J=7 Hz			
m	Br	H	Me	4.65(d) J=7 Hz	3.53(m)	1.40(d) J=7 Hz	5.15(d) J=9 Hz	1.16(d) J=7 Hz			
n	OMe	H	Me	4.66(d) J=7 Hz	3.56(m)	1.41(d) J=7 Hz	5.17(d) J=8.5 Hz	1.15(d) J=7 Hz			

a) The *cis*-isomer, which was a minor component of the mixture of products, was detectable only by the ^{1}H NMR spectrum. (A) AB type: J=15 Hz, (B) Chemical shifts were not determined because of overlapping of the signal with those of other protons. (C) Not detected. (D) δ 2.69(dd), J=8.5 and 15 Hz, 1H), δ 2.98 (dd, J=5 and 15 Hz, 1H).

4i containing minor components with acetic anhydride in pyridine solution gave only the single monoacetate **6b**, **6d**, **6f**, and **6i**, respectively. The minor components are therefore presumed to be the stereoisomers of the thermodynamically stable major products. In the ^{1}H NMR spectra, the coupling constants due to C-2 and C-3 protons of 2,3-disubstituted 2,3-dihydrobenzofuran are $J_{cis}>J_{trans}$[11] as predicted by the Karplus equation.[12] The most striking differences between the ^{1}H NMR spectra of the *cis* and *trans* isomers of 2,3-disubstituted 2,3-dihydrobenzofuran, other than the values of $J_{2,3}$ are the different values for the chemical shift of the C-2 proton. The ^{1}H NMR signal of the C-2 proton of the *trans* isomers is located upfield at about δ 0.3 compared to the corresponding proton of the *cis* isomers. The major product **4** (δ 4.63—4.77, J=5—7 Hz) is concluded to be *trans*, and the minor to be *cis* (δ 5.14—5.17, J=8.5—9 Hz) as shown in Table 2.

On the other hand, the photolysis of quinone **3e** did not afford a dihydrobenzofuran derivative, but methyl 2-(2,5-dihydroxy-4-methylphenyl)-3-methyl-3-butenoate **4e** as the major product.

The proposed mechanism of these photochemical reactions is given in Scheme 2. γ-Hydrogen abstraction by photoexcited carbonyl of the quinone **3** forms the biradical intermediate **A**[13] and subsequently yields the spirocyclopropyl ketone **B-1**[3] and/or spirocyclopropyl zwitter-ion intermediate **B-2**;[3] then the cyclopropane

ring opens to afford the observed product **4**. However it is difficult to anticipate a ring-opened zwitter-ion intermediate,[14] because the three-membered ring may cleave to give a positive charge at the α position to the methoxycarbonyl group. From the present results preferential cleavage of bond **a** can be recognized **B-1** to give phenyl migrated products **4** with exception of only one case **3e** (R_2=R_3=Me). In the latter case cleavage of bond **b** may be the preferential course to give **4e**, in which no phenyl migration occurs. Thus, among the alkyl substituted *p*-benzoquinones examined, the trend of phenyl migration initiated by photochemical γ-hydrogen abstraction reaction may be explained in terms of the stability of the radical intermediates involved. The present results indicate the stability of the radical to be

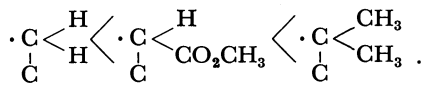

Of course, this trend should be applied under the very limited conditions, for a contribution of a dipolar intermediate, such as **B-2**, could not be excluded in the present reactions.

Experimental

Melting points and boiling points were uncorrected. Bulb to bulb distillations were carried out on a Kugelrohr-type apparatus. IR spectra were measured on a JASCO IRA-1 spectrophotometer. ^{1}H NMR spectra were measured on a JEOL PS-100 instrument with tetramethylsilane as an internal standard and the chemical shifts are reported in δ values. Mass spectra were obtained with a Hitachi M-52 mass spectrometers (20 eV). Elemental analyses were performed by the Kyoto University Microanalytical Laboratories. Column chromatography was performed using Wako reagent grade silica gel (200 mesh). The irradiation was carried out in a Pyrex vessel at 0—10 °C, using an Eikosha 300-W high pressure Hg lamp.

Materials. 3-(Methoxycarbonyl)propionyl chloride[15] and 5-(methoxycarbonyl)pentanoyl chloride[16] were prepared from the corresponding methyl hydrogen succinate and methyl hydrogen adipate, respectively. 6-Phthalimidohexanoyl chloride[17] and 6-(trifluoroacetamido)hexanoyl chloride[18] were prepared from 6-aminohexanoic acid. Other acid chlorides were commercially available.

Preparation of Starting Materials. All of the compounds **1a**—**n**, except for **1k**, were prepared by the Friedel-Crafts acylation according to the previous reported methods.[5a]

Physical Properties of the Starting Materials. 2',5'-Dimethoxy-4'-methylpropiophenone ***1a***: 96%; mp 78 °C,[5a] (lit,[19] mp76—77 °C).

2',5'-Dimethoxy-4'-methylbutyrophenone ***1b***: 96%; bp 129—130 °C at 3 Torr (1 Torr=133.322 Pa); mp 46—46.5 °C (hexane–ether); IR (KBr): 1660 cm^{-1}; ^{1}H NMR ($CDCl_3$) δ: 0.93 (t, 3H), 1.67 (m, 2H), 2.23 (s, 3H), 2.92 (t, 2H), 3.80 (s, 3H), 3.84 (s, 3H), 6.74 (s, 1H), and 7.20 (s, 1H); Found: C, 69.99; H, 8.21%. Calcd for $C_{13}H_{18}O_3$: C, 70.24; H, 8.16%.

2',5'-Dimethoxy-2,4'-dimethylpropiophenone ***1c***: 99%; bp 125—127 °C at 3 Torr; mp 38—39 °C (petroleum ether); IR (neat): 1675 cm^{-1}; ^{1}H NMR ($CDCl_3$) δ: 1.14 (d, 6H), 2.25 (s, 3H), 3.57 (m, 1H), 3.82 (s, 3H), 3.86 (s, 3H), 6.78 (s, 1H), and 7.14 (s, 1H); Found: C, 69.96; H, 8.20%. Calcd for $C_{13}H_{18}O_3$: C, 70.24; H, 8.16%.

2',5'-Dimethoxy-4'-methylvalerophenone ***1d***: 95%; bp 140—143 °C at 3 Torr; mp 33.5—34 °C (petroleum ether); IR (KBr): 1670 cm^{-1}; ^{1}H NMR ($CDCl_3$) δ: 1.92 (t, 3H,) 1.20—1.90 (m, 4H), 2.25 (s, 3H), 2.97 (t, 2H), 3.80 (s, 3H), 3.85 (s, 3H), 6.77 (s, 1H), and 7.21 (s, (1H); Found: C, 71.21; H, 8.75%. Calcd for $C_{14}H_{20}O_3$: C, 71.16; H, 8.53%.

2',5'-Dimethoxy-3,4'-dimethylbutyrophenone ***1e***: 88%; bp 140—143 °C at 3 Torr; mp 48—48.5 °C (petroleum ether); IR (KBr): 1600 cm^{-1}; ^{1}H NMR ($CDCl_3$) δ: 0.97 (d, 6H), 2.08—2.41 (m, 1H), 2.26 (s, 3H), 2.84 (d, 2H), 3.81 (s, 3H), 3.85 (s, 3H), 6.76 (s, 1H), and 7.19 (s, 1H); Found: C, 71.42; H, 8.69%. Calcd for $C_{14}H_{20}O_3$: C, 71.16; H, 8.53%.

2',5'-Dimethoxy-4'-methylhexanophenone ***1f***: 85%; bp 183 °C at 3 Torr; IR (neat): 1665 cm^{-1}; ^{1}H NMR ($CDCl_3$) δ: 0.90 (t, 3H), 1.22—1.82 (m, 6H), 2.26 (s, 3H), 2.98 (t, 2H), 3.84 (s, 3H), 3.88 (s, 3H), 6.81 (s, 1H), and 7.27 (s, 1H); Found: C, 72.25; H, 8.87%. Calcd for $C_{15}H_{22}O_3$: C, 71.97; H, 8.86%.

Methyl 3-(2,5-Dimethoxy-4-methylbenzoyl)propionate ***1g***: 90%; mp 89—90 °C (petroleum ether–dichloromethane); IR (KBr): 1735 and 1660 cm^{-1}; ^{1}H NMR ($CDCl_3$) δ: 2.26 (s, 3H), 2.69 (t, 2H), 3.32 (t, 2H), 3.70 (s, 3H), 3.81 (s, 3H), 3.88 (s, 3H), 6.77 (s, 1H), and 7.30 (s, 1H); Found: C, 63.33; H, 6.86%. Calcd for $C_{14}H_{18}O_3$: C, 63.14; H, 6.81%.

Methyl 5-(2,5-Dimethoxy-4-methylbenzoyl)pentanoate ***1h***: 73%; mp 80—81 °C (petroleum ether–dichloromethane); IR (KBr): 1730 and 1660 cm^{-1}; ^{1}H NMR ($CDCl_3$) δ: 1.64—1.86 (m, 4H), 2.26 (s, 3H), 2.36 (m, 2H), 3.00 (m, 2H), 3.67 (s, 3H), 3.82 (s, 3H), 3.87 (s, 3H), 6.78 (s, 1H), and 7.23 (s, 1H); Found: C, 65.33; H, 7.58%. Calcd for $C_{16}H_{22}O_5$: C, 65.29; H, 7.53%.

2',5'-Dimethoxy-4'-methyl-6-(phthalimido)hexanophenone ***1i***: 71%; mp 156—157 °C (methanol–dichloromethane); IR (KBr): 1775, 1715, and 1660 cm^{-1}; ^{1}H NMR ($CDCl_3$) δ: 1.31—1.87 (m, 6H), 2.25 (s, 3H), 2.97 (t, 2H), 3.69 (t, 2H), 3.81 (s, 3H), 3.86 (s, 3H), 6.75 (s, 1H), 7.21 (s, 1H), and 7.63—7.77 (m, 4H); Found: C, 69.92; H, 6.39, N, 3.54%. Calcd for $C_{23}H_{25}O_5N$: C, 69.85; H, 6.37; N, 3.54%.

2',5'-Dimethoxy-4'-methyl-6-(trifluoroacetamido)hexanophenone ***1j***: 56%; mp 87.5—89 °C (petroleum ether–dichloromethane); IR (KBr): 3300, 1730, and 1640 cm^{-1}; ^{1}H NMR ($CDCl_3$) δ 1.20—1.84 (m, 6H), 2.25 (s, 3H), 3.00 (t, 2H), 3.39(q, 2H), 3.82 (s, 3H), 3.86 (s, 3H), 6.80 (s, 1H), 6.90 (bs, 1H), and 7.24 (s, 1H); Found: C, 56.43; H, 6.12; N, 4.00%. Calcd for $C_{17}H_{22}O_4NF_3$: C, 56.50; H, 6.14; N, 3.88%.

2',5'-Dimethoxy-4'-methyl-4-(phenoxycarbonyloxy)butyrophenone ***1k***: was prepared from **1g** in the following three steps. Reduction of the **1g** with excess lithium aluminum hydride in THF followed by reaction of the obtained 1-(2,5-dimethoxy-4-methylphenyl)-1,4-butanediol (1 mol equiv.) in dichloromethane with phenyl chloroformate (1.2 mol equiv.) in the presence of pyridine at 0 °C afforded 1-(2,5-dimethoxy-4-methylphenyl)-4-(phenoxycarbonyloxy)-1-butanol, which on oxidation with excess Cr–Pyr complex in dichloromethane yield **1k**, total yield: 30%; IR (neat): 1760 and 1660 cm^{-1}; ^{1}H NMR ($CDCl_3$) δ: 2.00—2.36 (m, 2H), 2.21 (s, 3H), 3.12 (t, J=7 Hz, 2H), 3.81 (s, 3H), 3.87 (s, 3H), 4.31 (d, J=6.5 Hz, 2H), 6.78 (s, 1H), and 7.12—7.46 (m, 6H); Found: C, 66.81; H, 6.30%. Calcd for $C_{20}H_{22}O_6$: C, 67.02; H, 6.19%.

2',5'-Dimethoxybutyrophenone ***1l***: 90%; bp 121—123 °C at 3 Torr, (lit,[20] bp 172—175 °C at 25 Torr).

2',4',5'-Trimethoxybutyrophenone ***1n***: 88%; mp 79 °C (petroleum ether–dichloromethane), (lit,[21,22] mp 77 °C, 78.5—80 °C).

The following esters **2a**—**n**, except for **2m**, were prepared according to the reported methods.[5]

Methyl 2-(2,5-Dimethoxy-4-methylphenyl)propionate ***2a***: was

prepared from **1a** with $Tl(NO_3)_3$–TMOF–MeOH as described previously[5a] (90%): bp 162—165 °C at 4 Torr (bulb to bulb).

Methyl 2-(2,5-Dimethoxy-4-methylphenyl)butyrate **2b**: was prepared from **1b** with $Tl(NO_3)_3$–TMOF–MeOH following by the general procedure (96%): bp 150—152 °C at 3 Torr (bulb to bulb); IR (neat): 1735 cm^{-1}; ^1H NMR ($CDCl_3$) δ: 0.87 (t, 3H), 1.56—2.20 (m, 2H), 2.20 (s, 3H), 3.64 (s, 3H), 3.77 (s, 6H), 3.90 (t, 1H), 6.68 (s, 1H), and 6.74 (s, 1H); Found: C, 66.49; H, 8.17%. Calcd for $C_{14}H_{20}O_4$: C, 66.64; H, 7.99%.

Methyl 2-Methyl-2-(2,5-dimethoxy-4-methylphenyl)propionate **2c**: was prepared from **1c** with $Tl(NO_3)_3$–TMOF–MeOH following by the same general procedure (95%): bp 154—156 °C at 4 Torr (bulb to bulb); IR (neat): 1740 cm^{-1}; ^1H NMR ($CDCl_3$) δ: 1.49 (s, 6H), 2.18 (s, 3H), 3.60 (s, 3H), 3.68 (s, 3H), 3.78 (s, 3H), 6.63 (s, 1H), and 6.74 (s, 1H); Found: C, 66.50; H, 8.27%. Calcd for $C_{14}H_{20}O_4$: C, 66.64; H, 7.99%.

Methyl 2-(2,5-Dimethoxy-4-methoxy-4-methylphenyl)pentanoate **2d**: was prepared from **1d** with $Tl(NO_3)_3$–TMOF–MeOH following by the general reaction procedure (98%): bp 158—159 °C at 3 Torr (bulb to bulb); IR (neat): 1730 cm^{-1}; ^1H NMR ($CDCl_3$) δ: 0.90 (t, 3H), 1.09—2.10 (m,4H), 2.19 (s, 3H), 3.63 (s, 3H), 3.77 (s, 3H), 4.00 (t, 1H), 6.67 (s, 1H), and 6.76 (s, 1H); Found: C, 67.79; H, 8.49%. Calcd for $C_{15}H_{22}O_4$: C, 67.64; H, 8.33%.

Methyl 2-(2,5-Dimethoxy-4-methylphenyl)-3-methylbutyrate **2e**: was prepared from **1e** with $Tl(NO_3)_3$–TMOF–MeOH following by the usual manner (81%): bp 133—135 °C at 3 Torr (bulb to bulb); mp 78—79 °C (petroleum ether); IR (KBr): 1735 cm^{-1}; ^1H NMR ($CDCl_3$) δ: 0.71 (d, 3H), 1.03 (d, 3H), 2.00—2.26 (m, 1H), 2.20 (s, 3H), 3.65 (s, 3H), 3.79 (s, 6H), 3.84 (d, 1H), 6.71 (s, 1H), and 6.91 (s, 1H); Found: C, 67.69; H, 8.41%. Calcd for $C_{15}H_{22}O_4$: C, 67.64; H, 8.33%.

Methyl 2-(2,5-Dimethoxy-4-methylphenyl)hexanoate **2f**: was prepared from **1f** with $Tl(NO_3)_3$–TMOF–MeOH following by the general method (90%): bp 135—140 °C at 0.1 Torr (bulb to bulb); IR (neat): 1735 cm^{-1}; ^1H NMR ($CDCl_3$) δ: 0.86 (t, 3H), 1.00—2.19 (m, 6H), 2.19 (s, 3H), 3.64 (s, 3H), 3.78 (s, 6H), 3.98 (t, 1H), 6.68 (s, 1H), and 6.75 (s, 1H); Found: C, 68.30; H, 8.77%. Calcd for $C_{16}H_{24}O_4$: C, 68.54; H, 8.63%.

Dimethyl 2-(2,5-Dimethoxy-4-methylphenyl)succinate **2g**: was prepared from **1g** with $Tl(NO_3)_3$–TMOF–MeOH following by the general procedure (95%): mp 93—94 °C (petroleum ether–dichloromethane); IR (KBr): 1735 cm^{-1}; ^1H NMR ($CDCl_3$) δ: 2.18 (s, 3H), 2.54 (dd, 1H), 3.14 (dd, 1H), 3.65 (s, 6H), 3.75 (s, 6H), 4.35 (dd, 1H), 6.62 (s, 1H), and 6.67 (s, 1H); Found: C, 60.57; H, 6.86%. Calcd for $C_{15}H_{20}O_6$: C, 60.80; H, 6.80%.

Dimethyl 2-(2,5-Dimethoxy-4-methylphenyl)hexanedioate **2h**: was prepared from **1h** with $Tl(NO_3)_3$–TMOF–MeOH by the same method (99%): bp 129—131 °C at 0.06 Torr (bulb to bulb); IR (neat): 1735 cm^{-1}; ^1H NMR ($CDCl_3$) δ: 1.40—2.20 (m, 4H), 2.22 (s, 3H), 2.34 (t, 2H), 3.66 (s, 6H), 3.80 (s, 6H), 4.02 (t, 1H), 6.72 (s, 1H), and 6.75 (s, 1H); Found: C, 62.68; H, 7.40%. Calcd for $C_{17}H_{24}O_6$: C, 62.95; H, 7.46%.

Methyl 2-(2,5-Dimethoxy-4-methylphenyl)-6-(phthalimido)hexanoate **2i**: was prepared from **1i** with $Tl(NO_3)_3$–TMOF–MeOH by the usual method (84%): mp 96—97.5 °C (methanol); IR (KBr): 1775, 1720, and 1710 cm^{-1}; ^1H NMR ($CDCl_3$) δ: 1.16—1.84 (m, 6H), 2.14 (s, 3H), 3.60 (s, 3H), 3.60 (m, 2H), 3.73 (s, 6H), 3.95 (t, 1H), 6.62 (s, 1H), 6.68 (s, 1H), and 7.58—7.84 (m, 4H); Found: C, 67.70; H, 6.39; N, 3.28%. Calcd for $C_{24}H_{27}O_6N$: C, 67.75; H, 6.40; N, 3.29%.

Methyl 2-(2,5-Dimethoxy-4-methylphenyl)-6-(trifluoroacetamido)hexanoate **2j**: was prepared from **1j** with $Tl(NO_3)_3$–TMOF–MeOH following by the general procedure (93%): mp 86.5—88 °C (petroleum ether–ether); IR (KBr): 3340, 1725, and 1710 cm^{-1}; ^1H NMR ($CDCl_3$) δ: 1.20—2.20 (m, 6H), 2.20 (s, 3H), 3.34 (q, 2H), 3.66 (s, 3H), 3.79 (s, 6H), 6.56 (bs, 1H), and 6.71 (s, 2H); Found: C, 55.27; H, 6.30; N, 3.52%. Calcd for $C_{18}H_{24}O_5NF_3$: C, 55.24; H, 6.18; N, 3.58%.

Methyl 2-(2,5-Dimethoxy-4-methylphenyl)-4-(phenoxycarbonyloxy)butyrate **2k**: was prepared from **1k** with $Tl(NO_3)_3$–TMOF–MeOH following by the same procedure (70%): IR (neat): 1760 and 1735 cm^{-1}; ^1H NMR ($CDCl_3$) δ: 1.92—2.71 (m, 2H), 2.21 (s, 3H), 3.67 (s, 3H), 3.77 (s, 6H), 4.07—4.33 (m, 3H), 6.73 (s, 2H), and 7.13—7.42 (m, 5H); Found: C, 65.13; H, 6.25%. Calcd for $C_{21}H_{24}O_7$: C, 64.93; H, 6.23%.

Methyl 2-(2,5-Dimethoxyphenyl)butyrate **2l**: was prepared from **1l** with $Tl(NO_3)_3$–TMOF–MeOH following by the general procedure (91%): bp 120—121 °C at 3 Torr (bulb to bulb); IR (neat): 1730 cm^{-1}; ^1H NMR ($CDCl_3$) δ: 0.88 (t, 3H), 1.57—2.19 (m, 2H), 3.64 (s, 3H), 3.75 (s, 3H), 3.77 (s, 3H), 3.89 (t, 1H), and 6.77—6.83 (m, 3H); Found: C, 65.81; H, 7.80%. Calcd for $C_{13}H_{18}O_4$: C, 65.53; H, 7.61%.

Methyl 2-(4-Bromo-2,5-dimethoxyphenyl)butyrate **2m**: was prepared from **2l** with bromine in chloroform (96%): bp 136—140 °C at 0.05 Torr (bulb to bulb); IR (neat): 1730 cm^{-1}; ^1H NMR ($CDCl_3$) δ: 0.88 (t, 3H), 1.56—2.18 (m, 2H), 3.66 (s, 3H), 3.84 (s, 3H), 3.89 (s, 3H), 3.89 (m, 1H), 6.86 (s, 1H), and 7.04 (s, 1H); Found: C, 49.24; H, 5.52; Br, 25.18%. Calcd for $C_{13}H_{17}O_4Br$: C, 49.22; H, 5.40; Br, 25.20%.

Methyl 2-(2,4,5-Trimethoxyphenyl)butyrate **2n**: was prepared from **1n** with $Tl(NO_3)_3$–TMOF–MeOH following by the general method (60%): mp 60—62 °C (petroleum ether); IR (KBr): 1735 cm^{-1}; ^1H NMR ($CDCl_3$) δ: 0.87 (t, 3H), 1.60—2.12 (m, 2H), 3.64 (s, 3H), 3.80 (s, 3H), 3.82 (s, 3H), 3.88 (s, 3H and m, 1H), 6.49 (s, 1H), and 6.80 (s, 1H); Found: C, 62.91; H, 7.60%. Calcd for $C_{14}H_{20}O_5$: C, 62.67; H, 7.51%.

Preparation of Quinones **3**. Quinones **3a**—**n** were prepared from the corresponding **2a**—**n** with ceric ammonium nitrate (CAN) in aq acetonitrile by the method of Jacob *et al.*[6a]

Methyl 2-(4-Methyl-3,6-dioxo-1,4-cyclohexadienyl)propionate **3a**: (CAN oxidation of **2a**): 88%; mp 59—60 °C.[5a]

Methyl 2-(4-Methyl-3,6-dioxo-1,4-cyclohexadienyl)butyrate **3b**: (CAN oxidation of **2b**): 98%; bp 130—131 °C at 3 Torr (bulb to bulb); IR (neat): 1735 and 1655 cm^{-1}: ^1H NMR ($CDCl_3$) δ: 0.92 (t, J=7 Hz, 3H), 1.60—2.00 (m, 2H), 2.04 (d, J=1.6 Hz, 3H), 3.70 (s, 3H), 3.70—3.98 (m, 1H), 6.64 (q, J=1.6 Hz, 1H), and 6.70 (s, 1H); Found: C, 64.98; H, 6.60%. Calcd for $C_{12}H_{14}O_4$: C, 64.85; H, 6.35%.

Methyl 2-Methyl-2-(4-methyl-3,6-dioxo-1,4-cyclohexadienyl)propinate **3c**: (CAN oxidation of **2c**): 95%; mp 111—112 °C (petroleum ether); IR (KBr): 1740 and 1650 cm^{-1}; ^1H NMR ($CDCl_3$) δ: 1.42 (s, 6H), 2.03 (d, J=1.6 Hz, 3H), 3.62 (s, 3H), 6.56 (q, J=1.6 Hz, 1H), and 6.59 (s, 1H); Found: C, 64.56; H, 6.35%. Calcd for $C_{12}H_{14}O_4$: C, 64.85; H, 6.35%.

Methyl 2-(4-Methyl-3,6-dioxo-1,4-cyclohexadienyl)pentanoate **3d**: (CAN oxidation of **2d**): 96%; bp 143—145 °C at 3 Torr (bulb to bulb); IR (neat): 1735 and 1655 cm^{-1}; ^1H NMR ($CDCl_3$) δ: 0.92 (t, J=7 Hz, 3H), 1.15—2.04 (m, 4H), 2.04 (d, J=1.6 Hz, 3H), 3.68 (s, 3H), 3.90 (t, J=7 Hz, 1H), 6.62 (q, J=1.6 Hz, 1H), and 6.69 (s, 1H); Found: C, 66.05; H, 6.89%. Calcd for $C_{13}H_{16}O_4$: C, 66.08; H, 6.83%.

Methyl 3-Methyl-2-(4-methyl-3,6-dioxo-1,4-cyclohexadienyl)butyrate **3e**: (CAN oxidation of **2e**): 96%; bp 140—143 °C at 3 Torr (bulb to bulb); IR (neat): 1735 and 1655 cm^{-1}; ^1H NMR ($CDCl_3$) δ: 0.83 (d, J=7 Hz, 3H), 0.99 (d, J=7 Hz, 3H), 2.03 (d, J=1.6 Hz, 3H), 1.91—2.38 (m, 1H), 3.65 (s, 1H), 3.74 (t, J=7 Hz, 1H), 6.60 (q, J=1.6 Hz, 1H), and 6.84 (s, 1H); Found: C, 66.04; H, 6.96%. Calcd for $C_{13}H_{16}O_4$: C, 66.08; H, 6.83%.

Methyl 2-(4-Methyl-3,6-dioxo-1,4-cyclohexadienyl)hexanoate **3f**: (CAN oxidation of **2f**): 90%; IR (neat): 1735 and 1655 cm^{-1};

^{1}H NMR ($CDCl_3$) δ: 0.88 (t, J=7 Hz, 3H), 1.00—2.04 (m, 6H), 3.68 (s, 3H), 3.82 (t, J=7 Hz, 1H), 6.60 (q, J=1.6 Hz, 1H), and 6.68 (s, 1H); Found: C, 66.95; H, 7.38%. Calcd for $C_{14}H_{18}O_4$: C, 67.18; H, 7.25%.

Dimethyl 2-(4-Methyl-3,6-dioxo-1,4-cyclohexadienyl)succinate ***3g***: (CAN oxidation of **2g**): 80%; mp 85—86 °C (methanol–petroleum ether); IR (KBr): 1735 and 1640 cm^{-1}; ^{1}H NMR ($CDCl_3$) δ: 2.06 (d, J=1.6 Hz, 3H), 2.61 (dd, J=6 and 17 Hz, 1H), 3.06 (dd, J=6 and 17 Hz, 1H), 3.66 (s, 3H), 3.68 (s, 3H), 4.12 (t, J=7 Hz, 1H), and 6.63 (m, 2H); Found: C, 58.57; H, 5.36%. Calcd for $C_{13}H_{14}O_6$: C, 58.64; H, 5.30%.

Dimethyl 2-(4-Methyl-3,6-dioxo-1,4-cyclohexadioenyl)hexanediate ***3h***: (CAN oxidation of **2h**): 88%; bp 169—172 °C at 0.03 Torr (bulb to bulb); IR (neat): 1735 and 1655 cm^{-1}; ^{1}H NMR ($CDCl_3$) δ: 1.36—2.05 (m, 4H), 2.05 (d, J=1.6 Hz, 3H), 2.33 (t, J=7.5 Hz, 2H), 3.64 (s, 3H), 3.67 (s, 3H and m, 1H), 6.60 (q, J=1.6 Hz, 1H), and 6.64 (s, 1H); Found: C, 61.18; H, 6.30%. Calcd for $C_{15}H_{18}O_6$: C, 61.21; H, 6.17%.

Methyl 2-(4-Methyl-3,6-dioxo-1,4-cyclohexadienyl)-6-(phthalimido)hexanoate ***3i***: (CAN oxidation of **2i**): 88%; IR (neat): 1775, 1735, 1710, and 1655 cm^{-1}; ^{1}H NMR ($CDCl_3$) δ: 1.18—1.88 (m, 6H), 2.03 (d, J=1.6 Hz, 3H), 3.61 (s, 3H), 3.56—3.7 (m, 2H), 3.87 (m, 1H), 6.58 (q, J=1.6 Hz, 1H), 6.64 (d, J=1.2 Hz, 1H), and 7.60—7.82 (m, 4H); Found: C, 66.77; H, 5.42; N, 3.58%. Calcd for $C_{22}H_{21}O_6N$: C, 66.82; H, 5.35; N, 3.54%.

Methyl 2-(4-Methyl-3,6-dioxo-1,4-cyclohexadienyl)-6-(trifluoroacetamido)hexanoate ***3j***: (CAN oxidation of **2j**): 80%; IR (neat): 3320, 1710, and 1650 cm^{-1}; ^{1}H NMR ($CDCl_3$) δ: 1.00—2.00 (m, 6H), 2.04 (d, J=1.6 Hz, 3H), 3.35 (q, J=7 Hz, 2H), 3.68 (s, 3H), 3.76 (m, 1H), 6.63 (q, J=1.6 Hz, 1H), 6.67 (s, 1H), and 6.68 (bs, 1H); Found: C, 52.87; H, 5.13; N, 3.84%. Calcd for $C_{16}H_{18}O_5NF_3$: C, 53.18; H, 5.02; N, 3.88%.

Methyl 2-(4-Methyl-3,6-dioxo-1,4-cyclohexadienyl)-4-(phenoxycarbonyloxy)butyrate ***3k***: (CAN oxidation of **2k**): 71%; IR (neat): 1750 and 1655 cm^{-1}; ^{1}H NMR ($CDCl_3$) δ: 2.05 (d, J=1.6 Hz, 3H), 2.05—2.59 (m, 2H), 3.72 (s, 3H), 3.88 (t, J=7.5 Hz, 1H), 4.28 (t, J=6.5 Hz, 2H), 6.63 (q, J=1.6 Hz, 1H), 6.71 (s, 1H), and 7.11—7.46 (m, 5H); Found: C, 63.29; H, 5.19%. Calcd for $C_{19}H_{18}O_7$: C, 63.68; H, 5.06%.

Methyl 2-(3,6-Dioxo-1,4-cyclohexadienyl)butyrate ***3l***: (CAN oxidation of **2l**): 54%; bp 131—134 °C at 3 Torr (bulb to bulb); IR (neat): 1730 and 1655 cm^{-1}; ^{1}H NMR ($CDCl_3$) δ: 0.95 (t, J=7 Hz, 3H), 1.56—2.13 (m, 2H), 3.68 (s, 3H and m, 1H), 6.69 (m, 1H), and 6.75 (s, 2H); Found: C, 63.17; H, 6.06%. Calcd for $C_{11}H_{12}O_4$: C, 63.45; H, 5.81%.

Methyl 2-(4-Bromo-3,6-dioxo-1,4-cyclohexadienyl)butyrate ***3m***: (CAN oxidation of **2m**): 68%; bp 140—145 °C at 0.05 Torr (bulb to bulb); IR (neat): 1735 and 1660 cm^{-1}; ^{1}H NMR ($CDCl_3$) δ: 0.95 (t, J=7 Hz, 3H), 1.56—2.15 (m, 2H), 3.62 (t, J=7.5 Hz, 1H), 3.68 (s, 3H), 6.88 (s, 1H), and 7.27 (s, 1H); Found: C, 45.81; H, 3.87; Br, 28.07%. Calcd for $C_{11}H_{11}O_4$-Br: C, 46.06; H, 3.86; Br, 27.83%.

Methyl 2-(4-Methoxy-3,6-dioxo-1,4-cyclohexadienyl)butyrate ***3n***: (CAN oxidation of **2n**): 60%; mp 70—72 °C (petroleum ether); IR (KBr): 1740 and 1665 cm^{-1} ^{1}H NMR ($CDCl_3$) δ: 0.94 (t, J=7 Hz, 3H), 1.55—2.13 (m, 2H), 3.69 (s, 3H and m, 1H), 3.83 (s, 3H), 5.95 (s, 1H), and 6.64 (s, 1H); Found: C, 60.29; H, 5.99%. Calcd for $C_{12}H_{14}O_5$: C, 60.50; H, 5.92%.

Irradiation of Quinones ***3***. *Irradiation of* ***3a***: A solution of **3a** (416 mg, 2 mmol) in dry benzene (200 ml) was purged with nitrogen for 20 min and irradiated for 1 h. Evaporation of the solvent and column chromatography of the residue on silica gel with 10% ether–benzene as eluant gave methyl 2,3-dihydro-5-hydroxy-6-methylbenzofuran-2-carboxylate **4a** (171 mg, 41%); mp 153—154 °C (dichloromethane–petroleum ether); IR (KBr): 3420 and 1740 cm^{-1}; ^{1}H NMR ($CDCl_3$) δ: 2.20 (s, 3H), 3.26 (dd, J=7 and 15 Hz, 1H), 3.51 (dd, J=10 and 15 Hz, 1H), 3.80 (s, 3H), 4.50 (s, 1H), 5.12 (dd, J=7 and 10 Hz, 1H), 6.60 (s, 1H), and 6.74 (s, 1H); MS, *m/e* (rel intensity), 208 (M^+, 65), 176 (42), 149 (100); Found: C, 63.18; H, 5.89%. Calcd for $C_{11}H_{12}O_4$: C, 63.45; H, 5.81%.

Irradiation of ***3b***: A solution of **3b** (444 mg, 2 mmol) in dry benzene (200 ml) was purged with nitrogen for 20 min and irradiated for 1 h. After evaporation of the solvent, the residue was purified by chromatography on silica gel with 10% ether–benzene to give methyl 2,3-dihydro-5-hydroxy-3,6-dimethylbenzofuran-2-carboxylate **4b** (289 mg, 65%): mp 99—101 °C (dichloromethane–petroleum ether); IR (KBr): 3440 and 1745 cm^{-1}; ^{1}H NMR ($CDCl_3$) δ: 1,40 (d, J=7 Hz, 3H), 2.18 (s, 3H), 3.40—3.68 (m, 1H), 3.79 (s, 3H), 4.63 (d, J=7 Hz, 1H), 4.71 (bs, 1H), 6.56 (s, 1H), and 6.63 (s, 1H); MS, *m/e* (rel intensity), 222 (M^+, 100). 191 (17), 190 (17), 163 (68), 162 (91); Found: C, 64.85; H, 6.34%. Calcd for $C_{12}H_{14}O_4$: C, 64.85; H, 6.35%.

Irradiation of ***3c***: A solution of **3c** (222 mg, 1 mmol) in dry benzene (100 ml) was purged with nitrogen for 20 min and irradiated for 1 h. The solvent was evaporated, and the residue was chromatographed on silica gel with 10% ether–benzene to give methyl 2,3-dihydro-5-hydroxy-2,6-dimethylbenzofuran-2-carboxylate **4c** (100 mg, 45%): bp 170—180 °C at 0.01 Torr (bulb to bulb); IR (neat): 3420 and 1735 cm^{-1}; ^{1}H NMR ($CDCl_3$) δ: 1.64 (s, 3H), 2.16 (s, 3H), 3.00 (d, J=15 Hz, 1H), 3.50 (d, J=15 Hz, 1H), 3.75 (s, 3H), and 6.56 (s, 2H); MS, *m/e*, 222 (M^+); Found: C, 68.69; H, 6.21%. Calcd for $C_{12}H_{14}O_4$: C, 68.85; H, 6.35%.

Irradiation of ***3d***: A solution of **3d** (473 mg, 2 mmol) in dry benzene (200 ml) was purged with nitrogen for 15 min and irradiated for 1 h. After evaporation of the solvent, the residue was chromatographed on silica gel with 10% ether–benzene to give methyl 3-ethyl-2,3-dihydro-5-hydroxy-6-methylbenzofuran-2-carboxylate **4d** (322 mg, 68%): mp 101—102 °C (dichloromethane–petroleum ether); IR (KBr): 3440 and 1740 cm^{-1}; ^{1}H NMR ($CDCl_3$) δ: 1.00 (t, J=7 Hz, 3H), 1.40—2.00 (m, 2H), 2.19 (s, 3H), 3.42 (m, 1H), 3.76 (s, 3H), 4.51 (s, 1H), 4.74 (d, J=5 Hz, 1H), 6.58 (s, 1H), and 6.63 (s, 1H); MS, *m/e* (rel intensity), 236 (M^+, 100), 205 (31), 204 (55); Found: C, 66.36; H, 7.07%. Calcd for $C_{13}H_{16}O_4$: C, 66.08; H, 6.83%.

Irradiation of ***3e***: A solution of **3e** (473 mg, 2 mmol) in dry benzene (200 ml) was purged with nitrogen for 20 min and irradiated for 1 h. The solvent was removed, and the crude oil was chromatographed on silica gel with 20% ether–benzene to give methyl 4-methyl-2-(2,5-dihydroxy-4-methylphenyl)-3-butenoate **4e** (189 mg, 40%): mp 130—131 °C (dichloromethane–petroleum ether); IR (KBr): 3400, 3340, 1715, and 900 cm^{-1}; ^{1}H NMR ($CDCl_3$) δ: 1.78 (s, 3H), 2.15 (s, 3H), 3.77 (s, 1H), 4.38 (bs, 1H), 4.84 (s, 1H), 5.02 (bs, 1H), 6.60 (s, 1H), and 6.64 (s, 1H); MS, *m/e* (rel intensity), 236 (M^+, 3), 204 (57), 175 (100).

Irradiation of ***3f***: A solution of **3f** (500 mg, 2 mmol) in dry benzene (200 ml) was purged with nitrogen for 10 min and irradiated for 1 h. Removal of the solvent left a dark oil which was subjected to column chromatography on silica gel with 10% ether–benzene. The only component isolated was methyl 2,3-dihydro-5-hydroxy-6-methyl-3-propylbenzofuran-2-carboxylate **4f** (300 mg, 60%): IR (neat): 3440 and 1745 cm^{-1}; ^{1}H NMR ($CDCl_3$) δ: 0.94 (t, J=7 Hz, 3H), 1.20—1.82 (m, 4H), 2.18 (s,1H), 3.46 (m, 1H), 3.77 (s, 3H), 4.54 (bs, 1H), 4.76 (d, J=5 Hz, 1H), 6.57 (s, 1H), and 6.63 (s, 1H); Found: C, 67.14; H, 7.50%. Calcd for $C_{14}H_{18}O_4$: C, 67.18; H, 7.25%.

Irradiation of ***3g***: A solution of **3f** (532 mg, 2 mmol) in dry

benzene (200 ml) was purged with nitrogen for 20 min and irradiated for 2 h. The solvent was removed, and the residue was subjected to column chromatography on silica gel with 10% ether–chloroform. The product isolated was dimethyl 2,3-dihydro-5-hydroxy-6-methylbenzofuran-2,3-dicarboxylate **4g** (299 mg, 56%): 180—181 °C (dichloromethane–petroleum ether); IR (KBr): 3340, 1735, and 1695 cm^{-1}; ^1H NMR ($CDCl_3$) δ: 2.17 (s, 3H), 3.77 (s, 3H), 3.80 (s, 3H), 4.41 (d, J=6 Hz, 1H), 5.32 (bs, 1H), 5.56 (d, J=6 Hz, 1H), 6.65 (s, 1H), and 6.78 (s, 1H); MS, *m/e* (rel intensity), 266 (M^+, 8), 264 (100); Found: C, 58.35; H, 5.24%. Calcd for $C_{13}H_{14}O_6$: C, 58.64; H, 5.30%.

Irradiation of ***3h***: A solution of **3h** (589 mg, 2 mmol) in dry benzene (300 ml) was purged with nitrogen for 10 min and irradiated for 1 h. The solution was concentrated, and the crude residue was purified by column chromatography on silica gel with 10% ether-chloroform to give methyl 2,3-dihydro-5-hydroxy-3-[2-(methoxycarbonyl)ethyl]-6-methylbenzofuran-2-carboxylate **4h** (300 mg, 51%): mp 136—137 °C (dichloromethane–petroleum ether); IR (KBr): 3480, 1750, and 1730 cm^{-1}; ^1H NMR ($CDCl_3$) δ: 2.02 (m, 2H), 2.20 (s, 3H), 2.46 (t, J=7 Hz, 2H), 3.44—3.69 (m, 1H), 3.69 (s, 3H), 3.78 (s, 3H), 4.77 (d, J=6 Hz, 1H), 4.88 (s, 1H), 6.60 (s, 1H), and 6.67 (s, 1H); MS, *m/e* (rel intensity), 294 (M^+, 26), 174 (100); Found: C, 60.93; H, 6.13%. Calcd for $C_{15}H_{18}O_6$: C, 61.21; H, 6.17%.

Irradiation of ***3i***: A solution of **3i** (791 mg, 2 mmol) in dry benzene (300 ml) was purged with nitrogen for 15 min and irradiated for 1 h. The solvent was removed, and the residue was chromatographed on silica gel with 10% ether–chloroform to give methyl 2,3-dihydro-5-hydroxy-6-methyl-3-[3-(phthalimido)propyl]benzofuran-2-carboxylate **4i** (593 mg, 75%): mp 180—181 °C (dichloromethane–petroleum ether); IR (KBr): 3480, 1775, 1745, and 1705 cm^{-1}; ^1H NMR ($CDCl_3$) δ: 1.40—2.00 (m, 4H), 2.17 (s, 3H), 3.30—4.00 (m, 3H), 3.76 (s, 3H), 4.76 (d, J=5 Hz, 1H), 5.56 (bs, 1H), 6.63 (s, 2H), and 7.60—7.90 (m, 4H); MS, *m/e* (rel intensity), 395 (M^+, 61), 203 (100); Found: C, 66.50; H, 5.40; N, 3.56%. Calcd for $C_{22}H_{21}O_6N$: C, 66.82; H, 5.35; N, 3.54%.

Irradiation of ***3j***: A solution of **3j** (723 mg, 2 mmol) in dry benzene (300 ml) was purged with nitrogen for 10 min and irradiated for 1 h. Removal of the solvent left a crude oil which was purified by column chromatography on silica gel using 10% ether–chloroform. The only component isolated was identified as methyl 2,3-dihydro-5-hydroxy-6-methyl-3-[3-(trifluoroacetamido)propyl]benzofuran-2-carboxylate **4j** (499 mg, 69%): IR (neat): 3300 and 1740—1700 cm^{-1}; ^1H NMR ($CDCl_3$) δ: 1.69 (m, 4H), 2.17 (s, 3H), 3.38 (m, 3H), 3.77 (s, 3H), 4.71 (d, J=5 Hz, 1H), 6.57 (s, 1H), 6.63 (s, 1H), and 6.95 (bs, 1H); MS, *m/e*, 361 (M^+); Found: C, 52.80; H, 5.16; N, 3.82%. Calcd for $C_{16}H_{18}O_5NF_3$: C, 53.18; H, 5.02; N, 3.88%.

Irradiation of ***3k***: A solution of **3k** (300 mg, 0.83 mmol) in dry benzene (150 ml) was purged with nitrogen for 5 min and irradiated for 1 h. The solution was concentrated. The residue was chromatographed on silica gel with 10% ether–chloroform to give methyl 2,3-dihydro-5-hydroxy-6-methyl-3-(phenoxycarbonyloxymethyl) benzofuran-2-carboxylate **4k** (117 mg, 39%): IR (neat): 3440 and 1750 cm^{-1}; ^1H NMR ($CDCl_3$) δ: 2.17 (s, 3H), 3.79 (s, 3H), 3.90 (m, 1H), 4.35 (m, 2H), 5.02 (d, J=5.1 Hz, 1H), 5.55 (bs, 1H), 6.61 (s, 1H), 6.67 (s, 1H), and 7.08—7.43 (m, 5H); Found: C, 63.50; H, 5.20%. Calcd for $C_{19}H_{18}O_7$: C, 63.68; H, 5.06%.

Irradation of ***3l***: A solution of **3l** (416 mg, 2 mmol) in dry benzene (200 ml) was purged with nitrogen for 20 min and irradiated for 1 h. Removal of the solvent left an oil which was subjected to chromatography on silica gel with 10% ether–benzene. The product obtained was methyl 2,3-dihydro-5-hydroxy-3-methylbenzofuran-2-carboxylate **4l** (250 mg, 60%): IR (neat): 3400 and 1735 cm^{-1}; ^1H NMR ($CDCl_3$) δ: 1.38 (d, J=7 Hz, 3H), 3.53 (m, 1H), 3.79 (s, 3H), 4.64 (d, J=7 Hz, 1H), and 6.60 (s, 3H and bs, 1H); Found: C, 63.19; H, 5.81%. Calcd for $C_{11}H_{12}O_4$: C, 63.45; H, 5.81%.

Irradiation of ***3m***: A solution of **3m** (574 mg, 2 mmol) in dry benzene (200 ml) was purged with nitrogen for 20 min and irradiated for 1 h. Evaporation of the solvent gave a dark oil. The oil was chromatographed on silica gel to give methyl 6-bromo-2,3-dihydro-5-hydroxy-3-methylbenzofuran-2-carboxylate **4m** (178 mg, 31%): IR (neat): 3420 and 1735 cm^{-1}; ^1H NMR ($CDCl_3$) δ: 1.41 (d, J=7 Hz, 3H), 3.53 (m, 1H), 3.78 (s, 3H), 4.65 (d, J=7 Hz, 1H), 6.74 (s, 1H), and 6.90 (s, 1H); MS, *m/e* (rel intensity), 287 (M^+, 67); Found: C, 45.79; H, 3.95%. Calcd for $C_{11}H_{11}O_4Br$: C, 46.01; H, 3.86%.

Irradiation of ***3n***: A solution of **3n** (476 mg, 2 mmol) in dry benzene (200 ml) was purged with nitrogen for 10 min and irradiated for 1 h. Evaporation of the solvent and chromatographic separation of the crude oil by column chromatography on silica gel with 20% ether–benzene gave two compounds: The first fractions gave methyl 5-hydroxy-6-methoxy-3-methylbenzofuran-2-carboxylate (76 mg, 16%): mp 179—180 °C (dichloromethane–petroleum ether); IR (KBr): 3510 and 1720 cm^{-1}; ^1H NMR ($CDCl_3$) δ: 2.51 (s, 3H), 3.94 (s, 6H), 5.58 (s, 1H), 6.98 (s, 1H), and 7.04 (s, 1H), Found: C, 60.72; H, 5.24%. Calcd for $C_{12}H_{12}O_5$: C, 61.01; H, 5.12%. The second fractions gave methyl 2,3-dihydro-5-hydroxy-6-methoxy-3-methylbenzofuran-2-carboxylate **4n** (200 mg,42%): IR (neat): 3500 and 1735 cm^{-1}; ^1H NMR ($CDCl_3$) δ: 1.41 (d, J=7 Hz, 3H), 3.56 (m, 1H), 3.80 (s, 3H), 3.83 (s, 3H), 4.66 (d, J=7 Hz, 1H), 5.32 (s, 1H), 6.49 (s, 1H), and 6.68 (s, 1H); Found: C, 60.25; H, 5.87%. Calcd for $C_{12}H_{14}O_5$: C, 60.50; H, 5.92%.

Preparation of Quinones ***5*** *by Oxidative Cleavage*[6b] *of Photoproducts* ***4***. *Methyl 2-Hydroxy-3-(4-methyl-3,6-dioxo-1,4-cyclohexadienyl)propionate* ***5a***: A solution of **4a** (208 mg, 1 mmol) in 70% aq cetonitrile (5 ml) was treated with ceric ammonium nitrate 1.21 g, 2.2 mmol) in water (3 ml). The mixture was stirred at 0 °C for 30 min, poured into water (100 ml), and extracted with chloroform (2 × 20 ml). The extract was washed with water, dried, and evaporated to give **5a** (174 mg, 78%): IR (neat): 3500, 1735, and 1650 cm^{-1}; ^1H NMR ($CDCl_3$) δ: 2.03 (d, J=1.6 Hz, 3H), 2.69 (dd, J=8.5 and 15 Hz, 1H), 2.98 (dd, J=5 and 15 Hz, 1H), 3.81 (s, 3H), 4.18 (dd, J=5 and 8.5 Hz, 1H), 6.61 (q, J=1.6 Hz, 1H), and 6.71 (s, 1H); MS, *m/e* (rel intensity), 224 (M^+, 6), 206 (12), 164 (86), 136 (100); Found: C, 58.79; H, 5.50%. Calcd for $C_{11}H_{12}O_5$: C, 58.92; H, 5.40%.

Methyl 2-Hydroxy-3-(4-methyl-3,6-dioxo-1,4-cyclohexadienyl)-butyrate ***5b***: A solution of **4b** in aq acetonitrile was treated with CAN by the general procedure to give **5b** (80%): mp 104.5—105.5 °C (dichloromethane–petroleum ether); IR (KBr): 3480, 1725, and 1650 cm^{-1}; ^1H NMR ($CDCl_3$) δ: 1.28 (d, J=7 Hz, 3H), 2.04 (d, J=1.6 Hz, 3H), 3.00 (bs, 1H), 3.46 (dq, J=7 and 4 Hz, 1H), 3.76 (s, 3H), 4.30 (bs, 1H), 6.60 (q, J=1.6 Hz, 1H), and 6.71 (s, 1H); Found: C, 60.54; H, 6.12%. Calcd for $C_{12}H_{14}O_5$: C, 60.50; H, 5.92%.

Methyl 2-Hydroxy-2-methyl-3-(4-methyl-3,6-dioxo-1,4-cyclohexadienyl)propionate ***5c***: A solution of **4c** in aq acetonitrile was treated with CAN by the same method to give **5c** (67%): mp 78 °C (petroleum ether); IR (KBr): 3480, 1720, and 1655 cm^{-1}; ^1H NMR ($CDCl_3$) δ: 1.47 (s, 3H), 2.04 (d, J=1.6 Hz, 3H), 2.70 (d, J=13.5 Hz, 1H), 2.97 (d, J=13.5 Hz, 1H), 3.34 (s, 1H), 3.78 (s, 3H), 6.59 (q, J=1.6 Hz, 1H), and 6.70 (s, 1H); Found: C, 60.74; H. 5.98%. Calcd for $C_{12}H_{14}O_5$: C, 60.50; H, 5.92%.

Methyl 2-Hydroxy-3-(4-methyl-3,6-dioxo-1,4-cyclohexadienyl)-

pentanoate ***5d***: A solution of **4d** in aq acetonitrile was treated with CAN by the usual method to give **5d** (97%): mp 97—98 °C (petroleum ether); IR (KBr): 3420, 1720, and 1650 cm^{-1}; ^1H NMR ($CDCl_3$) δ: 0.94 (t, J=7.5 Hz, 3H), 1.57—1.94 (m, 2H), 2.04 (d, J=1.6 Hz, 3H), 2.98 (d, J=7.6 Hz, 1H), 3.27 (dt, J=3.5 and 7 Hz, 1H), 3.74 (s, 3H), 4.36 (dd, J=3.5 and 7.6 Hz, 1H), 6.58 (q, J=1.6 Hz, 1H), and 6.71 (s, 1H); Found: C, 61.64; H, 6.38%. Calcd for $C_{13}H_{16}O_5$: C, 61.89; H, 6.39%.

Methyl 2-Hydroxy-3-(4-methyl-3,6-dioxo-1,4-cyclohexadienyl)-hexanoates ***5f***: A solution of **4f** in aq acetonitrile was treated with CAN by the usual manner to give **5f** (80%): mp 75—76 °C; IR (KBr): 3470, 1720, 1650, and 1645 cm^{-1}; ^1H NMR ($CDCl_3$) δ: 0.90 (t, J=7 Hz, 3H), 1.31 (m, 2H), 1.64 (m, 2H), 2.02 (d, J=1.6 Hz, 3H), 2.87 (d, J=7 Hz, 1H), 3.31 (m, 1H), 3.92 (s, 3H), 4.31 (dd, J=3.5 and 7 Hz, 1H), 6.55 (q, J=1.6 Hz, 1H), and 6.68 (s, 1H); Found: C, 62.87; H, 6.73%. Calcd for $C_{14}H_{18}O_5$: C, 63.14; H, 6.81%.

Dimethyl 2-Hydroxy-3-(4-methyl-3,6-dioxo-1,4-cyclohexadienyl)-succinate ***5g***: A solution of **4g** in aq acetonitrile was treated with CAN by the general procedure to give **5g** (50%): IR (neat): 3470, 1735, and 1650 cm^{-1}; ^1H NMR ($CDCl_3$) δ: 2.03 (d, J=1.6 Hz, 3H), 3.75 (s, 6H and 1H), 4.32 (d, J=4.2 Hz, 1H), 4.86 (d, J=4.2 Hz, 1H), 6.62 (q, J=1.6 Hz, 1H), and 6.87 (s, 1H); Found: C, 55.03; H, 5.23%. Calcd for $C_{13}H_{14}O_7$: C, 55.32; H, 5.00%.

Dimethyl 2-Hydroxy-3-(4-methyl-3,6-dioxo-1,4-cyclohexadienyl)-hexanedioate ***5h***: A solution of **4h** in aq acetonitrile was treated with CAN according to the general method to give **5h** (98%): IR (neat): 3460, 1730, and 1650 cm^{-1}; ^1H NMR ($CDCl_3$) δ: 2.04 (d, J=1.6 Hz, 3H), 2.00—2.42 (m, 4H), 3.07 (bd, J=8 Hz, 1H), 3.38 (m, 1H), 3.68 (s, 3H), 3.37 (s, 3H), 4.35 (bs, 1H), 6.59 (q, J=1.6 Hz, 1H), and 6.74 (s, 1H); Found: C, 58.30; H, 6.01%. Calcd for $C_{15}H_{18}O_7$: C, 58.06; H, 5.85%.

Acetylation of Photoproducts ***4b***, ***4d***, ***4f***, *and* ***4i***. *Methyl 5-Acetoxy-2,3-dihydro-3,6-dimethylbenzofuran-2-carboxylate* ***6b***: The compound **4b** (111 mg, 0.5 mmol) was acetylated with acetic anhydride (5 ml) in the presence of pyridine (1 ml) to give **6b** (80%): mp 86—87 °C (petroleum ether); IR (KBr): 1750 cm^{-1}; ^1H NMR ($CDCl_3$) δ: 1.45 (d, J=7 Hz, 3H), 2.13 (s, 3H), 2.30 (s, 3H), 3.64 (m, 1H), 3.83 (s, 3H), 4.73 (d, J=7.2 Hz, 1H), 6.75 (s, 1H), and 6.78 (s, 1H). Found: C, 63.50; H, 6.04%. Calcd for $C_{14}H_{16}O_5$: C, 63.62; H, 6.10%.

Methyl 5-Acetoxy-3-ethyl-2,3-dihydro-6-methylbenzofuran-2-carboxylate ***6d***: Acetylation of **4d** as described above gave **6d** (85%): mp 98—98.5 °C (dichloromethane–petroleum ether); IR (KBr): 1760 and 1745 cm^{-1}; ^1H NMR ($CDCl_3$) δ: 1.01 (t, J=7.5 Hz, 3H), 1.78 (m, 2H), 2.13 (s, 3H), 2.31 (s, 3H), 3.50 (dt, J=5.5 and 7 Hz, 1H), 3.80 (s, 3H), 4.84 (d, J=5.5 Hz, 1H), 6.77 (s, 1H), and 6.82 (s, 1H); Found: C, 64.79; H, 6.49%. Calcd for $C_{15}H_{18}O_5$: C, 64.73; H, 6.52%.

Methyl 5-Acetoxy-2,3-dihydro-6-methyl-3-propylbenzofuran-2-carboxylate ***6f***: The compound **4f** was treated with acetic anhydride–pyridine to give **6f** (82%): IR (neat): 1760 and 1735 cm^{-1}; ^1H NMR ($CDCl_3$) δ: 0.96 (t, J=7 Hz, 3H), 1.06—1.84 (m, 4H), 2.08 (s, 3H), 2.21 (s, 3H), 3.46 (m, 1H), 3.72 (s, 3H), 4.67 (d, J=5 Hz, 1H), 6.59 (s, 1H), and 6.65 (s, 1H); MS, *m/e* (rel intensity), 292 (M^+, 4), 250 (100). Found: C, 65.59; H, 6.97%. Calcd for $C_{16}H_{20}O_5$: C, 65.74; H, 6.90%.

Methyl 5-Acetoxy-2,3-dihydro-6-methyl-3-[3-(phthalimido)-propyl]benzofuran-2-carboxylate ***6i***: The title compound was prepared from **4i** by acetylation with acetic anhydride in pyridine (77%): mp 128—129 °C (methanol); IR (KBr): 1760 and 1710 cm^{-1}; ^1H NMR ($CDCl_3$) δ: 1.40—2.00 (m, 4H), 2.10 (s, 3H), 2.28 (s, 3H), 3.47—4.00 (m, 3H), 3.76 (s, 3H), 4.81 (d, J=5 Hz, 1H), 6.72 (s, 1H), 6.80 (s, 1H), and 6.80 (s, 1H), and 7.60—7.90 (m, 4H); Found: C, 65.62; H, 5.24; N, 3.11%. Calcd for $C_{24}H_{23}O_7N$: C, 65.89; H, 5.30; N, 3.20%.

Methyl 2-Acetoxy-3-(2,5-diacetoxy-4-methylphenyl)hexanoate ***7***: A solution of **5f** (133 mg, 0.5 mmol) in ether (50 ml) was reduced with excess aq sodium dithionite to give methyl 2-hydroxy-3-(2,5-dihydroxy-4-methylphenyl)hexanoate, which was acetylated with acetic anhydride (2 ml) in the presence of pyridine (0.1 ml) to afford **7** (118 mg, 60%): IR (neat): 1760 cm^{-1}; ^1H NMR ($CDCl_3$) δ: 0.86 (t, J=7 Hz, 3H), 1.27 (m, 2H), 1.64 (m, 2H), 2.10 (s, 3H), 2.16 (s, 3H), 2.33 (s, 6H), 3.46 (m, 1H), 3.65 (s, 3H), 5.18 (d, J=5 Hz, 1H), 6.96 (s, 1H), and 7.09 (s, 1H); MS, *m/e* (rel intensity), 394 (M^+, 1), 352 (38), and 310 (100); Found: C, 60.66; H, 6.87%. Calcd for $C_{20}H_{26}O_8$: C, 60.90; H, 6.64%.

The author is grateful to Professor Kazuhiro Maruyama for his invaluable suggestions to this work and his continuous encouragement.

References

1) A. G. Shultz, Y. K. Yee, and M. H. Berger, *J. Am. Chem. Soc.*, **99**, 8065 (1977) and references cited therein.

2) For reviews of quinones and their chemistry, see: "The Chemistry of the Quinonid Compounds," ed by S. Patai, Wiley, New York (1974), Parts 1 and 2; J. M. Bruce, *Quart. Rev.*, **21**, 405 (1967).

3) a) C. M. Orland., Jr, H. Mark, A. K. Bose, and M. S. Manhas, *J. Org. Chem.*, **32**, 2512 (1968); b) J. M. Bruce and K. Dawes, *J. Chem. Soc., C*, **1970**, 645; c) J. M. Bruce and D. Creed *ibid.*, **1970**, 649; d) J. M. Bruce, D. Creed, and K. Dawes, *ibid.*, **1971**, 2244; e) J. M. Bruce, D. Creed, and K. Dawes, *ibid.*, **1971**, 3748; f) J. M. Bruce and A.-u.-h. Chaudhry *J. Chem. Soc., Perkin Trans. 1*, **1972**, 372.

4) In a preliminary report of this work, the author erroneously assigned the positions of substituent groups for dihydrobenzofuran structure of these several photoproducts, it should be corrected to the photorearranged dihydrobenzofuran structure **4**: K. Maruyama and T. Kozuka, *Chem. Lett.*, **1980**, 341.

5) a) K. Maruyama and T. Kozuka, *Bull. Chem. Soc. Jpn.*, **51**. 3586 (1978); b) E. C. Taylor, R. L. Robey, K.-T. Liu, B. Favre, H. T. Bozino, R. D. Conley, C.-S. Chiang, A. McKillop, and M. E. Ford, *J. Am. Chem. Soc.*, **98**, 3037 (1976); c) E. C. Taylor, C.-S. Chiang, A. McKillop, and J. F. White, *ibid.*, **98**, 750 (1976).

6) a) P. Jacob, III, P. S. Callery, A. T. Shulgin, and N. Catagnoli, Jr., *J. Org. Chem.*, **41**, 3627 (1976); b) R.L. Hannan, R. B. Barker, and H. Rapoport, *ibid.*, **44**, 2153 (1979).

7) Ref. 3d and references cited therein the 2- and 3-substituted 2,3-dihydrobenzofuran compounds have $J_{3A,3B}$=*ca.* 15 and $J_{2A,2B}$=*ca.* 8 Hz, respectively.

8) Ref 3e.

9) L. M. Jackman, "Applications of Nuclear Magnetic Resonance Spectroscopy in Organic Chemistry," 2nd ed, Pregamon Press, New York (1967), p. 316.

10) a) J. Gripenberg and T. Hase, *Acta Chem. Scand.*, **20**, 1561 (1966); b) C. H. Ludwig, B. J. Nist, and J. L. McCarthy, *J. Am. Chem. Soc.*, **86**, 1186 (1964); c) G. Aulin-Erdtman and Y. Tomita, *Acta Chem. Scand.*, **17**, 535 (1963).

11) a) D. P. Brust, D. S. Tarbell, S. M. Hecht, E. C. Hayward, and L. D. Colebook, *J. Org. Chem.*, **31**, 2196 (1966); b) E. C. Hayward, D. S. Tarbell, and L. D. Colebook, *ibid.*, **33**, 399 (1968); c) L. H. Zalkow and M. Ghosal, *ibid.*, **34**, 1646 (1969); d) M. P. Mertes and L. J. Powes, *ibid.*, **36**, 1805 (1971). The coupling constans for 2,3-dialkyl 2,3-dihydrobenzofuran were J_{cis}=7.0 Hz and J_{trans}=4.8 Hz.

12) M. Karplus, *J. Am. Chem. Soc.*, **85**, 2870 (1963).
13) S. Farid, *J. Chem. Soc., Chem. Commun.*, **1971**, 73.
14) S. Farid, *J. Chem. Soc., Chem. Commun.*, **1970**, 303
15) *Org. Synth.*, Coll. Vol. III, 169 (1955).
16) *Org. Synth.*, Coll. Vol. IV, 556 (1963).
17) S. Gabriel and J. Colman, *Chem. Ber.*, **41**, 2014 (1908).
18) E. E. Schallenberg and M. Calvin, *J. Am. Chem. Soc.*, **77**, 2779 (1955).
19) B.-T. Ho, L. W. Tansey, and W. M. McIssac, *J. Med. Chem.*, **13**, 1022 (1970).
20) T. R. Ingle, N. L. Phalnikar, and B. V. Bhide, *J. Indian Chem. Soc.*, **26**, 569 (1949).
21) E. Hardegger, H. P. Knowpfel, E. Widmer, H. Corrodi, Th. Schmidt, H. P. Knoepfel, W. Reder, H. J. Meyer, F. Kugler, and H. Gempeler, *Helv. Chem. Acta*, **47**, 1996 (1964).
22) R. B. Moffett, A. R. Hanze, and P. H. Seay, *J. Med. Chem.*, **7**, 178 (1964).

 © 1982 The Chemical Society of Japan Bull. Chem. Soc. Jpn., 55, 2424—2427 (1982) [Vol. 55, No. 8

Structure of Epilubimin, Epioxylubimin, and Isolubimin, Spirovetivane Stress Metabolites in Diseased Potato[1]

Nobukatsu KATSUI, Fujio YAGIHASHI, Akio MURAI, and Tadashi MASAMUNE*
Department of Chemistry, Faculty of Science, Hokkaido University, Sapporo 060
(Received December 3, 1981)

The isolation and structure elucidation of the title spirovetivane sesquiterpenes, stress metabolites produced in diseased potato tubers, are described.

In recent preliminary communications,[2,3] we reported the isolation and structure of three spirovetivane sesquiterpenes named epilubimin (**1**), epioxylubimin (**2**), and isolubimin (**3**), stress metabolites produced in diseased potato tubers. In the present paper we describe details of the modified isolation procedure and structure elucidation of these metabolites.

Isolation. The metabolites were isolated from tuber tissues of potatoes (Rishiri, *Solanum tuberosum*×*S. demissum*) infected with an incompatible race of *Phytophthora infestans* as follows. Neutral chloroform extracts[4] (83 g), obtained from the diseased potato tubers (300 kg), were roughly separated into five fractions (I—V) by chromatography. The fraction II (8.5 g) was again separated by chromatography to yield a "lubimin-rich" fraction (690 mg), containing epilubimin (**1**), isolubimin (**3**), and oxyglutinosone[5] (**4**) beside lubimin[6] (**5**) as its major component. This fraction was further separated by chromatography into "epilubimin-rich" and "oxyglutinosone and isolubimin-rich" fractions. Preparative TLC of the former gave **1** (59 mg), oil, $[\alpha]_D$ 0°, in pure state, and acetylation of the latter followed by preparative TLC afforded **4** and **3** as the respective acetates (**4a**)[5] (43 mg) and (**3a**) (37 mg), mp 49—50 °C, $[\alpha]_D$ +26.3°. The latter acetate (**3a**) was hydrolyzed smoothly to give **3**, oil, $[\alpha]_D$ +34.4°, in pure state. On the other hand, the fraction IV (5.0 g), including oxylubimin[6] (**6**) as its major constituent, contained two other metabolites, lubiminol[6] (**7**) (=dihydrolubimin) and epioxylubimin (**2**). This was separated and purified by repeated chromatography and recrystallization to give **2** (294 mg), mp 123—124 °C, $[\alpha]_D$ −12.1°, in pure state.

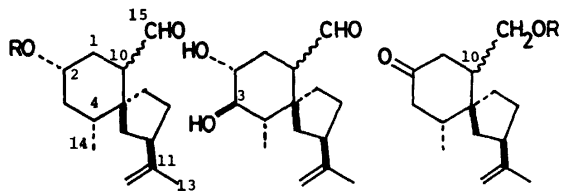

1 10αH, R=H **2** 10αH, R=H **3** 10βH, R=H
1a 10αH, R=Ac **6** 10βH, R=H **3a** 10βH, R=Ac
5 10βH, R=H **9** 10αH, R=H
9a 10αH, R=Ac

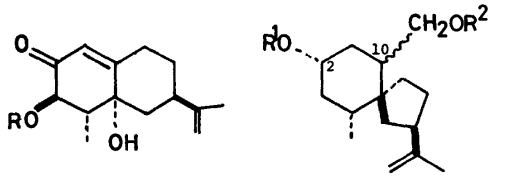

4 R=H
4a R=Ac

7 10βH, $R^1=R^2=H$
7a 10βH, $R^1=H$, $R^2=Ac$
8 10αH, $R^1=R^2=H$
8a 10αH, $R^1=R^2=Ac$
8b 10αH, $R^1=H$, $R^2=Ac$

Epilubimin. Epilubimin (**1**) had the same molecular formula $C_{15}H_{24}O_2$ [*m/e* 236 (M^+)] as **5** and gave its monoacetate (**1a**), oil, $[\alpha]_D$ 0°. Hydride reduction of **1** afforded its dihydro derivative, epilubiminol[7,8] (**8**), mp 135—136 °C, which also formed its diacetate (**8a**), oil. The mass, IR, and ^1H and ^{13}C NMR spectra of these compounds indicated the presence of the following structural units: $CH_3\dot{C}H$– [**1**, δ 0.94 (3H, d, J=6.5 Hz); **8**, 0.85 (3H, d, J=7 Hz)]: CH_2=C(CH_3)– [**1**, IR, 1640 and 891 cm^{-1}; δ 1.72 (3H, s) and 4.64(2H, s); **8**, IR, 1640 and 891 cm^{-1}; δ 1.68 (3H, s) and 4.64 (2H, s)]: –CHO [**1**, IR, 1715 cm^{-1}; δ 9.81 (1H, s),; **1a**, IR, no absorption near 3400 cm^{-1}; δ near 9.8]: –CH(OH)– [**1**, IR, 3300 cm^{-1}; δ 3.69 (1H, br, W_H=25 Hz); **1a**, IR, 1740 cm^{-1}; δ 4.64 (1H, br, W_H=25 Hz)]: a quaternary carbon atom (■)† of spiro type (**8**, δ 46.2, in Table 1). Addition of 0.25 mol equiv of the shift reagent Eu(dpm)$_3$ to the chloroform-*d* solution of **1** effected down-field shift of the ^1H NMR signals, leading to separation of most of the protons (Fig. 1), and spin-decoupling studies on the spectrum elucidated the following structural moiety: (■ ?)–CH(CH_3)–CH_2–CH(OH)–CH_2–CH(CHO ?)–(■). All the results strongly suggested that **1** would be an epimer (with an axial formyl group) of **5** (with an equatorial one). Compound **1** was treated with base under mild conditions to give a mixture of **1** and **5**, from which **5**, oil, $[\alpha]_D$ +31°, identical with natural lubimin, oil, $[\alpha]_D$ +36°, in the mass, IR, and ^1H NMR spectra, was isolated in 60% yield. Hence epilubimin is represented by formula **1**.

Epioxylubimin. Epioxylubimin (**2**) had the same molecular formula $C_{15}H_{24}O_3$ as **6**[6] and displayed the mass spectrum similar closely to that of **6**. The IR, and ^1H and ^{13}C spectra (see Experimental and Table 1) indicated the presence of the following structural units: $CH_3\dot{C}H$–, CH_2=C(CH_3)–, two –CH(OH)–, –CH(CHO)–, and (■). While the ^1H NMR spectrum differed in multiplicity of the formyl methine protons from that of **6** [**2**, δ 9.87 (1H, s) and 2.41 (1H, t, J=4 Hz); **6**,[6] δ 9.80 (1H, d, J=2.5 Hz) and 2.58 (1H, ddd, J=10, 4, and 2.5 Hz)], it also resembled as a whole closely to that of **6**. These facts, combined with the coocurrence of **1** and **5**, suggested that **2** would probably be a 10-epimer of **6**. Indeed, **2**, when treated with base, gave a mixture of **2** and **6** in 92% yield, from which

† The abbreviation denotes a carbon atom bearing no hydrogen atom.

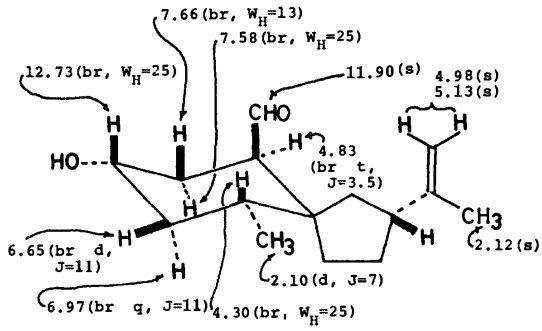

Fig. 1.

Table 1. The ^{13}C NMR spectra of epilubiminol (**8**), epioxylubimin (**2**), and isolubimin (**3**)[a]

Carbon No.	Chemical shift δ		
	8[b]	**2**	**3**[b]
1	42.1(42.1)	42.8	42.4(42.4)
2	66.0(66.6)	71.4	211.0(211.6)
3	40.0(40.4)	76.9	46.7(46.7)
4	35.2(35.4)	43.1	43.0(43.0)
5	46.2(46.4)	46.7	46.8(46.8)
6	35.2(34.0)	31.2	40.2(40.0)
7	47.8(47.9)	47.9	47.1(47.2)
8	31.1(31.2)	30.9 or 30.0	32.5(32.5)
9	31.1(31.3)	30.0 or 30.9	25.0(25.0)
10	48.9(49.1)	57.9	50.1(50.1)
11	147.9(148.4)	147.1	147.6(147.6)
12	107.8(108.2)	108.4	108.5(108.6)
13	21.3(21.5)	21.4	21.5(21.5)
14	17.1(17.2)	11.7	16.7(16.7)
15	61.2(62.1)	204.7	64.2(64.3)

a) Measured in chloroform-*d* at 25.2 MHz. b) The figures in the parentheses denote the chemical shifts reported by Stoessl *et al.*, *cf.*, Ref. 8.

6, mp 83—85 °C, $[\alpha]_D$ +52.6°, identical with natural oxylubimin, mp 85—86 °C, $[\alpha]_D$ +55.6°, was isolated in 60% yield.

Isolubimin and Epiisolubimin. Isolubimin (**3**), with the same molecular formula $C_{15}H_{24}O_2$ as that of **1**, exhibited the IR, ^1H and ^{13}C NMR spectra (Experimental and Tables 1 and 2), indicating the presence of the following structural units: CH_3CH–, CH_2=C(CH_3)–, $HOCH_2$–, O=C–, and (■). The structure of **3** was elucidated by correlation with **5** as follows. Lubiminol[6] (**7**), derived from **5**, was converted by treatment with acetic anhydride and pyridine in benzene into its 15-*O*-monoacetate (**7a**), oil, in 70% yield, which on Collins oxidation gave keto acetate in 60% yield, which was identified as acetylisolubimin (**3a**), in all respects. The same structure (**3**) had been proposed for "isolubimin" isolated from infected potato tubers independently by Kalan,[9] Stoessl,[8] and coworkers. In fact, the ^{13}C NMR spectrum of **3** was indistinguishable from that of Stoessl's isolubimin (Table 1).[10] However, the ^1H NMR spectrum appeared to be different from that reported by Kalan and Osman[9] (Table 2). Thus we prepared epiisolubimin (**9**), a 10-epimer of **3**, from epilbiuminol (**8**); namely, **8** underwent partial acetylation under the aforementioned conditions to give its 15-*O*-monoacetate (**8b**), $[\alpha]_D$ −9.0°, which on Collins oxidation afforded keto acetate (**9a**), oil, $[\alpha]_D$ −2.7°, isomeric from **3a**, in 60% yield. Interestingly, epiisolubimin (**9**), oil, obtained by hydrolysis of **9a**, exhibited the ^1H NMR spectrum, which resembled closely to that of "isolubimin" reported by Kalan and Osman (Table 2)[11].

Experimental

All the melting points were uncorrected. The purity of each compound was always checked by TLC over silica gel (Wakogel B-5 or Merck GF-254) with various solvent systems, and the spots were developed with cerium(IV) sulfate in dil sulfuric acid, iodine, and/or concd sulfuric acid. The optical rotations, UV, IR, and NMR (100 MHz) were measured in ethanol, in ethanol, in liquid state (oil) or in Nujol (crystals), and in chloroform-*d*, respectively, unless otherwise stated. The preparative TLC was carried out over silica gel (Merck GF-254), and the column chromatography over silca gel (Mallinckrodt AR-100) or silicic acid (Kiesel gel 60), respectively.

Isolation of Epilubimin (1), Epioxylubimin (2), and Isolubimin (3). The neutral chloroform extracts (83 g), corresponding to "neutral syrup" described in the section of "Isolation of rishitin,"[4] obtained from the diseased potato tubers (300 kg), were separated roughly into five fractions I—V by column chromatography over silica gel (1.8 kg), benzene, benzene–ethyl acetate (1 : 1), ether, ethyl acetate, and methanol being used as eluents, successively.

Fraction II (8.5 g), yellow oil, corresponding to "fraction E,"[4] was separated by chromatography over silica gel (100 g). Fractions (5.9 g) eluted with hexane–ethyl acetate (100 : 1) contained sterols as main components, which were not further examined. Successive elution with hexane–ethyl acetate (3 : 1) gave a "lubimin-rich" fraction (688 mg), which contained epilubimin (**1**), isolubimin (**3**), and oxyglutinosone (**4**) besides lubimin (**5**). This fraction was further separated into five fractions with hexane–ethyl acetate (5 : 1) as an eluent. Preparative TLC of the second fraction afforded epilubimin

Table 2. Comparison of the ^1H NMR spectra of isolubimin (**3**) and epiisolubimin (**9**) with that of Kalan's isolubimin (K–I)[a]

Proton	Chemical shift (δ) and splitting pattern (Hz)		
	3	**9**	K–I[b]
14-H	0.99(3H, d, J=7)	0.93(3H, d, J=6)	0.90(3H, d)
13-H	1.73(3H, s)	1.75(3H, s)	1.69(3H, s)
15-H	3.41(1H, dd, J=11, 8)	3.52(1H, dd, J=10, 8)	3.70(2H, m)
	3.85(1H, dd, J=11, 3)	3.79(1H, dd, J=10, 3)	
12-H	4.67(2H, s)	4.72(2H, s)	4.68(2H, s)

a) Measured in carbon tetrachloride at 100 MHz. b) Ref. 9.

(**1**) (59 mg), oil, $[\alpha]_D$ 0°, in pure state, showing a single spot on TLC; MS, *m/e* 236 (M^+), 218, 193, 175, 161, 149, 147, 145, 119, 107 (base), and 93; IR, 3300, 2730, 1715, 1640, and 891 cm^{-1}; ^1H NMR, δ 0.94 (3H, d, J=6.5 Hz), 1.72 (3H, s), 3.69 (1H, br, W_H=25 Hz), 4.64 (2H, br s), and 9.81 (1H, s). The third fraction, showing a single spot on TLC, was identified as slightly crude lubimin (**5**) (450 mg). The fifth, most polar fraction (160 mg) was an inseparable mixture of isolubimin and oxyglutinosone and treated with acetic anhydride and pyridine at room temperature overnight. The resulting acetate mixture (167 mg) was separated into two components by column chromatography over silica gel (4.0 g) with hexane–ethyl acetate (10 : 1) to give isolubimin acetate (**3a**) (37 mg), mp 49—50 °C, $[\alpha]_D$ +26.3°; MS, *m/e* 278 (M^+), 218, 203, 175, 146, 133, 107, 93, and 43 (base); IR, 1745, 1725, 1645, 1240, 1040, and 885 cm^{-1}; ^1H NMR, δ 1.00 (3H, d, J=6 Hz), 1.75 (3H, s), 2.04 (3H, s), 3.87 (1H, dd, J=11 and 9), 4.41 (1H, dd, J=11 and 3 Hz), and 4.73 (2H, s), and oxyglutinosone acetate[5] (**4a**) (43 mg) in pure state. The former (**3a**) was hydrolyzed to give isolubimin (**3**) as follows. A solution of **3a** (11 mg) in 50% aqueous methanol (2 ml) containing potassium carbonate (20 mg) was stirred at room temperature for 1 h under nitrogen. After removal of the solvent, the mixture was extracted with ether (25 ml), and the ether solution was washed with saturated brine (10 ml), dried and evaporated to leave an oily residue, which was purified by chromatography over silica gel with hexane–ethyl acetate (1 : 1) to give isolubimin (**3**) (8 mg) in pure state, oil, $[\alpha]_D$ +34.4°; MS, *m/e* 236 (M^+), 218, 205, 193, 175, 165, 149, 147, 135, 108 (base), and 93; IR, 3300, 3080, 1725, 1645, and 889 cm^{-1}; ^1H and ^{13}C NMR, in Tables 2 and 1.

Fraction IV (5.0 g), corresponding to "fraction H,"[4] was separated by column chromatography over silica gel (200 g), benzene and benzene–ethyl acetate mixtures being used as eluents. Fractions eluted with benzene–ethyl acetate (5 : 1) yielded a crystalline substance, which was recrystallized from diisopropyl ether to give epioxylubimin (**2**) (294 mg) in pure state, mp 123—124 °C, $[\alpha]_D$ −12.1°; MS, *m/e* 252 (M^+), 234, 219, 209, 191, 177, 165, 136, 135, 121, 107, and 93 (base); IR, 3390, 1720, 1640, and 893 cm^{-1}; ^1H NMR, δ 1.06 (3H, d, J=7Hz), 1.75 (3H, s), 2.411 H, d, J=4 Hz, 10-H), 3.08 (1H, t, J=9 Hz, 3-H), 3.49 (1H, dt, J=4 and 9 Hz, 2-H), 4.77 (2H, s) and 9.87 (1H, s): ^{13}C NMR, in Table 1. The follwing fractions eluted with benzene–ethyl acetate(3 : 1)gave oxylubimin[6] (**6**) (415 mg), mp 85—86 °C, $[\alpha]_D$ +55.6°. The more polar fractions eluted with benzene–ethyl acetate (2 : 1) afforded crystalline material (112 mg), showing a single spot, which on recrystallization from ether afforded lubiminol[6] (**7**) (dihydrolubimin), mp 129—130 °C, $[\alpha]_D$ +33°.

*Acetylepilubimin (**1a**).* Epilubimin (**1**) (25 mg) was treated with acetic anhydride (0.5 ml) and pyridine (0.5 ml) at room temperature for 14 h. The mixture was diluted with water and extracted with ether. The ether solution was washed with 1 M (1 M=1 mol dm^{-3}) hydrochloric acid, 5% aqueous sodium hydrogencarbonate, and saturated brine, dried, and evaporated to yield **1a** (26 mg), showing a single spot on TLC, oil, $[\alpha]_D$ 0°; MS, *m/e* 278 (M^+), 234, 218, 149 (base), 147, 107, 105, 93, and 91; IR, 1740, 1720, 1642, 1240, 1030, and 888 cm^{-1}; ^1H NMR, δ 0.96 (3H, d, J=7 Hz, 14-H), 1.71 and 1.95 (each 3H, s, 13-H and $OCOCH_3$), 4.64 (2H, s, 12-H), 4.64 (1H, br m, W_H=25 Hz, 2-H), and 9.78 (1H, s, 15-H).

*Epilubiminol (**8**) and Its Diacetate (**8a**).* A solution of **1** (20 mg) in methanol (2 ml) was stirred with sodium borohydride (50 mg) at room temperature for 6 h under nitrogen. After being diluted with water (10 ml), the mixture was extracted with ether. The ether solution was worked up as usual to give **8** (16 mg), mp 135—136 °C (from ether), $[\alpha]_D$ +3.4°; MS, *m/e* 238 (M^+), 220, 202, 177, 107, and 93; IR, 3400, 1640, 1030, 1010, and 891 cm^{-1}; ^1H NMR, δ 0.85 (3H, d, J=7 Hz, 14-H), 1.68 (3H, s, 13-H), 6.75 (3H, br m, 2- and 15-H), and 4.64 (2H, s, 12-H); ^{13}C NMR, in Table 1.

Compound **8** (25 mg) was treated with acetic anhydride (0.5 ml) and pyridine (0.5 ml) at room temperature for 16 h. The reaction mixture was worked up as usual to leave an oily residue (28 mg), which was purified by preparative TLC to give **8a** (22 mg), oil; MS, *m/e* 322 (M^+), 279, 262, 202 (base), 159, 107, and 93; IR, 1742, 1639, 1244, and 888 cm^{-1}; ^1H NMR, δ 0.89 (3H, d, J=7 Hz, 14-H), 1.69 (3H, s, 13-H), 1.90 and 1.97 (each 3H, s, $OCOCH_3$), 4.04 (2H, br m, W_H= 26 Hz, 15-H), 4.62 (2H, s, 12-H), and 4.64 (1H, br m, W_H= 25 Hz, 2-H); ^{13}C NMR, δ 16.8 and 20.9 (each q), 30.4, 31.1, and 31.5 (each t), 35.2 and 35.2 (each d), 36.0 and 41.3 (each t), 46.2 (s), 47.5 and 69.1(each d), 63.9 and 108.0(each t), and 147.3 (s).

*Epimerization of Epilubimin (**1**) into Lubimin (**5**) and That of Epioxylubimin (**2**) into Oxylubimin (**6**).* A solution of **1** (10 mg) in 5% methanolic potassium hydroxide (5 ml) was stirred at room temperature for 30 min under nitrogen. The reaction mixture was diluted with water (10 ml) and extracted repeatedly with ether (total 50 ml). The combined ether extracts were worked up as usual to leave an oily residue (11 mg), which was separated by column chromatography over silica gel. Elution with benzene–ether (5 : 1) gave the unchanged starting material (**1**) (3 mg) and its 10-epimer (**5**) (6 mg), oil, $[\alpha]_D$ +31°, which was identical with natural lubimin,[6] oil, $[\alpha]_D$ +36°, in the mass, IR, and ^1H NMR spectra.

Compound **2** (26 mg) was treated in the same manner as described above. The mixture, after being worked up as usual, left to oily substance (23 mg), which was separated by column chromatography over silica gal. Elution with benzene–ethyl acetate (1 : 1) gave the starting material (**2**) (6 mg) and its 10-epimer (**6**) (14 mg), mp 85—86 °C (from diisopropyl ether), $[\alpha]_D$ +52.6°, which was identical with natural oxylubimin,[6] mp 85—86 °C, $[\alpha]_D$ +55.6°, in the mass, IR, and ^1H NMR spectra.

*Conversion of Lubimin (**5**) into Isolubimin (**3**).* A solution of lubiminol[6] (**7**) (50 mg), obtained from **5**, in benzene (1 ml) was stirred with acetic anhydride (42 μl) and pyridine (0.2 ml) at room temperature for 5 h. The reaction mixture was mixed with methanol (1 ml) under cooling, stirred at room temperature for 10 min, and evaporated to leave an oily residue, which was extracted with ether (30 ml). The ether solution was worked up as usual to give an oily mixture (53 mg), which was separated into three fractions by chromatography over silica gel with benzene–ethyl acetate (1 : 1). Middle fractions gave crude 15-*O*-monoacetate (**7a**) (37 mg), showing a single spot on TLC, oil; ^1H NMR, δ 0.92 (3H, d, J=7 Hz, 14-H), 1.73 and 2.06 (each 3H, 13-H and $OCOCH_3$), 3.70 (1H, br, W_H=25 Hz, 2-H), 3.79 (1H, dd, J=11 and 9 Hz, 15-H), 4.35 (1H, dd, J=11 and 4 Hz), and 4.65(2H, s, 12-H). This was used for the next reaction without further characterization.

A solution of **7a** (37 mg) in dichloromethane (1 ml) was stirred with chromiun(VI) oxide (92 mg) and pyridine (68 μl) at room temperature for 30 min. The reaction mixture was mixed with ether (50 ml) and filtered. The filtrate was washed with 5% aqueous sodium hydrogencarbonate (15 ml) and saturated brine (15 ml), dried, and evaporated to yield oily substance (35 mg), which was purified by preparative TLC to give **3a** (28 mg), mp 45—48 °C, $[\alpha]_D$ +20.0°, identical with natural isolubimin acetate, mp 49—50 °C, $[\alpha]_D$ +26.3°, in the mass, IR, and ^1H NMR spectra.

Conversion of Epilubimin (1) into Epiisolubimin (9). A solution of epilubiminol (**8**) (19 mg), obtained from **1**, in benzene (20 μl) was treated with acetic anhydride (21 μl) and pyridine (60 μl) for 3 h at room temperature under stirring. The reaction mixture was mixed with methanol, stirred for 10 min, and evaporated to leave an oily residue, which was extracted with ether (30 ml). The ether solution was worked up as usual to give a colorless oil (22 mg), showing three spots on TLC, which was separated by column chromatography over silica gel. Elution with hexane–ethyl acetate (1 : 1) afforded diacetylepilubiminol (**8a**) (5 mg), the starting material (**8**) (2 mg), and 15-*O*-acetylepilubiminol (**8b**) (12 mg), oil, $[\alpha]_D$ −9.0°; MS, *m/e* 280 (M^+), 262, 220, 202, 187, 107 (base); IR, 3600, 3440, 3080, 1730, 1645, 1254, 1032, 1020, and 890 cm^{-1}; ^1H NMR, δ 0.89 (3H, d, J=6 Hz, 14-H), 1.71 (3H, s, 13-H), 2.05 (3H, s, $OCOCH_3$), 3.86 (1H, m, W_H= 20 Hz, 2-H), 4.12 (2H, d, J=7 Hz, 15-H), and 4.68 (2H, s, 12-H).

To a solution of pyridine (43 μl) and dichloromethane (1 ml) was added chromium(VI) oxide (30 mg), and the mixture was stirred for 15 min at room temperature under nitrogen. A solution of **8b** (12 mg) in dichloromethane (0.5 ml) was added into the above deep-red colored reaction mixture. After being stirred for 15 min, the mixture was diluted with ether (30 ml) and filtered. The ethereal filtrate was worked up as usual to leave an oily residue (12 mg), showing two spots on TLC, which was purified by preparative TLC over silica gel with hexane–ethyl acetate (10 : 1) to give the unreacted alcohol (**8b**) (3 mg) and acetylepiisolubimin (**9a**) (7 mg), oil, $[\alpha]_D$ −2.7°; MS, *m/e* 278 (M^+), 236, 218, 203 ,107, 105, 93, and 91; IR, 3090, 1735, 1712, 1646, 1238, 1034, and 895 cm^{-1}; ^1H NMR, δ 0.95 (3H, d, J=6 Hz, 14-H), 1.75 (3H, s, 13-H), 2.03 (3H, s, $OCOCH_3$), 3.86 (1H, dd, J=9 and 11 Hz, 15-H), 4.27 (1H, dd, J=3 and 11 Hz, 15-H), and 4.37 (2H, s, 12-H).

A solution of **9a** (5 mg) in methanol (1 ml) was stirred with potassium carbonate (5 mg) at room temperature for 1.5 h under nitrogen. The reaction mixture was diluted with ether (30 ml) and washed with water (10 ml) and saturated brine (10 ml), dried, and evaporated to give **9** (3 mg), oil; MS, *m/e* 236 (M^+), 218, 205, 149, 135, 107, 105 (base), 93, and 91; ^1H NMR, in Table 2.

References

1) Part XXXIV of "Studies on the Phytoalexins." Part XXXIII, A. Murai, M. Ono, and T. Masamune, *Bull. Chem. Soc. Jpn.*, **55**, 1202 (1982).

2) N. Katsui, F. Yagihashi, A. Matsunaga, K. Orito, A. Murai, and T. Masamune, *Chem. Lett.*, **1977**, 723.

3) N. Katsui, F. Yagihashi, A. Murai, and T. Masamune, *Chem. Lett.*, **1978**, 1205.

4) T. Masamune, A. Murai, M. Takasugi, A. Matsunaga, N. Katsui, N. Sato, and K. Tomiyama, *Bull. Chem. Soc. Jpn.*, **50**, 1201 (1977). The extracts corresponded to "neutral syrup," described in the section of "Isolation of rishitin" of this reference.

5) A. Murai, H. Taketsuru, F. Yagihashi, N. Katsui, and T. Masamune, *Bull. Chem. Soc. Jpn.*, **53**, 1045 (1980).

6) N. Katsui, A. Matsunaga, H. Kitahara, F. Yagihashi, A. Murai, T. Masamune, and N. Sato, *Bull. Chem. Soc. Jpn.*, **50**, 1217 (1977).

7) This compound must be the same as dihydroepilubimin, mp 138—140 °C, which was recently isolated from diseased potato tubers by Stoessl and coworkers, though direct comparison has not been carried out; *cf.*, Ref. 8.

8) A. Stoessl, J. B. Stothers, and E. W. Ward, *Can. J. Chem.*, **56**, 645 (1978).

9) E. B. Kalan and S. F. Osman, *Phytochemistry*, **15**, 775 (1976).

10) The mass, IR, and ^1H NMR spectra of "isolubimin" isolated by Stoessl *et al.*[8] were not fully described.

11) Direct comparison of a Kalan's sample of isolubimin with our samples of isolubimin and epiisolubimin was not performed.

Structure of Rishitinone, a Valencane Stress Metabolite in Diseased Potato[1)]

Nobukatsu KATSUI, Fujio YAGIHASHI, Akio MURAI, and Tadashi MASAMUNE*
Department of Chemistry, Faculty of Science, Hokkaido University, Sapporo 060
(Received December 3, 1981)

The isolation and structure elucidation of the title valencane sesquiterpene, a stress metabolite produced in diseased potato tubers, are described.

In a recent communication,[2)] we reported the isolation and structure of a valencane sesquiterpene named rishitinone (**1**), a stress metabolite produced in diseased potato tubers. In view of the fact that all stress metabolites so far isolated from the Family Solanaceae differ in planar structure and/or stereochemistry from usual naturally occurring sesquiterpenes, the sesquiterpene (**1**) with the valencane skeleton stands unique on biogenetic grounds as stress compounds.[3)] In the present paper we describe details of the isolation and structure elucidation of the compound.

Isolation. The metabolite was isolated from tuber tissues of potatoes (Rishiri, *Solanum tuberosum*×*S. demissum*) infected with an incompatible race of *Phytophthora infestans* as follows. Neutral chloroform extracts[4)] (83 g), obtained from the diseased potato tubers (300 kg), were separated as described previously[1)] to give "rishitin-rich" fractions (Fraction III,[1)] 5.5 g), which on acetylation followed by chromatography over silica gel afforded a semi-crystalline mixture of acetates. Fractional recrystallization of the mixture gave pure rishitin diacetate[4)] (3.3 g), mp 65—67 °C, and crude oily rishitinone acetate (**1a**) (0.11 g), which was purified by chromatography to yield **1a** (68 mg), oil, $[\alpha]_D$ −2.4°, in pure state. The acetate (**1a**) was then hydrolyzed smoothly to give rishitinone (**1**), mp 72—75 °C, $[\alpha]_D$ +10.1°.

Planar Structure. Rishitinone (**1**) was analyzed for $C_{15}H_{24}O_2$ (*m/e* 236, M^+) and converted by hydrogenation over palladium into dihydrorishitinone (**2**), mp 80—82 °C, $[\alpha]_D$ +7.2°, and by acetylation into the acetate (**1a**). The latter (**1a**) was reduced with sodium borohydride to give hydroxy acetate (**3**), $C_{17}H_{28}O_3$ (*m/e* 280, M^+), mp 96—98 °C, $[\alpha]_D$ −6.9°, as a sole product (90%). The IR and ^{1}H NMR spectra of these compounds indicated the presence of the following structural units: CH_3-(■)-[5)] [**1**, δ 0.76 (3H, s)]: $CH_3\overset{|}{C}H$- [**1**, δ 0.84 (3H, d, J=7 Hz)]: CH_2-C(CH_3)- [**1**, IR, 1651 and 900 cm^{-1}; δ 1.76 (3H, s) and 4.77 (2H, br s); **2**, IR, 1388 and 1372 cm^{-1}, δ 0.91 (6H, d, J=6 Hz)]: -C(=O)- [**1**, IR, 1710 cm^{-1}]: -CH(OH)- [**1**, IR, 3500 cm^{-1}; δ 3.65 (1H, br m, W_H=25 Hz); **1a**, IR, 1739 and 1248 cm^{-1}; δ 2.02 (3H, s) and 4.77 (1H, br m, W_H=25 Hz)]. The ^{13}C NMR spectra of **1**, obtained under proton-noise decoupled and single-frequency off-resonance decoupled conditions, provided additional information of the other carbon atoms, four $-CH_2$- [δ 30.2, 39.3, 42.8, and 46.0 (each t)] and two -CH- [δ 41.3 or 41.5 and 56.1 (each d)], indicating that the ketone (**1**) possesses a bicyclic skeleton.

The ^{1}H NMR spectra of **1** in the presence of the shift reagent Eu(dpm)$_3$ (0.2 and 0.4 mol equiv.) led to downfield shift of all the signals and revealed one-proton signals (W_H=25 Hz) at δ 6.80 and 10.50 in the respective spectra, which were reasonably assigned to the proton on the carbon atom bearing the hydroxyl group. The spectra, coupled with spin-decoupling studies (Table 1), strongly suggested that the ketone (**1**) would probably involve partial formula A. In view of the remaining nine carbon units (formula B) deduced from the afore-mentioned spectra, specially from the ^{13}C NMR spectra [only two (■) at δ 40.7 and 211.1, and one -CH- and one $-CH_2$- at low field, δ 69.5 and 46.0], formula C was presented as one of the most plausible planar structures for **1**. The following comments on the stereochemistry are based on the formula (C).

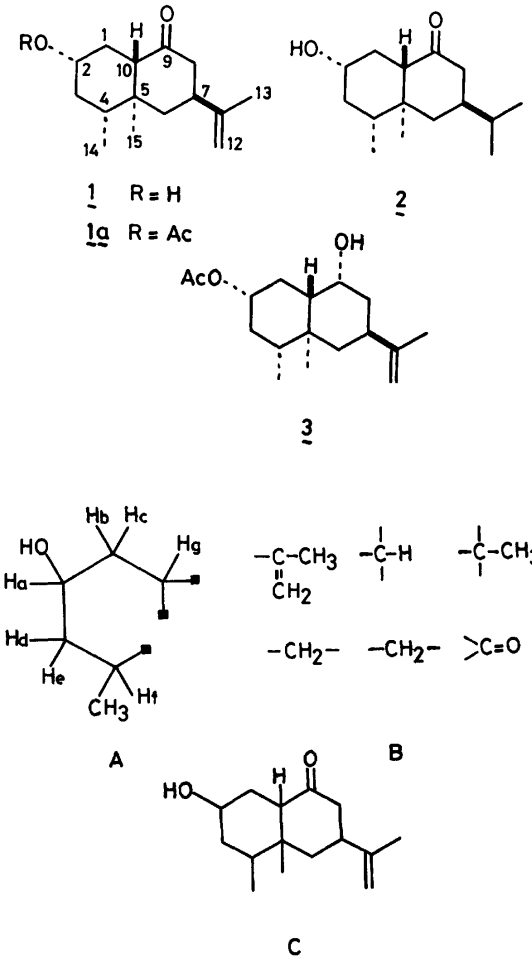

1 R = H
1a R = Ac
2
3

Stereochemistry. The presumption that rishitinone (**1**) would possess two *trans*-fused rings with 5α-axial

Table 1. The ^{1}H NMR spectra of rishitinone (**1**) in the presence of the shift reagent Eu(dpm)$_3$ (CCl_4, 100 MHz) and the results of the spin-decoupling studies

Protons irradiated (δ and Hz)	Observed multiplicity change (δ and Hz)
Mole ratio of **1**: Eu(dpm)$_3$ 5 : 1	
6.80 [Ha (C-2), br (W_H=25)	4.00[Hb, dt → dd(J=12 and 4)]
	3.20—3.80[Hc—He, br m → changed]
4.00[Hb(C-1), dt(J=12 and 4)]	6.80[Ha, br → changed]
3.50[Hc—He(C-1—C-3), br m]	6.80[Ha, br → changed]
	2.30[Hf, br → changed]
2.34[Hf(C-4), br]	1.23[CH_3, d → s]
1.23[CH_3(C-4), d(J=7)]	2.30[Hf, br → dd(J=11 and 3)]
Mole ratio of **1**: Eu (dpm)$_3$ 5 : 2	
10.5[Ha(C-2), br(W_H=25)]	5.6—6.4[Hb—He, br m → changed]
6.12[Hb and Hc(C-1), br m]	4.12[Hg, dd → s]
4.12[Hg(C-10), dd(J=12 and 4)]	6.0—6.3[Hb—Hc, br m → changed]

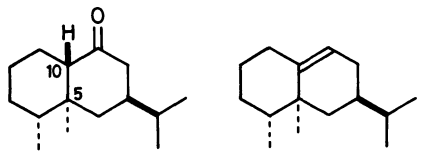

4 **5**

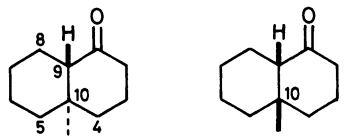

6 **7**

methyl group and 10β-hydrogen atom was deduced from the following facts: (i) dihydrorishitinone (**2**) showed a typical positive Cotton effect with a=+25.7, and the value was in good accord with that reported[6] (a=+26) for ketone **4**, which had been derived from natural (−)-aristolochene[6] (**5**), a valencane sesquiterpene with the established configurations. (ii) Angular methyl protons of *trans*-10-methyl-1-decalones (**6**) are usually observed at higher fields than the corresponding protons of the *cis*-analogues (**7**): *trans*, δ 0.7—0.9; *cis*, δ 1.0—1.2.[7] The observed chemical shifts (δ 0.76, 0.73, and 0.67) of **1**, **1a**, and **2** were in good agreement with those of the *trans*-fused model compounds (**6**).

The hydroxyl at C-2 and methyl groups at C-4 were assigned equatorial conformation and hence α-configuration on the basis of the spectral data. The signal multiplicities in Table 1 (*cf.*, formula A) revealed the following coupling constants: $J_{g\text{-}b}$, $J_{g\text{-}c}$, $J_{a\text{-}b}$, $J_{b\text{-}c}$, and $J_{f\text{-}e}$ (or $J_{f\text{-}d}$)=4, 12, 4, 12, and 11 Hz, respectively. Since the ring A must take a chair conformation, these values, combined with the large half-width value (25 Hz) of the signal due to the C-2 proton (Ha), not only support the axially oriented β-configuration of the C-10 hydrogen atom but also confirm the afore-mentioned stereochemical assignment to the relevant groups at C-2 and C-4.

The presumption that the isopropenyl group would be located at C-7 and possess β-configuration was deduced from interpretation of the ^{1}H NMR spectrum of the hydroxy acetate (**3**), in which two new well-resolved signals were observed at δ 3.95 (1H, q, J=4 Hz) and 2.52 (1H, tt, J=12 and 4 Hz). The former was ascribed readily to the hydroxy-methine proton at C-9, and its coupling constants indicated that the hydrogen is oriented equatorial (β-configuration). On the other hand, the latter would be attributed reasonably to the proton on the carbon adjacent to the isopropenyl group. The observed multiplicity accounting for two axial-axial (J=12 Hz) and two equatorial-axial (J=4 Hz) coupling constants indicated that the carbon atom in question must be flanked by two unsubstituted methylene groups, and hence the isopropenyl group must be disposed at C-7 (neither C-6 nor C-8). Moreover, the splitting pattern revealed that the relevant C-7 proton is oriented axial, and hence the isopropenyl group must take β-configuration. It follows that the angular methyl group at C-5, the hydrogen atom at C-7, and the hydroxyl group at C-9 all have 1,3-diaxial relationship each other on the ring B with a chair conformation. In accordance with this conformational assignment, the hydroxy acetate (**3**) exhibited the signal due to the C-5 angular methyl protons at lower field (δ 1.02) than the corresponding oxo acetate (**1a**) (δ 0.73).[8] Furthermore, in the ^{1}H NMR spectrum in pyridine-d_5, remarkable down-field shifts were observed for the C-7 proton ($\Delta\delta$ 0.35) and the C-5 angular methyl protons ($\Delta\delta$ 0.25) (Table 2) (the solvent-induced NMR shift correlation).[9] In summary, all the chemical evidence and spectral data strongly suggested that rishitinone would probably be represented by formula **1**. This presumption was confirmed by correlation of **1** with (+)-nootkatone[10] (**8**), a well-known sesquiterpene with the established configurations, as described below.

Transformation of Nootkatone into Dihydrorishitinone. (+)-Nootkatone[10] (**8**), mp 28—30 °C, $[\alpha]_D$ +172°, was submitted to partial hydrogenation in benzene, containing tris(triphenylphosphine)chlororhodium[11] at room temperature for 14 h to give dihydronootkatone (**9**), oil, $[\alpha]_D$ +167°, in 81% yield. The compound (**9**) was converted by a modification of the Edwards procedure[12] into the corresponding dienol acetate (**10**), oil, $[\alpha]_D$ +45.3°, in 69% yield, showing the following

TABLE 2. THE SOLVENT EFFECT IN THE CHEMICAL SHIFTS OF HYDROXY ACETATE (3) IN CHLOROFORM-*d* AND PYRIDINE-d_5

Proton	Chemical shift δ		
	$CDCl_3$	C_5D_5N	$\Delta\delta$
14-H (4-CH_3)	0.79 (3H, d, J=6 Hz)	0.76	−0.03
15-H (5-CH_3)	1.02 (3H, s)	1.27	0.25
13-H (11-CH_3)	1.72 (3H, s)	1.76	0.04
$OCOCH_3$	2.02 (3H, s)	2.04	0.02
7-H	2.52 (1H, tt, J=12 and 4 Hz)	2.87	0.35
9-H	3.95 (1H,q, J=4 Hz)	4.05	0.10
12-H(11-CH_2)	4.75 (2H, s)	4.87	0.12
2-H	4.77 (1H, m, W=25 Hz)	4.96	0.10

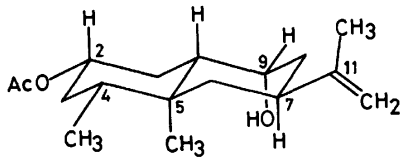

3

spectra: IR, 1759 and 1664 cm^{-1}; NMR, δ 2.12 (3H, s, $OCOCH_3$), 5.42 (1H, W_H=10 Hz, 9-H), and 5.71 (1H, s, 1-H). Reduction of **10** with sodium borohydride produced a 1 : 5 mixture of stereoisomeric homoallyl alcohols (**11**) and (**12**), which were separated by preparative TLC. The minor (**11**) (9%), oil, $[\alpha]_D$ −30.7°, and the major alcohols (**12**) (45%), oil, $[\alpha]_D$ −34.2°, were assigned 2-axial and 2-equatorial alcohols respectively, on the basis of the NMR spectra: **11**, δ 3.99 (1H, m, W_H=8 Hz, 2-H) and 5.43 (1H, m, W_H= 12 Hz, 9-H); **12**, δ 3.56 (1H, m, W_H=25 Hz, 2-H) and 5.38 (1H, m, W_H=12 Hz, 9-H). The hydroxyl group of the latter (**12**) was then protected by treatment with *t*-butyldimethylsilyl (TBS) chloride and imidazole in *N*,*N*-dimethylformamide. The resulting silyl ether (**12a**), oil, $[\alpha]_D$ −16.3°, obtained in 76% yield, underwent hydroboration followed by oxidation with alkaline hydrogen peroxide, producing a mixture of the starting alkene (**12a**) and two stereoisomeric alcohols (**13**) and (**14**), which were separated by column chromatography in 23, 8 (crude), and 42% (pure) yields, respectively. The major product (**14**), oil, $[\alpha]_D$ +38.0°, was assigned 9β-hydroxy-*trans*-valencane structure on the basis of the spectral data: MS, *m*/*e* 354(M^+); IR, 3360 cm^{-1}; NMR, δ 0.72 (3H, s, 15-H), 3.49 (1H, dt, J=4.5 and 10 Hz, 9-H), and 3.58 (1H, m, W_H=25 Hz, 2-H). Supporting this assignment, the acetate (**14a**), oil, $[\alpha]_D$ +35.5°, of **14** displayed the following NMR spectrum: δ 0.76 (3H, s, 15-H), 3.76 (1H, m, W_H=25 Hz, 2-H), and 4.74 (1H, dt, J=4 and 11 Hz, 9-H). The assigned stereostructure to the major alcohol (**14**) was also consistent with the currently accepted steric manner of hydroboration; namely, the reaction of the alkene (**12a**) took place mainly in a *cis*-addition manner at the less-hindered β-side opposite to the angular methyl group,[6,13] in contrast with formation of *cis*-eremophilane from dihydroeremophilene.[14] On the other hand, the minor crude alcohol (**13**) was submitted to acetylation followed by purification by chromatography. The resultant pure acetate (**13a**), oil, $[\alpha]_D$ −2.8°, exhibited two signals due to the C-2 and C-9 protons at δ 3.60 (1H, m, W_H=25 Hz) and 5.00 (1H, q, J=4 Hz), respectively, in the NMR spectrum, indicative of the axial conformation of the relevant hydroxyl group at C-9.

The *trans*-decalol (**14**) was oxidized with Collins reagent at room temperature for 15 h to yield the corresponding ketone (**15**), mp 51—53 °C, $[\alpha]_D$ +2.1°, in a quantitative yield, showing the IR absorption at 1717 cm^{-1}. Hydrolysis of the silyloxy ketone (**15**)

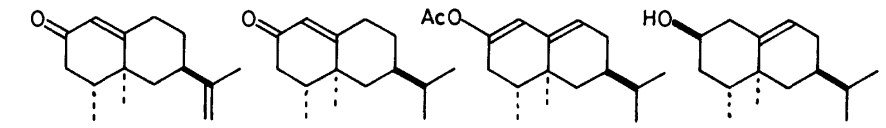

8 9 10 11

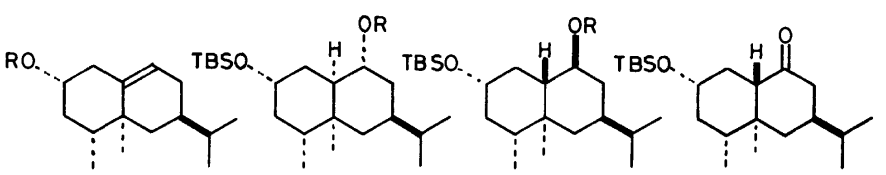

12 R = H
12a R = TBS
13 R = H
13a R = Ac
14 R = H
14a R = Ac
15

TBS = t-Bu$(CH_3)_2$Si

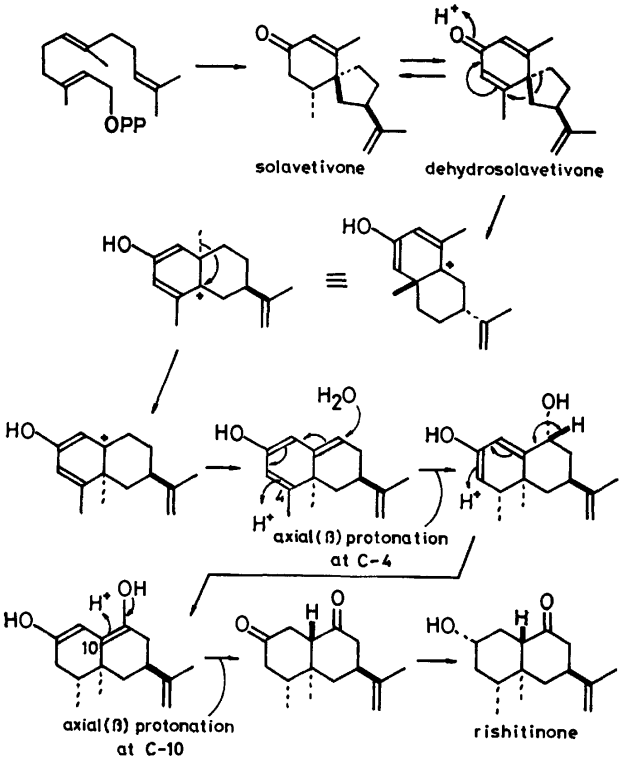

Scheme 1.

without epimerization at C-10 was effected by treatment with a 3 : 1 : 1 mixture of acetic acid, water, and tetrahydrofuran to give hydroxy ketone, mp 82—83 °C, $[\alpha]_D$ +7.8°, in 95% yield, which was identical with an authentic specimen of natural dihydrorishitinone (**2**) in all respects. All these results establish that the structure and configuration of (+)-rishitinone are represented by formula **1**.

Rishitinone (**1**), a stress metabolite with the valencane skeletone from diseased potato tubers, has a comparable fungitoxicity as rishitin, and would be qualified as a phytoalexin. In view of the facts that the phytoalexins (stress metabolites) produced in the Solanaceae plants possess structures which differ from usual sesquiterpenes in planar structure and/or configuration,[3] the following scheme 1 is proposed as one of plausible biogeneses for formation of the compound (**1**), considering the biosynthetic pathway of rishitin.[15]

Experimental

All the melting points were uncorrected. The purity of each compound was always checked by TLC over silica gel (Wakogel B-5 or Merck GF-254) with various solvent systems, and the spots were developed with cerium(IV) sulfate in dil sulfuric acid, iodine, and/or concd sulfuric acid. The optical rotations, UV, IR, and NMR (100 MHz) were measured in ethanol, in ethanol, in liquid state (oil) or in Nujol (crystals), and in chloroform-*d*, respectively, unless otherwise stated. The preparative TLC was carried out over silica gel (Merck GF-254), and the column chromatography over silica gel (Mallinckrodt AR-100) or silicic acid (Kiesel gel 60), respectively.

Isolation of Rishitinone (1). The neutral chloroform extracts[4] (83 g), obtained from the diseased potato tubers[4] (300 kg) were separated roughly into five fractions I—V by column chromatography over silica gel (1.8 kg), benzene, benzene–ethyl acetate (1 : 1), ether, ethyl acetate, and methanol being used as eluents, successively. Fraction III (5.5 g), yellow oil, corresponding to "fraction F,"[4] was treated with acetic anhydride and pyridine, and the acetate mixture was separated by column chromatography over silica gel to give a semi-crystalline mixture (3.4 g), composing of rishitin diacetate[4] and rishitinone acetate (**1a**). Fractional recrystallization of the mixture from hexane afforded pure rishitin diacetate (3.3 g), mp 65—67 °C, and crude **1a** (112 mg). The latter was again purified by chromatography over silica gel (5.0 g) with a 10 : 1 mixture of hexane–ethyl acetate as an eluent to yield a crude semi-crystalline acetate mixture (82 mg), which was subjected to repeated crystallization from hexane, the resulting crystals being removed by filtration. Pure rishitinone acetate (**1a**) (68 mg) was obtained from the filtrate as an oil, $[\alpha]_D$ −2.4°, which on hydrolysis with potassium carbonate in methanol at room temperature for 1 h under nitrogen gave rishitinone (**1**), mp 72—75 °C (from diisopropyl ether), $[\alpha]_D$ +10.1°; MS, *m/e* 236 (M^+), 221, 218, 203, 193, and 153 (base); IR, 3500, 3400, 1710, 1651, and 900 cm^{-1}; ^1H NMR, δ 0.76 (3H, s, 15-H), 0.84 (3H, d, J=7 Hz, 14-H), 1.76 (3H, s, 13-H), 3.65 (1H, m, W_H=25 Hz, 2-H), and 4.77 (2H, br s, 12-H); ^{13}C NMR, δ 12.9, 15.5, and 20.4 (each q), 30.2, 39.3, 42.8, 46.0, and 109.9 (each t), 41.3, 41.5, 56.1, and 69.5 (each d), 40.7, 147.4, and 211.1 (each s). Found: C, 76.38; H, 10.01%. Calcd for $C_{15}H_{24}O_2$: C, 76.22; H, 10.24%.

Acetylation and Hydrogenation of 1. Compound **1** (14 mg) was treated with acetic anhydride (0.2 ml) and pyridine (1 ml) at room tem erature for 6 h. The reaction mixture was worked up as usual to give rishitinone acetate (**1a**) (16 mg), oil, $[\alpha]_D$ −2.4°; MS, *m/e* 278 (M^+), 236, 218, 203 ,195, and 135 (base); IR, 1739, 1717, 1644, 1248, 1030, and 893 cm^{-1}; ^1H NMR, δ 0.73 (3H, s, 15-H), 0.89 (3H, d, J=6 Hz, 14-H), 1.75 (3H, s, 13-H), 2.02 (3H, s, $OCOCH_3$), 4.77 (1H, m, W_H= 25 Hz, 2-H), and 4.80 (2H, s, 12-H).

A solution of **1** (13 mg) in ethanol (1.0 ml) was hydrogenated over 5% palladized charcoal (1.5 mg) at room temperature for 20 h under stirring. After removal of the catalyst the reaction mixture was evaporated *in vacuo* to leave a colorless crystalline substance, which was recrystallized from diisopropyl ether to afford dihydrorishitinone (**2**) (12 mg), mp 80—82 °C, $[\alpha]_D$ +7.2°; ORD, $[\Phi]_{310}^{peak}$ +1140°, $[\Phi]_{268}^{trough}$ −1430°, a= 25.7; MS, *m/e* 238 (M^+), 223, 205, 195, 177, 166, 153, 140, and 97; IR, 3580, 3440, 1702, 1388, 1372, 1063, and 1027 cm^{-1}; ^1H NMR, δ 0.67 (3H, s, 15-H), 0.90 (3H, d, J=6 Hz, 14-H), 0.91 (6H, d, J=6 Hz, 12- and 13-H), and 3.61 (1H, m, W_H= 25 Hz, 2-H).

Reduction of 1a with Sodium Borohydride ($NaBH_4$). A solution of **1a** (12 mg) in ethanol (1.5 ml) was stirred with $NaBH_4$ (20 mg) at room temperature for 30 min under nitrogen. The reaction mixture was diluted with ether (30 ml), and the whole mixture was washed with water (10 ml) and saturated brine (10 ml), dried, and evaporated to leave a colorless oil (12 mg), showing a single spot on TLC, which crystallized on trituration with hexane. Recrystallization from hexane–diisopropyl ether afforded hydroxy acetate (**3**) (10 mg), mp 96—98 °C, $[\alpha]_D$ −6.9°; MS, *m/e* 280 (M^+), 262, and 220; IR, 3620, 3480, 1728, 1645, 1259, 1028, and 895 cm^{-1}; ^1H NMR in $CDCl_3$ and C_5D_5N, in Table 2.

Hydrogenation of Nootkatone (8). A solution of **8** (653 mg), mp 28—30 °C, $[\alpha]_D$ +172° (lit,[10] mp 28—30 °C, $[\alpha]_D$ +170°), and tris(triphenylphosphine)chlororhodium (450 mg) in benzene (90 ml) was stirred with hydrogen at room temperature for 14 h, and the mixture was passed through an activated alumina column (Merck, activity II—III, 30 g). The column

was eluted with benzene–ethyl acetate (1 : 1) (0.5 l), and the eluate was evaporated to give dihydronootkatone (**9**) (523 mg), showing a single spot on TLC, colorless oil, $[\alpha]_D$ +167°; MS, *m/e* 220 (M^+), 178, 177, and 135 (base); IR, 1670, 1621, 1435, 1414, 1383, 1372, 1355, and 1290 cm^{-1}; ^1H NMR, δ 0.69, 0.72, and 0.78 (each 3H, d, J=7 Hz, 12-, 13-, and 14-H, or *vice versa*), 1.08 (3H, s, 15-H), and 5.78 (1H, s, 1-H). Found: C, 81.45; H, 11.23%. Calcd for $C_{15}H_{24}O$: C, 81.76; H, 10.16%.

Treatment of ***9*** *with Acetic Anhydride and Perchloric Acid.* The Edwards reagent A,[12] an absolute ethyl acetate solution (50 ml) containing acetic anhydride (4.8 ml) and 60% perchloric acid (0.06 ml), was prepared according to the reported procedure. Compound **9** (350 mg) was dissolved in the soltion and stirred at room temperature for 10 min. The reaction mixture was mixed with 5% aqueous sodiumhydrogencarbonate (20 ml), shaken, and separated. The aqueous solution was extracted with ethyl acetate (2 × 10 ml). The combined acetate solution was washed with 2 M hydrochloric acid (10 ml), 5% aqueous sodium hydrogencarbonate (10 ml), and saturated brine (10 ml), dried, and evaporated to yield an oily substance (362 mg), which was purified by column chromatography over silica gel (15 g). Elution with hexane–ethyl acetate (20 : 1) afforded dienol acetate (**10**) (353 mg), showing a single spot on TLC, oil, $[\alpha]_D$ +45.3°; MS, *m/e* 262 (M^+), 236, 220, and 177; IR, 1759, 1664, and 1212 cm^{-1}; ^1H NMR, δ 0.90 (12H, br s, 12-, 13-, 14-, and 15-H), 2.12 (3H, s, $OCOCH_3$), 5.42 (1H, m, W_H=10 Hz, 9-H), and 5.71 (1H, s, 1-H).

Reduction of ***10*** *with* $NaBH_4$. A solution of **10** (300 mg) in ethanol (20 ml) was stirred with $NaBH_4$ (300 mg) at room temperature for 3 h. The reaction mixture was evaporated *in vacuo*, mixed with water (30 ml), and extracted with ether (50 ml). The ether solution was worked up as usual to leave an oily substance, consisting of two components on TLC, which were successively separated by column chromatography over silica gel (20 g) with hexane–ethyl acetate (5 : 1) as an eluent to give two epimeric homoallyl alcohols (**11**) (22 mg) and (**12**) (118 mg): **11**, oil, $[\alpha]_D$ −30.7°; MS, *m/e* 222 (M^+), 204, 189, 175, and 161; IR, 3300, 1382, 1365, 1060, 1024, and 1002 cm^{-1}; ^1H NMR, δ 0.90 (12H, br s, 12-, 13-, 14-, and 15-H), 2.58 (1H, dt, J=14 and 2 Hz, 1-H), 3.99 (1H, m, W_H=8 Hz, 2-H), and 5.43 (1H, m, W_H=12 Hz, 9-H): **12**, oil, $[\alpha]_D$ −34.2°; MS, *m/e* 222 (M^+), 204, 189, 179, and 161; IR, 3320, 1381, 1368, and 1021 cm^{-1}; ^1H NMR, δ 0.90 (12H, br s, 12-, 13-, 14-, and 15-H), 3.56 (1H, m, W_H=25 Hz, 2-H), and 5.38 (1H, m, W_H=12 Hz).

t-*Butyldimethylsilylation of* ***12***. A solution of **12** (104 mg) in *N*,*N*-dimethylformamide (4 ml) was stirred with *t*-butyldimethylsilyl (TBS) chloride (200 mg) and imidazole (180 mg) at room temperature for 8 h. The reaction mixture was cooled, diluted with water (30 ml), and extracted with ether (4 × 20 ml). The combined ether solutions were washed with water (2 × 30 ml), dried, and evaporated to give practically pure silyl ether (**12a**) (120 mg), showing a single spot on TLC, oil, $[\alpha]_D$ −16.3°; MS, *m/e* 337 (M^+ +1), 279, 203, and 147 (base); IR, 1460, 1370, 1258, 1100, 1060, 910, 883, 850, and 839; ^1H NMR, δ 0.90 (12H, br s, 12-, 13-, 14- and 15-H), 3.49 (1H, m, W_H=25 Hz, 2-H), and 5.35 (1H, m, W_H=12 Hz, 9-H).

Hydroboration of ***12a*** *Followed by Oxidation.* To a cooled solution of **12a** (110 mg) in tetrahydrofuran (THF) (0.5 ml) at 0 °C was added a 1.87 M solution of diborane in THF (0.5 ml). The mixture was stirred at room temperature for 1 h and cooled at 0 °C, and water (2 ml) was then added to decompose the excess reagent. The aqueous mixture was stirred with 3 M aqueous sodium hydroxide (0.1 ml) and 30% hydrogen peroxide (0.2 ml) at 0 °C for 1 h. The reaction mixture was diluted with water (20 ml) and extracted with ether (5 × 10 ml). The combined ether solution was worked up as usual to leave an oily residue (113 mg), which was separated into three fractions by column chromatography over silica gel with hexane–ethyl acetate (1 : 1) as an eluent. The most mobile fraction (25 mg) gave the practically pure starting alkene (**12a**). The middle fraction (8 mg) showed three spots on TLC and was then treated with acetic anhydride (0.1 ml) and pyridine (1 ml) at room temperature overnight for purification. The reaction mixture was purified by preparative TLC over silica gel with hexane–ethyl acetate (10 : 1) as a solvent. A fraction with R_f value of 0.36 afforded 9*α*-acetate (**13a**) (4 mg) in pure state, oil, $[\alpha]_D$ −2.8°; MS, *m/e* 395 (M^+ −1), 339, 335, 279, and 205; IR, 1721, 1252, 1100, 1051, 1020, 855, and 836 cm^{-1}; ^1H NMR, δ 0.05 (6H, s), 0.88 (9H, s), and 0.90 (br s, 12-, 13-, 14-, and 15-H), 2.04 (3H, s, $OCOCH_3$), 3.60 (1H, m, W_H=25 Hz), and 5.00 (1H, q, J=4 Hz, 9-H). The least mobile fraction (49 mg), showing a single spot on TLC, was purified by preparative TLC to give 9*β*-alcohol (**14**), oil, $[\alpha]_D$ +38.0°; MS, *m/e* 354 (M^+), 229, 205, and 75 (base); IR, 3360, 1258, 1100, 1077, 1050, 1038, 859, 837, and 773 cm^{-1}; ^1H NMR, δ 0.05 (6H, s), 0.72 (3H, s, 15-H), 0.88 (9H, s), 0.90 (9H, br s, 12-, 13-, and 14-H), 3.49 (1H, dt, J=4.5 and 10 Hz, 9-H), and 3.58 (1H, m, W_H= 25 Hz, 2-H). Compound **14** (49 mg) was converted by treatment with acetic anhydride (0.5 ml) and pyridine (2 ml) at room temperature for 14 h into the corresponding 9*β*-acetate (**14a**) (52 mg), oil, $[\alpha]_D$ +35.5°; MS, *m/e* 395 (M^+ −1), 335, 279, and 205 (base); IR, 1740, 1240, 1238, 1100, 1077, 1053, 1030, 856, 833, and 770 cm^{-1}; ^1H NMR, δ 0.05 (6H, s), 0.76 (3H, s, 15-H), 0.88 (9H, s), 0.90 (9H, br s, 12-, 13-, and 14-H), 2.02 (3H, s, $OCOCH_3$), 3.76 (1H, m, W_H= 25 Hz, 2-H), and 4.74 (1H, dt, J=4 and 11 Hz).

Collins Oxidation of ***14***. A mixture of chromium(VI) oxide (54 mg) and pyridine (54 μl) in dichloromethane (0.8 ml) was stirred at room temperature for 15 min under nitrogen. To the mixture was added a solution of **14** (16 mg) in dichloromethane (0.2 ml) under stirring. The mixture was further stirred at room temperature for 15 h, and diluted with ether (40 ml) and filtered. The filtrate was washed with 5% aqueous sodium hydrogencarbonate (2 × 30 ml), dried, and evaporated to yield a crystalline substance, which on recrystallization from diisopropyl ether gave ketone (**15**) (15 mg), mp 51—53 °C, $[\alpha]_D$ +2.1°; MS, *m/e* 352 (M^+), 337, 309, and 295 (base); IR, 1717, 1468, 1390, 1380, 1372, 1362, 1258, 1101, 1080, 1057, 860, 839, and 778 cm^{-1}; ^1H NMR, δ 0.05 (6H, s), 0.66 (3H, s, 15-H), 0.88 (9H, s), 0.90 (9H, br s, 12-, 13-, and 14-H), 3.78 (1H, m, W_H=25 Hz, 2-H).

Hydrolysis of ***15***. A solution of **15** (14 mg) in a 3 : 1 : 1 mixture (2 ml) of acetic acid, water, and THF was stirred at room temperature for 17 h. The reaction mixture was diluted with ether (40 ml) and washed with 5% aqueous sodium hydrogencarbonate (15 ml), dried, and evaporated to leave a crystalline substance, which on recrystallization from diisopropyl ether afforded hydroxy ketone (7 mg), mp 82—83 °C, $[\alpha]_D$ +7.8°; MS, *m/e* 238 (M^+), 223, 220, 205, 195, 177, 168, 167, 166, 153, 140, and 97; IR, 3580, 3440, 1702 1063, and 1027 cm^{-1}; ^1H NMR, δ 0.66 (3H, s, 15-H), 0.89 (6H, d, J=6 Hz, 12- and 13-H), 0.91 (3H, d, J=6 Hz, 14-H), and 3.62 (1H, m, W_H=25 Hz, 2-H). The compound was identical with an authentic sampel of dihydrorishitinone (**2**) derived from natural rishitinone (**1**) in all respects (TLC, $[\alpha]_D$, MS, IR, ^1H NMR, and mixed mp).

References

1) Part XXXV of "Studies on the Phytoalexins." Part XXXIV, N. Katsui, F. Yagihashi, A. Murai, and T. Masamune, *Bull. Chem. Soc. Jpn.*, **55**, 2424 (1982).

2) N. Katsui, F. Yagihashi, A. Murai, and T. Masamune, *Chem. Lett.*, **1980**, 1455.

3) T. Masamune, A. Murai, and N. Katsui, *Kagaku To Seibutsu*, **16**, 648 (1978).

4) T. Masamune, A. Murai, M. Takasugi, A. Matsunaga, N. Katsui, N. Sato, and K. Tomiyama, *Bull. Chem. Soc. Jpn.*, **50**, 1201 (1977). The extracts corresponded to "neutral syrup," described in the section of "Isolation of rishitin" of this reference.

5) The abbreviation (■) denotes a carbon atom bearing no hydrogen atom.

6) T. R. Govindachari, P. A. Mohamed, and P. C. Parthasarathy, *Tetrahedron*, **26**, 615 (1970).

7) C. H. Heathcock and T. R. Kelly, *Tetrahedron*, **24**, 1801 (1968); J. A. Mareall and A. R. Hochstetler, *J. Am. Chem. Soc.*, **91**, 648 (1969); J. D. Godfrey and A. G. Schultz, *Tetrahedron Lett.*, **1979**, 3241.

8) *Cf.*, R. F. Zürcher, *Helv. Chim. Acta*, **44**, 1380 (1961); **46**, 2054 (1963); N. S. Bhacca and D. H. Williams, "Application of NMR Spectroscopy in Organic Chemistry," Holden-Day, San Francisco (1964), p. 14.

9) P. V. Demarco, E. Farkas, D. Doddrell, B. L. Mylari, and E. Wenkert, *J. Am. Chem. Soc.*, **90**, 5480 (1968).

10) Y. Takagi, Y. Nakahara, and M. Matsui, *Tetrahedron*, **34**, 517 (1978), and references cited therein.

11) M. Brown and L. W. Piszkiewicz, *J. Org. Chem.*, **32**, 2013 (1967).

12) B. E. Edwards and P. N. Rao, *J. Org. Chem.*, **31**, 324 (1966).

13) H. C. Brown and G. Zweifel, *J. Am. Chem. Soc.*, **83**, 2544 (1961).

14) K. Naya, M. Kawai, and T. Kasai, *Chem. Lett.*, **1972**, 241.

15) A. Murai, S. Sato, A. Osada, N. Katsui, and T. Masamune, *J. Chem. Soc., Chem. Commun.*, **1982**, 32.

Synthesis of Paracyclo(1,8)napthalenophane and Paracyclo(5,6)acenaphthenophane[1]

Akira KASAHARA,* Taeko IZUMI, Iwao SHIMIZU, Masahiro SATOU, and Takao KATOU
Department of Applied Chemistry, Faculty of Engineering, Yamagata University, Yonezawa 992
(Received December 5, 1981)

[2]Paracyclo[2]paracyclo[2](1,8)naphthalenophan-9-ene-1,17-diyne, [0]paracyclo[2]paracyclo[0](5,6)acenaphthenophan-7-ene, and [2]paracyclo[2]paracyclo[2](5,6)acenaphthenophan-9-ene-1,17-diyne, were synthesized by intramolecular reductive coupling reaction of the corresponding carbonyl compounds with low-valent titanium reagent. The structures of the compounds were elucidated by NMR analyses, and the transannular π-electronic interactions between two benzene rings were examined on the basis of electronic spectra.

Recently, a wide variety of [2.2]phanes containing benzene or heteroaromatic rings has been synthesized in order to study the effect of transannular π-electronic interactions on their physical and chemical properties.[2] However, there are only a few investigations of paracyclonaphthalenophane having a bridged system in a peri-position of the naphthalene ring: the only compounds of this class which have been described are [0]paracyclo[2]paracyclo[0](1,8)naphthalenophane[3](**1**) and [0]paracyclo[2]paracyclo[0](1,8)naphthalenophan-7-ene[3] (**2**). The distance between atoms 1 and 8 in naphthalene is 2.44 Å, while the van der Waals separation in the parallel π-system is 3.4 Å.[4] Thus, in compounds **1** and **2**, substantial repulsive interactions must exist between the two peri-aryl rings, which are bound closely by ethano bridges at both ends. These results have prompted us to study the synthesis of [2]paracyclo[2]paracyclo[2](1,8)naphthalenophan-9-ene-1,17-diyne (**3**), [0]paracyclo[2]paracyclo[0](5,6)-acenaphthenophane (**4**), [0]paracyclo[2]paracyclo[0]-(5,6)acenaphthenophan-7-ene (**5**), and [2]paracyclo-[2]paracyclo[2](5,6)acenaphthenophan-9-ene-1,17-diyne (**6**).

Experimental

Materials and Measurement. All the melting points are uncorrected. 1,8-Diiodonaphthalene (**7**),[5] 5,6-dibromoacenaphthene (**8**),[6] 5,6-diiodoacenaphthene (**9**),[7] 5-iodoacenaphthene (**10**),[7] (*p*-bromophenylethynyl)trimethylsilane (**11**),[8] and *p*-bromobenzaldehyde ethylene acetal (**12**)[9] were prepared as described in the literature. The IR, NMR, mass, and electronic spectra were recorded with a Hitachi 260-10, a Hitachi R-22, a Hitachi RMU-6M, and a Hitachi 200-10 spectrometer, respectively.

*p-Ethynylbenzaldehyde Diethyl Acetal (**15**).* The Grignard reagent prepared from **11** (10.2 g, 0.04 mol) and 1.0 g (0.042 mol) of magnesium turning in 80 ml of dry THF was cooled to 20 °C; a solution of 2.8 g (0.038 mol) of anhydrous *N,N*-dimethylformamide in 20 ml of dry THF was then added dropwise over a 0.5 h period. After the addition was complete, the reaction was stirred for 4 h and then was allowed to remain overnight under a nitrogen atmosphere. The mixture was hydrolyzed with a saturated aqueous solution of ammonium chloride, the organic layers were separated, and the aqueous layers were extracted twice with a 50 ml portion of ether. The organic layers and ether extracts were combined and dried over anhydrous $MgSO_4$. After removal of the solvent under reduced pressure, the residue was chromatographed in benzene on silica gel. Colorless crystals of (*p*-formylphenylethynyl)-trimethylsilane (**13**), mp 56—58 °C, were obtained in 80% yield (6.5 g). IR (KBr): 2150 (–C≡C–), 1700 cm^{-1} (–CHO). NMR ($CDCl_3$): δ=0.18 (s, 9H, –C<u>H</u>$_3$), 7.47 (d, 2H, Ar–<u>H</u>), 7.68 (d, 2H, Ar–<u>H</u>), 9.87 ppm (s, 1H, –C<u>H</u>O). Found: C, 71.08; H, 6.86%. Calcd for $C_{12}H_{14}OSi$: C, 71.23; H, 6.97%.

A solution of **13** (5.6 g, 0.028 mol), triethyl orthoformate (5.5 g, 0.037 mol), and *p*-toluenesulfonic acid (0.16 g) in ethanol (20 ml) was refluxed for 5 h under stirring. After pouring into an aqueous solution of ammonia (50 ml), the mixture was extracted with ether. The extracts were then washed successively with aqueous ammonia and a saturated sodium chloride solution, dried over potassium carbonate, and evaporated to give a dark red liquid: [*p*-(diethoxymethyl)phenylethynyl]trimethylsilane (**14**). The liquid shows no IR absorption due to a formyl group, but it does show that due to an acetal. IR (neat): 1100, 1070, 1050 cm^{-1}.

The crude product (**14**) in methanol (200 ml) was stirred with a solution of potassium hydroxide (3.6 g) in water (36 ml). The mixture was then heated under reflux for an additional 3 h, poured into water (1000 ml), and extracted with ether. The extracts were washed with a saturated sodium chloride solution and dried over potassium carbonate. The dark red liquid which remained after the evaporation of the solvents was distilled under reduced pressure to give **15**, a colorless liquid, bp 98—103 °C/2 mmHg,† 4.1 g (72% yield based on **13**). IR (neat): 3350 (–C≡C–H), 2150 (–C≡C–), 1100, 1040 cm^{-1} (–C–O–C–). NMR ($CDCl_3$): δ=1.16 (t, 6H, –C<u>H</u>$_3$), 3.02 (s, 1H, –C≡C–<u>H</u>), 3.54 (q, 4H, –C<u>H</u>$_2$–), 5.47 (s, 1H, –C–<u>H</u>), 7.06 (d, 2H, Ar–<u>H</u>), and 7.68 ppm (d, 2H, Ar–<u>H</u>). Found: C, 76.35; H, 7.81%; M^+, 204. Calcd for $C_{13}H_{16}O_2$: C, 76.44; H, 7.89%; M, 204.

*1,8-Bis(p-formylphenylethynyl)naphthalene (**17**).* A mixture of **7** (9.6 g, 25 mmol), **15** (10.2 g, 50 mmol), copper(I) iodide (0.048 g, 0.25 mmol), dichlorobis(triphenylphosphine)palladium(II) (0.70 g, 1 mmol), and diethylamine (180 ml) was heated under nitrogen in an autoclave at 80 °C for 10 h. After the removal of diethylamine under reduced pressure, ether and water were added to the residue. The ether phase was separated, washed thoroughly with 10% hydrochloric acid, a saturated sodium hydrogencarbonate solution, and a saturated sodium chloride solution, dried over anhydrous magnesium sulfate, filtered, and concentrated. The residue was purified by column chromatography (silica gel–benzene). First elution with benzene gave 1-(*p*-formylphenylethynyl)-8-iodonaphthalene (**16**), colorless needles, mp 113—115 °C in 42% yield (4.05 g): IR (KBr): 2200 (–C≡C–), 1700 cm^{-1} (–CHO). NMR ($CDCl_3$): δ=7.36—7.93 (m, 10H, Ar–<u>H</u>), 9.95 ppm (s, 1H, –C<u>H</u>O). Found: C, 59.55; H, 2.78%; M^+ 382. Calcd for $C_{19}H_{11}IO$: C, 59.70; H, 2.90%; M, 382.

A second elution with benzene afforded 3.39 g (35% yield) of **17**, colorless needles, mp 168—169 °C. IR (KBr): 2200

† 1 mmHg ≈ 133.322 Pa.

(-C≡C-), 1700 cm^{-1} (-CHO). NMR ($CDCl_3$): δ=7.42—7.95 (m, 14H, Ar-H), 9.98 ppm (s, 2H, -CHO). Found: C 87.40; H, 4.68%; M^+, 384. Calcd for $C_{28}H_{20}O_2$: C, 87.48; H, 4.79%; M, 384.

5,6-Bis(p-formylphenyl)acenaphthene (19). Under a nitrogen atmosphere, the Grignard reagent prepared from **12** (9.1 g, 40 mmol) and magnesium turnings (1.2 g, 49 mmol) in dry THF (60 ml) was dropwise added to a mixture of **8** (2.5 g, 8 mmol) and dichloro[1,3-bis(diphenylphosphino)propane]-nickel(II) (0.9 g, 1.6 mmol) in dry THF (60 ml) at 0 °C with stirring over 2.5 h. The reaction mixture was stirred for 4 h at 0 °C and then was allowed to remain overnight at room temperature. The mixture was hydrolyzed with 10% hydrochloric acid under cooling with an ice bath. The organic layers and ether extracts from the aqueous layer were combined, washed with 10% hydrochloric acid, water, a saturated sodium hydrogencarbonate solution, and water again, and then dried over anhydrous $MgSO_4$. After removal of the solvents, the residue was purified by column chromatography (silica gel–benzene). The first elution with benzene gave 5-(*p*-formylphenyl)-6-bromoacenaphthene (**18**), colorless needles, mp 115—116 °C, in 37% yield (1.00 g). IR (KBr): 1690 (-CHO), 1600, 810 cm^{-1}. NMR ($CDCl_3$): δ=3.36 (s, 4H, -CH$_2$-), 7.09 (d, J=7 Hz, 2H, Ar-H), 7.47 (d, J=8 Hz, 2H, Ar-H), 7.62 (d, J=7 Hz, 2H, Ar-H), 7.83 (d, J=8 Hz, 2H, Ar-H), 10.02 ppm (s, 1H, -CHO). Found: C, 67.58; H, 3.80%; M^+, 337. Calcd for $C_{19}H_{13}BrO$: C, 67.67; H, 3.88%; M, 337.

The second elution with benzene afforded 0.37 g (13% yield) of **19**, colorless needles, mp 244—245 °C. IR (KBr): 1695 (-CHO), 1600, 810 cm^{-1}. NMR ($CDCl_3$): δ =3.49(s, 4H, -CH$_2$-), 7.07 (d, J=7 Hz, 4H, Ar-H), 7.33 (d, J=8 Hz, 2H, Ar-H), 7.39 (d, J=7 Hz, 4H, Ar-H), 7.45 (d, J=8 Hz, 2H, Ar-H), 9.97 ppm (s, 2H, -CHO). Found: C, 86.02; H, 4.88%; M^+, 362. Calcd for $C_{26}H_{18}O_2$: C, 86.16; H, 5.01%; M, 362.

5,6-Bis(p-formylphenylethynyl)acenaphthene (21). In the presence of $(Ph_3P)_2PdCl_2$ and CuI, the palladium-catalyzed substitution of **9** with **15** was carried out in the same way as described for **17**, and 5-(*p*-formylphenylethynyl)-6-iodoacenaphthene (**20**) (colorless needles, mp 154—155 °C) and **21** (pale yellow needles, mp 175—176 °C) were obtained in 24 and 50% yields, respectively.

20: IR (KBr): 2190 (-C≡C-), 1690 cm^{-1} (-CHO). NMR ($CDCl_3$): δ=3.33 (s, 4H, -CH$_2$-), 7.05—7.77 (m, 8H, Ar-H), 9.96 ppm (s, 1H, -CHO). Found: C, 61.63; H, 3.13%; M^+, 408. Calcd for $C_{21}H_{13}IO$: C, 61.78; H, 3.21%; M, 408.

21: IR (KBr): 2200 (-C≡C-), 1690 cm^{-1} (-CHO). NMR ($CDCl_3$): δ=3.41 (s, 4H, -CH$_2$-), 7.29 (d, J=7 Hz, 2H, Ar-H), 7.41 (d, J=8 Hz, 4H, Ar-H), 7.55 (d, J=7 Hz, 2H, Ar-H), 7.78 (d, J=8 Hz, 4H, Ar-H), 9.90 ppm (s, 2H, -CHO). Found: C, 87.70; H, 4.33%; M^+, 410. Calcd for $C_{30}H_{18}O_2$: C, 87.78; H, 4.42%; M, 410.

The Intramolecular Reductive Coupling of 17 with $TiCl_4$–$LiAlH_4$. To a solution of $TiCl_4$ (9.5 g, 0.05 mol) in dry THF (200 ml) was added $LiAlH_4$ (0.90 g, 0.024 mol) with cooling under a nitrogen atmosphere. The mixture was refluxed for 2 h; to the metal complex solution thus obtained, was added dropwise a solution of **17** (3.84 g, 0.01 mol) and tributylamine (1.86 g, 0.01 mol) in dry THF (250 ml) over 8 h under refluxing, followed by an additional 10 h period of reflux. The reaction mixture was then cooled to room temperature and quenched with 20% aqueous K_2CO_3 solution. After filtration, the filtrate was extracted with chloroform. The chloroform extracts were washed with water and dried over anhydrous $MgSO_4$. After removal of the solvents, the residue was dissolved in hexane and chromatographed on silica gel.

The first fraction, eluted with hexane, gave colorless needles, mp 115—117 °C, in 35% yield, which were identified as 1,8-bis(*p*-tolylethynyl)naphthalene (**22**) by a comparison of the IR, NMR, and mass spectra and by a mixed-melting-point determination with an authentic sample (lit,[10] mp 116—117 °C).

The second fraction, eluted with hexane, gave 1,8-bis[[(*p*-hydroxymethyl)phenyl]ethynyl]naphthalene (**23**) (from CH_3-OH), colorless needles, mp 166—167 °C, in 11% yield. IR (KBr): 3300 (-OH), 2150 (-C≡C-), 1600, 1500, 860 cm^{-1} *p*-disubstituted benzene ring). NMR ($CDCl_3$): δ=2.32 (br-s, 2H, -OH), 4.58 (s, 4H, -CH$_2$-), 7.14—7.54 ppm (m, 10H, Ar-H). Found: C, 86.46; H, 5.07%; M^+, 388. Calcd for $C_{28}H_{20}O_2$: C, 86.57; H, 5.19%; M, 388.

The third fraction, eluted with hexane, gave **3** (from benzene–hexane), pale yellow needles, mp 239—241 °C (decomp), in 7.5% yield. IR (KBr): 1660, 1600, 1500, 830, 770, 750, 720, 690 cm^{-1}. Found: C, 95.28; H, 4.51%; M^+, 352. Calcd for $C_{28}H_{16}$: C, 95.42; H, 4.58%; M, 352.

The Intramolecular Reductive Coupling of 19 with $TiCl_4$–Zn. To a solution of $TiCl_4$ (2.6 g, 14 mmol) in dry THF (70 ml) was added Zn dust (1.8 g, 28 mmol) with cooling. The mixture was refluxed 1.5 h under a nitrogen atmosphere to give a deep black solution. To the metal complex solution thus obtained was added a solution of **19** (1.0 g, 2.8 mmol) and dry pyridine (0.20 g) in dry THF (150 ml) over 9.5 h under refluxing, followed by an additional 10 h period of refluxing. The reaction mixture was then cooled to room temperature and quenched with 20% K_2CO_3 solution. After filtration, the filtrate was extracted with $CHCl_3$. The $CHCl_3$ extracts were washed with water and dried over $MgSO_4$. After removal of the solvents, the residue was dissolved in hexane and chromatographed on silica gel.

The first fraction, eluted with hexane, gave 5,6-di-*p*-tolylacenaphthene (**24**), colorless needles, mp 142—144 °C, in 12.5% yield. IR (KBr): 1600, 1510, 820, 800 cm^{-1}. Found: C, 93.32; H, 6.57%; M^+, 334. Calcd for $C_{26}H_{22}$: C, 93.37; H, 6.63%; M, 334. The compound **24** is identical in all respects with 5,6-di-*p*-tolylacenaphthene, which was prepared by the nickel-phosphine catalyzed Grignard cross coupling reaction of **8** with *p*-tolylmagnesium bromide.

The second fraction, eluted with hexane, gave **5**, pale yellow needles, mp 186—188 °C, in 24% yield. IR (KBr): 1600, 1490, 825, 805, 720, 690 cm^{-1}. Found: C, 94.44; H, 5.40%; M^+, 330. Calcd for $C_{26}H_{18}$: C, 94.51; H, 5.49%; M, 330.

The third fraction, eluted with benzene, gave [0]paracyclo-[2]paracyclo[0](5,6)acenaphthenophane-7,8-diol (**25**), colorless needles, mp 210—211 °C (decomp), in 2.5% yield. IR (KBr): 3420 (-OH), 1610, 1600, 1500, 835, 810, 715, 690 cm^{-1}. Found: C, 85.60; H, 5.45%; M^+, 364. Calcd for $C_{26}H_{20}O_2$: C, 85.69; H, 5.53%; M, 364.

The Catalytic Hydrogenation of 5 to 4. In the mixture of THF (10 ml) and ethanol (70 ml), **5** (0.4 g) was hydrogenated with PtO_2 (0.1 g) at room temperature under ordinary pressure. The reaction mixture was filtered to remove the catalyst and the filtrate was evaporated. The residue was chromatographed on silica gel with hexane to give 0.35 g (87.5% yield) of **4**, colorless needles, mp 263—265 °C. IR (KBr): 1600, 1500, 820, 800, 725, 695 cm^{-1}. Found: C, 93.87; H, 6.58%; M^+, 332. Calcd for $C_{26}H_{20}$: C, 93.94; H, 6.06%; M, 332.

The Intramolecular Reductive Coupling of 21 with $TiCl_4$–Zn. The reductive coupling of **21** was carried out in the same way as described for the reaction of **19** with $TiCl_4$–Zn, and the products were separated by chromatography on silica gel. The first fraction, eluted with hexane, gave 5,6-bis(*p*-tolylethynyl)acenaphthene (**26**), pale yellow needles, mp 179—180 °C, in 8.5% yield. IR (KBr): 1590, 1490, 830, 800 cm^{-1}.

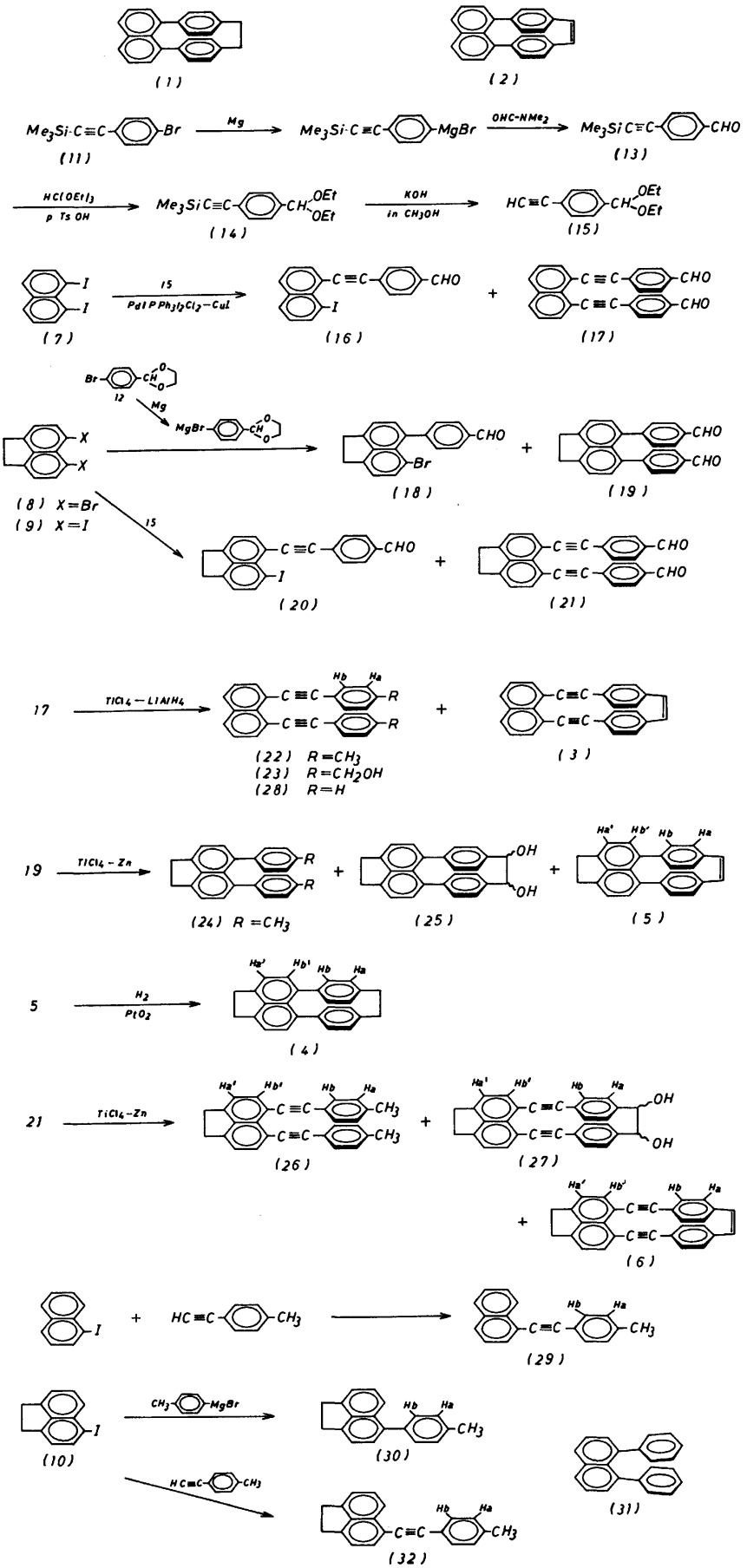

Scheme 1.

Found: C, 94.07; H, 5.71%; M+, 382. Calcd for $C_{30}H_{22}$: C, 94.20; H, 5.80%; M, 382. The compound **26** is identical in all respects with 5,6-bis(*p*-tolylethynyl)acenaphthene, which was prepared by the palladium-catalyzed substitution of **9** with *p*-tolylacetylene.

The second fraction, eluted with hexane, gave **6**, yellow needles, mp 219—220 °C, in 32% yield. IR (KBr): 1630, 1600, 1500, 900, 840, 810, 765, 720, 690 cm^{-1}. Found: C, 95.08; H, 4.68%; M+, 378. Calcd for $C_{30}H_{18}$: C, 95.21; H, 4.79%; M, 378.

The third fraction, eluted with benzene–$CHCl_3$ (4 : 1), gave [2]paracyclo[2]paracyclo[2](5,6)acenaphthenophane-9,10-diol (**27**), yellow needles, mp 219—221 °C, in 15% yield. IR (KBr): 3350 (-OH), 1590, 1490, 1020, 820, 715, 690 cm^{-1}. Found: C, 87.24; H, 4.80%; M+, 412. Calcd for $C_{30}H_{20}O_2$: C, 87.35; H, 4.89%; M, 412.

1-p-Tolylethynylnaphthalene (29). In the presence of $(Ph_3P)_2PdCl_2$ and CuI, the palladium-catalyzed substitution of 1-iodonaphthalene with *p*-tolylacetylene was carried out in the same way as described for **17**, and the compound **29**, colorless needles, mp 61—63 °C (from CH_3OH), was obtained in 78% yield. IR (KBr): 1600, 1500, 810, 790, 765 cm^{-1}. Found: C, 94.04; H, 5.77%; M+, 242. Calcd for $C_{19}H_{14}$: C, 94.18; H, 5.82%; M, 242.

5-p-Tolylacenaphthene (30). In the presence of dichloro-[1,3-bis(diphenylphosphino)propane]nickel(II), the cross coupling reaction of **10** with *p*-tolylmagnesium bromide in dry THF was carried out in the same way as described for **19**, and the compound **30**, colorless needles, mp 55—57 °C (from CH_3OH) was obtained in 63% yield. IR (KBr): 1600, 1500, 840, 790, 760, 720 cm^{-1}. Found: C, 93.28; H, 6.51%; M+, 244. Calcd for $C_{19}H_{16}$: C, 93.40; H, 6.60%; M, 244.

5,6-Di-p-tolylacenaphthene (24). In the presence of nickel phosphine complex, the cross coupling reaction of **8** with *p*-tolylmagnesium bromide in dry THF was carried out in the same way as described for **19**, and the compound **24**, mp 142—144 °C, was obtained in 65% yield.

5-p-Tolylethynylacenaphthene (32). In the presence of $(Ph_3P)_2PdCl_2$ and CuI, the palladium-catalyzed substitution of **10** with *p*-tolylacetylene was carried out in the same way as described for **17**, and the compound **32**, colorless needles, mp 116—118 °C (from ethanol) was obtained in 67% yield. IR (KBr): 1600, 1500, 830, 800 cm^{-1}. Found: C, 93.92; H, 5.89%; M+, 268. Calcd for $C_{21}H_{16}$: C, 93.99; H, 6.01%; M, 268.

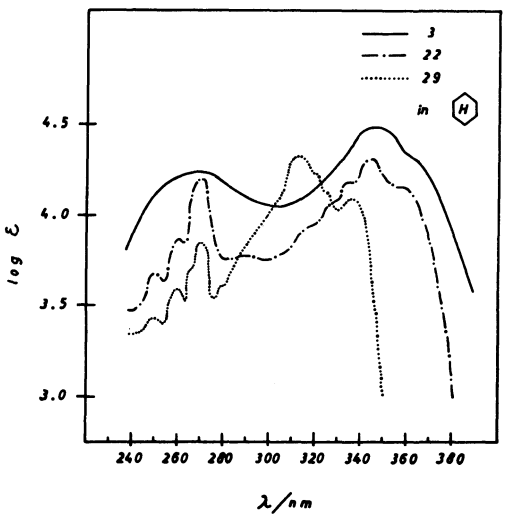

Fig. 1. Electronic spectra of **3**, **22**, and **29**.

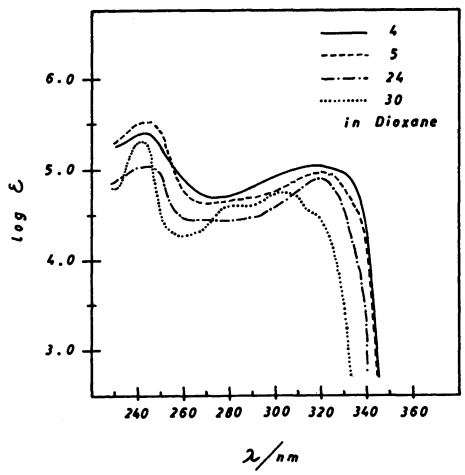

Fig. 2. Electronic spectra of **4**, **5**, **24**, and **30**.

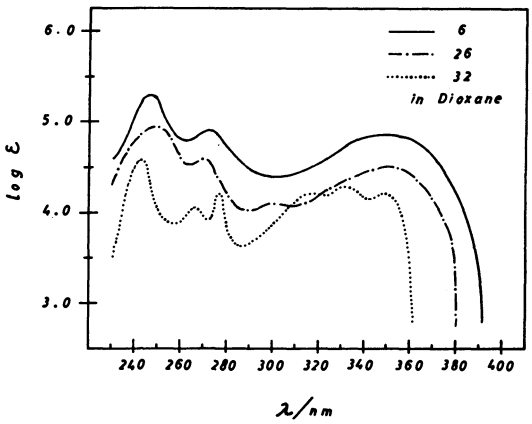

Fig. 3. Electronic spectra of **6**, **26**, and **32**.

Table 1. IR spectra of cyclophanes around 700 cm^{-1}

Compound	Wave number/cm^{-1}
3	720, 690
4	725, 700
5	700, 690
6	720, 690
25	715, 690
27	715, 690

5,6-Bis(p-tolyethynyl)acenaphthene (26). In the presence of $(Ph_3P)_2PdCl_2$ and CuI, the palladium-catalyzed substitution of **9** with *p*-tolylacetylene was carried out in the same way as described for **17**, and the compound **26**, mp 179—180 °C, was obtained in 58% yield.

Results and Discussion

A number of synthetic methods have been recently developed for [2.2]cyclophane.[11] The naphthalenophane **1** has been prepared by pyrolytic method of sulfone derivative **31**.[3] But a reductive coupling of carbonyl compounds with low valent titanium reagents[12] is still very convenient and advantageous for the synthesis of cyclophane because of the facile availability of the intermediary compounds.[13]

In the present work, we applied the same method for

TABLE 2. NMR SPECTRA OF THE CYCLOPHANE AND REFERENCE COMPOUNDS (δ, IN $CDCl_3$)

Compound	Aromatic protons	Naphthalene or acenaphthene ring	Other protons
3	$\underline{H}_a$, $\underline{H}_b$ } 6.39(s, 8H)	7.40—7.76(m, 6H, Ar-$\underline{H}$)	7.18(s, 2H, -C$\underline{H}$=C$\underline{H}$-)
22	$\underline{H}_a$ 6.91(d, J=8 Hz, 4H) $\underline{H}_b$ 7.23(d, J=8 Hz, 4H)	7.12—7.81(m, 6H, Ar-$\underline{H}$)	2.28(s, 6H, -C$\underline{H}_3$)
29	$\underline{H}_a$ 7.17(d, J=8 Hz, 2H) $\underline{H}_b$ 7.53(d, J=8 Hz, 2H)	7.31—7.88(m, 7H, Ar-$\underline{H}$)	2.35(s, 3H, -C$\underline{H}_3$)
4	H_a 6.41(d, J=8 Hz, 4H) H_b 6.54(d, J=8 Hz, 4H)	$\underline{H}_a$, 7.31(d, J=7 Hz, 2H) $\underline{H}_b$, 7.49(d, J=7 Hz, 2H) $\underline{H}$-$_{CH_2}$-3.44(s, 4H)	3.07(s, 4H, bridged-C$\underline{H}_2$-)
5	$\underline{H}_a$ 6.56(d, J=8 Hz, 4H) $\underline{H}_b$ 6.62(d, J=8 Hz, 4H)	$\underline{H}_a$, 7.34(d, J=7 Hz, 2H) $\underline{H}_b$, 7.51(d, J=7 Hz, 2H) $\underline{H}$-$_{CH_2}$-3.43(s, 4H)	7.24(s, 2H, -C$\underline{H}$=C$\underline{H}$-)
24	$\underline{H}_a$ 6.65(d, J=8 Hz, 4H) $\underline{H}_b$ 6.74(d, J=8 Hz, 4H)	$\underline{H}_{a'}$, $\underline{H}_{b'}$ } 7.30(br-s, 4H) $\underline{H}$-$_{CH_2}$-3.43(s, 4H)	2.16(s, 6H, -C$\underline{H}_3$)
25[a]	$\underline{H}_a$ 6.77(d, J=8 Hz, 4H) $\underline{H}_b$ 6.95(d, J=8 Hz, 4H)	$\underline{H}_a$, 7.35(d, J=7 Hz, 4H) $\underline{H}_b$, 7.41(d, J=7 Hz, 4H) $\underline{H}$-$_{CH_2}$-3.46(s, 4H)	2.75(br-s, 2H, -O$\underline{H}$) 4.78(br-s, 2H, -C$\underline{H}$-)
30	$\underline{H}_a$ 7.26(d, J=7 Hz, 2H) $\underline{H}_b$ 7.68(d, J=7 Hz, 2H)	7.27—7.50(m, 5H, Ar-$\underline{H}$) $\underline{H}$-$_{CH_2}$-3.45(s, 4H)	2.38(s, 3H, -C$\underline{H}_3$)
6	$\underline{H}_a$ 6.58(d, J=8 Hz, 4H) $\underline{H}_b$ 7.07(d, J=8 Hz, 4H)	$\underline{H}_a$, 7.21(d, J=7 Hz, 2H) $\underline{H}_b$, 7.67(d, J=7 Hz, 2H) $\underline{H}$-$_{CH_2}$-3.38(s, 4H)	7.31(s, 2H, -C$\underline{H}$=C$\underline{H}$-)
26	$\underline{H}_a$ 6.88(d, J=8 Hz, 4H) $\underline{H}_b$ 7.20(d, J=8 Hz, 4H)	$\underline{H}_a$, 7.22(d, J=7 Hz, 2H) $\underline{H}_b$, 7.71(d, J=7 Hz, 2H) $\underline{H}$-$_{CH_2}$-3.37(s, 4H)	2.24(s, 6H, -C$\underline{H}_3$)
27[a]	$\underline{H}_a$ 6.45(d, J=8 Hz, 4H) $\underline{H}_b$ 6.90(d, J=8 Hz, 4H)	$\underline{H}_a$, 7.35(d, J=7 Hz, 4H) $\underline{H}_b$, 7.70(d, J=7 Hz, 4H) $\underline{H}$-$_{CH_2}$-3.42(s, 4H)	2.78(br-s, 2H, -O$\underline{H}$) 4.86(br-s, 2H, -C$\underline{H}$-)
32	$\underline{H}_a$ 7.17(d, J=8 Hz, 2H) $\underline{H}_b$ 7.52(d, J=8 Hz, 2H)	7.08—8.04(m, 5H, Ar-$\underline{H}$) $\underline{H}$-$_{CH_2}$-3.38(s, 4H)	2.34(s, 3H, -C$\underline{H}_3$)

a) The spectra of **25** and **27** were observed in acetone-d_6.

the synthesis of cyclophanes **3**, **5**, and **6**. The synthesis of intermediates, dialdehydes **17** and **21**, were carried out by the palladium-catalyzed substitution[14] of diiodo compounds **7** and **9** with acetylene derivative **15**; in the presence of phosphino nickel complex, dialdehyde **19** was obtained by the cross coupling reaction[15] of **8** with a Grignard reagent prepared from **12**.

The intramolecular reductive coupling of **17** with a low valent titanium reagent ($TiCl_4$-$LiAlH_4$[12d]) afforded a mixture of the reduction products (**22** and **23**) of carbonyl group and cyclophane **3**. On the other hand, the intramolecular reductive coupling of **19** or **21** with a low valent titanium reagent ($TiCl_4$-Zn[12a]) gave a mixture of the reduction products (**24** or **26**), cyclophanes (**5** or **6**), and dihydroxycyclophane derivatives (**25** or **27**), respectively. It has already been reported that aldehydes and ketones were reduced by low valent titanium compounds, produced from $TiCl_4$ and Zn, to give the corresponding pinacols and olefins in high yields.[12a] The cyclophane **4** was also obtained by the catalytic hydrogenation of **5**.

The structures of the compounds were assigned on the basis of the IR, NMR, and mass spectra and the elementary analyses.

The IR spectra of [2.2]paracyclophane system show these two obvious features. One is the increase of the intensity of the band in 1600—1580 cm^{-1}, which is related to the increased double bond character due to the distortion of the benzene rings.[16] The other is the appearance of a strong new maximum near 710 cm^{-1} region. Longone and Warren[17] reported that the strong maximum at 725 cm^{-1} in [2.2]paracyclophane and at 710 cm^{-1} in 4,7,12,15-tetramethyl[2.2]paracyclophane might be a characteristic band associated with the distorted benzene rings in the [2.2]paracyclophane system. Otsubo *et al.*[18] reported the same phenomena in the multilayered [2.2]paracyclophane system. In practice, besides the strong peak around 1600 cm^{-1}, the cyclophanes (**3**—**6**, **25**, and **27**) also exhibit two strong peaks near 720 and 690 cm^{-1} (Table 1). This result indicates that the compounds all bear strained benzene rings.

The NMR spectral data of all the cyclophanes and the reference compounds are summarized in Table 2. The most remarkable feature is that the chemical shifts of all the benzene ring protons appear at high field, as in the case of [2.2]paracyclophane.[19] For example, in the NMR spectrum of **3**, the signal of benzene protons (δ, 6.38 ppm) is shifted upfield by 0.53 and 0.84 ppm compared with that of the reference compound **22**

(δ, 6.93 and 7.23 ppm). Since the benzene ring protons of **3** are probably deshielded by the bridging vinylene group, this phenomenon indicates that the two benzene rings in **3** are held face to face in more close proximity by the vinylene bridge than in **22**. Staab and Ipaktschi[10] have previously reported from the X-ray analysis of 1,8-bis(phenylethynyl)naphthalene (**28**) that the nonbonding interaction between the two phenylethynyl groups of **28** results in a splaying out of the two phenylethynyl groups and, as a result, that the distance between the centers of two triple bonds is near the sum of van der Waals radii of π-systems. Similar to the case of **28**, the tolyl groups in **22** are relatively more distant from one another, compared with those of **3** in which the tolyl groups are bound together by vinylene bridges at both ends. Moreover, as in the electronic spectra of other cyclophanes, the electronic spectrum of **3** shows a general broadening of all bands in the spectrum and hyperchromic and bathochromic shifts of the long wavelength bands, compared with that of **22** (see Fig. 1). This result may be due to a more strong transannular π-electronic interaction in **3** than in **22**. On the other hand, the NMR signals of benzene ring protons in **22** are shifted somewhat upfield, compared with those of monosubstituted analog, 1-(*p*-tolylethynyl)naphthalene (**29**). In addition, in the electronic spectrum of **22**, the longest wavelength bands appear at a wavelength longer by 32 nm than those of **29**. This bathochromic shift and an increase of intensity in the spectrum of **22** may be caused by the transannular π-electronic interaction between the two chromophores in **22**.

The structures of **4** and **5** can be also assigned to cyclophane structure by a comparison of their NMR data with those of the reference compounds: **24** and 5-*p*-tolylacenaphthene (**30**). Similar to the case of **3**, the upfield shifts of benzene ring protons in **4** (Δ, 0.24 and 0.20 ppm) and in **5** (Δ, 0.09 and 0.12 ppm), compared with those in **24**, are explained by cyclophane structure, in which the benzene ring protons in **4** and **5** lie in more close proximity to the π-cloud of the opposed moiety than in **24**. House *et al.*[5] have previously reported that the molecule of 1,8-diphenylnaphthalene (**31**) should be deformed to alleviate the nonbonding interaction between the two phenyl rings and that the approximately parallel planes of the two phenyls are at an angle of approximately 70° to the plane of the naphthalene ring. Similar to the case of **31**, in **24** the nonbonding interaction between the two aryl rings results in a splaying out of the two aryl rings and as a result, the aryl rings in **24** are relatively more distant from one another, compared with those of **4**. Furthermore, the NMR spectrum of saturated cyclophane **4** showed H_a at 6.41 ppm and H_b at 6.54 ppm, indicating a marginal upfield shift (0.06 and 0.15 ppm) with respect to the unsaturated cyclophane **5**; this is characteristic of such pairs of cyclophanes (with saturated and unsaturated bridges).[20] On the other hand, similar to the case of **22**, the NMR signals of aryl ring protons in **24** are shifted upfield, compared with those of **30**. Additionally, in the electronic spectrum of **24**, compared with that of **30**, all the absorption curves exhibit broadening, and bathochromic and hyperchromic shifts, caused by the transannular π-electronic interaction between the two aryl moieties in **24** (see Fig. 2).

The NMR and electronic spectra of **6** are also consistent with a cyclophane structure. The chemical shifts for H_a and H_b protons of benzene rings of **6** are found respectively at 0.30 and 0.13 ppm upfield relative to those (H_a and H_b) of the reference compound **26**. These upfield shifts are due to the fact that, as in the case of **3**, the two benzene rings in **6** are held face to face in more close proximity by the vinylene bridge at both ends than in **26**. Furthermore, the electronic spectrum of **6** shows a general broadening of all bands in spectrum and hyperchromic and bathochromic shifts of the long wavelength bands, compared with that of **26** (see Fig. 3). It is probably due to more strong transannular π-electronic interaction between the two aryl moieties in **6** than in **26**. On the other hand, in the NMR spectrum of **26**, the upfield shifts of H_a (Δ, 0.29 ppm) and H_b (Δ, 0.32 ppm) are also observed, compared with the corresponding ones in the reference compound: 5-*p*-tolylacenaphthene (**32**). Moreover, in the electronic spectrum of **26**, the electronic absorption curve becomes even more structureless with bathochromic shift and increased intensity of the band, compared with those of **32**. It indicates that the two aryl moieties in **26** interact strongly with each other, similar to the case of **22**.

This research was supported by Grant-in-Aid for Scientific Research No 554137 from the Ministry of Education, Science and Culture.

References

1) A preliminary report dealing with a part of this work has appeared: A. Kasahara, T. Izumi, and T. Katou, *Chem. Lett.*, **1979**, 1373.

2) S. Misumi and T. Otsubo, *Acc. Chem. Res.*, **11**, 251 (1978).

3) W. Bieber and F. Vögtle, *Angew. Chem.*, **89**, 199 (1977).

4) L.Pauling, "The nature of the Chemical Bond," 3rd ed, Cornell University Press., Ithaca, N. Y. (1960), p. 262.

5) H. O. House, D. G. Koepsell, and W. J. Campbell, *J. Org. Chem.*, **37**, 1003 (1972).

6) R. L. Letsinger, J. A. Gilpin, and W. J. Vullo, *J. Org. Chem.*, **27**, 672 (1962).

7) R. L. Clough, P. Mison, and J. P. Roberts, *J. Org. Chem.*, **41**, 2252 (1976).

8) C. Eaborn, A. R. Thompson, and D. R. M. Walton, *J. Chem. Soc., C*, **1967**, 1364.

9) J. A. Landgrebe and R. H. Rynbrandt, *J. Org. Chem.*, **31**, 2585 (1966).

10) H. A. Staab and J. Ipaktschi, *Chem. Ber.*, **104**, 1170 (1971).

11) F. Vöglte and P. Neumann, *Synthesis*, **1973**, 85; S. Misumi, *Kagaku No Ryoiki*, **28**, 927 (1974); **32**, 651 (1978); Y. Sakata, *Yuki Gosei Kyokai Shi*, **38**, 164 (1980).

12) a) T. Mukaiyama, T. Sato, and J. Hanna, *Chem. Lett.*, **1973**, 1041; b) J. E. McMurry and M. P. Fleming, *J. Am. Chem. Soc.*, **96**, 4708 (1974): c) J. E. McMurry and L. R. Krepski, *J. Org. Chem.*, **41**, 3929 (1976); d) A. Ishida and T. Mukaiyama, *Chem. Lett.*, **1976**, 1127; e) J. E. McMurry, M. P. Fleming, K. L. Kees, and L. R. Krepski, *J. Org. Chem.*, **43**, 3255 (1978).

13) a) A. Kasahara and T. Izumi, *Chem. Lett.*, **1978**, 21;

b) A. Kasahara, T. Izumi, and I. Shimizu, *ibid.*, **1979**, 1119; c) A. Kasahara, T. Izumi, and H. Umezawa, *ibid.*, **1980**, 1039; d) D. Tanner and O. Wennerstrom, *Tetrahedron Lett.*, **1981**, 2313.

14) a) K. Sonogashira, Y. Tohda, and N. Hagihara, *Tetrahedron Lett.*, **1975**, 4467; b) S. Takahashi, Y. Kuroyama, K. Sonogashira, and N. Hagihara, *Synthesis*, **1980**, 627.

15) K. Tamao, K. Sumitani, Y. Kiso, M. Zembayashi, A. Fujioka, S. Kodama, I. Nakajima, A. Minato, and M. Kumada, *Bull. Chem. Soc. Jpn.*, **49**, 1958 (1976).

16) D. J. Cram and H. Steinberg, *J. Am. Chem. Soc.*, **73**, 5691 (1951).

17) D. T. Longone and C. L. Warren, *J. Am. Chem. Soc.*, **84**, 1507 (1962).

18) T. Otsubo, S. Mizogami, I. Otsubo, Z. Tozuka, A. Sakagami, Y. Sakata, and S. Misumi, *Bull. Chem. Soc. Jpn.*, **46**, 3519 (1973).

19) a) D. J. Cram, C. K. Dalton, and G. R. Knox, *J. Am. Chem. Soc.*, **85**, 1088 (1963); b) T. Otsubo, S. Mizogami, Y Sakata, and S. Misumi, *Bull. Chem. Soc. Jpn.*, **46**, 3831 (1973).

20) a) R. H. Mitchell and V. Boekelheide, *J. Am. Chem. Soc.*, **96**, 1547 (1974); b) J. R. Davy and J. A. Reiss, *Aust. J. Chem.*, **29**, 163 (1976); c) J. R. Davy, M. N. Iskander, and J. A. Reiss, *ibid.*, **32**, 1067 (1979).

 © 1982 The Chemical Society of Japan Bull. Chem. Soc. Jpn., 55, 2441—2444 (1982)

Ruthenium-catalyzed Reduction of Carbonyl Compounds Using Formic Acid

Yoshihisa WATANABE,* Tetsuo OHTA, and Yasushi TSUJI
Department of Hydrocarbon Chemistry, Kyoto University, Sakyo-ku, Kyoto 606
(Received November 19, 1981)

Carbonyl compounds were hydrogenated to the corresponding alcohols in excellent yields using formic acid with a ruthenium complex at 125 °C for 3 h. 2-Propanone was reduced to 2-propanol by $RuCl_2(PPh_3)_3$–HCOOH system in 94% yield with 98% selectivity. 3-Pentanone, cyclohexanone, acetophenone, and propiophenone were hydrogenated to the corresponding alcohols in 86, 78, 84, and 86% yields respectively. The ketone having the bulkier alkyl groups showed lower reactivity. The catalytic activity was found to decrease in the order $RuCl_2(PPh_3)_3$, $RuHCl(PPh_3)_3$, $RuHCl(CO)(PPh_3)_3$, and $RuH_2(PPh_3)_4$.

Catalytic transformation of carbonyl compounds to alcohols is an important unit processes in organic synthesis. Since the first report of Schrock and Osborn using a cationic rhodium complex as a catalyst, several methods have been reported for the homogeneous catalytic hydrogenation of carbonyl compounds.[1] On the other hand, catalytic transfer hydrogenation using organic compounds as hydrogen sources is of current interest and there have been several reports using iridium,[2] cobalt,[3] iron,[4] rhodium,[5] and ruthenium[6] complexes. In these reactions alcohols have most often been used as hydrogen sources.

Formic acid is easily derived from synthesis gas and its application to organic synthesis is worth pursuing; we found that the $RuCl_2(PPh_3)_3$–HCOOH system is effective for the homogeneous hydrogenation of carbonyl compounds to alcohols without solvent. The preliminary results have been reported[7] briefly. In this paper we will describe the detailed investigation of the optimum conditions and the scope of this catalyst system.

Results and Discussion

Ketones and aldehydes were reduced to the corresponding alcohols in excellent yields by formic acid with a ruthenium catalyst such as $RuCl_2(PPh_3)_3$ without solvent. In a representative example, an equimolar mixture of acetophenone (80 mmol) and formic acid was heated without solvent at 125 °C for 3 h in an autoclave in the presence of a catalytic amount of $RuCl_2(PPh_3)_3$ (0.10 mmol). As a reaction product, 1-phenylethanol was formed in 84% yield with 98% selectivity.

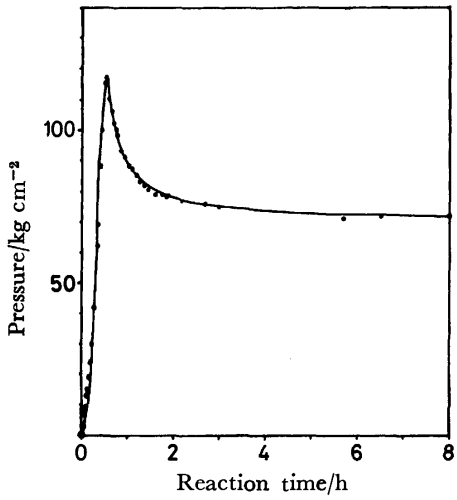

Fig. 1. Time dependence of the pressure in the hydrogenation of acetophenone by $RuCl_2(PPh_3)_3$–HCOOH.
The mixture of acetophenone (80 mmol), formic acid (97 mmol), and $RuCl_2(PPh_3)_3$ (0.10 mmol) was stirred at 125 °C for 3 h in 50 ml stainless steel autoclave.

$$R\text{–}\overset{O}{\overset{\|}{C}}\text{–}R' + HCOOH \xrightarrow{RuCl_2(PPh_3)_3} R\text{–}\overset{OH}{\overset{|}{C}}H\text{–}R' + CO_2 \quad (1)$$

Results of the hydrogenation of various ketones are listed in Table 1. Methyl alkyl ketones and methyl aryl ketones such as acetone, 2-butanone, 4-methyl-2-pentanone, and acetophenone were hydrogenated to the corresponding alcohols in excellent yields. Similarly, 3-pentanone, cyclohexanone, and propiophenone gave the corresponding alcohols in good yields. But 3-methyl-2-butanone and 3,3-dimethyl-2-propanone showed poor reactivity and 2,4-dimethyl-3-pentanone was not reduced under the conditions used. These results show that the ketones having the bulkier alkyl groups would have the lower reactivity.

α- and β-Keto esters were also reduced by this method. Ethyl pyruvate was reduced in *ca.* 100% conversion to give ethyl lactate in 78% isolated yield. Ethyl acetoacetate gave the mixture of ethyl 3-hydroxybutyrate and 1-methyl-2-(ethoxycarbonyl)ethyl 3-hydroxybutyrate. The latter seems to be formed by two steps, hydrogenation of ethyl acetoacetate followed by the ester exchange reaction between two molecules of ethyl 3-hydroxybutyrate.

$$2\ CH_3\overset{OH}{\overset{|}{C}}HCH_2COOEt \longrightarrow CH_3\overset{OH}{\overset{|}{C}}HCH_2COO\overset{CH_3}{\overset{|}{C}}HCOOEt + EtOH \quad (2)$$

2-Acetylpyridine was also reduced by this system to give 2-(1-hydroxyethyl)pyridine in 17% isolated yield, but 3-acetylpyridine was reduced very little.

When an equimolar mixture of 2,3-butanedione and formic acid was heated in the presence of $RuCl_2(PPh_3)_3$, 2-hydroxy-3-butanone and 2,3-butanediol were given in 35 and 28% yields respectively. When the ratio of formic acid/2,3-butanedione was two, 2-hydroxy-3-butanone was given in 6% yield and 2,3-butanediol was given in 54% yield. 2-Hydroxy-3-butanone was also reduced by this system to give a 57% yield of 2,3-

TABLE 1. THE HYDROGENATION OF KETONES BY $RuCl_2(PPh_3)_3$–HCOOH[a]

Run	Ketones	Ketone recovered/%	Products	Yield/%
1	2-Propanone	4	2-Propanol	94
2	2-Butanone	10	2-Butanol	85
3	3-Pentanone	12	3-Pentanol	86
4	2-Hexanone	13	2-Hexanol	72
5	4-Methyl-2-pentanone	15	4-Methyl-2-pentanol	80
6	3-Methyl-2-butanone	43	3-Methyl-2-butanol	50
7	3,3-Dimethyl-2-propanone	69	3,3-Dimethyl-2-propanol	30
8	2,4-Dimethyl-3-pentanone	100	2,4-Dimethyl-3-pentanol	0
9	Cyclohexanone	22	Cyclohexanol	78
10[c]	Cyclohexanone	23	Cyclohexanol	76
11[d]	Cyclohexanone	43	Cyclohexanol	57
12	Acetophenone	15	1-Phenylethanol	84
13	Propiophenone	14	1-Phenyl-1-propanol	86
14	Diphenyl ketone	36	Diphenyl methanol	64
15	Ethyl pyruvate	0	Ethyl lactate	(78)
16	Ethyl acetoacetate	0	Ethyl 3-hydroxybutyrate	(39)
			1-Methyl-2-(ethoxycarbonyl)ethyl 3-hydroxybutyrate	(23)

a) The mixture of a ketone (160 mmol), formic acid (160), and $RuCl_2(PPh_3)_3$(0.20 mmol) was stirred at 125 °C for 3 h. b) Determined by GLC and based on the amount of ketone used. The figures in parentheses show isolated yields. c) $RuCl_2(PPh_3)_3$ (0.10 mmol). d) $RuCl_2(PPh_3)_3$ (0.05 mmol).

butanediol.

A few examples of the transfer hydrogenation of ketones in the presence of ruthenium complexes are known; benzyl alcohol,[6c] 1-phenylethanol,[6b,f] and 2-propanol[6f] are used as hydrogen donors. These reactions, however, give products in lower yields and severer reaction conditions are required. These transfer hydrogenations of carbonyl compounds by alcohols are reversible and the maximum yield of the hydrogenated product is determined by the equilibrium unless the product is removed from the reaction mixture. Since carbon dioxide derived by the decomposition of the formic acid is not reduced to formic acid in the reverse direction in the present system, the yield of the product would be expected to be determined kinetically.

The present system, $RuCl_2(PPh_3)_3$–HCOOH, can be used for the hydrogenation of aldehydes such as benzaldehyde, 2-ethylhexanal and octanal (Table 2). The aldehydes were reduced to the corresponding alcohols in 80—63% yields accompanied by the formation of the corresponding formate in 5—20% yields.

Catalyst. Catalytic activities of several ruthenium complexes for the hydrogenation of acetophenone are shown in Table 3. Among the ruthenium complexes examined, $RuCl_2(PPh_3)_3$ exhibited the highest activity, followed by $RuHCl(PPh_3)_3$, $RuHCl(CO)(PPh_3)_3$, $RuH_2(CO)(PPh_3)_3$, $Ru(CO)_3(PPh_3)_2$, and $RuH_2(PPh_3)_4$. One cluster, $Ru_3(CO)_{12}$, showed no catalytic activity. Although $RuCl_3$ showed only low catalytic activity, an addition of PPh_3 markedly improved the activity (Fig. 2). When the ratio of $PPh_3/RuCl_3$ was 6, the reactivity was almost equal to that of $RuCl_2(PPh_3)_3$. The large excess of the PPh_3 resulted in the decrease of the yield of the alcohol. Tributylphosphine and triphenyl phosphite had much poorer effects as additives (3 mol/mol of $RuCl_3$) and gave the alcohols in 6 and 3% yields respectively.

Effects of Reaction Conditions. Effects of reaction temperature, reaction time, amounts of $RuCl_2(PPh_3)_3$, and the molar ratio of substrate/formic acid were examined. The effects of reaction temperature in the hydrogenation of acetophenone by the $RuCl_2(PPh_3)_3$–

TABLE 2. THE HYDROGENATION OF ALDEHYDES BY $RuCl_2(PPh_3)_3$–HCOOH[a]

Run	Aldehyde	Aldehyde recovered %	Products	Yield/%[b]
17	2-Ethylhexanal	15	2-Ethyl-1-hexanol	63
			2-Ethyl-1-hexyl formate	20
18	Octanal	3	1-Octanol	80
			1-Octyl formate	14
19	Benzaldehyde	9	Benzyl alcohol	79
			Benzyl formate	9

a) The mixture of an aldehyde (80 mmol), formic acid (80 mmol), and $RuCl_2(PPh_3)_3$ (0.10 mmol) was stirred at 125 °C for 3 h. b) Determined by GLC and based on the amount of aldehyde used.

TABLE 3. CATALYTIC ACTIVITIES OF RUTHENIUM COMPLEXES FOR THE REDUCTION OF ACETOPHENONE WITH FORMIC ACID

Run	Ru complexes	Acetophenone[b] recovered/%	Yield/% of 1-phenylethanol[b]
10	$RuCl_2(PPh_3)_3$	15	84
20	$RuHCl(PPh_3)_3$	39	56
21	$RuHCl(CO)(PPh_3)_3$	54	46
22	$RuH_2(PPh_3)_4$	81	17
23	$RuH_2(CO)(PPh_3)_3$	70	28
24	$Ru(CO)_3(PPh_3)_2$	80	20
25	$Ru_3(CO)_{12}$	100	0
26	$Ru_3(CO)_{12}+9PPh_3$	91	9

a) The mixture of acetophenone (160 mmol), formic acid (160 mmol), and a Ru complex (0.20 mmol) was stirred at 125 °C for 3 h. b) Determined by GLC and based on the amount of acetophenone used.

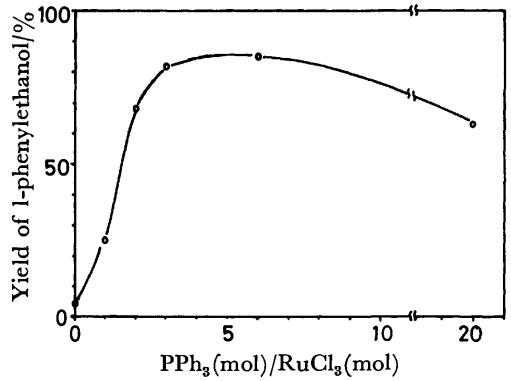

Fig. 2. Effect of the ratio of $PPh_3/RuCl_3$ on the hydrogenation of acetophenone with formic acid.
The mixture of acetophenone (80 mmol), formic acid 80 mmol), $RuCl_3 \cdot nH_2O$ (0.10 mmol), and PPh_3 (0—2.0 mmol) was stirred at 125 °C for 3 h. Yield was determined by GLC and based on the amount of acetophenone used.

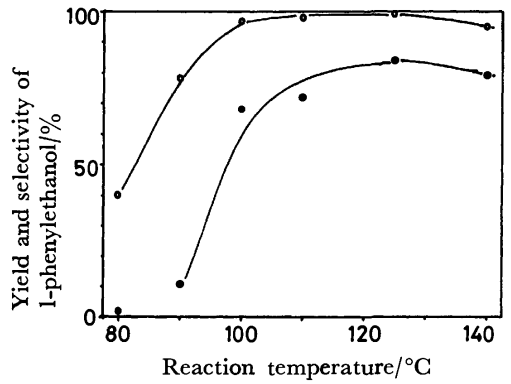

Fig. 3. The temperature dependence on the yield and selectivity of 1-phenylethanol in the hydrogenation of acetophenone by $RuCl_2(PPh_3)_3$ with formic acid.
●: Yield, ○: selectivity.
The mixture of acetophenone (80 mmol), formic acid (80 mmol), and $RuCl_2(PPh_3)_3$ (0.10 mmol) was stirred for 3 h. Yield was determined by GLC and based on the amount of acetophenone used.

HCOOH system are shown in Fig. 3. The yield of 1-phenylethanol and its selectivity had a peak at about 125 °C, because the formate and a small amount of condensation products were obtained at lower (95 and 110 °C) and higher (140 °C) temperatures respectively.

In this procedure, 0.10 mmol (0.063 mol%) of $RuCl_2(PPh_3)_3$ appears to be sufficient for the hydrogenation of cyclohexanone (Table 1: Runs 9, 10, and 11).

The effect of the amount of formic acid is shown in Table 4. Excellent yields and selectivities of the products can be achieved by using an equimolar amount of formic acid. The presence of an excess amount of the formic acid improves the yield of the alcohol but it decreases the selectivity of the alcohol by formation of the corresponding formate (See Runs 10, 28, and 29).

For the reduction of unsaturated compounds with formic acid, the Leukert-Wallach reaction is well known, but reducible substrates are limited. Formic acid is also used for conversion of benzaldehyde, acetophenone, and acetylpyridine to toluene, ethylbenzene, and ethylpyridine respectively[8] in the presence of heterogeneous catalysts. There have been only a few reports on hydrogenation by ruthenium complexes using formic acid.[9,10] They have been applied only for the hydrogenation of olefinic bonds.

The results obtained here clearly demonstrate that a $RuCl_2(PPh_3)_3$–HCOOH system is applicable for the transformation of carbonyl compounds to alcohols efficiently without solvent. This procedure has the following advantages. 1) As formic acid is liquid handling is easier than that of molecular hydrogen. 2) As the reaction is carried out without solvent and the formic acid used is completely decomposed through the reaction, products are easily separated. 3) The reaction proceeds with excellent yields and selectivities of the products.

The pressure *vs.* the reaction time through the reduction are shown in Fig. 1. At the maximum pressure, acetophenone was reduced to 1-phenylethanol in 39% yield and molecular hydrogen was produced in 36% yield, based on the formic acid used. It has been reported that the catalytic hydrogenation of carbonyl compounds by $RuHCl(CO)(PPh_3)_3$ using molecular hydrogen is accelated by the addition of water.[1a] In the present hydrogenation using formic acid, a considerable amount of molecular hydrogen was first evolved and then it was absorbed in the cource of the reaction. In this case the formic acid used contained some water. The fact that the reaction of acetophenone with molecular hydrogen in the presence of water without formic acid gave a 65% yield of 1-phenylethanol (Run 31) also supports the mechanism described above. Thus the main part of the present reaction can be explained as follows. First, formic acid is decomposed to hydrogen gas and carbon dioxide. Then the carbonyl compounds

Table 4. The hydrogenation of acetophenone by $RuCl_2(PPh_3)_3$[a]

Run	Hydrogen source	Reaction time/h	Acetophenone recovered/%	Yield/% of 1-phenylethanol[b]
10	HCOOH (160 mmol)	3	15	84
27	HCOOH (160 mmol)	5	8	91
28	HCOOH (200 mmol)	3	5	91 (4)
29	HCOOH (196 mmol)	8	Trace	94 (5)
30	H_2 (73 kg/cm² at 15 °C)	3	84	16
31[c]	H_2 (88 kg/cm² at 15 °C)	3	34	65

a) The mixture of acetophenone (160 mmol), hydrogen source, and $RuCl_2(PPh_3)_3$ was heated at 125 °C. b) Determined by GLC and based on the amount of acetophenone used. The figures in parentheses show the yields of 1-phenylethyl formate. c) Water (16 mmol) was added.

are catalytically hydrogenated in the presence of water by a ruthenium complex. However, since Sasson has reported, the transfer hydrogenation of α,β-unsaturated ketones by formic acid,[10] the transfer hydrogenation of the carbonyl compounds by formic acid may not be ruled out completely.

Experimental

GLC analysis was performed on a Shimadzu-GC 3BT. ^{1}H NMR spectra were obtained at 60MHz with a JEOL PM-60 and ^{13}C NMR spectra were obtained at 60 MHz with a JEOL PM-60 and ^{13}C NMR spectra were recorded at 25.05 MHz with a JEOL pulsed Fourier Transform spectrometer, model FX-100, using tetramethylsilane as an internal standard. IR spectra were measured on a Hitachi model 215 grating spectrophotometer.

Materials. All substrates used were commercial products. The aldehydes and ketones were distilled before use. Moist formic acid (*ca.* 90% aq solution) was used without further purification. $RuCl_3 \cdot nH_2O$, PPh_3, $P(n\text{-}Bu)_3$, $P(OPh)_3$, and $Ru_3(CO)_{12}$ were commercial products. $RuCl_2(PPh_3)_3$,[11] $RuHCl(PPh_3)_3$,[12] $RuHCl(CO)(PPh_3)_3$,[13] $RuH_2(PPh_3)_4$,[14] $RuH_2(CO)(PPh_3)_3$,[13] and $Ru(CO)_3(PPh_3)_2$[13] were prepared by published methods.

Procedures of Hydrogenation. A substrate (160 mmol), formic acid (160 mmol), and a ruthenium complex (0.20 mmol) were placed in a 100 ml stainless steel autocleave with a magnetic stirring bar. The air was replaced with argon. The autoclave was then heated at the appropriate temperature in an oil bath for 3 h. Reaction products were isolated by the usual method and identified by comparing the ^{1}H and/or ^{13}C NMR and IR spectra with those of the authentic samples. Amounts of the substrate recovered and of the products were determined by GLC (3 mm$\phi \times$3 m column packed with 10% Versamide 900 on Neopack 1A 60—80 mesh or with 20% DEGA on Uniport B 80—100 mesh) using internal standards.

In the reaction of benzophenone, amounts of benzophenone recovered and of diphenylmethanol formed were determined by ^{1}H NMR spectra.

Reduction of Acetophenone with Molecular Hydrogen. Acetophenone (160 mmol) and $RuCl_2(PPh_3)_3$ (0.20 mmol) were placed into a 100 ml stainless steel autoclave. The air was replaced with argon and then hydrogen was charged at room temperature. Then the autoclave was heated at 125 °C for 3 h.

References

1) a) R. R. Schrock and J. A. Osborn, *J. Chem. Soc., Chem. Commun.*, **1970**, 567; b) J. Tsuji and H. Suzuki, *Chem. Lett.*, **1977**, 1085; c) I. Ojima, T. Kogure, and K. Achiwa, *J. Chem. Soc., Chem. Commun.*, **1977**, 428; d) W. Stromeier and L. Weigelt, *J. Organomet. Chem.*, **171**, 121 (1979); e) R. A.Sanchez-Delgado and O. L. de Ochoa, *ibid.*, **202**, 427 (1980).

2) J. Trocha-Grimshaw and H. B. Henbest, *J. Chem. Soc., Chem. Commun.*, **1967**, 544; M. Gullotti, R. Ugo, and S. Colonna, *J. Chem. Soc., C*, **1971**, 2652; Y. M. Y. Haddad, H. B. Henbest, J. Husbands, T. R. B. Mitchell, and J. Trocha-Grimshaw, *J. Chem. Soc., Perkin Trans. 1*, **1974**, 596.

3) E. M. S. Tyrlik and Z. Lasocki, *J. Organomet. Chem.*, **72**, 269 (1974).

4) R. Noyori, I. Umeda, and T. Ishigami, *J. Org. Chem.*, **37**, 1542 (1972); T. Nishiguchi and K. Fukuzumi, *Bull. Chem. Soc. Jpn.*, **45**, 1656 (1972).

5) J. C. Orr, M. Mersereau, and A. Sanford, *J. Chem. Soc., Chem. Commun.*, **1970**, 162; T. Nishiguchi, K. Tachi, and K. Fukuzumi, *J. Org. Chem.*, **40**, 237 (1975).

6) a) Y. Sasson and J. Blum, *Tetrahedron Lett.*, **1971**, 2167; b) Y. Sasson and J. Blum, *J. Org. Chem.*, **40**, 1887 (1975); c) H. Imai, T. Nishiguchi, and K. Fukuzumi, *ibid.*, **41**, 665 (1976); d) H. Imai, T. Nishiguchi, and K. Fukuzumi, *ibid.*, **41**, 2688 (1976); e) M. Bianchi, U. Matteoli, G. Menchi, P. Frediani, S. Pratesi, and F. Piacenti, *J. Organomet. Chem.*, **198**, 73 (1980); f) V. Z. Sharf, L. Kh. Freidlin, I. S. Shekoyan, and V. N. Krutii, *Izv. Akad. Nauk SSSR, Ser. Khim.*, **1976**, 1064.

7) Y. Watanabe, T. Ota, and Y. Tsuji, *Chem. Lett.*, **1980**, 1585.

8) M. Ferles, O. Kocian, and S. Radl, *J. Chem. Soc., Chem. Commun.*, **43**, 1628 (1978); J. R. Weir, B. A. Patel, and R. F. Heck, *J. Org. Chem.*, **45**, 4926 (1980).

9) M. E. Vol'pin, V. P. Kukolev, V. O. Chernyshev, and I. S. Kolomnikov, *Tetrahedron Lett.*, **1971**, 4435.

10) J. Blum, Y. Sasson, and S. Iflah, *Tetrahedron Lett.*, **1972**, 1015.

11) P. S. Hallman, T. A. Stephenson, and G. Wilkinson, *Inorg. Synth.*, **12**, 237 (1970).

12) P. S. Hallman, B. R. McGarvey, and G. Wilkinson, *J. Chem. Soc., A*, **1968**, 3142.

13) N. Ahmad, J. J. Levison, S. D. Robinson, and M. F. Uttley, *Inorg. Synth.*, **15**, 48 (1974).

14) R. Young and G. Wilkinson, *Inorg. Synth.*, **17**, 75 (1977).

 © 1982 The Chemical Society of Japan Bull. Chem. Soc. Jpn., 55, 2445—2449 (1982)

The Transition Metal-catalyzed *N*-Heterocyclization. A Reductive Transformation of Aminonitroarenes and Dinitroarenes into Phenanthroline Derivatives Using Aliphatic Aldehydes under Carbon Monoxide Pressure

Yoshihisa WATANABE,* Naoki SUZUKI, and Yasushi TSUJI

Department of Hydrocarbon Chemistry, Faculty of Engineering, Kyoto University, Sakyo-ku, Kyoto 606

(Received December 21, 1981)

The Catalytic *N*-heterocyclization of aminoarenes and dinitroarenes using aliphatic *n*-C_3—C_5 aldehydes was carried out at 180 °C under the pressure of carbon monoxide (70 atm at room temperature) in the presence of $RhCl(PPh_3)_3$ and $PdCl_2$ as a binary catalyst system. The reaction of *p*-nitroaniline with propanal, butanal, and pentanal gave 3,8-diethyl-2,9-dimethyl-4,7-phenanthroline, 2,9-diethyl-3,8-dipropyl-4,7-phenanthroline, and 3,8-dibutyl-2,9-dipropyl-4,7-phenantroline in 43, 57, and 54% yields respectively. On the other hand, *m*-nitroaniline and *o*-nitroaniline gave 1,7-phenanthroline and imidazole derivatives in rather low yields (21 and 24%) under the reaction conditions employed.

Recently, novel methods have been developed for building up a quinoline nucleus using transition-metal complexes as catalysts under nonacidic conditions.[1,2] In previous papers, we have demonstrated that rhodium, ruthenium, and palladium complexes are effective catalysts for the *N*-heterocyclization of aminoarenes and nitroarenes.[3-6] μ,μ'-Dichlorobis(norbornadiene)dirhodium(I)($[RhCl(NBD)]_2$) was active for the *N*-heterocyclization of aminoarenes using aliphatic aldehydes.[3] Nitroarenes were reductively converted into quinolines and (dialkylamino)arenes using an aldehyde in the presence of a binary catalyst system, $RhCl(PPh_3)_3$–$PdCl_2$, under the pressure of carbon monoxide.[4] $RuCl_2(PPh_3)_3$ is also active for the *N*-heterocyclization of aminoarenes using $\Delta^{2,3}$-unsaturated alcohols[5] and for that of nitroarenes using saturated alcohols.[6] These methods provided a variety of methods for synthesizing quinoline derivatives.

In this paper, phenanthroline derivatives were prepared by the double *N*-heterocyclization of nitroanilines and dinitrobenzenes using *n*-C_3—C_5 aliphatic aldehydes in the presence of a binary catalyst system ($RhCl(PPh_3)_3$–$PdCl_2$) under the pressure of carbon monoxide.

1,7-Phenanthroline and imidazole derivatives were also obtained by the reaction of *m*-nitroaniline and *o*-nitroaniline respectively with propanal.

Results and Discussion

At the outset, *p*-nitroaniline was allowed to react with propanal at 180 °C in the presence of a rhodium and/or palladium complex under carbon-monoxide pressure. In this reaction, 3,8-diethyl-2,9-dimethyl-4,7-phenanthroline (**1**), 2-ethyl-3-methyl-6-(propylamino)quinoline (**2**), and 2-ethyl-3-methyl-6-nitroquinoline (**3**) were obtained as the products (Eq. 1). This reaction was examined in detail in order to determine the optimum conditions for the preparation of **1**.

A variety of rhodium and/or palladium complexes

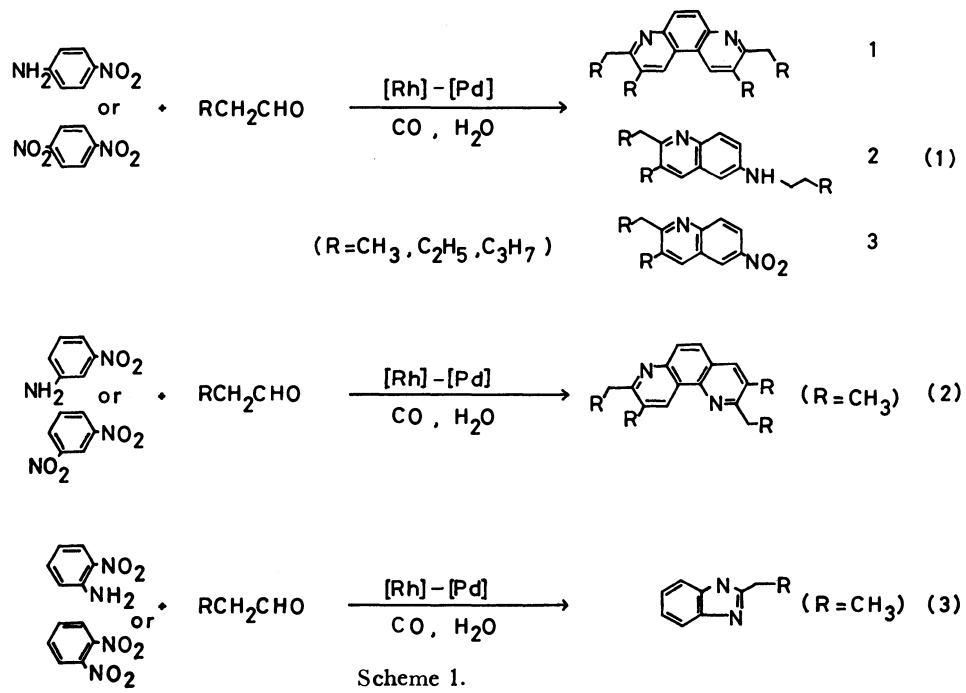

Scheme 1.

TABLE 1. *N*-HETEROCYCLIZATION OF *p*-NITROANILINE WITH PROPANAL USING RHODIUM AND/OR PALLADIUM COMPLEXES AS CATALYSTS[a]

Run No.	Rh and/or Pd complexes		Conversion[b] %	Product yield %[b,c] 1	2	3
1	$RhCl(PPh_3)_3$	(0.17 mmol)	100	43	19	4
	$PdCl_2$	(0.26 mmol)				
2	$RhCl_3 \cdot 3H_2O$	(0.17 mmol)	100	46	15	5
	$Pd(PPh_3)_4$	(0.26 mmol)				
3	$RhCl_3 \cdot 3H_2O$	(0.17 mmol)	100	44	27	3
	$PdCl_2$	(0.26 mmol)				
	PPh_3	(0.26 mmol)				
4	$RhCl_3 \cdot 3H_2O$	(0.17 mmol)	100	30	18	0
	$PdCl_2$	(0.26 mmol)				
5	$RhCl(PPh_3)_3$	(0.17 mmol)	99	11	2	0
	$PdCl_2$	(0.26 mmol)				
	PPh_3	(0.26 mmol)				
6	$RhCl_3 \cdot 3H_2O$	(0.17 mmol)	100	25	19	0
7	$RhCl_3 \cdot 3H_2O$	(0.43 mmol)	100	31	13	0
8	$RhCl(PPh_3)_3$	(0.17 mmol)	95	5	10	0
9	$[RhCl(COD)]_2$	(0.17 mmol)	100	3	14	2
10	$Rh_4(CO)_{12}$	(0.17 mmol)	100	3	3	3
11	$PdCl_2$	(0.43 mmol)	99	23	10	12
12	$Pd(PPh_3)_4$	(0.26 mmol)	90	4	1	1

a) A mixture of *p*-nitroaniline (20 mmol), propanal (90 mmol), water (2 ml), a rhodium and/or palladium complex, and ethanol (20 ml) was heated at 180 °C under the pressure of carbon monoxide (70 atm) for 4 h. b) Based on the amount of *p*-nitroaniline used. Determined by GLC. c) **1**: 3,8-Diethyl-2,9-dimethyl-4,7-phenanthroline, **2**: 2-ethyl-3-methyl-6-(propylamino) quinoline, **3**: 2-ethyl-3-methyl-6-nitroquinoline.

was examined as catalysts, the results are shown in Table 1. In these runs, the conversion of nitroaniline was high. In some cases, a tarry material was also formed.

The yields of the products depended greatly on the catalysts used. A binary catalyst system was effective for the double *N*-heterocyclization to give **1** in 43—46% yields (Runs 1, 2, and 3). The catalyst systems, such as $RhCl(PPh_3)_3$–$PdCl_2$ (Run 1), $RhCl_3$–$Pd(PPh_3)_4$ (Run 2), and $RhCl_3$–$PdCl_2$–PPh_3 (Run 3), gave almost the same yield of **1**. The presence of triphenylphosphines enhanced the yield of **1** (Runs 3 and 4), although the addition of triphenylphosphine to the combination of $RhCl(PPh_3)_3$–$PdCl_2$ retarded the formation of **1** (Run 5). On the other hand, when a rhodium catalyst was used alone, the yield of **1** decreased considerably. In those cases, $RhCl_3$–$3H_2O$ was effective for the formation of **1** (Run 6), followed by μ,μ'-dichlorobis(cyclooctadiene)dirhodium ($[RhCl(COD)]_2$) (Run 9), $Rh_4(CO)_{12}$ (Run 10), and $RhCl(PPh_3)_3$ (Run 8). An increase in the amount of the $RhCl_3 \cdot 3H_2O$, however, resulted in only a small increase in the yield of **1** (Runs 6 and 7). Palladium complexes alone, such as $PdCl_2$ and $Pd(PPh_3)_4$, also showed catalytic activities, but with low yields of **1** (Runs 11 and 12).

Next, the effects of other reaction variables were examined. The results are listed in Table 2. A binary system, $RhCl(PPh_3)_3$ (0.17 mmol) and $PdCl_2$ (0.26 mmol), was used as the catalyst. A four-fold molar quantity of propanal (80 mmol) is required for the double *N*-heterocyclization of nitroanilines (20 mmol) stoichiometrically. A moderate yield of **1** (43%) was obtained when 90 mmol of the aldehyde was used. An increase in the amount of the aldehyde to 120 or 160 mmol, however, resulted in a decrease in the yields of **1**, **2**, and **3** and an increase in the amouns of tarry materials. An aldol condensation may interfere with the reaction in these cases (Runs 13 and 14). Concerning the reaction temperature, an elevated temperature (180 °C) was needed for the reaction. Lower and higher temperatures gave poorer yields of **1** (Runs 15 and 16). Prolonging the reaction time from 4 h to 8 h slightly improved the yield of **1** and **2** (Run 18). Even a 2 h reaction time almost completed the reaction (Run 17). Among the solvents examined, ethanol was the best, followed by methanol, benzene, and tetrahydrofuran

TABLE 2. EFFECTS OF REACTION VARIABLES ON PRODUCTS DISTRIBUTION[a]

Run No.	Propanal (mmol)	Reaction temp/°C	Reaction time/h	Solvent	Conversion[b] %	Product yield/%[b,c] 1	2	3
1	90	180	4	EtOH	100	43	19	4
13	120	180	4	EtOH	98	26	10	3
14	160	180	4	EtOH	94	20	7	0
15	90	150	4	EtOH	96	12	6	1
16	90	200	4	EtOH	100	38	23	3
17	90	180	2	EtOH	100	39	21	1
18	90	180	8	EtOH	100	46	24	4
19	90	180	4	EtOH[d]	98	7	3	2
20	90	180	4	MeOH	98	35	17	1
21	90	180	4	THF	100	24	9	2
22	90	180	4	Benzene	95	26	17	4
23[e]	90	180	4	EtOH	100	11	15	8

a) A mixture of *p*-nitroaniline (20 mmol), propanal (90—160 mmol), water (2 ml), $RhCl(PPh_3)_3$ (0.17 mmol), $PdCl_2$ (0.26 mmol), and a solvent (20 ml) was treated at 150—200 °C under the pressure of carbon monoxide (70 atm) for 2—8 h. b) Based on the amount of *p*-nitroaniline used. Determined by GLC. c) **1**: 3,8-Diethyl-2,9-dimethyl-4,7-phenanthroline, **2**: 2-ethyl-3-methyl-6-(propylamino)-quinoline, **3**: 2-ethyl-3-methyl-6-nitroquinoline. d) Without water. e) Under the pressure of hydrogen (70 atm) instead of carbon monoxide.

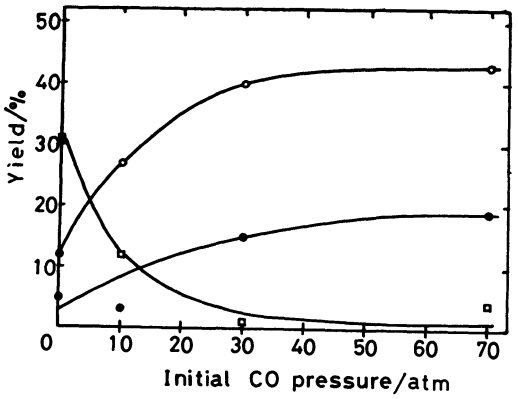

Fig. 1. Effects of pressure of carbon monoxide on products distribution.
A mixture of *p*-nitroaniline (20 mmol), propanal (90 mmol), water (2 ml), $RhCl(PPh_3)_3$ (0.17 mmol), $PdCl_2$ (0.26 mmol), and ethanol (20 ml) was treated at 180 °C for 4 h. Yields were based on an amount of *p*-nitroaniline used and determined by GLC. ○: 3,8-Diethyl-2,9-dimethyl-4,7-phenanthroline, ●: 2-ethyl-3-methyl-6-(propylamino)quinoline, □: 2-ethyl-3-methyl-6-nitroquinoline.

(Runs 1, 20, 21, and 22). The yields of **1** and **2** decreased considerably when the reaction was carried out without water (Run 19). Thus, water is indispensable for the reductive *N*-heterocyclization of nitroarene under carbon-monoxide pressure. Furthermore, under hydrogen pressure (70 atm) instead of carbon monoxide, **1** was also produced, but in only low yield (Run 23). These results indicated that the water-gas-shift reaction was operative for the reaction.

The relation between the initial pressure of carbon monoxide and the yield of the products is shown in Fig. 1. Under an argon atmosphere ($P_{CO}=0$), **3** was a dominant product in a yield of more than 30%, while **1** and **2** were given as minor products, indicating that carbon-monoxide pressure is not necessary for the *N*-heterocyclization of the aminoarene moiety, as was shown in previous paper.[3] However, with increases in the pressures of carbon monoxide to 10—70 atm, the yields of **3** decreased and then **1** and **2** became the major products, with a reduction of the nitroarene moiety. A pressure of carbon monoxide higher than 30 atm is required for the major production of **1**.

By inference from the result of the *N*-heterocyclization of aminoarene,[3] we first expected *p*-phenylenediamine to be a suitable substrate for the double *N*-heterocyclization. However, that is not the case. A mixture of *p*-phenylenediamine (20 mmol), $[RhCl(NBD)]_2$ (0.17 mmol), which was an excellent catalyst for the formation of quinoline derivatives from aminoarene and aldehyde,[3] propanal (90 mmol), ethanol (20 ml), and *p*-nitroaniline (30 mmol) or nitrobenzene (60 mmol) as oxidizing agents was heated at 180 °C under an argon atmosphere for 4 h. The yields of **1** were only 1—2%, based on the *p*-phenylenediamine used. In this case, one amino group may interfere with the *N*-heterocyclization of the other amino group in the same molecule.

This procedure can be applied to a variety of other aliphatic aldehydes and nitroarenes for the preparation of phenanthroline derivatives. The results are summarized in Table 3. *p*-Nitroaniline reacted with propanal, butanal, and pentanal to give the corresponding phenanthroline derivatives in fairly good yields of 43, 57, and 54% respectively (Runs 1, 24, and 25). The conbination of *p*-nitroaniline and ethanal, however failed to give the product, and a tarry material was formed. As the substrate, *p*-dinitrobenzene can be employed in this reaction, although the yield was rather low (Run 26).

As for the structure of the product mentioned above, two isomers were possible because of the two directions in the cyclization. In the reaction of *p*-nitroaniline or *p*-dinitrobenzene with the aldehyde, two isomers, 4,7-phenanthroline and 1,5-diazaanthracene derivatives, were possible (Scheme 2). The absence of J_{C-C-H} in the non-decoupling ^{13}C-NMR spectra clearly indicated that the products are not 1,5-diazaanthracene, but 4,7-phenanthroline derivatives, as is shown in Eq. 1. In the non-decoupling ^{13}C-NMR spectrum of the product, one of the aromatic carbon resonances, with a shoter T_1, appeared as a doublet ($J_{C-H}=163$ Hz) without any further long-range coupling. The resonance is assigned

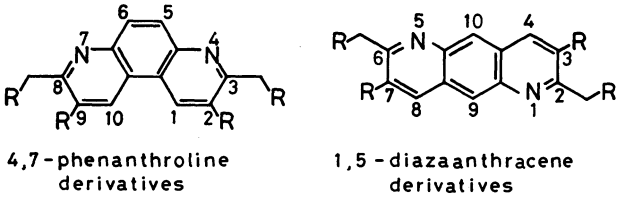

Scheme 2.

Table 3. Synthesis of phenanthroline derivatives from nitroarenes and aldehydes[a]

Run No.	Nitroarene	Aldehyde	Product	Yield/%[b]
1	*p*-Nitroaniline	Propanal	3,8-Diethyl-2,9-dimethyl-4,7-phenanthroline	43 (26)
24	*p*-Nitroaniline	Butanal	2,9-Diethyl-3,8-dipropyl-4,7-phenanthroline	57 (13)
25	*p*-Nitroaniline	Pentanal	3,8-Dibutyl-2,9-dipropyl-4,7-phenanthroline	54 (33)
26	*p*-Dinitrobenzene	Propanal	3,8-Diethyl-2,9-dimethyl-4,7-phenanthroline	14
27	*m*-Nitroaniline	Propanal	2,8-Diethyl-3,9-dimethyl-1,7-phenanthroline	21
28	*m*-Dinitrobenzene	Propanal	2,8-Diethyl-3,9-dimethyl-1,7-phenanthroline	15
29	*o*-Nitroaniline	Propanal	2-Ethylbenzimidazole	24
30	*o*-Dinitrobenzene	Propanal	2-Ethylbenzimidazole	10

a) A mixture of nitroarene (20 mmol), aldehyde (90 mmol), water (2 ml), $RhCl(PPh_3)_3$ (0.17 mmol), $PdCl_2$ (0.26 mmol), and ethanol (20 ml) was treated at 180 °C under the pressure of carbon monoxide (70 atm) for 4 h. b) GLC yield based on the amount of nitroarene used. Parentheses indicate isolated yields.

to C_5 (or C_6) of 4,7-phenanthroline derivatives, since $J_{C_5\text{-}C\text{-}C\text{-}H_1}$ is too small and since the C_5 (or C_6) carbon resonance does not show any long-range coupling in the spectra. If the product is the 1,5-diazaanthracene derivative, all the resonances of the aromatic carbon resonances having shorter T_1 values will appear as peaks with a long-range coupling of 4—5 Hz ($J_{C_9\text{-}C\text{-}H_8}$, $J_{C_8\text{-}C\text{-}H_9}$). The absence of such a long-range coupling clearly indicated the product was 4,7-phenanthroline derivative.

Subsequently this reaction is applied to other nitroaniline and dinitrobenzene isomers. In the reaction with propanal, *m*-nitroaniline and *m*-dinitrobenzene gave 1,7-phenanthroline derivative in yields of 21 and 15% respectively (Runs 27 and 28) (Eq. 2). In this case, there are also two possible structures of the product based on a direction of the cyclization. However, in this case two nonequivalent peaks of methyl and ethyl groups appeared in the ^1H and ^{13}C-NMR spectra. This fact clearly indicated that the product was a 1,7-phenanthroline derivative, not a synmetric 1,8-diazaanthracene derivative.

o-Nitroaniline and *o*-dinitrobenzene failed to give a 1,10-phenanthroline derivative, but 2-ethylbenzimidazole was produced in poor yields (Runs 29 and 30) (Eq. 3).

The mechanism of the binary catalyst system is not yet clear, but several palladium complexes have been reported to form a ortho-metalated complex easily.[7] We previously suggested that the ortho-metalated species was a key intermediate in the rhodium complex-catalyzed *N*-heterocyclization of aminoarenes with aldehydes.[3] In the present reaction, palladium complex might be operative in the ortho-metalated step in the catalytic cycle. However, another factor, the so-called synergism, might also work in the reaction.

Experimental

The melting points and boiling points are uncorrected. The melting points were taken on a Yanagimoto capillary melting-point apparatus. The IR spectra were measured on a Hitachi model 215 grating spectrophotometer. The ^1H-NMR-spectra were obtained at 60 MHz with a JEOL JNM-PMX 60 spectrometer or at 220 MHz with a Varian Model HR-220 spectrometer. ^{13}C NMR spectra were measured at 25.05 MHz with a JEOL JNM FX 100. Samples were dissolved in $CDCl_3$, and the chemical-shift values were expressed in δ relative to Me_4Si as the internal standerd. Elemental analyses were performed at the Microanalytical Center of Kyoto University. The mass spectra were recorded on a JMS OISG mass spectrometer.

The aldehydes, the nitroarenes, and the other materials employed in this study were commercial products. The aldehydes were distilled before use. Carbon monoxide was used without further purification. Anhydrous ethanol was dried by the usual method with Mg.

A 100 ml stainless steel autoclave equipped with a magnetic stirrer was used. The general experimental procedure is exemplified by the reaction of *p*-nitroaniline with propanal. A mixture of *p*-nitroaniline (2.76 g, 20 mmol), propanal (5.23 g, 90 mmol), water (2.0 ml), $RhCl(PPh_3)_3$ (0.17 mmol), $PdCl_2$ (0.26 mmol), and anhydrous ethanol (20 ml) was stirred at 180 °C under carbon monoxide (initial pressure, 70 atm at room temperature).

The autoclave was heated to 180 °C (20 min required) and then held at this temperature for 4 h. After cooling, the autoclave was discharged and the ethanol was evaporated from the reaction mixture under a vacuum. The GLC analysis of the reaction product was made using an internal standard (*N,N*-dibenzylaniline): A column (0.3 cmϕ × 3 m) packed with 5% Silicone GE SE-30 on Shimalite W 60—80 mesh. The reaction products were then subjected to fractional distillation or column chromatography (silica gel, $CHCl_3$). Recrystallization was done by means of ether. The identity of the compound was comfirmed by IR, ^1H-NMR, ^{13}C-NMR, mass spectra, and elemental analysis.

The analytical data of the phenanthroline derivatives and other products obtained here may be described as follows:

3,8-Diethyl-2,9-dimethyl-4,7-phenanthroline. Yellow crystals, mp 133—136 °C. ^1H-NMR (220 MHz) ($CDCl_3$): δ 1.39 (t, 6H, $2CH_3$), 2.55 (s, 6H, $2CH_3$), 3.01 (q, 4H, $2CH_2$), 8.08 (s, 2H), 8.46 (s, 2H). ^{13}C-NMR (25.05 MHz) ($CDCl_3$): δ 12.8 (q, $2CH_3$), 19.3 (q, $2CH_3$), 29.2 (t, $2CH_2$), 122.7 (s), 129.3 (s), 130.3 (d), 130.7 (d), 145.5 (s), 162.3 (s). MS: *m/e* 264 (M^+). Found: C, 80.79; H, 7.60; N, 10.49%. Calcd for $C_{18}H_{20}N_2$: C, 81.78; H, 7.63; N, 10.60%.

2,9-Diethyl-3,8-dipropyl-4,7-phenanthroline. Yellow crystals, mp 77—79 °C. ^1H-NMR (220 MHz) ($CDCl_3$): δ 1.09 (t, 6H, $2CH_3$), 1.41 (t, 6H, $2CH_3$), 1.87 (sex, 4H, $2CH_2$), 2.95 (q, 4H, $2CH_2$), 2.96 (t, 4H, $2CH_2$), 8.09 (s, 2H), 8.58 (s, 2H). ^{13}C-NMR (25.05 MHz) ($CDCl_3$): δ 14.4 (q, $2CH_3$), 15.1 (q, $2CH_3$), 23.0 (t, $2CH_2$), 25.7 (t, $2CH_2$), 37.5 (t, $2CH_2$), 122.9 (s), 129.1 (d), 130.5 (d), 135.5 (s), 145.4 (s), 161.1 (s). Found C, 82.52; H, 9.00; N, 8.66%. Calcd for $C_{22}H_{28}N_2$: C, 82.45; H, 8.81; N, 8.74%.

3,8-Dibutyl-2,9-dipropyl-4,7-phenanthroline. Yellow crystals, mp 79—81 °C. ^1H-NMR (220 MHz) ($CDCl_3$): δ 0.99 (t, 6H, $2CH_3$), 1.09 (t, 6H, $2CH_3$), 1.51 (sex, 4H, $2CH_2$), 1.46—1.56 (m, 8H, $4CH_2$), 2.87 (t, 4H, $2CH_2$), 3.02 (t, 4H, $2CH_2$), 8.08 (s, 2H), 8.54 (s, 2H). ^{13}C-NMR (25.05 MHz) ($CDCl_3$): δ 14.1 (q, $2CH_3$), 14.2 (q, $2CH_3$), 23.0 (t, $2CH_2$), 24.2 (t, $2CH_2$), 32.0 (t, $2CH_2$), 34.9 (t, $2CH_2$), 35.3 (t, $2CH_2$), 122.8 (s), 130.0 (d), 130.4 (d), 134.0 (s), 145.4 (s), 161.4 (s). Found: C, 83.01; H, 9.91; N, 7.32%. Calcd for $C_{26}H_{36}N_2$: C, 82.93; H, 9.64; N, 7.44%.

2,8-Diethyl-3,9-dimethyl-1,7-phenanthroline. Yellow crystals, mp 101—104 °C. ^1H-NMR (220 MHz) ($CDCl_3$): δ 1.40 (t, 3H, CH_3), 1.48 (t, 3H, CH_3), 2.48 (s, 3H, CH_3), 2.60 (s, 3H, CH_3), 3.02 (q, 2H, CH_2), 3.05 (q, 2H, CH_2), 7.74 (d, 1H), 7.83 (s, 1H), 7.93 (d, 1H), 9.24 (s, 1H). ^{13}C-NMR (25.05 MHz) ($CDCl_3$): δ 12.3 (q, CH_3), 13.0 (q, CH_3), 18.9 (q, CH_3), 19.2 (q, CH_3), 29.1 (t, CH_2), 29.3 (t, CH_2), 124.2 (s), 125.3 (s), 127.1 (d), 127.3 (d), 129.6 (s), 129.8 (s), 132.8 (d), 135.7 (d), 143.2 (s), 147.0 (s), 161.5 (s), 163.0 (s). Found: C, 80.49; H, 7.74; N, 10.53%. Calcd for $C_{18}H_{20}N_2$: C, 81.78; H, 7.63; N, 10.60%.

2-Ethylbenzimidazole. White crystals, mp 175—177 °C. ^1H-NMR (220 MHz) ($CDCl_3$): δ 1.42 (t, 3H, CH_3), 3.00 (q, 2H, CH_2), 7.17—7.21 (m, 2H), 7.53—7.57 (m, 2H), 9.29 (s, 1H, N-H). ^{13}C-NMR (25.05 MHz) ($CDCl_3$): δ 12.6 (q, CH_3), 22.6 (t, CH_2), 114.5 (d), 122.0 (d), 138.6 (s), 156.8 (s). Found: C, 74.08; H, 6.77; N, 19.38%. Calcd for $C_9H_{10}N_2$: C, 73.94; H, 6.89; N, 19.16%.

2-Ethyl-3-methyl-6-nitroquinoline. Yellow crystals, mp 118—120 °C. IR (KBr): 1340, 1520 cm^{-1}. ^1H-NMR (220 MHz) ($CDCl_3$): δ 1.41 (t, 3H, CH_3), 2.53 (s, 3H, CH_3), 3.03 (q, 2H, CH_2), 7.97 (s, 1H), 8.09 (d, 1H), 8.34 (d, 1H), 8.63 (s, 1H). ^{13}C-NMR (25.05 MHz) ($CDCl_3$): δ 12.2 (q, CH_3), 19.1 (q, CH_3), 29.6 (t, CH_2). MS (*m/e*): 216 (M^+). Found: C, 67.61; H, 5.48; N, 11.78%. Calcd for $C_{12}H_{12}N_2O_2$: C,

66.65; H, 5.59; N, 12.96%.

2-Ethyl-3-methyl-6-(propylamino) quinoline: Yellow crystals. IR (KBr): 3300 cm^{-1}. ^{1}H-NMR (220 MHz) ($CDCl_3$): δ 0.89 (t, 3H, CH_3), 1.19 (t, 3H, CH_3), 1.55 (sex, 2H, CH_2), 2.30 (s, 3H, CH_3), 2.84 (q, 2H, CH_2), 3.05 (t, 2H, CH_2), 3.73 (s, 1H, N–H), 6.50—7.73 (m, 4H).

This work was supported by a Grant-in-Aid, Ministry of Education, Science and Culture, Japan (No. 56550587).

References

1) S. E. Diamond, A. Szalkiewicz, and F. Mares, *J. Am. Chem. Soc.*, **101**, 490 (1979).

2) T. Joh and N. Hagihara, *Tetrahedron Lett.*, **1967**, 4199.

3) Y. Watanabe, M. Yamamoto, S. C. Shim, T. Mitsudo, and Y. Takegami, *Chem. Lett.*, **1979**, 1025; Y. Watanabe, S. C. Shim, and T. Mitsudo, *Bull. Chem. Soc. Jpn.*, **54**, 3460 (1981).

4) Y. Watanabe, N. Suzuki, S. C. Shim, M. Yamamoto, T. Mitsudo, and Y. Takegami, *Chem. Lett.*, **1980**, 429; Y. Watanabe N. Suzuki, and Y. Tsuji, *Bull. Chem. Soc. Jpn.*, **55**, 1116 (1982).

5) Y. Watanabe, Y. Tsuji, and Y. Ohsugi, *Tetrahedron Lett.*, **1981**, 2667.

6) Y. Watanabe, Y. Tsuji, and N. Suzuki, *Chem. Lett.*, **1981**, 1067.

7) I. Omae, *Chem. Rev.*, **79**, 287 (1979); A. D. Ryabov and A. K. Yatsimirsky, *Tetrahedron Lett.*, **1980**, 2757; J. M. Thompson and R. F. Heck, *J. Org. Chem.*, **40**, 2667 (1975).

Intramolecular 1,3-Dipolar Cycloadditions and Intramolecular Ene Reactions of 2-(Alkenyloxy)benzaldehyde Arylhydrazones[1]

Tomio SHIMIZU,* Yoshiyuki HAYASHI, Yoshitaka KITORA, and Kazuhiro TERAMURA
Department of Dyeing, Faculty of Industrial Arts, Kyoto Technical University, Matsugasaki, Sakyo-ku, Kyoto 606
(Received December 4, 1981)

2-(3-Aryl-2-propenyloxy)benzaldehyde (or 1-naphthaldehyde) arylhydrazones undergo an intramolecular cycloaddition reaction *via* their 1,3-dipolar tautomers, azomethine imines, to the alkenyl group. Initial cycloadducts were converted to dehydrogenated compounds under the reaction conditions. On the other hand, introduction of cyano or ethoxycarbonyl groups instead of the aryl group into 3-position of the ortho propenyloxy group gave 3-cyanomethyl-4-chromanone arylhydrazones or the corresponding ethoxycarbonyl derivatives, respectively. The formation of these hydrazones was interpreted in terms of intramolecular ene reaction. The course of the reactions depends on the nature of the alkenyl substituents.

1,3-Dipolar cycloaddition reactions provide the most versatile synthesis of 5-membered heterocycles.[2] The syntheses of a number of fused ring compounds using intramolecular cycloadditions have been reported.[3]

Hydrazones are ambident nucleophiles and can react with electrophiles at either carbon or nitrogen. Recent investigations show that monosubstituted hydrazones undergo ene reactions (and subsequent cyclization),[4] 1,3-dipolar cycloadditions *via* azomethine imine tautomer,[5] acid-catalyzed [3+2] cycloadditions,[6] and/or Michael additions (and subsequent cyclization)[4] with alkenes (the four reactions may provide a simple route to a variety of unusual pyrazoles). It is interesting to examine substituent effects on the competing processes of arylhydrazones in the presence of intramolecular olefins. As one of a series of benzopyranopyrazoles preparations,[7] we report here thermal transformations of 2-(alkenyloxy)benzaldehyde (or 1-naphthaldehyde) arylhydrazones to [1]benzo (or naphtho[1',2':5,6]) pyrano[4,3-*c*]pyrazoles or 3-substituted 4-chromanone arylhydrazones.

Results and Discussion

2-(Alkenyloxy)benzaldehyde (or 1-naphthaldehyde) arylhydrazones (**2**) were prepared from salicylaldehyde (or 2-hydroxy-1-naphthaldehyde) *via* 2-(alkenyloxy)-benzaldehydes (or 1-naphthaldehydes) (**1**) in two steps. Although the preparation of **1** was worked up in the usual manner[8a,b] by etherification with alkenyl bromides in the presence of potassium carbonate, some (**1d—e**, **1k—m**) of **1** underwent further base-promoted cyclization, giving furans (**3**) (see Eq. 1). On the other hand, the etherification in the presence of potassium fluoride (fluoride-assisted etherification[8c]) gave **1** in satisfactory yields (Table 1). The reaction of **1** with arylhydrazines gave hydrazones (**2**) in good yields (Table 2). Satisfactory spectral and analytical data for **1** and **2** were obtained. Though some of the hydrazones bearing an ethoxycarbonyl group were not isolated in a crystalline form, it was found from NMR spectra that these hydrazones were formed almost

TABLE 1. YIELDS, MELTING AND BOILING POINTS, AND SPECTRAL DATA OF 1[a]

	Yield %	Mp θ_m/°C (Bp θ_b/°C)[b]	IR $\tilde{\nu}$/cm^{-1}	NMR δ $CDCl_3$
1a	86	51	1680(CHO)	4.8(d, 2H, J=5 Hz), 6.1—8.0(m, 1H), 10.6(s, 1H)
1b	83	78—79	1690(CHO)	5.8(d, 2H, J=5 Hz), 6.1—8.0(m, 10H), 10.6(s,1H)
1c	72	90—91	1690(CHO)	2.3(s, 3H), 5.8(d,2H, J=5 Hz), 6.1—8.0(m, 10H), 10.6(s, 1H)
1d	32	95—96	2220(CN)	4.8(dd, 2H, J=2 and 3 Hz), 5.87(dt, 1H, J=16 and 2 Hz),
			1680(CHO)	6.67—8.0(m, 5H), 10.4(s, 1H)
1e	51	66—69	1720(COO)	1.3(t, 3H, J=7 Hz), 4.2(q, 2H, J=7 Hz), 4.7—5.0 (m, 2H)
			1680(CHO)	6.2(d, 1H, J=16 Hz), 6.7—8.0(m, 5H), 10.5(s, 1H)
1f	90	(142 / 17 mmHg)	1680(CHO)	4.5(d, 2H, J=5 Hz), 5.1—5.6(m, 2H), 5.7—6.4(m, 1H), 6.7—7.8(m, 4 H), 10.4(s, 1H)
1g	93	(120 / 4 mmHg)	1680(CHO)	1.73(d, 3H, J=4 Hz), 4.57(d, 2H, J=4 Hz), 5.4—6.3(m, 2H), 6.8—7.2(m, 2H), 7.3—8.0(m, 2H), 10.5(s, 1H)
1h	100	139—140	1670(CHO)	4.9(d, 2H, J=5 Hz), 6.1—8.2(m, 12H), 9.37(d, 1H, J=8 Hz), 11.0(s, 1H)
1i	78	136—137	1670(CHO)	4.8(d, 2H, J=5 Hz), 6.0—6.85(m, 2H), 7.05—8.1(m, 9H), 9.25(d, 1H, J=8 Hz), 10.9(s, 1H)
1j	65	116	1680(CHO)	2.3(s, 1H), 5.8(d, 2H, J=5 Hz), 6.0—8.1(m, 10H), 9.3(d, 1H, J=8 Hz), 10.9(s, 1H)
1k	75	129	2230(CN)	4.9(dd, 2H, J=2 and 3 Hz), 5.85(dt, 1H, J=16 and 2 Hz), 6.6—7.95(m, 5H),
			1670(CHO)	8.1(d, 1H, J=9 Hz), 9.2(d, 1H, J=8 Hz), 10.9(s, 1H)
1m	66	113—115	1720(COO)	1.25(t, 3H, J=7 Hz), 4.2(q, 2H, J=7 Hz), 4.75—4.9(m, 2H),
			1670(CHO)	6.15(dt, 1H, J=16 and 2 Hz), 6.9—8.1(m, 7H), 9.2(d, 1H, J=8 Hz), 10.9(s, 1H)

a) Satisfactory analytical data were obtained for these compounds. b) Recrystallized from ethanol.

TABLE 2. YIELDS, MELTING POINTS,[a] AND SPECTRAL DATA OF **2**[b]

	Yield %	Mp θ_m/°C	IR $\tilde{\nu}$/cm^{-1}	NMR δ[c]
2aq	70	105—107	3320(NH)	4.7(d, 2H, J=5 Hz), 6.1—7.6(m, 16H), 7.9—8.2(m, 1H), 8.1(s, 1H), 7.57(s, 1H)
2ar	62	126—128	3330(NH)	4.67(d, 2H, J=5 Hz), 6.1—7–5(m, 15H), 7.85—8.1(m, 1H), 8.07(s, 1H)
2at	100	201—202	3250(NH)	4.75(d, 2H, J=5 Hz), 6.2—8.5(m, 16H), 11.23(s, 1H)
2bq	56	118—120	3330(NH)	4.65(d, 2H, J=5 Hz), 6.0—7.5(m, 14H), 7.8—8.1(m, 1H), 8.1(s, 1H)
2cq	85	126—128	3330(NH)	2.3(s, 3H), 4.7(d, 2H, J=5 Hz), 6.1—7.5(m, 14H), 7.9(d, 1H, J=6 Hz), 8.3(s, 1H), 10.4(s, 1H)
2cr	33	d)	3330(NH)	2.3(s, 1H), 4.6(d, 2H, J=5 Hz), 6.0—7.65(m, 14H), 7.8—8.1(m, 1H), 8.05(s, 1H)
2dq	83	145—146	3280(NH) 2230(CN)	4.77(dd, 2H, J=2 and 4 Hz), 6.03(dt, 1H, J=2 and 17 Hz), 6.5—7.5(m, 9H), 7.9(dd, 1H, J=2 and 8 Hz), 8.3(s, 1H), 10.3(s, 1H)
2dr	81	170—171	3270(NH) 2230(CN)	4.79(dd, 2H, J=2 and 4 Hz), 5.98(dt, 1H, J=2 and 17 Hz), 6.8—7.45 (m, 8H), 7.9(dd, 1H, J=2 and 8 Hz), 8.25(s, 1H), 10.4(s, 1H)
2dt	100	248—250	3260(NH) 2240(CN)	4.75—4.95(m, 2H), 6.05(d, 1H, J=18 Hz), 6.95—7.4(m, 6H), 7.8—8.2(m, 3H), 8.35(s, 1H), 11.25(s, 1H)
2et	93	142—143	3240(NH) 1720(COO)	1.3(t, 3H, J=7 Hz), 4.2(q, 2H, J=7 Hz), 4.7(dd, 2H, J=2 and 4 Hz), 6.15(dt, 1H, J=2 and 16 Hz), 6.7—7.45(m, 6H), 7.85—8.3(m, 4H), 8.6(s, 1H)
2fq	100	63	3260(NH)	4.4—4.6(m, 2H), 5.1—5.6(m, 2H), 5.7—6.4(m, 1H), 6.6—7.3(m, 9H), 7.8—8.1(m, 1H), 8.0(s, 1H)
2ft	95	213—215	3270(NH)	4.6(d, 2H, J=5 Hz), 5.1—5.7(m, 2H), 5.75—6.4(m, 1H), 6.8—7.6 (m, 5H), 7.8—8.27(m, 3H), 8.4(s,1H), 11.23(s, 1H)
2gt	95	188—190	3360(NH)	1.7(d, 3H, J=5 Hz), 4.5(d, 2H, J=5 Hz), 5.7—5.9(m, 2H), 6.8—8.4(m, 9H), 11.3(s, 1H)
2gq	91	51—55	3300(NH)	1.7(d, 3H, J=5 Hz), 4.4(d, 2H, J=5 Hz), 5.4—6.1(m, 2H), 6.6—7.5(m, 8H), 7.8—8.1(m, 1H), 8.0(s, 1H)
2hq	86	122—123	3300(NH)	4.8(d, 2H, J=5 Hz), 6.1—8.0(m, 18H), 8.5(s, 1H), 9.33(d, 1H, J=8 Hz)
2hr	80	124—127	3300(NH)	4.8(d, 2H, J=5 Hz), 6.1—7.9(m, 17H), 8.4(s, 1H), 9.2(d, 1H, J=8 Hz)
2jq	90	139—141	3300(NH)	2.3(s, 3H), 4.8(d, 2H, J=5 Hz), 6.1—7.9(m, 17H), 8.46(s, 1H), 9.2(d, 1H, J=8 Hz)
2kq	78	168—169	3300(NH) 2240(CN)	4.85—5.1(m, 2H), 6.1(dt, 1H, J=2 and 16 Hz), 6.65—8.0(m, 11H), 8.7(s, 1H), 9.36(d, 1H, J=8 Hz)10.4(s, 1H)
2kr	95	139—140	3280(NH) 2230(CN)	4.9—5.1(m, 2H), 6.15(dt, 1H, J=2 and 8 Hz), 6.95—8.05(m, 10H), 8.64(s, 1H), 9.25(d, 1H, J=8 Hz), 10.45(s, 1H)
2kt	84	210—212	3300(NH) 2220(CN)	4.9—5.1(m, 2H), 6.2(d, 1H, J=7Hz), 6.85—8.4(m, 10H), 8.9(s, 1H), 9.35(d, 1H, J=7 Hz), 11.43(s, 1H)
2mt	90	144—145	3300(NH) 1730(COO)	1.25(t, 3H, J=7 Hz), 4.15(q, 2H, J=7 Hz), 4.8—5.1(m, 2H), 6.2(d, 1H, J=16 Hz), 6.9—8.3(m, 10H), 8.8(s, 1H), 9.25(d, 1H, J=8 Hz), 11.4(s, 1H)

a) Recrystallized from ethanol. b) Satisfactory analytical data were obtained for these compounds. c) **2at**, **cq**, **dq**, **dr**, **kq**, **kr**, **kt**, **dt**, and **2mt** were dissolved in DMSO-d_6, the others were dissolved in $CDCl_3$. d) This material is so hygroscopic that we could not determine the melting point.

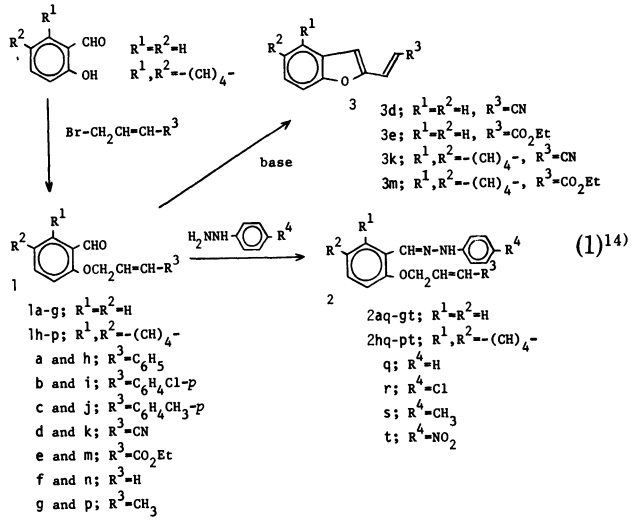

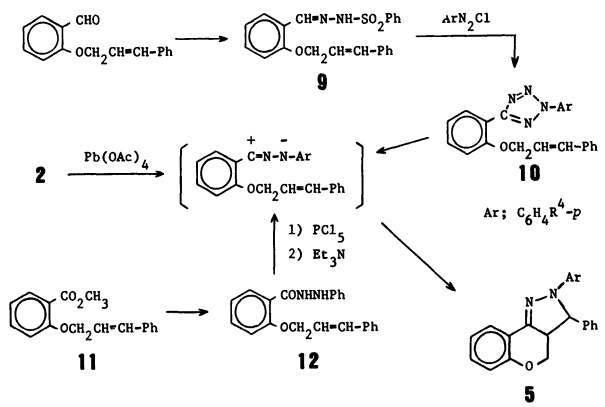

Scheme 1.

TABLE 3. YIELDS, MELTING POINTS[a], AND SPECTRAL DATA OF 5[b]

	Reaction[c] condition	Yield %	Mp θ_m/°C	NMR δ[d]
5aq	A	36	146—147	3.3—4.8(m, 4H), 6.6—7.5(m, 13H), 7.73—7.97(m, 1H)
5ar	A	12	180—183	3.3—4.8(m, 4H), 6.73—7.5(m, 12H), 7.73—7.95(m, 1H)
5as	C	10	148—150	2.2(s, 3H), 2.23—4.77(m, 4H), 6.7—7.5(m, 12H), 7.75—7.95(m, 1H)
5bs	C	52	191—193	2.2(s, 3H), 3.17—4.75(m, 4H), 6.4—7.5(m, 11H), 7.65—7.9(m, 1H)
5cq	A	50	145—146	2.3(s, 3H), 3.2—4.8(m, 4H), 6.5—7.5(m, 12H), 7.7—7.95(m, 1H)
5cr	A	13	190—192	2.25(s, 3H), 3.3—5.2(m, 4H), 6.8—7.5(m, 11H), 7.6—7.9(m, 1H)
5cs	C	34	187—188	2.15(s, 3H), 2.3(s, 3H), 3.2—5.2(m, 4H), 7.0—7.75(m, 11H), 7.8—8.1(m, 1H)
5hq	A	31	194—195	3.35—4.85(m, 4H), 6.55—7.8(m, 15H), 9.33(d, 1H, J=8 Hz)
5hr	A	50	206—208	3.35—4.87(m, 4H), 6.8—7.85(m, 14H), 9.3(d, 1H, J=8 Hz)
5hs	C	24	208—210	2.2(s, 3H), 3.3—4.8(m, 4H), 6.8—7.95(m, 14H), 9.4(d, 1H, J=8 Hz)
5iq	B	79	182—184	3.3—5.1(m, 4H), 6.5—8.0(m, 14H), 8.57(d, 1H, J=8 Hz)
5ir	B	64	239—240	3.3—5.0(m, 4H), 6.8—8.0(m, 13H), 9.45(d, 1H, J=8 Hz)
5is	C	35	230—231	2.2(s, 3H), 3.2—4.9(m, 4H), 6.7—7.9(m, 13H), 9.35(d, 1H, J=8 Hz)
5jq	A	26	188—191	2.35(s, 3H), 3.3—4.87(m, 4H), 6.5—7.9(m, 14H), 9.4(d, 1H, J=8 Hz)
5jr	B	62	217—218	2.33(s, 3H), 3.3—4.9(m, 4H), 6.8—7.9(m, 13H), 9.3(d, 1H, J=8 Hz)
5js	C	23	202—203	2.2(s, 3H), 2.4(s, 3H), 3.25—4.8(m, 4H), 6.7—7.8(m, 13H), 9.4(d, 1H, J=8 Hz)
5mq	D	55	134—136	1.27(t, 3H, J=7 Hz), 3.5—4.9(m, 6H), 6.5—7.8(m, 10H), 9.2(d, 1H, J= 8 Hz)
5mr	D	70	162—165	1.3(t, 3H, J=7 Hz), 3.9—5.0(m, 6H), 6.4—7.9(m, 9H), 9.2(d, 1H, J=8 Hz)
5ms	D	70	148—151	1.3(t, 3H, J=7 Hz), 2.2(s, 3H), 3.8—4.95(m, 6H), 6.87—7.9(m, 9H), 9.3(d, 1H, J=8 Hz)

a) Recrystallized from ethanol. b) Satisfactory analytical data were obtained for these compounds. c) A: Refluxing the solution of **2** in xylene for 24 h; B: Refluxing the ethanol solution of **1** and arylhydrazine for 24 h : C: Refluxing the pyridine solution of **1** and *p*-tolylhydrazine hydrochloride for 24 h; D: Refluxing the solution of **1** and arylhydrazine in ethanol containing acetic acid for 24 h. d) **5cr** and **5cs** were dissolved in DMSO-d_6, the others were dissolved in $CDCl_3$.

TABLE 4. YIELDS, MELTING POINTS[a], AND SPECTRALDATA OF 7 AND 8[b]

	Reaction[c] condition	Yield %	Mp θ_m/°C	IR $\tilde{\nu}$/cm^{-1}	NMR δ[d]
7dq	A	60	173—175	3310(NH) 2250(CN)	2.7(d, 2H, J=8 Hz), 3.4(t, 1H, J=8 Hz), 4.17(d, 1H, J=12 Hz), 4.58(d, 1H, J=12 Hz), 6.8—7.5(m, 8H), 7.9(s, 1H), 7.95—8.3(m, 1H)
7dr	A	38	216—218	3330(NH) 2250(CN)	2.73(d, 2H, J=8 Hz), 3.2—3.9(m, 2H), 4.12(d, 1H, J=12 Hz), 4.43(d, 1H, J=12 Hz), 6.7—7.35(m, 7H), 7.8—8.03(m, 1H)
7ds	C	42	181—185	3300(NH) 2250(CN)	2.2(s, 3H), 2.7(d, 2H, J=8 Hz), 3.3(s, 1H), 3.67(t, 1H, J=8 Hz), 4.1(d, 1H, J=12 Hz), 4.3(d, 1H, J=12 Hz), 6.7—7.3(m, 7H) 7.8—8.1(m, 1H)
7eq	B	45	129—130	3250(NH) 1700(COO)	1.27(t, 3H, J=7 Hz), 2.83—3.3(br, 1H), 4.27(q, 2H, J=7 Hz), 4.05—4.8(m, 5H), 6.5—7.3(m, 8H), 7.43—7.67(m, 1H)
7kq	A	58	209—212	3270(NH) 2240(CN)	4.05—4.8(m, 3H), 5.15(d, 1H, J=8 Hz), 5.9(d, 1H, J=12 Hz), 6.7—8.15(m, 10H), 8.37(d, 1H, J=8 Hz), 9.2(d, 1H, J=8 Hz)
7kr	A	31	240—241	3280(NH) 2240(CN)	4.3—5.2(m, 4H), 5.95(d, 1H, J=8 Hz), 7.1—8.15(m, 10H), 9.23(d, 1H, J=8 Hz)
8eq	C	49	159—162	1680(CON)	2.2—4.53(m, 5H), 6.67—7.7(m, 8H), 7.8—8.03(m, 1H)
8er	C	26	209—211	1670(CON)	2.5—4.7(m, 5H), 6.8—7.7(m, 7H), 7.9—8.15(m, 1H)
8es	C	43	165—166	1670(CON)	2.33(s, 3H), 2.5—4.6(m, 5H), 6.77—7.63(m, 7H), 7.83—8.1(m, 1H)

a) Recrystallized from ethanol. b) Satisfactory analytical data were obtained for these compounds. c) A: Refluxing the solution of **2** in xylene for 24 h; B: Refluxing the ethanol solution of **1** and aryl hydrazine for 24 h; C: Refluxing the pyridine solution of **1** and *p*-tolylhydrazine hydrochloride for 24 h. d) **7dr**, **ds**, **kq**, and **7kr** were dissolved in DMSO-d_6, the others were dissolved in $CDCl_3$.

quantitatively. The oily hydrazones were used for the thermal reaction without further purification.

The treatment of the arylhydrazones (**2**) in xylene at 150 °C for 20 h gave 2-aryl-2,3,3a,4-tetrahydro[1]-benzo (or naphtho[1′,2′:5,6])pyrano[4,3-*c*]pyrazoles (**5**). The structure of **5** was assigned on the basis of a comparison of its physical properties (Table 3) with those of specimens prepared by authentic methods[9] (see Scheme 1). On the other hand, 3-cyanomethyl-4-chromanone arylhydrazones (**7**) were the only isolable products from the reaction mixtures of hydrazones (**2**) bearing a 3-cyano-2-propenyloxy group at *o*-position and none of the corresponding cycloadducts (**5**) could be detected. The structure of **7** was determined on the basis of its spectral and analytical data (see Table 4). Reaction of the hydrazones (**2**) bearing an ethoxycarbonyl group as R^3 might occur by different mechanisms: for example, a) The reaction of **1e** with phenylhydrazine

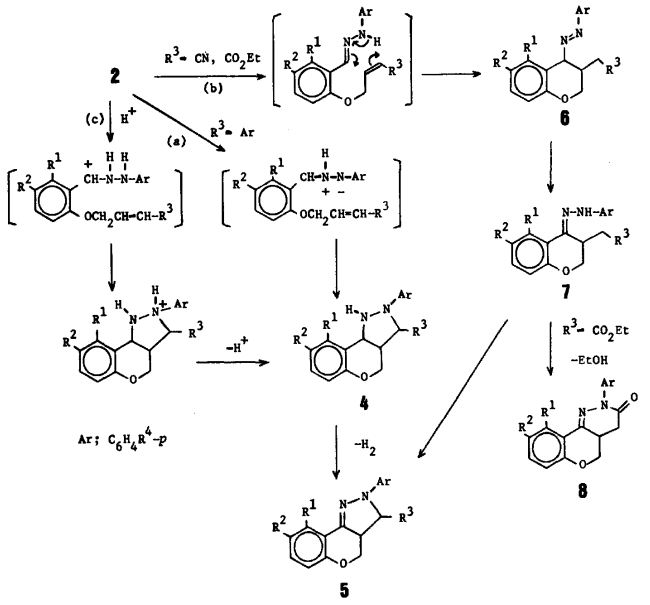

Scheme 2.

in neutral solvents such as ethanol or xylene at refluxing temperatures over 20 h resulted in the formation of ene type product **7eq** in 45% yield. The same reaction in a basic solvent such as pyridine gave **8eq** along with **7eq**. b) The reaction in ethanol containing a small amount of an acid such as acetic acid or sulfuric acid gave the cycloadduct **5mq** in 55% yield without contamination of the ene product.

One of the most plausible mechanisms of the formation of **5** is as follows: arylhydrazones (**2**) undergo intramolecular 1,3-dipolar cycloaddition reaction *via* their azomethine imine tautomer[5] to give pyrazolidines (**4**). which were dehydrogenated to pyrazolines (**5**) under the reaction conditions [route (a) in Scheme 2]. Several possible pathways for the reaction of aldehyde or ketone hydrazones with alkenes are shown in Scheme 2. The route (c) in Scheme 2 is an alternative mechanism, an acid-catalyzed concerted [3+2] cycloaddition reaction,[6] for the formation of **4**. Presence or absence of a base ($NaHCO_3$, Et_3N, or DABCO) has no effect on the reaction of **2jq** in refluxing xylene giving only **5jq**, but an addition of an acid in the reaction of some hydrazones even at room temperature induced a marked increase in yields of the cycloadducts (**5**). The temperatures (150 °C) used in our reactions are apparently high enough to permit substantial presence of the azomethine imine tautomer. If the cyclization reaction of **2** was carried out in solvents containing trace amounts of acid,

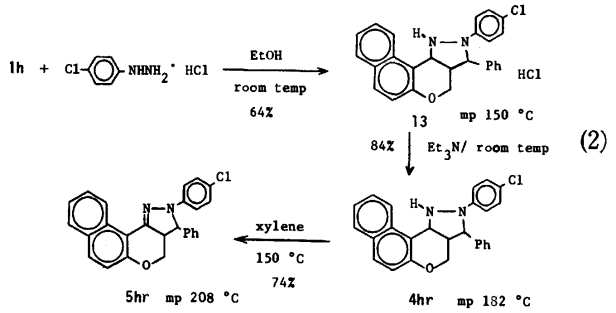

(2)

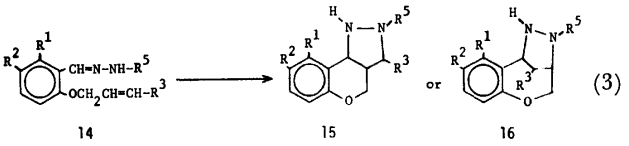

(3)

the [3+2] cycloaddition proceeds much faster than the azomethine imine cycloaddition. Therefore the treatment of **2** in the presence of acid is more convenient for the preparation of **5** (see Eq. 2) and we confirmed that the reaction was facilitated in order of $CO_2Et \approx CN > Ph > alkyl$ group at R^3. Another alternative pathway for the formation of **5** suggested by Snider *et al.*,[4a] intramolecular *N*-alkylation (**7**→**5**) of initial ene type product (**6**→**7**), would be excluded because **7** was stable under the reaction conditions. The intramolecular ene reaction [route (b) in Scheme 1] of the substrate bearing cyano or ethoxycarbonyl group as R^3 may proceed faster than the intramolecular 1,3-dipolar cycloaddition reaction, although we could not find a reasonable explanation of the competitive reactivity in the ene and 1,3-dipolar reaction studied here in terms of FMO theory.[10] Azo compound (**6**), apparent ene reaction products, would easily isomerize to hydrazone structure (**7**), which is a thermodynamically more stable structure under the reaction conditions.

In the case of the reaction with the substrate bearing electron-rich alkenyl group (**2fq** and **2gq**), neither cycloadducts nor ene reaction products was obtained from the reaction mixture, and starting materials were recovered unchanged. It is known[10] that these electron-rich olefins are more reluctant than electron-poor or conjugated olefines to either nucleophilic addition or 1,3-dipolar cycloaddition. Electron-withdrawing substituents on the hydrazone would lower its reactivity, because of the lowered HOMO energy. Thus, we examined the reactivity of phenyl-, *p*-tolyl-, and *p*-chlorophenylhydrazones in the reaction. The more electron-deficient mono- and dinitrophenylhydrazones should be less reactive toward electrophilic species[11] and we, in fact, could not obtain any **5**, **7**, or **8** from the thermal treatment of **2at**—**qt**. Intramolecular Michael type cyclization (Eq. 3) bearing electron deficient olefins would give a product (**16**) containing a seven-membered ring and we could isolate no such products. On the other hand, alkylhydrazones (R^5= alkyl at **14**) have higher reactivity at nitrogen than at carbon atom[12] and only a small amount of Michael adducts (the structure is not yet confirmed) were isolated from the reaction.

Our results show that the thermal intramolecular 1,3-dipolar and ene reactions of **2** proceed in a manner similar to the intermolecular 1,3-dipolar[5] and ene reactions,[4] giving good yields of complex heterocycles. We could obtain **5** in two or three steps from salicylaldehyde (or 2-hydroxy-1-naphthaldehyde) and our procedure is simpler than a reported one.[9b] Our procedure is also suitable for the preparation of 3-substituted 4-chromanone derivatives (**7** or **8**), which are generally difficult to prepare by other methods.

Experimental

Measurements. All the melting and boiling points are

uncorrected. The IR spectra were determined on a Hitachi 215 Infrared Spectrophotometer. The ^1H NMR spectra were measured on a Varian T-60A instrument with TMS as an internal standard.

Materials. 3-Bromo-1-*p*-tolyl-1-propene[13a] and 3-bromo-1-(*p*-chlorophenyl)-1-propene[13b] were prepared according to the method described in the literature.

Preparation of the 2-(Alkenyloxy)benzaldehydes (or 1-naphthaldehydes) (1). *General Procedure*: A mixture of salicylaldehyde (or 2-hydroxy-1-naphthaldehyde) (0.2 mol), 1-substituted 3-bromo-1-propenes (0.25 mol), and potassium fluoride (0.8 mol) in acetone (300 ml) was refluxed for 72 h. After filtration of inorganic salts, evaporation of the filtrate gave a viscous oil which solidified upon scratching with a glass rod. Recrystallization from ethanol gave colorless needles (**1a—m**) in the yields shown in Table 1. In the cases of **1d—e** and **1k—m**, 0.4 mol of KF was used.

Preparation of Hydrazones (2). *General Procedure*: Into a stirred ethanol solution (300 ml) of **1** (0.1 mol) was added first an ethanol solution (50 ml) of phenylhydrazine (or *p*-chlorophenylhydrazine) (0.1 mol) and then 3 ml of acetic acid at room temperature. After stirring the mixture for 6 h at room temperature, evaporation of the ethanol and acetic acid *in vacuo* gave hydrazones (**2**), which was recrystallized from ethanol. Yields and spectral data are shown in Table 2. *p*-Tolylhydrazones are apt to undergo subsequent cycloaddition under the conditions described above, and several attempts to isolate the *p*-tolylhydrazones failed because of subsequent thermal transformation of the hydrazones.

Thermal Reactions of Hydrazones (2) *General Procedure*: Hydrazones (5 mmol) shown in Table 2 and hydrazones bearing an ethoxycarbonyl group as R^3 were refluxed in xylene (50 ml) with a small amount of hydroquinone for 24 h. After distillation of the solvent, the residue was mixed with a small amount of ethanol and was allowed to stand for several days. The crystals which separated were recrystallized from ethanol to give colorless needles (**7**) or yellow crystals (**5**). A chloroform solution of **5** has a brilliant greenish fluorescence.

Specific Procedure. *A)*: A mixture of **1** (10 mmol) and *p*-tolylhydrazine hydrochloride (10 mmol) in pyridine (50 ml) was heated to reflux for 24 h. Then the reaction mixture was poured into water and extracted with ether several times. The ethereal layer was washed with a dilute hydrochloric acid solution, dried over anhydrous sodium sulfate, and evaporated to give **5** from **1a—c**, **1h**, and **1j** or **8** along with **7** from **1d** or **1e**, respectively. The results are shown in Tables 3 and 4.

B): A mixture of **1e** (or **1m**) (10 mmol) and arylhydrazines (10 mmol) was refluxed in ethanol (150 ml) for 24 h. The evaporation of the solvent gave a viscous oil without contamination of **5**. Crystallization from ethanol gave **7**.

C): An ethanol solution (150 ml) of **1m** (10 mmol), arylhydrazine (or arylhydrazine hydrochloride) (10 mmol), and acetic acid (3 ml) was allowed to stand for 10 h at 20—80 °C. Concentration of the reaction gave yellowish crystals, which were recrystallized from ethanol to give **5mq—ms** in 40—70% yields.

Intramolecular Condensation Reaction of 7 to 8. A solution of **7eq** (1 mmol) in acetic acid (10 ml) was heated to reflux for 6 h, then poured into water (50 ml), and extracted with ether several times. The combined ether layer was washed with a dilute sodium carbonate aqueous solution and dried over anhydrous sodium sulfate. Evaporation of the solvent gave **8eq** in 85% yield. Treatment of **7eq** in pyridine also gave **8eq** in 82% yield.

Independent Synthesis of 5aq and 5as. *A)*: 2-Phenyl-5-[2-(3-phenyl-2-propenyloxy)phenyl]-2*H*-tetrazole (**10a**) was prepared from 2-(3-phenyl-2-propenyloxy)benzaldehyde phenylsulfonylhydrazone (**9**)[7a] and benzenediazonium chloride according to a method analogous to that of Ito *et al.*[9a] in 34% yield; mp 104—105 °C (from ethanol). NMR ($CDCl_3$): δ 4.82 (d, 2H, J=4 Hz), 6.15—7.6 (m, 13H), and 8.0—8.3 (m, 3H). Found: C, 74.68; H, 5.13; N, 15.77%. Calcd for $C_{21}H_{18}N_4O$: C, 74.55; H, 5.12; N, 15.81%. 2-(*p*-Tolyl)-5-[2-(3-phenyl-2-propenyloxy)phenyl]-2*H*-tetrazole (**10b**) was prepared in the same manner as described above in 53% yield; mp 106—108 °C (from ethanol). NMR ($CDCl_3$): δ 2.37 (s, 3H), 4.80 (d, 2H, J=4 Hz), 6.12—7.8 (m, 10H), and 7.9—8.2 (m, 3H). Found: C, 74.97; H, 5.31; N, 15.38%. Calcd for $C_{22}H_{20}N_4O$: C, 74.98; H, 5.47; N, 15.21%. Pyrolysis of **10a** (or **10b**) at 140—160 °C for 5 h gave **5aq** (or **5as**) in 100 (or 83) % yields.

B): A mixture of methyl salicylate (0.1 mol), 3-bromo-1-propenyl-2-propene (0.11 mol) and potassium carbonate (0.1 mol) in acetone (400 ml) was set to reflux for 25 h. Filtration of inorganic salts and evaporation of the solvent gave a solid, which was recrystallized from ethanol to give methyl 2-(3-phenyl-2-propenyloxy)benzoate (**11**) in 71% yield; mp 67—68 °C. IR (Nujol): 1725 cm^{-1} ($COOCH_3$); NMR ($CDCl_3$): δ 3.9 (s, 3H), 4.95 (d, 2H, J=6 Hz), and 6.2—7.7 (m, 11H). A mixture of **11** (10 mmol) and phenylhydrazine (17 mmol) was heated at 80 °C for 10 h and subsequently allowed to stand at room tempetature for several days, giving crystals of 1-phenyl-2-[2-(3-phenyl-2-propenyloxy)benzoyl]hydrazine(**12**) as precipitate in 30% yield; mp 161—163 °C (from ethanol). IR (Nujol): 3360 and 3230 cm^{-1} (NH), 1635 cm^{-1} (CONH); NMR ($CDCl_3$): δ 4.95 (d, 2H, J=6 Hz), 6.23—7.70 (m, 16H), 8.17—8.40 (m, 1H) and 9.6 (s, 1H). Found: C, 76.69; H, 5.75; N, 8.00%. Calcd for $C_{22}H_{20}N_2O_2$: C, 76.72; H, 5.85; N, 8.13%. Chlorination of **12** with PCl_5 was carried out in ether at 35 °C for 6 h. The reaction mixture was poured into ice–water and extracted with ether several times. The combined ether layer was washed with water several times and dried over anhydrous sodium sulfate. Subsequent evaporation of the ether yielded a viscous oil (chlorohydrazone). To a stirred benzene solution of the oil was added dropwise an excess mole of triethylamine at 5 °C. The mixture was stirred at the same temperature for 1 h and then at room temperature for 5 h. The reaction mixture was washed with water and dried over sodium sulfate. Evaporation of the solvent gave a viscous oil, which was chromatographed (silica gel) with chloroform to give **5aq** in 5% yield.

The Reaction of 1h with p-*Chlorophenylhydrazine Hydrochloride at Room Temperature.* 0.7 g (3.91 mmol) of *p*-chlorophenylhydrazine hydrochloride was dissolved in hot ethanol (200 ml). The solution was allowed to cool to room temperature. We added an ethanol solution (20 ml) of **1h** (1 g, 3.48 mmol) into the ethanol solution of the hydrazine at room temperature and stirred for 2 h. Precipitated crystals (**13**) was filtered, 64% yield (1.0 g); mp 149—150 °C. After treatment of a chloroform solution (50 ml) of **13** (1.0 g, 2.23 mmol) with triethylamine (3 ml) at room temperature for 2 h, the mixture was washed with water several times. Subsequent evaporation of the solvent gave pyrazolidine (**4hr**) in 84% yield (0.77 g); mp 180—182 °C (from ethanol). Thermal treatment of **14** (0.5 g, 1.22 mmol) in xylene (50 ml) at 150 °C for 4 h yielded pyrazoline (**5hr**) in 74% yield (0.37 g).

References

1) Presented in part at the 42nd National Meeting of the Chemical Society of Japan, Sendai, September 1980, Abstr. Vol. II, 588.

2) R. Huisgen, *Angew. Chem., Int. Ed. Engl.*, **2**, 565, 633 (1963).

3) a) W. Oppolzer, *Angew. Chem., Int. Ed. Engl.*, **16**, 10 (1977); b) A. Padwa, *ibid.*, **15**, 123 (1976).

4) a) B. B. Snider, R. S. E. Conn, and S. Sealfon, *J. Org. Chem.*, **44**, 218 (1979); b) B. T. Gillis and F. A. Daniher, *J. Org. Chem.*, **27**, 4001 (1962); c) E. Fahr and H. D. Rupp, *Angew. Chem., Int. Ed. Engl.*, **3**, 693 (1964).

5) a) R. Grigg, J. Kemp, and N. Tompson, *Tetrahedron Lett.*, **1978**, 2827; R. Grigg and J. Kemp, *J. Chem. Soc., Chem. Commun.*, **1978**, 109; b) G. Le Fevre and J. Hamelin, *Tetrahedron Lett.*, **1978**, 4503; *Tetrahedron*, **36**, 887 (1980).

6) G. Le Fevre, S. Sinbandhit, and J. Hamelin, *Tetrahedron*, **35**, 1821 (1979); G. Le Fevre and J. Hamelin, *Tetrahedron Lett.*, **1979**, 1757.

7) a) T. Shimizu, Y. Hayashi, Y. Nagano, and K. Teramura, *Bull. Chem. Soc. Jpn.*, **53**, 429 (1980); b) T. Shimizu, Y. Hayashi, K. Yamada, T. Nishio, and K. Teramura, *ibid.*, **54**, 217 (1981).

8) a) L. Garanti, A. Sala, and G. Zecchi, *J. Org. Chem.*, **40**, 2403 (1975); b) J. Ide and I. Iwai, *Chem. Pharm. Bull.*, **11**, 1042 (1963); c) J. H. Clark and J. M. Miller, *J. Am. Chem. Soc.*, **99**, 498 (1977).

9) a) S. Ito, Y. Tanaka, A. Kakehi, and K. Kondo, *Bull. Chem. Soc. Jpn.*, **49**, 1920 (1976); b) G. Schmitt and B. Laude, *Tetrahedron Lett.*, **1978**, 3727.

10) a) I. Fleming, "Frontier Orbitals and Organic Chemical Reactions," John Wiley and Sons, New York (1976); b) K. N. Houk, J. Sims, R. E. Duke, Jr., R. W. Stronzier, and J. K. George, *J. Am. Chem. Soc.*, **95**, 7287 (1973); c) K. N. Houk, "Pericyclic Reaction. II," ed by R. E. Lehr and A. P. Marchand, Academic Press, New York (1977).

11) a) Yu. P. Kiteav and B. I. Buzykin, *Russ. Chem. Rev. (Engl. Transl.)*, **41**, 495 (1972); b) J. Buckingham, *Q. Rev., Chem. Soc.*, **23**, 37 (1969); c) H. M. R. Hoffmann, *Angew. Chem., Int. Ed. Engl.*, **8**, 556 (1969).

12) a) W. Sucrow, C. Mentzel, and M. Slopianka, *Chem. Ber.*, **107**, 1318 (1974); b) V. Bardakos, W. Sucrow, and A. Fehlauer, *ibid.*, **108**, 2161 (1975); c) R. Baumes, R. Jacquir, and G. Tarrago, *Bull. Soc. Chim. Fr.*, **1976**, 260.

13) a) H. Burton and C. K. Ingold, *J. Chem. Soc.*, **130**, 914 (1928); b) H. Burton, *ibid.*, **130**, 1653 (1928).

14) The notation of the suffix of **2** is as follows: the first alphabetical suffix (**a**—**p**) is same as for **1** and the second one (**q**—**t**) is for R^4. The notation of the suffixes for compounds used here is the same as for **2**.

Intramolecular 1,3-Dipolar Cycloaddition of Nitrilimines Bearing Alkenyl Groups[1]

Tomio SHIMIZU,* Yoshiyuki HAYASHI, Susumu ISHIKAWA, and Kazuhiro TERAMURA
Department of Dyeing, Faculty of Industrial Arts, Kyoto Technical University, Matsugasaki, Sakyo-ku, Kyoto 606
(Received December 4, 1981)

The reaction of the arylhydrazones of some 2-(alkenyloxy)benzaldehydes(or 1-naphthaldehydes) with $Pb(OAc)_4$ leads, *via* the nitrilimine intermediates, to intramolecular 1,3-dipolar cycloadducts, 3-substituted 2-aryl-2,3,3a,4-tetrahydro[1]benzopyrano(or naphtho[1′,2′:5,6]pyrano)[4,3-*c*]pyrazoles, in 10—80% yields. In the presence of an excess of $Pb(OAc)_4$, these cycloadducts were dehydrogenated to 3-substituted 2-aryl-2,4-dihydro[1]benzopyrano-(or naphtho[1′,2′:5,6]pyrano)[4,3-*c*]pyrazoles. In the presence of a large excess of $Pb(OAc)_4$, some of the pyrazoles were acetoxylated to give the corresponding 4-acetoxypyrazoles. The effect of substituents of the alkenyl group on reactivity of the reaction was interpreted in terms of the frontier molecular orbital (FMO) theory.

1,3-Dipolar cycloaddition reactions are one of the most useful methods for the preparation of five-membered heterocycles.[2] Intermolecular 1,3-dipolar cycloaddition reactions can be rationalized in terms of FMO theory.[3] In this decade, a number of applications for preparation of heterocycles *via* intramolecular cycloadditions have been reported.[4] But the explanation of electronic effects of substituents on the intramolecular cycloaddition in terms of FMO theory is not completely satisfactory, mainly owing to the large entropy term. It is therefore interesting to investigate in detail the substituent effects on the reaction. Besides these mechanistic points of interests, intramolecular 1,3-dipolar cycloaddition reactions are very convenient and useful ones for the preparation of complex polycyclic, annelated, and fused molecules, which are difficult to prepare by other methods. The intramolecular nitrilimine cycloaddition shown below[5] was reported for preparation of benzopyranopyrazoles (**3**), but the method is cumbersome because multi-step reactions are required for the preparation of chlorohydrazone (**1**), a precursor of nitrilimine (**2**). One of the aims of our work was to find a simpler preparative method for **3**.[6] We found that application of the method[7] reported by Gladstone for preparation of the nitrilimine to this system gave the corresponding cycloadducts (**3**) in satisfactory yields.

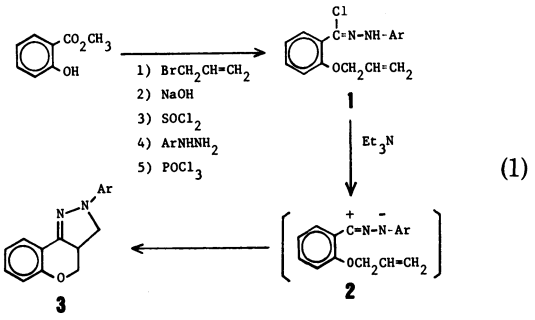

(1)

Results and Discussion

Arylhydrazones of 2-(alkenyloxy)benzaldehyde(or 1-naphthaldehydes) (**5**) are prepared in two steps from salicylaldehyde (or 2-hydroxy-1-naphthaldehyde) as shown in the preceding paper.[6c] The reaction of **5** with an equimolar or excess amount of $Pb(OAc)_4$ was carried out in chloroform for 3—6 h at room temperature or below. 2,4-Dihydro[1]benzopyrano[4,3-*c*]pyrazoles (**8**) were isolated from the reaction of **5** in the presence of three equivalents of $Pb(OAc)_4$, while an equimolar mixture of **5** and $Pb(OAc)_4$ gave pyrazolines (**7**). The results of the reaction are shown in Tables 1 and 2, respectively. The structures of **7** and **8** were established on the basis of elemental analyses and spectral data. The assignment of the structures was further supported

TABLE 1. 2-ARYL-2,3,3a,4-TETRAHYDRO[1]BENZOPYRANO(OR NAPHTHO[1′,2′:5,6]PYRANO)[4,3-*c*]PYRAZOLES (**7**)

Compd[a]	R^1	R^2	R^3	R^4	Yield %	Mp[b] θ_m/°C	IR $\tilde{\nu}$/cm^{-1}	NMR δ[c]
7a	H	H	CO_2Et	H	10	164—166	1740(COO)	1.3(t, 3H, J=7 Hz), 3.6—4.7(m, 6H), 6.6—7.4(m, 9H)
7b	H	H	CN	H	24	d)	2240(CN)	3.9—4.9(m, 4H), 6.8—8.0(m, 9H)
7c	H	H	CO_2Et	Cl	18	121—122	1750(COO)	1.3(t, 3H, J=7 Hz), 3.6—4.8(m,6H), 6.7—7.4(m, 7H), 7.75(dt, 1H, J=2 and 6 Hz)
7d	H	H	CN	Cl	10	130—132	2240(CN)	3.8—4.9(m, 4H), 6.8—7.9(m, 8H)
7e	H	H	CO_2Et	NO_2	60	165—166	1750(COO)	1.3(t, 3H, J=7 Hz), 3.75—4.9(m, 6H), 6.8—8.3(m, 8H)
7f	H	H	CN	NO_2	53	126—128	2240(CN)	4.25—5.5(m, 4H), 6.9—7.4(m, 8H)
7g	$-(CH)_4-$		CO_2Et	NO_2	80	205—207	1750(COO)	1.3(t, 3H, J=7 Hz), 4.0—5.0(m, 6H), 6.9—8.3(m, 9H), 9.1(d, 1H, J=8 Hz)
7h	H	H	C_6H_5	NO_2	10	238	—	3.5—5.4(m, 4H), 6.7—7.7(m, 13H)

a) **7a**—**g** were obtained from the equimolar reaction of **5** with $Pb(OAc)_4$. **7h** was isolated from the reaction mixture of **5** with three equivalents of $Pb(OAc)_4$. b) Recrystallized from ethanol. c) **7f** and **7h** were dissolved in DMSO-d_6; the others were dissolved in $CDCl_3$. d) The melting point range of **7b** was very broad because of contamination of a trace amount of **8b**; chromatographic purification failed.

TABLE 2. 2-ARYL-2,4-DIHYDRO[1] BENZOPYRANO(OR NAPHTHO[1′,2′:5,6]PYRANO)[4,3-*c*]PYRAZOLES (**8**)

Compd[a]	R^1	R^2	R^3	R^4	Yield %	Mp[b] θ_m/°C	IR $\tilde{\nu}$/cm^{-1}	NMR δ[c]
8a	H	H	CO_2Et	H	26	129—130	1730(COO)	1.2(t, 3H, J=7 Hz), 4.2(q, 2H, J=7 Hz), 5.45(s, 2H), 6.75—7.75(m, 9H)
8b	H	H	CN	H	39	159—160	2230(CN)	5.35(s, 2H), 6.85—7.9(m, 9H)
8c	H	H	CO_2Et	Cl	32	159—161	1740(COO)	1.25(t, 3H, J=7 Hz), 4.3(q, 2H, J=7 Hz), 5.45(s, 2H) 6.8—7.85(m, 8H)
8d	H	H	CN	Cl	41	183—185	2240(CN)	5.35(s, 2H), 6.8—7.9(m, 8H)
8e	H	H	CO_2Et	NO_2	38	204—205	1720(COO)	1.3(t, 3H, J=7 Hz), 4.3(q, 2H, J=7 Hz), 5.45(s, 2H), 6.8—8.4(m, 8H)
8f	H	H	CN	NO_2	38	184—185	2240(CN)	5.5(s, 2H), 6.95—8.6(m, 8H)
8g	$-(CH)_4-$		CO_2Et	NO_2	78	178—188	1740(COO)	1.3(t, 3H, J=7 Hz), 4.3(q, 2H, J=7 Hz), 5.5(s, 2H), 6.9—8.4(m, 9H), 9.1(d, 1H, J=8 Hz)
8h	H	H	C_6H_5	NO_2	21	174	——	5.3(s, 2H), 3.8—8.3(m, 13H)

a) **8a**—**f** and **8h** were obtained from the reaction of **5** with three equivalents of $Pb(OAc)_4$. **8g** was obtained from the oxidation of **7g** with DDQ. b) Recrystallized from ethanol. c) **8f** was dissolved in DMSO-d_6; the others were dissolved in $CDCl_3$.

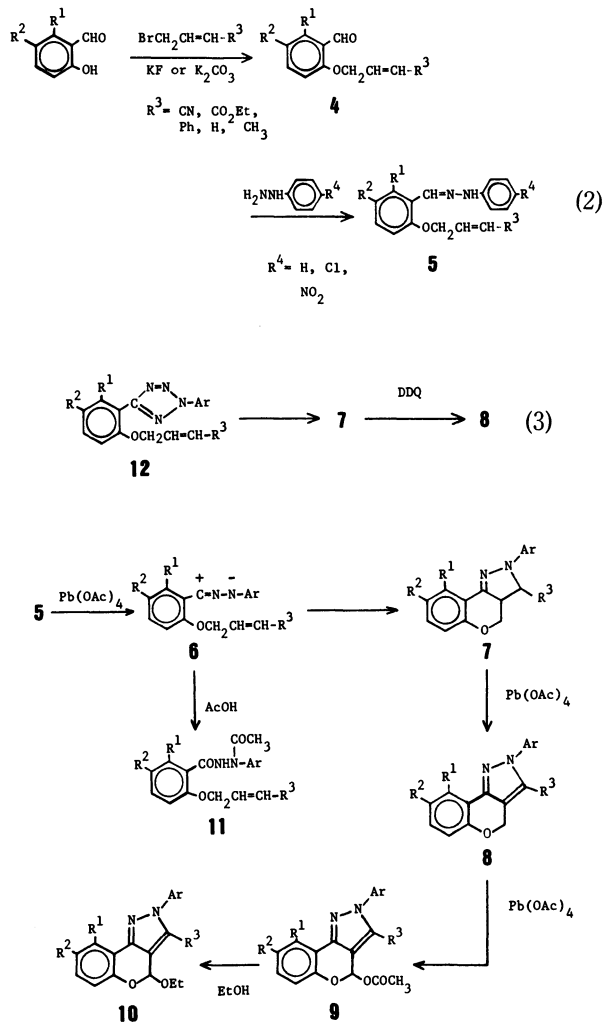

Scheme 1.

by comparison of the physical properties of **7d** and **8d** with those of the authentic samples prepared according to the published procedures:[8,9] **12**→**7d**→**8d**. The most plausible reaction mechanism for the reaction is shown in Scheme 1; formation of nitrilimines (**6**) was followed by intramolecular cycloaddition to give pyrazolines (**7**), which were further oxidised to **8**. The rates of the oxidation of hydrazones (**5**) to nitrilimines (**6**), the following intramolecular cycloaddition, and the oxidation of **7** to **8** were quite fast. It was found that **5** disappeared within ten minutes in the presence of three equivalents of $Pb(OAc)_4$ and the product was shown to be **8f** along with a trace amount of **7f**. Thus, it was rather difficult to isolate some of **7** in high yields from the equimolar reaction of **5** with $Pb(OAc)_4$. Phenylhydrazones bearing an alkenyl group may exhibit other intramolecular reactions besides the reaction mentioned here: a) thermal 1,3-dipolar cycloaddition *via* azomethine imine,[6c,10] b) ene reaction,[6c,11] and c) acid-catalyzed [3$^+$+2] cycloaddition.[6c,12] It was confirmed that none of the three intramolecular reactions occurred under our reaction conditions. Thus the starting materials (**5**) in chloroform were definitely stable at room temperature, even in the presence of acetic acid. The most remarkable substituent effects on the reaction products were observed in the case of the substituents of R^3 on **5**, as expected from the results of intermolecular nitrilimine cycloaddition, while relatively small substituent effects were observed in spite of the wide variation in R^1, R^2, and R^4. The reactivity in the cycloaddition has been rationalized in terms of FMO theory,[3] although some of the intramolecular cycloaddi-

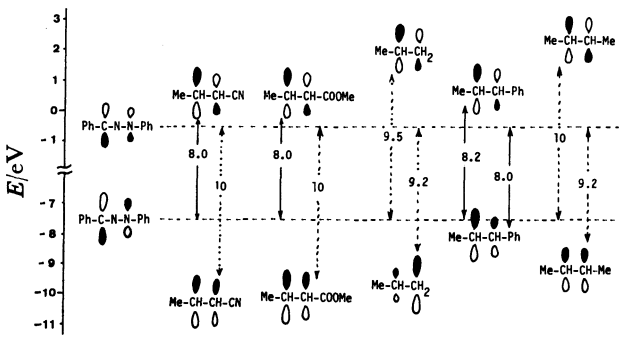

Scheme 2. Interaction scheme of diphenylnitrilinime with several 1-substituted 1-propenes (see Refs. 3a, 13, and 14).

TABLE 3. 2-ARYL-4-ETHOXY-2,4-DIHYDRO[1]BENZOPYRANO(OR NAPHTHO[1',2':5,6]PYRANO[4,3-*c*]PYRAZOLES (**10**)

Compd[a]	R^1	R^1	R^3	R^4	Yield %	Mp[b] θ_m/°C	IR $\tilde{\nu}$/cm^{-1}	NMR δ[c]
10a	H	H	CN	NO_2	82	176—180	2240(CN)	1.2(t, 3H, J=7 Hz), 3.7—4.25(m, 2H), 6.6(s, 1H), 7.0—8.6(m, 8H)
10b	$-(CH)_4-$		CO_2Et	H	63	165—167	1740(COO)	1.08(t, 3H, J=7 Hz), 1.17(t, 3H, J=7 Hz), 3.5—4.6(m, 2H), 4.32(q, 2H, J=7 Hz), 6.7(s, 1H), 7.2—8.0(m, 10H), 9.2(d, 1H, J=8 Hz)
10c	$-(CH)_4-$		CN	H	61	167—168	2240(CN)	1.27(t, 3H, J=7 Hz), 4.0(d, quintet, 2H, J=3 and 7 Hz), 6.57(s, 1H), 7.15—8.15(m, 10H), 9.5(d, 1H, J=8 Hz)
10d	$-(CH)_4-$		CO_2Et	Cl	49	197—198	1750(COO)	1.23(t, 3H, J=7 Hz), 1.3(t, 3H, J=7Hz), 4.3(q, 2H, J=7 Hz), 3.66—4.47(m, 2H), 6.6(s, 1H), 7.0—8.0(m, 9H), 9.3(d, 1H, J=8 Hz)
10e	$-(CH)_4-$		CN	Cl	35	180—181	2250(CN)	1.23(t, 3H, J=7 Hz), 3.95(d, quintet, 2H, J=3 and 7 Hz), 6.4(s, 1H), 7.0—7.95(m, 9H), 9.25(d, 1H, J=8 Hz)
10f	$-(CH)_4-$		CO_2Et	NO_2	60	174—176	1750(COO)	1.23(t, 3H, J=7 Hz), 3.66—4.5(m, 2H), 1.33(t, 3H, J=7 Hz), 4.33(q, 2H, J=7 Hz), 6.53(s, 1H), 7.0—7.9 (m, 7H), 8.3(d, 2H, J=9 Hz), 9.23(d, 2H, J=8 Hz)
10g	$-(CH)_4-$		CN	NO_2	46	196—197	2240(CN)	1.23(t, 3H, J=7Hz), 4.0(q, 2H, J=7Hz), 6.7(s, 1H), 7.0—8.3(m, 9H), 9.2(d, 1H, J=8 Hz)

a) **10a** was obtained from the reaction of **8f** with a large excess of $Pb(OAc)_4$. The others were obtained from the reaction of **5** with three equivalents of $Pb(OAc)_4$. b) Recrystallized from ethanol. c) **10b** and **10g** were dissolved in DMSO-d_6; the others were dissolved in $CDCl_3$.

tions take place easier than the intermolecular one because of an activation in entropy terms.[4] The interaction scheme of frontier orbitals of diphenylnitrilimine[3a,13] and several 1-substituted 1-propenes[3a,14] are shown in Scheme 2. Examination of the scheme led us to expect following general tendencies:

i) Dipole-HOMO controlled cycloaddition is the most probable route for the substrates bearing cyano or methoxycarbonyl group as R^3.

ii) Both dipole-HOMO and dipole-LUMO controlled cycloaddition may be allowed for the substrates bearing a phenyl group as R^3 but the rate of the reaction would be slower than that described in i).

iii) The substrates bearing H or CH_3 as R^3 would be less reactive, due to the relatively lowered HOMO energy of the dipolarophile by the substituents.

The qualitative reactivity of **5** was in accordance with the tendencies mentioned above. When R^3=Ph on **5**, the reaction gave pyrazoline (**7f**), pyrazole (**8h**), and *N*-acetyl hydrazide (**11a**), roughly in the ratio of 1 : 2 : 2. On the other hand, none of cycloadducts could be isolated when R^3=H or CH_3, and *N*-acetyl hydrazide (**11b**) was only isolable product. The reaction of aldehyde hydrazones with $Pb(OAc)_4$ generally gave *N*-acetyl hydrazides in the absence of suitable dipolarophiles.[15]

2-(Alkenyloxy)-1-naphthaldehyde arylhydrazones (**5**) gave better yields of cycloadducts (**8**), partly because of the ease of isolation from the reaction mixture. Whereas the cycloadducts, **8a**—**f** and **8h**, from 2-(alkenyloxy)benzaldehyde arylhydrazones are stable in the presence of an excess amount of $Pb(OAc)_4$, **8** from 2-(alkenyloxy)-1-naphthaldehyde aryhydrazones gave acetoxylated products (**9**) at position 4 under the same reaction conditions. Radical acetoxylation has been achieved wiht $Pb(OAc)_4$.[15b] Thus, when **8f** was treated with an excess of $Pb(OAc)_4$ in refluxing chloroform for 3 h, the susceptible position in **8**, the α-position of the ethers, was acetoxylated to give product (**9**). The acetoxyl group was easily displaced by the ethoxyl group, giving **10**, when **9** was recrystallized from ethanol.

Experimental

Measurements. All the melting and boiling points are uncorrected. The IR spectra were recorded on a Hitachi 215 Infrared Spectrophotometer. The NMR spectra were measured on a Varian T-60A instrument using suitable solvents and TMS as an internal standard.

Materials. Lead tetraacetate (90.6%) was commericallly available (Nakarai Chem. Co.,) and was used without further purification. The arylhydrazones of 2-(alkenyloxy)benzaldehydes (or 1-naphthaldehydes) (**5**) were prepared according to the method described in the preceding paper.[6c]

Reaction of Arylhydrazones (5) with Three Equivalents of Pb(OAc)$_4$. General Procedure: A mixture of **5** (5.4 mmol) and $Pb(OAc)_4$ (7.97 g, 16.2 mmol) was stirred in chloroform (300 ml) for 6 h at room temperature. The insoluble material thus precipitated was filtered off using a Celite bed. The filtrate was mixed with water, and the mixture was filtered using the Celite bed. The organic layer was washed with water several times and dried over magnesium sulfate. Evaporation of the organic layer yielded a viscous oil, which solidified upon being scratched with a glass rod. Recrystallization from ethanol gave colorless needles of the cycloadducts (**8**). Concentration of the filtrate and subsequent chromatography on silica gel with chloroform gave an additional amount of needles (**8**). The yields and some physical data are given in Table 2.

Reaction of 2-(3-Phenyl-2-propenyloxy)benzaldehyde p-*Nitrophenylhydrazone with Pb(OAc)$_4$.* The reaction was carried out by the General Procedure. The reaction mixture was chromatographed (silica gel) with chloroform to give cycloadducts (**7h** and **8h**) and *N*-acetylated compound (**11a**) in 10, 21, and 17% yield, respectively. The spectral data for **7h** and **8h** are shown in Tables 1 and 2, respectively. The

spectral data for **11a** (mp 114 °C from ethanol) was as follows: IR (Nujol): 3250 (NH), 1710 (CONH), and 1670 cm^{-1} (CON). NMR ($CDCl_3$): δ 2.25 (s, 3H), 4.9 (d, 2H, J=6 Hz), 6.5—8.3 (m, 13H), and 10.2 (s, 1H).

Reaction of 2-(3-Butenyloxy)benzaldehyde p-*Nitrophenylhydrazone with* $Pb(OAc)_4$. The reaction was carried out by the General Procedure. An *N*-acetylated compound (**11b**) was obtained from the reaction mixture in 41% yield; mp 159 °C (from ethanol). IR (Nujol): 3200 (NH), 1700 (CONH), and 1670 cm^{-1} (CON). NMR ($CDCl_3$): δ 2.7 (d, 3H, J=5 Hz), 3.3 (s, 3H), 5.5—5.8 (m, 2H), 6.7—7.0 (m, 2H), 8.0—9.3 (m, 8H), and 11.2 (s, 1H).

An Equimolar Reaction of Arylhydrazones with $Pb(OAc)_4$. A mixture of **5** (5.4 mmol) and $Pb(OAc)_4$ (2.66 g, 5.4 mmol) was stirred in chloroform for 6 h at room temperature. The reaction mixture was washed with water several times. The organic layer was dried over magnesium sulfate. Evaporation of the solvent yielded cycloadducts (**7**) in the yields shown in Table 1.

Oxidation of 7f to 8f with $Pb(OAc)_4$. A mixture of **7f** (1.0 g, 3.1 mmol) and $Pb(OAc)_4$ (1.37 g, 3.1 mmol) was stirred in chloroform for 6 h at room temperature. The reaction mixture was treated in a manner similar to the procedure described above to give **8f** in 76% yield.

Oxidation of 7g to 8g with DDQ (2,3-Dichloro-5,6-dicyano-p-benzoquinone). A mixture of **7g** (0.5 g, 1.3 mmol) and DDQ (0.29 g, 1.3 mmol) was heated to reflux in benzene (50 ml) for 12 h. The reaction mixture was washed with water and evaporation of the organic layer gave **8g**, 0.39 g (78%) (recrystallized from ethanol).

Reaction of 8f with $Pb(OAc)_4$. A mixture of **8f** (0.2 g, 0.65 mmol) and $Pb(OAc)_4$ (2.0 g, 4.1 mmol) was heated to reflux in chloroform (50 ml) for 3 h. The reaction mixture was treated in a manner similar to the General Procedure. Crystals obtained were shown to be 4-acetoxylated product (**9**) in 92% yield; IR (Nujol): 2230 (CN) and 1760 cm^{-1} (COO). NMR (DMSO-d_6): δ 2.1 (s, 3H) and 7.0—8.6 (m, 9H). Found: C, 60.03; H, 3.25; N, 14.62%. Calcd for $C_{19}H_{12}N_4O_5$: C, 60.64; H, 3.21; N, 14.89%. Recrystallization of this compound from ethanol gave the corresponding 4-ethoxy derivative quantitatively; Found: C, 62.88; H, 3.94; N, 15.26%. Calcd for $C_{19}H_{14}N_4O_4$: C, 62.98; H, 3.89; N, 15.46%.

Preparation of an Authentic Sample of 7d. 2-(*p*-Chlorophenyl)-5-[2-(3-cyano-2-propenyloxy)phenyl]-2*H*-tetrazole (**12**) was prepared from the reaction of 2-(3-cyano-2-propenyloxy)benzaldehyde *p*-tolylsulfonylhydrazone[6a] with *p*-chlorobenzenediazonium chloride according to a method analogous to that of Ito *et al.*,[8] in 73% yield; mp 192—193 °C (decomp). IR (Nujol): 2230 cm^{-1} (CN). Found: C, 60.43; H, 3.45; N, 20.69%. Calcd for $C_{17}H_{12}N_5OCl$: C, 60.45; H, 3.58; N, 20.73%. Pyrolysis of **12** at 200 °C for 3 h gave **7d** in 30% yield.

Oxidation of 7d to 8d with DDQ. A mixture of **7d** (1.0 g, 3.3 mmol) and DDQ (0.67 g, 3.3 mmol) was heated to reflux in benzene (50 ml) for 12 h. The reaction mixture was washed with water and evaporation of the organic layer gave **8d**, 0.58 g (58%) (recrystallized from ethanol).

References

1) Presented in part at 44th National Meeting of the Chemical Society of Japan, Okayama, October 1981, Abstr. Vol. II, p. 495.

2) R. Huisgen, *Angew. Chem., Int. Ed. Engl.*, **2**, 565 (1963).

3) a) K. N. Houk, J. Sims, C. R. Watts, and L. J. Luskus, *J. Am. Chem. Soc.*, **95**, 7301 (1973); K. N. Houk, J. Sims, R. E. Duke, Jr., R. W. Strozier, and J. K. George, *ibid.*, **95**, 7287 (1973); b) K. N. Houk, "Pericyclic Reacitions. II," ed by R. E. Lehr and A. P. Marchand, Academic Press, New York (1977); c) I. Fleming, "Frontier Orbitals and Organic Chemical Reactions," John Wiley and Sons, New York (1976),

4) a) W. Oppolzer, *Angew. Chem., Int. Ed. Engl.*, **16**, 10 (1977); b) A. Padwa, *ibid.*, **15**, 123 (1976).

5) G. Schmidt and B. Laude, *Tetrahedron Lett.*, **1978**, 3727.

6) a) T. Shimizu, Y. Hayashi, Y. Nagano, and K. Teramura, *Bull. Chem. Soc. Jpn.*, **53**, 429 (1980); b) T. Shimizu, Y. Hayashi, K. Yamada, T. Nishio, and K. Teramura, *ibid.*, **54**, 217 (1981); c) T. Shimizu, Y. Hayashi, Y. Kitora, and K. Teramura, *ibid.*, **55**, 2450 (1982).

7) W. A. F. Gladstone, *J. Chem. Soc., Chem. Commun.*,**1969**. 179; W. A. F. Gladstone, J. B. Aylward, and R. O. C. Norman, *J. Chem. Soc., C*, **1969**, 2587.

8) S. Ito, Y. Tanaka, A. Kakehi, and K. Kondo, *Bull. Chem. Soc., Jpn.*, **49**, 1920 (1976).

9) R. Huisgen, M. Siedel, G. Wallbillich, and H. Knupfer, *Tetrahedron*, **17**, 3 (1962).

10) R. Grigg, J. Kemp, and N. Tompson, *Tetrahedron Lett.*, **1978**, 2827; R. Grigg and J. Kemp, *J. Chem. Soc., Chem. Commun.*, **1978**, 109; G. Le Fevre and J. Hamelin, *Tetrahedron Lett.*, **1978**, 4503; *Tetrahedron*, **36**, 887 (1980).

11) a) B. B. Snider, R. S. E. Conn, and S. Sealfon, *J. Org. Chem.*, **44**, 218 (1979); b) B. T. Gillis and F. A. Daniher, *ibid.*, **27**, 4001 (1962); c) E. Fahr and H. D. Rupp, *Angew. Chem., Int. Ed. Engl.*, **3**, 693 (1964).

12) G. Le Fevre, S. Sinbandhit, and J. Hamelin, *Tetrahedron*, **35**, 1821 (1979); G. Le Fevre and J. Hamelin, *Tetrahedron Lett.*, **1979**, 1757.

13) M. Bonadeo, C. De Micheli, and R. Gandolfi, *J. Chem. Soc., Perkin Trans. 1*, **1977**, 939; G. Bianchi, R. Gandolfi, and C. De Micheli, *J. Chem. Res. (S)*, **1981**, 6; *J. Chem. Res. (M)*, **1981**, 0135.

14) J. Bastide, N. El Chandour, and O. Henri-Rousseau, and L. Aspart-Pascot, *Tetrahedron*, **30**, 3355 (1974); K. N. Houk, *J. Org. Chem.*, **43**, 3006 (1978); M. Joucla, F. Tonnard, D. Gree, and J. Hamelin, *J. Chem. Res. (M)*, **1978**, 2901; K. B. Lipkowitz, S. Scarpone, B. P. Mundy, and W. G. Bornmann, *J. Org. Chem.*, **44**, 486 (1979).

15) a) F. L. Scott and R. N. Butler. *J. Chem. Soc., C*, **1966**, 1202; b) R. N. Butler, F. L. Scott, and T. A. F. O'Mahony, *Chem. Rev.*, **73**, 93 (1973).

Substituent Effects on the Mesophase Stability for Cholesteryl Benzoylbenzoates

Mitsuhiro KODEN, Shunsuke TAKENAKA, and Shigekazu KUSABAYASHI*
Department of Applied Chemistry, Faculty of Engineering, Osaka University, Suita, Osaka 565
(Received December 7, 1981)

The thermal properties of cholesteryl esters of substituted benzoylbenzoic acids were examined. The substituent effects on the thermal stability of the chloesteric phase of these esters are quite striking. For cholesteryl 4-(4′-substituted benzoyl)benzoates, the Ch-I transition temperatures are slightly influenced by an electronic effect of the substituents, because the bond direction of the substituents is tilted with respect to the long molecular axis. For cholesteryl 4-(3′-substituted benzoyl)benzoates and cholesteryl 3-(4′-substituted benzoyl)benzoates, the Ch-I transition temperatures are influenced by the polarizability anisotropy of the terminal phenyl ring, which probably gives rise to a change in the ratio of the number of more-linear isomers to the number of less-linear isomers. For cholesteryl 4-(2′-substituted benzoyl)benzoates, the substituents increase the angle between the two phenyl rings, *i.e.*, the thickness of the benzophenone moiety, due to the repulsive interaction between the substituent(s) and ortho-hydrogens of the other phenyl ring, and therefore decrease the Ch-I transition temperature largely.

Recently we examined the mesomorphic properties of some cholesteryl esters of arylbenzoic acids incorporating the angular linkages, such as –CO–, –O–, –S–, and $-CH_2-$.[1,2] In spite of the angular geometry, these esters exhibit a cholesteric phase and their thermal stabilities are in the order of $-CO->-O->-CH_2->-S-$. These results indicate that the mesophase stability is strongly dependent on the electronic effect of the carboxylic acid moieties. But a replacement of the aryl ring by the cyclohexyl ring at the terminal position of cholesteryl 4-benzoylbenzoate gives rise to a depression of the Ch-I transition temperature by only 6 °C, and the replacement at the inner position enhances it by 7 °C,[2] though the replacement would decrease the electronic effect of the carboxylic acid moiety because of the reduced conjugative interactions among carbonyl and ester groups and rings. These results appear to be inconsistent. So we are interested in the role of the electronic effect of the carboxylic acid moiety on the mesophase stability. For this purpose, we have prepared two types of cholesteryl esters of substituted benzoylbenzoic acids with the following formula:

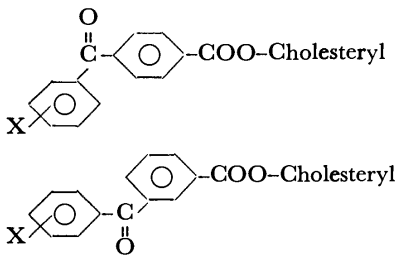

In this paper, the substituent effect on the mesophase stability will be discussed in terms of the structural features of the benzophenone moiety and the electronic effect of the substituents.

Experimental

Preparation of Materials. Substituted 4-methylbenzophenones were prepared by the Friedel-Crafts reaction[3] of toluene with the substituted benzoyl chloride, which was prepared from the substituted benzoic acid and thionyl chloride[4] or phosphorus pentachloride.[5]

3- And 4-(substituted benzoyl)benzoic acids, except for 3- and 4-(4′-alkylbenzoyl)benzoic acids, were prepared by sodium dichromate oxidation[6] of the substituted 4-methylbenzophenone.

4-(4′-Alkylbenzoyl)benzoic acids were prepared by the Friedel-Crafts reaction[3] of the alkylbenzene with terephthaloyl chloride, followed by hydrolysis.

3-(4′-Alkylbenzoyl)benzoic acids were prepared by the Friedel-Crafts reaction[3] of the alkylbenzene with isophthaloyl chloride, followed by hydrolysis.

3-(3′-Methylbenzoyl)benzoic acid was prepared by Grignard reaction[7] of dimethyl isophthalate with 3-methylphenylmagnesium bromide.

3- And 4-(substituted benzoyl)benzoyl chlorides were prepared from the 3- and 4-(substituted benzoyl)benzoic acid and phosphorus pentachloride.[5]

Cholesteryl esters were prepared from the 4- and 3-(substituted benzoyl)benzoyl chloride and chloesterol.[8] All esters were purified by column chromatography on silica gel, followed by recrystallization from a suitable solvent. The elemental analyses are listed in Table 3.

Physical Measurement. Identification of the mesophase and determination of the transition temperatures were made using a Nikon polarizing microscope in conjunction with a Mettler FP 52 heated stage and control unit. Transition enthalpies were determined using a Daini Seikosha differential scanning calorimeter, model SSC-560. Entropy values were calculated using the equation, $\Delta S=\Delta H/T$.

Results and Discussion

The thermal properties of cholesteryl 4-(substituted benzoyl)benzoates and cholesteryl 3-(substituted benzoyl)benzoates are summarized in Tables 1 and 2, respectively.

Cholesteryl 4-(4′-Substituted benzoyl)benzoates. Generally, terminal groups with a small, compact structure such as cyano, halogen, methoxy, nitro, methyl, raise the N-I or Ch-I transition temperature relative to hydrogen because of increased polarizability anisotropy.[9,10] As is evident from Table 1, although the melting points appreciably change by introduction of the substituent at the 4′-position of **1**, the effect on the Ch-I transition temperature is remarkably small. Generally, introduction of methyl or methoxyl groups at the terminal position of a molecule gives rise to an increase in the N-I or Ch-I transition temperature

Table 1. Thermodynamic properties of cholesteryl 4-(substituted benzoyl)benzoates

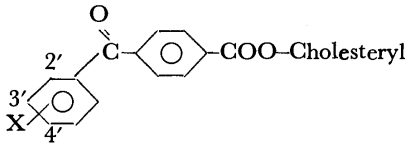

Graphical code	X	T_{MP} °C	$T_{Ch\text{-}I}$ °C	$\Delta H_{Ch\text{-}I}$ kJ mol^{-1}	$\Delta S_{Ch\text{-}I}$ J K^{-1} mol^{-1}
1[a]	H	134.2	210.3	0.51	1.01
2[b]	4′-CH_3	158.3	205.9	0.52	1.09
3	4′-C_2H_5	179.0	193.1	0.40	0.86
4	4′-C_3H_7	174.3	(169.2)	—	—
5	4′-F	154.2	227.1	0.52	1.04
6	4′-Cl	175.4	206.4	0.43	0.90
7	4′-Br	182.6	214.6	0.38	0.78
8	4′-CH_3O	158.5	205.4	0.44	0.92
9	4′-NO_2	200.1	215.6	0.54	1.11
10	3′-F	142.4	219.6	0.53	1.08
11	3′-Cl	165.0	213.8	0.44	0.90
12[c]	3′-NO_2	175.1	233.0	1.01	2.00
13[d]	3′,5′-Cl	161.0	194.4	0.56	1.18
14	2′-F	154.1	168.6	0.38	0.86
15	2′-Cl	157.7	[90]	—	—
16	2′,4′-Cl	151.3	[90]	—	—
17	2′,6′-Cl	185.6	[−10]	—	—

a) This compound underwent a change in crystal form at 119.5 °C. b) This compound also underwent a change in crystal form at 150.1 °C. c) This compound showed a smectic A phase ($T_{S_A\text{-}Ch}$=156.5 °C). d) This compound also underwent a change in crystal form at 149.1 °C. ( ): Monotropic transition. [ ]: "Virtual" transition temperature.

Table 2. Thermodynamic properties of cholesteryl 3-(substituted benzoyl) benzoates

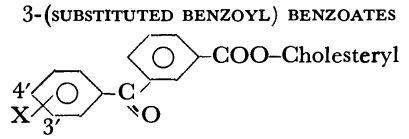

Graphical code	X	T_{MP} °C	$T_{Ch\text{-}I}$ °C	$\Delta H_{Ch\text{-}I}$ kJ mol^{-1}	$\Delta S_{Ch\text{-}I}$ J K^{-1} mol^{-1}
18	H	149.6	(71.7)[a]	0.15	0.44
19	4′-CH_3	141.4	(89.0)	0.64	1.77
20	4′-C_3H_7	144.0	(85.0)	—	—
21	3′-CH_3	153.3	(43.4)	0.16	0.51

a) ( ): Monotropic transition.

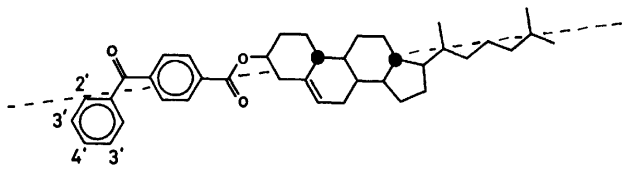

Fig. 1. Structural model of cholesteryl 4-benzoylbenzoates. The dotted line represents the long molecular axis.

by more than 50 °C.[11] For **1**, this trend is absent. Furthermore, when the number of the carbon atoms in the alkyl chain at the 4′-position is increased (**1**—**4**), the Ch-I transition temperatures decrease steeply without any distinct alternation between odd and even members.[12] These characteristics are quite striking and should be related to the angular geometry of the benzophenone moiety.

The molecular structure of cholesteryl 4-benzoylbenzoates is illustrated in Fig. 1. The valence angle between the C–C bonds linking two phenyl rings is *ca.* 120°.[13] Then, the substituent, X, located at the 4′-position contributes in two ways to the mesophase stability. One is that it increases the molecular breadth as well as the molecular length. These structural characteristics should depress the Ch-I transition temperature due to an action similar to that of the lateral substituents for ordinary mesogenic compounds. According to Gray's studies, the depression of the clearing points has a good correlation with the molecular diameter.[14] The efficiency order is reported to be H>F>CH_3>Cl>Br>NO_2. The other effect is to produce changes in conjugative interactions within the molecule, thus affecting factors such as polarizability and dipolarity. For example, the longitudinal substituent effect on the mesophase stability for cholesteryl benzoates is reported to be CN($T_{Ch\text{-}I}$=287.0 °C)>CH_3O(267.0 °C)>Cl(252.8 °C)>Br(251.6 °C)>CH_3(241.1 °C)>F(193.1 °C)>H(179.9 °C).[15] The dominant effect for the substituents is attributable to the increase in polarizability and dipolarity due to conjugation between aryl group and substituent. For cholesteryl 4-benzoylbenzoates, the substituent at the 4′-position also increases the molecular polarizability and dipolarity due to conjugative interactions between aryl and carbonyl groups. However, the anisotropy of these terms along the long molecular axis indicated by the dotted line in Fig. 1 should be smaller than that for cholesteryl benzoates, because the C–X bond is tilted by *ca.* 60° from the long molecular axis.

As is evident from Table 1, the Ch-I transition temperature in this series isn't very susceptible to changes in the effect of substituent, and the efficiency order is quite different from that for cholesteryl benzoates. Supposing that a methyl group at the 4′-position lowers the Ch-I transition temperature by 50 °C due to a steric repulsion similar to that from the methyl group at 3-position of cholesteryl benzoate,[16] and enhances it by 63 °C due to the electronic effect similar to that from the methyl group at the 4-position of cholesteryl benzoate,[15] we can expect the Ch-I transition temperature for **2** to be 223 °C. The observed Ch-I transition temperature for **2** appears to be considerably lower than the calculated one. The trend is also recognized in **6**—**9**. These facts indicate that the electronic effect of the substituent at the 4′-position isn't so large, compared with that for ordinary mesogens, because the directions of the polarizability and dipolarity arising from the terminal benzoyl portion including substituent intersect the long molecular axis.

Cholesteryl 4-(3′-Substituted benzoyl)benzoates. The effect of a substituent at the 3′-position on the

mesophase stability exhibits some interesting trends. Generally, a meta-substituent (lateral substituent) increases the molecular breadth, giving rise to a decrease in the lateral interaction. However, the substituent at 3′-position slightly enhances the Ch-I transition temperatures and the di-substitution gives rise to a depression of the Ch-I transition temperature (**13**). This unusual behavior should be related to the angular geometry of the benzophenone moiety. Let's consider the conformational equilibrium, as shown below:

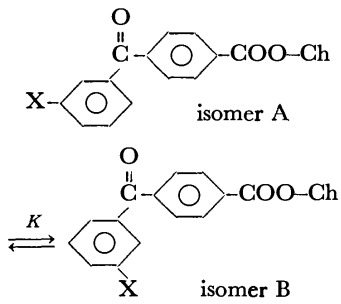

The energy of both isomers will be quite similar under usual conditions, such as in an isotropic medium ($K=1$). The substituent X in isomer A will elongate the molecular length and enhance a local polarizability arising from the C–X bond along the long molecular axis. The substituent X in isomer B, on the other hand, will increase the molecular breadth, causing the Ch-I transition temperature to decrease. Certainly, **11** and **12** exhibit higher Ch-I transition temperature than **6** and **9**, whereas the substituents are located at the meta-position with respect to the carbonyl group. Temperature differences for the transition between **5** and **10**, **6** and **11**, and **9** and **12** are −7.5 °C, 7.4 °C, and 17.4 °C, respectively. These tend to increase with increasing the bond polarizabilities, 0.5, 2.5, and 4.0 Å^3.[17] This fact indicates that polarizability and/or dipolarity of the C–X bond tends to move the equilibrium point toward isomer A in the mesophase. However, this contribution should be small, since we can't recognize it in the entropy change for the Ch-I transition. On the other hand, the disubstituted compound, **13**, exhibits a lower Ch-I transition temperature than that for **10**—**12**. This is caused by one of chlorine atoms inevitably occupying the unfavorable site in isomer B.

Cholesteryl 4-(2′-Substituted benzoyl)benzoates. As is evident from Table 1, the substituent effect at the 2′-position on the Ch-I transition temperature is striking. The 2′-substituted compounds, **15**—**17**, show no mesophase. So-called "virtual" Ch-I transition temperatures were determined from binary phase diagrams, as shown in Fig. 2. By mixing **15** with known amounts of **1**, and determining the Ch-I transition temperatures of the mixtures, a phase diagram for the binary system was constructed. The "virtual" Ch-I transition temperature for **15** was found, by extrapolation, to be 90 °C. Similar phase diagrams were constructed for **16** and **17**, the "virtual" ones being 90 and −10 °C, respectively. As one can assume from the structural model (Fig. 1), introduction of the substituent at 2′-position will increase not the molecular breadth but the thickness of the carboxylic acid moiety due to

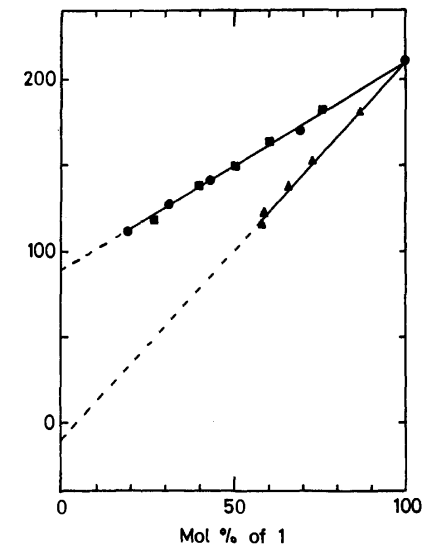

Fig. 2. Ch-I transition lines in the binary phase diagrams for (a) **1** and **15** (●), (b) **1** and **16** (■), and (c) **1** and **17** (▲).

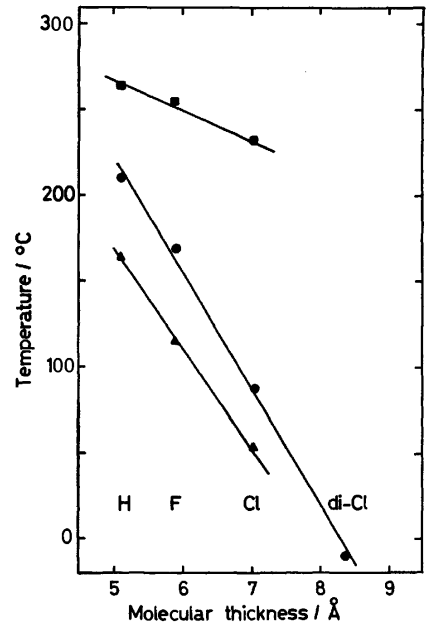

Fig. 3. A plot of molecular thickness of the benzophenone moiety[18] against the $T_{Ch\text{-}I}$ of cholesteryl 4-(2′-substituted benzoyl)benzoates (●), the $T_{N\text{-}I}$ of 2-substituted 4-*p*-(octyloxy)benzylideneaminobiphenyls (▲),[19,20] and the $T_{N\text{-}I}$ of 3′-substituted 4′-(octyloxy)biphenyl-4-carboxylic acids (■).[21]

increased interaction between the substituent(s) and ortho-hydrogens at the other ring, and also will decrease the molecular polarizability arising from the resonance between both aryl and carbonyl groups. Then, the Ch-I transition temperatures for **1** and **15**—**17** are plotted against the molecular thickness of the carboxylic acid moieties[18] (Fig. 3). Similar to the other cases, these exhibit linear correlation. The slope is close to that for 2-substituted 4-*p*-(octyloxy)benzylideneaminobiphenyls[19,20] rather than 3′-substituted 4′-(octyloxy)biphenyl-

Table 3. Elemental analyses of cholesteryl esters

Graphical code	Molecular formula	Calculated(%) C	Calculated(%) H	Found(%) C	Found(%) H
1	$C_{41}H_{54}O_3$	82.78	9.15	82.48	9.14
2	$C_{42}H_{56}O_3$	82.85	9.27	82.75	9.34
3	$C_{43}H_{58}O_3$	82.90	9.39	82.83	9.49
4	$C_{44}H_{60}O_3$	82.97	9.50	82.72	9.64
5	$C_{41}H_{53}FO_3$	80.35	8.72	80.17	8.80
6	$C_{41}H_{53}ClO_3$	78.25	8.49	78.09	8.53
7	$C_{41}H_{53}BrO_3$	73.09	7.93	72.98	7.87
8	$C_{42}H_{56}O_4$	80.73	9.03	80.55	8.91
9	$C_{41}H_{53}NO_5$	76.96	8.35	77.21	8.59
10	$C_{41}H_{53}FO_3$	80.35	8.72	80.33	8.70
11	$C_{41}H_{53}ClO_3$	78.25	8.49	78.18	8.58
12	$C_{41}H_{53}NO_5$	76.96	8.35	76.90	8.24
13	$C_{41}H_{52}Cl_2O_3$	74.19	7.90	73.94	7.88
14	$C_{41}H_{53}FO_3$	80.35	8.72	80.53	8.65
15	$C_{41}H_{53}ClO_3$	78.25	8.49	77.99	8.41
16	$C_{41}H_{52}Cl_2O_3$	74.19	7.90	74.02	7.94
17	$C_{41}H_{52}Cl_2O_3$	74.19	7.90	74.09	8.02
18	$C_{41}H_{54}O_3$	82.78	9.15	82.75	9.13
19	$C_{42}H_{56}O_3$	82.85	9.27	82.67	9.24
20	$C_{44}H_{60}O_3$	82.96	9.50	82.81	9.77
21	$C_{42}H_{56}O_3$	82.85	9.27	82.91	9.20

4-carboxylic acids,[21] indicating that an increased molecular thickness due to repulsion between the substituent(s) and the ortho-hydrogens is the major cause of rapid depression of the Ch-I transition temperatures.

Cholesteryl 3-(Substituted benzoyl)benzoates. Although **18** has a low Ch-I transition temperature relative to **1**, its derivatives exhibit an apparent substituent effect on the mesophase stability, *i.e.*, the substituent at the 4′-position enhances the Ch-I transition temperature, and that at the 3′-position depresses it. These trends are in contrast with the substituent effect for **1**. These results can be accounted for by considering the conformational models shown below:

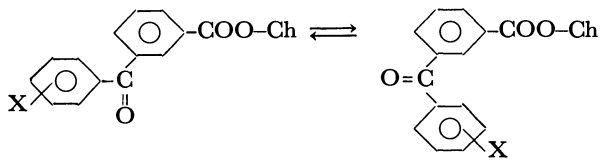

isomer C isomer D

The energy of these two isomers will be also equivalent in the isotropic state. For preservation of the parallel arrangement in the mesophase, isomer C will be preferable to isomer D, because the former is less wide than the latter. Furthermore, the substituent at the 4′-position in isomer C will increase the molecular length and anisotropy of polarizability along the long molecular axis. Then, the role of the substituent seems to be analogous to that of the substituent at the 3′-position in isomer A for **1**. The substituents at both 3′- and 4′-position in isomer D, on the other hand, give rise to an increase in molecular breadth. Then, the enhanced Ch-I transition temperatures for **19** and **20** must indicate that the position of the conformational equilibrium for **18** slightly inclines toward the left side, as the substituent is introduced at the 4′-position. We could recognize it in the entropy data (**18** and **19**). On the contrary, methyl group at the 3′-position is assumed to be inevitably unfavorable for the mesophase stability. **21** shows that case.

The present work was partially supported by a Grant-in-Aid for Scientific Research from the Ministry of Education, Science and Culture.

References

1) M. Koden, S. Takenaka, and S. Kusabayashi, *Chem. Lett.*, **1980**, 471.
2) M. Koden, S. Takenaka, and S. Kusayashi, to be published.
3) E. D. Hughes, C. K. Ingold, and N. A. Taher, *J. Chem. Soc.*, **1940**, 949.
4) B. Herferrich and W. Schaefer, *Org. Synth.*, Coll. Vol. I, 147 (1941).
5) R. Adams and R. L. Jenkins, *Org. Synth.*, Coll. Vol. I, 394 (1941).
6) O. Kamm and A. O. Matthews, *Org. Synth.*, Coll. Vol. I, 392 (1941).
7) D. S. Noyce and P. A. Kittle, *J. Org. Chem.*, **30**, 1896 (1965).
8) G. W. Gray, *J. Chem. Soc.*, **1956**, 3733.
9) G. W. Gray, "The Molecular Physics of Liquid Crystals," ed by G. R. Luckhurst and G. W. Gray, Academic Press, London, New York, San Francisco (1979), Chap. 1.
10) W. H. de Jeu and J. van der Veen, *Mol. Cryst. Liq. Cryst.*, **40**, 1 (1977).
11) D. Demus, H. Demus, and H. Zaschke, "Flüssige Kristalle in Tabellen," VEB Deutscher Verlag für Grundstoff Industrie, Leipzig (1974).
12) M. Koden, T. Yagyu, S. Takenaka, H. Terauchi, and S. Kusabayashi, *Chem. Lett.*, **1981**, 269.
13) E. B. Fleischer, N. Sung, and S. Hawkinson, *J. Phys. Chem.*, **72**, 4311 (1968).
14) G. W. Gray, *Mol. Cryst.*, **1**, 333 (1966).
15) M. J. S. Dewar and A. C. Griffin, *J. Chem. Soc., Perkin Trans. 2*, **1976**, 713.
16) Unpublished result for our laboratory.
17) J. van der Veen, *J. de Phys.*, **36**, Cl-375 (1975).
18) F. Zuccarello, S. Millelieri, and S. Trovato, *Can. J. Chem.*, **54**, 226 (1976).
19) G. W. Gray, J. B. Hartley, A. Ibbotson, and B. Jones, *J. Chem. Soc.*, **1955**, 4359.
20) D. J. Byron, G. W. Gray, A. Ibbotson, and B. M. Worrall, *J. Chem. Soc.*, **1963**, 2246.
21) G. W. Gray and B. M. Worrall, *J. Chem. Soc.*, **1959**, 1545.

Studies on Heteropentalenes. V.[1] Cycloadditions of 5-Aryl-3-methylimidazo-[5,1-*b*]thiazoles with Acetylenic Esters Leading to 5-Aryl-3-methylthiazolo[2,3-*c*]benzimidazoles and Related Heterocycles

Noritaka Abe,* Tarozaemon Nishiwaki, and Kotaro Ikeda
Department of Chemistry, Faculty of Sciences, Yamaguchi University, Yamaguchi 753
(Received December 10, 1981)

Cycloaddition of 5-aryl-3-methylimidazo[5,1-*b*]thiazoles with dialkyl acetylenedicarboxylate in an aprotic nonpolar solvent gives a number of products including epimeric thiazolo[2,3-*c*]benzimidazoles (**3** and **4**) [1:2-cycloadducts], epimeric 5,10b-ethenothiazolo[3′,2′:3,4]imidazo[1,5-*a*]pyridines (**5** and **6**) [1:3-cycloadducts], and thiazolo[3′,2′:3,4]imidazo[1,2-*a*]pyridines [1:3-adducts]. At higher temperature, formation of the 1:2-cycloadducts is favored over the 1:3-adducts, whereas the latter predominates at room temperature. In an aprotic polar medium, the 1:3-cycloadducts (**5** and **6**) and tetraalkyl 6-arylpyridine-2,3,4,5-tetracarboxylates are substantially produced. Epimerization of **3** and **4** has been found to compete well with fragmentation to 4*H*-1,4-benzothiazine.

Although the chemistry of aromatic azapentalenes has been dealt with from various angles,[2] studies on cycloadditions to them had been undeservedly neglected before we first reported the 1,4-cycloadditions[3] of imidazo-[2,1-*b*]thiazoles and of imidazo[2,1-*b*]benzothiazoles with acetylenic esters (*e.g.*, dimethyl acetylenedicarboxylate (DMAD)[4] and methyl propiolate[5]). The present paper is concerned with the 1,4-cycloadditions[3] of imidazo[5,1-*b*]thiazoles (**1**). The result will prove of some interest for the synthesis of thiazolo[2,3-*c*]benzimidazoles (**3** and **4**) and 4*H*-1,4-benzothiazine rings (**10**).

The reactions of imidazo[5,1-*b*]thiazoles with acetylenic esters are highly solvent dependent, like those of imidazo[2,1-*b*]thiazoles[4] and of imidazo[2,1-*b*]benzothiazoles.[4] With DMAD in acetonitrile, 3-methyl-5-phenylimidazo[5,1-*b*]thiazole (**1a**) produced tetramethyl 6-phenylpyridine-2,3,4,5-tetracarboxylate (**2**),[6] two diastereoisomers **3a** and **4a** of tetramethyl 3-methyl-5-phenylthiazolo[2,3-*c*]benzimidazole-7,8,9,10-tetracarboxylate [1:2-cycloadducts], and two diastereoisomers **5a** and **6a** of hexamethyl 3-methyl-5-phenyl-5,10b-ethenothiazolo[3′,2′:3,4]imidazo[1,5-*a*]pyridine-7,8,9,10,11,12-hexacarboxylate [1:3-cycloadducts]. However, use of benzene, xylene, or tetrahydrofuran (THF) as a solvent resulted in the formation of a new 1:3-adduct [dimethyl 2-(5,6,7,8-tetramethoxycarbonyl-3-methyl-4a-phenylthiazolo[3′,2′:3,4]imidazo]1,2-*a*]pyridin-10-yl)fumarate (**8a**)] in addition to **3a**, **4a**, **5a**, and **6a**, but did not yield the pyridine (**2**).

a series: E = CO_2Me, Ar = Ph
b series: E = CO_2Me, Ar = C_6H_4Me-p
c series: E = CO_2Et, Ar = Ph

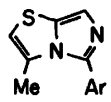

1a - b

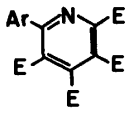

2a - b

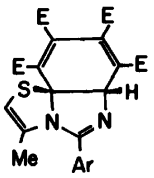

3a - c

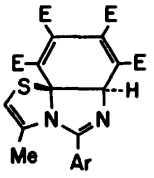

4a - c

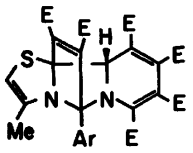

5a - b

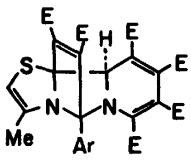

6a - b

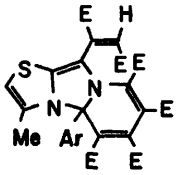

8a - b

Likewise, the reaction of **1b** with DMAD afforded a series of the compounds **2b**, **3b**, **4b**, **5b**, and **6b** in

Table 1. Conditions and yields for the reactions of 1 with acetylenic esters

Substrate	Reagent	Ratio	Solvent	Temp	Time/h	Products (%)						
1a	DMAD	1:1	MeCN	Reflux	1	**1a**(49)	**2a**(2)	**3a**(10)	**4a**(7)	**5a**(3)	**6a**(3)	
1a	DMAD	1:5	MeCN	Reflux	1		**2a**(10)	**3a**(21)	**4a**(5)	**5a**(22)	**6a**(34)	
1a	DMAD	1:5	MeCN	R.T.	20		**2a**(18)	**3a**(8)	**4a**(2)	**5a**(8)	**6a**(43)	
1a	DMAD	1:1	Benzene	Reflux	1	**1a**(47)		**3a**(10)	**4a**(9)	**5a**(4)	**6a**(4)	**8a**(6)
1a	DMAD	1:5	Benzene	Reflux	1			**3a**(27)	**4a**(26)	**5a**(14)	**6a**(20)	**8a**(7)
1a	DMAD	1:5	Benzene	R.T.	20			**3a**(4)	**4a**(4)	**5a**(10)	**6a**(34)	**8a**(3)
1a	DMAD	1:5	THF	Reflux	1			**3a**(21)	**4a**(7)	**5a**(10)	**6a**(18)	**8a**(9)
1a	DMAD	1:5	Xylene	Reflux	1			**3a**(22)	**4a**(20)	**5a**(5)	**6a**(7)	**8a**(5)
1b	DMAD	1:5	MeCN	Reflux	1		**2b**(11)	**3b**(7)	**4b**(16)	**5b**(19)	**6b**(37)	
1b	DMAD	1:5	Benzene	Reflux	1			**3b**(13)	**4b**(41)	**5b**(13)	**6b**(21)	**8b**(8)
1b	DMAD	1:5	Xylene	Reflux	1			**3b**(12)	**4b**(41)	**5b**(10)	**6b**(14)	**8b**(9)
1a	DEAD	1:5	MeCN	Reflux	1			**3c**(22)	**4c**(6)			
1a	DEAD	1:5	Benzene	Reflux	1			**3c**(51)	**4c**(5)			

acetonitrile, and a series of the products **3b**, **4b**, **5b**, **6b**, and **8b** in benzene or xylene. With diethyl acetylenedicarboxylate (DEAD), **1a** yielded the diastereoisomers **3c** and **4c** alone in either of acetonitrile or benzene, however. Irrespective of the polarity of the solvent, formation of the 1:2-cycloadducts seems to become favorable at higher temperature than that of the 1:3-adducts. These results are provided in Table 1.

Structures of these new compounds were deduced from their elemental analyses and spectroscopic behaviors. Elemental analyses of **3a** and **4a** gave the same elemental composition of $C_{24}H_{22}N_2O_8S$. The compound **3a** exhibits three ν(C=O) absorptions at 1705, 1725, and 1750 cm^{-1} in the IR spectrum, and the ^{13}C NMR signals for two sp^3-carbons of the ring at δ 47.1 (d) (C-6a) and 118.9 (s) (C-10a) and one easily identified sp^2-carbon flanked by two nitrogens at δ 166.6 (s). Specific ^1H NMR resonances observed for **3a** include four ester Me singlets at δ 3.47, 3.51, 3.77, and 3.79, and two 1H-singlets at δ 7.12 (H-2) and 6.68 (H-6a).

The ^{13}C NMR signals of the compound **4a** are very similar to those of the compound **3a**, and the ^1H NMR spectra of **3a** and **4a** resemble each other except for the resonance of one ester Me and H-6a protons. As to the differences, **3a** has an ester Me signal at δ 3.51 and a methine singlet at δ 6.68 (H-6a), whereas **4a** at δ 3.73 and 6.27 respectively. These significant changes strongly suggest that stereochemical disposition of the hydrogen at C-6a of differs from that of **4a**. As the hydrogen disposed *syn* must be susceptible to anisotropic deshielding effect of the ring sulfur atom, the compound whose H-6a proton is seen at lower field should be *syn*-isomer **3a** and the one displaying its H-6a proton at higher field *anti*-isomer **4a**.

Interconversion of **3a** and **4a**, though not attained thermally (*e.g.*, heating in xylene), takes place readily in the presence of base. Heating of either **3a** or **4a** with sodium methoxide in methanol or 1,8-diazabicyclo-[5.4.0]undec-7-ene (DBU) in benzene produced a mixture of **3a**, **4a**, and tetramethyl 3-methyl-4*H*-1,4-benzothiazine-5,6,7,8-tetracarboxylate (**10a**)[7] whose structure is delineated later. These observations firmly show the compounds **3a** and **4a** to be epimers. Similarly, the epimerization of **3c** to **4c** was found to compete significantly with the fragmentation to **10c**.

The structures **5a** and **6a**, both being analyzed as $C_{30}H_{28}N_2O_{12}S$, were assigned as follows. Their UV spectra resemble each other, possessing a maximum absorption even at the wavelength greater than 400 nm. As the ^{13}C NMR spectra of **5a** and **6a** also resemble each other, they must be stereoisomers. Besides signals for carbons associated with Me, Ph, and CO_2Me groups, eleven carbons are seen, among which six singlets at δ 120—150 are assigned to =C–CO_2Me groups by reference to the spectra of **3a** and **4a**. Signals at δ 117—118 and at δ 153—154 are assigned to a CH=CH–Me group. Two sp^3-carbons which appear at δ 56—58 and δ 71—72 are assigned to >CH and >C–Ph groups with the aid of proton-decoupled off resonance spectra. The remaining singlet observed at lower field (δ 113—114) must be due to a quarternary carbon flanked by sulfur and nitrogen atoms. This is supported by the ^{13}C NMR spectrum of **7** whose C-4a has been reported to resonate at δ 114.[8]

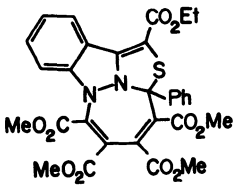

7

It is therefore deduced that a new six membered ring incorporating 2 mol of DMAD is annelated to **1** at the N(6)–C(7) bond and the remaining DMAD forms an etheno bridge whose termini are at C-5 and C-8 of **1**. The isomers **5a** and **6a** reveal their H-10a proton at δ 5.12 and 5.15 respectively. With the same reasonings for the stereochemical assignments of **3a** and **4a**, the *syn*-hydrogen at C-10a of a 5,10b-ethenothiazolo-[3′,2′:3,4]imidazo[1,5-*a*]pyridine ring must resonate at lower field than its counterpart, and hence the compound whose methine hydrogen is seen at δ 5.12 is assigned the *anti*-structure (**5a**) and the one displaying the methine hydrogen at δ 5.15 the *syn*-structure (**6a**).

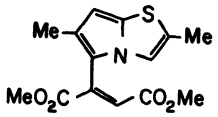

9

The ^1H NMR spectrum of **8a**, $C_{30}H_{28}N_2O_{12}S$, confirmed the presence of six ester Me groups and two olefinic protons, one Me group and a phenyl group. Of the two olefinic protons, the one has its chemical shift (δ 6.72) close to the olefinic proton of dimethyl fumarate (δ 6.83) and of the compound **9** (δ 6.79).[9] As both of the other olefinic singlet (δ 6.96) and a Me singlet at δ 2.38 broaden, as seen for the ^1H NMR spectra of **1a**, **3a**, **4a**, **5a**, and **6a**, the thiazole ring of **1a** would have remained intact. These observations, together with the disappearance of the H-7 proton of **1a** and complete difference of the UV spectrum of **8a** from those of the other 1 : 3-adducts **5a** and **6a**, allowed the structure to be proposed.

UV, IR, and ^1H NMR spectroscopic properties of the compounds **2a**—**2b**, **3a**—**3c**, **4a**—**4c**, **5a**—**5b**, **6a**—**6b**, and **8a**—**8b** are collected in Table 2 and full ^{13}C NMR spectral assignments of **3a**, **4a**, **4b**, **5a**, and **6a** in Table 3.

The structure **10a**, $C_{17}H_{17}NO_8S$, was determined as follows. The ^1H NMR spectrum shows a Me doublet at δ 2.41 which couples (J=0.5 Hz) with an olefinic proton at δ 6.74. Of the two singlets at δ 3.83 and 3.90 associated with four ester Me groups, the latter was found to be overlapped with an additional proton, which could be exchangeable. Furthermore, the spectrum indicated the absence of a benzene ring. The IR spectrum had ν(C=O) bands at 1695, 1715, and 1730 cm^{-1} and a broad ν(NH) band at 2300—2850 cm^{-1}

TABLE 2. SPECTROSCOPIC PROPERTIES OF **2**, **3**, **4**, **5**, **6**, AND **8**

Compound	λ_{max}/nm (log ε)	ν(C=O)/cm^{-1}	^{1}H MNR δ
2a	269 (4.22)	1740, 1730, 1715	3.68(3H, s), 3.93(3H, s), 3.95(3H, s), 3.98(3H, s), 7.25—7.75(5H, m)
2b	282 (4.06)	1740, 1725	2.38(3H, s), 3.70(3H, s), 3.89(3H, s), 3.92(3H, s), 3.96(3H, s), 7.21(2H, d, J=8 Hz), 7.48(2H, d, J=8 Hz),
3a	250^{sh} (4.21), 317 (4.32), 350^{sh} (4.16)	1750, 1725, 1705	2.45(3H, bs), 3.47(3H, s), 3.51(3H, s), 3.77(3H, s), 3.79(3H, s), 6.68(1H, s), 7.12(1H, bs), 7.2—7.6(5H, m)
3b	250 (4.08), 327 (4.31), 355^{sh} (4.17)	1750, 1725, 1710	2.38(3H, s), 2.47(3H, bs), 3.53(6H, s), 3.80(6H, s), 6.75(1H, s), 7.18(1H, bs), 7.25(2H, d, J=8 Hz), 7.44(2H, d, J=8 Hz)
3c	242(4.33), 313 (4.40), 345^{sh} (4.25)	1745, 1720, 1695	0.86(3H, t, J=7 Hz), 1.08(3H, t, J=7 Hz), 1.28(6H, t, J=7 Hz), 2.47(3H, bs), 3.90(2H, q, J=7 Hz), 3.96(2H, q, J=7 Hz), 4.24(2H, q, J=7 Hz), 4.25(2H, q, J=7 Hz), 6.70(1H, s), 7.13 (1H,bs), 7.25—7.6(5H, m)
4a	255 (4.28), 320 (4.13), 360 (4.16)	1740, 1725, 1695	2.42(3H, bs), 3.46(3H, s), 3.73(3H, s), 3.76(3H, s), 3.79(3H, s), 6.27(1H, s), 7.00(1H, bs), 7.3—7.6(3H, m), 7.9—8.2(2H, m)
4b	255 (4.31), 325 (4.26), 361 (4.26)	1750, 1740, 1720	2.42(6H, s), 3.47(3H, s), 3.75(3H, s), 3.78(3H, s), 3.82(3H, s), 6.27(1H, s), 7.03(1H, bs), 7.30(2H, d, J=8 Hz), 8.03(2H, d, J=8 Hz)
4c	253 (4.25), 320 (4.18), 360 (4.20)	1750, 1725, 1690	1.01(3H, t, J=7 Hz), 1.22(3H, t, J=7 Hz), 1.25(3H, t, J=7 Hz), 1.32(3H, t, J=7 Hz), 2.42(3H, bs), 3.97(2H, q, J=7 Hz), 4.26(2H, q, J=7 Hz), 4.27(2H, q, J=7 Hz), 4.30(2H, q, J=7 Hz), 6.12(1H, s), 7.03(1H, bs), 7.35—7.65(3H, m), 8.05—8.3(2H, m)
5a	260 (4.44), 405 (4.07)	1735, 1720	2.45(3H, bs), 3.10(3H, s), 3.38(3H, s), 3.48(3H, s), 3.57(3H, s), 3.84(3H, s), 3.94(3H, s), 5.12(1H, s), 7.15(1H, bs), 7.15—7.35(3H, m), 7.45—7.7(2H, m)
5b	261 (4.21), 406 (3.87)	1735, 1720	2.25(3H, s), 2.45(3H, bs), 3.12(3H, s), 3.36(3H, s), 3.48(3H, s), 3.55(3H, s), 3.81(3H, s), 3.91(3H, s), 5.10(1H, s), 6.98(2H, d, J=8 Hz), 7.13(1H, bs), 7.40(2H, d, J=8 Hz)
6a	262 (4.32), 290 (4.28), 408 (3.97), 430^{sh} (3.85)	1750, 1740, 1720, 1710	2.17(3H, bs), 3.20(3H, s), 3.48(3H, s), 3.77(3H, s), 3.80(3H, s), 3.87(6H, s), 5.15(1H, s), 6.61(1H, bs), 7.0—7.4(5H, m)
6b	263 (4.26), 300 (4.21), 410 (3.94), 430^{sh} (3.82)	1755, 1735, 1715	2.20(3H, bs), 2.26(3H, s), 3.26(3H, s), 3.50(3H, s), 3.79(3H, s), 3.82(3H, s), 3.88(6H, s), 5.16(1H, bs), 6.69(1H, bs), 6.90(2H, d, J=8 Hz), 7.23(2H, d, J=8 Hz)
8a	368 (3.56)	1755, 1730, 1720, 1700	2.38(3H, bs), 3.48(3H, s), 3.54(3H, s), 3.68(3H, s), 3.73(3H, s), 3.76(3H, s), 3.87(3H, s), 6.72(1H, s), 6.96(1H, bs),7.15—7.6(5H, m)
8b	362 (3.66)	1740, 1730, 1710	2.27(3H, s), 2.38(3H, bs), 3.47(3H, s), 3.54(3H, s), 3.63(3H, s), 3.70(3H, s), 3.74(3H, s), 3.82(3H, s), 6.65(1H, s), 6.92(1H, bs), 7.07(2H, d, J=8 Hz), 7.28(2H, d, J=8 Hz)

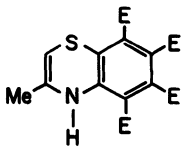

10a, c

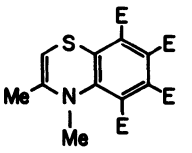

11a

indicative of hydrogen-bonding with the CO_2Me absorbing at 1695 cm^{-1}. This compound, though resistant toward acetylation, was found to react with methyl fluorosulfate giving the corresponding *N*-methyl derivative (**11a**). These data are accounted for in terms of the structure **10a**.

Plausible mechanisms for the reactions of imidazo-[5,1-*b*]thiazoles (**1**) with acetylenic esters are given in Scheme 1. Electrophilic attack of the acetylenic ester would occur at either C-5 or C-7 of **1**. The attack at C-7 gives an intermediate **A**, from which the 1:2-cycloadducts **3** and **4** are formed (Path a). When the attack takes place at C-5, the position presumed to be more electron-rich than C-7 due to electron release from the sulfur and the nitrogen at the 4-position, an intermediate **B** is generated. Cyclization of **B** to **C**

Table 3. ^{13}C NMR spectra of **3a**, **4a**, **4b**, **5a**, and **6a**

Carbon	3a	4a	4b	5a	6a
2	121.2d	117.5d	117.4d	118.5d	117.4d
3	152.8s	154.9s	154.8s	153.6s	152.9s
5	166.6s	166.8s	166.9s	71.2s	72.4s
6a	47.1d	52.6d	47.4d	—	—
7	141.3s	146.7s	147.0s	152.9s	148.8s
8	137.8s	134.5s	131.8s	137.4s	133.3s
9	138.8s	139.6s	139.4s	137.8s	138.3s
10	154.8s	150.5s	150.2s	144.8s	146.5s
10a	118.9s	116.4s	116.1s	57.9d	56.0d
10b	—	—	—	113.1s	114.2s
11	—	—	—	124.9s	126.6s
12	—	—	—	127.4s	126.8s
Me	17.1q	17.4q	17.3q	16.7q	16.6q
			21.5q		
OMe	52.3q	52.9q	52.6q	51.7q	51.5q
	52.9q[a]	53.0q[b]	52.9q[b]	51.8q	51.6q
		53.2q	53.2q	52.2q	52.3q
				52.7q[b]	52.6q
				52.8q	52.8q
					53.6q
C=O	163.7s	164.1s	163.8s	161.7s	162.8s
	164.6s	164.3s	164.3s	163.3s	163.5s
	167.0s	166.6s	166.7s	163.8s	165.4s
	167.8s	166.9s	167.2s	164.6s	166.8s
				166.1s	168.8s
				168.6s	170.2s
Ph	128.1d[b]	128.8d	129.7d[b]	127.0s	126.9s
	128.3d[b]	129.0d[b]	129.8d[b]	127.1d[b]	127.3d[b]
	129.0s	129.0d[b]	131.6s	127.6d[b]	129.6d
	129.7d	132.3d	139.4s	128.7d	130.4d[b]

a) Three peaks degenerate. b) Two peaks degenerate.

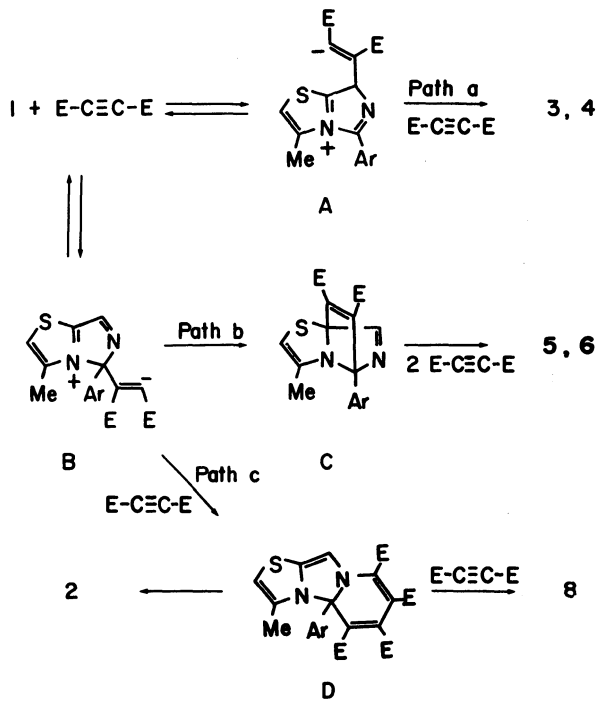

Scheme 1.

followed by a 1,4-dipolar cycloaddition[3] affords the 1:3-cycloadducts **5** and **6** (Path b). Alternatively, cycloaddition of **B** with an additional acetylenic ester would lead to an intermediate **D**, which undergoes either the Michael-type addition in a nonpolar solvent to produce **8** or fragmentation in polar medium to the pyridine **2** (Path c).

Conceivably, an equilibrium will be established between **1** and the dipolar species **A** and **B**. As cyclization of **A** leading to **3** or **4** (Path a) would be unfavorable because the acetylenic ester has to approach from a sterically crowded site, formation of **3** or **4** will require higher temperature. By comparison with the Path a, the pathways b and c would be easier to proceed because neither cyclizations of **B** to **C** nor **D** is sterically disturbed by the C-3-Me or C-5-Ar groups.

A likely mechanism for the base-promoted fragmentation of **3** or **4** to the benzothiazine (**10**) is depicted in Scheme 2. Abstraction of the hydrogen at C-6a by base gives rise to a carbanion **E** and a sulfide anion **F**, successively. Cyclization of the sulfide anion **F** leads to a new anion **G**, which subsequently undergoes loss of a nitrile followed by protonation to give **10**.

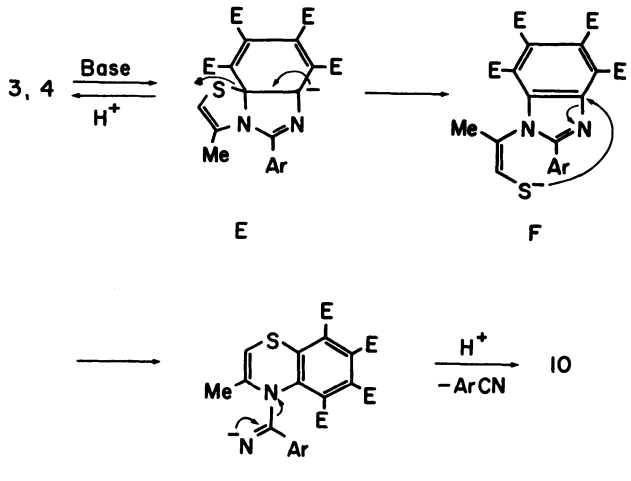

Scheme 2.

Experimental

Melting points were uncorrected. IR spectra were determined as Nujol mulls unless otherwise stated. ^1H NMR spectra were recorded in $CDCl_3$ with Me_4Si as internal standard with a Hitachi R-24B (60 MHz) or JEOL FX-100 (100 MHz) spectrometers, and ^{13}C NMR spectra with a Varian FT-80A instrument (20 MHz; solutions in $CDCl_3$ with Me_4Si as internal standard). Mass spectra were determined with a Hitachi M-80 spectrometer by means of either electron impact or field desorption ionization methods. Kieselgel 60 was used for chromatography.

3-Methyl-5-phenylimidazo[5,1-*b*]thiazole (**1a**) was prepared as reported.[10] **1a**: mp 105—106 °C (lit,[10] 106 °C), UV_{max} (chloroform) 303 nm (log ε 4.08), IR 775 and 700 cm^{-1} (phenyl), ^1H NMR δ=2.02 (3H, d, J=1 Hz), 6.27 (1H, q, J=1 Hz), 7.04 (1H, s), 7.15—7.6 (5H, m). Found: C, 67.20; H, 4.75; N, 13.12; S, 14.88%.

*3-Methyl-5-(p-tolyl)imidazo[5,1-*b*]thiazole (**1b**).* A mix-

TABLE 4. ANALYTICAL DATA OF **2**, **3**, **4**, **5**, **6**, AND **7**

Compound	Appearance	Mp θ_m/°C	Formula	Found (Calcd) (%) C	H	N	S	MS *m/e* (M^+)
2a	Colorless needles[a]	126—128[e]	$C_{19}H_{17}NO_8$	58.47 (58.91)	4.50 (4.42)	3.35 (3.62)		387
2b	Colorless needles[b]	85—87	$C_{20}H_{19}NO_8$	59.75 (59.85)	4.82 (4.77)	3.55 (3.49)		
3a	Yellow prisms[c]	191—193	$C_{24}H_{22}N_2O_8S$	57.90 (57.82)	4.42 (4.45)	5.61 (5.62)	6.46 (6.43)	498
3b	Yellow prisms[c]	176—178	$C_{25}H_{24}N_2O_8S$	58.82 (58.59)	4.79 (4.72)	5.52 (5.46)	6.12 (6.26)	
3c	Yellow needles[b]	140—142	$C_{28}H_{30}N_2O_8S$	60.82 (60.64)	5.53 (5.45)	5.16 (5.05)	5.66 (5.78)	554
4a	Yellow needles[c]	151—152	$C_{24}H_{22}N_2O_8S$	57.93 (57.82)	4.46 (4.45)	5.55 (5.62)	6.43 (6.43)	498
4b	Yellow needles[c]	196—198	$C_{25}H_{24}N_2O_8S$	58.77 (58.59)	4.63 (4.72)	5.44 (5.46)	6.21 (6.26)	
4c	Yellow needles[d]	57—61	$C_{28}H_{30}N_2O_8S$	60.78 (60.64)	5.62 (5.45)	5.28 (5.05)	5.48 (5.78)	554
5a	Yellow prisms[c]	180—181	$C_{30}H_{28}N_2O_{12}S$	56.48 (56.25)	4.46 (4.41)	4.33 (4.37)	5.30 (5.00)	640
5b	Yellow needles[d]	137—139	$C_{31}H_{30}N_2O_{12}S$	57.14 (56.88)	4.84 (4.62)	4.06 (4.28)	4.75 (4.90)	
6a	Yellow prisms[c]	180—181	$C_{30}H_{28}N_2O_{12}S$	56.12 (56.25)	4.54 (4.41)	4.09 (4.37)	4.81 (5.00)	
6b	Yellow prisms[d]	200—201	$C_{31}H_{30}N_2O_{12}S$	57.09 (56.88)	4.58 (4.62)	4.34 (4.28)	5.17 (4.90)	
8a	Yellow needles[c]	118—121	$C_{30}H_{28}N_2O_{12}S$	56.31 (56.25)	4.45 (4.41)	4.30 (4.37)	4.95 (5.00)	
8b	Yellow needles[c]	179—181	$C_{31}H_{30}N_2O_{12}S$	56.69 (56.88)	4.55 (4.62)	4.09 (4.28)	5.12 (4.90)	

a) Recrystallized from petroleum ether. b) Recrystallized from ligroine. c) Recrystallized from ethanol. d) Recrystallized from ligroine–dichloromethane. e) Lit,[6] mp 128—129 °C.

tuer of 4-methyl-2-(*p*-toluoylaminomethyl)thiazole (7.4 g) and $POCl_3$ (25 ml) in dry benzene (50 ml) was heated under reflux for 6 h and evaporated under reduced pressure. Water was added to the residue and the solution was neutralized with NH_3 to deposit **1b** (4.0 g, 58%), which crystallized as colorless prisms from ligroine [mp 123—124 °C, UV_{max} (chloroform) 300 nm (log ε 4.14), IR 825 cm^{-1} (phenyl), ^1H NMR δ=2.07 (3H, d, J=1 Hz), 2.42 (3H, s), 6.36 (1H, q, J=1 Hz), 7.10 (1H, s), 7.20 (2H, d, J=8 Hz), 7.42 (2H, d, J=8 Hz). Found: C, 68.50; H, 5.14; N, 12.13; S, 14.14%. Calcd for $C_{13}H_{12}N_2S$: C, 68.39; H, 5.30; N, 12.27; S, 14.04%].

General Procedure for the Reactions of ***1*** *with DMAD.* A mixture of **1** (2.0 mmol), DMAD, and the solvent (30 ml) was allowed to react under the conditions specified in Table 1 and evaporated to dryness under reduced pressure. Chromatography of the residue with benzene, benzene–chloroform (1 : 1), and chloroform, successively, gave the compounds, **1**, **2**, **3**, **4**, **5**, and **6**, in the order. Analytical data are collected in Table 4 and spectroscopic data in Tables 2 and 3.

Reaction of ***1a*** *with DEAD.* A mixture of **1a** (2.0 mmol), DEAD, and the solvent (30 ml) was allowed to react under the conditions specified in Table 1 and evaporated to dryness under reduced pressure. Chromatography of the residue with benzene–chloroform (1 : 1) gave **3c** and **4c**, successively. Analytical data are given in Table 4 and spectroscopic data in Table 2.

Epimerization of ***3*** *and* ***4****.* *a)*: **3a** (0.150 g) was added to a sodium methoxide solution prepared from sodium (0.069 g) and abs methanol (30 ml). The mixture was heated under reflux, cooled, acidified with dil hydrochloric acid, and extracted with chloroform. The extracts were washed with water, dried (Na_2SO_4), and evaporated. Chromatography of the residue with benzene–chloroform (2:1) gave **3a** followed by **4a**. Elution with chloroform gave **10a**, which crystallized as yellow needles from benzene and had mp 223—225 °C, UV_{max} (ethanol) 238 nm (log ε 4.28), 275 (4.42), 394 (4.37), IR (chloroform) 2300—2850 (NH), 1730, 1715, and 1695 cm^{-1} (C=O), ^1H NMR δ=2.41 (3H, d, J=0.5 Hz), 3.83 (6H, s), 3.90 (7H, s) (one proton is exchangeable), 6.74 (1H, q, J=0.5 Hz), δ (CF_3CO_2H)=2.72 (3H, bs), 3.93 (6H, s), 4.18 (6H, s), 7.70 (1H, bs), 10.47 (1H, bs) (exchangeable). Found: C, 51.94; H, 4.23; N, 3.55; S, 8.16%. Calcd for $C_{17}H_{17}NO_8S$: C, 51.64; H, 4.33; N, 3.54; S, 8.11%. MS *m/e* (rel intensity) 395 (9%, M^+), 363 (61), 332 (100). Treatment of **8a** with methyl fluorosulfate in $CDCl_3$ in an NMR tube produced **11a**; ^1H NMR δ=2.50 (3H, bs), 3.87 (12H, s), 3.96 (3H, s), 6.87 (1H, bs). Yields of **3a**, **4a**, and **8a** are given in Table 5.

b): A mixture of **3a** (0.100 g) and DBU (1 drop) in dry benzene (5 ml) was heated under reflux for 1 h and evaporated under reduced pressure. The residue was chromatographed with benzene–chloroform (1 : 1) to give **3a**, **4a**, and **8a**, successively, whose yields are given in Table 5.

c): A mixture of **3c** (0.300 g) and a sodium ethoxide solution prepared from sodium (0.124 g) and abs ethanol (30 ml) was heated under reflux for 5 h and worked up as dercribed above. Elution with benzene–chloroform (2 : 1) gave **3c**

Table 5. Conditions and yields for the reactions of **3** and **4** with base

Substrate	Conditions	Time/h	(Yield/%)		
3a	NaOMe/MeOH	1	**3a**(68)	**4a**(24)	**10a**(7)
3a	NaOMe/MeOH	4	**3a**(26)	**4a**(4)	**10a**(62)
3a	DBU/Benzene	1	**3a**(70)	**4a**(14)	**10a**(13)
4a	NaOMe/MeOH	1	**3a**(65)	**4a**(25)	**10a**(5)
4b	NaOMe/MeOH	1	**3b**(17)	**4b**(54)	**10a**(17)
4b	NaOMe/MeOH	4	**3b**(5)	**4b**(18)	**10a**(45)

(0.050 g, 17%) followed by **4c** (0.055 g, 18%). Elution with chloroform gave **8c** (0.030 g, 12%), which crystallized as yellow needles from ligroine–dichloromethane and had mp 155—156 °C, UV_{max} (ethanol) 232 nm (log ε 4.50), 271 (4.55), 395 (4.48). IR 2850—2300 (NH), 1725, 1715, and 1695 cm^{-1} (C=O). ^1H NMR δ=1.32 (6H, t, J=7 Hz), 1.35 (6H, *t*, J=7 Hz), 2.45 (3H, d, J=0.5 Hz), 3.47 (1H, s) (exchangeable), 4.25 (4H, q, J=7 Hz), 4.32 (4H, q, J=7 Hz), 6.62 (1H, q, J=0.5 Hz). Found: C, 55.72; H, 5.45; N, 3.18; S, 7.15%, M^+ *m/e* 451. Calcd for $C_{21}H_{25}NO_8S$: C, 55.86; H, 5.58; N, 3.10; S, 7.10%, M 451.

We thank Dr. Masafumi Yasunami, Tohoku University, and Akira Mori, Kyushu University, for NMR spectral determinations.

References

1) Part IV, N. Abe, T. Nishiwaki, T. Omori, and E. Harada, *Bull. Chem. Soc. Jpn.*, **55**, 200 (1982).
2) J. Elguero, R. M. Claramunt, and A. J. Summers, *Adv. Heterocycl. Chem.*, **22**, 183 (1978); C. A. Ramsden, *Tetrahedron*, **33**, 3203 (1977); H. Volz and H. Kowarsch, *Heterocycles*, **7**, 1319 (1977); Th. Pyl and K.-H., Wunsch, *Z. Chem.*, **5**, 361 (1965).
3) R. Huisgen, "Topics in Heterocyclic Chemistry," ed by R. N. Castle, Wiley, New York (1969), p. 223.
4) N. Abe, T. Nishiwaki, and N. Komoto, *Bull. Chem. Soc. Jpn.*, **53**, 3308 (1980).
5) N. Abe and T. Nishiwaki, *Heterocycles*, **16**, 537 (1981).
6) R. Huisgen and K. Herbig, *Justus Liebigs Ann. Chem.*, **688**, 98 (1965).
7) Earlier we incorrectly proposed the 8a*H*-1,4-benzothiazine structure for this compound: N. Abe, T. Nishiwaki, and K. Ikeda, 14th Symposium on Nonbenzenoid Chemistry, Okayama, October 1981, Abstr. No. 1X05. The structure is now revised as shown.
8) K. T. Potts and J. L. Marshall, *J. Org. Chem.*, **41**, 129 (1976).
9) O. Ceder and B. Beijer, *Tetrahedron*, **28**, 4341 (1972).
10) Th. Pyl, O. Seitz, and K. Steage, *Justus Liebigs Ann. Chem.*, **679**, 144 (1964).

Syntheses and Properties of the Polymethylenebis-(diphenylcyclopropenium) Dications[1)]

Koichi Komatsu, Katsuhisa Masumoto, Yoshinori Waki, and Kunio Okamoto*
Department of Hydrocarbon Chemistry, Faculty of Engineering, Kyoto University, Sakyo-ku, Kyoto 606
(Received December 26, 1981)

A series of polymethylenebis(diphenylcyclopropenium) dications with the polymethylene chain of one to six carbons ($\mathbf{4}_{n=1-6}$) were synthesized and characterized by spectral and analytical means. Among the dications $\mathbf{4}_{n=3-6}$ which were isolated as perchlorates, $\mathbf{4}_{n=3}$ was shown by the pK_{R^+} measurements to be destabilized by 1.3 pK units as compared with $\mathbf{4}_{n=4-6}$. The values of reduction potential exhibited the same tendency. The chromium(II) ion reduction of $\mathbf{4}_{n=6}$, a representative dication, afforded a polymeric material containing a hexylbenzene unit. The dication $\mathbf{4}_{n=2}$ was isolable only as a complex salt with $SbCl_6^-$ and Cl^-: the conventional hydride abstraction from 1,2-dicyclopropenylethane using trityl perchlorate resulted in rearrangements affording 4,9,10-triphenylphenanthrene and the unknown monocation $C_{32}H_{25}^+$ containing the tropylium ring. A possible mechanism for these rearrangements is presented. On the other hand, the dication $\mathbf{4}_{n=1}$ was observable only in a highly acidic solution due to the ready deprotonation yielding a new fully conjugated monocation **17**. This cation, characterized by remarkable stability (pK_{R^+} 8.9 in 50% aq acetonitrile), is formally represented as a triafulvene with a cyclopropenium ring substituted at the 4-position, but is shown to have a partially polarized electronic structure by ^{13}C NMR spectroscopy.

The divalent carbocations are typically classified into two groups, namely, the dipositive ions, in which the dipositive charge resides on one fully conjugated π-system, as exemplified by the cyclobutadienyl[2)] and cyclooctatetraenyl[3)] dipositive ions, and the carbodications, which contain two separate monocationic units in the same molecule.

In the latter class of dications, those having tertiary-alkyl cationic units are observable only in solution under stable-ion conditions,[4)] but those carrying nonbenzenoid aromatic cations are generally stable enough for isolation and for further investigation on their structure and reactivity. Thus, there have already been reported as stable species a variety of polyvalent cations containing two[5)] or more[6)] tropylium rings. Dications composed of two diaminocyclopropenium rings connected by a cyclopentadiene ring[7a)] and by various hetero-atom linkages[7b-d)] have also been synthesized, together with the directly bonded bis(diaminocyclopropenium) dications;[7e)] even the tetracation consisting of three diaminocyclopropenium rings bonded to the central cyclopropenium ring has been reported.[8)] However, studies on the dicyclopropenylio-dications carrying no stabilizing hetero atom seem to be quite limited; the reported examples are *p*-phenylenebis(diphenylcyclopropenium) dication (**1**) synthesized by Eicher and Berneth,[9)] and 1,8- (**2**) and 1,5-naphthylenebis(diphenylcyclopropenium) dication (**3**), synthesized by us.[10)]

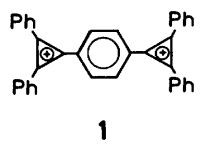

1

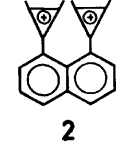

2

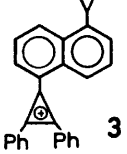

3

In connection with our previous work on the syntheses and both inter- and intramolecular reductive cyclization of the polymethylenebistropylium dications,[5h)] we have synthesized a series of new dicyclopropenylio-dications, *i.e.* the polymethylenebis(diphenylcyclopropenium) dications ($\mathbf{4}_{n=1-6}$), and examined their stability and reducibility with reference to the polymethylene chain length. In this paper, these results will be described, together with unusual molecular rearrangements observed during the course of syntheses.[1b)]

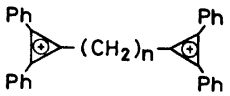

$\mathbf{4}_{n=1-6}$

Syntheses of Polymethylenebis(diphenylcyclopropenium) Dications ($\mathbf{4}_{n=1-6}$). It has been reported that chlorophenylcarbene thermally generated from chlorophenyldiazirine readily adds to mono- and diphenylacetylenes to give the chlorocyclopropene derivatives, which can be converted to the cyclopropenium ions.[11)] This method has been successfully applied to the synthesis of the dication **3** in our previous work.[10)] Thus, we first attempted the thermal reaction of two molar equivalents of chlorophenyldiazirine with 1,8-diphenyl-1,7-octadiyne as a representative alkadiyne. The product, however, was an intractable mixture of unwanted materials, and there was observed no indication of the formation of the cyclopropenyl or cyclopropenium ring. Apparently the first formed 1-alkyl-3-chloro-2,3-diphenylcyclopropene was unstable and was subjected to further reactions; several modifications of the reaction conditions did not improve the results.

Subsequently, we examined direct coupling of the di-Grignard reagent, α,ω-(bromomagnesio)alkanes, with the diphenylcyclopropenium ion as shown in Scheme 1, and obtained the corresponding α,ω-bis(2,3-diphenyl-2-

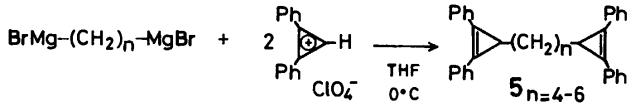

Scheme 1.

Table 1. Spectral properties of α,ω-bis(2,3-diphenyl-2-cyclopropenyl)alkanes ($\mathbf{5}_{n=1-6}$)

5	IR (KBr)[a] ν/cm^{-1}	UV ($CHCl_3$) λ_{max}/nm (log ε)	^{1}H NMR ($CDCl_3$) δ from Me_4Si
n=1	1815	317sh(4.66)	7.73 (m, 8H, *o*-H)
		327(4.74)	7.36 (m, 12H, *m*, *p*-H)
		344(4.61)	2.41 (t, 2H, >CH–)
			1.92 (t, 2H, –CH_2–)
n=2	1807	317sh(4.65)	7.61 (m, 8H, *o*-H)[b]
		326(4.72)	7.30 (m, 12H, *m*, *p*-H)
		344(4.57)	2.17 (m, 2H, >CH–)
			1.84 (d, 4H, –CH_2–)
n=3	1810	317sh(4.69)	7.63 (m, 8H, *o*-H)
		326(4.74)	7.33 (m, 12H, *m*, *p*-H)
		344(4.59)	2.17 (t, 2H, >CH–)
			1.72 (br s, 6H, –CH_2–)
n=4	1808	316sh(4.68)	7.64 (m, 8H, *o*-H)
		325(4.75)	7.34 (m, 12H, *m*, *p*-H)
		343(4.60)	2.14 (t, 2H, >CH–)
			1.60 (br s, 8H, –CH_2–)
n=5	1806	317sh(4.68)	7.61 (m, 8H, *o*-H)[b]
		325(4.74)	7.25 (m, 12H, *m*, *p*-H)
		344(4.59)	2.10 (t, 2H, >CH–)
			1.51 (br s, 10H, –CH_2–)
n=6	1810	316sh(4.68)	7.67 (m, 8H, *o*-H)
		325(4.74)	7.37 (m, 12H, *m*, *p*-H)
		343(4.60)	2.16 (t, 2H, >CH–)
			1.47 (br s, 12H, –CH_2–)

a) ν(cyclopropene). b) Taken in CCl_4.

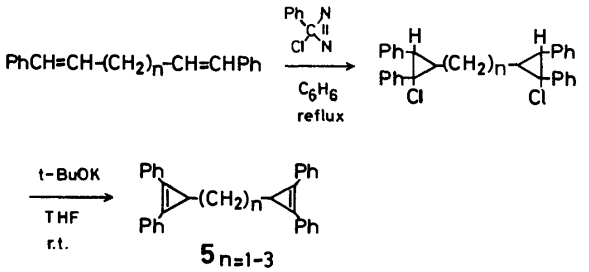

Scheme 2.

cyclopropenyl)alkanes ($\mathbf{5}_{n=4-6}$) in 37—60% yield. This method, however, is applicable only to the compounds with $n \geq 4$ due to the synthetic limitation for the di-Grignard reagent. For the syntheses of the dicyclopropenylalkanes $\mathbf{5}_{n=1-3}$, we adopted a stepwise method involving the addition of chlorophenylcarbene to the α,ω-alkadienes and the subsequent elimination of HCl, as shown in Scheme 2. The crude overall yield for $\mathbf{5}_{n=1-3}$ was 43—57%, based on the alkadienes. The dicyclopropenylalkanes $\mathbf{5}_{n=1-6}$ thus obtained were characterized by the spectral data listed in Table 1.

For the purpose of conversion to the polymethylenebiscyclopropenium dication **4**, the dicyclopropenylalkanes $\mathbf{5}_{n=1-6}$ were treated with two equivalents of trityl perchlorate. In the case with the polymethylene chain length of three to six carbons, the corresponding perchlorate salts of the dications $\mathbf{4}_{n=3-6}\cdot 2ClO_4^-$, were obtained as white powder in 70—94% yield. When the 1,2-dicyclopropenylethane $\mathbf{5}_{n=2}$ was treated with the trityl cation, an unexpected rearrangement occurred as a main reaction, as will be described later in detail. Among various other hydride-abstraction reagents examined, only antimony pentachloride[12] was effective to give a dicationic salt, which was analyzed as $\mathbf{4}_{n=2}\cdot 0.5SbCl_6^-\cdot 1.5Cl^-$, with no attendant rearrangement. On the other hand, the methylenebiscyclopropenium dication $\mathbf{4}_{n=1}$,[1b] obtained by the reaction of $\mathbf{5}_{n=1}$ with two equivalents of the trityl cation, was observable only in the highly acidic solution (*e.g.* in CF_3CO_2H–CF_3SO_3H (9 : 1)) owing to its ease in deprotonation which afforded the fully conjugated monocations, as will also be shown later.

Properties of the Polymethylenebis(diphenylcyclopropenium) Dications ($\mathbf{4}_{n=1-6}$). The dicyclopropenylio-dications $\mathbf{4}_{n=1-6}$ are characterized by the spectral properties shown in Table 2, which also includes the data for the related monocations $\mathbf{6}_{n=0-3}$ and **17** (*vide infra*) for

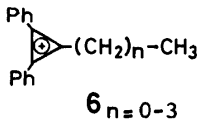

$\mathbf{6}_{n=0-3}$

comparison. All the di- and monocations (except **17**) exhibit strong IR absorption due to the cyclopropenium ring stretching near 1420 cm^{-1} and characteristic UV absorptions near 247, 293, and 307 nm. In the ^{1}H NMR spectra the methylene protons of the dications **4** are generally deshielded compared with the corresponding protons of the monocations **6**. Among the dications, the signals for each methylene proton are gradually shifted downfield as the chain length decreases. This tendency in methylene chemical shifts suggests the presence of some repulsive interaction between the two cationic rings through the polymethylene chain.

In order to examine the effect of such repulsive interaction, the pK_{R^+} and reduction potential of the purely isolated perchlorates of the dications $\mathbf{4}_{n=3-6}$ were determined by the use of the spectrophotometric method and cyclic voltammetry (CV), respectively. The results are shown in Table 3, together with the data for $\mathbf{6}_{n=2}$ as the representative monocation for comparison. For the dications, two pK_{R^+} values were determined, corresponding to the stepwise neutralization sequences for the two cationic units present at both ends of the polymethylene chain. The comparison of pK_{R^+} values for the first neutralization clearly shows that the dication $\mathbf{4}_{n=3}$, with the chain length of only three carbons, is destabilized by 1.3 pK units, *i.e.* *ca.* 1.8 kcal/mol at 25 °C, as compared with the dications with longer chain length.

The values of reduction potential also exhibit the same tendency; the dication $\mathbf{4}_{n=3}$ is most susceptible towards the electrochemical one-electron reduction. Notice here that the reduction wave observed at the potential listed in Table 3 is irreversible, and only corresponds to the first one-electron transfer to the dicationic species; this was determined from the comparison of the peak current with that of ferrocene determined under the identical conditions. The second reduction wave was not clearly observed in the sweep range of 0 to −2.0 V *vs.* Ag/Ag$^+$. This is presumably

Table 2. Spectral properties of the salts of polymethylenebis(diphenylcyclopropenium) dications ($\mathbf{4}_{n=1-6}$) and 1-alkyl-2,3-diphenylcyclopropenium ($\mathbf{6}_{n=0-3}$) and 1,2-diphenyl-3-(1,2-diphenyltriafulven-4-yl)cyclopropenium (**17**) monocations

Cation salt	IR (KBr) ν/cm^{-1}	UV (MeCN) λ_{max}/nm (log ε)	^{1}H NMR (CF_3CO_2H) δ from Me_4Si
$\mathbf{4}_{n=1}$	—	298(4.77)[a]	8.41 (m, 8H, *o*-H)[a]
		313(4.78)	7.90 (m, 12H, *m*, *p*-H)
			6.19 (s, 2H, $-CH_2-$)
$\mathbf{4}_{n=2}\cdot 0.5SbCl_6^-\cdot 1.5Cl^-$	1420[b]	247(4.53)	—[c]
		292(4.66)	
		308(4.63)	
$\mathbf{4}_{n=3}\cdot 2ClO_4^-$	1420[b]	247(4.53)	8.42 (m, 8H, *o*-H)
	1090[d]	292(4.80)	7.90 (m, 12H, *m*, *p*-H)
		306(4.81)	4.10 (t, 4H, α-CH_2-)
			3.27 (quint, 2H, β-CH_2-)
$\mathbf{4}_{n=4}\cdot 2ClO_4^-$	1420[b]	247(4.38)	8.38 (m, 8H, *o*-H)
	1090[d]	293(4.80)	7.90 (m, 12H, *m*, *p*-H)
		306(4.82)	3.87 (br t, 4H, α-CH_2-)
			2.62 (br m, 4H, β-CH_2-)
$\mathbf{4}_{n=5}\cdot 2ClO_4^-$	1420[b]	247(4.43)	8.39 (m, 8H, *o*-H)
	1090[b]	294(4.80)	7.92 (m, 12H, *m*, *p*-H)
		307(4.80)	3.77 (t, 4H, α-CH_2-)
			2.49 (m, 4H, β-CH_2-)
			2.10 (m, 2H, γ-CH_2-)
$\mathbf{4}_{n=6}\cdot 2ClO_4^-$	1420[b]	246(4.53)	8.36 (m, 8H, *o*-H)
	1090[d]	293(4.78)	7.91 (m, 12H, *m*, *p*-H)
		306(4.79)	3.72 (t, 4H, α-CH_2-)
			2.37 (m, 4H, β-CH_2-)
			1.90 (br m, 4H, γ-CH_2-)
$\mathbf{6}_{n=0}\cdot BF_4^-$[e]	1425[b]	243(4.16)	8.37 (m, 4H, *o*-H)[f]
	1060[g]	290(4.53)	7.87 (m, 6H, *m*, *p*-H)
		304(4.55)	3.20 (s, 3H, $-CH_3$)
$\mathbf{6}_{n=1}\cdot BF_4^-$	1420[b]	244(4.20)	8.37 (m, 4H, *o*-H)
	1055[g]	290(4.53)	7.92 (m, 6H, *m*, *p*-H)
		304(4.55)	3.63 (q, 2H, $-CH_2-$)
			1.80 (t, 3H, $-CH_3$)
$\mathbf{6}_{n=2}\cdot BF_4^-$[h]	1420[b]	244(4.20)	8.27 (m, 4H, *o*-H)
	1055[g]	290(4.50)	7.93 (m, 6H, *m*, *p*-H)
		304(4.52)	3.52 (t, 2H, α-CH_2-)
			2.25 (sext, 2H, β-CH_2-)
			1.27 (t. 3H, $-CH_3$)
$\mathbf{6}_{n=3}\cdot BF_4^-$[e]	1418[b]	244(4.23)	8.39 (m, 4H, *o*-H)[f]
	1055[g]	290(4.54)	7.91 (m, 6H, *m*, *p*-H)
		304(4.55)	3.62 (t, 2H, α-CH_2-)
			2.14 (quint, 2H, β-CH_2-)
			1.57 (sext, 2H, γ-CH_2-)
			1.04 (t, 3H, $-CH_3$)
17$\cdot ClO_4^-$	1435[b]	243(4.45)	8.17 (m, 8H, *o*-H)
	1090[d]	269(4.51)	7.73 (m, 12H, *m*, *p*-H)
		353(4.77)	

a) Observed in CF_3CO_2H–CF_3SO_3H (9 : 1). b) ν(cyclopropenium ring). c) Not measured due to poor solubility in the common solvents. d) $\nu(ClO_4^-)$. e) K. Komatsu, T. Niwa, and K. Okamoto; unpublished results. f) Taken in CD_3CN. g) $\nu(BF_4^-)$. h) Ref. 13.

due to the rapid coupling of the first formed cation-radical to give the dimeric dication, which upon further reduction and repeated coupling gives some polymeric material which accumulates at the electrode surface. Actually, this polymerization, which supposedly results in the coating of the working electrode, caused marked depression of the reduction wave (to less than one third of the peak height of each previous scan) at the second and subsequent scans.

Chromium(II) Ion Reduction of the Hexamethylenebis-(diphenylcyclopropenium) Dication ($\mathbf{4}_{n=6}$). The above-mentioned result of the electrochemical reduction led us to investigate the chemical reduction of the dicyclopropenylio-dication. In our previous kinetic

and product study, the 1,2-diphenyl-3-propylcyclopropenium ion was found to be reduced by the chromium(II) ion in 10% HCl at 75 °C smoothly to give the dimer of the corresponding cyclopropenyl radical in good yield (82.1%).[13] Thus, the chromium(II) ion reduction was carried out under similar reaction conditions on $\mathbf{4}_{n=6}$ as the representative dication. The product, obtained as a yellowish solid in 81% yield, exhibited the IR absorptions only for the polymethylene chain and the benzene nuclei, but no absorption for the cyclopropene structure near 1800 cm^{-1}; the ^1H NMR spectrum showed only two broad signals, one centered at δ 7.2 and the other ranging from δ 2.5 to 0.9, with an integrated ratio of 5 : 3. This product was developed on a TLC plate (SiO_2) as a streak with benzene–hexane (1 : 1) as a solvent but not as spots, as are commonly observed for polymeric hydrocarbons. Based on these findings, the product is supposed to be an oligomer or a polymer of the structure such as **7**, formed by repeated coupling of the cyclopropenyl radicals generated at both ends of the polymethylene chain, followed by the subsequent "bicyclopropenyl→benzene" rearrangement,[14] as shown

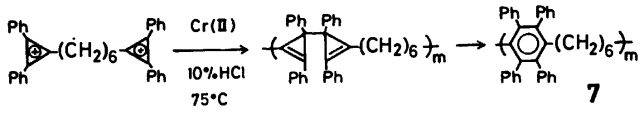

Scheme 3.

in Scheme 3. The same type of polymerization has already been observed upon the chromium(II) ion reduction of polymethylenebistropylium dications under similar reaction conditions.[5h]

Reaction of 1,2-Bis(2,3-diphenyl-2-cyclopropenyl)ethane ($\mathbf{5}_{n=2}$) with the Trityl Cation Accompanied by Molecular Rearrangements. As has been mentioned, unexpected rearrangements were observed upon hydride abstraction from the dicyclopropenylethane $\mathbf{5}_{n=2}$. When two equivalents of trityl perchlorate were allowed to react with $\mathbf{5}_{n=2}$ in dichloromethane at room temperature, a mild exothermic reaction took place, as shown by the immediate darkening of the reaction mixture. However, no dicationic salt was obtained but rather some unknown monocationic salt with the molecular formula $C_{32}H_{25}ClO_4$† (40.7% yield based on $\mathbf{5}_{n=2}$) upon

† This cation salt is yellow and exhibits no IR absorption for the cyclopropenium ring. From the ^1H and ^{13}C NMR data (see Experimental), the long-wave UV-Vis absorption (λ_{max} (MeCN) 433 nm), high stability (pK_{R^+} 6.89 in 23% EtOH),and the facile $NaBH_4$ reduction to the cycloheptatriene derivative, this cation is supposed to have a structure composed of the tropylium ring with a conjugative substituent. Assuming that this cation is derived as shown below from the same reaction intermediate (**13** in Scheme 6) as the one leading to the phenanthrene **15**, the structure **16** may be tentatively assigned to this cation.

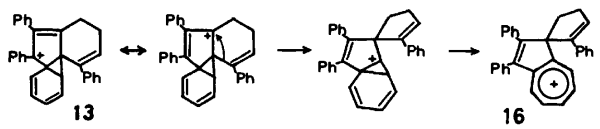

Table 3. The pK_{R^+} and reduction potential of the dications $\mathbf{4}_{n=3-6}$ and the monocation $\mathbf{6}_{n=2}$

Cation	pK_{R^+} [a]	Red'n potential[b] V *vs.* Ag/Ag^+
$\mathbf{4}_{n=3}$	2.06 (4.50)	−0.95
$\mathbf{4}_{n=4}$	3.38 (4.75)	−1.16
$\mathbf{4}_{n=5}$	3.35 (4.80)	−1.26
$\mathbf{4}_{n=6}$	3.35 (4.67)	−1.28
$\mathbf{6}_{n=2}$	3.52	−1.31

a) Measured in 50% aq MeCN at 25°C. The values for the second neutralization are given in the parentheses. b) The peak potential observed by CV in MeCN with $Bu_4N^+ClO_4^-$ as a supporting electrolyte.

precipitation with ether. After hydrolysis of the filtrate and the usual work-up, the rest of the products were separated and identified as a hydrocarbon with the molecular formula $C_{32}H_{22}$ (46.3% yield based on $\mathbf{5}_{n=2}$), triphenylmethane (50.9% yield based on Ph_3C^+), and triphenylmethanol (32.9% yield based on Ph_3C^+). The product distribution was not affected greatly, the variation in the yield being less than 15% of the above values, upon changes in reaction temperature (0 to 60 °C), in mode of addition (*i.e.* inverse addition), and in the solvent to more polar acetonitrile and even to trifluoroacetic acid. Triphenylmethanol is apparently derived from the unchanged trityl cation, since the product distribution was not changed when the reaction was carried out with only one equivalent of the trityl salt. These results suggest that some rearrangement of the dicyclopropenylethane structure took place immediately after abstraction of one equivalent of the hydride ion from $\mathbf{5}_{n=2}$.

The hydrocarbon $C_{32}H_{22}$, which exhibits the parent peak at *m/e* 406 in the mass spectrum, does not react with bromine, and no longer retains any cyclopropene ring, as is also shown by the absence of specific IR absorption near 1800 cm^{-1}; rather, the absorptions at 820 and 727 cm^{-1} suggest the presence of a phenanthrene framework. In the ^1H NMR spectrum taken in CCl_4, which exhibits signals for only the aromatic protons mainly at δ 7.47—7.10, two rather broad singlets are prominent at δ 7.42 (5H) and 7.15 (10H), together with a small doublet at δ 7.78 (1H, J=8.5 Hz). The two broad singlets seem to represent two types of phenyl groups, both of which are in a conformation that prevents effective conjugation with the other aromatic nucleus, and are thus reasonably correlated with the phenyl signals in 4-phenylphenanthrene (δ 7.36)[15] and in 9,10-diphenylphenanthrene (δ 7.20),[16] respectively. The doublet at δ 7.78, on the other hand, seems to correspond to 4-phenylphenanthrene's H-5 (δ 7.60),[15] which is markedly shielded by the oposing phenyl group as compared with H-4,5 (δ 8.55)[15] in phenanthrene itself. Based on these facts, together with other similarities in the UV spectrum (λ_{max} (cyclohexane) 264 nm (log ε, 4.59), 271 sh (4.57), 304 sh (4.18)) with that for 9,10-diphenylphenanthrene (λ_{max} (cyclohexane) 260 nm (log ε, 4.52), 271 (4.20), 302 (4.00)),[16,17] the hydrocarbon $C_{32}H_{22}$ is assigned to 4,9,10-triphenylphenanthrene (**15**) as the most probable structure.

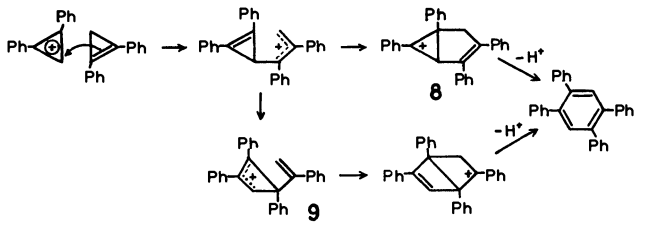

Scheme 4.

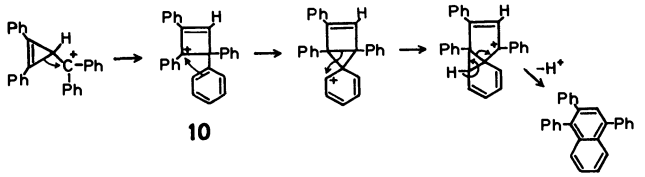

Scheme 5.

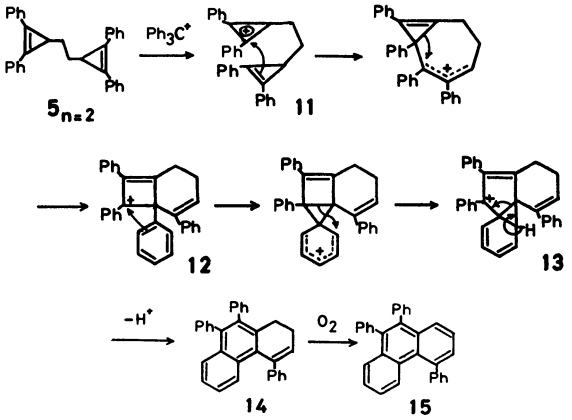

Scheme 6.

1,2-Diphenylcyclopropene is known to react with the diphenylcyclopropenium ion to give 1,2,4,5-tetraphenylbenzene according to Scheme 4.[18] The mechanism proceeding through the cation **9** seems more likely than the originally reported one involving the cation **8**, as judged from the results of later work by Moerck and Battiste[19] and by Weiss and Andrae.[14b] On the other hand, a unique rearrangement of the cyclobutenyl cation **10** giving the naphthalene derivative (Scheme 5) has also been reported by Breslow and Battiste.[20] Considering the mutual accessibility of the two three-membered rings connected by an ethylene linkage in $\mathbf{5}_{n=2}$, it seems reasonable to interpret the observed transformation of $\mathbf{5}_{n=2}$ to **15** in analogy with these two reported rearrangements, as shown in Scheme 6: the intramolecular cyclization of the first formed monocation **11**, followed by the subsequent rearrangement to the cyclobutenyl cation **12**, and the ring expansion of **12** to **14** through **13** are formally analogous to the rearrangements shown in Schemes 4 and 5, respectively. Since in the ^{1}H NMR spectrum of the crude product the presence of the ethylenic linkage was indicated by two rather broad multiplets at δ 2.45 and 2.15, the aromatization of **14** to the phenanthrene **15** is supposed to have occurred by air oxidation during the course of isolation procedures involving the repeated preparative TLC, in which exposure to air was inevitable.

The reaction of $\mathbf{5}_{n=2}$ with various other hydride abstraction reagents was surveyed to see if the rearrangement of **11** can be suppressed to allow the formation of the dication $\mathbf{4}_{n=2}$. However, the course of the reaction was not changed by the use of such reagents as: diphenylmethyl cation,[12] which is less stable and supposed to have stronger hydride abstracting ability than the trityl cation; 2,3-dichloro-5,6-dicyano-*p*-benzoquinone[21] with high complexing ability with the produced cation; and the Lewis acids, *e.g.* phosphorus pentachloride and boron trifluoride etherate.

*Reaction of Bis(2,3-diphenyl-2-cyclopropenyl)methane ($\mathbf{5}_{n=1}$) with the Trityl Cation——The Formation of the 1,2-Diphenyl-3-(1,2-diphenyltriafulven-4-yl)cyclopropenium Ion (**17**).*[1b] As has already been described briefly, when the dicyclopropenylmethane $\mathbf{5}_{n=1}$ was treated with two equivalents of trityl perchlorate, the perchlorate of the expected dication was not obtained but rather that of the monocation, which was yellow and analyzed as $C_{31}H_{21}ClO_4$. The spectral data are included in Table 2. While the presence of the cyclopropenium ring is clearly exhibited by the broad and strong IR absorption at 1435 cm^{-1}, in the ^{1}H NMR spectrum taken in CD_3CN (Fig. 1a) the signal for the proton of the central carbon appears as a singlet at the olefinic range (δ 6.52), and the signals for the phenyl protons are somewhat shifted upfield compared with those for the dications $\mathbf{4}_{n=3-6}$ implying an appreciable decrease of positive charge in the three-membered rings. The multiplicity of the phenyl signals also indicates the restricted rotation of the three-membered ring with respect to the bond

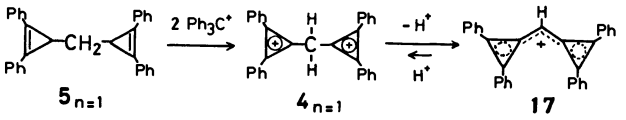

Scheme 7.

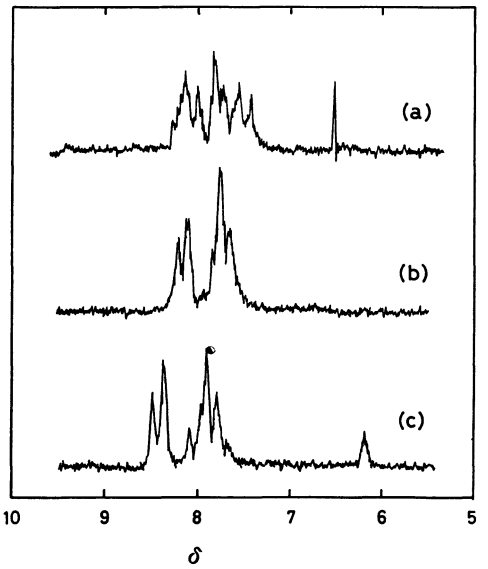

Fig. 1. The ^{1}H NMR spectra of the triafulvenylcyclopropenium ion **17** (a) in CD_3CN, (b) in CF_3CO_2H, and (c) in CF_3CO_2H–CF_3SO_3H (9 : 1).

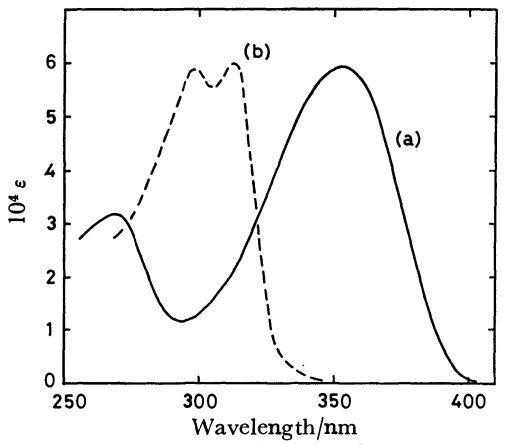

Fig. 2. The UV spectra of the triafulvenylcyclopropenium ion **17** (a) in MeCN and (b) in CF_3CO_2H–CF_3SO_3H (95: 5).

connecting the central carbon and the three-membered ring. These data are most compatible with the assignment of the fully conjugated structure **17**, formed by deprotonation of the first formed dication $\mathbf{4}_{n=1}$ (Scheme 7), to this new monocation. In the ^1H NMR spectrum taken in trifluoroacetic acid (Fig. 1b), the olefinic proton signal disappears, presumably owing to the rapid proton exchange process occurring in the equilibrium between **17** and $\mathbf{4}_{n=1}$. When the stronger acid, CF_3SO_3H, is added (*ca.* 10%), the equilibrium is shifted towards the dication $\mathbf{4}_{n=1}$, as shown by the appearance of a methylene singlet at δ 6.19 (2H) and the downfield shift of the phenyl protons (Fig. 1c). Similarly, the long-wavelength absorption of **17** at 353 nm in acetonitrile, reflecting the fully conjugated structure, is shifted upon addition of CF_3SO_3H to 313 nm (log ε, 4.78) and 298 nm (4.77), which is a characteristic absorption pattern for the cyclopropenium ion, as shown in Fig. 2.

The stable monocations having a similar type of cross-conjugated structure, such as **18**[22] and **19**,[23] have been synthesized by Kitahara *et al*, and the analogous anion **20** by Jutz and Amschler.[24] The

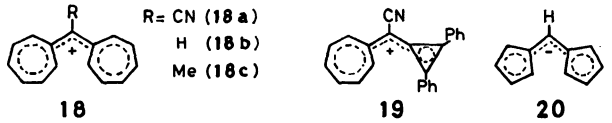

18 **19** **20**

monocation **17** is thus regarded as the smallest-ring member in the family of these cross-conjugated ionic systems, and its stability is of much interest. The preliminary measurement of its pK_{R^+} value was carried out spectrophotometrically in 23% ethanol. In this solvent a considerable decomposition of the cation was observed after partial hydrolysis commenced at pH 7.1. Based on the plot of absorbance of the cation at 350 nm recorded at 15 min after preparation of the sample solution against the pH value, the pK_{R^+} was determined to be 7.23; however, this value should be considered as somewhat smaller than the true value, when the partial decomposition is taken into account. In 50% aq acetonitrile, the cation was found to be more stable, not being neutralized appreciably until the pH of the solution reached 8.0. In the solution with the pH near 10, almost all of the cation was neutralized, but about 90% of the cation was regenerated upon acidification. From the absorbance-pH plot, the most probable value for pK_{R^+} was determined to be surprisingly high, *i.e.* 8.9±0.2, for such a strained molecule. This remarkable increase in stability, as compared with the cation **18b** (pK_{R^+} 7.49 in 10% ethanol),[22b] may have arisen from the increased aromatic character in **17** with four stabilizing phenyl substituents. This result is in good agreement with the ^{13}C NMR data shown below.

The ^{13}C NMR spectrum of **17** measured in CD_3CN exhibited the following signals (in the parentheses are given the peak multiplicity in the off-resonance spectrum, assignments,†† and the charge density calculated by simple HMO method using the following parameters; $\beta_{1,3}=\beta_{2,3}=0.9$, $\beta_{C-Ph}=0.8$): δ (ppm from Me_4Si) 144.0 (s), 145.0 (s) (C-1, C-2; charge density +0.1833); 148.4 (s) (C-3; +0.1955); 68.6 (d) (C-4; −0.2632); 122.6 (s), 123.0 (s) (C-*i*, C-*i'*; −0.0106); 133.4 (d), 134.4 (d) (C-*o*, C-*o'*; +0.0166); 130.5 (d), 131.0 (d) (C-*m*, C-*m'*; −0.0007); and 135.7 (d), 136.4 (d) (C-*p*, C-*p'*; +0.0134). The planarity of the whole π-system in **17** is clearly demonstrated by the appearance of C-1, C-2, and phenyl carbons in sets of pairs of signals. It should be noted here that the central carbon, C-4, is resonating at an unusually high field at δ 68.6. This marked upfield shift is attributable to the considerable amount of negative charge residing on this carbon, which is in agreement with the calculated result. This spectral feature thus demonstrates the significant contribution of the dipolar structure, **17c**, with both of the three-membered rings positively charged, to the

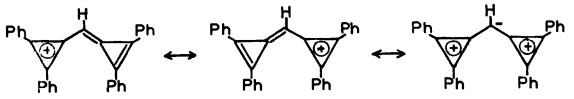

17a **17b** **17c**

Scheme 8.

resonance hybrid of **17** (Scheme 8). A similar type of polarization seems to be present also in cation **18**, as shown by the charge density (−0.1972) calculated by the same method for the central carbon of **18b** and the ^{13}C chemical shift (δ 100.1) observed for **18a**.[25] However, comparison of these values with those for the cation **17** indicates that the contribution of such a polar structure is greater in **17** than in **18**. Thus, it is supposed that this greater polarization in **17**, which forms the two Hückeloid aromatic rings, has caused a considerable

†† The numbering system is as follows:

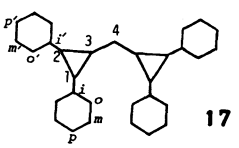

17

increase in the aromatic stabilization of the cation **17**, as has already been noted from its pK_{R^+} value.

Experimental

Melting and boiling points are uncorrected. Elemental analyses were performed by the Microanalytical Center, Kyoto University, Kyoto. IR and UV-Vis spectra were recorded with a Hitachi 215 and a Hitachi 200-10 spectrometers, respectively. ^{1}H NMR spectra were taken on a Hitachi R-24 (60 MHz) and on a Varian HA-100 (100 MHz) spectrometers, with Me_4Si as an internal standard. ^{13}C NMR spectra were obtained on a JEOL FX-100 spectrometer (25 MHz) operated in the pulse Fourier transform mode. Mass spectra were recorded with a JEOL JMS-01SG spectrometer.

All reagents were of reagent-grade quality unless otherwise noted. MeCN and CH_2Cl_2 were refluxed and distilled over P_2O_5, and THF was distilled over $LiAlH_4$. Merck SiO_2 type GF_{254} and type PF_{254} were used for analytical and preparative TLC, respectively.

Diphenylcyclopropenium Perchlorate. To a stirred solution of bis(2,3-diphenyl-2-cyclopropenyl) ether[11] (3.32 g; 8.33 mmol) in THF (10 ml) and ether (90 ml) was added dropwise 70% $HClO_4$ (3.62 g) at 0 °C. The resulting white precipitates were filtered, washed with ether, and dried under reduced pressure to give diphenylcyclopropenium perchlorate (4.01 g; 82.8%) as white powder: mp 148.5—150.0 °C (decomp) (lit, mp 149.5—150.5 °C (decomp)).[26]

Bis(2,3-diphenyl-2-cyclopropenyl)methane ($\mathbf{5}_{n=1}$). 1,5-Diphenyl-1,4-pentadiene was prepared by dehydration of 1,5-diphenyl-1,5-pentanediol, which had been obtained by Grignard reaction of phenylmagnesium bromide with pentanedial, by the use of $KHSO_4$[27] in 63.3% yield: bp 132—138 °C/0.2 Torr (1 Torr=133.322 Pa) (lit, bp 205—211 °C/12 Torr);[28] ^{1}H NMR (CCl_4) δ 7.17 (s, 10H, Ph), 6.41 (d, J=15.5 Hz, 2H, =CHPh), 6.07 (dt, 2H, =CH–), 3.03 (t, 2H, $-CH_2-$). A solution of 1,5-diphenyl-1,4-pentadiene (3.03 g; 13.7 mmol) and chlorophenyldiazirine[11] (6.75 g; 44.2 mmol) in dry C_6H_6 (180 ml) was heated to reflux with magnetic stirring for 4 h. After removal of the solvent *in vacuo*, the crude product was separated by the use of preparative TLC (R_f 0.34; C_6H_6–n-C_6H_{14}(1 : 4)/SiO_2) to give bis(2-chloro-2,3-diphenylcyclopropyl)methane (3.79 g; 58.9%) as a pale yellow solid: ^{1}H NMR (CCl_4) δ 7.30, 7.07 (br s×2, 20H, Ph), 2.9—1.5 (br m, 6H, >CH– +$-CH_2-$).

To a stirred solution of the bis(chlorocyclopropyl)methane (3.60 g; 7.68 mmol) in THF (250 ml) was added *t*-BuOK (17.2 g; 0.153 mol) in portions during 5 min under nitrogen. After stirring for 18 h at room temp, the mixture was poured into 1 dm^3 of cold water and extracted with ether. The ethereal extract was washed with 10% NaCl, dried ($MgSO_4$), and evaporated to give the crude dicyclopropenylmethane $\mathbf{5}_{n=1}$ (2.93 g; 96.2%) as a yellow solid. Recrystallization from C_6H_6–n-C_6H_{14} afforded white needles: mp 118.0—118.6 °C. Found: C, 94.17; H, 6.06%. Calcd for $C_{31}H_{24}$: C, 93.90; H, 6.10%.

1,2-Bis(2,3-diphenyl-2-cyclopropenyl)ethane ($\mathbf{5}_{n=2}$). 1,6-Diphenyl-1,5-hexadiene was prepared by dehydration of 1,6-diphenyl-1,6-hexanediol, derived from hexanedial, in 83.9% yield: bp 154—157 °C/0.5 Torr, mp 77.4—77.8 °C (lit, bp 115 °C/0.005 Torr, mp 80.5—81 °C);[29] ^{1}H NMR (CCl_4) δ 7.18 (s, 10H, Ph), 6.41 (d, J=15.5 Hz, 2H, =CHPh), 6.08 (dt, 2H, =CH–), 2.31 (d, 4H, $-CH_2-$). The reaction of 1,6-diphenyl-1,5-hexadiene (3.27 g; 14.0 mmol) with chlorophenyldiazirine (4.94 g; 32.4 mmol) in dry C_6H_6 (100 ml) afforded 1,2-bis-(2-chloro-2,3-diphenylcyclopropyl)ethane (2.87 g; 42.5%) as a pale yellow viscous oil: ^{1}H NMR ($CDCl_3$) δ 7.3—6.9 (m, 20H, Ph), 2.7—1.6 (br m, 8H, >CH–+$-CH_2-$). The reaction of the 1,2-bis(chlorocyclopropyl)ethane (4.61 g; 9.53 mmol) with *t*-BuOK (17.93 g; 0.160 mol) in THF (300 ml) gave the crude 1,2-dicyclopropenylethane $\mathbf{5}_{n=2}$ (3.95 g; 100.9%) as a yellow solid. Recrystallization from MeCN afforded white needles: mp 120.1—120.9 °C. Found: C, 93.32; H, 6.46%. Calcd for $C_{32}H_{26}$: C, 93.62; H, 6.38%.

1,3-Bis(2,3-diphenyl-2-cyclopropenyl)propane ($\mathbf{5}_{n=3}$). 1,7-Diphenyl-1,6-heptadiene was prepared by dehydration of 1,7-diphenyl-1,7-heptanediol, obtained from heptanedial, in 51.7% yield: bp 177—180 °C/0.6 Torr; ^{1}H NMR (CCl_4) δ 7.15 (s, 10H, Ph), 6.36 (d, J=15.5 Hz, 2H, =CHPh), 6.03 (dt, 2H, =CH–), 2.20 (dt, 4H, $-CH_2-$), 1.26 (quint, 2H, $>CH_2-$). The reaction of 1,7-diphenyl-1,6-heptadiene (1.16 g; 4.67 mmol) with chlorophenyldiazirine (2.14 g; 14.0 mmol) in dry C_6H_6 (65 ml) yielded 1,3-bis(2-chloro-2,3-diphenylcyclopropyl)propane (1.21 g; 52.0%) as a pale yellow viscous oil: ^{1}H NMR ($CDCl_3$) δ 7.3—6.9 (m, 20H, Ph), 2.6—1.4 (br m, 10H, >CH–+$-CH_2-$). The dehydrochlorination of the 1,3-bis(chlorocyclopropyl)propane (0.989 g; 1.99 mmol) with *t*-BuOK (4.63 g; 41.3 mmol) in THF (80 ml) gave the crude 1,3-dicyclopropenylpropane $\mathbf{5}_{n=3}$ (0.774 g; 91.6%) as a yellow-brown solid. Recrystallization from MeCN afforded white needles: mp 94.8—95.6 °C. Found: C, 93.65; H, 6.56%. Calcd for $C_{33}H_{28}$: C, 93.35; H, 6.65%.

1,4-Bis(2,3-diphenyl-2-cyclopropenyl)butane ($\mathbf{5}_{n=4}$). A solution of the di-Grignard reagent, 1,4-bis(bromomagnesio)-butane, was prepared from 1,4-dibromobutane (1.74 g; 8.06 mmol) and Mg (0.371 g; 15.3 mmol) in THF (40 ml). To the stirred solution of the di-Grignard reagent cooled at 0 °C was added diphenylcyclopropenium perchlorate (3.97 g; 13.7 mmol) slowly, at a rate such that the temperature did not exceed 5 °C, in portions under nitrogen during 15 min. After stirring for 15 h at 0 °C, the mixture was hydrolyzed with 10% HCl and extracted with C_6H_6. The extract was washed with 10% NaCl, dried ($MgSO_4$), and evaporated to give 3.19 g of the crude product, which afforded the 1,4-dicyclopropenylbutane $\mathbf{5}_{n=4}$ (1.52 g; 51.0%) as white needles after recrystallization from C_6H_6–n-C_6H_{14}: mp 122.1—123.1 °C. Found: C, 93.40; H, 7.00%. Calcd for $C_{34}H_{30}$: C, 93.11; H, 6.89%.

1,5-Bis(2,3-diphenyl-2-cyclopropenyl)pentane ($\mathbf{5}_{n=5}$). Similarly, the reaction of diphenylcyclopropenium perchlorate (2.01 g; 6.88 mmol) with 1,5-bis(bromomagnesio)pentane, prepared from 1,5-dibromopentane (0.960 g; 4.17 mmol) and Mg (0.188 g; 7.75 mmol) in THF (20 ml), gave 1.81 g of the crude product, which afforded, by the use of preparative TLC (R_f 0.47, C_6H_6–n-C_6H_{14} (1 : 9)/SiO_2), the 1,5-dicyclopropenylpentane $\mathbf{5}_{n=5}$ (0.574 g; 36.9%) as a colorless viscous oil. Found: C, 92.12; H, 7.12%. Calcd for $C_{35}H_{32}$: C, 92.88; H, 7.12%.

1,6-Bis(2,3-diphenyl-2-cyclopropenyl)hexane ($\mathbf{5}_{n=6}$). The reaction of diphenylcyclopropenium perchlorate (3.97 g; 13.8 mmol) with 1,6-bis(bromomagnesio)hexane, prepared from 1,6-dibromohexane (1.96 g; 8.03 mmol) and Mg (0.368 g; 15.2 mmol) in THF (40 ml), gave 5.00 g of the crude product, which afforded the 1,6-dicyclopropenylhexane $\mathbf{5}_{n=6}$ (1.89 g; 59.8%) as white needles after recrystallization from C_6H_6–n-C_6H_{14}: mp 126.0—126.9 °C. Found: C, 92.42; H, 7.61%. Calcd for $C_{36}H_{34}$: C, 92.66; H, 7.34%.

*The Hydride Abstraction from $\mathbf{5}_{n=1}$——Formation of 1,2-diphenyl-3-(1,2-diphenyltriafulven-4-yl)cyclopropenium Perchlorate (**17**·ClO_4^-).* A solution of trityl perchlorate ($Ph_3C^+ClO_4^-$)[30] (0.417 g; 1.22 mmol) in MeCN (7 ml) was slowly added to a stirred solution of the dicyclopropenylmethane $\mathbf{5}_{n=1}$ (0.234 g; 0.589 mmol) in dry C_6H_6 (2 ml) at room temp during 1 h under nitrogen, and the resulting dark red solution was heated at 65 °C for 10 min. To this solution was added, with stirring

and ice-bath cooling, dry AcOEt (2 ml) and dry ether (100 ml) to cause the formation of orange-colored precipitates. These were filtered, washed with dry ether, and dried *in vacuo* to give the triafulvenylcyclopropenium perchlorate **17**·ClO_4^- (0.220 g; 75.8%) as yellow powder: mp 227.0—228.0 °C (decomp) after recrystallization from MeCN. Found: C, 75.52; H, 4.14%. Calcd for $C_{31}H_{21}ClO_4$: C, 75.53; H, 4.29%.

The Methylenebis(diphenylcyclopropenium) Dication ($4_{n=1}$). The dication $4_{n=1}$ was observed by the use of ^1H NMR and UV spectra on the CF_3CO_2H solution of the triafulvenylcyclopropenium ion **17** with CF_3SO_3H added (*ca.* 10%) (see Figs. 1 and 2).

The Hydride Abstraction from $5_{n=2}$ *with the Trityl Cation—— Rearrangements to* **15** *and the Cation* $C_{32}H_{25}^+$. A solution of the dicyclopropenylethane $5_{n=2}$ (0.201 g; 0.489 mmol) in CH_2Cl_2 (3 ml) was slowly added during 10 min to a stirred solution of $Ph_3C^+ClO_4^-$ (0.339 g; 0.988 mmol) in CH_2Cl_2 (7 ml) at room temp. During the addition the color of the solution changed from orange to dark red with an increase of the temperature from 23.0 to 26.5 °C. After stirring the mixture for 30 min at room temp and for 10 min at 40 °C, dry ether (100 ml) was added to the stirred and ice-cooled mixture to cause the formation of yellow precipitates, which were then filtered, washed with dry ether, and dried *in vacuo* to give the yellow powder (0.101 g; 40.7% based on $5_{n=2}$) tentatively assigned as **16**·ClO_4^-: mp 215.5—218.0 °C (decomp) after recrystallization from MeCN; IR (KBr) 3070, 2930, 2860, 1600, 1500, 1483, 1450, 1440, 1358, 1250, 1148, 1090, 840, 763, 740, 700 cm^{-1}; UV-Vis (MeCN) λ_{max} 256 nm (log ε, 4.46), 280 sh (4.19), 433 (4.15); ^1H NMR (100 MHz) (CF_3CO_2H) δ 8.90—8.52 (br m centered at 8.66, 5H, ···CH···+), 7.58—7.06 (m, 15H, Ph), 7.02 (t, 1H, =CH–), 3.13—2.85 (m, 2H, $-CH_2-$), 2.73—2.54 (m, 2H, $-CH_2-$); ^{13}C NMR (CD_3CN) δ 177.4 (s), 170.0 (s), 168.9 (s), 152.2 (d), 149.7 (d), 149.2 (d), 144.6 (d), 144.3 (s), 144.1 (d), 140.7 (s), 140.0 (d), 135.3 (s), 133.7 (s), 133.0 (s), 131.4 (d), 130.6×2 (d), 130.5 (d), 130.3 (d), 129.8 (d), 129.5 (d), 129.3 (d), 126.4 (d), 75.4 (s), 36.6 (t), 33.1 (t). Found: C, 75.23; H, 4.91%. Calcd for $C_{32}H_{25}ClO_4$: C, 75.51; H, 4.95%.

The filtrate from the above procedure was washed with 10% NaCl, dried ($MgSO_4$), and evaporated to give 0.368 g of the crude product, which was then separated by preparative TLC (C_6H_6-*n*-C_6H_{14}(1 : 4)/SiO_2) repeated twice. From the fraction with R_f 0.55 was obtained triphenylmethane (0.123 g; 50.9% based on Ph_3C^+), identified by comparison of the IR and ^1H NMR spectra with those of the authentic sample. From the fraction with R_f 0.30 was isolated the hydrocarbon $C_{32}H_{22}$ (0.923 g; 46.3% based on $5_{n=2}$), determined to be the triphenylphenanthrene **15**, as white crystals: mp 219.1—219.6 °C; IR (KBr) 3060, 3030, 1600, 1592, 1575, 1495, 1480, 1440, 1160, 1070, 1025, 1000, 920, 820, 782, 763, 750, 727, 700 cm^{-1}; for UV, see text; ^1H NMR (CCl_4) δ 7.78 (d, J=8 Hz, 1H), 7.50—7.05 (m+br s×2, 21H); MS *m/e* 406. Found: C, 94.18; H, 5.77%. Calcd for $C_{32}H_{22}$: C, 94.54; H, 5.46%. From the fraction with R_f 0.1 was obtained triphenylmethanol (0.0846 g; 32.9% based on Ph_3C^+), identified by comparison of the IR and ^1H NMR spectra with those of the authentic sample.

The cation $C_{32}H_{25}ClO_4$ was reduced with $NaBH_4$ as follows. A solution of $C_{32}H_{25}ClO_4$ (0.116 g; 0.228 mmol) in MeCN (3 ml) was added dropwise to a stirred suspension of $NaBH_4$ (0.0182 g; 0.481 mmol) in MeCN (2 ml) with ice-bath cooling under nitrogen. After stirring for 30 min, the mixture was hydrolyzed with H_2O and worked up in the usual way to give 0.0985 g of the crude product, which showed mainly one spot at R_f 0.41 on an analytical TLC plate (C_6H_6-*n*-C_6H_{14} (1 : 4)/SiO_2). Purification with preparative TLC afforded a pale yellow solid (0.0741 g; 79.3%), supposed to be an isomeric mixture of substituted cycloheptatrienes ($C_{32}H_{26}$) corresponding to the cation $C_{32}H_{25}^+$ (supposedly **16**): IR (KBr) 3040, 2970, 2860, 1600, 1575, 1495, 1485, 1452, 1442, 1380, 1070, 1030, 755, 735, 705 cm^{-1}; ^1H NMR (CCl_4) δ 7.17 (br s, 10H, Ph), 6.95 (br s, 5H, Ph), 6.55—5.80 (br m, 4H, =CH–), 5.50—5.00 (br m, 1H, =CH–), 2.85—1.85 (br m, 6H, $-CH_2-$); MS *m/e* 410.

The Complex Salt of Ethylenebis(diphenylcyclopropenium) Dication ($4_{n=2}$). A solution of the 1,2-dicyclopropenylethane $5_{n=2}$ (0.411 g; 1.00 mmol) in CH_2Cl_2 (5 ml) was added dropwise to a stirred solution of $SbCl_5$ (1.44 g; 4.80 mmol) in CH_2Cl_2 (10 ml) with ice-bath cooling under nitrogen during 10 min. After stirring the resulting dark-gray suspension for 1 h, dry ether (180 ml) was added to the mixture to cause the formation of additional dark green precipitates. The precipitates were filtered, washed with dry ether, and dried *in vacuo* to give grayish powder (0.601 g; 93.2%) analyzed as $C_{32}H_{24}$·0.55$SbCl_6$·1.45Cl: mp>300 °C. Found: C, 59.62; H, 3.43%. Calcd for $C_{32}H_{24}Cl_{4.75}Sb_{0.55}$: C, 59.62; H, 3.75%.

Trimethylenebis(diphenylcyclopropenium) Perchlorate ($4_{n=3}$·$2ClO_4^-$). To a stirred suspension of the 1,3-dicyclopropenylpropane $5_{n=3}$ (0.145 g; 0.342 mmol) in MeCN (2 ml) was added $Ph_3C^+ClO_4^-$ (0.238 g; 0.695 mmol) in one portion at room temp. After stirring at room temp for 15 min and at 60 °C for 15 min, dry AcOEt (10 ml) and dry ether (30 ml) were added to the cooled mixture to cause the formation of yellowish white precipitates, which were then filtered, washed with dry ether, and dried *in vacuo* to give $4_{n=3}$·2ClO_4^- (0.200 g; 94.2%) as white powder: mp 214.0—215.0 °C (decomp) after recrystallization from MeCN; ^{13}C NMR (CD_3CN) δ 166.9 (s), 162.3 (s), 139.8 (d), 137.2 (d), 131.4 (d), 120.5 (s), 27.9 (t), 23.9 (t). Found: C, 63.60: H, 4.17%. Calcd for $C_{33}H_{26}Cl_2O_8$: C, 63.78; H, 4.23%.

Tetramethylenebis(diphenylcyclopropenium) Perchlorate ($4_{n=4}$·$2ClO_4^-$). In the same way, the reaction of the 1,4-dicyclopropenylbutane $5_{n=4}$ (0.0975 g; 0.222 mmol) with $Ph_3C^+ClO_4^-$ (0.155 g; 0.452 mmol) was carried out in MeCN (2 ml) to give $4_{n=4}$·2ClO_4^- (0.132 g; 93.7%) as white powder: mp 229.8—231.3 °C (decomp) after recrystallization from MeCN; ^{13}C NMR (CD_3CN) δ 167.9 (s), 162.2 (s), 139.6 (d), 137.0 (d), 131.4 (d), 120.5 (s), 27.7 (t), 26.6 (t). Found: C, 64.16; H, 4.35%. Calcd for $C_{34}H_{28}Cl_2O_8$: C, 64.26; H, 4.44%.

Pentamethylenebis(diphenylcyclopropenium) Perchlorate ($4_{n=5}$·$2ClO_4^-$). To a stirred solution of the 1,5-dicyclopropenylpentane $5_{n=5}$ (0.233 g; 0.515 mmol) in CCl_4 (1 ml) and MeCN (2 ml) was added $Ph_3C^+ClO_4^-$ (0.356 g; 1.04 mmol). After stirring at room temp for 20 min and at 60 °C for 30 min, dry AcOEt (15 ml) was added to the cooled mixture. The formed precipitates were filtered, washed with dry AcOEt and dry ether, and dried *in vacuo* to give $4_{n=5}$·2ClO_4^- (0.232 g; 69.2%) as white powder: mp 223.4—224.2 °C (decomp) after recrystallization from MeCN; ^{13}C NMR (CD_3CN) δ 168.3 (s), 162.2 (s), 139.5 (d), 137.0 (d), 131.4 (d), 120.6 (s), 29.7 (t), 28.0 (t), 26.3 (t). Found: C, 64.72; H, 4.90%. Calcd for $C_{35}H_{30}Cl_2O_8$: C, 64.84; H, 4.66%.

Hexamethylenebis(diphenylcyclopropenium) Perchlorate ($4_{n=6}$·$2ClO_4^-$). Similarly, the reaction of the 1,6-dicyclopropenylhexane $5_{n=6}$ (0.444 g; 0.950 mmol) with $Ph_3C^+ClO_4^-$ (0.652 g; 1.90 mmol) in MeCN (5 ml) afforded $4_{n=6}$·2ClO_4^- (0.545 g; 86.5%) as white powder: mp 229.6—230.3 °C (decomp) after recrystallization from MeCN; ^{13}C NMR (CD_3CN) δ 168.5 (s), 162.2 (s), 139.5 (d), 137.0 (d), 131.4 (d), 120.6 (s), 29.4 (t), 28.1 (t), 26.7 (t). Found: C, 64.88; H, 4.78%. Calcd for $C_{36}H_{32}Cl_2O_8$: C, 65.16; H, 4.86%.

The Chromium(II) Ion Reduction of Hexamethylenebis(diphenylcyclopropenium) Perchlorate ($4_{n=6}$·2ClO_4^-). A solution (28.6

ml; 28.6 mmol) of the chromium(II) ion (1.00 M, 1 M=1 mol dm^{-3}) in 10% HCl, which had been prepared as previously reported,[31] was added to a stirred solution of $\mathbf{4}_{n=6}\cdot 2ClO_4^-$ (0.122 g; 0.183 mmol) in 10% HCl (100 ml), which had been deaired by bubbling with nitrogen for 2 h. The mixture was stirred with heating at 75 °C for 3 h. The color of the mixture gradually changed from blue to greenish blue with the concomitant formation of white paste-like precipitates. The mixture was extracted with C_6H_6 and worked up in the usual manner to give the polymeric material (supposedly **7**) (0.0691 g; 81.0%) as a yellowish solid: mp 73.5—99.2 °C; IR (KBr) 3065, 3030, 2930, 2855, 1600, 1577, 1495, 1480, 1460, 1440, 1073, 1030, 917, 760, 700, 680 cm^{-1}; for ^1H NMR see text.

Determination of pK_{R^+} *Values.* Buffer solutions of slightly different acidities (pH 2—8) were prepared by mixing a citric acid solution (0.1 M) in 50% aq MeCN (1 : 1 by volume) and a saturated solution of Na_2HPO_4 in 50% aq MeCN, in various proportions. For the preparation of a sample solution, each 1-ml portion of the stock solution, prepared by dissolving 1—2 mg of the cation salt in MeCN (20 ml), was pipetted out and made up to 10 ml by adding H_2O (1 ml) and the buffer solution. The sample solution with higher or lower acidity was made by further addition of 1—3 drops of H_2SO_4 or 10% NaOH. The UV-Vis spectrum was recorded, using a 1-cm cell thermostated at 25 °C, on each cation in 15—20 solutions of buffers spaced through a pH range of about two units on each side of the pK_{R^+}. Immediately after recording the spectrum, the pH of each sample solution was determined on a Horiba Model H pH meter calibrated with standard buffers before use. After complete neutralization of each cation, the reversibility was confirmed by quantitative regeneration of the cation spectrum upon acidification of the solution with H_2SO_4. The observed absorbance at the specific absorption wavelength of each cation was plotted against the pH to give a classical titration curve, whose midpoint was taken as the pK_{R^+}.

Cyclic Voltammetry. The measurements were carried out with a Hokuto-Denko Model HA 104 potentiostat equipped with a Hokuto-Denko Model HB 107A function generator. A three-electrode cell was used, consisting of Pt wire working and auxiliary electrodes and a reference electrode, $Ag/AgNO_3$ (0.01 M) with $Bu_4N^+ClO_4^-$ (0.1 M) in MeCN. The reference electrode was connected to the bulk of the sample solution by a salt bridge made up with a $Bu_4N^+ClO_4^-$ solution (0.1 M) in MeCN. Ferrocene, used as a reference compound (*vide infra*), was found to exhibit $E_{1/2}$+0.083 V against this reference electrode.[32] All the sample solutions were 1 mM in the cation and 0.1 M in $Bu_4N^+ClO_4^-$ as a supporting electrolyte in MeCN, and were deaired by bubbling with nitrogen for 10 min. The measurements were made at the scan rate of 0.1 V/s, and the voltammograms recorded on a Hitachi Model 057 X-Y recorder. Immediately after the measurements. ferrocene (0.2 mM) was added as an internal standard,[33] and the observed cathodic peak potential was corrected with reference to this standard.

References

1) a) Presented at the 9th Symposium on Nonbenzenoid Aromatic Compounds, Sendai, December 1976; b) Part of this work has been published as a short communication: K, Komatsu, K. Masumoto, and K. Okamoto, *J. Chem. Soc., Chem. Commun.*, **1977**, 232.

2) G. A. Olah and J. S. Staral, *J. Am. Chem. Soc.*, **98**, 6290 (1976) and the references cited therein.

3) G. A. Olah, J. S. Staral, and L. A. Paquette, *J. Am. Chem. Soc.*, **98**, 1267 (1976).

4) G. A. Olah, G. K. S. Prakash, and T. N. Rawdah, *J. Am. Chem. Soc.*, **102**, 6127 (1980) and the references cited therein.

5) a) E. C. Kirby and D. H. Reid, *J. Chem. Soc.*, **1961**, 3579; b) R. W. Murray and M. L. Kaplan, *Tetrahedron Lett.*, **1965**, 2903; c) I. S. Akhrem, E. I. Fedin, B. A. Kvasov, and M. E. Vol'pin, *ibid.*, **1967**, 5265; d) R. E. Harmon, R. Suder, and S. K.Gupta, *J.Chem. Soc., D*,**1969**,1170; e) H.Volz and M. Volz-de Lecea, *Justus Liebigs Ann. Chem.*, **750**, 136 (1971); f) M.Yagihara, Y. Kitahara, and T. Asao, *Chem. Lett.*, **1972**, 653; g) S. Kuroda, M. Oda, and Y. Kitahara, *Angew. Chem.*, **85**, 93 (1973); h) K. Komatsu, M. Oshida, and K. Okamoto, *Tetrahedron Lett.*, **1974**, 4487; i) P. J. Stang, G. Maas, and T. E. Fisk, *J. Am. Chem. Soc.*, **102**, 6361 (1980); the preparation of bis(dipropylcyclopropenium) dication ether is also described in this paper.

6) R. W. Murray and M. L. Kaplan, *Tetrahedron Lett.*, **1967**, 1307; G. Manecke and M. Shoeneshoefer, *Makromol. Chem.*, **112**, 293 (1968).

7) a) Z. Yoshida, S. Araki, and H. Ogoshi, *Tetrahedron Lett.*, **1975**, 19; b) Z. Yoshida, S. Sawada, and H. Ogoshi, 33rd National Meeting of the Chemical Society of Japan, Fukuoka, October 1975, Abstr. II, p. 620; c) Z. Yoshida, H. Konishi, and H. Ogoshi, the 3rd Symposium on Organic Sulfur and Phosphorus Compounds, Abstr. p. 41 (1975); d) Z. Yoshida, H. Konishi, Y. Kamitori, and H. Ogoshi, *Chem. Lett.*, **1977**, 1341; e) Z. Yoshida, H. Konishi, S. Sawada, and H. Ogoshi, *J. Chem. Soc., Chem. Commun.*, **1977**, 850.

8) R. Weiss, M. Hertel, and H. Wolf, *Angew. Chem.*, **91**, 506 (1979).

9) T. Eicher and H. Berneth, *Tetrahedron Lett.*, **1973**, 2039.

10) K. Komatsu, M. Arai, and K. Okamoto, *Tetrahedron Lett.*, **23**, 91(1982).

11) A. Padwa and D. Eastman, *J. Org. Chem.*, **34**, 2728 (1969).

12) J. Holmes and R. Pettit, *J. Org. Chem.*, **28**, 1695 (1963).

13) K. Okamoto, K. Komatsu, and A. Hitomi, *Bull. Chem. Soc. Jpn.*, **46**, 3881 (1973).

14) a) R. Breslow, P. Gal, H. W. Chang, and L. J. Altman, *J. Am. Chem. Soc.*, **87**, 5139 (1965); b) R. Weiss and S. Andrae, *Angew. Chem.*, **85**, 145, 147 (1973); c) J. H. Davis, K. J. Shea, and R. G. Bergman, *ibid.*, **88**, 254 (1976) and the references cited therein.

15) A. H. A. Tinnemans and W. H. Laarhoven, *J. Chem. Soc., Perkin Trans. 2*, **1976**, 1115.

16) D. Y. Curtin and R. P. Quirk, *Tetrahedron*, **24**, 5791 (1968).

17) L. Friedman and P. W. Rabideau, *J. Org. Chem.*, **33**, 451 (1968).

18) D. M. Stehouwer and D. T. Longone, *Tetrahedron Lett.*, **1969**, 5311.

19) R. E. Moerck and M. A. Battiste, *Tetrahedron Lett.*, **1973**, 4421.

20) R. Breslow and M. Battiste, *J. Am. Chem. Soc.*, **82**, 3626 (1960).

21) D. H. Reid, M. Fraser, B. B. Molloy, H. A. S. Payne, and R. G. Sutherland, *Tetrahedron Lett.*, **1961**, 530.

22) a) Cation **18a**: T. Otomo, M. Oda, and Y. Kitahara, *J.Chem. Soc., D*, **1971**, 114; b) cation **18b**, **c**: Y. Kayama, M. Oda, and Y. Kitahara, *Chem. Lett.*, **1973**, 1169; c) the cation **18** (R=H, Cl, Ph) has also been prepared in solution: I. Fleming, *J. Chem. Soc., Perkin Trans. 1*, **1973**, 1019.

23) M. Oda, K. Tamate, and Y. Kitahara, *J. Chem. Soc., D*, **1971**, 347.

24) Ch. Jutz and H. Amschler, *Angew. Chem.*, **73**, 806 (1961).

25) Private communication from Professor M. Oda: we are grateful to Professor Oda for informing us of these unpub-

shed results.
26) D. G. Farnum and M. Burr, *J. Am. Chem. Soc.*, **82**, 2651 (1960).
27) C. G. Overberger and J. H. Saunders, *Org. Synth.*, Coll. Vol. III, 204 (1955).
28) G. Wittig, H. Eggers, and P. Duffner, *Justus Liebigs Ann. Chem.*, **619**, 10 (1958).
29) H. P. Koch, *J. Chem. Soc.*, **1948**, 1111.
30) H. J. Dauben, Jr., L. R. Honnen, and K. M. Harmon, *J. Org. Chem.*, **25**, 1442 (1960).
31) K. Okamoto, K. Komatsu, S. Tsukada, and O. Murai, *Bull. Chem. Soc. Jpn.*, **46**, 1780 (1973).
32) The literature value for the ferrocene/ferricenium potential is +0.043 V *vs.* $Ag/AgNO_3$ (0.1 M) with $Bu_4N^+ ClO_4^-$ (0.1 M) in MeCN (R. R. Gagné, J. L. Allison, R. S. Gall, and C. A. Koval, *J. Am. Chem. Soc.*, **99**, 7170 (1977)), which can be corrected to +0.089 V *vs.* $Ag/AgNO_3$ (0.01 M) with $Bu_4N^+ClO_4^-$ (0.1 M) in MeCN (C. K. Mann, "Electroanalytical Chemistry," ed by A. J. Bard, M. Decker, Inc., New York (1969), Vol. 3, p. 64).
33) R. R. Gagné, C. A. Koval, and G. C. Lisensky, *Inorg. Chem.*, **19**, 2854 (1980).

The Reaction of Isocyanides with Halogens or *N*-Halosuccinimides and Alcohols

Hideyo YAMADA,† Yasuo WADA,† Shigeo TANIMOTO, and Masaya OKANO*
Institute for Chemical Research, Kyoto University, Uji, Kyoto 611
(Received December 28, 1981)

The reaction of aliphatic isocyanides with bromine or chlorine in primary alcohols, followed by hydrolysis, afforded the corresponding carbamates in moderate yields, together with various amounts of amines. Bromine was superior to chlorine as a halogen source for the formation of carbamates. unexpectedly, the addition of $HgCl_2$ resulted in a decrease in the carbamate yield. When *N*-halosuccinimides were used in the place of halogens, an additional formation of the succinimide-incorporated product was observed to some extent.

Previously we reported that the reactions of isocyanides with *t*-butyl hypochlorite and with wet *N*-bromo amides in chlorinated methanes in either the presence or absence of the $ZnCl_2$ catalyst, followed by treatment with water, gave *t*-butyl carbamates and acylureas respectively, although the yields were low.[1] In order to know whether or not the combined use of halogens and alcohols in the place of the alkyl hypohalite is feasible for the former reaction, and also to determine to what extent the formation of carbamates may compete in the latter reaction using alcohols as solvents, we have examined the reaction of isocyanides with halogens or *N*-halosuccinimides and alcohols. Taking into account the nucleophilic nature of isocyanides, the reaction was carried out with or without an acid catalyst. The present paper deals with these results.

$$R\text{–}N{\equiv}C + X_2(\text{or } X\text{–}Y) + R'OH \longrightarrow \left[R\text{–}N{=}C(X)(OR')\right] \xrightarrow{H_2O} RNHCOOR' \quad (1)$$

X=Br or Cl, Y=N(CO–CH$_2$)$_2$(CO–CH$_2$)$_2$

In this connection, the facile addition of chlorine or bromine to both aliphatic and aromatic isocyanides to afford the corresponding carbonimidoyl dihalides (isocyanide dihalides) is well-known, except for the case of unstable alkylcarbonimidoyl dibromides, but studies of the alcoholysis and hydrolysis of carbonimidoyl dihalides has been confined to the *N*-aryl compounds, which afford *N*-arylcarbamates and/or arylamines as final products under neutral or acidic conditions.[2,3]

Results and Discussion

The treatment of isocyanides with bromine or chlorine in various alcohols without a catalyst for several hours at room or a higher temperature, followed by a work-up procedure with water, gave the expected carbamates (**1**) in moderate yields, along with various amounts of amines, as is shown in Table 1. A controlled experiment indicated that the amines were formed by the hydrolysis of the unreacted imidoyl dihalides (**2**) during the work-up procedure and that iminocarobates [R–N=C(OR')$_2$], if they are formed, did not give amines at least under the given work-up conditions.

When an equimolar reaction of cyclohexyl isocyanide with bromine was carried out in a small quantity of methanol, a yellowish-orange solid separated out in a considerable amount at an early stage of the reaction, leaving nearly a half equivalent amount of the isocyanide in the solution. Further, when a methanol solution of this solid was allowed to stand for several hours at room temperature, the expected **1** (R=cyclo-C_6H_{11}, R'=Me) was produced in a good yield (see Experimental). Based on these facts the solid was tentatively presumed to be a 1 : 1 molecular complex of **2** (R=cyclo-C_6H_{11}, X=Br) and bromine. The use of chlorine in place of bromine did not cause any formation of such a complex, but the conversion of **2** (R=cyclo-C_6H_{11}, X=Cl) into **1** (R=cyclo-C_6H_{11}, R'=Me) with methanol was also confirmed by another experiment. We may thus conclude that **2** is the initial intermediate of this reaction.

$$R\text{–}N{\equiv}C + X_2 \rightleftharpoons \underset{\mathbf{2}}{\left[R\text{–}N{=}C(X)_2\right]}$$

X=Br or Cl **3**

$$\xrightarrow{\text{slow}} [R\text{–}N{=}\overset{+}{C}\text{–}X + X^-]$$

$$\xrightarrow[\text{fast}]{R'OH} \underset{\mathbf{4}}{\left[R\text{–}N{=}C(X)(OR')\right]} \xrightarrow{H_2O} \underset{\mathbf{1}}{RNHCOOR'} \quad (2)$$

Relating to the transformation of **2** to **4**, it has been reported that both neutral and acidic hydrolyses of **2**, where R=aryl and X=Cl, in aqueous dioxane proceeds by means of the S_N1 mechanism, based on an aryl-substituent effect on the rate (the rate decreases in this order: *p*-Me>H>*p*-Cl>*m*-Cl).[3] This mechanism involving the rate-determining heterolysis to afford the cation, **3**, can be safely adapted for the case of R=alkyl; thus, the yields of **4**, and hence those of **1**, may be expected to decrease in this order: R=tertiary> secondary>primary and R=alkyl>aryl. The obtained data agree with this expectation. Further, the fact is known that the relative reactivity of acyl halides, the structure of which is similar to **2**, decreases in this order: X=Br>Cl in alcoholysis with ethylene glycol[4] and in the a cylation of active aromatics.[5] A similar feature may be expected for the ionization of one C–X bond, since the effect of another X (being not ionized) may not be so important on the ground that only a slight difference in polar (both inductive and resonance) effect between Br and Cl is known. Thus, in the reaction with bromine, the better the yields of **1** compared with

† Koei Chemical Co., Ltd., Joto-ku, Osaka 536.

Table 1. Reaction of isocyanides with halogens and alcohols
Isocyanides, 20 mmol; Br_2, 20 mmol; Cl_2, 60 mmol; alcohols, 20 ml.
Reaction conditions: near 5 °C, 1 h and 20—25 °C, 5 h.

RNC	X_2	R'OH	Additive (mol%)	Product and yield/%[a]	
				1	Amine[b]
cyclo-$C_6H_{11}NC$	Br_2	MeOH	—	76	4
cyclo-$C_6H_{11}NC$	Br_2	MeOH[c]	—	74	—[d]
cyclo-$C_6H_{11}NC$	Br_2	MeOH	$HgCl_2$(10)	64	0
cyclo-$C_6H_{11}NC$	Br_2	EtOH	—	65	—[d]
cyclo-$C_6H_{11}NC$	Br_2	*n*-PrOH	—	60	—[d]
cyclo-$C_6H_{11}NC$	Br_2	*i*-PrOH	—	33	—[d]
cyclo-$C_6H_{11}NC$	Br_2	*n*-BuOH	—	58	—[d]
cyclo-$C_6H_{11}NC$	Br_2	$PhCH_2OH$	—	47	—[d]
t-BuNC	Br_2	MeOH	—	70	—[d]
n-BuNC	Br_2	MeOH	—	43	—[d]
PhNC	Br_2	MeOH	—	3	55
cyclo-$C_6H_{11}NC$	Cl_2	MeOH[e]	—	43[g]	34
cyclo-$C_6H_{11}NC$	Cl_2	MeOH[f]	—	54[g]	27
cyclo-$C_6H_{11}NC$	Cl_2	MeOH[e]	$HgCl_2$(50)	25[g]	11[h]

a) Isolated yield (based on isocyanide). b) Isolated as its HCl salt. c) Reaction conditions: near 5 °C, 1 h and 20—25 °C, 1 h. d) Not determined, but it seems to be 5% or so. e) Reaction conditions: near 5 °C, 2 h and 20—25 °C, 7 h. f) Reaction conditions: near 5 °C, 2 h and 65 °C, 2 h. g) Determined by GLC. h) Other product, probably $C_6H_{11}N(HgCl)CCl_2(OMe)$, 38% (based on isocyanide).

the case of chlorine can be ascribed to the higher reactivity of **2** where X=Br, while the poorer yields of amine can be explained by the same reason.

The effect of the alcohol component on the yields of **1** was not so significant, except for one case. In the reaction with isopropyl alcohol, the considerable decrease in the yield of **1** may be due mostly to the decreased stability of the corresponding **4** (R=cyclo-C_6H_{11}, R'=*i*-Pr, X=Br). In connection with this, we previously observed a considerable formation of cyclohexyl isocyanate, which probably arose from the initially formed **4** (R=cyclo-C_6H_{11}, R'=*t*-Bu, X=Cl), in the reaction of cyclohexyl isocyanide with *t*-butyl hypochlorite.[1] Besides, in the hydrolysis of alkyl chloroformates (ClCOOR") where R"=secondary alkyls, such as *i*-Pr and cycloalkyls, their relatively sacile ionization by means of the S_N1 mechanism and the succeeding rapid decomposition leading to olefins and/or secondary alcohols have been cited, in contrast to the cases of R=primary alkyls.[6,7] Thus, a partial loss of **4** (R=cyclo-C_6H_{11}, R'=*i*-Pr, X=Br) by a limilar process is highly probable.

We also have to note the effect of a Lewis-acid catalyst on the reaction. When 10 mol% of $HgCl_2$ was added as a catalyst in the cyclohexyl isocyanide–bromine–methanol reaction, a 12% decrease in the yield of **1** (R=cyclo-C_6H_{11}, R'=Me) was observed. This result is somewhat surprising in view of our previous information that $HgCl_2$ is the most efficient catalyst for the formation of **1** from isocyanides and halogens in cyclic ethers.[9] Further, the addition of a larger amount of $HgCl_2$ resulted in the formation of another product, besides considerable decreases in the yields of both **1** and amine. That is, when 50 mol% of $HgCl_2$ was added, 18 and 23% drops in the yields of **1** and cyclohexylamine respectively were observed, while a white, solid product was formed in a considerable quantity. In this case, it was observed that the reaction mixture became homogeneous by the dissolution of $HgCl_2$ at an earlier stage, and that then a white solid separated out gradually. Here, the existence of an equilibrium (Eq. 3) may be presumed for the homogeneous system, because a marked solubility of $HgCl_2$ in alcohols and the existence of a similar equilibrium between $HgCl_2$ and HgCl(OH) in an aqueous $HgCl_2$ solution has been

$$HgCl_2 + MeOH \rightleftharpoons HgCl(OMe)\,HCl + HCl \quad (3)$$

known.[10] The same solid was also obtained by the reaction of **2** (R=cyclo-C_6H_{11}, X=Cl) with equimolar $HgCl_2$ in methanol. On the contrary, we previously observed that a similar treatment in tetrahydrofuran did not afford any product and that most of the **2** was recovered.[7] The above solid was soluble in dil. hydrochloric acid and was reprecipitated by adding aqueous potassium carbonate. This suggests the presence of a basic nitrogen other than the C=N group. The absence of this group was also confirmed by the IR spectrum. The result of the elemental analysis of the solid corresponded to that for $C_8H_{14}NCl_3Hg$. Based on these facts, it was supposed that the product was a 1 : 1 adduct of either **2** (R=cyclo-C_6H_{11}, X=Cl) and HgCl(OMe) or **4** (R=cyclo-C_6H_{11}, R'=Me, X=Cl) and $HgCl_2$ (see Experimental). Considering both the substantial decrease in the amine yield and the probably high reactivity of HgCl(OMe) compared with $HgCl_2$, the former structure, *i.e.*, $C_6H_{11}N(HgCl)CHCl_2(OMe)$, is highly probable. An analogous example which involves an electrophilic attack of $HgOAc^+$ on the methine N of aromatic aldehyde arylhydrazone has been reported in a recent article.[11]

Next, when *N*-bromo- and *N*-chlorosuccinimide (NBS and NCS respectively) were used as halogen sources, the yields of **1** were generally not so good as in the case of halogens, even when a large excess of alcohol was used. Besides, the formation of *N*-carbamoylsuccinamates (**7**), a succinimide-incorporated product,

TABLE 2. REACTION OF CYCLOHEXYL ISOCYANIDE WITH *N*-HALOSUCCINIMIDES AND ALCOHOLS

Isocyanide, 20 mmol; NBS or NCS, 20 mmol; alcohols, 10 ml. Reaction conditions: near 5 °C, 1 h and 20—25 °C, 1 h.

Halide	R'OH	Product and yield/%[a]		
		1(R=C_6H_{11})	**7**(R=C_6H_{11})	**9**(R=C_6H_{11})
NBS	MeOH	49	22	2
NBS	MeOH[b]	51	12	3
NBS	MeOH[c]	45	26	0
NBS	EtOH	40	29	1
NBS	*i*-PrOH	10	9	16[d]
NBS	$PhCH_2OH$	38	0	0
NCS	MeOH	34	26	10
NCS	EtOH	27	39	7
NCS	*n*-PrOH	29	39	6

a) Isolated yield (based on isocyanide). b) Thirty ml of MeOH was used. c) Reaction conditions: near 5 °C, 1 h and 20—25 °C, 6 h. d) Other product, *N*-(cyclohexylcarbamoyl)succinimide (**8**), 18%.

in lower yields was observed. In the cyclohexylamine–NBS–methanol reaction, a change in the amount of methanol from 10 ml (*ca.* 10 equiv.) to 30 ml (*ca.* 30 equiv.) resulted in a slight increase (only 2%) in the yield of **1** and a considerable decrease in that of **7**. Some results are shown in Table 2. The reaction proceeded readily even in the dark. Further, it is generally accepted that *N*-halo imides act as electrophiles in polar media. Thus, a pathway *via* the haloimidoyl cation, **3**, formed by the electrophilic attack of X^+ (or the highly polarized halo imide), may be suggested (Eq. 4). Here, both **8** and **9** are products formed from **5** during the work-up procedure.

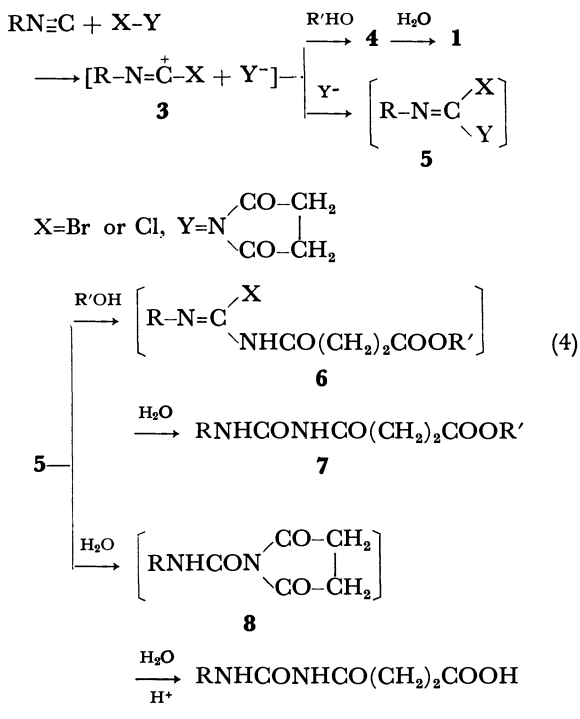

In the cyclohexyl isocyanide–NBS–isopropyl alcohol reaction, the marked decrease in the yield of the corresponding **1** is due to the lower stability of the corresponding **4** described above, and a steric hindrance in the ring-opening alcoholysis of the isocyanide–NBS adduct, **5**, resulted in a poor yield of the corresponding **7**. The reaction in benzyl alcohol appears to be somewhat complex, and none of products derived from **5** are found. The reason for this is not clear, but the competitive consumption of NBS for the oxidation of benzyl alcohol may be postulated, at least in part, since its facile oxidation with *N*-bromoacetamide is known.[12]

It is obvious from Table 2 that NBS is more effective than NCS as a halogen source for the formation of **1** from isocyanides, but no sufficient explanation of the observed different selectivities of the cation **3** (X=Br and Cl) can be offered at the present time, since the mechanistic details of the **3**-forming stage(s) and the relative stabilities of **3** are not yet available.

Experimental

The GLC analyses were carried out on a Shimadzu 5APTF apparatus, using EGSS-X(30%)-Chromosorb W(1 m) (with N_2 as the carrier gas). The ^1H NMR, IR, and mass spectra recorded on Varian A-60, Hitachi EPI-S2, and JEOL-01SG spectrometers respectively. The isocyanides (RNC) were prepared by the method of Ugi *et al.*[13] R=*n*-Bu, bp 119—120 °C (lit,[13] bp 116—117 °C/730 Torr); R=cyclo-C_6H_{11}, bp 69—71 °C/22 Torr (lit,[13] bp 56—58 °C/11 Torr); R=*t*-Bu, bp 91—92 °C (lit,[13] bp 91—92 °C/730 Torr); R=Ph, bp 60 °C/19 Torr (lit,[13] bp 50—51 °C/11 Torr). Commercial organic materials were used after distillation or recrystallization. Commercial inorganic materials were used without further purification.

Reaction of Isocyanides with Halogens and Alcohols. Some typical examples are shown below.

a): Into a stirred solution of bromine (3.20 g, 20 mmol) in methanol (16 ml), a solution of cyclohexyl isocyanide (2.18 g, 20 mmol) in methanol (4 ml) was added over a 0.5-h period, the temperature being maintained at near 5 °C by cooling with ice water. The mixture was stirred for an additional 0.5 h at that temperature and for 5 h at room temperature, and then added to a stirred suspension of $CaCO_3$ (4 g) in water. After the mixture had been stirred for 2 h at room temperature, the precipitated inorganic substance was filtered off and the filtrate was extracted with ether. Then the organic layer separated from the aqueous one washed with aqueous K_2CO_3 and water, and dried over anhydrous $MgSO_4$, and most of the solvent was evaporated. Distillation afforded crude methyl cyclohexylcarbamate (**1**, R=cyclo-C_6H_{11}, R'=Me) (2.40 g, 76% yield). The pure compound was obtained by redistillation; bp 82 °C/3 Torr, mp 72—74 °C (lit,[14] mp 75 °C); IR (KBr), 3380, 1530 (NH), 1690 (CO), and 1220, 1052 cm^{-1} (C–O–C); ^1H NMR ($CDCl_3$), δ=4.50 (1H, b), 3.50 (3H, s), 3.30 (1H, b), 2.1—0.9 (10H, m). The filtrate was made basic (pH *ca.* 10) with aqueous K_2CO_3 and steam-distilled. The aqueous distillate was made acidic with concd. HCl and dried up to afford cyclohexylamine hydrochloride (0.11 g, 4% yield) (mp 208—209 °C), which was identified by the mixed-melting-point method.

When the amount of methanol was reduced to a half volume (total 10 ml) in the above reaction, a yellowish-orange solid separated out from the reaction mixture during an early stage of the reaction, and finally the stirring became difficult. After

all the isocyanide had been added, the solid was filtered off, washed with a small amount of methanol, and dried. . The solid weighed 1.93 g. From the filtrate, the unreacted isocyanide (9 mmol) was recovered. Assuming that the above solid is a 1 : 1 complex of **3** (R=cyclo-C_6H_{11}, X=Br) and Br_2, the yield of the solid is estimated to be 82% (based on the isocyanide consumed). In addition, when the solid (0.43 g, 1 mmol) was dissolved in methanol (2 ml) and this solution was allowed to stand for 5 h at room temperature, the above carbamate (0.11 g, 70% yield) was obtained after the usual work-up procedure.

b): Chlorine gas (4.26 g, 60 mmol) was bubbled into a stirred solution of cyclohexyl isocyanide (2.18 g, 20 mmol) in methanol (20 ml) over a period of 1.5 h at near 5 °C. After being maintained for 0.5 h at the same temperature and for 7 h at room temperature with stirring, the mixture was poured into water. The resulting mixture was stirred for 2 h at room temperature and then worked-up as has been described in *a*). A GLC analysis of the evaporation residue, using bibenzyl as the internal standard, showed the formation of the expected carbamate (1.35 g, 43% yield). From the acidic aqueous layer, cyclohexylamine hydrochloride (0.92 g, 34%) was isolated.

When this reaction was carried out in the presence of $HgCl_2$ (2.72 g, 10 mmol), a light brown solid was separated out by pouring the reaction mixture into ice water. This solid was dissolved in dil. HCl, and the subsequent neutralization of this acidic solution afforded a white precipitate (3.41 g), which was soluble in acetic acid, but insoluble in ether, chloroform, and methanol. This solid gave analytical figures corresponging to a 1 : 1 adduct of either **2** (R=cyclo-C_6H_{11}, X=Cl) and HgCl(OMe) or **4** (R=cyclo-C_6H_{11}, R'=Me, X=Cl) and $HgCl_2$. Found: C, 20.77; H, 3.72; N, 3.88%. Calcd for $C_8H_{14}NC_{13}Hg$. C, 21.49; H, 3.16; N, 3.13%. The IR spectrum revealed the absence of any C=N bond.

The physical properties and analytical data of other pure **1** substances are as follows. cyclo-C_6H_{11}NHCOOR': R'=Et, bp 87 °C/3 Torr, mp 54—55 °C (lit,[15] bp 123 °C/11 Torr, mp 56 °C). R'=*n*-Pr, bp 96—98 °C/3 Torr, mp 39—40 °C (lit,[16] mp 40—41 °C). R'=*i*-Pr, bp 84—85 °C/3 Torr, mp 65—66 °C (lit,[17] mp 66.5—67 °C). R'=*n*-Bu, bp 110—112 °C/3 Torr, mp 50—52 °C (Found: C, 66.19; H, 10.59; N, 6.62%. Calcd for $C_{11}H_{21}NO_2$: C, 66.29; H, 10.62; N, 7.03%). ^{1}H NMR ($CDCl_3$) δ=4.40 (1H, b), 3.90 (2H, t, J=6.0 Hz), 3.35 (1H, b), 1.8—1.05 (4H, m), 0.9 (3H, t, J=6.0 Hz), 2.05—0.9 (10H, m). R'=CH_2Ph, mp 85—87 °C (from 50% aq. EtOH) (Found: C, 71.73; H, 8.32; N, 5.96%; M$^+$, 233 Calcd for $C_{14}H_{19}NO_2$: C, 72.07; H, 8.21; N, 6.00%; M, 233). ^{1}H NMR ($CDCl_3$) δ=7.05 (5H, s), 4.90 (2H, s), 4.40 (1H, b), 3.40 (1H, b), 2.1—0.8 (10H, m). RNHCOOMe: R=*n*-Bu, bp 96 °C/20 Torr (lit,[18] bp 92 °C/15 Torr). R=*t*-Bu, bp 64 °C/20 Torr (lit,[18] bp 63.3 °C/17 Torr). R=Ph, bp 125—126 °C/10 Torr, mp 44—46 °C (lit,[19] mp 47 °C).

Reaction of Isocyanides with N-*Halosuccinimides and Alcohols.* A typical example is given below. A solution of cyclohexyl isocyanide (2.18 g, 20 mmol) in methanol (4 ml) was stirred into a solution of NBS (3.56 g, 20 mmol) in methanol (6 ml) over a 0.5-h period at near 5 °C. After the mixture had been stirred for an additional 0.5 h at the same temperature and for 1 h at room temperature, the reaction mixture was poured into water and allowed to stand for 2 h at room temperature with stirring. The work-up procedure was the same as above. Distillation gave the expected carbamate (1.54 g, 49% yield), leaving a solid residue of crude methyl *N*-(cyclohexylcarbamoyl)succinamate (**7**, R=cyclo-C_6H_{11}, R'=Me) (1.13 g, 22% yield). The recrystallization of this residue from 50% aq EtOH afforded the pure compound; mp 95—96 °C (Found: C, 56.37; H, 8.09; N, 10.89%; M$^+$, 256. Calcd for $C_{12}H_{20}N_2O_4$: C, 56.24; H, 7.87; N, 10.93%; M, 256. IR (KBr) 3300, 3150, 1550 (NH), 1740 (ester CO), 1710 (urethane CO), 1685 (amide CO), 1220, 1175 cm^{-1} (C–O–C). ^{1}H NMR ($CDCl_3$) δ=9.70 (1H, s), 8.05 (1H, d, J=7.0 Hz), 3.60 (3H, s), 3.45 (1H, b), 2.70 (4H, s), 2.1—0.9 (10H, m). When the aqueous layer was allowed to stand for a few days, needles of crude *N*-(cyclohexylcarbamoyl)succinamic acid (**9**, R=cyclo-C_6H_{11}) (0.09 g, 2% yield) separated out. A pure compound was obtained by recrystallization; mp 170—173 °C (lit,[1] mp 162—164 °C).

The ^{1}H NMR ($CDCl_3$) data of other **7** and **8** substances are as follows. cyclo-C_6H_{11}NHCONHCO$(CH_2)_2$COOR': R'=Et, δ=9.70 (1H, s), 8.10 (1H, d, J=8.0 Hz), 4.05 (2H, q, J=7.0 Hz), 3.55 (1H, b), 2.60 (4H, s), 1.25 (3H, t, J=7.0 Hz), 2.1—0.9 (10H, m). R'=*n*-Pr, δ=9.80 (1H, s), 8.10 (1H, d, J=8.0 Hz), 3.90 (2H, t, J=6.0 Hz), 3.55 (1H, b), 2.60 (4H, s), 1.60 (2H, m, J=6.0 Hz), 0.90 (3H, t, J=6.0 Hz), 2.1—0.9 (10H, m). R'=*i*-Pr, δ=9.20 (1H, s), 8.05 (1H, d, J=7.8 Hz), 4.80 (1H, m, J=6.0 Hz), 3.55 (1H, b), 2.60 (4H, m), 1.20 (6H, d, J=6.0 Hz), 2.0—0.9 (10H, m). **8** (R=cyclo-C_6H_{11}); δ=7.0 (1H, s), 3.65 (1H, b), 2.70 (4H, s), 2.1—1.0 (10H, m).

References

1) M. Okano, Y. Ito, T. Shono, and R. Oda, *Bull. Chem. Soc. Jpn.*, **36**, 1314 (1963).
2) G. M. Dyson and T. Harrington, *J. Chem. Soc.*, **1942**, 150.
3) A. F. Hegarty and K. J. Dignam, *J. Chem. Soc., Perkin Trans. 2*, **1975**, 1046.
4) R. Leimu, *Ber.*, **70**, 1040 (1937).
5) Y. Yamase, *Bull. Chem. Soc. Jpn.*, **34**, 480 (1961).
6) M. Green and R. F. Hudson, *J. Chem. Soc.*, **1962**, 1076; A. Queen, *Can. J. Chem.*, **45**, 1619 (1967).
7) For the neutral hydrolysis of *N*-aryl chloroimidates, the S_N1 mechanism has been established.[8] Judging from the substituent effect in this reaction, the same mechanism would be expected for the *N*-alkyl compounds. In contrast to this, the hydrolysis of the usual chloroformates (where R''=primary alkyls) is known to proceed by means of the S_N2 mechanism even under neutral conditions.
8) A. F. Hegarty, J. D. Cronin, and F. L. Scott, *J. Chem. Soc., Perkin Trans. 2*, **1975**, 429.
9) T. Yamazaki, Y. Wada, S. Tanimoto, and M. Okano, *Bull. Chem. Soc. Jpn.*, **50**, 1094 (1977).
10) *Cf.* F. A. Cotton and G. Wilkinson, "Advanced Inorganic Chemistry," 3rd ed, Interscience Pub., New York, N. Y. (1972), p. 518.
11) R. N. Butler and A. M. O'Donohuo, *J. Chem. Soc., Perkin Trans. 2*, **1979**, 1387.
12) J. Lecomte and C. Dufour, *C. R. Acad. Sci.*, **234**, 1887 (1952).
13) I. Ugi and R. Meyer, *Chem. Ber.*, **93**, 239 (1960).
14) M. Barker, L. Hunter, and N. G. Reynolds, *J. Chem. Soc.*, **1948**, 874.
15) M. I. Gllibrand and A. H. Lamberton, *J. Chem. Soc.*, **1949**, 1883.
16) S. Tanaka, H. Kido, S. Uemura, and M. Okano, *Bull. Chem. Soc. Jpn.*, **48**, 3415 (1975).
17) Z. G. Hajos, D. R. Parrish, and M. W. Goldberg, *J. Org. Chem.*, **30**, 2849 (1965).
18) H. van Erp, *Rec. Trav. Chim.*, **14**, 17 (1895).
19) B. T. Dewey and N. F. Witt, *Ind. Eng. Chem. Anal.*, **12**, 459 (1940).

Oxidation of Unsymmetrical Disulfide and Thiosulfinic S-Esters with Peroxy Acids. Search for Formation of α-Disulfoxide as An Intermediate in the Electrophilic Oxidation of Thiosulfinic S-Ester[1]

Shigeru OAE,* Toshikazu TAKATA, and Yong Hae KIM[2]
Department of Chemistry, The University of Tsukuba, Sakura-mura, Ibaraki 305
(Received January 7, 1982)

Oxidation of an unsymmetrical disulfide, methyl phenyl disulfide, with peroxy acids takes place mainly at more electron-rich sulfur atom to form thiosulfinic *S*-ester at the first stage, while oxidation of unsymmetrical thiosulfinic *S*-ester with peroxy acids gives usually four thiosulfonic *S*-esters, together with sulfinic and sulfonic acids, further oxidation products. Oxidation of *S*-methyl benzenethiosulfinate **6** affords, as one of the products, *S*-phenyl methanethiosulfonate **11**, in which the original sulfinyl oxygen is brought into methanesulfonyl group. A small amount of *S*-phenyl benzenethiosulfonate **9** (or benzenesulfonic acid **15**) is obtained in the oxidation of *S*-phenyl methanethiosulfinate **7**. ^{18}O-Label of the starting thiosulfinic *S*-ester **6** was found to be incorporated to some extents into all four products, *i.e.* **8**—**11**, while a part of ^{18}O-label of *S*-phenyl methanethiosulfinate **7** was also observed in *S*-phenyl benzenethiosulfonate **9** and benzenesulfonic acid **15**, although most of ^{18}O-label of **7** was incorporated into *S*-phenyl methanethiosulfonate **11**. Thiosulfinic *S*-esters are stable and do not undergo disproportionation and ^{18}O-exchange under the conditions. These observations suggest the formation of α-disulfoxide as an intermediate in the oxidation of thiosulfinic *S*-ester to thiosulfonic *S*-ester, especially in the oxidation of **6**, although no peak corresponding to α-disulfoxide was observed directly in the NMR spectra taken during the oxidations of a few thiosulfinic *S*-esters with peroxy acids. Mechanism of the oxidation is discussed.

Oxidation of disulfide is considered to proceed *via* various stable intermediates as shown in Eq. 1. When the disulfide is unsymmetrical, oxidation with peroxy acids usually affords two regioisomeric thiosulfinic *S*-esters (thiolsulfinates) as the initial oxidation products, of which the ratio depends on the electron density of the sulfur atom, *i.e.* the more electron-rich sulfur atom is known to be oxidized predominantly.[3a,b] However, when the electron-rich sulfur atom is substituted by a bulky group, the ratio is known to be controlled by the steric effect instead of the electronic effect.[3]

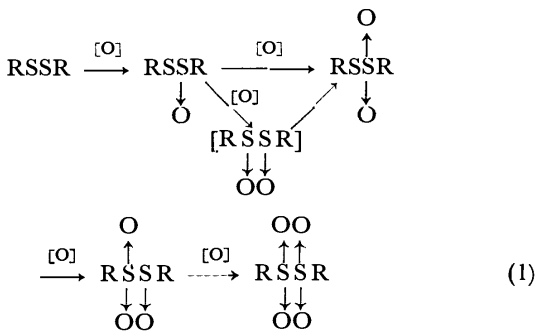
(1)

Mechanism of further oxidation of the thiolsulfinate has long been a matter of controversy, especially as to the question whether or not the oxidation of thiolsulfinate proceeds *via* forming "α-disulfoxide" as an intermediate. α-Disulfoxides have been long proposed as either stable products or intermediates in the oxidations of both disulfides[4,5] and thiolsulfinates.[5] Since the sulfenyl sulfur of thiolsulfinate is considered to be more prone to be oxidized than the sulfinyl sulfur, intermediary formation of α-disulfoxide has been believed in the oxidation of cystine.[5f-j] The fact that no one has succeeded in obtaining α-disulfoxide despite numerous attempts,[5k] by Barnard,[5b] Modena *et al.*,[5d,e] Kice and Chau,[5a] and others, is now explained in terms of the unusually small bond energy of "α-disulfoxide."[5a]

In order to understand the mechanism of oxidation of disulfide and thiolsulfinate with peroxy acids, the oxidations of unsymmetrical disulfide and thiolsulfinates have been investigated and evidence for formation of α-disulfoxide as an intermediate has now been obtained in the oxidation of thiolsulfinate. This paper describes our experimental observations and subsequent discussions.

Results

Methyl phenyl disulfide **3**, an unsymmetrical disulfide, was prepared by the reaction of methanesulfenyl chloride with thiophenol in the presence of pyridine (Eq. 2).[6] Unsymmetrical thiolsulfinates **6** and **7** were prepared by treating sulfinyl chloride with thiol (Eq. 3) according to the usual method.[7] In the same manner, authentic samples of thiosulfonic *S*-esters (thiolsulfonates) **9**, **10**, and **11** were synthesized by treating sulfenyl chloride with sulfinic acid in the presence of pyridine (Eq. 4).[7]

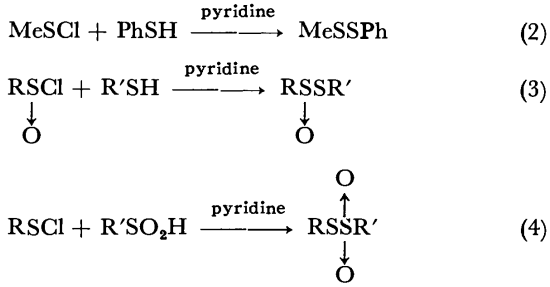
(2)

(3)

(4)

The disulfide and the thiolsulfinate thus prepared were oxidized with either H_2O_2 in AcOH or *m*-chloroperbenzoic acid (MCPBA) in CH_2Cl_2.

Product analysis was performed by using NMR, GLC, and HPLC. As shown in Fig. 1, fortunately all these compounds were able to be separated by HPLC. ^1H-

Table 1. NMR chemical shifts of compounds having methyl group (δ TMS, at *ca.* 27 °C)

Compound	Solvent			
	$CDCl_3$	CCl_4	CD_3COOD ($-D_2O$)	Others
MeSSMe **1**	2.40	2.30[a]		
MeSSMe **4**	[2.66 [2.98	[2.67[a] [3.00[a]	[2.36 [2.72	
MeSSMe **8**	[2.69 [3.30	[2.69[b] [3.28[b]	[2.36 [3.02	
PhSSMe **3**	2.37		2.05	
PhSSMe **6**	2.53		2.24	
PhSSMe **7**	2.90		2.72	
PhSSMe **10**	2.48		2.15	
PhSSMe **11**	3.15		2.90	
$MeSO_2H$ **12**	2.70	2.93[b]	[2.39 [2.44 ($+D_2O$)	2.48(D_2O)
$MeSO_2Na$				[2.30(D_2O) [2.34(D_2O)[b]
$MeSO_3H$ **14**	3.18 (2.90)[a]		2.68	[2.98(D_2O) [2.90(DMSO-d_6)[a]
$MeSO_3Na$				2.80(D_2O)

a) E. Block, "Reactions of Organic Sulfur Compounds," Academic Press, New York (1978), p. 297. b) R. O. Norton, G. M. Beverly, and I. B. Douglass, *J. Org. Chem.*, **32**, 3645 (1967).

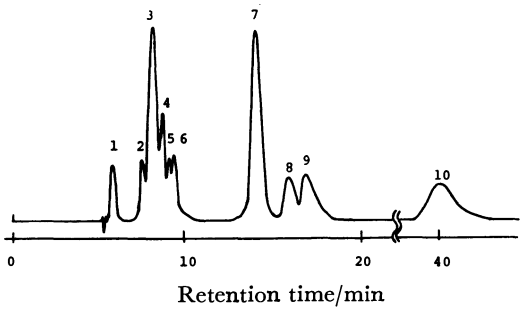

Fig. 1. High pressure liquid chromatography by Yanaco Model L-1030 at room temperature.
Column: Yanaco Gel 5510, carrier: MeOH, pressure: 125 kg/cm², flow rate: 16.1 ml/h.
Peak 1: $MeSS(O)_2Me$(**8**), 2: MeSSMe(**1**), 3: $PhSS(O)_2$-Me(**11**), 4: $PhS(O)_2SMe$(**10**), 5: PhSS(O)Me(**7**), 6: PhS(O)SMe(**6**), 7: $PhSS(O)_2Ph$(**9**), 8: PhSS(O)Ph-(**5**), 9: PhSSMe(**3**), 10: PhSSPh(**2**).
Peaks of $MeSO_2H$(**12**), $MeSO_3H$(**14**), $PhSO_2$(**13**), and $PhSO_3H$(**15**) appear earlier than that of peak of **8**, while peak of MeSS(O)Me(**4**) appears between peaks 1 and 2.

NMR chemical shifts of methyl groups of these compounds are listed in Table 1 together with the NMR data of the related compounds.

Oxidation of Disulfide **3**. When methyl phenyl disulfide **3** was treated with H_2O_2 in AcOH, *S*-phenyl methanethiosulfinate **7** was formed predominantly over *S*-methyl benzenethiosulfinate **6**, as shown in Figs. 2 and 3, which are drawn following the changes of NMR signals of methyl groups of **3** and the other products during the oxidation of **3** with 30% H_2O_2 in deuterated acetic acid (Eq. 5). When the oxidation of **3** was followed

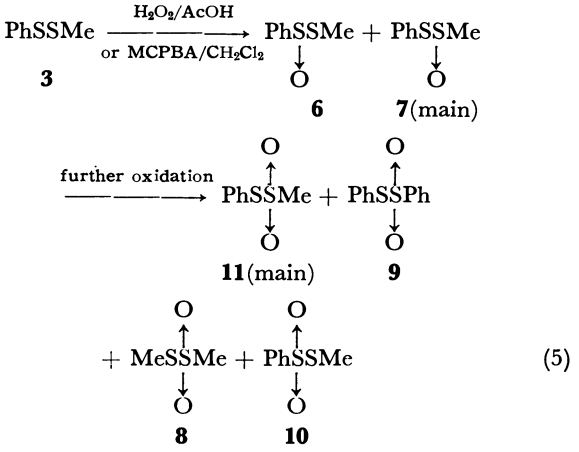

by HPLC, the products, which could not be detected in GLC, were detected in NMR. Comparison of Figs. 2 and 3 reveals that the rate of disappearance of **3** is very sensitive to the change of reaction temperature. Since the oxidant used was substantially in excess over the disulfide **3**, the oxidation proceeded further. In the oxidation of the following step, the major product isolated was *S*-phenyl methanethiosulfonate **11**, accompanied with quite a small amount of *S*-methyl benzenethiosulfonate **10**, as shown in Figs. 2 and 3. Besides the products having original S–S linkage (*i.e.* **10** and **11**), formations of symmetrical thiolsulfinates, both *S*-methyl

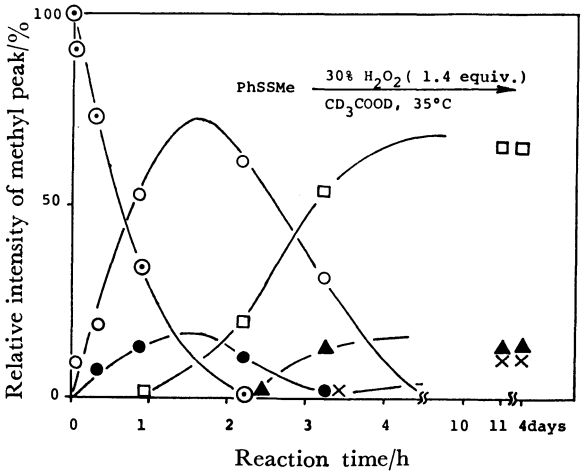

Fig. 2. Oxidation of PhSSMe (**3**) with 30% H_2O_2 (1.4 equiv.) in acetic acid at 35 °C.
Marks used in figures are common and as follows: ◑: MeSSMe (**1**), ⊙: PhSSMe (**3**), △: MeS(O)SMe (**4**), ●: PhS(O)SMe (**6**), ○: PhSS(O)Me (**7**), ▲: MeSS-$(O)_2$Me (**8**), ■: $PhS(O)_2SMe$ (**10**), □: $PhSS(O)_2Me$ (**11**), ◒: $MeSO_2H$ (**12**), ×: $MeSO_3H$(**14**).

TABLE 2. OXIDATION PRODUCTS OF PhSSMe (**3**)

Entry	Oxidation system	Temp/°C	Time/h	Product (mol%)[a]						
				3	**7**	**9**	**10**	**11**	**14**	**15**
1	30% H_2O_2(1.4 equiv.) CD_3COOD	35	10	0	0	17	11	61	10	≈0
2	30% H_2O_2(1.5 equiv.) CD_3COOD	18	77	0	31	13	5	26	≈0	≈0
3	30% H_2O_2(2.4 equiv.) CD_3COOD	35	5	0	0	27	2	30	38	—
4	MCPBA (1.0 equiv.) CH_2Cl_2	0	24	15	65	≈0	≈0	15	—	—[b]

a) Determined by NMR. b) Determined by HPLC.

TABLE 3. OXIDATION PRODUCTS OF PhSS(O)Me (**7**)

Entry	Oxidation conditions			Product (mol%)[a]					
	System	Temp/°C	Time/h	**7**	**8**	**9**	**11**	**14**	**15**
1	30% H_2O_2(1.2 equiv.) CD_3COOD	35	1	≈0	5	14	36	30	17
2	30% H_2O_2(1.2 equiv.) CD_3COOD	18	15	≈0	2	11	46	28	10
3	30% H_2O_2(1.0 equiv.) AcOH	50	2/3	—[c]	—	—	55[b]	—	—
4	30% H_2O_2(1.3 equiv.) AcOH	19	11	≈0	Trace	12	46	31	5
5	30% H_2O_2(1.5 equiv.) AcOH	25	13	≈0	Trace	20	27	45[d]	Trace
6	30% H_2O_2(10 equiv.) AcOH	70	5	0	0	0	0	50	50
7	MCPBA(1.2 equiv.) CH_2Cl_2	0	7.5	17	Trace	8	48	23[e]	Trace
8	MCPBA(1.3 equiv.) CH_2Cl_2	0	3	21	Trace	15	49	15	Trace

a) Yield was determined by NMR, GLC, and HPLC. b) Yield after recrystallization from hexane. c) —: Not determined. d) Containing $MeSO_2H$ (16%). e) Containing $MeSO_2H$(9%).

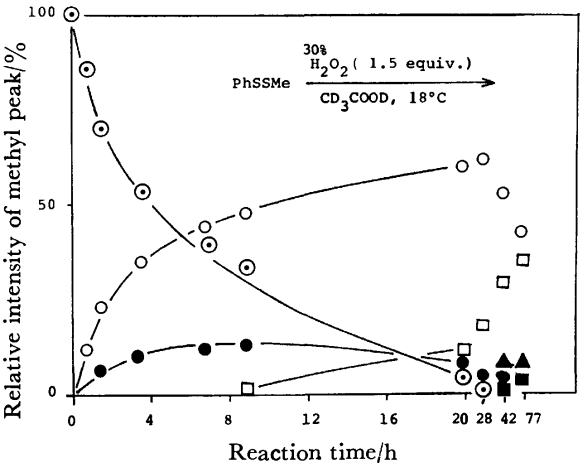

Fig. 3. Oxidation of PhSSMe with 30% H_2O_2 (1.5 equiv.) in acetic acid at 18 °C.
⊙: PhSSMe (**3**), ○: PhSS(O)Me (**7**), ●: PhS(O)SMe (**6**), □: $PhSS(O)_2Me$ (**11**), ■: $PhS(O)_2SMe$ (**10**).

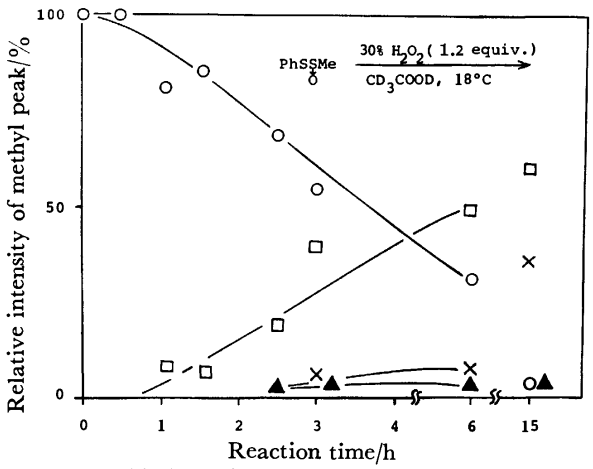

Fig. 4. Oxidation of PhSS(O)Me(**7**) with 30% H_2O_2 (1.2 equiv.) in acetic acid at 18 °C.
○: PhSS(O)Me (**7**), □: $PhSS(O)_2Me$ (**11**), ▲: $MeSS(O)_2Me$ (**8**), ×: $MeSO_3H$ (**14**).

methanethiosulfonate **8** and *S*-phenyl benzenethiosulfonate **9**, were also confirmed by GLC. Both methanesulfonic acid **14** and benzenesulfonic acid **15** were also detected by NMR and HPLC respectively, and found to be the end products upon oxidation with additional H_2O_2.

Oxidation products of **3** are listed in Table 2, which shows that nearly the same result is obtained in MCPBA oxidation of **3** (entry 4). In direct NMR study as shown in Figs. 2 and 3, the rate of the oxidation of **3** was comparable to those of **6** and **7**.[5d]

The methyl signal, corresponds to α-disulfoxide (PhS(O)S(O)Me, [A]) which may be formed by the oxidation of more electron-rich sulfenyl sulfur atom of thiolsulfinate (*e.g.* **6** or **7**), was not observed in the NMR spectra obtained during the oxidation of **3**.

On the other hand, in NMR study on the oxidation of symmetrical disulfide (dimethyl disulfide, **1**) with H_2O_2 in deuterated acetic acid, the products observed through NMR spectra were at first only *S*-methyl methanethiosulfinate **2**, then **8** and eventually **14**, in the final stage with no other methyl peak. The same transformation was observed in the oxidation of **1** to **8** with MCPBA in $CDCl_3$.

Oxidation of Thiosulfinic S-Esters **6** *and* **7**: In the oxidation of **7** with H_2O_2 in AcOH or *m*-chloroperbenzoic acid (MCPBA) in CH_2Cl_2, **11** was obtained as the major product, along with other thiolsulfonates such as **8** and **9**, and acids (**12**—**15**) (Table 3, Fig. 4) (Eq. 6). The

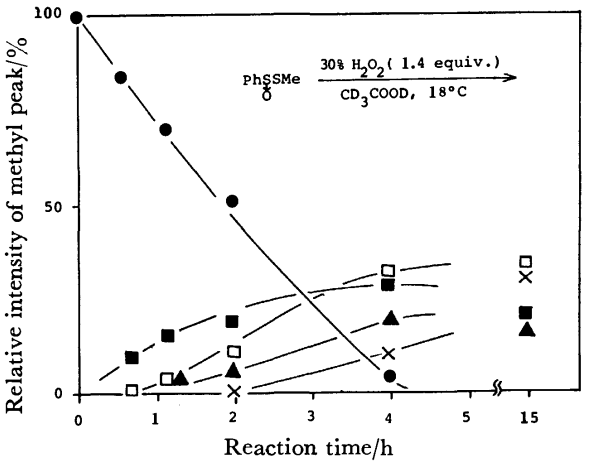

Fig. 5. Oxidation of PhS(O)SMe (**6**) with 30% H_2O_2 (1.4 equiv.) in acetic acid at 18 °C.
●: PhS(O)SMe (**6**), ■: $PhS(O)_2SMe$ (**10**), □: $PhSS(O)_2Me$ (**11**), ▲: $MeSS(O)_2Me$ (**8**), ×: $MeSO_3H$ (**14**).

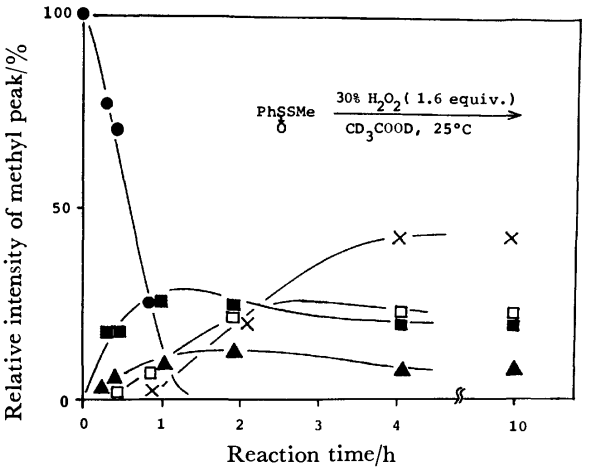

Fig. 6. Oxidation of PhS(O)SMe (**6**) with 30% H_2O_2 (1.6 equiv.) in acetic acid at 25 °C.
●: PhS(O)SMe (**6**), ■: $PhS(O)_2SMe$ (**10**), □: $PhSS(O)_2Me$ (**11**), ▲: $MeSS(O)_2Me$ (**8**), ×: $MeSO_3H$ (**14**).

Table 4. Oxidation products of PhS(O)SMe (**6**)

Entry	Oxidation conditions: System	Temp/°C	Time/h	Product (mol%)[a]: **6**	**8**	**9**	**10**	**11**	**14**	**15**
1	30% H_2O_2(1.2 equiv.) AcOH	22	5	—	13[b]	18[b]	—	22[b]	—	—
2	30% H_2O_2(1.4 equiv.) CD_3COOD	35	<1	0	8	21	12	21	28	7
3	30% H_2O_2(1.4 equiv.) CD_3COOD	18	<15	0	10	21	12	23	29	5
4	MCPBA(1.1 equiv.) CH_2Cl_2	20	20	≈0	14	14	25	34	0	—[c]
5	MCPBA(1.2 equiv.) CH_2Cl_2	0	4.5	6	7	7	27	32	10	—
6	MCPBA(1.2 equiv.) CH_2Cl_2	0	9	≈0	Trace	15	13	30	30[d]	—[c]

a) Yield was determined by NMR, GLC, and LLC. b) Isolated and purified yield. c) Unidentified methyl peak (14%) was observed. d) Containing $MeSO_2H$ (12%).

yield of **10** was only a trace or none in both oxidations. Although methyl signal of "α-disulfoxide" is expected to appear at 2.6—2.9 ppm (in CD_3COOD), no signal was observed in such a region during the oxidation of **7**. While the oxidation of **7** with 1.2 equiv. of 30% H_2O_2 was completed within 1 h at temperatures higher than 35 °C, the products obtained in the oxidation with ten equivalents of H_2O_2 in AcOH at 70 °C for 5 h, were only the sulfonic acids **14** and **15** as shown in Table 3 (entry 6).

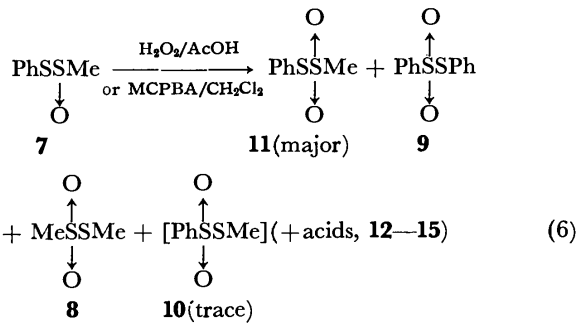

(6)

Figures 5 and 6 show the changes of the NMR signals of the methyl groups of the starting thiolsulfinate and the products during the oxidation of **6** with H_2O_2 in CD_3COOD. One of the final products was also found to be **14**, though thiolsulfonates still remained. The oxidation of **6**, during which considerably complex methyl peaks were observed in NMR spectra, gave eventually two symmetrical and two unsymmetrical thiolsulfonates (**8**—**11**), along with further oxidation products (*i.e.* acids: **12**—**15**) (Eq. 7). This result is in contrast to that in the oxidation of **7**, and the oxidation of **6** gave nearly the same amounts of the four thiol-

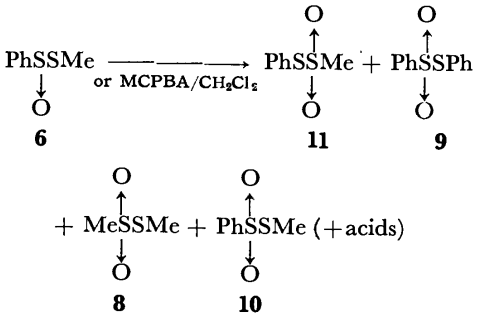

(7)

sulfonates.† Yields of products in the oxidation of **6** are listed in Table 4. Inspection of the data in Table 4

† *S*-Methyl benzenethiosulfonate (**10**) was not confirmed at first[1] but then identified, since we found later that the ^{1}H-NMR chemical shift of **10** was unusually *higher* than that of **6**. (T. Takata, Y. H. Kim, S. Oae, and K. T. Suzuki, *Tetrahedron Lett.*, **1978**, 4303).

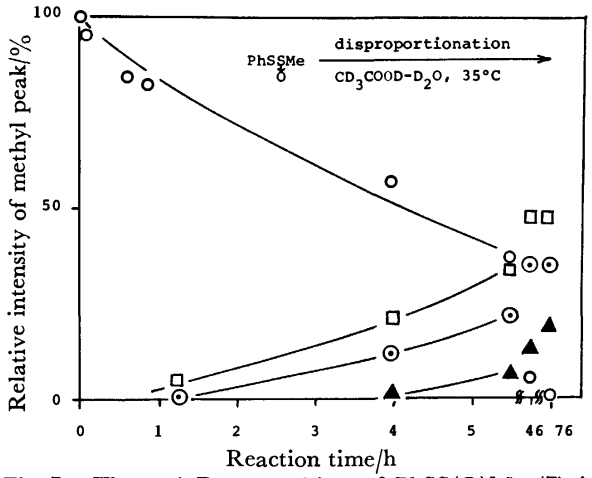

Fig. 7. Thermal Decomposition of PhSS(O)Me (**7**) in acetic acid–water at 35 °C.
○: PhSS(O)Me (**7**), □: PhSS(O)$_2$Me (**11**), ⊙: PhSSMe (**3**), ▲: MeSS(O)$_2$Me (**8**).

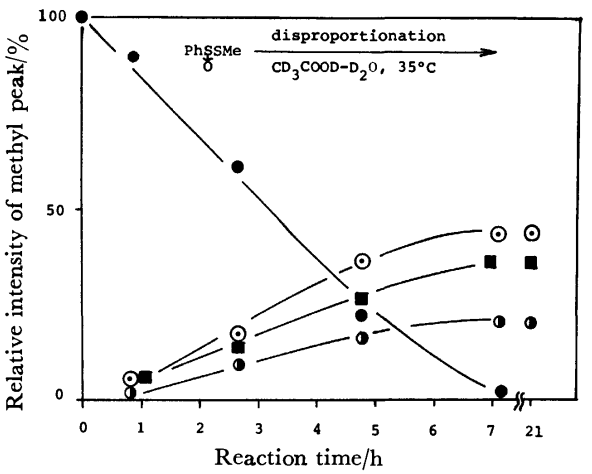

Fig. 8. Thermal Decomposition of PhS(O)SMe (**6**) in acetic acid–water at 35 °C.
●: PhS(O)SMe (**6**), ⊙: PhSSMe (**3**), ■: PhS(O)$_2$SMe (**10**), ◑: MeSSMe (**1**).

TABLE 5. ^{18}O-TRACER EXPERIMENTS IN THE OXIDATION OF PhSS(O)Me (**7**)

Entry	Excess ^{18}O content of **7** / %	Oxidant	Reaction Temp/°C	Reaction Time/h	Product	Excess[a] ^{18}O content / %	Incorporated ^{18}O %
1a	PhSSMe (O)	1.3 equiv. H_2O_2	25	13	**11**	0.376	122
	0.615				**9**	0.076	24
1b	0.549	10 equiv. H_2O_2	70	5	$PhSO_2NH_2$	0.037	6.7[b]
2a	0.615	1.2 equiv. MCPBA	0	7.5	**11**	0.342	112
					9	0.259	84
2b	0.451	1.3 equiv. MCPBA	0	3	**11**	0.211	94
					9	0.181	80

a) ^{18}O Content of CO_2. b) 20.1% for $PhSO_3H$ (Eq. 11).

reveals that the oxidation of **6** with MCPBA in CH_2Cl_2 gives nearly the same result as that with H_2O_2 in AcO H No methyl peak corresponding to *α*-disulfoxide (at 2.6—2.9 ppm) was also observed in NMR spectra during the oxidation.

Since thiolsulfinate has been known to disproportionate readily to afford mainly a mixture of disulfides and thiolsulfonates,[8] **7** was heated in NMR tube in CD_3COOD–D_2O system at 35 °C for *ca.* 76 h and the disproportionation of **7** was found to proceed so slowly (Eq. 8, Fig. 7) that its contribution in product distribution can be neglected during the oxidation. Main products in the disproportionation of **7** were **11** and **3**, together with **8** and **2** as minor products. It is interesting to note that in the disproportionation of *S*-phenyl methanethiosulfinate **7** neither *S*-methyl not *S*-phenyl benzenethiosulfonates **9** and **10** was obtained.

$$\underset{\mathbf{7}}{\text{PhSSMe}(\text{O})} \xrightarrow[\text{CD}_3\text{COOD-D}_2\text{O, 35 °C, 76 h}]{\text{disproportionation}} \underset{\mathbf{11}(42\%)}{\text{PhSSMe}(\text{O})} + \underset{\mathbf{8}(14\%)}{\text{MeSSMe}(\text{O})} + \underset{\mathbf{3}(31\%)}{\text{PhSSMe}} + \underset{\mathbf{2}(13\%)}{\text{PhSSPh}} + \underset{\mathbf{1}(\approx 0\%)}{\text{MeSSMe}} \quad (8)$$

In the disproportionation of **6** in CD_3COOD–D_2O system at 35 °C, the same trend was observed as in the case of **7** (Eq, 9, Fig. 8). Namely, there was no product having methanesulfonyl group but only benzenesulfonyl derivatives **9** and **10** are the oxidation products. As shown in Fig. 6, Fig. 8 and Table 4, the disproportionation of **6** at 35 °C was much slower than the oxidation of **6** at the same temperature (≈1 h, Table 4, entry 2). Meanwhile, disproportionation was confirmed not to occur at 18—20 °C for 10—20 h.

$$\underset{\mathbf{6}}{\text{PhSSMe}(\text{O})} \xrightarrow[\text{CD}_3\text{COO-D}_2\text{O, 35 °C}]{\text{disproportionation}} \underset{\mathbf{10}(30\%)}{\text{PhSSMe}(\text{O})_2} + \underset{\mathbf{9}(10\%)}{\text{PhSSPh}(\text{O})} + \underset{\mathbf{3}(36\%)}{\text{PhSSMe}} + \underset{\mathbf{1}(17\%)}{\text{MeSSMe}} + \underset{\mathbf{2}(7\%)}{\text{PhSSPh}} \quad (9)$$

^{18}O-Tracer Experiments. In order to examine the oxygen transfer of **6** or **7** to the products, **11** or **10**, ^{18}O-tracer experiments were carried out.

^{18}O-Labelled thiolsulfinate (**6** and **7**) were prepared (Eq. 3) by treating thiols with ^{18}O-labelled sulfinyl chlorides which were prepared according to the following reactions (Eq. 10), as described in detail in experimental section.

^{18}O-Labelled **6** and **7** were treated with an equimolar

Table 6. ^{18}O-Tracer experiments in the oxidation of PhS(O) SMe (**6**)

Entry	Excess ^{18}O content of **6** %	Oxidant	Reaction Temp/°C	Reaction Time/h	Product	Excess ^{18}O content %	Incorporated ^{18}O %
1a	PhSSMe ↓ O 0.636%	1.4 equiv. H_2O_2	20	5	**11**	0.186	58
					9	0.378	118
1b	0.578	1.2 equiv. H_2O_2	20	10	**11**	0.175	60
					9	0.354	122
1c	0.515	1.2 equiv. H_2O_2	20	6	**11**	0.178	70
					9	0.319	124
					8	0.170	68
1d	0.578	1.3 equiv. H_2O_2	20	9	**11**	0.188	66
					9	0.342	118
1e	0.578	1.3 equiv. H_2O_2	20	5.5	**11**	0.169	58
					10	0.294	102
2a	0.578	1.2 equiv. MCPBA	0	9	**11**	0.316	109
					9	0.397	137
2b	0.564	1.2 equiv. MCPBA	0	3	**11**	0.286	102
					9	0.311	110

amount of 30% H_2O_2 in AcOH or with an equivalent of MCPBA in CH_2Cl_2. After the disappearance of most

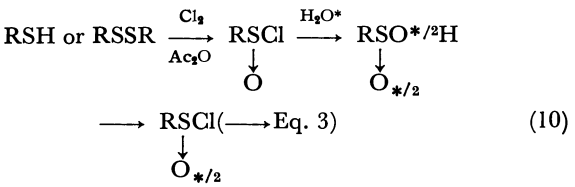

(10)

of **6** and **7** (monitored by TLC or HPLC), the reaction mixture was treated according to the usual work-up. The mixture of organic products was subjected directly to column chromatography (on silica gel, eluent : $CHCl_3$: EtOAc : hexane = 1 : 1 : 4) to separate into each product component. The products thus obtained and the starting materials were then subjected to the routine ^{18}O-analyses. The results are summarized in Tables 5 and 6.

While ^{18}O-labelled oxygen of **7** was found to be retained nearly completely in the major product **11**, the minor product **9** was also incorporated with a small amount of ^{18}O-label during the oxidation of **7** with 30% H_2O_2 in AcOH (Table 5, entry 1a). A similar trend was also seen in the ^{18}O distributions among the products formed in the oxidation of **7** with MCPBA (Table 5, entry 2). However, the ^{18}O incorporation of the minor product **9** was considerably larger in the oxidation with MCPBA than that with H_2O_2.

In another way to examine the possible oxygen transfer from methanesulfinyl group of **7** to the phenylthio moiety in the oxidation of **7** with H_2O_2, both acids **14** and **15** obtained under vigorous oxidation conditions (10 equiv. H_2O_2, 70 °C, 5 h: Table 5, entry 1b), were converted to the corresponding sulfonyl chlorides with $SOCl_2$ (eq. 11). Benzenesulfonyl chloride was purified by distillation and then treated with gaseous ammonia in dry ether to afford the sulfonamide. ^{18}O-Analysis of the sulfonamide showed that benzenesulfonic acid contained 20% of the original ^{18}O-label of **7**.

The ^{18}O-tracer experimental results in the oxidations

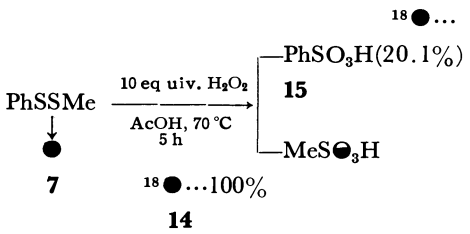

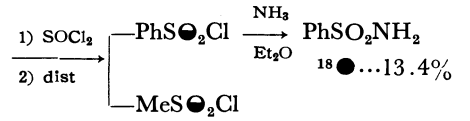

(11)

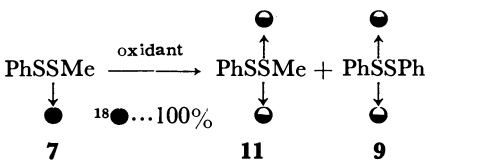

(12)

^{18}O-Incorporation

Oxidant	**11**	**9**
H_2O_2/AcOH	122%	24%
MCPBA/CH_2Cl_2	94—112%	80—84%

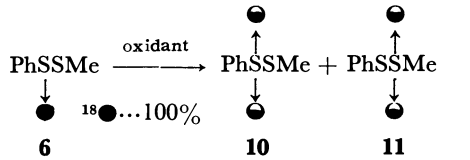

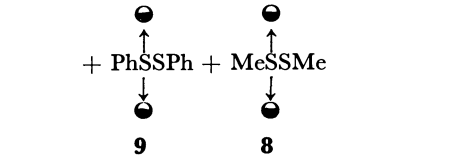

(13)

^{18}O-Incoroporation

Oxidant	**10**	**11**	**9**	**8**
H_2O_2/AcOH	102%	58—70%	108—124%	68%
MCPBA/CH_2Cl_2	—	102—109%	110—137%	—

TABLE 7. ^{18}O INCORPORATION % OF RECOVERED THIOLSULFINATE **6** IN THE OXIDATION OF **6** WITH H_2O_2 IN AcOH

Entry	Excess ^{18}O content of **6** / %	Oxidation system	Reaction Temp/°C	Reaction Time/h	Excess ^{18}O content of **6** recovered/% (Incorporated %)
1	0.53	No H_2O_2/AcOH–H_2O	19	3	0.56 (106)
2	0.53	1.2 equiv. 30% H_2O_2/AcOH	20	0.5	0.52 (98)
3	0.53	1.2 equiv. 30% H_2O_2/AcOH	20	2.5	0.50 (94)

of **7** are summarized in Eq. 12. Meanwhile, as summarized in Table 6 and Eq. 13, all four thiolsulfonates obtained in the oxidation of **6** were incorporated with considerable amounts of the original ^{18}O-label of the ^{8}O-labelled **6**. A significant product **11**, obviously oxygen-transfered oxidation product formed from **6**, contained 58—70% of the original ^{18}O-label in the oxidation of **6** with H_2O_2/AcOH, while, 100% of the original ^{18}O-label was incoroporated into **11** in the oxidation with MCPBA/CH_2Cl_2. More than 100% of the original ^{18}O-label of **6** was incorporated into **9** and the incorporation was a little greater in the oxidation with MCPBA/CH_2Cl_2 than in that with H_2O_2/AcOH.

In both oxidations of ^{18}O-labelled **6** and **7**, the following observations may be noteworthy. i) The thiolsulfonate which was formed by apparent simple oxidation of sulfinyl sulfur, keeping the original S–S bond of the thiolsulfinate, *i.e.* **10**, in the case of **6** or **11** in the case of **7**, retained completely the original ^{18}O-label in the starting materials, regardless of the oxidation conditions. ii) In the thiolsulfonates in which their sulfonyl groups are originally the sulfenyl groups of the starting thiolsulfinates, *i.e.* **9** (or **15**) from **7** and **8** and **11** from **6**, ^{18}O-incorporations of **9** from **7** and **11** from **6** in the oxidation with H_2O_2/AcOH dramatically increased in the oxidation with MCPBA/CH_2Cl_2.

Control experiments show that **6** is sufficiently stable in AcOH–H_2O system in the absence of oxidant for 20 h at 20 °C and no ^{18}O-label was lost under the conditions (Table 7). The thiolsulfinate **6** recovered after partial oxidation of ^{18}O-labelled **6** with H_2O_2 in AcOH retained almost completely the original ^{18}O-label of **6** (Table 7).

Discussion

The orientation in the oxidation of unsymmetrical disulfide **3** with peroxy acid or hydrogen peroxide was in complete accordance with the reported results in which the more electron-rich sulfur atom of disulfide is mainly oxidized,[3] since the oxidation of **3** with such an electrophilic oxidant as MCPBA or H_2O_2/AcOH is expected to take place on the sulfur atom attached to methyl group of **3**. In direct NMR study no detectable intermediate was observed and therefore the oxidation must proceed *via* usual electrophilic attack of the oxidant at sulfur atom attached to methyl group. Further continuous oxidation gave a mixture of thiolsulfonates which are well-known products in the oxidation of unsymmetrical thiolsulfinate.[5c] The formation of sulfinic and sulfonic acids was confirmed to be derived by further oxidation of thiolsulfonate (RSO_2SR) in the control experiments.[9] The fact that there was no observable peak corresponding either to α-disulfoxide ([A]) or other possible intermediates in the NMR spectra during the oxidation, may not rule out the formation of [A] as an intermediate because of the expected instability of [A].[5a]

Since the total amount of **11** is comparable to that of **7** in the oxidation of **3**, **11** seems to be formed *via* direct oxidation of sulfinyl sulfur of **7** without breaking the S–S bond. However, only a trace amount of **10** was detected (*e.g.* Fig. 3) in further oxidation of **3**, during which a substantial amount of **6** was formed. This observation suggests that the oxidation of **6** does not always give **10**. Then a question remains if there is any direct oxidation of the electron-*poor* sulfinyl sulfur of thiolsulfinate to corresponding thiolsulfonate. This question may now be answered by scrutinizing the various data accumulated on the product analyses, NMR studies, and ^{18}O-tracer experiments in the oxidations of thiolsulfinates, **6** and **7**.

The control experiments on the disproportionation of both **6** and **7** reveal that the oxidations of **6** and **7** are not complicated by the disproportionation. Neither the oxygen migration nor S–O bond fission, was found to occur, although cleavage of S–S bond usually takes place. Even when the cleavage of S–S bond takes place in the disproportionations of both **6** and **7**, there is no thiolsulfonate in which the sulfenyl sulfur of original thiolsulfinate is oxidized among the products (Eqs. 8 and 9). No ^{18}O-exchange was observed with ^{18}O-labelled thiolsulfinate under the conditions (Table 7). Thus, no side reaction was observed in the oxidations.

Formation of a trace or none of **10** in the oxidation of **7** is in keeping with the result of the oxidation of **3** with excess H_2O_2. Formation of **11** as the main product and little or no formation of **10** in the oxidation of **7** indicate that the oxidation appears to take place mainly at sulfinyl sulfur atom of **7**, although the electron-rich sulfenyl sulfur atom is usually oxidized more readily than the electron-poor sulfinyl sulfur. However, the formation of small amounts of **9** (Eq. 6) from **7** may indicate the possible formation of α-disulfoxide as an intermediate. Especially, formation of a considerable amount of **11** from **6** strongly suggests the intermediary formation of α-disulfoxide. The ^{18}O-tracer results also support the formation of α-disulfoxide (Tables 5—7).

However, the difference in the product distributions between the two oxidations of **6** and **7** with both H_2O_2/AcOH and MCPBA/CH_2Cl_2, clearly indicates that the mechanism of the oxidation of **6** is somewhat different from that of **7**. Namely, the *S*-substituent, *i.e.* phenyl *vs.* methyl, may affects substantially the distribution of products. Therefore, the oxidations of **6** and **7** cannot be explained simply by assuming the formation of a common intermediate (*i.e.* α-disulfoxide, [A]). In

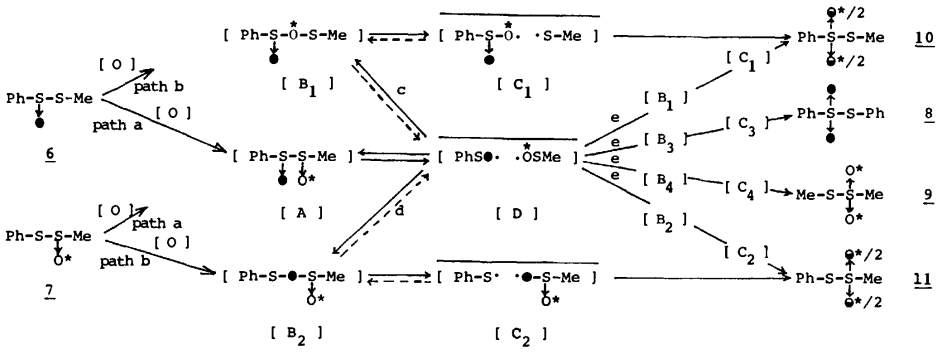

1. ●, O* ------ ^{18}O or ^{16}O(one of which is ^{18}O)
2. path e: diffusion path
3. [B_3](R= Ph), [B_4](R= Me) in [R-S(=O)-O· ·S-R]
4. [C_3](R= Ph), [C_4](R= Me) in [R-S(=O)-O-S-R]

Chart

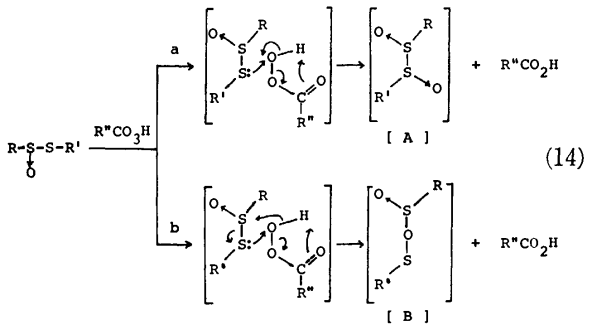

(14)

fact, the yields of the products formed by the cleavage of S–S bond (*i.e.* **8** and **9**) are greater in the oxidation of **6** than that of **7**. This may suggest that the oxidation of **6** proceeds *via* forming an intermediate of which S–S bond cleavage takes place more readily than that which would be formed in the oxidation of **7**.

Based on all these data on the product analyses and ^{18}O-tracer experiments, a few conceivable mechanistic pathways for the oxidation of unsymmetrical thiolsulfinates are illustrated in Chart. According to this chart, the initial oxidation step may involve the following two paths (Eq. 14). Path a involves the formation of α-disulfoxide *via* direct electrophilic attack of oxygen of oxidant, while path b involves the nucleophilic attack of oxygen on the sulfinyl sulfur to result in the oxygen insertion into S–S linkage to form *S*-sulfenyl sulfinate [B] which is considered to be more stable than α-disulfoxide. The oxidation of **6** may takes place mainly *via* path *a* to form α-disulfoxide, since sulfenyl sulfur of **6** is expected to be rather reactive to the electrophilic oxygen of peroxy acid. Actually, the rate of the oxidation of **6** seems to be slightly faster than that of **7**. This process is in good accordance with Kice's process on the product balance[5a] and explain the substituent effect in this oxidation.

In the mechanistic pathways, the ^{18}O-exchange process is neglected, since the homolytic cleavage of S–S bond of [A] thus formed would proceed very readily even at a low temperature to give a caged sulfinyl radical pair,[5a] which then recombines immediately to give *O*-sulfenyl sulfinate, [B_1] and [B_2]. The intermediate [B] must be also unstable and collapse to a caged radical pair [C] which recombines between both sulfur atoms to give thiolsulfonates. Since there is no energy barrier in the recombination of [C] to form stable S–S bond, the recombination of radical pair must be even faster than the diffusion of two radicals out of cage. In fact, no symmetrical disulfide was observed in our direct NMR studies, as reported earlier.[5a,e] On the other hand, since the recombination of two sulfinyl radicals [D] makes energy-rich S–O bond to form [B] (path c and d), some activation energy may be required for this process. Therefore, the diffusion of the radical pair may be faster than the recombination process. Sulfinyl radicals thus diffused may give finally two unsymmetrical thiolsulfonates (**10** and **11**) and two symmetrical thiolsulfonates (**8** and **9**), *via* [B] and [C].

The following concerted isomerization pathway cannot be completely excluded (Eqs. 15 and 16),

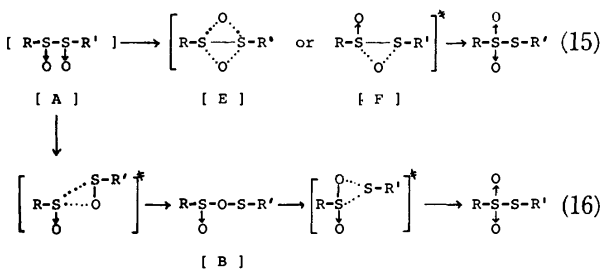

(15)

(16)

however, it is quite unlikely in view of a somewhat similar oxygen migration in the oxygen scrambling of aroyl alkyl carbonate.[10]

On the other hand, phenylthio group in **7** is a good leaving group and, the oxidation of **7** may proceed mainly *via* path b to form directly [B_2] which changes eventually to the thiolsulfonate **11** *via* [C_2]. This hypothesis may be supported by the following two observations: i) the formation of **11** predominates over those of other thiolsulfonates, *i.e.* **8**, **9**, and **10**, in the oxidation of **7**, ii) the ^{18}O-label of **11** retained nearly completely the original ^{18}O-label of **7** (Table 5).

There are following mechanistic pathways conceivable for the formation of ^{18}O-labelled **8** in the oxidation of ^{18}O-labelled **6** and that of ^{18}O-labelled **9** from ^{18}O-labelled **7**. i) If the homolytic fission-recombination

processes are all reversible as shown in Eq. 17, ^{18}O-scrambling should take place within the sulfinyl radical pair [D] and hence both **8** and **9** should be incorporated

$$[C_1] \rightleftharpoons [B_1] \rightleftharpoons [D] \rightleftharpoons [B_2] \rightleftharpoons [C_2] \quad (17)$$

with ^{18}O-label. ii) The following concerted oxygen scrambling in [A] as shown in Eq. 18 may be also

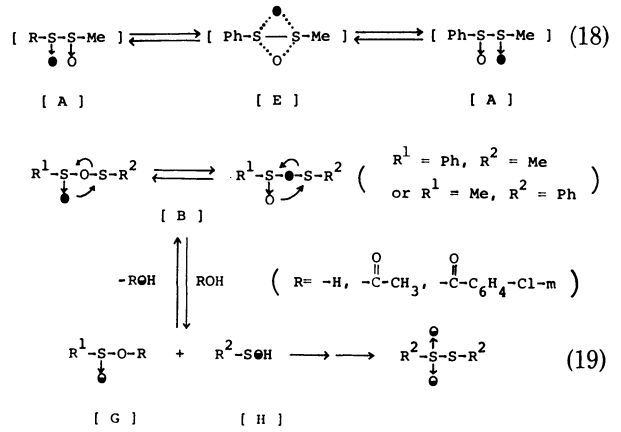

(18) (19)

conceivable. iii) The ionic path shown above is also conceivable in [B] (Eq. 19). According to this mechanistic path (iii), [B] may lose ^{18}O-label by the following reversible process, *i.e.* [B]⇄[G]+[H]. This ^{18}O-loss in [B] by this process must be greater in the oxidation system with H_2O_2/AcOH than in that with MCPBA/CH_2Cl_2. This hypothetical ^{18}O-exchange reaction between [B] and the medium can explain the fact that ^{18}O-incorporations in **11** obtained from **7** and both **9** and **11** from **6** (Eqs. 12 and 13) are greater in the oxidation with MCPBA/CH_2Cl_2 than those in the oxidation with H_2O_2/AcOH (Tables 5 and 6). Another explanation may be that the ionic ^{18}O-exchange process (Eqs. 18 and 19) is facilitated in less polar aprotic solvents while solvation of [B] and [C] does not promote the ^{18}O-exchange in a polar protic solvent.

Thus, all these hypotheses seem to be in accordance with all above experimental results in this study.

Our new selective oxidation of unsymmetrical thiolsulfinate with $NaIO_4$ gives quantitatively the corresponding unsymmetrical thiolsulfonate[11,12] by the selective oxidation of sulfinyl sulfur with IO_4^- ion without any cleavage of S–S linkage, in contrast to the oxidation with H_2O_2/AcOH or MCPBA/CH_2Cl_2 as mentioned in this paper.

Experimental

General. Melting points were taken on a Yanaco instrument and were uncorrected. NMR spectra were recorded on a Hitachi Perkin-Elmer R-20 spectrometer. Infrared spectra were obtained on a Hitachi 215 spectrometer and are uncorrected. Mass spectra were recorded on a Hitachi RMU-6MG mass spectrometer. Gas and liquid chromatographs were obtained by Shimadzu GC-6A and Yanaco L-1030 instruments, respectively.

Both oxidizing agents, 30% H_2O_2 and MCPBA were obtained from Kanto Chemicals and Wako Pure Chemicals, respectively. Deuterated acetic acid and water were of Merck.

Disulfide. Both diphenyl and dimethyl disulfides are commercially available (Tokyo Kasei Kogyo Co.). Methyl phenyl disulfide was prepared by the following procedure, according to the reported method.[7]

Methanesulfenyl chloride (0.03 mol) which was prepared by the reaction of dimethyl disulfide with gaseous chlorine in CCl_4,[13] according to the known method and purified by distillation, was dissolved in dry CCl_4 (100 ml) which was cooled to *ca.* −10 °C. To the CCl_4 solution of MeSCl, dry pyridine (0.033 mol) was added and then thiophenol (0.03 mol) in dry CCl_4 (*ca.* 50 ml) was added dropwise under cooling below 0 °C. After the addition of thiophenol, cooling bath was removed and the heterogeneous reaction mixture was stirred until the solution reached room temperature. The resulting reaction mixture was transfered into a separatory funnel, and washed with water, 5% $NaHCO_3$ aq solution, and again water. Organic layer was dried over $CaCl_2$ and CCl_4 was evaporated. The residual crude oil was purified by distillation under reduced pressure (71—72 °C/2.5—3.0 Torr, lit,[6] 79—81 °C/1.0 Torr, 1 Torr=133.322 Pa). Complete purification of unsymmetrical disulfide is very difficult. Methyl phenyl disulfide purified by the distillation also contained a small amount of diphenyl disulfide (≈5%) which was detected by GLC. Yield was *ca.* 85%. NMR ($CDCl_3$, δ, TMS) 2.40 (s, 3H, CH_3).

Thiolsulfinate. S-*Methyl methanethiosulfinate (4)*[14] used as an authentic sample, was prepared by direct oxidation of dimethyl disulfide **1** with H_2O_2 in AcOH and purified by distillation (46—47 °C/1.5 Torr). *S*-Phenyl benzenethiosulfinate (**5**), *S*-methyl benzenethiosulfinate (**6**), and *S*-phenyl methanethiosulfinate (**7**) were also prepared by the condensation of the corresponding sulfniyl chlorides and thiols in the presence of pyridine at low temperature (<0 °C), according to the usual method.[7] Yields were 80—95%. Purification of **5** was carried out by recrystallization from hexane–chloroform while **6** and **7** were purified carefully by column chromatography (silica gel, eluent: hexane: $CHCl_3$: EtOAc= 4 : 1 : 1).

S-*Phenyl Benzenethiosulfinate* **5**: Mp 69—70 °C (lit,[15] 69—70 °C).

S-*Methyl Benzenethiosulfinate* **6**: Mp 26—28 °C; NMR ($CDCl_3$, δ, TMS) 2.53 (s, 3H, CH_3), 7.30 (m, 5H, Ar); IR (neat, cm^{-1}) 3050, 2975, 2900, 1570, 1470, 1095, and 1060 (S=O), (lit,[16] 1088 ($CHCl_3$)).

S-*Phenyl Methanethiosulfinate* **7**: Mp 15—20 °C; IR (neat, cm^{-1}) 3050, 2980, 2900, 1570, 1470, 1090 (S=O), (lit,[16] 1079 ($CHCl_3$)).

Thiolsulfonate. S-*Methyl Methanethiosulfonate* **8** was prepared by the oxidation of dimethyl disulfide with H_2O_2 in AcOH and purified by distillation (59—61 °C/2.5 Torr, (lit,[17] 56.5 °C/1.0 Torr)); NMR (Table 1); IR (neat, cm^{-1}) 2925, 1430, 1410, 1335, and 1305 (SO_2), 1140 (S=O), 960, 755.

Other thiolsulfonates, **9**, **10**, and **11**, were synthesized by condensation of sulfenyl chlorides with free sulfinic acids in the presence of pyridine, as reported.[7] Products were purified by column chromatography, in a yield of 80—95%. Purification of **11** was performed also by recrystallization from hexane.

S-*Phenyl Benzenethiosulfonate* **9**: Colorless crystals from EtOH; mp 44—45 °C (lit,[18] 44—45 °C).

S-*Methyl Benzenethiosulfonate* **10**: Colorless oil, IR (neat, cm^{-1}) 3050, 3000, 2920, 1580, 1475, 1445, 1330, and 1302 (SO_2), 1042 (S=O); NMR (Table 1). Found: C, 44.92; H, 4.18%. Calcd for $C_7H_8O_2S_2$: C, 44.66; H, 4.28%.

S-*Phenyl Methanethiosulfonate* **11**: Colorless crystals from hexane having mp 85—86.5 °C; IR (KBr, cm^{-1}) 3050, 3000, 2905, 1565, 1465, 1310 (SO_2), 1130 (S=O); NMR (Table 1). Found: C, 44.78; H, 4.25%. Calcd for $C_7H_8O_2S_2$: C, 44.66; H, 4.28%.

Sulfinic and Sulfonic Acids. Methanesulfinic acid **12** was prepared by hydrolysis of methanesulfinyl chloride.[19] Free benzenesulfinic acid **13** was obtained by acidification of commercial sodium benzenesulfinate (Tokyo Kasei Kogyo Co.) with concd HCl and purified by recrystallization from water. Both methanesulfonic (**14**) and benzenesulfonic acids (**15**) were obtained commercially.

^{18}O-Labelled Thiolsulfinates, 6 and 7. ^{18}O-Labelled **6** and **7** were prepared using both ^{18}O-labelled benzenesulfinyl and methanesulfinyl chlorides, respectively, as starting materials. ^{18}O-Labelled sulfinyl chlorides were derived from non-labelled sulfinyl chlorides and ^{18}O-enriched water (*ca.* 1.5%) (eqs. 10 and 3).

To a dry ether solution (30 ml) of benzenesulfinyl chloride (0.03 mol) which was purified by distillation (72 °C/2.0 Torr), was added dropwise ^{18}O-enriched water (0.05 mol) under ccoling with ice-water bath. The reaction was considerably exothermic, with evolution of HCl gas. Benzenesulfinic acid obtained after evaporation of ether and excess water under reduced pressure, was dissolved again in ether (*ca.* 20 ml). To the stirring ether solution of the free sulfinic acid, excess distilled thionyl chloride (0.067 mol) was added then a vigorous endothermic reaction took place evolving gaseous SO_2 and HCl. The residual oil after evaporation of ether and excess thionyl chloride was purified by distillation.

^{18}O-Labelled thiolsulfinate (**6**) was prepared by treating ^{18}O-labelled benzenesulfinyl chloride with methanethiol in the presence of pyridine,[7] as mentioned above. ^{18}O-Labelled methanesulfinyl chloride was also prepared by the same method. Since the crude thiolsulfinate decomposes readily, the crude thiolsulfinate thus obtained were immediately subjected to purification by careful column chromatography (on silica gel, eluent: hexane: $CHCl_3$: EtOAc=4 : 1 : 1), in order to avoid the fast catalytic decomposition by impurities. Purified ^{18}O-labelled thiolsulfinates (**6** and **7**) were fairly stable for several days under cooling below 0 °C and contained *ca.* 0.7—0.8 atom% of ^{18}O.

Oxidation of Disulfide and Thiolsulfinate. Oxidation with H_2O_2 in AcOH: Acetic acid (*ca.* 15 ml) dissolving *ca.* 1.0 g of the substrate (disulfide or thiolsulfinate) was cooled down to nearly freezing, by an ice-water bath. Thirty percent H_2O_2 (amount shown in Tables 2—7) was added slowly dropwise to the cooled and stirred solution of the substrate and the temperature of the solution rose up by the addition. After the whole addition of H_2O_2 the mixture was warmed up to a set temperature and stirred further at the same temperature until the starting material disappeared upon monitoring by TLC or HPLC. After the reaction, the reaction mixture was diluted with 50 ml of water, transfered into a separatory funnel and extracted three times with $CHCl_3$ (≈100 ml). The combined organic layer was washed with water, sat. $NaHCO_3$ aq solution, and then water again to remove AcOH and other acid species. $CHCl_3$ was evaporated and NMR spectrum of the residue was taken. The residue was, then, subjected to separation by column chromatography (silica gel, eluent: hexane: $CHCl_3$: EtOAc=4 : 1 : 1). First fraction gave *S*-phenyl benzenethiosulfonate, **9**, second one gave *S*-methyl benzenethiosulfonate **10**, then *S*-phenyl methanethiosulfonate **11** was eluted and the last fraction contained *S*-methyl methanethiosulfonate **8**. Thiolsulfinates, **5**, **6**, and **7** were eluted between **11** and **8**, while **4** appeared after **8**. **10** and **11** were separated completely by repeated column chromatography in which first fraction gave colorless solid **11** and the following fraction afforded colorless oil **10**. They were identified by comparing their NMR, IR, GLC, HPLC, and melting points with those of authentic samples prepared independently.

Meanwhile, the combined aqueous layer which was neutralized by sat. $NaHCO_3$ solution was concentrated by complete evaporation of water. Sulfinic and sulfonic acids (salts) were determined by NMR spectra in D_2O in which methyl signals of both sodium salts of **12** and **14** appeared in the range of 2.15—2.30 and 2.75—2.82 ppm, respectively, depending on the pH of the solution.

Oxidation with MCPBA in CH_2Cl_2: To a cooled (*ca.* 0 °C) solution of *ca.* 1.0 g of the substrate in CH_2Cl_2 (*ca.* 20 ml) was added powdered MCPBA (1.0—2.0 equiv., amount are shown in Tables 2—7) slowly. The reaction mixture was warmed and stirred at a set temperature until the starting material disappeared upon monitoring by TLC or HPLC. The reaction mixture was washed with 5% $NaHCO_3$ aq. solution and water after the reaction. Both the organic and aqueous layers were treated with the same procedures as described above.

Yields of the products which were determined in connection with the data of NMR, GLC, and HPLC, are shown in Tables 2—7.

Oxidation in NMR Sample Tube: An NMR spectrum of the substrate (0.4—0.5 mmol) was measured in CD_3COOD or $CDCl_3$ (430 μl). To the solution in NMR sample tube 30% H_2O_2 or powdered MCPBA (amount listed in Tables 2—7) was added at a set temperature and immediately MNR spectra of the resulting mixture were taken at a few time intervals. After the reaction completed, GC and HPLC of the reaction mixture were measured to determine the yields of the products.

^{18}O-Tracer Experiments: Products thus obtained and purified were well dried *in vacuo* with slightly heating. ^{18}O-Labelled *S*-methyl benzenethiosulfinate **6** recovered during the oxidation was purified by column chromatography (silica gel, eluent: hexane: $CHCl_3$: EtOAc=4 : 1 : 1). It was eluted as a colorless oil after **9**, **10**, and **11**.

^{18}O-Tracer analysis was carried out by the method developed by Rittenberg and Ponticorvo,[20] with a slight modification, using $Pb(OAc)_2$ to remove H_2S gas formed by the thermolysis of the sample.

Twenty mg of sample was pyrolyzed with 300 mg of purified $HgCl_2$ and $Hg(CN)_2$, respectively, in an evacuated, sealed Pyrex tube at *ca.* 500 °C for 12 h. Then the tube was broken in a vacuum line and CO_2 gas formed was purified by distillation and the mass peaks of *m/e* 44 and 46 which correspond to $C^{16}O_2$ and $C^{16}O^{18}O$, respectively, were recorded on a mass spectrometer.

Derivation of Benzenesulfonamide from Benzenesulfonic Acid in the Oxidation of ^{18}O-Labelled Thiolsulfinate 7 with H_2O_2/AcOH: The reaction mixture resulted by the complete oxidation of ^{18}O-labelled *S*-phenyl methanethiosulfinate **7** (437 mg) with ten equivalents of 30% H_2O_2 (2.65 g) in AcOH (9 ml) at 70 °C for 5 h, contained only both methane- and benzenesulfonic acids. To the reaction mixture a small amount of MnO_2 was added to decompose excess H_2O_2. After filtration, acetic acid and water were evaporated by heating. Into the residue containing two sulfonic acids, was added excess thionyl chloride (10 mmol). The resulting mixture, after evaporation under reduced pressure to remove excess thionyl chloride, was distilled to separate two fractions (bp 62 °C/21 Torr and 70 °C/1 Torr) which were methane- and benzenesulfonyl chlorides, respectively. Distilled benzenesulfonyl chloride was dissolved in dry ether and gaseous ammonia was introduced into the solution. The white solid of NH_4Cl was filtered. The solid residure after evaporation of ether was benzenesulfonamide (43 mg) which was purified by recrystallization from ether–ethyl acetate mixed solvent (30 : 1) and then subjected to the routine ^{18}O-analysis.

References

1) S. Oae, Y. H. Kim, T. Takata, and D. Fukushima, *Tetrahedron Lett.*, **1977**, 1195.

2) Address correspondence to Department of Chemistry, The Korea Advanced Institute of Science, P. O. Box 150, Chongyangni, Seoul, Korea.

3) a) G. Leandri, and A. Tundo, *Ann. Chim. (Rome)*, **44**, 74 (1964); b) W. Walter and P.-M. Hell, *Justus Liebigs Ann. Chem.*, **727**, 35 (1969); c) E. Block and J. O'Connor, *J. Am. Chem. Soc.*, **96**, 3291 (1974).

4) a) H. Kawasaki and H. Yonemoto, *Yakugaku Zasshi*, **77**, 640 (1957); b) I. Utsumi, T. Watanabe, K. Harada, and G. Tsukamoto, *Chem. Pharm. Bull.*, **15**, 1485 (1967).

5) a) M. M. Chau and J. L. Kice, *J. Am. Chem. Soc.*, **98**, 7711 (1976); b) D. Barnard, *J. Chem. Soc.*, **1957**, 4637; c) D. Barnard and E. J. Percy, *Chem. Ind.*, **1960**, 1332; d) U. Marangelli, G. Modena, and P. E. Todesco, *Gazz. Chim. Ital.*, **90**, 681 (1960); e) G. Modena and P. E. Todesco, *Ric. Sci.*, **30**, 1788 (1960); f) T. F. Lavine, G. Toennies, and E. C. Wagner, *J. Am. Chem. Soc.*, **56**, 242 (1934); g) W. E. Savige, J. Eager, J. A. Maclaren, and C. M. Ruxburgh, *Tetrahedron Lett.*, **1964**, 3289; h) G. Toennies and T. F. Lavine, *J. Biol. Chem.*, **113**, 57 (1936); i) T. F. Lavine, *ibid.* **113**, 583 (1936); j) G.E. Utzinger, *Experientia*, **16**, 136 (1960); **17**, 374 (1961); k) After completion of this work, Freeman *et al.* reported the detection of α-disulfoxide in direct NMR study at low temperature: F. Freeman and C. N. Angeletakis, *J. Am. Chem. Soc.*, **103**, 6232 (1981).

6) S. Oae, Y. H. Kim, D. Fukushima, and K. Shinhama, *J. Chem. Soc., Perkin Trans. 1*, **1978**, 913.

7) S. Oae, T. Takata, and Y. H. Kim, *Tetrahedron*, **37**, 37 (1981).

8) P. Koch, E. Ciuffarin, and A. Fava, *J. Am. Chem. Soc.*, **92**, 5971 (1970).

9) S. Oae and T. Takata, *Chem. Lett.*, **1981**, 845.

10) S. Oae, Y. Uchida, K. Fujimori, and S. Kozuka, *Bull. Chem. Soc. Jpn.*, **46**, 1741 (1973).

11) Y. H. Kim, T. Takata, and S. Oae, *Tetrahedron Lett.*, **1978**, 2305.

12) S. Oae and T. Takata, *Tetrahedron Lett.*, **21**, 3213 (1980).

13) C. J. M. Stirling, *J. Chem. Soc.*, **1957**, 3597.

14) L. D. Small, J. H. Baily, and C. J. Cavallito, *J. Am. Chem. Soc.*, **69**, 1710 (1947).

15) S. Oae, Y. Yoshikawa, and W. Tagaki, *Bull. Chem. Soc. Jpn.*, **42**, 2899 (1969).

16) G. Ghersetti and G. Modena, *Spectrochim. Acta*, **19**, 1809 (1963).

17) E. Block and J. O'Connor, *J. Am. Chem. Soc.*, **96**, 3929 (1974).

18) S. Oae, R. Nomura, Y. Yoshikawa, and W. Tagaki, *Bull. Chem. Soc. Jpn.*, **42**, 2903 (1969).

19) F. Wudl, D. A. Lightner, and D. J. Cram, *J. Am. Chem. Soc.*, **89**, 4099 (1967).

20) D. Rittenberg and L. Ponticorvo, *J. Appl. Rad. Isotopes*, **1**, 208 (1956).

An Application of Molecular Mechanics Calculations on Thermal Reactions of Ten-membered Ring Sesquiterpenes

Yukimasa TERADA* and Shosuke YAMAMURA†

Faculty of Pharmacy, Meijo University, Tenpaku-ku, Nagoya 468

†*Department of Chemistry, Faculty of Science and Technology, Keio University, Hiyoshi, Kohoku-ku, Yokohama 223*

(Received January 28, 1982)

Molecular mechanics calculations were successfully carried out to evaluate relative stabilities of each conformation of germacrenes in their ground states and transition states. In the calculation of such a transition state model as shown in Scheme 1, the parameters for partial bonds were taken as mean values of those for a reactant and a product. Thus, the calculation results on each transition state model indicate that the elemenes are formed from the corresponding germacrenes through the most stable transition state (CC), regardless of the most stable conformers in ground state. Calculations were also carried out on ground and transition states of acoragermacrone and isoacoragermacrone, both of which have an α,β-unsaturated carbonyl system. The calculation results on each transition state model indicate that shyobunone (**5**) and epishyobunone (**6**) both are formed from acoragermacrone through the corresponding transition states [**5** from CC; **6** from C'C' and C'T] in relative ratio (**5**/**6**=87/13) which is in good agreement with that of the experimental result (**5**/**6**=84/16). In the case of isoacoragermacrone, molecular mechanics calculations indicate that the preisocalamendiol-type transition state model is more favorable than the models corresponding to the Cope rearrangement products.

Conformation of ten-membered ring sesquiterpenes has been studied extensively, in connection with biosyntheses of many other types of sesquiterpene. Frequently, the ground state conformation of ten-membered ring sesquiterpenes was discussed in relation to the structure of their reaction products,[1] while it was also pointed out that the crown-like transition state is most favorable and determines the configuration of products.[2]

From the pioneering work by Hammond, a number of theoretical consideration to deduce the transition state structure have been made.[3] Moreover recently, semi-empirical[4] and non-empirical[5] molecular orbital methods have also been used to predict the transition states and reaction processes. At present, however, these theoretical methods can be applied to relatively small molecules and simple reactions.

On the other hand, the frontier orbitals method[6] and the Woodward-Hoffmann rule,[7] both are extremely convenient and effective for deducing the structure of reaction product, but these methods are inefficient if the reaction conformer differs from the most stable conformer in the ground state.

The molecular mechanics calculations can be carried out easily and inexpensively, even on relatively large organic molecules, therefore, this calculation method has been widely used. Essentially, however, this method can only be used to such a molecule which consists of atomic groups with experimentally determined parameters. On this condition, there have been made some efforts to apply the molecular mechanics method on treatment of the transition states of oxidation reactions.[8] In the present paper, independently of these attempts, we wish to describe a successful application of the molecular mechanics calculations to a transition state model in thermal reactions of ten-membered ring sesquiterpenes. In this calculation method the transition state model was represented by a plausible structure with partial bonds, the parameters for which were taken as mean values of those for a reactant and a product.

Method of Calculation

Inspection of molecular models shows that each plane of the endocyclic double bond must be placed approximately perpendicular to the average plane of the ten-membered ring. Consequently, several stable conformers are possible for individual sesquiterpene. Steric energies of these conformers in ground state were calculated by means of the program COORD[9] with bond lengths, bond angles, and torsional angles obtainable from Dreiding molecular models, and then iterative calculations were made to minimize the steric energy of each conformer by means of the program MMI and MMPI.[10] Relative populations of these conformers at given temperature were calculated with energy values so far obtained, assuming they are in an equilibrium.

Transition State Model of Cope Rearrangement. In the reaction process of Cope rearrangement from germacrenes (**1**) to elemenes (**3**), we have proposed such a transition state model (**2**)[11] as shown in Scheme 1, and have applied molecular mechanics calculations to this model.[12]

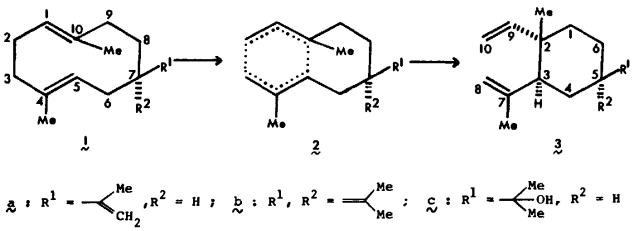

Scheme 1. Thermal isomerizations of germacrenes.

Several modifications were required for application of program MMI to such a transition state model. Thus, in the energy minimize calculations of the transition state model (**2**), iterative calculations were made starting from the co-ordinate set corresponding to the each stable conformer in ground state, except for the co-ordinates of C_{10}. The position of C_{10} in **2** was located

TABLE 1. STERIC ENERGY AND RELATIVE POPULATION OF GERMACRENES IN EACH GROUND AND TRANSITION STATE

		Ground state		Transition state	
		Steric energy kcal mol^{-1}	Relative population % at 25 °C	Steric energy kcal mol^{-1}	Relative population[a] %
Germacrene-A	CC	22.91	62.3	33.47	at 25 °C 100.0
	TC	23.24	35.7	40.61	0.0
	T'C	25.09	1.6	39.36	0.0
	C'T	25.97	0.4	38.31	0.0
Germacrene-B	CC	23.13	34.7	35.85	at 120 °C 86.3
	CT	22.91	50.5	37.29	13.6
	TT'	23.94	8.8	41.57	0.1
	TC'	24.17	6.0	41.66	0.1
Hedycaryol	CC	25.57	28.8	37.56	at 400 °C 95.8
	C'T	26.45	6.5	42.38	2.6
	TC	25.11	62.0	44.44	0.6
	T'C	26.98	2.6	43.64	1.0

a) Experimentally, each thermal isomerization has been carried out at thecited temperature.

on a line between C_5 and C_{10} in **1**, assuming that the partially formed bond length ($C_5 \cdots C_{10}$) in **2** is equal to a mean value between the distance from C_5 to C_{10} in **1** and bond length $C_2—C_3$ in the product (**3**). The energy minimize calculations were executed fixing the positions of C_5 and C_{10} at the given positions and releasing all other part of molecule.

The parameters for the unusual bonds, which are characteristic of the transition state model (**2**) and not included originally in program MMI, were calculated by means of a simple arithmetical procedure. Accordingly, the parameters for the partial bonds were regarded as mean values of those of initial and final states: *e.g.* parameters for C···C in **2** were assumed to be mean values of C=C and C–C. Similarly, parameters for C···C were regarded as the half of C–C. The partially splitting bond length of $C_2 \cdots C_3$ was assumed to be 3.36 Å, which roughly corresponds to a mean value of the bond length C_2–C_3 in germacrenes and the average intramolecular distance between C_8 and C_{10} in elemenes.[13]

We supposed, furthermore, the steric energy calculated for the transition state model, corresponds or is at least proportional to the height of the energy barrier of the Cope rearrangement, and the probability of the reaction can be substituted by the relative population of the transition state models in each conformation, under assumption of the Boltzmann's distribution.

Transition State Model for Preisocalamendiol-type Rearrangement. On thermal rearrangement of preisocalamendiol, such a transition state model (**A**) as shown in Scheme 4 was proposed,[14] and application of molecular mechanics calculations to this type of transition state model revealed to be in good agreement with the experimental results.[15] The co-ordinates of C_1 in **A** was calculated according to the same manner as that of the Cope rearrangement-type transition state. Each position of the remaining atoms except for C_1 and C_6 varied in the course of energy minimization.

Of the plausible conformers which arise from calculations of the ground state, some of them can adopt such a transition state as **A**, in which the carbonyl group and the methyl group on vinylic carbon C_{10} both are located on the same side of a plane of the ten-membered ring.

The partial bond lengths of O···H and C_{15}···H both are assumed approximately to be 1.7 Å, on the basis of the distance between O and C_{15} in the initial and final states of the reaction, as well as of an assumption in which this proton is nearly placed at the equidistant point from both O and C_{15} in the transition state model.

Parameters for the partial bonds were estimated according to the same procedure as described above.

Results and Discussion

Germacrene-A (1a). Germacrene-A (**1a**), a ten-membered ring sesquiterpene isolated from a sea fan, is an unstable compound and spontaneously converted into the corresponding elemene (**3a**),[16] as shown in Scheme 1. Molecular mechanics calculations on the four conformers of **1a** were carried out to deduce the main conformations with energy minima and their results were summarized in Table 1.

Further calculations were also made on the transition state models corresponding to the conformers in each ground state, as shown in Scheme 2. The resulting

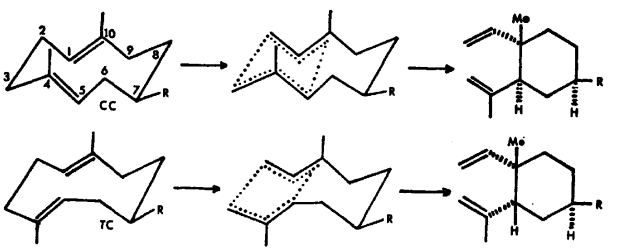

Scheme 2. Two possible isomerization of germacrenes.

structures of CC and TC in their transition states are shown in Fig. 1 and their steric energies and relative populations are also summarized in Table 1.

From these data, it is evident that the most stable conformation of **1a** in a ground state is directly related to the corresponding elemene (**3a**) through the most stable transition state CC.

Germacrene-B (1b). Molecular mechanics calculations were carried out on germacrene-B (**1b**) which

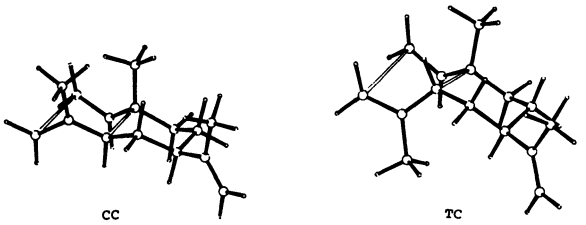

Fig. 1. Calculated minimum energy structures of two conformations of germacrene-A (**1a**) in transition states. The hollow bonds depict the partial bonds $C_5 \cdots C_{10}$ and $C_2 \cdots C_3$.[17]

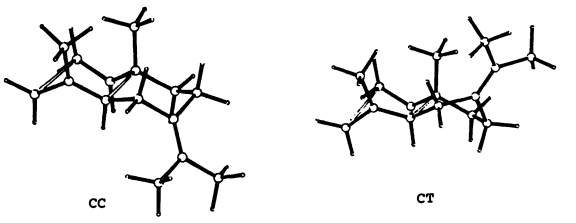

Fig. 2. Calculated minimum energy structures of two stable conformations of germacrene-B (**1b**) in transition states.

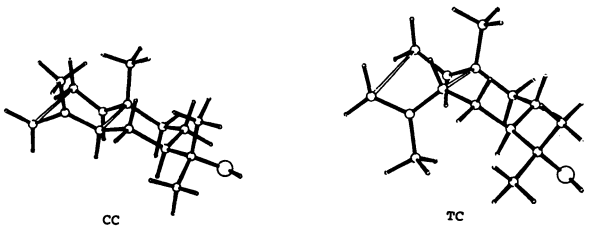

Fig. 3. Calculated minimum energy structures of two conformations of hedycaryol (**1c**) in transition states.

was also known to be thermally converted into the corresponding elemene (**3b**),[2b] indicating that the conformation CT is most stable,[18] although an X-ray crystallographic analysis revealed that a 1 : 1 silver nitrate adduct of **1b** adopts the conformation CC in a crystal state.[19] Of the two transition state models CC and CT (see Fig. 2), it is noteworthy that the former is more stable than CT,[20] as shown in Table 1. However, the same elemene must be derived from both CC and CT.

Hedycaryol (1c). In the case of hedycaryol (**1c**), its molecular mechanics calculations revealed that the favorable conformation in a ground state does not correspond to the structure of elemene (**3c**).[21] Therefore, we also applied the molecular mechanics calculations to such transition state models as shown in Scheme 2. The resulting structures of CC and TC in their transition states are shown in Fig. 3 and their steric energies and relative populations are also shown in Table 1. The conformation CC in the ground state is less stable than another conformation TC by 0.46 kcal/mol.[21] In their transition states, however, the conformation CC is more stable than the latter TC by 6.9 kcal/mol.

Acoragermacrone (4). Acoragermacrone (**4**) and isoacoragermacrone (**7**) both have an α,β-unsaturated carbonyl group. From a biogenetic point of view, acoragermacrone (**4**), an attractant of fruit-fly species,[22] is regarded as an important precursor of many sesquiterpenes which have been isolated from the plant *Acorus calamus* L.[11,23] In fact, Cope rearrangement of **4** affords shyobunone (**5**) and epishyobunone (**6**), both of which co-occur in the same plant, as shown in Scheme 3.[11,23]

Molecular mechanics calculations on the plausible conformers of **4** were carried out using program MMPI to deduce the main conformations with energy minima

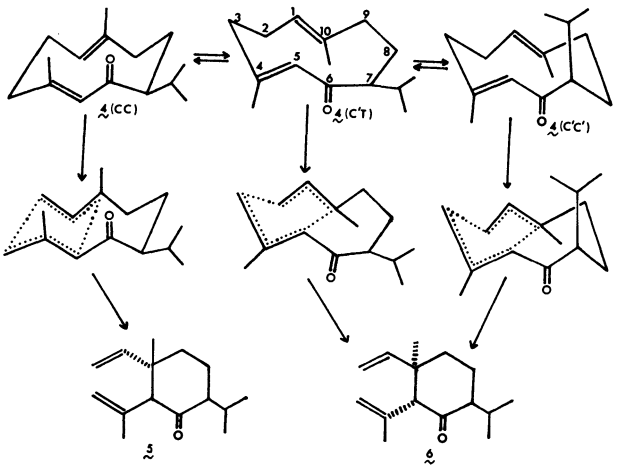

Scheme 3. Thermal isomerization of acoragermacrone (**4**).

Table 2. Relative population of each conformation of **4** in both ground and transition states

Conformer	Ground state		Transition state		Product
	Steric energy[a] / kcal mol^{-1}	Relative population / % at 25 °C	Steric energy / kcal mol^{-1}	Relative population / % at 110 °C	
CC	25.17(−39.22)	80.8	36.40	87.0	Shyobunone (**5**)
C'C'	26.11(−38.29)	16.6	38.14	10.4	
C'T	27.25(−37.14)	2.4	39.11	2.5	Epishyobunone (**6**)
C'T'	30.76(−33.63)	0.0	50.21	0.0	
TT'	29.35(−35.04)	0.1	44.91	0.0	
T'C'	29.33(−35.06)	0.1	42.35	0.0	
T'C	30.67(−33.72)	0.0	51.39	0.0	

a) Heat of formation is also shown in parenthesis.

TABLE 3. HEATS OF FORMATION (kcal mol^{-1}) OF PLAUSIBLE CONFORMATIONS OF **7** IN TWO DIFFERENT TRANSITION STATES

Conformer	Ground state[a)]	Transition state	
		Preisocalamendiol-type	Cope rearrangement type
TC	−43.09(74.6)	−8.99	−0.21
C'T	−42.09(13.8)		−7.36
CT	−41.82(8.7)		−6.05
T'T'	−41.15(2.8)	−6.53	2.60
T'C'	−37.77(0.0)	−3.34	2.48

a) Relative population(%) at 25 °C is also shown in parenthesis.

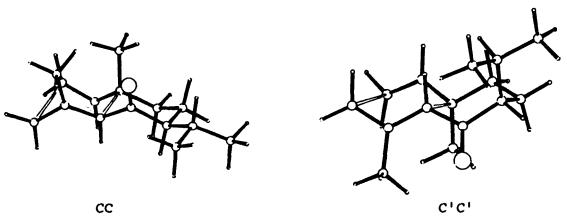

Fig. 4. Calculated minimum energy structures of two conformations of acoragermacrone (**4**) in transition states.

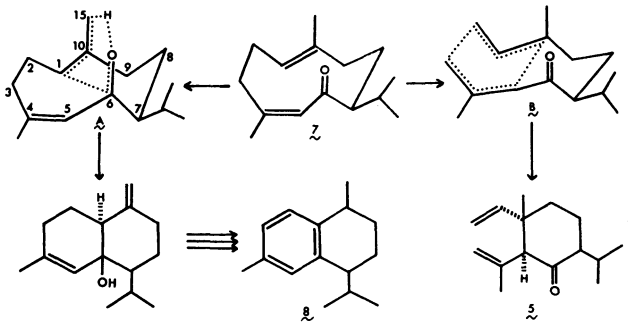

Scheme 4. Thermal isomerization of isoacoragermacrone (**7**).

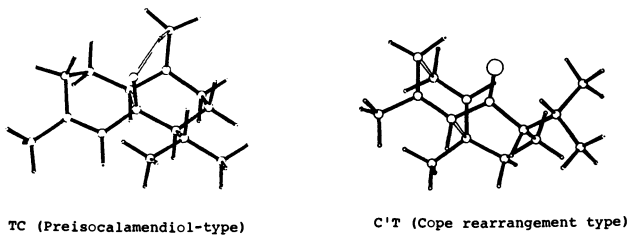

Fig. 5. Calculated minimum energy structures of most stable conformers in each different transition state model of **7**.

and their results were summarized in Table 2. Further calculations were also made on the transition state models corresponding to the conformers in each ground state (see Table 2). Thus, of seven transition state models, the most stable one is CC (see Fig. 4), from which shyobunone (**5**) must be produced. On the other hand, it is noted that epishyobunone (**6**) can be formed mainly from C'C' (see Fig. 4) and slightly from C'T, as seen in Table 2. Furthermore, the relative ratio (**5**/**6**=87/13) is in good agreement with that of the experimental result (**5**/**6**=84/16).

Isoacoragermacrone (7). We further applied molecular mechanics calculations to the possible conformers of isoacoragermacrone (**7**), in each ground state, and these results were summarized in Table 3. As expected from the base-catalyzed reactions of **7**,[11] clearly, isoacoragermacrone (**7**) is more stable than acoragermacrone (**4**) (see Tables 2 and 3). In the case of **7**, furthermore, two possible transition state models were considered as follows.

One of them is a presiocalamendiol-type transition state model (**A**)[15] leading to the formation of cadinene (**8**), as shown in Scheme 4. The remaining one is such a model as shown in Scheme 3, leading to the formation of Cope rearrangement products (see Scheme 4). Thus, molecular mechanics calculations were made on these two different models, and their results were summarized in Table 3. In addition, the most stable conformers in each different transition state model are shown in Fig. 5. As judged from these calculation data, clearly, the preisocalamendiol-type transition state model is more favorable than the models corresponding to each Cope rearrangement product.[24] This is compatible with the experimental results of thermal reaction of isoacoragermacrone (**7**).[25]

Conclusion

Although, germacrenes having an (*E*,*E*)-1,5-cyclodecadiene system are known to prefer the crossed conformation,[1a,2c,26] it has been proved that the stability of this system is affected by the substituent at C_7. Moreover, all sesquiterpenes calculated in this report exist in more than two conformers.[1a,21,27]

In the case of Cope rearrangement, however, the elemenes are formed from the corresponding germacrenes through the most stable transition state, regardless of the stable conformers in each ground state.[28] Moreover, the most favorable transition state of (*E*,*E*)-cyclodecadiene system is always CC, as pointed out before.[2] When the 1,5-cyclodecadiene system has carbonyl group at C_6 and one of the double bonds is *Z*-type or exocyclic,[15] the preisocalamendiol-type transition state is preferred rather than the Cope rearrangement type one. But, in the case of (*E*,*E*)-1,5-cyclodecadiene, large strain energy to form the $C_1 \cdots C_6$ partial bond prevents the preisocalamendiol-type transition state, resulting mainly in the formation of Cope rearrangement products.

Finally, our procedure, to which the ordinarily used programs are applied taking modified parameters

calculated by means of simple arithmetic way for partial bonds, has been proved to be quite useful in order to estimate the stereochemistry and the reaction product's ratio in thermal reactions of germacrenes and germacrones.

The authors wish to thank Professor N. L. Allinger (University of Georgia) and Professor E. Osawa (Hokkaido University) for their kind permission to use their MMI/MMPI programs. They are also indebted to Professor K. Sasaki (Nagoya University) for his helpful discussion. The molecular mechanics calculations were carried out using a FACOM 230-75 computer at Nagoya University Computation Center.

References

1) a) K. Takeda, *Tetrahedron*, **30**, 1525 (1974); b) N. S. Zefirov, *ibid.*, **33**, 2719 (1977).

2) a) J. K. Sutherland, *Tetrahedron*, **30**, 1651 (1974); b) E. D. Brown, T. W. Sam, J. K. Sutherland, and A. Torre, *J. Chem. Soc., Perkin Trans. 1*, **1975**, 2326; c) N. S. Bhacca and N. H. Fisher, *Chem. Commun.*, **1969**, 68.

3) G. S. Hammond, *J. Am. Chem. Soc.*, **77**, 334 (1955); T. Ando and H. Yamataka, *Kagaku No Ryoiki*, **35**, 483 and 584 (1981) and references cited therein.

4) M. J. S. Dewar, *Chem. Brit.*, **1975**, 97.

5) H. F. Schaefer, "The Electronic Structure of Atoms and Molecules: A Survey of Rigorous Quantum Mechanical Results," Addison-Wesley, Reading, Mass. (1972).

6) I. Fleming, "Frontier Orbitals and Organic Chemical Reactions," William Clowes and Sons, London (1976).

7) R. B. Woodward and R. Hoffmann, "The Conservation of Orbital Symmetry," Academic Press, New York (1970).

8) J. Perlberger and P. Muller, *J. Am. Chem. Soc.*, **99**, 6136 (1977); W. T. Wipke and P. Gund, *ibid.*, **98**, 8107 (1976).

9) J. Rhee, COORD program, QCPE, # 226.

10) N. L. Allinger and Y. H. Yuh, MMI/MMPI program (1973), QCPE, # 318.

11) M. Niwa, A. Nishiyama, N. Iguchi, and S. Yamamura, *Bull. Chem. Soc. Jpn.*, **48**, 2930 (1975).

12) Y. Terada and S. Yamamura, *Tetrahedron Lett.*, **1979**, 3303.

13) For a few conformers of acoragermacrone (**4**), a series of calculations were made changing the $C_2 \cdots C_3$ partial bond length, namely 2.2, 2.5, 2.7, and 3.36 Å in order. Although the length of 2.5 Å afforded the smallest strain energy value for each conformer, 3.36 Å was chosen, because this length gave best fit to experimental product's ratio. Therefore, it can be thought that the bond length of $C_2 \cdots C_3$ has some ambiguity.

14) M. Niwa, M. Iguchi, and S. Yamamura, *Bull. Chem. Soc. Jpn.*, **49**, 3148 (1976).

15) Y. Terada and S. Yamamura, *Tetrahedron Lett.*, **1979**, 1623.

16) A. J. Weinheimer, W. W. Youngblood, P. H. Washecheck, T. K. B. Karns, and L. S. Ciereszko, *Tetrahedron Lett.*, **1970**, 497.

17) ORTEP drawing was carried out using a program made by C. K. Johnson and revised by K. Sasaki.

18) Identical result has been reported; H. Shirahama, E. Osawa, and T. Matsumoto, *Tetrahedron Lett.*, **1979**, 2245.

19) F. H. Allen and D. Rogers, *J. Chem. Soc., B*, **1971**, 257.

20) This is compatible with the result in which cyclization of germacrene-B to selinane derivatives proceeds through the crown conformer.[2b]

21) E. Osawa, K. Shimada, M. Kodama, and S. Ito, *Tetrahedron Lett.*, **1979**, 2353.

22) M. Jacobson, I. Keiser, D. Miyashita, and E. J. Harris, *Lloydia*, **39**, 412 (1976).

23) S. Yamamura, M. Iguchi, A. Nishiyama, M. Niwa, H. Koyama, and Y. Hirata, *Tetrahedron*, **27**, 5419 (1971); M. Niwa, Y. Terada, M. Iguchi, and S. Yamamura, *Chem. Lett.*, **1977**, 1415.

24) Calculations for preisocalamendiol-type transition state model of acoragermacrone (**4**), revealed that the heat of formation of the lowest energy transition state is about 15 kcal/mol higher than corresponding one of Cope rearrangement. In fact, thermal reaction of accoragermarone (**4**) afforded exclusively the Cope rearrangement product, as shown in Table 2.

25) M. Iguchi, A. Nishiyama, S. Yamamura, and Y. Hirata, *Tetrahedron Lett.*, **1969**, 4295.

26) F. H. Allen and D. Rogers, *Chem. Commun.*, **1967**, 558; J. McClure, G. A. Sim, P. Coggon, and A. T. McPhail, *ibid.*, **1970**, 128; F. Sǒrm, M. Suchý, M. Holub, A. Línec, I. Hodinec, and C. Novák, *Tetrahedron Lett.*, **1970**, 1893; F. A. L. Anet and A. J. R. Bourn, *J. Am. Chem. Soc.*, **87**, 5250 (1965); see also Ref. 25.

27) H. Yoshioka, T. J. Mabry, and H. E. Miller, *Chem. Commun.*, **1968**, 1679; R. K. Bently, J. G. St. C. Buchanan, T. G. Halsall, and V. Thaller, *ibid.*, **1970**, 435.

28) The energy barrier of the interchange between the conformational isomers in the ground state is much lower than the activation energy of the rearrangement. Therefore, it can be thought that the relative stabilities of conformers in the ground state are not so important for the consideration of the subsequent reaction process.

The Synthesis of Racemic Fomannoxin, Anodendroic Acid, and 5-Acetyl-2-[1-(hydroxymethyl)vinyl]-2,3-dihydrobenzofuran

Seiji YAMAGUCHI, Seizo KONDO, Keiko SHIMOKAWA, Osamu INOUE, Michiko SANNOMIYA, and Yoshiyuki KAWASE*

Department of Chemistry, Faculty of Science, Toyama University, Gofuku 3190, Toyama 930

(Received February 4, 1982)

2-Isopropenyl-2,3-dihydrobenzofuran was effectively prepared by two new methods. Fomannoxin and 5-acetyl-2-[1-(hydroxymethyl)vinyl]-2,3-dihydrobenzofuran were synthesized from 2-isopropenyl-2,3-dihydrobenzofuran, while anodendroic acid was synthesized from 2-(1-hydroxy-1-methylethyl)-2,3-dihydrobenzofuran.

Three optically active 2,3-dihydrobenzofuran derivatives, fomannoxin (**1**),[1] anodendroic acid (**2**),[2] and (−)-5-acetyl-2-[1-(hydroxymethyl)vinyl]-2,3-dihydrobenzofuran (**3**),[3] have been isolated from natural sources. We have already reported the synthesis of these three compounds in two short communications.[4,5] Now, we wish to report the details and some added data.

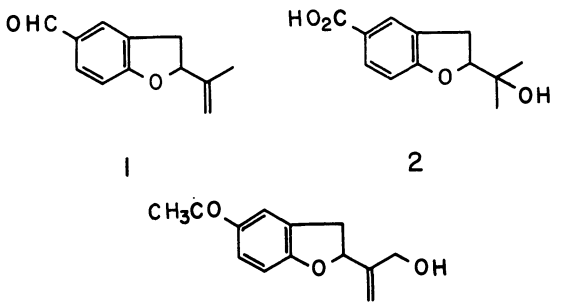

1 2 3

Chart 1.

For the synthesis of **1** and **3**, an effective method of preparing 2-isopropenyl-2,3-dihydrobenzofuran (**7**) is required. In 1963, DeGraw *et al.* reported the preparation of **7**.[6] They prepared **7** by two methods, the Wittig reaction of 2-acetyl-2,3-dihydrobenzofuran (**4**) and the dehydration of 2-(1-hydroxy-1-methylethyl)-2,3-dihydrobenzofuran (**5**). However, the dehydration of **5** with phosphoryl chloride–pyridine gave a mixture of **7** and 2-isopropylbenzofuran, the components of which were difficult to separate. Also, the Wittig reaction of **4** gave only a 6% yield. We studied other dehydration methods. **7** was obtained in a 49% yield by refluxing in phenyl isocyanate for 16 h. In this dehydration reaction, longer refluxing caused a isomerization to 2-isopropylbenzofuran; 2-isopropylbenzofuran was only obtained after refluxing for 60 h, while a mixture of **7** and 2-isopropylbenzofuran was obtained after 22 h. In 1958, Nickl reported that a 2-isopropenyl-2,3-dihydrobenzofuran derivative was obtained from 2,4,6-trihydroxyacetophenone and 1,4-dibromo-2-methyl-2-butene.[7] Now, we have applied this reaction to phenol, thus obtaining **7** in one step in a 43% yield.

Hirotani *et al.* isolated (+)-2-isopropenyl-2,3-dihydrobenzofuran-5-carbaldehyde from *Fomes annosus*; they named it fomannoxin.[1] Fomannoxin had a structure very similar to that of tremetone (**16**), but it showed the opposite optical rotation and the opposite absolute

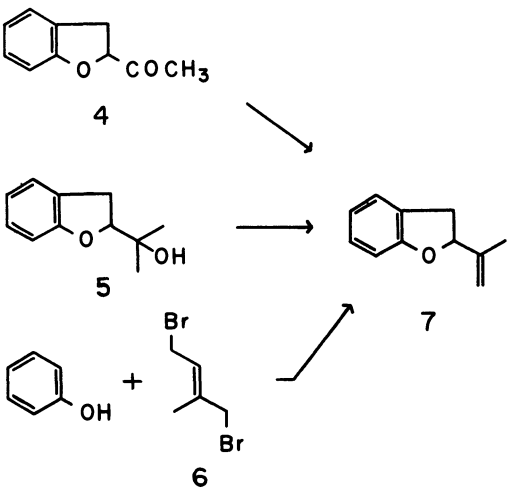

Chart 2.

configuration. This shows the existence of different biosynthetic cyclizations in different families of plants.[8] First, when Nickl's method was applied to *p*-hydroxybenzaldehyde, fomannoxin was not obtained. Next, it was used in an attempt to convert 5-bromo- and 5-iodo-2-isopropenyl-2,3-dihydrobenzofuran (**8a**, **b**), obtained from *p*-bromo- and *p*-iodophenol by Nickl's method, to **1** or 2-isopropenyl-2,3-dihydrobenzofuran-5-carboxylic acid (**13**) through the corresponding Grignard reagents. However, these attempts were all unsuccessful because of the inactivity of **8a** and **8b** to magnesium metal. Then, we tried to formylate **7** to **1**; the formylation of **7** with *N*-methylformanilide–phosphoryl chloride gave the desired aldehyde (**1**) in a 41% yield. The IR and ^{1}H-NMR spectra were identical with those of natural fomannoxin.[1]

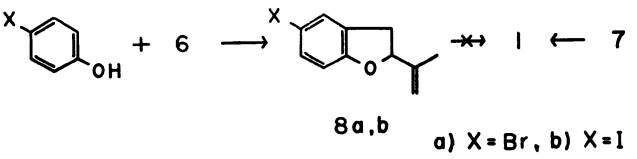

Chart 3.

Shima *et al.* isolated (−)-2-(1-hydroxy-1-methylethyl)-2,3-dihydrobenzofuran-5-carboxylic acid (**2**) from *Anodendron affine* and named it anodendroic acid.[2] The Vilsmeyer formylation of the acetate (**9**) with *N*-methylformanilide–phosphoryl chloride gave a mixture

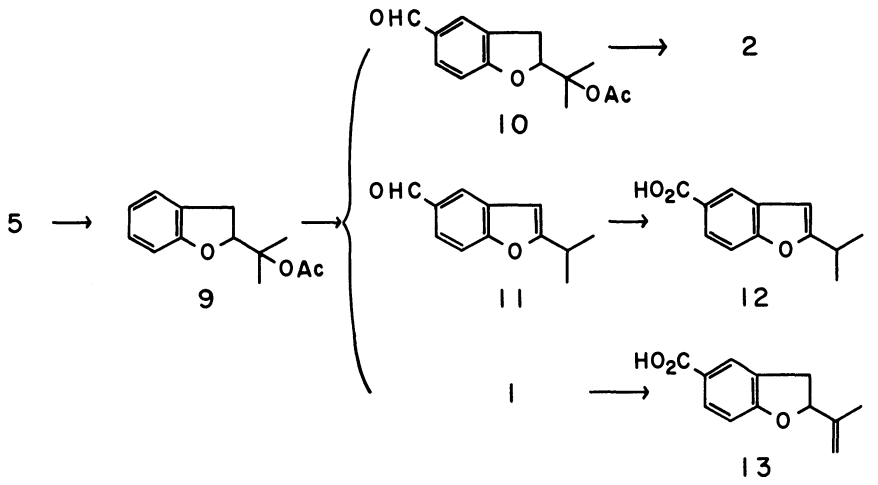

Chart 4.

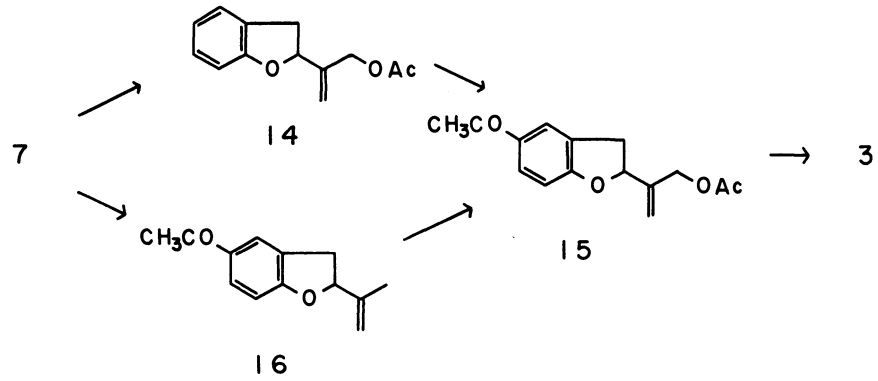

Chart 5.

of three aldehydes (**10**, **11**, and **1**; 4 : 3 : 3), which was separated to components by silica-gel chromatography. Then, these three aldehydes were oxidized to the corresponding carboxylic acids (**2**, **12**, and **13**) with silver oxide. The IR and ^{1}H-NMR spectra were identical with those of natural anodendroic acid.[2]

López and González isolated (−)-5-acetyl-2-[1-(hydroxymethyl)vinyl]-2,3-dihydrobenzofuran (**3**).[3] The acetylation of **7** with acetic acid–trifluoroacetic anhydride at room temp gave 5-acetyl-2-isopropenyl-2,3-dihydrobenzofuran (tremetone) (**16**). The spectral data of **16** were identical with those previously reported.[6] Then, **16** was converted to **15** by treatment with selenium dioxide in acetic anhydride at 130 °C. The ^{1}H-NMR spectrum was identical with that of natural **3**.[3] The keto acetate (**15**) was also prepared in a better yield from **7** by treatment with selenium dioxide in acetic anhydride to **14**, followed by acetylation with acetic acid–trifluoroacetic anhydride. The alkaline hydrolysis of **15** gave **3**, whose spectral data were identical with those previously reported.[3]

Experimental

The boiling points and melting points were uncorrected (in boiling points: 1 mmHg=133.322 Pa); the IR spectra were measured on a Hitachi EPI-S2 spectrophotomether, and the ^{1}H-NMR spectra, on a JEOL JNM-MH-60 spectrometer.

Preparation of **7**. *Method A). The Dehydration of* **5**: A mixture of **5** (1.42 g, 7.98 mmol) and phenyl isocyanate (9.50 g, 79.8 mmol) was refluxed for 16 h. The subsequent fractional distillation of the reaction mixture gave **7** (0.55 g, 44%); bp 105—106 °C/18 mmHg; IR (neat): 1650 cm^{-1}; ^{1}H-NMR (neat): δ=1.7 (3H, s), 3.0 (1H, dd, J=16+10 Hz), 3.1 (1H, dd, J=16+10 Hz), 5.1 (1H, broad s), 5.2 (1H, t, J=10 Hz), 5.3 (1H, broad s), 6.9—8.1 ppm (4H, m). Found: C, 82.67; H, 7.60%. Calcd: C, 82.46; H, 7.55%.

Method B). From Phenol and 1,4-Dibromo-2-methyl-2-butene: Sodium metal (10 g) was added by small portion, into a solution of phenol (9.4 g, 0.10 mol) in dry ether (100 ml). After the addition, stirring was continued for 30 min. Then, 1,4-dibromo-2-methyl-2-butene[7] (23.4 g, 0.10 mol) was added with vigorous stirring, drop by drop, into this suspended mixture. The mixture was then refluxed for 4.5 h with stirring. After the reaction, the ether layer was decanted, and the residual sodium metal was carefully treated with ethanol. The

ethanol was removed from the ethanolic solution, and the residue was acidified with 10% hydrochloric acid and then extracted with ether. The two ethereal layer obtained by the decantation and the extraction were combined and washed with a 5% aqueous sodium hydroxide solution. After drying over anhydrous sodium sulfate, the ether was removed. The resulting oil was distilled to give **7** (6.9 g, 43%) (bp 68—76 °C/2 mmHg), whose IR spectrum was identical with that of the product of the dehydration described above.

5-Bromo-2-isopropenyl-2,3-dihydrobenzofuran (8a). Upon treatment similar to that in the preparation of **7** described above, *p*-bromophenol (8.58 g, 49.6 mmol), sodium metal (5.0 g), and 1,4-dibromo-2-methyl-2-butene (11.3 g, 49.6 mmol) gave **8a** (1.9 g, 16%); bp 122—124 °C/4.5 mmHg; IR (neat): 1650 cm^{-1}; ^{1}H-NMR (in CCl_4): δ=1.7 (3H, s), 2.9 (1H, dd, J=16+9 Hz), 3.1 (1H, dd, J=16+9 Hz), 4.8 (1H, broad s), 5.0 (1H, broad s), 5.0 (1H, t, J=9 Hz), 6.6 (1H, d, J=9 Hz), 6.9—7.4 ppm (2H, m). Found: C, 55.14; H, 4.90%. Calcd: C, 55.25; H, 4.64%.

5-Iodo-2-isopropenyl-2,3-dihydrobenzofuran (8b). Upon treatment similar to that in the preparation of **7** described above, *p*-iodophenol (3.0 g, 13.6 mmol), sodium metal (1.4 g), and 1,4-dibromo-2-methyl-2-butene (3.1 g, 13.6 mmol) gave **8b** (1.3 g, 33%); bp 118—119 °C/3 mmHg; IR (neat): 1655 cm^{-1}; ^{1}H-NMR (in CCl_4): δ=1.8 (3H, s), (1H, dd, J=16+9 Hz), 3.3 (1H, dd, J=16+9 Hz), 5.0 (1H, broad s), 5.2 (1H, broad s), 5.2 (1H, t, J=9 Hz), 6.6 (1H, d, J=9 Hz), 7.5—7.7 ppm (2H, m). Found: C, 46.43; H, 3.60%. Calcd: C, 46.17; H, 3.88%.

2-Isopropenyl-2,3-dihydrobenzofuran-5-carbaldehyde (1). To a mixture of *N*-methylformanilide (4.46 g; 33.0 mmol) and phosphoryl chloride (5.05 g, 33.0 mmol), **7** (2.63 g, 16.4 mmol) was added. The mixture was then heated at 85—90 °C for 1 h with stirring. After cooling, the mixture was boiled with an aqueous sodium hydroxide solution (4 g in 20 ml) for 1 min and then extracted with ether. The ethereal layer was washed with 10% hydrochloric acid and a 5% sodium hydroxide solution, and then dried over anhydrous sodium sulfate. After the removal of the ether, the resulting oil was distilled to give **1** (1.26 g, 41%); bp 114—117 °C/2.5 mmHg; IR (neat): 1685 cm^{-1}; ^{1}H-NMR (in CCl_4): δ=1.8 (3H, s), 3.2 (1H, dd, J=16+9 Hz), 3.4 (1H, dd, J=16+9 Hz), 5.1 (1H, broad s), 5.2 (1H, broad s), 5.4 (1H, t, J=9 Hz), 7.0 (1H, d, J=9 Hz), 7.7—8.0 (2H, m), 10.2 ppm (1H, s). Found: C, 76.38; H, 6.42%. Calcd: C, 76.57; H, 6.43%.

The Formylation of 9. Upon treatment similar to that in the preparation of **1** described above, **9**[9] (3.26 g, 14.8 mmol), *N*-methylformanilide (5.0 g, 37.0 mmol), and phosphoryl chloride (4.5 g, 29.3 mmol) gave a mixture of three aldehydes, which were subsequently separated into components by silica-gel chromatography. The fractions eluted with benzene gave **11** (0.40 g, 14%); bp 215—225 °C/18 mmHg; IR (neat): 1690 cm^{-1}; ^{1}H-NMR (in CCl_4): δ=1.4 (6H, d, J=7 Hz), 3.2 (1H, m, J=7 Hz), 6.6 (1H, s), 7.7 (1H, d, J=9 Hz), 8.0 (1H, dd, J=9+2 Hz), 8.2 (1H, d, J=2 Hz), 12.1 ppm (1H, s). Found: C, 76.29; H, 6.43% (Calcd: C, 76.57; H, 6.43%); and **1** (0.42 g, 15%). The fractions eluted by chloroform gave **10** (0.75 g, 20%); bp *ca.* 130 °C/2 mmHg (bath temperature); IR (neat): 1740, 1695 cm^{-1}; ^{1}H-NMR (in CCl_4): δ=1.4 (3H, s), 1.5 (3H, s), 2.0 (3H, s), 3.3 (2H, d, J=9 Hz), 5.2 (1H, t, J=9 Hz), 7.2 (1H, d, J=9 Hz), 7.9 (1H, d, J=2 Hz), 7.9 (1H, dd, J=9+2 Hz), 10.1 ppm (1H, s). Found: C, 67.73; H, 64.41%. Calcd: C, 67.73; H, 6.50%.

The Oxidation of 10 to 2. To a solution of silver nitrate (0.70 g, 41.2 mmol) in water (7 ml), sodium hydroxide (0.4 g) was added. To this silver oxide suspension, a solution of **10** (0.44 g, 17.7 mmol) in ethanol (4 ml) was added. The mixture was then refluxed for 2 h. After the reaction, the mixture was filtered, and the filtrate was washed with ether and then acidified with 10% hydrochloric acid. The crystals thus obtained were collected and recrystallized from ethanol to give **1** (0.11 g, 28%); mp 231—232 °C; IR (KBr disk): 3425, 1690 cm^{-1}; ^{1}H-NMR (in DMSO-d_6): δ=1.2 (6H, s), 3.3 (2H, d, J=9 Hz), 4.7 (1H, t, J=9 Hz), 6.9 (1H, d, J=9 Hz), 7.9 (1H, d, J=2 Hz), 7.9 ppm (1H, dd, J=9+2 Hz); ^{1}H-NMR (in pyridine-d_5): δ=1.4 (3H, s), 1.5 (3H, s), 3.3 (1H, dd, J=16+9 Hz), 3.5 (1H, dd, J=16+9 Hz), 4.9 (1H, t, J=9 Hz), 7.1 ppm (1H, d, J=9 Hz). Found: C, 70.78; H, 5.90%. Calcd: C, 70.57; H, 5.92%.

2-Isopropylbenzofuran-5-carboxylic Acid (12). Upon treatment similar to that in the oxidation of **2** described above, **11** (0.40 g, 21.3 mmol), silver nitrate (0.75 g, 44.2 mmol), and sodium hydroxide (0.4 g) gave **12** (0.14 g, 32%); mp 136.5—137.5 °C (recrystallized from ethanol–water); IR (KBr disk): 1675 cm^{-1}; ^{1}H-NMR (in CCl_4): δ=1.4 (6H, d, J=7 Hz), 3.2 (1H, m, J=7 Hz), 6.6 (1H, s), 7.7 (1H, d, J=9 Hz), 8.4 (1H, dd, J=9+2 Hz), 8.6 (1H, d, J=2 Hz), 13.1 ppm (1H, s). Found: C, 70.78; H, 5.90%. Calcd: C, 70.57; H, 5.92%.

2-Isopropenyl-2,3-dihydrobenzofuran-5-carboxylic acid (13). Upon treatment similar to that in the oxidation of **2** described above, **1** (1.29 g, 6.85 mmol), silver nitrate (2.43 g, 14.3 mmol), and sodium hydroxide (1.1 g) gave **13** (0.68 g, 49%); mp 140.5—142.5 °C (recrystallized from benzene–cyclohexane); IR (KBr disk): 1675 cm^{-1}; ^{1}H-NMR (in $CDCl_3$): δ=1.8 (3H, s), 3.1 (1H, dd, J=15+9 Hz), 3.3 (1H, dd, J=15+9 Hz), 4.9 (1H, broad s), 5.1 (1H, broad s), 5.3 (1H, t, J=9 Hz), 6.8 (1H, d, J=9 Hz), 7.8 (1H, d, J=2 Hz), 8.0 (1H, dd, J=9+2 Hz), 10.6 ppm (1H, s). Found: C, 70.82; H, 5.79%. Calcd: C, 70.57; H, 5.92%.

2-[1-(Acetoxymethyl)vinyl]-2,3-dihydrobenzofuran (14). A mixture of **7** (6.7 g, 41.9 mmol), acetic anhydride (110 ml), and finely powdered selenium dioxide (4.3 g, 38.8 mmol) was refluxed for 45 min. Then, the mixture was diluted with ether and filtered. The filtrate was evaporated under reduced pressure to remove the ether and the acetic anhydride. The subsequent distillation of the residue gave **14** (1.42 g, 16%); bp 100—115 °C/4 mmHg; IR (neat): 1740 cm^{-1}; ^{1}H-NMR (in CCl_4): δ=2.0 (3H, s), 3.1 (1H, dd, J=16+9 Hz), 3.4 (1H, dd, J=16+9 Hz), 4.7 (2H, broad s), 5.2 (1H, t, J=9 Hz), 5.2 (1H, broad s), 5.4 (1H, broad s), 6.7—7.4 ppm (4H, m). Found: C, 71.49; H, 6.53%. Calcd: C, 71.54; H, 6.47%.

5-Acetyl-2-isopropenyl-2,3-dihydrobenzofuran (Tremetone) (16). Under cooling in an ice-water bath, trifluoroacetic anhydride (7.7 g, 36.7 mmol) was added to a solution of **7** (2.9 g, 18.1 mmol) in acetic anhydride (2.2 g, 36.7 mmol). The mixture was then allowed to stand for 6 h at room temperature. After the reaction, the mixture was treated with ice water, and alkalified with a sodium hydrogencarbonate aqueous solution, and extracted with ether. The ether extracts were dried over anhydrous sodium sulfate. After the removal of the ether, the resulting oil was distilled to give **16** (1.67 g, 46%); bp 102—105 °C/2 mmHg; IR (neat): 1670 cm^{-1}; ^{1}H-NMR (in CCl_4): δ=1.9 (3H, s), 2.5 (3H, s), 3.2 (1H, dd, J=16+9 Hz), 3.4 (1H, dd, J=16+9 Hz), 5.1 (1H, broad s), 5.3 (1H, broad s), 5.4 (1H, t, J=9 Hz), 7.1 (1H, d, J=9 Hz), 8.0—8.3 ppm (2H, m). Found: C, 76.96; H, 6.74%. Calcd: C, 77.20; H, 6.98%.

2-[1-(Acetoxymethyl)vinyl]-5-acetyl-2,3-dihydrobenzofuran (15). *Acetylation of 14*: Upon treatment similar to that in the preparation of **16** described above, **14** (1.42 g, 6.51 mmol) was acetylated with acetic acid (0.78 g, 13.0 mmol) and trifluoroacetic anhydride (2.73 g, 13.0 mmol) to give **15** (0.79 g, 47%); bp 120—135 °C/4 mmHg; IR (neat): 1740, 1670 cm^{-1}; ^{1}H-

NMR (in CCl_4): δ=2.1 (3H, s), 2.6 (3H, s), 3.4 (1H, dd, J=15+8 Hz), 3.6 (1H, dd, J=15+8 Hz), 4.9 (2H, broad s), 5.5 (1H, broad s), 5.6 (1H, t, J=8 Hz), 7.2 (1H, d, J=10 Hz), 8.1—8.4 ppm (2H, m). Found: C, 69.31; H, 6.25%. Calcd: C, 69.21; H, 6.20%.

Selenium Dioxide Oxidation of **16**: Upon treatment similar to that in the preparation of **14** described above, **16** (1.41 g, 6.98 mmol) was oxidized with selenium dioxide (0.72 g, 6.49 mmol) in acetic anhydride (18 ml) to give **15** (0.099 g; 5.4%); bp 120—130 °C/4 mmHg; it was identical with the sample prepared from **14** in all its spectral data.

5-Acetyl-[1-(hydroxymethyl)vinyl]-2,3-dihydrobenzofuran (3). A mixture of **15** (0.27 g, 1.04 mmol), a 10% aqueous potassium hydroxide solution (5 ml), and ethanol (10 ml) was gently refluxed for 20 min. The mixture was then diluted with ice water and extracted with ether. The removal of the ether gave an oily residue, which was subsequently purified by silica-gel chromatography to give **3** as ethanol eluents; bp 103—105 °C/3 mmHg (bath temperature); IR (neat): 3400, 1655 cm^{-1}; ^{1}H-NMR (in $CDCl_3$): δ=2.6 (3H, s), 3.0 (1H, broad s), 3.3 (1H, dd, J=19+10 Hz), 3.5 (1H, dd, J=19+10 Hz), 4.3 (2H, broad s), 5.4 (2H, broad s), 5.5 (1H, t, J=10 Hz), 7.0 (1H, d, J=10 Hz), 7.9—8.2 ppm (2H, m). Found: C, 71.26; H, 6.62%. Calcd: C, 71.54; H, 6.47%.

We wish to thank Professor Hisashi Ishii (Chiba Univ.) for his valuable information about the dehydration with phenyl isocyanate. We also wish to thank Dr. Katsuhito Kondo (Tokushima University of Arts and Science) for providing a copy of the IR spectrum of natural anodendroic acid.

This paper is dedicated to Emeritus Professor Takeo Sakan on his 70th birthday.

References

1) M. Hirotani, J. O'Reilly, D. M. X. Donnelly, and J. Polonsky, *Tetrahedron Lett.*, **1977**, 651.

2) K. Shima, S. Hisada, and I. Inagaki, *Yakugaku Zasshi*, **92**, 1410 (1972).

3) S. V. López and B. R. González, *An. Quim.*, **67**, 879 (1971).

4) Y. Kawase, S. Yamaguchi, S. Kondo, and K. Shimokawa, *Chem. Lett.*, **1978**, 253.

5) Y. Kawase, S. Yamaguchi, O. Inoue, M. Sannomiya, and K. Kawabe, *Chem. Lett.*, **1980**, 1581.

6) J. I. DeGraw, Jr., D. M. Bowen, and W. A. Bonner, *Tetrahedron*, **19**, 19 (1963).

7) J. Nickl, *Chem. Ber.*, **91**, 553 (1958).

8) Allan *et al.* isolated (+)-5-acetyl-4-hydroxy-2-isopropenyl-6-methoxy-2,3-dihydrobenzofuran (remirol) and (+)-5-acetyl-4,7-dihydroxy-2-isopropenyl-6-methoxy-2,3-dihydrobenzofuran (remiridiol) from *Remirea martima* Aubl.: R. D. Allan, R. L. Correll, and R. J. Wells, *Tetrahedron Lett.*, **1969**, 4673; R. D. Allan, R. J. Wells, and J. K. MacLeod, *ibid.*, **1970**, 3945.

9) D. M. Bowen, J. I. DeGraw, Jr., V. S. Shah, and W. A. Bonner, *J. Med. Chem.*, **6**, 315 (1963).

Fluoride Salts on Alumina as Reagents for Alkylation of Phenols and Alcohols

Takashi Ando,* Junko Yamawaki, Takehiko Kawate, Shinjiro Sumi, and Terukiyo Hanafusa

The Institute of Scientific and Industrial Research, Osaka University, Mihogaoka, Ibaraki, Osaka 567

(Received February 27, 1982)

The effectiveness of alkali metal fluorides impregnated on alumina as a reagent for promoting alkylation was optimized with respect to the metal cation, the amount of impregnation, and the reaction solvent. Potassium or caesium fluoride on alumina in acetonitrile or 1,2-dimethoxyethane was concluded to be the best reaction system for general use. *O*-Alkylation of substituted phenols, primary and secondary alcohols, and a glycol was carried out mostly in good yields under mild conditions with simple experimental procedures.

Increasing interest has been shown in the use of fluoride salts as potential bases to fascilitate a variety of synthetic reactions.[1,2] In recent studies by Clark, Miller, and their coworkers,[3,4] the effectiveness of alkali metal fluorides has been recognized in various types of alkylations with alkyl halides. According to them, nucleophilicity of protic organic compounds, *e.g.*, carboxylic acids or phenols, is greatly enhanced by the formation of strong hydrogen bonds with the fluoride anion; nucleophilic substitution proceeds with hydrogen bond assistance (Eq. 1). However, the low solubility

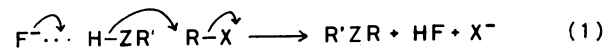

(1)

of alkali fluorides in ordinary solvents disturbs their wide application in organic synthesis. In order to overcome this difficulty, the reactions have been carried out at high temperatures with preformed hydrogen-bonded complexes or in a high-boiling solvent such as *N,N*-dimethylformamide,[4] but these methods are rather inconvenient.

On the other hand, there has been rapidly increasing use of organic and inorganic solids as supports of reagents or as reaction media in recent years.[5–8] In general, several advantages can be expected for their use: (1) work-up and purification of products are quite simple, (2) reactivity of functional groups can be modified, *i.e.*, enhanced or reduced, and (3) selectivity in the courses of reactions may be different from that in solution. These advantages may arise from the large effective surface area, the presence of pores, and the adsorption of reactants on the surface. In 1979, we communicated the preliminary results that potassium fluoride supported on diatomaceous earth (KF–Celite) is more efficient for promoting alkylations of various types of protic compounds than unsupported KF.[9] In this paper, we describe our detailed study on the scope and limitations of supported fluoride reagents for promoting *O*-alkylation of phenols and alcohols.

Results and Discussion

In order to optimize the efficiency of supported fluoride reagents, it is important to investigate the effects of the support, metal cation, amount of impregnation, and reaction solvent. We have previously discussed the efficiency of various inorganic solids as a support to enhance the reactivity of potassium fluoride,[10] and will not repeat that discussion here. In *O*-methylation of phenol with methyl iodide, the order of the effectiveness of supports has been found to be alumina>molecular sieves (MS) 13X and SK-40>montmorillonite>MS 4A and 5A>Celite.[10] Therefore, we used alumina as a support throughout this study.

The effect of varying the metal cation and the ratio of fluorides *vs.* alumina on the reactivity of alkali fluoride–alumina reagents was first studied. Various amounts of alkali metal fluorides (MF) and tetrabutylammonium fluoride (Bu_4NF) were impregnated on alumina; Classes I, II, III, and IV reagents were prepared with 0.1, 0.2, 0.5, and 1.0 mol of MF, respectively, impregnated on 100 g of alumina. Methylation of phenol with methyl iodide in acetonitrile was chosen as a reference

Table 1. Methylation of phenol with MF–alumina[a]

Reagent	Class[b]	Yield/%[c]		
		1 h	24 h	48 h
LiF–Alumina	I	0	1.3	2.5
	II	0.1	0.7	1.5
	IV	0	0.2	0.3
NaF–Alumina	I	1.5	6.1	9.6
	II	1.8	12.5	15.2
	IV	3.6	11.0	12.4
KF–Alumina	I	17.4	41.8	41.9
	II	57.7	97.0	
	IV	98.8		
CsF–Alumina	I	69.3	90.4[d]	
	II	99.6		
	III	100		
	IV	100[e]		
Bu_4NF–Alumina	I	100		
LiF[f]				0
NaF[f]				0
KF[f]				7.6
CsF[f]		19.5[e]		100
Bu_4NF[g]		98.3[e]		

a) Reaction of phenol (0.5 mmol) with methyl iodide (1 mmol) and MF–alumina (*ca.* 2.5 mmol MF) in 5 cm^3 of acetonitrile was carried out at room temperature. b) For Classes of reagents, see text. c) Yields were determined by GLPC using dodecane as an internal standard after a reaction time shown in Table. d) After 6 h. e) After 0.5 h. f) Without alumina. g) Trihydrate (Fluka) without alumina.

reaction, and the effectiveness of supported reagents was evaluated in terms of the yields of anisole after a definite time of reaction. The results are summarized in Table 1.

It is apparent from Table 1 that all the MF–alumina reagents are more effective than MF without a support and that the cation is a governing factor of the reactivity of the supported reagents. The order of effectiveness of MF–alumina is CsF>KF≫NaF>LiF. This is just the same as the reactivity order of MF without a support for the alkylation of phthalimide in *N,N*-dimethylformamide reported by Clark and Miller.[4] Although in general tetraalkylammonium fluorides are known as the most effective sources of the fluoride anion, they are expensive, hygroscopic, and thermally unstable. Clark reported that Bu_4NF supported on silica gel can be used as a non-hygroscopic source of the fluoride ion promoting various base-catalyzed reactions.[11] Bu_4NF–alumina prepared by us was somewhat easier to handle but not more effective than Bu_4NF alone. Although this Bu_4NF–alumina was most reactive among the supported reagents studied, CsF–alumina and KF–alumina can be regarded as more practical reagents than the Bu_4NF reagent when ease of handling and, especially for KF–alumina, economy of the reagents are taken into consideration. For these two reagents, the reactivity increased as the ratio of the fluoride *vs.* alumina was increased. However, as too much loading of the fluoride salts makes the reagents hygroscopic and thus cancels out their merit of easy handling, Class IV of KF–alumina and Class III of CsF–alumina are concluded to be the most practical reagents for general use.

The effect of varying the reaction solvent on the reaction rate was studied for these two reagents and for KF and CsF without a support (Table 2). Among the aprotic solvents used, the reaction became faster as the polarity of the solvent was increased. However, it was rather unexpected that the reaction was almost completed even in a nonpolar solvent such as hexane, although it took a longer reaction time. The adsorption of the reactants on the solid surface is obviously an important factor for the reaction. This is, to our knowledge, the first systematic study of the solvent effect on the reaction of supported reagents. KF and CsF both without alumina were effective only in very polar solvents; the effectivenesss might be due to the fact that they are slightly soluble in these solvents.[12] In conclusion, acetonitrile and 1,2-dimethoxyethane are adequate solvents for practical use with respect to their moderate boiling points and sufficient polarities.

Here we have reported that the effectiveness of the MF-support reagents is strongly affected by the metal cation, the amount of impregnation, and the reaction solvent. We have already reported that the kind and the form of solid supports and the drying conditions of the reagents are also important as factors which govern the efficiency of the supported fluoride reagents.[10] In this respect, the specific reactivities observed for "freeze-dried" and "spray-dried" potassium fluorides reported by Ishikawa and his coworkers is noteworthy;[13] the former is effective for alkylation and the latter is for fluorination. Although the role of the crystal structures of the supported fluorides and the role of a trace of the water remained in the reagents are not clear, the idea of the simple "hydrogen-bond-assistance" by the fluoride anion proposed by Clark and Miller[4] might be inapplicable in our case. Detailed study on the mechanism of the reaction promoted with MF–supports is now under way.

Applications of the most practical reagent, KF–alumina, were studied in some cases. As shown in

Table 2. Methylation of phenol in various solvents[a]

Solvent	Time/h	Yield/%[b] KF	CsF	KF–Alumina[c]	CsF–Alumina[d]
DMF	1	10	100	100	100
Diglyme	1	1	97	100	100
CH_3CN	1	1	31	95	92
DME	1	0	22	98	92
THF	1	0	3	53	49
Ether	1	0	0	0.3	5
	24	0	0	17	79
CH_2Cl_2	1	0.3	0.1	0.7	5
	48	0	0.7	41	93
Benzene	1	0	0.2	0.5	4
	24	0	0.3	13	64
Hexane	1	0	0	0.7	7
	24	0	0	30	80

a) Reaction of phenol (2.5 mmol) with methyl iodide (5 mmol) and MF or MF–alumina (12.5 mmol MF) in a solvent (5 cm^3) was carried out at room temperature. b) Yields were determined by GLPC using dodecane as an internal standard. c) Class IV reagent. d) Class III reagent.

Table 3. *O*-Alkylation of phenols with KF–alumina[a]

Phenol	Halide	Yield/% (Time/h) GLPC[b]		Isolated
C_6H_5OH	MeI	84(0.25)	100(0.5)	
2-$CH_3C_6H_4OH$	MeI	100(0.25)		
4-$CH_3C_6H_4OH$	MeI	100(0.25)		
2,6-$(CH_3)_2C_6H_3OH$	MeI	100(0.25)		
2,6-(*t*-Bu)$_2C_6H_3OH$	MeI			78(2.0)
4-ClC_6H_4OH	MeI	100(0.5)		
2-$NO_2C_6H_4OH$	MeI	2(1.0)	8(20)	
3-$NO_2C_6H_4OH$	MeI	46(1.0)	88(20)	
4-$NO_2C_6H_4OH$	MeI	2(1.0)	10(20)	
C_6H_5OH	*n*-BuI	68(1.0)		
C_6H_5OH	*n*-BuBr	95(24)		80(24)
C_6H_5OH	*n*-BuCl			62(162)[c]
C_6H_5OH	*s*-BuBr	26(24)	63(142)	30(144)
C_6H_5OH	*t*-BuBr	1(24)		

a) Unless otherwise mentioned, reaction of a phenol (1 equiv.) with an alkyl halide (1.2—1.5 equiv.) and KF–alumina (*ca.* 5 equiv. KF) was carried out in acetonitrile at room temperature. b) Yields determined with internal standards. c) Reaction was carried out in 1,2-dimethoxyethane at 60 °C.

Table 4. *O*-Alkylation of Alcohols with KF–alumina[a)]

Alcohol	Halide	Product	Yield/%(Time/h) GLPC[b)]	Yield/%(Time/h) Isolated
$CH_3(CH_2)_7OH$	MeI	$CH_3(CH_2)_7OMe$	90(40)	
$CH_3(CH_2)_3OH$	$PhCH_2Br$	$CH_3(CH_2)_3OCH_2Ph$	86(20)	66(30)
$CH_3CH_2CH(OH)CH_3$	$PhCH_2Br$	$CH_3CH_2CH(OCH_2Ph)CH_3$	33(20)	
$PhCH_2CH_2OH$	MeI	$PhCH_2CH_2OMe$	82(20)	66(43)
$PhCH_2CH_2OH$	BuI	$PhCH_2CH_2OBu$		62(124)
$PhCH_2CH(OH)CH_3$	MeI	$PhCH_2CH(OMe)CH_3$	52(20)	72(42)
$HO(CH_2)_2O(CH_2)_2OH$[c)]	MeI	$MeO(CH_2)_2O(CH_2)_2OMe$	96(16)	

a) Reaction of an alcohol (1 equiv.) with an alkyl halide (1.2—1.5 equiv.) and KF–alumina (*ca.* 5 equiv. KF) was carried out in acetonitrile at room temperature. b) Yields determined with internal standards. c) Reagents were doubled for ethylene glycol.

Table 3, KF–alumina was effective for methylation of alkyl-substituted phenols with methyl iodide. Even methylation of sterically hindered 2,6-di-*t*-butylphenol proceeded quantitatively at room temperature in 2 h. When the substituent was electron attracting, the rate of methylation decreased. Methylation of *p*-Cl and *m*-NO_2 derivatives proceeded at room temperature, but *o*- and *p*-NO_2 derivatives were only slightly methylated under the same conditions. Alkylation of phenol with a variety of butyl halides was also examined (Table 3). The reaction with butyl bromide proceeded smoothly, although not as fast as with butyl iodide. The alkylation with *s*-butyl bromide proceeded with partial elimination to give a moderate yield of butyl phenyl ether. However, the reaction with *t*-butyl bromide gave only a trace of the product because of the elimination.

Alkylation of a less acidic hydroxyl group of an alcohol than that of a phenol by use of the fluoride anion has scarcely been reported.[1,14)] Nevertheless, KF–alumina was found to give satisfactory yields of alkyl ethers from alcohols (Table 4). It is noteworthy that methylation and benzylation of even secondary alcohols and a glycol proceeded smoothly at room temperature. Thus KF–alumina manifested the characteristic reactivity promoting alkylation of neutral alcohols under mild conditions.

In all cases studied, isolation procedures of reaction products were quite simple and nonaqueous: filtration, washing the solid with ether, evaporation of the solvent, and distillation or column chromatography when necessary. In conclusion, as reaction conditions are mild, yields are good in most cases, and work-up is simple, KF on alumina is a useful and practical supported reagent for promoting *O*-alkylation of phenols and alcohols.

Experimental

General. Unless otherwise mentioned, reagents were obtained commercially and used without further purification. Solvents were dried with molecular sieves 3A and 4A. Neutral alumina was purchased from Merck Japan Ltd. (Type 90 for column chromatography, activity I, 70—230 mesh) and used as obtained. Alkali metal fluorides were dried *in vacuo* at 120 °C for several hours. KF, CsF, and $Bu_4NF \cdot 3H_2O$ (Fluka, mp 60—61 °C) without a support were handled under nitrogen. GLPC analysis of product mixtures was carried out with a Varian Aerograph Model 2850-30 gas chromatograph with a flame ionization detector and a Hewlett-Packard 3370B digital integrator. A column packed with 20% Silicone DC 550 on Celite 545 was used. Yields were determined using internal standards.

Preparation of MF–Alumina Reagents. Alumina was mixed with metal fluoride in water, and the water was removed at 50—60 °C in a rotary evaporator. This impregnated alumina was further dried in a vacuum drying oven for several hours at 75 °C. Classes I, II, III, and IV of MF–alumina reagents were prepared from 100 g of alumina with 0.1, 0.2, 0.5, and 1.0 mol of MF, respectively. The typical KF–alumina reagent used for the alkylation of phenols and alcohols was prepared at the weight ratio of 2 : 3 which corresponds to 1.15 mol of KF on 100 g of alumina.

All these MF–alumina reagents except CsF–alumina (Class IV) and Bu_4NF–alumina can be handled in the atmosphere without special care. The effectiveness of the typical reagents remained unaltered after several months' storage in bottles kept in a desiccator.

Effectivity Determination of Supported Reagents. Methylation of phenol was carried out with methyl iodide and MF–alumina in a solvent, whose quantities are as shown below. Methylation of phenol with MF–alumina: phenol (47 mg, 0.5 mmol), methyl iodide (140 mg, 1.0 mmol), and MF–alumina (*ca.* 2.5 mmol MF) in 5 cm^3 of acetonitrile. Methylation of phenol in various solvent: phenol (0.24 g, 2.5 mmol), methyl iodide (0.71 g, 5.0 mmol), and MF–alumina (*ca.* 12.5 mmol MF) in 5 cm^3 of a solvent. The reaction mixture placed in a test tube with a Teflon-coated screw-cap was vigorously agitated at room temperature by a Vapor Mix S-10 vibrating apparatus (Tokyo Rikakikai Co., Ltd.). Yields of anisole formed after a definite reaction time were determined by GLPC with dodecane as an internal standard.

Alkylation with Supported Reagents. Experimental procedures for alkylation of phenols and alcohols in a preparative scale are given in the following typical examples. All the products are known compounds and gave ^1H NMR and IR spectra consistent with their structures and, when reported data are available, with those shown in the literature.

Methyl 2,6-Di-t-butylphenyl Ether: A mixture of 2,6-di-*t*-butylphenol (0.83 g, 4 mmol), methyl iodide (0.79 g, 5.6 mmol), and KF–alumina (3.00 g, *ca.* 20 mmol KF) in 6 cm^3 of acetonitrile was magnetically stirred at room temperature for 2 h. The solid material was filtered and washed with ether, and the solvent was evaporated. Purification by column chromatography (silica gel, hexane) gave 0.68 g of the product (78%): purity by GLPC 95%.

Butyl Phenyl Ether: Reaction of phenol (0.41 g, 4.4 mmol)

with butyl bromide (0.75 g, 5.5 mmol) and KF–alumina (3.3 g, *ca.* 22 mmol KF) in 6.5 cm^3 of acetonitrile was carried out at room temperature for 24 h. Work-up as above and purification by column chromatography (silica gel, chloroform) gave 0.52 g of the product (80%): purity by GLPC 99.7%.

Benzyl Butyl Ether: Reaction of 1-butanol (1.55 g, 20.9 mmol) with benzyl bromide (4.28 g, 25.0 mmol) and KF–alumina (15.8 g, *ca.* 104 mmol KF) in 30 cm^3 of acetonitrile was carried out at room temperature for 30 h. Work-up as above and purification by distillation gave 2.25 g of the product (66%): bp 92—94 °C/1.20—1.33 kPa (lit,[15] bp 88 °C/0.80—0.93 kPa); purity by GLPC 98.6%.

2-Methoxy-3-phenylpropane: A mixture of 3-phenyl-2-propanol (0.54 g, 4.0 mmol), methyl iodide (0.96 g, 6.8 mmol), and KF–alumina (3.0 g, *ca.* 20 mmol KF) in 6 cm^3 of acetonitrile was vigorously agitated at room temperature for 42 h. Work-up as above and purification by column chromatography (silica gel, chloroform) gave 0.43 g of the product (72%): purity by GLPC 97.9%.

The present work was supported in part by a Grant-in-Aid for Scientific Research No. 56740211 from the Ministry of Education, Science and Culture.

References

1) J. H. Clark, *Chem. Rev.*, **80**, 429 (1980).
2) T. Ando and J. Yamawaki, *J. Synth. Org. Chem. Jpn.*, **39**, 14 (1981).
3) J. H. Clark and J. M. Miller, *J. Am. Chem. Soc.*, **99**, 498 (1977).
4) J. H. Clark and J. Emsley, *J. Chem. Soc., Dalton Trans.*, **1973**, 2154, 1125; **1975**, 2129.
5) J. M. J. Fréchet, *Tetrahedron*, **37**, 663 (1981).
6) A. Akelah, *Synthesis*, **1981**, 413.
7) A. McKillop and D. W. Young, *Synthesis*, **1979**, 401, 481.
8) G. H. Posner, *Angew. Chem., Int. Ed. Engl.*, **17**, 487 (1978).
9) T. Ando and J. Yamawaki, *Chem. Lett.*, **1979**, 45.
10) J. Yamawaki and T. Ando, *Chem. Lett.*, **1979**, 755.
11) J. H. Clark, *J. Chem. Soc., Chem. Commun.*, **1978**, 789.
12) The solubility of KF in *N,N*-dimethylformamide was reported as less than 0.025 wt% under reflux; M. Mingin and R. Huisgen, *Tetrahedron Lett.*, **1979**, 719.
13) a) N. Ishikawa, T. Kitazume, and M. Nakabayashi, *Chem. Lett.*, **1980**, 1089; b) N. Ishikawa, T. Kitazume, T. Yamazaki, Y. Mochida, and T. Tatsuno, *ibid.*, **1981**, 761.
14) A. Chollet, J.-P. Hagenbuch, and P. Vogel, *Helv. Chim. Acta*, **62**, 511 (1979).
15) M. J. Murray and F. F. Cleveland, *J. Chem. Phys.*, **9**, 129 (1941).

Restricted Rotation Involving the Tetrahedral Carbon. XLII. Barriers to Rotation and Populations of Rotamers in 9-[2-(Substituted methyl)-1-napthyl]fluorenes[1)]

Ryo SAITO and Michinori ŌKI*

Department of Chemistry, Faculty of Science, The University of Tokyo, Bunkyo-ku, Tokyo 113

(Received March 30, 1982)

Rotational barriers in 9-[2-(substituted methyl)-1-naphthyl]fluorenes are found not significantly affected by the substituent on the methyl group, $\Delta G^{\ddagger}$'s being *ca.* 29 kcal/mol at 373 K. Populations of *sp*- and *ap*-rotamers at equilibriums show that the *sp* form is favored to some extent and the results are attributed to entropy factor. OH···π interaction is detected in the *ap* form of 9-(2-hydroxymethyl-1-naphthyl)fluorene.

In the classical work of Adams and his collaborators on restricted rotation of biphenyls,[2)] it was established that barriers to rotation are determined by the first atom with which substituents in the 2,2′,6,6′-positions are connected to the biphenyl skeleton. The results are understood by assuming that, in the transition state for rotation, atoms which are in a substituent but are not directly connected to the skeleton will avoid further interactions with those in other substituents to minimize the transition state energy.

While biphenyls give stable, enantiomeric atropisomers, 9-arylfluorenes give diastereomeric atropisomers.[3)] The interactions in the transition state for rotation in diastereomers are expected to be the same with the cases in biphenyls but the populations of diastereomeric atropisomers may be affected by a substituent which is not directly attached to the parent skeleton. Thus this work was undertaken 1) to confirm that the barrier to rotation in 9-arylfluorenes is not affected significantly by a remote substituent and 2) to examine whether the populations of rotamers can be affected by a substituent which is not directly attached to the skeleton.

Syntheses of the compounds examined are straightforward. 9-(2-Methyl-1-naphthyl)fluorene (**1**)[4)] was brominated with *N*-bromosuccinimide to give 9-(2-bromomethyl-1-naphthyl)fluorene (**2**) which was hydrolyzed with water in dimethyl sulfoxide to afford 9-(2-hydroxymethyl-1-naphthyl)fluorene (**3**). 9-(2-Methoxymethyl-1-naphthyl)fluorene (**4**) was prepared by substitution reactions of **2** in methanol with the aid of silver perchlorate. *sp*-**4** could be prepared by methanolysis of *sp*-**2** as well.[5)]

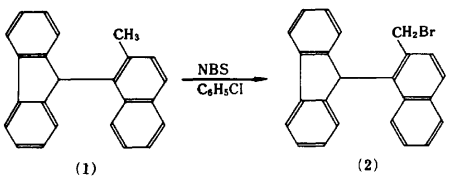

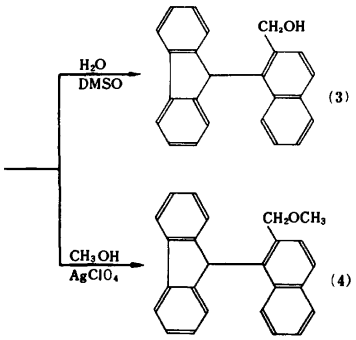

The rate constants for rotation about the C_{naph}–C_9 bond obtained at various temperatures are given in Tables 1—3 together with equilibrium constants. Activation parameters calculated from these rate constants are listed in Table 4 together with those of the rotation in **1** for comparison.

The results indicate that the barriers to rotation in compounds **1**—**4** are about the same, thus confirming that a substituent on the methyl group has little effect on the height of the barrier to rotation: the CH_2 group determines the barrier to the first approximation in these compounds. Although the hydroxy compound (**3**)

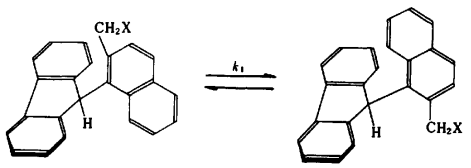

(Designation of stereochemistry is reversed if X=H.)

Table 1. Rate constants of rotation about the C_9–C_{naph} bond and equilibrium constants in 9-(2-bromomethyl-1-naphthyl)fluorene (**2**) in hexachlorobutadiene

Temp/°C	k_1/s^{-1}	$K(sp/ap)$
95.1	1.53×10^{-5}	2.78
106.0	4.24×10^{-5}	2.98
114.0	1.11×10^{-4}	2.83
124.0	2.62×10^{-4}	2.76

Table 2. Rate constants for rotation about the C_9–C_{naph} bond and equilibrium constants in 9-(2-hydroxymethyl-1-naphthyl)fluorene (**3**) in hexachlorobutadiene

Temp/°C	k_1/s^{-1}	$K(sp/ap)$
77.0	6.40×10^{-6}	1.80
95.0	4.37×10^{-5}	1.73
104.0	1.18×10^{-4}	1.70
114.0	2.97×10^{-4}	1.80

Table 3. Rate constants for rotation about the C_9–C_{naph} bond and equilibrium constants in 9-(2-methoxymethyl)-1-naphthyl)fluorene (**4**) in hexachlorobutadiene

Temp/°C	k_1/s^{-1}	$K(sp/ap)$
77.0	4.09×10^{-6}	2.40
95.0	3.12×10^{-5}	2.35
104.0	8.47×10^{-5}	2.33
114.0	2.32×10^{-4}	2.25

Table 4. Activation parameters for rotation about the C_9–C_{naph} bond in 9-[2-(substituted methyl)-1-naphthyl]fluorenes

Compound	Subst.	$\Delta H^{\ddagger}$ / kcal mol^{-1}	$\Delta S^{\ddagger}$ / e.u.	$\Delta G^{\ddagger}_{373}$ / kcal mol^{-1}
1[5]	H	25.6	−9.7	29.0
2	Br	28.3±0.8	−4.3±2.0	29.9
3	OH	27.4±0.6	−4.5±1.7	29.0
4	OCH_3	28.7±0.1	−1.5±0.3	29.3

Table 5. Rate constants for rotation about the C_9–C_{naph} bond and equilibrium constants in 9-(2-bromomethyl-1-naphthyl)-fluorene (**2**) in toluene-d_8

Temp/°C	k_1/s^{-1}	$K(sp/ap)$
87.3	6.74×10^{-6}	3.13
96.0	1.73×10^{-5}	3.06
105	4.43×10^{-5}	3.05
114	1.03×10^{-4}	2.92

Table 6. Infrared O–H stretching spectra of rotameric 9-(2-hydroxymethyl-1-naphthyl)fluorene (**3**)[a]

State		ν_{OH} Frequencies/cm^{-1}	
		sp	*ap*
Solid		3320(s) broad	3570(m) sharp 3450(s) broad
Solution	9.8 mM	3620(62.4)	3580(44.4) 3630(33.5)
	0.20 M	3610(26.8) 3320(24.8)	3630(14.4) 3580(29.8) 3480(13.3)

a) Numericals in parentheses are molecular extinction coefficients. Those in parentheses for the solid state are as follows. s: Strong, m: medium.

gives a little low barrier, if we compare the rate constant at a given temperature with that of **4**, the reason for this lowering is not well understood at the moment.

In contrast, we see that the equilibrium constants are appreciably larger than 1.0 which is the value reported for compound **1** in tetrachloroethene.[4] In hexachlorobutadiene the *sp*/*ap* ratio of **1** becomes 1.14,[6] which is still close to unity. Therefore the increase in the equilibrium constants on substitution of a substituent for hydrogen of the methyl group is significant. One of the possibilities which favor the *sp* form is the dipolar interaction between the C-substituent bond and the C–Cl in the solvent molecule. We therefore determined the barrier to rotation and the equilibrium constants in compound **2** in toluene-d_8. The results shown in Table 5 yield $\Delta H^{\ddagger}$ 27.6±0.2 kcal/mol (1 cal=4.18 J) and $\Delta S^{\ddagger}$ −5.9±0.5 e.u. (1 e.u.=4.18 J mol^{-1} K^{-1}) for the *ap*→*sp* process. Thus $\Delta G^{\ddagger}$ at 373 K is 29.8 kcal/mol. Interestingly the equilibrium constants are 3.0 which are not different from those in hexachlorobutadiene. Independence of the population ratios from the solvent nature may mean that the solvation is not an important factor in determining the *sp*/*ap* ratio.

We wish to attribute the large equilibrium constants for compounds **2**—**4**, from the above results, to the entropy effect. If one considers conformations which change by rotation about the XCH_2–naphthyl bond, there is a restriction in some of the conformations in the *ap* form. Since X is larger than hydrogen, a conformation in which X is close to the fluorene ring is strongly disfavored due to the steric effect. That kind of steric effect is less severe in the *sp* form. This factor should contribute to decrease in entropy in the *ap* form relative to the *sp* form.

Close examination of the *sp*/*ap* ratios reveals that the *ap* form of the hydroxy compound (**3**) is slightly favored relative to other *ap* forms. One of the possibilities that favor the *ap* conformation in **3** is the presence of OH···π interactions. If the aryl group in 9-arylfluorenes is either 2-hydroxy-1-naphthyl or 2-hydroxy-4,6-dimethylphenyl, strong stabilization of the *ap* form is reported.[7] Thus infrared ν_{OH} spectra of these compounds were recorded. The results are shown in Table 6.

Since the frequencies are not calibrated, the absorption at *ca.* 3620 cm^{-1} may be considered to correspond to the benzylic OH···π type band.[8] We may call this band "free," since its shift is small from the really free band and there is another bonded band in *ap*-**3**. Then the *sp* form shows only a free band in 9.8 mM solution and, in more concentrated solution and in the solid state, it shows a polymeric band. In contrast, the *ap* form shows two ν_{OH} bands in 9.8 mM solution: the band due to a free form at 3630 cm^{-1} and that due to an OH···π bonded form at 3580 cm^{-1}. In 0.2 M solution, the *ap* form is present as free, OH···π bonded, and polymeric forms, whereas in the solid state it is still possible to see a band due to monomeric species. In the sterically hindered alcohols, the monomeric form is often observed even in the condensed phase,[9] and *ap*-**3** is another example of such a case.

The above results clearly indicate that there is an OH···π interaction in the *ap* form at the concentration (0.2 M) of the NMR measurement. We may attribute the favoredness of *ap*-**3** relative to other *ap*-forms to the OH···π interaction. It is interesting to note that the OH···π interaction is detected even though the OH group and the π-system are separated by 4 carbon atoms. Among 4-phenyl-1-butanol derivatives, even *p*-aminophenylbutanol, which should facilitate the interaction because of the high electron density of the phenyl group, failed to show an OH···π bond.[10] *o*-(2-Phenylethyl)phenol shows a weak intramolecular OH···π interaction, whereas such an interaction is not detected

in *o*-(3-butenyl)phenol:[11] the results are partly attributed to the entropy effect because the π-system in the former distributes widely relative to the latter. The skeleton of *ap*-**3** is fixed except the $HOCH_2$ part. Therefore the presence of the fairly strong intramolecular OH···π interaction in *ap*-**3** can be attributed to the favorable entropy factor. If the conformation of a molecule is fixed favorably, the intramolecular interaction may be found even though the two groups are separated by more than 4 carbons.

We may now compare the effect of a 1-naphthyl group with that of *o*-tolyl on the barrier to rotation, because a pair of compounds both of which carry a bromomethyl group next to the carbon connected to fluorene is available. Activation parameters for rotation in 9-(2-bromomethyl-6-methylphenyl)fluorene in hexachlorobutadiene are as follows for the *ap*→*sp* process: $\Delta H^{\ddagger}$ 26.3 kcal/mol, $\Delta S^{\ddagger}$ −9.3 e.u., and $\Delta G^{\ddagger}_{373}$ 29.8 kcal/mol.[6] Comparing these data with those for **2**, we see that the enthalpy of activation is definitely larger for **2** than for 9-(2-bromomethyl-6-methylphenyl)fluorene, although the free energy for activation at 373 K is the same. This enthalpy difference must be the reflection of the rigidity of the 1-naphthyl group relative to the *o*-tolyl, as suggested before.[6]

Experimental

9-(2-Bromomethyl-1-naphthyl)fluorene (2). A solution of 13.0 g (43 mmol) of a mixture of rotamers of 9-(2-methyl-1-naphthyl)fluorene (**1**)[4] and 18 g (100 mmol) of *N*-bromosuccinimide in 400 mL of chlorobenzene was refluxed for 1 h with stirring. After cooling, succinimide was removed by filtration and chlorobenzene was distilled off *in vacuo*. The residue was chromatographed on silica gel with hexane. *sp*-**1**, *ap*-**1**, *ap*-**2**, and *sp*-**2** were eluted successively. A typical run gave 0.8 g of *ap*-**2** and 3.6 g of *sp*-**2** with 2.7 g of a mixture containing *sp*-**2**, *ap*-**2**, and starting materials.

ap-**2**, mp 132—133.5 °C. Found: C, 74.99; H, 4.32; Br, 21.13%. Calcd for $C_{24}H_{17}Br$: C, 74.81; H, 4.45; Br, 20.74%. ^{1}H NMR ($CDCl_3$, δ): 3.56 (2H, s), 6.12 (1H, s), 7.0—8.0 (13H, m), 8.37—8.57 (1H, m).

sp-**2**, mp 123—124 °C. Found: C, 75.07; H, 4.29; Br, 21.05%. Calcd for $C_{24}H_{17}Br$: C, 74.81; H, 4.45; Br, 20.74%. ^{1}H NMR ($CDCl_3$, δ): 4.96 (2H, s), 5.81 (1H, s), 6.47 (1H, d, J=8.7 Hz), 6.7—8.0 (13H, m).

9-(2-Hydroxymethyl-1-naphthyl)fluorene (3). To a solution of 4.0 g of the bromo compound (**2**) in 50 mL of dimethyl sulfoxide, was added 20 mL of water with heating and stirring. The heating and the stirring were continued for 2 h. The mixture was poured into water and the organic material was extracted with ether. The ethereal layer was thoroughly washed with water and dried over magnesium sulfate. After evaporation of the solvent, the residue was chromatographed on silica gel with benzene. *ap*-**3** and *sp*-**3**, eluted in this order, were obtained in 0.4 g and 2.0 g yield with 2.0 g of a mixture of rotamers of **3**.

ap-**3**, mp 134—135.5 °C. Found: C, 89.18; H, 5.44%. Calcd for $C_{24}H_{18}O$: C, 89.41; H, 5.63%. ^{1}H NMR ($CDCl_3$, δ): 0.87 (1H, t, J=6.0 Hz), 3.55 (2H, d, J=6.0 Hz), 6.10 (1H, s), 7.0—8.0 (13H, m), 8.40—8.60 (1H, m).

sp-**3**, mp 103—105 °C. Found: C, 89.29; H, 5.52%. Calcd for $C_{24}H_{18}O$: C, 89.41; H, 5.63%. ^{1}H NMR ($CDCl_3$, δ): 2.07 (1H, t, J=6.0 Hz), 5.05 (2H, d, J=6.0 Hz), 5.76 (1H, s), 6.45 (1H, d, J=9.0 Hz), 6.6—8.0 (13H, m).

9-(2-Methoxymethyl-1-naphthyl)fluorene (4). To a solution of 0.30 g (0.78 mmol) of *ap*-**2** in 30 mL of methanol was slowly added 0.16 g (0.77 mmol) of silver perchlorate in 5 mL of methanol. A small amount of chloroform may be used to facilitate dissolution of *ap*-**2** in methanol. After excess of silver perchlorate was decomposed by adding aqueous lithium chloride, the precipitate was removed by filtration and the filtrate was poured into water. The organic material was extracted with ether. The ethereal extract was washed with water and dried over magnesium sulfate. Evaporation of the solvent afforded almost pure *ap*-**4**, oil, in 96% yield. High resolution mass spectrum showed a molecular ion peak at *m/e* 336.1544, whereas the calculated mass of the molecule for $C_{25}H_{20}O$ is 336.1514. ^{1}H NMR ($CDCl_3$, δ): 2.53 (3H, s), 3.33 (2H, s), 6.12 (1H, s), 7.1—8.0 (13H, m), 8.43—8.60 (1H, m).

sp-**4**, mp 114—115 °C, was prepared similarly in 94% yield. Found: C, 89.22; H, 5.89%. Calcd for $C_{25}H_{20}O$: C, 89.25; H, 5.99%. ^{1}H NMR ($CDCl_3$, δ): 3.45 (3H, s), 4.93 (2H, s), 5.82 (1H, s), 6.47 (1H, d, J=9.0 Hz), 6.7—8.0 (13H, m).

sp-**4** was also prepared by methanolysis of *sp*-**2**. A solution of 0.30 g of *sp*-**2** in 30 mL of methanol was refluxed for 15 h. After evaporation of the solvent, the residue was recrystallizaed from 1 : 5 benzene–hexane to give 0.21 g of *sp*-**4**. A small amount of *ap*-**4** was detected in the reaction mixture before recrystallization. Methanolysis of *ap*-**3** was too slow to be practical.

Determination of Barriers to Rotation. A solution was prepared by dissolving 30 mg of the *ap* form of arylfluorenes in 0.4 mL of hexachlorobutadiene or toluene-d_8 and was placed in an NMR sample tube. The tube was immersed in an appropriate boiling-solvent bath, the temperature of which was directly measured by a thermometer. The rate of isomerization was followed by ^{1}H NMR spectroscopy and was treated assuming a reversible first-order reaction. The rate constants thus obtained were put into the Eyring equation to obtain activation parameters. The following solvents were used for the bath (solvent and approximate boiling points given): benzene (77 °C), 1 : 1 benzene–toluene (87 °C), dioxane (95 °C), toluene (104 °C), 1 : 1 chlorobenzene–toluene (114 °C), chlorobenzene (124 °C).

Determination of Infrared Spectra. The spectra were recorded on a Hitachi EPI-G spectrometer. The wave numbers reported are not calibrated. The spectra of solid were obtained as KBr discs. The spectra of solution were obtained with a KBr cell of variable length. With solutions of *ca.* 0.2 M in carbon tetrachloride, the cell length was 0.25 mm and, with those of 9.8 mM, the cell length was 5.0 mm.

^{1}H NMR spectra were obtained with either a Hitachi R-20B or a Varian EM 390 spectrometer.

References

1) For Part XLI, see S. Murata, T. Mori, and M. Ōki, *Chem. Lett.*, **1982**, 271.

2) R. Adams and H. C. Yuan, *Chem. Rev.*, **12**, 261 (1933).

3) M. Ōki, *Angew. Chem., Int. Ed. Engl.*, **15**, 87 (1976).

4) T. H. Siddall, III, and W. E. Stewart, *J. Org. Chem.*, **34**, 233 (1969).

5) Solvolysis of the CH_2Br group in a similar environment is very slow: S. Murata, S. Kanno, Y. Tanabe, M. Nakamura, and M. Ōki, *Angew. Chem., Int. Ed. Engl.*, **20**, 606 (1981).

6) S. Murata, S. Kanno, Y. Tanabe, M. Nakamura, and M. Ōki, *Bull. Chem. Soc. Jpn.*, **55**, 1522 (1982).

7) M. Nakamura and M. Ōki, *Bull. Chem. Soc. Jpn.*, **53**, 3248 (1980).

8) M. Ōki and H. Iwamura, *Bull. Chem. Soc. Jpn.*, **32**, 955 (1959) and papers cited therein.
9) R. N. Jones and C. Sandorfy, "Infrared and Raman Spectrometry: Applications," in "Chemical Applications of Spectroscopy," ed by W. West, Interscience Publisher, New York (1956), pp. 247—580.
10) M. Ōki and H. Iwamura, *Bull. Chem. Soc. Jpn.*, **32**, 1135 (1959).
11) M. Ōki and H. Iwamura, *Bull. Chem. Soc. Jpn.*, **33**, 681 (1960).

Restricted Rotation Involving the Tetrahedral Carbon. XLIII. Buttressing Effect on Rotational Barriers in Bromine-substituted 9-(2-Methoxy-4,6-dimethylphenyl)fluorenes[1]

Masahiro Aoki, Mikio Nakamura,† and Michinori Ōki*

Department of Chemistry, Faculty of Science, The University of Tokyo, Bunkyo-ku, Tokyo 113

†*Department of Chemistry, School of Medicine, Toho University, Omorinishi, Ota-ku, Tokyo 143*

(Received March 30, 1982)

9-(2-Methoxy-4,6-dimethylphenyl)fluorenes carrying one or two bromo groups on the phenyl ring were prepared and the buttressing effect on the rotational barrier about the C_9–C_{ph} bond were investigated. The free energies of activation for rotation were 26.5, 25.9, and 27.2 kcal/mol at 56 °C for 3-bromo, 5-bromo, and 3,5-dibromo compounds, respectively. The buttressing effect was enhanced when the bromo group was next to the methoxyl group relative to that given to the methyl group. The results were attributed to the fact that a methoxyl group, which gives its steric effect by the oxygen atom in the normal cases, has to take conformations, not coplanar with the phenyl ring, caused by the presence of the bromo group.

Buttressing effect was found in biphenyls: barrier to rotation is raised if a substituent is introduced next to a substituent which gives direct interaction with others in the transition state for rotation. Thus in biphenyls, the barriers are enhanced by the buttressing effect.[2] However, buttressing effect does not always enhance the barrier to rotation. There is a case in which buttressing effect lowers the barrier in a triptycene system.[3] Since both triptycenes and 9-arylfluorenes are congested systems in the ground state, it is worthwhile to see whether the buttressing effect enhances the barrier to rotation in the 9-arylfluorene system. This paper reports the results of such an investigation.

Syntheses of required compounds were carried out in the following way. 2,4,6-Tribromo-3,5-dimethylanisole (**1d**) was prepared according to a known method. 2,4-Dibromo-3,5-dimethylanisole (**1b**) had been prepared by a cumbersome method but we found that bromination of 3,5-dimethylanisole with 2 mol of bromine gave a satisfactory result. Preparation of 2,6-dibromo-3,5-dimethylphenol was described in a patent which utilizes the isomerization of a 2,4-dibromo isomer.[4] However, tracing the method revealed that it was not satisfactory for the preparative purpose. Thus we utilized a method which had been used for preparation of 2,6-dibromophenol.[5] The method, when applied to 3,5-dimethylphenol, gave a satisfactory yield of 2,6-dibromo, -3,5-dimethylphenol which was methylated to afford 2,6-dibromo-3,5-dimethylanisole (**1c**). The bromoanisoles (**1**) were converted to Grignard reagents which were allowed to react with fluorenone. The products (**2**) were reduced to give the desired monobromo or dibromo derivatives (**3**) of 9-(2-methoxy-4,6-dimethylphenyl)-fluorene.

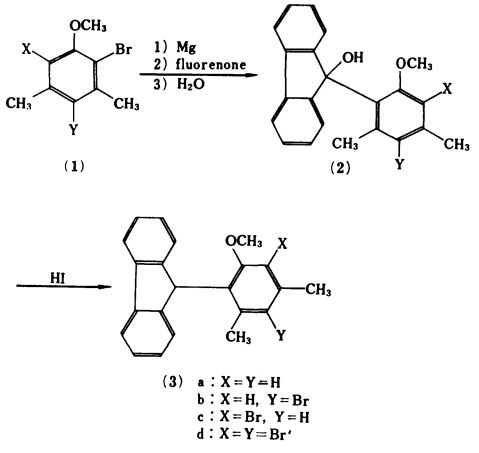

(1) (2)

(3) a : X=Y=H
b : X=H, Y=Br
c : X=Br, Y=H
d : X=Y=Br

The assignment of the stereostructures of the products (**2** and **3**) was performed in the usual way. The *ap* forms exhibited a high field signal due to the methoxyl group in ^{1}H NMR spectroscopy relative to the *sp*, because the methoxyl group is located over the fluorene ring in the *ap*. The reverse is true for the 6-methyl protons: they give a low field signal in the *ap* conformation and a high field signal in the *sp*.

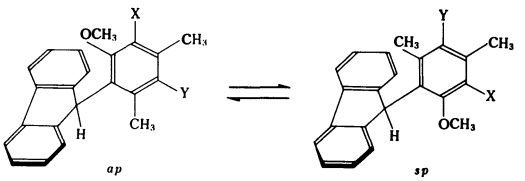

ap *sp*

Rates of isomerization of compounds **3b—d** at various temperatures are summarized in Tables 1—3. Kinetic parameters obtained by putting the rate data into the Eyring equation are shown in Table 4 together with those for the unsubstituted compound (**3a**),[6] for comparison. The data clearly show that there is the buttressing effect operating in compounds **3b—d**. We may call now the buttressing effect which raises the

Table 1. Rates of isomerization and equilibrium constants of rotamers in 9-(5-bromo-2-methoxy-4,6-dimethylphenyl)fluorene (**3b**) in tetrachloroethene

Temp/°C	$k(sp \rightarrow ap)/s^{-1}$	$K(sp/ap)$
49.4	2.14×10^{-5}	5.71
56.5	4.73×10^{-5}	5.38
64.2	1.02×10^{-4}	5.29
69.4	1.73×10^{-4}	5.11

Table 2. Rates of isomerization and equilibrium constants of rotamers in 9-(3-bromo-2-methoxy-4,6-dimethylphenyl)fluorene (**3c**) in tetrachloroethene

Temp/°C	$k(sp\rightarrow ap)/s^{-1}$	$K(sp/ap)$
56.3	1.73×10^{-5}	5.43
64.3	4.20×10^{-5}	5.30
68.9	6.68×10^{-5}	5.21
78.4	1.73×10^{-4}	5.11

Table 3. Rates of isomerization and equilibrium constants of rotamers in 9-(3,5-dibromo-2-methoxy-4,6-dimethylphenyl)fluorene (**3d**) in tetrachloroethene

Temp/°C	$k(sp\rightarrow ap)/s^{-1}$	$K(sp/ap)$
56.3	6.13×10^{-6}	7.08
64.3	1.56×10^{-5}	6.92
69.0	2.67×10^{-5}	6.82
78.4	7.52×10^{-5}	6.70

Table 4. Activation parameters for rotation ($sp\rightarrow ap$) in 9-(2-methoxy-4,6-dimethylphenyl)-fluorene and its bromo derivatives in tetrachloroethene

Compound	Substituent 3-	Substituent 5-	$\Delta H^{\ddagger}$ / kcal mol^{-1}	$\Delta S^{\ddagger}$ / e.u.	$\Delta G^{\ddagger}_{329}$ / kcal mol^{-1}
3a[a]	H	H	24.4±0.1	−1.9±0.1	25.0
3b	H	Br	22.2±0.3	−11.3±0.8	25.9
3c	Br	H	23.2±0.0	−10.0±0.0	26.5
3d	Br	Br	25.4±0.1	−5.4±0.4	27.2

a) Chloroform-*d* solvent.

Table 5. Rates of rotation, free energy of activation for rotation and equilibrium constants of rotamers in 9-(2-methoxy-4,6-dimethylphenyl) fluorene and its bromo derivatives in chloroform-*d* at 56.5 °C

Compound	Substituent 3-	Substituent 5-	$k(sp\rightarrow ap)$ / s^{-1}	$K(sp/ap)$	$\Delta G^{\ddagger}$ / kcal mol^{-1}
3a[a]	H	H	1.74×10^{-4}	3.3	24.9
3b	H	Br	5.39×10^{-5}	3.6	25.8
3c	Br	H	1.83×10^{-5}	5.3	26.5
3d	Br	Br	6.02×10^{-6}	7.0	27.2

a) At 56.3 °C.

barrier to rotation as positive. An interesting point is that the magnitude of the positive buttressing effect is different according to the position of the bromo group. When a bromo group is introduced to the ortho position of the 6-methyl group (**3a**→**3b** or **3c**→**3d**), the barrier is enhanced by less than 1 kcal/mol (1 cal=4.18 J). In contrast, if a bromo group is introduced ortho to the methoxyl group (**3a**→**3c** or **3b**→**3d**), the barrier is raised by *ca.* 1.5 kcal/mol.

The difference in the magnitude of buttressing effect caused by the same substituent may deserve further mention here. Electronic effect[7] may be neglected because a bromo group in the 3-position of the phenyl is ortho to the methoxyl and para to the 6-methyl, whereas that in the 6-position is para to the methoxyl and ortho to the 6-methyl. Probably the most important point is that a methoxyl group has an additional bond which can be involved in forming varieties of conformations: that is the CH_3–O bond. Anisole is known to be an almost planar molecule,[8] which can be interpreted that maximum stabilization is obtained in this conformation because of delocalization of electrons. However, if both ortho positions of the methoxyl group are occupied by substituents, the planar structure is no longer stable owing to the steric effect. There are some examples known in the literature.[9] If the methoxyl group in compound **3** is not coplanar with the phenyl group, the transition state for rotation rather than the ground state will be affected, as molecular models suggest. In conclusion, there are two facets of buttressing effect: prevention of angle deformation and the increase in relative bulkiness of a group by preventing certain conformations. In the methoxyl group, both factors are operative. By preventing the planar structure of the methoxyl group with the phenyl, the buttressing effect may even play a role of lengthening the C_{ar}–O bond, although the effect of this lengthening is not well understood. In contrast, the 6-methyl group suffers the buttressing effect of the neighboring group by being prevented from its angle deformation only.

The equilibrium constants suggest that the *sp* conformation is favored in every case. The reason for this is not well understood at the moment but it is possible that the solute-solvent interaction which is more favorable in the *sp* conformation than the *ap* is one of important reasons.

The kinetic and equilibrium data were obtained with chloroform-*d* solutions to see the effect of a weak hydrogen bonding.[10] The results are shown in Table 5. The free energies of activation were almost the same for the two kinds of solutions, *viz.* tetrachloroethene and chloroform-*d*. However, it is interesting to note that the *sp* form of **3c** and **3d** which carry the 3-bromo group shows larger K values (sp/ap) than **3a** and **3b** which lack the 3-bromo. It is possible that the hydrogen bond stabilization is more effective in the *sp* forms of **3c** and **3d** because their *ap* forms are really congested.

Experimental

*2,4,6-Tribromo-3,5-dimethylanisole (**1d**)* was prepared as described in the literature.[11]

*2,4-Dibromo-3,5-dimethylanisole (**1b**).* To a solution of 14 g (0.10 mol) of 3,5-dimethylanisole[12] in 50 mL of acetic acid, was added a solution of 32 g (0.20 mol) of bromine in 30 mL of acetic acid with stirring and cooling. The mixture was poured into water and crystals were collected by filtration. Although the product contained some monobrominated compounds, recrystallization of the mixture from benzene afforded 22.5 g (76.6%) of pure **1b**, mp 108—109 °C (lit,[13] mp 108—109 °C). ^{1}H NMR ($CDCl_3$, δ): 2.39 (3H, s), 2.61 (3H, s), 3.84 (3H, s), 6.63 (1H, s).

*2,6-Dibromo-3,5-dimethylanisole (**1c**).* To a cooled solu-

tion of 14.7 g (0.20 mol) of *t*-butylamine in 250 mL of toluene, 16.0 g (0.10 mol) of bromine was added at −20——−30 °C in about 10 min. To the mixture cooled at −70——−75 °C was added 6.1 g (0.05 mol) of 3,5-dimethylphenol in 30 mL of dichloromethane in 5 min with vigorous stirring. The stirring was continued for 9 h at that temperature and then the mixture was allowed to warm up to room temperature. The organic layer was extracted with 10% aqueous sodium hydroxide and the extract was acidified. Extraction of the mixture with dichloromethane and evaporation of the solvent left a solid residue. Treatment of the residue with hexane separated the desired product as an insoluble part. The crude yield was 58.6%. Recrystallization of the product from hexane afforded pure 2,6-dibromo-3,5-dimethylphenol, mp 93.5—94 °C. Found: C, 34.03; H, 2.95; Br, 57.05%. Calcd for $C_8H_8Br_2O$: C, 34.32; H, 2.88; Br, 57.08%. ^{1}H NMR ($CDCl_3$, δ): 2.34 (6H, s), 5.93 (1H, s), 6.74 (1H, s).

Treatment of the phenol (2.8 g) with 0.4 g of sodium hydroxide in 30 mL of water and 0.94 mL of dimethyl sulfate afforded 52.0% **1c** as a waxy solid. This compound was directly used for the next reaction. ^{1}H NMR ($CDCl_3$, δ): 2.34 (6H, s), 3.85 (3H, s), 6.93 (1H, s).

*9-(5-Bromo-2-methoxy-4,6-dimethylphenyl)fluoren-9-ol (**2b**).* To a vigorously stirred solution of 5-bromo-2-methoxy-4,6-dimethylphenylmagnesium bromide, prepared from 14.7 g (0.050 mol) of **1b** and 1.20 g (0.050 mol) of magnesium in tetrahydrofuran, was added 7.0 g (0.039 mol) of fluorenone in portions at 0 °C. The reaction mixture was stirred for 1 h at room temperature and was then heated under reflux for 2 h. The mixture was cooled and decomposed with aqueous ammonium chloride. The organic layer was separated and dried over magnesium sulfate. After evaporation of the solvent, the products were separated by chromatography on alumina, benzene–hexane mixtures being used as eluent. **2b**, mp 147—149 °C, was eluted first and then came a mixture of **2b** and 9-(3-bromo-4-methoxy-2,6-dimethylphenyl)fluoren-9-ol, as judged by its ^{1}H NMR spectrum ($CDCl_3$, δ): *sp*, 1.32 (3H, s), 1.75 (1H, s), 2.84 (3H, s), 3.75 (3H, s), 6.52 (1H, s), 7.0—7.6 (8H, m); *ap*, 1.13 (3H, s), 1.84 (1H, s), 3.01 (3H, s), 3.64 (3H, s), 6.13 (1H, s), 7.0—7.6 (8H, m). The *sp*/*ap* ratio of the latter was 0.5. The ratio of **2b** to 9-(3-bromo-4-methoxy-2,6-dimethylphenyl)fluoren-9-ol was 3 : 1 as ^{1}H NMR spectra indicated. The yield of **2b** was 57% based on fluorenone. Found: C, 67.03; H, 4.70; Br, 19.96%. Calcd for $C_{22}H_{19}BrO_2$: C, 66.84; H. 4.84; Br, 20.21%. ^{1}H NMR ($CDCl_3$ δ) indicated that **2b** was a mixture of *sp* and *ap* rotamers (8 : 1). *sp*: 1.45 (3H, s), 2.40 (3H, s), 4.03 (3H, s), 6.82 (1H, s), 6.90 (1H, s), 7.1—7.7 (8H, m). *ap*: 2.10 (1H, s), 2.40 (3H, s), 2.85 (3H, s), 3.12 (3H, s), 6.45 (1H, s), 7.1—7.7 (8H, m).

*9-(3,5-Dibromo-2-methoxy-4,6-dimethylphenyl)fluoren-9-ol (**2d**)*, mp 159—161 °C, was similarly prepared by treating 3,5-dibromo-2-methoxy-4,6-dimethylphenylmagnesium bromide, which was prepared from **1d**, with fluorenone. The yield was 43%. Found: C, 55.89; H, 3.68; Br, 33.67%. Calcd for $C_{22}H_{18}Br_2O_2$: C, 55.72; H, 3.83; Br, 33.67%. ^{1}H NMR ($CDCl_3$, δ) indicated that the compound was a 4 : 1 mixture of *sp* and *ap* forms: *sp*, 1.45 (3H, s), 2.70 (3H, s), 4.16 (3H, s), 6.57 (1H, s), 7.1—7.8 (8H, m); *ap*, 2.18 (1H, s), 2.65 (3H, s), 2.70 (3H, s), 3.10 (3H, s), 7.1—7.8 (8H, m).

*9-(3-Bromo-2-methoxy-4,6-dimethylphenyl)fluoren-9-ol (**2c**)* was similarly prepared from **1c** in 47% yield. ^{1}H NMR ($CDCl_3$, δ) indicated that the product was a 3.4 : 1 mixture of *sp* and *ap* forms: *sp*, 1.19 (3H, s), 2.36 (3H, s), 4.17 (3H, s), 6.85 (1H, s), 6.66 (1H, s), 7.1—7.8 (8H, m); *ap*, 2.06 (1H, s), 2.32 (3H, s), 2.65 (3H, s), 2.88 (3H, s), 6.93 (1H, s), 7.1—7.8 (8H, m). The product was directly used for reduction which is described below.

*9-(5-Bromo-2-methoxy-4,6-dimethylphenyl)fluorene (**3b**).* To a solution of 1.35 g (3.4 mmol) of **2b** in 50 mL of acetic acid was added 10 mL of 57% hydriodic acid. The solution was stirred for 3 h at 20 °C and poured into water. The organic materials were extracted with ether and the extract was washed with aqueous sodium hydrogencarbonate and then with aqueous sodium sulfite. The ethereal solution was dried over sodium sulfate. The solvent was evaporated and the residue was submitted to chromatography on alumina, hexane being used as an eluent. The chromatographed product was recrystallized from hexane to give pure *sp* form of **3b** in 92% yield. The melting point was 149—150 °C. Found: C, 69.83; H, 4.87; Br, 21.39%. Calcd for $C_{22}H_{19}BrO$: C, 69.67; H, 5.05; Br, 21.07%. ^{1}H NMR ($CDCl_3$, δ): 1.26 (3H, s), 2.43 (3H, s), 3.91 (3H, s), 6.02 (1H, s), 6.85 (1H, s), 7.1—7.9 (8H, m).

A rotameric mixture, which was obtained as the result of isomerization works, was submitted to TLC on alumina with hexane eluent. The *sp* form had a larger R_f value than the *ap*. Rechromatography afforded pure *ap*-**3b**, mp 132.2—133.0 °C. High resolution mass spectrum showed molecular ion peaks at 378.0675 and 380.0583, whereas $C_{22}H_{19}BrO$ requires 378.0620 and 380.0598. The relative intensities of the two peaks agreed well with those expected from the natural abundance of ^{79}Br and ^{81}Br. ^{1}H NMR ($CDCl_3$, δ): 2.38 (3H, s), 2.85 (3H, s), 2.88 (3H, s), 5.32 (1H, s), 6.45 (1H, s), 7.1—7.9 (8H, m).

*9-(3,5-Dibromo-2-methoxy-4,6-dimethylphenyl)fluorene (**3d**)*, mp 149—151 °C, was prepared similarly in 35% yield. Found: C, 57.57; H, 3.75; Br, 34.62%. Calcd for $C_{22}H_{18}Br_2O$: C, 57.67; H, 3.60; Br, 34.88%. ^{1}H NMR ($CDCl_3$, δ) data indicated that the product was pure *sp*-**3d**: 1.23 (3H, s), 2.66 (3H, s), 3.99 (3H, s), 5.87 (1H, s), 7.1—7.9 (8H, m). Since the population ratio at the equilibrium was very large, the isolation of the *ap*-form was not attempted. The following ^{1}H NMR ($CDCl_3$, δ) data for the *ap* form were recorded: 2.62 (3H, s), 2.65 (3H, s), 2.87 (3H, s), 5.39 (1H, s), 7.1—7.9 (8H, m).

*9-(3-Bromo-2-methoxy-4,6-dimethylphenyl)fluorene (**3c**)* was prepared similarly. Unlike other related compounds, reduction of 0.92 g of **2c** afforded 0.30 g of *sp*, mp 136.5—137.0 °C, and 0.28 g of *ap*, mp 115.5—116.5 °C, the total yield being 66.5%. The following ^{1}H NMR data ($CDCl_3$, δ) and analytical data were obtained.

sp. Found: C, 69.59; H, 5.00; Br, 21.39%. Calcd for $C_{22}H_{19}BrO$: C, 69.67; H, 5.05; Br, 21.07%. NMR: 1.04 (3H, s), 2.36 (3H, s), 4.03 (3H, s), 5.78 (1H, s), 6.64 (1H, s), 7.1—7.9 (8H, m).

ap. High resolution mass spectrum showed molecular ion peaks at 378.0604 and 380.0581, while $C_{22}H_{19}BrO$ requires 378.0620 and 380.0598. NMR: 2.35 (3H, s), 2.63 (3H, s), 2.63 (3H, s), 2.66 (3H, s), 5.22 (1H, s), 6.97 (1H, s), 7.1—7.9 (8H, m).

Determination of Barriers to Rotation. A pure sample (*ca.* 40 mg) of *sp*-**3** was dissolved in *ca.* 0.5 mL of tetrachloroethene or chloroform-*d* and placed in an NMR sample tube. The tube was immersed in an appropriate boiling-solvent bath, temperature being checked by a thermometer, and the appearance of *ap*-**3** was followed by ^{1}H NMR spectroscopy. The data were treated by assuming a reversible first-order reaction and the rate constants were put into the Eyring equation to obtain activation parameters. The following solvents were used for the bath (solvents and approximate temperatures given): methanol–hexane azeotrope (49.4 °C), acetone (56.5 °C), methanol (64 °C), hexane (69 °C), and ethanol (78 °C).

NMR Measurement. The spectra were obtained with

either a Varian EM 390 spectrometer or a Hitachi R-20B spectrometer. Integration was carried out 8—10 times and the average was used for the kinetic measurement.

References

1) For Part XLII, see R. Saito and M. Ōki, *Bull. Chem. Soc. Jpn.*, **55**, 2508 (1982).
2) S. L. Chen and R. Adams, *J. Am. Chem. Soc.*, **56**, 1787 (1934).
3) G. Yamamoto, M. Suzuki, and M. Ōki, *Chem. Lett.*, **1980**, 1523.
4) E. J. O'Bara, Brit. Patent 1269521; *Chem. Abstr.*, **76**, 15335g (1972); See also E. J. O'Bara, R. B. Balsley, and I. Starter, *J. Org. Chem.*, **35**, 16 (1970).
5) D. E. Pearson, R. D. Wysong, and C. V. Breder, *J. Org. Chem.*, **32**, 2358 (1967).
6) M. Nakamura and M. Ōki, *Bull. Chem. Soc. Jpn.*, **53**, 3248 (1980).
7) M. Ōki and G. Yamamoto, *Bull. Chem. Soc. Jpn.*, **44**, 266 (1971).
8) H. M. Seip and R. Seip, *Acta Chem. Scand.*, **27**, 4024 (1973).
9) M. J. Aroney, M. G. Corfield, and R. J. W. Le Ferve, *J. Chem. Soc.*, **1964**, 2954.
10) G. C. Pimentel and A. L. McClellan, "The Hydrogen Bond," W. H. Freeman and Co., San Francisco (1960), p. 197.
11) M. Kohn and M. K. Feldmann, *Monats. Chem.*, **49**, 170 (1982).
12) G. S. Hiers and F. D. Hager, *Org. Synth.*, Coll. Vol. I, 58 (1958).
13) K. V. Awers, *Justus Liebigs Ann. Chem.*, **421**, 1 (1920).

The Influence of Molecular Conformation on the Electronic Relaxation Processes. Biphenyl in Solution

Tsuneo Fujii,* Shigeru Komatsu,† and Satoshi Suzuki
Department of Industrial Chemistry, Faculty of Engineering, Shinshu University, Wakasato, Nagano 380
(Received January 20, 1981)

The fluorescence spectra of biphenyl in an isopentane and methylcyclohexane mixture, in propylene glycol, and in glycerol have been observed as a function of temperature and excitation wavelength. The temperature dependence of the fluorescence spectra is interpreted in terms of the intramolecular geometric relaxation. The fluorescence spectra of biphenyl have been observed in various solvents at room temperature. The Ham effect was found in the biphenyl fluorescence.

The influence of molecular structure on photophysical processes has been investigated by several authors. Lim and Chakrabarti have studied the phosphorescence lifetimes and polarization of various aromatic amines and of phenoxide ion.[1] Kasha and Rawls have studied the phosphorescence lifetimes of twisted anilines.[2] They suggested that the enhanced spin-orbit coupling in heteroaromatic molecules should be attributed to the pseudo non-bonding character of the lone-pair electrons of the substituent. Huber *et al.* showed that the rate constant of $S_1 \rightarrow T_i$ intersystem-crossing, k_{TM}, and the radiative rate constant of $T_1 \rightarrow S_0$ decrease rapidly on going from diphenylamine to 9,10-dihydroxyacridine (acridan) and carbazole, while the radiative rate constant of $S_1 \rightarrow S_0$ is only slightly altered.[3]

The influence of molecular conformations on electronic relaxation processes is an interesting problem in photophysics. Two benzene rings of biphenyl are connected with a C-C single bond and vibrate torsionally around the C-C bond. It was reported that the planes of the two benzene rings of biphenyl are inclined at an angle of 20—40° in the ground state, while they are inclined at an angle of 0—20° in the excited states.[4-8] Electronic excitation and deexcitation processes of biphenyl inevitably include conformational changes.

Hughes *et al.* and Naqvi *et al.* studied the excitation-wavelength dependence of the fluorescence spectra of biphenyl[9] and polyphenyls,[10] but little attention has been directed to the effect of conformation on the electronic relaxation processes.

The preceding paper[11] presented the excitation-wavelength dependence of the fluorescence and phosphorescence quantum yields and of the phosphorescence lifetime of biphenyl in propylene glycol and discussed the influence of molecular conformations on the rate constants of the radiative and radiationless processes of biphenyl. It was shown that the intramolecular geometric relaxation[12] plays an important role in the temperature dependence of the photophysical processes of biphenyl.

This paper presents the experimental findings of the influence of solvent, temperature, excitation wavelength, and viscosity on the fluorescence spectra of biphenyl. The difference of the distribution of conformers in the ground and excited states of biphenyl satisfactorily explains the observed spectral changes.

Experimental

Biphenyl was purified by repeated recrystallizations from ethanol and passed 1000 times through a zone refiner. Methanol (Wako Pure Chemical Industries, Inc., Luminasol grade) and acetonitrile (Wako, Spectrosol grade) were used without further purification. Cyclohexane, isopentane, methylcyclohexane, glycerol, propylene glycol (Wako, JIS S grade), and ethanol (Wako, Super special grade) were dehydrated by the use of molecular sieves 3A and passed through a silica-gel column. Isopropyl alcohol, *N*-methylformamide, and tetrahydrofuran (Wako, JIS S grade) were used without further purification. The absorption and emission spectra were recorded on a Hitachi EPS-3 recording spectrophotometer and a Hitachi MPF-2A fluorescence spectrophotometer respectively. The concentrations of the sample solutions used in fluorescence measurements at room temperature are less than 10^{-3} mol dm^{-3} and the solutions were not degassed. The degree of polarization, P, was measured by the method of photoselection.[13,14] The temperature of solutions was varied from 77 to 300 K by the use of a metal cryostat (Torisha Laboratory, Ltd.).

Results

Figure 1 shows the fluorescence spectra of biphenyl in isopentane (dielectric constant $\varepsilon = 1.843$ at 20 °C), isopropyl alcohol ($\varepsilon = 19.92$ at 25 °C), methanol ($\varepsilon = 32.70$ at 25 °C), and *N*-methylformamide ($\varepsilon = 182.4$ at 25 °C). The spectrum of biphenyl in isopentane shows a sharp vibrational structure but has no 0-0 band. The spectra observed in cyclohexane, in methylcyclohexane, and in an isopentane–methylcyclohexane mixture (3 : 1) are almost the same as those in isopentane. Biphenyl shows less sharp fluorescence spectra in ethanol, methanol, and isopropyl alcohol than in isopentane. The shoulder which is assigned to the 0-0 band is observed. The spectrum in *N*-methylformamide exhibits a diffuse vibrational structure and has an obvious 0-0 band. Spectra similar to that in *N*-methylformamide are observed in propylene glycol, glycerol, acetonitrile, and tetrahydrofuran. These findings indicate that the appearance of the 0-0 band depends on the solvent polarity and the spectral sharpness decreases with an increase in the dielectric constant of the solvent.

The temperature and excitation-wavelength dependence of the fluorescence spectra in an isopentane–

† Present address: Semiconductor Engineering Department, Semiconductor Division, Tokyo Shibaura Electric Co., Ltd., Kawasaki 210.

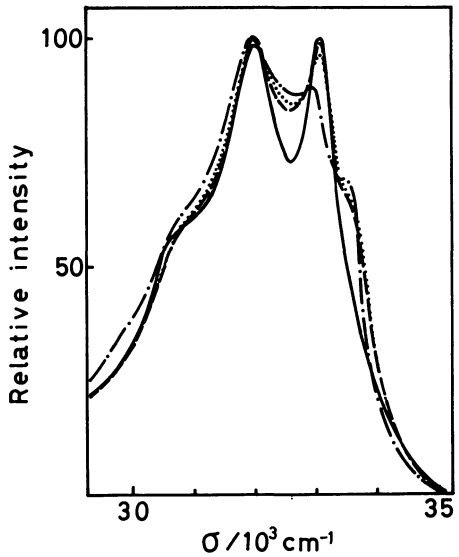

Fig. 1. The fluorescence spectra of biphenyl in isopentane (—), isopropyl alcohol (------), methanol (·····), and *N*-methylformamide (—·—) at room temperature. Excitation wavelength: 270 nm.

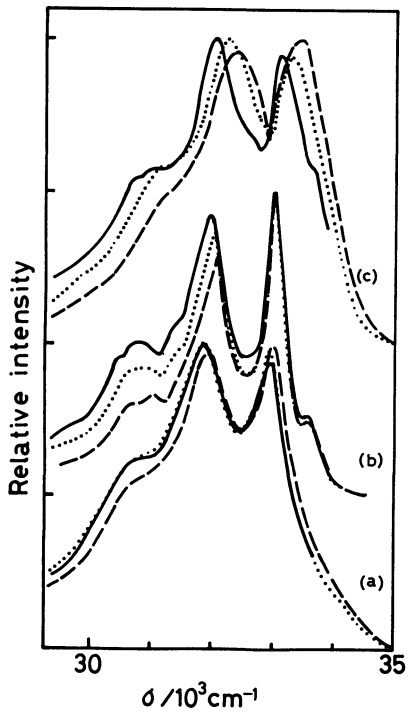

Fig. 2. The excitation-wavelength and temperature dependence of the fluorescence spectra of biphenyl in isopentane–methylcyclohexane mixture (3: 1).
a: 288 K, b: 128 K, c: 83 K. ------, ·····, and —— correspond to the spectra excited at 250 nm, 270 nm, and 290 nm respectively.

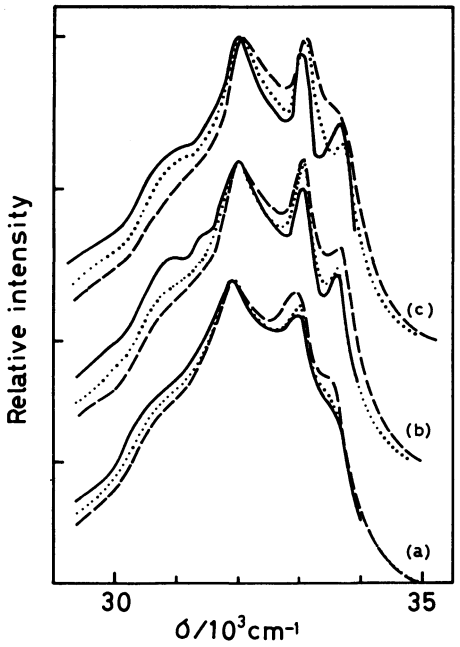

Fig. 3. The excitation-wavelength and temperature dependence of the fluorescence spectra of biphenyl in propylene glycol.
a: 291 K, b: 198 K, and c: 127 K. ------, ·····, and —— have the same meaning as in Fig. 2.

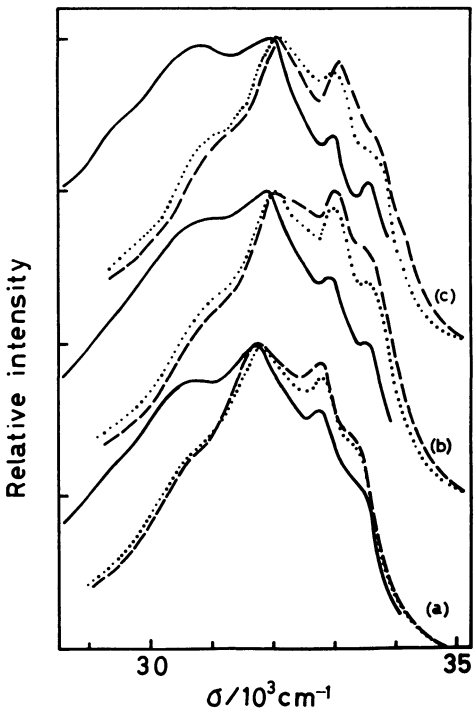

Fig. 4. The excitation-wavelength and temperature dependence of the fluorescence spectra of biphenyl in glycerol.
a: 287 K, b: 233 K, and c: 168 K. ------, ·····, and —— have the same meaning as in Fig. 2.

methylcyclohexane mixture, propylene glycol, and glycerol are shown in Figs. 2, 3, and 4 respectively. Figure 2 shows that the fluorescence spectra in a hydrocarbon solvents are slightly dependent on the excitation wavelength at room temperature. The spectra at 128 K has the sharpest vibrational bands among the observed fluorescence spectra. At 83 K, the vibrational bands become wide again. The freezing point of isopentane is

113 K; the mixed solvent appears to be rigid at 83 K and fluid at 128 K. The broadening of the vibrational structure with lowering temperature from 128 K to 83 K can be related to the freezing of the solvent. The width of vibrational bands is broader at 173 K and 83 K than at 128 K. The width of vibrational bands increases with increasing the excitation energy. The individual vibrational bands observed at 83 K are displaced more to the blue than those observed at higher temperature. The increase in excitation energy also shifts the individual vibrational bands to the blue. Figure 3 shows that the 0-0 vibrational band is obvious in propylene glycol at room temperature. The excitation-wavelength dependence of the biphenyl fluorescence increases with lowering the temperature. Figure 4 shows that the excitation-wavelength dependence of biphenyl fluorescence is also obvious in viscous solvents such as glycerol even at room temperature.

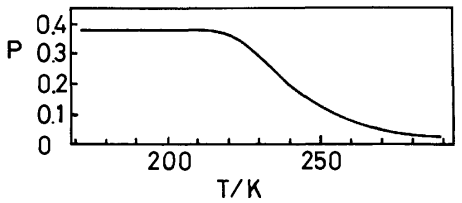

Fig. 5. The temperature dependence of the fluorescence polarization excited at 270 nm and monitored at the peak of 0-1 vibrational band.

The temperature dependence of P of the biphenyl fluorescence in propylene glycol is shown in Fig. 5. Figure 5 shows that the value of P of the biphenyl fluorescence reaches a maximum at 210 K in propylene glycol. The value of the fluorescence spectra for naphthalene derivatives also reaches a maximum at 210 K in the same solvent.[15]

Discussion

Effect of Molecular Conformations on the Fluorescence Spectra of Biphenyl. At high temperature, the fluorescence spectra of biphenyl in an isopentane–methylcyclohexane mixture are not dependent on the excitation wavelength and no 0-0 band is observed (Fig. 2). The spectrum observed at 128 K is more structured than that at 288 K and the 0-0 band becomes obvious. The spectrum at 83 K has more diffuse vibrational bands than those at 128 K.

The temperature and excitation-wavelength dependences in propylene glycol and glycerol are shown in Figs. 3 and 4. The spectral sharpness in the two solvents is different from that in hydrocarbon solvents but the energies of the individual vibrational bands are almost the same in these solvents. Figures 2—4 show that the temperature and viscosity of sample solutions, as well as the excitation wavelength, have an important effect upon the biphenyl fluorescence. This complex behavior may be interpreted in terms of the intramolecular geometric relaxation.[12]

We can classify the processes of the intramolecular

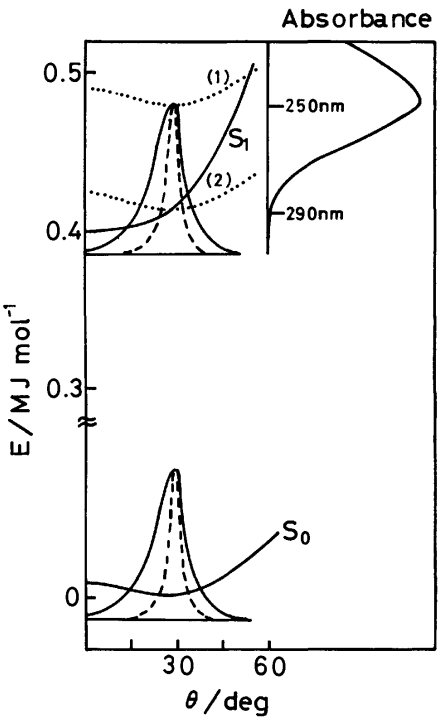

Fig. 6. A schematic potential energy curves of biphenyl for the angle of twist.
Curves (1) and (2) plot the potential curves which are higher in energy by an amount corresponding to 250 and 290 nm radiation respectively. Absorption and Boltzmann distribution at 300 K (——) and 77 K (·····) are also indicated.

geometric relaxation of biphenyl into five categories. (1) Vibrational relaxation, (2) emission without geometric relaxation, (3) geometric relaxation along the angle of twist between the planes of two benzene units of biphenyl(θ), (4) emission from incompletely relaxed conformers, (5) emission from the completely relaxed conformers in the excited state. Process (3) is considered to be rate-determing. When solvent viscosity increases with lowering the temperature, process (3) is gradually prevented and process (4) gradually increases. At sufficiently low temperature, process (3) is prevented completely due to high viscosity of solvent and emission occurs only *via* process (2). Under such conditions emission emerges only from the conformers having the same conformation as in the ground state. Figure 6 illustrates such a situation. The ground- and excited-state potential curves as a function of θ and the Boltzmann distribution of conformational population were estimated from the calculations by Imamura and Hoffmann[6] and Golebiewski and Parczewski.[7] Curves (1) and (2) indicate the energy levels obtained by exciting the ground-state biphenyl with 250-nm and 290-nm radiations respectively. The potential curve of the ground state has two minimums at about $\theta = \pm 30°$, while that of the S_1 has a minimum at $\theta = 0°$. The energy required to excite biphenyl to the S_1 excited state is larger at large θ than at small θ. The 290-nm radiation excites only biphenyl whose θ is smaller than about 30°, while the 250-nm radiation makes it possible to excite

all possible conformers of biphenyl in the ground state This leads to different distributions of conformers dependent on the excitation wavelength in the excited state and results in the fluorescence spectra being dependent on the excitation wavelength.

If process (3) is completed before emission, fluorescence emerges from the well-relaxed excited conformers. Under such conditions, a fluorescence spectrum independent of the excitation wavelength is expected to be observed. As the temperature decreases, the distribution about the equilibrium conformation becomes narrow due to the Boltzmann distribution law. This makes the fluorescence spectrum sharpen on lowering the temperature down to the freezing point of the solvent.

The fluorescence spectrum of biphenyl varies slightly with the excitation wavelength even at room temperature (Fig. 2). This implies that the fluorescence from the incompletely relaxed conformers can not be neglected at room temperature.

When process (3) is gradually hindered with decrease in temperature, biphenyl molecules tends to fluoresce from the imcompletely relaxed or unrelaxed conformers in the excited state. When process (3) in completely hindered, the distribution of excited conformers is the same as that of the ground-state conformers. The fluorescence under such conditions is the superposition of various fluorescences corresponding to different conformations and is broader than at higher temperature. Berlman also found that nonplanar conformers of polyphenyls show diffuse fluorescence spectra and planar conformers show structured ones.[16]

The above discussion is supported by the results in Fig. 2. The isopentane–methylcyclohexane mixture is fluid at 128 K and rigid at 83 K. Intramolecular geometric relaxation occurs effectively at 128 K and is prevented completely at 83 K. The features of the fluorescence spectra at 128 K are determined by the distribution of conformers which attain equilibrium fitting to the S_1 state, while those at 83 K are determined by a conformational distribution identical to that in the ground state. In addition to this, the potential curve for S_1 is steeper around $\theta=30°$ than that for S_0. As a consequence of these facts, biphenyl shows a more broad and blue-shifted fluorescence in an isopentane–methylcyclohexane mixture at 83 K than at 128 K. In the case of the fluorescence spectra in propylene glycol and glycerol, the solution is viscous to a certain extent even at room temperature. Since viscousness of the solvent prevents the complete intramolecular geometric relaxation of excited-state biphenyl even at higher temperature, the excitation-wavelength dependence of the biphenyl fluorescence in viscous solvents is larger than that in fluid solvents. The viscosity of the solvents such as propylene glycol and glycerol gradually increase with lowering the temperature; no drastic change with lowering the temperature is observed in these solvents, unlike the result for the isopentane–methylcyclohexane mixture (Figs. 3 and 4).

The above interpretation is also supported by considering the temperature dependence of the intersystem-crossing rate constants. The values of k_{TM} for biphenyl in propylene glycol by 250-nm and 290-nm excitations are almost the same in the temperature range from 303 to 200 K. There is a difference in the k_{TM} values based on the two excitations at 250 and 290 nm below 200 K.[11] These findings indicate that propylene glycol is completely rigid below 200 K against any molecular rotation including the relaxation along θ during the lifetime of the fluorescent state. The rigidity of propylene glycol is also confirmed by the result of Fig. 5. The P of the biphenyl fluorescence in the solvent reaches a maximum at 210 K. At the temperature below 200 K the distribution of conformers in the fluorescent state is the same as in the ground state. In conclusion, the effects of temperature, viscosity, and excitation-wavelength on biphenyl fluorescence can be interpreted by considering the intramolecular geometric relaxation.

The Ham Effect on the Fluorescence Spectra of Biphenyl. The symmetry-forbidden 0-0 band appears in the absorption spectra of benzene[17,18] and in the fluorescence spectra of pyrene.[19] The band is known as the Ham band. The MO calculations[5,6,20] and experimental findings[21] revealed that the lowest absorption band of biphenyl is symmetry-forbidden regardless of θ. It is seen from Fig. 1 that the appearance and the intensity of the 0-0 band of biphenyl fluorescence are related to the solvent polarity. The 0-0 band is also affected by the change of temperature. The lowering of temperature changes the solvent polarity, solvent viscosity, and the dispersion forces between biphenyl and solvent molecules. Figures 2—4 indicate that the 0-0 band becomes obvious with lowering the temperature. It is therefore concluded that the intensity change of the 0-0 band of biphenyl fluorescence in various solvents is attributable to the Ham effect.

References

1) E. C. Lim and S. K. Chakrabarti, *Chem. Phys. Lett.*, **1**, 28 (1967); *J. Chem. Phys.*, **47**, 4726 (1967).
2) M. Kasha and H. R. Rawls, *Photochem. Photobiol.*, **7**. 561 (1968).
3) J. E. Adams, W. W. Mantulin, and J. R. Huber, *J. Am. Chem. Soc.*, **95**, 5477 (1973); J. R. Huber and J. E. Adams, *Ber. Bunsenges. Phys. Chem.*, **78**, 217 (1974); H. J. Haink and J. R. Huber, *Chem. Phys. Lett.*, **44**, 117 (1967).
4) H. Suzuki, *Bull. Chem. Soc. Jpn.*, **32**, 1340 (1959).
5) Y. Gondo, *J. Chem. Phys.*, **32**, 3928 (1964).
6) A. Imamura and R. Hoffman, *J. Am. Chem. Soc.*, **90**, 5379 (1968).
7) A. Golebiewski and A. Parczewski, *Z. Naturforsch., Teil A*, **25**, 1710 (1970).
8) A. d'Annibale, L. Lunazzi, A. C. Boicelli, and D. Nacciantelli, *J. Chem. Soc., Perkin Trans. 2*, **69**, 1396 (1973).
9) E. Hughes, Jr., J. H. Wharton, and R. V. Nauman, *J. Phys. Chem.*, **75**, 3097 (1971).
10) K. R. Naqvi, J. Donatsch, and U. P. Wild, *Chem. Phys. Lett.*, **34**, 285 (1976).
11) T. Fujii, S. Suzuki, and S. Komatsu, *Chem. Phys. Lett.*, **57**, 175 (1978).
12) M. A. El-Bayoumi, *J. Phys. Chem.*, **80**, 2259 (1976).
13) A. C. Albrecht, *J. Mol. Spectrosc.*, **6**, 84 (1961).
14) T. Azumi and S. P. McGlynn, *J. Chem. Phys.*, **37**, 2413 (1962).
15) S. Suzuki, T. Fujii, A. Imai, and H. Akahori, *J. Phys. Chem.*, **81**, 1592 (1977).

16) I. B. Berlman, *J. Phys. Chem.*, **74**, 3084 (1970).
17) J. S. Ham, *J. Chem. Phys.*, **21**, 756 (1953).
18) M. Koyanagi, *J. Mol. Spectrosc.*, **25**, 273 (1969).
19) A. Nakajima, *Bull. Chem. Soc. Jpn.*, **44**, 3272 (1971).
20) A. Gamba, G. F. Rantardine, and M. Simonetta, *Spectrochim. Acta*, **28A**, 1877 (1972).
21) R. M. Hochstrasser, R. D. McAlpine, and J. D. Whiteman, *J. Chem. Phys.*, **58**, 5078 (1973).

The Electric-field Analyses of a System with an Axial Symmetry and Its Application to the Infrared Intensity

Isao KANESAKA,* Yoshihiro HIROYA, and Kiyoyasu KAWAI
Faculty of Science, Toyama University, Gofuku, Toyama 930

(Received April 25, 1981)

The method of solving the Laplace equation for a system with axial symmetry is formulated in terms of the finite element method. The molecule having C_{3v} point symmetry is assumed to have axial symmetry, and the van der Waals radii of the component atoms are used to estimate the shape of the central molecule. The method is applied to the IR intensity of the C≡N stretching mode of acetonitrile in various states. The observed intensities are adequately explained by the use of the local and reaction fields, except for the intensity in a solution diluted infinitely in chloroform. The intensity in chloroform can, however, reasonably be explained by taking the hydrogen bond into consideration.

It should be possible to determine the electric properties relevant to the estimation of the IR intensity in a liquid phase with a polar molecule by means of the Laplace equation. Ordinarily, however, the Laplace equation under a boundary condition is not easy to solve analytically, except for a system with spherical symmetry, (spherical model). The finite element method, which has been developed for just such a problem,[1,2] is used for the present study.

In this paper we regard a system with a central molecule with C_{3v} point symmetry as having axial symmetry. Under this assumption, we can treat any system by the finite element method; the difficulty in placing the precise shape of the central molecule into the Laplace equation is thereby eliminated. The present study is, thus, more general than that previously reported for a uniformly polarized ellipsoid.[3]

Since the quantities obtained directly from the Laplace equation are the potential, Ψ, and the macroscopic field, E_m, we propose a method of obtaining the local radiation field, E_L, or the reaction field, E_R, derived by the permanent dipole moment; E_L depends partially on the polarization charge stored on the boundary between the central molecule and the media, while E_R depends completely on it.

The absolute infrared intensity, Γ_a, is given by:[4]

$$\Gamma_a = \frac{8\pi^3}{3hc} N_a m_1^2, \tag{1}$$

where h is the Planck constant, c is the velocity of light, N_a is the Avogadro constant, and m_1 is the transition dipole moment, defined as follows:

$$m_1 = \mu_1 + \alpha_1 E_R, \tag{2}$$

where μ_1 and α_1 originate from the dipole moment and the polarizability derivatives respectively. It is well known that Γ_a is related to the observed intensity, Γ, as follows:

$$\Gamma = \Gamma_a E_L^2/n, \tag{3}$$

where n is the refractive index.

The value of E_L has been estimated mainly from the spherical model, and a quantitative discussion of Eq. 2 has been undertaken by several authors.[5,6] Kakimoto and Fujiyama[5] have calculated E_R on the basis of the model of dipole-dipole interaction and referred to the values of μ_1 and α_1. Since their method is essentially different from ours, the values of E_R obtained from their method should also differ from ours.

The intensity of the IR band of the C≡N stretching mode of acetonitrile diluted infinitely in chloroform (≈0% chloroform solution) has been reported to be stronger[7] than that to be expected qualitatively. Since our method can easily be expanded to a hydrogen-bonded system, it is also applicable to a quantitative treatment of this abnormal behavior.

Method

The Laplace equation for a system with axial symmetry is given, in terms of the cylindrical coordinates as follows:

$$\varepsilon_r \frac{1}{r}\frac{\partial}{\partial r}\left(r\frac{\partial \Psi}{\partial r}\right) + \varepsilon_z\left(\frac{\partial^2 \Psi}{\partial z^2}\right) = 0, \tag{4}$$

where ε_r and ε_z are the dielectric constants of the r and z directions respectively; in the present system, we have the following conditions: $\varepsilon_r \neq \varepsilon_z$ in the central molecule and $\varepsilon_r = \varepsilon_z = \varepsilon_2$ in the media. The functional equivalent to Eq. 4 in one of the elements is given by:[1]

$$\chi_e = \frac{1}{2}\iiint\left[\varepsilon_r\left(\frac{\partial \Psi}{\partial r}\right)^2 + \varepsilon_z\left(\frac{\partial \Psi}{\partial z}\right)^2\right] r dr dz. \tag{5}$$

On the basis of the isoparametric elements,[1,2] the trial function, Ψ, and the variables, r and z, are assumed to be:

$$\Psi = (2L_1-1)L_1\Psi_1 + (2L_2-1)L_2\Psi_2 + (2L_3-1)L_3\Psi_3 + 4L_1L_2\Psi_4 + 4L_2L_3\Psi_5 + 4L_3L_1\Psi_6 = \mathbf{N}\Psi_e, \tag{6}$$

and:

$$r = \mathbf{N}|r_1r_2r_3r_4r_5r_6| = \mathbf{N}\mathbf{r}_e, \tag{7}$$

and:

$$z = \mathbf{N}|z_1z_2z_3z_4z_5z_6| = \mathbf{N}\mathbf{z}_e \tag{8}$$

where $\mathbf{N}$ is the displacement model, where L_i is defined as $\Delta L_i/\Delta ABC$, and where Ψ_j, r_j, and z_j are the nodal values of the potential, r and z respectively, as is shown in Fig. 1. According to the definition of L_i, we can introduce the transformation $\xi = L_1$, $\eta = L_2$, and $1-\xi-\eta = L_3$. By the use of $\mathbf{N}$, ξ, and η, we obtain the derivatives in Eq. 5 as follows:

$$\begin{vmatrix} \frac{\partial \Psi}{\partial r} \\ \frac{\partial \Psi}{\partial z} \end{vmatrix} = \mathbf{J}^{-1} \begin{vmatrix} \frac{\partial \mathbf{N}}{\partial \xi} \\ \frac{\partial \mathbf{N}}{\partial \eta} \end{vmatrix} \Psi_e, \tag{9}$$

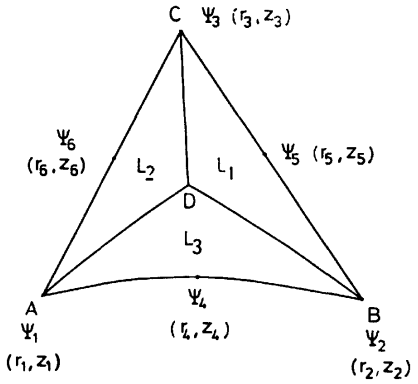

Fig. 1. The isoparametric element and the definition of Ψ_i, r_i, or z_i.

where:

$$\mathbf{J} = \begin{vmatrix} \frac{\Sigma \partial N_i}{\partial \xi} r_i & \frac{\Sigma \partial N_i}{\partial \xi} z_i \\ \frac{\Sigma \partial N_i}{\partial \eta} r_i & \frac{\Sigma \partial N_i}{\partial \eta} z_i \end{vmatrix}. \tag{10}$$

By substituting Eq. 9 into Eq. 5, we obtain the functional as a function of $\boldsymbol{\Psi}_e$:

$$\chi_e = \frac{1}{2} \tilde{\boldsymbol{\Psi}}_e \mathbf{Q}_e \boldsymbol{\Psi}_e, \tag{11}$$

where:

$$\mathbf{Q}_e = \iint \left(\varepsilon_r \frac{\partial \tilde{\mathbf{N}}}{\partial \xi} \tilde{\mathbf{J}}^{-1} \mathbf{J}^{-1} \frac{\partial \mathbf{N}}{\partial \xi} + \varepsilon_z \frac{\partial \tilde{\mathbf{N}}}{\partial \eta} \tilde{\mathbf{J}}^{-1} \mathbf{J}^{-1} \frac{\partial \mathbf{N}}{\partial \eta} \right) \mathbf{N} r_e \det[\mathbf{J}] d\xi d\eta. \tag{12}$$

According to the stationary condition of $\delta \chi_e = 0$, we obtain this equation:

$$\mathbf{Q}_e \boldsymbol{\Psi}_e = 0. \tag{13}$$

Since Eq. 13 holds for all elements, we obtain a final equation constructed from all the nodal values (see Appendix) as follows:

$$\mathbf{A} \boldsymbol{\Psi} = 0. \tag{14}$$

Equation 14 is solved under a given boundary condition, and we get the electric field from Eq. 9. E_m is obtained under the boundary condition of $\Psi_\infty = E_\infty z (= z)$ at r, $|z| \to \infty$.

Analyses of E_L and E_R

Although E_m is a field already compensated for by that of polarization, E_S, the extent of the compensation depends on the shape of the central molecule. Generally, the extent of a prolate top molecule is smaller than that of an oblate one.[3] This is reflected in E_L through the self-field of polarization, E_S^v, in a vacuum. For instance, the value of E_L in the present study is smaller than that to be expected from the spherical model, especially in liquid acetonitrile; E_L in the spherical model[8] is: $E_L = (\varepsilon_\infty + 2) E_\infty / 3$ ($\varepsilon_\infty = n^2$). Since this discrepancy is inevitable, we define E_L as follows:

$$E_L = E_m - E_S^v. \tag{15}$$

We calculate E_S^v by means of the general method, which corresponds to the field analysis of permanent polarization or of a magnet with axial symmetry.

The polarization charge, ρ_p, stored on a boundary results from induced polarization, so that ρ_p is given according to Gauss' expression as follows:

$$\rho_p = \mathbf{P} \cdot \mathbf{n} = \{(\varepsilon_r - 1) E_r + (\varepsilon_z - 1) E_z\} \cdot \mathbf{n}, \tag{16}$$

where $\mathbf{n}$ is the normal vector at the boundary. In the present problem, Eq. 16 is, thus, the boundary condition, and the functional is given by:

$$\chi_e = \frac{1}{2} \iint \left[\varepsilon_r \left(\frac{\partial \Psi}{\partial r} \right)^2 + \varepsilon_z \left(\frac{\partial \Psi}{\partial z} \right)^2 \right] r dr dz + \int_C \rho_p \Psi r dC, \tag{17}$$

where the linear integral is carried out along the boundary, C, between the central molecule and the media. The formulation of Eq. 17 is similar to that of Eq. 5; accordingly, we obtain the following equation (see Appendix):

$$\mathbf{A} \boldsymbol{\Psi} = \mathbf{B}, \tag{18}$$

where $\mathbf{A}$ is the matrix given in Eq. 14, except that $\varepsilon_r = \varepsilon_z = 1$ in all regions, and $\mathbf{B}$ is the column matrix determined from the linear integral in Eq. 17. Since $\mathbf{B}$ is known from the boundary condition of Eq. 16, E_S^v can be obtained from $\boldsymbol{\Psi}$ in Eq. 18.

The polarization charge, ρ_μ, stored on the boundary by the dipole-moment field is obtained from an equation similar to Eq. 16. Then we get E_R from Eq. 18. However, since E_R is zero if $\varepsilon_1 = \varepsilon_2$ and depends on $\varepsilon_1 - \varepsilon_2$, where ε_1 represents the dielectric constant of the central molecule, E_R can be obtained by the simple method to be described below.

We first calculate the potentials of $\Psi_{\varepsilon\infty}$ and $\Psi_{\varepsilon s}$, which are obtained, respectively, under the conditions of $\varepsilon_1 = \varepsilon_2 = \varepsilon_\infty$ and $\varepsilon_1 \neq \varepsilon_2 = \varepsilon_S$ (static dielectric constant). Second, we calculate this equation:

$$\Psi_R = \Psi_{\varepsilon s} - \Psi_{\varepsilon\infty}. \tag{19}$$

Ψ_R may be regarded as the potential, as for E_R. This method is simple because we have an analytical solution of $\Psi_{\varepsilon\infty}$; we assume the position of the point dipole to be the center of the C≡N bond of acetonitrile. $\Psi_{\varepsilon s}$ is obtained under the boundary condition of $\frac{\mu}{\varepsilon_1} \frac{z}{(r^2+z^2)}$ at r, $z \to 0$. It should be noted that the central molecule interacts with the media through the static dielectric constant;[9] the molecules around the central molecule are oriented so as to produce ε_s.

Since E_L and E_R in the central molecule are generally heterogeneous, it is necessary to average them. As long as we regard α_1 in Eq. 2 as the molecular constant, it is clear that the average of E_R over the z axis of the central molecule should be used as the reaction field. This process is given by:

$$\bar{E}_R = \frac{\int_b^a E_R dz}{D} = -\frac{\Psi(a) - \Psi(b)}{D}, \tag{20}$$

where a and b are the coordinates of the boundary on the z axis and where D is the distance between them. The average of the E_L values, $\bar{E}_L$, is also given by Eq. 20.

Equation 20 does not have a serious influence on E_L and E_R under the boundary conditions described above, but it does play an important role if E_R varies drastically.

Results and Discussion

The shape of acetonitrile, as estimated from the van der Waals radii[10] of the component atoms, is given in Fig. 2. The values of ε_∞ are obtained from the refractive indices,[11] and those of ε_s from the standard Table;[12] apart from the formulation, we use the condition of $\varepsilon_r=\varepsilon_z=\varepsilon_l$. The dipole moment of acetonitrile, 3.39 D,[13] is used.

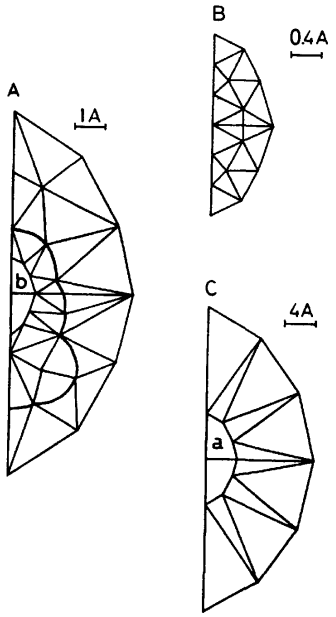

Fig. 2. The molecular shape (broad solid line) and the elements used for E_R. A and B are the expansion of a and b, respectively.

Table 1. Observed and calculated intensities (cm^2/mol) of the C≡N stretching of acetonitrile

State	$\Gamma^{a)}$	$\bar{E}_L/E_\infty$	Γ_a	$\bar{E}_R\times10^{-5}$	Γ_c
Liquid	444	1.20	415	0.906	396
≈0% In CCl_4	222	1.25	208	0.125	240
Gas	159	1.00	159	−0.493	144
≈0% In $CHCl_3$	500	1.24	470	0.535	317
H. B.[b)]	500	1.27	448	1.080	436

$\bar{E}_R$ in D/cm^3. a) From Ref. 7. b) From the hydrogen-bondmodel.

The intensities of the C≡N stretching mode in various states[5,7] are given in Table 1. As has been mentioned above, E_∞ is assumed to be 1.0, and the value of $\bar{E}_L$ in a liquid is smaller than that of 1.27 obtained from the spherical model. Accordingly, the values of $\bar{E}_L$ in Table 1 vary more gently with the dielectric constants than those to be expected from the spherical model. Since E_R is taken to be zero if $\varepsilon_1=\varepsilon_2$, the value of $\bar{E}_R$ in the gaseous state becomes negative. The value of $\bar{E}_R$ in a liquid is also smaller than that to be expected from the spherical model, 0.11×10^6 D/cm^3.

In order to estimate the values of the two parameters, μ_1 and α_1, we use the values of Γ_a defined by Eq. 3 and obtained using $\bar{E}_L$ in Table 1, except for the value of Γ_a for a ≈0% chloroform solution; the values thus obtained, $\mu_1=0.0295$ (D) and $\alpha_1=0.113$ (A^3), are used to calculate the intensity of $\Gamma_c=8\pi^3/(3hc)N_a\cdot(\mu_1+\alpha_1E_R)^2$ in Table 1. The agreement between Γ_a and Γ_c is satisfactory in each state, except for a ≈0% chloroform solution. The most important features are that the intensity in the gaseous state is explained simultaneously and that the value of α_1 agrees well with the observed value.[5,14]

The value of $\bar{E}_R$ for a ≈0% chloroform solution in Table 1 is reasonable if the interaction between the central molecule and the media takes place through the static electric force. However, Table 1 shows the imperfection in this static electric model. On the other hand, it is reasonable to expect that the hydrogen bond is formed between the nitrogen atom of actonitrile and the hydrogen atom of chloroform in a dilute solution and that, accordingly, the two molecules coordinate, as is shown in Fig. 3.

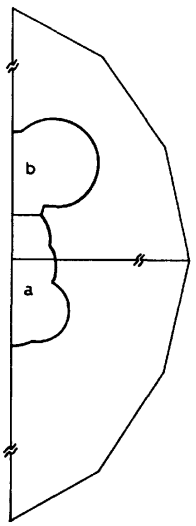

Fig. 3. The hydrogen-bond model of acetonitrile with chloroform. The shapes of acetonitrile and chloroform are given in a and b, respectively.

According to this hydrogen-bond model, the dipole-moment field, $\bar{E}_\mu$, which arises from the chloroform is added to $\bar{E}_R$; $\bar{E}_s$ should be recalculated under the condition of $\varepsilon_s=\varepsilon_\infty$ in the region of the chloroform. To calculate $\bar{E}_\mu$, the dipole moment of the chloroform, 1.55 debye,[13] is set at the center of the hydrogen and chlorine atoms on the z axis in the region of b in Fig. 3. The distance of the hydrogen bond of [C-H···N] is assumed to be 2.8 Å.

In the molecular shape of acetonitrile shown in Fig. 3, $\bar{E}_L$ and $\bar{E}_R$ are 1.27 and 0.331×10^5 D/cm^3 respectively, and $\bar{E}_\mu$ is 0.750×10^5 D/cm^3, resulting in $\Gamma_c=436$ (cm^2/mol) by the use of the same values of μ_1 and α_1 as have been presented above; they are also

given in Table 1. The refinement of Γ_c shows that E_μ is quite important in the intensity of the hydrogen-bonded system. The conclusion to be drawn from the fact that μ_1 is constant in various states is that the intensity in the present system depends only on the electric properties.

The numerical calculations were carried out by the use of the computer, FACOM 230-45S, of Toyama University.

Appendix

We will here outline in more detail the matrix **A** or **B** in Eq. 18 according to our computer program. **A** is constructed by the interconnection of each element. We define the nodal points for two elements (a and b), as is shown in Fig. A-1; the

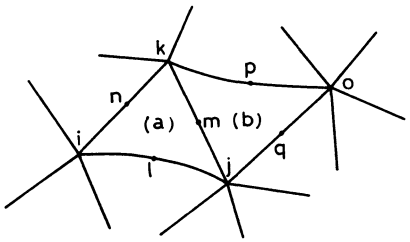

Fig. A-1. The two adjacent elements a and b. The numberings of the nodes (●) are given by i, j, ….

nodal points are numbered arbitrarily. The matrices, $\mathbf{Q}(6\times 6)$, of these elements, a and b, are denoted, respectively, by $\mathbf{Q}'$ and $\mathbf{Q}''$, which are defined as follows:

$$\mathbf{Q}' = \begin{vmatrix} i\ j\ k\ l\ m\ n \\ Q'_{rs} \end{vmatrix} \qquad \text{(A-1)}$$

and:

$$\mathbf{Q}'' = \begin{vmatrix} j\ o\ k\ q\ p\ m \\ Q''_{rs} \end{vmatrix} \qquad \text{(A-2)}$$

where $1\leq r,s\leq 6$. According to the condition of $\delta\chi=\sum\delta\chi_e$, we have a matrix element of **A** as follows:

$$\mathbf{A}\Psi =$$

i	j	k	m	
Q'_{11} ·····	Q'_{12} ·····	Q'_{13} ·····	Q'_{15} ·····	Ψ_i
	$Q'_{22}+Q''_{11}$ ···	$Q'_{23}+Q''_{13}$ ···	$Q'_{25}+Q''_{16}$ ···	Ψ_j
Sym.		$Q'_{33}+Q''_{33}$ ···	$Q'_{35}+Q''_{36}$ ···	Ψ_k
			$Q'_{55}+Q''_{66}$ ···	Ψ_m

(A-3)

All the matrix elements of **A** in Eq. A-3 are obtained in a similar manner.

We get the **B** column matrix by means of numerical integration. We define the following linear integral in an element:

$$\chi_B = \int_C \rho_p \Psi r dC \qquad \text{(A-4)}$$

It then follows that:

$$\delta\chi_B/\delta\Psi_e = \int_C \rho_p \mathbf{N} r dC$$

$$= \int_C \rho_p |(2L_1-1)L_1\ (2L_2-1)L_2\ 0\ 4L_1L_2\ 0\ 0\ |rdC \qquad \text{(A-5)}$$

where C is the boundary defined in Fig. A-2. This process is carried out for the elements with the C boundary in the central molecule.

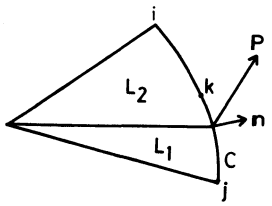

Fig. A-2. Linear integral along the boundary C. **P** is the induced polarization in the central molecule on C, and **n** is the normal vector. L_1 and L_2 are defined in Fig. 1.

References

1) O. C. Zienkiewicz, "The Finite Element Method in Engineering Science," McGraw-Hill, Maidenhead (1971).
2) C. S. Desai and J. F. Abel, "Introduction to the Finite Element Method," Van Nostrand, New York (1974).
3) I. G. Ross and A. R. Sack, *Proc. Phys. Soc. B*, **63**, 983 (1950).
4) G. Turrell, "Infrared and Raman Spectra of Crystals," Academic Press, London (1972).
5) M. Kakimoto and T. Fujiyama, *Bull. Chem. Soc. Jpn.*, **48**, 2258 (1975).
6) G. W. F. Pardoe, *Trans. Faraday Soc.*, **66**, 2699 (1970).
7) B. H. Thomas and W. J. Orville-Thomas, *J. Mol. Struct.*, **7**, 123 (1971).
8) For example, H. Fröhlich, "Theory of Dieletrics," The Clarendon Press, Oxford (1958).
9) A. D. Buckingham, *Proc. R. Soc. London, Ser. A*, **248**, 169 (1958).
10) L. Pauling, "The Nature of the Chemical Bond," Cornell University Press, New York (1960).
11) "International Critical Tables,' McGraw-Hill, New York (1930), Vol. VII.
12) "Landolt-Börnstein," Springer-Verlag, Berlin (1959) II/6.
13) A. L. McClellan, "Tables of Experimental Dipole Moments," W. H. Freeman and Company, San Francisco (1963).
14) H. W. Schrötter and H. J. Bernstein, *J. Mol. Spectrosc.*, **12**, 1 (1964).

The Interaction of a Neutral Polymer with Small Ions in Solution. I. A Method for the Analysis of Ion Binding to a Neutral Polymer

Hiroshi Awano, Katsumichi Ono,* and Kenkichi Murakami
Chemical Research Institute of Non-Aqueous Solutions, Tohoku University, Katahira, Sendai 980
(Received October 28, 1981)

A method for the analysis of ion binding to a neutral polymer, such as poly(oxyethylene) (POE), based on the one-dimensional lattice model has been proposed. The grand partition function for the one-dimensional lattice has been given by the product of the statistical weight matrix. Interaction between the ions bound to the lattice points has been well approximated by the Debye-Hückel pair-by-pair potential, and the distance between the bound ions has been assumed to be the root mean square end-to-end distance of the partial chain. Based on the model, an equilibrium constant has been defined which is referred to the *binding constant.*

It has been well known that a neutral polymer, such as poly(oxyethylene) (POE), forms complexes with a variety of metal salts in organic solvents.[1-6] In our previous paper,[6] we have given a method for elucidating the quantitative aspects of the ion binding to POE by means of conductometry. This method, which is based on a discrete site-binding model, enables us to calculate the minimum separation between two adjacent bound charges as a function of the ionic strength. The stoichiometry of the potassium ion complex in a methanol solution was determined to be four monomer units per ion from the intrinsic value of the charge separation at a high concentration limit.

The next important step in the investigation is the interpretation of the binding behavior in terms of the electrostatic potential set up by bound cations. The investigation along this line has been developed extensively for the potentiometric titration of polyacid,[7] but, because of the high charge density on the polymer chain, the straightforward application of the screened Debye-Hückel potential fails to reproduce the experimental titration curves in most cases. For the POE–salt systems, however, the charge density on a polymer chain is far lower than in the cases of typical polyelectrolyte systems. Thus the electrostatic interaction can be expected to be represented by the sum of the Debye-Hückel pair-by-pair interactions between bound cations.

In this paper, we propose a method for analyzing ion binding to POE based on the one-dimensional lattice model. It is therein assumed that a lattice point is composed of four monomer units; that is to say, a bound cation is surrounded by four ether-oxygen atoms.[6] The grand partition function for the one-dimensional lattice is expressed by means of a matrix method. In calculating the Debye-Hückel pair-by-pair potential, the distance between bound cations is approximated by the root mean square end-to-end distance of the partial chain, which is given by the Porod-Kratky model. The concrete application of the method will be discussed in the following paper.[8]

Treatment of Binding Equilibria. It can be considered that there are three approaches to treat the binding equilibria of linear polymer and small ions in solutions.

The first approach is to treat the equilibrium as a usual chemical equilibrium, regarding each polymer and its complexes as a different chemical species. In general, however, a ligand containing n sites can be completely characterized by $2^{n-1}n$ equilibrium constants.[9] For a very large n, an infinite number of species must be considered, and the problems becomes quite complicated and no effective results are obtained. Therefore, we must abandon this approach.

The second approach is to assume that binding sites supposed to be arranged on a polymer chain are uniformly distributed in the solution and behaved like low-molecular ligand; this is the so called *low-molecular analogy*. Many workers in this field have used this approach, but it has several defects. The assumption of a uniform distribution of binding sites becomes less tenable as the solution is more dilute, since the binding sites are connected with one another on a polymer chain. Next, since all the thermodynamic quantities are usually defined as adopting an infinite dilution as the reference state, these quantities, including the equilibrium constant, have an ambiguous physical meaning in the case of these polymer systems. In dilute solutions, the interaction between bound ions are, in general, greater than those between unbound ones. As a result, a marked anti-cooperativity appears on ion binding. In this approach, therefore, the equilibrium constant does not only depend intensely on the concentrations of the polymer and of the ion, but also has itself an ambiguous physical meaning, whereas the treatment is very easy. An example will be discussed in the following paper.[8]

The third approach is to regard the polymer chain as a one-dimensional lattice and to consider the binding equilibrium as the equilibrium between the *bulk* solution and the lattice (*one-dimensional lattice model*). The equilibrium constant can be defined as a measure of the tendency of the occupation of the lattice points, as will be discussed below, and the equilibrium constant has no ambiguity in its physical meaning, unlike the equilibrium in low-molecular analogy. If the interaction between the ions occupying the lattice points can be estimated by any method, analysis can be performed without difficulty. This approach, which keeps of the connectivity of the polymer, seems to be the most appropriate. Liem *et al.*[7] analyzed the potentiometric titration curves of polyacid using this approach, but they confused the one-dimensional lattice model with the low-molecular analogy throughout their discussion. In this paper, we overcome this type of confusion and develop a systematic discussion based on the one-dimensional lattice model.

The One-dimensional Lattice Model. We consider a one-dimensional lattice having N lattice points, where the total energy of the system may be expressed by the following equation:

$$\Phi(N,M) = \sum_{i=1}^{N} E\sigma_i + \sum_{i=1}^{N} \sum_{j=i+1}^{N} J_{ij}\sigma_i\sigma_j, \quad (1)$$

$$M = \sum_{i=1}^{N} \sigma_i, \quad (2)$$

where E is the binding energy; J_{ij}, the interaction energy between the particles occupying the ith and jth lattice points, and σ_i, the index whose value is 1 or 0 when the ith lattice point is occupied or unoccupied respectively. Thus, the partition function of the system is given by:

$$Z(N,M) = \sum_{\text{all}} \exp[-\Phi(N,M)/RT], \quad (3)$$

where $\sum_{\text{all}}$ means the summation over all the states in which M out of N lattice points are occupied. Introducing the chemical potential, μ, of the particle, we have the grand partition function given by:

$$\Xi = \sum_{M=0}^{N} Z(N,M)\exp(M\mu/RT). \quad (4)$$

Now we alter the form of Eq. 3 to:

$$Z(N,M) = \exp(-ME/RT) \times \sum_{\text{all}} \exp\left(-\sum_{i=1}^{N} \sum_{j=i+1}^{N} J_{ij}\sigma_i\sigma_j/RT\right). \quad (5)$$

If we define the normalized activity of the particle as:

$$\xi = \exp[(\mu-E)/RT], \quad (6)$$

then Eq. 4 becomes:

$$\Xi = \sum_{M=0}^{N} \xi^M \sum_{\text{all}} \exp\left(-\sum_{i=1}^{N} \sum_{j=i+1}^{N} J_{ij}\sigma_i\sigma_j/RT\right). \quad (7)$$

If we calculate Ξ, then the degree of binding, that is, probability that a lattice point is occupied, will be given by:

$$\theta = \frac{RT}{N}\frac{\partial \ln \Xi}{\partial \mu} = \frac{1}{N}\frac{\partial \ln \Xi}{\partial \ln \xi}. \quad (8)$$

Calculation of the Grand Partition Function by the Matrix Method. It is actually impossible to calculate the grand partition function straightforwardly using Eq. 7, particularly in the case of a very large N, so we shall use the matrix method as follows.

Let us first truncate the range of the interaction, supposing that, for a positive integer, k:

$$J_{ij} = \begin{cases} -RT\ln A_m, & \text{for } m \equiv j-i \leqslant k. \\ 0, & \text{for } j-i > k. \end{cases} \quad (9)$$

Thus, Ξ is given by the product of a statistical weight matrix:[7]

$$\Xi = \boldsymbol{e}\boldsymbol{U}_k^N \boldsymbol{e}', \quad (10)$$

where $\boldsymbol{e}$ and $\boldsymbol{e}'$ are the end vectors, as follows:

$$\boldsymbol{e} = (1,1,\cdots,1), \quad \boldsymbol{e}' = \begin{pmatrix} 1 \\ 0 \\ \vdots \\ 0 \end{pmatrix}.$$

$\boldsymbol{U}_k$ is a statistical weight matrix with dimensions of $2^k \times 2^k$, as follows:

For $k=1$,

$$\boldsymbol{U}_1 = \begin{bmatrix} 1 & 1 \\ \xi & \xi A_1 \end{bmatrix}.$$

For $k=2$,

$$\boldsymbol{U}_2 = \begin{pmatrix} 1 & 1 & 0 & 0 \\ 0 & 0 & 1 & 1 \\ \xi & \xi A_2 & 0 & 0 \\ 0 & 0 & \xi A_1 & \xi A_1 A_2 \end{pmatrix}.$$

For $k=3$,

$$\boldsymbol{U}_3 = \begin{pmatrix} 1 & 1 & 0 & 0 & 0 & 0 & 0 & 0 \\ 0 & 0 & 1 & 1 & 0 & 0 & 0 & 0 \\ 0 & 0 & 0 & 0 & 1 & 1 & 0 & 0 \\ 0 & 0 & 0 & 0 & 0 & 0 & 1 & 1 \\ \xi & \xi A_3 & 0 & 0 & 0 & 0 & 0 & 0 \\ 0 & 0 & \xi A_2 & \xi A_2 A_3 & 0 & 0 & 0 & 0 \\ 0 & 0 & 0 & 0 & \xi A_1 & \xi A_1 A_3 & 0 & 0 \\ 0 & 0 & 0 & 0 & 0 & 0 & \xi A_1 A_2 & \xi A_1 A_2 A_3 \end{pmatrix}.$$

Similarly, $\boldsymbol{U}_k$ can be expressed for $k>3$.

Equation 8 can be rewritten in the following form in obtaining θ:

$$\theta = \frac{\xi}{\Xi}\frac{\partial \Xi}{\partial \xi} = \frac{\xi \sum_{m=0}^{N-1} \boldsymbol{e}\boldsymbol{U}_k^m \boldsymbol{U}_k' \boldsymbol{U}_k^{N-m-1}\boldsymbol{e}'}{\boldsymbol{e}\boldsymbol{U}_k^N \boldsymbol{e}'}, \quad (11)$$

where

$$\boldsymbol{U}_k' = \frac{\partial \boldsymbol{U}_k}{\partial \xi}.$$

The values of θ can be calculated with a computer using the method of Jernigan.[10] The above method, which is based on the one-dimensional lattice model, follows the method discussed by Liem *et al.*[7] Since, However, a few mistakes regarding thermodynamics appear in their discussion, we have developed the discussion above.

Calculation of the Interaction Energy and Estimation of the Distance between Bound Ions. We shall confine ourselves to the POE–metal salt system as a model one. As has been stated before, it can be expected that, for the present system, the electrostatic interaction is represented by the sum of Debye-Hückel pair-by-pair interactions between bound cations. We therefore suppose that the statistical weight factor, A_m, in Eq. 9 can be expressed by:

$$RT\ln A_m = -\frac{e^2 \exp(-\kappa r_m)}{4\pi\varepsilon r_m}, \quad (12)$$

where e is the elementary charge; ε, the permittivity of the solvent; r_m, the distance between the ions bound to the ith and the $(i+m)$th sites (lattice points), and κ, the Debye's parameter, which is given by:

$$\kappa^2 = \frac{2N_A e^2 I}{\varepsilon k_B T}, \quad (13)$$

in which N_A is the Avogadro constant; I, the ionic strength, and k_B, the Boltzmann constant.

In order to obtain the Debye-Hückel pair-by-pair interaction from Eq. 12, it is necessary to estimate the distance between the bound ions, r_m. Let us now assume that r_m is given by the root mean square end-to-end distance, $\langle R^2_m\rangle^{1/2}$, for a partial chain of POE corresponding to m binding sites.

In the first place, let us estimate the mean square end-to-end distance in the unperturbed state, $\langle R^2_m\rangle_0$. According to Maeda *et al.*,[11] the real chain can be well approximated by a stiff chain, even in the case of a fairly short chain. Therefore, we will use the following equation for the stiff chain:

$$\langle R^2\rangle_0 = 2a_0L\left[1 - \frac{a_0}{L}(1-e^{-L/a_0})\right], \tag{14}$$

in which we take a contour length, L, in the following form:

$$L = nl\sin(\theta/2), \tag{15}$$

where a_0 is the persistence length; n, the number of bonds; l, the bond length, and θ, the bond angle. We thus obtain this relation:

$$\frac{2a_0}{l}\sin(\theta/2) = C_\infty, \tag{16}$$

in which C_∞ is the characteristic ratio. C_∞ is given by the following Flory-Fox relation:

$$C_\infty = \left(\frac{K}{\Phi}\right)^{2/3}\frac{M_b}{l^2}, \tag{17}$$

where $\Phi = 2.6\times10^{21}$ (universal constant), M_b is the molecular weight per bond, and K is the viscosity constant, which is given by $K = [\eta]_\theta/M^{1/2}$ if $[\eta]_\theta$ is the intrinsic viscosity in a theta solvent and M is the molecular weight of the polymer. Thus, Eq. 14 becomes:

$$\langle R^2_m\rangle_0 = C_\infty nl^2 \times\left[1 - \frac{C_\infty}{2n\sin^2(\theta/2)}\left\{1 - \exp\left(-\frac{2n\sin^2(\theta/2)}{C_\infty}\right)\right\}\right]. \tag{18}$$

If we suppose that a binding site is composed of four monomer units,[6] then we obtain:

$$\langle R^2_m\rangle_0 = 132.7\,m \times\left[1 - \frac{0.3150}{m}\{1 - \exp(-3.174\,m)\}\right]\text{Å}^2,** \tag{19}$$

by substituting the following values in Eq. 18:

$$n = 12\,m,$$
$$l = 1.46\text{ Å},**$$
$$\theta = 111.5°,$$
$$K = 1.7\times10^{-3}\text{ dl g}^{-1.12)}**$$

Next, let us estimate the expansion factor, α. Since α depends on m in general, we will express the expansion factor as $\alpha(m)$. If $\alpha(m)$ follows the fifth power law, then:

$$\alpha(m)^5 - \alpha(m)^3 = Cm^{1/2}, \tag{20}$$

where the constant, C, is determined from the value of m corresponding to the total number of binding sites on a polymer chain, m_0 (for example, $m_0 = 140.2$ for a chain of $M = 2.47\times10^4$), and from:

$$\alpha(m_0) = ([\eta]/[\eta]_\theta)^{1/3}, \tag{21}$$

that is,

$$C = \frac{\alpha(m_0)^5 - \alpha(m_0)^3}{m_0^{1/2}}. \tag{22}$$

By substituting Eq. 22 in Eq. 20, the value of $\alpha(m)$ corresponding to an arbitrary m is obtained. Finally, we obtain the distance between bound ions in the perturbed state from this relation:

$$\langle R^2_m\rangle = \alpha(m)^2\langle R^2_m\rangle_0. \tag{23}$$

Introduction of the Binding Constant. The chemical potential of the ion is written in the following form:

$$\mu = \mu^\ominus + ET\ln a, \tag{24}$$

where $\mu^\ominus$ is the standard chemical potential and a, the relative activity of the ion. Hence, experimentally the degree of binding θ, is obtained as a function of a. On the other hand, the degree of binding is calculated as a function of ξ. Let us now introduce the *binding constant* defined as follows:

$$K_0 = \exp[(\mu^\ominus - E)/RT]. \tag{25}$$

Thus, the normalized activity is expressed as:

$$\xi = K_0a. \tag{26}$$

Therefore, we can obtain a shift factor, $\log K_0$, which best fits the observed plots of θ *vs.* $\log a$ to the calculated curve of θ *vs.* $\log\xi$.

Discussion

Expansion Factors. We have calculated the mean square end-to-end distances for a partial chain of POE both in the unperturbed state and in the 2 mmol dm^{-3} KSCN-methanol system ($\alpha(m_0) = 1.386$). The dependence of these quantities on the number of bonds is shown in Fig. 1. In a perturbed state such as this system, the polymer chain is expanded to a great extent. However, for $m=6$, that is, $\log n = 1.86$ below the point at which

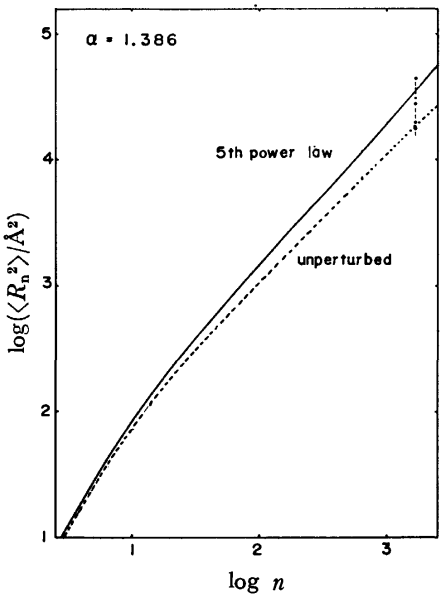

Fig. 1. Dependences of the mean square end-to-end distances for poly(oxyethylene) on the number of bonds, n, in the unperturbed state and in 2 mmol dm^{-3} KSCN–methanol system.

** 1 Å = 1×10^{-10} m; 1 dl = 1×10^{-4} m^3.

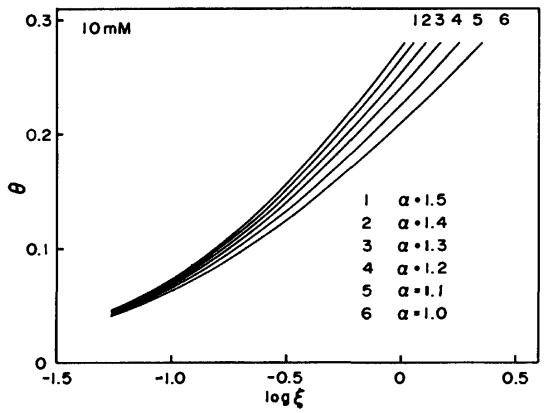

Fig. 2. Dependence of θ *vs.* log ξ curves on the expansion factor, α, for 10 mmol dm^{-3} KSCN–methanol system.

we are concerned, α is less than 1.15, and it is expected that the binding curve (θ *vs.* log ξ) is not very sensitive to the variation in α.

In Fig. 2, the dependence of the binding curve on $\alpha(m_0)$ is shown for the 10 mmol dm^{-3} KSCN–methanol system. As is suggested in Eq. 21, α is proportional to $[\eta]^{1/3}$, so the binding curve is quite insensitive to the variation in $[\eta]$.

Electrostatic Repulsion as a Long-range Interaction. In the foregoing discussion, the electrostatic interaction between bound ions has been assumed to range over only k sites. However, since the electrostatic interaction is a long-range one it is necessary to take a sufficiently large k. Figure 3 shows the binding curves for $k=0$—6, together with the extrapolated curve for $k\rightarrow\infty$ (see below). The degree of binding θ, decreases with an increase in k because of the long range electrostatic repulsion. Apparently, the convergence of the binding curve seems to be bad even for $k=6$. As k increases, however, the order of the statistical weight matrices exponentially increases. Hence it is actually impossible to obtain the degree of binding for a very large k in a

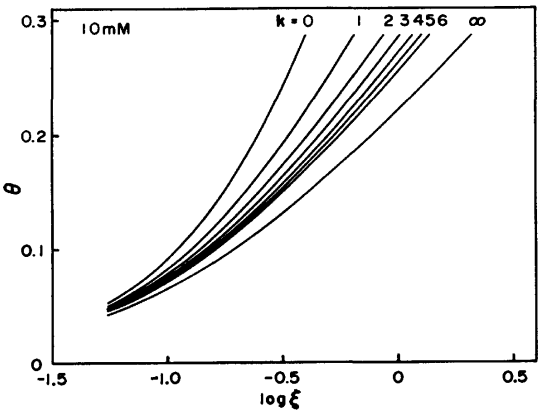

Fig. 3. Dependence of θ *vs.* log ξ curves on the number of sites over which the interaction ranges, k, for 10 mmol dm^{-3} KSCN–methanol system. The curve corresponding to $k\rightarrow\infty$ has been estimated from the extrapolation procedure shown in Fig. 4.

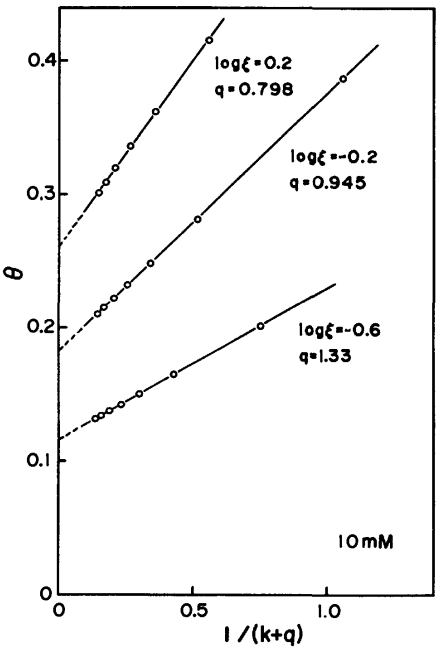

Fig. 4. Extrapolation procedure with the use of parameter, q, for 10 mmol dm^{-3} KSCN–methanol system.

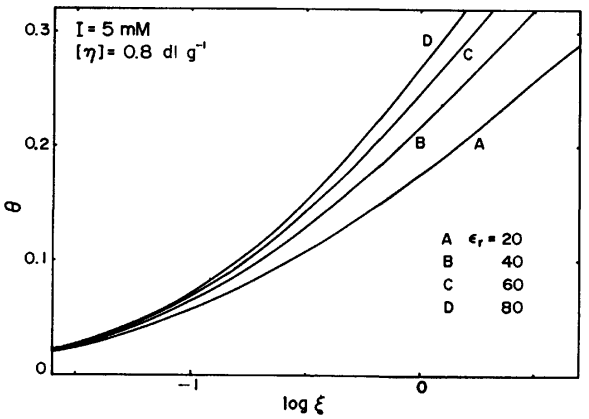

Fig. 5. Dependence of θ *vs.* log ξ curves of the relative permittivity of the solvent for an imaginary system.

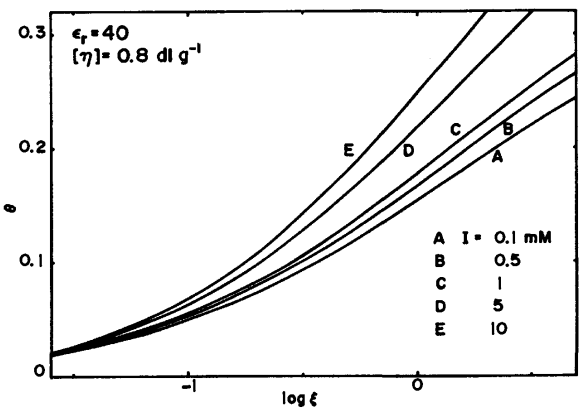

Fig. 6. Dependence of θ *vs.* log ξ curves on the ionic strength for an imaginary system.

straightforward manner.

For the extrapolation, we plotted θ against $1/(k+q)$, where q is a parameter which has been determined so that the correlation coefficient of the plot takes a maximum value. Figure 4 shows the plot thus obtained for several sets of log ξ and q for a fixed ion concentration. The degree of binding corresponding to $k\rightarrow\infty$ is determined as the intercept on the θ axis. This procedure seems to give a more precise extrapolated value than that of Liem *et al.*,[7] who have plotted the degree of the dissociation of polyacids against the reciprocal of the number of sites over which the interaction ranges.

The dependences of the binding curve on the relative permittivity, ε_r, of the solvent and on the ionic strength, I, are shown in Figs. 5 and 6 respectively for an imaginary model system. Both figures show that the degree of binding is less and the binding curve has a smaller slope when the interaction range is longer, that is, when the permittivity or the ionic strength is smaller, as has been expected.

References

1) R. D. Lundberg, F. E. Bailey, and R. W. Callard, *J. Polym. Sci., A1*, **4**, 1563 (1966).
2) K. J. Liu, *Macromolecules*, **1**, 308 (1968).
3) D. E. Fenton, J. M. Parker, and P. V. Wright, *Polymer*, **14**, 589 (1973).
4) A. Ricard, *Eur. Polym. J.*, **15**, 1 (1979).
5) J. A. Ibemesi and J. B. Kinsinger, *J. Polym. Sci., Polym. Chem. Ed.*, **18**, 1123 (1980).
6) K. Ono, H. Konami, and K. Murakami, *J. Phys. Chem.*, **83**, 2665 (1979).
7) R. K. Liem, D. Poland, and H. A. Scheraga, *J. Am. Chem. Soc.*, **92**, 5717 (1970).
8) H. Awano, K. Ono, and K. Murakami, *Bull. Chem. Soc. Jpn.*, **55**, 2530(1980). Part II of this series.
9) K. Bunger and B. Noszal, "Advances in Solution Chemistry," ed by I. Bertini, L. Lunazzi, and A. Dei, Plenum, New York (1981), pp. 139—148.
10) This method is explained in detail in the Appendix of D. Poland and H. A. Scheraga, *Biopolymers*, **7**, 887 (1969).
11) H. Maeda, N. Saitô, and W. H. Stockmayer, *Polym. J.*, **2**, 94 (1971).
12) D. R. Beech and C. Booth, *J. Polym. Sci., A2*, **7**, 575 (1969).

The Interaction of a Neutral Polymer with Small Ions in Solution. II. The Binding of Alkali Metal Ions to Poly(oxyethylene) in Several Organic Solvents

Hiroshi Awano, Katsumichi Ono,* and Kenkichi Murakami
Chemical Research Institute of Non-Aqueous Solutions, Tohoku University, Katahira, Sendai 980
(Received October 28, 1981)

The conductivities for several solutions of alkali metal salts, such as potassium thiocyanate, containing poly(oxyethylene) (POE) have been measured as functions of the POE concentration, C_p. A decrease in the conductivity with an increase in C_p has been observed, particularly in methanol, acetonitrile, propylene carbonate, and sulfolane. For these systems, the binding of the cation has been evaluated from the decrease in conductivity and analyzed by a method based on the one-dimensional lattice model. As well as the solvent effects, the effects of the salt concentration and the effect of the alteration of salt on the binding constant have been discussed.

In the preceding paper in this series,[1] we have established a method for the theoretical prediction of the ion binding to a neutral polymer, such as poly(oxyethylene) (POE), in solution.

In this paper, the binding of alkali metal ions to POE is observed by means of conductometry, and the results are analyzed by applying this method, which is based on the one-dimensional lattice model. Also discussed are the solvent effects on the binding of potassium ion, the effects of the salt concentration on the binding of the potassium ion in propylene carbonate (PC), and the effects of the alteration of salt on the binding of the cation in PC.

Experimental

Reagents. The poly(oxyethylene) sample, with an average molecular weight of 2.47×10^4, was obtained from Wako Pure Chemicals and was used without further purification. Methanol (Wako, >99.6%) was dried over calcium hydride, followed by distillation. The conductivity of the purified substance, κ, was 7×10^{-7} S cm^{-1}. Acetonitrile (Wako) was stirred with calcium hydride to dryness and then distilled in the presence of calcium hydride; $\kappa=3\times10^{-8}$ S cm^{-1}. Propylene carbonate (Wako) was stirred with a molecular sieve, 4A, to dryness, and then distilled under reduced pressure (87 °C at 2 mmHg†); $\kappa<10^{-8}$ S cm^{-1}. Sulfolane (Wako) was stirred with sodium hydroxide and distilled in the presence of sodium hydroxide under reduced pressure (105 °C at 4 mmHg) until a small amount of the sample did not show any development of visible color within 5 min after the addition of an equal volume of 100% sulfuric acid.[2] $\kappa<10^{-8}$ S cm^{-1}. *N,N*-Dimethylformamide (Kanto) was stirred with a molecular sieve, 4A, and distilled under reduced pressure; $\kappa=2\times10^{-8}$ S cm^{-1}. Dimethyl sulfoxide (Wako) was stirred with calcuim hydride and distilled under reduced pressure; $\kappa=2\times10^{-8}$ S cm^{-1}. Deionized water was used; $\kappa=3\times10^{-6}$ S cm^{-1}. All the salts used were reagent-grade and were dried under a vacuum.

Viscosity Measurements. The viscosity of a POE solution containing a salt was measured with a Ubbelohde viscometer. The effect of the shear rate was disregarded.

Conductivity Measurements. The conductiovity of the solution was measured in a fashion similar to the method of Ono *et al.*[3]

† 1 mmHg ≈ 133.322 Pa.

Results and Discussion

Evaluation of the Cation Binding. Procedure: In order to evaluate the degree of binding of the cation from the relationships between the equivalent conductivity of the salt, Λ, and the POE concentration (monomer base mole), C_p, we make the following assumptions: the decrease in the conductivity of the solution with the increase in C_p is solely due to the binding of the cation to POE, and the bound cations make no contribution to the conductivity. The reasonability of this assumption will be later checked in detail. According to Ono *et al.*,[4] the fraction of the unbound, free cation is given by:

$$\alpha = \frac{\Lambda - \Lambda_{ps}}{\Lambda_s - \Lambda_{ps}}, \tag{1}$$

where Λ_s is the equivalent conductivity at $C_p=0$ and Λ_{ps} is that supposing all the cations are bound. Λ_{ps} may be the ionic equivalent conductivity of the anion, based on the above assumption, and we assume, as a zeroth-order approximation, that:

$$\Lambda_{ps} = \Lambda_s[\lambda_-^\infty/(\lambda_+^\infty + \lambda_-^\infty)], \tag{2}$$

where λ_+^∞ and λ_-^∞ are the limiting ionic equivalent conductivities of the cation and the anion respectively. The values of λ_+^∞ and λ_-^∞ used here, together with those of $\lambda_-^\infty/(\lambda_+^\infty+\lambda_-^\infty)$ for the salts, are shown in Table 1. If we assume that a binding site is composed of four successive monomer units on a POE chain,[3] then the degree of binding θ, is:

$$\theta = \frac{(1-\alpha)C_s}{C_p/4}, \tag{3}$$

where C_s is the salt concentration. On the other hand, the relative activity of the cation in the bulk solution phase is given by:

$$a = \alpha y C_s, \tag{4}$$

where y is the activity coefficient on the molar concentration basis, which is regarded as equal to the activity coefficient on the molarity basis, γ, for a dilute solution. Hence, it is estimated using the Debye-Hückel extended equation for an activity coefficient. We thus obtain experimentally the relation of θ *vs.* log a.

Reasonability of Some Assumptions in the Evaluation of the Cation Binding. Although the assumptions presented above seem to be very daring, we shall verify

Table 1. Limiting ionic equivalent conductivity, λ_+^∞ and λ_-^∞, and $\lambda_-^\infty/(\lambda_+^\infty+\lambda_-^\infty)$ at 298.15 K

Solvent	Ion	λ_+^∞ or λ_-^∞ / S cm^2 mol^{-1}	Electrolyte	$\lambda_-^\infty/(\lambda_+^\infty+\lambda_-^\infty)$
Methanol[a]	Na^+	42.5	KSCN	0.565
	K^+	50.2	NaI	0.608
	Rb^+	53.0	KI	0.568
	Cs^+	59.2	RbI	0.555
	SCN^-	65.2	CsI	0.527
	I^-	66.0		
Acetonitrile[a]	K^+	85.9	KSCN	0.620
	SCN^-	140	KI	0.540
	I^-	101.0		
Propylene carbonate[b]	Na^+	9.45	$KClO_4$	0.623
	K^+	11.17	KSCN	0.665
	Rb^+	11.90	KBr	0.629
	Cs^+	12.66	KI	0.622
	ClO_4^-	18.44	NaI	0.660
	SCN^-	22.12	RbI	0.607
	Br^-	18.91	CsI	0.592
	I^-	18.35		
Sulfolane[c] (303.15 K)	K^+	4.04	KSCN	0.705
	SCN^-	9.63		

The values of λ_+^∞ and λ_-^∞ are cited in: a) Ref. 4; b) Ref. 5; Ref. 6.

in detail that these assumptions bring about no fatal results and that the derived conclusions are virtually correct.

In the first place, we have assumed that all the cations and anions behave freely and are independent of each other in the solution. If ionic association should occur, then, in addition to the equilibrium of binding of the cation to the POE lattice, another chemical equilibrium would have to be considered. According to the analysis of the equivalent conductivity data in the literature,[7] however, the ionic association constant is sufficiently small for the salt–solvent systems studied in this paper. Therefore, the influence of the ionic association is practically negligible. Moreover, since the degree of ion binding is not very large and the charge density on the polymer chain is small, the binding of the anion to the POE–cation complex can not be expected to occur.

Secondary, we have measured the equivalent conductivity by diluting a salt–POE solution with a salt solution which does not contain POE. If the volume changed on the dilution of POE, accurate values of the equivalent conductivity could not be obtained in this manner. Searching the literature for examples of the measurements of volume change on the dilution of ion–polymer solution systems, we find a few data for aqueous solutions of maleic acid–olefin copolymer[8,9] and of poly(acrylic acid).[9] The volume change accompanied by the protonation of the polyanion is, for both systems, in the order of $\Delta V \approx 10$ cm^{-3} mol^{-1} (monomer base mole). If, in our systems, the volume change is in this order, then $\Delta V\ C_p \approx 10^{-3}$ in the concentration of $C_p \approx 10^{-1}$ mol dm^{-3} and the error of the equivalent conductivity accompanied by the volume change is in the order of 0.1%. Although it will be necessary, in the future, to investigate this problem in detail, neglecting the influence of the volume change would not bring about any serious errors.

Thirdly, let us discuss the influence of the increase in the viscosity of the solution. It has been well known that, in a solution containing a polymer, the relationship between the equivalent conductivity and the viscosity of the solvent (a solution composed of a pure solvent and a polymer, in this case) deviates enormously from the Walden rule.[3,10] We have measured the equivalent conductivity as a function of C_p for the tetrapropylammonium iodide(TPrAI)–POE–PC system, in which the cation is expected not to be bound to POE. As may be seen in Fig. 1, the decrease in Λ with an increase in C_p is found to be very small. It is impossible, however, to conclude whether the decrease is caused by the binding of the cation or by the increase in the viscosity of the solvent. Even if the decrease in Λ were caused by an increase in the viscosity of the solvent in this case, neglecting the descent of Λ would bring about no serious errors in the systems in which the binding of the cation occurs to a large extent, because the contribution of the increase in the viscosity of the solvent to the decrease of Λ is expected to be very small. As long as no quantitative law has been established for the relationship between equivalent conductivity and viscosity in a system containing a polymer, we unavoidably neglect the influence of the increase in viscosity.

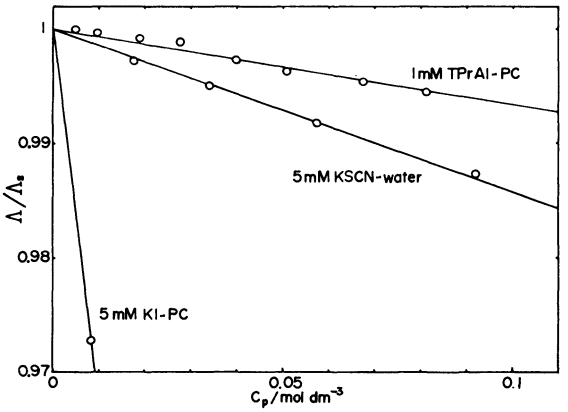

Fig. 1. The relation between Λ/Λ_s and C_p for 1 mmol dm^{-3} tetrapropylammonium iodide (TPrAI)–PC system, together with 5 mmol dm^{-3} KI–PC and 5 mmol dm^{-3} KSCN–water systems.

Fourthly, we shall examine the reasonability of Eq. 2. For ionic equivalent conductivity on the right-hand side of Eq. 2, it must be better to use the values of ionic equivalent conductivity in the salt concentration studied than to use those in the limit of $C_s \to 0$. For the KI–PC system, the limiting ionic equivalent conductivities of K^+ and I^- are, respectively, 11.17 and 18.35 S cm^2 mol^{-1},[5] so that $\lambda_-^\infty/(\lambda_+^\infty+\lambda_-^\infty)=0.6216$. On the other hand, if the Onsager limiting law holds, then the ionic equivalent conductivities of K^+ and I^- are, respectively, 10.09 and 17.12 S cm^2 mol^{-1} at 5 mmol dm^{-3}, so that $\lambda_-^\infty/(\lambda_+^\infty+\lambda_-^\infty)=0.6290$. Using these values, we analyzed the binding curve by a method to be described below; we found that the logarithmic binding constant is 1.99 in the

former case and 2.02 in the latter case. As this difference is very small, it is concluded that the approximation in Eq. 2 causes no essential errors.

Finally, we shall refer to the assumption that the bound cations make no contribution to the conductivity. As was observed by Ono *et al.*,[3] the conductivity of the solution at a given C_p decreases with an increase in the molecular weight of POE, M, but for $M>10^4$ the conductivity becomes independent of M. This finding implies that the assumption is reasonable.

In conclusion, the assumption in question does not reverse the quantitativity of the results which will be presented below.

The Solvent Effects on the Binding of the Potassium Ion. Binding Behavior in Various Solvents. Figure 2 shows η_{sp}/c *vs.* c relationships for POE in 5 mmol dm^{-3} KSCN solutions. The curves have a maximum in the methanol (MeOH), acetonictrile (AN), PC, and sulfolane (tetramethylene sulfone, TMS) systems, similar to the behavior of polyelectrolytes in added salt systems. These results imply that the polymer chain has some charges for these systems. The value of the intrinsic viscosity of the polymer, $[\eta]$, obtained by extrapolation to $c\rightarrow 0$, are shown in Table 2. As has been stated in the preceding paper,[1] these values can be used for the estimation of the intrinsic distance in a POE chain forming a one-dimensional lattice.

Table 2. Intrinsic viscosity of POE in the 5 mmol dm^{-3} KSCN system at 298.15 K

Solvent	$[\eta]$/dl g^{-1}
Methanol	0.57
Acetonitrile	0.72
Propylene carbonate	0.87
Sulfolane[a)]	0.54
DMF	0.44
DMSO	0.44
Water	0.47

a) 303.15 K.

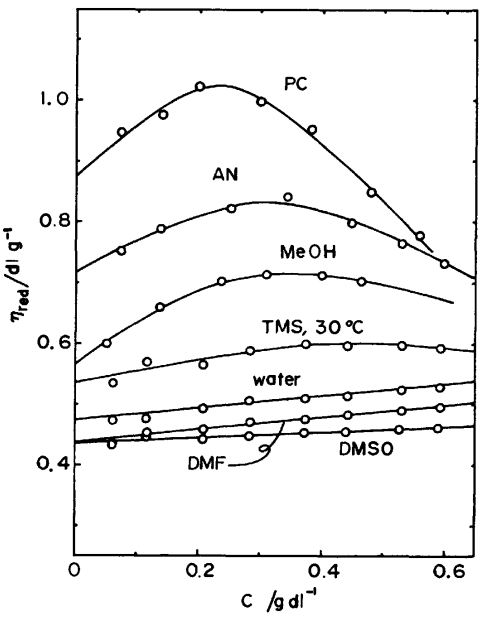

Fig. 2. Dependence of the reduced viscosity of POE, η_{red}, on POE concentration, c, in 5 mmol dm^{-3} KSCN solutions at 25 °C.

Figure 3 shows the relation between Λ/Λ_s and C_p for 5 mmol dm^{-3} of KSCN in seven solvent systems. In MeOH, AN, PC, and TMS systems, the degrees of the decrease in Λ/Λ_s with the increase in C_p are very large compared with other solvent systems. Thus, it can be qualitatively said that, in the MeOH, AN, PC, and TMS systems, ions are bound to the polymer. The preceding paper[1] states that log K_0 is a shift factor obtained by fitting the observed plots of θ *vs.* log a to the calculated curve of θ *vs.* log ξ, where ξ is the normalized activity.[1] Figure 4 shows the binding data obtained from the conductance values as well as the calculated binding curves. These binding data are in excellent agreement with the calculated curves over a wide range of activity of the potassium ion, using a single choice of the parameter, K_0. The binding constants obtained through this procedure are shown in Table 3. σ^2 is a measure of fitting (see Footnotes to Table 3). By the way, for the DMF, DMSO, and aqueous systems, the decrease in the conductivity with an increase in C_p is small, so the data are difficult to analyze with precision.

Comparison with the Method Based on the Low-molecular Analogy. As has been seen above, the analysis based on the one-dimensional lattice model seems to be most appropriate. We shall now compare this method with the method based on the low-molecular

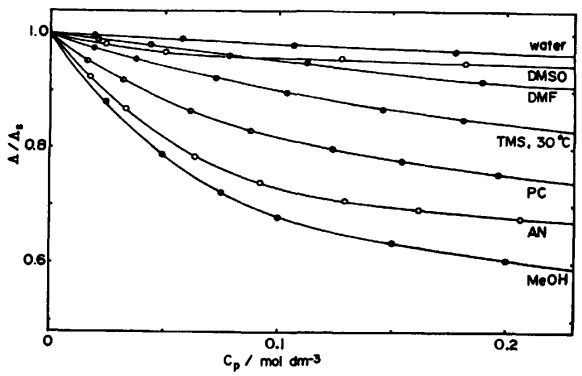

Fig. 3. The relation between the equivalent conductivity of KSCN, Λ, and POE concentration, C_p, at 25 °C.

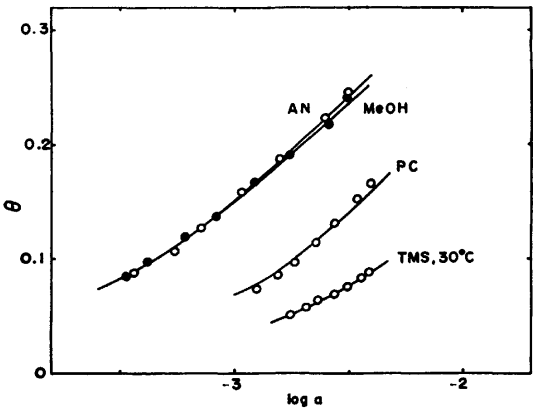

Fig. 4. Plots of the degree of binding, θ, against the logarithm of relative activity of potassium ion at 25 °C, together with the calculated curves.

Table 3. Binding constant of the potassium ion to POE determined for the 5 mmol dm^{-3} KSCN systems at 298.15 K

Solvent	log K_0	σ^{2} a)
Methanol	2.74	0.000173
Acetonitrile	2.68	0.000400
Propylene carbonate	1.97	0.00150
Sulfolane b)	1.63	0.000133

a) $\sigma^2=\frac{1}{n}\sum_{i=1}^{n}[(\theta_i^{\text{calcd}}-\theta_i^{\text{obsd}})/\theta_i^{\text{calcd}}]^2$. b) 303.15 K.

analogy. Based on the low-molecular analogy, we consider the following equilibrium:

$$\underset{(1-\theta)C_p/4}{\text{Site}} + \underset{C_s a}{\text{Ion}} \rightleftarrows \underset{\theta(C_p/4)}{\text{Site-ion complex.}} \quad (5)$$

We define the equilibrium constant, K, as in the following equation:

$$K=\frac{\theta}{(1-\theta)C_s a}. \quad (6)$$

Each simbol has the same meaning as that used in the preceding sections. In the system containing a polymer, however, the equilibrium constant defined in Eq. 6 intensively depends on θ, and K becomes greater as θ is smaller, in general. That is the problem that we brought forward in the introducion in the preceding paper.[1] The procedure often used in analyzing the proton dissociation of polyacids is to regard the intrinsic equilibrium constant as the value of K extrapolated to $\theta\rightarrow 0$, in which there is no interaction between the sites. Let us apply this procedure to our present systems. The relation of log K *vs.* θ is shown in Fig. 5. The degree of binding, θ, ranges widely, and the extrapolation to $\theta\rightarrow 0$ is then considerably easy in the MeOH and AN systems, whereas there is uncertainty in the extrapolation in PC and TMS systems. Even if the extrapolated value of log K can be accurately obtained, its physical meaning is ambiguous. As a result, it can be concluded that it is not effective to apply the method based on the low-molecular analogy to these systems.

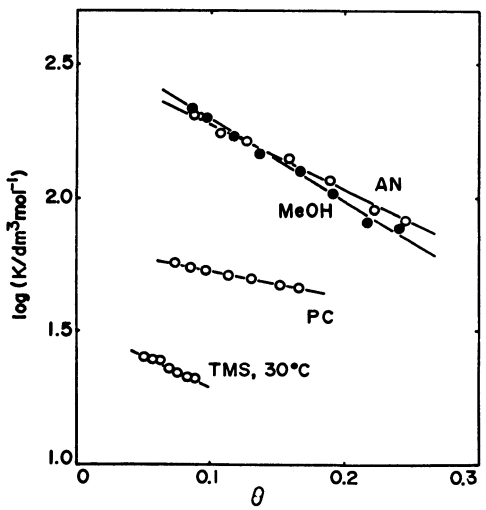

Fig. 5. Dependence of the equilibrium constant, K, which is defined in Eq. 6 based on the low-molecular analogy, on the degree of binding, θ, for 5 mmol dm^{-3} KSCN systems at 25 °C.

Interpretation of the Solvent Effects on the Binding Constant. We have obtained the binding constant, K_0, a quantity closely related to the intrinsic interaction between the site and the cation. Our next task is to discuss the solvent effects on K_0. In our treatment based on the one-dimensional lattice model, it is postulated that the solvent is to be regarded as a continuum. From the molecular-theoretical point of view, however, the cation binding to POE involves a process in which the solvent molecules coordinating to the cation are released. Thus, it can be said qualitatively that the cation binding to POE is less favorable as the solvent becomes a stronger solvator, *i.e.*, a stronger electron donor, to the cation. One of the parameters which represents the electron donicity of a solvent is the donor number (*DN*), proposed by Gutmann.[11] The *DN* values for several solvents are shown in Table 4. Roughly speaking, the binding of the potassium ion to POE occurs significantly in the solvents which have comparatively small *DN* values. By the way, the *DN* of diethyl ether, which is the low-molecular analog of POE, is 19.2. It might be noted that, in a solvent whose *DN* is larger than that of diethyl ether, the cation binding to POE is no longer observed. These quantitative considerations tell us that, in the interpretation of the solvent effects on K_0, we must pay attention to the problem of the solvation of the cation. However, the correlation between K_0 and *DN* is found to be bad.

Table 4. Correlation among the binding constant, K_0; the donor number of the solvent, *DN*, and the standard chemical potential of the potassium ion, $\mu^{\ominus}$

Solvent	*DN* a)	$\Delta\mu^{\ominus}$ b,c) / kJ mol^{-1}	$\Delta\log K_0$ b,c)
Nitromethane	2.7	9.64	
Ethanol		5.45	
Methanol	19.0	2.51	0.06
Acetonitrile	14.1	0	0
Propylene carbonate	15.1	−4.19	−0.71
Sulfolane e)	14.8	−6.70	−1.05
Diethyl ether	19.2		
Water	18.0 f)	−13.8	
DMF	26.6	−20.1	
DMSO	29.8	−25.1	

a) Ref. 11. b) Δ means that AN is chosen as the reference solvent. c) Ref. 13. d) This work (from Table 3). e) 303.15 K. For other solvent systems, 298.15 K. f) It is said that, although there is no theoretical ground for it, the value of 30 often explains experimental findings better for water as a solvent.[12]

Next let us try to correlate K_0 and the standard chemical potential of the potassium ion in each solvent, $\mu^{\ominus}$, which is a thermodynamic quantity reflecting the strength of the solvation of this ion as a whole. K_0 is composed of two factors, exp $(\mu^{\ominus}/RT)$ and exp$(-E/RT)$,

where E is the binding energy to the site (for details, see the preceding paper[1]). We introduce a rough assumption that E is constant, independent of the solvent. The binding energy, E can be expected to contain the complexation energy of the binding site and the desolvation energy of the polymer, the latter being dependent on the solvent. This assumption, however, seems to be sufficient as a zeroth-order approximation. According to this assumption, if we consider the ratio of the binding constant in an arbitrary solvent, S, $K_0(S)$, to that in a reference solvent, R, $K_0(R)$, then:

$$\begin{aligned}\Delta\log K_0 &\equiv \log[K_0(S)/K_0(R)] \\ &= [\mu^\ominus(S) - \mu^\ominus(R)]/2.303\,RT \\ &\equiv \Delta\mu^\ominus/2.303\,RT, \end{aligned} \quad (7)$$

where $\mu^\ominus(R)$ and $\mu^\ominus(S)$ are the standard chemical potential of the cation in the R and S solvents respectively. The $\Delta\mu^\ominus$'s of the potassium ion when AN is chosen as the reference solvent have been measured by Owensby *et al.***[13] They have measured the $\Delta\mu^\ominus$'s by several kinds of methods. We adopt the values obtained by assuming a negligible liquid-junction potential, which is believed to be the most reliable method. If we plot $\Delta\log K_0$ against $\Delta\mu^\ominus/2.303RT$, we find that Eq. 7 holds roughly, as is shown in Fig. 6. In the DMF, DMSO, and aqueous systems, we can say that, since $\Delta\mu^\ominus$ is very small, the cation is not bound in fact. As has been seen above, the solvent effects on the binding constant are mainly governed by the standard chemical potential of the cation in the solvent.

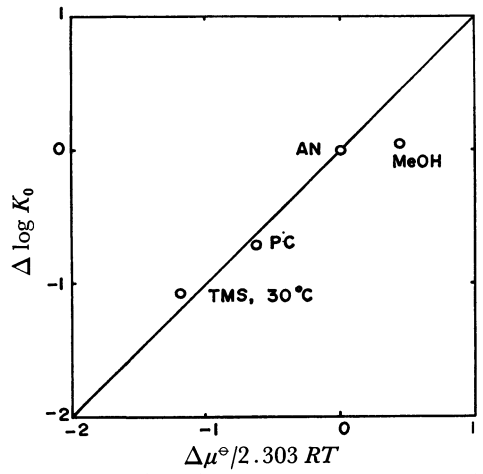

Fig. 6. The relationship between $\Delta\log K_0$ obtained in this study and $\Delta\mu^\ominus$ cited in Ref. 13. Acetonitrile (AN) is chosen as a reference solvent.

The Effects of the Salt Concentration on the Binding Constant. Figures 7 and 8 show the η_{sp}/c *vs.* c relationships for POE in various concentrations, C_s, of the KI-AN and -PC solutions. The curve is more raised in the region of small c values as C_s becomes smaller. This behavior closely resembles that of polyelectrolytes in salt-added systems.

** Owensby *et al.* have quantitatively discussed the relationship between $\Delta\mu^\ominus$ and the molecular structure of a solvent.

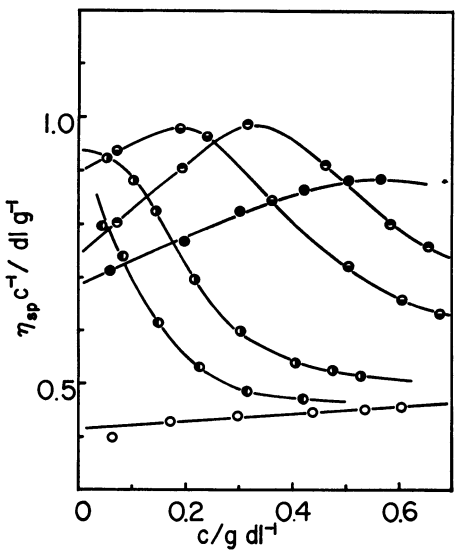

Fig. 7. η_{sp}/c *vs.* c relationships for POE in various concentration, C_s, of KI-AN solution at 25 °C.
●: C_s=10 mM, ◓: 5 mM, ◒: 3 mM, ◑: 1 mM, ◐: 0.5 mM, ○: salt-free.

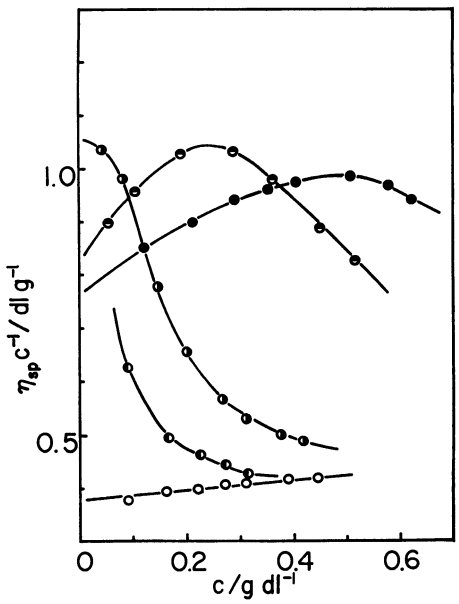

Fig. 8. η_{sp}/c *vs.* c relationships for POE in various concentration, C_s, of KI-PC solution at 25 °C.
●: C_s=10 mM, ◓: 5 mM, ◑: 1 mM, ◐: 0.4 mM, ○: salt-free.

We shall now investigate the dependence of the binding constant on the salt concentration. Plots of the degree of binding, θ, against log a and the calculated curves for the KI-POE-AN and KI-POE-PC systems are shown in Figs. 9 and 10 respectively. The binding constants for these systems are tabulated in Table 5. These results show that the binding constant, K_0, depends markedly on C_s in PC, whereas K_0 depends on it only a little in AN. As is illustrated in Fig. 11, K_0 increases with a decrease in C_s in both systems. The increase in K_0 can be explained by one of the following two ideas: (a) The cation is bound to a delocalized site

by nature, while our model has assumed a localized site, so that the entropy increment caused by the delocalized binding might result in an increase in K_0. (b) The factor of which K_0 is composed, $\exp(-E/RT)$, increases. The (a) idea will be discussed in the future. We will now verify phenomenologically that the (b) idea is valid.

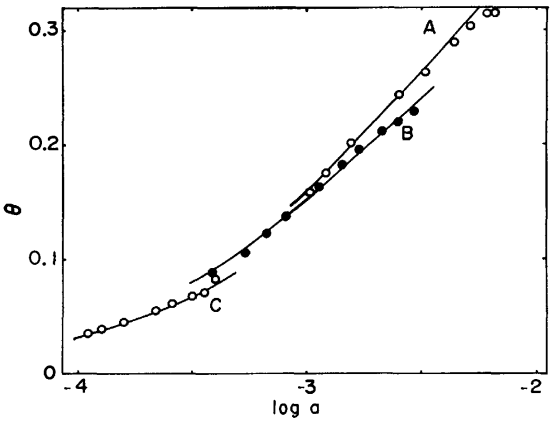

Fig. 9. Plots of θ *vs.* log a, together with the calculated curves, for KI–POE–acetonitrile systems at 25 °C.
A: C_s=10 mM, B: C_s=5 mM, C: C_s=1 mM.

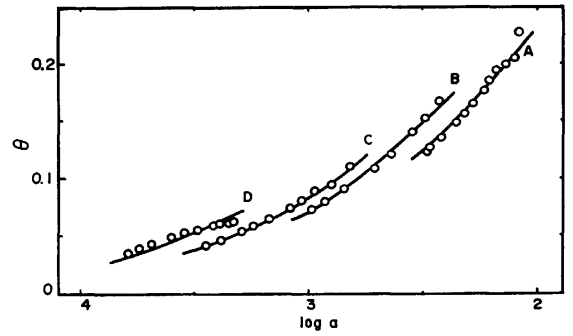

Fig. 10. Plots of θ *vs.* log a, together with the calculated curves, for KI–POE–propylene carbonate systems at 25 °C.
A: C_s=10 mM, B: C_s=5 mM, C: C_s=2 mM, D: C_s=0.5 mM.

Table 5. Dependence of the binding constant, K_0, on the salt concentration, C_s, at 298.15 K

KI–Acetonitrile		KI–Propylene carbonate	
C_s / mmol dm^{-3}	log K_0	C_s / mmol dm^{-3}	log K_0
0.1	2.86	0.5	2.38
0.5	2.70	1	2.28
1	2.63	2	2.15
5	2.56	5	1.99
10	2.42	10	1.83

In the preceding paper,[1] the binding constant, K_0, has been defined as follows:

$$K_0 = \exp[(\mu^\ominus - E)/RT]. \quad (8)$$

Let us differentiate the logarithm of Eq. 8 with respect to $1/T$. If we assume that:

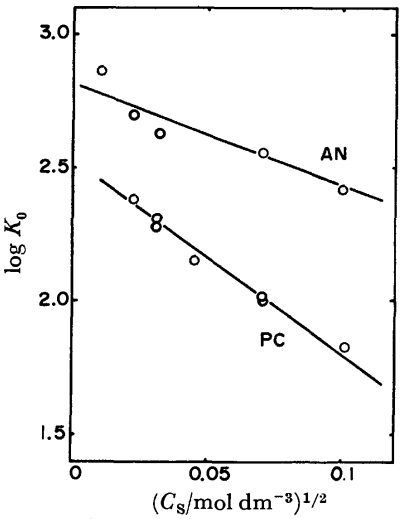

Fig. 11. Dependence of the binding constant, K_0, on the salt concentration, C_s, for KI–POE–AN and –PC systems at 25 °C.

$$\frac{\partial E}{\partial T} = 0, \quad (9)$$

then:

$$\frac{\partial \log K_0}{\partial (1/T)} = \frac{h^\ominus - E}{2.303RT}, \quad (10)$$

where $h^\ominus$ is the standard partial molar enthalpy of the cation. Figure 12 shows the plots of log K_0 against $1/T$ for 5 mmol dm^{-3} and 1 mmol dm^{-3} KI–POE–AN and –PC systems. The values of $h^\ominus - E$ obtained from the slope are tabulated in Table 6. Since $h^\ominus$ is common in both solvents, the differences between E in the 5 mmol dm^{-3} KI system and in the 1 mmol dm^{-3} KI system are 0.3 kJ mol^{-1} and 3.3 kJ mol^{-1} in AN and PC respectively. This finding phenomenologically supports

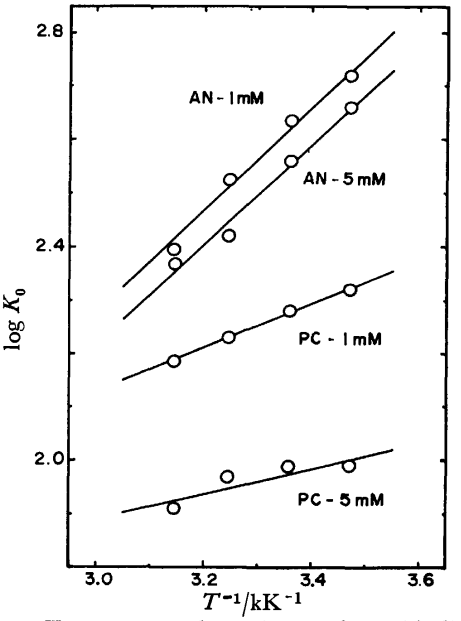

Fig. 12. Temperature dependence of the binding constant, K_0, for 1 mM and 5 mM KI–POE–AN and –PC systems.

the ideas that, as C_s grows smaller, E becomes smaller, that is, K_0 becomes greater, and that this tendency is notable in PC. The differences in the log K_0 calculated from the difference in E which has been just obtained are found to be 0.05 for the AN system and 0.58 for the PC system. These values do not agree with the observed values (AN, 0.07; PC, 0.26) very well. Taking account of the quality of the data, however, this result can be regarded as in rather better agreement and seems to support the idea (b).

Table 6. Values of $h^\ominus - E$ obtained from the slope of the plot of log K_0 against $1/T$.

Solvent	C_s/mmol dm^{-3}	$(h^\ominus - E)$/kJ mol^{-1}
Acetonitrile	1	18.2
	5	17.9
Propylene carbonate	1	7.9
	5	4.6

The Effects of the Variety of Salt. Table 7 shows the binding constants for various potassium salt–POE–PC systems. It is found that K_0 is little dependent on the variety of anion, as has been expected.

Table 7. Binding constants for potassium salt–POE–propylene carbonate systems at 298.15 K

Salt	log K_0
$KClO_4$	1.98
KSCN	1.97
KBr	1.91
KI	1.99

Table 8 shows the binding constants for various alkali metal iodide–POE–MeOH and –PC systems. It is clear that a large difference is found between the NaI and KI systems in MeOH, but not in PC. The differences between log K_0 values in the PC and MeOH systems are also shown in Table 8. $\Delta \log K_0$ is positive for NaI, but negative for other alkali metal iodides. The standard transfer Gibbs energies, $\Delta\mu^\ominus$, of the alkali metal ions from MeOH to PC[14] are added to Table 8 in the form of $\Delta\mu^\ominus/2.303\,RT$. The reason for the different behavior of NaI and KI is that $\Delta\mu^\ominus$ is negative for the potassium ion, but positive for the sodium ion.

Table 8. Binding constants for alkali metal iodide–POE–methanol and –propylene carbonate systems at 298.15 K

Salt	log K_0		$\Delta\log K_0$[a]	$\frac{\Delta\mu^\ominus}{2.303RT}$[b]
	Methanol	Propylene carbonate		
NaI	1.43	1.85	0.42	1.17
KI	2.72	1.99	−0.73	−0.74
RbI	2.77	1.93	−0.84	−2.28
CsI	2.58	1.80	−0.78	−3.82

a) $\Delta\log K_0 = \log K_0(\text{PC}) - \log K_0$ (MeOH). b) $\Delta\mu^\ominus$ is the standard transfer Gibbs energy from methanol to propylene carbonate (Ref. 11).

Conclusion

As has been seen above, the present method, which is based on the one-dimensional lattice model, is of great help in obtaining a unified understanding of the binding behavior on the solvent, the salt concentration, and the variety of salt.

This method, however, can be applied only to a system in which a strong interaction exists between POE and the ion and in which no specific interaction exists between the cation and the anion. If ionic association and/or binding of the anion to the polymer cation complex occurs, a modified method is required. The treatments for such systems will be discussed in the following paper.[15]

This work was partially supported by a Grant-in-Aid for Scientific Research No. 56550618 from the Ministry of Education, Science and Culture of Japan.

References

1) H. Awano, K. Ono, and Murakami, *Bull. Chem. Soc. Jpn.*, **55**, 2525 (1982). Part I of this series.
2) E. M. Arnett and C. F. Douty, *J. Am. Chem. Soc.*, **86**, 409 (1964).
3) K. Ono, H. Konami, and K. Murakami, *J. Phys. Chem.*, **83**, 2665 (1979).
4) "Landolt-Börnstein Tabellen," II band, 7 Teil, Elektrische Eigenschaften II, Springer-Verlag (1960), p. 653 for methanol; p. 664 for acetonitrile.
5) M. L. Jansen and H. L. Yeager, *J. Phys. Chem.*, **77**, 3089 (1973).
6) M. D. Monica, U. Lamanna, and L. Senatore, *J. Phys. Chem.*, **72**, 2124 (1968).
7) The data of equivalent conductivity *vs.* concentration are cited in: for the KSCN–methanol system, P. C. Sears, R. R. Holmes, and L. R. Dawson, *J. Electrochem Soc.*, **192**, 145 (1955); for the KSCN–acetonitrile system, H. L. Yeager and B. Kratochvil, *J. Phys. Chem.*, **74**, 963 (1970); for the KI–acetonitrile system, G. J. Janz, A. E. Marcinkowsky, and I. Ahmad, *Electrochim. Acta*, **9**, 1687 (1964); for the KSCN–sulfolane system, M. D. Monica and U. Lamanna, *Gazz. Chim.*, **98**, 256 (1968). For the propylene carbonate systems, see Ref. 5. Walden has measured the equivalent conductivities for various systems (P. Walden, *Z. Phys. Chem.*, **54**, 129 (1906)), but the reliability of his data is questionable.
8) J. C. Fenyo, F. Delben, S. Paoletti, and V. Crescenzi, *J. Phys. Chem.*, **81**, 1900 (1977).
9) J. Skerjanc, *J. Phys. Chem.*, **82**, 2313 (1978).
10) R. H. Stokes and R. Mills, "Viscosity of Electrolytes and Related Properties," Pergamon, Oxford (1965), Chap. 6.
11) V. Gutmann, "Coordination Chemistry in Non-Aqueous Solutions," Springer-Verlag (1968).
12) M.Tanaka, N. Matsuura, T. Tomonaga, M. Yamamoto, and Y. Yamamoto, *Kagaku Sosetsu*, **11**, 151 (1976), footnote to Tabel 9.1.
13) D. A. Owensby, A. J. Parker, and J. W. Diggle, *J. Am. Chem. Soc.*, **96**, 2682 (1974).
14) B. G. Cox, G. R. Hedwig, A. J. Parker, and D. W. Watts, *Aust. J. Chem.*, **27**, 477 (1974).
15) H. Awano, K. Ono, and K. Murakami, in preparation for publication. Preliminary results are published in: H. Awano, K. Ono, and K. Murakami, *Chem. Lett.*, **1982**, 149.

 © 1982 The Chemical Society of Japan Bull. Chem. Soc. Jpn., 55, 2537—2540 (1982)

Theoretical Considerations of the Dimer-formation Energy and Electronic Structures of the Monomer and Dimer of the 2-Pyridone by the Molecular Orbital Method

Kozo Inuzuka* and Akira Fujimoto

Department of Applied Science, Faculty of Technology, Tokyo Denki University, Kanda, Chiyoda-ku, Tokyo 101

(Received October 30, 1981)

When the dimer-formation energy of 2-pyridone was measured by means of ^{1}H-NMR spectroscopy, the value of 65.3 kJ mol^{-1} was obtained. It is much larger than the hydrogen-bond energies which are generally observed for the C=O···H–N system. The dimer-formation energy of 2-pyridone was calculated by means of the CNDO/2 method; its formation energy ($-\Delta H$) was estimated to be 68.2 kJ mol^{-1}. The electronic structures of the monomer and dimer of 2-pyridone were calculated by means of the CNDO method with configuration interaction (CNDO/CI) in order to clarify the previous band assignment of the UV spectrum of 2-pyridone. According to the calculated results, the absorption bands at 305 and 228 nm in isooctane (2,2,4-trimethylpentane) were assigned to the monomer, while those at 297.5 and 230.5 nm were assigned to the dimer.

In the previous paper[1] the longest-wavelength UV absorption of 2-pyridone in isooctane (2,2,4-trimethylpentane) was ascribed to π-π^* electronic transitions of the monomer and dimer. The dimer-absorption band appears at a wavenumber higher than that of the monomer by *ca.* 830 cm^{-1}. The dimer band corresponds to the π-π^* transition from the ground ^1A_g state to the excited ^1B_u state. No π-π^* transition absorption from the ground ^1A_g state to the excited ^1A_g state could be observed.

In this paper, the previous experimental considerations of the UV spectrum of 2-pyridone[1] were examined and further clarified by means of the CNDO method with CI. In addition, the formation energy of 2-pyridone dimer was evaluated by the CNDO/2 method; also, the dimer-formation energy was measured by the method of ^{1}H-NMR spectroscopy. The calculated energy was compared with the observed value.

Experimental

2-Pyridone was purified in the way described previously.[1] Tetrahydrofuran (THF) was refluxed with solid potassium hydroxide for at least 24 h, distilled from it, and again distilled from lithium aluminum hydride immediately before use. Benzene-d_6, Canada Merck (99.5% purity), was used as the solvent without further purification. The measurement of the ^{1}H-NMR spectrum was carried out with a JEOL FX-90Q NMR spectrometer at each of four temperatures, 8, 19, 32, and 42 °C. The concentration of the 2-pyridone solution was changed twelve times in the range of 10^{-3} to 10^{-1} mol dm^{-3}. The UV absorption spectrum was obtained at room temperature with a Hitachi Model 323 spectrophotometer.

Methods of Calculation and Molecular Models

The formation energy of the dimer, the π-bond orders, and the charge densities of 2-pyridone in the ground state were calculated by the CNDO/2 method[2,3] using the same parameter as in the previous paper.[1] The values of the bond distance and bond angle of 2-pyridone as measured by Penfold[4] were used. The data of 1-methyl-2-pyridone were the same as in the previous paper.[1]

For the dimer, the following planar model was used:

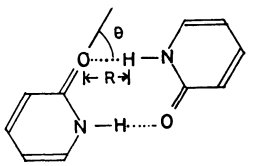

The present dimer model without the C_{2h} symmetry has the two parameters of R and θ, which correspond to the distance between the O atom of the C=O group and the H atom of the N–H group, and to the angle between the C=O axis and the direction of hydrogen bond of the O···H–N, respectively. The dimer-formation energy was calculated under an assumption that the ring framework of the 2-pyridone monomer and its N–H distance are invariant on the dimer formation. The enthalpy change ($-\Delta H$) for the dimerization of 2-pyridone was obtained by changing the R and the θ until the value of $-\Delta H$ reaches its maximum.

The CNDO method with CI (CNDO/CI) using the parameter given by Jaffé *et al.*[5,6] was employed for the calculation of the transition energies, transition oscillator strengths, charge densities, and π-bond orders in the lower-excited states. The Mataga-Nishimoto approximation[7] was used for the calculation of two-center Coulomb integrals. All the π molecular orbitals were built into the singly excited configuration interactions, while the two bonding σ-MO's of the highest and next-highest energies and one anti-bonding σ-MO of the lowest energy were taken into account for the CI of the 2-pyridone monomer. For the CI of the 2-pyridone dimer, all the π-MO's, the four bonding σ-MO's in the order of energy from the highest occupied σ-MO, and the two anti-bonding σ-MO's in the order of energy from the lowest energy were taken into account. The oscillator strength of the n-π^* transition was calculated according to Jaffé *et al.*[6]

Results and Discussion

Dimer-formation Energy of 2-Pyridone. Experimental: It was assumed that the following equilibrium between the monomer and the dimer of 2-pyridone exists:

$$2A \rightleftharpoons A_2. \quad (1)$$

The equilibrium constant for the above reaction was

defined by the following equation:

$$K = [A_2]/[A]^2, \quad (2)$$

where $[A_2]$ is the equilibrium concentration of the dimer and [A] is that of the monomer. The chemical shift of the N–H group moves to a lower magnetic field side as the concentration of 2-pyridone increases. The chemical shift, δ^i, of 2-pyridone in benzene-d_6 was represented by the following equation:

$$\delta^i = (1 - x^i)\delta_M + x^i\delta_D \quad (3)$$

where x^i corresponds to the mole fraction of the dimer and where δ_M and δ_D stand for the chemical shift of the monomer and dimer of 2-pyridone. The superscript, i, represents the i-th concentration of 2-pyridone. To bring the value of δ^i close to the observed value, δ^i_{obsd}, the next equation was used:

$$S = \sum_i (\delta^i_{obsd} - \delta^i)^2 \qquad (i = 1,2,\cdots,n) \quad (4)$$

The K and δ_M values were determined by the trial-and-error method using Eqs. 2, 3, and 4 and the assumed value of 14.20 ppm for δ_D. In the present calculation, the value of 11.61 ppm was obtained for the chemical shift of the monomer of 2-pyridone. In Fig. 1 the values of the chemical shift, calculated by means of Eq. 3 with the assumed values of δ_M and δ_D, are plotted with the observed values for the various concentrations and temperatures. The agreement between the calculated and observed δ values seems relatively good except for the results at 42 °C. The enthalpy change, $-\Delta H$, that is, the hydrogen-bond dimer-formation energy, was obtained by plotting $\ln K$ *versus* $1/T$, as is shown in Fig. 2. The value of $-\Delta H_{obsd}$, 65.3 kJ mol^{-1}, was evaluated from Fig. 2 using the least-squares method.

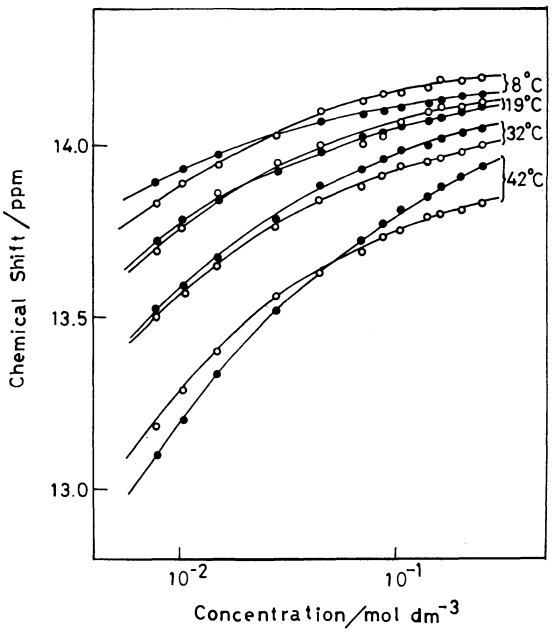

Fig. 1. The observed chemical shift (—○—) of NH proton of 2-pyridone *versus* total concentration of 2-pyridone and the calculated chemical shift (—●—) by Eq. 3. See Text.

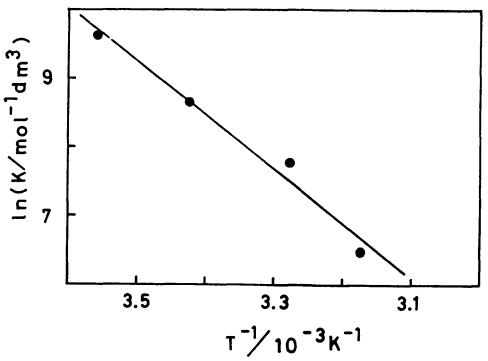

Fig. 2. Plots of $\ln K$ *vs.* $1/T$.

Theoretical: The dimer-formation energy, the π-bond order of the C=O group, the equilibrium distance, R_e, and angle, and the dipole moment of the dimer, which were obtained after the optimization of the parameters, R and θ, are given in Table 1. The optimized dimer model suggests that the 2-pyridone dimer belongs to the point group of the C_{2h} symmetry. The charge densities and π-bond orders of the 2-pyridone dimer are shown in Fig. 3. The dimer-formation energy $-\Delta H$, was 147.7 kJ mol^{-1}; the equilibrium distance, 1.35 Å, and the angle, 58.75°. The CNDO/2 method tends to overestimate the value of $-\Delta H$ and to underestimate Re.

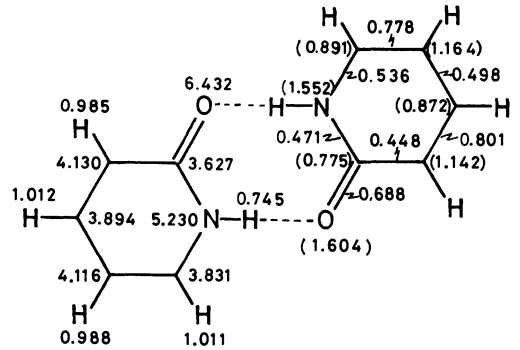

Fig. 3. Several molecular properties of 2-pyridone dimer calculated by the CNDO/2 method; the total charge densities of valence electron, π-charge densities, and π-bond orders. The values of π-charge densities are shown in parentheses.

Table 1. The calculated hydrogen-bond energy ($-\Delta H$), corrected hydrogen-bond energy ($-\Delta H_c$), equilibrium distance (R_e), and angle (θ), π-bond order of the carbonyl group ($p_{C=O}$), and dipole moment (μ) of the 2-pyridone dimer with observed hydrogen-bond energy

Dimer	Sym.	R_e/Å	θ/°	$p_{C=O}$	μ/D	$-\Delta H$ / kJ mol^{-1}	$-\Delta H_c$ / kJ mol^{-1}	$-\Delta H_{obsd}$ / kJ mol^{-1}
2-Pyridone	C_{2h}	1.35	58.75	0.688	0	147.7	68.2	65.3

The π-bond order of the C=O group of the dimer (0.688) is smaller than that of the monomer (0.782).[1] The IR band at 1654 cm^{-1} was assigned to the stretching vibration of the C=O group of the dimer, and the band at 1676 cm^{-1}, to that of the monomer in carbon tetrachloride.[1] This is in line with the calculated π-bond orders of the carbonyl groups of the dimer and monomer of 2-pyridone.

The charge density of the H atom of the N–H group of the dimer is smaller than that of the monomer (0.886).[1] This implies that the ^{1}H-NMR spectrum of the N–H group of the dimer may appear at a lower magnetic field than that of the monomer. The chemical shifts of the N–H group are 11.61 and 14.20 ppm for the monomer and dimer of 2-pyridone, respectively. This experimental result is in line with the theoretical result.

The present calculated value of the hydrogen-bond dimer-formation energy seems very large, although the hydrogen-bond energy calculated by the CNDO/2 method generally gives rise to values larger than the observed values.[9,10] In order to assess the reliability to be expected from the hydrogen-bond energy calculation by means of the CNDO/2 method and in order to obtain a correction factor by which to evaluate a desirable dimer-formation energy for 2-pyridone, the hydrogen-bond energies of several organic compounds were obtained theoretically by means of the CNDO/2 method and experimentally by means of the UV spectroscopic method. In the experiment, ethanol was used, but in the case of calculation, methanol was employed for the sake of simplicity.

The calculated and experimental results are listed in Table 2. When the calculated energy values are plotted against the experimental energy values, there is a good linear relationship between the calculated and experimental values. The line was determined by the least-squares method. The dimer-formation energy of 2-pyridone was obtained from the line using the calculated value of 147.7 kJ mol^{-1}. The present value of $-\Delta H_c$ was evaluated as 68.2 kJ mol^{-1}. The value of 68.2 kJ mol^{-1} is very close to the observed value. This value is larger than the dimer-formation energy of acetic acid (44.8 kJ mol^{-1}).[14] However, Hammes and Park,[15] by means of the ultrasonic absorption method, obtained 25 kJ mol^{-1} for the dimer-formation energy of 2-pyridone in chloroform. The values of 68.2 and 65.3 kJ mol^{-1} are much larger than Hammes and Park's value.[15] Chloroform is known to form a hydrogen bond. As 2-pyridone in chloroform is stabilized by a hydrogen-bond formation with the solvent, the dimer-formation energy of 2-pyridone may be smaller than it is in benzene. Another reason may be a difference in the experimental means for the measurement of the dimer-formation energy. The values of 68.2 and 65.3 kJ mol^{-1} are larger than the hydrogen-bond energy between the C=O and N–H groups which is generally observed.

The charge density of the O atom of the C=O group of the 2-pyridone monomer[1] is larger than that of the [1]benzopyrano[3,4-*c*]pyridine derivatives[9] and aldehydes.[10] The large charge density of the O atom of 2-pyridone may result in the large Coulombic interaction between the C=O and N–H groups of the 2-pyridone dimer.

Table 2. The hydrogen-bonding energies obtained theoretically by means of the CNDO/2 method and experimentally by means of the UV spectroscopic method for several hydrogen-bonding complexes

No.	H-Bonded complex	$-\Delta H_{calcd}$ / kJ mol^{-1}	$-\Delta H_{obsd}$ / kJ mol^{-1}
1	Aniline–Methanol	17.11[a]	8.8[a]
2	Crotonaldehyde –Methanol	29.37[b]	14.2[b]
3	Benzaldehyde –Methanol	29.87[b]	14.2[b]
4	Cinnamaldehyde –Methanol	29.41[b]	13.0[b]
5	Pyridine–Methanol	34.69[a]	17.6[a]
6	1-Methyl-2-pyridone –Methanol	40.71[b]	18.0[c]
7	2-Aminopyridine –Acetic acid	74.48[b]	34.7[b]
8	Acetic acid dimer	96.19[b]	44.8[d]

a) Ref. 11. b) Ref. 12. c) Ref. 13. d) Ref. 14.

Table 3. Calculated transition energies (E), wavelengths (λ), and oscillator strengths (f) of the 2-pyridone monomer

State	Sym.	E/eV	λ/nm	f	λ_{obsd}/nm
1	A″	3.595	345	0.000	
2	A′	4.330	286	0.248	305
3	A″	5.475	226	0.000	
4	A′	5.553	223	0.377	228

Electronic Structures of 2-Pyridone. In order to clarify the n,π^* state of 2-pyridone, the calculation of the transition energies and oscillator strengths of the 2-pyridone monomer was carried out by means of the CNDO/CI method. The calculated results are given in Table 3, along with the experimental values.[1] It is noteworthy that the lowest excited singlet state is of an n,π^* character and that the n-π^* transition band is expected near 350 nm for 2-pyridone. However, we could not observe any band in this region. It may be difficult to observe the corresponding band near 350 nm for the following reasons: (1) a low intensity as suggested by the calculated f value, and (2) the band position near 350 nm is too close to the strong π-π^* band in the vicinity of 300 nm, and so the n-π^* band may overlap with the first π-π^* band.

As is shown in Fig. 4, the addition of THF to the 2-pyridone in isooctane separated the monomer bands from the dimer bands. As the addition of THF results in the red-shift of the absorption band of the 2-pyridone monomer, the peak at 228 nm in isooctane may be assigned to the band maximum of the second π-π^* system of the monomer, which corresponds to the peak at 230 nm in the THF-isooctane solvent.

In order to clarify the previous assertions that the band with the maximum at 297.5 nm belongs to the dimer and that the band maximum at 305 nm corre-

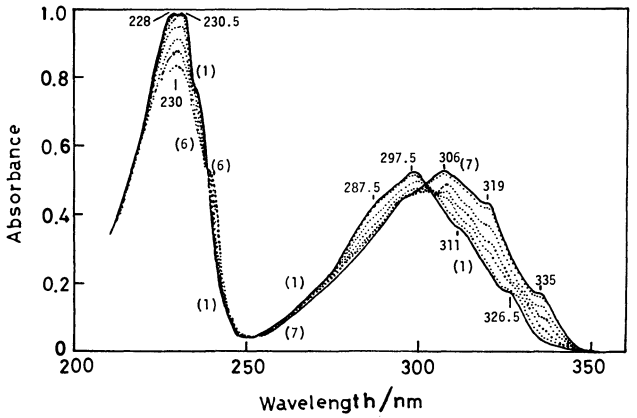

Fig. 4. The UV absorption spectrum of 2-pyridone in isooctane–THF mixed solvents at room temperature. Concentration of 2-pyridone: 1.22×10^{-4} mol dm^{-3}, concentrations of THF (mol dm^{-3}): (1) 0, (2) 4.89×10^{-2}, (3) 1.96×10^{-1}, (4) 4.98×10^{-1}, (5) 9.78×10^{-1}, (6) 4.89, (7) 7.33.

sponds to the monomer in isooctane,[1] and in order to clarify the assignment of the second band near 230 nm, the transition energy and oscillator strength of the dimer were calculated by the CNDO/CI method. The CI of 96th-orders was taken into account, including all π-MO's and six σ orbitals. The optimized equilibrium distance of 1.35 Å seems to be so short that it gives too large a hydrogen-bond energy. The equilibrium distance corresponding to the value of $-\Delta H_{obsd}$, 65.3 kJ mol^{-1}, should be longer than 1.35 Å. In the present calculation, the distances of 1.80 and 1.90 Å, which give rise to 76.27 and 61.34 kJ mol^{-1} for the values of $-\Delta H$ calculated by the CNDO/2 method, were used. The distance of the dimer with the formation energy of 65.3 kJ mol^{-1} lies between 1.80 and 1.90 Å.

The calculated transition energies and oscillator strengths for the dimer model (1.80 Å) are both listed in Table 4, because there is no essential difference between the two models with respect to the results of the CNDO/CI calculation. All the π,π^* excited states of the dimer are split into the two states of the A_g and B_u symmetries, while the n,π^* excited states are split into the two states of the B_g and A_u symmetries. A comparison of Table 3 with Table 4 shows that the 1st π-π^* transition energy of the dimer is higher than that of the monomer, but the 2nd π-π^* transition energy of the former is lower than that of the latter.

Table 4. Calculated transition energies (E), wavelengths(λ), and oscillator strengths (f) of the 2-pyridone dimer

State	Model (1.80 Å)				λ_{obsd}/nm
	Sym.	E/eV	λ/nm	f	
1	B_g	3.769	328	0	
2	A_u	3.771	328	0.000	
3	A_g	4.284	289	0	
4	B_u	4.412	281	0.469	297.5
5	B_g	5.252	236	0	
6	A_u	5.252	236	0.000	
7	B_u	5.515	224	0.893	230.5
8	A_g	5.567	222	0	
9	B_u	5.687	218	0.000	
10	A_g	5.688	218	0	

The present results, calculated by means of the CNDO/CI method and obtained by the use of the UV spectrum of 2-pyridone in the THF–isooctane system, agree with the previous band assignment of the 2-pyridone monomer and dimer.[1] Further, the calculation has clarified that the peak at 228 nm is to be assigned to the second π-π^* transition of the A′ symmetry of the monomer, and the peak at 230.5 nm, to that of the B_u symmetry of the dimer, although the assignments of those bands were unclear in the previous paper.[1]

Table 5. Energy difference between the ^{1}A′ state of the monomer and the ^1B_u state of the dimer in the first and second π-π^* regions

	Energy difference between ^{1}A′ and ^1B_u states in 1st- and 2nd-regions/cm^{-1}	
	(1st)	(2nd)
Dimer model (1.80 Å)	660	−310
Obsd	830	−480

In Table 5 the energy differences between the first ^{1}A′ state of the monomer and the first ^1B_u state of the dimer and between the second ^{1}A′ and ^1B_u states are given. The calculated energy differences between ^{1}A′ and ^1B_u states for the monomer and dimer are in good agreement with the observed values.

This work was supported by grants from the Research and Development Center of Engineering of Tokyo Denki University. One of the authors (K.I) also acknowledges his gratitude for the assistance of the staff of the T. D. U. Computing Center.

References

1) A. Fujimoto, K. Inuzuka, and R. Shiba, *Bull. Chem. Soc. Jpn.*, **54**, 2802 (1981).
2) J. A. Pople, D. P. Santry, and G. A. Segal, *J. Chem. Phys.*, **43**, 129 (1965).
3) J. A. Pople and G. A. Segal, *J. Chem. Phys.*, **43**, 136 (1965); **44**, 3289 (1966).
4) B. R. Penfold, *Acta Crystallogr.*, **6**, 591 (1953).
5) J. Del Bene and H. H. Jaffé, *J. Chem. Phys.*, **48**, 1807 (1968).
6) R. L. Ellis, G. Kuehnlenz, and H. Jaffé, *Theor. Chim. Acta*, **26**, 131 (1972).
7) N. Mataga and K. Nishimoto, *Z. Phys. Chem.*, **13**, 140 (1957).
8) F. Inagaki, M. Tasumi, and T. Miyazawa, *Bull. Chem. Soc. Jpn.*, **48**, 1427 (1975).
9) K. Inuzuka and A. Fujimoto, *Bull. Chem. Soc. Jpn.*, **51**, 2786 (1978).
10) K. Inuzuka, *Nippon Kagaku Kaishi*, **1978**, 1118.
11) A. Fujimoto and K. Inuzuka, *Bull. Chem. Soc. Jpn.*, **51**, 2781 (1978).
12) K. Inuzuka, to be published.
13) A. Fujimoto and K. Inuzuka, *Bull. Chem. Soc. Jpn.*, **52**, 1816 (1979).
14) H. E. Affsprung, S. D. Christlan, and A. M. Melnick, *Spectrochim. Acta*, **20**, 285 (1964).
15) G. G. Hammes and A. C. Park, *J. Am. Chem. Soc.*, **91**, 956 (1969).

Multidentate Ligand Kinetics. IV. Computer Simulation of the Steady State of the Free Ligands in a Coordination Chain Reaction

Tetsuo KATSUYAMA* and Toshihiko KUMAI

Department of Basic Technology, Faculty of Engineering, Yamagata University, Yonezawa, Yamagata 992

(Received November 2, 1981)

The ligand-substitution reactions between two multidentate ligand complexes in the presence of free ligands proceed by means of a coordination chain-reaction mechanism. The reaction was simulated on a computer under various conditions. The character of the steady state of the free ligands in the coordination chain reaction was discussed. The conditions under which the coordination chain reaction proceeds with the steady state of the free ligands were determined. The diagrams of the time development of the free ligands were found to be useful for studies using the coordination chain reaction.

In previous works,[1-3] the ligand-substitution reactions between two multidentate ligand complexes were studied in the presence of free ligands:

$$ML + ZX \longrightarrow MX + ZL, \quad (R1)$$

where ML, ZX, MX, and ZL are multidentate ligand complexes; the charges will be omitted hereafter for the sake of simplicity.

The reactions were shown to proceed by means of a coordination chain-reaction mechanism:

$$ML + X \underset{k_{-2}}{\overset{k_2}{\rightleftharpoons}} MX + L, \quad (R2)$$

$$ZX + L \underset{k_{-3}}{\overset{k_3}{\rightleftharpoons}} ZL + X, \quad (R3)$$

where X and L denote free ligands.

In the course of our studies, the rate law was derived from a steady-state treatment on the assumption that the concentrations of the free ligands (X and L) remain constant throughout the substitution. This assumption, however, was not examined.

Coordination chain reactions can be applied to the determination of trace metal ions.[4-6] In the analytical applications, the above assumption is taken to hold. However, in general, a coordination chain-reaction system can not necessarily be expected to satisfy the above assumption.

If the time development of the free-ligand concentration in the system can be known, it is useful for the studies using a coordination chain reaction. In this paper, coordination chain reactions were simulated on a computer under various conditions, and the concentration-time profiles for all the components were calculated. The purpose of this paper is to ascertain the conditions under which the reaction proceeds with the steady state of the free ligands.

Computational Method

The six-variable, four-rate constant isothermal model represented by Reactions R2 and R3 can be described by the following differential equations:

$$\frac{d[ML]}{dt} = -k_2[ML][X] + k_{-2}[MX][L], \quad (1)$$

$$\frac{d[ZX]}{dt} = -k_3[ZX][L] + k_{-3}[ZL][X], \quad (2)$$

$$\frac{d[MX]}{dt} = k_2[ML][X] - k_{-2}[MX][L], \quad (3)$$

$$\frac{d[ZL]}{dt} = k_3[ZX][L] - k_{-3}[ZL][X], \quad (4)$$

$$\frac{d[X]}{dt} = -k_2[ML][X] + k_{-2}[MX][L] + k_3[ZX][L] - k_{-3}[ZL][X], \quad (5)$$

$$\frac{d[L]}{dt} = k_2[ML][X] - k_{-2}[MX][L] - k_3[ZX][L] + k_{-3}[ZL][X]. \quad (6)$$

Using the known starting conditions and rate constants, the six above simultaneous differential equations were integrated by the numerical integration method of Runge-Kutta-Gill.[7] The starting conditions in the integration were as follows:

$$[ML]_0 = a\ \mathrm{M}(1\ \mathrm{M}=1\ \mathrm{mol\ dm^{-3}}), \quad (7)$$

$$[ZX]_0 = b\ \mathrm{M}, \quad (8)$$

$$[MX]_0 = [ZL]_0 = 0\ \mathrm{M}, \quad (9)$$

$$\begin{matrix}[X]_0 = c\ \mathrm{M} \\ [L]_0 = 0\ \mathrm{M}\end{matrix} \quad \text{or} \quad \begin{matrix}[X]_0 = 0\ \mathrm{M} \\ [L]_0 = c\ \mathrm{M}\end{matrix}, \quad (10)$$

where $[\ ]_0$ indicates the initial concentration of the species and where a, b, and c are not zero. In these calculations, it has been premised that $k_3 \geqq k_2$ and $[ZX]_0 \geqq [ML]_0$.[8]

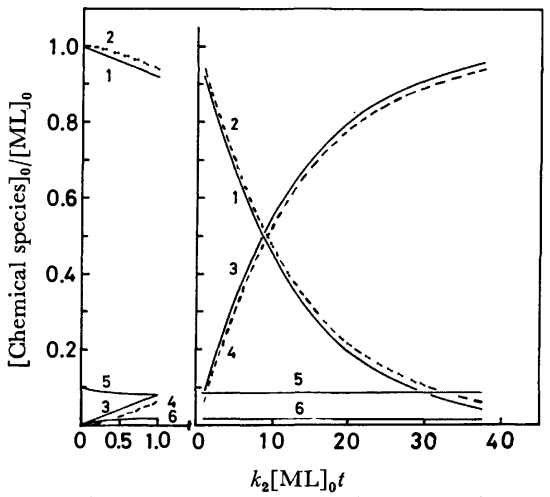

Fig. 1. An example of computer simulation of coordination chain reaction.[11]
Conditions: $[ML]_0=[ZX]_0=1$ M, $[MX]_0=[ZL]_0=0$ M, $[X]_0=0.1$ M, $[L]_0=0$ M; $k_2=1\ M^{-1}\ s^{-1}$, $k_3=4\ M^{-1}\ s^{-1}$, $k_{-2}=k_{-3}=0\ M^{-1}\ s^{-1}$. 1: ML, 2: ZX, 3: MX, 4: ZL, 5: X, 6: L.

The concentration-time profiles for all the components were obtained from the integration. The relative concentrations, expressed in terms of $[ML]_0$ as a unit, were then plotted against $k_2[ML]_0t$ (Fig. 1); this representation is convenient for the general treatment of the concentration-time profiles, since the ordinate and abscissa have no dimensions.[9]

In the studies using the coordination chain reaction, the reaction is usually run in the presence of the free ligand, and the relative concentration of the free ligand presented initially is ordinarily smaller than 0.1. Therefore, in this study, the simulations were carried out under the condition that $\frac{[\text{free ligand}]_0}{[ML]_0} \leqq 0.1$.

Calculations were carried out with an ACOS 900 computer of the Tohoku University Computation Center.

Results and Discussion

In order to clarify the nature of the coordination chain reaction, the reaction system was classified into the several cases shown in Table 1; *e.g.*, in the case of the I_1 system, the rate constants, k_{-2} and k_{-3}, can be regarded as zero, while the initial concentrations of ML and ZX are equal to one another.

The total free ligand concentration ([X]+[L]) is equal to the initial ligand concentration, c, throughout the substitution reaction. Therefore, if the X ligand reaches a steady state, the L ligand also reaches a steady state; the steady state of the free ligands can, then, be studied by examining the concentration-time profile for one of the two free ligands. In this study, the concentration-time profile for the X ligand was noted.

Reaction System I. *System* I_1 ($k_{-2}=k_{-3}=0$, $[ZX]_0=[ML]_0$): Figure 2 shows the time development of the concentration of X with the following specifications: $[X]_0/[ML]_0=0.1$ for Fig. 2.A and $[L]_0/[ML]_0=0.1$ for Fig. 2.B.

It may be seen that the greater the k_3/k_2 ratio, the closer the concentration of X comes to the steady state, and that the steady-state approximation in Fig. 2.A is superior to that in Fig. 2.B.

The concentration of the X ligand in the steady state can be estimated as follows. From $d[X]/dt=0$, the following relationship is obtained:

$$-k_2[ML][X] + k_3[ZX][L] = 0. \quad (11)$$

Since the $[X] \gg [L]$ inequality and the $[ML]_0=[ZX]_0$ equation hold, the following relation can be derived:

$$[ML] \approx [ZX]. \quad (12)$$

On the other hand, the following relationship also holds:

$$[X] + [L] = c. \quad (13)$$

Thus, from Eqs. 11, 12, and 13, the concentration of the X ligand in the steady state is obtained as

$$[X] \approx \frac{k_3/k_2}{1+k_3/k_2}c. \quad (14)$$

The concentration of X as estimated by means of Eq. 14 agrees very well with the concentration of X in the leveling-off range of Fig. 2.

Figure 3 shows the effect of variations in the initial concentration of the free ligand on the time development of the concentration of X.

It appears that the smaller the initial concentration of the free ligand, the more precise the steady-state

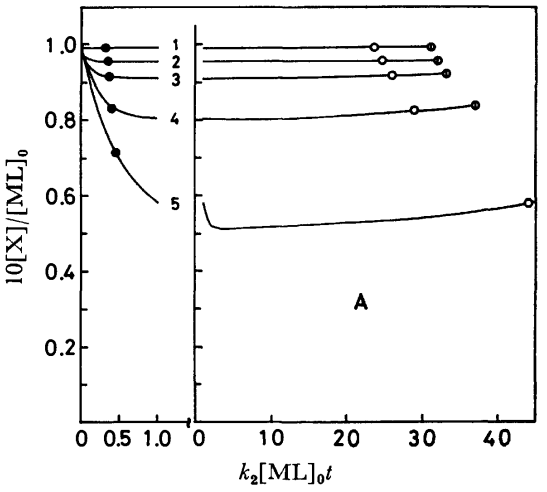

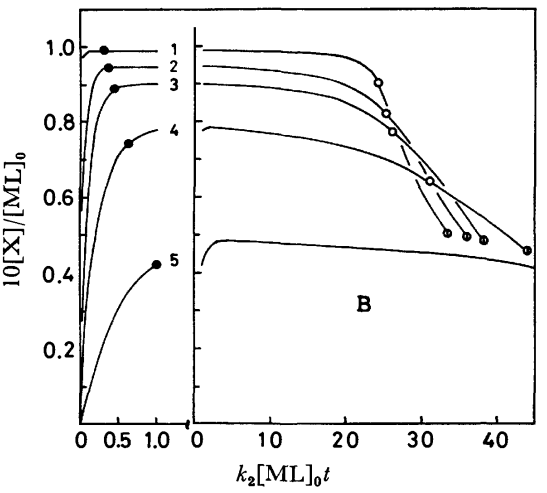

Fig. 2. The time development of the concentration of X for the system I_1 ($k_{-2}=k_{-3}=0$, $[ZX]_0=[ML]_0$). k_3/k_2; (1): 100, (2): 20, (3): 10, (4): 4, (5): 1. A shows the case in which $[X]_0/[ML]_0=0.1$, and B the case in which $[L]_0/[ML]_0=0.1$. Circles indicate the points of 3% (●), 90% (○), and 95% (◑) of the reaction proceeding, here and in the following figures.

Table 1. Classification of coordination chain-reaction system

I		II		III	
I_1	I_2	II_1	II_2	III_1	III_2
$k_{-2}=k_{-3}=0$	$k_{-2}=k_{-3}=0$	$k_{-2}=0$	$k_{-2}=0$	$k_{-3}=0$	$k_{-3}=0$
$[ZX]_0=[ML]_0$	$[ZX]_0 \geqq 2[ML]_0$	$[ZX]_0=[ML]_0$	$[ZX]_0 \geqq 2[ML]_0$	$[ZX]_0=[ML]_0$	$[ZX]_0 \geqq 2[ML]_0$

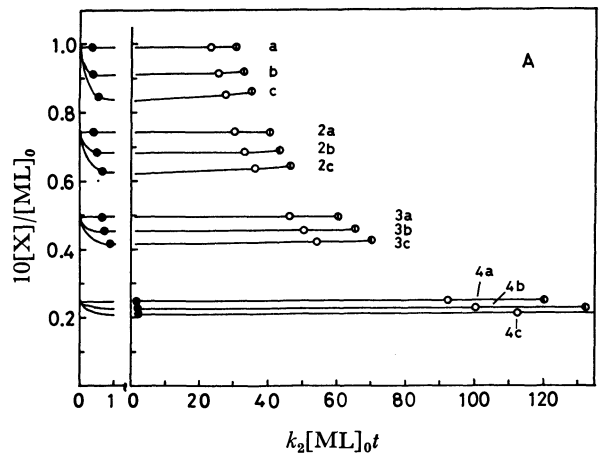

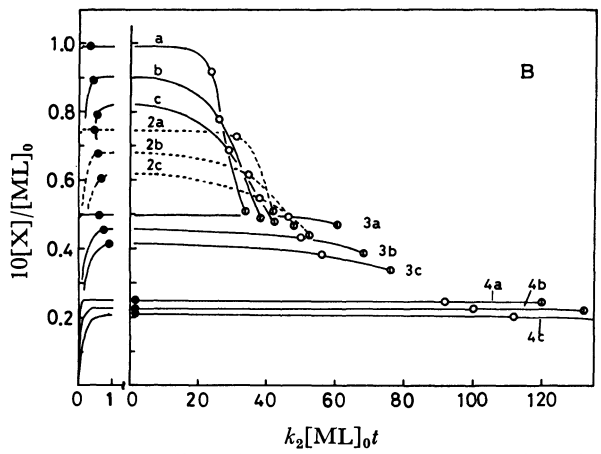

Fig. 3. The effect of the initial concentration of the free ligand on the development of the concentration of X for the system I_1 ($k_{-2}=k_{-3}=0$, $[ZX]_0=[ML]_0$). k_3/k_2, ([ligand]$_0$/[ML]$_0$); a: 100 (0.1), b: 10 (0.1), c: 5 (0.1),2a: 100 (0.075),2b: 10 (0.075),2c: 5 (0.075), 3a: 100 (0.050), 3b: 10 (0.050), 3c: 5 (0.050), 4a: 100 (0.025), 4b: 10 (0.025), 4c: 5 (0.025). A shows the case in which the ligand present initially is X, and B the case in which the ligand present initially is L.

approximation of X becomes, and that when the initial concentration of L is large, a good steady-state approximation of X can not be obtained (Fig. 3.B); moreover, the smaller the initial concentration of the free ligand, the longer the reaction time.

System I_2 ($k_{-2}=k_{-3}=0$, $[ZX]_0 \geqq 2[ML]_0$): Figure 4 shows the time dependence of the concentration of X for the I_2 system.

Where the X ligand is present initially (Case A), the concentration of X decreases at first, but very soon the concentration begins to increase. On the other hand, where L is present initially, the concentration of X increases rapidly at first, and later comes close to that in Case A. These modes differ from those of the I_1 system. Figure 5 shows the effect of the initial concentration of the free ligand on the time development of the concentration of X.

In system I, if the calculated curve of X is expressed as $([X]/[ML]_0)/c$ *vs.* $ck_2[ML]_0t$, the curve is little affected by the variations in the initial concentration

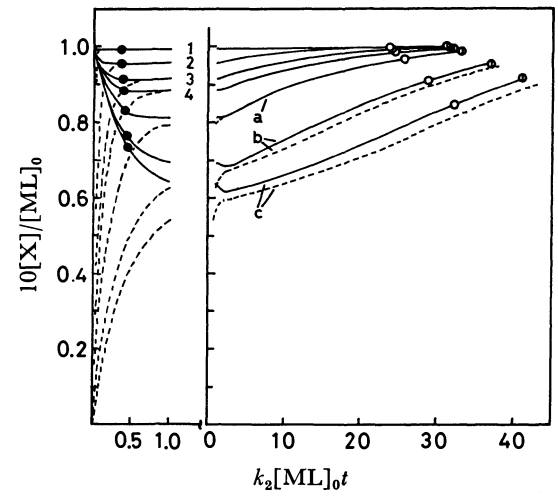

Fig. 4. The time development of the concentration of X for the system I_2 ($k_{-2}=k_{-3}=0$, $[ZX]_0 \geqq 2[ML]_0$).[12] $k_3/k_2 \cdot [ZX]_0/[ML]_0$; (1): 100, (2): 20, (3): 10, (4): 7. $[ZX]_0/[ML]_0$, (k_3/k_2); a: 4 (1.0), b: 2 (1.0), c: 1.5 (1.0). Full lines show the case in which $[X]_0/[ML]_0=0.1$, and dotted lines the case in which $[L]_0/[ML]_0=0.1$.

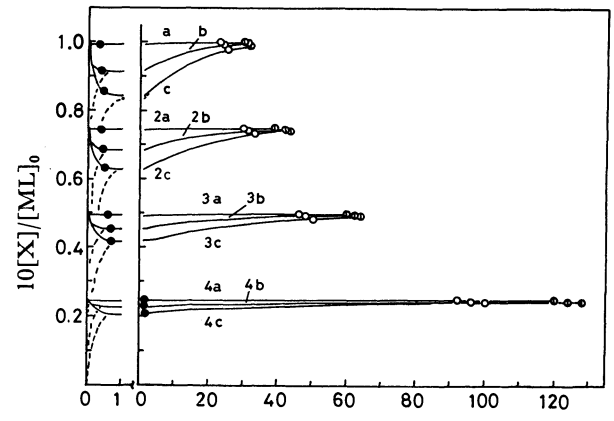

Fig. 5. The effect of the initial concentration of the free ligand on the time development of the concentration of X for the system I_2 ($k_{-2}=k_{-3}=0$, $[ZX]_0 \geqq 2[ML]_0$).[12] $k_3/k_2 \cdot [ZX]_0/[ML]_0$, ([ligand]$_0$/[ML]$_0$); a: 100 (0.1), b: 10 (0.1), c: 5 (0.1), 2a: 100 (0.075), 2b: 10 (0.075), 2c: 5 (0.075), 3a: 100 (0.050), 3b: 10 (0.050), 3c: 5 (0.050), 4a: 100 (0.025), 4b: 10 (0.025), 4c: 5(0.025). Full lines show the case in which the ligand presented initially is X, and dotted lines the case in which the ligand presented initially is L.

of the free ligand, except where $c=[L]_0$ and $[ZX]_0=[ML]_0$.

Therefore, X was henceforth used as the ligand present initially, and the concentration was set at $[X]_0/[ML]_0=0.1$; by these settings, the treatment of the system would be simplified.

Reaction System II. System II_1 ($k_{-2}=0$, $[ZY]_0=[ML]_0$): Figure 6 shows the time development of the concentration of X for the II_1 system. In this system, the time development of X is affected very much by the reverse reaction of R3; only when the k_3/k_{-3} ratio becomes more than 10^4, can the reverse reaction of R3

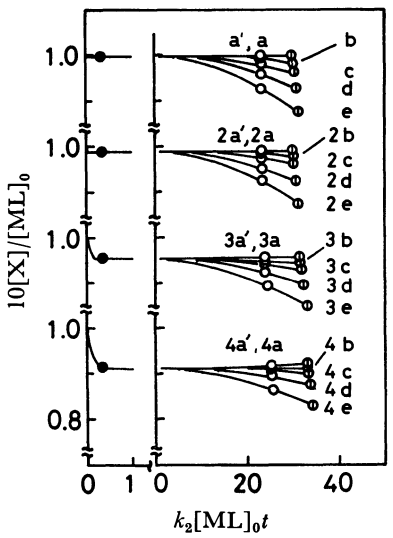

Fig. 6. The time development of the concentration of X for the system II_1 ($k_{-2}=0$, $[ZX]_0=[ML]_0$).
k_{-3}/k_{-2}, (k_3/k_2); a': 0 (1000), a: 0.1 (1000), b: 1 (1000), c: 2 (1000), d: 5 (1000), e: 10 (1000), 2a': 0 (100), 2a: 0.01 (100), 2b: 0.1 (100), 2c: 0.2 (100), 2d: 0.5 (100), 2e: 1.0 (100), 3a': 0 (20), 3a: 0.002 (20), 3b: 0.02 (20), 3c: 0.04 (20), 3d: 0.10 (20), 3e: 0.20 (20), 4a': 0 (10), 4a: 0.001 (10), 4b: 0.01 (10), 4c: 0.02 (10), 4d: 0.05 (10), 4e: 0.10 (10). The initial free ligand concentration ($[X]_0/[ML]_0$) is 0.1.

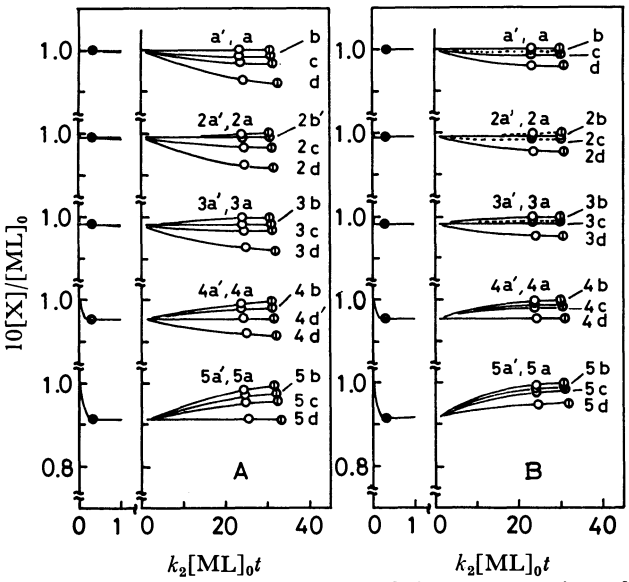

Fig. 7. The time development of the concentration of X for the system II_2 ($k_{-2}=0$, $[ZX]_0\geqq 2[ML]_0$).[12]
k_{-3}/k_2, ($k_3/k_2\cdot[ZX]_0/[ML]_0$); a': 0 (1000), a: 1 (1000), b: 10 (1000), c: 20 (1000), d: 50 (1000), 2a': (100), 2a: 0.1 (100), 2b': 0.5 (100), 2b: 1 (100), 2c: 2 (100), 2d: 5 (100), 3a': 0 (50), 3a: 0.05 (50), 3b: 0.5 (50), 3c: 1.0 (50), 3d: 2.5 (50), 4a': 0 (20), 4a: 0.02 (20), 4b: 0.2 (20), 4c: 0.4 (20), 4d': 0.5 (20), 4d: 1.0 (20), 5a': 0 (10), 5a: 0.01 (10), 5b: 0.1 (10), 5c: 0.2 (10), 5d: 0.5 (10). The initial free ligand concentration ($[X]_0/[ML]_0$) is 0.1. A shows the case in which $[ZX]_0/[ML]_0=2$, and B the case in which $[ZX]_0/[ML]_0\geqq 10$.

be neglected.

System II_2 ($k_{-2}=0$, $[ZY]_0\geqq 2[ML]_0$): Figure 7 shows the time development of the concentration of X for the II_2 system. In Fig. 7.A ($[ZX]_0=2[ML]_0$), it may be seen that, when the k_{-3}/k_2 ratio is equal to 0.5 (2b', 3b, 4d', 5d), the concentration of X is in a steady state.

The concentration of X in the steady state can be calculated as follows. From $d[X]/dt=0$, the following equation is obtained:

$$-k_2[ML][X] + k_3[ZX][L] - k_{-3}[ZL][X] = 0. \quad (15)$$

Combining Eqs. 13 and 15, the following equation is derived:

$$[X] = \frac{k_3[ZX]}{k_2[ML]+k_{-3}[ZL]+k_3[ZX]}c. \quad (16)$$

If the $k_{-3}/k_2=0.5$ and $[ZX]_0/[ML]_0=2$ equations hold, Eq. 16 can be rewritten as[10]

$$[X] = \frac{2k_3/k_2}{(2[ML]+[ZL])/[ZX]+2k_3/k_2}c \approx \frac{2k_3/k_2}{1+2k_3/k_2}c. \quad (17)$$

On the other hand, in Fig. 7.B ($[ZX]_0/[ML]\geqq 10$) it may be seen that, when the k_{-3}/k_2 ratio is equal to unity (a, 2b, 3c, 4d), the concentration of X is in a steady state.

The concentration of X in the steady state can also be calculated as follows. From Eq. 16, the following equation is obtained:

$$[X] = \frac{(k_3/k_2)([ZX]/[ML]_0)}{([ML]+(k_{-3}/k_2)[ZL])/[ML]_0+(k_3/k_2)([ZX]/[ML]_0)}c. \quad (18)$$

Since the $[X]\gg[L]$ inequality holds, the form of $[ML]_0=[ML]+[MX]\approx[ML]+[ZL]$ is obtained; moreover, the $k_{-3}/k_2=1$ equation holds under these conditions; thus, the following relationship is derived:

$$\frac{[ML]+(k_{-3}/k_2)[ZL]}{[ML]_0} \approx 1. \quad (19)$$

From Eqs. 18 and 19, and $[ZX]/[ML]_0\approx[ZX]_0/[ML]_0$, the following equation is derived:

$$[X] \approx \frac{(k_3/k_2)([ZX]_0/[ML]_0}{1+(k_3/k_2)([ZX]_0/[ML]_0)}c. \quad (20)$$

The concentrations of X, as estimated by Eqs. 17 and 20, agree very well with those of the steady state of X in Figs. 7.A and 7.B respectively.

Reaction System III ($k_{-3}=0$). Figure 8 shows the time development of the concentration of X for the III_1 system ($k_{-3}=0$, $[ZX]_0=[ML]_0$). As is shown in Fig. 8, the shape of the diagram for the time development of the concentration of X is not appreciably affected by the reverse reaction of R2. However, the reaction rate is greatly affected by it. These tendencies also appear in the III_2 system ($k_{-3}=0$, $[ZX]_0\geqq 2[ML]_0$), as is shown in Fig. 9.

From Figs. 8 and 9, it can be said that, in the III_1 system, when the k_3/k_{-2} ratio is greater than about 10^3, the III_1 system is approximately equal to the I_1 system, and that, in the III_2 system, when the $(k_3/k_{-2})([ZX]_0/[ML]_0)$ value is greater than about 10^2, the III_2 system is close to the I_2 system.

On the other hand, from Figs. 6 and 7, it can be said that, in the II_1 system, when the k_3/k_{-3} ratio is greater than about 10^4, the II_1 system is close to the I_1 system,

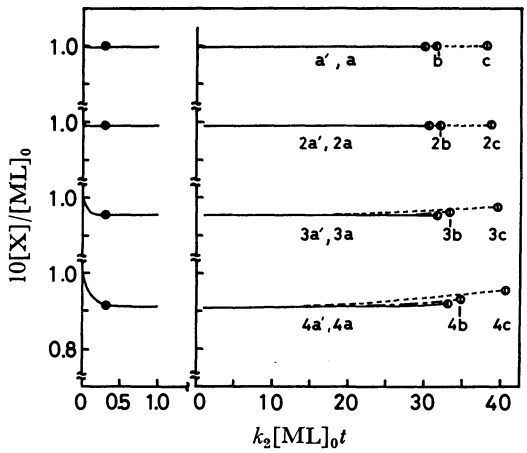

Fig. 8. The time development of the concentration of X for the system III_1 ($k_{-3}=0$, $[ZX]_0=[ML]_0$). k_{-2}/k_2, (k_3/k_2); a': 0 (1000), a: 1 (1000), b: 10: (1000), c: 50 (1000), 2a': 0 (100), 2a: 0.1 (100), 2b: 1 (100), 2c: 5 (100), 3a': 0 (20), 3a: 0.02 (20), 3b: 0.2 (20), 3c: 1.0 (20), 4a': (10), 4a: 0.01 (10), 4b: 0.1 (10), 4c: 0.5 (10). The initial free ligand concentration ($[X]_0/[ML]_0$) is 0.1.

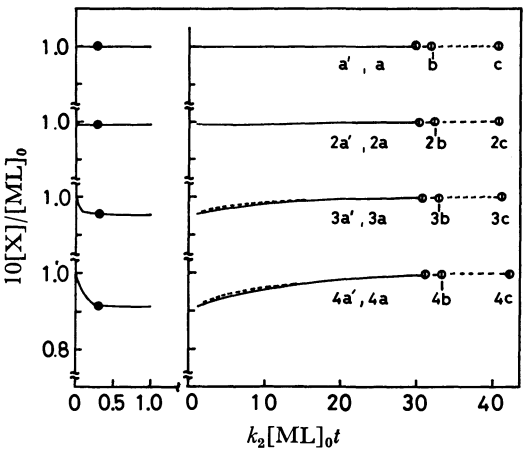

Fig. 9. The time development of the concentration of X for the system III_2 ($k_{-3}=0$, $[ZX]_0\geqq 2[ML]_0$).[12] k_{-2}/k_2, (k_3/k_2 $[ZX]_0/[ML]_0$); a': 0 (1000), a: 10(1000), b: 100 (1000), c: 500 (1000), 2a': 0 (100), 2a: 1 (100), 2b: 10 (100), 2c: 50 (100), 3a': 0 (20), 3a: 0.2 (20), 3b: 2 (20), 3c: 10 (20), 4a': 0 (10), 4a: 0.1 (10), 4b: 1 (10), 4c: 5 (10). The initial concentrations of X and ZX are as follows: $[X]_0/[ML]_0=0.1$ and $[ZX]_0/[ML]_0\geqq 10$.

and that, in the II_2 system, when the $(k_3/k_{-3})([ZX]_0/[ML]_0)$ value is greater than about 10^3, the II_2 system is close to the I_2 system.

In the II and III systems, one of the reverse reactions of R2 and R3 was considered to be negligible. From the above considerations, criteria for the omission of the reverse reaction may be presented as follows: $k_3/k_{-2}\approx 10^3$ for the II_1 system, $(k_3/k_{-2})([ZX]_0/[ML]_0)\approx 10^2$ for the II_2 system, $k_3/k_{-3}\approx 10^4$ for the III_1 system, and $(k_3/k_{-3})([ZX]_0/[ML]_0)\approx 10^3$ for the III_2 system; *i.e.*, for example, when $[ML]_0=[ZX]_0$, if the k_3/k_{-2} ratio is greater than 10^3, the system may be taken as the II_1 system, and when $[ZX]_0\geqq 2[ML]_0$, if the value $(k_3/k_{-2})([ZX]_0/[ML]_0)$ is greater than 10^2, the system may be taken as the II_2 system.

Reaction Rate. When the reaction rate of R1 is defined as the rate of the decrease in ML, the reaction rate of R1 can be written as

$$-\frac{d[ML]}{dt}=k_2[X]_s[ML]-k_{-2}[L][ZX]. \quad (21)$$

Therefore, if k_{-2} is negligibly small and if the concentration of X is constant throughout the reaction, the reaction can be regarded as a pseudo first-order reaction:

$$-\frac{d[ML]}{dt}=k_2[X]_s[ML]=k_o[ML], \quad (22)$$

where $[X]_s$ represents the concentration of X in the steady state.

It should be emphasized that the concentration of X in the steady state is not always equal to that of the ligand present initially. As is shown in Eqs. 14, 17, and 20, the ratio $[X]_s/c$ is little changed by the variations in the initial concentration of the free ligand. Thus, the following equation can be written:

$$\frac{[X]_s}{c}=a \quad (a\leqq 1), \quad (23)$$

where a is constant. Therefore, Eq. 22 can be rewritten as

$$-\frac{d[ML]}{dt}=k_2[X]_s[ML]=ack_2[ML]=k_o[ML]. \quad (24)$$

Consequently,

$$k_o=ack_2. \quad (25)$$

Therefore, if the pseudo first-order rate constant, k_o, is plotted against the free-ligand concentration present initially, the slope of the straight line represents, ak_2; only when $[X]_s=c$, is the value of the slope equal to k_2.

In the previous works,[1-3] it was a little laborious to derive Eq. 24. However, the conditions under which Eq. 24 is derived can be obtained from the diagrams presented above. Thus, the diagrams are useful for studies using a coordination chain reaction. One important fact is that a desired coordination chain reaction can be designed from the individual reactions (R2 and R3) on the basis of the diagrams presented above.

Simulation of the Practical Coordination Chain Reaction. As an example, the ligand-substitution reaction between the ethylenediaminetetraacetatocuprate(II) ion (Cu-(II)-edta) and the triethylenetetraminelead(II) ion (Pb(II)-trien) was undertaken. The reaction was considered to proceed by means of a coordination chain reaction mechanism:

$$\text{Cu(II)-edta} + \text{trlien} \underset{k_{-2}}{\overset{k_2}{\rightleftharpoons}} \text{Cu(II)-trien} + \text{edta}, \quad (R4)$$

$$\text{Pb(II)-trien} + \text{edta} \xrightarrow{k_3} \text{Pb(II)-edta} + \text{trien}. \quad (R5)$$

The known information about these reactions at pH 9.0 is as follows. The conditional equilibrium constant (K) of R4 is 4.2×10, while the conditional rate constant, k_2, is $1.17\times 10^4\ M^{-1}\ s^{-1}$ (this was measured at pH 9.0, 25.0 °C and $I=0.2$); hence, if follows that $k_{-2}=k_2/K=$

2.8×10^{2} M^{-1} s^{-1}. The conditional equilibrium constant of R5 is so large ($K=4.8\times10^{7}$) that the reverse reaction of R5 can be neglected in the kinetic study. Furthermore, the reaction of R5 is very fast; this fact was taken into account by setting k_3 large (*e.g.*, $k_3=1\times10^{7}$ M^{-1} s^{-1}).

In accordance with the above classification, this system can be taken as the III system. Moreover, this system can also be treated as the I system, since the k_3/k_{-2} ratio is larger than 10^3.

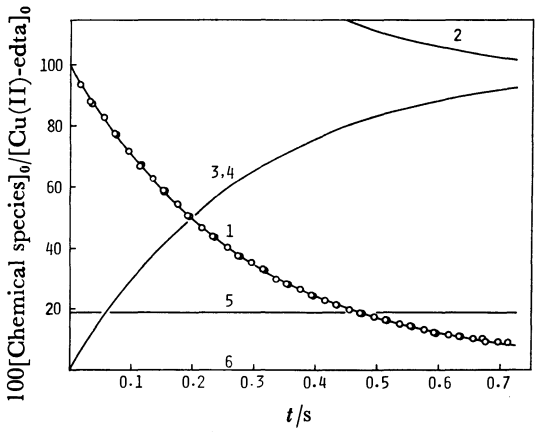

Fig. 10. Computer simulation of the Cu(II)-edta–Pb(II)trien system.[13]
Conditions: $[Cu(II)\text{-edta}]_0=1.86\times10^{-3}$ M, $[Pb(II)\text{-trien}]_0=3.62\times10^{-3}$ M, $[Cu(II)\text{-trien}]_0=[Pb(II)\text{-edta}]_0=0$ M, $[trien]_0=3.5\times10^{-4}$ M, $[edta]_0=0$ M; $I=0.2$ M, pH=9.0, 25.0 °C; $k_2=1.01\times10^{4}$ M^{-1} s^{-1}, $k_{-2}=k_2/K=2.8\times10^{2}$ M^{-1} s^{-1}, $k_3=1.0\times10^{7}$ M^{-1} s^{-1}, $k_{-3}=0$ M^{-1} s^{-1}.
1: Cu(II)-edta, 2: Pb(II)-trien, 3: Cu(II)-trien, 4: Pb(II)-edta, 5: trien, 6: edta. The circles indicate the experimental values.[14]

Figure 10 shows the results of the computer simulation of the Cu(II)-edta–Pb(II)-trien system (under the above conditions).[15] The experimental values (points of circle) agree with the calculated values. The calculated concentration of free trien is constant throughout the reaction and is nearly equal to the concentration of added free trien; these facts can also be predicted from Fig. 4, from which it follows that

$$\frac{k_3}{k_2}\frac{[ZX]_0}{[ML]_0}=\frac{k_3}{k_2}\frac{[Pb(II)\text{-trien}]_0}{[Cu(II)\text{-edta}]_0}=1.9\times10^{3}.$$

Using the diagrams stated above, the reaction of the practical system may be predicted.

References

1) T. Katsuyama and T. Kumai, *Bull. Chem. Sco. Jpn.*, **48**, 3581 (1975).
2) T. Katsuyama and T. Kumai, *Bull. Chem. Soc. Jpn.*, **51**, 1072 (1078).
3) T. Katsuyama and T. Kumai, *Bull. Chem. Soc. Jpn.*, **55**, 1050 (1982).
4) D. W. Margerum and R. K. Steinhaus, *Anal. Chem.*, **37**, 222 (1965).
5) R. H. Stehl, D. W. Margerum, and J. J. Latterll, *Anal. Chem.*, **39**, 1346 (1967).
6) D. W. Margerum and R. H. Stehl, *Anal. Chem.*, **39**, 1351 (1967).
7) J. Yamauchi, S. Moriguchi, and S. Hitotsumatsu "Denshi Keisanki No Tame No Suchi Keisan-ho," Baifukan, Tokyo (1975), Vol. 1, p. 123.
8) The rate determining step in the reaction model represented by Reactions R2 and R3 is defined as R2.
9) If the values of $[ZX]_0/[ML]_0$, $[\text{free ligand}]_0/[ML]_0$, and k_n/k_2 ($n=-2, \pm3$) in one system are equal to the respective values in the other system, these systems give the same relative concentration-$k_2[ML]_0t$ curve.
10) $(2[ML]+[ZL])/[ZX]=N/D\approx1$ can be derived as follows. N is written as $N=2[ML]+[ZL]=2([ML]+[ZL])-[ZL]$. As the $[X]\gg[L]$ inequality holds, [ZL] is approximately equal to [MX]. Consequently, $N\approx2[ML]_0-[ZL]$. On the other hand, $D=[ZX]=[ZX]_0-[ZL]=2[ML]_0-[ZL]$. Thus, $N/D\approx1$.
11) In the diagram, the following relationships hold: $[X]+[L]=c$ and $[L]=c-[X]=[MX]-[ZL]=[ZX]-[ML]$. In general, the following relationships also hold: $[X]+[L]=c$ and $[L]=c-[X]=|[MX]-[ZL]|=|([ZX]-(n-1)[ML]_0)-[ML]|$, where n ($n\geqq1$) is equal to the $[ZX]_0/[ML]_0$ ratio; these relationships were confirmed to hold from the simulations.
12) If the $[ZX]_0/[ML]_0$ ratio is greater than about r(r: 5 for Figs. 4 and 5, and 10 for Figs. 7 and 9),the reactions which have the same value of the product of k_3/k_2 and $[ZX]_0/[ML]_0$ give almost the same time development of the concentration of X.
13) In the simulation, the time developments of all the species were little affected by the variation in k_3.
14) In the kinetic measurements, a stopped-flow technique was employed with a Hitachi Model RSP-2 Rapid-scan Spectrophotometer. The reactions were followed at 575 nm.
15) In this simulation, the value of $k_2=1.01\times10^{4}$ M^{-1} s^{-1} was used. This value agrees closely with that obtained from other experiments.

 © 1982 The Chemical Society of Japan Bull. Chem. Soc. Jpn., 55, 2547—2550 (1982)

A Kinetic Study of the Interaction of Sodium Dodecyl Sulfate with Bovine Serum Albumin by Means of a Pressure-jump Method

Kunio TAKEDA

Department of Applied Chemistry, Faculty of Science, Okayama University of Science, 1-1 Ridai-cho, Okayama 700

(Received November 18, 1981)

A single relaxation was found in the system of sodium dodecyl sulfate and bovine serum albumin using a pressure-jump method with conductivity detection. The relaxation was observed in the concentration range of the surfactant below the critical micelle concentration. The relaxation time becomes fast with the stepwise formation of a complex between them and finally attains values compatible with those in the system of the pure surfactant micelle. This suggests a correlation of the relaxation phenomena with the partial breakdown and reformation of the complex. The similarity of the complex to the surfactant micelle was discussed on the basis of the kinetic aspects of the interaction of the surfactant with the protein.

The interactions between proteins and surfactants have been extensively investigated.[1] Quite recently, the present author and others have studied the interaction between sodium dodecyl sulfate (SDS) and bovine serum albumin (BSA).[2] They have found that an electric conductivity method is very useful in detecting the formation of complexes between them. This is because the measurement is highly sensitive to changes in the concentrations of surfactant ions. On the other hand, a pressure-jump method with conductivity detection has been used in many studies of micellization kinetics.[3] Therefore, it would be interesting to apply the pressure-jump method to the study of the surfactant-protein interactions. It is believed that further studies from a new aspect would be helpful in understanding the interactions.

It is worth noting that a similarity of the complex to the surfactant micelle is also found in the kinetic phenomena of the interaction. This paper will report the presence of a single relaxation process in the SDS–BSA system, which is strongly correlated with the stepwise growth of the complexes formed between them.

Experimental

The sources of SDS and BSA have been described previously.[2] The concentration of the protein was determined spectrophotometrically using $E^{1\%}_{1cm}=6.8$ at 280 nm.[4]

Kinetic measurements were made using a handmade pressure-jump apparatus similar to that described elsewhere.[5,6] However, it has been a little improved as follows. It is driven by water-pressure and a brass diaphragm bursts at a pressure of approximately 100 atm (1 atm=101.3 kPa). The triggering of the recording is done using a piezoelectricity of $PbTiO_3$ (see Acknowledgments). Circular dichroism measurements were carried out with a JASCO J-500A spectropolarimeter equipped with a DP-501 data processor.[2] A 1.0 mm light-pass-length cell was used in the measurements. The static conductivity was measured with a Universal Bridge 4265B of Yokogawa-Hewlett-Packard. Details of the conductivity measurements have been described elsewhere.[2]

All the measurements were made at 15 °C, because the accuracy of the relaxation time obtained by the pressure-jump method was greater at lower temperatures (see Fig .3 in Ref. 6). The only available solvent in high-precision conductometry has been limited to pure water in the pressure-jump measurements,[5] and so all the measurements were carried out in a non-buffered system, using water prepared by passing redistilled water through a mixed-bed ion-exchange column. The specific conductivity of the water used was above 1×10^{-6} Ω^{-1} cm^{-1}. The BSA concentration was held constant, 1.0×10^{-5} M (as the concentration unit, 1 M=1 mol/dm^3 is used).

Results

Prior to the application of the pressure-jump method to the study of the SDS–BSA interaction, the SDS-induced conformational change of the protein was examined by the circular dichroism measurements and the conductance changes with the complex formation were also measured. Figure 1 shows the SDS concentration dependence of the difference of residue ellipticity at 222 nm, $[\theta]_{222}$, which is one of the characteristic wavelengths for the helical structure of polypeptides. The addition of SDS caused a decrease of the helix-like structure, as may be seen in the insert of Fig. 1. The helix content decreased with an increase of the SDS concentration.

A conductivity method has so far been used in order to detect the micelle formation of ionic surfactants.[7] When the method was applied to the present SDS–BSA

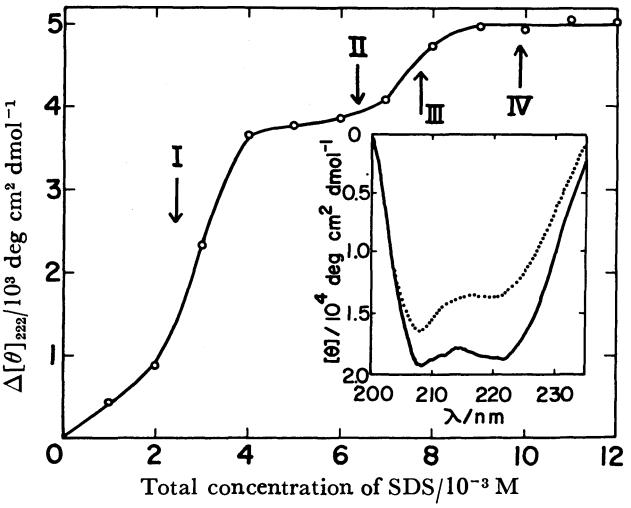

Fig. 1. The dependence of the residue ellipticity, $[\theta]_{222}$ on the SDS concentration. The typical circular dichroic spectra of BSA solutions in the absence (solid curve) and in the presence (dotted curve) of 12 mM SDS are shown in the insert. The arrows indicate the SDS concentrations where the inflection points appear in a plot such as Fig. 2.

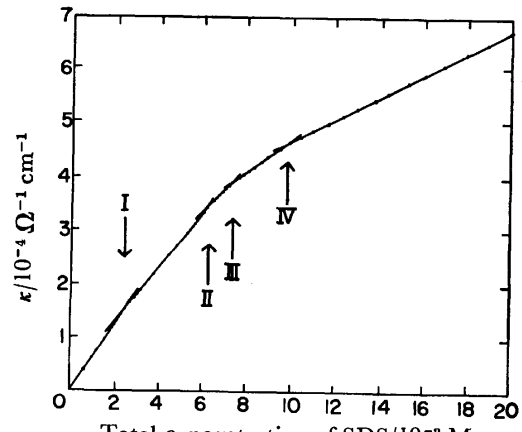

Fig. 2. The specific conductance, κ, of solutions of various SDS concentrations in the presence of 1.0×10^{-5} M BSA.

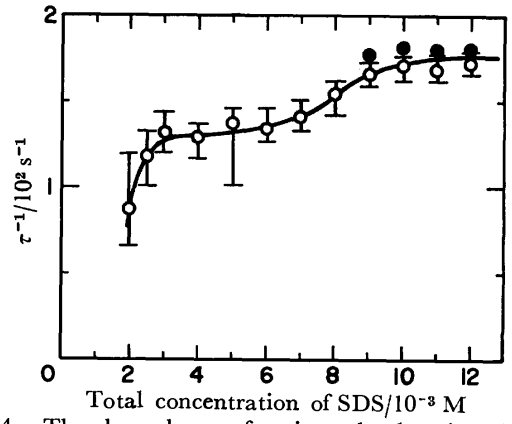

Fig. 4. The dependence of reciprocal relaxation time, τ^{-1}, on the SDS concentration (open circle). The vertical lines were drawn through the experimental points. Solid circles show the values of τ^{-1} in the pure SDS system.

system, four inflection points were observed in the plot of the specific conductance versus the concentration of SDS added to an aqueous BSA solution, as is shown in Fig. 2. These inflections can be demonstrated more clearly through an enlarged plot (not shown), as has been discussed before.[2] These inflection points appeared around 2.5, 6.5, 7.5, and 9.9 mM SDS. In comparing the SDS concentration dependence of the conformational change with the results of the conductivity measurements mentioned above, the first and the third inflections (corresponding to those at 2.5 and 7.5 mM SDS) appear in the courses of the first predominant conformational change and the subsequent one respectively, as is indicated by arrows in Fig. 1. The second and the fourth inflections (at 6.5 and 9.9 mM SDS) correspond to the beginning and the end of the second conformational change respectively (also shown by the arrows).

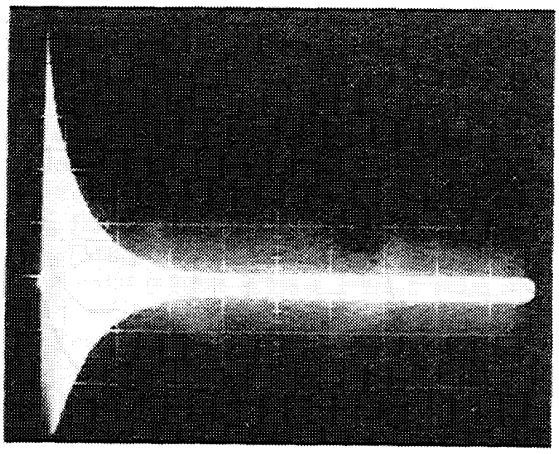

Fig. 3. The representative relaxation curve of 6.0 mM SDS solution containing 1.0×10^{-5} M BSA at 15 °C. The sweep rate is 10 m s/div.

The conductivity pressure-jump method was applied to the study of the SDS–BSA interaction. A representative relaxation curve is shown in Fig. 3. The relaxation phenomena in the presence of the protein were observed even in low SDS concentrations below the critical micelle concentration (CMC), although they had been observed only above the CMC in the pure SDS system.[3] The SDS concentration dependence of the relaxation time, τ, is presented in Fig. 4. The value of τ^{-1} gradually increased at first, attained a plateau between 3 and 7 mM SDS, and increased again up to about 9 mM SDS. The final values of τ^{-1} are compatible with those obtained in a solution containing only SDS micelles, indicating that the phenomena are not completely independent of those of micellization.

Discussion

The BSA has been proposed to have a few fairly independent domains.[8-11] The results obtained by the limited proteolysis of the protein strongly indicate that the protein consists of, at least, two independent domains.[8-10] It has been suggested by Jones *et al.*, in the light of the domain-structure theory, that the binding of surfactants initially occurs mainly to the C-terminal section of the protein molecule, bringing about its unfolding, and that the more stable N-terminal part then begins to unfold exposing new binding sites with an increase of the surfactant concentration.[11] At the same time, it is generally accepted that the surfactant molecules cooperatively bind to the protein by hydrophobic interaction following the first binding of approximately 8—10 molecules by electrostatic interaction.[1,12] In the interaction of the BSA with surfactants, the stepwise and all-or-none nature of the complex formation has been emphasized,[13] that is, there exist only complexes which consist of, at most, a few particular binding ratios (surfactants/protein), depending on the surfactant concentration ranges.[14-18] The binding isotherm has so far been explained in terms of the following expression;[12,18-20]

$$P \rightleftharpoons PS_{8-10} \rightleftharpoons PS_n \rightleftharpoons PS_{2n} \rightleftharpoons PS_{>2n} \quad (n = 40\text{—}50),$$

where P and S denote the protein and a surfactant, respectively, and n is the binding number of the surfactants (mol/mol). As has been discussed before,[2] and also as has been mentioned above, the profile of the conduc-

tance change is also reflected by the stepwise formation of complexes and the concomitant conformational changes of the protein with clearly separate domains. The binding of SDS to BSA and the accompanying conformational changes of the protein have previously been examined under experimental conditions[2] different from those of this work. In taking account of the SDS concentration dependence of the ellipticity at 222 nm[21] and the SDS concentration where the first inflection of the conductance change appears, it seems that there exist the complexes with bound surfactants above 40—50 molecules in the SDS concentration range where the relaxation has been observed. Thus, the discussion given below will be limited to the behavior of the complexes which have been considered to be formed cooperatively.

Three important facts should be taken into consideration in discussing the relaxation mechanism of the present system. The first is the fact that the contribution of the protein to the conductance is negligibly small compared with that of the surfactant, as has been stated previously.[2] This is also to be expected from the fact that the conductivity curve actually starts from the origin in Fig. 2 in spite of the existence of the protein. Naturally, the behavior of the surfactant molecules seems to be primarily related to the relaxation phenomena observed here. This may indeed be reasonable, when a similarity of the values of τ in the present system to those in the pure SDS system is taken into account. The second is that only complexes with particular binding ratios can exist at a certain SDS concentration, as has been stated above. Since the complexes are formed in the low SDS concentration range where the concentration of unbound surfactants is lower than the CMC,[1] the ordinary micelle does not exist in the total concentration range of SDS below about 10 mM (=about 8 mM (CMC) of unbound SDS+about 2 mM of SDS bound to 1.0×10^{-5} M BSA[2]). Therefore, the participating species of the surfactant may be limited to both free monomers and those bound to the protein with particular binding ratios. The nature of the latter participating species may critically change with the shift of the SDS concentration range.[11-16] Thirdly, it has been reported that the surfactant molecules bound to proteins are not easily removed from the proteins, so their removal needs specially designed techniques.[22] The difficulty of the removal of such surfactants is reminiscent of the long period necessary to attain the dialysis equilibrium which has frequently been utilized in studies of the binding of surfactants to proteins.[1,23-25] Therefore, it is improbable to assume a reversible process of a large-scale formation and complete dissociation of the complex such as $nS+P\rightleftharpoons PS_n$. This situation is also reminiscent of a previous experimental finding that only the relaxation process with relaxation times in the milli-second range exists in an emulsion system consisting of SDS and pentadecane.[26] In such an emulsion system, it would be impossible to assume a reversible process of a large-scale formation and complete dissociation of the emulsified particle. These facts might appear to contradict the previously proposed assumptions of micellization kinetics that the relaxation process with relaxation times in the milli-second range is related to the formation and complete dissociation of surfactant micelles.[3,27,28] Because of the reasons mentioned above, nevertheless, the formation and complete dissociation of the complex cannot be assumed, at least, in the present complexes system. Therefore, in the surfactant–protein system, a probable reversible process is the partial breakdown and reformation of the complex as follows;

$$mS + P_iS_{n-m} \underset{k_{21}}{\overset{k_{12}}{\rightleftharpoons}} P_iS_n, \tag{1}$$

where $m \ll n$, P_i indicates the protein with the i-th conformation in the stepwise conformational change, and k_{12} and k_{21} are the corresponding apparent rate constants.

The rate of Reaction 1 is expressed as follows;

$$\frac{d[P_iS_n]}{dt} = k_{12}[S]^m[P_iS_{n-m}] - k_{21}[P_iS_n], \tag{2}$$

where [ ] designates instantaneous concentrations during the perturbation of the equilibrium. The following relationship can be defined between the instantaneous concentrations and the equilibrium ones designated by the subscript, e;

$$x=[S]-[S]_e,\ y=[P_iS_{n-m}]-[P_iS_{n-m}]_e, \text{ and}$$
$$z = [P_iS_n] - [P_iS_n]_e. \tag{3}$$

By substituting Eq. 3 into Eq. 2, and by then expanding it in a power series, we obtain;

$$\frac{d[P_iS_n]}{dt} = k_{12}([S]_e^m[P_iS_{n-m}]_e + m[S]_e^{m-1}[P_iS_{n-m}]_e x + [S]_e^m y) - k_{21}([P_iS_n]_e + z). \tag{4}$$

Here, by introducing both the definition of the equilibrium condition and these relations; $x=-mz$ and $y=-z$ obtained from the stoichiometry of Reaction 1, we obtain;

$$\frac{dz}{dt} = -\{k_{12}(m^2[S]_e^{m-1}[P_iS_{n-m}]_e + [S]_e^m) + k_{21}\}z. \tag{5}$$

Then, we obtain;

$$\tau^{-1} = k_{12}(m^2[S]_e^{m-1}[P_iS_{n-m}]_e + [S]_e^m) + k_{21}. \tag{6}$$

Since

$$K_{12} = \frac{k_{12}}{k_{21}} = \frac{[P_iS_n]_e}{[S]_e^m[P_iS_{n-m}]_e},$$

we obtain;

$$k_{12}[S]_e^m = k_{21}\frac{[P_iS_n]_e}{[P_iS_{n-m}]_e}. \tag{7}$$

By assuming

$$[P_iS_{n-m}]_e = [P_iS_n]_e, \tag{8}$$

and by neglecting the magnitude of the first term compared with the second one in parentheses of Eq. 6, we obtain;

$$k_{21} = \frac{\tau^{-1}}{2}. \tag{9}$$

Therefore, we can substantially evaluate 50—80 s^{-1} as the magnitudes of k_{21} depending on the SDS concentration. This treatment apparently indicates that the rate constant of the dissociation becomes faster with

the complex growth, as has been anticipated from Fig. 4. However, the apparent dependence of k_{21} on the SDS concentration range should be considered to be mainly due to changes in the $[P_iS_n]_e/[P_iS_{n-m}]_e$ ratio. Strictly considered, it is considered that the ratio becomes greater than 1 in higher SDS concentrations, because the average amounts of the surfactants bound to the protein increase with the total SDS concentration, as judged from the binding isotherms.[1,2] Such a change in the ratio with the complex growth leads to smaller values of k_{21} than those straightforwardly obtained by Eq. 9. Therefore, the present author considers that the magnitudes of k_{21} hardly change at all with the complex growth in the SDS concentration range discussed here.

The magnitudes of k_{21} can be connected with those of the elementary steps of Reaction 1 as follows. It should be assumed that Reaction 1 consists of these succesive bimolecular steps;

$$\begin{aligned} &P_iS_{n-m} + S \underset{k_-}{\overset{k_+}{\rightleftharpoons}} P_iS_{n-m+1} \\ &\qquad\vdots \\ &P_iS_{n-2} + S \rightleftharpoons P_iS_{n-1} \\ &P_iS_{n-1} + S \rightleftharpoons P_iS_n, \end{aligned} \tag{10}$$

where k_+ and k_- are forward and backward rate constants, respectively. If each bimolecular step has the same activation energy, we obtain;

$$\prod_{j=1}^{m} K_j = \frac{k_+^m}{k_-^m} = \frac{k_{12}}{k_{21}} = K_{12} (1 \leq j \leq m), \tag{11}$$

where K_j is the equilibrium constant of each elementary step. Then, we obtain;

$$k_+ = k_{12}^{1/m} \text{ and } k_- = k_{21}^{1/m}. \tag{12}$$

The m value has been assumed to be very small. Therefore, we can substantially evaluate the rate constant, k_-, of the elementary dissociation process to be in orders of 1 to 10.[29]

Kinetic studies have so far been neglected with regard to the surfactant-protein interactions. Needless to say, further studies are required in order to discuss the relaxation mechanism of the system in detail.

The micelle-like properties of the surfactant-protein complexes have previously been demonstrated.[30] It is worth noting that a similarity of the complexes to the surfactant micelle also appears in the kinetic aspects of the interactions.

The author wishes to express his thanks to Dr. T. Nagata of Wireless Research Laboratory of Matsushita Denki (Electric Co.) for his kind donation of the $PbTiO_3$ element. Thanks are also due to Mr. H. Takahashi for his cooperation in the construction of the pressure-jump apparatus. This work was partly supported by a Grant-in-Aid for Scientific Research No. 56540270 from the Ministry of Education, Science and Culture of Japan.

References

1) J. Steinhardt and J. A. Reynolds, "Multiple Equilibria in Protein," Academic Press, New York (1969), pp. 239—302.

2) K. Takeda, M. Miura, and T. Takagi, *J. Colloid Interface Sci.*, **82**, 38 (1981).

3) N. Muller, "Solution Chemistry of Surfactants," ed by K. L. Mittal, Plenum Press, New York (1979), Vol. 1, pp. 267—295.

4) "Handbook of Biochemistry (Selected Data for Molecular Biology)," 2nd ed, ed by H. A. Sober and R. A. Harte, CRC Press, Cleveland, Ohio (1973), p. C-71.

5) K. Takeda, and T. Yasunaga, *J. Colloid Interface Sci.*, **40**, 127 (1972).

6) K. Takeda, T. Yasunaga, and H. Uehara, "Micellization, Solubilization, and Microemulsions," ed by K. L. Mittal, Plenum Press, New York (1977), Vol. 1, pp. 305—327.

7) K. Shinoda, T. Nakagawa, B. Tamamushi, and T. Isemura, "Colloidal Surfactants," Academic Press, New York (1969).

8) T. P. King, *Arch. Biochem. Biophys.*, **156**, 509 (1973).

9) M. C. Hilak, B. J. M. Harmsen, W. G. M. Braam, J. J. M. Joordens, and G. A. J. Van Os, *Int. J. Pept. Protein Res.*, **6**, 95 (1974).

10) R. C. Feldhoff and T. Peters, Jr., *Biochemistry*, **14**, 4508 (1975).

11) M. N. Jones, H. A. Skinner, and E. Tipping, *Biochem. J.*, **147**, 229 (1975).

12) J. A. Reynolds, S. Herbert, H. Polet, and J. Steinhardt, *Biochemistry*, **6**, 937 (1967).

13) M. J. Pallansch and D. R. Briggs, *J. Am. Chem. Soc.*, **76**, 1396 (1954).

14) K. Aoki and J. F. Foster, *J. Am. Chem. Soc.*, **79**, 3385 (1957).

15) K. Aoki, *J. Am. Chem. Soc.*, **80**, 4904 (1958).

16) R. V. Decker and J. F. Foster, *Biochemistry*, **5**, 1242 (1966).

17) R. V. Decker and J. F. Foster, *J. Biol. Chem.*, **242**, 1526 (1967).

18) J. Oakes, *J. Chem. Soc., Faraday Trans. 1*, **70**, 2200 (1974).

19) A. Ray, J. A. Reynolds, H. Polet, and J. Steinhardt, *Biochemistry*, **5**, 2606 (1966).

20) J. A. Reynolds, J. P. Gallacher, and J. Steinhardt, *Biochemistry*, **9**, 1232 (1970).

21) The residue ellipticity at 222 nm sharply changes at 40—50 mol/mol binding ratios, as can be seen by comparing Fig. 7 with Fig. 5 in Ref. 2. In this work, the relaxation begins to be observed at SDS concentrations where the ellipticity changes in a manner similar to the above.

22) D. A. Hager and R. R. Burgess, *Anal. Biochem.*, **109**, 76 (1980).

23) K. Birdi, *Anal. Biochem.*, **74**, 620 (1976).

24) J. C. Dohnal and J. E. Garvin, *Biochim. Biophys. Acta*, **575**, 393 (1979).

25) B. R. Vijayendran, *J. Colloid Interface Sci.*, **60**, 418 (1977).

26) K. Takeda, *J. Sci. Hiroshima Univ., Ser. A*, **40**, 69 (1976).

27) E. A. G. Aniansson and S. N. Wall, *J. Phys., Chem.* **78**, 1024 (1974).

28) E. A. G. Aniansson and S. N. Wall, *J. Phys. Chem.*, **79**, 857 (1975).

29) Through Eq. 12, we obtain k_-=50—80 s^{-1} (if m=1), 7.1—8.9 s^{-1} (m=2), 3.7—4.3 s^{-1} (m=3), and 2.2—2.4 s^{-1} (m=5). Equations 11 and 12 will not hold when the m value is large, because it may become impossible for each elementary step to have the same activation energy in such a case.[6]

30) J. Steinhardt, N. Stocker, D. Carrol, and K. Birdi, *Biochemistry*, **13**, 4461 (1974).

The Molecular Structure of Trimethylphosphine-Boron Triiodide as Studied by Gas-phase Electron Diffraction

Kinya IIJIMA, Eiichi KOSHIMIZU, and Shuzo SHIBATA*

Department of Chemistry, Faculty of Science, Shizuoka University, Oya, Shizuoka 422

(Received December 9, 1981)

The molecular structure of trimethylphosphine-boron triiodide $(CH_3)_3P \cdot BI_3$ has been determined by means of gas-electron diffraction. The molecular parameters and their uncertainties were r_g(B–I)$=2.233\pm0.003$ Å, r_g(P–B)$=1.947\pm0.011$ Å, r_g(C–P)$=1.809\pm0.003$ Å, r_g(C–H)$=1.094\pm0.008$ Å, $\angle$IBI$=111.6\pm0.3°$, and $\angle$CPC$=106.0\pm0.5°$. The gaseous molecule was rigid with respect to the rotational vibration around the P–B bond.

Trimethylphosphine readily forms complexes with boron trihalides. The molecular structures of the boron trichloride, boron tribromide, and boron triiodide complexes have been determined in the solid phase,[1] and the first two complexes have also been determined in the gas phase.[2,3] In the solid phase, the P–B distances of the complexes decrease with the increase in the atomic numbers of halogen atoms in the boron trihalides, though in the gas phase, the P–B distances in the chloro and bromo complexes are nearly equal. On the other hand, the rotational barrier about the P–B bond of $(CH_3)_3P \cdot BBr_3$[3] is larger than that of $(CH_3)_3P \cdot BCl_3$[2] in the gas phase. Thus, it is of interest to study the molecular structure of trimethylphosphine-boron triiodide $(CH_3)_3P \cdot BI_3$ in the gas phase in order to determine the P–B bond distance and the rotational barrier about this bond, and to compare the molecular structures of trimethylphosphine complexes with one another.

Experimental

Trimethylphosphine-silver iodide was prepared by the procedure described elsewhere.[4] The complex was decomposed at 200 °C under a vacuum, and the trimethylphosphine was collected in a trap cooled by liquid nitrogen after the benzene solution of boron triiodide has previously been condensed. The mixture in the trap was warmed up to room temperature and then allowed to react. Activated charcoal was added to the acetone solution of the crude complex, and sublimations were repeated to remove any impurities. The purity of the complex was confirmed by a study of the IR spectra.[5]

In the electron-diffraction experiment, the sample was vaporized at 200 °C through a high-temperature nozzle. The photographs were taken using an r^3-sector on Kodak Electron-Image plates at camera distances of 293.5 and 143.6 mm. The accelerating voltage was 40 kV. The exposure times were 12 s for the long camera distance and 21 s for the short camera distance with an electron-beam current of 0.7 μA. The pressure in the diffraction chamber was below 1×10^{-5} Torr (1 Torr$=$133.322 Pa) during the experiment. The electron wavelength was determined from the diffraction patterns of thallium chloride.[6] The optical densities of four long camera-distance plates and four short-camera-distance plates were measured at 0.4 mm intervals by means of a digital microphotometer. The electron-diffraction unit and the digital microphotometer used in the present study have been described previously.[7]

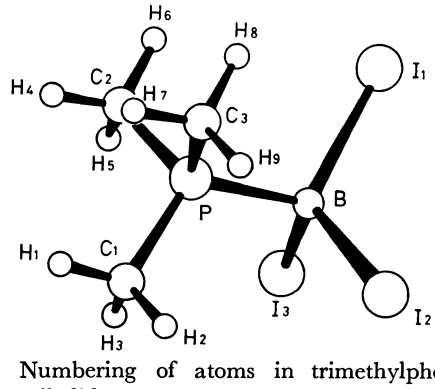

Fig. 1. Numbering of atoms in trimethylphosphine-boron triiodide.

Analysis and Results

The scattering intensities were obtained in the ranges of $s=2.5$—16.2 Å^{-1} and 7.5—34.2 Å^{-1} from the long- and short-camera-distance plates respectively. The intensities were leveled by means of theoretical backgrounds, and then the intensities for each camera distance were averaged. The elastic and inelastic scattering factors were taken from the tables prepared by Schäfer *et al.*[8] and by Cromer and Mann[9] respectively. The inelastic scattering factor for the hydrogen atom was taken from the table by Tavard *et al.*[10]

The background curves were drawn smoothly,[11] and the molecular intensities thus obtained are shown in Fig. 2.[12] The experimental radial distribution function,

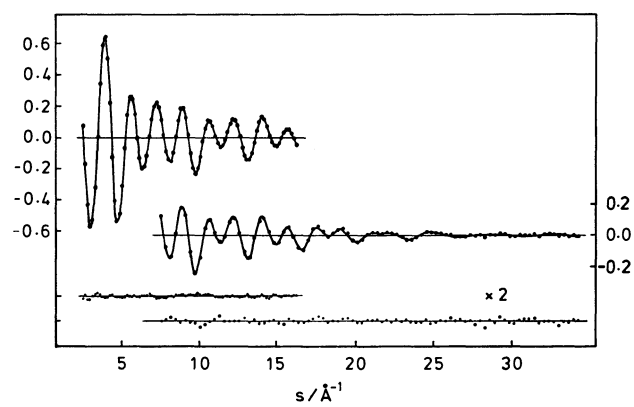

Fig. 2. Molecular intensities for trimethylphosphine-boron triiodide. The upper two curves are long and short camera-distance data. Dots represent observed ones, solid curves calculated ones, and two times the residuals are shown in below.

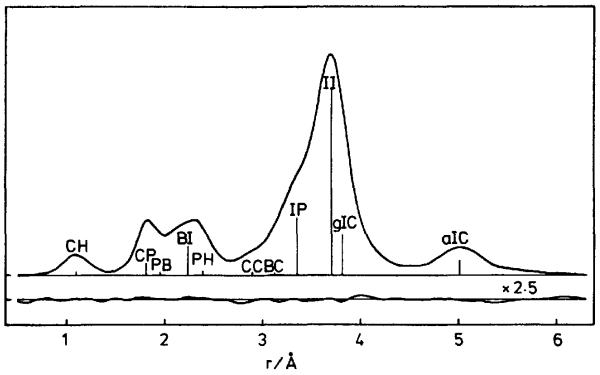

Fig. 3. Radial distribution curve for trimethylphosphine–boron triiodide. Solid curve represents the experimental curve, and lower curve 2.5 times the residuals.

shown in Fig. 3, was calculated from the observed molecular intensities of the range of $s=2.5$—34.2 Å^{-1}, where the long- and the short-camera-distance data were averaged in the overlapped region. A non-nuclear correction for the large difference between the atomic numbers of iodine and the other atom was made.[13,14]

The geometrical parameters listed in Table 3 and the mean amplitudes in Table 4 were determined by a least-squares analysis of the molecular intensities. It was assumed that the $(CH_3)_3P\cdot BI_3$ molecule has the C_{3v} symmetry in as taggered form, and that the methyl group has also C_{3v} symmetry in a staggered form with respect to the C–P bond. The asymmetry parameter, κ, for the C–H bond was assumed to be 1.2×10^{-5} Å^3, given by a diatomic approximation.[15] The asymmetry parameters for the other atomic pairs were neglected. The mean amplitudes and the shrinkage effects,[16] r_a-r_α, were calculated on the basis of the force field for $(CH_3)_3P\cdot BI_3$.[5]

The mean amplitudes for the B–I and I···I atomic pairs obtained in the least-squares analysis disagreed with those calculated from the force field given by Drake *et al.*[5] (see Table 4). On the basis of the fact that

Table 1. Force field for $(CH_3)_3P\cdot BI_3$

f(CH)	4.756	H(IBI)	0.20
f(HCH)	0.438	F(II)	0.27†
f(HCP)	0.639	F(PI)	0.18
f(CPC)	0.82	f(CH/CH′)	0.045
f(CPB)	0.99	f(HCP/HCP′)	−0.107
f(CP)	3.32	f(CP/CP′)	0.36
K(PB)	2.22	f(CPB/CPB′)	−0.045
K(BI)	1.2†	f(PBI/PBI′)	−0.19
H(PBI)	0.22	Y(CP)	0.081†

In the present normal-coordinate calculations, the general-valence force constants, f, and the Urey-Bradley force constants, K, H, F, and Y, were used. The units are 10^2 N m^{-1} for the stretching and repulsion constants, 10^{-18} J rad^{-2} for the bending constants, and 10^{-18} N m for the torsional constants. The linear constant, F' was assumed to be $-0.1F$. The values of the force constants were taken from Ref. 5, but those indicated by daggers were estimated for the gaseous molecule in the present study.

Table 2. Root-mean-square amplitudes and shrinkage effects for $(CH_3)_3P\cdot BI_3$ (in 10^{-4} Å units)

Atomic pair	l_{calcd}	r_a-r_α	Atomic pair	l_{calcd}	r_a-r_α
B–I_1	721	51	P–C_1	537	85
P–B	607	39	P···H_1	1162	317
B···C_1	1012	71	C_1···C_2	1085	66
B···H_1	1244	249	C_1–H_1	784	536
B···H_2	2132	101	C_1···H_4	2221	105
I_1···I_2	1268	−13	C_1···H_5	2276	82
I_1···P	1264	−6	C_1···H_6	1265	225
I_1···C_1	1199	31	H_1···H_2	1319	833
I_1···C_2	1997	−35	H_1···H_4	3134	62
I_1···H_1	1670	132	H_1···H_5	3571	−48
I_1···H_2	1907	86	H_1···H_6	2271	261
I_1···H_4	2499	69	H_2···H_5	2264	244
I_1···H_5	3150	−92	H_2···H_6	1521	320
I_1···H_6	3057	−73	H_2···H_9	3284	14

The numbering of atoms is shown in Fig. 1.

the force constants of K(BI) and F(II) are mainly related to l(B–I) and l(I···I) respectively, these constants were estimated to be $K(BI)=1.2\times10^2$ N m^{-1} and $F(II)=0.27\times10^2$ N m^{-1} respectively, so that the calculated values of l(B–I) and l(I···I) might be equal to the respective observed values.

In this calculation, the torsional vibration about the P–B bond was disregarded, for the mean amplitude for the *gauche* I···C atomic pair obtained from the least-squares analysis was nearly equal to that calculated from the force field neglecting this vibration. The force constant for the torsional vibration about the C–P bond was assumed to be 0.08×10^{-18} N m, which was estimated from the potential barrier of 2.6 kcal mol^{-1} for trimethylphosphine.[17] The force constants for gaseous $(CH_3)_3P\cdot BI_3$ modified in the present study are given in Table 1, while the calculated mean amplitudes and the shrinkage corrections for this molecule are given in Table 2.

The r_α parameters determined by the least-squares analysis are listed in Table 3, where the r_g parameters and the limits of error are also listed. The random errors are 2.6 times the standard errors in the least-squares calculations. The systematic errors were estimated from the errors in the measurement of the

Table 3. Molecular parameters obtained from least-squares analysis for $(CH_3)_3P\cdot BI_3$

	r_α	r_g	ε[a]
B–I	2.226	2.233	0.003
P–B	1.941	1.947	0.011
C–P	1.799	1.809	0.003
C–H	1.035	1.094	0.008
I···I	3.691	3.694	0.004
C···C	2.879	2.890	0.011
∠PCH	109.2		1.4
∠IBI[b]	112.0	111.6	0.3
∠CPC[b]	106.3	106.0	0.5

Bond distance: Å units; bond angle: degree units.
a) Limits of error. b) Calculated from independent parameters.

Table 4. Root-mean-square amplitudes for $(CH_3)_3P \cdot BI_3$ (in Å unit)

	Obsd[a]	Calcd[b]	Calcd[c]
B–I	0.074 (9)	0.072	0.087
C–P	0.055 (5)	0.054	0.054
C–H	0.075(10)	0.078	0.078
I···I	0.126 (2)	0.122	0.091
I···P	0.111 (5)	0.126	0.128
anti I···C	0.111(14)	0.120	0.125
gauche I···C	0.184(19)	0.199	0.195

a) Results obtained from least-squares analysis of electron-diffraction data. Limits of error are shown in parentheses. b) Values calculated from the force constants in Table 1. c) Values calculated from the force constants in Ref. 5.

camera distance (0.04%) and the wavelength (0.07%). The mean amplitudes, their limits of error, as obtained by least-squares analysis, and the calculated mean amplitudes are listed in Table 4. The correlation matrix is listed in Table 5, while the best-fit theoretical molecular intensities are shown in Fig. 2. The calculations of the mean amplitudes and the shrinkage effects and the least-squares analysis were carried out on a HITAC M-200H computer in the Computer Center of the University of Tokyo.

Discussion

The molecular parameters for gaseous trimethylphosphine-boron trihalides are listed in Table 6, where the molecular parameters in the solid phase[1] and those for component molecules[18–21] are also listed. The fractional changes in the parameters, $\Delta f/f$, between the complexes and the component molecules are shown in Fig. 4. The electronegativity of halogen atoms[22] is tentatively taken as the abscissa. It is apparent that, on the complex formation, the $|\Delta f|/f$ ratios systematically increase with the increase in electronegativity, that is, with the decrease in the atomic number of halogen atoms, though the P–B bond distances are equal to each other. On the other hand, the calorimetric study has shown that the complexes are stable in the order of $(CH_3)_3P \cdot BF_3 < (CH_3)_3P \cdot BCl_3 < (CH_3)_3P \cdot BBr_3$,[23] though there are no data for $(CH_3)_3P \cdot BI_3$. These results show that the stability of trimethylphosphine–boron trihalides decreases with an increase in the magnitude

Table 5. Correlation matrix of $(CH_3)_3P \cdot BI_3$

	r(BI)	r(PB)	r(CP)	r(CH)	r(II)	r(CC)	∠PCH	l(BI)	l(II)	l(IP)	l(*a*IC)	l(*g*IC)	l(CP)	l(CH)	R_1[a]	R_2[a]
r(BI)	1.0															
r(PB)	−0.67	1.0														
r(CP)	−0.05	0.04	1.0													
r(CH)	0.05	−0.02	−0.05	1.0												
r(II)	0.30	0.37	−0.13	0.05	1.0											
r(CC)	0.02	0.29	0.62	−0.04	0.22	1.0										
∠PCH	−0.13	0.11	0.09	−0.25	0.05	0.10	1.0									
l(BI)	−0.01	0.06	−0.34	−0.05	0.09	−0.23	−0.54	1.0								
l(II)	−0.10	−0.11	−0.23	0.04	0.02	−0.32	0.04	0.13	1.0							
l(IP)	0.06	0.26	−0.20	0.04	0.66	−0.13	0.16	0.07	0.42	1.0						
l(*a*IC)	0.05	−0.03	−0.09	0.09	0.07	−0.10	−0.18	0.16	0.13	0.08	1.0					
l(*g*IC)	0.32	0.18	−0.21	0.08	0.86	−0.05	−0.01	0.14	0.15	0.73	0.13	1.0				
l(CP)	0.42	−0.48	−0.11	0.04	0.01	−0.23	−0.04	−0.01	0.30	0.10	0.09	0.16	1.0			
l(CH)	0.07	−0.05	0.00	−0.04	0.08	−0.06	0.00	0.05	0.17	0.13	0.04	0.13	0.19	1.0		
R_1	0.23	−0.08	−0.26	0.15	0.50	−0.39	−0.03	0.18	0.53	0.61	0.21	0.73	0.34	0.19	1.0	
R_2	0.00	0.00	−0.15	0.05	0.14	−0.26	0.03	0.16	0.61	0.31	0.17	0.29	0.34	0.20	0.49	1.0

a) R_1 and R_2 are the indices of resolution for the long- and short-camera-distance data respectively. The indic of resolution and their uncertainties are $R_1 = 0.93 \pm 0.02$ and $R_2 = 0.94 \pm 0.03$.

Table 6. Comparison of molecular parameters

		r(P–B)/Å	r(B–X)/Å	r(C–P)/Å	∠XBX/°	∠CPC/°
$(CH_3)_3P \cdot BCl_3$	gas[a]	1.941 (16)	1.851 (7)	1.800 (4)	109.4 (4)	109.3 (3)
	solid[b]	1.957 (5)	1.855 (5)	1.80 (1)	111.2 (2)	107.9 (3)
$(CH_3)_3P \cdot BBr_3$	gas[c]	1.946 (29)	2.010 (9)	1.804 (4)	111.7 (7)	108.0 (7)
	solid[b]	1.924 (12)	2.022 (7)	1.81 (1)	110.4 (5)	107.2 (5)
$(CH_3)_3P \cdot BI_3$	gas[d]	1.947 (11)	2.233 (3)	1.809 (3)	111.6 (3)	106.0 (5)
	solid[b]	1.918 (15)	2.249 (12)	1.845 (12)	110.7 (6)	107.8 (6)
$(CH_3)_3P$[e]				1.846 (3)		98.6 (3)
BCl_3[f]			1.742 (4)		120	
BBr_3[g]			1.893 (5)		120	
BI_3[h]			2.118 (5)		120	

The values in the gas phase represent r_g parameters. The values in parentheses are the limits of error attached to the last significant digits. a) Ref. 2. b) Ref. 1. c) Ref. 3. d) Present study. e) Ref. 18. f) Ref. 19. g) Ref. 20. h) Ref. 21.

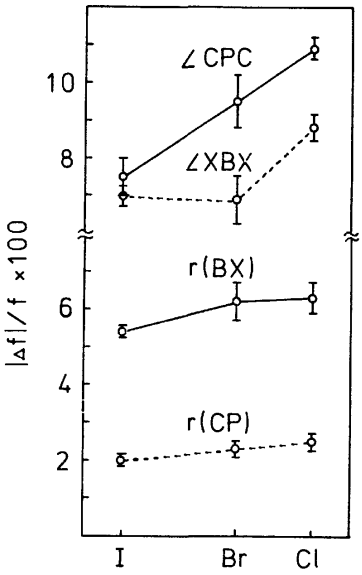

Fig. 4. Parameter changes on complex formation *versus* electronegativities for halogen atoms. Solid lines represent positive Δf and dashed lines negative Δf.

of the structural changes.

By comparing the parameters of the molecules in the solid phase with those of the gaseous molecules, we see that the dative bonds of $(CH_3)_3P\cdot BBr_3$ and $(CH_3)_3P\cdot BI_3$ seem to be enhanced in the solid phase in the order of $(CH_3)_3P\cdot BBr_3 < (CH_3)_3P\cdot BI_3$, while the dative bond of $(CH_3)_3P\cdot BCl_3$ is unchanged in the solid and gas phases.

The gaseous molecule of $(CH_3)_3P\cdot BI_3$ is rigid with respect to the torsional vibration about the P–B bond, while the potential barriers for $(CH_3)_3P\cdot BCl_3$[2] and $(CH_3)_3P\cdot BBr_3$[3] are 3.8 ± 0.7 and about 10 kcal mol^{-1} respectively. Accordingly, the potential barriers about the P–B bonds of $(CH_3)_3P\cdot BX_3$ are in the order of $(CH_3)_3P\cdot BCl_3 < (CH_3)_3P\cdot BBr_3 < (CH_3)_3P\cdot BI_3$, *i.e.*, in the order of the increasing size of the halogen atoms in the complexes. The height of the rotational barriers of these complexes may be controlled by the repulsion due to the nonbonded atomic pairs, such as $X_1\cdots H_6$ (see Fig. 1). The $X_1\cdots H_6$ distances are, however, nearly equal to each other in the above trimethylphosphine complexes; therefore, the above order for the rotational barrier heights is understandable if the large van der Waals radii for halogen atoms with large atomic numbers are taken into consideration.

References

1) D. L. Black and R. C. Taylor, *Acta Crystallogr., Sect. B*, **31**, 1116 (1975).
2) K. Iijima and S. Shibata, *Bull. Chem. Soc. Jpn.*, **52**, 3204 (1979).
3) K. Iijima, E. Koshimizu, and S. Shibata, *Bull. Chem. Soc. Jpn.*, **54**, 2255 (1981).
4) R. T. Markham, E. A. Dietz, Jr., and D. R. Martin, *J. Inorg. Nucl. Chem.* **35**, 2659 (1973).
5) J. E. Drake, J. L. Hencher, and B. Rapp, *Inorg. Chem.*, **16**, 2289 (1977).
6) W. Witt, *Z. Naturforsch., Teil A*, **19**, 1363 (1964).
7) S. Shibata, K. Iijima, R. Tani, and I. Nakamura, *Rep. Fac. Sci. Shizuoka Univ.*, **9**, 33 (1974).
8) L. Schäfer, A. C. Yates, and R. A. Bonham, *J. Chem. Phys.*, **55**, 3055 (1971).
9) D. T. Cromer and J. B. Mann, *J. Chem. Phys.*, **47**, 1892 (1967); D. T. Cromer, *ibid.*, **50**, 4857 (1969).
10) C. Tavard, D. Nicolas, and M. Rouault, *J. Chim. Phys.*, **64**, 540 (1967).
11) J. Karle and I. L. Karle, *J. Chem. Phys.*, **18**, 957 (1950).
12) Numerical experimental data of the leveled total intensity and the background have been deposited with the Chemical Society of Japan (Document No. 8237).
13) R. M. Gavin and L. S. Bartell, *J. Chem. Phys.*, **48**, 2460 (1968).
14) K. Iijima and S. Shibata, *Bull. Chem. Soc. Jpn.*, **47**, 1393 (1974).
15) K. Kuchitsu, *Bull. Chem. Soc. Jpn.*, **40**, 505 (1967).
16) K. Kuchitsu and S. J. Cyvin, "Molecular Structures and Vibrations," ed by S. J. Cyvin, Elsevier, Amsterdam (1972), Chap. 12.
17) "Kagaku Binran," 2nd ed, ed by the Chemical Society of Japan, Maruzen, Tokyo (1975), p. 1330.
18) L. S. Bartell and L. O. Brockway, *J. Chem. Phys.*, **32**, 512 (1960).
19) S. Konaka, Y. Murata, K. Kuchitsu, and Y. Morino, *Bull. Chem. Soc. Jpn.*, **39**, 1134 (1966).
20) S. Konaka, T. Ito, and Y. Morino, *Bull. Chem. Soc. Jpn.*, **39**, 1146 (1966).
21) H. Kakubari, S. Konaka, and M. Kimura, *Bull. Chem. Soc. Jpn.*, **47**, 2337 (1974).
22) L. Pauling, "The Nature of the Chemical Bond," 3rd ed, Cornell University Press, Ithaca, New York (1960).
23) D. C. Mente, J. L. Mills, and R. E. Mitchell, *Inorg. Chem.*, **14**, 123 (1975); D. C. Mente and J. L. Mills, *ibid.*, **14**, 1862 (1975).

 © 1982 The Chemical Society of Japan Bull. Chem. Soc. Jpn., 55, 2555—2559 (1982)

The Conversion of Methanol into Hydrocarbons over Dodecatungstophosphoric Acid

Toshihide Baba, Junya Sakai, Hideki Watanabe, and Yoshio Ono*

Department of Chemical Engineering, Tokyo Institute of Technology, Ookayama, Meguro-ku, Tokyo 152

(Received December 16, 1981)

Dodecatungstophosphoric acid (TPA) is a very effective catalyst for the conversion of methanol into hydrocarbons. The effects of the reaction parameters, such as the temperature or the methanol partial pressure, were therefore examined. The kinetic features of the conversion over TPA are quite different from those over ZSM-5 zeolites. This difference is caused by the unique nature of the conversion over TPA; methanol molecules are sorbed and undergo the conversion in the bulk of solid TPA.

Zeolites, especially ZSM-5, are very effective catalysts for converting methanol into hydrocarbons.[1-3] Ono and Mori[4] have studied the mechnism of the conversion in detail and have concluded that Brönsted acid sites are responsible for the conversion, refuting the mechanism which involves a carbene-like intermediate.[1] According to this mechanism,[4] the first carbon-carbon bond is formed in the following manner:

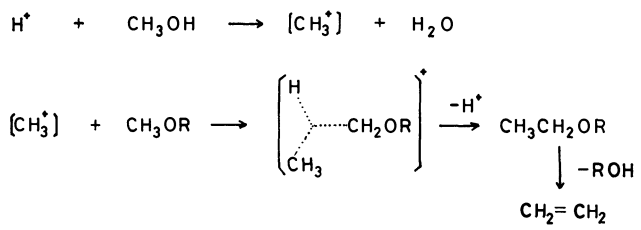

The subsequent fast reactions of lower olefins and methanol lead to the formation of a higher molecular weight. The overall reaction proceeds autocatalytically.[4-6] Thus, the yield of the hydrocarbons shows an abrupt increase with a small increase in the reaction temperature,[6] or the rate of hydrocarbon formation is accelerated as the reaction proceeds.[4,5]

Judging from the above mechanism, it seems that the methanol conversion should proceed over solid substances other than zeolites, if they are highly acidic. In fact, Ono *et al.* have reported that heteropolyacids such as dodecatungstophosphoric acid (TPA) are quite effective catalysts for the conversion.[4,7,8] Some heteropolyacids are known to have a high solid acidity and to be very active catalysts for various acid-catalyzed reactions.[9] Thus, TPA has a much higher activity than hydrogen-Y zeolite for the dehydration of 2-propanol.[9] In this work, the influences of the various reaction variables on the methanol conversion over TPA will be described, and the mechanistic characteristics will be discussed with reference to those of the conversion over zeolites.

Experimental

Dodecatungstophosphoric acid (TPA), obtained from Wako Pure Chemicals Ind., was made into pellets, crushed, and sorted into 9—16 mesh. The reaction was carried out with a continuous-flow reactor operating at atmospheric pressure. The catalyst was packed into a reactor of silica-tubing (10 mm i.d.) and placed in a vertical furnace. Methanol was delivered by means of a motor-driven syringe and vaporized in the preheating zone of the reactor, containing 10 cm^3 of quartz. The gas from the outlet of the reactor was analyzed by means of a gaschromatograph equipped with a flame-ionization detector. A 2-m Porapak Q column separated the hydrocarbon products efficiently. The yield or distribution of the products was calculated on a carbon-number basis.

Results and Discussion

Table 1 shows the product and hydrocarbon distribution in the conversion of methanol and dimethyl ether over TPA. The reaction conditions were as follows: reaction temperature, 573 K; methanol pressure, 50.7 kPa, and contact time $(W/F)=72.0$ g h mol^{-1}, where W and F denote the catalyst weight (g) and the total molar flow rate (mol h^{-1}) respectively. As is shown in Table 1, the two reactants gave similar hydrocarbon distributions except that a higher propylene/propane ratio was obtained when dimethyl ether was used as the starting material. At this temperature, the main products are lower aliphatic hydrocarbons, among which isobutane is most predominant. The formation of carbon monoxide

Table 1. Product distribution in the conversion of methanol and dimethyl ether

	Reactant	
	CH_3OH	CH_3OCH_3
Reaction conditions		
Reaction temperature/K	573	573
(W/F)/g mol^{-1} h	72	75
Pressure/kPa	50.7	50.7
Product distribution/%		
CH_3OH	Trace	0.0
CH_3OCH_3	55.1	55.8
Hydrocarbons	44.9	44.2
Hydrocarbon distribution/%		
CH_4	2.6	1.9
C_2H_4	11.9	12.5
C_2H_6	0.6	0.4
C_3H_6	8.3	11.9
C_3H_8	17.9	10.6
C_4	40.0	39.8
C_5	11.9	12.6
C_6	5.3	6.2
C_7^{+} a)	1.5	4.1

a) C_7^+ shows the hydrocarbons with more than six carbon atoms.

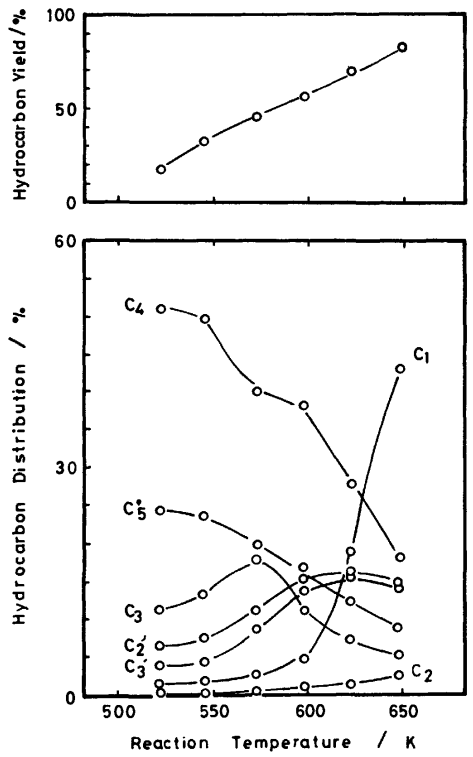

Fig. 1. Effect of the reaction temperature on the total hydrocarbon yield and the distribution of produced hydrocarbons.
Reaction conditions: methanol pressure 50.7 kPa, W/F = 72 g h mol^{-1}.

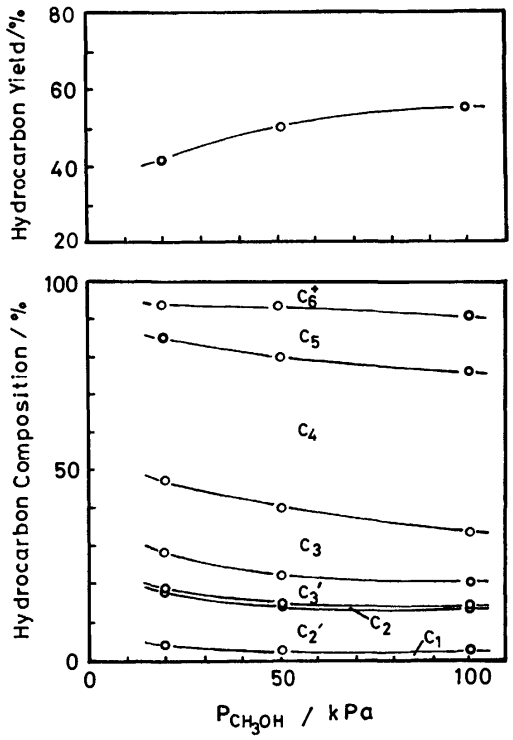

Fig. 2. Effect of the partial pressure of methanol on the total hydrocarbon yield and the composition of the produced hydrocarbons.
Reaction conditions: 573 K, W/F=71 g h mol^{-1}.

and carbon dioxide is negligible. In contrast to the conversion over ZSM-5, only a small amount of aromatic compounds is produced. The loss of the catalytic activity with the process time was small in spite of the accumulation of coke. Thus, under the conditions of 573 K, W/F=140 g h mol^{-1}, and a methanol pressure of 101 kPa, the hydrocarbon yields were 62.8 and 50.2% at 1 and 15 h of process time respectively.

Figure 1 shows the temperature dependence of the yield of hydrocarbons and their distribution in methanol conversion. The hydrocarbon yield increased gradually with the reaction temperature. In contrast to the conversion over ZSM-5,[6] no abrupt increase in the hydrocarbon yield was observed; that is, the reaction seems not to be an autocatalytic one. Among the products, C_4 (hydrocarbons with four carbon atoms) and C_5 hydrocarbons were the predominant products at lower temperatures, and their fractions decreased with the reaction temperature. The fractions of lower olefins (ethylene+propylene) increased with the reaction temperature up to 623 K and decreased at higher temperatures. The fraction of methane was small below 570 K, but increased sharply over 620 K. The optimum temperature for the conversion lies around 570—600 K.

Figure 2 shows the effect of the methanol partial pressure on the hydrocarbon yield and the hydrocarbon

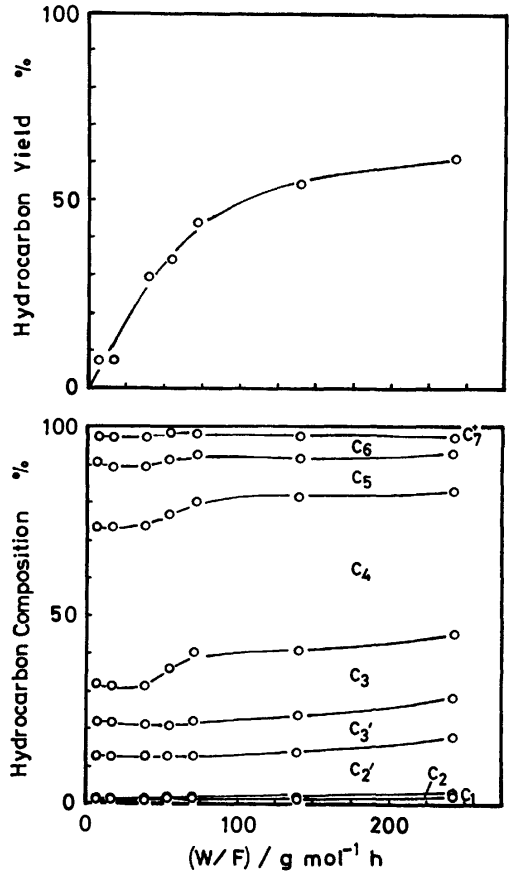

Fig. 3. Effect of the contact time (W/F) on the total hydrocarbon yield and the composition of the produced hydrocarbons.
Reaction conditions: 573 K, methanol pressure 50.7 kPa.

distribution. The yield of hydrocarbons increased only slightly with the methanol partial pressure, indicating that the overall rate of methanol conversion has a slightly higher order than one with respect to the methanol pressure. By lowering the methanol partial pressure, the fraction of lower hydrocarbons in the hydrocarbon products increased slightly.

Figure 3 shows the effect of the contact time (W/F) on the yield of hydrocarbons and their distribution at 573 K. The hydrocarbon yield increased gradually with the increase in the contact time. No acceleration in the rate of hydrocarbon formation was observed, in contrast to the conversion over ZSM-5.[4,5] This again indicates that the methanol conversion over TPA is not an autocatalytic reaction. For the conversion over ZMS-5, the autocatalytic phenomena were explained by assuming that Reaction 2 proceeds much faster than Reaction 1, according to the following reaction scheme:[4,5]

$$CH_3OH \longrightarrow \text{olefins (ethylene)} \quad (1)$$

$$CH_3OH + \text{olefins} \longrightarrow \text{olefins} + \text{paraffins}. \quad (2)$$

The lack of autocatalytic phenomena suggests that this assumption is not valid for the conversion over TPA. In conformity with this, the hydrocarbon distribution does not change appreciably with the total hydrocarbon yield. This is more clearly illustrated in Figs. 4—6, where the yield of each hydrocarbon species is plotted against the total hydrocarbon yield. The yield of each hydrocarbon species increases proportionally with the total hydrocarbon yield until the latter reaches *ca.* 50%, implying that all the hydrocarbon species are produced concurrently. Therefore, the following reaction scheme is plausible, assuming carbonium-ion intermediates.

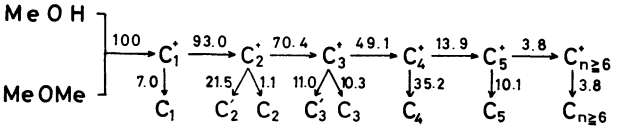

The numbers in the scheme represent the relative rates of the individual steps, which were calculated from the initial distribution of hydrocarbons.

The distinct difference between the mechanism over heteropolyacids and that over ZSM-5 is that olefins once desorbed from the catalyst surface hardly react at all with methanol in the former catalyst, while over ZSM-5 olefins react with methanol rapidly, as has been described above.

The high catalytic activity of TPA seems to be rather unusual, considering the small surface area of TPA ($\approx 2\ m^2\ g^{-1}$). To determine the effective number of active sites of TPA, the effect of pyridine sorption was examined. The reaction was started by feeding methanol and nitrogen at 573 K. After 2 h, pyridine was added to the feed, and then finally the feed was changed back to the starting mixture. Most of the pyridine introduced was retained by the catalyst. As

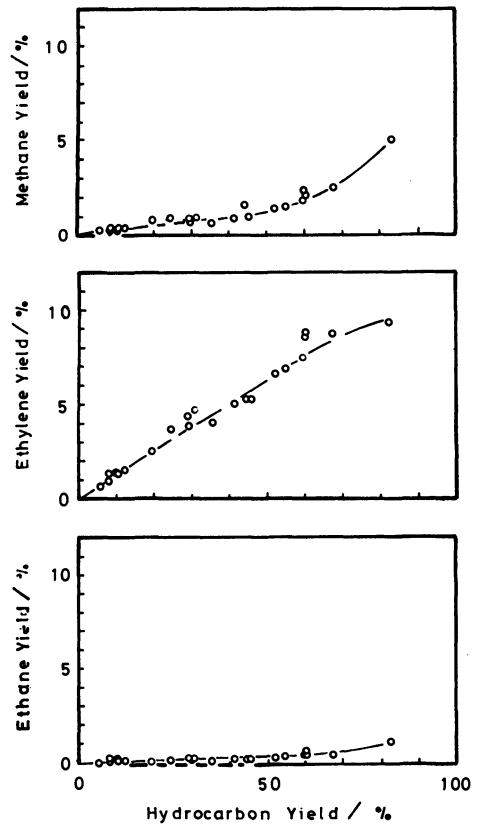

Fig. 4. Yields of methane, ethylene, and ethane as a function of the total hydrocarbon yield.
Reaction conditions: 573 K, methanol pressure 50.7 kPa.

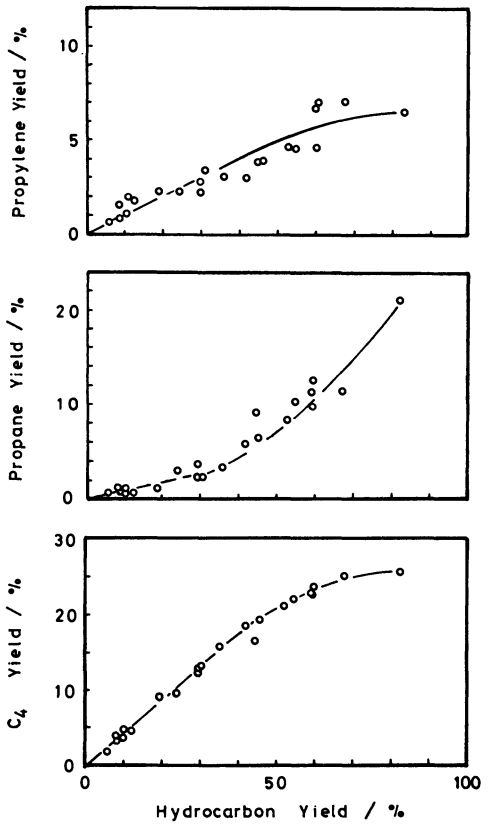

Fig. 5. Yields of propylene, propane and C_4-hydrocarbons as a function of the total hydrocarbon yield.
Reaction conditions, see Fig. 4.

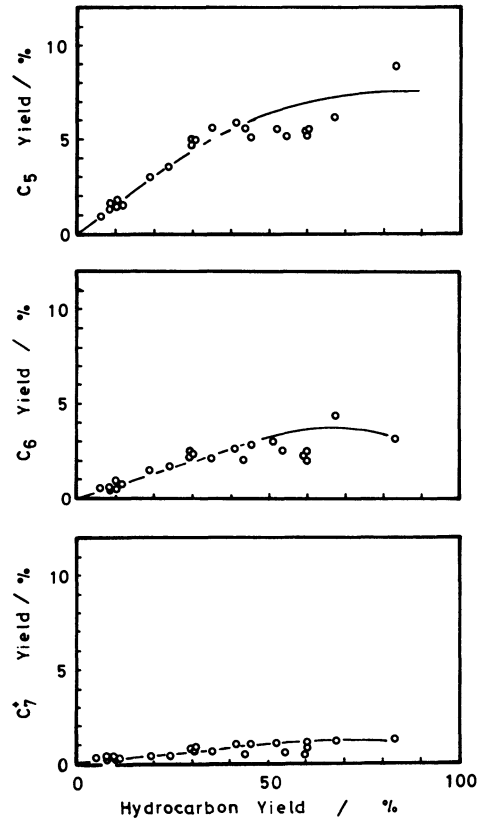

Fig. 6. Yields of C_5-, C_6-, and C_7^+-hydrocarbons as a function of the total hydrocarbon yield.
Reaction conditions, see Fig. 4.

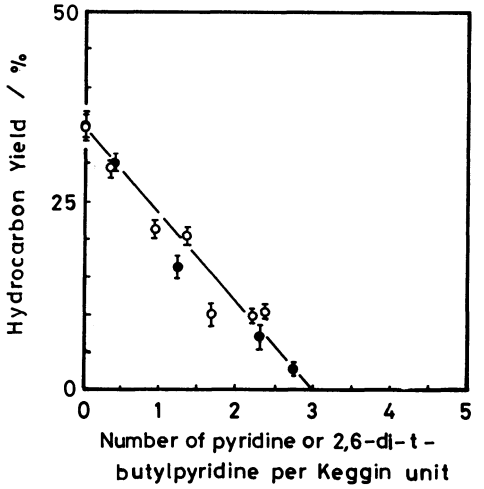

Fig. 7. Change in the hydrocarbon yield with the amount of the sorbed pyridine (○) and 2,6-di-*t*-butylpyridine (●).
Reaction conditions: 573 K, methanol pressure 50.7 kPa, $W/F=55.0$ g h mol^{-1}.

is shown in Fig. 7, the catalytic activity after pyridine sorption decreased linearly with the amount of the sorbed pyridine, a complete loss of the activity being attained when the molar ratio of the sorbed pyridine and the TPA used as a catalyst was three. The use of 2,6-di-*t*-butylpyridine instead of pyridine as a base has the same effect, as is shown in Fig. 7. Since the former poisons

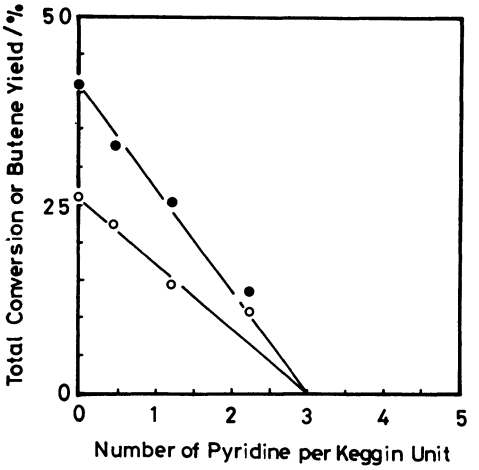

Fig. 8. Change in the conversion of 1-butanol (●) and the yield of butenes (○) in the dehydration of 1-butanol over TPA. The difference between the conversion and butene yield corresponds the formation of dibutyl ether.
Reaction conditions: 433 K, 1-butanol pressure, 24.3 kPa, $W/F=24.0$ g hmol^{-1}.

Brönsted-acid sites, but not Lewis-acid sites, the type of acid responsible for the conversion is Brönsted acid.

The amount of acid thus estimated indicates that all the protons in the solid TPA are accessible to pyridine molecules. The stoichiometric absorption of pyridine by heteropolyacids at 573 K was reported earlier.[10-12] Since methanol and other polar molecules are known to be absorbed by TPA, even at room temperature,[13,14] we presume that methanol molecules penetrate into the bulk of the solid TPA at the reaction temperature and react in the bulk. This explains the high activity of TPA, irrespective of its small surface area. Okuhara *et al.*,[12] on the basis of the correlation of the activity with the bulk acidity, recently proposed that the conversion of methanol occurred also in the bulk.

Methanol conversion was carried out with TPA (50 wt%) supported on three kinds of silica-gel with surface areas of 14.6, 37.5, and 80.9 m^2 g^{-1}. The yield of hydrocarbons depended only slightly on the surface area of the silica-gel. Thus, under the conditions of 573 K, $W/F=48.0$ g mol^{-1} h and a methanol pressure of 101 kPa, the hydrocarbon yields were 10.0, 9.1, and 10.6%. This again indicates that the reaction proceeds in the bulk; otherwise, the yield would depend on the surface area of silica-gel.

To confirm that the phenomenon is not specific to the conversion of methanol, the number of acid sites for the dehydration of 1-butanol to dibutyl ether and butenes was determined in a similar manner. As is shown in Fig. 8, the amount of acid sites responsible for the dehydration of 1-butanol is again three times as large as the amount of TPA used as a catalyst. Thus, the dehydration of 1-butanol is also presumed to proceed in the bulk of the solid. It has been reported that the dehydration of ethanol[13] and 2-propanol proceeds in the bulk of heteropolyacids.

Olefins, nonpolar molecules, cannot penetrate into the bulk of the solid TPA. Therefore, the reaction of olefins

with methanol occurs only on the surface of the solid, while the reaction between methanol molecules can proceed even in the bulk of the solid. This explains why Reaction 2 is not much faster than Reaction 1, and why the autocatalytic phenomena are not observed in the conversion of methanol over TPA.

The authors are deeply grateful to Professor Tominaga Keii for his fruitful discussion and his continuous encouragement throughout the present work.

References

1) S. L. Meisel, J. P. McCullough, C. H. Lechtler, and P. B. Weisz, *Chem. Tech.*, **6**, 86 (1976).
2) C. D. Chang and A. J. Silvestri, *J. Catal.*, **47**, 249 (1977).
3) E. G. Derouane, J. B. Nagy, P. Dejaifve, J. H. C. van Hooff, B. P. Spekman, J. C. Vedrine, and C. Naccache, *J. Catal.*, **53**, 40 (1978).
4) Y. Ono and T. Mori, *J. Chem. Soc., Faraday Trans. 1*, **77**, 2209 (1981).
5) N. Y. Chen and W. J. Reagan, *J. Catal.*, **59**, 123 (1979),
6) Y. Ono, E. Imai, and T. Mori, *Z. Phys. Chem. Neue Folge*, **115**, 99 (1979).
7) Y. Ono, T. Mori, and T. Keii, *Proc. 7th Int. Congr. Catal., 1980, Tokyo*, Kodansha-Elsevier (1981), p. 1414.
8) Y. Ono, T. Baba, J. Sakai, and T. Keii, *J. Chem. Soc., Chem. Commun.*, **1981**, 400.
9) M. Otake and T. Onoda, *Shokubai*, **18**, 169 (1976).
10) M. Misono, K. Sakata, Y. Yoneda, and W. Y. Lee, *Proc. 7th Int. Congr. Catal., 1980, Tokyo*, Kodansha-Elsevier (1981), p. 1047.
11) M. Furuta, K. Sakata, M. Misono, and Y. Yoneda, *Chem. Lett.*, **1979**, 31.
12) T. Okuhara, N. Hayakawa, A. Kasai, M. Misono, and Y. Yoneda, Preprint of the Meeting of the Catalysis Society of Japan, *Shokubai*, **22**, 226 (1980).
13) T. Okuhara, A. Kasai, N. Hayakawa, M. Misono, and Y. Yoneda, *Chem. Lett.*, **1981**, 391.
14) Y. Saito, N. Yoneda, H. Niiyama, and E. Echigoya, Preprint of the Meeting of the Catalysis Society of Japan, Sendai, 1980, Section A, p. 18.

Tris(2,2'-bipyridine)ruthenium(II)-photosensitized Reductions of Methyl Viologen and Molecular Oxygen in a Network of Water-swollen Cation-exchange Resin

Yoshimi KURIMURA* and Kimiyo KATSUMATA
Department of Chemistry, Ibaraki University, Mito, Ibaraki 310

(Received January 5, 1982)

The visible-light-induced reduction of methyl viologen was found to occur in water-swollen cation-exchange resin, which adsorbed both $Ru(bpy)_3^{2+}$ and methyl viologen (RMCA resin) with the aid of triethanolamine (TEA) as a donor. With illumination, the generation of hydrogen peroxide proceeds in an oxygenated TEA solution containing RMCA resin. Hydrogen peroxide is produced *via* the superoxide ion, which is itself formed by the reaction of the methyl viologen radical in the resin with the oxygen molecule in the bulk of the solution. The $Ru(bpy)_3^{2+}$-photosensitized reaction processes leading to the generation of methyl viologen radical and hydrogen peroxide in the heterogeneous systems are discussed on the basis of the results obtained.

Many recent investigations[1-11] have been focussed on the quenching processes and visible-light-induced reactions *via* the photosensitized reactions of this type:

$$*Ru(bpy)_3^{2+} + A \longrightarrow Ru(bpy)_3^{3+} + A^-,$$

where $*Ru(bpy)_3^{2+}$ (bpy=2,2'-bipyridine) is the lowest excited state of $Ru(bpy)_3^{2+}$. The micellar systems have been examined with an eye to enhancing the charge-separation of this type of reaction.[1,7,10] In the case of a micellar solution, the kinetic features are considered to be different from those in a homogeneous solution. It has been suggested that, in a micellar system, no intermicellar exchange of $*Ru(bpy)_3^{2+}$ and the acceptor molecules can take place; thus, the electron-transfer will occur within groups of only a few molecules that are compartmented within their host aggregate.[7]

Relatively little attention seems to have been paid to such heterogeneous reactions as those which occur in the networks of ion-exchange resins. The quenching of $*Ru(bpy)_3^{2+}$ by various metal ions has been investigated in water-swollen cation-exchange resin (Shphadex-SP)[12] or in a cluster network of perfluorosulfonate membrane (Nafion 120).[13] However, little investigation of the $Ru(bpy)_3^{2+}$ photosensitized reduction in the network of the ion-exchange resin has been reported except for that in water-swollen iminodiacetic acid type chelate resin bead adsorbing $Ru(bpy)_3^{2+}$ and methyl viologen (MV^{2+}).[14] If we use a cation-exchange resin, photosensitizer and acceptor ions having more than two positive charges, such as $Ru(bpy)_3^{2+}$ and MV^{2+} respectively, could be accumulated in the domain of the resin. In such a system, an efficient electron-transfer from $*Ru(bpy)_3^{2+}$ to the acceptor can be expected to occur if the resin is relatively transparent, and the back-reaction can be prevented by scavenging the oxidized species of the Ru(II) complex by a suitable donor, because the electron-transfer efficiency from the excited state of the chromophore to the acceptor should be enhance as a result of the intimate contact of these species in the domain of the resin.

In the present work, we have studied the photosensitized reduction of methyl viologen and the activation of the dissolved oxygen by use of a cation-exchange resin which adsorbs both $Ru(bpy)_3^{2+}$ and MV^{2+} (abbreviated as RMCA resin).

Experimental

The chloride salt of methyl viologen was recrystallized from methanol. The $[Ru(bpy)_3]Cl_2 \cdot 6H_2O$[15] was prepared according to the literature method. The triethanolamine (TEA) and other reagents were of the best commercial grade available. The cation-exchange resin (Dowex 50-W-X-8, 100—200 mesh; sodium form) was used after conditioning by means of a column exchange, washing with water until the effluent was transparent in the UV region, and drying at 60 °C. The exchange capacity of the resin was determined to be 4.51 mequiv. g^{-1}. The concentrations of $Ru(bpy)_3^{2+}$ and MV^{2+} were determined by means of solution spectrometry at 456 nm (ε 13600 M^{-1} cm^{-1}, 1 M=1 mol dm^{-3}) and 257 nm (ε 21000 M^{-1} cm^{-1}) respectively. The cation-exchange resin adsorbing both $Ru(bpy)_3^{2+}$ and MV^{2+} was prepared as follows. The resin beads (5.0 g) in a 100-ml portion of the solution containing the Ru(II) and MV^{2+} were stirred for 1 h. By determining the concentrations of the Ru(II) and MV^{2+} remaining in the solution, the amounts of the adsorbed ions could be ascertained. The resulting resin beads were filtered, washed with water, and dried at 60 °C in the dark. The absorption spectra werer ecorded on a Hitachi Model 320 spectrophotometer. The reflectance spectral change in the RMCA resin was recorded as follows. A mixture of the RMCA resin beads (*ca.* 3 ml) and about 10-ml of the phosphate buffer (pH 7.0, 0.02 M) were bubbled with nitrogen gas for 30 min, and then the resin beads (*ca.* 2 ml) and small amounts of the buffer solution were packed into a photometer cell (10 mm × 10 mm) with a ground-glass cap in a thermostated cell holder at 30± 0.2 °C under nitrogen. The cell was illuminated with a 150-W slide projector with a UV cut-off filter (Kenko Skylight, L-40, UV). The reflectance spectra were recorded on a Hitachi Model 320 spectrometer equipped with an integrating sphere accessory (Model 210-2102), with aluminum oxide as the reference.

A typical procedure for the illumination of a mixture of the RMCA resin and aqueous solution was as follows. The pH of a mixture of 0.50 g of the RMCA resin and 30.0 ml of water in a 100-ml Ehrenmayer flask was adjusted to about 7 by the addition of several drops of dilute hydrochloric acid and, if necessary, dilute sodium hydroxide, by then adding 5.0 ml of a phosphate buffer (0.2 M), and ,finally, by adjusting the volume of the solution to 50.0 ml. The flask was kept in a thermostated water bath, made of transparent polyacrylic acid resin, at 30±0.2 °C. Oxygen or air was flushed through the mixture for 20 min. The mixture was illuminated with a 150-W slide projector located below the water bath. During

the illumination, the mixture was stirred by bubbling in oxygen or air. The concentration of hydrogen peroxide in the illuminated solution was determined colorimetrically using titanium oxalate.[16]

Results and Discussion

The cation-exchange resin adsorbs both Ru(bpy)$_3^{2+}$ and MV^{2+} in an aqueous solution well. When the total amounts (equiv. g^{-1} of the resin) of the adsorbed Ru(bpy)$_3^{2+}$ and MV^{2+} ions were less than 10% of the exchange capacity of the resin, no appreciable amounts of the adsorbed ions were eluted into the solution when the RMCA resin was kept in a 0.1 M TEA solution at pH 8.0 for 3 h at 30 °C. It was also ascertained that no detectable amounts of TEA were found to be adsorbed on the cation-exchange resin when 0.50 g of the cation-exchange resin was stirred in 50 ml of a 0.10 M TEA solution at pH 7 and 30 °C for 2 h.

When RMCA resin was illuminated in a deoxygenated aqueous solution of TEA, the resin turned from the original light brown through light green to dark blue. In the absence of TEA, however, no such color change was observed at all upon illumination.

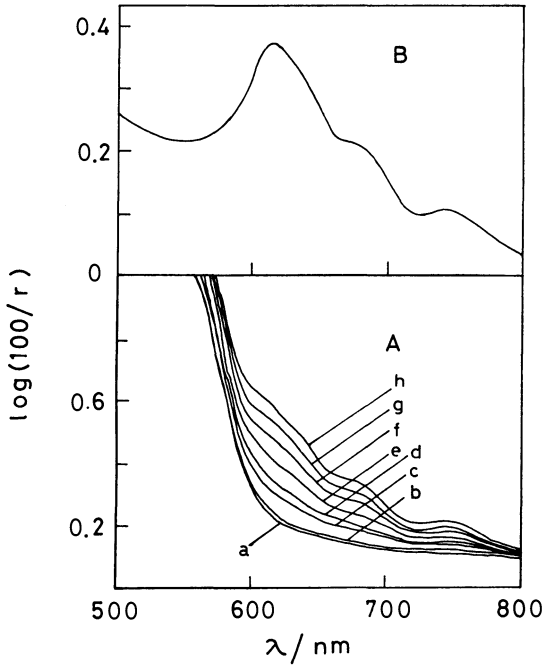

Fig. 1. Reflectance spectral change of the illuminated RMCA resin ([Ru(II)]=2.3×10^{-5} mol g^{-1}, [MV^{2+}]=1.1×10^{-4} mol g^{-1}) in N_2-saturated 0.10 M TEA solution with the illumination time (min) of 0 (a), 5 (b), 15 (c), 20 (d), 30 (e), 40 (f), 50 (g), and 60 (h) (A) and the differential spectrum of the 60 min illuminated RMCA resin (B) at pH 7.0 and 30 °C.

The reflectance spectral change in the RMCA resin in a deoxygenated solution (Fig. 1A) and the differential spectrum of the illuminated resin is essentially the same as the absorption spectrum of the methyl viologen radical in an aqueous solution in the region of 550—800 nm. It may be concluded that the *Ru(bpy)$_3^{2+}$ produced by the photoexcitation of the adsorbed Ru(bpy)$_3^{2+}$ reacts with MV^{2+} to give the methyl viologen radical, MV^{+},[17] in the interior of the domain of the resin and that the oxydized psecies of the chromophore is scavenged by the TEA molecule present in the bulk of the solution. A bead of the illuminated (*ca.* 5 min) RMCA resin in a deoxygenated solution was cut into two hemispheres and then the cut surface was examined under a microscope. The dark blue color of the methyl viologen radical was found to spread homogeneously on the surface. This seems to indicate that the reaction proceeds almost homogeneously in the resin bead.

The photosensitized reduction of methyl viologen using RMCA resin can be explained by the scheme given in Eqs. 1—5. In these equations, the chemical species written in branckets with the suffix *r* represent those adsorbed on the resin, while *m* denotes the ratio of the average number of the MV^{2+} to one Ru(bpy)$_3^{2+}$:

$$[(Ru(II))(MV^{2+})_m]_r \xrightarrow{h\nu} [(*Ru(II))(MV^{2+})_m]_r \quad (1)$$

$$[(*Ru(II))(MV^{2+})_m]_r \longrightarrow [(Ru(II))(MV^{2+})_m]_r + \Delta + h\nu' \quad (2)$$

$$[(*Ru(II))(MV^{2+})_m]_r \longrightarrow [(Ru(III))(MV^{+})(MV^{2+})_{m-1}]_r \quad (3)$$

$$[(Ru(III))(MV^{+})(MV^{2+})_{m-1}]_r \longrightarrow [(Ru(II))(MV^{2+})_m]_r \quad (4)$$

$$[(Ru(III))(MV^{+})(MV^{2+})_{m-1}]_r + TEA \longrightarrow [(Ru(II))(MV^{+})(MV^{2+})_{m-1}]_r + TEA_{ox}, \quad (5)$$

where TEA_{ox} is the oxidized species of triethanolamine. The charge separation, *i.e.*, generation of MV^{+}, takes place as a result of the reduction of the Ru(III) by the TEA molecule *via* Eq. 5.

When RMCA resin was illuminated in an oxygenated solution of TEA, only a slight color change or, in some cases, no color change at all was seen, while the formation of hydrogen peroxide was observed in the bulk of the solution. These facts indicate that the hydrogen peroxide is produced by the reaction of the methyl viologen radical with the oxygen molecule.

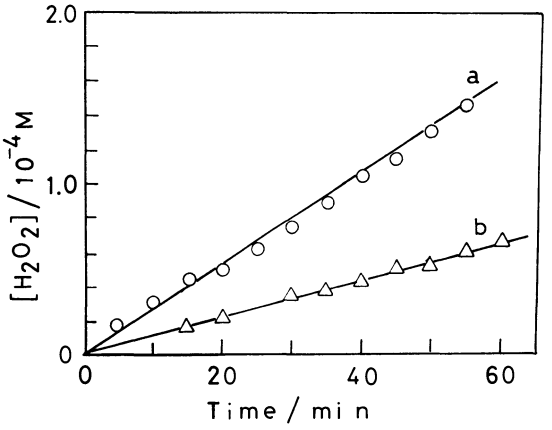

Fig. 2. Plots of the concentration of hydrogen peroxide with the illumination time in the mixture of 0.50 g of RMCA resin ([Ru(II)]=2.3×10^{-5} mol g^{-1}, [MV^{2+}]=1.1×10^{-4} mol g^{-1}) and 50 ml of the O_2-saturated (a) and air-saturated (b) 0.10 M TEA solutions at pH 7.0 and 30 °C.

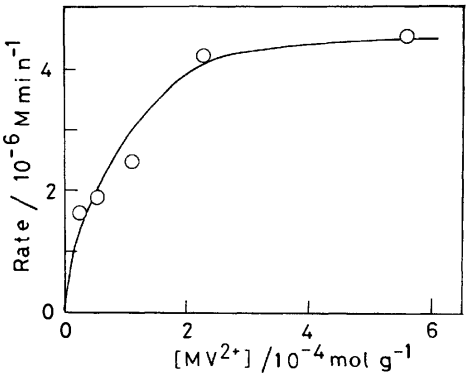

Fig. 3. Dependence of the rate of hydrogen peroxide formation on the concentration of MV^{2+} in the mixture of 0.50 g of RMCA resin ([Ru(II)]$=2.3\times10^{-5}$ mol g^{-1}) and 50 ml of O_2-saturated 0.10 M TEA solution at pH 7.0 and 30 °C.

The concentration of hydrogen peroxide is plotted as a function of the illumination time in Fig. 2. The rate of hydrogen peroxide formation was determined from the slope of the plots of the hydrogen peroxide concentration *vs.* the illumination time. The results shown in Fig. 2 demonstrate that the rate depends on the concentration of the dissolved oxygen: the rate in the oxygen-saturated solution is about two times greater than that in the air-saturated solution under the conditions employed.

The rate also depends on the "concentrations"[19] of the adsorbed $Ru(bpy)_3^{2+}$ and MV^{2+}. The rate dependence on the concentration of MV^{2+} shows that the rate increases sharply at lower [MV^{2+}] values and reaches the saturated value at [MV^{2+}] values higher than about 2×10^{-4} mol g^{-1} (Fig. 3).

The rate is also affected by the concentration of the TEA: the rate increases with the concentration of the TEA and is hardly saturated even at 0.5 M (Fig. 4). The dependence of the rate on the concentration of the

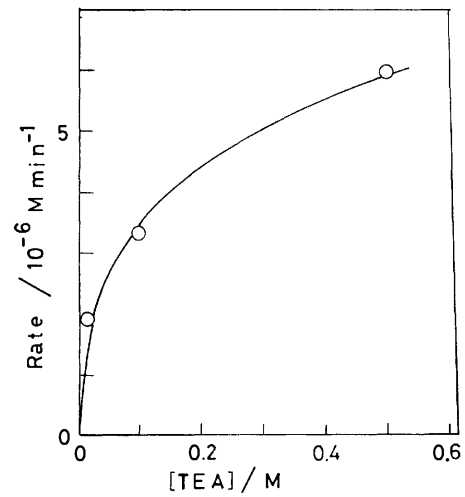

Fig. 4. Dependence of the rate of hydrogen peroxide formation on the concentration of TEA in the mixture of 0.50 g of RMCA resin ([Eu(II)]$=2.3\times10^{-5}$ mol g^{-1}, [MV^{2+}]$=1.1\times10^{-4}$ mol g^{-1}) and 50 ml of O_2-saturated TEA solution at pH 7.0 and 30 °C.

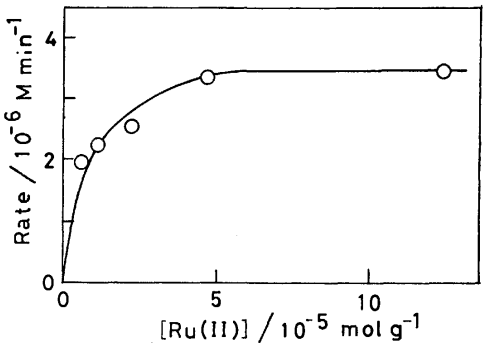

Fig. 5. Dependence of the rate of hydrogen peroxide formation on the concentration of $Ru(bpy)_3^{2+}$ in the mixture of 0.50 g RMCA resin ([MV^{2+}]$=1.1\times10^{-4}$ mol g^{-1}) and 50 ml of O_2-saturated 0.10 M TEA solution at pH 7.0 and 30 °C.

Ru(II) is presented in Fig. 5.

The reaction scheme for the formation of hydrogen peroxide responsible for the results can be explained by Eqs. 1—5, 6, and the subsequent reduction of the superoxide ion, by Eqs. 7—9. Hydrogen peroxide is,

$$[(Ru(II))(MV^{+})(MV^{2+})_{m-1}]_r + O_2 \longrightarrow [(Ru(II))(MV^{2+})_m]_r + O_2^- \quad (6)$$

probably, formed by the disproportionation reaction of the superoxide ions and the reaction of O_2^- with $*Ru(bpy)_3^{2+}$, and/or MV^+. The rate dependence on the

$$O_2^- + O_2^- + 2H^+ \longrightarrow H_2O_2 + O_2 \quad (7)$$

$$[*Ru(II)]_r + O_2^- + 2H^+ \longrightarrow [Ru(III)]_r + H_2O_2 \quad (8)$$

$$[MV^+]_r + O_2^- + 2H^+ \longrightarrow [MV^{2+}]_r + H_2O_2 \quad (9)$$

oxygen concentration may be explained by the fact that the rate of the reaction of MV^+ with O_2 is relatively slow at low O_2 concentrations relative to that of the methyl viologen-radical formation: thus, the rate of hydrogen peroxide increases with an increase in the O_2 concentration in the lower-concentration region.

When 0.50 g of the RMCA resin ([Ru(II)]$=2.3\times10^{-5}$ mol g^{-1} and [MV^{2+}]$=1.1\times10^{-5}$ mol g^{-1}) in 50 ml of 0.10 M TEA was illuminated at 30 °C for 10 h, 1.4×10^{-3} M H_2O_2 was generated: thus, the turnover number for the Ru(II) and MV^{2+} were estimated to be about 10 and 2 respectively in this case (Fig. 6).

A experiment aimed at comparing the efficiencies of hydrogen peroxide formation in the heterogeneous system with the corresponding homogeneous one was

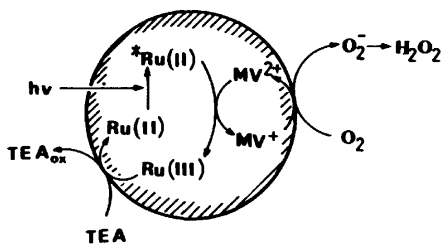

Fig. 6. Schematic representation of the generation of hydrogen peroxide in RMCA resin/O_2/TEA/H_2O system.

TABLE 1. COMPARISON OF THE RATE OF HYDROGEN PEROXIDE FORMATION IN THE RMCA RESIN SYSTEM WITH THE CORRESPONDING HOMOGENEOUS SYSTEM AT pH 7.0 AND 30 °C [a]

System		$[Ru(bpy)_3^{2+}]$	$[MV^{2+}]$	[TEA]/M	$(d[H_2O_2]/dt)$/mol min^{-1}
Heterogeneous[b]	1A	2.3×10^{-5}	1.1×10^{-4}	0.10	2.4×10^{-6}
	1B	5.9×10^{-6}	2.8×10^{-5}	0.012	1.3×10^{-6}
Homogeneous[c]	2A	2.3×10^{-4}	1.1×10^{-3}	0.10	1.4×10^{-5}
	2B	5.9×10^{-5}	2.8×10^{-4}	0.012	1.5×10^{-6}

a) 1A and 1B correspond to 2A and 2B respectively. O_2-saturated solution at pH 7.0 and 30 °C. b) 0.50 g of the RMCA resins in 50 ml of the solution. The unit of the "concentrations" of the Ru(II) and MV^{2+} is represented by mol g^{-1}. c) The volume of the illuminated solutions was 50 ml. The unit of the concentrations of the Ru(II) and MV^{2+} is represented by mol dm^{-3}.

carried out; the results are presented in Table 1. In higher-concentration regions of the Ru(II), MV^{2+}, and TEA, the relative rate in the resin system is lower than that of the corresponding homogeneous system. However, in the lower-concentration regions of those species, the rate in the heterogeneous system was almost the same with that of the corresponding homogeneous system.

A system similar to that used in the present study may be used as a model for the visible light-induced generation of high-energy substances. It seems possible to make a system consinsting of an ion-exchange resin in which the photosensitizer, acceptor, and donor are all localized in its cluster network. When we use such a system, a more efficient model for solar-energy conversion may be designed. Moreover, if we could use a transparent thin film made of ion-exchange resin which adsorbed $Ru(bpy)_3^{2+}$ and a donor such as MV^{2+} instead of the RMCA resin, a more efficient charge-separation system than the present one could be made. Further experiments in this direction are now being undertaken.

References

1) C. R. Bock, T. J. Meyer, and D. G. Whitten, *J. Am. Chem. Soc.*, **96**, 4710 (1974).

2) C. Creutz and N. Sutin, *Proc. Natl. Acad. Sci. U.S.A.*, **72**, 2858 (1975).

3) K. Takuma, M. Kajiwara, and T. Matsuo, *Chem. Lett.*, **1977**, 1199.

4) W.E. Ford, J. W. Otvos, and M. Calvin, *Nature (London)*, **274**, 507 (1978).

5) D. Meisel, M. S. Matheson, and J. Rabani, *J. Am. Chem. Soc.*, **100**, 117 (1978).

6) J. M. Lehn, J.-P. Sauvage, and R. Ziessel, *Nouv. J. Chim.*, **3**, 423 (1979).

7) G. Rothenberger, P. P. Ingelta, and M. Gratzel, *J. Phys. Chem.*, **83**, 1879 (1979).

8) Y. Kurimura and R. Onimura, *Inorg. Chem.*, **19**, 3516 (1980).

9) Y. Kurimura, H. Yokota, and Y. Muraki, *Bull. Chem. Soc. Jpn.*, **54**, 2450 (1981).

10) R. H. Schehl, L. G. Whitesell, and D. G. Whitten, *J. Am. Chem. Soc.*, **103**, 3761 (1981).

11) Y. Kurimura, N. Shinozaki, F. Ito, Y. Uratani, T. Shigehara, E. Tsuchida, M. Kaneko, and A. Yamada, *Bull. Chem. Soc. Jpn.*, **55**, 380 (1982).

12) A. T. Thornton and G. S. Laurence, *J. Chem. Soc., Chem. Commun.*, **1978**, 408.

13) P. C. Lee and D. Meisel, *J. Am. Chem. Soc.*, **102**, 5477 (1980).

14) Y. Kurimura, M. Nagashima, K. Takato, E. Tsuchida, M. Kaneko, and A. Yamada, *J. Phys. Chem.*, **86**, 2432 (1982).

15) R. A. Palmer and T. S. Piper, *Inorg. Chem.*, **5**, 864 (1966).

16) E. B. Sandell, "Colorimetric Determination of Traces of Metals," 2nd ed, Interscience, New York (1950), p. 572.

17) No appreciable amount of the MV^+ was eluted into the bulk of the solution during the illumination. Such a large adsorbability of the monopositive charged species of MV^+ on the cation-exchange resin may be attributable to both the electrostatic and hydrophobic interactions between the MV^+ and the resins.[18]

18) Y. Kurimura, H. Yokota, T. Shigehara, and E. Tsuchida, *Bull. Chem. Soc. Jpn.*, **55**, 55 (1982).

19) The amounts of $Ru(bpy)_3^{2+}$, MV^{2+}, and MV^+ adsorbed on the cation-exchange resin are conveniently represented as [Ru(II)], $[MV^{2+}]$, and $[MV^+]$ respectively, while the unit of the "concentration" is denoted by mol g^{-1}.

The Lowest Triplet State of 2-Methylpyrazine

Takeshi WATANABE, Hiroko SHIMADA,† and Ryoichi SHIMADA*

Department of Chemistry, Faculty of Science, Kyushu University 33, Hakozaki, Higashi-ku, Fukuoka 812

†Department of Chemistry, Faculty of Science, Fukuoka University, Nanakuma, Nishi-ku, Fukuoka 814

(Received February 1, 1982)

The infrared and Raman spectra of 2-methylpyrazine were studied. An assignment was given for all fundamental vibrations based on the polarization behavior of the spectral bands and on the normal coordinate analysis. The magnetic effect on the phosphorescence lifetime and the time-resolved and polarized phosphorescence spectra of this molecule were investigated at 1.4 K. From the analysis of the phosphorescence, (1) the short lifetime phosphorescence was assigned to the emission arising from the most emissive y″ sublevel, as in the case of pyrazine, (2) the long lifetime phosphorescence was assigned to the emissions arising from the x and z″ sublevels, whose lifetimes were roughly equal to each other and (3) the 0-0 and totally symmetric vibronic bands, and the out-of-plane vibronic bands observed in the long lifetime phosphorescence, were ascribed to the z″ and x sublevel emissions, respectively.

The lowest triplet state of pyrazine was assigned to a $^3B_{3u}(n, \pi^*)$ state by Goodman and Kasha[1] and Innes and Gidding.[2] Zalewski, McClure, and Narva[4] pointed out that the lowest triplet state was strongly perturbed by low lying $^3(\pi, \pi^*)$ states through H wagging ν_5 and ν_{10a} vibrations. Through phosphoresscence microwave double resonance (PMDR) and microwave induced delayed phosphorescence (MIDP), a number of workers have discussed the molecular structure of pyrazine in the lowest triplet state and suggested that the molecule, whose equilibrium structure belongs to the point group D_{2h}, whould be distorted to C_{2h} or lower symmetry.[4-7]

Lim *et al.*[8] carried out the vibrational analyses of the phosphorescence spectra of pyrazine and its methyl derivatives at 4.2 K and studied the proximity effects on the $T_1 \rightsquigarrow S_0$ radiationless transitions. The enhancement of the radiationless $T_1 \rightsquigarrow S_0$ rate due to methyl substitution was attributed to the distorsion of the potential surface for the T_1 state due to the decrease of energy separation between vibronically coupled states.

The study of the phosphorescence process of 3-methylpyrazine should be very interesting because the energy separations between $^3W(n, \pi^*)$ and $^3L_a(\pi, \pi^*)$ states, and $^3W(n, \pi^*)$ and $^3L_b(\pi, \pi^*)$ states are closer than in the case of pyrazine due to methyl substitution. In this paper, an assignment for the normal vibrations of 2-methylpyrazine will be given and then the phosphorescence process, vibronic coupling between (n, π^*) and (π, π^*) states, and distorsion of the molecular structure in the lowest triplet state will be discussed.

Experimental

Material. 2-Methylpyrazine obtained from Aldrich Chemical Company was purified by repeated vacuum distillation followed by zone-refining (about 60 passages). Methylcyclohexane of Dotite Spectrosol grade and *m*-xylene of Merck Reference Substance for gas chromatography were used without further purification. *p*-Dibromobenzene obtained from Wako Chemical Industry was purified by zone-refining (about 60 passages), followed by sublimation under reduced pressure.

Optical Measurement. The Raman spectrum was observed in the liquid and solid phases with a JEOL 400T Laser Raman Spectrophotometer. The sample was excited with the 514.5 nm line from an Ar^+ ion laser of Toshiba Model LAI-104-A. The depolarization measurement of the individual Raman bands was also made in the liquid.

The infrared spectrum was measured with a Hitachi Infrared Spectrophotometer Model 345 over the range of 4000—250 cm^{-1} in the vapor, liquid, and solid phases. The vapor spectrum was observed at 50 °C with a gas cell 10 cm in optical path. The polarized infrared spectrum was observed in the single crystal with an AgBr wire-grid polarizer by the method described in the previous paper.[9]

The phosphorescence lifetime and spectrum were studied at 1.4 K in methylcyclohexane and *p*-dibromobenzene by the method described in the previous paper.[10] The polarized phosphorescence spectrum of 2-methylpyrazine doped in a *p*-dibromobenzene single crystal was observed at 1.4 K along a, b, and c crystal axes. The single crystal grown in the Bridgman furnace was cut along the cleavage bc plane with a razor. The b and c crystal axes were determined optically with polarized light. Then the crystal was cut along the ac and ab planes. The crystal specimen was held in the dewar so that the normal of the ab or bc plane coincided with the optical axis of the spectrophotometer. The phosphorescence spectra polarized along the a and b axes, or along the b and c axes, were observed. Thus, the relative intensities of individual phosphorescence bands polarized along the a, b, and c axes were obtained.

The magnetic effect of the phosphorescence lifetime of 2-methylpyrazine doped in a *p*-dibromobenzene single crystal was studied at 1.4 K. The sample was set between two poles of a Komatsu Type 100 Electromagnet, which applied a constant magnetic field of 3 K Gauss to the sample. Excitation light from a xenon short arc lamp of Ushio Type UXL-500D was focused on the sample through a Corning glass filter and a solution filter, which acted as a thermal radiation cut filter. The decay of the 0-0 band of the phosphorescence was observed with an oscilloscope by rotating the sample about the crystal axes. The angle between the crystal axis and the magnetic field was calibrated in the following way. After a measurement of the lifetime was over, the xenon lamp was replaced by a miniature lamp. Weak light from the miniature lamp was reflected by the crystal surface in the dewar. The crystal was rotated about the vertical axis, that is, the axis perpendicular to both the magnetic field and the excitation (and phosphorescence) beam, so that the light reflected from the crystal surface went back to the miniature lamp. In this case, the normal of the crystal surface was to coincide with the direction of the excitation beam. The angle of rotation of the crystal directly gave the orientation of

the crystal under measurement.

Procedure of Normal Coordinate Calculation. A normal coordinate calculation was performed through the standard GF matirx method with a FACOM M-200 computer at the computer center of Kyushu University. Although the molecular structure of 2-methylpyrazine was not determined yet, it was assumed that the molecular structure belongs to roughly the C_s point group and that the geometric parameters of the ring and the CH_3 group were nearly identical with those of pyrazine[11] and toluene,[12] respectively. The F matrix elements for the in-plane and out-of-plane vibrations were evaluated with an improved modification of the Urey-Bradley force field given by Cossee and Schachtschneider[13] and with the valence force field, respectively, as described in the previous paper.[9]

Results and Discussion

Normal Vibration. Force constants for the in-plane and out-of-plane vibrations finally obtained after several iterative calculations are given in Tables 1 and 2, respectively. The internal coordinates for the in-plane and out-of-plane vibrations are illustrated in Fig. 1. The calculated vibrational frequencies and modes are given in Table 3.

The infrared spectrum observed in the single crystal and the Raman spectrum observed in the liquid phase are shown in Figs. 2 and 3, respectively. The polarized infrared spectrum measured with the incident light beams polarized parallel and perpendicular to the direction of the crystal growth of the single crystal will be referred to as // and ⊥ spectra, respectively: these are drawn with solid and dotted lines, respectively.

The polarized infrared bands observed in the single crystal could be classified into two types according to their polarization character. The bands belonging to the first type appear strongly in the // spectrum and weakly in the ⊥ spectrum, while the second type bands appear strongly in the ⊥ spectrum and weakly in the // spectrum. These two types of the bands will be referred to as types A and B, respectively.

Table 1. In-plane force constants

$K_{N-C}=K_{N-C'}$	5.60	$F_{C\cdots C''}$	0.65
$K_{C-C'}=K_{C-C}$	4.45	$F_{C\cdots H}=F_{C'\cdots H'}$	0.50
$K_{C'-C''}$	3.20	$F_{N\cdots H}=F_{N\cdots H'}$	0.41
$K_{C-H}=K_{C-H'}$	4.50	ρ	0.32
$K_{C''-H''}$	4.56	$k^o_{r,r}$	0.07
H_{C-N-C}	0.30	$k^o_{r,r''}$	0.30
$H_{C'-N-C}$	0.30	$k^o_{r'',r''}$	0.20
$H_{N-C'-C}$	0.48	$k^m_{r,r}$	0.06
$H_{N-C-C}=H_{N-C-C'}$	0.45	$h^m_{R,\alpha}$	−0.10
$H_{N-C'-C''}=H_{C-C'-C''}$	0.15	$h^m_{R,\alpha'}$	−0.02
$H_{C-C-H}=H_{C'-C-H}$	0.25	$h^m_{R,\beta}=h^m_{R,\beta'}$	0.03
H_{N-C-H}	0.24	$f^o_{\alpha,\alpha}=f^o_{\alpha,\alpha'}$	0.06
H_μ	0.45	$f^o_{\beta,\beta}=f^o_{\beta,\beta'}$	0.10
H_ν	0.53	$f^o_{\mu,\mu}$	0.005
$F_{C\cdots C}=F_{C\cdots C'}$	0.90	$f^o_{\nu,\nu}$	−0.04
$F_{N\cdots C}=F_{N\cdots C'}$	0.70	$f_{\tau,\mu}$	0.30
$F_{N\cdots C}$	0.90	$f_{\tau,\nu}$	0.35

Force constants denoted by K, H, F, and k are given in J/dm²(=mdyn/Å) units, and those denoted by h and f are in pJ/dm·rad(=mdyn/rad) and aJ/rad² (=mdynÅ/rad²) units, respectively.

Table 2. Out-of-plane force constants

$Q_{C-N}=Q_{C'-N}$	0.20 aJ/rad²
$Q_{C-C}=Q_{C'-C}$	0.22
$Q_{C'-C''}$	0.077
P_H	0.31
$P_{H'}$	0.24
$P_{C''}$	0.22
$q^o_{\tau,\tau}$	−0.06
$q^o_{\tau,\tau'}$	−0.01
$q^m_{\tau,\tau}$	−0.008
$p^o_{H,H}$	0.075
$p^o_{H',C''}$	0.055
$p^m_{H,H'}=p^m_{C'',H}$	−0.055
$t^o_{\tau,H}=t^o_{\tau,H'}$	−0.02
$t^m_{\tau,H}=t^m_{\tau,H'}=t^m_{\tau',H'}$	−0.02
$t^m_{\tau,C''}$	−0.005
$f^o_{\tau',\mu}$	0.30
$f^o_{\tau',\nu}$	0.35

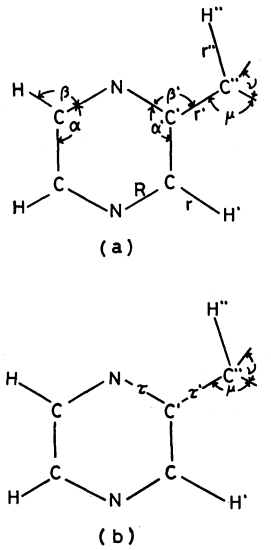

Fig. 1. Internal coordinates for the in-plane (a) and out-of-plane (b) vibrations.

Calculation of the principal moments of inertia indicates that the c axis of the moment is perpendicular to the molecular plane, the a axis is directed nearly along the C–CH_3 bond, and the b axis is perpendicular to both a and c axes. These axes will be referred to as the molecular axes. Careful observation of the rotational band envelopes of the infrared bands observed in the vapor phase showed that the bands could be classified into three types: A, B, and C, according to Ueda and Shimanouchi.[14]

In-plane Vibration: Bands observed at 342, 1031, and 1065 cm^{-1} in the infrared vapor spectrum showed a typical B band envelope and the corresponding bands in the single crystal showed type B character. Bands observed at 631, 1255, 1308, and 1408 cm^{-1} in the vapor showed a typical A band envelope and the corresponding single crystal bands showed type A

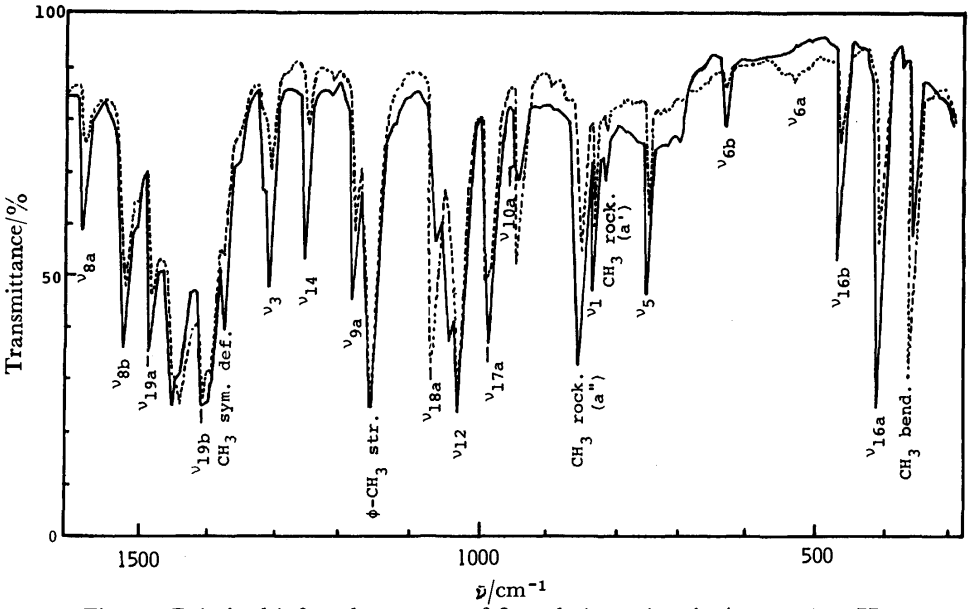

Fig. 2. Polarized infrared spectrum of 2-methylpyrazine single crystal at 77 K.

character. Normal coordinate and INDO calculations suggested that the transition moments of CH_3 bending, ν_{12} and ν_{18a} vibrations lie nearly along the molecular b axis, while those of ν_{6b}, ν_{14}, ν_3, and ν_{19b} vibrations nearly along the molecular a axis. These results definitely indicate that the bands at 342, 1031, and 1065 cm^{-1} should be assigned to CH_3 bending, ν_{12} and ν_{18a}, respectively, and the bands at 631, 1255, 1308, and 1408 cm^{-1} to ν_{6b}, ν_{14}, ν_3, and ν_{19b} vibrations, respectively.

The in-plane vibrations, which correspond to the vibrations belonging to the a_1 and b_2 species in the point group C_{2v}, are the totally symmetric vibrations in 2-methylpyrazine. However, it is expected that the bands which come from the a_1 species will show strongly polarized character and the bands which come from the b_2 species will show somewhat depolarized character in the depolarization measurement of the Raman spectrum. Therefore, the strongly polarized Raman bands at 3056, 3038, 1580, 1480, 1176, 1058, 1022, 826, and 556 cm^{-1} were assigned to ν_2, ν_{13}, ν_{8a}, ν_{19a}, ν_{9a}, ν_{18a}, ν_{12}, ν_1, and ν_{6a}, respectively, and the depolarized Raman band at 1529 cm^{-1} to ν_{8b}. Polarized Raman bands at 1247, 1154, and 635 cm^{-1} could be assigned to ν_{14}, C–CH_3 stretching, and ν_{6b} vibrations, respectively, since calculation suggested that these vibrations have the transition moments nearly along the C–CH_3 bond.

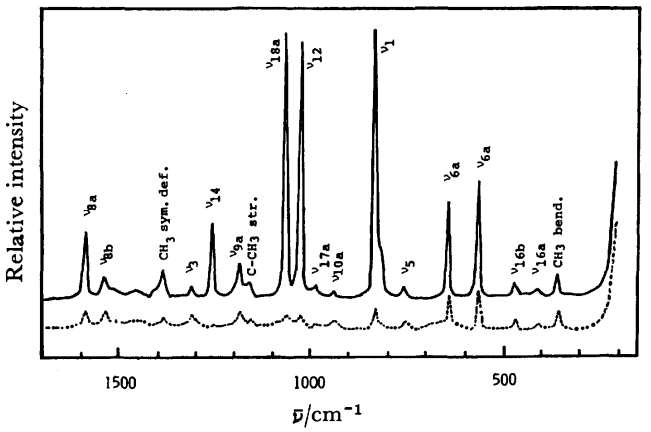

Fig. 3. Raman spectrum at room temperature.

Out-of-plane Vibration: Infrared bands observed at 404, 462, 751, and 831 cm^{-1} in the vapor showed quite clearly a C band envelope and the corresponding infrared single crystal bands showed type A polarization character. Hence, these bands were assigned to the out-of-plane ν_{16a}, ν_{16b}, ν_5, and CH_3 rocking vibrations (a″ species), respectively. The corresponding infrared single crystal bands showed type A polarization character. The other five out-of-plane vibrations of ν_{17a}, ν_{10a}, ν_4, CH_3 wagging, and C–CH_3 torsional vibrations were assigned to depolarized Raman bands observed at 975, 929, 720, 203, and 169 cm^{-1}, respectively. The corresponding infrared single crystal bands at 985 and 948 cm^{-1} showed type A character.

The characteristic vibrations for the CH_3 group were determined based on the observed polarization characters as well as on the normal coordinate calculation. The normal vibrations assigned are summarized in Table 3. The agreement between observed and calculated frequencies is satisfactory.

Phosphorescence. Magnetic Effect on the Phosphorescence Lifetime: Analysis of the phosphorescence decay observed at 1.4 K gave lifetimes of 6.2 and 80 ms in methylcyclohexane and 14 and 37 ms in *p*-dibromobenzene. We tried to identify the three sublevel decays through the MIDP technique, but the MIDP signals were too weak to detect the decays clearly. Therefore, the magnetic effect on the phosphorescence lifetime was studied in the *p*-dibromobenzene host single crystal at 1.4 K in order to investigate the emitting sublevels and to find the unknown third lifetime phosphorescence.

It is necessary to know what orientation a 2-methylpyrazine molecule takes in the *p*-dibromobenzene host crystal. The *p*-dibromobenzene single crystal is known to belong to the space group $P2_{1/a}$ with $Z=2$ and the

TABLE 3. NORMAL VIBRATIONS OF 2-METHYLPYRAZINE

Sym. species	Vibrational mode	Raman Liquid $\bar{\nu}$/cm^{-1}	Rel. int.	Pol.	Infrared Single crystal $\bar{\nu}$/cm^{-1}	Rel. int.	Pol.	Vapor Pol.	Calcd $\bar{\nu}$/cm^{-1}
a′	ν_2 C–H str.	3056	0.5	p					3058
	ν_{13} C–H str.	3038	1	p					3034
	ν_{8a} Ring	1580	2	p	1587	4	A		1573
	ν_{19a} Ring	1480	0.1	p	1487	5	A	A	1489
	ν_{9a} H bend.	1176	1	p	1183	6	A		1170
	ν_{18a} H bend.	1058	10	p	1063	7	B	B	1070
	ν_{12} Ring	1022	8	p	1027	9	B	B	1022
	ν_1 Ring	826	10	p	830	5	A		820
	ν_{6a} Ring	556	4	p	557	1	B		552
	ν_{7b} C–H str.	3005	0.1	?	3003[a]	3			3004
	ν_{8b} Ring	1529	0.5	dp	1530	7	A		1518
	ν_{19b} Ring	1395	0.3	dp	1405	9	A	A	1397
	ν_3 H bend.	1300	0.5	dp	1309	6	A	A	1303
	ν_{14} Ring	1247	3	p	1254	5	A	A	1249
	ν_{20b} C–CH_3 str.	1154	0.5	p	1156	9	A?		1154
	ν_{6b} Ring	635	4	p	640	2	A	A	637
	ν_{15} CH_3 bend.	352	1	dp	359	9	B	B	356
a″	ν_{17a} H wag.	975	0.5	dp	985	6	A		977
	ν_{10a} H wag.	929	0.5	dp	948	2	A		925
	ν_{16a} Ring	405	0.3	dp	409	10	A	C	407
	ν_5 H wag.	748	0.5	dp	752	6	A	C	750
	ν_4 Ring	720	0.1	?					718
	ν_{16b} Ring	464	0.5	dp	467	6	A	C	461
	ν_{11} CH_3 wag.	203	4	dp					202
	C–CH_3 tor.	169	0.2	?					169
Characteristic vibrations of CH_3 group									
a′	Sym. C–H str.	2928	2	p	2930[a]	2			2931
a′	Antisym. C–H str.	2865	0.2	?	2867[a]	0.5			2860
a′	CH_3 sym. def.	1377	1	p	1376	4	A		1377
a′	CH_3 degen. def.	1440	0.1	dp	1438	6	B		1441
a″	CH_3 degen. def.	1450	0.2	dp	1448	6	A		1456
a′	CH_3 rock.	813	1	dp	816	2	A		814
a″	CH_3 rock.	840[b]	0.2		847	7	A	C	838

a) Vapor. b) Solid.

site group C_i. The van der Waals radii of the methyl group and of hydrogen and bromine atoms may suggest that a *p*-dibromobenzene molecule in the crystal is replaced by a 2-methylpyrazine molecule with the C–CH_3 bond parallel to the Br–Br direction. Thus, the 2-methylpyrazine molecule could take four different orientations; two of these are the same due to the C_i site group symmetry. Therefore, the 2-methylpyrazine molecule could take two different orientations in the *p*-dibromobenzene crystal.

If the 2-methylpyrazine molecule could take two orientations equally, the intensity ratio of the 0-0 bands of the phosphorescences polarized along the b and a crystal axes would be calculated to be 1.9 from the crystal data given by Bezzi and Croatto.[15] The observed ratio was greater than 4 and no splitting of the 0-0 band of the unpolarized phosphorescence spectrum was observed under high resolution. These facts prove that the 2-methylpyrazine molecule could take only one orientation in the *p*-dibromobenzene host crystal.

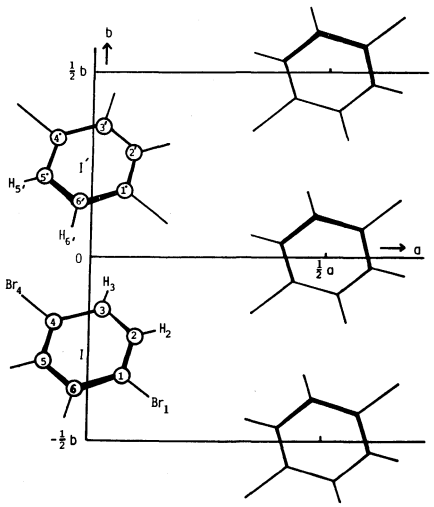

Fig. 4. Projection of *p*-dibromobenzene single crystal on the ab crystal plane.

The two nearest neighbor molecules, labeled I and I′, are shown in Fig. 4. The calculation of the intermolecular atomic distances using the crystal data showed that the distance of H_3–$H_{6'}$ is shorter than that of H_3–$H_{5'}$ and the distance of H_3–$C_{6'}$ is also shorter than that of H_3–$C_{5'}$. Thus, the hydrogen-hydrogen repulsion force between H_3 and $H_{6'}$ would be stronger than that between H_3 and $H_{5'}$ and the hydrogen bonding attraction between H_3 and $C_{6'}$ would be stronger than that between H_3 and $C_{5'}$, if $C_{6'}$ and $C_{5'}$ atoms are replaced with N atoms. These considerations clearly suggest that N atoms of 2-methylpyrazine should occupy the positions of $C_{3'}$ and $C_{6'}$, and thus, the N–N axis and the normal of the 2-methylpyrazine plane are nearly parallel to the b and c crystal axes, respectively.

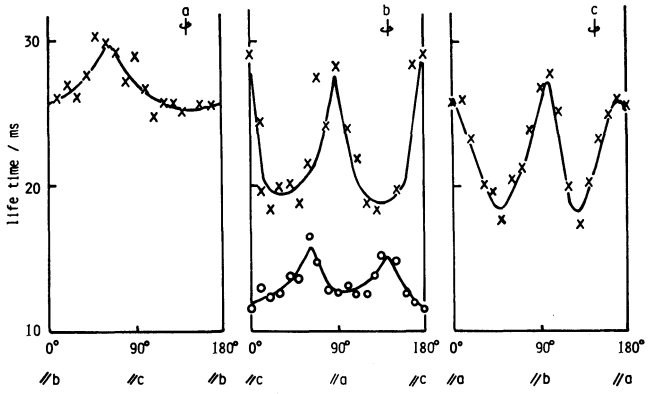

Fig. 5. Magnetic effect on the phosphorescence lifetime. a indicates rotation of the crystal about the a crystal axis. × and ○ indicate long and short lifetimes, respectively.

The magnetic effect on the phosphorescence lifetime is shown in Fig. 5. A remarkable change of the lifetime was observed for the long lifetime phosphorescence by rotation of the crystal about the a, b, and c crystal axes. If the third lifetime, which could not be resolved, were nearly equal to the short lifetime 14 ms, the observed long lifetime would become longer only when the spin axis of the long lifetime sublevel is parallel to the magnetic field. In other orientations of the spin axis, the long lifetime sublevel would mix with the short lifetime sublevels and the observed lifetime would become shorter. In other words, the observed long lifetime would become longer only at two orientations of the crystal, where the spin axis of the long lifetime sublevel is parallel to the magnetic field. But the observed results showed that the long lifetime became longer at more than two orientations of the crystal, as can be seen in Fig. 5. That is, the observed magnetic effect on the long lifetime phosphorescence did not support the assumption that the third lifetime is nearly equal to the short lifetime.

If the third lifetime is nearly equal to the long lifetime, 37 ms, the observed long lifetime would become longer whenever the spin axis of one of the two long lifetime sublevels is parallel to the magnetic field or whenever the spin axes of both the long lifetime sublevels are perpendicular to the magnetic field. In other words, a longer lifetime will be observed when any one of the three spin axes is parallel to the magnetic field. This is exactly consistent with the observation. Thus, it was concluded that the phosphorescence consists of three emission components: one is short and the others are long in lifetime, as in the cases of pyrazine[16] and 2,6-dimethylpyrazine.[17]

The magnetic effect on the short lifetime phosphorescence will be discussed next. An appreciable change of the lifetime was observed only for the rotation of the crystal sample about the b axis. This may suggest that the short lifetime sublevel would not be so sensitive to the mixing, compared with the long lifetime sublevel. Let the decay rate constants of the short and long lifetime sublevels be k_s and k_l, respectively. If the two sublevels mix with each other with a mixing ratio of a/b, the rate constants k_s and k_l may change to $k_{s'}=ak_s+bk_l$ and $k_{l'}=ak_l+bk_s$, respectively, where $a+b=1$. Thus, the new short and long lifetimes are given by $\tau_{s'}=1/(ak_s+bk_l)$ and $\tau_{l'}=1/(ak_l+bk_s)$, respectively. The observed ratio of the rate constants k_s/k_l was approximately 3/1. In our experiment, the magnetic perturbation was not strong enough and thus a would be greater than b. Hence, the magnetic dependence on the short lifetime phosphorescence is expected to be much less sensitive than that on the long lifetime phosphorescence.

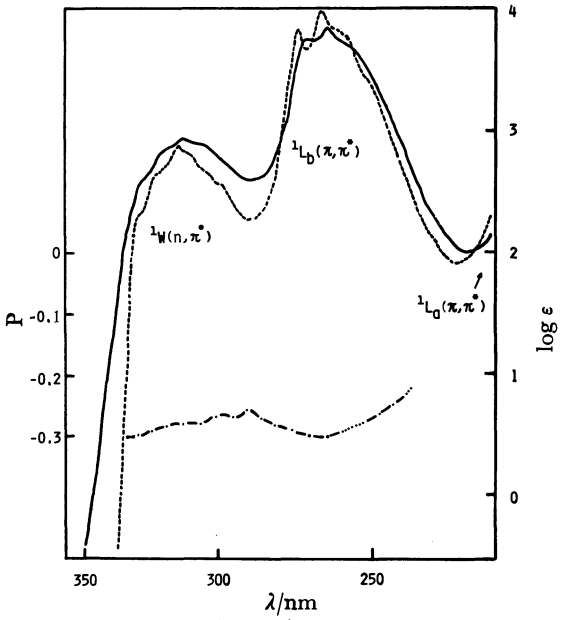

Fig. 6. Near ultraviolet absorption spectrum (—— at 20 °C, ------ at 77 K) and excitation polarization spectrum (-·-·-) monitoring the intensity of the 0-0 band of the phosphorescence at 77 K in EPA.

Phosphorescence Process: The excitation polarization spectrum obtained by the photoselection experiment in EPA at 77 K is shown in Fig. 6, together with the absorption spectrum. These spectra clearly indicate that the lowest triplet state is a $^3W(n, \pi^*)$ perturbed by the $^1L_a(\pi, \pi^*)$ state, as in the case of pyrazine. The coordinate axis for this molecule was taken in such a

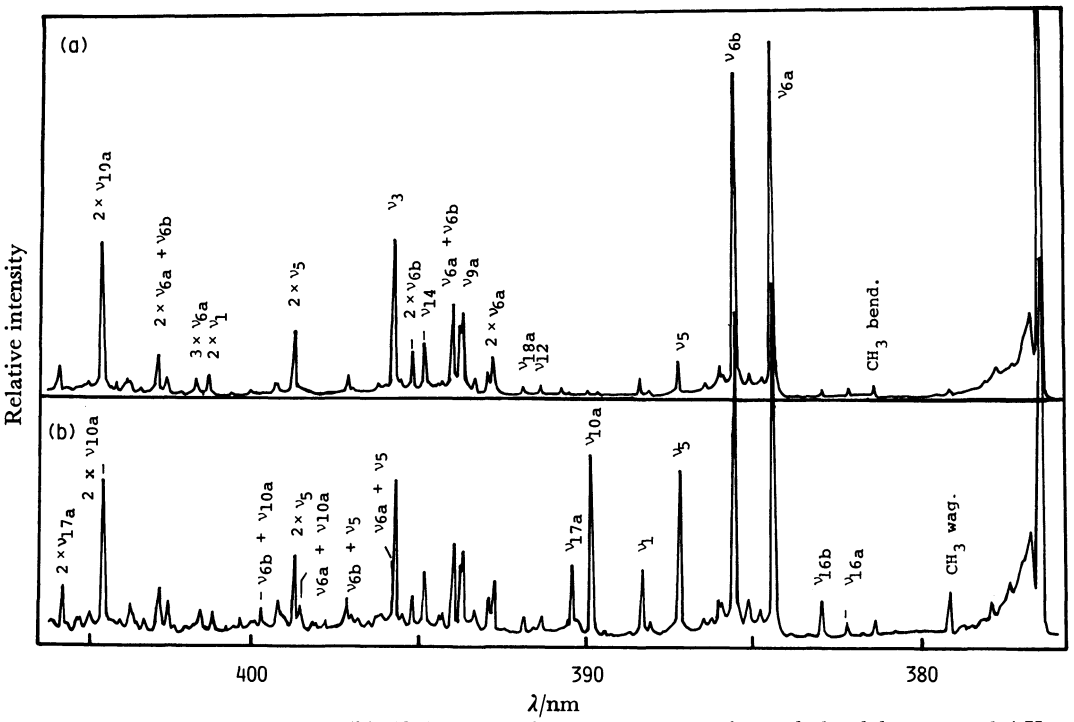

Fig. 7. Short (a) and long (b) lifetime phosphorescence spectra in methylcyclohexane at 1.4 K.

way that the x axis is perpendicular to the molecular plane and the z axis is along the N–N direction. Althrough the axis of the diagonalized spin functions of this molecule is not known, we could suppose that the x″ spin axis may coincide with the x axis and y″ and z″ spin axes would be roughly parallel to the y and x axes, respectively. The spin-orbit coupling matrix element between the $^1L_a(\pi, \pi^*)$ and $^3W(n, \pi^*)$ states gives the atomic integral of $\langle p_z|Hso|p_x\rangle$, where the most effective angular momentum operator is L_y. Hence, we may conclude that the short lifetime phosphorescence may arise from the y″ sublevel of the lowest triplet state, as in the case of pyrazine.

The time-resolved phosphorescence spectrum in methylcyclohexane at 1.4 K is shown in Fig. 7. The short lifetime phosphorescence spectrum was observed in the following way. The sample was excited for 5 ms and the excitation was cut off. 1 ms after ceasing the excitation, the phosphorescence was sampled for 5 ms. The observed spectrum might contain the bands due to the long lifetime phosphorescence, but their intensity is expected to be very weak; hence, all bands of the spectrum except for extremely weak bands could be safely ascribed to the short lifetime phosphorescence. The long lifetime phosphorescence was observed with 100, 100, and 100 ms of the excitation, waiting, and sampling times, respectively. Intensity ratio of the 0-0 bands of the long and short lifetime phosphorescence spectra at $t=0$, when the excitation of the sample was cut off, was calculated to be about 1/30. The spectra shown in Fig. 7 are drawn after normalizing the observed intensities of the 0-0 bands of the short and long lifetime phosphorescences to unity.

The vibrational analysis of the short lifetime phosphorescence will be discussed first. The shortest wavelength band at 376.55 nm, whose intensity is the strongest in the spectrum, was taken as the 0-0 band. Strong bands separated by 557, 636, 1175, 1248, and 1303 cm^{-1} from the 0-0 band were assigned to ν_{6a}, ν_{6a}, ν_{9b}, ν_{14}, and ν_3 vibrations, respectively. The overtone and combination bands of these vibrations were observed with medium intensity.

Medium intense bands separated by 750 and 926 cm^{-1} from the 0-0 band were ascribed to ν_5 and ν_{10a} vibrations, respectively. Progressions of the ν_5 and ν_{10a} vibrations extending up to four quanta were observed with strong intensity in the even quanta and weak intensity in the odd quanta. Extremely weak bands assigned to CH_3 wagging, ν_{16a}, ν_{16b}, and ν_{17a} vibrations were also observed.

Although the long lifetime phosphrescence gave essentially the same spectral structure as that of the short lifetime phosphorescence, the most characteristic feature of the long lifetime spectrum was the remarkable intensification of the bands assigned to the out-of-plane CH_3 wagging, ν_{16b}, ν_5, ν_{10a}, ν_{17a}, and the totally symmetric ν_1 vibrations. The bands assigned to the totally symmetric ν_{6a}, ν_{6b}, ν_{9a}, ν_{14}, and ν_3 vibrations were also observed with strong intensity in the long lifetime spectrum.

The short lifetime phosphorescence cannot sneak into the long lifetime spectrum, because the population of the y″ sublevel must decay out during 100 ms of the waiting time for sampling the phosphorescence. Therefore, the bands assigned to the totally symmetric vibrations observed in the long lifetime spectrum should be ascribed to the bands arising from the x and/or z″ sublevels.

The time-resolved phosphorescence spectrum was also studied in *p*-dibromobenzene at 1.4 K. The short and

long lifetime phosphorescence showed essentially the same spectral structures as those observed in methylcyclohexane. The polarized long lifetime phosphorescence spectrum of 2-methylpyrazine doped in a *p*-dibromobenzene host single crystal was observed at 1.4 K. The phosphorescence spectra polarized along the a, b, and c crystal axes are shown in Fig. 8, where the intensity of the band polarized along the c axis was normalized to unity.

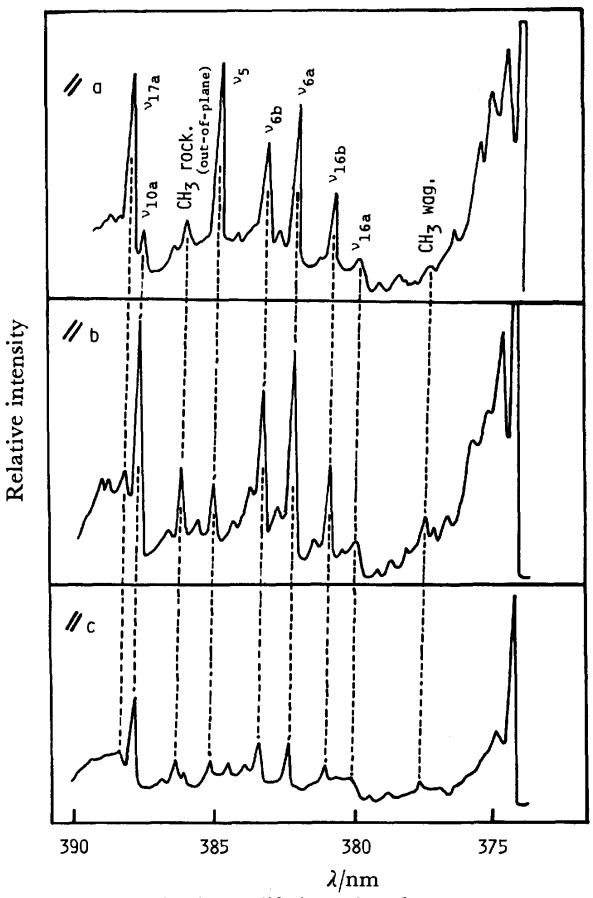

Fig. 8. Polarized long lifetime phosphorescence spectrum in *p*-dibromobenzene single crystal at 1.4 K.

Let the direction of the transition moments of the $^1W(n, \pi^*)\leftarrow S_0$, $^1L_b(\pi, \pi^*)\leftarrow S_0$, and $^1L_a(\pi, \pi^*)\leftarrow S_0$ absorptions be x, y′, and z′, respectively. The INDO calculation indicates that the z′ axis is in between the N–N and C–CH_3 axes and that the y′ axis is perpendicular to both x and z′ axes. Thus, we could suppose that the x, y′, and z′ axes are roughly parallel to the c, a, and b crystal axes, respectively.

Observed polarized spectra showed that the ν_5 and ν_{17a} bands were strongly polarized along the a crystal axis, the bands ascribed to CH_3 wagging, ν_1 and ν_{10a} vibrations were strongly polarized along the b axis, and the 0-0, ν_{6a}, ν_{6b}, ν_{16a}, and ν_{16b} bands were equally polarized along the b and a axes. These observations indicate that the first two y′ polarized vibronic bands get their intensities from the $^1L_b\leftarrow S_0$, the second three z′ polarized bands from the $^1L_a\leftarrow S_0$, and the last five y′ and z′ polarized bands from the $^1L_a\leftarrow S_0$ as well as the $^1L_b\leftarrow S_0$ transitions.

TABLE 4. POLARIZATION DIRECTION OF THE PHOSPHORESCENCE BAND EMITTED FROM EACH SUBLEVELS OF THE LOWEST TRIPLET STATE

Band	Sublevel	Polarization direction
0-0 and in-plane vibronic	x	x
	y″	y′, z′
	z″	y′, z′
Out-of-plane vibronic	x	y′, z′
	y″	x
	z″	x

Polarization directions of the phosphorescence bands emitted from each sublevel of the lowest triplet state are given in Table 4. It was already concluded that the long lifetime phosphorescence consists of two emissions arising from x and z″ sublevels whose lifetimes are roughly equal. Table 4 definitely indicates that the y′ and z′ polarized 0-0 and totally symmetric vibronic bands should be attributed to the emission arising from the z″ sublevel, and the y′ and/or z′ polarized out-of-plane vibronic bands to the emission arising from the x sublevel.

The observed long progressions of the ν_5 and ν_{10a} vibrations extending up to four quanta with strong intensity in the even quanta and relatively weak intensity in the odd quanta suggest that the potential surfaces for these normal coordinates would not be harmonic in the lowest triplet state. Such remarkable ν_5 and ν_{10a} progressions are not observed in pyrazine, and thus the unharmonicity of the potentials for 2-methylpyrazine is expected to be much greater than that for pyrazine.

It should be noted that the observed long lifetime of about 80 ms for 2-methylpyrazine is much shorter than the longest lifetime of about 300 ms for pyrazine. This may be due to the low symmetry of the 2-methylpyrazine molecule caused by methyl substitution.

The authors wish to express their thanks to Dr. Motohiko Koyanagi for his valuable discussions. They are also indebted to Mr. Yoshinori Nibu for his help in the experimental work.

References

1) L. Goodman and M. Kasha, *J. Mol. Spectrosc.*, **2**, 58 (1958).
2) K. K. Innes and L. E. Gidding, *Discuss. Faraday Soc.*, **35**, 192 (1963).
3) E. F. Zalewski, D. S. McClure, and D. L. Narva, *J. Chem. Phys.*, **61**, 2964 (1974).
4) A. A. Gwaiz and M. A. El-Sayed, *Chem, Phys. Lett.*, **19**, 11 (1973).
5) K. Matsuzaki, M. Sasaki, and T. Azumi, *J. Chem. Phys.*, **65**, 3326 (1976).
6) K. Matsuzaki and T. Azumi, *J. Chem. Phys.*, **69**, 3907 (1978).
7) N. Nishi, M. Kinoshita, T. Nakashima, R. Shimada, and Y. Kanda, *Mol. Phys.*, **33**, 31 (1979).
8) S. L. Madej, G. D. Gillispie, and E. C. Lim, *Chem. Phys.*, **32**, 1 (1978).
9) S. Kizuki, Y. Ishibashi, H. Shimada, and R. Shimada,

Mem. Fac. Sci. Kyushu Univ., Ser. C, **13**, 7 (1981).
10) Y. Urabe, T. Watanabe, Y. Ishibashi, H. Shimada, and R. Shimada, *Mem. Fac. Sci. Kyushu Univ., Ser. C*, **13**, 1 (1981).
11) M. Scrocco, C. di Lauro, and S. Califano, *Spectrochim. Acta*, **21**, 571 (1965).
12) F. A. Keidel and S. H. Bauer, *J. Chem. Phys.*, **25**, 1218 (1965).
13) P. Cossee and J. H. Schachtschneider, *J. Chem. Phys.*, **44**, 97 (1966).
14) T. Ueda and T. Shimanouchi, *J. Mol. Spectrosc.*, **28**, 350 (1968).
15) S. Bezzi and V. Croatto, *Gazz. Chim. Ital.*, **72**, 318 (1942).
16) D. M. Burland and J. Schmidt, *Mol. Phys.*, **22**, 19 (1971).
17) K. Niimori, K. Fukuda, N. Nishi, and M. Kinoshita, Symposium on the Molecular Structure and Molecular Electronic Structure, Tokyo, October 1974, Abstr. No. 20A10.

Direct Measurement of the Interaction Energy between Solids and Gases. VIII. A High-temperature Calorimeter for the Determination of Heats of Adsorption from Room Temperature to 700 K

Kazuo Tsutsumi,* Seiichi Hagiwara,† Yoshio Mitani,†† and Horoshi Takahashi††

Toyohashi University of Technology, Tempaku-cho, Toyohashi 440

†*Tokyo Riko Co. Ltd., 3-2-16 Kita-machi, Hoya, Tokyo 188*

††*Institute of Industrial Science, The University of Tokyo, Roppongi, Minato-ku, Tokyo 106*

(Received February 4, 1982)

A high-temperature calorimeter of the twin conduction type was designed with the capability of measuring heats of adsorption of gases on solids in the temperature range RT to 700 K. A chromel-alumel thermopile was used as the detector and a volumetric adsorption apparatus was equipped. Its calibration and preliminary experiments on heats of adsorption of ammonia on zeolites are described.

Adsorption of gases on solids at higher temperature occurs, in many cases, by specific interaction of gases with solid surfaces. The energetical analysis of the interaction provides informations on activity and reactivity of solids, and permits effective use of catalysts, adsorbents, fillers and so on. Calorimetric studies on high temperature adsorption have been made mainly by means of dynamic methods such as DTA, TGA, DSC, or TPD. However, these methods are less satisfactory from the standpoint of quantitative analysis and difficult to examine active sites of surfaces in detail. Measurements of isosteric heats of adsorption from temperature change of adsorption are not adequate in view of the possibility that the characteristics of active sites vary with temperature. In particular, as chemisorption depends to a great extent on temperature and is often characterized by hysteresis, its mechanism and capacity cannot be estimated from equilibrium theory.[1] The temperature change of heats of chemisorption is often different from that expected from heat capacity.[2]

The present authors have already designed the adsorption calorimeter available near room temperature[3] and measured heats of adsorption of ammonia on solid acids.[4–9] However, evaluation of active sites must be the most useful when made at the same temperature as the working one. Therefore, direct measurement of heats of adsorption at higher temperature is indispensable.

This paper reports a newly designed microcalorimeter available from room temperature to 700 K for measurements of interaction energy between solids and gases. Heats of adsorption of ammonia on zeolites are measured as a preliminary experiment to illustrate the applications of this calorimeter.

Experimental

Apparatus. The calorimeter of the twin-conduction type; the detector part and cell are schematically illustrated in Fig. 1. Thermal effects were detected by use of a chromel-alumel thermopile (D) made of 128 thermocouples, amplified and recorded. The thermocouples are connected in series, placed in 8 directions and in 16 steps, insulated by alumina, and attached to the stainless-steel cell container (C). Two detectors are arranged in a differential and similar way in order to eliminate thermal effects other than the intended ones. Detectors and cell containers are set in a heat sink (E) made of

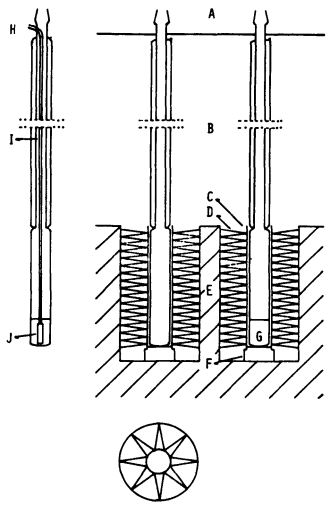

Fig. 1. Schematics of the calorimeter cell and detector. A: Volumetric adsorption line and manometer, B: thermal insulator, C: stainless-steel container, D: thermopile, E: heat sink, F: thermal insulator, G: sample, H: constant voltage circuit, I: platinum lead wire, J: platinum heater.

stainless-steel, the temperature of which is controlled to within $\pm 10^{-3}$K by monitering temperatures and operating noninductively wound Kanthal heaters at three different positions, bottom, side, and top regions. These parts are thermally insulated from the surroundings by bricks and ceramic fibers (B).

Sample and reference cells are made of pyrex or quartz glass, the upper part of which is of dewar-type for thermal insulation. They are symmetrically placed in the stainless-steel container (C) and the thermal insulator (F) in such a way that a good thermal contact is established between them. Both cells are joined together at the top and connected to the volumetric adsorption apparatus (A) outside the calorimeter through vacuum joints and stopcocks, then the dose of gases is introduced simultaneously into both cells. The pressure can be maintained below 1 mPa. Samples (G) in the cell can be heated under vacuum outside the calorimeter and reset in the calorimeter without being exposed to air.

The calibration cell is designed in the same way as for the sample or reference cell, in which a platinum heater (J) (176.7 Ω at 473 K) sealed in a glass tube was inserted, joined to a platinum lead wire (I) and connected to a constant voltage supply (H).

Calibration. In order to ascertain the reliability of the calorimeter, a known amount of electric voltage was fed to the heater and the saturation electromotive force obtained was plotted against the power. The calibration was carried out by feeding a Joule heat and measuring the area under the thermogram, *i.e.* time (t) *vs.* recorder response due to the temperature difference between the calibration cell and the reference cell (ΔT).

Heats of Adsorption. The adsorbent was NH_4–$Y_{4.7}$ zeolite, $0.93(NH_4)_2O \cdot 0.07Na_2O \cdot 4.7SiO_2 \cdot Al_2O_3$, which was obtained by conventional ion-exchange of Na-type zeolite. One gram (dehydrated and decationated basis) of the zeolite was placed in a sample cell and pretreated at 673 K under a pressure of 1 mPa for 10 h. The sample cell was set in a calorimeter and connected to a volumetric line. After the thermal equilibrium was established, a small quantity of adsorbate gas, ammonia, was admitted. The heat evolution was recorded and when the thermal equilibrium was reestablished, another dose of gas was admitted. The adsorption amount was determined by the pressure change before and after adsorption. Since the temperature gradient existed between the thermostated lower part and the top part of the cell, the dead volume of the system was determined by helium under the same conditions as those of calorimetric measurement. The minor temperature change at the gas reservoir which is placed outside the calorimeter was corrected for. The amount of heat evolved was determined by comparison of the area with the area under a calibration curve obtained as mentioned above.

Infrared Spectra. Infrared spectra of adsorbed ammonia which were obtained by the *in situ* method described elsewhere[7] were analyzed in order to interprete the calorimetric data.

Results and Discussion

Calibration of the Calorimeter. The calibration was carried out at 313, 373, 473, 573, and 673 K and the results are shown in Fig. 2. The test at 473 K was carried out under several conditions in order to examine influences of the heat capacity and the heat transfer: the heater was burried in different quantities of inert quartz powder and/or different amount of helium was maintained in the cell.

A linear correlation was obtained between the electrical power and the saturated electromotive force irrespective of calibration conditions; therefore the calibration can be separately carried out by use of the calibration cell. A quantitative determination of the heat by means of a conduction calorimeter is based on Tian's equation,[10]

$$dQ/dt = C \cdot d(\Delta T)/dt + \sigma \cdot \Delta T,$$

where dQ/dt refers to the heat evolved or absorbed in a unit time within the cell, C the heat capacity of the cell and detector, ΔT the temperature difference between the cell and the heat sink, and σ the apparent heat transfer coefficient. Therefore, the calorimeter cell should be devised in such a way that the heat evolved in the cell flows only through the detector to the heat sink. A linear relation of Fig. 2 implies that thermal leak along the wall of the cell could be neglected and that Tian's equation can be considered to hold in this system.

After the saturation, the electric current was turned off and then the cooling curve was obtained from which the time constant was calculated. The time constants with 6.5 g of quartz under 6.67 kPa of helium were 28.0, 22.7, 16.2, 12.2, and 9.0 min at 313, 373, 473, 573, and 673 K, respectively. The decrease with temperature may be explained on the basis of the possibility that, as temperature rises, the thermal flux becomes liable to transfer from the cell to the heat sink by means of radiation, convection or conduction through the thermopile, resulting in an increase in the value of σ.

An electrical energy was supplied through this heater during an appropriate length of time and areas obtained under the thermogram were plotted against the Joule heat in Fig. 3. In this temperature range, the area is proportional to the generated heat, which fact suggests that this calibration is applicable to determine quantitatively the heat evolved in the adsorption cell. A change of the time constant calculated from a change of the area by use of Tian's equation was consistent with that

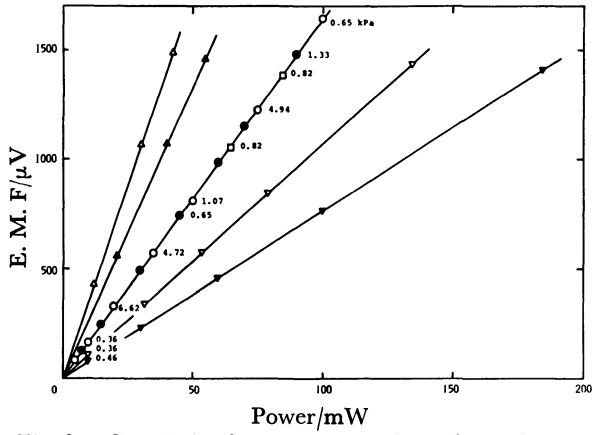

Fig. 2. Correlation between thermal powder and electromotive force.
△: At 313 K with 6.5 g of quartz and 6.67 kPa of He, ▲: at 373 K with 6.5 g of quartz and 6.67 kPa of He, ▽: at 573 K with 6.5 g of quartz and 6.67 kPa of He, ▼: at 673 K with 6.5 g of quartz and 6.67 kPa of He, ○: at 473 K with 21.5 g of quartz, □: at 473 K with 10.8 g of quartz, ●: at 473 K without quartz. The figures represent He pressure in the measurements at 473 K.

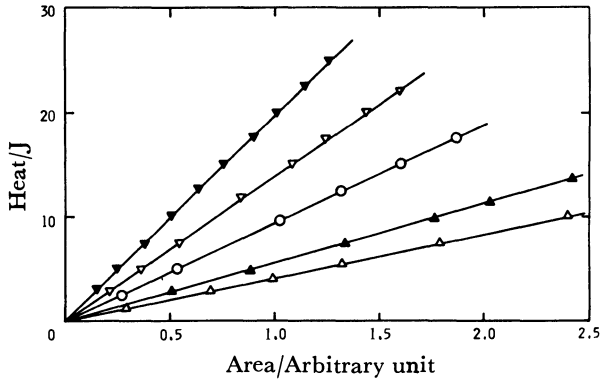

Fig. 3. Electrical calibration of the calorimeter.
△: 313 K, ▲: 373 K, ○: 473 K, ▽: 573 K, ▼: 673 K.

obtained from the cooling curve as mentioned above. When this calorimeter was used at lower temperature, calibration became more reliable, whereas an increase in the time constant resulted in the tailing phenomenon in the recorder response.

The sensitivity of this calorimeter at 473 K was 300 μJ/s within the error of 1% and the fluctuation below 0.25 μW/h. In favor of the twin system, the calorimeter response was not disturbed by thermal effects other than the intended reaction or adsorption. Such thermal effects were brought about by a temperature change of the surrounding or by a dose of gas. Two kinds of errors must result from the latter effect: the first is due to the work delivered to the cell by dosed gas and the second due to the temperature difference between dosed gas and the adsorbent. The simultaneous introduction of helium into adsorption and reference cells, the former of which contained one gram of zeolite, gave no appreciable thermal response, then the work delivered by dosed gas could be considered to be energetically cancelled. As to the second, although the upper part of the cell served to preheat an adsorbate, its temperature should be still different from that of the adsorbent. However, when the gas was preheated outside the calorimeter before being introduced, the heat value obtained was not different from the corresponding one obtained by the measurement without preheating. Therefore, the gas temperature effect was not corrected.

Heats of Adsorption of Ammonia on Decationated Zeolite. Acidic properties of decationated zeolites have been extensively studied by means of IR spectroscopy, amine titration and so on.[11,12] Calorimetric studies on acidities have also been made by many workers including the present authors.[1,3,7,13-15] The measurement of heats of adsorption of ammonia on zeolites can, therefore, be considered to be a good example to illustrate the application of the calorimeter.

The Brønsted acidity is formed on heating NH_4-type zeolites and originates from the hydroxyl groups. Heating the decationated zeolites to higher temperature results in a decrease in the concentration of Brønsted acid sites, accompanied by the formation of Lewis acid sites.[12]

In this study, NH_4–$Y_{4.7}$ zeolite was evacuated at 673 K and heats of adsorption of ammonia were measured at 473 K. An example of the thermogram of the heat evolved on adsorption of 0.071 mmol of ammonia is shown in Fig. 4 with the calibration thermogram. This adsorption amount corresponds to about one-three hundredth of the total adsorption capacity and about one-sixtieth of acid sites. Therefore, this calorimeter can provide information on fine structure of about one-several hundredth of active sites by considering the precision. The time required for one measurement depended on the adsorption amount as well as the temperature. The measurement at 473 K required from 100 to 150 min.

Differential heats of adsorption are given in Fig. 5. A lower curve shows the results of readsorption of ammonia on the same sample which was evacuated overnight at 473 K at 1 mPa after the first run of the adsorption measurement. Since the number of total

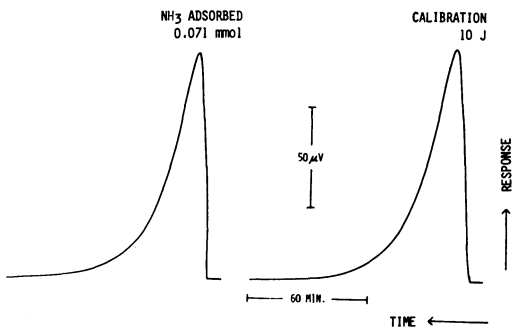

Fig. 4. An example of the recorder response of ammonia adsorption.
Initial pressure of ammonia: 1.098 kPa, equilibrium pressure: 0.007 kPa.

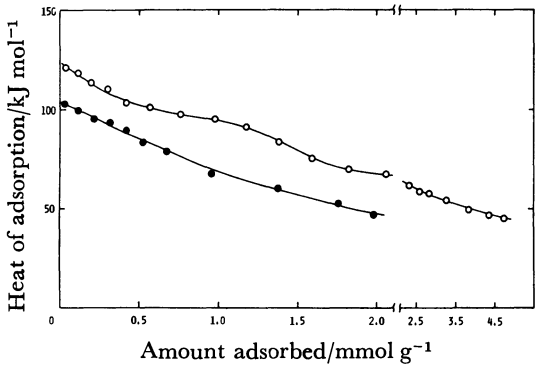

Fig. 5. Differential heats of adsorption of ammonia on decationated zeolites.
○: Original zeolite, ●: ammonia-preadsorbed zeplite

protons contained in the zeolite is 4.6 mmol/g which was calculated under the assumption that ammonium ions were converted into protons during the course of heat treatment at 673 K, the mutual interactions of adsorbed ammonia can be neglected and the heat should be evolved by the interaction of ammonia with the proton in this experimental condition. In the original sample, heats decrease from the initial value of about 120 kJ/mol, attain a plateau region of about 100 kJ/mol and decrease again. The presence of the plateau region is also observed in the measurement at room temperature.[3,4] The differential heats on the ammonia-preadsorbed sample are lower even in the initial region and decrease in monotonic way. The amount of ammonia which was irreversibly adsorbed after evacuation at 473 K was determined volumetrically to be 0.45 mmol/g, which agrees with the value obtained by comparison of two heat curves. Then relatively strong acid sites can be considered to evolve heats with ammonia adsorption higher than 105 kJ/mol.

The surface adsorption site distribution which was obtained by graphical differentiation of Fig. 5 is given in Fig. 6. The maximum of the distribution is observed at about 100 kJ/mol in the original sample, indicating the existence of considerably homogeneous active sites. About one-fifth of the total protons corresponded to adsorption sites contained in the maximum. However, this distribution was less significant than that observed at 298 K.[4] On the other hand, no maximum is observed

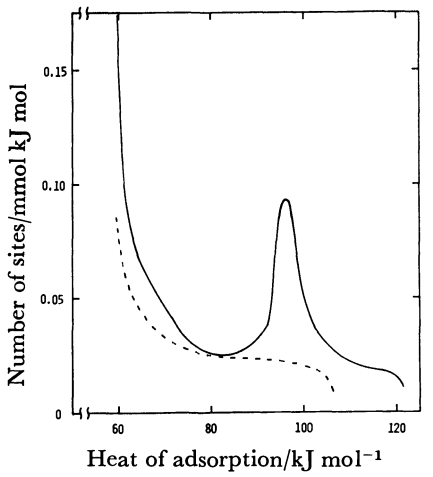

Fig. 6. Adsorption energy distribution on decationated zeolites.
——: Original zeolite, ------: ammonia-preadsorbed zeolite

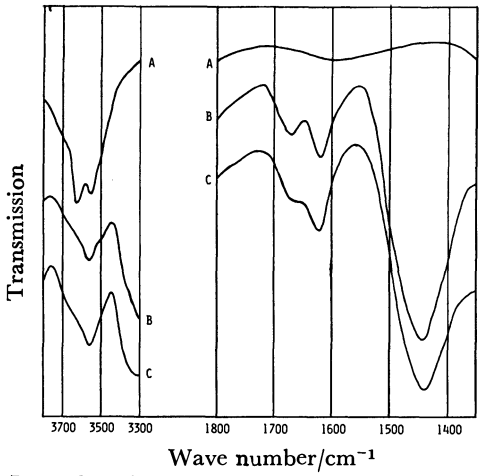

Fig. 7. Infrared spectra of OH and NH bands.
A: Decationated zeolite evacuated at 673 K, B: after ammonia adsorption and evacuation at 298 K, C: after ammonia adsorption and evacuation at 473 K.

in the ammonia-preadsorbed sample and more active sites having heats of adsorption above 105 kJ/mol are completely poisoned.

Infrared spectra of hydroxyl groups of the zeolite and adsorbed ammonia are shown in Fig. 7. The elimination of NH bands was completed by evacuation of the NH_4–$Y_{4.7}$ zeolite at 673 K, accompanied by the appearance of OH bands as shown in Fig. 7A, which is consistent with many previous results.[12] Ammonia was adsorbed at 298 K on this sample at the equilibrium pressure of 4 kPa and evacuated at the same temperature, then the spectrum was recorded (Fig. 7B). The reformation of bands from ammonium ion vibrations (1440 and 1670 cm^{-1}) was observed and also Lewis acid-bonded ammonia was detected at 1670 cm^{-1}. The hydroxyl band at 3650 cm^{-1} simultaneously disappeared, which fact indicates that ammonia interacted with these hydroxyl groups. The spectrum in Fig. 7C was taken after the treatment as follows; ammonia was adsorbed at 473 K at the equilibrium pressure of 40 kPa, which corresponded to the adsorbed amount of 4.83 mmol/g and desorbed overnight at the same temperature at 1 mPa. The intensities of bands at 1440 and 1670 cm^{-1} became weaker, whereas the intensity at 1620 cm^{-1} remained constant. This observation suggests that the irreversibly adsorbed ammonia on Brønsted acid sites decreases at higher temperature. In comparison with calorimetric data, the adsorption with heats higher than 105 kJ/mol can be suggested to occur mainly on Lewis acid sites.

In conclusion, this type of adsorption calorimeter is available at higher temperature and capable of providing information on fine structure of active sites of solid surfaces near their working temperature. The results of heats of adsorption of several bases on solids in the temperature range up to 673 K will be presented in another paper.

References

1) A. Auroux, V. Bolis, P. Wierzchowski, P. C. Gravelle, and J. C. Vedrine, *J. Chem. Soc., Faraday Trans. 2*, **75**, 2544 (1979).
2) Y.-Y. Huang, *J. Catal.*, **25**, 131 (1972).
3) K. Tsutsumi, H. Q. Koh, S. Hagiwara, and H. Takahashi, *Bull. Chem. Soc. Jpn.*, **48**, 3575 (1975).
4) T. Masuda, H. Taniguchi, K. Tsutsumi, and H. Takahashi, *Bull. Chem. Soc. Jpn.*, **51**, 1965 (1978).
5) H. Taniguchi, T. Masuda, K. Tsutsumi, and H. Takahashi, *Bull. Chem. Soc. Jpn.*, **51**, 1970 (1978).
6) H. Taniguchi, T. Masuda, K. Tsutsumi, and H. Takahashi, *Bull. Chem. Soc. Jpn.*, **52**, 2195 (1979).
7) T. Masuda, H. Taniguchi, K. Tsutsumi, and H. Takahashi, *Bull. Chem. Soc. Jpn.*, **52**, 2849 (1979).
8) H. Taniguchi, T. Masuda, K. Tsutsumi, and H. Takahashi, *Bull. Chem. Soc. Jpn.*, **53**, 362 (1980).
9) H. Taniguchi, T. Masuda, K. Tsutsumi, and H. Takahashi, *Bull. Chem. Soc. Jpn.*, **53**, 2463 (1980).
10) P. C. Gravelle, *Adv. Catal.*, **22**, 191 (1972).
11) R. M. Barrer, "Zeolite and Clay Minerals," Academic Press, London (1978), p. 342.
12) J. W. Ward, "Zeolite Chemistry and Catalysis," ed by J. A. Rabo, ACS Monograph 171, Washington (1979), p. 118.
13) F. S. Stone and L. Whalley, *J. Catal.*, **8**, 173 (1967).
14) J. C. Vedrine, A. Auroux, V. Bolis, P. Dejaifve, C. Naccache, P. Wierzchowski, E. C. Derouane, and J. H. C. Van Hoof, *J. Catal.*, **59**, 248 (1979).
15) A. Auroux, P. C. Gravelle, and J. C. Verdine, *Proc. 5th Int. Conf. Zeolites*, Napoli (1980), p. 433.

Syntheses of Sodium-Calcium Zeolites at Atmospheric Pressure and 80 °C. I. Reagents Used: Na_4SiO_4, $Al(OH)_3$, $Ca(NO_3)_2$

Kazuko KATSUKI* and Kyunosuke MAJIMA
Department of Chemistry, Faculty of Science, Toho University, 2-2-1 Miyama, Funabashi, Chiba 274
(Received May 18, 1981)

Sodium-calcium zeolite minerals were synthesized in an electric oven at 80 °C for 1—5 weeks from suspensions of a suitable combination of the starting materials, which had a chemical composition of $2n Na_2O \cdot 2CaO \cdot Al_2O_3 \cdot nSiO_2 \cdot xH_2O$ ($4 \leqq n \leqq 20$, $x = 83$—610). All of the synthetic products were obtained as massive products in the gel. X-Ray and IR analyses and a quantitative analysis of the principal ingredients showed these massive products to be well-crystallized hydroxycancrinites which contained 0—4.9% calcium oxide.

Zeolite minerals have been studied for a long time and have been synthesized extensively by many investigators, because they have useful properties, such as ion-exchange and molecular-sieve. Barrer and his co-workers have reported that the crystallization from active gel of sodium and potassium aluminosilicates could occur at 100 °C or below, but less reactive materials (*e.g.*, calcium and lithium aluminosilicates) were crystallizable only above about 150 °C.[1,2] Most calcium zeolites including sodium-calcium zeolites have thus been far synthesized only above 150 °C. It is now well known, however, that the crystallization of zeolite minerals is considerably influenced by the particular combination of the starting materials. It is also known that either water or salt, singly or in combination, aids the formation of aluminosilicate.[3] If suitable combinations of the starting materials, including salts and excess water, are chosen, sodium-calcium zeolite minerals can therefore be expected to crystallize at atmospheric pressure and at temperatures lower than 150 °C.

Our aim is to examine the reactivity of the starting materials and to make clear what kinds of sodium-calcium zeolite minerals can be synthesized under these mild conditions. In this paper it is reported that the sodium-calcium hydroxycancrinite has been synthesized at 80 °C and under atmospheric pressure from a suspension of sodium silicate (ortho), aluminium hydroxide, and calcium nitrate.

Experimental

Reagents Used. *Sources*: *Silicon*: 1 mol dm^{-3} solution of sodium silicate (ortho); *Aluminium*: finely powdered aluminium hydroxide; *Calcium*: 1 mol dm^{-3} solution of calcium nitrate.

Synthetic Method. The starting materials, composed of $2n Na_2O \cdot 2CaO \cdot Al_2O_3 \cdot nSiO_2 \cdot xH_2O$ ($1 \leqq n \leqq 20$, $x = 83$—610), were prepared as follows. Aluminium hydroxide was stirred well into the source of silicon, and then a calcium nitrate solution was added slowly. After this mixture had been stirred enough, the suspensions finally obtained were placed in 100 cm^3 polyethylene bottles and allowed to stand overnight. These bottles were kept for 1—5 weeks in an electrically heated oven, thermostatically controlled at 80±1 °C, and then the bottles were cooled in air. The reaction products were washed in hot water until the washings were free from alkali. Massive products present in the gel were separated from the gel by decantation and filtered off. All the products were air dried and powdered by the use of a porcelain mortar and 200-mesh sieves.

Analytical Apparatus and Method. *X-Ray*: A powder diffractometer (Rigaku Co.) was used with filtered Cu *Kα* radiation. It was operated at 30 kV; 15 mA; time constant, 1 s, and count range, 1000 cps.

IR: An infrared spectrophotometer of the JASCO DS701-G type was used. Samples were measured by the KBr-wafer method.

Quantitative Analysis of Principal Ingredients: The method of "Speedy Analysis of Silicate"[4] was used.

Results and Discussion

Sodium-calcium zeolite minerals have been synthesized from suspensions having the chemical composition of $2n Na_2O \cdot 2CaO \cdot Al_2O_3 \cdot nSiO_2 \cdot xH_2O$ ($1 \leqq n \leqq 20$, $x = 83$—610). They were obtained in three different states.

Two of them were in gel-like states (these will be referred to as "Gel 1" and "Gel 2" hereafter), while the other was in a massive form. The "Gel 1" minerals were obtained from suspensions with n values from 1 to 3. Mixtures of "Gel 2" and massive products were obtained from suspensions with n values from 4 to 20. X-Ray analysis revealed that the crystallinities of "Gel 1," "Gel 2," and the massive products were very low, low, and high respectively, as is shown in Fig. 1. We can also see in Fig. 1 that "Gel 2" has some peaks in

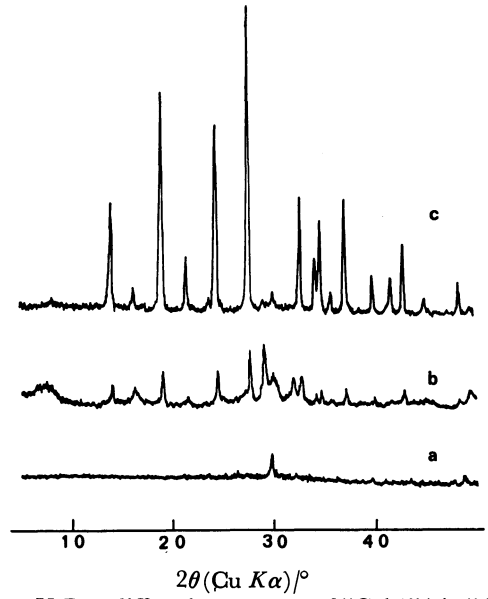

Fig. 1. X-Ray diffraction patterns of "Gel 1"(a), "Gel 2" (b), and massive product (c).

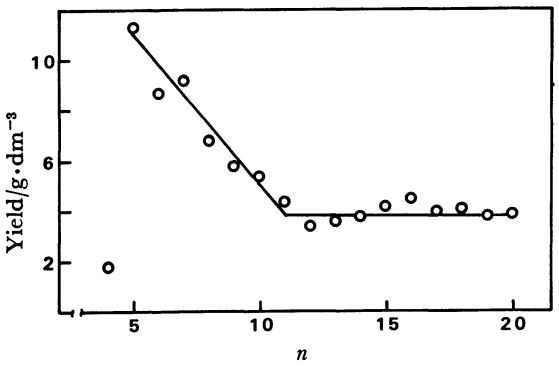

Fig. 2. The relation between the value of n and the yield of massive products.

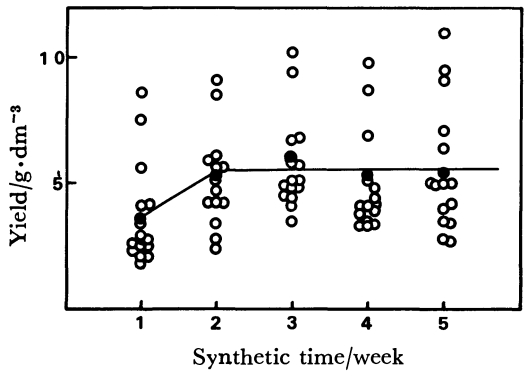

Fig. 3. The relation between the synthetic time and the yield of massive products.
●: The mean value of the yield.

Table 1. X-Ray powder-diffraction data for hydroxycancrinite

Natural cancrinite[a]			Massive product (hydroxy-cancrinite)		Synthetic hydroxy-cancrinite[b]	
hkl	*d*/Å	I/I_1	*d*/Å	I/I_1	*d*/Å	I/I_1
100	10.92	40				
110	6.23	5	6.46	33	6.30	65
200	5.45	5	5.57	7	5.46	14
101	4.64	90	4.75	68	4.60	66
210	4.11	15	4.21	19	4.12	15
			3.82	5	3.72	7
300	3.64	70	3.71	65	3.63	76
211	3.21	100	3.27	100	3.21	100
310	3.02	10	3.02	5	3.04	8
301	2.950	10			2.963	10
400	2.730	40	2.763	33	2.724	56
311	2.607	30	2.644	15	2.601	33
002	2.560	30	2.614	27	2.551	23
320,102	2.498	20	2.543	7	2.500	11
401	2.408	40	2.442	49	2.404	28
112	2.536	1				
202	2.321	1				
321	2.249	25	2.276	11	2.250	14
330,302	2.099	70	2.127	26	2.098	37
501,222	2.010	20	2.031	6		
132,331	1.953	2				
421	1.914	10				
420	1.868	20	1.895	15		

a) "Mineral Powder Diffraction File," (JCPDS International Diffraction Data 1980). b) Synthesis by Aoki and Abe. I/I_1: calculated from their pattern.

Table 2. IR data for hydroxycancrinite

Material	SiO_2/Al_2O_3	Asym. Stretch		Sym. Stretch		Dobl. Ring		T-O Bend		Pore Opening?	
Hydroxy-cancrinite	2	1095mw 1000s	1035msh 965msh	755w	680m	624m	567m	498mw 458m	429m	390mw	353wb
Massive product[a]	2.6	1115mw 997s	1035ms 965msh	820w 687m	757wsh 670wsh	624m	575m	500mw 462m	430m	390mw	346wb
Massive product[b]	2.6	1117mw 1002s	1037s 965s	820w 685m	760ws 669wsh	624m	575m	498mw 465m	428m	393mw	342wb
Massive product[c]		1120mw 990wsh	1040w 950s	820w 685m	668wsh	620m	573m	492mw 460m	422m	387mw	340w

a) n=20, synthetic time=5 weeks, CaO=0%. b) n=5, synthetic time=3 weeks, CaO=3.0%. c) n=5, synthetic time=1 week, starting materials involving sodium nitrate instead of calcium nitrate. s=strong, m=medium, w=weak, sh=shoulder, b=broad

addition to those of the massive products. "Gel 2" is possibly a mixture of the massive product and another material. As a result, we studied the massive products in detail.

The optimum conditions for the syntheses of massive products are determined from the n values and the synthetic-time dependence of the yield (g dm^{-1}) and the crystallinity. As may be seen from Figs. 2 and 3, the yield is more dependent on the n value than on the synthetic time. In Fig. 3, the data scatter widely because the yield is strongly dependent on the n value, and from the mean value of them it is clear that the yield becomes approximately constant after two weeks. On the other hand, the crystallinity becomes better with the increase in the synthetic time, but has little relation with the n value. From these examinations it may be concluded that the n values 5, 6, and 7 and a synthetic time of more than two weeks are the most suitable conditions for the synthesis.

We analyzed the massive products by means of X-Ray, IR, and quantitative analyses to ensure their identification. The X-Ray results are shown in Table 1. From Table 1, it is clear that the diffraction data of the massive product agree with those of cancrinite[5] and with those of the synthetic hydroxycancrinite reported by Aoki and Abe.[6]

The IR results are shown in Table 2. The data agree with those of the hydroxycancrinite reported

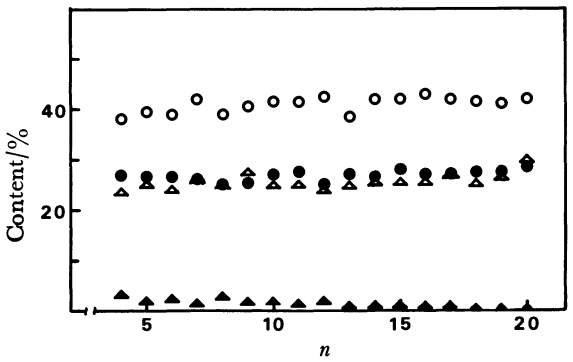

Fig. 4. The relation between the value n in starting materials and quantity of ingredients of massive products.
○: SiO_2, ●: Al_2O_3, △: Na_2O, ▲: CaO.

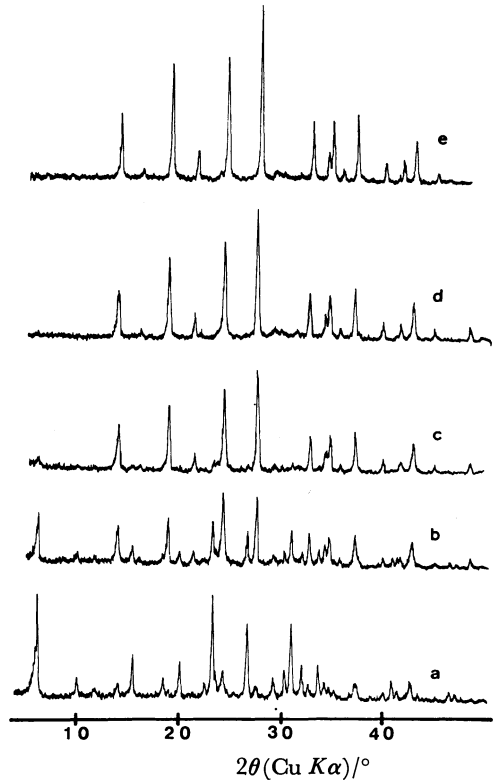

Fig. 5. X-Ray diffraction patterns of massive products which were synthesized in 1 d run (a), 2 d run (b), 3 d run (c), 4 d run (d), 5 d run (e).

previously,[7] except for small differences in the regions of 950—1200 and 750—820 cm^{-1} caused by asymmetric and symmetric stretching.

The amounts of the ingredients in massive products as a function of the n value have been determined by quantitative analysis, they are shown in Fig. 4. The dependence of the quantity of the ingredients on the n value is rather weak. Calcium oxide of 0.2—4.0% has been detected in all massive products except for those obtained by synthetic times between 4 and 5 weeks and when the n value equals 20. The mean values of the contents of Na_2O, CaO, Al_2O_3, and SiO_2 for 84 products are 27.5%, 1.5%, 26.7%, and 40.9% respectively. The experimental formula determined by the use of these values is $Na_9Ca_{0.25}Al_5Si_7O_{24}(NO_3)_{4.5}\cdot xH_2O$. The existence of the NO_3^- ion in this formula is deduced from the IR data, which has two characteristic absorption bands caused by the NO_3^- ion at 1384 and 820 cm^{-1}. In this deduction of the existence of the NO_3^- ion, we also referred to the report by Guth.[8] The experimental formula determined here agrees with that of cancrinite. From these three analyses, the massive products obtained here are identified as examples of hydroxycancrinite.

TABLE 3. X-RAY POWDER-DIFFRACTION DATA FOR MASSIVE PRODUCTS SYNTHESIZED FOR SHORTER SYNTHETIC TIMES

1 d Run		2 d Run		3 d Run	
d/Å	I/I_1	d/Å	I/I_1	d/Å	I/I_1
14.98	100	15.24	85		
9.03		9.11			
7.69					
7.46		6.46		6.46	35
5.83		5.87		5.57	5
4.87					
		4.77	69	4.75	67
4.48		4.48			
		4.21		4.19	16
4.00					
3.85	100	3.84			
		3.82		3.82	5
3.69		3.71	100	3.69	65
3.38	79	3.38			
		3.27	96	3.27	100
3.08		3.08		3.07	5
2.969		2.979		3.02	5
2.912	64	2.912			
2.814		2.823			
2.763		2.772		2.763	38
		2.691			
2.644		2.644		2.644	16
		2.614		2.607	29
				2.536	6
2.430		2.442		2.442	37
2.222		2.222		2.281	13
		2.196		2.186	13
2.132		2.127		2.127	25
				2.031	6
				1.895	10

Comparing with the conditions of the conventional synthetic way of hydroxycancrinite, such as a temperature higher than 80 °C and the limited n value of the starting materials, it is remarkable that only hydroxycancrinite has been synthesized over such a wide range of n values as n=4—20 and under such mild conditions as 80 °C and the atmospheric pressure used in this study. This suggests that the present combination of starting materials is especially effective in the synthesis of hydroxycancrinite. It seemed, therefore, that it would be to make clear the facility and characteristics of the present combination of starting materials. Thus, we have performed the following experiments using the most suitable n values 5, 6, and 7.

First we made experiments at shorter synthetic times in order to elucidate the initial crystallization. The

Table 4. X-Ray powder-diffraction data for synthetic results from the starting materials without calcium nitrate

1 d Run		2 d Run	
d/Å	I/I_1	d/Å	I/I_1
14.98	(1)		
9.03			
6.46		6.46	44
5.83			
		4.72	53
4.48			
		4.19	17
3.85	(3)		
3.71	(4)	3.68	100
3.38	(2)		
		3.27	81
3.08			
2.974			
2.912			
2.867			
2.814			
		2.755	33
2.698			
2.614		2.607	39
2.270			
2.132			
		2.122	39
1.941			

Table 5. X-Ray powder-diffraction data for the synthetic results from starting materials containing sodium nitrate instead of calcium nitrate

1 d Run		2 d Run		3 d Run	
d/Å	I/I_1	d/Å	I/I_1	d/Å	I/I_1
14.98	(1)	14.98	100		
9.03		9.03			
7.69		7.69			
		6.42		6.46	30
5.76		5.76		5.57	6
		4.87			
		4.72		4.77	67
4.46		4.46			
				4.19	18
3.85	(2)	3.85	61	3.80	6
		3.69		3.71	56
3.36	(3)	3.36	64		
		3.25		3.27	100
3.08		3.08			
2.919	(4)	2.967		3.02	4
2.876		2.912			
2.814		2.814			
		2.755		2.763	22
2.683		2.683			
				2.644	15
				2.607	26
				2.536	7
		2.430		2.442	34
				2.276	10
2.227		2.222		2.186	10
2.137					
				2.122	21
				2.031	4
				1.895	8

results are shown in Table 3 and Fig. 5. In a one-day run, a faujasite-type zeolite with a strong peak at nearly d(Å)=14.73 was synthesized. In a two-day run, a mixture of the faujasite-type zeolite and hydroxycancrinite was detected. From the four-day run, only hydroxycancrinite was observed in the X-Ray diffraction pattern. From these results, it is clear that the hydroxycancrnite has been synthesized almost completely in such a short time as four days under these mild conditions.

Secondly, we examined the effect of calcium salts on the crystallization. The results of the synthesis without calcium nitrate are shown in Table 4. As may be seen in Table 4, only the faujasite-type zeolite was synthesized in a one-day run. From the second-day run, the zeolite was changed from the faujasite-type into a mixture of sodalite-type zeolite and hydroxycancrinite. The crystallinities of these zeolites were very low. Therefore, we can guess that calcium nitrate as a calcium source plays a very important role in the formation of hydroxycancrinite. It had been believed that the existence of calcium would tend to hinder the formation of the aluminosilicate framework under mild conditions. Our experiment, however, revealed that if the $CaO/(CaO+Na_2O)$ ratio is limited within the range between 0.05—0.2, calcium tends to promote the formation of zeolite.

Lastly, we performed a synthesis experiment using sodium nitrate instead of calcium nitrate in order to make sure of the role of the NO_3^- ion. The results shown in Table 5 are almost the same as those in Table 3, thus indicative that calcium nitrate and sodium nitrate lead to the same effect. Therefore, it is confirmed that the characteristics of the present combination of starting materials are mainly due to the NO_3^- ion. This result is consistent with the report by Guth,[8] who pointed out that AO_m^{n-} favored the hexagonal derivation of cancrinite.

The success of the present synthesis suggests the possibility of preparing other sodium-calcium zeolite minerals under mild conditions if suitable combinations of starting materials are chosen.

We would like to thank Professor Isamu Shinno of Kyushu University for his critical reading of the manuscript. A part of this research was supported by a Grant-in-Aid for Scientific Research from the Ministry of Education, Science and Culture (264191).

References

1) R. M. Barrer and P. J. Denny, *J. Chem. Soc.*, **1961**, 983.
2) R. M. Barrer and E. A. D. White, *J. Chem. Soc.*, **1951**, 1267.
3) D. W. Breck, "Zeolite Molecular Sieves," A Wiley-Interscience Publication, U. S. A. (1974), p. 410.

4) I. Iwasaki, *Yogyo Kyokai Zasshi*, **66**, 148 (1958).
5) "Mineral Powder Diffraction File," Data Book, JCPDS International Center for Diffraction Data, U. S. A. (1980), p. 151.
6) M. Aoki and H. Abe, *Ganseki Kobutsu Kosho Kaishi*, **70**, 295 (1975).
7) E. M. Flanigen, H. A. Szymanski, and H. Khatami "Molecular Sieve Zeolite-1, Advances in Chemistry, Series 101," ed by Robert F. Gould, Am. Chem. Soc, Washington, D. C. (1971), p. 206.
8) J. L. Guth, *Rev. Chim. Mineral*, **2**, 127 (1965).

 © 1982 The Chemical Society of Japan Bull. Chem. Soc. Jpn., 55, 2581—2587 (1982)

Reactions of Chloroiron(III) Schiff Base Complexes with Superoxide Ion in Dimethyl Sulfoxide

Takayuki MATSUSHITA,* Hiroshi KONO, Mitsuru NISHINO, and Toshiyuki SHONO

Department of Applied Chemistry, Faculty of Engineering, Osaka University, Yamadaoka, Suita, Osaka 565

(Received August 10, 1981)

A series of monomeric chloroiron(III) complexes with the quadridentate or quinquedentate Schiff bases such as *N,N'*-disalicylideneethylenediamine or bis[3-(salicylideneamino)propyl]amine react with superoxide ions, O_2^-, in dimethyl sulfoxide to give the corresponding μ-oxo dimers. The polymeric chloroiron(III) complexes with the polymeric (oligomeric) Schiff bases derived from 5,5'-methylenedisalicylaldehyde and triamines react with O_2^- in dimethyl sulfoxide to give the oxygenated complexes, probably dioxygen adducts, Fe^{III}–O_2^-. This is suggested by the absorption spectra and the polarographic measurements.

The reactions of iron complexes with superoxide ions, O_2^-, are of interest in connection with the biological processes: the disproportionation of O_2^- by the iron-containing superoxide dismutases (Fe–SOD) and the catalytic utilization of molecular oxygen by the hemoproteins.

Hill *et al.* reported that $Fe^{III}(ppde)ClO_4$ reacts with O_2^- in *N,N*-dimethylformamide (DMF) to give Fe(ppde)–O_2 at low temperature (−50 °C).[1,2] McClune *et al.* proposed the formation of the peroxo complex, $[Fe^{III}(edta)-O_2]^{2-}$, by the reaction of $[Fe^{III}(edta)]^-$ with O_2^- in water on the basis of a stopped-flow spectrophotometry.[3] Recently, McCandlish *et al.* have reported that four different reaction pathways occurred in the reactions of O_2^- with iron porphyrins, as follows:

$$Fe^{III}(por)^+ + O_2^- \longrightarrow Fe^{II}(por) + O_2$$
$$2\,Fe^{III}(por)^+ + O_2^- \longrightarrow [Fe^{III}(por)]_2O$$
$$Fe^{III}(por)^+ + O_2^- \longrightarrow Fe(por)(O_2)$$
$$Fe^{II}(por) + O_2^- \longrightarrow Fe^{III}(por)(O_2^{2-}).$$

These reactions depend on conditions such as the solvent, the concentration, the presence or absence of traces of water, and the temperature.[4]

We have previously reported on the reactions of the monomeric and polymeric chloromanganese(III) Schiff base complexes with O_2^- in dimethyl sulfoxide (DMSO). With the monomeric complexes, they can be classified into two types in the reactivity toward O_2^-: one gives the oxygenated complexes and the other is reduced to the corresponding manganese(II) complexes. The reactivities toward O_2^- are found to be correlated to the polarographic half-wave potentials corresponding to the reduction from Mn(III) to Mn(II).[5] In the reactions of the polymeric complexes, the formation of their oxygenated complexes has been found.[6]

This paper describes the reactions between O_2^- and the monomeric and polymeric chloroiron(III) Schiff base complexes in DMSO. Some of the polymeric complexes showed a clearly different behavior in the changes of the absorption spectra and polarograms

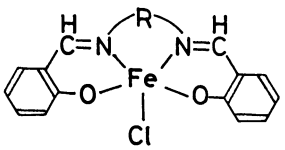

R	Abbreviation of ligands
CH_2CH_2	salen
C_6H_4	salphen
$CH(CH_3)CH_2$	salpln
C_6H_{10}	salchxn
$(CH_2)_2NH(CH_2)_2$	saldien
$(CH_2)_3NH(CH_2)_3$	saldpt
$(CH_2)_3N(CH_3)(CH_2)_3$	salMedpt

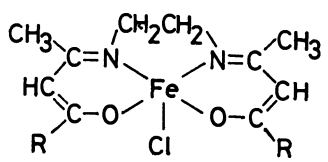

R	Abbreviation of ligands
CH_3	acacen
C_6H_5	bzacen

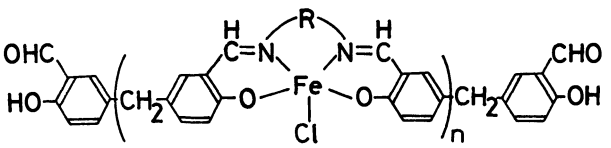

R	Abbreviation of ligands	R	Abbreviation of ligands
CH_2CH_2	p-salen	$(CH_2)_2NH(CH_2)_2$	p-saldien
C_6H_4	p-salphen	$(CH_2)_3NH(CH_2)_3$	p-saldpt
$CH(CH_3)CH_2$	p-salpln	$(CH_2)_3N(CH_3)(CH_2)_3$	p-salMedpt
C_6H_{10}	p-salchxn		

during the reactions with O_2^-, as compared with those observed for the monomeric complexes which react with O_2^- to give μ-oxo dimers.

Experimental

Preparation of Monomeric Chloroiron(III) Schiff Base Complexes Chloro(N,N'-disalicylideneethylenediaminato)iron(III), Fe(salen)Cl: This complex was obtained by a modified method described in the literature[7] as follows. Anhydrous iron(III) chloride (0.81 g) was added to an absolute ethanol solution (100 cm^3) containing *N,N'*-disalicylideneethylenediamine (salenH_2, 1.34 g) and triethylamine (1.01 g). The mixture was stirred at 70 °C for 1 h, and then allowed to stand overnight in a refrigerator. The resulting precipitates were collected on a glass filter, washed with ethanol and ether, and then dried *in vacuo*. They were recrystallized from dichloromethane. The yield was 1.1 g.

The other monomeric chloroiron(III) Schiff base complexes were prepared in a similar manner. The analytical data for some of the complexes are given in Table 1.

Preparation of Polymeric (Oligomeric) Schiff Base Ligands. The oligomers of the Schiff bases were prepared by the polycondensation of 5,5'-methylenedisalicylaldehyde with diamine or triamines under the controlled conditions: the molar ratio of 5,5'-methylenedisalicylaldehyde to amines was maintained at 1.25; the temperature was kept below 20 °C; the reaction was stopped within 5 min; a dichloromethane was used as solvent for the polycondensation.

Polymeric Schiff Base, p-saldienH_2: A dichloromethane solution (20 cm^3) of bis(2-aminoethyl)amine (1.4 g, 0.016 mol) was added to a dichloromethane solution (50 cm^3) of 5,5'-methylenedisalicylaldehyde (5.2 g, 0.02 mol) with stirring below 20 °C. After the solution had been stirred for 5 min, it was poured into a large volume of ether (300 cm^3) with vigorous stirring. The resulting yellow precipitates were collected on a glass filter, washed with ether, and then dried *in vacuo*. They were reprecipitated twice from a mixture of dichloromethane and ether. The yield was 3.1 g. Found: C, 69.95; H, 6.40; N, 11.63%. Calcd for a hexamer: C, 70.54; H, 6.33; N, 11.45%. ^{1}H NMR ($CDCl_3$) δ=12.2 (br, OH), 9.70 (s, CHO), 8.27 (s, CH=N), *ca.* 7 (m, ϕ), 3.80 (s, ϕ-CH_2-ϕ), 3.65 (t, CH_2N=), 2.95 (t, CH_2N–). The specific viscosity (η_{sp}) measured in chloroform (0.4 g/100 cm^3) at 25±0.1 °C was 0.037. The degree of condensation (n) was estimated to be six from the analytical data, the ratios of the peak intensities in the ^{1}H NMR spectra, and the specific viscosity.

The polymeric Schiff bases, p-salplnH_2, p-salchxnH_2, p-saldptH_2, and p-salMedptH_2, prepared previously[6] were used. They were found to be oligomers (n=3 to 5) on the basis of the above measurements. The other polymeric Schiff bases, p-salenH_2 and p-salphenH_2, were prepared in a similar manner. However, their NMR spectra and viscosities could not be measured owing to their poor solubility in organic solvents.

Preparation of Polymeric Chloroiron(III) Schiff Base Complexes. Fe(p-saldien)Cl: To a dichloromethane (50 cm^3)–methanol (20 cm^3) solution containing p-saldienH_2 (1.1 g) and triethylamine (0.6 g), anhydrous iron(III) chloride (0.5 g) was added with stirring at room temperature. The precipitated wine-red solids were collected on a glass filter, washed with water, ethanol, and then ether, and then dried *in vacuo*. They were partly soluble in DMSO or *N,N*-dimethylformamide (DMF) and were insoluble in dichloromethane or methanol. They were extracted with DMF (300 cm^3). The DMF solution was concentrated to *ca.* 30 cm^3 under reduced pressure, and poured into methanol (200 cm^3). The precipitates were collected on a glass filter, washed with ether, and dried *in vacuo*. The yield was 0.2 g.

The other polymeric iron(III) complexes were prepared in a similar manner. They are slightly soluble in DMSO or DMF (*ca.* 0.1 g/100 cm^3) and are insoluble in methanol or dichloromethane. Therefore, the viscosity for them could not be measured. The infrared spectra of the polymeric complexes indicate that the Schiff base ligands coordinate to iron ions in the same features as the corresponding monomeric complexes. The magnetic moments of the polymeric complexes were determined on the basis of their iron contents.

Isolation of the Reaction Products of Monomeric Complexes with KO_2. [Fe(acacen)]$_2O$: To a dichloromethane solution (50 cm^3) containing Fe(acacen)Cl (0.63 g, 0.002 mol) and 18-crown-6 (0.56 g, 0.002 mol), potassium superoxide, KO_2, (0.22 g, 0.003 mol) was added. The mixture was stirred for 1 h at room temperature. The wine-colored solution turned gradually orange. The mixture was filtered, and the filtrate was evaporated under reduced pressure to yield orange solids. They were collected on a glass filter, washed with a little volume of water and methanol, and then ether, and dried *in vacuo*. They were recrystallized from dichloromethane to give orange crystals. The yield was 0.3 g. Found: C, 50.20; H, 6.37; N, 9.84; Fe, 19.23%. Calcd for $Fe_2C_{24}H_{36}N_4O_5$: C, 50.37; H, 6.34; N, 9.79; Fe, 19.52%.

The reaction product of Fe(bzacen)Cl with KO_2 was obtained in a similar manner. The reaction products of the other monomeric complexes with KO_2 were obtained similarly, using DMSO in place of dichloromethane as reaction solvent.

Preparation of KO_2 DMSO Solution. DMSO solutions of KO_2 (*ca.* 10^{-2} M, 1 M=1 mol dm^{-3}) were prepared by dissolving KO_2 (0.018 g) into dry DMSO (25 cm^3) in the presence of 18-crown-6 (0.10 g). The O_2^- concentration of the KO_2 DMSO solution was determined by spectrophotometry.[8] The reactions of the iron(III) complexes with KO_2 in DMSO were carried out in a nitrogen atmosphere.

TABLE 1. ELEMENTAL ANALYSES OF IRON(III) SCHIFF BASE COMPLEXES

Complex	Found (%)				Calcd (%)			
	C	H	N	Fe	C	H	N	Fe
Fe(salchxn)Cl	57.84	5.07	6.94	13.35	58.35	4.90	6.80	13.57
Fe(bzacen)Cl	59.77	5.13	6.49	12.62	60.37	5.07	6.40	12.76
Fe(acacen)Cl	45.65	5.89	8.81	18.34	45.96	5.79	8.93	17.81
Fe(saldien)Cl·H_2O	51.68	4.80	10.23	14.43	51.64	5.06	10.05	14.44
Fe(saldpt)Cl·$(H_2O)_{0.5}$	54.88	5.30	9.73	13.03	54.88	5.53	9.60	13.06
Fe(salMedpt)Cl·$(CH_2Cl_2)_{0.9}$	50.73	5.26	8.11	10.97	50.67	5.20	8.09	10.76

TABLE 2. PHYSICAL PROPERTIES OF IRON(III) SCHIFF BASE COMPLEXES

Ligand	μ_{eff}[a] / BM		λ_{max}[b] / nm		$-E_{1/2}$[c] *vs.* Hg pool / V	
	Monomer	Polymer	Monomer	Polymer	Monomer	Polymer
salen	5.29	5.25	482	506	0.20	0.22
salphen	5.64	5.72	560	572	0.11	−0.01
salpln	5.49	5.73	486	510	0.24	−0.03
salchxn	5.41	5.38	482	510	0.21	−0.04
saldien	5.99	5.82	502	524	0.25	−0.03
saldpt	6.05	5.17	496	512	0.06	−0.02
salMedpt	5.57	5.56	516	528	0.03	−0.01
acacen	5.92		510		0.28	
bzacen	5.99		512		0.21	

a) Measured at room temperature. b) Measured in DMSO. c) Measured in DMSO containing 0.1 M Bu_4NClO_4 at 25 °C.

Material. Iron(III) chloride was of reagent grade. Potassium superoxide, KO_2, was purchased from Alfa Products Inc. (above 96.5%). Dimethyl sulfoxide was distilled twice under reduced pressure prior to use. Other solvents were purified by a usual method.

Measurements. All the physical measurements were made by the methods described elsewhere.[5]

Results and Discussion

The monomeric and polymeric chloroiron(III) Schiff base complexes were synthesized and their reactions with O_2^- in DMSO were investigated. The degree of the condensation (n) of the polymeric iron(III) complexes could not be determined by the molecular weight and the viscosity measurements owing to their poor solubility. However, they are considered to be oligomers ($n=3$ to 6) from the degree of the condensation of the Schiff base ligands.

Table 2 includes the magnetic moments, the absorption maxima in the visible region, and the polarographic half-wave potentials corresponding to the reduction from Fe(III) to Fe(II). The magnetic moments of the monomeric complexes fall within the range of 5.29 to 6.05 BM, indicating that these complexes have a d^5 high-spin electron configuration.[7,9] The magnetic moments of the polymeric complexes also fall within the range of 5.17 to 5.85 BM. The low value (5.17 BM) observed for the Fe(p-saldpt)Cl complex may be caused by antiferromagnetic interactions between iron atoms in the complex. No further investigation on the magnetic properties was made in the present work.

The absorption spectra of the monomeric and polymeric complexes in DMSO show an intense absorption band ($\varepsilon \fallingdotseq 4000$) around 500 nm, which can be assigned to a charge-transfer transition.[10] The absorption maxima of the polymeric complexes were observed at lower energies than those of the corresponding monomeric complexes. Similar behavior was observed for the monomeric and the polymeric chloromanganese(III) Schiff base complexes.[6] The monomeric chloroiron(III) complexes with the quadridentate ligands (N_2O_2) in DMSO may have a weak six-coordinate structure by coordination of a DMSO molecule to the central iron atom. It was reported that the Fe(salen)Cl complex is nonelectrolyte in pyridine (py) and has a six-coordinate structure of Fe(salen)Cl–py.[9] The monomeric chloroiron(III) complexes with the quinquedentate ligands (N_3O_2) may have a six-coordinate structure of a donor set of N_3O_2Cl in DMSO. Wilson *et al.* have reported that the Fe(saltrien)$^+$ cation has a six-coordinate structure (N_4O_2) and that the solvent effect on its spin-equilibrium in solution can be attributed to the hydrogen-bonding interactions between the NH groups of saltrien and solvents, where saltrien denotes the dianion of *N,N'*-disalicylidenetriethylenetetramine.[10,11] On the other hand, the coordination features of the polymeric chloroiron(III) complexes are considered to be similar to those of the monomeric complexes. However, the coordination or interaction of DMSO with the polymeric complexes may be weaker than that of the monomeric complexes, because the iron atoms in the former complexes are not so isolated from the surroundings as are the latter complexes. This may be one reason why the lower energy shifts were observed in the polymeric complexes.

The polarograms of the chloroiron(III) Schiff base complexes in DMSO show the cathodic wave at the half-wave potential around −0.1 V (*vs.* Hg pool) in Table 2, which can be assigned to the one-electron reduction of Fe(III) to Fe(II).[12] The reduction of the polymeric complexes occurred at more positive potentials than those for the corresponding monomeric complexes. These results are consistent with the absorption spectral data mentioned above on the basis of the electron density in the central iron atoms of the complexes.

Visible Absorption Spectra. Figure 1 shows the absorption spectral changes of a DMSO solution of Fe(salen)Cl caused by the addition of a KO_2 DMSO solution in different molar ratios. The intensity of the absorption band at 490 nm decreased with increasing the molar ratio of KO_2 to the complex, showing an isosbestic point at 458 nm. The absorption spectrum at the $[KO_2]/[complex]=3$ is almost the same as that of the μ-oxo dimer, $[Fe(salen)]_2O$. This indicates that Fe(salen)Cl reacts with O_2^- in DMSO at room temper-

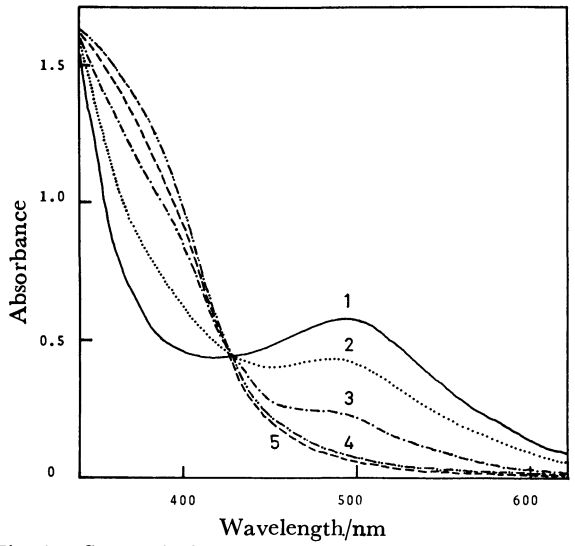

Fig. 1. Spectral changes on the addition of KO_2 to a DMSO solution of 6×10^{-5} M Fe(salen)Cl in different molar ratios.
1): No addition, 2): $[KO_2]/[complex]=1$, 3): 2, 4): 3, 5): spectrum of 3×10^{-5} M $[Fe(salen)]_2O$ in DMSO. Cell length: 1.0 cm.

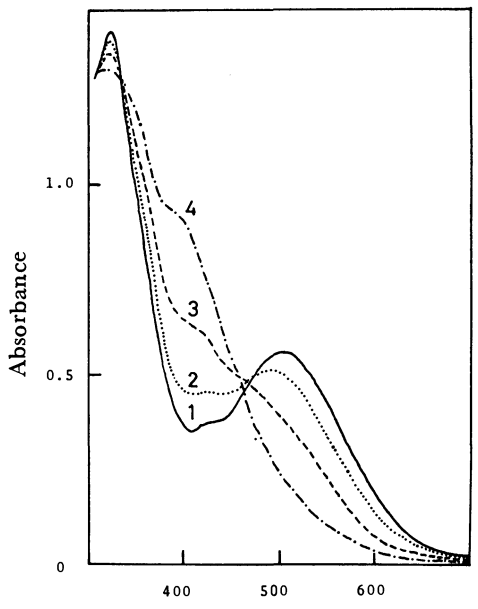

Fig. 2. Spectral changes on the addition of KO_2 to a DMSO solution of 1×10^{-4} M Fe(saldien)Cl in different molar ratios.
1): No addition, 2): $[KO_2]/[complex]=1$, 3): 2, 4): 4. Cell length: 1.0 cm.

ature to give a μ-oxo dimer.

All the monomeric chloroiron(III) complexes investigated here showed similar spectral changes to those observed for the above Fe(salen)Cl complex.

Figures 2 and 3 show the comparison of the spectral changes caused by the addition of the KO_2–DMSO solution to the DMSO solutions of Fe(saldien)Cl and Fe(p-saldien)Cl, respectively. The spectral changes for

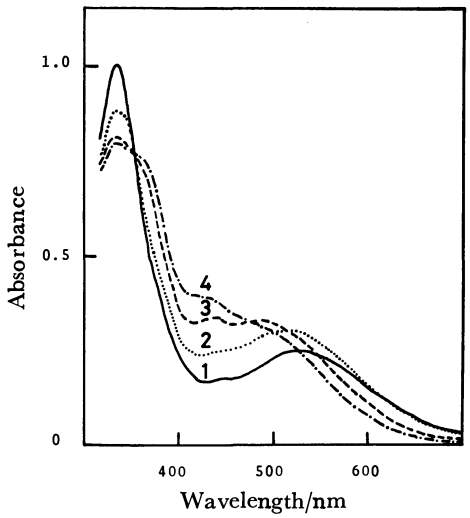

Fig. 3. Spectral changes on the addition of KO_2 to a DMSO solution of 1×10^{-4} unit M Fe(p-saldien)Cl in different molar ratios.
1): No addition, 2): $[KO_2]/[Fe]=2$, 3): 3, 4): 5. Cell length: 1.0 cm.

Fe(saldien)Cl are similar to those for Fe(salen)Cl, indicating the formation of the μ-oxo dimer. On the other hand, the spectral changes for the polymeric complex, Fe(p-saldien)Cl, are clearly different from those for the monomeric complex, Fe(saldien)Cl. At the $[KO_2]/[Fe]=2$, the absorption maximum was shifted to higher energy from 524 to 516 nm and the intensity increased slightly. At the $[KO_2]/[Fe]=3$, the absorption maximum was shifted to 492 nm and its intensity increased even more. By the further addition of KO_2 ($[KO_2]/[Fe]=5$), the intensity of the absorption band at 492 nm decreased and a new absorption band appeared around 420 nm. This new absorption band at 420 nm can be assigned to the anion of the Schiff base ligand. This is confirmed by the absorption spectrum of p-saldienH_2 in a KOH–DMSO solution. These spectral changes can be explained as follows. The Fe(p-saldien)Cl reacts with O_2^- in the DMSO solutions ($[KO_2]/[Fe]<3$) to give the oxygenated complex, probably a dioxygen adduct, and it reacts with O_2^- added in excess over the complex ($[KO_2]/[Fe]>3$) to decompose with some dissociation of the Schiff base ligand.

The polymeric iron(III) complexes of Fe(p-saldpt)Cl and Fe(p-salMedpt)Cl showed similar spectral changes to the above Fe(p-saldien)Cl complex. However, the other polymeric complexes, Fe(p-salen)Cl, Fe(p-salphen)Cl, Fe(p-salpln)Cl, and Fe(p-salchxn)Cl, showed the spectral changes similar to those observed for the corresponding monomeric complexes. These results may be attributed to the configurations of the reaction sites in the complexes. As discussed above, the former complexes may have a six-coordinate configuration, while the latter complexes may be taken to have essentially a five-coordinate configuration by neglecting the weak interaction between DMSO molecules and central iron atoms in these polymeric

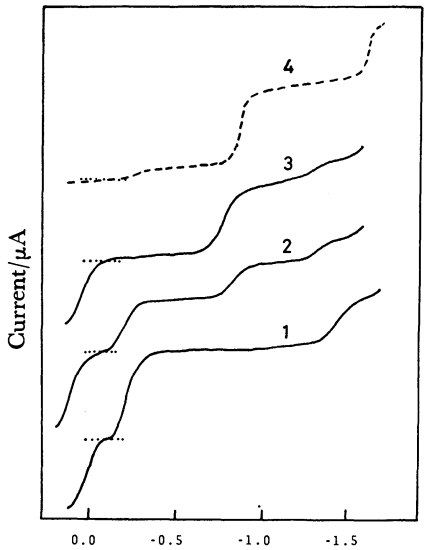

Fig. 4. Polarograms during the reactions of Fe(salen)Cl (5×10^{-4} M) with KO_2 in DMSO at 25 °C.
1): No addition, 2): $[KO_2]/[complex]=1$, 3): 2, 4): polarogram of $[Fe(salen)]_2O$ (2.5×10^{-4} M) in DMSO.

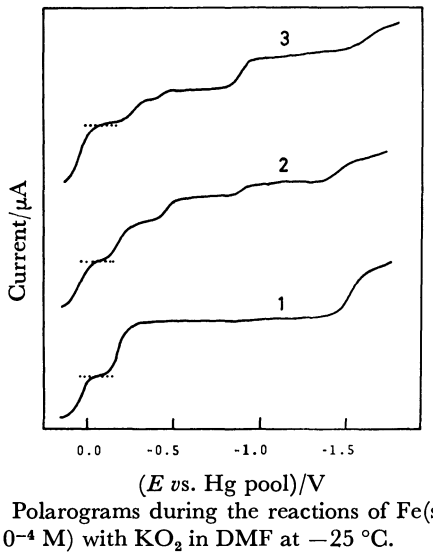

Fig. 5. Polarograms during the reactions of Fe(salen)Cl (5×10^{-4} M) with KO_2 in DMF at −25 °C.
1): No addition, 2): $[KO_2]/[complex]=0.5$, 3): 1.

complexes.

Polarographic Measurements. Figure 4 shows the changes in the polarograms during the reaction of Fe(salen)Cl with KO_2 in DMSO at 25 °C. At the molar ratio of $[KO_2]/[complex]=1$, the wave height at −0.20 V due to the reduction of Fe(III) to Fe(II) decreased and a new cathodic wave appeared around −0.8 V. By the further addition of KO_2 ($[KO_2]/[complex]=2$), the first cathodic wave disappeared and the wave height at −0.8 V increased. The half-wave potential of this cathodic wave is nearly equal to that (−0.89 V) of the μ-oxo dimer, $[Fe(salen)]_2O$. These results indicate that the reaction of Fe(salen)Cl with KO_2 in DMSO at 25 °C produces the μ-oxo dimer. The polarographic observations are consistent with those obtained in the absorption spectra mentioned above. Similar polarographic behavior was observed for all the monomeric iron(III) complexes investigated in this work.

It was reported that the dioxygen adduct of iron(II) porphyrin complexes can be stabilized at low temperature.[13] Thus, we carried out the reaction of Fe(salen)Cl with KO_2 in DMF at −25 °C. Figure 5 shows the changes in the polarograms of Fe(salen)Cl in DMF at −25 °C caused by the addition of a KO_2 DMSO solution. The half-wave potential (−0.19 V) of the first cathodic wave due to the reduction of Fe(III) to Fe(II) is nearly equal to that (−0.20 V) observed in DMSO at 25 °C. At the molar ratio of $[KO_2]/[complex]=0.5$, two new cathodic waves appeared at the half-wave potentials of −0.48 and −0.88 V and the height of the first cathodic wave decreased. By the further addition of KO_2 ($[KO_2]/[complex]=1$), the wave heights of both the first and the second cathodic waves decreased and the third cathodic wave height increased. The second cathodic wave observed at −0.48 V may be attributed to the reduction of the oxygenated complex, Fe(salen)–O_2 or Fe(salen)–O_2·–Fe(salen), formed in the solution. This may further react with O_2^- to give the μ-oxo dimer. Similar polarographic behavior was observed in the reaction of Fe(salphen)Cl with KO_2 in DMF at −25 °C. From the available data we propose this scheme for the reactions of Fe(salen)Cl with O_2^-:

$$FeLCl + O_2^- \longrightarrow FeL\text{–}O_2 + Cl^-$$
$$FeL\text{–}O_2 + FeLCl \longrightarrow FeL\text{–}O_2\text{·–}FeL + Cl^-$$
$$FeL\text{–}O_2\text{·–}FeL + O_2^- \longrightarrow FeL\text{–}O_2\text{–}FeL + O_2$$
$$FeL\text{–}O_2\text{–}FeL \longrightarrow FeL\text{–}O\text{–}FeL,$$

where L denotes the dianion of *N,N'*-disalicylideneethylenediamine. Recently, Chin *et al.* have reported on the mechanism of autoxidation of Fe^{II}(por) and proposed that the intermediate (por)Fe–O_2–Fe(por) can be stabilized at low temperature (−50 °C). This oxygenated complex reacts with Fe^{II}(por) to give (por)Fe–O–Fe(por) or decomposes thermally to (por)-Fe–O–Fe(por) *via* iron(IV) complex, (por)Fe^{IV}=0, in the absence of Fe^{II}(por).[14]

Figures 6 and 7 show the changes in the polarograms during the reactions of Fe(p-saldien)Cl with KO_2 in DMSO. In Fig. 6, the KO_2– DMSO solution was added successively to the DMSO solution of the complex, whereas in Fig. 7, it was added step by step after passing nitrogen gas through the mixed solutions. The changes in the polarograms (in Fig. 6) are clearly different from those observed for Fe(salen)Cl (in Fig. 4). The cathodic wave at the half-wave potential of +0.01 V is due to the reduction of Fe(III) to Fe(II). The addition of KO_2 ($[KO_2]/[Fe]=1$) caused the appearance of a new cathodic wave around −0.3 V. At the $[KO_2]/[Fe]=2$, this wave height decreased slightly and a new cathodic wave appeared at the half-wave potential of −0.6 V; this new wave can be assigned to the reduction of free molecular oxygen liberated during the reactions on the basis of its potential. At the $[KO_2]/[Fe]=3$, the wave height around −0.3 V decreased and the wave

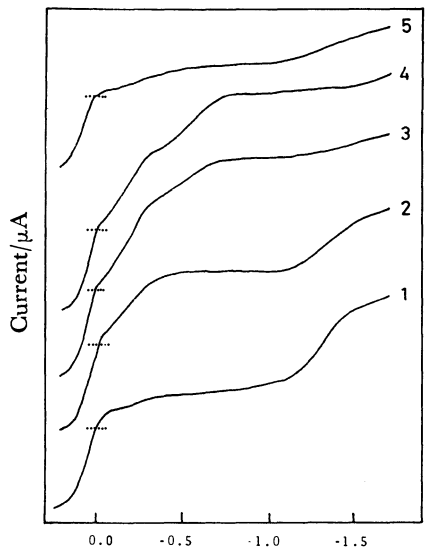

Fig. 6. Polarograms during the reactions of Fe(p-saldien)Cl (5×10^{-4} unit M) with KO_2 in DMSO at 25 °C.
1): No addition, 2): $[KO_2]/[Fe]=1$, 3): 2, 4): 3, 5): after passing nitrogen gas through the solution shown by the curve 4.

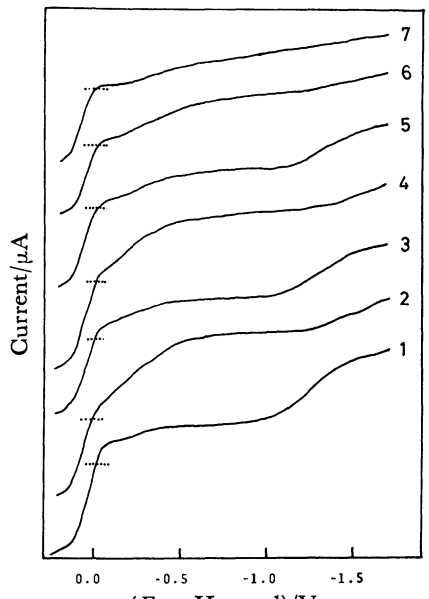

Fig. 7. Polarograms during the reactions of Fe(p-saldien)Cl (5×10^{-4} unit M) with KO_2 in DMSO at 25 °C.
1): No addition, 2): $[KO_2]/[Fe]=1$, 4): 2, 6): 4, 3), 5), and 7): after passing nitrogen gas through the solutions shown by the curves 2, 4, and 6, respectively.

height around −0.6 V increased. By passing nitrogen gas through the mixed solution, both cathodic waves disappeared. The cathodic wave which appeared around −0.3 V may be due to the oxygenated complex, Fe(p-saldien)–O_2. This is confirmed by the observations shown in Fig. 7. The polarograms observed at the $[KO_2]/[Fe]=1$ was identical to that shown by curve 2 in Fig. 6. By passing nitrogen gas through the solution, the wave height around −0.3 V decreased. Such a cycle (adding KO_2 and passing N_2) was made three times. The polarograms shown by curves 2, 4, and 6 in Fig. 7 did not show any cathodic wave at the half-wave potential around −0.6 V. Moreover, the degree of increase in the wave height around −0.3 V lowered gradually by repeating the cycle. These results indicate that the oxygenated complex, Fe(p-saldien)–O_2, may decompose to Fe^{II}(p-saldien) and molecular oxygen by passing nitrogen gas through the mixed solutions. Similar polarographic behavior was observed for the polymeric complexes, Fe(p-saldpt)Cl and Fe(p-sal-Medpt)Cl.

From the observations in the absorption spectra and the polarographic measurements, the reactions of the polymeric iron(III) complexes with O_2^- may occur as follows:

$$\text{(p-L)FeCl} + O_2^- \longrightarrow \text{(p-L)Fe–}O_2 + Cl^- \quad ([KO_2]/[Fe] < 2)$$

$$\text{(p-L)Fe–}O_2 + O_2^- \longrightarrow \text{(p-L)Fe–}O_2^- + O_2 \quad ([KO_2]/[Fe] > 2)$$

$$\text{(p-L)Fe–}O_2^- \longrightarrow \text{(p-L)}Fe^- + O_2$$

$$\text{(p-L)}Fe^- \longrightarrow \text{Decomposition,}$$

where (p-L) denotes the dianion of the polymeric Schiff base ligands.

The reversible oxygenation of the iron(II) porphyrin complexes can be established by preventing the formation of μ-peroxo diiron complex in one or more of the following ways: (1) steric effects, (2) immobilization in rigid surfaces, and (3) low-temperature measurements. In addition, it has been proposed that (4) a five-coordinate structure and (5) a nonpolar, hydrophobic environment around iron(II) complex play an important role for the synthesis of iron(II) porphyrin dioxygen adduct.[13] Recently, Niswander *et al.* have reported that Fe^{II}(salen)·py[15] and Fe^{II}(5-NO_2saldpt)[16] react with molecular oxygen to give only the corresponding μ-oxo dimers.

In the present work, the monomeric chloroiron(III) Schiff base complexes react with O_2^- to give only the μ-oxo dimers. On the other hand, the polymeric complexes of Fe(p-saldien)Cl, Fe(p-saldpt)Cl, and Fe(p-

Table 3. Physical properties of the reaction products of the monomeric iron(III) complexes with KO_2 in DMSO

Formula	μ_{eff}[a] BM	ν(Fe–O–Fe) cm^{-1}	$-E_{1/2}$[b] *vs.*Hg pool V
$[Fe(salen)]_2O$	1.91	825	0.89
$[Fe(salphen)]_2O$	2.05	820	0.86
$[Fe(salpln)]_2O$	2.02	815	0.97
$[Fe(salchxn)]_2O$	1.87	820	0.98
$[Fe(acacen)]_2O$[c]	1.88	838	1.18
$[Fe(bzacen)]_2O$[c]	2.50	820	1.22

a) Measured at room temperature. b) Measured in DMSO containing 0.1 M Bu_4NClO_4 at 25 °C. c) In dichloromethane.

salMedpt)Cl form the dioxygen adduct in DMSO solution at room temperature by the reaction with O_2^-. Such behavior suggests that these polymeric complexes may satisfy the above requirements (1), (2), and (4).

Reaction Products of the Iron(III) Complexes with KO_2. The reaction products of the monomeric iron(III) complexes, Fe(acacen)Cl, Fe(bzacen)Cl, Fe(salen)Cl, Fe(salphen)Cl, Fe(salpln)Cl, and Fe(salchxn)Cl, were confirmed to be their μ-oxo dimers from the analytical data and physicochemical properties (in Table 3). However, for the other monomeric complexes, Fe(saldien)Cl, Fe(saldpt)Cl, and Fe(salMedpt)Cl, their μ-oxo dimers could not be characterized. On the other hand, the reaction products of the polymeric iron(III) complexes have not been identified with their oxygenated complexes by the analytical data and the physicochemical measurements. This may be caused by the instability of the oxygenated complexes. Further investigation is now in progress.

References

1) Abbreviations used in this work: ppde, protoporphyrin IX dimethyl ester dianion; H_4edta, ethylenediaminetetraacetic acid; por, tetraphenyl porphyrin dianion.

2) H. A. O. Hill, D. R. Turner, and G. Pellizer, *Biochem. Biophys. Res. Commun.*, **56**, 739 (1974).

3) G. J. McClune, J. A. Fee, G. A. McCluskey, and J. T. Groves, *J. Am. Chem. Soc.*, **99**, 5220 (1977).

4) E. McCandlish, A. R. Miksztal, M. Nappa, A. Q. Sprenger, J. S. Valentine, J. D. Stong, and T. G. Spiro, *J. Am. Chem. Soc.*, **102**, 4268 (1980).

5) T. Matsushita and T. Shono, *Bull. Chem. Soc. Jpn.*, **54**, 3743 (1981).

6) T. Matsushita, M. Nishino, and T. Shono, *Bull. Chem. Soc. Jpn.*, **55**, 2663 (1982).

7) M. Gerloch, J. Lewis, F. E. Mabbs, and A. Richards, *J. Chem. Soc., A*, **1968**, 112.

8) S. Kim, R. DiCosimo, and J. San Filippo, Jr., *Anal. Chem.*, **51**, 679 (1979).

9) M. Gullotti, L. Casella, A. Pasini, and R. Ugo, *J. Chem. Soc., Dalton Trans.*, **1977**, 339.

10) M. F. Tweedle and L. J. Wilson, *J. Am. Chem. Soc.*, **98**, 4824 (1976).

11) E. Sinn, G. Sim, E. V. Dose, M. F. Tweedle, and L. J. Wilson, *J. Am. Chem. Soc.*, **100**, 3375 (1978).

12) K. M. Kadish, K. Das, D. Schaeper, C. L. Merrill, B. R. Welch, and L. J. Wilson, *Inorg. Chem.*, **19**, 2816 (1980).

13) R. D. Jones, D. A. Summerville, and F. Basolo, *Chem. Rev.*, **79**, 139 (1979).

14) D-H. Chin, G. N. La Mar, and A. L. Balch, *J. Am. Chem. Soc.*, **102**, 4344 (1980).

15) R. H. Niswander and A. E. Martell, *Inorg. Chem.*, **17**, 2341 (1978).

16) R. H. Niswander and A. E. Martell, *Inorg. Chem.*, **17** 1511 (1978).

The Temperature Dependence of the Peak Height of the Lead Ion in Square-wave Polarography

Nobuko HATANAKA

Osaka Environmental Pollution Control Center, Nakamichi 1-3, 62, Higashinari-ku, Osaka 537

(Received September 16, 1981)

The peak height of the square-wave (s.w.) polarogram of lead increased markedly upon the addition of anions forming insoluble compounds with lead, and the temperature coefficient of the peak height showed a negative value, different from the theoretical value in a diffusion-controlled or an electrode-reaction-rate-controlled process at the following concentrations of anions; $[Cl^-]=1$ M†, $[Br^-]=10^{-2}$ M, $[SCN^-]=10^{-1}$ M for 10^{-4} M lead. In the case of the addition of iodide, the s.w. peak height of lead increased at concentrations of iodide above 10^{-4} M for 10^{-4} M lead but the temperature coefficient of the peak height was always positive. Moreover, another peak due to lead appeared superimposed on the oxidation peak of iodide at a more positive potential, and this peak had a negative temperature coefficient. It was found that these phenomena were attributable to a specific adsorption of lead on mercury electrodes, induced by the foremost adsorbed anions. However in the case of the addition of iodide or in that of a high concentration of bromide or thiocyanate, the reversibility of the electrode process decreased and the temperature coefficient varied to a positive value in spite of the increase in adsorbed depolarizers.

The influence of the temperature on polarographic currents has not been much reported on since the theoretical consideration by Ilkovič[1] and the experimental report by Nejedlý[2] using direct-current (d.c.) polarography.

The temperature coefficient of d.c., alternating current (a.c.), s.w., and other polarographic currents has generally been accepted as positive in a reversible or an irreversible process, for it depends on the temperature dependence of the diffusion coefficient of a depolarizer and that of the rate constant of the electrode reaction, too, in an irreversible process.

We reported in a previous paper[3] that, when a chloride ion coexisted as a supporting electrolyte, the temperature coefficient of the s.w. polarographic peak height of lead showed a negative value, different from the theoretical temperature coefficient in a reversible or an irreversible process, on the other hand, the temperature coefficient of the d.c. polarographic wave height agreeded well with the theoretical value in a reversible process.

In this paper, the temperature dependence of the s.w. peak height of lead was studied in the presence of a chloride, bromide, thiocyanate, or iodide ion, as it is known that these anions are adsorbed on dropping mercury electrodes[4] and then give various influences on the electrode reaction.[5-7]

Theoretical

In d.c. polarography, the temperature coefficient of a diffusion-controlled current, $(1/I_{d.c.})\mathrm{d}I_{d.c.}/\mathrm{d}T$, can be expressed theoretically[1] thus;

$$(1/I_{d.c.})\mathrm{d}I_{d.c.}/\mathrm{d}T = (1/2D)\mathrm{d}D/\mathrm{d}T - (1/2\eta_{Hg})\mathrm{d}\eta_{Hg}/\mathrm{d}T, \quad (1)$$

in which D is the diffusion coefficient of the depolarizer and η_{Hg} is the viscosity of mercury.

In s.w. polarography, $(1/I_{s.w})\mathrm{d}I_{s.w.}/\mathrm{d}T$ at the reversible half-wave potential ($E=E_{1/2}$) in the case of a diffusion-controlled process can be expressed theoretically as;

$$(1/I_{s.w.})\mathrm{d}I_{s.w}/\mathrm{d}T = (1/2D)\mathrm{d}D/\mathrm{d}T - 1/T, \quad (2)$$

because $I_{s.w.}$ can be expressed as follows, as reported by Barker,[8]

$$I_{s.w.} = k\,\Delta E\, n^2\, A\, c\, D^{1/2} T^{-1}\, P/(1+P)^2, \quad (3)$$

where k=a constant varing with the apparatus, ΔE= the amplitude of the superimposed square-wave voltage, n= the number of electrons in an electrode reaction, c= the concentration of a depolarizer, A= the electrode area, $P=\exp[(E-E_{1/2})nF/RT]$, and $P=1$ when $E=E_{1/2}$.

It has been reported that the temperature coefficient of the d.c. wave height was in the range of 1.3—2.3%,[2] while that of the a.c. peak height, which should be the same as that of the s.w. peak height, was experimentally found in the range of 0.4—1.6%.[9]

It was reported by Imai and Adachi[10] that, in the case of a reaction-rate-controlled process, the temperature coefficient of the a.c. peak height was much higher than that of a diffusion-controlled process. Kambara and Kunimatsu[11] showed that, in the case of a redox system of a fairly low reversibility, the temperature coefficient decreased with an increase in the temperature, and that when the rate of the electrode process has become fast enough at higher temperatures, the coefficient approached that of the completely reversible system.

Experimental

Square-wave polarographic curves were recorded by a Yanagimoto high-frequency polarograph, Model PF-500, using a mercury pool at the bottom of an electrolysis cell as an anode.

Experiments were carried out under the following conditions; the span voltage =2 V, the gate range=2 to 7, the time constant=5.5.

Direct-current polarographic curves were recorded by a Yanagimoto voltammetric analyzer, P-1000 type, using a spiral platinum wire electrode as an anode and a saturated calomel electrode as a reference electrode.

The electrolysis cell was held in a Tajiri electronic thermo-water bath, ECW-108 type, with an accuracy of ±0.2 °C.

All the chemicals used were guaranteed-grade reagents. As the standard solution of lead, lead nitrate was used. For the addition of anions, potassium chloride, sodium chloride,

† 1 M=1 mol dm^{-3}.

sodium bromide, sodium thiocyanate, and sodium iodide were used.

Results and Discussion

Increased Sensitivity and Negative Temperature Coefficient. The peak height of the s.w. polarogram of lead increased markedly upon the addition of a smaller amount of iodide, bromide or thiocyanate than that of chloride, as is shown in Figs. 1—4. This increase was remarkable at lower temperatures, therefore, the temperature coefficient of the s.w. peak height of lead began to decrease from the theoretical value with an increase in the concentration of anions, except in the case of iodide, and was negative in the presence of the following concentrations, varing with each anion; $[Cl^-]=1$ M, $[Br^-]=10^{-2}$ M, $[SCN^-]=10^{-1}$ M. However, with still more increasing anions, the coefficient changed again to a positive value larger than the theoretical value.

Concerning the influence of the addition of anions

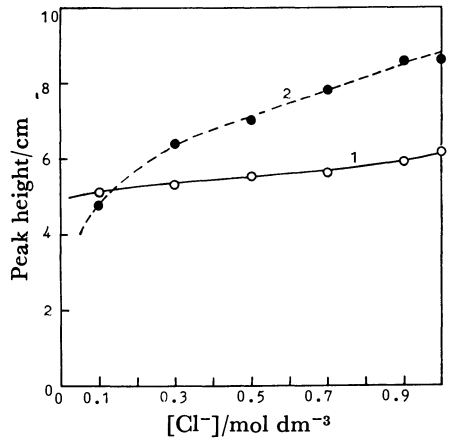

Fig. 1. Influence of the concentration of KCl on the peak height of 10^{-4} M Pb^{2+} in the s. w. polarogram. (HNO_3 acidic, pH 3—4).
1: 25.0 °C, 2: 1.0 °C, ΔE: 5 mV, sens.: 1/20, 0.200 μA/mm.

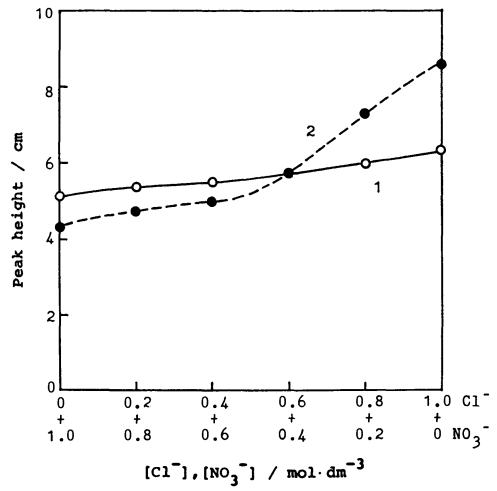

Fig. 2. Influence of the concentration of KCl summed with KNO_3 to 1.0 M on the peak height of 10^{-4} M Pb^{2+} in the s. w. polarogram. (HNO_3 acidic, pH 3—4)
1: 25.0 °C, 2: 0.8 °C, ΔE: 5 mV, sens.: 1/20, 0.200 μA/mm.

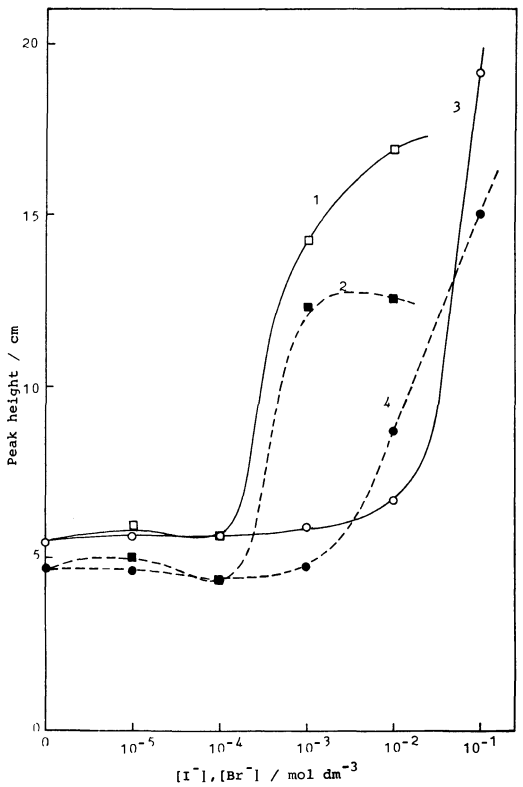

Fig. 3. Influence of I^- (1, 2) or Br^- (3, 4) concentration on the peak height of 10^{-4} M Pb^{2+} in 0.1 M $HClO_4$ in the s. w. polarogram.
1, 3: 25.0 °C, 2, 4: 0.2 °C, ΔE: 5 mV, sens.: 1/20, 0.200 μA/mm.

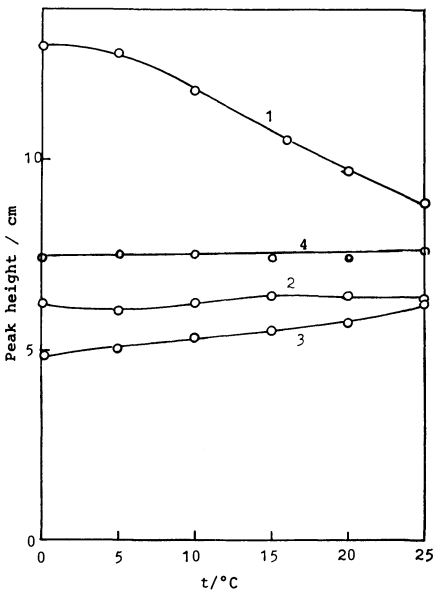

Fig. 4. Temperature dependence of the peak height in the s. w. polarograms of 10^{-4} M Pb^{2+} in 0.1 M $HClO_4$ with 10^{-1} M SCN^- (1), 10^{-2} M SCN^- (2), 10^{-3} M SCN^- (3), and 0.01 M $HClO_4$ with 1.0 M SCN^- (4). ΔE: 5 mV, sens.: 1/20, 0.200 μA/mm.

on the d.c. polarogram, the wave height of lead was constant, and the temperature coefficient coincided with the theoretical value, regardless of the addition of anions, unlike as in the case of the s.w. polarogram.

These experimental results seem to suggest the adsorption of the depolarizer.

In d.c. polarography, in which the mean current in a drop life is measured, a small quantity of adsorbed depolarizer has hardly any influence on the wave height, as the current occasioned by the reduction of an adsorbed depolarizer decreases with the growth of a drop in proportion to $t^{-1/3}$, where t is the time from the beginning of the drop.

In s.w. polarography, in which the electrode potential changes with the frequency of 200 Hz, even a small quantity of adsorbed depolarizer results in an increase in the peak height. The peak height is then increased by this approximate factor;[7]

$$1+\frac{(\gamma_{E_{1/2}})^2\sum_{m=0}^{\infty}(-1)^m(m+\beta)^{-3/2}}{8D_e\tau\sum_{m=0}^{\infty}(-1)^m(m+\beta)^{-1/2}}, \qquad (4)$$

where $\gamma_{E1/2}$ is the adsorption coefficient, which refers to the half-wave potential, τ is the half-period of the square-wave, and $\beta=t/\tau$, t now being the time elapsed since the last sudden potential change. The current occasioned by the reduction of adsorbed depolarizers decreases more rapidly than that occasioned by the reduction of diffusing depolarizers with the elapsed time t. Nevertheless, the current occasioned by the reduction of adsorbed depolarizers is considerably retained, even at the latter half-period of each square pulse, as the τ of 1/400 s is very short.

A temperature coefficient of the adsorption quantity always has a negative value in a physical adsorption, and frequently in a chemical adsorption as well and so

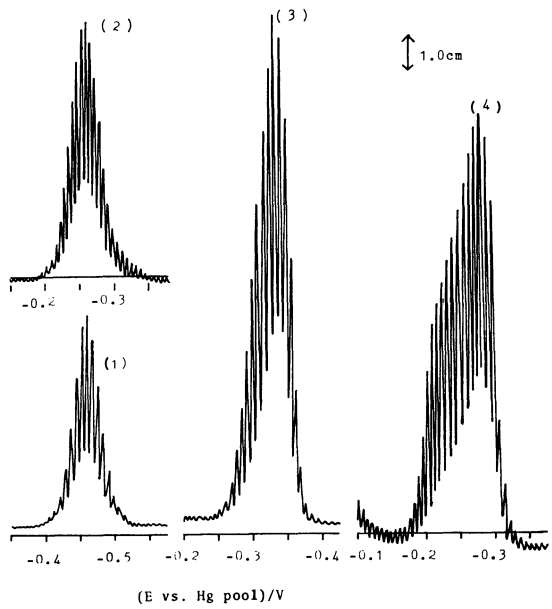

Fig. 5. Square wave polarograms of 10^{-4} M Pb^{2+} in 1.0 M NaCl (1), NaSCN (2), NaBr (3), and NaI (4) at 25.0 °C.
ΔE: 5 mV, sens.: 1/20, 0.200 μA/mm.

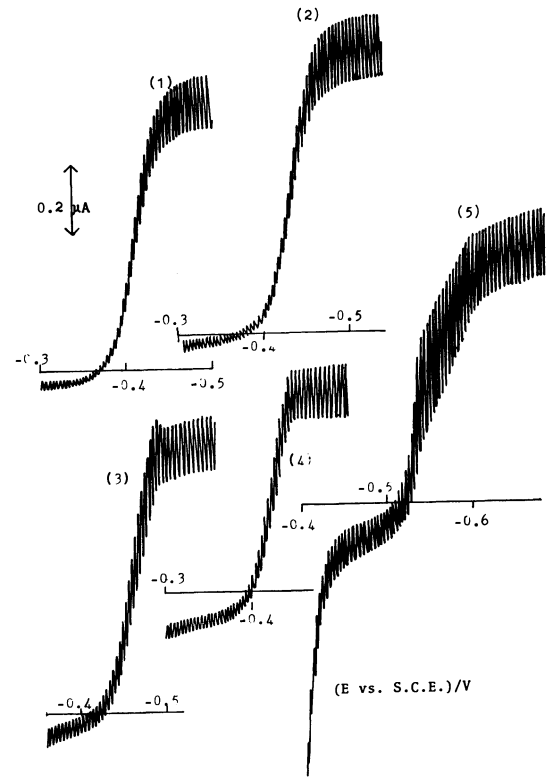

Fig. 6. Direct current polarograms of 10^{-4} M Pb^{2+} in 1.0 M NO_3^- (1), Cl^- (2), Br^- (3), SCN^- (4), and I^- (5) at 25.0 °C.

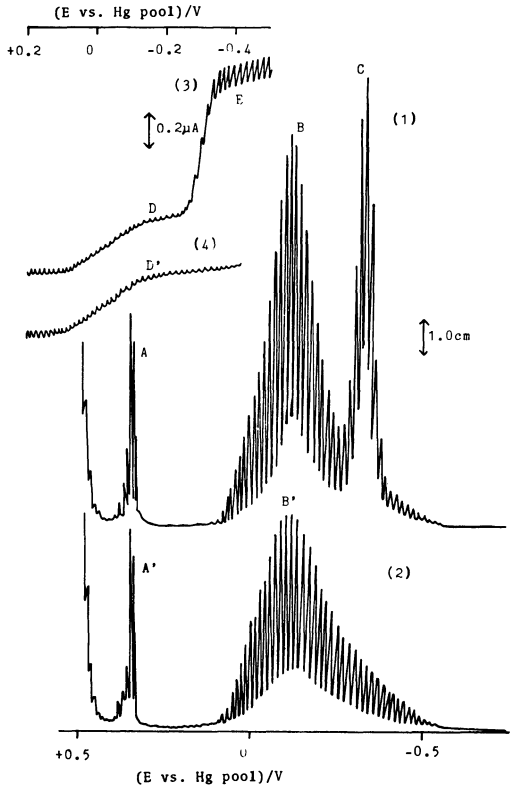

Fig. 7. Square wave and direct current polarograms.
1, 3: 2×10^{-4} M Pb^{2+} in 0.1 M $HClO_4$ with 2×10^{-4} M I^-, 2, 4: 2×10^{-4} M I^- in 0.1 M $HClO_4$, 1, 2: ΔE: 5 mV, sens.: 1/20, 0.200 μA/mm.

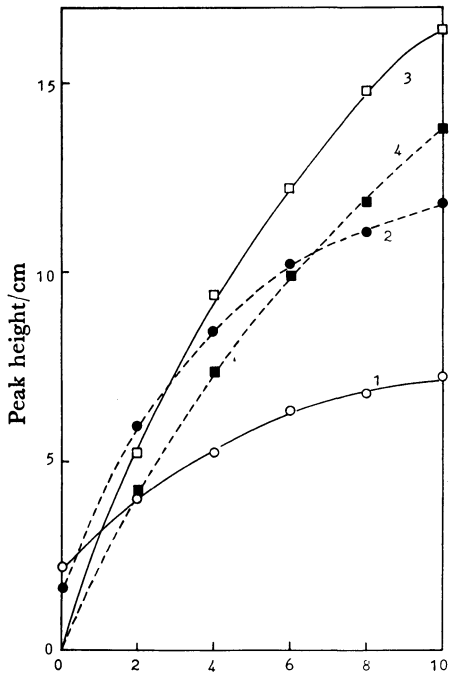

Fig. 8. Relation between the peak height of B, C, and Pb^{2+} concentration.
1: B, 25.0 °C, 2: B, 0.2 °C, 3: C, 25.0 °C, 4: C, 0.2 °C.
ΔE: 5 mV, sens.: 1/50, 0.200 μA/mm.

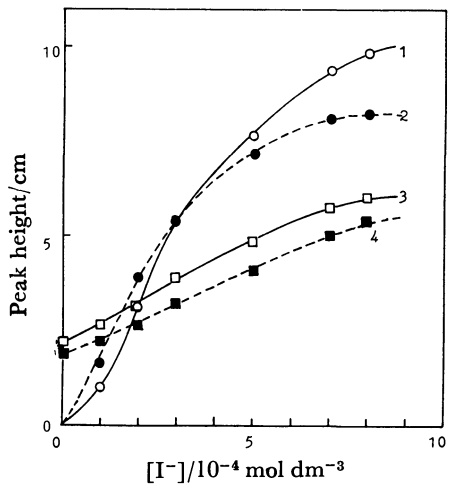

Fig. 9. Influence of I^- concentration on the peak heights of B and C.
1: B, 25.0 °C, 2: B, 0.8 °C, 3: C, 25.0 °C, 4: C, 0.8 °C.
ΔE: 5 mV, sens.: 1/50, 0.200 μA/mm.

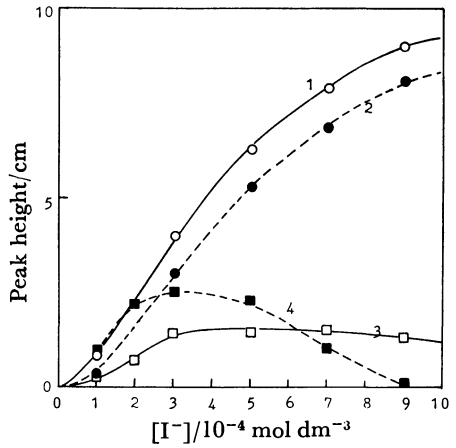

Fig. 10. Relation between I^- concentration and the peak height of B′ and B-B′.
1: B′, 25.0 °C, 2: B′, 1.0 °C, 3: B-B′, 25.0 °C, 4: B-B′, 0.2 °C. ΔE: 5 mV, sens.: 1/50, 0.200 μA/mm.

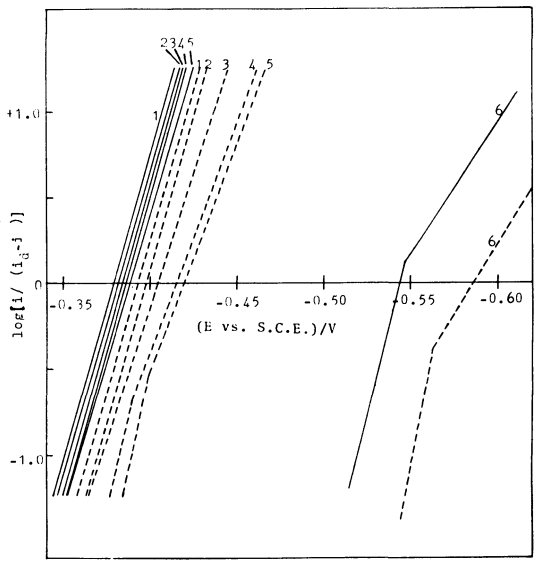

Fig. 11. Log plot analysis of the d. c. polarogram of 10^{-4} M Pb^{2+} in 0.1 M $HClO_4$.
Added I^-: 1) 0, 2) 2×10^{-4} M, 3) 4×10^{-4} M, 4) 6×10^{-4} M, 5) 8×10^{-4} M, 6) 1.0 M.
—— 25.0 °C, ------ 0 °C.

these experimental results may be considered reasonable.

Moreover, the following facts support adsorption of the depolarizer. In the presence of high concentrations of anions, s.w. polarograms of lead became noticeably asymmetric, as is shown in Fig. 5. In the presence of 1 M Br^-, a maximum which characterized the adsorption of the depolarizer appeared in the d.c. polarogram of 10^{-4} M lead. The surface-active substances, such as gelatin, Methyl Red, camphor, Eosin, thymol, and Alizarin S, changed the temperature coefficient of the peak height in the s.w. polarogram of lead from negative to positive, as has been shown in a previous paper.[3]

Increased Sensitivity and Positive Temperature Coefficient. Upon the addition of iodide, the temperature coefficient was always positive in spite of the increased peak height of lead in the s.w. polarogram caused by the adsorbed depolarizer, this was different from the cases of the addition of bromide, thiocyanate, and chloride.

However, it was found that another peak attributable to lead, which was superimposed on the oxidation peak of iodide, had a negative temperature coefficient.

When iodide was added to a 10^{-4} M Pb^{2+} solution of 0.1 M $HClO_4$, three peaks appeared in the s.w. polarogram, as is shown in Fig. 7. The first peak, A, at about +0.4 V (*vs.* Hg pool), apparently depends

on the tensammetric process. The height of the second peak, B, which was, at first sight, thought to be the oxidation peak of iodide, was higher than the oxidation peak, B′, of iodide in the absence of lead, and increased progressively with an increase in the concentration of lead or iodide, as is shown in Figs. 8 and 9. The temperature coefficient of B was negative, whereas that of B′ was positive, as is shown in Fig. 10. By substracting the peak height of the oxidation of iodide, B′, from the peak height of B, the plot of (B-B′) against the concentration of iodide shown in Fig. 10 was obtained. At a low concentration of iodide, (B-B′) increased with an increase in the iodide concentration, and the temperature coefficient of (B-B′) was negative. On the other hand, at higher concentrations of iodide, (B-B′) decreased with an increase in the iodide concentration and the temperature coefficient of (B-B′) was positive.

In the d.c. polarogram, the D and D′ corresponding to B and B′ were equal in wave height, so both D and D′ were only the oxidation waves of the iodide ion.

Therefore, (B-B′), which was superimposed on the peak of the iodide oxidation, must be a peak attributable to the adsorbed lead ion, the same as the C peak.

Next, the plot of $E_{d.e.}$ (a potential of a dropping mercury electrode) *vs.* log $[i/(i_d-i)]$ in the d.c. polarogram of lead (E corresponding to Peak C in the s.w. polarogram) was analyzed; the results are shown in Fig. 11.

In a reversible process, a plot of $E_{d.e.}$ *vs.* log $[i/(i_d-i)]$ shows a straight line, with a slope equal to $0.0591/n$ V at 25.0 °C and $0.0550/n$ V at 0 °C.

The presence of 2×10^{-4}—8×10^{-4} M I^- at 25 °C did not influence the slope, but at 0 °C, with an increase in the concentration of iodide, the slope was larger than the theoretical value and the half-wave potential was more negative.

These results show that the process becomes irreversible with an increase in the concentration of iodide at low temperatures.

In s.w. polarography, which requires a faster electrode reaction than d.c. polarography for an electrode reaction to be reversible because of the frequent periodic change in the electrode potential, the electrode processes in this case should be far more irreversible than in d.c. polarography. In an irreversible process, the temperature coefficient of a Peak height should be positive and larger than in a diffusion-controlled process.

Therefore, in spite of the electrode process accompanied by the depolarizer adsorption, the temperature coefficient of the peak (C) height of lead in the addition of iodide in the s.w. polarogram was positive.

Moreover, the positive temperature coefficient in the presence of bromide or thiocyanate of a high concentration may be attributable to the same reason.

The accelerating effect of halide ions on the electrode reactions of bismuth,[12] copper,[12] and zinc[13] has been reported. Breyer *et al.* suggested that the presence of halide ions decreased the repulsion of the aqueous Bi^{3+} or Cu^{2+} from the positively charged electrode, either because of the formation of a halo-complex or because of the adsorption of negatively charged halide ions on the electrode. Therefore, similar accelerating effects of iodide on the electrode reaction may be expected in the case of lead. Nevertheless, a decreasing reversibility with an increase in the concentration of iodide was observed. It may be that this decreasing reversibility is related to the dissociation rate of the complex preceeding the electrode reaction. A more detailed investigation is, however, necessary to clarify the cause of the decreasing reversibility.

Complex Formation and Adsorption. The half-wave potential shifted to a more negative potential upon the addition of anions in the order of; SCN^-, Cl^-, Br^-, I^- at 25 °C, and in the order of; Cl^-, SCN^-, Br^-, I^- at 0 °C, as is shown in Fig. 12. This order of the shift of a half-wave potential to a negative potential shows a tendency to form complexes of the depolarizer with anions or a tendency to form insoluble compounds. This order coincided with the ability to adsorb lead found from the degree of the increase in the peak height in the s.w. polarogram and also approximately with the ability to adsorb anions on mercury electrodes which was calculated by Grahame[14] and which is shown in Table 1. Therefore, the ability to adsorb lead may depend on both the adsorbed ability of anions on mercury electrodes and the complex-forming ability of lead with anions.

In the case of cadmium, which forms an insoluble

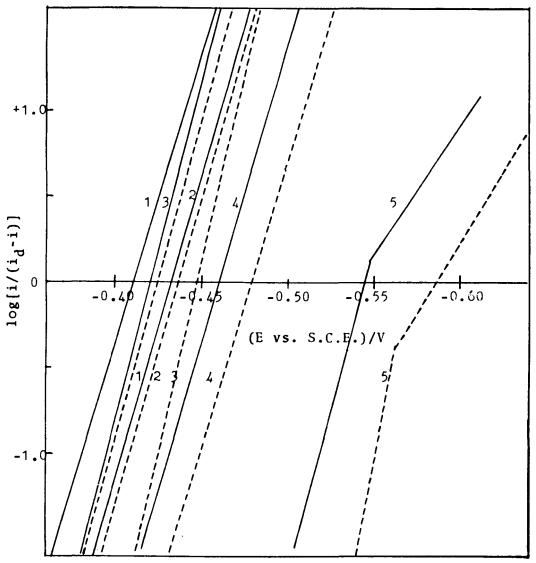

Fig. 12. Log plot analysis of the d. c. polarogram of 10^{-4} M Pb^{2+} in 1.0 M NO_3^- (1), Cl^- (2), SCN^- (3), Br^- (4), and I^- (5) with 0.01 M $HClO_4$.
—— 25.0 °C, ------ 0 °C.

Table 1. The quantities of the electrolytes adsorbed per unit of area of the mercury interface at the electrocapillary maximum[14]

Electrolyte	$\Gamma_m/\mu C\ cm^{-2}$
1 M NaCl	3.6
1 M KBr	10.6
1 M KI	15.2
1 M NaSCN	14.0
1 M KNO_3	5.5

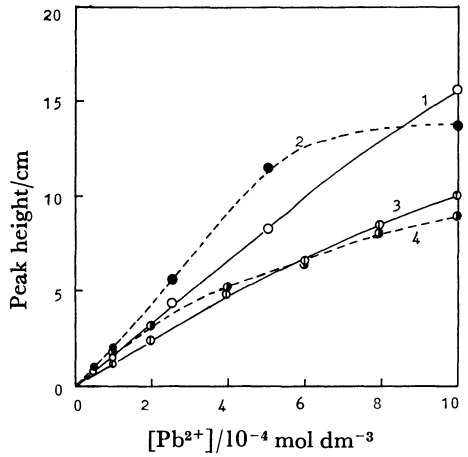

Fig. 13. Relation between the peak height in the s. w. polarogram and the concentration of lead in the presence of 1.0 M Cl^- (1, 2) and 0.5 M Cl^- (3, 4).
1, 3: 25.0 °C, 2, 4: 0 °C, ΔE: 5 mV, sens.: 1/100, 0.200 μA/mm.

compound with these anions only with difficulty, no adsorption of cadmium was found by means of s.w. polarography[3] in the presence of chloride, but it was reported in the presence of iodide on the basis of the experimental result from differential-pulse polarography.[15]

In the case of thallium, which forms an insoluble compound with chloride, the adsorption of thallium[16] was found by means of s.w. polarography[3] in the presence of chloride.

Moreover, the adsorption of lead decreased upon the addition of nitrate to chloride, as may be seen in Figs. 1 and 2. These results can be explained as follows; the adsorption of chloride on mercury was decreased by the nonspecific adsorption of nitrate, which did not induce so much adsorption of lead as chloride did.

These facts show that lead is induced by a covalent bonding force with adsorbed anions and adsorbed on mercury electrodes; in other words, lead adsorption is a specific adsorption induced by the foremost adsorbed anions. Therefore, upon the increase in the depolarizer over the inducing ability of anions, the temperature coefficient of the peak height of the depolarizer approached the theoretical value in a diffusion-controlled process, as is shown in Fig. 13.

The auther wishes to express her thanks to Professor Toyokichi Kitagawa of Osaka City University for his continuous encouragement and for his kind guidance in this work.

References

1) D. Ilkovič, *Collect. Czech. Chem. Commun.*, **10**, 249 (1938).
2) V. Nejedlý, *Collect. Czech. Chem. Commun.*, **1**, 319 (1929).
3) N. Akashi-Hatanaka and Y.Kumazawa, *Rev. Polarogra., phy*, **15**, 28 (1968).
4) J. Lawrence, R. Parsons, and R. Payne, *J. Electroanal. Chem. Interfacial Electrochem.*, **16**, 193 (1968).
5) J. Kuta and I. Smoler, *Collect. Czech. Chem. Commun.*, **33**, 1656 (1968).
6) J. E. B. Randles and K. W. Somerton, *Trans. Faraday Soc.*, **48**, 951 (1952).
7) G. C. Barker and J. A. Bolzan, *Z. Analyt. Chem. Bd.*, **1966**, 216.
8) G. C. Barker, R. L. Faircloth, and A. W. Gardner, Atomic Energy Research Establishment Report C/R 1786, H. M. Stationary Office, London (1956).
9) B. Breyer and H. H. Bauer, "Alternating Current Polarography and Tensammetry," Interscience, New York (1963), Chap. 2.
10) H. Imai and N. Adachi,Paper presented at the National Meeting of the Chem. Soc. Japan, Tokyo (1964).
11) T. Kambara and K. Kunimatsu, *Rev. Polarogr.*, **13**, 20 (1960).
12) B. Breyer, F. Gutmann, and S. Hacobian, *Aust. J. Sci. Res.*, **A5**, 595 (1951).
13) J. E. B. Randles, *Faraday Soc. Discuss.*, **1**, 11 (1947).
14) D. C. Grahame, *Chem. Rev.*, **41**, 441 (1947) (translated by S. Watanabe, K. Nishizawa, K. Kanata, and K. Takubo), *Hyomen*, **10**, 98 (1972).
15) F. C. Anson, J. B. Flanagan, K. Takahashi, and A. Yamada, *J. Electroanal. Chem.*, **67**, 253 (1976).
16) A. Frumukin, "Surface Phenomena in Chemistry and Biology," Pergamon Press, London(1958), p. 189.

Sublimation Behavior of Actinoid Chelates of 2,2,6,6-Tetramethyl-3,5-heptanedione

Ryohei AMANO,* Akiko SATO,† and Shin SUZUKI†

School of Paramedicine, Kanazawa University, Kodatsuno 5, Kanazawa 920

†*The Research Institute for Iron, Steel and Other Metals, Tohoku University, Katahira 2, Sendai 980*

(Received December 11, 1981)

Vacuum sublimation-recrystallizing temperatures were determined for a tracer amount of actinoid chelates of 2,2,6,6-tetramethyl-3,5-heptanedione in order to obtain information about their sublimation behavior. The influence of the amount of sample (in tracer scale or in milligram scale) on its sublimation-recrystallizing temperature was also examined. The sublimation-recrystallizing zone temperature of the tracer amount of chelate was lower than that of the milligram amount. In addition, the sublimation-recrystallizing zone temperatures of the actinoid chelates were found to be in the following sequence: UO_2^{2+}>Am(III), Cm(III)>Th(IV), Np(IV), Pu(IV)>Cf-(III). These results suggest that the sublimation technique can be applied to separate the actinoid elements in a carrier-free state.

A number of workers have studied the volatility of lanthanoid β-diketone chelates. They reported that 2,2,6,6-tetramethyl-3,5-heptanedione makes a highly volatile and thermally stable lanthanoid chelate.[1-4] In previous work,[5,6] we have studied the sublimation behavior of tris(2,2,6,6-tetramethyl-3,5-heptanedionato)-lanthanoid(III) (La(III)$(thd)_3$) in detail, and have shown that the behavior can be divided into three groups (La to Gd, Tb and Dy, and Ho to Lu) and that the middle lanthanoid chelates (Tb and Dy) change thermally in solid phase at various fixed temperatures. Their volatilities have also been found to affect the two different crystallographic forms. It is therefore important to study the sublimation behavior of actinoid chelates of 2,2,6,6-tetramethyl-3,5-heptanedione. Among the actinoid metal chelates, uranyl(UO_2^{2+}) and thorium-(Th(IV)) chelates of β-diketone have already been examined as to volatility by using a milligram amount of sample.[7,8] Sakanoue and Amano have prepared some other actinoid β-diketonato chelates in tracer scale and described their volatilities.[9]

In the present study, in order to obtain the sublimation-recrystallizing temperatures of actinoid chelates of 2,2,6,6-tetramethyl-3,5-heptanedione, we examined the influence of sample amount (milligram amount or tracer amount) on their sublimation-recrystallizing temperatures. In addition, their sublimation behavior was determined for a tracer amount of actinoid chelates, and this was compared with those of lanthanoid chelates.

Experimental

Reagents. *Actinoid Metal*: Uranyl nitrate and thorium nitrate were purchased commercially in gram quantities, and used without delicate handling because of their low specific radioactivities. Other actinoid metals were used in tracer scale. Some actinoid radioisotopes: ^{227}Ac, ^{241}Am, ^{243}Am, and ^{242}Cm, were purchased from The Radiochemical Centre (England) and from New England Nuclear corporation (U. S. A.). The daughter nuclides, ^{228}Ac and ^{234}Th, were obtained by a milking procedure from the parent nuclides, ^{228}Ra and ^{238}U. Californium radioisotope, ^{252}Cf, was recovered from a nickel foil which had covered a ^{252}Cf neutron source; was obtained enough to prepared its chelate and determine its radioactivity. The plutonium radioisotope, ^{239}Pu, was obained by Inoue.[10] The radioactivities and metal amounts of actinoids used in preparation and their specific radioactivities are summarised in Table 1.

Table 1. Radioactivities, metal amounts, and specific activities of actionoid and gadolinium nuclides, which are used in one preparative procedure[a)]

Radio-nuclide	Radio-activity/μCi	Metal amount/mg	Specific activity/μCi mg^{-1}
^{228}Ac	10	4.5×10^{-9}	2.2×10^{9}
^{228}Th	5	6.1×10^{-6}	8.2×10^{5}
^{232}Th[b)]	3.3×10^{-2}	300	1.1×10^{-4}
^{234}Th	2	8.6×10^{-8}	2.3×10^{7}
^{238}U[b,c)]	1.0×10^{-1}	300	3.4×10^{-4}
^{239}Np	10	4.3×10^{-8}	2.3×10^{8}
^{239}Pu	1.0×10^{-2}	1.6×10^{-4}	6.2×10^{1}
^{241}Am	1	2.9×10^{-4}	3.4×10^{3}
^{242}Cm	2	6.0×10^{-7}	3.3×10^{6}
^{252}Cf	1.0×10^{-3}	1.9×10^{-3}	5.4×10^{-1}
^{153}Gd[d)]	5	2.2×10^{-3}	2.3×10^{3}

a) One-tenth of the amounts in this table was used in one sublimation procedure. b) Thorium and uranium are weighable. c) A depleted uranium sample was used. d) The purchased Gd radioisotope is not carrier-free, and contains other stable Gd isotopes.

Lanthanoid Carriers and Radioisotope: The purified lanthanoid oxides (99.9%) of La_2O_3, Gd_2O_3, and Sc_2O_3 were used as a carrier for the preparation of actinoid chelates in tracer scale. Gadolinium radioisotope, ^{153}Gd, were purchased from The Radiochemical Centre (England).

Preparation of Actinoid Chelates of 2,2,6,6-Tetramethyl-3,5-heptanedione. Macro amounts of thorium and uranyl chelates, $Th(thd)_4$ and $UO_2(thd)_2\cdot2H_2O$, were prepared by mixing 90% methanol solutions of the neutralized 2,2,6,6-tetramethyl-3,5-heptanedione chelating agent and thorium nitrate or uranyl nitrate. The chelates precipitated immediately upon mixing the solutions and were purified by recrystallization from dichloromethane and vacuum sublimation. The purified uranyl chelate was found to be unhydrous form, $UO_2(thd)_2$, by elemental and thermochemical (TG, DTA) analyses.

Tracer amounts of other actinoid chelates of 2,2,6,6-tetramethyl-3,5-heptanedione were prepared according to the preparative method for $Ln(thd)_3$ (Ln=lanthanoid metal) of Eisentraut and Sievers[1] with a slight modification, by the use of about 100 mg of lanthanoid metal as a non-isotopic

carrier. The mixed solution of the lanthanoid salt solution and tracer amounts of each actinoid metal were heated to dryness. The residue was dissolved in a minimum amount of 99% methanol, and the pH of the resultant solution was adjusted between 3 and 5 by dropwise addition of 2 M NH_4OH solution. A solution of Hthd chelating agent was then added to the above solution. The mixture was adjusted to the desired pH. The precipitate was filtered off and then purified by recrystallization from dichloromethane. Several sets of the chelates were prepared as follows: $(La+^{228}Th)(thd)_3$, $(La+^{234}Th)(thd)_3$, $(UO_2+^{234}Th)(thd)_2$, $(La+^{228}Ac+^{228}Th+^{239}Np+^{239}Pu+^{241}Am+^{252}Cf)(thd)_3$, $(UO_2+^{234}Th+^{239}Pu)(thd)_2$, $(La+^{153}Gd)(thd)_3$, $(Sc+^{153}Gd)(thd)_3$, and $(La+^{241}Am+^{242}Cm+^{252}Cf)(thd)_3$.

Measurements of Vacuum Sublimation-recrystallizing Temperatures. Specifications for the vacuum sublimation apparatus for the measurement of the vaccum sublimation-recrysrallizing temperature were reported in the previous paper.[6] Briefly, the apparatus consists of a Pyrex tube (0.8 cm in outer diameter and 100 cm in length) with a continuous temperature gradient (1—3 °C/cm) maintained along its length, and evacuated to $(1-10)\times10^{-3}$ Torr) (1 Torr≈133.322 Pa). Samples were placed in small aluminum or porcelain boat and inserted into the high temperature end of the Pyrex sublimation tube. The samples then heated at 180 °C for 2 h under reduced pressure ($(1-10)\times10^{-3}$ Torr)). Their recrystallizing positions were determined by the scanning of the radioactivity along the sublimation tubes.

Special care has been paid in comparing the recrystallizing position of each actinoid chelate. Two sublimation tubes were inserted in an outer tube to sublimate each sample under the same conditions. The small differences between the sublimation-recrystallizing temperatures of each sample were clearly detected.

Radioactivity Measurement. While the gross gamma and characteristic X-ray were measured with a well-type NaI(Tl) scintillation counter, the gamma ray spectra were taken by using a Ge(Li) semiconductor detector connected with a 4096-channel pulse-height analyzer. Alpha spectra were taken with a Si(Au) semiconductor detector coupled to a 4096-channel pulse-height analyzer. The detection of alpha particles was also done by an α-track method by using a cellulose nitrate film. The ^{252}Cf radioactivity was measured by using Indian mica as a fission track detector. Both track methods (α-track and fission track methods) were very useful for locating clearly the sublimation-recrystallized chelate.

Results and Discussion

Vacuum Sublimation-recrystallizing Temperatures of Tracer Amounts of Metal Chelates of 2,2,6,6-Tetramethyl-3,5-heptanedione. In general, vacuum sublimation-recrystallizing temperature zones for macro amounts of metal chelates (more than 5 mg) can be observed discretely and reproducibly at the higher temperature site of the deposition zone, while the tailing appears in its lower temperature site.[6] In this experiment, the influence of the amount of sample on its sublimation-recrystallizing temperature was examined by the use of $Gd(thd)_3$ and $Th(thd)_4$. Figures 1 and 2 show these results. The peak position of the recrystallizing temperature zone for tracer amounts of $Gd(thd)_3$ or $Th(thd)_4$ shifted to a temperature position lower than that of macro amounts of $Gd(thd)_3$ or $Th(thd)_4$. On the other hand, the recrystallizing range of tracer amounts of

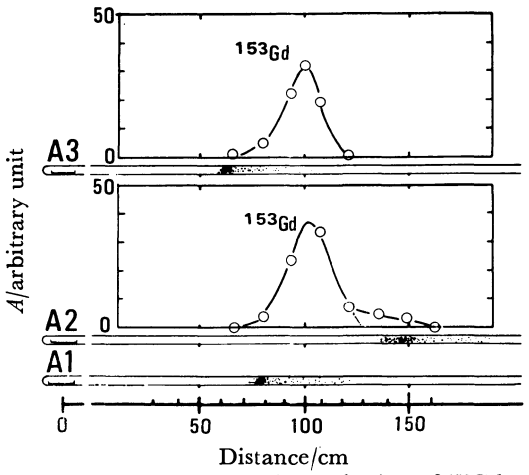

Fig. 1. Deposition zone and distribution of ^{153}Gd radioactivity along sublimation tube.
Sample, A1: $Gd(thd)_3$; A2: $(Sc+^{153}Gd)(thd)_3$; A3: $(La+^{153}Gd)(thd)_3$.

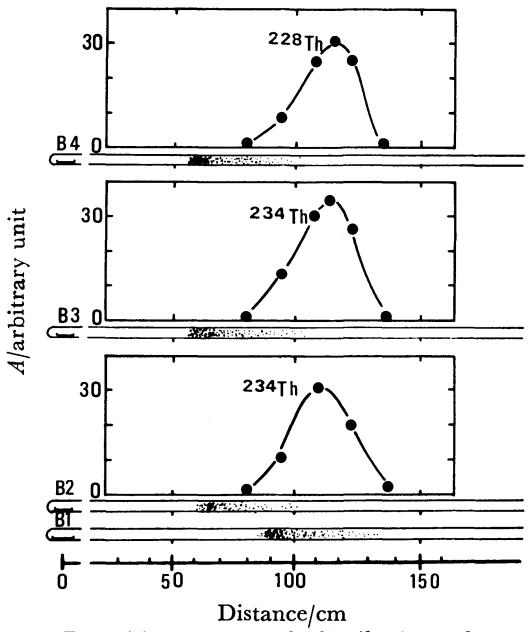

Fig. 2. Deposition zone and distribution of thorium radionuclide along sublimation tube.
Sample, B1: $Th(thd)_4$; B2: $(UO_2+^{234}Th)(thd)_2$; B3: $(La+^{234}Th)(thd)_3$; B4: $(La+^{228}Th)(thd)_3$.

chelate was also found to be equal to those of macro amounts of chelate. The tracer amounts of the sublimated chelates were located in discrete and reproducible temperature ranges. These reasons allow the sublimation behavior of tracer amounts of actinoid thd chelates to be expressed conveniently in terms of the sublimation-recrystallizing temperature range.

Sublimation Behavior of Actinoid Chelates of 2,2,6,6-Tetramethyl-3,5-heptanedione. The shape of the sublimatographic distribution of each actinoid thd chelate was that of tracer amounts of $Gd(thd)_3$ and $Th(thd)_4$. The sublimation-recrystallizing temperatures for the various actinoid thd chelates are graphically presented and compared in Fig. 3. In this figure, the depositing

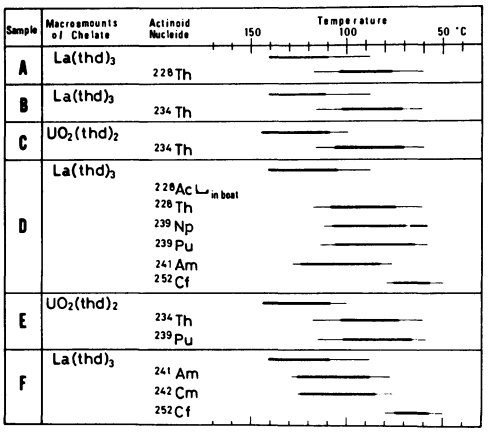

Fig. 3. Vacuum sublimation-recrystallizing temperature for tracer amounts of actinoid thd chelate.
Sample, A: (La+^{228}Th)(thd)$_3$; B: (La+^{234}Th)(thd)$_3$; C: (UO_2+^{234}Th)(thd)$_2$; D: (La+^{228}Ac+^{228}Th+^{239}Np+^{239}Pu+^{241}Am+^{252}Cf)(thd)$_3$; E: (UO_2+^{234}Th+^{239}Pu)-(thd)$_2$; F: (La+^{241}Am+^{242}Cm+^{252}Cf)(thd)$_3$.

TABLE 2. VACUUM SUBLIMATION-RECRYSTALLIZING TEMPERATURE RANGES OF ACTINOID thd CHELATES

Actinoid thd chelate	Temperature range/°C
$Th(thd)_4$	60—118
$UO_2(thd)_2$	100—145
$Np(thd)_4$	59—113
$Pu(thd)_4$	59—115
$Am(thd)_3$	77—129
$Cm(thd)_3$	76—126
$Cf(thd)_3$	50—80

zones in a large portion(80%) of sublimated chelate are shown as a thicker line. Table 2 summarizes the sublimation-recrystallizing temperature ranges obtained for actinoid thd chelates. Many actinoid metals, The U, Np, Pu, Am, Cm, and Cf, made a highly volatile, and thermally stable chelate by using 2,2,6,6-tetramethyl-3,5-heptanedione chelating agent. However, Ac(III) thd chelate was not sublimed under the same sublimation conditions. The Ac(III) thd chelate will be unstable on heating.

It is difficult to estimate the valence state of tracer amounts of solid actinoid sublimates. The valence states of Am, Cm, and Cf ions in each starting solution were tervalent, and those of Th, Np, and Pu ions were quadrivalent. In general, valence states of Am, Np, and Pu ions tend to change in various solutions. Therefore special care was paid in each preparative step of these actinoid chelates. On the other hand, according to solvent extraction data of these actinoid chelates of β-diketone agents, β-diketonato chelates of Am(III), Np(IV), and Pu(IV) gives the highest values of formation constants in each actinoid β-diketonato chelates. In this experiment, the recrystallizing positions of these actinoid thd chelates were compared with those of other actinoid and lanthanoid chelates. Under these conditions, the coordination forms between the actinoid metals and the thd chelating ligands were estimated. The estimated chemical forms are shown in the first column in Table 2.

By comparing the above results, it is found that the sublimation-recrystallizing temperature range of actinoid thd chelates decreases in the following order:

$$UO_2(thd)_2 > \begin{matrix} Th((thd)_4 \\ Am(thd)_3 \\ Cm(thd)_3 \\ Pu(thd)_4 \end{matrix} > Np(thd)_4 > Cf(thd)_3$$

The recrystallizing temperature ranges of tervalent $Am(thd)_3$, $Cm(thd)_3$ and $Cf(thd)_3$ were compared with those of the tervalent lanthanoid chelates, $Ln(thd)_3$. The recrystallizing temperature range of Cf(III)$(thd)_3$ was found to resembles those of the heavier lanthanoid (Ho–Lu) chelates, while the recrystallizing temperature ranges of Am(III)$(thd)_3$ and Cm(III)$(thd)_3$ chelates resemble those of the lighter lanthanoid (La, Pr–Gd) chelates.[5,6] Therefore the structures of the Am(III) and Cm(III) thd chelates should be different from that of the Cf(III)chelate. The Am(III) and Cm(III) thd chelates are estimated to be a dimer form, and the Cf(III) thd chelate may be a monomer form. As the dimer chemical forms of $Am_2(thd)_6$ and $Cm_2(thd)_6$ are improbable owing to very low metal concentrations, as shown in Table 1, $LaAm(thd)_6$ and $LaCm(thd)_6$ are possible forms.

The quadrivalent chelates of Th(IV)$(thd)_4$, Np(IV)-$(thd)_4$, and Pu(IV)$(thd)_4$ recrystallized in a similar position of the sublimation tube. Since there are little difference in structure and molecular weight of $M(thd)_4$ (M=Th, Np, Pu), their van der Waals' forces will be equal and their sublimation behaviors would be similar. The recrystallizing temperature of $UO_2(thd)_2$ chelate was found to be higher than those of the other actinoid chelates. This sublimation behavior will be due to the structural characteristic of "nyl" ion.

The actinoid thd chelates gave a high thermal stability during sublimation, but showed a considerable difference in the sublimation-recrystallizing temperature. The differences of their sublimation behaviors may be due to the difference in vapor pressure, molecular weight, heats of sublimation, and surface area of these chelates. The differences in heats of sublimation can be regarded as significant, because the heats of sublimation are correlated with the space arrangement. However, a number of fundamental experiments must be undertaken in order to determine the sublimation behavior of tracer amounts of chelate compound.

The reproducibility of sublimation-recrystallizing temperatures suggests that the sublimation technique can be applied to separate the actinoid elements in a carrier-free state. It is proposed that the ^{238}U–^{234}Th, ^{243}Am–^{239}Np radioactive equilibrium mixture and the Am(Cm)–Cf mixture can be separated by a sublimation technique.

The authors wish to express their deep thanks to Professor Masanobu Sakanoue of the Faculty of Science, Kanazawa University for his continuous encouragement throughout this study.

The present work was partially supported by Grants-

in-Aid for Scientific Research Nos. 574227 and 56040004 from the Ministry of Education, Science and Culture.

References

1) K. J. Eisentraut and R. E. Sievers, *J. Am. Chem. Soc.*, **87**, 5254 (1965).
2) J. E. Sicre, J. T. Dubois, K. J. Eisentraut, and R. E. Sievers, *J. Am. Chem. Soc.*, **91**, 3476 (1969).
3) E. W. Berg and J. J. C. Acosta, *Anal. Chim. Acta*, **40**, 101 (1965).
4) R. E. Sievers and J. E. Sadlowski, *Science*, **201**, 217 (1978). In this paper, a number of works on volatile metal complexes and their applications are reviewed.
5) R. Amano, A. Sato, and S. Suzuki, *Chem. Lett.*, **1980**, 537.
6) R. Amano, A. Sato, and S. Suzuki, *Bull. Chem. Soc. Jpn.*, **54**, 1368 (1981).
7) R. C. Young, C. Goodman, and J. Kovitz, *J. Am. Chem. Soc.*, **61**, 876 (1936).
8) H. A. Swain, Jr., and D. G. Karraker, *Inorg. Chem.*, **9**, 1766 (1970).
9) M. Sakanoue and R. Amano, "Transplutonium 1975," ed by W. Müller and R. Lindner, North-Holland Publ. (1976), p. 123.
10) Y. Inoue, private communication.

The Stereochemistry and Reactivity of Metal-Schiff Base Complexes. V. The Solvent Effect on the Stereoselectivity of Cobalt(III) Complexes Containing a sal_2en-type Schiff Base and L-Amino Acid

Yuki Fujii,* Yasuo Kuwana, Sozo Takahashi,†† Keiko Shimizu, and Kumiko Hiroi
Department of Chemistry, Faculty of Science, Ibaraki University, Bunkyo-cho, Mito, Ibaraki 310
††*Department of Chemistry, Ibaraki Technical College, Nakane, Katsuta, Ibaraki 312*
(Received December 12, 1981)

The solvent effect on the stereoselectivity between Λ- and Δ-β_2-diastereoisomers of cobalt(III) complexes with the general formula of [Co(Schiff base)(L-aa)], where Schiff base represents sal_2en^{2-}, α-Me-sal_2en^{2-}, and 5,6-benzo-sal_2en^{2-}, and where L-aa denotes L-alaninate, L-valinate, L-methioninate, and L-phenylalaninate, was studied. Generally, the Λ-β_2-isomer was more stable than the Δ-β_2-isomer in solution, and the stereoselectivity of all the L-ala-complexes and of the L-met-complex with 5,6-benzo-sal_2en increased in the following order of solvents : acetone=DMF$\leqq$*t*-BuOH<*s*-BuOH<*i*-PrOH<*n*-BuOH<*n*-PrOH<EtOH<MeOH. On the other hand, the stereoselectivity of L-val- and L-phe-complexes with sal_2en and 5,6-benzo-sal_2en increased in the following order : acetone=DMF<MeOH<EtOH<*n*-PrOH<*n*-BuOH<*i*-PrOH<*s*-BuOH<*t*-BuOH. In the case of 5,6-benzo-sal_2en complexes with L-val and L-ile, the Δ-β_2-isomer was preferred rather than the Λ-β_2-isomer in acetone and DMF with 8—13% stereoselectivity. From the spectroscopic evidence, a hydrogen bonding between the OH group of alcoholic solvents and phenolic oxygen atoms of a Schiff base ligand was assummed, and the above phenomena were explained in terms of the steric difference between the Λ- and Δ-β_2-isomers for the solvation with the alcoholic solvents by means of the hydrogen bonding.

Detailed studies have been directed toward the thermodynamic stereoselectivity of $Co(N_4)$-complexes with a chiral amino acid. In these studies, the energy differences among the diastereoisomers have been explained mainly in terms of the intramolecular steric interaction (nonbonded interactions, bond deformations, angle deformations, and torsional strain) of the diastereoisomers.[1-3] However, the results of energy-minimization calculations have sometimes disagreed with the observed values. In such cases, an intermolecular interaction between the diastereoisomers and solvent molecules has been suggested.[2-4] In fact, it is well known that racemic *cis*-$[Co(en)_2Cl_2]^+$ and racemic α-$[Co(trien)Cl_2]^+$ antiracemize in an optically active solvent.[5] It has been pointed out recently for *trans*-$[Co((R)\text{-pn})_2X_2]^+$ (X=Cl^- and Br^-) that the conformation of the (*R*)-pn chelate ring changes depending on the nature of the solvents.[6] It has also reported that solvents affect the conformation of the 3,2,3-tet chelate ring of *trans*-$[Co(3,2,3\text{-tet})(N_3)_2]^+$ and the conformation of 1,3-diamine of *trans*-$[Co(1,3\text{-diamine})_2X_2]^{+n}$ (X=Cl^-, CN^-, and NH_3).[7,8] These facts suggest that solvents play an important role in the thermodynamic stereoselectivity of metal complexes.

In the course of our study of the stereoselectivity of Co(III)-Schiff base complexes with a chiral amino acid,[9] we found that the stereoselectivity of Co(III)-Schiff base complexes is much higher than that of $Co(N_4)$-complexes. In order to explain the high stereoselectivity, an X-ray study of $(-)_{435}$-Λ-β_2-[Co(α-Me-sal_2en)(L-ile)]·$1.5H_2O$ was carried out;[10] however, no steric factor stabilizing this configuration has been found. In this paper, the solvent effect on the stereoselectivity of a series of β_2-[Co(Schiff base)(L-aa)] complexes will be investigated in detail.[11]

Experimental

Preparation of Complexes. β_2-[Co(sal_2en)(L-aa)] and β_2-[Co(α-Me-sal_2en)(L-aa)] were prepared as previously repoted.[9] β_2-[Co(5,6-benzo-sal_2en)(L-aa)] was prepared as follows. (Since the preparation is similar for all the amino acids used here, the method for only the L-ala-complex is described.) L-Alanine (0.5 g, 5.5×10^{-3} mol) in a mixed solvent of water (20 cm^3) and methanol (100 cm^3) was added to a slurry of [Co(5,6-benzo-sal_2en)] (2.3 g, 5.4×10^{-3} mol) in 250 cm^3 of chloroform. The mixture was stirred vigorously in the open air for about 3 h to give a green solution. This solution was then filtered, and the filtrate was concentrated to a small volume at room temperature to give green crystals. In the cases of L-alanine, L-threonine, and L-isoleucine, the green crystals were recrystallized from methanol. In the cases of L-valine, L-leucine, L-methionine, and L-phenylalanine, the green crystals were washed with methanol. Yields, about 2.0 g (75%). The elemental analyses data are given in Table 1.

[Co(5,6-benzo-sal_2en)] was prepared as follows: 2-Hydroxy-1-naphthaldehyde (5.2 g, 3×10^{-2} mol) in 50 cm^3 of methanol was mixed with ethylenediamine (0.9 g, 1.5×10^{-2} mol); the Schiff base separated out as an yellow powder in about a 95% yield. $Co(CH_3COO)_2\cdot4H_2O$ (2.5 g, 1×10^{-2} mol), dissolved in methanol (100 cm^3), was added to a slurry of the ligand (3.7 g, 1×10^{-2} mol) in chloroform (200 cm^3). The mixture was heated at about 80 °C for 1 h to give a red complex, [Co(5,6-benzo-sal_2en)] in about an 80% yield. Found: C, 67.67; H, 6.74; N, 6.47%. Calcd for $CoC_{24}H_{18}N_2O_2$: C, 67.78; H, 6.62; N, 6.59%.

Preparation of Solutions. Extra-pure solvents were used after distillation. About 5×10^{-4} mol dm^{-3} solutions of the complexes were used for the AB and CD measurements. The establishment of equilibrium was confirmed from the mutarotation at 435 nm of the complex solutions. In acetone, the isomerization of the complexes was very slow. Therefore, activated charcoal was added to the acetone solutions, and the mixtures were warmed at about 50 °C until the solutions showed a constant rotation at 435 nm. The AB and CD measurements were carried out after the filtration of the activated charcoal. The concentration of the acetone solutions was calibrated by the use of the absorbance at 580 nm. No decomposition was found from the ^1H NMR spectra in the DMF-d_7 of the complexes recovered from acetone solutions. Also, the isomerization in DMF (*N*,*N*-dimethylformamide) was fairly slow; the solutions were warmed at about 40 °C to establish the isomerization equilibrium. No decomposition

Table 1. Elemental analyses data

Complex	Found(%)			Calcd(%)		
	C	H	N	C	H	N
[Co(5,6-benzo-sal$_2$en)(L-ala)]·H_2O	61.03	4.87	8.13	61.02	4.93	7.91
[Co(5,6-benzo-sal$_2$en)(L-met)]	60.87	4.72	7.49	60.73	4.92	7.33
[Co(5,6-benzo-sal$_2$en)(L-val)]·H_2O	61.81	5.11	7.60	62.25	5.40	7.51
[Co(5,6-benzo-sal$_2$en)(L-thr)]·1.5H_2O	59.43	5.31	7.23	58.95	5.12	7.37
[Co(5,6-benzo-sal$_2$en)(L-leu)]·2H_2O	60.72	5.58	7.12	60.91	5.79	7.10
[Co(5,6-benzo-sal$_2$en)(L-ile)]·2H_2O	60.51	5.54	7.34	60.91	5.79	7.10
[Co(5,6-benzo-sal$_2$en)(L-phen)]·2H_2O	63.22	4.96	6.76	63.36	5.16	6.72

was found from the ^{1}H NMR spectra of the complexes in DMF-d_7 at 35 °C.

Measurements. The absorption (AB) and circular dichroism (CD) spectra were measured with a Hitachi 200-10 Spectrophotometer at 23 °C and with a JASCO J-20 Spectropolarimeter ar room temperature respectively. The optical rotation at 435 nm was measured with a JASCO DIP-140 Polarimeter. The ^{1}H NMR spectra were recorded with a Hitachi R-20 Spectrometer (60 MHz) or a Varian CFT-20 Spectrometer (80 MHz) at 35 °C.

Results and Discussion

Structure and Properties of Complexes. In a previous paper,[9] the *cis*-β_1-structure was assigned tentatively to [Co(sal$_2$en)(L-aa)] and [Co(α-Me-sal$_2$en)(L-aa)] (L-aa= L-ala, L-met, L-val, L-leu, L-ile, L-thr, L-phe, L-tyr, and L-trp). However, it has been found recently, in our X-ray study of $(-)_{435}$-[Co(α-Me-sal$_2$en)(L-ile)]·1.5H_2O, that the complex takes the *cis*-β_2-structure.[10] As is shown in Fig. 1, the AB and CD spectra of the L-ile-complex in methanol closely resemble those in the solid state (KBr disk), and the AB and CD spectra of Co(sal$_2$en)- and Co(α-Me-sal$_2$en)-complexes with various L-amino acidates in methanol are very similar to those of the L-ile-complex in methanol.[9] Accordingly, the *cis*-β_2-structure can be assigned to all the Co(sal$_2$en)- and Co(α-Me-sal$_2$en)-complexes with L-amino acidates in methanol.

As has been mentioned previously,[9] [Co(sal$_2$en)(L-aa)] and [Co(α-Me-sal$_2$en)(L-aa)] are isolated as a 1 : 1

Table 2. Abbreviations and structures of Schiff-base ligands

Structure	Abbreviation
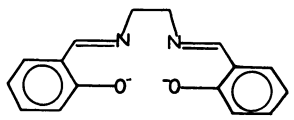	sal$_2$en
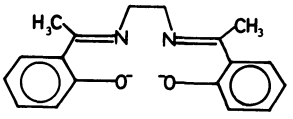	α-Me-sal$_2$en
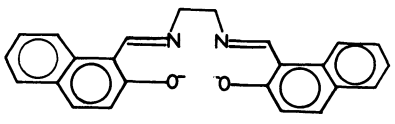	5,6-Benzo-sal$_2$en

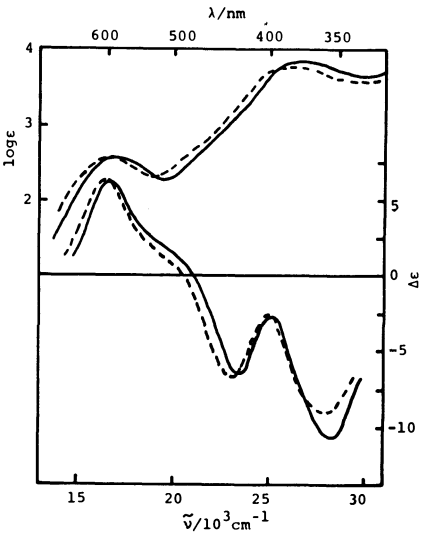

Fig. 1. AB and CD spectra of [Co(α-Me-sal$_2$en)(L-ile)].
——: In methanol under the equilibrium conditions,
------: in KBr disk (arbitrary scale).

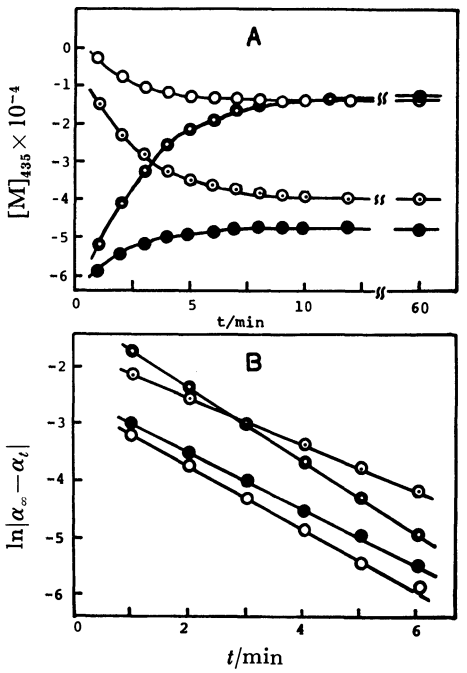

Fig. 2. Mutarotation at 435 nm of β_2-[Co(5,6-benzo-sal$_2$en)(L-aa)] in methanol at 23 °C (A) and the ln-plot (B).
—○—: L-ala-complex, —⊙—: L-thr-complex,
—○—: L-val-complex, —●—: L-phe-complex.

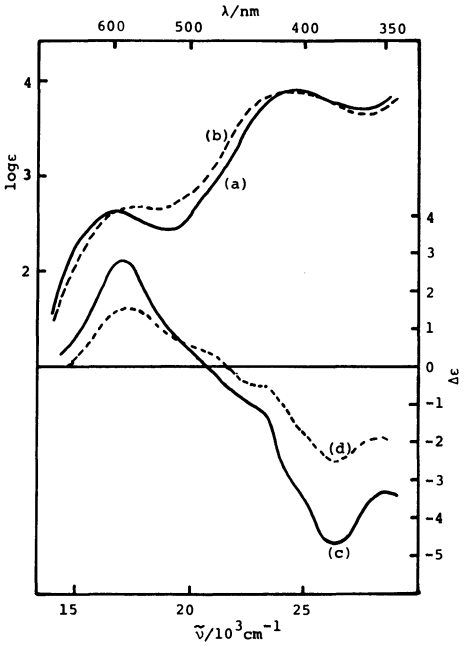

Fig. 3. AB and CD spectra of β_2-[Co(5,6-benzo-sal$_2$en)-(L-ala)] in methanol ((a) and (c)) and in DMF ((b) and (d)) under the equilibrium conditions.

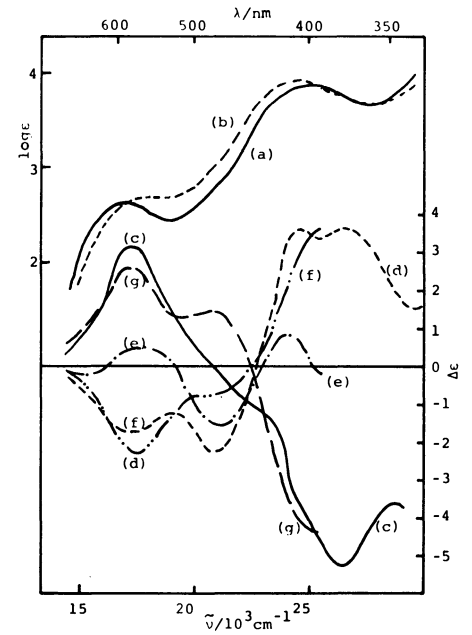

Fig. 4. AB and CD spectra of β_2-[Co(5,6-benzo-sal$_2$en)-(L-val)] in methanol ((a) and (c)) and in DMF ((b) and (d)) under the equilibrium conditions. (e): Vicinal CD of L-val of β_2-[Co(sal$_2$en)(L-val)], (f): CD curve rectified vicinal CD (e) for CD (d), (g): CD curve rectified vicinal CD (e) for CD (c).

mixture of Λ- and Λ-β_2-isomers or as a pure Λ-β_2-isomer. This difference in the isolated form comes from the solubility of the complexes. On the other hand, the isolated complexes exhibit mutarotation in methanol to show a minus rotation at 435 nm under equilibrium conditions.[9] These facts indicate that: 1) the complexes

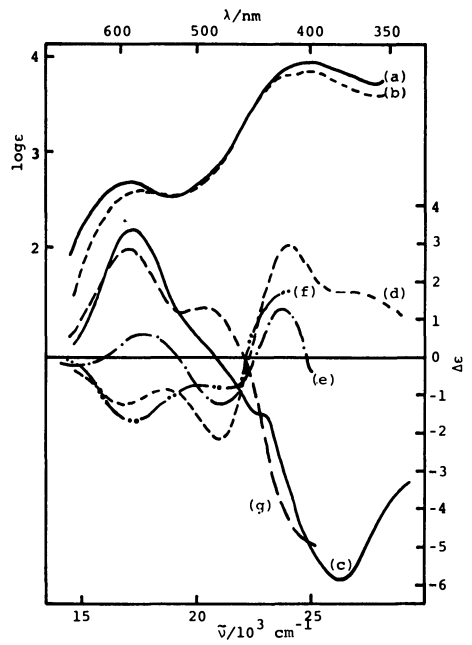

Fig. 5. AB and CD spectra of β_2-[Co(5,6-benzo-sal$_2$en)-L-ile)] in methanol ((a) and (c)) and in DMF ((b) and (d)) under the equilibrium conditions. (e): Vicinal CD of L-ile, (f): CD curve rectified vicinal CD (e) for CD (d), (g): CD curve rectified vicinal CD (e) for CD (c).

are labile in isomerization between Λ- and Λ-β_2-isomers in methanol, 2) the complexes exist as an equilibrium mixture of the two isomers in methanol, and 3) the Λ-β_2-isomer ($(-)_{435}$-isomer) is thermodynamically more stable than the Λ-β_2-isomer ($(+)_{435}$-isomer) in methanol. Also, in the cases of the [Co(5,6-benzo-sal$_2$en)(L-aa)] newly prepared here, they exhibit mutarotation in methanol to show a minus rotation at 435 nm under equilibrium conditions. Some representative mutarotations are shown in Fig. 2. The numerical data are given in Table 3. The plots of $\ln(\alpha_\infty - \alpha_t)$ *vs.* the time gave a straight line, indicating that two species of isomers, $(-)_{435}$- and $(+)_{435}$-isomers, are involved in each mutarotation. On the other hand, the AB spectra showed no clear change during the mutarotation. These facts suggest that: 1) [Co(5,6-benzo-sal$_2$en)(L-aa)] is also labile in isomerization and exists as an equilibrium mixture of $(-)_{435}$- and $(+)_{435}$-isomers in methanol; 2) the $(-)_{435}$-isomer is more stable than the $(+)_{435}$-isomer in methanol, and 3) both isomers have the same geometrical structure with respect to the coordinated atoms around the Co(III) ion.

Figures 3—5 show the AB and CD spectra of the representative 5,6-benzo-sal$_2$en complexes under the equilibrium conditions. The numerical data are listed in Table 4. The AB spectra and the CD spectral patterns of all the 5,6-benzo-sal$_2$en complexes in methanol closely resemble each other and are very similar to those of Λ-β_2-[Co(α-Me-sal$_2$en)(L-ile)] in methanol. Thus, it becomes clear that 1) all the 5,6-benzo-sal$_2$en complexes take the *cis*-β_2-structure, and 2) they favor the Λ-β_2-configuration over the Δ-β_2-configuration in methanol.

TABLE 3. MUTAROTATION DATA AND ISOLATION FORM OF β_2-[Co(5,6-BENZO-sal$_2$en)(L-aa)]

L-aa	Solvent	Temp °C	$[M]_{435}$ ° mol dm^{-3} m^{-1} (soon after dissolution)[a]	$[M]_{435}$ ° mol dm^{-3} m^{-1} (under equilibrium conditions)	Isomerization rate constant from Δ-β_2- to Λ-β_2- isomers k_{obsd}/s^{-1}, 23 °C	Isolation form Λ-β_2-isomer: Δ-β_2-isomer
L-ala	MeOH	23.5	−4000	−14000	$(9.3\pm0.2)\times10^{-3}$	
L-met	MeOH	23.5	−5500	−21000	$(7.6\pm0.2)\times10^{-3}$	
L-val	MeOH	23.5	−52000	−13000	$(6.2\pm0.1)\times10^{-3}$ [b]	
L-thr	MeOH	23.5	−15000	−40000	$(6.6\pm0.1)\times10^{-3}$	
L-leu	MeOH	23.5	−4000	−18000	$(8.5\pm0.2)\times10^{-3}$	
L-ile	MeOH	23.5	0	−12000	$(1.0\pm0.3)\times10^{-2}$	
L-phe	MeOH	23.5	−58800	−48000	$(8.4\pm0.2)\times10^{-3}$ [b]	
L-ala	DMF	36.0	+2000	−12000	$(1.3\pm0.1)\times10^{-5}$	1 : 1
L-met	DMF	36.0	+2600	−17000	$(2.1\pm0.1)\times10^{-5}$	1 : 1
L-val	DMF	36.0	−110000	+12000	$(2.1\pm0.1)\times10^{-5}$ [b]	pure Λ-β_2-isomer
L-thr	DMF	36.0	−4700	−41000	$(4.9\pm0.5)\times10^{-5}$	1 : 1
L-leu	DMF	36.0	+1400	−18000	$(9.2\pm0.2)\times10^{-6}$	1 : 1
L-ile	DMF	36.0	+3000	+12000	$(2.4\pm0.5)\times10^{-5}$	1 : 1
L-phe	DMF	36.0	−59800	−18300	$(3.2\pm0.1)\times10^{-5}$ [b]	3 : 1

a) About 1 min after dissolution. b) Isomerization constant (observed value) from the Λ-β_2-isomer to the Δ-β_2-isomer.

TABLE 4. AB AND CD SPECTRAL DATA OF β_2-[Co(5,6-BENZO-sal$_2$en)(L-aa)] [a]

L-aa	Solvent	1st band		CT and π-π^* bands	
		$\tilde{\nu}/10^3$ cm^{-1} (log ε)	$\tilde{\nu}/10^3$ cm^{-1} ($\Delta\varepsilon$)	$\tilde{\nu}/10^3$ cm^{-1} (log ε)	$\tilde{\nu}/10^3$ cm^{-1} ($\Delta\varepsilon$)
L-ala	MeOH	16.81(2.66)	16.95(+2.77) 20.00(+0.36)	23.92(3.86) 24.88(3.91)	22.73(−1.18) 24.39(−3.02) 26.32(−4.73)
	DMF	17.54(2.68)	17.33(+1.85) 20.41(+0.53)	23.64(3.85) 24.75(3.90)	22.22(−0.62) 23.81(−1.77) 25.97(−3.51)
L-met	MeOH	16.81(2.71)	17.04(+4.42) 20.41(+0.75)	24.10(3.93) 25.00(3.98)	22.73(−1.68) 24.69(−5.77) 26.67(−6.33)
	DMF	17.39(2.68)	17.37(+2.37) 20.20(+0.85)	23.61(3.90) 24.75(3.95)	22.22(−0.79) 24.10(−2.16) 26.32(−4.77)
L-val	MeOH	16.86(2.66)	17.15(+3.22)	24.10(3.86) 25.00(3.90)	22.73(−1.20) 24.39(−3.69) 26.46(−5.33)
	DMF	17.54(2.67)	16.95(−1.85) 21.05(−2.75)	23.64(3.89) 24.81(3.93)	24.10(+4.16) 26.67(+3.05)
L-leu	MeOH	16.84(2.67)	16.81(+3.38) 20.41(+0.72)	24.10(3.92) 25.00(3.96)	22.73(−1.43) 24.10(−3.51) 26.32(−6.02)
	DMF	17.39(2.66)	17.39(+2.88) 20.41(+0.89)	23.64(3.88) 24.69(3.93)	22.22(−0.93) 23.81(−2.24) 26.32(−6.02)
L-ile	MeOH	16.89(2.67)	17.24(+3.39) 20.00(+0.41)	24.10(3.93) 25.00(3.96)	22.73(−1.42) 24.10(−3.54) 26.32(−6.01)
	DMF	17.54(2.64)	16.81(−1.28) 21.05(−2.24)	23.81(3.86) 25.00(3.91)	23.98(+3.07) 27.03(+1.84)
L-thr	MeOH	16.84(2.62)	16.81(+9.46) 20.62(+2.19)	23.92(3.85) 24.94(3.90)	22.47(−3.70) 24.39(−13.30) 26.32(−16.18)
	DMF	17.64(2.65)	17.33(+6.51) 20.62(+2.55)	23.81(3.88) 24.88(3.92)	22.47(−1.42) 24.10(−8.52) 26.11(−13.38)
L-phe	MeOH	16.81(2.67)	16.86(+7.58) 20.57(+2.10)	24.10(3.91) 25.00(3.95)	22.83(−3.99) 24.69(−10.43) 26.53(−12.46)
	DMF	17.45(2.67)	17.39(+2.59) 20.00(+0.88)	23.92(3.90) 25.00(3.94)	22.22(−0.82) 24.39(−2.72) 26.32(−5.34)

a) Data are those under the equilibrium conditions.

The mutarotation of representative complexes in DMF is shown in Fig. 6. The numerical data are given in Table 3. Although the mutarotation in DMF is slow, the curves are very similar to those in methanol, and the plots of $\ln(a_\infty - a_t)$ *vs.* the time give a straight line. The AB spectra show no clear time dependence during the mutarotation. These facts indicate that the complexes have properties in DMF similar to those in methanol. However, L-val- and L-ile-complexes exhibit a plus rotation under the equilibrium conditions in DMF, suggesting that they favor the Δ-β_2-configuration in DMF more than the Λ-β_2-configuration.

The AB and CD spectra of representative complexes in DMF under the equilibrium conditions are shown in Figs. 3—5. Although some shift of the AB and CD spectra is observed as compared with those in methanol, the AB and CD spectra in DMF of L-ala-, L-met-, L-leu-, L-thr-, and L-phe-complexes closely resemble those in methanol, indicating that the complexes take the *cis*-β_2-structure and prefer the Λ-β_2-isomer rather than the Δ-β_2-isomer in DMF. In the case of the L-val- and L-ile-complexes, the AB spectra in DMF are similar to those in methanol, while the CD spectra in DMF show signs different from those in methanol. When the vicinal effect of the coordinated L-amino acidates is subtracted from the CD curves of the L-val- and L-ile-complexes in DMF, it becomes clear that the resulting CD curves ((f) in Figs. 4 and 5) are almost in a mirror-image relation with the rectified CD curves ((g) in Figs. 4 and 5) in methanol. From these facts, it can be concluded that the L-val- and L-ile-complexes prefer the Δ-β_2-isomer in DMF rather than the Λ-β_2-isomer. It is interesting that the stereoselectivity changes depending upon the kind of solvent.

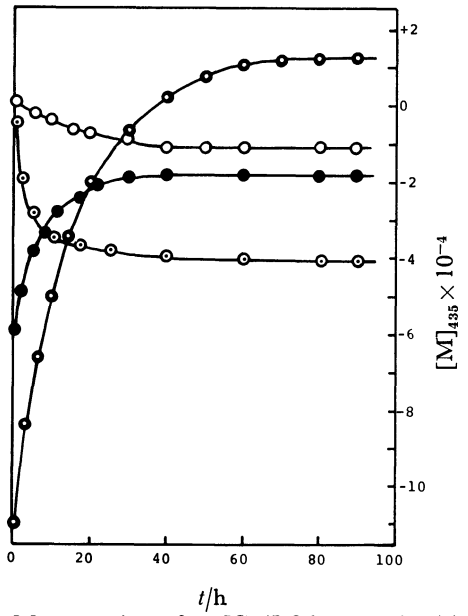

Fig. 6. Mutarotation of β_2-[Co(5,6-benzo-sal$_2$en)(L-aa)] in DMF at 36 °C.
—○—: L-ala-complex, —⊙—: L-thr-complex, —O—: L-val-complex, —●—: L-phe-complex.

From the molar rotation of the 5,6-benzo-sal$_2$en complexes soon after dissolution in DMF (Table 3), it can be assummed that: 1) the L-ala-, L-met-, L-leu-, L-ile-, and L-thr-complexes were isolated as a 1 : 1 mixture of Λ- and Δ-β_2-isomers, 2) the L-val-complex was isolated as the pure Λ-β_2-isomer, and 3) the L-phe-complex was isolated as a 3 : 1 mixture of Λ- and Δ-β_2-isomers. The isomeric ratios of the L-ala-, L-met-, L-thr-, and L-val-complexes will be confirmed below from the ^{1}H NMR spectra of the complexes in DMF.

Stereoselectivity of 5,6-Benzo-sal$_2$en Complexes. Figure 7 shows the representative ^{1}H NMR spectra of the complexes in DMF-d_7 and in a mixed solvent of CD_3OD and DMF-d_7. The numerical data are listed in Table 5. Since the 5,6-benzo-sal$_2$en complexes are not so fully soluble in CD_3OD, the mixed solvent of CD_3OD and DMF-d_7 (20%) was used here in place of CD_3OD. The CD spectra of the complexes in the mixed solvent of methanol and DMF (20%) are almost the same as those in methanol. Thus, we regarded the ^{1}H NMR spectra in the mixed solvent as close to those in CD_3OD.

Table 5. ^{1}H NMR spectral data of β_2-[Co(5,6-benzo-sal$_2$en)(L-aa)] under the equilibrium conditions δ [a]

L-aa	HC=N	$-CH_2-CH_2-$[b]	R (Amino acid)		Others
L-ala	8.45[1] 9.30[1]	4.1	1.36 1.48[1.4]	1.56 1.68[1.6]	c)
L-met	8.40[1] 9.30[1]	4.1	2.13[1.2]	2.01[1.8]	2.15—2.75 (broad multiplet of $-C\underline{H}_2-C\underline{H}_2-S-CH_3$), c)
L-val	8.48[1] 9.30[1]	4.1	0.84[0.8] 0.95[1.7]	1.06[2.2] 1.15[1.3]	c)
	8.58[1][d] 9.38[1][d]	4.4[d]	0.86[1.5][d] 0.89[3.0][d]	1.11[1.5][d]	c)
L-thr	8.47[1] 9.30[1]	4.1	1.19 1.30[1.1]	1.25 1.36[1.9]	c)
L-leu	8.44[1] 9.25[1]	4.1	0.95[b]		1.75 (broad multiplet of $-C\underline{H}_2-C\underline{H}(CH_3)_2$), c)
L-ile	8.53[1] 9.35[1]	4.1	0.85[0.2] 0.97[2.2]	1.07[2.9] 1.18[0.7]	c)
L-phe	8.19[1] 9.31[1]	4.1	3.3 (multiplet of $-C\underline{H}_2-\phi$)		6.7—8.5 (multiplets of naphtyl and phenyl signals)

a) Data in CD_3OD+DMF-d_7 (20%), [ ] represents the relative peak area. b) Broad multiplet. c) 6.8—8.4 (multiplet of naphtyl signal). d) Soon after dissolution in DMF-d_7.

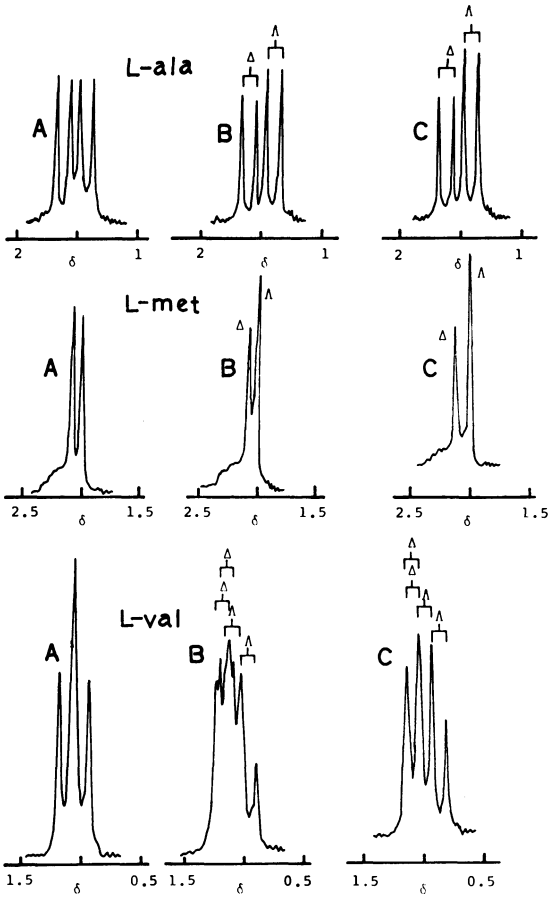

Fig. 7. The representative ^{1}H NMR spectra of β_2-[Co(5,6-benzo-sal$_2$en)(L-aa)].
A: Soon after dissolution in DMF-d_7, B: under the equilibrium conditions in DMF-d_7, C: under the equilibrium conditions in CD_3OD+DMF-d_7 (20%).

Table 6. Stereoselectivity of β_2-[Co(5,6-benzo-sal$_2$en)(L-aa)]

L-aa	[Λ]/[Δ] (in MeOH)	SS(%)[a]	[Λ]/[Δ] (in DMF)	SS(%)[a]
L-ala	1.25 (1.2—1.3)[b]	11.5	1.15 (1.1—1.2)[c]	6.9
L-met	1.45 (1.4—1.5)[b]	18.4	1.17 (1.1—1.2)[c]	8.0
L-val	1.27 (1.2—1.3)[b]	11.8	1.32[d]	−13.7
L-thr	2.61 (2.6—2.8)[b]	44.6	1.85 (1.7—1.9)[c]	29.8
L-leu	1.37	15.6	1.30	13.1
L-ile	1.39	16.2	1.18[d]	−8.2
L-phe	2.20	36.9	1.27	11.6

a) Value of $([\Lambda]-[\Delta])/([\Lambda]+[\Delta])\times 100(\%)$ from the CD spectra. b) Isomeric ratio from the ^{1}H NMR spectra in CD_3OD+DMF-d_7(20%). c) Isomeric ratio from the ^{1}H NMR spectra in DMF-d_7. d) Value of [Δ]/[Λ].

The signal of the coordinated 5,6-benzo-sal$_2$en ligand showed no observable time dependence, and the signals of all the complexes are very similar to each other. On the other hand, as is shown in Fig. 7, the alkyl signal of the coordinated L-amino acidates exhibits a time dependence. From the time dependence, it is confirmed that only two species of isomer are involved in the mutarotation of the L-ala-, L-met-, L-val-, and L-thr-complexes. Further, by a comparison with the mutarotation at 435 nm, the assignment of the alkyl peaks for Λ- and Δ-β_2-isomers becomes possible. From the relative peak area of the alkyl peaks soon after dissolution in DMF-d_7, it can be confirmed that the L-ala-, L-met-, and L-thr-complexes were isolated as a 1 : 1 mixture of the two isomers, but the L-val-complex was isolated as the pure Λ-β_2-isomer. On the other hand, from the relative peak areas of the alkyl peaks under the equilibrium conditions, the isomeric ratio between the two isomers under the equilibrium conditions can be estimated in the cases of L-ala-, L-met-, and L-thr-complexes; the values are listed in Table 6.

In the case of the L-val-complex, the alkyl signal under the equilibrium conditions is somewhat complicated due to the overlap of the peaks of the two isomers, although it is confirmed from a careful inspection that the Λ-β_2-isomer somewhat predominates over the Δ-β_2-isomer in the mixed solvent of CD_3OD and DMF-d_7, while the selectivity is reversed in DMF-d_7.

In the cases of the L-leu-, L-ile-, and L-phe-complexes, the alkyl signal is complicated due to the overlap of the peaks. Therefore, the isomeric ratio of these complexes was estimated from the $\Delta\varepsilon$ value of the main CD band in the 1st-absorption-band region of the complexes by the use of the following equation:

$$([\Lambda]-[\Delta])/([\Lambda]+[\Delta]) = (\Delta\varepsilon^A-\Delta\varepsilon^B)/(\Delta\varepsilon^C-\Delta\varepsilon^B), \quad (1)$$

where [Λ] and [Δ] represent the concentrations of the Λ- and Δ-β_2-isomers under the equilibrium conditions respectively; $\Delta\varepsilon^A$ denotes the CD intensity of the complexes at the main CD band near 580 nm under the equilibrium conditions; $\Delta\varepsilon^B$ stands for the vicinal effect of the coordinated L-amino acidates at the same wave length as that of $\Delta\varepsilon^A$, and $\Delta\varepsilon^C$ represents the CD intensity of the pure Λ-β_2-isomer at the main CD band near 580 nm. In this study, as the $\Delta\varepsilon^C$ value of various L-amino acidato complexes with 5,6-benzo-sal$_2$en, we used the $\Delta\varepsilon$ value of the pure Λ-β_2-isomer of the [Co(5,6-benzo-sal$_2$en)(L-val)] complex soon after dissolution in DMF. This is because: 1) it is only in the L-val-complex that the pure Λ-β_2-isomer can be isolated, however, 2) the $\Delta\varepsilon^C$ value can be regarded as almost a constant for the following reasons: 1) as is shown in Fig. 8, the vicinal effect of the coordinated L-amino acidates is almost a constant in the 1st-absorption region for various L-amino acidato complexes, and it is small in value as compared with the configurational effect of the complexes, and 2) as is shown in Table 7, the $\Delta\varepsilon^C$ value is almost a constant in sal$_2$en and in α-Me-sal$_2$en complexes. Indeed, as is shown in Table 6, the isomeric ratios of the L-ala-, L-met-, and L-thr-complexes, which were estimated from the CD intensity of the complexes and the $\Delta\varepsilon^C$ value of the L-val-complex, well fitted with the isomeric ratios estimated from the ^{1}H NMR spectra of the complexes.

Figure 8 shows the CD spectra of the 1 : 1 mixture of Λ- and Δ-β_2-isomers soon after dissolution in DMF; these spectra correspond to the vicinal effect of the coordinated

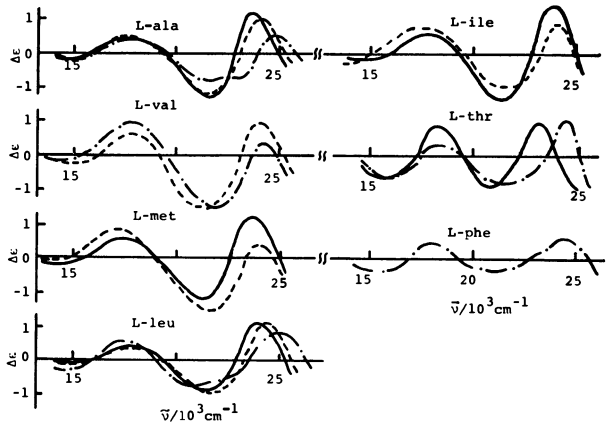

Fig. 8. Vicinal CD of β_2-[Co(Schiff base)(L-aa)] in DMF.
------: sal$_2$en complex, -·-·-: α-Me-sal$_2$en complex, ——: 5,6-benzo-sal$_2$en complex.

Table 7. The CD intensity of pure Λ-β_2-isomers in DMF

Complex	$\bar{\nu}/10^3$ cm^{-1}($\Delta\varepsilon$)
Λ-β_2-[Co(sal$_2$en)(L-thr)]·H$_2$O	17.24(+14.99)
Λ-β_2-[Co(sal$_2$en)(L-phe)]·4.5H$_2$O	17.15(+15.21)
Λ-β_2-[Co(α-Me-sal$_2$en)(L-ile)]·1.5H$_2$O	16.95(+14.08)
Λ-β_2-[Co(α-Me-sal$_2$en)(L-met)]·2H$_2$O	16.95(+14.14)
Λ-β_2-[Co(5,6-benzo-sal$_2$en)(L-val)]·H$_2$O	17.45(+20.71)

L-amino acidates. The vicinal CD's in the 1st-absorption-band region are very similar to each other; therefore, in the calculation of Eq. 1, we used the vicinal CD's of β_2-[Co(sal$_2$en)(L-val)] and β_2-[Co(α-Me-sal$_2$en)-(L-phe)] for the $\Delta\varepsilon^B$ values of the 5,6-benzo-sal$_2$en complexes with L-val and L-phe respectively. From the similarity in the vicinal CD spectra, it is assumed that all the L-amino acidates take conformations quite similar to each other.

From Table 6, the following conclusions can be drawn: 1) the 5,6-benzo-sal$_2$en complexes have an inclination to prefer the Λ-β_2-isomer rather than the Δ-β_2-isomer in methanol and in a mixed solvent of methanol and DMF, 2) the stereoselectivity of 5,6-benzo-sal$_2$en complexes in methanol increases in the following order of L-amino acidates: L-ala=L-val<L-ile=L-leu<L-met<L-phe<L-thr, 3) this order is not parallel with the increasing order of steric bulkness of the alkyl group of amino acidates, as has been observed for sal$_2$en and α-Me-sal$_2$en complexes,[9] 4) the degree of the stereoselectivity of 5,6-benzo-sal$_2$en complexes in methanol is somewhat lower than that of sal$_2$en and α-Me-sal$_2$en complexes,[9] 5) the stereoselectivity of 5,6-benzo-sal$_2$en complexes in DMF is lower than that in methanol, and 6) in the case of L-val- and L-ile-complexes, which have the secondary β-carbon atom at the alkyl group of amino acid, they exhibit an inclination to prefer the Λ-β_2-isomer rather than the Λ-β_2-isomer in DMF.

Solvent Effect on the Stereoselectivity of Complexes. In order to get information about the stereoselectivity of Co(Schiff base)-complexes with L-amino acidates in various solvents, we measured the AB and CD spectra of Co(sal$_2$en)-, Co(α-Me-sal$_2$en)-, and Co(5,6-benzo-sal$_2$en)-complexes with L-ala, L-met, L-val, and L-phe in H$_2$O, MeOH, EtOH, PrOH, BuOH, DMF, and acetone. The numerical data are given in Tables 8—10, while representative AB and CD spectra in various solvents are shown in Figs. 9 and 10. Although some extent of shift (within 20 nm) with the variation of solvents is observed for the absorption and the associated CD bands in all the complexes, the AB spectral pattern and the intensity of each complex are very similar to those in methanol; this indicates that each complex takes the *cis*-β_2-structure in these solvents. The CD

Table 8. AB and CD spectral data (1st band) and stereoselectivity of β_2-[Co(5,6-benzo-sal$_2$en) (L-aa)] in various solvents

Solvent (pK_a)[20]		L-ala λ/nm (ε or $\Delta\varepsilon$)	SS(%)	L-met λ/nm (ε or $\Delta\varepsilon$)	SS(%)	L-val λ/nm (ε or $\Delta\varepsilon$)	SS(%)	L-phe λ/nm (ε or $\Delta\varepsilon$)	SS(%)
H$_2$O[a] (14.0)	AB	592(496)	7.3	592(495)	10.4	592(490)	2.9	592(477)	34.4
	CD	587(1.94)		589(2.84)		579(1.48)		593(7.07)	
MeOH (15.1)	AB	594(457)	11.5	594(508)	18.4	594(455)	11.8	594(469)	37.0
	CD	589(2.77)		587(4.42)		583(3.22)		593(7.58)	
EtOH (15.9)	AB	588(478)	9.3	593(510)	13.2	592(520)	15.6	594(484)	41.2
	CD	586(2.34)		585(3.40)		581(3.97)		590(8.42)	
n-PrOH (16.1)	AB	588(492)	7.8	591(509)[b]	12.5	590(505)	15.1	593(501)	41.8
	CD	583(2.04)		583(3.26)[b]		579(3.87)		588(8.53)	
n-BuOH (16.1)	AB	588(468)	7.6	592(489)[b]	11.4	590(505)	14.0	590(531)	42.3
	CD	583(2.00)		582(3.05)[b]		579(3.65)		588(8.73)	
i-PrOH (17.1)	AB	587(497)	5.4	587(536)[b]	9.1	588(521)	15.9	590(504)	44.0
	CD	583(1.56)		581(2.60)[b]		577(4.03)		585(8.96)	
s-BuOH (17.6)	AB	583(485)	4.0	585(529)[b]	9.7	588(473)	17.0	587(479)	44.0
	CD	578(1.29)		578(2.71)[b]		577(4.24)		586(8.97)	
t-BuOH (19.2)	AB	580(491)	2.5	582(516)[b]	9.0	587(531)	22.2	589(509)	46.6
	CD	576(0.99)		575(2.58)[b]		575(5.28)		586(9.48)	
DMF	AB	570(479)	6.9	575(475)	8.0	573(476)	−13.7	573(467)	11.6
	CD	577(1.85)		575(2.37)		590(−1.80)		575(2.59)	
Acetone	AB	575(496)	6.9	578(533)[b]	8.1	576(514)	−16.4	577(467)	9.4
	CD	575(1.86)		575(2.40)[b]		595(−2.35)		570(2.14)	

a) 40% DMF is present. b) 20% DMF is present.

Table 9. AB and CD spectral data (1st band) and stereoselectivity of β_2-[Co(sal$_2$en)(L-aa)] in various solvents

Solvent (pK_a)[20]		L-ala λ/nm (ε or Δε)	SS(%)	L-met λ/nm (ε or Δε)	SS(%)	L-val λ/nm (ε or Δε)	SS(%)	L-phe λ/nm (ε or Δε)	SS(%)
H_2O (14.0)	AB	586(308)	0.7	580(405)[a]	13.2	590(289)	3.7	585(299)	42.1
	CD	586(0.66)		594(2.35)[a]		580(0.94)		603(6.53)	
MeOH (15.1)	AB	585(401)	17.2	584(447)[b]	20.6	585(399)	18.5	585(398)	53.2
	CD	588(2.95)		593(3.44)[b]		585(3.14)		592(8.18)	
EtOH (15.9)	AB	585(408)	14.2	582(440)[b]	17.6	585(400)	20.9	585(388)	52.7
	CD	588(2.50)		593(3.00)[b]		585(3.49)		592(8.05)	
n-PrOH (16.1)	AB	585(435)	13.8	582(454)[b]	16.6	585(408)	24.1	585(435)	60.4
	CD	587(2.44)		590(2.85)[b]		584(3.97)		590(9.24)	
n-BuOH (16.1)	AB	584(410)	11.7	580(445)[b]	16.8	583(398)	21.5	584(430)	56.8
	CD	587(2.13)		590(2.89)[b]		584(3.58)		590(8.70)	
i-PrOH (17.1)	AB	585(435)	8.4	582(448)[b]	16.6	585(436)	30.4	584(433)	59.9
	CD	586(1.64)		590(2.85)[b]		584(4.90)		588(9.16)	
s-BuOH (17.6)	AB	584(427)	6.9	580(446)[b]	16.5	583(429)	34.4	583(415)	64.8
	CD	583(1.42)		588(2.84)[b]		584(5.49)		588(9.89)	
t-BuOH (19.2)	AB	583(480)	1.0	580(464)[b]	16.4	582(435)	37.2	583(460)	66.9
	CD	575(0.95)		586(2.82)[b]		584(5.90)		586(10.20)	
DMF	AB	579(435)	6.4	577(532)	17.0	579(431)	0.0	578(435)	22.6
	CD	580(1.35)		587(2.91)		560(0.34)		583(3.64)	
						635(−0.31)			
Acetone	AB	577(415)	5.5	575(430)	16.0	577(429)	−3.0	575(431)	27.3
	CD	575(1.21)		586(2.76)		555(0.06)		582(4.95)	
						618(−0.66)			

a) DMF (30%) is added. b) DMF (10%) is added.

Table 10. AB and CD spectral data (1st band) and stereoselectivity of β_2-[Co(α-Me-sal$_2$en)(L-aa)] in various solvents

Solvent (pK_a)[20]		L-ala λ/nm (ε or Δε)	SS(%)	L-met λ/nm (ε or Δε)	SS(%)	L-val λ/nm (ε or Δε)	SS(%)	L-phe λ/nm (ε or Δε)	SS(%)
H_2O (14.0)	AB	580(370)	4.3	584(370)	3.8	585(346)	40.0	585(350)	69.9
	CD	600(0.88)		604(3.84)		611(6.02)		612(9.65)	
MeOH (15.1)	AB	580(397)	25.4	582(358)	24.9	581(383)	41.5	583(356)	65.4
	CD	601(3.77)		602(3.90)		607(6.37)		616(9.03)	
EtOH (15.9)	AB	580(395)	19.2	581(360)	26.7	580(390)	41.4	582(367)	68.2
	CD	601(2.92)		598(4.15)		606(6.36)		616(9.41)	
n-PrOH (16.1)	AB	579(405)	17.9	580(372)	25.8	580(394)	41.2	580(377)	67.2
	CD	600(2.73)		598(4.02)		603(6.32)		614(9.28)	
n-BuOH (16.1)	AB	577(397)	17.9	580(362)	25.2	580(392)	39.5	580(368)	67.6
	CD	599(2.72)		598(3.94)		603(6.00)		613(9.33)	
i-PrOH (17.1)	AB	577(405)	11.9	580(356)	21.5	580(362)	41.8	580(374)	64.9
	CD	600(1.93)		596(3.43)		603(6.41)		612(8.96)	
s-BuOH (17.6)	AB	573(407)	9.3	579(367)	20.5	577(390)	39.2	577(362)	66.4
	CD	598(1.57)		594(3.00)		600(5.95)		600(9.17)	
t-BuOH (19.2)	AB	572(400)	5.0	578(382)	21.2	577(392)	41.5	577(380)	67.3
	CD	596(0.98)		590(3.40)		600(6.37)		600(9.29)	
DMF	AB	575(389)	7.5	578(391)	16.2	575(401)	6.3	577(378)	25.6
	CD	585(1.32)		585(2.71)		576(1.56)		586(3.59)	
Acetone	AB	574(395)	8.1	575(389)	16.8	573(404)	7.5	575(373)	27.5
	CD	580(1.41)		585(2.80)		573(1.72)		585(3.85)	

pattern of each complex in various solvents is also very similar to that in methanol; however, the CD intensity varies depending upon the kind of solvent in some complexes. Especially in the case of [Co(5,6-benzo-sal$_2$en)(L-val)], the CD spectra in DMF and acetone are almost in a mirror-image relation with that in methanol when the vicinal effect is rectified, as has been mentioned previously.

In order to certify that the variation in the CD intensity in various solvents comes mainly from the variation in the isomeric ratio between the *Λ*- and *Δ*-β_2-isomers, the ^{1}H NMR spectra of several complexes were measured in various solvents. Some representative ^{1}H NMR spectra are shown in Fig. 11. Indeed, the relative isomeric ratio changes depending upon the solvent, and the isomeric ratios estimated from the ^{1}H NMR spectra fit well with the isomeric ratios estimated from the CD intensity by the use of Eq. 1. On the other hand, the CD intensity of *Λ*$_{SS}$-β_2-[Co(α-Me-sal$_2$en)(*N*-Bz-L-ala)][12] and *Λ*-β_2-Co(sal$_2$-(*S*,*S*)-chxn)-complexes with L-ala and D-ala,[13] the stereoselectivity of which reaches almost 100% for stereochemical reasons, was nearly constant (the variation in the CD intensity in the 1st-absorption-band region in various

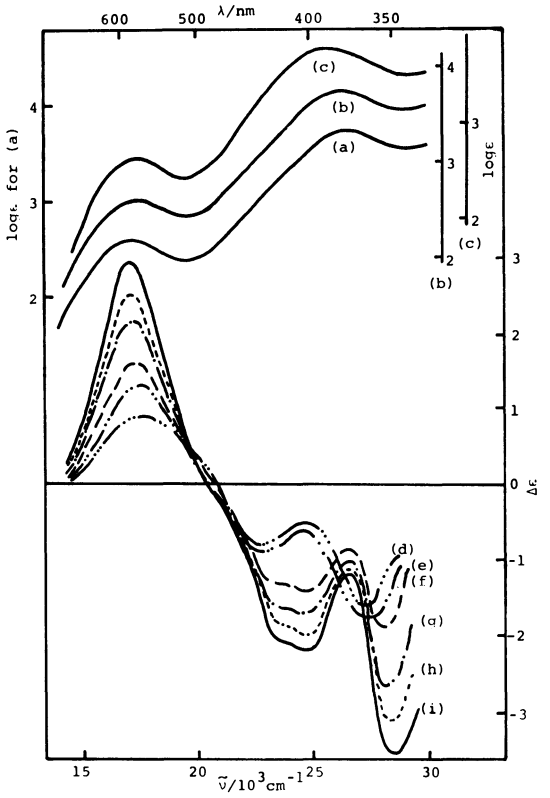

Fig. 9. AB and CD spectra of β_2-[Co(sal$_2$en)(L-ala)] in various solvents under the equilibrium conditions.
(a): MeOH, (b): *i*-PrOH, (c): DMF, (d): *t*-BuOH, (e): DMF, (f): *i*-PrOH, (g): *n*-BuOH, (h): EtOH, (i): MeOH.

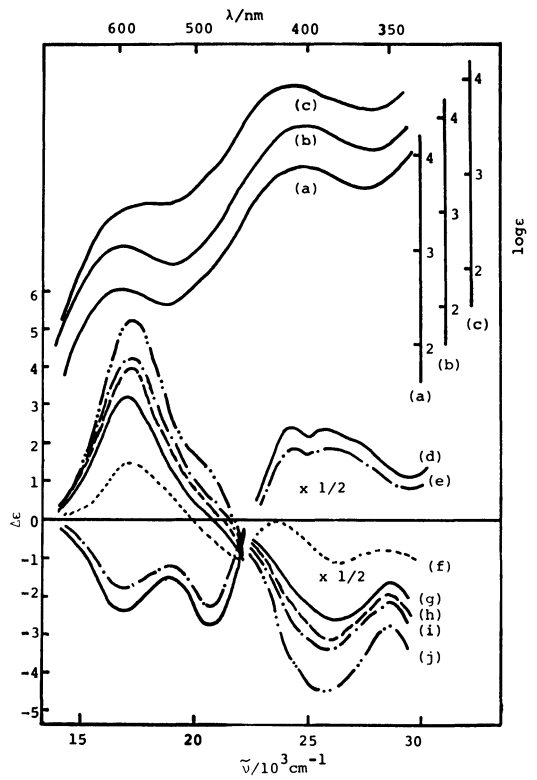

Fig. 10. AB and CD spectra of β_2-[Co(5,6-benzo-sal$_2$en)-(L-val)] in various solvents under the equilibrium conditions.
(a): MeOH, (b): *n*-BuOH, (c) DMF, (d): acetone, (e): DMF, (f): H_2O (40% DMF), (g): MeOH, (h): EtOH, (i): *s*-BuOH, (j): *t*-BuOH.

solvents was within a few %) even when the solvent was changed. These facts indicate that: 1) the effect of the solvent on the CD intensity of a pure isomer (so-called solvent effect) is very small in [Co(Schiff base)-(L-aa)] complexes, and thus 2) the CD variation in the equilibrium mixtures of Λ- and Δ-β_2-isomers with the variation in the solvents can be safely ascribed to the change in the isomeric ratio of the complexes. The stereoselectivities of the complexes in various solvents, which were estimated from the CD intensity, are given in Tables 8—10.

It becomes clear from Tables 8—10 that 1) the stereoselectivity in DMF and acetone is generally lower than that in alcoholic solvents, 2) the stereoselectivity of all the L-ala-complexes and of the 5,6-benzo-sal$_2$en complex with L-met increases with a decrease in the pK_a value of alcoholic solvents, whereas 3) the stereoselectivity of the L-val- and L-phe-complexes with sal$_2$en and 5,6-benzo-sal$_2$en increases with the increase in the pK_a value, and 4) the stereoselectivity of the L-met-complex with sal$_2$en and of the L-met-, L-val-, and L-phe-complexes with α-Me-sal$_2$en is almost constant in all the alcoholic solvents.

As may be seen in Figs. 9 and 10 and Tables 8—10, the 1st absorption band and the associated CD band at about 580 nm of all the complexes shift to the lower-energy side in the order of DMF = acetone < *t*-BuOH < *s*-BuOH < *i*-PrOH ≦ *n*-BuOH ≦ *n*-PrOH ≦ EtOH < MeOH ≦ H_2O. On the other hand, the CT and π-π*

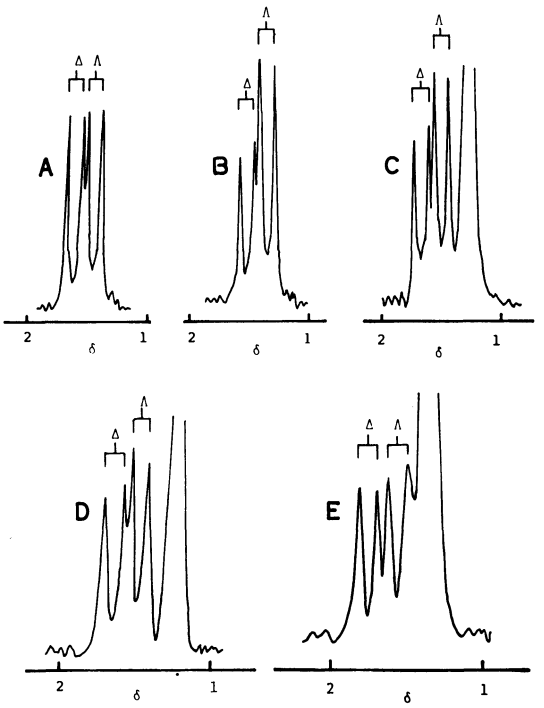

Fig. 11. ^{1}H NMR spectra of β_2-[Co(sal$_2$en)(L-ala)] in various solvents under the equilibrium conditions.
A: D_2O (20% DMF), B: CD_3OD, C: C_2D_5OD, D: *i*-C_3D_7OD, E: *t*-C_4D_9OD.

bands from 440 to 360 nm and the associated CD bands shift to the higher-energy side in the same order of solvents. These spectral shifts are characteristic of the alcoholic solvents, and are proportional to the decrease in the pK_a values of alcoholic solvents. Therefore, it can be assummed that the alcoholic solvents interact with the complexes by making a hydrogen bond with their OH group. It is known that the coordinated phenolic oxygen atoms of metal-Schiff base complexes act as proton acceptors[14] and as Lewis bases.[15-17] Accordingly it may be mainly at the phenolic oxygen atoms that the hydrogen bonding with alcoholic solvents occurs. When the hydrogen bonding is the stronger, the more the ligand-field strength of the phenolic oxygen atoms can be expected to decrease. It may be as the result of this effect that the 1st absorption band and the associated CD band shift to the lower-energy side, in parallel with the decrease in the pK_a value of the alcoholic solvents, that is, in parallel with the increase in the hydrogen-bonding ability of alcoholic solvents. The higher energy shift of the CT and π-π^* bands and the associated CD bands with the increase in the hydrogen-bonding ability may be due to the stabilization of the π-conjugate system of the Schiff-base ligand by the hydrogen bonding and the alternative instabilization of the π^*-orbital.[18]

The molecular models suggest that: 1) when complexes take the Δ-β_2-structure, the alkyl group of the coordinated L-amino acidates faces one of the phenolic oxygen atoms (O_1 in Fig. 12) of the Schiff-base ligand, whereas 2) when they take the Λ-β_2-structure, the alkyl group somewhat faces one of the Schiff-base chelate rings (B in Fig. 12), which inclines about 30° from the O–Co–N plane.[10,19] However, in either case, the alkyl group does not approach them so closely that any quite strong intramolecular steric interaction seems to exist in either isomer. This corresponds to the finding that the stereoselectivity in DMF and acetone, in which the solvation by the hydrogen bonding is not expected, is generally very small, as has been observed above. In the case of 5,6-benzo-sal$_2$en complexes with L-val and L-ile, as is shown in Fig. 13, the alkyl group has a bulky secondary β-carbon atom, so that the alkyl group approaches the 5,6-benzo-group of the chelate ring B when the complexes take the Λ-β_2-structure. Therefore, the L-val and L-ile-complexes with 5,6-benzo-sal$_2$en favor the Δ-β_2-isomer more than the Λ-β_2-isomer in DMF and acetone.

On the other hand, in alcoholic solvents, solvation at the phenolic oxygen atoms by the hydrogen bonding should be considered. As has been mentioned above, one of the phenolic oxygen atoms (O_1 in Fig. 12) of the Δ-β_2-isomer faces the alkyl group of the coordinated L-amino acidates, but the phenolic oxygen atom of the Λ-β_2-isomer does not. This corresponds to the fact that the alkyl group of L-amino acidates in the Δ-β_2-isomers sterically hinders the alcoholic solvents from approaching to one of the phenolic oxygen atoms, but there is no such steric hindrance in the Λ-β_2-isomer. Therefore, in alcoholic solvents, the Λ-β_2-isomer is more stabilized by the hydrogen bonding than the Δ-β_2-isomer is. A plausible presentation of the difference in hydrogen-bond formation is shown in Fig. 14. Since the steric bulkiness of alkyl groups of L-aa increases generally in the order of L-ala<L-met<L-val<L-phe, it is assummed that the steric hindrance of the alkyl groups for the solvation of alcoholic solvents increases in the order of L-ala<L-met<L-val<L-phe. In fact, the stereoselectivity in alcoholic solvents does indeed increase in this order.

From the above results and discussion, the free energy difference for the isomerization equilibrium between Δ- and Λ-β_2-isomers can be written as follows:

$$\Delta G = -RT\ln([\Lambda]/[\Delta]) = \Delta G^{I} + \Delta G^{S}, \qquad (2)$$

where $[\Lambda]$ and $[\Delta]$ represent the concentrations of Λ- and Δ-β_2-isomers respectively under the equilibrium conditions, ΔG^{I} denotes the free energy difference between the two isomers for the intramolecular steric interaction, and ΔG^{S} means the free energy difference for the hydrogen bonding with alcoholic solvents. In DMF and acetone, the ΔG value comes mainly from

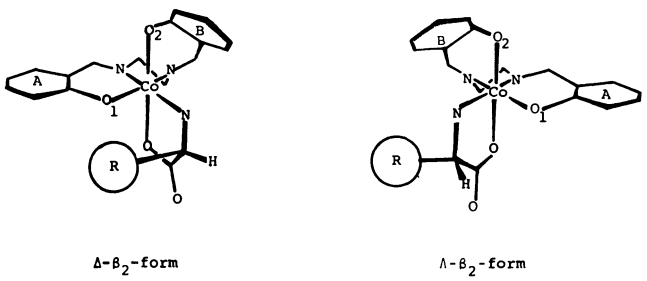

Fig. 12. Steric structure of β_2-[Co(Schiff base)(L-aa)].

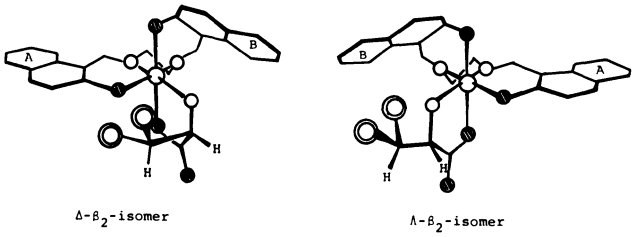

Fig. 13. Steric structure of β_2-[Co(5,6-benzo-sal$_2$en)(L-val)].
●: Represents oxygen atom, ○: represents nitrogen atom, ◎: represents methyl group.

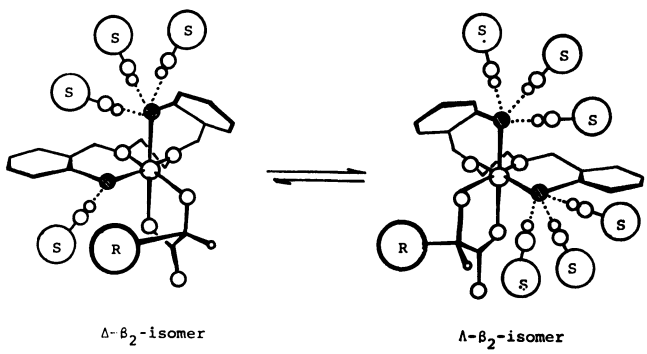

Fig. 14. Plausible feature for hydrogen bond formation with alcoholic solvent.
●: Represents phenolic oxygen atom, and S represents solvent molecule.

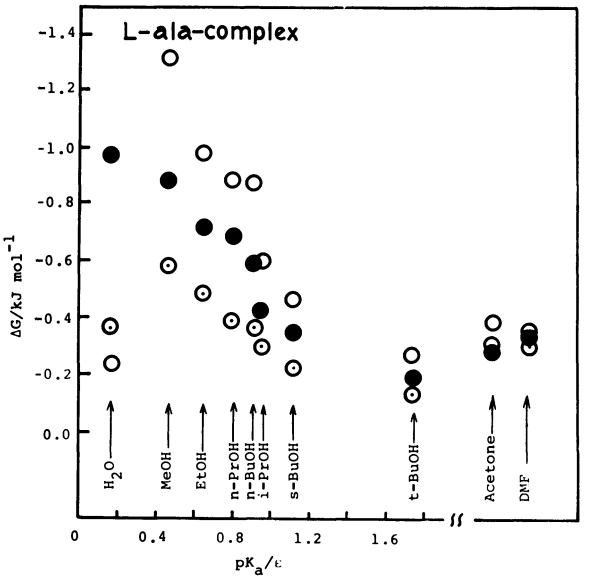

Fig. 15. Plot of ΔG value *vs.* pK_a/ε of alcoholic solvents (L-ala-complex).
⊙: 5,6-Benzo-sal$_2$en, ●: sal$_2$en, ○: α-Me-sal$_2$en.

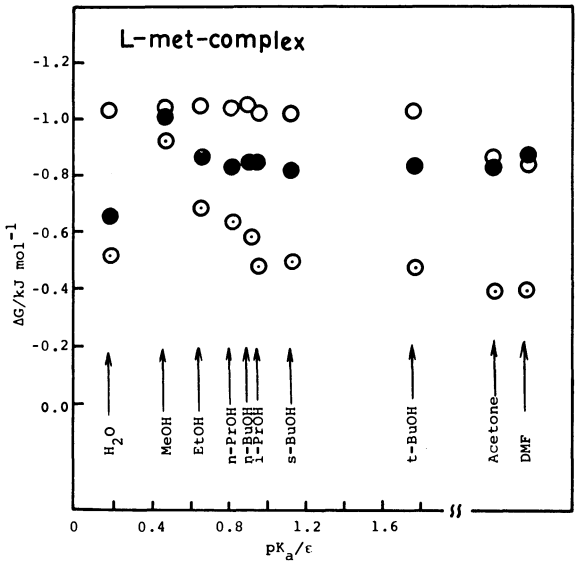

Fig. 16. Plot of ΔG value *vs.* pK_a/ε of alcoholic solvents (L-met-complex).
⊙: 5,6-Benzo-sal$_2$en, ●: sal$_2$en, ○: α-Me-sal$_2$en.

ΔG^I. On the other hand, in alcoholic solvents, the ΔG value comes from both ΔG^I and ΔG^S. However, the degree of stereoselectivity of all the complexes in DMF and acetone is generally much lower than that in alcoholic solvents. Therefore, in alcoholic solvents, the contribution of ΔG^I is assummed to be much smaller than that of ΔG^S.

When the entropy term is neglected and the hydrogen bonding is assummed to be electrostatic,[21] ΔG^S can be written as follows:

$$\Delta G^S = (q_1 q_2 N_\Lambda)/\varepsilon r_\Lambda - ((q_1 q_2 N_\Delta)/\varepsilon r_\Delta, \quad (3)$$

where q_1 and q_2 represent the charge of the phenolic oxygen atom (q_1) and that of the OH-proton of alcoholic solvents (q_2) respectively, ε denotes the dielectric

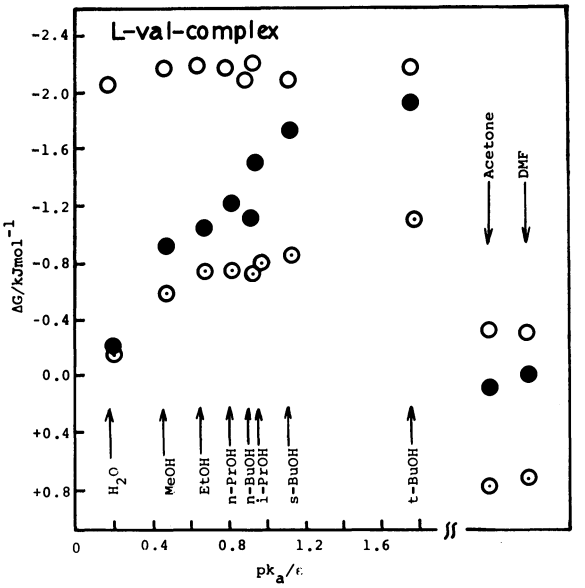

Fig. 17. Plot of ΔG value *vs.* pK_a/ε of alcoholic solvents (L-val-complex).
⊙: 5,6-Benzo-sal$_2$en, ●: sal$_2$en, ○: α-Me-sal$_2$en.

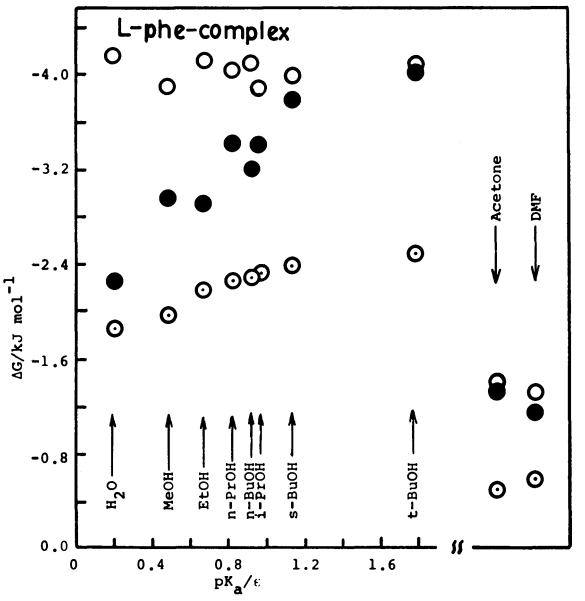

Fig. 18. Plot of ΔG value *vs.* pK_a/ε of alcoholic solvents (L-phe-complex).
⊙: 5,6-Benzo-sal$_2$en, ●: sal$_2$en, ○: α-Me-sal$_2$en.

constant of alcoholic solvents, and N_Λ and N_Δ represent the number of hydrogen-bonded solvent molecules at the phenolic oxygen atoms of Λ- and Λ-β_2-isomers at the mean distances of r_Λ and r_Δ respectively. Here, in order to simplify the explanation, we will use the following assumptions: 1) the hydrogen-bonding distance, r, is the same in both Λ- and Λ-β_2-isomers, and only the number of the hydrogen-bonding solvent molecules differs between the Λ- and Λ-β_2-isomers; 2) the distance, r, is the same for all the L-amino acidato complexes, and 3) the distance is the same for all the alcoholic solvents, and only the number of the hydrogen-bonding

solvent molecules differs among the alcoholic solvents. On the basis of the above assumptions, Eq. 3 is written as follows:

$$\Delta G^{s} = q_1 q_2 (N_\Lambda - N_\Delta)/\varepsilon r. \quad (4)$$

In this paper, as the measure of q_2, we used the pK_a values of the alcoholic solvents. Figures 15—18 show the plots of the ΔG value, calculated from the isomeric ratios in Tables 8—10, *vs.* the pK_a/ε value.

The pK_a/ε value increases in the order of $H_2O <$ MeOH $<$ *n*-PrOH $<$ *n*-BuOH $<$ *i*-PrOH $<$ *s*-BuOH $<$ *t*-BuOH; this order corresponds to the decreasing order of the hydrogen-bonding ability of the solvents. Hence, if the term of q_2 in Eq. 4 is related predominantly to the stereoselectivity of complexes, the ΔG value in alcoholic solvents decreases in parallel with the increasing order of the pK_a/ε value. It may be that, in this case, the ΔG values of all the L-ala-complexes and the L-met-complex with 5,6-benzo-sal_2en decrease in parallel with the increasing order of the pK_a/ε value of alcoholic solvents. Since a water molecule is very small and has quite a strong hydrogen-bonding ability, when the alkyl group of L-aa is not so bulky as those of L-ala and L-met, the value of $(N_\Lambda - N_\Delta)$ in Eq. 4 is expected to be small in water; indeed, the estimated ΔG values of the L-ala- and L-met-complexes are small in water. As may be seen in Fig. 15, the degree of variation in the ΔG value *vs.* the pK_a/ε value of alcoholic solvents becomes greater in the order of 5,6-benzo-sal_2en $<$ sal_2en $<$ α-Me-sal_2en; this suggests that the q_1 value of Schiff-base ligands increases in this same order. This order corresponds to the electron-donating ability of the substituent on the Schiff-base skeleton.

On the other hand, it can also be expected from Eq. 4 that, when the steric bulkiness of solvent molecule is higher, it becomes difficult to make the effective hydrogen bonding at the phenolic oxygen atoms of the Schiff-base ligand. This corresponds to the fact that the higher is the steric bulkiness of the solvent molecule, the larger is the value of $(N_\Lambda - N_\Delta)$. It may be that, in this case, the ΔG values of the sal_2en and 5,6-benzo-sal_2en complexes with L-val and L-phe increase with the increase in pK_a/ε, as may be seen in Figs. 17 and 18. This is because the increasing order of the steric bulkiness of alcoholic solvents is $H_2O <$ MeOH $<$ EtOH $<$ *n*-PrOH $<$ *n*-BuOH $<$ *i*-PrOH $<$ *s*-BuOH $<$ *t*-BuOH, and this order is parallel with the increasing order of their pK_a/ε values.

As has been observed above, the hydrogen-bonding ability and the steric bulkiness of alcoholic solvents affect the stereoselectivity of the complexes as if they were the reverse of each other. Therefore, if both effects are cancelled out, the ΔG value can be expected to be almost constant. It may be that, in this case, the α-Me-sal_2en complexes with L-met, L-val, and L-phe, sal_2en complex with L-met, and 5,6-benzo-sal_2en complex with L-phe, show a nearly constant ΔG value in various alcoholic solvents.

From these results and discussion, the following conclusion can be drawn: 1) the difference in steric hindrance between Λ- and Λ-β_2-isomers for the hydrogen-bond formation with alcoholic solvents plays an important role in the stereoselectivity of [Co(Schiff base)(L-aa)] complexes. 2) The higher the steric bulkiness of the alkyl group of coordinated L-aa, the higher the steric hindrance for the hydrogen-bond formation. 3) When the hydrogen-bonding ability of alcoholic solvents is higher, the stereoselectivity of the complexes becomes higher. 4) When the steric bulkiness of the alcoholic solvents is higher, the stereoselectivity of the complexes becomes higher. 5) However, the effects of 3) and 4) are reversed in the case of usual alcoholic solvents.

The authors wish to express their deep thanks to Professor J. Hidaka and Dr. K. Okamoto of Tsukuba University and to Professor K. Sone and Dr. Y. Fukuda of Ochanomizu University for their kind assistance with the CD spectral measurements. This work was partly supported by a Grant-in-Aid for Scientific Research (No. 547038) from the Ministry of Education, Science and Culture.

References

1) B. F. Anderson, D. A. Buckingham, G. J. Gainsford, G. B. Robertson, and A. M. Sargeson, *Inorg. Chem.*, **14**, 1658 (1975).
2) M. Yamaguchi, S. Yamamatsu, T. Furusawa, S. Yano, M. Saburi, and S. Yoshikawa, *Inorg. Chem.*, **19**, 2010 (1980).
3) M. Yamaguchi, S. Yano, M. Saburi, and S. Yoshikawa, *Bull. Chem. Soc. Jpn.*, **53**, 691 (1980).
4) M. Saburi and S. Yoshikawa, "Chemistry of Octahedral Complexes," Kagaku Sosetsu, **13**, Gakkai Shuppan Center, Tokyo (1976), p. 109.
5) B. Bosnich, *J. Am. Chem. Soc.*, **89**, 6143 (1967).
6) C. J. Hawkins, G. A. Lawrance, R. M. Peachey, *Aust. J. Chem.*, **30**, 2115 (1977); C. J. Hawkins and M. L. McEniery, *ibid.*, **32**, 1433 (1979).
7) B. Bosnich and J. M. Harrowfield, *J. Am. Chem. Soc.*, **94**, 989 (1972).
8) K. Kashiwabara, M. Kojima, and J. Fujita, *Bull. Chem. Soc. Jpn.*, **52**, 772 (1979).
9) Y. Fujii, T. Isago, M. Sano, N. Yanagibashi, S. Hirasawa, and S. Takahashi, *Bull. Chem. Soc. Jpn.*, **49**, 3509 (1976).
10) Y. Kushi, R. Tamura, M. Kuramoto, T. Yoshizawa, H. Yoneda, and Y. Fujii, *J. Chem. Soc., Chem. Commun.*, **1978**, 266.
11) The following abbreviations are used: L-ala=L-alaninate, L-met=L-methioninate, L-val=L-valinate, L-leu=L-leucinate, L-ile=L-isoleucinate, L-phe=L-phenylalaninate, L-thr=L-threoninate, L-tyr=L-tyrosinate, L-trp=L-tryptophanate, L-aa=L-amino acidate, Those of Schiff-base ligands are shown in Table 2.
12) Y. Fujii, M. Matsufuru, A. Saito, and S. Tsuchiya, *Bull. Chem. Soc. Jpn.*, **54**, 2029 (1981).
13) Y. Fujii, M. Sano, and Y. Nakano, *Bull. Chem. Soc. Jpn.*, **50**, 2609 (1977).
14) J. R. Thornback and G. Wilkinson, *J. Chem. Soc., Dalton Trans.*, **1978**, 110.
15) M. D. Hobday and T. D. Smith, *J. Chem. Soc., A*, **1971**, 1453.
16) M. D. Hobday and T. D. Smith, *J. Chem. Soc., A*, **1971**, 3424.
17) L. F. Lindoy and W. E. Moody, *J. Am. Chem. Soc.*, **97**, 2275 (1975); L. F. Lindoy, H. C. Lip, and H. W. Louie,

J. Am. Chem. Soc., **101**, 841 (1979).
18) B. Bosnich, *J. Am. Chem. Soc.*, **90**, 627 (1968).
19) M. Calligaris, G. Manzini, G. Nardin, and L. Ransaccio, *J. Chem. Soc., Dalton Trans.*, **1972**, 543; N. A. Bailey, B. M. Higson, and E. D. McKenzie, *ibid.*, **1972**, 503.
20) E. P. Serjieant and B. Dempsey, "Inoization Constants of Organic Acids in Aqueous Solution," IUPAC Chemical Data Series-No. 23, Pergamon Press, Oxford (1979).
21) J. E. Huheey, "Inorganic Chemistry," Harper and Row, New York (1972), p. 193.

Sorption Behavior of Aromatic Compounds in Water on β-Cyclodextrin Polyurethane Resins

Yoshihiro KAWAGUCHI, Yoshikazu MIZOBUCHI, Minoru TANAKA, and Toshiyuki SHONO*
Department of Applied Chemistry, Faculty of Engineering, Osaka University, Yamada-oka, Suita, Osaka 565
(Received December 12, 1981)

The sorption behavior of aromatic compounds in water on β-cyclodextrin polyurethane resins was evaluated by batch and column procedures. The values of their sorption capacities obtained in the batch experiments were comparable to those of Amberlite XAD-2 and/or -7. In the column experiments, β-H6XDI-P-6.0-M showed a quantitative collection of the aromatic compounds at low concentrations, while Amberlite XAD-7 did not.

Since various organic pollutants exist at relatively low concentrations in water, pre-concentration is generally required before their qualitative and quantitative analyses. For this purpose, commercially available porous polymer sorbents (*i.e.*, Amberlite XAD,[1,2] Tenax GC,[2] Separon,[3] and Hitachi gel[4]) have been widely used. In water, the degree of interaction between solutes and these polymers generally increases with increasing hydrophobicity of the solutes because these polymers are hydrophobic. Therefore, it is difficult for these polymers to sorb specific organic solutes selectively. We have been interested in developing sorbents that can collect the solutes in water selectively.

It is well known that cyclodextrins form stable inclusion complexes with specific organic compounds. The polyurethane resins containing cyclodextrin units as specific sorption sites were prepared by cross-linking β-cyclodextrin with diisocyanates.[5] In gas-solid chromatography these cyclodextrin resins exhibited strong interactions with organic compounds containing π-electrons or heteroatoms. It was found that these cyclodextrin resins interact strongly with benzene vapor in a nitrogen or an air stream and that one of these, β-H6XDI-P-6.0-M, retains the polar volatile organic compounds (*i.e.*, methyl and ethyl alcohols, acetone, and ethyl methyl ketone) more than Amberlite XAD-7 does in the gas stripping experiments.[6]

In the present paper we describe the application of β-cyclodextrin polyurethane resins to sorbents which concentrate aromatic compounds in artificial water samples. The sorption capacities of these resins are compared with that of Amberlite XAD-2 and/or -7 in order to evaluate the possibility of using these cyclodextrin resins as sorbents to collect aromatic compounds dissolved in water.

Experimental

Materials. β-Cyclodextrin polyurethane resins were prepared by cross-linking β-cyclodextrin with diisocyanate (hexamethylene diisocyanate (HDI), 1,3-bis(isocyanatomethyl)benzene (XDI), or 1,3-bis(isocyanatomethyl)cyclohexane (H6XDI)).

Amberlite XAD-2 and -7 resins were obtained from Rohm and Hass (Philadelphia, PA, U. S. A.).

These resins were granulated to particle sizes of 80—100 mesh (for batch method) and 100—200 mesh (for column method), purified by Soxhlet extraction with ethyl alcohol, dried *in vacuo* for 8 h at 80 °C, and then used as sorbents.

The reagents for uptake studies were obtained from Wako (Osaka, Japan) or from Aldrich (U. S. A.) and used without further purification.

Procedure. Sorption capacities of β-cyclodextrin polyurethane resins and Amberlite XAD-2 and -7 were determined by the following batch (static) method. A resin (0.1 g) and 100 ml aqueous solution containing one of the model organic compounds at various concentrations (0.08—1 mM; 1 mM= 10^{-3} mol dm^{-3}) in a 300 ml conical flask with a glass stopper was shaken in a thermostated water bath (25±0.1 °C) for 4 h. The resin was then removed by filtration. The concentration of solute in the filtrate was determined spectrophotometrically (Hitachi Model 340 Recording Spectrophotometer) and from this value the sorption capacity (mmol/g resin) and percent uptake were calculated.

The column (dynamic) experiments were carried out by using a 10 cm×0.52 cm I. D. glass column packed by a slurry packing technique with a sorbent bed volume of 2.1 cm^3. The sample solutions (1 mM) were allowed to pass through the column at a flow-rate of 55.3 ml/h using an Adzuma Model MF-1 microfeeder equipped with a 200 ml cylinder. The absorbance of the effluent was monitored at 254 nm (Atto Model SJ-1541 UV Monitor).

Results and Discussion

Sorption Capacities in Batch System. The sorption capacities of the resins for the disubstituted benzenes (0.2 mM) in the bath system are shown in Table 1. The β-cyclodextrin polyurethane resins (β-H6XDI-P-6.0-M, β-HDI-P-5.5-A, and β-XDI-P-5.8-A; see Ref. 5) have much larger capacities than that of the BDOL-HDI-P-M polyurethane resin. Since it was prepared from 1,4-butanediol and HDI, BDOL-HDI-P-M contains no β-cyclodextrin units. This suggests that the inclusion process by β-cyclodextrin units acts efficiently on the sorption of the solutes on the cyclodextrin resins. The sorption capacities of the cyclodextrin resins decrease in the order β-H6XDI-P-6.0-M>β-XDI-P-5.8-A>β-HDI-P-5.5-A, which indicates that the interaction between the resins and the solutes depends upon the cross-linking diisocyanate, in a way similar to the interaction with the organic vapors.[5] Roughly speaking, the β-cyclodextrin resins take up the solutes as well as the commercially available sorbents, Amberlite XAD-2 and -7, do, except for three dinitrobenzene isomers. It is assumed that dinitrobenzene, much more hydrophobic than the other solutes, is taken up more by the latter resins because their hydrophobicity is stronger than that of the β-cyclodextrin resins.

For each given disubstituted benzene solute, the amount of *o*-, *m*-, or *p*-isomer taken up by each β-cyclodextrin resin decreases in one of three orders: *p*>*m*>*o*

TABLE 1. SORPTION CAPACITIES FOR DISUBSTITUTED BENZENES IN WATER BY BATCH METHOD

Solute[a)]	Sorption capacity/10^{-2} mmol per g resin					
	β-H6XDI-P-6.0-M	β-HDI-P-5.5-A	β-XDI-P-5.8-A	BDOL-HDI-P-M	Amberlite XAD-2	Amberlite XAD-7
o-Nitroaniline	8.6	5.5	7.3	1.2	8.6	13.9
m-	6.4	5.2	5.1	0.8	4.7	11.6
p-	11.6	10.0	9.5	1.2	2.6	11.5
o-Aminobenzoic acid	5.1	2.8	3.7	0.6	0.3	5.8
m-	2.0	1.0	1.5	0.6	0.0	1.4
p-	5.9	4.6	6.0	1.1	0.8	4.8
o-Dinitrobenzene	9.0	5.8	7.1	1.8	14.7	14.9
m-	5.1	3.1	5.3	0.0	15.2	13.4
p-	5.9	4.2	5.8	1.3	13.5	13.7
o-Toluidine	4.6	2.8	4.1	0.3	6.5	5.7
m-	6.4	3.8	5.3	0.1	7.0	6.9
p-	8.1	5.7	7.2	0.0	6.3	6.4
o-Cresol	6.6	5.0	6.5	1.9	4.0	10.0
m-	7.0	5.4	7.1	2.1	3.7	9.2
p-	9.7	7.7	8.6	2.0	4.1	9.7
o-Ethylphenol	10.2	7.7	9.4	2.7	8.4	14.9
m-	11.9	8.9	10.8	2.8	10.3	10.8
p-	14.1	11.3	11.6	1.2	7.7	13.3

a) Concentration of solute: 0.2 mM.

TABLE 2. SORPTION CAPACITIES FOR PHENOL, AROMATIC ALCOHOLS, AND CARBOXYLIC ACIDS IN WATER BY BATCH METHOD

Solute[a)]	Sorption capacity/10^{-2} mmol per g resin					
	β-H6XDI-P-6.0-M	β-HDI-P-5.5-A	β-XDI-P-5.8-A	BDOL-HDI-P-M	Amberlite XAD-2	Amberlite XAD-7
Phenol	6.0	5.3	5.5	0.0	2.8	7.5
Benzyl alcohol	4.7	3.3	4.0	0.4	2.9	3.2
2-Phenylethanol	9.5	5.9	6.6	0.0	4.7	6.0
3-Phenyl-1-propanol	13.9	9.4	8.8	0.3	8.6	12.4
Benzoic acid	9.0	6.2	7.5	0.9	2.8	6.9
Phenylacetic acid	7.3	3.6	3.6	0.4	2.0	3.2
3-Phenylpropionic acid	11.4	7.3	6.9	1.4	4.5	9.7
4-Phenylbutyric acid	14.0	11.9	10.3	1.8	9.2	11.0
5-Phenylvaleric acid	16.6	12.3	10.7	3.5	13.5	15.6

a) Concentration of solute: 0.2 mM.

for toluidine, cresol, and ethylphenol; $p>o>m$ for nitroaniline and aminobenzoic acid; $o>p>m$ for dinitrobenzene. It is of great interest that just the same order is observed in the retention of each isomer on the chemically bonded β-cyclodextrin phase.[7] Except for dinitrobenzene, the *p*-isomers give the largest sorption capacities. This may be reasonably interpreted because the *p*-isomers can enter deep into the cyclodextrin cavity and can participate in the strongest hydrophobic interaction with the cavity. The irregularity of the order for dinitrobenzene is still unexplainable.

Table 2 shows sorption capacities for phenol, aromatic alcohols, and carboxylic acids. Concerning these substances, the β-cyclodextrin resins also have sorption capacities comparable to those of Amberlite XAD-2 or -7. In this case, β-H6XDI-P-6.0-M also exhibits the largest values among these cyclodextrin resins. Therefore, β-H6XDI-P-6.0-M was further investigated.

Effect of Solute Concentration on Sorption Capacities. Percent uptakes (u %) are determined by the equation:

$$u = \left(1 - \frac{\text{concentration of solute in water (filtrate) after sorption}}{\text{initial concentration of solute in water}}\right) \times 100.$$

Figure 1 shows the percent uptakes for phenol, benzyl alcohol, and 3-phenyl-1-propanol in the concentration range of 0.08—1 mM. Phenol is taken up more by Amberlite XAD-7 than by β-H6XDI-P-6.0-M, though slightly, while the reverse is observed for benzyl alcohol and 3-phenyl-1-propanol. The results of similar measurements for three aromatic carboxylic acids are shown in Fig. 2. Compared with Amberlite XAD-7, β-H6XDI-P-6.0-M exhibits the stronger ability to collect these compounds, particularly in the low concentration regions. This phenomenon is presumably attributable to the formation of inclusion complex where the solutes

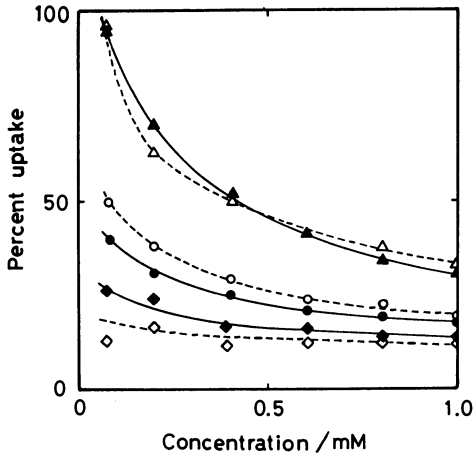

Fig. 1. Uptake of phenol, benzylalcohol, and 3-phenyl-1-propanol in water by β-H6XDI-P-6.0-M (——) and Amberlite XAD-7 (------).
△▲: 3-Phenyl-1-propanol, ○●: phenol, ◇◆: benzyl alcohol.

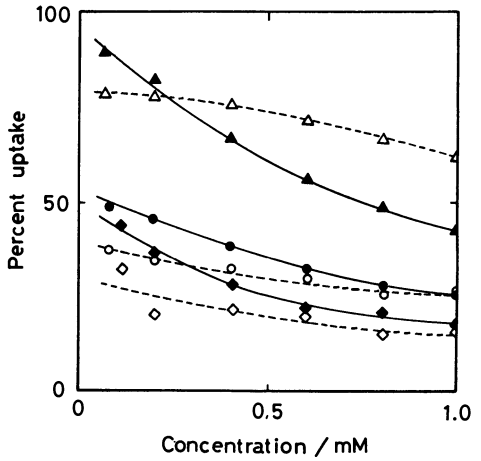

Fig. 2. Uptake of aromatic carboxylic acids in water by β-H6XDI-P-6.0-M (——) and Amberlite XAD-7 (------).
△▲: 5-Phenylvaleric acid, ○●: benzoic acid, ◇◆: phenylacetic acid.

are strongly retained in the β-cyclodextrin cavities. Accordingly, it is expected that the β-H6XDI-P-6.0-M resin will be used as sorbent to collect those compounds in water at trace concentrations.

Sorption Capacities in Column System. In order to achieve practical applications, the breakthrough experiments using the column method were performed, and the breakthrough capacities of the β-cyclodextrin polyurethane resins and Amberlite XAD-7 were compared.

Figure 3 shows the breakthrough curves for phenol (1 mM) on these resins packed separately into 10 cm × 0.52 cm I.D. columns. Ideally, a breakthrough curve should be steep and a solute concentration in an effluent should rise rapidly from zero to that in the influent.[8] The breakthrough curves on the β-cyclodextrin resins are not so steep as the ideal one on Amberlite XAD-7; this is presumably due to slower sorption rates of the solute into the β-cyclodextrin cavities. The breakthrough

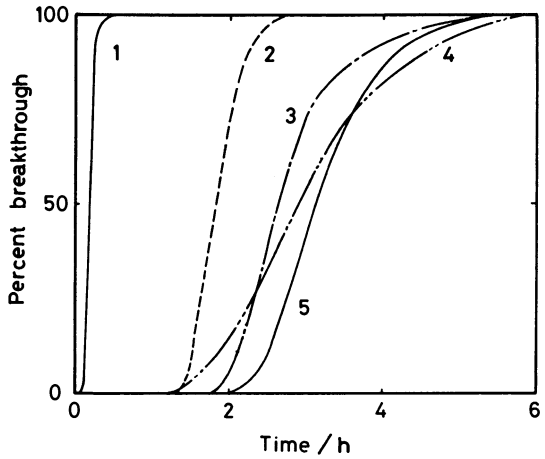

Fig. 3. Breakthrough curves for 1 mM phenol.
1: BDOL-HDI-P-M, 2: Amberlite XAD-7, 3: β-XDI-P-5.8-A, 4: β-HDI-P-5.5-A, 5: β-H6XDI-P-6.0-M.

times for phenol, the points where the tangents of the breakthrough curves intersect the time abscissa, are decreasing in the order β-H6XDI-P-6.0-M>β-XDI-P-5.8-A>β-HDI-P-5.5-A>Amberlite XAD-7>BDOL-HDI-P-M. BDOL-HDI-P-M has only a small breakthrough time. On the other hand, the breakthrough times on the β-cyclodextrin resins are larger than that on Amberlite XAD-7. The β-H6XDI-P-6.0-M resin, which shows the largest breakthrough time of all the three β-cyclodextrin polyurethane resins, was compared in more detail with Amberlite XAD-7.

Table 3. Breakthrough capacities for several aromatic compounds

Solute	Breakthrough capacity/10^{-2} mmol per g resin		
	β-H6XDI-P-6.0-M	BDOL-HDI-P-M	Amberlite XAD-7
p-Nitroaniline	20.0	5.0	44.5
Phenol	13.2	1.7	19.2
p-Cresol	16.2	2.2	41.6
Benzoic acid	10.7	3.6	31.7
Phenylacetic acid	6.6	1.6	23.6

Table 3 shows that the breakthrough capacities (expressed in mmol/g resin) on Amberlite XAD-7 for the aromatic compounds are larger than those on β-H6XDI-P-6.0-M. The weight of β-H6XDI-P-6.0-M and Amberlite XAD-7 per unit bed volume are 0.453 and 0.203 g/ml, respectively; thus there is not much difference in the breakthrough capacities per unit bed volume between β-H6XDI-P-6.0-M and Amberlite XAD-7. In practice, it is of great importance to investigate the sorption behavior of the resins for solutes at lower concentrations than 1 mM.

Each aqueous solution of the four solutes (model concentrations of 0.1, 0.05 or 0.01 mM) was passed at a flow-rate of 55.3 ml/h for 3 h through the column used for the breakthrough studies. The effluent from the column was collected in a graduated cylinder. The concentration of the solute in it was determined spectro-

photometrically, and then the percent uptake by β-H6XDI-P-6.0-M or Amberlite XAD-7 was evaluated (Table 4). In the case of Amberlite XAD-7, the percent uptake for benzoic acid decreases with the concentration of the solute. The β-cyclodextrin polyurethane resin, however, shows a perfectly quantitative collection at these low concentrations. The same statement is true for the percent uptake for phenylacetic acid. *p*-Nitroaniline or phenol is perfectly collected on both β-H6XDI-P-6.0-M and Amberlite XAD-7, as shown in Table 4.

TABLE 4. PERCENT UPTAKE BY COLUMN METHOD

Solute	Concentration/mM	Percent uptake	
		β-H6XDI-P-6.0-M	Amberlite XAD-7
p-Nitroaniline	0.10	100	100
	0.05	100	100
	0.01	100	100
Phenol	0.10	100	100
	0.05	100	100
	0.01	100	100
Benzoic acid	0.10	100	93
	0.05	100	89
	0.01	100	63
Phenylacetic acid	0.10	100	89
	0.05	100	77
	0.01	100	67

In this way, it is found that β-H6XDI-P-6.0-M can quantitatively collect the aromatic solutes at low concentrations and is superior to widely used Amberlite XAD-7. In addition, the β-cyclodextrin resins used in this study can be easily regenerated by Soxhlet extraction with ethyl alcohol and the collecting abilities of the resins after several regenerations remain unchanged. These results suggest that the β-cyclodextrin polyurethane resins will be used satisfactorily as sorbents to collect aromatic compounds at low concentrations in water.

This work was partially supported by a Grant-in-Aid for Scientific Research from the Ministry of Education, Science and Culture.

References

1) J. D. White and D. P. Schwarz, *J. Chromatogr.*, **196**, 303 (1980).
2) N. Picer and M. Picer, *J. Chromatogr.*, **193**, 357 (1980).
3) Z. Vozňáková and M. Popl, *J. Chromatogr. Sci.*, **17**, 682 (1979).
4) L. M. Majid and O. Samuelson, *J. Chromatogr.*, **193**, 197 (1980).
5) Y. Mizobuchi, M. Tanaka, and T. Shono, *J. Chromatogr.*, **194**, 153 (1980).
6) Y. Mizobuchi, M. Tanaka, Y. Kawaguchi, and T. Shono, *Bull. Chem. Soc. Jpn.*, **54**, 2487 (1981).
7) M. Tanaka, Y. Mizobuchi, T. Sonoda, and T. Shono, *Anal. Lett.*, **14**, 281 (1981).
8) S. E. Jorgensen, "Industrial Waste Water Management," Elsevier, Amsterdam (1979), p. 71.

 © 1982 The Chemical Society of Japan Bull. Chem. Soc. Jpn., 55, 2615—2617 (1982)

Stepwise Reduction of Samarium and Ytterbium in the Polarographic Reduction Process in the Presence of 1,4,7,10,13,16-Hexaoxacyclooctadecane[1)]

Hajimu YAMANA,† Toshiaki MITSUGASHIRA,* Yoshinobu SHIOKAWA, and Shin SUZUKI
The Research Institute for Iron, Steel and Other Metals, Tohoku University, Katahira 2-1-1, Sendai 980
(Received December 25, 1981)

Polarographic reduction of La, Pr, Nd, Sm, Gd, Dy, Er, and Yb was investigated in the aqueous solutions containing 1,4,7,10,13,16-hexaoxacyclooctadecane (18-CROWN-6). It is shown that Sm(III) and Yb(III) are reduced stepwisely *via* the divalent state in the presence of 18-CROWN-6. The divalent state is stabilized by the complex formation with 18-CROWN-6.

From the view point of f-series element chemistry, it is of great interest to investigate abnormal oxidation states. We are interested in low oxidation states found in aqueous solutions. For lanthanoids, Eu(II) and Yb(II) are farely stable in aqueous solutions. The findings of Sm(II) and Tm(II) were also reported[2,3)] but they are so unstable that they are rapidly oxidized in aqueous solutions. Because of this instability, the findings of Sm(II) and Tm(II) in aqueous solutions are not recognized widely.

Among many experimental techniques, polarographic reduction seems to be most promising for the investigation of low oxidation states of f-series elements in aqueous solutions. It affords useful information about the reduction process and we can inspect whether they are reduced directly to the metallic state or stepwisely *via* an intermediate lower oxidation state. In addition, it can be applied to the investigation of actinoids in tracer concentrations by the use of the radiopolarographic method.[4,5)]

1,4,7,10,13,16-Hexaoxacyclooctadecane(18-CROWN-6) has size selectivity for cations on complex formation.[6,7)] Taking into consideration the facts that the radii of some dipositive cations of lanthanoids(Ln^{2+}) and actinoids(An^{2+}) are very close to the radius of the ring of 18-CROWN-6, we expected that 18-CROWN-6 stabilizes Ln^{2+} and An^{2+} in aqueous solutions by complex formation.

In this report, we describe the stabilization of Sm(II) and Yb(II) by 18-CROWN-6 observed in stepwise reduction waves on a polarogram.

Experimental

Apparatus. Yanagimoto PA-102 was used as a direct current polarograph. An ordinary polarographic cell was used and connected to the standard calomel electrode(SCE) through an agar gel bridge.

Reagents. 18-CROWN-6 produced by Nippon Soda Co., LTD was used without purification. After drying in a vacuum desiccator, 18-CROWN-6 was dissolved into pure water. A 1 M (1 M=1 mol/dm^3) 18-CROWN-6 solution was used as a stock solution. Lanthanoid oxides of 99.99% purity were obtained from the Rare Earth Elements Purification Facility of our institute and converted to trichlorides before use.

Procedures. *Preparation of Sample Solutions*: Tetramethylammonium chloride(TMACl) was used as a supporting electrolyte in the concentration of 0.1 M. Because of the inertness of TMACl toward reduction, the reduction of Ln(II) can be investigated without disturbance by the discharge of the supporting electrolyte. The concentration of lanthanoids in the sample solutions was 4 mM. Sample solutions containing 18-CROWN-6 were prepared by the addition of the stock solution. Sample solutions of Ba(II) and Pb(II), which make stable complexes with 18-CROWN-6, were also prepared and the reduction behaviors were examined.

Determination of Half Wave Potentials. Direct current polarograms were obtained according to the ordinary method. Argon gas was bubbled into the sample solution for 10—15 min. in order to eliminate dissolved oxygen. The half wave potentials were determined after subtracting the back ground current induced by hydrogen discharge, which was observed at more positive potentials than the potentials for the reduction of Ln(II).

Results and Discussion

Reduction of Sm(III). Several authors have reported the stepwise reduction of Sm(III) *via* a divalent state in weakly acidic solutions. Timnic reported the stepwise reduction under experimental conditions very similar to ours using tetramethylammonium iodide for the supporting electrolyte.[8)] However, the ratio of the

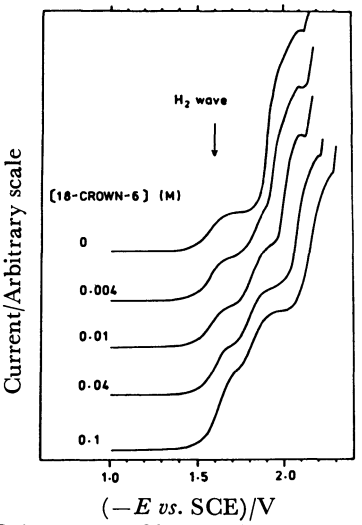

Fig. 1. Polarograms of Sm as a function of the concentration of 18-CROWN-6.

† Present address: Tokai Laboratory of Power Reactor and Nuclear Fuel Developement Corporation, Tokai, Naka-gun, Ibaraki 319-11.

diffusion current of the first wave to that of the second wave estimated from his data was not consistent with his conclusion. The ratio should be 1 : 2 for the reduction *via* the divalent state, while his data for the ratio varied with the concentration of Sm.

Polarograms of Sm are shown in Fig. 1. The small wave at about −1.55 V (*vs.* SCE) is the hydrogen discharge wave. The polarogram exhibits a deformed single wave at −1.8 V (*vs.* SCE) in the absence of 18-CROWN-6. We did not observe stepwise reduction with respect to the sample solutions without 18-CROWN-6. In contrast with this finding, the polarograms of Sm(III) in the presence of 18-CROWN-6 showed two well-defined reduction waves, as shown in Fig. 1. This fact was clearly observed as the splitting of a deformed single wave. The splitting was enhanced by the shift of the first wave to more positive potentials and the second wave to more negative potentials with the increase in the concentration of 18-CROWN-6. The ratio of the diffusion current of the two waves remained at 1 : 2. Therefore, it is quite reasonable to conclude that the first wave is due to a one-electron reduction of Sm(III) and the second wave is due to a two-electron reduction of Sm(II). And the direction of the shift of the second wave, along with the increase in the concentration of 18-CROWN-6, shows qualitatively the stabilization of Sm(II) by 18-CROWN-6.

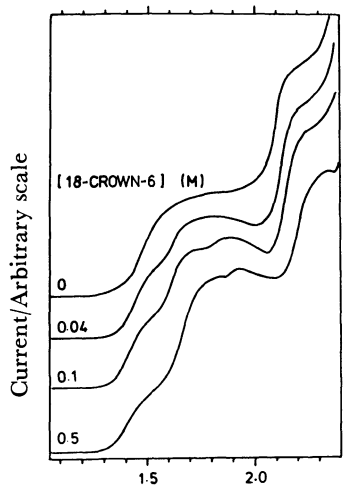

Fig. 2. Polarograms of Yb as a function of the concentration of 18-CROWN-6.

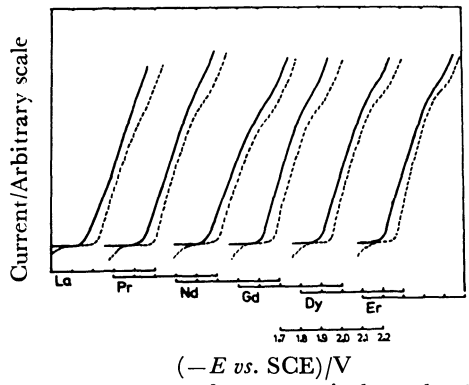

Fig. 3. Polarograms of some trivalent lanthanoids. Polarograms for the samples free from 18-CROWN-6 are shown by solid lines and for the samples of 0.48 M 18-CROWN-6 solutions by dotted lines.

Reduction of Yb(III). Polarograms of Yb are shown in Fig. 2. Yb(II) is more stable than Sm(II) in aqueous solutions. Two reduction waves were observed with respect to the solutions without 18-CROWN-6. The first wave, at about −1.4 V (*vs.* SCE), overlaps with the hydrogen discharge wave when the sample solution does not contain 18-CROWN-6. This wave shifts to more positive potentials with the increase in the concentration of 18-CROWN-6. The second wave, at about −2.1 V (*vs.* SCE), is attributable to the reduction of Yb(II) to Yb(0). The ratio of the diffusion currents of these two waves in the presence of 18-CROWN-6 is 1 : 2. Therefore, the first wave can be assigned to the reduction of Yb(III) to Yb(II). The other wave observed between the hydrogen discharge wave and the second wave seems to be a catalytic wave of hydrogen induced by the presence of 18-CROWN-6 in the sample solution.

Reduction of La(III), Nd(III), Pr(III), Gd(III), Dy(III), and Er(III). Divalent state of La, Nd, Pr, Gd, Dy, and Er are not yet known in aqueous solutions. For comparison to Sm and Yb, the reduction of these six elements were examined under the same condition. The polarograms are shown in Fig. 3. Only a single wave, due to the reduction of trivalent cation to the metallic state, was observed for every element. The presence of 18-CROWN-6 has little influence to the reduction wave. The results indicate that these six elements are reduced directly even in the presence of 18-CROWN-6. A small shift was observed but the magnitude of the shift did not exceed about 20 mV even in the sample solutions of 0.48 M 18-CROWN-6, the highest concentration used in this experiment.

The Influence of 18-CROWN-6 to the Reduction of Ba(II) and Pb(II). The influence of 18-CROWN-6 to the polarograms of Ba(II) and Pb(II) was examined in 0.1 M TMACl, pH 3.0 solutions. A well defined single reduction wave was observed. It was found that the addition of 18-CROWN-6 had no influence on the shape of the reduction wave. But the addition of 18-CROWN-6 induced a very large shift of the reduction wave to more negative potentials, which suggested a strong interaction between Ba(II) or Pb(II) and 18-CROWN-6.

The Relation between the Shift of the Reduction Wave and the Concentration of 18-CROWN-6. The stepwise reduction of the complex is represented by the following reactions.

1st reduction:

$$MX_p^{m+} + rX + (m-n)e^- \longrightarrow MX_q^{n+} + (p+r-p)X \quad (1)$$

2nd reduction (reduction to metallic state in Hg phase):

$$MX_q^n + ne^- \longrightarrow M(Hg) + qX \quad (2)$$

In these expression, X represents a ligand, p and q are the coordination numbers, and $(m-n)$ and n are the numbers of the electrons involved in the reduction. When complex formation proceeds reversibly and the electron transfer is rapid, the magnitude of the shift

induced by the addition of X is expressed as follows for the second reduction.[9]

$$-\Delta E_{1/2} = (E_{1/2})_c - (E_{1/2})_s = \frac{RT}{nF} \cdot q \cdot \ln[X] + \frac{RT}{nF} \cdot \ln \beta_{MX_q} \quad (3)$$

In this equation, $(E_{1/2})_c$ and $(E_{1/2})_s$ represent the half wave potentials of complex and hydrated cation, respectively. β represents the formation constant of the complex. The value of RT/F is 0.059 V under the present experimental condition. The shifts for Ba(II) and Pb(II) are also represented by Eq. 3.

The relation between the shift of the reduction waves and the logarithm of the concentration of 18-CROWN-6 is shown in Fig. 4 for the second waves of Sm and Yb. In the figure, the shifts of the waves of Pb and Ba are also shown. As shown in Fig. 4, an almost linear dependency between $-\Delta E_{1/2}$ and the logarithm of the concentration of 18-CROWN-6 was observed and the slope showed that n was equal to q. Undoubtedly n is equal to 2. Therefore, the coordination number was determined to be 2. Thus, the complex is probably of the sandwich type. From the intercepts, we estimated the values of log $\beta_{MX_2^{2+}}$ to be 3.8—4.3, 5.9—6.2, 6.3—6.9, and 4.1—4.9 for Yb(II), Pb(II), Sm(II), and Ba(II), respectively.

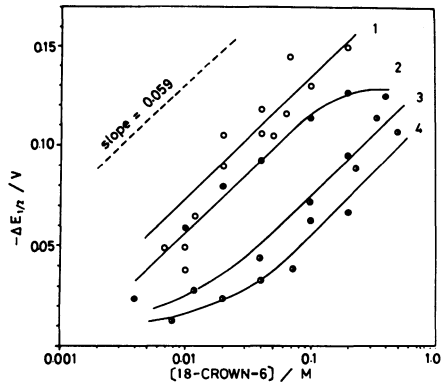

Fig. 4. $\Delta E_{1/2}$ *vs.* log [18-CROWN-6].
1: Sm(II), 2: Pb(II), 3: Ba(II), 4: Yb(II).

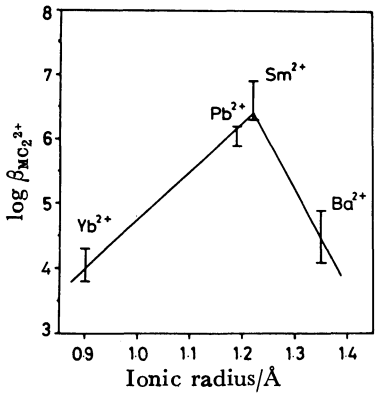

Fig. 5. Plot of log $\beta_{MX_2^{2+}}$ *vs.* cation crystal radius.

Considering that the formation constants of 18-CROWN-6 complexes exhibit a simple relation with the size of the central cations, we examined the dependence of log $\beta_{MX_2^{2+}}$ on the ionic radii of the four divalent cations We cited the ionic radii reported by Shanon.[10] The relation is shown in Fig. 5. A maximum of the stability is clearly observed at 1.2 Å. A similar tendency was reported by Izatt for 1 : 1 complexes of divalent cations.[6,7]

Consequently, we can say that Sm(III) and Yb(III) form stable complexes with 18-CROWN-6 and that Sm(III) is reduced stepwisely *via* divalent states in the presence of 18-CROWN-6.

A part of the expense for this work has been defrayed by Grant-in-Aid for Scientific Research No. 505002 from the Ministry of Education, Science and Culture.

References

1) H. Yamana, Ph. D. Thesis, Department of Nuclear Engineering, Tohoku University, 1981.
2) A. F. Clifford and H. C. Beachell, *J. Am. Chem. Soc.*, **70**, 2730 (1948).
3) L. B. Asprey and F. H. Kruse, *J. Inorg. Nucl. Chem.*, **13**, 32 (1960).
4) F. David, *Radiochem. Radioanal. Lett.*, **5**, 279 (1970).
5) F. David, "Proceedings of the Moscow Symposium on the Chemistry of Transuranium Elements," ed by V. I. Spitsyn and J. J. Katz, (*J. Inorg. Nucl. Chem., Supplement* **1976**) pp. 197—200.
6) R. M. Izatt, R. E. Terry, B. L. Haymore, N. K. Dalley, L. D. Hansen, A. G. Avamdet, and J. J. Christensen, *J. Am. Chem. Soc.*, **98**, 7620 (1976).
7) R. M. Izatt, R. E. Terry, D. P. Nelson, Y. Chan, D. J. Eatough, J.S. Bradshow, and L.D. Hansen, *J. Am. Chem. Soc.*, **98**, 7626 (1976).
8) A. Timnic and G. Glockler, *J. Am. Chem. Soc.*, **70**, 1347 (1948).
9) D. W. Crow, "Polarography of Metal Complexes," Academic Press, London (1969).
10) R. D. Shanon, *Acta Crystallogr., Sect. A*, **32**, 751 (1976).

Characterization of Nitrogen-containing Active Carbon Catalysts for SO_2 Removal

Akio Nishijima,* Hiroyuki Hagiwara,† Minoru Kurita, Akifumi Ueno,††
Toshio Sato, Yoshimichi Kiyozumi, and Naoyuki Todo
National Chemical Laboratory for Industry 1-1, Higashi, Yatabe, Ibaraki 305
(Received December 10, 1981)

Physical and chemical properties of nitrogen-containing active carbons (ACs), having a much higher activity and capacity for SO_2 adsorption than commercial ACs, were investigated to define suitable properties for SO_2 removal. The capacity of nitrogen-containing ACs for SO_2 adsorption correlates with the amount of their surface basic groups. However, the amount of basic surface groups for the ACs is practically the same as that for commercial ACs, indicating that the ACs have another characteristic property effective for SO_2 removal. A study on the chemical state of surface nitrogen atoms by means of an X-ray photoelectron spectrometer has revealed that surface nitrogen species are effective for SO_2 adsorption.

Recently active carbons (ACs) have been used for simultaneous removal of sulfur oxides (SO_x) and nitrogen oxides (NO_x) from flue gas discharged from stationary combustion equipments.[1-3] In this process SO_x is adsorbed on AC and removed as ammonium sulfate through reaction with NH_3 added in the flue gas,[3] NO_x being reduced to N_2 and H_2O by NH_3. However, those ACs developed so far are available only at low space velocities below 1000 h^{-1}, because of their low catalytic activity for SO_2 adsorption at temperatures effective for NO_x removal. Some of the present authors[3] found a new type of AC effective for SO_2 removal and developed a novel catalyst for the simultaneous removal of SO_x and NO_x by allowing AC to support metal salts effective for NO reduction with NH_3. The ACs developed were prepared from nitrogen-containing compounds such as polyacrylonitrile so as to contain some amounts of nitrogen atoms. It was also found, however, that the capacity of ACs for SO_2 removal is dependent highly on their activating conditions.

A number of mechanisms have been proposed for the catalytic oxidation of SO_2 on AC.[4-8] Daytyan[4] has indicated that the oxygen reversibly adsorbed on AC will oxidize SO_2 to SO_3. Siedlewski[5] has shown that free radicals on AC act as active centers in the chemisorption of SO_2. Kitagawa *et al.*[6] have found that the capacity for SO_2 removal does not depend on the surface area of AC but on the amount of oxygen atoms in AC. The work by Yamamoto *et al.*[7,8] has also shown that the capacity is dependent on preparation conditions and raw materials for AC rather than on the surface area of AC. Then, it was estimated by Kamino *et al.*[9,10] that basic surface group functions are activation points of oxidative chemisorption for SO_2 adsorption. Sano and Ogawa[11] have shown that for AC catalysts with higher activity for SO_2 removal, certain impurities on AC, such as surface nitrogen species, seem to have a good effect on catalytic activity.

The ACs studied in this work are designed to contain a few percent nitrogen atoms. Accordingly, nitrogen species in AC seem to play an important role in the process of SO_2 removal. Activating processes have been known to have an effect on physical and chemical properties of AC.[12,13] It is considered that various properties, especially the chemical state of nitrogen species in AC, are also affected by activating processes. In this work, physical and chemical properties of ACs prepared from polyacrylonitrile were investigated to characterize appropriate surface properties of AC for SO_2 removal.

Experimental

Catalysts. Polyacrylonitrile (100 g) was placed in a reactor made of quartz (length: 500 mm; diam.: 60 mm). The reactor was capable of rotating at desired speeds. Carbonization treatments were performed at 250 °C in an N_2 flow (1 l/h). Activation treatments were performed in the temperature range 400—1000 °C in the presence of water vapor. In the activating process, water (80 ml/h) was vaporized with a conventional vaporizer and supplied into the reactor with

Table 1. Activating conditions and nitrogen content of the AC catalyst used for SO_2 removal

Run	Activating temp/°C	Activating time/min	Nitrogen content/%	
			Bulk	Surface
1	400	60	—[a]	—[a]
2	500	30	14.6	7.8
3	600	30	10.3	5.1
4	700	30	8.4	3.7
5	750	30	8.0	3.0
6	800	15	11.0	3.4
7	800	30	7.4	2.4
8	800	40	5.5	—
9	800	50	4.5	—
10	800	60	3.7	1.4
11	850	30	—	—
12	900	15	—	—
13	900	30	5.1	1.5
14	900	60	—	—
15	950	30	—	—
16	1000	10	4.7	1.2
17	1000	15	4.1	0.9
18	1000	30	2.9	0[b]

a) No analysis was performed. b) No nitrogen atoms were detected by XPS.

† Present address: New Energy Development Organization, Sunshine 60 (29F), 3-1-1, Higashi Ikebukuro, Toshima-ku, Tokyo 170.

†† Present address: Toyohashi University of Technology, 1-1, Hibarigaoka, Tenpaku, Toyohashi 440.

nitrogen (600 ml/h). The duration of activation was in the range 10—60 min. Some ACs now in commercial use for SO_2 removal were also used as reference. The AC catalysts studied are summarized in Table 1.

Activity and Capacity Measurement. The following reaction conditions for activity and capacity measurement was previously established as suitable for development of new processes which make higher space velocities available for SO_2 removal. An AC sample (diam.: about 1.2 mm) of 20 ml was placed in a flow reactor made of stainless steel (length: 300 mm; diam.: 20 mm). Activity and capacity measurements were then carried out at 200 °C at a space velocity of 5000 h^{-1}.[3] The gas mixture used consisted of 500 ppm SO_2, 500 ppm NH_3, 5 vol% O_2, 10 vol% H_2O, and N_2 balance. The analysis for SO_2 was made by means of an NDIR type SO_x analyzer.

Measurement of Catalytic Properties. Measurements of surface area and pore size distribution were carried out by the BET method (CARLO ERBA Sorptomatic 1800) and with a porosimeter (AMINCO 60000 PSI). Benzoic and hydrochloric acids were used to measure the amount of basic groups in AC, sodium hydroxide being used to measure that of acidic groups. For measuring the amount of benzoic acid adsorbed, 0.5 g of sample was dried under vacuum at 110 °C and then immersed in 50 ml of ethyl alcohol solution of benzoic acid (10 mol m^{-3}) for 48 h at room temperature. The amount of benzoic acid adsorbed was determined by titration with sodium hydroxide standard solution (10 mol m^{-3}).[9,14] Similar methods were used to measure amounts of hydrochloric acid and sodium hydroxide adsorbed. Surface chemical properties of AC such as chemical composition and chemical state were obtained by using an X-ray photoelectron spectrometer (Dupont 650 B) and Al anode. Measured areas of spectra, or measured heights in some cases, were used for determing surface elemental compositions, as demonstrated in several recent papers.[15-17] A CHN Corder (Yanaco MT-2) was also used to determine the chemical composition of AC.

Results and Discussion

Activity and Capacity of AC. Figure 1 shows the activity and capacity of ACs for SO_2 removal. The ACs prepared from polyacrylonitrile are superior in activity and capacity to the commercial ACs. However, their capacity is dependent highly on activating conditions. In this work the capacity of AC is defined as the shortest reaction time that brings about 100% SO_2 removal in the activity measurement. For the commercial ACs the capacity is defined as the shortest reaction time for 40% SO_2 removal, because of their lower catalytic activity for SO_2 removal.

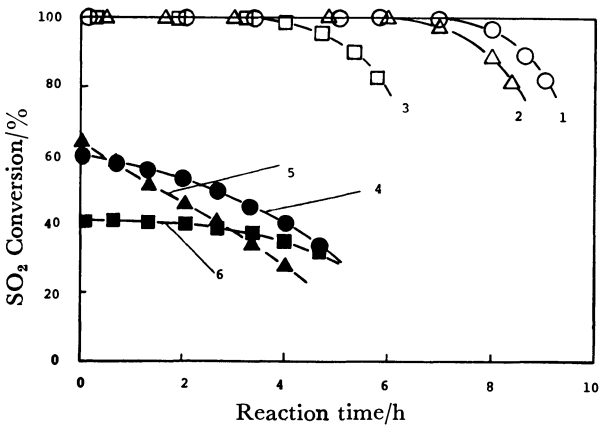

Fig. 1. Activity and capacity of AC used for SO_2 removal.
○, △, □: AC prepared from polyacrylonitrile, ●, ▲, ■: commercial AC.
Activating conditions: 1) 800 °C, 30 min, 2) 900 °C, 30 min, 3) 700 °C, 30 min,

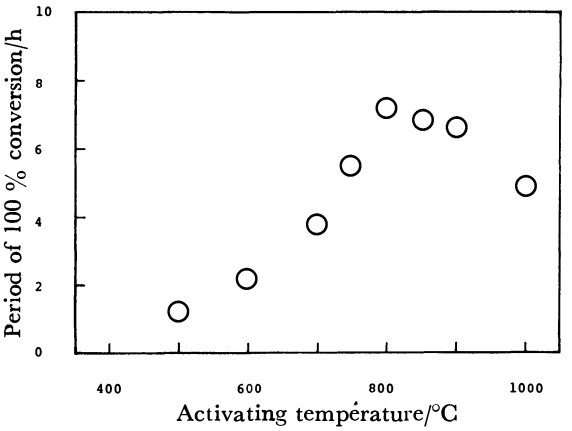

Fig. 2. Effect of activating temperature on capacity of the AC.
Activating conditions: activating time: 30 min, H_2O (vapor): 100 l/h, N_2: 600 ml/h

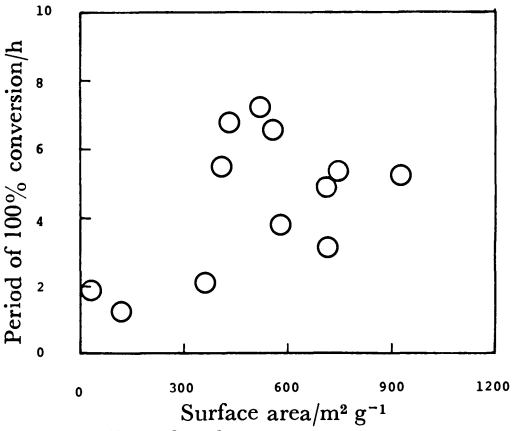

Fig. 3. Effect of surface area on capacity of the AC.

Physical Properties. Figure 2 shows the relationship between the capacity and activating temperature of AC. The activating time used was 30 min. The highest capacity is obtained when the AC is activated at 800 °C. A change in capacity of AC with surface area of AC is shown in Fig. 3. The capacity does not correlate with the surface areas, though the surface area is dependent on activating conditions. Figure 4 shows pore size distributions for the ACs and commercial ACs. Similar pore size distributions are shown between these ACs. No correlation is found between the capacity and pore size distribution. These results seem to indicate that the SO_2 removal capacities of the ACs as well as usual AC catalysts depend on surface chemical propeties rather than on surface physical properties. Thus chemical properties of the ACs were then studied.

Basic and Acidic Surface Group. Figure 5 shows the

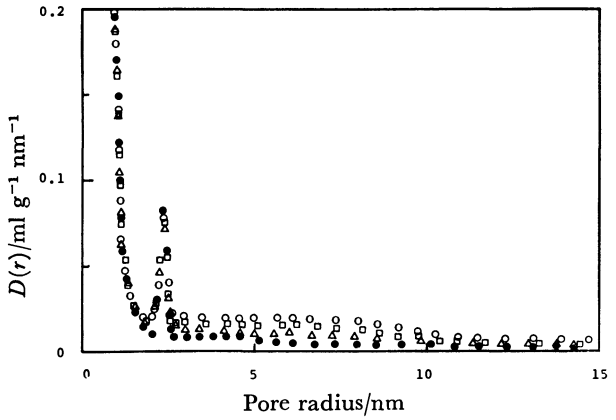

Fig. 4. Pore size distribution of AC used for SO_2 removal.
$D(r)$: Pore size distribution function, ○, △, □: AC prepared from polyacrylonitrile. ●: Commercial AC.

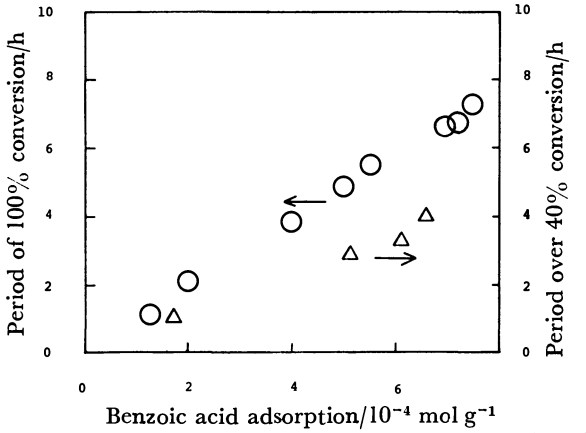

Fig. 5. Effect of benzoic acid adsorption on capacity of the AC.
○: AC prepared from polyacrylonitrile, △: commercial AC.
Capacities of the AC and commercial AC were defined as periods of 100% and over 40% conversion for SO_2 removal, respectively.

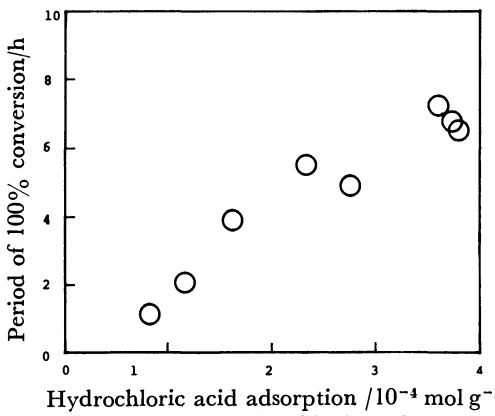

Fig. 6. Effect of hydrochloric acid adsorption on capacity of the AC.

correlation between the capacity and the amount of basic surface groups of the ACs as measured by using benzoic acid. The capacity increases with increase in benzoic acid adsorption, indicating that basic surface groups of AC are effective for the SO_2 adsorption. A similar trend was observed in a case using hydrochloric acid (Fig. 6), though with lowered correlation as compared with that shown in Fig. 5. On the other hand, the amount of acidic surface groups of the ACs decreases with increase in the capacity as shown in Fig. 7, indicating that acidic surface groups are not effective for the capacity. Amounts of benzoic acid adsorbed for the commercial ACs are $1.7—6.5\times10^{-4}$ mol/g-AC and almost the same as those obtained for the ACs which have much higher activities and capacities for SO_2 removal (Fig. 5). These results seem to indicate that the ACs have another characteristic property effective for SO_2 removal, though the presence of basic surface groups is one of important necessities for the high performance catalyst for SO_2 removal. Amounts of sodium hydroxide adsorbed for the commercial ACs are $1—4\times10^{-5}$ mol/g-AC, less than those for the ACs prepared (Fig. 7).

Nitrogen and Oxygen Species. As already mentioned, the ACs studied are designed to contain some amounts of nitrogen species, and hence it is considered that the nitrogen species in the ACs furnishes another property effective for SO_2 removal. A recent work by Kobayashi[18] has indicated that nitrogen species in ACs prepared from polyacrylonitrile exist in the states of C–N and N–N chemical bonds. A previous study[3] using an X-ray photoelectron spectrometer (XPS) has shown existence of two possible surface chemical states C–N and N–N, with the third state, more effective for SO_2 removal, left undefined.

Figure 8 shows change in nitrogen content in the ACs with activating temperature. The nitrogen content decreases with increase in activating temperature. When the same activating temperature is used, the nitrogen content decreases with increasing activating time as shown in Fig. 9. On the other hand, the capacity of the ACs increases up to the maximum with increasing

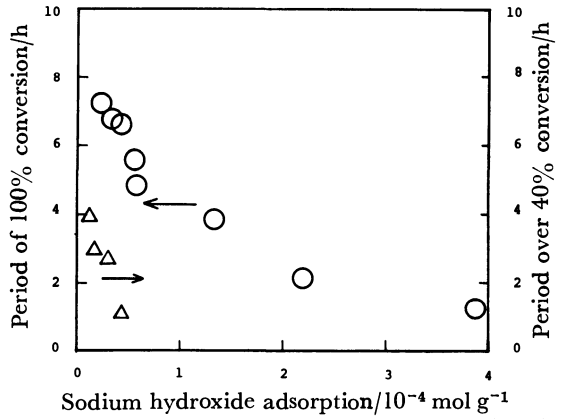

Fig. 7. Effect of hydroxide adsorption on capacity of the AC.
○: AC prepared from polyacrylonitrile, △: commercial AC.
Capacities of the AC and commercial AC were defined as periods of 100% and over 40% conversion for SO_2 removal, respectively.

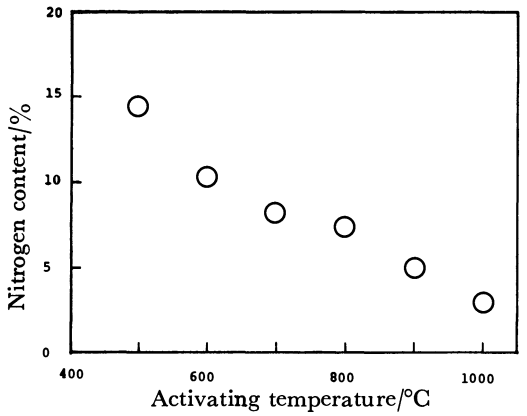

Fig. 8. Effect of activating temperature on nitrogen content in the AC.
Activating conditions: activating time: 30 min, H_2O (vapor): 100 l/h, N_2: 600 ml/h.

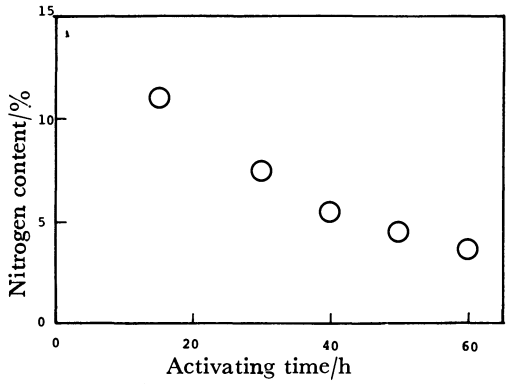

Fig. 9. Effect of activating time on nitrogen content in the AC.
Activating conditions: activating temperature: 800 °C. H_2O (vapor): 100 l/h, N_2: 600 ml/h.

reaction time and then decreases gradually.

Two peaks on N 1s photoelectron spectra were observed for the surface of the ACs, their binding energies being 396.1 and 397.5 eV. The higher binding energy peak (397.5 eV) seems to correspond to the chemical state of C–N bond, from a comparison with XPS spectra of polyacrylonitrile and other compounds which involve the chemical state of C–N bond,[19] whereas the lower binding energy peak seems to correspond to the chemical state of N–N bond.[20] The AC activated at 800 °C for 30 min has the highest capacity for SO_2 removal and gives a lower binding energy peak of maximum intensity (peak area). With the ACs having lower capacity for SO_2 removal, the intensity of lower binding energy peak is lower than that of the ACs with higher capacity. These results seem to indicate that the chemical state of N–N bond is more effective for SO_2 adsorption than that of C–N bond.

Table 1 also shows a comparison of amounts of nitrogen atoms present on the surface and in the bulk as measured by using XPS and CHN Corder, respectively. These results indicate that nitrogen species still exist on outer surface layers of AC particles though the amount of nitrogen atoms on surface layers is much less than that in the bulk. The amount of nitrogen atoms on surface layers decreases with increase in activating temperature. XPS shows that there is no detectable amount of nitrogen atoms on outer surface layers of the AC particles activated at 1000 °C for 30 min.

Oxygen species on surface are also known to affect the activity and capacity of AC for SO_2 removal.[6] No correlation is, however, found between the oxygen content on surface layers as measured by XPS and the capacity for SO_2 removal. Amounts of oxygen atoms on surface layers increase with increasing surface area. No chemical state of oxygen in surface functional groups is clear because of smaller chemical shifts in O 1s photoelectron spectra. Broader peaks of O 1s spectra on the ACs seem to support existence of more than two kinds of oxygen functional groups (acidic and basic) on the surface of the ACs.

References

1) H. Nishino, *Kankyo Sozo*, **4**, 25, (1976).
2) R. Yamada, 4th Symposium of Environmental Techniques, Tokyo, March 1977, 7—35.
3) A. Nishijima, M. Kurita, Y. Kiyozumi, R. Kobayashi, H. Hagiwara, A. Ueno, T. Sato, and N. Todo, *Bull. Chem. Soc. Jpn.*, **53**, 3356 (1980).
4) O. K. Daytyan, *Zh. Fiz. Khim.*, **35**, 992 (1961).
5) J. Siedlewski, *Int. Chem. Eng.*, **5**, 608 (1965).
6) H. Kitagawa, N. Yuki, Y. Sanada, S. Watari, and H. Honda, *Kogyo Kagaku Zasshi*, **72**, 2260 (1969).
7) K. Yamamoto, K. Kaneko, and M. Seki, *Kogyo Kagaku* Zasshi, **74**, 1582 (1971).
8) K. Yamamoto and M. Seki, *Kogyo Kagaku Zasshi*, **74**, 1576 (1971).
9) Y. Kamino, S. Onitsuka, and K. Yasuda, *Bull. Jpn. Petrol. Inst.*, **14**, 141 (1972).
10) Y. Kamino, S. Onitsuka, and K. Yasuda, *Bull. Jpn. Petrol. Inst.*, **14**, 147 (1972).
11) H. Sano and H. Ogawa, *Sangyo Kogai*, **10**, 2245, (1974).
12) F. Watanabe, Y. Yamada, M. Hasatani, and S. Sugiyama, *J. Chem. Eng. Jpn.*, **9**, 319 (1976).
13) S. Kasaoka, Y. Sakata, M. Umeno, Y. Adachi, and H. Morishita, *Nippon Kagaku Kaishi*, **1979**, 1569.
14) S. Yoshizawa, Z. Takehara, A. Katagiri, and M. Yamazaki, *Denki Kagaku*, **37**, 710 (1969).
15) N. S. Mclntyre, "American Society for Testing and Materials," (1978), pp. 31—64.
16) J. M. Adams, E. Evans, P. I. Reid, J. M. Tomas, and M. S. Walters, *Anal. Chem.*, **49**, 2001 (1977).
17) G. M. Bancroft, R. P. Gupta, A. H. Hardin, and M. Ternan, *Anal. Chem.*, **51**, 2102 (1979).
18) R. Kobayashi, 25th Summer Seminor of the Society of Polymer Science, Japan, 1977, Abstr. 155.
19) D. N. Hendrickson, J. M. Hollander, and W. L. Jolly, *Inorg. Chem.*, **8**, 2642 (1969).
20) B. J. Lindberg and J. Hedeman, *Chemica Scripta*, **7**, 155 (1975).

The Oxidation Behavior of Various Organic Compounds on the Determination of Chemical-oxygen Demand by Means of Flow-injection Analysis with Acidic Permanganate

Takashi KORENAGA,* Hisayoshi IKATSU, and Tosio MORIWAKE
School of Engineering, Okayama University, Tsushima-naka, Okayama 700
(Received December 21, 1981)

Forty-five organic compounds have been oxidized with an acidic permanganate solution under various oxidation conditions. In an attempt to determine the standard substance for chemical oxygen demand (COD), their oxidation behavior is analyzed in detail with respect to the reaction temperature and the reaction time by means of flow-injection analysis using ammonium iron(II) sulfate as the internal standard. The compounds used are classified into three groups according to the oxidation values obtained by the standard COD_{Mn} method. The results show that the compounds with oxidation values of more than 50% are easily oxidized with acidic permanganate, even under relatively mild conditions; those with oxidation values of 5—50% are severely influenced by the reaction temperature and the reaction time, and those with oxidation values of less than 5% are seldom oxidized at below 100 °C or for less than 30 min. As a standard substance for COD, it has been established that a mixture of the compounds has to be properly chosen from the aforementioned three groups according to the oxidation behavior of the water sample. The addition of silver nitrate to the oxidation system accelerates the oxidation reaction with acidic permanganate, whereas that of phosphoric acid suppresses the oxidation of organic compounds.

There is a growing interest on the part of environmental researchers in determining the contribution of organic substances to water pollution. For measurements of the chemical oxygen demand (COD), however, there is no specific substance to be used as a standard. Hence, skillful and complicated procedures have been established based on the standard methods with permanganate (COD_{Mn})[1,2] and dichromate (COD_{Cr}).[2,3] It is, however, difficult to obtain correct values of COD in water samples, because of the lack of a standard substance for COD.[4] To select a proper standard substance for the COD measurements, therefore, the oxidation behavior of D-glucose[5,6] and lactose[7] has been studied in detail with dichromate and permanganate. Also, the oxidation values of various organic compounds[8-10] have been examined to some extent with the standard method previously established,[1-3] but their oxidation behavior has not yet been determined in detail with regard to the reaction temperature and the reaction time.

Recently, the present authors have developed a useful method, based on flow-injection analysis (FIA),[11] for the simple and continuous determination of COD (COD_{FIA}) using potassium permanganate ($COD_{FIA\cdot Mn}$)[12-18] or potassium dichromate ($COD_{FIA\cdot Cr}$).[19] These methods for the COD determination always need a standard substance for COD, so sodium oxalate,[12] D-glucose,[13-19] lactose,[17,18] *etc.* were used to obtain the calibration curves. However, the oxidation behavior of these standards did not always accord with those of various organic pollutants in environmental water samples. Hence, the oxidation behavior with permanganate and dichromate should be investigated further in connection with various fundamental organic compounds in order to design a more complete FIA apparatus for COD measurements.

Therefore, this paper will mainly described the oxidation behavior of forty-five organic compounds as determined by means of the $COD_{FIA\cdot Mn}$ method developed in this laboratory,[12-18] and the effects of silver nitrate[17] and phosphoric acid,[18] added to the FIA system with acidic permanganate. It will also describe some problems of the present official Japanese method using COD_{Mn},[2] as considered in view of the oxidation behavior of the organic compounds obtained in this work.

Experimental

Materials. All the reagents used were of an analytical reagent grade except antipyrine, *o*-cresol (guaranteed), disodium dihydrogen ethylenediaminetetraacetate (EDTA), soluble starch (guaranteed), and sodium dodecylbenzesulfonate (DBS; standard for the determination of alkylbenzenesulfonate). These reagents were used as received after dissolution with distilled water. Preparations of potassium permanganate and sulfuric acid solutions were the same as those reported previously.[17]

Apparatus. The FIA apparatus used in this work is basically the same as those used in the previous works,[13-17] as is shown in Fig. 1. To obtain flexible operating conditions, however, it was composed of a double reciprocating micropump (Kyowa-Seimitsu Model KHU-W-52), a sampling valve (Kusano, sampling volume: 20 mm^3), a water bath (Yamato Model BM-41), a spectrophotometer (Shimadzu Model UV-100-01), a quartz tubular flow-through cell (path length: 10 mm, inner volume: 18 mm^3), a multirange recorder (Nippon-Denshi-Kagaku Model U-228), and poly(tetrafluoroethylene) (PTFE) tubings with various inner diameters (i. d.) and lengths.

Procedure. Both a suitable concentration of potassium permanganate solution (*ca.* 1 mol m^{-3}) and a 10% v/v sulfuric

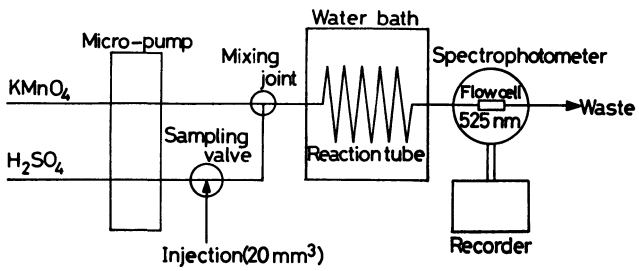

Fig. 1. Schematic diagram of a basic composition of the apparatus for COD_{FIA}.

Table 1. Operating conditions of the FIA apparatus for evaluating oxidation behavior

Parameter	Change in reaction temperature				Change in reaction time			
Temperature of water bath/°C	38	59	79	98	98	98	98	98
Residence time of sample/min	30	30	30	30	2	10	30	45
Flow rate of $KMnO_4$ solution/cm^3 min^{-1}	0.32	0.32	0.32	0.32	0.24	0.48	0.32	0.21
Flow rate of H_2SO_4 solution/cm^3 min^{-1}	0.32	0.32	0.32	0.32	0.24	0.48	0.32	0.21
Flow rate of carrier stream/cm^3 min^{-1}	0.64	0.64	0.64	0.64	0.48	0.96	0.64	0.42
Inner diameter of PTFE reaction tube/mm	1.0	1.0	1.0	1.0	0.5	1.0	1.0	1.0
Length of PTFE reaction tube/m	20	20	20	20	4	10	20	20
Peak height of Mohr's salt[a)]/mm	54.5	61.5	77.0	96.0	169.5	82.5	96.0	98.0
Peak height of water blank[b)]/mm	2.0	1.5	1.0	0.5	6.0	0.5	0.5	0.0

a) Mohr's salt can be completely oxidized in spite of changes in the reaction temperature and time. The flowing and mixing patterns of the sample zones are variable according to the viscosities of the carrier streams, so that peak heights are stably changed to some extent only with a change in the reaction temperature. However, the peak areas of Mohr's salt are almost equal in all FIA systems in this work. b) For the same reason as in a), the peak heights of the water blank are changed according to the peak-broadening phenomena based on the flowing and mixing patterns of their FIA systems.

acid solution are individually pumped up with the micro-pump in a 1 : 1 ratio. The concentrations of the potassium permanganate solution are adjusted to obtain absorbances of about 0.9 at 525 nm when this FIA apparatus system is operated.[17] Also, the flow rates of the two solutions are constant at the 1 : 1 flow-ratio and are adjusted between the potassium permanganate and sulfuric acid solutions in order to obtain a proper residence time of the injected samples. Twenty-mm^3 portions of sample solutions are continuously injected into the stream of the sulfuric acid solution by means of the sampling valve just before a PTFE mixing joint. The sample is merged with the mixing joint and carrier solutions and then introduced into the PTFE reaction tube. The tube is properly selected from the various PTFE tubings with many inner diameters and lengths in order to minimize the dispersion of the sample zones and to keep a suitable residence time of the samples. The reaction tube is placed in an accurately thermostated water bath to control the oxidation reaction. The reaction mixture is detected by means of a spectrophotometer with a flow cell at 525 nm. The absorbances are continuously recorded with the recorder; the peaks in the recordings are then compared with that of an internal standard substance (Mohr's salt: ammonium iron(II) sulfate). The peak-height ratio of each organic compound (see below) is used to evaluate its oxidation behavior. The operating conditions of the apparatus, such as the temperature of the water bath, the flow rates, the kind of PTFE reaction tube, and the residence time, are given in Table 1.

Calculation of Peak-height Ratio. To symbolize the extent of oxidation for various fundamental organic compounds, the idea of the peak-height ratio is used for each organic compound in this work. The peak height of a certain organic compound is widely changed when the operating conditions are changed in the apparatus, according to the parameters in Table 1. Hence, ammonium iron(II) sulfate, which is readily and quantitatively oxidized with potassium permanganate, even at room temperature, is used as the internal standard substance to obtain a standardized peak value. The calculation of the peak-height ratio is as follows;

$$\textit{Peak-height ratio} = \frac{H_{\text{organic compound}}(\text{mm}) - H_{\text{blank}}(\text{mm})}{H_{\text{Mohr's salt}}(\text{mm}) - H_{\text{blank}}(\text{mm})}, \quad (1)$$

where H is the peak height using 20-mm^3 portions of organic compounds or an ammonium iron(II) sulfate solution as 200 mg-COD_{Mn} dm^{-3} and 20 mm^3 of distilled water (blank) in the recordings.

Results and Discussion

Choice of Organic Compounds. From the previous papers,[5-10] forty-five organic compounds were chosen and classified into three groups according to their oxidation values with acidic permanganate by means of the standard COD_{Mn} method.[2] Fifteen of the forty-five compounds (Group 1 in Table 2), all of which showed oxidation values of more than 50% in comparison with the theoretical oxidation values (COD_{Th}) of the compounds,[8] were first examined in order to evaluate their oxidation behavior with permanganate at various reaction temperatures and reaction times. Fourteen compounds (Group 2 in Table 2), all of which showed oxidation values of from 5 to 50% in comparison with the COD_{Th} values, were then examined. Sixteen compounds (Group 3 in Table 2), which showed oxidation values of less than 5%, were also examined. Almost all the organic compounds are adjusted to 200 mg-COD_{Mn} dm^{-3} solutions according to their own oxidation values by means of the standard COD_{Mn} method in use, but several compounds showing oxidation values of less than 1% were prepared to make them as close to 200 mg-COD_{Mn} dm^{-3} as possible.

Oxidation Behavior of Group 1. In the ten organic compounds in Group 1, the effect of the reaction temperature was examined in order to evaluate their oxidation behavior at a residence time of 30 min; the results are shown in Figs. 2a and 2b. The effect of the reaction time on the oxidation behavior (reaction temperature: 98 °C) is also shown in Figs. 2c and 2d. The organic compounds used in Group 1 have turned out to be easily oxidizable. Figures 2a and 2b show that the oxidation reactions with acidic permanganate easily occurred at a relatively low temperature and were seldom changed in the temperature range between 80 and 100 °C except soluble starch, lactose, and glycine. As for the reaction time (Figs. 2c and 2d), the oxidation with permanganate at 98 °C occurred at a relatively short residence time (2—10 min), so that almost all the values of the peak-height ratio were apparently constant, even with a change in residence time.

TABLE 2. CLASSIFICATION OF FORTY-FIVE ORGANIC COMPOUNDS USED

Group 1[a)]	Group 2[a)]	Group 3[a)]
Sodium oxalate (1)	Acetaldehyde (1)	Ethyl acetate (1)
Citric acid (2)	Ethanol (2)	1-Propanol (2)
EDTA (3)	1-Butanol (3)	Urea (3)
Saccharose (4)	Methanol (4)	DBS (4)
Starch, soluble (5)	Acetic acid (5)	Butyric acid (5)
Glycerol (6)	1-Propanol (6)	Acetone (6)
o-Cresol (7)	Formic acid (7)	Pyridine (7)
Aniline (8)	Lactic acid (8)	Benzoic acid (8)
D-Glucose (9)	L-Glutamic acid (9)	Glycine (9)
Lactose (10)	Propionic acid (10)	Valeric acid (10)
Tartaric acid	Isobutyric acid	Isovaleric acid
Malic acid	Formaldehyde	Diethyl ether
Phenol	2-Butanol	2-Propanol
Salicylic acid	L-Cystine	Isobutyl acetate
Antipyrine		*β*-Alanine
		L-Methionine

a) Number in parenthesis denotes those compounds in Groups 1, 2, and 3 in Figs. 2, 3, and 4 respectively.

Oxidation Behavior of Group 2. Of ten organic compounds in Group 2, the effects of the reaction temperature (residence time: 30 min) and the reaction time (reaction temperature: 98 °C) are shown in Figs. 3a and 3b, and Figs. 3c and 3d, respectively. The compounds in Group 2 are considered oxidizable in the middle region of many of the organic compounds used in this work. Of the reaction temperature, all the compounds except acetaldehyde, acetic acid, and propionic acid gave an almost linear relationship, obtained by means of the increases in the peak-height ratio values with increases in the reaction temperature, as is shown in Figs. 3a and 3b. From Figs. 3c and 3d, it was found that the residence time severely affected methanol, ethanol, 1-propanol, 1-butanol, formic acid, and glutamic acid, but not acetaldehyde, lactic acid, acetic acid, and propionic acid. Also, the peak-height-ratio values of acetic and propionic acids were found to be very small in the absence of silver salt. Acetaldehyde, ethanol, 1-propanol, 1-butanol, and formic acid gave very large peak-height-ratio values of more than 1.5 in this work. Therefore, the values in Figs. 3a—d were plotted on a reduced scale of from 1 to 2 or 4.

Oxidation Behavior of Group 3. Of ten organic compounds in Group 3, the effects of the reaction temperature and the reaction time were also examined in a similar way (Figs. 4a—d). The compounds in Group 3 were generally considered to be difficult to oxidize by the use of an acidic permanganate solution. As for the effect of the reaction temperature on oxidation behavior, all the compounds in Figs. 4a and 4b gave exponential increases in the peak-height-ratio value when the reaction temperature increased. Therefore, the compounds in Group 3 were found to be much less oxidizable than those in Groups 1 and 2 in the low-temperature region. Of course, the former were further oxidized by acidic permanganate at a temperature of more than 100 °C, since the slopes of the oxidation-behavior curves were very abrupt between the reaction

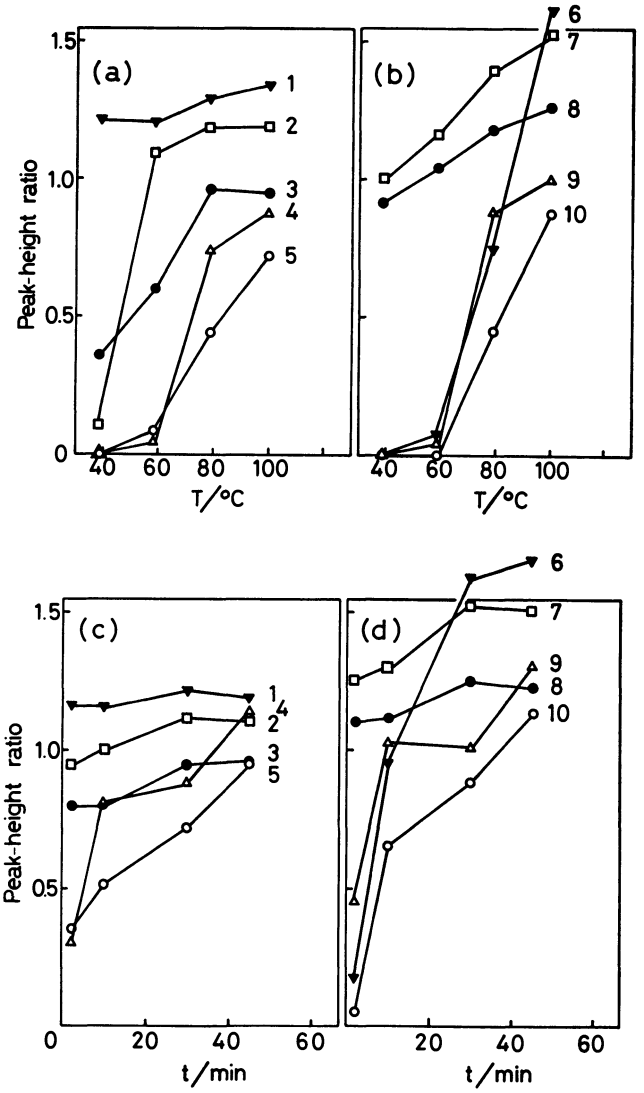

Fig. 2a—d. Effect of the reaction temperature (a, b) and the reaction time (c, d) on oxidation behavior of Group 1.
(a) and (b): Change in reaction temperature for a residence time of 30 min, (c) and (d): change in reaction time at a reaction temperature of 98 °C, 1: sodium oxalate, 2: citric acid, 3: EDTA, 4: saccharose, 5: soluble starch, 6: glycerol, 7: *o*-cresol, 8: aniline, 9: D-glucose, 10: lactose.

temperature and the peak-height ratio. As for the reaction time, almost all the compounds except butyric acid and glycine gave abruptly sloped relationships between the reaction time and the peak-height ratio at 98 °C, as is shown in Figs. 4c and 4d. In Figs. 4a—d, however, ethyl acetate, 2-propanol, and acetone gave outstandingly large peak-height-ratio values of more than 1.5, so those values in these figures had to be plotted on a reduced scale of from 1 to 4 or 8. Moreover, the peak-height-ratio values of butyric acid, glycine, and valeric acid showed oxidation behavior typical of much less oxidizable compounds when an acidic permanganate solution was used at more or less than 100 °C in the absence of silver salt.

As a result of these oxidation-behavior studies,

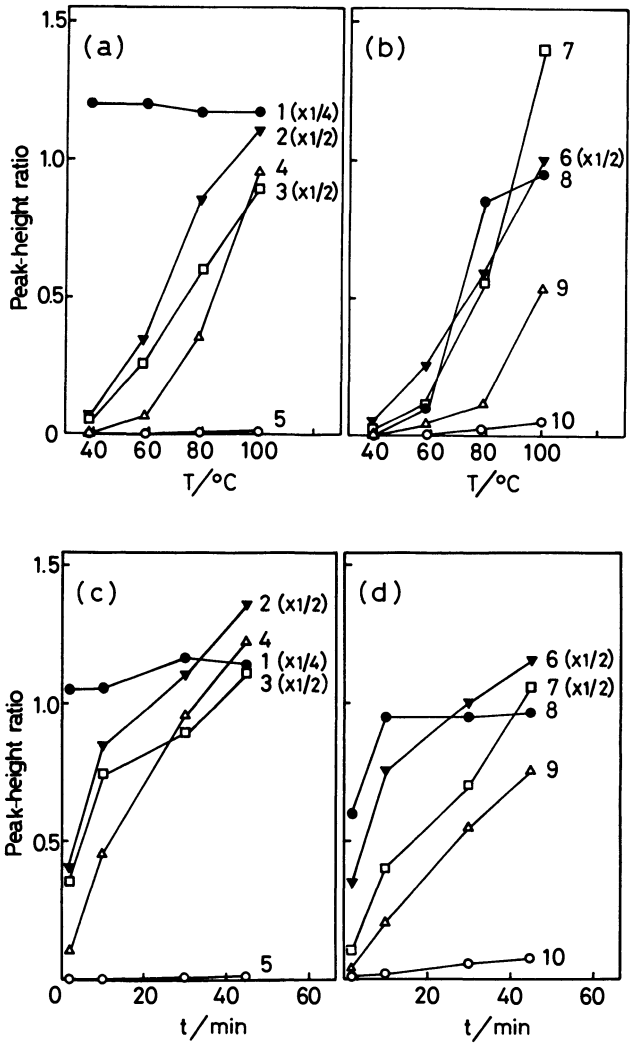

Fig. 3a—d. Effect of the reaction temperature (a, b) and the reaction time (c, d) on oxidation behavior of Group 2.
(a) and (b): Change in reaction temperature for a residence time of 30 min, (c) and (d): change in reaction time at a reaction temperature of 98 °C, 1: acetaldehyde, 2: ethanol, 3: 1-butanol, 4: methanol, 5: acetic acid, 6: 1-propanol, 7: formic acid, 8: lactic acid, 9: L-glutamic acid, 10: propionic acid.

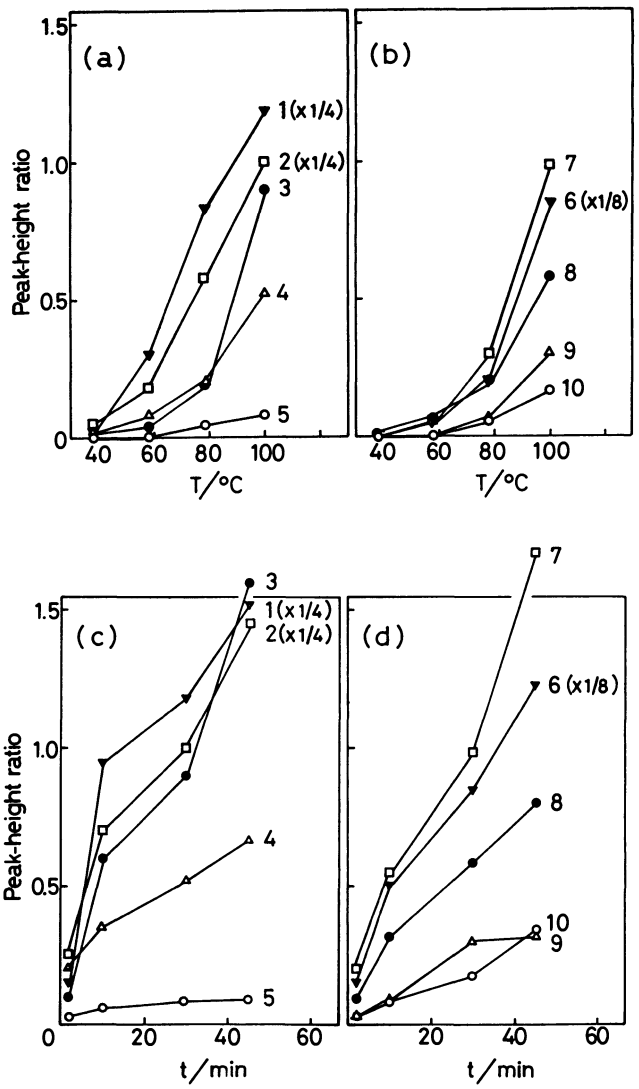

Fig. 4a—d. Effect of the reaction temperature (a, b) and the reaction time (c, d) on oxidation behavior of Group 3.
(a) and (b): Change in reaction temperature for a residence time of 30 min, (c) and (d): change in reaction time at a reaction temperature of 98 °C, 1: ethyl acetate, 2: 1-propanol, 3: urea, 4: DBS, 5: butyric acid, 6: acetone, 7: pyridine, 8: benzoic acid, 9: glycine, 10: valeric acid.

although the COD_{Mn} values[2] of the eight organic compounds with large peak-height-ratio values in Groups 2 and 3 were precisely adjusted to 200 mg dm^{-3}, the peak-height-ratio values were inconceivably large in comparison with those of the ammonium iron(II) sulfate used as the internal standard. Accordingly, it is noteworthy that organic compounds with small oxidation values[8] really had quite large COD_{Mn} values. Consequently, organic compounds with relatively low boiling points (*e.g.*, acetaldehyde, methanol, ethanol, propanols, butanols, formic acid, acetone, and ethyl acetate) potentially exhibit amazingly high peak-height-ratio values in this closed-flow injection system with acidic permanganate,[12-18] even when the permanganate values are precisely measured after digestion with acidic permanganate at about 100°C by means of the manual-titration method.[1,2] It was, therefore, considered that these organic compounds almost evaporated from the opened Erlenmeyer flask when the mixed solution was heated with a boiling-water bath in the official Japanese method for COD_{Mn}.[2]

Oxidation Behavior of Actual Waste Waters. As for actual waste water samples (*ca.* 200 mg-COD_{Mn} dm^{-3}) from civil sewage, the chemical industry, the food industry, the textile industry, and university laboratories, their oxidation behavior was also investigated with this useful methodology; the results are shown in Figs. 5a and 5b. Figure 5a shows the results on the reaction temperature obtained for the five samples at a residence time of 30 min. Figure 5a shows that waste waters from the food and textile industries gave almost linear increases in the peak-height-ratio values when the reaction temperature increased, while civil sewage and

waste water from the chemical industry reacted with acidic permanganate beyond 80 °C, but not up to 60 °C. Figure 5b also shows the effect of the reaction time at 98 °C for the same samples. The civil-sewage sample gave almost constant peak-height-ratio values for more than 30 minutes' residence time, while the waste water from the chemical industry showed a linear increase with an increase in the reaction time. Waste water from the food and textile industries gave constant peak-height-ratio values between 10 and 30 min of reaction time and then proceeded to a new oxidation step for more than 30 min. As is shown in both Figs. 5a and 5b, waste water from university laboratories gave very large peak-height-ratio values which were far beyond 1.0, so it was considered that the water sample contained some volatile organic compounds, such as methanol, ethanol, or acetone. However, it should be noted that the oxidation behavior on the samples used in this work was not found in each sample of the waste water of the same industrial groups, but was particular to their own waste-water samples.

As for a standard substance for COD measurements, it can, therefore, be considered that oxidation behavior of the series of samples has to be first examined with regard to the effects of the reaction temperature and the time with acidic permanganate; an optimum substance (single or mixture) is then chosen according to these oxidation-behavior studies. Of course, the correlation between $COD_{FIA\cdot Mn}$ and standard COD_{Mn} methods shall also be considered whenever the substance chosen is used as a standard for $COD_{FIA\cdot Mn}$ measurement.

Effect on the Addition of Silver Nitrate or Phosphoric Acid. Table 3 shows the results of the additions of silver nitrate or phosphoric acid to a sulfuric acid stream when the reaction temperature and reaction time of the present FIA system were 98 °C and 30 min respectively. With waste-water samples, the peak-height-ratio values increased when 0.05% silver nitrate was added to a carrier solution containing 5% sulfuric acid and potassium permanganate, whereas they decreased when 10% phosphoric acid was added to the carrier solution, as is shown in Table 3. Of the organic substances used in this work, D-glucose, citric acid, ethanol, *o*-cresol, *etc.* were not affected by the addition of silver nitrate or phosphoric acid. However, lactose, starch, glycine, urea, 1-butanol, benzoic acid, *etc.* obviously showed the same phenomena as waste-water samples. These results prove the catalytic effect of silver(I) salt and the formation of manganese(III) phosphate. These effects on oxidation behavior with acidic permanganate are important for deciding on a standard substance for measuring the $COD_{FIA\cdot Mn}$ values in a series of waste-water samples.

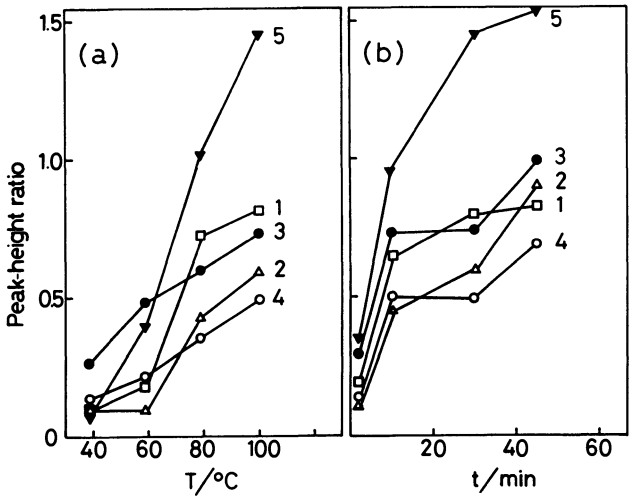

Fig. 5a—b. Effect of the reaction temperature (a) and the reaction time (b) on oxidation behavior of actual waste waters.
(a): Change in reaction temperature for a residence time of 30 min, (b): change in reaction time at a reaction temperature of 98 °C, 1: civil sewage, 2: waste water from the chemical industry, 3: waste water from the food industry, 4: waste water from the textile industry, 5: waste water from university laboratories.

Table 3. Effect of addition of silver nitrate or phosphoric acid on the determination of peak-heicht-ratio values
(98 °C × 30 min)

Sample	Peak-height-ratio value: Reaction medium (5% H_2SO_4)	Reaction medium (5% H_2SO_4 0.05% $AgNO_3$)	Reaction medium (5% H_2SO_4 10% H_3PO_4)
Waste water from			
Chemical industry	0.60	0.93	0.49
Textile industry	0.49	0.54	0.45
Food industry	0.73	0.92	0.85
University lab.	1.45	1.62	1.37
Civil sewage	0.80	0.78	0.60
D-Glucose	1.29	1.34	1.39
Lactose	1.04	1.13	0.82
Starch, soluble	0.73	0.77	0.52
Citric acid	1.18	0.96	1.04
Glycine	0.31	0.46	0.04
Urea	0.89	0.69	0.51
Ethanol	2.18	2.03	2.42
1-Butanol	1.76	1.91	1.68
o-Cresol	1.55	1.30	1.32
Benzoic acid	0.58	1.36	0.68

Conclusion

The present study fundamentally proves various aspects of the oxidation behavior of common organic substances with an acidic permanganate solution with reference to COD measurements based on the value of the permanganate consumed. By applying a continuous $COD_{FIA\cdot Mn}$ analyzer[18] to the monitoring of industrial and municipal waste water, a standard substance containing one or a mixture of organic substances can easily be found out from Groups 1, 2, and 3 after the oxidation behavior of each waste water sample has been analyzed in detail.

Besides, this paper has provided concomitant useful suggestions for preparing a standard substance for the

official COD_{Mn} method now being studied in the Japanese Ministry of International Trade and Industry.[20]

This work has also established the orders of oxidizability to sugars, alcohols, carboxylic acids, and benzene derivatives for reference in considering oxidation behavior. The oxidizability to sugars is in this order: D-glucose>saccharose>lactose≈starch; that to alcohols is in this order: ethanol>1-propanol≈2-butanol≳1-butanol>2-propanol≳methanol; that to carboxyl acids is in this order: formic acid>isovaleric acid≳valeric acid>isobutyric acid≈butyric acid>propionic acid>acetic acid, and that to benzene derivatives is in this order: *o*-cresol>phenol>salicylic acid≳aniline≫benzoic acid≈dodecylbenzenesulfonic acid. These results show that the activity of the α-hydrogen in alcohols and carboxylic acids may affect their oxidation behavior.

The authors wish to express their thanks to Professors Kyoji Tôei and Teruo Takahashi of Okayama University for their helpful suggestions and encouragement. The present work was partially supported by a Grant-in-Aid for Scientific Research from the Japanese Ministry of Education, Science and Culture, and also the Nissan Science Foundation.

References

1) JIS K 0101 (1979).
2) JIS K 0102 (1974).
3) ASTM D 1252 (1978).
4) Nippon Kankyo Sokutei Bunseki Kyokai, "Kyotsu Shiryo Ni Yoru Cross Check," Nippon Kankyo Sokutei Bunseki Kyokai, Tokyo (1978).
5) J. E. Shriver and J. C. Young, *J. Water Pollut. Control Fed.*, **44**, 2140 (1972).
6) A. Yamasaki, Y. Tanaka, Y. Kuge, and S. Asada, *Kogai To Taisaku*, **14**, 1133 (1978).
7) H. Namiki, E. Nakamura, and H. Katsumata, *Kogyo Yosui*, **242**, 25 (1978).
8) JIS K 0102, Instruction Manual (1974).
9) H. Yamada, K. Kawamura, and T. Kono, *Mizu-shori Gijutsu*, **14**, 1229 (1973).
10) M. Omori, *Kankyo Gijutsu*, **8**, 589 (1979).
11) J. Růžička and E. H. Hansen, *Anal. Chim. Acta*, **78**, 145 (1975).
12) T. Korenaga, *Bunseki Kagaku*, **29**, 222 (1980).
13) T. Korenaga, *Chem. Biomed. Environ. Instrum.*, **10**, 273 (1980).
14) T. Korenaga, *Anal. Lett.*, **13A**, 1001 (1980).
15) T. Korenaga and H. Ikatsu, *Bunseki Kagaku*, **29**, 497 (1980).
16) T. Korenaga and H. Ikatsu, *Analyst*, **106**, 653 (1981).
17) T. Korenaga and H. Ikatsu, *Nippon Kagaku Kaishi*, **1981**, 616.
18) T. Korenaga and H. Ikatsu, *Bunseki Kagaku*, **31**, 135 (1982).
19) T. Korenaga, *Bull. Chem. Soc. Jpn.*, **55**, 1033 (1982).
20) H. Namiki, Yokohama National University, private communication (1981).

Conformational Characterization of *S*-Methyl Dithiocarbazate by Infrared Spectra and Vibrational Assignments

Sadasivam MANOGARAN and Dixit Narayanarao SATHYANARAYANA*

Department of Inorganic and Physical Chemistry, Indian Institute of Science, Bangalore 560012, India

(Received November 9, 1981)

Infrared spectra are recorded for *S*-methyl dithiocarbazate and its *N*-deuterated compound in two molecular conformations in the solid state and in solution between 4000 and 30 cm^{-1}. The assignments have been supported from a complete normal coordinate analysis; the conformation sensitive bands of the $-CSNHNH_2$ grouping are discussed. The assignments are compared with those of related molecules to check the internal consistency and to obtain the pattern of the characteristic bands of thiocarbazoyl ($-CSNHNH_2$) group. The magnitudes of the C–N and S–CH_3 torsional barriers are estimated from the force constants.

The structural and spectroscopic studies[1-6] of the methyl ester of dithiocarbazic acid and its *N*-substituted derivatives are currently of interest. The impetus for this and similar work arises from the wide ranging applications of these compounds in industry and medicine[7,8] and their varying ligational[9] and conformational properties.[1,10] *S*-methyl dithiocarbazate (SMDTCZ) is itself a very interesting compound which has been isolated as solid in two planar molecular conformations[1,2] shown below (Fig. 1).

(a) *cis-trans* (b) *trans-cis*

Fig. 1.

The infrared spectra of SMDTCZ have been reported;[2,6] some assignments have been made empirically. In order to note more precisely the conformation-sensitive vibrations and discuss the vibrational spectra of SMDTCZ more fully, we have investigated the infrared spectra of SMDTCZ in two molecular conformations as well as their *N*-deuterated species. Based upon the force function previously developed,[11,12] normal coordinate analyses have been accomplished. The results are compared with those of chemically and structurally related molecules[11-15] for which detailed vibrational assignments have recently become available to provide a test for the general validity of the assignments derived and to obtain a pattern characteristic of the bands arising from thiocarbazoyl $-C(=S)NHNH_2$ grouping. The magnitude of the torsional barriers about the C–N and S–CH_3 bonds is estimated from the force constants.

Experimental

SMDTCZ having *cis-trans* and *trans-cis* conformation was prepared according to the literature methods.[16,17] Recrystallization from aqueous solution of the *trans-cis* conformer yields the *cis-trans* conformer of SMDTCZ. The purity of the compounds was checked by microanalyses. The *N*-deuterated samples were obtained by repeated exchange reaction with D_2O.

The infrared spectra from 4000 to 200 cm^{-1} were measured on a Perkin-Elmer 580 spectrophotometer in KBr pellets and nujol mulls which yielded identical spectra. The observed spectra are shown in Fig. 2. The solution spectra

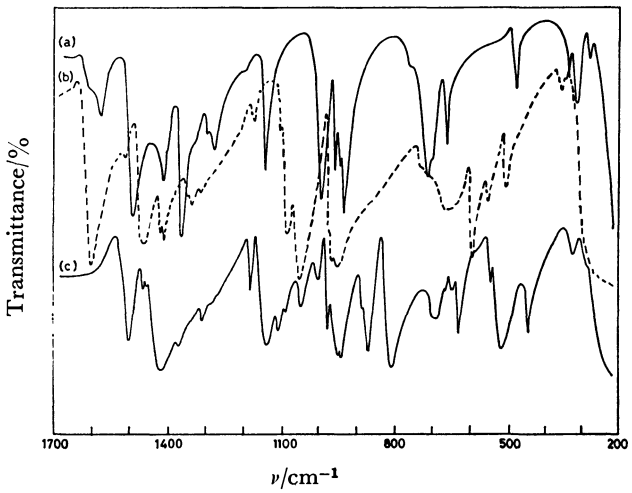

Fig. 2. Infrared spectra of SMDTCZ in (a) *cis-trans*, (b) *trans-cis*, and (c) of SMDTCZ-d_3 in *cis-trans* conformations.

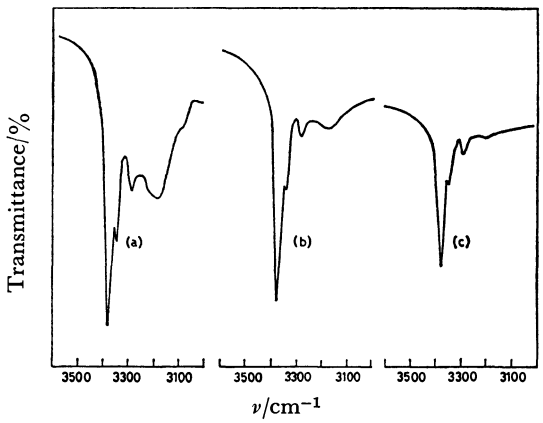

Fig. 3. Infrared spectra of *S*-methyl dithiocarbazate in $CHCl_3$ at concentrations of (a) 1.0×10^{-1} M, (b) 0.6×10^{-1} M, and 0.3×10^{-1} M (1M = 1 mol dm^{-3}).

were run on the same instrument using NaCl cells of path length of 0.4 mm (Figs. 3 and 4). The spectra between 400 and 30 cm^{-1} were recorded on a Polytec FIR 30 Michelson interferometer as polyethylene disks. The instruments were calibrated with usual standards.

Normal Coordinate Analysis

The conformations adopted for the calculations are shown in Fig. 1. In the molecular symmetry C_s, the 30 normal modes of vibration of SMDTCZ span

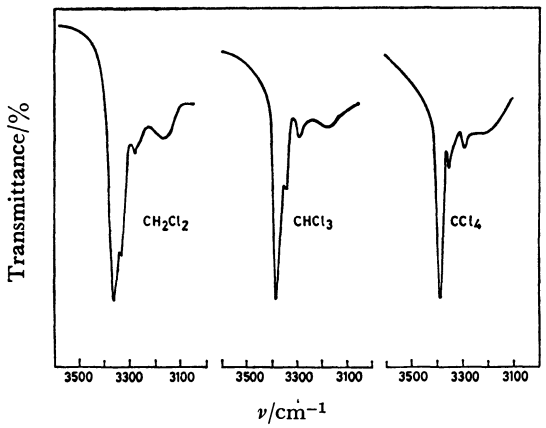

Fig. 4. Infrared spectra of *S*-methyl dithiocarbazate in different solvents.

19 of species a′ (in-plane) and 11 of species a″ (out-of-plane) vibrations. The internal and symmetry coordinates were selected in the usually accepted form. The bond length and valence angle values for SMDTCZ, were transferred from the X-ray crystal structure data.[1,2] The potential energy was expressed in terms of a Urey-Bradley force function employing valence force field type constants for the out-of-plane and torsional coordinates. The initial values of the force constants were transferred from thiosemicarbazide[11] (hydrazinecarbothioamide) and *S*-methyl *N*-methyldithiocarbamate.[12] The refinement of the force constants was carried out as already described.[11,12] The computations were made on a DEC 1090 digital computer employing a program similar in form to that of Schachtschneider.[18]

The final force constants of SMDTCZ listed in Table 1 are considered physically reasonable. Good fit reached between the observed and calculated frequencies for SMDTCZ and its deuterium labelled molecule also lends confidence to the values of the force constants and the assignments derived (Tables 2 and 3).

Results and Discussion

We noted that recrystallization of the *trans-cis* conformer of SMDTCZ from aqueous solution transformed it to the *cis-trans* form, while recrystallization from organic solvents including alcohols did not effect any conformational change, contrary to an earlier report.[2] Further, heating the *trans-cis* isomer to its melting and then cooling it also did not bring about any conformational change. The *N*-deuterated product of both isomeric forms of SMDTCZ interestingly yielded identical infrared spectrum; it was found to correspond to that of the *cis-trans* conformer which is the stablest form.

The frequencies of the observed infrared bands of SMDTCZ are listed in Table 2, together with the calculated vibrational frequencies along with approximate descriptions of the modes in terms of the potential energy distributions (PED) amongst the symmetry coordinates including only terms having greater than 15 percent for simplicity. Similar data for the *N*-deuterated compound are presented in Table 3. Despite the general asymmetry of the molecule, most of the fundamental frequencies may be described as group vibrations. A perusal of Table 2 shows that most of the frequencies for the two conformers differ, to a lesser or a greater extent.

N–H Stretching. The characteristic N–H stretching frequencies are sensitive to structural and electronic variations. The existence of conformational isomers in solution is clearly manifested in the infrared spectra of SMDTCZ (Figs. 3 and 4) which possess

Table 1. Force constants[a] of SMDTCZ in (a) *cis-trans* and (b) *trans-cis* conformations

(1) Urey-Bradley type constants

	(a)	(b)		(a)	(b)		(a)	(b)
K(C=S)	3.80	4.05	H(NC=S)	0.46	0.40	F(NC=S)	1.15	1.15
K(C–S)	2.70	3.05	H(NC–S)	0.30	0.30	F(NC–S)	0.90	0.90
K(S–C)	2.10	1.90	H(SCS)	0.20	0.06	F(SCS)	0.40	0.45
K(CN)	6.15	5.45	H(CSC)	0.14	0.18	F(CSC)	0.15	0.15
K(NN)	3.60	4.20	H(CNN)	0.27	0.40	F(CNN)	0.35	0.35
K(N′H)	5.45	5.50	H(CNH)	0.27	0.27	F(CNH)	0.45	0.50
K(NH)	5.30	5.40	H(HNN)	0.12	0.08	F(HNN)	0.50	0.54
K(CH)	4.52	4.50	H(NNH)	0.09	0.06	F(NNH)	0.54	0.35
k(CH_3)	−0.08	−0.04	H(HNH)	0.60	0.64	F(HNH)	0.08	0.07
			H(SCH)	0.20	0.17	F(SCH)	0.40	0.40
			H(HCH)	0.40	0.36	F(HCH)	0.05	0.14

(2) Valence type constants

	(a)	(b)		(a)	(b)
f(πCS)	0.090	0.150	f(τCN)	0.085	0.060
f(πNH)	0.044	0.060	f(τCS)	0.180	0.220
f(tNH_2)	0.550	0.570	f(τCH_3)	0.008	0.007
f(τNH_2)	0.030	0.024	f(πCS, τNH_2)	−0.012	0.014

a) Units: K, H, F are in N cm^{-1} (=mdyn Å^{-1}) and k, f in 10^{-16} N cm rad^{-2} (=mdyn Å rad^{-2}); meaning of t, π, τ as in Table 3.

TABLE 2. OBSERVED AND CALCULATED FUNDAMENTALS (cm^{-1}) AND POTENTIAL ENERGY DISTRIBUTION(PED) FOR SMDTCZ IN TWO CONFORMATIONS

Species	*cis-trans* Obsd	Calcd	Description[a] (PED/%)	*trans-cis* Obsd	Calcd	Description[a] (PED/%)
a′	3280	3282	νNH(99)	3305	3311	νNH(100)
	3155	3157	νNH_2(99)	3175	3162	νNH_2(100)
	2960	2966	$\nu_a CH_3$(100)	2975	2973	$\nu_a CH_3$(100)
	2890	2886	$\nu_s CH_3$(100)	2920	2947	$\nu_s CH_3$(100)
	1598	1597	δNH_2(86)	1610	1608	δNH_2(92)
	1507	1502	νCN(54), δNH(27)	1465	1467	δNH(45), νCN(31)
	1420	1431	$\delta_a CH_3$(82)	1412	1412	$\delta_a CH_3$(88)
	1373	1385	δNH(47), νCN(25), νC=S(15)	1340	1344	νCN(54), δNH(25)
	1290	1288	$\delta_s CH_3$(96)	1312	1309	$\delta_s CH_3$(97)
	1155	1159	δNCS(28), νNN(20), νC=S(16)	1170	1183	δNCS(24), νC=S(21), νC-S(18)
	1005	1003	νNN(45), νC-S(30)	1080	1080	νNN(58), νC=S(30)
	955, 945	950	rCH_3(73)	949	947	rCH_3(83)
	780	789	wNH_2(60)	727	724	νS-C(67), νC-S(17)
	725	728	νS-C(95)	655	662	wNH_2(30), νS-C(29), νC-S(23)
	705	693	νC=S(34), wNH_2(29)	582	585	wNH_2(63), νC-S(18)
	465	461	νC-S(45), δNCS(24)	496	499	δNNC(25), δNCS(24), νC=S(24)
	315	314	δSCS(62)	350	347	δSCS(50), δCSC(24)
	230	230	δNNC(60), δNCS(16)	222	222	δNNC(44), δNCS(31), δCSC(19)
	149	150	δCSC(71)	150	151	δCSC(53), δSCS(34)
a″	3180	3160	νNH_2(100)	3240	3246	νNH_2(100)
	2975	2966	νCH_3(100)	2975	2972	νCH_3(100)
	1430	1431	δCH_3(82), rCH_3(18)	1421	1412	δCH_3(88)
	1120	1119	tNH(100)	1047	1042	tNH_2(99)
	970	949	rCH_3(76), δCH_3(23)	964	945	rCH_3(84), δCH_3(15)
	665	666	τCN(47), τNH_2(32), πNH(21)	635	648	τCN(39), πNH(38), τNH_2(21)
	338	337	τNH_2(60), πNH(20)	290	297	πC=S(53), τNH_2(38)
	278	279	πC=S(53), τCN(22), τC-S(16)	260	270	τNH_2(41), πC=S(25), τCN(19)
	148	150	τC-S(62), πNH(17)	205	204	τC-S(73), τCN(18)
	135	133	τCH_3(42), πC=S(18), τC-S(16)	115	115	τCH_3(88)
	110	112	τCH_3(45), πC=S(22), πNH(21)	115	111	πNH(39), τCN(25), τC-S(18)

a) Meaning of ν, δ, r, t, w, π, τ as in Table 3.

two distinguishable bands in the N–H frequency region. The first band observed in the 3365—3390 cm^{-1} range is attributable to a *trans* –CS–NH– grouping and the second appearing in the 3340—3350 cm^{-1} interval to a *cis* –CS–NH– conformation. If we assume the extinction coefficients of the *cis* and *trans* forms to be nearly equal as is usually done, it is seen that the *cis-trans* conformer (a) with *trans* –NH–CS– grouping predominates in solution. Further, the relative intensities of the doublet peaks were found to be concentration independent (Fig. 3) ruling out the doublets being ascribed to molecular association. The infrared spectra of SMDTCZ in a series of solvents were obtained to note the influence of solvent dielectric on the spectra. The experimental data are presented in Fig. 4. It is observed that changing the solvent causes considerable alterations in the relative intensities of the two bands, which supports the presence of a conformational equilibrium. Increasing the solvent polarity favours transition to a *trans-cis* form (with *cis* –CS–NH– grouping). The spectra (Figs. 3 and 4) further exhibit a weak band around 3285 cm^{-1} and another weak but broad absorption centred around 3180 cm^{-1}. The former band has the characteristics of the intermolecularly hydrogen-bonded N–H stretching band; the region being same as in the solid. The latter absorption arise from the $-NH_2$ stretching motions.

According to the literature data, and as already pointed out, in the infrared spectra, of the two N–H stretching bands, a high frequency band is assigned to the *trans*(–NH–CS–) form and a low frequency band for the *cis* conformation. Interestingly, a reverse situation—the *trans* NH stretching band occurring at a lower frequency than the *cis* NH stretching mode—is realised for SMDTCZ in the solid phase. It may be ascribed essentially to intermolecular hydrogen bonding. Both rotamers exist as intermolecularly hydrogen bonded dimers. In the *cis-trans* isomer, N–H···N hydrogen bonds exist while in the *trans-cis* conformation N–H···S hydrogen bonds are present.[1,2] Since the former hydrogen bonds are stronger than the latter ones, the greater downward shift of the –NH stretching frequency may be expected pro-

Table 3. Observed and calculated fundamentals (cm^{-1}) and potential energy distribution (PED) for SMDTCZ-d_3

Species	Obsd	Calcd	Description[a](PED/%)	Species	Obsd	Calcd	Description[a](PED/%)
a′	2950	2966	$\nu_a CH_3$(100)		210	216	δNNC(59)
	2890	2886	$\nu_s CH_3$(100)		140	147	δCSC(67), δNCS(16)
	2420	2400	νND(98)	a″	2950	2966	νCH_3(100)
	2270	2284	νND_2(98)		2350	2335	νND_2(100)
	1490	1477	νCN(72)		1420	1431	δCH_3(82)
	1420	1431	$\delta_a CH_3$(82)		955	949	rCH_3(76), δCH_3(23)
	1286	1288	$\delta_s CH_3$(96)		815	836	tND_2(98)
	1240	1247	δNCS(26), νC=S(25), νNN(15)		520	484	τCN(46), τND_2(29), πND(24)
	1180	1175	δND_2(76)		310	295	πCS(40), τND_2(25), πND(16)
	982	992	νC-S(32), νNN(28)				
	955	948	rCH_3(69), $\delta_a CH_3$(21)		232	226	τND_2(47), τCN(28), πCS(17)
	945	936	δND(63), νNN(23)				
	712	728	νS-C(94)		—	149	τC-S(65), πND(15)
	700	719	νC=S(49)		133	130	τCH_3(57)
	625	588	wND_2(65)		105	108	τCH_3(30), πND(27), πCS(25)
	446	439	νC-S(38), δNCS(27)				
	305	311	δSCS(62)				

a) ν: Stretching, δ: deformation, r: rocking, t: twisting, w: wagging, π: out of plane bending, τ: torsion, a: asymmetric, s: symmetric.

Table 4. Comparison of the assignments of SMDTCZ with those of its related molecules

TSC	MMTU	TCH[a]	DMTU	MMDTC	SMDTCZ		Main assignments
					cis-trans	*trans-cis*	
3260 3180	3350 3139	3200	—	—	3180 3155	3240 3175	NH_2 stretching
3180	3230	3170	3305	3260	3280	3305	NH stretching
800	778	768	725	468	705	490	C=S stretching
1643	—	1620	—	—	1598	1610	NH_2 bend
1480	1302	1333	1355 1287	1349	1373	1465	NH bend+C-N stretching
1530	1500	1530[t] 1488[c]	1560 1506	1519	1507	1340	C-N stretching+NH bend
1160	1125	1140[c] 1078[t]	—	—	1005	1080	NN/CN stretching
995	—	1010[c] 932[t]	—	—	1120	1047	NH_2 twist
725	—	680[c] 754[t]	—	—	780	655	NH_2 wag
—	—	—	—	721	725	727	S-CH_3 stretching
570	—	579	662 642	556	665	635	N-H out-of-plane bend
408	496	468	445	356	465	496	C=S bend
353	—	307	445	440	278	290	C=S out-of-plane bend
—	—	—	—	174	149	150	CSC bend
206	—	253 194	—	—	230	228	NNC/CNC bend
				2930	2960	2975	CH_3 stretching
				2885	2890	2920	
				1409	1420	1412	CH_3 asymmetric bend
				1309	1290	1312	CH_3 symmetric bend
				946	955 945	949	CH_3 rock
				946	970	964	CH_3 wag
				106	110	115	CH_3 torsion

Abbrs. and (Refs.): TSC; thiosemicarbazide (11), NMTU; *N*-methylthiourea (15), TCH; thiocarbonohydrazide (13), DMTU; *N,N′*-dimethylthiourea (14), MMDTC; *N*-methyl *S*-methyldithiocarbamate (12), SMDTCZ; *S*-methyl dithiocarbazate (present work).

a) c and t refer to *cis* and *trans* groups to C=S bond.

ducing *cis*-NH band at a frequency higher than the *trans*-NH band.

Comparison. The assignments for SMDTCZ are compared with those available for related compounds[11-15] in Table 4. It is satisfactory that most of the assignments for SMDTCZ are compatible with the general features of the spectra of thiosemicarbazide and thiocarbonohydrazide and the pertinent portions from their isoelectronic thioureas and from *S*-methyl *N*-methyldithiocarbamate. Some of the differences in the characteristic frequencies could be explained on the basis of the different nature of the coupling with other vibrations. On the whole, there is internal consistency in the assignments and some pattern characteristic of –CSHN– grouping as well as those of the $-HNNH_2$ vibrations could be recognized. A brief discussion of the spectra of SMDTCZ will now be given.

$-CSNHNH_2$ Group Vibrations. An important band in the spectra of hydrazo derivatives is the N–N stretching band. The stretching frequency of N–N bond *cis* to C=S group is found 80 cm^{-1} lower than that for the *trans* N–N group. This is compatible with a similar assignment for *trans* and *cis* N–N bond stretching in thiosemicarbazide[11,21] but a reverse situation is found in thiocarbonohydrazide.[13] This may partly be explained on the basis of the mixing of the other vibrations.

The other bands of interest are those arising from the thioureide vibrations. The thioamide II and III bands arise from coupled modes of in-plane NH bending and C–N stretching; the former band is predominantly due to NH bending while the latter one arises chiefly from C–N stretching. These bands are conformation-sensitive. For SMDTCZ, the *trans* –CSNH– group has CN stretching band at a higher frequency than N–H in-plane bending. Similar findings have been made in other related systems.

The thioamide I band corresponding to C=S stretching is sensitive to the molecular environment and conformation. SMDTCZ provides a dramatic example of this; both rotamers have however no bands which could be attributed unequivocally to the C=S stretching mode.

The wagging and twisting modes of the $-NNH_2$ group appear to be conformation-sensitive. The vibrations of the $-NH_2$ group *cis* to the C=S moiety occur at higher wave numbers compared to $-NH_2$ group bands trans to the C=S grouping. A similar trend is noticeable for NH_2 torsional mode but is complicated by the more extensive mixing with other vibrations.

Torsional Barriers. From the value of the torsional force constants we may roughly estimate the potential barriers for C–N and S–C bonds. Following the procedures of Uno *et al.*,[22,23] we obtained 6.4 and 5.6 kJ mol^{-1} (1.53 and 1.34 kcal mol^{-1}) as barriers to internal rotation for $S-CH_3$ bond for the *cis-trans* and *trans-cis* conformers respectively. The values obtained are similar to that of acetamide[22] and *N*-methylurea[23] (5.4—7.1 kJ mol^{-1}). The C–N barrier is calculated to be 100.7 and 70.6 kJ mol^{-1} (24.06 and 16.87 kcal mol^{-1}) respectively for the *cis-trans* and *trans-cis* isomers, assuming an energy difference of 6.7 kJ mol^{-1} (1.6 kcal mol^{-1}) between the *cis* and *trans* NH_2 forms.[10] The estimates of the barrier heights over the amide C–N bond from torsional force constants in related thioamides and thioureas are similar and are usually higher than those determined by NMR methods.[24]

References

1) A. M. Manotti-Lanfredi, A. Tiripicchio, M. Tiripicchio Camellini, A. Monaci, and F. Tarli, *J. Chem. Soc., Dalton Trans.*, **1977**, 417.
2) R. Mattes and H. Weber, *J. Chem. Soc., Dalton Trans.*, **1980**, 423.
3) D. Gattegno and A. M. Giuliani, *Tetrahedron*, **30**, 701 (1974).
4) A. A. Bonapasta, C. Battistoni, and A. Lapiccirella, *J. Mol. Struct.*, **63**, 93 (1980).
5) C. Battistoni, M. Bossa, C. Furlani, and G. Mattogno, *J. Electron Spectrosc.*, **2**, 355 (1973).
6) D. F. Michalska and B. Kedzia, *Bull. Pol. des. Sci.*, **24**, 393 (1976).
7) S. Kubota, M. Uda, Y. Mori, F. Kametani, and H. Terada, *J. Med. Chem.*, **21**, 591 (1978).
8) V. V. Doulatyan and F. V. Avetysian, *Arm. Khim. Zh.*, **26**, 240 (1973).
9) M. A. Ali and S. G. Teoh, *J. Inorg. Nucl. Chem.*, **40**, 451 (1978); and references therein.
10) M. V. Andreocci, M. Bossa, G. Ramunni, M. Scazzocchio, D. Gattegno, and A. M. Giuliani, *J. Chem. Soc., Dalton Trans.*, **1974**, 41.
11) D. N. Sathyanarayana, K. Volka, and K. Geetharani, *Spectrochim. Acta, Part A*, **33**, 517 (1977).
12) K. R. Gayathri Devi, D. N. Sathyanarayana, and S. Manogaran, *Spectrochim. Acta, Part A*, **37**, 633 (1981).
13) K. Dwarakanath, D. N. Sathyanarayana, and K. Volka, *Bull. Soc. Chim. Belg.*, **87**, 667 (1978).
14) K. R. Gayathri Devi and D. N. Sathyanarayana, *Bull. Chem. Soc. Jpn.*, **53**, 2990 (1980).
15) K. Dwarakanath and D. N. Sathyanarayana, *Bull. Chem. Soc. Jpn.*, **52**, 2084 (1979).
16) G. Bahr and G. Schleitzer, *Z. Anorg. Chem.*, **280**, 161 (1955).
17) L. F. Audrieth, E. S. Scott, and P. S. Kippur, *J. Org. Chem.*, **19**, 733 (1954).
18) J. H. Schachtschneider, Technical Report, Shell Development Company, Emeryville, California, U.S.A. (1964).
19) W. Walter and H. P. Kubersky, *J. Mol. Struct.*, **11**, 207 (1972).
20) B. Galabov, G. Vassilev, N. Neykova, and A. Galabov, *J. Mol. Struct.*, **44**, 15 (1978).
21) K. Geetharani and D. N. Sathyanarayana, *Aust. J. Chem.*, **30**, 1617 (1977).
22) T. Uno, K. Machida, and Y. Saito, *Spectrochim. Acta, Part A*, **27**, 833 (1971).
23) Y. Saito, K. Machida, and T. Uno, *Spectrochim. Acta, Part A*, **31**, 1237 (1975).
24) W. E. Stewart and T. H. Siddall, III, *Chem. Rev.*, **70**, 517 (1970).

Spectrophotometric Determination of Osmium by Ternary Complex Formation with Thiocyanate and Rhodamine 6G

Sambamurthy JAYA and Tiruvesaloor Venkatrama RAMAKRISHNA*
Department of Chemistry, Indian Institute of Technology, Madras-600036, India
(Received June 18, 1981)

Osmium in trace amounts is determined by use of its reaction with thiocyanate and Rhodamine 6G to form an ion-association complex at pH 3.0. Aided by stabilization with gelatin, measurement of absorbance at 565 nm permits the determination of osmium in the range 0.04—1.2 ppm. The colour system is very stable and provides a molar absorptivity of 6.84×10^4 l mol^{-1} cm^{-1}. A few elements interfere and methods are suggested for handling them except ruthenium and rhodium.

Although many spectrophotometric methods have been suggested for the determination of osmium in the literature, the most often used are based on its reaction with thiourea[1-2] or thiocyanate.[3-4] These methods, besides being insensitive, call for considerable skill on the part of analysts as they are unselective and hence subjected to many sources of errors.

A highly sensitive method based on reaction of osmium with diphenyl carbazide[5] ($\varepsilon=1.5\times10^5$ l mol^{-1} cm^{-1}) has been described. This method lacks adequate selectivity and is not reliable because of its dependence on various experimental parameters such as acid concentration, temperature, and duration of heating. Prior extraction of OsO_4 into chloroform and subsequent colour development in the organic phase have been attempted to improve the selectivity,[6] but this caused considerable dimunition in the sensitivity ($\varepsilon=3.1\times10^4$ l mol^{-1} cm^{-1}). We ourselves had examined the osmium-diphenyl carbazide reaction and found that the determination can be made highly selective by extracting the complex into isobutyl methyl ketone at pH 5.0.[7]

The investigation reported here is based on the interaction of Rhodamine 6G cation with the anionic osmium–thiocyanate complex. The introduction of Rhodamine 6G in the reaction medium resulted in formation of a new coloured species with a molar absorptivity of 6.84×10^4 l mol^{-1} cm^{-1}. A detailed study indicated that under certain conditions most other ions do not duplicate the colour reaction, concluding that the analytical method may facilitate the determination of osmium with high degree of selectivity.

Experimental

Reagents. *Osmium (VIII) Solution*: This solution was prepared by dissolving 1 g of osmium tetroxide in 250 cm^3 of water as described elsewhere.[2] A working solution containing 10 μg cm^{-3} of osmium was prepared by suitably diluting the stock solution with water.

Potassium Thiocyanate Solution (5%): This solution was prepared by dissolving 5 g of potassium thiocyanate in water and diluting the solution to 100 cm^3.

Rhodamine 6G Solution (0.005%): This solution was prepared by dissolving 0.05 g of the reagent (BDH) in water and diluting the solution to 1 dm^3 with water.

Buffer Solution: This solution was prepared by dissolving 34 g of sodium aecetate trihydrate in water, adding 15 cm^3 of glacial acetic acid, adjusting to pH 3.0 with dilute HCl, and diluting to 250 cm^3.

Gelatin Solution (1%): This solution was prepared by dissolving 1 g of gelatin in boiling water and diluting the solution to 100 cm^3.

Apparatus. A Carl Zeiss PMQ-II Spectrophotometer with 10 mm quartz cells was used.

Procedure. To an aliquot of sample solution upto 15 cm^3 containing not more than 30 μg of osmium were added 2.5 cm^3 each of the thiocyanate and buffer solutions. The solution was heated on a boiling water bath for 20 minutes and cooled. The solution was transferred to a 25 cm^3 volumetric flask, 5 cm^3 of Rhodamine 6G solution added, 1 cm^3 of gelatin mixed, and distilled water was added to the mark. Absorbence was measured at 565 nm with 10 mm cells against a reagent blank.

Results and Discussion

The addition of Rhodamine 6G to a weakly acidic solution of osmium containing excess thiocyanate resulted in formation of a pink coloured complex. Maximum intensity was developed about an hour after the addition. Further standing of the mixture caused the colour to begin to fade owing to gradual separation of the ion-associate as a precipitate. The addition of gelatin retarded the precipitation since, in its presence, the colour system was found to remain stable for at least 24 h. Later experiments showed that the reaction can be made to proceed rapidly by first heating the osmium solution with thiocyanate for about 20 min on a boiling water bath and then adding Rhodamine 6G and gelatin to the cooled so-

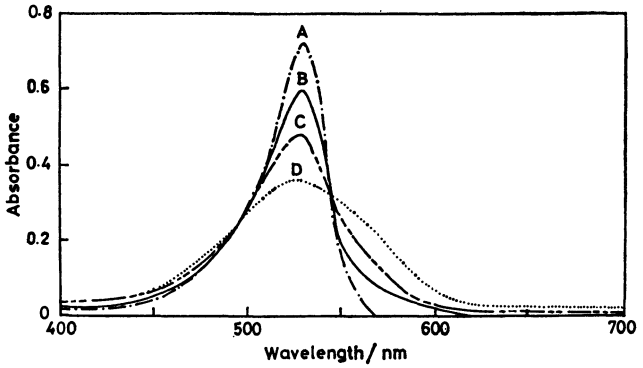

Fig. 1. Absorption spectra (2.5 cm^3 each of 1 mol dm^{-3} acetate buffer and 5% potassium thiocyanate, 1 cm^3 of 1% gelatin).
A: 2 cm^3 of 1.07×10^{-4} mol dm^{-3} Rhodamine 6G, total volume 25 cm^3, reference water 10 mm cells, B, C, and D: as in A with 0.5, 1.0, and 2 cm^3 of 1.07×10^{-4} mol dm^{-3} osmium.

lution. The resulting complex was characterised by its absorption maximum at 565 nm as taken against that of the reagent blank at 530 nm (Fig. 1).

Effect of Experimental Variables. Two sets of experiments were carried out to investigate the influence of acidity of the colour development in the range 2 mol dm^{-3} HCl to pH 9.0. In one set, solutions containing osmium and thiocyanate were adjusted to various acidities and then heated to expedite the formation of the binary complex. The solutions were then adjusted to pH 3.0 before treating with Rhodamine 6G and gelatin for colour development. In the other, the binary complex was first formed at pH 3.0 and then adjustment was made to varying acidities before the binary complex was brought into reaction with Rhodamine 6G. It is apparent from Fig. 2 that the interaction with Rhodamine 6G proceeds over a wide range of pH from 1 to 9, provided the binary complex is formed in the pH range 1—3.5. The most favourable pH for the colour development is 3.0.

Experiments were then made to ascertain the optimal concentrations of potassium thiocyanate and Rhodamine 6G for obtaining the maximum and constant absorbance. The results indicate that the absorbance increases with increasing concentration of potassium thiocyanate and Rhodamine 6G and that it reaches a limiting value when the concentrations are 2 cm^3 of 5% thiocyanate and 4 cm^3 of 0.005% Rhodamine 6G. The presence of the reagents in excess of the amounts indicated did not affect the absorbance.

The effect of temperature on the formation of the anionic thiocyanate complex was studied by thermostating reaction mixtures for 30 min at various temperatures ranging from 40 to 98 °C. Colour was developed after the solutions were cooled to room temperature. The results indicate that a constant and maximum absorbance is obtainable for the solutions that have been kept at 65 °C and above. Further studies using a boiling water bath showed that 15-min heating was sufficient to provide maximum absorbance and that prolonged heating upto 40 min did not affect the recovery of osmium.

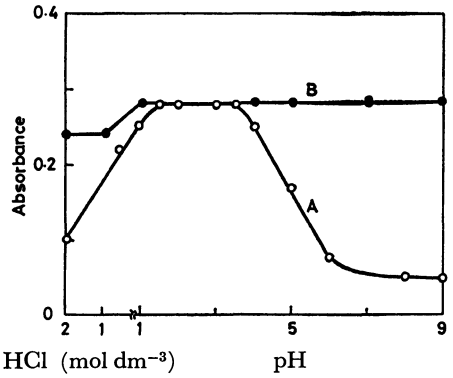

Fig. 2. Effect of pH/acidity (20 μg of osmium, 2.5 cm^3 each of 5% potassium thiocyanate and buffer, 5 cm^3 of 0.005% Rhodamine 6G, 1 cm^3 of 1% gelatin, final volume 25 cm^3, 565 nm, 10 mm cells). A: Formation of Os-SCN^- complex, B: association of SCN^- with Rhodamine 6G.

With the above optimal conditions a linear calibration graph was obtained over the range of 0—30 μg of osmium. The molar absorptivity was calculated to be 6.84×10^4 l mol^{-1} cm^{-1} at 565 nm and the sensitivity of the reaction was 0.0028 μg cm^{-1}.

Ten replicate determinations of standard osmium solutions each containing 20 μg of osmium gave an average recovery of 100.4% with a relative standard deviation of 1.8%.

Nature of the Complex. Experiments were then conducted to find reaction ratios between osmium and Rhodamine 6G by the mole-ratio and continuous var-

TABLE 1. EFFECTS OF DIVERSE IONS
(Amount of osmium = 20 μg in 25 cm^3)

Diverse ion	Amount added/μg	Absorbance
None	—	0.285
Pt(IV)	20	0.550
	—[a]	0.285
	250[a]	0.285
	500[a]	0.320
Pd(II)	20	0.580
	500[a]	0.285
	1000[a]	0.360
Rh(III)	1	0.310
	20	0.510
Ir(IV)	20	0.315
	—[b]	0.280
	200[b]	0.280
	500[b]	0.500
Ru(III)	1	0.340
	20	0.570
Fe(III)	20	0.440
	1000[b]	0.280
Co(II)	250	0.285
	500	0.315
	1000[a]	0.280
Hg(II)	20	0.285
	100	0.390
	1000[a]	0.290
Cu(II)	20	0.345
	50[a]	0.285
	100[a]	0.340
Zn(II)	50	0.285
	100	0.410
	—[c]	0.285
	1000[c]	0.280
Zr(IV)	100	0.285
	500	0.335
	—[d]	0.285
	1000[d]	0.285
W(VI)	100	0.285
	500	0.335
	1000[d]	0.285

a) Two cm^3 of 2% thiourea added before addition of Rhodamine 6G. b) In the presence of 1 cm^3 of 5% ascorbic acid. c) One cm^3 of 0.1 mol dm^{-3} EDTA added before addition of Rhodamine 6G. d) In the presence of 2 cm^3 of 2% sodium fluoride.

iation methods. The equilibrium shift method was employed to establish combining ratios of osmium and thiocyanate. The results indicate the empirical formula of the complex as $R^+[Os^{II}(SCN)_3]^-$ where R^+ represents the Rhodamine 6G cation.

Though 0.5 cm^3 of 1% solution of gelatin was found to be sufficient to stabilize the system, a significant effect was observed when gelatin was added prior to the addition of Rhodamine 6G solution. In this instance the sensitivity of the colour reaction diminished considerably. It was also noticed that the ion-associate breaks down when heated to higher temperature or treated with miscible organic solvent like acetone. Since Rhodamine 6G is known to exist as aggregates in aqueous solution,[8] and from the fact that acetone raises the "critical micelle concentration" of the dye and that the addition of gelatin or increase in temperature can cause deaggregation of the dye,[9] it appeared reasonable to conclude that the resulting colour change was due to interaction of the thiocyanate complex of osmium with micelles of Rhodamine 6G. The addition of gelatin after the addition of Rhodamine 6G prevents further aggragation of ion-associates, thus stabilising the colour system. The observed spectral shift possibly arises due to short range electrostatic interaction of the π-cloud of the dye with the polarising anion or π-cloud of another dye molecule or both, which can lower the energy gap between the highest occupied and lowest unoccupied molecular orbitals.

Effects of Diverse Ion. The influence of amounts of several ions were studied on the determination of 20 μg of osmium. No interference was noticed in the presence of 1 mg amount of Br^-, NO_3^-, ClO_4^-, I^-, SeO_3^{2-}, $B_4O_7^{2-}$, AsO_4^{3-}, PO_4^{3-}, Li^+, Be^{2+}, Ca^{2+}, Sr^{2+}, Ba^{2+}, Cd^{2+}, Pb^{2+}, Mn^{2+}, Ni^{2+}, UO_2^{2+}, Cr^{3+}, Al^{3+}, Bi^{3+}, La^{3+}, Tl^{3+}, Th^{4+}, Ce^{4+}, or Sb^{5+}. Other metal ions, which interfered, were dealt with as summarised in Table 1. The data clearly show that only ruthenium and rhodium interfere seriously with the determination.

Table 2. Analysis of synthetic samples[a]

	Absorbance
None	0.285
Pt^{4+}(0.25 mg) + Pd^{2+}(0.5 mg)	0.280
Pt^{4+}(0.25 mg) + Pd^{2+}(0.5 mg) + Ir^{4+}(0.2 mg)	0.285
Pt^{4+}(0.25 mg) + Fe^{3+}(1 mg) + Ni^{2+}(1 mg)	0.275
Pd^{2+}(0.5 mg) + Fe^{3+}(1 mg) + Cu^{2+}(0.05 mg)	0.285
Pd^{2+}(0.5 mg) + MoO_4^{2-}(1 mg) + La^{3+}(1 mg)	0.280
Fe^{3+}(1 mg) + Cu^{2+}(1 mg) + Ni^{2+}(1 mg)	0.285
WO_4^{2-}(1 mg) + Fe^{3+}(1 mg) + UO_2^{2+}(1 mg)	0.280

a) Determinations were carried out after adding appropriate masking agents as given in Table 1.

Analyses of several composite mixtures by the proposed method are given in Table 2.

One of us (S. J.) is thankful to C. S. I. R., New Delhi for the financial assistance.

References

1) K. J. Jensen, *Anal. Chem.*, **37**, 1430 (1965).
2) E. B. Sandell, "Colorimetric Determination of Traces of Metals," Interscience Publishers, New York (1959), p. 705.
3) J. H. Wiersma and P. F. Lott, *Anal. Chem.*, **39**, 674 (1967).
4) N. Quershi and N. K. Mathur, *Z. Anal. Chem.*, **242**, 159 (1968).
5) G. Goldstein, D. L. Manning, O. Menis, and J. A. Dean, *Talanta*, **7**, 307 (1961).
6) G. Goldstein, D. L. Manning, and O. Menis, *Talanta*, **7**, 301 (1961).
7) S. Jaya and T. V. Ramakrishna, a paper submitted to *Talanta*.
8) L. V. Levshin, A. P. Golovina, and E. A. Bobrovskaya, *Vestn. Mosk. Univ. Ser. III: Fiz. Astron.*, **21**, 67 (1966); *Chem. Abstr.*, **65**, 13029e (1966).
9) M. J. Rosen, "Surfactants and Interfacial Phenomena," Wiley Interscience, New York (1978), p. 102.

Synthesis, Ion Exchange Properties, and Analytical Applications of a Novel Tin(IV)-edta Ion Exchanger

Syed Ashfaq Nabi* and Rifaqat Ali Khan Rao
Department of Chemistry, Aligarh Muslim University, Aligarh-202001, India

(Received June 11, 1981)

Tin(IV)-edta compound has been synthesized by mixing aqueous solutions of tin(IV) chloride and disodium salt of ethylenediaminetetraacetic acid (EDTA=H_4 edta) in different conditions. The most stable sample is prepared by mixing 0.1 mol dm^{-3} solution of tin(IV) chloride with 0.1 mol dm^{-3} solution of disodium salt of edta in the volume ratio of 3:2 at pH 2.5 and refluxing the mixture for 16 h. Ion exchange capacities of the material for alkali metals are significantly smaller (0.26—0.20 mequiv./g) than for alkaline earths (0.74—0.40 mequiv./g). The thermal and chemical stability of this material has been compared with amine-tin hexacyanoferrate-(II). Analytical importance of this material has been established by achieving a number of quantitative separations on its columns.

The advancement in the field of synthetic inorganic ion exchangers has been reviewed by various authors.[1,2] Their importance in analytical chemistry has been firmly established. It has been found that inorganic ion exchangers often exhibit their own characteristic properties. It is therefore, always of interest to synthesize new ion exchange materials and to utilize them to solve analytically difficult problems of specific nature.

Of the various ion exchangers studied earlier, have been synthesized either by interaction of pure organic or inorganic compounds. As far as we are aware only limited efforts have been made to develop this new class of ion exchange material which is based on the interaction of metal ions with organic compounds. Amine-tin hexacyanoferrate(II) and zirconium(IV)-bis(carboxymethanephosphonate)[3,4] have been found to exhibit exchange properties. However, detailed studies have not been made on these materials due to their limited chemical and thermal stability.

Crystalline edta complexes of zirconium, hafnium, thorium and tin at pH 1.5 have been described fairly stable.[5] However these compounds have not been studied for their ion exchange properties. In continuation to our studies in these directions we have been able to synthesize amorphous tin(IV)-edta compound as a new cation exchanger. EDTA has been chosen because of its enormous usefulness as an analytical reagent. The present paper deals with the preparation, properties and applications of tin(IV)-edta compounds.

Experimental

Reagents. Tin(IV) chloride pentahydrate (Poland) and ethylenediaminetetraaceticacid disodium salt (E. Merck, Germany) were used. All the other chemicals were of reagent grade.

Apparatus. pH was measured with an Elico LI-10 pH meter. A spectronic 20 colorimeter and a Perkin Elmer 137 spectrophotometer were used for spectrophotometric and IR studies respectively. An electric temperature controlled shaker (SICO) was used for shaking. X-Ray studies were performed on a philips diffractometer and Stanton-Thermobalance type H_4 was used for thermogravimetric studies.

Synthesis. Tin(IV)-edta precipitates were prepared by mixing 0.1 mol dm^{-3} aqueous solution of ethylenediaminetetraacetic acid disodium salt to 0.1 mol dm^{-3} aqueous solution of tin(IV) chloride in different volume ratio as indicated in Table 1. The desired pH was adjusted by adding either dilute hydrochloric acid or dilute sodium hydroxide solution. The precipitate formed, was allowed to settle for 24 h at room temperature. It was then filtered off, washed with distilled water and dried at 40 °C. Sample 1, 2, and 3 so prepared were powder like and yellowish white in appearance. Sample 4 was prepared by adding 0.1 mol dm^{-3} aqueous solution of disodium salt of edta gradually to 0.1 mol dm^{-3} aqueous solution of tin(IV) chloride in volume ratio 2:3 while continuously stirring the mixture. The pH was adjusted to 2.5 by adding dilute solution of sodium hydroxide. The white precipitate obtained was refluxed for 16 h with mother liquor. It was then filtered off under suction, washed several times with distilled water and then dried at 40 °C. This dirty yellow substance when immersed in water, broke down into smaller particles with cracking. Out of these four samples, sample 4 was found to be fairly stable in water and some mineral acids and further studies were therefore, performed on sample 4. The material was immersed in 1 mol dm^{-3} nitric acid solution for 24 h to convert it into H^+ form. Excess of acid was removed by repeated washing with demineralized water. The conditions of synthesis and few properties are summarized in Table 1.

Chemical Stability. Sample 4 was washed several times to remove excess of tin or EDTA adhered to the surface of the particles. 0.5 g of the material was then treated with 50 cm^3 of the solvent in a 250 cm^3 Erlenmeyer flask. The mixture was shaken for 6 h in a shaker incubator at 25±2 °C and then kept for 24 h. Tin released was determined spectrophotometrically using hematoxylin as a colouring reagent[6] and edta in the solution was determined volumetrically using magnesium nitrate solution.[7] These results are given in Table 2.

Chemical Composition. Since the material is not completely soluble in concentrated hydrochloric acid and EDTA is damaged by hot concentrated sulfuric acid, potassium hydroxide was utilized for its dissolution. A 0.2 g of the exchanger was dissolved in 1.0 mol dm^{-3} potassium hydroxide solution. The pH of the solution was decreased by adding hydrochloric acid drop by drop till precipitation was complete. It was then filtered off. The precipitate was dried and tin was estimated as tin dioxide. The filtrate left was made to 100 cm^{-3} and edta was determined titrimetrically against a standard solution of mangnesium nitrate.[7]

Ion Exchange Capacity. Ion exchange capacities of some uni- and bivalent ions are shown in Table 3. 0.5 g

Table 1. Synthesis of tin(IV)-edta

Sample No.	Conditions of synthesis: $SnCl_4 5H_2O$ (mol dm^{-3})	Conditions of synthesis: edta (mol dm^{-3})	Conditions of synthesis: Mixing ratio (v/v)	Adjusted pH	Time of refluxing / h	Appearance H^+ form	Chemical composition Tin/edta
1	0.1	0.1	1 : 1	2.0	—	Yellow powder	—
2	0.1	0.1	2 : 1	2.1	—	Yellowish white powder	—
3	0.1	0.1	3 : 2	2.0	—	Yellowish white powder	1.0
4	0.1	0.1	3 : 2	2.5	16	Dark yellow shiny particles	2.5

Table 2. Comparison of few properties of tin(IV)-edta and amine-tin hexacyanoferrate(II)

Effect of drying temperature on ion exchange capacity (meqiv./g): Temp / °C	Tin(IV)-edta	Amine-tin hexacyanoferrate(II)	Solvent	Chemical stability: Tin(IV)-edta: Tin released (mg/50 cm^3)	Tin(IV)-edta: edta released (mg/50 cm^3)	Amine-tin hexacyanoferrate(II): Iron released (mg/50 cm^3)	Amine-tin hexacyanoferrate(II): Tin released (mg/50 cm^3)
			H_2O	0.00	0.00	0.10	0.20
60	0.74	1.2	0.05 M HNO_3	0.00	0.00	0.25	0.00
100	0.74	1.2	0.1 M HNO_3	0.00	0.00	—	—
200	0.48	0.8	0.5 M HNO_3	0.00	0.00	0.20	0.10
300	0.24	—	1.0 M HNO_3	0.00	0.00	0.40	0.15
400	0.13	0.10	0.1 M NaOH	6.00	6.50	Complete dissolution	
500	0.12	0.00					
600	0.10	0.00					

Table 3. Ion exchange capacity (pH=6) of tin(IV)-edta (sample 4) at room temperature

Exchanging ion	Solution used	Ion exchange capacity (mequiv./g)
Li^+	Lithium chloride	0.20
Na^+	Sodium nitrate	0.20
K^+	Potassium nitrate	0.24
Rb^+	Rubidium chloride	0.20
Mg^{2+}	Magnesium nitrate	0.70
Ca^{2+}	Calcium nitrate	0.74
Sr^{2+}	Strontium nitrate	0.60
Ba^{2+}	Barium chloride	0.40

of the exchanger in H^+ form was taken into the column with glass wool support. The H^+ ions eluted by passing 1 mol dm^{-3} of the electrolyte solutions (pH=6) through the column. The eluted H^+ ions in the effluent were determined volumetrically using standard sodium hydroxide solution as titrant.

pH Titrations. pH titrations were performed using Topp and Papper's method[8] for LiCl–LiOH, NaCl–NaOH, and KCl–KOH systems at 25±2 °C (Fig. 1).

Distribution Coefficient. The K_d values of metal ions in different solvent systems were determined with the method reported earlier.[9] The results are given in Tables 4 and 5.

Quantitative Separations of Metal Ions. Quantitative separations of some metal ions were achieved on a 0.3 cm diameter (id) glass column using 2.0 g of exchanger (mesh size 100—200) in H^+ form. The cation mixture was poured on the top of the column. The stop cock open so that the mixture passed through the column with a very slow rate. The column was rinsed with distilled water. The cations

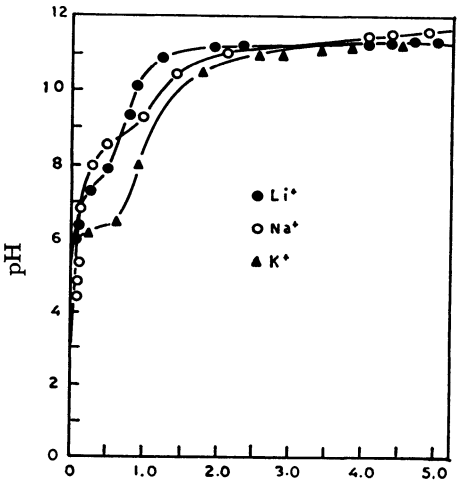

$\overline{OH}$ added (mequiv./0.5 g exchanger)

Fig. 1. pH titration curves of tin(IV)-edta.

adsorbed were then eluted with suitable eluting agents. The flow rate during elution was maintained 1.0 cm^3/min. The 10 cm^3 fraction of the effluent was collected and the metal ions were determined by standard methods.[6,7] Quantitative separations of metal ions achieved on the columns of tin(IV)-edta are summarized in Table 6.

X-Ray Analysis. Nickel-filtered Cu $K\alpha$ radiation was used for X-ray analysis of sample 4.

Infrared Spectra. IR spectrum of tin(IV)-edta compound in H^+ form was performed using Nujol technique and compared with IR spectrum of disodium salt of EDTA (Fig. 2).

Thermal Treatment. Thermogravimetric analysis of 0.3310 g of sample 4 in Mg^{2+} form was performed at a heating rate of 10 °C/min (Fig. 3). To examine the effect of

Table 4. Distribution coefficients of metal ions on tin(IV)-edta sample 4 in different solvent systems

Metal ions	K_d/cm^3 g^{-1}					
	Water pH=6	10^{-3} mol dm^{-3} HNO_3	10^{-2} mol dm^{-3} HNO_3	10^{-1} mol dm^{-3} HNO_3	10^{-1} mol dm^{-3} NH_4Cl	10^{-1} mol dm^{-3} NH_4Cl + 10^{-2} mol dm^{-3} HNO_3
Mg^{2+}	308±17	85±1	45±2	27±2	70±3	36±1
Ca^{2+}	270±8	120±2	90±2	32±2	38±2	18±2
Sr^{2+}	140±6	78±1	45±2	22±1	28±3	32±8
Ba^{2+}	100±8	65±1	36±1	19±1	22±2	20±1
Al^{3+}	117±12	52±2	17±1	00±0	52±1	00±0
Fe^{3+}	1080±134	880±9	200±33	74±4	85±4	64±6
Co^{2+}	448±17	284±7	140±3	65±2	67±2	20±1
Ni^{2+}	970±92	430±15	270±2	165±4	93±5	31±2
Zn^{2+}	316±16	240±1	178±1	12±1	246±5	43±1
Pb^{2+}	1900±182	640±29	263±3	77±1	400±2	176±4
Cd^{2+}	526±6	410±2	88±2	21±1	120±7	17±5
Mn^{2+}	1660±73	190±2	91±1	25±2	63±2	76±2
VO^{2+}	8100±400	1210±56	550±7	64±1	370±8	134±1
Cu^{2+}	2020±82	2020±43	430±8	92±1	324±2	35±2
Zr^{4+}	120±10	110±2	68±4	00±0	86±22	60±5
Hg^{2+}	368±18	64±1	36±1	6±1	157±3	32±2
Ce^{4+}	320±36	210±3	77±2	61±1	310±6	40±2
Ho^{3+}	1280±120	1020±20	530±30	200±4	530±30	510±10
Dy^{3+}	3580±130	720±22	600±5	140±6	4330±20	360±3
Sm^{3+}	660±33	620±2	230±2	82±3	420±9	196±5
La^{3+}	286±24	200±4	130±1	100±5	110±5	58±4
Tm^{3+}	496±28	460±4	440±7	350±10	200±32	230±8
Eu^{3+}	220±14	210±3	170±1	94±2	210±62	200±12
Pr^{3+}	450±12	430±1	280±5	140±4	270±10	150±7
Nd^{3+}	428±28	330±24	250±7	210±6	431±31	271±4

Table 5.

Metal ions	K_d/cm^3 g^{-1}			
	10^{-2} mol dm^{-3} $HClO_4$	10^{-1} mol dm^{-3} $HClO_4$	10^{-1} mol dm^{-3} $NaClO_4$	10^{-2} mol dm^{-3} $HClO_4$ + 10^{-1} mol dm^{-3} $NaClO_4$
Mg^{2+}	51±1	46±1	70±1	36±2
Ca^{2+}	70±3	46±2	70±6	42±1
Ba^{2+}	80±4	50±3	80±6	63±5
Al^{3+}	20±2	3±1	260±20	00±0
Fe^{3+}	526±15	10±1	660±5	276±36
Co^{2+}	29±1	10±1	57±2	10±3
Ni^{2+}	86±2	24±1	348±4	80±6
Zn^{2+}	340±7	100±6	1750±40	214±11
Pb^{2+}	12000±1200	104±4	15200±101	508±2
Cd^{2+}	700±11	60±1	220±1	200±8
Mn^{2+}	72±3	32±5	55±2	40±6
VO^{2+}	71±9	33±3	1100±23	60±36
Cu^{2+}	2040±20	850±13	9450±545	881±79
Th^{4+}	60±5	31±1	210±10	50±1
Hg^{2+}	12200±300	1400±51	11250±100	1900±140
Ce^{4+}	20±1	15±1	53±3	15±1
UO^{2+}	11±2	00±0	40±2	22±6
Ho^{3+}	61±4	22±2	82±2	66±1
Dy^{3+}	30±3	11±3	39±5	22±1
Sm^{3+}	65±1	24±3	120±1	53±2
Pr^{3+}	28±1	20±4	45±5	28±2
Nd^{3+}	20±1,	14±1	44±13	17±1

Table 6. Separations of metal ions achieved on tin(IV)-edta columns

Sample No.	Separations achieved	Amount loaded μg	Total elution volume[a] (cm^3)	% of metal ion eluted	Eluent used
1	Ca^{2+}	240	30	98	0.01 M HNO_3
	UO_2^{2+}	2000	30	95	0.05 M HNO_3
2	Ba^{2+}	520	30	96.1	0.01 M HNO_3
	UO_2^{2+}	2000	30	95	0.05 M HNO_3
3	UO_2^{2+}	2000	30	95	0.05 M HNO_3
	Cu^{2+}	370	50	95.5	1.0 M $HClO_4$+0.1 M $NaClO_4$
4	Mg^{2+}	134	40	95.5	0.01 M HNO_3
	UO_2^{2+}	2000	30	95.5	0.05 M HNO_3
5	Ni^{2+}	293	60	98.6	0.05 M $HClO_4$+0.1 M $NaClO_4$
	Pb^{2+}	1035	50	96.2	0.5 M $HClO_4$+0.1 M $NaClO_4$
6	Mn^{2+}	265	50	97	0.05 M $HClO_4$+0.1 M $NaClO_4$
	Pb^{2+}	1035	50	96.4	0.5 M $HClO_4$+0.1 M $NaClO_4$
7	Mg^{2+}	134	50	97	0.01 M HNO_3
	Pb^{2+}	952	60	97	0.1 M HNO_3
8	Ca^{2+}	240	40	95.8	0.01 M HNO_3
	Pb^{2+}	952	60	96.1	0.1 M HNO_3
9	Zn^{2+}	340	50	94.7	0.05 M $HClO_4$+0.1 M $NaClO_4$
	Pb^{2+}	1035	50	97.2	0.5 M $HClO_4$+0.1 M $NaClO_4$
10	Cd^{2+}	562	40	97.5	0.05 M $HClO_4$+0.1 M $NaClO_4$
	Pb^{2+}	1035	50	96.6	0.5 M $HClO_4$+0.1 M $NaClO_4$
11	Ba^{2+}	520	30	94.6	0.01 M HNO_3
	Pb^{2+}	952	60	92.4	0.1 M HNO_3
12	Ba^{2+}	520	30	98	0.01 M HNO_3
	Cu^{2+}	330	50	100	1.0 M $HClO_4$+0.1 M $NaClO_4$
13	Ca^{2+}	240	40	96.6	0.1 M HNO_3
	Cu^{2+}	330	50	98.4	1.0 M $HClO_4$+0.1 M $NaClO_4$
14	Mg^{2+}	134	50	97	0.01 M HNO_3
	Cu^{2+}	330	50	99	1.0 M $HClO_4$+0.1 M $NaClO_4$
15	Co^{2+}	280	50	92.8	0.05 M HNO_3
	Cu^{2+}	330	50	99.6	1.0 M $HClO_4$+0.1 M $NaClO_4$
16	Zn^{2+}	340	50	98.5	0.05 M $HClO_4$+0.1 M $NaClO_4$
	Cu^{2+}	330	50	100	1.0 M $HClO_4$+0.1 M $NaClO_4$
17	Pb^{2+}	950	60	94.6	0.1 M HNO_3
	Cu^{2+}	330	50	96.4	1.0 M $HClO_4$+0.1 M $NaClO_4$
18	Cd^{2+}	562	40	99.6	0.05 M $HClO_4$+0.1 M $NaClO_4$
	Cu^{2+}	330	50	98.4	1.0 $HClO_4$+0.1 M $NaClO_4$
19	Ni^{2+}	293	60	95.2	0.05 M $HClO_4$+0.1 M $NaClO_4$
	Cu^{2+}	330	50	100	1.0 M $HClO_4$+0.1 M $NaClO_4$
20	Mn^{2+}	265	50	94.3	0.05 M $HClO_4$+0.1 M $NaClO_4$
	Cu^{2+}	330	50	95.4	1.0 M $HClO_4$+0.1 M $NaClO_4$

Cation mentioned first has been eluted first. a) Volume of eluent for total elution of metal ions.

drying temperatures on the ion exchange capacity, the material was dried at various temperatures in a muffle furnace for 1 h. The exchange capacities at various temperatures are given in Table 2.

Discussion

It is apparent from Tables 1 and 2 that the mixing ratio of the reactants and conditions of reaction greatly affects the chemical stability and physical appearance of the product. It has been observed that when the precipitate is refluxed for several hours, the chemical stability of the product is significantly increased. The optimum pH for the precipitation of the material which can exhibit exchange properties has been found to be 2.5. However, if the precipitation is done below this pH value, the product obtained is

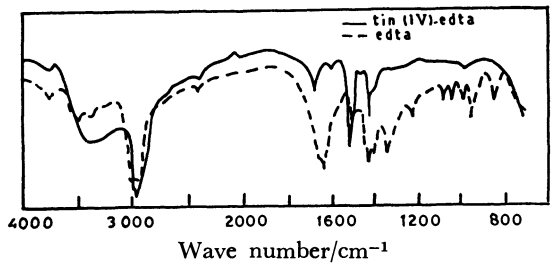

Fig. 2.

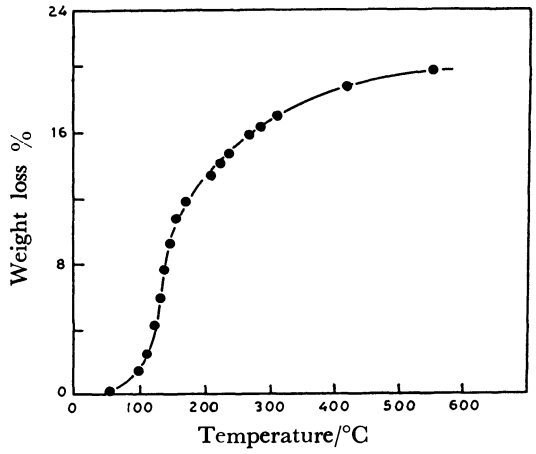

Fig. 3. Thermogram of tin(IV)-edta in Mg^{2+} form.

unstable and therefore has not been studied in detail.

The ion exchange capacities of tin(IV)-edta sample 4 varies with different metal ions (Table 3). The maximum ion exchange capacity is recorded as 0.74 mequiv./g for Ca^{2+} ion. The values of ion exchange capacity for alkali metals are almost constant and small as compare to the ion exchange capacities for alkaline earth metals. However, the ion exchange capacities for alkaline earths has been found to be in the order $Ca^{2+} \geqslant Mg^{2+} > Sr^{2+} > Ba^{2+}$. The peculiar feature which has been noticed regarding this material is that the ion exchange capacities for the univalent ions differ significantly from the ion exchange capacities for the bivalent ions. These data (Table 3) suggest the potentiality of the ion exchanger for the separation of almost all the alkali metals from alkaline earth series.

The pH-titration curves reveal some interesting features regarding the uptake of alkali metals which is affected by pH. The uptake of these metals below pH 6 is almost equal which is supported by ion exchange capacity data (Table 3). However, in the pH range 6 to 8.5 the uptake order is $K^+ > Li^+ > Na^+$. In the pH range 8.5 to 11.2, Na^+ ions are more strongly adsorbed than Li^+ ions and beyond pH 11.2 again the uptake of Li^+ ions becomes higher than Na^+ ions. The two inflection points in all the curves show the bifunctional behaviour of the ion exchanger.

The specificity of inorganic ion exchangers for metal ions is greatly dependent on the nature of the material. Thus tin(IV) antimonate[10] and titanium(IV) antimonate[11] are selective for alkaline earths while zirconium(IV) antimonate[12] and tin(IV) selenite[13] for alkali metals. Tin(IV)-edta is found to be selective for alkaline earth metals when compared to alkali metals as it is evident from ion exchange capacity data. K_d values of some important metal ions on tin(IV)-edta in different solvent systems are given in Tables 4 and 5. The adsorption sequence for some metal ions in water is found to be $Mg^{2+} > Ca^{2+} > Sr^{2+} > Ba^{2+}$: $Pb^{2+} > Mn^{2+} > Fe^{3+} > Ni^{2+}$: $Sm^{3+} > Pr^{3+} > Ce^{4+}$. It is clear from Table 4 that K_d values decreases gradually with the increase in nitric acid concentration as expected. A marked difference in K_d values of metal ions has been observed in perchloric acid and sodium perchlorate system. K_d values for bivalent ions in general, are found to be higher then ter and quadrivalent ions. The sequence of adsorption in 0.01 mol dm^{-3} perchloric acid is found to be $Hg^{2+} > Pb^{2+} > Cu^{2+} > Cd^{2+} > Ni^{2+} > Mn^{2+} > Co^{2+} > Al^{3+}$: $Sm^{3+} > Ho^{3+} > Dy^{3+} > Pr^{3+} > Ce^{4+} > UO_2^{2+}$. K_d values reveal the possibility of numerous separations of metal ions. Some of the binary separations achieved on the columns of tin(IV)-edta are listed in Table 6.

The usual interferences which are encountered in the determination of Mg are Fe, Cu, Co, Ni, Zn, Pb, *etc*, and are frequently removed by precipitation with diethyldithiocarbamate.[14] However, separation of Mg from these metal ions using this ion exchange material offers additional advantages being a simple and inexpensive method.

The X-ray analysis of sample 4 in H^+ form indicates amorphous nature of the material.

The infrared absorption spectrum of tin(IV)-edta in H^+ form when compared with infrared spectrum of disodium salt of EDTA, tin(IV) selenite and those explained by Sawyer and Paulsen[15] yield the following interpretations.

IR spectrum of disodium salt of EDTA shows four important peaks. The different peaks at 1630 cm^{-1}, 1390 cm^{-1}, 1360 cm^{-1} to 1310 cm^{-1}, and 1000 cm^{-1} to 900 cm^{-1} are due to -COO- groups. Infrared spectrum of tin(IV)-edta shows three strong peaks. A broad peak in the 3400—3000 cm^{-1} region represents the interstitial water and OH groups. Another strong peak in the 1700—1500 cm^{-1} region with a maximum at 1650 cm^{-1} may be due to interstitial water molecules. The peaks appearing at 1380, 1500, and 3000 cm^{-1} are also the standard peaks of nujol mull.

The thermogram of tin(IV)-edta sample 4 in Mg^{2+} form (Fig. 3) shows that there is continuous loss in weight upto 170 °C which can be attributed to loss of water molecules. If temperature is raised further, decomposition of the material starts which continues upto 550 °C. This conclusion is also confirmed by the ion exchange capacity data (Table 2). The exchange capacity decreases gradually as the drying temperature is increased. The capacity of the exchanger however completely lost beyond 500 °C.

The authors thank Prof. W. Rahman for research facilities. Thanks also due to C. S. I. R. (INDIA) for financial assistance to one of us (R. A. K. Rao).

References

1) C. B. Amphlett, "Inorganic Ion Exchangers," Elsevier, New York (1964).
2) Y. Inoue, *J. Inorg. Nucl. Chem.*, **26**, 2241 (1964).
3) K. G. Varshney and S. Naheed, *J. Inorg. Nucl. Chem.*, **39**, 2075 (1977).
4) G. Alberti, U. Costantino, and M. L. Luciani Giovagnotti, *J. Chromatogr.*, **45**, 180 (1979).
5) G. H. Langer, *J. Inorg. Nucl. Chem.*, **26**, 59 (1964).
6) F. D. Snell and C. Snell, "Colorimetric Methods of Analysis," Princeton, New Jersey (1959), Vol. II.
7) F. J. Welcher, "The Analytical Uses of Ethylene Diamine Tetraacetic acid," Princeton, New Jersey (1958).
8) N. E. Topp and K. W. Pepper, *J. Chem. Soc.*, **1949**, 3299.
9) H. Hamaguchi, R. Kuroda, K. Aoki, R. Sngisita, and N. Onuma, *Talanta*, **10**, 153 (1963).
10) M. Qureshi, V. Kumar, and N. Zhra, *J. Chromatogr.*, **67**, 351 (1972).
11) M. Qureshi and V. Kumar, *J. Chem. Soc.*, **1970**, 1488.
12) H. O. Phillips and K. A. Kraus, *J. Am. Chem. Soc.*, **84**, 2267 (1962).
13) M. Qureshi and S. Ashfaq Nabi, *Talanta*, **19**, 1033 (1972).
14) I. M. Kolthoff and P. J. Elving, "Treatise on Analytical Chemistry," Interscience Publishers, New York (1961), Part II, Vol. 3, p. 61.
15) D. T. Sawyer and P. J. Paulsen, *J. Am. Chem. Soc.*, **80**, 1597 (1958).

A Comparative Study on the Synthesis and Ion-exchange Behaviour of Tin(IV) Salts of Different Heteropolyanions. Separations of Metal Ions on Tin(IV) Boratomolybdate Columns

Syed Ashfaq Nabi,* Zia Mahmood Siddiqi, and Wajahat Umar Farooqi
Department of Chemistry, Aligarh Muslim, University, Aligarh-202001, India
(Received October 9, 1981)

Various samples of tin(IV) boratomolybdate, tin(IV) boratotungstate, tin(IV) boratophosphate, tin(IV) arsenatoborate and tin(IV) boratosulfate has been synthesized by mixing aqueous solutions of appropriate reagents in different volume ratios at pH=1. One of the samples of tin(IV) boratomolybdate has been studied in greater detail for its ion-exchange capacity, thermal and chemical stability, pH-titration and chemical composition. A comparison of few properties of tin(IV) boratomolybdate has been made with other tin(IV) salts of different heteropolyanions. Distribution coefficients of 24 metal ions on tin(IV) boratomolybdate in water, nitric acid, water–dioxane, and nitric acid–dioxane systems have been determined. The effect of temperature on the sorption behaviour of metal ions has also been studied. It has been found that K_d value increases in general with the increase in temperature. The differential selectivity of metal ions on tin(IV) boratomolybdate reveals that tin(IV) boratomolybdate is a useful ion exchanger for the separation of metal ions. As a result ten important separations have been quantitatively achieved on the columns of this ion-exchange material.

The wide spread applications of synthetic inorganic ion-exchangers has now been well established.[1] Recently they have been found useful in portable renal dialysis units. Simple salts of metals as ion-exchanger have been much studied as compared to double salts. Earlier studies[2-4] show that mixed salts usually exhibit higher ion-exchange capacities and better thermal and chemical stability as compared to simple salts. A literature survey shows that a number of tin(IV) salts[5-8] have been studied as ion-exchangers. But no systematic comparison has been made on the ion exchange properties of these materials. In the present paper we therefore describe a comparative study on the synthesis and ion-exchange behaviour of a new series of tin(IV) ion-exchangers based on boron. Tin(IV) boratomolybdate have been chosen for detailed study owing to its high exchange capacity and better chemical stability.

Experimental

Reagents. Tin(IV) chloride pentahydrate (Reachim U.S.S.R.), potassium tetraborate (B. D. H.), ammonium molybdate (B. D. H.) sodium tungstate (B. D. H.); sodium arsenate (B. D. H.); sodium sulfate (E. Merck) and potassium dihydrogenphosphate (E. Merck) were used. Other chemicals were of analytical reagent grade.

Apparatus. The spectrophotometry and pH-measurements were performed using Bausch & Lomb Spectronic 20 Colorimeter, Elico LI-10 pH-meter respectively. A temperature controlled shaker "SICO" was used for shaking.

Synthesis. Samples of tin(IV) boratophosphate, tin(IV) boratosulfate, tin(IV) arsenatoborate, tin(IV) boratotungstate, tin(IV) boratomolybdate were prepared by mixing aqueous solutions of appropriate reagents under the conditions indicated in Table 1a—e. The desired pH was adjusted by adding either dilute hydrochloric acid solution or dilute sodium hydroxide solution. The precipitate so formed was allowed to settle down for 24 h washed several times with demineralized water (DMW) and filtered under suction. It was then dried at 40 °C in an oven. The dried material was then treated with DMW resulting cracking of the substance into smaller particles with slight evolution of heat. To convert the sample in hydrogen ion form, the material was kept for 48 h in 1 mol dm^{-3} nitric acid solutions. It was then washed with DMW to remove excess acid. Tin(IV) boratomolybdate sample (TBM_1) has been chosen for detailed study owing to its higher ion-exchange capacity and higher chemical stability as compared to other materials.

Ion-exchange Capacity. To determine the ion-exchange capacity of the sample, 0.5 g of the ion-exchanger material in hydrogen form was placed in column with glass wool support. The hydrogen ions were eluted with 1 mol dm^{-3} solution of different salt (Table 2). The hydrogen ions released from the exchanger were then determined by titrating the effluent with standard solution of sodium hydroxide. The ion-exchange capacities for Cu(II), Al(III), and Fe(III) were determined as follows.

10 cm^3 solution of the metal ion of known strength was passed through 1 g exchanger in hydrogen form with a flow rate of 1.2 cm^3 min^{-1}. The effluent was passed through the column several times to ensure replacement of maximum hydrogen ion of the exchanger. The column was then

Table 1a. Synthesis and properties of tin(IV) boratophosphate (TBP)

Sample No.	Conditions of synthesis					Appearance of precipitate	Appearance of beads after drying at 40 °C	IEC[a] for K^+ (mequiv./dry g)
	$SnCl_4 \cdot 5H_2O$ (mol dm^{-3})	$K_2B_4O_7$ (mol dm^{-3})	KH_2PO_4 (mol dm^{-3})	Mixing ratio (v/v/v)	pH			
TBP_1	0.05	0.05	0.05	1:2:1	0—1	White gelatinous	White opaque	0.77
TBP_2	0.05	0.05	0.05	1:1:2	0—1	White gelatinous	White opaque	1.10
TBP_3	0.05	0.05	0.05	2:1:1	0—1	White gelatinous	White opaque	0.73
TP	0.05	—	0.05	1:2	0—1	White gelatinous	White opaque	0.20

Yield order: $TP > TBP_2 > TBP_3 > TBP_1$. a) Ion exchange capacity.

Table 1b. Synthesis and properties of tin(IV) boratosulfate (TBS)

Sample No.	Conditions of synthesis					Appearance of precipitate	Appearance of beads after drying at 40 °C	IEC for K^+ (mequiv./dry g)
	$SnCl_4 \cdot 5H_2O$ (mol dm^{-3})	$K_2B_4O_7$ (mol dm^{-3})	Na_2SO_4 (mol dm^{-3})	Mixing ratio (v/v/v)	pH			
TBS_1	0.05/2	0.05	0.05	1:2:1	0—1	White gelatinous	White opaque	0.55
TBS_2	0.05/2	0.05	0.05	1:1:2	0—1	White gelatinous	White opaque	0.40
TBS_3	0.05/2	0.05	0.05	2:1:1	0—1	White gelatinous	White opaque	0.22
TBS_4	0.05	0.05	0.05	1:2:1	0—1	White gelatinous	White opaque	0.35
TS	0.05	—	0.05	1:1	0—1	White gelatinous	White opaque	0.17

Yield order: $TBS_3 > TBS_1 > TBS_2 > TBS_4 > TS$.

Table 1c. Synthesis and properties of tin(IV) arsenatoborate (ABA)

Sample No.	Conditions of synthesis					Appearance of precipitate	Appearance of beads after drying at 40 °C	IEC for K^+ (mequiv./dry g)
	$SnCl_4 \cdot 5H_2O$ (mol dm^{-3})	$K_2B_4O_7$ (mol dm^{-3})	Na_2AsO_4 (mol dm^{-3})	Mixing ratio (v/v/v)	pH			
TBA_1	0.05	0.05	0.05	1:2:1	0—1	White gelatinous	White opaque	0.96
TBA_2	0.05	0.05	0.05	1:1:2	0—1	White gelatinous	White opaque	0.96
TBA_3	0.05	0.05	0.05	2:1:1	0—1	White gelatinous	White opaque	0.73
TA	0.05	—	0.05	1:1	0—1	White gelatinous	White opaque	0.99

Yield order: $TBA_3 > TBA_2 > TBA_1 > TA$.

Table 1d. Synthesis and properties of tin(IV) boratotungstate (TBT)

Sample No.	Conditions of synthesis					Appearance of precipitate	Appearance of beads after drying at 40 °C	IEC for K^+ (mequiv./dry g)
	$SnCl_4 \cdot 5H_2O$ (mol dm^{-3})	$K_2B_4O_7$ (mol dm^{-3})	Na_2WO_4 (mol dm^{-3})	Mixing ratio (v/v/v)	pH			
TBT_1	0.05	0.05	0.05	1:2:1	0—1	White gelatinous	Dirty white shiny	1.1
TBT_2	0.05	0.05	0.05	1:1:2	0—1	White gelatinous	Yellowish green	1.3
TBT_3	0.05	0.05	0.05	2:1:1	0—1	White gelatinous	White shiny	0.88
TT	0.05	—	0.05	1:2	0—1	White gelatinous	Yellowish green	1.15

Yield order: $TBT_3 > TBT_1 > TT > TBT_2$.

Table 1e. Synthesis and properties of tin(IV) boratomolybdate (TBM)

Sample No.	Conditions of synthesis					Appearance of precipitate	Appearance of beads after drying at 40 °C	IEC for K^+ (mequiv./dry g)
	$SnCl_4 \cdot 5H_2O$ (mol dm^{-3})	$K_2B_4O_7$ (mol dm^{-3})	$(NH_4)_6Mo_7O_{24}$ (mol dm^{-3})	Mixing ratio (v/v/v)	pH			
TBM_1	0.05	0.05	0.05	1:2:1	0—1	Gelatinous yellowish	Yellowish shiny	1.12
TBM_2	0.05	0.05	0.05	1:1:2	0—1	White granular	White fine powder dispersed when immersed in water	—
TBM_3	0.05	0.05	0.05	2:1:1	0—1	Gelatinous yellowish	Yellowish shiny	0.88
TM_1	0.05	—	0.05	1:2	0—1	White granular	White fine powder dispersed when immersed in water	—
TM_2	0.05	—	0.05	1:1	0—1	Gelatinous yellowish	Yellowish	0.68
TB	0.05	0.05	—	1:2	0—1	White gelatinous	White opaque	0.11

Yield order: $TBM_1 = TBM_3 > TM_2 > TB$.

washed with water till the effluent free from metal ions. The whole effluent is titrated with standard EDTA solution. The amount of metal ions adsorbed by the exchanger was calculated. The ion-exchange capacity for different metal ions is reported in Table 2.

Thermal Treatment. To examine the effect of drying temperature on the ion-exchange capacity the materials were heated at different temperatures in Muffle Furnace for 1 h. The ion-exchange capacity for potassium ion at different drying temperatures is given in Table 3.

pH-titration. pH-titrations for sample TBM_1 was performed by the earlier method[9] using sodium chloride–sodium hydroxide system. The pH titration curve is shown in Fig. 1.

Chemical Stability. A 0.5 g of the exchanger material (sample TBM_1) was equilibrated with 50 cm^3 of the solution of analytical interest at room temperature (25±2 °C) and kept for 24 h with occasional shaking. Tin and molybdenum released in the solution were determined spectrophotometrically using hematoxylin[10] and thiocyanate[11] as colouring reagents respectively. The amount of boron released in the solvent was determined titrimetrically[12] using sodium hydroxide as titrant. The results are summarized in Table 4.

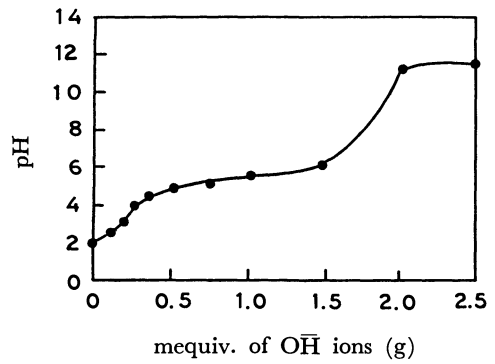

Fig. 1. pH titration curve of tin(IV) boratomolybdate.

Chemical Composition. For the determination of chemical composition of sample TBM_1, 0.2 g of exchanger was dissolved in hot concentrated hydrochloric acid. Then the solution was diluted to 100 cm^3 with water. Tin and molybdenum were determined spectrophotometrically[10,11] while boron is determined titrimetrically.[12] The mole ratio of Sn, B, and Mo is found to 1:1:1.

Distribution Coefficient. The distribution coefficient (K_d) for 24 metal ions in different solution system were determined. 0.5 g of exchanger in hydrogen form (150—200 mesh size) was treated with 50 cm^3 of cation solution in 250 cm^3 Erlenmeyer flask. The mixture was then shaken for 6 h at 25±2 °C in a shaker incubator. The ionic strengths of various metal ion solutions lies between 0.0006 to 0.0057. The amount of cation left in the solution was then determined by titrating against the standard solution of EDTA. The K_d values were calculated according to the formula,

$$K_d = \frac{I-F}{F \times W} \times 50,$$

where F is the volume of EDTA consumed by the solution after equilibrium, I is the volume of EDTA consumed by the original solution (*i.e.* before equilibrium) and W is the weight of ion exchanger in g.

The results of K_d values are summarized in Table 5. The adsorption of metal ions was also studied at different temperatures. The effect of temperature on K_d (values) are described in Table 6 and in Fig. 2.

Quantitative Separations. For separation purpose the column was prepared using 2.0 g of exchanger (150—200

Table 2. Ion exchange capacity (mequiv./dry g) of different tin(IV) based ion exchangers for various cations

Sample No.	Cations	Salt used	pH	Hydrated radii[17] Å	TBP_2	TBS_4	TBT_2	TBM_1
1	Li^+	LiCl	6.8	10.0	0.26	0.18	0.37	0.84
2	Na^+	$NaNO_3$	6.8	7.9	0.42	0.33	0.62	0.90
3	K^+	KCl	6.8	5.3	1.10	0.35	1.30	1.12
4	Mg^{2+}	$Mg(NO_3)_2$	6.2	10.8	0.41	0.42	0.40	0.52
5	Ca^{2+}	$Ca(NO_3)_2$	6.2	9.6	0.54	0.40	0.44	0.77
6	Sr^{2+}	$Sr(NO_3)_2$	6.2	9.6	0.34	0.36	0.21	0.46
7	Ba^{2+}	$Ba(NO_3)_2$	6.2	8.8	0.48	0.35	0.41	0.68
8	Cu^{2+}	$Cu(NO_3)_2$	—	—	0.40	0.91	0.28	0.79
9	Al^{3+}	$Al(NO_3)_3$	—	—	0.23	0.24	0.23	0.29
10	Fe^{3+}	$FeCl_3$	—	—	0.68	0.72	0.68	0.71

Table 3. Effect of drying temperature on the ion exchange capacity (mequiv./dry g for K^+) for tin(IV) based ion exchangers

Sample No.	Temp/°C	TBP_2	TBS_4	TBT_2	TBM_1
1	40	1.10 (white)	0.35 (white)	1.30 (light yellow)	1.12 (yellow)
2	100	0.50 (white)	0.33 (white)	1.20 (light yellow)	0.33 (yellow)
3	200	0.46 (white)	0.32 (white)	0.19 (brown)	0.22 (greenish yellow)
4	300	0.41 (light yellow)	0.31 (white)	0.18 (brownish black)	0.17 (greenish)
5	400	0.36 (light yellow)	0.28 (yellowish)	0.17 (brownish black)	0.13 (grey)
6	500	0.29 (yellowish)	0.22 (yellowish green)	0.14 (brownish black)	0.08 (dark grey)
7	600	0.23 (yellow)	0.14 (light green)	0.13 (brownish black)	0.04 (dark grey)
8	800	0.21 (grey)	0.08 (green)	0.09 (brownish black)	0.00 (greyish white)

TABLE 4. CHEMICAL STABILITY OF SAMPLE TBM_1

Sample No.	Solvents	Tin(IV) released (mg/50 cm^3)	Mo released (mg/50 cm^3)	B released (mg/50 cm^2)
1	Water	0.40	0.18	0.22
2	0.1 mol dm^{-3} HNO_3	0.55	—	0.54
3	0.5 mol dm^{-3} HNO_3	0.60	0.60	0.74
4	1 mol dm^{-3} HNO_3	0.70	0.75	0.83
5	0.1 mol dm^{-3} HCl	0.55	—	0.44
6	0.5 mol dm^{-3} HCl	1.45	0.38	0.69
7	1 mol dm^{-3} HCl	1.55	0.63	0.93
8	0.1 mol dm^{-3} $HClO_4$	0.55	—	0.43
9	0.5 mol dm^{-3} $HClO_4$	1.05	0.38	0.65
10	1 mol dm^{-3} $HClO_4$	1.20	0.91	0.91
11	0.1 mol dm^{-3} H_2SO_4	0.80	—	0.67
12	0.5 mol dm^{-3} H_2SO_4	1.45	0.35	0.79
13	1 mol dm^{-3} H_2SO_4	1.70	0.61	1.35
14	0.05 mol dm^{-3} NaOH	3.15	0.75	1.52
15	0.1 mol dm^{-3} NaOH		Completely dissolved	
16	0.05 mol dm^{-3} KOH	2.20	0.64	1.21
17	0.1 mol dm^{-3} KOH		Completely dissolved	
18	0.05 mol dm^{-3} LiOH	1.55	0.60	0.78
19	0.1 mol dm^{-3} LiOH		Completely dissolved	
20	1 mol dm^{-3} KCl	0.0	0.0	0.0
21	1 mol dm^{-3} $NaNO_3$	0.40	0.18	0.42

TABLE 5. DISTRIBUTION COEFFICIENTS (ml/g) OF METAL IONS ON TIN(IV) BORATOMOLYBDATE (SAMPLE TBM_1) AT 25±2 °C

Sample No.	Metal ion	Water	0.01 mol dm^{-3} HNO_3	Dioxane: Water (1:4)	Dioxane: Water (4:1)	Dioxane: 0.01 mol dm^{-3} HNO_3 (1:1)
1	Ni^{2+}	309±5	70±5	800±20	71±5	100±5
2	Fe^{3+}	47±7	29±5	62±5	36±5	24±5
3	Cu^{2+}	497±12	10±2	856±30	335±5	49±5
4	Mn^{2+}	300±5	71±5	380±5	160±5	100±5
5	Co^{2+}	167±5	60±5	182±6	101±5	60±5
6	Vo^{2+}	461±10	79±5	490±5	1375±40	353±5
7	Hg^{2+}	11400±12	70±5	5650±50	383±5	1433±35
8	Zn^{2+}	257±5	55±5	89±5	99±5	62±5
9	Pb^{2+}	24900±240	245±5	733±20	257±5	2400±44
10	Cd^{2+}	28900±300	152±5	318±8	32±5	59±5
11	Ca^{2+}	860±20	153±5	380±5	380±5	4700±136
12	Mg^{2+}	184±5	26±5	145±5	78±5	29±5
13	Ba^{2+}	500±20	58±5	1400±50	650±8	25±5
14	Ce^{4+}	200±5	140±5	100±5	200±5	20±5
15	Al^{3+}	300±5	188±5	136±5	1200±40	136±5
16	Zr^{4+}	1600±25	1550±20	1600±50	410±5	1175±30
17	Th^{4+}	2500±32	165±5	1225±42	1225±45	440±5
18	Sr^{2+}	174±5	33±5	209±5	152±5	32±5
19	Ho^{3+}	265±5	90±5	133±5	71±5	105±5
20	Dy^{3+}	135±5	132±5	115±5	67±5	104±5
21	Nd^{3+}	583±12	162±5	229±8	67±5	104±5
22	Sm^{3+}	560±11	450±10	132±5	210±5	209±5
23	Pr^{3+}	580±15	390±8	156±5	97±5	412±5
24	La^{3+}	695±14	420±10	306±20	76±5	97±5

Table 6. Distribution coefficients (ml/g) of metal ions on tin(IV) boratomolybdate (TBM_1) in 0.005 mol dm^{-3} HNO_3 at different temperatures

Sample No.	Metal ions	22±1 °C	50±1 °C	75±1 °C
1	Ni^{3+}	57±5	157±5	463±12
2	Fe^{3+}	33±5	62±5	100±5
3	Cu^{2+}	49±5	1812±50	9460±180
4	Mn^{2+}	107±5	700±10	2900±84
5	Co^{2+}	125±5	1988±52	10340±156
6	Vo^{+2}	60±5	136±5	136±5
7	Hg^{2+}	10±2	17±5	54±5
8	Zn^{2+}	112±5	507±5	2328±45
9	Pb^{2+}	1900±50	24900±170	49900±200
10	Cd^{2+}	181±5	1080±36	3943±60
11	Ca^{2+}	109±5	1100±22	3100±50
12	Mg^{2+}	75±5	657±10	3686±84
13	Ba^{2+}	300±5	650±12	3650±80
14	Ce^{4+}	150±5	320±6	443±10
15	Al^{3+}	30±5	73±5	420±5
16	Zr^{4+}	53±5	628±5	750±5
17	Th^{4+}	152±5	382±5	430±5
18	Sr^{2+}	109±5	860±20	3100±80
19	Ho^{3+}	80±5	5020±145	25500±163
20	Dy^{3+}	117±5	6420±120	32500±145
21	Nd^{3+}	328±5	8460±60	42200±210
22	La^{3+}	527±5	13700±150	68900±320
23	Sm^{3+}	225±5	12900±135	64900±316
24	Pr^{3+}	553±5	5020±120	25500±225

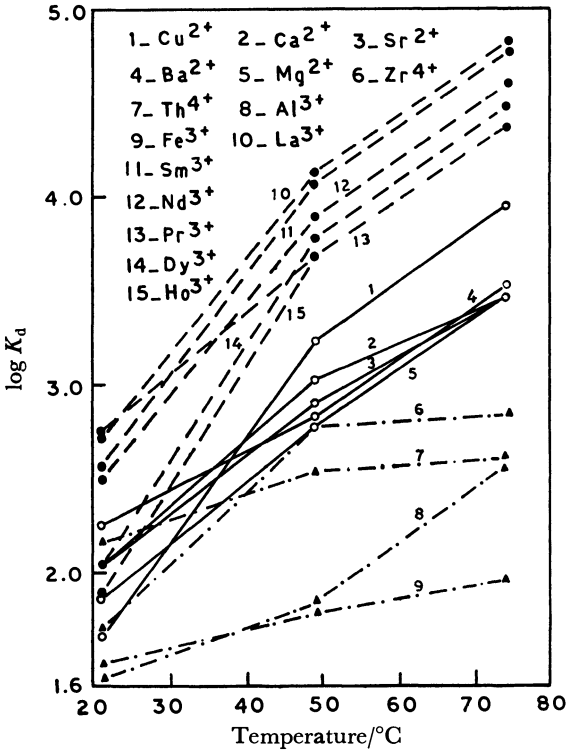

Fig. 2. Plot log K_d *vs.* temperature.

mesh size) in hydrogen form in a glass tube of internal diameter 0.6 cm in each case. A mixture of metal ion solution was applied on the column. The solution was allowed to flowdown very slowly through the column as a result metal ions are adsorbed at the top of exchanger bed forming initial zone. The column was washed with water. The metal ions were then eluted by appropriate eluting reagent. The flow rate of effluent was maintained 1.4 cm^3 min^{-1} throughout the elution process. The effluent was collected in 10 cm^3 fractions and titrated with 0.002 mol dm^{-3} EDTA solution. Ten important separations of metal ions have been quantitatively achieved. The elution curves for each set of separation are shown in Figs. 3(a)—(c).

Results and Discussion

Tables 1a to 1e describe the preprations of samples of tin(IV) salts of different heteropolyanions under identical conditions. Ion exchange capacity of each samples has been compared with single salts prepared under the same conditions. It has been observed that capacity of double salts is higher than the single salts with the exception of tin(IV) boratophosphate and tin(IV) arsenatoborate. An interesting feature is emerged when tin(IV) boratosulfate is compared with tin(IV) sulfate, the latter has a negligible ion-exchange capacity (0.17 mequiv./dry g). Moreover the capacity is significantly increased for sample TBS_1 (0.55 mequiv./dry g). It is important to note that mixing volume ratio of different components affect the ion-exchange capacity of the final product. Also in the case of tin(IV) boratomolybdate the exchange capacity becomes almost two times as high as the exchange capacity of single salts namely tin(IV) molybdate and tin(IV) borate prepared under the same conditions. The order of ion-exchange capacity (for K^+ ions) for tin(IV) salts of different heteropolyanions is as follows:

> Tin(IV) boratotungstate (TBT_2)>Tin(IV) boratomolybdate (TBM_1)>Tin(IV) boratophosphate(TBP_2) >Tin(IV) arsenatoborate (TBA_1, TBA_2)> Tin(IV) boratosulfate (TBS_1).

Results of Table 4 show that tin(IV) boratomolybdate is quite stable in water, hydrochloric acid, perchloric acid, nitric acid, sulfuric acid, and in common salts of moderate concentrations. This material appreciably dissolves in 0.01 mol dm^{-3} solutions of LiOH, NaOH, and KOH on prolonged shaking. The material is apparently stable in various common organic solvents like acetone, dioxane, ethanol, acetaldehyde, formic acid, acetic acid, tartaric acid, and citric acid. Tin(IV) boratomolybdate is relatively more chemically stable than tin(IV) molybdate prepared earlier.[13,14]

Results of Table 2 show that the exchange capacity of all the compounds increases with the decrease in hydrated radii. The ion exchange capacity followed the order $K^+>Na^+>Li^+$ for alkali metals. However, for alkaline earths the exchange capacity remains almost the same as hydrated radii do not vary appreciably.

It is apparent from Table 3 that tin(IV) boratophosphate, tin(IV) boratosulfate, tin(IV) boratomolybdate, and tin(IV) boratotungstate loose ion exchange capacity as the drying temperature of the material is subsequently increased. The thermal stability of these materials can be represented in the order TBS_4>

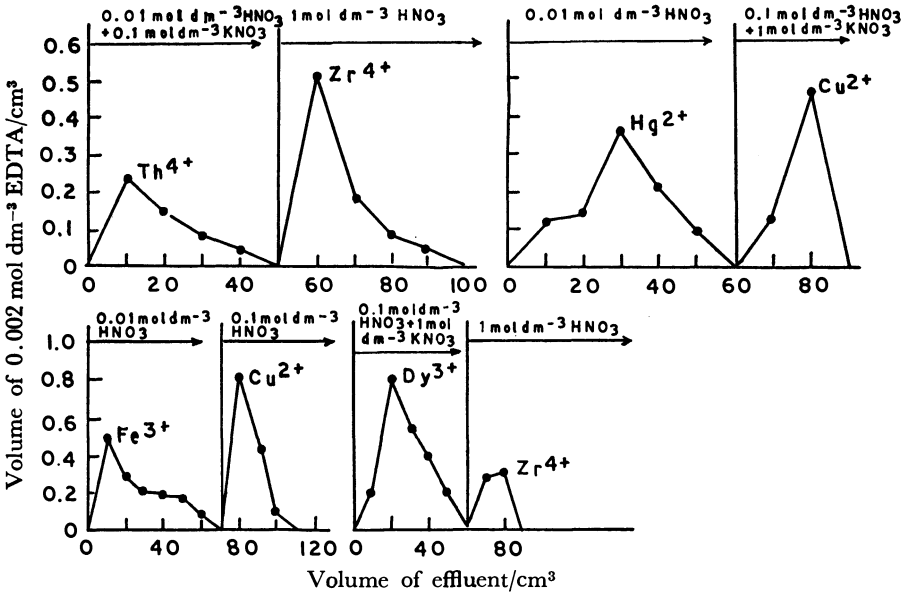

Fig. 3(a). Separation of Th^{4+}-Zr^{4+}, Hg^{2+}-Cu^{2+}, Fe^{3+}-Cu^{2+}, and Dy^{3+}-Zr^{4+}.

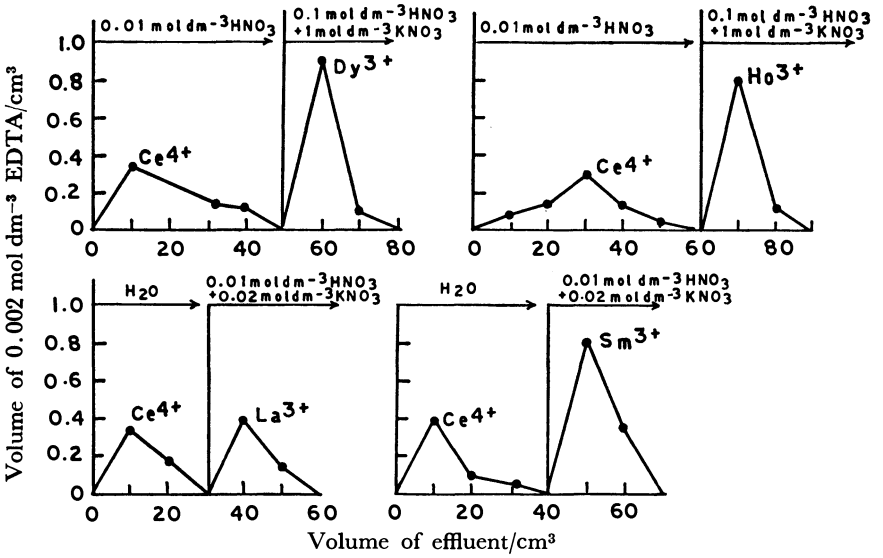

Fig. 3(b). Separation of Ce^{4+}-Dy^{3+}, Ce^{4+}-Ho^{3+}, Ce^{4+}-La^{3+}, and Ce^{4+}-Sm^{3+}.

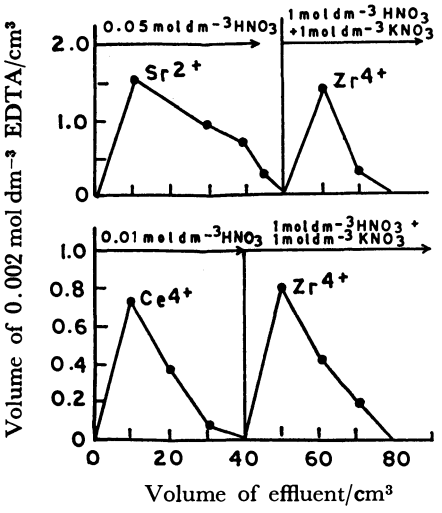

Fig. 3(c). Separation of Sr^{2+}-Zr^{4+} and Ce^{4+}-Zr^{4+}.

$TBP_2 > TBM_1 > TBT_2$. It is observed however, in the case of tin(IV) boratosulfate, the increasing temperature does not affect the capacity significantly. Tin(IV) boratotungstate and tin(IV)boratomolybdate lost their exchange capacity more than 70% when their drying temperature increased to 100 °C. The capacity falls to a negligible value when the drying temperature is raised upto 500 °C (0.08 mequiv./dry g for tin(IV) boratomolybdate and 0.14 mequiv./dry g for tin(IV) boratotungstate). This may be due to conversion of material into their oxides as is also indicated by their colors at these temperatures. Tin(IV) boratotungstate is more thermally stable than tin(IV) tungstate[15] and also tin(IV) boratomolybdate is more stable than tin(IV) molybdate.[13] Tin(IV) boratosulfate and tin(IV) boratophosphate retain their exchange capacity to a greater extent. The capacity of boratosulfate remains almost the same up to 300 °C. Tin(IV) boratophosphate and tin(IV) boratosul-

fate can be conveniently used as ion exchangers even when the drying temperature is raised up to 500 °C. However, when these materials (dried at 40 °C) are heated at 95±5 °C in the presence of water no loss in ion-exchange capacity is observed in all the cases.

pH titration curve (Fig. 1) for NaCl–NaOH system indicates two breaks in the curve showing thereby that tin(IV) boratomolybdate behaves as a bifunctional weak cation exchanger.

It is clear from Table 5 that values of distribution coefficients vary with the composition and nature of solvent system. The K_d values of metal ions are decreasing in general with the increase in dioxane content of the medium. The increased amount of dioxane in dioxane–water system decreases the dielectric constant and thus decreases the K_d value. This is probably due to the fact that the ions of an electrolyte are more ionized in a solvent of relatively high dielectric constant. However, a definite conclusion can only be drawn in the presence of other experimental data. An increase in the K_d value for most metal ions are also observed as one goes from pure dilute acid (0.01 mol dm^{-3}) to a mixture of dioxane+0.01 mol dm^{-3} HNO_3 in 1:1 volume ratio and the increase in the pH of the solvent causes higher adsorption of metal ions as expected.

A study of the adsorption of metal ions on tin(IV) boratomolybdate at different temperatures reveals that extent of adsorption increases with the increase in temperature (Table 6). Thus K_d values are found to be highest in 75±1 °C. From Fig. 2 it can be concluded that the K_d value for quadrivalent and rare earth metal ions increases sharply below 50 °C and then slowly after this temperature.

The sequence of K_d values of some important metal ions in different solvent systems and at different temperatures on tin(IV) boratomolybdate can be shown as follows:

Water	$Th^{4+}>Zr^{4+}>La^{3+}>Nd^{3+}>Pr^{3+}>Sm^{3+}>Ho^{3+}>Ce^{4+}>Dy^{3+}$
0.01 mol dm^{-3} HNO_3	$Zr^{4+}>Sm^{3+}>La^{3+}>Pr^{3+}>Th^{4+}>Nd^{3+}>Ce^{4+}>Dy^{3+}>Ho^{3+}$
Dioxane:Water (1:4)	$Zr^{4+}>Th^{4+}>La^{3+}>Nd^{3+}>Pr^{3+}>Ho^{3+}>Sm^{3+}>Dy^{3+}>Ce^{4+}$
Dioxane:Water (4:1)	$Th^{4+}>Zr^{4+}>Sm^{3+}>Ce^{4+}>Pr^{3+}>Nd^{3+}>La^{3+}>Ho^{3+}>Dy^{3+}$
Dioxane:0.01 mol dm^{-3} HNO_3 (1:1)	$Zr^{4+}>Th^{4+}>Pr^{3+}>Sm^{3+}>Nd^{3+}>Ho^{3+}>Dy^{3+}>La^{3+}>Ce^{4+}$
0.005 mol dm^{-3} HNO_3 (22±1 °C)	$Pr^{3+}>La^{3+}>Nd^{3+}>Sm^{3+}>Th^{4+}>Ce^{4+}>Dy^{3+}>Ho^{3+}>Zr^{4+}$
0.005 mol dm^{-3} HNO_3 (50±1 °C)	$La^{3+}>Sm^{3+}>Nd^{3+}>Dy^{3+}>Ho^{3+}=Pr^{3+}>Zr^{4+}>Th^{4+}>Ce^{4+}$
0.005 mol dm^{-3} HNO_3 (75±1 °C)	$La^{3+}>Sm^{3+}>Nd^{3+}>Dy^{3+}>Ho^{3+}=Pr^{3+}>Zr^{4+}>Ce^{4+}>Th^{4+}$

The sorption studies on tin(IV) boratomolybdate for different metal ions reveal many important separations. As a result ten binary separations of analytical and industrial importance have been achieved successfully on small columns of tin(IV) boratomolybdate (Figs. 3(a)—3(c)). Separation of iron from copper may be utilized in the removal of iron impurities from chalcopyrite ($CuFeS_2$) and Bornite (Cu_5FeS_4) ores.

In the determination of thorium as oxalate good separation from zirconium can not be achieved because of the possible hydration of zirconium.[16] Zirconium also seriously interferes probably in all the spectrophotometric determination of thorium by various coloring reagents such as thoron, dinitrosochromotropic acid, quercetin, SPADN, and Di SNADNS.[16] Therefore columns of tin(IV) boratomolybdate can be conveniently used for separating zirconium impurities prior to the determination of thorium. Tin(IV) boratomolybdate can also be utilized for the recovery of zirconium free thorium from thorianite.

The authors are thankful to Prof. W. Rahman, Head, Department of Chemistry for providing research facilities. C. S. I. R., New Delhi is also acknowledged for financial assistance to one of us (ZMS).

References

1) A. Clearfield, G. H. Nancollas, and R. H. Blessing, "Ion Exchange and Solvent Extraction," ed by J. A. Marinsky and Y. Marcus, Marcel Dekker, New York (1973), Vol. 5, p. 2.
2) V. Pekarek and V. Vesely, *Talanta*, **19**, 1245 (1972).
3) H. F. Walton, *Anal. Chem.*, **42**, 86R (1970).
4) C. B. Amphlett, "Inorganic Ion Exchangers," Elsevier, Amsterdam, (1964).
5) M. Qureshi, R. Kumar, V. Sharma, and T. Khan, *J. Chromotogr.*, **118**, 175, (1976).
6) M. Qureshi, R. Kumar, and R. C. Kaushik, *Sep. Sci. Technol.*, **13**, 185 (1978).
7) M. Qureshi and R. C. Kaushik, *Anal. Chem.*, **49**, 165 (1977).
8) K. G. Varshney and A. A. Khan, *J. Inorg. Nucl. Chem.*, **41**, 241, (1979).
9) N. F. Topp and K. W. Pepper, *J. Chem. Soc.*, **1949**, 3299.
10) F. D. Snell and C. T. Snell, "Colorimetric Methods of Analysis," Princeton, New Jersey (1959), Vol. IIA, p. 135.
11) Ref. 10, pp. 370.
12) N. H. Furman, "Standard Methods of Chemical Analysis," 6th ed, Van Nostrand, Princeton (1963), Vol. I, p. 215.
13) M. Qureshi and J. P. Rawat, *J. Inorg. Nucl. Chem.*, **30**, 305 (1968).
14) M. Qureshi, K. Husain, and J. P. Gupta, *J. Chem. Soc., A*, **1971**, 29.
15) M. Qureshi and K. G. Varshney, *J. Chem. Soc., A*, **30**, 3081 (1968).
16) I. M. Kolthoff, Philip J. Elving, and Ernest B. Sandell, "Treatise on Analytical Chemistry," Interscience Publisher, New York and London (1961), Part II, Vol. 5, pp. 159—189.
17) Wiklander, *Annals Roy. Agr. Coll. Sweden*, **14**, 1—171 (1946).

 © 1982 The Chemical Society of Japan Bull. Chem. Soc. Jpn., 55, 2649—2652 (1982)

A Convenient Synthesis of Linear 2-Methylpyranochromones

Vinod Kumar AHLUWALIA,* Anjula JAIN, and Ranjna GUPTA
Department of Chemistry, University of Delhi, Delhi-110007, India
(Received November 5, 1981)

A convenient synthesis of linear 2-methylpyranochromones, *viz.*, spatheliachromen(5-hydroxy-2,2,8-trimethyl-2*H*,6*H*-benzo[1,2-*b*:5,4-*b'*]dipyran-6-one), *O*-methylspatheliachromen (5-methoxy-2,2,8-trimethyl-2*H*,6*H*-benzo[1,2-*b*:5,4-*b'*]dipyran-6-one) (**8**) and *O*-methylallopteroxylin (5-methoxy-2,8,8-trimethyl-4*H*,8*H*-benzo[1,2-*b*:3,4-*b'*]dipyran-4-one) is described by blocking the eighth position of the corresponding 7-propargyl ether derivative 7-(1,1-dimethyl-2-propynyloxy)-8-iodo-5-methoxy-2-methyl-4*H*-1-benzopyran-4-one with iodine followed by thermal cyclization. The linear pyranochromones 2,2,8-trimethyl-2*H*,6*H*-benzo[1,2-*b*:5,4-*b'*]dipyran-6-one and **8** are also synthesized starting with the easily available appropriate 3,4-dihydro-2,2-dimethyl-2*H*-1-benzopyran-7-ols following the steps of Claisen condensation with ethyl acetate, cyclization with ethanolic sulfuric acid followed by dehydrogenation with NBS.

The occurrence[1] of 2-methyl linear pyranochromones, *viz.*, spatheliachromen prompted us to devise a convenient method for their synthesis. A few syntheses of these chromones are known[2,3] but these involve a number of steps and the overall yield is poor.

Attempts have now been made for the synthesis of linear pyranochromones by using our earlier finding[4] that if position-8 of a coumarin ring is blocked by an iodo group, the cyclization of the corresponding 7-propargyl ethers of 2*H*-1-benzopyran-2-ones (coumarins) on heating with *N,N*-dimethylaniline gives rise to linear pyranocoumarins, cyclization taking place at position 6 with simultaneous removal of iodine. As a test case 7-hydroxy-2-methyl-4*H*-1-benzopyran-4-one[5] (**1**) was used. Its iodination with iodine and periodic acid gave 7-hydroxy-8-iodo-2-methyl-4*H*-1-benzopyran-4-one[6] (**2**), which on propargylation with 3-chloro-3-methyl-1-butyne gave 7-(1,1-dimethyl-2-propynyloxy)-8-iodo-2-methyl-4*H*-1-benzopyran-4-one (**3**). Compound **3** on heating with *N,N*-dimethylaniline gave a mixture of two products which were separated by preparative TLC. The lower band on elution gave the linear product *i.e.* 2,2,8-trimethyl-2*H*,6*H*-benzo[1,2-*b*:5,4-*b'*]dipyran-6-one (**4**). Its structure was assigned on the basis of ^{1}H NMR spectral data which showed besides other signals, two singlets at δ 6.65 and 7.65 for the two para aromatic protons. The upper band on elution gave the angular pyranochromone, *viz.*, 2,8,8-trimethyl-4*H*,8*H*-benzo[1,2-*b*:3,4-*b'*]dipyran-4-one (**5**). Its structure was assigned on the basis of its ^{1}H NMR spectral data which showed two doublets at δ 6.89 and 8.00 (J=10 Hz each) for two ortho-coupled aromatic protons. It was also found to be identical (mp, mixed mp, superimposed IR) with an authentic sample[1] prepared by cyclization of 7-(1,1-dimethyl-2-propynyloxy)-2-methyl-4*H*-1-benzopyran-4-one (**6**).

Using the above method, spatheliachromen (**7**) and *O*-methylspatheliachromen (**8**) have now been synthesized starting from 7-(1,1-dimethyl-2-propynyloxy)-8-iodo-5-methoxy-2-methyl-4*H*-1-benzopyran-4-one (**9**), which was prepared as follows: 2-Hydroxy-4-benzyloxy-6-methoxyacetophenone[7] on Claisen condensation with ethyl acetate in the presence of pulverized sodium followed by the cyclodehydration with concd sulfuric acid in ethanol gave 7-benzyloxy-5-methoxy-2-methyl-4*H*-1-benzopyran-4-one (**10**). Its catalytic debenzylation afforded 7-hydroxy-5-methoxy-2-methyl-4*H*-1-benzopyran-4-one (**11**). Iodination of **11** with iodine and periodic acid gave 7-hydroxy-8-iodo-5-methoxy-2-methyl-4*H*-1-benzopyran-4-one (**12**), which on propargylation afforded **9**. Its thermal cyclization by heating with *N,N*-dimethylaniline gave a product which showed the absence of iodine indicating that iodine was knocked out in the above reaction. It was found to be a mixture of three products. The slowest moving band on elution gave a product which gave a green iron(III) chloride reaction indicating that the 5-hydroxyl was free. It gave positive Gibbs' test, indicating that the para position to the hydroxyl group was free. On the basis of this, it was assigned the linear chromone structure, *viz.*, 5-hydroxy-2,2,8-trimethyl-2*H*,6*H*-benzo[1,2-*b*:5,4-*b'*]dipyran-6-one (**7**). It was identical in mp and ^{1}H NMR spectral data with spatheliachromen isolated from *Spathelia sorbifolia*.[1] The middle band on elution gave a product, which was identical with the product obtained by the methylation of **7**. On the basis of this, it was assigned the structure *O*-methylspatheliachromen (**8**). The upper band on elution gave a product which gave a negative iron(III) chloride reaction and Gibbs' test. On the basis of this it was assigned the angular chromone structure, *viz.*, 5-methoxy-2,8,8-trimethyl-4*H*,8*H*-benzo-[1,2-*b*:3,4-*b'*]dipyran-4-one (**13**). It was found to be identical with *O*-methylallopteroxylin isolated from *Ptaeroxylon obliquum*.[8]

In another convenient approach 6-acetyl-3,4-dihydro-2,2-dimethyl-2*H*-1-benzopyran-7-ol (**17**) (obtained[9] in one step by the reaction of isoprene with 2,4-dihydroxyacetophenone) on Claisen condensation with ethyl acetate in the presence of pulverized sodium gave 6-acetoacetyl-3,4-dihydro-2,2-dimethyl-2*H*-1-benzopyran-7-ol (**18**). Its cyclization with ethanolic sulfuric acid afforded 2,2,8-trimethyl-3,4-dihydro-2*H*,6*H*-benzo-[1,2-*b*:5,4-*b'*]dipyran-6-one (**19**). Dehydrogenation of **19** with NBS gave the required linear pyranochromone **4**, identical in all respects with the product obtained above.

Similarly 6-acetyl-3,4-dihydro-5-methoxy-2,2-dimethyl-2*H*-1-benzopyran-7-ol (**20**) (obtained[9] by the reaction of 2,4-dihydroxy-6-methoxyacetophenone with isoprene) on Claisen condensation with ethyl acetate in the presence of pulverized sodium gave 6-acetoacetyl-3,4-dihydro-5-methoxy-2,2-dimethyl-2*H*-1-benzopyran-7-ol (**21**). Its cyclization with ethanolic sul-

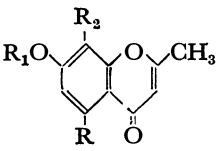

	R	R_1	R_2
1	H	H	H
2	H	H	I
3	H		I
6	H		H
9	$-OCH_3$		I
10	$-OCH_3$	$-CH_2C_6H_5$	H
11	$-OCH_3$	H	H
12	$-OCH_3$	H	I
15	H	$-CH_2C_6H_5$	H

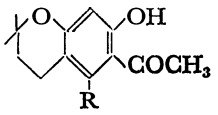

17 R=H
20 R=OCH_3

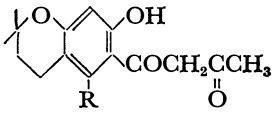

18 R=H
21 R=OCH_3

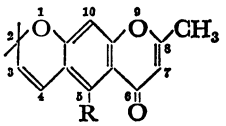

4 R=H
7 R=OH
8 R=OCH_3

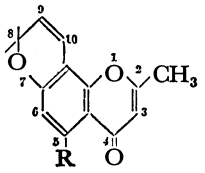

5 R=H
13 R=OCH_3

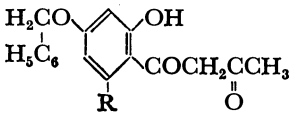

14 R=H
16 R=OCH_3

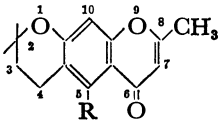

19 R=H
22 R=OCH_3

furic acid gave 2,2,8-trimethyl-3,4-dihydro-5-methoxy-2*H*,6*H*-benzo[1,2-*b*:5,4-*b*']dipyran-6-one (**22**). Dehydrogenation of **22** with NBS gave the required linear pyranochromone **8**, identical with the sample obtained above.

Discussion

A synthesis of linear pyranochromones lacking an oxygen function at 5-position has not previously been available. Blocking the more reactive 8-position by iodine represents the potential route for achieving the same. In the preparation of linear pyranochromones the thermal cyclization of **3** and **9** gives a mixture of the linear and the angular pyranochromones. It shows that the reaction is nonregiospecific, as compared to the thermal cyclization in coumarins[4] which is regiospecific. A possible explanation for the nonregiospecificity in the case of chromones is due to more fixation of double bonds as compared to that of coumarins. It is believed that in this case, the loss of iodine and its cyclization are competing reactions. All attempts to make the above cyclization regiospecific, using a variety of conditions, are unsuccessful.

The alternate route employed for the synthesis of linear pyranochromones involving the use of the corresponding 3,4-dihydro-2*H*,6*H*-benzo[1,2-*b*:5,4-*b*']-dipyran-6-ones (**17** and **20**) is more convenient.

Experimental

Melting points are uncorrected. The NMR spectra were recorded on Perkin Elmer R-32 instrument with TMS as an internal standard.

*2,2,8-Trimethyl-2*H,*6*H-*benzo*[*1,2*-b:*5,4*-b']*dipyran-6-one* (**4**) *1-(4-Benzyloxy-2-hydroxyphenyl)-1,3-butanedione* (**14**): A solution of 4-benzyloxy-2-hydroxyacetophenone[8] (1 g, 4.1 mmol) in dry ethyl acetate (5 ml) was added to pulverized sodium (0.5 g), the mixture being shaken and cooled. After the initial vigorous reaction had subsided, the reaction mixture was heated in a boiling water bath for 3 h. The mixture was cooled, diluted with water and extracted with ether to remove excess of ethyl acetate. The clear alkaline solution was acidified in cold with dilute acetic acid when yellow solid separated. It crystallized from benzene–petroleum ether as shining needles of **14** (0.6 g, 1.75 mmol) (46%) mp 120—121 °C. Found: C, 71.8; H, 5.7%. Calcd for $C_{17}H_{16}O_4$: C, 71.9; H, 5.6%. ^{1}H NMR($CDCl_3$) δ=2.12 (s, CH_3 of enol); 2.30(s, CH_3 of keto); 4.02(s, $-\underset{\underset{O}{\|}}{C}-\underline{CH_2}-\underset{\underset{O}{\|}}{C}-$ of keto) 5.10(s, 2H, $-O\underline{CH_2}C_6H_5$); 6.08(s, $-CH=\underset{\underset{OH}{|}}{C}-$ of enol); 6.55(m, 2H, H3 and H5); 7.45(s, 5H, $-OCH_2C_6\underline{H_5}$); 7.60 (d, J=10 Hz, 1H, H6); 12.50(s, 1H, –OH exchangeable with D_2O). The integration of the spectrum showed that the ratio of keto-enol forms is 1:2.

*7-Benzyloxy-2-methyl-4*H-*1-benzopyran-4-one* (**15**): **14** (0.2 g, 0.64 mmol) in absolute ethanol (15 ml) containing concd sulfuric acid (few drops) was refluxed for 20 min on a water bath. The mixture was cooled, diluted with water (30 ml) and rendered alkaline by adding few drops of sodium hydroxide solution (5%). The separated solid was filtered and crystallized from methanol as cream-colored crystals of **15** (0.15 g; 0.67 mmol) (88%) mp 115—116 °C. Found: C, 76.8; H, 5.3%. Calcd for $C_{17}H_{14}O_3$: C, 76.7; H, 5.3%. ^{1}H NMR($CDCl_3$) δ=2.29(s, 3H, CH_3); 5.05(s, 2H,

$-OCH_2C_6H_5$); 6.02(s, 1H, H3); 6.90(m, 2H, H6 and H8); 7.25(s, 5H, $-OCH_2C_6H_5$); 7.95(d, J=10 Hz, 1H, H5).

7-Hydroxy-2-methyl-4H-1-benzopyran-4-one (1): Palladium charcoal (0.5 g, 5%) in ethyl acetate (30 ml) was saturated with hydrogen gas with stirring. A solution of the above chromone **15** (0.5 g) in ethyl acetate (40 ml) was then added and hydrogenation continued till the rapid absorption ceased. The reaction mixture was freed from catalyst by filtration and solvent distilled to give required product **1** (0.2 g; 1.14 mmol) (60.6%) mp 254—255 °C (lit,[5] 254—255 °C).

7-Hydroxy-8-iodo-2-methyl-4H-1-benzopyran-4-one (2): It was prepared following the method described in literature.[6]

7-(1,1-Dimethyl-2-propynyloxy)-8-iodo-2-methyl-4H-1-benzopyran-4-one (3): A solution of **2** (1 g, 3.90 mmol) in dry acetone (175 ml) was refluxed with 3-chloro-3-methyl-1-butyne (4 ml, 39.2 mmol) in the presence of anhydrous potassium carbonate (3 g) and anhydrous potassium iodide (1.9 g) for 24 h. The solvent was distilled off and the residue treated with ice. The separated solid was filtered, washed with a dilute solution of sodium carbonate and water and crystallized from benzene–petroleum ether to give **3** (0.65 g, 2.14 mmol) (54%) as colorless needles mp 144—145 °C. Found: C, 56.1; H, 4.2%. Calcd for $C_{15}H_{13}O_3I$: C, 56.0; H, 4.0%. ^{1}H NMR($CDCl_3$) δ=1.75(s, 6H, $C(CH_3)_2$); 2.40 (s, 3H, CH_3); 2.62(s, 1H, C≡CH); 6.05(s, 1H, H3); 7.54 (d, J=10 Hz, 1H, H6); 8.00(d, J=10 Hz, 1H, H5).

2,2,8-Trimethyl-2H,6H-benzo[1,2-b:5,4-b']dipyran-6-one (4): The above 1,1-dimethyl-2-propynyl ether (**3**) (0.5 g, 1.65 mmol), was refluxed with *N,N*-dimethylaniline (3 ml) for 12 h. The cooled reaction mixture was poured over ice cold hydrochloric acid. The solution was extracted thrice with ethyl acetate (150 ml); washed with 5% HCl, 5% NaOH, and finally with water and dried (Na_2SO_4). Distillation of ethyl acetate yielded a mixture of two products, which were separated by preparative TLC (benzene–acetone, 9:1). Elution of lower band with ether yielded **4** which crystallized from benzene–petroleum ether to give shining white crystals (0.15 g, 0.61 mmol) (38%) mp 163—164 °C. Found: C, 74.5; H, 5.8%. Calcd for $C_{15}H_{14}O_3$: C, 74.3; H, 5.79%. ^{1}H NMR($CDCl_3$) δ=1.45(s, 6H, $C(CH_3)_2$); 2.35(s, 3H, CH_3); 5.65(d, J=10 Hz, 1H, H4); 6.00(s, 1H, H7); 6.35(d, J=10 Hz, 1H, H3); 6.65(s, 1H, H10); 7.65 (s, 1H, H5). The compound **4** is identical (mp, mixed mp, superimposed IR) with the sample obtained below.

The upper band on elution with ether gave a product which was crystallized from benzene–petroleum ether to give colorless needles of 2,8,8-trimethyl-4*H*,8*H*-benzo[1,2-*b*:3,4-*b'*]dipyran-4-one (**5**) (0.25 g, 1.0 mmol) (64%) mp 130—131 °C (lit,[10] mp 130—132 °C). Found: C, 74.2; H, 5.6%. Calcd for $C_{15}H_{14}O_3$: C, 74.3; H, 5.79%. ^{1}H NMR($CDCl_3$) δ=1.45(s, 6H, $C(CH_3)_2$); 2.35(s, 3H, CH_3); 5.70(d, J=10 Hz, 1H, H10); 6.05(s, 1H, H3); 6.89(m, 2H, H6 and H9); 8.00(d, J=10 Hz, 1H, H5).

2,2,8-Trimethyl-2H,6H-benzo[1,2-b:5,4-b']dipyran-6-one (4). *6-Acetoacetyl-3,4-dihydro-2,2-dimethyl-2H-1-benzopyran-7-ol (18)*: 6-Acetyl-3,4-dihydro-2,2-dimethyl-2*H*-1-benzopyran-7-ol[9] (**17**), (1 g, 4.5 mmol) dissolved in dry ethyl acetate (20 ml) was treated with pulverized sodium (0.5 g). The mixture was refluxed on a boiling water bath for 4 h, cooled and treated with crushed ice very slowly. The brownish alkaline layer was separated and extracted with ether to remove excess of ethyl acetate and unreacted ketone. Acidification of cold alkaline solution with dilute acetic acid (10%) gave a white solid. It was crystallized from benzene–petroleum ether (0.75 g, 2.8 mmol) (75%) mp 108—109 °C. Found: C, 68.5; H, 6.8%. Calcd for $C_{15}H_{18}O_4$: C, 68.7; H, 6.9%). ^{1}H NMR ($CDCl_3$) δ=1.31(s, 6H, $C(CH_3)_2$); 1.75 and 2.70 (t, each, J=7 Hz, 2H each, H3 and H4); 2.05(s, CH_3 of enol); 2.25(s, CH_3 of keto); 3.95(s, –C(=O)–C$\underline{H}_2$–C(=O)– of keto); 5.98(s, –CH=C(OH)– of enol); 6.28(s, 1H, H8); 7.30(s, 1H, H5); 13.8(s, 1H, –OH exchangeable with D_2O). The integration of the spectrum showed that the ratio of keto-enol is 1:2.

2,2,8-Trimethyl-3,4-dihydro-2H,6H-benzo[1,2-b:5,4-b']dipyran-6-one (19): The diketone **18** (0.2 g, 0.76 mmol) in absolute ethanol (25 ml) containing concd sulfuric acid (2 ml) was refluxed for 2 h on a boiling water bath. The mixture was cooled, diluted with water (25 ml) and rendered alkaline with aq sodium hydroxide. The separated solid was filtered and crystallized from ethanol as pale yellow needles of **19** (75%) (0.15 g, 0.61 mmol), mp 149—150 °C. Found: C, 74.3; H, 6.4%. Calcd for $C_{15}H_{16}O_3$: C, 74.4; H, 6.8%. ^{1}H NMR($CDCl_3$) δ=1.35(s, 6H, $C(CH_3)_2$) 1.82 and 2.85(t, each, J=7 Hz, 2H each, H3 and H4); 2.32(s, 3H, CH_3); 6.01(s, 1H, H7); 6.7(s, 1H, H10), 7.86(s, 1H, H5).

2,2,8-Trimethyl-2H,6H-benzo[1,2-b:5,4-b']dipyran-6-one (4): A solution of the chroman **19** (0.1 g, 0.41 mmol), *N*-bromosuccinimide (0.07 g) and benzoyl peroxide (0.008 g) in anhydrous carbon tetrachloride (10 ml) was refluxed for 6 h. The solution was filtered. The solvent was removed and the residue on column chromatography and elution with benzene gave **4** which crystallized from benzene–petroleum ether as light yellow needles (0.05 g, 0.20 mmol) (50%), mp and mixed mp, 163—164 °C.

5-Hydroxy-2,2,8-trimethyl-2H,6H-benzo[1,2-b:5,4-b']dipyran-6-one (spatheliachromen) (7). *1-(4-Benzyloxy-2-hydroxy-6-methoxyphenyl)-1,3-butanedione (16)*: A solution of 4-benzyloxy-2-hydroxy-6-methoxyacetophenone[7] (1 g, 3.70 mmol) in dry ethyl acetate (5 ml) was added to pulverized sodium (0.5 g). The mixture was shaken and cooled. After the initial vigorous reaction had subsided, the reaction mixture was heated in a boiling water bath for 3 h. The mixture was cooled, diluted with water and extracted with ether to remove an excess of ethyl acetate. The clear brownish alkaline solution was acidified in cold with dilute acetic acid when a yellow solid separated. It crystallized from benzene–petroleum ether as pale yellow shining needles of **16** (0.6 g, 1.89 mmol) (52%), mp 135—136 °C. Found: C, 68.9; H, 5.7%. Calcd for $C_{18}H_{18}O_5$: C, 68.7; H, 5.9%. ^{1}H NMR($CDCl_3$) δ=2.08(s, CH_3 of enol); 2.15(s, CH_3 of keto); 3.85(s, 3H, $-OCH_3$); 3.92(s, –C(=O)–C$\underline{H}_2$–C(=O)– of keto); 4.95(s, 2H, $-OC\underline{H}_2C_6H_5$); 5.85(s, –C$\underline{H}$=C(OH)– of enol); 6.00 and 6.15(d, each, J=2.5 Hz each, 2H, H3 and H5); 7.35 (s, 5H, $-OCH_2C_6\underline{H}_5$); 13.50(s, –OH at C-2 of enol, exchangeable with D_2O); 13.80(s, –OH at C-3 of keto, exchangeable with D_2O). The integration of the spectrum showed that the ratio of keto and enol forms is 3:1.

7-Benzyloxy-5-methoxy-2-methyl-4H-1-benzopyran-4-one (10): **16** (0.2 g, 0.63 mmol) in absolute ethanol (15 ml) containing concd sulfuric acid (few drops) were refluxed for 30 min on a water bath. The mixture was cooled, diluted with water (30 ml) and rendered alkaline by adding few drops of sodium hydroxide solution (5%). The separated solid was filtered and crystallized from methanol as colorless shining needles of **10** (0.16 g, 0.61 mmol) (80%) mp 90—91 °C. Found: C, 73.1; H, 5.3%. Calcd for $C_{18}H_{16}O_4$: C, 73.0; H, 5.4%. ^{1}H NMR($CDCl_3$) δ=2.20(s, 3H, CH_3); 3.85(s, 3H, $-OCH_3$); 5.00(s, 2H, $-OC\underline{H}_2C_6H_5$); 5.90(s, 1H, H3); 6.29 and 6.32 (d, each, J=2 Hz each, 1H each, H6

and H8); 7.25 (s, 5H, $-OCH_2C_6\underline{H}_5$).

*7-Hydroxy-5-methoxy-2-methyl-4*H*-1-benzopyran-4-one (**11**)*: Palladium charcoal (0.5 g, 5%) in ethyl acetate (20 ml) was saturated with hydrogen gas with stirring. A solution of the above chromone **10** (0.5 g, 1.70 mmol) in ethyl acetate (40 ml) was then added and hydrogenation continued till the rapid absorption ceased. The reaction mixture was freed from catalyst by filtration and solvent distilled to give **11** (0.2 g, 0.98 mmol) (57%) mp 215—216 °C. Found: C, 64.2; H, 4.9%. Calcd for $C_{11}H_{10}O_4$: C, 64.0; H, 4.85%.

Its acetate (prepared by acetic anhydride–pyridine) melted at 114—115 °C. ^{1}H NMR($CDCl_3$) δ=2.32(s, 3H, CH_3); 2.38(s, 3H, $-COCH_3$); 3.95(s, 3H, $-OCH_3$); 6.08(s, 1H, H3); 6.55 and 6.82(d, each, J=2.5 Hz each, 1H each, H5 and H8).

*7-Hydroxy-8-iodo-6-methoxy-2-methyl-4*H*-1-benzopyran-4-one (**12**)*: **11** (2 g, 6.80 mmol) was dissolved in a minimum amount of ethanol and to this solution iodine (1.20 g) and periodic acid (0.38 g in water) were added. The mixture was stirred for 2 h at a room-temperature and then diluted with water to give chromone **12** (2.5 g, 8.75 mmol) (89%). It crystallized from ethanol as light yellowish needles, mp 225—226 °C. Found: C, 46.5; H, 3.10%. Calcd for $C_{11}H_9O_4I$: C, 46.3; H, 3.15%.

Its acetate (prepared by acetic anhydride–pyridine) melted at 145—146 °C. ^{1}H NMR($CDCl_3$) δ=2.39(s, 3H, CH_3); 2.43(s, 3H, $-COCH_3$); 3.95(s, 3H, $-OCH_3$); 6.10(s, 1H, H3); 6.65(s, 1H, H6).

*7-(1,1-Dimethyl-2-propynyloxy)-8-iodo-5-methoxy-2-methyl-4*H*-1-benzopyran-4-one (**9**)*: A solution of **12** (1 g, 3.50 mmol) in dry acetone (200 ml) was refluxed with 3-chloro-2-methyl-1-butyne (4 ml, 38.9 mmol) in the presence of anhydrous potassium carbonate (3 g) and anhydrous potassium iodide (1.5 g) for 24 h. Working up of the reaction mixture yielded **9** (0.7 g, 1.99 mmol) (58.3%) which crystallized from benzene–petroleum ether as white needles mp 185—186 °C. Found: C, 54.8; H, 4.30%. Calcd for $C_{16}H_{15}O_4I$: C, 54.7; H, 4.27%. ^{1}H NMR($CDCl_3$) δ=1.80(s, 6H, $C(CH_3)_2$); 2.25(s, 3H, CH_3); 2.70(s, 1H, C≡CH); 3.90(s, 3H, $-OCH_3$); 6.00(s, 1H, H3); 7.29(s, 1H, H6).

*5-Hydroxy-2,2,8-trimethyl-2*H*,6*H*-benzo[1,2-b:5,4-b']dipyran-6-one (Spatheliachromen) (**7**)*: The above 1,1-dimethyl-2-propynyl ether (**9**) (0.5 g, 0.7 mmol) was refluxed with *N,N*-dimethylaniline (3 ml) for 12 h. The cooled reaction mixture was poured over ice cold hydrochloric acid and worked up (as in case of **4**) to yield a mixture of three products, which were separated by preparative TLC. The slowest moving band on elution with ether gave **7**. It crystallized from ethyl acetate–petroleum ether to give colorless needles (0.100 g, 0.39 mmol) (27%), mp 139—140 °C (lit,[1] mp 139—140 °C). Found: C, 70.0; H, 5.60%. Calcd for $C_{15}H_{14}O_4$: C, 69.75; H, 5.50%. ^{1}H NMR($CDCl_3$) δ=1.45 (s, 6H, $C(CH_3)_2$); 2.32(s, 3H, CH_3) 5.60(d, J=10 Hz, 1H, H4); 6.01(s, 1H, H7); 6.28(s, 1H, H10); 6.71(d, J=10 Hz, 1H, H3); 13.06(s, 1H, –OH, exchangeable with D_2O).

The middle band on elution gave a product which was assigned the structure *O*-methylspatheliachromen (**8**). It crystallized from benzene–petroleum ether (0.150 g, 0.455 mmol) (37.5%), mp 121—122 °C (lit,[1] mp 120—122 °C). Found: C, 70.35; H, 6.0%. Calcd for $C_{16}H_{16}O_4$: C, 70.6; H, 5.9%). ^{1}H NMR($CDCl_3$) δ=1.47(s, 6H, $C(CH_3)_2$); 2.28 (s, 3H, CH_3); 3.90(s, 3H, $-OCH_3$); 5.71(d, J=10 Hz, 1H, H4); 6.00(s, 1H, H7); 6.58(s, 1H, H10) and 6.75(d, 1H, J=10 Hz, H3). The compound **8** was identical (mp, mixed mp, superimposed IR) with the sample obtained below.

The upper most band on elution with ether gave a solid product which was crystallized from benzene–petroleum ether to give *O*-methylallopteroxylin (**13**) (0.100 g; 0.39 mmol) (25%) mp 152—154 °C (lit,[8] mp 150—152 °C). Found: C, 70.35; H, 6.09%. Calcd for $C_{16}H_{16}O_4$: C, 70.6; H, 5.9%. ^{1}H NMR($CDCl_3$) δ=1.48(s, 6H, $C(CH_3)_2$); 2.29 (s, 3H, CH_3); 3.93(s, 3H, $-OCH_3$); 5.56(d, J=10 Hz, 1H, H10); 6.01(s, 1H, H3); 6.31(s, 1H, H6) and 6.71(d, J=10 Hz, 1H, H9).

*5-Methoxy-2,2,8-trimethyl-2*H*,6*H*-benzo[1,2-b:5,4-b']dipyran-6-one (**8**).* *6-Acetoacetyl-3,4-dihydro-5-methoxy-2,2-dimethyl-2*H*-1-benzopyran-7-ol (**21**)*: 6-Acetyl-3,4-dihydro-5-methoxy-2,2-dimethyl-2*H*-1-benzopyran-7-ol[9] (**20**) (0.5 g, 2.0 mmol) dissolved in dry ethyl acetate (10 ml) was treated with pulverized sodium (0.25 g). The mixture was refluxed on a boiling water bath for 4 h. The reaction mixture was worked up as usual and the solid obtained was crystallized from benzene–petroleum ether as pale yellow needles (0.35 g, 1.2 mmol) (70%) mp 104—105 °C. Found: C, 60.2; H, 7.91%. Calcd for $C_{16}H_{20}O_5$: C, 60.23; H, 7.94%. ^{1}H NMR($CDCl_3$) δ=1.34(s, 6H, $C(CH_3)_2$), 1.75 and 2.7(t, each, J=7 Hz, each 2H, H3, and H4); 2.13(s, CH_3 of enol); 2.22(s, CH_3 of keto), 3.75(s, 3H, OCH_3), 4.02(s, $-\underset{\underset{O}{\|}}{C}-C\underline{H}-\underset{\underset{O}{\|}}{C}-$ of keto); 5.86(s, $-CH=C-$); 6.1(s, 1H, H8); 13.7(s, 1H, $-\underset{|}{\underset{OH}{}}$ –OH exchangeable with D_2O). The integration of the spectrum showed that the ratio of keto and enol is 1:2.

*5-Methoxy-2,2,8-trimethyl-3,4-dihydro-2*H*,6*H*-benzo[1,2-b:5,4-b']dipyran-6-one (**22**)*: The diketone **21** (0.2 g, 0.68 mmol) in ethanol (25 ml) containing concd sulfuric acid (2 ml) was refluxed for 2 h on a boiling water bath. Working up of the reaction mixture as in the case of **19** gave **22** which crystallized from ethanol as yellow needles (0.15 g, 0.55 mmol) (75%) mp 114—115 °C. Found: C, 70.54; H, 6.52%. Calcd for $C_{16}H_{18}O_4$: C, 70.59; H, 6.57%. ^{1}H NMR($CDCl_3$) δ=1.34(s, 6H, $C(CH_3)_2$), 1.78 and 2.76(t, each, J=7 Hz, 2H each H3, and H4), 2.23(s, 3H, CH_3); 3.81 (s, 3H, $-OCH_3$); 5.85(s, 1H, H7); 6.44(s, 1H, H10).

*5-Methoxy-2,2,8-trimethyl-2*H*,6*H*-benzo[1,2-b:5,4-b']dipyran-6-one (**8**)*: Dehydrogenation of **22** (0.1 g, 0.36 mmol) with NBS as in the case of **4** gave **8** (0.06 g, 0.22 mmol) (60%) mp 120—121 °C.

References

1) D. R. Taylor, J. M. Warner, and J. A. Wright, *J. Chem. Soc., Perkin Trans. 1*, **1977**, 397.

2) B. S. Bajwa, P. Lal, and T. R. Seshadri, *Indian J. Chem.*, **9**, 17 (1971).

3) A. C. Jain, V. K. Khanna, P. Lal, and T. R. Seshadri, *Indian J. Chem.*, **8**, 480 (1970).

4) V. K. Ahluwalia, Mrs. Krishna Bhat, Chandra Prakash, and Shashi Bala, *Bull. Chem. Soc. Jpn.*, **53**, 1070 (1980).

5) C. Bheemasankara Rao, G. Subramanyam, and V. Venkateswarlu, *J. Org. Chem.*, **24**, 683 (1959).

6) V. K. Ahluwalia, Krishan Kumar, and Chandra Prakash, *Gazz. Chim. Ital.*, Accepted for publication.

7) V. V. S. Murti and T. R. Seshadri, *Proc. Ind. Acad. Sci.*, **29A**, 1 (1949).

8) F. M. Dean and D. A. H. Taylor, *J. Chem. Soc., C*, **1969**, 114.

9) V. K. Ahluwalia and K. K. Arora, *Tetrahedron*, **37**, 1437 (1981).

10) V. K. Ahluwalia, Chandra Prakash, and Shashi Bala, unpublished work.

11) S. K. Mukerjee, S. C. Sarkar, and T. R. Seshadri, *Indian J. Chem.*, **10**, 374 (1972).

The Promotion Effect of Rare Earth Oxides on the Hydrogenation of Carbon Monoxide over Rh-Al_2O_3 Catalyst

Yusaku TAKITA,* Tamiyasu YOKO-O, Naoyoshi EGASHIRA, and Fumiaki HORI
Department of Environmental Chemistry and Engineering, Faculty of Engineering, Oita University, Dannohara, Oita 870-11

(Received June 1, 1981)

Synopsis. The addition of Dy_2O_3, Nd_2O_3, Yb_2O_3, La_2O_3, or Gd_2O_3 to the Rh–Al_2O_3 catalyst enhanced the activity of the hydrogenation of CO to methane. There was the linear relationship between the carbon skeleton propagation of the hydrocarbons formed and the basicity of the rare earth oxides.

Catalytic behaviors of rare earth oxides have been explored for many reactions and a wide variety of catalytic properties has been known.[1] Rare earth oxides are hardly reducible, La_2O_3 and Ce_2O_3, for example, remain three valent oxides after treatment in hydrogen at 673 K,[2] and Lu_2O_3 generates two valent ions even at 823—973 K by treatment in hydrogen.[3] These character is suited for the catalyst support which is applied under reducing atmosphere, there is, however, only a few paper investigated rare earth oxides as a catalyst support. It has been known that the incorporation of a small amount of La_2O_3 or Ce_2O_3 to supported Ni, Ni–Rh, and Ni–Ru catalysts brought about considerable increase of activity in the methanation of carbon oxides[4]. It was reported that the Rh carbonyl clusters dispersed on La_2O_3, Nd_2O_3, and CeO_2 were the effective catalysts for ethanol and C_2 oxygenated products formation as well as the catalysts dispersed on TiO_2, ZrO_2, and ThO_2.[5] However the effect of rare earth oxides other than these three oxides on the catalytic property of noble metals has remained obscure. The present paper dealt with the effect of rare earth oxides on the catalytic property of Rh–Al_2O_3 catalyst in the hydrogenation of carbon monoxide.

The results are given in Table 1 together with apparent activation energies. The products formed over these catalysts were similar to those over Rh–Al_2O_3 catalyst. The CO conversion at the temperatures below 573 K slightly decreased by the addition of Dy, Nd, Yb, or La, but it increased at above 613 K. The addition of Gd oxide and Ho oxide gave positive effect on the conversion only at 633 K. The addition of Pr oxide gave no significant effect on the CO conversion, while Tm or Eu oxide reduced the conversion over the temperature range examined.

The selectivity of CO_2 was raised by the addition of any rare earth oxide, especially high over the Nd and La containing catalysts.

Since water vapor should be formed during the reaction by the amount counterbalanced with the formation of hydrocarbons, there must be two possible reactions for CO_2 formation, *viz.*, water gas shift reaction and disproportionation of CO. The reaction were achieved in a good carbon balance (100±3%) at

Table 1. Product distributions on the hydrogenation of carbon monoxide

Promoter[a]	Temp K	Conversion %	Selectivity/% CH_4	C_2H_6	C_3H_8	C_4H_{10}	C_4H_8	CO_2	E_a
None	593	42.7	87.8	7.40	1.80	0.44	0.12	2.27	
	613	60.7	89.9	5.90	0.57	0.06	—	3.60	66.1
	633	80.7	89.6	2.76	0.11	—	—	7.55	
Dy_2O_3	593	43.8	84.9	5.90	1.63	0.30	0.12	6.90	
	613	82.9	83.5	3.90	0.19	—	—	12.4	92.0
	633	100.0	88.9	—	—	—	—	11.1	
Nd_2O_3	593	44.4	71.0	4.54	1.11	0.16	—	23.0	
	613	86.0	72.0	1.90	0.20	—	—	25.9	102.9
	633	100.0	87.3	—	—	—	—	12.7	
Yb_2O_3	593	47.9	83.7	5.28	1.32	0.23	0.07	9.45	
	613	83.1	82.8	3.26	0.17	—	—	13.1	92.5
	633	100.0	87.4	—	—	—	—	12.5	
La_2O_3	593	42.3	80.8	6.84	1.75	0.31	0.10	10.2	
	613	74.8	78.7	4.55	0.39	0.03	—	16.3	84.9
	633	100.0	84.5	—	—	—	—	15.5	
Gd_2O_3	613	59.8	85.0	4.13	—	0.03	0.03	10.7	90.0
	633	99.1	95.4	—	—	—	—	4.51	
Ho_2O_3	633	82.4	89.2	0.05	0.03	—	—	10.7	93.7
Pr_6O_{11}	633	83.0	87.3	—	0.02	—	—	12.6	109.2
Tm_2O_3	633	84.0	88.4	2.63	0.01	0.01	—	8.98	103.8
Eu_2O_3	633	59.4	83.8	2.78	0.08	—	0.01	13.3	96.7

Catalyst: Rh(1 wt%)–rare earth oxide(5%)–Al_2O_3, 1.50 g; reactant gas composition: CO 10 mol%, H_2 30 mol%, N_2 60 mol%; SV: 1970+30 cm^3 STP $g\text{-}cat^{-1}$ h^{-1}. a) Starting material, E_a: apparent activation energy of methanation (kJ mol^{-1}).

least within initial 12 h even on the catalyst containing Nd oxide which showed the highest selectivity of CO_2. A small amount of carbon deposition was observed on the catalysts after the reaction for 3 d or more, so that the latter reaction is believed to be dominant under these reaction conditions.

The apparent activation energy was calculated to 66 kJ mol^{-1} for Rh–Al_2O_3 and those for the catalysts containing rare earth oxides were distributed in 85—110 kJ mol^{-1}. Although these values are considerably small comparing with those in references,[6] a distinction of activation energy between Rh supported on an acidic support such as Al_2O_3 and the basic catalysts containing rare earth oxides strongly suggests the direct interaction of Rh with rare earth oxide on Al_2O_3. The following facts would support this speculation. Specific surface area of the catalysts including Dy and Yb oxides, 197 and 247 m^2 g^{-1} respectively, were not smaller than 280 m^2 g^{-1} of the Rh–Al_2O_3 catalyst. Assuming that La_2O_3 makes a monolayer on Al_2O_3 as oriented its (0001) plane to the Al_2O_3 surface, the coverage of La_2O_3 is calculated to 27—40% of the surface.

The formation of CO_2 reduces the yield of hydrocarbons, the oder of the effect of the oxides as evaluated from the yield of hydrocarbons is

Dy, Nd, Yb>La>Gd>Ho, Pr, none>Tm>Eu.

This order is essencially the same as reported for hydrogenation of ethene.[7]

The selectivity of methane was relatively less sensitive to the reaction temperature over the catalysts, and it remained about 70—85% even at 573 K. As for the hydrocarbons with carbon-carbon bond, the lowering of temperature from 633 to 573 K resulted in a passable increase of selectivity. $\sum n_i S_i$ was plotted in Fig. 1 against logarithmic solubility product constant (log K) of hydroxides of tervalent rare earth metals[8] which is regarded as a scale of the basicity of the oxides. Where n_i represents the number of carbon-carbon bond of hydrocarbon i among hydrocarbons produced, so that $\sum n_i S_i$ is an index of chain growth over catalyst.[9] The figure shows an approximately linear relationship. Due to explaine the wide diversity of the products in the hydrogenation of CO, many reaction mechanisms have

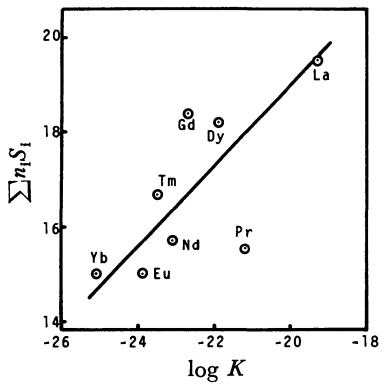

Fig. 1. The relation between carbon-carbon bond formation and the basicity of rare earth oxides.
n_i: The number of carbon-carbon bond in hydrocarbon i, S_i: selectivity of hydrocarbon i among the hydrocarbons produced in the reaction at 573 K, K: solubility product constants in aqueous solution at 291—298 K.

been proposed. These are divided broadly into three categories.[10] In the first category it is assumed that the CO dissiciates completely on adsorption and carbon chain is formed by the linking up of CH_2 or CHR. In the second category it is presumed that the CO chemisorbs associatively and chain growth occurs by H_2O elimination between neighbouring species such as R–C(=M)–OH and R–CH(=M)–OH where M represents a catalyst surface site and R represents H or alkyl. The associative CO chemisorption and CO insertion into M–H or M–CH_2R bond are assumed in the third category. Seeing the steps of the carbon chain propagation, carben type intermediates[11] take part in the first two categories, while the surface alkyl participates in the third one. It can not be decided which mechanism is dominant on the catalyst used in this work. However, it would be expected the stronger the basicity of the rare earth oxides added, the weaker the bond between surface carben or alkyl and Rh metal. Therefore the addition of strongly basic rare earth oxides to the catalyst would bring about the encouragement of either aggregation of the carben type intermediates or CO insertion into Rh–alkyl bond.

Experimental

Rh–Al_2O_3 catalyst was prepared by impregnation method. Al_2O_3 (Sunbead AN from Catalysts and Chemicals Ind. Co., 24—32 mesh) was poured into the solution of $RhCl_3 \cdot 3H_2O$ and the solution was then evaporated to dryness at about 363 K. The catalyst was calcined at 573 K for 4 h in air and it was then reduced in hydrogen stream at 723 K for 4 h.

Rh–rare earth oxide–Al_2O_3 catalysts were prepared as following procedure. Rare earth nitrate was supported on Al_2O_3 using its acidic solution. After the calcination at 823 K for 5 h, the catalyst was subjected to impregnation of Rh in the same manner as above.

Reactions were carried out using ordinary flow type reactor under atmospheric pressure. Reaction products were analyzed by gas chromatograph. Surface areas of the catalysts were determined by nitrogen adsorption at 77 K using BET method.

References

1) M. P. Rosynek, *Catal. Rev.*, **16**, 111 (1977).
2) T. Inui, M. Funabiki, M. Suehiro, T. Sezume, and T. Iwana, *Nippon Kagaku Kaishi*, **1978**, 517.
3) J. A. Arias and P. W. Selwood, *J. Catal.*, **33**, 284 (1974).
4) T. Inui and M. Funabiki, *Chem. Lett.*, **1978**, 251; *Chem. Eng. News*, Oct. 13, **1980**, 21.
5) M. Ichikawa, *J. Catal.*, **59**, 67 (1979).
6) M. A. Vannice, *J. Catal.*, **37**, 462 (1975); B. A. Sexton and G. A. Somorjai, *ibid.*, **46**, 167 (1977).
7) Yu. S. Khodakov, V. S. Nakhshunov, and Kh. M. Minachev, *Kinet. Katal.*, **12**, 535 (1971).
8) Bjerrum, Shuwarzenbach, Sillen, "Stability Constants of Metal Complexes," Chemical Society, London (1958), Part II.
9) H. Arai, M. Uchida, and H. Tominaga, *Shokubai*, **20**, 242 (1978).
10) J. R. Anderson and M. Boudart, "Catalysis, Science and Technology," Springer-verlag, Berlin, Heidelberg, New York (1981), Vol. 1, p. 159.
11) D. J. Dwyer, K. Yoshida, and G. A. Somorjai, "Hydrocarbon Synthesis from Carbon Monoxide and Hydrogen," ed by E. L. Kugler and F. W. Steffgen, Am. Chem. Soc., Washington D. C. (1979), p. 65.

The Effect of Ultraviolet Radiation on Wettability of Silane Coupling Agents Coated on Glass

Kunio Esumi,* Kenjiro Meguro, Anthony M. Schwartz,† and Albert C. Zettlemoyer†

Department of Applied Chemistry, Faculty of Science, Science University of Tokyo, Kagurazaka, Shinjuku-ku, Tokyo 162

† *Center for Surface and Coating Research, Sinclair Laboratory, Lehigh University, Bethlehem, Pa 18015, U.S.A.*

(Received December 16, 1981)

Synopsis. The effect of ultraviolet irradiation on wettability of silane coupling agents coated on glass was studied by using contact angle measurements. The water contact angle for the silane coupling agents decreased due to photooxidation as the irradiation progressed. It was found that silane coupling agents which contain vinyl, allyl, or phenyl groups were easily photooxidated by the irradiation.

Silane coupling agents are well known to alter surfaces from hydrophilic to hydrophobic. There are many papers[1-4] about wettability of silane coupling agents coated on silica particles or glass; these attempt to understand the adhesion mechanism between a matrix and reinforcing medium. Lee[5] determined critical surface tensions for silane coupling agents on glass and found a relationship between the wettability of functional groups of silanes and their solubility parameters.

Silane coupling agents coated on substrates, under normal condition, were put in contact with atmospheric oxygen and exposed to various temperatures, humidities, and lights. It is expected that silane coupling agents on substrates would undergo a photochemical change at their surfaces. Indeed, vinyl and [3-(methacryloyloxy)-propyl] silane agents on glass[6] were found to change very readily in the presence of air at room temperature or at 80 °C and their critical surface tensions increased, presumably due to increase in polarity. Accordingly, it is very interesting to study the stability of silane coupling agents on substrates against different exposure conditions, especially light exposure. To evaluate the change in a surface composition, contact angle measurements have often been used. This work describes the effect of ultraviolet radiation on the wettability of silane coupling agents coated on glass by using contact angle technique.

The silane coupling agents used in this study were chloromethylphenylvinylsilane, chlorodimethylvinylsilane, allyltriethoxysilane, trichloro(1-methyl-2-phenylethyl)silane, chlorotrimethylsilane, and hexamethyldisilazane, which were supplied by Petrarch Systems, Inc. The liquid used for contact angle measurement was deionized water.

A micro slide glass was used as a substrate. The slide glass was cleaned by chromium trioxide solution, washed with distilled water and then dried carefully.

Coating of silanes on slide glass was carried out with about 3 wt% solution of silanes in 2-propanol. The

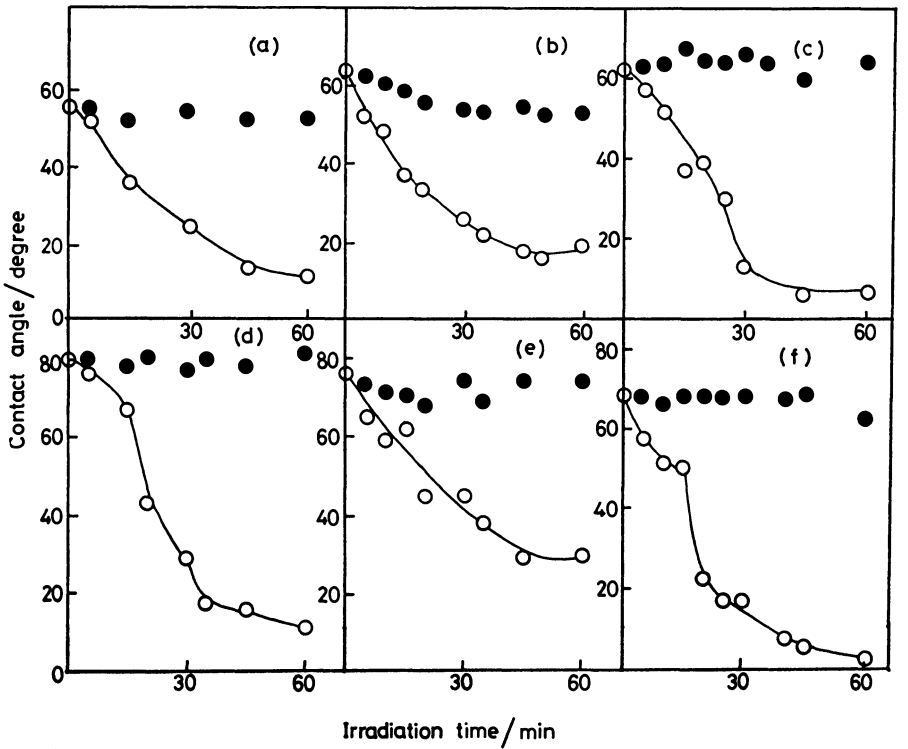

Fig. 1. Water contact angle *vs.* irradiation time.
(○) Water contact angle on irradiated portion, (●) on unirradiated portion. (a) Chloromethylphenylvinylsilane, (b) chlorodimethylvinysilane, (c) allyltriethoxysilane, (d) trichloro(1-methyl-2-phenylethyl)silane, (e) chlorotrimethylsilane, and (f) hexamethyldisilazane.

clean slide glass was dipped into the solution for 30 min, this was followed by washing with 2-propanol and drying *in vacuum*. In the case of hexamethyldisilazane, coating was conducted in vapor state on the slide glass. After exposing the slide glass to the vapor, the treated glass was heated at 100 °C for 20 min to eliminate ammonia generated during the coating.

Contact angles were measured on sessile drops of water by using a goniometer at 20 °C. Three drops for water were measured on both sides of the drops and the six values were averaged. The overall variation in the contact angle measurement was about ± 3 degrees.

Exposures were carried out in air in a hood with a unfiltered radiation from 55.2 W low pressure mercury lamp supplied by Oriel Co. The distance between the sample and the lamp was 5 cm.

The contact angle of water for the silanes on the slide glass was measured as a function of exposure time of ultraviolet irradiation. The results are shown in Fig. 1.

Chloromethylphenylvinylsilane. The initial contact angle of water was 55°. The contact angle decreased with increasing the exposure time and reached to about 10° in 60 min exposure.

Chlorodimethylvinylsilane. The contact angle of water was 60° at initial stage and became 20° during 60 min exposure. During irradiation, however, the unirradiated portion of sample lost hydrophobicity significantly, so that the contact angle on this unirradiated sample went to about 50°.

Allyltriethoxysilane. The contact angle was 60° initially and reached 10° after 30 min exposure.

Trichloro(1-methyl-2-phenylethyl)silane. The initial contact angle was 80°. Irradiation for 30 min dramatically dropped the contact angle to 15°.

Chlorotrimethylsilane. The initial contact angle was 75°. Irradiation for 40 min brought the contact angle down to 30°. This result is somewhat unexpected because methyl groups seem to be stable against ultraviolet irradiation.

Hexamethyldisilazane. The initial contact angle was 65°. The contact angle decreased remarkably to 10° after 40 min exposure.

Generally, the use of a monohalogenosilane[7] prevents the formation of polymeric films on substrates and the coating by the monohalogenosilane is envisioned as a monolayer of silane monomers. On the other hand, trialkoxysilane or trihalogenosilanes undergo the hydrolysis and polymerization to form a polysiloxane network structure, which is much thicker than a monolayer of monomer. Lee[6] studied the conformation of hydrolyzed silanes on glass and concluded that the interaction between the hydrolyzed silanes and the glass surface could take place with the attachment of one hydroxysilyl group to the surface.

In this study, all the silanes except trichloro(1-methyl-2-phenylethyl)silane and allyltriethoxysilane are considered not to form polymeric films on the glass. If chlorotrimethylsilane as a monohalogenosilane is coated on a glass, the water contact angle on the surface would be predicted[8] to be about 73°, while the water contact angle on a fully methylated surface like paraffin wax is taken as 110°. This predictable value of 73° was in good agreement with the experimental value. The above difference of water contact angle between that on monolayer film and that on polymeric film depends on the surface coverage of silane on glass. That is, the polymeric film of silane would give a larger water contact angle than the monolayer of silane.

From Fig. 1, it is seen that by using different silane coupling agents, a variety of functional groups can be exposed on the surface of glass, and each functional group shows a different water contact angle value. When all the samples were irradiated in air by ultraviolet light, the water contact angles decreased as a function of irradiation time. Furthermore, it was found that the water contact angles of silane coupling agents which contain vinyl, phenyl, or allyl groups changed very readily over a short irradiation time.

It is interesting to compare the results obtained with the silane coupling agents on the glass irradiated in air and *in vacuum*. All the silane coupling agents in this study on the glass irradiated *in vacuum* showed no changes in the water contact angles after exposures up to 60 min. This result supports the assertion that during irradiation in air the surface of silane coupling agents on the glass is photooxidated to yield hydrophilic products on the surface.

References

1) P. W. Erickson and E. P. Plueddemann, "Composite Materials," Academic Press, New York (1974), Vol. 6, Chap. 6, 1.
2) W. D. Bascom, *Adv. Chem. Ser.*, **1968**, 87.
3) H. Inoue and S. Kohama, *J. Appl. Polym. Sci.*, **19**, 1939 (1975).
4) E. P. Plueddemann, *Soc. Plastic Ind.*, 19A (1965).
5) L. H. Lee, "Adhesion Science and Technology," Plenum Publ., New York (1975), Vol. 9B.
6) L. H. Lee, *J. Colloid Interface Sci.*, **27**, 751 (1968).
7) M. R. Rosen, *J. Coat. Technol.*, **50**, 70 (1978).
8) J. Laskowski and J. A. Kitchener, *J. Colloid Interface Sci.*, **29**, 670 (1969).

The Conversion of Methanol into Hydrocarbons over Metal Salts of Heteropolyacids

Toshihide BABA, Junya SAKAI, and Yoshio ONO*

Department of Chemical Engineering, Tokyo Institute of Technology, Ookayama, Meguro-ku, Tokyo 152

(Received December 16, 1981)

Synopsis. Metal salts of heteropolyacids are active catalysts for the conversion of methanol into hydrocarbons. Though the activity depends on the kind of metal salt, the reaction mechanism for the conversion is common to most of the metal salts, and the active centers are probably Brönsted acid centers.

Heteropolyacids such as dodecatungstophosphoric acid (TPA) have a high catalytic activity for the conversion of methanol into hydrocarbons.[1,2] This high activity is caused by the high Brönsted acidity of the heteropolyacids.[2,3] The metal salts of heteropolyacids are effective catalysts for many reactions, for which Brönsted acid sites are supposed to be responsible.[4-8] In this paper, the catalytic activities of various metal salts of TPA and dodecatungstosilicic acid (TSiA) for the conversion of methanol into hydrocarbons will be examined. The mechanistic features of the conversion over the salts will also be discussed.

Metal salts of heteropolyacids were prepared as follows. To the aqueous solution of TPA or TSiA, a stoichiometric amount of metal carbonate in the powder form was added slowly. For metals of which carbonates were not available, metal nitrates in an aqueous solution were used instead. When the metal salts of the heteropolyacids were obtained as precipitates (metal salts of TPA: Al, K, Ag, Cd, Cs, La, and Tl; metal salts of TSiA: Rb, Ag, Cs, La, and Tl), they were filtered, washed with water and dried. To obtain metal salts of heteropolyacid soluble in water, the aqueous solutions were heated to dryness over a water-bath.

The metal salts thus prepared were made into pellets, crushed, and sorted into grains of 9—16 mesh. The reaction was carried out at 573 K with a continuous-flow reactor at atmospheric pressure. The catalyst (3 g) was packed in a reactor of silica tubing (10 mm i.d.), placed in a vertical furnace, and then heated under a nitrogen stream at the reaction temperature. Methanol was delivered at the rate of 2.12×10^{-2} mol h^{-1} by means of a motor-driven syringe; it was vaporized by the preheating zone of the reactor, containing 10 cm^3 of quartz. The gas from the outlet of the reactor was analyzed by means of gas chromatography.

Table 1. Product distribution of the conversion of methanol into hydrocarbons

	Catalyst					
	Cu-TPA[a]	Fe-TPA	Al-TPA	Cu-TSiA[a]	Fe-TSiA	Al-TSiA
Product distribution/%[b]						
CH_3OH	1.4	0	0	4.6	1.8	2.1
CH_3OCH_3	37.3	51.7	64.2	34.7	74.0	83.4
Hydrocarbons	61.3	48.3	35.8	60.7	24.2	14.5
Hydrocarbon distribution/%[b]						
CH_4	5.2	2.3	5.6	8.2	3.2	4.3
C_2H_4	9.5	9.5	8.4	14.8	10.3	12.4
C_2H_6	0.8	0.5	0.8	0.4	0.4	0.6
C_3H_6	8.5	7.5	7.1	7.9	9.5	13.8
C_3H_8	13.4	13.0	16.0	12.2	12.4	13.1
C_4	39.2	41.4	38.7	36.0	36.1	32.4
C_5	13.7	14.3	11.0	14.3	16.1	14.5
C_6^+	9.7	11.5	12.4	6.2	12.0	8.9

a) TPA and TSiA indicate dodecatungstophosphate and dodecatungstosilicate respectively. b) Calculated on a carbon-number basis.

In Table 1, the product and the hydrocarbon distribution for several metal salts of TPA and TSiA are listed. In every case, methanol is converted into dimethyl ether and hydrocarbons, the formation of carbon monoxide and carbon dioxide being negligible. The main hydrocarbon products are lower aliphatic hydrocarbons; the fraction of aromatic hydrocarbons in the products was very low. The catalytic activities of most of the metal salts did not change appreciably with the running time, though the rather high fraction of paraffins in the products indicates coke deposition in the catalyst bed. Thus, in the case of the conversion over copper(II) salts of TPA, the hydrocarbon yields were 63.1% and 62.4% at the running times of 2.5 h and 32 h respectively.

The activities of the series of metal salts of TPA and TSiA are listed as follows:

For salts of TPA:

Ag (98.0) > Cu (61.3) > Cd (61 0) > H (60 1) > Fe (48 3) > Tl (37.3) > Al (35.8)

Cs (35.4) > Pb (25.6) > La (23 6) > Na (23 5) > K (20 9) > Cr (20.4) > Zn (12.8)

Li (12.0) > Ni (11.8) > Mn (10.7) > Co (7.7) > Mg (6.9) > Ca (4.1) > NH_4 (2.6)

For salts of TSiA

Ag (78.9) > Cu (60.7) > H (38.6) > Cs* (38.4) > Rb (28.7) > Fe (24 2) > Na (22.2)

Al (14.5) > Zn (7.3) > Tl (5.5) > La (2.4) > Mg (1 2)

* $HCs_3SiW_{12}O_{40}$[9]

The numbers in parentheses indicate the hydrocarbon yield at a running time of 2—6 h except for the cadmium salt of TPA, for which the yield at 1 h was adopted because of the rapid deactivation. In general, the metal salt of TPA is more active than the same metal salt of TSiA. As has been reported previously,[10] silver and copper salts are most active among the metal salts; they are even more active than the protonic forms.

In Figs. 1 and 2, the yields of specific hydrocarbons over metal salts are plotted against the total hydrocarbon yield. It is worthy of note that the points obtained for a variety of catalysts fall onto one common line for each hydrocarbon species. Moreover, when the hydrocarbon yield over Cu(II) salt of TPA was reduced by decreasing the contact time, the yield of each hydrocarbon species was decreased, as was to be expected from the lines

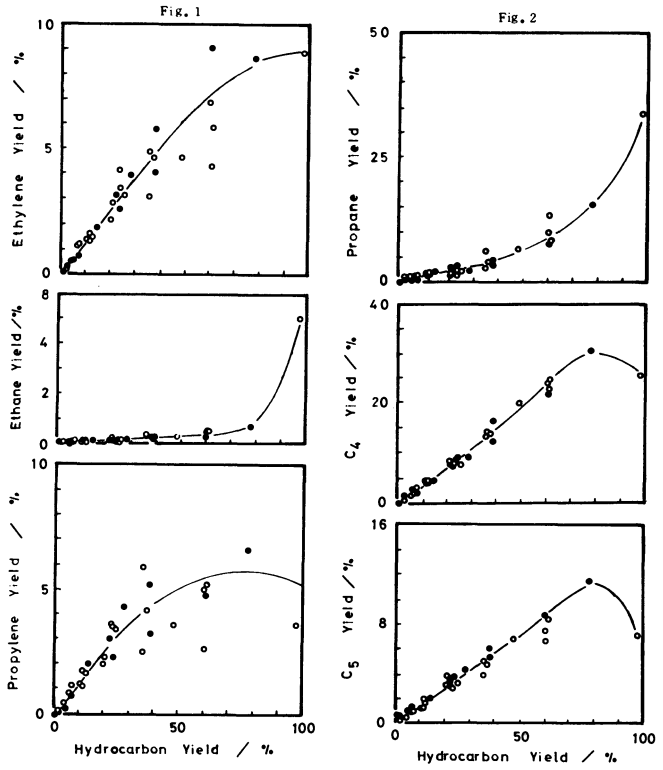

Fig. 1. The yields of ethylene, ethane, and propylene, as a function of the total yields of hydrocarbons obtained over metal salts of dodecatungstophosphoric acid (○) and dodecatungstosilicic acid (●).

Fig. 2. The yields of propane, C_4-, and C_5-hydrocarbons, as a function of the total yields of hydrocarbons obtained over metal salts of dodecatungstophosphoric acid (○) and dodecatungstosilicic acid (●).

drawn in Figs. 1 and 2. These facts strongly suggest that the reaction mechanism is common for most of the metal salts, although the activity depends on the kind of metal salt. Thus, the active centers for the methanol conversion should be common, and they are presumably Brönsted acid sites. In fact, the activities of copper and silver salts of TPA were poisoned by the addition of pyridine under the present reaction conditions. Presumably, Brönsted acid is produced by the reduction of metal cations by hydrogen molecules or atoms formed by the decomposition of methanol:

$$Ag^+ + 1/2H_2(H) \longrightarrow Ag^0 + H^+.$$

This explains why the salts with highly reducible metal cations, like Ag(I) or Cu(II), have high catalytic activities. The formation of Brönsted acid by the dissociation of water[5] could also be operative for salts with less reducible metals.

Figures 1 and 2 also show that the yield of each hydrocarbon is nearly proportional to the total hydrocarbon yield until the latter reaches 30%, indicating that the hydrocarbon products are formed concurrently at the first stage of the reaction; the products once desorbed from the catalysts do not react easily with methanol or other products. Thus, the reaction scheme of the reaction may be expressed as follows:

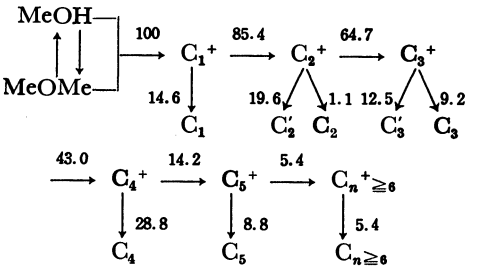

Furthermore, one can estimate the relative rate of each reaction step from the initial distribution of hydrocarbons given in the above scheme.

Figures 1 and 2 indicate that the situation is different at the later stage of the conversion. The fraction of propane in the product hydrocarbons increases at the expense of the fractions of light olefins, especially propylene. This change in the product distribution is apparently caused by the presence of water, one of the products, since the addition of water to the starting methanol has a similar effect on the product distribution. Thus, when the feed was composed of methanol (20.2 kPa) and nitrogen (80.8 kPa), the conversion of methanol over copper(II) salt of TPA gave the propane/propylene and butanes/butenes ratio of 0.99 and 2.9 respectively, while the ratios were 4.8 and 8.7 when water (80.8 kPa) was added to the feed instead of nitrogen.

The great difference in the conversion over heteropolyacids from that over zeolites is that olefins, once formed, react with methanol only slowly,[3] while, over zeolites, the reaction of olefins with methanol is so fast that the overall reaction proceeds autocatalytically.[11,12]

The authors are deeply grateful to Professor Keii Tominaga for his fruitful discussions and for his continuous encouragement throughout the present work.

References

1) Y. Ono, T. Mori, and T. Keii, *Proc. 7th Int. Congr. Catal., 1980, Tokyo*, Kodansha-Elsevier (1981), p. 1414.
2) Y. Ono and T. Mori, *J. Chem. Soc., Faraday Trans. 1*, **77**, 2209 (1981).
3) T. Baba, J. Sakai, and H. Watanabe, *Bull. Chem. Soc. Jpn.*, **55**, 2555(1982).
4) M. Otake and T. Onoda, *Shokubai*, **18**, 169 (1976).
5) H. Niiyama, Y. Saito, and E.Echigoya, *Proc. 7th Int. Congr. Catal., 1980, Tokyo*, Kodansha-Elsevier (1981), p. 1416.
6) M. Misono, K. Sakata, Y. Yoneda, and W. Y. Lee, *Proc. 7th Int. Congr. Catal., 1980, Tokyo*, Kodansha-Elsevier (1981), p. 1047.
7) T. Matuda, M. Sato, T. Kanno, H. Miura, and K. Sugiyama, *J. Chem. Soc., Faraday Trans. 1*, **77**, 3107 (1981).
8) H. Niiyama, Y. Saito, S. Yoshida, and E. Echigoya, *Nippon Kagaku Kaishi*, **1982**, 569.
9) G. A. Tsigdinos, "Molybdenum Chemicals," Chemical Data Series Bulletin Cdb-12a (1969).
10) Y. Ono, T. Baba, J. Sakai, and T. Keii, *J. Chem. Soc., Chem. Commun.*, **1981**, 400.
11) N. Y. Chen and W. J. Reagan, *J. Catal.*, **59**, 123 (1979).
12) Y. Ono, E. Imai, and T. Mori, *Z. Phys. Chem. Neue Folge*, **115**, 99 (1979).

Efficient Photoreduction of Methylviologen Sensitized by Chlorophyll Derivatives and Hydrogen Evolution by Visible Light

Takashi Koiso, Masataka Okuyama,* Tadayoshi Sakata,*,† and Tomoji Kawai†

Depatrment of Engineering Chemistry, Nagoya Institute of Technology, Showa-ku, Nagoya 466

†*Institute for Molecular Science, Myodaiji, Okazaki 444*

(Received December 22, 1981)

Synopsis. The photoreduction of methylviologen sensitized by chlorophyll derivatives and porphines was investigated using EDTA as a reducing agent. The quantum yield of the photoreduction depends greatly on the kind of central metal ion of chlorophyll derivatives and porphines. Zn–chlorophyll-a and Zn–tetraphyenylporphine show a high quantum efficiency amounting 0.4, which is higher than that of chlorophyll-a.

Redox reactions induced by photoexcitation of chlorophyll play an important role in the photosynthesis in green plants and some bacteria. Much work has been done to construct an artificial system having such a function by making use of photochemical reactions of chlorophyll, its derivatives and porphyrins.[1-9] Here we would like to report an efficient photoreduction of methylviologen (MV^{2+}) by chlorophyll derivatives.

Methylviologen was used as an electron acceptor and EDTA as an electron donor. Photochemical reactions were carried out in the mixture of dimethyl sulfoxide (DMSO) and water (9 : 1 in volume ratio) which dissolves chlorophylls and porphines. The solution of MV^{2+} and EDTA in a quartz cell was deaerated to remove oxygen before illumination. A Xe lamp (500 W, Ushio) and a monochromator (Nikon, p-250) were used for monochromatic illumination (≈1 mW) at the peak wavelength of the visible absorption band of each dye molecule. A strong absorption band at 610 nm of the reduced methylviologen, $MV^{+\cdot}$, was monitored by a spectrophotometer to follow the reaction. The quantum yield of the reaction (the number of $MV^{+\cdot}$ formed/the number of absorbed photons) was determined by using a thermopile (Eppley Lab. Inc.).

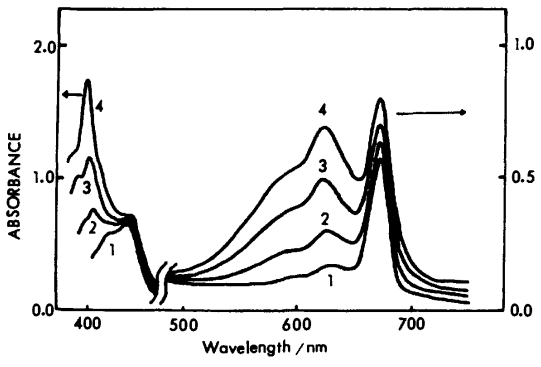

Fig. 1. Spectral changes of the solution (photocatalyst: Chl-a, electron donor: EDTA, electron acceptor: MV^{2+}) due to the reduction of MV^{2+} during illumination by a monochromatic light (≈ 1 mW) at 665 nm.
1) 0.0 min, 2) 2.0 min, 3) 12.0 min, 4) 37.0 min.
$[MgChl\text{-}a] = 9.4 \times 10^{-6}$ M, $[EDTA] = 1.0 \times 10^{-2}$ M, $[MV^{2+}] = 2.0 \times 10^{-3}$ M. Solvent; DMSO: water= 1: 1 (in volume ratio).

When chlorophyll-a was excited by visible light, it turned out to oxidize EDTA and reduce methylviologen. The net reaction is considered to be as follows.[9]

$$EDTA + 2MV^{2+} + H_2O \longrightarrow C_2H_4N_2(CH_2COOH)_3H + 2\,MV^{+\cdot} + CH_2O + CO_2 + 2H^+$$

$$\Delta G^0 = 20 \text{ kcal/mol.}$$

Due to the formation of reduced methylviologen the deaerated solution colored blue by illumination. Besides (Chl-a, its derivatives such as ZnChl and CuChl were found to work well as a photocatalyst for the reduction of methylviologen (MV^{2+}). Figure 1 shows the spectral change of the solution (photocatalyst: Chl-a, electron donor: EDTA, electron acceptor: MV^{2+}) during illumination with a monochromatic light at 665 nm. The introduction of air into the solution after illumination extinguished the blue color of the reduced methylviologen ($MV^{+\cdot}$) but did not cause any change of the absorption intensity of photocatalysts such as Chl-a and its derivatives, which indicates that they work reversibly as photocatalysts. Table 1 shows the quantum yield of the photoreduction for chlorophyll derivatives and porphines determined spectrophotometrically. One interesting thing is that the quantum yield depends remarkably on the kind of the central metal and is comparatively high, as seen in this table. Another interesting thing is that the quantum yield of an artificial compound such as ZnChl and ZnTPP is higher than that of MgChl, Chlorophyll-a (a natural compound). This suggests a possibility of constructing an artificial photosysnthetic device which is superior to the photosysnthetic system in the nature.

As is shown in Table 1, TPP derivatives have a similar tendency with Chl derivatives in the dependence of the quantum yield on the kind of central metal ion. Since the fluorescence intensity of Chl-a and ZnTPP is hardly influenced by adding EDTA and MV^{2+}, the triplet

Table 1. Quantum yield of phoreduction of methylviologen by chlorophyll derivatives, porphines, and dyes. They were excited by a monochromatic light at the peak wavelength of the visible absorption band

$[MV^{2+}] = 2.0 \times 10^{-3}$ M, $[EDTA] = 1.0 \times 10^{-2}$ M,
Solvent; DMSO: Water=9 : 1.
The concentration of each dye is about 1×10^{-5} M.

	Dye	Quantum yield/%
a	MgChl-a (Chl-a)	23
	ZnChl-a	40
	CuChl-a	13
b	MgTPP	10
	ZnTPP	40
	CuTPP	1

state is considered to be responsible for the above reaction. MgTPP has the longest lifetime (46 ms[11]). ZnTPP the next one (25 ms[11]) and CuTPP the shortest one (0.6 ms[11]) at liq. N_2 temperature. Although the life-time was measured at liq. N_2 temperature, the order of their magnitude would be the same at room temperature. Therefore, it seems reasonable to attribute the lowest quantum yield of photoreduction for CuTPP to the shortest triplet life-time. However, it can not be explained in terms of the triplet life-time (τ_T) that the quantum yield for MgTPP is smaller than that for ZnTPP. Another factor to be taken into consideration would be the rate of triplet population (γ_T: the quantum yield of intersystem crossing). It is 0.97 for ZnTPP,[11] 0.84 for MgTPP[11] and 1.0 for CuTPP.[12] Since the reactivity would depend on the product, $\tau_T\gamma_T$, we compared its value for ZnTPP with that for MgTPP. The value for MgTPP (39 ms) is still larger than that for ZnTPP (24 ms). Therefore these factors could not explain the fact that ZnTPP is better than MgTPP for photoreduction of MV^{2+}. Another important factor to be taken into consideration is the energetical relation. Since the oxidation potential of ZnTPP (0.95 V *vs.* NHE) is more positive than that of MgTPP (0.78 V *vs.* NHE),[13] the cation radical of ZnTPP would oxidize EDTA more efficiently than that of MgTPP would if the reaction rate of the recombination between the dye cation and $MV^{+\cdot}$ is assumed not to depend on the kind of the central metal ions.

We tried hydrogen evolution by adding Pt or Pt/TiO_2 catalyst which is already a popular method.[9,14-16] After Pt catalyst was added to the solution of EDTA, MV^{2+}, and Chl-a (or ZnTPP) either in DMSO–water (1 : 1) mixture or in MeOH–water (8 : 2) mixture, it was irradiated by visible light (λ>440 nm) for 3 h. The hydrogen evolution was confirmed by a quadrupole mass spectrometer. The hydrogen evolution rate was about 5 μmol/h in MeOH–water mixture for ZnTPP.

This work was supported by the Joint Studies Program (1979) of the Institute for Molecular Science.

References

1) M. Calvin, *Acc. Chem. Res.*, **10**, 369 (1978).
2) T. Miyasaka, T. Watanabe, A. Fujishima, and K. Honda, *Nature*, **277**, 638 (1979).
3) F. K. Fong and L. Galloway, *J. Am. Chem. Soc.*, **100**, 3594 (1978).
4) T. Miyasaka, T. Watanabe, A. Fujishima, and K. Honda, *J. Am. Chem. Soc.*, **100**, 6657 (1978).
5) I. Okura and N. Kim-Thuan, *J. Mol. Catal.*, **6**, 227 (1979).
6) K. Takuma, M. Kajiwara, and T. Matsuo, *Chem. Lett.*, **1977**, 1199.
7) T. Watanabe, T. Miyasaka, A. Fujishima, and K. Honda, *Chem. Lett.*, **1978**, 443.
8) H. Tributsch and M. Calvin, *Photochem. Photobiol.*, **14**, 95 (1971).
9) A. Harriman, G. Porter, and M. C. Richoux, *J. Chem. Soc., Faraday Trans. 2*, **77**, 833 (1981).
10) W. E. Ford, J. W. Otvos, and M. Calvin, "Extended Abstracts of 2nd International Conference on the Photochemical Conversion and Storage of Solar Energy," Department of Physical Chemistry, University of Cambridge (1978), p. 149.
11) A. T. Gradyushko and M. P. Tsvirko, *Opt. Spectrosk.*, **31**, 548 (1971).
12) D. Eastwood and M. Gouterman, *J. Mol. Spectrosc.*, **30**, 437 (1969).
13) "Techiques of Chemistry," ed by A. Weissberger, John Wiley and Sons, Inc., New York (1975), Vol. 5, Part II, p. 1014.
14) T. Kawai and T. Sakata, *Chem. Lett.*, **1979**, 137.
15) J. Kiwi and M. Grätzel, *J. Am. Chem. Soc.*, **101**, 7214 (1979).
16) A. I. Krasna, *Photochem. Photobiol.*, **29**, 269 (1979).

Liquid Crystals of Binary Mixtures. Induction of Nematic Phase by Intermolecular Charge-transfer Interaction and Application of Solid-solution Model

Yôichi IIDA

Department of Chemistry, Faculty of Science, Hokkaido University, Sapporo 060

(Received February 15, 1982)

Synopsis. Nematic phase induced by binary mixture consisting of electron donor and acceptor was examined by using modified solid-solution model. The experimental results of Araya and Matsunaga were explained by this approach, and the charge-transfer interaction energy between donor and acceptor in the nematic phase was estimated by analyzing their phase diagrams.

Much attention has been paid to a great number of liquid crystals, which show intermediate state between crystalline solid and isotropic liquid.[1] Binary systems have been often used to achieve extended liquid crystalline temperature ranges. In binary mixtures consisting of electron donors and acceptors, parallel molecular arrangement required by liquid crystal formation becomes observable if an electron donor-acceptor charge-transfer interaction acts as the orientational forces.[2-5] Park *et al.* examined nematic phase→isotropic liquid transition temperature (T_{NI}) in the binary system of *N*-(*p*-methoxybenzylidene)-*p*-butylaniline (MBBA) and 4-cyano-4′-pentylbiphenyl (CPB), because there was a weak charge-transfer interaction between a donor of MBBA and an acceptor of CPB.[2] In this case, although both components of MBBA and CPB exhibit nematic phase→isotropic liquid phase transition, the relation of T_{NI} to the composition of MBBA–CPB mixture shows a broad curve whose maximum is located near 1 : 1 mole ratio, and T_{NI} of mixture is higher than the straight line joining T_{NI} of the two components. In order to understand the thermodynamic properties of the nematic phase, we applied a modified solid-solution model to the binary mixture of electron donor and acceptor, and explained well the relation of T_{NI} to composition.[5]

In binary mixture of donor and acceptor, even if the components show no liquid crystalline state, they may be considered to be potentially mesomorphic. Then, there is a possibility of induction of mesophase if those components are mixed. This was achieved by Araya and Matsunaga,[3] who observed nematic phase in the binary mixtures of potentially-mesomorphic electron donors and acceptors of the type *N*-(*p*-X-benzylidene)-*p*-Y-aniline. It acts as a donor if X or Y is dimethylamino group, and as an acceptor if X or Y is nitro group. The remaining substituents are methoxy, ethoxy or propoxy groups. For the binary systems of ethoxy derivatives, the experimental relations of T_{NI} to composition are given in Fig. 2 of Ref. 3, where nematic liquid crystals are stable in the hatched areas. In the present paper, for purposes of comparison with theoretical results, the T_{NI} *versus* composition curves of those combinations are reproduced in Fig. 1, where curves (a) show the experimental relation. It is to be noted that the relationship also shows a broad curve whose maximum is located near 1 : 1 mole ratio.

Let us consider these experimental results on the basis of our previous theoretical approach of binary solid-

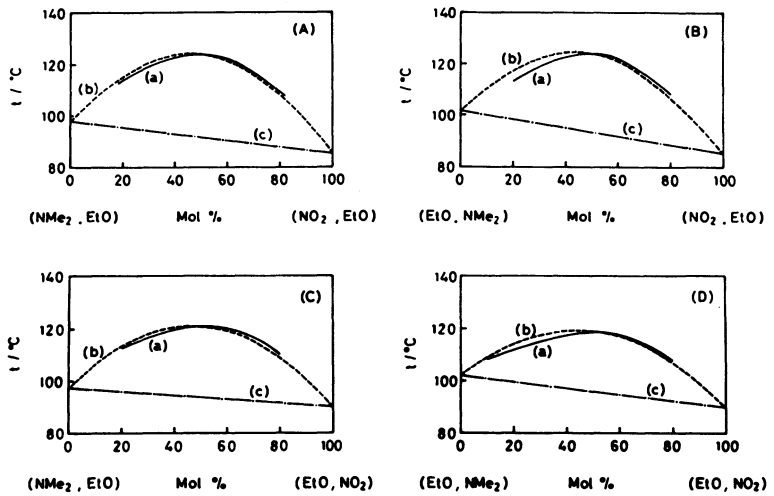

Fig. 1. Nematic phase→isotropic liquid transition temperature (T_{NI}) in the binary mixtures of *N*-(*p*-X-benzylidene)-*p*-Y-anilines, where the compounds are indicated by (X, Y). Curves (a) show experimental relation of T_{NI} to composition as reported by Araya and Matsunaga;[3] curves (b), theoretical relation of transition temperature (T_c) of order-disorder phase transition to composition as given by our modified solid-solution model; curves (c), straight lines joining T_{NI} of the two components. For further details, see text.

solution model. We examine binary mixtures of electron donor and acceptor, where donor is (X, Y)=(NMe_2, EtO) or (EtO, NMe_2), and where acceptor is (NO_2, EtO) or (EtO, NO_2). The mole fractions of donor and acceptor are x_D and x_A, respectively, where $x_D+x_A=1$. The model assumes that each of the components has nematic phase→isotropic liquid phase transition. In our compounds, however, each of the donor and acceptor shows no apparent nematic phase, but is considered to be potentially nematic. Araya and Matsunaga estimated the latent T_{NI} of the components as 97.5 °C for (NMe_2, EtO), 102 °C for (EtO, NMe_2), 85 °C for (NO_2, EtO) and 90 °C for (EtO, NO_2).[3] Let us denote the latent T_{NI} of pure donor or acceptor as T_D or T_A, respectively. Our model also assumes that the nematic phase of binary mixture is taken as three dimensional lattice, which is divided into two sublattices D and A, and the effect of mixing of donor and acceptor was only discussed.[5] For mixture with composition ($x_D \geq x_A$), when all acceptor molecules occupy sites of A sublattice, the system is called in order state. When donor and acceptor molecules occupy sites of D and A sublattices randomly, it is in disorder state. The situation is similar in the case of the composition ($x_D \leq x_A$). Then, if the charge-transfer interaction between donor and acceptor is essential for parallel molecular arrangement to induce nematic phase, the order→disorder phase transition with respect to mixing of donors and acceptors should correspond to nematic→isotropic phase transition. In other words, if the order of molecular arrangement of donors and acceptors remains, the system is supposed to be in nematic phase, while if the order is lost, it goes to isotropic liquid.

According to our previous study,[5] the temperature at which the order→disorder phase transition of such a binary system occurs is given by $T_C=x_DT_D+x_AT_A+4x_Dx_AT_C^\circ$, where $T_C^\circ=zv/2k$. Here, it is assumed that one site of D or A sublattice is surrounded by z equivalent nearest neighbor sites of A or D sublattice, respectively, and v is given by $v=(1/2)(v_{DD}+v_{AA})-v_{DA}$. The terms v_{DD}, v_{AA}, and v_{DA} indicate the energies between a pair of donor-donor, acceptor-acceptor and donor-acceptor molecules in nearest neighbor sites, respectively. Note that v_{DD} and v_{AA} arise from weakly attractive van der Waals forces between the same kind of molecules, while v_{DA} comes from rather strongly attractive forces due to the charge-transfer interaction between donor and acceptor. When the charge-transfer interaction is strong enough, we have $|v_{DA}| \gg (1/2)(|v_{DD}|+|v_{AA}|)$ and $v \approx -v_{DA} > 0$. In this case, $T_C^\circ=zv/2k(>0)$ increases considerably, and the relation of T_C to composition shows a broad curve whose maximum is located near 1 : 1 mole ratio. If the order→disorder phase transition corresponds to the nematic phase→isotropic liquid transition, we can observe considerable induction of the nematic phase upon mixing donors and acceptors. On the other hand, when the charge-transfer interaction is so small as $v_{DA} \approx (1/2)(v_{DD}+v_{AA})$, we have $v \approx 0$, $T_C^\circ \approx 0$ and $T_C=x_DT_D+x_AT_A$. Then, T_C *versus* composition is simply a straight line joining T_D at $x_D=1$ and T_A at $x_A=1$, and no stability enhancement of the nematic phase occurs.

In the following, we discuss how the relation of T_C to composition agrees with the observed T_{NI} *versus* composition curve. For example, we take the binary system of (NMe_2, EtO) donor and (NO_2, EtO) acceptor. The experimental relation between T_{NI} and composition is given by curve (a) of Fig. 1 (A). Here, curve (c) shows $x_DT_D+x_AT_A$, a straight line connecting T_D=97.5 °C and T_A=85 °C. Curve (b) represents $T_C=x_DT_D+x_AT_A+4x_Dx_AT_C^\circ$ with parameter value of T_C°=32 °C, which was chosen so as to obtain best fit between T_{NI} and T_C. Agreement between the curvatures of (a) and (b) is fairly good. The maximum value of T_{NI} occurs at x_D=0.50, while that of T_C, at x_D=0.45. This agreement is also satisfactory. In view of these results, the relation of T_C to composition corresponds well to that of T_{NI} to composition, and we can conclude that the charge-transfer interaction is essential for parallel molecular arrangement to induce nematic phase. From the estimated value of T_C°, zv is calculated as 0.53 kJ mol^{-1}.

In a similar way, the combination of the donor (EtO, NMe_2) with the acceptor (NO_2, EtO) gave values of T_C°=31 °C and zv=0.52 kJ mol^{-1}; the combination of (NMe_2, EtO) with (EtO, NO_2), T_C°=27 °C and zv=0.45 kJ mol^{-1}; the combination of (EtO, NMe_2) with (EtO, NO_2), T_C°=23 °C and zv=0.38 kJ mol^{-1}. For these systems, the relations of T_C to composition are compared with the experimental relations of T_{NI} to composition in Figs. 1 (B)—(D). In each case, the agreement between the two relations is satisfactory. Since the charge-transfer interaction is considerably strong, it appears that $|v_{DA}| \gg (1/2)(|v_{DD}|+|v_{AA}|)$ and that $zv_{DA} \approx -zv$ in each case. In order to estimate the v_{DA} value, it is necessary to determine the z value, but no further information has yet been obtained in the nematic phase of such binary mixtures.

References

1) See, for example, S. Chandrasekhar, "Liquid Crystals," Cambridge University Press, London, New York, New Rochelle, Melbourne, Sydney (1980).

2) J. W. Park, C. S. Bak, and M. M. Labes, *J. Am. Chem. Soc.*, **97**, 4398 (1975).

3) K. Araya and Y. Matsunaga, *Bull. Chem. Soc. Jpn.*, **53**, 3098 (1980).

4) A. C. Griffin, R. F. Fisher, and S. J. Havens, *J. Am. Chem. Soc.*, **100**, 6329 (1978); M. Domon and J. Billard, *J. Phys. (Paris), Colloq.*, **40**, C3-413 (1979); N. K. Sharma, G. Pelzl, D. Demus, and W. Weissflog, *Z. Phys. Chem. (Leipzig)*, **261**, 579 (1980).

5) Y. Iida, *Bull. Chem. Soc. Jpn.*, **55**, 313 (1982).

Reactions of Polymeric Chloromanganese(III) Schiff Base Complexes with Superoxide Ion in Dimethyl Sulfoxide

Takayuki MATSUSHITA,* Mitsuru NISHINO, and Toshiyuki SHONO
Department of Applied Chemistry, Faculty of Engineering, Osaka University, Yamadaoka, Suita, Osaka 565
(Received April 30, 1981)

Synopsis. The polymeric Mn(III) Schiff base complexes react with superoxide ions (O_2^-) in dimethyl sulfoxide (DMSO) to give the oxygenated complexes, while the corresponding monomeric Mn(III) complexes are reduced with O_2^- to the Mn(II) complexes.

Manganese ions play an important role in biological redox processes, the disproportionation of O_2^- by manganese-containing superoxide dismutases, and the photosynthetic water oxidation in green plants.[1-3] In the previous paper,[4] the monomeric Mn(III) Schiff base complexes are classified into two types according to their reactivity toward O_2^-: one gives the oxygenated complexes and the other is reduced to the Mn(II) complexes. This behavior can be correlated to the polarographic half-wave potentials for the reduction of Mn(III) to Mn(II). In this Note, the reactions of the polymeric Mn(III) complexes (shown below) with O_2^- in DMSO will be reported.

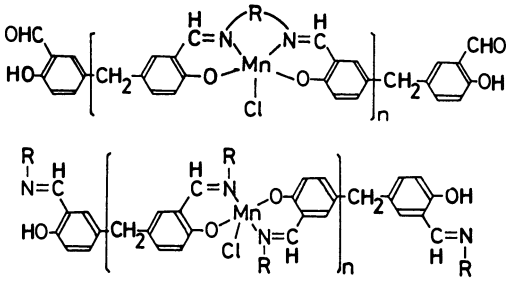

R	Abbreviation
$CH(CH_3)CH_2$	Mn(p-salpln)Cl
C_6H_{10}	Mn(p-salchxn)Cl
$(CH_2)_3NH(CH_2)_3$	Mn(p-saldpt)Cl
$(CH_2)_3N(CH_3)(CH_2)_3$	Mn(p-salMedpt)Cl
n-C_3H_7	Mn(*N*-Prdisai)Cl
n-C_4H_9	Mn(*N*-Budisai)Cl
c-C_6H_{11}	Mn(*N*-*c*-Hxdisai)Cl

Polymeric Mn(III) Schiff base complexes studied.

Experimental

The monomeric Mn(III) complexes, Mn(salpln)Cl, Mn(salchxn)Cl, Mn(saldpt)Cl, Mn(salMedpt)Cl, and chlorobis(*N*-alkylsalicylideneaminato)manganese(III), Mn(*N*-Rsai)$_2$Cl (R=*n*-C_3H_7 (Pr), *n*-C_4H_9 (Bu), and *c*-C_6H_{11} (*c*-Hx)), were prepared by a modification of the method described elsewhere;[4] salplnH$_2$: *N*,*N*′-disalicylidenepropylenediamine, salchxnH$_2$: *N*,*N*′-disalicylidene-1,2-cyclohexanediamine, saldptH$_2$: bis[3-(salicylideneamino)propyl]amine, salMedptH$_2$: bis[3-(salicylideneamino)propyl]methylamine.

Polymeric Schiff Bases. The polymeric Schiff base, p-salplnH$_2$ was obtained by polycondensation of 5,5′-methylenedisalicylaldehyde (disalH$_2$) with propylenediamine in dichloromethane (CH_2Cl_2). This was reprecipitated from a mixture of CH_2Cl_2–ether. The other polymeric Schiff bases, p-salchxnH$_2$, p-saldptH$_2$, and p-salMedptH$_2$, were obtained in a similar manner. The analytical data, specific viscosities (Table 1), and ^{1}H NMR data indicate that these polymeric Schiff bases are oligomers whose degrees of condensation (n) are within a range of three to five.

N,*N*′-Dibutyl-5,5′-methylenedisalicylideneamine, *N*-BudisaiH$_2$, was obtained by the condensation of disalH$_2$ with *n*-butylamine in tetrahydrofuran. This was recrystallized from a mixture of ether–petroleum ether. The other Schiff bases, *N*-PrdisaiH$_2$ and *N*-*c*-HxdisaiH$_2$ were obtained in a similar manner.

Preparation of Polymeric Mn(III) Complexes. The polymeric Mn(III) complex, Mn(p-salpln)Cl, was obtained by reacting p-salplnH$_2$ with Mn(CH$_3$COO)$_3$·2H$_2$O and LiCl in a mixture of CH_2Cl_2–MeOH, and was reprecipitated from a mixture of MeOH–ether. Mn(p-salchxn)Cl, Mn(p-saldpt)Cl, and Mn(p-salMedpt)Cl were obtained in a similar manner. The other polymeric complexes, Mn(*N*-Rdisai)Cl (R=Pr, Bu, and *c*-Hx), were obtained in a manner similar to that used for Mn(p-salpln)Cl, and were reprecipitated from a mixture of CH_2Cl_2–ether. These polymeric complexes are soluble in MeOH and DMSO. The analytical data and specific viscosities (Table 1) indicate that they are oligomers whose degrees of condensation are within a range of three to five.

Measurements. ^{1}H NMR spectra were taken on a JEOL JNM-PS 100 spectrometer using TMS as the internal standard. The specific viscosities were determined using an Ostwald's viscometer at 25±0.1 °C (0.40 g/solvent 100 cm^3). The other physical measurements were carried out by the method described elsewhere.[4]

Reactions of the Mn(III) complexes with KO_2 in DMSO were made by the procedure described elsewhere.[4]

Results and Discussion

We have previously found that the absorption spectral and polarographic changes can be used to distinguish clearly between the formation of the oxygenated complexes and the reduction of Mn(III) to Mn(II)

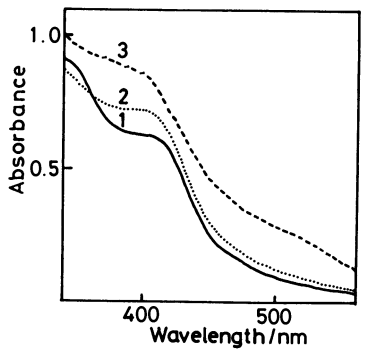

Fig. 1. Spectral changes of a DMSO solution of Mn(p-salpln)Cl (1×10^{-4} unit mol dm^{-3}) caused by the addition of KO_2.
1): No addition, 2): $[KO_2]/[Mn]=1$, 3): 3. Cell length: 1 cm.

Table 1. Properties of polymeric Mn(III) complexes, Mn(p-L)Cl and Mn(*N*-Rdisai)Cl, and of corresponding monomeric Mn(III) complexes, Mn(L)Cl and Mn(*N*-Rsai)$_2$Cl

Ligand		η_{sp}[b]	μ_{eff}[e] / BM	λ_{max}[f] / nm		$-E_{1/2}$ *vs.* Hg pool[g] / V
p-L	η_{sp}[a]			DMSO	Solid	
p-salpln	0.049	0.051	4.92 (5.03)	620sh (605)	630sh (618sh)	0.07 (0.18)
p-salchxn	0.057	0.058	4.97 (4.96)	605 (588)	628sh (612sh)	0.00[h] (0.21)
p-saldpt	0.028	0.033	4.96 (5.14)	595 (584)	618 (610)	0.01 (0.05)
p-salMedpt	0.035	0.044[c]	5.10 (4.77)	592 (570)	616 (608)	−0.01 (0.16)
N-Prdisai	—	0.028[c]	5.04 (4.86)	596 (580)	670 (666)	0.02[h] (0.05)
N-Budisai	—	0.028[d]	4.94 (5.03)	584 (579)	670 (658)	0.02 (0.02)
N-*c*-Hxdisai	—	0.020[d]	5.06 (4.89)	566 (572)	636sh (679)	0.02 (0.00)

Values in parentheses correspond to the monomeric complexes. a) Specific viscosities of polymeric Schiff bases measured in $CHCl_3$. b) Specific viscosities measured in DMSO. c) In MeOH. d) In $CHCl_3$. e) Magnetic susceptibilities measured at room temperature and calculated from manganese content for the polymeric complexes. f) Absorption maxima. g) Reduction potentials measured in CH_3CN containing 0.1 mol dm^{-3} Bu_4NClO_4. h) In DMSO.

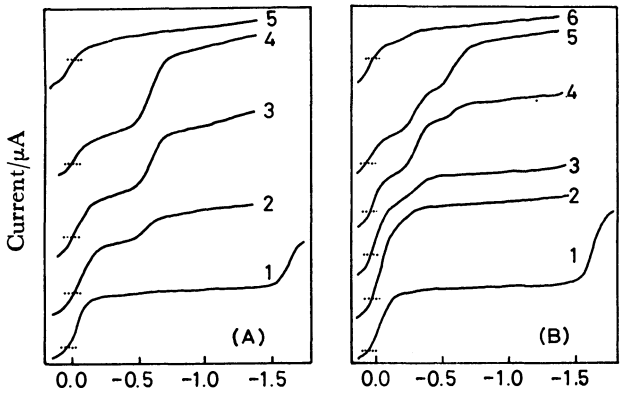

Fig. 2. Polarograms in the reactions of Mn(*N*-Prsai)$_2$Cl (A) and of Mn(*N*-Prdisai)Cl (B) with KO_2 in DMSO containing 0.1 mol dm^{-3} Bu_4NClO_4 at 25 °C.
(A); [Complex]$=2\times10^{-4}$ mol dm^{-3}, 1): no addition, 2): [KO_2]/[Mn]$=1$, 3): 3, 4): 6, 5): after passing N_2 through the solution shown by the curve 4. (B); [Complex]$=2\times10^{-4}$ unit mol dm^{-3}, 1): no addition, 2): [KO_2]/[Mn]$=1$, 3): 2, 4): 3, 5): 4, 6): after passing N_2 through the solution shown by the curve 5.

in the reactions of the Mn(III) Schiff base complexes with O_2^- in DMSO.[4] Figure 1 shows the spectral changes of a DMSO solution of Mn(p-salpln)Cl caused by the addition of a KO_2 DMSO solution. A broad absorption band appeared around 500 nm at the KO_2/Mn$=3$, indicating the formation of the oxygenated complex. The other polymeric Mn(III) complexes show spectral changes similar to the above.

Figures 2-A and 2-B show the changes in polarograms in the reactions of O_2^- with the monomeric Mn(*N*-Prsai)$_2$Cl and polymeric Mn(*N*-Prdisai)Cl in DMSO, respectively. In the case of Mn(*N*-Prsai)$_2$Cl, as the ratio of KO_2/Mn increased, the wave height at −0.03 V due to the reduction of Mn(III) to Mn(II) decreased and a new cathodic wave appeared at −0.55 V; this can be assigned to the reduction of free molecular oxygen. This indicates that Mn(*N*-Prsai)$_2$Cl is reduced to the Mn(II) complex and O_2^- is oxidized to O_2. In the case of Mn(*N*-Prdisai)Cl, a new cathodic wave was observed at *ca.* −0.25 V by the addition of KO_2 (KO_2/Mn$=$ 1—3), indicating the formation of the oxygenated complex. The other polymeric Mn(III) complexes show polarograms similar to the above. These results indicate that all the polymeric Mn(III) complexes investigated here react with O_2^- to give the oxygenated complexes, although the corresponding monomeric Mn(III) complexes are reduced with O_2^- to the Mn(II) complexes, with the exception of Mn(salchxn)Cl which gives the oxygenated complex.[4]

The polymeric complexes showed slightly positive reduction potentials compared with those for the monomeric complexes (Table 1). Nevertheless, the oxygenated complexes are found to be stabilized in the polymeric complexes. This may be caused by a polymeric sturcture in which the central manganese atoms are not isolated from the surroundings, unlike the monomeric complexes. In such an environment, interaction between DMSO molecules and the central manganese atom may be weakened by steric repulsion and thus the oxygenated complex may be protected from dissociation into the Mn(II) complex and O_2, because the dissociation should proceed *via* displacement of coordinated dioxygen with DMSO molecules. This consideration is not inconsistent with the spectral data (Table 1): the ligand field bands assignable to the $d_{xy}\rightarrow d_{x^2-y^2}$ transition[5] are observed at lower energies in the polymeric complexes than those for the monomeric complexes.

References

1) G. D. Lawrence and D. T. Sawyer, *Coord. Chem. Rev.*, **27**, 173 (1978).
2) W. M. Coleman and L. T. Taylor, *Coord. Chem. Rev.*, **32**, 1 (1980).
3) D. T. Sawyer, M. E. Bodini, L. A. Willis, T. L. Riechel, and K. D. Magers, *Adv. Chem. Ser.*, **162**, 330 (1977).
4) T. Matsushita and T. Shono, *Bull. Chem. Soc. Jpn.*, **54**, 3743 (1981).
5) L. J. Boucher and V. W. Day, *Inorg. Chem.*, **16**, 1360 (1977).

The Color Isomerism of Oxovanadium(IV) Complexes with Tetradentate Schiff Base

Kuninobu KASUGA,* Takeo NAGAHARA,† and Yasuo YAMAMOTO
Department of Chemistry, Faculty of Science, Shimane University, Matsue 690

(Received November 24, 1981)

Synopsis. An oxovanadium(IV) complex with *N,N'*-bis(1-methyl-2-bromo-3-oxobutylidene)ethylenediamine gave green and yellow forms in the solid state, depending upon the solvents used for recrystallization. A polymeric structure was proposed for the yellow form.

As has been reviewed elsewhere,[1-3] there have been a considerable number of spectroscopic and magnetic studies of oxovanadium(IV) complexes. Almost all complexes are blue or blue-green and exhibit strong V=O stretching frequencies around 1000 cm^{-1}. On the other hand, oxovanadium(IV) complexes of salicylideneamine, β-thioxo ketones, and dithiophosphinic acids with electron-withdrawing substituents,[4-6] and *N,N'*-disalicylidenepropylenediamine,[7,8] are yellow and shift their V=O bands to lower frequencies (around 900 cm^{-1}). The shift in the V=O stretching frequencies has been considered to be an indication of an oxygen bridging, V–O–V, polymeric-chain formation.[5,7,9] Recently, the yellow color and low V=O frequencies of oxovanadium(IV) complexes with some bidentate Schiff bases were explained in terms of distorted trigonal bipyramidal structure.[10] In the trigonal bipyramid, the three oxygen and vanadium atoms are on the equatorial plane, while the two nitrogen donors occupy axial positions. We wish to report here that an oxovanadium(IV) complex with *N,N'*-bis(1-methyl-2-bromo-3-oxobutylidene) ethylenediamine (VO(L-Br)) yields two color isomers in the solid state.

Experimental

Syntheses. [*N,N'*-Bis(1-methyl-3-oxobutylidene)ethylenediaminato]oxovanadium(IV) (VO(L)) was synthesized according to the method reported by Martin *et al.*[11]

[N,N'-Bis(1-methyl-2-bromo-3-oxobutylidene)ethylenediaminato]-oxovanadium(IV) (VO(L-Br)): *N*-Bromosuccinimide (1.8 g) was added to 20 cm^3 of a dichloromethane solution of VO(L) (1.4 g) at 0 °C, and the mixture was stirred below 0 °C for 20 min. After small amounts of precipitates had been filtered off, the filtrate was concentrated to 2—3 cm^3 under reduced pressure. The precipitates were subsequently obtained by the addition of adequate amounts of methanol. The yellow needles were recrystallized from dichloromethane (yield, 65%); IR: 902 cm^{-1} (V=O). Found: C, 32.51; H, 3.59; N, 6.69%. Calcd for $C_{12}H_{16}N_2O_3Br_2V$: C, 32.24; H, 3.66; N, 6.27%. An yellow [*N,N'*-bis(1-methyl-2-chloro-3-oxobutylidene)ethylenediaminato]oxovanadium(IV) (VO(L-Cl)) complex was synthesized using *N*-chlorosuccinimide instead of *N*-bromosuccinimide (yield, 67%); IR: 892 cm^{-1} (V=O). Found: C, 39.94; H, 4.13; N, 7.53%. Calcd for $C_{12}H_{16}N_2O_3Cl_2V$: C, 40.24; H, 4.51; N, 7.82%. Hydrogen chloride was bubbled through a dichloromethane solution of VO(L-Cl) for a few min to obtain a free ligand. The ligand thus precipitated was separated out; it was washed with water and subsequently with ethanol. On the other hand, no free L-Br ligand was obtained because of the decomposition of VO(L-Br) with hydrogen chloride.

Adducts of VO(L-Br) and VO(L-Cl) with 1-Methylimidazole: A 5 cm^3 portion of 1-methylimidazole was added to 20 cm^3 of a dichloromethane solution containing 1.3 g of VO (L-Br). After the solution had been refluxed for a few min, it was condensed to 2—3 cm^3. The brown adduct was precipitated by the addition of adequate amounts of hexane and subsequently washed with ether (yield, 68%); IR: 959 cm^{-1} (V=O). Found: C, 35.94; H, 4.14; N, 10.90%. Calcd for $C_{16}H_{22}N_4O_3Br_2V$: C, 36.31; H. 4.20; N, 10.59%. A brown adduct of the chloro derivative was obtained by a method similar to that described above (yield, 75%); IR: 959 cm^{-1} (V=O). Found: C, 43.36; H, 4.95; N, 12.67%. Calcd for $C_{16}H_{22}N_4O_3Cl_2V$: C, 43.65; H, 5.04: N, 12.73%.

Measurements. The infrared spectra were measured using nujol mull methods, on a Hitachi 215 spectrophotometer. The electronic spectra in sloution and in the solid state were measured on a Hitachi 124 spectrotometer and a Shimadzu spectrophotometer Model MPS-5000 respectively. The NMR spectra were recorded with a JEOL-MH 100 spectrophotometer at a frequancy of 100 MHz. The chemical shifts were determined in ppm, using TMS as the internal standard. The ESR spectra (X-band) of polycrystalline samples were obtained on a JEOL-1X apparatus. The X-ray powder diffraction analyses were carried out on a Toshiba ADG-301 apparatus.

Results and Discussion

Structures of Schiff-base Ligands. An NMR spectrum of the free L-Cl ligand eliminated from VO(L-Cl) shows three proton signals in 1,1,2,2-tetrachloroethane-d_2 (TCE-d_2); δ=2.16 (12H, d, CH_3), 3.36 (4H, m, CH_2), and 11.40 ppm (2H, broad s, OH). An unsubstituted free ligand, L, also shows four proton signals in TCE-d_2 at 1.86 (12H, d, CH_3), 3.30 (4H, m, CH_2), 4.92 (2H, s, CH), and 10.92 ppm (2H, broad s, OH). The signals of the methine protons in L disappeared in the chloro derivative, indicating the chlorination on the 2-position carbon of the complex. All the proton signals of the chloro derivative were shifted to a lower magnetic field compared with those of L. This tendency is attributable to an inductive effect of the chlorine atom. The bromination must also occur on the 2-position carbon.

Isolation of the Green and Yellow Forms. The yellow form was obtained by the recrystallization of the VO(L-Br) complex from dichloromethane, and the green, from tetrahydrofuran. However, the VO(L-Cl) complex only gave the yellow form upon recrystallization from both dichloromethane and tetrahydrofuran. On the other hand, the green form of VO(L) was easily recrystallized from common organic solvents, though the yellow was not obtained at all. The yellow forms seem to be easily isolated according to an increase in the electron negativities of the substituents. In the case of

† Present address: Izumo Technical High School, Izumo, Shimane 693.

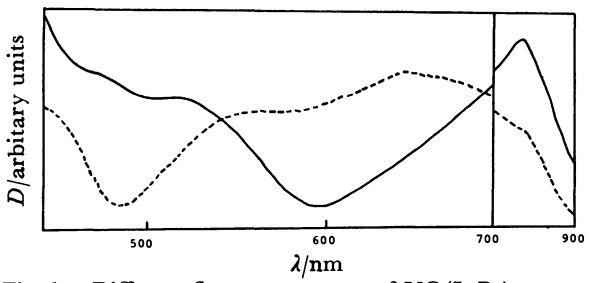

Fig. 1. Diffuse-reflectance spectra of VO(L-Br).
——: Yellow form, ------: green form.

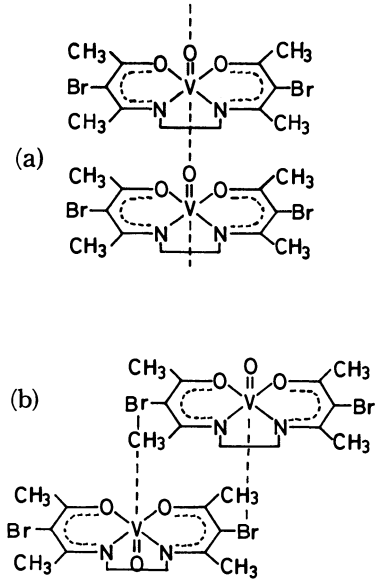

Fig. 2. The proposed structures for the yellow VO(L-Br) form.

VO(L-Br), the thermodynamic stabilities of the green and yellow forms might be similar, so that the two forms can be individually isolated by selecting appropriate solvents for recrystallization.

IR, Electronic, ESR, and X-Ray Powder Spectra. The V=O stretching frequencies of the green and yellow forms appear at *ca.* 980 and *ca.* 900 cm^{-1} respectively. This shift to lower frequencies for the yellow forms is in accord with the previously reported data for the yellow polymeric oxovanadium(IV) complexes.[4-8] The V=O stretching frequencies (959 cm^{-1}) of the 1-methylimidazole adducts lie between the values for the green and yellow forms. Both the green and yellow forms of the bromo derivative are dark green in common organic solvents, and they exhibit the same electronic spectra. The diffuse-reflectance spectra of VO(L-Br) are shown in Fig. 1. The spectrum of the yellow form significantly differs from that of the green in the solid state; the absorption band around 660 nm of the green form disappears in the yellow. The spectrum of the yellow VO(L-Br) form is similar in pattern to that of the yellow polymeric oxovanadium(IV) complex with β-thioxo ketone.[5] The ESR spectra for the green and yellow forms of VO(L-Br) were obtained in the powdered solid state at room temperature with no hyperfine structures. The g_0 value (1.972) of the yellow form is smaller than that of the green (g_0=1.984). This suggests that the electron delocalization increases in going from the green form to the yellow. The ESR spectra of VO(L-Br) diluted with Ni(II)(L) were also measured, but no clear hyperfine structures were obtained. In the X-ray powder-diffraction spectra of VO(L-Br), the peak at 14.5° of the green form became weak and a new intense peak appeared at 9.3° in the yellow. This shows different crystal forms between the green and yellow isomers.

Structure of the Yellow Form. A polymeric or distorted trigonal bipyramidal structure might be proposed for the yellow form, judging from previous reports.[5,7,9,10] The distorted trigonal bipyramid reported for the bidentate Schiff-base complexes seems difficult for the present tetradentate Schiff-base complex because of its steric hindrance. Either of the structures in Fig. 2 would be possible for the yellow form. The nitrogen atom of 1-methylimidazole must be coordinated to the vanadium(IV) ion more strongly than the bromine atom. Thus, the V=O stretching frequency of the adduct should be shifted to a lower frequency compared with that of the dimer, in which the vanadium(IV) ion is coordinated by bromine (Fig. 2b). However, the V=O stretching frequency of the adduct is higher than that of the yellow form of VO(L-Br). Therefore, the (a) structure seems more reasonable for the yellow form.

The authors wish to thank Dr. Kunihisa Sogabe of this University for his measurements of the ESR and Dr. Yuzo Nishida of Kyushu University for his measurements of the diffuse-reflectance spectra. This work was partially supported by a Grant-in-Aid for Scientific Research No. 00547042 of the Ministry of Education, Science and Culture.

References

1) J. Selbin, *Chem. Rev.*, **65**, 153 (1965).
2) J. Selbin, *Coord. Chem. Rev.*, **1**, 293 (1966).
3) A. Syamal, *Coord. Chem. Rev.*, **16**, 309 (1975).
4) A. P. Ginberg, E. Koubek, and H. J. Williams, *Inorg. Chem.*, **5**, 1656 (1966).
5) B. J. McCormick and R. A. Bozis, *Inorg. Chem.*, **10**, 2806 (1971).
6) R. G. Cavell, E. P. Day, W. Dyers, and P. M. Watkins, *Inorg. Chem.*, **11**, 1591 (1972).
7) M. Mathew, A. J. Carty, and G. J. Palenik, *J. Am. Chem. Soc.*, **92**, 3197 (1970).
8) G. A. Kolawole and K. S. Patel, *J. Chem. Soc., Dalton Trans.*, **1981**, 1241.
9) R. L. Farmer and F. L. Urbach, *Inorg. Chem.*, **13**, 587 (1974).
10) M. Pasquali, F. Marchetti, and C. Floviani, *J. Chem. Soc., Dalton Trans.*, **1977**, 139.
11) D. F. Martin and K. Ramiak, *J. Inorg. Nucl. Chem.*, **27**, 2027 (1965).

Gas-chromatographic Measurements of Dinitrogen Oxide in Surface Air

Michio HIROTA* and Hisafumi MURAMATSU
Meteorological Research Institute, Nagamine, Yatabe-machi, Tsukuba-gun, Ibaraki 305
(Received September 30, 1981)

Synopsis. The mixing ratio of N_2O in surface air was measured at Tsukuba between July and September, 1980. The mean was 0.32_5 ppm, and the standard deviation was 0.00_8 ppm. No difference in the N_2O content was found between the air blowing from the northeast or south and calm air.

Recently many measurements of atmospheric dinitrogen oxide have been performed by gas-chromatographic (GC) methods using an electron-capture detector (ECD),[1] and the mixing ratio of the tropospheric N_2O has been found to be almost constant in the range from 0.31 to 0.34 ppm, within about a 10% systematic error among many laboratories.[2-7] In this study, the results of measurements of N_2O in the surface air at the Meteorological Research Institute, Tsukuba, will be reported, since the major source of the atmospheric N_2O is the activity of microorganisms in soils and waters, and since the diurnal variation has, for example, previously been reported in surface air.[8,9]

Experimental

Air 1 m above a ground surface covered with weeds was sampled by means of an air pump into a 2-ml gas sampling tube and was then transferred into a stainless steel column (6 ft× 1/8″ o. d.) filled with Porapak Q or QS (50—80 mesh, 35 °C). GC measurements were performed using a Perkin-Elmer Gas Chromatograph Sigma 1-Sigma 10 system equipped with an ECD (350 °C). A 95% Ar–5% CH_4 mixture was used as the carrier gas at a flow rate of 25 ml min^{-1}. The reference air, which was compressed into a 50-l stainless steel container up to 7 kg cm^{-2} and which could be used for 40—50 d, was first analyzed; then, after one hour, the outdoor air was sampled and analyzed. Such a pair of measurements was repeated every 6 h. The mixing ratio of N_2O in the reference air was determined by a previously reported method.[7] The error in the repeating measurements of the reference air was about 1%, and the detection limit was about 0.00_4 ppm. The total error in the measurements was estimated to be about ±5%.

Results and Discussion

Figure 1 shows the measurement results at Tsukuba from July to September, 1980, together with the temperature and wind data, which were obtained from the Aerological Observatory. The mean value for 60 measurements was 0.32_5 ppm, and the standard deviation (*SD*) was 0.00_8 ppm. Similar results have been obtained in many measurements of surface air in the U.S.A.,[2-5] Japan,[10,11] New Zealand,[2] Australia,[6] and England;[12] *i.e.*, the mixing ratio of N_2O in surface air is almost constant, more than 0.30 ppm.

In Fig. 2, the results are plotted for each wind direction. Figures 1 and 2 show that no difference in the mixing ratio of N_2O was found between the air blowing from the northeast or south and calm air, though a high mixing ratio of N_2O was expected to be observed under calm meteorological conditions at Tsukuba, a suburban agricultural area. The mixing ratios also showed no correlation with the temperature, even under calm conditions. Accordingly, no diurnal variation was observed. Similar results were obtained in Yokohama[13] and Kobe.[11] This must be due to the height of the air sampling;[9] 1 m above the ground surface, N_2O would be well mixed.

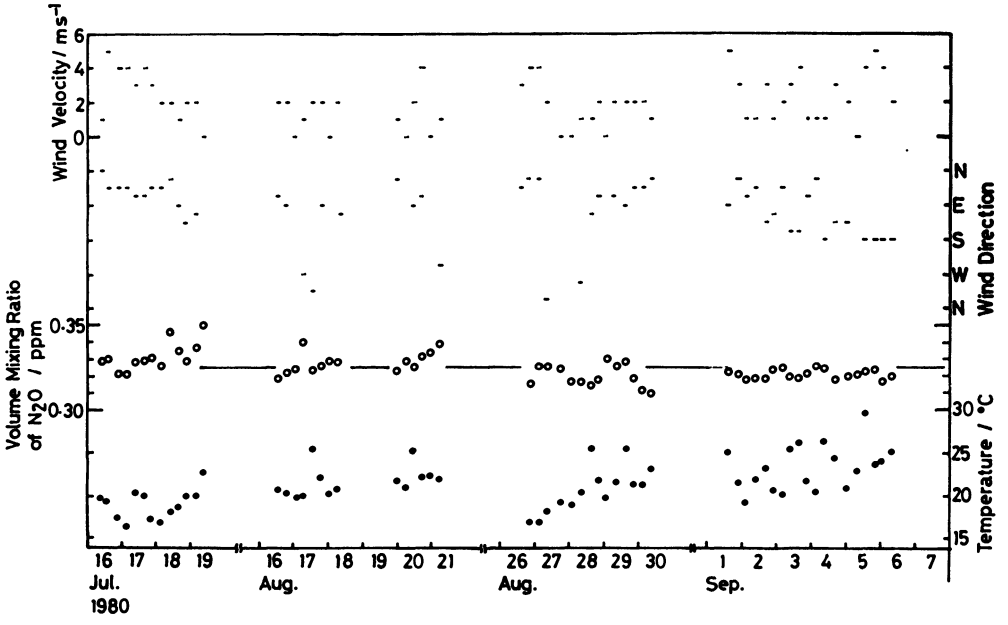

Fig. 1. The mixing ratio of N_2O in the surface air at Tsukuba between July and September, 1980.
——: Mean value (0.32_5 ppm). Wind and temperature data are also shown.

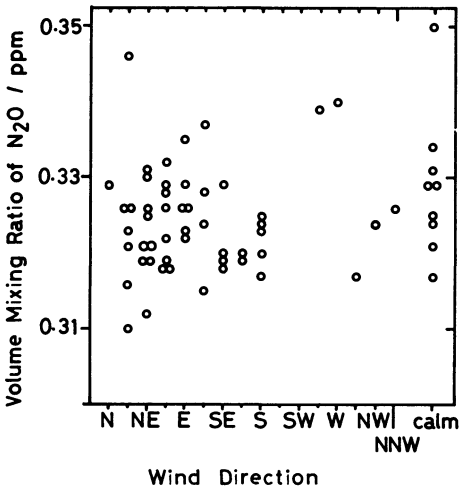

Fig. 2. The dependence of the mixing ratio of N_2O on the wind direction at Tsukuba.

The mean mixing ratio of N_2O observed at Tsukuba was almost equal to that of urban air at Kobe in the same year (mean value=0.319 ppm; *SD*=0.011 ppm).[11] Nearly the same mixing ratios were also observed from several measurements at Koenji, Tokyo, in the previous year (1979). The mean value was 0.32_7 ppm, and the *SD* was 0.00_9 ppm for 16 measurements between March and June.† This also shows that no difference in the mixing ratio of N_2O between urban and suburban air was found.

Much lower mean mixing ratios have been reported: 0.26 ppm in the summer of 1976[14] and 0.25 ppm in the summer of 1977[13] at Yokohama. The analytical method was improved from a GC-TCD one to a GC-MS one without preconcentration, and the *SD* of the measurement values decreased from 0.04 ppm to 0.015 ppm. One reason for the discrepancy between the GC-ECD method in the present study and the GC-MS one[13] would be that the calibration gas was composed of pure N_2 instead of purified air in the latter study. It is known at least that the sensitivity of ECD is raised by the presence of O_2.[15]

† Measurements were performed using a column filled with molecular sieve 5A.[7]

References

1) R. A. Rasmussen and D. Pierotti, *Geophys. Res. Lett.*, **5**, 353 (1978).
2) D. Pierotti and R. A. Rasmussen, *J. Geophys. Res.*, **82**, 5823 (1977).
3) H. A. Singh, L. Salas, H. Shigeishi, and A. Crawford, *Atmos. Environ.*, **11**, 819 (1977).
4) P. D. Goldan, Y. A. Bush, F. C. Fehsenfeld, D. A. Albritton, P. J. Crutzen, A. L. Schmeltekopf, and E. E. Ferguson, *J. Geophys. Res.*, **83**, 935 (1978).
5) R. J. Cicerone, J. D. Shetter, D. H. Stedman, T. J. Kelly, and S. C. Liu, *J. Geophys. Res.*, **83**, 3042 (1978).
6) C. R. Roy, *J. Geophys. Res.*, **84**, 3711 (1979).
7) H. Muramatsu, M. Hirota, and Y. Makino, *Bull. Chem. Soc. Jpn.*, **55**, 117 (1982).
8) K. A. Brice, A. E. Eggleton, and S. A. Penkett, *Nature*, **268**, 127 (1977).
9) A. D. Matthias, A. M. Blackmer, and J. M. Bremner, *Geophys. Res. Lett.*, **6**, 441 (1979).
10) S. Araki, S. Suzuki, M. Yamada, H. Suzuki, and T. Hobo, *J. Chromatogr. Sci.*, **16**, 249 (1978).
11) T. Hiraki, M. Tamaki, and H. Watanabe, *Rep. Environ. Sci. Inst. Hyogo Pref.*, **12**, 1 (1980).
12) J. C. Ryden, *Nature*, **292**, 235 (1981).
13) Y. Hanai, T. Katou, and T. Arai, *Bull. Inst. Environ. Sci. Tech., Yokohama National Univ.*, **5**, 35 (1979).
14) T. Katou, Y. Hanai, and M. Mimura, *Bull. Inst. Environ. Sci. Tech., Yokohama National Univ.*, **3**, 5 (1977).
15) E. P. Grimsrud and D. A. Miller, *Anal. Chem.*, **50**, 1141 (1978).

Substitution Reaction of In-plane Ligand in Bis(dimethylglyoximato)-cobalt(II) Complex with *N,N'*-Disalicylideneethylenediamine

Keisuke MITA,* Kazuhiko HOTTA, and Shoji WATANABE
Osaka Municipal Technical Research Institute, Morinomiya, Joto-ku, Osaka 536

(Received November 30, 1981)

Synopsis. A spectrophotometric study of the reaction $Co(dmgH)_2+salenH_2 \rightarrow Co(salen)+2\ dmgH_2$, in which $dmgH_2$ is dimethylglyoxime and $salenH_2$ is *N,N'*-disalicylideneethylenediamine, was carried out in methanol at 22 °C. The reaction rate decreased with increased amounts of added pyridine, and reached a stationary value at the molar ratio [pyridine]/[$Co(dmgH)_2$]=1. The form of the rate expression was $d[Co(salen)]/dt=k[Co(dmgH)_2]$ where the rate constant $k=0.023\ min^{-1}$.

In vitamin B_{12}, it has been reported that the 5,6-dimethylbenzimidazole axial base dissociates from the central cobalt atom very easily and that probably the base-off form contributes as a reactive intermediate during enzymatic reactions.[1] Therefore it is significant to study the properties of the base-off form in vitamin B_{12} or in a suitable model system. The high reactivity of the base-off form has been known in the electrochemical reduction of central cobalt atom[2] or in the cleavage of carbon-cobalt bond for vitamin B_{12} or for the model compounds.[3] However there have been few reports concerning the difference between the base-off form and base-on form in the reactivity of the in-plane ligand.

In the present work the substitution reaction of in-plane ligand in $Co(dmgH)_2$ complex (dmgH is the monoanion of dimethylglyoxime), which has been known as a good model compound of vitamin B_{12r}, was carried out in the presence and in the absence of axial base pyridine. $SalenH_2$ (*N,N'*-disalicylideneethylenediamine) was chosen as the substrate for the substitution reaction, because the reaction with $salenH_2$ was found to be a clean reaction, as expressed by

$$Co(dmgH)_2 + salenH_2 \longrightarrow Co(salen) + 2dmgH_2 \quad (1)$$

and it proceeds at an appropriate reaction rate in methanol solution at room temperature.

Experimental

A 30 cm^3 deoxygenated methanol solution of $Co(dmgH)_2$ complex was prepared at 2.0 mM† with 14.94 mg (0.06 mmol) of cobalt acetate tetrahydrate, 13.92 mg (0.12 mmol) of dimethylglyoxime, 4.8 mg (0.12 mmol) of sodium hydroxide and an appropriate amount of pyridine by the method of Schrauzer.[4] *N,N'*-Disalicylideneethylenediamine and Co(salen)was prepared by the method of Pfeiffer.[5]

The substitution reaction of $Co(dmgH)_2$ with $salenH_2$ was initiated by the injection of the deoxygenated methanol solution of $salenH_2$, which was prepared just before use, into the solution of $Co(dmgH)_2$ complex. After a small quantity of the reaction mixture was transferred to a 1 mm quartz cell, which was joined to the reaction vessel, the reaction progress was monitored by the measurement of the change in the visible absorption spectra in the thermostated cell compartment. The concentration of $Co(dmgH)_2$, $salenH_2$ and Co(salen) could then be determined by solving the equation described elsewhere.[6]

† 1 M=1 mol dm^{-3}.

Results and Discussion

Methanol solutions of $Co(dmgH)_2$ were prepared from cobalt acetate tetrahydrate and dimethylglyoxime without pyridine in concentrations ranging from 1 to 3 mM, and the visible absorption spectra were measured. When pyridine was added to the solutions no detectable change in the spectra was observed. When the absorbances of the spectra of those solutions at 472 nm were plotted against the amount of cobalt acetate tetrahydrate used for the complexation reaction, the plot showed a straight line with zero intercept. The results exhibit that, both in the presence and in the absence of pyridine, the complexation reaction between cobalt acetate tetrahydrate and dimethylglyoxime is complete in the present experimental conditions and that in both cases the spectra are almost the same. Similarly, at the concentrations ranging from 1 to 3 mM, cobalt acetate tetrahydrate and $salenH_2$ formed the 1 : 1 complex completely and the spectra of the solution showed no detectable change with the addition of pyridine.

The time-dependent change of spectra in the reaction between $Co(dmgH)_2$ and $salenH_2$ at equimolar ratio was measured in the molar ratios of pyridine to Co-$(dmgH)_2$, [py]/[$Co(dmgH)_2]_o$, =0.5, 0.8, 1.0, and 2.0 respectively. All of them showed distinct isosbestic points at 449 and 488 nm. A typical example is shown in Fig. 1. After the reaction was completed, the spectrum, for example of in Fig. 1, was found to be

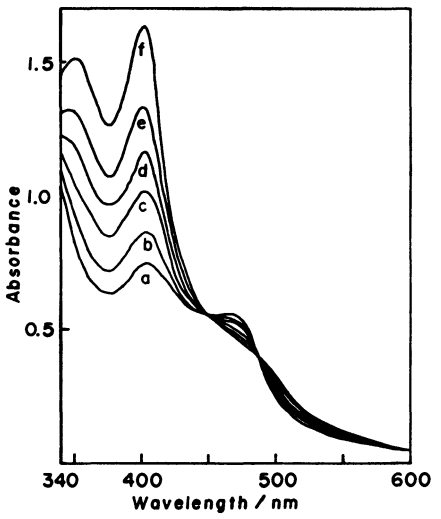

Fig. 1. Visible absorption spectra in the reaction between $Co(dmgH)_2$·py and $salenH_2$ in methanol at 22 °C after mixing 10(a), 15(b), 25(c), 35(d), 55(e), and 120 min(f) respectively.
Initial concentration: $Co(dmgH)_2$; 1.80, $salenH_2$; 1.80, and pyridine; 1.80 mM.

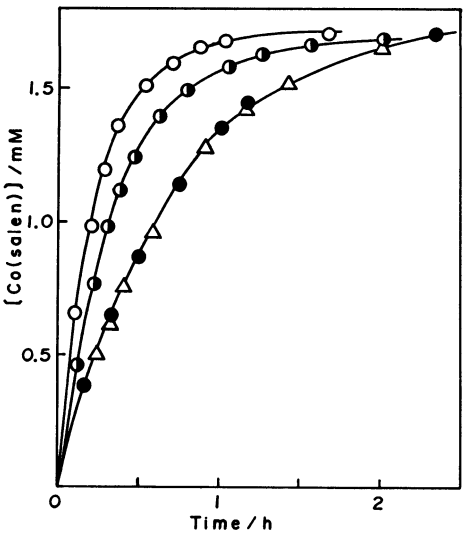

Fig. 2. Plots of the concentration of Co(salen) against reaction time for the substitution reaction at 22 °C.
Initial concentration of $Co(dmgH)_2$: 1.71 (○), 1.75 (◑), and 1.80 mM (△, ●).
$[py]/[Co(dmgH)_2]_o$=0.5 (○), 0.8 (◑), 1.0 (△), and 2.0 (●).

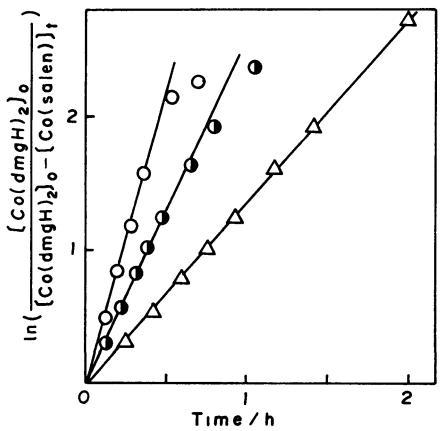

Fig. 3. First-order plots for the substitution reaction.
$[py]/[Co(dmgH)_2]_o$=0.5 (○), 0.8 (◑), and 1.0 (△).

similar to that of Co(salen) which was prepared in the same concentration as that of $Co(dmgH)_2$ at the reaction time t=0. The results of stoichiometry and the presence of isosbestic points indicate that they are clean reactions as expressed by Eq. 1.

The change of concentration of Co(salen) during the reaction was determined by using the above mentioned time-dependent change of the spectra. The results are shown in Fig. 2. In the absence of pyridine the reaction rate is so rapid that the result is not shown in the figure. From this result and Fig. 2 it was found that the reaction rate decreased with an increase of pyridine concentration and reached a stationary value at $[py]/[Co(dmgH)_2]_o$= 1.

Then $\ln(C_o/(C_o-C_t'))$, where C_o is the concentration of $Co(dmgH)_2$ at reaction time 0 and C_t' is the concentration of Co(salen) at reaction time t, was plotted against reaction time for the reaction between $Co(dmgH)_2$ and $salenH_2$ at $[py]/[Co(dmgH)_2]_o$=0.5, 0.8, and 1.0 respectively. Each of the plots, as is shown in Fig. 3, gives a straight line with a slope of 0.075, 0.042 and 0.023. Especially in the case of $[py]/[Co(dmgH)_2]_o$ =1, the plot showed linearity over at least 90% reaction. When $salenH_2$ was used in 2 times the concentration of $Co(dmgH)_2$ for the reaction, no detectable change was observed in the reaction rate. These results indicate that the reaction is first-order with respect to the concentration of $Co(dmgH)_2$ and zero-order with respect to the entering ligand concentration and that the rate equation is given by Eq. 2.

$$d[Co(salen)]/dt = k[Co(dmgH)_2] \quad (2)$$

in which rate constant k=0.023 at 22 °C in $[py]/[Co(dmgH)_2]_o$=1.

Recently Corey *et al.* have proposed a mechanism for the catalytic action of vitamin B_{12}.[1] A key feature of the proposal is the cleavage of the bond between carbon 1 and 19, which directly joins the A and D ring, and tridentate ligation of the seco-corin, by prior axial base ligand dissociation. The authors[7] and Tyrlik *et al.*[8] have proposed a mechanism involving lability of an in-plane dimethylglyoxime ligand for the hydrogenation of benzil catalyzed by $Co(dmgH)_2py$. These results do not contradict the present results.

References

1) E. J. Corey, N. J. Cooper, and M. L. H. Green, *Proc. Natl. Acad. Sci. U. S. A.*, **74**, 811 (1977).
2) N. R. de Tacconi, D. Lexa, and J. M. Saveant, *J. Am. Chem. Soc.*, **101**, 467 (1979).
3) T. Okamoto, M. Goto, and S. Oka, *Inorg. Chem.*, **20**, 899 (1981).
4) G. N. Schrauzer, "Inorganic Synthesis," ed by W. L. Jolly, New York, N. Y. (1968), Vol. XI, p. 64.
5) P. Pfeiffer, E. Breith, E. Lubbe, and T. Tsumaki, *Justus Liebigs Ann. Chem.*, **503**, 84 (1933).
6) K. Mita, K. Hotta, and S. Watanabe, *Bull. Chem. Soc. Jpn.*, **54**, 2341 (1981).
7) K. Mita, K. Hotta, and S. Watanabe, *Nippon Kagaku Kaishi*, **1979**, 1299.
8) S. Tyrlik, M. M. Kucharska, and I. Wolochowicz, *J. Mol. Catal.*, **6**, 393 (1979).

Syntheses and Configurations of Copper(II) and Nickel(II) Complexes of *trans*-1,2-Dicyano-1,2-cyclohexanediamine

Hisashi ŌKAWA,* Miyuki KAKIMOTO, Tatsuo IZUMITANI, and Sigeo KIDA
Department of Chemistry, Faculty of Science, Kyushu University 33, Hakozaki, Higashi-ku, Fukuoka 812
(Received March 12, 1982)

Synopsis. Complexation of the solid and oily isomers of 1,2-dicyano-1,2-cyclohexanediamine (abbreviated as s-cychd and o-cychd respectively) with nickel(II) and copper(II) ions have been investigated. Only s-cychd formed the complexes Ni(s-cychd)$_2$Cl$_2$ and Cu(s-cychd)$_2$X$_2$ (X=Cl, Br, NO$_3$, ClO$_4$). Based on the configuration of the nickel complex, s-cychd was shown to be the (*E*)-isomer and thence o-cychd the (*Z*)-isomer. Configurations of the copper complexes have been dicussed on the basis of electronic spectra of DMF solution and of powder sample.

Recently we have shown that the Schiff bases derived from 1,2-bis(aminomethyl)-1,2-cyclohexanediamine and salicylaldehydes are novel binucleating ligands, which can form "strati-bis" metal complexes.[1,2] However, we have not yet determined if the geometrical structure of 1,2-bis(aminomethyl)-1,2-cyclohexanediamine is (*Z*) or (*E*); the amine having been prepared by reducing the solid form of two isomers (crystal melting at 170 °C and oily substance) of 1,2-dicyano-1,2-cyclohexanediamine. It is known that the *trans*-1,2-cyclohexanediamine differs from the *cis*-isomer in complexation with nickel(II) chloride.[3] Thus, in order to determine the geometrical structures of the solid and oily isomers of 1,2-dicyano-1,2-cyclohexanediamine (abbreviated as s-cychd and o-cychd respectively), we attempted to synthesize nickel(II) and copper(II) complexes of s-cychd and o-cychd and to examine their configurations.

Experimental

Preparations. *Ni(s-cychd)$_2$Cl$_2$*: A solution of s-cychd (0.50 g) and nickel(II) chloride hexahydrate (0.36 g) in ethanol (40 cm^3) was stirred at a temperature lower than 25 °C. Pale blue crystalline powder, which was deposited, was collected, washed with ethanol, and dried *in vacuo*.

Cu(s-cychd)$_2$X$_2$ (X=Cl, Br, NO$_3$, ClO$_4$). These complexes were obtained as purple to bluish purple crystalline powder by the reaction of s-cychd and a copper(II) salt in ethanol.

Elemental analyses of the complexes are given in Table 1.

Measurements. Electronic spectra were recorded on a Shimadzu MPS-5000 spectrometer in *N,N*-dimethylformamide (DMF) and on powder sample. Infrared spectra were recorded on a Hitachi 215 spectrometer on KBr disks. magnetic susceptibilities were measured by the Faraday method and magnetic moments were calculated by the equation, $\mu_{eff}=2.828(\chi_A \times T)^{1/2}$.

Results and Discussion

By the reaction of s-cychd with nickel(II) chloride hexahydrate, blue-colored Ni(s-cychd)$_2$Cl$_2$ was prepared. However, the reaction of s-cychd with nickel(II) bromide, nitrate or perchlorate afforded a white amorphous compound, which is free from nickel and practically insoluble in water and most organic solvents. Infrared spectrum of this compound reveals a band at 1640 cm^{-1} attributable to amide group. We presume that this compound is a self-condensation product of s-cychd. On the other hand, s-cychd reacted with copper(II) salts to form copper(II) complexes with chloride, bromide, nitrate, and perchlorate.

All the attempts to obtain a metal complex from o-cychd and a nickel(II) salt or a copper(II) salt were unsuccessful. Instead, a white amorphous compound was produced, which is supposed to be a self-condensation product of o-cychd.

Infrared spectrum of Ni(s-cychd)$_2$Cl$_2$ showed two CN stretching bands at 2240 and 2150 cm^{-1}, while the spectra of the copper complexes showed one band near 2300 cm^{-1}. Nitrate and perchlorate ions are not coordinated to the metal in the copper complexes

Table 2. Magnetic moments and spectral data of complexes

	μ_{eff}/BM (T/K)	d-d and CT/10^3 cm^{-1} Absorption in DMF (ε/mol^{-1} dm^3 cm^{-1})		Reflectance
Ni(s-cychd)$_2$Cl$_2$	3.07 (286.1)	8.9 (5.1)	14.7 (6 2)	9.1 15.2
		16.0 (5.5)	24.3 (14.6)	16.1 25.0
Cu(s-cychd)$_2$Cl$_2$	1.83 (288.6)	14.1 (69)	22.9 (216)	15.6
Cu(s-cychd)$_2$Br$_2$	1.83 (288.5)	14.0 (143)	22.2 (86)	16.0
Cu(s-cychd)$_2$(NO$_3$)$_2$	1.84 (290.5)	14.6 (24)		17.9
Cu(s-cychd)$_2$(ClO$_4$)$_2$	1.76 (287.0)	14.6 (53)		17.5

Concentratiosn of the solutions are *ca.* 1×10^{-3} mol dm^{-3}.

Table 1. Elemental analyses of complexes

	Found(%)				Calcd (%)			
	C	H	N	M	C	H	N	M
Ni(s-cychd)$_2$Cl$_2$·1/2H$_2$O	41.44	5.32	24.00	11.95	41.15	5.40	23.99	12.57
Cu(s-cychd)$_2$Cl$_2$	41.29	5.30	23.94	13.70	41.52	5.23	24.21	13.73
Cu(s-cychd)$_2$Br$_2$·1/2H$_2$O	34.44	4.37	19.98	10.81	34.26	4.49	19.98	11.33
Cu(s-cychd)$_2$(NO$_3$)$_2$·C$_2$H$_5$OH	38.33	5.37	25.25	11.26	38.47	5.38	24.92	11.31
Cu(s-cychd)$_2$(ClO$_4$)$_2$·1/2H$_2$O	32.26	4.20	18.34	10.74	32.04	4.20	18.68	10.59

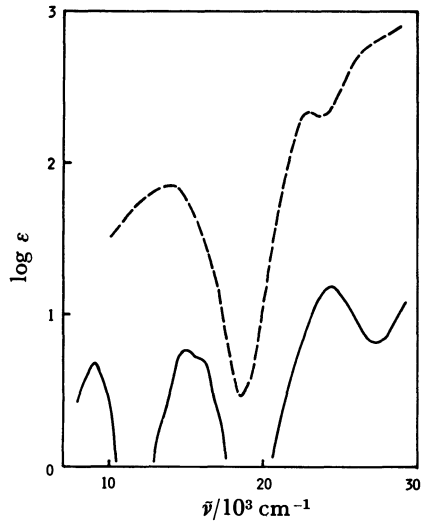

Fig. 1. Electronic spectra of (——) $Ni(s\text{-}cychd)_2Cl_2$ and (------) $Cu(s\text{-}cychd)_2Cl_2$.

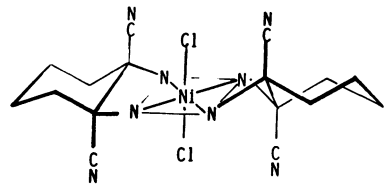

Fig. 2. Possible structure of $Ni(s\text{-}cychd)_2Cl_2$.

judging from their ν(NO) and ν(ClO) bands (NO_3^- 1360; ClO_4^- 1100 cm^{-1}).[4]

Magnetic moments and band frequencies of electronic spectra are given in Table 2. The electronic spectra of $Ni(s\text{-}cychd)_2Cl_2$ and $Cu(s\text{-}cychd)_2Cl_2$ in DMF are shown in Fig. 1. Electronic spectra of the nickel complex in DMF and on powder clearly indicate that the geometry around the metal is essentially octahedral. Splitting of the band $^3T_{1g} \leftarrow {}^3A_{2g}$ into two components may be attributed to the lowering of symmetry. The magnetic moment of this complex is quite normal for an octahedral nickel(II) complex.

Saito and Kidani[3] have shown that *trans*-1,2-cyclohexanediamine forms an octahedral nickel(II) complex, while the *cis*-isomer forms a planar complex. Hence, isolation of octahedral $Ni(s\text{-}cychd)_2Cl_2$ indicates that s-cychd is of the (*E*)-form. Thus, we may conclude that o-cychd is of the (*Z*)-form. A plausible structure of the nickel complex is shown in Fig. 2. The amino groups of s-cychd are equatorial when s-cychd coordinates to a metal and hence cyano groups are axial. Judging from the orientation of the cyano groups in $Ni(s\text{-}cychd)_2Cl_2$, it seems that there is little steric hinderance between the cyano groups and the chloride ion coordinated at the apical position.

Reflectance spectra of the copper complexes showed a broad band around $(15—18) \times 10^3$ cm^{-1} attributable to the d-d band. Relatively high frequencies of the bands for the nitrate and perchlorate complexes indicate the planar configuration around the metal ion, being consistent with the infrared spectral data implying non-coordination of the anions. On the other hand, the coordination geometry of the chloride and bromide copper complexes was assumed to be of a five-coordination with a halide ion at the apical position. Absorption spectra of all the copper complexes in DMF showed d-d band centered at $(14—15) \times 10^3$ cm^{-1}. This suggests that an anion or a solvent molecule coordinates to the metal to form a five- or six-coordinate configuration in DMF. Notably, the spectra of the complexes with halide ions in DMF showed an additional band at $(22—23) \times 10^3$ cm^{-1}, which was not clearly recognized in the reflectance spectra owing to the poor resolution. It seems reasonable to assign this band to the CT transition from halide ion to copper(II) ion. The molar extinction coefficient (ε) of the band of $Cu(s\text{-}cychd)_2Cl_2$ was practically independent of the concentration examined in this study (3.36×10^{-3}–1.03×10^{-4} mol dm^{-3}). On the other hand, that of the band of $Cu(s\text{-}cychd)_2Br_2$ was remarkably dependent on the concentration; ε decreased upon dilution and the band almost disappeared at the concentration 9.05×10^{-5} mol dm^{-3}. Thus, it is likely that the bromide ion is readily replaced by the solvent molecule in DMF.

References

1) T. Izumitani, M. Nakamura, H. Ōkawa, and S. Kida, *Bull. Chem. Soc. Jpn.*, **55**, 2122 (1982).

2) T. Izumitani, H. Ōkawa, and S. Kida, *Chem. Lett.*, **1981**, 483..

3) R. Saito and Y. Kidani, *Chem. Lett.*, **1976**, 123.

4) K. Nakamoto, "Infrared Spectra of Inorganic and Coordination Compounds," John Wiley and Sons, New York (1970), pp. 98, 111.

Photoredox Chemistry of Copper(II) Perchlorate in Methanolic Medium

Paulo Augustro Correa da SILVA and Pazhayirayyathu Geeverghese DAVID*
Departamento de Quimica, Universidade de Brasilia, Brasilia-DF, Brazil
(Received November 16, 1981)

Synopsis. Ultraviolet irradiation of copper(II) perchlorate in methanol yields copper(I) and formaldehyde as the products. The primary photoprocess is believed to be the homolytic cleavage of copper(II)-methanol bond. Secondary reactions of oxidized solvent species with copper(II), copper(I), and solvent molecules affect the product quantum yields. Variation of the quantum yield for copper(I) as a function of irradiating wavelength indicates the existence of methanol-to-copper(II) charge transfer band in the 200—250 nm region.

Most of the reports on the photochemistry of copper(II) salts such as copper(II) chloride, bromide, perchlorate, *etc.*, describe only qualitative observations. Eventhough the observation of the photoxidation of organic solvents by copper(II) chloride dates back to 1804,[1] no report on the quantitative aspects has appeared hitherto. Kochi reported the use of UV irradiation of methanolic solutions of copper(II) chloride in the chlorination of organic compounds.[2] Qualitative observation of the photochemistry of methanolic solutions of copper(II) perchlorate to 254 nm radiations were reported by Murai and Tsutsumi.[3] The present report deals with the quantitative aspects of the photoreduction of copper(II) perchlorate in methanolic medium.

Experimental

Copper(II) perchlorate hexahydrate (Alfa Inorganics) and benzoic acid were purified by recrystallization from hot water and dried under vacuum. Methanol and methyl methacrylate were purified by published procedures.[4-6] Copper(I) solution was prepared by exhaustive photolysis of methanolic solution of copper(II) perchlorate (2.0×10^{-3} M, 1 M = 1 mol dm^{-3}) deaerated by bubbling oxygen-free nitrogen. A Rayonet Photochemical Reactor fitted with RPR 2540 Å lamps was used for this photolysis. All the quantum yields were determined at 25 ± 0.2 °C using deaerated solutions. Photochemical techniques[4] and chemical scavenging experiments[4-6] have been described. Copper(I) was determined spectrophotometrically as the $[Cu(dmp)_2]^+$ complex (dmp=2,9-dimethyl-1,10-phenanthroline). Formaldehyde and ethylene glycol were determined by the literature procedures.[7,8]

Results and Discussion

The electronic absorption spectrum of copper(II) perchlorate in anhydrous methanol is presented in Fig. 1 along which the variation of quantum yields for the formation of copper(I) ($\Phi_{Cu(I)}$) and formaldehyde (Φ_{CH_2O}) as a function of irradiating wavelength. Being a weak ligand coordination of ClO_4^- to copper(II) may be excluded and, hence, the broad absorption in the 200—250 nm region may reasonably be attributed to the charge transfer from methanol to copper(II). The existence of the CT absorption in this region is substantiated by the variation of the photoredox quantum yield as a function of irradiating wavelength (Fig. 1). The quantum yields show a tendency to level off for $\lambda<230$ nm and exhibit a threshold energy at approximately 333 nm.

In addition to copper(I), formaldehyde was formed during the irradiation at all wavelengths studied and its quantum yield was half of that of copper(I). It is important to point out that, contrary to the report of Murai and Tsutsumi,[3] we did not detect the formation of any precipitate of copper metal during or after the irradiations. It is quite probable that the disproportionation of copper(I) reported by these authors might be a consequence of its higher concentration (approximately 0.5 M copper(I) produced by exhaustive photolysis of copper(II) perchlorate). Copper(I) is apparently stable in methanol at the lower concentrations ($<10^{-1}$ M) encountered in our system.[9]

The primary photoprocess in the photolysis of methanolic solutions of copper(II) perchlorate may be represented as given below.

$$[Cu(CH_3OH)_6]^{2+} \longrightarrow [Cu(CH_3OH)_5]^+ + [CH_3OH]^+ \quad (1)$$

The $[CH_3OH]^+$ may be converted to $CH_3O\cdot$ or $\cdot CH_2OH$ by the following reactions.

$$[CH_3OH]^+ \longrightarrow CH_3O\cdot + H^+ \quad (2)$$

$$^*CH_3O\cdot + CH_3OH \longrightarrow {}^*CH_3OH + \cdot CH_2OH \quad (3)$$

The formation of $CH_3O\cdot$ during the photolysis of copper(II) perchlorate in methanol has been substantiated by Murai and Tsutsumi,[3] while our chemical scavenging experiments using methyl methacrylate clearly indicate the incorporation of $-CH_2OH$ end group in the polymer as was shown by the strong positive test for the OH end group in the photopolymer obtained by irradiating methanolic solutions of copper(II) perchlorate at 254 nm in the presence of methyl methacrylate. Polymer obtained from methanol solution which did not contain copper(II) perchlorate gave a negative test for OH end group.

In addition to Reaction 3, $CH_3O\cdot$ radical may disproportionate according to Reaction 4. Since Reaction 4 is second order, it may be considered insignificant due to the insufficient rate of production of $CH_3O\cdot$ during the photolysis of methanolic solutions of copper(II) perchlorate. Hence, we consider that Reaction 3 is the only significant thermal reaction in which $CH_3O\cdot$ disappears.

$$2CH_3O\cdot \longrightarrow CH_2O + CH_3OH \quad (4)$$

In methanolic medium $\cdot CH_2OH$ may dimerize, disproportionate, or reduce copper(II).[10,11] Ethylene glycol was not detected in our system after the photolysis and, hence, Reaction 5 may be considered insignificant. It is known that Reaction 6 has a second order rate constant slower than that of Reaction 5 by approximately a factor of ten.[12] Consequently, we consider the disproportionation reaction (6) insignificant. Therefore, the principal reaction of the reducing radical $\cdot CH_2OH$ is (7) leading to the formation of copper(I) and formaldehyde. This is further substantiated by our quantum yield data in the

$$2\cdot CH_2OH \longrightarrow (CH_2OH)_2 \quad (5)$$

$$2\cdot CH_2OH \longrightarrow CH_2O + CH_3OH \quad (6)$$

$$\cdot CH_2OH + [Cu(CH_3OH)_6]^{2+} \longrightarrow [Cu(CH_3OH)_6]^+ + CH_2O + H^+ \quad (7)$$

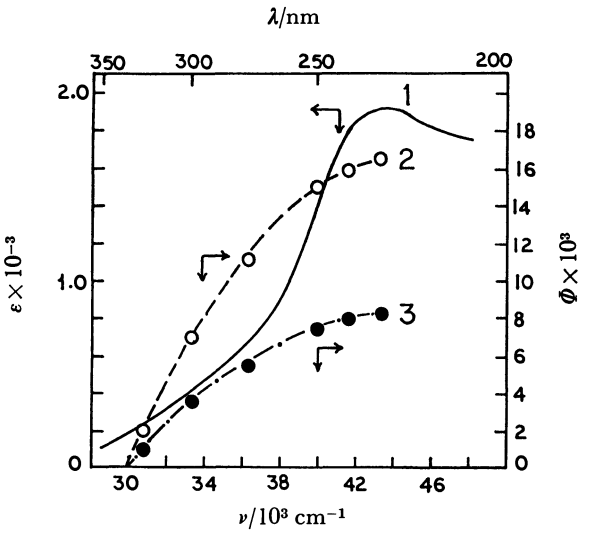

Fig. 1. Electronic absorption spectrum of copper(II) perchlorate in methanol (1), and the quantum yields for the formation of copper(I) (2), and formaldehyde (3) as a function of wavelength of irradiation. The quantum yields were determined for an initial concentration of copper(II) perchlorate 2.0×10^{-3} M, incident intensity $1.5\pm0.1\times10^{14}$ photons s^{-1}, and time of irradiation 10 h.

presence of added concentrations of benzoic acid for an initial concentration of copper(II) perchlorate 2.0×10^{-3} M, wavelength of irradiation 300 nm, incident intensity 1.5×10^{14} photons s^{-1}, and time of irradiation 10 h. The 300 nm irradiating wavelength was chosen to avoid the partial absorption of light by benzoic acid which absorbs at $\lambda<300$ nm. Gradual decreases in $\Phi_{Cu(I)}$ and Φ_{CH_2O} occur with increase in the concentration of benzoic acid. At benzoic acid concentrations 0.05 M or higher $\Phi_{Cu(I)}$ dropped to half of the value 0.007 obtained in the absence of benzoic acid and the Φ_{CH_2O} dropped to zero. This is in agreement with our prediction that, in the absence of benzoic acid which is known to act as a scavenger for $CH_3O\cdot$ and $\cdot CH_2OH$ radicals,[5] $\cdot CH_2OH$ reacts with copper(II) leading to copper(I) and formaldehyde (Reaction 7). If the thermal reactions (2), (3), and (7) follow Reaction 1, Φ_{CH_2O} should be half of $\Phi_{Cu(I)}$. Suppression of Reaction 7 by added $\cdot CH_2OH$ scavengers will affect $\Phi_{Cu(I)}$ and Φ_{CH_2O} and their relative values. Complete scavenging of $\cdot CH_2OH$ by benzoic acid will lead to $\Phi_{CH_2O}=0$ and $\Phi_{Cu(I)}$ equal to half of that in the absence of added radical scavengers, as was observed.

Quantum yields (wavelength of irradiation 250 nm, incident intensity 1.5×10^{14} photons s^{-1}, and time of irradiation 5 h) for the formation of copper(I) for initial concentrations of copper(II) perchlorate ($M\times10^5$) 1000, 500, 100, 50, 10, and 5 were, respectively, 0.006, 0.010, 0.016, 0.030, 0.102, and 0.120 (all± 0.002). The decrease in the product quantum yield with the increase in the initial copper(II) concentration suggests the importance of the reoxidation of copper(I) by the radicals generated in the reaction. Assuming a steady-state concentration for $CH_3O\cdot$ (or $[CH_3OH]^+$), the recombination $Cu^+ + CH_3O\cdot + H^+ \rightarrow [Cu(CH_3OH)]^{2+}$ (or $Cu^+ + [CH_3OH]^+ \rightarrow [Cu(CH_3OH)]^{2+}$) depends on the effective concentration of Cu^+. Increase in the concentration of copper(II) increases the absorbed intensity of light and/or decreases the pathlength of the solution absorbing light. This amounts to the increase in the photoreduction and/or restriction of the photoreduction to a narrower and narrower region of the photolysis cell nearest to the source (depth effect) with the consequent increase in the effective concentration of Cu^+. We have also observed decreases in the product quantum yields with the increase in time of irradiation indicating further the probable importance of the reoxidation of copper(I) by $CH_3O\cdot$ or $[CH_3OH]^+$. For 250 nm irradiating wavelength (incident intensity 1.5×10^{14} photons s^{-1} and initial concentration of copper(II) perchlorate 2.0×10^{-3} M) $\Phi_{Cu(I)}$ for time of irradiation 5, 10, 15, 20, and 40 h were, respectively, 0.014 (6.27), 0.012 (10.76), 0.010 (13.45), 0.008 (14.34), and 0.005 (17.93), the numbers in parentheses indicating the concentrations (mmol$\times10^5$) of copper(I) in 4.5 cm^3 of the solution after the irradiation. As we may observe, increase in the copper(I) concentration occurs with increasing time of irradiation, thus rendering the second order recombination (see above) more probable.[4] The quantum yields determined in the presence of added initial concentrations of copper(I) (mmol$\times10^5$) 0, 5, 10, 15, 20, and 25 in 4.5 cm^3 of the solution (other experimental conditions remaining same as indicated above) support this hypothesis. The quantum yields ($\Phi_{Cu(I)}$) were, respectively, 0.014, 0.012, 0.008, and 0.002 (all±0.002) for the first four solutions while it was zero for the last two. Photolysis appears to reach a steady-state for copper(I) concentrations higher than 1.5×10^{-4} mmol in 4.5 cm^3 (3.33×10^{-5} mol dm^{-3}).

The authors thank the National Research Council of Brazil (CNPq) for partial support to this work.

References

1) V. Balzani and V. Carassiti, "Photochemistry of Coordination Compounds," Academic Press, New York (1970).
2) J. K. Kochi, *J. Am. Chem. Soc.*, **84**, 2121 (1962).
3) S. Murai and T. Tsutsumi, *Bull. Chem. Soc. Jpn.*, **39**, 198 (1966).
4) F. David and P. G. David, *J. Phys. Chem.*, **80**, 579 (1976).
5) P. G. David and E. L. Wehry, *Mol. Photochem.*, **5**, 21 (1973).
6) P. G. David, J. G. Richardson, and E. L. Wehry, *J. Inorg. Nucl. Chem.*, **34**, 1333 (1972).
7) C. E. Bricker and H. R. Johnson, *Ind. Eng. Chem., Anal. Ed.*, **17**, 400 (1945).
8) N. N. Lichtin, *J. Phys. Chem.*, **63**, 1449 (1959).
9) F. A. Cotton and G. Wilkinson, "Advanced Inorganic Chemistry," Wiley-Interscience, New York (1980).
10) W. Brackman, F. V. D. Craats, and P. J. Smit, *Recueil*, **83**, 1253 (1964).
11) G. E. Adams and J. H. Baxendale, *J. Am. Chem. Soc.*, **80**, 4215 (1958).
12) F. S. Dainton, G. A. Salmon, and P. Wardman, *Proc. R. Soc. London, Ser. A*, **313**, 1 (1969).

The Preparation and Catalytic Properties of the Silica-supported Rhodium Complex

Tamon OKANO,* Teruyuki KOBAYASHI, Hisatoshi KONISHI, and Jitsuo KIJI*
Department of Environmental Chemistry and Technology, Faculty of Engineering, Tottori University, Tottori 680
(Received September 21, 1981)

Synopsis. The $RhH_2(O_2COH)[P(i\text{-}Pr)_3]_2$ complex is attached to the phosphinated silica prepared from a new linking agent, $Ph_2PCH_2CH_2CH_2Si(OCH_3)_3$. The supported complex is an active catalyst for the hydrogenation of methyl cinnamate with CO and H_2O, and it can be used repeatedly with little loss of activity, whereas the polystyrene-supported one is not recoverable because of the insufficient complexation of the rhodium.

Recently, much attention has been focused on the chemistry of polymer-supported complex catalysts[1] because of their potential advantages. Functionalized polystyrenes have widely been studied as support, but few reports on silica have appeared. In contrast with polystyrene, silica is rigid and hydrophilic, and it is superior in thermal stability. Making good use of these characteristics, we have tried utilizing the silica-supported rhodium catalyst in the hydrogenation, using H_2O and CO as reducing agents.

The phosphinated silica[2] was synthesized by the following reactions.

$$ClCH_2CH_2CH_2Si(OCH_3)_3 \xrightarrow{Ph_2PH,\ NaH} Ph_2PCH_2CH_2CH_2Si(OCH_3)_3$$

$$Ph_2PCH_2CH_2CH_2Si(OCH_3)_3 \xrightarrow[HCl\ aq]{silica} Ph_2PCH_2CH_2CH_2Si\text{–}O\text{–}SiO_2$$

The linking agent, $Ph_2PCH_2CH_2CH_2Si(OCH_3)_3$, was prepared by the reaction of 3-chloropropyltrimethoxysilane with diphenylphosphine in the presence of sodium hydride. This reaction is a convenient alternative to the general synthetic method, which is based on the slow photochemical addition of diphenylphosphine to vinylsilanes.[3] The phosphination of silica was achieved by the hydrolysis of the linking agent in the presence of hydrochloric acid. The IR spectrum of the phosphinated silica thus prepared showed strong absorptions (3600—3200, 1200—1000, 960, 800 cm^{-1}) attributed to silica and weak absorptions (2930, 2870, 1420, 720, 685 cm^{-1}) attributed to the organofunctional group. The elemental analysis for phosphorus showed the content of the phosphine group to be 0.56 mmol/g. The hydrogen content observed was higher than the value calculated on the basis of the phosphorous content. This may be attributed to ≡Si–OH groups and/or adsorbed water on the silica surface. Since the surface area of the parent silica is 362 m^2/g, the average distance between the phosphino groups is estimated to be about 10 Å (1.8×10^{-6} mol/m^2).[4] Possessing some flexibility attributed to the trimethylene chain, the adjacent phosphines may act as a bidentate ligand with regard to the coordination to metals.

We have previously reported that halide-free rhodium phosphine complexes, such as $RhH_2(O_2COH)[P(i\text{-}Pr)_3]_2$ and $RhH(CO)(PPh_3)_3$, are efficient catalysts for the homogeneous hydrogenation of olefins with CO and H_2O.[5] The catalytic properties of the silica-supported catalyst were examined in hydorgenation of methyl cinnamate with CO in aqueous THF, in comparison with a polystyrene-supported one. The polystyrene support, which contains a diphenylphosphinomethyl group (7.9×10^{-4} mol/g, 1.7×10^{-6} mol/m^2), was prepared from a highly cross-linking polystyrene (divinylbenzene content, >30%; surface area, 590 m^2/g). The results are shown in Fig. 1. In the first run (R-0), a mixture of the silica or polystyrene support and $RhH_2(O_2COH)[P(i\text{-}Pr)_3]_2$ was used as a catalyst without any prior isolation of the supported complex. The catalysts were recovered by filtration and then reused in the succeeding runs. It seems that the homogeneous

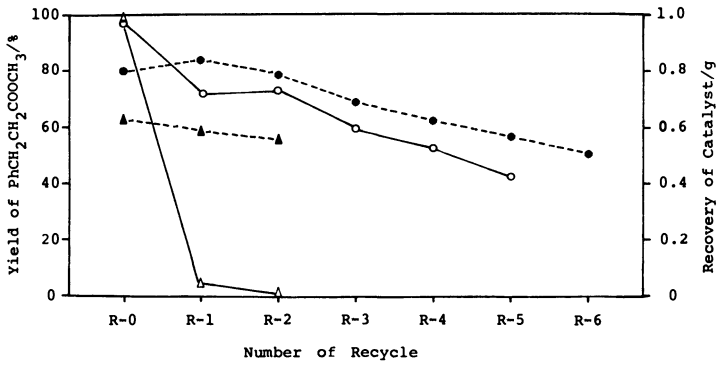

Fig. 1. Recycling of silica- and polystyrene-supported rhodium catalysts.
——: Yield, ------: recovery, ○, ●: silica-supported complex, △, ▲: polystyrene-supported complex. The weight of catalyst in R-0 is represented by the sum of the weight of support and $RhH_2(O_2COH)[P(i\text{-}Pr)_3]_2$.

catalyst is anchored on the supports during the first reaction (R-0), and that the anchoring complex, which is able to exist stably under these reaction conditions, remains on the supports. The high activities of both fresh catalysts (R-0) may be attributed to the presence of some rhodium species uncomplexed on the supports. The polystyrene-based catalyst recovered after the first run was no longer active. In fact, the filtrate of the first run using the silica support was slightly pale yellow, while that using the polystyrene support was deeply colored. The leach of the rhodium from the pre-supported catalyst, which had been prepared by immersing the phosphinated polystyrene in a toluene solution of $RhH_2(O_2COH)[P(i\text{-}Pr)_3]_2$ at room temperature for 20 h, was not repressed by the use of double the amount of the support. Therefore, the complexation of the rhodium complex on the polystyrene support was insufficient. On the other hand, the loss of activity in the silica-supported catalyst was still gradual for several repeated uses. The amount of the supported catalyst recovered was also gradually decreased due to the loss in manipulation, except for the first recovery, where the weight was increased by the adsorption of water. Consequently, the corrected activities (R-0, 11.9; R-1, 7.8; R-2, 8.8; R-3, 8.5; R-4, 8.4; R-5, 7.4 mol of product/g of catalyst) of R-2, R-3, and R-4 suggest that the true activity was scarcely affected by the repeated uses. Additionally, the silica-supported catalyst was stable in air for a short time. The catalyst for the last use (R-5) was handled in air, but the loss of activity was small.

The supported complex prepared by immersing the phosphinated silica in a toluene solution of $RhH_2(O_2COH)[P(i\text{-}Pr)_3]_2$ at room temperature for 20 h did not show any observable IR absorptions attributed to the anchoring complex. On exposure to carbon monoxide (1 atm), three weak bands (2020, 1975, 1945 cm^{-1}) appeared. Therefore, the active species on the support may be mononuclear because these IR bands are in the region of the stretching vibrations of terminal metal carbonyls and metal hydrides containing phosphine ligands.

Experimental

Unless otherwise noted, all reactions and manipulations were carried out under an atmosphere of nitrogen. Literature methods were employed for the preparations of diphenylphosphine, $PHPh_2$,[6] and bis(triisopropylphosphine)dihydrido(hydrogencarbonato)rhodium(III), $RhH_2(O_2COH)[P(i\text{-}Pr)_3]_2$.[7] The IR spectra were recorded on a JASCO IRA-1 spectrometer.

Preparation of $Ph_2PCH_2CH_2CH_2Si(OCH_3)_3$. A suspension of NaH (1.7 g, 71 mmol) in diphenylphosphine (12 g, 64 mmol) and Dimethyl Carbitol (30 ml) was heated at 120 °C for 1 h. The resulting red solution was cooled, and then $ClCH_2CH_2CH_2Si(OCH_3)_3$ (10.8 g, 54 mmol) was added. The mixture was heated at 130 °C for 1 h and subsequently, distilled under reduced pressure to give a viscous liquid (14 g, 150—180 °C/1 mmHg, 1 mmHg≈133.322 Pa). The crude product was redistilled to give the pure linking agent (10 g, 157—160 °C/0.5 mmHg) in a 53% yield.

Phosphination of Silica. Silica gel (Wakogel C-300, for column chromatography) was used without further purification. To a suspension of the silica (25 g) in toluene (150 ml) and concd hydrochloric acid (5 ml), we added $Ph_2PCH_2CH_2CH_2Si(OCH_3)_3$ (26 g, 75 mmol). The mixture was then slowly stirred with refluxing for 20 h. After cooling, the silica was collected by filtration, washed successively with water, methanol, benzene, methanol, water, methanol, benzene, and hexane, and then dried in a vacuum oven at 50 °C for 20 h to give white powder of phosphinated silica (28 g). Found: C, 11.70; H, 1.78; P, 1.72%.

Preparation of Phosphinated Polystyrene. Cross-linking polystyrene (Mitsubishi Chemical Ind., Ltd., Dia-ion HP-50: was purified by previously reported methods.[8] Chloromethylation was achieved according to literature methods[9] under the following condition: polystyrene (10 g), CH_3OCH_2Cl (9 ml), $SnCl_4$ (1.1 ml), in CH_2Cl_2 (50 ml), at 25 °C, for 1 h. The resulting chloromethylated polystyrene, which contained 4.41%. of chlorine, was phosphinated by previously reported methods[10] with a large excess of $LiPPh_2$ ($LiPPh_2/-CH_2Cl$= 50 mol/mol) in THF at room temperature for 60 h.

Hydrogenation of Methyl Cinnamate. A stainless steel autoclave (65 ml in capacity)was charged with phosphinated silica (724 mg, $-PPh_2$; 0.4 mmol), $PhH_2(O_2COH)[P(i\text{-}Pr)_3]_2$ (97 mg, 0.2 mmol) methyl cinnamate (1.62 g, 10 mmol), H_2O (0.9 g, 50 mmol), and THF (15 ml). The reactor was pressurized with CO (15 atm) and then heated at 130 °C for 20 h. After cooling, the suspension was filtered, and the silica-supported catalyst was washed with benzene. The filtrate was analyzed by GC, using naphthalene as the internal standard The silica was dried at room temperature under reduced presure and then weighed. The silica was used as the catalyst for the next run.

We wish to thank Mitsubishi Chemical Ind., Ltd., for its generous gift of polystyrene.

References

1) D. C. Bailey and S. H. Langer, *Chem. Rev.*, **81**, 109 (1981); R. H. Grubbs, *CHEMTECH*, **1977**, 512.

2) A similar phosphinated silica prepared from $ClCH_2CH_2CH_2(SiO_2)_n$ and $KPPh_2$ has been reported: a) K. G. Allum, R. D. Hancock, I. V. Howell, S. Mckenzie, R. C. Pitkethly, and P. J. Robinson, *J. Organomet. Chem.*, **87**, 203 (1975); b) H. Knozinger and E. Rumpf, *Inorg. Chim. Acta*, **30**, 51 (1978).

3) Ref. 2a.

4) The value was calculated from the following equation: $5.6\times10^{-4}/362[1-5.6\times10^{-4}$ (mol wt of $Ph_2PCH_2CH_2CH_2Si)]$.

5) T. Okano, T. Kobayashi, S. Konishi, and J. Kiji, *Bull. Chem. Soc. Jpn.*, **54**, 3799 (1981).

6) W. Kuchen and H. Buchwald, *Chem. Ber.*, **91**, 2875 (1958).

7) T. Yoshida, D. L. Thorn, T. Okano, J. A. Ibers, and S. Otsuka, *J. Am. Chem. Soc.*, **101**, 4212 (1979).

8) M. J. Farrall, *J. Org. Chem.*, **41**, 3877 (1976).

9) K. W. Pepper, H. M. Paisley, and M. A. Young, *J. Chem. Soc.*, **1953**, 4097.

10) G. O. Evans, C. U. Pittman, Jr., R. McMillan, R. T. Beach, and R. J. Jones, *J. Organomet. Chem.*, **67**, 295 (1974).

Ozonization of Organic Compounds. VI. Relative Reactivity of Protic Solvents toward Carbonyl Oxide

Yorihiro YAMAMOTO, Etsuo NIKI,* and Yoshio KAMIYA

Department of Reaction Chemistry, Faculty of Engineering, The University of Tokyo, Hongo, Bunkyo-ku, Tokyo 113

(Received October 8, 1981)

Synopsis. Tetramethylethylene was ozonized at 0 °C in several binary protic solvents and the relative reactivities of the solvents toward acetone carbonyl oxide were measured. The reactivity was found to decrease in the order methanol, ethanol, propyl alcohol, isopropyl alcohol, water, *t*-butyl alcohol, and acetic acid.

Carbonyl oxide is a key intermediate in the ozonolysis of olefinic compounds. It reacts with protic solvent (SH) to give hydroperoxide according to Eq. 1.[1] To understand the reactions of carbonyl oxide it is interesting and fundamental to know how the rate changes with solvents. For example, we reported previously[2]

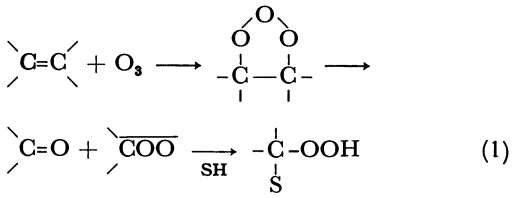

(1)

that the anomalous ozonolysis of α,β-unsaturated carbonyl compounds proceeded in protic solvents mainly by the rearrangement of carbonyl oxide substituted by carbonyl or carboxyl group (Eq. 2) and that the ratio of anomalous ozonolysis to total ozonolysis depend on the solvents. These results suggest that the rate of reaction of carbonyl oxide with protic solvent varies with solvents.

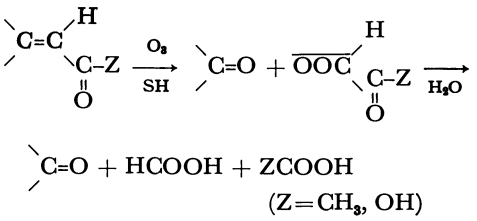

(2)

($Z=CH_3$, OH)

We wish to report here the relative reactivities of several protic solvents toward carbonyl oxide. We ozonized tetramethylethylene in binary protic solvents at 0 °C and measured the relative reactivities of protic solvents toward acetone carbonyl oxide, $(CH_3)_2\overline{COO}$ (Eqs. 3, 4).

The relative reactivity of S_1H and S_2H toward $(CH_3)_2\overline{COO}$, k_1/k_2, is expressed by Eq. 5 when the initial concentrations of S_1H and S_2H are high enough. It was difficult to measure the amounts of hydroperoxides **A** and **B** separately, so the relative reactivity k_1/k_2 was estimated from Eq. 6, where ΔS_1H and ΔS_2H represent the amount of S_1H and S_2H reacted, respectively.

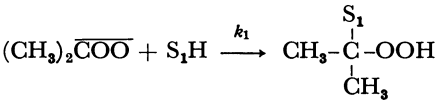

(3)

A

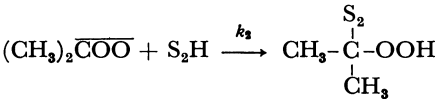

(4)

B

$$\frac{k_1}{k_2}=\frac{\Delta A\cdot[S_2H]_0}{\Delta B\cdot[S_1H]_0} \quad (5) \qquad \frac{k_1}{k_2}=\frac{\Delta S_1H\cdot[S_2H]_0}{\Delta S_2H\cdot[S_1H]_0} \quad (6)$$

5 mmol of tetramethylethylene, S_1H, S_2H, and 15 ml of inactive solvent such as carbon tetrachloride, nitromethane, and ethyl methyl ketone were mixed in a reactor and O_3/O_2 gas was introduced into the reactor at 0 °C. Total amount of hydroperoxide was measured by iodometric titration. Both production of acetone and decrease of S_1H and S_2H were followed by GLC using PEG 20M, Porapak Q, and Apiezon Grease L columns. A part of tetramethylethylene was missed because of its high vapor pressure, so the amount of tetramethylethylene decreased was more than that of ozone introduced. Nevertheless, the ozonation was controlled so that some tetramethylethylene remained in the reaction mixture even at the end of ozonolysis in

Table 1. Relative reactivities of protic solvents (S_1H and S_2H) toward carbonyl oxide $(CH_3)_2\overline{COO}$ in the ozonolysis of 5 mmol of tetramethylethylene at 0 °C

Run No.	1	2	3	4	5	6	7	8	9	10
S_1H	MeOH	MeOH	MeOH	MeOH	MeOH	EtOH	*n*-PrOH	*n*-PrOH	*n*-PrOH	*t*-BuOH
S_2H	EtOH	EtOH	*n*-PrOH	*i*-PrOH	H_2O	*n*-PrOH	*i*-PrOH	*t*-BuOH	AcOH	AcOH
Solvent[a]	CH_3NO_2	CCl_4	CH_3NO_2	CH_3NO_2	MEK[b]	CH_3NO_2	CCl_4	CCl_4	CCl_4	CCl_4
S_1H_0[c] (mmol)	16.37	8.43	14.41	14.58	8.74	7.52	10.75	11.06	8.92	6.31
S_2H_0[c] (mmol)	13.22	6.36	9.20	8.51	19.50	7.35	8.04	6.63	9.10	10.95
ΔS_1H (mmol)	1.85	1.40	1.48	1.40	1.05	0.89	0.76	1.64	1.46	0.85
ΔS_2H (mmol)	0.76	0.50	0.38	0.29	0.65[g]	0.61	0.52	0.19	0.25	1.10
ΔSH[d] (mmol)	2.61	1.90	1.74	1.69	1.70	1.50	1.28	1.83	1.71	1.95
ΔHPO[e] (mmol)	2.36	1.85	1.84	1.40	1.65	1.46	1.40	1.93	1.85	1.90
k_1/k_2[f]	2.0	2.1	2.5	2.8	3.6	1.4	1.1	5.2	6.0	1.3

a) 15 ml. b) Ethyl methyl ketone. c) Initial amounts of S_1H and S_2H in mmol. d) $\Delta SH=\Delta S_1H+\Delta S_2H$.
e) Hydroperoxides. f) See text. g) Estimated by the amount of acetone formed.

Table 2. Polarity parameters and physical properties of protic solvents

	E_T[a]	Z[a]	S[a]	pK_{auto}[b]	BDE[c]
MeOH	55.5	83.6	0.0499	17.20	104.4
EtOH	51.9	79.6	0.0000	18.88	104.2
n-PrOH	50.7	78.3	−0.0158	19.43	
i-PrOH	48.6	76.3	−0.0413	20.80	
t-BuOH	43.9	71.3	−0.1047	26.8	105.1
H_2O	63.1	94.6	0.1540	14.00	119
AcOH	51.2	79.2	0.0050	14.45	112

a) Empirical parameter of solvent polarity based on solvatochromism, Ref. 4. b) Autoprotolysis constants, Ref. 4. c) Bond dissociation energy of O–H bond in kcal/mol, Ref. 5.

order to avoid overozonization. Conversion of S_1H and S_2H was kept below 15%. It should be noted that α-methoxyalkyl hydroperoxide, $(CH_3)_2C(OCH_3)OOH$ decomposed to acetone quantitatively on GLC and that methanol was not detected.

It is necessary to confirm that the protic solvents react with carbonyl oxide quantitatively and peroxides, **A** and **B**, are the sole products in the reaction. As shown in Table 1, the amounts of peroxide formed (ΔHPO) and those of protic solvents reacted ($\Delta SH = \Delta S_1H + \Delta S_2H$) are in satisfactory agreement, which suggests that the hydroperoxides **A** and **B** are formed exclusively and that other peroxides such as diperoxide, triperoxide, and oligomers were not formed under the present conditions. It may be safely assumed that the inactive solvents used in Table 1 have little effect on the *relative* reactivities of protic solvents toward carbonyl oxides. From Table 1, the ratio $k_{MeOH}/k_{n\text{-}PrOH}$ is obtained as 2.5 in Run 3, which is in satisfactory agreement with the ratio calculated from the results of Runs 1 and 6, $2.0 \times 1.4 = 2.8$. Similarly, Run 4, and Runs 3 and 7 show that $k_{MeOH}/k_{i\text{-}PrOH}$ is 2.8.

Table 1 indicates that the reactivity of protic solvents toward $(CH_3)_2\overline{COO}$ decreased in the order of MeOH (1) > EtOH (0.50) > *n*-PrOH (0.40) > *i*-PrOH (0.36) > H_2O (0.28) > *t*-BuOH (0.077) > AcOH (0.063). The numbers in parentheses are the calculated reactivities of various protic solvents toward $(CH_3)_2\overline{COO}$ relative to methanol. The reactivity of alcohols has a close relation with the solvent polarity parameters, E_T, Z, S, and pK_{auto} as shown in Table 2. This suggests that the ionic transition state (**C**) plays an important role in the reaction of carbonyl oxide with protic solvent. In fact, the *ab initio* calculations[3] for carbonyl oxide suggest that the zwitterions (**D**, **E**) are favored over biradical (**F**) in protic solvents. However, the low reactivities of water and acetic acid toward carbonyl oxide in spite of their strong protic character (Table 2) suggest that this is not the only factor that determines the reactivity. Table 2 also shows that the bond dissociation energies of O–H bonds of water and acetic acid are much larger than those of alcohols. This might imply some contribution of homolytic scission of O–H bond (**G**) as well as the ionic one. Recent report by Sawaki, Kato, and Ogata[6] on the hydrogen atom abstraction by carbonyl oxide from toluene, cumene, and cyclohexane also suggests the importance of biradical character of carbonyl oxide.

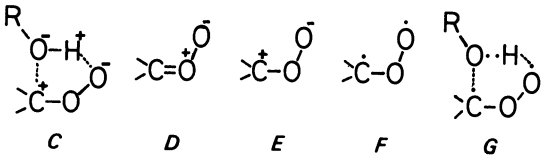

C D E F G

References

1) P. S. Bailey, "Ozonation in Organic Chemistry, Olefinic Compounds," Academic Press, New York (1978), Vol. 1.

2) Y. Yamamoto, E. Niki, and Y. Kamiya, *J. Org. Chem.*, **46**, 250 (1981).

3) L. B. Harding and W. A. Goddard III, *J. Am. Chem. Soc.*, **100**, 7180 (1978).

4) C. Reichardt, "Solvent Effects in Organic Chemistry," Verlag Chemie, New York (1979), pp. 238, 242, 283.

5) J. A. Kerr and A. F. Trotman-Dickenson, "Handbook of Chemistry and Physics," CRC Press, Cleveland (1975), Vol. 57, p. F-232.

6) Y. Sawaki, H. Kato, and Y. Ogata, *J. Am. Chem. Soc.*, **103**, 3832 (1981).

CIDNP Studies of the Oxidation of *N*-(*p*-Tolylsulfonyl)-*N'*-triphenylmethylhydrazine

Masato Yoshida,* Akira Yano, and Michio Kobayashi
Department of Chemistry, Faculty of Science, Tokyo Metropolitan University, Fukazawa, Setagaya-ku, Tokyo 158
(Received October 8, 1981)

Synopsis. The ^{13}C-CIDNP spectra were observed during the oxidation of *N*-(*p*-tolylsulfonyl)-*N'*-triphenylmethylhydrazine. The formation of sulfone and sulfinic ester as recombination products in a solvent cage was established from the signs of polarization.

In continuing the studies of the decomposition mechanism of the arylazo aryl sulfone,[1] we are interested in the reaction of *p*-tolyl triphenylmethylazo sulfone (**1**). Although *N*-(*p*-tolylsulfonyl)-*N'*-triphenylmethylhydrazine (**2**) is oxidized fairly easily by various oxidizing agents, such as mercury(II) oxide or potassium permanganate, the expected azo sulfone (Ph_3C–N=N–SO_2–Tol-*p*) is too unstable to be isolated as such; it decomposes immediately, with the evolution of nitrogen. The main product is *p*-tolyl triphenylmethyl sulfone (**3**; yield 51.7%), whose formation has been ascribed to the recombination of the *p*-toluenesulfonyl and triphenylmethyl radicals.[2] In order to clarify the details of the decomposition mechanism of *p*-tolyl triphenylmethylazo sulfone, we have studied the ^{13}C-CIDNP spectra observed during the oxidation of *N*-(*p*-tolylsulfonyl)-*N'*-triphenylmethylhydrazine.

Results and Discussion

CIDNP signals appeared when a mixture of *N*-(*p*-tolysulfonyl)-*N'*-triphenylmethylhydrazine (**2**) and yellow mercury(II) oxide in benzene or toluene was inserted into an NMR probe heated to 60—90 °C and the ^{13}C-NMR was measured. One of the spectra thus obtained is shown in Fig. 1. The signals were assigned by comparison with the chemical shifts of the authentic samples. Triphenylmethyl *p*-toluenesulfinate (**4**) was expected to isomerize quickly to the sulfone (**3**) at room temperature, so its chemical shifts were determined as follows: *p*-toluenesulfinyl chloride was added to a solution of triphenylmethanol in carbon tetrachloride in the presence of pyridine in an NMR sample tube at −30 °C, and then its ^{13}C-NMR spectrum was immediately determined at −30 °C. Strong, new ^{13}C-NMR signals assigned to sulfinate (**4**) were observed; when this solution was subsequently warmed to room temperature, though, different signals corresponding to sulfone (**3**) began to appear:

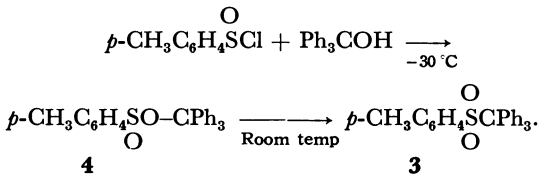

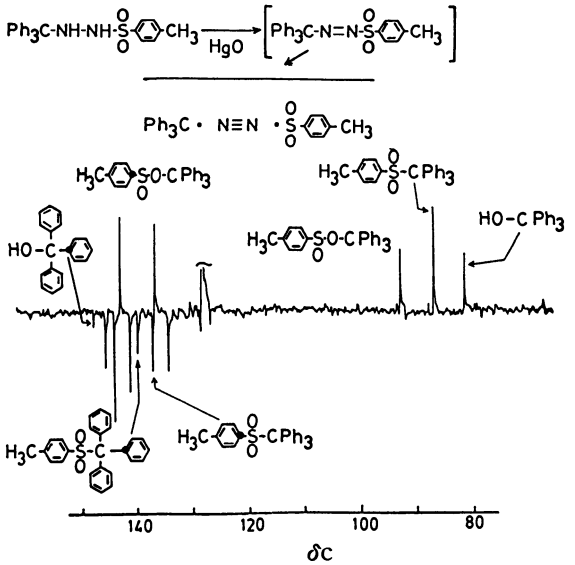

Fig. 1. ^{13}C-CIDNP spectrum in the oxidation of *N*-(*p*-toluenesulfonyl)-*N'*-triphenylmehtylhydrazine in benzene at 60 °C.

The formation of sulfone (**3**) and the sulfinic ester (**4**) as geminate recombination products in a solvent cage is established from the signs of polarization, as is shown in Fig. 1. The generated sulfonyl radical is ambident and acts as either an S- or O-centered radical to give both sulfone and the sulfinic ester, with triphenylmethyl radicals. The azo sulfone (**1**) did not show polarization. This indicates that hydrazine (**2**) is oxidized by mercury(II) oxide to the azo sulfone (**1**), which might decompose to the sulfonyl radical, the triphenylmethyl radical, and nitrogen simultaneously. On the other hand, it has been established that phenylazo *p*-tolyl sulfone (**5**) decomposes to the aryldiazenyl radical and the sulfonyl radical.[1] When a mixture of *N*-phenyl-*N'*-(*p*-tolylsulfonyl)hydrazine (**6**) and yellow mercury(II) oxide in toluene was warmed at 90 °C, the CIDNP signals of not only sulfone and the sulfinic ester, but also of azo sulfone (**5**), were observed. The obtained spectrum was identical with that observed in the thermal decomposition of

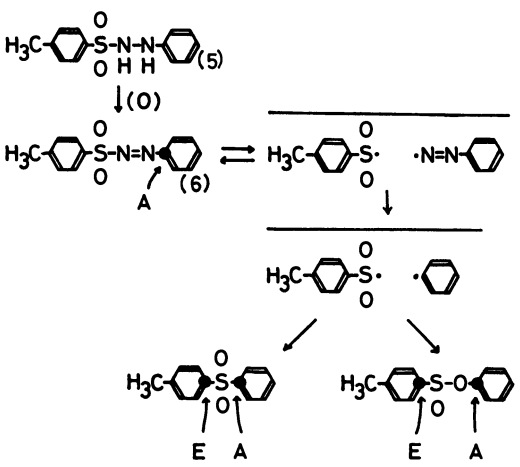

Scheme 1.

phenylazo *p*-tolyl sulfone in toluene.

In order to examine the possibility of the recombination of the sulfonyl radical and the triphenylmethyl radical escaped from the solvent cage, the following two experiments were carried out.

(i) When the ^{13}C-NMR of a mixture of phenylazo *p*-tolyl sulfone and phenylazotriphenylmethane (PAT) in toluene at 90 °C was measured, CIDNP signals assignable to *p*-tolyl triphenylmethyl sulfone (**3**) and triphenylmethyl *p*-toluenesulfinate (**4**) were observed, besides the signals observed in the thermal decomposition of the azosulfone or PAT alone.

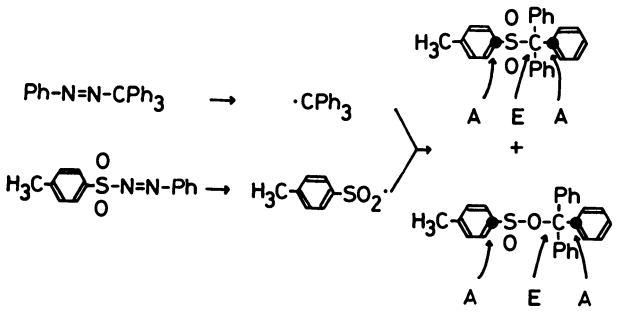

Scheme 2.

(ii) When the ^{13}C-NMR spectrum of a mixture of *p*-toluenesulfonyl iodide and PAT in toluene was measured at 90 °C, the CIDNP signals of *p*-tolyl triphenylmethyl sulfone (**3**) were obtained. The formation of the sulfone can be explained by the following reaction Scheme;

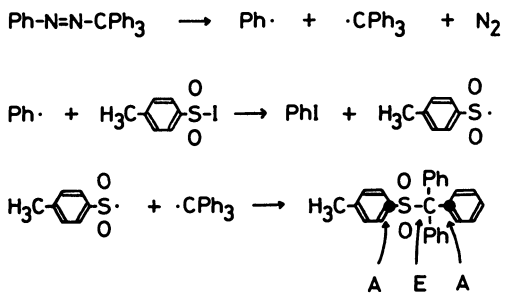

Scheme 3.

The sulfone and the sulfinic ester must be the result of the encounter of free radicals escaped from the original solvent cage, as has been shown before, and the signs of polarization should be the opposite of those obtained in the oxidation of hydrazine (**2**). The predicted signs of the recombination of the encounter of free radical, according to Kaptein's rule[3] are shown below:

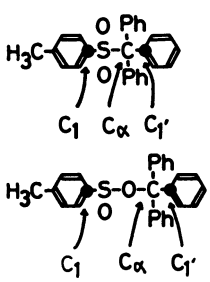

	μ	ε	Δg	a	Γ_{ne}
C_1	+	+	+	(+)[4]	(+)
C_α	+	+	−	+[5]	−
$C_{1'}$	+	+	−	−[5]	+
C_1	+	+	+	(+)[4]	(+)
C_α	+	+	−	+[5]	−
$C_{1'}$	+	+	−	−[5]	+

$g = 2\ 0041(\cdot SO_2C_6H_4CH_3\text{-}p)$, $g = 2\ 0026(\cdot CPh_3)$.

Experimental

The ^{13}C-NMR spectra were taken with a JEOL Fx-60 FT-NMR spectrometer. The *N*-(*p*-tolylsulfonyl)-*N'*-triphenylmethylhydrazine was prepared from triphenylmethyl chloride and *p*-tolylsulfonylhydrazine and recrystallized from ethanol. The details have been described in Ref. 1. The *p*-tolyl triphenylmethyl sulfone was obtained from the reaction mixture of *N*-(*p*-tolylsulfonyl)-*N'*-triphenylmethylhydrazin and yellow mercury(II) oxide; it was recrystallized from benzene–ether (mp, 175—178 °C, lit, 171 °C[2]).

References

1) M. Yoshida, N. Furuta, and M. Kobayashi, *Bull. Chem. Soc. Jpn.*, **54**, 2356 (1981).

2) M. Kojima, N. Kamigata, H. Minato, and M. Kobayashi, *Bull. Chem. Soc. Jpn.*, **46**, 2501 (1973).

3) R. Kaptein and J. Osterhoff, *Chem. Phys. Lett.*, **4**, 195, 214 (1969).

4) If one assumes that the hyperifine splitting constant "*a*" of C_1 is positive, the sign in the net polarization, (Γ_{ne}), as calculated according to Kaptein's rule, agrees with the observed mode.

5) M. Karplus and G. K. Frankel, *J. Chem. Phys.*, **35**, 1312 (1961).

The Thermal Decomposition of *N,O*-Diacyl-*N*-*t*-butylhydroxylamines. IV. A Novel Acyloxyl Migration in *N,O*-Diacyl-*N*-*t*-butylhydroxylamines

Yuzuru UCHIDA* and Seizi KOZUKA†

Department of Applied Chemistry, Osaka Institute of Technology, Asahi-ku, Osaka 535

†*Department of Applied Chemistry, Faculty of Engineering, Osaka City University, Sumiyoshi-ku, Osaka 558*

(Received November 2, 1981)

Synopsis. Several *N,O*-diacyl-*N*-*t*-butylhydroxylamines were prepared, and their thermal decompositions were studied. *N*-Propionyl-*O*-benzoyl-*N*-*t*-butylhydroxylamine gave *N*-*t*-butyl-2-benzoyloxypropanamide, together with the decomposition products, *N*-*t*-butylpropanamide and benzoic acid, upon thermal decomposition in tetralin. Similar benzyloxyl migrations were found in the thermal decomposition of *N*-butyryl, *N*-valeryl, and *N*-(3-phenylpropionyl) derivatives.

In the previous papers, we have reported that *N,O*-diaroyl-*N*-*t*-butylhydroxylamines gave amides and carboxylic acids upon the thermolysis in tetralin.[1] On the other hand, *N*-[2-(methylthio)benzoyl]-*O*-acyl-*N*-*t*-butylhydroxylamines gave rearranged products, *N*-*t*-butyl-2-(acyloxymethylthio)benzamides.[2] As a continuation of those studies, we have now studied the thermal decomposition of *N*-acyl-*O*-benzoyl-*N*-*t*-butylhydroxylamines (**1**) and found a novel benzoyloxyl migration reaction.

Results and Discussion

Several *N*-acyl-*O*-benzoyl-*N*-*t*-butylhydroxylamines (**1a**—**g**) were prepared by the reaction of *O*-benzoyl-*N*-*t*-butylhydroxylamine and the corresponding acyl chlorides in the presence of pyridine in benzene at 70 °C. However, the reaction of *O*-benzoyl-*N*-*t*-butylhydroxylamine with phenylacetyl chloride under the same conditions did not afford the corresponding *N*-phenylacetyl-*O*-benzoyl-*N*-*t*-butylhydroxylamine (**1h**), but *N*-*t*-butyl-2-chloro-2-phenylacetamide (**3**), as the major product. When the reaction was carried out in diethyl ether at room temperature, **1h** was detected as the product, together with **3**, but the attempted isolation of **1h** from the mixture was unsuccessful.

The thermal decomposition of **1** was carried out in tetralin at 210 °C in a degassed ampule. In the thermal decomposition of *N*-acetyl-*O*-benzoyl-*N*-*t*-butylhydroxylamine (**1a**), the products isolated were *N*-*t*-butylacetamide (**4a**), benzoic acid (**5**), acetic acid (**6a**), *N*-*t*-butylbenzamide (**7**), and carbon dioxide. 1,1′-Bitetralyl (**8**) and 1,2-dihydronaphthalene (**9**) were formed from the solvent. The yields of the products are summarized in Table 1. Similar results were also obtained in the thermal decomposition of *N*-isopropionyl-*O*-benzoyl-*N*-*t*-butylhydroxylamine (**1b**) and *N*-cyclohexylcarbonyl-*O*-benzoyl-*N*-*t*-butylhydroxylamine (**1c**).

Table 1. Thermal decomposition of *N*-acyl-*O*-benzoyl-*N*-*t*-butylhydroxylamines in tetralin at 210 °C

	Compd		Time	Products yields/mol%[a]							
	R_1	R_2	h	2	4[b]	5[c]	6[d]	7[e]	CO_2[f]	8[g]	9[g]
1a	H	H	24	0	48	61	[h]	30	9	30	43
1b	CH_3	CH_3	40	0	47	58	14[f]	13	7	42	15
1c	$-(CH_2)_5-$		40	0	57	73	18	18	3	44	16
1d	CH_3	H	24	27	47	60	[h]	10	4	31	22
1e	C_2H_5	H	25	24	60	67	18[f]	12	3	36	25
1f	C_3H_7	H	25	10	70	70	[h]	11	1	[h]	[h]
1g	$PhCH_2$	H	25	23	64	63	8	11	5	[h]	[h]

a) The yields were estimated by GLC. b) RCONHBu^t. c) $PhCO_2H$. The yields were estimated after methylation with diazomethane. d) RCO_2H. e) $PhCONHBu^t$. f) Estmated by titration. g) Based on 1. h) Not determined.

The results given in Table 1 show that two kinds of amides and acids, originating from the two acyl groups of the starting materials, were formed in each decomposition. The mode of decomposition is quite similar to that previously reported for the thermolysis of *N,O*-diaroyl-*N*-*t*-butylhydroxylamines.[1] The minor acid (**6**) and the amide (**7**) must be formed by means of an acyl-exchange reaction between the major acid (**4**) and the amide (**5**).[1]

On the other hand, *N*-propionyl-*O*-benzoyl-*N*-*t*-butylhydroxylamine (**1d**) gave the rearranged product, *N*-*t*-butyl-2-benzoyloxypropanemide (**2d**), together with the decomposition products: *N*-*t*-butylpropanamide (**4d**), **5**, propionic acid (**6d**), **7**, and a small amount of carbon dioxide. A similar benzoyloxyl migration from the nitrogen atom to the α-carbon atom of the *N*-acyl group was found in the thermal decompositions of *N*-butyryl- (**1e**), *N*-valeryl- (**1f**), and *N*-(3-phenylpropionyl)-*O*-benzoyl-*N*-*t*-butylhydroxylamine (**1g**), all of which have α-methylene in the *N*-acyl group. The products were identified by a comparison of their physical properties with those of authentic samples. The structures of the rearranged products (**2**) were established by means of elemental and spectral analyses. The IR spectra of **2** showed bands at 3300—3320 (N–H), 1720—1725, and 1660—1665 cm^{-1} (C=O). The yields of the products were estimated by means of GLC analysis.

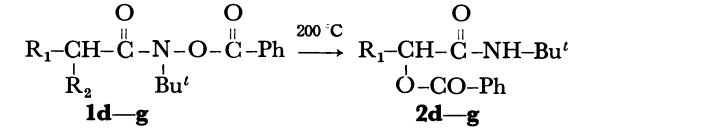

1d—g **2d—g**

1d, 2d; $R_1 = CH_3$, $R_2 = H$ **1e, 2e**; $R_1 = C_2H_5$, $R_2 = H$
1f, 2f; $R_1 = C_3H_7$, $R_2 = H$ **1g, 2g**; $R_1 = PhCH_2$, $R_2 = H$

When the thermal decomposition of **1e** was carried out in the presence of an equimolar amount of *p*-toluic acid, both the benzoate (**2e**) and the toluate (**2i**) were formed. These results suggest that the rearrangement is an intermolecular reaction.

Baumgarten[3] reported that *N*-*t*-butylphenylacetamide gave *N*-*t*-butyl-2-*t*-butoxy-2-phenylacetamide on treatment with potassium *t*-butoxide and *t*-butyl hypochlorite. The formation of 1-*t*-butyl-3-phenylaziridinone (**10h**) *via* *N*-*t*-butyl-*N*-chlorophenylacetamide as an intermediate was suggested.

Although, a strong base was not used in the present thermolysis of **1**, α-lactam (**10**) may also contribute to the benzoyloxyl migration reaction as an intermediate. In previous papers,[1,2] we have proposed that nucleophilic displacement at the nitrogen atom was involved in the thermal decomposition of *N,O*-diacyl-*N*-*t*-

butylhydroxylamines. By analogy, the following scheme can be presented for the reaction involving the initial abstraction of the α-proton by the carboxylate ion; the resulting anion would cyclize to give **10**. Another possibility is the intramolecular elimination of benzoic acid from **1**, by either a 5- or 7-membered transition state, directly giving **10**. The α-lactam would react with carboxylic acid to give the rearranged product (**2**).

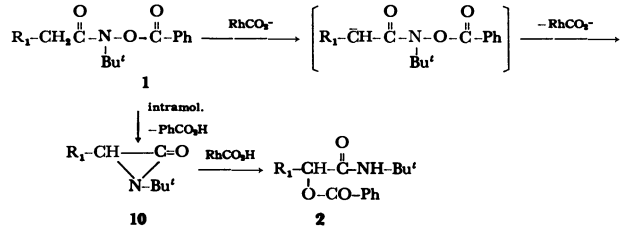

The unexpected results of the reaction of *O*-benzoyl-*N*-*t*-butylhydroxylamine with phenylacetyl chloride, which gave **3** instead of **1h** in benzene, may also proceed by a similar process involving the reaction of the α-lactam with hydrogen chloride.[4]

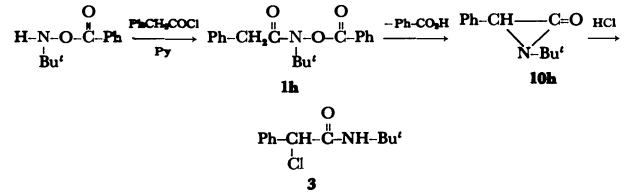

The absence of the rearranged products in the thermal decompositions of **1a**—**c** may be due to the instability of the intermediate (**10**). 1-*t*-Butylaziridinone (**10a**) is an unknown compound, and 1-*t*-butyl-3,3-dimethylaziridinone (**10b**)[5] and 1-*t*-butyl-3,3-pentamethyleneaziridinone (**10c**)[6] are known to decompose under milder conditions (above 75 °C). Thus, **2a**—**c** if formed, would decompose under the conditions employed for the thermolysis of **1**.

Experimental

All the melting points and boiling points are uncorrected. The IR spectra were recorded on a Shimadzu IR-430 infrared spectrometer. The NMR spectra were recorded on a Varian EM-360 spectrometer, using TMS as the internal standard.

Preparation of N-*Acyl*-O-*benzoyl*-N-t-*butylhydroxylamine* (*1*). A typical procedure was as follows: A mixture of propionyl chloride (9.3 g, 100 mmol), *O*-benzoyl-*N*-*t*-butylhydroxylamine (19.3 g, 100 mmol),[1] and pyridine (7.9 g, 100 mmol) in benzene (100 cm³) was stirred at 70 °C for 6 h. The reaction mixture was washed with dil HCl, aq $NaHCO_3$, and water, and then dried over Na_2SO_4. The benzene was removed *in vacuo* to give crude *N*-propionyl-*O*-benzoyl-*N*-*t*-butylhydroxylamine (**1d**) (24.7 g), which was recrystallzed from petroleum ether (17.9 g, 72%): mp 56.5—57.5 °C. Found: C, 67.60; H, 7.83; N, 5.60%. Calcd for $C_{14}H_{19}NO_3$: C, 67.45; H, 7.68; N, 5.62%. By the same procedure, **1a**—**c** and **1e**—**g** were prepared by the reactions of *O*-benzoyl-*N*-*t*-butylhydroxylamine with the corresponding acyl chlorides. The results were as follows: **1a**; 86%, bp 125 °C/3 mmHg.†† Found: C, 66.49; H, 7.49; N, 5.98%. Calcd for $C_{13}H_{17}NO_3$: C, 66.36; H, 7.28; N, 5.95%. **1b**: 87%, mp 79—80 °C. Found: C, 68.44; H, 8.25; N, 5.22%. Calcd for $C_{15}H_{21}NO_3$: C, 68.41; H, 8.04; N, 5.32%. **1c**: 92%, mp 118.5—119.5 °C. Found: C, 71.26; H, 8.49; N, 4.42%. Calcd for $C_{18}H_{25}NO_3$: C, 71.26; H, 8.31; N, 4.62%. **1e**: 68%, bp 136 °C/4 mmHg. Found: C, 68.13; H, 8.19; N, 5.21%. Calcd for $C_{15}H_{21}NO_3$: C, 68.41; H, 8.04; N, 5.32%. **1f**: 67%, mp 41—42 °C. Found: C, 69.32; H, 8.37; N, 4.90%. Calcd for $C_{16}H_{23}NO_3$: C, 69.28; H, 8.36; N, 5.05%. **1g**: 71%, mp 76—77 °C. Found: C, 74.00; H, 7.22; N, 4.13%. Calcd for $C_{20}H_{23}NO_3$: C, 73.82; H, 7.12; N, 4.30%.

Reaction of O-*Benzoyl*-N-t-*butylhydroxylamine with Phenylacetyl Chloride*. A mixture of phenylacetyl chloride (15.4 g, 100 mmol), *O*-benzoyl-*N*-*t*-butylhydroxylamine (19.3 g, 100 mmol), and pyridine (7.9 g, 100 mmol) in benzene (300 cm³) was stirred at 70 °C for 3 h. The reaction mixture was washed with dil HCl, aq $NaHCO_3$, and water, and then dried over Na_2SO_4. The benzene was removed *in vacuo* and the residue was recrystallized from petroleum ether–dichloromethane to give *N*-*t*-butyl-2-chloro-2-phenylacetamide (**3**) (37%); mp 125.5—126.5 °C. NMR (CCl_4): δ 1.38 (9H, s), 5.14 (1H, s), 6.38 (1H, broad), 7.35 (5H, s). IR (KBr); 3300, 1550 (N–H), and 1655 cm⁻¹ (C=O). Found: C, 64.04; H, 7.38; N, 6.12%. Calcd for $C_{12}H_{16}ClNO$: C, 63.85; H, 7.15; N, 6.21%.

Thermal Decomposition of N-*Acyl*-O-*benzoyl*-N-t-*butylhydroxylamine* (*1*). A solution of **1** (2 mmol) in tetralin (20 cm³) was sealed in a degassed tube and heated at 210 °C in a constant-temperature bath. The product analyses and isolation were the same as those reported previously.[1] The properties of the rearranged products (**2**) were as follows: **2d**; mp 160—161 °C. IR (KBr); 3300 (N–H), 1720, 1660 cm⁻¹ (C=O). NMR (CCl_4): δ 1.35 (9H, s), 1.54 (3H, d, J=7 Hz), 5.28 (1H, q, J=7 Hz), 6.0 (1H, broad), 7.2—8.2 (5H, m). Found: C, 67.42; H, 7.91; N, 5.84%. Calcd for $C_{14}H_{19}NO_3$: C, 67.45; H, 7.68; N, 5.62%. **2e**; mp 124—125 °C. IR (KBr): 3300 (N–H), 1725, 1665 cm⁻¹ (C=O). NMR (CCl_4): δ 0.98 (3H, t, J=7 Hz), 1.34 (9H, s), 1.98 (2H, m), 5.14 (1H, t, J=7 Hz), 5.8 (1H, broad), 7.2—8.2 (5H, m). Found: C, 68.50; H, 8.34; N, 5.06%. Calcd for $C_{15}H_{21}NO_3$: C, 68.41; H, 8.04; N, 5.32%. **2f**; mp 98—99 °C. IR (KBr): 3300 (N–H), 1720, 1660 cm⁻¹ (C=O). NMR (CCl_4): δ 0.97 (3H, t, J=7 Hz), 1.33 (9H, s), 1.4—2.3 (4H, m), 5.18 (1H, t, J=6 Hz), 5.8 (1H, broad), 7.2—8.2 (5H, m). Found: C, 69.23; H, 8.51; N, 4.92%. Calcd for $C_{16}H_{23}NO_3$: C, 69.28; H, 8.36; N, 5.05%. **2g**; mp 153—154 °C. IR (KBr): 3320 (N–H), 1720, 1665 cm⁻¹ (C=O). NMR (CCl_4): δ 1.23 (9H, s), 3.25 (2H, d, J=6 Hz), 5.38 (1H, t, J=6 Hz), 5.6 (1H, broad), 7.20 (5H, s), 7.2—8.1 (5H, m). Found: C, 73.66; H, 7.21; N, 4.13%. Calcd for $C_{20}H_{23}NO_3$: C, 73.82; H, 7.13; N, 4.30%. **2i**; mp 123—124 °C. IR (KBr): 3300 (N–H), 1720, 1660 cm⁻¹ (C=O). NMR (CCl_4): δ 0.95 (3H, t, J=7 Hz), 1.32 (9H, s), 1.88 (2H, m), 2.24 (3H, s), 5.10 (1H, t, J=6 Hz), 5.8 (1H, broad), 7.21 (2H, d, J=10 Hz), 7.90 (2H, d, J=10 Hz). Found: C, 69.19; H, 8.58; N, 4.95%. Calcd for $C_{16}H_{23}NO_3$: C, 69.28; H, 8.36; N, 5.05%.

†† Throughout this paper 1 mmHg≈133.322 Pa.

References

1) Y. Uchida, Y. Hashimoto, and S. Kozuka, *Bull. Chem. Soc. Jpn.*, **53**, 2309 (1980).

2) Y. Uchida, Y. Kobayashi, and S. Kozuka, *Bull. Chem. Soc. Jpn.*, **54**, 1781 (1981).

3) H. E. Baumgarten, *J. Am. Chem. Soc.*, **84**, 4975 (1962).

4) H. E. Baumgarten, J. F. Fuerholzer, R. D. Clark, and R. D. Thompson, *J. Am. Chem. Soc.*, **85**, 3303 (1963).

5) J. C. Sheehan and I. Lengyel, *J. Am. Chem. Soc.*, **86**, 1356 (1964); J. C. Sheehan and J. H. Beeson, *ibid.*, **89**, 362 (1967).

6) J. C. Sheehan and I. Lengyel, *J. Am. Chem. Soc.*, **86**, 746 (1964).

Information Chemistry and Molecular Evolution of Protein. Evolutionary Tree of Calmodulin

Yôichi IIDA

Department of Chemistry, Faculty of Science, Hokkaido University, Sapporo 060

(Received December 10, 1981)

Synopsis. The amino acid sequences of calmodulin, one of calcium-binding proteins, taken from bovine brain, scallop, sea anemone, and tetrahymena were compared to examine its molecular evolution. By the use of maximum parsimony method, its evolutionary tree was constructed, It was found that this protein has changed much more slowly than have such proteins as cytochrome c.

Origin and evolution of life is one of the most important problems in biology and biochemistry. One of the best ways to approach this problem is to study molecular evolution of proteins.[1] In the course of evolution, natural selection improved the functions of protein molecules and preserved the improvements. However, it has been known that there are rapidly changing and slowly changing proteins against evolution. An advantage of studying the molecular evolution arises from this phenomenon. If the broad outlines of the history of life are wanted, then a widely distributed, slowly evolving protein must be studied. On the other hand rapidly changing proteins such as fibrinopeptides are most useful to study the details of one branch of the evolutionary tree of living organisms.

So far, cytochrome c has been known to be a typical example of widely distributed, slowly evolving proteins, and its evolutionary tree has been constructed.[1] In the present paper, we examine the molecular evolution of calmodulin (CM). It is also widely distributed throughout eukaryotes, and changes much more slowly than does cytochrome c. This implies that the evolution of CM is useful to measure the history of life with much longer time scale than that of cytochrome c. By applying maximum parsimony method (a technique of information chemistry) to the primary amino acid sequence, we construct an evolutionary tree of CM taken from various biological species.

CM is one of the calcium-binding proteins.[2,3] It has four calcium-binding sites, and interacts reversibly with Ca^{2+} to form a calmodulin–Ca^{2+} complex, whose activity is controlled by the cellular flux of Ca^{2+}. Once bound to Ca^{2+}, CM assumes a more helical conformation to become the active form. Thus, CM plays an important role in regulating other enzymatic reactions or cellular processes. The complete amino acid sequence of bovine brain CM was determined by Watterson *et al.*[4] and by Kasai *et al.*[5] It contains 148 amino acids and has a trimethylated lysine at position 115. The primary structure of CM appears to be highly conservative throughout the phylogenetic scale. For example, the amino acid sequence of CM from bovine brain is virtually identical with the partially completed sequences of CM from rat testis and bovine uterus.[3] Recently, in order to examine such a highly conservative structure, Toda *et al.*,[6] Takagi *et al.*,[7] and Yazawa *et al.*[8] determined the amino acid sequences of CM from phylogenetically more distant species, such as scallop (*Patinopecten*), sea anemone (*Metridium senile*), and tetrahymena (*Tetrahymena pyriformis*).

For the complete amino acid sequences of CM from (A) bovine brain, (B) scallop, (C) sea anemone, and (D) tetrahymena, refer to those references. In the following, we discuss only the positions and the species of amino acid residues which are different from each other. For this purpose, we take an expression of {position, (a), (b), (c), (d)}, where (a), (b), (c), or (d) indicates the amino acid residue of CM from the biological species of (A), (B), (C), or (D) at the corresponding position, respectively. Using this expression, we can only find the following differences; {70, Thr, Thr, Thr, Ser}, {71, Met, Met, Met, Leu}, {85, Ile, Ile, Ile, Leu}, {86, Arg, Arg, Arg, Ile}, {90, Arg, Arg, Arg, Lys}, {94, Lys, Lys, Lys, Arg}, {99, Tyr, Phe, Phe, Leu}, {101, Ser, Ser, Ser, Thr}, {135, Gln, Gln, Gln, His}, {136, Val, Val, Val, Ile}, {143, Gln, Thr, Lys, Arg}, {146, Thr, Thr, Thr, Deletion}, and {147, Ala, Ser, Ser, Ala}. The amino acids at the other positions are common with the four biological species. Highly conservative property of the amino acid sequence of CM is well demonstrated, if we compare the difference of the amino acid residues at the same position. For example, only three amino acid differences are found between bovine brain and sea anemone. Concerning the sequences of bovine brain and tetrahymena, only eleven amino acid changes and one lack of amino acid residue at position 146 are found in tetrahymena.

It is generally known that codons of m RNA are translated into amino acids of protein.[1] Any codon is composed of a series of three nucleotides and is expressed by "the genetic code." Therefore, the observed difference of amino acid residues of CM between two biological species is attributable to the difference of nucleotides between the corresponding codons. Referring to the genetic code, we assume that the difference of amino acids of CM between the two species is given

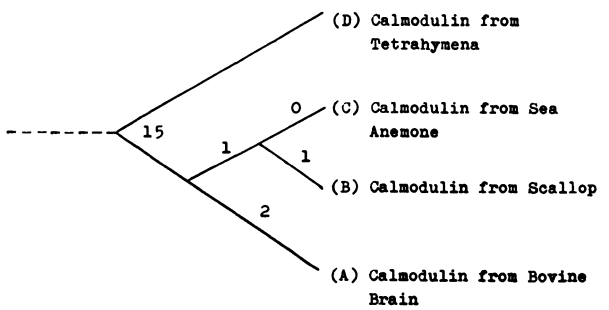

Fig. 1. The evolutionary tree estimated by applying maximum parsimony method to the difference in the amino acid sequences of calmodulin taken from (A) bovine brain, (B) scallop (*Patinopecten*), (C) sea anemone (*Metridium senile*), and (D) tetrahymena (*Tetrahymena pyriformis*). Numbers indicate nucleotide replacements.

by the least number of nucleotide replacements of the codons. This approach is called "maximum parsimony method." It is considered that the distance between two biological species may be also expressed by such a number of replacements. According to this method, the number of nucleotide replacements in CM between two biological species of (A) and (B) is 4, that between (A) and (C) is 3, that between (A) and (D) is 17, that between (B) and (C) is 1, that between (B) and (D) is 17, and that between (C) and (D) is 16. Here, the lack of amino acid residue at position 146 of (D) is counted as three nucleotide replacements. From these data, an evolutionary tree of CM is constructed as is shown in Fig. 1, where numbers indicate nucleotide replacements. Using this evolutionary tree together with the data on the difference of amino acid residues given previously, we can reconstruct the amino acid sequence of the common ancestor of (A), (B), and (C) as ···-$\overset{99}{\text{Phe}}$-··· -$\overset{143}{\text{Lys}}$-···-$\overset{147}{\text{Ala}}$-···, where the remaining amino acid residues are common to those of the three species. In order to reconstruct the amino acid sequence of the common ancestor of (A), (B), (C), and (D), it is necessary to know the amino acid sequences of CM of fungi and plants, which had diverged earlier than the common ancestor of (A), (B), (C), and (D) diverged. However, no such data are available at present.

Next, we compare evolutionary rate of CM with that of cytochrome c, which contains 104 amino acid residues. In cytochrome c, the primates differ from other mammals by 8—12 residues; mammals and birds differ by an average of 9.9; mammals and reptiles and amphibia by 14; the vertebrates of all kinds differ from insects by 26.[1] On the other hand, as was mentioned, only three amino acid differences were found in CM between bovine brain and sea anemone. Biologically speaking, these two biological species are phylogenetically more distant from each other than those species given in cytochrome c. Therefore, CM appears to be much more conservative against evolution than cytochrome c. Why CM is so conservative? One of the reasons for this is that CM is a finely tooled molecule which must mesh with a number of other macromolecules to regulate various enzymatic reactions or cellular processes.[2,3] This means that a slight structural change in CM will have great influence upon such reactions and processes and that the vast majority of chance alternations are intolerable. On the other hand, cytochrome c, although it meshes with some other proteins, has less influence upon other reactions, and a chance mutation which is tolerable will occur more frequently. In this respect, if the primary amino acid sequences of CM are determined with more variety of biological species, we can measure the history of life with considerably longer time scale.

The author would like to express his appreciation to Professor Koichi Yagi for his kind advice and stimulating discussion regarding this work.

References

1) See, for example, M. O. Dayhoff, "Atlas of Protein Sequence and Structure," National Biomedical Research Foundation, Washington, D. C. (1972), Vol. 5.

2) See, for example, "Calcium Binding Proteins and Calcium Function," ed by R. H. Wasserman *et al.*, North Holland, New York (1977).

3) W. Y. Cheung, *Science*, **207**, 19 (1980).

4) D. M. Watterson, F. Sharief, and T. C. Vanaman, *J. Biol. Chem.*, **255**, 962 (1980).

5) H. Kasai, Y. Kato, T. Isobe, H. Kawasaki, and T. Okuyama, *Biomed. Res.*, **1**, 248 (1980).

6) H. Toda, M. Yazawa, K. Kondo, T. Honma, K. Narita, and K. Yagi, *J. Biochem.*, **90**, 1493(1981).

7) T. Takagi, T. Nemoto, K. Konishi, M. Yazawa, and K. Yagi, *Biochem. Biophys. Res. Commun.*, **96**, 377 (1980)

8) M. Yazawa, K. Yagi, H. Toda, K. Kondo, K. Narita, R. Yamazaki, K. Sobue, S. Kakiuchi, S. Nagano, and Y. Nozawa, *Biochem. Biophys. Res. Commun.*, **99**, 1051 (1981).

Anormalous Halogen to Dimethylamino Replacement with *N,N*-Dimethylformamide Catalyzed by Ethylenediamine or 2-Aminoethanol

Hiroshi YAMAMOTO

Department of Chemistry, Faculty of Science, Okayama University, Tsushima, Okayama 700

(Received January 11, 1982)

Synopsis. 1- And 2-chloroanthraquinone and 2-amino-4-chloro-6-hydroxypyrimidine exclusively gave the dimethylamino derivatives upon heating in DMF at 90 °C in the presence of ethylenediamine or ethanolamine. A possible reaction pathway for this unusual exchange reaction was discussed.

The active chlorine atoms that are attached to an acyl group[1] or certain aromatic and heteroaromatic nuclei[2-7] (*e.g.*, nitrobenzene[2] and pyridine[6]) are replaced by dimethylamino groups upon boiling with *N,N*-dimethylformamide (DMF) for a prolonged period according to Scheme 1. We will describe here a similar type of exchange reaction which is, however, characteristically catalyzed by ethylenediamine (EDA) or 2-aminoethanol at *ca.* 90 °C.

$$RCl + Me_2NCHO \longrightarrow RNMe_2 + HCl\ (or RN^+HMe_2Cl^-) + CO$$

Scheme 1.

The treatment of 1- and 2-chloroanthraquinone (**1** and **2**) and the chloropyrimidines (**3** and **4**) with 1.0—2.0 mol equiv. of EDA or 2-aminoethanol in DMF at 90 °C afforded exclusively the dimethylamino compounds (**5**—**8**) instead of the normally expected substitution products (*e.g.*, **9**—**11**), as is recorded in Entry 1 of Table 1. Since all these chloro compounds were stable in DMF alone at this temperature, EDA and 2-aminoethanol are thought to act as catalysts for the dimethylamination. The catalytic efficiency was shown best by EDA or 2-aminoethanol, moderately by 1,3-propanediamine, and only slightly by 1,4-butanediamine, *N,N*- and *N,N'*-dimethylethylenediamine, 2-(methylamino)ethanol, or butylamine (Entry 2). No catalytic effect was found with triethylamine or ethylene glycol.

N-Methylformamide and *N*-formylmorpholine afforded a moderate yield of the corresponding exchange products (**12**—**15**), along with an appreciable amount of the substitution products (**9**, **10**), whereas, with *N,N*-diethylformamide and *N,N*-dimethylacetamide, the chloro compounds (**1**—**3**) either remained unreactive or preferably produced **9** and **10**. Thus, the reactivities of the aminating reagents depended upon the combination of the amines and the *N*-acyl groups (Entry 3).

The use of ethanol as a solvent in the reaction of **1** with DMF–2-aminoethanol (2 mol equiv. each) suppressed the formation of both **5** and **9** (Entry 4). It should also be noticed that the reaction temperature plays an important role, as was observed in the predominant formation of **9** when **1** was heated with DMF or *N*-formylmorpholine in the presence of 2-aminoethanol at a lower temperature, such as 60 °C (Entry 4).

Benzoyl chloride, bearing a chlorine atom highly reactive towards nucleophiles, reacted with EDA in DMF, even at 0 °C, to give solely the *bis*-compound (**16**); without EDA, *N,N*-dimethylbenzamide is slowly produced upon heating in DMF only above 150 °C.[1] On the other hand, 2,4-diamino-6-chloropyrimidine (**17**), with a less reactive chlorine atom than **3** or **4**, remained almost unchanged, even on heating with DMF–EDA at 120 °C (Entry 4).

Chlorine atoms in hydroxy- or amino-chloropyrimidines are known to be replaced by alcoholic solution of amines, usually at relatively elevated temperatures in a sealed tube;[8] *e.g.*, 6-methylaminouracil is obtained from **4** at 130 °C, and 2,4,6-triaminopyrimidine, from **17** at 200 °C. However, such nucleophilic substitution with liberated dimethylamine is not conceivable in the present, unusual exchange reaction, since no dimethylamine was produced upon the heating of a 1 : 1 mixture of DMF and EDA (or 2-aminoethanol) at 90—100 °C for 2—20 h (by ^{1}H-NMR and GLC). Instead, DMF is likely to form a certain complex with EDA or 2-aminoethanol at *ca.* 90 °C; this complex subsequently reacts with chloro compounds (**1**—**4**) to give the dimethylamino derivatives at much faster rates than those of the exchange reaction (without using such catalysts) as are illustrated in Scheme 2. The predominant formation of the substitution products (**9**, **16**) with the catalysts at 0—60 °C can be explained in terms of the sluggish formation of such an intermediate complex at low temperatures.

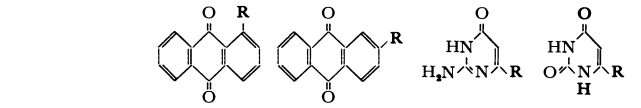

R	1	2	3	4
Cl	1	2	3	4
NMe_2	5	6	7	8
$NH(CH_2)_2OH$	9	10		
$NMe(CH_2)_2OH$	11			
NHMe	12	13		
Morpholino	14	15		

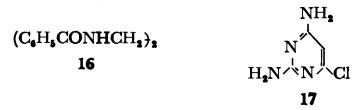

$(C_6H_5CONHCH_2)_2$ **16**

17

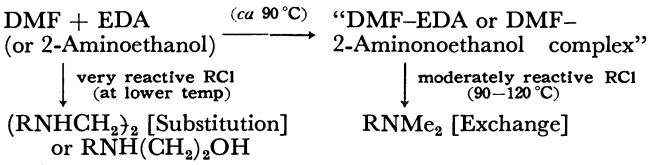

Scheme 2.

Although the exact nature of the complex and the reaction mechanism remain to be clarified further, the present procedure is apparently a convenient method for the dimethylamination of some aromatic and heteroaromatic compounds bearing a reactive chlorine atom. The results also demonstrate the necessity of

Table 1. Active chlorides to amines

Entry	Starting matl.	Reagent[a]	Catalyst[b]	Reaction temp/°C (Time/h)	Exchange product; Yield[c]/%	Substitution product; Yield[c]/%	Yield[c] of the recovered starting matl./%
1	**1—4**	DMF	None	90 (22)			100
	1	**DMF**	EDA	90 (9)	**5**[d] ; 60		18
	1	DMF	AE	90 (22)	**5** ; 75	**9**[e] ; 15	
	2	DMF	EDA	90 (30)	**6**[d] ; 63		20
	2	DMF	AE	90 (22)	**6** ; 84		
	3[f]	DMF	EDA	90 (3)	**7**[g] ; 90		
	4[h]	DMF	EDA	90 (5)	**8**[i] ; 45		28
2	**1, 3**	DMF	TEA	90 (10)			100
	1, 2	DMF	EG	90 (22)			95
	1	DMF	MAE	90 (20)	**5** ; 5	**11**[j] ; 70	17
	2	DMF	DME	90 (22)	**6** ; 14		65
	2	DMF	DMED	90 (24)	**6** ; 8		80
	3	DMF	PDA	90 (7)	**7** ; 31		28
	3	DMF	BDA	90 (6)	**7** ; 3		67
	3	DMF	BA	90 (9)	**7** ; 4		55
3	**1**	MeNHCHO	AE	90 (19)	**12**[d] ; 41	**9** ; 28	20
	2	MeNHCHO	AE	100 (60)	**13**[d] ; 36		25
	1	FM	AE	90 (22)	**14**[k] ; 45	**9** ; 33	
	2	FM	AE	90 (22)	**15**[l] ; 37	**10**[l] ; 4	45
	1	Et_2NCHO	AE	90 (22)		**9** ; 63	25
	2	Et_2NCHO	AE	90 (22)		**10** ; 5	90
	1	Me_2NAc	AE	90 (22)	**5** ; 2	**9** ; 73	12
	2	Me_2NAc	AE	100 (40)	**6** ; 21	**10** ; 60	7
	3	Me_2NAc	EDA	90 (5)			100
4	**1**	DMF+EtOH	AE	90 (22)	**5** ; 18	**9** ; 12	65
	1	DMF	AE	60 (10)	**5** ; Trace	**9** ; 38	40
	1	FM	AE	60 (10)	**14** ; Trace	**9** ; 27	56
	PhCOCl	DMF	EDA	0 (0.5)		**16**[m]; 71	
	PhCOCl	DMF	None	150 (6)	$PhCONMe_2$[n]; 85		
	17[o]	DMF	EDA	120 (10)			90

a) Used as the solvent; DMF, *N,N*-dimethylformamide; FM, *N*-formylmorpholine. b) 1.0—2.0 mol equiv. to the substrate; EDA, ethylenediamine; AE, 2-aminoethanol; TEA, triethylamine; EG, ethylene glycol; MAE, 2-(methylamino)ethanol; DME, *N,N*-dimethylethylenediamine; DMED, *N,N'*-dimethylethylenediamine; PDA, 1,3-propanediamine; BDA, 1,4-butanediamine; BA, butylamine. c) Yield referred to isolated, pure (TLC) products. d) Ref. 3. e) H. W. Coover, J. B. Bickey, and E. B. Towne, U. S. Patent 2459149, *Chem. Abstr.*, **43**, 3205 (1949). f) Ref. 8, p. 575. g) R. Huegi and W. Pfleiderer, *Justus Liebigs Ann. Chem.*, **759**, 76 (1972). h) Ref. 8, p. 602. i) Ref. 8, p. 559. j) V. V. Russkikh and E. P. Fokin, *Izv. Sib. Otd. Akad. Nauk SSSR, Ser. Khim. Nauk*, **1966**, 91. k) K. Bredereck, M. Diamantoglou, and F. Sommermann, *Chem. Ber.*, **103**, 1748 (1970). l) New compound. m) P. Ruggli, R. Patti, and E. Henzi, *Helv. Chim. Acta*, **12**, 347 (1929). n) Ref. 1. o) Ref. 8, p. 544.

taking precaution in employing DMF as a solvent in combination with certain amines, such as EDA and 2-aminoethanol.

Expermiental

The ^{1}H-NMR Spectra were measured with a Hitachi High-resolution NMR Spectrometer, R 20A (60 MHz), at 27 °C, using TMS as the internal standard, and the IR spectra, with a JASCO IRA-1 Spectrophotometer. Column chromatograhpy was carried out with alumina (Merck, Activity I, basic) or silica gel (Wako C-200), with ether–benzene or methanol–chloroform as the eluant. All the reactions were monitored by means of TLC.

Materials. The starting materials and products cited in this study are all known compounds except for **10** and **15**; thus, they are either commercially availabel or are prepared according to the literature methods (*cf.* Table 1) and purified before use.

General Procedures. A mixture of 50 mg of the active chloro compounds (**1**—**4**, PhCOCl, and **17**), 1.0 mol equiv. of the ethylenediamines (or 2.0 mol equiv. of 2-amonoethanol or other amines), and 1 ml of freshly distilled DMF (or the aminating reagent) was heated under nitrogen (or, in some cases, in a sealed tube); the reaction time and temperature are shown in Table 1. In many cases, the pure product was precipitated and subsequently isolated simply by filtration. The dilution of the filtrate with water gave the second crop. When the reaction products were a mixture, they were extracted with benzene after being diluted with water. The combined organic extracts were concentrated, and the residue was chromatographed. The products were characterized by a mixed-melting-point determination and by means of comparative TLC with authentic specimens prepared by alternative routes (Table 1) as well as by means of their ^{1}H-NMR and IR spectra.

*2-(2-Hydroxyethylamino)anthraquinone (**10**)*: Brown prisms; mp 206—207 °C (from EtOH); IR (Nujol) 3390, 3280 (OH, NH), 1660 (C=O), 1595 and 1560 cm^{-1} (C=C); ^{1}H-NMR δ ($CDCl_3$–DMSO-d_6, 1 : 1) 3.29† (1H, s, HO-2'), 3.40 (2H, brt, J=5.0 Hz, H_2-1'), 3.80 (2H, brt, J=5.0 Hz, H_2-2'), 4.91† (1H, m, NH), 6.90 (1H, dd, J=9.0, 2.5 Hz, H-3), 7.40 (1H, d, J=2.5 Hz, H-1), 7.80 (2H, m, H-6,7), 8.15 (1H, d, J=9.0 Hz, H-4), and 8.25 (2H, m, H-5,8), Found: C, 72.08; H, 4.82; N, 4.93%. Calcd for $C_{16}H_{13}NO_3$: C, 71.89; H, 4.91; N, 5.25%.

*2-Morpholinoanthraquinone (**15**)*: Reddish orange needles; mp 223—224 °C (from benzene); IR ($CHCl_3$) 1670 (C=O), 1595 (C=C), 1325, 1290 and 915 cm^{-1}; ^{1}H-NMR δ ($CDCl_3$–DMSO-d_6) 3.3—3.8 (8H, m, morpholino) and 7.0—8.3 (7H, m, aromatic). Found: C, 73.65; H, 5.28; N, 4.43%. Calcd for $C_{18}H_{15}NO_3$: C, 73.70; H, 5.15; N, 4.77%.

The author wishes to thank to Professor Wolfgang Pfleiderer of Universität Konstanz, West Germany, for his valuable discussions and encouragement.

References

1) G. M. Coppinger, *J. Am. Chem. Soc.*, **76**, 1372 (1954).
2) W. Wakabe and K. Hamano, *Bull. Chem. Soc. Jpn.*, **36**, 230 (1963).
3) W. M. Lord and A. T. Peters, *J. Chem. Soc., C*, **1968**, 783; *Chem. Ind. (London)*, **1973**, 227.
4) J. J. D'Aminom, S. T. Webster, R. H. Campbell, and C. E. Twine, *J. Org. Chem.*, **30**, 3618 (1965).
5) L. Joseph and A. M. Albert, *J. Heterocycl. Chem.*, **3**, 107 (1966).
6) N. D. Heindel and P. D. Kennewell, *Chem. Commun.*, **1969**, 38.
7) S. Nishigaki, K. Senga, and F. Yoneda, *Chem. Pharm. Bull. (Tokyo)*, **19**, 1526 (1971).
8) See, *e. g.*, D. J. Brown, "The Pyrimidines," Interscience, New York (1962), p. 197.

† Signals being D_2O exchangeable.

Copper(II) Halide Catalyzed Cyclopropanation of Olefins Involving Dehydrobromination of Bromomalonic Ester by Amine

Nariyoshi KAWABATA,* Shinji YANAO, and Jun-ichi YOSHIDA
Department of Chemistry, Faculty of Polytechnic Science, Kyoto Institute of Technology, Matsugasaki, Sakyo-ku, Kyoto 606
(Received January 21, 1982)

Synopsis. The reaction of olefins with bromomalonic ester and 1,8-diazabicyclo[5.4.0]undec-7-ene (DBU) proceeded in the presence of a catalytic amount of copper(II) halide to give 1,1-bis(alkoxycarbonyl)cyclopropane derivatives. DBU was converted into DBU-hydrobromide during the reaction. The reaction was electrophilic and proceeded nonstereospecifically.

Cyclopropane derivatives activated by two electron-withdrawing substituents at geminal position are called electrophilic cyclopropanes, and have recently been recognized as useful intermediates in organic synthesis.[1] Their inter- and intramolecular ring opening reactions by various nucleophiles have been investigated intensively, and applied to the synthesis of several natural products.[1] Recently we have reported a new cyclopropanation reaction of olefins with *gem*-dibromides such as dibromomalonic ester using a stoichiometric amount of copper[2] or copper(I) salt.[3] In this paper we wish to describe that electrophilic cyclopropanes were obtained by use of only a catalytic amount of copper(II) salt in the reaction of olefins with bromomalonic ester and amine (Eq. 1).

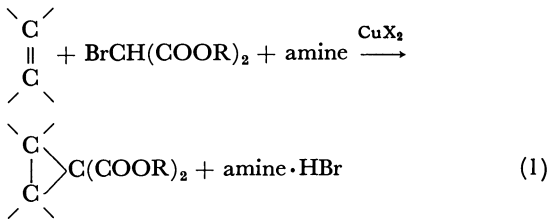

(1)

When bromomalonic ester was allowed to react with 1,8-diazabicyclo[5.4.0]undec-7-ene (DBU) and olefins in the presence of a catalytic amount of copper(II) bromide, 1,1-bis(alkoxycarbonyl)cyclopropane derivatives were obtained. For example, the reaction with styrene proceeded smoothly at room temperature in benzene to give 1,1-bis(ethoxycarbonyl)-2-phenylcyclopropane in 87% yield. During the course of the reaction, a solid material precipitated which was identified as DBU-hydrobromide by comparison of its IR spectrum with that of an authentic sample.

The effect of a variety of amines on the yield of the cyclopropane derivative was examined in the reaction with styrene (Table 1). DBU (pK_a 11.5) was the most effective amine among the examined. Triethylamine (pK_a 10.7), diethylamine (pK_a 10.9), and butylamine (pK_a 10.6) were less effective. 1,4-Diazabicyclo[2.2.2]-octane (DABCO) (pK_{a1} 3.0; pK_{a2} 8.6), pyridine (pK_a 5.2), and aniline (pK_a 4.6) were scarcely effective. In the absence of amine, the cyclopropane derivative was not formed. These results seemed to indicate that basicity of the added amine was of major importance. It should be noted, however, that sodium hydride was inactive in spite of its higher basicity than that of DBU.

Table 1. Effect of amine on the copper(II) bromide catalyzed cyclopropanation of styrene involving dehydrobromonation of diethyl bromomalonate by the amine[a]

Amine	Yield of cyclopropane/%[b]	
DBU	87	
Triethylamine	Trace[c]	(26)
Diethylamine	47	(59)
Butylamine	16	(25)
DABCO	Trace[c]	(Trace[c])
Pyridine	0	(0)
Aniline	0	(Trace[c])
Sodium hydride	Trace[c]	(Trace[c])

a) Reactions were carried out with styrene (2.0 mmol), diethyl bromomalonate (3.0 mmol), amine or sodium hydride (3.6 mmol), copper(II) bromide (0.10 mmol), and benzene (2.0 ml) at room temperature for 1 h. b) Determined by GLC, based on the olefin. Yields after 24 h are given in parentheses. c) GLC analysis of the reaction mixture showed a very small peak having the identical retention time with that of the cyclopropane derivative, but the product was not fully identified.

Table 2. Synthesis of 1,1-bis(alkoxycarbonyl)-cyclopropanes from various olefins[a]

Olefin	Yield of cyclopropane/%[b]	
Styrene	87	(Trace[c])
p-Methylstyrene	76	(Trace[c])
m-Trifluoromethylstyrene	27	(Trace[c])
p-Chlorostyrene	53	(Trace[c])
Acrylonitrile	62	(63)
Methyl vinyl ketone	56	(56)
Ethyl acrylate	18	(20)

a) Reactions were carried out with an olefin (2.0 mmol), diethyl bromomalonate (3.0 mmol), DBU (3.6 mmol), and benzene (2.0 ml) in the absence or presence of copper(II) bromide (0.10 mmol). b) Determined by GLC, based on the olefin. Yields obtained in the absence of copper(II) bromide are given in parentheses. c) See footnote (c) in Table 1.

Presumably the amine played some important role, *e.g.*, coordination to the copper ion and accelerating the reaction, in addition to functioning as a simple base.

Copper(II) bromide was the catalyst of choice for the reaction of styrene with diethyl bromomalonate and DBU in benzene, and the yield of the cyclopropane derivative was 87%. Copper(II) chloride (50% yield), copper(I) chloride (76%), and copper(I) iodide (51%) were somewhat less effective. Use of copper(II) acetate and copper(II) acetylacetonate resulted in very low yields. In the absence of catalyst, the cyclopropane derivative was not obtained. The yield was also greatly

influenced by the nature of the solvent. In methanol and hexane, the cyclopropane derivative was not obtained in an appreciable amount. Polar aprotic solvents such as dimethyl sulfoxide (82%), *N,N*-dimethylformamide (54%), and acetonitrile (52%) were effective, but benzene was the most suitable solvent among the examined.

Other examples of the reaction (Eq. 1) are summarized in Table 2. The reaction with substituted styrenes gave the corresponding cyclopropane derivatives in moderate to high yields. Electron-deficient olefins such as acrylonitrile and methyl vinyl ketone also reacted smoothly to give the cyclopropane derivatibes in good yields. Electron-rich olefins such as isobutyl vinyl ether were inactive under the conditions. The reaction with alkyl-substituted olefins such as 1-octene and cyclooctene gave the cyclopropane derivatives only in very low yields.

The cyclopropanation reactions of (*E*)- and (*Z*)-β-methylstyrene were studied to determine the stereospecificity of the reaction. From both olefins were obtained the (*E*)- and (*Z*)-cyclopropane derivatives in essentially the same ratio (*E*/*Z*=95/5), indicating that the reaction proceeded in a non-stereospecific way. Isomerization of (*E*)- and (*Z*)-β-methylstyrene and that of (*E*)- and (*Z*)-cyclopropane derivatives were not observed under the conditions.

The relative reactivity of substituted styrenes was also investigated. The logarithm of relative reactivity was plotted against Hammett σ value to obtain a straight line with good correlation. A slope of −0.8 indicates that the reaction is electrophilic.

It should be noted that the reaction with electron-deficient olefins such as acrylonitrile proceeded even in the absence of the catalyst, whereas the reaction with styrene derivatives essentially required the copper salt as catalyst. Therefore it seems reasonable to consider that the reaction with electron-deficient olefins proceeded through a different reaction pathway from that with styrene derivatives. A mechanism involving Michael type addition of the carbanion of bromomalonic ester may be plausible for the reaction with electron-deficient olefins.[4] For the copper(II) bromide catalyzed reaction with styrene derivatives, a mechanism involving a free radical intermediate or an organocopper intermediate seems to be plausible. Relatively low reactivity of unconjugated olefins such as isobutyl vinyl ether or 1-octene may accommodate the free radical mechanism. Further mechanistic studies will hopefully delineate the detailed mechanism.

Experimental

Infrared spectra were measured with a Hitachi Model 215 grating spectrophotometer. ^{1}H NMR spectra were obtained with a Varian Model T-60A spectrometer in CCl_4 using Me_4Si as the internal standard. GLC analysis and preparative purification were performed by a Shimadzu GC-4C gas chromatograph equipped with a 1 m×3 mm column (Silicone DC-550 5% on Celite 545, 60—80 mesh) and a thermal conductivity detector. Diethyl bromomalonate was prepared by light-induced bromination of diethyl malonate[5] and purified by fractional distillation under reduced pressure. *p*-Methylstyrene,[6] *p*-chlorostyrene,[6] *m*-trifluoromethylstyrene,[6] (*E*)-β-methylstyrene,[6] and (*Z*)-β-methylstyrene[7] were prepared according to the literature procedures with minor modifications. Other olefins were commercially available and were distilled before use. An authentic sample of DBU-hydrobromide was prepared by treatment of DBU with dry hydrogen bromide in benzene. All solvents were dried in a usual manner and distilled before use. Other chemicals including copper salts and amines were used as obtained commercially.

General Reaction Procedure for Synthesis of 1,1-Bis(alkoxycarbonyl)cyclopropanes from Olefins. A mixture of an olefin (2.0 mmol), DBU (548 mg, 3.6 mmol), and anhydrous copper(II) bromide (22 mg, 0.10 mmol) in benzene (2.0 ml) was placed in a 20-ml one-necked flask fitted with a magnetic stir bar and a stopcock. Diethyl bromomalonate (717 mg, 3.0 mmol) was added dropwise with stirring under cooling in a water bath (15—25 °C). An exothermic reaction took place and DBU-hydrobromide gradually precipitated. After the addition was completed, the mixture was stirred for 1 h. An appropriate hydrocarbon internal standard was added and the mixture was analyzed by GLC. The products were isolated by preparative GLC and identified by comparison of their IR and ^{1}H NMR spectra with those of authentic samples.[2] DBU-hydrobromide was separated from the reaction mixture by filtration, washed with ether, dried under vacuum, and identified by comparison of its IR spectrum with that of an authentic sample (88% yield based on diethyl bromomalonate).

The reaction with other amines, sodium hydride, or other copper salts, and the reaction in other solvents were carried out in a similar fashion.

References

1) S. Danishefsky, *Acc. Chem. Res.*, **12**, 66 (1979).
2) N. Kawabata and M. Tanimoto, *Tetrahedron*, **36**, 3517 (1980).
3) N. Kawabata, S. Yano, J. Hashimoto, and J. Yoshida, *Bull. Chem. Soc. Jpn.*, **54**, 2539 (1981).
4) It has been reported that an anion of α-halo ester reacted with α,β-unsaturated carbonyl compounds to give the corresponding cyclopropane derivatives. See: L. L. McCoy, *J. Am. Chem. Soc.*, **80**, 6568 (1958).
5) T. Wakui, Y. Otsuji, and E. Imoto, *Nippon Kagaku Kaishi*, **1974**, 1686.
6) C. G. Overberger and J. H. Saunders, *Org. Synth.*, Coll. Vol. III, 204 (1955).
7) J. R. Johnson, *Org. React.*, **1**, 210 (1942); R. H. Wiley, N. R. Smith, R. T. Arnold, W. E. Parham, and D. D. Davis, *Org. Synth.*, Coll. Vol. IV, 731 (1963).

An Experimental Approach to the Prebiotic Synthesis of α-Amino Acids under UV Irradiation in Aqueous Medium

Masato NISHIZAWA* and Fujio EGAMI
Mitsubishi-Kasei Institute of Life Sciences, 11 Minamiooya, Machida, Tokyo 194
(Received March 3, 1982)

Synopsis. *N*-Oxaloglycine obtained from a glyoxylic acid and ammonia mixture was allowed to produce various α-amino acids under UV irradiation using an alkylating agent such as an olefin in the presence of acetone as the initiator. Aspartic acid, norvaline, valine, leucine, phenylalanine, and tyrosine were identified by TLC, amino acid analysis, GC, and GCMS techniques.

On the basis of a generally accepted working hypothesis that life originated in the primeval sea, research at our laboratory has been directed toward the synthesis of biomolecules in modified sea medium from primitive compounds such as formaldehyde and hydroxylamine.[1] Particular attention has been paid to synthetic pathways of amino acid formation in the primeval sea. An understanding of these pathways of amino acid formation may possibly provide a clue to the origin of genetic code, in view of the relation between amino acid and nucleic bases. Our purpose has been to find possible synthetic routes of amino acids prebiotically in a neutral aqueous medium. Besides the well-known Strecker synthesis,[2] we found a new route through *N*-acyl amino acid from α-oxo acid and ammonia.[3] *N*-Oxaloglycine is synthesized from a glyoxylic acid and ammonia mixture simply by combining it with a neutral or weak acidic aqueous solution to obtain a yield of about 20% even at room temperature. The reactions involved are as follows:

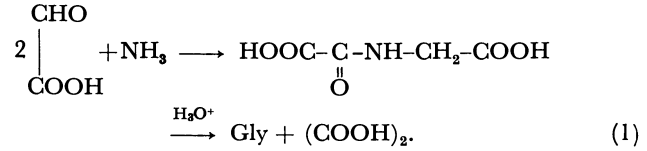

This general reaction scheme was demonstrated in the synthesis of sarcosine, alanine, glutamic acid, and phenylalanine.[3,4] In this paper, our effort has been directed to the conversion of *N*-oxaloglycine into other α-amino acids by introducing C_n moieties on the α-carbon of the glycine residue photochemically.

Experimental

Materials. Disodium salt of *N*-oxaloglycine was prepared by two methods. By one method, this compound was isolated from a reaction mixture of glyoxylic acid and ammonia.[3] The other method was the traditional organic synthesis.[5] The purity was determined by elemental analysis, UV, IR, and NMR. And the results were as follows; Calcd for $C_4H_3N_1O_5Na_2 \cdot 1/2\ H_2O$: C, 24.16; H, 1.78; N, 6.74%. Found: C, 23.80; H, 1.55; N, 6.46%. λ_{max} (ε)=214 nm (4.5×10^3 cm^{-1} M^{-1} (1 M=1 mol dm^{-3})) in 0.6 M HCl. 1680—1600, 1550 cm^{-1}. δ=4.29 (s). Research grade propylene, isobutylene and 2-butene (*cis* and *trans*) were purchased from Seitetsu Kagaku Co. Ltd. *N,N*-Bis(trimethylsilyl)trifluoroacetamide (BSTFA) was obtained from Pierce Chemical Co. Acetonitrile was refluxed with phosphorus pentaoxide and distilled.

Method. An aqueous solution containing 20—40 mg of disodium salt of *N*-oxaloglycine, 10—20% (v/v) of acetone and an alkylating agent was made up, deaerated by charging it with nitrogen gas using the syringe technique and irradiated with a high pressure Hg-lamp (Ushio electric Co. UM-102, 100 W) through a Pyrex-filter. When using a gas as an alkylating agent, it was made to pass through the reaction mixtures under irradiation. After 20 h irradiation, the reaction mixture was evaporated and hydrolyzed with 6 M HCl at 105 °C in Dri-block DB-3H (M & S instrument) over night. A hydrolysate was used to determine what amino acids were present. The spots on silica gel TLC (ethanol : water=6 : 4, 1-butanol: acetic acid : water=4 : 1 : 1, and 1-propanol : ammonia= 3 : 1) were investigated with UV light and ninhydrin spraying. Amino acid analysis was performed with a Hitachi KLA-5 automatic analyzer.

Analysis of Trimethylsililated Amino Acid (TMS-Amino Acid). An aqueous solution of hydrolysate was treated with an appropriate amount of $CaCl_2$ to remove calcium oxalate, and the supernatant was lyophilized and dried at 80 °C under vacuum. A 5—10 mg of residue was heated with 0.5 ml distilled acetonitrile and 0.5 ml of BSTFA at 140 °C for 2 h. After concentrated under vacuum, a 0.5—5 μl sample was charged on a GC (Shimadzu GC-4M) and GCMS (Shimadzu 7000) using an OV-11 (10%) column. The technical data obtained were as follows. I) Reaction with acetonitrile: GC, col. temp 195 °C, inj. temp 250 °C. Retention time was 4.51 min (TMS-aspartic acid). GCMS *m/e* 349 (M^+), 232, 218. II) Reaction with propylene: GC, col. temp 80—200 °C at 5 °C/min, inj. temp 220 °C. Peaks appeared at 14.56 (TMS-valine) and 15.43 min (TMS-norvaline). GCMS *m/e* 218, 144 for both peaks. III) Reaction with isobutylene: GC, col. temp 80—200 °C at 5 °C/min, inj. temp 220 °C. Retention time was 17.55 min (TMS-leucine). GCMS *m/e* 218, 158. IV) Reaction with toluene: GC, col. temp 190 °C, inj. temp 250 °C. A peak corresponding to TMS-phenylalanine appeared at 5.50 min. GCMS *m/e* 218, 192, 91. V) Reaction with *p*-cresol: GC, col. temp 240 °C, inj. temp 280 °C. A peak of 5.05 min corresponded to TMS-tyrosine. GCMS *m/e* 280, 218, 179. The carrier gas flow rates were 40 ml/min and 15—20 ml/min for nitrogen (GC) and helium (GCMS), respectively.

Results and Discussion

N-Oxaloglycine was useful as a starting material in this experiment, since it could be obtained simply by mixing glyoxylic acid and ammonia in a neutral or weak acidic aqueous solution at room temperature.

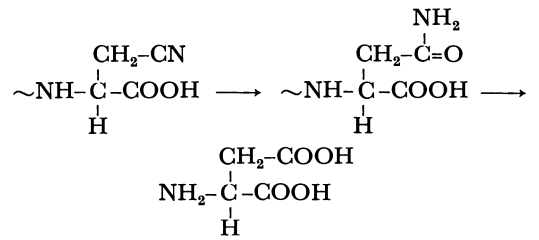

The introduction of a C_2 unit to *N*-oxaloglycine was achieved with the use of acetonitrile. Since aspartic acid was found to be one of the final product following acid hydrolysis, following scheme has been proposed

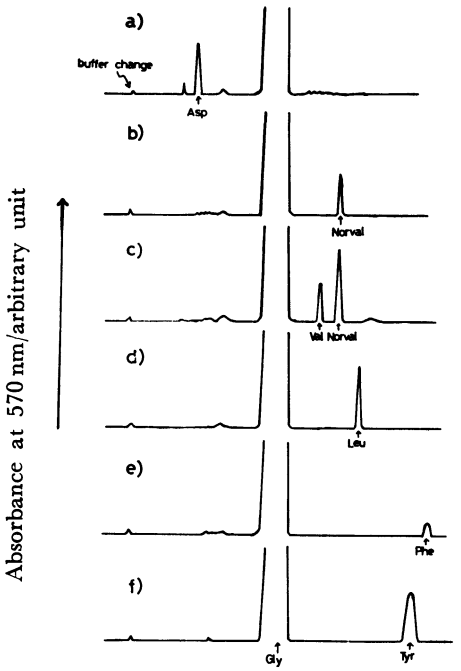

Fig. 1. Amino acid analyses of acid hydrolysates from reaction mixtures.
a): Reaction with acetonitrile, b): reaction with propylene, c): reaction with propylene in the presence of 10^{-4} M palladium(II) chloride, d): reaction with isobutylene, e): reaction with toluene, f): reaction with *p*-cresol.

as a plausible hydrolysis route. The cyanoalanine residue is finally hydrolysed to asparagine and aspartic acid. Acetate could not be introduced onto *N*-oxaloglycine in this experiment.

Norvaline was formed using propylene in the absence of metal ions (Fig. 1-(b)). The formation of valine (Fig. 1-(c)) may be inconsistent with the anti-Markownikov mode, if a radical mechanism is operative. However, added metal ions can react with propylene under the experimental conditions to result in a different product. This phenomenon was observed when either $PdCl_2$, $CoCl_2$, or $MnCl_2$ was added. Other metal ions such as Fe^{2+}, Cu^{2+} gave no valine peak. When acrylonitrile was put into the reaction system, the resulting considerable precipitation under UV irradiation precluded an analysis of glutamic acid.

The C_4 unit was inserted onto *N*-oxaloglycine by using isobutylene as an alkylating agent. Except glycine only a leucine peak is evident in Fig. 1-(d). Only a trace amount of *cis* and *trans*-2-butene resulted in the formation of isoleucine as indicated by amino acid analysis sensitivity. Decisive identification was not possible under our experimental conditions.

In the system which included *p*-cresol as an alkylating agent, tyrosine was obtained from *N*-oxaloglycine. The hydroxyl group of *p*-cresol probably had no need of protection since there was no ninhydrin-positive by-product as evident from Fig. 1-(f). Since toluene is not very soluble in the aqueous-acetone mentioned above, *N*-oxaloglycine was suspended in a 1 : 1 aqueous acetone mixture under vigorous stirring, resulting in the formation of phenylalanine.

When using a low pressure Hg-lamp to excite *N*-oxaloglycine ($\varepsilon_{254}=450\ cm^{-1}\ M^{-1}$) and alkylating agents, no expected amino acids were produced. Acetone was then introduced into the system so as to initiate a photochemical process. Similar photochemical reactions were reported by Elad *et al.*[6] in organic solvents. The n-π^* transition of a carbonyl compound brings about a biradical expressed as $>\dot{C}-\dot{O}$, which can abstract a active hydrogen on α-carbon of glycine residue. The radical species can react with an alkylating agent to possibly form a branched α-amino acid. On the other hand, it is necessary for the rather stable radicals to combine with the glycine residue. In fact, when this combination occurs, unsaturated bonds are situated close to the radical site. When glycine was used as a starting material, no converted amino acid was found. In this connection, *N*-oxaloglycine synthesized from glyoxylic acid and ammonia is suitable for conversion to other amino acids, in view of prebiotic synthesis and the organic chemistry involved. In strong acidic or basic media, the above reaction was found to be negligibly. In a non-deaerated system ninhydrin-positive by-products were formed to a considerable extent and the production of expected amino acids decreased by about one third. This may possibly confirm that a prebiotic neutral aqueous medium is suitable for forming amino acids photochemically, though the conversion yield was *ca.* 1% at this stage.

Also of interest is the relation between the synthetic route of amino acids and the origin of genetic code, for which a working hypothesis has been proposed by Egami.[7] The most important aspect of this matter is the interdependent genesis of protein amino acids and nucleic bases. According to Egami, synthetic route is reasonable in the case of aspartic acid from a glycine residue plus a C_2 unit, and valine from a glycine residue plus a C_3 unit.

In conclusion, several protein amino acids were formed from common materials such as glyoxylic acid, ammonia, nitrile, and hydrocarbons under UV light.

We should like to express our sincere appreciation to Miss Yumiko Makino for her technical assistance in the amino acid analysis.

References

1) H. Hatanaka and F. Egami, *Bull. Chem. Soc. Jpn.*, **50**, 1147 (1977); T. Ochiai, H. Hatanaka, M. Ventilla, H. Yanagawa, Y. Ogawa, and F. Egami, "Origin of Life, Proc. 5th Intern. Cong. Origin of Life", ed by H. Noda, Center Acad. Publ. Japan (1978), p. 135; H. Yanagawa, Y. Kobayashi, and F. Egami, *J. Biochem.*, **87**, 359 (1980).

2) J. Oró, A. Kimball, R. Firtz, and F. Master, *Arch. Biochem. Biophys.*, **85**, 115 (1959).

3) F. Egami, Y. Makino, K. Sato, M. Nishizawa, and H. Yanagawa, *Viva Origino*, **9**, 66 (1981); H. Yanagawa, Y. Makino, K. Sato, M. Nishizawa, and F. Egami, *J. Biochem.*, **91**, 2087 (1982).

4) F. Egami, Y. Makino, K. Sato, and M. Nishizawa, *Proc. Jpn. Acad., Ser. B*, **57**, 329 (1981).

5) W. Kerp and K. Unger, *Ber. Dtsch. Chem. Ges.*, **30**, 579 (1897).

6) D. Elad, *Fortschr. Chem. Forsch.*, **7**, 428 (1967), and references therein.

7) F. Egami, *Nippon Nōgei Kagaku Kaishi*, **53**, 173 (1979); *Origins of Life*, **11**, 197 (1981).

Trimethylsilyl Triflate Induced Reaction of Humulene 6,7-Epoxide. Cyclization to 5-Hydroxy-4,8,11,11-tetramethyltricyclo[6.3.0.0^{2,4}]undec-9-ene

Haruhisa SHIRAHAMA,* Shizuaki MURATA,† Terunori FUJITA, Baldev R. CHHABRA, Ryoji NOYORI,† and Takeshi MATSUMOTO

Department of Chemistry, Faculty of Science, Hokkaido University, Sapporo 060

†*Department of Chemistry, Faculty of Science, Nagoya University, Chikusa-ku, Nagoya 464*

(Received January 30, 1982)

Synopsis. Humulene 6,7-epoxide was converted by treatment with trimethylsilyl triflate to 5-hydroxy-4,8,11,11-tetramethyl[6.3.0.0^{2,4}]undec-9-ene in 81% yield.

Recently we reported a conversion of humulene 9,10-epoxide (**1**) to africanol (**2**) and bicyclohumulenone (**3**) through a "conformationally selective reaction"[1] (Scheme 1). The conversion means achievement of a high grade simulation of cyclohumulanoid biosynthesis.[1] In this paper we would like to describe a conversion of humulene 6,7-epoxide (**4**) by means of trimethylsilyl triflate (TMSOTf)[2] into a tricyclic alcohol, 5-hydroxy-4,8,11,11-tetramethyltricyclo[6.3.0.0^{2,4}]undec-9-ene (**5**) in good yield. The transannular cyclization (**4**→**5**) was first described by Takahashi *et al.*[3] who treated **4** with sulfuric acid and obtained a hydrated form of **5**, namely, **7** in 25% yield with several other products. Our reaction was quite clean and gave **5** as an essentially sole product.

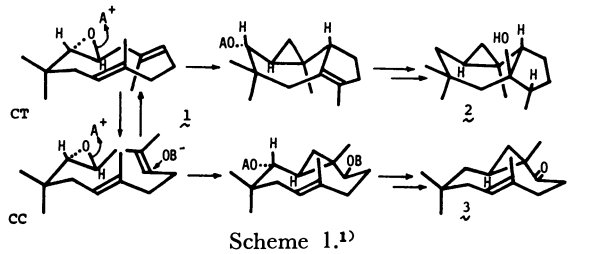

Scheme 1.[1]

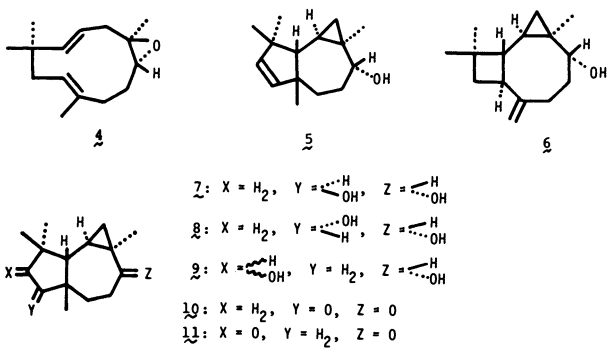

The epoxide **4**[4] was treated with TMSOTf in toluene at −78 °C to give a crystalline mass. Chromatographic separation of the products gave tricyclic alcohol **5** in 81% yield accompanied by a small amount (8%) of another tricyclic alcohol **6**. The alcohol **6** was previously obtained by acid treatment of a tricyclohumuladiol by Naya and Kotake.[5]

The compound **5** exhibited the same molecular weight as that of the original epoxide (M^+=220) and an OH band (3300 cm^{-1}) in its Mass and IR spectra respectively. The NMR spectrum displayed signals at δ 0.1—0.8 (3H, m, cyclopropane), 1.00, 1.10, 1.12, 1.14 (each 3H, s, Me×4), 3.39 (1H, dd, J=6, 10 Hz, H+OH), 5.24 (2H, s, olefinic). These observations together with consideration of the reaction course led to structure **5** for this compound. Stereochemistry of **5** was determined through its chemical conversion to known compounds. Treatment of **5** with B_2H_6 in THF followed by oxidation with H_2O_2 gave a mixture to alcohols which was separated by column chromatography into three diols **A**, **B**, and **C** in 39, 14, and 12% respectively. The IR and NMR spectra of diol **C** were superimposable with those of compound **7** which was previously obtained by Takahashi *et al.*[3] by the reaction of **4** with H_2SO_4 in acetone. On oxidation with Collins reagent diols **B** and **C** gave the same diketone **10**[3] and diol **A** yielded a new diketone **11**. Therefore, the configuration of **B** is represented by the formula **8** and that of **A** by **9**. The original olefinic alcohol is hence formulated as **5**.

Humulene is at equilibrium between two strain minimum conformers, CT and CC.[6] Assuming that these two stable conformers are effective for the epoxide **4**, the stereochemistry of the present transannular reaction was reasonably figured as Scheme 2, based on the configuration of the products **5** and **6**.

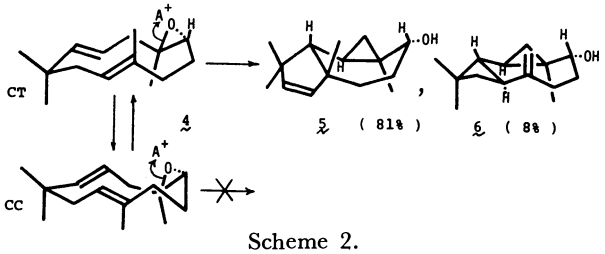

Scheme 2.

Experimental

All melting points were uncorrected. IR spectra were recorded on a JASCO IR-S spectrometer. NMR spectra were measured with HITACHI R-20B (60 MHz) and JEOL JNM PS-100 (100 MHz) instruments in $CDCl_3$ using TMS as an internal standard. Mass spectra were obtained on a HITACHI M-52 spectrometer.

TMSOTf Induced Cyclization of Humulene 6,7-Epoxide (4). A solution of TMSOTf (1.86 ml) and 2,6-lutidine (1.39 ml) in toluene (40 ml) was stirred and cooled at −78 °C under argon. To this solution was added a solution of **4** (2.324 g) in toluene (12 ml) by portions. The mixture was stirred at this temperature for 5 h till the epoxide **4** was completely consumed. After removal of the cooling bath, DBU (2.8 ml) was added and the mixture was stirred for 2 h at room temperature. By addition of 1 mol dm^{-3} HCl the mixture was neutralized at

0 °C and extracted with hexane four times. The combined extracts were evaporated *in vacuo* to leave a brown mass which was dissolved in MeOH (10 ml). Mixing the solution with 1 mol dm^{-3} HCl (0.5 ml) for a few minutes effected desilylation. The methanol was removed and the residue was extracted with $CHCl_3$ four times. The combined extracts were dried and evaporated to leave a crystalline mass (2.331 g) which was subjected to silica gel chromatography. Elution of the column with 2.5% AcOEt–hexane afforded tricyclohumulenol (**6**)[5] (186 mg, 8%) first and then 5-hydroxy-4,8,11,11-tetramethyltricyclo[6.3.0.$0^{2,4}$]undec-9-ene (**5**) (1.822 g, 81%); mp 120—122 °C. Spectral data were described in the text.

Found: C, 81.75; H, 10.95%. Calcd for $C_{15}H_{24}O$: C, 81.76; H, 10.98%.

Hydroboration-Oxidation of **5**. To a solution of borane–THF (1.5 ml, 1 mol dm^{-3}) was added **5** (220 mg) in THF (3 ml) under argon at 0 °C. After standing for 3 h at 0 °C, the reaction mixture was quenched by the successive addition of ice, NaOH aq (10 ml, 3 mol dm^{-3}) and H_2O_2 (1.5 ml, 30%). The reaction mixture was stirred at room temperature for further 1.5 h till the oxidation was complete. After usual workup it gave a colorless liquid (200 mg) which was chromatographed on a column of $AgNO_3$ impregnated silica gel. Elution with hexane–ether (7 : 3) gave successively three crystalline diols, A (93 mg, 39%), B (33 mg, 14%), and C (29 mg, 12%). Further elution with ether gave a mixture which was not studied. Diol **C** showed the IR and NMR spectra superimposable with those of an authentic sample of **7**.[3]

Diol ***A*** *(**9**)*: Mp 150 °C; IR 3200—3400 cm^{-1}; NMR δ 1.02 (9H, s), 1.08 (3H, s), 3.40 (1H, t, J=6 Hz), 3.86 (1H, dd, J=8, 6 Hz).

Found: C, 75.57: H, 11.17%. Calcd for $C_{15}H_{26}O_2$: C, 75.58; H, 11.00%.

Diol ***B*** *(**8**)*: Mp 140 °C; IR 3200—3400 cm^{-1}; NMR δ 0.95, 1.05, 1.12, 1.20 (each 3H, s), 3.38 (1H, dd, J=10, 7 Hz), 3.70 (1H, br).

Found: C, 75.65; H, 11.44%. Calcd for $C_{15}H_{26}O_2$: C, 75.58; H, 11.00%.

Collins Oxidation of Diol ***A*** *(**9**), **B** (**8**), and **C** (**7**)*. To a solution of dry pyridine (1 ml) in dry dichloromethane (15 ml) at 0 °C was added dry chromium trioxide (600 mg) under argon. The temperature of the mixture was raised to room temperature and the solution was stirred until it colored wine-red (20 min). At the end of this period a solution of diol ***A*** (**9**, 150 mg) in dry dichloromethane (5 ml) was added dropwise. A tarry black deposit separated immediately. After stirring for 20 min, the reaction mixture was worked up as usual and evaporation of the solvent gave a crystalline diketone (**11**); mp 149 °C. IR 1693, 1735, 1450 cm^{-1}; NMR δ 1.00, 1.12, 1.18, 1.32 (each 3H, s), 2.25 (2H, s).

Found: C, 76.86; H, 9.47%. Calcd for $C_{15}H_{22}O_2$: C, 76.88; H, 9.46%.

Oxidation of Diol ***B*** *(**8**)* in the same manner gave an oily diketone whose IR and NMR spectra were superimposable with those of an authentic sample of **10**.[3]

Diol ***C*** *(**7**)* was converted to the same diketone (**10**) by the same procedure as above.

The authors are grateful to Dr. T. Murae (The University of Tokyo) for sending spectra of compounds **7** and **10**.

References

1) H. Shirahama, K. Hayano, Y. Kanemoto, S. Misumi, T. Ohtsuka, N. Hashiba, A. Furusaki, S. Murata, R. Noyori, and T. Matsumoto, *Tetrahedron Lett.*, **1980**, 4835.

2) S. Murata, M. Suzuki, and R. Noyori, *J. Am. Chem. Soc.*, **101**, 2738 (1979); R. Noyori, S. Murata, and M. Suzuki, *Tetrahedron*, **37**, 3899 (1981).

3) M. Namikawa, T. Murae, and T. Takahashi, *Bull. Chem. Soc. Jpn.*, **51**, 3616 (1978).

4) N. P. Damodaran and S. Dev, *Tetrahedron*, **24**, 4123 (1968).

5) Y. Naya and M. Kotake, *Nippon Kagaku Zasshi*, **91**, 275 (1970).

6) H. Shirahama, E. Osawa, and T. Matsumoto, *J. Am. Chem. Soc.*, **102**, 3208 (1980).

Phase Transitions of the 1 : 2 Complex of *N*-Ethyl-*N*-methylmorpholinium and 7,7,8,8-Tetracyanoquinodimethan, MEM(TCNQ)$_2$ above Room Temperature

Hayao KOBAYASHI

Department of Chemistry, Faculty of Science, Toho University, Funabashi, Chiba 274

(Received July 21, 1981)

The thermal expansion coefficient, the electrical conductivity, and the crystal structure (at 325 K) of MEM-(TCNQ)$_2$ were examined. A new phase transition was observed at 315 K, where the thermal expansion coefficient jumps. This second-order transition may be triggered by the molecular motion of MEM cations and can be regarded as a precursor of the first-order transition around 62 °C. The molecular motion of MEM cations reduces the electrostatic lattice energy and leads to a structural change. The structural instability of TCNQ columns around 335 K is not attributable to the electron-electron correlation effect in the one-dimensional system, but to the change in the energy balance between the charge-transfer interaction and the electrostatic energy.

In the crystals of anion radical salts of 7,7,8,8-tetracyanoquinodimethan(TCNQ), TCNQ molecules stack to form one-dimensional columns. The periodicity of TCNQ columns frequently reflects a lattice instability characteristic of one-dimensional electronic systems. The "$2k_F$-structure" is associated with the Peierls instability, which has been observed in such well-known one-dimensional metals as TTF–TCNQ and KCP.[1] The "$4k_F$-instability" has also been observed in TTF–TCNQ. Sawatzky, Huizinga and their co-workers[2] have performed extensive studies of the physical properties of the 1:2 complex of *N*-ethyl-*N*-methylmorpholinium and TCNQ (MEM(TCNQ)$_2$) and found a series of the phase transitions. When $T>335$ K, MEM(TCNQ)$_2$ has nearly uniform columns of TCNQ and shows metallic behavior. The nearly uniform columns are transformed to diadic ones at 335 K, below which point MEM(TCNQ)$_2$ is semiconductive. The diadic columns change to tetradic ones at 19 K, where a non-magnetic spin-Peierls state appears. Although the 335 K transition has been reported to be a (electronic) Peierls transition,[2] the electrical conductivity of the "metallic phase" is relatively small (50 $(\Omega\,\mathrm{cm})^{-1}$). Therefore, it may be worthwhile to try to make clear the lattice instability which causes the 335 K transition.

The thermal expansion, the electrical resistivity, and the crystal structure of MEM(TCNQ)$_2$ at 325 K were studied.

Experimental

Black crystals were grown from a mixture of hot solutions of TCNQ and *N*-ethyl-*N*-methylmorpholinium iodide in acetonitrile. X-Ray oscillation and Weissenberg photographs showed that the well-developed plane of the crystal is (010). The maximum dimensions of the specimen are about 10 mm × 2 mm × 1 mm.

Thermal Expansion. The thermal expansion was measured over the temperature range of 293—363 K along the c and b* directions, which are parallel and perpendicular respectively to the TCNQ stacks. The results are shown in Figs. 1 and 2. The values of $L_\perp(\alpha_\perp)$ are less accurate than those of $L_{//}(\alpha_{//})$ because of the diffculty of the crystal alignment ($L_{//}(L_\perp)$ is the length of the crystal parallel (perpendicular) to TCNQ columns, and $\alpha_{//}(\alpha_\perp)$ is the corresponding thermal expansion coefficient). The typical crystals used had the dimensions of 7 mm and 0.7 mm along the c (//)

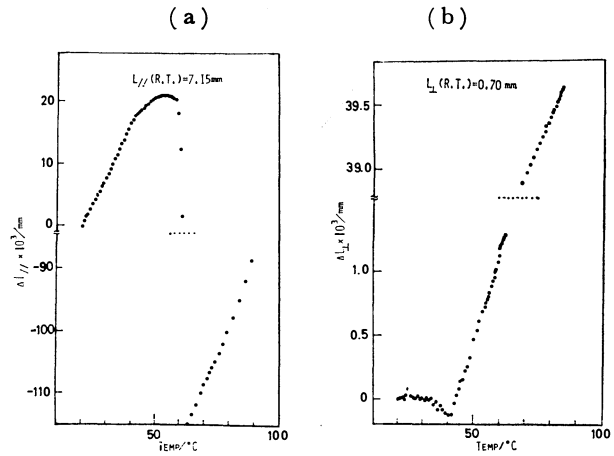

Fig. 1. Thermal expansion parallel to c(a) and b*(b).

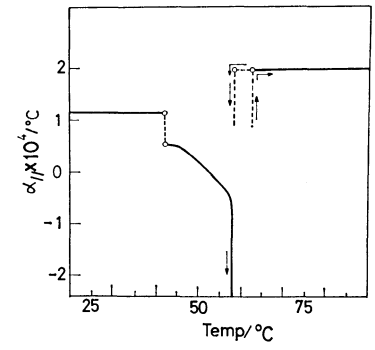

Fig. 2. Thermal expansion coefficient $\alpha_{//}$ (parallel to c).
The arrows indicate the cooling and heating processes. The hysteresis are observed around 60 °C.

and b* ($\perp$) directions respectively.

The discontinuous change in $L_{//}(L_\perp)$ at 335 K (Tc_1) and $\alpha_{//}(\alpha_\perp)$ at 315 K (Tc_2) show the first-order phase transition at Tc_1 and the second-order phase transition at Tc_2. Above Tc_2, the thermal expansion coefficient ($\alpha_{//}$) decreases with the temperature and becomes negative above 326 K. Thus, the second-order phase transition is a precursor of the discontinuous contraction of the crystal at Tc_1. The transition temperature, Tc_1 agrees well with that obtained from the electrical conduction experiment.[2] The temperature dependences of $\alpha_{//}$ and $\alpha_\perp$ are as follows:

(i) $T>Tc_1$: Around Tc_1, $L_{//}$, $L_\perp$, $\alpha_{//}$, and $\alpha_\perp$ show hysteresis. Since the crystals were cracked at Tc_1, it was difficult to obtain accurate data above Tc_1. The transition

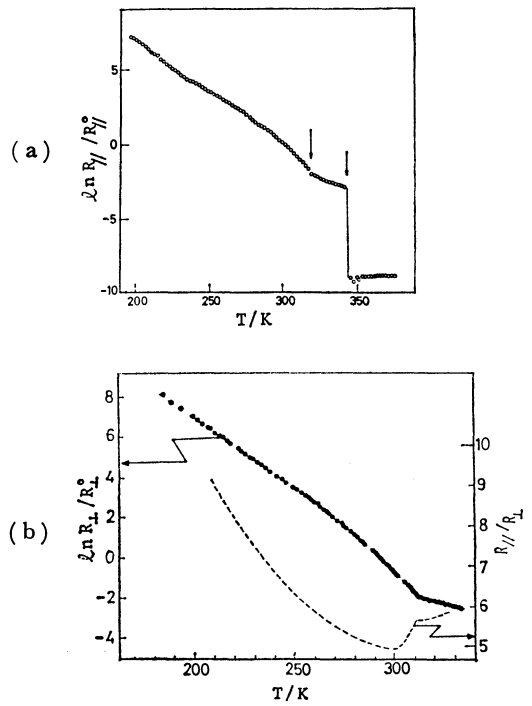

Fig. 3. (a) Electrical resistivities parallel to the TCNQ columns ($R_{//}$). The room-temperature value of $R_{//}$ ($=R^{\circ}_{//}$) is $10^4\,\Omega$ cm. (b) Electrical resistivities perpendicular to the TCNQ columns ($R_{\perp}$) and anisotropy of the resistivities ($R_{//}/R_{\perp}$). The room-temperature value of $R_{\perp}(R^{\circ}_{\perp})$ is $5\times10^4\,\Omega$ cm.

temperature, Tc_1 determined from the heating process is 335 K, but that determined from the cooling process is about 328 K. The crystal shrinks along the TCNQ column (//c) and elongates along the direction perpendicular to it (//b*). The thermal expansion coefficients above Tc_1 are $\alpha_{//}=2\times10^{-4}$/deg and $\alpha_{\perp}=9\times10^{-5}$/deg.

(ii) $Tc_2<T<Tc_1$: With an increase in the temperature, $\alpha_{//}$ decreases and becomes negative, while $\alpha_{\perp}$ is almost constant (9.6×10^{-5}/deg).

iii) 293 K$<T<Tc_2$: $\alpha_{//}$ is 1.15×10^{-4}/deg, and $\alpha_{\perp}$ is much smaller than $\alpha_{//}$ ($<10^{-5}$/deg).

Electrical Resistivity. Huizinga and Sawatzky[2] have reported a "metal-semiconductor transition" at 335 K (Tc_1). The conductivity of the ' metallic state" is 10^3 times larger than that of the semiconducting state. Since the thermal-expansion experiments revealed a second-order phase transition, the d. c. electrical resistivities were measured around the transition temperature by the use of a standard four-probe technique. Gold wires 0.025 mm in diameter were bonded to the crystal by means of silver conducting paint. The results are shown in Fig. 3. The room-temperature resistivities were $R_{//}=10^4$ cmΩ and $R_{\perp}=5\times10^4\,\Omega$ cm, where $R_{//}$ and $R_{\perp}$ indicate the resistivities parallel (//c) and perpendicular (//a*) to the c axis. Since the crystals were cracked at Tc_1, it was difficult to obtain the resistivities accurately above Tc_1. As has previously been reported,[2] the parallel resistivity, $R_{//}$, jumps at Tc_1 by a factor of 10^2—10^3. A slight anomaly was observed at Tc_2, where $d\ln(R_{//}/R^{\circ}_{//})/dT^{-1}$ becomes very large (>1500 K). The perpendicular resistivity, $R_{\perp}$, shows a similar temperature dependence.

Crystal Structure at 325 K. Since the new phase transition has been found at Tc_2, the crystal-structure analysis was made to obtain the structure information above Tc_2.

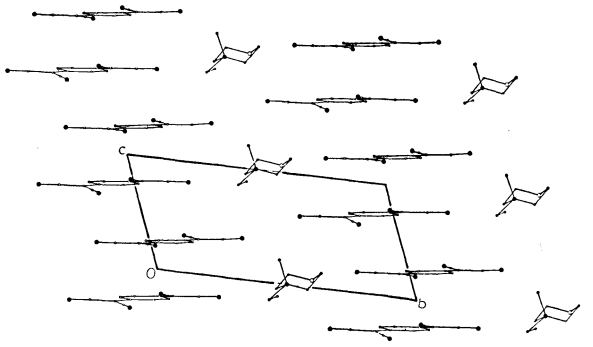

Fig. 4. The crystal structure of MEM(TCNQ)$_2$ at 325 K.

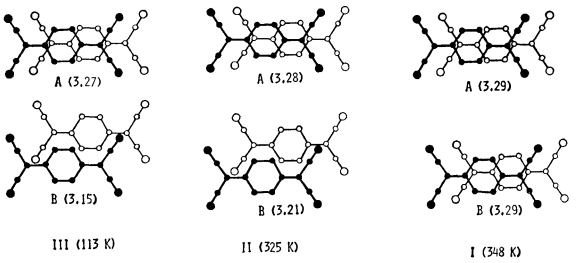

Fig. 5. The mode of intermolecular overlappings of TCNQ of the three phases (at 325 (this work), 113[3] and 348 K.[6] The interplanar distances are given in parentheses.

The lattice constants were determined by the use of a Rigaku automated four-circle diffractometer. The crystal data are: $(C_7H_6NO)^+(C_{12}H_4N_4)^-$, $F.W.=538.6$, triclinic, $P\bar{1}$, $a=7.796(5)$, $b=15.308(8)$, $c=6.993(5)$ Å, $\alpha=111.96(6)$, $\beta=74.87(4)$, $\gamma=111.82(6)^{\circ}$, $U=711.3$ Å^3, $F=(000)=281$, $Z=1$, and $\mu(\text{Mo }K\alpha)=0.9$ cm^{-1}. The intensity data were collected at 52 °C with monochromated Mo $K\alpha$ radiation up to $2\theta=55^{\circ}$. The number of the significant reflections ($|F_o|>3\sigma(|F_o|)$ is 1710.[3,4]

Starting with the atomic parameters of the low-temperature structure reported by Bosh and Bodegom,[3] the crystal structure was refined. The hydrogen atoms of TCNQ were included; however, those of MEM could not be located. The final R value was 0.088. The atomic parameters are given in Table 1.*

The crystal structure, shown in Fig. 4, is almost identical to the structure at 113 K[3] and that at 323 K reported very recently.[5] The TCNQ columns have a diadic structure. The TCNQ molecules the centers of the coordinates of which lie at $z=0.27$ and those with centers $z=-0.27$ form a dimer. The least-squares plane through two crystallographically independent TCNQ molecules are: $0.0168X+0.1106Y-0.9441Z+1.6284=0.0$ and $0.0350X+0.1002Y-0.9382Z-1.6513=0.0$, where X, Y, and Z are the coordinates(Å) referred to the crystal axes, a, b, and c respectively. These two planes are almost parallel to each other (the dihedral angle between the planes is *ca.* 1.1°). The angles between the normals to TCNQ planes and c are 19.2 and 20.2°, slightly smaller than those observed at 113 K (20.5 and 21.3°).[3] The mode of overlapping between adjacent TCNQ molecules is shown in Fig. 5, together with those obtained at different temperatures.[3,6] The interplanar distances between

* A list of the observed and calculated structure factors and a table of anisotropic thermal parameters are kept as Document No. 8231 at the Chemical Society of Japan.

Table 1. The final atomic coordinates ($\times 10^4$)

Atom	x	y	z	B_{eq}/Å^2 a)
N(1)	3061(18)	4283(8)	3708(22)	6.86
C(2)	3327(18)	3573(11)	3489(23)	5.40
C(3)	3490(17)	2641(9)	3175(21)	4.72
C(4)	5419(21)	2697(11)	3252(27)	6.43
N(5)	6801(18)	2676(10)	3358(25)	7.86
C(6)	2135(16)	1794(9)	2937(18)	3.97
C(7)	2285(18)	818(10)	2629(22)	4.93
C(8)	892(15)	21(8)	2463(17)	3.16
C(9)	−915(17)	−11(9)	2419(20)	4.28
C(10)	−1177(16)	904(10)	2663(21)	4.65
C(11)	205(16)	1759(10)	2863(20)	4.36
N(12)	−5763(16)	−878(10)	2103(26)	7.79
C(13)	−4314(19)	−912(11)	2229(23)	5.39
C(14)	−2452(17)	−903(9)	2153(18)	3.97
C(15)	−2206(17)	−1791(9)	2008(21)	4.38
N(16)	−2036(16)	−2495(8)	1851(21)	6.40
N(17)	−3009(20)	−4298(10)	−3584(25)	8.05
C(18)	−3203(18)	−3552(9)	−3425(21)	4.71
C(19)	−3510(17)	−2643(9)	−3279(19)	4.35
C(20)	−5277(17)	−2692(9)	−3462(22)	4.63
N(21)	−6746(17)	−2782(11)	−3707(25)	7.72
C(22)	−1943(16)	−1744(9)	−2901(19)	4.02
C(23)	−2270(15)	−872(9)	−2730(17)	3.58
C(24)	−821(19)	4(10)	−2476(22)	5.39
C(25)	1064(15)	23(8)	−2401(17)	3.63
C(26)	1280(16)	−917(9)	−2628(20)	4.37
C(27)	−212(17)	−1765(8)	−2847(19)	4.22
N(28)	5771(16)	893(10)	−2329(26)	7.45
C(29)	4365(17)	883(9)	−2193(23)	5.02
C(30)	2497(16)	858(9)	−2227(21)	4.44
C(31)	2343(18)	1808(10)	−1946(21)	4.82
N(32)	2172(18)	2554(8)	−1748(20)	6.17
N(33)	107(34)	5023(15)	119(33)	8.06
C(34)	2358(23)	4970(11)	−460(33)	8.13
C(35)	3425(28)	5830(11)	1039(32)	8.73
C(36)	1710(26)	6810(13)	1478(48)	13.38
C(37)	348(22)	5873(13)	−173(50)	13.74
C(38)	−489(36)	4851(25)	2142(35)	14.78
C(39)	−812(31)	3974(23)	−1595(43)	16.98
C(40)	−2983(38)	3925(18)	−1103(43)	13.57
O	3521(15)	6710(8)	622(22)	8.72

a) Equivalent isotropic temperature factor as defined by H. C. Hamilton (*Acta Crystallogr.*, **12**, 609 (1959)).

the neighbouring TCNQ molecules are 3.21 Å (interdimer) and 3.28 (intradimer). They are 3.15 and 3.27 Å at 113 K.[3] The interdimer distance increases by 0.06 Å with an increase in the temperature from 113 K to 325 K, while the intradimer distance stays nearly constant. That is, the difference in the interplanar distances decreases. The bond lengths and angles are shown in Fig. 6.

The anomalous molecular structure and thermal parameters indicate a large thermal motion of MEM, which is consistent with the NMR observation of the onset of molecular motion around 300 K.[2] Since no significant structural change in TCNQ columns occurs at Tc_2, the second-order phase transition is considered to be triggered by the thermal motion of the MEM cations.

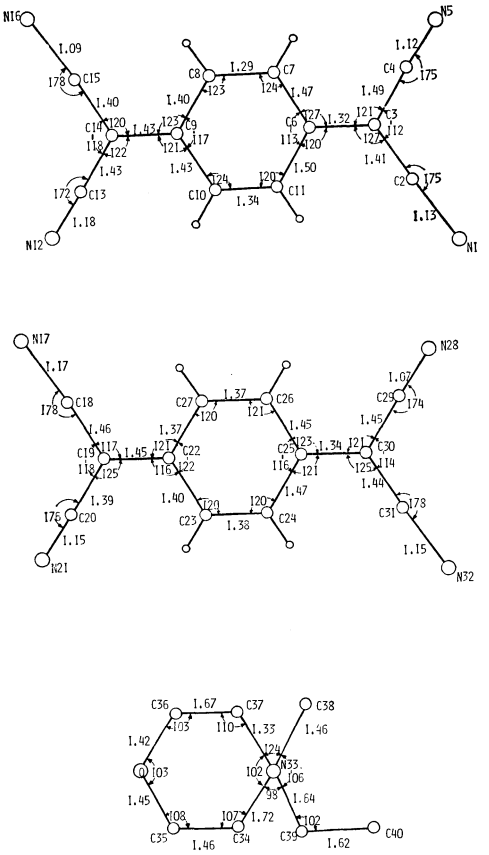

Fig. 6. The bond lengths and the bond angles. The e.s.d's of the bond lengths are 0.02 Å(TCNQ) and 0.02—0.04 Å(MEM) and those of the bond angles are 1—2°(TCNQ) and 1—3°(MEM). The bond lengths of C–H is 0.98—1.06 Å.

Discussion

In a quarter-filled system like MEM(TCNQ)$_2$, the diadic and tetradic columns of TCNQ correspond to the $4k_F$- and $2k_F$-structures respectively. The $4k_F$-structure has been frequently discussed in connection with the electron correlation. Sumi[7] has proposed a series of possible structural-phase transitions in a highly correlated linear-chain system: a uniform-$4k_F$ transition and $4k_F$-$2k_F$ transition. Since both types of transitions have been found, MEM(TCNQ)$_2$ has been regarded as a typical high-U material. The origin of the $2k_F$- and $4k_F$-structures has been considered to be correlated with the general principle of the periodical instability of the one-dimensional electronic system.[2]

However, as has been shown in this paper, the "$4k_F$-phase" contains an additional second-order phase transition at Tc_2. The thermal-expansion anomalies suggest that the second-order phase transition at Tc_2 is a precursor of the first-order phase transition at Tc_1. The diadic structure of TCNQ columns is transformed into an almost regular one at Tc_1.[2] Since the phase transition does not alter the intermolecular overlapping between intradimer molecules, TCNQ molecules are considered to move in pairs on passing through Tc_1. The change in the mode of the intradimer overlapping indicates the rotation of the TCNQ

dimer about 20°.

The thermal expansion experiments showed that the length of the crystal ($L_{//}$) is shortened by about 4.5% at Tc_1.[8] If the transition does not change the interplanar distances, the crystal must be shortened along the TCNQ columns by the rotation. The magnitude of the contraction is estimated as $\Delta L_{//}/L_{//}=1-\cos 20°$ (=0.05). Since the observed contraction (4.5%) agrees well with the estimated value, the discontinuous contraction of the crystal is considered to be mainly due to the rotation of the TCNQ dimers.

Each TCNQ dimer has an excess electron. The structure is stabilized by the Coulomb interaction between the MEM cations and the excess electrons in dimers. The small interplanar distance between TCNQ molecules indicates that the charge-transfer interaction also plays an important role. At high temperatures ($T>Tc_2$), the Coulomb interaction is reduced by the large thermal motion of MEM cations. Then, the MEM cations cannot restrain the movement of the excess electrons along the column. The interdimer charge-transfer interaction becomes importants. Figure 5 shows that in a diadic structure, the interdimer charge-transfer interaction is negligibly small, but it becomes as large as the intradimer one in a nearly uniform structure. This indicates that the diadic structure is transformed to a uniform one to gain a larger charge-transfer stabilization energy. As has been mentioned before, the crystal contracts along the direction parallel to the TCNQ columns (//c) and expands along the direction perpendicular to it (//b*). The expansion suggests a decrease in the Coulomb interaction between MEM cations and the excess electrons in TCNQ columns (see Fig. 4), while the contraction implies an increase in the charge-transfer interaction along the columns.

Lacoe, Gruner, and Chaikin have reported on the thermoelectric power(TEP) of MEM(TCNQ)$_2$.[9] Above Tc_1, TEP is $-65\ \mu$V/K, which suggests that the spin entropy of the excess electron makes the dominant contribution, as in other highly correlated quarter-filled band TCNQ salts. This indicates that the excess electrons are uniformly distributed in the TCNQ columns above Tc_1. As the temperature is lowered, the TEP increases faster, suggesting a change in the semiconducting gap.

However, the temperature dependence of $R_{//}$ (see Fig. 3) shows that the semiconducting gap does not alter around Tc_2. The anomaly around Tc_2 may be attributable to the change in $\mu(T)$. The mobility, $\mu(T)$, is considered to change by an order of magnitude. In other words, the mobility depends strongly on the thermal motion of MEM.

References

1) "Quasi One-Dimensional Conductors," ed by S. Barisic, A. Bjeris, J. R. Cooper, and B. Leontic, Springer-Verlag, Berlin, Heidelberg, and New York (1979); "Highly Conducting One-Dimensional Solids," ed by J. T. Devreese, R. P. Evrard, and V. E. van Doren, Plenum Press, New York and London (1979).

2) S. Huizinga, J. Kommandeur, G. A. Sawatzky, K. Kopinga, and W. J. M. de Jonge, "Quasi One-Dimensional Conductors," ed by S. Barisic, A. Bjelis, J. R. Cooper, and B. Leontic, Springer-Verlag, Berlin, Heidelberg, and New York (1979); S. Huizinga, J. Kommandeur, G. A. Sawatzky, B. T. Thole, K. Kopinga, W. J. M. de Jonge, and J. Rose, *Phys. Rev. B*, **19**, 4723 (1979); M. Morrow, W. N. Hardy, J. F. Carolan, A. J. Berlinsky, L. Weiler, V. K. Gujral, A. Janossy, K. Holczer, G. Mihlay, G. Gruner, S. Huizinga, A. Verwey, and G. A. Sawatzky, *Can. J. Phys.*, **58**, 334 (1980).

3) A. Bosch and B. van Bodegom, *Acta Crystallogr., Sect. B*, **33**, 3013 (1977).

4) Bosch and Bodegom have collected 4239 non-zero reflections ($2\theta<68°$) at -160 °C (Ref. 3).

5) B. van Bodegom, *Acta Crystallogr., Sect. B*, **37**, 857 (1981).

6) B. van Bodegom and A. Bosch, *Acta Crystallogr., Sect. B*, **37**, 863 (1981).

7) H. Sumi, *Solid State Commun.*, **21**, 17 (1977).

8) Very Recently, Bodegom have reported the crystal data at 113, 294, 303, 313, 323, and 348 K, which indicate that the magnitude of $\Delta L_{//}/L_{//}$ is about 0.057.

9) R. C. Lacoe, G. Gruner, and P. M. Chaikin, *Solid State Commun.*, **36**, 599 (1980).

 © 1982 The Chemical Society of Japan Bull. Chem. Soc. Jpn., 55, 2697—2705 (1982)

Synthesis, Luminescence Quantum Yields, and Lifetimes of Trischelated Ruthenium(II) Mixed-ligand Complexes Including 3,3′-Dimethyl-2,2′-bipyridyl

Katsumi NAKAMARU

Department of Chemistry, Faculty of Science, Hirosaki University, Bunkyo, Hirosaki, Aomori 036

(Received October 28, 1981)

New five complexes of the type of $[RuL_{3-x}(dmby)_x]X_2$(x=1,2,3, L=2,2′-bipyridyl or 1,10-phenanthroline, dmby=3,3′-dimethyl-2,2′-bipyridyl, X=halide ion) have been synthesized in order to investigate the effects of two methyl groups of dmby on the absorption and emission spectra, luminescence quantum yields, and lifetimes. Values of the radiative and nonradiative rate constants have been calculated from these data at 77 K. Although the absorption and emission maxima and the lifetimes are not much affected by the dmby ligand substitution, the molar extinction coefficients and emission quantum yields are decreased compared with trischelated complexes of the parent bipyridyl or phenanthroline ligands. At 25 °C the emission yields of the complexes containing dmby decrease by 3—4 orders of magnitude than at 77 K. Possible causes of the decrease in the quantum yields are discussed.

Tris(2,2′-bipyridyl)ruthenium(II) ion, $[Ru(bpy)_3]^{2+}$, has attracted widespread attention in recent years because of its strong charge transfer (CT) luminescence[1,2] even in fluid solutions at room temperature as well as at 77 K and because of higher redox ability in the excited state than in the ground state.[3-5] In particular, the latter property has accelerated many investigations on photoredox chemistry of this ion and related complexes in the hope of possible catalytic activity in solar energy conversion to chemical potential energy.[6-10]

There have been a few studies on the effects of ligand substituents on the spectral and excited state properties of bipyridyl or 1,10-phenanthroline (phen) complexes with ruthenium(II). Phenyl substitution on the 4,4′-positions of bipyridyl and 4,7-positions of phenanthroline ligands has been shown to produce an increase in the luminescence quantum yields and a slight decrease in the measured lifetimes. These effects have been interpreted on the basis of a model of intensity borrowing *via* spin-orbit coupling interaction between a luminescing triplet state and a lending singlet state.[11-13] Temperature dependence of the quantum yields and lifetimes of ruthenium(II) complexes with the unsubstituted and methyl- or phenyl-substituted ligands at low temperature has been reported[14,15] (at higher temperatures, only for the $[Ru(bpy)_3]^{2+}$ [16,17]). Recently, some sterically hindering bi- and tridentate ligand complexes have been prepared and their effects on the relaxation processes of the excited state have been discussed.[18-20]

3,3′-Dimethyl-2,2′-bipyridyl(dmby), which was first synthesized by Case,[21] is an interesting ligand in that upon coordination to metal it is expected to take a twisted, and hence non-coplanar conformation owing to the steric hindrance of the two methyl groups.[22,23] Photophysical and photochemical studies, however, on the transition metal complexes with this dmby have scarcely been found. This paper reports the preparation of several trischelated ruthenium(II) complexes including dmby and bipyridyl (or phenanthroline); also the effects of dmby on the absorption and emission spectra, emission quantum yields, and lifetimes of these complexes.

Experimental

Materials. $RuCl_3 \cdot 3H_2O$ (Aldrich Chemical Co.), 2,2′-bipyridyl and 1,10-phenanthroline (Wako Pure Chemicals Co.), and substituted ligands (G. Frederick Smith Chemical Co.) other than dmby were used as obtained. 2-Amino-3-methylpyridine was prepared by reflux of 3-methylpyridine with sodium amide in xylene.[24] 2-Bromo-3-methylpyridine was synthesized from 2-amino-3-methylpyridine by the Sandmeyer reaction.[25]

Preparation of 3,3′-Dimethyl-2,2′-bipyridyl. A slight modification of the method of Case[21] was used. A dried mixture of 200 ml of *p*-cymene, 75 g of copper powder, and 75 g of sodium chloride was refluxed with stirring in an oil bath. To this 120 g of 2-bromo-3-methylpyridine was added slowly and the reflux continued for two hours at 180—200 °C. After cooling to 100 °C, 200 ml of 6 mol dm^{-3} HCl was added. This reaction mixture was made alkaline with NaOH and distilled with steam. About 10 L of the aqueous distillate was extracted with chloroform. After the chloroform was removed, the remainder was distilled under reduced pressure. On redistillation 26 g of pale yellow liquid boiling at 157—158 °C (20 mmHg, 1 mmHg≈133.322 Pa) was obtained (yield, 40%). Purification of the crude product was accomplished by conversion of the base to its hydrochloric acid salt and repeated recrystallization from 330 ml of the mixture of ethanol and concentrated HCl (90:10%, v/v). 19 g of the pure white crystals (yield, 21%) were again converted to the base with NaOH and the liberated product was extracted with diethyl ether. Evaporation of the ether gave 12 g of viscous, colorless liquid (final yield, 19%). Its absorption spectrum agreed well with the authentic sample.[23]

cis-$[Ru(bpy)_2Cl_2] \cdot 2H_2O$ and *cis*-$[Ru(phen)_2Cl_2] \cdot 3H_2O$ were prepared by the method described in the literature.[26]

Preparation of cis-$[Ru(dmby)_2Cl_2] \cdot 3H_2O$. Since all attempts to prepare this compound according to the method described in literature were unsuccessful, the following procedure was adopted. 3.0 g of $RuCl_3 \cdot 3H_2O$ and 4.3 g of dmby in 104 ml of *N,N*-dimethylformamide and 12 ml of 0.2 M (1 M=1 mol dm^{-3}) phosphate buffer solution (pH 6.8—7.0) were refluxed together for 6 h. The solvent was distilled off, and the residue was dissolved in about 400 ml of hot water containing 10 ml of phosphate buffer solution. The dark red brown solution was quickly filtered and 57 g of LiCl added to the filtrate. The product, which precipitated on standing overnight in refrigerator, was collected by suction filtration, washed several times with cold water and

TABLE 1. ANALYTICAL RESULTS

Compound	C (%)		H (%)		N (%)	
	Calcd	Found	Calcd	Found	Calcd	Found
$[Ru(bpy)_3]Cl_2 \cdot 3H_2O$	49.32	48.88	4.69	4.51	11.50	11.67
$[Ru(bpy)_2(dmby)]I_2 \cdot 2H_2O$	43.31	43.14	3.63	3.42	9.47	9.30
$[Ru(bpy)(dmby)_2]I_2 \cdot 3H_2O$	43.74	43.84	4.10	3.88	9.00	8.95
$[Ru(dmby)_3]Br_2 \cdot 7H_2O$	46.01	46.17	5.36	5.02	8.94	8.96
$[Ru(phen)_3]Cl_2 \cdot 7H_2O$	51.55	51.34	4.57	4.17	10.02	10.00
$[Ru(phen)_2(dmby)]Cl_2 \cdot 8H_2O$	50.23	49.94	5.15	4.89	9.76	10.05
$[Ru(phen)(dmby)_2]Cl_2 \cdot 7H_2O$	51.06	50.58	5.48	5.07	9.92	9.89
$[Ru(4,4'\text{-dimethylbpy})_3]Cl_2 \cdot 7H_2O$	50.82	50.85	5.92	5.56	9.87	9.75
$[Ru(4,7\text{-diphenylphen})_3]Cl_2 \cdot 5H_2O$	68.67	69.11	4.64	4.33	6.67	6.83
cis-$[Ru(dmby)_2Cl_2] \cdot 3H_2O$	48.49	48.55	5.09	4.37	9.47	9.76

dried. The dark, almost black, fine powder product was obtained in 44% yield (4.0 g).

$[Ru(bpy)_3]Cl_2 \cdot 5H_2O$ was prepared according to the method reported.[27] $[Ru(4,4'\text{-dimethylbpy})_3]Cl_2 \cdot 7H_2O$, $[Ru(4,4'\text{-diphenylbpy})_3]Cl_2 \cdot 5H_2O$, $[Ru(dmby)_3]Br_2 \cdot 7H_2O$, $[Ru(phen)_3]Cl_2 \cdot 7H_2O$, and $[Ru(4,7\text{-diphenylphen})_3]Cl_2 \cdot 5H_2O$ were prepared analogously.

Preparation of $[RuL_{3-x}(dmby)_x]X_2 (x=1,2)$. The preparation of this type of compounds all follows the same procedure as described for $[Ru(phen)_2(dmby)]Cl_2 \cdot 8H_2O$.

$[Ru(phen)_2(dmby)]Cl_2 \cdot 8H_2O$: 2.0 g of *cis*-$[Ru(phen)_2Cl_2] \cdot 3H_2O$ (3.2 mM) and 0.7 g of dmby (3.8 mM) in 200 ml of ethanol and 15 ml of 0.2 M phosphate buffer solution were refluxed for 72 h. The dark red brown solution was filtered and then evaporated to dryness. The residue was first purified on a column of silica gel eluting with acetone–ethanol (1:2, v/v). Final purification was achieved by repeated recrystallization from water. The pure chloride product is a deep red brown crystalline material.

For the preparation of the other trischelated complexes, *cis*-$[Ru(bpy)_2Cl_2] \cdot 2H_2O$ or *cis*-$[Ru(dmby)_2Cl_2] \cdot 3H_2O$ was used as the starting material instead of *cis*-$[Ru(phen)_2Cl_2] \cdot 2H_2O$. The chloride and bromide salts of $[Ru(bpy)_2(dmby)]^{2+}$ and $[Ru(bpy)(dmby)_2]^{2+}$ were too soluble to crystallize from water. Hence, for the purpose of elemental analysis, they were converted to the iodide salts by treatment with KI. For the same reasons, the chloride salt of $[Ru(dmby)_3]^{2+}$ was converted to the bromide salt by KBr. Elemental analysis was performed by Chem. Dept., Fac. Sci., Tohoku Univ. and the results are listed in Table 1.

Spectroscopic Measurements. Absorption spectra were measured with a Hitachi 124 double-beam spectrophotometer thermostated at 25 °C. All luminescence measurements were made with a Hitachi MPF-4 fluorescence spectrophotometer. Emission spectra were corrected using 2-naphthol in (0.020± 0.001) mol dm^{-3} sodium acetate–acetic acid buffer solution, *N,N*-dimethyl-*m*-nitroaniline in benzene–hexane (30:70%, v/v), and 4-dimethylamino-4'-nitrostilbene in *o*-dichlorobenzene as the standard. The true emission spectra of these substances were reported by Lippert *et al.*[28] For emission measurements at 77 K the complexes were dissolved in methanol–ethanol (1:4, v/v) mixed-solvent and frozen in liquid nitrogen by immersion of a 5-mm quartz tube. The sample absorbance at an exciting wavelength was kept as low as possible to avoid fluorescence errors. The usual concentrations were $(3—5) \times 10^{-6}$ M. For excitation at 436 nm, light from a 150 W xenon lamp was passed through a monochromater and a Toshiba V-Y43 cut-off filter. For the emission intensity measurements a Toshiba V-O58 cut-off filter was further placed in front of the PM tube.

Quantum yields were measured by the modified Parker and Rees method.[29] As the quantum yield standard, $[Ru(4,7\text{-diphenylphen})_3]Cl_2$ was used assuming a value of 0.682.[13] Preliminary measurements using $[Ru(4,4'\text{-diphenylbpy})_3]Cl_2$ as a test sample gave a value of 0.563±0.014, in good agreement with the reported value of 0.573±0.032.[13]

Measurements at 25 °C were done in aqueous solutions with the same apparatus and procedures except that the usual fluorescence cell was used and that the emission quantum yield standard was fluorescein in 0.1 mol dm^{-3} NaOH or $[Ru(bpy)_3]Cl_2$ in air saturated aqueous solution. Each yield is 0.90[13] and 0.028,[30] respectively. All the ruthenium(II) complexes in H_2O were thermally stable, but the samples were daily prepared prior to use. If necessary, nitrogen was bubbled through the sample solutions for 15 min. More details have been described previously.[30]

For the lifetime measurements, an apparatus constructed by Kokubun (Chem. Dept., Fac. Sci., Tohoku Univ.) was used. The sample was excited at 337 nm with a pulsed nitrogen laser. Lifetimes were determined from the slope of a linear plot of ln intensity *vs.* time.

The absorption spectra of the iodide salts of $[Ru(bpy)_2(dmby)]^{2+}$ and $[Ru(bpy)(dmby)_2]^{2+}$ differ in the ultraviolet region from their chloride or bromide salts owing to the iodide absorption. Therefore the chloride salts of these complexes were used for the absorption measurements. For the emission measurements, however, the iodide salts of these complexes and the bromide salt of $[Ru(dmby)_3]^{2+}$ were used since no effect of the counterions was observed on the emission spectra and intensities.

Results

The absorption and luminescence spectra of the ruthenium(II) complexes studied are shown in Figs. 1—3. The wavelengths of the absorption maxima and the corresponding molar extinction coefficients as well as the wavelengths of the emission maxima for all the ruthenium(II) complexes are summarized in Table 2.

The quantum yields and lifetimes for all the complexes at 77 K are tabulated in Table 3. A value of the quantum yield, 0.328, for the $[Ru(bpy)_3]Cl_2$ is smaller than that of 0.376 reported by Demas and Crosby.[11] A once recrystallized sample also gave the same value. When $[Ru(4,4'\text{-diphenylbpy})_3]Cl_2$ was used as the quantum yield standard with a value of 0.563 measured in this study, again the same result

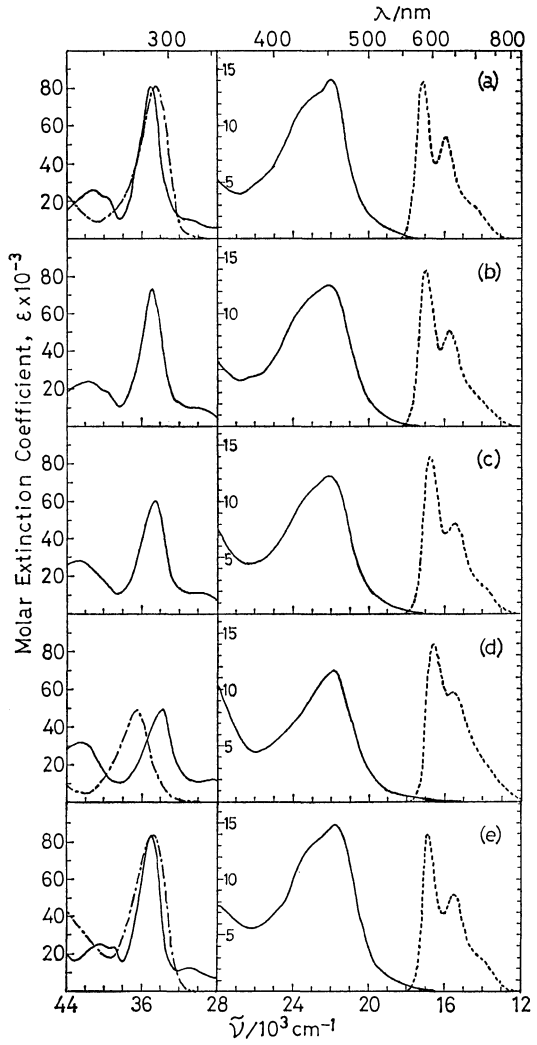

Fig. 1. Absorption and emission spectra of (a) [Ru(bpy)$_3$]Cl$_2$, (b) [Ru(bpy)$_2$(dmby)]Cl$_2$, (c) [Ru(bpy)(dmby)$_2$]Cl$_2$, (d) [Ru(dmby)$_3$]Br$_2$, (e) [Ru(4,4′-dimethylbpy)$_3$]Cl$_2$: (——) and (— — —) absorption spectra of complexes in H_2O and ligands in 50% H_2SO_4 at 25 °C, respectively; (----) emission spectra in methanol–ethanol (1:4, v/v) glass at 77 K. ε of bpy and dmby free ligands is multiplied by 5.07 and 3.54, respectively.

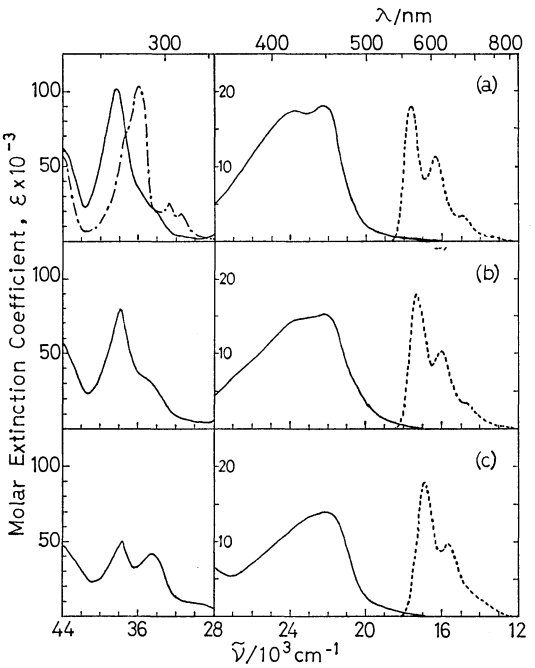

Fig. 2. Absorption and emission spectra of (a) [Ru(phen)$_3$]Cl$_2$, (b) [Ru(phen)$_2$(dmby)]Cl$_2$, (c) [Ru(phen)(dmby)$_2$]Cl$_2$: (——) and (— — —) absorption spectra of complexes in H_2O and ligands in 50% H_2SO_4 at 25 °C, respectively; (- - -) emission spectra in methanol–ethanol (1:4, v/v) glass at 77 K. ε of phen and dmby free ligands is multiplied by 2.52 and 3.54, respectively.

was obtained. The quantum yield, 0.328, for the [Ru(bpy)$_3$]Cl$_2$ complex is acceptable in view of the fact that the present quantum yields for the [Ru(phen)$_3$]Cl$_2$ (0.578) and [Ru(4,4′-diphenylbpy)$_3$]Cl$_2$ (0.563) agree well with the values of 0.584 and 0.573 measured by Demas and Crosby,[11,13] respectively, and the lifetimes for [Ru(bpy)$_3$]Cl$_2$, [Ru(4,4′-diphenylbpy)$_3$]Cl$_2$, [Ru(phen)$_3$]Cl$_2$, and [Ru(4,7-diphenylphen)$_3$]Cl$_2$ (5.1, 4.8, 9.9, and 10.2 μs, respectively) are also in good agreement with the values reported for these complexes (5.21, 4.68, 9.79, and 9.58 μs, respectively[11,13]).

Radiative (k_r) and nonradiative (k_{nr}) rate constants were calculated using the following expressions,

$$Q = k_r/(k_r+k_{nr}) = k_r\tau_m, \quad (1)$$

$$k_{nr} = \tau_m^{-1} - \tau_r^{-1}, \quad (2)$$

where Q is the emission quantum yield, τ_m is the measured lifetime, and τ_r is the radiative lifetime ($=1/k_r$). In Eq. 1 the efficiency of populating the emitting CTTL excited state (see Discussion) is assumed to be unity as is generally accepted.[2,31] The results are included in Table 3.

At 25 °C the emission intensity largely decreases, especially for the complexes including the dmby ligand. This is the reason why the lifetimes of the complexes including dmby (except that of [Ru(bpy)$_2$(dmby)]Cl$_2$) and the quantum yield of [Ru(dmby)$_3$]Br$_2$ could not be measured. As for the two complexes of [Ru(bpy)(dmby)$_2$]I$_2$ and [Ru(phen)(dmby)$_2$]Cl$_2$, it was difficult to obtain the exact corrected emission spectra because of their low intensities. The yields were estimated, however, by an assumption that the ratio of the integrated area under the corrected emission spectrum to the intensity in height at the observed wavelength (600 nm)[29] is equal to those of [Ru(bpy)$_2$(dmby)]I$_2$ and [Ru(phen)$_2$(dmby)]Cl$_2$, respectively. The errors in these procedures mainly stem from the estimate of the height in the ratio because the area is almost the same within the bipyridyl or phenanthroline complex series. Since the red shift in the emission spectra on introduction of dmby is evident but small (Table 2), the errors caused by the above assumption seem not so large that the order in the yield is varied. The results are listed in Table 4. The quantum yields using the excitation wavelength of 480 nm agreed well with those at 436 nm. Moreover, an excellent coincidence was seen between the yields obtained by means of fluorescein and [Ru(bpy)$_3$]Cl$_2$ as the standard.

TABLE 2. ABSORPTION AND EMISSION SPECTRAL DATA FOR LIGANDS AND Ru(II) COMPLEXES

Compound	Absorption[a] λ_{max}/nm	$\varepsilon_{max}\times10^{-4}$ / $M^{-1}cm^{-1}$	δ[b] / cm^{-1}	f[c]	Emission[a] λ_{max}/nm	Emission[d] λ_{max}/nm
$[Ru(bpy)_3]Cl_2$	452	1.40	2300	0.15	628	582, 629
	286, 243	8.14, 2.55				
$[Ru(bpy)_2(dmby)]Cl_2$	453	1.26	2700	0.16	630	588, 636
	287, 239	7.14, 2.43				
$[Ru(bpy)(dmby)_2]Cl_2$	454, 342	1.23, 1.09	2700	0.15		597, 641
	289, 235	6.06, 2.82				
$[Ru(dmby)_3]Br_2$	456, 348	1.16, 1.18	2800	0.15		601, 638
	296, 236	4.94, 3.23				
$[Ru(phen)_3]Cl_2$	447, 420	1.81, 1.74	2500	0.21	604	566, 610
	262, 222	10.8, 7.89				
$[Ru(phen)_2(dmby)]Cl_2$	450, 423	1.52, 1.47	3000	0.21	611	576, 623
	264, 224	7.96, 6.04				
$[Ru(phen)(dmby)_2]Cl_2$	451, 423	1.40, 1.24	2800	0.18		591, 638
	289, 265, 226	4.22, 5.08, 4.53				
$[Ru(4,4'\text{-dimethylbpy})_3]Cl_2$	459	1.49	2600	0.18	642	593, 641
	285, 247	8.00, 2.52				
bpy[e]	289 (280)	1.61 (1.29)				
dmby[e]	274 (271, 266)	1.40 (0.85, 0.85)				
4,4'-Dimethylbpy[e]	286 (279)	1.58 (1.24)				
phen[e]	278 (264)	4.28 (2.91)				

a) In water at 25 °C. b) Bandwidth at half-height of CT-absorption band estimated by drawing gaussian curves eliminating shoulders. c) Oscillator strengths, f, were calculated using the expression, $f=4.60\times10^{-9}\varepsilon_{max}\delta$, from C. J. Ballhausen, *Prog. Inorg. Chem.*, **2**, 251 (1960). d) In methanol-ethanol(1:4, v/v) rigid glass at 77 K. e) In 50% H_2SO_4. Values in 0.1 M NaOH were indicated in parentheses.

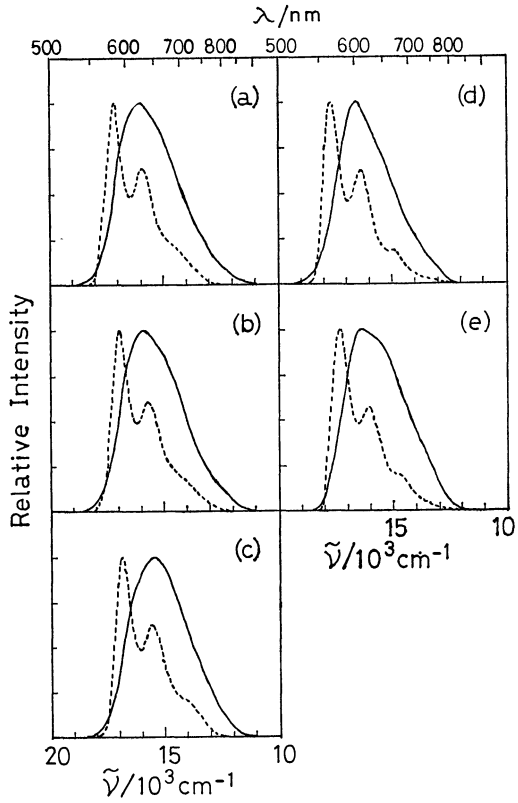

Fig. 3. Emission spectra of (a) $[Ru(bpy)_3]Cl_2$, (b) $[Ru(bpy)_2(dmby)]I_2$, (c) $[Ru(4,4'\text{-dimethylbpy})_3]Cl_2$, (d) $[Ru(phen)_3]Cl_2$, (e) $[Ru(phen)_2(dmby)]Cl_2$: (——) in H_2O at 25 °C; (- - -) in methanol–ethanol (1:4, v/v) glass at 77 K.

Discussion

Absorption and Emission Spectra. The intense visible absorption bands of the tris-type ruthenium(II) complexes of bipyridyl,[2] phenanthroline,[2,32] and 4,4'-dimethylbipyridyl[14] have been all assigned to the spin-allowed charge transfer transitions from the metal d orbitals to the ligand π^* orbitals (CTTL), while the more intense bands below 300 nm have been assigned to intraligand π-π^* transitions.[14,33] Because of the similarities in the spectra of the complexes containing the dmby ligand, the same band assignments can be made for the new complexes reported here.

The following features can be seen from Figs. 1 and 2 or Table 2. First, the absorption spectra of the parent complexes of $[Ru(bpy)_3]^{2+}$ or $[Ru(phen)_3]^{2+}$ regularly change to that of $[Ru(dmby)_3]^{2+}$ without any appearance of new bands in the mixed-ligand complexes other than the characteristic bands already present in these three homotrischelated complexes. Moreover, a slight red shift is seen except for the 240 nm band in the bipyridyl complex series which shows a blue shift. Secondly, the π-π^* absorption maximum of the dmby free ligand lies in a considerable shorter wavelength than that of the parent bipyridyl. This contrasts with 4,4'-dimethylbipyridyl in which the position and intensity of the absorption maximum are comparable with the parent ligand, and hence suggests that due to the steric interactions of the two methyl groups of dmby the delocalization of π-electrons is limited to a narrow range. Such hypsochromic effect of a substituent(s) at the sterically hindering

Table 3. Quantum yields, lifetimes, and rate constants for Ru(II) complexes at 77 K[a]

Complex	Q[b]	τ_m[c] μs	τ_r[d] μs	k_r[e] μs^{-1}	k_{nr}[f] μs^{-1}	Q_h[g]
$[Ru(bpy)_3]Cl_2$	0.328±0.011	5.1±0.2	16	0.064	0.14	
$[Ru(bpy)_2(dmby)]I_2$	0.252±0.008	5.2±0.1	21	0.048	0.14	0.255
$[Ru(bpy)(dmby)_2]I_2$	0.192±0.003	5.4±0.2	28	0.036	0.15	0.205
$[Ru(dmby)_3]Br_2$	0.113±0.014	6.4±0.2	57	0.018	0.14	0.114
$[Ru(phen)_3]Cl_2$	0.578±0.007	9.9±0.3	17	0.058	0.042	
$[Ru(phen)_2(dmby)]Cl_2$	0.422±0.011	9.4±0.2	22	0.045	0.065	0.517
$[Ru(phen)(dmby)_2]Cl_2$	0.281±0.013	9.3±0.2	33	0.030	0.080	0.417
$[Ru(dmby)_3]Br_2$	0.113±0.014	6.4±0.2	57	0.018	0.14	0.300
$[Ru(4,4'\text{-dimethylbpy})_3]Cl_2$	0.283±0.007	4.6±0.2	16	0.062	0.093	0.307

a) Measured in methanol-ethanol(1:4, v/v) rigid glass. b) Luminescence quantum yields. Excited at 436 nm. c) Measured lifetimes. Excited at 337 nm. d) Radiative lifetimes calculated from τ_m/Q. e) Radiative rate constant calculated from $1/\tau_r$. f) Nonradiative rate constants calculated from $\tau_m^{-1}-\tau_r^{-1}$. g) Hypothetical quantum yield (see context).

Table 4. Luminescence quantum yields for Ru(II) complexes at 25 °C[a]

Complex	N_2-saturated[b]		Air-saturated[b]	
	Q(F)	Q(R)	Q(F)	Q(R)
$[Ru(bpy)_3]Cl_2$[c]	0.042±0.002		0.028±0.002	
$[Ru(bpy)_2(dmby)]I_2$	$(3.6\pm0.2)\times10^{-4}$	$(3.6\pm0.3)\times10^{-4}$	$(3.0\pm0.2)\times10^{-4}$	$(3.1\pm0.2)\times10^{-4}$
$[Ru(bpy)(dmby)_2]I_2$[d]	$(1.3\pm0.3)\times10^{-5}$	$(1.9\pm0.8)\times10^{-5}$	$(0.8\pm0.2)\times10^{-5}$	$(1.1\pm0.3)\times10^{-5}$
$[Ru(phen)_3]Cl_2$[c]	0.058±0.005	0.058±0.004	0.032±0.002	0.030±0.002
$[Ru(phen)_2(dmby)]Cl_2$	$(4.0\pm0.5)\times10^{-5}$	$(4.0\pm0.4)\times10^{-5}$	$(4.6\pm0.6)\times10^{-5}$	$(4.9\pm0.7)\times10^{-5}$
$[Ru(phen)(dmby)_2]Cl_2$[d]	$(6\pm3)\times10^{-6}$	$(9\pm3)\times10^{-6}$	$(5\pm2)\times10^{-6}$	$(8\pm2)\times10^{-6}$
$[Ru(4,4'\text{-dimethylbpy})_3]Cl_2$[c]	0.026±0.002	0.025±0.002	0.021±0.002	0.021±0.002

a) In water at 25 °C. b) Luminescence quantum yields. Excited at 436 nm. Q(F) and Q(R) denote the yields measured by using fluorescein and $[Ru(bpy)_3]Cl_2$ as the standard, respectively. c) Value from Ref. 30. d) As for the procedures to obtain these values, see Results.

positions of various organic compounds is well known (for example, biphenyl, a similar compound to 2,2'-bipyridyl).[34] The π-π^* absorption maximum of dmby (274 nm), however, greatly shifts to the longer wavelength (296 nm) upon coordination to ruthenium, contrasted with that of phenanthroline (278 nm) which shifts to shorter wavelength (262 nm). Finally, as the number of the dmby ligand increases, maximum molar extinction coefficients decrease step by step except also for the 240 nm band, where an increase rather than a decrease is observed. This decrease can be explained, at least in part, by a broadening of the visible CT band.[18] The oscillator strengths in Table 2, though by a rough calculation, are almost the same; a reduction in the extinction coefficients is recovered by an increase in the bandwidths.

The emission at 77 K from the trischelated ruthenium(II) complexes with the unsubstituted and substituted bipyridyl or phenanthroline arises from a CTTL excited state.[11,13,14] However, a discussion about the assignment of a spin multiplicity is inappropriate due to strong spin-orbit coupling.[35] As is similar to these complexes, the emission spectra reported here clearly show the vibrational progression indicative of a CT luminescence[2] although the vibrational structure is somewhat obscure in the tris(dmby) complex. It is therefore concluded that the observed luminescence of the complexes including dmby is also due to the radiative transitions from the CTTL excited state. It should be pointed out that the red shift of the emission peak of $[Ru(dmby)_3]^{2+}$ from that of $[Ru(bpy)_3]^{2+}$ is larger than any other ruthenium(II) complexes of substituted bipyridyls reported until now.

The emission spectra at 25 °C (Fig. 3) are broader and indicate red shifts in comparison with those at 77 K. These large changes in the shape of the spectra when the solvent medium is transformed from a rigid glass to a fluid have been used as an evidence for the argument that in fluid solutions charge transfer to solvent (CTTS) configurations interact with the CTTL excited state of $[Ru(bpy)_3]^{2+}$.[16,17]

Lifetimes and Quantum Yields. The observed lifetimes for the bipyridyl complex series produce only a relatively minor variation as well as for the phenanthroline series. The longer lifetimes for the latter are plain enough.

The most notable effect of dmby is seen in a large decrease in the emission quantum yield of its tris complex, that is, 66% and 80% decreases compared with the parent complexes of bipyridyl and phenanthroline, respectively. Dimethyl substitution on the normal (sterically not hindering) positions such as 4,4'- for bipyridyl or 4,7- and 5,6-positions for phenanthroline has been known to result in relatively slight changes in the yields (3—12%), whereas diphenyl substitution causes a larger increase (20—50%).[14,15,36] However,

TABLE 5. REPRODUCTION OF THE EMISSION QUANTUM YIELDS OF THE MIXED LIGAND Ru(II) COMPLEXES

	$k_r/\mu s^{-1}$		$k_{nr}/\mu s^{-1}$		$\tau/\mu s$		Q	
	Calcd[a]	Obsd	Calcd[b]	Obsd	Calcd[c]	Obsd	Calcd[d]	Obsd
$[Ru(bpy)_2(dmby)]I_2$	0.0486	0.048	0.140	0.14	5.29	5.2	0.257	0.252
$[Ru(bpy)(dmby)_2]I_2$	0.0333	0.036	0.140	0.15	5.78	5.4	0.192	0.192
$[Ru(phen)_2(dmby)]Cl_2$	0.0446	0.045	0.0747	0.065	8.40	9.4	0.375	0.422
$[Ru(phen)(dmby)_2]Cl_2$	0.0313	0.030	0.107	0.080	7.25	9.3	0.227	0.281

a) Calculated using the values of 0.0213 for a bpy, 0.0193 for a phen, and 0.006 μs^{-1} for a dmby. These values were obtained by division of k_r for the corresponding parent tris complexes by 3. b) Calculated using the values of 0.0467 for a bpy, 0.014 for a phen, and 0.0467 μs^{-1} for a dmby obtained by division of k_{nr} for the corresponding parent tris complexes by 3. c) Calculated from $1/(k_r+k_{nr})$. d) Calculated from $k_r\tau$.

methyl- or dimethyl-substitution on the sterically hindering positions such as 6,6'- for bipyridyl or 2,9-positions for phenanthroline has been shown to bring about a great decrease in the yields (72% for the monomethyl and 92% for the dimethyl ligands).[20] It should be noted that the latter values are comparable to the present case.

A perusal of Table 3 shows that introduction of the dmby ligand into the parent tris complexes causes a decrease in the yields at almost the same rate for both series of complexes. According to Hipps and Crosby,[37] the lowest CTTL excited state of the ruthenium(II) complexes is viewed as the one in which an electron has been essentially promoted from the central metal core to an antibonding orbital delocalized over the three ligands. Therefore the electronic properties of the excited state are described as weighted averages of the properties of the individual ligands. In line with this point of view, the quantum yields of the mixed-ligand complexes can be calculated as follows. An assumption that the values of radiative and nonradiative rate constant for the tris(bipyridyl) complexes can be alloted equally to each of three bipyridyl molecules gives the values of 0.0213 and 0.0467 μs^{-1}, respectively. An analogous procedure for the tris-(phenanthroline or dmby) complexes gives 0.0193 and 0.014 μs^{-1} for a phenanthroline, 0.006 and 0.0467 μs^{-1} for a dmby. Then using these values the quantum yields are computed by Eq. 1 and the results are listed in Table 5. It is seen that the calculated and observed quantum yields agree well although somewhat low calculated values are obtained for the phenanthroline mixed-ligand complexes.

As Eq. 1 shows, the observed decrease of the emission quantum yield is due both to the decrease in k_r and to the increase in k_{nr}. The relative contributions of these two factors to the decrease in the yield are illustrated in Fig. 4. The line on the left of each diagram represents the quantum yield of the parent complex while the line on the right represents the observed quantum yield of the complex including dmby. The line in the middle represents the hypothetical quantum yield (Q_h) that the dmby complex would have if only a change in the radiative rate constant (Δk_r) were caused by the dmby ligand substitution (the values of Q_h are also listed in Table 3). Δk_{nr} represents the change in the quantum yield due to the change in k_{nr}. The figure shows that both factors

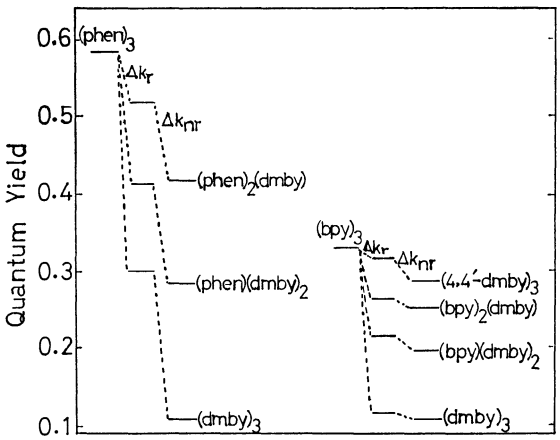

Fig. 4. Dmby substitution-induced changes in quantum yields resolved into radiative(Δk_r) and nonradiative(Δk_{nr}) factors for Ru(II) complexes in methanol–ethanol (1:4, v/v) glass at 77 K.

comparably contribute to the decrease in the yield for the phenanthroline complexes, although a detailed examination indicates that as the number of dmby increases the role of Δk_r factor becomes more important while the role of Δk_{nr} factor decreases. In sharp contrast to the phenanthroline complexes, however, the decrease in the yield for the bipyridyl complexes is almost ascribed to the decrease in k_r. Similar results have been also reported for the other ruthenium(II) complexes.[38]

The decrease in k_r can be, at least qualitatively, explained by the model by Demas and Crosby[11] which assumes that the emitting (triplet) state (the energy, E_T) borrows intensity from the lending, highly spin-allowed (singlet) state (the energy, E_S) through the spin-orbit coupling interaction (magnitude, $K|M_{SO}|^2$). On the basis of this model, they have expressed the radiative rate constant as follows:

$$k_r = \varepsilon(S)K|M_{SO}|^2(E_T^3/E_S)/(E_T-E_S)^2, \quad (3)$$

where $\varepsilon(S)$ is the maximum molar extinction coefficient of the first visible CT band. E_S is taken as the energy of the first absorption maximum of the highly allowed CT band, and E_T is assumed to be the energy of the shortest wavelength emission peak.[11] In calculating the radiative rate constant by Eq. 3, two additional approximations are made. First, the values of $\varepsilon(S)$ at 25 °C in Table 2 are used because the absorption spectra have not been measured at 77

Table 6. Caculated and experimental radiative rate constants of Ru(II) complexes at 77 K*)

Complex	ε(S)[a]	E_S[b]	E_T[c]	k_r(calcd)[d] / μs^{-1}	k_r(exptl)[e] / μs^{-1}
$[Ru(bpy)_3]Cl_2$	1.40	22.1	17.2	0.064 (1.00)	0.064 (1.00)
$[Ru(bpy)_2(dmby)]I_2$	1.26	22.1	17.0	0.053 (0.83)	0.048 (0.75)
$[Ru(bpy)(dmby)_2]I_2$	1.23	22.0	16.8	0.046 (0.72)	0.036 (0.56)
$[Ru(dmby)_3]Br_2$	1.16	21.9	16.6	0.042 (0.66)	0.018 (0.28)
$[Ru(phen)_3]Cl_2$	1.81	22.4	17.7	0.058 (1.00)	0.058 (1.00)
$[Ru(phen)_2(dmby)]Cl_2$	1.52	22.2	17.4	0.044 (0.75)	0.045 (0.78)
$[Ru(phen)(dmby)_2]Cl_2$	1.40	22.2	16.9	0.032 (0.55)	0.030 (0.52)
$[Ru(dmby)_3]Br_2$	1.16	21.9	16.6	0.025 (0.43)	0.018 (0.31)
$[Ru(4,4'\text{-dimethylbpy})_3]Cl_2$	1.49	21.8	16.9	0.066 (1.03)	0.062 (0.97)

a) Maximum molar extinction coefficient of the first visible CT band (in unit of $10^4\,M^{-1}\,cm^{-1}$). b) Singlet state energy of the absorption maximum of the first visible CT band(in unit of $10^3\,cm^{-1}$). c) Triplet state energy assumed to be the energy of the shortest emission peak at 77 K(in unit of $10^3\,cm^{-1}$). d) Calculated radiative rate constant using a value of $K|M_{SO}|^2$ of 4.87×10^{-7} for the bipyridyl complexes and 2.87×10^{-7} ($M\,cm\,\mu s^{-1}$) for the phenanthroline complexes. e) Experimentally obtained radiative rate constant (see Table 3). *) Normalized figures of k_r for the bipyridyl and phenanthroline complexes are shown in parentheses.

K. Secondly, value of $K|M_{SO}|^2$ is assumed not to be so much affected by dmby substitution. Hence, a value of 4.87×10^{-7} and 2.87×10^{-7} ($M\,cm\,\mu s^{-1}$) is used as $K|M_{SO}|^2$ for the bipyridyl and phenanthroline complexes, respectively, in order to normalize the calculated values to the experimentally obtained radiative rate constants for the parent complexes (the latter value reasonably agrees with 2.43×10^{-7} for $[Ru(phen)_3]^{2+}$, but the former is somewhat larger than 3.78×10^{-7} for $[Ru(bpy)_3]^{2+}$ reported by Demas and Crosby[11]). The results in Table 6 show that agreement between the calculated and experimental radiative rate constant is excellent for the phenanthroline complexes, whereas poor agreement is observed for the bipyridyl complexes. However, it may safely be said that the observed decrease in k_r is, at least qualitatively, due to the decrease in ε(S) and E_T^3/E_S term and the increase in the energy gap term for both the complex series as is expected from Eq. 3.

The larger nonradiative rate constant for the parent bipyridyl complex than for the parent phenanthroline complex is attributed to the difference between the structure of the two ligands; the rigid ring system and planarity of phenanthroline considerably slow down the nonradiative processes. The effect of dmby substitution on the nonradiative rate constant would be largely observed for the complex which has a small value of k_{nr}, *i.e.* the phenanthroline complexes as compared with the bipyridyl complexes. In such a case the values of k_{nr} for the bipyridyl complexes are hardly influenced by dmby if the effect is not large. Nearly the constant values of k_{nr} observed for the bipyridyl complexes may be a reflection of such circumstances.

The above discussion reveals that methyl substituents on the 3,3'-positions of the bipyridyl ligand decrease the visible CTTL absorption intensity and increase the energy gap between the intensity-lending singlet and the emitting triplet state, and that this leads to the decrease in k_r and hence the emission quantum yield. On the contrary, methyl substitution on the 4,4'-positions of the parent ligand, which is considered not to change chelate conformation of the parent ligand

Table 7. Lifetimes of $[Ru(bpy)_3]Cl_2$ and $[Ru(bpy)_2(dmby)]Cl_2$ in various solvents at 25 °C[a]

Solvent	$[Ru(bpy)_3]Cl_2$[b] $\tau_m/\mu s$	$[Ru(bpy)_2(dmby)]Cl_2$ $\tau_m/\mu s$	AN[c]
Water	0.65±0.02	0.41±0.03	54.8
Methanol	0.72±0.03	0.44±0.02	41.3
Ethanol	0.74±0.02	0.39±0.02	37.1
Acetonitrile	0.89±0.03	0.59±0.02	19.3
Pyridine	0.92±0.05	0.63±0.03	14.2

a) In nitrogen-bubbled solutions. Excited at 337 nm. b) Ref. 40. c) Gutmann's acceptor number from Ref. 39.

believed to be coplanar, produces only a minor change in these factors and thus a relatively small decrease in the yield. Fabian, *et al.*,[20] have reported more marked decreases in the absorption intensities and emission yields of the ruthenium(II) complexes caused by methyl substituents on the sterically hindering 6,6'-positions for bipyridyl and 2,9-positions for phenanthroline than the complexes reported here, and have pointed out that the effects can be reduced to some extent by relief of the steric hindrance by twisting of the ligands. From these comparisons with the other substituted ligand complexes, it may be reasonable to consider that 3,3'-dimethyl-2,2'-bipyridyl in the ruthenium(II) complexes studied takes a twisted, noncoplanar conformation owing to the steric hindrance of the two methyl groups.

At 25 °C, only the lifetime of $[Ru(bpy)_2(dmby)]Cl_2$ in the dmby-mixed complexes can be measured because of the low emission intensities. As is seen from Table 7, the lifetimes of the bis(bipyridyl) complex in several solvents are about 2/3 compared with those of the tris(bipyridyl) complex and increase with the decrease in the Gutmann's acceptor number[39] as in the parent complex. This may suggest that the emitting state of the bis(bipyridyl) complex is similar to that of the tris(bipyridyl) complex, *i.e.* CTTL excited state contributed by the CTTS configurations.[16,17]

Values of the radiative (k_r) and nonradiative (k_{nr}) rate constants calculated from Eqs. 1 and 2 using the data in H_2O are 0.065, 1.5 μs^{-1} for $[Ru(bpy)_3]Cl_2$ and 8.8×10^{-4}, 2.4 μs^{-1} for $[Ru(bpy)_2(dmby)]Cl_2$, respectively; namely, the drastical decrease in the yield of the bis(bipyridyl) complex at 25 °C is due mainly to the large decrease in k_r. However, such a result does not agree with the usual understanding that the radiative rate constant is characteristic of a molecule and not dependent on the surrounding conditions, such as temperature or solvent properties. In fact, the value of k_r for $[Ru(bpy)_3]Cl_2$ is nearly the same both at 77 K and 25 °C. On the other hand, the above calculations show another important point that the nonradiative rate constant of the bis(bipyridyl) complex at 25 °C is only slightly larger than that of the parent tris complex, and thus the large decrease in the yield of the bis(bipyridyl) complex cannot be ascribed to the increase in k_{nr}. Consequently two reasons are possible for the decrease in the yield of the bis(bipyridyl) complex at 25 °C; (i) decrease of the formation efficiency of the emitting state (φ_{isc}) and (ii) changes of the circumstances of the excited states in contrast with those at 77 K. According to the first alternative, Eq. 1 does not hold any more and must be replaced by the following expression:

$$Q = \varphi_{isc}k_r/(k_r+k_{nr}) = \varphi_{isc}k_r\tau_m. \quad (4)$$

φ_{isc} can be estimated if k_r at 25 °C is assumed to be the same as that at 77 K (0.048 μs^{-1}). The value of φ_{isc} obtained in this way is 1.8×10^{-2}, *i.e.* decreased by two orders of magnitude. The cause of the large decrease in φ_{isc}, however, is not obvious at this stage. In order to argue about the second alternative, it is necessary to know about various aspects such as the contributions of the CTTS configurations to the emitting state,[16,17] equilibrium between the CTTL and d-d excited state (this problem is neglected at 77 K),[17,41] as well as the detailed knowledge of the energy levels of each excited states. These data, however, are also insufficient. It is likely that changes in the excited state features result in the decrease of φ_{isc}, but further experiments are needed to establish this view.

Finally it should be noted that the quenching effect of dissolved oxygen in the solvent reported for the tris(bipyridyl)ruthenium(II) complex[42] is also seen in the complexes studied here (Table 4).

The author wishes to thank Associate Professor Hiroshi Kokubun and Dr. Koichi Kikuchi of Tohoku University for their kindness in allowing the use of their apparatus for lifetime measurements, and Dr. Toshishige Suzuki of the Government Industrial Research Institute of Tohoku, Sendai, for kindly supplying his authentic sample of the dmby ligand.

References

1) J. Paris and W. W. Brandt, *J. Am. Chem. Soc.*, **81**, 5001 (1957).
2) D. M. Klassen and G. A. Crosby, *J. Chem. Phys.*, **48**, 1853 (1968).
3) C. R. Bock, T. J. Meyer, and D. G. Whitten, *J. Am. Chem. Soc.*, **97**, 2909 (1975).
4) C. P. Anderson, D. J. Salmon, T. J. Meyer, and R. C. Young, *J. Am. Chem. Soc.*, **99**, 1980 (1977).
5) R. C. Young, J. K. Nagle, T. J. Meyer, and D. G. Whitten, *J. Am. Chem. Soc.*, **100**, 4773 (1978).
6) C. Creutz and N. Sutin, *Proc. Natl. Acad. Sci. U.S.A.*, **72**, 2858 (1975).
7) V. Balzani, L. Moggi, M. F. Manfrin, F. Bolletta, and M. Gleira, *Science*, **189**, 852 (1975).
8) W. D. K. Clark and N. Sutin, *J. Am. Chem. Soc.*, **99**, 4676 (1977).
9) G. Sprintschnik, H. W. Sprintschnik, P. P. Kirsch, and D. G. Whitten, *J. Am. Chem. Soc.*, **99**, 4947 (1977).
10) G. M. Brown, B. S. Brunschwig, C. Creutz, J. F. Endicott, and N. Sutin, *J. Am. Chem. Soc.*, **101**, 1298 (1979).
11) J. N. Demas and G. A. Crosby, *J. Am. Chem. Soc.*, **93**, 2841 (1971).
12) R. J. Watts and G. A. Crosby, *J. Am. Chem. Soc.*, **93**, 3184 (1971).
13) R. J. Watts and G. A. Crosby, *J. Am. Chem. Soc.*, **94**, 2606 (1972).
14) G. D. Hager and G. A. Crosby, *J. Am. Chem. Soc.*, **97**, 7031 (1975).
15) G. D. Hager, R. J. Watts, and G. A. Crosby, *J. Am. Chem. Soc.*, **97**, 7038 (1975).
16) J. Van Houten and R. J. Watts, *J. Am. Chem. Soc.*, **97**, 3843 (1975).
17) J. Van Houten and R. J. Watts, *J. Am. Chem. Soc.*, **98**, 4853 (1976).
18) D. M. Klassen, C. W. Hudson, and E. L. Shaddix, *Inorg. Chem.*, **14**, 2733 (1975).
19) D. M. Klassen, *Inorg. Chem.*, **15**, 3166 (1976).
20) R. H. Fabian, D. M. Klassen, and R. W. Sonntag, *Inorg. Chem.*, **19**, 1977 (1980).
21) F. H. Case, *J. Am. Chem. Soc.*, **68**, 2574 (1946).
22) F. W. Cagle, Jr., and G. F. Smith, *J. Am. Chem. Soc.*, **69**, 1860 (1947).
23) T. M. Suzuki and T. Kimura, *Bull. Chem. Soc. Jpn.*, **50**, 391 (1977).
24) O. Seide, *Ber.*, **57**, 1802 (1924).
25) *Org. Synth.*, Coll. Vol. III, 136 (1955).
26) P. J. Giordano, C. R. Bock, and M. S. Wrighton, *J. Am. Chem. Soc.*, **100**, 6960 (1978).
27) I. Fujita and H. Kobayashi, *J. Chem. Phys.*, **59**, 2902 (1973).
28) E. Lippert, W. Nägele, I. Seibold-Blankenstein, U. Staiger, and W. Voss, *Z. Anal. Chem.*, **17**, 1 (1959).
29) C. A. Parker and W. T. Rees, *Analyst (London)*, **85**, 587 (1960).
30) K. Nakamaru, K. Nishio, and H. Nobe, *Sci. Rept. Hirosaki Univ.*, **26**, 57 (1979).
31) J. N. Demas and D. G. Taylor, *Inorg. Chem.*, **18**, 3177 (1979).
32) G. A. Crosby, W. G. Perkins, and D. M. Klassen, *J. Chem. Phys.*, **43**, 1498 (1965).
33) F. E. Lytle and D. M. Hercules, *J. Am. Chem. Soc.*, **91**, 253 (1969).
34) W. R. Remington, *J. Am. Chem. Soc.*, **67**, 1838 (1945).
35) G. A. Crosby, K. W. Hipps, and W. H. Elfring, *J. Am. Chem. Soc.*, **96**, 629 (1974).
36) W. H. Elfring, Jr., and G. A. Crosby, *J. Am. Chem. Soc.*, **103**, 2683 (1981).
37) K. W. Hipps and G. A. Crosby, *J. Am. Chem. Soc.*, **97**, 7042 (1975).
38) Fabian, *et al.*,[20] have stated that both factors contribute about equally to the decrease in the quantum yields for 6-methyl or 6,6'-dimethylbpy complexes, while for 2-

methyl or 2,9-dimethylphen complexes the decrease in the quantum yields is due more to the increase in the nonradiative rate constant. However, recalculations of Q_h using their data suggest that these conclusions seem not to be correct.
39) V. Gutmann, *Electrochim. Acta*, **21**, 661 (1976).
40) K. Nakamaru, *Bull. Chem. Soc. Jpn.*, **55**, 1639 (1982).
41) J. Van Houten and R. J. Watts, *Inorg. Chem.*, **17**, 3381 (1978).
42) J. N. Demas, D. Diemente, and E. W. Harris, *J. Am. Chem. Soc.*, **95**, 6864 (1973).

The Oxidation of Carbon Monoxide on Pt/Al_2O_3 Containing a Metal Oxide

Yukio Kosaki,* Akira Miyamoto, and Yuichi Murakami
Department of Synthetic Chemistry, Faculty of Engineering, Nagoya University, Furo-cho, Chikusa-ku, Nagoya 464
(Received November 25, 1981)

By using a three-way catalyst containing a metal oxide, CO is removed as CO_2 even in the "rich" region of the air/fuel ratio. In order to elucidate the mechanism of this action of the added metal oxide, the reaction of CO with O_2 on a $Pt–V_2O_5/Al_2O_3$ catalyst was investigated using a rectangular pulse-reaction apparatus. In the $CO–O_2$ reaction on a Pt/Al_2O_3 catalyst, a significant amount of unreacted CO was exhausted in the "rich" region of the reactants. Furthermore, the conversion of CO decreased markedly with an increase in the CO/O_2 ratio in the reactants. In the $CO–O_2$ reaction on the $Pt–V_2O_5/Al_2O_3$ catalyst, on the other hand, the conversion of CO was high and did not decrease markedly with an increase in the CO/O_2 ratio in the "rich" region. As for the reaction on the $Pt–V_2O_5/Al_2O_3$ at 558 K and above, the CO was completely removed as CO_2 at any of the CO/O_2 ratios examined. These effects of the added V_2O_5 were found to be due to: (i) the reaction of CO with an oxygen of V_2O_5 in the $Pt–V_2O_5/Al_2O_3$ catalyst and (ii) the enhanced oxidation of CO with a gaseous O_2 on the Pt/Al_2O_3 catalyst upon the addition of V_2O_5. On the basis of the kinetics of the oxidation of CO with the oxygen of V_2O_5 in the $Pt–V_2O_5/Al_2O_3$ and Pt black–V_2O_5 mixtures, its mechanism was proposed to be as follows; the oxygen of V_2O_5 at the $Pt–V_2O_5$ interface is activated by contact with Pt (this activated oxygen is denoted by [Pt···O···V]). The oxidation of CO with the oxygen of the $Pt–V_2O_5/Al_2O_3$ and Pt black–V_2O_5 mixtures proceeds according to the following two steps. Step I is the reaction of a gaseous CO with the active oxygen at the $Pt–V_2O_5$ interface, [Pt···O···V], to form CO_2 and a reduced site, [Pt V]. Step II is the oxidation of the reduced site with the bulk oxygen in V_2O_5 to reproduce [Pt···O···V]. The enhanced oxidation of CO with a gaseous O_2 caused by the addition of V_2O_5 to Pt/Al_2O_3 was found also to be understandable in terms of the active site, [Pt···O···V], where the reduced site, [Pt V], is oxidized by the gaseous O_2 to reproduce [Pt···O···V] instead of the bulk oxygen in V_2O_5.

The three-way catalyst system is used for the simultaneous removal of nitrogen monoxide, carbon monoxide, and hydrocarbons in automotive exhaust emissions.[1–5] Furthermore, attention has been focused on finding a three-way catalyst containing a metal oxide in order to deal with the fluctuation in the air/fuel ratio and broaden the "window" width.[6,7] It has been found, for the reaction of synthetic exhaust gas, that the conversion of CO in the "rich" region is much increased by the addition of a metal oxide to a three-way catalyst.[7,8] Although the mechanisms of the $CO–O_2$ reaction on precious metal[9–17] and metal oxide[18–21] catalysts have been the subject of many investigations, the mechanism of the action of a metal oxide added to a three-way catalyst in the $CO–O_2$ reaction has scarcely been investigated. The purpose of this study, then, was to establish the mechanism of the action of V_2O_5 in the $CO–O_2$ reaction on a $Pt–V_2O_5/Al_2O_3$ catalyst, particularly the mechanism of the reaction in the "rich" region. The $CO–O_2$ reaction was investigated, since this reaction is one of the most important reactions involved in the real three-way catalyst system.[22,23] The reason why V_2O_5 was chosen as the metal oxide has already been described in a previous paper,[24] where a mechanism of the action of the V_2O_5 in the $NO–H_2$ reaction on the $Pt–V_2O_5/Al_2O_3$ catalyst has been proposed. It should also be noted that a rectangular pulse-reaction technique was employed in this study in order to investigate the kinetics of the reaction more precisely than the conventional pulse-reaction technique makes possible. The pulse-reaction technique is considered to be useful for the investigation of the effect of the addition of a metal oxide to a three-way catalyst.[24] Furthermore, it seemed interesting to compare the synergistic effect between Pt and V_2O_5 in the $CO–O_2$ reaction with that in the $NO–H_2$ reaction.

Experimental

Catalysts. A Pt/Al_2O_3 catalyst (the Pt loading was 0.5 wt%) was purchased from Nippon Engelhard, Ltd. The $Pt–V_2O_5/Al_2O_3$ (the Pt loading was 0.5 wt%, and, unless otherwise specified, the content of V_2O_5 in the catalyst was 9 wt%, although a catalyst with a 36 wt% V_2O_5 loading was also used), $Pt/Al_2O_3–V_2O_5$(M) (the ratio of Pt/Al_2O_3 to V_2O_5 was 1/1 in weight), and Pt black–V_2O_5(P) (the ratio of Pt black to V_2O_5 was 1/1 in weight) were the same as the catalysts used in the previous study.[24] The Pt black and Pd black were purchased from Mitsuwa's Pure Chemicals Co. The Rh black was prepared using the method employed by Feulgen.[25] The precious metal black–metal oxides(M), that is, Pt black–V_2O_5(M), Pd black–V_2O_5(M), Rh black–V_2O_5(M), Pt black–MoO_3(M), Pt black–WO_3(M), and Pt black–Cr_2O_3(M), were prepared by mixing powders of the precious metal black and the metal oxide in a mortar for 20 min without water.

Characterizations of the catalysts were made by means of X-ray diffraction on a GFD-35, by scanning-electron microscope on JSM-T 20, by ESR on JES ME 1X, by IR on JASCO EDR-31,[26] and by UV on UVIDEC-505. The number of surface Pt atoms on the Pt/Al_2O_3 catalyst was determined using a conventional hydrogen adsorption apparatus.

Reagents. Commercial CO (99.9% purity) and O_2 (99.9% purity) were used without further purification. The helium used as a carrier gas was purified with a titanium metal sponge heated at 1073 K and a Molecular Sieve column at room temperature.

Apparatus and Procedure. Experiments were conducted using the rectangular pulse-reaction apparatus shown in Fig. 1. Reactants of given compositions were prepared and stor-

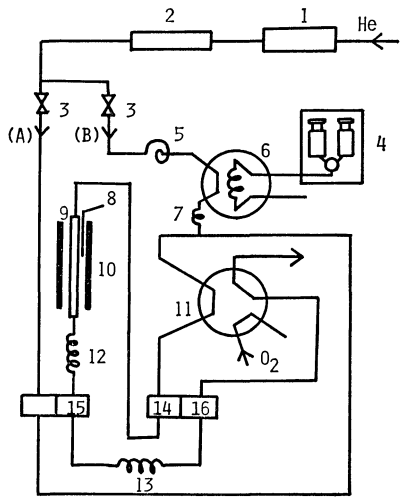

Fig. 1. A rectangular pulse reaction apparatus.
1: Titanium metal sponge deoxygenizer, 2: Molecular Sieve, 3: pressure regulator; 4: 200 ml syringes, 5: cupper tube, 6: 6-way valve for sampling, 7: stainless steel capillary, 8: thermocouple, 9: reactor, 10: electric furnace, 11: 6-way valve for O_2 treatment, 12: Porapak Q column, 13: Molecular Sieve type 13X column, 14: TCD for detecting an inlet shape of a mixture of CO and O_2, 15: TCD for detecting the shape of outlet CO_2, 16: TCD for measuring the amount of the outlet CO or O_2, (A), main stream of the carrier gas; (B), stream of the pusher gas.

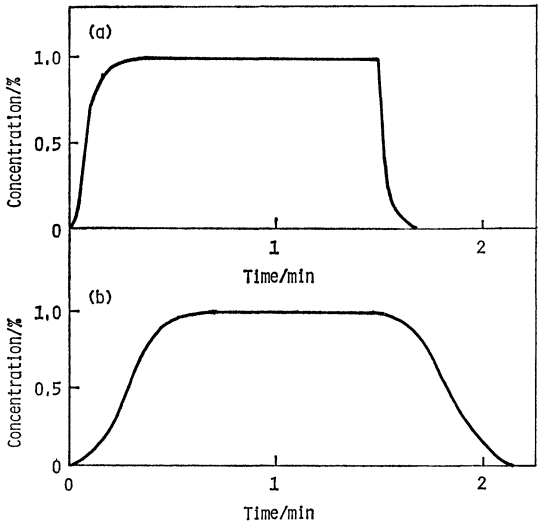

Fig. 2. Shapes of the inlet reactants and outlet CO_2.
(a): Concentration profile for the inlet mixture of CO and O_2 detected by TCD (14) (inlet concentration of the mixture=1.0%), (b): concentration profile for the CO_2 detected by TCD (15) when CO_2 is introduced (inlet concentration of CO_2=1.0%). Carrier gas flow rate=31 cm³/min. Pulse width=90 s (total amount of a single pulse=5 cm³-STP).

ed in two syringes (4), and the sampling loop of a 6-way valve (6) was filled by means of them. The 6-way valve was turned so that the reactant gas in the sampling loop could be pushed out through a stainless steel capillary (7) to the main stream of the carrier gas (Stream A) and then carried to the reactor (9). Before all of the reactant gas in the sampling loop had been pushed out from the sampling loop, the 6-way valve (6) was returned. In such a way, the rectangular pulse could be obtained. The concentration was varied by changing the composition of the sample gas and the flow rates of the carrier gas and pusher gas. The pulse width was varied by changing the time interval between turning and returning the 6-way valve (6). The shape of the input pulse was recorded by means of a thermal conductivity detector, TCD, (14). The shape of the CO_2 produced by the oxidation of CO was observed by means of TCD (15). The carrier-gas flow rate and the length of the Porapak Q column (12) were regulated so that the shape of the CO_2 detected by means of TCD (15) gave the best rectangular pulse. The conversions of the unreacted CO and O_2 were also measured by using TCD (16). Unless otherwise specified, experiments were carried out under the following conditions. The carrier gas flow rate was 31 cm³-STP/min, and the length of the Porapak Q column was 2 m. The pulse width was 1.5 min, and the total amount of a single pulse was 5 cm³-STP. The concentrations of CO were 0.26—10.3%. The reaction temperatures were 341—773 K.

Results

Shapes of the Inlet Reactants and Outlet CO_2. Figure 2(a) shows an example of the Shape of the inlet mixture of CO and O_2. It was almost rectangular except for a small tailing at the front and tail of the pulse. This indicates a constant concentration of individual reactants in a pulse, a behavior significantly different from that of a conventional pulse technique. Figure 2(b) shows the shape of the CO_2 pulse detected by TCD (15) when CO_2 was pulsed instead of a mixture of CO and O_2. The concentration of CO_2 detected was independent of the time except for that at the front and tail of the pulse. This means that the shape of CO_2 is not deformed by the Porapak Q column [(12) in Fig. 1] except for the front and tail of the pulse. This also means that the rate of CO_2 formation, R_{CO_2}, can be measured from the shape of the outlet CO_2; for example, a constant concentration of CO_2 indicates a constant R_{CO_2}, because the flow rate of the carrier gas was constant. It was found that the dispersion at the front and tail of the outlet CO_2 is mainly caused when the CO_2 pulse passes through the Porapak Q column.

The CO–O_2 Reaction on the Pt/Al_2O_3 and Pt–V_2O_5/Al_2O_3 Catalysts. Figures 3 and 4 show the results of the CO–O_2 reaction on the Pt/Al_2O_3 and Pt–V_2O_5/Al_2O_3 catalysts at various inlet CO/O_2 ratios. The unsupported V_2O_5 or V_2O_5/Al_2O_3 was inactive for the CO–O_2 reaction under the experimental conditions used in this study. As is shown in Fig. 3, the conversion of CO (X_{CO}) for the Pt–V_2O_5/Al_2O_3 catalyst was larger than that of X_{CO} for the Pt/Al_2O_3 catalyst under any conditions shown in this figure. Although the X_{CO} for the Pt/Al_2O_3 catalyst decreased abruptly in the "rich" region (*i.e.*, CO/O_2>2) with an increase in the CO/O_2 ratio, the X_{CO} for the Pt–V_2O_5/Al_2O_3 catalyst did not decrease markedly with an increase in the CO/O_2 ratio. Even in the absence of gaseous O_2 (CO/O_2=∞), the X_{CO} for the Pt–V_2O_5/Al_2O_3 catalyst was quite high, indicating a significant contribu-

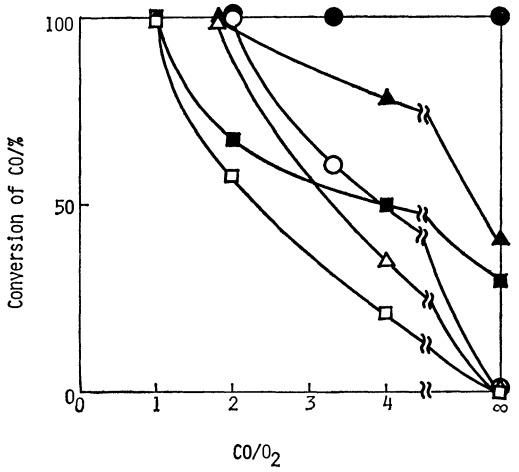

Fig. 3. Effect of the CO/O_2 ratio on the conversion of CO (X_{CO}) in the CO–O_2 reaction on the Pt/Al_2O_3 and $Pt–V_2O_5/Al_2O_3$ catalysts at various temperatures. ○,●: 558 K, △,▲: 448 K, □,■: 423 K (open symbols, Pt/Al_2O_3; closed symbols, $Pt–V_2O_5/Al_2O_3$). Catalyst weight; Pt/Al_2O_3=200 mg, $Pt–V_2O_5/Al_2O_3$=218 mg (Pt weight in catalysts=1 mg). Concentration of CO=1.0%.

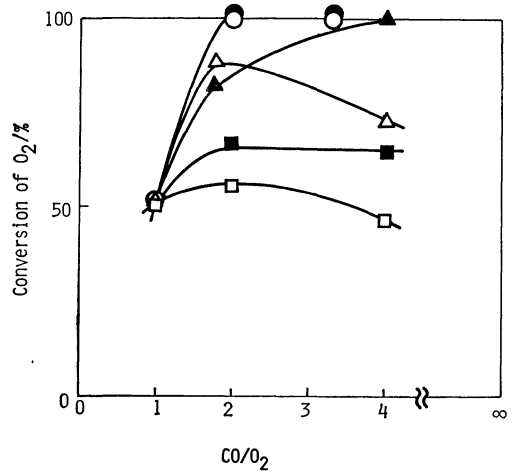

Fig. 4. Effect of the CO/O_2 ratio on the conversion of O_2 (X_{O_2}) in the CO–O_2 reaction on the Pt/Al_2O_3 and $Pt–V_2O_5/Al_2O_3$ catalysts at various temperatures. ○,●: 558 K, △,▲: 448 K, □,■: 423 K (open symbols, Pt/Al_2O_3; closed symbols, $Pt–V_2O_5/Al_2O_3$). Catalyst weight; Pt/Al_2O_3=200 mg, $Pt–V_2O_5/Al_2O_3$=218 mg (Pt weight in catalysts=1 mg). Concentration of CO=1.0%.

tion of the oxygen of V_2O_5 to the oxidation of CO. For the reaction on this catalyst at temperatures above 558 K, CO was completely oxidized (*i.e.*, X_{CO}=100%), irrespective of the inlet CO/O_2 ratio. These data clearly indicate that the added V_2O_5 plays an important role in the oxidation of CO on the $Pt–V_2O_5/Al_2O_3$ catalyst. As is shown in Fig. 4, the conversion of O_2 (X_{O_2}) in the "rich" region for the $Pt–V_2O_5/Al_2O_3$ catalyst was higher than X_{O_2} for the Pt/Al_2O_3 catalyst. This indicates that the oxidation of CO with a gaseous O_2 on Pt/Al_2O_3 is also promoted by the addition of V_2O_5 to Pt/Al_2O_3.

Concentration Profiles of the CO_2 Produced by the Oxidation of CO on the Pt/Al_2O_3 and $Pt–V_2O_5/Al_2O_3$ Catalysts. Figure 5 shows the concentration profiles of the CO_2 produced by the oxidation of CO under various conditions. Since the flow rate of the carrier gas was constant, the measured concentration of CO_2 at a given time is proportional to R_{CO_2} at this same time. As is shown in Fig. 5(a), the R_{CO_2} on Pt/Al_2O_3 at the stoichiometric point (*i.e.* CO/O_2=2) decreased markedly with the time after its maximum. On the other hand, the R_{CO_2} on the $Pt–V_2O_5/Al_2O_3$ catalyst decreased only slightly with the time; in fact, it was almost independent of the time. As for the reaction in the "rich" region (*i.e.*, CO/O_2=4)[Fig. 5(b)], the R_{CO_2} on the Pt/Al_2O_3 catalyst was significantly slower than the R_{CO_2} on the $Pt–V_2O_5/Al_2O_3$ catalyst. It is also noted that the R_{CO_2} for the $Pt–V_2O_5/Al_2O_3$ catalyst decreases slightly with an increase in the time. As for the reaction in the absence of gaseous O_2(*i.e.*, $CO/O_2=\infty$)[Fig. 5(c)], the R_{CO_2} on the $Pt–V_2O_5/Al_2O_3$ catalyst decreased markedly with the time; on the other hand, no CO_2 was produced on the Pt/Al_2O_3 catalyst, irrespective of the time. It can also be noted in Fig. 5(c) that the R_{CO_2} for the reaction on $Pt–V_2O_5/Al_2O_3$ in the absence of O_2 is independent of the concentration of CO.[27] This can also be seen in the relationship between the yield of CO_2(Y_{CO_2}) and the concentration of CO(C_{CO}; 1%=2.24 μmol/cm³ under the experimental conditions in this study) shown in Fig. 6; Y_{CO_2} was independent of C_{CO} at both 341 and 423 K.[27]

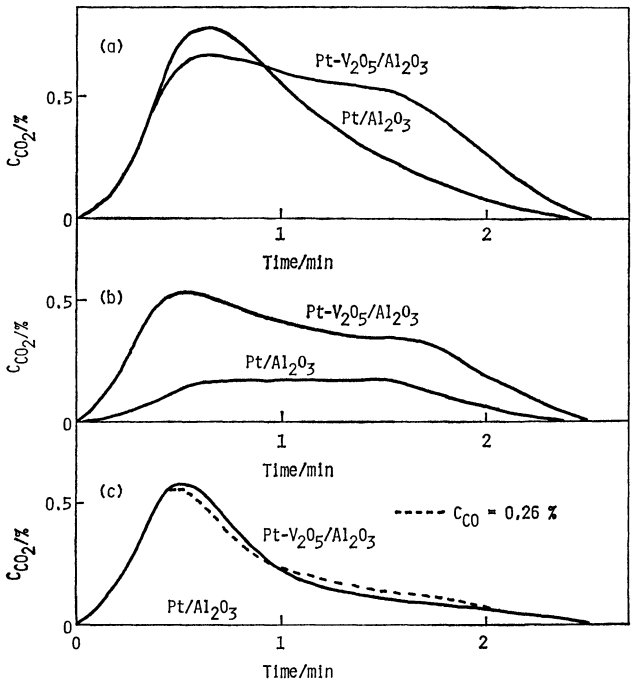

Fig. 5. Shapes of the outlet CO_2 in the CO–O_2 reaction on the Pt/Al_2O_3 and $Pt–V_2O_5/Al_2O_3$ catalysts at 423 K.
(a): CO/O_2=2.0, (b): CO/O_2=4.0, (c): $CO/O_2=\infty$ (concentration of CO=1.0%). Catalyst weight; Pt/Al_2O_3=200 mg, $Pt–V_2O_5/Al_2O_3$=218 mg (Pt weight in catalysts=1 mg).

Kinetics of the Oxidation of CO with the Oxygen of Metal

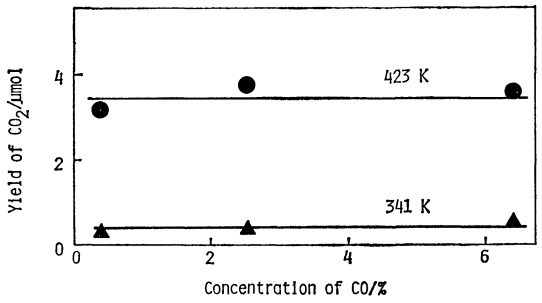

Fig. 6. Effect of the concentration of CO on the reaction of CO with the Pt–V_2O_5/Al_2O_3 catalyst at various temperatures.
●: 423 K, ▲: 341 K. Catalyst weight=218 mg.

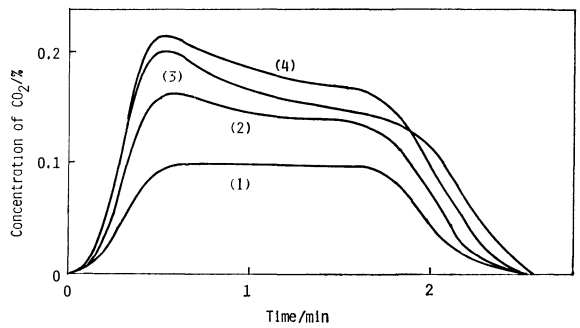

Fig. 7. Shapes of the outlet CO_2 in the reaction of CO with the 5 wt% Pt black–V_2O_5(M) catalyst at 504 K.
(1): Concentration of CO=1.0%, (2): concentration of CO=2.0%, (3): concentration of CO=5.0%, (4): concentration of CO=6.5%. Catalyst weight=40 mg.

Oxides. Since the unsupported V_2O_5 or V_2O_5/Al_2O_3 was inactive for the reaction with CO, the formation of CO_2 observed for the Pt–V_2O_5/Al_2O_3 [Fig. 5(c)] is due to the oxidation of CO with the oxygen of V_2O_5 promoted by Pt. However, as is shown in Fig. 5(c), the R_{CO_2} for the Pt–V_2O_5/Al_2O_3 catalyst changes greatly with the time, which makes it difficult to investigate the mechanism of the synergistic effect between Pt and V_2O_5. This is the reason why various mixtures of precious metal and metal oxide were used in this study as catalysts for investigating the mechanism of the reaction of CO with the oxygen of metal oxides promoted by precious metals.[28] The Pt/Al_2O_3–V_2O_5(M) or Pt black–V_2O_5 (P) did not oxidize CO to CO_2 under the present experimental conditions. Pt black–V_2O_5(M) was active for the oxidation of CO, and, as is shown in Fig. 7, R_{CO_2} did not change significantly with the time. Similarly, the R_{CO_2} on Pd black–V_2O_5(M), Rh black–V_2O_5(M), and Pt black–MoO_3(M) was almost independent of the time. The Pt black–WO_3(M) or Pt black–Cr_2O_3(M) was inactive for the reaction. Therefore, the Pt black–V_2O_5(M), Pd black–V_2O_5(M), Rh black–V_2O_5(M), and Pt black–MoO_3(M) are considered to be catalysts which can be used for detailed investigations of the mechanism of the synergistic effect between a precious metal and a metal oxide on the oxidation of CO with the oxygen of the metal oxide.

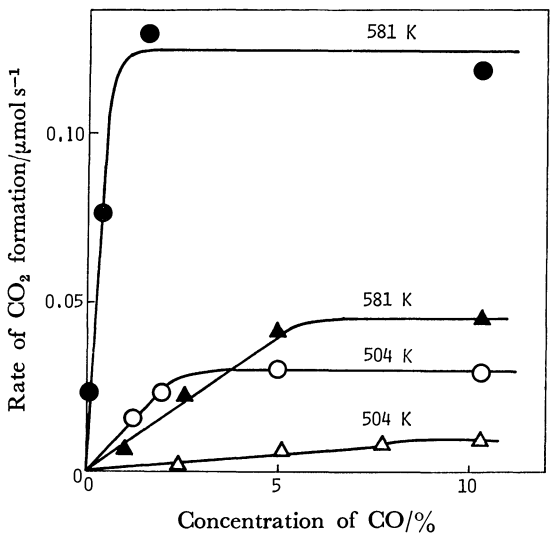

Fig. 8. Effect of the concentration of CO on the reaction of CO with 1 and 5 wt% Pt black–V_2O_5(M) catalysts at various temperatures.
●,▲: 581 K, ○,△: 504 K [circle symbols, 5 wt% Pt black–V_2O_5(M); triangle symbols, 1 wt% Pt black–V_2O_5(M)]. Catalyst weight=40 mg.

Figure 8 shows some of the findings regarding R_{CO_2} for the reaction of CO with Pt black–V_2O_5(M) at various C_{CO} values. Here, R_{CO_2} is calculated from the average value of R_{CO_2} at the plateau of the concentration profile shown in Fig. 7. As is shown in Fig. 8, R_{CO_2} was of the first order with respect to C_{CO} when C_{CO} was low(this region will hereafter be referred to as R1). When C_{CO} was high, R_{CO_2} was of the zeroth order with respect to C_{CO}(this region will hereafter be referred as R0). The boundary between R1 and R0 for 1 wt% Pt black–V_2O_5(M) was located at C_{CO}, higher than that for 5 wt% Pt black–V_2O_5(M). It may also be noted in Fig. 8 that the boundary between R1 and R0 moves to a lower C_{CO} with an increase in the reaction temperature. From the observed R_{CO_2} values at various C_{CO} levels, the first-order and zeroth-order rate constants were determined. These rate constants, measured at various temperatures, satisfied the Arrhenius equations, and the activation energies(E_1 and E_0) and pre-exponential factors(A_1 and A_0) were determined to be as is shown in Table 1. Here, A_1 and A_0 are normalized to have a unit weight of the precious metal. The Arrhenius parameters were also determined for the Pd black–V_2O_5(M), Rh black–V_2O_5(M), and Pt black–MoO_3(M) catalysts; these are also shown in Table 1. The E_1 for 1 wt%Pt black–V_2O_5(M) was almost the same as the E_1 for 5 wt% Pt black–V_2O_5(M); on the other hand, both values are larger than the E_1 for Pd black–V_2O_5(M) or Rh black–V_2O_5(M). The E_0 for 1 and 5 wt% Pt black–V_2O_5(M), Pd black–V_2O_5(M), and Rh black–V_2O_5(M) was almost constant and independent of the kind of catalyst. However, the E_0 for Pt black–MoO_3(M) was larger than the E_0 for the former catalysts. The A_1 or A_0 did not change markedly with the kind of catalyst; that is, the A_1 and A_0 changed at the maximum by factors of only

Table 1. The activation energies and pre-exponential factors in the reaction of CO with the cataly

Catalyst	R1		R0	
	E_1 / kcal mol^{-1}	A_1 / cm^3 s^{-1} g-metal^{-1}	E_0 / kcal mol^{-1}	A_0 / mol s^{-1} g-metal^{-1}
1 wt% Pt black-V_2O_5(M)	17.3	1.4×10^8	11.5	2.6
5 wt% Pt black-V_2O_5(M)	16.4	1.7×10^8	11.8	2.2
1 wt% Pd black-V_2O_5(M)	13.6	0.2×10^8	12.2	12
1 wt% Rh black-V_2O_5(M)	13.7	0.6×10^8	12.6	7.1
1 wt% Pt black-MoO_3(M)	—a)	—a)	15.0	4.9
Pt-V_2O_5/Al_2O_3	—a)	—a)	10.3b)	40b)
			(10.4)c)	(116)c)

a) The R1 region did not appear under the experimental conditions used in this study. b) Values calculated from the average R_{CO_2}. c) Values calculated from the maximum R_{CO_2}.

7 and 5 respectively. The A_0 and E_0 for Pt-V_2O_5/Al_2O_3 were similarly determined, though these values are considered not to be correct for the reasons presented above. The E_0 for Pt-V_2O_5/Al_2O_3 was slightly lower than the E_0 for Pt black-V_2O_5(M), while the A_0 for Pt-V_2O_5/Al_2O_3 was about 20 times larger than the A_0 for Pt black-V_2O_5(M).

Characterizations of the Pt-V_2O_5/Al_2O_3 and Pt Black-V_2O_5(M) Catalysts. The number of surface Pt atoms on the Pt/Al_2O_3 catalyst was determined, by using the H_2 adsorption technique, to be 5.0 μmol/g-cat, which leads to an average Pt diameter of 30 Å. The X-ray diffraction pattern of Pt black-V_2O_5(M) indicated that it is a mixture of Pt metal and V_2O_5 crystallines; therefore, no other compound was detected. On the basis of the SEM measurements of Pt black-V_2O_5(M), the average diameters of Pt and V_2O_5 in the catalyst were determined to be 5000 and 2000 Å respectively. ESR, IR, and UV measurements of Pt-V_2O_5/Al_2O_3 and Pt black-V_2O_5(M) indicated that the vanadium oxides in these catalysts are mainly in the highest oxidation state, *i.e.*, V^{5+}. The structure of V_2O_5 in V_2O_5/Al_2O_3 catalysts with various contents of V_2O_5 has been determined by using the NO-NH_3 rectangular pulse technique, coupled with the IR, ESR, and UV techniques.[29]

Discussion

Removal of CO in the "Rich" Region Using the Pt-V_2O_5/Al_2O_3 Catalyst. As is shown in Fig. 3, CO is almost completely removed in the "lean" region of the reactants (*i.e.*, $CO/O_2<2$) by using the Pt/Al_2O_3 catalyst. However, the X_{CO} in the CO-O_2 reaction in the "rich" region (*i.e.*, $CO/O_2>2$) decreases markedly with an increase in the CO/O_2 ratio. This means that a considerable amount of unreacted CO is exhausted in the "rich" region. This behavior in the CO-O_2 reaction on the Pt/Al_2O_3 catalyst is similar to that in the reactions of synthetic exhaust gas in three-way catalysts without metal oxides.[22,23] The X_{CO} in the reaction on the Pt-V_2O_5/Al_2O_3 catalyst is high even in the "rich" region. As for the reaction at temperatures above 558 K, X_{CO} is 100% at any CO/O_2 ratio, indicating a complete removal of CO. This behavior in the CO-O_2 reaction on the Pt-V_2O_5/Al_2O_3 catalyst is similar to that in the reactions of synthetic exhaust gas on three-way catalysts containing metal oxides.[7,8]

The Amounts of Gaseous O_2 and Oxygen of V_2O_5 Consumed for the Oxidation of CO on the Pt-V_2O_5/Al_2O_3 Catalyst. In addition to a gaseous O_2, the oxygen of V_2O_5 participates in the oxidation of CO on the Pt-V_2O_5/Al_2O_3 catalyst (Fig. 3). Also, as is shown in Fig. 4, the oxidation of CO with a gaseous O_2 on the Pt/Al_2O_3 catalyst is promoted by the addition of V_2O_5 to the catalyst. It is, therefore, necessary to calculate the amounts of gaseous O_2 [Q_G(Pt) and Q_G(Pt-V)] and the oxygen of V_2O_5 [Q_V(pt) and Q_V(Pt-V)] consumed for the oxidation of CO on the Pt/Al_2O_3 and Pt-V_2O_5/Al_2O_3 catalysts before discussing in detail the mechanism of the action of the added V_2O_5. In the pulse experiment, material balances with respect to the oxygen atoms lead to the following equations:

$$Q_G(\text{Pt}) = 2Q^\circ_{O_2}\cdot X_{O_2}(\text{Pt}), \quad (1)$$

$$Q_V(\text{Pt}) = Q_{CO_2}(\text{Pt}) - Q_G(\text{Pt}), \quad (2)$$

$$Q_G(\text{Pt-V}) = 2Q^\circ_{O_2}\cdot X_{O_2}(\text{Pt-V}), \quad (3)$$

$$Q_V(\text{Pt-V}) = Q_{CO_2}(\text{Pt-V}) - Q_G(\text{Pt-V}), \quad (4)$$

where Q_G is the number of oxygen atoms in O_2 consumed for the oxidation of CO; Q_V is the number of the oxygen of V_2O_5 consumed for the oxidation of CO; $Q^\circ_{O_2}$ is the number of gaseous O_2 injected as a reactant of the pulse experiment; X_{O_2} is the conversion of O_2; Q_{CO_2} is the number of CO_2 molecules produced; and (Pt) and (Pt-V) refer to the Pt/Al_2O_3 and Pt-V_2O_5/Al_2O_3 catalysts respectively. On the basis of the experimental results for the Pt/Al_2O_3 catalyst shown in Figs. 3 and 4, Eq. 2′ is obtained for Q_V(Pt):

$$Q_V(\text{Pt}) = 0. \quad (2')$$

This relationship is reasonable, since the Pt/Al_2O_3 catalyst does not contain V_2O_5. From Eqs. 1 and 3, the increase in Q_G caused by the addition of V_2O_5 to Pt/Al_2O_3(ΔQ_G) is given by Eq. 5:

$$\Delta Q_G = Q_G(\text{Pt-V}) - Q_G(\text{Pt}). \quad (5)$$

Similarly, from Eqs. 2′ and 4 the increase in $Q_V(\Delta Q_V)$

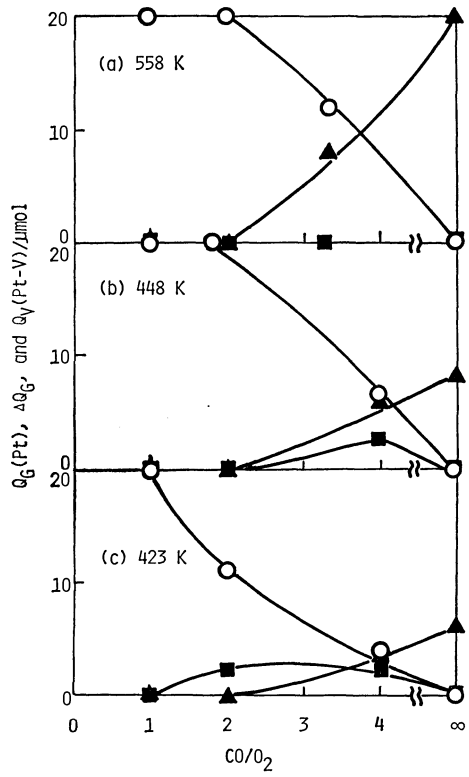

Fig. 9. Relationship between the CO/O_2 ratio and $Q_G(Pt)$, ΔQ_G, and $Q_V(Pt\text{-}V)$ in the $CO\text{-}O_2$ reaction on the $Pt\text{-}V_2O_5/Al_2O_3$ catalyst.
○: $Q_G(Pt)$, ■: ΔQ_G, ▲: $Q_V(Pt\text{-}V)$. Concentration of CO=1.0%. Catalyst weight=218 mg.

is given by Eq. 6:

$$\Delta Q_V = Q_V(Pt\text{-}V). \quad (6)$$

Figure 9 shows the results for $Q_G(Pt)$, ΔQ_G, and $Q_V(Pt\text{-}V)$, which were calculated from the experimental results shown in Figs. 3 and 4. As is shown in Fig. 9, $Q_G(Pt)$ mainly contributes to the $CO\text{-}O_2$ reaction on the $Pt\text{-}V_2O_5/Al_2O_3$ catalyst in the "lean" region ($CO/O_2<2$), and the synergistic effect between Pt and V_2O_5, *i.e.*, ΔQ_G or $Q_V(Pt\text{-}V)$, is not important. As the CO/O_2 ratio increases in the "rich" region ($CO/O_2>2$), $Q_G(Pt)$ decreases, but $Q_V(Pt\text{-}V)$ and ΔQ_G become significant. In particular, $Q_V(Pt\text{-}V)$ mainly contributes to the reaction in the "rich" region. It should also be noted that ΔQ_G plays an important role in the reaction in the "rich" region at temperatures as low as 423 K.

Structures of $Pt\text{-}V_2O_5/Al_2O_3$ and Pt Black-V_2O_5(M). On the basis of the above-mentioned characterizations of $Pt\text{-}V_2O_5/Al_2O_3$ and Pt black-V_2O_5(M), the structures of these catalysts shown in Fig. 10 can be proposed. The average diameter of Pt particles on $Pt\text{-}V_2O_5/Al_2O_3$ is about 30 Å, which has been determined by the H_2 adsorption measurement. In the V_2O_5/Al_2O_3 catalyst(V_2O_5 loading is 9 wt%), 1—2 layers of V_2O_5 lamellae cover a small percentage of the Al_2O_3 surface.[29] Since the content of Pt is very low (0.5 wt%), the V_2O_5 in the $Pt\text{-}V_2O_5/Al_2O_3$ catalyst is considered to be almost the same as the V_2O_5 in the V_2O_5/Al_2O_3 catalyst. The coverage of V_2O_5 and the particle size of Pt thus determined lead to

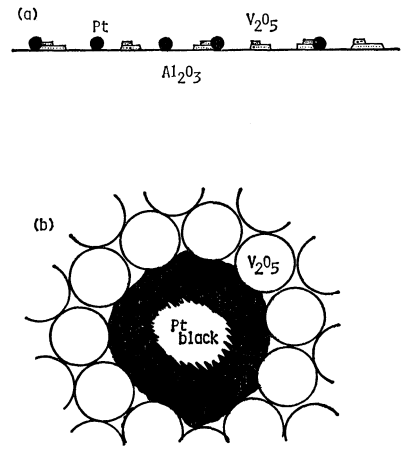

Fig. 10. Structures of $Pt\text{-}V_2O_5$ mixed catalysts.
(a): $Pt\text{-}V_2O_5/Al_2O_3$; the average diameter of Pt particles is about 30 Å, 1—2 layers of V_2O_5 lamella cover a few percentage of the Al_2O_3 surface, (b): Pt black-V_2O_5(M); a Pt black particle (about 5000 Å in diameter) is surrounded by many V_2O_5 particles [about 2000 Å in diameter (about 500 layers of V_2O_5 lamella)].

the structure of V_2O_5 and Pt on Al_2O_3, indicating that Pt particles are partly in contact with V_2O_5 and are partly separated from V_2O_5. The vanadium oxides in the $Pt\text{-}V_2O_5/Al_2O_3$ catalyst are mainly in the highest oxidation state, *i.e.*, V^{5+}, judging from the ESR and UV measurements of $Pt\text{-}V_2O_5/Al_2O_3$. On the basis of the SEM and XRD investigations of Pt black-V_2O_5(M), the structure shown in Fig. 10(b) can be proposed; Pt black-V_2O_5(M) is a mixture of Pt black(about 5000 Å in diameter) and V_2O_5 particles(about 2000 Å in diameter). The V_2O_5 in Pt black-V_2O_5(M) is composed of about 500 layers of V_2O_5 lamellae.

Mechanism of the Oxidation of CO with the Oxygen of V_2O_5 in Pt Black-V_2O_5(M). From the experimental results shown in Table 1 and in Figs. 7 and 8, the mechanism of the oxidation of CO with the oxygen of V_2O_5 in Pt black-V_2O_5(M) shown in Fig. 11(a) can be proposed. According to this mechanism, the oxygen of V_2O_5 at the $Pt\text{-}V_2O_5$ interface is activated by contact with Pt; this is a new type of active site and will hereafter be denoted by [Pt···O···V]. Also, the oxidation of CO with the oxygen of Pt black-V_2O_5(M) proceeds according to the following two steps. Step I is the reaction of a gaseous CO with the active oxygen at the $Pt\text{-}V_2O_5$ interface, [Pt···O···V], to form CO_2 and a reduced site, [Pt V]. Step II is the oxidation of the reduced site, [Pt V], with the bulk oxygen in V_2O_5 to reproduce [Pt···O···V]. The validity of this mechanism can be proved as follows.

Kinetics: Since Step I is the reaction of a gaseous CO with the activated surface oxygen, its rate will increase with the increase in the concentration of CO. Since a gaseous CO does not participate in Step II, on the other hand, the rate of Step II will be independent of C_{CO}. Therefore, the rate of Step I relative to Step II would decrease with a decrease in C_{CO}. In other words, Step I becomes the rate-

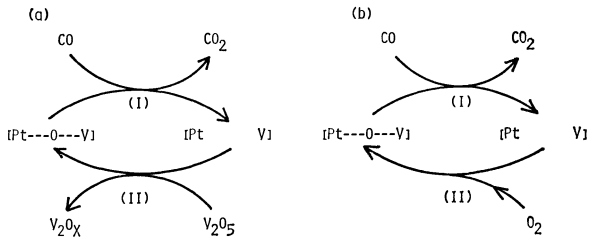

Fig. 11. Mechanism of the CO–O_2 reaction on Pt–V_2O_5 mixed catalysts.
(a): Mechanism of the oxidation of CO with the oxygen of V_2O_5 in the Pt black–V_2O_5(M) catalyst, (b): mechanism of the oxidation of CO with a gaseous O_2 caused by the synergistic effect between Pt and V_2O_5 [ΔQ_G].

determining step when C_{CO} is low. On the other hand, when C_{CO} is high, Step II becomes the rate-determining step. This is in accordance with the observed kinetics shown in Fig. 8, because the rate is of the first order with respect to C_{CO} when C_{CO} is low, while it is of the zeroth order when C_{CO} is high.

Activation Energies: Judging from the above-mentioned discussion on the kinetics of the reaction, E_1 and E_0 can be regarded as the activation energies of Steps I and II respectively. Since a precious metal plays an important role in Step I of the mechanism shown in Fig. 11(a), E_1 should vary depending on the kind of precious metal used. Step II is the migration of the bulk oxygen atom of a metal oxide to its surface, followed by the interaction of the surface oxygen atom with Pt. Since the adsorption of an atomic oxygen on the Pt surface is considered to be a non-activated process, the migration of the bulk oxygen to the surface may limit the rate of Step II. This leads to the value of E_0, which should be independent of the kind of precious metal, but which should change with the kind of metal oxide. This inference is in accordance with the experimental results shown in Table 1.

Boundary between R1 and R0: According to the mechanism shown in Fig. 11(a), the boundary between R1 and R0 is determined by the rate of Step I relative to Step II. Judging from the structure of Pt black–V_2O_5(M), the number of [Pt···O···V] sites can be expected to increase in proportion to the content of the Pt black. This leads to the increase in the rate of Step I in proportion to the content of the Pt black in the catalyst. Since the quantity of oxygen atoms consumed for the reaction in the R0 region was much larger than the amount of the surface oxygen atoms of V_2O_5,[29] the rate in the R0 region may refer to the rate of the diffusion of oxygen in the bulk of V_2O_5 particles, but not to the rate of the diffusion of the subsurface oxygen atoms to the reduced active site, [Pt V]. This means that the rate of Step II is less sensitive to the increase in the content of Pt black than the rate of Step I, suggesting that the rate of Step I relative to Step II increases with an increase in the content of the Pt black in the catalyst. The boundary between R1 and R0 for 5 wt% Pt black–V_2O_5(M) is thus considered to be located at a C_{CO} point lower than the C_{CO} for 1 wt% Pt black–V_2O_5(M). This is in accordance with the experimental results shown in Fig. 8.

The above discussion indicates that all of the experimental data shown in Table 1 and Figs. 7 and 8 can reasonably be understood in terms of the mechanism shown in Fig. 11(a). In order to establish the validity of the mechanism, however, a discussion of possible alternative mechanisms is indispensable.

AM-1: CO is activated on the Pt surface, migrates onto V_2O_5, and reacts with the oxygen of V_2O_5 to form CO_2.[30]

CO is not dissociatively, but molecularly, adsorbed on the Pt surface[31–34] under the present experimental conditions. V_2O_5 is not active for the reaction with a molecular CO; CO is scarcely oxidized by the oxygen of V_2O_5, even at a temperature as high as 773 K. These data indicate that AM-1 does not play an important role in the oxidation of CO with Pt black–V_2O_5(M).

AM-2: The oxygen of V_2O_5 migrates onto the surface of Pt and reacts with CO to form CO_2.

The reaction of CO with an adsorbed oxygen atom on Pt proceeds so rapidly that the activation energy for this process is low.[9,11,35] and every 10 collisions of CO molecules with the oxygen atom adsorbed on Pt lead to the formation of one CO_2 molecule, even at room temperature.[31] This is not consistent with the observed activation energy shown in Table 1.

AM-3: The CO adsorbed on the Pt surface reacts with the oxygen of V_2O_5 at the Pt–V_2O_5 interface; therefore, the R_{CO_2}–C_{CO} curves are determined by the coverage of CO on the Pt surface.

The amount of CO adsorbed on Pt decreases with an increase in the temperature.[31–33] If the boundary between R1 and R0 is determined by the coverage of the adsorbed CO, then it should move to a higher C_{CO} value as the temperature increases. However, this is not consistent with the experimental results shown in Fig. 8.

Mechanism of the Oxidation of CO on the Pt–V_2O_5/Al_2O_3 Catalyst. As has been mentioned above, the amount of CO_2 molecules produced by the CO–O_2 reaction on the Pt–V_2O_5/Al_2O_3 catalyst is determined by following three factors: Q_G(Pt), ΔQ_G, and Q_V (Pt–V). The mechanisms of the reactions responsible for the individual factors will be discussed below.[36]

The CO–O_2 Reaction on the Pt Surface[Q_G(Pt)]: The mechanism of the CO–O_2 reaction on the Pt surface has already been investigated extensively.[9–11,13,37] According to the mechanism, the CO adsorbed on Pt retards the CO–O_2 reaction at low temperatures.[9,10,38–41] In accordance with this mechanism, the observed rate of the CO–O_2 reaction on the Pt/Al_2O_3 catalyst decreases markedly with an increase in the CO/O_2 ratio at low temperatures, especially at 423 K (Fig. 3). The concentration profile of CO_2 produced by the CO–O_2 reaction on Pt/Al_2O_3 shows that the rate of CO_2 formation decreases significantly with the time [Fig. 5(a)]. This phenomenon may be interpreted in terms of the proposed mechanism of the CO–O_2 reaction on the Pt surface as follows; as the time increases, the coverage of CO on the Pt surface in-

creases, which then leads to the decrease in the rate of the reaction with an increase in the time.

The Oxidation of CO with the Oxygen of V_2O_5 Promoted by Pt [Q_V(Pt–V)]: Since the electronic state of V_2O_5 supported on Al_2O_3 is almost the same as that of the unsupported V_2O_5, the mechanism shown in Fig. 11(a) can be applied to the reaction of CO with the oxygen of V_2O_5 in the Pt–V_2O_5/Al_2O_3 catalyst. Although the kinetics for Pt–V_2O_5/Al_2O_3 is different from that for Pt black–V_2O_5(M), this difference can be explained in terms of the structures of Pt–V_2O_5/Al_2O_3 and Pt black–V_2O_5(M) as follows. As is shown in Fig. 10, both Pt and V_2O_5 for Pt–V_2O_5/Al_2O_3 are much better dispersed than those for Pt black–V_2O_5-(M). The number of the active sites, [Pt···O···V], for Pt–V_2O_5/Al_2O_3 is thus considered to be greater than that for Pt black–V_2O_5(M). This in turn leads to a rate of Step I for Pt–V_2O_5/Al_2O_3 which is faster than that for Pt black–V_2O_5(M). On the other hand, the amount of V_2O_5, which can supply oxygen atoms to the active site, is limited for Pt–V_2O_5/Al_2O_3, because the V_2O_5 on Al_2O_3 is highly dispersed. This is the reason the rate of CO_2 formation decreases markedly with the time for Pt–V_2O_5/Al_2O_3 [Fig. 5(c)] and why the R1 region does not appear in the R_{CO_2}–C_{CO} curves for Pt–V_2O_5/Al_2O_3 (Fig. 6). The A_0 for Pt–V_2O_5/Al_2O_3 is larger than the A_0 for Pt black–V_2O_5(M) (Table 1). This may also be due to the high dispersion of Pt and V_2O_5 on Al_2O_3 in Pt–V_2O_5/Al_2O_3. The E_0 for Pt–V_2O_5/Al_2O_3 is a little lower than the E_0 for Pt black–V_2O_5(M); this difference may be ascribable to the lack of a supply of the bulk oxygen in V_2O_5 at high temperatures for Pt–V_2O_5/Al_2O_3. Although the results for Pt–V_2O_5/Al_2O_3 can well be understood on the basis of the mechanism shown in Fig. 11(a), a discussion of a following alternative mechanism is indispensable:

AM-4: The oxygen of V_2O_5 migrates to the Pt surface through Al_2O_3 and reacts with CO on Pt.

As for Pt/Al_2O_3–V_2O_5(M), Pt is considered to be separated from V_2O_5 by Al_2O_3, and CO is not oxidized with the oxygen of this catalyst. Therefore, AM-4 is not important in the reaction on Pt–V_2O_5/Al_2O_3.

The Oxidation of CO with a Gaseous O_2 Caused by the Synergistic Effect between Pt and V_2O_5[ΔQ_G]: According to the mechanism of the reaction of CO with the oxygen of V_2O_5 in the Pt black–V_2O_5(M) and Pt–V_2O_5/Al_2O_3 catalysts shown in Fig. 11(a), [Pt V] is formed by the reaction of CO with the [Pt···O···V] site. If a gaseous O_2 is present in the system, [Pt V] can be expected to be oxidized by the gaseous O_2 to reproduce the [Pt···O···V] site, which may in turn increase the rate of the oxidation of CO with a gaseous O_2 on Pt–V_2O_5/Al_2O_3 more than that on Pt/Al_2O_3. This means that ΔQ_G can be explained in terms of the mechanism of the CO–O_2 reaction shown in Fig. 11(b). This mechanism is similar to the mechanism of the oxidation of CO with the oxygen of V_2O_5 shown in Fig. 11(a), but the reduced site, [Pt V], is reoxidized to [Pt···O···V] by a gaseous O_2, not by the bulk oxygen in V_2O_5. As is evident from the mechanism shown in Fig. 11(b), the reaction of CO with [Pt···O···V] is not retarded by the adsorbed CO, behavior which is different from the behavior in the CO–O_2 reaction on the Pt surface. This explains why ΔQ_G mainly contributes to the reaction in the "rich" region at low temperatures (Fig. 9). In the practical three-way catalyst system, the fluctuation in the air/fuel ratio takes place rapidly with a frequency of 1—10 Hz;[42,43] therefore a part of the CO adsorbed on Pt on the "rich" side may still remain on Pt even on the "lean" side. This suggests that the CO–O_2 reaction on Pt, [Q_G(Pt)], is retarded by the CO remaining on Pt under practical three-way catalyst conditions. Since the reaction of CO at the [Pt···O···V] site, [Q_V(Pt–V) and ΔQ_G], is not retarded by CO remaining on Pt, it may play an important role under certain conditions.

Synergistic Effect between Pt and V_2O_5 in the CO–O_2 Reaction as Compared with That in the NO–H_2 Reaction. The conversion of CO in the CO–O_2 reaction on the Pt/Al_2O_3 catalyst in the "rich" region has been markedly enhanced by the addition of V_2O_5 to Pt/Al_2O_3. This effect of V_2O_5 has been found to be brought about by the formation of a new type of active site, [Pt···O···V], at the Pt–V_2O_5 interface, which plays an important role in the oxidation of CO with the oxygen of V_2O_5 and the enhanced oxidation of CO with a gaseous O_2 on Pt/Al_2O_3 caused by the addition of V_2O_5 to Pt/Al_2O_3. The mechanism of the action of V_2O_5 in the oxidation of CO is much different from that in the NO–H_2 reaction found in the previous study.[24] In the NO–H_2 reaction on the Pt–V_2O_5/Al_2O_3 catalyst, the selective reduction of NO to N_2 or N_2O in the "rich" region is brought about by the "hydrogen spillover"—the dissociation of H_2 on Pt, followed by the spillover of the dissociated hydrogen from Pt to Al_2O_3 and then to V_2O_5 and the subsequent reduction of V_2O_5 with the spilled-over hydrogen. The synergistic effect between Pt and V_2O_5 in the NO–H_2 reaction can, therefore, appear even if Pt and V_2O_5 are separated from each other by Al_2O_3; this behavior is different from that in the CO–O_2 reaction. This means that the mechanism of the action of a metal oxide added to a three-way catalyst can change greatly depending on the kind of reaction. Since the real three-way catalyst system is composed of various types of reactions, the accumulation of investigations such as the present one can lead to the scientific development of a three-way catalyst with a sufficiently broad "window". In addition, the activity of the Pt/Al_2O_3 catalyst for the oxidation of CO with the gaseous O_2 enhanced by the addition of V_2O_5 suggests the possibility that the amount the precious metals used for the three-way catalyst system can be saved by the addition of a metal oxide to a three-way catalyst.

References

1) M. Shelef, *Catal. Rev.*, **11**, 1 (1975).
2) J. Wei, *Adv. Catal.*, **24**, 57 (1975).
3) T. Ono, *Shokubai*, **19**, 142 (1977).
4) E. Echigoya, *Kagaku*, **33**, 338 (1978).
5) H. Ohara, S. Kondo, and Y. Fujitani, *Paper of Society of Automotive Engineers of Japan*, **16**, 9 (1978).

6) J. E. Hunter, *SAE Paper*, 720201 (1972).
7) H. S. Gandhi, A. G. Pikin, M. Shelef, and R. G. Delosh, *SAE Paper*, 760201 (1976).
8) J. C. Schlatter and P. J. Mitchell, *Ind. Eng. Chem., Prod. Res. Dev.*, **19**, 288 (1980).
9) H. P. Bonzel and R. Ku, *Surf. Sci.*, **33**, 91 (1972).
10) H. P. Bonzel and R. Ku, *J. Vac. Sci. Technol.*, **9**, 633 (1972).
11) T. Matsushima, D. B. Almy, and J. M. White, *Surf. Sci.*, **67**, 89 (1977).
12) C. T. Campbell and J. M. White, *J. Catal.*, **54**, 289 (1978).
13) T. Matsushima, *Surf. Sci.*, **79**, 63 (1979).
14) T. Engel and G. Ertl, *Adv. Catal.*, **28**, 1 (1979).
15) K. Kunimori and T. Uchijima, *Hyomen*, **19**, 143 (1981).
16) E. Miyazaki, *Shokubai*, **22**, 301 (1980).
17) M. Kawai, T. Onishi, and K. Tamaru, *Shokubai*, **22**, 304 (1980).
18) F. S. Stone, *Adv. Catal.*, **13**, 1 (1962).
19) S. Yoshida, Y. Miyata, H. Niiyama, and E. Echigoya, *Shokubai*, **23**, 284 (1981).
20) K. Sakata, F. Ueda, M. Misono, and Y. Yoneda, *Bull. Chem. Soc. Jpn.*, **53**, 324 (1980).
21) T. Nakamura, M. Misono, T. Uchijima, and Y. Yoneda, *Nippon Kagaku Kaishi*, **1980**, 1679.
22) K. C. Taylor, "The Catalytic Chemistry of Nitrogen Oxides," ed by R. L. Klimisch and J. G. Larson, Plenum Press, New York, N. Y. (1975), p. 173.
23) J. Wei, *Adv. Catal.*, **24**, 57 (1976).
24) Y. Kosaki, A. Miyamoto, and Y. Murakami, *Bull. Chem. Soc. Jpn.*, **55**, 1719 (1982).
25) R. Feulgen, *Ber.*, **54**, 360 (1921).
26) M. Niwa, T. Hattori, M. Takahashi, and K. Shirai, *Anal. Chem.*, **51**, 46 (1979).
27) Similar phenomena were also observed in the reaction of CO with the Pt–V_2O_5(36 wt%)/Al_2O_3 catalyst.
28) The precious metal black–metal oxide(M) catalyst was used as a model catalyst of the Pt–V_2O_5/Al_2O_3 because it was difficult to prepare a Pt/V_2O_5 (impregnation) catalyst.
29) Y. Murakami, M. Inomata, A. Miyamoto, and K. Mori, *Proc. 7th Int. Congr. Catal., Tokyo*, 1980, Kodansha (Tokyo) and Elsevier (Amsterdam-Oxford-New York) (1981), p. 1344.
30) G. C. Bond, M. J. Fuller, and L. R. Molloy, *Proc. 6th Int. Congr. Catal., London*, 1976, The Chemical Society (1977), p. 356.
31) Y. Nishiyama and H. Wise, *J. Catal.*, **32**, 50 (1974).
32) G. K. Hori and L. D. Schmidt, *J. Catal.*, **38**, 335 (1975).
33) R. G. Donnelly, M. Modell, and R. F. Baddour, *J. Catal.*, **53**, 239 (1978).
34) T. Okuhara and M. Misono, *Hyomen*, **18**, 357 (1980).
35) H. P. Bonzel and J. J. Burton, *Surf. Sci.*, **52**, 223 (1975).
36) According to our preliminary ^{18}O-tracer experiments, a considerable amount of $C^{16}O^{16}O$ was obtained by the reaction of $C^{16}O$ with $^{18}O_2$ on the Pt–V_2O_5/Al_2O_3 catalyst. This means that the reduced site, [Pt V], is considerably reoxidized by the bulk oxygen of V_2O_5 and that the V^{4+} in V_2O_5 thus produced is oxidized by $^{18}O_2$. The details of the results will be reported in a subsequent paper.
37) R. L. Palmer and J. N. Smith, Jr., *J. Chem. Phys.*, **60**, 1453 (1974).
38) A. W. Sklyarov, J. Voelter, and I. I. Tretjakov, *Z. Anorg. Allg. Chem.*, **396**, 129 (1973).
39) H. D. Cochran, R. G. Donnelly, M. Modell, and R. F. Baddour, *Colloid Interface Sci.*, **3**, 131 (1976).
40) N. W. Cant, P. C. Hicks, and B. S. Lennon, *J. Catal.*, **54**, 372 (1978).
41) A. Golchet and J. M. White, *J. Catal.*, **53**, 266 (1978).
42) P. Öser, *SAE Paper*, 790306 (1979).
43) W. M. Wang, *SAE Paper*, 800052 (1980).

 © 1982 The Chemical Society of Japan Bull. Chem. Soc. Jpn., 55, 2715—2720 (1982)

Electronic Structures of Pyridinols and of Their Anions and Cations

Hiroshi Morita,* Józef S. Kwiatkowski,† and Anna Tempczyk††

Department of Image Science and Technology, Faculty of Engineering, Chiba University, Chiba 260

† *Institute of Physics, Nicholas Copernicus University, 87-100 Toruń, Poland*

†† *Institute of Chemistry, University of Gdańsk, 80-952 Gdańsk, Poland*

(Received December 9, 1981)

Electronic structures of the lactim and lactam forms of 2-, 3-, and 4-pyridinols, and of their anions and protonated cations were calculated by a modified CNDO-CI (mCNDO-CI), CNDO/S-CI, and a modified π-SCF-MO-CI methods. The theoretical results agree well with the observed spectra of both the neutral and ionic species, and predict satisfactorily the shorter wavelength shift of lower excited π-π^* and n-π^* bands of the lactim form compared to the corresponding bands of the lactam form. The π-π^* assignment to the lowest triplet states of 2- and 4-pyridones, and of 2- and 3-pyridinols, together with the n-π^* assignment to the lowest singlet state of 4-pyridone was predicted by the mCNDO-CI method, in agreement with the suggestion based on emission properties. The orbital energies calculated by the mCNDO method were compared with the observed photoelectron spectra; the results show that the fourth highest occupied orbital is π-orbital in 2- and 3-pyridinols, and σ-orbital in 4-pyridinol and 4-pyridone.

N-heterocyclic compounds having hydroxy substituents show the lactim-lactam tautomerism. This is important in photochemical reaction and in molecular biology. The electronic structure of uracil has recently been studied theoretically in our previous paper.[1] For pyridinols which are the simplest hydroxy-substituted *N*-heterocyclic compounds, quantum mechanical studies have been devoted to the estimation of the relative stabilities of the tautomers and to the assignment of the electronic spectra using the semiempirical methods considering π-electrons[2-6] or all-valence electrons,[6-9] as well as the nonempirical SCF-LCAO-MO method.[8,10] However, as far as we are aware, the neutral and ionic forms of pyridinols have not been studied systematically by any all-valence electron (AVE) SCF-MO-CI methods. The aim of the present paper is to apply both the AVE-SCF-MO-CI and π-SCF-MO-CI methods to understand the electronic structures and spectra of different forms of pyridinols and of their ions. Ultraviolet photoelectron spectra (UPS) of neutral forms of the molecules are also discussed in comparison with the calculated orbital energies.

Theoretical

The details of a modified CNDO-CI (mCNDO-CI) method and a modified π-SCF-MO-CI (mPPP) method, as well as the semiempirical parametrization in these methods are described in previous papers.[1,11,12] In the mPPP method a polarizable σ-core is introduced in the evaluation of the π-electron Hartree-Fock matrix elements.[1]

The molecular structures of the lactim and lactam forms of isomeric pyridinols were the same as in a previous paper[10] and they are shown in Fig. 1, together with the coordinate system. The molecular structures of the anions were assumed to be the same as those of the corresponding neutral forms except that the proton of either N–H (in the lactam forms) or O–H (in the lactim forms) was removed. In the case of protonated cations the additional proton was located at either the nitrogen atom (in the lactim forms) or at the oxygen atom (in the lactam forms) with the assumed distance of the proton-protonated atom to be equal to 1.03 or 1.00 Å, respectively.

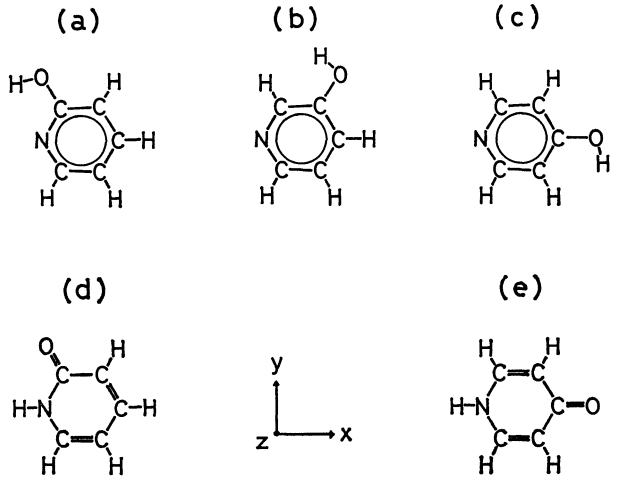

Fig. 1. Molecular structures of (a) 2-pyridinol, (b) 3-pyridinol, (c) 4-pyridinol, (d) 2-pyridone, and (e) 4-pyridone, and coordinate system.

Results and Discussion

Electronic Structures of Pyridinols. Electronic structures of the lactam and lactim forms of 2-, 3-, and 4-pyridinols have been calculated by the mCNDO-CI, the original CNDO/S-CI,[13] and the mPPP methods. The theoretical results calculated by the mCNDO-CI and mPPP methods are compared with the corresponding experimental data[2,9,14-16] in Tables 1—3. Electronic spectra of the lactam form (*i.e.*, 2- and 4-pyridones) are predicted well by all the three methods. In the case of 4-pyridone, the first π-π^* absorption band is predicted to be composed of two π-π^* bands. Both the AVE methods predict the weak first π-π^* band to appear on the longer wavelength side of the strong 2nd π-π^* band, whereas the mPPP method predicts the reverse order of the two π-π^* states.

Electronic structures of the lactim form of 2- and

Table 1. Singlet and triplet transition energies ($^1\Delta E$/eV and $^3\Delta E$/eV) and oscillator strengths (f) calculated and observed for 2-pyridone and 2-pyridinol

Assignment	mCNDO-CI			mPPP		Obsd[b]	
	$^1\Delta E$	$^3\Delta E$	f[a]	$^1\Delta E$	f	$^1\Delta E$	f
2-Pyridone							
n-π^*		2.73	0.001 (z)				
π-π^*	4.07	2.14	0.211 (y)	4.53	0.325	4.09—4.28	0.12
n-π^*		4.56	0.002 (z)				
π-π^*	5.40	3.10	0.308 ($x\bar{y}$)	5.48	0.148	5.40—5.60	0.14
σ-π^*		5.75	0.001 (z)				
π-σ^*		6.39	0.019 (z)				
σ-π^*		6.69	0.004 (z)				
n-π^*		6.89	0.000_3 (z)				
π-π^*	6.92	4.54	0.009 ($x\bar{y}$)	6.58	0.301		
σ-π^*		7.00	0.001 (z)				
π-σ^*		7.07	0.015 (z)				
π-π^*	7.29	5.85	0.241 ($\bar{x}$Y)	6.92	0.156		
2-Pyridinol							
n-π^*		3.90	0.005 (z)				
n-π^*		5.07	0.000 (z)				
π-π^*	5.38	3.52	0.096 (y)	4.59	0.099	4.54—4.59	0.11
π-π^*	6.11	4.40	0.171 (X$\bar{y}$)	5.85	0.136	5.72—5.79	0.14
σ-π^*		6.39	0.001 (z)				
σ-π^*		6.97	0.000 (z)				
n-π^*		7.01	0.004 (z)				
π-π^*	7.09	4.80	0.480 (Xy)	6.84	1.014	6.77	(26000)[c]
π-π^*	7.35	5.99	0.682 ($\bar{x}$Y)	6.92	0.939		
π-σ^*		7.83	0.000_2 (z)				

a) Oscillator strength is calculated for the singlet manifold. The direction of transition moment is shown in parentheses, x-, y-, and z-axes being taken as is shown in Fig. 1. When the transition moment has both x- and y-components, the larger one is designated by capital letter. x-Component with negative sign is designated as $\bar{x}$, and y-component, as $\bar{y}$. b) Refs. 2, 6, 9, 14, and 15. c) Molar extinction coefficient at the band maximum is shown in parentheses.

Table 2. Singlet and triplet transition energies ($^1\Delta E$/eV and $^3\Delta E$/eV) and oscillator strengths (f) calculated and observed for 4-pyridone and 4-pyridinol

Assignment	mCNDO-CI			mPPP		Obsd[b]	
	$^1\Delta E$	$^3\Delta E$	f[a]	$^1\Delta E$	f	$^1\Delta E$	f
4-Pyridone							
n-π^*		2.06	0				
n-π^*		4.26	0.005 (z)				
π-π^*	4.65	2.08	0.029 (y)	4.85	0.557	4.77—4.86	0.21
π-π^*	4.84	3.08	0.559 (x)	4.99	0.050		
σ-π^*		5.50	0.001 (z)				
n-π^*		5.87	0				
π-π^*	6.42	4.13	0.128 (y)	5.93	0.143	>6.2	
π-σ^*		6.46	0.005 (z)				
σ-π^*		6.76	0				
π-π^*	7.09	5.26	0.064 (x)	7.30	0.575		
4-Pyridinol							
n-π^*		3.95	0.006 (z)				
n-π^*		5.10	0.000 (z)				
π-π^*	5.58	3.54	0.003 (y)	4.71	0.015	5.17—5.27[c]	
σ-π^*		5.81	0.000 (z)				
π-π^*	6.14	4.69	0.055 (x)	5.79	0.063	5.58	0.15
σ-π^*		6.22	0.000 (z)				
π-π^*	6.86	4.80	0.598 (y)	6.63	0.908		
π-π^*	6.89	5.42	0.724 (x)	6.69	1.148		
n-π^*		7.36	0.007 (z)				
σ-π^*		7.95	0.001 (z)				

a) See footnote (a) in Table 1. b) Refs. 2, 14, and 15. c) Shoulder.

Table 3. Singlet and triplet transition energies ($^1\Delta E$/eV and $^3\Delta E$/eV) and oscillator strengths (f) calculated and observed for 3-pyridinol

Assignment	mCNDO-CI			mPPP		Obsd[b]	
	$^1\Delta E$	$^3\Delta E$	f[a]	$^1\Delta E$	f	$^1\Delta E$	f
σ-π^*	3.68		0.005 (z)				
σ-π^*	4.94		0.000 (z)				
π-π^*	5.34	3.45	0.090 ($\bar{x}$Y)	4.56	0.091	4.44—4.51	0.07
π-π^*	5.98	4.32	0.130 (xy)	5.76	0.125	5.64—5.77	0.13
σ-π^*	6.29		0.002 (z)				
σ-π^*	6.67		0.001 (z)				
π-π^*	6.93	4.74	0.518 (x)	6.76	0.989		
σ-π^*	7.07		0.004 (z)				
π-π^*	7.19	5.82	0.647 (y)	6.85	0.931		
π-σ^*	7.71		0.000 (z)				
π-π^*	8.16	6.54	0.038 (xY)				

a) See footnote (a) in Table 1. b) Refs. 2, 9, and 14.

3-pyridinols are predicted satisfactorily by the mPPP and CNDO/S-CI methods. The mCNDO-CI method predicts the first π-π^* band to be 0.4—0.8 eV higher than the observed values. This is due to overestimation ($\approx$0.8 eV) in transition energy of the first π-π^* band of the reference molecules (*i.e.*, of benzene, phenol, and pyridine)[17] by the use of the semiempirical parameters adopted in the present calculation. Electronic structure of 4-pyridinol is predicted less satisfactorily by all the three methods compared with the ones of 2- and 3-pyridinols. Absorption bands of lower excited π-π^* (and n-π^*) states of the lactim form shift to shorter wavelengths than the corresponding bands of the lactam form. This is well reproduced by the three methods as is listed in Tables 1 and 2.

The assignment of the lowest excited state is important to understand the photophysical properties of substituted pyridines. In mCNDO-CI method, calculated transition energy for n-π^* state corresponds to that of the triplet manifold.[11] Considering the underestimation ($\approx$0.7 eV) of transition energy of the ^{3}n-π^* state,[1] calculated results by mCNDO-CI method listed in Tables 1—3 clearly predict the lowest triplet state is π-π^* state for 2-pyridone, 2-pyridinol, 3-pyridinol, and 4-pyridone in agreement with the suggestion based on phosphorescence quantum yield and lifetime.[22] In mCNDO-CI method, transition energy of the first ^{1}n-π^* state may be estimated to be $\approx$1.7 eV (or less) higher than the calculated value for the triplet manifold when we consider the singlet-triplet separation energy[1] of $\approx$1 eV (or less) and underestimation of ^{3}n-π^* transition energy ($\approx$0.7 eV).[1] In 2-pyridone, 2-pyridinol, and 3-pyridinol, energy separation between the first $^1\pi$-π^* and the first ^{3}n-π^* states is calculated to be 1.3—1.7 eV. Therefore, the calculation shows that the first $^1\pi$-π^* state locates near to the first ^{1}n-π^* state. However, owing to the approximations employed, it is difficult to decide which is the lowest excited singlet state. In 4-pyridone, the lowest excited singlet state is safely assigned to n-π^* state in agreement with the suggestion based on fluorescence properties.[22]

Electronic Structures of the Anions and Cations of Pyridinols. Two different molecular structures based on the neutral parent molecules of either the lactam or lactim forms were assumed for each ionic species. Difference in calculated results between the two structures is due to the changes in geometrical structure and in mesomeric structure. As is shown in Tables 4 and 5, the difference in calculated π-π^* transition energies is more significant for the mPPP method (0.1—0.5 eV) than for the AVE method (0—0.2 eV). This is due to the fact that the electronic structures calculated by π-SCF-MO-CI method are much more sensitive to the assumed mesomeric structure of a system, *i.e.*, to the assumed numbers of π-electrons on each atom. However, in mPPP method, the mesomeric effect is reduced in some extent compared to the original PPP method, because consideration of σ-polarizable core in mPPP method partly cancels the effect of change in mesomeric structures.

In Table 4, the calculated results by the mCNDO-CI and mPPP methods are tabulated for the anions which are derived from the lactim forms of pyridinols. Compared with the results of the neutral molecules listed in Tables 1—3, the first n-π^* states of 2-, 3-, and 4-pyridinolate anions in Table 4 are shifted toward longer wavelengths (by $\approx$0.8 eV by mCNDO-CI method) by deprotonation. n-Orbitals pertinent to the first n-π^* states of the anions are localized on O atom, while those of pyridinols on N atom, thus the character of the first n-π^* state being changed. The third n-π^* states in 2-, 3-, and 4-pyridinolate anions have essentially n(N)-π^* character (calculated at 4.89, 4.37, and 4.21 eV, respectively, by mCNDO-CI method). Therefore, by deprotonation, n(N)-π^* state shifts toward shorter wavelength (by 0.3—1.0 eV by mCNDO-CI method). In the case of 4-pyridone and its anion, the first n-π^* states correspond to n(O)-π^* state. As in the case of n(N)-π^* state, n(O)-π^* state also shifts toward shorter wavelength (by 0.8 eV by mCNDO-CI method) by deprotonation. The first two π-π^* bands of the lactim forms were observed to shift toward longer wavelengths (by 0.3—0.5 eV) by deprotonation.[14-16] This is correctly predicted by the present calculations.

Table 4. Singlet and triplet transition energies ($^1\Delta E$/eV and $^3\Delta E$/eV) and oscillator strengths (f) calculated and observed for 2-, 3-, and 4-pyridinolate anions[a)]

Assignment	mCNDO-CI			mPPP		Obsd[c)]	
	$^1\Delta E$	$^3\Delta E$	f[b)]	$^1\Delta E$	f	$^1\Delta E$	ε[d)]
2-Pyridinolate anion[a)]							
n-π^*		3.11 (2.73)	0.000_4 (z)				
n-π^*		3.50	0.000_1 (z)				
π-π^*	3.97	2.88	0.093 (xy)	4.28 (4.10)	0.140 (0.152)	4.26	5070
n-π^*		4.89	0.013 (z)				
π-π^*	4.93	3.04	0.422 ($\bar{x}$Y)	5.40 (5.18)	0.383 (0.407)	5.39	9000
n-π^*		5.38	0.000 (z)				
σ-π^*		5.93	0.006 (z)				
σ-π^*		6.24	0.001 (z)				
π-σ^*		6.57	0.000_1 (z)				
π-π^*	6.68	4.25	0.008 (y)	6.40 (6.48)	0.148 (0.482)		
π-π^*	6.80	5.12	0.022 ($\bar{x}$Y)				
3-Pyridinolate anion							
n-π^*		2.91	0.000_2 (z)				
n-π^*		3.33	0.000_1 (z)				
π-π^*	3.84	2.63	0.103 ($\bar{x}$y)	4.16	0.126	4.16	4960
n(σ)-π^*		4.37	0.014 (z)				
π-π^*	4.70	2.91	0.361 (xY)	5.19	0.352	5.25	11000
n(σ)-π^*		5.56	0.001 (z)				
σ-π^*		6.15	0.000_1 (z)				
π-σ^*		6.39	0.008 (z)				
π-π^*	6.54	4.24	0.009 (y)	6.17	0.299		
σ-π^*		6.58	0.003 (z)				
π-π^*	6.74	5.09	0.112 (Xy)				
π-π^*	6.88	5.70	0.056 (y)				
4-Pyridinolate anion[a)]							
n-π^*		3.18 (2.84)	0				
n-π^*		4.02	0.001 (z)				
n-π^*		4.21	0.012 (z)				
π-π^*	4.26	2.92	0.071 (y)	4.59 (4.40)	0.014 (0.064)	4.77	2200
n-π^*		4.75	0				
π-π^*	4.92	3.32	0.421 (x)	5.23 (4.84)	0.360 (0.612)	5.19	14150
n-π^*		6.45	0				
σ-π^*		6.47	0.000 (z)				
π-π^*	6.57	4.22	0.113 (y)	6.06 (6.53)	0.514 (0.103)		
π-σ^*		6.64	0.017 (z)				
π-π^*	6.71	5.38	0.198 (x)				
π-π^*	6.94	5.38	0.258 (x)				

a) Molecular structures based on the corresponding lactim forms were employed in the calculations. For the purpose of comparison, calculated results for the ions, molecular structures of which are based on the lactam forms were listed in part in parentheses. b) See footnote (a) in Table 1. c) Refs. 2 and 16. d) Molar extinction coefficient at the band maximum.

As is shown in Table 5, theoretical calculations for the protonated cations predict satisfactorily the shorter wavelength shift of the first n(σ)-π^* state by protonation. The first two π-π^* bands of the lactam forms are correctly predicted to shift to shorter wavelengths by protonation in agreement with observations.[16)]

Orbital Assignment in UPS of Pyridinols. Ionization potentials (IP's) of the lactam and lactim forms of pyridinols were evaluated by the mCNDO method according to Koopmans' theorem.[23)] The results are shown in Fig. 2, compared with the observed values in ultraviolet photoelectron spectra (UPS).[24)] In the

Table 5. Singlet and triplet transition energies ($^1\Delta E$/eV and $^3\Delta E$/eV) and oscillator strengths (f) calculated and observed for the protonated cations of 2-, 3-, and 4-pyridinols[a)]

Assignment	mCNDO-CI			mPPP		Obsd[c)]	
	$^1\Delta E$	$^3\Delta E$	f[b)]	$^1\Delta E$	f	$^1\Delta E$	ε[d)]
Cation of 2-pyridinol[a)]							
π-π*	4.94 (4.87)	3.57 (3.42)	0.245 (y) (0.281)	4.37 (4.55)	0.280 (0.424)	4.48	6950
σ-π*	5.29		0.001 (z)				
σ-π*	6.06		0.000_3 (z)				
π-π*	6.12 (6.04)	3.84 (3.82)	0.117 (x) (0.154)	5.83 (5.71)	0.110 (0.112)	5.93	3600
σ-π*	6.41		0.001 (z)				
σ-π*	7.14		0.000_4 (z)				
π-π*	7.24	4.97	0.694 (x)	6.71	0.913		
π-σ*	7.36		0.001 (z)				
π-π*	7.79	6.00	0.311 (y)				
σ-π*	7.88		0.002 (z)				
Cation of 3-pyridinol							
π-π*	4.84	3.25	0.211 (y)	4.37	0.248	4.38	5840
σ-π*	4.97		0.001 (z)				
σ-π*	5.75		0.000 (z)				
π-π*	5.91	3.77	0.057 (xy)	5.67	0.048	5.58	3730
σ-π*	6.13		0.000 (z)				
π-π*	6.80	4.61	0.704 (Xy)	6.63	0.908		
σ-π*	7.00		0.000_2 (z)				
π-σ*	7.20		0.001 (z)				
π-π*	7.55	5.78	0.450 (y)				
π-σ*	7.90		0.001 (z)				
Cation of 4-pyridinol[a)]							
σ-π*	5.07		0.000 (z)				
π-π*	5.44 (5.56)	4.00 (3.96)	0.141 (y) (0.101)	4.64 (4.81)	0.142 (0.446)	5.30	9800
π-π*	5.91 (5.68)	4.02 (4.12)	0.188 (x) (0.317)	5.60 (5.34)	0.095 (0.018)		
σ-π*	5.94		0.000_2 (z)				
σ-π*	6.24		0.000_2 (z)				
π-π*	6.88	4.40	0.392 (y)	6.59	1.081		
σ-π*	6.92		0.000_3 (z)				
π-π*	6.99	5.39	0.766 (x)				
σ-π*	7.79		0.000_2 (z)				
π-σ*	7.83		0.000 (z)				

a) See footnote (a) in Table 4. b) See footnote (a) in Table 1. c) Refs. 2, 14, and 16. d) Molar extinction coefficient at the band maximum.

figure, the calculated and observed values for pyridine[25)] are also shown for the purpose of comparison. A good correlation between observed and calculated values for pyridinols (Fig. 2a) and pyridones (Fig. 2b) clearly indicates that the order of the first three highest occupied molecular orbitals is $\pi > n > \pi$ for 2- and 3-pyridinols, and 2- and 4-pyridones in agreement with the assignment by Cook, *et al.*[24)] Assignments to the fourth and fifth bands in UPS have not yet been established for pyridinols and pyridones. In pyridine, the fifth IP (which is from π-orbital)[25)] was calculated to be $\approx$2.5 eV higher by the present calculation. When we adjust the relative shift of the calculated fourth and fifth IP's, a good correlation can be obtained in Fig. 2a between the observed and calculated IP's for pyridinols, indicating that the fourth and fifth bands in UPS are π- and σ-orbitals, respectively, for both 2- and 3-pyridinols, and that the fourth band of 4-pyridinol is σ-orbital. From the correlation diagram in Fig. 2b, the fourth band of 4-pyridone can safely be assigned to σ-orbital, and the one of 2-pyridone, plausibly to σ-orbital, too.

From the orbital energy calculations by the CNDO/S method, a correlation diagram which is qualitatively similar to the one in Fig. 2 was obtained. Although the sequence in the calculated molecular orbitals by the CNDO/S method is partly incorrect, the argument mentioned to Fig. 2 also holds in the results by the CNDO/S method, and the same conclusion as to the orbital assignment in UPS could be drawn.

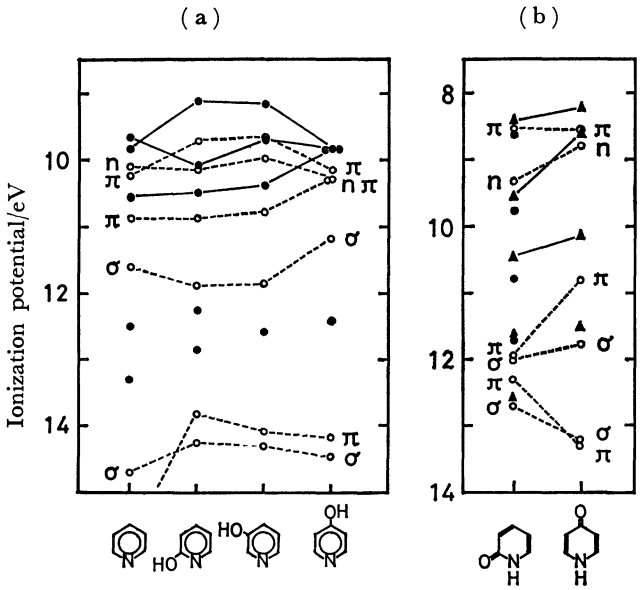

Fig. 2. Ionization potentials (IP's/eV) observed in UPS (●) and calculated by mCNDO method (○) for (a) pyridine, and 2-, 3-, and 4-pyridinols, and (b) 2- and 4-pyridones. ▲; IP's observed for 1-methyl-2(or 4)-pyridone.

This work was initiated during the stay of J. S. K. at the Institute for Solid State Physics, the University of Tokyo. J. S. K. wishes to thank the Japan Society for the Promotion of Sciences for support of his stay in Japan. This work was also supported in part by the Ministry of Science and Higher Education/Poland/ within the project MR. I. 5.

References

1) H. Morita, J. S. Kwiatkowski, and A. Tempczyk, *Bull. Chem. Soc. Jpn.*, **54**, 1797 (1981).
2) M. Berndt and J. S. Kwiatkowski, *Theor. Chim. Acta*, **17**, 35 (1970).
3) J. S. Kwiatkowski, *J. Mol. Struct.*, **10**, 245 (1971).
4) A. Tempczyk and J. S. Kwiatkowski, *Bull. Acad. Pol. Sci., Ser. Sci. Chim.*, **27**, 161 (1979).
5) Yu. V. Morozov and L. P. Cherkashina, *Mol. Photochem.*, **8**, 45 (1977); V. T. Grachev, B. E. Zaicev, E. M. Ickovich, B. N. Licyutenko, K. M. Dyumaev, and G. V. Scheban, *Teor. Eksp. Khim.*, **13**, 94 (1977).
6) A. Fujimoto, K. Inuzuka, and R. Shiba, *Bull. Chem. Soc. Jpn.*, **54**, 2802 (1981).
7) W. Fabian, *Z. Naturforsch., Teil B*, **34**, 266 (1979).
8) C. Krebs, H. J. Hofmann, H. J. Köhler, and C. Weiss, *Chem. Phys. Lett.*, **69**, 537 (1980).
9) A. Kaito and M. Hatano, *Bull. Chem. Soc. Jpn.*, **53**, 3069 (1980).
10) J. S. Kwiatkowski, *Acta Phys. Pol. A*, **55**, 923 (1979).
11) H. Morita, K. Fuke, and S. Nagakura, *Bull. Chem. Soc. Jpn.*, **49**, 922 (1976).
12) J. S. Kwiatkowski and B. Lesyng, *Int. J. Quantum Chem., QBS*, **6**, 391 (1979).
13) J. Del Bene and H. H. Jaffé, *J. Chem. Phys.*, **48**, 1807, 4050 (1968); **49**, 1221 (1968).
14) G. Favini, M. Raimondi, and C. Gandolfo, *Spectrochim. Acta, Part A*, **24**, 207 (1968).
15) I. Jonáš and J. Michl, *J. Am. Chem. Soc.*, **100**, 6828 (1978).
16) S. F. Mason, *J. Chem. Soc.*, **1957**, 5010; **1959**, 1253.
17) Calculated transition energies from the ground to excited states for benzene are (in eV; observed values are given in parentheses) 5.67 (4.89)[18] for $^1B_{2u}$, 6.25 (6.17)[18] for $^1B_{1u}$, 6.97 (6.98)[18] for $^1E_{1u}$, 3.54 (3.66)[19] for $^3B_{1u}$, 4.83 (4.69)[19] for $^3E_{1u}$, and 5.67 (5.76)[19] for $^3B_{2u}$. The first π-π^* bands calculated for phenol and pyridine are 5.43 (Obsd[20] 4.59) and 5.68 (Obsd[21] 4.8) eV, respectively, by mCNDO-CI method.
18) K. Kimura, H. Tsubomura, and S. Nagakura, *Bull. Chem. Soc. Jpn.*, **37**, 1336 (1964).
19) D. R. Kearns, *J. Chem. Phys.*, **36**, 1608 (1962).
20) K. Kimura and S. Nagakura, *Mol. Phys.*, **9**, 117 (1965).
21) J. E. Perkin and K. K. Innes, *J. Mol. Spectrosc.*, **15**, 407 (1965).
22) K. Kimura and R. Nagai, *Bull. Chem. Soc. Jpn.*, **49**, 3343 (1976).
23) T. Koopmans, *Physica*, **1**, 104 (1934).
24) M. J. Cook, S. El-Abbady, A. R. Katritzky, C. Guimon, and G. Pfister-Guillouzo, *J. Chem. Soc., Perkin Trans. 2*, **1977**, 1652.
25) C. Utsunomiya, T. Kobayashi, and S. Nagakura, *Bull. Chem. Soc. Jpn.*, **51**, 3482 (1978).

 © 1982 The Chemical Society of Japan Bull. Chem. Soc. Jpn., 55, 2721—2729 (1982)

Association of Inclusion Compounds of β-Cyclodextrin in Aqueous Solution

Sanyo Hamai

Department of Physics, Miyazaki Medical College, Kiyotake, Miyazaki 889-16

(Received December 9, 1981)

Inclusion compounds in the systems naphthalene–β-cyclodextrin (CDx) and 2-methoxynaphthalene (MN)–o-dicyanobenzene (DB)–β-cyclodextrin in aqueous solution were studied by means of absorption and fluorescence spectra. In the former system a naphthalene excimer fluorescence was observed. By the analyses of the concentration dependence of the absorption spectra and the excimer fluorescence intensities, the species responsible for the excimer fluorescence is identified as a 2:2 inclusion compound which is formed by association of two 1:1 naphthalene–CDx inclusion compounds, not a 2:1 inclusion compound in which two naphthalene molecules enter into the cavity of one CDx molecule. In the latter system, absorption and fluorescence spectra due to a charge transfer complex of MN with DB were observed. By analyses similar to the naphthalene case, the existence of a 1:1:2 association compound formed between a MN–CDx inclusion compound and a DB–CDx inclusion compound is confirmed. Fluorescence quenching by I^- and IO_3^- was also studied for the inclusion compounds in both systems.

Recently, much attention has been focused on cyclodextrin as a model compound for enzymatic processes. It is interesting to note that such a relatively small molecule can promote a stereospecific reaction although in organisms much larger molecules act catalytically. This catalytic action is based on the fact that cyclodextrin forms inclusion compounds with many kinds of organic compounds in aqueous solution. The component ratios of substrates to β-cyclodextrin are 1:1 for most compounds.[1–5] However, 1:2 or 2:1 inclusion compounds have been reported for α-, β-, γ-, and capped cyclodextrins.[6–8] Ueno *et al.*[9] suggested that γ-cyclodextrin forms a 2:1 inclusion compound with 1-naphthyl acetate in aqueous solution by observing an excimer fluorescence of 1-naphthyl acetate. For some systems, formation of a 2:2 inclusion compound by association of two 1:1 inclusion compounds has been speculated,[10,11] but ambiguity remains as to whether such an association really occurs. By study of fluorescence quenching in the system in which two kinds of 1:1 inclusion compounds can exist, Kano *et al.*[12] predicted the existence of a 1:1:1 inclusion compound. Thus it appears that the compositions of the inclusion compounds other than the 1:1 compounds depend critically on the types of cyclodextrin and the physicochemical properties of the substrates involved.

In the present study, we have investigated inclusion compounds in the systems naphthalene–β-cyclodextrin and 2-methoxynaphthalene–o-dicyanobenzene–β-cyclodextrin in aqueous solution by analyses of the absorption and fluorescence spectra.

Experimental

β-Cyclodextrin (CDx) purchased from Nakarai Chemical Co. was recrystallized three times from water and the molecular weight of CDx was calculated as the dodecahydrate.[13] Naphthalene (Nakarai Chemical Co.) and 2-methoxynaphthalene (MN) (Tokyo Kasei Kogyo Co.) were recrystallized three times from ethanol. o-Dicyanobenzene (DB) (Tokyo Kasei Kogyo Co.) was recrystallized first from water and then from cyclohexane. Potassium iodide (Wako Pure Chemical Industries) and potassium iodate (Nakarai Chemical Co.) were used without further purification. Water was doubly distilled.

Absorption spectra were measured with a Hitachi 124 spectrophotometer and fluorescence spectra with a Shimadzu RF-501 fluorescence spectrophotometer (modified by employing a cooled EMI 9789QA photomultiplier). Both instruments were equipped with thermostatically controlled sample compartments. Fluorescence was detected at right angles to the direction of excitation. Fluorescence spectra were corrected for the spectral sensitivity of the detection system.[14]

Absorption and fluorescence spectra were measured at (25±0.1) °C unless otherwise stated. Aerated sample solutions were used throughout the present work because nitrogen bubbling caused considerable decreases in the concentrations of naphthalene and MN in aqueous solution (containing no CDx).

Fluorescence decay times were determined by means of an Ortec 9200 nanosecond decay time fluorescence spectrometer. Light from a nanosecond light pulser (filled with H_2 or air) was passed into a 0.3 m Ritsu MC-30 monochromator and the 270 nm (for naphthalene–CDx system, H_2 gas) or the 316 nm (for MN–DB–CDx system, air) exciting light was isolated. Fluorescence from sample solutions was collected through appropriate filters.

Results

Inclusion Compounds in Naphthalene–β-Cyclodextrin System. Absorption spectra of naphthalene aqueous solutions containing varying concentrations of CDx are shown in Fig. 1. At concentrations of CDx between 0 and $\approx 3\times10^{-3}$ M (1 M=1 mol dm^{-3}), isosbestic points are observed at 267, 271, 276, and 283 nm, indicating the following 1:1 equilibrium in this concentration range:

$$\mathrm{N} + \mathrm{CDx} \overset{K_1}{\rightleftharpoons} \mathrm{NC}, \tag{1}$$

where N and NC represent naphthalene and the 1:1 inclusion compound of CDx with naphthalene, respectively, and K_1 is the equilibrium constant for the formation of NC. The Benesi-Hildebrand relation for such an equilibrium is[1]

$$\frac{1}{A-A_0} = \frac{1}{(\varepsilon_1-\varepsilon_0)[\mathrm{N}]_0} + \frac{1}{(\varepsilon_1-\varepsilon_0)[\mathrm{N}]_0K_1}\frac{1}{[\mathrm{CDx}]_0}, \tag{2}$$

where A and A_0 are the absorbances per cm of the naphthalene aqueous solutions in the presence and absence of CDx, ε_1 and ε_0 are the molar absorption coefficients of NC and naphthalene, and $[\mathrm{N}]_0$ and $[\mathrm{CDx}]_0$

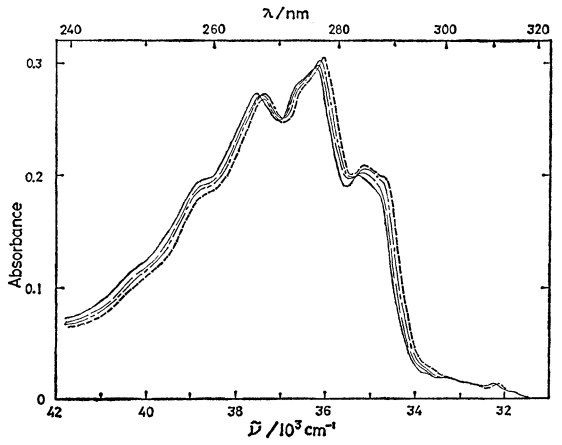

Fig. 1. Absorption spectra of naphthalene (5.80×10^{-5} M) in aqueous solution in the presence of CDx. Initial concentration of CDx, ——: 0 M, — —: 8.40× 10^{-4} M, — — —: 2.52×10^{-3} M, - - - -: 8.40×10^{-3} M.

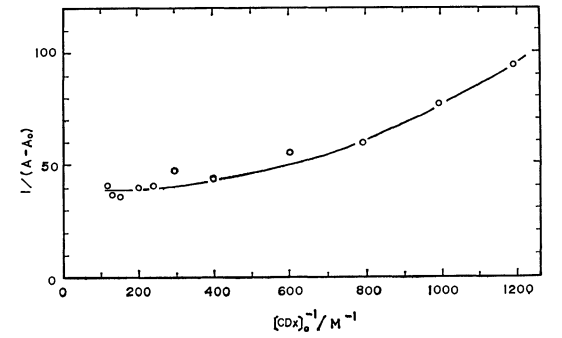

Fig. 2. Benesi-Hildebrand plot for absorbance changes at 277 nm of naphthalene aqueous solutions containing varying concentrations of CDx. $[N]_0=5.80\times10^{-5}$ M.

are the initial concentrations of naphthalene and CDx, respectively. We choose 277 nm as the analyzing wavelength for the absorbance changes. A plot of $1/(A-A_0)$ *vs.* $1/[CDx]_0$ gives a concave upward curve as shown in Fig. 2. This combined with the fact that the spectral curves no longer pass through the isosbestic points at higher CDx concentrations (see Fig. 1) suggests the existence of another species other than NC in the naphthalene–CDx system.

Figure 3 shows the fluorescence spectra of naphthalene in the absence and presence of CDx in aqueous solution. By addition of CDx the fluorescence band at around 330 nm is enhanced, and at the same time a broad structureless band having λ_{max} at 410 nm appears. This new band grows in intensity at the expense of the 330 nm band with decreasing temperature as shown in Fig. 4. The enhancement of the 330 nm band seen in Fig. 3 can be interpreted as due to the formation of NC having the higher fluorescence yield than naphthalene. The new band is assignable to the well-known naphthalene excimer fluorescence.[15,16] The appearance of this band indicates the existence of another species beside NC because the excimer cannot be formed from uncomplexed naphthalene molecules at the concentrations as low as $\approx6\times10^{-5}$ M.

As the species responsible for the excimer fluorescence, two kinds of inclusion compounds represented by the following two mechanisms can be considered:

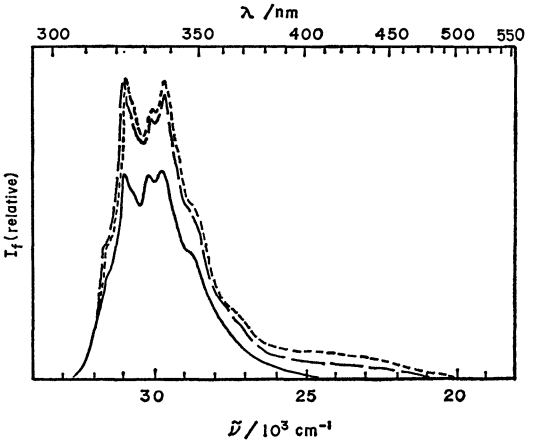

Fig. 3. Fluorescence spectra of naphthalene (5.80×10^{-5} M) in aqueous solution in the presence of CDx. Initial concentration of CDx, ——: 0 M, — —: 2.52×10^{-3} M, - - - -: 8.40×10^{-3} M. $\lambda_{exc}=283$ nm.

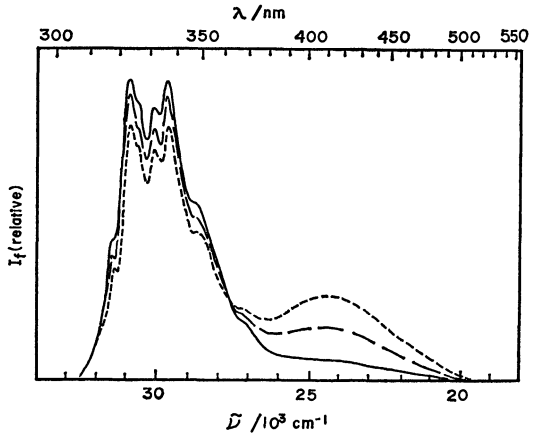

Fig. 4. Temperature dependence of the fluorescence spectra of naphthalene (4.90×10^{-5} M) in aqueous solution in the presence of CDx (8.40×10^{-3} M). ——: 25 °C, — —: 12 °C, ----: 3 °C. $\lambda_{exc}=283$ nm.

Mechanism 1) $$N + NC \overset{K_2'}{\rightleftharpoons} N_2C, \quad (3)$$

Mechanism 2) $$NC + NC \overset{K_2}{\rightleftharpoons} N_2C_2. \quad (4)$$

One of these is a 2:1 inclusion compound N_2C which is composed of two naphthalene molecules entering into the cavity of a CDx molecule. The other is a 2:2 inclusion compound N_2C_2 which is formed by association of two 1:1 inclusion compounds. For Mechanism 1, the relation that the concentration of the uncomplexed naphthalene [N] should satisfy is

$$2K_1K_2'[CDx]_0[N]^2 + (1+K_1[CDx]_0)[N]-[N]_0 = 0, \quad (5)$$

whereas for Mechanism 2, it is

$$2K_1^2K_2[CDx]_0^2[N]^2 + (1+K_1(CDx]_0)[N]-[N]_0 = 0. \quad (6)$$

The concentration of N_2C or N_2C_2 can be evaluated after obtaining [N] from Eq. 5 or 6. To solve these equations for [N] we must first know the equilibrium constant K_1. The value of K_1 was determined as following.

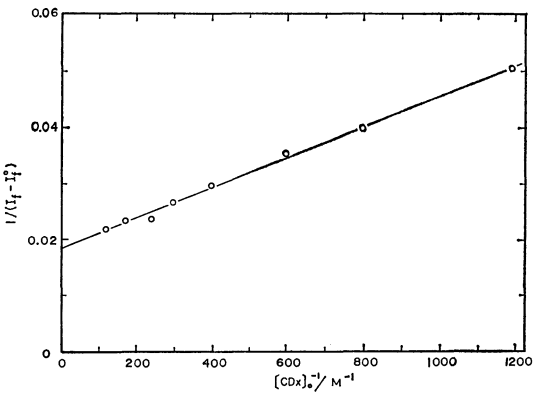

Fig. 5. Benesi-Hildebrand plot for fluorescence increments at 336 nm of naphthalene aqueous solutions containing varying concentrations of CDx. $[N]_0=6.10\times10^{-6}$ M.

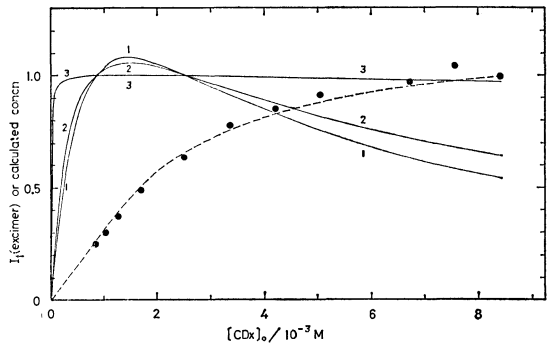

Fig. 6. Comparison of the observed excimer intensities, I_f(excimer), with calculated concentrations $[N_2C]$ and $[N_2C_2]$.
●: I_f(excimer), ——: $[N_2C]$ calculated with $K'_2=1\ M^{-1}$ (curve 1); $K'_2=10^4\ M^{-1}$ (curve 2); $K'_2=10^7\ M^{-1}$ (curve 3), - - - -: $[N_2C_2]$ calculated with $K_2=4000\ M^{-1}$. $[N]_0=5.80\times10^{-5}$ M. I_f(excimer) and $[N_2C_2]$ are normalized to unity at the highest concentration of $[CDx]_0$, and $[N_2C]$ at the lowest concentration of $[CDx]_0$.

The fluorescence intensity was measured at a naphthalene concentration of 6×10^{-6} M at which no excimer fluorescence appears and thus only NC exists as the inclusion compound. For our experimental geometry in the fluorescence measurements, the observed intensity was always proportional to the concentration of the emitting species. Under these conditions, the following relation holds:[7]

$$\frac{1}{I_f-I_f^0}=\frac{1}{a[N]_0}+\frac{1}{a[N]_0K_1}\frac{1}{[CDx]_0}, \tag{7}$$

where I_f and I_f^0 are the fluorescence intensities of the 330 nm band in the presence and absence of CDx, and a is a proportionality constant. A plot of $1/(I_f-I_f^0)$ *vs.* $1/[CDx]_0$ yields a good straight line as shown in Fig. 5, and from the intercept-to-slope ratio $K_1=685\ M^{-1}$ is obtained.

The value of [N] for Mechanism 1 can then be calculated from Eq. 5 for an assumed value of K'_2 from which the concentration of N_2C can be evaluated. The concentration of N_2C_2 will be similarly evaluated for an assumed value of K_2 through Eq. 6. Figure 6 shows the dependence of the observed excimer fluorescence intensity on CDx concentration and the calculated concentrations of N_2C and N_2C_2 using various values of K'_2 or K_2. As seen in Fig. 6 even when K'_2 is varied from 1 M^{-1} to 10^7 M^{-1}, none of the concentration curves for N_2C fit the intensity curve of the excimer fluorescence. On the other hand, the calculated curve for N_2C_2 fits the data quite well when K_2 is taken equal to 4000 M^{-1}. These findings strongly support Mechanism 2. We will therefore assume in the following that N_2C_2 is the species responsible for the excimer emission in the naphthalene–CDx system.

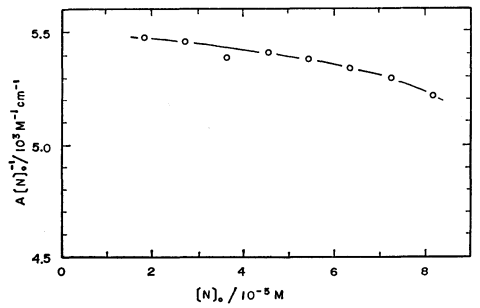

Fig. 7. Plot of $A/[N]_0$ at 277 nm *vs.* $[N]_0$. $[CDx]_0=8.40\times10^{-3}$ M.

So far, we have dealt with the spectroscopic data which were obtained at a fixed concentration of naphthalene with varying amounts of CDx. We will now examine the dependence of the naphthalene concentration (at a fixed CDx concentration) on the absorption and fluorescence spectra. No appreciable spectral change was observed in the absorption spectra when the varying concentrations of naphthalene were added to the solution containing a fixed concentration of CDx. However, as displayed in Fig. 7, the apparent molar absorption coefficient ($A/[N]_0$) at 277 nm decreases with increasing $[N]_0$. Obviously, the molar absorption coefficient of N_2C_2 per naphthalene molecule, $\varepsilon_2/2$, must be smaller than ε_1.

The data shown in Fig. 7 can further be analyzed as following. The absorbance A at 277 nm is given by

$$A=\varepsilon_0[N]+\varepsilon_1[NC]+\varepsilon_2[N_2C_2], \tag{8}$$

which can be rewritten using the equilibrium constants K_1 and K_2 as

$$\frac{A}{[N]}=(\varepsilon_0+\varepsilon_1K_1[CDx]_0)+\varepsilon_2K_1^2K_2[CDx]_0^2[N]. \tag{9}$$

The concentration of uncomplexed naphthalene [N] can be calculated from Eq. 6 as functions of $[N]_0$ and $[CDx]_0$ since K_1 and K_2 have already been determined. A plot of $A/[N]$ *vs.* [N] gives a straight line as presented in Fig. 8, and from this plot the values $\varepsilon_1=5690\ M^{-1}\ cm^{-1}$ and $\varepsilon_2=9160\ M^{-1}\ cm^{-1}$ are obtained using the known value of ε_0 (4870 $M^{-1}\ cm^{-1}$). As expected, $\varepsilon_1>\varepsilon_0$ and $\varepsilon_2/2<\varepsilon_1$. These relationships amongst ε_0, ε_1, and $\varepsilon_2/2$ explain the temperature variation of the absorption spectra given in Fig. 9 which shows the decrease of the absorbance at 277 nm on cooling. As is apparent from the temperature depend-

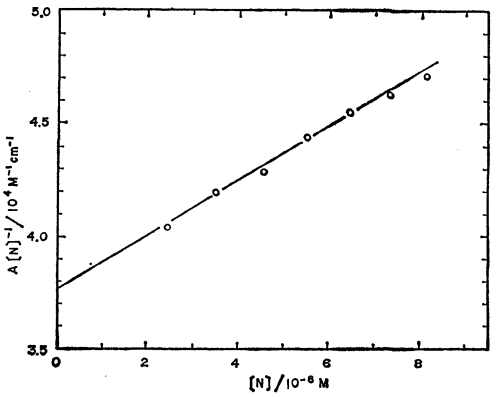

Fig. 8. Plot of $A/[N]$ at 277 nm *vs.* [N]. [N] is calculated from Eq. 6.

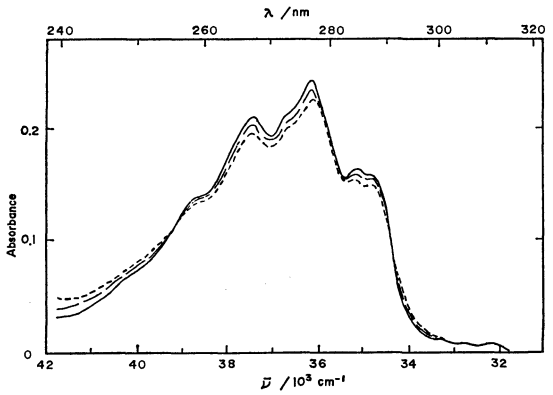

Fig. 9. Temperature dependence of the absorption spectra of naphthalene (4.90×10^{-5} M) in aqueous solution in the presence of CDx (8.40×10^{-3} M). ——: 25 °C, — —: 12 °C, - - - -: 3 °C.

ence of the fluorescence spectra (Fig. 4), $[N_2C_2]$ increases on lowering temperature, accompanied by the decrease in [NC].

The good linearity obtained in Fig. 8 indicates that any aggregates higher than a 2:2 adduct (N_nC_n, $n>2$) do not exist at least in the concentration range we have examined. That the species other than NC in the naphthalene–CDx system is indeed the 2:2 inclusion compounds, and is not a higher aggregate can also be shown from the dependence of the excimer intensity, I_f(excimer), on the naphthalene concentration at a fixed CDx concentration. For Mechanism 2,

$$I_f(\text{excimer}) = b'[N_2C_2] = b'K_1^2K_2[\text{CDx}]_0^2[N]^2 = b[N]^2, \tag{10}$$

where b' is an instrumental constant. Taking logarithm of both sides of Eq. 10,

$$\log I_f(\text{excimer}) = 2\log[N] + \log b. \tag{11}$$

A plot of $\log I_f$(excimer) *vs.* log [N], [N] being calculated from Eq. 6, gives a good straight line with the slope 1.9 ($\simeq2$) as shown in Fig. 10, indicating the square dependence of I_f(excimer) on [N].

By measuring I_f(330 nm) over the temperature range from 3 to 25 °C and obtaining the value of K_1 at each temperature from the plot as shown in Fig. 5, the enthalpy and entropy changes for the equilibrium constant K_1 were determined to be -19 kJ mol^{-1} and

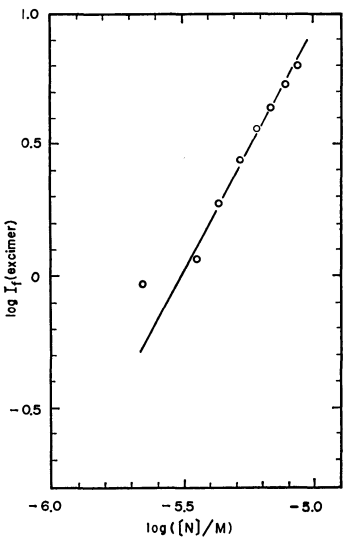

Fig. 10. Plot of $\log I_f$(excimer) *vs.* log [N].

-10 J mol^{-1} K^{-1}, respectively. These thermodynamic quantities are similar to those obtained for other 1:1 inclusion compounds with CDx.[1,17] Unfortunately, these quantities could not be obtained for K_2 since the shape of the I_f(excimer) curve shown in Fig. 6 was relatively insensitive to the temperature change.

Fluorescence decay times and fluorescence quenching by I^- and IO_3^- were also studied for the three components in the naphthalene–CDx system. An aqueous solution of naphthalene alone for the uncomplexed naphthalene and a solution of naphthalene (6.0×10^{-5} M) and CDx (8.4×10^{-3} M) for NC and N_2C_2 were examined. With the 283 nm excitation the quenching of the 330 nm fluorescence bands for N and NC and the 410 nm band for N_2C_2 was studied by adding varying amounts of KI or KIO_3. Strictly speaking, the 330 nm band of the naphthalene–CDx solution contains the fluorescence from the uncomplexed naphthalene, but since its contribution was calculated to be only about 10%, no corrections were applied for the quenching data for NC. The results were analyzed by the usual Stern-Volmer relation:

$$\frac{I_f^0}{I_f} = 1 + k_q\tau'[Q], \tag{12}$$

where I_f^0 and I_f represent the fluorescence intensities in the absence and presence of a quencher Q (using the same notations for N, NC, and N_2C_2 for simplicity), k_q is the rate constant for quenching, and τ' is the fluorescence lifetime of each species in aerated solution. As an example, the Stern-Volmer plots for quenching by IO_3^- are shown in Fig. 11. In Table 1 are summarized the fluorescence lifetimes and the rate constants k_q.[18,19] The reduction of the quenching efficiencies by forming the 1:1 inclusion compounds has already been shown for many other systems and has been attributed to the CDx molecule partly preventing the quencher molecule to penetrate into its cavity.[10,20] The further reduction of the quenching efficiencies for N_2C_2 indicates that it is more difficult for the quencher molecule to approach the naphthalene molecules contained in the two CDx molecules

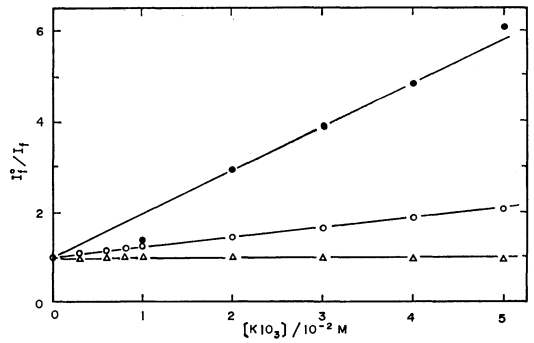

Fig. 11. Stern-Volmer plots for fluorescence quenching of naphthalene (●), NC (○), and N_2C_2 (△) by IO_3^-.

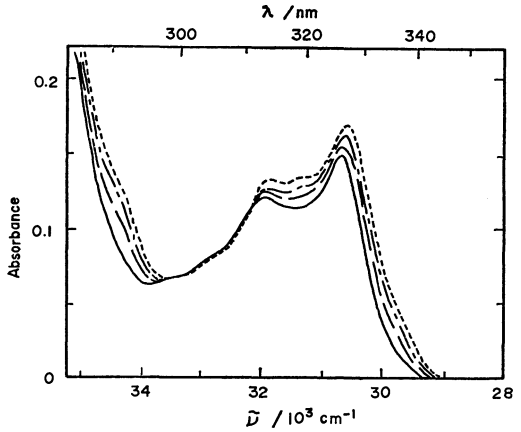

Fig. 12. Absorption spectra of MN (9.60×10^{-5} M) in aqueous solution in the presence of CDx.
Initial concentration of CDx, ——: 0 M, — —: 8.40×10^{-4} M, — — —: 2.52×10^{-3} M, - - -: 8.40×10^{-3} M.

Table 1. Fluorescence lifetimes (τ') in aerated solution and rate constants for fluorescence quenching (k_q) for N, NC, and N_2C_2 in the naphthalene-CDx system

		N	NC	N_2C_2
τ'/ns		40 (39)[a] (35)[b]	48	68
$k_q/10^9$ M^{-1} s^{-1}	I^-	6.0	3.9	1.8
	IO_3^-	2.4	0.45	0

a) R. R. Hautala, N. E. Schore, and N. J. Turro, *J. Am. Chem. Soc.*, **95**, 5508 (1973). b) M. Van Bockstaele, J. Gelan, H. Martens, J. Put, J. C. Dederen, N. Boens, and F. C. de Schrijver, *Chem. Phys. Lett.*, **58**, 211 (1978).

than in NC, the extreme case being that no quenching was observed by IO_3^- ion which is bulkier than I^-.

Inclusion Compounds in 2-Methoxynaphthalene–o-Dicyanobenzene–β-Cyclodextrin System. Absorption spectra of 2-methoxynaphthalene (MN) aqueous solutions containing varying concentrations of CDx are shown in Fig. 12. Isosbestic points observed at 310 nm and ≈300 nm indicate the following equilibrium:

$$MN + CDx \overset{K_3}{\rightleftharpoons} MC, \qquad (13)$$

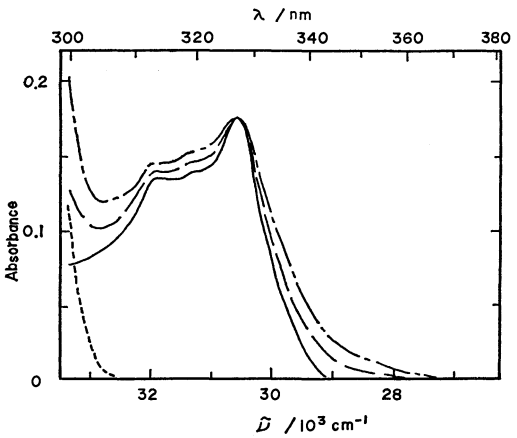

Fig. 13. Absorption spectra of MN (9.60×10^{-5} M)–CDx (8.40×10^{-3} M) in aqueous solution in the presence of DB.
Initial concentration of DB, ——: 0 M, — —: 7.0×10^{-4} M, — — —: 2.0×10^{-3} M. - - - -: absorption spectrum of DB (2.0×10^{-3} M) in the presence of CDx (8.40×10^{-3} M).

where MC is the 1:1 inclusion compound of CDx with MN and K_3 is the equilibrium constant for the formation of MC. The value of K_3 was determined from the Benesi-Hildebrand plot (Eq. 2) using the absorbance changes at 330 nm. $K_3=630$ M^{-1} was obtained.

Very little changes were observed in the absorption spectrum of an *o*-dicyanobenzene (DB) aqueous solution on adding CDx. However, the fluorescence intensity of DB ($\lambda_{max}=307$ nm) decreased with increasing the CDx concentration. We attribute this change as being due to the formation of a 1:1 inclusion compound, DC, *i.e.*,

$$DB + CDx \overset{K_4}{\rightleftharpoons} DC. \qquad (14)$$

From the Benesi-Hildebrand plot for the change in fluorescence intensity (Eq. 7), the value of the equilibrium constant K_4 was determined to be 15 M^{-1}.

Figure 13 shows the absorption spectra of the MN–CDx solutions containing varying amounts of DB. The appearance of a new band extending to longer wavelengths is seen on adding DB. This band is most plausibly due to an MN–DB charge transfer (CT) complex since MN is an electron donor and DB an electron acceptor. Such a CT band, however, could not be observed for the solutions containing only MN and DB in 1,4-dioxane, ethyl ether, and toluene (up to the DB concentrations of 0.2 M, 0.1 M, and 0.1 M, respectively) or in water ($<4\times10^{-3}$ M).

Figure 14 shows the fluorescence spectra of the aqueous solutions of MN alone, MN with CDx, and MN with DB and CDx. The enhancement of the 350 nm band with the addition of CDx indicates that the fluorescence quantum yield of MC is higher than that of MN.[21,22] On adding DB, a structureless band having λ_{max} at 480 nm appears at the expense of the 350 nm band. The excitation spectrum of this band is found to coincide with the long wavelength tail of the absorption spectrum, and thus this band can be assigned to the fluorescence from the CT complex of

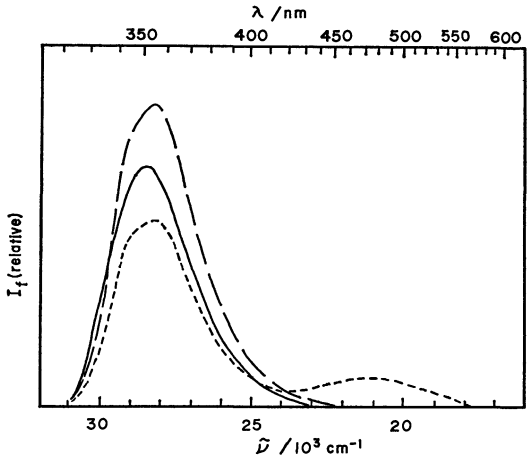

Fig. 14. Fluorescence spectra of MN (——), MN-CDx (— —), and MN–DB–CDx (- - - -) in aqueous solution.
$[MN]_0=9.60\times10^{-5}$ M; $[CDx]_0=8.40\times10^{-3}$ M; $[DB]_0=2.0\times10^{-3}$ M. $\lambda_{exc}=310$ nm.

MN and DB. This assignment is supported by our findings that the fluorescence from an exciplex formed between MN and DB in 1,4-dioxane, the dielectric constant of which is almost the same as that in the CDx cavity,[1] peaks at 480 nm.

Since, as mentioned above, MN and DB alone do not form a CT complex in their ground states in the solvents we have examined, the two substrate molecules are obviously forced to approach each other by virtue of the presence of CDx. Two alternatives can be considered as the species which forms the CT complex in the ground state and which emits the CT fluorescence in the excited state. One is a 1:1:1 inclusion compound, MDC, which is composed of one CDx molecule filled with an MN molecule and a DB molecule. The other is a 1:1:2 inclusion compound, MDC_2, formed by association of MC and DC. The formation of such species is represented by

Mechanism 3) $$MC + DB \overset{K'_5}{\rightleftharpoons} MDC, \quad (15)$$

$$MN + DC \overset{K'_6}{\rightleftharpoons} MDC, \quad (16)$$

and

Mechanism 4) $$MC + DC \overset{K_5}{\rightleftharpoons} MDC_2. \quad (17)$$

In the following, we will examine which of the two species, MDC or MDC_2, is the real species present in the MN–DB–CDx system using analyses somewhat similar to those employed for the naphthalene–CDx system. The fluorescence intensity of MC, I_f(MC), which is proportional to [MC] in the MN–DB–CDx system, should satisfy the following relations for Mechanism 3 and 4, respectively:[23]

$$\frac{1}{I_f(MC)}=\frac{K_3K'_5[CDx]_0}{c[MN]_0(1+K_4[CDx]_0)}[DB]_0 + \frac{(1+K_3[CDx]_0)}{c[MN]_0}, \quad (18)$$

and

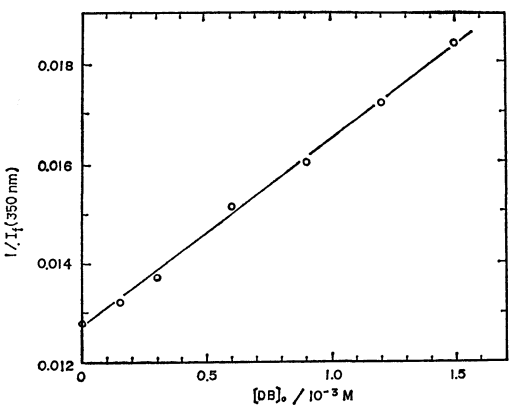

Fig. 15. Plot of $1/I_f$(350 nm) *vs.* $[DB]_0$.
$[MN]_0=9.60\times10^{-5}$ M; $[CDx]_0=8.40\times10^{-3}$ M.

$$\frac{1}{I_f(MC)}=\frac{K_4K_5[CDx]_0}{c[MN]_0(1+K_4[CDx]_0)}[DB]_0 + \frac{(1+K_3[CDx]_0)}{cK_3[MN]_0[CDx]_0}, \quad (19)$$

where $[MN]_0$, $[DB]_0$, and $[CDx]_0$ refer to the initial concentration of each substrate, and c is an instrumental constant. When I_f(MC) is measured as a function of the DB concentration at fixed concentrations of MN and CDx, both Eq. 18 and Eq. 19 predict the plots of $1/I_f$(MC) *vs.* $[DB]_0$ to be linear. We cannot, therefore, discriminate between the two mechanisms from such plots alone. However, we should be able to determine the values of K'_5 and K_5, since the equilibrium constants K_3 and K_4 have already been obtained ($K_3=630$ M^{-1}, $K_4=15$ M^{-1}). Our next step is the following. Whichever of the two mechanisms is operating, we should be able to calculate the expected concentration of MDC or MDC_2 as a function of the CDx concentration through the relation containing either K'_5 or K_5 with the common values of K_3 and K_4. We will then compare the measured intensity of the CT fluorescence, I_f(CT), with the calculated curves of [MDC] and [MDC_2] and see which of the concentration curves better reproduce the observed I_f(CT) curve.

As a first step of the analysis, the reciprocal of the fluorescence intensities of the 350 nm band, $1/I_f$(350 nm), is shown plotted against $[DB]_0$ in Fig. 15. Simple kinetics shows that I_f(350 nm), which contains the fluorescence from the uncomplexed MN too (amounting to $\approx10\%$ of I_f(350 nm)), is proportional to I_f(MC), and thus the analyses by Eqs. 18 and 19 are possible. The values we obtain from Fig. 15 are: $K'_5=400$ M^{-1}, $K_5=3200$ M^{-1}. We now advance to the second step.

In order to make a comparison with the naphthalene–CDx system easier, it will be preferable to keep the concentrations of the two kinds of inclusion compound, MC and DC, approximately the same at each CDx concentration. We therefore employed the system in which $[MN]_0$ was fixed but $[DB]_0$ was varied according to the relation: $[DB]_0/[MN]_0=K_3/K_4(1+K_3[CDx]_0)$. (If the equilibriums involving MN–CDx and DB–CDx stop at the first stage of forming 1:1 inclusion compounds, [MC]=[DC] when $[DB]_0$ is varied by this relation.)

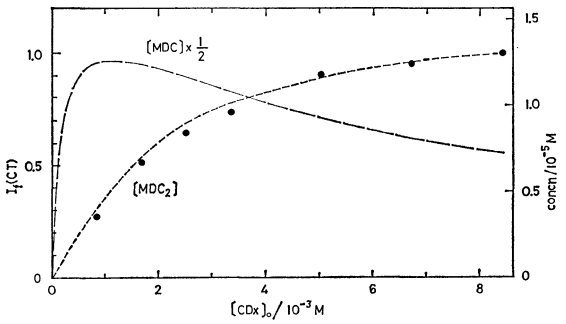

Fig. 16. Comparison of the observed CT fluorescence intensities, I_f(CT), with calculated concentrations [MDC] and [MDC_2].
●: I_f(CT), ——: [MDC], - - - -: [MDC_2].
$[MN]_0=5.0\times10^{-5}$ M. I_f(CT) is normalized to match the calculated [MDC_2] at the highest concentration of $[CDx]_0$.

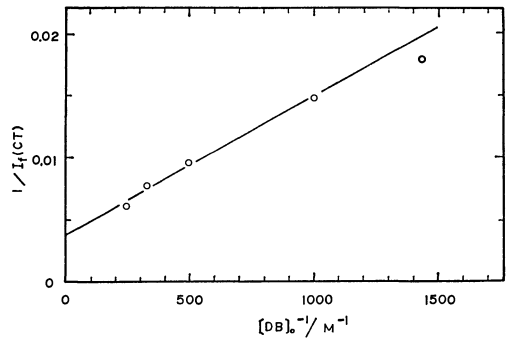

Fig. 17. Plot of $1/I_f$(CT) *vs.* $1/[DB]_0$.
$[MN]_0=9.60\times10^{-5}$ M; $[CDx]_0=8.40\times10^{-3}$ M.

The comparison of the variation of the experimentally observed I_f(CT) with $[CDx]_0$ under such conditions with the calculated curves of [MDC] and [MDC_2] is displayed in Fig. 16. It is immediately apparent that the calculated [MDC_2] curve reproduces the I_f(CT) curve fairly well, whereas the [MDC] curve nowhere matches the experimental curve. We are therefore led to conclude that MDC_2, not MDC, is the species responsible for the CT absorption and CT fluorescence in the MN–DB–CDx system.

Once Mechanism 4 is established, a simpler analysis of the CT fluorescence than that used above can be made. Namely, if we measure the CT fluorescence intensities as a function of $[DB]_0$ at fixed concentrations of MN and CDx, I_f(CT) can be expressed by

$$\frac{1}{I_f(CT)}=\frac{(1+K_3[CDx]_0)(1+K_4[CDx]_0)}{dK_3K_4K_5[MN]_0[CDx]_0^2}\frac{1}{[DB]_0}+\frac{1}{d[MN]_0}, \quad (20)$$

where d is an instrumental constant. A plot of $1/I_f$(CT) *vs.* $1/[DB]_0$ should give a linear relationship. Figure 17 shows such a plot, and with the known values of K_3 and K_4, the value $K_5=3700$ M^{-1} is obtained.[24] The K_5-value can also be determined from the absorbance of the CT absorption band, A(CT), of the same system which should have the same dependence on $[DB]_0$ as in Eq. 20. The value of K_5 evaluated from this type of analysis was 3300 M^{-1}.

Table 2. Equilibrium constants K_3, K_4, and K_5 at 25 °C, and enthalpy changes (ΔH) and entropy changes (ΔS) for K_3, K_4, and K_5 in the MN-DB-CDx system

	M^{-1} (at 25 °C)	ΔH / kJ mol^{-1}	ΔS / J mol^{-1} K^{-1}
K_3	630	−17	−5.0
K_4	15	−11	−16
K_5	3200[a]	−41	−16

a) The value obtained from I_f(MC) by Eq. 19.

These values of K_5 are close to the equilibrium constant obtained for the association of the 1:1 inclusion compounds in the naphthalene–CDx system ($K_2=4000$ M^{-1}). The previously determined value of K_5(=3200 M^{-1}) from Eq. 19 is solely from the intensity variation of the MC fluorescence (at 350 nm). The fairly good agreement between this K_5 and those obtained above from the CT bands implies that an exciplex type fluorescence is not involved in the observed 480 nm band which we have attributed to the CT type fluorescence.

The temperature dependence of the equilibrium constants, K_3, K_4, and K_5 was examined by measuring, respectively, the absorption spectra of the MC–CDx system, the fluorescence intensities of the DB–CDx system, and I_f(MC) of the MC–DB–CDx system in the temperature range from 3 to 25 °C, and by obtaining at each temperature the equilibrium constants as was done at 25 °C. The enthalpy changes ΔH and the entropy changes ΔS for K_3, K_4, and K_5 obtained from such measurements are summarized in Table 2.

It will be noted that the values of both $-\Delta H$ and ΔS for K_4 are smaller than those for K_3. This is consistent with the much smaller value of K_4 than K_3. The relatively inefficient formation of DC from DB and CDx may be due probably to the fact that the solubility of DB in water is about an order of magnitude larger than that of MN, and also that the steric effect of the two ortho-substituted linear cyano groups of DB may hinder the efficient complexing with CDx. The smaller value of $-\Delta S$ for K_3 than those for K_4 and K_5 indicates the less rigid structure of MC than DC and MDC_2.

As in the case of the naphthalene–CDx system, fluorescence decay times and fluorescence quenching by I^- and IO_3^- were studied for MN, MC, and MDC_2. Aqueous solutions of MN alone, MN–CDx, and MN–DB–CDx ($[MN]_0=9.6\times10^{-5}$M, $[CDx]_0=8.4\times10^{-3}$M, and $[DB]_0=2.0\times10^{-3}$ M) were examined. With the 316 nm excitation, the quenching of the 350 nm bands for MN and MC and of the 480 nm band for MDC_2 was measured by adding varying amounts of KI or KIO_3. No corrections were applied for quenching of the 350 nm band of MC which contains about 10% of MN fluorescence. The fluorescence lifetimes and the quenching rate constants for each species are presented in Table 3. One immediately finds upon comparison with Table 1 that the quenching behavior of these ions for MN, MC, and MDC_2 is very similar to that for the corresponding species in the naphthalene–CDx system. Thus, nearly the same structure of

TABLE 3. FLUORESCENCE LIFETIMES (τ') IN AERATED SOLUTION AND RATE CONSTANTS FOR QUENCHING (k_q) FOR MN, MC, AND MDC_2 IN THE MN-DB-CDx SYSTEM

		MN	MC	MDC_2
τ'/ns		11	12	39
$k_q/10^9\ M^{-1}\ s^{-1}$	I^-	6.0	2.6	1.7
	IO_3^-	2.8	0.60	−0.06

the 1:1:2 inclusion compound as that of the 2:2 inclusion compound (N_2C_2) is implicated from these quenching results.

Discussion

Sodium 1-naphthyl acetate (electron donor) and picric acid (electron acceptor) do not form a complex under usual conditions, but recently Kobayashi *et al.*[25] reported the formation of a charge transfer complex (CT) between them in the presence of γ-cyclodextrin but not significantly in the presence of β-cyclodextrin. They attributed these results to the capability of γ-cyclodextrin to include both electron donor and acceptor molecules in its cavity simultaneously.[26] What we have found in the MN–DB–CDx study is a similar promotion of the CT complex formation between MN and DB, but in this case by virtue of the association of two β-cyclodextrin molecules each of which accommodates one electron donor or acceptor molecule in its cavity. Much less efficient complex formation by β-cyclodextrin found in the Kobayashi *et al.*'s system appears to imply the incapability of the β-cyclodextrin molecule to hold the two molecules in its cavity, probably due to its smaller cavity size than in γ-cyclodextrin. Their results are thus consistent with our interpretation assigning the species responsible for the CT absorption and CT fluorescence to the 1:1:2 inclusion compound, not to the 1:1:1 inclusion compound.

Our results on the naphthalene–CDx system show that a similar type of association of two 1:1 inclusion compounds can occur when an aromatic hydrocarbon molecule is included in the CDx molecule. We did not find an excimer-type emission in the benzene–CDx system. Solubility restrictions prevented us from pursuing the same type of experiment for an anthracene–CDx or pyrene–CDx system. We therefore do not know at present whether the deciding factor for the formation of the 2:2 inclusion compound in an aromatic–CDx system is merely the molecular size of the substrate or if some other specific physicochemical properties of the substrate are involved. Such an association may be hindered for inclusion complexes containing a molecule larger than naphthalene by its protrusion out of the CDx cavity.

What remains to be discussed here is the problem of what kind of binding force brings the two 1:1 inclusion compounds together. One possible explanation is that the CDx molecules in aqueous solution (in the absence of any substrates) may be capable of forming a dimer by themselves. To the author's knowledge, however, there has been no experimental evidence pointing to the occurrence of such phenomena in cyclodextrin systems. Another explanation is to consider such an association as a first stage of the precipitation process. This idea comes from the fact that the solubility of the inclusion compounds is generally smaller than that of CDx. Once a 2:2 or 1:1:2 adduct is formed by adhesion of two 1:1 adducts in the course of precipitation, its unique structure of two CDx shells shielding completely the substrate molecules within them may prevent the attack of other 1:1 adducts to form a higher aggregate. That is, the first stage of the precipitation process may persist over a fairly wide range of concentration owing to the peculiar properties of the CDx inclusion compounds. Of course, this is only a speculation. Elucidation of further details in various aspects of 2:2 or 1:1:2 inclusion compounds will require more systematic studies using a variety of substrate materials and will have to wait for future study.

The author wishes to thank Professor Fumio Hirayama for his valuable comments and critical review of the manuscript.

References

1) R. L. VanEtten, J. F. Sebastian, G. A. Clowes, and M. L. Bender, *J. Am. Chem. Soc.*, **89**, 3242 (1967).
2) C. J. Seliskar and L. Brand, *Science*, **171**, 799 (1971).
3) K. Harata and H. Uedaira, *Bull. Chem. Soc. Jpn.*, **48**, 375 (1975).
4) N. Ikeda and H. Yamaguchi, *Chem. Phys. Lett.*, **56**, 167 (1978).
5) I. Tabushi, K. Yamamura, K. Fujita, and H. Kawakubo, *J. Am. Chem. Soc.*, **101**, 1019 (1979).
6) F. Cramer, W. Saenger, and H. -Ch. Spatz, *J. Am. Chem. Soc.*, **89**, 14 (1967).
7) H. Kondo, H. Nakatani, and K. Hiromi, *J. Biochem.*, **79**, 393 (1976).
8) A. Ueno, H. Yoshimura, R. Saka, and T. Osa, *J. Am. Chem. Soc.*, **101**, 2779 (1979).
9) A. Ueno, K. Takahashi, and T. Osa, *J. Chem. Soc., Chem. Commun.*, **1980**, 921.
10) H. E. Edwards and J. K. Thomas, *Carbohydr. Res.*, **65**, 173 (1978).
11) M. Otagiri, K. Uekama, and K. Ikeda, *Chem. Pharm. Bull.*, **23**, 188 (1975).
12) K. Kano, I. Takenoshita, and T. Ogawa, *Chem. Lett.*, **1980**, 1035.
13) K. Lindner and W. Saenger, *Angew. Chem., Int. Ed. Engl.*, **17**, 694 (1978).
14) The technique for determining the spectral response of the analyzing system has been described in: S. Hamai and F. Hirayama, *J. Chem. Phys.*, **71**, 2934 (1979).
15) J. B. Aladekomo and J. B. Birks, *Proc. R. Soc. London, Ser. A*, **284**, 551 (1965).
16) E. A. Chandross and C. J. Dempster, *J. Am. Chem. Soc.*, **92**, 3586 (1970).
17) M. Otagiri, T, Miyaji, K. Uekama, and K. Ikeda, *Chem. Pharm. Bull.*, **24**, 1146 (1976).
18) CDx also forms inclusion compounds with inorganic anions. Rohrbach *et al.* (*J. Phys. Chem.*, **81**, 944 (1977)) reported that the equilibrium constant for the formation of an inclusion compound with I^- is 18.0 M^{-1} in aqueous so-

lution at 25 °C. They employed a competition method in which the indicator was an azo dye. We obtained, however, the values of 4.1 and 4.7 M^{-1} for I^- using neutral substances, 2-naphthol and 1,4-naphthoquinone, respectively, by a similar competition method. It is not apparent why such a discrepancy occurs between our values and their value. The equilibrium constant for IO_3^- was determined to be 1.0 M^{-1} using 1,4-naphthoquinone. Because of these small values of the equilibrium constants, formation of the inclusion compounds of CDx with I^- and IO_3^- does not seriously change the concentration of CDx in the quenching experiments.

19) The viscosity of water increases only about 2% on adding 8.4×10^{-3} M of CDx. Thus, the viscosity effect on the quenching constant k_q is negligible.

20) H. Kobashi, M. Takahashi, Y. Muramatsu, and T. Morita, *Bull. Chem. Soc. Jpn.*, **54**, 2815 (1981).

21) The equilibrium constant K_3 for formation of MC can also be determined from the Benesi-Hildebrand plot for the fluorescence increment (Eq. 7). The value obtained is 660 M^{-1} which is close to 630 M^{-1} determined from the absorption spectra.

22) In more concentrated solutions of MN ($>5\times10^{-4}$ M), an excimer-like fluorescence appeared at around 420 nm. Although this emission is not as pronounced as in the case of naphthalene–CDx system, this observation suggests the possibility of the presence of a 2:2 inclusion compounds in the MN–CDx system in the high MN concentration region.

23) In deriving Eqs. 18 and 19, the fluorescence intensity of MC is regarded as that solely from the 1:1 inclusion compound MC, *i.e.*, a monomer-like emission from the MC part of MDC or MDC_2 is assumed not to occur. Since we define here MDC or MDC_2 as the species which exhibits the CT absorption, and the CT interaction is generally stronger in the excited state than in the ground state, this assumption seems reasonable.

24) The plots of $1/I_f(CT)$ *vs.* $1/[DB]_0$ shown in Fig. 17 can also be analyzed by Mechanism 3 which we have already discarded. Such an analysis gives $K'_5=8.7$ M^{-1} whereas the K'_5-value obtained from $I_f(MC)$ by Eq. 18 is 400 M^{-1} as stated before. This vast inconsistency further supports the inadequacy of Mechanism 3.

25) N. Kobayashi, A. Ueno, and T. Osa, *J. Chem. Soc., Chem. Commun.*, **1981**, 340.

26) The capability of γ-cyclodextrin to include two molecules of different kinds has also been reported in: A. Ueno, T. Takahashi, Y. Hino, and T. Osa, *J. Chem. Soc., Chem. Commun.*, **1981**, 194.

Freezing-Thawing Hysteresis Phenomena of Biological Systems by the New Method of Proton Magnetic Resonance

Ei-ichiro Suzuki* and Nobuya Nagashima

Central Research Laboratories, Ajinomoto Co. Inc., 1-1 Suzuki-cho, Kawasaki-ku, Kawasaki 210

(Received December 11, 1981)

An automatic recording system was developed for unfrozen water content and spin-spin relaxation time measurements as continuous functions of temperature, by using a broad-line pulsed NMR spectrometer and a minicomputer. The advantages of this system are that the exact quantitative measurements can be done by calibrating the nonlinearity of the NMR sensitivity, and that for high sensitivity temperature measurement the thermocouple with special device is directly immersed in a sample. Three types of freezing-thawing hysteresis phenomena, (1) recrystallization of solute(hydroxy-L-proline, D-mannitol) and refreezing of released hydrated water molecules in frozen aqueous solutions, and (2) hysteresis as the characteristic feature of gels(gelatin, α_{s1}-casein), and (3) supercooling of capillary water in water-insoluble materials(zein, yeast RNA, cellulose) were analysed. The usefulness of this system as an analytical instrument of hydration properties of biological materials is emphasized.

The state of water in biological systems has been one of the most important subjects in life science studies. Proton magnetic resonance gives most useful information in the study of water motions,[1,2] although there are many other methods, for example, dielectric relaxation, thermal analysis, and neutron scattering[3] *etc.* There have been many publications concerning the application of proton magnetic resonance to studies of the state of water in biological systems or food.[4,5] At room temperature, a distinction between the state of water, *i.e.* bound or free, is given by a graphical resolution of the triple exponential decay curve due to the three kinds of spin-spin relaxation times(T_2) as observed using the Carr-Purcell/Meiboom-Gill method.[6] However this method presents experimental difficulties and is not applicable to homogeneous aqueous solutions, which have both bound and free water but show only the averaged T_2. Then the measurements of unfrozen water(UFW) content and its relaxation times as functions of temperature are effective for the investigation of wider range of samples.[2,7] We have developed a convenient system for some purposes; it involves a broad-line pulsed NMR spectrometer and an X-Y analogue recorder.[8] By using this system, only the variation of the free induction decay(FID) amplitude in the voltage value at about 40 μs with temperature change can be measured. This is acceptable as a qualitative method for the measurement of the UFW content as a function of temperature, which is called the freezing curve.

A quantitative method was developed for the freezing curve measurement, by adding a minicomputer system and a special thermocouple device which is directly immersed in a sample. By this means the UFW content and the spin-spin relaxation time as functions of temperature can be recorded automatically.[9] This new freezing curve method is a powerful tool for the investigation of the state of water in biological systems, especially those which show freezing-thawing hysteresis phenomena. The essencial cause of freezing-thawing hysteresis is only supercooling, but it was found by this method that there are three types of supercooling. In this study, water systems of sugar alcohols(D-sorbitol, D-mannitol[9]), and amino acids(glycine, L-alanine, L-methionine, L-proline, hydroxy-L-proline), and proteins(gelatin,[9] α_{s1}-casein, glycinin, bovin serum albumin, ovalbumin, zein) and other polymers(cellulose, polyethylene glycols, yeast RNA) were measured. In this paper, some aspects of freezing-thawing hysteresis are described to illustrate the usefulness of our freezing curve method.

Experimental

Sample Preparation. All samples were commercially available, except for α_{s1}-casein and glycinin (soybean protein 11s unit), which were obtained by preparative gel filtration chromatography.

Freezing Curve Measurements. The block diagram of the system, which consists of a broad-line pulsed NMR spectrometer with proton Larmor frequency of 20 MHz (Bruker, minispec p 20) and a disc based minicomputer system (Yokogawa-Hewlett-Packard, HP 1000) is shown in Fig. 1. Each sample of about 250 mg in a 6.8 mm inner diameter glass tube is cooled or warmed at the usual rate of about three degrees per minute, by using gas and liquid nitrogen, if necessary, whose temperature can be controlled by a variable temperature unit (Bruker B-ST 100/700). The freezing-thawing processes are observed using the NMR spectrometer and the chromel-constantan thermocouple.

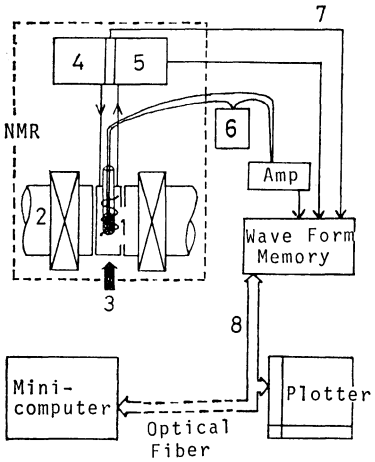

Fig. 1. Block diagram of the system.
1: Sample, 2: parmanent magnet, 3: nitrogen gas flow, 4: transmitter, 5: receiver, 6: cold junction of ice for thermocouple, 7: sampling trigger, 8: HP-IB interface bus with fiber optic link.

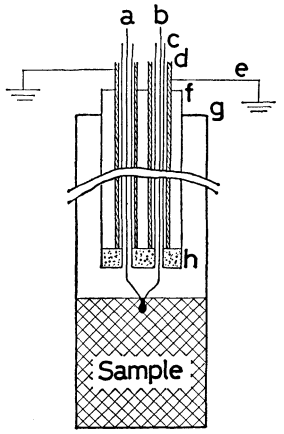

Fig. 2. The measurement of sample temperature with the special thermocouple device.
a,b: Chromel and constantan wires, c,f: teflon tubes, d: aluminum metal, e: ground to the NMR spectrometer body, g: sample tube of glass, h: thermal insulater.

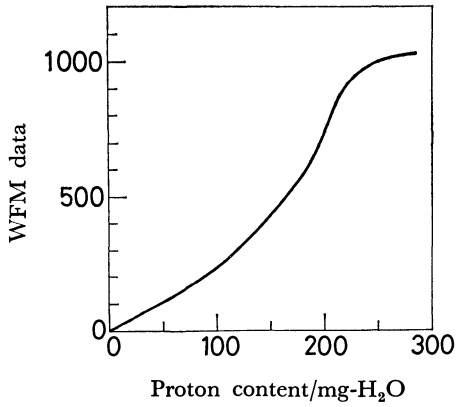

Fig. 3. The sensitivity of the NMR spectrometer. Proton content shows the water amount in the cupric sulfate solution whose sample volume is constant at about 0.27 cm³. A WFM datum is a digital value, which ranges from 0 to 1023.

The signal values at intervals of two μs of free induction decay (FID) curve after a 90° pulse and the sample temperature are A/D converted and memorized at every few seconds by a two channel wave form memory (WFM) apparatus (Kikusui, modified 8702S). The data are transferred to the minicomputer by a fiber optic Hewlett-Packard interface bus(HP-IB) link system (HP, 12050A).

One of the advantages of this system is that the special thermocouple device is directly immersed in a sample as shown in Fig. 2. High sensitivity measurement of the temperature change of a sample can be achieved with this thermocouple. The WFM apparatus and the NMR spectrometer generate the electric clock pulses from quartz oscillators. The noise so generated make it impossible to detect the FID curve; the thermocouple acts like an antenna here. For shielding from this noise, grounded aluminum tape is used. A thermal insulator is necessary to reduce the heat conduction to the sample through the aluminum metal.

Another advantage is that the exact quantitative measurement can be done by calibrating of the FID curve at each 90° pulse. The real FID curves are obtained after calibrating the sensitivity of NMR by using fifteen standards of 0.65 M (1 M=1 mol dm^{-3}) cupric sulfate solutions in water–heavy water mixtures which have various proton concentrations and the same sample volume of about 0.27 cm³ at the bottom of a sample tube. This calibration is required because of the nonlinear relationship between the proton content and the signal intensity, as shown in Fig. 3. This calibration curve is stored in our system memory and is used in every measurement of each FID curve.

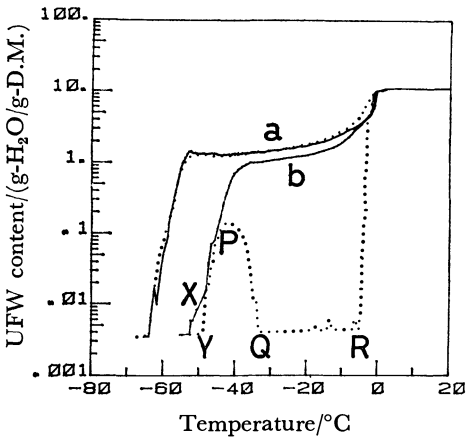

Fig. 4. Freezing (——) and thawing (·····) curves of 9.1% aqueous solutions of L-proline(a) and hydroxy-L-proline(b).
X and *Q* are the liquid signal vanishing temperatures, and *Y* and *R* are the liquid signal appearing temperatures, and *P* shows the top of the peak.

On the measurement of FID curves, it generally occurs that a sample exhibits at least two different spin-spin relaxation times T_{2s} and T_{2l}, which correspond to solid (short T_2) and liquid (long T_2) state protons, respectively. The shape of the FID curve of liquid state protons is exponential, but that of solid state protons is Gaussian. The population of liquid state or unfrozen protons (UFP) is obtained by extrapolating the FID curve from 40 to 100 μs back to zero time. Then this point is corrected according to the well-known Curie law; the lower the temperature, the greater the sensitivity. For practical purposes, this UFP value is reduced to a UFW content and converted to a dry basis, *i.e.* gram water per gram dry matter (g-H_2O/g-D.M.), using the dry matter value obtained by drying a sample for about 8 h at 115 °C. The UFW content is plotted as a function of temperature on a semilogarithmic graph by a graphic plotter (HP, 9872A). This function was named the freezing curve (liquid content curve). The solid content versus temperature can be obtained in a similar way. Also T_{2s} versus temperature and T_{2l} versus temperature can be obtained.

All of the programs used were written in FORTRAN language of the software package (HP, RTE IVB) of the minicomputer system.

Results and Discussions

Recrystallization of Solutes in Frozen Aqueous Solutions. It has been found that freezing curves of some aqueous solutions show peculiar freezing-thawing hysteresis. The example of D-mannitol aqueous solution has been reported previously.[9] Figure 4(b) shows the remarkably large hysteresis of hydroxy-L-proline aqueous solution, in contrast with the case of L-proline (a). The following mechanism is suggested for this large hysteresis of hydroxy-L-proline. In the cooling process,

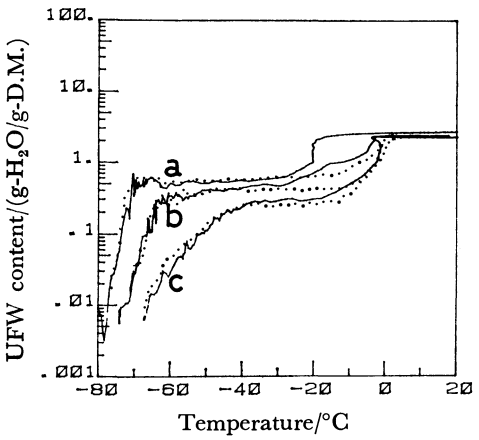

Fig. 5. Freezing (——) and thawing (·····) curves of 32% aqueous colloids of gelatin(a), α_{s1}-casein(b), and glycinin(c).

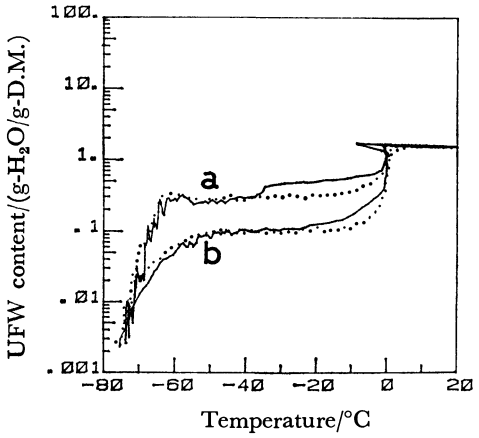

Fig. 6. Freezing (——) and thawing (·····) curves of aqueous suspensions of zein(a, 37%) and cotton cellulose(b, 39%).

free water in aqueous solution is frozen at near 0 °C, and water hydrated(bound) to solute remains as UFW until about −40 °C, and vitrification of the cluster which consists of solute and hydrated water molecules occurs(point *X*). In the warming process, after beginning of thawing(point *Y*), hydrated water molecules are released from the cluster with the beginning of recrystallization of solute, and their refreezing takes place at the point *P*. The difference between D-mannitol and hydroxy-L-proline is that the *X* and *Y* points are not the same in the former case.

Materials such as L-proline and D-sorbitol, which have comparatively high water solubilities, showed no hysteresis loops, at any cooling rates. At the usual cooling rate of about three degrees per minute, materials of low water solubilities such as glycine, L-alanine, L-methionine *etc.* do not show this type of hysteresis loop, but show simple hysteresis without a peak in the thawing curve, due to completion of recrystallization in the cooling process. The solubilities of hydroxy-L-proline and D-mannitol are medium, and these substances also show simple hysteresis loops, at the cooling rate of one degree per minute or more slowly.

The shape of the thawing curves of polyethylene glycols depends upon their molecular weight or crystallinity. In the case of low molecular weight, the shape of the thawing curve is almost the same as that of the freezing curve. But in the high molecular weight(about 6000) case, a remarkably large hysteresis can be observed. This hysteresis loop is similar to that of hydroxy-L-proline, but the rehydration temperature *R* is about −20 °C.

Characterization of Biopolymer Colloids——Gels and Sols. Figure 5 shows the freezing and thawing curves of 32% aqueous colloids of three kinds of proteins; α_{s1}-casein, glycinin, and gelatin. The UFW content of glycinin, which is known as a "cold-precipated protein,"[10] is much lower than that of gelatin, which forms a viscous aqueous gel. The freezing-thawing curve of gelatin has a remarkably large hysteresis loop, but that of glycinin has a very small hysteresis loop; that of α_{s1}-casein is situated between the two.

It is thought that water molecules in gelatin gel are structured in a gel network and supercooled until about −20 °C, and then a phase separation occurs due to freezing, and micro ice crystals are formed, which do not melt until 0 °C during thawing. Hence the freezing-thawing curve of gelatin has large hysteresis, and that of α_{s1}-casein has hysteresis of a medium value, due to the high viscosity and comparatively large UFW content of the liquid.

Table 1. UFW contents and signal vanishing temperatures for several proteins

Proteins	Concentrations/%	UFW[a] g-H_2O/g-D.M.	SVT[b]/°C
Glycinin	32	0.24	−68
Ovalbumin	31	0.32	−78
Bovine serum albumin	29	0.38	−80
α_{s1}-Casein	32	0.41	−72
Gelatin	32	0.60	−77

a) At about −30 °C. b) Signal vanishing temperature, which is defined as the temperature at which the apparent UFW content becomes lower than 0.01 g-H_2O/g-D.M.

The UFW values at −30 °C, which correspond to tightly-bount water content,[8] and signal vanishing temperatures(SVT) are shown for several proteins in Table 1. The freezing-thawing curve of an aqueous colloid of bovine serum albumin has no hysteresis, although its UFW content at −30 °C is near to that of α_{s1}-casein. The viscosity of this colloid is much smaller than that of α_{s1}-casein. This suggests that the measurement of weakly-bound water, which is frozen between 0 and −30 °C and does not melt in this case until near 0 °C, is very important to characterize the hydration properties of biopolymers, and that the freezing curve method is very useful for this purpose. The SVT data show the vitrification points of the clusters, which consist of protein and unfrozen water molecules. This data are also useful for the characterization of biopolymers.

Special Problems for Water-insoluble Biopolymers——Cellulose and Corn Protein etc. Figure 6(a) shows the freezing-thawing hysteresis phenomenon of aqueous sus-

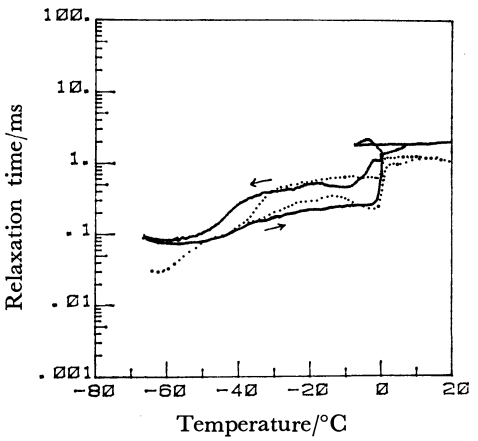

Fig. 7. Temperature dependence of spin-spin relaxation time of aqueous suspensions of zein (·····, 37%) and cotton cellulose (——, 39%).

pension of corn protein(zein). It is shown that a part of the UFW is frozen at about −37 °C in the cooling process. Freeze-drying from the homogeneous solution in 90% ethanol gave fine powder, which does not show such a phenomenon. Hence the cause of this hysteresis is thought to be the freezing of weakly-bound water in capillaries of water-insoluble materials. A similar phenomenon was observed for water-insoluble yeast RNA powder. A related type of freezing-thawing hysteresis is studied in relation to the mechanism of frost avoidance in plant tissues by Burke *et al.*,[11] using NMR and thermal analysis. We think that our method is more convenient and powerful for these studies.

Figure 6(b) shows the freezing-thawing curve of cotton cellulose, which has no obvious hysteresis loop. But the remarkable hysteresis phenomenon of spin-spin relaxation time (T_{21}) was observed, which is similar to the case of zein, as shown in Fig. 7. By the thermal analysis for cotton cellulose suspension with a differential scanning calorimeter(DSC; Daini Seikosha, SSC 560U), a broad exothermic peak was observed at about −42 °C. The cause of this phenomenon is not clear but it is obvious from Fig. 6(b) that no water is frozen at about −42 °C. One of the possible speculations is that the mobility of UFW is lowered by the change of surroundings accompanied with the crystal transformation of cotton cellulose at about −42 °C, because cellulose has polymorphism. In general, the freezing curve method would be powerful to elucidate the mechanism of an exothermic or endothermic peak observed in a DSC curve.

Conclusion

The new freezing curve method is a useful tool for the analysis of hydration properties of biological materials, from the viewpoint of freezing-thawing hysteresis phenomena. Three types of phenomena, (1) recrystallization of solutes and refreezing of released hydrated water in frozen aqueous solutions, (2) hysteresis as the characteristic feature of biopolymer gels, (3) supercooling of capillary water in water-insoluble biopolymers, were discussed and useful information was obtained. Our method can be applied to many practical problems in the food and drug industry *etc.*

The authors are grateful to Professor Masamichi Tsuboi of Tokyo University for his keen interest and valuable discussions.

References

1) J. M. Harvey, M. C. R. Symons, and R. J. Naftalin, *Nature (London)*, **261**, 435 (1976).
2) A. Zipp, I. D. Kuntz, and T. L. James, *J. Magn. Reson.* **24**, 411 (1976).
3) J. Randall, H. D. Middendorf, H. L. Crepsi, and A. D. Taylor, *Nature (London)*, **276**, 636 (1978).
4) "Water Relations of Foods," ed by R. B. Duckworth Academic Press, London (1975).
5) J. A. Walter and A. B. Hope, *Prog. Biophys.*, **23**, 3 (1971).
6) P. S. Belton, R. R. Jackson, and K. J. Packer, *Biochim. Biophys. Acta*, **286**, 16 (1972).
7) B. M. Fung and T. W. McGauchy, *Biochim. Biophys. Acta*, **343**, 663 (1974).
8) N. Nagashima and E. Suzuki, "Water Activity: Influences on Food Quality," ed by L. B. Rockland and G. F. Stewart, Academic Press, London (1981), p. 247.
9) E. Suzuki and N. Nagashima, *Chem. Lett.*, **1981**, 181 (1981).
10) D. R. Briggs and R. L. Mann, *Cereal Chem.*, **27**, 243 (1950).
11) M. J. Burke, M. F. George, and R. G. Bryant, p. 111 in Ref. 4.

Elementary Patterns in Protein-Nucleic Acid Interactions. IV.† Crystal Structure of 3-(Adenin-9-yl)propionamide : 1-Methylthymine (1 : 1) Complex Dihydrate

Midori Takimoto,* Akio Takenaka, and Yoshio Sasada
Laboratory of Chemistry for Natural Products, Tokyo Institute of Technology, Nagatsuta, Midori-ku, Yokohama 227
(Received December 21, 1981)

As a ternary interaction model between adenine:thymine base pair and carbamoyl group, 3-(adenin-9-yl)-propionamide: 1-methylthymine complex was prepared and its crystal structure was examined. The crystal exhibits a disordered structure, and the structure unit is a monoclinic cell with dimensions $a=11.368(1)$, $b=6.909(1)$, $c=12.708(2)$ Å, and $\beta=114.49(1)°$. The space group is $P2_1$ and the unit cell contains two complexes and four water molecules. The base pairing pattern between adenine and thymine is the Hoogsteen type. The carbamoyl group is hydrogen-bonded to N(A1) of adenine in this base pair, the distance NH···N(A1) being 2.94(2) Å. With two kinds of hydrogen bonds of the carbamoyl group, NH···N(A1) above-mentioned and NH···O(carbamoyl), the 3-(adenin-9-yl)propionamide molecules form a sheet extending perpendicular to the c axis; the base-paired thymine molecules extrude alternately from the sheet. Diffused spots along c* with half integers of l can be interpreted as a stacking disorder of the sheets.

In the studies of the elementary patterns in protein: nucleic acid interactions, we have reported several modes of hydrogen bonding between cytosine and carboxyl group,[1-4] between adenine and indolyl group,[5,6] between adenine and carboxyl group,[7,8] and between adenine and carbamoyl group.[9]

It is well-known that nucleic acid tends to form double strands by the hydrogen bonds between the complementary bases. Rich *et al.* proposed a recognition pattern between the carbamoyl group and base-paired adenine.[10] It is interesting to examine whether some base pair shows special affinity to the carbamoyl group, and where is the preferential binding site of the bases.

We have succeeded in preparing crystals of 3-(adenin-9-yl)propionamide : 1-methylthymine complex as one of the ternary interaction models between purine:pyrimidine base pair and the side chain of amino acid, and an X-ray analysis of the crystal structure has been performed. In this paper, we will report a mode of hydrogen bonding between adenine: thymine base pair and the carbamoyl group, and discuss the capability of the interaction of carbamoyl group with a double-stranded polynucleotides.

Experimental

Equimolar quantities of 3-(adenin-9-yl)propionamide[9] and 1-methylthymine (purchased from Cyclo Chem. Co.) were dissolved in a water–methanol (1:1) solution. Thick plate crystals of the 1:1 complex were obtained after standing the solution for 10 d. Density was measured by flotation in a mixture of cyclohexane and carbon tetrachloride. Preliminary X-ray photographs indicated the space group to be $P2_1$ or $P2_1/m$, but on the upper-layer Weissenberg photographs diffused spots extending along c* appeared at the positions with half-integer of l, as shown in Fig. 1. It apparently suggests the stacking disorder with two kinds of sheets along c. To obtain the crystals without such disorder, we tried crystallization from water-methanol solutions of the adenine and thymine with different molar ratios (1:2, 1:3, 2:1 and 3:1) at different temperatures (2—25 °C), but failed.

A crystal from the solution with 1:1 molar ratio, $0.2\times0.2\times0.05$ mm³ in size, was used for data collection. The intensities for 2767 independent reflexions in the range $4°<2\theta<122°$ were measured on a Rigaku automated four-circle diffractometer with nickel filtered Cu $K\alpha$ radiation ($\lambda=1.54184$ Å). A scan speed was 4° (in 2θ) min^{-1} and a scan width was 1.2° (in ω) plus α_1-α_2 divergence. After every 50 reflexions, five standard reflexions were monitored, the intensities of which showed no significant change. The intensities were corrected for Lorentz and polarization effects, but not for absorption. Only 73 reflexions had no net intensities; the observational threshold value, F_{11m}, was 1.98. The standard deviations were estimated by the equation of $\sigma^2(F_o)=\sigma_P^2(F_o)+qF_o^2$, where q, 8.1×10^{-6}, was derived from the variations of the monitored reflexions.[11]

Crystallographic data are summarized in Table 1.

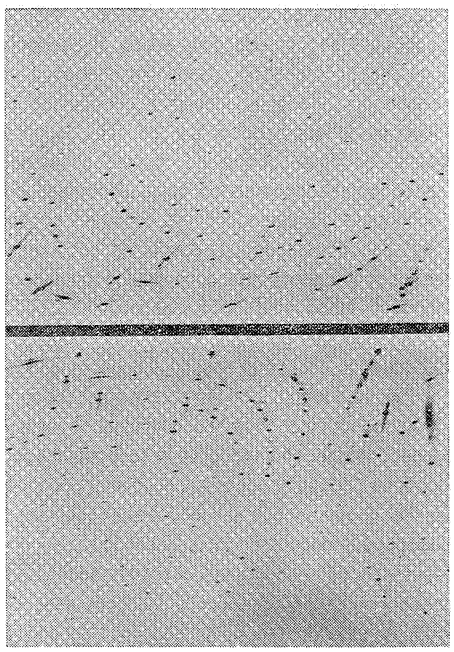

Fig. 1. An hll layer Weissenberg photograph of the title crystal.

Structure Determination and Refinement

Structure determination was unsuccessful on the basis of the space group $P2_1$ and $P2_1/m$. As stated in the

† Part III of this series is Ref. 8.

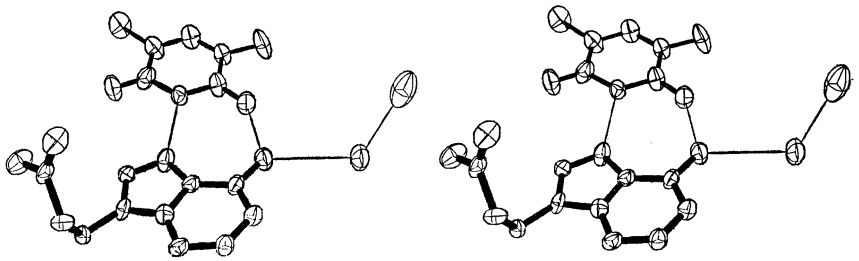

Fig. 2. Stereoview of 3-(adenin-9-yl)propionamide:1-methylthymine complex dihydrate with 50% probability ellipsoids.

Table 1. Crystal data

3-(Adenin-9-yl)propionamide: 1-Methylthymine Complex Dihydrate	
$C_8H_{10}N_6O : C_6H_8N_2O_2 : 2H_2O$	
Space group: $P2_1$	
$a=11.368(1)$ Å	$U=907.0$ (1) Å^3
$b=6.909(1)$ Å	$Z=2$
$c=12.708(2)$ Å	$D_x=1.41$ g cm^{-3}
$\beta=114.49(1)°$	$D_m=1.40$ g cm^{-3}

previous section, diffused spots appeared at the positions with half-integer of l, but the spreads of these spots were rather small. If these spots were regarded to be Bragg reflexions, the space group should be $P2_1/c$. Values of l for all normal spots became even and those for diffused ones were odd. On the basis of the space group $P2_1/c$, however, the analysis by the use of the MULTAN 74 Programme[12] was not straightforward. As E values of reflexions with odd l's were much less than those with even l's, the former reflexions were not included in the data set for phase determinations, if the normal criterion for the magnitudes of E was applied. So, we prepared a starting data set by picking up the largest 30 reflexions in each parity group. An E map with the fifth lowest R value revealed a reasonable molecular skeleton. Successive refinement of the structural parameters, however, was not successful in getting a reasonably low R value. Therefore, we tried to modify the refinement process from the view of rather special character of the present crystal including some stacking disorder along the c axis. As will be described in the later section, the molecules related by 2_1 symmetry form a sheet parallel to the ab plane by the hydrogen bonds. If such a sheet is represented by P, the stacking mode in the space group $P2_1/c$ is $P\bar{P}\bar{P}P\cdots$, where $\bar{P}$ stands for an inversed sheet. The unit cell for P contains equivalent positions x, y, z, and $\bar{x}$, $1/2+y$, $\bar{z}$, and that for $\bar{P}$ $\bar{x}$, $\bar{y}$, $\bar{z}$ and x, $1/2-y$, z (the unit cell dimensions are those given in Table 1). Therefore, a reasonable model of disorder was constructed by putting the stacking mode $PP\cdots$ or $\bar{P}\bar{P}\cdots$ into the alternate P's and $\bar{P}$'s. Intensity profiles of the diffused spots on hll Weissenberg photographs were measured with a microdensitometer (SAKURA PDM-5) and interpreted on such a disordered model by the use of Wilson's equation.[13] The probability α of finding P after P was estimated to be 0.16 from half-value width of a diffused spot (2,1,3/2), after correction for spot size. Low value of α means that the major part of the crystal consists of the $P2_1/c$ domains. So, intensities can be approximately expressed as a sum of the intensity from the $P2_1/c$ domains and that from the $P2_1$ domains. Refinement on such approximation is equivalent to the improvement of the structural parameters and w in the equation:

$$F = K[wF_P + (1-w)F_{\bar{P}}],$$

Table 2. Fractional coordinates and isotropic temperature factors

The B values accompanied with $\langle\ \rangle$ are the equivalent isotropic temperature factors calculated from anisotropic thermal parameters using the equation $B=8\pi^2(U_1+U_2+U_3)/3$, where U_1, U_2, and U_3 are the principal components of mean square displacement matrix $\boldsymbol{U}$. Values in $\langle\ \rangle$ are anisotropicity defined by $(\sum(B-8\pi^2U_i)^2/3)^{1/2}$. The e.s.d.'s in ( ) refer to last decimal places.

Atom	x	y	z	B/Å^2
N(A1)	0.6478(8)	0.166(2)	0.5857(7)	2.8⟨8⟩
C(A2)	0.564(1)	0.167(2)	0.473(1)	3.0⟨7⟩
N(A3)	0.4344(8)	0.184(2)	0.4280(7)	2.7⟨8⟩
C(A4)	0.393(1)	0.208(2)	0.5130(9)	2.8⟨3⟩
C(A5)	0.4702(9)	0.207(2)	0.6320(8)	2.6⟨7⟩
C(A6)	0.603(1)	0.186(2)	0.668(1)	2.9⟨8⟩
N(A6)	0.6899(7)	0.190(2)	0.7803(7)	3.6⟨17⟩
N(A7)	0.3931(7)	0.240(4)	0.6921(6)	3.3⟨19⟩
C(A8)	0.2745(8)	0.253(4)	0.6109(8)	2.9⟨11⟩
N(A9)	0.2685(6)	0.244(4)	0.4996(6)	2.5⟨13⟩
C(A11)	0.1535(9)	0.263(4)	0.3899(8)	2.6⟨7⟩
C(A12)	0.114(1)	0.058(2)	0.335(1)	3.1⟨9⟩
C(A13)	0.064(1)	−0.068(3)	0.409(1)	3.2⟨20⟩
N(A13)	0.1066(8)	−0.256(4)	0.4322(8)	3.7⟨16⟩
O(A13)	−0.0199(8)	0.001(2)	0.4383(7)	4.3⟨18⟩
N(T1)	0.3505(8)	0.247(4)	1.0715(7)	4.9⟨33⟩
C(T1M)	0.233(1)	0.215(5)	1.101(1)	7.0⟨56⟩
C(T2)	0.326(1)	0.255(4)	0.9551(9)	4.1⟨18⟩
O(T2)	0.2195(6)	0.250(4)	0.8778(6)	6.4⟨52⟩
N(T3)	0.4361(7)	0.263(4)	0.9340(6)	3.1⟨9⟩
C(T4)	0.562(1)	0.262(4)	1.0175(9)	3.5⟨17⟩
O(T4)	0.6519(6)	0.270(4)	0.9865(6)	4.7⟨27⟩
C(T5)	0.5801(9)	0.260(4)	1.1343(7)	3.2⟨17⟩
C(T5M)	0.716(1)	0.269(5)	1.2266(9)	5.6⟨43⟩
C(T6)	0.474(1)	0.245(4)	1.1570(8)	4.0⟨16⟩
O(W1)	1.0719(7)	−0.242(4)	0.9350(6)	6.7⟨40⟩
O(W2)	0.9731(7)	0.140(2)	0.8638(7)	5.8⟨37⟩

Table 3. Hydrogen bond distances and angles of 3-(adenin-9-yl)propionamide: 1-methylthymine complex dihydrate

Standard deviations are given in parentheses. * and † indicate PP̄ and PP junctions, respectively.

	l/Å		ϕ/°
N(A1)···N(A13)[a]	2.94(2)	C(A8)-N(A7)···N(T3)	120(1)
N(A13)···O(A13)[e]	2.80(2)	C(T2)-N(T3)···N(A7)	116(1)
N(A6)···O(W2)	2.96(2)	C(T4)-N(T3)···N(A7)	119(1)
O(T2)···O(W2)[h]	2.83(2)	C(T4)-O(T4)···N(A6)	137(1)
O(T4)···O(W1)[g]	2.88(3)*	C(T4)-O(T4)···O(W1)[g]	144(1)*
N(T3)···N(A7)	2.91(2)	C(T4)-O(T4)···O(W1)[c]	145(1)†
O(T4)···N(A6)	2.88(2)	N(A6)···O(T4)···O(W1)[g]	75(1)*
O(T4)···O(W1)[c]	2.87(3)†	N(A6)···O(T4)···O(W1)[c]	76(1)†
O(W1)···O(W2)[g]	2.90(2)*	N(A6)···O(W2)···O(W1)[g]	74(1)*
O(W1)···O(W2)	2.86(2)	N(A6)···O(W2)···O(W1)[c]	74(1)†
O(W1)···O(W2)[i]	2.93(2)†	O(T4)···O(W1)[c]···O(W2)	105(1)†
		O(T4)···O(W1)[g]···O(W2)	106(1)*
	ϕ/°	O(T4)···O(W1)[g]···O(W2)[g]	114(1)*
		O(T4)[i]···O(W1)···O(W2)	108(1)†
C(A13)-O(A13)···N(A13)[b]	154(1)	O(W1)[g]···O(W2)···O(W1)	98(1)*
C(A13)-N(A13)···O(A13)[e]	121(1)	O(W1)[c]···O(W2)···O(W1)	100(1)†
C(A13)-N(A13)···N(A1)[f]	115(1)	O(W2)···O(W1)···O(W2)[g]	82(1)*
O(A13)[e]···N(A13)···N(A1)[f]	121(1)	O(W2)···O(W1)···O(W2)[i]	110(1)†
C(A2)-N(A1)···N(A13)[a]	101(1)	N(A6)···O(W2)···O(T2)[d]	153(1)
C(A6)-N(A1)···N(A13)[a]	136(1)	N(A6)···O(W2)···O(W1)	116(1)
C(A6)-N(A6)···O(W2)	125(1)	O(T2)[d]···O(W2)···O(W1)	89(1)
C(A6)-N(A6)···O(T4)	130(1)	C(T2)-O(T2)···O(W2)[h]	134(2)
O(T4)···N(A6)···O(W2)	104(1)	O(T2)[d]···O(W2)···O(W1)[c]	113(1)†
C(A5)-N(A7)···N(T3)	136(1)	O(T2)[d]···O(W2)···O(W1)[g]	114(1)*

Symmetry codes

(a) $1-x$, $1/2+y$, $1-z$, (b) $-x$, $1/2+y$, $1-z$, (c) $2-x$, $1/2+y$, $2-z$, (d) $1+x$, y, z, (e) $-x$, $-1/2+y$, $1-z$, (f) $1-x$, $-1/2+y$, $1-z$, (g) $2-x$, $-y$, $2-z$, (h) $-1+x$, y, z, (i) $2-x$, $-1/2+y$, $2-z$.

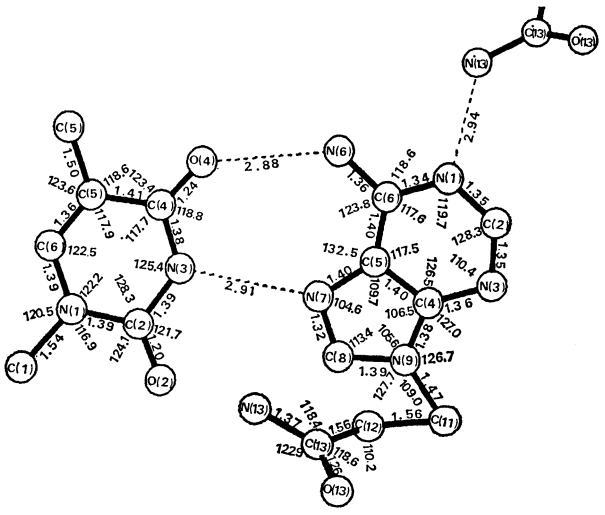

Fig. 3. Atomic numbering and bond distances (l/Å) and angles (ϕ/°) in 3-(adenin-9-yl)propionamide:1-methylthymine complex.

Numbers for the atoms in 3-(adenin-9-yl)propionamide and 1-methylthymine should be prefixed by A and T, and methyl carbon atoms, C(1) and C(5), should be read C(T1M) and C(T5M), respectively. E.s.d's for the bond distances and angles are 0.03 Å and 1.2—2.1°, respectively.

where F_P and $F_{\bar{P}}$ are structure factors for P and $\bar{P}$, respectively, and K scale factor. The value of w is related to the volume fraction W of the $P2_1/c$ domain by equation

$$(1-W)/W = \pm(1-2w)/2\sqrt{w(1-w)}.$$

The parameters were refined by the full-matrix least-squares method. The quantity minimized was $\Sigma\omega(|F_o|-|F_c|)^2$, where $\omega=1/(\sigma^2(F_o))$. As the adenine-thymine pair lies near the plane at $y=1/4$, the matrix became ill-conditioned. In order to resolve such difficulty, only F_P was differentiated in the least-squares calculations. The R value converged to 0.091. The maximum shift of parameters in the last cycle was 0.1σ for C, N, and O atoms. From the final w of 0.763, the volume fraction of the $P2_1/c$ domains was estimated to be 0.62, which is compatible to the expectation from the value of α.

Atomic scattering factors used were taken from "International Tables for X-Ray Crystallography."[14] The final atomic parameters are listed in Table 2.[15]

Results and Discussion

Molecular Structure. Figure 2 gives stereoscopic view of 3-(adenin-9-yl)propionamide:1-methylthymine complex dihydrate. Bond distances and angles are shown in Fig. 3, together with the atomic numbering

Table 4. Deviations of atoms from the least-squares planes

Plane 1: carbamoyl plane, Plane 2: adenine plane, Plane 3: thymine plane.

Deviations l/Å					
Plane 1		Plane 2		Plane 3	
C(A12)*	−0.007	N(A1)*	0.024	N(T1)*	0.002
C(A13)*	0.024	C(A2)*	0.013	C(T2)*	0.007
N(A13)*	−0.008	N(A3)*	−0.029	N(T3)*	0.001
O(A13)*	−0.009	C(A4)*	−0.021	C(T4)*	−0.017
C(A11)	1.055	C(A5)*	−0.029	C(T5)*	0.027
		C(A6)*	−0.001	C(T6)*	−0.020
		N(A7)*	0.006	C(T1M)	−0.151
		C(A8)*	−0.006	O(T2)	−0.029
		N(A9)*	0.043	O(T4)	−0.016
		N(A6)	0.044	C(T5M)	0.082
		C(A11)	0.101		

* Atoms included in the calculations of the least-squares plane.

Dihedral angles between the planes ϕ/°

No.	2	3
1	69.2(6)	70.8(7)
2		10.8(5)

system, and the geometries of hydrogen bonds in Table 3. The displacements of atoms from the least-squares planes of adenine, thymine and carbamoyl moieties are given in Table 4.

The dimensions of 3-(adenin-9-yl)propionamide in the present complex are in good agreement with those in the crystal of 3-(adenin-9-yl)propionamide.[9] The N(A6) atom is almost on the purine ring plane and the C(A11) atom deviates by 0.1 Å from it. The conformation of the ethyl chain with the carbamoyl group is different from that of 3-(adenin-9-yl)propionamide. In the present crystal the torsion angle of N(A9)–C(A11)–C(A12)–C(A13) and C(A11)–C(A12)–C(A13)–N(A13) are 78.1 and −135.1°, respectively, while in 3-(adenin-9-yl)propionamide they are −170.0 and 173.3°.

In 1-methylthymine, the C(T4)–O(T4) bond is longer than C(T2)–O(T2). Such difference is also found in 1-methylthymine:9-methyladenine complex.[16] The methyl carbon atoms, C(T1M) and C(T5M), deviate by 0.15 and 0.08 Å from the pyrimidine plane, respectively.

Crystal Structure. As seen in Fig. 3, the adenine and thymine moieties form a pair through the two hydrogen bonds between N(A6) and O(T4) and between N(A7) and N(T3), their distances being 2.88(2) and 2.91(3) Å, respectively. This pattern is the "Hoogsteen" pairing found in 1-methylthymine:9-methyladenine complex.[16] The purine and pyrimidine planes are twisted to each other by 10.8(5)°, as commonly observed in the other Hoogsteen base pairs.[16,17] Such a twisting is favourable to relieve the bending of hydrogen bonds.

The crystal structure viewed along the b axis is shown in Fig. 4. The carbamoyl group branching from the adjacent base pair related by 2_1 around (1/2, y,1/2) is hydrogen-bonded to the adenine moiety; in the NH···N(A1) hydrogen bond, the NH···N(A1) distance is 2.94(2) Å and the dihedral angle between the carbamoyl group and the adenine moiety is 106.7(6)°. The adenine moieties in the molecules connected by this hydrogen bond are, at the same time, stacked to form a molecular column around the 2_1 axis at $x=1/2$ and $z=1/2$. The remaining carbamoyl hydrogen atom participates in hydrogen bond to the carbamoyl group, the O(A13) atom in the complex related by 2_1 around (0,y,1/2) being an acceptor. This hydrogen bond links the molecular columns to form a sheet parallel to the ab plane.

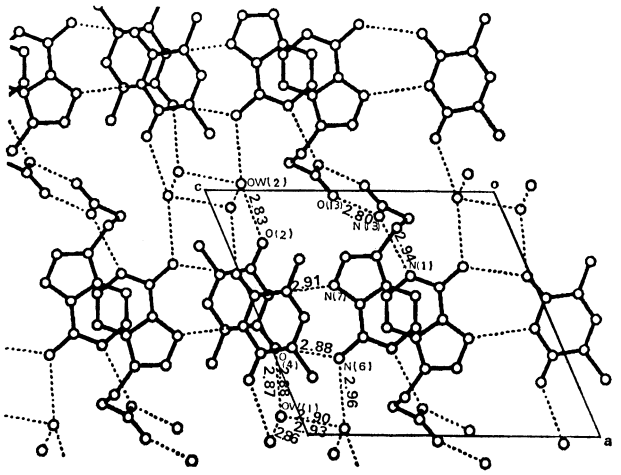

Fig. 4. Crystal structure of 3-(adenin-9-yl)propionamide : 1-methylthymine complex dihydrate projected along the b axis.
In hydrogen bond distances (l/Å) doubly indicated, the upper one corresponds to the value in the PP̄ junction and the lower one in the PP junction.

As shown in Fig. 5, the molecular sheets are joined along the direction of c by the alternate stacking of the 1-methylthymine molecules extruded perpendicular to the sheets. Although there are two kinds of stacking in PP and PP̄ junctions, the spacings are almost the same. In the latter junction, however, the N(A6) atom at $1-x$, $-y$, $2-z$ is close to the C(T1M) atom, the distance being 3.13(3) Å.

In addition, there are two different hydrogen bonding patterns for PP and PP̄ junctions. In both junctions, the water oxygen atoms, O(W1) and O(W2), are hydrogen bonded to O(T4) and O(T2), respectively, and the O(W2) atom is an acceptor of hydrogen bond from N(A6) of adenine moiety. In PP junction, two water molecules are connected by hydrogen bonds, to form a chain around the 2_1 axis at $x=0$, and $z=1$. In PP̄ junction, the hydrogen bonding scheme between waters is a loop around the inversion centre. There is no significant difference in hydrogen bond distances and angles between the two junctions.

Interaction between Carbamoyl Group and Adenine:Thymine Base-pair. In the present model crystal, it is found that the carbamoyl group interacts with the Hoogsteen base pair of adenine and thymine through the hydrogen bond between the adenine N(A1) and the car-

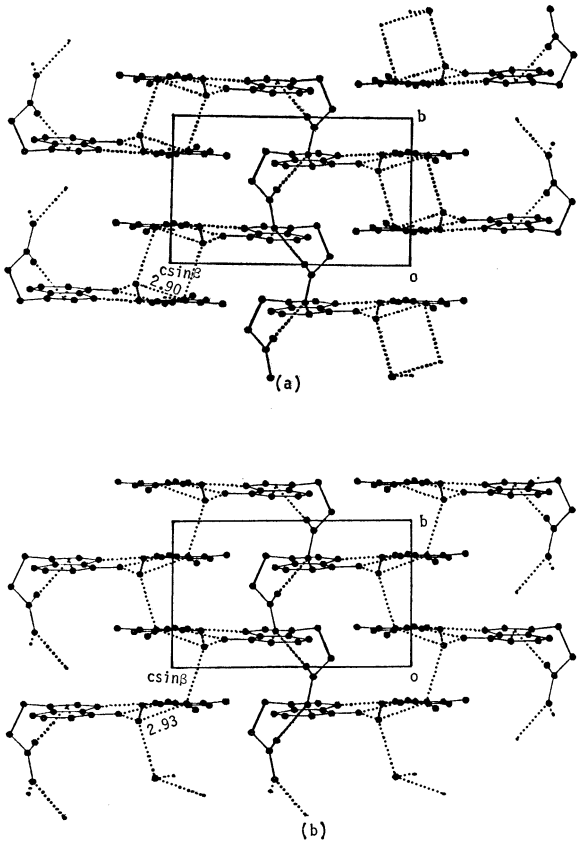

Fig. 5. Crystal structure of 3-(adenin-9-yl)propionamide : 1-methylthymine complex dihydrate projected along the a axis.
(a) $P\bar{P}$ junction and (b) PP junction.

bamoyl N(A13) atoms, as shown in Fig. 3. For adenine: thymine pair in Hoogsteen type, the carbamoyl group seems to have a preferential interaction with adenine.

To examine whether the present mode is possible in the protein:nucleic acid interaction, we need geometrical data of the Hoogsteen base pair in the nucleic acids. This type of base pair has been found to occur actually between Uracil 8 and Adenine 14 in tRNA,[18–20] though it is reversed. Model building by computer graphics[21] proves that the observed interaction geometry can be incorporated into $tRNA^{Phe}$ [22] at Adenine 14, with minor adjustment. It is indicated that ethidium bromide[23] and magnesium ion[24] bind to tRNA in the vicinity of this pair. Enzymes involved in protein synthesis would also possibly interact with this region. If glutamine or asparagine residue in the protein would participate in such an interaction, the carbamoyl group might combine to tRNA in a mode shown in Fig. 3.

The authors are grateful to Professor Yoshito Takaki of Osaka Kyoiku University for the valuable suggestion on treating the disordered structure, and to Professor Jumpei Tsujiuchi of this Institute for the use of the microdensitometer (SAKURA PDM-5). The present work was supported in part by a Grant-in-Aid for Scientific Research from the Ministry of Education, Science and Culture, to which the authors' thanks are due.

References

1) M. Ohki, A. Takenaka, H. Shimanouchi, and Y. Sasada, *Bull. Chem. Soc. Jpn.*, **48**, 848 (1975).
2) C. Tamura, T. Hata, S. Sato, and N. Sakurai, *Bull. Chem. Soc. Jpn.*, **45**, 3254 (1972).
3) A. Takenaka, M. Ohki, and Y. Sasada, *Bull. Chem. Soc. Jpn.*, **53**, 2724 (1980).
4) T. Hata, M. Yoshioka, S. Sato, and C. Tamura, *Acta Crystallogr., Sect. B*, **31**, 312 (1975).
5) M. Ohki, A. Takenaka, H. Shimanouchi, and Y. Sasada, *Bull. Chem. Soc. Jpn.*, **50**, 2573 (1977).
6) M. Ohki, A. Takenaka, H. Shimanouchi, and Y. Sasada, *Acta Crystallogr., Sect. B*, **33**, 2954 (1977).
7) A. Takenaka and Y. Sasada, 38th National Meeting of the Chemical Society of Japan, Nagoya, October 1978, Abstr., p. 1004.
8) A. Takenaka and Y. Sasada, *Bull. Chem. Soc. Jpn.*, **55**, 680 (1982).
9) M. Takimoto, A. Takenaka, and Y. Sasada, *Bull. Chem. Soc. Jpn.*, **54**, 1635 (1981).
10) N. C. Seeman, J. M. Rosenberg, and A. Rich, *Proc. Natl. Acad. Sci. U.S.A.*, **73**, 804 (1976).
11) L. E. McCandlish and G. H. Staut, *Acta Crystallogr., Sect. A*, **31**, 245 (1975).
12) P. Main, M. M. Woolfson, L. Lessinger, G. Germain, and J. P. Declercq, MULTAN 74. A System of Computer Programs from X-Ray Diffraction Data. Univs. of York, England, and Louvain-la-Neuve, Belgium.
13) A. J. C. Wilson, *X-Ray Optics.*, London: Methuen. (1962).
14) "International Tables for X-Ray Crystallography," Kynoch Press, Birmingham (1974), Vol. IV, p. 71.
15) Lists of structure factors and anisotropic thermal parameters have been deposited as Documents No. 8243, at the Office of the Chemical Society of Japan.
16) K. Hoogsteen, *Acta Crystallogr.*, **16**, 907 (1963).
17) A. E. V. Haschemeyer and H. M. Sobell, *Acta Crystallogr.*, **18**, 525 (1965).
18) C. D. Stout, H. Mizuno, S. T. Rao, P. Swaminathan, J. Rubin, T. Brennan, and M. Sundaralingam, *Acta Crystallogr., Sect. B*, **34**, 1529 (1978); J. L. Sussman, S. R. Holbrook, R. W. Warrant, G. M. Church, and S. -H. Kim, *J. Mol. Biol.* **123**, 607 (1978); A. Jack, J. E. Ladner, A. Klug, *ibid.*, **124**, 523 (1978).
19) N. H. Woo, B. A. Roe, and A. Rich, *Nature*, **286**, 346 (1980).
20) D. Moras, M. B. Comarmond, J. Fisher, R. Weiss, J. C. Tierry, J. P. Ebel, and T. Giegé, *Nature*, **288**, 669 (1980).
21) A. Takenaka and Y. Sasada, *J. Cryst. Soc. Jpn.*, **22**, 214 (1980).
22) F. C. Bernstein, T. F. Koetzle, G. J. B. Williams, E. F. Meyer, J. M. D. Brice, J. R. Rodgers, O. Kennard, T. Shimanouchi, and M. Tasumi, *J. Mol. Biol.* **112**, 535 (1977).
23) M. Liebman, J. Rubin, and M. Sundaralingam *Proc. Natl. Acad. Sci. U.S.A.*, **74**, 4821 (1977).
24) G. J. Quigley, M. M. Teeter, and A. Rich, *Proc. Natl. Acad. Sci. U.S.A.*, **75**, 64 (1978).

Steric Effect on Carbon-13 Nuclear Magnetic Resonance Shifts in Poly(vinylnaphthalene)s

Kazuhiko Seki, Shinji Mori, and Yoshio Imamura*

Department of Chemistry, Faculty of Science, Science University of Tokyo, Kagurazaka, Shinjuku-ku, Tokyo 162

(Received January 12, 1982)

From the point of view of the rotational isomeric state for the side groups (π- and o-conformation), the steric compression effect on the ^{13}C chemical shift of the aliphatic carbons in poly(1-vinylnaphthalene)(P1VN) and poly(2-vinylnaphthalene)(P2VN) were evaluated according to H. J. Schneider's method. In addition to the steric compression effect, the ring current effect by the naphthyl groups in P1VN and P2VN was taken into account. The numerical results suggested that the marked higher field shifts of the methine carbon of P1VN in comparison with that of P2VN, was attributed to the strong steric compression with the 1-naphthyl group (occupied the stable π-conformation) in the same monomer units. While in the P2VN chain, the resonances of the aliphatic carbons were calculated to be in the vicinity of those of polystyrene. Naphthyl ring current contribution to ^{13}C-NMR chemical shifts was found to be small in comparison to the dominant steric compression effect.

The two isomeric polymers of vinylnaphthalene (PVN), poly(1-vinylnaphthalene)(P1VN) and poly(2-vinylnaphthalene)(P2VN), differ from each other in some solution properties and the latter polymer behaves rather similar to polystyrene (PS) in a transition phenomenon[1,2] or ^1H-NMR spectral pattern.[3] In a previous paper,[4] we reported the results of evaluations of the steric energy of the RIS (Rotational Isomeric State) of the pendant groups in P1VN and P2VN. Since the naphthyl groups in P1VN or P2VN have no symmetry axis along the plane of the ring, there are distinguished two RIS (π- and o-conformation, see Fig. 1) of the side groups. The conclusions from the result are as follow; a) in the P1VN chain, the π-conformation is preferred but in paticular conditions, there are possibilities of formation of the o-conformations, and b) in P2VN chain, both the π- and o-conformations are stable; the choice of the RIS would not have a great influence upon the total stability of the P2VN chain and there are little conformational differences in the rotational states of P2VN and PS. We also pointed out a characteristic nonbonded interaction between the hydrogen atoms of a rotating 1-naphthyl ring and the methine hydrogen, found in the same monomer unit of P1VN chain.

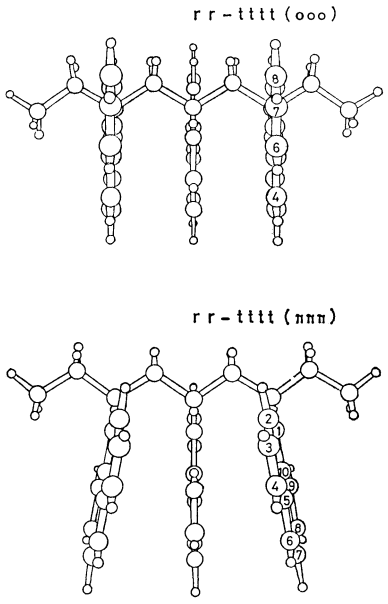

Fig. 1. Schematic representation of the rotational isomeric states of the side groups in (rr)-P1VN chain: (top) o-conformation; (bottom) π-conformation. In the P2VN chain, the α-carbon is bonded to the C(2) atom in the naphthyl group.

Recently, Tonelli[5] revealed that the ^{13}C-NMR chemical shifts of the aliphatic carbons in PS were attributable to a "γ-effect" (steric interaction between carbon atoms in the gauche arrangement) and to the ring current shielding effect (RCSE) of the aromatic groups. The γ-effect in PS depended on the stereoregularity or the skeletal conformations of the polymer chain. The apparent resemblance of the conformational situation between P2VN and PS described above suggests that the ^{13}C chemical shift of the former would be elucidated by γ-effect and RCSE of the aromatic rings, as reported by Tonelli for PS.[5] In the P1VN chain, the characteristic steric compression produced by the π-conformation would control the chemical shifts of the methine carbons. This effect depends only on the range accesible to the rotation of the 1-naphthyl ring, so that it would not depend on the steric regularity of the chain.

In this paper, we will discuss the distinct differences of the observed ^{13}C-NMR spectral patterns between P1VN and P2VN, based on the steric compression effect. In this spectra of P2VN and PS, there is no such unique effect as in P1VN, in addition to the γ-effect and RCSE.

Experimental

Instead of PVN polymers of high molecular weight, we used polymer samples of relatively low molecular weight, to obtain better resolved NMR spectra. The monomer of P1VN and P2VN were prepared from methyl naphthyl ketones,[6] and polymerized[7] in THF at -78 °C, using sodium naphthalenide as an initiator. The polymers were precipitated in about 10 times their volume of methanol in order to free them from any residual monomer and initiator, and were dried *in vacuo*.

The number-average molecular weights of these polymers were determined using a "KUNAUAR's Vapor Pressure

Osmometer" in chloroform solutions at 37 °C. The number-average degrees of polymerization ($\overline{DP}$) of the polymer samples were 80 for P1VN and 60 for P2VN. The molecular weight distributions of the polymers were determined by gel permeation chromatography ($\overline{Mw}/\overline{Mn}$: 1.90 for P1VN and 1.22 for P2VN).

^{13}C-NMR spectra were obtained using a JEOL JNM PS-100 spectrometer equipped with a PFT-100 Fourier transform system operating at 25.03 MHz, and a EC-100 computer with a memory capacity of 16 kilo words. samples were contained in 8 mm O.D. glass tubes and were degassed. The solvent used was chloroform-d_1, obtained from E. Merck A. G. The polymer concentration was *ca.* 30%. The 45° pulse width was about 13 μs. The apparatus was equipped with an internal ^{2}D field-frequency lock and a noise-modulated proton decoupler. The time-domain signal was digitized in 8192 channels, to provide 4096 data points after Fourier transformation. All spectra were observed at 30 °C.

Calculation

The chemical shifts of sterically perturbed carbon atoms are generally found at higher magnetic fields than those of unperturbed carbons which are not spatially crowded by neighboring atoms. The magnitude of these shifts exhibits a strong dependence upon the repulsive interactions between the ^{13}C–H bond and its surrounding groups. In order to evaluate the extent of the steric compression effect on ^{13}C-NMR chemical shifts, some equations of the steric force vector were proposed.[8,9] The steric compression effect was found to be directly related to the force component along the direction of the ^{13}C–H bond associated with nonbonded repulsive interaction. The repulsive interactions between nonbonded atoms or groups are sensitive to small changes in their separation distances and are produced not only by the hydrogen atom but also by the carbon atom. The numerical results reported here were obtained according to the H. J. Schneider's method[9] which has been applied to the fully relaxed molecular model in Force Field Method (FFM).[10] In defining the force vector F on the ^{13}C–H bond, H. J. Schneider *et al.*,[9] proposed an equation which was derived from a potential for nonbonded interactions:[11]

$$F = 0.6952\times10^{-5}(18\varepsilon/r^*)((r^*/r)^{10} - (r^*/r)^7)\times\cos\theta, \quad (1)$$

where r represents the distance of the hydrogen atom attached to ^{13}C from the interacting H or C; θ is the angle between the force vector and the perturbed ^{13}C–H bond. Equation 1 was applied to the hydrogen-hydrogen interaction ($\varepsilon=0.004109$, $r^*=3.632$) and also to the carbon-hydrogen interaction ($\varepsilon=0.026102$, $r^*=3.575$).[11] ε is an energy parameter which measures the depth of the van der Waals energy minimum, and r^* is the parameter which is correlated to the combined van der Waals radii of atoms. The steric compression effect on the methine and methylene carbons for P1VN was estimated by using a pentamer and a tetramer model, respectively, in which the terminal naphthyl groups were replaced by methyl groups.

To estimate the steric compression effect on the methylene carbon, the conformations of a relaxed tetramer model were chosen by the following procedure. A set of the initial models of trial conformations were obtained by combinations of each RIS for side groups (π- and o-conformations) and the backbone bonds (t, g, and $\bar{g}$). Before optimization[4] was completed (mainly in terms of the variation of the internal rotation for side groups and main chain, and bond angles for CH_2–αC–CH_2 and αC–CH_2–αC of the energy of these conformers), we carried out several examinations of the rotational angle of the naphthyl ring from the plane made by the adjoining backbone bonds. If the rotational angle in the conformer exceeded 10°, the subsequent optimization was rejected and this model of conformation was excluded from the relaxed conformations. In the pentamer model, the conformation of the relaxed model and their steric energies were adopted from the results in the previous paper.[4]

In addition to the steric compression effect, the ring currents of the naphthyl groups in PVN may also affect the ^{13}C-NMR chemical shift. The shift parameter $(\delta)_{RC}$ for this effect can be approximately calculated from the equation of McConnell,[12]

$$\delta_{RC} = \Delta\chi(1-3\cos^2\Omega)/3r^3, \quad (2)$$

where r is the distance of ^{13}C from the center of each ring, Ω is the angle made by the r vector and the plane of the ring, and $\Delta\chi$ is the anisotropy of the magnetic susceptibility. In naphthalene, the intensity of the ring current of each ring will be 1.093 times[13] larger than that of the benzene ring.[14] Therefore, we used -65.5×10^{-6} cm^3 mol^{-1} as the values of $\Delta\chi$ for each ring of naphthalene. The ring anisotropic effects on the methine and the methylene carbon were evaluated by using a pentamer and a hexamer model, respectively. In previously calculated results[4] of steric energies for pentamer models, the optimized rotational angles of the 1- and 2-naphthyl ring did not exceed ±4.5°, from the perpendicular position. Accordingly, it is resonable to consider that the naphthyl planes are almost perpendicular to the plane defined by adjoining skeletal bonds. The skeletal chains were assumed to have the same set of conformations which are generally preferred for vinyl polymers.[15]

Results and Discussion

Based on the calculation described above, we obtained six conformations as the relaxed conformations of PS, P1VN and P2VN, respectively. The steric energies of the relaxed conformations were shown in Table 1. The rotational angles for backbone bonds were denoted by the convention of Flory *et al.*[16] The steric interactions involving the bulky naphthyl group precluded $\bar{g}$ conformation. The backbones in PVN were limited to just two rotational states, the trans (t) and gauche (g) conformations, as in the case of PS.[16] The steric energy of the P2VN chain was hardly influenced by the change of RIS of the side groups. The steric energy of the P2VN chain, (except meso-tt conformer), was 0.5—0.9 kcal mol^{-1}**

** 1 kcal mol^{-1}=4.184 kJ mol^{-1}.

Table 1. Steric energies[a] of the tetramer model of P1VN, P2VN, and PS with terminal methyl groups (kcal mol^{-1})

		Meso			Racemic		
		tt[b]	tg	gg	tt	tg	gg
PS		−0.71	1.24	3.64	0.0	2.10	2.59
P2VN	$\pi\pi$[c]	−2.29	1.77	4.23	0.0	3.04	3.19
	πo	−1.96	1.74	4.34	0.27	3.20	3.19
	$o\pi$	−1.96	1.74	4.40	0.27	2.84	3.19
	oo	−2.34	1.70	4.16	0.37	2.82	3.19
P1VN	$\pi\pi$	0.12	3.76	6.98	0.0	4.54	5.58
	πo	2.47	5.16	7.63	3.37	5.91	6.79
	$o\pi$	2.47	5.19	7.44	3.39	6.47	6.79
	oo	3.02	6.77	10.3	6.18	7.69	7.87

a) All values are evaluated relative to the each racemic-tt($\pi\pi$) state. b) Rotational Isomeric States (RIS) for backbone bonds are denoted by the convention of Flory *et al.* c) RIS for side groups in tetramer models.

larger than that of PS. The difference in the energy was attributed to the steric interaction of the bulky 2-naphthyl groups. In the meso-tt conformer, the 2-naphthyl planes are parallel to the adjoining one, and oriented in the same direction; the distance between the two planes was estimated to be about 2.87—3.64 Å. The nonbonded interaction energies between the two 2-naphthyl groups are mainly attributable to the attractive van der Waals force. The steric energy of the meso-tt conformer for P2VN was found to be smaller than that of PS.

The difference of the steric energies between racemic-tt($\pi\pi$) and other conformers of P1VN was obviously larger than that of PS and P2VN. In the conformers with the same skeletal conformation, $\pi\pi$-conformer is more stable than πo-, $o\pi$- and oo-conformer (represented by full line in Fig. 3). However, the $\pi\pi$-conformer may not always be of lower energy in comparison with another conformer, which has the skeletal conformation different from that of $\pi\pi$-conformer: m-tt(oo)<m-tg($\pi\pi$) and r-tt($o\pi$)<r-gg($\pi\pi$). In case of the tetramer model, in which the terminal naphthyl groups were replaced by methyl groups, the steric repulsion produced by o-conformation (the steric interaction of the adjacent naphthyl groups) was appreciably relaxed, and the total steric energy was underestimated. When the tetramer model containing four naphthyl groups was used, the curves in Fig. 3 might slope to the right. On the other hand, the summation of the force components, F_{sum}, along the methine or methylene bond, will not be affected by the choice of model. This is because the total steric energy would not be so much influenced by the steric interaction with respect to the F_{sum} values in this model.

Figure 2 shows the correlation of the steric energy E_{steric} for the pentamer model with the steric force F_{sum} directed along the methine bond, where F_{sum} is the arithmetical average of the steric forces directed along each methine bond in the same model chain.

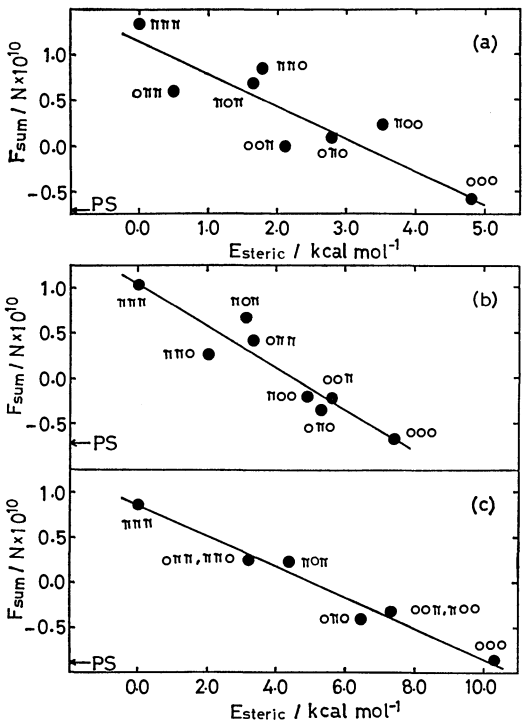

Fig. 2. Correlation of the steric energy E_{steric} of P1VN chain with the steric force F_{sum} directed along the methine bond. An arrow designates the calculated values of F_{sum} for PS chain.
(a): mm-tgtg conformer, (b): mr-tttg conformer, and (c): mm-tgtg conformer.

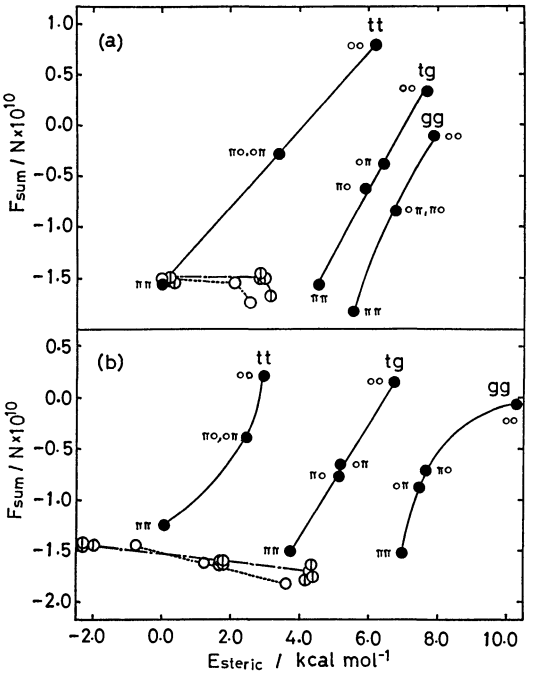

Fig. 3. Correlation of the steric energy E_{steric} for the tetramer model with the steric force F_{sum} directed along the central methylene bond.
●: P1VN chain, ⓘ: P2VN chain, and ○: PS chain.
(a): Racemic and (b): meso.

Table 2. Ring current shielding effect on the central methine and methylene carbon in model chain for the respective conformation

Chain conform.		Methine carbon (CH)			Methylene carbon (CH_2)		
		δ_{PS}[a]	$\delta_{P1VN}-\delta_{PS}$ $\pi\pi\pi\pi\pi$[b]	$\delta_{P2VN}-\delta_{PS}$[c] (h) (l)	δ_{PS}	$\delta_{P1VN}-\delta_{PS}$ $\pi\pi\pi\pi\pi\pi$	$\delta_{P2VN}-\delta_{PS}$ (h) (l)
iso	*gtgt[d]	−1.25	−0.54	−0.40 — −0.44	−0.46	0.25	−0.18 — −0.38
	*ttgg	−1.48	−0.92	−0.46 — −0.52	−1.15	−0.76	−0.39 — −0.67
	ggtt	−1.59	−0.93	−0.51 — −0.62	−0.85	−0.57	−0.41 — −0.66
syndio	*tttt	−0.63	−0.48	−0.30 — −0.31	−0.35	−0.30	−0.20 — −0.27
	ggtt	−1.72	−0.94	−0.55 — −0.70	−0.67	−0.55	−0.32 — −0.39
	ttgg	−1.34	−0.91	−0.42 — −0.44	−1.63	−0.60	−0.58 — −0.92
hetero*	tgtt	−1.11	−0.49	−0.36 — −0.41	0.36	−0.03	0.26 — 0.10
	gttt	−0.86	−0.64	−0.37 — −0.37	0.36	−0.03	0.26 — 0.10

a) The minus and plus signs represent paramagnetic and diamagnetic shielding, respectively. b) Rotational isomeric states for side groups in the P1VN chain. c) (h) and (l) represent ($\delta_{P2VN}-\delta_{PS}$) for the most upfield conformer and for the most downfield conformer, respectively. d) * represents the preferred conformation.

An arrow in Fig. 2 designates the calculated value of F_{sum} for the PS chain. When all RIS of the side groups in the model chain occupied the stable π-conformation ($\pi\pi\pi$-conformer), the methine group undergoes the maximum repulsive force in comparison with other conformers. The methine group in the *ooo*-conformer of this model experiences the same force as in the PS chain. The calculated values of F_{sum} for the P2VN model were located in the vicinity of that of the PS chain. Thus, the steric force directed along the methine bond in the P1VN chain was estimated to be $(1.73—2.08)\times10^{-10}$ N larger than that of PS or P2VN. As described above, whenever the P1VN chain occupies a π-conformation, the steric compression effect on the methine carbon was mainly caused by the intramolecular interaction of 1-naphthyl hydrogen in the same monomer unit. This effect was almost independent of the tacticity of the polymer chain. The methine group was slightly affected by other steric compression effects (*e.g.* γ-effect and detailed descriptions of γ-effect on the methine carbon in PS were given by Tonelli[5]). The backbones in PS are restricted to the trans and gauche states, excluding $\bar{g}$ state, and the methine carbons are always in the gauche arrangement with $C_{aromatic}$ connected to αC or CH_2 without regard to stereosequences, and should not exhibit any stereosequence-sensitive γ-effect. As the backbones in PVN are also restricted to the t and g, the methine carbons in PVN are not affected by the γ-effect and by the chain stereoregularity, as well as in PS.

The correlation of the steric energy E_{steric} for the tetramer model with the steric force F_{sum} directed along the central methylene bond is shown in Fig. 3. The numerical results of the γ-effect on methylene bond were excluded due to the interaction of the backbone atoms in the special case of the tetramer model. In contrast, with methine bond in P1VN chain, the methylene bond undergoes a repulsive force when the RIS of the side groups are in *o*-conformation. The repulsive force was produced by the steric overlap between the hydrogen in a rotating naphthyl ring and one of the methylenes. The magnitude of the steric force directed along the methylene bond in P1VN (occupied by the π-conformation) was not very different from that of the PS or the P2VN chain.

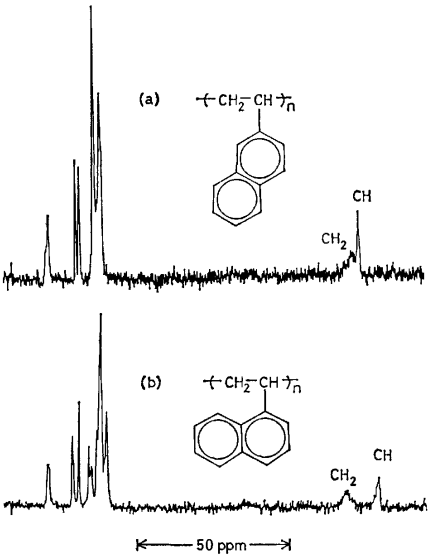

Fig. 4. Proton-decoupled, natural abundance ^{13}C FT NMR spectra of (a) P2VN and (b) P1VN in chloroform-d_1 at 25.03 MHz and 30 °C.

The correlation between the chemical shift and the steric force F_{sum} can be interpreted as follows, a) In the P1VN chain, the resonance of the methine carbon shifts to higher field in comparison with that of PS, owing to the steric interaction of the 1-naphthyl group (π) in the same monomer unit. The chemical shift of the methylene carbon is attributed to the γ-effect,[5] and the resonance peak is located in the vicinity of the position of PS. b) The resonance of the aliphatic carbons in the P2VN chain would appear at the same positions as the resonance of PS.

Figures 4a and 4b show the proton-decoupled ^{13}C-NMR spectra of P2VN ($\overline{DP}=60$) and P1VN ($\overline{DP}=80$), respectively. The experimental values of the chemical shifts of methine carbon or methylene carbon for PVN at 30 °C are represented relative to the chemical shifts of PS ($\overline{DP}=20$), and are summarized as follow.

$(\delta_{P1VN}-\delta_{PS})_{CH} = 6.83$, $(\delta_{P1VN}-\delta_{PS})_{CH_2} = 0.43$ ppm,

$(\delta_{P2VN}-\delta_{PS})_{CH} = -0.37$, $(\delta_{P2VN}-\delta_{PS})_{CH_2} = 0.85$ ppm.

The spectrum of the aliphatic region in the P2VN chain shows a similar pattern as that of PS. The resonance of the methine carbon in the P1VN chain appears at higher field in comparison with that of PS and P2VN. These experimental results correspond to the conclusion derived from Figs. 2 and 3.

The calculated results for ring anisotropic effect on methine and methylene carbon are given in Table 2. In RCSE on methylene carbon, the numerical results of those polymer chain (PS, P1VN, and P2VN) depend slightly on the chain regularity and conformation, indicating that the resonance of the methylene carbon spread to a broad band. On the other hand, the numerical results for RCSE on the methine carbon were little affected by the chain stereoregularity and backbone conformation. RCSE shifts of P2VN relative to PS, $(\delta_{P2VN}-\delta_{PS})_{CH,\,RCSE}$ for the preferred conformation were about -0.30——-0.44 ppm. The resonance of the methine carbon for the P2VN chain was not influenced by the steric interaction, resulting in an upfield shift of the methine in the P1VN chain, and was simply governed by the anisotropy of the 2-naphthyl ring. The experimental value of -0.37 ppm was in the range of the calculated values (-0.30——-0.44 ppm). For methine carbon in the P1VN chain, $(\delta_{P1VN}-\delta_{PS})_{CH,\,RCSE}$ the values for preferred conformations were about -0.48——-0.54 ppm. Evidently, the RCSE contributions to the observed ^{13}C chemical shift of methine carbon in P1VN are found to be small in comparison to the dominant steric compression effect.

Finally, we are tried to obtain the proportional constant between the magnitude of the steric compression force of methine bond in a P1VN chain and the chemical shift values. The shift values which depend on the steric compression effect only, could be obtained from substracting the $(\delta_{P1VN}-\delta_{PS})_{CH,\,RCSE}$ value from the experimental values. The constant obtained was $(3.5—4.2)\times10^{10}$ ppm N^{-1}. H. J. Schneider's constant was 20×10^{10} ppm N^{-1},[9] which was obtained for deshielded carbon atoms in substituted cyclohexane and in norbornane derivatives. D. M. Grant's constant for shielded carbon obtained from the non-relaxed model (*o*-xylene and methyl cyclohexane) was 1.30×10^{10} ppm N^{-1}.[8] Taking into account that the extent of the shift by the shielding force is smaller than that of the deshielding force, and that our constant was derived from shielding carbon in a relaxed model, the value of the calculated constant is considered to be resonable.

In ^{1}H-NMR spectra of P1VN, in addition to the RCSE by the 1-naphthyl ring, such a steric compression effect on the methine proton would also be revealed. However, it is difficult to estimate numerically this steric compression effect on the chemical shift of the proton in P1VN. The deshielding associated with the steric compression increases with increasing the repulsive interaction, but the distance between the hydrogen atoms does not simply relate to the extent of deshielding. Moreover, the nature of the deshielding mechanism by the steric interaction on the chemical shift of the proton is not very apparent at present.[17]

References

1) L. A. Utracki and R. Simha, *Makromol. Chem.*, **117**, 94 (1968).
2) J. B. Helms and G. J. Challa, *J. Polym. Sci., Part A-2*, **10**, 1447 (1972).
3) J. Heller and D. B. Miller, *J. Polym. Sci., Part A-1*, **5**, 2323 (1967).
4) K. Seki, Y. Ichimura, and Y. Imamura, *Macromolecules*, **14**, 1831 (1981).
5) A. E. Tonelli, *Macromolecules*, **12**, 252, 255 (1979).
6) S. Loshaek, E. Broderick, and P. Bernstein, *J. Polym. Sci.*, **39**, 223 (1959).
7) S. Loshack, *J. Polym. Sci.*, **39**, 241 (1959).
8) B. V. Cheney and D. M. Grant, *J. Am. Chem. Soc.*, **89**, 5319 (1967); D. M. Grant and B. V. Cheney, *ibid.*, **89**, 5315 (1967).
9) H. J. Schneider and E. F. Weigand, *J. Am. Chem. Soc.*, **99**, 8362 (1977).
10) N. L. Allinger, M. T. Tribble, M. A. Miller, and D. H. Wertz, *J. Am. Chem. Soc.*, **93**, 1637 (1971); N. L. Allinger and J. T. Sparague, *ibid.*, **95**, 3893 (1973); N. L. Allinger, J. T. Sparague, and T. Liljefors, *ibid.*, **96**, 5100 (1974); D. H. Wertz and N. L. Allinger, *Tetrahedron*, **30**, 1579 (1974).
11) A. Warshel and S. Lifson, *J. Chem. Phys.*, **53**, 582 (1970); O. Ermer and S. Lifson, *J. Am. Chem. Soc.*, **94**, 4121 (1973).
12) H. M. McConnell, *J. Chem. Phys.*, **27**, 226 (1957).
13) N. Jonathan, S. Gordon, and B. P. Dailey, *J. Chem. Phys.*, **36**, 2443 (1962).
14) T. G. Schmalz, C. L. Norris, and W. H. Flygare, *J. Am. Chem. Soc.*, **95**, 7961 (1973).
15) D. Doskocilova, J. Stokr, B. Schneider, H. Pivcova, M. Kolinsky, J. Petranek, and D. Lim, *J. Polym. Sci., Part C*, **16**, 215 (1967).
16) D. Y. Yoon, P. R. Sundararajan, and P. J. Flory, *Macromolecules*, **8**, 776 (1975).
17) W. Nagata, T. Terasawa, and K. Tori, *J. Am. Chem. Soc.*, **86**, 3746 (1964); S. Winstein, D. Carter, F. A. L. Anat, and A. J. R. Bourn, *ibid.*, **87**, 5247 (1965); E. M. Arnett and J. M. Bolliner, *ibid.*, **86**, 4729 (1964).

Temperature Effect on the Adsorption of Ionic Surfactants at Water/Hexane Interface from Micellar Solutions

Michio YAMANAKA,* Makoto ARATONO, Hidemi IYOTA,
Kinsi MOTOMURA, and Ryohei MATUURA
Department of Chemistry, Faculty of Science, Kyushu University 33, Higashi-ku, Fukuoka 812
(Received January 16, 1982)

The adsorption behavior of dodecylammonium chloride (DAC) and sodium dodecyl sulfate (SDS) at their aqueous micellar solution/hexane interface has been studied by measuring the interfacial tension as a function of temperature at concentrations around the critical micelle concentration (cmc). The derivative of the interfacial tension with respect to temperature has been observed to change abruptly at the cmc and very little thereafter with increasing concentration in a limited range above the cmc. By applying the thermodynamic treatment of adsorption from micellar solution developed previously to the present experimental results, the entropy changes associated with the adsorption of DAC and SDS from monomeric state and from micellar state and the corresponding energy changes have been calculated. Further, the entropy and energy changes of micelle formation have been obtained from these quantity changes. These values have been compared with those obtained for DAC at water/air interface. It has been observed that the behavior of the micelle in the limited concentration range is controlled solely by temperature and pressure and bears resemblance to that of the adsorbed film at the interface. It has also been observed that the entropy and energy of micelle and adsorbed film are lowered by the hexane existing in the system.

In a recent paper,[1] we have investigated the adsorption of dodecylammonium chloride (DAC) at water/air interface by measuring the surface tension of the solution as a function of temperature at various concentrations around critical micelle concentration (cmc). It has been clarified with the aid of the entropy and energy changes associated with the adsorption of DAC evaluated by applying the thermodynamic treatment of adsorption[2-5] that the thermodynamic properties of the micelle of DAC in the aqueous solution are closely related to those of adsorbed film of DAC at water/air interface. It is now interesting to see if a similar conclusion is obtained at water/oil interface by measurement of the interfacial tension.

The purposes of the present work are to confirm the validity of our thermodynamic treatment of the adsorption from micellar solution[1] and to reveal the difference of the behavior of adsorbed film at water/hexane interface from that of micelle. In order to attain these purposes, we adopt as surfactants DAC and sodium dodecyl sulfate (SDS), of which the adsorbed films at water/hexane interface have well been investigated in the range of concentration below cmc.[3,6] The interfacial tension is measured as a function of temperature at various concentrations around cmc. The thermodynamic quantity changes associated with adsorption from micellar solution are evaluated by applying the thermodynamic equations and compared with corresponding changes of DAC at water/air interface.

Experimental

DAC and SDS were synthesized and purified by the method described in the previous papers.[3,6] Water was distilled three times from alkaline permanganate solution. Hexane was purified by distillation after passing through an activated alumina column.

The equilibrium interfacial tension was measured as a function of temperature at constant total concentration around cmc under atmospheric pressure. The value of the interfacial tension of the system of aqueous SDS solution and hexane was determined by the pendant drop technique[7,8] within the experimental error of 0.05 mN m^{-1}. Since the system of aqueous DAC solution and hexane had a very small interfacial tension (about 2 mN m^{-1}) in the neighborhood of cmc, we adopted the sessile drop technique[8,9] for the determination of the equilibrium interfacial tension.

The sessile drop of hexane made in the DAC solution in the glass cell was allowed to stand for about an hour in order to establish the thermal equilibrium. The enlarged photograph of the sessile drop was taken by the camera and the shape and size of the drop on the photographic film were determined to a precision of μm by Nikon Measurescope. The value of the interfacial tension γ was calculated by the equation

$$\gamma = (1/2)g\Delta d a^2, \quad (1)$$

where g is the acceleration of gravity, Δd the difference in density between aqueous solution and hexane, and a the capillary constant. The value of a^2 is obtained from the experimental values of the radius r of the sessile drop in the equatorial plane and the height h from this plane to the top of the drop:

$$a^2 = r^2 f(h/r),$$

where $f(h/r)$ is a function of h/r. We took the value of $f(h/r)$ from the tables of Tawde and Parvatikar.[10-12] In the case where the value of h/r is too small and deviates from these tables, we calculated it by the equations presented by Blaisdell.[13] The error estimated for the value of the interfacial tension was 0.05 mN m^{-1}.

The densities of pure hexane and water were used instead of those of hexane and aqueous solutions, because the mutual solubility between hexane and water was small and the concentrations of the solution were low. Temperature was kept constant within 0.05 K by circulating thermostated water around the cell.

Results and Discussion

The variation of the interfacial tension γ with temperature T at constant total molality $m_t^{\ddagger}$ of surfactant around cmc under atmospheric pressure is shown in Figs. 1a and 1b for DAC and SDS, respectively. The γ *vs.* T curve of the pure water/hexane interface is

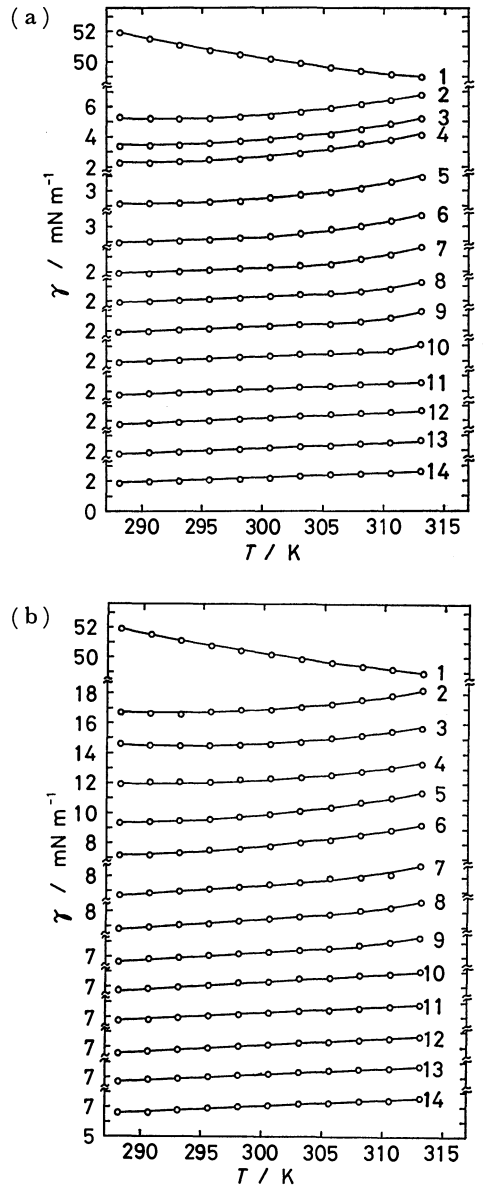

Fig. 1. Interfacial tension *vs.* temperature curves of DAC (a) and SDS (b) at constant total molality under atmospheric pressure.
(a): (1) $m_1^t = 0$ mmol kg^{-1}; (2) 11.08; (3) 12.04; (4) 12.51; (5) 12.65; (6) 12.80; (7) 12.98; (8) 13.04; (9) 13.14; (10) 13.29; (11) 15.04; (12) 16.53; (13) 18.03; (14) 20.13. (b): (1) $m_1^t = 0$ mmol kg^{-1}; (2) 3.99; (3) 4.59; (4) 5.49; (5) 6.36; (6) 7.20; (7) 7.40; (8) 7.54; (9) 7.67; (10) 7.70; (11) 8.46; (12) 9.97; (13) 11.29; (14) 12.69.

included for comparison. These figures seem to resemble each other. The γ *vs.* T curve at a concentration below cmc is slightly concave upward, while at a concentration above cmc γ increases linearly with increasing T in the range of 288.15 K to 313.15 K in contrast with that of the pure water/hexane interface. Examining the γ *vs.* T curve at a concentration near cmc, it is found that the curve consists of linear and curved portions and the linear portion is made longer by the increase of m_1^t. This fact suggests that the values of cmc of DAC and SDS vary with temperature.

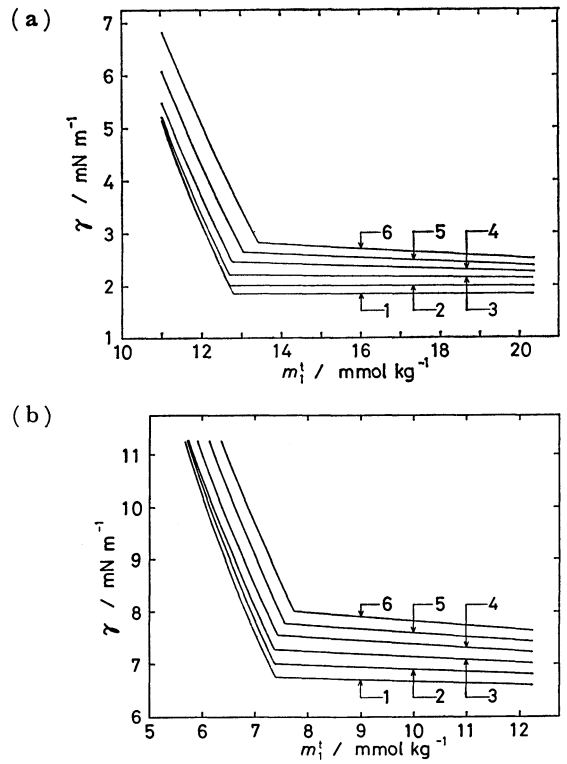

Fig. 2. Interfacial tension *vs.* total molality curves of DAC (a) and SDS (b) at constant temperature under atmospheric pressure.
(a): (1) 288.15 K; (2) 293.15 K; (3) 298.15 K; (4) 303.15 K; (5) 308.15 K; (6) 313.15 K. (b): (1) 288.15 K; (2) 293.15 K; (3) 298.15 K; (4) 303.15 K; (5) 308.15 K; (6) 313.15 K.

The values of the interfacial tension taken from Figs. 1a and 1b are plotted against m_1^t at constant temperature in Figs. 2a and 2b for DAC and SDS, respectively. The γ *vs.* m_1^t curve has a visible break point at a certain concentration which provides the value of cmc. In the concentration range above cmc, γ is observed to decrease linearly and slightly with m_1^t. When we are concerned with a limited range of m_1^t close to the cmc, we may say that γ remains constant.

In Fig. 3, the cmc *vs.* T curves of DAC and SDS obtained from Figs. 2a and 2b are shown together with the curve, for comparison, of the system of aqueous DAC solution and air taken from our previous paper.[1] It is found that the curves are concave upward and have a distinct minimum; the temperature of minimum is near 295 K for the curves of DAC and SDS in this work and near 300 K for the curve of DAC in the previous paper. Further, the value of cmc of DAC measured by the interfacial tension is different from that measured by the surface tension. This fact may be attributable to the difference of the phase coexisting with the DAC solution.

Next, we will consider the derivative of the interfacial tension with respect to temperature at constant concentration under atmospheric pressure. The values of $-\partial\gamma/\partial T$, which are evaluated from Figs. 1a and

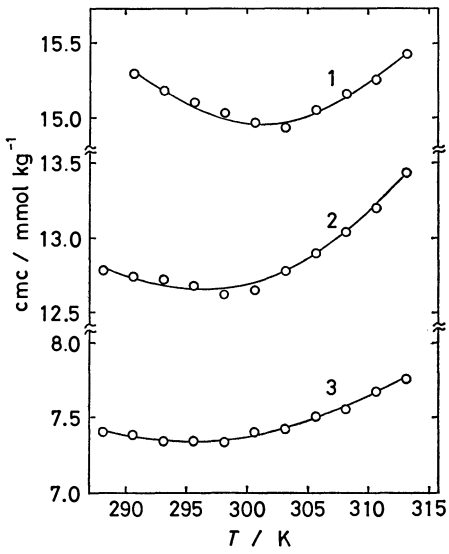

Fig. 3. Critical micelle concentration *vs.* temperature curves under atmospheric pressure.
(1): DAC water/air, (2): DAC water/hexane, (3): SDS water/hexane.

1b, are plotted against m_1^t in Figs. 4a and 4b for DAC and SDS, respectively. It is seen clearly that $-\partial\gamma/\partial T$ varies discontinuously at the cmc. Above cmc it has a negative and almost constant value in the limited range of concentration near cmc. The same observation has been obtained with the adsorption of DAC at water/air interface.[1] The constancy of $-\partial\gamma/\partial T$ and γ in the limited range of m_1^t suggests that the concentration of monomeric surfactant is not varied significantly by m_1^t and the behavior of the micelle in this concentration range is controlled solely by temperature and pressure.

According to our thermodynamic treatment of the adsorption from micellar solution developed previously,[1] we can evaluate the two types of the thermodynamic quantity changes denoted by $\Delta y(1)$ and $\Delta y(\mathrm{M})$, which are associated with the adsorption of surfactant from its monomeric state and micellar state, respectively. Let us assume that the surfactant is a strong electrolyte and that the behavior of micelle is described by using thermodynamic properties of an imaginary micelle particle which contains the surrounding counterions so as to satisfy the condition of electroneutrality. Since the total differential of its chemical potential μ^{M} is expressed as a function of T and p:

$$\mathrm{d}\mu^{\mathrm{M}} = -s^{\mathrm{M}}\mathrm{d}T + v^{\mathrm{M}}\mathrm{d}p, \tag{2}$$

where s^{M} and v^{M} are the molar entropy and volume of micelle, respectively, $\Delta y(1)$ and $\Delta y(\mathrm{M})$ are defined by the equations

$$\Delta y(1) = y^{\mathrm{H}} - \Gamma_1^{\mathrm{H}} y_1^{\mathrm{W}}, \tag{3}$$

and

$$\Delta y(\mathrm{M}) = y^{\mathrm{H}} - \Gamma_1^{\mathrm{H}}(y^{\mathrm{M}}/N_1^{\mathrm{M}}), \tag{4}$$

where Γ_1^{H} is the interfacial density of surfactant, y^{H} the interfacial excess quantity per unit area, y_1^{W} the partial molar quantity of surfactant in the solution, and N_1^{M} the number of surfactant ions in the micelle.

In the first place, the entropy changes, $\Delta s(1)$ and

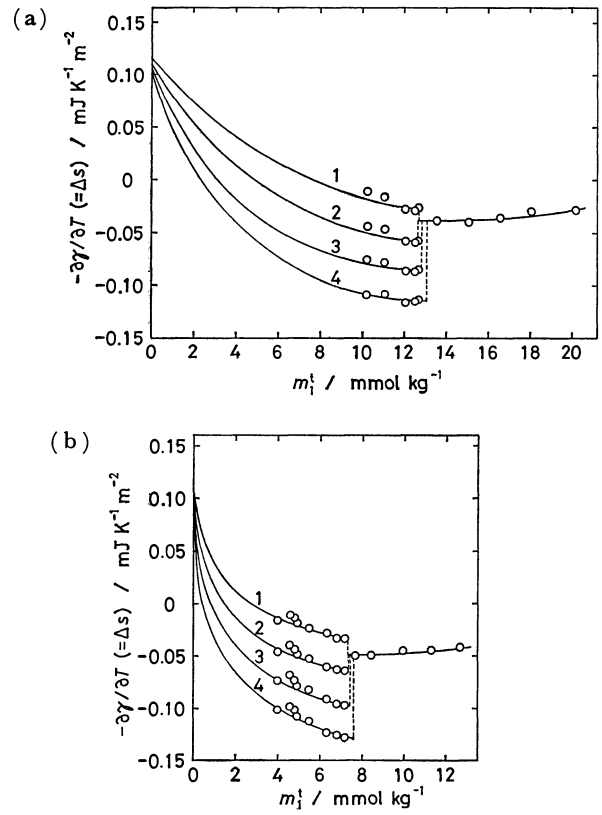

Fig. 4. Derivative of interfacial tension with respect to temperature *vs.* total molality curves of DAC (a) and SDS (b) at constant temperature under atmospheric pressure.
(a): (1) 293.15 K; (2) 298.15 K; (3) 303.15 K; (4) 308.15 K. (b): (1) 293.15 K; (2) 298.15 K; (3) 303.15 K; (4) 308.15 K.

$\Delta s(\mathrm{M})$, can be calculated by applying the following equations to the present experimental results:

$$\Delta s(\mathrm{M}) = -(\partial\gamma/\partial T)_{p,m_1^t}, \tag{5}$$

and

$$\Delta s(1) = -(\partial\gamma/\partial T)_{p,m_1^t} - 2(RT/\mathrm{cmc})\Gamma_1^{\mathrm{H}}(\partial\mathrm{cmc}/\partial T)_p, \tag{6}$$

where it is presumed that the micellar solution behaves ideally and the concentration of monomeric surfactant is equal to the value of cmc. On the other hand, in the case where the system is free from micelle, $\Delta s(1)$ is provided directly by the equation

$$\Delta s(1) = -(\partial\gamma/\partial T)_{p,m_1^t}. \tag{7}$$

Thus, it is evident from Eqs. 5 and 7 that the value of $-\partial\gamma/\partial T$ in Figs. 4a and 4b provides $\Delta s(\mathrm{M})$ at the concentration above cmc and $\Delta s(1)$ at the concentration below cmc. Therefore, the discontinuous change in $-\partial\gamma/\partial T$ at the cmc corresponds to the difference between $\Delta s(1)$ and $\Delta s(\mathrm{M})$ and its value is related to the temperature dependence of cmc by the equation

$$\Delta s(1) - \Delta s(\mathrm{M}) = -2(RT/\mathrm{cmc})\Gamma_1^{\mathrm{H}}(\partial\mathrm{cmc}/\partial T)_p \text{ at cmc.} \tag{8}$$

The right side of Eq. 8 is calculated easily, since the value of Γ_1^{H} is estimated by applying the equation

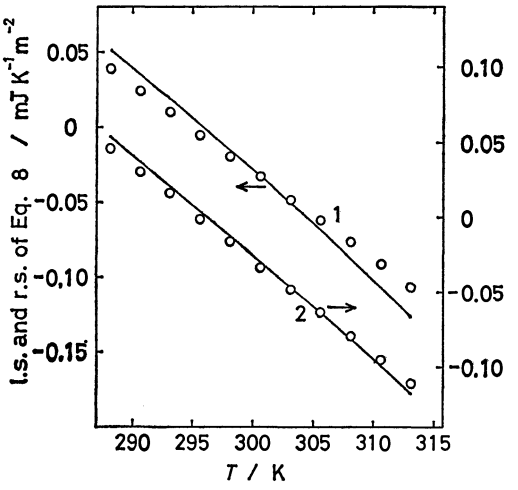

Fig. 5. Comparison between left side $(\Delta s(1)-\Delta s(M))$ and right side $(-2(RT/\text{cmc})\Gamma_1^H(\partial \text{cmc}/\partial T)_p)$ of Eq. 8. Left side ○ and right side ——; (1) DAC; (2) SDS.

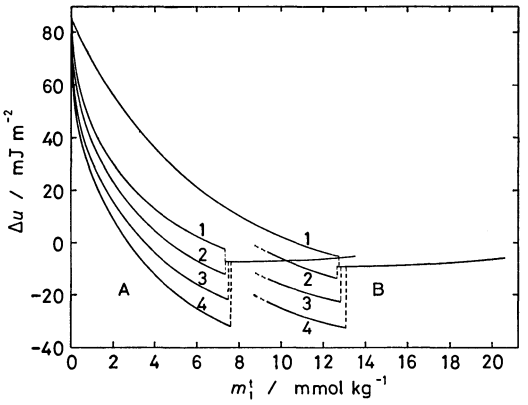

Fig. 6. Energy change associated with adsorption *vs.* total molality curves of DAC and SDS at constant temperature under atmospheric pressure.
(A): SDS; (B): DAC; (1) 293.15 K; (2) 298.15 K; (3) 303.15 K; (4) 308.15 K.

$$\Gamma_1^H = -(m_1^t/2RT)(\partial\gamma/\partial m_1^t)_{T,p}, \quad (9)$$

to the γ *vs.* m_1^t curves in Figs. 2a and 2b, and the values of cmc and $\partial \text{cmc}/\partial T$ are obtained from the cmc *vs.* T curves in Fig. 3. The left side of Eq. 8 is evaluated by extrapolating the values of $\Delta s(1)$ and $\Delta s(M)$ to the cmc. Both sides of Eq. 8 are compared in Fig. 5. They seem to be in fair agreement with each other. A similar result has been obtained for the system of aqueous solution of DAC and air.[1] This fact indicates that Eq. 2 is a useful approximation for the behavior of micelle in a limited concentration range near the cmc.

Next, let us evaluate the energy changes, $\Delta u(1)$ and $\Delta u(M)$, by the use of the relations

$$\Delta u(1) = \gamma + T\Delta s(1) - p\Delta v(1), \quad (10)$$

and

$$\Delta u(M) = \gamma + T\Delta s(M) - p\Delta v(M). \quad (11)$$

Since the terms of $p\Delta v(1)$ and $p\Delta v(M)$ on the right sides of these equations are usually negligible compared with the other terms under atmospheric pressure,[3,6,14]

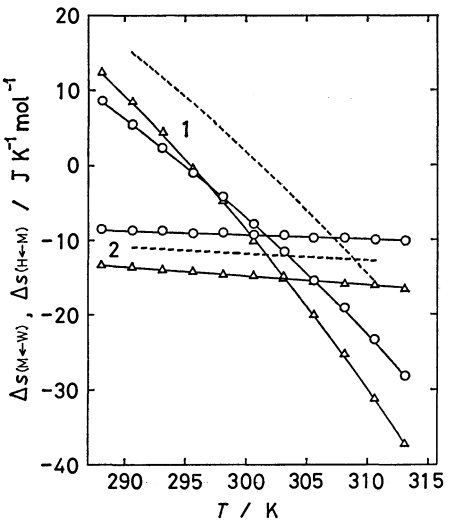

Fig. 7. Entropy change of micelle formation $(\Delta s(M\leftarrow W))$ *vs.* temperature curves and entropy change associated with adsorption from micellar state $(\Delta s(H\leftarrow M))$ *vs.* temperature curves under atmospheric pressure.
(1): $\Delta s(M\leftarrow W)$, (2): $\Delta s(H\leftarrow M)$, ○: DAC water/hexane, △: SDS water/hexane, - - - -: DAC water/air.

the numerical values of $\Delta u(1)$ and $\Delta u(M)$ can be obtained by making use of Figs. 2a, 2b, 4a, and 4b. They are plotted against m_1^t in Fig. 6 for both DAC and SDS. It is apparent that the values of $\Delta u(1)$ and $\Delta u(M)$ depend on m_1^t in a similar manner as the corresponding entropy changes in Figs. 4a and 4b.

Now, it is instructive to look more closely at the behavior of DAC and SDS molecules in the adsorbed film and micelle. In order to do this, it is convenient to introduce the thermodynamic quantity changes per mole of surfactant, which are defined by the equations

$$\Delta y(H\leftarrow M) = y^H/\Gamma_1^H - y^M/N_1^M = \Delta y(M)/\Gamma_1^H, \quad (12)$$

and

$$\Delta y(M\leftarrow W) = y^M/N_1^M - y_1^W = [\Delta y(1)-\Delta y(M)]/\Gamma_1^H, \quad (13)$$

where Eqs. 3 and 4 have been used.

In Fig. 7, the entropy changes, $\Delta s(H\leftarrow M)$ and $\Delta s(M\leftarrow W)$, which are obtained from Figs. 4a, 4b, and 5, are plotted against temperature. Included in this figure for comparison are those obtained for the system of DAC solution and air.[1] Their values are found to be fairly different between DAC and SDS and between the water/hexane and water/air interfaces. It is also seen that the value of $\Delta s(H\leftarrow M)$ is negative and slightly dependent on T while the value of $\Delta s(M\leftarrow W)$ decreases from a positive value to a negative one with increasing T.

The corresponding energy changes, $\Delta u(H\leftarrow M)$ and $\Delta u(M\leftarrow W)$, obtained from Fig. 6 and the previous paper,[1] are shown in Fig. 8. It is noteworthy that the $\Delta u(H\leftarrow M)$ has nearly equal negative values for DAC and SDS at water/hexane interface and has a positive value for DAC at water/air interface. It is also seen that $\Delta u(H\leftarrow M)$, likely $\Delta s(H\leftarrow M)$, depends slightly on T. These facts indicate that the tempera-

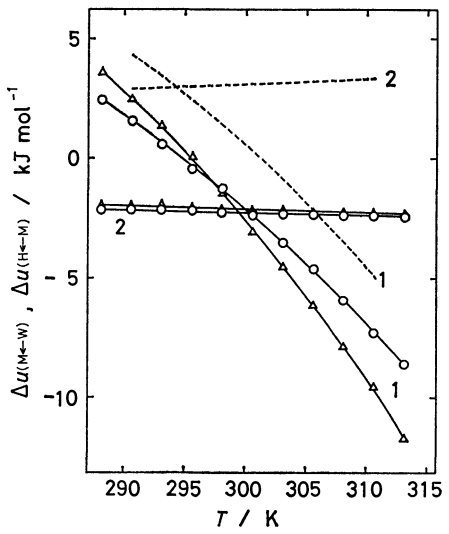

Fig. 8. Energy change of micelle formation (Δu(M←W)) *vs.* temperature curves and energy change associated with adsorption from micellar state (Δu(H←M)) *vs.* temperature curves under atmospheric pressure.
(1): Δu(M←W), (2): Δu(H←M), ○: DAC water/hexane, △: SDS water/hexane, ----: DACwater/air.

ture dependence of energy and entropy of the micelle bears resemblance to that of the adsorbed film. The resemblance of the behavior between the adsorbed film and the micelle will be further confirmed by evaluating the corresponding volume changes from the pressure dependence of the interfacial tension, which will be reported in the near future.[14]

Finally, let us examine the temperature dependence of Δu(M←W) and Δs(M←W). According to Eq. 13, they may be respectively referred to as the energy and entropy changes of micelle formation. As can be seen in Figs. 7 and 8, the values of Δu(M←W) and Δs(M←W) vary with temperature in a similar manner. It is also seen that the temperature dependence of Δu(M←W) and Δs(M←W) of DAC at water/hexane interface is smaller than that of SDS. This result may be attributable to the difference in charge and size of the ionic head group and counterion of surfactant between DAC and SDS. Furthermore, we notice that the values of Δu(M←W) and Δs(M←W) for the aqueous DAC solution–hexane system are fairly smaller than those for the aqueous DAC solution–air system. We may conclude that such a behavior results from the lowering of the energy and entropy of micelle of DAC by the solubilization of hexane into the micelle.

The present work was supported by a Grant-in-Aid for Scientific Research No. 547009 from the Ministry of Education, Science and Culture.

References

1) K. Motomura, S. Iwanaga, M. Yamanaka, M. Aratono, and R. Matuura, *J. Colloid Interface Sci.*, **86**, 151 (1982).
2) K. Motomura, *J. Colloid Interface Sci.*, **64**, 348 (1978).
3) K. Motomura, M. Aratono, N. Matubayasi, and R. Matuura, *J. Colloid Interface Sci.*, **67**, 247 (1978).
4) K. Motomura, S. Iwanaga, Y. Hayami, S. Uryu, and R. Matuura, *J. Colloid Interface Sci.*, **80**, 32 (1981).
5) K. Motomura, *Adv. Colloid Interface Sci.*, **12**, 1 (1980).
6) M. Aratono, M. Yamanaka, N. Matubayasi, K. Motomura, and R. Matuura, *J. Colloid Interface Sci.*, **74**, 489 (1980).
7) N. Matubayasi, K. Motomura, S. Kaneshina, M. Nakamura, and R. Matuura, *Bull. Chem. Soc. Jpn.*, **50**, 523 (1977).
8) J. F. Padday, "Surface and Colloid Science," ed by E. Matijević, Wiley, New York (1969), Vol. 1, p. 101.
9) J. F. Padday, *Phil. Trans. R. Soc. London, A*, **269**, 265 (1971).
10) N. R. Tawde and K. G. Parvatikar, *Indian J. Phys.*, **25**, 473 (1951).
11) N. R. Tawde and K. G. Parvatikar, *Indian J. Phys.*, **28**, 345 (1954).
12) K. G. Parvatikar, *Indian J. Phys.*, **32**, 174 (1958).
13) B. E. Blaisdell, *J. Math. Phys.*, **19**, 186 (1940).
14) M. Yamanaka, M. Aratono, K. Motomura, and R. Matuura, unpublished data.

Photon Echo of Pentacene Molecules Introduced in Crystals with High Concentration

Yuzo Yoshikuni,† Arao Nakamura,†† and Shigeo Shionoya*

The Institute for Solid State Physics, The University of Tokyo, Roppongi, Minato-ku, Tokyo 106

(Received January 20, 1982)

Photon echo decay time is measured for pentacence molecules introduced in naphthalene and *p*-terphenyl crystals with rather high concentrations (10^{-6}—10^{-5} mol/mol) at temperatures between 1.6 K and 4.1 K, using a tunable picosecond laser system consisting of a mode-locked YAG laser and a parametric oscillator. In naphthalene echo decay time increases with lowering temperature approaching a constant value below 2 K, but in *p*-terphenyl it is almost constant. The phase relaxation time at very low temperature is much shorter than twice the population relaxation time in both crystals, indicating that pure dephasing processes exist. Analyzing the results it turns out that there exsists a pure dephasing process which is temperature-independent and is very probably due to interactions between pentacene molecules, in addition to the temperature-dependent dephasing process due to the scattering of pseudolocalized phonons.

Recently, with the progress of coherent transient techniques in the optical region, for example photon echo observation, much information on optical dephasing processes associated with electronic transitions has been obtained for organic molecules introduced in crystals. From the optical line shape, useful information on phase relaxation can be obtained, but usually the optical homogeneous line shape is masked by inhomogeneous line broadening. Coherent transient techniques enable to obtain homogeneous line width buried in inhomogeneous line width.

Photon echo measurements were performed recently by Wiersma and his coworkers for a number of organic molecules, such as pyrene,[1] pentacene,[2-4] and naphthalene[5] introduced in organic crystals. Especially, for pentacene molecules very dilutely introduced (10^{-8}—10^{-7} mol/mol) in naphthalene and *p*-terphenyl crystals as hosts, detailed studies were made using nanosecond and picosecond lasers. It turned out[2] in the case of *p*-terphenyl host that at very low temperature of 1.5 K where phonons are not active, the phase relaxation time (T_2) is determined by the population relaxation time (T_1), in other words T_2 is equal to $2T_1$. The temperature dependence of the phase relaxation time was measured in a wide range above 4.2 K up to 20 K.[3,4] It was found that the homogeneous line width is exponentially activated with phonon-like activation energy. This exponential activation of the homogeneous line width was interpreted by assuming optical dephasing due to the scattering of pseudolocalized phonons,[4,6] and the energy and the lifetime of such phonons were determined.

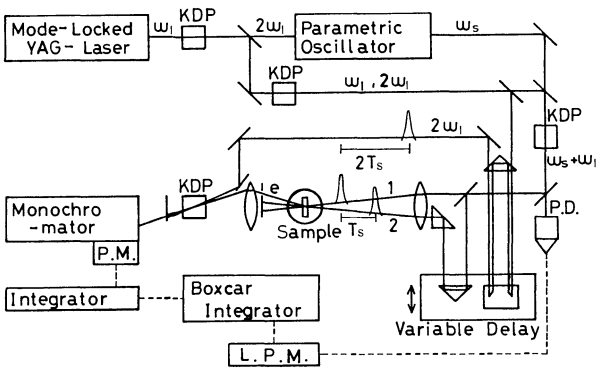

Fig. 1. Experimental set-up for photon echo measurements using a parametric oscillator (output frequency: ω_s) pumped by second harmonics of a mode-locked YAG laser (output frequency: ω_1). 1: first excitation pulse, 2: second excitation pulse, e: echo signal, T_s: separation of the first and second pulse, P.D.: photodetector, P.M.: photomultiplier, L.P.M.: laser power monitor.

If pentacene molecules are introduced in host crystals with high concentration, interactions between guest molecules would influence optical dephasing. The temperature dependence of T_2 in such cases are not yet studied. In this paper, we report picosecond photon echo measurements for pentacene molecules introduced in naphthalene and *p*-terphenyl crystals with rather high concentrations (10^{-6}—10^{-5} mol/mol) at temperatures between 1.6 and 4.2 K. As will be mentioned below, the temperature dependence of T_2 is observed, and it is found that at very low temperature, T_2 is independent of temperature, but is much shorter than $2T_1$.

Experimental

Pentacence-doped naphthalene and *p*-terphenyl crystals were grown by the Bridgman technique. In the case of naphthalene zone-refined reagent was used as the starting material. In the case of *p*-terphenyl, zone-refined reagent is not available, so ordinary reagent was vacuum-sublimed, zone-refined and then used. Crystals were cleaved in parallel to the *ab* cleavage plane to thickness of about 1 mm with a sharp razor blade.

Pentacene molecule in naphthalene has the zero-phonon absorption line of the S_0-S_1 transition at 602.7 nm. In the case of *p*-terphenyl host there exist four zero-phonon absorption lines originating from different sites. Measurements were made for the lowest energy line located at 592.2 nm. The spectral width of these absorption lines is about 1 cm^{-1} in both host crystals. The transition dipole moment for these absorption lines is known to be about 1 D.[7] The concentration of pentacene molecules in a sample was determined combining the absorption intensity and the transition dipole moment of this value.

In photon echo experiments a tunable picosecond laser

† Present address: Musashino Electrical Communication Laboratory, NTT, Musashino, Tokyo 180.

†† Present address: Department of Applied Physics, Faculty of Engineering, Tohoku University, Sendai 980.

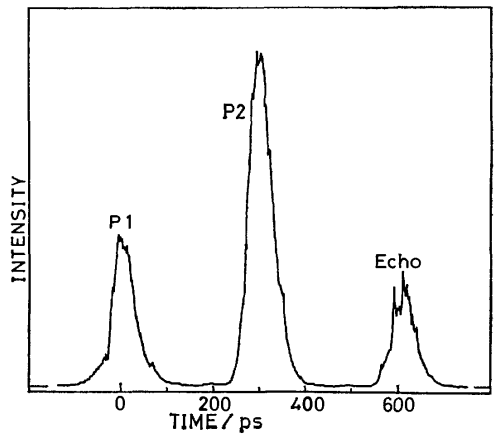

Fig. 2. Photon echo observation for pentacence in naphthalene (5×10^{-6} mol/mol) at 1.6 K. P1 and P2 are the first and second excitation pulses observed in the direction of the echo signal as leaked light. The pulse separation T_s is 300 ps.

system consisting of a repetitively mode-locked YAG:Nd^{3+} laser and a parametric oscillator was used.[8] Figure 1 shows the experimental set-up employed. The parametric oscillator using a temperature-controlled $LiNbO_3$ crystal was pumped by 532 nm second harmonic pulses of the YAG laser output. Excitation pulses tunable in the range around 600 nm were generated by the sum-frequency mixing of tunable pulses around 1300 nm produced by the parametric oscillator with 1064 nm fundamental pulses of the YAG laser by using a KDP crystal. Their characteristics are duration of about 20 ps, spectral width of about 2 cm^{-1} and peak power of about 200 kW.

The two pulses needed for the photon-echo experiments were generated by a beam splitter, and one pulse was delayed by an optical delay to obtain variable pulse separation (T_s). The intensity ratio of the first to second pulse was made to be almost 1:4 according to the standard way in photon echo experiments. Two excitation pulses were focused on the sample at an angle of about 0.5 degree. The size of the excitation spot was about 300 μm in diameter, and excitation densities of the first and the second pulses were 20 and 80 MW/cm^2, respectively. These power densities nearly correspond to the conditions of the $\pi/2$ and π pulses, respectively, since the transition dipole moment in the present case is about 1 D. The echo was emitted in a direction separated from the second pulse by the same angle as that between the first and second pulses as expected. It is sure that this configuration is useful to reduce the background by spatially separating the echo signal from the excitation pulses.

The echo signal was made to pass through a diaphragm to remove the excitation pulses as much as possible. Then the echo signal was mixed with the second harmonic pulse of the YAG laser output to generate the sum-frequency pulse. This second harmonic pulse acts as the time-gate pulse, which selects the echo signal from the excitation pulses. The gate pulse was delayed by the variable optical-delay so as to coincide with the echo in time. The optical delay consists of two prisms located on a moving stage driven by a pulse motor. The second excitation pulse passes one prism and the gate pulse passes the other prism. The gate pulse passes the delay twice, so that the time delay of the gate pulse is double that of the second pulse from the first pulse. Thus the synchronization of the gate pulse with the echo is maintained. The mixed pulse of the echo and gate pulse

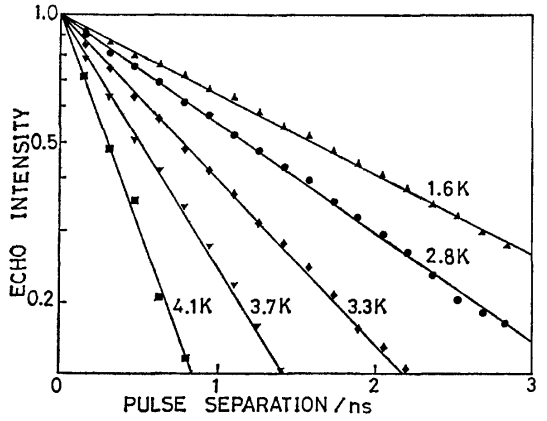

Fig. 3. Logarithmic plots of photon echo decay of pentacene in naphthalene (5×10^{-6} mol/mol) at temperatures between 1.6 and 4.1 K. Solid lines are the least square fitting to the experimental data.

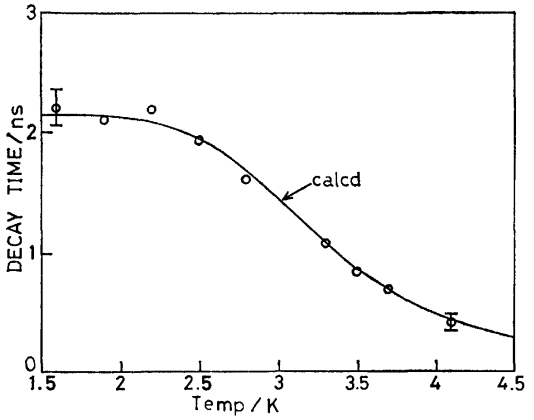

Fig. 4. Temperature change of echo decay time of pentacene in naphthalene (5×10^{-6} mol/mol). Solid line is calculated curve; see the text.

was made to pass through a monochromator, and then was detected by a photomultiplier. The output of the photomultiplier was integrated and held by an integrator. On the other hand, a part of excitation pulses were detected by a phototube, and the power was checked by a laser power monitor. Only when the power is within $\pm5\%$ for a certain fixed value, the echo signal held in the integrator was accumulated by a Boxcar integrator.

Results and Discussion

Figure 2 demonstrates an observation of photon echo for pentacene molecules in a naphthalene crystal (5×10^{-6} mol/mol) at 1.6 K. This data was obtained by changing the arriving time of the gate pulse but fixing the separation of the two excitation pulses at 300 ps. P1 and P2 are the first and second excitation pulses observed in the direction of the photon echo signal as leaked light through the diaphragm. It is seen that the photon echo appears after the second pulse with the interval the same as that between the first and second pulses.

To obtain the relaxation time of photon echo, the echo intensity was measured as a function of the separation of the two excitation pulses. The separation was changed by scanning the variable optical delay,

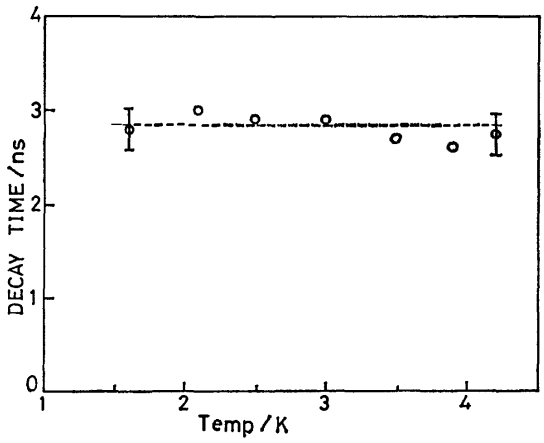

Fig. 5. Temperature change of echo decay time of pentacene in *p*-terphenyl (1×10^{-5} mol/mol).

maintaining the synchronization of the gate pulse with the echo signal. The echo intensity as a function of the excitation pulse separation is given by

$$I(T_s) = I_0\exp(4T_s/T_2). \quad (1)$$

Figure 3 shows logarithmic plots of the relative echo intensity versus the pulse separation for pentacene in naphthalene (5×10^{-6} mol/mol) at temperatures between 1.6 K and 4.1 K. The functional form of the photon echo decay is exponential at the whole temperature range. The echo decay time decreases with elevating temperature.

Decay times obtained, *i.e.* $T_2/4$, are plotted in Fig. 4 as a function of temperature. It is seen that the decay time becomes constant at temperature below 2 K. Figure 5 shows results of the echo decay time in the case of pentacene in *p*-terphenyl (1×10^{-5} mol/mol). It is found that the decay time is almost constant in the whole temperature range and is slightly longer than that in the case of the naphthalene host below 2 K.

The echo decay time is governed by the phase relaxation time T_2 given by

$$1/T_2 = 1/2T_1 + 1/T_2^*, \quad (2)$$

where T_1 is the population relaxation time and T_2^* is the pure dephasing time. T_1 in the present case was reported to be 19.5 ns in naphthalene and 23.5 ns in *p*-terphenyl.[4]

As shown in Fig. 5, the decay time of the echo in the *p*-terphenyl host is almost constant below 4.1 K and is about 2.9 ns giving the value of about 11.6 ns as T_2. This value of T_2 is much shorter than $2T_1$. This suggests that the pure dephasing process that is independent of temperature exists below 4.1 K in this host. From Eq. 2, the pure dephasing time T_2^* is obtained to be 15 ns.

In the case of the naphthalene host, T_2 increases with lowering temperature but approaches a constant value which is much shorter than $2T_1$. One may consider that the temperature-independent, pure dephasing process exists also in this host at very low temperature. As mentioned already, it is known that in dilutely doped crystals T_2 is dominated by the dephasing process due to the scattering of pseudolocalized phonons at temperature above 4.2 K.[4] Such a dephasing process dominated by phonons should exist also in highly doped crystals.

One may assume that T_2^* in the present case of the naphthalene host consists of two components, one T_{2c}^* which is temperature-independent and the other T_{2ph}^* which is temperature-dependent and is dominated by phonon scattering, that is

$$1/T_2^* = 1/T_{2c}^* + 1/T_{2ph}^*. \quad (3)$$

The temperature-dependence of T_{2ph}^* may be expressed by

$$T_{2ph}^* = \tau_{ph}\exp(E_{ph}/kT), \quad (4)$$

where τ_{ph} is the lifetime of relevant phonons and E_{ph} is their energy. The observed temperature change of the decay time in Fig. 4 was attempted to fit with the calculation based on the assumption of Eqs. 3 and 4. Adjustable parameters are τ_{ph}, E_{ph}, and T_{2c} which is the temperature-independent component of T_2 given by

$$1/T_{2c} = 1/T_{2c}^* + 1/2T_1. \quad (5)$$

The result of the calculation is shown by the solid curve in the figure. It is seen that observed decay times are well represented by the calculation. The values of the adjustable parameters used are $\tau_{ph}=7.4$ ps, $E_{ph}=16.1$ cm^{-1} and $T_{2c}=8.7$ ns. It is noted that these values of τ_{ph} and E_{ph} well coincide with those obtained in the dilutely doped naphthalene host at temperature above 4.2 K.[4] It is sure that also in the highly doped host the same kind of the pseudolocalized phonon is active for dephasing. Further from the above value of T_{2c}, T_{2c}^* is obtained to be 11.2 ns.

Also in the case of the dilutely doped *p*-terphenyl host, the values of τ_{ph} and E_{ph} are known from the temperature dependence of T_2 above 4.2 K. If T_2 is calculated using such values for temperatures below 4.2 K, it is found that T_2 becomes constant below about 3 K. Therefore, the results shown in Fig. 5 for the highly doped *p*-terphenyl host are regarded as reasonable.

From the above-mentioned discussion, it is definitely concluded that when pentacene molecules are introduced with high concentration, a pure dephasing process, represented by T_{2c}^*, exists and dominates dephasing at very low temperature where phonon-dominated processes are not active. This fact is a distinct difference of the high concentration case from the low concentration case, and allows us to consider that the origin of this pure dephasing is interactions between pentacence molecules.

Cooper *et al.*[9] observed the photon echo of pentacence molecules introduced in naphthalene crystals with rather high concentrations (10^{-7}—10^{-5} mol/mol) at 1.4 K, and found that concentration-dependent, pure dephasing takes place. Although they did not measure the temperature dependence of this process, it is certain that the same kind of origin as that of the present case dominates this process, considering the concentration and the temperature in their experiments.

They explained this concentration-dependent dephasing as caused by the fluctuation of the dipole-dipole interaction between pentacene molecules due to phonons. According to this phonon-modulated dipolar in-

teraction model, T_{2c}^* is given by[9]

$$1/\pi T_{2c}^* = \{(dE/dr) \times \Delta r\}^2/h^2\nu, \quad (6)$$

where E is the excitation energy of molecules, Δr is fluctuation of intermolecular distance and ν is the rate of the fluctuation. The value of ν should be comparable to the thermal average acoustic phonon frequency, so that it is expected to increase linearly with temperature. On the other hand, the value of Δr is known to be almost constant in the temperature range below 4.2 K in the present case.[10] Then T_{2c}^* given by Eq. 6 should be temperature-dependent, increasing linearly with temperature. According to our experimental results, T_{2c}^* is temperature-independent in this temperature range. Therefore, the model proposed by Cooper *et al.* can not account for the dephasing process in the case of the high pentacene concentration.

Morsink *et al.*[11] also found concentration-dependent dephasing in photon echo measurements of naphthalene molecules in durene. This dephasing was interpreted as the effect of dipolar broadening due to energy migration among resonant molecules. However, this interpretation was based on the assumption, which has no solid experimental evidence, that the crystal consists of large domains of resonant molecules.

Anyway we need more detailed information on the temperature- and concentration-dependence of the dephasing time to discuss the mechanism of dephasing in the high concentration case as observed here. Measurements of the concentration depnedence for pentacene molecules in naphthalene and *p*-terphenyl are now in progress, and results will be reported shortly.**

References

1) T. J. Aartsma and D. A. Wiersma, *Phys. Rev. Lett.*, **36**, 1360 (1976).
2) J. B. W. Morsink, T. J. Aartsma, and D. A. Wiersma, *Chem. Phys. Lett.*, **49**, 34 (1977).
3) W. H. Hesselink and D. A. Wiersma, *Chem. Phys. Lett.*, **56**, 227 (1978).
4) W. H. Hesselink and D. A. Wiersma, *J. Chem. Phys.*, **73**, 648 (1980).
5) T. J. Aartsma and D. A. Wiersma, *Chem. Phys. Lett.*, **54**, 415 (1978).
6) P. de Bee and D. A. Wiersma, *J. Chem. Phys.*, **70**, 790 (1979).
7) T. E. Orlowski and A. H. Zewail, *J. Chem. Phys.*, **70**, 1390 (1979).
8) Y. Tanaka, T. Kushida, and S. Shionoya, *Opt. Commun.*, **25**, 278 (1978).
9) D. E. Cooper, R. W. Olson, and M. D. Fayer, *J. Chem. Phys.*, **72**, 2332 (1980).
10) D. W. J. Cruickshank, *Acta Crystallogr.*, **9**, 1005 (1956).
11) J. B. W. Morsink, B. Kruizinga, and D. A. Wiersma, *Chem. Phys. Lett.*, **76**, 218 (1980).

** **Note added in proof.** See: Y. Yoshikuni, A. Nakamura, S. Shionoya, and M. Aihara, *J. Phys. Soc. Jpn.*, **51**, 2604 (1982).

 © 1982 The Chemical Society of Japan Bull. Chem. Soc. Jpn., 55, 2753—2759 (1982)

Electron Transfer in the Quenching of Triplet States of Zinc Phthalocyanine and Methylene Blue by the Use of Fe(III), Co(III), and Organic Oxidants

Takeshi Ohno,* Shunji Kato, and Norman N. Lichtin†

Chemistry Department, College of General Education, Osaka University, Toyonaka, Osaka 560

† *Department of Chemistry, Boston University, Commonwealth Avenue, Boston, Massachusetts 02215, U. S. A.*

(Received December 14, 1981)

The mechanism of the quenching of the triplet state of zinc phthalocyanine (ZnPc) and Methylene Blue (MB^+) by low-spin complexes of Fe(III) and Co(III) and aromatic oxidants was studied. The quenchers studied included $Fe^{III}(CN)_6^{3-}$, $Fe^{III}(CN)_4$(2,2-bipyridyl)$^-$, $Fe^{III}(CN)_2$(2,2-bipyridyl)$^+$, ferrocenium ion, Co^{III}(2,2′: 6′-2″-terpyridyl)$^{3+}$, Co^{III}(1,10-phenanthroline)$^{3+}$, dimethylviologen, 1,4-benzoquinone, and 2,4,7-trinitro-9-fluorenone (TNF). The rate constants of the quenching of ^{3}ZnPc varied from a diffusion-controlled one to 6×10^5 dm^3 mol^{-1} s^{-1} in the mixed solvent of dimethylacetamide (DMA) and water (7:3 by volume). The metal complexes quenched $^3MB^+$ and the triplet state of protonated MB^+ with a rate constant of more than 2×10^6 dm^3 mol^{-1} s^{-1} in an aqueous solution with 0.5 mol dm^{-3} of $MgCl_2$. The fractions of electron transfer yielding $ZnPc^{+\cdot}$ in the quenching process (F_1) were high except for TNF and the iron(III) compounds. The F_1 fractions were also obtained in the quenching of $^3MB^+$ and the triplet state of the protonated MB^+. The absence of radical production in the quenching by the doublet iron(III) compounds can be explained in terms of spin-allowed reverse electron transfer in the life of the geminate radical pair. Fractions of the reverse electron transfer between the half-reduced quencher and $ZnPc^{+\cdot}$ or $MB^{2+\cdot}$ were also measured; they are very close to those of $1-F_1$. The data reported in this study are consistent with the following mechanistic features. (1) Every quenching encounter produces a geminated radical pair. (2) The geminated pair is common to the quenching of the triplet excited state by oxidants and to the reverse electron transfer between the free radicals formed in the quenching. The molar extinction coefficient of $ZnPc^{+\cdot}$ was determined to be 2.9×10^4 dm^3 mol^{-1} cm^{-1} at 520 nm.

Electron transfer between an excited molecule and a quencher to produce redox products is a necessary step in the conversion of solar into chemical energy. Either the dissociation of the radicals or the reverse electron transter may follow the electron-transfer quenching of the excited state within the lifetime of the geminate radical pair, the former of which yields redox products. The fraction of the radical formation in quenching has been called "the efficiency of electron transfer in the quenching process,"[1,2] which corresponds to "the cage-escape probability"[3,4] provided every quenching yields a geminate radical pair. Reverse electron transfer in a singlet radical pair reproducing the singlet reactant pair is spin-allowed,[5,6] so F_1 is nil unless the reverse electron transfer is unfavourable with respect to the free-energy change. On the other hand, reverse electron transfer in a triplet radical pair is spin-forbidden,[5-7] so F_1 is high except multiplicity restriction is broken by means of spin-orbit interaction.[2,8] The rate of the reverse electron transfer can be estimated by using Marcus' equation[9] or an empirical equation proposed by Rehm and Weller,[10] which is written in terms of the free-energy change and rearrangement energy involved in the electron transfer, provided the electron-transfer process is spin-allowed.

This paper will describe a study of electron-transfer quenching rates and the efficiency of electron transfer in the quenching of the triplet state of zinc phthalocyanine (ZnPc) and Methylene Blue (MB^+) by a substitution-inert coordination compound of iron(III) and cobalt(III) and some aromatic oxidants, such as 1,4-benzoquinone and dimethylviologen. The efficiency of the reverse electron transfer between the half-reduced quencher and half-oxidized ZnPc or MB^+ is also studied in order to make the quenching mechanism clear.

Metal phthalocyanine compounds are regarded as inert and stable metal complexes in which photoexcitation energy may not be dissipated before the conversion of solar to chemical energy. Since the phthalocyanine compounds resemble porphyrins in both geometrical and electronic structures, they have been studied by several workers. More recently, different results with respect to the efficiency of photo-electron transfer has been reported. Harriman and Richoux[11] reported F_1 to be less than 5% in the quenching of zinc phthalocyanine tetrasulfate by methylviologen in water. On the other hand, Tanno, Wöhrle, Kaneko, and Yamada[12] reported a high quantum yield of the production of the methylviologen radical on exciting magnesium phthalocyanine in a mixed solvent of dimethylsulfoxide and water.

MB^+ is a photosensitizer of the photogalvanic cell proposed by Rabinowitch[13] and developed by the present author (N. N. L.);[14] in the method, the reduction of MB^+ to $MBH^{+\cdot}$ is coupled by the oxidation of Fe^{II} to Fe^{III}. Recently, $Fe^{III}(H_2O)_6^{3+}$ was reported to oxidize the singlet excited state of MB^+ with a very small yield.[15] The unfavorable process of MB^+-oxidation by iron(III) compound is worth examining.

Experimental

Materials. Water was purified by passage through a Millipore deionizer and a filter. Dimethylacetamide (DMA) was purified by vacuum distilation. The Puriss-grade $MB^+Cl^-\cdot3H_2O$ (Fluka), $HClO_4$ (Wako Junyaku), dimethylvio-

logen** (Tokyo Kasei), 2,4,7-trinitro-9-fluorenone** (Tokyo Kasei), and 2,3,5,6-tetrachloro-1,4-benzoquinone** (Wako Junyaku) were used as supplied. The ZnPc (Tokyo Kasei), 1,4-benzoquinone** (Wako Junyaku), and 1,4-naphthoquinone (Wako Junyaku) were purified by vacuum sublimation immediately before use. The Co^{III}(2,2′:6′-2″-terpyridyl**)$_2$-$(ClO_4)_3$ and Co^{III}(1,10-phenanthroline**)$_3(ClO_4)_3$ were prepared by the method of Maki.[16] The ferrocenium ion was prepared immediately before use by the oxidation of ferrocene with iron(III) nitrate in 0.01 mol dm^{-3} of a $HClO_4$ aqueous solution. Fe^{III}(2,2′-bipyridyl**)$_2(CN)_2(NO_3)$ and $H[Fe^{III}(CN)_4(bpy)]$ were prepared by the method of Schilt.[17] The solvent for ZnPc was a mixture of DMA and water (7:3 by volume). The ionic strengths of the sample solution were kept to be 1—1.5 mol/dm^3 by using $MgCl_2$ or $NaClO_4$. All the test solutions were deaerated by purging nitrogen for 15—20 min.

Apparatus. A *NEC* ruby laser *SLG*-2018 with a *Q*-switch capable of providing up to 0.85 J per flash at 694.3 nm with a pulse width of 20 ns was used. The laser beam (ϕ=10 mm) is vertically converged and longtudinally expanded by means of two cylindrical lenses to 6 mm×12 mm on the photolysis cell (10 mm×10 mm). The laser intensity was stabilized within a fluctuation of a few percent by controlling the temperature of the circulating water for the ruby rod. The absorption changes in the sample were measured by the use of the monitoring beam of a 150 W Xenon arc lamp, which was operated at 20 V (8 A) and which could be pulsed to 30—70 V by the use of a transistor-switched discharging circuit, made by Dr. N. Tatebe. The probe-beam is also focussed by a means of a convex lens on the sample cell with a pin hole (ϕ=1 mm). A shutter driven by a pulse motor is put between the focusing lens and the sample cell to minimize photolysis. The intensity of the monitoring beam was measured by means of a Hamamatsu R955 photomultiplier tube and a Tektronix 456 synchroscope. Another ruby apparatus was used for the study of the MB^+-oxidation; it has been described in the literature.[18]

Measurements. The decay of ^{3}ZnPc was monitored at 450 or 490 nm. The decays of $^3MBH^{2+}$ and $^3MB^+$ were monitored at 710 and 820 nm respectively.[1] The yields of ZnPc† were measured at 520 nm (ε_{520}=2.9×10^4 dm^3 mol^{-1} cm^{-1}). The yields of MB^{2+} were measured at 520 nm (ε_{520}=5.7×10^4 dm^3 mol^{-1} cm^{-1} [19]). The rate of disappearance of ZnPc† were monitored through the decay of its absorbance at 835 nm. The rates of the disappearance of MB^{2+} were monitored through its absorbance at 520 nm or through its increase in absorbance due to MB^+.

Results and Discussion

T-T Absorption. On exposure to 694.3 nm light, the S_1-S_0 absorption of ZnPc was reduced and a transient species was observed with a lifetime of 200 μs. Its absorption spectrum, shown in Fig. 1, is very similar to the absorption spectrum of the triplet excited state of ZnPc in neutral 2-propanol previously reported.[20] The conversion of ZnPc to its triplet state can be estimated from the decrease in the peak absorbance of ZnPc at 672 nm almost completely disappeared for several hundred nano seconds on exposure to a laser beam intensified by means of a cyclindrical convex lens. The molar extinction coefficient of the triplet state at 490 nm can be calculated to be 3.25×10^4 mol^{-1} dm^3 cm^{-1}, which is very close to that reported in 2-propanol.

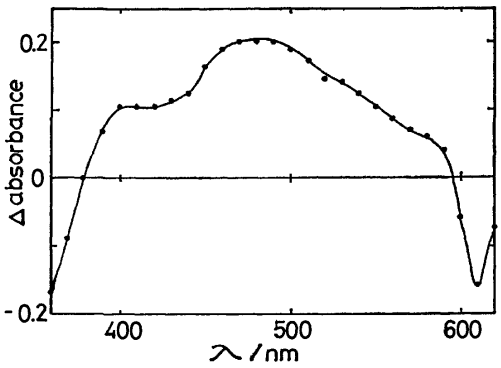

Fig. 1. Transient spectrum of ^{3}ZnPc in 70% DMA aqueous solution.
[ZnPc]=5×10^{-6} mol/dm^3.

Table 1. Quenching-rate constants and fractions of electron transfer in the quenching of ^{3}ZnPc in DMA aqueous solution

Quencher	[$HClO_4$] / mol dm^{-3}	k_q / 10^9 dm^3 mol^{-1} s^{-1}	F_1
Ferrocenium ion	0.01	1.0	0
$Fe^{III}(CN)_6^{3-}$	0.01	0.286	0
	0	0.019	0
TCBQ	0.01	1.3	0.27
	0	0.83	0.75
TNF	0.01	1.0	0
BQ	0.01	0.50	0.90
	0	0.50	0.78
1,4-Naphthoquinone	0.01	0.03	—
MV^{2+}	0.01	0.0005	0.43
	0	0.0036	1.0
$Co^{III}(tpy)_2^{3+}$	0.01	0.14	0.37
	0	0.53	0.70

The absorption spectra and molar extinction coefficients of $^3MB^+$ and the triplet state of protonated MB^+ ($^3MBH^{2+}$) have already been measured by the present authors, S.K.,[20] T.O., and N.N.L.[18] The decay-rate constants of $^3MBH^{2+}$ and $^3MB^+$ in the presence of a charged compound of iron(III) or cobalt(III) were measured in an aqueous solution with $MgCl_2$ of 0.5 mol/dm^3, where the electrostatic effect on the rate constant of the bimolecular process between $^3MBH^{2+}$ and the metal compound can be neglected.

Quenching Reactions of ^{3}ZnPc, $^3MBH^{2+}$, and $^3MB^+$. ^{3}ZnPc is quenched by an oxidant, such as the ferrocenium ion, $Fe^{III}(CN)_6^{3-}$, $Co^{III}(tpy)_2^{3+}$, BQ, 1,4-naphthoquinone, TNF, TCBQ, and MV^{2+}. The addition of the quencher did not change the ^{3}ZnPc

** The following abbreviations are used; dimethylviologen:MV^{2+}, 2,4,7-trinitro-9-fluorenone:TNF, 2,3,5,6-tetrachloro-1,4-benzoquinone:TCBQ, 1,4-benzoquinone:BQ, 2,2′:6′-2″-terpyridyl:tpy, 1,10-phenanthroline:phen, 2,2′-bipyridyl:bpy.

Table 2. Relevant properties of ZnPc, MB^+, and the quenchers

Species[a]	pK_a	E°_{redox}, *vs.* NHE
ZnPc	—	1.02($ZnPc^+/ZnPc$)[c]
^{3}ZnPc(1.13 eV[b])	—	−0.11($ZnPc^+/^3ZnPc$)
MB^+	—	1.08(MB^{2+}/MB^+)[e]
$^3MB^+$(1.44 eV[d])	—	−0.36($MB^{2+}/^3MB^+$)
MBH^{2+}	0.0[g]	1.06(MBH^{3+}/MBH^{2+})
$^3MBH^{2+}$(1.02 eV[f])	7.2[f]	0.04($MBH^{3+}/^3MBH^{2+}$)
$Fe^{III}(CN)_2(bpy)_2^+$	—	0.78[h]
$Fe^{III}(H_2O)_6^{3+}$	—	0.77[k]
$Fe^{III}(CN)_4(bpy)^-$	—	0.56[l]
Ferrocenium ion	—	0.54[j]
$Fe^{III}(CN)_6^{3-}$	—	0.36[k]
$Co^{III}(phen)_3^{3+}$	—	0.40[l]
$Co^{III}(tpy)_2^{3+}$	—	0.31[l]
TCBQ	—	0.26[m]
TNF	—	−0.08[n]
BQ	—	−0.27[m]
1,4-Naphthoquinone	—	−0.34[m]
MV^{2+}	—	−0.22[o]

a) S_0 state unless otherwise indicated. Excitation energy to the lowest triplet state is shown in parentheses. b) P. S. Vincent, E. M. Voigt, and K. E. Rieckhoff, *J. Chem. Phys.*, **55**, 4131 (1971). c) A. B. P. Lever and J. P. Wilshire, *Can. J. Chem.*, **54**, 2514 (1976). d) Ref. 23. e) T. Takizawa, T. Watanabe, and K. Honda, *J. Phys. Chem.*, **82**, 1391 (1978). f) Ref. 18. g) J. P. Keene, E. J. Land, and A. J. Swallow, "Pulse Radiolysis," ed by M. Evert, J. P. Keene, A. J. Swallow, and J. H. Baxendale, Academic Press, London (1965), p. 227. h) A. A. Schilt, *Anal. Chem.*, **35**, 1599, (1963). i) P. George, G. I. H. Hanavia, and D. H. Irvine, *J. Chem. Soc.*, **1959**, 2548. j) J. G. Mason and M. Rosenblum, *J. Am. Chem. Soc.*, **82**, 4216 (1960). k) W. M. Latimer, "The Oxidation States of the Elements and Their Potentials in Aqueous Solutions," 2nd ed, Prentice Hall, N. J. (1952). l) R. Farina and R. G. Wilkins, *Inorg. Chem.*, **7**, 514 (1968). m) C. K. Mann and K. K. Barness, "Electrochemical Reactions in Nonaqueous Systems," Marcell Deckker, N. Y. (1970). n) Estimated from the electron affinity (1.01 eV) by using this equation: $EA = -1.04E^\circ + 1.39$ (G. Briegleb, *Angew. Chem.*, **76**, 326 (1964)). o) S. Hunig, J. Gross, and W. Schenk, *Justus Liebigs Ann. Chem.*, **1973**, 324.

production immediately after flashing, but it did increase the decay rate of ^{3}ZnPc. However, TNF of more than 50 μmol/dm^3 reduced both the fluorescence and the ^{3}ZnPc production; this effect is ascribed to complex formation in the ground state.[22] An analysis of the pseudo-first order decay of ^{3}ZnPc in the presence of the oxidant gives the quenching-rate constant listed in Table 1. The quenching-rate constant with a charged quencher was changed in an acidic solution by $HClO_4$ of 0.01 mol/dm^3; *i.e.*, that with a cation, MV^{2+} or $Co^{III}(tpy)_2^{3+}$, decreased and that with an anion, $Fe^{III}(CN)_6^{3-}$, increased compared to those in the neutral solution. No change in the quenching rate was observed with BQ in the $HClO_4$ solution. The dependence of the rate constants on the charge of the quencher suggests that ^{3}ZnPc in a 0.01 mol/dm^3 $HClO_4$ solution takes a proton, so electrostatic interaction between the cation triplet state and the charged quencher modifies the quenching-rate constant.

The largest rate constant was obtained using TCBQ as a quencher; it is assumed to quench ^{3}ZnPc at the rate of the encounter. The decreasing order of the quenching rate constants is: TCBQ > TNF > BQ > 1,4-naphthoquinone > MV^{2+}, which agrees with the decreasing order of the redox potential ($E^\circ(Q/Q^-)$ except for MV^{2+} (see Table 2). Since the free-energy change in the electron-transfer reaction between ^{3}ZnPc and the quencher (Q) is written by Eq. 1:

$$-\Delta G = F \times [E^\circ(Q/Q^-) - E^\circ(ZnPc^+/ZnPc)], \quad (1)$$

where $E^\circ(ZnPc^+/^3ZnPc)$ is the redox potential of ^{3}ZnPc and F is the Faraday constant, the quenching can be ascribed to electron transfer. The abnormally small rate constant with MV^{2+} can be explained by the large reorganization energy involved in electron transfer,[23] which Marcus,[9] Rehm and Weller[10] have introduced in explanation of the rate of an adiabatic electron-transfer reaction. The quenching-rate constants with the metal compounds studied in this work were much slower than that expected from the free-energy change. The rate constant observed with $Co^{III}(tpy)_2^{3+}$ can be explained by the fairly large reorganization energy involved in the electron transfer:[24] it is very close to the one estimated by using the equations of Marcus (Eq. 2) and Rehm and Weller (Eq. 3) to get the free energy of activation (ΔG^*_{12}) by using the self-exchange rate constants, electrostatically corrected, of 800 dm^3 mol^{-1} s^{-1} for $Co^{III}(tpy)_2^{3+} - Co^{II}(tpy)_2^{2+}$ and of 1×10^9 dm^3 mol^{-1} s^{-1} for $ZnPc^+$–^{3}ZnPc and by assuming that the electron-transfer rate constant (k) is written as in Eq. 4:

$$\Delta G^*_{12} = \frac{\Delta G^*_1(0) + \Delta G^*_2(0)}{4} + \frac{\Delta G_{12}}{2} + \frac{(\Delta G_{12})^2}{8 \times [\Delta G^*_1(0) + \Delta G^*_2(0)]}, \quad (2)$$

$$\Delta G^*_{12} = \frac{\Delta G_{12}}{2} + \left\{ \frac{(\Delta G_{12})^2}{4} + \frac{[\Delta G^*_1(0) + \Delta G^*_2(0)]^2}{4} \right\}^{1/2}, \quad (3)$$

where $\Delta G^*_1(0)$, $\Delta G^*_2(0)$, and ΔG_{12} are the free energies of activation for the self-exchange reaction of Reactants 1 and 2, and the free-energy change of the cross reaction between Reactants 1 and 2, and,

$$k = \kappa Z \exp(-\Delta G^*_{12}/RT), \quad (4)$$

where κ and Z are the adiabatic parameter and the collision frequency (-10^{11} s^{-1}) respectively. The estimated rate constants are shown in Table 3. However, the estimated rate constant with $Fe^{III}(CN)_6^{3-}$ is still sixty times as large as the observed one, so some non-adiabaticity in the electron transfer may exist.

Spin restriction on any dynamic phenomenon of transition-metal compounds is still effective; for example, the rate constant of an exchange-type energy transfer between a triplet excited state of an organic compound

Table 3. Rate constants of electron-transfer processes (in $dm^3\ mol^{-1}\ s^{-1}$) observed and estimated by means of the Marcus equation and the Rehm and Weller equation

Reactants		$k_q^{ob}(k_{ret})\times10^{-8}$	$k_2^{EEa)}\times10^{-8}$	$k^{cal}(RW)^{b)}\times10^{-8}$	$k^{cal}(M)^{c)}\times10^{-8}$	$k_q^{ob}/k^{cal}(RW)$
^{3}ZnPc	$^2Fe^{III}(CN)_6^{3-}$	0.19	3.5×10^{-4} d)	11	53	0.017
^{3}ZnPc	MV^{2+}	0.036	0.06e)	0.013	0.019	2.77
^{3}ZnPc	$Co^{III}(tpy)_2^{3+}$	5.3	8×10^{-6} f)	1.6	4.2	3.3
^{2}ZnPc†	$^2Co^{II}(tpy)_2^{2+}$	4.6	8×10^{-6} f)	13.8	135	0.33
$^3MBH^{2+}$	$^2Fe^{III}(CN)_6^{3-}$	4.5	3.5×10^{-4} d)	11	32	0.42
$^3MBH^{2+}$	$Co^{III}(phen)_3^{2+}$	0.20	6.5×10^{-7} f)	0.38	0.066	0.53
$^3MBH^{2+}$	$Co^{III}(tpy)_2^{3+}$	0.05	8×10^{-6} f)	0.42	98	0.12
$^2MB^{2+}$	$^4Co^{II}(phen)_3^{2+}$	1.3	6.5×10^{-7} f)	8.2	0.66	0.16

a) The self-exchange electron-transfer rate constant of the second reactant is electrostatically corrected and normalized at 25 °C. b) Estimated by using Eqs. 3 and 4. c) Estimated by using Eqs. 2 and 4. d) Ref. 23. e) M. Shporer, G. Ron, A. Loewenstein, and G. Navon, *Inorg. Chem.*, **4**, 361 (1965). f) Ref. 24.

and a quartet ground state of the chromium(III) compound, yielding the singlet ground state of the organic compound and the doublet excited state of chromium(III), is limited to the spin-statistical factor of the process.[25] Therefore, it is reasonable to think that the spin non-conserved channel of electron transfer is still non-adiabatic ($\kappa<1$). In the quenching by the doublet $Fe^{III}(CN)_6^{3-}$, the formation of the encounter complex preceeds the electron transfer, which has the spin multiplicity of the doublet or quartet. The doublet complex is converted to ^{2}ZnPc† and $^1Fe^{II}(CN)_6^{3-}$, but the quartet complex dissociates into the original reactants, ^{3}ZnPc and $^2Fe^{III}(CN)_6^{3-}$, without spin-inverted conversion into the redox products. Consequently, this kind of non-adiabaticity may reduce the quenching-rate constant to one quarter (the spin-statistical factor of the process), provided the spin restriction is firm. Another kind of non-adiabaticity may come from some specific hindrance to electron-exchange interaction between the reactants.

The decay rates of $^3MBH^{2+}$ and $^3MB^+$ increased in the presence of the oxidant; this did not, however, affect the triplet production immediately after flashing. The quenching rate constants of $^3MB^+$ in an ammonia alkaline aqueous solution by $Fe^{III}(CN)_6^{3-}$ and $Fe^{III}(CN)_4(bpy)^-$ are 4.3×10^9 and 4.5×10^9 $dm^3\ mol^{-1}\ s^{-1}$ respectively; these values are close to the diffusion-controlled rate constant of the bimolecular process in water. Each of the cobalt(III) compounds quenched $^3MB^+$ at a slower rate than did $Fe^{III}(CN)_6^{3-}$ as Table 4 shows. All the oxidants studied quenched $^3MBH^{2+}$ at a slower rate in an acidic solution than in the ammonia alkaline solution. It is reasonable to assume that $^3MB^+$, with the excitation energy of 1.44 eV,[26] is more susceptible to electron-transfer quenching than $^3MBH^{2+}$ with an excitation energy of 1.02 eV,[18] because $E°(MB^{2+}/{}^3MB^+)$ is more positive than $E°(MBH^{3+}/{}^3MBH^{2+})$. The smaller quenching rate constant by the cobalt(III) compounds can not be explained without reference to the self-exchange rates being smaller than those with the iron(III) compounds (see Table 3). Though $Fe^{III}(H_2O)_6^{3+}$ of 0.04 mol/dm^3 quenched MB^+ fluorescence, the decay of $^3MBH^{2+}$ was not effectively quenched, so the increase in the decay rate with $Fe^{III}(H_2O)_6^{3+}$ of 1 mmol/dm^3 is one hundredth of the spontaneous decay rate of $^3MBH^{2+}$. This means that the $Fe^{III}(H_2O)_6^{3+}$ produced in the reduction of MB^+ has practically no effect on the photoreduction of MB^+ in the MB^+–$Fe^{II}(H_2O)_6^{2+}$ photogalvanic cell.

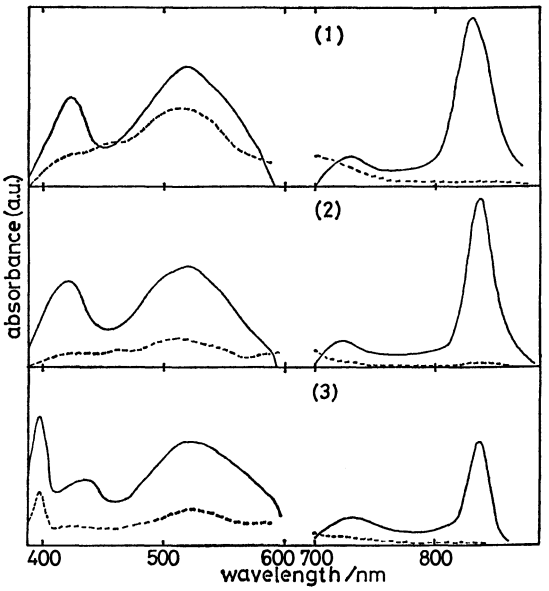

Fig. 2. Transient spectra of ZnPc solution containing an oxidant after the disappearance of ^{3}ZnPc. (1): $[ZnPc]=2\times10^{-5}$ mol/dm^3 and $[Co^{III}(tpy)_2^{3+}]=2.4\times10^{-4}$ mol/dm^3. ——: 10 μs after flashing, - - -: 1 ms after flashing. (2): $[ZnPc]=4\times10^{-6}$ mol/dm^3 and $[BQ]=2\times10^{-3}$ mol/dm^3. ——: 25 μs after flashing, - - -: 0.6 ms after flashing. (3): $[ZnPc]=2\times10^{-6}$ mol/dm^3 and $[MV^{2+}]=1\times10^{-2}$ mol/dm^3. ——: 300 μs after flashing, - - -: 2.5 ms after flashing.

Production of Half-oxidized ZnPc and MB^+. An intermediate was produced in the quenching of ^{3}ZnPc by TCBQ, BQ, 1,4-naphthoquinone, MV^{2+}, and $Co^{III}(tpy)_2^{3+}$. A transient absorption with maxima at 420, 530, 730, and 840 nm was observed immediately after the decay of ^{3}ZnPc, irrespective of the kind of oxidant, as Fig. 2 shows, so it can be identified as the half-oxidized form of ZnPc ($ZnPc^+$). In Fig. 2, the band at 394 nm can also be ascribed to the half-reduced form of MV^{2+}, which is well known to have absorp-

Table 4. Quenching-rate constants and fractions of electron transfer in the quenching of $^3MBH^{2+}$ or $^3MB^+$ in an aqueous solution with $MgCl_2$ of 0.5 mol/dm^3

Quencher	$[H_2SO_4]$[a]	$[NH_4OH]$[a]	$k_q/10^9$ dm^3 mol^{-1} s^{-1}	F_1
$Fe^{III}(CN)_2(bpy)_2^+$	5	0	2.0	0
$Fe^{III}(CN)_4(bpy)^-$	5	0	2.1	0
	0	5	4.5	0
$Fe^{III}(CN)_6^{3-}$	5	0	0.45	0
	0	5	4.3	0
$Co^{III}(phen)_3^{3+}$	5	0	0.02	0.71
	0	5	1.7	0.07
$Co^{III}(tpy)_2^{3+}$	5	0	0.005	0.17
	0	5	1.16	0
$Fe^{III}(H_2O)_6^{3+}$	10[b]	0	0.005	—

a) The concentration of the acid or base is 10^{-3} mol/dm^3. b) H_2SO_4 is replaced by HNO_3.

tion maxima at 394 and 604 nm in water.[27] The molar extinction coefficient of $ZnPC^+$ is calculated to be 2.9×10^4 dm^3 mol^{-1} cm^{-1} at 520 nm by assuming that MV^+ has the same molar extinction coefficient at 394 nm as that in water. Assuming that the conversion of ZnPc to $ZnPc^+$ can be estimated from the decrease in the strong absorbance of ZnPc ($\varepsilon_{672}=2.3\times10^5$ dm^3 mol^{-1} cm^{-1}), the same extinction coefficient of $ZnPc^+$ was obtained at 520 nm. The production of half-reduced quinone was not clearly observed, for the molar extinction coefficients are in the order of 10^3 dm^3 mol^{-1} cm^{-1}.[28] Since the extinction coefficient of $Co^{II}(tpy)_2^{2+}$ is less than 1.6×10^3 dm^3 mol^{-1} cm^{-1} in the visible region,[29] the transient absorption spectrum observed with the cobalt complex can be fully ascribed to $ZnPc^+$. It is a little different from the spectra of either chemically oxidized forms of ZnPc in crystal[30] or of magnesium phthalocyanine in dichloromethane,[31] the former of which has been reported to exhibit three bands at 446, 550, and 730 nm.

The half-oxidized form of MB^+ (MB^{2+}) was also produced in the quenching of $^3MBH^{2+}$ and $^3MB^+$ by the cobalt(III) compounds, which have an absorption maximum at 520 nm, like that observed in the self-quenching reaction of $^3MBH^{2+}$ [19] and in the electrolytic oxidation of MB^+.[32] The iron(III) compounds produced no MB^{2+} in the quenching.

The production of $ZnPc^+$ in the quenching process can be written as Eq. 5;

$$[ZnPc^+]_0 = [^3ZnPc]_0\frac{k_{et}[Q]}{k_d} \quad (5)$$

where $[^3ZnPc]_0$ and $[ZnPc^+]_0$ are productions in mol/dm^3 per flash, k_{et} is the rate constant of overall electron transfer, and k_d is the decay-rate constant of ^3ZnPc in the presence of a quencher. As Fig. 3 shows, the ratio of $[ZnPc^+]_0$ to $[^3ZnPc]_0$ is proportional to $[Q]/k_d$ so the value of k_{et} can be obtained. The ratio of k_{et} to the quenching-rate constant can be regarded as the fraction of free-radical formation in the quenching, which is expressed as k_{et}/k_g and designated as F_1. F_1 can also be defined as a fraction dissociating to

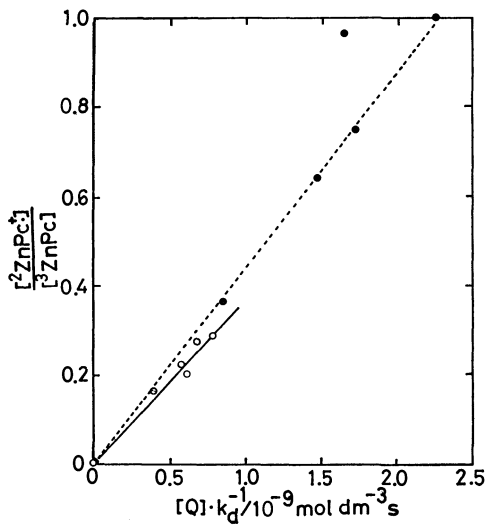

Fig. 3. Determination of k_{et} in the quenching of ^3ZnPc by BQ, ●, and by TCBQ, ○. $[ZnPc]=2\times10^{-5}$ mol/dm^3 and $[HClO_4]=0.01$ mol/dm^3.

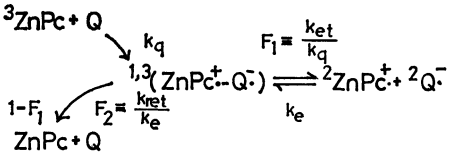

Fig. 4. Reaction scheme.

two free radicals, and the residue $(1-F_1)$, as a fraction performing a reverse electron-transfer reaction, as is shown in Fig. 4. F_1s are fairly high with BQ, MV^{2+}, TCBQ, and $Co^{III}(tpy)_2^{3+}$. However, the iron(III) compounds did not yield $ZnPc^+$ in the quenching of ^3ZnPc, nor did TNF produced $ZnPc^+$ in the quenching of the excited singlet and the excited triplet states of ZnPc.

Two of the present authors (T.O. and N.N.L.) have previously demonstrated that the fraction, F_1, in a homogeneous solution can be explained in terms of the rate of reverse electron transfer in the life of cage complex with triplet multiplicity.[1,2] The rate of reverse electron transfer can be estimated from : (i) the breaking down of spin-conservation, (ii) the free energy change involved in electron transfer, and (iii) the reorganization energy of the reactants involved in electron transfer. If the spin-multiplicity restriction is firm for the reverse electron-transfer, F_1 is unity. However, intersystem crossing from the triplet complex to the singlet one occurs by means of two mechanisms, hyperfine interaction in a weakly interacting cage complex[33] and the spin-orbit interaction of the cage complex on the surrounding reaction surface, the latter of which may be strengthened by a heavy atom and σ-π and/or n-π interaction.

The small value of F_1 with TNF can be explained by means of the spin-orbit interaction of the cage complex on the surrounding reaction surface. The three nitro groups of TNF may induce intersystem crossing through charge transfer and/or σ-π interac-

tion. It has also been reported that no nitro aromatic compound produces $Ru^{III}(bpy)_3^{3+}$ in the quenching of the excited state of $Ru^{II}(bpy)_3^{2+}$.[23] The high efficiencies with BQ, TCBQ, and MV^{2+} can be explained in terms of the spin-multiplicity restriction of reverse electron transfer within the life-time of the geminate pair. The dissociation rate of the geminate pair is too fast, compared to spin-inverted reverse electron transfer, to generate the free radicals in these cases. This is contrary to the fact that the radical yield in the quenching of excited $Ru^{II}(bpy)_3^{2+}$ depends on the charges of half-reduced oxidants; the yield of $Ru^{III}(bpy)_3^{3+}$ and $MV^{+\cdot}$ is 0.4, but that of $Ru^{III}(bpy)_3^{3+}$ and $BQ^{-\cdot}$ is only 0.05.[34] The much larger dependence on the reactant charge may be interpreted in terms of a faster spin-inverted geminate recombination which is caused by a heavy atom (ruthenium) of the reactant pair. The high F_1 of $MV^{+\cdot}$ formation in the ^{3}ZnPc quenching is consistent with a high yield of $MV^{+\cdot}$ with magnesium phthalocyanine in a 90% dimethyl sulfoxide aqueous solution containing of 10^{-3} mol/dm^3 of EDTA.[12]

The highly efficient production of $ZnPc^{+\cdot}$ and $MB^{2+\cdot}$ with the cobalt(III) compounds is attributable to the larger reorganization energy of the $Co^{III}(tpy)_2^{3+}$–$Co^{II}(tpy)_2^{2+}$ reaction or the $Co^{III}(phen)_3^{3+}$–$Co^{II}(phen)_3^{2+}$ reaction, since the large reorganization energy hinders the reverse electron transfer in the geminate radical pair, even though the free-energy change involved in the reverse process is so largly negative.

On the other hand, the reverse electron transfer from the iron(II) compounds to $ZnPc^{+\cdot}$ or $MB^{2+\cdot}$ in the geminate pair is a spin-allowed process, because both the total spin multiplicity of reactants and products are doublet;

$$^2[^2ZnPc^{+}\cdots{}^1ferrocene] \rightarrow {}^2[^1ZnPc\cdots{}^2ferrocenium\ ion]. \quad (6)$$

In this case, the rate of electron transfer can be estimated only from the free energy change and the reorganization energy. This situation is the same as that in the electron-transfer quenching of a singlet excited state. The singlet excited state of chlorophyll-a yields no cation radical in the quenching reaction by BQ.[5]

Decay of $ZnPc^{+\cdot}$ and $MB^{2+\cdot}$. The $ZnPc^{+\cdot}$ produced in the quenching of ^{3}ZnPc decayed in a complex way, resulting in a complete recovery of ZnPc within 0.1 s. The absorption spectrum of $ZnPc^{+\cdot}$ was changed to a broader one (shown in Fig. 2), which can be ascribed to a product in the decay of $ZnPc^{+\cdot}$, because the broad band around 700 nm appeared with the disappearance of the 835 nm band of $ZnPc^{+\cdot}$ in several milliseconds. The fact that both the disappearance rate of $ZnPc^{+\cdot}$ of the 700 nm band increased proportionally to the $ZnPc^{+\cdot}$ production suggests a bimolecular reaction of $ZnPc^{+\cdot}$, dimerization and/or disproportionation, although a single run of the decay of the absorbance at 835 nm could be analysed by means of the first-order kinetics. The recovery of ZnPc was accompanied by not only the disappearance of $ZnPc^{+\cdot}$, but also the decay of the second intermediate. An electron-transfer reaction may take place between oxidized species, $ZnPc^{+\cdot}$, and the second intermediate of ZnPc, and the reduced species of the oxidant. Actually, when $Co^{II}(tpy)_2^{2+}$ ($1\text{—}5\times10^{-5}$ mol/dm^3) was added to a sample solution containing ZnPc and $Co^{III}(tpy)_2^{3+}$, which is one of the products in the electron-transfer quencing, $ZnPc^{+\cdot}$ was completely converted to ZnPc without the appearance of the second intermediate. The rate constant of the electron-transfer reaction shown in Eq. 7 was obtained as 4.55×10^8 dm^3 mol^{-1} s^{-1} by analysing the pseudo-first-order decay of $ZnPc^{+\cdot}$ monitored at 835 nm:

$$^2ZnPc^{+\cdot} + {}^2Co^{II}(tpy)_2^{2+} \rightarrow ZnPc + Co^{III}(tpy)_2^{3+}. \quad (7)$$

The reverse electron transfer from the bulk proceeds via encounter complexes with either singlet or triplet multiplicity, the latter of which needs spin-inversion to the singlet complex on the surrounding reaction surface just as the reverse electron transfer in the geminate pair needs spin-inversion, triplet→singlet. Therefore, the second-order rate constant of the reverse reaction (k_{ret}) is expected to be correlated to the rate of the reverse electron transfer from the geminate pair in the forward process. It is conveinent to define the fraction of the reverse electron transfer (F_2) as the ratio of k_{ret} to the encounter-rate constant (k_e), which is assumed to be equal to the largest quenching-rate constant of ^{3}ZnPc (1.3×10^9 dm^3 mol^{-1} s^{-1}); *i.e.*, F_2 calculated as k_{ret}/k_e with $Co^{III}(tpy)_2^{3+}$ is 0.35, which is close to the fraction of geminate recombination ($1-F_1=0.30$). After $^3MBH^{2+}$ was converted to $MB^{2+\cdot}$ by $Co^{III}(phen)_3^{3+}$, $MB^{2+\cdot}$ disappeared *via* second-order kinetics with a rate constant of 1.3×10^9 dm^3 mol^{-1} s^{-1} in a solution with a high ionic strength: this process coincides with that of the product between $1-F_1$ (0.29) and the encounter-rate constant (k_e) of 4.5×10^9 dm^3 mol^{-1} s^{-1} in water.

The coincidence between the fractions of geminate recombination ($1-F_1$) and bulk recombination (F_2) supports mechanistic conclusions which have already been reached in the reductive quenching of $^3MBH^{2+}$ and $^3MB^{+}$ by iron(II) compounds[1] and aromatic compounds[2] and in the oxidative quenching of $^3Ru^{II}(bpy)_3^{2+}$ by $Cu^{II}(H_2O)_6^{2+}$.[35] On the basis of these studies, we can conclude that: (1) every quenching of the triplet state produces a geminate radical pair, unless the free energy change involved in electron transfer is largely positive and energy transfer to the quencher is possible; (2) the fraction of free-radical formation in the quenching is limited to the "cage escape probability," and (3) the fraction of geminate recombination, $1-F_1$, in the quenching process is close to k_{ret}/k_e. Consequently, we can predict F_1 from the rate constant of the thermal reverse electron-transfer process, which is itself possibly estimated from the free-energy change and the reorganization energy. Unfortunately, k_{ret} values estimated by using the equations of Marcus or Rehm and Weller are a little smaller than those observed for $^2ZnPc^{+\cdot}$–$^2Co^{II}(tpy)_2^{2+}$ and $^2MB^{2+}$–$^4Co^{II}(phen)_3^{2+}$. Though the estimated rate constants of the reverse process are considerably scat-

tered (see Table 3), the smaller rate constants estimated are consistent with the spin-statistical factor of the reverse process, as may be seen in the following reaction scheme;

$$^2ZnPc^{\dagger} + {}^2Co^{II}(tpy)_2^{2+} \begin{cases} \xrightarrow{1/4} {}^1(ZnPc^{\dagger}\text{--}Co^{II}(tpy)_2^{2+}) \\ \xrightarrow{3/4} {}^3(ZnPc^{\dagger}\text{--}Co^{II}(tpy)_2^{2+}) \end{cases} \rightarrow {}^1ZnPc + {}^1Co^{III}(tpy)_2^{3+}. \quad (8)$$

This work was partly supported by the U.S. Department of Energy, Contract EY-76-S-02-2889.

References

1) T. Ohno and N. N. Lichtin, *J. Am. Chem. Soc.*, **102**, 4636 (1980).
2) T. Ohno and N. N. Lichtin, *J. Phys. Chem.*, **86**, 354 (1982).
3) H. Sana and M. Tachiya, *J. Chem. Phys.*, **71**, 1276 (1979).
4) S.-F. Chan, M. Chou, C. Creuts, T. Matsubara, and N. Sutin, *J. Am. Chem. Soc.*, **103**, 369 (1981).
5) D. Holten, M. Gouterman, W. W. Parson, M. W. Windsor, and M. G. Rockley, *Photochem. Photobiol.*, **23**, 415 (1976).
6) G. R. Seely, *Photochem. Photobiol.*, **27**, 639 (1978).
7) U. Steiner and G. Winter, *Chem. Phys. Lett.*, **55**, 364 (1978).
8) U. Steiner, M. Hafner, S. Schreiner, and H. E. A. Kramer, *Photochem. Photobiol.*, **9**, 119 (1974).
9) R. A. Marcus, *J. Phys. Chem.*, **67**, 853 (1963).
10) D. Rehm and A. Weller, *Ber. Bunsenges. Phys. Chem.*, **73**, 834 (1969).
11) A. Harriman and M. -C. Richoux, *J. Chem. Soc., Faraday Trans. 2*, **76**, 1618 (1980).
12) T. Tanno, D. Wohrle, M. Kaneko, and A. Yamada, *Ber. Bunsenges. Phys. Chem.*, **84**, 1032 (1980).
13) E. Rabinowitch, *J. Chem. Phys.*, **8**, 551 (1940).
14) N. N. Lichtin, P. D. Wildes, T. L. Osif, and D. E. Hall, *Adv. Chem. Ser.*, **173**, 296 (1979).
15) T. Ohno and N. N. Lichtin, *J. Phys. Chem.*, **84**, 3485 (1980).
16) N. Maki, *Bull. Chem. Soc. Jpn.*, **42**, 2295 (1969).
17) A. A. Schilt, *J. Am. Chem. Soc.*, **82**, 3000 (1969).
18) T. Ohno, T. L. Osif, and N. N. Lichtin, *Photochem. Photobiol.*, **30**, 541 (1979).
19) P. Kamat and N. N. Lichtin, *J. Phys. Chem.*, **85**, 814 (1981).
20) M. P. Tuirko, V. V. Sapunov, and K. N. Salovev, *Opt. Spectrosk.*, **34**, 1094 (1973).
21) S. Kato, M. Morita, and M. Koizumi, *Bull. Chem. Soc. Jpn.*, **37**, 117 (1962).
22) P. J. McCartin, *J. Am. Chem. Soc.*, **85**, 2021 (1963).
23) C. R. Bock, J. A. Conner, A. R. Gutierrez, T. J. Meyer, D. G. Whitten, B. P. Sullivan, and J. K. Nagle, *J. Am. Chem. Soc.*, **101**, 4815 (1979).
24) T. Ohno and N. N. Lichtin, *J. Phys. Chem.*, **84**, 3019 (1980).
25) F. Wilkinson and C. Tsiamis, *J. Chem. Soc., Faraday Trans. 2*, **77**, 1681 (1981).
26) K. Gollnick, *Ann. N. Y. Acad. Sci.*, **171**, 89 (1970).
27) J. A. Farrington, M. Evert, E. J. Land, and K. Fletcher, *Biochim. Biophys. Acta*, **314**, 372 (1973).
28) K. B. Patel and R. L. Willson, *Trans. Faraday Soc.*, **69**, 814 (1973).
29) R. Hogg and R. G. Wilkins, *J. Chem. Soc.*, **1962**, 341.
30) J. F. Meyers, G. W. R. Canham, and A. B. P. Lever, *Inorg. Chem.*, **14**, 461 (1975).
32) T. Watanabe, M. Kimura, and K. Honda, to be published.
31) D. Lexa and M. Reix, *J. Chim. Phys.*, **71**, 517 (1970).
33) K. Shulten, H. Staerk, A. Weller, H. -J. Werner, and B. Nickel, *Z. Phys. Chem. (Wiesbaden)*, **101**, 371 (1976).
34) J. R. Darwent and K. Kalyanasundaram, *J. Chem. Soc., Faraday Trans. 2*, **77**, 373 (1981).
35) H. A. Hoselton, C. -T. Lin, H. A. Schwarz, and N. Sutin, *J. Am. Chem. Soc.*, **100**, 2383 (1978).

The Dehydrogenation of Cyclohexane by the Use of a Porous-glass Reactor††

Osamu SHINJI,† Makoto MISONO,* and Yukio YONEDA

Department of Synthetic Chemistry, Faculty of Engineering, The University of Tokyo, Hongo, Bunkyo-ku, Tokyo 113

(Received January 22, 1982)

The dehydrogenation of cyclohexane was studied by the use of a double tubular reactor; the inner tube was made of porous glass, and the outer tube, of non-porous glass. The Pt/Al_2O_3 catalyst was placed inside the inner tube. It was demonstrated that dehydrogenation proceeded beyond the equilibrium conversion to be expected in the absence of a porous tube, by separating the hydrogen produced from the central reaction zone through the porous tube. When the reaction rate was so high that the reactant gas reached equilibrium near the inlet of the reactor, the dehydrogenation conversion became greater (more than twice the equilibrium conversion) as the flow rate in the inner path decreased and the flow rate in the outer path increased. The experimental data obtained by using the porous reactor were well reproduced by a computer simulation based on a simple model, in which such parameters as the flow rate, the gas permeability, and the reaction rate, were considered. The potential application of the present porous-reactor system was also discussed.

The dehydrogenation reaction, which usually requires a high reaction temperature because of the restriction caused by equilibrium, can be expected to proceed seemingly beyond equilibrium if the hydrogen produced by the reaction is removed selectively. Based on this idea, a palladium-alloy membrane was successfully applied to hydrogenation and dehydrogenation reactions.[1,2] Palladium acts as a barrier through which only hydrogen penetrates, and also as a catalyst. However, this membrane may not be used when palladium causes undesirable side-reactions and when poisons to palladium like sulfur are present. In these cases, porous glass[3] is sometimes very useful as the separation medium, since porous glass is fairly inert against chemicals and still has considerable physical strength. The permeability of gases can be controlled to some extent by changing the size and number of pores. Because of these advantages, the permeability of gases through porous glass has already been studied,[4] and application to isotope separation has been attempted.[5] Recently a porous-glass reactor was used to increase the hydrogen yield in the thermal decomposition of hydrogen sulfide.[6,7]

In the present study, a porous-glass reactor was constructed and the effectiveness of the reactor was experimentally examined by applying it to the dehydrogenation of cyclohexane. To confirm the effectiveness, the observed results were semi-quantitatively compared with the results of a computer simulation. On the basis of this comparison, the desirable properties of porous glass and the operation conditions are discussed.

Experimental

The porous reactor used in the present study was a double tubular reactor, as is illustrated in Fig. 1. The inner tube was made of porous Vycor glass (Corning Code No. 7930, outer diameter: 17.3 mm, wall thickness: 1.4 mm), with a mean pore size of 40 Å. The outer tube was ordinary non-porous Pyrex glass. Additional non-porous glass tubes were inserted tightly inside the upper and lower parts of the inner tube in order to minimize the permeation of gases outside the reaction zone (catalyst bed). By the insertion of these two tubes, the gas permeation outside the reaction zone was made negligible. 11 g of a Pt/Al_2O_3 catalyst (Pt: 0.38 wt%) in the form of 1.6 mm beads were packed in the inner tube (the length of the catalyst bed was 14 cm). Prior to the reaction, the catalyst was treated at 400 °C in an oxygen stream for 1 h and then reduced in a hydrogen stream for 1 h. No change in the catalytic activity during the reaction was detectable. Nitrogen, to which 16.0±0.5 mol% cyclohexane was mixed by passing it through an evaporator-saturator kept at 31 °C, was fed into the inner tube (inner path), and pure nitrogen into the outer path (path between the two tubes). The reaction temperature, as measured by an iron-constantan thermocouple, was 215—218 °C at the center of the catalyst bed. The outlet gases of the inner and outer paths were sampled by operating the valves and analyzed by two gas chromatographs directly connected to the valves. The material balance of the reaction was above 90%. The total pressures in the inner and outer paths were both close to 1 atm. A non-porous reactor, both tubes of which were non-porous glass of the same sizes as those of the porous reactor, was also used for purposes of comparison.

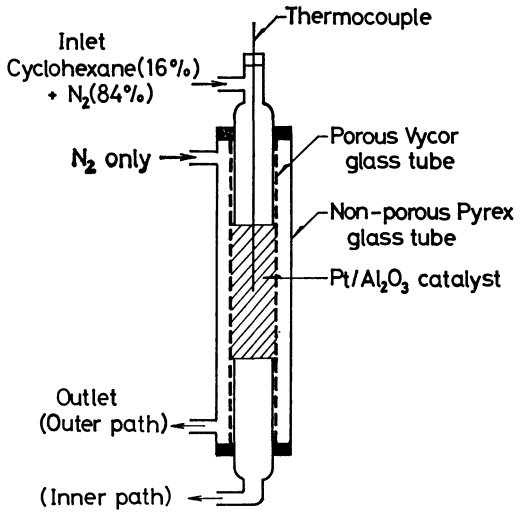

Fig. 1. Schematic diagram of porous reactor.

Results and Discussion

Permeability of Gases. If the diffusion of gases through the porous glass tube is effusion (Knudsen

† Present address: Showa Electric Wire and Cable Co. Ltd., Minamihashimoto, Sagamihara, Kanagawa 229.

†† This paper has been presented at the 45th Symposium on Catalysis, Sendai, Oct. 1980.

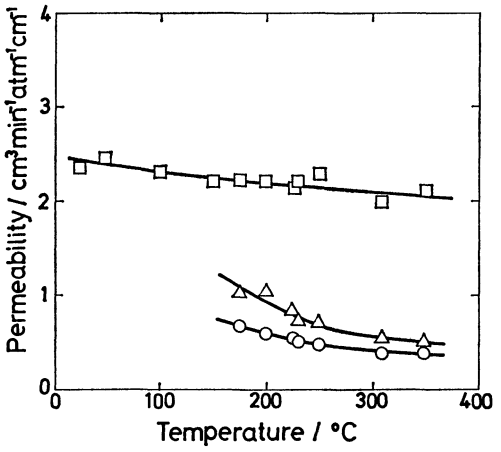

Fig. 2. Gas permeability of the porous tube as a function of temperature.
○: Cyclohexane, △: benzene, □: hydrogen.

flow), the rate of gas permeation can be described by:[4,5,8]

$$N_i = Q_i(P_i - p_i) \tag{1}$$

where N_i is the molar flow rate of the i component per unit of length of the porous glass tube, Q_i is the permeability of the i component, and P_i and p_i are the partial pressures of the inner and outer paths respectively. The permeability, Q_i, depends on the molecular weight, M_i, as in Eq. 2:

$$Q_i = \frac{a}{\sqrt{M_i T}}, \tag{2}$$

where T is the absolute temperature and a is a constant which depends on the properties of the porous barrier. The permeabilities, Q_i, of cyclohexane, benzene, and hydrogen for the porous glass tube used in the present work were measured in the following way. Mixtures of the three gases diluted with nitrogen were conducted into the inner tube loaded with glass beads in the same form as the catalyst, and then the outlet compositions of the reactor were analyzed. The Q_i value was calculated by means of Eq. 3:

$$f_{iL} = Q_i\left(\frac{P_{i0}+P_{iL}}{2} - \frac{p_{iL}}{2}\right)L, \tag{3}$$

where f_{iL} is the flow rate of the i component in the outlet gas of the outer path. The suffixes 0 and L indicate the inlet and outlet respectively, and L is the length of the reactor zone (catalyst bed). By increasing the flow rates in both paths, the changes in the flow rates along the reactor caused by gas permeation were made negligible. In this case, Eq. 3 is readily obtained by integrating Eq. 1 from l (the distance from the inlet of the catalyst bed)=0 to L.

Figure 2 shows the temperature dependence of the permeability. The permeation of hydrogen was obviously dominant, and hydrogen was effectively separated from the other two gases at higher temperatures. The Q_i ratio, as calculated from the molecular weight by means of Eq. 2, is cyclohexane:benzene:hydrogen= 1.00:1.04:6.48, while the observed ratio at 230 °C was 1.0:1.4:4.4. Hydrogen permeation was less preferential than was expected from Eq. 2. Moreover, the permeabilities of cyclohexane and benzene increased rapidly at low temperatures, indicating that diffusion processes other than effusion (probably surface diffusion[4]) increase for cyclohexane and benzene at lower temperatures.

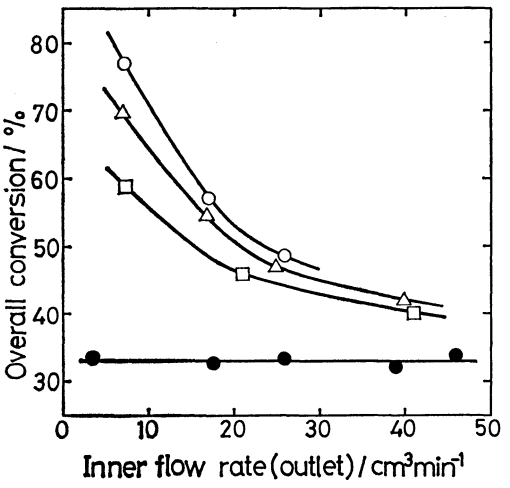

Fig. 3. Comparison of porous and non-porous reactors as applied to dehydrogenation of cyclohexane at 215 °C.
Open symbols: porous reactor [outer flow rate (outlet) was ○: 110 cm³ min⁻¹, △: 60 cm³ min⁻¹, and □: 20 cm³ min⁻¹]. ●: Non-porous reactor.

Dehydrogenation of Cyclohexane by the Use of a Porous Reactor. Comparison of Porous and Non-porous Reaction: The overall conversions obtained with the porous and non-porous reactors are compared in Fig. 3 as functions of the inner and outer flow rates. The overall conversion, X, for the porous reactor is defined and calculated by means of:

$$X = \frac{F_L P_{BL} + f_L p_{BL}}{F_L(P_{CL}+P_{BL}) + f_L(p_{CL}+p_{BL})}, \tag{4}$$

where F and f are the inner and outer flow rates respectively. The suffixes C and B denote cyclohexane and benzene components respectively, while the suffix L indicates the values at the outlet. The relation of the conversion *vs.* W/F obtained with the non-porous reactor showed that the catalytic activity was so high that the reactant gas reached equilibrium within 2 cm from the inlet of the catalyst bed. Consequently, the conversion for the non-porous reactor was constant in Fig. 3 and independent of the inner flow rate. Figure 3 shows clearly that the conversion for the porous reactor was higher than that for the non-porous reactor, which gave an equilibrium conversion. The lower the inner flow rate was, and the higher the outer flow rate was, the greater the overall conversion became. The highest conversion was more than twice the equilibrium conversion which would be expected in the absence of the preferential separation of hydrogen.

Effects of Inner and Outer Flow Rates. The outlet-gas compositions in the inner and outer paths are plotted against the inner flow rate in Fig. 4, together with the conversion. In these experiments, the outer

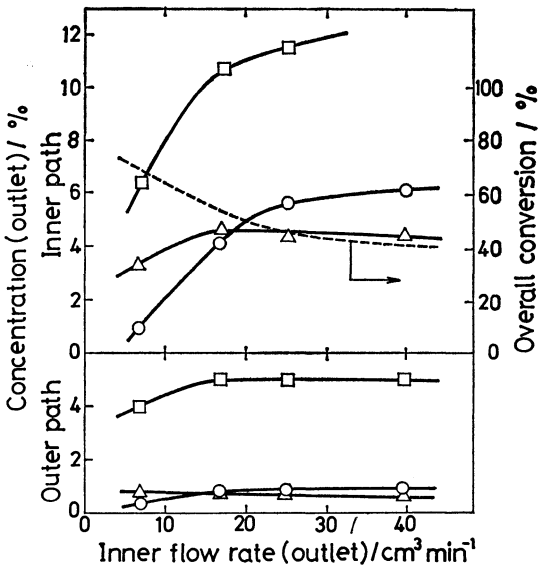

Fig. 4. Effects of inner flow rate on the composition at outlet and overall conversion.
Temperature: 215 °C, outer flow rate (outlet): 60 $cm^3\ min^{-1}$. ——: Composition, - - -: overall conversion, ○: cyclohexane, △: benzene, □: hydrogen.

flow rate was kept constant at 60 $cm^3\ min^{-1}$. The following things may be noted in this figure: (i) The hydrogen concentration in the outer path was much higher than the concentrations of cyclohexane and benzene in the outer path. This dominant permeation of hydrogen into the outer path is the reason why higher conversions were obtained for the porous reactor. (ii) At low inner flow rates, the conversion was high, and the concentrations of hydrogen and cyclohexane in the inner path were very low. The residence time of the reactant gas was probably so high as to remove sufficiently the produced hydrogen from the reaction zone, resulting in the marked increase in the conversion. (iii) The hydrogen concentration in the outer path decreased at a low inner flow rate, in spite of the sufficient removal of hydrogen from the inner path to the outer. This was, however, due to the insufficient supply of the reactant; therefore, it is not contradictory.

The higher conversions at high outer flow rates shown in Fig. 3 are apparently caused by the dilution of hydrogen in the outer path; hydrogen permeation is accelerated by the greater difference in the partial pressure of hydrogen between the inner and outer paths (see Eq. 1). In fact, the hydrogen concentration in the outer path decreased constantly with an increase in the outer flow rate.

Effectiveness of Porous Reactor when the Catalytic Activity is Low. Another experiment was carried out in which the apparent reaction rate was reduced by diluting the Pt/Al_2O_3 catalyst with glass beads of the same size as the catalyst. At 230 °C, the conversion for the porous reactor was 65% (inner flow rate: 7.0 $cm^3\ min^{-1}$, outer flow rate: 90 $cm^3\ min^{-1}$, while that for the non-porous was 40% (flow rate: 7.0 $cm^3\ min^{-1}$). Those results demonstrate that dehydrogenation, even in the case of a low catalytic activity,

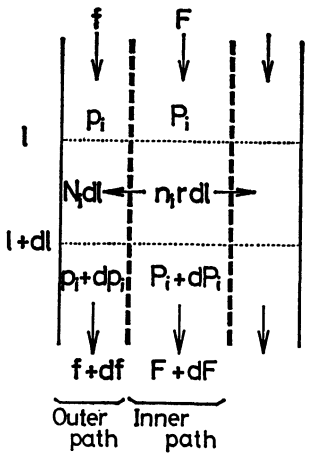

Fig. 5. Material balance in differential length of reactor, l—$l+dl$. F, f, *etc.*: See text.

proceeds beyond the equilibrium conversion (50% at 230 °C) which is to be expected in the absence of the hydrogen permeation, when the porous reactor is used.

Simulation of Reaction with Porous Reactor. A computer simulation was attempted to clarify further the characteristics of the porous reactor obtained experimentally, as has been described in the preceding sections.

Method of Calculation. (i) The rate equation for dehydrogenation was empirically approximated by:

$$r = k\left(P_C - \frac{P^2_{H,e}}{K} P_B P_H\right), \tag{5}$$

where r is the rate of benzene produced; P_i, the partial pressures of cyclohexane (C), benzene (B), and hydrogen (H) respectively; K, the pressure equilibrium constant; $P_{H,e}$, the partial pressure of hydrogen at equilibrium, and k, the rate constant. The k value was experimentally determined as a function of the temperature by the use of the non-porous reactor. The values of K were calculated as a function of the temperature and were experimentally justified in the present temperature region. The conversion calculated by Eq. 5 agreed well with those observed in the W/F range from 0.004 to 0.06 g min cm^{-3} at 200—230 °C. Because the total mass in the inner path changes along the catalyst bed, $P_{H,e}$ was calculated from the gas composition and the K value at every position of the reactor. (ii) The temperature distribution along the catalyst bed was measured (see Fig. 7) and approximated by a biquadratic function of l, the distance from the inlet of the catalyst bed. (iii) The permeation of the three gases was calculated by means of Eq. 1, where the permeabilities, Q_i, measured at 230 °C were used. The permeation of nitrogen was neglected because the reactant gases were very dilute. (iv) By assuming a plug flow in the reactor, a set of equations are obtained from the material balance for the three components in a differential length of the reactor, dl (see Fig. 5). For the inner path,

$$FP_i = (F+dF)(P_i+dP_i) + N_i dl + n_i r dl, \tag{6}$$

where $n_i = 1$, -1, and -3 for i=C, B, and H respec-

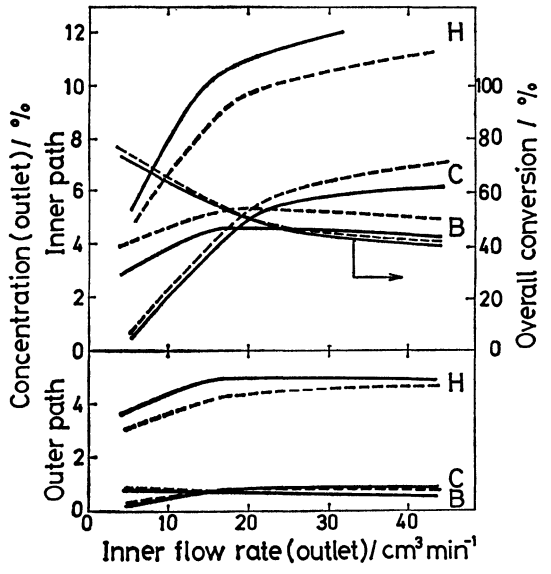

Fig. 6. Comparison of the experimental and simulated results for dehydrogenation of cyclohexane with the porous reactor.
Temperature: 215 °C, outer flow rate (outlet): 60 $cm^3\ min^{-1}$. ——: Experimental, - - -: simulated, C: cyclohexane, B: benzene, H: hydrogen.

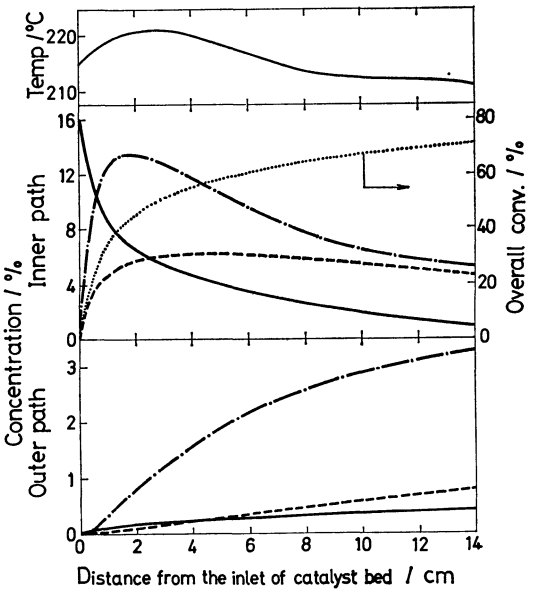

Fig. 7. Change of compositions and overall conversion along the catalyst bed for the porous reactor (simulated).
Inner flow rate (inlet): 7.0 $cm^3\ min^{-1}$, outer flow rate (inlet) 60 $cm^3\ min^{-1}$.
——: Cyclohexane, - - -: benzene, —·—: hydrogen, ·····: overall conversion.

tively. For the outer path,

$$fp_i = (f+df)(p_i+dp_i) - N_i dl \quad (i=C, B, H,). \qquad (7)$$

The flow rates, F and f, in Eqs. 6 and 7 are described in terms of P_i and p_i:

$$F = \frac{F_N}{1-\sum P_i} \text{ and } f = \frac{f_N}{1-\sum p_i} \quad (i=C, B, H,), \qquad (8)$$

where F_N and f_N are the flow rates of nitrogen (constant) in the inner and outer paths respectively. Equations 6, 7, and 8 are rewritten into six simultaneous differential equations in terms of P_i and p_i (i=C, B, and H); they were solved numerically by the Runge-Kutta method.

Results of Calculation. The calculated results are compared with the observed data in Fig. 6. A good agreement is seen in conversion, and the trend of the outlet compositions is essentially reproduced by the simulation. The simulation data given in Fig. 7 show how the compositions change in the reactor from the inlet to the outlet. Equilibrium is reached within 2 cm from the inlet of the catalyst bed. The hydrogen concentration decreases in the inner path, and increases in the outer path, along the reactor, as expected.

Conclusion

Both the experiments and the simulation proved that the dehydrogenation of cyclohexane proceeds beyond the equilibrium (expected in the absence of a porous tube) by means of the selective separation of hydrogen from the reaction zone by the use of a porous reactor. For example, the conversion for the porous reactor was 80% at 215 °C as compared with the equilibrium conversion of 35% for the non-porous reactor. Since the 80% conversion corresponds to the equilibrium conversion at 255 °C, the porous reactor reduces the reaction temperature by 40 °C. However, a low inner flow rate and a high outer flow rate are necessary to obtain a high conversion. The former is disadvantageous for the reaction efficiency, and the latter for the recovery of hydrogen, because of its low concentration. Thus, the efficiency of the porous reactor is significantly dependent on the permeation rate. It is, therefore, important, for the improvement of efficiency, to select a material with a high and highly selective permeability and to design a reactor with a large area for gas permeation. When such factors as the reaction rate, the permeability, *etc.* are once known, a computer simulation such as is shown in this study may be helpful for the design of a more efficient reactor and the optimization of the operation conditions.

With the aid of a porous reactor, characterized by simultaneous reaction and separation, the reaction temperature can be lowered. By taking advantage of this, the porous reactor may be used for the conversion of low-temperature thermal energy to hydrogen or other chemical energies. The reduction of the reaction temperature is also suitable for reactions that use thermally unstable catalysts or reactants.

The authors are grateful to Professor Toshio Uchijima (The University of Tsukuba), Mr. Hiromitsu Takeyasu, and Mr. Koichi Katamura for the preliminary experiments and discussions; they also wish to acknowledge the helpful advice of Dr. Masayuki Dokiya (National Chemical Laboratory for Industry) for the helpful discussions.

References

1) V. M. Gryaznov, V. S. Smirnov, and M. G. Slinko, "Proc. 5th Int. Congr. Catal., Miami Beach, 1972," North-Holland, Amsterdam (1973), p. 1139; "Proc. 7th Int. Congr. Catal., Tokyo, 1980," Kodansha, Tokyo, and Elsevier, Amsterdam (1981), p. 224.

2) B. J. Wood, *J. Catal.*, **11**, 30 (1968).

3) T. Kyono and A. Makishima, *Zairyo Kagaku*, **12**, 33 (1975).

4) S-T. Hwang and K. Kammermeyer, *Separation Science*, **1**, 629 (1966); *Can. J. Chem. Eng.*, **44**, 82 (1966).

5) K. Higashi, H. Ito, and J. Oishi, *J. Nucl. Sci. Technol.*, **1**, 298 (1964); K. Higashi, A. Oya, and J. Oishi, *ibid.*, **3**, 51 (1966).

6) M. E. D. Raymont, *Hydrocarbon Process.*, **54**, 139 (1975).

7) M. Dokiya, T. Kameyama, and K. Fukuda, *Denki Kagaku*, **45**, 701 (1977).

8) J. Shacter, E. Von Halle, and R. L. Hoglund, "Diffusion Separation Methods," in "Kirk-Othmer Encyclopedia of Chemical Technology," 2nd ed, ed by A. Standen, Interscience, New York (1965), Vol. 7, p. 91.

 © 1982 The Chemical Society of Japan Bull. Chem. Soc. Jpn., 55, 2765—2770 (1982)

Polarized Raman Spectrum of Maleic Anhydride Crystal

Yoshimi Ishibashi, Ryoichi Shimada,*,† and Hiroko Shimada

Department of Chemistry, Faculty of Science, Fukuoka University, Nanakuma, Nishi-ku, Fukuoka 814

† *Department of Chemistry, Faculty of Science, Kyushu University 33, Hakozaki, Higashi-ku, Fukuoka 812*

(Received January 25, 1982)

The polarized Raman spectrum of the maleic anhydride single crystal was studied. Prominent polarization behavior of the Raman bands was observed. Assuming the oriented gas model, the relative intensities of the non-totally symmetric intramolecular vibrations in various polarized Raman spectra were studied based on the data of the crystal structure. The assignments of the fundamental vibrational frequencies for maleic anhydride were reinvestigated through the polarization behavior of the Raman bands as well as the normal coordinate calculation.

The infrared and Raman spectra of maleic anhydride were first studied by Mirone and Chiorboli.[1] Most of their assignments were confirmed by the study of the polarized infrared spectrum of the single crystal observed by Di Lauro *et al.*[2] They also carried out the normal coordinate analysis for the in-plane vibrations.[2] Rogstad *et al.*[3] reexamined the vibrational analyses made by earlier workers on the basis of the band contours of the infrared vapor spectrum as well as the isotopic product and sum rules for deuterated molecules.

In this work, the fundamental vibrational assignments are reinvestigated based on the study of the polarized Raman spectrum of the single crystal of maleic anhydride as well as the normal coordinate analyses for in-plane and out-of-plane vibrations.

Experimental

Material. Maleic anhydride obtained from Nakarai Chemicals, Ltd. was purified by zone-refining of about 60 passages followed by sublimation under reduced pressure.

Optical Measurement. The polarized Raman spectrum of maleic anhydride was observed in the single crystal with a JEOL 400T Laser Raman Spectrophotometer. The sample was excited with the 514.5 nm line from an Ar^+ ion laser of Toshiba Model LAI-104-A.

Single crystals were grown in a closed tube by sublimation. Cubic crystals, about $(3\ mm)^3$, were obtained. A well-grown single crystal was selected and the crystal axes were determined by the observation of the birefringence under a polarization microscope. The direction of the crystal growth was selected as the c axis and the two-fold axis of the crystal as the b axis.

The crystal sample was excited with the laser beam polarized along the y axis in the z direction and the Raman scattering was observed in the x direction. The two polarized components of the scattering were analyzed by a polarizer inserted between the sample and the condenser lens. A compensator was placed between the condenser lens and the entrance slit in order to compensate the preferential sensitivity of the spectrophotometer for the light beams polarized along the y and z axes. The crystal was placed in the sample holder equipped with a goniometer in such a way that the crystal axes a, b, and c were parallel to the space-fixed axes x, y, and z. Thus, there are six ways of orientation of the crystal cube and a pair of polarized spectra are observed by the use of the polarizer for each orientation.

Twelve polarized Raman spectra were measured in total. The polarized Raman spectrum was denoted with four symbols following the notation adopted by Porto *et al.*,[4] such as a(ba)c. The letters inside the parentheses refer to the polarization directions of the excitation and scattering light beams in order, and the first and last letters refer to the propagation directions of the excitation and scattering light beams, respectively.

Depolarization measurements of the Raman spectrum were also made in the molten phase.

Calculation of Derived Polarizability Tensors

The crystal structure of maleic anhydride has been determined by Marsh *et al.*[5] Maleic anhydride crystallizes in the orthorhombic system of the space group D_2^4 with four molecules in the unit cell. The projection of the crystal structure on the ab plane is shown in Fig. 1. The correlation among the molecular point group C_{2v}, the factor group D_2, and the site group C_1 of the crystal is given in Table 1. No factor group splitting was observed for the bands due to the molecular vibrations. Thus, the relationship between the two derived polarizability tensors, for the free molecule and the crystal, was derived based on the sim-

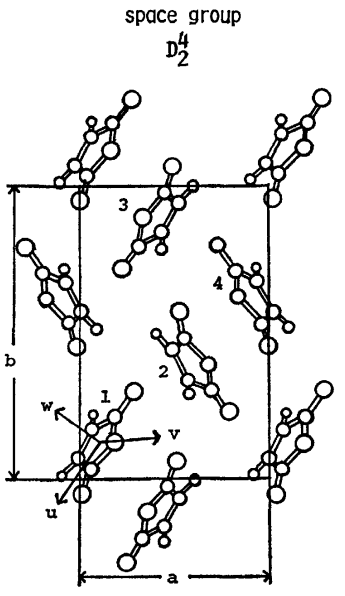

Fig. 1. Projection of the maleic anhydride crystal on the ab plane.

Table 1. Correlation diagram for maleic anhydride crystal

	Molecular group C_{2v}	Site group C_1	Factor group D_2
a_1	α_{uu}, α_{vv}, α_{ww}	a	a
a_2	α_{uv}		b_1
b_1	α_{uw}		b_2
b_2	α_{vw}		b_3

plified oriented gas model.

The evaluation of the matrix elements of the derived polarizability tensors of maleic anhydride was made following the procedures applied for naphthalene and anthracene crystals by Ito *et al.*[6] If the transformation matrix between the molecular-fixed coordinates u, v, w and the crystal fixed a, b, c is expressed by

$$T_1 = \begin{vmatrix} a_u & a_v & a_w \\ b_u & b_v & b_w \\ c_u & c_v & c_w \end{vmatrix}$$

for molecule 1, then the matrices for molecules 2, 3, and 4 are given for the D_2^4 crystal by

$$T_2 = \begin{vmatrix} -a_u & -a_v & -a_w \\ -b_u & -b_v & -b_w \\ c_u & c_v & c_w \end{vmatrix}, \quad T_3 = \begin{vmatrix} -a_u & -a_v & -a_w \\ b_u & b_v & b_w \\ -c_u & -c_v & -c_w \end{vmatrix},$$

and

$$T_4 = \begin{vmatrix} a_u & a_v & a_w \\ -b_u & -b_v & -b_w \\ -c_u & -c_v & -c_w \end{vmatrix},$$

respectively, where a_u is the direction cosine of the a and u axes, and so on. The derived polarizability tensor of a free molecule with respect to a normal vibration Q is given by

$$\alpha'_m(Q) = \begin{vmatrix} \alpha'_{uu} & \alpha'_{uv} & \alpha'_{uw} \\ \alpha'_{vu} & \alpha'_{vv} & \alpha'_{vw} \\ \alpha'_{wu} & \alpha'_{wv} & \alpha'_{ww} \end{vmatrix},$$

where $\alpha'_{uu}=\partial\alpha_{uu}/\partial Q$, and so on. The molecular tensors with respect to the crystal-fixed coordinates are given by

$$\alpha'_{m_1} = T_1\alpha'_m\tilde{T}_1$$

for molecule 1, and

$$\alpha'_{m_2} = T_2\alpha'_m\tilde{T}_2$$

for molecule 2, and so on. Under the assumption of the oriented gas model, the polarizability tensor of the unit cell, α_u, is assumed to be

$$\alpha_u = \alpha'_{m_1}Q_1 + \alpha'_{m_2}Q_2 + \alpha'_{m_3}Q_3 + \alpha'_{m_4}Q_4.$$

Using the symmetry coordinates S_{A_1}, S_{B_1}, S_{B_2}, and S_{B_3} appropriate to the four molecule unit cell, the derived polarizability tensors with respect to the unit cell vibrations are given for each symmetry species by

$$\alpha'_u(S_{A_1}) = \begin{vmatrix} A_{aa} & 0 & 0 \\ 0 & A_{bb} & 0 \\ 0 & 0 & A_{cc} \end{vmatrix} \quad \alpha'_u(S_{B_1}) = \begin{vmatrix} 0 & A_{ab} & 0 \\ A_{ba} & 0 & 0 \\ 0 & 0 & 0 \end{vmatrix}$$

Table 2. Elements of the derived polarizability tensors of maleic anhydride

	b_1	b_2
A_{aa}	$2a_ua_w\alpha'_{uw}$	$2a_va_w\alpha'_{vw}$
A_{bb}	$2b_ub_w\alpha'_{uw}$	$2b_vb_w\alpha'_{vw}$
A_{cc}	$2c_uc_w\alpha'_{uw}$	$2c_vc_w\alpha'_{vw}$
A_{ab}	$(a_ub_w+a_wb_u)\alpha'_{uw}$	$(a_vb_w+a_wb_v)\alpha'_{vw}$
A_{ac}	$(a_uc_w+a_wc_u)\alpha'_{uw}$	$(a_vc_w+a_wc_v)\alpha'_{vw}$
A_{bc}	$(b_uc_w+b_wc_u)\alpha'_{uw}$	$(b_vc_w+b_wc_v)\alpha'_{vw}$
	a_2	a_1
A_{aa}	$2a_ua_v\alpha'_{uv}$	$a_u^2\alpha'_{uu}+a_v^2\alpha'_{vv}+a_w^2\alpha'_{ww}$
A_{bb}	$2b_ub_v\alpha'_{uv}$	$b_u^2\alpha'_{uu}+b_v^2\alpha'_{vv}+b_w^2\alpha'_{ww}$
A_{cc}	$2c_uc_v\alpha'_{uv}$	$c_u^2\alpha'_{uu}+c_v^2\alpha'_{vv}+c_w^2\alpha'_{ww}$
A_{ab}	$(a_ub_v+a_vb_u)\alpha'_{uv}$	$a_ub_u\alpha'_{uu}+a_vb_v\alpha'_{vv}+a_wb_w\alpha'_{ww}$
A_{ac}	$(a_uc_v+a_vc_u)\alpha'_{uv}$	$a_uc_u\alpha'_{uu}+a_vc_v\alpha'_{vv}+a_wc_w\alpha'_{ww}$
A_{bc}	$(b_uc_v+b_vc_u)\alpha'_{uv}$	$b_uc_u\alpha'_{uu}+b_vc_v\alpha'_{vv}+b_wc_w\alpha'_{ww}$

$$\alpha'_u(S_{B_2}) = \begin{vmatrix} 0 & 0 & A_{ac} \\ 0 & 0 & 0 \\ A_{ca} & 0 & 0 \end{vmatrix} \quad \alpha'_u(S_{B_3}) = \begin{vmatrix} 0 & 0 & 0 \\ 0 & 0 & A_{bc} \\ 0 & A_{cb} & 0 \end{vmatrix},$$

where the A's are the functions of the direction cosines and of the elements of the derived polarizability tensor of the free molecule.

According to the character table and selection rules for the C_{2v} molecule, we derived simple analytical expressions of A's for the vibrations belonging to the different species of the molecule. These results are given in Table 2.

Normal Coordinate Calculation

A normal coordinate calculation was performed through the standard ***GF*** matrix method with a Facom M-200 computer at the computer center of Kyushu University. Heiderbrandt *et al.*[7] showed that the maleic anhydride molecule is planar and gave geometric parameters for this molecular structure. We used their geometric parameters for the construction of the ***G*** matrix elements.

The ***F*** matrix elements for the in-plane vibrations were evaluated with the potential field of an improved modification of the Urey-Bradley force field as described in the previous paper.[8] The potential field is given by

$$\begin{aligned} 2V = 2V_{UB} &+ \sum k^o(\Delta r, \Delta r) \\ &+ \sum k^m(\Delta r, \Delta r) + \sum k^m(\Delta R, \Delta R) \\ &+ \sum h^m(\Delta R, \Delta\alpha) + \sum h^m(\Delta R, \Delta\beta) \\ &+ \sum f^o(\Delta\alpha, \Delta\alpha) + \sum f^o(\Delta\beta, \Delta\beta), \end{aligned}$$

where V_{UB} is the basic Urey-Bradley force field, and k, h, and f are due to the valence force field. k^o and k^m are the interaction terms between two stretching coordinates oriented in the ortho and meta positions to each other, respectively, h^m is the interaction term between stretching and bending coordinates oriented in the meta position, and f^o is the interaction term between two bending coordinates oriented in the ortho position. R and α refer to the bond distances and angles constructing the ring, and r and β to the bond

distances and angles relating to the C=O and C–H side bonds, respectively.

For the out-of-plane vibrations, the valence force field and ϕ-type torsional coordinates were used. The notations of the force constants Q, q, P, p, and t are the same as those given by Whiffen.[9] The procedure of the calculation was exactly the same as described in the previous paper.[8]

Table 3. Force constants for in-plane vibrations of maleic anhydride

$K_{C'=C'}$ [a]	8.34	$F_{C'\cdots H}$	0.53
$K_{C'-C}$	3.67	$F_{C\cdots H}$	0.25
K_{C-O}	2.60	$F_{C'\cdots O}$	0.30
$K_{C'-H}$	4.82	$F_{O\cdots O}$	0.84
$K_{C=O}$	10.46	$k^o_{r_H,r_H}$	0.02
$H_{C'-C'-C}$	0.28	$k^o_{r_H,r_O}$	0.02
$H_{C'-C-O}$	0.49	$k^m_{r_O,r_O}$	0.06
H_{C-O-C}	0.50	$k^m_{R,R}$	−0.02
$H_{C'-C'-H}$	0.20	h^m_{R,α_O}	0.03
$H_{C-C'-H}$	0.08	h^m_{R,α_C}	0.01
$H_{C'-C-O}$	0.28	h^m_{R,β_O}	−0.02
H_{O-C-O}	0.66	h^m_{R,β_H}	−0.03
$F_{C\cdots C'}$	0.60	$f^o_{\alpha,\alpha}$	0.03
$F_{C'\cdots O}$	0.70	$f^o_{\beta_H,\beta_O}$	0.03
$F_{C\cdots C}$	0.96	$f^o_{\beta_H,\beta_H}$	0.06

Force constants denoted by K, H, F, and k are given in J/dm² (=mdyn/Å) units, and those denoted by h and f are in pJ/dm·rad (=mdyn/rad) and aJ/rad² (=mdyn·Å/rad²) units, respectively. a) C′ is a carbon atom bonded to H.

Results and Discussion

The force constants finally obtained after several iterative calculations for the in-plane and out-of-plane vibrations of maleic anhydride are given in Tables 3 and 4, respectively. The calculated frequencies and modes are given in Table 5, together with the experimental results.

The direction cosines were calculated using the X-ray diffraction data given by Marsh *et al.*[5] and the matrix elements of the derived polarizability tensors given in Table 2 were evaluated. The squares of the calculated elements of the derived polarizability tensors, which are proportional to the Raman intensities, are given in Table 6 for the non-totally symmetric vibrations. In this calculation, the values of α'_{uw}, α'_{vw}, and α'_{uv} are taken to be 1.

Table 4. Force constants for out-of-plane vibrations of maleic anhydride (in aJ/rad²=mdyn·Å/rad²)

$Q_{C=C}$	0.35	$p^o_{H,H}$	0.045
Q_{C-C}	0.30	$p^o_{H,O}$	0.02
Q_{C-O}	0.42	$p^m_{O,O}$	0.01
$q^o_{C=C,C-C}$	−0.05	$p^m_{H,O}$	0.02
$q^o_{C-C,C-O}$	−0.02	$t^o_{C=C,H}$	−0.14
$q^o_{C-O,C-O}$	−0.03	$t^o_{C-O,O}$	−0.14
q^m	0.02	$t^o_{C-C,O}$	−0.14
P_H	0.39	$t^o_{C-C,H}$	−0.10
P_O	0.30		

Table 5. Fundamental vibrations of maleic anhydride

Sym. species	Vibrational mode	Raman				Infrared		Calcd	Obsd Rogstad *et al.*
		Liquid			Crystal	Crystal[a]	Vapor[b]		
		$\bar{\nu}$/cm⁻¹	Int.	Pol.	Pol.	Pol.	Type	$\bar{\nu}$/cm⁻¹	$\bar{\nu}$/cm⁻¹
a_1	ν_1 C–H str.	3124	m	p		//		3124	3117
	ν_2 C=O str.	1843	vs	p		//	B	1851	1852
	ν_3 C=C str.	1592	vs	p		//	B	1591	1592
	ν_4 C–O str.	1240	m	p		//		1236	1235
	ν_5 C–H bend.	1056	s	p		//		1054	1060
	ν_6 C–C str.	870	s	p		//		876	864
	ν_7 ring def.	638	vs	p		//[c]		641	632
	ν_8 C=O bend.	409	m	p		//		408	403
b_2	ν_9 C–H str.					⊥	A	3120	3117
	ν_{10} C=O str.	1785	m	dp	bc	⊥	A	1774	1782
	ν_{11} C–C str.	1306	w	dp	bc	⊥		1309	1054
	ν_{12} C–H bend.	1065	m		bc	⊥		1070	1305
	ν_{13} C–O str.	890	vw		bc	⊥	A	897	889
	ν_{14} ring def.	700	w	dp	bc	⊥	A	696	697
	ν_{15} C=O bend.	564	w	dp	bc	⊥	A	574	557
a_2	ν_{16} H wag.	766	m	dp	bb, aa			771	959
	ν_{17} ring def.	548	w	dp	bb, aa			544	768
	ν_{18} C=O wag.	269	s	dp	bb, aa			271	275
b_1	ν_{19} H wag.	838	vw		cc, aa	⊥	C	840	839
	ν_{20} ring def.	632	m		cc, aa	⊥		631	642
	ν_{21} C=O wag.	188	vw		cc, aa			190	173

a) Observed by Di Lauro *et al.* b) Observed by Rogstad *et al.* c) Observed in this work.

Table 6. Squared values of the elements of the derived polarizability tensors for maleic anhydride

	b_1	b_2	a_2
$(A_{aa})^2$	0.50	0.15	0.45
$(A_{bb})^2$	0.	0.	0.75
$(A_{cc})^2$	0.55	0.20	0.05
$(A_{ab})^2$	0.05	0.15	0.20
$(A_{ac})^2$	0.30	0.10	0.15
$(A_{bc})^2$	0.20	0.60	0.05

It is well known that all Raman bands belonging to one and the same symmetric species, except for the totally symmetric species, show the same polarization behavior in the various different polarized Raman spectra. Thus, the non-totally symmetric Raman bands were clearly classified into the specific symmetry species through the observation of the polarization behavior of the Raman bands. It is expected from Table 6 that the b_1 vibrations appear strongly in the (cc) and (aa) spectra, the b_2 vibrations in the (bc) spectrum, and the a_2 vibrations in the (bb) and (aa) spectra.

The six polarized Raman spectra observed in the different orientations of the single crystal are shown in Fig. 2. The vibrational frequencies observed in the crystal agreed well with the frequencies observed in the liquid.

a_1 Species. The totally symmetric vibrations were straightforwardly identified by depolarization measurements of the Raman bands observed in the molten state. The assignments given for the totally symmetric vibrations were the same as those given by earlier workers,[2,3] except for the C=O stretching (ν_1), C–H bending (ν_5), and ring deformation (ν_7) vibrations. The strong and polarized Raman bands observed at 1848, 1069, and 638 cm^{-1} in the molten state split into doublets, 1856 and 1843, 1065 and 1056, and 638 and 632 cm^{-1}, respectively, in the solid and single crystal. The 1843, 1056, and 638 cm^{-1} bands are stronger in intensity than the other components of the doublets, and do not show the polarization behavior characteristic to the non-totally symmetric species. Therefore, these bands were assigned to ν_2, ν_5, and ν_7 vibrations, respectively, although earlier workers have assigned the weaker components of the doublets, 1856, 1065, and 632 cm^{-1} to ν_2, ν_5, and ν_7 vibrations, respectively. As discussed later, the 1065 and 632 cm^{-1} bands should be assigned to the b_2 and b_1 vibrations, respectively, because of the polarization behavior of the Raman bands. The 1856 cm^{-1} band does not show polarization character of the non-totally symmetric vibrations, and thus, this band was assigned to the combination band of $\nu_{11}+\nu_{15}$ of the a_1 species.

b_1 Species. The non-totally symmetric Raman bands observed in the polarized Raman spectrum were divided into three types according to their relative intensities. The Raman bands of the first type, observed at 838, 632, and 188 cm^{-1}, are characterized by stronger intensity in the (cc) and (aa) spectra

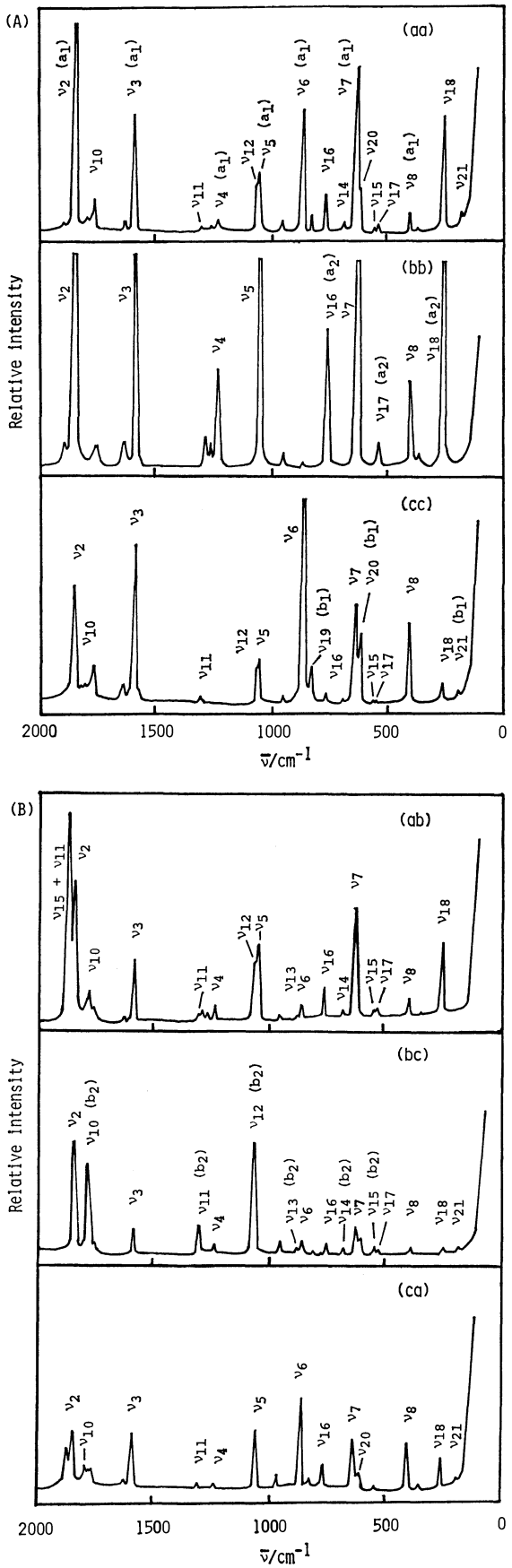

Fig. 2. Polarized Raman spectrum of the maleic anhydride crystal.
(A): (aa), (bb), and (cc) spectra, (B): (ab), (bc), and (ca) spectra.

Table 7. Vibrational analysis of the Raman spectrum of maleic anhydride

Liquid (60 °C)			Solid		Crystal		Assignment
$\tilde{\nu}$/cm^{-1}	Int.	Pol.	$\tilde{\nu}$/cm^{-1}	Int.	$\tilde{\nu}$/cm^{-1}	Pol.	
			28	vs	28	aa, bb	lattice
			43	sh	43	bc	lattice
			52	vs	52	aa, bb	lattice
			65	vs	65	ab	lattice
			95	sh	95	cc, aa	lattice
			115	sh	115	ac	lattice
			188	vw	188	cc, aa	ν_{21}
270	s	dp	269	s	269	bb, aa	ν_{18}
			371	vw	371	bb, aa	$\nu_7-\nu_{18}$
408	m	p	409	m	409	bb, cc	ν_8
548	w	dp	548	w	548	bb, aa	ν_{17}
564	w	dp	564	w	564	bc	ν_{15}
638	vs	p	632	m	632	cc, aa	ν_{20}
			638	vs	638	bb, aa	ν_7
698	w	dp	700	w	700	bc	ν_{14}
770	m	dp	766	m	766	bb, aa	ν_{16}
			818	vw			$2\times\nu_8$
			838	w	838	cc, aa	ν_{19}
870	s	p	870	s	870	cc, aa, ca	ν_6
			890	vw	890	bc	ν_{13}
956	w	dp	955	w	956	bb, aa	$\nu_8+\nu_{17}$
1069	s	p	1056	s	1056	bb	ν_5
			1065	m	1065	bc	ν_{12}
1237	m	p	1240	m	1240	bb	ν_4
1267	w	p	1267	w	1267	bb	$\nu_8+\nu_6$
1285	w	p	1285	w	1285	bb	$2\times\nu_7$
1310	w	dp	1306	w	1306	bc	ν_{11}
			1567	w	1567	bb, cc	
1591	vs	p	1592	vs	1592	bb	ν_3
1624	m	p	1624	w	1624	bb, cc	$\nu_{15}+\nu_{12}$
1628	w	p	1632	w	1632	bb, cc	$\nu_4+\nu_8$
1737	w		1737	w	1737	bb	$2\times\nu_6$
1748	w		1748	sh	1748	aa, cc	
1754	sh	dp	1753	m	1754	bc	$\nu_5+\nu_{14}$
					1762	bb	$\nu_{14}+\nu_{12}$
1780	m	dp	1785	m	1785	bc	ν_{10}
			1802	vw	1800	bc	$\nu_{15}+\nu_4$
1848	vs	p	1843	vs	1843	bb, aa	ν_2
			1856	m	1856	ab	$\nu_{15}+\nu_{11}$
			1875	vw	1875	bb	$\nu_4+\nu_7$
			1932	vw			
			2110	vw			$2\times\nu_5$
			2118	vw			$\nu_5+\nu_{12}$
			2124	m			$2\times\nu_{12}$
3121	m	p	3124	m	3124	bb, aa	ν_1
			3132	m	3132	cc, bb, bc	$\nu_2+2\times\nu_7$
3180	w	p	3184	w			$2\times\nu_3$

compared with the intensity in the other polarized spectra. The 838, 632, and 188 cm^{-1} bands were observed with weak intensity in the (ca) spectrum and with very weak intensity in the (bc) spectrum, and were hardly detectable in the (bb) and (ab) spectra. The polarization behavior of these bands is consistent with b_1 vibrations according to Table 6. Therefore, these Raman bands were assigned to ring deformation (ν_{19}), H wagging (ν_{20}), and C=O wagging (ν_{21}) vibrations of the b_1 species, respectively.

a_2 Species. The Raman bands of the second type are those appearing strongly in the (bb) and (aa) spectra. A strong Raman band observed at 269 cm^{-1}, a medium intense band at 766 cm^{-1}, and a weak band at 548 cm^{-1} belong to this type. These Raman bands decrease their intensities in the order

of the (bb)>(aa)>(ab)>(ac)>(cc)>(bc) spectra, as can be seen in Fig. 2. Table 6 indicates that these bands should definitely be assigned to the a_2 bands. Therefore, these bands were to be assigned to C=O wagging (ν_{18}), H wagging (ν_{16}), and ring deformation (ν_{17}) vibrations of the a_2 species, respectively. Although Rogstad *et al.* have assigned a Raman band observed at 959 cm^{-1} to the ν_{16} vibration, which shows the a_2 polarization character, we assigned this band to the combination band of $\nu_8+\nu_{17}$, based on the weak intensity of this band as well as the normal coordinate calculation.

b_2 Species. The Raman bands of the third type are characterized by stronger intensity in the (bc) spectrum compared with the intensity in the other spectra. Medium intense bands observed at 1785 and 1065 cm^{-1}, a weak band at 1306 cm^{-1}, and very weak bands at 890, 700, and 564 cm^{-1} belong to this type, as can be seen in Fig. 2. According to Table 6, the Raman bands appearing strongly only in the (bc) spectrum should be assigned to the b_2 bands. Thus, these bands were assigned to the C=O stretching (ν_{10}), C–H bending (ν_{12}), C–C stretching (ν_{11}), C–O stretching (ν_{13}), ring deformation (ν_{14}), and C=O bending (ν_{15}) vibrations of the b_2 species, respectively.

Polarization behavior of these bands in the various polarized Raman spectra is consistent with the predicted ones except for ν_{10} and ν_{14} vibrations. Although the vibrations belonging to the b_2 species are expected to appear with about equal intensity in the (aa), (cc), (ab), and (ac) spectra according to Table 6, the intensity of the ν_{10} Raman band is weaker in the (aa) and (cc) spectra compared with that in the (ab) and (ac) spectra. The intensity of ν_{14} Raman band is expected to be strongest in intensity in the (bc) spectrum, but this is not the case in our spectrum. One of the reasons for these discrepancies is considered to be that the oriented gas model is not quite suitable for the prediction of the intensity of the off-diagonal spectra, such as (ab) and (ac), as discussed by Ito *et al.*[6]

The detailed vibrational analysis of the polarized Raman spectrum is given in Table 7.

The assignments given for the fundamental bands based on the polarized Raman spectra are consistent with the polarization behavior and band envelope of the infrared spectrum observed in the crystal and vapor phases, respectively. The agreement between the observed and calculated frequencies is satisfactory.

References

1) P. Mirone and P. Chiorboli, *Spectrochim. Acta*, **18**, 1425 (1962).
2) C. Di Lauro, S. Califano, and G. Adembri, *J. Mol. Struct.*, **2**, 173 (1968).
3) A. Rogstad, P. Klaboe, H. Baranska, E. Bjarnov, D. H. Christensen, F. Nicolaisen, O. F. Nielsen, B. N. Cyvin, and S. J. Cyvin, *J. Mol. Struct.*, **20**, 403 (1974).
4) T. C. Damen, S. P. S. Porto, and S. B. Tell, *Phys. Rev.*, **142**, 570 (1966).
5) R. E. Marsh, E. Ubell, and H. E. Wilcox, *Acta Crystallogr.*, **15**, 35 (1962).
6) M. Suzuki, T. Yokoyama, and M. Ito, *Spectrochim. Acta, Part A*, **24**, 1091 (1968).
7) R. L. Hilderbrandt and E. M. A. Peixoto, *J. Mol. Struct.*, **12**, 31 (1972).
8) S. Kizuki, Y. Ishibashi, H. Shimada, and R. Shimada, *Mem. Fac. Sci. Kyushu Univ. Ser. C*, **13**, 7 (1981).
9) D. H. Whiffen, *Phil. Trans. R. Soc., Ser. A*, **248**, 131 (1955).

 © 1982 The Chemical Society of Japan Bull. Chem. Soc. Jpn., 55, 2771—2778 (1982)

Estimation of Compressibility and Volume of Electrostriction Layer in Water–Methanol System and Its Application to the Partial Molar Volumes of LiCl, KCl, and CsCl in This System

Fumio KAWAIZUMI,* Hiroshi SUZUKI, Hiroyasu NOMURA, and Yutaka MIYAHARA

Department of Chemical Engineering, Faculty of Engineering, Nagoya University, Chikusa-ku, Nagoya 464

(Received January 25, 1982)

A theory of electrostriction based on the spherical symmetry of electric field around ion and the dielectric continuum of solvent has been applied to the mixed solvent of water–methanol. The isothermal compressibility, κ_T, and the volume decrease, ΔV of primary solvation layer have been calculated for univalent ions. Calculation procedure consists of two steps; 1) calculation of the variation of electric field strength and dielectric constant with the distance from ion, 2) calculation of the compressibility and the volume decrease of electrostriction layer. In step 2), the calculation method proposed by Desnoyers *et al.* (*J. Chem. Phys.*, **43**, 243 (1965)) was used. Parameters necessary for the calculation were estimated in an appropriate manner and the results of calculation are shown as plots of κ_T and ΔV, *vs.* the distance from the center of ion. Partial molar volumes of LiCl, KCl, and CsCl in water–methanol system have been measured and the disordered part of partial molar volume has been determined after taking account of the values of κ_T and ΔV of the primary solvation layer.

The problem of electrostriction in solutions of electrolyte has an intimate relation to those of ionic hydration and partial molar volume of ion. Since the pioneering work of Webb,[1] numerous investigators have discussed the theories of electrostriction of aqueous solutions, most important of which are, in our opinion, those proposed by Padova[2] and Desnoyers *et al.*[3] The electrostriction is a universal phenomenon and it is not inherent to aqueous media. However, only a few works[4,5] have been reported dealing with the theoretical estimation of electrostriction effects in nonaqueous solution.

On the other hand, in recent years much progress has been achieved in the determination of various physicochemical properties of ion in nonaqueous solvent. The data obtained are now summarized in the form of review.[6,7] For the discussion of these data, the consideration on the effects of electrostriction in nonaqueous solvents should be required. Generally speaking, the interpretation of the differences among the data found in different solvents is often disputable. The sound comparison of the data on the behavior of ions in different solvents or different compositions of the solvent system can only be possible after the electrostriction effects are subtracted from what has been observed in each solvent. This is one of our fundamental points of view. The purposes of this work consist of two parts; one is to develop a method to estimate the electrostriction effects in mixed solvent system for which the reliable physical constants necessary for the estimation are often lacking, while the other is to discuss the numerical values obtained by applying the results of the present calculation to the actual system. In this study we have chosen the mixed solvent consisting of water and methanol and have estimated the compressibility and the volume decrease of the primary solvation layer in this system at 25 °C. The study of the solution properties in mixed aqueous solvents leads to the firm interpretation of the behavior of the ion in nonaqueous solvents. In addition, this mixed solvent system is widely used for inorganic solute species and a limited number of physical constants are known.

Desnoyers *et al.*,[3] concentrating attention on the local behavior of the solvent itself, assumed that the only role of the ions is to provide the polarizing electrostatic field which acts on the solvent and that an ion is a hard incompressible sphere surrounded by a spherical primary coordination shell whose thickness is equal to the diameter of the solvent. In their treatment the volume decrease due to the electrostriction was given as a function of the distance from the center of ion and the total electrostriction volume was evaluated for some particular ions such as Na^+ and F^- after considering the number of the coordinated (hydrated) water. The validity of the present calculation of the electrostriction effects in the mixed solvent system is limited in the frame of the idea and the procedure proposed by Desnoyers *et al.*[3] It should be stressed that this work is a macroscopic approach for the elucidation of the solute-solvent interactions. In addition to the calculation, the partial molar volumes of three kinds of alkali chlorides, LiCl, KCl, and CsCl in water–methanol mixture have been measured and the results of the present calculation have been applied to obtain the disordered part of the partial molar volumes. The reason for the choice of these alkali chlorides will be mentioned in the section of the discussion of this paper.

Theory and Calculation

The calculation of the electrostriction effects will be divided into two part; one is the calculation of the dielectric saturation effects, namely the variation of field strength and dielectric constant with the distance from the center of ion, while the other is that of the compressibility and volume decrease of the electrostriction layer. In what follows, each part will be described separately.

Throughout the calculation, the spherical symmetry of the electric field around ion and the dielectric continuum of the solvent are assumed. A controversy may exist for the application of the dielectric continuum model to the mixed solvent such as water-methanol mixture, as the preferential hydration is often observed in mixed aqueous solvent. If the preferential

hydration (more generally, solvation) occurs in a mixed solvent system, this obviously contradicts the basic assumption of the dielectric continuum of the solvent. Nevertheless, we would like to employ the spherical symmetry of the electric field and continuum model of solvent on the ground of the conviction that the *macroscopic* approach can give information on the *microscopic* level of solute-solvent interactions, as for the case of the application of the Debye-Hückel theory to the evaluation of association constant and interionic distance parameter from the conductivity data.

Calculation of Dielectric Saturation Effects. Calculation procedure is the same as given by Laidler.[8] The dielectric behavior in the vicinity of ions can be expressed in terms of differential dielectric constant, ε_d, which is defined and given by the relation[3,8,9]

$$\varepsilon_d \equiv d\boldsymbol{D}/dE = [(\varepsilon_o - n^2)/(1+bE^2)] + n^2, \quad (1)$$

where $\boldsymbol{D}$ is the dielectric displacement, E, the field strength, ε_o, the dielectric constant at zero field strength, n^2, the square of refractive index, and b a constant as described below. The electric displacement $\boldsymbol{D}$ at a distance r from the center of an ion of charge ze is ze/r, which should be equal to $\boldsymbol{D}$ obtained by the integration of Eq. 1. It follows then that

$$\frac{ze}{r^2} = n^2E + [(\varepsilon_o - n^2)/b^{1/2}]\tan^{-1}b^{1/2}E. \quad (2)$$

Equation 2 can not give the explicit solution of E as a function of r, but it can afford tabulated values of r for assumed values of E. Then, the substitution of the numerical values of $E=E(r)$ into Eq. 1 permits to show the variation of ε_d with the distance from the center of ion. Values used in calculation are as follows:

ε_o; given or estimated from the data found in Ref. 10.

b; 1.08×10^{-8} e.s.u. for water[3,8] and 2.2×10^{-8} e.s.u. for methanol.[5] Values in the mixture are calculated on the assumption of linear variation of b with mole fraction of the component in the solvent.

n^2; determined by the present authors.

Results of calculation are illustrated as a series of curves in Fig. 1 (E *vs.* r) and Fig. 2 (ε_d *vs.* r) for univalent ion at various compositions of water–methanol system at 25 °C. Figure 1 shows that the field strength at a certain distance from the center of the ion becomes higher with the content of methanol. Figure 2 is essentially the same as Fig. 1 but it has an advantage to give us an explicit image of the dielectric saturation effects and the extent of the dielectric saturation layer. In Fig. 2, the smallest values of ε_d is determined by the relation that $\varepsilon_d=n^2$, which is approximately 1.8 for both water and methanol at 25 °C. If the distance at which ε_d begins to be effectively field-dependent is determined on the criterion of $\varepsilon_d=1.9$, following values are obtained: 1.68, 1.74, 1.96, 2.19, 2.52, 2.87, and 3.00×10^{-8} cm for the contents of methanol equal to 0, 10, 30, 50, 70, 90, and 100 mol%, respectively. The dielectric saturation layer becomes larger with the content of methanol in the mixed solvent. The distinction between bulk solvent and dielectric saturation layer is less clear in methanol than in water as is seen in Fig. 2.

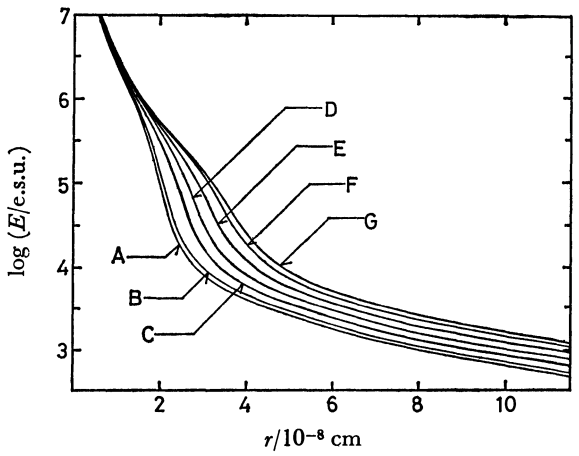

Fig. 1. Relation between the logarithm of the field strength, E, and the distance from the center of univalent ion in water–methanol system at 25 °C.
Symbols A, B, C, D, E, F, and G correspond to the mole per cent of methanol equal to 0, 10, 30, 50, 70, 90, and 100, respectively.

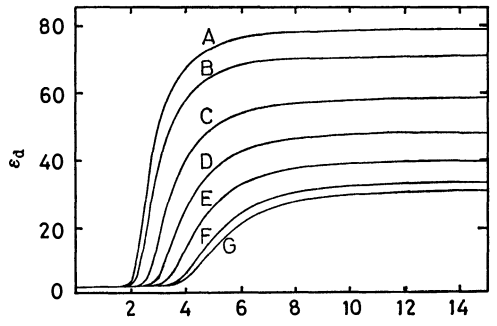

Fig. 2. Variation of differential dielectric constant with the distance from univalent ion in water–methanol system at 25 °C.
Symbols A—G are the same as in Fig. 1.

Calculation of the Compressibility of Electrostriction Layer. According to Desnoyers *et al.*,[3] the relation between the field strength and the effective pressure, defined as the pressure which, in the absence of the field E, would produce the same volume change of the solvent that E produces is expressed as (Eq. 13 in Ref. 3),

$$dP = [4\pi D(1+bE^2)]^{-1} \times \left[\varepsilon_o A\left(1+\frac{P}{B}\right)^A - n^2C\left(1+\frac{P}{B}\right)^C\right]EdE + \frac{n^2C}{4\pi D}\left(1+\frac{P}{B}\right)^C EdE, \quad (3)$$

where parameters, A, B, C, and D are the constants involved in the following equations:

$$\frac{1}{\varepsilon}\left(\frac{\partial\varepsilon}{\partial P}\right)_{T,E} = \frac{A}{B+P}, \quad (4)$$

$$\frac{1}{n^2}\left(\frac{\partial n^2}{\partial P}\right)_{T,E} = \frac{C}{B+P}, \quad (5)$$

$$\kappa_T = -\frac{1}{v}\left(\frac{\partial v}{\partial P}\right)_{T,E} = \frac{D}{B+P}. \quad (6)$$

In other words, the pressure dependence of dielectric constant, square of the refractive index, and isothermal compressibility can be represented in terms of so-called Tait equation.[11] The use of the Tait-form equation and the adoption of the same value of B through Eqs. 4—6 for such high pressures as in the electrostriction layer are the two essential points employed by Desnoyers *et al.* in deriving Eq. 3 which made the calculation very tractable. The expression of pressure dependence of dielectric constant and square of refractive index in terms of Tait-form equation is understandable if we consider that the variation of these properties with pressure is mainly ascribed to the variation of volume with pressure, as seen by Clausius-Mosotti and Lorenz-Lorentz equations.

In order to carry out the integration of Eq. 3 values of the parameters A, B, C, and D must be known for the solvent composition under consideration. However, in water–methanol mixture, limited data are available on the pressure dependence of the dielectric constant,[12] and for the (P, n) and (P, κ_T) relations, no reliable data can be found at present. Therefore, we are obliged to do much effort for the estimation of the values of these parameters in the mixture. A rather expounded description of the estimation procedure may be permitted in the light of the future application for other solvent systems.

Parameter B: In the first step of the estimation procedure, the parameter B is to be considered. As B is assumed to be the same in Eqs. 4—6, its value can be otained from any one of the three sets of relationships, (P, ε), (P, n), and (P, κ_T). Even with excellent data, to obtain a set of unique parameter (A, B), (C, B), and (D, B), is not an easy task. Several sets of parameters may equally well represent the available data for a fluid. For example, as shown in Table 1, values of B and D have been known for water,[3,13] and methanol.[13] But this value of B for water differs considerably from the value reported by other investigators from the variation of dielectric constant with pressure ($B=4.547\times10^8$ Pa and $A=0.1916$).[14] As it will be shown later, the parameter A plays only a minor role in the calculation of the electric field of practical interest ($E\geqq5\times10^5$ e.s.u.). On considering this factor along with the fact that the Tait equation was originally derived to express the volume change with pressure, the value of B in the set (B, D) was preferred.

For mixture of water and methanol, Schadow and Steiner[12] have given the data of the pressure dependence of dielectric constant at 30 °C for weight per cent of methanol equal to 0, 20, 40, 60, 80, and 100. Their data are, however, not accurate enough to be usable for the simultaneous determination of the parameters B and A. No theory has been proposed for the estimation of the value of B in mixture from its value in pure component. Therefore, values of B in mixture were estimated on the simple assumption of the linear variation of parameter B with mole fraction of the component in the mixed solvent system, without taking account of the values of other parameters.

Parameter D: Values of D in the mixed solvent were calculated from the data of isothermal compressibility. Under the condition of $B\gg P$, Eq. 6 should lead to the compressibility at ordinary pressures. In fact, the relation $\kappa_T(P=10^5\text{ Pa})=D/B$ holds for the reported values of B and D for water and methanol, as seen in Table 1. It is remembered that errors involved in the estimated values of B are largely compensated for by the evaluation process of the parameter D.

Values of κ_T necessary for the estimation of D were obtained by the aid of the thermodynamic relation,

$$k_T=\kappa_s+\left(\frac{Tv\alpha^2}{C_p}\right). \tag{7}$$

Meaning of the symbols used in Eq. 7 and the values used are;

κ_s; adiabatic compressibility, whose values are given from the measurements of ultrasonic propagation velocity and density. For the measurements of ultrasonic velocity, an ultrasonic interferometer was used.

v; volume.

α; thermal expansion coefficient. The value at 25 °C is calculated from the density at 20 and 30 °C.

C_p; specific heat capacity, whose values are found in the literature.[15]

Parameter A: Slightly different values of B have been given for water and methanol for the pressure dependence of dielectric constant.[17] Therefore, the parameters A in water and methanol were recalculated using the value of B obtained from the pressure dependence of the isothermal compressibility. For mixture, values of parameter A were determined by the fitting of experimental results of (P, ε) relation[12] using the estimated values of B. Average values of A determined for pressures higher than 7×10^7 Pa were adopted. Surprisingly values of A thus determined vary linearly with mole fraction of the component. To illustrate the validity of the estimated values of A and B in the mixture, the comparison between (P, ε) relation determined experimentally and that calculated from Eq. 4 using the estimated values of A and B is represented in Table 2. The agreement is satisfactory.

Parameter C: Two reports have been published on the pressure dependence of the refractive index of water.[18,19] These results were combined and recalculated to obtain the parameter C in Eq. 5, irrespective of the difference in the experimental conditions in two works (in Ref. 18, at 25 °C and up to 1.50×10^8 Pa, while in Ref. 19, at 24.8 °C and *ca.* to 1.1×10^8 Pa). Recalculation yields $C=0.0678$ for $B=2.996\times10^8$ Pa. This value is in fair accordance with the one used by Desnoyers *et al.* ($C=0.0685$).[3] Data on methanol[20] were similarly recalculated as for the case of water. Values of C in the mixture were estimated on the assumption of the linear variation of parameter C with the mole fraction of the component. This assumption seems reasonable in view of the linear variation of parameter A and the small difference in the value of C in water and methanol.

Final results of the numerical values of the parameters A, B, C, and D as well as κ_T are summarized in Table 1. Once the values of these parameters are determined, the integration of Eq. 3 reduces to a problem of mathematics.

At low field intensities ($bE^2\ll1$) or at high field

TABLE 1. VALUES OF THE PARAMETERS A, B, C, AND D USED IN CALCULATION AND THE ISOTHERMAL COMPRESSIBILITY OF WATER–METHANOL MIXTURE AT 25 °C

MeOH / mol %	κ_T / 10^{-11} Pa^{-1}	B / 10^8 Pa	A	C	D
0	45.23, 45.7[15]	2.996[3,13]	0.1818	0.0678	0.1368[3,13]
10	43.54	2.773	0.175	0.0671	0.1207
30	50.60	2.327	0.159	0.0656	0.1177
50	66.10	1.880	0.142	0.0641	0.1243
70	83.86	1.434	0.126	0.0626	0.1201
90	110.30	0.987	0.110	0.0611	0.1088
100	124.50, 125.5[15]	0.764[3,13]	0.0998	0.0604	0.09589[3,13]

TABLE 2. COMPARISON BETWEEN EXPERIMENTAL (30 °C) AND CALCULATED (P, ε) RELATIONS OF WATER–METHANOL MIXTURE

MeOH wt%	$P/10^5$ Pa					
	0.980	257	505	717	913	1107
20	69.01	69.75	70.50	71.52	72.73	73.51
		69.97	70.84	71.55	72.17	72.79
40	60.48	61.10	61.75	62.72	63.71	64.69
		61.38	62.18	62.84	63.40	63.94
60	53.02	53.60	54.28	55.13	56.10	57.00
		53.96	54.80	55.46	56.03	56.56
80	43.72	44.20	44.75	45.61	46.54	47.52
		44.68	45.50	46.14	46.68	47.18

Values in upper and lower rows correspond respectively to experimental[12] and calculated results.

($bE^2 \gg 1$), Eq. 3 can be simplified and the integration leads to low-field limit (Eq. 6 of Ref. 3) and high-field limit solutions (Eq. 14 or Ref. 3), respectively. In high-field limit solution, the parameter A has little effect. Low-field limit corresponds to Born approximation in which dielectric saturation effects are neglected. It has been shown that the field near ordinary ions in water is of such value as to make the simplification of Eq. 3 inapplicable.[3] In the present work dealing with water–methanol system, Eq. 3 was directly integrated by means of a digital computer FACOM M-200 of Nagoya University Computer Center. Runge-Kutta-Gill method was used. Results of the integration of Eq. 3 are represented in Fig. 3, where the curves related to 10, 30, 70, and 90 mol% of methanol are eliminated for the sake of simplicity. The slope in low-field limit is independent of the composition of the solvent, taking the value of 2, while the slope in high-field limit depends weakly on the properties of the solvent concerned.

Experimental

The determination of the partial molar volumes of LiCl, KCl, and CsCl which was done as a part of the present study is briefly mentioned here. Salts used are of guaranteed grade reagent supplied from Nakarai Chemicals and they were used without further purification. Densities of solutions containing the salt were measured with pycnometer of 20 cm^3.

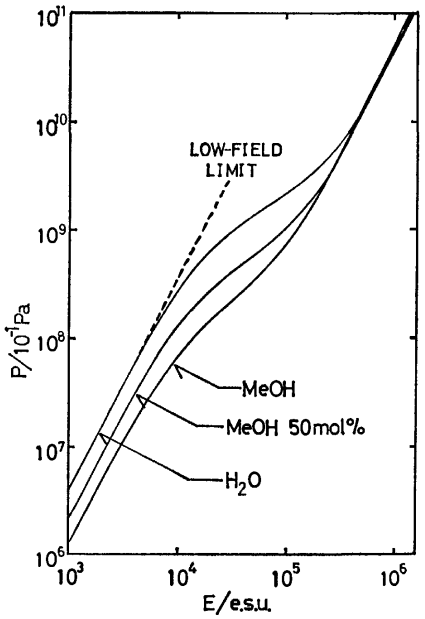

Fig. 3. Numerical solutions to pressure-field relationships in Eq. 3 for univalent ion in water, 50 mol% of methanol, and pure methanol.

Results and Discussion

Results of Calculation. In Fig. 3, the high-field limit approximation holds for $E > 4 \times 10^5$ e.s.u., which corresponds to $r < 2.5 \times 10^{-8}$ cm in methanol in Fig. 1. It follows then that the calculation of electrostriction effects in methanol must at least be done on high-field approximation for the familiar alkali metal and halide ions. Figure 3 also indicates that in methanol the low-field approximation which corresponds to the simple Born approximation holds only for $E < 10^4$ e.s.u., a value equivalent to $r > ca.\ 5 \times 10^{-8}$ cm in Fig. 1, namely, the Born approximation is generally unacceptable in the solvent methanol. On the other hand, the combination of the results shown in Figs. 1 and 3 enables P to be expressed as a function or r. Substitution of the pressure given as $P(r)$ along with the numerical values of parameters B and D into Eq. 6 can offer the relation between κ_T and the distance from the ion, which is represented in Fig. 4. Desnoyers *et al.*[3] have shown the variation of κ_T with the field strength in water, but to discuss the dependence of ionic hydration on the dimension of ion, the relation

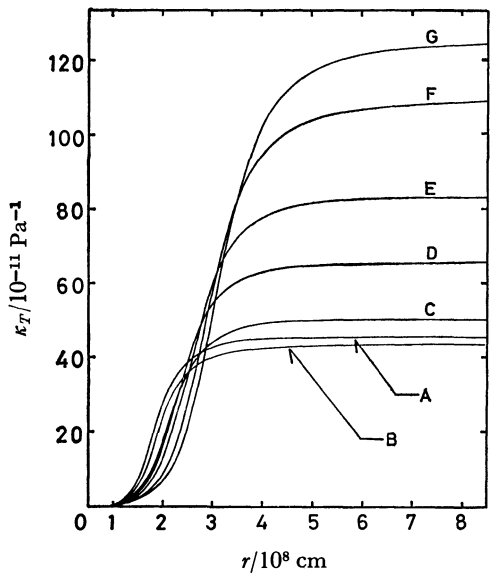

Fig. 4. Variation of the compressibility of solvent with the distance from the center of univalent ion in water–methanol system.
Symbols A—G are the same as in Fig. 1.

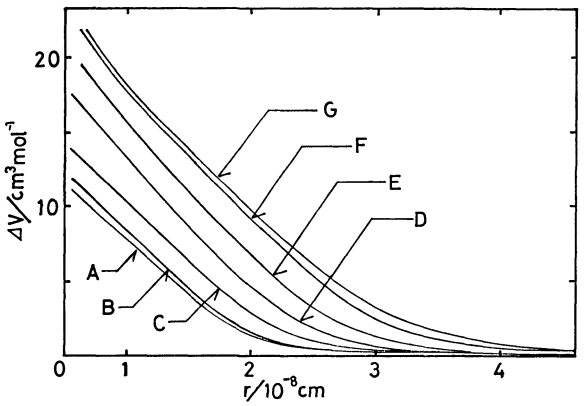

Fig. 5. Volume decrease of one molar of solvent expressed as a function of the distance from the center of univalent ion in water–methanol system at 25 °C.
Symbols A—G are the same as in Fig. 1.

as shown by Fig. 4 is preferable. As a consequence of the estimation procedure of the parameters B and D, the value of κ_T approaches asymptotically that of the pure solvent with increasing distance from the center of ion.

The volume decrease of solvent defined as $\Delta V = v^\circ - v(P)$, where $v(P)$ is the molar volume of the solvent at the effective pressure P, can be evaluated from the relation,

$$\ln (v^\circ/v(P)) = D \ln\left(1+\frac{P}{B}\right). \quad (8)$$

This equation derives from the integration of Eq. 6. It should be noted that the quantity ΔV does not refer to the absolute amount of volume decrease of the solvent but to the relative decrease of volume assigned to one molar of solvent at distance r from the center of the univalent ion. The variation of the volume decrease ΔV for univalent ion in mixed solvent system of water–methanol at 25 °C is illustrated in Fig. 5.

Table 3. Partial molar volumes of CsCl, KCl, and LiCl in water-methanol system at 25 °C

MeOH mol%	$\overline{V}_2^\circ$/cm^3 mol^{-1}		
	CsCl	KCl	LiCl
0	39.1	26.8	18.2
30	39.2	27.7	15.9
50	37.5	27.3	13.4
70	32.6	22.4	8.5[a)]
90	25.3	13.4	4.2[a)]
100	23.6[b)]	5.9[b)]	−4.9[b)]

a) Owing to the limited solubility of LiCl, uncertainties are larger than the other cases. b) Values found in Ref. 21.

At this point it seems worth while to sum up ambiguities involved in the estimation and the results obtained:

I) Can Tait-form equation containing only two parameters really represent the pressure dependence of ε, n^2, and κ_T in such high pressure regions as in electrostriction layer with the same accuracy?

II) Even if the Tait-form equation is correct, should the parameter B be the same for three physical quantities? Nearly the same numerical values have been found for B associated with ε and that associated with κ_T.[17] But is the fact a mere coincidence?

III) Parameters A, B, C, and D have not been known with the same precision. Moreover, errors involved in estimating the values of these parameters in the mixed solvent differ for each parameter.

Authors admit that the present treatments of electrostriction are not free from the controversy on the ambiguities mentioned just above. None the less, the result of calculation can afford much information on the order and the magnitude of electrostriction in the mixed solvent system as described below. For example, Fig. 4 shows that for many ordinary univalent ions the compressibility of the primary solvation layer in methanol can be neglected in comparison with that of bulk solvent if the electrostriction layer is assumed to correspond to the primary solvation layer.

Application of the Calculated Results to the Partial Molar Volumes of LiCl, KCl, and CsCl. As mentioned at the begining of this paper, the partial molar volumes of ions are discussed in their relation to electrostriction effects. In order to apply the results of the calculation, the partial molar volumes, $\overline{V}_2^\circ$, of salts LiCl, KCl, and CsCl have been determined in water–methanol system. The reasons for the choice of these salts are as follows: Throughout the present work, the continuum model of the solvent has been assumed. This assumption does not hold well for transition metal ions in mixed aqueous solvent, because the ligand-field is generally strong for these ions and the preferential hydration occurs, which contradicts our basic assumption. For alkali metal, in particular for lithium, and chloride ions, preferential hydration may occur, but to much lesser extent than for the case of transition metal

TABLE 4. EFFECTIVE RADIUS AND VOLUME DECREASE OF ONE MOLAR OF SOLVENT FOR IONS Cs^+, K^+, Li^+, AND Cl^- IN WATER–METHANOL SYSTEM AT 25 °C

MeOH mol%	$r_e/10^{-8}$ cm				$\Delta V/cm^3\ mol^{-1}$			
	Cs^+	K^+	Li^+	Cl^-	Cs^+	K^+	Li^+	Cl^-
0	1.91	1.42	1.10	2.15	1.6	4.6	7.0	0.8
10	1.94	1.47	1.18	2.17	1.9	4.6	6.9	1.0
30	1.99	1.58	1.31	2.20	2.9	5.7	7.8	1.8
50	2.05	1.68	1.47	2.23	4.3	7.0	8.9	3.2
70	2.10	1.78	1.60	2.27	5.9	8.4	9.9	4.6
90	2.15	1.89	1.74	2.30	7.9	10.1	11.3	6.7
100	2.18	1.94	1.81	2.32	8.3	10.1	11.2	7.2

ions, and ionic associations are seldom observed for alkali chlorides. Thus alkali chlorides are considered to be the best salts for the present work. In pure methanol, the determination of the reliable values of $\overline{V}_2^\circ$ was difficult on account of the low solubility of the salts and the values in the literature[21] were adopted. Results of the determination of $\overline{V}_2^\circ$ are given in Table 3. For three alkali chlorides investigated, the variation of $\overline{V}_2^\circ$ is small up to 50 mol% of methanol but in concentration of methanol above 70 mol%, $\overline{V}_2^\circ$ decreases remarkably with the content of methanol in the solvent.

In the application of the theoretically estimated electrostriction effects to the actual ions in solution, a problem of crucial importance is how to evaluate the effective radius of the solvated ion. This problem is inherent to any theory dealing with the electrostriction effects. It is not the ion but the solvent around ion which contracts under electrostrictive pressures. Therefore, the effective radius of the solvated ion concerned in the present treatment must be larger than the crystallographic radius, r_c. In this respect, the use of Stokes radius, r_s, derived from the hydrodynamic consideration of ion in solution, is inappropriate, as $r_s/r_c<1$ has been observed for large alkali and halide ions. On the same ground, Gourary-Adrian radii[22] are rejected, though sometimes they have been used. Desnoyers *et al.*[3] considered the distance from the center of ion to the center of a neighboring water molecule. Their consideration, however, is not free from the disputation. We have evaluated the effective ionic radius, r_e, by the aid of the relationship between $\overline{V}_{ion}^\circ$ and r_e given by Padova.[2,5] In his papers,[2,5] r_e was defined as the intrinsic radius of ion and the intrinsic volume of the ion in solution $\overline{V}_{int}$, was expressed as $\overline{V}_{int}=4/3\pi N_0 r_e^3$, where N_0 is the Avogadro number. On the contrary, we have used the value of r_e as a *literal* effective radius of the solvated ion, without taking account of the original physical significances of r_e in the Padova's model for the calculation of $\overline{V}_{ion}^\circ$. As Padova used incorrect values of $\overline{V}_{ion}^\circ$,[2,5] effective ionic radii have been determined using the generally accepted values of $\overline{V}_{ion}^\circ$ in water[23] and methanol.[21] The estimated values of r_e are given in Table 4. In both solvents values of r_e are larger than those of r_c and the variation of r_e with the ionic species seems to be reasonable. In the mixed solvent system, it was assumed that r_e varies linearly with the mole fraction of the component. Corresponding to each value of r_e, the amount of volume decrease of one molar of solvent, ΔV, is determined from Fig. 5. Table 4 shows the numerical values of r_e and ΔV thus determined for ions Cs^+, K^+, Li^+, and Cl^- in water–methanol system. Padova,[5] using the theoretical coefficients of the concentration dependence of the partial molar volume and partial molar compressibility, estimated the average theoretical electrostriction volume per mole of solvent methanol, which is equal to 7.54 $cm^3\ mol^{-1}$. In comparison with this value, the results of the present calculation are larger by 1—4 $cm^3\ mol^{-1}$ for cations, while the agreement is satisfactory for Cl^- ion. The total electrostriction volume arising from the addition of one molar of 1-1 type salt into solvent, expressed as $\overline{V}_e$, is given by the relation,

$$\overline{V}_e = \Delta V(M^+)n_s(M^+) + \Delta V(X^-)n_s(X^-), \quad (9)$$

where $n_s(M^+)$ and $n_s(X^-)$ are solvation numbers for cation and anion, respectively. However, the solvation number is experimentally determined for salt MX and the assignment of solvation number to cationic and anionic components requires further assumptions. Accordingly, instead of Eq. 9 we have adopted the following relation to calculate $\overline{V}_e$ of the salt MX:

$$\overline{V}_e = [\Delta V(M^+)+\Delta V(X^-)]\bar{n}_s(M^+, X^-), \quad (10)$$

where $\bar{n}_s(M^+, X^-)$ is the solvation number averaged over cation and anion and it is assumed to be equal to a half of n_s for the salt MX. The determination of solvation number in taking account of the volume decrease and the compressibility of the primary solvation layer can be attained by the use of an expression,[24]

$$\bar{\kappa}_2^\circ = \kappa_2 + \frac{n_s v_s}{\bar{v}_2}(\kappa_{sol}-\kappa_1) \quad (11)$$

In Eq. 11, κ stands for the compressibility and $\bar{v}_2$ is the partial specific volume of solute, and the subscripts s and sol (to avoid the confusion with κ_s used in Eq. 8) refer to the solvation layer, while subscripts 1 and 2 refer to solvent and solute, respectively. The derivation of Eq. 11 and the determination of the value of $\bar{\kappa}_2^\circ$ from the data of compressibility and density of solution is described elsewhere.[24] For the measurements of the compressibility of solutions, an ultrasonic interferometer was used.[25]

In the calculation of n_s of salt MCl from Eq. 11, the compressibility of the solvation layer, κ_{sol}, was not considered for each ion but a mean value of κ_{sol} for salt MCl was considered and a value of κ_T at r equal

Table 5. Compressibility of solvation layer, solvation number, total electrostriction volume, $\overline{V}_e$, and disordered partial molar volume, $\overline{V}_d$, of CsCl, KCl, and LiCl in water-methanol system at 25 °C

MeOH	$\kappa_{sol}/10^{-11}$ Pa^{-1}			n_s/mol mol^{-1}			$\overline{V}_e$/cm^3 mol^{-1}			$\overline{V}_d$/cm^3 mol^{-1}		
mol%	CsCl	KCl	LiCl	CsCl	KCl	LiCl	CsCl	KCl	LiCl	CsCl	KCl	LiCl
0	29.0	19.1	12.4	1.3	2.8	4.6	1.6	7.6	18.0	13.6	13.6	20.8
10	25.1	15.6	10.7	—	—	—	—	—	—	—	—	—
30	21.9	13.7	9.4	0.6	1.4	3.2	1.4	5.3	15.4	13.5	12.2	15.9
50	22.4	14.9	11.2	0.6	1.8	3.7	2.3	9.2	22.4	12.7	15.7	20.4
70	20.4	14.2	11.4	0.8	2.6	4.7	4.2	16.9	34.1	9.7	18.5	27.2
90	16.2	12.1	9.7	1.3	3.5	5.9	9.5	29.4	53.1	7.7	22.0	41.9
100	13.0	9.9	8.6	1.6	3.5	5.8	12.4	30.3	53.4	8.9	15.4	33.1

The numerical values of $\overline{V}$(crystal)/cm^3 mol^{-1} for CsCl, KCl, and LiCl are 27.1, 20.8, and 15.4 respectively.

to $1/2(r_e(M^+)+r_e(Cl^-))$ was taken. This step of calculation corresponds to the use of Eq. 10 in place of Eq. 9. As mentioned above, it has been assumed that no preferential solvation occurs in the mixed solvents, n_s being the average solvation number.

It is generally admitted that the partial molar volume of an ion at infinite dilution, $\overline{V}_{ion}^{\circ}$, can be attributed to the following components:

$$\overline{V}_{ion}^{\circ} = \overline{V}(\text{crystal}) - \overline{V}(\text{electrostriction}) + \overline{V}(\text{disordered}) \quad (12)$$

$\overline{V}$(crystal) can be evaluated using the radius of the ion. Pauling radius was used in the evaluation of $\overline{V}$(crystal). Upon substituting into Eq. 12 the values of $\overline{V}$(crystal) and $\overline{V}$(electrostriction) obtained in the present calculation, the $\overline{V}$(disordered) is evaluated. According to the treatment of Padova,[2,5] the following relation should hold and the amount of $\overline{V}$(disordered) is calculated without recourse to Eq. 12;

$$\overline{V}(\text{disordered}) = \overline{V}_{int} - \overline{V}(\text{crystal}) = \frac{4}{3}\pi N_0(r_e^3 - r(\text{crystal})^3), \quad (13)$$

However, we do not calculate $\overline{V}$(disordered) in this manner. As mentioned earlier, the numerical value of r_e was evaluated as to be a mere effective radius of the solvated ion. Moreover, the fundamental point of the present study lies to see to what extent the consideration of the electrostriction effects can explain the observed fact, and for this purpose the contribution of the electrostriction effects must be substracted from the values determined by experiments. If the consideration of the electrostriction term suffices to the interpretation of $\overline{V}_{ion}^{\circ}$, then the contribution of $\overline{V}$(disordered) disappears, otherwise it will appear as a correction term.

Final results are shown in Table 5 along with the value of n_s. In Table 5, three significant figures are used to express the values of $\overline{V}_e$ and $\overline{V}_d$. But apart from the problem related with the estimation procedure of the effective radius of the solvated ion, r_e, on account of the cumulation of various kinds of assumptions and ambiguities involved in the present calculation, physical significance of the figures of $\overline{V}_e$ and $\overline{V}_d$ is not so much reliable. However, we can mention and discuss the general features of the variation of $\overline{V}_e$, $\overline{V}_d$, and n_s with the composition of the solvent system as follows.

1) The variation of partial molar volume with composition of the solvent is rather small up to 50 mol% of methanol but in methanol-rich regions partial molar volume decreases rapidly with the content of methanol in the solvent (see Table 3). Corresponding to this fact, the amount of total electrostriction volume increases remarkably in the same concentration ranges of methanol for three chlorides investigated.

2) Values of $\overline{V}_d$ are smaller for CsCl and larger for LiCl than the corresponding values in water, while values of $\overline{V}_d$ for KCl are comparable in both solvents. Smaller value of $\overline{V}_d$ of CsCl in methanol than in water is compatible with the finding of Kawaizumi and Zana[21] that the void space around ions appears to be smaller in methanol than in water. Results related to KCl and LiCl may be interpreted as follows: In an early paper[21] and in many other references[26] the contributions of electrostriction volume and void space to the partial molar volume of ions are evaluated as the parameters A and B of Hepler equation,[27]

$$\overline{V}_{ion}^{\circ} = Ar^3 - \frac{B}{r}, \quad (13)$$

and A and B are determined independently, while in the present estimation the disordered part of the partial molar volume of the salt is determined through the subtraction of $\overline{V}$(crystal) and $\overline{V}_e$ from the value of $\overline{V}_{ion}^{\circ}$. For K^+ and Li^+ ions, the present estimation of electrostriction effects seems to give somewhat larger electrostriction volume than the actual volume decrease in solutions, as is seen from the comparison of the values of ΔV of Table 4 with the value of 7.54 cm^3 mol^{-1} estimated by Padova.[5] The small differences of ΔV can affect largely the values of $\overline{V}_d$ as a result of the multiplication of ΔV by n_s, this being especially the case for LiCl. It is noteworthy that the value of $\overline{V}_{ion}^{\circ}$ allotted to Li^+ ion in methanol clearly departs from the relationships given by Hepler equation and observed for all small univalent ions.[21] Also we would like to say that the result relative to CsCl seems to support the conclusion drawn by Kawaizumi and Zana,[21] but one should retain prudence in discussing $\overline{V}_d$ and $\overline{V}_e$ separately, as they are essentially interrelated in the present treatment.

3) Values of $\overline{V}_e$ and $\overline{V}_d$ are the largest for LiCl, then for KCl, and the smallest for CsCl at any compositions of the solvent system. In other words, the quantities $\overline{V}_e$ and $\overline{V}_d$ are inversely proportional to the cationic size.

4) For three alkali chlorides investigated, the average solvation number of the salt, n_s, first decreases, then increases, with increasing amount of methanol in the solvent and finally in pure methanol values of n_s are larger than those in water.

5) As for $\overline{V}_2^\circ$ of LiCl, the contribution of $\overline{V}$(crystal) is minor than that of $\overline{V}_e$ and $\overline{V}_d$ in the solvents containing more than 50 mol% of methanol.

To be free from the speculation, further discussion of the results of present study is postponed until more data are available on this mixed solvent system.

The authors wish to express their thanks to Professor Keizo Suzuki of Ritsumeikan University and Associate Professor Takashi Moriyoshi of Tokushima University for their kindness of informing them the source of the pressure dependence of dielectric constant and refractive index of the system concerned in the present work.

References

1) T. J. Webb, *J. Am. Chem. Soc.*, **48**, 2589 (1926).
2) J. Padova, *J. Chem. Phys.*, **39**, 1552 (1963).
3) J. E. Desnoyers, R. E. Verrall, and B. E. Conway, *J. Chem. Phys.*, **43**, 243 (1965).
4) W. C. Vosburgh, L. C. Connell, and J. A. V. Butler, *J. Chem. Soc.*, **1933**, 933.
5) J. Padova, *J. Chem. Phys.*, **56**, 1606 (1972).
6) B. E. Conway, *J. Solution Chem.*, **7**, 721 (1978).
7) B. E. Conway, "Ionic Hydration in Chemistry and Biophysics," Elsevier, Amsterdam (1981), Chap. 31.
8) K. J. Laidler, *Can. J. Chem.*, **37**, 138 (1959).
9) D. C. Grahame, *J. Chem. Phys.*, **21**, 1054 (1953).
10) "Water, A Comprehensive Treatise," ed by F. Franks, Plenum Press, New York and London (1973), Vol. 2, p. 421.
11) In some cases, expressions somewhat different from Eqs. 4—6 are cited as Tait equation:

$$1-\frac{\varepsilon^\circ}{\varepsilon}=A\ln\left(1+\frac{P}{B}\right) \tag{4'}$$

$$1-\frac{v}{v^\circ}=D\ln\left(1+\frac{P}{B}\right), \tag{6'}$$

where superscript ° indicates the value at ordinary pressure. Equations 4′ and 6′ are respectively equivalent to Eqs. 4 and 6 under the condition that $\varepsilon^\circ\simeq\varepsilon$, and $v^\circ\simeq v$. The differences between values of dielectric constant and volume calculated from two different forms of Tait equation become gradually significant with increase in pressure. However, the errors arising from two different forms of Tait equation are within the uncertainties arising from various kinds of physical assumption used in the present calculation.
12) E. Schadow and R. Steiner, *Z. Phys. Chem. (Frankfurt am Main)*, **66**, 105 (1969).
13) H. S. Harned and B. B. Owen, "The Physical Chemistry of Electrolytic Solutions," 3rd ed, Reinhold, New York (1958), p. 380.
14) K. R. Srinivasan and R. L. Kay, *J. Chem. Phys.*, **60**, 3645 (1974).
15) Landolt-Börnstein, "Zahlenwerte und Funktionen aus Naturwissenschaften und Technik," Springer, Berlin (1977), Neue Serie, VI 1b.
16) "Handbook of Chemistry and Physics," 48th ed, Chemical Rubber Company, Cleaveland (1968).
17) B. B. Owen and S. R. Brinkley, *Phys. Rev.*, **64**, 32 (1943).
18) J. S. Rosen, *J. Opt. Soc. Am.*, **37**, 932 (1947).
19) R. M. Waxler and C. E. Wier, *J. Res. Natl. Bur. Std.*, **67A**, 163 (1963).
20) K. Vedam and P. Limsuwan, *J. Chem. Phys.*, **69**, 4762, 4772 (1978).
21) F. Kawaizumi and R. Zana, *J. Phys. Chem.*, **78**, 627 (1974).
22) B. S. Gourary and F. J. Adrian, *Solid State Phys.*, **10**, 127 (1960).
23) Calculated from the data tabulated by F. J. Millero, *Chem. Rev.*, **71**, 147 (1971) with $\overline{V}_2^\circ(Cl^-)=23.5$ cm^3 mol^{-1}.
24) H. Nomura and Y. Miyahara, *J. Appl. Polym. Sci.*, **3**, 1643 (1964).
25) The compressibility determined directly from the data of ultrasonic velocity and density is the adiabatic one. However, the use of the values of adiabatic compressibility in place of isothermal compressibility in Eq. 11 does not affect the conclusion significantly.
26) For example, R. Zana, G. A. Lage, and C. M. Criss, *J. Solution Chem.*, **9**, 667 (1980).
27) L. G. Hepler, *J. Phys. Chem.*, **61**, 1426 (1957).

 © 1982 The Chemical Society of Japan Bull. Chem. Soc. Jpn., 55, 2779—2782 (1982)

Temperature Dependence of Raman Spectra of Pyridine in Hydrogen Bonding Solvents

Kunio FUKUSHIMA* and Masahiro YAMAJI

Department of Chemistry, Faculty of Science, Shizuoka University 836, Oya, Shizuoka 422

(Received February 2, 1982)

Raman spectra of pyridine in solvents of various hydrogen bonding powers were recorded and frequency shifts of some bands were measured. With methanol as solvent, Raman spectra recorded at temperatures between 128 and 293 K exhibit a remarkable change with temperature. Results are interpreted on the basis of possible existence of a $\sigma\pi$-complex.

It was found by Takahashi *et al.*,[1] that some infrared bands of pyridine will shift to higher frequencies by its hydrogen bonding with solvents. They ascribed the frequency shifts to formation of σ-complexes (one-to-one and one-to-two complexes) by hydrogen bonding to the nitrogen atom of pyridine, and also to change in state of electrons in the molecule. On the other hand, Stidham and DiLella[2] measured frequency shifts of Raman bands of pyridine in various hydrogen bonding solvents. Infrared spectral change due to change in pyridine concentration in aqueous solution was investigated by Takahashi *et al.*,[1] but no works have been done on change in the above mentioned bands with temperature, although a temperature dependence of infrared spectra of hydrogen-bonded pyridine at 3 μ region was reported by Wolff *et al.*[3] On the other hand, a series of recent studies[4-7] on one-to-one σ-complexes by *ab initio* molecular orbital calculation made it clear that the π electron density on the nitrogen atom in the complexes is larger than that in pyridine itself,[8] and, therefore, existence of $\sigma\pi$-complex, in which a molecule is hydrogen-bonded to a one-to-one σ-complex by π-bonding, is probable. If $\sigma\pi$-complex coexists with one-to-one σ-complex, some peculiar temperature dependence of Raman spectra of pyridine in methanol is expected. In the present study, Raman spectra of pyridine in methanol were measured at various temperatures, and results were examined along with those of Raman spectral measurements at various concentrations, with the possibility of formation of $\sigma\pi$-complex taken into consideration.

Experimental

Raman spectra of pyridine and its aqueous and methanol solutions at various concentrations and those of pyridine in other hydrogen bonding solvents were measured. For a methanol solution (a mixture of pyridine and methanol in a mole ratio of 1 to 0.526), Raman spectra were measured at various temperatures between 128 and 293 K. Raman spectra of solutions at room temperature were measured using 0.3 ml Raman cells, while those at lower temperatures were measured by use of an Oxford-type cryostat using liquid nitrogen for cooling. Raman spectra were recorded on a Model R-800T Raman Spectrophotometer (Japan Spectroscopic Co., Ltd.) and the 514.5 nm line (300 mW) of a Spectra Physics argon ion laser (model 165).

Results and Discussion

(a) Raman Spectral Change Associated with Concentration Change. Change in spectra of pyridine in its aqueous solution with concentration is shown in Figs. 1, 2, and 3, in comparison with spectra of pure pyridine ((A) in the figures). In Figs. 1(B), (C), and (D), with decreasing concentration of pyridine, the intensity of the band at 1585 cm^{-1} (Fig. 1(B)) decreases and a new band at 1591 cm^{-1} (Fig. 1(B)) increases its intensity. At lower concentrations (Fig. 1(D)), the former almost disappears and changes into the band at 1594 cm^{-1} (Fig. 1(D)). This change confirms that the band at 1585 cm^{-1} forms a couple with the band at 1591 cm^{-1} (Fig. 1(B)), as the authors of Refs. 1 and 2 described. The reason why the intensity of the band at 1576 cm^{-1} (Fig. 1(B)) is not affected much by concentration change of pyridine is that a new band appears at 1578 cm^{-1} increasing its intensity with decreasing concentration of pyridine. In the same way as Fig. 1, Figs. 2 and 3 show that the bands at 998 and 992 cm^{-1} (Fig. 2(B)) and those at 612 and 605 cm^{-1} (Fig. 3(B)) form two couples. The

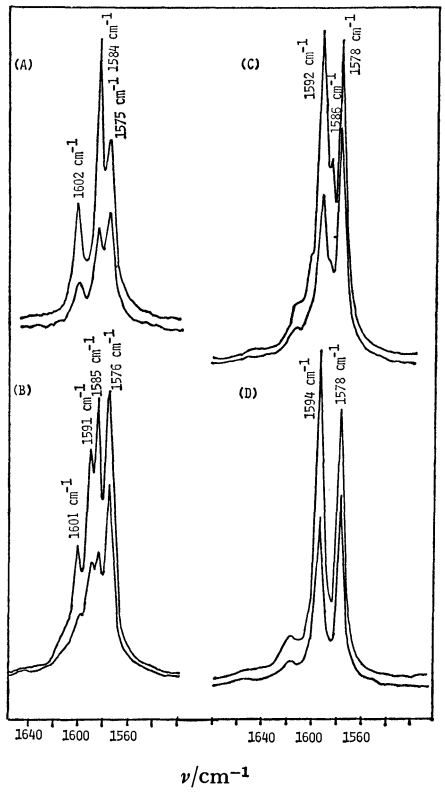

Fig. 1. Raman spectra (1540—1640 cm^{-1}, $I_{//}$ and $I_{\perp}$) of aqueous solutions of pyridine at room temperature. (A): Pyridine, (B): X_P=0.746, (C): X_P=0.574, (D): X_P=0.214, X_P: mole fraction of pyridine.

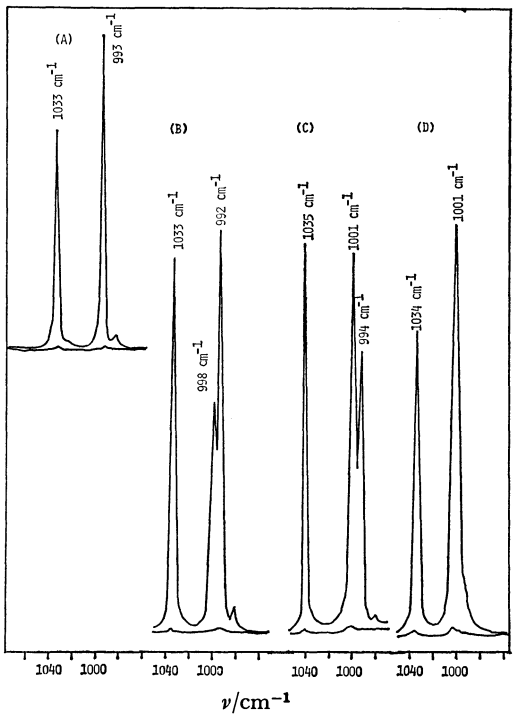

Fig. 2. Raman spectra (980—1060 cm^{-1}, $I_{//}$ and $I_{\perp}$) of aqueous solutions of pyridine at room temperature. (A): Pyridine, (B): X_P=0.746, (C): X_P=0.574, (D) X_P=0.214.

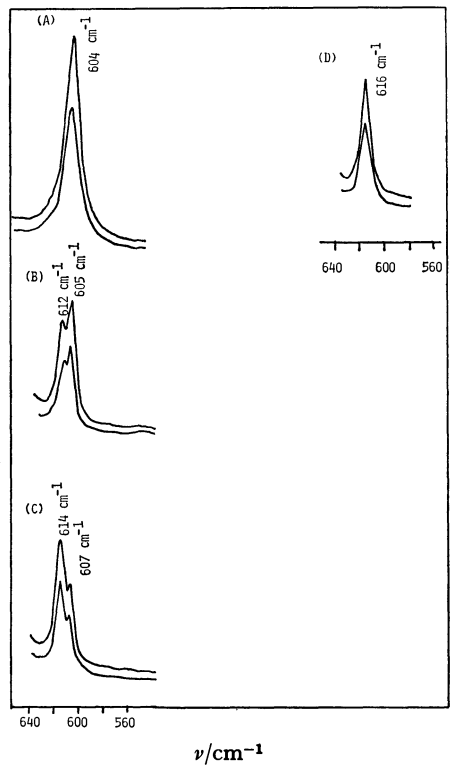

Fig. 3. Raman spectra (560—640 cm^{-1}, $I_{//}$ and $I_{\perp}$) of aqueous solutions of pyridine at room temperature. (A): Pyridine, (B): X_P=0.746, (C): X_P=0.574, (D): X_P=0.214.

same type of spectral change was observed for methanol solutions of pyridine.

(b) Raman Spectral Change with Temperature. Results of measurement are shown in Figs. 4(A), (B), and (C). In the spectrum at 293.0 K in Fig. 4(A), the band at 1576 cm^{-1} is an overlapped band composed of a pyridine band and bands of bonded pyridine as discussed in *(a)*. As temperature falls, the intensity of this band increases greatly, as compared with those of other bands. The band at 1591 cm^{-1} also increases its intensity. However, its degree of change is smaller than that of the band at 1576 cm^{-1}. Moreover, the real increase in intensity of the band of bonded pyridine at 1576 cm^{-1} is far greater than it appears, because the band of nonbonded pyridine overlapping with the bands of bonded pyridine decreases its intensity. Therefore, the band at 1576 cm^{-1} is concerned with a larger enthalpy difference, while the band at 1591 cm^{-1} is concerned with a smaller enthalpy difference. As the band at 1591 cm^{-1} forms a couple with the band at 1585 cm^{-1}, the smaller increase in intensity of the former band relative to the latter band suggests that the couple bands correspond to a species whose enthalpy difference is very small. Thus, the band at 1585 cm^{-1} is not due to only nonbonded pyridine, but to both bonded and nonbonded pyridines. However, it is not the same bonded pyridine that corresponds to the band at 1591 cm^{-1}. For other band couples, as shown in Figs. 4(B) and (C), the bands at 992 and 605 cm^{-1} behave like the one at 1585 cm^{-1}, and those at 998 and 612 cm^{-1} behave as the one at 1591 cm^{-1}. The above results can be interpreted as follows: It is expected that the enthalpy difference for the reaction, pyridine+CH_3OH→σ-complex (one-to-one complex), has a negative value whose absolute value is greater than that of the enthalpy difference for the reaction, σ-complex (one-to-one complex)+CH_3OH→$\sigma\pi$-complex. In accordance with this expectation, as shown in Figs. 4(A), (B), and (C), the degree of relative intensity increase of the bands assigned to $\sigma\pi$-complex (1591, 998, and 612 cm^{-1}), compared with their partner bands (1585, 992, and 605 cm^{-1}), is far smaller than that of the band at 1576 cm^{-1} assigned to σ-complexes, $\sigma\pi$-complex, and pyridine. Thus, the band at 1576 cm^{-1} is assigned to nonbonded pyridine, σ-complexes, and $\sigma\pi$-complex, while the band at 1585 cm^{-1} corresponds to nonbonded pyridine and σ-complexes. The band at 1591 cm^{-1} is assigned to $\sigma\pi$-complex. The bands at 992 and 605 cm^{-1} are assigned to nonbonded pyridine and σ-complexes, while those at 998 and 612 cm^{-1} correspond to $\sigma\pi$-complex.

(c) Raman Spectra of Pyridine in Carboxylic Acids. Acetic acid solutions: Though the band of pyridine at 1575 cm^{-1} shifts only by 1 cm^{-1} in aqueous solution, it shifts by 5 cm^{-1} in acetic acid solution. Shift of the band at 1584 cm^{-1} is 16 cm^{-1}, which is larger than that in aqueous solution (10 cm^{-1}). A similar large shift (15 cm^{-1}) is observed for the band of pyridine at 993 cm^{-1}. In acetic acid solution, pyridinium ion coexists with hydrogen bonded pyridines since the bands at 646 and 617 cm^{-1} appearing in the spectrum of the solution correspond to the bands at 642 and 614 cm^{-1} of pyridine dissolved in hydrochloric

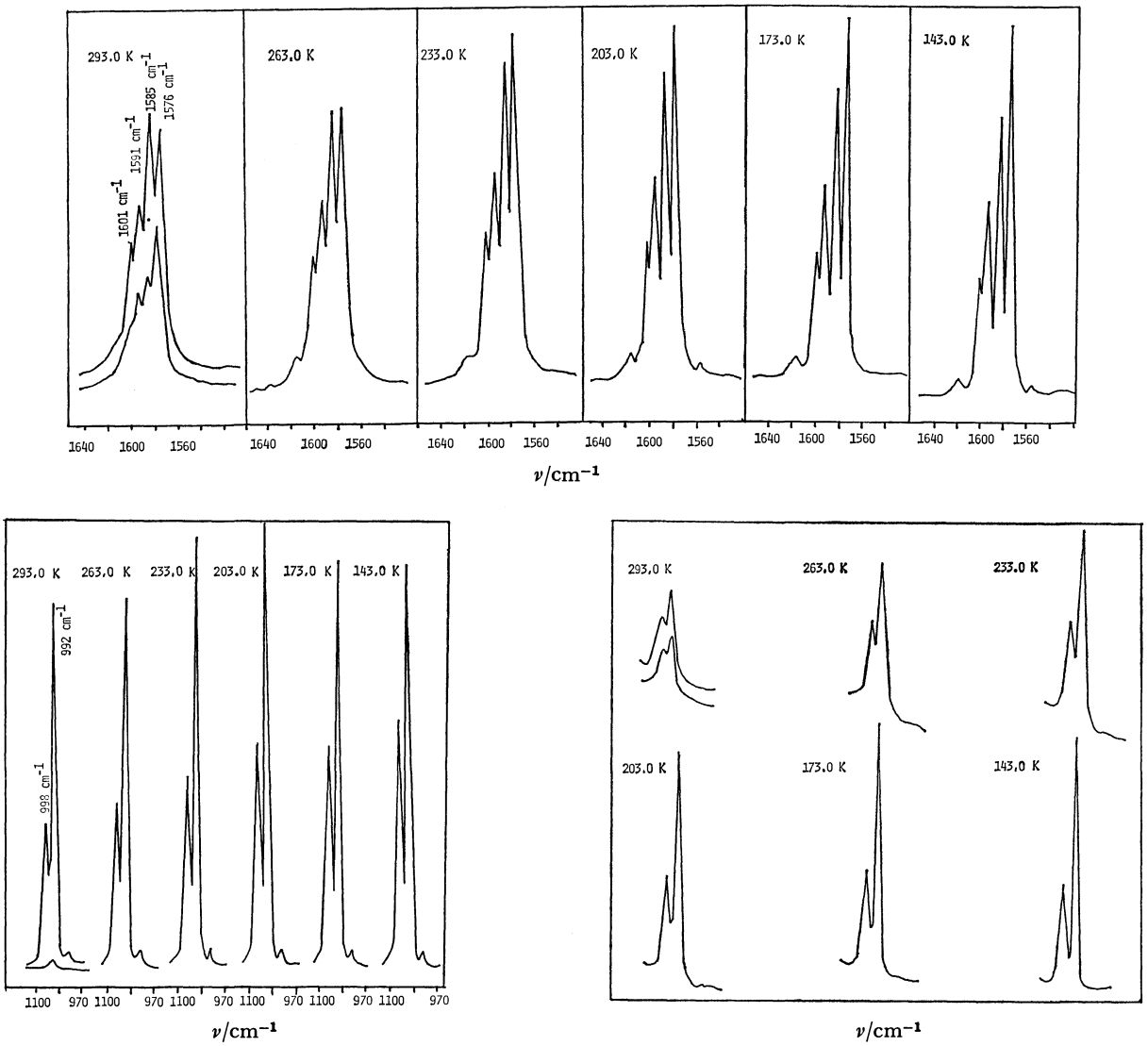

Fig. 4. Raman spectra of a methanol solution of pyridine (a mixture of pyridine and methanol in mol ratio of 1 to 0.526) at various temperatures.
(A): 1540—1640 cm^{-1} region, (B): 970—1100 cm^{-1} region, (C): 580—620 cm^{-1} region.

acid (refer to Table 1 for the solution with a mixing mole ratio of pyridine 1: hydrogen chloride 1.451: water 5.239). Results of measurement are shown in Table 1.

Among the bands of pyridine which shift by hydrogen bond formation, those at 1584, 993, and 605 cm^{-1} are assigned to the C–C ring stretching vibration, the ring breathing vibration, and the CCC and CNC deformation vibration, respectively.[9] As the bonds in the ring are formed primariliy by π-electron bonding, the ring vibrations may be affected by hydrogen bonding to π electrons, and the strength of the bonding may be influenced by the hydrogen bonding power of proton donors. The experimental results in Table 1 show that the shifts of the three bands differ in compliance with the hydrogen bonding power of the two acids. This is consistent with the assignment of the above-mentioned bands to $\sigma\pi$-complex.

(d) Propriety of the Band Assignment. The following calculation suggests that the band assignment discussed in *(a)* and *(b)* above is reliable.

Expressing the peak intensity of a band having frequency f by I_f, we have

$$I_{1576} = I_{1576,\sigma} + I_{1576,\sigma\pi} + I_{1576,P}, \quad (1)$$

$$I_{1585} = I_{1585,\sigma} + I_{1585,P}, \quad (2)$$

$$I_{992} = I_{992,\sigma} + I_{992,P}, \quad (3)$$

$$I_{998} = I_{998,\sigma\pi}, \quad (4)$$

where σ, $\sigma\pi$, and P denote σ-complexes, $\sigma\pi$-complex, and pyridine, respectively. Denoting the ratio $I^{\circ}_{1575}/I^{\circ}_{1585}$ for pure pyridine by r and assuming that $I_{1576,\sigma}+I_{1576,P}=(I_{1585,\sigma}+I_{1585,P})r$, the quantity $r_{\sigma\pi}$, proportional to the mole fraction of $\sigma\pi$-complex, will be obtained from Eqs. 1 and 2 for the solution corresponding to Fig. 1(B):

$$r_{\sigma\pi} = (I_{1576}-I_{1585}r)/I_{1576} = 0.38,$$

for which the observed value of r=0.638 is used. On the other hand, $r_{\sigma\pi}$ can be obtained by Eqs. 3 and 4 for the same solution as

$$r_{\sigma\pi} = I_{998}/(I_{998}+I_{993}) = 0.36.$$

TABLE 1. RAMAN SHIFT FREQUENCIES OF PYRIDINE IN ACIDS AND PYRIDINIUM ION (in cm^{-1})[a]

Pyridine	CH_3COOH soln[b]	HCOOH soln[c]	Pyridinium ion
379 (0)	385 (0)	385 (1)	
	403 (1)	407 (2)	400 (2)
409 (1)	414 (1)	415 (2)	
	610 (sh, ?)	608 (2)	614 (6)
605 (1)	617 (2)	627 (2)	
	645 (sh, ?)	642 (sh, ?)	642 (8)
655 (4)	655 (10)	655 (13)	
980 (4)	983 (4)	983 (6)	
993 (100)	1008 (100)	1012 (100)	
	1011 (sh, ?)		1011 (100)
	1035 (sh, ?)		1029 (35)
1031 (75)	1038 (28)	1035 (81)	
	1065 (sh, ?)	1063 (sh, ?)	1063 (6)
1072 (1)	1070 (2)	1068 (3)	
1148 (1)	1154 (1)	1156 (1)	
	1204 (sh, ?)	1204 (sh, ?)	1204 (4)
1218 (3)	1217 (5)	1220 (8)	
	1240 (1)	1247 (sh, ?)	1247 (1)
	1260 (1)	1260 (1)	1258 (1)
1485 (1)	1489 (1)	1490 (2)	
1575 (2)	1580 (2)	1580 (sh, ?)	
1584 (3)	1600 (2)	1603 (3)	
	1625 (1)	1625 (1)	1625 (1)
1602 (1)	1631 (1)	1638 (1)	
	1644 (1)	1644 (sh, ?)	1644 (3)

a) Figures in parentheses represent relative intensity. b) Mixture of pyridine and acetic acid in a mole ratio of 1 to 1.487 (pH=4.17). c) Mixture of pyridine and formic acid in a mole ratio of 1 to 1.519 (pH= 3.65).

In the same way, $r_{\sigma\pi}$ for the solution corresponding to Fig. 1(C) is obtained as 0.60 and 0.58 from Eqs. 1 and 2 and from Eqs. 3 and 4, respectively. This good agreement of the $r_{\sigma\pi}$ values from the two sets of equations suggests a reliability of the assignment of the band at 1576 cm^{-1} to σ-complexes, $\sigma\pi$-complexes, and pyridine, and those at 1585, 993, and 606 cm^{-1} to σ-complexes and pyridine, and those at 1591, 998, and 616 cm^{-1} to $\sigma\pi$-complex.

(e) Quantitative Relation between the Relative Intensities of the Bands at 992 and 998 cm^{-1} and Temperatures. As shown in Fig. 5, an almost linear relation holds between $\ln(I_{992}/I_{998})$ and $(1/T)$. Although equilibria in the solution are not known, this result suggests that (I_{992}/I_{998}) is approximately proportional to an equilibrium constant. The quantity ΔH obtained from the straight line in the figure on the basis of the equation

$$\ln (I_{992}/I_{998}) = -\frac{\Delta H}{RT} + \text{const.}$$

may be related to the enthalpy difference for the reaction concerning the equilibrium constant. The value for the ΔH is 0.9 ± 0.2 kJ mol^{-1}, whose absolute value is very small compared with those of enthalpy differences for ordinary σ-type hydrogen bonds. Therefore, the equilibrium which predominates the temperature change in (I_{992}/I_{998}) might be the equilibrium between $\sigma\pi$-complex and σ-complexes.

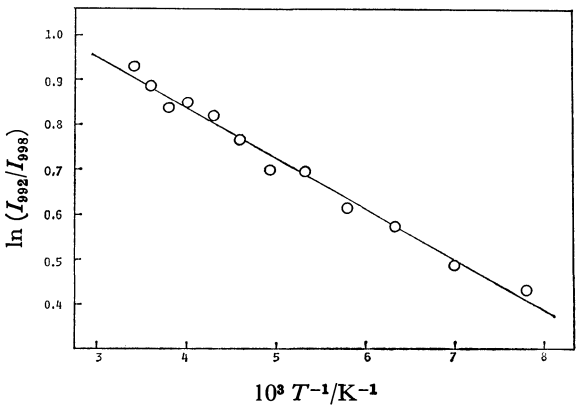

Fig. 5. Relation between $\ln(I_{992}/I_{998})$ and $(1/T)$. T in K.

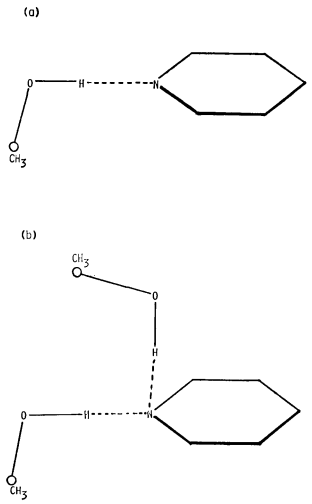

Fig. 6. σ-Complex (a) and $\sigma\pi$-complex (b).

References

1) H. Takahashi, K. Mamola, and E. K. Plyler, *J. Mol. Spectrosc.*, **21**, 217 (1966).
2) H. D. Stidham and D. P. DiLella, *J. Raman Spectrosc.*, **8**, 180 (1979).
3) H. Wolff, W. Hagedorn, D. Rethel, E. Millermann, and L. Leidner, *J. Phys. Chem.*, **82**, 2404 (1978).
4) W. Adam, A. Grimson, R. Hoffmann, and C. Zuazaga de Oritz, *J. Am. Chem. Soc.*, **90**, 1509 (1968).
5) J. E. DelBene, *J. Am. Chem. Soc.*, **97**, 5330 (1975).
6) J. E. DelBene, *J. Am. Chem. Soc.*, **101**, 7146 (1979).
7) J. E. DelBene, *J. Am. Chem. Soc.*, **102**, 5191 (1980).
8) I. G. John, G. L. Ritchie, and L. Radom, *J. Chem. Soc., Perkin Trans. 2*, **1977**, 1601.
9) D. A. Long, E. L. Thomas, *Trans. Faraday Soc.*, **59**, 783 (1963).

Laser Flash Photolysis of Benzene. IV. Physicochemical Properties of Mist Produced by Laser Excitation†

Nobuaki NAKASHIMA and Keitaro YOSHIHARA*
Institute for Molecular Science, Myodaiji, Okazaki 444
(Received February 3, 1982)

Mist formation is observed when gaseous benzene (8—75 Torr) (1 Torr=133.322 Pa) with oxygen ($\lesssim 10^{-5}$—860 Torr) is irradiated by a KrF excimer laser. By measuring the falling speed, the size of droplets in the mist is determined to be 2 to 6 μm depending on gas pressure. The number of droplets produced by irradiation with a 100 mJ/cm² pulse is estimated to be 1×10^5/cm³ by measuring the benzene pressure change and by turbidity measurement. The disappearance yield of benzene is 0.1 and phenol is identified with a quantum yield of 0.01. The nucleus is produced by two-photon excitation of benzene and allowed to grow into mist through a subsequent oxidation and/or polymerization reaction.

During the course of a laser-flash photolytic study of gaseous benzene,[1,2] we observed that laser beam will often cause mist to appear. The mist causes intense Mie scattering of monitor laser light and is easily visible in the form of falling "mist" or "rain." This laser-induced mist or particle formation seems to be the first observation with organic systems.

In this paper we report some physical and chemical properties of the mist studied with light scattering and transient absorption. The size of droplets in the mist was determined by measuring the falling speed. The number of droplets was estimated by observing the benzene pressure change and also by turbidity measurement. A possible mechanism for the photochemical formation of nucleus and for the enhancement of mist formation with oxygen is discussed.

Laser-induced solid particle formation has recently been observed in several other systems with simple molecules and/or metal vapors. Formation of solid alkali hydrides from alkali metal vapor and H_2 (Refs. 3 and 4) is induced by irradiation with a CW laser. Produced particles are called "laser snow," because they are white solid and fall down by gravity. Evolution of particles from NO_2 and SO_2 (Ref. 5) and of sulfur or aerosols from SF_6+H_2, CS_2, and Cl_2CS (Refs. 6,7, and 8) are also recognized.

Experimental

Gaseous benzene was excited by a KrF excimer laser (Lambda Physik EMG 500), at 248 nm, with typical output energy of 100 mJ and a pulse halfwidth of 15 ns. The laser beam with an area of 2.5×0.5 cm² was not focused for most experiments unless otherwise indicated. Transient absorption[2] and light scattering were measured in the perpendicular direction with a pulsed Xe lamp (EG & G 265UV) and a He–Ne laser, respectively. The intensity of light from a He–Ne laser scattered by mist was monitored with a photomultiplier at right angles through an $f=1.5$ lens and recorded on an X-T recorder.

A monitoring light at 260 nm was obtained from a D_2 lamp through a Shimadzu-Bausch & Lomb monochromator and was used for determining the concentration (pressure) of benzene. The output signal, run through a Nikon P250 monochromator and two Ortec Brookdeal 9503 lock-in amplifiers, was further normalized with a ratio meter model 5043. The linearity of absorbance at 260 nm held up to 0.9 in absorbance units, corresponding to 100 Torr cm of gaseous benzene, when the smallest slit width ($\Delta\lambda\approx$ 0.15 nm) of the monochromator was used. Absorption spectra were measured on a Cary 17 spectrophotometer.

A conventional greaseless vacuum line was used for sample preparation with a Baratron pressure gauge 310BHS-1000. Back pressure was 1×10^{-5} Torr. A quartz cell was closed with a J. Young greaseless stopcock. Our "oxygen free" sample was prepared by complete degassing with freeze-pump-thaw cycles and closed off by fusing the tubing. Quartz cells were baked at about 490 °C for several hours before use. Usually the sample was excited at intervals of 15 min and was renewed after 5 laser shots.

Benzene (J. T. Baker, stated purity of 99.98%), oxygen (99.98%), nitrogen (99.9995%), SF_6 (99.9%), and *cis*-2-butene (99%) were used without further purification. All the gases were produced by Nippon Sanso.

Results

Observation of Mist Formation. In the flash photolysis experiment with a KrF excimer laser we visually observed mist formation when the sample was viewed under room light. Scattering from a He–Ne laser makes the presence of mist much clearer as shown in Fig. 1. Figure 2 shows the intensity of 90° light scattering by mist produced from a sample with 20 Torr of benzene and 0.08 Torr of oxygen. The mist formation is enhanced by oxygen; it is observable even in an "oxygen free" condition with the same pressure of benzene.

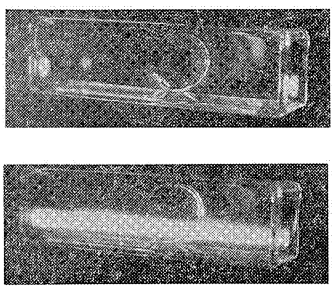

Fig. 1. Mie scattering by mist produced from gaseous benzene excited by a KrF laser.
a): Sample cell before irradiation, b): after irradiation of 40 Torr of benzene and 2 Torr of oxygen. The size of the sample cell is $4.0\times1.0\times1.0$ cm³. The area of the laser beam is 2.5×0.5 cm². The sample is irradiated without focusing the beam.

† Part III of this series is Ref. 2.

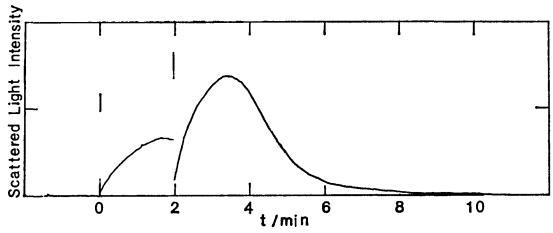

Fig. 2. Time course of the light scattered at 90° with 20 Torr of benzene and 0.08 Torr of oxygen.
The spikes indicate noise due to laser pulses. The light scatterings are quenched very quickly by subsequent laser excitations and then regenerated slowly.

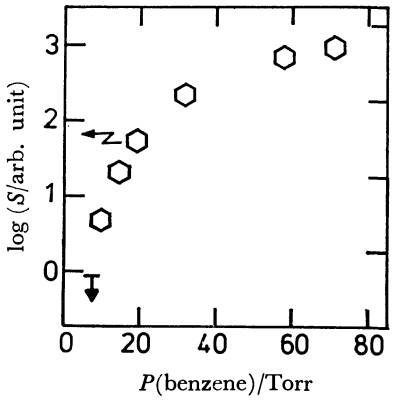

Fig. 3. Dependence of pressure of benzene on the scattered light intensity.
Peak height of the scattered light is plotted by ○; each sample contains 2 Torr of oxygen. A bar with an arrow at 7.5 Torr shows that the scattered signal was lower than the detection limit (the bar).

It takes the signal about 50 s to reach its peak and about the same time to decay. The rise time of the scattered light intensity is related to the rate of the nucleation process. Decay times simply depend on the falling speed of droplets, as discussed in the next section.

The scattered light intensity is decreased immediately by subsequent laser shots as shown in Fig. 2. This indicates that the mist absorbs the subsequent laser pulse and is destroyed easily. It is suggested that component molecules of the mist are relatively small and bound together by a small molecular interaction.

The scattered light intensity is increased more than 300 times upon increasing the pressure of benzene from 8 to 75 Torr. Figure 3 shows scattered light intensity *vs.* pressure of benzene in the presence of 2 Torr of oxygen. We do not observe any signal if the benzene pressure is less than 7.5 Torr. The concentration of nuclei is suggested to be too low to start nucleation at pressures less than 7.5 Torr.

The size of droplets has been determined to be 2—6 μm by measurement of the falling speed. The size can be evaluated using the equations[9]

$$mg = 6\pi\eta rv, \quad m = \frac{4}{3}\pi r^3\rho, \tag{1}$$

where η is viscosity of mixed gas, r is radius of droplet, v is falling speed, ρ is density of droplet, and g is gravity. For the system consisting of 21 Torr of benzene, 2.1 Torr of oxygen, and 207 Torr of nitrogen, η is evaluated to be 1.57×10^{-4} P (1 P=0.1 Pa s). We do not know all of the compositions of the droplets, so that ρ cannot be given any accurate value. However, we presume $\rho=1.0$ g/cm^3. This seems to be a feasible approximation since the starting materials for the droplets are benzene and oxygen and densities of most organic hydrocarbons are close to unity. For example, the density of benzene is 0.88 g/cm^3 and that of phenol (one of photoproducts) 1.07 g/cm^3. If we measure v, the size will be given by Eq. 1.

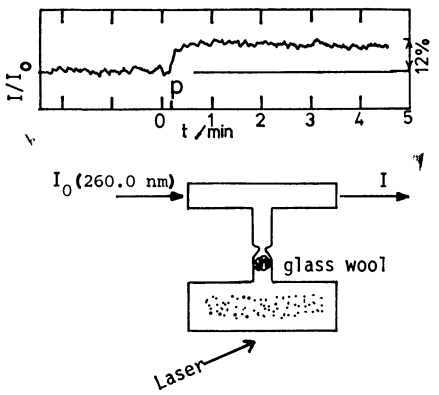

Fig. 4. Junction cell experiment. The larger cell was irradiated with 20 laser shots at 2 Hz.
Irradiation started at 0 min and stopped at p in the figure. Pressure change was monitored at 260 nm ($6_0^1 16_1^1$ transition). The actual change in transmittance was 3%, which corresponds to a quantum yield of 0.12 after correcting the volume of irradiation and the laser energy. The sample cell contains 23.2 Torr of benzene and 2.3 Torr of oxygen.

The mist produced by irradiation begins to fall. The speed is so low as to be measured visually. The position of the fastest droplet is plotted as a function of time. For the above case v was $(1.8\pm0.5)\times10^{-2}$ cm/s. Then, the diameter ($2r$) of the droplets is $(2.3\pm0.3)\times10^{-4}$ cm. The size of 2—6 μm is obtained in the benzene pressure range 8—75 Torr. An increase in the size accompanies an increase in the pressure of benzene.

By knowing the approximate size of droplets, we can determine an approximate number of the droplets produced, in two independent ways: one uses pressure change of gaseous benzene due to mist formation and the other is based on turbidity measurement of mist. Decrease in benzene pressure can be determined by change in absorbance at 260 nm, which corresponds to the $6_0^1 16_1^1$ transition. As shown in Fig. 4, two quartz cells are connected by a thin neck, one being the sample cell for excitation of benzene and the other being the monitoring cell.

The yield for the decrease in benzene pressure is 0.13 ± 0.02 with and without oxygen. Taking into account the size of droplet (2.5 μm), the number of droplets is obtained to be 1.3×10^5 /cm^3 at a laser excitation of 125 mJ/cm^2. Experimental details are as follows: A mixture of benzene (23.2 Torr) and oxygen (2.3 Torr) is irradiated by 20 pulses of a 156

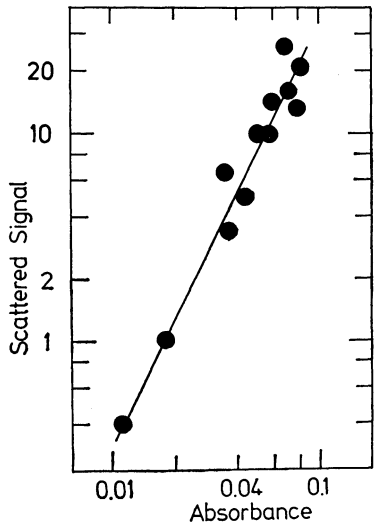

Fig. 5. Scattered light intensity *vs.* absorbance of the excited singlet state observed at 256 nm.
Pressure of benzene is 20 Torr with 0.08 Torr of oxygen. The straight line shows a slope of 2.0.

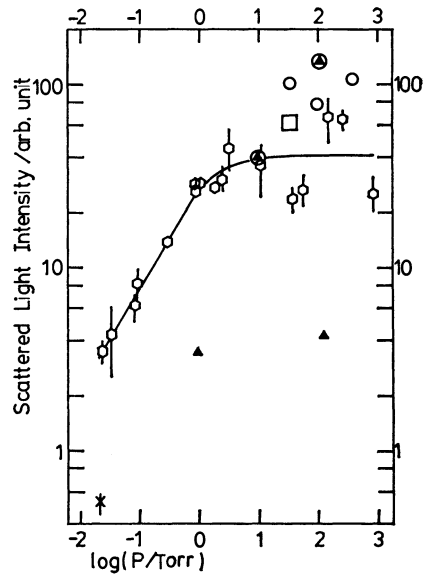

Fig. 6. Dependence of foreign gases on the scattered light intensity.
The benzene pressure for all experiments is 20 Torr. ⬡: Pressure of oxygen is denoted on the abscissa, □, ◭, ○: effects of *cis*-2-butene, SF_6, and nitrogen, respectively are given. In these cases 2 Torr of oxygen is included and the total pressures of foreign gases are denoted on the abscissa. x: 20 Torr of benzene with an oxygen pressure less than 10^{-5} Torr, ▲: benzene and SF_6 with oxygen pressure also less than 10^{-5} Torr.

mJ laser with a cross section of 1.25 cm^2 at 2 Hz. About 2×10^{18} photons are absorbed in a total volume of 5 cm^3. In order to estimate the number of droplets, it is necessary to assume the volume of component molecules. The approximate volume of phenol (0.53 nm^3 is used here as that of the component molecules. Glass wool was inserted at the neck of the quartz cell in order to prevent photoproducts from flowing into the monitoring cell. If the glass wool was not added, photoproducts canceled out the change in absorbance due to mist formation.

During the sample irradiation at 2 Hz, the signal shows no change. Just after stopping the irradiation (denoted as p in Fig. 4), the pressure of benzene begin to decrease, reaching the minimum value within 10 s. This observation indicates that the mist is destroyed by the subsequent laser shots as seen in Fig. 2. The slow increase after a few minutes indicates a flowing-in of photoproducts.

Turbidity was measured in order to estimate the number of droplets. Extinction change due to scattering by droplets is expressed as

$$\tau = \frac{1}{a}\ln\frac{I_0}{I} = \pi r^2 KN, \qquad (2)$$

where a is the path length of the monitoring cell (2.5 cm), r is the radius of the droplet (1.25 μm), and K is the average total Mie scattering cross section (2.0 used here). In the case of 45 Torr benzene with 2 Torr of oxygen, τ was 1×10^{-2} /cm for the first laser shot of 100 mJ/cm^2 and then the number (N) is given as 1×10^5 /cm^3, which is in agreement with that obtained by the pressure change of benzene in the previous section. The value K=2.0 is a good approximation, considering the size parameter of Mie scattering.[10]

Power Dependence, Effect of Foreign Gases, and Photoproducts. Figure 5 shows scattered light intensity *vs.* absorbance of the excited state of benzene. The scattered light intensity clearly gives a quadratic dependence on the S_1 concentration. The latter quantity was obtained by observing the intensity of the $S_n\leftarrow S_1$ absorption at 256 nm.[1,2] The absorbance of 0.1 corresponds to *ca.* 0.4 Torr of the S_1 concentration.

We could not observe any scattered signal when a Xe lamp was used as an exciting light source instead of the laser. These results indicates clearly that multiphoton excitation makes the mist formation possible, but that one-photon excitation does not. The energy of the Xe lamp was 1.3 mJ in the range of 220—250 nm at the sample cell. In order to avoid exciting benzene into the S_3 state and heating it up by IR light, methanol in a 2 cm cell was used as a filter.[11] A sample with 42 Torr of benzene and 8 Torr of oxygen was excited at 0.7 Hz and a total energy of 200 mJ was dumped in.

Pressure effect of foreign gases on scattered light intensity makes the role of oxygen clear. An oxygen-free sample shows a very weak signal as shown in Fig. 6 (denoted by ×). An increase in oxygen pressure (denoted by ⬡) is accompanied by an enhancement of scattered light intensity in the range from 2×10^{-2} to 2 Torr. This observation indicates that oxidation reaction is the major reaction which causes the mist formation.

cis-2-Butene, SF_6, or nitrogen does not seem to have any significant effect on the intensity when added to a system of 20 Torr of benzene and 2 Torr of oxygen. It is worth noting that only SF_6 makes aerosol. This may occur according to a mechanism similar to that for other sulfur-containing compounds.[6-8] This is the

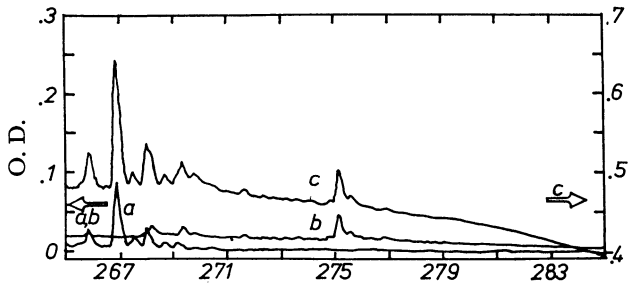

Fig. 7. Absorption spectra of 48 Torr of benzene with 5 Torr of oxygen after irradiation with 15 shots of 150 mJ laser energy.
a: Benzene (reference spectrum), b: reference absorption spectrum of phenol with a pressure of 0.35 Torr, and c: after laser irradiation.

reason that the oxygen free sample with SF_6 shows a larger signal than the ones without SF_6.

The consumption yield of benzene upon excitation was 0.08 ± 0.02 with and without oxygen after several hours. In order to avoid photolysing mist, the sample was irradiated only every 4 min so that most of the droplets fell down to the bottom of the cell before the subsequent laser shot came. The comsumption yield of 0.08 roughly coincides with the yield of pressure change of 0.13 obtained in the previous section. This reasonable agreement suggests that the major part of the pressure change due to mist formation can be ascribed to the nucleation of permanent photoproducts of benzene and not to aggregation of pure benzene.

Phenol was observed with a quantum yield of 0.01 as shown in Fig. 7. In addition to phenol, we obtained volatile species with absorption spectra shorter than 230 nm and nonvolatile species with a shoulder around 290 nm. The latter was observed only in the sample with oxygen. Phenol has been reported as a major photo-oxidation product in the gas phase,[12,13] though there is no report on the quantum yield of phenol formation. The shoulder around 290 nm might be for mucondialdehyde, which has been detected as a photo-oxidation product in the gas phase[13] as well as in pure liquid benzene.[14] A larger yield of polymer formation was observed in the sample without oxygen.

Discussion

Two-photon Absorption and Primary Photoproducts. There are a few possible processes for the two-photon mechanism leading to the formation of nuclei: 1) simultaneous two-photon absorption; 2) two-step excitation by energy transfer between excited singlet and/or triplet molecules, 3) consecutive two-step absorption *via* excited state. The major process is suggested to result from effects of foreign gases. Oxygen quenches the lowest excited singlet state of benzene with a rate constant of 1.02×10^{11} M^{-1} s^{-1} and the triplet state with 9.5×10^{9} M^{-1} s^{-1} (the same order of magnitude as that of *cis*-2-butene) (Refs. 15 and 16). Then the lifetime in the presence of 860 Torr of oxygen is expected to be 0.12 ns for the singlet state and 1.2 ns for the triplet state. These lifetimes are too short for excited molecules to collide among themselves and not long enough to absorb the second photon consecutively. The scattered signal intensity does not decrease at higher pressures of oxygen. Therefore, two-step excitation by energy transfer between two excited molecules can be excluded. The consecutive two-step excitation mechanism *via* excited states may be included to a small extent. The major process is suggested to be the simultaneous two-photon absorption.

In any two-photon processes, benzene is excited in the VUV region of 8.6—10 eV. The photochemistry of benzene by continuous light sources in the VUV region suggests that precursors for the mist produced by two-photon absorption are likely to be radicals with linear structure. With Kr (116.5 nm) and Xe (147 nm) lines, polymer formation is the major process and acetylene is produced with a quantum yield of *ca.* 0.1. The photochemical consumption yield has been estimated to be almost 1.0 at lower pressures.[17,18] On the other hand, the photochemical consumption yield is 0.1 by laser excitation in our experiment. The cross section of the absorption at the laser wavelength is expected to be larger under higher power irradiation. Several percent of increase in the cross section was observed at 80 Torr of benzene when incident laser power is varied from 40 to 150 mJ/cm^2. Hexatriene is accumulated easily by irradiation of benzene in cyclohexane with a KrF laser,[19] and the yield of polymer is higher in the absence of oxygen. These observations also support that the major primary photoproducts are linear radicals. The major processes are suggested to be

$$\mathrm{B} \xrightarrow{2h\nu} \mathrm{B^{**}} \longrightarrow \mathrm{R\cdot} \begin{cases} \nearrow \text{polymer} \\ \searrow \text{oxygenated compound} \end{cases} \searrow \text{mist}, \qquad (3)$$

where B** is a higher excited state of benzene and R· is a linear radical. Other minor photoproducts are also conceivable, *i.e.*, cationic species (monomer or dimer cations) and phenyl radicals, which may be a primary source of phenol.

Effect of Oxygen on Mist Formation. Organic mist formation requires accumulation of condensable species in excess of their gas-phase saturation conditions. Linear radicals are known to react with one another as well as to react with benzene and produce various derivatives by photolysis in solution.[20] All of these photoproducts are expected to show vapor pressures lower by several orders of magnitude than those of six-carbon parent molecules. Thus they would form mist even in the absence of oxygen according to the upper process of Scheme 3.

Linear biradicals formed by ring cleavage will be very easily oxidized and will give many kinds of bifunctional oxygenated compounds. Rates of addition reaction of oxygen have been reported as a few percent of the collisional frequency for simple radicals and equilibrium constants are very large, of the order of 10^{10} $Torr^{-1}$ (Ref. 21). Oxidation makes volatility

lower by more than several orders of magnitude; in particular, those of dicarboxylic acids are about 9 orders of magnitude lower than those of the parent molecules. The nucleation is much enhanced in the presence of oxygen according to the lower process of Scheme 3.

Formation of phenol was observed as shown in Fig. 7. In the course of formation of phenol, atomic oxygen (^3P) can be produced upon excitation of gaseous benzene.[12,22] It is well known that atomic oxygen reacts with benzene to produce phenol and also allows linear radicals to be oxidized.[23] These oxidation reactions contribute to the enhancement of mist formation.

The mechanism for the photochemical aerosol formation in urban atomosphere has been studied in detail.[24] Hydrocarbons are oxidized by ozone and/or hydroxyl radicals to form aldehydes, alcohols, or carboxylic acids. These oxygenated compounds have a low volatility. Then, no polymerization is necessary to form aerosols from cyclic olefins, even when they are present at trace concentrations (below 10^{-6} Torr) in ambient air.[24] These processes are similar to what we observed with benzene.

We reported that the initial stage of light-induced condensation of benzene was found in nanosecond time-resolved difference spectra.[1] However, we have recently found that these spectra can also be explained in terms of temperature rise due to nonradiative transitions.[25] The observations presented in this report, *i.e.*, the effects of foreign gas and laser power on mist formation and the results from the junction cell experiment, do not support the tentative explanation given in the previous report.

We thank Dr. I. Chabay for critical reading of the manuscript and valuable suggestions and Dr. N. Washida for discussion on the mechanism of aerosol formation. The present work was supported in part by the Grant-in-Aid from the Ministry of Education, Science and Culture of Japan.

References

1) N. Nakashima, H. Inoue, M. Sumitani, and K. Yoshihara, *J. Chem. Phys.*, **73**, 4693 (1980).
2) N. Nakashima, H. Inoue, M. Sumitani, and K. Yoshihara, *J. Chem. Phys.*, **73**, 5976 (1980).
3) A. Tam, G. Moe, and W. Happer, *Phys. Rev. Lett.*, **35**, 1630 (1975).
4) T. Yabuzaki, T. Sato, and T. Ogawa, *J. Chem. Phys.*, **73**, 2780 (1980).
5) K. Iwamoto, N. Presser, and J. Ross, *J. Chem. Phys.*, **68**, 663 (1978).
6) S. T. Lin and A. M. Ronn, *Chem. Phys. Lett.*, **56**, 414 (1978).
7) K. Ernst and J. J. Hoffman, *Chem. Phys. Lett.*, **68**, 40 (1979); **75**, 388 (1980).
8) H. Sato, M. Kawasaki, K. Kasatani, and S. Yoshida, *Research Reports, Fuculty of Engneering, Mie Univ.*, **5**, 109 (1980).
9) R. A. Millikan, *Phys. Rev.*, **32**, 349 (1911).
10) Since the diameter ($2r$) is 2—6 μm, this gives a size parameter, $q=2\pi rn/\lambda=15$—45 at refractive index of 1.5 and wavelength $\lambda=0.633$ μm, so that the integrated scattering cross section K converges to 2 at all q's within this region. [M. Born and E. Wolf, "Principles of Optics," Pergamon Press, Oxford and New York (1975), pp. 647—664; F. T. Gucker and R. L. Rowell, *Faraday Discuss. Chem. Soc.*, **30**, 185 (1965).]
11) Dr. T. Yabuzaki (Kyoto Univ.) informed us that particles are formed by an irradiation with a D_2 lamp (The First Conference on Laser Science, Osaka, Japan, Feb. 12, 1981). We suppose that it is possible, if photoproducts are accumulated in excess over their vapor pressure by excitation to the S_2 and S_3 electronic states (the formation yield of linear radical has been known as ≈ 0.5) or by prolonged excitation to S_1.
12) P. S. Gukasyan, A. S. Saakyan, A. A. Mantashyan, and A. B. Nalbandyan, *Dokl. Akad. Nauk SSSR*, **213**, 978 (1973) (English Transl.); *Arm. Khim. Zh.*, **27**, 83 (1974).
13) J. Irina and K. C. Kurien, *J. Chem. Soc., Chem. Commun.*, **1973**, 738.
14) K. Wei, J. C. Mani, and J. N. Pitts, Jr., *J. Am. Chem. Soc.*, **89**, 4225 (1967).
15) R. G. Brown and D. Phillips, *J. Chem. Soc., Faraday Trans. 2*, **70**, 630 (1974).
16) A. Morikawa and R. J. Cvetanovic, *J. Chem. Phys.*, **52**, 3237 (1970).
17) W. M. Jackson, J. L. Faris, and B. Donn, *J. Phys. Chem.*, **71**, 3346 (1967).
18) R. R. Hentz and S. J. Rzad, *J. Phys. Chem.*, **71**, 4096 (1967).
19) N. Nakashima, M. Sumitani, I. Ohmine, and K. Yoshihara, *J. Chem. Phys.*, **72**, 2226 (1980). Some of the absorption peaks of photoproducts in cyclohexane solution are in good agreement with those of hexatriene.
20) K. H. Grellmann and W. Kühnle, *Tetrahedron Lett.*, **20**, 1537 (1969).
21) R. W. Walker, "Gas Kinetics and Energy Transfer," ed by P. G. Ashmore, The Chemical Society London, London (1975/1977), p. 161/p. 296.
22) T. F. Hunter, D. Rumbles, and M. G. Stock, *Chem. Phys. Lett.*, **45**, 145 (1977).
23) R. E. Huie and J. T. Herron, "Progress in Reaction Kinetics," ed by K. R. Jennings and R. B. Cundull, Pergamon Press, Oxford and New York (1975), Vol. 8, p. 60.
24) "Ozone and Other Photochemical Oxidants," ed by National Research Council, Div. Medical Sciences, Medical, and Biologic Effects of Environmental Pollutants. Natl. Acad. Press, Washington (1977), pp. 45—125.
25) N. Nakashima and K. Yoshihara, *J. Chem. Phys.*, in press.

The Structure of Liquid Water by Neutron Scattering. II. Temperature Dependence of the Liquid Structure

Norio Ohtomo,† Kazuo Tokiwano,† and Kiyoshi Arakawa*
Research Institute of Applied Electricity, Hokkaido University, Sapporo 060
† *Faculty of Engineering, Hokkaido University, Sapporo 060*
(Received March 1, 1982)

The structure factors for heavy water at 25, 50, 70, and 95 °C were determined in the range of Q, 1.4—20 Å^{-1}, by means of the time-of-flight (TOF) neutron diffraction method using the electron linear accelerator (LINAC). An analysis of the neutron diffraction data was made by applying a new general theoretical procedure of analysis for the fluid system composed of molecular clusters with various sizes. Structure factors were calculated according to the general procedure for the pentamer-monomer mixture model as a mixture of regular tetrahedral pentamers and non-bonded monomers with a due assignment of pentamer fraction at each temperature. Excellent agreement was obtained between the calculated and observed structure factors at temperatures in 25—95 °C. Combined with the preceding result (N. Ohtomo, K. Tokiwano, and K. Arakawa, *Bull. Chem. Soc. Jpn.*, **54**, 1802 (1981)), it was concluded that the pentamer-monomer mixture model is the best one for water from room temperature to near the boiling point.

In the preceding paper[1]# we reported an analysis of the liquid structure of water by combining neutron and X-ray diffraction data, and showed that liquid water at room temperature has a basic structure as an aggregate of regular tetrahedral pentamers. The analysis was performed concerning the structure of water only at a temperature, 15 °C. Then, we attempt here to perform structure analysis of liquid water at more elevated temperatures. For this purpose, we have carried out a neutron diffraction measurement on water at 25—95 °C, and further, have made an analysis of the data by applying a newly devised theoretical procedure of analysis for the fluid system composed of molecular clusters with various sizes.

Neutron Diffraction Data

Measurement. Neutron scattering intensities were measured for liquid water at 25, 50, 70, and 95 °C by means of the LINAC-TOF neutron diffraction method. Basic architecture of the diffractometer and experimental procedures were reported elsewhere.[2] In the present study measurements were made simultaneously at two scattering angles (2θ=40° and 65°). Neutrons scattered towards two directions were detected in a bifurcated array of two counters (Fig. 1). The angular divergence of the Soller slit as a collimator, which governs primarily the resolving power, was 30′ and 38′ for the slit used at lower and higher scattering angles, respectively.

A sample of 99.9% deuterium oxide contained in a thin-walled cylindrical quartz vessel (100 mm long, 10 mm internal diameter, and 0.1 mm wall thickness) was placed within a thin aluminum cylindrical reflector of an elliptical contour (Fig. 1). A Digital Thermometer (FLUKE Model 2190A) and a rod heater were used, and the vertical axis of the heating rod and the cylindrical sample container are placed exactly at the two focussing points of the elliptic contour. Temperature measurement was made by thermocouples inserted into the top and bottom of the sample. The temperature was controlled within the fluctuation of 1 °C through all the measurements in the present experiment (Fig. 2).

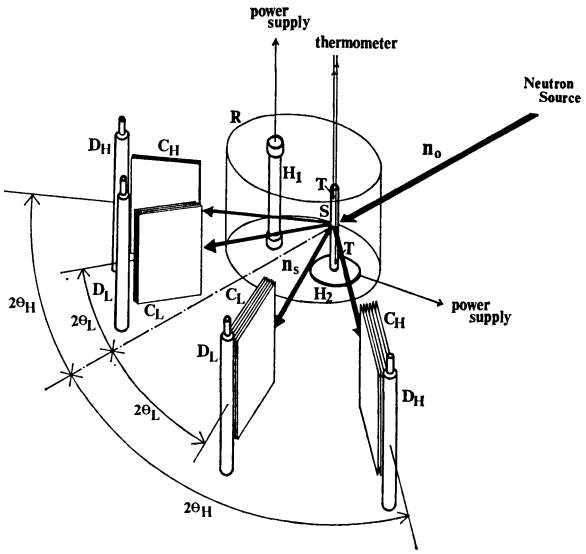

Fig. 1. A perspective view of the diffractometer. n_0: Incident neutron beam, n_s: scattered neutron beam, S: sample, H_1: heater rod, H_2: auxiliary heater, R: reflector, T: thermocouple, C: Soller collimator, D: detector, 2θ: scattering angle. Suffixs H and L denote higher and lower scattering angles, respectively.

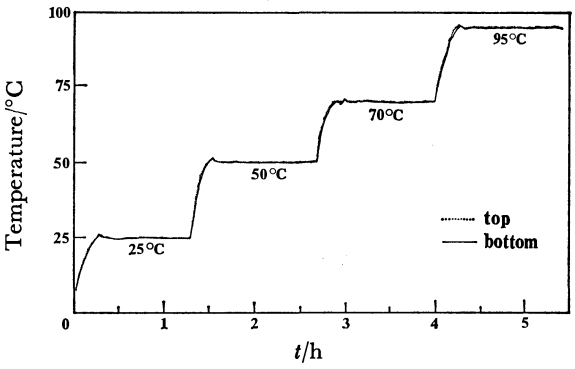

Fig. 2. Temperature of D_2O sample through all the measurements.

Correction Procedures and Structure Factors. For obtaining the structure factors $S_m(Q)$ from the measured raw data, several corrections (multiple scattering, ab-

We cite Ref. 1 as paper I in the following.

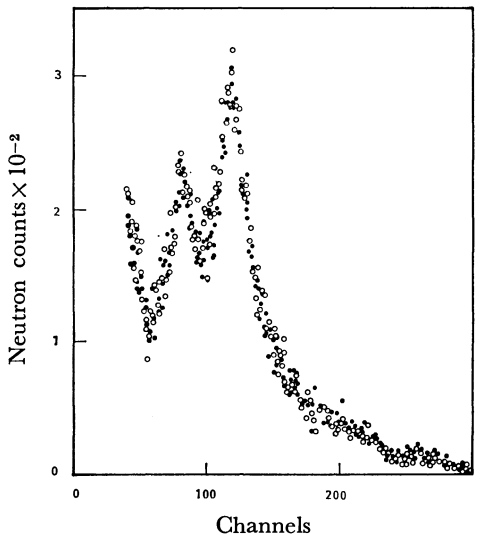

Fig. 3. Temperature variation of background counting including the scattering from the container ($2\theta=65°$).
○: 25 °C, ●: 95 °C.

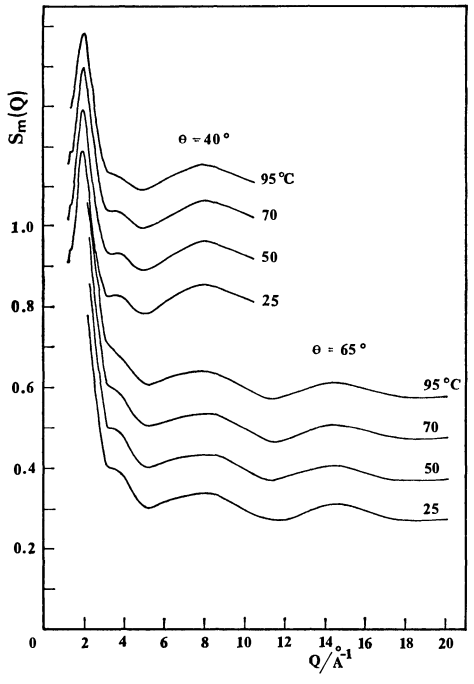

Fig. 4. Partially-corrected neutron structure factors $S_m(Q)$ (corrected with respect to background counting, multiple scattering, and absorption).

sorption, background counting, inelastic scattering, and incoherent scattering) and absolute normalization of data were carried out according to similar procedures as made in the preceding studies.[2-4] In applying these correction procedures to the present raw data, however, a due consideration on the influence of temperature variations must have been taken into account. In order to examine the temperature variation of background counting including the scattering from the container, we measured the intensity of neutrons scattered from the empty container at two temperatures (25 and 95 °C). It was found that differences between the

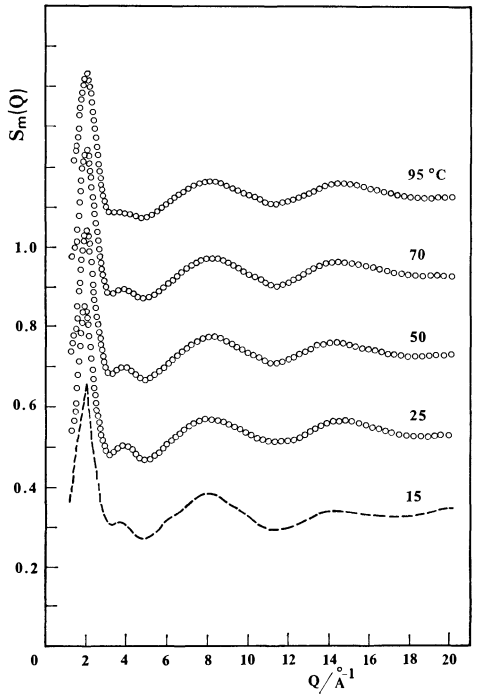

Fig. 5. Observed neutron structure factors $S_m(Q)$ for heavy water at 25, 50, 70, and 95 °C, together with the previous data at 15 °C.

two temperatures were negligibly small (Fig. 3). This is attributed to the thin wall-width of the container. Then, for the background counting, we could safely use the value at 25 °C through all the temperatures. With respect to multiple scattering and absorption, the temperature-dependent variation was assumed to be negligible for the temperature range in the present study. The partially-corrected $S_m(Q)$ curves after corrected with respect to background counting, multiple scattering, and absorption are shown in Fig. 4.

With respect to inelastic scattering which is important for D_2O, the following feature is clearly seen in Fig. 4. All the $S_m(Q)$ data at the same scattering angle at different temperatures are in full agreement with each other except the first peak and the hump at 4 $Å^{-1}$. This indicates that the inelastic correction is insensitive to temperature variation within the range of the present experiment. The $S_m(Q)$ data at $2\theta=65°$ in Fig. 4 exhibit a larger effect due to inelastic scattering than the data at $2\theta=40°$. This is explained theoretically as follows: the greater descending trend in the $S_m(Q)$ curve with increasing Q at larger scattering angle is typical of the Placzek corrections[5] and is almost entirely due to the self-scattering by the deuterons.[5,6] It can be said that the inelastic correction contributes a temperature-independent monotonic variation as a function of Q. Thus, the Placzek and Wick correction methods used in the previous studies at room temperature[2-4] were safely applied to the present data in lower and higher Q region, respectively, at 25—95 °C.

Absolute normalization of data was carried out with the use of scattering data from a vanadium standard. Calibration of absolute values for high Q data was performed according to the limiting procedure that

$S_m(Q)\to\Sigma b_n^2/(\Sigma b_n)^2$ as $Q\to\infty$, where incoherent scattering is duely considered. Calibration for low Q data was done by overlapping the $S_m(Q)$ curves in the Q range of 3—5 Å^{-1}. Combining the two corrected data at each scattering angle, the final $S_m(Q)$ curves for a range of Q=1.4—10.5 Å^{-1} and those for a range of Q=2.5—20 Å^{-1} were obtained from the data sets of $2\theta=40°$ and from those of $2\theta=65°$, respectively. The values are tabulated in Table 1. These data at two angles at the same temperature agree very well in the region of Q=2.5—10.5 Å^{-1} (Table 1). Thus, by combining these data at two angles, we obtain the final $S_m(Q)$ curves at each temperature as shown in Fig. 5, together with the curve at 15 °C obtained previously.[1] A marked feature of the structure factors obtained is a gradual falling of the hump at *ca.* 4 Å^{-1} as the temperature is raised.

Experimental accuracy has been improved at more satisfactory level in this study. The statistical error for values of $S_m(Q)$ is smaller than 0.5% in the range of Q=2—6 Å^{-1}, and the resolving power $\Delta Q/Q$ less than a few % in the whole range of Q.

Theoretical Procedure of Analysis

Theory. In paper I we derived a formula of $S_m(Q)$ for liquid consisting of identical clusters (Eqs. 7—11 in I). For the analysis of the present data, the $S_m(Q)$ formula for liquid composed of molecular clusters of various sizes including monomers is required. In the following, we will state the details of derivation of the formula, which is an extension of the theory reported in I, with the addition of due assumptions.

The coherent neutron structure factor $S_m(Q)$ is given in general by

$$S_m(Q) = N_m^{-1}\Sigma^{-2}\langle\sum_{i,j}\sum_{n_i,n_j} b_{n_i}b_{n_j}\exp(i\vec{Q}\cdot\vec{r}_{n_in_j})\rangle, \quad (1)$$

where i and j label molecules in a liquid and n_i denotes the n-th nucleus in the molecule i. $\vec{r}_{n_in_j}$ is the vector distance between the nuclei n_i and n_j, b_{n_i} the scattering length of nucleus n_i, $\vec{Q}$ the scattering vector, and $\Sigma=\sum_n b_n$. We sum over all the scatterers in the N_m molecules in the system.

We now consider the case of a fluid system consisting of molecular cluster of various sizes including monomers, where the number of clusters composed of ν molecules is N_ν, and its fraction in molecular number x_ν.

$$x_\nu = \frac{\nu N_\nu}{N_m}, \quad \text{and} \quad \sum_\nu \nu N_\nu = \sum_\nu x_\nu N_m = N_m, \quad (\nu=1, 2, \cdots).$$

Then, Eq. 1 is written as follows,

$$S_m(Q) = N_m^{-1}\Sigma^{-2}\langle\sum_\nu\sum_{\alpha_\nu}\sum_{l,l'}\sum_{n_l,n_{l'}} b_{n_l}b_{n_{l'}}\exp(i\vec{Q}\cdot\vec{r}_{n_ln_{l'}})\rangle + N_m^{-1}\Sigma^{-2}\langle\sum_{\nu,\mu}\sum_{\substack{\alpha_\nu,\beta_\mu\\(\alpha_\nu\neq\beta_\mu)}}\sum_{l,\kappa}\sum_{n_l,n_\kappa} b_{n_l}b_{n_\kappa}\exp(i\vec{Q}\cdot\vec{r}_{n_ln_\kappa})\rangle, \quad (2)$$

α_ν denotes the α-th cluster in the clusters composed of ν molecules, β_μ the β-th one in the ones composed of μ molecules ($\alpha_\nu=1,\cdots,N_\nu$ and $\beta_\mu=1,\cdots,N_\mu$), l and l′ the l-th and l′-th molecule within the cluster α_ν (l, l′: $1,\cdots,\nu$) respectively, and κ the κ-th molecule within the cluster β_μ($\kappa=1,\cdots,\mu$). The first term in Eq. 2 is the contribution of atom pairs within clusters and the second term the one of inter-cluster atom pairs.

Let us use $\vec{r}_{cll'}$ to denote the vector distance from the center of the l-th molecule to that of the l′-th one within the cluster α_ν, and $\vec{r}_{cl\kappa}$ the vector distance from the center of the l-th molecule in the cluster α_ν to the center of the κ-th molecule in the cluster β_μ. Then, $\vec{r}_{n_ln_{l'}}=\vec{r}_{cll'}-\vec{r}_{cn_l}+\vec{r}_{cn_{l'}}$ and $\vec{r}_{n_ln_\kappa}=\vec{r}_{cl\kappa}-\vec{r}_{cn_l}+\vec{r}_{cn_\kappa}$, where $\vec{r}_{cn_l}$ is the vector distance from the center of the molecule l to its n_l-th nucleus, and Eq. 2 is rewritten as follows,

$$S_m(Q) = N_m^{-1}\Sigma^{-2}\langle\sum_\nu\sum_{\alpha_\nu}\sum_{l,l'}\exp(i\vec{Q}\cdot\vec{r}_{cll'})\sum_{n_l,n_{l'}} b_{n_l}b_{n_{l'}} \times\exp\{i\vec{Q}\cdot(-\vec{r}_{cn_l}+\vec{r}_{cn_{l'}})\}\rangle + N_m^{-1}\Sigma^{-2}\langle\sum_{\nu,\mu}\sum_{\substack{\alpha_\nu,\beta_\mu\\(\alpha_\nu\neq\beta_\mu)}}\sum_{l,\kappa}\exp(i\vec{Q}\cdot\vec{r}_{cl\kappa})\sum_{n_l,n_\kappa} b_{n_l}b_{n_\kappa} \times\exp\{i\vec{Q}\cdot(-\vec{r}_{cn_l}+\vec{r}_{cn_\kappa})\}\rangle. \quad (3)$$

We adopt here the following assumption: all clusters of equal size have an identical structure on the average (assumption I). Then, the first term of Eq. 3 becomes as follows,

the first term in Eq. 3

$$= N_m^{-1}\Sigma^{-2}\sum_\nu N_\nu\langle[\sum_{l,l'}\exp(i\vec{Q}\cdot\vec{r}_{cll'})\sum_{n_l,n_{l'}} b_{n_l}b_{n_{l'}} \times\exp\{i\vec{Q}\cdot(-\vec{r}_{cn_l}+\vec{r}_{cn_{l'}})\}\rangle, \quad (4)$$

and further, with respect to the second term in Eq. 3, we assume that $\vec{r}_{cl\kappa}$, $\vec{r}_{cn_l}$, $\vec{r}_{cn\kappa}$ are all statistically independent. That is, the molecules belonging to different clusters are assumed to be orientationally-uncorrelated (assumption II). Then,

the second term in Eq. 3

$$= N_m^{-1}\Sigma^{-2}\sum_{\nu,\mu}\sum_{\alpha_\nu,\beta_\mu}\langle\sum_{l,\kappa}\exp(i\vec{Q}\cdot\vec{r}_{cl\kappa})\rangle \times\langle\sum_{n_l} b_{n_l}\exp(-i\vec{Q}\cdot\vec{r}_{cn_l})\rangle\langle\sum_{n_\kappa} b_{n_\kappa}\exp(i\vec{Q}\cdot\vec{r}_{cn_\kappa})\rangle - N_m^{-1}\Sigma^{-2}\sum_\nu N_\nu\sum_{l,l'}\langle\exp(i\vec{Q}\cdot\vec{r}_{cll'})\rangle \times\langle\sum_{n_l} b_{n_l}\exp(-i\vec{Q}\cdot\vec{r}_{cn_l})\rangle\langle\sum_{n_{l'}} b_{n_{l'}}\exp(i\vec{Q}\cdot\vec{r}_{cn_{l'}})\rangle. \quad (5)$$

From Eqs. 3—5, the $S_m(Q)$ for the liquid becomes

$$S_m(Q) = \sum_\nu\frac{x_\nu}{\nu}f^\nu(Q) + N_m^{-1}\Sigma^{-2}\sum_{\nu,\mu}\sum_{\alpha_\nu,\beta_\mu}\sum_{l,\kappa}\langle\exp(i\vec{Q}\cdot\vec{r}_{cl\kappa})\rangle \times\langle\sum_{n_l} b_{n_l}\exp(-i\vec{Q}\cdot\vec{r}_{cn_l})\rangle\langle\sum_{n_\kappa} b_{n_\kappa}\exp(i\vec{Q}\cdot\vec{r}_{cn_\kappa})\rangle, \quad (6)$$

where

$$f^{\nu}(Q) = \Sigma^{-2}[\langle \sum_{l,l'} \exp(i\vec{Q}\cdot\vec{r}_{cll'}) \sum_{n_l, n_{l'}} b_{n_l} b_{n_{l'}} \times \exp\{i\vec{Q}\cdot(-\vec{r}_{cn_l}+\vec{r}_{cn_{l'}})\}\rangle - \sum_{l,l'} \langle \exp(i\vec{Q}\cdot\vec{r}_{cll'})\rangle \langle \sum_{n_l} b_{n_l} \exp(-i\vec{Q}\cdot\vec{r}_{cn_l})\rangle \times \langle \sum_{n_{l'}} b_{n_{l'}} \exp(i\vec{Q}\cdot\vec{r}_{cn_{l'}})\rangle]_{\nu}. \quad (7)$$

In order to express the second term in Eq. 6 as a practically applicable form, we take the factor $\langle \sum_{n_l} b_{n_l} \exp(i\vec{Q}\cdot\vec{r}_{cn_l})\rangle$ to be independent of ν and replace it by the averaged value

$$\left\{\sum_{\nu} \frac{x_{\nu}}{\nu}\left[\sum_{l}[\sum_{n_l} b_{n_l}\langle \exp(i\vec{Q}\cdot\vec{r}_{cn_l})\rangle]^2\right]_{\nu}\right\}^{1/2}, \quad \text{(assumption III)}. \quad (8)$$

Thus, we obtain finally the formula for the $S_m(Q)$ in the form

$$S_m(Q) = \sum_{\nu} \frac{x_{\nu}}{\nu} f^{\nu}(Q) + S_c(Q)\cdot \bar{f}_{2U}(Q), \quad (9)$$

$$S_c(Q) = N_m^{-1}\langle \sum_{i,j} \exp(i\vec{Q}\cdot\vec{r}_{cij})\rangle = 1 + N_m^{-1}\langle \sum_{i\neq j} \exp(i\vec{Q}\cdot\vec{r}_{cij})\rangle, \quad (10)$$

$$\bar{f}_{2U}(Q) = \Sigma^{-2} \sum_{\nu} \frac{x_{\nu}}{\nu}\left[\sum_{l}[\sum_{n_l} b_{n_l}\langle \exp(i\vec{Q}\cdot\vec{r}_{cn_l})\rangle]^2\right]_{\nu}. \quad (11)$$

The Eqs. 7—11 are an extension of the formula Eqs. 7—11 in I, which are applicable to the liquid consisting of molecular clusters of various sizes including monomer molecules. For $x_{\mu}=1$ and $x_{\nu(\neq\mu)}=0$, Eq. 9 reproduces Eq. 7 in I.

Further, in order to elucidate the physical meaning of Eqs. 7—11, we rewrite Eq. 9 and obtain, separating the intramolecular contribution from the intermolecular one, in the form

$$S_m(Q) = \sum_{\nu} \frac{x_{\nu}}{\nu} f_1^{\nu}(Q) + \bar{f}_{2U}(Q)[S_c(Q)-1] + \sum_{\nu\geqq 2} \frac{x_{\nu}}{\nu} f_c^{\nu}(Q), \quad (12)$$

$$f_1^{\nu}(Q) = \Sigma^{-2}[\langle \sum_{l} |\sum_{n_l} b_{n_l} \exp(i\vec{Q}\cdot\vec{r}_{cn_l})|^2\rangle]_{\nu}, \quad (13)$$

and

$$f_c^{\nu}(Q) = \Sigma^{-2}[\langle \sum_{l\neq l'} \exp(i\vec{Q}\cdot\vec{r}_{cll'}) \sum_{n_l, n_{l'}} b_{n_l} b_{n_{l'}} \times \exp\{i\vec{Q}\cdot(-\vec{r}_{cn_l}+\vec{r}_{cn_{l'}})\rangle - \sum_{l\neq l'} \langle \exp(i\vec{Q}\cdot\vec{r}_{cll'})\rangle \langle \sum_{n_l} b_{n_l} \exp(-i\vec{Q}\cdot\vec{r}_{cn_l})\rangle \times \langle \sum_{n_{l'}} b_{n_{l'}} \exp(i\vec{Q}\cdot\vec{r}_{cn_{l'}})\rangle]_{\nu}, \quad (14)$$

where $f_1^{\nu}(Q)$ is the intramolecular contribution within the cluster composed of ν molecules. The first sum $\sum_{\nu}(x_{\nu}/\nu)f_1^{\nu}(Q)$ $(\equiv f_1(Q))$ is the overall averaged intramolecular contribution in the liquid. The Eqs. 12—14 are compared to Eqs. 176—179 in a text by Hansen and McDonald[7] (originally derived by Gubbins *et al.*[8,9]), though the latters are impractical except for very simple cases because of the difficulties arising from the calculation of higher order spherical harmonics expansions. The third term $\sum_{\nu}(x_{\nu}/\nu)f_c^{\nu}(Q)$ in Eq. 12 corresponds to the sum of the higher order expansion terms in Gubbins *et al.*'s formula.

In the expression of Eq. 9, it can be seen that for $Q\to 0$ $S_m(Q)\to S_c(Q)$ because $f^{\nu}(Q)\to 0$ and $\bar{f}_{2U}(Q)\to 1$. On the other hand, in the expression of Eq. 12, $S_m(Q)\to f_1(Q)$ when $Q\to\infty$ as is directly seen.

Structure Factor $S_m(Q)$ for the Pentamer–Monomer Mixture Model. From Eqs. 7—11, we can give here the formula of $S_m(Q)$ for the pentamer–monomer mixture model[10,11] for the later analysis of neutron diffraction data, where the form of the pentamer is such as shown in Fig. 3 of paper I. In this case, we put $x_1\neq 0$ and $x_5\neq 0$ (others=zero). Eq. 9 becomes

$$S_m(Q) = x_1 f^1(Q) + \frac{x_5}{5} f^5(Q) + \bar{f}_{2U}(Q) S_c(Q), \quad (15)$$

where the factors $f^1(Q)$ and $f^5(Q)$ are expressed by applying Eq. 7 for the case of $\nu=1$ and $\nu=5$, respectively, as

$$f^1(Q) = f_1^1(Q) - f_{2U}^1(Q) = f_1^1(Q) - \Sigma^{-2}[\sum_{n} b_n\langle \exp(i\vec{Q}\cdot\vec{r}_{cn})\rangle]^2_{\nu=1} \quad (16)$$

and

$$\frac{1}{5}f^5(Q) = S_m^p(Q) - f_{2U}^5(Q)[S_{m,p}^{(00)}(Q)+1] = S_m^p(Q) - \Sigma^{-2}\frac{1}{5}\sum_{l}^{5}[\sum_{n_l} b_{n_l}\langle \exp(i\vec{Q}\cdot\vec{r}_{cn_l})\rangle]^2_{\nu=5} \times [S_{m,p}^{(00)}(Q)+1]. \quad (17)$$

The factor $f_1^1(Q)$ is the intramolecular structure factor for monomer molecules and the two factors, $f_{2U}^1(Q)$ and $f_{2U}^5(Q)$, are the molecular form factor for monomers and pentamers, respectively, which are given in relation to the assumption II. $S_m^p(Q)$ is the intrapentamer structure factor (Eq. 13 in I) and $S_{m,p}^{(00)}(Q)$ the contribution from intra-pentamer O–O pairs only (Eq. 16 in I). For $x_5=1$ and $x_1=0$, Eq. 9 becomes Eq. 12 in I and for $x_1=1$ and $x_5=0$ we obtain a formula for the completely-uncorrelated orientation model proposed by Egelstaff, Page, and Powles.[12,13]

Eq. 12 becomes

$$S_m(Q) = x_1 f_1^1(Q) + \frac{x_5}{5} f_1^5(Q) + \bar{f}_{2U}(Q)[S_c(Q)-1] + \frac{x_5}{5} f_c^5(Q). \quad (18)$$

The first two terms in Eq. 18 are the averaged intramolecular structure factor for the pentamer–monomer mixture and are grouped as $f_1(Q)$ according to the definition described above,

$$x_1 f_1^1(Q) + \frac{x_5}{5} f_1^5(Q) = f_1(Q). \quad (19)$$

$f_1^5(Q)$ $(\equiv 5S_m^{(1)}(Q)$, Eq. 15 in I) in Eq. 18 is the intramolecular contribution within the pentamer and $f_c^5(Q)$ is obtained from Eq. 14 for the case of $\nu=5$ as

$$\frac{x_5}{5} f_c^5(Q) = x_5[S_m^p(Q) - \frac{1}{5}f_1^5(Q) - f_{2U}^5(Q) S_{m,p}^{(00)}(Q)]. \quad (20)$$

Interpretation of Experimental Data

Procedure of Calculation of the $S_m(Q)$ of Pentamer–Monomer Mixture Model. Now, we can determine the liquid structure of water at each temperature by making the calculated $S_m(Q)$ curve fit with the observed curve shown in Fig. 5. In the preceding study (paper I) it has turned out that the liquid structure of water at 15 °C can be regarded as an aggregate of the regular tetrahedral pentamers. This is the case $x_5=1$ and $x_1=0$ in Eqs. 15—17. At more elevated temperatures, a part of the pentamers is supposed to be destroyed. Then, we can use here Eqs. 15—17 for the calculation of the $S_m(Q)$ of the pentamer-monomer mixture model with due assignment of x_5 values as parameter.

In applying Eqs. 15—17, the structure of the pentamer is taken to be identical with that shown in Fig. 3 in I ($r_{OD}=0.98$ Å, $r_{DD}=1.60$ Å, and DOD angle= 109.5°) and the molecular structure of the monomer is that for the vapour ($r_{OD}=0.96$ Å, $r_{DD}=1.52$ Å, and DOD angle=104.5°).[1,2,14] For the molecular-centers structure factor of the liquid, $S_c(Q)$, the observed X-ray intensity data reported by Narten and Levy (25, 50, 75, and 100 °C)[15] were used, together with the data by Hajdu *et al.* (25 and 50 °C)[16] when required for comparison. Some appreciable differences are observed in these X-ray data, especially with respect to the first peak, and a discussion for the X-ray data will be made in the later section.

Figure 5 shows that a monotonous falling of the main peak at 2 Å^{-1} and the neighboring hump at *ca.* 4 Å^{-1} is produced by increasing temperature while the $S_m(Q)$ curves are quite unchanged in the range of $Q\gtrsim 6$ Å^{-1}. This latter fact is explained as: the $S_m(Q)$ in higher Q region is determined primarily by the intramolecular contribution only. The main interest in recent studies of liquid water has been, thus, concentrated upon the behaviors of the $S_m(Q)$ curves in the region of $Q\lesssim 6$ Å^{-1}.[1,13,17]

Determination of the Best Fit Model by Comparison of $S_m(Q)_{calcd}$ with $S_m(Q)_{obsd}$. We first determined the value of pentamer fraction x_5 by fitting the calculated $S_m(Q)$ curves with the experimental data. The calculated $S_m(Q)$ associated with the variation of x were compared with the observed neutron $S_m(Q)$ data at 25, 50, 70, and 95 °C, respectively, in Fig. 6. For the experimental data at 25 °C, the best fit $S_m(Q)$ curve was obtained in the case of $x_5=0.85$, at 50 °C $x_5=0.75$, at 70 °C $x_5=0.65$, and 95 °C $x_5=0.55$. The agreement of the calculated $S_m(Q)$ curves with the experimental ones is very excellent at all temperatures. Taking account of experimental errors, the deviations of x_5 are found to be ±0.05 for all cases. The x_5 values determined are shown in Fig. 7 including the result for the data at 15 °C reported in I.

Thus, the variation of the structure of liquid water with temperature is fundamentally explained by the pentamer-monomer mixture model with appropriate pentamer fractions according to Eqs. 15—17. It is concluded that liquid water is regarded as a mixture of regular tetrahedral pentamers and non-hydrogen-bonded monomers at 25—95 °C.

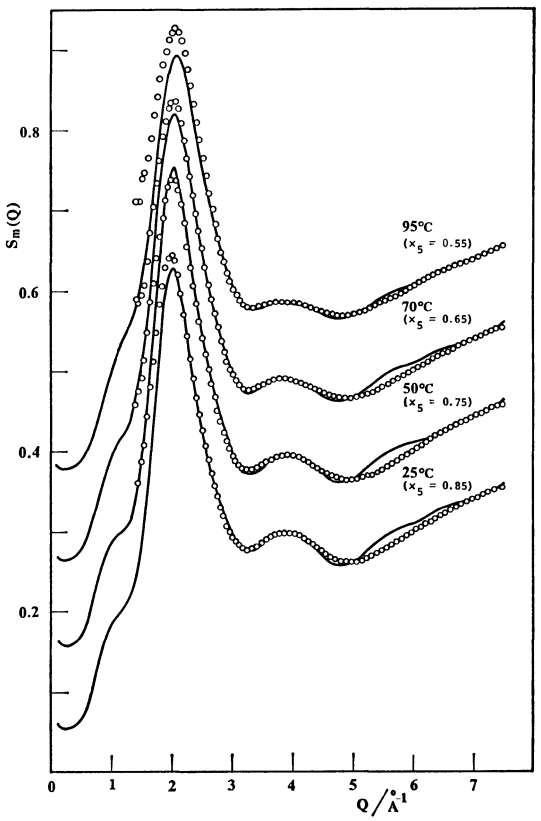

Fig. 6. The comparison between the calculated $S_m(Q)$ for the pentamer-monomer mixture model and the observed neutron structure factors $S_m(Q)$.
○: Observed, ——: calculated.

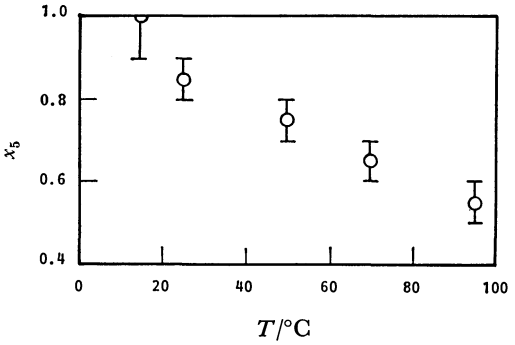

Fig. 7. Pentamer fraction x_5 determined by fitting the $S_m(Q)_{calcd}$ with the $S_m(Q)_{obsd}$ at each temperature. The vertical rod indicates the range of deviations of x_5.

Change of the Principal Peak at 2 Å^{-1} with Temperature. As seen in Table 1, when the temperature is raised, the intensity of the principal peak at *ca.* 2 Å^{-1} is found to decrease gradually, while the position of that to shift slightly to the higher Q-value side. Temperature dependence of the peak intensity and that of its position are shown in Figs. 8(a) and (b), respectively. The trend of the intensity change of the calculated result agrees with that of the experimental data, and the absolute intensity is in agreement with the measured one within the spread of the X-ray data used for $S_c(Q)$. With respect to the shift in the position

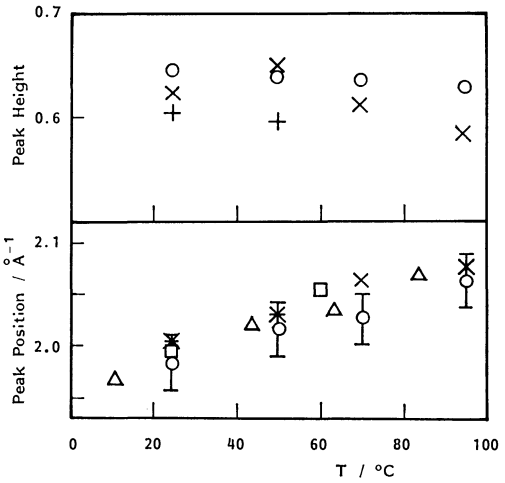

Fig. 8. The change of the intensity and the position of the principal peak at 2 Å^{-1} with the variation of temperature.
○: Observed by the authors, △: observed by Walford and Dore ($\lambda_0=1.13$ Å),[17] □: observed by Walford and Dore ($\lambda_0=0.84$ Å),[17] ×: calculated by the authors with the use of Narten and Levy's X-ray intensity data,[15] +: calculated by the authors with the use of Hajdu *et al.*'s X-ray intensity data.[16]

of the peak, the agreement between the calculated and observed results is very good as a whole within the experimental accuracy.

X-Ray Intensity Data. We used the observed X-ray intensity data mainly provided by Narten and Levy[15] for the calculation of $S_c(Q)$. The X-ray data are shown in Fig. 9, together with the data by Hajdu *et al.*[16] As clearly seen in Fig. 9, the two intensity data show some appreciable discrepancies certainly. However, with respect to the intensity and position of the principal peak of $S_m(Q)_{calcd}$, the influence of the discrepancies on the final $S_m(Q)$ for neutrons through the calculated values of $S_c(Q)$ is within the range of experimental errors: concerning the peak intensities of $S_m(Q)$, it is within the range of circles and concerning the positional shift, within the range of vertical rod (Fig. 8). It is certain that this discrepancies does not affect the conclusion of the present study, and we have used the data by Narten and Levy on the whole.

The values of $x_5[1+S^{(00)}_{m,p}(Q)]$ calculated are shown together in Fig. 9. The overall agreement of the values with the experimental data is fairly good except in the range of $Q \lesssim 2$ Å^{-1}, though the factor $x_5[1+S^{(00)}_{m,p}(Q)]$ is the intra-pentamer contribution only. This shows that it is a main contribution to total intensities in the case of X-rays. And, to see in details, the calculated curves are in better agreement with the data of Narten at various temperatures on the whole, except for the deviation in the first peak[1] and that in the range of $Q=4.5$—6 Å^{-1}. Thus, the X-ray data also is expected to support the essential effectiveness of the pentamer-monomer mixture model as a whole.

Discussion and Conclusions

Physical Meaning of the Ingredient of $S_m(Q)$. In the preceding sections we have shown that the pentamer–monomer mixture model with a due assignment of x_5 value is a best structure model in the interpretation of neutron diffraction data at 25—95 °C. Here, overall features of the temperature variation of $S_m(Q)_{calcd}$ for the model are shown in Fig. 10. It is clear in the figure that the intensities in the hump at *ca.* 4 Å^{-1} as well as those in the main peak at 2 Å^{-1} decrease gradually with increasing temperature.

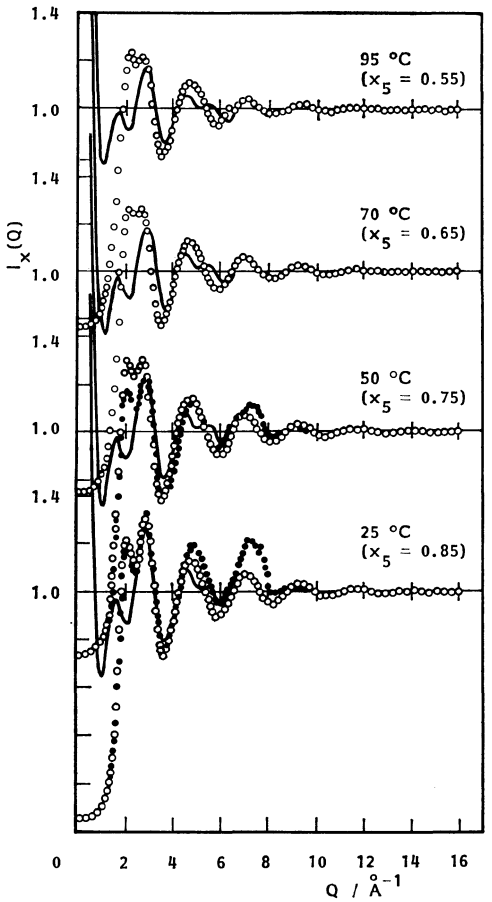

Fig. 9. The comparison between the calculated curves of $x_5[1+S^{(00)}_{m,p}(Q)]$ with the determined values of x_5 and the observed X-ray intensity data $I_x(Q)$.
○: Observed $I_x(Q)$ by Narten and Levy,[15] ●: observed $I_x(Q)$ by Hajdu *et al.*,[16] ——: $x_5[1+S^{(00)}_{m,p}(Q)]$.

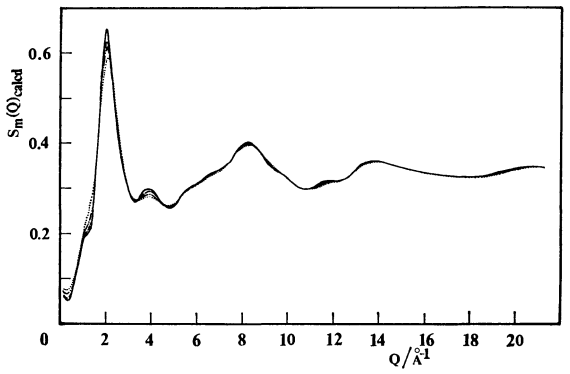

Fig. 10. Calculated $S_m(Q)$ for the pentamer–monomer mixture model.
——: $x_5=0.85$ (25 °C), - - -: $x_5=0.75$ (50 °C), —·—: $x_5=0.65$ (70 °C), ·····: $x_5=0.55$ (95 °C).

Table 1. The observed absolute neutron scattering factor $S_m(Q)$ as a function of scattering vector $Q/Å^{-1}$ for heavy water

$Q/Å^{-1}$	25 °C		50 °C		70 °C		95 °C	
	$2\theta=40°$	$2\theta=65°$	$2\theta=40°$	$2\theta=65°$	$2\theta=40°$	$2\theta=65°$	$2\theta=40°$	$2\theta=65°$
1.40	0.362		0.358		0.389		0.412	
1.45	0.361		0.374		0.386		0.411	
1.50	0.387		0.391		0.394		0.439	
1.55	0.407		0.413		0.407		0.448	
1.60	0.444		0.448		0.436		0.467	
1.65	0.479		0.485		0.472		0.490	
1.70	0.512		0.510		0.505		0.519	
1.75	0.548		0.542		0.533		0.542	
1.80	0.583		0.566		0.562		0.565	
1.85	0.607		0.590		0.592		0.582	
1.90	0.630		0.612		0.610		0.598	
1.95	0.642		0.629		0.629		0.614	
2.00	0.645		0.638		0.638		0.622	
2.05	0.638		0.637		0.636		0.627	
2.10	0.621		0.626		0.626		0.625	
2.15	0.597		0.608		0.608		0.613	
2.20	0.570		0.585		0.587		0.598	
2.25	0.544		0.557		0.565		0.576	
2.30	0.515		0.530		0.542		0.555	
2.35	0.490		0.507		0.519		0.533	
2.40	0.467		0.484		0.497		0.510	
2.45	0.446		0.462		0.475		0.488	
2.50	0.426	0.454	0.442	0.461	0.453	0.478	0.466	0.492
2.55	0.407	0.431	0.422	0.428	0.430	0.454	0.444	0.467
2.60	0.390	0.411	0.402	0.402	0.409	0.431	0.421	0.442
2.65	0.373	0.389	0.384	0.386	0.390	0.409	0.402	0.417
2.70	0.358	0.377	0.366	0.373	0.371	0.395	0.384	0.405
2.75	0.344	0.363	0.351	0.360	0.354	0.375	0.366	0.387
2.80	0.330	0.348	0.336	0.344	0.337	0.358	0.349	0.367
2.85	0.319	0.331	0.323	0.331	0.323	0.334	0.335	0.347
2.90	0.308	0.312	0.312	0.315	0.311	0.316	0.322	0.328
2.95	0.300	0.299	0.303	0.305	0.301	0.301	0.311	0.311
3.00	0.293	0.287	0.294	0.295	0.295	0.291	0.303	0.296
3.05	0.287	0.282	0.288	0.284	0.288	0.284	0.295	0.287
3.10	0.284	0.280	0.283	0.279	0.283	0.280	0.289	0.283
3.15	0.280	0.277	0.280	0.275	0.279	0.277	0.284	0.277
3.20	0.278	0.277	0.278	0.273	0.276	0.276	0.281	0.275
3.25	0.278	0.278	0.277	0.274	0.275	0.277	0.280	0.273
3.30	0.279	0.279	0.277	0.278	0.275	0.278	0.280	0.272
3.35	0.282	0.282	0.278	0.281	0.277	0.280	0.280	0.272
3.40	0.284	0.283	0.278	0.284	0.278	0.281	0.281	0.272
3.45	0.286	0.287	0.282	0.287	0.281	0.283	0.282	0.272
3.50	0.288	0.291	0.284	0.289	0.283	0.286	0.283	0.276
3.55	0.291	0.293	0.285	0.291	0.284	0.288	0.284	0.277
3.60	0.292	0.295	0.287	0.292	0.285	0.290	0.285	0.277
3.65	0.293	0.294	0.289	0.293	0.287	0.291	0.285	0.278
3.70	0.295	0.295	0.291	0.294	0.289	0.290	0.286	0.279
3.75	0.296	0.296	0.292	0.295	0.290	0.290	0.286	0.279
3.80	0.296	0.297	0.293	0.296	0.289	0.290	0.286	0.279
3.85	0.297	0.299	0.283	0.296	0.290	0.290	0.287	0.279
3.90	0.297	0.299	0.293	0.296	0.289	0.290	0.287	0.280
3.95	0.297	0.298	0.294	0.295	0.289	0.288	0.286	0.280
4.00	0.297	0.298	0.294	0.294	0.287	0.287	0.286	0.280
4.05	0.296	0.297	0.293	0.292	0.286	0.286	0.285	0.281
4.10	0.295	0.296	0.292	0.291	0.285	0.284	0.284	0.281
4.15	0.293	0.295	0.290	0.288	0.283	0.284	0.283	0.281
4.20	0.290	0.293	0.288	0.287	0.281	0.282	0.282	0.280
4.25	0.288	0.290	0.285	0.284	0.280	0.279	0.281	0.280
4.30	0.286	0.288	0.283	0.281	0.278	0.279	0.278	0.276
4.35	0.284	0.285	0.281	0.278	0.277	0.276	0.278	0.276
4.40	0.281	0.282	0.279	0.276	0.276	0.274	0.277	0.274
4.45	0.278	0.278	0.276	0.273	0.274	0.272	0.275	0.274
4.50	0.275	0.274	0.274	0.271	0.272	0.270	0.274	0.272
4.55	0.273	0.271	0.272	0.268	0.270	0.268	0.274	0.271
4.60	0.270	0.268	0.271	0.266	0.269	0.266	0.273	0.270
4.65	0.268	0.267	0.269	0.263	0.268	0.265	0.271	0.269
4.70	0.266	0.265	0.268	0.262	0.267	0.264	0.270	0.268
4.75	0.265	0.263	0.267	0.260	0.266	0.263	0.270	0.267
4.80	0.263	0.262	0.267	0.260	0.266	0.263	0.270	0.267
4.85	0.262	0.260	0.266	0.259	0.265	0.263	0.269	0.266
4.90	0.262	0.260	0.265	0.259	0.265	0.264	0.270	0.265
4.95	0.263	0.259	0.264	0.259	0.265	0.264	0.270	0.265
5.00	0.263	0.260	0.264	0.259	0.266	0.264	0.271	0.264
5.10	0.263	0.262	0.265	0.261	0.266	0.266	0.273	0.265
5.20	0.265	0.265	0.268	0.264	0.269	0.268	0.275	0.267
5.30	0.289	0.265	0.271	0.266	0.271	0.270	0.279	0.269
5.40	0.272	0.270	0.274	0.271	0.274	0.274	0.282	0.273
5.50	0.276	0.276	0.278	0.276	0.278	0.280	0.285	0.277
5.60	0.281	0.281	0.283	0.281	0.282	0.284	0.289	0.281
5.70	0.286	0.287	0.287	0.286	0.286	0.289	0.293	0.286
5.80	0.290	0.292	0.291	0.290	0.290	0.294	0.297	0.291
5.90	0.295	0.297	0.295	0.295	0.295	0.299	0.302	0.297
6.00	0.300	0.301	0.300	0.300	0.300	0.303	0.306	0.302
6.10	0.304	0.305	0.304	0.305	0.303	0.307	0.310	0.307
6.20	0.309	0.309	0.309	0.309	0.308	0.311	0.313	0.312
6.30	0.314	0.312	0.313	0.314	0.313	0.314	0.318	0.316
6.40	0.318	0.316	0.318	0.317	0.318	0.322	0.322	0.321
6.50	0.322	0.320	0.322	0.322	0.321	0.322	0.326	0.325
6.60	0.325	0.323	0.326	0.325	0.324	0.325	0.329	0.330
6.70	0.330	0.326	0.330	0.328	0.328	0.328	0.333	0.334
6.80	0.334	0.329	0.334	0.331	0.331	0.331	0.336	0.337
6.90	0.337	0.332	0.338	0.335	0.335	0.333	0.339	0.340
7.00	0.341	0.336	0.342	0.338	0.339	0.337	0.342	0.344
7.10	0.344	0.339	0.346	0.340	0.342	0.339	0.344	0.346
7.20	0.347	0.342	0.349	0.342	0.345	0.342	0.347	0.348
7.30	0.350	0.345	0.352	0.345	0.348	0.344	0.351	0.351
7.40	0.353	0.348	0.355	0.346	0.351	0.357	0.353	0.353
7.50	0.355	0.351	0.357	0.349	0.354	0.349	0.356	0.355
7.60	0.358	0.353	0.360	0.351	0.356	0.351	0.358	0.358
7.70	0.360	0.354	0.362	0.353	0.358	0.353	0.360	0.359
7.80	0.361	0.357	0.364	0.354	0.359	0.354	0.361	0.361
7.90	0.361	0.359	0.366	0.356	0.361	0.355	0.362	0.362
8.00	0.362	0.360	0.367	0.357	0.362	0.357	0.363	0.363
8.10	0.362	0.361	0.368	0.358	0.362	0.358	0.363	0.363
8.20	0.362	0.362	0.369	0.359	0.363	0.356	0.363	0.363
8.30	0.362	0.362	0.369	0.359	0.363	0.358	0.363	0.363
8.40	0.361	0.361	0.368	0.359	0.362	0.358	0.362	0.362
8.50	0.360	0.360	0.367	0.359	0.361	0.358	0.361	0.362
8.60	0.359	0.360	0.366	0.359	0.359	0.357	0.360	0.360
8.70	0.357	0.358	0.364	0.359	0.358	0.356	0.358	0.360
8.80	0.355	0.357	0.363	0.358	0.356	0.355	0.355	0.358
8.90	0.354	0.355	0.361	0.357	0.355	0.353	0.353	0.357
9.00	0.352	0.353	0.359	0.355	0.353	0.352	0.351	0.356
9.10	0.350	0.350	0.356	0.353	0.351	0.350	0.348	0.355
9.20	0.348	0.347	0.354	0.351	0.349	0.348	0.346	0.353
9.30	0.346	0.345	0.352	0.348	0.346	0.345	0.344	0.350
9.40	0.344	0.342	0.350	0.345	0.344	0.342	0.342	0.347
9.50	0.342	0.339	0.348	0.342	0.339	0.339	0.340	0.344
9.60	0.340	0.336	0.345	0.339	0.340	0.336	0.338	0.341
9.70	0.338	0.334	0.343	0.337	0.338	0.333	0.335	0.338
9.80	0.336	0.331	0.341	0.335	0.335	0.330	0.333	0.336
9.90	0.333	0.329	0.340	0.333	0.333	0.328	0.332	0.334
10.00	0.331	0.326	0.337	0.330	0.331	0.325	0.330	0.331
10.10	0.330	0.323	0.335	0.327	0.328	0.322	0.328	0.329
10.20	0.328	0.321	0.333	0.325	0.326	0.320	0.326	0.327
10.30	0.326	0.319	0.331	0.323	0.324	0.318	0.324	0.325
10.40	0.324	0.317	0.328	0.321	0.322	0.317	0.322	0.324
10.50	0.321	0.315	0.325	0.319	0.319	0.316	0.319	0.315

In order to elucidate further the physical meaning of temperature dependence of the structure factor $S_m(Q)$, we examine ingredients of the $S_m(Q)$, by considering the terms in Eq. 18. As clearly seen in Fig. 11, the first peak is mainly composed of the sum of the curve (a)$\equiv f_1(Q)$ and the curve (c)$\equiv \bar{f}_{2U}(Q)[S_c(Q)-1]$, expressing the averaged separation between two adjacent centers of water molecules to be about 3 Å, and, on the other hand, the hump at *ca.* 4 $Å^{-1}$ is originated from the curve (b)$\equiv (x_5/5)f_c^5(Q)$, which is ascribed to the presence of the tetrahedral pentamer. The sum of curves (a) and (c) ($\equiv f_1(Q)+\bar{f}_{2U}(Q)[S_c(Q)-1]$) corresponds to the $S_m(Q)$ for completely-uncorrelated (at molecular level) orientation model, as described by Egelstaff, Page and Powles.[12,13] Hence, it is stated that the contribution of curve (b) (Eq. 20) originated from the presence of the tetrahedral pentamers forms the essential character of the liquid structure of water, producing the hump at *ca.* 4 $Å^{-1}$ in the $S_m(Q)$ curves.

Concluding Remarks. Neutron structure factors $S_m(Q)$ of D_2O were determined at 25, 50, 70, and 95 °C. The diffraction data were analyzed by using a general expression of $S_m(Q)$ derived from a new

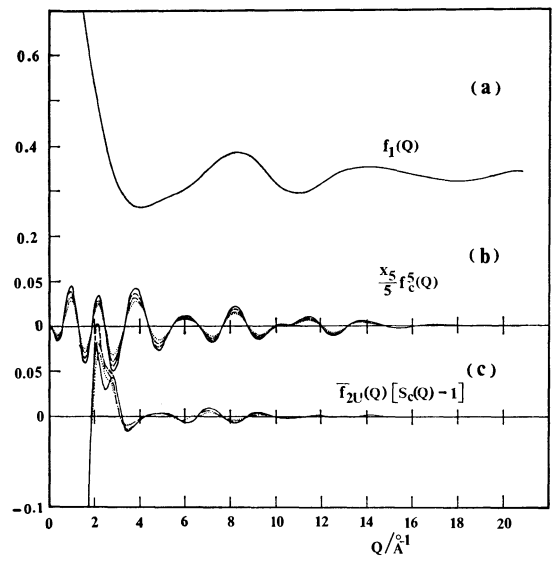

Fig. 11. Contributions of (a) $f_1(Q)$ (Eq. 19), (b) $\frac{x_5}{5}f_c^5(Q)$ (Eq. 20), and (c) $\bar{f}_{2U}(Q)[S_c(Q)-1]$ to the $S_m(Q)_{calcd}$ (Eq. 18).
——: $x_5=0.85$, - - -: $x_5=0.75$, —·—: $x_5=0.65$, ……: $x_5=0.55$.

theoretical procedure of analysis which is generally applicable to the fluid system composed of molecular clusters with various sizes. The following conclusions were obtained:

1) The pentamer–monomer mixture model with the due value of pentamer fraction x_5 assigned is the best one as a fundamental structure model of water at temperatures, 25—95 °C, for the explanation of diffraction data.

2) The x_5 values determined by fitting the $S_m(Q)_{calcd}$ with the $S_m(Q)_{obsd}$ at each temperature are $x_5=0.85\pm0.05$ at 25 °C, $x_5=0.75\pm0.05$ at 50 °C, $x_5=0.65\pm0.05$ at 70 °C, and $x_5=0.55\pm0.05$ at 95 °C, respectively.

3) The decrease of x_5 with temperature rise indicates the destruction of pentamers expected at elevated temperatures and the effect of the destruction appears mainly as the gradual decrease of intensities in the first peak at 2 Å^{-1} and the hump at *ca.* 4 Å^{-1} in the neutron structure factor curves.

4) The hump at *ca.* 4 Å^{-1} in the $S_m(Q)$ curves is originated from the presence of the tetrahedral pentamers forming the essential character of the liquid structure of water.

References

1) N. Ohtomo, K. Tokiwano, and K. Arakawa, *Bull. Chem. Soc. Jpn.*, **54**, 1802 (1981).
2) N. Ohtomo and K. Arakawa, *Bull. Chem. Soc. Jpn.*, **51**, 1649 (1978).
3) N. Ohtomo and K. Arakawa, *Bull. Chem. Soc. Jpn.*, **53**, 1510 (1980).
4) N. Ohtomo, K. Arakawa, M. Takeuchi, T. Yamaguchi, and H. Ohtaki, *Bull. Chem. Soc. Jpn.*, **54**, 1314 (1981).
5) J. G. Powles, *Mol. Phys.*, **26**, 1325 (1973): **36**, 1181 (1978).
6) J. G. Powles, *Mol. Phys.*, **42**, 757 (1981).
7) J. P. Hansen and I. R. McDonald, "Theory of Simple Liquids," Academic Press, London (1976), Chap. 5.
8) K. E. Gubbins, C. G. Gray, P. A. Egelstaff, and M. S. Ananth, *Mol. Phys.*, **25**, 1353 (1973).
9) J. J. Weis and D. Levesque, *Phys. Rev. A*, **13**, 450 (1976).
10) K. Arakawa, K. Tokiwano, and K. Kojima, *Bull. Chem. Soc. Jpn.*, **50**, 65 (1977).
11) K. Arakawa, "Water and Metal Cations in Biological System," ed by B. Pullman and K. Yagi, Japan Scientific Societies Press, Tokyo (1980), pp. 13—29.
12) P. A. Egelstaff, D. I. Page, and J. G. Powles, *Mol. Phys.*, **20**, 881 (1971).
13) D. I. Page and J. G. Powles, *Mol. Phys.*, **21**, 901 (1971).
14) With respect to the assignment of Debye-Waller factors, the magnitude of mean-square variation $2\gamma_{nn'}$ is estimated to be 0.06 Å per 1 Å of interatomic distance $r_{nn'}$, assuming $\gamma_{nn'} \propto r_{nn'}$, throughout all the present calculations.[2])
15) A. H. Narten and H. A. Levy, *J. Chem. Phys.*, **55**, 2263 (1971).
16) F. Hajdu, S. Lengyel, and G. Pálinkás, *J. Appl. Cryst.*, **9**, 134 (1976).
17) G. Walford and J. C. Dore, *Mol. Phys.*, **34**, 21 (1977): In this work, they have reported neutron diffraction data for heavy water at temperatures, 11—79 °C, in which the same trend as seen in our present data has been observed. However, their data are unreliable for its experimental inaccuracy because "it was discovered that the incident beam was contaminated by a contribution from 2.26 Å neutrons (arising from second-order reflections in the monochrometor) which was estimated to be 28 per cent" as they stated in their article.

One-photon and Two-photon Electronic Spectra of Two Caged Amines

Narishi GONOHE, Norio YATSUDA, Naohiko MIKAMI, and Mitsuo ITO*

Department of Chemistry, Faculty of Science, Tohoku University, Sendai, 980

(Received March 1, 1982)

The one-photon fluorescence excitation and two-photon resonant multiphoton ionization spectra of the $S_1 \leftarrow S_0$ transition of 1,4-diazabicyclo[2.2.2]octane (DABCO) in a supersonic free jet have been obtained and analyzed. It was found from the vibrational analysis that the $S_1 \leftarrow S_0$ transition is one-photon forbidden, two-photon allowed and the one-photon absorption appears by the vibronic interaction between the S_1 and S_2 states through the e′ vibrations. In addition, from the fluorescence spectrum and the polarization studies of the two-photon spectrum using the two linearly polarized laser beams of different wavelengths, it was concluded that the S_1 state is $^1A_1'$. The sequence structure involving the low-frequency cage torsional vibration has been observed in the two-photon resonant multiphoton ionization spectra of DABCO and 1-azabicyclo[2.2.2]octane (ABCO). The potential functions with respect to the torsional motion for both ground and excited states have been determined by utilizing the observed vibrational levels. It was found that the torsional potential has a broad minimum near the D_{3h} (for DABCO) and C_{3v} (for ABCO) conformations.

The electronic spectra of 1,4-diazabicyclo[2.2.2]octane (DABCO) and 1-azabicyclo[2.2.2]octane (ABCO) (Fig. 1) have been studied by many workers[1–6] with special interest in their cage structures. The spectra of these molecules with the rigid structure generally show a well-resolved vibrational structure compared with the broad and structureless spectra of non-rigid saturated amines such as trimethylamine and triethylamine. However, the one-photon absorption spectra of DABCO and ABCO due to the $S_1 \leftarrow S_0$ transition (280—260 nm for DABCO and 250—230 nm for ABCO) are still broad and show only a faint vibrational structure. Recently, Parker and Avouris[7] have observed the corresponding two-photon absorption spectra by means of fluorescence excitation (FE) and multiphoton ionization (MPI) techniques and found a rich vibronic structure. They concluded from their laser polarization studies that the S_1 state is a totally symmetric Rydberg state which is one-photon forbidden and two-photon allowed in the transition from the S_0 state. The two-photon absorption spectrum of DABCO is characteristic of extensive sequence bands involving the low-frequency torsional vibration in which the two N pyramids are twisted in the opposite sense about the C_3 symmetry axis. Although the potential of the torsional motion has been discussed by several workers[8–10] for DABCO, no conclusive result is obtained yet. The corresponding potential for ABCO has never been studied.

In the present paper, we report the one-photon fluorescence excitation spectra and the two-photon resonant multiphoton ionization spectra of the $S_1 \leftarrow S_0$ transition of DABCO seeded in a supersonic free jet. On account of temperature cooling effect through the free expansion, most of the hot bands in the room temperature spectrum disappeared and a well resolved vibrational structure showed up. Vibrational analysis of the one-photon and two-photon absorption spectra thus obtained and the $S_1 \leftarrow S_0$ fluorescence spectrum as well as the laser polarization studies of the two-photon absorption spectrum led us to a definite assignment of the S_1 state of DABCO. The torsional potential was also obtained for both S_0 and S_1 states of DABCO and ABCO from the two-photon resonant multiphoton ionization spectra of the vapor and the supersonic free jets.

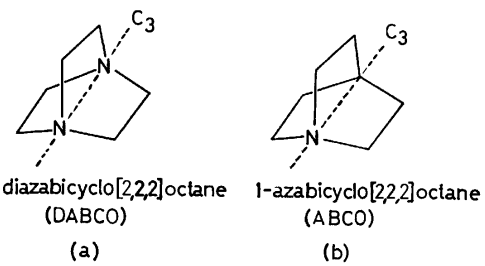

1,4-diazabicyclo[2,2,2]octane (DABCO) (a)

1-azabicyclo[2,2,2]octane (ABCO) (b)

Fig. 1. Structures of (a) 1,4-diazabicyclo[2.2.2]octane (DABCO) and (b) 1-azabicyclo[2.2.2]octane (ABCO).

Experimental

The experimental setup for measurements of the FE and MPI spectra of a supersonic free jet was already described elsewhere.[11,12] A Molectron scanning dye laser (DL-14) pumped by a nitrogen laser (UV-22) was used as an exciting light source for measurements of the two-photon resonant MPI spectrum and the second harmonic of the dye laser for the one-photon resonant FE spectrum. The FWHM of the dye laser light was about 0.5 cm^{-1}. Coumarin 540 (Exciton) was used to cover the spectral region of the $S_1 \leftarrow S_0$ transition. The MPI spectra of the vapor at room temperature were measured with a metal gas cell equipped with windows and a pair of electrodes instead of the supersonic jet cell. The fluorescence spectrum of DABCO vapor at room temperature excited by the frequency-doubled dye laser was obtained with a Nikon grating monochromator having reciprocal dispersion of 3 nm/mm in the second order and recorded by photon counting method. The fluorescence decay was also measured by the use of a boxcar integrator (Brookdeal 9415).

In polarization studies of the two-photon resonant MPI spectrum of DABCO at room temperature, two linearly polarized laser beams of different wavelengths were used; the second harmonic of the Nd:YAG laser (Quanta-Ray) and dye laser pumped by the same second harmonic. The laser beam was depolarized by passing through a polarization scrambler and then the linear polarization was achieved by a polaroid sheet. The two linearly polarized light beams thus obtained were focussed from opposit directions into the center of the metal gas cell described above. The ions produced by MPI process were detected by biassed parallel electrodes equipped inside the cell. In order to avoid the MPI process by the single beam, the laser power was sup-

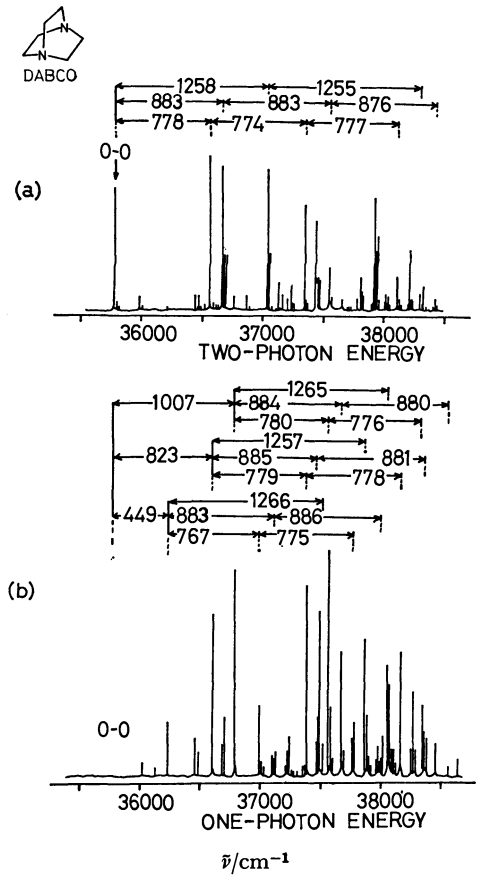

Fig. 2. (a) Two-photon resonant MPI and (b) one-photon fluorescence excitation spectra of the $S_1 \leftarrow S_0$ transition of DABCO in a supersonic free jet. The spectra are corrected for laser intensity variation.

pressed to such an extent that the ions are not produced by the signle beam.

The samples used were obtained from Tokyo-kasei Co. Ltd. DABCO was sublimed several times in vacuum. ABCO was prepared from its hydrochloride and purified by sublimation in vacuum.

Results and Discussion

One-photon and Two-photon Absorption Spectra of DABCO in a Supersonic Free Jet. The two-photon resonant MPI spectrum of DABCO in a supersonic free jet of He carrier gas at 2.5 atm. is shown in Fig. 2a. First ionization potential of DABCO is 7.2 eV. Therefore, using the dye laser in the visible region (≈540 nm), four photons are necessary to excite the molecule into the ionization continuum. Since the S_1 state of DABCO is located at around 270 nm, the spectrum shown in Fig. 2a is due to two-photon resonant four-photon ionization process. It is seen from the figure that the spectrum exhibits a well-resolved vibrational structure. Comparing with the two-photon spectrum of the vapor at room temperature reported by Parker and Avouris,[7] the individual vibronic bands become extremely sharp (with FWHM of 4 cm^{-1}) and most of the vibrational hot bands are swept out in the supersonic jet spectrum, indicating very low rotational and vibrational temperatures of the jet. The observed main vibronic bands are listed in Table 1 together

Table 1. Vibrational assignments of the main bands in the two-photon resonant MPI spectrum for the $S_1 \leftarrow S_0$ transition of DABCO in a supersonic free jet

$\tilde{\nu}$ / cm^{-1}	$\Delta\tilde{\nu}$ / cm^{-1} a)	Intensity	Analysis	Assignment
35783	0	vs		0-0
36561	778	vs	0+778	ν_3' b)
36666	883	vs	0+883	ν_2' b)
36672	889	m	0+889	ν_α' c)
36685	902	m	0+902	ν_β' c)
37041	1258	vs	0+1258	ν_1' b)
37052	1269	m	0+1269	ν_γ' c)
37335	1552	s	0+778×2=1556	$2\nu_3'$
37439	1656	s-m	0+778+883=1661	$\nu_3'+\nu_2'$
37447	1664	m-w	0+889+778=1667	$\nu_\alpha'+\nu_3'$
37459	1676	m-w	0+902+778=1680	$\nu_\beta'+\nu_3'$
37549	1766	m-w	0+883×2=1766	$2\nu_2'$
37553	1770	w(sh)	0+889+883=1772	$\nu_\alpha'+\nu_2'$
37567	1784	w	0+902+883=1785	$\nu_\beta'+\nu_2'$
37822	2039	m-w	0+778+1258=2036	$\nu_3'+\nu_1'$
37830	2047	w	0+1269+778=2047	$\nu_\gamma'+\nu_3'$
37921	2138	s	0+883+1258=2141	$\nu_2'+\nu_1'$
37927	2144	m(sh)	0+889+1258=2147	$\nu_\alpha'+\nu_1'$
37932	2149	m	0+1269+883=2152	$\nu_\gamma'+\nu_2'$
37943	2160	m-w	0+902+1258=2160	$\nu_\beta'+\nu_1'$
38112	2329	w	0+778×3=2334	$3\nu_3'$
38215	2432	m	0+778×2+883=2439	$2\nu_3'+\nu_2'$
38222	2439	w	0+889+2×778=2445	$\nu_\alpha'+2\nu_3'$
38238	2455	w	0+902+2×778=2458	$\nu_\beta'+2\nu_3'$
38296	2513	w	0+1258×2=2516	$2\nu_1'$
38312	2529	w	0+1269+1258=2527	$\nu_\gamma'+\nu_1'$
38322	2539	w	0+778+2×883=2544	$\nu_3'+2\nu_2'$
38425	2642	w	0+883×3=2649	$3\nu_2'$

a) Frequency difference from the 0-0 transition at 35783 cm^{-1}. b) We follow the notations given in Ref. 7. c) We tentatively designate these vibrations as ν_α' (889 cm^{-1}), ν_β'(902 cm^{-1}), and ν_γ'(1269 cm^{-1}), respectively.

with their assignments. The overall spectral pattern is rather simple. The longest wavelength band at 35783 cm^{-1} [13] is readily assigned to the 0-0 band and most of other intense bands are interpreted as the vibronic bands involving the fundamentals, overtones and combinations of three excited-state totally symmetric vibrations of 778, 883, and 1258 cm^{-1}.

The one-photon absorption spectrum of the same $S_1 \leftarrow S_0$ transition of DABCO in a supersonic free jet is shown in Fig. 2b, which was taken by FE method. In contrast with the broad spectrum in vapor at room temperature, the supersonic jet spectrum exhibits a well-resolved vibrational structure. The vibrational structure is similar to that of the two-photon absorption spectrum with respect to repeated appearance of the excited-state vibrations of 778, 883, and 1258 cm^{-1}. A great difference between the two spectra is that the 0-0 band at 35783 cm^{-1} appearing strongly in the two-photon spectrum is completely missing in the one-photon spectrum. Moreover, in the one-photon spectrum, the progressions and combinations of

Table 2. Vibrational assignment of the main bands in the one-photon fluorescence excitation spfctrum for the $S_1 \leftarrow S_0$ transition of DABCO in a supersonic free jet

$\tilde{\nu}$ / cm^{-1}	$\Delta\tilde{\nu}$ / cm^{-1} a)	Intensity	Analysis	Assignment
(35783)				0-0
36232	449	w-m	0+449	$\nu'_{27}(e')$ b)
36606	823	s	0+823	$\nu'_{26}(e')$ b)
36704	921	w-m	0+921	ν'_{ω} c)
36792	1007	vs	0+1007	$\nu'_{20}(e')$ b)
37000	1217	m	0+449+778=1227	$\nu'_{27}+\nu'_3$
37116	1333	w	0+449+883=1332	$\nu'_{27}+\nu'_2$
37388	1605	vs	0+823+778=1601	$\nu'_{26}+\nu'_3$
37482	1699	w	0+921+778=1699	$\nu'_{\omega}+\nu'_3$
37492	1709	s	0+823+883=1706	$\nu'_{26}+\nu'_2$
37498	1715	w	0+449+1258=1707	$\nu'_{27}+\nu'_1$
37573	1790	vs	0+1007+778=1785	$\nu'_{20}+\nu'_3$
37584	1801	w-m	0+921+883=1804	$\nu'_{\omega}+\nu'_2$
37674	1892	m	0+1007+883=1890	$\nu'_{20}+\nu'_2$
37774	1991	w	0+449+778×2=2005	$\nu'_{27}+2\nu'_3$
37867	2084	m-s	0+823+1258=2081	$\nu'_{26}+\nu'_1$
37962	2179	w	0+921+1258=2179	$\nu'_{\omega}+\nu'_1$
38001	2218	w	0+449+883×2=2215	$\nu'_{27}+2\nu'_2$
38049	2266	m	0+1007+1258=2265	$\nu'_{20}+\nu'_1$
38159	2376	m	0+823+778×2=2379	$\nu'_{26}+2\nu'_3$
38261	2478	m	0+921+778×2=2477	$\nu'_{\omega}+2\nu'_3$
38349	2566	m	0+1007+778×2=2563	$\nu'_{20}+2\nu'_3$
38374	2591	w	0+823+883×2=2589	$\nu'_{26}+2\nu'_2$
38556	2773	w	0+1007+883×2=2773	$\nu'_{20}+2\nu'_2$

a) Frequency difference from the 0-0 transition at 35783 cm^{-1} (which is observed in the two-photon spectrum). b) The assignments of these vibrations were carried out on the basis of the fluorescence spectrum in Fig. 3. The numbering of the vibbration is in accord with that in Ref. 15. c) The assignment of this vibration is not established yet. We designate this vibration as ν'_{ω}.

the totally symmetric vibrations start from the bands at 36232, 36606, and 36792 cm^{-1}, which act as false origins of the spectrum. The detailed vibrational analysis is listed in Table 2.

The vibrational structures of the one-photon and two-photon spectra mentioned above are typical for one-photon forbidden and two-photon allowed transition. It is concluded, therefore, that the S_1 state of DABCO should be of either A'_1 or E'' symmetry from the optical selection rule for D_{3h} point group. Based on this conclusion, the frequency differences between the 0-0 band and the three false origins of the one-photon spectrum (449, 823, and 1007 cm^{-1}) must represent some non-totally symmetric vibrations in the excited state which make the one-photon forbidden transition allowed by vibronic coupling. Determination of the symmetry species of these excited state vibrations will lead to unambiguous assignment of the S_1 state. With this aim in mind, we measured the fluorescence spectrum of DABCO in vapor, which will be described in the next section.

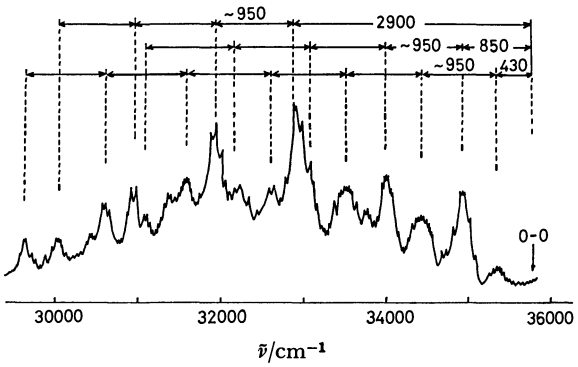

Fig. 3. Fluorescence spectrum of DABCO vapor at room temperature.

Fluorescence Spectrum of DABCO. The fluorescence spectrum of DABCO vapor was excited by frequency-doubled dye laser light at 271.7 nm, which coincides with the strongest band at 36792 cm^{-1} of the one-photon absorption spectrum. In order to obtain the fluorescence spectrum originating from the vibrationless level of the S_1 state, 2-methylbutane vapor (≈5300 Pa) was added to DABCO vapor to accelerate vibrational relaxation. The fluorescence spectrum thus obtained is shown in Fig. 3. The effective vibrational relaxation is proved by absence of band in the region of shorter wavelength than 0-0 band position.

As is seen from the figure, the 0-0 band does not appear as in the case of the one-photon absorption spectrum. There are long progressions of 950 cm^{-1} starting from 0—430, 0—850, and 0—2900 cm^{-1} bands.[14] Assignments of the ground state vibrations of DABCO are fairly well established from the IR and Raman studies.[9,15,16] According to their assignments, the ground-state frequencies of 430, 850, and 2900 cm^{-1} may be identified as $\nu_{27}(e')$, NC_3 deformation mode), $\nu_{26}(e')$, NC_3 stretching mode), and $\nu_{20}(e')$, C–H stretching mode), respectively. The frequency of 950 cm^{-1} should be a totally symmetric vibration and assigned to $\nu_4(a'_1)$ of a cage squashing mode in which the two N pyramids move along the C_3 axis in the opposite directions. The corresponding excited-state vibrational frequency is 882 cm^{-1}. Thus, the bands at 0—430, 0—850, and 0—2900 cm^{-1} are assigned as the false origins involving the ground-state e′ vibrations. The vibrations of 430 and 850 cm^{-1} correspond to the excited-state vibrations of 449 and 823 cm^{-1}, respectively, which make the false origins in the one-photon absorption spectrum. The excited-state vibration corresponding to the $\nu_{20}(e')$ of 2900 cm^{-1} is hard to find in the one-photon absorption spectrum. Remained excited-state vibration forming the false origin in the absorption spectrum is of 1007 cm^{-1}. This suggests that the 1007 cm^{-1} vibration corresponds to the ground-state vibration of 2900 cm^{-1}. If it would be the case, a drastic frequency decrease should occur for $\nu_{20}(e')$ in the transition from the ground state to the excited state.

It is established from the above results that the perturbing vibrations of the one-photon forbidden $S_1 \leftarrow S_0$ transition are of e′ symmetry. Taking into account the results obtained in a previous section, this leads

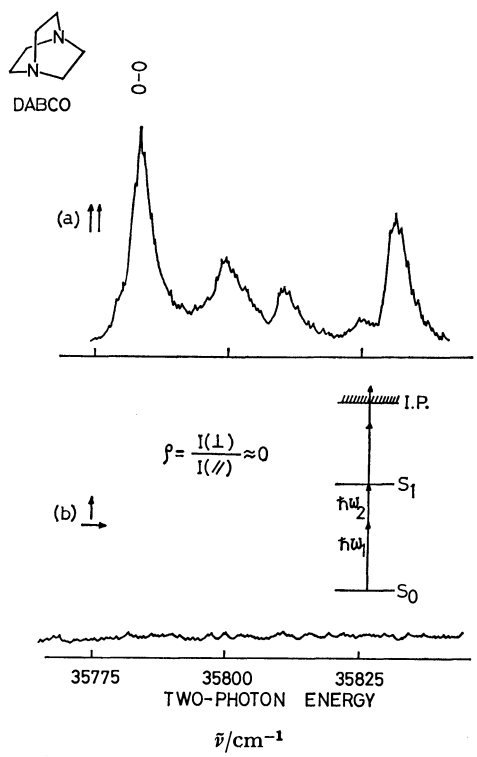

Fig. 4. Polarized two-photon resonant MPI spectrum of the $S_1 \leftarrow S_0$ transition of DABCO in the region around the 0-0 band at room temperature.
(a): Parallel polarization, (b): perpendicular polarization.

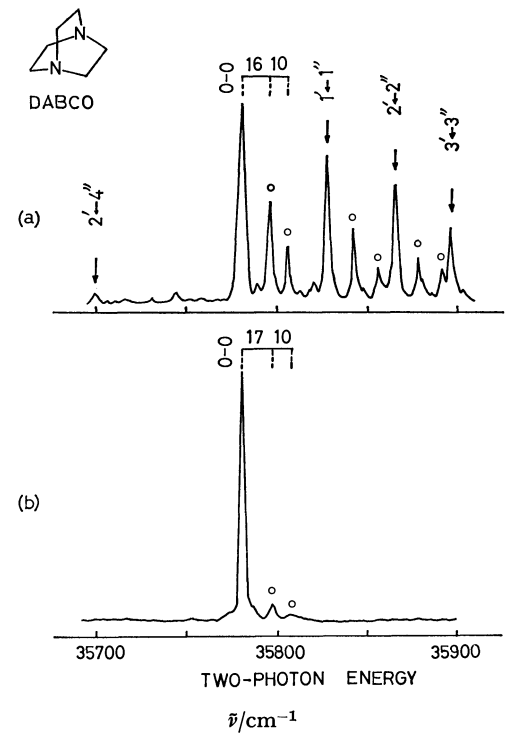

Fig. 5. Sequence structures for the 0-0 band region of DABCO in the two-photon resonant MPI spectrum.
(a): At room temperature, (b): in a supersonic free jet.

to the conclusion that the S_1 state is A_1'. The $S_1(A_1') \leftarrow S_0(A_1')$ transition should appear in the one-photon spectrum by borrowing intensity from the one-photon allowed $S_n(E') \leftarrow S_0(A')$ transition through vibronic coupling between $S_1(A_1')$ and $S_n(E')$. The $S_n(E')$ state is probably the second excited state (S_2) around 39813 cm^{-1}, which has been assigned to E' symmetry by Parker *et al.*[5,7]

Laser Polarization Studies. It was found from the vibrational analysis described in a previous section that the S_1 state is A_1'. This result is in agreement with the conclusion derived by Parker and Avouris[7] from their laser polarization studies of the two-photon absorption spectrum. In their polarization studies, they used two identical photons and measured the ratio of the two-photon absorption signal from a circularly polarized source to that from a linearly polarized source of the same intensity. We carried out a different polarization measurement. In our measurement, two linearly polarized laser beams of different frequencies were used; the frequency of one laser beam was fixed at 530 nm (second harmonic of YAG laser) and that of another beam was varied between 590 and 583 nm to observe the 0-0 band region. Two-photon resonant MPI spectrum of DABCO at room temperature was taken for both parallel and perpendicular polarizations of the two laser beams. The results obtained is shown in Fig. 4. It is seen from the figure that the spectrum appears strongly in the parallel polarization while it is extremely weak in the perpendicular polarization. The ratio ρ of the intensity of perpendicular polarization to that of parallel one (which corresponds to depolarization ratio in Raman scattering) is nearly zero. Since ρ should be 3/4 for non-totally symmetric state and less than 3/4 for totally symmetric state,[17,18] it is concluded that the S_1 state is A_1' in agreement with the result derived from the vibrational analysis.

Low Frequency Torsional Motion of DABCO and ABCO. The two-photon absorption spectrum of DABCO vapor at room temperature has been studied in detail by Parker and Avouris.[7] They found the presence of extensive sequence structure in the spectrum. The sequence structure was attributed by them to the $\Delta v = 0$ and ± 2 transitions of the $\nu_{13}(a_1'')$ low-frequency torsional motion in which the two N pyramids are twisted in the opposite sense about the C_3 symmetry axis. We also observed the identical sequence structure which is shown in Fig. 5a for the 0-0 band region. In order to confirm the assignments given by Parker and Avouris, the two-photon resonant MPI spectrum was measured for DABCO in a supersonic free jet. The result is shown in Fig. 5b. It is seen that the bands assigned to the torsional motion (which are indicated by arrows in Fig. 5a) completely disappear in the supersonic jet spectrum, supporting their assignment. Our supersonic jet spectrum adds nothing more than the results obtained by Parker and Avouris about the sequence of the a_1'' torsional vibration.

In the two-photon absorption spectrum of DABCO vapor at room temperature, Parker and Avouris also noted the presence of a minor sequence in addition to the major sequence described above. The bands belonging to the minor sequence are indicated by

TABLE 3. OBSERVED AND CALCULATED TRANSITION ENERGIES ASSOCIATED WITH THE TORSIONAL VIBRATION IN THE TWO-PHOTON RESONANT MPI SPECTRUM OF DABCO AND THE CALCULATED VIBRATIONAL LEVELS

Transition	Observed $\tilde{\nu}$/cm^{-1}	Calculated $\tilde{\nu}$/cm^{-1}	v	Ground state $\tilde{\nu}$/cm^{-1}	Excited state $\tilde{\nu}$/cm^{-1}
0-0	35780		1	54	99
1′←1″	35826	35825	2	119[a)]	204[a)]
2′←2″	35865	35865	3	196	315
3′←3″	35897	35899	4	284[a)]	431[a)]
4′←4″	35927	35927	5	384	553
5′←5″	35952	35949	6	479	681
2′←0	35984	35984			
3′←1″	36043	36041	ν_0	42	93
4′←2″	36092	36092			
5′←3″	36134	36137			
0←2″	35661	35661			
1′←3″	35681	35683			

a) These are the observed values.

TABLE 4. OBSERVED AND CALCULATED TRANSITION ENERGIES ASSOCIATED WITH THE TORSIONAL VIBRATION IN THE TWO-PHOTON RESONANT MPI SPECTRUM OF ABCO AND THE CALCULATED VIBRATIONAL LEVELS

Transition	Observed $\tilde{\nu}$/cm^{-1}	Calculated $\tilde{\nu}$/cm^{-1}	v	Ground state $\tilde{\nu}$/cm^{-1}	Excited state $\tilde{\nu}$/cm^{-1}
0-0	39095		1	37	63
1′←1″	39125	39121	2	87[a)]	134[a)]
2′←2″	39142	39142	3	150	215
3′←3″	39159	39159	4	227[a)]	304[a)]
4′←4″	39172	39172	5	317	403
5′←5″	39188	39181	6	420	510
2′←0	39229	39229			
3′←1″	39282	39273	ν_0	24	54
4′←2″	39312	39312			
5′←3″	39346	39347			
0←2″	39008	39008			
1′←3″	39006	39007			

a) These are the observed values.

open circles in Fig. 5a. Most of these bands disappear or appear weakly in the supersonic jet spectrum, indicating that they are also hot bands. These bands may be assigned to the $\Delta v=0$ transitions of a low-frequency vibration. By assuming same Franck-Condon factor for these bands as that for the 0-0 band, the frequency of the ground-state vibration involved is estimated to be about $\approx$150 cm^{-1} for a non-degenerate vibration and about $\approx$300 cm^{-1} for a degenerate vibration from the intensities of these bands relative to that of the 0-0 band of the room temperature spectrum. It is known from the vibrational spectra that the lowest-frequency fundamental vibration except the torsional vibration $\nu_{13}(a_1'')$ is $\nu_{36}(e'')$ of the rocking mode of N pyramids with the frequency of 332 cm^{-1}. Therefore, we assign the minor sequence as the $\Delta v=0$ transitions of $\nu_{36}(e'')$. It is noticed in Fig. 5 that in the supersonic jet spectrum 1′←1″ and 2′←2″ bands of $\nu_{36}(e'')$ still remain with weak intensity, while the $\Delta v=0$ and ±2 bands of $\nu_{13}(a_1'')$ are absent. Since the ground-state vibrational frequency of $\nu_{36}(e'')$ is higher than that of $\nu_{13}(a_1'')$, the above result indicates a non-Boltzmann distribution between the levels of $\nu_{13}(a_1'')$ and $\nu_{36}(e'')$ in a supersonic free jet.

Table 3 summarizes the observed transitions of DABCO associated with $\nu_{13}(a_1'')$, which will be used later for determination of the potentials of the torsional mode in the ground and excited states.

The two-photon resonant MPI spectrum of ABCO was also observed for the vapor at room temperature as well as for the supersonic jet and they are shown in Fig. 6 for the 0-0 band region. An extensive sequence structure similar to that of DABCO was found in the room temperature spectrum. The bands of the major sequence indicated by arrows in the figure are assigned to the $\Delta v=0$ and ±2 transitions of the torsional motion corresponding to $\nu_{13}(a_1'')$ of DABCO. The band indicated by the open circle is probably due to the 1′←1″ transition of the rocking motion similar to $\nu_{36}(e'')$ of DABCO. The observed transitions are summarized in Table 4. In a supersonic free jet, the intensities of all these sequence bands greatly decrease, but the 1′←1″, 2′←2″, and 3′←3″ transitions for the torsional mode and the 1′←1″ transition for the rocking mode still seen with weak intensities. This suggests that ABCO is less efficient in the vibrational cooling than DABCO.

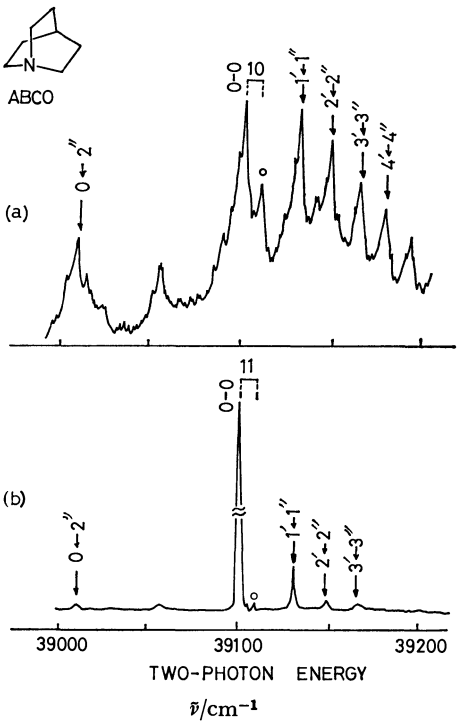

Fig. 6. Sequence structures for the 0-0 band region of ABCO in the two-photon resonant MPI spectrum. (a): At room temperature, (b): in a supersonic free jet.

By utilizing the observed transitions associated with the torsional motion given in Tables 3 and 4, we can obtain the potentials and the vibrational levels for

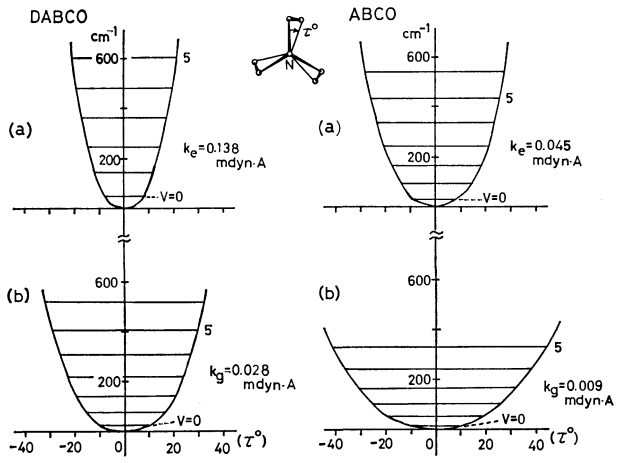

Fig. 7. The calculated potential function of the torsional vibration (a) in the excited state and (b) in the ground state of DABCO (left side) and ABCO (right side). The observed values for $v=2$ and $v=4$ are used as a reference of the calculation for the other levels.

both ground and excited states. Since only the transitions accompanying with even quantum changes are allowed in the two-photon absorption spectrum, the vibrational levels of even quantum number states are directly obtained from the experiment. We attempted to determine the torsional potentials and energy levels by assuming an anharmonic potential of $V(Q)=(1/2)kQ^2+bQ^4$, where Q is the normal coordinate of the torsional motion, $k(=4\pi^2\nu_0^2m)$ is the force constant, ν_0 and m being the zeroth-order harmonic frequency and reduced mass, respectively. Applying the first-order perturbation theory, the vibrational energy[19] is given by

$$w=\left(v+\frac{1}{2}\right)h\nu_0+\frac{3}{64\pi^4}(2v^2+2v+1)\frac{h^2b}{m^2\nu_0^2},$$

where v is the vibrational quantum number. The calculation was carried out by using the observed values of $v=2$ and $v=4$ levels for the ground and excited states with the effective reduced mass of 26.8 amu A^2/rad^2 [10] for both ground and excited states. The calculated transition energies are compared with the observed ones in Tables 3 and 4, where the values of the vibrational levels and ν_0 obtained from the calculation are also given. It is found that the calculated transition energies agree very well with the observed energies. Figure 7 shows the potential energies as a function of the "twist angle" τ about the C_3 axis. The ground-state potential is considerably flat and has a broad minimum near D_{3h} or C_{3v} conformation. Yokozeki and Kuchitsu[10] determined the ground-state potential of DABCO from their electron diffraction studies and obtained a double minimum potential with the barrier of $\approx 35\ cm^{-1}$. Since our potential without the barrier reproduces the observed energies very well, the deviation from D_{3h} or C_{3v} conformation seems to be not significant.

As is seen from Fig. 7, the torsional potential becomes sharp in the excited state. In fact, the force constant for the excited state is five times larger than that for the ground state. The sharpening may qualitatively be explained from the electronic character of the S_1 state. According to Parker and Avouris, the S_1 state of DABCO or ABCO is a totally symmetric Rydberg state arising through the excitation of a non-bonding electron localized on the nitrogen atom to the 3s nitrogen atomic orbital. Thus, the s character of the nitrogen atom increases in the S_1 state compared with that in the ground state, leading to a more rigid cage.

Conclusion

We have obtained and analyzed the one-photon FE and two-photon resonant MPI spectra due to the $S_1 \leftarrow S_0$ transition of DABCO in a supersonic free jet. It was found from the vibrational analysis that the $S_1 \leftarrow S_0$ transition is one-photon forbidden, two-photon allowed and the one-photon absorption appears by the vibronic interaction between the S_1 and S_2 states through the e′ vibrations. The S_1 state was definitely assigned to A_1' from the vibrational analyses of the absorption and fluorescence spectra as well as from the laser polarization studies. The sequence structures appearing in the two-photon absorption spectra of DABCO and ABCO have been analyzed and the potentials of the torsional motion have been determined for both ground and excited states. It has been found that the torsional potential has a broad minimum in the ground state and it becomes sharp in the excited state.

References

1) A. M. Halpern, J. L. Roebber, and K. Weiss, *J. Chem. Phys.*, **49**, 1348 (1968).
2) A. M. Halpern, *Chem. Phys. Lett.*, **6**, 296 (1970).
3) A. M. Halpern and R. M. Danziger, *Chem. Phys. Lett.*, **16**, 72 (1972).
4) Y. Hamada, A. Y. Hirakawa, and M. Tsuboi, *J. Mol. Spectrosc.*, **47**, 440 (1973).
5) D. H. Parker and Ph. Avouris, *Chem. Phys. Lett.*, **53**, 515 (1978).
6) H. Kuno, K. Kasatani, M. Kawasaki, and H. Sato, *Bull. Chem. Soc. Jpn.*, (to be published).
7) D. H. Parker and Ph. Avouris, *J. Chem. Phys.*, **71**, 1241 (1979).
8) G. S. Weiss, A. S. Parkes, E. R. Nixon, and R. E. Hughes, *J. Chem. Phys.*, **41**, 3759 (1964).
9) M. P. Marzocchi, G. Sbrana, and G. Zerbi, *J. Am. Chem. Soc.*, **87**, 1429 (1964).
10) A. Yokozeki and K. Kuchitsu, *Bull. Chem. Soc. Jpn.*, **44**, 72 (1971).
11) N. Mikami, A. Hiraya, I. Fujiwara, and M. Ito, *Chem. Phys. Lett.*, **74**, 531 (1980).
12) J. Murakami, K. Kaya, and M. Ito, *J. Chem. Phys.*, **72**, 3263 (1980).
13) The wavenumber of the 0-0 band (35783 cm^{-1}) does not agree with that (35794 cm^{-1}) reported by Parker and Avouris (Table 1 in Ref. 7), latter being the value uncorrected for vacuum.
14) The strong intensities of 0—2900 cm^{-1} band and the long progression of 950 cm^{-1} starting from 0—2900 cm^{-1} band suggested that they are due to the phosphorescence. We observed the lifetime for these bands and found that

it is about 200 ns at the vapor pressure of *ca.* 67 Pa, which is same for the other bands. It was concluded that the emission is almost certainly fluorescence.

15) P. Brüesch and H. H. Günthard, *Spectrochim. Acta*, **22**, 877 (1966).

16) J. R. McDivitt and G. L. Humphrey, *Spectrochim. Acta, Part A*, **30**, 1021 (1974).

17) E. B. Wilson, J. C. Decius, and P. C. Cross, "Molecular Vibrations, The Theory of Infrared and Raman Vibrational Spectra," McGraw-Hill, New York (1955), pp. 34—53.

18) G. Placzek, "The Rayleigh and Raman Scattering," translation from "Handbuch der Radiologie," Heftb, Teil 2 (1934) by NTIS (1959), pp. 40—55.

19) L. Pauling and E. B. Wilson, "Introduction to Quantum Mechanics," McGraw-Hill, New York (1935), pp. 160—162.

 © 1982 The Chemical Society of Japan Bull. Chem. Soc. Jpn., 55, 2803—2807 (1982)

Thermochemical Studies on 2,4,6-Triisopropylbenzophenone and Its Photo-isomer, 3′,5′-Diisopropyl-4,4-dimethyl-3-phenyl-1,2-benzocyclobuten-3-ol. Evaluation of Magnitude of Light Energy Stored in the Latter Molecule**

Sadayasu INAGAKI,†† Shigeo MURATA, Minoru SAKIYAMA,* Yoshikatsu ITO,† Yasutoshi UMEHARA,† Toyoto HIJIYA,† and Teruo MATSUURA†

Chemical Thermodynamics Laboratory and Department of Chemistry, Faculty of Science, Osaka University, Toyonaka 560

† *Department of Synthetic Chemistry, Faculty of Engineering, Kyoto University, Kyoto 606*

(Received March 8, 1982)

Standard energy of combustion and standard enthalpy of sublimation were determined for the title compounds with static bomb combustion calorimetry and with sublimation calorimetry, respectively. Derived standard enthalpies of combustion and of formation at 298.15 K were as follows: $\Delta H_c^\circ(c) = -(12354.3 \pm 1.8)$, $\Delta H_f^\circ(c) = -(304.6 \pm 3.4)$, and $\Delta H_f^\circ(g) = -(189 \pm 8)$ kJ mol^{-1}, respectively, for 2,4,6-triisopropylbenzophenone(**1**), and $\Delta H_c^\circ(c) = -(12440.6 \pm 1.6)$, $\Delta H_f^\circ(c) = -(218.3 \pm 3.3)$, and $\Delta H_f^\circ(g) = -(101 \pm 10)$ kJ mol^{-1}, respectively, for 3′,5′-diisopropyl-4,4-dimethyl-3-phenyl-1,2-benzocyclobuten-3-ol(**2**). The enthalpy change for the reaction: **1**(g)→**2**(g), of 88 kJ mol^{-1}, which may be supposed to be the magnitude of light energy stored in the latter molecule, has been discussed.

2,4,6-Triisopropylbenzophenone (**1**) undergoes photo-isomerization under irradiation in solution to afford 3′,5′-diisopropyl-4,4-dimethyl-3-phenyl-1,2-benzocyclobuten-3-ol (**2**) in quantitative yield[1] and the latter compound is converted to the former quantitatively, when it is heated above 120 °C or reacted with base catalyst.[2] The mechanism of the photo-isomerization has been elucidated,[2] and the hindered rotation of **1**,[3] the effect of 4′-substitution on the life-time of the triplet state of **1**,[4] and the influence of ring substitution on the life-time of the biradical from **1**[5] have been studied. Crystal structure of **1** has been determined by X-ray diffraction method.[21]

In the present study, standard energies of combustion and standard enthalpies of sublimation were determined for **1** and **2** by calorimetric methods, in order to evaluate the magnitude of light energy, stored in the latter molecule as a result of the photo-isomerization reaction. The stored energy has been discussed in terms of the strain energy of the molecule.

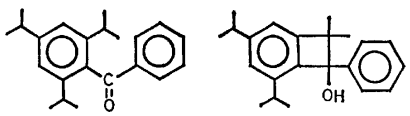

1 **2**

Experimental

Materials. **1**[6] and **2**[1] were prepared according to the procedure described previously. **1** was purified by recrystallization from ethanol solution followed by vacuum fractional sublimation. **1** was treated throughout with minimum exposure to light. **2** was purified by recrystallization from petroleum ether solution followed by vacuum fractional sublimation. The procedure for **2** was undertaken at temperatures below 60 °C.

Combustion Calorimetry. An isoperibol rotating bomb calorimeter with a platinum-lined bomb, described elsewhere,[7,8] was used without rotating the bomb. The calorimeter was calibrated by burning thermochemical standard benzoic acid(U.S. National Bureau of Standards SRM 39i) under certificate conditions. The certified specific energy of combustion of the benzoic acid Δu_c(ba) is $-(26434 \pm 1)$ J g^{-1}, where uncertainty is our estimate of the standard deviation of the mean. Mean and standard deviation of the mean for the energy equivalent of the empty calorimetric system ε(calor)[12] were determined to be (15157.32 ± 0.67) J K^{-1} from seven calibration experiments. A pellet of **1** was ignited in a deep crucible with a small lid[9] together with a pellet of the thermochemical standard benzoic acid(approximately 0.25 g) in order to prevent incomplete combustion of **1**. The auxiliary benzoic acid contributed to approximately one fourth of total energy change. **2** was pressed into pellets and a pellet was burnt in an ordinary open crucible without a promoter at 3.040 MPa of oxygen pressure.

Nitric acid was determined by measuring the absorbance at 202 nm of the bomb solutions. Carbon dioxide recovery was determined for **2** by the method described elsewhere[8] in order to examine the purity and/or completeness of combustion.

Sublimation Calorimetry. Sublimation enthalpy was measured as a function of temperature with the sublimation calorimetric system described elsewhere,[10] in which a Calvet microcalorimeter (DAM, ambient to 473 K type), homemade sublimation apparatuses, and Knudsen-type sample containers were incorporated. Sublimation apparatus Mark II and sample containers Mark C were employed. Both the diameter and the depth of the effusion orifice were 1.0 mm. Thin-walled Pyrex glass tubes with a closed end were used for both compounds in order to prevent the samples from contact with the metallic container.

Auxiliary Quantities. Relative atomic masses were taken from the recommendation of IUPAC Commission on Atomic Weights (1977). Densities, specific heat capacities, $(\partial U/\partial p)_T$ values, and other auxiliary quantities, which were used to reduce weights to masses in vacuum and to deduce standard energies of combustion from calorimetric data, are collected in Table 1.

** Contribution No. 30 from Chemical Thermodynamics Laboratory, Faculty of Science, Osaka University.

†† Present address: Chofu Factory, Kobe Steel, Ltd., Shimonoseki, Yamaguchi 752.

TABLE 1. AUXILIARY PHYSICAL QUANTITIES OF 2,4,6-TRIISOPROPYLBENZOPHENONE(**1**), 3′,5′-DIISOPROPYL-4,4-DIMETHYL-3-PHENYL-1,2-BENZOCYCLOBUTEN-3-OL(**2**), BENZOIC ACID, AND COTTON

Compound	Formula	ρ / g cm^{-3}	c_p / J K^{-1} g^{-1}	$-(\partial U/\partial p)_T$ / J MPa^{-1} g^{-1}	$-\{\Delta U_c^\circ/M\}$ / J g^{-1}
1	$C_{22}H_{28}O$	(1.11) a)	(1.601) a)	(0.052) a)	—
2	$C_{22}H_{28}O$	(1.11) a)	(1.601) a)	(0.052) a)	—
Benzoic acid	$C_7H_6O_2$	1.320	1.21	0.052	26413.6
Fuse	$CH_{1.86}O_{0.93}$	1.5	1.70	0.29	16507

V(bomb) = 0.3469 dm^3. a) Parenthesized values were estimated.

TABLE 2. RESULTS OF COMBUSTION CALORIMETRIC EXPERIMENTS ON 2,4,6-TRIISOPROPYLBENZOPHENONE(**1**)

	Experiment						
	1	2	3	4	5	6	7
m'(compd)/g	0.51199	0.50934	0.50935	0.50622	0.51282	0.52518	0.52314
m''(auxil)/g	0.26424	0.25506	0.25192	0.25663	0.25306	0.24586	0.24904
m'''(fuse)/g	0.00214	0.00234	0.00258	0.00219	0.00243	0.00227	0.00254
$m^i(H_2O)$/g	1.150	1.131	1.096	1.117	1.092	1.108	1.116
p^i(gas)/MPa	3.040	3.030	3.040	3.040	3.040	3.040	3.040
θ_i/°C	23.14333	23.14841	23.15025	23.15616	23.14868	23.15248	23.14701
θ_f/°C	24.97957	24.96276	24.95958	24.96517	24.96893	24.99102	24.98630
$\Delta\theta_{corr}$/°C	0.02374	0.02451	0.02446	0.02438	0.02431	0.02299	0.02325
ΔU_{ign}/J	3.8	4.4	4.8	4.9	4.3	4.6	4.8
ε^i(cont)/J K^{-1}	20.46	20.33	20.21	20.30	20.20	20.28	20.31
ε^f(cont)J K^{-1}	21.84	21.69	21.57	21.66	21.57	21.67	21.70
ΔU_Σ/J	15.0	14.7	14.8	14.8	14.9	15.1	15.1
$-U_{IBP}$/J	27506.2	27160.7	27085.5	27081.3	27253.5	27551.5	27558.6
$-\{\Delta U_c^\circ/M\}$/kJ g^{-1}	39.9937	39.9937	39.9999	40.0058	40.0029	39.9956	39.9961
$-\Delta U_c^\circ$/kJ mol^{-1}	12336.8	12336.8	12338.7	12340.5	12339.6	12337.4	12337.5

TABLE 3. RESULTS OF COMBUSTION CALORIMETRIC EXPERIMENTS ON 3′,5′-DIISOPROPYL-4,4-DIMETHYL-3-PHENYL-1,2-BENZOCYCLOBUTEN-3-OL(**2**)

	Experiment					
	1	2	3	4	5	6
m'(compd)/g	0.67759	0.67176	0.66857	0.66276	0.66979	0.67304
m'''(fuse)/g	0.00232	0.00206	0.00208	0.00184	0.00222	0.00182
$m^i(H_2O)$/g	1.094	1.122	1.123	1.121	1.100	1.102
θ_i/°C	23.12603	23.14599	23.14867	23:14726	23.14819	23.15170
θ_f/°C	24.95129	24.95521	24.94995	24.93364	24.95284	24.96429
$\Delta\theta_{corr}$/°C	0.02307	0.02302	0.02341	0.02408	0.02321	0.02305
ΔU_{ign}/J	3.9	4.3	4.0	4.0	4.3	4.3
ε^i(cont)/J K^{-1}	17.51	17.62	17.61	17.59	17.52	17.53
ε^f(cont)/J K^{-1}	18.93	19.02	19.01	18.98	18.92	18.94
ΔU_Σ/J	12.9	12.8	12.7	12.6	12.7	12.8
$-\Delta U_{IBP}$/J	27344.0	27101.0	26974.9	26738.6	27029.9	27151.9
$-\{\Delta U_c^\circ/M\}$/kJ g^{-1}	40.2791	40.2735	40.2768	40.2795	40.2808	40.2785
$-\Delta U_c^\circ$/kJ mol^{-1}	12424.8	12423.1	12424.1	12424.9	12425.3	12424.6
$\{m(CO_2, obsd)\}/\{m(CO_2, calcd)\}$	0.9993	0.9998	—	0.9995	0.9999	1.0001

Results

Results of combustion calorimetric experiments are presented in Tables 2 and 3 for **1** and **2**, respectively. Molar standard energies of combustion given in these tables refer to the following idealized combustion reaction at 298.15 K:

$$C_{22}H_{28}O(c) + (57/2)O_2(g) = 22CO_2(g) + 14H_2O(l).$$

Most of the symbols in these tables are essentially similar to those used by Hubbard *et al.*[12] ΔU_Σ denotes the sum of contributions from items 81—85 and 87—94 as defined by Hubbard *et al.*[12] $\{m(CO_2, obsd)/$

Table 4. Summary of sublimation calorimetric results on 2,4,6-triisopropylbenzophenone(**1**) and 3′,5′-diisopropyl-4,4-dimethyl-1,2-benzocyclobuten-3-ol(**2**)

T/K	m/mg	E_{calib}/J	$\{S_T/S_B\}$	$\Delta H_s^\circ(T)$/kJ mol^{-1}
		1		
353.5	36.15	1.594	7.8843	107.3
353.4	29.13	2.941	5.4596	107.8
363.7	64.83	4.258	5.2257	105.9
363.9	90.57	4.866	6.4016	106.1
		2		
353.2	25.21	1.477	5.9252	107.1
353.5	26.07	1.546	5.8885	107.7
363.1	56.17	4.864	4.0756	108.9
363.1	54.90	3.756	5.1570	108.8
364.0	83.54	4.564	6.4538	108.8
364.0	65.34	4.709	4.9787	110.6

$m(CO_2, calcd)\}$ is the ratio of the observed total mass of recovered carbon dioxide to the calculated one. Mean and standard deviation of the mean for the ratio were (0.9997±0.0001) for five experiments on **2**. While trace of soot was found in the crucibles in experiments Nos. 1, 3, 5, 6, and 7 for **1** and No. 3 and 5 for **2**, no correlation was found between the soot formation and the resultant standard energy of combustion. In addition, carbon monoxide was barely detected in the bomb gas. Mean and standard deviation of the mean for molar standard energy of combustion ΔU_c°(c) were −(12338.18±0.55) and −(12424.48±0.32) kJ mol^{-1} for **1** and **2**, respectively.

Results of sublimation calorimetric experiments are summarized in Table 4. Molar standard enthalpy of sublimation ΔH_s° (T)was calculated with the equation:

$$\Delta H_s^\circ(T) = E_{calib}(S_T/S_B)(M/m),$$

where E_{calib} is the electrical energy used for calibration, (S_T/S_B) is the ratio of the sublimation enthalpy to the calibration energy, which was determined by the calorimetric experiment, m is the mass of material that effused from the sample container, and M is the molar mass of the material.

For **1**, measurements were performed at two temperatures. Observed enthalpies of sublimation were subjected to a regression analysis for linear relations between two variables.[11] The derived function was as follows: ΔH_s° (T)/kJ mol^{-1} = −0.1452(T/K) +158.8, with standard deviation from the fit of 0.3 kJ mol^{-1}. Standard enthalpy of sublimation at 298.15 K was evaluated by extrapolating the function to the reference temperature, since no heat capacity anomaly was found over the relevant temperature range in DSC heating curves of **1**. Derived standard enthalpy of sublimation at 298.15 K was (116±7) kJ mol^{-1}, where uncertainty is the one at the 95 per cent level.

The temperature dependence of $\Delta H_s^\circ(T)$ for **2** does not seem to be normal, although the observed values themselves are of reasonable magnitude: $\Delta H_s^\circ(T)$ should decrease with temperature rise. The observed values are supposed to include experimental errors of considerable magnitude, since the output voltage from the microcalorimeter was small. Although the output voltage could be increased by rising the temperature, this is not desirable for **2** owing to its thermal instability. Consequently, the observed values for **2**, given in Table 4, were averaged with equal weights, and the mean value was taken to be the value at the mean temperature. The value at 298.15 K was then estimated by assuming that the temperature dependence of $\Delta H_s^\circ(T)$ for **2** is identical with that of **1**. No heat capacity anomaly was detected in the DSC heating curves of **2** over the relevant temperature range. The estimated value at 298.15 K was (117±9) kJ mol^{-1}, where uncertainty was assigned rather arbitrarily.

Table 5. Derived thermodynamic quantities of 2,4,6-triisopropylbenzophenone(**1**) and 3′,5′-diisopropyl-4,4-dimethyl-3-phenyl-1,2-benzocyclobuten-3-ol(**2**) at 298.15 K

Compound	**1**	**2**
$-\Delta U_c^\circ$(c)/kJ mol^{-1}	12338.2±1.8	12424.5±1.6
$-\Delta H_c^\circ$(c)/kJ mol^{-1}	12354.3±1.8	12440.6±1.6
$-\Delta H_f^\circ$(c)/kJ mol^{-1}	304.6±3.4	218.3±3.3
ΔH_s°/kJ mol^{-1}	116±7	117± 9
$-\Delta H_f^\circ$(g)/kJ mol^{-1}	189±8	101±10

Derived thermodynamic quantities are presented in Table 5. Uncertainties in this table are the overall values. The overall uncertainties for ΔU_c°(c) and ΔH_c°(c) are twice the overall standard deviation of the mean for ΔU_c°(c), $\{2s(\bar{U})_\Sigma\}$. $s(\bar{U})_\Sigma$ was calculated according to:

$$s(\bar{U})_\Sigma = [s(\bar{U})^2 + \{\Delta U_c^\circ(c)s(\varepsilon)/\varepsilon(calor)\}^2 + \{\Delta \bar{U}_c^\circ(c)s(ba)/\Delta u_c(ba)\}^2 + \{M(compd)\bar{m}(ba)s(ba)/\bar{m}(compd)\}^2]^{1/2},$$

where $s(\bar{U})$, $s(\varepsilon)$, and s(ba) are the standard deviations of the mean for ΔU_c°(c), ε(calor), and Δu_c°(ba), respectively, and $\bar{m}$(ba) and $\bar{m}$(compd) are the mean masses of the benzoic acid as used as the promoter and of the compound, respectively. For **2**, m(ba)=0, and so the fourth term in the bracket of the equation is deleted. $s(\bar{U})_\Sigma$ amounted to 0.9 and 0.8 kJ mol^{-1} for **1** and **2**, respectively. Standard enthalpies of formation in the crystalline state were calculated by use of the following CODATA key values for thermodynamics:[13] $\Delta H_f^\circ(CO_2, g) = -(393.51\pm0.13)$ and $\Delta H_f^\circ(H_2O, l) = -(235.830\pm0.042)$ kJ mol^{-1}, respectively, where uncertainties are those at the 95 per cent confidence level. Overall uncertainties for ΔH_f°(c) and ΔH_f°(g), $\delta(\Delta H_f^\circ, c)$ and $\delta(\Delta H_f^\circ, g)$, respectively, were calculated as follows:

$$\delta(\Delta H_f^\circ, c) = [\delta(\Delta U_c^\circ, c)^2 + \{22\times0.13\}^2 + \{14\times0.042\}^2]^{1/2}$$

and

$$\delta(\Delta H_f^\circ, g) = [\delta(\Delta H_f^\circ, c)^2 + \delta(\Delta H_s^\circ)^2]^{1/2},$$

where $\delta(\Delta H_s^\circ)$ is the uncertainty assigned to ΔH_s°(298.15 K).

Table 6. Comparison between calculated and observed values of $\Delta H_f^\circ(g)$ for 2,4,6-triisopropylbenzophenone(**1**), 3′,5′-diisopropyl-4,4-dimethyl-3-phenyl-1,2-benzocyclobuten-3-ol(**2**), and related compounds

Compound	$\Delta H_f^\circ(g)$/kJ mol^{-1}			Δ[d] / kJ mol^{-1}	
	Obsd	Calcd			
		Laidler[a]	Group[b]	Laidler[a]	Group[b]
Benzene	82.9±0.3[c]	83.1	82.8	−0.2	0.1
Isopropylbenzene	4.0±1.0[c]	0.5	3.1	3.5	0.9
Benzophenone	59.0±1.7[c]	43.9	61.1	16.1	−2.1
1	−189±8[e]	−203.9	−178.2	15	−11
Cyclobutene	156.7±1.5[c]	31.0	31.2	125.7	125.0
2	−101±10[e]	−241.9	−233.8	141	123

a) Calculated values based on the Laidler sheme of bond energy:[15,16] E(C-C) = −0.1, E(C_b-C_b) = 37.7, E(C_b-C) = −14.5, E(C_b-C_{co}) = −57.2, E(C=C) = 158.6, E(C-H)$_p$ = −14.1, E(C-H)$_s$ = −10.2, E(C-H)$_t$ = −7.1, E(C_b-H) = −23.9, E(C-O) = −77.5, E(C=O) = −55.6, and E(O-H) = −108.6 kJ mol^{-1}. b) Calculated values based on the group contribution method:[22,23] [**C**$_B$-(H)] = 13.8, [**C**$_B$-(C)] = 23.5, [**C**-(C_B)(C)$_2$(H)] = −4.3, [**C**-(C)(H)$_3$] = −42.3, [**CO**-(C_B)$_2$] = −107.9, [**C**$_B$-(CO)] = 15.5, [**C**$_d$-(C)(H)] = 36.2, [**C**-(C_d)(C)(H)] = −20.6, [**C**-(C)$_3$(C_B)] = 11.8, [**C**-(C_B)$_2$(C)(O)] = −27.9 (assumed), and [**O**-(C)(H)] = −158.4 kJ mol^{-1}. c) Selected value given in Ref. 20. d) Destabilization energy: $\Delta = \Delta H_f^\circ$(g, obsd) − ΔH_f°(g, calcd). e) Present result.

Discussion

Comparison between the standard enthalpies of formation in gaseous state of **1** and **2**, given in Table 5, leads to the standard enthalpy change of 88 kJ mol^{-1} for the isomerization reaction: **1**(g)→**2**(g). Since combustion and sublimation calorimetric experiments were carried out for **1** and **2** quite similarly, part of the uncertainties assigned to ΔH_f°(g) of **1** and **2** would be cancelled in calculating the difference in ΔH_f°(g) between **1** and **2**. Uncertainty for the difference is estimated to be around 10 kJ mol^{-1}. This enthalpy change may be identified with the magnitude of light energy stored in a molecule of **2** as a result of the reaction. Note that this enthalpy change is twice as large as that for the reaction: norbornadiene(g)→quadricyclane(g), with standard enthalpy change of 41.6 kJ mol^{-1} at 298.15 K.[14]

In order to interpret the large enthalpy change for the present isomerization, destabilization (strain) energy was evaluated for **1** and **2**, by use of the Laidler scheme of bond energy[15,16] and the group contribution method.[22,23] Calculated and observed standard enthalpies of formation in gaseous state are presented and compared with each other in Table 6, together with those of related compounds. As is shown in the table, both the schemes are capable of reproducing ΔH_f°(g) for benzene and isopropylbenzene reasonably well. The same is true by the group contribution method for benzophenone, but the Laidler scheme gives ΔH_f°(g) which is by 15 kJ mol^{-1} less negative than the experimental value. Destabilization energy for **1** was estimated to be 15 and −11 kJ mol^{-1} by the Laidler scheme and the group method, respectively. In view of the large uncertainty assigned to the experimental value of ΔH_f°(g) and possible uncertainty of at least 4 kJ mol^{-1} for the calculated values, these destabilization energies appear to be barely significant.

The destabilization energy of **2** amounts to 141 and

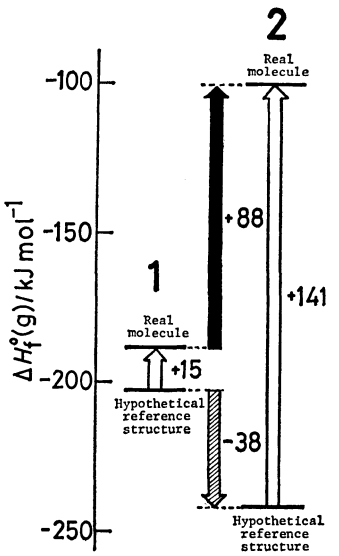

Fig. 1. Enthalpy diagram, based on the Laidler scheme of bond energy, of the gas phase photo-isomerization: 2,4,6-triisopropylbenzophenone(**1**)→3′,5′-diisopropyl-4,4-dimethyl-3-phenyl-1,2-benzocyclobuten-3-ol(**2**). Black and shaded arrows denote real and hypothetical enthalpy changes, respectively, for the reaction, and blank arrows denote estimated destabilization energies.

123 kJ mol^{-1} by the Laidler scheme and the group method, respectively. It is to be noted that these values are of similar magnitude with the destabilization energy of cyclobutene. The molecular structure of **2** has not been reported. However, according to X-ray diffraction studies on *cis*-3,4-dihalo-1,2-benzocyclobutenes (halogen=Cl, Br, and I)[17] and *cis*-1,2-benzocyclobuten-3,4-diol dinitrate,[18] carbon atoms in these molecules are almost coplanar, bond angles of the four-membered ring are similar with the corresponding ones of a cyclobutene molecule,[19] and the benzene ring is slightly elongated along the line connecting 3′ and 6′ carbon atoms. The presence of a highly strain-

ed four-membered ring and the concomitant distortion of the benzene ring seem to be among the principal origins of the enhanced destabilization observed for **2**. Another posible contribution would come from the steric hindrance between the substituents of the four-membered ring. If this contribution is neglegibly small, the destabilization energy of 123 kJ mol^{-1} would be identified with the ring correction for a 1,2-benzocyclobutene ring in the group method.[23]

In the meantime, if both **1** and **2** were neither stabilized nor destabilized as compared with each hypothetical reference structure, enthalpy change for the reaction: **1**(g)→**2**(g), would have been −38 kJ mol^{-1} (the Laidler scheme) or −46 kJ mol^{-1} (the group method), in contrast to the real value of 88 kJ mol^{-1}. The large positive enthalpy change for the real reaction is brought about by the large destabilization energy of **2**, which is far superior to the destabilization energy of **1** and also to the enthalpy change for the reaction between the hypothetical reference structures, as illustrated in Fig. 1, by use of the Laidler scheme. A similar diagram based on the group contribution method may be drawn.

References

1) Y. Kitaura and T. Matsuura, *Tetrahedron*, **27**, 1597 (1971).

2) Y. Ito, Y. Umehara, T. Hijiya, Y. Yamada, and T. Matsuura, *J. Am. Chem. Soc.*, **102**, 5917 (1980).

3) Y. Ito, Y. Umehara, K. Nakamura, Y. Yamada, T. Matsuura, and F. Imashiro, *J. Org. Chem.*, **46**, 4359 (1981).

4) Y. Ito, Y. Umehara, Y. Yamada, and T. Matsuura, *J. Chem. Soc., Chem. Commun.*, **1980**, 1160.

5) Y. Ito, H. Nishimura, T. Matsuura, and H. Hayashi, *J. Chem. Soc., Chem. Commun.*, **1981**, 1187.

6) R. C. Fuson, E. M. Bottorff, R. E. Foster, and S. B. Speck, *J. Am. Chem. Soc.*, **64**, 2573 (1942).

7) M. Sakiyama, T. Nakano, and S. Seki, *Bull. Chem. Soc. Jpn.*, **48**, 1705 (1975).

8) K. Nishiyama, M. Sakiyama, S. Seki, H. Horita, T. Otsubo, and S. Misumi, *Bull. Chem. Soc. Jpn.*, **53**, 869 (1980).

9) A. Kamaguchi, T. Sato, M. Sakiyama, and S. Seki, *Bull. Chem. Soc. Jpn.*, **48**, 2203 (1975).

10) S. Murata, M. Sakiyama, and S. Seki, *J. Chem. Thermodyn.*, **14**, 707 (1982).

11) "Statistical Method in Research and Production with Special Reference to Chemical Industry," ed by O. L. Davies and P. L. Goldsmith, 4th ed, Longman, London (1977).

12) W. N. Hubbard, D. W. Scott, and G. Waddington, "Experimental Thermochemistry," ed by F. D. Rossini, Interscience, New York (1956), Vol. 1, Chap. 5.

13) CODATA Task Group on Key Values for Thermodynamics, 1977, *CODATA Bulletin*, **1978**, 28.

14) H. K. Hall, C. D. Smith, and J. H. Baldt, *J. Am. Chem. Soc.*, **95**, 3197 (1973).

15) K. J. Laidler, *Can. J. Chem.*, **34**, 626 (1956).

16) J. D. Cox and G. Pilcher, "Thermochemistry of Organic and Organometallic Compounds," Academic, London (1970), p. 592.

17) G. L. Hardgrove, L. K. Templeton, and D. H. Templeton, *J. Phys. Chem.*, **72**, 668 (1970).

18) F. H. Allen and J. Trotter, *J. Chem. Soc., B*, **1970**, 1551.

19) B. Bak, J. L. Led, L. Nygaard, J. Rastrup-Andersen, and G. O. Soerensen, *J. Mol. Struct.*, **3**, 369 (1969).

20) J. B. Pedley and J. Rylance, "Sussex-N.P.L. Computer Analysed Thermochemical Data: Organic and Organometallic Compounds," University of Sussex, Brighton (1977).

21) Y. Ito, Y. Umehara, T. Matsuura, Y. Katsube, and K. Fukuyama, 41st National Meeting of the Chemical Society of Japan, Higashi-Osaka, April 1980, Abstr., 2M34.

22) S. W. Benson, "Thermochemical Kinetics," 2nd ed, Wiley Interscience, New York (1976).

23) a) S. W. Benson and J. H. Buss, *J. Chem. Phys.*, **29**, 546 (1958); b) S. W. Benson, F. R. Cruickshank, D. M. Golden, G. R. Hougen, H. E. O'Neal, A. S. Rodgers, R. Shaw, and R. Walsh, *Chem. Rev.*, **69**, 279 (1969); c) H. K. Eigenmann, S. W. Benson, and D. M. Golden, *J. Phys. Chem.*, **77**, 1687 (1973).

Thermochemical Studies on Thioacetamide and Tetramethylthiourea. Estimation of Stabilization Energies Due to Interaction between Thiocarbonyl Group and Neighbouring Nitrogen Atom**

Sadayasu INAGAKI,† Shigeo MURATA, and Minoru SAKIYAMA*

Chemical Thermodynamics Laboratory and Department of Chemistry, Faculty of Science, Osaka University, Toyonaka 560

(Received March 10, 1982)

Standard energy of combustion at 298.15 K and standard enthalpy of sublimation as a function of temperature were determined for thioacetamide and tetramethylthiourea by oxygen bomb combustion calorimetry and sublimation calorimetry. Derived standard enthalpies of formation in crystalline and gaseous states at 298.15 K are $-(70.6\pm1.1)$ and (12.7 ± 1.2) kJ mol^{-1}, respectively, for thioacetamide, and $-(38.3\pm2.3)$ and (44.7 ± 2.4) kJ mol^{-1}, respectively, for tetramethylthiourea. Stabilization energies of these molecules were evaluated by estimating the standard enthalpies of formation in gaseous state for the hypothetical reference structures by use of the group contribution method.

While ketones are usually stable substances, thioketones are very unstable at ambient temperatures. This suggests the inherent instability of a thiocarbonyl group as compared with a carbonyl group. However, when a thiocarbonyl group neighbours a nitrogen atom in a molecule, the group is substantially stabilized: Thioamides and thioureas are fairly stable at room temperatures. The stabilization seems to be caused by the interaction of a thiocarbonyl π-electrons with nitrogen lone pair electrons. Analogous but more enhanced stabilization is observed in amides and ureas.

In this paper, standard enthalpies of combustion and of sublimation at 298.15 K are reported on thioacetamide and tetramethylthiourea. Derived standard enthalpies of formation in gaseous state are compared with those estimated for the hypothetical reference structures to evaluate the stabilization energies for these molecules.

Experimental

Materials. Thianthrene, which was used to test the reliability of our combustion calorimetric equipment and procedure for sulfur-containing organic compounds, was synthesized by the method of Fries and Vogt,[1] and was purified by recrystallization from benzene solution followed by vacuum fractional sublimation and zone-melting. Commercial thioacetamide (Nakarai, G. R.) and tetramethylthiourea (Tokyo Kasei, G. R.) were purified by recrystallization from benzene and ligroine solutions, respectively, followed by vacuum fractional sublimation. The purity of the samples was assessed from DSC heating curves in the melting region as follows: thianthrene, 99.93; thioacetamide, 99.99; and tetramethylthiourea, 99.97 mol%, respectively.

Combustion Calorimetry. An isoperibol rotating bomb calorimeter, described elsewhere,[2,3] was employed. The calorimeter was calibrated by burning thermochemical standard benzoic acid (U. S. National Bureau of Standards, SRM 39i) in the presence of 10 g of water at 3.040 MPa of oxygen pressure. The certified value for the specific energy of combustion of the benzoic acid is $-(26434\pm1)$ J g^{-1} under certificate conditions and it follows[4] that the specific energy of combustion is $-(26414\pm1)$ J g^{-1}, where uncertainties are our estimates of standard deviation of mean. The calibration experiments were carried out in the bomb rotation mode to be described below. Mean and standard deviation of the mean for the energy equivalent of the empty calorimetric system ε(calor),[7] derived from nine experiments, were (15162.31 ± 0.55) J K^{-1}.

Thianthrene, thioacetamide and tetramethylthiourea were pressed into pellets. The bomb was charged with a sample, water (10 g), and oxygen (3.040 MPa at 298.15 K). The bomb was not flushed before charging the oxygen in thianthrene and thioacetamide experiments. Every sample was ignited in an ordinary platinum crucible by discharging a 7.184 mF capacitor bank, previously charged to 36.5 V, through a platinum wire.

Both calibration and combustion experiments were designed to include successive four rating periods, denoted with $i(=1\text{—}4)$. Each period is composed of twelve 101.5 s intervals. At the end of each interval, a temperature reading displayed on a Hewlett-Packard quartz thermometer (2801A with option M40) with the resolution of 1×10^{-5} K was recorded. Although the temperature reading is the mean during a 100 s duration in the interval, it was taken to be the mean temperature for the whole interval. A sample was ignited at the end of the first rating period. Bomb rotation was started at the end of the first interval of the second rating period and continued to the end of the third rating period.

Temperature readings of the first and fourth rating periods and of the third rating period were fitted to the following integrated forms of the Newton's cooling law equation: For $i=1$ or 4,

$$\theta = \theta_\infty^s - (\theta_\infty^s - \theta_i^0)\exp[-k(t-t_i^0)], \quad (1)$$

and for $i=3$,

$$\theta = \theta_\infty^r - (\theta_\infty^r - \theta_i^0)\exp[-k(t-t_i^0)], \quad (2)$$

where θ_∞^r and θ_∞^s are the convergence temperatures for the calorimeter in which the bomb is rotating and not rotating, respectively, θ_i^0 is the temperature at time t_i^0, which is the starting time of the i-th rating period, and k is the cooling constant throughout an experiment.

In the first step of analysis, an appropriate value was assumed for k and a least squares procedure for linear relation between θ and $\exp[-k(t-t_i^0)]$ was conducted for the temperature readings of the first and fourth rating periods, respectively, to determine θ_∞^s and θ_i^0. By use of the derived equations, temperature and rate of temperature change were calculated for the midtimes of the first and fourth rat-

** Contribution No. 31 from Chemical Thermodynamics Laboratory, Faculty of Science, Osaka University.

† Present address: Chofu Factory, Kobe Steel, Ltd., Shimonoseki, Yamaguchi 752.

Table 1. Auxiliary quantities

	Formula	ρ / g cm^{-3}	c_p / J K^{-1} g^{-1}	$-(\partial U/\partial p)_T$ / J MPa^{-1} g^{-1}	$-(\Delta U_c^\circ/M)$ / J g^{-1}
Thioacetamide	C_2H_5NS	1.273	(1.21)	(0.052)	—
Tetramethylthiourea	$C_5H_{12}N_2S$	1.17	(1.21)	(0.052)	—
Fuse	$CH_{1.86}O_{0.93}$	1.5	1.70	0.29	16507

ing period. Then, k was calculated with the following equation:

$$k = [(d\theta/dt)_1^m - (d\theta/dt)_4^m]/(\theta_4^m - \theta_1^m),$$

where θ_1^m and θ_4^m are the tempertures at the midtimes of the first and fourth rating periods, respectively, and $(d\theta/dt)_1^m$ and $(d\theta/dt)_4^m$ are the corresponding rates of temperature change. By using successively renewed k values, the procedure described above was repeated, until a consistent set of k and θ_∞^s was obtained. The temperature readings of the third period were fitted to Eq. 2 by the least squares procedure by use of the final k value to determine θ_∞^r and $\theta_3{}^0$.

Corrected temperature rise, $\Delta\theta_c$, was calculated with the following equation:

$$\Delta\theta_c = \theta_e - \theta_b - 101.5k[\theta_\infty^s + 11\theta_\infty^r - \sum_1^{12} \theta_2(j)],$$

where θ_b and θ_e are the temperatures at the start and end of the second rating period, respectively, and $\theta_2(j)$ is the j-th reading of the period. θ_b was calculated from Eq. 1 with $i=1$ by letting $(t-t^0{}_1)=1218$ s, and θ_e is equal to $\theta^0{}_3$.

Nitric acid in the bomb solution was converted to ammonia with Devarda's alloy and the ammonia was absorbed in aqueous sulfuric acid of known concentration. The unreacted sulfuric acid was determined with aqueous sodium hydroxide. Nitrous acid was determined by use of Griess-Ilosvay reagent. The amount of nitrous acid was less than 0.1% of nitric acid. Carbon monoxide was scarcely detected from the bomb gas after combustion experiments.

Sublimation Calorimetry. Sublimation enthalpy was measured as a function of temperature with a sublimation calorimetric system described elsewhere,[5] in which a Calvet microcalorimeter (DAM, ambient to 473 K type), homemade sublimation apparatus (Mark II) and sample containers (Mark C) were incorporated. Both the diameter and the depth of the effusion orifice were 1.0 mm.

Auxiliary Quantities. Relative atomic masses were taken from the recommendation of IUPAC Commission on Atomic Weights (1977). Densities, specific heat capacities, $(\partial U/\partial p)_T$ values, and other auxiliary quantities, which were used to reduce weights to masses in vacuum and to deduce standard energies of combustion from observed calorimetric data, are collected in Table 1. The internal volume of the bomb was 0.3469 dm^3.

Results

Molar standard energies of combustion given in this paper refer to the following idealized combustion reaction at 298.15 K:

$$C_aH_bN_cS_d(c) + [(4a+b+6d)/4]O_2(g) + (116d-b/2)H_2O(1) = aCO_2(g) + (c/2)N_2(g) + d[H_2SO_4 + 115H_2O](1),$$

where $a=12$, $b=8$, $c=0$, and $d=2$ for thianthrene, $a=2$, $b=5$, $c=1$, and $d=1$ for thioacetamide, and finally $a=5$, $b=12$, $c=2$, and $d=1$ for tetramethylthiourea.

Table 2. Comparison of the present result on thianthrene with literature values

Investigator	$-\Delta H_c^\circ(c)$ / kJ mol^{-1}
Hubbard *et al.*[10]	7251.5±2.2
Keith and Mackle[11]	7250.3±2.9
Sunner and Lundin[12]	7252.1±1.2
Hu *et al.*[13]	7252.6±2.2
Johnson[14]	7253.6±1.4
Recommened value[15]	7252.0
Present result	7255.7±1.8

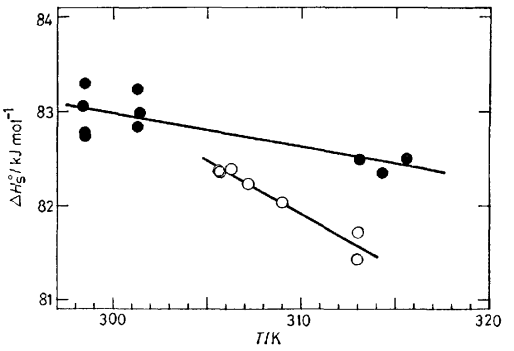

Fig. 1. Standard enthalpy of sublimation versus temperature plot of thioacetamide(○) and tetramethylthiourea(●).

Standard energies of combustion of thianthrene obtained from four experiments were −7241.71, −7245.19, −7242.42, and −7244.05 kJ mol^{-1} with the mean and standard deviation of the mean of −(7243.34±0.79) kJ mol^{-1}. Derived standard enthalpy of combustion is compared with literature values in Table 2. The uncertainty assigned to the present value given in Table 2 is twice the overall standard deviation of mean, to be described below.

Six combustion experiments were carried out for thioacetamide and tetramethylthiourea, respectively. Clean combustion was achieved in every combustion experiment. Combustion calorimetric results on thioacetamide and tetramethylthiourea are presented in Tables 3 and 4, respectively. Most of the symbols in these tables are essentially similar to those used by Hubbard *et al.*[7] ΔU_Σ denotes the contribution from items 81—85, 87—91, and 93—94 defined by Hubbard *et al.*[7] The mean and standard deviation of the mean for molar standard energies of combustion were −(2027.79±0.17) and −(4238.05±0.40) kJ mol^{-1} for thioacetamide and tetramethylthiourea, respectively.

Sublimation calorimetric results are summarized in

TABLE 3. SUMMARY OF COMBUSTION CALORIMETRIC RESULTS ON THIOACETAMIDE

	Experiment					
	1	2	3	4	5	6
m'(compd)/g	1.19724	1.01014	1.01226	1.01446	1.00841	1.01502
m'''(fuse)/g	0.00190	0.00190	0.00219	0.00229	0.00184	0.00224
$m^{i}(H_2O)$/g	9.822	9.800	10.027	9.834	9.924	9.996
θ_i/°C	23.12846	23.13300	23.13625	23.13091	23.12903	23.13003
θ_f/°C	25.27055	24.95798	24.96516	24.96313	24.95129	24.96262
$\Delta\theta_{corr}$/°C	0.01239	0.02654	0.02654	0.02614	0.02731	0.02599
$n^{f}(HNO_3)$/mmol	1.262	1.241	1.173	1.260	1.225	1.260
$n^{f}(HNO_2)$/μmol	0.1	0.0	0·1	0.1	0.1	0.0
ΔU_{ign}/J	4.0	4.9	4.4	4.3	4.8	4.8
ε^{i}(cont)/J K^{-1}	54.1	53.8	54.7	53.9	54.3	54.6
ε^{f}(cont)/J K^{-1}	54.9	54.4	55.3	54.5	54.9	55.2
$\Delta U_{dec}(HNO_3+HNO_2)$/J	74.3	73.1	69.1	74.2	72.1	74.2
$-\Delta U_{dil}(H_2SO_4)$/J	19.1	13.2	12.9	13.3	13.0	13.1
$-\Delta U_{\Sigma}$/J	16.8	11.3	10.8	11.3	10.9	11.0
$-\Delta U_{IBP}$/J	32402.2	27360.4	27421.7	27477.6	27307.7	27486.0
$-\{\Delta U^{\circ}_{c}/M\}$/kJ g^{-1}	26.9898	26.9936	26.9963	26.9867	26.9892	26.9806
$-\Delta U^{\circ}_{c}$/kJ mol^{-1}	2027.82	2028.10	2028.31	2027.59	2027.77	2027.13

TABLE 4. SUMMARY OF COMBUSTION CALORIMETRIC RESULTS ON TETRAMETHYLTHIOUREA

	Experiment					
	1	2	3	4	5	6
m'(compd)/g	1.04506	0.86498	0.85530	0.85992	0.86037	0.86476
m'''(fuse)/g	0.00251	0.00243	0.00233	0.00256	0.00196	0.00211
$m^{i}(H_2O)$/g	10.019	9.947	9.984	9.948	9.964	9.945
θ_i/°C	23.12913	23.13125	23.13736	23.13179	23.12721	23.13513
θ_f/°C	25.34762	24.98626	24.97193	24.97671	24.97241	24.98906
$\Delta\theta_{corr}$/°C	0.00892	0.02504	0.02629	0.02627	0.02583	0.02491
$n^{f}(HNO_3)$/mmol	1.378	1.047	1.022	1.007	1.061	1.054
$n^{f}(HNO_2)$/μmol	0.2	0.4	0.2	0.6	0.6	0.9
ΔU_{ign}/J	5.0	4.8	4.8	4.8	4.9	4.9
ε^{i}(cont)/J K^{-1}	54.7	54.2	54.4	54.2	54.3	54.2
ε^{f}(cont)/J K^{-1}	56.5	55.6	55.8	55.6	55.7	55.6
$\Delta U_{dec}(HNO_3+HNO_2)$/J	81.1	61.6	60.2	59.3	62.5	62.0
$-\Delta U_{dil}(H_2SO_4)$/J	3.6	1.9	1.8	1.8	1.8	1.9
ΔU_{Σ}/J	7.6	7.6	7.6	7.6	7.5	7.6
$-\Delta U_{IBP}$/J	33618.7	27840.4	27511.0	27668.6	27680.0	27826.4
$-\{\Delta U^{\circ}_{c}/M\}$/kJ g^{-1}	32.0446	32.0599	32.0411	32.0489	32.0534	32.0575
$-\Delta U^{\circ}_{c}$/kJ mol^{-1}	4237.21	4239.24	4236.75	4237.79	4238.36	4238.92

Tables 5 and 6 for thioacetamide and tetramethylthiourea, respectively. The sublimation enthalpies are plotted against temperature in Fig. 1 in the temperature range below 320 K. Molar standard enthalpy of sublimation $\Delta H^{\circ}_{s}(T)$, was calculated with the following equation:

$$\Delta H^{\circ}_{s}(T) = E_{calib}(S_T/S_B)(M/m),$$

where E_{calib} is the electrical energy used in the calibration, (S_T/S_B) is the ratio of sublimation enthalpy to the electrical energy, as determined by calorimetry, and m and M are the mass and the molar mass, respectively, of the material effused from the sample container.

Observed enthalpies of sublimation for each substance were subjected to a regression analysis for linear relations between two variables.[8] Derived results are as follows: ΔH°_{s}/kJ mol^{-1} $= -(0.11314\pm0.03179)(T/\mathrm{K}) + (116.99\pm9.81)$ with estimated standard deviation from the fit s_f of 0.10 kJ mol^{-1} for thioacetamide, and ΔH°_{s}/kJ mol^{-1} $= -(0.03534\pm0.00965)(T/\mathrm{K}) + (93.57 \pm2.93)$ with s_f of 0.21 kJ mol^{-1} for tetramethylthiourea, where uncertainties are those at the 95% confidence level. Three values at 320.8 K of thioacetamide were not employed in the analysis, since they showed significant deviations from the fit.

Standard enthalpies of sublimation at 298.15 K were obtained by extrapolation of the smoothed functions to the reference temperature. Derived values were (83.26±0.34) and (83.04±0.20) kJ mol^{-1} for thioacet-

Table 5. Summary of sublimation calorimetric results on thioacetamide

T / K	t / ks	m / mg	E_{calib} / J	S_T / S_B	$\Delta H_s^\circ(T)$ / kJ mol^{-1}
305.6	17.04	7.91	1.1225	7.728	82.38
305.7	15.00	6.61	0.9283	7.803	82.37
306.3	54.80	22.65	14.760	1.683	82.39
307.2	127.20	64.57	1.6570	42.656	82.24
309.0	142.60	77.65	26.753	3.169	82.04
313.0	52.00	41.25	8.4759	5.275	81.43
313.0	104.60	86.96	4.4871	21.082	81.72
320.8	45.80	84.64	20.124	4.649	83.05
320.8	95.70	174.92	8.6817	22.407	83.56
320.8	72.45	131.63	24.474	5.984	83.60

Table 6. Summary of sublimation calorimetric results on tetramethylthiourea

T / K	t / ks	m / mg	E_{calib} / J	S_T / S_B	$\Delta H_s^\circ(T)$ / kJ mol^{-1}
298.5	24.45	28.89	2.2374	8.084	82.78
298.4	23.70	27.74	2.4405	7.140	83.06
298.5	20.40	23.87	2.2371	6.721	83.30
298.5	24.60	29.09	2.8476	6.393	82.74
301.3	31.90	52.20	2.8236	11.638	83.24
301.3	21.60	35.36	2.8235	7.847	82.84
301.4	21.70	35.37	4.8003	4.625	82.98
313.1	16.40	107.49	13.185	5.086	82.49
314.3	14.80	113.39	15.180	4.653	82.35
315.6	11.40	101.74	14.604	4.346	82.50

amide and tetramethylthiourea, respectively, where uncertainties are those at the 95% confidence level.

Derived standard thermodynamic quantities are presented in Table 7. Uncertainties given in this table are the overall values. The following contributions were taken into consideration in assigning uncertainties to $\Delta U_c^\circ(c)$: (1) Calculated standard deviation of mean (sdm) for the experimental values of $\Delta U_c^\circ(c)$, $s(\bar{U})$; (2) calculated sdm for those of ε(calor), $s(\varepsilon)$; (3) estimated sdm for the certified specific energy of combustion of the thermochemical standard benzoic acid Δu_c(ba), s(ba); and (4) likely systematic error of 0.05%. The former three were used to calculate the overall standard deviation of mean for $\Delta U_c^\circ(c)$, $s(\bar{U})_\Sigma$:

$$s(\bar{U})_\Sigma = [s(\bar{U})^2 + \{\Delta U_c^\circ(c)s(\varepsilon)/\varepsilon(\text{calor})\}^2 + \{\Delta U_c^\circ(c)s(\text{ba})/\Delta u_c(\text{ba})\}^2]^{1/2}.$$

$s(\bar{U})_\Sigma$ was 0.20 and 0.46 kJ mol^{-1} for thioacetamide and tetramethylthiourea, respectively. The overall uncertainty for $\Delta U_c^\circ(c)$, $\delta(\Delta U_c^\circ, c)$, was calculated by combining $\{2s(\bar{U})\}$ with the likely systematic error, mentioned above, by use of the following equation:

$$\delta(\Delta U_c^\circ, c) = [\{2s(\bar{U})_\Sigma\}^2 + \{0.0005\Delta U_c^\circ(c)\}^2]^{1/2}.$$

The overall uncertainty for $\Delta H_c^\circ(c)$ is equal to that for $\Delta U_c^\circ(c)$ and that for ΔH_s° is the uncertainty at the 95% confidence level.

The following CODATA recommended key values for thermodynamics[9] and the value[6] compatible with them were used to calculate standard enthalpies of formation in the crystalline state: $\Delta H_f^\circ(CO_2, g) = -(393.51 \pm 0.13)$,[9] $\Delta H_f^\circ(H_2O, l) = -(285.830 \pm 0.042)$,[9] and $\Delta H_f^\circ(H_2SO_4 \text{ in } 115H_2O) = -(888.263 \pm 0.042)$[6] kJ mol^{-1}, respectively, where uncertainties are those at the 95% confidence level for the former two, and that for the latter one is an estimated value.

Table 7. Standard thermodynamic quantities at 298.15 K of thioacetamide and tetramethylthiourea

Compound	Thioacetamide	Tetramethylthiourea
$-\Delta U_c^\circ(c)$ / kJ mol^{-1}	2027.8 ±1.1	4238.1 ±2.2
$-\Delta H_c^\circ(c)$ / kJ mol^{-1}	2033.4 ±1.1	4246.7 ±2.2
$-\Delta H_f^\circ(c)$ / kJ mol^{-1}	70.6 ±1.1	38.3 ±2.3
ΔH_s° / kJ mol^{-1}	83.26±0.34	83.03±0.20
$\Delta H_f^\circ(g)$ / kJ mol^{-1}	12.7 ±1.2	44.7 ±2.3

The overall uncertainties for $\Delta H_f^\circ(c)$ and for $\Delta H_f^\circ(g)$, $\delta(\Delta H_f^\circ, c)$ and $\delta(\Delta H_f^\circ, g)$, respectively, were calculated according to:

$$\delta(\Delta H_f^\circ, c) = [\delta(\Delta U_c^\circ, c)^2 + \{a\delta(CO_2)\}^2 + \{(b/2-d)\delta(H_2O)\}^2 + \{d\delta(H_2SO_4)\}^2]^{1/2},$$

and

$$\delta(\Delta H_f^\circ, g) = [\delta(\Delta H_f^\circ, c)^2 + \delta(\Delta H_s^\circ)^2]^{1/2},$$

where $\delta(CO_2)$, $\delta(H_2O)$, $\delta(H_2SO_4)$ and $\delta(\Delta H_s^\circ)$ are the uncertainties assigned to $\Delta H_f^\circ(CO_2, g)$, $\Delta H_f^\circ(H_2O, l)$, $\Delta H_f^\circ(H_2SO_4 \text{ in } 115H_2O)$, and ΔH_s°, respectively.

Discussion

Thianthrene is a test substance for combustion calorimetry of organic sulfur compounds, recommended by IUPAC.[15] The standard enthalpy of combustion of thianthrene, obtained in this study, agrees with the value of Hu *et al.*[13] and that of Johnson[14] within the sum of each uncertainty, among the literature values given in Table 2. The difference between the recommended value[15] and the present value amounts to 3.7 kJ mol^{-1}, which is 0.05% of total. The relative deviation of 0.05% was assumed to be the relative systematic error for $\Delta H_c^\circ(c)$ and the contribution from this source has been included in the overall uncertainties for $\Delta U_c^\circ(c)$ and $\Delta H_c^\circ(c)$, $\delta(\Delta U_c^\circ, c)$, as described in the preceding section. Standard enthalpy of combustion has not been reported so far for thioacetamide and tetramethylthiourea.

As was pointed out briefly, amides are stabilized considerably due to interaction between a carbonyl group and a neighbouring nitrogen atom, as compared with the hypothetical reference structures, where no such interaction exerts. Stabilization energy may be evaluated by comparing observed and calculated standard enthalpies of formation in gaseous state, for example, as shown in Table 8 for normal alkanamides, $CH_3(CH_2)_{n-1}CONH_2$. The calculated values were obtained by means of the group contribution method[16] as follows:

Table 8. Estimated stabilization energies, U_s, of normal alkanamides, $CH_3(CH_2)_{n-1}CONH_2$

n	$-\Delta H_f^\circ$(g)/kJ mol^{-1}		U_s[c]
	Obsd[a]	Calcd[b]	kJ mol^{-1}
1	238.3	155.5	82.8
2	258.9	176.1	82.8
3	278.1	196.7	81.4
4	290.2	217.3	73.0
5	328.1	237.8	90.3
6	—	258.4	—
7	362.7	279.0	83.7

a) Ref. 20. b) See the text. c) $U_s=\Delta H_f^\circ$(g, calcd)$-\Delta H_f^\circ$(g, obsd).

$$\Delta H_f^\circ(\text{g, calcd}) = [\mathbf{C}\text{-}(C)(H)_3] + (n-1)[\mathbf{C}\text{-}(C)_2(H)_2] + [\mathbf{CO}\text{-}(C)_2] + [\mathbf{N}\text{-}(C)(H)_2],$$

where [**C**-(C)(H)$_3$], [**C**-(C)$_2$(H)$_2$], [**CO**-(C)$_2$], and [**N**-(C)(H)$_2$] are the contributions from methyl, methylene, ketonic carbonyl, and amino groups, respectively. These contributions are such that standard enthalpies of formation in gaseous state at 298.15 K for normal alkanes, normal alkanones, and normal alkylamines are reproduced satisfactorily as an appropriate sum of these contributions. Values selected by Cox and Pilcher[21] were used for these contribution terms. Table 8 shows that the normal alkanamides are stabilized as much as 83 kJ mol^{-1} in average, as compared with the corresponding reference structures.

In order to achieve a similar analysis for thioacetamide and tetramethylthiourea, it is necessary to know the value of an additional contribution, [**CS**-(C)$_2$], which is the contribution from a thioketonic thiocarbonyl group. Since thioketones are very unstable compounds, this value has not been presented. Only thermochemical data that is available for unstabilized thiocarbonyl compounds is the standard enthalpy of formation in gaseous state of thioformaldehyde, $\Delta H_f^\circ(H_2C{=}S, g)$, of (100±11) kJ mol^{-1}, which was determined by electron impact method.[17] Consequently, the value of [**CS**-(C)$_2$] was estimated by adding the difference $\{\Delta H_f^\circ(H_2C{=}S, g)-\Delta H_f^\circ(H_2C{=}O, g)\}$ to [**CO**-(C)$_2$] (= −132.47 kJ mol^{-1}).[21] By adopting −(108.7±0.7) kJ mol^{-1} [20] for $\Delta H_f^\circ(H_2C{=}O, g)$, [**CS**-(C)$_2$] was estimated to be 77 kJ mol^{-1}.

Standard enthalpies of formation in gaseous state were calculated for hypothetical reference structures:[21] For thioacetamide,

$$\begin{aligned}\Delta H_f^\circ(\text{g, calcd}) &= [\mathbf{C}\text{-}(C)(H)_3] + [\mathbf{CS}\text{-}(C)_2] + [\mathbf{N}\text{-}(C)(H)_2] \\ &= (-42.34) + (77) + (19.33) \\ &= 54\ \text{kJ mol}^{-1},\end{aligned}$$

and for tetramethylthiourea,

$$\begin{aligned}\Delta H_f^\circ(\text{g, calcd}) &= 4[\mathbf{C}\text{-}(N)(H)_3]^{ass} + 2[\mathbf{N}\text{-}(C)_3] + [\mathbf{CS}\text{-}(C)_2] \\ &= 4\times(-42.34) + 2\times(103.30) + (77) \\ &= 114\ \text{kJ mol}^{-1},\end{aligned}$$

where [**C**-(N)(H)$_3$]^{ass} and [**N**-(C)$_3$] are the contributions from a methyl group attached to a nitrogen atom and from a tertiary nitrogen atom, respectively.

Comparison of the observed values of ΔH_f°(g), given in Table 7, with these calculated values leads to stabilization energies of 41 and 69 kJ mol^{-1} for thioacetamide and tetramethylthiourea, respectively. The stabilization energy of thioacetamide amounts to about 50% of the corresponding value of acetamide and the value for tetramethylthiourea is 1.7 times as large as that of thioacetamide. Although uncertainties approaching 15 kJ mol^{-1} should be assigned to the estimated stabilization energies, in view of the large uncertainty of $\Delta H_f^\circ(H_2C{=}S, g)$ and the assumption made in the course of estimation of [**CS**-(C)$_2$], it may be stated conclusively that thioacetamide and tetramethylthiourea are stabilized considerably, as compared with the corresponding reference structures. This fact may be the reason why these compounds are fairly stable at ambient temperatures, while thioketones are not. This stabilization is possibly due to the interaction between thiocarbonyl π-electrons and nitrogen lone pair electrons.

According to an X-ray diffraction study, a thioacetamide molecule is almost planar except for methyl hydrogen atoms.[18] Although the molecular structure is not known for tetramethylthiourea, sulfur, carbon and nitrogen atoms in a thiourea molecule are coplanar.[19] These findings seem to be an indication of possible intramolecular interaction between thiocarbonyl π-electrons and nitrogen lone pair electrons.

References

1) K. Fries and W. Vogt, *Ann.*, **381**, 320 (1911).
2) M. Sakiyama, T. Nakano, and S. Seki, *Bull. Chem. Soc. Jpn.*, **48**, 1705 (1975).
3) K. Nishiyama, M. Sakiyama, S. Seki, H. Horita, T. Otsubo, and S. Misumi, *Bull. Chem. Soc. Jpn.*, **53**, 869 (1980).
4) J. D. Cox and G. Pilcher, "Thermochemistry of Organic and Organometallic Compounds," Academic Press, London (1970), p. 70.
5) S. Murata, M. Sakiyama, and S. Seki, *J. Chem. Thermodyn.*, **14**, 707 (1982).
6) V. B. Parker, D. D. Wagman, and D. Garvin, "Selected Thermochemical Data Compatible with the CODATA Recommendations," *NBSIR* 75-968, NTIS (1975).
7) W. N. Hubbard, D. W. Scott, and G. Waddington, "Experimental Thermochemistry," ed by F. D. Rossini, Interscience, New York (1956), Vol. 1, Chap. 5.
8) "Statistical Method in Research and Production with Special Reference to Chemical Industry," 4th ed, ed by O. L. Davies and P. L. Goldsmith, Longman, London (1977).
9) CODATA Task Group on Key Values for Thermodynamics, 1977, *CODATA Bull.*, **1978**, 28; *J. Chem. Thermodyn.*, **10**, 903 (1978).
10) W. N. Hubbard, C. Katz, and G. Waddington, *J. Phys. Chem.*, **58**, 142 (1954).
11) W. A. Keith and H. Mackle, *Trans. Faraday Soc.*, **54**, 353 (1958).
12) (a) S. Sunner and B. Lundin, *Acta Chem. Scand.*, **7**, 1112 (1953); (b) S. Sunner, *ibid.*, **17**, 728 (1963).
13) J-H. Hu, H-K. Yen, and Y-L. Geng, *Acta Chim. Sin.*, **32**, 242 (1966).
14) W. H. Johnson, *J. Res. Natl. Bur. Stds.*, **79A**, 561

(1975).
15) J. D. Cox, *Pure Appl. Chem.*, **40**, 399 (1974).
16) S. W. Benson and J. H. Buss, *J. Chem. Phys.*, **29**, 546 (1958).
17) A. Jones and F. P. Lossing, *J. Phys. Chem.*, **71**, 4111 (1967).
18) M. R. Truter, *J. Chem. Soc.*, **1960**, 997.
19) N. R. Kunchur and M. R. Truter, *J. Chem. Soc.*, **1958**, 2558.
20) J. B. Pedley and J. Rylance, "Sussex-N.P.L. Computer Analysed Thermochemical Data: Organic and Organometallic Compounds," University of Sussex, Brighton (1977).
21) Ref. 4, p. 590.

Specific Anion Effects on Water Structure at Polypeptide Monolayer-Water Interface

Akira SHIBATA,* Shinsuke YAMASHITA, and Takuya YAMASHITA
Faculty of Pharmaceutical Sciences, Tokushima University, Shomachi, Tokushima 770
(Received March 8, 1982)

The specific anion effects on water structure at the polypeptide monolayer-water interface were investigated. It was found that the effects of anions on increasing the film transition pressure were in the order of $SCN^->Br^->Cl^->F^-$ in line with that of those anions as breakers of water structure. The SCN^- ion disrupts the hydrophobic hydration surrounding the hydrocarbon moieties of polypeptides and lipids at the interface. On the other hand, the presence of F^- ion as a structure maker tends to stabilize the hydrophobic bonding. The increase of the film transition pressure on KSCN subsolution was associated with a difference in the conformation between poly(γ-benzyl L-glutamate) and poly(γ-benzyl DL-glutamate). The infrared spectra of polymers obtained from single and mixed films were practically identical with the collapsed films in the presence and the absence of SCN^- and F^- ions.

In recent years, a number of attentions have been focused on the structure of water in living cells and the role of hydration of water around protein molecules in life processes. It is currently believed that the structure of water at biosurface is significantly influenced and ordered by constituent macromolecules.[1] In other words, water adjacent to biosurface differs appreciably from bulk water.[2]

A wide variety of electrolyte effects on biological systems has been found to give rise to the same sequence observed by Hofmeister.[3] The unifying principle underlying the effects of electrolytes on macromolecules and on water itself is that the order of effectiveness of anions is nearly the same for all. The anions are considered to exert their effects by altering the structure of water, thus weakening the tendency toward hydrophobic bonding. Recent evidence suggests that the electrolyte effects are associated with the structure of water at an interface.[2]

The structure breaking and structure making effects of electrolytes on the water structure should have application to interfacial water structure. One way of enhancing water structure at the interface is the application of monolayer technique. Weil[4] and Goddard *et al.*[5] reported on the effects of electrolytes on the interfacial water structure at "ionized" monolayers. It is necessary to use "un-ionized monolayer to emphasize the specific electrolyte effects on water structure at the interfaces. Ralston and Healy[6] have studied the effects of cations on 1-octadecanol monolayers in connection with the interfacial water structure.

In relation to the structure of water in the surface region, we have reported the effects of monovalent anions on the surface pressure-area(π-A) curves of poly(N^ϵ-benzyloxycarbonyl-L-lysine) monolayer.[7] The effects of anions on increasing the surface pressure were in the order of $SCN^->Br^->Cl^->F^-$ in line with that of these anions as breakers of water structure.[8]

The purpose of this work is to clarify the effects of anions on the conformation of polypeptide and on the interaction of polypeptide and lipid in relation to the structure of water in the interfacial region.

Experimental

Poly(N^δ-benzyloxycarbonyl-L-ornithine) (PLO(Z)), poly(N^ϵ-benzyloxycarbonyl-L-lysine) (PLL(Z)), poly(γ-benzyl L-glutamate) (PBLG), and poly(γ-benzyl DL-glutamate) (PBDLG) were prepared by the polymerization of the *N*-carboxy anhydrides of respective amino acids. The molecular weights determined from the viscosities in *N*,*N*-dimethylformamide (DMF)[9] or dichloroacetic acid[10] are 3.5×10^5 for PLO(Z), 3.8×10^5 for PLL(Z), 3.1×10^5 for PBLG, and 6.0×10^4 for PBDLG, respectively. Infrared spectra indicated that PLO(Z), PLL(Z) and PBLG are in the α-helical conformation in the solid state. The helical content of PBDLG was 13% regular α-helix and 60% perturbed α-helix. Lipids used were myristic acid(C_{14} acid) and stearic acid(C_{18} acid). These materials were purified by fractional distillation, and were chromatographycally pure.

The spreading solvents (DMF, dichloromethane (DCM)) were distilled under nitrogen atmosphere. The subsolution, 0.01 M HCl, was made up from twice distilled water and distilled 6 M HCl (1 M = 1 mol dm^{-3}). The spreading solvents were DCM for PBLG- and PBDLG-lipid systems and a 9:1 (v/v) mixture of DCM and DMF for PLO(Z)- and PLL(Z)-lipid systems. The solutions of polypeptide and lipid were prepared separately, and mixed in the desired ratio immediately before spreading. The spreading solution was deposited from a micrometer syringe onto the surface of subsolution, and left to stand for 15 min. The initial spreading-area was 0.5 nm^2/residue or molecule. The trough (60 cm × 15 cm × 1 cm) and compressing barrier were made of Teflon.

Electrolyte solutions (KSCN, KBr, KCl, and KF) were treated with activated charcoal in order to remove surface active contaminants, and were used as a subsolution after being adjusted to contain 0.01 M HCl. A 10 to 1 compression of the surface of the electrolyte subsolutions, after standing for 10 min, produced less than 0.1 mN m^{-1} film pressure. The surface pressure was measured by the Wilhelmy method at 25±0.5 °C. The film was compressed at a rate of 10 mm/min (0.01 nm^2 min^{-1} per residue or molecule).

The polarized infrared spectra of collapsed films were measured by JASCO-701G instrument. The monolayer was spread and compressed until collapse under the same conditions as in the case of surface pressure measurements. In order to remove the monolayer, it was compressed between two Teflon barriers, until the separation was about 1.5 cm. The polymer was then removed by drawing a stainless steel net across the trough between the barriers.

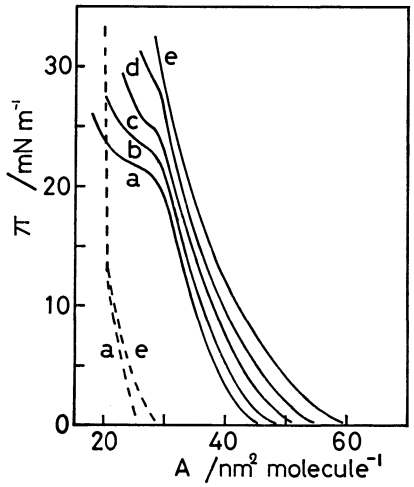

Fig. 1. Surface pressure-area curves of C_{14} acid (——) and C_{18} acid (- - -) on HCl and KSCN subsolutions. 1 dyn=10^{-5} N, 1 Å=0.1 nm. a: 0.01 M HCl, b: 1 M KSCN, c: 2 M KSCN, d: 3 M KSCN, e: 4 M KSCN.

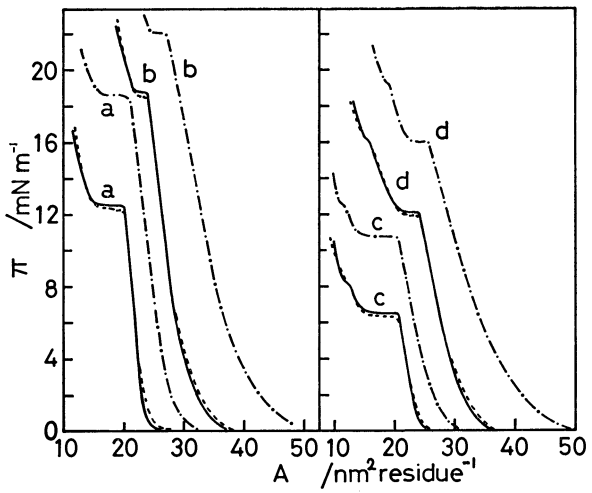

Fig. 2. Surface pressure-area curves of single and mixed monolayers on 0.01 M HCl(——), 2 M KSCN (—·—) and 2 M KF(- - -) subsolutions.
a: PLO(Z), b: PLO(Z)-C_{14} acid(1:1(residue mol: mol)), c: PLL(Z), d: PLL(Z)-C_{14} acid(1:1(residue mol:mol)).

The transferred collapsed films were dried at a room temperature.

Results

Figure 1 shows the π-A curves for C_{14} acid and C_{18} acid monolayers on 0.01 M HCl and KSCN subsolutions containing 0.01 M HCl. The increasing concentration of KSCN causes the increase of transition pressure and the expansion of C_{14} acid monolayer. The transition point of C_{14} acid monolayer tends to disappear with increasing concentration of KSCN, and is no longer detectable at 4 M KSCN. The expansion of C_{18} acid monolayer on KSCN subsolution is considerably small compared with C_{14} acid monolayer.

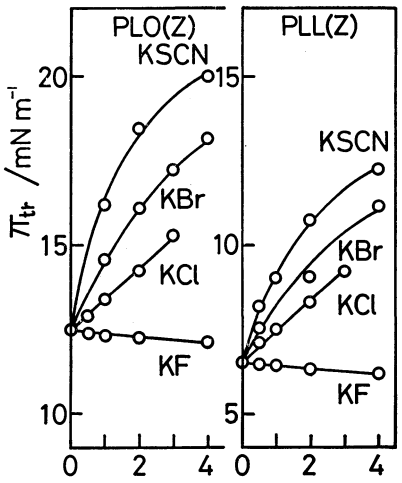

Fig. 3. Transition pressures of PLO(Z) and PLL(Z) monolayers as a function of electrolyte concentration.

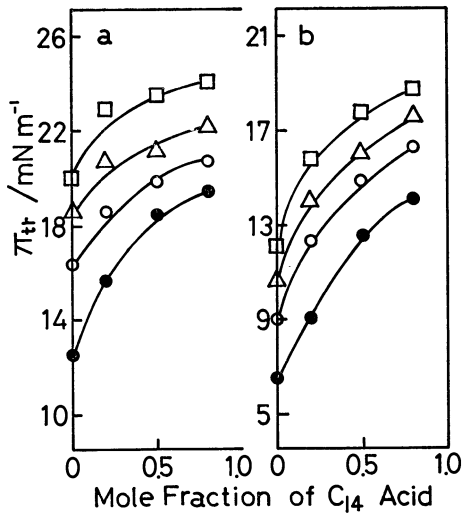

Fig. 4. Transition pressures of mixed monolayers of C_{14} acid with PLO(Z) (a) or PLL(Z) (b) as a function of C_{14} acid mole fraction on HCl and KSCN subsolutions.
●: 0.01 M HCl, ○: 1 M KSCN, △: 2 M KSCN, □: 4 M KSCN.

Figure 2 shows the π-A curves for PLO(Z), PLL(Z), PLO(Z)-C_{14} acid and PLL(Z)-C_{14} acid mixtures(1:1 (residue mol:mol)) spread on 0.01 M HCl, and on 2 M KSCN and 2 M KF subsolutions containing 0.01 M HCl. In the π-A curves of PLO(Z) and PLL(Z) monolayers, the height of plateau which is associated with the transition pressures is much higher on the subsolution containing KSCN than 0.01 M HCl. On the other hand, in the presence of KF, the film transition pressure becomes slightly lower. The film expansion is observed for PLO(Z) and PLL(Z) in the presence of KSCN. The effect of KF on expansion is quite small.

Figure 3 shows the transition pressures of PLO(Z) and PLL(Z) monolayers as a function of electrolyte concentration. The transition pressures of PLO(Z) and PLL(Z) increase with electrolyte concentration

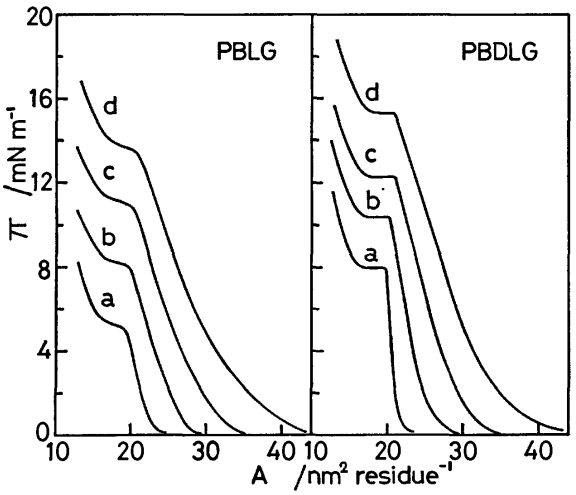

Fig. 5. Surface pressure-area curves of PBLG and PBDLG monolayers on HCl and KSCN subsolutions. a: 0.01 M HCl, b: 2 M KSCN, c: 4 M KSCN, d: 6 M KSCN.

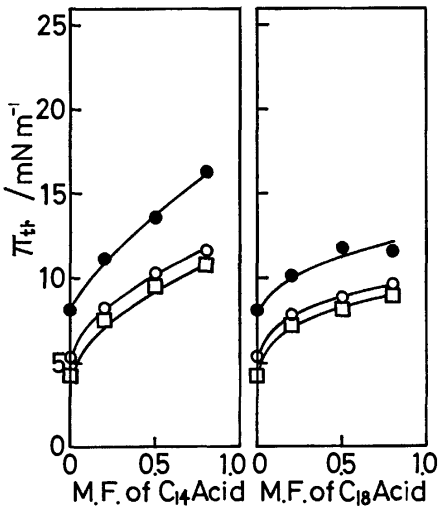

Fig. 7. Transition pressures of mixed monolayers of PBLG with C_{14} acid or C_{18} acid as a function of lipid mole fraction on 0.01 M HCl(○), 2 M KSCN(●), and 2 M KF(□) subsolutions.

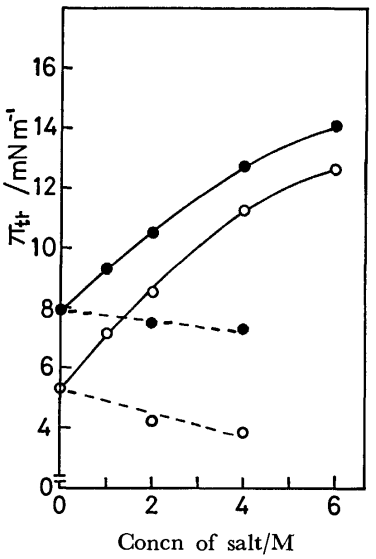

Fig. 6. Transition pressures of PBLG(○) and PBDLG (●) as a function of electrolyte concentration. ——: KSCN, – – –: KF.

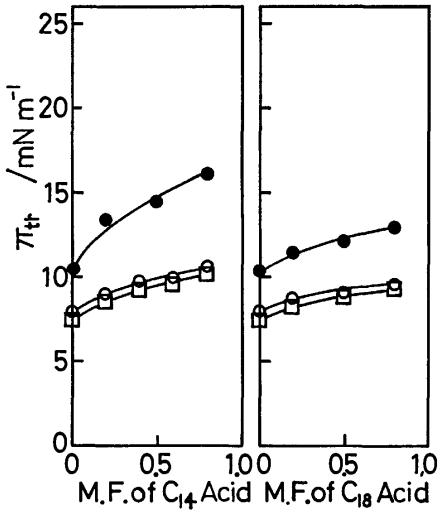

Fig. 8. Transition pressures of mixed monolayers of PBDLG with C_{14} acid or C_{18} acid as a function of lipid mole fraction on 0.01 M HCl(○), 2 M KSCN (●), and 2 M KF(□) subsolutions.

except for KF. In the lower concentration of KSCN or KBr, in particular, the transition pressures show the marked increase.

Figure 4 shows the transition pressures of mixed monolayers of C_{14} acid with PLO(Z) or PLL(Z) on 0.01 M HCl and KSCN subsolutions as a function of the mole fraction of C_{14} acid. The phase rule of the surface predicts that two film components are miscible in the presence and the absence of KSCN in the subsolution.[11,12] The increasing concentration of KSCN causes the increase of transition pressure. The effect of KSCN on the transition pressure for mixed PLO(Z)–C_{14} acid monolayer is smaller than for mixed PLL(Z)–C_{14} acid monolayer.

Figure 5 shows the π-A curves for PBLG and PBDLG monolayers on 0.01 M HCl and KSCN subsolutions containing 0.01 M HCl. As such case of benzyloxycarbonyl derivatives of basic poly(α-amino acid), PLO(Z) and PLL(Z), the film expansion is also observed on KSCN subsolution.

The transition pressures of PBLG and PBDLG monolayers as a function of KSCN and KF concentration is shown in Fig. 6. The transition pressures of PBLG and PBDLG monolayers increase with KSCN concentration, and in the presence of KF, decrease linearly.

Figures 7 and 8 show the relationship between transition pressure and lipid mole fraction for mixed PBLG–fatty acid and PBDLG–fatty acid monolayers on 0.01 M HCl, and 2 M KSCN and 2 M KF subsolutions, respectively. The transition pressures for both mixed PBLG–fatty acid and PBDLG–fatty acid systems increase with the mole fraction of C_{14} acid or C_{18} acid. The increments of transition pressure for mixed PBLG–fatty acid systems are larger than for mixed PBDLG–fatty acid systems. The effect of

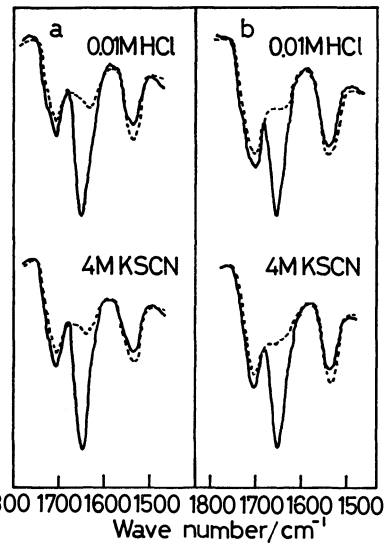

Fig. 9. Polarized IR spectra of collapsed films of PLL(Z) (a) and 4:1 (residue mol:mol) mixture of PLL(Z) and C_{14} acid(b) formed on 0.01 M HCl and 4 M KSCN subsolutions.
——: Electric vector parallel to the barrier used to collapse the film, - - -: electric vector perpendicular.

C_{14} acid on the transition pressure is larger compared with C_{18} acid.

As typical examples, the polarized infrared spectra for collapsed films of PLL(Z) and a 4:1 (residue mol: mol) mixture of PLL(Z) and C_{14} acid are shown in Fig. 9. The spectra which are characteristic of polypeptide designated as a α-helix form have major diagnostic peaks at about 1650 cm^{-1} (amide I band) and 1550 cm^{-1} (amide II band). Dichroism is also observed at about 1700 cm^{-1}(assignable to streching of C=O bond of the side chain). A similar tendency was observed for other single and mixed films.

Discussion

Mixed PLO(Z)–C_{14} Acid and PLL(Z)–C_{14} Acid Systems. C_{14} acid and C_{18} acid monolayers are of expanded and condensed type at 25 °C, respectively (Fig. 1).[13] The transition is seen in the π-A curves of C_{14} acid. The transition region becomes short with increasing KSCN concentration, and ultimately disappears at 4 M. A similar tendency is also recognized for the effect of temperature on transition pressure of C_{14} acid.[14] If the monolayer expansion is due to the flexibility of the hydrophobic moieties of C_{14} acid, the rotation of the flexible hydrophobic moieties may be hindered with compressing monolayer. The hindered molecular rotation may lead to the discontinuity of compressibility associated with the onset of the transition.[15] In analogy with the effect of temperature, the addition of SCN^- ion as a breaker of water structure may favor the molecular rotation of C_{14} acid at the interface.

A complex polymer like a protein will be sheathed in a complex hydration envelope consisting of regions of differing local water structure at the interface.[16] The polypeptides used in this work will also have two types of water structure arising from the hydrophobic and Coulombic hydrations. The nonpolar moieties will be encased by the same hydrophobic hydration that one associates with nonpolar solutes and neutral interface, whereas polar regions will be surrounded by the same Coulombic hydration that surrounds ion in solution.

There exist plateaux in the π-A curves for PLO(Z) and PLL(Z) monolayers(Fig. 2). The plateau was found for a number of synthetic polypeptide monolayers, and ascribed to the transition from a two-dimensional ordered state to a three-dimensional disordered state.[17,18] The height of plateau can be regarded as a measure of the adhesion force of monolayer to water. As shown in Fig. 3, the transition pressures increase with concentration of electrolyte, and the effects of anions on the transition pressure are in the order of $SCN^- > Br^- > Cl^- > F^-$ in accordance with that of these anions as breakers of water structure.[8] A structure breaker like SCN^- is more easily accomodated in the interface than F^-, a structure maker, due to the fact that it introduces more disorder in the structure region at the air-water interface.[19] The hydration atmosphere of SCN^- ion is compatible with the Coulombic hydration surrounding the polar group of polypeptide and enable SCN^- ion to penetrate, and profoundly alter the hydration. In addition, the hydrophobic hydration surrounding the polypeptide side chain is disrupted by the action of SCN^- ion. This will be accompanied by a decrease in adhesion of the hydrophobic moieties of the side chains to water, followed by an increase in the surface pressure.[20]

Comparing the π-A curves of PLO(Z) with PLL(Z) monolayers, the difference in height of the transition pressures is accounted for as arising essentially from the additional methylene group (Fig. 2). The effects of anions on the transition pressure of PLO(Z) are larger than PLL(Z) (Fig. 3). If the α-helix form can be stable at the air–water interface, the geometry of the α-helix is such that the side chains of adjacent helices can interpenetrate to form good hydrophobic contacts.[18]

It can be assumed that the hydrophobic and Coulombic hydrations surrounding polypeptide monolayers are in equilibrium with the Coulombic hydration for electrolyte in the presence of electrolyte. As the electrolyte is added. In other words, hydrophobic hydration is disrupted, the equilibrium indicated in the scheme (1) is shifted to right along the dotted line, and after that, shifted to left along the full line. Therefore, the compatibility of Coulombic hydration between polypeptide and electrolyte may cause the increase of transition pressure.

In the presence of F^- ion, the transition pressure decreases slightly with increasing concentration(Fig. 3). Increasing concentration of F^- ion as a maker of water structure, the equilibrium in the scheme (1) will be shifted to the direction of the stabilization of hydrophobic hydration. In the present case, the effect of F^- ion on the transition pressure may imply the stabilization of hydrophobic hydration surrounding the monolayers.

For mixed monolayers of C_{14} acid and either PLO-(Z) or PLL(Z) on 0.01 M HCl subsolution, the increase of transition pressure is due to the hydrophobic bonding between polypeptide side chain and C_{14} acid (Fig. 4).[21] The effect of C_{14} acid on the transition pressure caused by PLL(Z) is larger than that of PLO(Z). This is caused by the additional methylene group for PLL(Z).[21] A similar tendency was also recognized on KSCN subsolutions (Fig. 4).

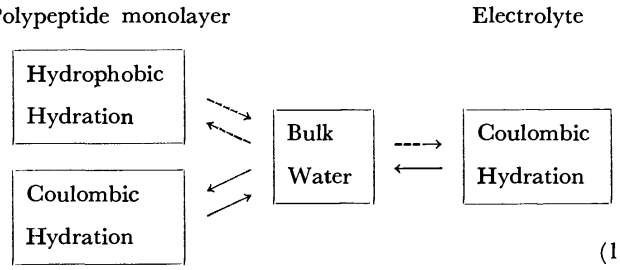

(1)

In the presence of KSCN, the relationship between transition pressure and the mole fraction of C_{14} acid gives a parallel shift to the direction of the increase of transition pressure in the range of 1 to 4 M KSCN concentration. This parallel shift suggests that the hydrophobic hydration surrounding polypeptide–C_{14} acid complex is "partially" disrupted with increasing concentration of SCN^- ion. If, however, the hydrophobic bonding between polypeptide and C_{14} acid is "essentially" disrupted by the action of SCN^-, the value of transition pressure caused by polymer will have of coming close to that of polypeptide itself or the lower value compared with that of mixed monolayer different from our results.

Mixed PBLG–Fatty Acid and PBDLG–Fatty Acid Systems. The perturbed helix portion of PBDLG is unfolded at the interface owing to relatively weak stability of the helix.[22] As is shown in Fig. 5, the difference in shape of the π-A curves between PBLG and PBDLG is accounted for as arising essentially from the conformation of these polymers at the interface.[21] The more increase of the transition pressure of PBDLG compared with PBLG may be caused by the hydration surrounding the perturbed helix portion of PBDLG. The water structure beneath the monolayer must be also reflected to the monolayer compressibility. We have reported that the compressibilities at closed packed area are 0.027 for PBLG and 0.015 for PBDLG.[21] The film expansion on KSCN subsolution suggests that SCN^- ion is transferred into the interface relative to the surface without monolayer(Fig. 5).

The change in the transition pressures of mixed monolayers is larger for PBLG than for PBDLG(Figs. 7 and 8). The flexible side chains of PBLG in α-helical conformation might undergo rearrangement more easily into the position favorable to the interaction with hydrophobic moieties of fatty acids. Chatelain *et al.*[23] reported that the maximum interaction of lipid monolayer with polypeptides occurs when the polypeptides dissolved in the subsolution in α-helical conformation.

Comparing the transition pressures of mixed PBLG–C_{14} acid and PBLG–C_{18} acid monolayers, the state of fatty acid monolayers(expanded and condensed films) seems to affect the degree of interaction (Fig. 7). The C_{14} acid interacts more strongly than C_{18} acid with PBLG.

The transition pressures of mixed PBLG– and PBDLG–fatty acid monolayers on 2 M KSCN subsolution become higher compared with those on KSCN free subsolution (Figs. 7 and 8). The increase of transition pressure is larger for mixed PBDLG–fatty acid systems than for mixed PBLG–fatty acid systems. In the presence of SCN^- ion, the hydrophobic hydration surrounding mixed monolayer is disrupted, and then, the increase of the compatibility of Coulombic hydration around unfolded PBDLG may be caused. Therefore, this may be associated with a difference in the conformation between PBLG and PBDLG in mixed monolayers.

As shown in Figs. 7 and 8, the transition pressures of mixed monolayers on 2 M KF subsolution become low compared with those on KF free subsolution. In the presence of F^- ion as a maker of water structure, the adhesion force of polypeptide to water becomes weak with the formation of hydrated structure surrounding the mixed films. The effect of F^- ion on the transition pressure of mixed monolayer is slightly large for PBLG compared to PBDLG. This suggests that the hydrophobic hydration around PBLG–C_{14} acid complex tends to be stabilized by the action of F^-. PBLG is expected to be more hydrophobic than PBDLG since the polypeptide main chain is considerably shielded from the interaction with water molecules.

Infrared Spectra of Collapsed Films. The parallel dichroism of the amide I band and the perpendicular dichroism of the amide II are those known to be characteristic of the α-helix, with the molecules showing alignment parallel to the barrier used to collapse the monolayer (Fig. 9). Similar spectra of the collapsed films were obtained in the presence and the absence of electrolyte. This is an evidence that as mentioned above, SCN^- ion disrupts partially hydrophobic hydration surrounding the monolayers, and that, in other words, the monolayers are stabilized by the hydrophobic bonding. The dichroism for the side chains suggests that the side chains are considerably ordered at the interface. This might favor the polypeptide-lipid interaction at close packed state in monolayers.

References

1) R. D. Schultz and S. K. Asunmaa, "Prog. Surface Sci.," Academic Press, New York (1971), Vol. 3, p. 291.
2) W. Drost-Hansen, "Chemistry of the Cell Interface," ed by H. D. Brown, Academic Press, New York (1971), Part B, p. 1.
3) F. Hofmeister, *Arch. Exp. Pathol. Pharmakol.*, **24**, 247 (1888).
4) I. Weil, *J. Phys. Chem.*, **70**, 133 (1966).
5) E. D. Goddard, O. Kao, and H. C. Kung, *J. Colloid Sci.*, **27**, 616 (1968).
6) J. Ralston and T. W. Healy, *J. Colloid Interface Sci.*, **42**, 629 (1973).
7) T. Yamashita, A. Shibata, and S. Yamashita, *Chem.*

Lett., **1978**, 11.
8) R. W. Gurney, "Ionic Processes in Solution," McGrow-Hill, New York (1953), Chap. 9.
9) E. Daniel and E. Kachalsky, "Polyamino Acids, Polypeptides and Proteins," ed by M. A. Stahmann, The University of Wisconsin Press, Madison (1962), p. 188.
10) P. Doty, J. H. Bradbury, and A. M. Holtzer, *J. Am. Chem. Soc.*, **78**, 947 (1956).
11) D. J. Crisp, "Surface Chemistry Suppl. Research," London (1949), p. 17.
12) R. Defay, I. Prigogine, A. Bellemans, and D. H. Everett, "Surface Tension and Adsorption," Longmans, London (1966) p. 71.
13) G. L. Gaines, Jr., "Insoluble Monolayers at Liquid-Gas Interfaces," Interscience, New York (1966), p. 208.
14) N. K. Adam and G. Jessop, *Proc. R. Soc. London, Ser. A*, **112**, 364 (1926).
15) G. L. Gaines, Jr., "Insoluble Monolayers at Liquid-Gas Interfaces," Interscience, New York (1966), p. 184.
16) R. A. Horne, *J. Colloid Interface Sci.*, **35**, 77 (1971).
17) B. R. Malcolm, *Proc. R. Soc. London, Ser. A*, **305**, 363 (1968).
18) B. R. Malcolm, *Prog. Surf. Membr. Sci.*, **7**, 183 (1973).
19) R. Aveyard and D. A. Haydon, "An Introduction to the Principles of Surface Chemistry," Cambridge University Press (1973), p. 102.
20) A. Shibata, S. Yamashita, and T. Yamashita, *Bull. Chem. Soc. Jpn.*, **51**, 2757 (1978).
21) T. Yamashita, A. Shibata, and S. Yamashita, *Bull. Chem. Soc. Jpn.*, **51**, 2751 (1978).
22) M. Tsuboi, Y. Mitsui, A. Wada, T. Miyazawa, and N. Nagashima, *Biopolymers*, **1**, 297 (1963).
23) P. Chatelain, C. Berliner, J. -M. Ruysschaert, and J. Jaffe, *J. Colloid Interface Sci.*, **51**, 239 (1975).

Tunnel Electrode I. Electron Transfer Process at Highly Doped SnO_2 Electrode with Ce^{4+} in High Overvoltage Region

Kenkichiro KOBAYASHI,* Yoshihiro AIKAWA, and Mitsunori SUKIGARA
Institute of Industrial Science, The University of Tokyo,
7-22-1 Roppongi, Minato-ku, Tokyo 106
(Received February 24, 1982)

Electron transfer theory at tunnel semiconductor electrode was derived from the double adiabatic perturbation theory. The cathodic current of Ce^{4+} with very positive redox potential was measured at highly doped SnO_2 electrode. The rearrangement energy of 0.65 eV for Ce^{4+} was estimated from the relationship of transfer coefficient *vs.* electrode potential. Large electron transfer rate in the high overvoltage region can be explained in terms of the contribution of excited vibrational states in the first coordination sphere into electron transfer.

The effect of electrode potential on the characteristics of an usual semiconductor electrode is such that the electrode potential cannot modify the energy of electrons and holes at the surface, but can change the surface density of electrons and holes through the band bending. When the carrier density of a semiconductor is very large, the thickness of the space charge layer is so small that electrons or holes can move through the depletion layer by tunneling. If such a highly doped semiconductor is used as an electrode, the electron transfer by tunneling through the space charge layer and the Helmholtz layer may occur in a certain potential range.[1-3] Thus, such a electrode may be called "tunnel semiconductor electrode." The electrochemical characteristic of a tunnel electrode is that the energy of a transferring electron or hole can be easily varied by the electrode potential.

For the rate of electron transfer reactions, Marcus[4] predicted that, in the so called normal region where the energy change of a reaction, $|\Delta E|$, is smaller than the rearrangement energy λ_s, the reaction rate should increase with $|\Delta E|$, while in the abnormal region where $|\Delta E|>\lambda_s$, the reaction rate should decrease with $|\Delta E|$. Rhem and Weller,[5,6] however, reported that such a decrease in the reaction rate was not observed in the abnormal region. Although their experimental results are significant, the electron transfer rate in the abnormal region could not be quantitatively discussed because of the diffusion limit of their reactions. The electrochemical electron transfer rate in the abnormal region has not been studied with metal electrode, because the electrons are distributed over a wide energy range in a metal. On the other hand, a tunnel electrode has an electron distribution in a definite and narrow energy range, so that the observed current directly reflects on the transition probability of electron with the semiconductor Fermi level. Therefore, the tunnel electrode is especially a useful tool for the measurement of electron transfer rate in the abnormal region.[7] The tunnel electrode has another advantage that the tunneling probability is usually not so high that the current may not be limited by diffusion even in a high overvoltage region.

In the present work, a theory for the cathodic tunnel current is derived and, by measuring the cathodic tunnel current at a highly doped tin oxide electrode, the electron transfer mechanism of Ce^{4+} at high overvoltage is discussed.

Theoretical

The cathodic and anodic current density at n-type tunnel electrode are respectively given by[8]

$$i_c = -ed\Omega C_{ox}\int W_c(E)\rho_{sc}(E)f(E)\mathrm{d}E, \quad (1)$$

and

$$i_a = ed\Omega C_{red}\int W_a(E)\rho_{sc}(E)[1-f(E)]\mathrm{d}E, \quad (2)$$

where W_c and W_a are respectively the transition probability for cathodic and anodic processes, $\rho_{sc}(E)$ is the state density in the semiconductor bulk, $f(E)$ is the Fermi distribution function, C_{ox} and C_{red} are respectively the concentration of the oxidant and that of reductant, d is the distance from the electrode surface, at which the transition probability is the greatest, E denotes the energy of transferring electron, e is the elementary charge, and Ω is the volume of the electrode.

The transition probability, $W_c(E)$, can be derived from the adiabatic perturbation theory considering the vibration in the first coordination sphere and given by[9-11]

$$W_c(E) = \frac{2\pi}{\hbar}|\langle\psi_f|V_{int}|\psi_i\rangle|^2\rho_{red}(E), \quad (3)$$

where ρ_{red} corresponds to the state density which is given by,[9-11]

$$\rho_{red}(E) = \left(\frac{1}{4\pi kT\lambda_s}\right)^{1/2} \times \sum_{m=-\infty}^{\infty}\exp\left[-(E-E^\circ_{redox}-\lambda_s-m\hbar\omega_c)^2/4kT\lambda_s\right] \times \exp\left[-Z_c\cosh\left(\frac{\hbar\omega_c}{2kT}\right)+\frac{m\hbar\omega_c}{kT}\right]I_m(Z_c), \quad (4)$$

where $Z_c=(1/2)\Delta_c^2\ \mathrm{cosec}\ (\hbar\omega_c/2kT)$, $I_m(Z_c)=(Z_c/2)_m\times\sum_{k=0}^{\infty}(Z_c/2)^{2k}/[k!\times(m+k)!]$, ψ_f denotes the unperturbed electronic wave function for the final state where an electron is located at an ion in solvent, ψ_i denotes the unperturbed electronic wave function for the initial state where an electron is located in semiconductor, V_{int} is the electronic interaction causing electron transfer, $\hbar\omega_c$ is the vibrational energy of the first coordination sphere, λ_s represents the rearrangement energy of solvent, E°_{redox} is the electronic energy corresponding to the standard redox potential, V°, and Δ_c is the difference between the equilibrium normal

coordinates of the vibration in the first coordination sphere in the initial state and those in the final state.

Similarly, the transition probability for anodic current, $W_a(E)$, is given by[9-11]

$$W_a(E) = \frac{2\pi}{\hbar}|\langle\phi_f|V_{int}|\phi_i\rangle|^2\rho_{ox}(E), \quad (5)$$

where

$$\rho_{ox}(E) = \left(\frac{1}{4\pi kT\lambda_s}\right)^{1/2} \times \sum_{m=-\infty}^{\infty} \exp\left[-(E^\circ_{redox}-E-\lambda_s-m\hbar\omega_c)^2/4kT\lambda_s\right] \times \exp\left[-Z_c\cosh\left(\frac{\hbar\omega_c}{2kT}\right)+\frac{m\hbar\omega_c}{2kT}\right]I_m(Z_c). \quad (6)$$

The square of the matrix element $|\langle\phi_f|V_{int}|\phi_i\rangle|^2$ can be rewritten as[12]

$$|\langle\phi_i|V_{int}|\phi_f\rangle|^2 = Pr|\langle\phi_f|V'_{int}|\phi'_i\rangle|^2, \quad (7)$$

where Pr represents the tunneling probability through the space charge layer, and $\langle\phi_f|V'_{int}|\phi'_i\rangle$ denotes approximately the matrix element causing electron transfer through the Helmholtz layer.

The tunneling probability Pr was calculated with the WKB approximation, assuming the Schottky type barrier and the two band model[13] for the energy-complex momentum relationship in the forbidden gap. In the case of a semiconductor with wide gap energy, the probability for the direct tunneling through the space charge layer is given by[14]

$$Pr = C_1\exp\left[-\frac{2}{\hbar}\left(\frac{m^*\varepsilon_{sc}}{n}\right)^{1/2}\phi_{sc}\right], \quad (8)$$

where m^* is the effective mass, ε_{sc} is the permittivity of semiconductor, ϕ_{sc} denotes the band bending, n is the electron density in the semiconductor bulk,[15] and C_1 is slowly varying function of the band bending, *etc.* With the decrease of carrier density, the probability for the direct tunneling decrease quickly, and thus the indirect tunneling *via* trapping states in the space charge layer becomes important. If the indirect tunneling occurs *via* one trapping state, the tunneling probability for this process is given by[14]

$$Pr = C_2\exp\left[-\frac{1}{\hbar}\left(\frac{m^*\varepsilon_{sc}}{n}\right)^{1/2}\phi_{sc}\right], \quad (9)$$

where C_2 is slowly varying function of the band bending, *etc.*

Figure 1 shows the energy relationship at a semiconductor/electrolyte interface. We consider then a highly doped SnO_2 electrode as an example. In the case of parabolic model for $\rho_{sc}(E)$, the Fermi level of SnO_2 with $n=10^{19}$ cm^{-3}, $m^*=0.22\,m$ and $\varepsilon_{sc}=10\,\varepsilon_0$ is located at 0.07 eV above the bottom of conduction band, and electrons are distributed in a narrow energy range near the Fermi level. Thus, if the tunneling through the space charge layer is dominant, $\rho_{sc}(E)f(E)$ can be approximated by

$$\rho_{sc}(E)f(E) = n\delta(E+eV), \quad (10)$$

where n is the carrier density, V is the electrode potential, and δ is the Dirac δ function. The validity of this approximation will be discussed later.

Substituting Eq. 10 and the relation of $E_{redox}=-eV^\circ$ into Eq. 1, the cathodic current density is written as

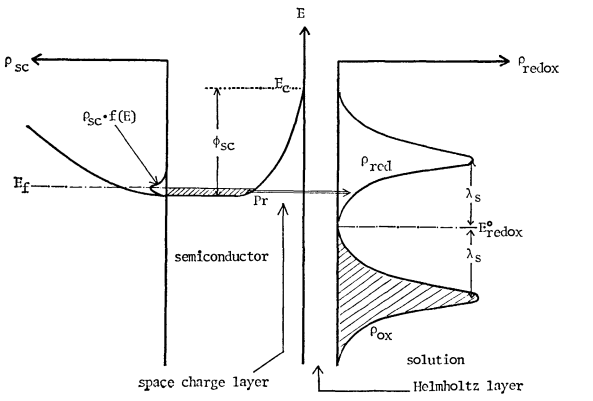

Fig. 1. Schematic representation of electron transfer under more positive potential than flat band potential at a highly doped semiconductor/electrolyte interface.

$$i_c = -edn\Omega C_{ox} \times \frac{2\pi}{\hbar}|\langle\phi_f|V'_{int}|\phi'_i\rangle|^2 \times Pr \times \rho_{red}(-eV), \quad (11)$$

where

$$\rho_{red}(-eV) = \left(\frac{1}{4\pi KT\lambda_s}\right)^{1/2} \times \sum_{m=-\infty}^{\infty} \exp\left[-(-eV+eV^\circ-\lambda_s-m\hbar\omega_c)^2/4kT\lambda_s\right] \times \exp\left[-Z_c\cosh\left(\hbar\omega_c/2kT\right)+m\hbar\omega_c/2kT\right]I_m(Z_c). \quad (12)$$

Equation 11 indicates that the magnitude of tunnel current directl reflects the transition probability at semiconductor Fermi level which can be defined by the electrode potential. On the other hand, the integral in Eq. 2 cannot be removed by the use of Eq. 10; the anodic current at an n-type semiconductor tunnel electrode contains all the electron transfer processes at various energy levels. Then, it is difficult to determine the transition probability from the experimental anodic tunnel current. In the present work, only the cathodic tunnel current at tunnel n-type semiconductor electrode is discussed.

The band bending, ϕ_{sc}, at more positive potential than the flat band potential is a function of the electrode potential, V, as follows:[3]

$$\phi_{sc}^{1/2} = \frac{1}{2}[-K+(K^2+4V-4V_{fb})^{1/2}]. \quad (13)$$

Here,

$$K = \frac{d_H}{\varepsilon_H}(2\varepsilon_{sc}nq)^{1/2}, \quad (14)$$

where V_{fb} is the flat band potential, d_H is the thickness of the Helmholtz layer, and ε_H is the permittivity of the Helmholtz layer. Then, the transfer coefficient, α, is given by

$$\alpha \equiv -\frac{kT}{e}\frac{\partial\ln(-i_c)}{\partial V} = \alpha_T + \alpha_\rho, \quad (15)$$

where $\alpha_T\equiv(-kT/e)(\partial\ln Pr/\partial V)$ is the transfer coefficient due to the tunneling through the space charge layer and is given by

$$\alpha_T \equiv \frac{kT}{e}\frac{2}{\hbar}\left(\frac{m^*\varepsilon_{sc}}{n}\right)^{1/2}\{1-K(K^2+4V-4V_{fb})^{-1/2}\}, \quad (16)$$

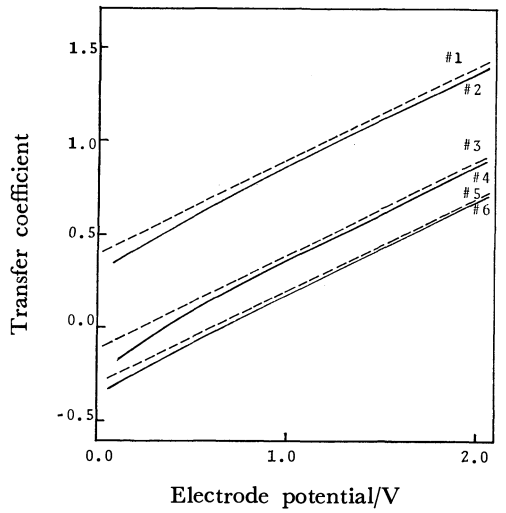

Fig. 2. Relationship between transfer coefficient and electrode potential in high temperature limiting case (T=300 K, λ_s=0.6 eV, $\hbar\omega_c$=0.002 eV, Δ_c=20, λ_c=0.4 eV, $V°$=2.0 V, V_{fb}=0.0 V, $\varepsilon_{sc}=10\varepsilon_o$, m^*=0.2 m, $\varepsilon_H=6\varepsilon_o$, d_H=0.3 nm). #1 and #2: $n=5\times10^{18}$ cm^{-3}, #3 and #4: $n=2.7\times10^{19}$ cm^{-3}, #5 and #6: $n=1.0\times10^{20}$ cm^{-3}. Solid lines are α-V curves considering potential drop across the Helmholtz layer, ϕ_H. Broken lines are α-V curves neglecting ϕ_H.

for the direct tunneling, and

$$\alpha_T \equiv \frac{kT}{e}\frac{1}{\hbar}\left(\frac{m^*\varepsilon_{sc}}{n}\right)^{1/2}\{1-K(K^2+4V-4V_{fb})^{-1/2}\}, \quad (17)$$

for the indirect tunneling with one trapping state, and $\alpha_\rho \equiv (-KT/e)(\partial \ln \rho_{red}/\partial V)$ is the transfer coefficient depending on the state density for acceptor state.

In case of $\hbar\omega_c \ll kT$, the transfer coefficient α_ρ is written as[16]

$$\alpha_\rho = \frac{eV-eV°+\lambda_s+(1/2)\hbar\omega_c\Delta_c^2}{2(\lambda_s+(1/2)\hbar\omega_c\Delta_c^2)}. \quad (18)$$

In case of $\hbar\omega_c \gg kT$, the transfer coefficient α_ρ in the normal region, *i.e.* $V > V°-\lambda_s/e$, is given by

$$\alpha_\rho = \frac{eV-eV°+\lambda_s}{2\lambda_s}, \quad (19)$$

while in the abnormal region, *i.e.* $V < V°-\lambda_s/e$,

$$\alpha_\rho = -\frac{kT}{e}\frac{\partial \ln}{\partial V}\left\{\sum_{m=0}^{\infty}\exp\left[-\frac{(-eV+eV°-\lambda_s-m\hbar\omega_c)^2}{4kT\lambda_s}\right]\times\frac{1}{m!}\left(\frac{\Delta_c^2}{2}\right)^m\right\}, \quad (20)$$

and it oscillates with the period, $V_p=\hbar\omega_c/e$, when the electrode potential is swept. In the intermediate case, *i.e.* $\hbar\omega_c \approx kT$,[9]

$$\alpha_\rho = \frac{e(V-V°)+\lambda_s}{2\lambda_s}+\frac{kT}{\lambda_s}\frac{\Delta_c^2}{2}\frac{\hbar\omega_c}{2kT}\operatorname{cosech}\left(\frac{\hbar\omega_c}{2kT}\right)\times\sinh\left[\frac{\hbar\omega_c(-eV+eV°)}{2kT\lambda_s}\right] \quad (21)$$

Broken lines in Figs. 2, 3, and 4 show the α-V curves neglecting the potential drop across the Helmholtz layer for $\hbar\omega_c \ll KT$, $\hbar\omega_c \gg KT$, and $\hbar\omega_c \approx KT$, respectively. In the high temperature limiting case, the slope of α-V curves is $(2\lambda_s+\hbar\omega_c\Delta_c^2)^{-1}$, and

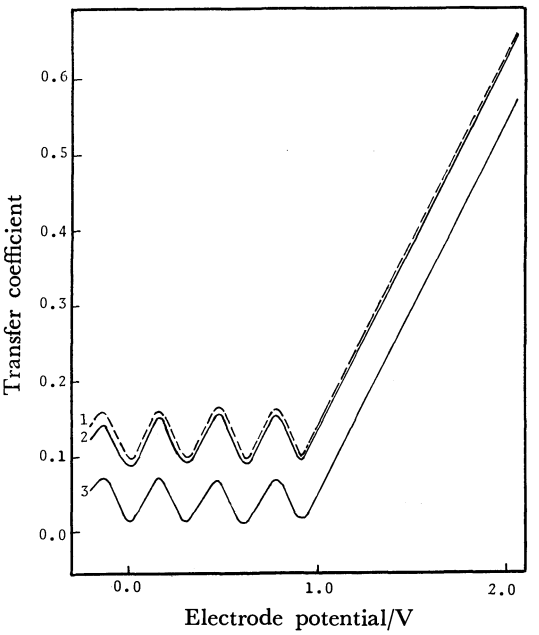

Fig. 3. Relationship between transfer coefficient and electrode potential in low temperature limiting case (T=30 K, $\hbar\omega_c$=0.3 eV, λ_s=1.0 eV, $\varepsilon_H=6\varepsilon_o$, d_H=0.3 nm, $\Delta_c=2^{1/2}$, $V°$=2.0 V). Curves of 1 and 2 are α-V curves at semiconductor with V_{fb}=0.0 V, m^*=0.1 m, $\varepsilon_{sc}=5\varepsilon_o$, and $n=10^{19}$ cm^{-3} in case of neglecting ϕ_H and that in case of considering ϕ_H, respectively. Curve 3 corresponds to α_T=0.

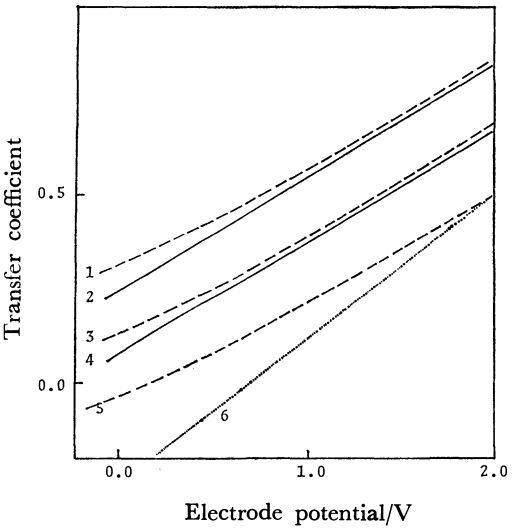

Fig. 4. Relationship between transfer coefficient and electrode potential in intermediate case (T=300 K, $\hbar\omega_c$=0.06 eV, λ_s=0.6 eV, m^*=0.2 m, $\varepsilon_{sc}=10\varepsilon_o$, Δ_c=2, V_{fb}=0.0 V, $V°$=2.0 V).
1 and 2: $n=2.7\times10^{19}$ cm^{-3}, 3 and 4: $n=1.0\times10^{20}$ cm^{-3}, 5: α_T=0.0. Dotted line is α-V curve neglecting ϕ_H and change of Δ_c (Δ_c=0). Broken lines are α-V curves neglecting ϕ_H. Solid lines are α-V curves considering ϕ_H.

there is not difference in α-V curve between the normal and abnormal regions. In the low temperature limiting case, electron transfer is accompanied by the nuclear tunneling in the first coordination sphere. Then, the slope of α-V curves in the normal region

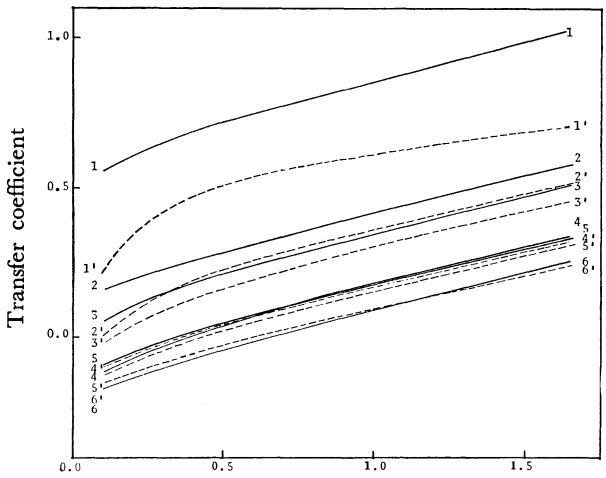

Fig. 5. Relationship between transfer coefficient and electrode potential ($T=300\,K$, $\lambda_s=1.0$ eV, $\lambda_c=1.0$ eV, $\lambda_c=1.0$ eV, $\hbar\omega_c=0.002$ eV, $\Delta_c=22.3$, $V^\circ=3.0$ V, $V_{fb}=0.0$ V, $\varepsilon_{sc}=10\varepsilon_o$, $m^*=0.2\,m$). Solid lines are α-V curves calculated with Eq. 10. Broken lines are α-V curves calculated without Eq. 10. 1,1′,3,3′,5,5′: direct tunneling; 2,2′,4,4′,6,6′: indirect tunneling. 1,1′,2,2′: $n=5\times10^{18}$ cm^{-3}; 3,3′,4,4′: $n=2.7\times10^{19}$ cm^{-3}; 5,5′,6,6′: $n=1.0\times10^{20}$ cm^{-3}.

is $(2\lambda_s)^{-1}$ because both the initial vibrational state and the final state are the ground states, while α-V curves in the abnormal region oscillate with the period, $\hbar\omega_c$, because of the significant contribution of an excited vibrational state in the final state. In the intermediate case, the nuclear tunneling in the first coordination sphere occurs to some extent, and the slope of α-V curves in small overvoltage region is approximately $(2\lambda_s)^{-1}$.

The solid lines in Figs. 2, 3, and 4 show the α-V curves considering the potential drop across the Helmholtz layer. In determing the rearrangement energy of solvent from the α-V curve, the effect of the potential drop across the Helmholtz layer on the transfer coefficient is not significant, except for the region near the flat band potential.

Here we consider the validity of the approximation in Eq. 10. Figure 5 shows the α-V curves corresponding to the high temperature limiting case. The broken lines in Fig. 5 are α-V curves calculated numerically without using the approximation given in Eq. 10. The α-V curves calculated with Eq. 10 are also shown by solid lines in Fig. 5. The good agreement between the solid lines of 3 to 6 and the broken lines of 3′ to 6′ indicates that the approximation of Eq. 10 is reasonable under the condition, $n\geqq2.7\times10^{19}$ cm^{-3}, $m^*=0.2\,m$, and $\varepsilon_{sc}=10\,\varepsilon_o$, at room temperature. However, the broken line (1′) deviates from the solid line (1). This deviation is interpreted in terms of a considerable contribution of the thermal excitation in the total current. This result means that the approximation given by Eq. 10 is no longer applicable when the carrier concentration is less than 5×10^{18} cm^{-3} at room temperature.

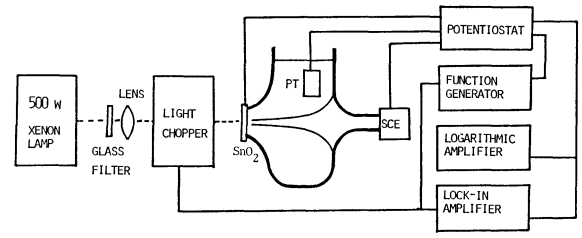

Fig. 6. Diagram of the experimental setup.

Experimental

Tin oxide coated glasses supplied from Matsuzaki Vacuum Co. and those from Asahi Glass Co. were made by the spray and vacuum evaporation methods, respectively. The former tin oxide layer has been doped with Sb and the latter has a high density O_2-vacancy. The surface area of each electrode was about 0.8 cm^2. The thickness of the SnO_2 layer was measured by a surface roughness meter. Ceric sulfate of commercially available reagent grade was used without further purification. The experimental setup is shown in Fig. 6. A saturated calomel electrode and a large area platinum disk electrode were used as the reference electrode and the counter electrode, respectively. In order to determine the flat band potential at various pH values, photocurrents by the band gap excitation were measured with a chopped light and a lock-in amplifier. Buffered solutions of pH 3, 5, and 7 were prepared with 0.2 M (1 M=1 mol dm^{-3}) citric acid and sodium dihydrogenphosphate. Differential capacitance measurements were made by modulating the electrode potential with a 10 mV sine wave of 120—1000 Hz and by balancing the bridge. The transfer coefficient was obtained by using a logarithmic amplifier and a lock-in amplifier by modulating the electrode potential with a 0.2 mV square wave of 2 Hz. The steady state current was measured with the potential sweep rate of 2 mV/s.

Results and Discussion

The Measurement of the Properties of Tin Oxide Electrode. Figure 7 shows the relation between differential capacitance per unit area, C, and the electrode potential. As seen in Fig. 7, the plots of C^{-2} *vs.* applied potential show good linearity. This result indicates that the spatial distribution of the dopant in SnO_2 electrode is uniform, and that the depletion layer is formed under the anodic polarization. A frequency dependence in the capacitance was observed as shown in Fig. 7, but this may be interpreted in terms of the CR dispersion at the semiconductor/electrolyte interface[1] and the structural irregularity of the electrode surface.[17] The slopes of the plots in Fig. 7 should be proportional to N_D^{-1}, but the accurate carrier density could not be obtained from Fig. 7 without the knowledge of the surface factor.

The carrier density was determined directly by the Hall effect measurement. The carrier density of the SnO_2 electrodes thus obtained was in the range from 2.7×10^{19} to 3×10^{20} cm^{-3}. The large carrier density shows that the distribution of the carrier of those electrodes is degenerate. The surface factor was determined by comparing the carrier density obtained from the Hall effect with that from the slope of Mott-Schottky plot in Fig. 7.

TABLE 1. PROPERTIES OF TUNNEL SnO_2 ELECTRODES

Electrode #	Thickness[a] Å	Apparent carrier[b] concentration cm^{-3}	Carrier[c] concentration n cm^{-3}	Surface factor	Flat band[d] potential V_{fb} *vs.* SCE V
1	1450	4.5×10^{21}	3.1×10^{20}	3.8	0.20
2	3000	3.7×10^{22}	1.0×10^{20}	19.2	0.22
3	400	1.0×10^{21}	2.7×10^{19}	6.0	0.24

a) Thickness of the SnO_2 layers measured by Dr. R. Kimura of the Institute of Molecular Science in Japan. b) Values obtained from Mott-Schottky plot at 120 Hz. c) Values obtained from Hall effect. d) Values obtained at pH=0.3.

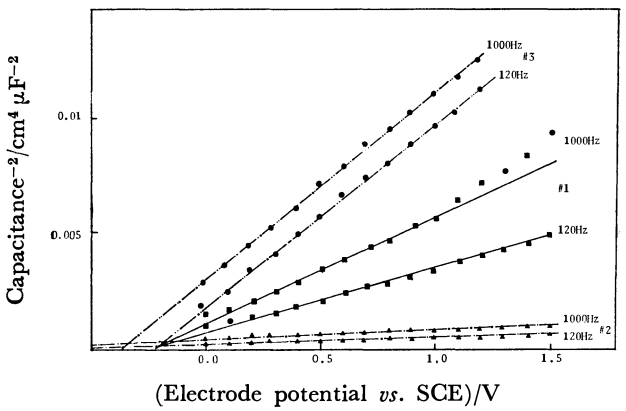

Fig. 7. Mott-Schottky plots for SnO_2 electrodes in a 0.25 M H_2SO_4.

The flat band potential, V_{fb}, of the SnO_2 electrode was determined from the onset potential of the anodic photocurrent[18] corresponding to O_2 evolution. The onset potential thus obtained agrees with the literature value.[19]

In Table 1 are listed the thickness of the tin oxide layer, the apparent carrier density from the slope of Mott-Schottky plot, the carrier density by the Hall effect, the surface factor and the flat band potential. The thickness of the electrode #3 is rather thin but is thicker than that of the depletion layer, *e.g.* 64 Å at 1.2 V *vs.* SCE. Table 1 also shows that the flat band potential shifts more negative with the increase of the carrier density, *i.e.* the Fermi level moves upper with the carrier density. The Fermi energy calculated by the parabolic model with $m^*=0.22m^{20}$ lies above the bottom of the conduction band, E_c: for the electrode #1; $E_F=E_c+0.66$ eV, #2; $E_c+0.39$ eV, and #3; $E_c+0.16$ eV. The difference among the above mentioned Fermi levels of these electrodes is significantly larger than the difference among the flat band potentials shown in Table 1. The discrepancy between the Fermi level thus calculated and the measured one has been often observed in the study of the tunnel diode,[21] and it was interpreted in terms of impurity band model.[22] Thus, the impurity band is formed in the SnO_2 electrode in this work. When the donor is O_2-vacancy or Sb, the relation between the donor density N_D and the donor ionization energy E_D for SnO_2 crystal has been given as[20]

$$E_D = 0.15 - 8.7\times10^{-8}N_D^{1/3} \quad [\text{eV}] \qquad (22)$$

The above relation means that the donor ionization energy approaches zero at a donor density of 5.5×10^{18} cm^{-3}. Since the carrier density of SnO_2 used in this work is larger than 10^{19} cm^{-3}, the shallow donor impurity band has been merged near the bottom of conduction band.

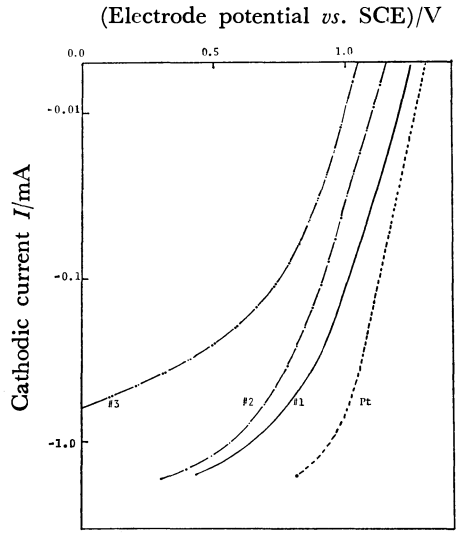

Fig. 8. Plots of cathodic tunnel current for the system of highly doped SnO_2–Ce^{4+} in a 0.25 M H_2SO_4 aqueous solution against electrode potential. #1: $n=3.1\times10^{20}$ cm^{-3}, #2: $n=1.0\times10^{20}$ cm^{-3}, #3: $n=2.7\times10^{19}$ cm^{-3}.

Cathodic Tunnel Current for Highly Doped SnO_2/Ce^{4+}. The steady state tunnel current was measured for Ce^{4+} which has very positive standard redox potential; $V^\circ(Ce^{4+/3+})=1.3$ V *vs.* SCE. In order to extend the potential region where the current is controlled by the electron transfer rate, a concentrated Ce^{4+} solution (0.5 M) was used. Figure 8 shows the curves of the cathodic current *vs.* electrode potential (*i-V*) for Ce^{4+} at SnO_2 electrodes in a 0.25 M H_2SO_4 aqueous solution. An *i-V* curve at a Pt electrode was also shown in Fig. 8 for comparison. As shown in Fig. 8 the magnitude of the current increases with the carrier density in SnO_2. The diffusion limited current is observed in the large current density region. In order to study the electron transfer mechanism in high overvoltage region, it is not suitable to use a too heavily doped semiconductor electrode because the current tends to become diffusion limited. However, a high carrier density is needed to ignore the thermal excitation current.

In Fig. 9 experimental values of the transfer coefficient, $\alpha(V)$, are plotted against electrode potential.

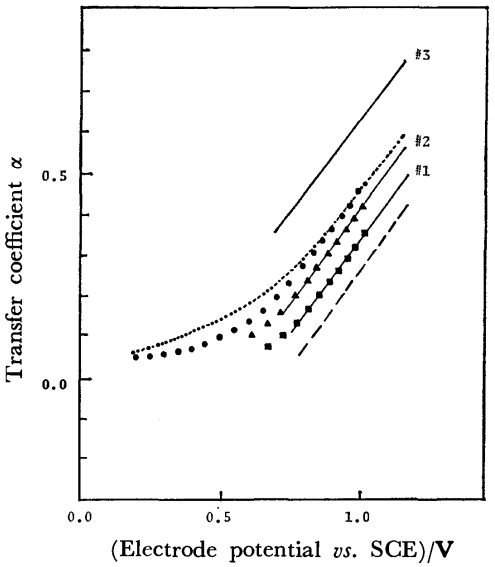

Fig. 9. Curves of transfer coefficient vs. electrode potential for 0.5 M Ce^{4+} at tunnel SnO_2 electrodes in a 0.25 M H_2SO_4 aqueous solution.
■,▲,●: Experimental values, ■ corresponds to #1, ▲ to #2 and ● to #3; solid lines: theoretical curves calculated with $m^*=0.21\,m$, $\lambda_s=0.65$ eV, and $V^\circ=1.3$ *vs.* SCE, broken line: solvent term, $1/2+e(V-V^\circ)/\lambda_s$, dotted line: theoretical curve for indirect tunneling at the electrode #3. #1: $n=3.1\times10^{20}$ cm^{-3}, #2: $n=1.0\times10^{20}$ cm^{-3}, #3: $n=2.7\times10^{19}$ cm^{-3}.

Since the amplitude of the modulation in obtaining α was such small value as 0.2 mV, higher order differential terms were negligible, and the pretty accurate values for $\partial \ln i/\partial V$ could be obtained. It seems from Fig. 8 that one can get constant values for the transfer coefficient in the potential range more positive than 1.0 V. However, in such region where the potential becomes near the equilibrium electrode potential, the contribution of the anodic process to the total current becomes so large that the effect of the anodic process on the transfer coefficient can not be neglected. Under such condition, α-V curve deviates from the theoretical one.

The plots in Fig. 9 show linearity in the potential region, $V>0.65$ V *vs.* SCE, and the slopes of these plots are almost same for three electrode. The plots shift with the carrier density of SnO_2 electrode. The slope of an α-V curve begins to change near $V=0.6$: the slope of an experimental α-V curve in the potential region, $V<0.6$, is much smaller. As mentioned in theoretical part, this α-V relationship implies that the electron transfer of Ce^{4+} corresponds to the intermediate case at room temperature. Thus, the rearrangement energy $\lambda_s=0.65$ eV for Ce^{4+} was determined from the slope of α-V in the small overvoltage region.

The rearrangement energy, λ_s, for Ce^{4+} or Ce^{3+} has been estimated by various methods. For instance, $\lambda_s=2.06$ eV[23] was determined from the electron transfer rate constant at a metal electrode by assuming the adiabatic electron transfer. Memming and Möller[19] estimated $\lambda_s=1.75$ eV by analyzing the anodic tunnel current at SnO_2. However, the Marcus theory[24] using the ion radius of Ce^{4+}, $R=3.77$ Å, has given $\lambda_s=0.5$ eV,[25] and the above values of λ_s seems too large. The overestimation of λ_s value determined from an electron transfer rate at a metal electrode is attributed to the break-down of the adiabatic electron transfer approximation: Ce^{4+} is so powerful oxidant that even a noble metal electrode is covered with a thin oxide layer in the potential region where the rates are measured. The electron transfer rate is mainly governed by the tunneling probability through the thin oxide film,[26] and the assumption of adiabatic electron transfer is not longer applied in this case. In addition, the nonadiabatic behaviour would be expected for the reduction of Ce^{4+} because the 4f orbitals involved in the reduction are strongly shielded by the 5s and 5p orbitals and the matrix element in Eq. 11 is expected to be very small.[27] In fact, the nonadiabatic electron transfer was found in the homogeneous redox reaction of $Eu^{2+/3+}$ in which 4*f* electron takes part in the electron transfer.[28]

The large λ_s-value reported by Memming and Möller[19] seems to be attributed to the complicated electron transfer mechanism of the anodic tunnel current at SnO_2 electrode: They calculated the anodic tunnel current by assuming the state density ρ_{ox} to be Gaussian function including the rearrangement energy, λ_s, as the parameter, and they determined the λ_s value by comparing the experimental tunnel i-V curve with the calculated one. In their calculation, however, they neglected the factors which might affect the tunnel i-V characteristics, that is, the indirect tunneling process, the excited vibrational states in the first coordination sphere, and the potential dependence of the state density in the conduction band, and the tunnel i-V characteristics were interpreted only in terms of the change in the rearrangement energy. Then, λ_s value thus estimated includes the rearrangement energy of the vibration in the first coordination sphere $(1/2)\hbar\omega_c\Delta_c^2$ as well as the contribution of the outersphere.

Three solid lines in Fig. 9 are the theoretical α-V curves, each of which is the sum of α_T in Eq. 16 and $\alpha_\rho=(eV-eV_0+0.65)/(2\times0.65)$. Two lines for the electrode #1 and #2 fit well will the experimental values, while for the electrode #3, the theoretical α-V curve does not fit with the experimental one. The small α_T for the electrode #3 indicates that the indirect tunneling process becomes significant in the tunneling through the space charge layer as expected in Eq. 17.

According to the values of standard redox potential for $Ce^{4+/3+}$, $V^\circ=1.3$ V *vs.* SCE and $\lambda_s=0.65$ eV for the cerium ion in an aqueous solution, the potential region more positive than 0.65 V *vs.* SCE corresponds to the normal region, and the region less than 0.65 V corresponds to the abnormal region. Linear relationship of α-V in the normal region leads to the Gaussian function for the acceptor state density, ρ_{red}. The dotted line in Fig. 9 was calculated with $\hbar\omega_c=400$ cm^{-1}, $\Delta_c=2.6$ by assuming the indirect tunneling (two step process). Those values of $\hbar\omega_c$ and Δ_c are typical ones[29] for the hydrated ions. Therefore, the small slope of α-V in the abnormal region is explained

by the contribution of the excited vibrational state in the first coordination sphere. If the λ_s-value is estimated formally from the potential dependence of the tunnel cathodic current in this abnormal region, one may obtain a unreasonably large value.[30]

Conclusion

The tunnel electrode appeared to be the very useful tool to study the electron transfer rate at high overvoltage. The λ_s-value of 0.65 eV for Ce^{4+} proved that this electron transfer process is nonadiabatic. Large electron transfer rate in the abnormal region could be explained by the significant contribution of the excited vibrational state in the first coordination sphere. The small tunnel transfer coefficient at SnO_2 #3 ($n = 2.7 \times 10^{19}$ cm^{-3}) implied that, in this case, the tunneling through the space charge layer involved the indirect tunneling *via* trapping states in the space charge layer.

The support of this research by Grant-in-Aid for Scientific Research, and Asahi Glass Foundation for Industrial Technology, is gratefully acknowledged.

References

1) D. Elliot, D. L. Zellmer, and H. A. Laitinen, *J. Electrochem. Soc.*, **117**, 1343 (1970).
2) B. Pettinger, H. R. Schöppel, and H. Gerischer, *Ber. Bunsenges. Phys. Chem.*, **78**, 450 (1974).
3) B. Pettinger, H. R. Schöppel, T. Yokoyama, and H. Gerischer, *Ber. Bunsenges. Phys. Chem.*, **78**, 1024 (1974).
4) R. A. Marcus, *J. Chem. Phys.*, **43**, 2654 (1965).
5) D. Rehm and A. Weller, *Israel J. Chem.*, **8**, 259 (1970).
6) H. Schonburg, H. Stark, and A. Weller, *Chem. Phys. Lett.*, **22**, 1 (1973).
7) K. Kobayashi, Y. Aikawa, and M. Sukigara, *J. Electroanal. Chem.*, **134**, 11 (1982).
8) V. G. Levich, "Advances in Electrochem. and Electrochem. Eng.," ed by P. Delahay and C. W. Tobias, Interscience New York (1966), Vol. 4, p. 249.
9) N. R. Kestner, J. Logan, and J. Jortner, *J. Phys. Chem.*, **78**, 2148 (1974).
10) J. Ulstrup and J. Jortner, *J. Chem. Phys.*, **63**, 4358 (1975).
11) V. G. Levich, "Physical Chemistry," ed by H. Eyring, D. Henderson, and W. Jost, Academic Press New York (1970), IXB 985.
12) W. A. Harrison, *Phys. Rev.*, **123**, 85 (1961).
13) W. Frang, "Handbuch der Physik, ed by S. Flugge, Springer Verlag, Berlin (1956), Vol. 17.
14) G. H. Parker and C. A. Mead, *Phys. Rev.*, **184**, 780 (1969).
15) If carrier in semiconductor is produced by the shallow donor level, donor is completely ionized at room temperature. Under the condition, the donor density N_D is identical with the electron density n in semiconductor bulk. Then, the tunneling probability in Eq. 8 was expressed with the electron density n instead of the donor density N_D.
16) R. R. Dogonadze, A. M. Kuznetsov, and V. G. Levich, *Electrochimica. Acta*, **13**, 1025 (1968).
17) E. C. Dutoit, R. L. van Meihaeghe, and F. Cardon, *Ber. Bunsenges. Phys. Chem.*, **79**, 1206 (1975).
18) J. M. Bolts and M. S. Wrighton, *J. Phys. Chem.*, **80**, 2641 (1976).
19) R. Memming and R. Möller, *Ber. Bunsenges. Phys. Chem.*, **76**, 475 (1972).
20) J. A. Mauley and R. C. Dockerty, *Phys. Rev. A*, **140**, 304 (1965).
21) A. G. Chynoweth, W. L. Feldmann, G. A. Lee, R. A. Rogan, and G. L. Person, *Phys. Rev.*, **118**, 425 (1960).
22) T. P. Brody, *J. Appl. Phys.*, **33**, 100 (1962).
23) R. Greef and H. Aulich, *J. Electroanal. Chem.*, **18**, 295 (1968).
24) R. A. Marcus, *Ann. Rev. Phys. Chem.*, **15**, 155 (1964).
25) J. O'M. Bockris and S. U. M. Khan, "Quantum Electrochemistry," Plenum Press, New York (1979).
26) J. W. Schultze, *Z. Phys. Chem.*, **73**, 29 (1970); P. Kohl and J. W. Schultze, *Ber. Bunsenges. Phys. Chem.*, **77**, 953 (1973).
27) H. Taube, *Adv. Chem. Ser.*, **162**, 127 (1977).
28) V. Balzani, F. Scandola, G. Orlandi, N. Sabbatini, and M. T. Indelli, *J. Am. Chem. Soc.*, **103**, 3370 (1981).
29) I. Nagasawa and T. Shimanouchi, *Spectrochim. Acta*, **20**, 429 (1964).
30) K. E. Heusler and Kyung Suk Yun, *Electrochim. Acta*, **22**, 977 (1977).

 © 1982 The Chemical Society of Japan Bull. Chem. Soc. Jpn., 55, 2827—2830 (1982)

Temperature Effect on the Hydrophobic Hydration in Aqueous Solution of Nonpolar Molecule by Monte Carlo Calculation

Susumu Okazaki, Hidekazu Touhara, Koichiro Nakanishi,* and Nobuatsu Watanabe

Department of Industrial Chemistry, Faculty of Engineering, Kyoto University, Sakyo-ku, Kyoto, 606

(Received March 13, 1982)

Monte Carlo calculations have been carried out for pure water and aqueous solution of Lennard-Jones particle at infinite dilution between 273.15 K and 353.15 K in order to examine temperature effect on the hydrophobic hydration. It is found that internal energy of mixing ΔU due to the introduction of the solute into water becomes less negative monotonously with increasing temperature. It is in good correspondence with the tendency obtained from solubility measurement, and represents that heat capacity of mixing ΔC_v is positive. Furthermore the dissolution proceeds no longer exothermically at 353.15 K, where water behaves as a normal solvent. Several structural and energetical distribution functions have been calculated for the deep understanding of these observations.

In a previous paper,[1] it was shown that the energetic stabilization and free energy increase due to the hydrophobic hydration in dilute aqueous solution of methane can be reproduced by Monte Carlo (MC) calculations adopting the ST-2 model[2] for water and Lennard-Jones (LJ) potential for methane. The MC calculation was later extended to other LJ solutes having larger sizes and the size effect in hydrophobic hydration has been clarified.[3] In principle, the energetic stabilization can be directly evaluated by calorimetry; however extremely low solubility of nonpolar solutes in water prevents the establishment of accurate and reliable value for the energy change from ordinary laboratory experiments. Thus, we are at present forced to rely on the information from the temperature dependence of solubility. The solubility of nonpolar gas into water decreases with increasing temperature, and this anomaly is not observed in other solute and solvent systems.[4] It must be related to the temperature dependence of the hydrophobic hydration.

Computer experiment may be more favourable in studying these phenomena of the hydrophobic hydration. Although many MC or MD (molecular dynamics) studies have been reported recently for aqueous solution of nonpolar solute,[5] no extensive calculation has been hitherto made on the temperature effect in hydrophobic hydration. We will present here MC results for aqueous methane solutions at 273.15, 333.15, and 353.15 K. Temperature effect on hydrophobic hydration will be discussed based upon these calculations together with the results in the previous calculation at 298.15 K.[1]

Model and Method of Computation

The model and method of computation used here are the same as those in preceding papers.[1,3] They are summarized briefly as follows.

Monte Carlo calculations have been carried out with the ordinary Metropolis method[6] in NVT-ensemble where $N=64$ (64 water molecules or 63 water molecules+one LJ particle whose potential parameters are those of methane), $T=273.15$, 333.15, and 353.15 K, and $V=18.02$, 18.32, and 18.54 $cm^3\ mol^{-1}$ at the above three temperatures, respectively. The volume of each system is determined from the molar volume of pure water at each temperature, no correction being made for the volume change due to the introduction of the solute. The total number of configurations generated is $(5-9)\times10^5$ for pure water and $(6-12)\times10^5$ for methane solutions.

Table 1. Internal energy and internal energy of mixing at each temperature for aqueous solution of methane. The standard state of the solute is assumed to be ideal gas

		T/K			
		273.15	298.15	333.15	353.15
U/kJ mol^{-1}	Pure	−38.5	−35.1	−31.7	−30.4
	Soln	−40.2	−36.1	−32.1	−29.1
ΔU/kJ mol^{-1}		−2.3	−1.5	−0.9	0.9

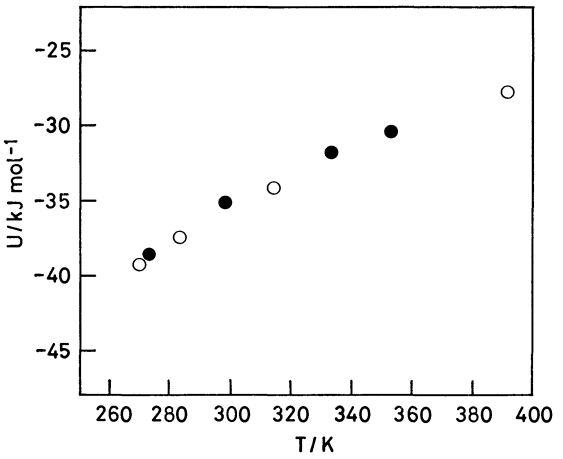

Fig. 1. Internal energies U of pure water as a function of temperature.
Closed circle: this work, open circle: Stillinger and Rahman.[2]

Results and Discussion

The convergence characteristics of the system to an equilibrium state are the most important problem in the MC calculation. This has been already discussed in detail elsewhere[3] and enough convergence has been also confirmed for the present systems.

Internal Energies. The internal energies U of

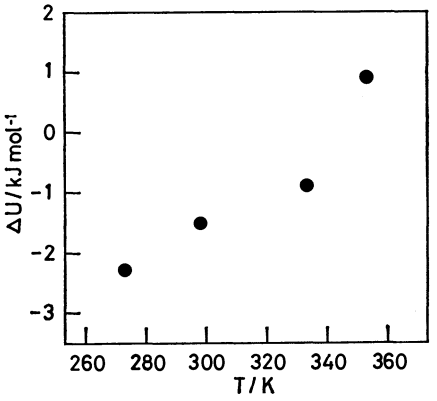

Fig. 2. Internal energies of mixing ΔU of aqueous solution of methane as a function of temperature. The standard state of the solute is assumed to be ideal gas.

both pure water and aqueous methane solution have been calculated as a function of temperature and the results are given in Table 1.

First the temperature dependence of U for pure water shown in Fig. 1 is examined. This kind of calculation has already been carried out with the MD method by Stillinger and Rahman[2] in a wide range of temperature, and their results are also given in the figure. The present calculations are concerned with a narrower temperature range in detail and the results are in good agreement with those obtained by Stillinger and Rahman.[2] Although U increases with increasing temperature as expected, the U *vs.* T curve is convex upward, which means that the heat capacity C_v decreases with increasing temperature. This result coincides with experimental observation.[7] The C_v value evaluated from the present result of the temperature gradient is 80 J K^{-1} mol^{-1} at 298.15 K. The agreement with the experimental value (75 J K^{-1} mol^{-1})[7] is reasonable in view of the present status of computer experiment.

It must be noted here that the fluctuation of internal energies for pure water and the solution at 273.15 K is so large that the values are less reliable than those at higher temperatures. This uncertainty in the present calculation is unavoidable. It may be caused by the continuous phase transition from liquid state to ice in computer experiment owing to the restriction of initial phase condition. Then the thermodynamic properties and distribution functions at 273.15 K are limited only to the comparison with those at other temperatures. For this reason, we present here only the results of internal energy at 273.15 K, and do not discuss the distribution functions in detail.

In Table 1 are given the internal energies of mixing ΔU,

$$\Delta U = U_{\text{soln}} - (x_{\text{water}}U_{\text{water}} + x_{\text{solute}}U_{\text{solute}}),$$

where the reference state of the solute is an ideal gas state and x refers to mole fraction. The ΔU *vs.* T relation is plotted in Fig. 2. Except at 353.15 K, the dissolution proceeds exothermically which is evidence for hydrophobic hydration.

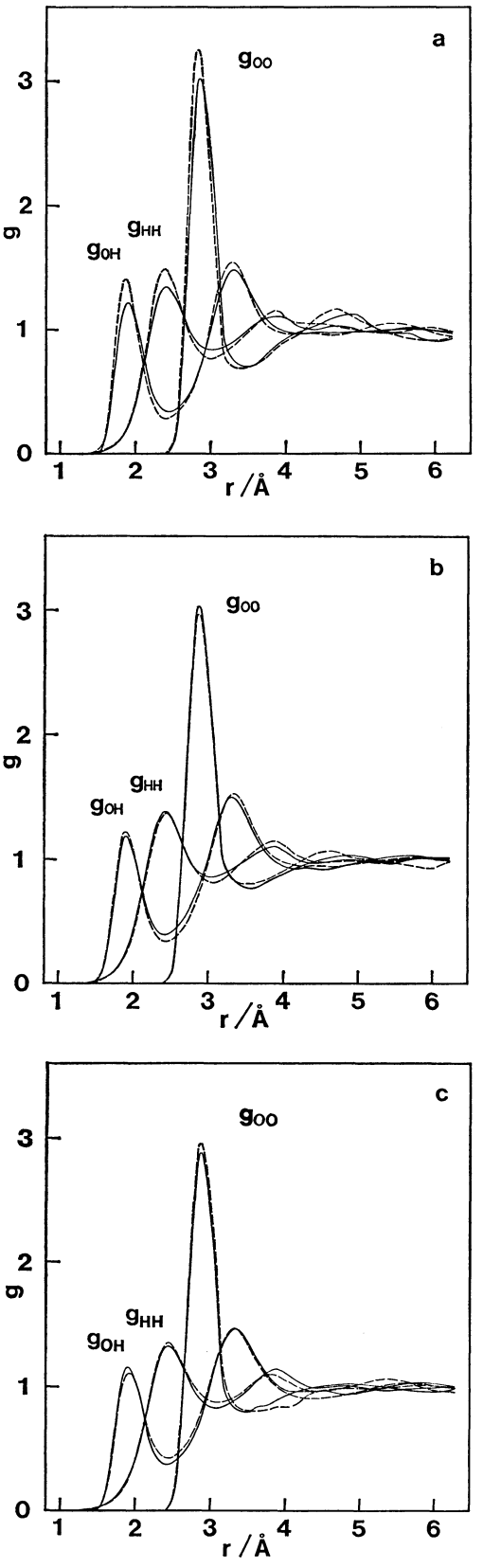

Fig. 3. Atom-atom pair correlation functions, g_{OO}, g_{OH}, and g_{HH} at (a) 298.15 K, (b) 333.15 K, (c) 353.15 K.
Solid line: pure water, broken line: aqueous solution of methane.

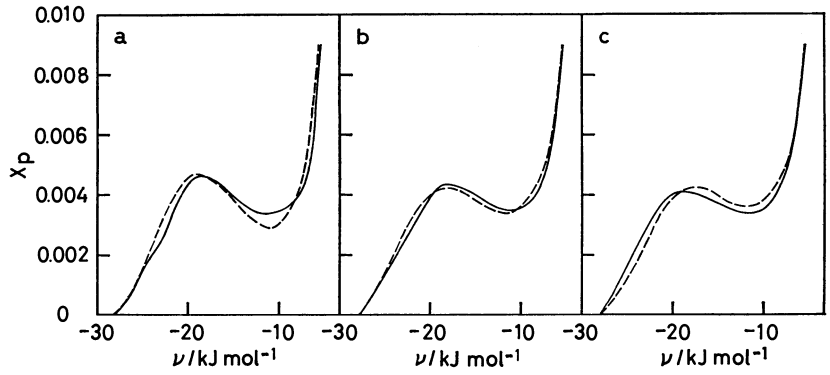

Fig. 4. Pair interaction distribution function x_p at (a) 298.15 K, (b) 333.15 K, and (c) 353.15 K.
Solid line: pure water, broken line: aqueous solution of methane.

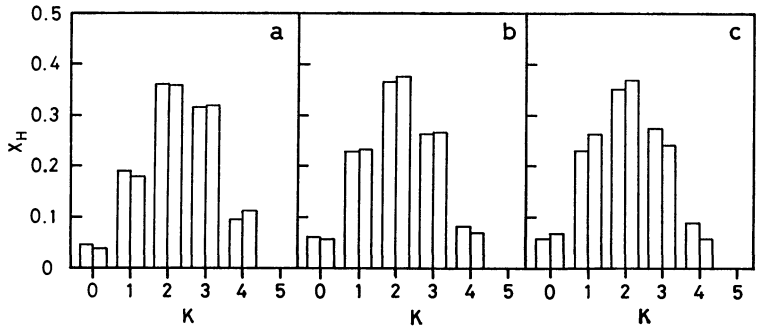

Fig. 5. Hydrogen bonding number distribution function x_H for $\nu_H = -16$ kJ mol^{-1} at (a) 298.15 K, (b) 333.15 K, and (c) 353.15 K.
Left: pure water, right: aqueous solution of methane.

The solubilities of nonpolar molecules in water decrease regularly as temperature increases; then the change in partial molar enthalpies $\Delta\bar{H}^\circ$ associated with dissolution is negative and its absolute values become smaller as temperature increases.[4] The temperature dependence of ΔU obtained from the present MC calculations is in good accordance with that of $\Delta\bar{H}^\circ$. From the positive slope of the internal energy of mixing it becomes clear that the heat capacity of mixing is positive.

Radial Distribution Functions. In order to explore the behaviour of ΔU which reflects hydrophobic hydration in aqueous solutions, we have calculated various distribution functions. In the first place, atom-atom radial distribution functions, g_{OO}, g_{OH}, and g_{HH} are presented and discussed in this subsection. Figure 3 shows the three rdf's as a function of temperature. Among these rdf's, g_{OH} is very important in discussing the structuration of water near the solute because higher positional correlation between oxygen and hydrogen atoms corresponds to stronger hydrogen bonding and is evidence for structuration of water molecules around a nonpolar solute. As is clearly seen in Fig. 3, the height of the first peak of g_{OH} for aqueous solution of methane is much larger than that for pure water only at 298.15 K. At 333.15 K, the correlation is still higher in the case of aqueous solution, though the difference becomes smaller. However, the reverse of this order is observed at 353.15 K, where the correlation is smaller for the aqueous solution. This suggests that water behaves as a normal solvent at this temperature.

Other Distribution Functions. The results of radial distribution functions presented above show a good correspondence with the internal energy of mixing ΔU for the solution at each temperature. It is now interesting to examine the temperature dependence of other distribution functions, such as hydrogen bonding number distribution function (HBNDF) and pair interaction distribution function (PIDF). The former function represents fractions of water molecules which make hydrogen bondings with other K water molecules and the latter function represents fraction of molecular pair which interacts with each other by ν kJ mol^{-1}. The detailed definitions are given elsewhere.[3,8] The results for PIDF are shown in Fig. 4, whereas those for HBNDF are plotted in Fig.5.

We first discuss the PIDF results. It is seen from Fig. 4 that the peak at about -20 kJ mol^{-1} indicates the hydrogen bonding. With the increase in temperature, the peak of PIDF gradually shifts to higher energy direction both for pure water and aqueous solution. The value of ν at the peak for aqueous solution is lower than that for pure water at 298.15 K and 333.15 K. This is the region where the structuration of water due to nonpolar solute takes place significantly. On the contrary, the peak for aqueous solution shifts slightly to higher energy compared with that for pure water at 353.15 K. At this rather higher temperature, most of water molecules seem to behave

as an ordinary molecular liquid, though a considerable number of hydrogen-bonded species are still retained.

The above picture can be further confirmed by the information from HBNDF which counts the number of hydrogen bonds in the system. Although we have calculated the distribution functions with different criteria for the hydrogen bonding strength, it is enough for the present purpose to give only the HBNDF at $v_H = -16$ kJ mol^{-1}. Figure 5 clearly shows that the number of water molecules with the hydrogen bonding number $K=3$ or 4 in pure water at 353.15 K is evidently larger than that in aqueous solution at the same temperature, indicating overall decrease in hydrogen bonding structure by the introduction of the solute molecule. On the other hand, the fractions of molecules with $K=3$ and especially $K=4$ for aqueous solution are larger than those in pure water at 298.15 K. The fractions for $K=1$, 2, and 3 in aqueous solution are slightly larger than those in pure water at 333.15 K.[9] These are also in the same situation with other distribution functions.

The mole fraction of the nonpolar solute in the present systems is as large as 0.015, which is much more concentrated than that in the gas solubility equilibrium of methane and related compounds in water. In spite of this different situation, one can depict a fairly consistent picture on the temperature effect on the hydrophobic hydration as below.

1) The value for internal energy of mixing ΔU is negative except at 353.15 K.

2) The heat capacity of mixing ΔC_v is positive at all temperatures.

3) Radial distribution function and other distribution functions show that the structuration of water due to apolar solute is significant at 298.15 K and 333.15 K. These are in good correspondence to those observed in solubility measurements of nonpolar molecule in water.

4) At 353.15 K, unique structural properties of water are lost and the introduction of nonpolar solute is energetically unfavourable.

The authors thank the Computer Center, Institute for Molecular Science and the Data Processing Center, Kyoto University for the use of the facilities, HITAC M-200H and FACOM M200, respectively.

References

1) S. Okazaki, K. Nakanishi, H. Touhara, and Y. Adachi, *J. Chem. Phys.*, **71**, 2421 (1979), **72**, 4253 (1980).

2) F. H. Stillinger and A. Rahman, *J. Chem. Phys.*, **60**, 1545 (1975).

3) S. Okazaki, K. Nakanishi, H. Touhara, N. Watanabe, and Y. Adachi, *J. Chem. Phys.*, **74**, 5863 (1981).

4) F. Franks and D. S. Reid, "Water—A Comprehensive Treatise," ed by F. Franks, Plenum, New York (1973), Vol. 2, p. 323; A. Ben-Naim, "Hydrophobic Interactions," Plenum, New York (1980); E. Wilhelm, R. Battino, and R. J. Wilcock, *Chem. Rev.*, **77**, 219 (1977).

5) V. G. Dashevsky and G. N. Sarkisov, *Mol. Phys.*, **27**, 1272 (1974); J. C. Owicki and H. A. Scheraga, *J. Am. Chem. Soc.*, **99**, 7413 (1977); S. Swaminathan, S. W. Harrison, and D. L. Beveridge, *ibid.*, **100**, 5705 (1978); A. Geiger, A. Rahman, and F. H. Stillinger, *J. Chem. Phys.*, **70**, 263 (1979); C. Pangali, M. Rao, and B. J. Berne, *ibid.*, **71**, 2982 (1979); G. Alagona and A. Tani, *ibid.*, **72**, 580 (1980).

6) N. Metropolis, A. W. Rosenbluth, M. N. Rosenbluth, A. H. Teller, and E. Teller, *J. Chem. Phys.*, **21**, 1087 (1953).

7) D. Eisenberg and W. Kauzmann, "The Structure and Properties of Water," Oxford University Press, Oxford (1969).

8) A. Ben-Naim, "Water and Aqueous Solutions—Introduction to a Molecular Theory," Plenum, New York (1974).

9) It must be noted that the negative ΔU value at 273.15 K is not due to the increase in the number of hydrogen bonds with larger interaction energy, but due to the enhancement of smaller dipole-dipole interactions. Thus energetical stabilization at 273.15 K is quite different from those at higher temperatures. However, the statistical error in the calculation for 273.15 K is so large that we cannot reach a final conclusion here.

 © 1982 The Chemical Society of Japan Bull. Chem. Soc. Jpn., 55, 2831—2834 (1982)

Observation of Spin Sublevel Excitation Spectra. An Application to Vibrational Analysis of T←S Absorption

Kazuhiko SUGA,† Nobuyuki NISHI,†† and Minoru KINOSHITA*

The Institute for Solid State Physics, The University of Tokyo, Roppongi, Minato-ku, Tokyo 106

(Received April 9, 1982)

A new application of the $T_1 \leftarrow S_0$ excitation spectroscopy is presented by which absorptions to one or two of the three spin sublevels can be measured separately. This method has been applied to the $T_1 \leftarrow S_0$ excitation of crystalline 1,2,4,5-tetrachlorobenzene and 9*H*-xanthen-9-one at 1.4 K. The vibrational structures of the excitation spectra are analyzed in view of the spin selectivity observed.

The photoexcitation spectroscopy has achieved a considerable success in studying absorptions of aromatic compounds at low temperatures. In particular, the method using phosphorescence for detection has been applied successfully to observation of $T_1 \leftarrow S_0$ absorptions in crystalline aromatic compounds. In this case, triplet excitons in a crystal are formed by direct $T_1 \leftarrow S_0$ absorption and then the triplet excitation is transferred to guest or trap molecules having a lower T_1 energy, from which emission originates.

Since $T_1 \leftarrow S_0$ absorption requires anisotropic spin-orbit interactions, the absorption cross sections of the individual spin sublevels in a particular vibronic level are quite different from one another, resulting in formation of the state of spin alignment of triplet excitons in the crystal. It is well established that the triplet-triplet energy transfer occurs through the exchange mechanism[1] and that the spin angular momentum is conserved during energy transfer.[2] Consequently, at very low temperature, where the spin-lattice relaxation is negligible, the high degree of spin alignment in the excitons can be replicated on the guest or trap molecules in accordance with the relative orientation of the principal spin axes.

Then, if the spin alignment thus prepared in the guest or trap molecules is analyzed by applying the MIDP (microwave induced delayed phosphorescence) method to the trap emission, the spin selectivity in the $T_1 \leftarrow S_0$ excitation processes may be inferred. In fact, this technique has been developed previously[3] and applied successfully to the analyses of the spectra of *p*-chloroaniline,[4] pyrazine,[5] triphenylene,[6] and *p*-dichlorobenzene.[7]

In the present paper, a new method is described by which the $T_1 \leftarrow S_0$ spin sublevel excitation spectra can be obtained. This method is applied to neat crystals of 1,2,4,5-tetrachlorobenzene (TCB) and 9*H*-xanthen-9-one (xanthone) for the purpose of analyzing the vibrational structures of the $T_1 \leftarrow S_0$ absorptions. For successful application of this technique, some requirements have to be satisfied by the system selected. These conditions will be first described below.

Description of the Method

Excitation spectroscopy provides information on excited states through the properties of the monitored emission. Therefore, when the emission which originates predominantly from one of the spin sublevels of the trap is monitored, the resulting spectrum would reflect the absorption cross section of the corresponding spin sublevel in the triplet state of the crystal to be examined, provided that the spin alignment produced in the triplet excitons by direct $T_1 \leftarrow S_0$ excitation is almost exactly replicated on the trap molecules. This is the essential point of the method presented in this paper. To populate the spin sublevels of the excitons in proportion to the absorption cross sections of the individual spin sublevels, it may be appropriate to use the pulse excitation method.

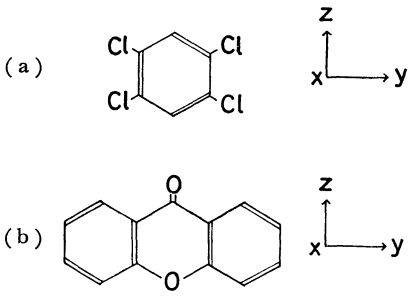

Fig. 1. Molecular structure and choice of the axis system; (a) 1,2,4,5-tetrachlorobenzene and (b) 9*H*-xanthen-9-one.

The spin alignment produced by T←S excitation plays a crucial role in this method; it should be maintained throughout the experiment which involves the processes of vibrational relaxation, energy transfer, trapping, and emission from the trap molecules. The first three processes are usually fast compared with the spin-lattice relaxation process at very low temperature. Therefore, molecules having a relatively short lifetime, such as halogenated aromatics and aromatic carbonyls, may be chosen as a trap to minimize the spin-lattice relaxation effect.

Another requirement to be satisfied by the trap molecules is that the individual spin sublevels should contribute quite differently to an emission band which is energetically resolvable for monitoring. Most of the compounds having a symmetry of C_{2v} or higher are known to fulfill this requirement and may be used as a trap.

In addition, the trap molecules should enter into the crystal in such a way that the orientation of the principal spin axes of the trap relative to that of the triplet excitons can be inferred. The simplest case is an experiment on the system in which the directions

† Present address: Technical Research Center, Nippon Mining Co., Ltd., Niiso-Minami, Toda, Saitama 335.

†† Present address: Institute for Molecular Science, Myodaiji, Okazaki, Aichi 444.

of the spin axes of the trap triplet state are, at least approximately, coincident with those of the excitonic triplet state. In such a system, the populations of the spin sublevels in the emitting trap molecules are almost exactly proportional to the absorption cross sections of the spin sublevels in the excitons pumped by pulse excitation ($N_i \propto P_i$). Accordingly, the intensity of the phosphorescence to a selected vibrational band, ν, is given by $I(\nu)=c\Sigma k_i^r(\nu)P_i$, where the sum is taken over the spin sublevels(i), $k_i^r(\nu)$ refers to the relative radiative decay rates to ν, P_i is the relative absorption cross sections of the individual spin sublevels, and c is a proportional constant which also corrects for the sensitivity of the detection system. On the basis of the values of $k_i^r(\nu)$, the values of P_i may be determined by observing the intensities of the emission to different vibrational bands. In an ideal case where the vibrational band having contribution only from one of the spin sublevels could be selected for monitoring, an absorption spectrum of that spin sublevel would be obtained. In a real system, however, contributions from the other two sublevels would not be eliminated completely, but the following examples demonstrate the usefulness of the method.

Experimental

1,2,4,5-Tetrachlorobenzene (TCB) was purified by recrystallization and vacuum sublimation, followed by extensive zone-refining. 9*H*-Xanthen-9-one (xanthone) was recrystallized and then zone-refined. Single crystals were grown by the standard Bridgman technique.

Excitation of the crystals was performed with a Molectron DL-200 tunable dye laser equipped with a Molectron UV-1000 1 MW N_2 laser. Phosphorescence was monitored at right angle to excitation path through a Spex 1700 III 3/4 m monochromator. A PAR 162 boxcar integrator was used to acquire the average emission intensity for 2 ms. Other equipment for optical experiments was essentially the same as reported in the previous paper.[8]

1,2,4,5-Tetrachlorobenzene

A TCB crystal is triclinic below 188 K and belongs to the space group $P_{\bar{1}}$ with two molecules in a unit cell.[9] The molecules in the translationally inequivalent lattice sites are interchanged by the action of inversion so that the molecular axes of these two are parallel. Therefore, the principal spin axes of the excitons are coincident with those of the molecule. The selection rules for the isolated molecule are expected to hold for the excitons.

The translationally equivalent molecules stack nearly plane-to-plane along the a axis with the out-of-plane molecular axis almost parallel to the a axis. Because of this card pack array of the molecules, together with the small value of the *a* lattice constant relative to the *b* and *c* lattice constants, the exchange interaction for the π,π^* triplet state is largest along the a axis. In fact, the Davydov splitting, which is a measure of the interchain interaction, has been estimated to be about 1 MHz, that is orders of magnitude less than the intrachain matrix element of 0.35 cm^{-1}.[10] All these lead to the conclusion that the exciton migration in this system is essentially one-dimensional along the a axis and probably coherent at liquid helium temperatures. The manifestation of this nature has been discussed in great detail in the literature.[11]

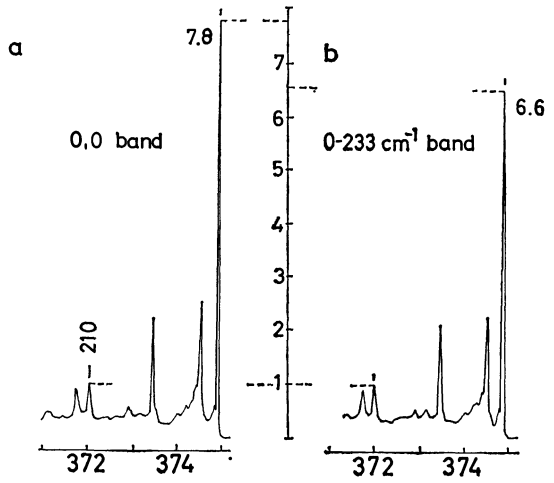

Fig. 2. The $T_1 \leftarrow S_0$ phosphorescence excitation spectra of the TCB neat crystal at 1.4 K, monitored (a) at the 0,0 band and (b) at the 0−233 cm^{-1} band of the Y trap emission.

In addition to the exciton, TCB crystals show phosphorescence from traps with the origin at 26626 cm^{-1} (Y trap).[12] Francis and Harris[13] have reported that the electron spin transitions associated with the excitons are also observed by monitoring the Y trap emission. This evidently results from the spin selectivity of the exciton-trap interaction and, furthermore, indicates that the spin alignment in the excitons is transferred, for the most part, with electronic energy to the molecules in the Y trap site.

Figure 2 shows the excitation spectra of the TCB crystal at 1.4 K obtained by separately monitoring the 0,0 band and 0−233 cm^{-1} band in the phosphorescence emission from the Y trap. There is a significant difference between the two spectra. The intensity of the 0+210 cm^{-1} band relative to the intensity of the origin band is larger in the spectrum monitored at the 0−233 cm^{-1} band than that at the 0,0 band. Since the emission of the Y trap originates mainly from the y sublevel at the 0,0 band and, on the other hand, predominantly from the z sublevel at the 0−233 cm^{-1} band,[14] this difference can be attributed to the difference in the populations of the y and z sublevels. As mentioned above, the spin alignment in the excitons can be replicated on the Y trap without serious population rearrangement. Therefore, the observed results above indicate that the absorption to the 0+210 cm^{-1} band occurs in the y sublevel in preference to the z sublevel, whereas the situation is opposite for the origin band.

A number of studies[14,15] on the phosphorescence of TCB have revealed that besides the vibronic bands due to the a_g modes, only the band due to the C–Cl out-of-plane bending mode of b_{2g} appears strongly in the phosphorescence spectrum and that the main mech-

Table 1. The important mechanisms for phosphorescence of TCB

Band[a]	k_z^r/k_y^r [a]	k_x^r/k_y^r [a]	Mechanisms for the radiative decay[b]
0,0	0.2	<0.02	T_y $^3B_{1u} \xrightarrow{so} {}^1B_{3u}$
0−233 cm^{-1} (b_{2g})	3.0	<0.1	T_z $^3B_{1u} \xrightarrow{b_{2g}} {}^3B_{3u} \xrightarrow{so} {}^1B_{2u}$
			T_y $^3B_{1u} \xrightarrow{b_{2g}} {}^3B_{3u} \xrightarrow{so} {}^1B_{1u}$

a) Data for the Y trap of a TCB neat crystal; taken from Ref. 14. b) From Ref. 15.

Table 2. The important mechanisms for phosphorescence of xanthone[a]

Band	k_z^r/k_y^r	k_x^r/k_y^r	Mechanisms for the radiative decay
0,0	≃0.8		T_y $^3A_1 \xrightarrow{so} {}^1B_1(\sigma, \pi^*)$
			T_z $^3A_1 \xrightarrow{so} {}^1A_2(n, \pi^*)$
0−674 cm^{-1} (b_1)	6.5	0.3	T_y $^3A_1 \xrightarrow{so} {}^1B_1(\sigma, \pi^*) \xrightarrow{b_1} {}^1A_1(\pi, \pi^*)$
			T_z $^3A_1 \xrightarrow{so} {}^1A_2(n, \pi^*) \xrightarrow{b_1} {}^1B_2(\pi, \pi^*)$

a) Taken from Ref. 18; data for the trap named site I in the neat crystal.

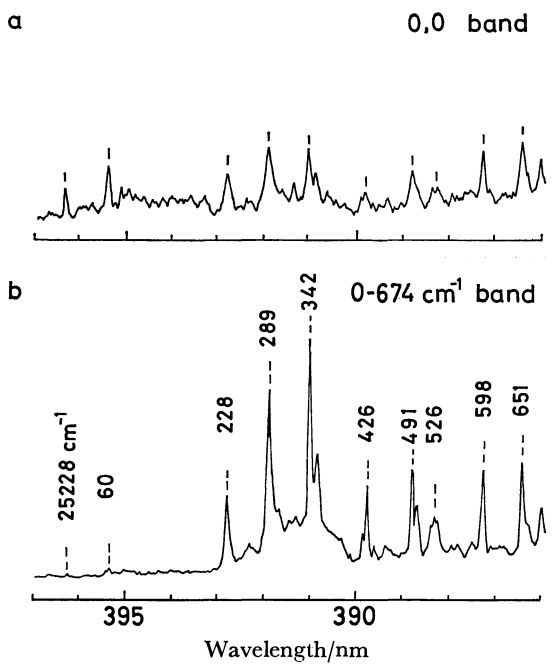

Fig. 3. The $T_1 \leftarrow S_0$ phosphorescence excitation spectra of the xanthone neat crystal at 1.4 K, monitored (a) at the 0,0 band and (b) at the 0−670 cm^{-1} band of the trap emission of site I.

anisms for the radiative decay are those listed in Table 1. A similar situation can be expected to hold for the absorption processes. Accordingly, the 0+210 cm^{-1} band can be assigned as being due to the C−Cl out-of-plane bending mode of b_{2g}, corresponding to that of 233 cm^{-1} in the ground state.

9*H*-Xanthen-9-one

A xanthone crystal is orthorhombic with four molecules in a unit cell.[16] The translationally equivalent molecules stack plane-to-plane along the a axis, with the out-of-plane molecular axis almost parallel to the a axis. The *a* lattice constant is small (4.894 Å) compared with the *b*(13.651 Å) and *c*(14.127 Å) lattice constants. The exciton motion in this system is therefore considered to be essentially one-dimensional along the a axis. No Davydov splitting has been resolved in the $T_1 \leftarrow S_0$ absorption, implying that the interaction between linear molecular chains is small. Therefore, the spin alignment of the excitons created by direct $T_1 \leftarrow S_0$ excitation is assumed to be appreciably preserved during the exciton migration. In addition, since the molecules in the trap sites have the orientations close to those in the host lattice, the populations of the spin sublevels of the trap molecules populated by the excitation trapping are considered to be just a replica of those of the excitons.

The $T_1 \leftarrow S_0$ absorption of the xanthone crystal was studied at 1.4 K by phosphorescence excitation method with short pulses. Some of the vibronic bands are found to behave in quite different ways from the 0,0 band as the wavelength for monitoring is changed. Figure 3 compares, as an example, the spectra obtained by monitoring the emission from the trap, named as site I, at the 0,0 band and 0−670 cm^{-1} band. These two bands have been reported to differ largely in the radiative activity of the z sublevel, whereas the x and y sublevels make similar contributions.[17,18] The remarkable difference between the two spectra can be attributed to the change in the relative population of the z sublevel of the site I trap as the wavelength of the excitation is changed. Furthermore, this indicates that both the spin-lattice relaxation and population rearrangement according to the relative orientation of the spin axes of donor and acceptor molecules have a little effect during the energy transfer process and is in good agreement with the expectation mentioned above that the excitation transfer may occur essentially in a one-dimensional manner.

Accordingly, the observed results imply that for excitation to the vibronic bands in the triplet manifold, such as 0+228, 0+289, and 0+342 cm^{-1}, the z sublevel has preferable activity whereas the y sublevel is

probably most active for the 0,0 band excitation. The y and z sublevels have been reported to gain the activity in the $T_1 \rightarrow S_0$ radiative decay through the mechanisms listed in Table 2, and similar mechanisms are expected to play a role in the $T_1 \leftarrow S_0$ absorption process. In fact, the experimental finding that the absorption cross section of the y sublevel is larger than that of the z sublevel in the case of the 0,0 band excitation is consistent with this expectation, and also the vibronic bands such as 0+228, 0+289, and 0+342 cm^{-1} can be assigned as being due to the b_1 species in view of the intensity behavior. In addition, the vibronic bands probably due to the a_2 modes such as 0+670 cm^{-1} are found to appear with considerable intensity at upward of 600 cm^{-1} from the origin, although the bands involving a_2 species appear with little intensity in the phosphorescence spectrum. This is a consequence of the increased importance of the vibronic coupling with intermediate $^3A_2$ (n,π^*) state resulting from the reduction of energy separation.

The present work was partly supported by a Grant-in-Aid for Scientific Research from the Ministry of Education, Science and Culture (Nos. 56340019 and 56340026).

References

1) D. L. Dexter, *J. Chem. Phys.*, **21**, 836 (1953).
2) M. A. El-Sayed, *J. Chem. Phys.*, **54**, 680 (1971).
3) M. Kinoshita, N. Iwasaki, and N. Nishi, *Rev. Appl. Spectrosc.*, **17**, 1 (1981).
4) N. Nishi and M. Kinoshita, *Bull. Chem. Soc. Jpn.*, **49**, 1221 (1976).
5) N. Nishi, M. Kinoshita, T. Nakashima, R. Shimada, and Y. Kanda, *Mol. Phys.*, **33**, 31 (1977).
6) N. Nishi, K. Matsui, M. Kinoshita, and J. Higuchi, *Mol. Phys.*, **38**, 1 (1979).
7) N. Iwasaki, N. Goto, and M. Kinoshita, in preparation.
8) E. Kanezaki, N. Nishi, and M. Kinoshita, *Bull. Chem. Soc. Jpn.*, **52**, 2836 (1979).
9) F. H. Herbstein, *Acta Crystallogr.*, **18**, 997 (1965).
10) A. H. Zewail and C. B. Harris, *Chem. Phys. Lett.*, **28**, 8 (1974), *Phys. Rev. B*, **11**, 935, 952 (1975).
11) C. B. Harris and D. A. Zwemer, *Ann. Rev. Phys. Chem.*, **29**, 473 (1978) and references therein.
12) G. A. George and G. C. Morris, *Mol. Cryst. Liq. Cryst.*, **11**, 61 (1970).
13) A. H. Francis and C. B. Harris, *J. Chem. Phys.*, **57**, 1050 (1972).
14) A. H. Francis and C. B. Harris, *Chem. Phys. Lett.*, **9**, 188 (1971), *J. Chem. Phys.*, **55**, 3595 (1971).
15) C. R. Chen and M. A. El-Sayed, *Chem. Phys. Lett.*, **10**, 303 (1971).
16) D. M. Burland, *Chem. Phys. Lett.*, **70**, 508 (1980).
17) A. Chakrabarti and N. Hirota, *J. Phys. Chem.*, **80**, 2966 (1976).
18) K. Suga and M. Kinoshita, *Bull. Chem. Soc. Jpn.*, **54**, 1651 (1981).

 © 1982 The Chemical Society of Japan Bull. Chem. Soc. Jpn., 55, 2835—2839 (1982)

The Group Coordinate Force Field of Oxymethylene and Thiomethylene Chain Molecules

Hiroatsu MATSUURA* and Hiromu MURATA

Department of Chemistry, Faculty of Science, Hiroshima University, Higashisenda-machi, Naka-ku, Hiroshima 730

(Received May 12, 1982)

Force field was systematically determined in terms of the group symmetry coordinates for series of $CH_3(OCH_2)_mOCH_3$ ($m=1$—3), the polymer $(-OCH_2-)_n$, and their deuterated derivatives, and of $CH_3(SCH_2)_mSCH_3$, $(-SCH_2-)_n$, and their deuterated derivatives. Twenty-five force constants for the oxymethylene molecules and twenty-two force constants for the thiomethylene molecules were adjusted by using 178 and 126 observed wavenumbers, respectively. The force constants obtained were compared with those for related molecules. The results of the normal coordinate treatment on the polymers were discussed in comparison with the results in previous works.

The intramolecular force field is one of the essential factors that characterize the properties of a molecule. The data concerning the force field are, therefore, of great importance in various fields of chemistry and physics, and the accumulation of such data is highly desired. In fact, systematic researches to establish the molecular force constants have been initiated by Shimanouchi *et al.* and the results so far obtained have been compiled as standard reference data.[1-3] The force constants thus published include those for unbranched chain molecules of alkanes, dialkyl ethers, dialkyl sulfides,[1] fluoroalkanes, chloroalkanes, bromoalkanes, and iodoalkanes.[2]

The force constants in these studies have been expressed in terms of the symmetry coordinates of the atomic groups constituting the molecule. This type of force field, called the group coordinate force field (GCFF)[3] or the local symmetry force field, has been proved to be suitable for describing the intramolecular potential of such classes of molecules as those mentioned above.

Having established the force field for dialkyl ethers ROR′, where R and R′ are alkyl groups,[1] and studied closely a conformational stability of dimethoxymethane $CH_2OCH_2OCH_3$,[4] it seems timely to work thoroughly on the GCFF for a series of $CH_3(OCH_2)_mOCH_3$ and the polymer $(-OCH_2-)_n$. In the present work, therefore, the force constants in the GCFF were derived for the oxymethylene chain molecules and the sulfur analogues, namely the thiomethylene chain molecules. The force constants determined and the results of the normal coordinate calculations are reported in the present paper.

Normal Coordinate Treatment

The force constants in the GCFF were calculated for the oxymethylene and thiomethylene chain molecules by means of the normal coordinate treatment.[5] The calculations were carried out by using a computer program MVIB[3] which has been developed for treating vibrations of chain molecules.

Molecules Treated. The calculations were performed on the following molecules; the oxymethylene series: $CH_3OCH_2OCH_3$ *gauche-gauche* form (to be abbreviated as G_2), $CH_3OCD_2OCH_3$ G_2, $CD_3OCH_2OCD_3$ G_2, $CD_3OCD_2OCD_3$ G_2, $CH_3(OCH_2)_2OCH_3$ G_4, $CH_3(OCH_2)_3OCH_3$ G_6, $(-OCH_2-)_n$ G_∞, and $(-OCD_2-)_n$ G_∞, and the thiomethylene series: $CH_3SCH_2SCH_3$ G_2, $CH_3SCD_2SCH_3$ G_2, $CH_3(SCH_2)_2SCH_3$ G_4, $CH_3(SCH_2)_3SCH_3$ G_6, $(-SCH_2-)_n$ G_∞, and $(-SCD_2-)_n$ G_∞. The observed infrared and Raman wavenumbers were taken from the literature: $CH_3OCH_2OCH_3$,[4,6] $CH_3OCD_2OCH_3$,[6] $CD_3OCH_2OCD_3$,[6] $CD_3OCD_2OCD_3$,[6] $CH_3(OCH_2)_2OCH_3$,[7] $CH_3(OCH_2)_3OCH_3$,[7] $(-OCH_2-)_n$,[8-10] $(-OCD_2-)_n$,[8-10] $CH_3SCH_2SCH_3$,[11] $CH_3SCD_2SCH_3$,[12] $CH_3(SCH_2)_2SCH_3$,[11] $CH_3(SCH_2)_3SCH_3$,[11] $(-SCH_2-)_n$,[13] and $(-SCD_2-)_n$.[14]

Table 1. Atomic masses for the oxymethylene and thiomethylene molecules

Atom	Atomic mass[a]/u
Hydrogen, protium	1.007825
Hydrogen, deuterium	2.014102
Carbon	12.011[b]
Oxygen	15.9994[b]
Sulfur	32.06[b]

a) Atomic mass in units of unified atomic mass unit. $1\ u \approx 1.660531 \times 10^{-27}$ kg. b) Isotope-abundance weighted atomic mass.

Atomic Masses and Structural Parameters. The values of the atomic masses and the structural parameters used in the normal coordinate treatment are listed in Tables 1 and 2. Isotope-abundance weighted atomic masses were used for carbon, oxygen, and sulfur, since the experimental vibrational wavenumbers were not resolved into components of individual isotopic species except for hydrogen under the spectral resolution utilized.

The structural parameters for the polymers are based on the results of the X-ray diffraction analyses,[15,16] and are in conformity with the 9/5 helix for poly(oxymethylene) and the 17/9 helix for poly(thiomethylene). Some of the structural parameters were recalculated by making use of equations for helix parameters.[17] The geometries of the oligomer molecules, $CH_3(OCH_2)_mOCH_3$ and $CH_3(SCH_2)_mSCH_3$ ($m=1-3$), were deduced from those of related molecules.[18]

Group Symmetry Coordinates. The symmetry coordinates in the methyl group, $CH_3(O)$ or $CH_3(S)$, and the methylene group, $(O)CH_2(O)$ or $(S)CH_2(S)$,

TABLE 2. STRUCTURAL PARAMETERS FOR THE OXYMETHYLENE AND THIOMETHYLENE MOLECULES

Structural parameter	Values			
	$CH_3(OCH_2)_mOCH_3$ ($m=1$—3)	$(-OCH_2-)_n$	$CH_3(SCH_2)_mSCH_3$ ($m=1$—3)	$(-SCH_2-)_n$
Bond lengths				
r(C–H)/Å[a]	1.100	1.100	1.100	1.100
r(C–O)/Å	1.410	1.4219	—	—
r(C–S)/Å	—	—	1.816	1.816
Valence angles				
∠(C–O–C)/°	111.8	112.40	—	—
∠(O–C–O)/°	110.8	110.82	—	—
∠(O–C–H)/°	109.8	109.8	—	—
∠(C–S–C)/°	—	—	98.6	97.1
∠(S–C–S)/°	—	—	117.4	117.40
∠(S–C–H)/°	—	—	108.8	108.8
Dihedral angles				
τ(O–C–O–C)/°	60.0	78.005	—	—
τ(S–C–S–C)/°	—	—	60.0	66.866

a) 1 Å = 1×10^{-10} m.

TABLE 3. FORCE CONSTANTS IN THE GCFF FOR THE OXYMETHYLENE AND RELATED MOLECULES

Intragroup force constants		Values[a,b]		
Symbol[c]	Description	X=Y=O	X=CH_2, Y=O[d]	X=Y=CH_2[d]
$f_{(X)CH_2(Y)\text{-}2}$	CH_2 scissor.	0.596(6)	0.590(4)	0.589(2)
$f_{(X)CH_2(Y)\text{-}4}$	CH_2 rock.	1.088(45)	0.820(31)	0.766(5)
$f_{(X)CH_2(Y)\text{-}5}$	CH_2 wag.	0.812(17)	0.764(11)	0.622(3)
$f_{(X)CH_2(Y)\text{-}6}$	CH_2 twist.	0.756(9)	0.699(16)	0.639(4)
$f_{(X)CH_2(Y)\text{-}D}$	XCY deform.	1.356(16)	1.153(26)	0.941(8)
$f_{(X)CH_2(Y)\text{-}2D}$	CH_2 scissor./XCY deform.	−0.049(20)	0.076(21)	0.047(12)
Intergroup force constants		Values[b,e]		
Symbol[c]	Description	X=O	X=CH_2[d]	
$f_{(X)CH_2O(CH_2)\text{-}S}$	CH_2–O stretch.	4.673(24)	5.037(22)	
$f_{(X)CH_2O(CH_2)\text{-}2S}$	CH_2 scissor./CH_2–O stretch.	−0.223(16)	−0.176(24)	
$f_{(X)CH_2O(CH_2)\text{-}5S}$	CH_2 wag./CH_2–O stretch.	−0.551(27)	−0.588(22)	
$f_{(X)CH_2O(CH_2)\text{-}DS}$	XCO deform./CH_2–O stretch.	0.214[f]	0.386(18)	
$f_{(X)CH_2O(CH_2)\text{-}SB}$	CH_2–O stretch./COC bend.	0.177(31)	0.363(16)	
$f_{(X)CH_2(O)\text{-}SS}$	X–CH_2 stretch./CH_2–O stretch.	0.663(20)	0.314(28)	

a) Force constant values in units of aJ=mdyn Å. b) Errors in the force constants, given in parentheses, apply to the last significant figure(s). c) Ref. 3. d) Ref. 1. e) Force constant values in units of aJ $Å^{-2}$=mdyn $Å^{-1}$ for $f_{(X)CH_2O(CH_2)\text{-}S}$ and $f_{(X)CH_2(O)\text{-}SS}$, and of aJ $Å^{-1}$=mdyn for the others. f) Constrained in the final least-squares calculation.

were constructed in accordance with the group symmetry of C_{3v} and C_{2v}, respectively. General expressions to give the group symmetry coordinates with arbitrary valence angles have been formulated.[3] The coordinates and their signs were thus defined on the basis of these formulations, with the structural parameters given in Table 2. The group coordinates for the molecules treated in this work are similar to those for ROR′ and RSR′ molecules[1] with different coefficients only for the CH_2 scissoring, CH_2 wagging, and OCO or SCS deformation coordinates. Full details of the coordinate definition are found in Table 1 of Ref. 3.

Force Constants. The force constants in the GCFF are given in terms of the group symmetry coordinates given above and are classified into intragroup force constants and intergroup force constants.[1-3] The intragroup force constants for the terminal methyl group and the intergroup force constants between the methyl group and the adjoining oxygen or sulfur atom were constrained to those determined previously for CH_3OR or CH_3SR[1] and were not adjusted further in the present work. Other force constants were refined by the least-squares method in order that the calculated wavenumbers of normal vibrations agreed more closely with the observed ones. In the course of the refinement calculations, some of the force constants were found to be ill-determined with large errors. Such force constants were eventually assumed to be equiv-

Table 4. Force constants in the GCFF for the thiomethylene and related molecules

Intragroup force constants		Values[a,b]		
Symbol[c]	Description	X=Y=S	X=CH_2, Y=S[d]	X=Y=CH_2[d]
$f_{(X)CH_2(Y)-2}$	CH_2 scissor.	0.534(5)	0.551(5)	0.589(2)
$f_{(X)CH_2(Y)-4}$	CH_2 rock.	0.921(48)	0.804(15)	0.766(5)
$f_{(X)CH_2(Y)-5}$	CH_2 wag.	0.571(27)	0.607(11)	0.622(3)
$f_{(X)CH_2(Y)-6}$	CH_2 twist.	0.571(3)	0.626(4)	0.639(4)
$f_{(X)CH_2(Y)-D}$	XCY deform.	1.115(18)	0.846(41)	0.941(8)
$f_{(X)CH_2(Y)-2D}$	CH_2 scissor./XCY deform.	0.031(30)	0.161(35)	0.047(12)
Intergroup force constants		Values[b,e]		
Symbol[c]	Description	X=S	X=CH_2[d]	
$f_{(X)CH_2S(CH_2)-S}$	CH_2-S stretch.	2.955(51)	2.959(57)	
$f_{(X)CH_2S(CH_2)-2S}$	CH_2 scissor./CH_2-S stretch.	0.0[f]	0.0[f]	
$f_{(X)CH_2S(CH_2)-5S}$	CH_2 wag./CH_2-S stretch.	−0.271(84)	−0.217(44)	
$f_{(X)CH_2S(CH_2)-DS}$	XCS deform./CH_2-S stretch.	0.226[f]	0.226(30)	
$f_{(X)CH_2S(CH_2)-SB}$	CH_2-S stretch./CSC bend.	−0.239(54)	0.058(27)	
$f_{(X)CH_2(S)-SS}$	X-CH_2 stretch./CH_2-S stretch.	0.629(50)	0.473(26)	

a), b), c), d) See footnotes a), b), c), d), respectively, to Table 3. e) Force constant values in units of aJ Å^{-2} = mdyn Å^{-1} for $f_{(X)CH_2S(CH_2)-S}$ and $f_{(X)CH_2(S)-SS}$, and of aJ Å^{-1} = mdyn for the others. f) Assumed.

Table 5. Observed and calculated wavenumbers for $(-OCH_2-)_n$

Symmetry species	$\tilde{\nu}_{obsd}$/cm^{-1}	$\tilde{\nu}_{calcd}$/cm^{-1} and P.E.D.[a]			
		This work	Sugeta[b]	Piseri and Zerbi[c]	Tadokoro *et al.*[d]
a_1		2869 1(99)	2897	2920	2924
	1491	1484 2(100)	1501	1491	1508
	1339	1334 6(96)	1342	1324	1330
	920	932 S(85)	928	962	916
	539	528 D(57), B(57)	536	499	587
a_2	2978	2961 3(99)	2978	2971	2977
	1381	1378 5(94)	1385	1419	1425
	1097	1093 4(84)	1109	1110	1118
	903	923 S(110), 5(25)	905	928	922
	235	227 T(96)	234	223	237
e_1	2980	2969 3(99)	2984	2979	2982
	2924	2868 1(99)	2896	2919	2926
	1471	1465 2(100)	1481	1486	1506
	1434	1440 5(88)	1446	1418	1407
	1286	1291 6(92)	1289	1303	1318
	1235	1240 4(63), 5(24)	1240	1224	1169
	1091	1093 S(78)	1098	1077	1072
	932	938 S(111)	938	916	930
	630	633 D(74)	633	649	634
	455	472 B(80)	453	466	483
		20 T(92)	21	26	22

a) Potential-energy distributions (P.E.D.) calculated in this work are given in parentheses following the symmetry coordinates; 1: CH_2 symmetrical stretching, 2: CH_2 scissoring, 3: CH_2 antisymmetrical stretching, 4: CH_2 rocking, 5: CH_2 wagging, 6: CH_2 twisting, D: OCO deformation, B: COC bending, S: C-O stretching, and T: C-O torsion. b) Ref. 7. c) Ref. 19. d) Ref. 8.

alent to those for similar atomic groups so that the remaining constants converged properly. The calculations also revealed that the interaction force constants between the coordinates belonging to the second-neighboring atomic groups were required for satisfactory fitting of the observed and calculated wavenumbers. These constants include the interactions between the CH_2 rocking and CH_2 rocking coordinates, CH_2 wagging and CH_2 wagging, *etc.* of the neighboring methylene groups with an oxygen or sulfur atom in between, and the interaction between the COC (or CSC) bending and COC (or CSC) bending coordinates of the neighboring COC (or CSC) groups. The constants associated with the CH_2 symmetrical and antisymmetrical stretching coordinates were not refined in the present study.

TABLE 6. OBSERVED AND CALCULATED WAVENUMBERS FOR $(-OCD_2-)_n$

Symmetry species	$\tilde{\nu}_{obsd}$ / cm^{-1}	$\tilde{\nu}_{calcd}/cm^{-1}$ and P.E.D.[a]				
		This work		Sugeta[b]	Piseri and Zerbi[c]	Tadokoro *et al.*[d]
a_1		2107	1 (97)	2123	2140	2121
	1120	1102	2 (88)	1112	1126	1126
	1015	1018	6 (66), S (23)	1017	1031	1013
	850	836	S (51), 6 (30)	838	838	828
	508	501	D (56), B (54)	511	470	557
a_2	2235	2209	3 (98)	2225	2220	2193
	1050	1050	5 (57), S (11)	1046	1106	1154
	970	973	S (89), 5 (70)	973	974	1026
	835	822	4 (73), S (29)	819	813	769
	212	207	T (97)	213	205	212
e_1	2235	2232	3 (95)	2243	2241	2207
	2106	2106	1 (97)	2122	2138	2121
	1156	1146	4 (40), B (19)	1144	1142	1178
	1128	1118	S (61), 2 (25)	1121	1131	1145
	1078	1072	5 (90), S (73)	1071	1078	1047
	1064	1057	2 (69)	1058	1045	1044
	909	900	6 (79)	906	896	916
	838	838	S (55), 4 (22)	836	806	810
	618	616	D (70)	615	632	618
	363	373	B (72), 4 (20)	365	369	372
		19	T (93)	20	25	21

a), b), c), d) See footnotes a), b), c), d), respectively, to Table 5.

A full list of the force constants finally determined for the oxymethylene and thiomethylene chain molecules, together with the calculated results for all the molecules treated, has been deposited with the Chemical Society of Japan (Document No. 8247). In Tables 3 and 4, some important force constants are compared with those for related molecules. The calculated wavenumbers and assignments are given in this article only for the polymers.

Results and Discussion

In the present study, twenty-five force constants in the GCFF were determined for the oxymethylene chain molecules from 178 observed wavenumbers and twenty-two force constants for the thiomethylene chain molecules from 126 observed wavenumbers. The calculations with these force constants gave overall root-mean-square deviations of 9.6 and 8.2 cm^{-1}, respectively, for the oxymethylene and thiomethylene molecules, between the observed and calculated wavenumbers.

Table 3 shows that the values of the diagonal force constants for the $(X)CH_2(Y)$ group increase systematically in going from $(CH_2)CH_2(CH_2)$ to $(CH_2)CH_2(O)$ and $(O)CH_2(O)$. For the sulfides in Table 4, on the other hand, the values of the CH_2 scissoring, CH_2 wagging, and CH_2 twisting force constants decrease in going from $(CH_2)CH_2(CH_2)$ to $(CH_2)CH_2(S)$ and $(S)CH_2(S)$, but the value of only the CH_2 rocking constant increases. The CH_2–O stretching constant for the $(O)CH_2$–$O(CH_2)$ group (4.67 mdyn $Å^{-1}$) is found to be considerably smaller than that for the $(CH_2)CH_2$–$O(CH_2)$ group (5.04 mdyn $Å^{-1}$). This contrasts with the essentially same value (2.96 mdyn $Å^{-1}$) of the CH_2–S stretching constant for the $(S)CH_2$–$S(CH_2)$ and $(CH_2)CH_2$–$S(CH_2)$ groups.

The calculated results for poly(oxymethylene) and poly(oxymethylene-d_2) are given in Tables 5 and 6 in comparison with those reported previously.[7,8,19] The agreement between the observed and calculated wavenumbers is less satisfactory in the earlier studies. The nature of the normal modes is represented by the potential-energy distributions (P.E.D.).† The P.E.D.'s for the undeuterated species is almost the same among the studies, but some of the P.E.D.'s for the deuterated species differ considerably from one another. For example, the vibration at 1156 cm^{-1} (e_1) is assigned in this work to the CD_2 rocking, but was assigned to the CD_2 wagging and CD_2 scissoring,[7] to the C–O stretching and CD_2 scissoring,[19] or to the C–O stretching and CD_2 wagging,[8] and the vibration at 1078 cm^{-1} (e_1) is assigned in this work to the CD_2 wagging and C–O stretching, but was assigned to the CD_2 rocking,[7] to the CD_2 rocking and C–O stretching,[19] or to the CD_2 scissoring and C–O stretching.[8] We believe that the present assignment based on the systematic treatment is more likely than the previous ones.

The assignment of the observed bands of poly(thiomethylene) and poly(thiomethylene-d_2) is now estab-

† The potential-energy distribution, as defined by (P.E.D.)$_{ji} = 100 \times L_{ji}^2 f_{jj}/\lambda_i$,[3] may exceed 100 because of neglecting the contribution of off-diagonal force constants. This effect is particularly enhanced for polymers.

Table 7. Observed and calculated wavenumbers for $(-SCH_2-)_n$ and $(-SCD_2-)_n$

Symmetry species	$(-SCH_2-)_n$			$(-SCD_2-)_n$		
	$\tilde{\nu}_{obsd}/cm^{-1}$	$\tilde{\nu}_{calcd}/cm^{-1}$	P.E.D.[a]	$\tilde{\nu}_{obsd}/cm^{-1}$	$\tilde{\nu}_{calcd}/cm^{-1}$	P.E.D.[a]
a_1	2905	2905	1(100)		2128	1(98)
	1373	1386	2(99)		1025	2(92)
	1180	1179	6(99)		844	6(96)
	648	658	S(90)		618	S(83)
	355	340	D(99), B(47)		330	D(101), B(46)
a_2		2940	3(100)		2183	3(99)
	1225	1231	5(109)	962	954	5(108), S(25)
	882	886	4(95)	752	732	4(51), S(40)
	729	738	S(104)		670	4(47), S(45)
		117	T(98)		103	T(99)
e_1	2965	2938	3(100)		2178	3(99)
	2910	2905	1(100)		2128	1(98)
	1361	1372	2(99)	1012	1014	2(92)
	1173	1180	5(108)	908	902	5(113), S(30)
	1120	1117	6(99)		797	6(97)
	743	743	S(87)	697	700	S(95)
	711	712	4(95), S(35)	648	653	S(66), D(22)
	674	688	S(66), D(23)		529	4(136)
	299	300	D(75)		298	D(76)
	299	291	B(176), 4(57)		264	B(171), 4(40)
		3	T(95)		3	T(95)

a) Potential-energy distributions (P.E.D.) are given in parentheses following the symmetry coordinates; 1: CH_2 symmetrical stretching, 2: CH_2 scissoring, 3: CH_2 antisymmetrical stretching, 4: CH_2 rocking, 5: CH_2 wagging, 6: CH_2 twisting, D: SCS deformation, B: CSC bending, S: C–S stretching, and T: C–S torsion.

lished, as given in Table 7, in the light of the force field determined in the present work. The vibrational assignment of this polymer was first made by Hendra *et al.*,[13] who acknowledged, however, that their assignment based on empirical basis was very tentative. The normal coordinate treatment of poly(thiomethylene) and the deuterated derivative has been reported by Ohsaku.[14] His calculation is unfortunately erroneous as evidenced by the unlikely number of normal vibrations belonging to each symmetry species.

The group coordinate force field derived in this work for the $-OCH_2O-$ and $-SCH_2S-$ groups may be applied to other molecules consisting of similar atomic groups. The accumulation of the force constants for various types of atomic groups will eventually make possible the calculation of normal vibrational wavenumbers and modes of a large number of molecules.

The authors wish to thank Mr. Tomoya Takuwa for his assistance in the computational work. Numerical computations were carried out with a HITAC M-200H computing system at Hiroshima University.

References

1) T. Shimanouchi, H. Matsuura, Y. Ogawa, and I. Harada, *J. Phys. Chem. Ref. Data*, **7**, 1323 (1978).
2) T. Shimanouchi, H. Matsuura, Y. Ogawa, and I. Harada, *J. Phys. Chem. Ref. Data*, **9**, 1149 (1980).
3) H. Matsuura and M. Tasumi, "Force Fields for Large Molecules," in "Vibrational Spectra and Structure," ed by J. R. Durig, Elsevier, Amsterdam (1982), Vol. 12, Chap. 2, in press.
4) M. Sakakibara, Y. Yonemura, H. Matsuura, and H. Murata, *J. Mol. Struct.*, **66**, 333 (1980).
5) T. Shimanouchi, "The Molecular Force Field," in "Physical Chemistry, An Advanced Treatise," ed by H. Eyring, D. Henderson, and W. Jost, Academic Press, New York (1970), Vol. IV, Chap. 6, p. 233.
6) K. Nukada, *Spectrochim. Acta*, **18**, 745 (1962).
7) H. Sugeta, Ph. D. Thesis, Osaka University (1969).
8) H. Tadokoro, M. Kobayashi, Y. Kawaguchi, A. Kobayashi, and S. Murahashi, *J. Chem. Phys.*, **38**, 703 (1963).
9) G. Zerbi and P. J. Hendra, *J. Mol. Spectrosc.*, **27**, 17 (1968).
10) H. Sugeta, T. Miyazawa, and T. Kajiura, *J. Polym. Sci., Pt. B*, **7**, 251 (1969).
11) M. Ohsaku, Y. Shiro, and H. Murata, *Bull. Chem. Soc. Jpn.*, **45**, 113 (1972).
12) M. Sakakibara, unpublished work.
13) P. J. Hendra, D. S. Watson, and M. Mammi, *Spectrochim. Acta, Part A*, **28**, 351 (1972).
14) M. Ohsaku, *Bull. Chem. Soc. Jpn.*, **47**, 965 (1974).
15) T. Uchida and H. Tadokoro, *J. Polym. Sci., A-2*, **5**, 63 (1967).
16) G. Carazzolo and G. Valle, *Makromol. Chem.*, **90**, 66 (1966).
17) T. Miyazawa, *J. Polym. Sci.*, **55**, 215 (1961).
18) Structure Data of Free Polyatomic Molecules, "Landolt-Börnstein, Numerical Data and Functional Relationships in Science and Technology," New Series, Group II: Atomic and Molecular Physics, Springer-Verlag, Berlin (1976), Vol. 7.
19) L. Piseri and G. Zerbi, *J. Chem. Phys.*, **48**, 3561 (1968).

The Structure and Properties of the Triaquahexakis(methylthioacetato)-dineodymium(III) Polymer, $[Nd_2(C_3H_5SO_2)_6(H_2O)_3]_n$, and the Same-ligand Complexes of Lanthanoid Elements

Satoshi KONDO, Mamoru SHIMOI, Akira OUCHI,* and Toshio TAKEUCHI†

Department of Chemistry, College of General Education, The University of Tokyo, Komaba 3-8-1, Meguro-ku, Tokyo 153

† *Department of General Sciences, Faculty of Science and Technology, Sophia University, Kioi-cho 7, Chiyoda-ku, Tokyo 102*

(Received August 25, 1981)

The crystal and molecular structure of the title complex has been determined by the X-ray diffraction method. The crystal was triclinic, space group $P\bar{1}$, $a=12.80(1)$, $b=16.65(1)$, $c=8.659(9)$ Å, $\alpha=104.6(1)$, $\beta=93.7(2)$, $\gamma=107.5(1)°$, $Z=2$, $D_x=1.892(3)$, $D_m=1.91(2)$ Mg m^{-3}, μ(Mo $K\alpha$)$=3.45$ mm^{-1}, and the final R value was 0.051 for 3577 reflections. The coordination number of both neodymium atoms is nine, although the coordinated atoms around one neodymium atom are arrayed in a tri-capped trigonal prism, and those around the other neodymium atom, in a mono-capped tetragonal antiprism. The neodymium atoms are arrayed on a linear chain bridged by the ligand; however, no metal-metal interaction is observed. The corresponding complexes of cerium(III), praseodymium(III), and europium(III) form isomorphous crystals with the title complex, but the complex of lanthanum(III) has the formula of $ML_3\cdot 4.5H_2O$ (HL=(methylthio)acetic acid), and the complexes of dysprosium(III) and ytterbium(III), $ML_3\cdot 2H_2O$.

Many synthetic works were already published about the (alkylthio)acetato** complexes of 3d elements,[1-11] and we have already reported about these structures.[12-15] According to our results, in general, one oxygen atom as well as a sulfur atom are coordinated with the central metal atom, thus forming a five-membered chelate ring. However, in the case of bis(isopropylthioacetato)copper(II) dihydrate, two oxygen atoms of a carboxyl group of the ligand are coordinated to separate metal atoms.[14] In the case of the bis(propylthioacetato)cobalt(II) hexamer, there are two kinds of ligands acting in different modes of coordination.[15] Although no structural analysis was done, in the case of bis(alkylthioacetato)triphenylantimony(III) the ligand is expected to be coordinated to the metal atom by only one oxygen atom.[11]

The methylthioacetato complexes of lanthanoid elements now obtained were found to have the formula of $ML_3\cdot nH_2O$ (where HL=methylthioacetic acid, and $n=4.5$, 1.5, or 2 for their hydrated complexes). The lanthanoid elements generally show a high coordination number, and the sulfur atom of a ligand is hardly coordinated at all to the metal because of its "hard" character. Consequently, it is not probable that the five-membered chelate ring found in the 3d element complexes exists also in the lanthanoid complexes. On the other hand, a linear polymer structure has been reported for some carboxylato complexes of 4f and 5f metals, such as cerium(III) acetate[16] and uranium(IV) acetate.[17] Therefore, for the alkylthioacetato complexes of lanthanoid elements, too, such a type of interesting polymerized structure was expected. Thus, we have attempted to determine their crystal and molecular structure by means of X-ray diffraction. The methylthioacetato complexes of other lanthanoid elements were also obtained and were compared with the titled complex with regard to their analytical, spectral, and thermochemical properties, as well as their X-ray powder patterns in order to classify them.

** The parentheses in the name of the ligand are neglected hereafter.

Experimental

Synthesis of Triaquahexakis(methylthioacetato)dineodymium(III), $[Nd_2(CH_3SCH_2CO_2)_6(H_2O)_3]_n$. The ligand was obtained by means of a slight modification of the method of Larsson;[18] a condensation reaction between dimethyl sulfate (in place of methyl iodide) and mercaptoacetic acid in the presence of sodium hydroxide in an aqueous solution. The aqueous solutions of sodium methylthioacetate (2.4 g (19 mmol) in 5 cm^3 of water) and of neodymium(III) chloride hexahydrate (2.0 g (5.5 mmol) in 5 cm^3 of water) were mixed and the mixture was left standing for one day or more at 6 °C. The first crop of the product was thus obtained; the yield was 1.1 g (41%). The filtered mother liquor was concentrated to 5 cm^3 and then left standing; a second crop which was almost as pure as the first one was also obtained; the total yield was 1.8 g (66%). The complex could be recrystallized from water, although the crystal appeared slowly, and the yield was low because of its fairly high solubility. The crystals thus obtained were submitted to the X-ray diffraction after being checked by means of their Weissenberg photograph. Found: Nd, 29.76; C, 22.08; H, 3.69%. Calcd for $Nd_2C_{18}H_{36}S_6O_{15}$: Nd, 29.64; C, 22.21; H, 3.73%.

Syntheses and Analyses of the Methylthioacetato Complexes of Lanthanoid Elements. These complexes were obtained in almost the same way as the neodymium complex. Among them, the cerium(III), praseodymium(III), and europium(III) complexes have the same type of chemical formula, $ML_3\cdot 1.5H_2O$ (HL=methylthioacetic acid). 1) Cerium(III) complex, Found: Ce, 28.78; C, 22.30; H, 3.67%. Calcd for $CeC_9H_{18}O_{7.5}S_3$: Ce, 29.04; C, 22.42; H, 3.76%. 2) Praseodymium(III) complex, Found: Pr, 29.15; C, 22.24; H, 3.70%. Calcd for $PrC_9H_{18}O_{7.5}S_3$: Pr, 29.15; C, 22.37; H, 3.75%. 3) Europium(III) complex, Found: Eu, 30.73; C, 21.80; H, 3.63%. Calcd for $EuC_9H_{18}O_{7.5}S_3$: Eu, 30.74; C, 21.87; H, 3.67%. The lanthanum(III) complex of the ligand has the chemical formula of $ML_3\cdot 4.5H_2O$. Found: La, 25.67; C, 19.81; H, 4.17%. Calcd for $LaC_9H_{24}O_{10.5}S_3$: La, 25.95; C, 20.19; H, 4.52%. The dysprosium(III) and ytterbium(III) complexes have the chemical formula of $ML_3\cdot$

$2H_2O$. 1) Dysprosium(III) complex, Found: Dy, 31.61; C, 21.02; H, 3.68%. Calcd for $DyC_9H_{18}O_8S_3$: Dy, 31.62; C, 21.03; H, 3.73%. 2) Ytterbium(III) complex, Found: Yb, 33.01; C, 20.54; H, 3.57%. Calcd for $YbC_9H_{18}O_8S_3$: Yb, 32.99; C, 20.61; H, 3.65%.

X-Ray Measurements. *X-Ray Powder Pattern*: Their X-ray powder patterns were obtained by the use of the diffractometer, Model DX-GO-F JEOL, using Cu $K\alpha$ radiation, in the range from 6° to 30° in 2θ.

Single-crystal X-Ray Analysis: Almost all single crystals of the title complex obtained were thin-plate ones; the crystal grew poorly in the a axis direction. As it was brittle, a crystal of 0.3 mm × 0.2 mm × 0.3 mm was used for the measurement, without any reshaping process.

The crystallographic data are: $Nd_2C_{18}H_{36}O_{15}S_6$, F.W.= 973.34, triclinic, space group $P\bar{1}$, $Z=2$, $a=12.80(1)$, $b=16.65(1)$, $c=8.659(9)$ Å $\alpha=104.6(1)$, $\beta=93.7(2)$, $\gamma=107.5(1)$°, $D_x=1.892(3)$, $D_m=1.91(2)$ Mg m^{-3}, μ(Mo $K\alpha$)=3.45 mm^{-1}.

The reflections with 2θ less than 55° were collected on a Philips PW 1100 automated four-circle diffractometer with Mo $K\alpha$ radiation, the θ-2θ scan technique being employed. We used 3577 independent reflections with $|F_o|>3\sigma(|F_o|)$ for the structure refinement. The intensities were corrected for Lorentz and polarization factors, but no correction was made for absorption and extinction.

All the calculations were carried out on a HITAC M-200H computer at The Computer Center of The University of Tokyo, using the local version of the UNICS program.[19] The atomic-scattering factors were taken from the tables.[20]

Structure Determination. The structure was solved by the heavy-atom method. The positions of neodymium atoms were deduced from a three-dimensional Patterson map, while all the other non-hydrogen atoms were located by means of successive Fourier syntheses. Their positional and thermal parameters were refined by the block-diagonal least-squares method. The positions of 20 hydrogen atoms were obtained from a difference Fourier synthesis and were also refined. The position of a sulfur atom, S(4), was divided into two, and the probability of the occupancy of each position was approximately assigned from the Fourier map and refined by the full-matrix procedure with regard to the positions of the atoms of the ligand. The final values are 46.7 and 53.3% respectively. Although it is not necessary to divide the position of the methyl carbon atom of each ligand, it has a relatively large amplitude of thermal vibration, just as in the case of some ligands in the hexamer of the propylthioacetato complex of cobalt(II).[15] In the last cycle of the refinement with anisotropic temperature factors for all non-hydrogen atoms, all the parameter shifts were less than one-third of the corresponding standard deviations. The final R value obtained was 0.051.[21]

Other Measurements. The magnetic moments of the solid samples were measured using a Gouy balance at 25 °C.

The simultaneous thermogravimetric (TG) and differential thermal analysis (DTA) were carried out with a Rigaku Denki "Thermoflex" M-8075 using a sample weighing about 10 mg in each operation, at the heating rate of 10 °C min^{-1} in air, using α-alumina as the reference.

The infrared spectra of the samples were obtained by means of a JASCO 403G infrared spectrophotometer, using Nujol and hexachloro-1,3-butadiene mull.

Results and Discussion

The crystal structure of the triaquahexakis(methylthioacetato)dineodymium(III) polymer will now be summarized. The final atomic parameters are listed in Table 1,[22] while the interatomic distances as well as the bond angles are tabulated in Table 2. A projection of the structure along the c axis is shown in Fig. 1, and a perspective drawing of the complex around Nd(1) and Nd(2), together with the numbering scheme of neodymium, oxygen, and carbon atoms, is presented in Fig. 2.

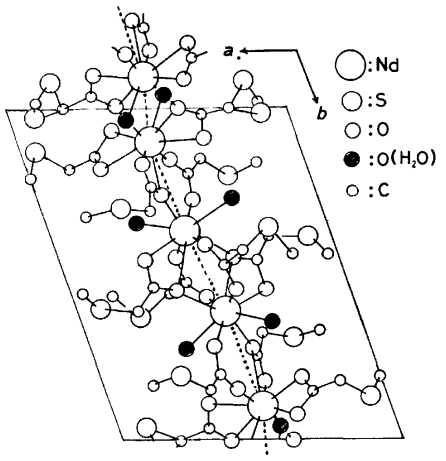

Fig. 1. Crystal packing diagram of $[Nd_2(CH_3SCH_2CO_2)_6(H_2O)_3]_n$ projected along c.

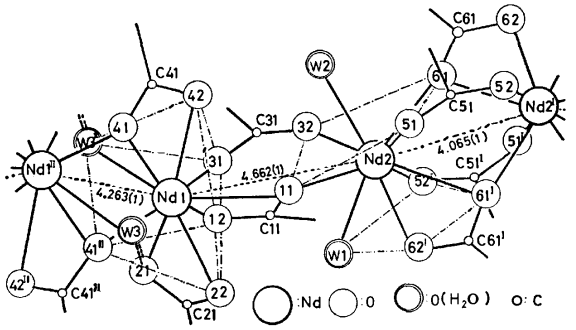

Fig. 2. A perspective drawing of $[Nd_2(CH_3SCH_2CO_2)_6(H_2O)_3]_n$, and the numbering scheme of neodymium, oxygen, and carboxyl carbon atoms. Each coordination polyhedron around neodymium atom is shown by —·—.

The crystal consists of the linear polymer of $[Nd(CH_3SCH_2CO_2)_3(H_2O)$–$Nd(CH_3SCH_2CO_2)_3(H_2O)_2]_n$, nearly parallel to the b axis. Each chain is connected with a hydrogen bond between O(W3) atom and the O(21) atom of the neighbouring chain in the c axis direction. No other bonds were observed between chains except for van der Waals interactions. As is shown in Fig. 1, the coordination number of both the neodymium atoms in the complex is nine. Their coordination polyhedrons are, however, different from each other; that around Nd(1) is a distorted tri-capped trigonal prism, while that around Nd(2) is, rather, a mono-capped tetragonal antiprism, as is shown by the —·— line in Fig. 2. Each water molecule is coordinated to one of the neodymium atoms, and, as is shown above, one of them forms a hydrogen bond with the carboxyl oxygen atom of a neighbouring chain. Each methylthioacetato ligand is coordinated to neodymium atoms through the oxygen

Table 1. Final atomic coordinates ($\times 10^4$ for non-hydrogen atoms, and $\times 10^3$ for hydrogen atoms), equivalent isotropic (for non-hydrogen atoms), and isotropic temperature factors (for hydrogen atoms), with estimated standard deviations in parentheses

Atom	x	y	z	B_{eq}/Å^2 a)
Nd (1)	5352.0 (4)	967.4 (3)	3724.1 (6)	2.2
Nd (2)	5203.7 (4)	3800.4 (3)	4435.4 (6)	2.0
S (1)	7308 (3)	3046 (2)	9564 (3)	5.0
S (2)	9466 (3)	1355 (3)	2249 (5)	6.7
S (3)	2918 (3)	1949 (2)	−1449 (4)	4.9
S (4A)****	1013 (8)	187 (8)	4163 (15)	9.4
S (4B)****	1246 (5)	−745 (4)	3142 (8)	4.9
S (5)	2169 (2)	3611 (2)	7939 (4)	3.8
S (6)	942 (3)	3960 (2)	1506 (4)	4.4
O (11)	5594 (5)	2618 (4)	5456 (7)	2.3
O (12)	5888 (6)	1671 (4)	6639 (8)	3.3
O (21)	6619 (6)	751 (4)	1638 (8)	3.5
O (22)	7277 (5)	1926 (4)	3676 (8)	3.1
O (31)	4822 (7)	1555 (6)	1775 (10)	5.2
O (32)	4408 (7)	2742 (5)	1774 (8)	4.1
O (41)	3918 (5)	23 (4)	5241 (7)	2.7
O (42)	3496 (6)	1000 (4)	4360 (10)	3.7
O (51)	4676 (6)	4200 (4)	7077 (8)	3.0
O (52)	4288 (6)	5438 (4)	7613 (8)	3.5
O (61)	3836 (5)	4503 (4)	4193 (7)	2.8
O (62)	3006 (5)	5375 (4)	3536 (8)	3.0
O (W1)	6879 (6)	3491 (5)	3338 (9)	4.1
O (W2)	3330 (6)	2687 (4)	4626 (8)	3.4
O (W3)	5838 (6)	412 (4)	8248 (8)	3.4
C (11)	6872 (8)	2421 (6)	6709 (11)	2.6
C (12)	6188 (8)	3155 (6)	8315 (11)	2.7
C (13)	8368 (13)	3288 (13)	8340 (23)	8.1
C (21)	7351 (9)	1465 (6)	2266 (13)	3.6
C (22)	8387 (11)	1792 (9)	1565 (17)	5.8
C (23)	9959 (13)	2044 (11)	4316 (19)	6.6
C (31)	4349 (8)	1997 (6)	1156 (12)	2.9
C (32)	3810 (10)	1514 (7)	−594 (13)	4.0
C (33)	1784 (13)	1654 (10)	−393 (27)	8.0
C (41)	3204 (8)	355 (6)	4939 (11)	2.4
C (42)	2015 (10)	−24 (8)	5115 (14)	4.1
C (43)	1247 (16)	−108 (17)	2036 (25)	10.7
C (51)	4199 (8)	4707 (7)	7806 (11)	3.1
C (52)	3478 (8)	4378 (6)	9036 (10)	2.6
C (53)	1507 (12)	4380 (11)	7487 (21)	7.1
C (61)	3033 (7)	4626 (6)	3414 (10)	2.1
C (62)	2139 (9)	3810 (6)	2392 (12)	3.0
C (63)	383 (12)	4417 (10)	3243 (18)	5.9

Atom	x	y	z	B_{iso}/Å^2
H (W11)	716 (8)	300 (6)	368 (11)	3.01 (1)
H (W21)	386 (8)	220 (6)	465 (12)	3.01 (1)
H (W31)	615 (8)	89 (6)	818 (12)	3.01 (1)
H (W32)	605 (8)	66 (6)	947 (12)	3.01 (1)
H (11)	557 (8)	289 (6)	872 (12)	3.01 (1)
H (12)	610 (8)	390 (6)	863 (11)	3.01 (1)
H (13)	851 (8)	404 (6)	780 (12)	2.94 (1)
H (14)	771 (8)	288 (6)	728 (12)	2.93 (1)
H (21)	845 (8)	228 (6)	142 (12)	3.01 (1)
H (22)	800 (8)	173 (6)	27 (11)	3.01 (1)
H (31)	336 (7)	106 (6)	−42 (11)	3.01 (1)
H (33)	187 (8)	103 (6)	−10 (12)	2.93 (1)
H (41)	160 (8)	−14 (6)	594 (12)	3.01 (1)
H (43)	196 (8)	12 (6)	168 (11)	2.93 (1)
H (44)	60 (8)	9 (6)	186 (12)	2.93 (1)
H (51)	337 (8)	480 (6)	1017 (12)	3.01 (1)
H (52)	411 (8)	404 (6)	940 (12)	3.01 (1)
H (53)	206 (8)	491 (6)	692 (11)	2.93 (1)
H (61)	226 (8)	412 (6)	123 (12)	3.01 (1)
H (62)	191 (8)	353 (6)	313 (11)	3.01 (1)

a) The equivalent isotropic temperature factors for non-hydrogen atoms were computed using the following expression: $B_{eq}=(4/3)(B_{11}a^2+B_{22}b^2+B_{33}c^2+B_{12}ab\cos\gamma+B_{13}ac\cos\beta+B_{23}bc\cos\alpha)$. The B_{ij}'s are defined by: $\exp[-(h^2B_{11}+k^2B_{22}+l^2B_{33}+2klB_{23}+2hlB_{13}+2hkB_{12})]$.

**** The probability of the occupancy of each position was 46.7% for S(4A) and 53.3% for S(4B).

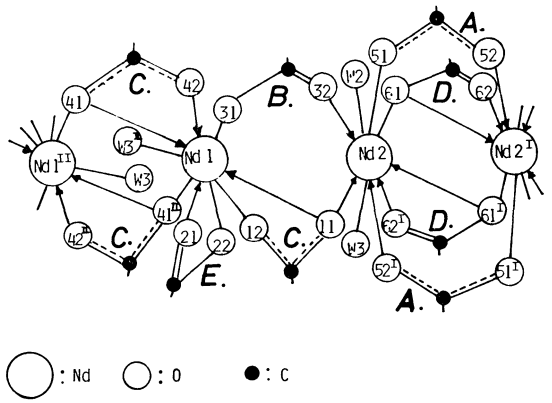

Fig. 3. Schematic presentation of the bonding modes of ligands. The mode of each carboxyl group is presented by *A*—*E*. The Nd–O bond without arrow mark is the shortest one of those from the carboxyl group.

atoms, not through its sulfur atom. As is shown in Fig. 3, there are five kinds of ligands, as considered in terms of their coordination modes; they are tentatively named *A*—*E*-mode ligands.

The *A* and *B* ligands span two neodymium atoms through both the oxygen atoms of a carboxyl group. The C–O distances of *A* ligand are almost the same (C(51)–O(51)=1.256(14), C(51)–O(52)=1.258(14) Å), and the corresponding Nd–O distances are not much different (Nd(2)–O(51)=2.415(7), Nd(2)–O(52^{I})=2.456(9) Å). In the case of the *B* ligand, one C–O is longer than the other one (C(31)–O(31)=1.272(16), C(31)–O(32)=1.198(13) Å), while the Nd–O from the oxygen atom of the shorter C–O is longer than the other one (Nd(2)–O(32)=2.454(8), Nd(1)–O(31)=2.312(10) Å). The *C* and *D* ligands bridge two neodymium atoms by one oxygen atom, and, at the same time, the other oxygen atom of the ligand is coordinated to one of the bridged neodymium at-

TABLE 2. INTERATOMIC DISTANCES AND BOND ANGLES WITH ESTIMATED STANDARD DEVIATIONS IN PARENTHESES

Interatomic distance	l/Å		l/Å
Nd (1) ···Nd (2)	4.662 (1)	O (22) - C (21)	1.294 (13)
Nd (2) ···Nd (2^{I})	4.065 (1)	C (21) - C (22)	1.503 (19)
Nd (1) ···Nd (1^{II})	4.263 (1)	C (22) - S (2)	1.850 (18)
Nd (1) - O (11)	2.691 (7)	S (2) - C (23)	1.818 (15)
Nd (1) - O (12)	2.452 (7)	O (31) - C (31)	1.272 (16)
Nd (1) - O (21)	2.536 (9)	O (32) - C (31)	1.198 (13)
Nd (1) - O (22)	2.512 (7)	C (31) - C (32)	1.528 (14)
Nd (1) - O (31)	2.312 (10)	C (32) - S (3)	1.744 (15)
Nd (1) - O (41)	2.681 (8)	S (3) - C (33)	1.777 (21)
Nd (1) - O (42)	2.488 (8)	O (41) - C (41)	1.247 (14)
Nd (1) - O (41^{II})	2.441 (8)	O (42) - C (41)	1.265 (13)
Nd (1) - O ($W3^{II}$)	2.468 (8)	C (41) - C (42)	1.497 (15)
Nd (2) - O (61)	2.405 (8)	C (42) - S (4A)	1.651 (19)
Nd (2) - O (32)	2.454 (8)	C (42) - S (4B)	1.835 (12)
Nd (2) - O (11)	2.513 (8)	S (4A) - C (43)	1.851 (25)
Nd (2) - O (W1)	2.541 (9)	S (4B) - C (43)	1.598 (30)
Nd (2) - O (51)	2.415 (7)	O (51) - C (51)	1.256 (14)
Nd (2) - O (W2)	2.599 (8)	O (52) - C (51)	1.258 (14)
Nd (2) - O (52^{I})	2.456 (9)	C (51) - C (52)	1.552 (15)
Nd (2) - O (61^{I})	2.633 (8)	C (52) - S (5)	1.799 (10)
Nd (2) - O (62^{I})	2.568 (9)	S (5) - C (53)	1.838 (20)
O (11) - C (11)	1.269 (13)	O (61) - C (61)	1.289 (13)
O (12) - C (11)	1.241 (13)	O (62) - C (61)	1.236 (12)
C (11) - C (12)	1.538 (12)	C (61) - C (62)	1.505 (11)
C (12) - S (1)	1.820 (12)	C (62) - S (6)	1.782 (13)
S (1) - C (13)	1.789 (19)	S (6) - C (63)	1.800 (16)
O (21) - C (21)	1.236 (11)	O (W3) ··· O (21^{III})	2.894 (11)
Bond angle	θ/°		θ/°
Nd (1) ···Nd (2) ···Nd (2^{I})	171.58 (2)	O (W2) -Nd (2) - O (W1)	128.6 (2)
Nd (1^{II}) ···Nd (1) ···Nd (2)	137.38 (2)	O (W2) -Nd (2) - O (62^{I})	132.1 (2)
O (11) -Nd (1) - O (21)	118.3 (2)	O (W2) -Nd (2) - O (61^{I})	132.9 (2)
O (11) -Nd (1) - O (41)	101.4 (2)	O (W2) -Nd (2) - O (52^{I})	131.6 (2)
O (21) -Nd (1) - O (41)	139.5 (2)	O (11) -Nd (2) - O (51)	82.2 (2)
O (11) -Nd (1) - O (12)	50.2 (2)	O (51) -Nd (2) - O (61)	73.2 (3)
O (11) -Nd (1) - O (22)	72.0 (2)	O (61) -Nd (2) - O (32)	90.5 (2)
O (11) -Nd (1) - O (31)	77.8 (3)	O (32) -Nd (2) - O (11)	90.3 (2)
O (11) -Nd (1) - O (42)	72.5 (2)	O (W1) -Nd (2) - O (62^{I})	67.8 (2)
O (21) -Nd (1) - O (22)	51.0 (2)	O (62^{I}) -Nd (2) - O (61^{I})	97.1 (2)
O (21) -Nd (1) - O (41^{II})	83.1 (2)	O (61^{I}) -Nd (2) - O (52^{I})	69.6 (2)
O (21) -Nd (1) - O (31)	75.8 (3)	O (52^{I}) -Nd (2) - O (W1)	68.8 (3)
O (21) -Nd (1) - O ($W3^{II}$)	79.0 (2)	O (11) -Nd (2) - O (W1)	70.4 (3)
O (41) -Nd (1) - O (12)	71.9 (2)	O (11) -Nd (2) - O (62^{I})	76.4 (2)
O (41) -Nd (1) - O (41^{II})	67.4 (2)	O (51) -Nd (2) - O (62^{I})	72.7 (2)
O (41) -Nd (1) - O ($W3^{II}$)	70.7 (2)	O (51) -Nd (2) - O (61^{I})	70.4 (2)
O (41) -Nd (1) - O (42)	49.0 (2)	O (61) -Nd (2) - O (61^{I})	72.5 (2)
O (12) -Nd (1) - O (42)	82.3 (2)	O (61) -Nd (2) - O (52^{I})	76.4 (3)
O (41^{II}) -Nd (1) - O ($W3^{II}$)	83.2 (2)	O (32) -Nd (2) - O (52^{I})	72.4 (2)
O (22) -Nd (1) - O (31)	84.9 (3)	O (32) -Nd (2) - O (W1)	76.8 (2)
O (12) -Nd (1) - O (41^{II})	74.7 (2)	Nd (1) - O (11) - C (11)	88.1 (6)
O (12) -Nd (1) - O (22)	83.0 (2)	Nd (1) - O (11) -Nd (2)	127.2 (2)
O (22) -Nd (1) - O (41^{II})	91.0 (2)	Nd (1) - O (12) - C (11)	100.2 (6)
O (42) -Nd (1) - O (31)	79.0 (3)	Nd (2) - O (11) - C (11)	144.5 (7)
O (42) -Nd (1) - O ($W3^{II}$)	79.9 (2)	O (11) - C (11) - O (12)	121.5 (8)
O (31) -Nd (1) - O ($W3^{II}$)	81.4 (3)	O (11) - C (11) - C (12)	116.8 (9)
O (W2) -Nd (2) - O (11)	71.4 (2)	O (12) - C (11) - C (12)	126.6 (9)
O (W2) -Nd (2) - O (51)	68.7 (2)	C (11) - C (12) - S (1)	109.4 (7)
O (W2) -Nd (2) - O (61)	74.1 (2)	C (12) - S (1) - C (13)	98.4 (7)
O (W2) -Nd (2) - O (32)	70.4 (2)	Nd (1) - O (21) - C (21)	95.1 (6)

Table 2. Continued

Bond angle	θ/°		θ/°
Nd(1)-O(22)-C(21)	94.7(6)	S(4A)-C(43)-S(4B)	58.6(9)
O(21)-C(21)-O(22)	118.4(10)	S(4A)-C(42)-S(4B)	58.2(6)
O(21)-C(21)-C(22)	123.7(10)	Nd(1)-O(41)-Nd(1^{III})	112.6(3)
O(22)-C(21)-C(22)	117.5(9)	Nd(1^{III})-O(41)-C(41)	155.6(7)
C(21)-C(22)-S(2)	109.4(11)	Nd(2)-O(51)-C(51)	137.5(7)
C(22)-S(2)-C(23)	103.2(7)	Nd(2^{I})-O(52)-C(51)	96.7(6)
Nd(1)-O(31)-C(31)	157.4(8)	O(51)-C(51)-O(52)	126.8(10)
Nd(2)-O(32)-C(31)	134.7(7)	O(51)-C(51)-C(52)	115.8(9)
O(31)-C(31)-O(32)	125.4(10)	O(52)-C(51)-C(52)	117.4(9)
O(31)-C(31)-C(32)	112.1(9)	C(51)-C(52)-S(5)	108.3(6)
O(32)-C(31)-C(32)	122.0(10)	C(52)-S(5)-C(53)	99.8(7)
C(31)-C(32)-S(3)	116.4(8)	Nd(2)-O(61)-C(61)	153.4(7)
C(32)-S(3)-C(33)	99.5(8)	Nd(2^{I})-O(61)-C(61)	92.3(6)
Nd(1)-O(41)-C(41)	91.7(6)	Nd(2^{I})-O(62)-C(61)	96.7(6)
Nd(1)-O(42)-C(41)	100.6(6)	Nd(2)-O(61)-Nd(2^{I})	107.5(2)
O(41)-C(41)-O(42)	117.7(9)	O(61)-C(61)-O(62)	121.0(7)
O(41)-C(41)-C(42)	122.6(9)	O(61)-C(61)-C(62)	116.8(8)
O(42)-C(41)-C(42)	119.6(10)	O(62)-C(61)-C(62)	123.0(8)
C(41)-C(42)-S(4A)	122.0(11)	C(61)-C(62)-S(6)	116.7(8)
C(41)-C(42)-S(4B)	108.6(8)	C(62)-S(6)-C(63)	102.7(7)
C(42)-S(4A)-C(43)	90.9(24)	O(12)···O(W3)···O(21^{III})	126.2(3)
C(42)-S(4B)-C(43)	97.9(28)		

Key to symmetry operations: I. $1.0-x$, $1.0-y$, $1.0-z$; II. $1.0-x$, $-y$, $1.0-z$; III. x, y, $1.0+z$

oms. The two C–O distances of the *D* ligand are different from each other (C(61)–O(61)=1.289(13), C(61)–O(62)=1.236(12) Å); the difference is a little larger than those of *C* ligands (C(11)–O(11)=1.269(13), C(11)–O(12)=1.241(13) Å; C(41)–O(41)=1.247(14), C(41)–O(42)=1.265(13) Å). In the *D* ligand, the oxygen atom of the longer C–O, O(61), forms the bridge, and both the bridging Nd–O distances are a little shorter than the one-oxygen-atom-bridging Nd–O distances of the *C* ligands (Nd(2)–O(61)=2.405(8), and Nd(2^{I})–O(61)=2.633(8) Å, *vs.* Nd(2)–O(11)=2.513(8), Nd(1)–O(11)=2.691(7); Nd(1^{II})–O(41)=2.441(8), Nd(1)–O(41)=2.681(8) Å). The Nd–O distance of the non-bridged oxygen atom of the *D* ligand (Nd(2)–O(62^{I})=2.568(9) Å) is longer than the corresponding Nd–O distance of the *C* ligands (Nd(1)–O(12)=2.452(7), Nd(1)–O(42)=2.488(8) Å). The *E* ligand forms a four-membered chelate ring by being coordinated its two oxygen atoms to the same neodymium atom. Its two C–O distances are different from each other (C(21)–O(21)=1.236(11), C(21)–O(22)=1.294(13) Å).

Consequently, as is shown in Fig. 3, there are three kinds of bridging modes between neodymium atoms in a polymer chain; *i.e.* Nd(1^{II})···Nd(1) (4.236(1) Å), where two *C* bridges exist; Nd(1)···Nd(2) (4.662(1) Å), connected with one each of the *B* and *C* bridges, and Nd(2)···Nd(2^{I}) (4.065(1) Å), with two each of the *A* and *D* bridges. From these Nd···Nd distances, the *B* bridge is found to be weaker than the *C* one in the ability of bridging neodymium atoms, while Nd(2)···Nd(2^{I}) is the shortest because of the existence of four bridges between them. This type of complicated polymeric linear-chain structure, including many types of coordination modes of the ligands, has not previously known.

Each complex has a normal magnetic moment as the metal salt of each elements,[23] and no metal-metal interaction was found. The found magnetic moments of the methylthioacetato complexes of lanthanum(III), diamagnetic; and cerium(III) was 2.4_2; praseodymium(III), 3.5_8; neodymium(III), 3.5_4; europium(III), 3.3_8; dysprosium(III), 10.6_5; ytterbium(III), 4.4_4 BM,*** at 25 °C.

The powder X-ray diffraction patterns of synthesized methylthioacetato complexes of lanthanoid elements are shown in Fig. 4. They are divided into three groups according to their patterns; the grouping is the same as that when they are divided by their chemical composition: *i.e.*, Group 1 (lanthanum(III) complex $ML_3 \cdot 4.5H_2O$), Group 2 (cerium(III), praseodymium(III), neodymium(III) and europium(III) complexes; $ML_3 \cdot 1.5H_2O$), and Group 3 (dysprosium(III) and ytterbium(III) complexes; $ML_3 \cdot 2H_2O$). The same grouping was also observed with regard to their infrared absorption spectra, as well as with regard to TG and DTA, as will be shown later. The complexes belonging to the same group give similar powder X-ray diffraction patterns, and the intensity ratios of their main peaks are nearly the same. Therefore, they are found to be isomorphous with each other, and the structure given to the neodymium(III) complex can be expected to be the same as those of light lanthanoid elements, although exceptionally, lanthanum(III) makes a different type of hydrate. On the other hand, as Group 3 elements make the $ML_3 \cdot 2H_2O$ type of hydrated complexes, they are likely to be like those of heavy lanthanoid elements. In fact, this kind of difference in hydration number and this type of difference in structure between the complexes of light

*** 1 BM=9.274078(36) 10^{-24} J T^{-1}.

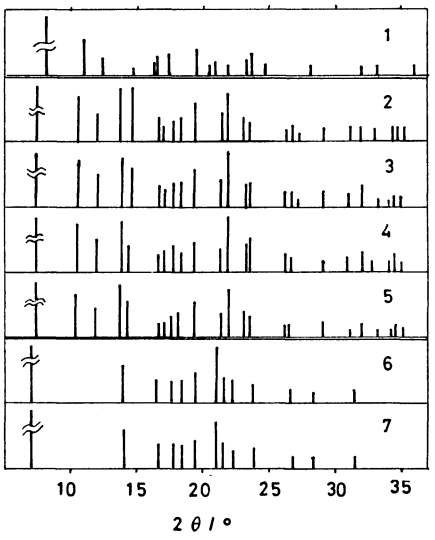

Fig. 4. X-Ray powder patterns of methylthioacetato complexes of lanthanoid elements (Cu $K\alpha$).
1: $LaL_3 \cdot 4.5\ H_2O$, 2: $CeL_3 \cdot 1.5\ H_2O$, 3: $PrL_3 \cdot 1.5\ H_2O$, 4: $NdL_3 \cdot 1.5\ H_2O$, 5: $EuL_3 \cdot 1.5\ H_2O$, 6: $DyL_3 \cdot 2\ H_2O$, 7: $YbL_3 \cdot 2\ H_2O$ (HL=methylthioacetic acid).

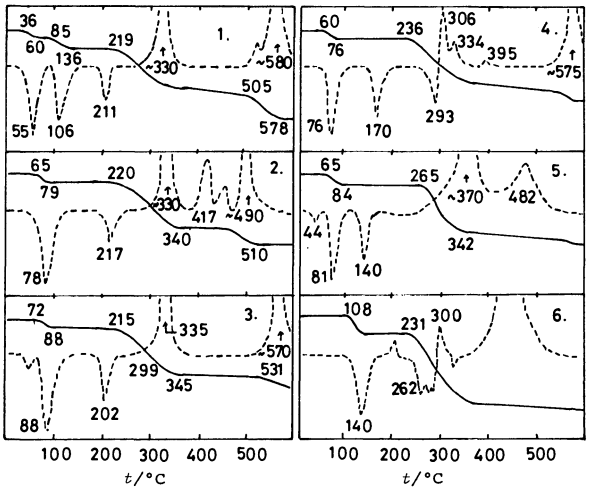

Fig. 5. TG(——) and DTA(- - -) curves of the methylthioacetato complexes.
1: $LaL_3 \cdot 4.5\ H_2O$, 2: $CeL_3 \cdot 1.5\ H_2O$, 3: $NdL_3 \cdot 1.5\ H_2O$, 4: $DyL_3 \cdot 2\ H_2O$, 5: $YbL_3 \cdot 2\ H_2O$, 6: $CoL_2 \cdot 2\ H_2O$. (HL = methylthioacetic acid) (10 °C min^{-1})
Mass loss of TG was taken downwards, and the exothermal change of DTA was taken upwards.

and heavy lanthanoid elements are often observed; for example, the hydrated oxalates of the light lanthanoid metals are commonly decahydrates, while the heavy lanthanoid metals make stable hexa- or heptahydrates.[23]

The results of the simultaneous TG and DTA of these complexes, together with that of diaquabis(methylthioacetato)cobalt(II), are shown in Fig. 5. As is shown by Pattern 3 of the figure, the dehydration of the neodymium(III) complex is in one step, even in the each coordination mode of O(W1) and O(W2) is different from that of O(W3). It is characteristic that the dehydration occurs at a low temperature;

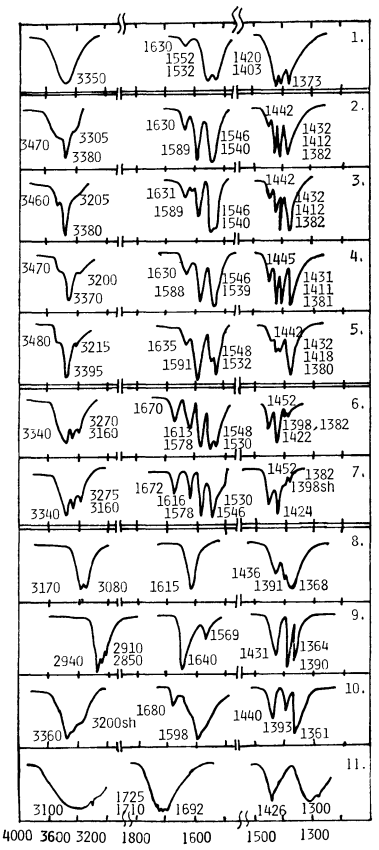

Fig. 6. Infrared absorption spectra of the methylthioacetato complexes and the related compounds.
1: $LaL_3 \cdot 4.5\ H_2O$, 2: $CeL_3 \cdot 1.5\ H_2O$, 3: $PrL_3 \cdot 1.5\ H_2O$, 4: $NdL_3 \cdot 1.5\ H_2O$, 5: $EuL_3 \cdot 1.5\ H_2O$, 6: $DyL_3 \cdot 2\ H_2O$, 7: $YbL_3 \cdot 2\ H_2O$, 8: $CoL_2 \cdot 2\ H_2O$, 9: bis(propylthioacetato)cobalt(II) hexamer–xylene, 10: bis(isopropylthioacetato)copper(II) dihydrate (violet isomer), 11: HL (HL=methylthioacetic acid).

lower than that of the corresponding hydrated complexes of cobalt(II) and of other 3d elements (*cf.* Pattern 6). A drastic mass loss due to the decomposition of the ligand occurs at about 200—300 °C, and the temperature is about the same as that of 3d-complexes.

The hydrated methylthioacetato complexes of the other Group 2 elements show almost the same TG and DTA patterns as are shown by Patterns 2 and 3 in the figure.

Although the general features of the TG and DTA curves of the other-group complexes are nearly the same, and although the low dehydration temperature is characteristic of all of them, there are some differences between them, as will be shown below. The lanthanum(III) complex (Group 1) gives two steps of dehydration, as is shown in Pattern 1 of the figure, and the Group 3 complexes give an endothermic peak of DTA, due to the isomerization and not the melting, between the dehydration and the ligand degradation temperatures, when the complexes are kept in the solid state (see Patterns 4 and 5).

Their infrared absorption spectra of the ν(OH), ν_{as}(COO), and ν_s(COO) regions are shown in Fig. 6, together with the maximum wave numbers of the peaks. The corresponding charts of some related com-

plexes and of methylthioacetic acid are also shown. These spectra, too, are divided into Groups 1, 2, and 3 in terms of their general features, as well as in terms of the wave numbers of the split peaks in the range, as is shown in the figure. This splitting of the peak of ν_{as}(COO) and of ν_{s}(COO) is probably due to the existence of multi-modes of the coordination of the carboxyl groups, although the assignment of each splitting peak is difficult. The ν_{as}(COO) peak of the methylthioacetato complexes of lanthanoid elements appears in rather a little lower wave number region than that of the common 3d-metal complexes.[24] This is probably due to the "hard" character of lanthanoid elements, which makes the coordination bond more ionic. The bridging of the carboxyl group in these complexes may be another reason.

The authors wish to thank Professor Yoichi Iitaka, Faculty of Pharmaceutical Sciences, the University of Tokyo, for the collection of the intensity data.

References

1) A. Ouchi, Y. Ohashi, T. Takeuchi, and Y. Yoshino, *Bull. Chem. Soc. Jpn.*, **43**, 1088 (1970).
2) Y. Ohashi, T. Takeuchi, A. Ouchi, and Y. Yoshino, *Bull. Chem. Soc. Jpn.*, **43**, 2845 (1970).
3) A. Ouchi, T. Takeuchi, and Y. Ohashi, *Bull. Chem. Soc. Jpn.*, **44**, 731 (1971).
4) A. Ouchi, T. Takeuchi, and Y. Ohashi, *Bull. Chem. Soc. Jpn.*, **44**, 3461 (1971).
5) K. Suzuki and K. Yamazaki, *J. Inorg. Nucl. Chem.*, **24**, 1093 (1962).
6) L. D. Pettit, A. Poyston, and R. J. Whewell, *J. Chem. Soc., A*, **1968**, 2009.
7) L. D. Pettit and C. Sherrington, *J. Chem. Soc., A*, **1968**, 3078.
8) M. M. Jones, A. J. Banks, and C. H. Brown, *J. Inorg. Nucl. Chem.*, **37**, 761 (1975).
9) M. M. Jones, H. D. Coble, T. H. Partt, and R. D. Harbison, *J. Inorg. Nucl. Chem.*, **37**, 2409 (1975).
10) Y. Ueda, *J. Chem. Soc. Jpn.*, **44**, 1061 (1923); **50**, 687 (1929).
11) A. Ouchi, H. Honda, and S. Kitazima, *J. Inorg. Nucl. Chem.*, **37**, 2559 (1975).
12) A. Ouchi, M. Shimoi, T. Takeuchi, and H. Saito, *Bull. Chem. Soc. Jpn.*, **54**, 2290 (1981).
13) T. Ogawa, M. Shimoi, and A. Ouchi, *Bull. Chem. Soc. Jpn.*, **55**, 126 (1982).
14) T. Ogawa, M. Shimoi, and A. Ouchi, *Acta Crystallogr., Sect. B*, **36**, 3114 (1980).
15) M. Shimoi, F. Ebina, A. Ouchi, Y. Yoshino, and T. Takeuchi, *J. Chem. Soc., Chem. Commun.*, **1979**, 1132.
16) G. G. Sadikov, G. A. Kukina, and M. A. Poraikoshits, *Zh. Strukt. Khim.*, **8**, 551 (1967).
17) I. Jelenic, D. Grdenic, and A. Bezjak, *Acta Crystallogr.*, **17**, 758 (1964).
18) E. Larsson, *Chem. Ber.*, **63**, 1347 (1930).
19) "The Universal Crystallographic Computation Program System (UNICS)," ed by T. Sakurai, Crystallographic Society of Japan, Tokyo (1967).
20) "International Tables for X-Ray Crystallography," Kynoch Press, Birmingham, U. K. (1974), Vol. IV.
21) $R=\Sigma||F_o|-|F_c||/\Sigma|F_o|$
22) The final thermal parameters and the final F_o-F_c table are kept at the Chemical Society of Japan as Document No. 8240.
23) T. Moeller, "Comprehensive Inorganic Chemistry," Pergamon Press, Oxford, U. K. (1973), Vol. 4, pp. 94, 51, and 10.
24) D. T. Sawyer and P. J. Paulsen, *J. Am. Chem. Soc.*, **80**, 1597 (1958); **81**, 816 (1959).

Simple Approximate Approaches for the Determination of Circular Dichroism Spectra in Multiple Scattering Systems

Yutaka TANIGUCHI* and Yoichi SHIMURA

Department of Chemistry, Faculty of Science, Osaka University, Toyonaka, Osaka 560

(Received October 24, 1981)

A convenient method for the determination of CD spectra in multiple scattering systems is demonstrated. The formula of approximation, which gives the molar CD in terms of the values observable with commercial spectrometers by using a plate of opal glass, is presented based on some assumptions. The resulting solid-state CD spectrum of Λ-$[Co(en)_3]Br_3 \cdot H_2O$ is reported and compared with the solution CD spectrum.

Circular dichroism (CD) spectra have proved very useful in the studies of the structure of molecules. The measurements of CD spectra have recently been extended to the suspensions of particulate biological matters.[1,2] However, the CD spectra obtained are contributed by unequal scattering of left- and right-circularly polarized light, and this effect has not been well elucidated.

In the preceding paper[3] we demonstrated the method for determining the approximate molar CD in a multiple scattering system, a Nujol mull of cobalt(III) complex. In our method, the ellipticity (Θ) and the transmittance (T) are measured with conventional spectrometers by only setting a plate of opal glass on the unilluminated sides of a sample and a blank cell. The molar CD ($\Delta\varepsilon$) of a particulate sample is evaluated based on appropriate assumptions and approximations from the values of Θ and T by somewhat lengthy calculations. The resulting molar CD is well reproducible. The $\Delta\varepsilon$ of Λ-$[Co(en)_3]Br_3 \cdot H_2O$ obtained by our method at the peak position of the first absorption band is almost equal in magnitude to that in aqueous solution.

In order to obtain the CD spectrum in such a multiple scattering particulate system, lengthy calculating operations, which are inconvenient for rapid analysis of spectra, need to be carried out at every wavelength. In this paper a simple approximation method for such a CD spectrum will be described, and the resulting CD spectrum of solid-state Λ-$[Co(en)_3]Br_3 \cdot H_2O$ will be shown.

Calculation Methods

The variation of the intensity and polarization state of a light beam in a multiple scattering medium is written by the equation of radiative transfer in the vector form.[4] In the preceding paper the intensity of light transmitted through the plane-parallel scattering medium containing optically active particles has been analyzed by using the Kubelka-Munk model.[5] When the optical activity of the scatterers is weak, as is often the case with the d-d transition of cobalt(III) complexes, the transmittance constituents for the left (L) and right (R) circularly polarized light are approximately given by[3]

$$T_i = 4\beta_i(I_0)_i/[(1+\beta_i)^2 e^{\alpha_i l} - (1-\beta_i)^2 e^{-\alpha_i l}]I_0;\ i=L,R, \quad (1)$$

where

$$\alpha_i = [k_i(k_i+2s_i)]^{1/2}, \quad (2)$$

$$\beta_i = [k_i/(k_i+2s_i)]^{1/2}, \quad (3)$$

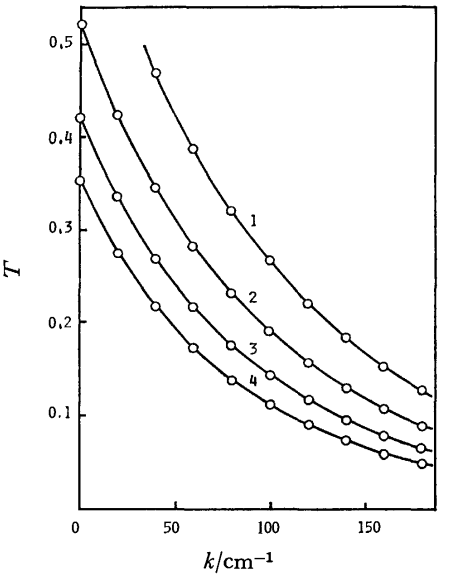

Fig. 1. Variation of T with k.
The value of s: (1) 50 cm^{-1}, (2) 100 cm^{-1}, (3) 150 cm^{-1}, and (4) 200 cm^{-1}.

and

$$I_0 = \Sigma_i(I_0)_i. \quad (4)$$

The letters k and s denote the absorption and scattering coefficients, respectively, l the path length, and I_0 the intensity of incident light. Hereinafter, l is always taken to be 9.15×10^{-3} cm (path length of our sample cell). Figure 1 shows the variation of T with k plotted when s remains constant.

The angular dependence of the scattering contribution to CD has been investigated by Bohren[6] and Gitter-Amir *et al.*[7] It has been shown that the difference between scattering of left- and right-circularly polarized light by optically active spheres is significant only in the forward scattering directions. The difference in scattering is negligible in the backward directions. In the Kubelka-Munk model, s is the back-scattering coefficient. It is, therefore, assumed in this study that the scattering coefficients s_L and s_R are equal, and hence their value is equal to that for natural light:

$$s_L = s_R = s. \quad (5)$$

In a conventional Grosjean-Legrand type CD instrument,[8] the polarization state of incident light varies with time alternately between left- and right-circular polarizations. As shown in the preceding paper,[3] the recorded ellipticity Θ in radians is related to the trans-

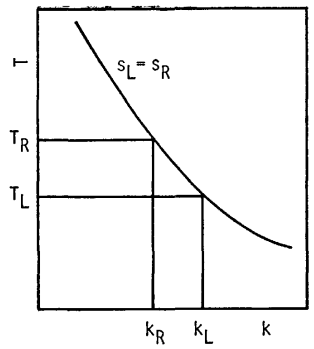

Fig. 2. Diagram showing the relation between ΔT and Δk in the case of $s_L = s_R$.

mittances for the periodical incidence of left- and right-circularly polarized light, T_L and T_R, by

$$\Theta = -(1/4)\Delta T/T, \tag{6}$$

where

$$\Delta T = T_L - T_R, \tag{7}$$

and

$$T = (T_L + T_R)/2. \tag{8}$$

Consequently, T_L and T_R are separately given by

$$T_L = (1-2\Theta)T, \tag{9}$$

and

$$T_R = (1+2\Theta)T. \tag{10}$$

Thus the values of T_L and T_R which are defined in the Kubelka-Munk model can be determined by measuring Θ and T with conventional spectrometers using a plate of opal glass.

Since the scattering coefficients s_L and s_R are considered equal in the Kubelka-Munk model, the T_L and T_R are given by the ordinates of two points on a certain k-T curve (see Fig. 2). Then the distance between the two points along the horizontal axis gives the experimental value of circular dichroism:

$$\Delta k = k_L - k_R. \tag{11}$$

The experimental value of ΔT being generally small, about the order of 10^{-3} in our measurements, the ratio $\Delta T/\Delta k$ approaches the differential coefficient dT/dk, *i.e.*, the slope of the k-T curve. In practice we may let

$$\Delta T/\Delta k = dT/dk. \tag{12}$$

Rearranging this equation we have

$$\Delta k = (dk/dT)\Delta T. \tag{13}$$

According to Eq. 6 we can rewrite Eq. 13 in the form

$$\Delta k = -4\Theta(dk/dT)T. \tag{14}$$

Thus, in order to obtain the CD spectrum, we must evaluate dk/dT for the set of T and s values found at every wavelength. But this is a big operation.

Now we consider the value of $(dk/dT)T$. In the Kubelka-Munk model, k, s, and T are associated with one another as has been represented by Eqs. 1—4. When s remains constant, log T is plotted against k in Fig. 3. Figure 3 shows these plots are approximately aligned in a straight line. In other words, the slopes of the plots are not exactly but nearly constant regardless of the value of k. Therefore, as a

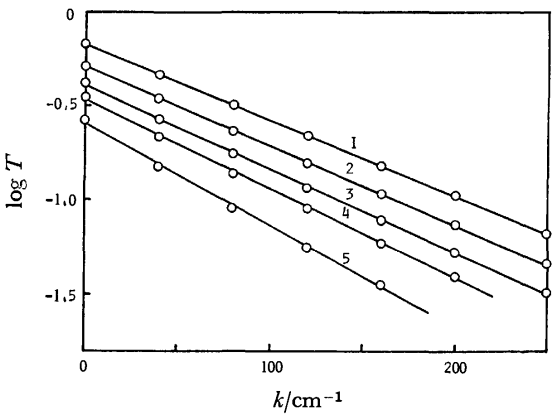

Fig. 3. Plots of log T against k.
The value of s: (1) 50 cm^{-1}, (2) 100 cm^{-1}, (3) 150 cm^{-1}, (4) 200 cm^{-1}, and (5) 300 cm^{-1}.

first approximation, we may let

$$\log T = Ak + B, \tag{15}$$

where A and B are constants.

Differentiating log T with respect to k, we have

$$(1/2.303T)(dT/dk) = A. \tag{16}$$

Rearranging this equation we have

$$(dk/dT)T = 1/2.303A. \tag{17}$$

Since A is a constant in the above approximation, the value of $(dk/dT)T$ can be considered constant, too.

It is also found from Fig. 3 that the slopes of the lines are not sensitive to their s values. In particular, when the values of s are not so different from each other, the slopes are nearly equal.

The scattering coefficient usually increases in magnitude with decreasing wavelength, but its variation should be small in the region of the d-d transitions of cobalt(III) complexes,[9] which we are now concerned about. Consequently, as a first approximation, the value of $(dk/dT)T$ can be taken as constant in such a region, though k, s, and T may vary with wavelength. In our studies a certain value of $(dk/dT)T$ associated with the first absorption maximum will be chosen for convenience.

In the preceding paper the molar CD of a microcrystalline sample has been determined based on the assumption that the molar absorbance is equal both in crystal and in solution in the region of d-d transitions. By using the molar absorbance ε(soln) and the absorption coefficient k at a peak position, which will be marked by asterisks, the molar CD in crystal is related to the experimentally determinable Δk as follows:

$$\Delta\varepsilon(\text{cryst}) = \varepsilon^*(\text{soln})\Delta k/k^*. \tag{18}$$

Substituting Eq. 14 in Eq. 18 we have

$$\Delta\varepsilon(\text{cryst}) = -4\Theta(dk/dT)_{s^*,T^*}T^*\varepsilon^*(\text{soln})/k^*, \tag{19}$$

where the subscripts s^* and T^* denote the restriction of (dk/dT) to the value for the case of $s=s^*$ and $T=T^*$. The values of Θ, ε^*(soln), and T^* are measurable by conventional instruments. Further, the values of k^* and $(dk/dT)_{s^*,T^*}$ can be calculated if s^* and T^* are fixed. Although s^* cannot be measured directly, but estimated from the data of transmittance

Table 1. Spectral properties of Λ-$[Co(en)_3]Br_3 \cdot H_2O$

Absorption (soln)		CD (soln)		Solid-state CD (Nujol mull)	
$\sigma/10^3$ cm^{-1}	log (ε/mol^{-1} dm^3 cm^{-1})	$\sigma/10^3$ cm^{-1}	$\Delta\varepsilon$/mol^{-1} dm^3 cm^{-1}	$\sigma/10^3$ cm^{-1}	$\Delta\varepsilon$/mol^{-1} dm^3 cm^{-1}
21.5	1.95	20.4	+1.89	20.2	+1.83
		22.4	0	22.1	0
		23.3	−0.14	23.0	−0.26
25.9	0.99	25.8	0	25.7	0
29.6	1.91	28.8	+0.24	28.9	+0.24

in the wavelength region without absorption.[3] Thus the quantities other than Θ are fixed irrespective of wavelengths, and hence the CD curve can be readily obtained by only multiplying Θ by a definite value associating with an absorption maximum:

$$-4(dk/dT)_{s^*,T^*}T^*\varepsilon^*(\text{soln})/k^*. \quad (20)$$

Experimental

Materials. Λ-$[Co(en)_3]Br_3 \cdot H_2O$ was prepared by the method of Werner.[10] Commercial Nujol was used as the mulling agent.

Measurements. The principles and the validity of our measurements have been described in the preceding paper.[3] The transmittance and the absorbance were measured by a Shimadzu UV-200 spectrophotometer, and the ellipticity by a JASCO MOE-1 spectropolarimeter(detector: end-window photomultiplier tube, HTV-R376). Measurements on Nujol mulls were carried out by the opal glass technique,[11] where a plate of opal glass was placed just after the sample cell, and the diffused light penetrating behind the plate was detected by a photomultiplier.

A quartz cell with demountable window (path length 9.15×10^{-3} cm) was used in the measurements on mulls. A mull was prepared by grinding the complex salt (5—11 mg) and mixing it with Nujol (40—50 mg) in an agate mortar.

Since the intensity of light after passage of a plate of opal glass was very weakened in the wavelength region shorter than *ca.* 320 nm, the CD measurements were unable to be carried out in this region.

Results and Discussion

The CD spectra of Λ-$[Co(en)_3]Br_3 \cdot H_2O$ in Nujol and in water are shown in Fig. 4. Table 1 gives the intensities of $\Delta\varepsilon$ at peak positions. Both the CD curves are roughly similar in pattern and intensity. This shows the effects of molecular orientation and crystal anisotropy, which are usually observed in the single-crystal CD, are cancelled out in a randomly oriented particulate system, microcrystallines in Nujol. The solid-state CD spectrum obtained by our method is, therefore, regarded as an isotropic CD spectrum, and hence can be compared directly with a solution CD spectrum.

Figure 4 shows the solid-state CD spectrum is slightly changed in intensity compared to the solution CD spectrum. There are a decrease in the rotational strength, proportional to the area of a CD peak, of E_a band and an increase in that of A_2 band. These changes are similar to the changes well-known as the ion-pairing effects,[12] which are usually observed in

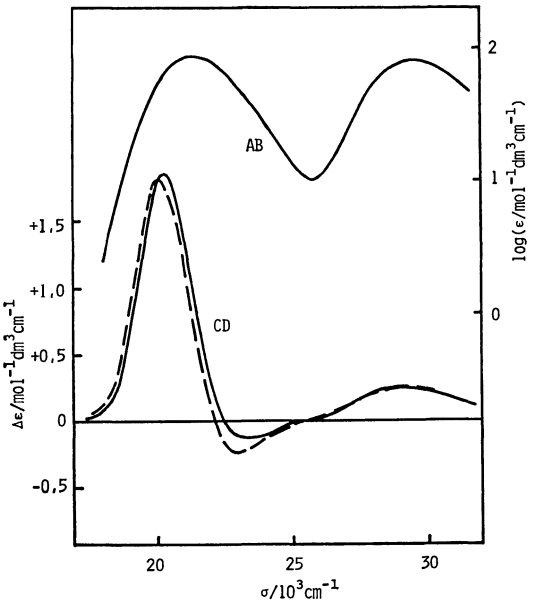

Fig. 4. Absorption (AB) and CD spectra of Λ-$[Co(en)_3]Br_3 \cdot H_2O$.
- - -: Nujol mull, ——: aqueous solution.

the CD spectrum of Λ-$[Co(en)_3]^{3+}$ on addition of anions. Thus the solid-state CD measurements may provide some significant informations regarding the ion-pairing effects.

Single-crystal CD spectra are generally attended by experimental difficulties owing to the crystal anisotropies.[13] Solid-state CD spectra are readily obtained by the KBr method, but there are some questions in the resulting CD spectra. Even if disks are clear, there may exist optical artifacts more or less by the effects of light scattering arising from optical fluctuation in disks. The counter ions of complex ions may be substituted by the matrix ion K^+ or Br^- in disks; so essential informations may not be obtained.

On the other hand, there is no fear of the exchange of counter ions in Nujol mulls. A Nujol mull method will give good results in this connection. Another advantage of our Nujol mull method is that the isotropic solid-state CD spectrum can be obtained by easy procedures of experimentation and calculation.

References

1) M. Glaser and S. J. Singer, *Biochemistry*, **10**, 1780 (1971).
2) M. F. Maestre and C. Reich, *Biochemistry*, **19**, 5214

(1980).
3) Y. Taniguchi and Y. Shimura, *Bull. Chem. Soc. Jpn.*, **55**, 754 (1982).
4) S. Chandrasekhar, "Radiative Transfer," Dover Publications, New York (1960), p. 38.
5) P. Kubelka, *J. Opt. Soc. Am.*, **38**, 448 (1948).
6) C. F. Bohren, *Chem. Phys. Lett.*, **40**, 391 (1976).
7) A. Gitter-Amir, K. Rosenheck, and A. S. Schneider, *Biochemistry*, **15**, 3131, 3138 (1976).
8) M. Grosjean and M. Legrand, *C. R. Acad. Sci.*, **251**. 2150 (1960).
9) The scattering coefficient of a colored particle depends on the complex refractive index. When its absorption is weak, as is often the case with the d-d transition bands, the scattering coefficient is mainly governed by the real part of the complex refractive index. The variation of the real part should not be so large in the d-d absorption region because the normal dispersion of the real part is almost determined by far apart intense bands in the ultraviolet region. The anomalous dispersion should be small in the d-d absorption region, because the absorption in such a region is generally small. Therefore, we can suppose the scattering coefficient is not so changed in such a d-d absorption region.
10) A. Werner, *Ber. Dtsch. Chem. Ges.*, **45**, 121 (1912).
11) K. Shibata, A. A. Benson, and M. Calvin, *Biochim. Biophys. Acta*, **15**, 461 (1954).
12) S. F. Mason and B. J. Norman, *Proc. Chem. Soc.*, **1964**, 339.
13) H. P. Jensen, *Acta Chem. Scand., Ser. A*, **30**, 137 (1976).

 © 1982 The Chemical Society of Japan Bull. Chem. Soc. Jpn., 55, 2851—2853 (1982)

Spectrophotometric Determination of Hexacyanoferrate(III) by Use of Coagulated Material Prepared from Finely Divided Anion and Cation Exchange Resins

Kin-ya Suzuki, Guee-deuk Park,** Kunio Ohzeki,* and Tomihito Kambara

Department of Chemistry, Faculty of Science, Hokkaido University, Sapporo 060

***Division of Environmental Conservation, Graduate School of Environmental Science, Hokkaido University, Sapporo 060*

(Received November 2, 1981)

A simple and sensitive method for the determination of hexacyanoferrate(III) is described. This method is based on the preconcentration of hexacyanoferrate(III) ion on the coagulated material prepared from finely divided anion and cation exchange resins. The mixed resin is collected on a filter paper, forming a disk of thin layer. The hexacyanoferrate(III) fixed on the resin is converted to Turnbull's Blue by treating with iron(II) ammonium sulfate solution. The colored compound in the resin phase is determined by a densitometer equipped with a linearizer. The working range is 0.4—3.0 μmol dm^{-3} hexacyanoferrate(III). Among cations likely to be present, only copper(II) interferes, however, the interference is removed by the addition of EDTA. Hexacyanoferrate(II) ion shows the same coloration as hexacyanoferrate(III), and the total amount is determined when both ions are present.

Mutual coagulation takes place when a suspension of finely divided anion and cation exchanger is mixed with each other.[1] The resulting coagulated material is bulky and easily separated from the solution by filtration. By use of a cylindrical filter holder, a disk of thin layer of the mixed resin is prepared on a filter paper. Metal complexes with negative and/or positive charge are much more effectively fixed on the mixed resin than simple ions. When a colored complex is retained on the resin, the resulting thin layer is directly subjected to spectrophotometric analysis. In this manner, chromium(VI) was determined as the diphenylcarbazide compound,[2] and phosphate as the Molybdenum Blue complex,[3] both in ppb range.

The determination of hexacyanoferrate(III) is important in environmental analysis. Yogo *et al.*[4] reported a method in which hexacyanoferrate(II) and (III) were converted to the 1,10-phenanthroline complex and determined spectrophotometrically, in which, after adding mercury(II) heating was required for accelerating the ligand exchange reaction. In the present report, hexacyanoferrate(III) is selectively concentrated on the mixed resin and determined as Turnbull's Blue.

Experimental

Reagents. All chemicals used were of analytical reagent grade.

Standard hexacyanoferrate(III), 10^{-2} mol dm^{-3} solution was prepared by dissolving potassium salt in water.

Standard hexacyanoferrate(II), 10^{-2} mol dm^{-3} solution was also made by dissolving potassium hexacyanoferrate(II) trihydrate in water containing 0.05% of sodium carbonate.

Iron(II) ammonium sulfate, 0.5 mol dm^{-3} solution was prepared by dissolving Mohr's salt in water containing 0.06 mol dm^{-3} hydrochloric acid.

Sodium chloride, 1 mol dm^{-3} solution was used to adjust the ionic strength of sample solutions.

Ion exchange resin suspension. The ion exchangers used were macroreticular type Amberlyst 15 and A-27 (both Rohm and Haas Co.) in RSO_3H and $RN(CH_3)_3Cl$ forms, respectively. The cation exchange resin suspension (CRS) and the anion exchange resin suspension (ARS) were prepared according to the method already reported.[1] The ion exchange capacities of CRS and ARS were determined by conductometric titration with the sodium hydroxide and silver nitrate solutions, respectively. The exchange capacities were 9.73 μequiv. ml^{-1} for CRS and 2.43 μequiv. mol^{-1} for ARS. When one part of CRS was mixed with two parts of ARS, both resins were almost completely coagulated.[1]

Apparatus. A Shimadzu Chromatoscanner CS-920 was used for absorption measurement. A Shimadzu UV-visible recording spectrophotometer, type UV-240, was used for measuring absorption spectra. A Toyo KG-25 filter holder was used for the preparation of thin layer of the mixed resin by filtration. Filter papers of No. 5A (Toyo Roshi) were used.

All experiments were carried out at room temperature.

Procedure. An aliquot of sample solution containing more than 20 nmol of hexacyanoferrate(III) is placed in a 100-ml beaker. A 5-ml portion of 1 mol dm^{-3} of sodium chloride is added for controlling the ionic strength and the volume is adjusted to 50 ml with water. A 3-ml portion of CRS and 6 ml of ARS are added. The mixture is stirred for 5 min by means of a magnetic stirrer. The resulting coagulated resins are collected on the filter paper by suction with a running water. A disk of thin layer of the mixed resin of 17 mm in diameter and about 0.3 mm in thickness is prepared. It is then dipped into the iron(II) ammonium sulfate solution for 1 h to develop the coloration. The wet filter paper holding the colored resin is placed on a white plastic plate fixed on the scanning board in the apparatus. The center of the disk of thin layer is exposed by a light beam, the section area is 1.44 mm^2. The board is periodically moved from side to side in a range of 24 mm wide, so that the absorbance of the thin layer is determined against the filter paper substrate. The absorbance is measured at 630 nm and the value is printed out automatically.

Another disk of resin is prepared without addition of hexacyanoferrate(III). The absorbance corresponding to the reagent blank including the resin matrices is also measured. The net absorbance of the complex in the resin phase is obtained as the difference.

Results and Discussion

Preparation of Thin Layer. During the course of stirring, hexacyanoferrate(III) ion is fixed on the anion

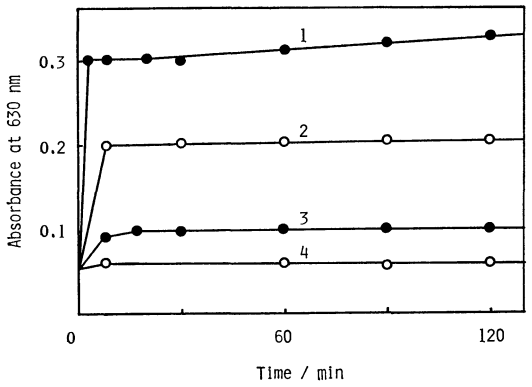

Fig. 1. Rate of color development at various concentrations of hexacyanoferrate(III).
(1): 2.0 μM, (2): 1.2 μM, (3): 0.4 μM, (4): blank. Sample volume: 50 ml.

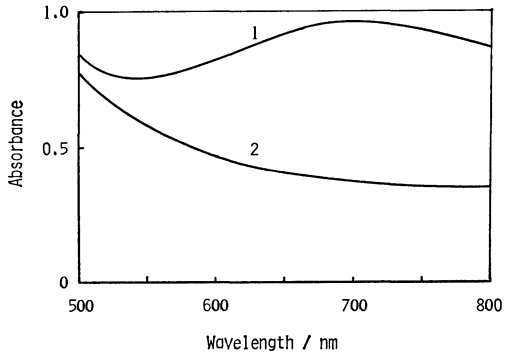

Fig. 2. Absorption spectra of the Turnbull's Blue on the thin layer of mixed resin prepared from 50 ml of solution.
(1): 2.0 μM of hexacyanoferrate(III), (2): blank, reference: wet filter paper.

exchanger and the latter is simultaneously combined with the cation exchanger, forming a coagulated material. The homogeneous dispersion of the mixed resin in the sample solution is essential for preparing the thin layer with a smooth surface. The degree of dispersion depends on the ionic strength of the sample solution. The finely dispersed mixed resin was obtained from the solution containing sodium chloride in 0.1—0.3 mol dm^{-3}. The average rate of filtration was about 30 ml min^{-1}. When sodium chloride was added too much, a long time was required for collecting the coagulated material.

Color Development. The color producing reagent used was 0.5 mol dm^{-3} of iron(II) ammonium sulfate. With decreasing concentration of the reagent, a longer dipping time was needed for the coloration of Turnbull's Blue. The dependence of coloration on the soaking time was examined with varying concentrations of hexacyanoferrate(III). A rapid coloration was found at the higher hexacyanoferrate(III) concentration, while at the lower concentration more than 20 min were necessary for obtaining a constant coloration (Fig. 1). The blue coloration was stable at least for 1.5 h in the iron(II) salt solution.

Absorption Measurement. The absorbance of Turnbull's Blue in the resin phase was determined by

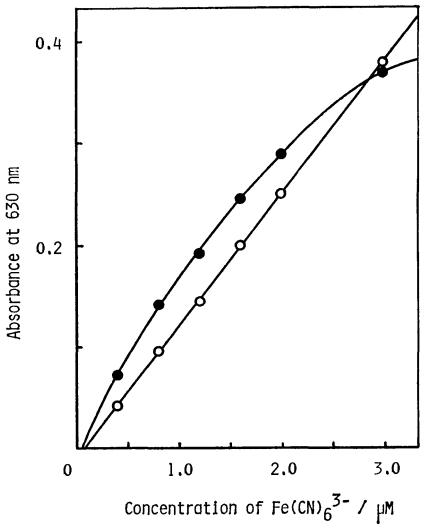

Fig. 3. Calibration curve.
○: Linearizer on, ●: linearizer off. Sample volume: 50 ml.

the densitometer at 630 nm, that is the upper limit of measurable wavelength of the apparatus. Since the complex has an absorption maximum at around 700 nm, higher sensitivity would be obtainable, if the measurement at the maximum wavelength is possible (Fig. 2).

Collection of Hexacyanoferrate(III). A trace amount of hexacyanoferrate(III) was effectively fixed on the mixed resin by stirring the sample mixture for 5 min, even in the presence of 0.3 mol dm^{-3} of sodium chloride. The recovery was considered to be quantitative, since the hexacyanoferrate(III) was not found in the filtrate. A 100-nmol portion of hexacyanoferrate(III) was quantitatively collected from 50—200 ml of sample solution.

Effect of pH. The pH of test solution was adjusted with the addition of hydrochloric acid or sodium hydroxide solution. A constant absorbance was obtained for the given amount of hexacyanoferrate(III) in the pH range of 1—12.

Calibration Curve. The calibration curve deviated from the linearity. By use of the linearizer a good linearity was obtained, however, the line did not go through the origin (Fig. 3). The relative standard deviation was 2.4% (n=6) for 1.2 μmol dm^{-3} of hexacyanoferrate(III).

Effect of Foreign Ions. Among the diverse ions studied, copper(II) interfered with the determination of 1 μmol dm^{-3} of hexacyanoferrate(III) even in the same concentration level (Table 1). When the concentration of foreign ions was 100 times hexacyanoferrate(III), copper(II), mercury(II), and zinc(II) gave negative error, while silver(I) a positive one. The interference from copper(II) was successfully eliminated by EDTA. The addition of EDTA was also effective for masking zinc(II), manganese(II), and lead(II) even in 1000 times concentration of hexacyanoferrate(III).

Effect of Hexacyanoferrate(II). As well known, hexacyanoferrate(II) combines with iron(III) to form

Table 1. Effct of foreign ions on the determination of hexacyanoferrate(III)[a]

Ion	Concentration/M			
	10^{-6}	10^{-5}	10^{-4}	10^{-3}
	Relative error/%			
Ca(II), Mg(II), Cd(II), Ni(II), Co(II), Fe(II), Fe(III), Cr(III), Al(III)				none[b]
Zn(II)		none	−7	−10 (none)[c]
Cu(II)	−8	−56	−93 (none)	−88 (−24)
Mn(II)			none	−14 (none)
Pb(II)			none	−17 (none)
Hg(II)		none	−9 (−8)	−64 (−75)
Ag(I)		none	+11	>+100

a) $Fe(CN)_6^{3-}$: 10^{-6} M. b) None: within 5% error. c) ( ): In the presence of EDTA.

the familiar Prussian Blue. The spectrophotometric determination of hexacyanoferrate(II) as the Prussian Bule was reported.[5,6] Galik and Vopravilova extracted the Prussian Blue into chloroform in the presence of a quaternary ammonium ion.[6]

Hexacyanoferrate(II) was found to be fixed on the mixed resin and showed a blue coloration as well as hexacyanoferrate(III); namely, the Prussian Blue and Turnbull's Blue are the same compound.[7] In the presence of hexacyanoferrate(II) and (III), the sum of them was determined (Table 2).

Table 2. Determination of hexacyanoferrate(II) and (III)

$Fe(CN)_6^{3-}$ taken (nmol)	$Fe(CN)_6^{4-}$ taken (nmol)	Total taken (nmol)	Total found (nmol)	Relative error %
0	50	50	51.0	+2.0
0	80	80	80.7	+0.9
0	100	100	99.7	−0.3
50	30	80	78.7	−1.6
50	50	100	99.7	−0.3

Sample volume: 50 ml.

The present work was partially supported by Grant-in-Aid for Scientific Research from the Ministry of Education, Science and Culture.

References

1) M. Abe, K. Ohzeki, and T. Kambara, *Bull. Chem. Soc. Jpn.*, **51**, 1090 (1978).
2) K. Ohzeki, T. Sakuma, and T. Kambara, *Bull. Chem. Soc. Jpn.*, **53**, 2878 (1980).
3) K. Matsuhisa, K. Ohzeki, and T. Kambara, *Bull. Chem. Soc. Jpn.*, **54**, 2675 (1981).
4) T. Yogo, G. Nakagawa, and K. Kodama, *Bunseki Kagaku*, **24**, 677 (1975).
5) J. R. Marier and D. S. Clark, *Analyst*, **85**, 574 (1960).
6) A. Galik and J. Vopravilova, *Talanta*, **21**, 307 (1974).
7) F. Umland, "Charakteristische Reaktionen anorganischer Stoffe," Akademische Verlagsges., Frankfurt am Main (1975), pp. 152—153.

Spectroscopic Properties for High-pressure Polymorphs of Calcium and Strontium Metasilicates

Ken-ichi MACHIDA, Gin-ya ADACHI,* and Jiro SHIOKAWA
Department of Applied Chemistry, Faculty of Engineering, Osaka University, Yamadaoka, Suita, Osaka 565

(Received November 4, 1981)

The IR spectra for the high-pressure polymorphs of alkaline-earth metasilicates, *viz.* α-$CaSiO_3$, δ-$CaSiO_3$, α-$SrSiO_3$, δ-$SrSiO_3$, and δ′-$SrSiO_3$, which consist of cyclic anions, $(Si_3O_9)^{6-}$ or $(Si_4O_{12})^{8-}$ rings, were studied over a range of 1200—400 cm^{-1}. These silicates gave absorption bands in wavenumbers of about 1050—820 cm^{-1}, 750—620 cm^{-1}, and below about 580 cm^{-1}, based on symmetrical and anti-symmetrical stretches of Si–O bonds and Si–O bending modes for tetrahedral SiO_4 units, and Ca–O or Sr–O stretches. Among them, the bands characteristic of the silicate anions with ring structure in the $SrSiO_3$ polymorphs were found to shift to lower wavenumber with transformation into the δ′ form. This suggests that the $(Si_4O_{12})^{8-}$ ring in δ′-$SrSiO_3$ is less flexible than the $(Si_3O_9)^{6-}$ ring in the α or δ form. The experimental result that the quenching temperature of δ′-$SrSiO_3$:Eu^{2+} phosphor is higher than that of the δ form supports this consideration.

For most of silicates, the structure elements in crystal lattices are tetrahedral SiO_4 units, which are either isolated or connected with one another by sharing oxygens. The infrared absorption (IR) spectra of those silicates result from the stretching and bending modes for the Si–O bonds of SiO_4 units.[1] Lazarev and coworkers[2] have estimated the structures of silicate anions from the measurements of IR spectra.

Alkaline-earth metasilicates show various polymorphisms under high-temperature and high-pressure.[3] For example, α- and β-$CaSiO_3$ (atmospheric high- and low-temperature forms) transform into δ-$CaSiO_3$ above 30 kbar and 900 °C.[4] The strontium metasilicate, α-$SrSiO_3$, also give high-pressure phases, δ- and δ′-$SrSiO_3$, at 34—120 kbar and 750—1400 °C.[5] Recently we have studied the luminescence properties for the high-pressure polymorphs of $CaSiO_3$:Eu^{2+} and $SrSiO_3$:Eu^{2+}, and their emission intensities have been found to increase when the host lattice transforms into the high-pressure phases.[6] Lattice vibrations of phosphors can be pointed out as one of quenching effects on luminescences.

In this paper, we study the IR spectra for the high-pressure polymorphs of $MSiO_3$ (M=Ca and Sr) and the temperature dependence for the luminescences of $SrSiO_3$:Eu^{2+} polymorphs.

Experimental

Sample Preparation. The preparation methods for the atmospheric and high-pressure phases of $MSiO_3$ and $MSiO_3$:Eu^{2+} are described in Ref. 6.

Optical Measurements. The IR spectra of samples were obtained with a Hitachi Perkin-Elmer 225 grating spectrophotometer covering the range of 1200—400 cm^{-1}. Dry air was circulated through the spectrometer to eliminate the interference from atmospheric moisture. The samples dispersed in potassium bromide were examined using the pressed disk technique, and the mixtures containing 1.0 wt% samples were generally employed. Ultraviolet luminescence spectra were obtained with a Shimadzu recording absolute spectrofluorophotometer according to the techniques described elsewhere.[7] The temperature dependence of luminescences was measured over the range between liquid N_2 temperature (77.4 K) and about 450 K in a stream of dry N_2 gas.

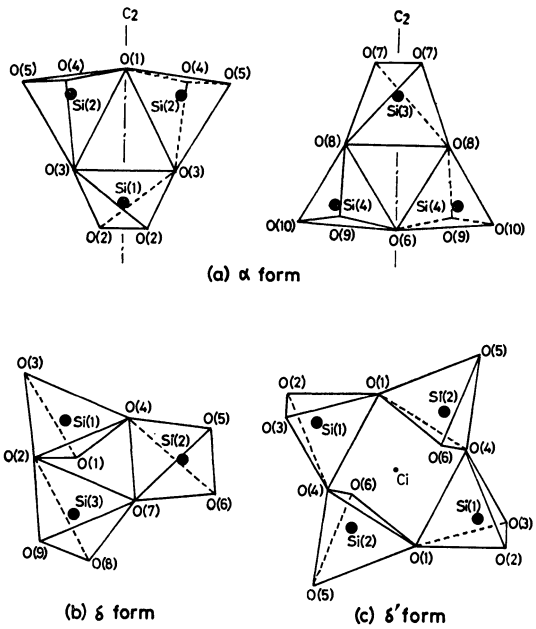

Fig. 1. Illustrations of silicate anions in the high-pressure polymorphs of $SrSiO_3$. These crystal structures have been reported in Refs. 5b and 6.

Results and Discussion

Silicate Anions. In Table 1, we show the silicate anions in the high-pressure polymorphs of $CaSiO_3$ and $SrSiO_3$. Among these polymorphs, α- and δ-$CaSiO_3$ correspond to α- and δ-$SrSiO_3$, and hence the α or δ forms of $CaSiO_3$ and $SrSiO_3$ are approximately or entirely isostructural with each other. However, the δ′ form is a characteristic phase of $SrSiO_3$ because δ′-$CaSiO_3$ has not been obtained. The crystal lattices consist of $(Si_3O_9)^{6-}$ rings for the α or δ form and $(Si_4O_{12})^{8-}$ rings for the δ′ form, respectively. The symmetries of these silicate anions are generally low.

In Fig. 1, we illustrate the silicate anions in $SrSiO_3$ polymorphs, of which the crystal structures have been reported in our previous papers.[5b,6] The $(Si_3O_9)^{6-}$ rings of the α form show the symmetry of twofold rotation around an axis of Si(1)–O(1) or Si(3)–O(6) and the $(Si_4O_{12})^{8-}$ rings have inversion centers, but

Table 1. Silicate anions in the high-pressure polymorphs of $MSiO_3$ (M=Ca and Sr)

Phase	Symmetry of crystal lattice[a)]	Silicate anion	Point group of anion	Ref.
α-$CaSiO_3$[b)]	Triclinic (P1 or $P\bar{1}$)	$(Si_3O_9)^{6-}$ ring	$\overline{\quad}$ (pseudo D_{3h})	8
δ-$CaSiO_3$	Triclinic ($P\bar{1}$)	$(Si_3O_9)^{6-}$ ring	C_1	9
α-$SrSiO_3$	Monoclinic (C2)	$(Si_3O_9)^{6-}$ ring	C_2 (pseudo D_{3h})	5b
δ-$SrSiO_3$	Triclinic ($P\bar{1}$)	$(Si_3O_9)^{6-}$ ring	C_1	6
δ′-$SrSiO_3$	Monoclinic ($P2_1/c$)	$(Si_4O_{12})^{8-}$ ring	Ci	6

a) The space groups of polymorphs are given in parentheses. b) The detailed structure analysis of this phase has not been performed, but α-$CaSiO_3$ is approximately isostructural with α-$SrSiO_3$.

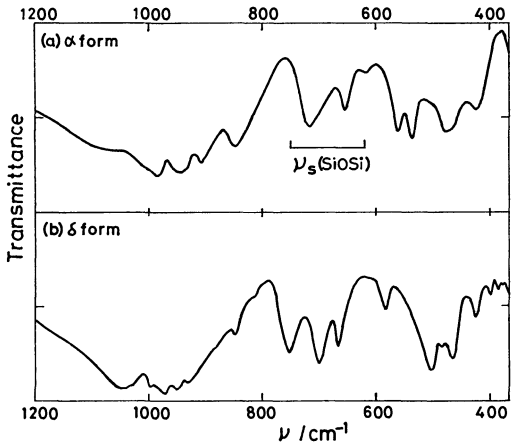

Fig. 2. IR spectra for the high-pressure polymorphs of $CaSiO_3$.

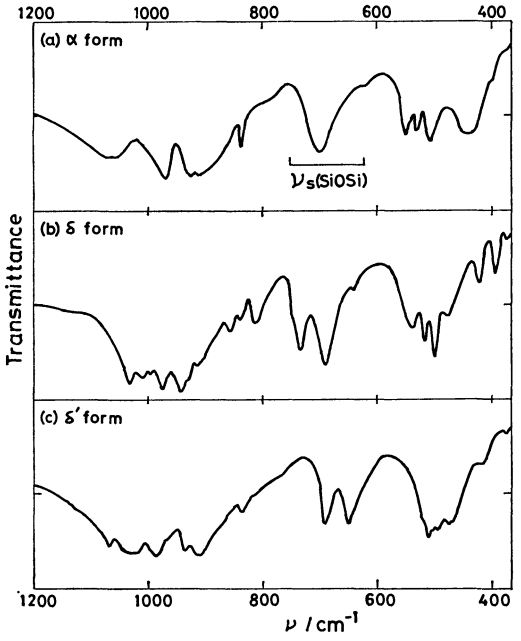

Fig. 3. IR spectra for the high-pressure polymorphs of $SrSiO_3$.

no symmetry element can be found out about the $(Si_3O_9)^{6-}$ rings of the δ form. Their point groups are C_2 (pseudo D_{3h}), C_1, and Ci for the α, δ, and δ′ forms, respectively. Consequently, the IR spectrum patterns of $CaSiO_3$ and $SrSiO_3$ polymorphs are expected to be very complex.

IR Spectra. For an isolated tetrahedral SiO_4 anions with a symmetry Td, there are four fundamental modes of vibrations, *viz.* a normally inactive symmetric stretch (800 cm^{-1}), an inactive doubly degenerate bend (500 cm^{-1}), a strongly active triply degenerate stretch (1050 cm^{-1}), and another active bending mode (625 cm^{-1}).[1)] When the SiO_4 units are connected with one another by sharing oxygens, the symmetric stretch of SiO_4 unit becomes an infrared active mode.

In Figs. 2 and 3, we show the IR spectra for the high-pressure polymorphs of $CaSiO_3$ and $SrSiO_3$, and in Table 2, their spectrum patterns are interpreted according to the assignments of some silicates attempted by Lazarev and co-workers.[2)] These metasilicates give strong absorptions over three regions around ≈580 cm^{-1}, 615—750 cm^{-1}, and 815—1070 cm^{-1}. The absorption bands of 815—1070 cm^{-1} are derived from $\nu_{as}(O^-SiO^-)$, $\nu_{as}(SiOSi)$, and $\nu_s(O^-SiO^-)$, where ν_{as} and ν_s correspond to the antisymmetric and symmetric stretching modes of SiO_4 unit, and $\nu(O^-SiO^-)$ and ν(SiOSi) represent the Si–O bonds of oxygens non-shared and shared with the other SiO_4 units, respectively. The bands below 580 cm^{-1} are responsible for the Si–O bending and Ca–O or Sr–O stretching modes. The group of bands in the regions of 615—750 cm^{-1} corresponds to the mode originated from the ν_s(SiOSi), which has been suggested to be a characteristic mode of the silicates containing cyclic anions by some workers.[10)] From the absorption bands around 615—750 cm^{-1}, consequently, we can obtain information for the ring structures of silicate anions in the high-pressure polymorphs of $CaSiO_3$ and $SrSiO_3$.

The IR spectrum patterns of δ-$CaSiO_3$ and δ-$SrSiO_3$, of which the crystal structures have been found to be entirely isostructural from the previous X-ray analyses,[6,9)] are closely similar to each other. For the α form, however, the spectrum profile around 615—750 cm^{-1} for $CaSiO_3$ somewhat differs from that of $SrSiO_3$. The former silicate consists of three bands: 616, 653, and 717 cm^{-1} whereas two bands: 622 and 705 cm^{-1} are observed on the latter silicate. This suggests that the shapes of $(Si_3O_9)^{6-}$ rings in α-$CaSiO_3$ and α-$SrSiO_3$

TABLE 2. IR SPECTRA (cm^{-1})[a] FOR THE HIGH-PRESSURE POLYMORPHS OF $MSiO_3$ (M=Ca and Sr)

	$CaSiO_3$		$SrSiO_3$		
	α	δ	α	δ	δ'
	1050 m	1046 vs	1067 s	1033 vs	1067 s
ν_{as}(O-SiO)	1003 s	1031 s	1053 s	1007 s	1025 vsb
	985 vs	1004 s	970 vs	997 s	985 vs
ν_{as}(SiOSi)	948 vs	994 s	925 vs	976 vs	968 s
	940 vs	972 vs	910 vsb	943 vs	938 vs
ν_s(O-SiO-)	906 s	949 vs	840 m	929 s	910 vsb
	846 s	933 s		915 s	840 w
		882 w		858 m	816 vw
		847 w		842 w	
		817 w		816 m	
	717 s	753 s	705 vsb	749 m	690 s
ν_s(SiOSi)	653 m	700 vs	622 vw	734 vs	648 s
	616 w	666 s		692 vs	
				643 w	
Si-O bending and M-O	560 s	581 m	549 m	535 m	526 m
stretching vibrations	538 vs	509 vs	529 m	519 s	511 vs
	474 sb	484 m	504 s	502 vs	505 s
	421 w	466 s	436 sb	485 s	495 s
		425 m		480 s	474 s
		400 w		476 s	470 s
				421 m	417 vw
				305 m	

a) The characters of spectrum bands are represented as follows: v, very; s, strong; m, medium; w, weak; b, broad.

TABLE 3. LUMINESCENCE DATA FOR THE HIGH-PRESSURE POLYMORPHS OF $SrSiO_3$: Eu^{2+} (1 atom%)

Phase	λ_{max}/nm[a]	(λ/2)/nm[b]	*Q.E.*/%[c]	T_{50}/K[d]
α	498	75—80	<1	380
δ	503	63	6	300
δ'	466	58	37	360

a) λ_{max}=peak position of the emission band at 300 K. b) λ/2=half-width of emission band. c) *Q.E.*=quantum efficiency under an optimum excitation at 300 K. d) T_{50}=quenching temperature at which the intensity of the luminescence is half of that at 77 K.

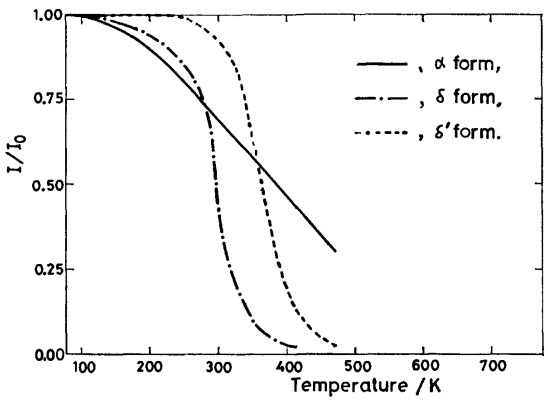

Fig. 4. Temperature dependences of the light output of $SrSiO_3$: Eu^{2+} (1 atom%) polymorphs.

are similar but their symmetries are distinct from each other. The symmetries of crystal structures are generally higher than those of structure elements, *e.g.* silicate anions, in crystal lattices. From Table 1, the symmetry for the $(Si_3O_9)^{6-}$ ring in α-$CaSiO_3$ is expected to be low compared with that for α-$SrSiO_3$, and possibly the silicate anion in α-$CaSiO_3$ does not show the symmetry of two-fold rotation. This must be confirmed if the detailed structure analysis of α-$CaSiO_3$ is performed.

For the δ' form, the IR spectrum profile responsible for the mode of ν_s(SiOSi) consists of two strong bands at about 648 and 690 cm^{-1}, which shift to longer wavenumber compared with the main absorption bands of α- or δ-$SrSiO_3$. This observation suggests that the ring of $(Si_4O_{12})^{8-}$ anion is less flexible than that of the $(Si_3O_9)^{6-}$ anion in α- or δ-$SrSiO_3$.

Luminescence Properties of $SrSiO_3$:Eu^{2+}. In Table 3, we summarize the luminescence properties of $SrSiO_3$: Eu^{2+} modifications. The polymorphs of $SrSiO_3$:Eu^{2+} give various emissions colored with blue or green,[6] and the emission intensity considerably increases when the host lattice has transformed into high-pressure phases. As one of quenching effects on luminescences, we can point out the lattice vibration of phosphors, and the luminescences are generally quenched when the temperature of phosphors is raised. The temperature dependences for the emission intensities of $SrSiO_3$: Eu^{2+} polymorphs are shown in Fig. 4. The shape of quenching curve observed on α-$SrSiO_3$:Eu^{2+} differs from those for the δ and δ' forms. Since the emission of the α form is very weak and the quenching curve is unreliable, however, we are possibly unable to obtain any information from this observation. The δ

and δ' forms give the shapes of quenching curves similar to each other, of which the results are reasonable and well reliable.

It is noticeable that the T_{50} value of δ'-$SrSiO_3$:Eu^{2+} (*ca.* 360 K) is higher than that of δ-$SrSiO_3$:Eu^{2+} (*ca.* 300 K). This means that, in δ'-$SrSiO_3$:Eu^{2+}, the quenching effect caused by the lattice vibration is to be smaller than that in the δ form. Since the silicate anions can be regarded as mainly taking part in the lattice vibration of the crystals, the $(Si_4O_{12})^{8-}$ ring in the δ' form must be hard to vibrate compared with the $(Si_3O_9)^{6-}$ ring in the δ form. This agrees with the information obtained form the IR spectrum measurements. Therefore, δ'-$SrSiO_3$:Eu^{2+}, which consists of the rigid $(Si_4O_{12})^{8-}$ rings give the relatively strong emission. The experimental result that the emission intensity of α-$SrSiO_3$:Eu^{2+} has been very weak is interpreted on the basis of a quenching effect *via* energy transfers between the neighboring Eu^{2+} ions.[6]

References

1) K. Nakamoto, "Infrared Spectra of Inorganic and Coordination Compounds," John Wiley and Sons, Inc., New York (1963), Part II, pp. 103—110.

2) a) A. N. Lazarev, *Opt. Spektrosk.*, **9**, 195 (1960); b) A. N. Lazarev and T. F. Tenisheva, *ibid.*, **11**, 584 (1961); c) A. N. Lazarev, *ibid.*, **12**, 60 (1962); d) A. N. Lazarev and T. F. Tenisheva, *Zh. Strukt. Khim.*, **4**, 703 (1963); e) A. N. Lazarev and V. A. Kolesova, *Izv. Akad. Nauk SSSR, Neorg. Mater.*, **6**, 1445 (1970); f) A. N. Lazarev and I. S. Ignatyev, *Opt. Spektrosk.*, **28**, 971 (1970).

3) N. A. Toropov, V. P. Barzakovskii, V. V. Lapin, and N. N. Kurtseva, "Handbook of Phase Diagrams of Silicate Systems; Binary Systems," 2nd ed, ed by N. A. Toropov, Israel Program for Scientific Transitions, Jerusalem (1972), Vol. I, pp. 20—44.

4) A. E. Ringwood and A. Major, *Earth Planet. Sci. Lett.*, **2**, 106 (1967).

5) a) Y. Shimizu, Y. Syono, and S. Akimoto, *High Temp.-High Pressures*; **2**, 113 (1970); b) K. Machida, G. Adachi, J. Shiokawa, M. Shimada, and M. Koizumi, *Acta Crystallogr., Sect. B*, **38**, 386 (1982).

6) K. Machida, G. Adachi, J. Shiokawa, M. Shimada, M. Koizumi, K. Suito, and A. Onodera, *Inorg. Chem.*, **21**, 1512 (1982).

7) a) K. Machida, G. Adachi, and J. Shiokawa, *J. Lumin.*, **21**, 101 (1979); b) K. Machida, G. Adachi, J. Shiokawa, M. Shimada, and M. Koizumi, *Inorg. Chem.*, **19**, 983 (1980).

8) J. W. Jeffery and L. Heller, *Acta Crystallogr.*, **6**, 807 (1953).

9) F. J. Trojer, *Z. Kristallogr.*, **130**, 185 (1969).

10) F. Matossi and H. Krüger, *Z. Phys.*, **99**, 1 (1936).

Nitrosyliron Complexes Containing 8-Quinolinolate or Its Derivatives**

Eiichi Miki,* Masaaki Motonaga, Kunihiko Mizumachi,
Tatsujiro Ishimori, and Motomi Katada†

Department of Chemistry, College of Science, Rikkyo University, 3-Chome, Nishi-Ikebukuro, Toshima-ku, Tokyo 171

† *Department of Chemistry, Faculty of Science, Tokyo Metropolitan University, Fukasawa, Setagaya-ku, Tokyo 158*

(Received November 11, 1981)

New nitrosyls, $[Fe(C_9H_6NO)_2(NO)]_2$($C_9H_6NO^-$=8-quinolinolate ion), $[Fe(C_{10}H_8NO)(NO)_2]$ ($C_{10}H_8NO^-$= 2-methyl-8-quinolinolate ion), and $[Fe(C_9H_5NOCl)_2(NO)(DMF)]$ ($C_9H_5NOCl^-$=5-chloro-8-quinolinolate ion) were isolated by the reaction of nitrogen monoxide with a mixture of iron(II) perchlorate and the corresponding quinolinol in methanol or methanol/DMF. They were characterized by IR, ^{57}Fe-Mössbauer, and magnetic measurements.

One of the present authors reported that $[Co(C_9H_6NO)_2(NO)]$ prepared by the reaction of nitrogen monoxide with a mixture of cobalt(II) chloride and 8-quinolinol in methanol, reacted further with nitrogen monoxide in dichloromethane at room temperature to precipitate $[NO][Co(C_9H_6NO)_2(NO_3)(NO_2)]$ with liberation of dinitrogen oxide. The reaction involved disproportionation of nitrogen monoxide and electrophilic attack by nitrogen monoxide on the coordinating nitrosyl group of the nitrosylcobalt complex.[1]

In this paper, we report the syntheses and characterization of some new nitrosyliron complexes containing 8-quinolinolate ion, and its derivatives, 2-methyl-, or 5-chloro-8-quinolinolate ion, and also examine whether the obtained nitrosyliron complexes react further with nitrogen monoxide, as reported for $[Co(C_9H_6NO)_2(NO)]$.

Experimental

Materials. The nitrosyl complexes were synthesized and manipulated under nitrogen atmosphere or in a vacuum line. Commercial iron(II) perchlorate hexahydrate was treated with zinc powder in methanol to reduce any iron (III) present and dried over Zeorum A-4(Toyo Soda Ind. Co., Ltd.) before using. Organic solvents were dried over anhyd calcium sulfate or Zeorum A-4, distilled or deoxygenated in nitrogen or argon stream, and then degassed in a reaction vessel by a repetitive freeze-pump-thaw cycle. Nitrogen monoxide was derived from the reaction of potassium nitrate with mercury and concd sulfuric acid.

Preparation. Two mmol of iron(II) perchlorate in methanol (40 cm^3) was brought into contact with 5 mmol of nitrogen monoxide, which resulted in an instant color change to dark brown. Four mmol of 8-quinolinol or 2-methyl-8-quinolinol in methanol or DMF (10 cm^3) was poured into the dark brown solution; it was then stirred at *ca.* 0 °C for 1 h to precipitate the nitrosyl complexes. In the case of using 5-chloro- or 5-nitro-8-quinolinol, DMF was used instead of methanol as a solvent because they are sparingly soluble in methanol. A mixture of the dark brown solution and 4 mmol of the quinolinol in DMF(10 cm^3) was stirred at *ca.* −20 °C for 1 h. The product was collected by filtration, washed with diethyl ether, dried under vacuum for a minute, and then stored in nitrogen atmosphere. The ^{15}NO-substituted complexes(^{15}N atom% in NO=99.4) were prepared by the use of ^{15}NO derived from $K^{15}NO_3$. The elementary analyses and the yields of the obtained nitrosyls are shown in Table 1. The C, H, N, and Cl contents were analyzed by the Organic Analysis Center of the Institute of Physical and Chemical Research. The content of the iron was obtained by colorimetric determination.[2]

Reaction of the Nitrosyl Complexes with Nitrogen Monoxide in Dichloromethane. Dichloromethane(20 cm^3) and 5 mmol of nitrogen monoxide were trapped into a reaction vessel containing *ca.* a half mmol of the nitrosyl complexes with the aid of liquid nitrogen. The frozen solution was melted and stirred at room temperature for several days. Gaseous materials in the reaction vessel were collected and identified by their IR bands. After the unreacted original nitrosyl had been filtered, the dichloromethane was removed from the filtrate at *ca.* −20 °C, and the residual product was characterized.

Measurements. The IR spectra in the solid state as Nujol and poly(chlorotrifluoroethylene) oil mulls, and of the dichloromethane solution were measured in the regions 200—4000 cm^{-1}, and 1500—2000 cm^{-1}, respectively. The gaseous materials were trapped into a calcium difluoride gas cell with the aid of liquid nitrogen, and identified on the basis of their IR bands.[3] The magnetic susceptibility at room temperature was measured by the Gouy method.

Table 1. Elementary analyses and yields of the nitrosyls

	Compound	Color	Yield/%		Fe(%)	C(%)	H(%)	N(%)	Cl(%)
1	$[Fe(C_9H_5NOCl)_2(NO)(DMF)]$	Dark khaki	34	Found	10.7	47.5	2.9	10.0	15.7
				Calcd	10.8	48.5	3.3	10.9	13.7
2	$[Fe(C_{10}H_8NO)(NO)_2]$	Chocolate	24	Found	20.0	44.9	3.1	14.4	—
				Calcd	20.4	43.8	2.9	15.3	—
3	$[Fe(C_9H_6NO)_2(NO)]_2$	Dark green	20	Found	14.8	57.8	3.2	10.8	—
				Calcd	14.9	57.8	3.2	11.2	—

**Partly presented at 43rd National Meeting of the Chemical Society of Japan, Tokyo, April 1981, Abstr., No. 3C02.

The magnetic susceptibility for $[Fe(C_9H_6NO)_2(NO)]_2$ was measured by the Faraday method in the temperature range from 83 K to room temperature. The apparatus was calibrated by $[Fe(H_2O)_6]SO_4\cdot(NH_4)_2SO_4$. The ^{57}Fe-Mössbauer spectra were measured at 80 K under vacuum by using a ^{57}Co(Pt) source moving in a constant acceleration mode. The isomer shift are relative to metallic iron foil.

Results and Discussion

It is very remarkable that different types of the nitrosyl complexes were isolated under the same preparative conditions. Nitrosyliron containing 5-nitro-8-quinolinolate ion could not be isolated under the present experimental conditions, dark green $[Fe(C_9H_5N_2O_3)_3]\cdot 1/2DMF$ being precipitated instead. Found: Fe, 8.3; C, 49.3; H, 2.8; N, 13.4%. Calcd: Fe, 8.5; C, 51.8; H, 2.8; N, 13.8%.

All the nitrosyls in the solid state were stable in nitrogen atmosphere, but compounds **1** and **2** were unstable at room temperature in a vacuum and nitrogen monoxide was liberated. The nitrosyls were also unstable in deoxygenated organic solvents such as dichloromethane, chloroform, acetone, THF, and DMSO, giving off nitrogen monoxide. Hence, they could not be recrystallized.

IR Spectra. *[Fe(C$_9$H$_5$NOCl)$_2$(NO)(DMF)] (1)*: Upon ^{15}NO-substitution, the IR bands at 1710(vs)[4] and 440(w) cm^{-1} shifted to 1679 and 434 cm^{-1}, respectively. The former was assigned to the N–O stretching vibration and the latter to one of the FeNO skeletal vibrations.[5] A shoulder band at 1655 cm^{-1} overlapping with the N–O stretching band was observed for both the ^{14}NO- and ^{15}NO-complexes, and was assigned to the C–O stretching vibration of DMF. It has been reported that the C–O stretching band at 1670 cm^{-1} for free DMF shifted to 1625—1650 cm^{-1} on coordination.[6,7] Thus, the DMF of the present nitrosyl seems to coordinate to the iron.

[Fe(C$_{10}$H$_8$NO)(NO)$_2$] (2): The IR bands at 1758 (vs), 1685(vs), 543(w), 519(s), 511(w), and 379(s) cm^{-1} shifted to 1722, 1649, 539, 515, 500, and 369 cm^{-1}, respectively, upon ^{15}NO-substitution, which suggests the presence of a $Fe(NO)_2$ skeleton. Although the wave numbers of the N–O stretching bands in the region 1760—1650 cm^{-1} shifted upwards by *ca.* 7 cm^{-1} at 80 K, relative intensity of the bands at room temperature did not change at 80 K.

Four-coordinate compounds containing a monopositive dinitrosyliron group such as the present nitrosyl have already been reported. $[N(PPh_3)_2][FeX_2(NO)_2]$ (X=Cl, Br, or I)[8] and $[Fe(L'H)(NO)_2]$ (L'=$^-$SCH$_2$-CH$_2$N(CH$_3$)CH$_2$CH$_2$CH$_2$N(CH$_3$)CH$_2$CH$_2$S$^-$)[9] show two N–O stretching bands in the region 1700—1780 cm^{-1} as observed for the present nitrosyl. X-Ray diffraction studies show that four-coordinate compounds with monopositive dinitrosyliron have flattened tetrahedral geometry with two equivalent nitrosyl groups, and the Fe–N–O angles are in the range 160—175°.[9,10] Thus, the present nitrosyl also is probably a pseudo-tetrahedral complex with almost linear Fe–N–O groups.

[Fe(C$_9$H$_6$NO)$_2$(NO)]$_2$ (3): Upon ^{15}NO-substitution, the IR bands at 1740(vs), 1667(vs), and 373(m) cm^{-1} shifted to 1711, 1643, and 362 cm^{-1}, respectively,

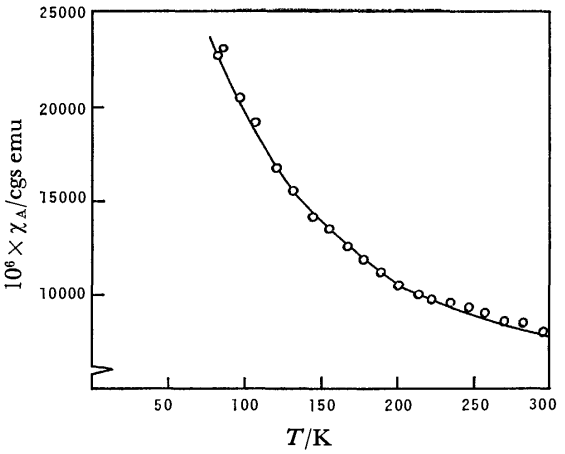

Fig. 1. Temperature dependence of atomic susceptibility of $[Fe(C_9H_6NO)_2(NO)]_2$.
The solid curve was calculated from Eq. 1 with $g=2.25\pm0.01$ and $-J=4.4\pm0.5$ cm^{-1}.

and the 540 cm^{-1} band(sh) also shifted and became concealed by the foot of the very strong band at 520 cm^{-1}, due to the coordinating 8-quinolinolate ions. The bands at 1740 and 1667 cm^{-1} could be assigned to the N–O stretching vibrations, and the bands at 540 and 373 cm^{-1} to the FeNO skeletal ones.

In the case of a dimer complex, $[Fe(TDBM)_2(NO)]_2$ (TDBM$^-$ = diphenylpropane-1-onate-3-thionate ion), where two of the iron atoms are bridged through the sulfur atoms of two TDBM and each iron atom has a coordination number of six, the N–O stretching vibrations are observed at 1675 and 1780 cm^{-1}.[11] For a spin-equilibrium complex, [Fe(salen)(NO)] (salen^{2-}= *N,N'*-disalicylideneethylenediaminate ion) with two N–O stretching bands, the relative intensity of the N–O bands changes with lowering temperature.[12,13] Geometry-equilibrium complexes, $[CoCl_2(NO)L_2]$ (L= phosphine derivatives) also show two N–O stretching bands; their relative intensity changes with temperature.[14,15]

On the other hand, the relative intensity of the N–O stretching bands for the present nitrosyl at 80 K was almost equal to that at room temperature although the bands shifted upwards by *ca.* 5 cm^{-1} at 80 K. The separation of the two bands is too large to be due to the solid state effect. The wave numbers of the two bands show that both nitrosyl groups are terminal.[16] Thus, the two N–O stretching bands suggest that the terminal nitrosyl groups are in different chemical environments.

Magnetism. According to the notation introduced by Enemark and Feltham,[17] both compounds, **1** and **3**, contain $\{Fe(NO)\}^7$, and compound **2** contains $\{Fe(NO)_2\}^9$; here the superscripts show the number of the *d*-electrons in the iron when the nitrosyl ligand is formally assumed to be NO$^+$.

The effective magnetic moment of compound **2** was 1.97 BM (at 292 K), which was comparable to that of $[N(PPh_3)_2][FeX_2(NO)_2]$ where the dinitrosyliron is the $\{Fe(NO)_2\}^9$ species.[8] The effective magnetic moments of compounds **1** and **3** were 4.21 (at 291 K) and 4.43 BM (at 285 K), respectively, and the values correspond to those observed for first row transition-

Table 2. Mössbauer parameters of the nitrosyls at 80 K

	Compound	δ[a,b) mm s^{-1}	ΔE_Q[b) mm s^{-1}	Γ_1[b) mm s^{-1}	Γ_2[b) mm s^{-1}
1	$[Fe(C_9H_5NOCl)_2(NO)(DMF)]$	0.68	1.32	0.49	0.36
2	$[Fe(C_{10}H_8NO)(NO)_2]$	0.47	0.88	0.28	0.30
3	$[Fe(C_9H_6NO)_2(NO)]_2$	0.45	0.69	0.48	0.49

a) The isomer shift is relative to metallic iron foil. b) The values are accurate within ± 0.03 mm s^{-1}. Γ_1, line width of a lower energy peak; Γ_2, line width of a higher energy peak.

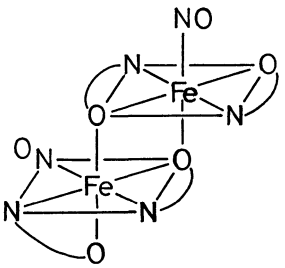

Fig. 2. One of the possible structures for $[Fe(C_9H_6NO)_2(NO)]_2$.
N-O: 8-Quinolinolate ion.

metal ions with high-spin d^7 configurations.[18] The magnetic moment of compound **3** decreased gradually with lowering temperature from 4.4 (at 285 K) to 4.0 BM (at 83 K); this decrease suggests the presence of antiferromagnetic exchange interaction between the iron ions.[19] The temperature dependence of the magnetic susceptibility is shown in Fig. 1.

The molecular weight of compound **3** could not be measured because it is unstable in the examined organic solvents. The two N–O stretching bands of compound **3** can not deny the possibility that it is a dimer. Thus, by assuming that compound **3** was a binuclear complex containing two iron ions with $S=3/2$, the susceptibility data were fit to Eq. 1, which was reported by Earnshaw and Lewis:[20]

$$\chi_A = \frac{Ng^2\beta^2}{kT}\left[\frac{14+5\exp(-6J/kT)+\exp(-10J/kT)}{7+5\exp(-6J/kT)+3\exp(-10J/kT)+\exp(-12J/kT)}\right] + N\alpha. \quad (1)$$

$N\alpha$ was neglected in the fitting. The experimental data fit Eq. 1 with $g=2.25\pm0.01$ and the exchange integral, $-J=4.4\pm0.5$ cm^{-1}. The negative J suggests that there is some antiferromagnetic interaction between the two iron ions in the assumed binuclear complex, $[Fe(C_9H_6NO)_2(NO)]_2$.

The value of J for compound **3** was comparable to those reported for $[Fe(salen)Cl]_2$ and its analogs with a binuclear moiety, $Fe^{III}\langle O \rangle Fe^{III}$.[19] On the other hand, the value of $-J$ for $[Fe(salen)]_2O$ and its analogs containing a Fe^{III}-O-Fe^{III} system with an Fe–O–Fe angle of *ca.* 160° have been reported to be 87—100 cm^{-1}.[21] This value of J shows that the $Fe\langle O \rangle Fe$ system is less favorable for transmitting the exchange interaction than the Fe–O–Fe one. The formal oxidation number of the iron for compound **3** is considered to be +I as discussed later. There is no

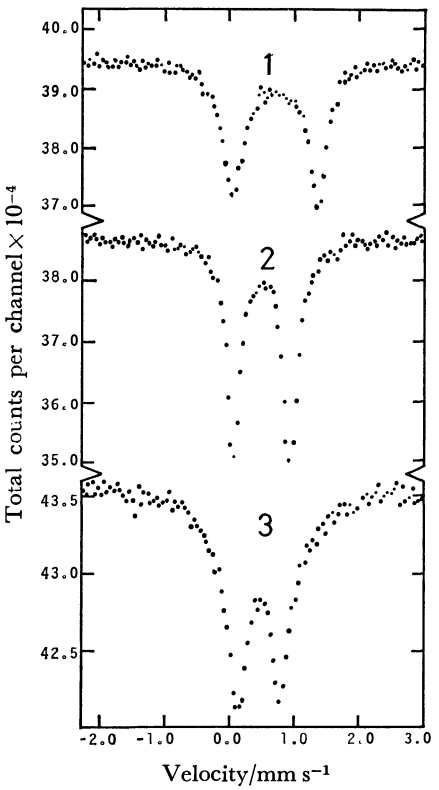

Fig. 3. Mössbauer spectra of the nitrosyls at 80 K.
1: $[Fe(C_9H_5NOCl)_2(NO)(DMF)]$, **2**: $[Fe(C_{10}H_8NO)(NO)_2]$, **3**: $[Fe(C_9H_6NO)_2(NO)]_2$.

data for the J value of the iron(I) complexes. Although the J value for the iron(I) complex can not be directly compared with those for the iron(III) complexes, the J value suggests the possibility that compound **3** is a dimer in which two of the iron atoms are bridged through the oxygen atoms of two 8-quinolinolate ions to form a $Fe^{I}\langle O \rangle Fe^{I}$ moiety. One of the possible structures for compound **3** is shown in Fig. 2.

^{57}Fe-Mössbauer Spectra. The Mössbauer spectra and the derived parameters of the nitrosyls are shown in Fig. 3 and Table 2, respectively. The spectrum of compound **2** consisted of a single and symmetrical doublet with line widths of *ca.* 0.3 mm s^{-1}, whereas that of compound **1** consisted of an unsymmetrical doublet with line widths of more than 0.3 mm s^{-1}. This suggests the presence of some impurity that may be derived from compound **1** which is not stable under these conditions. Compound **3** showed a symmetrical doublet but its line widths are broader than those of

compound **2**. The line broadening can be reasonably explained by supposing that compound **3** is a dimer, as shown in Fig. 2; the two sites of the irons are in very similar chemical environments, so the Mössbauer spectra are expected to be almost equal to each other. Such spectra are overlapped to give the line broadening.

Studies on the wave numbers of the N–O stretching vibration and its ^{15}N-isotopic shift for transition-metal nitrosyls indicate that the nitrosyl ligand of the present nitrosyls formally coordinates as NO^+ to the iron.[5] Thus, the formal oxidation number of the iron for both compounds **1** and **3** is +I, and that for compound **2** is −I. One might expect that the isomer shift observed for the iron compounds with such electronic structures are higher than those for high-spin iron(III) compounds (d^6, $S=2$). The isomer shift for $[Fe(H_2O)_5(NO)]SO_4$ (Fe^+, $S=3/2$) has been observed at *ca.* 1.3 mm s^{-1} at room temperature.[22] However, the isomer shifts for the present nitrosyls were observed in the region of those for Fe^{2+} ($S=0$), Fe^{3+} ($S=1/2$), or Fe^{3+} ($S=5/2$) ions.[23] The results can be explained as follows; strong π-acidity of NO^+ causes a decrease of the 3d-electron density of iron, and thus the isomer shifts for the nitrosyls decreases.[23] The smaller isomer shifts of compounds **1** and **3**, compared with that of $[Fe(H_2O)_5(NO)]SO_4$, indicate the increase in π-acceptor ability of the ligands in compounds **1** and **3**. The close values of the isomer shifts for compound **2** and compounds **1** and **3** may be due to strong π-back donation of two nitrosyl groups in compound **2**. The value of the isomer shift for compound **2** is comparable to those reported for dinitrosyliron compounds, $LYFe(NO)_2$ (L=$C_5H_{11}N$, Ph_3P, Ph_3As, or Ph_3Sb; Y=Br or I).[24]

The quadrupole splittings for the present nitrosyl compounds arise not only from the extra electrons in 3*d* orbitals, which can distort the symmetry of the total environment of iron atom, but also from the differences in strength of the π-acceptor of the ligands. Therefore, the larger quadrupole splitting for compound **1**, compared with that of compound **3**, indicates that the distortion from the octahedral symmetry in compound **1** is larger than that in compound **3**. Although compounds **1** and **3** seem to have the high-spin configuration from the magnetic results, the Mössbauer data shows the presence of strong π-back donation leading to low-spin configuration. This discrepancy seems worthy of further investigation.

. *Reaction of the Nitrosyl Complexes with Nitrogen Monoxide in Dichloromethane.* It has been reported that nitrogen monoxide disproportionates by reacting with transition-metal complexes to give nitrosyl nitrite and hyponitrito complexes, and that nitrosyl complexes with a NO^- group reacts with nitrogen monoxide to form nitro complexes with liberation of dinitrogen oxide.[1,25]

Compound **3** was stable in dichloromethane saturated with nitrogen monoxide, and the product from the filtrate was identified to be the original compound **3**. Compounds **1** and **2** decomposed to give unidentified products, but dinitrogen oxide could not be observed in the reaction vessel. Products from compounds **1** and **2** showed no N–O stretching bands assignable to $[NO]^+$, coordinating nitrosyl, nitrite or hyponitrite groups.

Thus, for all the present nitrosyl compounds, the disproportionation of nitrogen monoxide or the electrophilic attack by nitrogen monoxide on a coordinating nitrosyl group could not be observed. These facts are consistent with the idea that the present nitrosyls are formally NO^+-complexes.

The authors wish to express their thanks to Mr. Takashi Nagai of Rikkyo University for calculating the values of *g* and *J* from the magnetic data.

The present work was supported in part by a Grant-in-Aid for Scientific Research No. 564199 from the Ministry of Education, Science and Culture.

References

1) E. Miki, *Chem. Lett.*, **1980**, 835.
2) E. B. Sandell, "Colorimetric Determination of Traces of Metals," 3rd ed, Interscience Publishers, Inc., New York (1959), pp. 537—542.
3) S. Pinchas and I. Laulight, "Infrared Spectra of Labelled Compounds," Academic Press, London (1971), Chap. 6.
4) The signs in parentheses indicate the abbreviations of the strength and shape of the IR bands; vs=very strong, s=strong, m=medium, w=weak, sh=shoulder.
5) E. Miki, H. Okamura, K. Mizumachi, and T. Ishimori, *Bull. Chem. Soc. Jpn.*, **51**, 1768 (1978) and references therein.
6) M. L. Larson and F. W. Moore, *Inorg. Chem.*, **5**, 801 (1966).
7) V. S. Khain and V. P. Val'krova, *Russ. J. Inorg. Chem.*, **23**, 1870 (1978).
8) N. G. Connelly and C. Gardner, *J. Chem. Soc., Dalton Trans.*, **1976**, 1525.
9) L. M. Baltusis, K. D. Karlin, H. N. Rabinowitz, J. C. Dewan, and S. J. Lippard, *Inorg. Chem.*, **19**, 2627 (1980).
10) R. D. Feltham and J. H. Enemark, "Structures of Metal Nitrosyls," in "Topics in Stereochemistry," ed by N. L. Allinger, E. L. Eliel, and G. Geoffroy, Interscience Publishers, New York (1981), Vol. 12, pp. 155—215.
11) P. Thomas, L. Beyer, K. Hennig, E. Hoyer, V. I. Nefedov, and E. K. Žumadilov, *Z. Anorg. Allg. Chem.*, **437**, 299 (1977).
12) A. Earnshaw, E. A. King, and L. F. Larkworthy, *J. Chem. Soc., Inorg. Phys. Theor.*, **1969**, 2459.
13) K. J. Haller, P. L. Johnson, R. D. Feltham, J. H. Enemark, J. R. Ferraro, and L. J. Basile, *Inorg. Chim. Acta*, **33**, 119 (1979).
14) J. P. Collman, P. Farnham, and G. Dolcetti, *J. Am. Chem. Soc.*, **93**, 1788 (1971).
15) C. P. Brock, J. P. Collman, G. Dolcetti, P. H. Farnham, J. A. Ibers, J. E. Lester, and C. A. Reed, *Inorg. Chem.*, **12**, 1304 (1973).
16) B. F. G. Johnson and J. A. McCleverty, "Nitric Oxide Compounds of Transition Metals," in "Progress in Inorganic Chemistry," ed by F. A. Cotton, Interscience Publishers, New York (1966), Vol. 7, pp. 277—359.
17) J. H. Enemark and R. D. Feltham, *Coord. Chem. Rev.*, **13**, 339 (1974).
18) B. N. Figgis and J. Lewis, "The Magnetochemistry of Complex Compounds," in "Modern Coordination Chem-

istry: Principles and Methods," ed by J. Lewis and R. G. Wilkins, Interscience Publishers New York (1960), Chap. 6.
19) M. Gerloch, J. Lewis, F. E. Mabbs, and A. Richards, *J. Chem. Soc., Inorg. Phys. Theor.*, **1968**, 112.
20) A. Earnshaw and J. Lewis, *J. Chem. Soc.*, **1961**, 396.
21) J. Lewis, F. E. Mabbs, and A. Richards, *J. Chem. Soc., Inorg. Phys. Theor.*, **1967**, 1014.
22) J. Danon, *J. Chem. Phys.*, **41**, 3378 (1964).
23) H. Sano, "Mössbauer Bunkohgaku Gairon," Kohdansha, Tokyo (1972), pp. 125—171; G. M. Bancroft and R. H. Platt, "Mössbauer Spectra of Inorganic Compounds: Bonding and Structure," in "Advances in Inorganic Chemistry and Radiochemistry," ed by H. J. Emeléus and A. G. Sharpe, Academic Press, New York and London (1972), Vol. 15, pp. 59—258.
24) J. P. Crow, W. R. Cullen, F. G. Herring, J. R. Sams, and R. L. Tapping, *Inorg. Chem.*, **10**, 1616 (1971).
25) J. A. McCleverty, *Chem. Rev.*, **79**, 53, (1979).

 © 1982 The Chemical Society of Japan Bull. Chem. Soc. Jpn., 55, 2863—2865 (1982)

Copper(II) Complex of 2,2′-Bi-8-quinolinol

Youichi DEMURA,* Kazuyoshi HIRAKAWA,† and Ichiro MURASE

Laboratory of Chemistry, College of General Education, Kyushu University, Ropponmatsu, Chuo-ku, Fukuoka 810

† *Department of Electronics, Faculty of Engineering, Kyushu University, Hakozaki, Higashi-ku, Fukuoka 812*

(Received April 23, 1982)

A copper(II) complex of 2,2′-bi-8-quinolinol was prepared. The structure has been determined by means of infrared and electronic spectra, magnetic susceptibility under temperature variation, and molecular weight measurement. It was found to be a binuclear chelate having a tetrahedral arrangement around each copper ion.

8-Quinolinol functions as a bidentate ligand and forms stable chelates with a variety of metal ions as well as copper(II). The high stability of the complexes is mainly attributable to the fixed planar ligand structure containing a phenolic oxygen and a heteroaromatic nitrogen atom. On the other hand, 2,2′-biquinoline is known as a specific ligand for copper(I), and this property is due to the steric fitness of the ligand structure together with the stabilization of low oxidation state by the α-diimine coordination. It is of interest to prepare the compound in which these two functions are combined in one molecule. We thus have synthesized 2,2′-bi-8-quinolinol (**1**) and examined its complex formation with transition metal ions, and well defined crystals have been obtained with copper(II). In this paper we will deal with the synthesis of the ligand and the copper complex, and will discuss its structure by means of electronic and infrared spectroscopy and of magnetic measurement at various temperature.

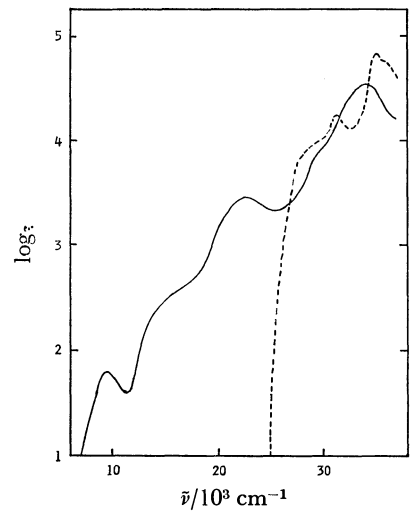

Fig. 1. Electronic spectrum of the free ligand (**1**) (- - -), and the Cu(II) complex (——).

Results and Discussion

2,2′-Bi-8-quinolinol (**1**) was prepared in poor yield by the dimerization of 2-bromo-8-tosyloxyquinoline with palladium-calcium carbonate catalyst in the presence of hydrazine according to the method developed by Nakano.[1] The tosyl group was hydrolyzed simultaneously during the dimerization reaction.

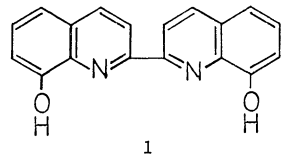

1

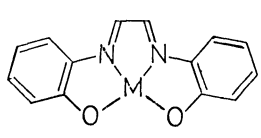

2

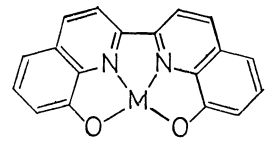

3

1 is considered as a heterocyclic analogue of *N,N′*-bis(*o*-hydroxyphenyl)-1,2-ethanediimine[2] in which the azomethine linkages are incorporated into heteroaromatic rings. *N,N′*-Bis(*o*-hydroxyphenyl)-1,2-ethanediimine functions as a planar quadridentate ligand and forms deep blue chelates **2** with copper(II) and other transition metal ions. Provided that **1** forms a copper chelate in the similar manner as shown in **3**, a molecular model reveals that the Cu–N and Cu–O distances are about 0.2 nm and 0.3 nm respectively, unless the quinoline moieties bend towards the central metal ion. The Cu–O distance will be too long to achieve stable coordination as compared with those in bis(8-quinolinolato)copper(II) in which the Cu–N and the Cu–O distances are 0.19 nm and 0.21 nm respectively.[3]

The copper(II) complex is deep brown fine crystals and the elemental analysis agrees with the metal-ligand ratio of 1:1. However, the molecular weight determined in chloroform was 708 and it is very close to the calculated value as a dimer (700).

The infrared spectral pattern in KBr resembles that of bis(8-quinolinolato)copper(II) in many respects, especially showing a sharp absorption at 1105 cm^{-1} which is characteristic for a C–O stretching vibration in metal 8-quinolinolates.[4] No absorption is observed for the OH stretching which appears as a sharp band at 3350 cm^{-1} in the free ligand. The electronic spectrum in chloroform exhibits an absorption maximum at 34000 cm^{-1}(ε=35500), 22200(ε=2900), 14300(ε=300), and 9300(ε=90) as seen in Fig. 1. The spectral pattern is quite different from those usually associated with bivalent copper in square-planar arrangements. Similar spectrum has been observed for bis(2,2′-biquinoline)copper(II) perchlorate, which exhibited d-d transition at 19230 cm^{-1}(ε=950), 13300(ε=170), and 9300

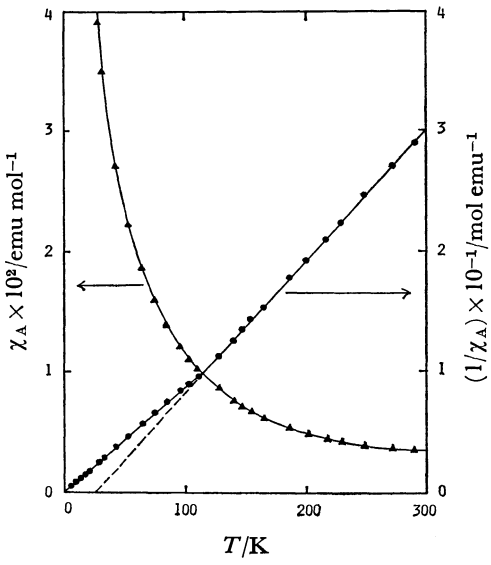

Fig. 2. Temperature variation of molar and inverse magnetic susceptibilities of the complex. The diamagnetic correction was -3.11×10^{-4}.

(ε=90) in nitrobenzene.[5] {2,2'-[1,1'-Biphenyl-2,2'-diyldinitrilomethylidyne]bisphenolato}copper(II) also showed absorptions at 20800 cm^{-1}(ε=790), 15200(ε=340), and 11500(ε=50).[6] These complexes have been assumed to have a pseudo tetrahedral structure and the latter was confirmed by X-ray crystallography.[7]

The variation of the magnetic susceptibility under temperature change is shown in Fig. 2. The susceptibility obeys Curie-Weiss' law in the temperature range 118—290.8 K with a value of θ=20.5 K, while it obeys Curie's law between 5.7—118 K. This temperature dependence of χ_A suggests that the copper(II) ions are not magnetically isolated but under some magnetic interaction. Provided a binuclear structure exists, the χ_A is given as the Bleaney-Bowers' equation,[8]

$$\chi_A = \frac{Ng^2\beta^2}{3kT}\left[1+\frac{1}{3}\exp(-2J/kT)\right]^{-1} + N_\alpha,$$

where N is the Avogadro constant, β the Bohr magneton, k the Boltzman constant, T the temperature, J the exchange integral, and the N_α the temperature-independent paramagnetism. The experimental $|J|$/K value which fits this equation best is 200 K below 118 K, and 120 K at higher temperature, where N_α is 1×10^{-4} emu/mol. The μ_{eff} values for one copper ion are 2.02 BM(290.8 K), 2.15(118.3 K), and 2.29 (5.7 K). The room temperature value is slightly lower than that (2.2 BM) predicted for copper(II) in a tetrahedral environment.[9] However, distortion can appreciably lower it, if low symmetry ligand fields produced are large compared to the spin-orbit coupling, and similar values (1.9—2.0 BM) have been reported for bis(2,2'-biquinoline)copper(II).[5]

Judging from the dimeric molecular weight, the electronic spectrum, and the magnetic evidence, the copper(II) complex prepared is binuclear and the ligands are tetrahedrally arranged around the copper ions. A molecular model can be sketched as shown in Fig. 3. Here one quinolinol plane is nearly perpendicular to the other in one biquinolinol molecule,

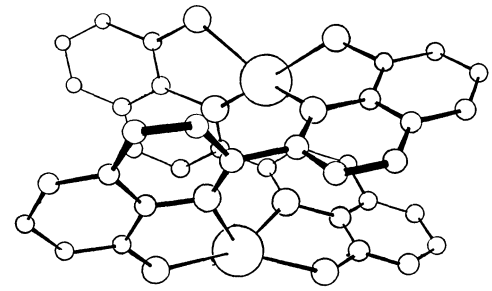

Fig. 3. Probable structure of the complex.

and each quinolinol moiety is individually coordinated to each of the two copper ions. The data obtained so far support the proposed structure, though the definite conclusion must wait for X-ray crystallography.

Experimental

2-Bromo-8-tosyloxyquinoline. A mixture of 8-tosyloxy-2(1*H*)-quinolinone (22.5 g) and phosphoryl bromide (50 g) in 40 cm^3 chloroform was refluxed with stirring in an oil bath at 110 °C for 4 h. The reaction mixture was poured into crashed ice and the water layer was neutralized with 5% aqueous sodium hydrogencarbonate. The chloroform layer was collected and the aqueous layer was extracted twice with 150 cm^3 of chloroform. The combined extracts were dried over anhydrous sodium sulfate and the solvent was removed by distillation. The crude residual product was recrystallized from ethanol and 24 g of the compound were obtained as colorless crystals, mp 133 °C, yield 80%.

Found: C, 50.55; H, 3.19; N, 3.70%. Calcd for $C_{16}H_{12}BrNO_3S$: C, 50.80; H, 3.18; N, 3.70%.

2,2'-Bi-8-quinolinol. 2-Bromo-8-tosyloxyquinoline (5 g) was dissolved in 200 cm^3 of methanol containing 5% potassium hydroxide and 3 g of 2% palladium on calcium carbonate was added. The mixture was heated at 50 °C and to this was added dropwise with stirring 6 cm^3 of hydrazine hydrate in 50 cm^3 methanol. The addition took 4 h and 3 g of the catalyst was newly added after 2 h during the reaction. After the addition of hydrazine, the reaction mixture was further heated at 80 °C for 1 h. The catalyst was filtered off and the mixture was treated with 500 cm^3 of hot 5% potassium hydroxide–methanol solution. The filtrate and the extract were combined and acidified with concentrated hydrochloric acid. Methanol was removed under reduced pressure and the residue was neutralized with aqueous sodium hydrogencarbonate. The resulting white precipitate was collected by filtration and boiled with 500 cm^3 of chloroform. The chloroform was removed from the extracts under reduced pressure and the residue was recrystallized from dioxane. The compound crystallized as colorless plates, mp 264 °C, yield 0.5 g.

Found: C, 74.78; H, 4.18; N, 9.76%. Calcd for $C_{18}H_{12}N_2O_2$: C, 75.01; H, 4.16; N, 9.72%.

Copper(II) Complex. 2,2'-Bi-8-quinolinol (0.1 g) was dissolved in minimum amount of hot dioxane and to this was added copper acetate monohydrate (0.065 g) in a dioxane–ethanol mixture (1:1). The mixture was heated on a water bath for 10 minutes and the resulting deep brown needles were collected by filtration and washed with methanol and dried at 100 °C under vacuum. The complex can be recrystallized from pyridine, but it is pure enough without recrystallization.

Found: C, 61.75; H, 2.87; N, 7.87; Cu, 18.22%. Calcd

for $C_{18}H_{10}N_2O_2Cu$: C, 61.80; H, 2.88; N, 8.01; Cu, 18.16%.

Measurements. Molecular weight was determined by vaper pressure equilibrium method with a Hitachi Osmometer Type-115 using chloroform as a solvent. Infrared spectra were recorded in KBr disks with a Hitachi EPI-S2, and electronic spectra were taken with a Hitachi EPS-3T spectrophotometer. The magnetic moments were measured bv means of a recording magnetometer especially designed by Hirakawa *et al.*[10]

References

1) S. Nakano, *Yakugaku Zasshi*, **79**, 310 (1959).
2) I. Murase, *Bull. Chem. Soc. Jpn.*, **33**, 607 (1956); E. Bayer, *Ber.*, **90**, 2325 (1957).
3) R. C. Hoy and R. H. Morriss, *Acta Crystallogr.*, **22**, 476 (1967); G. J. Palenic, *ibid.*, **17**, 687 (1964).
4) R. G. Charles, H. Freiser, R. Friedel, L. E. Hilliard, and W. D. Johnston, *Spectrochim. Acta*, **8**, 1 (1956).
5) C. M. Harris, H. R. H. Patil, and E. Sinn, *Inorg. Chem.*, **6**, 1102 (1967).
6) T. P. Cheeseman, D. Hall and T. N. Waters, *J. Chem. Soc.*, **1966**, 694.
7) T. P. Cheeseman, D. Hall, and T. N. Waters, *Proc. Chem. Soc.*, **1963**, 379.
8) B. Bleaney and K. D. Bowers, *Proc. R. Soc. London, Ser. A*, **214**, 451 (1952).
9) B. N. Figgis, *Nature*, **182**, 1568 (1958).
10) K. Hirakawa, Ka. Hirakawa, and S. Yoneyama, *Jpn. J. Appl. Phys.*, **2**, 816 (1963).

Studies of the Cobalt(III) Complexes of 8-Amino-3,6-diazaoctanate Ion. IV.[1] Preparations and Some Properties of [Co(ADAO)XY] Type Complexes: XY=Cl(NH_3), Cl(py), (H_2O)(py), Cl(H_2O), (NO_2)(H_2O), and Cl(NO_2)

Kiyokatsu WATANABE

Department of Chemistry, Faculty of Science, Ehime University, Matsuyama, Ehime 790

(Received January 14, 1982)

The following new cobalt(III) complexes containing the 8-amino-3,6-diazaoctanate ion (adao[2]) have been isolated: two isomers of *β-mer(N)-trans(Cl,*O_{adao})-[Co(adao)(Cl)(NH_3)]ClO_4, two isomers of *β-mer(N)-trans(Cl,* O_{adao})-[Co(adao)(Cl)(py)]ClO_4, *β-mer(N)-trans(O)*-[Co(adao)(H_2O)(py)]ClO_4·bcs,[2] *β-mer(N)-trans(Cl,*O_{adao})-[Co(adao)(Cl)(H_2O)]ClO_4, *β-fac(N)*-[Co(adao)(Cl)(H_2O)]ClO_4, *β-mer(N)-cis(O)*-[Co(adao)(NO_2)(H_2O)]ClO_4, and *β-fac(N)*-[Co(adao)(Cl)(NO_2)]. The geometrical structures have been determined on the basis of the absorption spectra, the proton NMR spectra, and the consideration of their preparative processes.

In the case of [Co(adao)XY] type complex, in which two different unidentate ligands (X and Y) occupy the residual two coordination sites, seven geometrical isomers, two *α*, two *β-mer(N)*, two *β-fac(N)*, and *trans*,[3] are possible, as shown in Fig. 1. The isolation of [Co(adao)XY] type complex has not been performed so far. It is necessary to isolate the complexes of [Co(adao)XY] type for the establishment of the stereochemistry of adao-Co(III) complex. In a previous paper,[1] it was reported that the deep crimson [Co(adao)(Cl)(H_2O)]ClO_4 was used as the starting material for the preparation of [Co(adao)X_2] type complexes. However, the structure of the deep crimson aquachloro isomer could not be decided yet. For its structural determination, it is essential to isolate many various kinds of [Co(adao)XY] isomers as well as the other aquachloro isomers.

In addition, two kinds of *β-mer(N)* racemic isomers with different configurations of the adao's secondary amine (*s*-N) were isolated in some complexes of [Co(adao)X_2] type (X=NO_2^- and Cl^-), as was described in the previous paper.[1] When the configurations of *s*-N in [Co(adao)XY] type complexes are considered, twelve kinds of racemic isomers are possible: namely, two *α*, four *β-mer(N)*, *four β-fac(N)*, and two *trans* ones. As an example, the *s*-N configurations of *Λ-β-mer(N)*-[Co(adao)XY] are shown in Fig. 2. Thus, the following four *β-mer(N)* racemic isomers are able to exist: *trans*(X,O_{adao})-($R_{N_1^s}S_{N_2^p},S_{N_1^s}R_{N_2^p}$), *trans*($X,O_{adao}$)-($R_{N_1^s}$-$R_{N_2^p},S_{N_1^s}S_{N_2^p}$), *cis*($X,O_{adao}$)-($R_{N_1^s}S_{N_2^p},S_{N_1^s}S_{N_2^p}$), *cis*($X,O_{adao}$)-($R_{N_1^s}R_{N_2^p},S_{N_1^s}S_{N_2^p}$).[4-6] Therefore, the isolations of isomers with the different *s*-N configurations are attempted also in [Co(adao)XY] type complex.

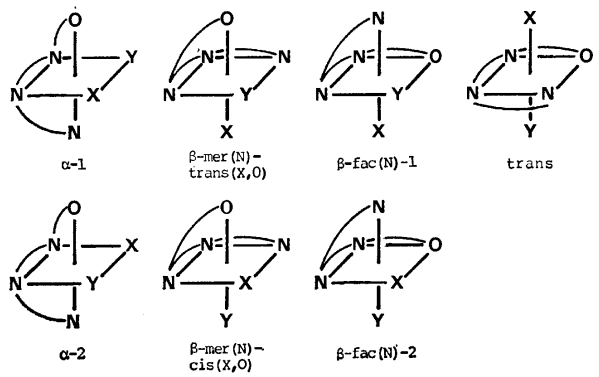

Fig. 1. The possible geometrical isomers of [Co(adao)-XY] type complex.

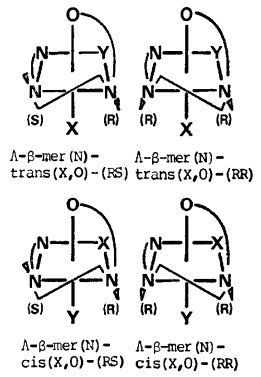

Fig. 2. The possible isomers of *Λ-β-mer(N)*-[Co(adao)-XY] under consideration of *s*-N configurations.

Experimental

Preparations of Complexes. *(1) β*-mer(N)-[*Co(adao)(Cl)(*H_2O*)*]ClO_4: The crude [Co(adao)Cl_2] (50 g)[1] was suspended in 400 cm^3 of 1 M (1 M=1 mol dm^{-3}) $HClO_4$, and the suspension was heated at about 65 °C in a water bath. The gray starting materials began to dissolve, at the same time the deep crimson crystals appeared. After the reaction mixture was allowed to stand at 65 °C for 20 min, it was cooled in an ice bath, and then filtered. The crystals were washed with a mixture of ethanol and ether (1:1). Upon recrystallization from 0.1 M $HClO_4$, *β-mer(N)*-[Co(adao)-Cl)(H_2O)]ClO_4 precipitated as deep crimson crystals. Yield, 40 g.

Found: C, 19.32; H, 4.35; N, 11.28%. Calcd for [Co(adao)(Cl)(H_2O)]ClO_4=$CoC_6H_{16}N_3O_7Cl_2$: C, 19,37; H, 4.33; N, 11.29%.

(2) β-fac(N)-[*Co(adao)(Cl)(*H_2O*)*]ClO_4: Method A, from the crude *β-fac(N)*-[Co(adao)Cl_2]; The reserved filtrate, which was obtained in the preparation of the crude [Co(adao)Cl_2] as described in the previous paper,[1] was concentrated on a water bath with the aid of an air stream, whereupon the brown material appeared. After the product was cooled, the brown material was filtered off. The procedures of concentration and removal were repeated two or three times. When the last deep blue filtrate obtained was further evaporated with the same method mentioned

above, tarry material was obtained. To this tarry material, ethanol (≈100 cm³) was added. When the mixture was stirred with a glass rod, the spherical oily material was sedimented. The blue supernatant solution was decanted. When the oily material was washed two times with 50 cm³ portions of ethanol by decantation, it changed to a crystalline material. These crystals were collected on a filter, and then washed with ethanol. Yield, 3 g. Although recrystallization was repeated, it was found that the blue crystals were not composed of pure *β-fac(N)*-dichloro isomer. This blue crystal will be named as the "crude *β-fac(N)*-[Co(adao)-Cl_2]" in the subsequent part.

The crude *β-fac(N)*-[Co(adao)Cl_2] (3 g) was suspended in 10 cm³ of water, and then 5 cm³ of 2 M $HClO_4$ was added to the suspension. The mixture was concentrated on a water bath with the aid of an air stream. Furthermore, 10 cm³ of water and 5 cm³ of 2 M $HClO_4$ were added to this concentrated product, and then the mixture was concentrated by the method mentioned above. When the treatment was repeated two or three times, pink red crystals began to appear. These crystals were dissolved in about 10 cm³ of water, and the solution was filtered once. The filtrate was concentrated by the same method until the crystals appeared. The pink red crystals were separated by filtration, and then washed with ethanol and ether. Yield, 0.15 g.

Found: C, 18.46; H, 4.49; N, 10.83%. Calcd for [Co(adao)(Cl)(H_2O)]$ClO_4 \cdot H_2O = CoC_6H_{18}N_3O_8Cl_2$: C, 18.48; H, 4.65; N, 10.77%.

Method B, from *β-fac(N)*-[Co(adao)(Cl)(NO_2)]; To the suspension of *β-fac(N)*-[Co(adao)(Cl)(NO_2)] (0.3 g) in 5 cm³ of water (whose preparative method will be described in the following procedure (*6*)) was added 1 cm³ of 1 M $HClO_4$ drop by drop. The suspension was concentrated to dryness on a water bath under an air stream. After the product was allowed to stand at room temperature for some time, 5 cm³ of water and 2 cm³ of 1 M $HClO_4$ were added to the product, and then the mixture was concentrated to dryness again. This treatment was repeated once more to force the aquation of the starting material to completion. The product was dissolved in 10 cm³ of water, and then filtered. The filtrate was evaporated until pink red crystals began to deposit out. After cooling, the crystals were collected on a filter, and then washed with ethanol and ether. Yield, 0.25 g. The identity of this crystal and the pink red isomer obtained in the Method A was checked by the absorption spectra.

Method C, the chromatographic separation of the product obtained from the crude *β-fac(N)*-[Co(adao)Cl_2]; The crude *β-fac(N)*-[Co(adao)Cl_2] (3 g) was suspended in 10 cm³ of water, and then 5 cm³ of 2 M $HClO_4$ was added. The mixture was treated with the method described in the Method A. After the violet precipitate obtained was removed by filtration, the filtrate was diluted with 10 cm³ of water. To the diluted solution was added ethanol, whereupon pink red crystals were deposited. After the removal of these crystals by filtration, the filtrate obtained was poured into a column (ϕ 50 mm × l 400 mm) containing a gel ion-exchange (SP-Sephadex C-25, Na^+ form). The column was swept with water, and then the adsorbed band at top of the column was eluted with an aqueous sodium perchlorate solution. By elution with 0.01—0.06 M $NaClO_4$, the adsorbed band was progressively separated into six bands, which were deep crimson (I), pink red (II), red (III), violet red (IV), red (V), and red (VI), in the order of elution. From their absorption spectra, it was found that these eluates contained the following isomers. Of the earlier two eluates, (I) consisted of *β-mer(N)*-[Co(adao)(Cl)(H_2O)]$^+$, and (II), *β-fac(N)*-[Co(adao)(Cl)(H_2O)]$^+$. In the case of the middle two eluates, it was certain that (III) was composed of *β-mer(N)*-[Co(adao)(H_2O)$_2$]$^{2+}$, although the structure of the isomer contained in (IV) could not be determined. Each of the latter two eluates ((V) and (VI)) consisted of an isomer with the dimeric structure. For the isolation of *β-fac(N)*-[Co(adao)(Cl)(H_2O)]ClO_4, (II) (≈3 dm³), which was eluted with 0.01 M $NaClO_4$, was concentrated to about 5 cm³ in a rotary evaporator below 40 °C. This concentrated solution was allowed to stand overnight in a refrigerator, whereupon the pink red needles were precipitated. After filtration, these were washed with ethanol, and then with ether. Yield, 0.1 g.

It was found that the visible absorption spectrum of the isolated isomer is identical to that of the pink red one in Method A or B.

(3) *β*-mer(N)-trans(Cl,O_{adao})-[*Co(adao)(Cl)(NH_3)*]ClO_4: To the suspension of *β-mer(N)*-[Co(adao)(Cl)(H_2O)]ClO_4 (3.8 g) in 20 cm³ of water was added 2 cm³ of 14% ammonia, and then the mixture was heated at 75 °C for 3 h with stirring. After cooling, deposited crystals were filtered off. The filtrate was evaporated at 50 °C with the aid of an air stream until the pale brown crystals began to appear. The product was cooled and filtered. The crystals collected on a filter were washed with ethanol and ether. Yield, 0.5 g. The filtrate which was obtained in this stage was reserved for the isolation of another isomer.

Recrystallization of the pale brown crystals was carried out by the method of fractional extraction with hot (≈75 °C) 0.1 M $HClO_4$ as follows. The first and the second extracts were cooled in an ice bath, whereupon the pale brown crystals with enough purity deposited out. They were washed with ethanol and ether. The total yield was about 0.3 g.

When the reserved filtrate (≈5 cm³) was further evaporated, reddish brown crystals deposited out. After cooling, they were collected on a filter, and then washed with ethanol. Yield, 1.5 g. They were recrystallized by a method similar to that described above. The total yield was about 0.2 g.

Found: C, 19.35; H, 4.70; N, 15.45% for the pale brown isomer; C, 19.10; H, 4.70; N, 15.57% for the reddish brown one. Calcd for [Co(adao)(Cl)(NH_3)]$ClO_4 = CoC_6H_{17}N_4O_6Cl_2$: C, 19.42; H, 4.62; N, 15.10%.

The reaction in the presence of active charcoal was also carried out. However, only one reddish brown isomer could be isolated together with *β-mer(N)*-[Co(adao)(NH_3)$_2$](ClO_4)$_2$.[7]

(4) *β*-mer(N)-trans(Cl,O_{adao})-[*Co(adao)(Cl)(py)*]ClO_4: To the suspension of *β-mer(N)*-[Co(adao)(Cl)(H_2O)]ClO_4 (1.9 g) in 10 cm³ of water was added 1 cm³ of pyridine, and then the mixture was stirred at ≈80 °C for 2 h. After that, the product was cooled in an ice bath, whereupon reddish brown needles precipitated. The crystals were separated by filtration, and then washed with ethanol. The yield of first precipitate was about 0.9 g.

When the filtrate was concentrated furthermore at 40 °C, massive crystals with a dull reddish brown color began to deposit out. After cooling, they were filtered and washed with ethanol. The yield of second precipitate was about 0.4 g.

Recrystallization was carried out by the fractional extraction as follows; the first precipitate was extracted with three 3 cm³ portions of hot (≈75 °C) 0.1 M $HClO_4$. Of these three extracts, the first and second extracts gave the pure reddish brown needles. The total yield was about 0.15 g. The second precipitate was extracted with five 2 cm³ portions of hot 0.1 M $HClO_4$. All these extracts

gave pure dull reddish brown massive crystals. The total yield was about 0.3 g.

Found: C, 30.33; H, 4.71; N, 13.39% for the reddish brown isomer; C, 30.09; H, 4.65; N, 13.40% for the dull reddish brown one. Calcd for $[Co(adao)(Cl)(py)]ClO_4$= $CoC_{11}H_{19}N_4O_6Cl_2$: C, 30.50; H, 4.42; N, 12.94%.

(5) β-mer(N)-trans(O)-*[Co(adao)(H_2O)(py)]ClO_4·bcs·$2H_2O$*:*[2] The author's carbonato complex (3 g)[8] was suspended in 15 cm³ of water. After 3.5 cm³ of 6 M $HClO_4$ was added to the suspension, pyridine (3.5 cm³) and active charcoal (0.5 g) were added in this order. The mixture was heated at 55 °C for 7 h with mechanical stirring. After the charcoal was separated on a filter, it was washed with two 10 cm³ portions of hot water (≈80 °C). The washings and filtrate were combined, and the combined solution was evaporated to about 25 cm³ at 55 °C in an air stream. After cooling, the first precipitate was filtered off. The filtrate was evaporated again, and then the second precipitate was also removed. On further concentrating, the third precipitate began to appear. After cooling, the precipitate was collected on a filter, and then washed with an ethanol–ether mixture (1:1). Yield, 0.7 g.

The above procedure was repeated three times to get enough crude *trans(O)*-aquapyridine complex deposited as the third precipitate. This crude complex (≈2 g) was dissolved in 20 cm³ of water, and then 10 cm³ of solution containing NH_4bcs (1.3 g)[2] was added to it. After the mixture was heated at 55 °C for 5 min, it was allowed to stand for about 6 h at room temperature. Brown orange crystals deposited out. They were collected on a filter, and then washed with a ethanol–ether (1:1) and with ether. Yield, 0.18 g. The filtrate was kept overnight in a refrigerator, whereupon the same crystals were obtained. Yield, 0.36 g.

Upon recrystallization from 3 cm³ of hot water (≈70 °C) containing the crude diastereoisomer (0.25 g), the pure brown orange crystals were precipitated. Yield, 0.1 g.

Found: C, 33.12; H, 5.18; N, 7.40%. Calcd for $[Co(adao)(H_2O)(py)]ClO_4$·bcs·$2H_2O$ = $CoC_{21}H_{39}N_4O_{13}ClBrS$: C, 33.11; H, 5.16; N, 7.35%.

(6) β-fac(N)-*[Co(adao)(Cl)(NO_2)]*: To the solution of *β-fac(N)*-$[Co(adao)(Cl)(H_2O)]ClO_4$·$H_2O$ (0.1 g) dissolved in 20 cm³ of water was added $NaNO_2$ (0.1 g), and then the mixture was heated at 75 °C for 15 min, whereupon orange crystals began to deposit gradually. After the heating was continued for 10 min more to achieve the complete reaction, the product was cooled. The crystals precipitated were separated by filtration, and then washed with ethanol and with ether. Yield, 0.05 g.

Found: C, 24.25; H, 4.44; N, 18.92%. Calcd for $[Co(adao)(Cl)(NO_2)]$= $CoC_6H_{14}N_4O_4Cl$: C, 23.98; H, 4.70; N, 18.64%.

(7) β-mer(N)-cis(O)-*[Co(adao)(NO_2)(H_2O)]ClO_4*:* The sparingly soluble *β-mer(N)*-$[Co(adao)(NO_2)_2]$ (1.3 g), of which preparative procedure was reported in the previous paper,[1] was covered with 5 cm³ of 2 M $HClO_4$, and then the mixture was heated at about 80 °C on a water bath. When the mixture was heated for 5 min, the starting material began to dissolve, and soon orange crystals began to appear. It was heated for 15 min more to complete the reaction, and then cooled. The crystals were filtered, then washed with ethanol and with ether. Yield, 1.1 g.

They were recrystallized from 5 cm³ of hot water (≈80 °C) by fractional extraction. The first and second extracts gave the pure crystals. The total yield was 0.6 g.

Although the reaction of Collman's dinitro complex[3] and $HClO_4$ afforded also the same isomer, the yield is lower than that in the reaction using this sparingly soluble *β-mer(N)*-dinitro isomer[1] as the starting material.

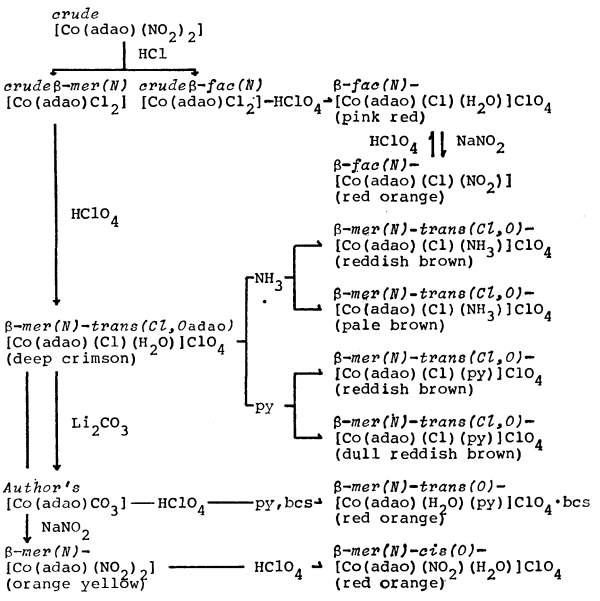

Fig. 3. The preparation scheme of [Co(adao)XY].

Found: C, 18.42; H, 4.47; N, 14.55%. Calcd for $[Co(adao)(NO_2)(H_2O)]ClO_4$= $CoC_6H_{16}N_4O_9Cl$: C, 18.84; H, 4.22; N, 14.64%.

Analyses. The carbon, hydrogen, and nitrogen in the isolated complexes were analyzed at the Microanalysis Center of Osaka University.

Measurements. The visible and ultraviolet absorption spectra were measured with a Shimadzu UV-200 Recording Spectrophotometer using 1 cm or 10 cm silica cells. The IR spectra were recorded with a JASCO IRA-1 Spectrophotometer by a Nujol mull method. The proton NMR spectra were recorded with a Varian XL-100 Spectrometer or a JEOL JNM-4H-100 Spectrometer in deuterium oxide, with *t*-butyl alcohol as the internal reference.

Results and Discussion

Preparative Remarks. As seen in Fig. 3, which shows the preparative scheme of [Co(adao)XY], the two aquachloro isomers with an deep crimson color or a pink red one were mainly used as the starting materials. The deep crimson isomer was isolated from crude *β-mer(N)*-$[Co(adao)Cl_2]$ by the treatment with 1 M $HClO_4$ (*1*), and the pink red one was precipitated from the last blue filtrate containing the crude *β-fac(N)*-dichloro isomer (Method A in *2*) or the *β-fac(N)*-$[Co(adao)(Cl)(NO_2)]$ (Method B in *2*) by using 6 M $HClO_4$ as the selective precipitant or reactant. Similar substitution reactions to that of the crude *β-mer(N)*-$[Co(adao)Cl_2]$ and 1 M $HClO_4$ were observed in the synthesizing reactions of *β-mer(N)-trans(O)*-$[Co(adao)(H_2O)(py)]ClO_4$·bcs (*5*) and *β-mer(N)-cis(O)*-$[Co(adao)(NO_2)(H_2O)]ClO_4$ (*7*). These facts suggest that in the substitution reaction of *β-mer(N)* isomer, the dissociation rates for the two unidentate ligands which are situated in the different coordination sites are different: that is, the unidentate ligand occupying the *cis* site to the "O_{adao}" is more dissociative than the other unidentate ligand occupying the *trans* site.

TABLE 1. ELECTRONIC SPECTRAL DATA OF [Co(adao)XY]

Complex	Color	Ia		Ib		II	
		$\tilde{\nu}_{max}$ / cm^{-1}	ε / (mol^{-1} dm^3 cm^{-1})	$\tilde{\nu}_{max}$ / cm^{-1}	ε / (mol^{-1} dm^3 cm^{-1})	$\tilde{\nu}_{max}$ / cm^{-1}	ε / (mol^{-1} dm^3 cm^{-1})
β-mer(N)-trans(Cl,O)-[Co(adao)(Cl)(NH_3)]ClO_4 [a]	Reddish brown	17500	(66)	21730	(69)	27340	(125)
β-mer(N)-trans(Cl,O)-[Co(adao)(Cl)(NH_3)]ClO_4 [a]	Pale brown	17540	(56)	21670	(84)	sh.	
β-mer(N)-trans(Cl,O)-[Co(adao)(Cl)(py)]ClO_4 [a]	Reddish brown	17580	(65)	21550	(83)	26880	(132)
β-mer(N)-trans(Cl,O)-[Co(adao)(Cl)(py)]ClO_4 [a]	Dull reddish brown	17570	(59)	21510	(89)	sh.	
β-mer(N)-trans(O)-[Co(adao)(H_2O)(py)]ClO_4·bcs	Brown orange	≈18900		21790	(98)	28140	(110)
β-mer(N)-trans(Cl,O_{adao})-[Co(adao)(Cl)(H_2O)]ClO_4 [b]	Deep crimson	≈17200		19830	(94)	25830	(132)
β-fac(N)-[Co(adao)(Cl)(H_2O)]ClO_4 [a]	Pink red	19140	(137)			27030	(149)
β-mer(N)-cis(O)-[Co(adao)(NO_2)(H_2O)]ClO_4	Red orange	20750	(182)			29760 (1652) [c]	
β-fac(N)-[Co(adao)(Cl)(NO_2)]	Red orange	20830	(180)			30490 (2000) [c]	

a) Measured in 0.1 M $HClO_4$. b) Measured in 0.1 M HCl. c) Nitro specific band.

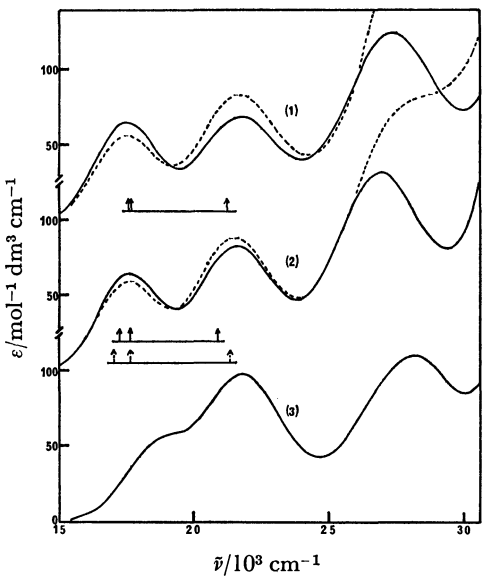

Fig. 4. The absorption spectra of [Co(adao)XY] type complexes and the predicted first band components.
(1): *β-mer(N)-trans(Cl,O_{adao})*-[Co(adao)(Cl)(NH_3)]ClO_4.
——: Reddish brown, - - -: pale brown. a) $\delta(N)=+330$ cm^{-1}, $\delta(O)=-3800$ cm^{-1}, and $\delta(Cl)=-10070$ cm^{-1} are used in the case of solid arrows.
(2): *β-mer(N)-trans(Cl,O_{adao})*-[Co(adao)(Cl)(py)]ClO_4.
——: Reddish brown, - - -: dull reddish brown. b) $\delta(N)=+330$ cm^{-1}, $\delta(O)=-3800$ cm^{-1} are used in the case of solid arrows, and $\delta(N_{adao})=+970$ cm^{-1}, $\delta(O_{adao})=-5190$ cm^{-1}, in the case of dotted arrows.
(3): *β-mer(N)-trans(O)*-[Co(adao)(H_2O)(py)]ClO_4·bcs.
——: Brown orange.

Furthermore, it was recognized that under only the mild reaction conditions, pairs of isomers with the different *s*-N configuration can be isolated in *β-mer(N)-trans(Cl,O_{adao})*-[Co(adao)(Cl)(NH_3)]ClO_4 and *β-mer(N)-trans(Cl,O_{adao})*-[Co(adao)(Cl)(py)]ClO_4, respectively.

The Structures of [Co(adao)(Cl)(NH_3)]ClO_4. As mentioned in procedure (*3*), the reddish brown and pale brown isomers were isolated. Their elemental analyses corresponded well to the composition of [Co(adao)(Cl)(NH_3)]ClO_4. Although there are small differences between their absorption spectra, which are shown in Fig. 4, the spectra show a similar pattern in the region of their first absorption bands. Namely, the positions of two split components are located at 17500 cm^{-1} and 21730 cm^{-1} for the reddish brown isomer, and at 17540 cm^{-1} and 21670 cm^{-1} for the pale brown one (Table 1).

When the following shift parameters, $\delta(N)=+330$ cm^{-1},[9] $\delta(O)=-3800$ cm^{-1},[9] $\delta(Cl)=-10070$ cm^{-1},[10] and $\delta(NH_3)=0$,[9] which were used in the previous paper,[1] are used, the first band components of *β-mer(N)-trans(Cl,O_{adao})*-[Co(adao)(Cl)(NH_3)]$^+$ can be predicted as is shown with the solid arrows in Fig. 4. These predicted components fit approximately to the observed first band maxima. Therefore, the reddish brown and pale brown isomers can be assigned to the *β-mer(N)-trans(Cl,O_{adao})* structure.

However, it is recognized from Fig. 4 that the observed higher wave number components (21730 cm^{-1} for the reddish brown and 21670 cm^{-1} for the pale brown) are located at the higher wave number than the predicted highest one (21220 cm^{-1}). These discrepancies suggest that the practical $\delta(N_{adao})$ in [Co(adao)(Cl)(NH_3)]ClO_4 is larger than $\delta(N)=+330$ cm^{-1} which was used in the above calculation. In order to estimate new adao shift parameter values ($\delta(N_{adao})$ and $\delta(O_{adao})$), the following calculations are made by using the mean value of the corresponding observed split band's positions for two kinds of *β-mer(N)-trans(Cl,O_{adao})*-[Co(adao)(Cl)(NH_3)]ClO_4. In the higher wave number component, the following equa-

tion is written:

$$3/4\,\delta(N_{adao}) + 1/4\,\delta(NH_3) = 21700 - 20970 = +730\ (cm^{-1}) \quad (1)$$

When it is assumed that the lower wave number maximum is observed as the mean of two lower wave number component positions, the following equation also holds.

$$1/2[\{2/4\,\delta(N_{adao}) + 1/4\,\delta(O_{adao}) + 1/4\,\delta(Cl)\} + \{1/4\,\delta(N_{adao}) + 1/4\,\delta(NH_3) + 1/4\,\delta(O_{adao}) + 1/4\,\delta(Cl)\}] = 3/8\,\delta(N_{adao}) + 1/8\,\delta(NH_3) + 1/4\,\delta(O_{adao}) + 1/4\,\delta(Cl) = 17520 - 20970 = -3450\ (cm^{-1}) \quad (2)$$

Because $\delta(NH_3)=0$,[9] the value of $\delta(N_{adao})$ is obtained as $+970\ cm^{-1}$ from Eq. 1. Substituting this value into Eq. 2, the value of $\delta(O_{adao})$ is also obtained as $-5190\ cm^{-1}$. Here, the value of $\delta(Cl)=-10070\ cm^{-1}$ [10] is used.

The Structures of [Co(adao)(Cl)(py)]ClO$_4$. In the case of [Co(adao)(Cl)(py)]ClO$_4$, two isomers with a reddish brown color and dull reddish brown one were isolated. Their absorption spectra are shown in Fig. 4. From their marked splitting patterns, these two isomers are assigned as taking the *β-mer(N)-trans(Cl, O$_{adao}$)* structure.

In Fig. 4, two sets of the predicted first band components of *β-mer(N)-trans(Cl,O$_{adao}$)*-[Co(adao)(Cl)(py)]-ClO$_4$ are represented with the solid arrows and the dotted arrows. The former is predicted by using the following shift parameters: $\delta(N)=+330\ cm^{-1}$, $\delta(O)=-3800\ cm^{-1}$, $\delta(Cl)=-10070\ cm^{-1}$, and $\delta(py)=-1300\ cm^{-1}$ (estimated from *trans*-[CoCl$_2$(py)$_4$]$^+$ [11]). The latter is predicted by the use of new adao shift parameters, $\delta(N_{adao})=+970\ cm^{-1}$, and $\delta(O_{adao})=-5190\ cm^{-1}$. When their predicted first band components are compared with the observed ones, better correspondence is observed between the latter predicted pattern and the observed one. Then, it is attempted to estimate the value of $\delta(py)$ in [Co(adao)(Cl)(py)]ClO$_4$ by using the following equation:

$$3/4\,\delta(N_{adao}) + 1/4\,\delta(py) = 21530 - 20970 = +580\ (cm^{-1}) \quad (3)$$

Substituting the value of $\delta(N_{adao})=+970\ cm^{-1}$ into Eq. (3), $\delta(py)$ is obtained as $-670\ cm^{-1}$.

The Structure of [Co(adao)(H$_2$O)(py)]ClO$_4$·bcs·2H$_2$O. By the use of NH$_4$bcs, this complex could be obtained as the crystalline form for the first time. The measurement of its circular dichroism spectrum suggests that the complex is an optically active one. Its IR spectrum in a Nujol mull shows a band due to bcs$^-$ at 1760 cm^{-1} and a strong broad band due to ClO$_4^-$ around 1100 cm^{-1}.

The first absorption band of brown orange isomer exhibits a sub-peak at the lower wave number side ($\approx$18900 cm^{-1}) of major peak (21790 cm^{-1}), as seen in Fig. 4 and Table 1. From this large splitting pattern, the isomer can be identified as the *trans(O)* one.[12,13] It is found from Fig. 1 that the coordinated adao in the *trans(O)* isomer takes necessarily the *β-mer(N)* coordination mode, and hence [Co(adao)(H$_2$O)-(py)]ClO$_4$·bcs is assigned to the *β-mer(N)-trans(O)* structure. It is an interesting behavior that the intensity of the higher wave number split component is stronger than that of the lower wave number one, which is thought to consist of two components.

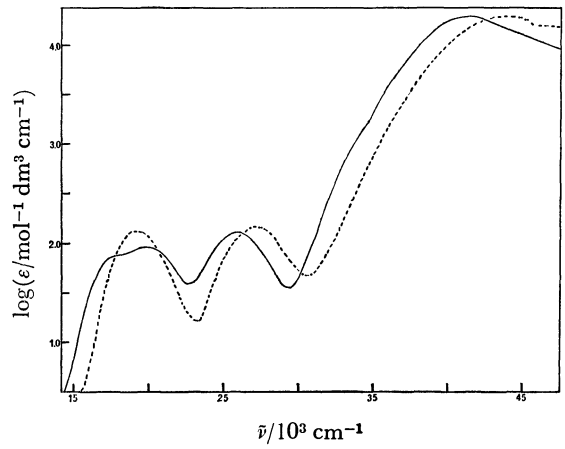

Fig. 5. The absorption spectra of [Co(adao)(Cl)-(H$_2$O)]ClO$_4$.
——: *β-mer(N)*-[Co(adao)(Cl)(H$_2$O)]ClO$_4$ (deep crimson), - - -: *β-fac(N)*-[Co(adao)(Cl)(H$_2$O)]ClO$_4$ (pink red).

In order to estimate the shift parameter of aqua ligand ($\delta(H_2O)$), new shift parameters, $\delta(N_{adao})=+970\ cm^{-1}$, $\delta(O_{adao})=-5190\ cm^{-1}$, and $\delta(py)=-670\ cm^{-1}$, are used. Then, the value of $\delta(H_2O)$ is obtained as $-4210\ cm^{-1}$.

The Structures of [Co(adao)(Cl)(H$_2$O)]ClO$_4$. For the aquachloro complex, two isomers, deep crimson and pink red isomers, were isolated. The elemental analyses of these isomers showed the following compositions: [Co(adao)(Cl)(H$_2$O)]ClO$_4$ for the deep crimson isomer, [Co(adao)(Cl)(H$_2$O)]ClO$_4$·H$_2$O for the pink red one. As seen in Fig. 5 and Table 1, the deep crimson isomer shows the first band with two split components ($\approx$17200 cm^{-1} and 19830 cm^{-1}); the intensity of the higher wave number component is stronger than that of the lower wave number one. The pink red isomer shows the first band without splitting (19140 cm^{-1}). The second absorption maximum of the deep crimson isomer is located at a lower wave number (25830 cm^{-1}) than that of the pink red isomer (27030 cm^{-1}).

When the configuration of *s*-N is ignored, seven geometrical isomers are possible in the complex of [Co-(adao)(Cl)(H$_2$O)]$^+$ (in Fig. 1). In order to predict the first split components for these seven geometrical isomers, the new estimated shift parameters, $\delta(N_{adao})=+970\ cm^{-1}$, $\delta(O_{adao})=-5190\ cm^{-1}$, $\delta(H_2O)=-4210\ cm^{-1}$, which were mentioned above, and $\delta(Cl)=-10070\ cm^{-1}$,[10] are used. In Fig. 6, their predicted components are shown with the solid arrows together with the absorption spectrum of deep crimson isomer.

When the predicted split patterns are compared with the observed first band of deep crimson isomer, the predicted split patterns of three structures, *β-mer(N)-trans(Cl,O$_{adao}$)*, *β-mer(N)-cis(Cl,O$_{adao}$)*, and *trans*, agree with the split pattern of the observed first band. Among the three possible structures, the best coinci-

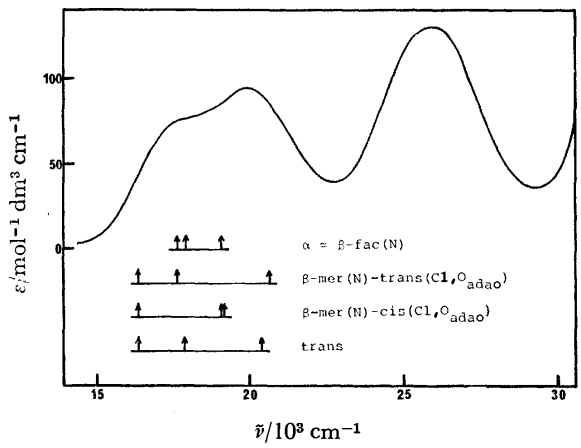

Fig. 6. The absorption spectrum of deep crimson [Co(adao)(Cl)(H_2O)]ClO_4 and the predicted first band components (solid arrows) for the possible geometrical isomers of [Co(adao)(Cl)(H_2O)]$^+$.

dence is observed between the predicted first band components of *trans* structure and the observed first band. However, the possibility of a *trans* structure is excluded, because it was already found that the treatment of this deep crimson isomer with hydrochloric acid gave only *β-mer(N)*-[Co(adao)Cl_2], as was reported in the previous paper.[1] Furthermore, as is shown in Fig. 7, the proton NMR spectrum of deep crimson isomer shows one AB quartet in the range of 2.09 ppm to 3.18 ppm, although the two resonances at the lower field split into two doublets. The value of $\delta_{AB}(=\delta_A-\delta_B)$ is about 0.7 ppm (J_{AB}=18 Hz). As was reported in the previous papers,[1,7,8] this observation of AB quartet pattern due to the adao glycinate ring protons suggests that the deep crimson isomer takes the α or the *β-mer(N)* structure. From the consideration of these proton NMR and absorption spectral patterns, the coordination mode of deep crimson isomer is assigned to the *β-mer(N)* one.

As was mentioned above, the reaction of deep crimson *β-mer(N)*-[Co(adao)(Cl)(H_2O)]ClO_4 and ammonia or pyridine gave *β-mer(N)-trans(Cl,*O_{adao}*)*-[Co(adao)(Cl)(NH_3)]ClO_4 or *β-mer(N)-trans(Cl,*O_{adao}*)*-[Co(adao)(Cl)(py)]ClO_4. These facts indicate that the chloro ligand in the deep crimson isomer occupies the *trans* position to "O_{adao}." Thus, it can be concluded that the structure of deep crimson isomer is the *β-mer(N)-trans(Cl,*O_{adao}*)* one.

In Fig. 5, the absorption spectrum of pink red isomer is shown. From the narrow first absorption band shape, it is recognized that the pink red isomer takes the α or the *β-fac(N)* structure. The proton NMR spectrum of the pink red isomer is shown in Fig. 7. The proton NMR spectrum shows the strong doublet peaks at 1.64 ppm and 1.69 ppm, due to the adao glycinate ring protons. These resonance peaks are located at higher field than those of *β-fac(N)*-[Co(adao)CO_3] (located at 2.73 ppm and 2.41 ppm) and *β-fac(N)*-[Co(adao)mal] (located at 2.35 ppm and 2.29 ppm).[8] In the proton NMR studies of [Co(Hedta)X]$^{n-}$ (X= NO_2^- and H_2O),[14-16] [Co(edta)en]$^-$,[17] and [Co(H_2dtpa)NO_2]$^-$,[18] the resonance peaks of the unco-

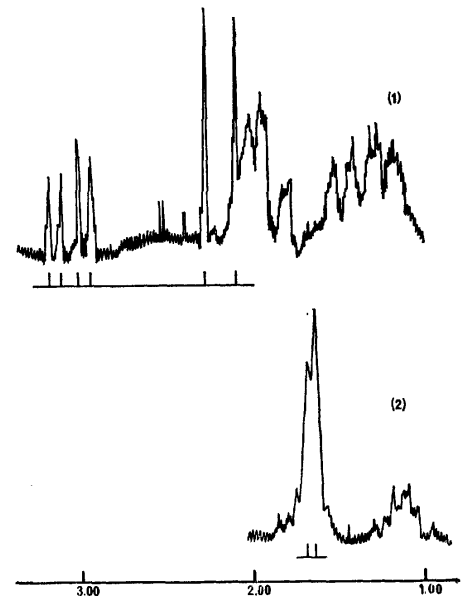

Fig. 7. The proton NMR spectra of [Co(adao)(Cl)(H_2O)]ClO_4.
(1): *β-mer(N)*-[Co(adao)(Cl)(H_2O)]ClO_4 (deep crimson), (2): *β-fac(N)*-[Co(adao)(Cl)(H_2O)]ClO_4 (pink red).

ordinated glycinate ring protons are observed as the singlet or AB quartet pattern in the field region lower than 2.0 ppm. Therefore, some doubts as to whether the adao glycinate ring in the pink red isomer is coordinated to the Co(III) ion or not, still remain.

To clarify the above doubts, a few preparations using the pink red isomer had been achieved as were described in procedure (*5*) and the previous paper.[1] Their isolated complexes have the compositions of [Co(adao)(Cl)(NO_2)] and [Co(adao)Cl_2]. From the facts, it is inferred that the adao glycinate ring is coordinated to the Co(III) ion. As the other experiment, the chromatographic separation was also performed (Method C in *2*). The chromatographic behavior of pink red isomer was similar to that of *β-mer(N)*-[Co(adao)(Cl)(H_2O)]ClO_4. This fact suggests that the pink red isomer is an univalent cation and that the adao glycinate ring is not free. Then, the pink red isomer is tentatively assigned to the *β-fac(N)* structure. However, it is difficult to decide the position of the chloro ligand in the pink red isomer.

The Structure of [Co(adao)(NO_2)(H_2O)]ClO_4.
The reaction of orange yellow *β-mer(N)*-[Co(adao)(NO_2)$_2$][1] and $HClO_4$ gave [Co(adao)(NO_2)(H_2O)]ClO_4. The reaction of α-[Co(adao)(NO_2)$_2$][1] and $HClO_4$ was attempted, but no crystalline complex could be obtained. In Fig. 8, the absorption spectrum of [Co(adao)(NO_2)(H_2O)]ClO_4 is shown.

The proton NMR spectrum of [Co(adao)(NO_2)(H_2O)]ClO_4 shows one AB quartet pattern at 2.01, 2.19, 2.81, and 2.99 ppm. From this observation, the adao coordination mode is the α or the *β-mer(N)* one. The reaction of α-[Co(adao)(NO_2)$_2$] and $HClO_4$ gave no crystals. The structure can thus be assigned to the *β-mer(N)* one. For *β-mer(N)*-[Co(adao)(NO_2)-

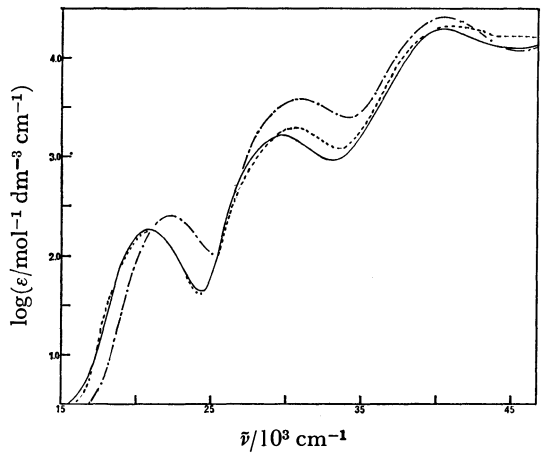

Fig. 8. The absorption spectra of $[Co(adao)(NO_2)(H_2O)]ClO_4$ and $[Co(adao)(Cl)(NO_2)]$.
——: *β-mer(N)*-$[Co(adao)(NO_2)(H_2O)]ClO_4$ (red orange), – – –: *β-fac(N)*-$[Co(adao)(Cl)(NO_2)]$ (red orange), —·—: *β-mer(N)*-$[Co(adao)(NO_2)_2]$ (orange yellow).

$(H_2O)]ClO_4$, the *cis(O)* and *trans(O)* isomers are possible. When $[Co(adao)(NO_2)(H_2O)]ClO_4$ is regarded as a complex of $[CoN_4O_2]$ type, the *trans(O)* isomer shows the more split first absorption band than that of the *cis(O)* one.[12,13] Because the isolated aquanitro isomer exhibits the first absorption band with no remarkable splitting, it is concluded that $[Co(adao)(NO_2)(H_2O)]ClO_4$ takes the *β-mer(N)-cis(O)* structure. The production of *β-mer(N)-cis(O)*-$[Co(adao)(NO_2)(H_2O)]ClO_4$ by the treatment of $[Co(adao)(NO_2)_2]$ with $HClO_4$ indicates that the reactivities of two nitro ligands in *β-mer(N)*-$[Co(adao)(NO_2)_2]$ are different.

The Structure of [Co(adao)(Cl)(NO₂)]. As was mentioned in (*5*), $[Co(adao)(Cl)(NO_2)]$ was obtained as the slightly soluble crystal from *β-fac(N)*-$[Co(adao)(Cl)(H_2O)]ClO_4$ by the treatment with $NaNO_2$. Table 1 (ε=2000 for the chloronitro complex and ε=1652 for the aquanitro one) shows that the isolated complex contains one coordinated nitro ligand. It is also observed that its first absorption maximum is located at a similar wave number region to that of *β-mer(N)-cis(O)*-$[Co(adao)(NO_2)(H_2O)]ClO_4$. The similar absorption band shifts to the higher wave number side are observed as an anomalous absorption spectral behavior also in the other *β-fac(N)* complexes.

Furthermore, it was found that the treatment of $[Co(adao)(Cl)(NO_2)]$ with $HClO_4$ gave *β-fac(N)*-$[Co(adao)(Cl)(H_2O)]ClO_4$. The fact suggests that the reaction of *β-fac(N)*-$[Co(adao)(Cl)(H_2O)]ClO_4$ and $NaNO_2$ proceeds with the configurational retention of adao. This retention reaction supports that the isolated chloronitro isomer takes the *β-fac(N)* structure.

Summary. From the successful isolations of two isomers of *β-mer(N)-trans(Cl,O*$_{adao}$*)*-$[Co(adao)(Cl)(NH_3)]ClO_4$, reddish brown, pale brown, and two isomers of *β-mer(N)-trans(Cl,O*$_{adao}$*)*-$[Co(adao)(Cl)(py)]ClO_4$, reddish brown, dull reddish brown, the existence of two kinds of *β-mer(N)* isomers with the different *s*-N configurations was proved.

By using their definitive split first band maxima, furthermore, the shift parameters of the adao ligating atoms were estimated as $\delta(N_{adao})=+970\ cm^{-1}$ and $\delta(O_{adao})=-5190\ cm^{-1}$ at present. The pyridine shift parameter ($\delta(py)=-670\ cm^{-1}$) and the aqua one ($\delta(H_2O)=-4210\ cm^{-1}$) could also be calculated. On the basis of the absorption band components predicted by the use of these shift parameters and the considerations of the preparative results, the deep crimson $[Co(adao)(Cl)(H_2O)]ClO_4$ could be assigned to the *β-mer(N)-trans(Cl,O*$_{adao}$*)* structure.

Besides the one kind of isolated *β-fac(N)*-$[Co(adao)Cl_2]$,[1] it was also found that the respective *β-fac(N)* isomers can be isolated in $[Co(adao)(Cl)(H_2O)]ClO_4$ and $[Co(adao)(Cl)(NO_2)]$.

The author is sincerely grateful to Professor Yoichi Shimura of Osaka University for the guidance of this work. He also thanks Professor Kashiro Kuroda of Ehime University for his continuing interest and encouragement during the work.

References

1) K. Watanabe, Part III of this series: *Bull. Chem. Soc. Jpn.*, **55**, 427 (1982).
2) The following abbreviations are used for ligands: adao ($^-OOCCH_2NHCH_2CH_2NHCH_2CH_2NH_2$), 8-amino-3,6-diazaoctanate; edta, ethylenediaminetetraacetate; dtpa, diethylenetriaminepentaacetate; en, ethylenediamine; py, pyridine; bcs, $(+)_{589}$-(1*R*,3*S*,4*S*,7*R*)-3-bromocamphor-9-sulfonate.
3) P. W. Schneider and J. P. Collman, *Inorg. Chem.*, **7**, 2010 (1968).
4) R. S. Cahn, C. K. Ingold, and V. Prelog, *Angew. Chem.*, **5**, 385 (1966).
5) The two kinds of *s*-N of adao are discriminated by numbering as follows: $O-N_1-N_2-N$.
6) The two *s*-N dispositions, angular and planar, are represented by using the superscripts of a (angular) and p (planar): N^a or N^p.
7) K. Watanabe and K. Kuroda, *Nippon Kagaku Kaishi*, **1972**, 1409.
8) K. Watanabe, *Bull. Chem. Soc. Jpn.*, **49**, 3068 (1976).
9) J. Fujita and Y. Shimura, *Bull. Chem. Soc. Jpn.*, **36**, 1281 (1963).
10) Y. Shimura and R. Tsuchida, *Bull. Chem. Soc. Jpn.*, **28**, 572 (1955).
11) A. Werner and R. Feenstra, *Ber.*, **39**, 1538 (1906); T. Baba and Y. Shimura provided *trans*-$[CoCl_2(py)_4]Cl$ and its absorption spectral data.
12) Y. Shimura and R. Tsuchida, *Bull. Chem. Soc. Jpn.*, **29**, 311 (1956).
13) K. Kuroda, Y. Mori, H. Matsunaga, K. Kunigita, and K. Watanabe, *Bull. Chem. Soc. Jpn.*, **48**, 234 (1975).
14) J. B. Terril and C. N. Reilley, *Inorg. Chem.*, **5**, 1988 (1966).
15) B. B. Smith and R. H. Betts, *Inorg. Chem.*, **9**, 2858 (1970).
16) G. L. Blackmer and J. L. Sudmeier, *Inorg. Chem.*, **10**, 2019 (1971).
17) M. K. Doh, H. Ogino, J. Fujita, K. Saito, and N. Tanaka, *Chem. Lett.*, **1974**, 1233.
18) B. B. Smith and R. H. Betts, *J. Am. Chem. Soc.*, **91**, 7749 (1969).

Oxidative Synthesis, Optical Resolution, and Characterization of Mixed Sulfenato and Sulfinato Cobalt(III) Complexes

Masakazu KITA,* Kazuaki YAMANARI, and Yoichi SHIMURA

Department of Chemistry, Faculty of Science, Osaka University, Toyonaka, Osaka 560

(Received January 20, 1982)

Twelve new mixed sulfenato and sulfinato cobalt(III) complexes were prepared via successive H_2O_2 oxidation of $[Co(SCH_2CH_2NH_2)_3]$, $[Co\{SCH_2CH(COOCH_3)NH_2\}_3]$, and related complexes. These oxidation products, $[Co(sulfenato\text{-}N,S)_n(sulfinato\text{-}N,S)_{3-n}]$ ($n=3$, 2, 1, and 0), were optically resolved by means of column chromatography or preferential crystallization of a diastereomeric molecular compound with *d*-tartaric acid. The mixed sulfenato and sulfinato complexes show characteristic variation of absorption spectra with the change of "*n*" in $[Co(sulfenato\text{-}N,S)_n(sulfinato\text{-}N,S)_{3-n}]$ ($n=3$, 2, 1, and 0). It is concluded that the (*R*) configuration of the sulfenato group is more stable than the (*S*) one in the *fac*(*S*)-*Λ*-$[Co(sulfenato\text{-}N,S)_n(sulfinato\text{-}N,S)_{3-n}]$.

Owing to the high nucleophilicity of the thiolato sulfur atom coordinated to cobalt(III) ion, the reaction of the thiolato complex with other metal ion, Co^{3+}, Zn^{2+}, Ag^+, *etc.*,[1] or with carbonium ion, CH_3^+, $C_2H_5^+$, $C_6H_5CH_2^+$, *etc.*,[2] yielded easily μ-thiolato or thioether complex, respectively. Furthermore, it has been reported that the successive oxidation of the thiolato cobalt(III) complex generates several sulfur-bonded sulfenato and sulfinato complexes.[3] These complexes are of interest in connection with their kinetic and spectrochemical behaviors. However, no optically active sulfenato or sulfinato complex except $[Co\{S(O)CH_2CH(COOH)NH_2\}(en)_2]^{2+}$ has been reported so far and consequently their stereochemical aspects have not been investigated systematically.

Present study is concerned with the preparation and optical resolution of mixed sulfenato and sulfinato complexes, $[Co(sulfenato\text{-}N,S)_n(sulfinato\text{-}N,S)_{3-n}]$ ($n=3$, 2, 1, and 0), and related complexes. These optically active complexes were obtained by means of three methods, preferential crystallization of a diastereomeric molecular compound, column chromatography, and stereospecific substitution reaction. The complexes were identified from their visible and ultraviolet absorption, circular dichroism (CD), and ^{13}C NMR spectra, and their spectrochemical and stereochemical features were discussed. A preliminary report has been presented.[4]

Abbreviations used for ligands are as follows: Haet, 2-aminoethanethiol $HSCH_2CH_2NH_2$; Haese, 2-aminoethanesulfenic acid $HS(O)CH_2CH_2NH_2$; Haesi, 2-aminoethanesulfinic acid $HS(O)_2CH_2CH_2NH_2$; L-Hcym, L-cysteine methyl ester $HSCH_2CH(COOCH_3)NH_2$; L-cyme, (*R*)-2-amino-2-(methoxycarbonyl)ethanesulfenic acid $HS(O)CH_2CH(COOCH_3)NH_2$; L-Hcymi, (*R*)-2-amino-2-(methoxycarbonyl)ethanesulfinic acid $HS(O)_2CH_2CH(COOCH_3)NH_2$; L-$H_2$cys, L-cysteine $HSCH_2CH(COOH)NH_2$; L-H_2cyse, (*R*)-2-amino-3-sulfenopropanoic acid $HS(O)CH_2CH(COOH)NH_2$; L-H_2cysi, (*R*)-2-amino-3-sulfinopropanoic acid $HS(O)_2CH_2CH(COOH)NH_2$; L-H_2pene, (*R*)-2-amino-3-methyl-3-sulfenobutanoic acid $HS(O)C(CH_3)_2CH(COOH)NH_2$; en, ethylenediamine $NH_2CH_2CH_2NH_2$; *d*-H_2tart, *d*-tartaric acid *d*-$C_4H_6O_6$.

Experimental

Preparation, Separation, and Optical Resolution of Complexes.

(1) $[Co(aese)_n(aesi)_{3-n}]$ *(n=3, 2, 1, and 0)*: To a solution of 3.5 g (30 mmol) of 2-aminoethanethiol hydrochloride in 30 cm^3 of water was gradually added 3.6 g (10 mmol) of $Na_3[Co(CO_3)_3]\cdot 3H_2O$ and the mixture was stirred at 95 °C for 1 h. The blue-green curdy precipitate of $[Co(aet)_3]$ was filtered and washed with water. A stoichiometric amount (21 mmol) of 2.86% aqueous H_2O_2 was added dropwise to suspension of 2.0 g (7 mmol) of $[Co(aet)_3]$ in 25 cm^3 of water with stirring below 5 °C, leading to an orange-red solution instantly. This solution was filtered in order to remove a little amount of unreacted $[Co(aet)_3]$. On addition of acetone (200 cm^3) and ether (200 cm^3) to the filtrate, an orange precipitate was obtained. This was dissolved in a small amount of water, adsorbed on a column (2 cm × 100 cm) of anion-exchange resin (QAE-Sephadex A-25, *d*-tartrate form) and eluted with water. Five colored bands, orange(I), orange(II), orange(III), yellow orange(**IV**), and orange yellow(**V**), were eluted in this order. Bands, II, III, and **IV**, were major products, and I and **V** minor ones. At this stage each of the bands was partially resolved: the earlier eluted fractions of band II, III, **IV**, or **V** showed negative CD at the longest wavelength region of the first d-d absorption band.

The oxidation of eluate II or III by diluted H_2O_2 (*ca.* 2%) produced bands **IV** and V which were separated by column chromatography. Similarly, eluate **IV** generated band **V** and a new yellow band **VI**, and eluate **V** did single band **VI**. The sparingly soluble yellow complex **VI** could also be obtained *via* oxidation of eluate II, III, **IV**, or **V** by an excess 30% H_2O_2. These results indicate that the oxidation process is stepwise in a series of II (or III)→**IV**→**V**→**VI**.

Each eluate was concentrated in a vacuum rotatory evaporator at *ca.* 8 °C to yield the precipitate. The precipitate was collected by filtration and washed with acetone and ether. But the precipitate could not be isolated from eluate I because of the low yield and very hygroscopic property. Complex II partially isomerized into complex III during the crystallization, which was identified by column chromatographic treatment and ^{13}C NMR spectra. It was confirmed from the absorption measurement and the following elemental analyses that complexes II (and III), **IV**, **V**, and **VI** correspond to $n=3$, 2, 1, and 0 of $[Co(aese)_n(aesi)_{3-n}]$, respectively.

Found for II: C, 21.08; H, 5.56; N, 12.25%. Calcd for $[Co(aese)_3]\cdot 0.5H_2O = C_6H_{19}N_3O_{3.5}S_3Co$: C, 20.93; H, 5.56; N, 12.20%. Found for III: C, 19.08; H, 6.12; N, 11.22%. Calcd for $[Co(aese)_3]\cdot 2.5H_2O = C_6H_{23}N_3O_{5.5}S_3Co$: C, 18.94; H, 6.09; N, 11.22%. Found for **IV**: C, 18.39; H, 5.62; N, 10.79%. Calcd for $[Co(aese)_2(aesi)]\cdot 2H_2O = C_6H_{22}N_3O_6S_3Co$: C, 18.61; H, 5.72; N, 10.48%. Found

for **V**: C, 18.50; H, 5.17; N, 10.84%. Calcd for [Co(aese)(aesi)$_2$]·H_2O=$C_6H_{20}N_3O_6S_3Co$: C, 18.70; H, 5.23; N, 10.90%. Found for VI: C, 18.80; H, 4.80; N, 10.90%. Calcd for [Co(aesi)$_3$]=$C_6H_{18}N_3O_6S_3Co$: C, 18.80; H, 4.73; N, 10.96%.

(2) Molecular Compound of III with d-*Tartaric Acid,* d-$C_4H_6O_6$·$(+)^{CD}_{500}$-[*Co(aese)*$_3$]·H_2O *and Its Derivatives*: The optical resolution of III was achieved using *d*-tartaric acid as a resolving agent. Racemate III, [Co(aese)$_3$]·2.5H_2O (1.0 g, 2.76 mmol), was dissolved in an ethanol–water (2:1) mixture and then *d*-H_2tart (0.42 g, 2.76 mmol) was added to the solution. After a few minutes, an orange-red diastereomeric molecular compound, *d*-H_2tart·$(+)^{CD}_{500}$-[Co(aese)$_3$]·H_2O began to deposit as needle-like crystals. The crystals were filtered and washed with ethanol. Found: C, 23.72; H, 5.22; N, 8.35%. Calcd for *d*-H_2tart·$(+)^{CD}_{500}$-[Co(aese)$_3$]·H_2O=$C_{10}H_{26}N_3O_{10}S_3Co$: C, 23.86; H, 5.21; N, 8.35%.

The diastereomeric molecular compound was converted into $(+)^{CD}_{500}$-[Co(aese)$_3$] by treating with an equimolar amount of $Ca(OH)_2$.

Optically pure complexes corresponding to IV, V, and **VI** were prepared by the oxidation of $(+)^{CD}_{500}$-[Co(aese)$_3$]. The CD spectra were measured with the eluates and their concentrations were calculated from the optical densities referring to those of the corresponding racemates. The oxidation products of $(+)^{CD}_{500}$-II were same as those of $(+)^{CD}_{500}$-III.

(3) Partial Resolution of [*Co(aet)*$_3$]: A solution of 1.0 g (2.0 mmol) of *Λ*-[Co(en)$_3$]Br_3·H_2O in 20 cm^3 of water was added to a solution of 0.5 g (6.5 mmol) of 2-aminoethanethiol and of 0.5 g (12 mmol) of sodium hydroxide in 20 cm^3 of water. The mixture was stirred at 70 °C. After a few minutes, the precipitate of [Co(aet)$_3$] which shows optical activity began to deposit. This was filtered and washed with water. Its oxidative derivatives, II, III, **IV**, **V** and **VI**, were obtained according to the same procedure mentioned above and separated by the column chromatography using anion-exchange resin (QAE-Sephadex A-25, Cl^- form). These oxidation products showed positive CD at the longest wavelength region of the first d-d transition band. Their $\Delta\varepsilon$ values were 13.0% compared with those of optically pure complexes $(+)^{CD}_{500}$-III, $(+)^{CD}_{485}$-**IV**, $(+)^{CD}_{468}$-**V**, and $(+)^{CD}_{440}$-**VI**, respectively, which were obtained from the previous two methods. This enantiomer ratio (+)/(−)=1.30 was used to the calculation of the optical purity of $(+)^{CD}_{500}$-II resolved by column chromatography, which was approximately optically pure.

(4) [*Co(*L*-cym)*$_3$]: The procedure employed for this preparation was analogous to that of [Co(aet)$_3$]. To a solution of 8.0 g (47 mmol) of L-cysteine methyl ester hydrochloride in 70 cm^3 of water was gradually added 5.6 g (15.6 mmol) of Na_3[Co(CO_3)$_3$]·3H_2O, and the mixture was stirred at 95 °C for an hour. The blue-green curdy precipitate of [Co(L-cym)$_3$] was filtered and washed with water. Found: C, 29.89; H, 5.32; N, 8.76%. Calcd for [Co(L-cym)$_3$]·H_2O=$C_{12}H_{26}N_3O_7S_3Co$: C, 30.06; H, 5.47; N, 8.76%.

(5) [*Co(*L*-cyme)*$_n$*(*L*-cymi)*$_{3-n}$] (n=*3, 2, 1, and 0*): These complexes were prepared *via* H_2O_2 oxidation of [Co(L-cym)$_3$] and isolated by the analogous column chromatographic technique used for [Co(aese)$_n$(aesi)$_{3-n}$] (*n*=3, 2, 1, and 0).

To a suspension of 2.0 g (4.2 mmol) of [Co(L-cym)$_3$]·H_2O in 30 cm^3 of water was added 20 cm^3 (12.6 mmol) of 6.43% aqueous H_2O_2 with stirring below 5 °C, leading to an orange-red solution. On addition of acetone and ether, an orange precipitate appeared. This was dissolved in a small amount of water, adsorbed on a column (QAE-Sephadex A-25, *d*-tartrate form) and eluted with water. Four colored bands, orange (II′, major), orange (III′, minor), yellow-orange (**IV′**, major), and orange-yellow (V′, minor), were eluted in this order. Each band was composed of single optical isomer. Therefore, this system showed the high stereoselectivity as well as that of tris(L-cysteinato-*N*,*S*)cobaltate(III) (3−).[6] Some yellow-orange bands remained on the column, which seem to be partially hydrolyzed products because of their negative charges. The absorption and CD spectra of bands II′, III′, **IV′**, and V′ correspond to *n*=3, 3, 2, and 1 of [Co(L-cyme)$_n$(L-cymi)$_{3-n}$], respectively. The insoluble yellow complex [Co(L-cymi)$_3$] (**VI′**) was prepared by oxidation of [Co(L-cym)$_3$] with excess 30% H_2O_2. After concentrating each eluate, a small amount of acetone and ether was added to the solution, and the precipitate was filtered off. Complex II′ as well as **II** partially changed into complex III′ during the crystallization, though the other eluates showed no isomerization. Found for II′: C, 26.48; H, 4.98; N, 7.37%. Calcd for [Co(L-cyme)$_3$]·2H_2O=$C_{12}H_{28}N_3O_{11}S_3Co$: C, 26.42; H, 5.17; N, 7.70%. Found for III′: C, 26.98; H, 4.88; N, 7.89%. Calcd for [Co(L-cyme)$_3$]·1.5H_2O=$C_{12}H_{27}N_3O_{9.5}S_3Co$: C, 26.87; H, 5.07; N, 7.83%. Found for **IV′**: C, 26.01; H, 4.78; N, 7.56%. Calcd for [Co(L-cyme)$_2$(L-cymi)]·1.5H_2O=$C_{12}H_{27}N_3O_{11.5}S_3Co$: C, 26.09; H, 4.93; N, 7.61%. Found for **V′**: C, 26.00; H, 4.61; N, 7.56%. Calcd for [Co(L-cyme)(L-cymi)$_2$]·0.5H_2O=$C_{12}H_{25}N_3O_{11.5}S_3Co$: C, 26.18; H, 4.58; N, 7.63%. Found for **VI′**: C, 25.78; H, 4.72; N, 7.52%. Calcd for [Co(L-cymi)$_3$]=$C_{12}H_{24}N_3O_{12}S_3Co$: C, 25.86; H, 4.34; N, 7.54%.

The complex [Co(L-cymi)$_3$] (**VI′**) was easily hydrolyzed in diluted sodium hydroxide solution (0.1 mol dm^{-3}) and the resulting complex had high solubility. The CD and absorption spectra of this hydrolyzed complex were quite similar to those of [Co(L-cysi)$_3$]$^{3-}$.

*(5) Λ-(*R*)- and Λ-(*S*)-*[*Co(aese)(en)*$_2$]$^{2+}$: *Λ*-[Co(aet)(en)$_2$](ClO_4)$_2$ was obtained according to the procedure previously reported.[5] The stoichiometric oxidation of the *Λ*-complex gave an orange solution. After addition of 2-propanol to the solution, an orange precipitate appeared, which showed almost the same CD spectrum as that of *Λ*-(*R*) isomer in [Co(L-cyse)(en)$_2$]$^+$. The filtrate contained *Λ*-(*S*) isomer predominantly. The concentrations of solutions used for CD spectral measurement were determined from the optical densities referring to that of the racemate.

(6) Na_3[*Co(*L*-cysi)*$_3$]: This compound was prepared *via* oxidation of green Na_3[Co(L-cys)$_3$] with excess 30% H_2O_2. The procedure forms the only one isomer stereoselectively.[6] Found: C, 13.63; H, 4.56; N, 5.31%. Calcd for Na_3[Co(L-cysi)$_3$]·11H_2O=$C_9H_{37}N_3O_{23}S_3CoNa_3$: C, 13.87; H, 4.78; N, 5.31%.

(7) K[*Co(aesi)*$_2$*(*L*-cysi)*]: The solution of 2-aminoethanethiol, L-cysteine, and KOH (2:1:4) was added to the solution of $[Co(NH_3)_6]Cl_3$ (a stoichiometric amount). The mixture was heated until no further evolution of ammonia could be detected. Then an excess of 30% H_2O_2 was added to the reaction mixture. After the column chromatography, the desired complex was obtained. Found: C, 16.07; H, 4.29; N, 7.93%. Calcd for K[Co(aesi)$_2$(L-cysi)]=$C_7H_{23}N_3O_{11}S_3CoK$: C, 16.18; H, 4.46; N, 8.07%.

Measurements. The visible and ultraviolet absorption spectra were measured on a Shimadzu UV-200 and a Hitachi 330 spectrophotometers. The CD spectra were recorded on a JASCO MOE-1 spectropolarimeter. The absorption and CD measurements of the complexes were made in aqueous solutions at ambient temperature. The ^{13}C NMR spectra were measured with a Varian XL-100-15 NMR spec-

trometer in D_2O containing dioxane as an internal standard.

Results and Discussion

Optical Resolution. So far only a limited number of neutral complexes have been optically resolved, where the available methods were stereoselective decomposition by bacteria,[7] circular dichromatic excitation,[8] and column chromatography,[9] no preferential crystallization of a diastereomer having been applied. In the present study, three techniques were applied effectively to the optical resolution of neutral complexes $[Co(aese)_n(aesi)_{3-n}]$ (n=3, 2, 1, and 0). The first method is a modification of column chromatography; the anion-exchange resin (QAE-Sephadex A-25) was used as *d*-tartrate form and the eluting solvent was water. In the course of separation, all eluates contain no salt advantageously. The second method is the preferential crystallization of a diastereomeric molecular compound *d*-H_2tart·$(+)^{CD}_{500}$-$[Co(aese)_3]\cdot H_2O$ (molecular compound of III). This is the first case of optical resolution of a neutral complex *via* diastereomer formation. The composition and structure of this diastereomeric molecular compound has been confirmed by the single crystal X-ray structure analysis.[10] The third method is the substitution reaction with partial retention of configuration (see Experimental).

Geometrical Isomerism. The unsymmetrical nature of bidentate ligands such as 2-aminoethanethiol, L-cysteine methyl ester, and L-cysteine leads to the possibility of two geometrical isomers, *fac*(*S*) and *mer*-(*S*), for the tris(bidentate)cobalt(III) complexes of $[Co(N)_3(S)_3]$ type. It has been shown by the investigations of trinuclear derivatives of $[Co(aet)_3]$[1a] that the complex exists only in the *fac*(*S*) form. The visible and ultraviolet absorption spectra of the present starting thiolato complexes $[Co(aet)_3]$, $[Co(L\text{-}cym)_3]$, and $[Co(L\text{-}cys)_3]^{3-}$ are quite similar as shown in Fig. 1. Furthermore, the ^{13}C NMR spectra of their oxidation products, which have a C_3 symmetry, suggest that the starting complexes have *fac*(*S*) geometry. The energy difference between the two isomers, *fac* and *mer*, has been discussed by Burdett, who concluded that the most stable geometry will be *fac* for a low spin d^6 configuration such as $[Co(CN)_3(H_2O)_3]$, $[Cr(CO)_3(PH_3)_3]$, and $[M(CO)_3(P_4S_3)_3]$ (M=Cr and Mo).[11] A similar trend is also found in the tris(bidentate-*N*,*S*)cobalt(III) complexes.

Characterization of $[Co(aese)_n(aesi)_{3-n}]$ *(n=3, 2, 1, and 0).* Table 1 shows the absorption spectral data of the complexes. The absorption spectra of the complexes containing thiolato groups exhibit a characteristic weak band at *ca.* 17000 cm^{-1}.[12] All the oxidation products did not show this band and therefore contain no thiolato group. The intense absorption bands appeared in the near-ultraviolet region (*ca.* 32000—37000 cm^{-1}) indicate that the coordination of sulfur-containing ligands occurs through the sulfur atoms.[3] Complexes II and III, both of which are the precursors of complexes IV, V, and VI in the oxidation reaction, gave the same absorption spectra (Fig. 2). Since the most intense band at *ca.* 27000 cm^{-1} is due to the sulfenato groups,[3] the two complexes

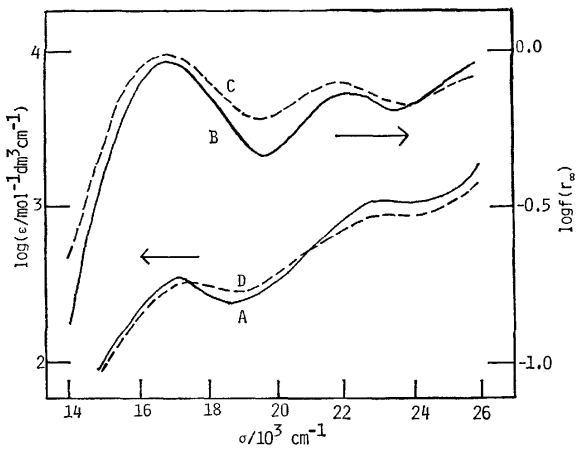

Fig. 1. Absorption spectra of A: $[Co(aet)_3]$ (in aqueous solution), B: $[Co(aet)_3]$ and C: $[Co(L\text{-}cym)_3]$ (in solid diluted by MgO), and D: $[Co(L\text{-}cym)_3]$ (in 0.1 mol dm^{-3} NaOH solution).

Table 1. Absorption data of the complexes

Complex	σ_{max}(log ε)[a]
$[Co(aet)_3]$[b]	17.2, 22.7, 30.8[sh], 36.4
$[Co(aet)_3]$[c]	16.9, 22.4
$[Co(L\text{-}cym)_3]$[c]	17.3, 22.2
$[Co(L\text{-}cym)_3]$[d]	17.4(2.59), 22.9(2.98), 28.7(3.51)[sh], 36.2(4.27)
$[Co(L\text{-}cys)_3]^{3-}$	17.5(2.48), 22.5(2.96), 36.4(4.27)
$[Co(aese)_3]$ (II or III)	21.5(2.92), 27.9(4.21), 37.0(3.76), 42.9(3.80)
$[Co(aese)_2(aesi)]$	22.0(2.96)[sh], 27.3(4.07), 35.6(4.09)
$[Co(aese)(aesi)_2]$	22.0(2.86)[sh], 27.0(3.91), 34.0(4.24)
$[Co(aesi)_3]$	24.4(2.71), 32.8(4.23), 35.7(4.00)[sh]
$[Co(L\text{-}cyme)_3]$ (II′ or III′)	20.9(3.07), 27.3(4.19), 36.1(3.76),
$[Co(L\text{-}cyme)_2(L\text{-}cymi)]$	21.0(2.97)[sh], 26.6(4.06), 35.0(4.07)
$[Co(L\text{-}cyme)(L\text{-}cymi)_2]$[d]	21.6(2.94)[sh], 26.7(4.01), 34.0(4.26)
$[Co(L\text{-}cymi)_3]$[d]	24.5(3.15)[sh], 32.7(4.43), 35.3(4.25)[sh]
$[Co(L\text{-}cysi)(aesi)_2]^-$	24.4(2.89), 32.7(4.50), 35.5(4.32)[sh]
$[Co(L\text{-}cysi)_3]^{3-}$	26.4(2.90), 32.5(4.43), 35.3(4.25)[sh]

a) Wave numbers are given in 10^3 cm^{-1} unit, log ε (in parentheses) in mol^{-1} dm^3 cm^{-1}, and sh means a shoulder. b) The absorption confficient of the complex could not be determined. c) Obtained by diffuse reflection method in 15000—25000 cm^{-1}. d) 0.1 mol dm^{-3} NaOH solution.

can be identified to the diastereomers of $[Co(aese)_3]$. The gradual decrease in molar extinction coefficients at 27000 cm^{-1} along a series of II (or III)→IV→V just corresponds to the decrease in the number of sulfenato groups. Complex VI does not exhibit the 27000 cm^{-1} band and therefore no sulfenato group exists in this complex. The assignments are well supported by the oxidation reaction scheme (Scheme 1). Thus, complexes II (and III), IV, V, and VI correspond to n=3, 2, 1, and 0 of $[Co(aese)_n(aesi)_{3-n}]$, respectively.

The CD spectra of complexes II, III, IV, V, and VI are shown in Figs. 3 and 4 and Table 2. The

a) $[Co(aet)_3] \xrightarrow{3(O)}$ II(or III) $\xrightarrow{(O)}$ IV $\xrightarrow{(O)}$ V $\xrightarrow{(O)}$ VI $\xrightarrow{(O)}$ —

b) $(+)^{CD}_{500}$-II, $(+)^{CD}_{500}$-III $\xrightarrow{(O)}$ $(+)^{CD}_{485}$-IV $\xrightarrow{(O)}$ $(+)^{CD}_{468}$-V $\xrightarrow{(O)}$ $(+)^{CD}_{440}$-VI

c) Λ-(*R*,*R*,*S*)-[Co(aese)$_3$] (II) Λ-(*R*,*R*,*R*)-[Co(aese)$_3$] (III)

Λ-(*R*,*R*)-[Co(aese)$_2$(aesi)] (IV)

Λ-(*R*)-[Co(aese)(aesi)$_2$] (V)

Λ-[Co(aesi)$_3$] (VI)

Scheme 1.

a): Oxidation scheme of racemate complex, b): oxidation scheme of optically active complex, c): assignments.

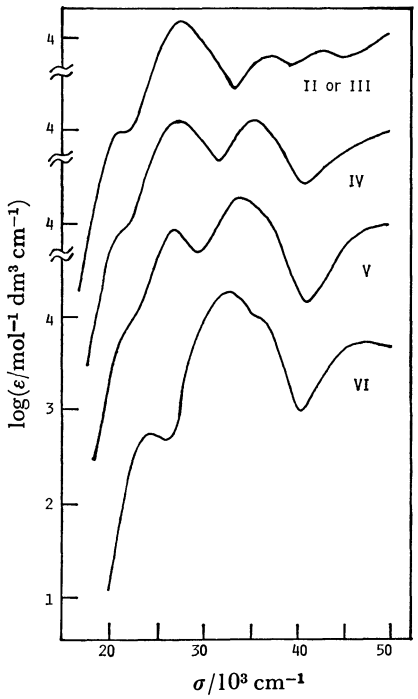

Fig. 2. Absorption spectra of the complexes [Co(aese)$_n$(aesi)$_{3-n}$]: II or III (n=3), IV (n=2), V (n=1), and VI (n=0).

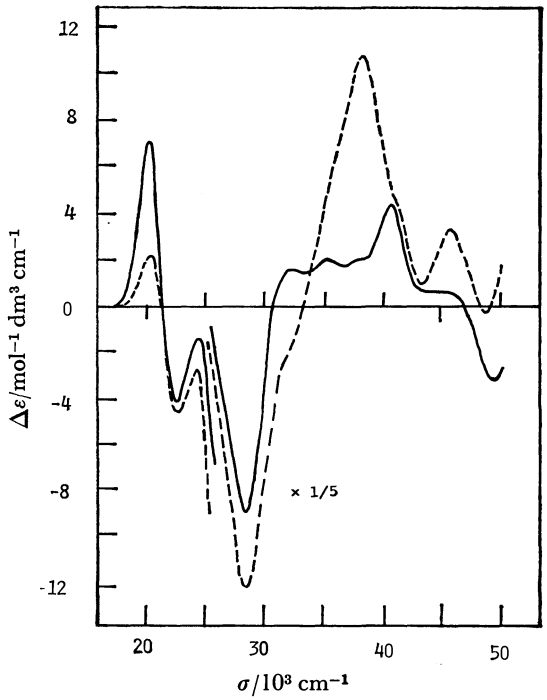

Fig. 3. CD spectra of the complexes $(+)^{CD}_{500}$-II (——) and $(+)^{CD}_{500}$-III (- - -).

complexes containing sulfenato groups should have two CD contributions, one from the configurational chirality based on the skew pair of chelate rings (Δ or Λ) and the other from the chirality based on the asymmetric sulfur donor atoms of sulfenato groups (*S* or *R*). The oxidation of Λ-[Co(aet)(en)$_2$]$^{2+}$ produced two sulfenato diastereomers Λ-(*R*) and Λ-(*S*), whose absorption and CD spectra are shown in Fig. 5. Both complexes showed a positive CD band at the longest wavelength region of the first d-d absorption band, whereas the almost enantiomeric CD patterns appeared in the remaining regions. Similar results have been reported for the oxidation products of Λ-[Co(L-cyse)(en)$_2$]$^+$;[3c] the configurational chirality dominates the CD band at the longest wavelength region of the first d-d absorption band but the CD bands at remaining regions depend on the chirality of sulfenato group. The complexes of $(+)^{CD}_{500}$-II, $(+)^{CD}_{500}$-III, $(+)^{CD}_{485}$-IV, $(+)^{CD}_{468}$-V, and $(+)^{CD}_{440}$-VI are tentatively assigned to the Λ-configuration on the basis of the sign of the longest wavelength CD band (Figs. 3 and 4). The absolute configuration of sulfur center can be characterized on the basis of the CD sign in the sulfenato absorption band region at *ca.* 27000 cm^{-1}; the (*R*) and (*S*) configurations correspond to a negative and a positive band, respectively. The ^{13}C NMR spectrum of complex III showed only two resonances and that complex II six resonances (Fig. 6 and Table 3). Therefore, the *fac*(*S*)-Λ-(*R*,*R*,*R*) configuration can be assigned for Λ-III and the *fac*(*S*)-Λ-(*R*,*R*,*S*) one for Λ-II. The fact that the oxidation of the com-

TABLE 2. CD DATA OF THE COMPLEXES

Complex	$\sigma_{ext}(\Delta\varepsilon)$[a]
Λ-(*R*)-[Co(aese)(en)$_2$]$^{2+}$	19.1(+1.39), 22.7(−2.84), 27.7(−16.90), 35.4(+11.48)
Λ-(*S*)-[Co(aese)(en)$_2$]$^{2+}$	19.8(+2.60), 26.6(+11.71), 35.4(−11.59)
$(+)^{CD}_{500}$-[Co(aese)$_3$] (II)	20.0(+6.96), 22.4(−4.12), 28.1(−44.16), 31.8(+7.58), 35.0(+9.84), 38.0(+10.03), 40.4(+21.78)
$(+)^{CD}_{500}$-[Co(aese)$_3$] (III)	20.0(+2.20), 22.6(−4.56), 28.2(−60.31), 31.4(−4.56)^{sh}, 38.2(+53.33), 41.0(+20.86)^{sh}, 45.6(+16.46), 48.5(−0.85)
$(+)^{CD}_{485}$-[Co(aese)$_2$(aesi)] (IV)	20.6(+1.46), 28.0(−14.04), 35.4(+12.64), 39.0(+11.84), 45.6(+4.90)
$(+)^{CD}_{468}$-[Co(aese)(aesi)$_2$] (V)	21.4(+3.91), 26.4(−19.43), 31.0(−4.98)^{sh}, 35.0(+18.45), 44.6(+7.15)
$(+)^{CD}_{440}$-[Co(aesi)$_3$] (VI)	22.7(+2.04), 25.6(−2.39), 31.7(−10.86), 36.4(+7.86), 46.2(+5.13)
[Co(L-cyme)$_3$] (II′)	19.8(−6.26), 22.1(+4.60), 27.8(+45.10), 30.3(−8.12), 40.4(−13.08), 42.8(−5.32)^{sh}
[Co(L-cyme)$_3$] (III′)	19.6(−0.71), 22.2(+3.90), 27.8(+49.30), 31.3(+7.01)^{sh}, 34.5(−18.80)^{sh}, 38.0(−28.60), 45.0(−19.70)
[Co(L-cyme)$_2$(L-cymi)] (IV′)	20.5(−2.43), 26.6(+24.24), 34.4(−21.74), 39.0(−11.25), 45.6(−7.39)
[Co(L-cyme)(L-cymi)$_2$][b] (V′)	21.1(−3.04), 26.2(+21.17), 30.5(+6.76)^{sh}, 34.4(−16.94), 38.3(−3.90)^{sh}, 41.7(+6.43)
[Co(L-cymi)$_3$][b] (VI′)	22.5(−2.91), 25.8(+5.74), 31.7(+15.11), 35.6(−14.81), 41.2(+6.04), 45.5(+2.42)
[Co(aesi)$_2$(L-cysi)]$^-$	22.7(−2.87), 25.6(+3.21), 31.7(+15.51), 35.7(−13.31), 41.3(+7.59)
[Co(L-cysi)$_3$]$^{3-}$	22.7(−3.16), 25.6(+3.48), 31.8(+17.98), 35.7(−17.20), 41.3(+7.59)

a) Wave numbers are given in 10^3 cm^{-1} unit, $\Delta\varepsilon$ (in parentheses) in mol^{-1} dm^3 cm^{-1}, and sh means a shoulder. b) 0.1 mol dm^{-3} NaOH solution.

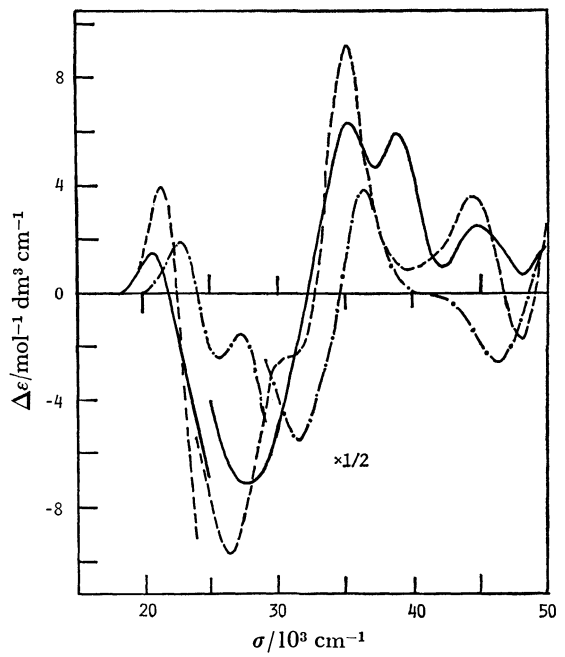

Fig. 4. CD spectra of the complexes $(+)^{CD}_{485}$-IV (——), $(+)^{CD}_{468}$-V (- - -), and $(+)^{CD}_{440}$-VI (—·—).

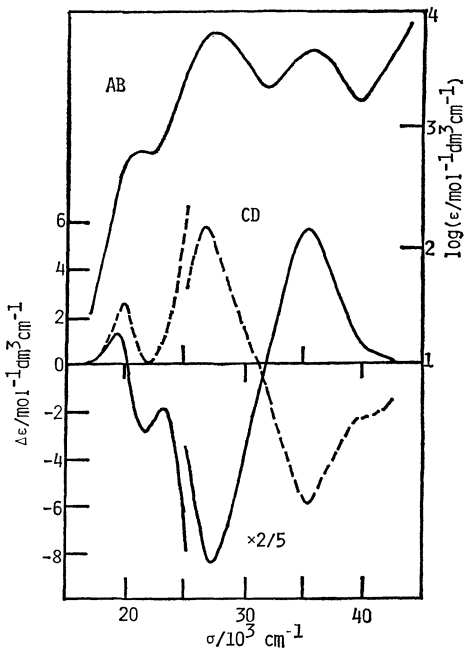

Fig. 5. Absorption and CD spectra of Λ-(*R*)-[Co(aese)-(en)$_2$]$^{2+}$ (——) and Λ-(*S*)-[Co(aese)(en)$_2$]$^{2+}$ (- - -).

plexes Λ-(*R,R,S*)-II and Λ-(*R,R,R*)-III generated the same products leads to an unequivocal assignment of complexes IV and V; $(+)^{CD}_{485}$-IV and $(+)^{CD}_{468}$-V have Λ-(*R,R*) and Λ-(*R*) configurations, respectively. This assignment is consistent with the result of the X-ray single crystal structure analysis of *d*-H$_2$tart·$(+)^{CD}_{500}$-[Co(aese)$_3$]·H$_2$O in which the cobalt(III) complex III has the *fac*(*S*)-Λ-(*R,R,R*) structure.[10]

[*Co*(L-*cyme*)$_n$(L-*cymi*)$_{3-n}$] (n=*3, 2, 1, and 0*). The absorption and CD spectra of complexes II′, III′, IV′, V′, and VI′ (Figs. 7 and 8, and Tables 1 and 2) are similar to those of $(-)^{CD}_{500}$-[Co(aese)$_3$] (II), $(-)^{CD}_{500}$-[Co(aese)$_3$] (III), $(-)^{CD}_{485}$-[Co(aese)$_2$(aesi)] (IV), $(-)^{CD}_{468}$-[Co(aese)(aesi)$_2$] (V), and $(-)^{CD}_{440}$-[Co(aesi)$_3$] (VI), respectively. Furthermore, complex III′ exhibited only four ^{13}C NMR resonances (Table 3), which indicate that complex III′ has the *fac*(*S*)-Λ-(*S,S,S*) structure with C_3 symmetry. The stepwise oxidation scheme of this system is entirely similar to Scheme 1. The assignment of structure is as follows; Λ-(*R,S,S*)-[Co(L-cyme)$_3$] for II′, Λ-(*S,S,S*)-[Co(L-cyme)$_3$] for III′, Λ-(*S,S*)-[Co(L-cyme)$_2$(L-cymi)] for IV′, Λ-(*S*)-[Co(L-

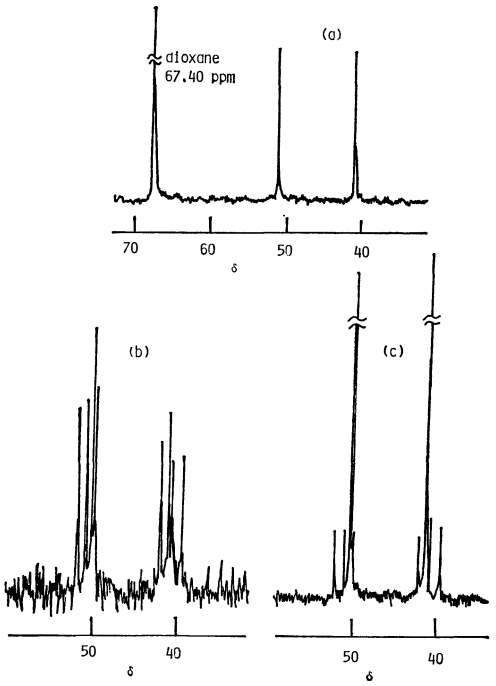

Fig. 6. ^{13}C NMR spectra of the tris(sulfenato) complexes.
(a): III, (b): II (partially isomerized), (c): II+III (1:1).

TABLE 3. CHEMICAL SHIFTS OF ^{13}C NMR SPECTRA[a)]

Complex	δ
$[Co(aese)_3]$ (II)	40.35, 41.65, (42.17), 43.10, 51.69, (52.07), 52.76, 53.97
$[Co(aese)_3]$ (III)	42.17, 52.07
$[Co(L\text{-}cyme)_3]$ (III′)	53.58, 54.34, 55.47, 173.55

a) In D_2O containing *ca.* 80 mg of dioxane (δ=67.40) as an internal standard.

cyme)(L-cymi)$_2$] for V′, and Δ-[Co(L-cymi)$_3$] for VI′. Assuming that the ester group $-COOCH_3$ in L-cym$^-$, L-cyme$^-$, or L-cymi$^-$ ligand takes an equatorial orientation, the chelate ring conformations of Δ- and Λ-complexes become $(lel)_3$ and $(ob)_3$, respectively. Because no Λ-isomer was detected in this [Co(L-cyme)$_n$-(L-cymi)$_{3-n}$] system, the experimental result means that the Δ-$(lel)_3$ conformation is of primary importance to the stability of these complexes.

$[Co(L\text{-}cysi)_3]^{3-}$ and $[Co(aesi)_2(L\text{-}cysi)]^-$ Complexes. The absorption and CD spectra of the complexes, $(-)^{CD}_{440}$-[Co(aesi)$_3$], $(-)^{CD}_{440}$-[Co(L-cysi)$_3$]$^{3-}$, and $(-)^{CD}_{440}$-[Co(aesi)$_2$(L-cysi)]$^-$, are shown in Fig. 9, and Tables 1 and 2. These three complexes and $(-)^{CD}_{440}$-[Co(L-cymi)$_3$] show quite similar absorption and CD spectra to one another. Since $(-)^{CD}_{440}$-[Co(aesi)$_3$] and $(-)^{CD}_{440}$-[Co(L-cymi)$_3$] complexes were assigned to the *fac*(*S*)-Δ structure as described above, two remaining complexes can be assigned reasonably to the same *fac*(*S*)-Δ configuration. The geometry of [Co(L-cysi)$_3$]$^{3-}$ assigned from ^{13}C NMR spectrum[13)] is identical with the present results. Thus, it is concluded that the *ac*(*S*) geometry is preferentially formed for the [Co(N)$_3$(S)$_3$] type complexes and Δ-configuration is significantly stable for the complexes containing L-cysteine or its derivatives.

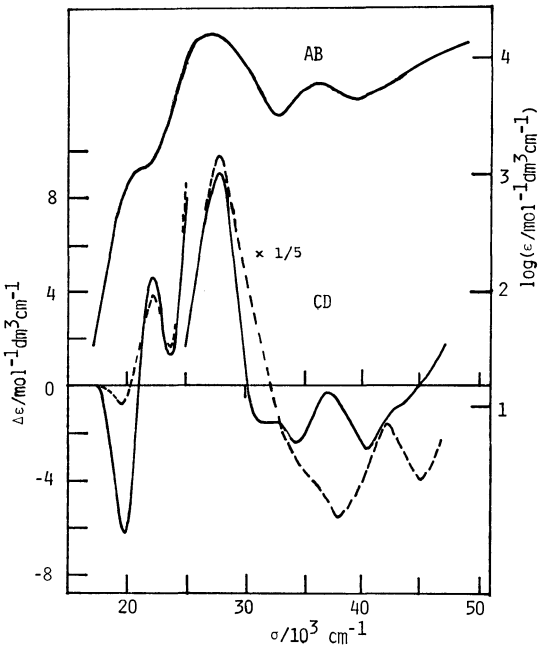

Fig. 7. Absorption and CD spectra of the complexes II′ (——) and III′ (- - -).

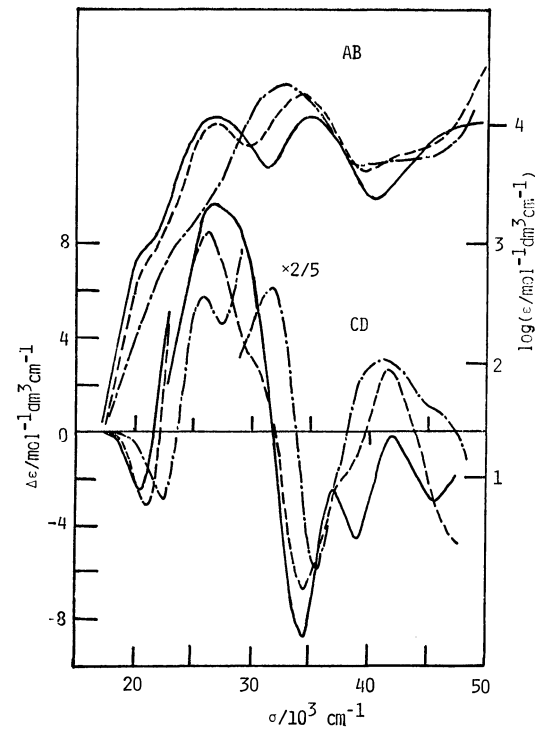

Fig. 8. Absorption and CD spectra of the complexes IV′ (——) in water; V′ (—) and VI′ (—·—) in 0.1 mol dm^{-3} NaOH solution.

Stereoselectivity of Chiral Sulfenato Sulfur Atoms. The $R \rightleftarrows S$ interconversion of sulfenato group was reported in diluted solution of Λ-(*R*)- or Λ-(*S*)-[Co(L-cyse-*N*,*S*)(en)$_2$]$^+$ complex and the equilibrium ratio *S*/*R* became 3.[3c)] The result was explained as fol-

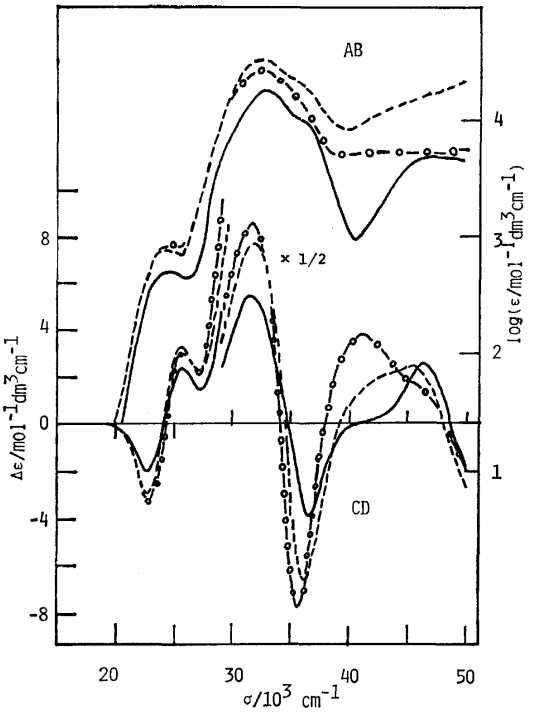

Fig. 9. Absorption and CD spectra of the tris(sulfinato) complexes $(-)^{CD}_{440}$-**VI** (——), $[Co(aesi)_2(L\text{-}cysi)]^-$ (- - -), and $[Co(L\text{-}cysi)_3]^{3-}$ (—○—).

lows; the cobalt–sulfur bond breaking and re-forming occurred to produce the (*S*) configuration, which has lesser steric hindrance toward the ethylenediamine chelate ring because of an equatorial orientation of carboxylate than the (*R*) one. Present systems also showed such interconversions. Complexes II and II′ partially isomerized into complexes III and III′, respectively, during the crystallization in a vacuum rotary evaporator at *ca.* 8 °C. This fact was confirmed by ^{13}C NMR spectra. The spectrum of crystallized complex II was identical to that of a mixture of complexes II and III (Fig. 6 and Table 3). This result was supported by the chromatographic separation. The isomerization of *Δ*-(*R*,*R*,*S*) configuration into *Δ*-(*R*,*R*,*R*) one occurs easily but the reverse does not. Similarily, the crystallized complex II′ was a mixture of complexes II′ and III′, this fact being detected by the ^{13}C NMR spectra (Table 3) and chromatographic separation. The isomerization of *Δ*-(*R*,*S*,*S*) configuration into *Δ*-(*S*,*S*,*S*) one takes place but its reverse change does not occur. Other complexes, *Δ*-(*R*,*R*)-$[Co(aese)_2(aesi)]$, *Δ*-(*R*)-$[Co(aese)_2(aesi)]$, *Δ*-(*S*,*S*)-$[Co(L\text{-}cyme)_2(L\text{-}cymi)]$, and *Δ*-(*S*)-$[Co(L\text{-}cyme)(L\text{-}cymi)_2]$, showed no change even after crystallization.

Figure 10 shows the view of *fac*(*S*)-*Δ*-$[Co(L\text{-}cym)_3]$ projected down the threefold axis. There are six lone pairs on the three sulfur donor atoms, they being divided into two groups, three axial and three equatorial. In the first oxidation process from *fac*(*S*)-$[Co(L\text{-}cym)_3]$ to *fac*(*S*)-$[Co(L\text{-}cyme)(L\text{-}cym)_2]$, the (*R*) and (*S*) configurations will be formed. In the second and third oxidation steps of the remaining sulfur atoms for (*R*)-$[Co(L\text{-}cyme)(L\text{-}cym)_2]$, however, oxygen atom

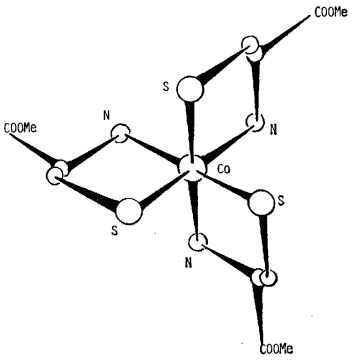

Fig. 10. A perspective view of the *fac*(*S*)-*Δ*-(*lel*)$_3$-$[Co(L\text{-}cym)_3]$ projected down the threefold axis of the complex, the axial or equatorial group on sulfur lone pairs denotes parallel or perpendicular one to the C_3 axis, respectively.

will take preferentially the equatorial position rather than the axial one to avoid the steric interaction with the first sulfenato oxygen. Consequently the (*R*,*S*,*S*) and (*S*,*S*,*S*) configurations will be formed. The consideration agrees with the fact that no *Δ*-(*R*,*R*,*S*) and *Δ*-(*R*,*R*,*R*) isomers occurred in *Δ*-$[Co(L\text{-}cyme)_3]$. The isomerization from *Δ*-(*R*,*S*,*S*) (II′) to *Δ*-(*S*,*S*,*S*) (III′) can be also explained; in the *Δ*-(*S*,*S*,*S*) isomer, all sulfenato oxygens occupy the equatorial positions and the mutual repulsion among them will be weak as compared with *Δ*-(*R*,*S*,*S*) isomer. This argument apparently conflicts with the experimental result that the yield of II′ is significantly higher than that of III′. However, the formation ratio does not reflect the relative stability because the equilibrium state was not realized in our experiment owing to very short reaction time. A similar argument can be also applied to *fac*(*S*)-*Δ*-$[Co(aese)_3]$, in which the *Δ*-(*R*,*R*,*R*) configuration becomes the most stable species.

It has been shown that the oxidation of $[Co(L\text{-}cyse)(en)_2]^+$ or $[Co(L\text{-}pene)(en)_2]^+$ complex proceeds approximately 10^3 times slower than that of the corresponding thiolato complex.[3c] In the present systems of $[Co(L\text{-}cym)_3]$ and $[Co(aet)_3]$, significant amounts of $[Co(L\text{-}cyme)_2(L\text{-}cymi)]$ (*ca.* 50%) and $[Co(aese)_2(aesi)]$ (*ca.* 30%) were nevertheless derived by the very short reaction time, further oxidation products, V′ and VI′ or V and VI, being in small yields. Product IV or IV′ is regarded as the superimposed one of II and III or II′ and III′, respectively. Four oxygen atoms occupy three equatorial and one axial positions and two axial positions remain unoccupied in both complexes. Therefore, the steric hindrance in IV (or IV′) is not largely different from that in II and III (or II′ and III′). On the other hand, complexes V and VI (or V′ and VI′) require the further oxygen attack to the remaining axial positions. Such a process seems to have a large energy barrier.

This work was partly supported by a Grant-in-Aid for Scientific Research No. 547041 from the Ministry of Education, Science and Culture.

References

1) a) D. H. Busch and D. C. Jicha, *Inorg. Chem.*, **1**, 884 (1962); b) M. J. Heeg, R. C. Elder, and E. Deutsch, *ibid.*, **18**, 2036 (1979).

2) R. C. Elder, G. J. Kennard, D. Payne, and E. Deutsch, *Inorg. Chem.*, **17**, 1296 (1978).

3) a) W. G. Jackson, A. M. Sargeson, and P. O. Whimp, *J. Chem. Soc., Chem. Commun.*, **1976**, 934; b) C. P. Sloan and J. H. Kruger, *Inorg. Chem.*, **14**, 1481 (1975); c) D. L. Herting, G. P. Sloan, A. W. Carbral, and J. H. Kruger, *ibid.*, **17**, 1649 (1978); d) I. K. Libson, J. D. Lydon, R. C. Elder, and E. Deutsch, *ibid.*, **18**, 303 (1979).

4) M. Kita, K. Yamanari, and Y. Shimura, *Chem. Lett.*, **1980**, 275.

5) K. Yamanari, J. Hidaka, and Y. Shimura, *Bull. Chem. Soc. Jpn.*, **50**, 2299 (1977).

6) L. S. Dollimore and R. D. Gillard, *J. Chem. Soc., Dalton Trans.*, **1973**, 933.

7) R. D. Gillard, J. R. Lyons, and C. Thorpe, *J. Chem. Soc., Dalton Trans.*, **1972**, 1584.

8) H. Yoneda, U. Sakaguchi, and Y. Nakashima, *Bull. Chem. Soc. Jpn.*, **48**, 1200 (1975).

9) R. C. Fay, A. Y. Girgis, and U. Klabunde, *J. Am. Chem. Soc.*, **92**, 7056 (1970); H. Yoneda and T. Yoshizawa, *Chem. Lett.*, **1976**, 707.

10) M. Kita, K. Yamanari, K. Kitahama, and Y. Shimura, *Bull. Chem. Soc. Jpn.*, **54**, 2995 (1981).

11) J. K. Burdett, *Inorg. Chem.*, **15**, 212 (1976).

12) V. M. Kothari and D. H. Busch, *Inorg. Chem.*, **8**, 2276 (1969).

13) R. D. Gillard, "Optical Activity and Chiral Discrimination," ed by S. F. Mason, D. Reidel Publishing Company, London (1978), Chap. XIV, p. 348.

Effect of Protolytic Behavior of Ligands on Formation Rates of Mono-complexes of Nickel(II) Ion with 2,2′-Bipyridine and 1,10-Phenanthroline in Aqueous Solution

Isao Ando, Shigeyoshi Nishijima,† Kikujiro Ujimoto, and Hirondo Kurihara*

Department of Chemistry, Faculty of Science, Fukuoka University, Nanakuma 11, Jonan-ku, Fukuoka 814-01

(Received January 22, 1982)

The mono-complex formation of nickel(II) ion with 2,2′-bipyridine(bpy) and 1,10-phenanthroline (phen) was studied in aqueous solution by means of a stopped-flow method. The apparent complex formation rates of the Ni(II)–bpy and Ni(II)–phen complexes depended on the pH of the solution. The rate constants of the mono-complex formation with the ligand in the free base form, k_f, and that with the monoprotonated ligand, k_{fh}, were evaluated from the rate-[H$^+$] profiles in the region of high hydrogen ion concentration where the pseudo-equilibrium of acid dissociation of the ligands was attained during the complex formation. The rate constants determined for the Ni(II)–phen were $k_f=(2.6\pm0.3)\times10^3$ mol^{-1} dm^3 s^{-1} and $k_{fh}=2.4\pm0.3$ mol^{-1} dm^3 s^{-1}, which are practically the same as those reported elsewhere. On the other hand, the rate constants for the Ni(II)–bpy were $k_f=(5.3\pm1.2)\times10^3$ mol^{-1} dm^3 s^{-1} and $k_{fh}=5.0\pm2.6$ mol^{-1} dm^3 s^{-1}, which are quite different from the values reported by other researchers. The validity of the present data was discussed in terms of slow proton-transfer reactions of the ligands.

Nickel(II) ion is one of the ions suitable for kinetic studies on complex formation because it has the slowest rate among metal ions which form labile octahedral complexes. In addition, the behavior of this nickel(II) ion is representative. Therefore, the complex formation reactions of nickel(II) ion have been investigated in detail by many workers.[1–17]

Cassatte *et al.*[18] studied the complex formation of nickel(II) ion with a number of ligands involving 2,2′-bipyridine (bpy) and 1,10-phenanthroline (phen). They reported that both the monoprotonated form and the free base form of the ligands take part in the complex formation and that the rate constant with the former is much smaller than that with the latter because of the shielding effect on the reaction site by a proton. The rate constants with the ligand in the two forms were evaluated separately from the rate-[H$^+$] profiles which were obtained by kinetic measurements of apparent rates at various pH, assuming that the pseudo-equilibrium between the two forms of the ligand is attained throughout the complex formation.[18–22]

On the other hand, we have recently found that ligands such as bpy and phen undergo an unexpectedly slow reaction with respect to the proton-transfer process.[23,24] This fact suggests that in the complex formation with bpy and phen there is a region of hydrogen ion concentration where the pseudo-equilibrium of acid dissociation of the ligands is no longer maintained and hence the proton-transfer process of the ligands is a rate-determining step. The rate constants evaluated from the kinetic data in such a hydrogen ion concentration range should be erroneous.

Therefore, this study was undertaken in order to confirm that the rate-determining step interchanges depending on hydrogen ion concentration for the mono-complex formation of nickel(II) ion with bpy and phen. The rate constants of the complex formation were determined in the region of hydrogen ion concentration where the pseudo-equilibrium of acid dissociation holds during the reaction.

Theoretical

With a ligand of weak acids such as bpy and phen, the mono-complex formation of nickel(II) ion in aqueous solution is thought to proceed through both reaction paths, 1 and 2:[18]

$$Ni^{2+} + L \xrightarrow{\text{(rate f)}} NiL^{2+}, \quad (1)$$

$$Ni^{2+} + HL^+ \xrightarrow{\text{(rate fh)}} NiL^{2+} + H^+, \quad (2)$$

where L and HL$^+$ represent the free base form and the monoprotonated form of the ligand, respectively, and (rate f) and (rate fh) denote the rates of the Reactions 1 and 2, respectively. Assuming that the diprotonated species of the ligand, H_2L^{2+}, is negligible and that the equilibrium between HL$^+$ and L,

$$HL^+ \overset{K_2}{\rightleftharpoons} L + H^+, \quad (3)$$

holds in the whole course of the complex formation, the acid dissociation constant, K_2, can be introduced into a rate expression. Since the backward reactions of Eqs. 1 and 2 can be ignored in the early stage of the reaction, the formation rate of the mono-complex is expressed by

$$\begin{aligned} d[NiL^{2+}]/dt &= (k_f[L]+k_{fh}[HL^+])[Ni^{2+}] \\ &= \{(k_f+k_{fh}[H^+]/K_2)/(1+[H^+]/K_2)\}[Ni^{2+}][L'], \end{aligned} \quad (4)$$

where k_f and k_{fh} denote the rate constants of the Reactions 1 and 2, respectively, and [L′] designates the analytical concentration of the ligand. Consequently, the apparent second order rate constant, k_{obsd}, can be correlated with k_f and k_{fh} by

$$k_{obsd}(1+[H^+]/K_2) = k_f + k_{fh}[H^+]/K_2. \quad (5)$$

As long as the equilibrium of Eq. 3 holds during the complex formation, the k_f and k_{fh} values can be evaluated from the k_{obsd} values at various hydrogen ion concentrations according to Eq. 5.

† Present address: Atom Chemical Paint Co. Ltd., Funado, Itabashi-ku, Tokyo 174.

However, Eq. 5 is not applicable when the deprotonation rate of HL^+, (rate dp), or the protonation rate of L, (rate p), in Reaction 3 is slower than the (rate f) or the (rate fh), that is, when the pseudo-equilibrium between HL^+ and L does not hold in progress of Reactions 1 and 2. Namely, the requirement for the applicability of Eq. 5 is

$$\text{(rate dp)} > \text{(rate f) and (rate p)} > \text{(rate fh)}. \quad (6)$$

These four rates for the mono-complex formation in acidic solution are given by

$$\text{(rate f)} = k_f[Ni^{2+}][L], \quad (7)$$

$$\text{(rate fh)} = k_{fh}[Ni^{2+}][HL^+], \quad (8)$$

$$\text{(rate dp)} = k_{dp}[HL^+], \quad (9)$$

and

$$\text{(rate p)} = k_p[H^+][L], \quad (10)$$

where k_{dp} and k_p are the rate constants of the forward and the backward reaction of Eq. 3, respectively. The contribution of hydroxide ion is negligibly small in acidic solution.[23,24] The (rate fh), (rate dp), and (rate p) decrease and the (rate f) increases with lowering hydrogen ion concentration. Therefore, the pseudo-equilibrium of the ligand holds in adequately high hydrogen ion concentration, but it might fail at lower hydrogen ion concentration.

Experimental

Materials and Sample Solutions. Nickel(II) perchlorate was synthesized with nickel(II) carbonate and perchloric acid in the usual way. 2,2′-Bipyridine was purchased from Wako Pure Chemical Ind. and 1,10-phenanthroline monohydrate from Nakarai Chemicals; these ligands were used without further purification. All other chemicals were of guaranteed reagent grade and used without further purification, unless otherwise noted.

The stock solution of nickel(II) ion was prepared by dissolving nickel(II) perchlorate in deionized-distilled water. The concentration was determined by a chelate titration with edta. The stock solution of bpy or phen was prepared by dissolving a weighed amount of it in water. These stock solutions were diluted appropriately for kinetic measurements. The ionic strength of the solution was adjusted to 0.20 mol dm^{-3} with sodium perchlorate except for the case of evaluating the effect of ionic strength on the formation rate constant of the Ni(II)–bpy complex.

Kinetic Measurements. The rates of the complex formation were measured by means of a Union RA-1300 stopped-flow spectrophotometer at 25.0 °C. In order to determine the formation rate of a mono-complex, the concentration of nickel(II) ion to be mixed in the stopped-flow apparatus was one hundred or more times that of the ligand. The pH values of both the nickel(II) ion and ligand solutions to be mixed were adjusted to be the same within the 0.05 pH unit with perchloric acid. The change in absorbance of the mixture was followed at the wavelength at which the absorbance change accompanied by the complex formation was most marked. The optimum wavelength varied slightly depending on the pH of the solution in the vicinity of 314 nm for bpy and 277 nm for phen, respectively.

Both of the nickel(II) ion and ligand solutions were thermally equilibrated at 25.0 °C in separate reservoirs of the stopped-flow apparatus. Equal volumes of them were mixed instantaneously by a pressure-drive device. The change in absorbance of the mixture at the optimum wavelength was stored in a high speed memory unit and displayed on an X-Y recorder as a function of time. The pseudo-first order rate constant was determined from the first order plot of the concentration of mono-complex, $[NiL^{2+}]$, against time. The apparent rate constant of the second order, k_{obsd}, was obtained by dividing the pseudo-first order rate constant by the concentration of nickel(II) ion existing in large excess.

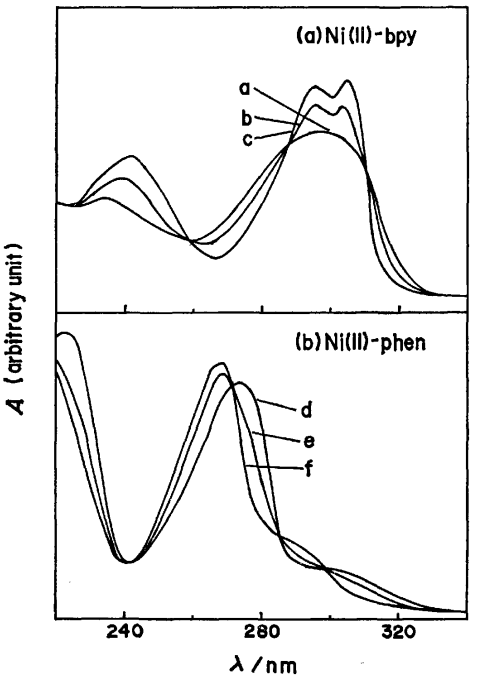

Fig. 1. Rapid scanning spectra of mono-complex of nickel(II) ion with bpy or phen at 25.0 °C. The pHs are 3.99 for the Ni(II)–bpy complex and 1.90 for the Ni(II)–phen complex. Times after mixing: a, 0—10 ms; b, 1.9—2.0 s; c, 7.9—8.0 s; d, 0—10 ms; e, 4.9—5.0 s; f, 10—20 s.

Results and Discussion

Figure 1 shows a typical example of the spectral change of the mixed solution of nickel(II) ion and bpy or phen, measured by a rapid scanning technique during the complex formation. The spectra of c and f in Fig. 1 were identical with those of the mixed solutions at equilibrium which contain nickel(II) ions in large excess to the respective ligands. This indicates that only the mono-complex formation of nickel(II) ion with bpy or phen can be followed spectrophotometrically under the experimental conditions.

The apparent second order rate constant for the Ni(II)–bpy complex formation tended to decrease slightly with the increasing ionic strength from 0.1 to 1.0 mol dm^{-3}. The k_{obsd} values for the Ni(II)–bpy and the Ni(II)–phen complex formations were almost independent of the concentration of nickel(II) ion, as can be seen in Figs. 2 and 3. In contrast to the insensitiveness to the ionic strength and the concentration of nickel(II) ion, the k_{obsd} values varied significantly depending on the pH of the solutions and increased markedly with increasing pH.

Figures 4 and 5 show the plots of $k_{obsd}(1+[H^+]/K_2)$

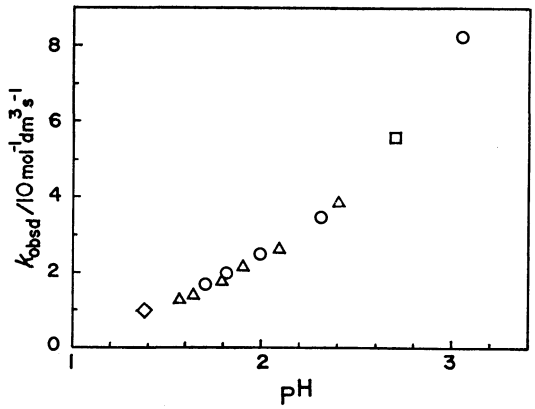

Fig. 2. pH dependence of k_{obsd} values for the Ni(II)–bpy complex. [Ni^{2+}]: □, 5.28×10^{-3}; ○, 9.26×10^{-3}; ◇, 1.06×10^{-2}; △, 2.11×10^{-2} mol dm^{-3}; [bpy]: 5.00×10^{-5} mol dm^{-3}. Temperature: 25.0 °C.

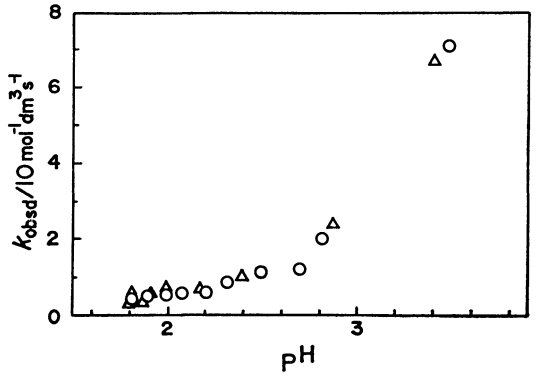

Fig. 3. pH dependence of k_{obsd} values for the Ni(II)–phen complex. [Ni^{2+}]: ○, 5.28×10^{-3}; △, 2.40×10^{-2} mol dm^{-3}; [phen]: 2.50×10^{-5} mol dm^{-3}. Temperature: 25.0 °C.

against $[H^+]/K_2$. For the Ni(II)–bpy system, the plot seems to consist of two straight lines: one in the region of high hydrogen ion concentration, the other in that of low concentration. The boundary of the two regions somewhat changes depending on the concentration of nickel(II) ion. On the other hand, the plot for the Ni(II)–phen system consists approximately of one straight line under the present experimental conditions.

As mentioned in Theoretical, it was assumed in this study that the ligands exist as the monoprotonated form and/or as the free base form. However, if bpy and phen exist partly as a diprotonated species in the range of high hydrogen ion concentration, the rates of the complex formation shall be reduced because of the unreactivity of H_2L^{2+}. Based on the pK_1 values of H_2L^{2+}, 1.5 for bpy and 1.9 for phen, reported by Condike and Martell,[25] the amount of H_2L^{2+} cannot be ignored in the acidic region. Other workers, however, reported the pK_1 values of −0.2——0.5 for bpy[26-30] and −0.9——1.7 for phen.[30-33] Hence, we also determined the pK_1 value of bpy by a spectrophotometric method under the present experimental conditions and obtained the value of −0.35. This pK_1 value, different from that of Condike and Martell, indicates that the H_2L^{2+} species of bpy is

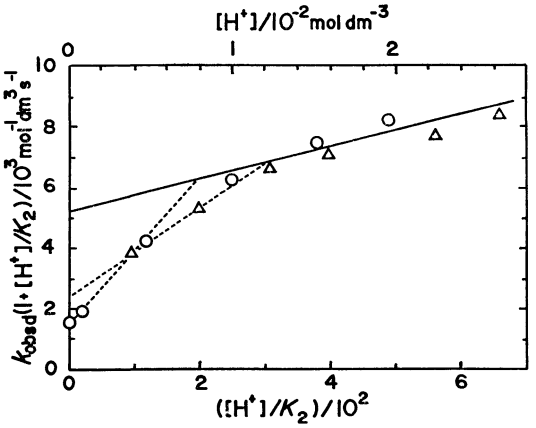

Fig. 4. Plots of k_{obsd} $(1+[H^+]/K_2)$ against $[H^+]/K_2$ for the Ni(II)–bpy complex. Data were taken from Fig. 2. Cross points of solid and broken lines indicate critical points (see text). [Ni^{2+}]: ○, 9.26×10^{-3}; △, 2.11×10^{-2} mol dm^{-3}; [bpy]: 5.00×10^{-5} mol dm^{-3}.

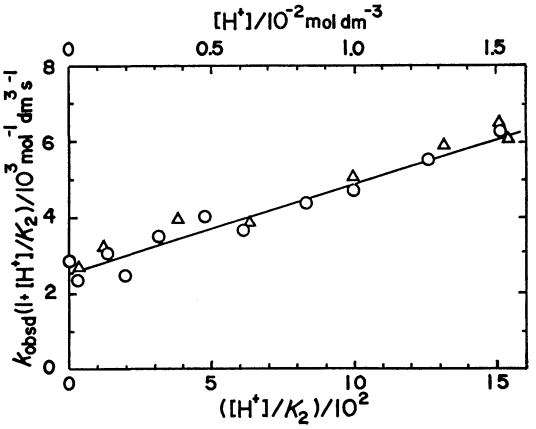

Fig. 5. Plot of k_{obsd} $(1+[H^+]/K_2)$ against $[H^+]/K_2$ for the Ni(II)–phen complex. Data were taken from Fig. 3.
[Ni^{2+}]: ○, 5.28×10^{-3}; △, 2.40×10^{-2} mol dm^{-3}; [phen]: 2.50×10^{-5} mol dm^{-3}.

negligible in the pH region of this study (pH 1.5—5.0). The H_2L^{2+} of phen can be also neglected, because of its pK_1 values of −0.9——1.7 given in the literature.

Consequently, it is concluded that the pseudo-equilibrium of the proton transfer on bpy holds in the region represented by the straight line in the higher hydrogen ion concentration in Fig. 4. The pseudo-equilibrium may fail in hydrogen ion concentrations lower than the cross point of the two straight lines. On the other hand, the pseudo-equilibrium of proton transfer on phen is established in the whole region of hydrogen ion concentration in Fig. 5. Table 1 lists the k_f and k_{fh} values obtained from the intercept and the slope of the linear plot in the high hydrogen ion concentration in Fig. 4 and from those in Fig. 5 by the least-squares method, together with the literature values.

In order to add support to the validity of k_f and k_{fh} determined in the present study, the establishment of the pseudo-equilibria of acid dissociation of the

Table 1. Rate constants of nickel(II) mono complex formation at 25.0 °C

k_f / $mol^{-1}\,dm^3\,s^{-1}$	k_{fh} / $mol^{-1}\,dm^3\,s^{-1}$	Ref.
Ni(II)-bpy		
$(5.3\pm1.2)\times10^3$ a)	5.0 ± 2.6 a)	This work
1.6×10^3		9
1.61×10^3		11
1.6×10^3		16
2.6×10^3	25	18
Ni(II)-phen		
$(2.6\pm0.3)\times10^3$ a)	2.4 ± 0.3 a)	This work
2.95×10^3		11
3.2×10^3		16
3.5×10^3	5.0	18
4.2×10^3	3.0	19

a) These values are shown together with the 0.95 confidence intervals.

ligands were confirmed as follows. The rates of the processes 1 to 3 at $t=0$ were calculated as functions of hydrogen ion concentration according to Eqs. 7 to 10 by use of the k_f and k_{fh} values in this study, the k_{dp} values of bpy and phen in the previous papers,[23,24] and the initial concentrations of the species participating in the reaction. An example of the results is shown in Fig. 6. The $(\text{rate p})_0$ is identical with the $(\text{rate dp})_0$ at $t=0$. Then the $(\text{rate p})_0$ is greater than the $(\text{rate fh})_0$ over the whole range of hydrogen ion concentration investigated. Accordingly, the inequality 6 is satisfied at $t=0$, in the high hydrogen ion concentration where the $(\text{rate dp})_0$ is larger than the $(\text{rate f})_0$. At $t>0$, the (rate p) and (rate dp) values will no longer be identical with each other, owing to the difference in the magnitude between the $(\text{rate f})_0$ and $(\text{rate fh})_0$. The (rate p) and (rate dp) values, however, do not presumably vary so much that the inequality 6 will also fail in the high hydrogen ion concentration. Consequently, the requirement 6 may be satisfied in the hydrogen ion concentrations higher than that at the cross point of the (rate f) and (rate dp) curves. For the Ni(II)–bpy system, the hydrogen ion concentrations at the cross points, $[H^+]_{cp}$, were calculated to be 4.0×10^{-3} mol dm^{-3} at $[Ni^{2+}]=9.26\times10^{-3}$ mol dm^{-3} and 9.2×10^{-3} mol dm^{-3} at $[Ni^{2+}]=2.11\times10^{-2}$ mol dm^{-3}. These values agree approximately with 8.2×10^{-3} mol dm^{-3} at $[Ni^{2+}]=9.26\times10^{-3}$ mol dm^{-3} and 1.2×10^{-2} mol dm^{-3} at $[Ni^{2+}]=2.11\times10^{-2}$ mol dm^{-3}, which were obtained from the critical points deviating from the straight line in the high hydrogen ion concentration in Fig. 4. For the Ni(II)–phen system, the $[H^+]_{cp}$ values were calculated to be 5.4×10^{-4} mol dm^{-3} at $[Ni^{2+}]=5.28\times10^{-3}$ mol dm^{-3} and 2.4×10^{-3} mol dm^{-3} at $[Ni^{2+}]=2.40\times10^{-2}$ mol dm^{-3}. However, no critical point was observed in Fig. 5. Since the $[H^+]_{cp}$ values calculated for the Ni(II)–phen system are small relative to the hydrogen ion concentration investigated, it is likely that the inequality 6 holds in all the hydrogen ion concentration region in Fig. 5. When the pseudo-equilibrium of acid dissociation of ligands is attained, Eqs. 7 and 9 give the following expression with respect to $[H^+]_{cp}$:

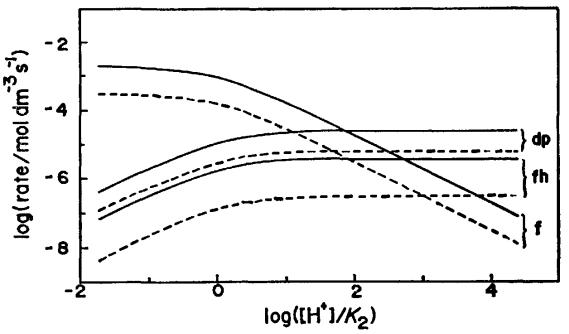

Fig. 6. Relationship between initial rates and $[H^+]/K_2$ at 25.0 °C.
Curve f, (rate f); curve fh, (rate fh); curve dp, (rate dp). Solid lines: for the Ni(II)–bpy complex, $[Ni^{2+}]=9.26\times10^{-3}$, $[bpy]=5.00\times10^{-5}$ mol dm^{-3}; broken lines: for the Ni(II)–phen complex, $[Ni^{2+}]=5.28\times10^{-3}$, $[phen]=2.50\times10^{-5}$ mol dm^{-3}.

$$[H^+]_{cp} = k_f K_2 [Ni^{2+}]/k_{dp}, \quad (11)$$

because the (rate f) is equal to the (rate dp) at the hydrogen ion concentration of $[H^+]_{cp}$. The $[H^+]_{cp}$ value obtained from the plot in Fig. 4 for the Ni(II)–bpy system increased with the increasing nickel(II) ion concentration, in agreement with the prediction of Eq. 11. The appearance of two regions in Fig. 4 can thus be interpreted in terms of the pseudo-equilibrium of acid dissociation of the ligand.

As can be seen in Table 1, the rate constants for the Ni(II)–phen complex obtained in this study agree well with the literature values.[11,16,18,19] In contrast, the k_f and k_{fh} values for the Ni(II)–bpy complex are considerably different from those reported by other workers.[9,11,16,18] This discrepancy is probably attributable to the fact that all the previous data were obtained under the conditions where the pseudo-equilibrium of acid dissociation of bpy failed during the mono-complex formation. Accordingly, it is concluded that the careful examination for the rate-determining step is necessary to evaluate the rate constant of the complex formation especially with ligands showing slow protolytic properties.

The authors wish to thank Professor S. Kida and Associate Professor H. Okawa of Kyushu University for valuable discussions.

References

1) D. W. Margerum, R. I. Bystoff, and C. V. Banks, *J. Am. Chem. Soc.*, **78**, 4211 (1956).
2) R. Hogg and R. G. Wilkins, *J. Chem. Soc.*, **1962**, 341.
3) G. Davies, K. Kustin, and R. F. Pasternack, *Trans. Faraday Soc.*, **64**, 1006 (1968).
4) D. Rablen and G. Gordon, *Inorg. Chem.*, **8**, 395 (1969).
5) K. Kustin and J. Swinhart, *Prog. Inorg. Chem.*, **13**, 107 (1970).
6) R. G. Wilkins, *Acc. Chem. Res.*, **3**, 408 (1970).

7) W. J. Mackellar and D. B. Rorabacher, *J. Am. Chem. Soc.*, **93**, 4379 (1971).
8) D. B. Rorabacher and C. A. Melendez-Cepeda, *J. Am. Chem. Soc.*, **93**, 6071 (1971).
9) H. P. Bennetto and E. F. Caldin, *J. Chem. Soc., A*, **1971**, 2191.
10) F. R. Shu and D. B. Rorabacher, *Inorg. Chem.*, **11**, 1496 (1972).
11) W. S. Melvin, D. P. Rablen, and G. Gordon, *Inorg. Chem.*, **11**, 488 (1972).
12) T. S. Turan and D. B. Rorabacher, *Inorg. Chem.*, **11**, 288 (1972).
13) C.-T. Lin and D. B. Rorabacher, *Inorg. Chem.*, **12**, 2402 (1973).
14) J. F. Coetzee and D. N. Gilles, *Inorg. Chem.*, **15**, 405 (1976).
15) J. F. Coetzee and C. G. Karakatsanis, *Anal. Chem.*, **52**, 59 (1980).
16) R. H. Holyer, C. D. Hubbard, S. F. A. Kettle, and R. G. Wilkins, *Inorg. Chem.*, **4**, 929 (1965).
17) R. H. Holyer, C. D. Hubbard, S. F. A. Kettle, and R. G. Wilkins, *Inorg. Chem.*, **5**, 622 (1966).
18) J. C. Cassatte, W. A. Johnson, L. M. Smith, and R. G. Wilkins, *J. Am. Chem. Soc.*, **94**, 8399 (1972).
19) M. L. Sanduja and W. M. Smith, *Can. J. Chem.*, **47**, 3773 (1969).
20) J. E. Letter, Jr., and R. B. Jordan, *Inorg. Chem.*, **10** 2692 (1971).
21) R. W. Taylor, H. K. Stepien, and D. B. Rorabacher, *Inorg. Chem.*, **13**, 1282 (1974).
22) R. B. Jordan, *Inorg. Chem.*, **15**, 748 (1976).
23) I. Ando, J. Saito, K. Ujimoto, and H. Kurihara, *Fukuoka Univ. Sci. Reports*, **11**, 47 (1981).
24) I. Ando, K. Ujimoto, and H. Kurihara, *Bull. Chem. Soc. Jpn.*, **55**, 713 (1982).
25) G. F. Condike and A. E. Martell, *J. Inorg. Nucl. Chem.*, **31**, 2445 (1969).
26) F. H. Westheimer and O. T. Benfey, *J. Am. Chem. Soc.*, **78**, 5309 (1956).
27) P. Krumholtz, *J. Phys. Chem.*, **60**, 87 (1956).
28) S. Raman, *J. Inorg. Nucl. Chem.*, **37**, 1747 (1975).
29) M. T. Beck and M. Halmos, *Nature*, **191**, 1090 (1961).
30) R. H. Linnell and A. Kaczmarczyk, *J. Phys. Chem.*, **65**, 1196 (1961).
31) O. T. Benfey and J. W. Mills, *J. Am. Chem. Soc.*, **93**, 922 (1971).
32) N. L. Babenko, A. I. Busev, and M. S. Blokh, *Russ. J. Inorg. Chem.*, **17**, 210 (1972).
33) W. A. E. McBryde, *Can. J. Chem.*, **43**, 3472 (1965).

Electron Transfer Activation in the Oxidative Addition of Iodine to Rhodium(I) Complexes

Shunichi Fukuzumi, Nobuaki Nishizawa, and Toshio Tanaka*

Department of Applied Chemistry, Faculty of Engineering, Osaka University, Suita, Osaka 565

(Received February 5, 1982)

The kinetics of the oxidative addition of iodine to the following isocyaniderhodium(I) monomers and dimers in MeCN has been examined; $[Rh(RNC)_4]^+$, $[Rh(RNC)_2(PPh_3)_2]^+$, $[Rh_2(dppm)_2(RNC)_4]^{2+}$, and $[Rh_2(dicp)_4]^{2+}$ (R=alkyl, aryl; dppm=bis(diphenylphosphino)methane; dicp=1,3-diisocyanopropane). The reaction proceeds *via* two consecutive steps which consist of the formation of the initial adduct followed by the intramolecular isomerization to yield the final *trans*-adduct. The kinetic results for the first step of the oxidative addition reactions suggest that there exist three kinds of intermediates formed between the Rh(I) complex and iodine with 1:1, 1:2, and 2:1 stoichiometry prior to the formation of the initial adduct. This mechanism coincides with that for the electron transfer reactions between the Rh(I) complexes and inorganic oxidants such as $[Fe(N\text{-}N)_3]^{3+}$ (N-N=1,10-phenanthroline and 2,2′-bipyridine). The values of the rate constants for the first step of the oxidative addition of iodine to dppm- or dicp-bridged Rh(I) dimers are found to agree with those for the electron transfer reactions between the same reactants by using linear free energy relationships. The possibility of electron transfer activation as the rate determining step in the oxidative addition to Rh(I) complexes is discussed.

Coordinatively unsaturated d^8 metal complexes are converted into octahedral d^6 metal complexes by the oxidative addition of polar or highly polarizable addenda such as alkyl halides RX and halogens X_2.[1,2] Despite extensive studies on the mechanism of the oxidative additions from the importance of their key role in various metal catalyzed processes,[1-3] there has been no simple generalization to predict the reactivities of the metal complexes. Such a situation in organo-transition metal chemistry is in a marked contrast to organic reaction systems, where reactivities of organic substrates have been summarized as a number of linear free energy relationships such as the Taft σ^* constant in electrophilic additions of X_2 to olefins and the Brown σ^+ constant in electrophilic aromatic substitutions with X_2.[4] These constants represent donor properties of substituents of the organic substrates, providing quantitative prediction on the change of reactivities of the substrates with different substituents.[5]

Our aim in this study is to understand the change of the reactivities of d^8 metal complexes in the oxidative addition reactions in terms of the donor properties of d^8 metal complexes with various ligands. The system we chose for study is the oxidative addition of iodine to Rh(I) (d^8) complexes.[6,7] Rhodium(I) complexes were selected since we have previously reported the electrochemistry of Rh(I) complexes as well as the electron transfer reactions with inorganic oxidants[8,9] which revealed the donor properties of the Rh(I) complexes. Thus, the kinetic study on the oxidative addition reactions of the same series of Rh(I) complexes with iodine allows the direct comparison of the reactivities as well as the mechanisms for the oxidative addition reactions with those for the electron transfer reactions of the Rh(I) complexes.

Experimental

Materials. Tetrakis(isocyanide)- and bis(isocyanide)-bis(triphenylphosphine)rhodium(I) perchlorates used in this study were prepared as described previously ($[Rh(RNC)_4]^+$: R=*p*-MeC_6H_4, 2,4,6-$Me_3C_6H_2$, Ph, $PhCH_2$, *t*-Bu, C_6H_{11}; $[Rh(RNC)_2(PPh_3)_2]^+$:R=*p*-$MeOC_6H_4$, 2,4,6-$Me_3C_6H_2$).[8,10] Ligand-bridged complexes of Rh(I) dimer of the $[Rh_2(dppm)_2(RNC)_4](ClO_4)_2$ (dppm=bis(diphenylphosphino)-methane; R=Ph, *p*-$MeOC_6H_4$, *t*-Bu, $PhCH_2$)[11] were prepared by the addition of dppm to a solution of the corresponding $[Rh(RNC)_4](ClO_4)$ in acetone by the procedure analogous to the literature.[7a,9] Another ligand-bridged complex of Rh(I) dimer, $[Rh_2(dicp)_4]Cl_2$ (dicp=1,3-diisocyanopropane),[12] was prepared by the reaction of dicp with [Rh(cyclooctadiene)Cl]$_2$[13] in chloroform. Since the chloride salt formed in the reaction is sparingly soluble in acetonitrile, the tetraphenylborate salt which is soluble in acetonitrile was prepared by methathesis in methanol. Iodine was sublimed three times prior to use. Acetonitrile used as a solvent for kinetic and electrochemical measurements was purified by a standard procedure.[14]

Kinetic Measurements. Acetonitrile solutions of the Rh(I) complexes as well as those of iodine were freshly prepared before use. The reactions of Rh(I) complexes with iodine were carried out at 298 K in the presence of a large excess of either Rh(I) complexes or iodine. Rates of the reactions were measured by monitoring the change of the absorbance (at 360 nm) due to the reaction by using a Union RA-103 stopped-flow spectrophotometer. The ionic strength of the reaction medium was adjusted to 0.1 with *n*-Bu_4NClO_4. The change of the absorbance at 360 nm was expressed as two consecutive pseudo-first-order steps with significantly different half-lives, *e.g.*, the half-life of the first step was 1.2×10^3 times shorter than the second step for the reaction of $[Rh(2,4,6\text{-}Me_3C_6H_2NC)_4]^+$ (2.43×10^{-4} mol dm^{-3}) with iodine (2.72×10^{-3} mol dm^{-3}) in MeCN at 298 K. The two steps were then well separated by changing the monitoring time scale; the first and the second steps were monitored for 50 ms—1 s and 200—1000 s, respectively. The pseudo-first-order rate constants $k^{(1)}$ and $k^{(2)}$ for the first and the second steps were determined from Eqs. 2 and 3, respectively, by the least squares curve fit, using a microcomputer Union System 77;

$$A^{(1)} = A_\infty^{(1)} + (A_0^{(1)} - A_\infty^{(1)}) \exp(-k^{(1)}t) \quad (2)$$

$$A^{(2)} = A_\infty^{(2)} + (A_0^{(2)} - A_\infty^{(2)}) \exp(-k^{(2)}t) \quad (3)$$

where $A^{(1)}$ and $A^{(2)}$ are the absorbances at 360 nm for the first and second steps, respectively, in the two different time scales, $A_0^{(1)}$ and $A_0^{(2)}$ are the initial absorbances, and $A_\infty^{(1)}$ and $A_\infty^{(2)}$ are the final absorbances due to the products in the first and second steps, respectively. It should be noted that $A_\infty^{(1)}=A_0^{(2)}$. It was confirmed that the pseudo-

first-order rate constants $k^{(1)}$ and $k^{(2)}$ were independent of the monitoring wavelengths in the range 340—450 nm.

Cyclic Voltammetry. The cyclic voltammograms (CV) of Rh(I) complexes were obtained as described previously.[9] The CV of iodine in MeCN containing 0.1 mol dm^{-3} *n*-Bu_4NClO_4 as a supporting electrolyte was measured on a Hokuto Denko Model HA-301 potentiostat/galvanostat at 298 K, using a platinum microelectrode and a Ag/Ag^+ ($AgNO_3$ 0.1 mol dm^{-3}) reference electrode. A reversible CV wave was observed at $E_{1/2}=0.34$ V *vs.* Ag/Ag^+ with the peak separation of 0.1 V, which corresponds to the two electron processes; $I_2 \overset{2e}{\rightleftharpoons} 2I^-$.

Results and Discussion

Kinetics and Mechanism of Oxidative Addition of Rh(I) Complexes with Iodine. The final products of the oxidative addition of I_2 to Rh(I) complexes have well been established as the *trans*-adducts (Eq. 4).[6,7] Typical decay curves of the absorbance at 360 nm

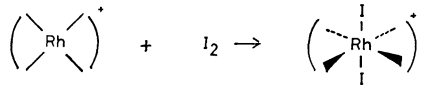

(4)

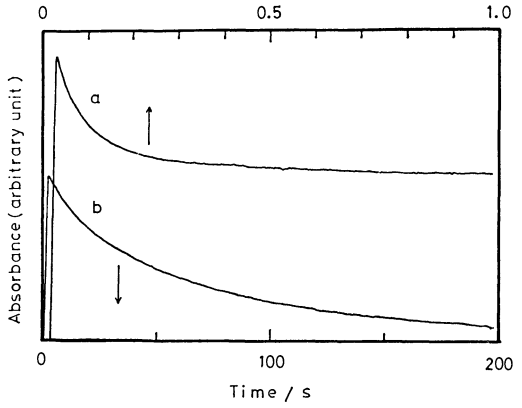

Fig. 1. Decay curves of the absorbance at 360 nm for the reaction of $[Rh(2,4,6\text{-}Me_3C_6H_2NC)_4]^+$ (2.4×10^{-4} mol dm^{-3}) with I_2 (2.7×10^{-3} mol dm^{-3}) in MeCN containing 0.1 mol dm^{-3} *n*-Bu_4NClO_4 at 298 K; a) monitored for 1 s, b) monitored for 200 s.

Table 1. Observed rate constants for the two consecutive steps for the reactions of Rh(I) complexes with excess I_2 in MeCN at 298 K

$[Rh(2,4,6\text{-}Me_3C_6H_2NC)_4]^+$ (mol dm^{-3})	I_2 (mol dm^{-3})	$k^{(1)}$ / s^{-1}	$k^{(2)}$ / s^{-1}
1.1×10^{-5}	1.2×10^{-4}	1.2	1.3×10^{-2}
1.8×10^{-5}	2.0×10^{-4}	2.0	1.3×10^{-2}
3.1×10^{-5}	3.3×10^{-4}	2.4	1.3×10^{-2}
5.1×10^{-5}	5.5×10^{-4}	3.6	1.2×10^{-2}
8.8×10^{-5}	5.9×10^{-4}	2.7	1.3×10^{-2}
8.8×10^{-5}	9.8×10^{-4}	5.1	1.3×10^{-2}
1.5×10^{-4}	1.6×10^{-3}	7.3	1.4×10^{-2}
$[Rh(PhCH_2NC)_4]^+$ (mol dm^{-3})			
5.7×10^{-5}	6.9×10^{-4}	1.7	1.0×10^{-2}
9.5×10^{-5}	1.2×10^{-3}	2.6	1.0×10^{-2}
1.6×10^{-4}	1.9×10^{-3}	3.5	1.0×10^{-2}
2.7×10^{-4}	3.2×10^{-3}	5.3	8.9×10^{-3}

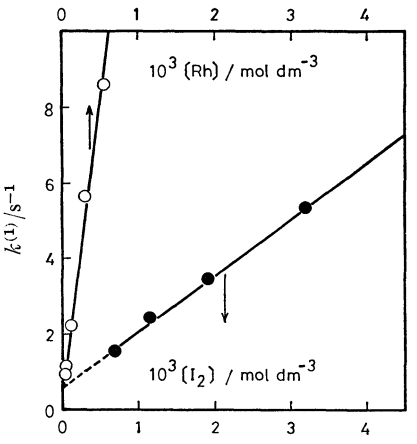

Fig. 2. Kinetics of the oxidative addition of $[Rh(PhCH_2NC)_4]^+$ with I_2; the pseudo-first-order rate constant $k^{(1)}$ for the first step as a function of large excess I_2 (●) or $[Rh(PhCH_2NC)_4]^+$ (○) in MeCN at 298 K.

after mixing $[Rh(2,4,6\text{-}Me_3C_6H_2NC)_4]^+$ and excess I_2 in MeCN at 298 K are shown in Fig. 1, which indicates that the reaction proceeds *via* two consecutive pseudo-first-order steps with different half-lives of 44 ms and 53 s. The reaction rates in the two steps differ from each other sufficiently to allow the determination of both rate constants separately. As shown in Table 1, the pseudo-first-order rate constant $k^{(2)}$ for the second step is independent of the I_2 concentration, while $k^{(1)}$ for the first step varies with the I_2 concentration. Thus, the second step is suggested as an intramolecular process. Since the final product is the *trans*-adduct, the two consecutive steps may consist of the formation of the initial *cis*-adduct followed by the isomerization to the *trans*-adduct (Eqs. 5 and 6). Such an intramolecular *cis-trans* isomerization has

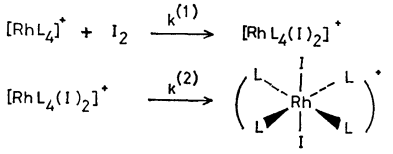

been reported also for transition metal complexes of $[Rh(I)_2(dtc)L_2]$ (dtc=S_2CNMe_2, L=2,4,6-$Me_3C_6H_2$-NC),[6a] $[Cr(CO)_4(C(OMe)Me)(PR_3)]$ (R=C_2H_5, C_6H_{11}),[15] $[Ru(CO)_4(SiCl_3)_2]$,[16] and $[Os(CO)_4$-$(SiMe_3)_2]$.[16]

On the other hand, the pseudo-first-order rate constant $k^{(1)}$ for the first step is linearly dependent on the I_2 concentration as shown in Fig. 2. Thus, the first step may involve a bimolecular process. However, the $k^{(1)}$ values in the presence of large excess Rh(I) complex differ significantly from those in the presence of large excess I_2 when they are compared at the same concentrations as seen in Fig. 2, where the reaction of $[Rh(PhCH_2NC)_4]^+$ with I_2 is illustrated as a typical example. Such different $k^{(1)}$ values suggest that the reactive species are different, depending upon the conditions where either I_2 or the Rh(I) complex is present in large excess. Since the extrapolated $k^{(1)}$ values to the zero concentration in both cases, *i.e.*, the intercepts in Fig. 2, are the same,

Table 2. Rate constants for the reactions of Rh(I) complexes with I_2 and inorganic oxidants in MeCN at 298 K[a)]

No.	Rh(I) Monomer	I_2		$[Fe(phen)_3]^{3+}$ [b)]		$[Co(bpy)_3]^{3+}$ [c)]	
		k_1 / s^{-1}	k_2K_2 / $mol^{-1}\,dm^3\,s^{-1}$	k_1' / s^{-1}	$k_2'K_2'$ / $mol^{-1}\,dm^3\,s^{-1}$	k_1' / s^{-1}	$k_1'K_2'$ / $mol^{-1}\,dm^3\,s^{-1}$
1	$[Rh(p\text{-}MeC_6H_4NC)_4]^+$	8.1×10^{-1}	1.3×10^3	4.6×10	8.5×10^5		
2	$[Rh(2,4,6\text{-}Me_3C_6H_2NC)_4]^+$	6.3×10^{-1}	5.5×10^3	2.0×10	4.3×10^5	1.0×10^{-6}	1.9×10^{-4}
3	$[Rh(PhNC)_4]^+$	9.3×10^{-1}	3.4×10^3	3.2×10	6.1×10^5		
4	$[Rh(PhCH_2NC)_4]^+$	8.5×10^{-1}	1.4×10^3	4.6×10	1.5×10^6		
5	$[Rh(t\text{-}BuNC)_4]^+$	2.8×10^{-1}	1.1×10^3	4.0×10	8.0×10^5	1.5×10^{-6}	1.9×10^{-4}
6	$[Rh(C_6H_{11}NC)_4]^+$	1.3	1.5×10^3	7.2×10	8.1×10^5		
7	$[Rh(p\text{-}MeOC_6H_4NC)_2(PPh_3)_2]^+$	2.3	1.3×10^3	4.0×10	3.5×10^5		
8	$[Rh(2,4,6\text{-}Me_3C_6H_2NC)_2(PPh_3)_2]^+$	2.1	1.7×10^3	6.5	1.4×10^5		
	Rh(I) Dimer						
9	$[Rh_2(dppm)_2(t\text{-}BuNC)_4]^{2+}$	6.8×10	4.4×10^5				
10	$[Rh_2(dppm)_2(p\text{-}MeC_6H_4NC)_4]^{2+}$	5.7×10	1.5×10^5			5.5×10^{-2}	4.4×10
11	$]Rh_2(dppm)_2(PhCH_2NC)_4]^{2+}$	1.1×10^2	2.7×10^5			6.3×10^{-2}	6.2
12	$[Rh_2(dppm)_2(PhNC)_4]^{2+}$	3.9×10^2	1.1×10^5			8.2×10^{-2}	1.1×10
13	$[Rh_2(dicp)_4]^{2+}$	4.8×10^2	5.8×10^5				

a) Containing 0.1 mol dm^{-3} n-Bu_4NClO_4. b) From Ref. 8. c) From Ref. 9.

$$[RhL_4]^+ + I_2 \overset{K_1}{\rightleftharpoons} ([RhL_4]^+\ I_2) \xrightarrow{k_1} [RhL_4(I)_2]^+ \quad (7)$$

I_2 in excess

$$([RhL_4]^+I_2) + I_2 \overset{K_2}{\rightleftharpoons} ([RhL_4]^+\ 2I_2) \xrightarrow{k_2} [RhL_4(I)_2]^+ + I_2 \quad (8)$$

$[RhL_4]^+$ in excess

$$([RhL_4]^+\ I_2) + [RhL_4]^+ \overset{K_3}{\rightleftharpoons} (2[RhL_4]^+\ I_2) \xrightarrow{k_3} [RhL_4(I)_2]^+ + [RhL_4]^+ \quad (9)$$

Scheme 1.

it is suggested that there exist three kinds of intermediates, one of which is common for both cases. Thus, the kinetics for the first step may best be interpreted by assuming three kinds of complexes formed between the Rh(I) cation and I_2 with 1:1, 1:2, and 2:1 stoichiometry (Scheme 1). According to Scheme 1, the pseudo-first-order rate constants $k_I^{(1)}$ and $k_{Rh}^{(1)}$ for the first step are expressed by Eqs. 10 and 11 in the presence of excess I_2 and $[RhL_4]^+$, respectively, when a steady state approximation is applied to the three complexes with 1:1, 1:2, and 2:1 mole ratios. When $K_1[I_2]$, $K_1[Rh] \gg 1$ and $K_2[I_2]$, $K_3[Rh] \ll 1$, Eqs. 10 and 11 are reduced to Eqs. 12 and 13, respectively.

$$k_I^{(1)} = \frac{k_1K_1[I_2] + k_2K_1K_2[I_2]^2}{1 + K_1[I_2] + K_1K_2[I_2]^2} \quad (10)$$

$$k_{Rh}^{(1)} = \frac{k_1K_1[Rh] + k_3K_1K_3[Rh]^2}{1 + K_1[Rh] + K_1K_3[Rh]^2} \quad (11)$$

Thus, the intercept of the plots of $k_I^{(1)}$ *vs.* $[I_2]$ and $k_{Rh}^{(1)}$ *vs.* [Rh] in Fig. 2 gives the k_1 value and the slopes of $k_I^{(1)}$ and $k_{Rh}^{(1)}$ yield the k_2K_2 and k_3K_3 values, respectively. The same kinetic formulation as Eq. 12 was applied to dppm- and dicp-bridged Rh(I)

$$k_I^{(1)} = k_1 + k_2K_2[I_2] \quad (12)$$

$$k_{Rh}^{(1)} = k_1 + k_3K_3[Rh] \quad (13)$$

dimers, $[Rh_2(dppm)_2(RNC)_4]^{2+}$ and $[Rh_2(dicp)_4]^{2+}$, as well as other $[RhL_4]^+$ monomers. The k_1 and k_2K_2 values for reactions of these complexes in the presence of excess I_2 are listed in Table 2.

Mechanistic Comparison for Reactions of Rh(I) Complexes between the Oxidative Addition of Iodine and the Electron Transfer with Inorganic Oxidants. The Rh(I) complexes employed in this study are readily oxidized by inorganic oxidants such as $[Fe(N\text{-}N)_3]^{3+}$ (N-N= 1,10-phenanthroline and 2,2′-bipyridine) and $[Co(bpy)_3]^{3+}$ (bpy=2,2′-bipyridine) (Eq. 14);[8,9]

$$[RhL_4]^+ + Ox \longrightarrow [RhL_4]^{2+} + Ox^- \quad (14)$$

where Ox represents the inorganic oxidants. Based on the kinetic study the following scheme has previously been presented for the electron transfer reactions between the Rh(I) complexes and inorganic oxidants;[8,9]

$$[RhL_4]^+ + Ox \overset{K_1'}{\rightleftharpoons} ([RhL_4]^+\ Ox) \xrightarrow[e.t.]{k_1'} \quad (15)$$

$$([RhL_4]^+\ Ox) + Ox \overset{K_2'}{\rightleftharpoons} ([RhL_4]^+\ 2Ox) \xrightarrow[e.t.]{k_2'} \quad (16)$$

$$([RhL_4]^+\ Ox) + [RhL_4]^+ \overset{K_3'}{\rightleftharpoons} (2[RhL_4]^+\ Ox) \xrightarrow[e.t.]{k_3'} \quad (17)$$

Scheme 2.

where e.t. represents the electron transfer reaction in Eq. 14. It is noteworthy that Scheme 1 for the oxidative addition of Rh(I) complexes with I_2 is equivalent to Scheme 2 for the electron transfer reactions of the same Rh(I) complexes with inorganic oxidants, as characterized by three kinds of complexes formed between the Rh(I) cation and I_2 or Ox with 1:1, 1:2, and 2:1 stoichiometry. Such complex formation may occur through the d_{z^2} HOMO orbital of the Rh(I) complex[17] since a given Rh(I) complex can interact with I_2, Ox, or another Rh(I) complex at both sides of the square-planar Rh(I) complex. The

Table 3. The $E^{p}_{ox}-E^{0}_{red}$ values for redox pairs between Rh(I) complexes and I_2 as well as inorganic oxidants ($[Fe(phen)_3]^{3+}$ and $[Co(bpy)_3]^{3+}$)[a]

	$(E^{p}_{ox}-E^{0}_{red})$/V		
	I_2	$[Fe(phen)_3]^{3+}$	$[Co(bpy)_3]^{3+}$
$[Rh(p\text{-}MeC_6H_4NC)_4]^+$	0.72	0.33	1.09
$[Rh(2,4,6\text{-}Me_3C_6H_2NC)_4]^+$	0.80	0.41	1.17
$[Rh(PhNC)_4]^+$	0.84	0.45	1.21
$[Rh(PhCH_2NC)_4]^+$	0.73	0.34	1.10
$[Rh(t\text{-}BuNC)_4]^+$	0.86	0.47	1.23
$[Rh(C_6H_{11}NC)_4]^+$	0.75	0.36	1.21
$[Rh_2(dppm)_2(t\text{-}BuNC)_4]^{2+}$	0.29	−0.10	0.66
$[Rh_2(dppm)_2(PhCH_2NC)_4]^{2+}$	0.28	−0.11	0.65
$[Rh_2(dppm)_2(PhNC)_4]^{2+}$	0.34	−0.05	0.71
$[Rh_2(dicp)_4]^{2+}$	0.22	−0.17	0.59

a) The E^{p}_{ox} values of Rh(I) complexes and the E^{0}_{red} values of inorganic oxidants were taken from Refs. 9 and 8, respectively.

kinetic formulation for the electron transfer reactions (Eqs. 18 and 19)[8] also is equivalent to that for the first step for the oxidative addition reactions (Eqs. 12 and 13);

$$k'_{Ox} = k'_1 + k'_2K'_2[Ox] \quad (18)$$

$$k'_{Rh} = k'_1 + k'_3K'_3[Rh] \quad (19)$$

where k'_{Ox} and k'_{Rh} are the pseudo-first-order rate constants in the presence of excess oxidant and Rh(I) complex, respectively. The k'_1 and $k'_2K'_2$ values for the electron transfer reactions of the Rh(I) complexes with the inorganic oxidants have been determined previously from the intercepts and the slopes of the plots between k'_{Ox} and [Ox] by the same manner as described above,[8] and relisted in Table 2 for comparison.

In addition to the similarity in the reaction scheme between the oxidative addition (Scheme 1) and the electron transfer reactions (Scheme 2), there can be seen similarities in the reactivity patterns of the Rh(I) complexes as well. In both oxidative additions and electron transfer reactions, the k_1 and k_2K_2 values as well as the k'_1 and $k'_2K'_2$ values for ligand bridged Rh(I) dimers $[Rh_2(dppm)_2(RNC)_4]^{2+}$ and $[Rh_2(dicp)_4]^{2+}$ are significantly larger than those for Rh(I) monomers $[Rh(RNC)_4]^+$. Moreover, the rate constants for Rh(I) monomers as well as Rh(I) dimers are approximately constant in both reactions, independent of the ligands. Such similarities in the reactivity patterns of Rh(I) complexes as well as the reaction scheme between the oxidative additions and the electron transfer reactions indicate that the activation process for the oxidative addition is analogous to that for the electron transfer shown in Eq. 20,

$$([RhL_4]^+ I_2) \xrightarrow{e.t.} ([RhL_4]^{2+} I_2^-)^* \quad (20)$$

where the double dagger represents the activated complex. Attachment of electron to I_2 is known to cause the dissociation of the I–I bond since the ground state energy of I_2 is 1.5 eV higher than the dissociation limit for I_2^- (Eq. 21).[18] Thus, electron transfer from

$$I_2 \xrightarrow{e} I\cdot + I^- \quad (21)$$

$[RhL_4]^+$ to I_2 would result in the facile dissociation of I–I bond, followed by the geminate recombination between the $[RhL_4]^{2+}$ and I· radicals to yield the adduct as the first step (Eq. 22). In the next section,

$$([RhL_4]^{2+}I_2^-)^* \longrightarrow [RhL_4(I)_2]^+ \quad (22)$$

the rate constants for the oxidative additions of Rh(I) complexes with I_2 are compared with those of the posturated electron transfer reactions (Eq. 20) in a quantitative manner with the aid of linear free energy relationships.

Quantitative Comparison of Rate Constants between the Oxidative Additions and the Electron Transfer Reactions of Rh(I) Complexes. Previously, we have established a linear free energy relationship (LFER) for the electron transfer reactions of Rh(I) complexes with inorganic oxidants (Eq. 14), which can be expressed as Eq. 23,[9,19]

$$\log k'_1 = -8.6(E^{p}_{ox}-E^{0}_{red}) + \text{Const.} \quad (23)$$

where k'_1 stands for the rate constant (Eq. 15), E^{p}_{ox} is the anodic current peak potential in the cyclic voltammogram of the Rh(I) complex at a constant sweep rate (100 mV s^{-1}), and E^{0}_{red} is the standard reduction potential of the oxidant. Thus, the rate constant for the electron transfer reaction from the Rh(I) complex to I_2 (Eq. 20) may be evaluated by substituting the reduction potential of I_2 into Eq. 23. The reduction potential may be approximated by the $E_{1/2}$ value of I_2 obtained in the Experimental section, since the peak separation (0.1 V) is close to that for one electron reversible process (0.06 V).[20,21] The $E^{p}_{ox}-E^{0}_{red}$ values for the redox pairs between the Rh(I) complexes and I_2 as well as the representative inorganic oxidants are listed in Table 3.

The plot of Eq. 23 is shown by open circles in Fig. 3a, where the plot of the log k_1 values for the oxidative additions of Rh(I) complexes with I_2 against the $E^{p}_{ox}-E^{0}_{red}$ values (Table 3) also is given by closed circles. The log k_1 values for the Rh(I) dimers (Nos. 9, 11—13) agree well with the solid line which represents the rate constant when electron transfer reactions between the cationic Rh(I) complexes and I_2 would occur (Eq. 20). The k_2K_2 values for the same

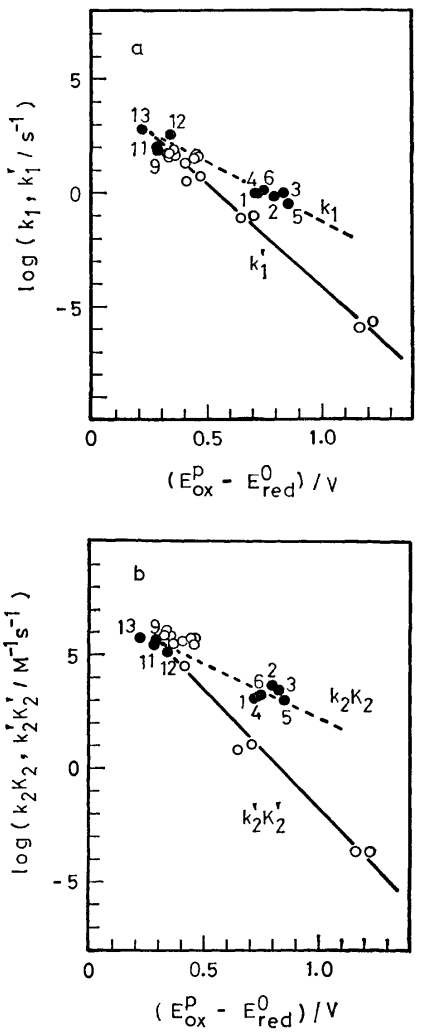

Fig. 3. Linear free energy relationships between logarithm of the rate constants ($\log(k_1, k_1')$ (a) and $\log(k_2K_2, k_2'K_2')$ (b)) and $E^p_{ox}-E^0_{red}$ for the reactions of Rh(I) complexes with I_2 (k_1, k_2K_2) and inorganic oxidants (k_1', $k_2'K_2'$); numbers refer to compounds in Table 2.

Rh(I) dimers also are in agreement with those for the electron transfer rate constant $k_2'K_2'$ drawn by the solid line in Fig. 3b, which barrs fortuitous coincidences. Such agreement of the absolute values of k_1 as well as k_2K_2 for the oxidative additions of I_2 to the Rh(I) dimers with those for the electron transfer reactions strongly suggests that the activation process in the first step of the oxidative additions is electron transfer from the Rh(I) complexes to I_2 as shown in Eq. 20.

The k_1 and k_2K_2 values decrease with increasing the $E^p_{ox}-E^0_{red}$ values as shown by the dotted lines in Figs. 3a and 3b. The differences between the Rh(I) dimers (Nos. 9, 11—13) and the Rh(I) monomers (Nos. 1—6) are remarkable both in k_1 and in k_2K_2. These values for the Rh(I) monomers, however, lie somewhat above the solid lines which represent the electron transfer rate constants. Accordingly the slopes of the linear free energy relationships for the oxidative additions are smaller than those for the electron transfer reactions. The linear free energy relationships in Figs. 3a and 3b themselves are not a definitive proof for the occurrence of complete electron transfer in the activation process of the oxidative addition reactions of I_2 to the Rh(I) complexes since the reaction *via* an intermediate with greater or lesser charge-transfer character is expected to show similar trends.[22,23] The description of the activation process as the complete electron transfer in Eq. 20, however, enables us to evaluate the rate constants for the oxidative additions of the Rh(I) dimers with I_2 as the rate constants for the electron transfer reactions in the same systems as shown in Figs. 3a and 3b. Since the solid lines in Figs. 3a and 3b represent the electron transfer rate constants, the larger rate constants for the oxidative additions of the Rh(I) monomers with I_2 than expected from the solid lines in Figs. 3a and 3b may be regarded as arising from the stronger interaction of the Rh(I) monomers with I_2 in the transition state of electron transfer in Eq. 20 than that with the inorganic oxidants.

A similar electron transfer mechanism has been presented by Tsou and Kochi[24] for the oxidative addition of aryl halides to tetrakis(triethylphosphine)-nickel, in which the second-order rate constant ($\log k$) were linearly related to the polarographic $E_{1/2}$ values of aryl halides. Our study has shown that there exists a mechanistic similarity between the oxidative addition of Rh(I) complexes with I_2 and the electron transfer reactions with inorganic oxidants $[Fe(N\text{-}N)_3]^{3+}$ and $[Co(bpy)_3]^{3+}$, and that the absolute values of the rate constants for the oxidative additions can be approximated by the rate constants for the electron transfer reactions from the Rh(I) complexes to I_2. The generalization of the electron transfer mechanism for the oxidative additions of Rh(I) complexes with I_2 described above or its utility to predict the rate constants for oxidative additions of other metal complexes with different substrates remains to be elaborated in further studies.

References

1) J. Halpern, *Acc. Chem. Res.*, **3**, 386 (1970); R. Cramer, *ibid.*, **1**, 186 (1968); R. Crabtree, *ibid.*, **12**, 331 (1979); L. Vaska, *ibid.*, **1**, 335 (1968); E. L. Muetterties and J. R. Bleeke, *ibid.*, **12**, 324 (1979); J. Halpern, *Inorg. Chim. Acta*, **50**, 11 (1981); R. D. W. Kemmit and M. A. R. Smith, *Inorg. React. Mech.*, **3**, 451 (1974).

2) J. K. Kochi, "Organometallic Mechanisms and Catalysis," Academic Press, New York, (1978).

3) F. A. Cotton and G. Wilkinson, "Advanced Inorganic Chemistry," 4th ed, Wiley-Interscience, New York (1980), p. 1243, and references cited therein.

4) N. B. Chapman and J. Shorter, "Correlation Analysis in Chemistry," Plenum Press, New York, (1978); L. M. Stock and H. C. Brown, *Adv. Phys. Org. Chem.*, **1**, 35 (1963); R. W. Taft, Jr., "Steric Effects in Organic Chemistry," ed by M. S. Newman, Wiley, New York (1956), p. 556; N. B. Chapman and J. Shorter, "Advances in Linear Free Energy Relationships," Plenem Press, London (1972).

5) S. Fukuzumi and J. K. Kochi, *J. Am. Chem. Soc.*, **103**, 2783, 7240 (1981).

6) a) R. Kuwae, T. Tanaka, and K. Kawakami, *Bull. Chem. Soc. Jpn.*, **52**, 437 (1979); b) R. Kuwae and T. Tanaka,

ibid., **52**, 1067 (1979).
7) a) A. L. Balch, *J. Am. Chem. Soc.*, **98**, 8049 (1976); b) N. S. Lewis, K. R. Mann, J. G. Gordon, II, and H. B. Gray, *ibid.*, **98**, 7461 (1976); c) J. T. Mague, M. O. Nutt, *Inorg. Chem.*, **16**, 1259 (1977).
8) S. Fukuzumi, N. Nishizawa, and T. Tanada, *Bull. Chem. Soc. Jpn.*, in press.
9) S. Fukuzumi, N. Nishizawa, and T. Tanaka, *Bull. Chem. Soc. Jpn.*, **55**, 2892 (1982).
10) T. Iinuma and T. Tanaka, *Inorg. Chim. Acta*, **49**, 79 (1981).
11) W. Hewertson and H. R. Watson, *J. Chem. Soc.*, **1962**, 1490.
12) W. P. Weber, G. W. Gokel, and I. K. Ugi, *Angew. Chem., Int. Ed. Engl.*, **11**, 530 (1972).
13) J. Chatt and L. M. Venanzi, *J. Chem. Soc.*, **1957**, 4735.
14) D. D. Perrin, W. L. F. Armarego, and D. R. Perrin, "Purification of Laboratory Chemicals," Pergamon Press, New York (1966).
15) H. Fischer, E. O. Fischer, and H. Werner, *J. Organomet. Chem.*, **73**, 331 (1974).
16) R. K. Pomeroy and W. A. G. Graham, *J. Am. Chem. Soc.*, **94**, 274 (1972).
17) H. Isci and W. R. Mason, *Inorg. Chem.*, **14**, 913 (1975).
18) A. D. McLean, O. Gropen, and S. Huzinaga, *J. Chem. Phys.*, **73**, 396 (1980); R. F. Barrow, D. F. Broyd, L. B. Pederson, and K. K. Yee, *Chem. Phys. Lett.*, **18**, 357 (1973).
19) The $E^{p}_{ox}-E^{0}_{red}$ value can be taken as the free energy change of electron transfer reaction from the Rh(I) complex to the oxidant, $\Delta G^{0}+\text{Const.}$[9]
20) W. M. Latimer, "Oxidation Potentials," 2nd ed, Prentice Hall, Englewood Cliffs, N. J. (1952), p. 62.
21) R. S. Nicholson and I. Shain, *Anal. Chem.*, **36**, 706 (1964).
22) I. E. Kochevar and P. J. Wagner, *J. Am. Chem. Soc.*, **94**, 3859 (1972); J. B. Gutteplan and S. G. Cohen, *ibid.*, **94**, 4040 (1972); B. M. Monroe, C. G. Lee, and N. J. Turro, *Mol. Photochem.*, **6**, 271 (1974); F. Wilkinson and A. Garner, *J. Chem. Soc., Faraday Trans. 2*, **73**, 222 (1977).
23) C. Walling, *J. Am. Chem. Soc.*, **102**, 6854 (1980).
24) T. T. Tsou and J. K. Kochi, *J. Am. Chem. Soc.*, **101**, 6319 (1979).

Cyclic Voltammetry of Rh(I) Complexes and the Oligomers. A Correlation between the Anodic Peak Potentials and the Rate Constants for the Electron Transfer Reactions with Inorganic Oxidants

Shunichi Fukuzumi, Nobuaki Nishizawa, and Toshio Tanaka*

Department of Applied Chemistry, Faculty of Engineering, Osaka University, Suita, Osaka 565

(Received February 5, 1982)

The cyclic voltammogram of a CH_3CN solution of $[Rh(p\text{-}MeOC_6H_4NC)_4]^+$ exhibits three anodic current peaks which correspond to the oxidations of the monomer, the dimer, and the trimer, with no cathodic wave on the reverse scan. The anodic peak potentials E^p_{ox} in such irreversible cyclic voltammograms were determined for various Rh(I) monomers and the oligomers such as $[Rh(RNC)_4]^+$, $[Rh_2(RNC)_8]^{2+}$, $[Rh_2(dppm)_2(RNC)_4]^{2+}$, $[Rh_2(dicp)_4]^{2+}$, $[Rh_3(RNC)_{12}]^{3+}$, and $[Rh_4(dicp)_8]^{4+}$ (R=*p*-$MeOC_6H_4$ and Ph, *etc*; dppm=bis(diphenylphosphino)methane, dicp=1,3-diisocyanopropane). The anodic peak potentials E^p_{ox} vary mainly with the degree of oligomerization of the Rh(I) complexes, decreasing in the order monomer>dimer>trimer>tetramer, in parallel with the energies of the highest occupied molecular orbitals E_{HOMO}. It has been found that the E^p_{ox} values are linearly correlated with logarithm of the rate constants for the electron transfer reactions with inorganic oxidants such as $[Fe(bpy)_3]^{3+}$ and $[Co(bpy)_3]^{3+}$ (bpy=2,2′-bipyridine) in the context of the Marcus theory as expected when the standard oxidation potentials E^0_{ox} would be used. It is thus suggested that the anodic peak potentials of the Rh(I) complexes in the irreversible system can be used as the standard oxidation potentials as far as the relative values are concerned.

Recently, Rh(I) complex oligomers such as $[Rh_2(dicp)_4]^{2+}$ (dicp=1,3-diisocyanopropane) have merited a special attention since Gray *et al.*[1] discovered that $[Rh_2(dicp)_4]^{2+}$ dissolved in 12 mol dm^{-3} aqueous HCl solution produces H_2 upon irradiation of visible light. It seems to be of importance to know the redox properties of the Rh(I) complexes in order to delineate the mechanism as well as to improve the efficacy of the system. However, the redox properties of Rh(I) complexes have scarcely been known in contrast with other conventional systems of photosensitized hydrogen production such as utilizing $[Ru(bpy)_3]^{2+}$ (bpy=2,2′-bipyridine)[2-4] whose redox properties have well been established.[5]

Previously, we have reported the kinetic study on the electron transfer reactions of tetrakis(isocyanide)-rhodium(I) and the oligomers, $[(RhL_4^+)_n]$ (n=1—3), with inorganic oxidants such as $[Fe(N\text{-}N)_3]^{3+}$ (N-N= 2,2′-bipyridine, 1,10-phenanthroline, and related ligands) and $[Co(bpy)_3]^{3+}$,[6] in which $[(RhL_4^+)_n]$ were found to undergo irreversible oxidation by these oxidants. In such irreversible systems, the thermodynamic redox properties of $[(RhL_4^+)_n]$ such as the redox potentials E^0 cannot be obtained directly. It seems, however, to be possible to relate the dynamic properties of $[(RhL_4^+)_n]$ in the redox reactions to the redox potential by utilizing the linear free energy relationship (LFER).

In the present study, we wish to report the relation between the dynamic properties of various Rh(I) complexes including $[Rh_2(dicp)_4]^{2+}$ in the electrochemical oxidation, obtained as the anodic peak potentials of the cyclic voltammograms (E^p_{ox}), and the standard oxidation potentials of the complexes (E^0_{ox}), by comparing the E^p_{ox} values with the electron transfer rate constants for the reactions with inorganic oxidants (k_1) reported previously.[6] It will be shown that the anodic peak potentials (E^p_{ox}) provide useful informations on the differences between the redox properties of the Rh(I) monomers and the oligomers.

Experimental

Materials. Preparations of tetrakis(isocyanide)rhodium(I) perchlorates used in this study were described previously.[6,7] Bis(diphenylphosphino)methane (dppm) was prepared according to the literature.[8] dppm-Bridged Rh(I) dimers of the $[Rh_2(dppm)_2(RNC)_4]^{2+}$ type (R=Ph, *p*-$MeOC_6H_4$, *t*-Bu, $PhCH_2$) were prepared by adding a stoichiometric amount of dppm to a solution of appropriate $[Rh(RNC)_4](ClO_4)$ in acetone by the procedure analogous to the preparation of $[Rh_2(dppm)_2(n\text{-}BuNC)_4]^{2+}$.[9] The product was collected by filtration and purified by recrystallization from acetone/ethanol, followed by drying in a vacuum. The elemental analysis was performed for a representative compound, $[Rh_2(dppm)_2(p\text{-}MeOC_6H_4NC)_4](ClO_4)_2$. Found: C, 57.25; H, 4.56; N, 3.23%. Calcd for $Rh_2C_{82}H_{72}N_4P_4Cl_2O_{12}$: C, 57.73; H, 4.25; N, 3.28%. 1,3-Diisocyanopropane (dicp) was prepared from 1,3-propanediamine, chloroform, and 50% aqueous sodium hydroxide by the procedure analogous to the preparation of phenyl isocyanide,[10] and the product was purified by vacuum distillation. The dicp-bridged Rh(I) dimer, $[Rh_2(dicp)_4]Cl_2$, was prepared by the reaction of dicp with $[Rh(cyclooctadiene)Cl]_2$[11] in chloroform according to the literature.[12] The tetraphenylborate salt, $[Rh_2(dicp)_4](BPh_4)_2$, was obtained by the addition of $NaBPh_4$ to a methanol solution of $[Rh_2(dicp)_4]Cl_2$. Tetrabutylammonium perchlorate used as a supporting electrolyte was prepared by the reaction of tetrabutylammonium bromide with perchloric acid, and purified by recrystallization from ethanol. Acetonitrile used as a solvent for electrochemical and kinetic experiments was purified by the standard method.[13]

Cyclic Voltammetry. Cyclic voltammetry measurements were performed on a Hokuto Denko Model HA-301 potentiostat/galvanostat at 298 K in CH_3CN containing 0.1 mol dm^{-3} $n\text{-}Bu_4NClO_4$ as a supporting electrolyte, using a platinum microelectrode and a standard NaCl calomel reference electrode (SCE) or a Ag/Ag^+ reference electrode ($Ag/AgNO_3$ 0.1 mol dm^{-3}). The electrochemical cell was constructed according to the literature.[14] The platinum microelectrode was routinely cleaned by soaking it in concentrated nitric acid, followed by repeated rinsing with water

and then acetone, and drying at 353 K prior to use. Two cm^3 of a CH_3CN solution of Rh(I) complexes (1.0×10^{-3}—1.0×10^{-2} mol dm^{-3}) was introduced into the cell and flashed with nitrogen prior to the measurements. The anodic peak potentials, E^p_{ox}, observed at the same sweep rate of 100 mV s^{-1} for the Rh(I) complexes employed in this study were always reproducible to within 50 mV. No aging of the electrode was observed on a week to week basis. There were no complications on the electrode arising from the deposition of the oxidized Rh(II) species for most Rh(I) complexes so that the repeated scans did not affect the appearance of the voltammograms. For some Rh(I) dimer complexes such as $[Rh_2(dicp)_4]^{2+}$ and $[Rh_2(dppm)_2(t\text{-BuNC})_4]^{2+}$, the anodic peak current decreased with repeating the scan, but the anodic peak potentials in the first scan were reproducible. The cyclic voltammetry of $[Rh_2(dicp)_4]^{2+}$ was measured in a methanol solution of the chloride salt containing 0.04 mol dm^{-3} KCl or 0.1 mol dm^{-3} LiCl, since the salt was not soluble enough in CH_3CN containing 0.1 mol dm^{-3} n-Bu_4NClO_4. The anodic peak potential of each Rh(I) complex in CH_3CN containing 0.1 mol dm^{-3} n-Bu_4NClO_4 *vs.* Ag/Ag^+ ($Ag/AgNO_3$ 0.1 mol dm^{-3}) was 0.34 V lower than that *vs.* SCE. The same difference between the redox potentials of ferrocene used as a reference compound *vs.* Ag/Ag^+ and SCE was always observed in accordance with the literature.[15]

Kinetic Measurements of Electron Transfer Reactions. The measurements of rates of the electron transfer reactions between Rh(I) complexes and $[Fe(N\text{-}N)_3]^{3+}$ were described previously.[6] Rates of the electron transfer reactions between dppm-bridged Rh(I) complexes, $[Rh_2(dppm)_2(RNC)_4]^{2+}$, and $[Co(bpy)_3]^{3+}$ in CH_3CN were measured at 298 K by monitoring the decay of the absorbances due to the Rh(I) dimers (λ_{max} listed in Table 1) in the presence of large excess $[Co(bpy)_3]^{3+}$ (2.19×10^{-3}—1.22×10^{-2} mol dm^{-3}), by using a Union SM-401 spectrophotometer. A mixing apparatus (Model MX-7, Union Giken) was used to ensure the fast and complete mixing of the two sample solutions. The ionic strength of the reaction medium was adjusted to 0.1 with n-Bu_4NClO_4.

Results

Cyclic Voltammetry of Rh(I) Complexes. The cyclic voltammograms (CV) of three representative Rh(I) complexes, $[Rh(p\text{-}MeOC_6H_4NC)_4]^+$, $[Rh(2,4,6\text{-}Me_3C_6H_2NC)_4]^+$, and $[Rh_2(dppm)_2(PhNC)_4]^{2+}$, are illustrated in Fig. 1, which shows anodic waves with current maxima but no cathodic wave on the reverse scan, as confirmed by changing the sweep rates in the range 20 mV s^{-1} to 1000 mV s^{-1}. The anodic oxidation of the Rh(I) complexes is thus irreversible, indicating that the follow-up chemical reactions are fast on the time scale of the CV experiments.

The CV of $[Rh(p\text{-}MeOC_6H_4NC)_4]^+$ shows three distinct anodic current peaks in the range 0.2—1.2 V *vs.* Ag/Ag^+ (Fig. 1a), which correspond to the fact that the $[Rh(p\text{-}MeOC_6H_4NC)_4]^+$ cation oligomerizes in CH_3CN to exist as an equilibrium mixture with the dimer $[Rh_2(p\text{-}MeOC_6H_4NC)_8]^{2+}$ and the trimer $[Rh_3(p\text{-}MeOC_6H_4NC)_{12}]^{3+}$, as shown in Eqs. 1 and 2,[6,16]

$$2[RhL_4]^+ \overset{K_D}{\rightleftharpoons} [Rh_2L_8]^{2+} \quad (1)$$

$$[Rh_2L_8]^{2+} + [RhL_4]^+ \overset{K_T}{\rightleftharpoons} [Rh_3L_{12}]^{3+} \quad (2)$$

where L represents p-$MeOC_6H_4NC$. Similar multi-

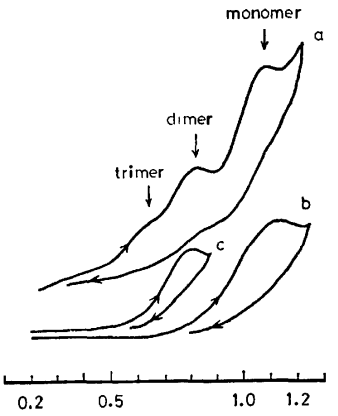

Fig. 1. Cyclic voltammograms of representative Rh(I) complexes in CH_3CN containing 0.1 mol dm^{-3} n-Bu_4NClO_4; (a) $[Rh(p\text{-}MeOC_6H_4NC)_4]^+$ 2.1×10^{-2} mol dm^{-3}, (b) $[Rh(2,4,6\text{-}Me_3C_6H_2NC)_4]^+$ 1.0×10^{-3} mol dm^{-3}, (c) $[Rh_2(dppm)_2(PhNC)_4]^{2+}$ 5.1×10^{-3} mol dm^{-3}.

CV peaks were observed for $[Rh(p\text{-}MeC_6H_4NC)_4]^+$ and $[Rh(PhNC)_4]^+$ which also are known to oligomerize in CH_3CN.[6,17] On the other hand, $[Rh(2,4,6\text{-}Me_3C_6H_2NC)_4]^+$ does not oligomerize appreciably because of the steric effect of the bulky ligand,[6] and there exists only the monomer as the predominant species in CH_3CN, *e.g.*, 99.9% monomer in 2.21×10^{-3} mol dm^{-3} where the CV was measured. Indeed, the CV of $[Rh(2,4,6\text{-}Me_3C_6H_2NC)_4]^+$ shows a single anodic current peak at 1.14 V (Fig. 1b) which is nearly the same as the position of the third anodic peak for $[Rh(p\text{-}MeOC_6H_4NC)_4]^+$. Similar single CV peaks were observed for $[Rh(C_6H_{11}NC)_4]^+$, $[Rh(2,6\text{-}Me_2C_6H_3NC)_4]^+$, $[Rh(t\text{-BuNC})_4]^+$, and $[Rh(PhCH_2NC)_4]^+$ which do not oligomerize appreciably either.[6] dppm-Bridged Rh(I) dimers of the $[Rh_2(dppm)_2(RNC)_4]^{2+}$ type (R=Ph, $PhCH_2$, t-Bu) do not oligomerize in CH_3CN either.[9] In accordance with this, the CV of $[Rh_2(dppm)_2(PhNC)_4]^{2+}$ exhibits a single anodic wave due to the oxidation of the dimer with a current maximum at 0.68 V (Fig. 1c) which corresponds to the second anodic peak of $[Rh(p\text{-}MeOC_6H_4NC)_4]^+$.

Based on the above results, the three anodic current peaks at 1.03, 0.79, and 0.56 V for the CV of $[Rh(p\text{-}MeOC_6H_4NC)_4]^+$ can be assigned to the oxidation of the monomer, the dimer, and the trimer, respectively. Anodic peak potentials E^p_{ox} of Rh(I) complexes determined at the same sweep rate (100 mV s^{-1}) are listed in Table 1. The peak potentials E^p_{ox} of the Rh(I) monomers (Nos. 1—8) are approximately constant, independent of the nature of isocyanide ligands. Those values of the Rh(I) dimers present in CH_3CN solutions of $[RhL_4]^+$ (Nos. 9—11) also are constant at 0.76 ± 0.03 V, but smaller by about 0.3 V than the Rh(I) monomers. Moreover, the E^p_{ox} values (Nos. 12—15) are slightly smaller than those of the Rh(I) dimers whose ligands are not bridged. The $[Rh_2(dicp)_4]^{2+}$ cation partly oligomerizes to form the tetramer in methanol (Eq. 3). The formation of the

$$2[Rh_2(dicp)_4]^{2+} \overset{K_D}{\rightleftharpoons} [Rh_4(dicp)_8]^{4+} \quad (3)$$

Table 1. Anodic peak potentials of CV for Rh(I) complexes (E^{p}_{ox})[a] and the electronic absorption maxima (λ_{max} and $h\nu_{max}$)

No.	Monomer	E^{p}_{ox} *vs.* Ag/Ag$^+$ V	λ_{max} nm	$h\nu_{max}$ eV
1	$[Rh(p\text{-}MeOC_6H_4NC)_4]^+$	1.03±0.01	403	3.08
2	$[Rh(p\text{-}MeC_6H_4NC)_4]^+$	1.06±0.02	407	3.05
3	$[Rh(PhNC)_4]^+$	1.18±0.02	411	3.02
4	$[Rh(2,4,6\text{-}Me_3C_6H_2NC)_4]^+$	1.14±0.04	405	3.06
5	$[Rh(C_6H_{11}NC)_4]^+$	1.09±0.01	385	3.22
6	$[Rh(2,6\text{-}Me_2C_6H_3NC)_4]^+$	1.03±0.02	409	3.03
7	$[Rh(t\text{-}BuNC)_4]^+$	1.20±0.01	383	3.24
8	$[Rh(PhCH_2NC)_4]^+$ Dimer	1.07±0.04	387	3.20
9	$[Rh_2(p\text{-}MeOC_6H_4NC)_8]^{2+}$	0.79±0.02	564	2.20
10	$[Rh_2(p\text{-}MeC_6H_4NC)_8]^{2+}$	0.74±0.04	563	2.20
11	$[Rh_2(PhNC)_8]^{2+}$	0.76±0.01	568	2.18
12	$[Rh_2(dppm)_2(PhNC)_4]^{2+}$	0.68±0.01	613	2.02
13	$[Rh_2(dppm)_2(PhCH_2NC)_4]^{2+}$	0.62±0.02	548	2.26
14	$[Rh_2(dppm)_2(t\text{-}BuNC)_4]^{2+}$	0.63±0.01	526	2.36
15	$[Rh_2(dicp)_4]^{2+}$ Trimer	0.58±0.02[b]	559[b]	2.22[b]
16	$[Rh_3(p\text{-}MeOC_6H_4NC)_{12}]^{3+}$ Tetramer	0.56±0.02	710	1.75
17	$[Rh_4(dicp)_8]^{4+}$	0.25±0.04[b]	778[b]	1.59[b]

a) Measured at the sweep rate of 100 mV s^{-1} in CH_3CN containing 0.1 mol dm^{-3} n-Bu_4NClO_4 at 298 K unless otherwise noted. b) Measured in methanol containing 0.04 mol dm^{-3} KCl.

tetramer, $[Rh_4(dicp)_8]^{4+}$, is characterized by the appearance of a new absorption band at 778 nm in the high concentrations in addition to absorption bands at 318, 342, and 559 nm observed in the low concentrations. The anodic current peak which is assignable to the tetramer appears at the smallest potential (No. 17) among the Rh(I) complexes in Table 1. Thus, the E^{p}_{ox} values for the Rh(I) monomers and the oligomers in Table 1 are concluded to increase in the order tetramer < trimer < dimer(bridged) < dimer(not bridged) < monomer.

Electron Transfer Reactions of Rh(I) Complexes with Inorganic Oxidants. The kinetics of the oxidation of Rh(I) monomers, $[Rh(RNC)_4]^+$, with inorganic oxidants such as $[Fe(N\text{-}N)_3]^{3+}$ (Eq. 4) were examined earlier,[6]

$$[RhL_4]^+ + [Fe(N\text{-}N)_3]^{3+} \longrightarrow [RhL_4]^{2+} + [Fe(N\text{-}N)_3]^{2+} \quad (4)$$

where N-N=2,2′-bipyridine, 1,10-phenanthroline, and substituted 1,10-phenanthrolines. The kinetic results in the presence of excess oxidants were best interpreted by the scheme,[6]

$$[RhL_4]^+ + Ox \overset{K_1}{\rightleftharpoons} ([RhL_4]^+\ Ox) \xrightarrow{k_1} \text{e. t.} \quad (5)$$

$$([RhL_4]^+\ Ox) + Ox \overset{K_2}{\rightleftharpoons} ([RhL_4]^+\ 2Ox) \xrightarrow{k_2} \text{e. t.} \quad (6)$$

Scheme

where Ox and e.t. represent the inorganic oxidants and the electron transfer reactions as the rate determining step, respectively. In order to compare the reactivity of Rh(I) dimers with Rh(I) monomers, the electron transfer reactions of $[Rh_2(dppm)_2(RNC)_4]^{2+}$ with $[Co(bpy)_3]^{3+}$ were examined kinetically in CH_3CN containing 0.1 mol dm^{-3} n-Bu_4NClO_4 at 298 K. The reactions were followed by monitoring the decay of the absorbance due to $[Rh_2(dppm)_2(RNC)_4]^{2+}$ (λ_{max} in Table 1).[18] The reactions obey pseudo-first-order kinetics in the presence of excess $[Co(bpy)_3]^{3+}$. According to the Scheme the pseudo-first-order rate constant k_{Co} is expressed as

$$k_{Co} = \frac{k_1K_1[Co] + k_2K_1K_2[Co]^2}{1 + K_1[Co] + K_1K_2[Co]^2} \quad (7)$$

When $K_1[Co] \gg 1$ and $K_2[Co] \ll 1$, Eq. 7 is reduced to Eq. 8.

$$k_{Co} = k_1 + k_2K_2[Co] \quad (8)$$

The plots of k_{Co} *vs.* [Co] are given in Fig. 2, which shows linear relations, in accordance with Eq. 8. The intramolecular electron transfer rate constant k_1 in Eq. 5 can thus be obtained from the extrapolated intercepts in Fig. 2 (compare with Eq. 8). The plot of k_{Fe} *vs.* [Fe] for the electron transfer reaction of $[Rh(PhCH_2NC)_4]^+$ with $[Fe(N\text{-}N)_3]^{3+}$ also is shown in Fig. 2 for comparison. The k_1 values for the reactions of Rh(I) complexes with $[Co(bpy)_3]^{3+}$ as well as $[Fe(N\text{-}N)_3]^{3+}$ are listed in Table 2, which gives the difference between the anodic peak potentials of Rh(I) complexes, E^{p}_{ox}, (Table 1) and the reduction potentials of the oxidants, E^{0}_{red},[6] as well for comparison. It can be seen that the electron transfer rate constants k_1 vary significantly from 1.0×10^{-6} to 1.2×10^{2} s^{-1}, approximately in parallel with the $E^{p}_{ox} - E^{0}_{red}$ values.

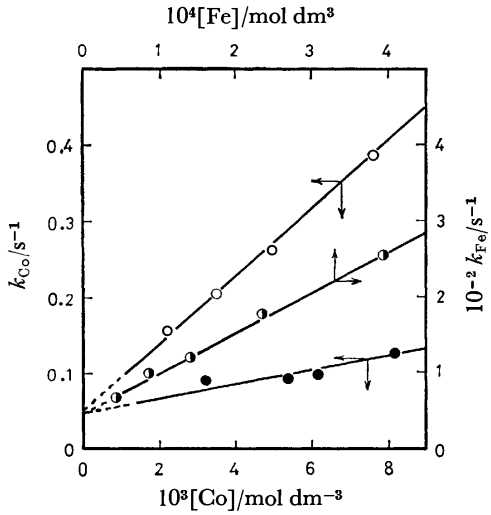

Fig. 2. Pseudo-first-order rate constants k_{Co} and k_{Fe} as a function of [Co] or [Fe] for the oxidations of $[Rh_2(dppm)_2(p\text{-}MeOC_6H_4NC)_4]^{2+}$ (○) and $[Rh_2(dppm)_2(PhCH_2NC)_4]^{2+}$ (●) with $[Co(bpy)_3]^{3+}$ and of $[Rh(PhCH_2NC)_4]^+$ (◑) with $[Fe(bpy)_3]^{3+}$, respectively, in CH_3CN containing 0.1 mol dm^{-3} n-Bu_4NClO_4 at 298 K.

Discussion

Peak Potentials of CV in Irreversible Systems. In

Table 2. Electron transfer rate constants k_1 for the reactions of Rh(I) complexes with $[Co(bpy)_3]^{3+}$ and $[Fe(N\text{-}N)_3]^{3+}$.[a]

Rh No.[b]	Oxidant	$E^p_{ox}-E^0_{red}$[c] / V	k_1[d] / s^{-1}	Rh No.[b]	Oxidant	$E^p_{ox}-E^0_{red}$[c] / V	k_1[d] / s^{-1}
Monomer				Monomer			
1	$[Fe(bpy)_3]^{3+}$	0.31	1.2×10^2	7	$[Fe(bpy)_3]^{3+}$	0.48	5.0
2	$[Fe(bpy)_3]^{3+}$	0.34	3.4×10		$[Fe(phen)_3]^{3+}$	0.47	4.0×10
	$[Fe(phen)_3]^{3+}$	0.33	4.6×10		$[Fe(5\text{-}Clphen)_3]^{3+}$	0.38	3.8×10
3	$[Fe(bpy)_3]^{3+}$	0.46	5.0×10		$[Fe(5\text{-}NO_2phen)_3]^{3+}$	0.27	3.8×10
	$[Fe(phen)_3]^{3+}$	0.45	3.2×10	8	$[Fe(bpy)_3]^{3+}$	0.35	4.3×10
4	$[Co(bpy)_3]^{3+}$	1.17	1.0×10^{-6}		$[Fe(phen)_3]^{3+}$	0.34	4.6×10
	$[Fe(4,7\text{-}Ph_2phen)_3]^{3+}$	0.47	4.6	Dimer			
	$[Fe(bpy)_3]^{3+}$	0.42	2.7	9	$[Co(bpy)_3]^{3+}$	0.82	
	$[Fe(phen)_3]^{3+}$	0.41	2.0×10	10	$[Co(bpy)_3]^{3+}$	0.77	1.5×10^{-3}
	$[Fe(5\text{-}Clphen)_3]^{3+}$	0.31	1.3×10	11	$[Co(bpy)_3]^{3+}$	0.79	1.6×10^{-3}
	$[Fe(5\text{-}NO_2phen)_3]^{3+}$	0.21	1.1×10^2	12	$[Co(bpy)_3]^{3+}$	0.71	8.2×10^{-2}[e]
5	$[Fe(bpy)_3]^{3+}$	0.37	4.3×10	13	$[Co(bpy)_3]^{3+}$	0.65	6.3×10^{-2}[e]
	$[Fe(phen)_3]^{3+}$	0.36	4.6×10	14	$[Co(bpy)_3]^{3+}$	0.66	
6	$[Fe(bpy)_3]^{3+}$	0.31	8.6×10	Trimer			
	$[Fe(phen)_3]^{3+}$	0.30	9.4×10	16	$[Co(bpy)_3]^{3+}$	0.59	5.4×10^{-1}
7	$[Co(bpy)_3]^{3+}$	1.23	1.5×10^{-6}	Tetramer			
	$[Fe(4,7\text{-}Ph_2phen)_3]^{3+}$	0.53	3.5	17	$[Co(bpy)_3]^{3+}$	0.28	

a) In CH_3CN containing 0.1 mol dm^{-3} n-Bu_4NClO_4 at 298 K. b) Numbers refer to compounds in Table 1. c) The E^0_{red} values are taken from Ref. 6. d) From Ref. 6 unless otherwise noted. e) This study.

reversible systems, an anodic current peak potential of CV is thermodynamically determined and the corresponding cathodic peak is observed in the reverse scan with the peak separation of 59 mV, irrespective of the sweep rate.[19] Thus, the redox potential E^0 is experimentally determined as $(E^p_{ox}+E^p_{red})/2$. When the oxidized species is unstable, however, the CV becomes irreversible since the oxidized species no longer exists on the electrode owing to the facile chemical reactions. Under such circumstances, the redox potential cannot be determined, and the anodic peak potential is dependent on a number of factors such as the electron transfer rate constant on the electrode, the reverse electron transfer rate constant, the sweep rate of the CV, and the rate constants of the follow-up chemical reactions. Recently, Klingler and Kochi[20] have, however, demonstrated that under the conditions where the follow-up chemical reactions are much faster than the reverse electron transfer, the anodic peak potential becomes independent of the follow-up chemical reactions since the forward electron transfer is the rate determining step. The anodic peak potential E^p_{ox} is then expressed in terms of the oxidation potential E^0_{ox}, the transfer coefficient β, and the electron transfer rate constants $k(E^p_{ox})$ and $k(E^0_{ox})$ at the peak potential and the oxidation potential, respectively,[20,21]

$$E^p_{ox} = E^0_{ox} + \frac{RT}{\beta F}\ln\frac{k(E^p_{ox})}{k(E^0_{ox})} \quad (9)$$

where $k(E^p_{ox})$ (in units of cm s^{-1}) is a function of the sweep rate v (in V s^{-1}) as given by Eq. 10,[19]

$$k(E^p_{ox}) = 2.18(D\beta Fv/RT)^{1/2} \quad (10)$$

where D (in cm^2 s^{-1}) is the diffusion coefficient and the other notations are conventional. It should be noted that the diffusion coefficient D is nearly constant irrespective of metal complexes.[20] Thus, if β and $k(E^0_{ox})$ are constant, the peak potential E^p_{ox} is linearly related to the standard oxidation potential E^0_{ox} with the slope of unity at a constant sweep rate as given by Eq. 11. Under such conditions, the peak potential

$$E^p_{ox} = E^0_{ox} + \text{Const.} \quad (11)$$

E^p_{ox} can be used as the thermodynamically defined oxidation potential E^0_{ox} as far as the relative values are concerned. In order to examine whether Eq. 11 is applicable to the anodic oxidation of Rh(I) complexes, the irreversibility of the CV wave is discussed in the following section.

Irreversibility in Oxidation of Rh(I) Complexes. The CV of Rh(I) complexes in Fig. 1 clearly demonstrates that the anodic oxidation of Rh(I) complexes is irreversible since no cathodic wave is observed in the reverse scan at the sweep rate as high as 1000 mV s^{-1}. The oxidized Rh(I) complexes, *i.e.*, Rh(II) species have well been regarded as radicals,[6,22] and dimerize rapidly (Eq. 12). An additional support for the irreversibility

$$2[RhL_4]^{2+} \xrightarrow{\text{fast}} [Rh_2L_8]^{4+} \quad (12)$$

in the anodic oxidation of Rh(I) complexes is given by the sweep rate dependence of the anodic peak potential E^p_{ox}. By combining Eqs. 9 and 10, one obtains Eq. 13 which shows that E^p_{ox} depends on the sweep rate v,[20]

$$E^p_{ox} = \frac{2.3RT}{2\beta F}\log v + \text{Const.} \quad (13)$$

where

$$\text{Const.} = E^0_{ox} + \frac{2.3RT}{\beta F}\log\frac{2.18D\beta F}{k(E^0_{ox})RT} \quad (14)$$

In Fig. 3, the E^p_{ox} values for some representative Rh(I) complexes are plotted against logarithm of the sweep rates. A linear correlation is obtained for each

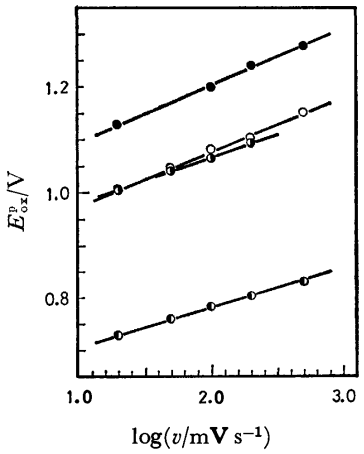

Fig. 3. Anodic peak potentials E^p_{ox} of $[Rh(t\text{-}BuNC)_4]^+$ (●), $[Rh(C_6H_{11}NC)_4]^+$ (○), $[Rh(p\text{-}MeOC_6H_4NC)_4]^+$ (◑), and $[Rh_2(p\text{-}MeOC_6H_4NC)_8]^{2+}$ (◐) as a function of the CV sweep rate v at a platinum microelectrode in CH_3CN containing 0.1 mol dm^{-3} n-Bu_4NClO_4 at 298 K.

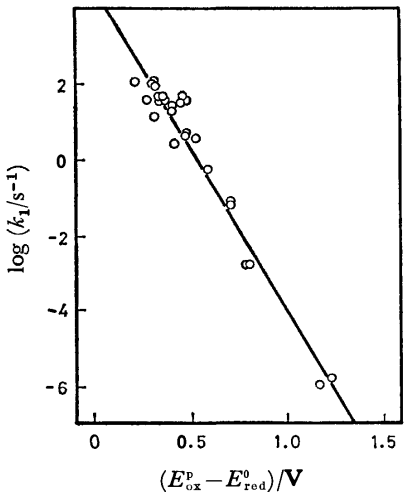

Fig. 4. Correlation between log k_1 for the oxidations of Rh(I) complexes with inorganic oxidants in CH_3CN and $E^p_{ox}-E^0_{red}$. Compare with Eq. 18 in text.

Rh(I) complex in accordance with Eq. 13. The slopes in Fig. 3 are almost the same for the present Rh(I) complexes, as 95±10 mV per decade, and are significantly larger than those of partially reversible electron transfer between the limits of 0 and 30 mV per decade.[19] Such large slopes may be characteristic of totally irreversible processes. Thus, from Eq. 13 the transfer coefficient β is obtained as 0.31±0.04 for the Rh(I) complexes studied here. The same β value was obtained from the analysis of the half-width of the CV wave in Fig. 1 by the use of Eq. 15 as well,[19]

$$E^p_{ox} - E^{p/2}_{ox} = 1.857\ (RT/\beta F) \qquad (15)$$

where $E^{p/2}_{ox}$ represents the electrode potential at the half peak current.

A Linear Free Energy Relationship (LFER) in the Irreversible Oxidation of Rh(I) Complexes. The foregoing section has established the conditions to use the E^p_{ox} values as the relative E^0_{ox} values (Eq. 11), such as the total irreversibility and the constant transfer coefficient β. In order to test the validity of Eq. 11 for the oxidation of Rh(I) complexes independently, the E^p_{ox} values have been compared with the electron transfer rate constants k_1 for the chemical oxidations of the Rh(I) complexes with inorganic oxidants by the following manner. Previously, the intramolecular electron transfer rate constants k_1 for reactions of a given Rh(I) complex with a series of inorganic oxidants whose reduction is reversible have been related to the reduction potentials of the oxidants by Eq. 16,[6] which accords with the Marcus relation (Eq. 17),[23]

$$\log k_1 = 8.5E^0_{red} + \text{Const.} \qquad (16)$$

$$\log k_1 = -8.5\Delta G^0 + \text{Const.} \qquad (17)$$

where ΔG^0 is the standard free energy change of electron transfer reactions given by $E^0_{ox}-E^0_{red}$ (in V). If Eq. 11 can be applied to the oxidations of Rh(I) complexes, the E^0_{ox} values which cannot be determined directly may be substituted by the experimentally accessible values of E^p_{ox}, and Eq. 17 is rewritten as Eq. 18. The relation of Eq. 18 is tested by plotting

$$\log k_1 = -8.5\ (E^p_{ox}-E^0_{red}) + \text{Const.} \qquad (18)$$

the log k_1 values for the oxidations of Rh(I) complexes with the inorganic oxidants against the $(E^p_{ox}-E^0_{red})$ values by taking the data in Table 2, as shown in Fig. 4. There is seen an excellent agreement between the experimental plot in Fig. 4 and the relation in Eq. 18 (the slope is −8.6 with the correlation coefficient ρ=0.98), which strongly supports the validity of Eq. 11. Thus, the LFER in Fig. 4 underscores the utility of the anodic peak potentials E^p_{ox} at a constant sweep rate for obtaining the relative oxidation potentials E^0_{ox} of Rh(I) complexes.

Variation of HOMO with Rh(I) Oligomerization. The E^p_{ox} values of Rh(I) complexes vary with the Rh(I) oligomerization (Table 1). Such variations of the E^p_{ox} value must reflect the change of the energy of the highest occupied molecular orbital (HOMO) from which electron is removed upon oxidation since the E^p_{ox} values are related to the standard oxidation potentials E^0_{ox} as discussed in the foregoing section. The variation of the E^p_{ox} values with the Rh(I) oligomerization may be understood by comparing the E^p_{ox} values with the electronic transition energies of the Rh(I) complexes which also reflect the HOMO energies, with the aid of the MO diagram of Rh(I) monomers and the oligomers shown in Fig. 5.[16] The HOMO energy, E^{HOMO}_n (n=1—4), increases with oligomerization, resulting in decrease of the transition energy in the order $h\nu_1 > h\nu_2 > h\nu_3 > h\nu_4$. Thus, the approximate relation between $h\nu_n$ and E^{HOMO}_n is given by Eq. 19 derived from the energy diagram (Fig. 5),

$$h\nu_n = -2E^{HOMO}_n + \text{Const.} \qquad (19)$$

where Const. is $h\nu_1+2E^{HOMO}_1$. The E^{HOMO}_n value is related to the oxidation potential E^0_{ox} by Eq. 20,[24]

$$E^{HOMO}_n = -E^0_{ox} + \Delta G^s - C' \qquad (20)$$

where ΔG^s is the free energy change of solvation in solutions, and C′ is a constant which includes the potential of the reference electrode on the absolute scale together with the liquid junction potential.[25] When

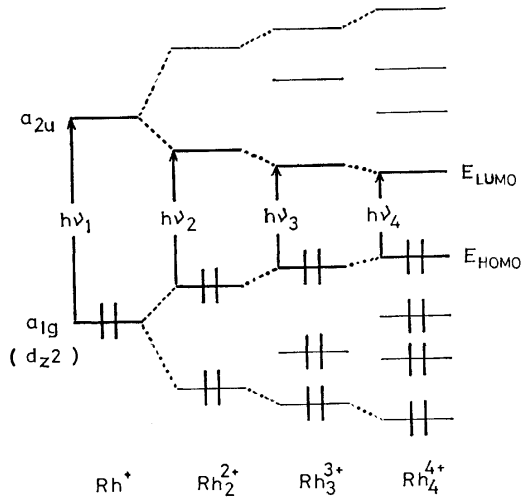

Fig. 5. MO diagram of the Rh(I) monomer and the oligomers.

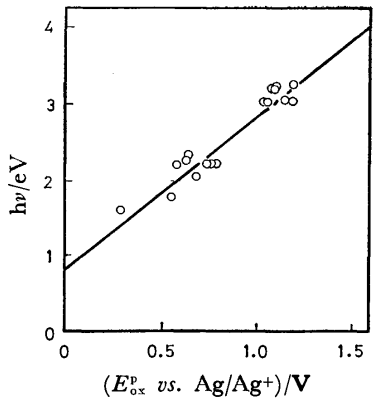

Fig. 6. Correlation between the electronic transition energies $h\nu$ of Rh(I) complexes and the anodic peak potentials E^{p}_{ox}.

ΔG^{s} is assumed as constant in the homologous series of Rh(I) complexes, Eq. 19 is rewritten by Eq. 21. Then, the relation between $h\nu_n$ and the anodic peak potential E^{p}_{ox} is obtained as Eq. 22, by substituting Eq. 11 into Eq. 21. The validity of Eq. 22 is confirmed from the plot between $h\nu$ and E^{p}_{ox} as shown in Fig. 6. Thus, the correlation between $h\nu$ and E^{p}_{ox} gives an additional support for the conclusion that the anodic peak potential E^{p}_{ox} can be taken as the relative thermodynamic quantity for the oxidation of Rh(I) complexes, E^{0}_{ox}, which cannot otherwise be obtained directly.

$$h\nu_n = 2E^{0}_{ox} + \text{Const.} \quad (21)$$

$$h\nu_n = 2E^{p}_{ox} + \text{Const.} \quad (22)$$

References

1) a) K. R. Mann, N. S. Lewis, V. M. Miskowski, D. K. Erwin, G. S. Hammond, and H. B. Gray, *J. Am. Chem. Soc.*, **99**, 5525 (1977); b) A. W. Maverick and H. B. Gray, *Pure Appl. Chem.*, **52**, 2339 (1980); c) H. B. Gray, K. R. Mann, N. S. Lewis, J. A. Thich, and R. M. Richma, *Adv. Chem. Ser.*, **168**, 44 (1978); d) K. R. Mann and H. B. Gray, *ibid.*, **173**, 225 (1979); e) V. M. Miscowski, I. S. Sigal, K. R. Mann, H. B. Gray, S. J. Milder, G. S. Hammond, and P. R. Ryason, *J. Am. Chem. Soc.*, **101**, 4383 (1979); f) I. S. Sigal, K. R. Mann, and H. B. Gray, *ibid.*, **102**, 7252 (1980).

2) K. Kalyanasundaram and M. Grätzel, *Angew. Chem., Int. Ed. Engl.*, **18**, 701 (1979); J. Kiwi, E. Borgarello, E. Pelizzetti, M. Visca, and M. Grätzel, *ibid.*, **19**, 646 (1980); A. Moradpour, E. Amouyal, P. Keller, and H. Kagan, *Nouv. J. Chim.*, **2**, 547 (1978).

3) J. M. Lehn and J. P. Sauvage, *Nouv. J. Chim.*, **1**, 449 (1977); M. Kirch, J. M. Lehn, and J. P. Sauvage, *Helv. Chim. Acta*, **62**, 1345 (1979); P. J. DeLaive, B. P. Sullivan, T. J. Meyer, and D. G. Whitten, *J. Am. Chem. Soc.*, **101**, 4007 (1979).

4) G. M. Brown, B. S. Brunschwig, C. Creutz, J. F. Endicott, and N. Sutin, *J. Am. Chem. Soc.*, **101**, 1298 (1979).

5) C. Creutz and N. Sutin, *Proc. Natl. Acad. Sci. U.S.A.*, **72**, 2858 (1975); N. Sutin and C. Creutz, *Adv. Chem. Ser.*, **168**, 1 (1978); D. G. Whitten, *Acc. Chem. Res.*, **13**, 83 (1980); C. T. Lin, W. Bottcher, M. Chou, C. Creutz, and N. Sutin, *J. Am. Chem. Soc.*, **98**, 6536 (1976).

6) S. Fukuzumi, N. Nishizawa, and T. Tanaka, *Bull. Chem. Soc. Jpn.*, in press.

7) T. Iinuma and T. Tanaka, *Inorg. Chim. Acta*, **49**, 79 (1981).

8) W. Hewertson and H. R. Watson, *J. Chem. Soc.*, **1962**, 1490.

9) A. L. Balch, *J. Am. Chem. Soc.*, **98**, 8049 (1976).

10) W. P. Weber, G. W. Gokel, and I. K. Ugi, *Angew. Chem., Int. Ed. Engl.*, **11**, 530 (1972).

11) J. Chatt, L. M. Vananzi, *J. Chem. Soc.*, **1957**, 4735.

12) N. S. Lewis, K. R. Mann, J. G. Gordon II, and H. B. Gray, *J. Am. Chem. Soc.*, **98**, 7461 (1976); K. Kawakami, M. Okajima, and T. Tanaka, *Bull. Chem. Soc. Jpn.*, **51**, 2327 (1978).

13) D. D. Perrin, W. L. F. Armarego, and D. R. Perrin, "Purification of Laboratory Chemicals," Pergamon Press, New York (1966).

14) R. P. Van Duyne and C. N. Reilley, *Anal. Chem.*, **44**, 142 (1972).

15) C. K. Mann, *Electroanal. Chem.*, **3**, 57 (1969).

16) K. Kawakami, M. Haga, and T. Tanaka, *J. Organomet. Chem.*, **60**, 363 (1973); K. R. Mann, J. G. Gordon II, and H. B. Gray, *J. Am. Chem. Soc.*, **97**, 3553 (1975); K. R. Mann, N. S. Lewis, R. M. Williams, H. B. Gray, and J. G. Gordon II, *Inorg. Chem.*, **17**, 828 (1978).

17) The third anodic current peak at 0.56 V due to the trimer was not observed clearly because of the smaller K_T.[6]

18) The rates of reactions between $[Rh_2(dppm)_2(RNC)_4]^{2+}$ and $[Fe(N\text{-}N)_3]^{3+}$ also were examined but too fast to be determined by the stopped-flow technique.

19) R. S. Nicholson and I. Shain, *Anal. Chem.*, **36**, 706 (1964).

20) R. J. Klingler and J. K. Kochi, *J. Am. Chem. Soc.*, **102**, 4790 (1980); **103**, 5839 (1981); *J. Phys. Chem.*, **85**, 1731 (1981).

21) The number of electrons transferred in the rate-determining step is taken as unity.[6]

22) T. L. Kelly and J. F. Endicott, *J. Am. Chem. Soc.*, **94**, 1797 (1972); B. B. Wayland and A. R. Newman, *ibid.*, **101**, 6472 (1979); H. Ogoshi, J. Setsune, and Z. Yoshida, *ibid.*, **99**, 3869 (1977).

23) R. A. Marcus, *Ann. Rev. Phys. Chem.*, **15**, 155 (1964); *J. Phys. Chem.*, **72**, 891 (1968).

24) M. E. Peover, *Electroanal. Chem.*, **2**, 1 (1967); B. Case, "Reactions of Molecules at Electrodes," ed by N. S. Hush, Wiley Interscience, New York (1971), p. 125.

25) R. E. Ballard, *Chem. Phys. Lett.*, **42**, 97 (1976).

Macrocyclic Enzyme Model System. Kinetic Activity of [20]Paracyclophane Bearing 1,4-Dihydronicotinamide and 2-Pyridinecarboxylic Acid Moieties as Effected by Zinc Ion†

Yukito Murakami,* Yasuhiro Aoyama,†† and Jun-ichi Kikuchi
Department of Organic Synthesis, Faculty of Engineering, Kyushu University, Hakozaki, Higashi-ku, Fukuoka 812

(Received March 1, 1982)

As regards the effect of zinc(II) ion on the reduction of hexachloroacetone, the kinetic activity of a [20]paracyclophane (PCP) bearing 1,4-dihydronicotinamide (HNA) and 2-pyridinecarboxylic acid (Py) moieties, HNA–PCP–Py, has been investigated as an alcohol dehydrogenase model in reference to that of PCP–HNA in the light of their metal-coordination behavior. The reduction ability of PCP–HNA was significantly lowered as it underwent complex formation with zinc. On the other hand, HNA–PCP–Py showed an apparent rate maximum in a relatively lower concentration range of $ZnCl_2$. The kinetic behavior was analyzed on the basis of the formation of two kinds of zinc complexes of HNA–PCP–Py: the 1:1 complex $\left(\begin{matrix}\text{Py}\\ \text{PCP}\\ \text{HNA}\end{matrix}\!\!>\!\text{Zn}^{\text{II}}\right)$, in which both Py and HNA moieties are simultaneously coordinated to the same zinc ion, showed a decreased reactivity relative to metal-free HNA–PCP–Py; while the 2:1 complex (HNA–PCP–Py–Zn^{II}–Py–PCP–HNA), in which HNA is free from metal-coordination, exercised a much enhanced activity, 7 times as reactive as metal-free HNA–PCP–Py. A plausible reaction mechanism for the enhanced reactivity has been discussed.

The NAD-dependent alcohol dehydrogenase contains zinc ion as an essential cofactor, and catalyzes the conversion of carbonyl compounds into alcohols and the reversed process. Such interconversion reactions are coupled with oxidation-reduction of the coenzyme. It is generally realized that direct coordination of the enzyme-bound zinc ion to an incorporated substrate promotes the hydrogen transfer between the coenzyme and the substrate,[1–3] and that there is no direct metal–coenzyme interaction in the enzyme active site.[3–5] In line with the participation of zinc ion in the enzyme system, metal ions have been observed to catalyze the reduction of *chelating* carbonyl substrates by simple NADH models[6–15] along with detailed kinetic analysis for relevant systems.[7,8,14] Recently, we have pointed out that a good alcohol dehydrogenase model needs to exhibit such a substrate–zinc interaction that arises from an enforced proximity effect even if the substrate has no or least intrinsic capability of coordination with zinc ion.[16] This situation can be attained if the dihydronicotinamide and the zinc ion are placed in an appropriate and fixed orientation owing to some rigid framework. Along this line, we have prepared a macrocyclic enzyme model involving both dihydronicotinamide and 2-pyridinecarboxylic acid moieties, the latter being an intramolecular zinc-binding site, and clarified its zinc-coordination behavior.[16] In the present work, we assessed the reactivities of zinc complexes of the [20]paracyclophane-based alcohol dehydrogenase model (HNA–PCP–Py) in the reduction of a simple carbonyl substrate in relation to that of a related compound having only a dihydronicotinamide moiety, PCP–HNA, in the light of their metal-coordination behavior.

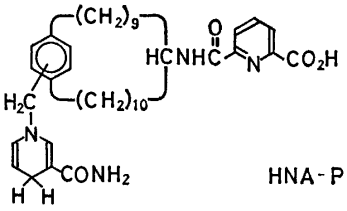

HNA-PCP-Py

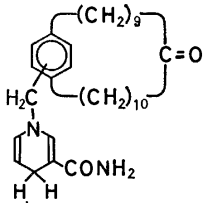

PCP-HNA

Experimental

Melting points were measured using capillary tubes with a Yamato MP-1 melting point apparatus (oil-bath type). Infrared spectra and ^1H NMR spectra were taken on a JASCO IR-E spectrophotometer and a Hitachi R-20 spectrometer, respectively. Electronic absorption spectra were obtained with a Union Giken SM-401 high-sensitivity spectrophotometer.

Materials. 1-[10(11)-(2-Carboxy-6-pyridylcarbonylamino)[20]paracyclophan-22-ylmethyl]-1,4-dihydronicotinamide (HNA–PCP–Py) and 1-[10(11)-oxo[20]paracyclophan-22-ylmethyl]-1,4-dihydronicotinamide (PCP–HNA) were prepared as described previously.[16] 1-Benzyl-1,4-dihydronicotinamide (BNAH) was prepared according to the published procedure.[17] Dichloromethane was fractionally distilled and stored over 4 Å molecular sieve. Hexachloroacetone was distilled (bp 110 °C/5.3×10^3 Pa) and zinc chloride of the highest quality was fused just before use.

Reduction of Hexachloroacetone with BNAH. A solution of BNAH (0.80 g, 3.7 mmol) and hexachloroacetone (1.0 g, 3.7 mmol) in dichloromethane (25 ml) was placed in a stoppered reaction vessel protected from room light, stirred for 9 h, and allowed to stand for 42 h at room temperature.

† Contribution No. 660 from this Department.

†† Present address: Department of Material Science and Technology, Technological University of Nagaoka, Nagaoka, Niigata 949-54.

Dilute hydrochloric acid (3%, 10 ml) was added to the solution, and the mixture was extracted with refluxing hexane (450 ml) for 7 h. The solvent was removed *in vacuo* and an oily residue was sublimed at 80 °C/1.1 × 10^4 Pa to recover colorless needles of 1,1,1,3,3,3-hexachloro-2-propanol (282 mg, 28%), mp 88.0—88.5 °C (lit,[18] 86—87 °C); IR spectrum being identical with that of the authentic sample obtained by LAH reduction of hexachloroacetone.[18]

The reaction behavior was monitored by ^{1}H NMR spectroscopy. Hexachloroacetone (30 μl, 2.0 × 10^{-4} mol) was added to a solution of BNAH (31 mg, 1.4 × 10^{-4} mol) in deuteriochloroform (300 μl), containing 5% toluene as an internal reference, in an NMR tube. After the reaction mixture was allowed to stand at room temperature for 1 h, ^{1}H NMR signals attributable to BNAH disappeared completely on one hand and a proton signal referred to the 2-proton of the alkoxide product (4.90 ppm downfield from Me_4Si) was observed to appear on the other. The latter signal was shifted to 4.81 ppm upon addition of deuterium oxide (30 μl). The signal intensity indicated quantitative formation of the alcohol.

Kinetic Measurements. A 30-μl sample of a stock solution of hexachloroacetone (1.0 mol dm^{-3}) in dichloromethane was injected into a reaction medium [dichloromethane–methanol (100:1 v/v), 3 ml], containing either PCP–HNA or HNA–PCP–Py (1.0 × 10^{-4} mol dm^{-3}) and an appropriate amount of $ZnCl_2$, placed in a thermostated cell (at 25.0 ± 0.1 °C) set in the spectrophotometer. The absorption intensity at 370 nm, characteristic of the dihydronicotinamide moiety, was measured to pursue the progress of reaction. An apparent first-order rate constant was obtained from the slope of the first-order plot for an early stage of the reaction. Control experiments indicated that no reaction took place in the absence of the carbonyl substrate. Hexachloroacetone having a broad absorption band at around 300 nm was independently shown to be practically free from spontaneous decomposition in dichloromethane–methanol (100:1 v/v), while underwent rapid decomposition (ketalization) in methanol. Kinetic measurements in methanol were not carried out due to such reason.

Results and Discussion

Hexachloroacetone is one of the activated carbonyl compounds which can be reduced with 1,4-dihydronicotinamides.[19,20] The reaction of hexachloroacetone with 1-benzyl-1,4-dihydronicotinamide in dichloromethane afforded 1,1,1,3,3,3-hexachloro-2-propanol quantitatively with concomitant formation of the oxidized nicotinamide salt, as shown below.

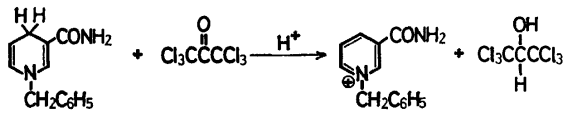

The reaction between the present cyclophane-1,4-dihydronicotinamide (PCP–HNA or HNA–PCP–Py, 1.0 × 10^{-4} mol dm^{-3}) and hexachloroacetone (1.0 × 10^{-2} mol dm^{-3}) in dichloromethane–methanol (100:1 v/v) was investigated kinetically both in the presence and absence of $ZnCl_2$. At lower concentrations of the zinc salt, the addition of water and/or methanol to the C_5–C_6 double bond of the dihydronicotinamide moiety also took place, leading to the formation of a solvolyzed product having an absorption maximum at around 290 nm. Since the solvolyzed product was not detected in the absence of the carbonyl substrate, it must be derived from the nicotinamide–substrate radical pair which was formed through one-electron transfer from the dihydronicotinamide moiety to the substrate.[21,22] The absorption maximum characteristic of the metal-free 1,4-dihydronicotinamide moiety appeared at 354.5 nm and shifted to somewhat longer wavelength as $ZnCl_2$ was added. Thus, the decrease in absorbance at 370 nm was measured to determine the reaction rate. The initial rate constants for reactions with PCP–HNA and HNA–PCP–Py are plotted in Fig. 1 against the total concentration of $ZnCl_2$. As described previously for the coordination equilibrium involving PCP–HNA and zinc ion,[16] the sole existing species in the concentration range of $[Zn^{II}] > 1 \times 10^{-3}$ mol dm^{-3} is a Zn^{II} complex at a 1:1 molar ratio of ligand to metal (PCP–HNA–Zn^{II}) and both the metal-free species and the zinc complex are present at the intermediate zinc

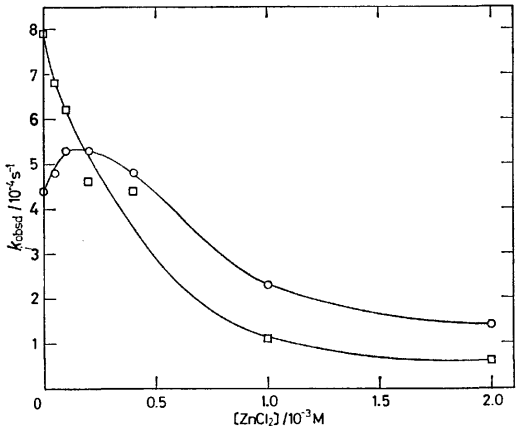

Fig. 1. Correlations between total concentration of $ZnCl_2$ and apparent first-order rate constant for reduction of hexachloroacetone (1.0 × 10^{-2} mol dm^{-3}) with HNA–PCP–Py (○) (1.0 × 10^{-4} mol dm^{-3}) and PCP–HNA (□) (1.0 × 10^{-4} mol dm^{-3}) in dichloromethane–methanol (100:1 v/v) at 25.0 °C.

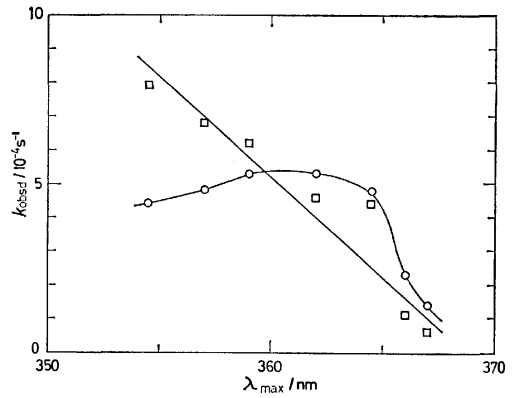

Fig. 2. Correlations between λ_{max} of the dihydronicotinamide moiety and rate constant for reduction of hexachloroacetone (1.0 × 10^{-2} mol dm^{-3}) in the presence of the same varying amounts of $ZnCl_2$: HNA–PCP–Py (○), 1.0 × 10^{-4} mol dm^{-3}; PCP–HNA (□), 1.0 × 10^{-4} mol dm^{-3}; in dichloromethane–methanol (100:1 v/v) at 25.0 °C.

Table 1. Specific first-order rate constants for reactions of dihydronicotinamide species with hexachloroacetone (1.0×10^{-2} mol dm^{-3}) at 25.0 °C

Dihydronicotinamide	Medium	k/s^{-1}
PCP-HNA	CH_2Cl_2-CH_3OH (100 : 1 v/v)	7.9×10^{-4}
PCP-HNA-Zn^{II}	CH_2Cl_2-CH_3OH (100 : 1 v/v)	0.6×10^{-4}
HNA-PCP-Py	CH_2Cl_2-CH_3OH (100 : 1 v/v)	4.4×10^{-4}
	CH_2Cl_2	2.9×10^{-4}
PCP$\langle^{Py}_{HNA}\rangle Zn^{II}$	CH_2Cl_2-CH_3OH (100 : 1 v/v)	1.4×10^{-4}
HNA-PCP-Py-Zn^{II}-Py-PCP-HNA	CH_2Cl_2-CH_3OH (100 : 1 v/v)	3×10^{-3}
	CH_2Cl_2	2×10^{-3}

concentration range. The rate constant for the reaction with PCP–HNA monotonously decreases as the concentration of zinc ion is raised until it levels off beyond $[Zn^{II}]>1\times10^{-3}$ mol dm^{-3}. It is apparent that PCP–HNA–Zn^{II} has a reduced reactivity (by a factor of 13) compared with PCP–HNA. A nearly linear correlation between rate constant and λ_{max} of the PCP–HNA species obtained by changing the zinc concentration (Fig. 2) also indicates that the formation of the zinc complex with the dihydronicotinamide moiety of PCP–HNA is responsible for the diminished rate, and the medium effect has no direct concern. Whatever the mechanistic details may be,[13,23-31] the reduction with dihydronicotinamide is an electron-donating process and the deactivation of PCP–HNA upon complex formation with Zn^{II} is readily understood on this basis.[20]

As for the HNA–PCP–Py system, the most remarkable aspect is that the rate constant reaches a maximum and then falls down as the concentration of $ZnCl_2$ increases (Fig. 1). This overall feature is completely reproducible in several sets of kinetic runs. The observed correlation of rate with $ZnCl_2$ concentration may be understood on the following basis: at least two kinds of zinc complexes are present in the reaction system to control the rate, the major one with a diminished (relative to HNA–PCP–Py) reactivity and the minor one with an enhanced reactivity. Figure 2 shows another aspect of the reaction behavior. In spite of an increase in the fraction of dihydronicotinamide–Zn^{II} species as the Zn^{II} concentration increases to a certain extent, the expected reduction in rate is compensated by contribution of rate-enhancement brought about by the active zinc species. In the light of the coordination behavior,[16] the major deactivated species and the minor activated one are referred to the 1:1 complex (PCP$\langle^{Py}_{HNA}\rangle Zn^{II}$), in which both Py and HNA moieties are simultaneously coordinated to the same zinc ion, and the 2:1 complex (HNA–PCP–Py–Zn^{II}–Py–PCP–HNA), in which HNA is free from metal-coordination, respectively. Consistent with this view, the highest reactivity is attained (Fig. 1) when the 2:1 complex reaches its maximum concentration at $[ZnCl_2]\cong1\times10^{-4}$ mol dm^{-3}. The rate constant at $[ZnCl_2]=2.0\times10^{-3}$ mol dm^{-3} may represent the specific reactivity of PCP$\langle^{Py}_{HNA}\rangle Zn^{II}$. The specific rate constant for the 2:1 complex, HNA–PCP–Py–Zn^{II}–Py–PCP–HNA, was calculated so that the observed rate–$[ZnCl_2]$ profile can be best reproduced by summation of rate contributions of the metal-free species (specific rate constant 4.4×10^{-4} s^{-1}), the 1:1 complex (specific rate constant 1.4×10^{-4} s^{-1}), and the 2:1 complex on the basis of their respective populations: a value of 3×10^{-3} s^{-1} (per HNA–PCP–Py unit) was obtained, larger by factor of 7 than that for the metal-free HNA–PCP–Py. The kinetic behavior of HNA–PCP–Py (5.1×10^{-5} mol dm^{-3}) was also investigated in dry dichloromethane, in which the addition reaction of water and/or methanol to dihydronicotinamide was not detected. The rate–$[ZnCl_2]$ profile, showing again a maximum at relatively lower concentration of zinc, was analyzed in a manner as described above under the assumption that the coordination behavior of HNA–PCP–Py in dichloromethane is the same as that in dichloromethane–methanol (100:1 v/v); the reactivity of HNA–PCP–Py–Zn^{II}–Py–PCP–HNA (per HNA–PCP–Py unit), 2×10^{-3} s^{-1}, 7 times as large as that of HNA–PCP–Py (2.9×10^{-4} s^{-1}). The specific rate constants for reduction of hexachloroacetone are summarized in Table 1.

The rate enhancement by HNA–PCP–Py–Zn^{II}–Py–PCP–HNA, even though not extremely large, should not be underestimated in reference to the more marked rate enhancement brought about by Zn^{II} in reduction of 2-pyridinecarbaldehyde,[6-12] its Schiff base,[12] 1,10-phenanthroline-2-carbaldehyde,[13] and pyridoxal phosphate[15] with dihydronicotinamide and its derivatives. These substrates are *specific* because, by virtue of their metal-chelating abilities, they readily form zinc complexes which are undoubtedly more susceptible to reduction with dihydronicotinamides. Not being limited to the nicotinamide chemistry, many investigators working on the metal-ion catalysis often choose *specific* substrates so as to be suited for given catalysts, which then undergo chelation with such substrates. However, we rather take a different approach; a catalyst should be chosen so as to be effective for a given *non-specific* substrate. It is generally realized that the role of zinc ion in the reduction of a carbonyl compound with alcohol dehydrogenase is to polarize the carbonyl group through metal-coordination and consequently facilitate the hydride transfer (in a formal sense) from the 1,4-dihydronicotinamide moiety of coenzyme NADH to the carbonyl carbon.[1-3] Hexachloroacetone, an electron-deficient carbonyl compound, may have the least tendency to coordinate to a metal ion. On the basis of these considerations, the ultimate goal of the present study has been to clarify whether or

not the zinc ion accelerates the reduction of hexachloroacetone, a *non-specific* substrate as regards the metal-coordination tendency, by a reaction mechanism schematically shown in **1**. The acceleration effect pro-

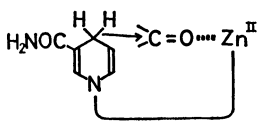

1

vided by the zinc ion, involved in the 2:1 complex (HNA–PCP–Py–Zn^{II}–Py–PCP–HNA), is the first successful example along this line, to the best of our knowledge. As for the overall rate effect provided by the zinc ion on the present reaction, the major complex formed with HNA–PCP–Py ($PCP\langle^{Py}_{HNA}\rangle Zn^{II}$) reduced the reactivity of HNA–PCP–Py itself. In order to improve this situation, a ligand for coordination with the zinc ion must have significantly larger metal-binding ability than the dihydronicotinamide moiety. Furthermore, dihydronicotinamide and ligand moieties need to be constrained in a certain limited space so that the cooperation of the former and the zinc ion bound to the latter toward a substrate molecule is geometrically possible under the condition: the zinc-binding with the ligand should not result ultimately in metal-bridging between the dihydronicotinamide and ligand moieties.

References

1) H. Sund and H. Theorell, "The Enzymes," 2nd ed, ed by P. D. Boyer, Academic Press, New York (1963), Vol. 7, p. 27.

2) R. H. Abeles, R. F. Hutton, and F. H. Westheimer, *J. Am. Chem. Soc.*, **79**, 712 (1957).

3) M. Hughes and R. H. Prince, *Bioorg. Chem.*, **6**, 137 (1977).

4) H. Dutler and C. -I. Brändén, *Bioorg. Chem.*, **10**, 1 (1981).

5) M. Hughes and R. H. Prince, *J. Inorg. Nucl. Chem.*, **40**, 719 (1978).

6) R. A. Hood and R. H. Prince, *J. Chem. Soc., Chem. Commun.*, **1979**, 163.

7) M. Hughes and R. H. Prince, *J. Inorg. Nucl. Chem.*, **40**, 703 (1978).

8) R. A. Gase, G. Boxhoorn, and U. K. Pandit, *Tetrahedron Lett.*, **1976**, 2889.

9) M. Shirai, T. Chisina, and M. Tanaka, *Bull. Chem. Soc. Jpn.*, **48**, 1079 (1975).

10) W. Tagaki, H. Sakai, Y. Yano, K. Ozeki, and Y. Shimizu, *Tetrahedron Lett.*, **1976**, 2541.

11) K. Watanabe, R. Kawaguchi, and H. Kato, *Chem. Lett.*, **1978**, 255.

12) S. Shinkai, H. Hamada, Y. Kusano, and O. Manabe, *Bull. Chem. Soc. Jpn.*, **52**, 2600 (1979).

13) D. J. Creighton, J. Hajdu, and D. S. Sigman, *J. Am. Chem. Soc.*, **98**, 4619 (1976).

14) A. Ohno, S. Yasui, R. A. Gase, S. Oka, and U. K. Pandit, *Bioorg. Chem.*, **9**, 199 (1980).

15) S. Shinkai and T. C. Bruice, *J. Am. Chem. Soc.*, **94**, 8258 (1972).

16) Y. Murakami, Y. Aoyama, and J. Kikuchi, *J. Chem. Soc., Perkin Trans. 1*, **1981**, 2809.

17) Y. Kurusu, K. Nakajima, and M. Okawara, *Kogyo Kagaku Zasshi*, **71**, 934 (1968).

18) M. Geiger, E. Usteri, and Ch. Gränacher, *Helv. Chim. Acta*, **34**, 1335 (1951).

19) D. C. Dittmer and R. A. Fouty, *J. Am. Chem. Soc.*, **86**, 91 (1964).

20) D. C. Dittmer, A. Lambardo, F. H. Batzold, and C. S. Greene, *J. Org. Chem.*, **41**, 2976 (1976).

21) P. van Eikeren, P. Kenney, and R. Tokmakian, *J. Am. Chem. Soc.*, **101**, 7402 (1979).

22) P. van Eikeren, D. L. Grier, and J. Eliason, *J. Am. Chem. Soc.*, **101**, 7406 (1979).

23) L. C. Kurz and C. Frieden, *J. Am. Chem. Soc.*, **97**, 677 (1975).

24) R. A. Hood, R. H. Prince, and K. A. Rubinson, *J. Chem. Soc., Chem. Commun.*, **1978**, 300.

25) F. M. Martens, J. W. Verhoeven, R. A. Gase, U. K. Pandit, and Th. J. de Boer, *Tetrahedron*, **34**, 443 (1978).

26) J. J. Steffens and D. M. Chipman, *J. Am. Chem. Soc.*, **93**, 6694 (1971).

27) J. Hajdu and D. S. Sigman, *J. Am. Chem. Soc.*, **98**, 6060 (1976).

28) P. van Eikeren and D. L. Grier, *J. Am. Chem. Soc.*, **99**, 8057 (1977).

29) E. M. Kosower, A. Teuerstein, H. D. Burrows, and A. J. Swallow, *J. Am. Chem. Soc.*, **100**, 5185 (1978).

30) A. Ohno, H. Yamamoto, and S. Oka, *J. Am. Chem. Soc.*, **103**, 2041 (1981).

31) A. Ohno, T. Shio, H. Yamamoto, and S. Oka, *J. Am. Chem. Soc.*, **103**, 2045 (1981).

Diarsenic Trioxide for Substituting Bridging Oxygen for Chlorine in Phosphorus Chlorides

Makoto WATANABE* and John R. VAN WAZER†

Department of Industrial Chemistry, Chubu Institute of Technology, Matsumoto-cho, Kasugai, Aichi 487

† *Department of Chemistry, Vanderbilt University, Nashville, Tennessee 37235, U. S. A.*

(Received November 24, 1981)

A preferential exchange of chlorines and bridging oxygens between phosphorus(III and V) chlorides and diarsenic trioxide was studied by adding diarsenic trioxide into phosphorus chlorides and then heating the mixtures at 50—60 °C with vigorous stirring under dried nitrogen (phosphorus(III) chlorides) or dried air (phosphorus(V) chlorides). ^{31}P NMR study showed that the exchange of chlorines and oxygens occurred between diarsenic trioxide and phosphorus trichloride, phosphoryl chloride, diethylphosphinic chloride, tetramethylphosphorodiamidic chloride, or diethylphosphinothioic chloride and that P–O–P bonds were formed in the products.

Diphosphorus trioxide is conventionally prepared by burning phosphorus under a reduced supply of oxygen. It is not easy to obtain pure diphosphorus trioxide by this method. One of us (J. R. Van Wazer) has pointed out the possibility of the exchange reaction of oxygen and halogen atoms for several pairs of different atoms. Among these exchange reactions, the enthalpy of the exchange between P–Cl and As–O bonds is the largest one, about 75 kJ/bond.[1] Therefore, we studied the exchange of oxygen and chlorine between diarsenic trioxide and several phosphorus(III and V) chlorides to investigate the formation of the P–O–P bond from the P–Cl bond.

Experimental

Materials. The diarsenic trioxide used in this study was purchased from J. T. Baker Chemical Co. and was ground for about 30 min by a miller, MIXER/MILL, made by Spex Co. Phosphorus trichloride, phosphoryl chloride, and carbon disulfide were Fisher Scientific Co. reagent grade. Phosphorus trichloride and phosphoryl chloride were distilled. Carbon disulfide was dried with calcium chloride and then distilled. Phenylphosphorous dichloride, diethylphosphinic chloride, diphenyl phosphorochloridate, tetramethylphosphorodiamidic chloride, and dimethylphosphinothioic chloride were purchased from Aldrich Chemical Co. and were used without any other purification. They were checked by ^{31}P NMR and gave the correct spectra.

^{31}P NMR Measurement. ^{31}P NMR measurements were carried out on Varian XL-100 spectrometer at 40.48 MHz. The chemical shifts in the phosphorus spectra are reported with respect to 85% phosphoric acid. In all cases, positive shifts were measured upfield.

Procedure. Diarsenic trioxide was added into a large excess of phosphorus(III) chloride in a three-necked round bottom flask under a stream of dried nitrogen. The mixtures were heated at 50—60 °C with vigorous stirring by using a hot-plate magnetic stirrer. The reaction mixtures were withdrawn at hourly intervals and analyzed for phosphorus compounds by the ^{31}P NMR instrument without any other solvent. The mixtures of diarsenic trioxide and a large excess of phosphorus(V) chloride were also reacted under dried air at 50—60 °C in the same way as that of the reaction of phosphorus(III) chloride. The progress of the reaction of the mixtures was checked by the same way as used for the reactions of phosphorus(III) chloride. The ^{31}P NMR analysis of the solid product in the system of phosphoryl chloride and diarsenic trioxide was also made by dissolving it in cold water.

Results and Discussion

As_2O_3–PCl_3 System. Typical NMR spectra of the reaction mixture are shown in Fig. 1. In the early stage of the reaction, the mixture gave a peak of PCl_3 at −220 ppm and unknown peaks at −183 and −193 ppm. The peak height of these unknown peaks did not change much with the passage of reaction time. Finally, the mixture gave a narrow peak of diphosphorus trioxide at −113 ppm and an unknown peak at −133 ppm. The intensity of these peaks increased as the reaction proceeded. The peak height of diphosphorus trioxide had a maximum; after

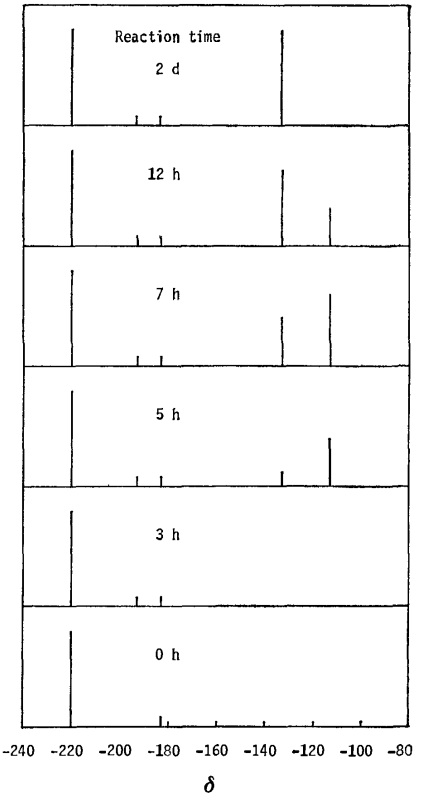

Fig. 1. ^{31}P NMR spectra of the reaction mixture of the As_2O_3–PCl_3 system.

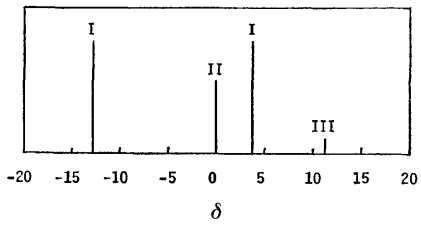

Fig. 2. ^{31}P NMR spectrum of the aqueous solution of the solid product of the As_2O_3–PCl_3 system.
I: Phosphonic acid, II: orthophosphoric acid, III: diphosphoric acid.

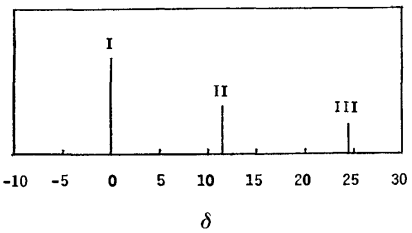

Fig. 3. ^{31}P NMR spectrum of the aqueous solution of the solid product of the As_2O_3–$POCl_3$ system.
I: Orthophosphoric acid, II: diphosphoric acid, III: *cyclo*-tetraphosphoric acid.

the maximum, it decreased gradually and finally disappeared. At this step of the reaction, the mixture gave a peak of phosphorus trichloride and unknown peaks at −133, −183, and −193 ppm. It was necessary to stir the reaction mixture vigorously to increase the rate of reaction. If the reaction mixture was stirred gently, it would take a much longer time to finish the reaction. When the reaction was stopped at the stage of maximum height of the ^{31}P NMR peak corresponding to diphosphorus trioxide, the reaction mixture contained a white precipitate. This precipitate was separated from the phosphorus trichloride solution by filtration and washed with phosphorus trichloride in a dry bag under nitrogen. Diphosphorus trioxide was obtained by a reduced distillation (667 Pa, 40 °C) of the phosphorus trichloride solution by using a trap cooled by Dry Ice–methanol; it had a melting point of around 23 °C and gave a narrow sharp ^{31}P NMR peak at −113 ppm. The yield of diphosphorus trioxide was about 35% relative to the amount of diarsenic trioxide used in this experiment. The liquid product in the trap gave boiling points of 75 and 130 °C at atmospheric pressure. The compound with a boiling point of 75 °C is unreacted phosphorus trichloride and that with a boiling point of 130 °C is arsenic trichloride. When the white precipitate was dissolved in cold water, a reddish brown precipitate was produced. The precipitate was filtered; the ^{31}P NMR spectrum of the filtrate is shown in Fig. 2. These peaks are due to phosphonic acid and ortho- and diphosphoric acids. The reddish brown precipitate was soluble in nitric acid and the solution gave the peak of phosphoric acid. So it could be concluded that the reddish brown precipitate is red phosphorus containing some phosphorus suboxides. Accordingly, the white precipitate mentioned above must be diphosphorus tetraoxide. Diphosphorus trioxide is oxidized very easily with oxygen, and the produced diphosphorus trioxide seems to be oxidized by slight amounts of oxygen in the reaction apparatus. It was difficult to prevent oxidation in the reaction apparatus used in this experiment. According to above results, one can write the following chemical equation for this reaction system:

$$4PCl_3 + 2As_2O_3 \xrightarrow{(N_2)} P_4O_6 + 4AsCl_3.$$
$$\downarrow (O_2)$$
$$P_4O_8$$

Diphosphorus trioxide was extracted from diphosphorus tetraoxide with carbon disulfide by mixing the tetraoxide with carbon disulfide and stirring the mixture under nitrogen. It took a long time to extract (a few days). The peak at −133 ppm seems to be due to diphosphorus trioxide, since one peak of diphosphorus trioxide shifts easily from −113 ppm to −133 ppm in arsenic trichloride. Diphosphorus trioxide gives the same peak at −133 ppm in phosphorus trichloride and the change is very slow.[2)]

As_2O_3–$C_6H_5PCl_2$ System. The reaction mixture was brown in the initial stage of the reaction. The reaction mixture did not give any peak other than that of phenylphosphonous dichloride. The reaction was stopped at the reaction time of 15 h and the brownish solid product was separated by filtration. The solid product was insoluble in any solvent, so it was impossible to study the phosphorus compounds contained in the solid product by the ^{31}P NMR instrument.

As_2O_3–$POCl_3$ System. The reaction mixture did not show any ^{31}P NMR spectrum other than that of phosphoryl chloride at any reaction time. At the reaction time of 50 h, the reaction mixture was cooled and the ashy solid product was filtered in a dry bag. The solid product was insoluble in any solvent. When the product was dissolved in water, the aqueous solution gave the spectrum shown in Fig. 3. The aqueous solution of diphosphorus pentaoxide gives the same spectrum and diphosphorus pentaoxide is insoluble in any solvent. So the ashy solid product must be diphosphorus pentaoxide. The liquid part of the reaction mixture was distilled at atmospheric pressure. It gave products with boiling points of 108 and 130 °C; these are unreacted phosphoryl chloride and arsenic trichloride. Therefore, the following equation can be written for this reaction system:

$$4POCl_3 + 2As_2O_3 \longrightarrow P_4O_{10} + 4AsCl_3.$$

As_2O_3–$(C_2H_5)_2POCl$ System. Diarsenic trioxide was soluble in diethylphosphinic chloride. The dissolution reaction is highly exothermic. So diarsenic trioxide was added carefully to diethylphosphinic chloride; the temperature of the mixture did not go beyond 60 °C. About 3 g of diarsenic trioxide was dissolved completely in 12 cm^3 of diethylphosphinic chloride. The reaction system seemed to reach equilibrium in less than 1 h, because the ^{31}P NMR spectrum of the reaction mixture gave the same spectrum at any reaction time longer than 1 h. The ^{31}P NMR spectrum

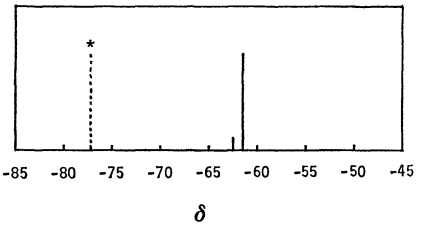

Fig. 4. Proton decoupled ^{31}P NMR spectrum of the reaction mixture of the As_2O_3–$(C_2H_5)_2POCl$ system at a reaction time of 1 h.
*: Diethylphosphinic chloride.

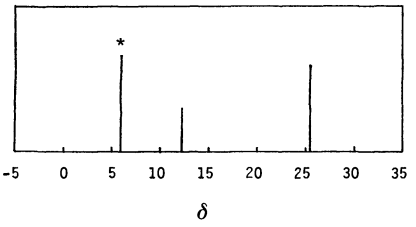

Fig. 5. ^{31}P NMR spectrum of the reaction mixture of the As_2O_3–$(C_6H_5O)_2POCl$ system at a reaction time of 15 h.
*: Diphenyl phosphorochloridate.

of the reaction mixture at the reaction time of 1 h is shown in Fig. 4. The mixture gave a strong peak at −61.5 ppm. This peak seems to be due to diethylphosphinic anhydride, $(C_2H_5)_2\overset{O}{P}O\overset{O}{P}(C_2H_5)_2$. There are no ^{31}P NMR data about diethylphosphinic anhydride, but P(α) of $(C_2H_5)_2\overset{O}{\underset{\alpha}{P}}O\overset{S}{\underset{\beta}{P}}(C_2H_5)_2$ gives a ^{31}P NMR peak at −60 ppm.[3] Accordingly, a preferential exchange of oxygen and chlorine between diarsenic trioxide and diethylphosphinic chloride seems to take place in this reaction system. Another new peak at −62.5 ppm could not be identified. Arsenic trichloride was not obtained by distillation of the reaction mixture.

As_2O_3–$(C_6H_5O)_2POCl$ System. Diarsenic trioxide does not dissolve in diphenyl phosphorochloridate. As is shown in Fig. 5, the reaction mixture gave two new peaks at 12.2 and 25.6 ppm other than that of diphenyl phosphorochloridate. The intensity of the new peaks increased with reaction time. Tetraphenyl diphosphate, $(C_6H_5O)_2\overset{O}{P}O\overset{O}{P}(C_6H_5O)_2$, gives a ^{31}P NMR peak at 23.3 ppm,[3] so the new peaks do not come from tetraphenyl diphosphate. There are no ^{31}P NMR data for these new peaks.

As_2O_3–$[(CH_3)_2N]_2POCl$ System. Diarsenic trioxide did not dissolve in tetramethylphosphorodiamidic chloride. The reaction mixture gradually changed into an ashy color with the elapse of reaction time. The ^{31}P NMR spectrum of the reaction mixture is shown in Fig. 6 and a strong new peak appears at −11 ppm. The height of the new peak increased as the reaction proceeded. The data listed in Ref. 3 show that octamethyldiphosphoramide, $[(CH_3)_2N]_2\overset{O}{P}O\overset{O}{P}[(CH_3)_2N]_2$, gives a ^{31}P NMR peak at −11 ppm. It can be concluded that the exchange of oxygen and chlorine between diarsenic trioxide and tetramethylphosphorodiamidic chloride occurs in this reaction system. We could not find from where the other weak new peaks come. Arsenic trichloride was not obtained by distillation of the reaction mixture.

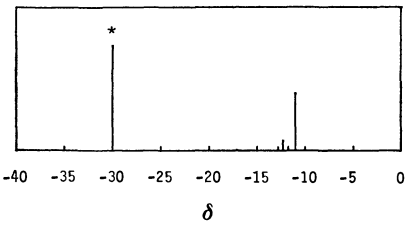

Fig. 6. Proton decoupled ^{31}P NMR spectrum of the reaction mixture of the As_2O_3–$[(CH_3)_2N]_2POCl$ system at a reaction time of 18 h.
*: Tetramethylphosphorodiamidic chloride.

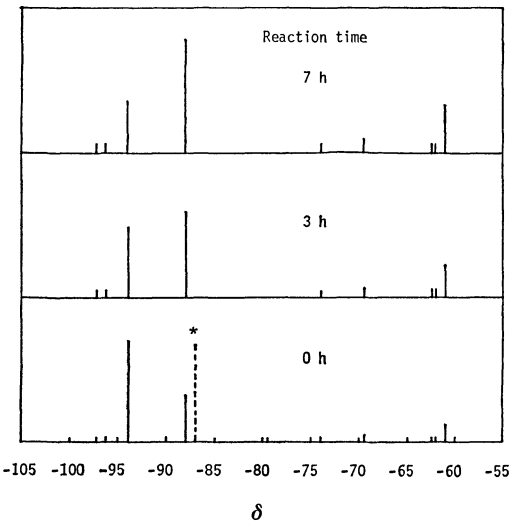

Fig. 7. Proton decoupled ^{31}P NMR spectrum of the reaction mixture of the As_2O_3–$(CH_3)_2PSCl$ system.
*: Dimethylphosphinothioic chloride.

As_2O_3–$(CH_3)_2PSCl$ System. Diarsenic trioxide dissolves in dimethylphosphinothioic chloride and the reaction is highly exothermic. Diarsenic trioxide was added into dimethylphosphinothioic chloride so slowly that the temperature of the mixture did not go beyond 60 °C. As is shown in Fig. 7, just after mixing, the mixture gave two strong new peaks at −94 and −88 ppm and several weak peaks in the region below −95 ppm and the region between −61 and −80 ppm. The peak at −94 ppm decreased and the peak at −88 ppm increased as the reaction proceeded. There are no ^{31}P NMR data about dimethylphosphinothioic anhydride, but the data in Ref. 3 give these results:

$$(C_6H_5)_2PSCl \longrightarrow (C_6H_5)_2\overset{S}{P}O\overset{S}{P}(C_6H_5)_2$$
$$-79.5 \text{ ppm} \qquad -79.3 \text{ ppm}$$

$$(CH_3)(C_2H_5)PSCl \longrightarrow (CH_3)(C_2H_6)\overset{O}{\underset{\alpha}{P}}O\overset{S}{\underset{\beta}{P}}(CH_3)(C_2H_5)$$
$$-98 \text{ ppm} \qquad P(\beta): -98.1 \text{ ppm}$$

$$(C_2H_5)_2PSCl \longrightarrow (C_2H_5)_2\overset{\alpha}{P}O\overset{\beta}{P}(C_2H_5)_2 \quad (O\ S)$$

-109 ppm P(β): -107 ppm

The result of this reaction system is

$$(CH_3)_2PSCl \longrightarrow \text{Product.}$$

-87 ppm -88 ppm

The new peak at -88 ppm may come from dimethylphosphinothioic anhydride, $(CH_3)_2\overset{S}{P}O\overset{S}{P}(CH_3)_2$. The other new peaks could not be identified. Arsenic trichloride was not obtained by distillation of the reaction mixture.

References

1) J. R. Van Wazer and K. Moedritzer, *J. Am. Chem. Soc.*, **90**, 47 (1968).

2) J. G. Riess and J. R. Van Wazer, *Inorg. Chem.*, **5**, 178 (1966).

3) M. M. Crutchfield, C. H. Dungan, J. H. Letcher, V. Mark, and J. R. Van Wazer, "^{31}P Nuclear Magnetic Resonance, Topics in Phosphorus Chemistry," Interscience Publishers, New York (1967), Vol. V, p. 227; and the references cited there.

 © 1982 The Chemical Society of Japan Bull. Chem. Soc. Jpn., 55, 2906—2910 (1982) [Vol. 55, No. 9

Substitution of Cyano Group by Hydroxyalkyl Group and of Ring Hydrogen by Alkoxyl Group in UV-Irradiation of 2-Pyridinecarbonitrile in Alcohols

Akira SUGIMORI,* Toshikazu FURIHATA, Shigeyuki MIKAYAMA, Makiko YOSHIDA, and Yasuo NAKANISHI

Department of Chemistry, Faculty of Science and Technology, Sophia University, Kioi-cho 7-1, Chiyoda-ku, Tokyo 102

(Received August 12, 1981)

The UV-irradiation of 2-pyridinecarbonitrile(**1**) in methanol and in ethanol brings about the replacement of the cyano group by the hydroxyalkyl groups and the replacement of the ring hydrogen by the alkoxyl group. Free base-form of **1** in ethanol undergoes exclusively photo-hydroxyethylation, while the pyridinium form of **1** in ethanol undergoes both photo-hydroxyethylation *via* a singlet excited state and -ethoxylation *via* a singlet-excited state complex, which is quenched by the electron transfer from the aromatic hydrocarbons to the excited complex.

Photochemical reactions of aromatic carbonitriles have been extensively investigated, especially from the viewpoint of the photoreactions *via* charge transfer complexes either in the ground state or in the excited state.[1,2] Concerning the photoreactions of quinolinecarbonitriles in alcohols, Hata *et al.* reported the substitution of the cyano group by the hydroxyalkyl groups derived from the solvent alcohols.[3] A similar photosubstitution has been reported for 4-pyridinecarbonitrile–triethylamine system.[4] Most of the reported photoreactions of aromatic and heteroaromatic nitriles are the substitution of CN in radical processes.

Another photoreactivity is expected for pyridinecarbonitriles: As a member of pyridinecarboxylic acid derivatives,[5,6] they are expected to undergo ionic type reactions. The main concern of our present study is to clarify in the photoreactions of pyridinecarbonitriles whether ionic processes similar to those of pyridinecarboxylic esters occur actually in parallel with radical processes or not and further what kinds of excited states are responsible for photoreactions.[7]

Results and Discussion

The UV-irradiation of 2-pyridinecarbonitrile (**1**) in alcohols brings about the replacement of the cyano group by the hydroxyalkyl group and the replacement of the ring hydrogen by the alkoxyl group (Table 1).

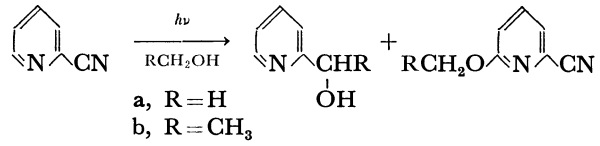

a, R=H
b, R=CH_3

1 **2** **3**

The former reaction is similar to that reported for quinolinecarbonitriles[3] and the latter to that reported for 2-pyridinecarboxylic ester.[6]

A detailed study was done mainly on the **1**–ethanol system. Which of the reactions is dominant is dependent on the reaction conditions: 1) the presence or the absence of the added acids, 2) the nature of the added acids, and 3) the concentration of **1**. Additives (quenchers) affect photo-ethoxylation and -hydroxyethylation differently.

Table 1 and Fig. 1 show the effect of sulfuric acid

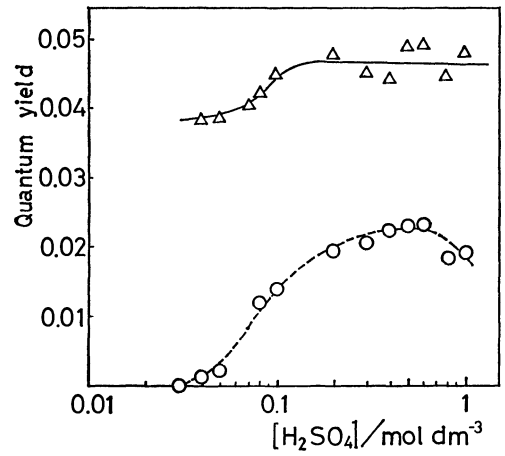

Fig. 1. Dependence of photo-hydroxyethylation and -ethoxylation of **1** on the concentration of sulfuric acid.
[**1**]=0.04 mol dm^{-3}, —△—: **2b**, --○--: **3b**.

on the photoreaction. In the absence of sulfuric acid, hydroxyethylation occurs exclusively. However, ethoxylation becomes significant as the concentration of sulfuric acid increases.

Like the photo-methoxylation of methyl 2-pyridinecarboxylate[6] and 2-pyridinecarboxylic acid,[8] the photo-ethoxylation of 2-pyridinecarbonitrile shows a remarkable concentration dependence (Fig. 2). Such behavior, *i.e.*, that alkoxylation is efficient at higher concentrations of the substrates, is an important common feature of 2-pyridinecarboxylic acid derivatives. A kinetic analysis for photo-methoxylation of methyl 2-pyridinecarboxylate shows that the concentration dependence is due to the formation of an excimer which undergoes alkoxylation.[6] A similar mechanism can be applied to the photo-ethoxylation of **1**.

An attempt to obtain direct evidence for the existence of an excimer by means of emission spectral measurement was unsuccessful because no fluorescence from **1** was observed either in lower or higher concentration of **1**.

In order to identify the excited species responsible for hydroxyethylation and ethoxylation, the effects of *trans*-1,3-pentadiene, anthracene, naphthalene, fluorene, and azulene were analyzed. Because some additives

Table 1. Yields of products in photoreaction of 2-pyridinecarbonitrile(**1**) in alcohols

Alcohol	[**1**] / mol dm^{-3}	[H_2SO_4] / mol dm^{-3}	Irr. time[a] / h	Yield of product[b] / % **2**	Yield of product[b] / % **3**	Recovery of **1** / %
Methanol	5×10^{-2}	5×10^{-2}	24	9	9	41
	1×10^{-2}	1×10^{-1}	24	8	15	52
Ethanol	4×10^{-2}	—	1	15	0	57
	4×10^{-2}	5×10^{-1}	1	15	7	82

a) Different light sources were used for the reactions in methanol and in ethanol.

b) $\text{Yield} = 100\times\frac{\text{Amount of product formed}}{\text{Amount of } \mathbf{1} \text{ consumed}}$.

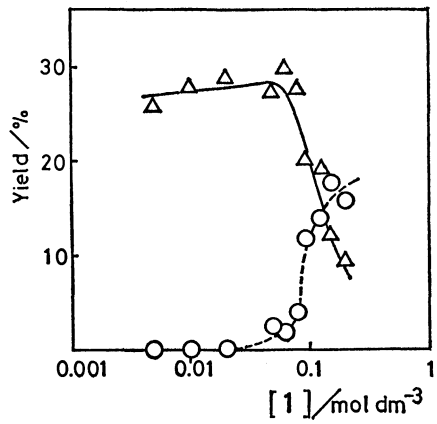

Fig. 2. Dependence of the yields of **2b** and **3b** on the concentration of **1**.
[H_2SO_4]=([**1**]+0.05) mol dm^{-3},
$\text{Yield} = 100\times\frac{\text{Amount of product formed}}{\text{Amount of } \mathbf{1} \text{ consumed}}$,
—△—: **2b**, --○--: **3b**.

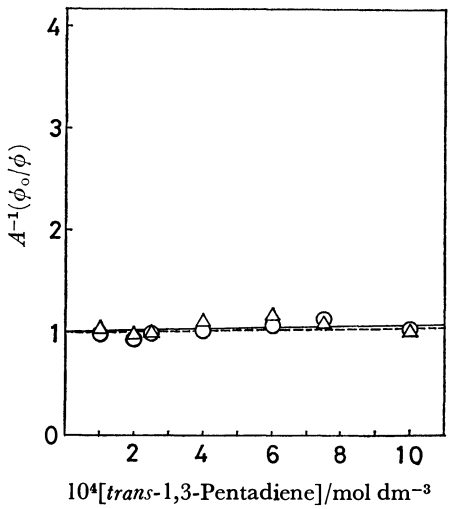

Fig. 3. Effects of *trans*-1,3-pentadiene on photo-hydroxyethylation and -ethoxylation of **1**.
[**1**]=0.04 mol dm^{-3}, [H_2SO_4]=0.2 mol dm^{-3}, —△—: **2b**, --○--: **3b**.

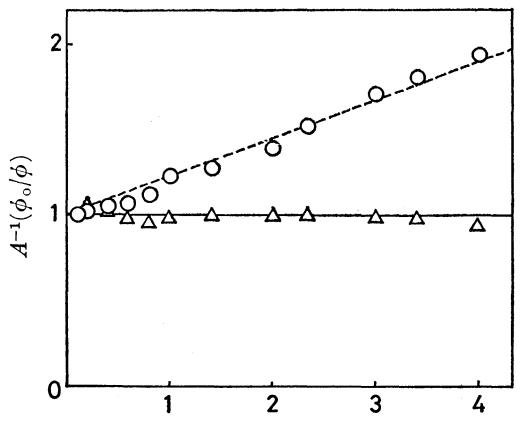

Fig. 4. Effects of fluorene on photo-hydroxyethylation and -ethoxylation of **1**.
[**1**]=0.04 mol dm^{-3}, [H_2SO_4]=0.2 mol dm^{-3}, —△—: **2b**, --○--: **3b**.

absorb the 254 nm light competitively with the substrate, the effects of the additives were analyzed by means of an index, A, the relative quantum yield calculated on the basis of the light absorbed by the substrate:

$$A = Y/L$$

$$Y = \frac{\text{Yield in the presence of additive}}{\text{Yield in the absence of additive}}$$

$$L = \frac{\varepsilon_1 c_1}{\varepsilon_1 c_1 + \varepsilon_Q c_Q},$$

where ε_1 and ε_Q are the molar absorption coefficients of **1** and the additive at 254 nm, respectively. Symbols c_1 and c_Q are the concentrations of **1** and the additive. A^{-1} corresponds to ϕ_0/ϕ for the Stern-Volmer equation in the quenching experiment (ϕ_0, quantum yield in the absence of a quencher; ϕ, quantum yield in the presence of a quencher).

trans-1,3-Pentadiene, an effective triplet quencher, (E_T=244 kJ/mol[9]), inhibits neither the photo-hydroxyethylation nor the photo-ethoxylation (Fig. 3). However, the quenching by fluorene (Fig. 4) shows a different feature from that by *trans*-1,3-pentadiene. Fluorene, the triplet energy of which is higher (E_T for fluorene, 284 kJ/mol[9]) than that of *trans*-1,3-pentadiene, inhibits photo-ethoxylation of **1**. On the other hand, fluorene exhibits no quenching during the photo-hydroxyethylation.

This characteristic of the quenching by fluorene is common for those by aromatic hydrocarbons, as are shown in the Stern-Volmer plots for the quenching by anthracene (Fig. 5), naphthalene (Fig. 6), and benzene (Fig. 7). Even benzene, which can be used as

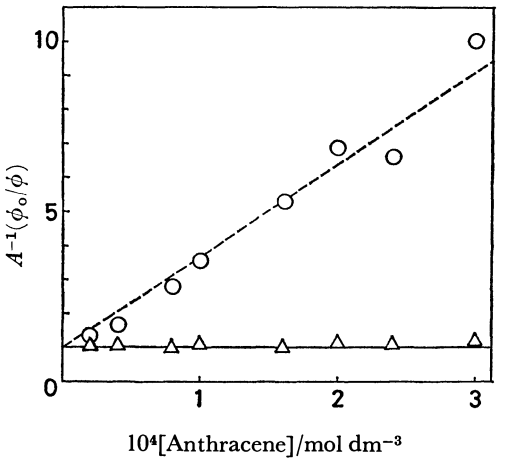

Fig. 5. Effects of anthracene on photo-hydroxyethylation and -ethoxylation of **1**.
[**1**]=0.04 mol dm^{-3}, [H_2SO_4]=0.2 mol dm^{-3}, —△—: **2b**, --○--: **3b**.

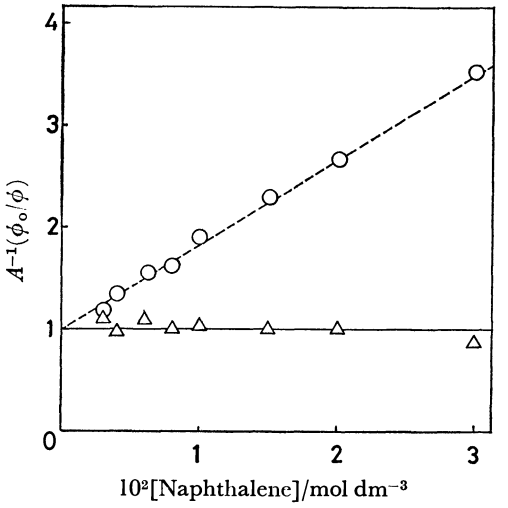

Fig. 6. Effects of naphthalene on photo-hydroxyethylation and -ethoxylation of **1**.
[**1**]=0.04 mol dm^{-3}, [H_2SO_4]=0.2 mol dm^{-3}, —△—: **2b**, --○--: **3b**.

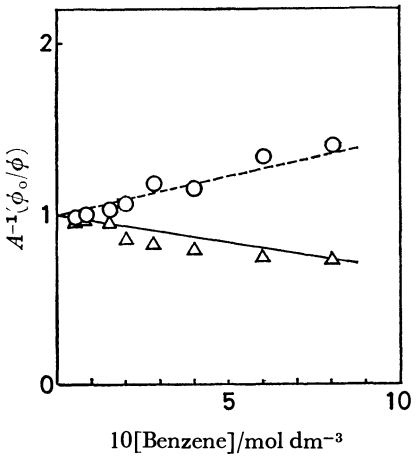

Fig. 7. Effects of benzene on photo-hydroxyethylation and -ethoxylation of **1**.
[**1**]=0.04 mol dm^{-3}, [H_2SO_4]=0.2 mol dm^{-3}, —△—: **2b**, --○--: **3b**.

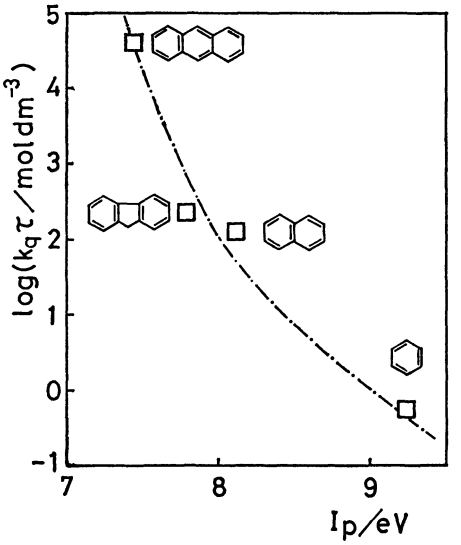

Fig. 8. Relation between $k_q\tau$ for the quenching of photo-ethoxylation and ionization potential of quencher.

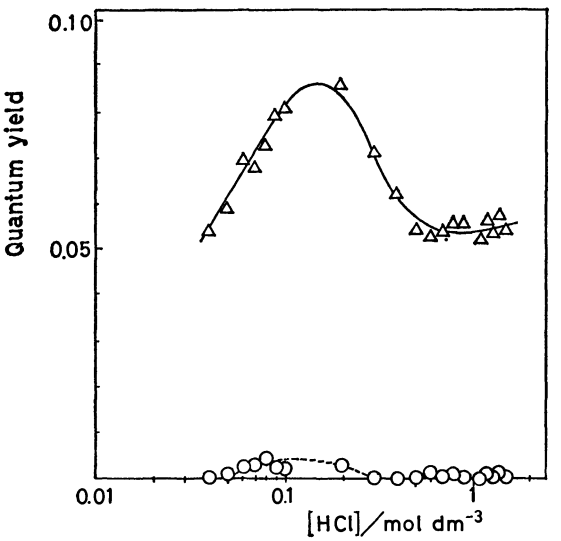

Fig. 9. Dependence of photo-hydroxyethylation and -ethoxylation of **1** on the concentration of hydrochloric acid.
[**1**]=0.04 mol dm^{-3}. —△—: **2b**, --○--: **3b**.

a triplet sensitizer because of its high triplet energy (E_T=347 kJ/mol[9]), inhibits the photo-ethoxylation of **1**. In contrast with the photo-ethoxylation, photo-hydroxyethylation is independent on the quenchers.

These facts indicate that: 1) the substitution of the cyano group by the hydroxyethyl group is ascribed to a singlet excited state and 2) the substitution of the ring hydrogen by the ethoxyl group is ascribed not to a triplet excited state but to a certain singlet excited state. This singlet excited state should be different from the one which gives the hydroxyethylated product.

When the fact that the photo-ethoxylation has a significant concentration dependence is taken into consideration, the quenching of the photo-ethoxylation by aromatic hydrocarbons can be explained by the quench-

ing of an excimer *via* the electron transfer mechanism proposed by Caldwell *et al.*[10]

The efficiencies for the quenching ($k_q\tau$ values obtained from the Stern-Volmer plots) of photo-ethoxylation by aromatic hydrocarbons correlate well with the ionization potentials of aromatic hydrocarbons[11] (Fig. 8). The lower the ionization potential, the higher the $k_q\tau$ value (k_q, rate constant for bimolecular quenching; τ, lifetime of the excited species). This shows that the excimer, which gives an ethoxylation product in the absence of quenchers, is quenched *via* the electron transfer from the quenchers. Alkoxylation is considered to involve a nucleophilic attack of alcohol to the electron-deficient moiety of the excited species. Therefore, the inhibition of ethoxylation by electron-rich aromatic hydrocarbons is reasonable. A similar quenching of photo-methoxylation by anthracene and benzene was observed for methyl 2-pyridinecarboxylate.[6]

Photo-ethoxylation is depressed by HCl (Fig. 9). A similar effect of HCl (or LiCl) on photo-methoxylation of 2-pyridinecarboxylic ester has been observed.[6] As in the case of 2-pyridinecarboxylic ester, the depression of photo-ethoxylation by HCl can be explained by the electron transfer from chloride ion to an electron-deficient excimer.

The conclusion that the hydroxyethylation occurs *via* a singlet excited state of **1** is similar to that reported by Hata *et al.* for the photo-hydroxyalkylation of quinolinecarbonitriles.[3] The mechanism proposed by Hata *et al.* can be applied to the corresponding reaction of 2-pyridinecarbonitrile.

The photoreactions of 2-pyridinecarbonitrile in acidic ethanolic solutions are summarized in Scheme 1.

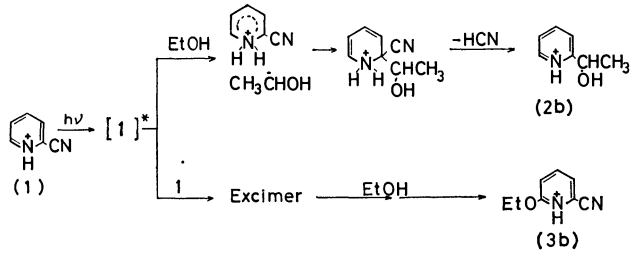

Scheme 1.

Experimental

Materials. 2-Pyridinecarbonitrile (**1**) supplied by Yuki Gosei Yakuhin Co. was purified by vacuum distillation; mp 28—29 °C. Commercial naphthalene was purified by recrystallization; mp 80.5—81.5 °C. Commercial anthracene (analytical standard reagent of BDH Chemicals Co.), fluorene (zone-refined U.P. grade reagent of Tokyo Kasei Co.), and *trans*-1,3-pentadiene (GR grade reagent of Wako Junyaku Co.) were used without further purification.

UV-Irradiation. The alcoholic solutions containing **1**, sulfuric or hydrochloric acid, and the additive if necessary, were deaerated by bubbling nitrogen or argon for 40 min before irradiation. For the quenching experiment with *trans*-1,3-pentadiene or benzene, the quencher was added after the deaeration of the substrate solutions in order to avoid the evaporation of the quenchers during the bubbling of inert gas.

The solutions were irradiated with a low pressure mercury lamp in a merry-go-round type photoreactor. For the normalization, standard and sample solutions were irradiated at the same time.

Isolation and Identification of Photo-products. After the irradiation the solution was concentrated under reduced pressure. The solution was neutralized with sodium carbonate and the products were extracted with dichloromethane. The products were separated by means of TLC (plate, GF_{254} (Type 60) of E. Merck Co.; developing solvent, ethyl acetate–dichloromethane 1:1 for the reaction products in methanol, hexane–dichloromethane–diethyl ether 2:20:3 for the reaction products in ethanol).

2-Pyridylmethanol (**2a**) was identified by the accordance of its spectral properties with those of the commercially available authentic specimen. 1-(2-Pyridyl)ethanol (**2b**) was identified by the accordance of its spectral and gas-chromatographic properties with those of the authentic sample prepared by the hydrogenation of 2-acetylpyridine over Raney nickel catalyst.

6-Methoxy-2-pyridinecarbonitrile (**3a**): mp 58.0—58.5 °C; IR (KBr disk) 3000, 2950, 2915, 2850, 2225 (C≡N), 1603, 1465, 1130, and 1030 cm^{-1}; NMR (CCl_4) δ=7.60 (1H, dd, J=8.4 and 7.4 Hz, H at 4-position), 7.16 (1H, dd, J=7.4 and 1.2 Hz, H at 3- or 5-position), 6.84 (1H, dd, J=8.4 and 1.2 Hz, H at 3- or 5-position), and 3.88 (3H, s, CH_3). Found: C, 61.6; H, 4.4; N, 20.4%. Calcd for $C_7H_6N_2O$: C, 62.7; H, 4.5; N, 20.9%.

6-Ethoxy-2-pyridinecarbonitrile (**3b**): mp 67.0—69.0 °C; IR (KBr disk) 3050, 2970, 2900, 2840, 2210 (C≡N), 1600, 1450, 1330, 1270, 1030, and 800 cm^{-1}; NMR ($CDCl_3$) δ=7.66 (1H, dd, J=8 and 6 Hz, H at 4-position), 7.21 (1H, dd, J=6 and 1 Hz, H at 3- or 5-position), 6.86 (1H, dd, J=8 and 1 Hz, H at 3- or 5-position), 4.34 (2H, q, J=7 Hz, CH_2), and 1.30 (3H, t, J=7 Hz, CH_3). Found: C, 64.9; H, 5.6; N, 19.4%. Calcd for $C_8H_8N_2O$: C, 64.9; H, 5.4; N, 18.9%.

Quantitative Analysis of Photoproducts. After the irradiation the reaction mixture was concentrated under reduced pressure and was neutralized with sodium hydroxide and/or sodium hydrogencarbonate. The products were extracted repeatedly with dichloromethane and submitted to GLC analysis (column, 2 m column of Triton QS 11 (15%) on Uniport B (60/80 mesh); column temperature, 160 °C).

Actinometry. Actinometry was performed with a potassium trioxalatoferrate(III) actinometer.[12]

Spectral Measurements. NMR spectra were recorded on a Hitachi R 22 NMR spectrometer (90 MHz), and IR spectra were recorded on a Hitachi 260-50 IR spectrometer.

References

1) M. Ohashi, *Kagaku No Ryoiki*, **32**, 703 (1978); A. Yoshino, K. Yamazaki, T. Yonezawa, and M. Ohashi, *J. Chem. Soc., Perkin Trans. 1*, **1975**, 735; M. Ohashi, K. Tsujimoto, and Y. Furukawa, *ibid.*, **1979**, 1147; M. Ohashi, K. Miyake, and K. Tsujimoto, *Bull. Chem. Soc. Jpn.*, **53**, 1683 (1980).

2) A. Sugimori, M. Nishijima, and T. Yashima, *Chem. Lett.*, **1981**, 303.

3) N. Hata, I. Ono, S. Matano, and H. Hirose, *Bull. Chem. Soc. Jpn.*, **46**, 942 (1973); N. Hata and T. Saito, *ibid.*, **47**, 942 (1974); N. Hata, I. Ono, and H. Suzuki, *ibid.*, **47**, 2609 (1974).

4) T. Caronna, S. Morrocchi, and B. M. Vittimberga, *Chim. Ind. (Milan)*, **60**, 806 (1978).

5) A. Sugimori, E. Tobita, Y. Kumagai, and G. P. Satô, *Bull. Chem. Soc. Jpn.*, **54**, 1761 (1981).

6) T. Sugiyama, T. Furihata, K. Takagi, M. Sato, S. Akiyama, G. P. Satô, and A. Sugimori, *Bull. Chem. Soc. Jpn.*, **54**, 3785 (1981).
7) A part of the work has been preliminarily reported: T. Furihata and A. Sugimori, *J. Chem. Soc., Chem. Commun.*, **1975**, 241.
8) H. Kurokawa, T. Furihata, F. Takeuchi, and A. Sugimori, *Tetrahedron Lett.*, **1973**, 2623.
9) S. L. Murov, "Handbook of Photochemistry," Marcel Dekker, New York (1973), pp. 27—35.
10) R. A. Caldwell, D. Creed, D. C. DeMarco, L. A. Melton, H. Ohta, and P. H. Wine, *J. Am. Chem. Soc.*, **102**, 2369 (1980).
11) S. L. Murov, "Handbook of Photochemistry," Marcel Dekker, New York (1973), pp. 199—200.
12) J. G. Calvert and J. N. Pitts, "Photochemistry," John Wiley & Sons, New York (1966), p. 783.

 © 1982 The Chemical Society of Japan Bull. Chem. Soc. Jpn., 55, 2911—2916 (1982)

Reaction of 1-Ethyl-3-methyl-4-imidazoline-2-thione with Methyl Iodide. Kinetic and Thermodynamic Aspects

Tetsuya YAMADA, Yasuhiko KONDO,* and Shigekazu KUSABAYASHI

Department of Applied Chemistry, Faculty of Engineering, Osaka University, Suita, Osaka 565

(Received August 29, 1981)

The reaction of 1-ethyl-3-methyl-4-imidazoline-2-thione with methyl iodide followed simple second order kinetics in polar solvents, whereas in less polar solvents the reverse process made a significant contribution to the overall rate. The solvent effects on the forward rate constant were linearly related to those on the rate of the reaction of tetramethylthiourea with methyl iodide. A plot of ΔV_0^* *vs.* $\Delta \overline{V}^\circ$ was linear with a slope of 0.33. From the volume changes and enthalpy changes measured, three transition state indices, $(\Delta_2 V^*/\Delta_2 \overline{V}^\circ)$, n_T and α were determined in acetonitrile, *ca.* 0.33, 0.32, and 0.41, respectively.

Much effort has recently been devoted to the rationalisation of solvent effects on kinetic and thermodynamic phenomena,[1-6] and it seems to have been commonly accepted that since the observed phenomena often result from combinations of various solvent characteristics, multiple parameter analysis is indispensable for such rationalisation. From another point of view, the relationships between kinetic and thermodynamic effects, especially those recently developed,[7-10] can be regarded as providing a theoretical basis for the characterisation of a solution reaction on terms of a transition state index.

As part of our continuing program to study any given process by as many different methods as possible, we analyse the reaction of 1-ethyl-3-methyl-4-imidazoline-2-thione (EMImdT) with methyl iodide which have a convenient rate,[11] from both kinetic and thermodynamic aspects, and then compare the results with those so far obtained for the reactions of the following thione derivatives with methyl iodide; 1,3-dimethyl imidazolidine-2-thione (DMIT),[12] *N,N,N',N'*-tetramethyl-thiourea (TMTU),[13] 3-isopropyl-4-methyl-4-thiazoline-2-thione (TT).[14]

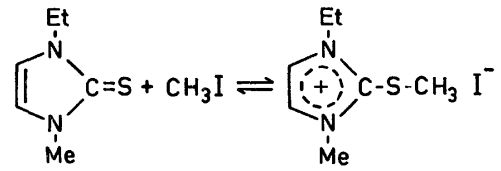

Experimental

Materials. 1,3-Dimethyl-4-imidazoline-2-thione, prepared as described,[15] was recrystallized three times from benzene and was then dried over phosphorus pentaoxide. 1-Ethyl-3-methyl-4-imidazoline-2-thione, prepared from *N*-methylimidazole and ethyl iodide by the same procedure as described,[15] was recrystallized three times from ether–pentane mixture and was dried over phosphorus pentaoxide (Found: C, 50.54; H, 7.09; N, 19.61; S, 22.59%. Calcd for $C_6H_{10}N_2S$: C, 50.67; H, 7.09; N, 19.70; S, 22.54%). 1,3-Dimethyl-2-methylthioimidazolium iodide, prepared by refluxing the corresponding thione with methyl iodide in acetonitrile was recrystallized twice from methanol–ether mixture, and was dried *in vacuo* over phosphorus pentaoxide at 65 °C. (Found: C, 26.75; H, 4.12; N, 10.28%. Calcd for $C_6H_{11}IN_2S$: C, 26.68; H, 4.10; N, 10.37%). 1-Ethyl-3-methyl-2-methylthioimidazolium iodide, prepared by refluxing the corresponding thione and methyl iodide in ether, was recrystallized twice from methanol–ether mixture and was dried *in vacuo* over phosphorus pentaoxide at 65 °C (Found: C, 29.66; H, 4.62; N, 9.90%. Calcd for $C_7H_{13}IN_2S$: C, 29.59; H, 4.61; N, 9.86%).

Solvents were purified as described elsewhere.[14,16] Kinetic measurements and density measurements (at 2.5×10^{-2} mol dm^{-3}) were performed as described elsewhere.[14,16]

Heat of Reaction Measurements. The heat of reaction was measured at 25° C with a Tokyo Riko MPC-11 calorimeter used as a conduction type vessel. A methyl iodide solution (5.5×10^{-2} mol dm^{-3}) in acetonitrile or in propylene carbonate (25 cm^3) and 1-ethyl-3-methyl-4-imidazoline-2-thione solution (0.1165 g in 1.2 cm^3 of the respective solvent) sealed in an ampoule were placed in the calorimeter cell. After thermal equilibration, the ampoule was broken, with stirring, and the temperature was recorded on a chart over 20 h. Calibration was achieved by introducing a measured quantity of electrical energy. Two to three determinations yielded a heat of reaction ΔH_r in acetonitrile of -59.8 ± 2 (kJ mol^{-1}) and in propylene carbonate of -51.9 ± 0.8 (kJ mol^{-1}).

Heat of solution Measurements. Heats of solution were measured at 25.0 °C with a twin isothermal calorimeter (Tokyo Riko TIC-2D) at 1.2×10^{-2} mol dm^{-3} for salts, 2.5×10^{-2} mol dm^{-3} for thione derivatives, and 1.3×10^{-1} mol dm^{-3} for methyl iodide. The experimental error was estimated to be *ca.* 1% from duplicate or triplicate runs.

Results and Discussion

Rate Laws. In polar solvents the reaction of 1-ethyl-3-methyl-4-imidazoline-2-thione with methyl iodide followed second order kinetics as expected,[11,14] *i.e.*, first order in both EMImdT and methyl iodide. In cyclohexanone an equilibrium was eventually reached. In bromobenzene the precipitation of the produced salt started at the point marked by an arrow in Fig. 1. In benzene the salt precipitated from the beginning of the reaction and the reaction was treated by second order kinetics. For a comprehensive treatment of the kinetic data which were measured in homogeneous phase, the scheme was postulated, and data have been treated, as described elsewhere.[13,14] The subscript, *e*, denotes the concentration at equilibrium.

$$\underset{a-x}{\text{EMImdT}} + \underset{b-x}{\text{MeI}^-} \underset{k_r}{\overset{k_f}{\rightleftharpoons}} \underset{x_{fl}}{\text{MEMImdT}^+} + \underset{x_{fl}}{\text{I}^-} \rightleftharpoons \underset{x_{ip}}{\text{MEMImdT}^+\text{I}^-}$$

$$2\,\underset{x_{ip}}{\text{MEMImdT}^+\text{I}^-} \rightleftharpoons \underset{x_q}{(\text{MEMImdT}^+\text{I}^-)_2}$$

Scheme 1.

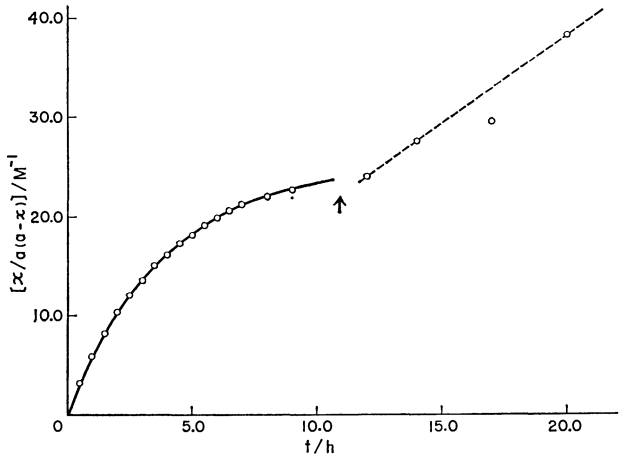

Fig. 1. Plots of $x/a(a-x)$ *vs.* t in bromobenzene at 30 °C.
○: Experimental, ——: calculated with $K_{obsd}=770$ $(dm^3mol^{-1})^{3/2}$ and $k_f=2.21\times10^{-3}$ $(dm^3\,mol^{-1}\,s^{-1})$. The arrow in the plots indicates the position where the precipitation of the salt started.

$$dx/dt = k_f(a-x)(b-x) - k_r x_{fl}^2 \quad (1)$$

$$K = k_f/k_r \quad (2)$$

$$K_{ip} = x_{ip}/x_{fl}^2 \quad (3)$$

$$K_q = x_q/x_{ip}^2 \quad (4)$$

$$x = x_{fl} + x_{ip} + 2x_q$$
$$= x_{fl} + K_{ip}x_{fl}^2 + 2K_qK_{ip}^2x_{fl}^4 \quad (5)$$

$$k_f(a-x_e)(b-x_e) = k_r x_{fl,e}^2 \quad (6)$$

In cyclohexanone the stoichiometric equilibrium constant, K_{sto}, determined analytically is rearranged to Eq. 8. From the set of x_e and K_{sto} values the equations were solved simultaneously to give $K=0.274$, $K_{ip}=1.25\times10^3$ dm³ mol⁻¹, $K_q=8.84$ dm³ mol⁻¹ (Fig. 2). The forward rate constant, k_f was calculated from Eq. 9 by the procedure described.[13,14]

$$K_{sto} = x_e^2/\{(a-x_e)(b-x_e)\} \quad (7)$$

$$(K_{sto}/K)^{1/2}$$
$$= 1 + K_{ip}(Kx_e^2/K_{sto})^{1/2} + 2K_qK_{ip}^2(Kx_e^2/K_{sto})^{3/2} \quad (8)$$

$$\int_0^x \frac{dx}{(a-x)(b-x)-x_{fl}^2/K} = \int_0^t k_f dt \quad (9)$$

In bromobenzene the assumption, $x_q \gg x_{fl}$ and x_{ip} seems plausible[12,13] and under the conditions the observed equilibrium constant as defined by the left hand side of Eq. 10 leads to the right hand side of Eq. 10. The forward rate constant, k_f was obtained

$$K_{obsd} \equiv x_e^{1/2}/[(a-x_e)(b-x_e)] = K(2K_qK_{ip}^2)^{1/2} \quad (10)$$

by performing the integration as described,[13,14] and the comparison of the experimental sets of x *vs.* t data

$$\int_0^x \frac{dx}{(a-x)(b-x)-K_{obsd}^{-1}x^{1/2}} = \int_0^t k_f dt \quad (11)$$

with the theoretical values calculated on the basis of the Scheme indicates fair agreement (Fig. 1). The kinetically determined equilibrium constant, $K_{obsd}=770$ $(dm^3\,mol^{-1})^{3/2}$ is in a comparable range with those observed previously (18.0—4400 $(dm^3\,mol^{-1})^{3/2}$),[12-14] though the value could not be verified analytically because of the precipitation of the produced salt.

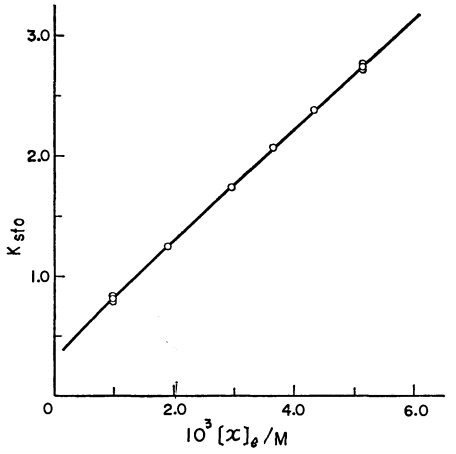

Fig. 2. Plots of K_{sto} *vs.* x_e at 30 °C.
○: Experimental, ——: calculated with $K=0.274$, $K_{ip}=1.25\times10^3$ $(dm^3\,mol^{-1})$ and $K_q=8.84$ $(dm^3\,mol^{-1})$.

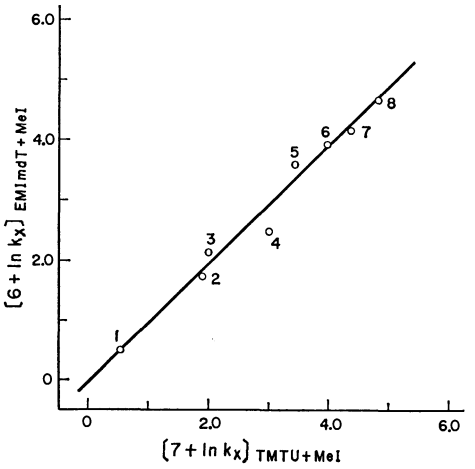

Fig. 3. Empirical correlations for rate constants.
○: Experimental, 1: benzene, 2: 2-propanol, 3: bromobenzene, 4: methanol, 5: cyclohexanone, 6: nitrobenzene, 7: acetonitrile, 8: propylene carbonate.

Table 1. Rate constants for the reaction of 1-ethyl-3-methyl-4-imidazoline-2-thione with methyl iodide (30 °C)

Solvents	$10^3\,k_f/dm^3\,mol^{-1}\,s^{-1}$	$10^2\,k_x/s^{-1}$
Propylene carbonate	22.3	26.1
Acetonitrile	8.36	15.7
N,*N*-Dimethylacetamide	12.9	13.8
Nitrobenzene	12.8	12.4
Cyclohexanone	9.25	8.83
Bromobenzene	2.21	2.08
Benzene	0.366	0.407
Methanol	1.21	2.96
2-Propanol	1.08	1.39

Table 2. Comparison of the kinetic and thermodynamic data (30 °C)

Reactions	$10^3 k_f$[a] / dm³ mol⁻¹ s⁻¹	K[a]	Slope[b]	ΔH^*[c] / kJ mol⁻¹	ΔH_r[c,d] / kJ mol⁻¹
EMImdT + MeI	9.25	0.274	0.97	55.2	−59.8
TMTU + MeI[13]	2.93	0.231	1.0	53.5	−70.3
DMIT + MeI[12]	0.721	1.35×10^{-3}	0.79	60.7	−49.8
TT + MeI[14]	0.640	1.08×10^{-2}	0.77	—	—

a) In cyclohexanone. b) Slope of Fig. 3 type correlation. c) In acetonitrile. d) At 25 °C.

Table 3. Apparent molal volumes, ϕ_v, the overall volume change of reaction, $\Delta\phi_v$, and activation volumes, ΔV_0^*, and their pressure derivatives (30 °C)

Solvents	ϕ_v/cm³ mol⁻¹			$\Delta\phi_v$ / cm³ mol⁻¹	ΔV_0^* / cm³ mol⁻¹	$(\partial\Delta V^*/\partial p)_0$ / cm⁵ mol⁻¹ N⁻¹
	EMImdT	MeI	MEMImdT+I⁻			
Acetonitrile	124.6	67.1	151.4	−40.3	−21.8	7.25×10^{-4}
Propylene carbonate	131.1	65.1	174.3	−21.9	−16.4	4.60×10^{-4}
N,*N*-Dimethylacetamide	127.0	64.7	161.0	−30.7	−16.7	5.35×10^{-4}
Acetonitrile	106.4[a]	67.1	133.6[b]	−39.9		

a) DMImdT. b) MDMImdT+I⁻.

Solvent Effects on the Rate Constants, k_f. The rate constants, k_f for the present reaction are summarized in Table 1, where k_x values calculated from the rate constant, k_f, and the molar volume of the solvent, V_s, expressed in dm³ mol⁻¹ by the equation, $k_x = k_f V_s^{-1}$ are also given.

There is a linear free energy relationship between the values of $\log k_x$ for the present reaction and the reaction of *N*,*N*,*N*′,*N*′-tetramethylthiourea with methyl iodide. (Fig. 3). The slope is 0.97.

In Table 2, typical values of the kinetic and thermodynamic data are summarized for comparison, where the reaction of TMTU with methyl iodide is taken as a standard reaction for comparison of the solvent effect.

The solvent effects on the rates of these ion forming reactions have been taken as giving the measure of the position of the transition state along the reaction coordinate, and were sometimes invoked as criteria for or against the operation of the reactivity-selectivity principles.[7-10] As far as these reactions are concerned, the first two reactions which proceed faster, have a larger sensitivity to solvent changes. In contrast to this observation, with respect to structural variations there seems to be some kind of correlation between kinetic and thermodynamic quantities, *i.e.*, a larger rate constant accompanies a larger equilibrium constant, and the activation enthalpy decreases with decreasing reaction enthalpy. Considering these trends, the interpretation of solvent effects on kinetics and thermodynamics needs deeper insights into the molecular processes operating in solution.

Activation Volumes and Volume Changes of Reaction. Activation volumes, ΔV_0^* and their pressure derivatives were determined by the least-squares method after expanding the rate constant into a power series of the pressure, Eqs. 12—14.

$$\ln k_p = \ln k_0 + Bp + Cp^2 \quad (12)$$

$$\Delta V_0^* = -1\ BRT \quad (13)$$

$$(\partial\Delta V^*/\partial p)_0 = -2\ CRT \quad (14)$$

The apparent molal volumes of the solutes, ϕ_v and the overall volume change in the reaction, $\Delta\phi_v$ are summarized in Table 3.

The volume behavior observed for the present reaction confirms the trends mentioned previously,[12] first, that molal volumes of thione derivatives and of ionic products are always larger in propylene carbonate than in acetonitrile and second, that the reaction in acetonitrile gives larger negative volume changes than in propylene carbonate, on activation as well as on reaction.

Recently, on the basis of the X-ray structural analysis[17] a polar structure with a partial negative charge on sulfur atom has been postulated for 1,3-dimethyl-4-imidazoline-2-thione. The apparent molal volume has also been measured for the compound for comparison. The molal volume difference of 7.7 cm³ mol⁻¹ between 1,3-dimethyl-4-imidazoline-2-thione (DMImdT) and 1,3-dimethylimidazolidine-2-thione (114.1 cm³ mol⁻¹ in acetonitrile[12]) would largely be ascribed to the molal volumes of two hydrogen atoms bonded to the ethylenic linkage of dimethylimidazolidine-2-thione. The estimation developed by Edwards and Bondi which relates the molal volumes to van der Waals volumes and surface areas,[18,19] gives 6.7 cm³ mol⁻¹ for the difference and this supports the above views. The methylene group contribution as deduced from molal volumes of two thione derivatives EMImdT and DMImdT, 18.2 cm³ mol⁻¹ agrees also with their estimation.[19] Thus, at this point, it is indeterminable to what extent the polarity of the solute manifests itself on the molal volume determined in dilute solution.

A fairly nice linear relationship, Eq. 15 exists be-

TABLE 4. ENTHALPY CHANGE OF SOLUTION, ΔH_s, AND OF REACTION, ΔH_r, AND ACTIVATION ENTHALPIES, ΔH^*

Solvents	ΔH_s/kJ mol^{-1} (25.0 °C)			ΔH_r	ΔH^*
	EMImdT	MeI	MEMImdT+I$^-$	kJ mol^{-1}	kJ mol^{-1}
Propylene carbonate	17.7	3.30	26.4	−51.9	53.5
Acetonitrile	17.5	3.64	21.2	−59.8	55.2
N,*N*-Dimethylacetamide	12.3	0.23	15.9	—	55.6
Methanol	22.0	2.59	38.4	—	—
N,*N*-Dimethylacetamide	17.8[a]	0.23	11.7[b]		
Methanol	26.6[a]	2.59	31.0[b]		

a) DMIT. b) MDMIT+I$^-$.

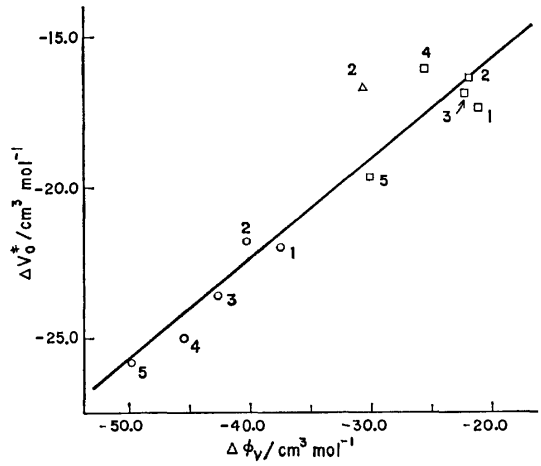

Fig. 4. Plots of ΔV_0^* *vs.* $\Delta\phi_v$.
Solvents: ○: acetonitrile, □: propylene carbonate, △: *N*,*N*-dimethylacetamide. Reactions: 1: TMTU+MeI, 2: EMImdT+MeI, 3: DMIT+MeI, 4: TT+MeI, 5: pyridine+MeI.

tween activation volumes and the overall volume changes of reactions studied by the authors, surprisingly including pyridine—methyl iodide reaction (Fig. 4). However, the possibility should be kept in mind

$$\Delta V_0^* = 0.33\Delta\phi_v - 9.2/\text{cm}^3\,\text{mol}^{-1} \quad (15)$$

that the linear relationship might be an artifact, since the points determined in propylene carbonate suggest a different trend from that obtained from the data in acetonitrile, though the regression line passes through the averaged point; also the point in dimethylacetamide largely deviates from the regression line. In the same vein as proposed previously,[12,13] the slope can be equated to the charge development index at the transition state, and the Eq. 16 can be derived,

$$\frac{\Delta V_0^* - \Delta_1 V^*}{\Delta\overline{V}^\circ - \Delta_1\overline{V}^\circ} = 0.33 \quad (16)$$

where the suffix, 1 indicates the structural volume changes on activation as well as on reaction. The combination of Eqs. 15 and 16 yields Eq. 17. In

$$\Delta_1 V^* - 0.33\Delta_1\overline{V}^\circ = -9.2/\text{cm}^3\,\text{mol}^{-1} \quad (17)$$

these derivations the apparent molal volumes were equated to the partial molal volumes ($\Delta\phi_v = \Delta\overline{V}^\circ$), taking into account the experimental conditions.

The structural volume changes have been estimated on various grounds, that is, for $\Delta_1 V^*$ they range from −6.5 to −11.7 cm^3 mol^{-1} [13,20-22] and for $\Delta_1\overline{V}^\circ$ from −4 to 0 cm^3 mol^{-1}.[13,14,20] Equation 17 does not give any preference to the respective set of values but serves as the criteria for the consistency of a given estimation. Considering these estimated values and also the relation (17), the set of central values, presumably the most plausible values, are taken as −10.1 and −2.8 cm^3 mol^{-1} for $\Delta_1\overline{V}^*$ and $\Delta_1 V^\circ$. The derived value, −10.1 cm^3 mol^{-1} for $\Delta_1 V^*$ is in fair agreement with the value, −10.7 cm^3 mol^{-1} estimated on completely different grounds.[21]

Enthalpy Measurements. Various enthalpies are summarized in Table 4. Throughout the two series of reactions, *i.e.*, DMIT with methyl iodide[12] and EMImdT with methyl iodide, the activation enthalpy has larger values in acetonitrile than in propylene carbonate, while the reaction enthalpy has larger negative values in acetonitrile than in propylene carbonate. With respect to structural variations there is observed some kind of relation between kinetics and thermodynamics as expected from the reactivity—selectivity pattern. In this regard also, the interpretation of the solvent effects on rates needs deeper insights. As a candidate, at least the cavity effect[23-25] would have to be invoked, though its' evaluation seems to present various problems.[23-25] On activation, as well as on reaction, reactants lose their volumes, *i.e.*, $\Delta_1 V^*$ and $\Delta_1\overline{V}^\circ$, and the work required to make a cavity in solution would differently affect activation enthalpies and reaction enthalpies. For rationalizing solvent effects on rates and on equilibria these would have to be evaluated on some basis. Abraham's way of taking an ion-pair as a final product[26] would provide one method for avoiding the complexity due to the cavity effect.

The thione derivatives as well as their methyl iodide salts give rise to characteristic transfer enthalpies. This might be ascribed to the polarity difference between the two thione derivatives DMIT and EMImdT, which could not be detected by the molal volume measurements. However, because of cancellations between reactants and products, a linear relation holds between the transfer reaction enthalpies, enthalpies of transfer from acetonitrile to other solvents of reaction, $\Delta H_{r,t} = \Delta H_{r,S} - \Delta H_{r,AN}$, of the two series (Fig. 5), and the slope of the plot, 0.86 is quite close to the ratio of the slopes of the linear free energy relationships

Table 5. Transition state indices for the reaction of 1-ethyl-3-methyl-4-imidazoline-2-thione with methyl iodide (30 °C)

Solvents	Slope	n_T	α
Acetonitrile	0.33	0.32	0.41
Propylene carbonate	0.33	0.34	0.42

as mentioned above, *i.e.*, (0.79/0.97)=0.82. This suggests that with respect to solvent variations, some sort of relation is operating between kinetics and thermodynamics as inferred from reactivity—selectivity pattern, though its direct proof would require much more effort.

Transition State Indices. Three kinds of transition state indices are compared in Table 5. The first is the charge development parameter which is defined as the slope of the plot of ΔV_0^* *vs.* $\Delta\overline{V}^\circ$. The second index has been calculated from the equation,

$$n_T = \frac{E_a}{(2E_a - \Delta E)} \tag{18}$$

where E_a and ΔE stand for the activation energy and the enthalpy change of the reaction.[8,9] The third index has been calculated by applying Marcus equations following the procedure as described by Albery and Kreevoy.[27,28] In the latter two calculations the activation enthalpy and the enthalpy change of the reaction have been directly substituted into these equations. Thus, judging from the experimental conditions, these indices would refer to the dissociated pair of ions as the final state.

$$\Delta G^* = \Delta G_0^* + (1/2)\Delta G^\circ + \Delta G^{\circ 2}/16\Delta G_0^* \tag{19}$$

$$\alpha = (1/2)(1+\Delta G^\circ/4\Delta G_0^*) \tag{20}$$

Recently Arnett *et al.*,[29] performed a complete kinetic and thermodynamic dissection of alkyl transfers. The Brönsted type plots gave linear relations and the slopes amount to 0.26 for the free energy correlation and to 0.23 for enthalpy correlation. On the other hand, the direct substitution of their enthalpies into Eq. 18, and Eqs. 19 and 20, and averaging afterwards lead to 0.30 and 0.39 for n_T and α. On the other hand Albery[30] calculated α ranging from 0.45 to 0.49 on the basis of the activation free energies and reaction free energies determined by Arnett *et al.*[29] Theoretical considerations demand the coincidence between the slope of the Brönsted type plots and the direct theoretical calculations as performed above.[10] In this regard for the Menschutkin reactions, n_T values indicate rather self-consistency. A similar situation holds for the present case, since n_T values obtained for the present reaction as well as for the previous reactions,[12-14] indicate close proximity to the charge development parameter as obtained from the volume correlation.

Here, again it should be pointed out that so far as we are concerned with a structurally related series of compounds, for a volume change correlation such as Fig. 4, structural volume changes, $\Delta_1 V^*$ and $\Delta_1\overline{V}^\circ$, could reasonably be assumed to be constant over the series. In contrast, for regular Brönsted type correlations such as ΔH^* *vs.* ΔH° or ΔG^* *vs.* ΔG°, the slope consists of two contributions, *i.e.*, a structural term and a solvational term accompanying structural variations. Thus the dissection of the slope into its constituent terms would be desirable for a more consistent comparison of the two types of slopes.

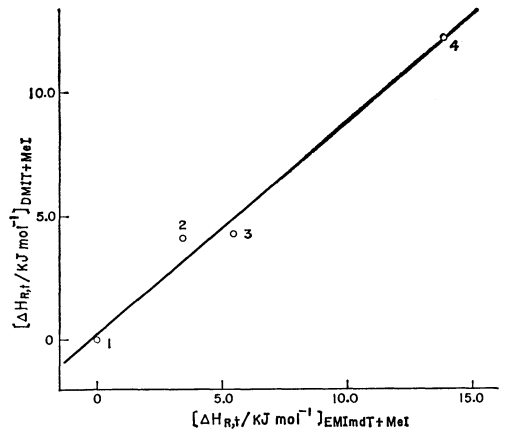

Fig. 5. Empirical correlations for the transfer reaction enthalpies (25 °C).
1: Acetonitrile, 2: *N,N*-dimethylacetamide, 3: propylene carbonate, 4: methanol.

The authors acknowledge their thanks to Dr. M. H. Abraham, University of Surrey, and Prof. T. Asano, Oita University for helpful discussions.

References

1) F. W. Fowler, A. R. Katritzky, and R. J. D. Rutherford, *J. Chem. Soc., B*, **1971**, 460.
2) I. A. Koppel and V. A. Palm, "Advances in Linear Free Energy Relationships," ed by N. B. Chapman and J. Shorter, Plenum Press, London (1972), Chap. 5.
3) V. Gutmann, *Chem. Tech.*, **1977**, 255.
4) A. G. Burden, N. B. Chapman, H. F. Duggua, and J. Shorter, *J. Chem. Soc., Perkin Trans. 2*, **1978**, 296.
5) M. J. Kamlet, T. N. Hall, J. Boykin, and R. W. Taft, *J. Org. Chem.*, **44**, 2599 (1979).
6) M. H. Abraham and R. J. Abraham, *J. Chem. Soc., Perkin Trans. 2*, **1975**, 1677.
7) R. A. Marcus, *J. Phys. Chem.*, **72**, 891 (1968).
8) N. Agmon, *J. Chem. Soc., Faraday Trans. 2*, **1978**, 388.
9) A. R. Miller, *J. Am. Chem. Soc.*, **100**, 1984 (1978).
10) R. D. Levine, *J. Phys. Chem.*, **83**, 159 (1979).
11) M. Arbelot, R. Gallo, M. Chanon, and J. Metzger, *Phosphorus and Sulfur*, **1**, 271 (1976).
12) Y. Kondo, T. Yamada, and S. Kusabayashi, *J. Chem. Soc., Pekin Trans. 2*, **1981**, 414.
13) Y. Kondo, S. Hirano, and N. Tokura, *J. Chem. Soc., Perkin Trans. 2*, **1979**, 1738.
14) Y. Kondo, M. Shinzawa, and N. Tokura, *Bull. Chem. Soc. Jpn.*, **50**, 713 (1977).
15) G. B. Ansell, D. M. Forkey, and D. W. Moore, *J. Chem. Soc., D*, **1970**, 56.
16) Y. Kondo, M. Ohnishi, and N. Tokura, *Bull. Chem. Soc. Jpn.*, **45**, 3579 (1972).
17) G. B. Ansell, *J. Chem. Soc., Perkin Trans. 2*, **1972**, 841.
18) A. Bondi, *J. Phys. Chem.*, **68**, 441 (1964).
19) J. T. Edward, P. G. Farrell, and F. Shahidi, *Can. J. Chem.*, **57**, 2585 (1979).

20) J. M. Stewart and K. E. Weale, *J. Chem. Soc.*, **1965**, 2854.
21) Y. Kondo, M. Uchida, and N. Tokura, *Bull. Chem. Soc. Jpn.*, **41**, 992 (1968).
22) T. Asano, *Rev. Phys. Chem. Jpn.*, **40**, 109 (1980).
23) M. H. Abraham and A. Nasehzadeh, *Can. J. Chem.*, **57**, 71 (1979).
24) M. H. Abraham, A. Nasehzadeh, J. J. M. Ramos, and J. Reisse, *J. Chem. Soc., Perkin Trans. 2*, **1980**, 854.
25) M. H. Abraham and A. Nasehzadeh, *J. Chem. Soc., Faraday Trans. 1*, **77**, 321 (1981).
26) M. H. Abraham, *Prog. Phys. Org. Chem.*, **11**, 1 (1974).
27) W. J. Albery, *Pure Appl. Chem.*, **51**, 949 (1979).
28) W. J. Albery, and M. M. Kreevoy, *Adv. Phys. Org. Chem.*, **16**, 87 (1978).
29) E. M. Arnett and R. Reich, *J. Am. Chem. Soc.*, **102**, 5892 (1980).
30) W. J. Albery, *Ann. Rev. Phys. Chem.*, **31**, 227 (1980).

 © 1982 The Chemical Society of Japan Bull. Chem. Soc. Jpn., 55, 2917—2921 (1982)

Synthesis of Sugar Derivatives of Tervalent Phosphorus Compounds and Their Application to Homogeneous Asymmetric Hydrogenation

Mitsuji YAMASHITA,* Koji HIRAMATSU, Manabu YAMADA,
Nobuyoshi SUZUKI, and Saburo INOKAWA†

Department of Synthetic Chemistry, Faculty of Engineering, Shizuoka University, Hamamatsu 432
† *Department of Chemistry, Faculty of Science, Okayama University, Okayama 700*

(Received October 23, 1981)

Diphenylphosphine and diphenylphosphinite derivatives of sugars such as methyl 6-deoxy-4-*C*-(diphenylphosphino)-2,3-*O*-isopropylidene-α-L-talopyranoside, methyl 4-*O*-(diphenylphosphino)-2,3-*O*-isopropylidene-α-L-rhamnopyranoside, methyl 4-*C*,4-*O*-(diphenylphosphino)-2,3-*O*-isopropylidene-α-L-talopyranoside, 6-deoxy-6-*C*-(diphenylphosphino)-1,2:3,5-di-*O*-isopropylidene-α-D-glucofuranose, and 6-*O*-(diphenylphosphino)-1,2:3,4-di-*O*-isopropylidene-α-D-galactopyranose were synthesized by the reaction of diphenylphosphine-sodium dihydrobis(2-methoxyethoxy)aluminate (SDMA) and/or diphenylphosphinous chloride–triethylamine with sugar derivatives. Homogeneous asymmetric hydrogenations of several prochiral olefins (α-acetylaminocinnamic acid, methyl α-acetylaminocinnamate, α-benzoylaminocinnamic acid, itaconic acid, and tiglic acid) were carried out using rhodium(I) catalysts with the tervalent chiral phosphorus derivatives of sugars. The highest optical yield for all the five substrates was obtained when di-μ-chloro-bis(cyclooctadiene)dirhodium(I) and 6-*O*-(diphenylphosphino)-1,2:3,4-di-*O*-isopropylidene-α-D-galactopyranose were used. The advantages of this method are the simplicity in the synthesis of the chiral phosphorus compound and the comparatively high optical yield in the asymmetric hydrogenation of olefins.

Homogeneous catalytic hydrogenation of olefins had been widely investigated since Wilkinson's works on chlorotris(triphenylphosphine)rhodium(I) were published.[1] The chirality of phosphine ligands of the reported rhodium catalysts appeared either on a phosphorus atom or on a carbon atom of the ligands. Various diphosphine ligands were often used for the asymmetric hydrogenation and they gave efficient results.[2] Monophosphines such as neomenthyldiphenylphosphine were used as the ligand of catalysts for asymmetric hydrogenation; these results, especially for monophosphines having a chiral center on the carbon atom,[3,4] were not always satisfactory.

Monosaccharides have several chiral carbon atoms in their skeletons; their applications to homogeneous asymmetric hydrogenation of prochiral materials are found in only a few papers. Iwami reported the asymmetric hydrogenation of olefins by rhodium complex with the ligand of 6-deoxy-6-(diphenylphosphino) derivative of galactose and 2-deoxy-2-(diphenylphosphino) derivative of altrose giving reduction products in optical yields of 2—39%.[5] Cullen and Sugi obtained an enantiomeric excess of 60—91% in the enantioselective hydrogenation of α-acetylaminoacrylic acid by rhodium catalyst having 2,3-bis(diphosphinite) derivative of glucopyranoside.[6,7] Recent studies on the efficiency of various tervalent diphosphorus derivatives of glucose and idose revealed that the ligand afforded up to 56% of enantiomeric excess *N*-acetylphenylalanine with *R* configuration in the hydrogenation.[8]

Our work on syntheses of carbohydrates having a phosphorus atom in the hemiacetal ring[9,10] suggested that we investigate the utility of chirality in the phosphorus-sugar skeleton as a chiral ligand. This paper deals with the synthesis of carbohydrates having a phosphorus-carbon linkage and the efficient application for asymmetric hydrogenation of olefins as a ligand of rhodium catalysts.

Results and Discussion

Synthesis of Chiral Phosphorus Ligands from Carbohydrates. Methyl 2,3-*O*-isopropylidene-α-L-rhamnopyranoside (**1**) was oxidized with phosphorus pentaoxide in dimethyl sulfoxide–pyridine to give methyl 6-deoxy-2,3-*O*-isopropylidene-α-L-*lyxo*-hexopyranosid-4-ulose (**2**) in 75% yield.[11] The reaction of glucosid-4-ulose **2** with diphenylphosphine in the presence of triethylamine under nitrogen atmosphere afforded methyl 6-deoxy-4-*C*-(diphenylphosphino)-2,3-*O*-isopropylidene-α-L-talopyranoside (**3**) in 13% yield.[12] The analogous reaction of glycosid-4-ulose **2** with diphenylphosphine oxide gave the corresponding 4-*C*-(diphenylphosphinyl) derivative of α-L-talopyranoside **4** in quantitative yield.

The reaction of compound **1** with diphenylphosphinous chloride in the presence of triethylamine under nitrogen atmosphere gave methyl 4-*O*-(diphenylphosphino)-2,3-*O*-isopropylidene-α-L-rhamnopyranoside (**5**) in 97% yield. The analogous reaction of compound **3** with diphenylphosphinous chloride gave methyl 4-*C*,4-*O*-bis(diphenylphosphino)-2,3-*O*-isopropylidene-α-L-talopyranoside (**6**) in 54% yield.

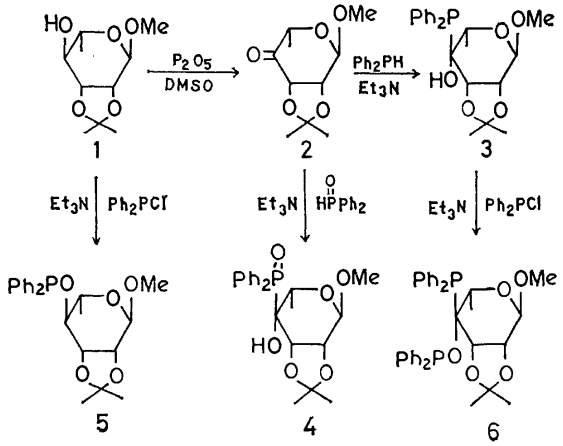

TABLE 1. HYDROGENATION OF OLEFINS WITH $RhCl(C_8H_{14})_2$-COMPOUND **3**

Substrate[a]	Ratio of substrate to Rh (I)	Solvent[b]	Temp °C	Time h	H_2 Pressure atm
α-Acetamidocinnamic acid	40[c]	EtOH	r. t.	48	1
	40[c]	EtOH	50	120	1
	100[d]	Benzene–EtOH (1:1)	50	12	50
Itaconic acid	100[d]	MeOH	50	120	1

a) 10 mmol of the substrate was used. b) 15 ml of the solvent was used. c) 1 mmol of compound **3** and 1.5 mmol of triethylamine was used. d) 0.5 mmol of compound **3** and 0.6 mmol of triethylamine was used.

The reaction of 1,2:3,5-di-*O*-isopropylidene-6-*O*-(*p*-tolylsulfonyl)-α-D-glucofuranose (**7**) with diphenylphosphine in the presence of SDMA gave 6-deoxy-6-*C*-(diphenylphosphino)-1,2:3,5-di-*O*-isopropylidene-α-D-glucofuranose (**8**) in 90% yield. The reaction of 1,2:3,4-di-*O*-isopropylidene-α-D-galactopyranose (**9**) with diphenylphosphinous chloride in the presence of triethylamine in tetrahydrofuran gave the corresponding phosphinite, 6-*O*-(diphenylphosphino)-1,2:3,4-di-*O*-isopropyridene-α-D-galactopyranose (**10**), in 46% yield. Oxidation of compounds **8** and **10** with hydrogen peroxide gave the oxides **11** and **12**. These tervalent phosphorus compounds were used as chiral ligands of rhodium catalysts.

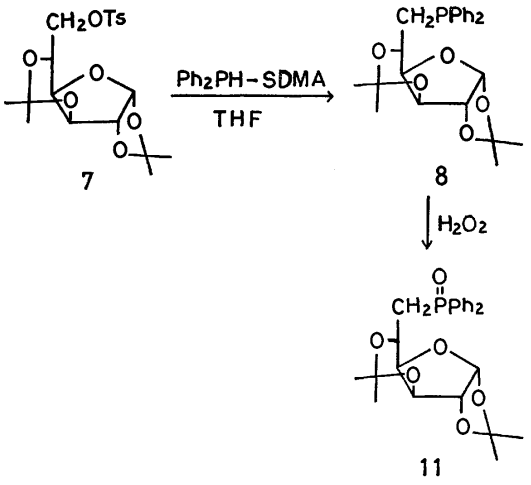

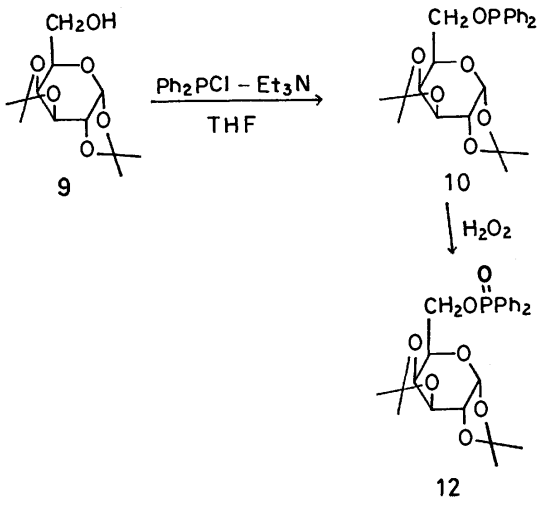

Asymmetric Hydrogenation of Prochiral Olefins. Asymmetric hydrogenations of α-acetylaminocinnamic acid and itaconic acid were carried out using compound **3** as a chiral ligand for chlorobis(cyclooctene)-rhodium(I) complex. The hydrogenation under the conditions shown in Table 1 afforded almost none of the corresponding products. This result shows that the ligand cannot contribute to the hydrogenation. The hydrogenation of α-acetylaminocinnamic acid in benzene–ethanol (1:1) under 50 atm. of hydrogen by chlorobis(cyclooctene)rhodium(I) and (1-hydroxy-1-methylethyl)diphenylphosphine (**13**) catalyst was also unsuccessful. The reaction of compound **3** with methyl iodide gave methyldiphenylphosphonium iodide (**14**) and glycosid-4-ulose **2**, instead of the methiodide of compound **3**. The same result was observed when compound **13** was treated with methyl iodide; the reaction product was compound **14**.

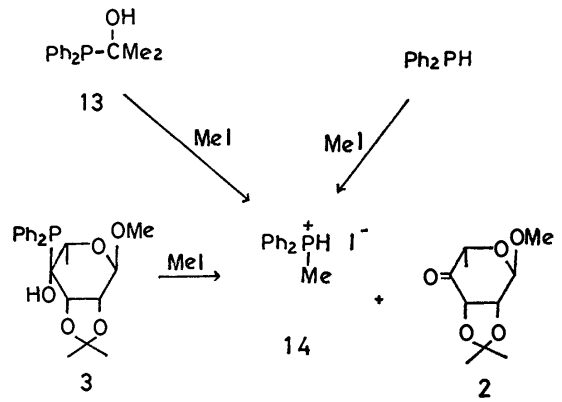

These findings suggest that the adducts of diphenylphosphine, *i.e.*, compounds **3** and **13**, are not so stable as to make complexes with the rhodium compound.

The asymmetric hydrogenation of α-acetylaminocinnamic acid by chlorobis(cyclooctene)rhodium(I) in the presence of compound **5** or **6** as a chiral ligand gave *N*-acetylphenylalanine with *R* configuration as a major product (Table 2). The dissociation of diphenylphosphine observed in adduct **3** should be depressed in making a rhodium complex with compound **6**.

The asymmetric hydrogenation of prochiral olefins in the presence of di-μ-chloro-bis(cyclooctadiene)dirhodium(I) and compound **8** gave the results summarized in Table 3. The same procedure using the rhodium complex and compound **10** for the prochiral olefins gave good results, as shown in Table 4. Table 5 summarizes the observed optical yield given by di-

Table 2. Asymmetric hydrogenation of α-acetamidicinnamic acid[a] with $RhCl(C_8H_{14})_2$-compound **5** or **6**

Phosphorus compound[b]	Ratio of substrate to Rh (I)	Temp °C	Time h	Conversion %	Optical yield/% (Configuration)
5	100	r. t.	24	100	13 (*R*)
6	100	r. t.	48	100	4.7(*R*)

a) 10 mmol of the acid, 40 ml of benzene-ethanol (1:1), and 0.6 mmol of triethylamine were used. b) 0.4 mmol of compound **5** and 0.1 mmol of compound **6** were used.

Table 3. Asymmetric hydrogenation of prochiral olefins with $Rh_2Cl_2(C_8H_{12})_2$-compound **8**[a]

Substrate	Reaction time h	Product	Chemical yield/%	$[\alpha]_D^{14}$/° (Solvent)	Optical yield/% (Configuration)
α-Acetylamino-cinnamic acid	24	*N*-Acetylphenylalanine ethyl ester	99	−1.3 (*c* 1.3, EtOH)	9 (*R*)
Methyl α-acetyl-aminocinnamate	24	*N*-Acetylphenylalanine methyl ester	99	−0.4 (*c* 1.0, MeOH)	2 (*R*)
α-Benzoylamino-cinnamic acid	24	*N*-Benzoylphenylalanine ethyl ester	72	−0.8 (*c* 1.0, MeOH)	2 (*S*)
Itaconic acid	24	Methylsuccinic acid	96	+2.4 (*c* 1.3, EtOH)	14 (*R*)
Tiglic acid	24	2-Methylbutyric acid	98	−0.3 (*c* 2.0, EtOH)	2 (*R*)

a) The ratios of substrate to Rh(I) complex and of compound **8** to Rh(I) complex were 25:1 and 4:1, respectively. All hydrogenations were carried out in 10 ml of benzene-ethanol (1:1) in the presence of 0.2 ml of triethylamine at room temperature under atmospheric pressure of hydrogen.

Table 4. Asymmetric hydrogenation of prochiral olefins with $Rh_2Cl_2(C_8H_{12})_2$-compound **10**[a]

Substrate	Reaction time h	Product	Chemical yield/%	$[\alpha]_D^{14}$/° (Solvent)	Optical yield/% (Configuration)
α-Acetylamino-cinnamic acid	24	*N*-Acetylphenylalanine ethyl ester	99	−8.9 (*c* 1.2, EtOH)	67 (*R*)
Methyl α-acetyl-aminocinnamate	24	*N*-Acetylphenylalanine methyl ester	99	−6.6 (*c* 2.2, MeOH)	29 (*R*)
α-Benzoylamino-cinnamic acid	24	*N*-Benzoylphenylalanine ethyl ester	85	−12.8 (*c* 1.0, MeOH)	32 (*S*)
Itaconic acid	24	Methylsuccinic acid	99	−8.4 (*c* 1.0, EtOH)	49 (*S*)
Tiglic acid	24	2-Methylbutyric acid	99	−11.9 (*c* 2.8, EtOH)	62 (*R*)

a) The ratios of substate to Rh(I) complex and of compound **10** to Rh(I) complex were 25:1 and 4:1, respectively. All hydrogenations were carried out in 10 ml of benzene-ethanol (1:1) in the presence of 0.2 ml of triethylamine at room temperature under atmospheric pressure of hydrogen.

μ-chloro-bis(cyclooctadiene)dirhodium(I) and chloro-bis(cyclooctene)rhodium(I) with compound **10** as the ligand.

These results indicate that efficiency of chiral phosphinite **10** is good enough for the asymmetric hydrogenation of prochiral olefins, since the reported enantiomeric excess of *N*-acetylphenylalanine is up to 56% in the homogeneous asymmetric hydrogenation of α-acetylaminocinnamic acid by a rhodium catalyst using chiral ligands of 5,6-bis(diphenylphosphino) derivatives of glucose and idose.[8] This procedure seems to be a simple and efficient way for the asymmetric hydrogenation of prochiral olefins, compared with the other methods reported in the literature,[8,13] owing to the convenience in the ligand synthesis and to comparably high optical yields.

Experimental

Measurements. Melting and boiling points were uncorrected. ^{1}H-NMR spectra were measured on Hitachi-Perkin-Elmer R-24 (60 MHz) spectrometer with tetramethylsilane as an internal standard, and IR spectra on a Japan Spectroscopic Co. Ltd. A-3 infrared spectrophotometer. Optical rotations were measured on Japan Spectroscopic Co. Ltd. DIP-4 digital polarimeter.

Materials. The following materials were synthesized according to reported methods: α-acetylaminocinnamic acid,[14] α-benzoylaminocinnamic acid,[15] methyl α-acetylam-

TABLE 5. ASYMMETRIC HYDROGENATION OF PROCHIRAL OLEFINS WITH $Rh_2Cl_2(C_8H_{12})_2$- OR $RhCl(C_8H_{14})_2$-COMPOUND **10**[a]

Rh(I) Complex	Substrate	Reaction time / h	Product	Chemical yield/%	$[\alpha]_D^{17}$/° (Solvent)	Optical yield/% (Configuration)
$Rh_2Cl_2(C_8H_{12})_2$	α-Acetylamino-cinnamic acid	96	*N*-Acetylphenyl-alanine ethyl ester	78	−3.3 (*c* 0.9, EtOH)	25 (*R*)
	Itaconic acid	96	Methylsuccinic acid	100	−3.8 (*c* 1.8, EtOH)	22 (*S*)
	Tiglic acid	120	2-Methylbutyric acid	100	−2.8 (*c* 1.6, EtOH)	15 (*R*)
$RhCl(C_8H_{14})_2$	α-Acetylamino-cinnamic acid	216	*N*-Acetylphenyl-alanine ethyl ester	88	−0.7 (*c* 1.1, EtOH)	6 (*R*)
	Itaconic acid	216	Methylsuccinic acid	100	−2.3 (*c* 1.6, EtOH)	14 (*S*)
	Tiglic acid	216	2-Methylbutyric acid	100	−1.0 (*c* 1.4, EtOH)	5 (*R*)

a) The ratios of substrate to Rh(I) complex and of compound **10** to Rh(I) complex were 100:1 and 4:1, respectively. All hydrogenations were carried out in 10 ml of benzene-ethanol (1:1) in the presence of 0.2 ml of triethylamine at room temperature under under atmospheric pressure of hydrogene.

inocinnamate,[16] diphenylphosphine (bp 108.5—113 °C/2 mmHg[17]),[18] diphenylphosphinous chloride (bp 110 °C/0.5 mmHg),[19] chlorobis(cyclooctene)rhodium(I),[20] di-μ-chlorobis(cyclooctadiene)dirhodium(I),[21] methyl 2,3-*O*-isopropylidene-α-L-rhamnopyranoside (**1**),[12] 1,2-*O*-isopropylidene-6-*O*-(*p*-tolylsulfonyl)-α-D-glucofuranose (**7**) (mp 108 °C),[22] 1,2:3,4-di-*O*-isopropylidene-α-D-galactopyranose (**9**),[23] (1-hydroxy-1-methylethyl)diphenylphosphine (13) (mp 140 °C).[24]

Methyl 6-Deoxy-2,3-O-isopropylidene-α-L-lyxo-hexopyranosid-4-ulose (2). Compound **1** (8.2 g) was oxidized with phosphorus pentaoxide (20.5 g) at room temperature for 4 d. The work-up, with addition of water and extraction with chloroform, gave compound **2** in 75% yield,[12] $[\alpha]_D^{15}$ −110° (*c* 0.7, EtOH). Mass spectrum, *m/e*, 216 (M^+).

Found: C, 55.08; H, 7.46%. Calcd for $C_{10}H_{16}O_5$: C, 55.55; H, 7.46%.

Addition of Diphenylphosphine to Compound 2. Addition of diphenylphosphine (0.30 g) to glycosid-4-ulose **2** (0.30 g) in the presence of triethylamine under nitrogen atmosphere at room temperature for 2 days gave methyl 6-deoxy-4-*C*-(diphenylphosphino)-2,3-*O*-isopropylidene-α-L-talopyranoside (**3**) (0.080 g) in 13% yield, mp 100—101.5 °C, $[\alpha]_D^{16}$ −97° (*c* 0.71, EtOH). ^{1}H-NMR ($CDCl_3$) δ 0.98, 1.30 (2×s, 6H, CMe_2), 1.36 (d, *J*=6.6 Hz, C_5–Me), 3.35 (s, 3H, C_1–OMe), 4.0—4.9 (m, 5H, C_1–, C_2–, C_3–, C_4–OH), 7.05—8.0 (m, 10H, Ph); IR ν_{max}^{KBr} 3200 cm^{-1} (OH); mass spectrum, *m/e*, 402 (M^+). Oxidation of compound **3** gave the oxide (compound **4**).

Found: C, 62.80; H, 6.31%. Calcd for $C_{22}H_{27}O_6P$: C, 63.15; H, 6.50%.

Addition of Diphenylphosphine Oxide to Compound 2. Addition of diphenylphosphine oxide (0.10 g) to glycosid-4-ulose **2** (0.10 g) in the presence of triethylamine under nitrogen flow at room temperature for 3 h gave a crystalline adduct **4**. Recrystallization of the product from methanol-ether gave 0.18 g of pure methyl 6-deoxy-4-*C*-(diphenylphosphinyl)-2,3-*O*-isopropylidene-α-L-talopyranoside (**4**), mp 117—118.5 °C, $[\alpha]_D^{25}$ −132° (*c* 1.0, $CHCl_3$). ^{1}H-NMR ($CDCl_3$) δ 1.00 (d, *J*=12 Hz, 3H, C_5–Me), 1.05, 1.31 (2×s, 6H, CMe_2), 3.45 (s, 3H, C_1–OMe), 3.96—5.0 (m, 5H, C_1–, C_2–, C_3–, C_5–H, C_4–OH), 7.0—8.5 (m, 10H, Ph); IR ν_{max}^{KBr} 3150 cm^{-1} (OH); mass spectrum, *m/e*, 418 (M^+).

Found: C, 63.06; H, 6.76%. Calcd for $C_{22}H_{27}O_6P$: C, 63.15; H, 6.50%.

Methyl 4-O-(Diphenylphosphino)-2,3-O-isopropylidene-α-L-rhamnopyranoside (5). Reaction of compound **1** (0.10 g) with diphenylphosphinous chloride (0.10 g) in triethylamine (4 ml) under nitrogen atmosphere at room temperature for 24 h, followed by work-up by adding water and extraction with chloroform, gave compound **5** (0.189 g) in 97% yield, $[\alpha]_D^{20}$ −8.3° (*c* 2.0, EtOH). ^{1}H-NMR ($CDCl_3$) δ 1.25 (d, *J*=6.0 Hz, 3H, C_5–Me), 1.30, 1.50 (2×s, 6H, CMe_2), 3.35 (s, 3H, C_1–OMe), 3.50—4.90 (m, 5H, C_1–, C_2–, C_3–, C_4–, C_5–H), 7.0—8.0 (m, 10H, Ph); mass spectrum, *m/e*, 402 (M^+).

Found: C, 65.52; H, 6.99%. Calcd for $C_{22}H_{27}O_5P$: C, 65.66; H, 6.76%.

Methyl 4-C,4-O-(Diphenylphosphino)-2,3-O-isopropylidene-α-L-talopyranoside (6). Reaction of compound **3** (0.080 g) with diphenylphosphinous chloride (0.050 g) in triethylamine (4 ml) at room temperature for 24 h, followed by purification by liquid chromatography, gave compound **6** (0.062 g) in 54% yield, $[\alpha]_D^{15}$ −28° (*c* 1.0, EtOH). ^{1}H-NMR ($CDCl_3$) δ 1.21 (d, *J*=13.6 Hz, 3H, C_5–Me), 1.21, 1.48 (2×s, 6H, CMe_2), 3.44 (s, 3H, C_1–OMe), 2.95—5.0 (m, 4H, C_1–, C_2–, C_3–, C_5–H), 7.0—8.5 (m, 20H, Ph); mass spectrum, *m/e*, 586.

The oxidation of compound **6** with hydrogen peroxide gave the dioxide, mp 104—106 °C, mass spectrum, *m/e*, 618 (M^+).

Found: C, 65.84; H, 6.33%. Calcd for $C_{34}H_{36}O_7P_2$: C, 66.01; H, 5.87%.

6-Deoxy-6-C-(diphenylphosphino)-1,2:3,5-di-O-isopropylidene-α-D-glucofuranose (8). Addition of compound **7** (1.5 g) in tetrahydrofuran (10 ml) to a mixture of diphenylphosphine (1.0 g) and SDMA (2.0 g) in tetrahydrofuran at room temperature, followed by refluxing for 4 h, gave compound **8**. Work-up by addition of water and neutralization, followed by filtration, concentration *in vacuo*, and isolation by liquid chromatography, gave 1.4 g of pure compound **8** (90% yield), $[\alpha]_D^{16}$ +2.1° (*c* 1.0, EtOH). ^{1}H-NMR ($CDCl_3$) δ 1.06, 1.26, 1.31, 1.45 (4×s, 12H, CMe_2), 2.02 (d, *J*=13.0 Hz, 2H, C_6–, $C_{6'}$–H), 3.3—5.0 (m, 4H, C_2–, C_3–, C_4–, C_5–H), 5.92 (d, 1H, *J*=4.0 Hz, C_1–H), 7.15—7.90 (m, 10H, Ph); mass spectrum, *m/e*, 428 (M^+)

Found: C, 67.35; H, 6.87%. Calcd for $C_{24}H_{29}O_5P$: C, 67.28; H, 6.82%.

*6-O-(Diphenylphosphino)-1,2:3,4-di-O-isopropylidene-α-D-galactopyranose (**10**).* Reaction of compound **9** (5.4 g) with diphenylphosphinous chloride (6.8 g) in the presence of triethylamine (13 ml) at room temperature for 24 h under nitrogen atmosphere, followed by filtration, concentration, and purification by liquid chromatography, gave compound **10** (4.1 g, 46% yield), $[\alpha]_D^{16}$ +47.0° (*c* 1.18, EtOH). ^{1}H-NMR ($CDCl_3$) δ 1.32, 1.42, 1.46 (4×s, 12H, CMe_2), 3.76—4.76 (m, 6H, C_2–, C_3–, C_4–, C_5–, C_6–, C_6'–H), 5.56 (d, *J*=5.0 Hz, 1H, C_1–H), 7.16—7.72 (m, 10H, Ph); mass spectrum, *m/e*, 444 (M^+).

Found: C, 64.35; H, 6.70%. Calcd for $C_{24}H_{29}O_6P$: C, 64.86; H, 6.58%.

*Asymmetric Hydrogenation of α-Acetylaminocinnamic Acid with Di-μ-chloro-bis(cyclooctadiene)dirhodium(I) and Compound **10**.* Asymmetric hydrogenation of α-acetylaminocinnamic acid (500 mg) in anhydrous benzene (5 ml)–absolute ethanol (5 ml) was carried out using di-μ-chloro-bis(cyclooctadiene)-dirhodium (I) (35 mg) and compound **10** (211 mg) as the catalyst in the presence of triethylamine (0.2 ml) under atmospheric pressure of hydrogen at room temperature for 24 h. Removal of the catalyst by passing a column peacked with ion exchange resine Dowex 50W (H^+), followed by decolorization with activated charcoal and removal of the solvent *in vacuo*, gave *N*-acetylphenylalanine ethyl ester (100% conversion). The identification of the product was performed by ^{1}H-NMR, whose spectrum was as follows: ($CDCl_3$) δ 1.21 (t, *J*=7.0 Hz, 3H, $OCH_2C\underline{H}_3$), 1.95 (s, 3H, Ac), 3.09 (d, *J*=6.0 Hz, 2H, $C\underline{H}_2Ph$), 4.15 (q, *J*=7.5 Hz, 2H, $OC\underline{H}_2CH_3$), 4.85 (dd, *J*=6.0 Hz, 1H, CH), 6.46 (bd, *J*=7.5 Hz, NH), 7.05—7.40 (m, 5H, Ph). The product had $[\alpha]_D^{16}$ −8.82° (*c* 1.2, EtOH) which showed 67% optical yield of the *R* configuration.

The asymmetric hydrogenation of methyl α-acetylaminocinnamate, *N*-benzoylaminocinnamic acid, itaconic acid, and tiglic acid were performed in a similar fashion. The optical yields of the products were calculated based on the reported values of optical rotation for *N*-acetyl-(*S*)-phenylalanine,[25] *N*-acetyl-(*S*)-phenylalanine ethyl ester,[26] *N*-acetyl-(*S*)-phenylalanine methyl ester,[26] *N*-benzoyl-(*R*)-phenylalanine ethyl ester,[27] (*R*)-methylsuccinic acid,[5] and (*S*)-2-methylbutyric acid.[28]

*Reaction of 6-Deoxy-4-C-(diphenylphosphino)-2,3-O-isopropylidene-α-L-talopyranoside (**3**) with Methyl Iodide.* Reaction of compound **3** (0.10 g) with an excess amount of methyl iodide in anhydrous ether (10 ml) under nitrogen atmosphere gave methyldiphenylphosphonium iodide (**14**) and glycosid-4-ulose **2** in 80% yield.

*Oxidation of Compound **10** with Hydrogen Peroxide.* Oxidation of compound **10** with 38% hydrogen peroxide (0.11 g) at room temperature, followed by work-up by treatment with sodium thiosulfate and extraction with chloroform, gave 6-*O*-(diphenylphosphinyl)-1,2:3,4-di-*O*-isopropylidene-α-D-galactopyranose (**12**) in 75% yield, mp 115—116 °C, $[\alpha]_D^{15}$ −40° (*c* 0.6, EtOH). ^{1}H-NMR δ 1.26, 1.33, 1.50 (4×s, 12H, CMe_2), 3.8—4.9 (m, 6H, C_2–, C_3–, C_4–, C_5–, C_6–, C_6'–H), 5.60 (d, *J*=8.0 Hz, 1H, C_1–H), 7.2—8.1 (m, 10H, Ph); mass spectrum, *m/e*, 460 (M^+).

Found: C, 62.80; H, 6.45%. Calcd for $C_{24}H_{29}O_7P$: C, 62.60; H, 6.35%.

*Oxidation of Compound **8**.* Oxidation of compound **8** in a similar way as described above gave 6-deoxy-6-*C*-(diphenylphosphinyl)-1,2:3,5-di-*O*-isopropylidene-α-D-glucofuranose (**11**), $[\alpha]_D^{16}$ +1.8° (*c* 1.2, EtOH), ^{1}H-NMR ($CDCl_3$) δ 1.16, 1.23, 1.40 (4×s, 12H, CMe_2), 2.02—2.75 (m, 2H, C_6–, C_6'–H), 3.25—4.46 (m, 3H, C_3–, C_4–, C_5–H), 4.50 (d, *J*=5.1 Hz, 1H, C_2–H), 5.89 (d, *J*=5.1 Hz, 1H, C_1–H), 6.80—7.93 (m, 10H, Ph); mass spectrum, *m/e*, 444 (M^+).

Found: C, 64.94; H, 6.40%. Calcd for $C_{24}H_{29}O_6P$: C, 64.86; H, 6.58%.

This work was partially supported by a Grant-in-Aid (475661) for Science Research from the Ministry of Education, Science and Culture.

References

1) J. A. Osborn, F. J. Jardive, J. F. Young, and G. Wilkinson, *J. Chem. Soc., A*, **1966**, 1711.
2) a) T.-P. Dang and H. B. Kagan, *J. Chem. Soc., Chem. Commun.*, **1971**, 481; b) H. B. Kagan and T.-P. Dang, *J. Am. Chem. Soc.*, **94**, 6429 (1972).
3) W. S. Knowles and M. J. Sabacky, *J. Chem. Soc., Chem. Commun.*, **1968**, 1445.
4) a) J. D. Morrison, R. E. Burnett, A. M. Aguiar, C. J. Morrow, and C. Phillips, *J. Am. Chem. Soc.*, **93**, 1301 (1971); b) G. Paiaro and L. Pandolofo, *Gazz. Chim. Ital.*, **107**, 467 (1977); *Chem. Abstr.*, **89**, 41984e (1978).
5) T. Iwami, T. Yoshida, and M. Sato, *Nippon Kagaku Kaishi*, **1976**, 1652.
6) W. R. Cullen and Y. Sugi, *Tetrahedron Lett.*, **1978**, 1635.
7) Y. Sugi and W. R. Cullen, *Chem. Lett.*, **1979**, 39.
8) T. H. Johnson and G. Rangarajan, *J. Org. Chem.*, **45**, 62 (1980).
9) H. Takayanagi, K. Seo, M. Yamashita, H. Yoshida, T. Ogata, and S. Inokawa, *Carbohydr. Res.*, **63**, 105 (1978).
10) M. Yamashita, Y. Nakatsukasa, H. Yoshida, T. Ogata, and S. Inokawa, *Carbohydr. Res.*, **70**, 247 (1979).
11) C. L. Stevens, R. R. Glinski, and K. G. Taylor, *J. Org. Chem.*, **33**, 1586 (1968).
12) M. Yamashita, P. T. Long, M. Shibata, and S. Inokawa, *Carbohydr. Res.*, **84**, 35 (1980).
13) V. Čaplar, G. Comisso, and V. Šunjić, *Synthesis*, **1981**, 85.
14) R. M. Herbst and D. Shemin, *Org. Synth.*, Coll. Vol. II, 1 (1950).
15) H. B. Gillespie and H. R. Snyder, *Org. Synth.*, Coll. Vol. II, 489 (1950).
16) E. Rothstein, *J. Chem. Soc.*, **1949**, 1968.
17) 1 mmHg=133.322 Pa.
18) W. Gee, R. A. Shaw, and B. C. Smith, *Inorg. Synth.*, **9**, 19 (1967).
19) M. P. Brown and H. B. Silver, *Chem. Ind. (London)*, **1961**, 24.
20) A. Van Der Ent and A. L. Onderdelinden, *Inorg. Synth.*, **14**, 92 (1973).
21) J. Chatt and L. M. Venanzi, *J. Chem. Soc.*, **1957**, 4735.
22) H. Ohle and E. Dickhäuser, *Ber. (Dtsch. Chem. Ges.)*, **58**, 2593 (1925).
23) O. T. Schmidt, "Method in Carbohydrates Chemistry," Academic Press Inc., New York (1963), Vol. II, p. 324.
24) L. Maier, "Organic Phosphorus Compound," Wiley-Interscience, New York (1972), Vol. II, p. 68.
25) J. Yoshimura, K. Sato, and H. Hashimoto, *Chem. Lett.*, **1977**, 1327.
26) R. Glaser and B. Vainas, *J. Organomet. Chem.*, **121**, 249 (1976).
27) M. D. Fryzuk and B. Bosnich, *J. Am. Chem. Soc.*, **99**, 6262 (1977).
28) Y. Asahina and T. Shimizu, *Nippon Yakugaku Kaishi*, **479**, 1 (1922).

Synthesis of 4,7-Indolequinones by Photoinduced Reaction of Azidoquinones

Tadashi KOZUKA

Department of Chemistry, Faculty of Science, Kyoto University, Sakyo-ku, Kyoto 606

(Received October 30, 1981)

Various azidoquinones were prepared from methyl 3-substituted 2,3-dihydro-5-hydroxy-6-methylbenzofuran-2-carboxylate. Irradiation of these azidoquinones gave methyl 3-substituted 6-methyl-4,7-dioxoindole-2-carboxylates, a model of mitomycin analogs, in a moderate yield.

Recently, the author found that *p*-benzoquinones having an ester group in the α position of alkyl side chains have a high reactivity toward γ-hydrogen abstraction reaction to give the rearranged product, *i.e.*, methyl 3-substituted 2,3-dihydro-5-hydroxybenzofuran-2-carboxylate derivatives **1**, in fairly good yields.[1] In this paper, as a further extension of these reactions, the present author reports a reaction of the corresponding azidoquinone **4** derived from the dihydrobenzofuran **1**. The investigations of the photolysis of azidoquinones have been centered on the exploitation of a new general synthetic method of 4,7-indolequinones, which are related to some natural products.[2] Pharmacologically interesting functionalized 4,7-indolequinones **5a**—**i** were obtained by photoinduced cyclization of the corresponding azidoquinones **4a**—**i** having a suitable side chain.

In general, the intramolecular cyclization of ortho-substituted aryl azide could be one of the most important synthetic routes to five-memberd nitrogen heterocycles.[3] However, research studies on simple alkyl-substituted azidoquinones so far reported have revealed that the reactions of azidoquinones were highly dependent upon the reaction conditions (acidic or thermal), and rearrangement products[4] or ring contraction products[5] were the major components of the reactions.[6] On the contrary, in the photoreaction of functionalized alkylazidoquinones as described in the following text, it was found that an intramolecular photoinduced cyclization reaction occurs without any difficulties to give 4,7-indolequinone derivatives **5**.

Results and Discussion

Preparation of Azidoquinones. All of the azidoquinones **4** were usually obtained from methyl 3-substituted 2,3-dihydro-5-hydroxy-6-methylbenzofuran-2-carboxylates **1**[1] by the subsequent reaction (Scheme 1). The dihydrobenzofuran **1** was treated with bromine in chloroform to give methyl 3-substituted 4-bromo-2,3-dihydro-5-hydroxy-6-methylbenzofuran-2-carboxylate **2**. Oxidation of this bromide **2** with ceric ammonium nitrate (CAN) in an aqueous acetonitrile[7] afforded bromoquinone **3**, which was reacted with sodium azide[8] in an aqueous methanol to provide azidoquinone **4** in an excellent overall yield from **1**. The structures of bromodihydrobenzofuran **2**, bromoquinone **3**, and azidoquinone **4** were identified on the basis of its spectroscopic properties (Table 2).

Table 1. Photoinduced formation of 4,7-indolequinone **5** from azidoquinone **4**

Entry	Azidoquinone	R	Product	Yield/%[a]
1	**4a**	H	**5a**	42
2	**4b**	Me	**5b**	62
3	**4c**	Et	**5c**	61
4	**4d**	$(CH_2)_2CH_3$	**5d**	60
5	**4e**	CO_2Me	**5e**	40
6	**4f**	$(CH_2)_2CO_2Me$	**5f**	64
7	**4g**	$(CH_2)_3NPht$	**5g**	56
8	**4h**	$(CH_2)_3NHCOCF_3$	**5h**	42
9	**4i**	$CH_2OCO_2C_6H_5$	**5i**	37

a) Reported yields are for isolated, purified products.

Irradiation of Azidoquinones. On irradiation of a solution of azidoquinone **4** (1 mmol) in methanol with a high pressure Hg arc lamp (300 W), the orange yellow color of the solution rapidly turned purple red with the evolution of nitrogen, and then gradually changed to dark yellow. The photochemical reaction was complete in several hours (2—5 h) at room temperature and gave methyl 3-substituted 6-methyl-4,7-dioxoindole-2-carboxylate **5** in a good yield after purification by column chromatography (Table 1). Methanol was the best solvent for the photochemical reaction. Although the same product was taken in benzene, hexane, and chloroform, the yield of the 4,7-indolequinone **5** was rather poor.

The salient feature of this result indicated that the formation of functionalized 4,7-indolequinones **5e**—**i** easily occures on irradiation of azidoquinone **4e**—**i** having various functional groups (ester, amide, imide, and protected alcohol) in the alkyl side chain.

The structures of the irradiation product **5** were established by their IR and ^1H NMR spectra and by their chemical reactions (Experimental). For ex-

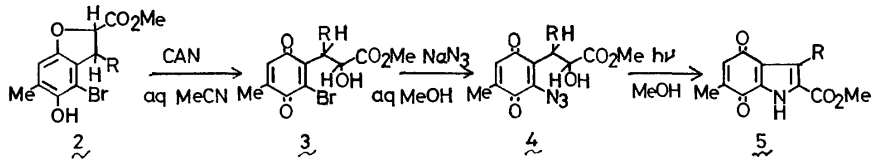

Scheme 1.

Table 2. ^{1}H NMR Spectra[a] of intermediates **2**, **3**, and **4**

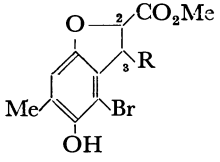

2

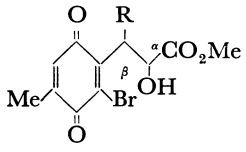

3

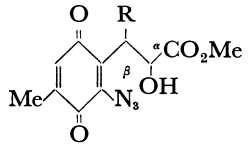

4

	R	C_2-H	C_3-H	OH	C_α-H	C_β-H	OH	C_α-H	C_β-H	OH
a	H	5.18(dd) J=7.2 Hz J=10 Hz	b)	3.92(s)	4.43(t) J=7 Hz	3.10(d) J=7 Hz	2.83(d) J=7 Hz	4.36(t) J=7 Hz	2.87(d) J=7 Hz	2.96(bs)
b	Me	4.68(d) J=4 Hz	3.62(m)	5.14(s)	4.64(t) J=8 Hz	3.53(m)	3.39(bd) J=8 Hz	4.46(d)	3.46(dq)	c)
c	Et	4.85(d) J=3.2 Hz	3.52(m)	5.17(s)	4.56(dd) J=7.5 Hz J=10 Hz	3.61(m)	3.70(d) J=10 Hz	4.47(t) J=8 Hz	3.34(dq) J=7.5 Hz J=8 Hz	3.94(bs)
d	$(CH_2)_2CH_3$	4.85(d) J=3.2 Hz	3.52(m)	5.16(s)	4.55(dd) J=7.5 Hz J=10 Hz	3.74(m)	3.74(d) J=10 Hz	4.45(dd) J=7 Hz J=9.5 Hz	3.43(m)	c)
e	CO_2Me	5.35(d) J=4.6 Hz	4.40(d) J=4.6 Hz	5.22(s)	4.84(dd) J=6 Hz J=8 Hz	4.55(d) J=6 Hz	3.39(d) J=8 Hz	4.83(dd) J=5.5 Hz J=7.5 Hz	4.32(d) J=5.5 Hz	3.38(bd) J=7.5 Hz
f	$(CH_2)_2CO_2Me$	4.83(d) J=3.3 Hz	3.52— 3.88(m)	5.23(s)	4.57(dd) J=7.5 Hz J=10 Hz	c)	c)	4.48(dd) J=7.5 Hz J=10 Hz	c)	c)
g	$(CH_2)_3NPht$	4.86(d) J=3.5 Hz	3.50— 3.90(m)	5.19(s)	4.52(dd) J=8 Hz J=10 Hz	c)	3.56(d) J=10 Hz	4.44(t) J=7.5 Hz	3.32— 3.80(m)	c)
h	$(CH_2)_3NHCOCF_3$	4.78(d) J=3 Hz	3.54(m)	5.13(s)	4.54(dd) J=8 Hz J=10 Hz	c)	c)	4.45(t) J=8 Hz	3.34(m)	3.92(bd) J=8 Hz
i	$CH_2OCO_2C_6H_5$	5.18(d) J=3.2 Hz	4.02(m)	5.19(s)	4.44— 4.85(m)	4.12(m)	3.59(d) J=8 Hz	4.35— 4.82(m)	c)	c)

a) ^{1}H NMR spectra were run on a 100 MHz instrument. b) ABX type: 3.29(dd, J=7.2 and 16 Hz, 1H); 3.53(dd, J=10 and 16 Hz, 1H). c) Chemical shifts and coupling constants were not determined due to overlap with the signal of other protons.

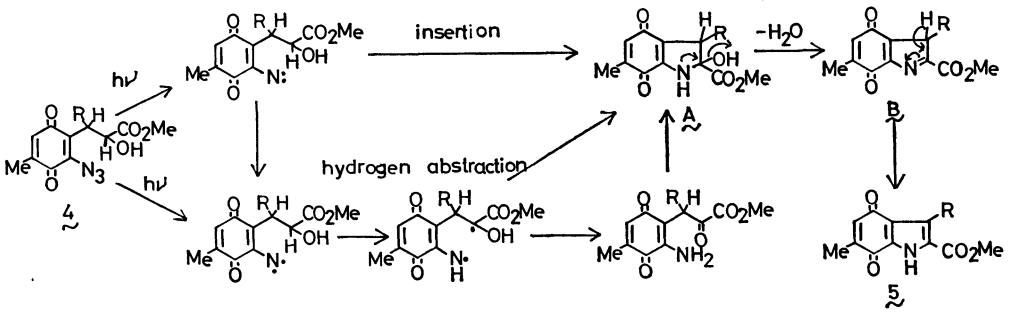

Scheme 2.

ample, evidence for the presence of N–H bond in photoproduct **5** was shown by the fact that the reaction of **5b** with 1 equiv of potassium *t*-butoxide,[9] followed by addition of the excess methyl iodide, gave methyl 1,3,6-trimethyl-4,7-dioxoindole-2-carboxylate **6a** in an excellent yield (90%). Additional evidence for the presence of the quinone ring in the product **5** was obtained by reduction-acetylation[10] of **5f** to methyl 4,7-diacetoxy-5-methylindole-2-carboxylate derivative **7** in an 80% yield. The structure of **5f** was further supported by the Thiele oxidation[11] to methyl 4,5,7-triacetoxy-6-methylindole 2-carboxylate **8**.

Thermal cyclization of azidoquinone **4** in benzene or toluene gave indolequinone **5** in a low yield (5—10%). The yield of **5** decreased further when **4** was heated in a high boiling solvent (xylene or decalin), and tars were obtained.

The photochemical conversion from **4** to **5** can be rationalized as proceeding *via* nitrene[12] (Scheme 2), but it is not clear whether the cyclization step takes place by direct intramolecular insertion of the singlet nitrene into a C–H bond or by intramolecular 1,5-hydrogen abstraction of the triplet nitrene.

The evidence for the reaction pathway outlined in Scheme 2 was obtained by studying UV spectra analysis during irradiation of **4b**. Irradiation of **4b** in methanol caused a rapid change in the absorption spectrum. The absorption maximum at 405 nm (**4b**) was shifted initially to 510 nm (**A** or **B**), but finally moved 346 nm (**5b**). That is to be expected for the intermediate corresponding to **A** or **B**.

In summary, these photochemical ring formations from the azidoquinone under mild conditions allow the facile synthesis of highly functionalized 4,7-indolequinones which have mitosane ring systems.

Experimental

Melting points were measured on a Yanagimoto micro melting point apparatus and are uncorrected. Infrared spectra were run on a JASCO IRA-1 spectrophotometer. Nuclear magnetic resonance spectra were obtained with JEOL PS-100 spectrometer with tetramethylsilane as an internal standard and the chemical shifts are recorded in δ values. Mass spectra were measured with Hitachi M-52 instrument (20 eV). Column chromatography was performed using Wako reagent grade silica gel (200 mesh). Preparative thin layer chromatography was performed using Merck silica gel F-254. Elemental analyses were performed by the Microanalytical Laboratory of Kyoto University. UV irradiations were carried out in a Pyrex tube at room temperature with an Eikosha 300 W high pressure Hg lamp.

Preparation of Starting Materials. All of the compounds **1a**—**i** described below were prepared according to the previously reported methods.[1] Methyl 2,3-dihydro-5-hydroxy-6-methylbenzofuran-2-carboxylate (**1a**), methyl 2,3-dihydro-5-hydroxy-3,6-dimethylbenzofuran-2-carboxylate (**1b**), methyl 3-ethyl-2,3-dihydro-5-hydroxy-6-methylbenzofuran-2-carboxylate (**1c**), methyl 2,3-dihydro-5-hydroxy-6-methyl-3-propylbenzofuran-2-carboxylate (**1d**), dimethyl 2,3-dihydro-5-hydroxy-6-methylbenzofuran-2,3-dicarboxylate (**1e**), methyl 2,3-dihydro-5-hydroxy-3-[2-(methoxycarbonyl)ethyl]-6-methylbenzofuran-2-carboxylate (**1f**), methyl 2,3-dihydro-5-hydroxy-3-[3-(phthalimido)propyl]-6-methylbenzofuran-2-carboxylate (**1g**), methyl 2,3-dihydro-5-hydroxy-6-methyl-3-[3-trifluoroacetamido)propyl]benzofuran-2-carboxylate (**1h**), and methyl 2,3-dihydro-5-hydroxy-3-(phenoxycarbonyloxymethyl)benzofuran-2-carboxylate (**1i**).

Methyl 4-Bromo-2,3-dihydro-5-hydroxy-6-methylbenzofuran-2-carboxylate (2a). (General Procedure for Bromination). To a well-stirred solution of **1a** (389 mg, 1.87 mmol) in chloroform (20 ml) at 0 °C was added dropwise (30 min) 1 M (1 M=1 mol dm^{-3}) bromine in chloroform (2 ml). After stirring for 30 min, the reaction mixture was treated with a diluted solution of sodium thiosulfate. The organic layer was washed twice with water, dried over $MgSO_4$, evaporated, and chromatographed (silica gel, benzene solvent) to give **2a** (484 mg, 90%): Mp 81.5—82.5 °C (dichloromethane–petroleum ether); IR (KBr): 3350 and 1740 cm^{-1}; ^{1}H NMR ($CDCl_3$) δ: 2.25 (s, 3H), 3.29 (dd, J=7.2 and 16 Hz, 1H), 3.53 (dd, J=10 and 16 Hz, 1H), 3.81 (s, 3H), 3.92 (bs, 1H), 5.18 (dd, J=7.2 and 10 Hz, 1H), and 6.62 (s, 1H); Found: C, 45.81; H, 3.94; Br, 28.17%. Calcd for $C_{11}H_{11}O_4Br$: C, 46.01; H, 3.86; Br, 27.83%.

Methyl 4-Bromo-2,3-dihydro-5-hydroxy-3,6-dimethylbenzofuran-2-carboxylate (2b). Reaction of **1b** (641 mg, 2.88 mmol) with bromine by the method described above gave **2b** (702 mg, 81%): Mp 70—73 °C (dichloromethane–petroleum ether); IR (KBr): 3420 and 1735 cm^{-1}; ^{1}H NMR ($CDCl_3$) δ: 1.46 (d, J=7 Hz, 3H), 2.23 (s, 3H), 3.72 (s, 3H), 3.62 (m, 1H), 4.68 (d, J=4 Hz, 1H), 5.14 (s, 1H), and 6.62 (s, 1H); Found: C, 47.62; H, 4.43; Br, 26.77%. Calcd for $C_{12}H_{13}O_4Br$: C, 47.86; H, 4.35; Br, 26.54%.

Methyl 4-Bromo-3-ethyl-2,3-dihydro-5-hydroxy-6-methylbenzofuran-2-carboxylate (2c). Reaction of **1c** (236 mg, 1 mmol) with bromine gave **2c** (230 mg, 73%): Mp 80—81 °C (petroleum ether); IR (KBr): 3460 and 1740 cm^{-1}; ^{1}H NMR ($CDCl_3$) δ: 0.96 (t, J=7 Hz, 3H), 1.66 (m, 2H), 2.26 (s, 3H), 3.52 (m, 1H), 3.78 (s, 3H), 4.85 (d, J=3.2 Hz, 1H), 5.17 (s, 1H), and 6.67 (s, 1H); Found: C, 49.26; H, 4.92; Br, 25.29%. Calcd for $C_{13}H_{15}O_4Br$: C, 49.54; H, 4.80; Br, 25.36%.

*Methyl 4-Bromo-2,3-dihydro-5-hydroxy-6-methyl-3-propylbenzofuran-2-carboxylate (**2d**).* Bromination of **1d** (250 mg, 1 mmol) gave **2d** as an oil (263 mg, 80%). IR (neat): 3460 and 1740 cm^{-1}; ^1H NMR ($CDCl_3$) δ: 0.96 (t, J=7 Hz, 3H), 1.20—2.20 (m, 4H), 2.25 (s, 3H), 3.52 (m, 1H), 3.76 (s, 3H), 4.85 (d, J=3.2 Hz, 1H), 5.16 (s, 1H), and 6.64 (s, 1H). Found: C, 50.94; H, 5.40%. Calcd for $C_{14}H_{17}O_4Br$: C, 51.08; H, 5.21%.

*Dimethyl 4-Bromo-2,3-dihydro-5-hydroxy-6-methylbenzofuran-2,3-dicarboxylate (**2e**).* A solution of **1e** (476 mg, 1.79 mmol) in chloroform was treated with bromine to give **2e** (405 mg, 66%): Mp 182—185 °C (methanol–petroleum ether); IR (KBr): 3340 and 1740 cm^{-1}; ^1H NMR ($CDCl_3$) δ: 2.27 (s, 3H), 3.80 (s, 3H), 3.82 (s, 3H), 4.40 (d, J=4.6 Hz, 1H), 5.22 (s, 1H), 5.35 (d, J=4.6 Hz, 1H), and 6.71 (s, 1H). Found: C, 45.10; H, 3.94%. Calcd for $C_{13}H_{13}O_6Br$: C, 45.24; H, 3.80%.

*Methyl 4-Bromo-2,3-dihydro-5-hydroxy-3-[2-(methoxycarbonyl)ethyl]-6-methylbenzofuran-2-carboxylate (**2f**).* Reaction of **1f** (589 mg, 2 mmol) with bromine afforded **2f** (642 mg, 86%): Mp 91—92 °C (petroleum ether–dichloromethane); IR (KBr): 3470, 1745, and 1720 cm^{-1}; ^1H NMR ($CDCl_3$) δ: 1.90—2.51 (m, 4H), 2.26 (s, 3H), 3.52—3.88 (m, 1H), 3.66 (s, 3H), 3.75 (s, 3H), 4.83 (d, J=3.3 Hz, 1H), 5.23 (s, 1H), and 6.64 (s, 1H). Found: C, 47.97; H, 4.76; Br, 21.59%. Calcd for $C_{15}H_{17}O_6Br$: C, 48.27; H, 4.59; Br, 21.41%.

*Methyl 4-Bromo-2,3-dihydro-5-hydroxy-3-[3-(phthalimido)propyl]-6-methylbenzofuran-2-carboxylate (**2g**).* Reaction of **1g** (395 mg, 1 mmol) with bromine gave **2g** (337 mg, 71%): Mp 153—154 °C (methanol–dichloromethane); IR (KBr): 3490, 1765, and 1705 cm^{-1}; ^1H NMR ($CDCl_3$) δ: 1.60—2.20 (m, 4H), 2.24 (s, 3H), 3.50—3.90 (m, 3H), 3.77 (s, 3H), 4.86 (d, J=3.5 Hz, 1H), 5.19 (s, 1H), 6.65 (s, 1H), and 7.66—7.90 (m, 4H). Found: C, 55.44, H, 4.17; N, 2.83; Br, 17.07%. Calcd for $C_{22}H_{20}O_6NBr$: C, 55.71; H, 4.25; N, 2.95; Br, 16.85%.

*Methyl 4-Bromo-2,3-dihydro-5-hydroxy-6-methyl-3-[3-(trifluoroacetamido)propyl]benzofuran-2-carboxylate (**2h**).* Prepared from **1h** (860 mg, 2.38 mmol) and bromine; (628 mg, 60%): Mp 93—94 °C (petroleum ether–dichloromethane); IR (KBr): 3420, 3290, 1735, and 1700 cm^{-1}; ^1H NMR ($CDCl_3$)δ: 1.45—2.20 (m, 4H), 2.25 (m, 3H), 3.40 (t, J= 7 Hz, 2H), 3.54 (m, 1H), 3.75 (s, 3H), 4.78 (d, J=3 Hz, 1H), 5.13 (s, 1H), 6.41 (bs, 1H), and 6.61 (s, 1H). Found: C, 43.50; H, 3.87; N, 3.30%. Calcd for $C_{16}H_{17}O_5NBr$: C, 43.65; H, 3.89; N, 3.18%.

*Methyl 4-Bromo-2,3-dihydro-5-hydroxy-6-methyl-3-(phenoxycarbonyloxymethyl)benzofuran-2-carboxylate (**2i**).* Treatment of **1i** (117 mg, 0.327 mmol) with bromine afforded **2i** (140 mg, 98%): Mp 103—104 °C (petroleum ether–dichloromethane); IR (KBr): 3470, 1760, and 1590 cm^{-1}; ^1H NMR ($CDCl_3$) δ: 2.27 (s, 3H), 3.79 (s, 3H), 4.02 (m, 1H), 4.31 (dd, J= 8.2 and 11 Hz, 1H), 4.72 (dd, J=3.8 and 11 Hz, 1H), 5.18 (d, J=3.2 Hz, 1H), 5.19 (s, 1H), 6.71 (s, 1H), and 7.20—7.44 (m, 5H). Found: C, 52.24; H, 4.09%. Calcd for $C_{19}H_{17}O_7Br$: C, 52.19; H, 3.92%.

*Methyl 3-(2-Bromo-4-methyl-3,6-dioxo-1,4-cyclohexadienyl)-2-hydroxypropionate (**3a**).* (General Procedure for Oxidation). To a solution of **2a** (287 mg, 1 mmol) in 70% aq acetonitrile (10 ml) at 0 °C was added dropwise over 15 min a solution of ceric ammonium nitrate (CAN)[7] (1.21 g, 2.2 mmol) in water (5 ml). The mixture was stirred for 15 min and then poured into water (100 ml). The aq suspension was extracted with chloroform (3×20 ml) and the organic phases were washed with water (3×20 ml), dried, passed through a short pad of silica gel using chloroform, and evaporated to give **3a** (220 mg, 98%): Mp 77—78 °C (dichloromethane–petroleum ether); IR (KBr): 3480, 1735, 1660, and 1650 cm^{-1}; ^1H NMR ($CDCl_3$) δ: 2.11 (d, J=1.6 Hz, 3H), 2.83 (d, J=7 Hz, 1H), 3.10 (d, J=7 Hz, 2H), 3.78 (s, 3H), 4.43 (q, J=7 Hz, 1H), and 6.61 (q, J=1.6 Hz, 1H). Found: C, 43.78; H, 3.69; Br, 26.60%. Calcd for $C_{11}H_{11}O_5Br$: C, 43.58; H, 3.66; Br, 26.37%.

*Methyl 3-(2-Bromo-4-methyl-3,6-dioxo-1,4-cyclohexadienyl)-2-hydroxybutyrate (**3b**).* (CAN Oxidation of **2b**): (86%); mp 116—118 °C (hexane–dichloromethane); IR (KBr): 3470, 1740, 1675, and 1650 cm^{-1}; ^1H NMR ($CDCl_3$) δ: 1.32 (d, J=7 Hz, 3H), 2.12 (d, J=1.6 Hz, 3H), 3.39 (bd, J=8 Hz, 1H), 3.53—3.80 (m, 1H), 3.80 (s, 3H), 4.64 (t, J=8 Hz, 1H), and 6.62 (q, J=1.6 Hz, 1H). Found: C, 45.53; H, 4.16; Br, 25.43%. Calcd for $C_{12}H_{13}O_5Br$: C, 45.44; H, 4.13; Br, 25.19%.

*Methyl 3-(2-Bromo-4-methyl-3,6-dioxo-1,4-cyclohexadienyl)-2-hydroxypentanoate (**3c**).* (CAN Oxidation of **2c**): (88%); IR (neat): 3460, 1740, 1670, and 1655 cm^{-1}; ^1H NMR ($CDCl_3$) δ: 0.90 (t, J=7 Hz, 3H), 1.70—1.92 (m, 2H), 2.12 (d, J=1.6 Hz, 3H), 3.61 (m, 1H), 3.70 (d, J=10 Hz, 1H), 3.74 (s, 3H), 4.56 (dd, J=7.5 and 10 Hz, 1H), and 6.63 (q, J=1.6 Hz, 1H). Found: C, 47.10; H, 4.66; Br, 24.38%. Calcd for $C_{13}H_{15}O_5Br$: C, 47.15; H, 4.57; Br, 24.13%.

*Methyl 3-(2-Bromo-4-methyl-3,6-dioxo-1,4-cyclohexadienyl)-2-hydroxyhexanoate (**3d**).* (CAN Oxidation of **2d**): (90%); mp 82—83 °C (petroleum ether); IR (KBr): 3460, 1735, 1670, and 1655 cm^{-1}; ^1H NMR ($CDCl_3$) δ: 0.90 (t, J=7 Hz, 3H), 1.28 (m, 2H), 1.77 (m, 2H), 2.16 (d, J=1.6 Hz, 3H), 3.74 (s, 3H and m, 2H), 4.55 (dd, J=7.5 and 10 Hz, 1H), and 6.63 (q, J=1.6 Hz, 1H). Found: C, 48.51; H, 5.01; Br, 23.43%. Calcd for $C_{14}H_{17}O_5Br$: C, 48.71; H, 4.96; Br, 23.15%.

*Dimethyl 3-(2-Bromo-4-methyl-3,6-dioxo-1,4-cyclohexadienyl)-2-hydroxysuccinate (**3e**).* (CAN Oxidation of **2e**): (96%); IR (neat): 3460, 1735, 1670, and 1650 cm^{-1}; ^1H NMR ($CDCl_3$) δ: 2.13 (d, J=1.6 Hz, 3H), 3.39 (d, J=8 Hz, 1H), 3.70 (s, 3H), 3.76 (s, 3H), 4.55 (d, J=6 Hz, 1H), 4.84 (dd, J=6 and 8 Hz, 1H), and 6.65 (q, J=1.6 Hz, 1H). Found: C, 43.02; H, 3.75%. Calcd for $C_{13}H_{13}O_7Br$: C, 43.23; H, 3.63%.

*Dimethyl 3-(2-Bromo-4-methyl-3,6-dioxo-1,4-cyclohexadienyl)-2-hydroxyhexanedioate (**3f**).* (CAN Oxidation of **2f**): (92%); mp 91—92 °C (hexane–dichloromethane); IR (KBr): 3440, 1735, 1725, 1665, and 1650 cm^{-1}; ^1H NMR ($CDCl_3$) δ: 2.13 (d, J=1.6 Hz, 3H), 2.13—2.46 (m, 4H), 3.64 (s, 3H), 3.75 (s, 3H and m, 2H), 4.57 (dd, J=8 and 10 Hz, 1H), and 6.64 (q, J=1.6 Hz, 1H). Found: C, 46.55; H, 4.44; Br, 20.68%. Calcd for $C_{15}H_{17}O_7Br$: C, 46.29; H, 4.40; Br, 20.53%.

*Methyl 3-(2-Bromo-4-methyl-3,6-dioxo-1,4-cyclohexadienyl)-2-hydroxy-6-phthalimidohexanoate (**3g**).* (CAN Oxidation of **2g**): (89%); mp 153—155 °C (dichloromethane–petroleum ether); IR (KBr): 3460, 3400, 1770, 1735, and 1650 cm^{-1}; ^1H NMR ($CDCl_3$) δ: 1.40—2.10 (m, 4H), 2.10 (d, J=1.6 Hz, 3H), 3.62—3.76 (m, 2H), 3.72 (s, 3H), 4.52 (dd, J= 8 and 10 Hz, 1H), 6.60 (q, J=1.6 Hz, 1H), and 7.69—7.82 (m, 4H). Found: C, 53.67; H, 4.34; N, 2.76%. Calcd for $C_{22}H_{20}O_7NBr$: C, 53.89; H, 4.11; N, 2.86%.

*Methyl 6-Trifluoroacetamido-3-(2-bromo-4-methyl-3,6-dioxo-1,4-cyclohexadienyl)-2-hydroxyhexanoate (**3h**).* (CAN Oxidation of **2h**): (42%); mp 124—125 °C (dichloromethane–petroleum ether); IR (KBr): 3450, 3330, 1750, 1700, and 1655 cm^{-1}; ^1H NMR ($CDCl_3$) δ: 1.30—2.10 (m, 4H), 2.12 (d, J=1.6 Hz, 3H), 3.35 (q, J=7 Hz, 2H), 3.73 (s, 3H and m, 1H), 4.54 (dd, J=4 and 5 Hz, 1H), and 6.60 (q, J=1.6 Hz, 1H). Found: C, 41.83; H, 3.82; N, 3.03; Br, 17.78%.

Calcd for $C_{16}H_{17}O_6NF_3Br$: C, 42.12; H, 3.76; N, 3.07; Br, 17.52%.

*Methyl 3-(2-Bromo-4-methyl-3,6-dioxo-1,4-cyclohexadienyl)-2-hydroxy-4-(phenoxycarbonyloxy)butyrate (**3i**).* (CAN Oxidation of **2i**): (80%); IR (neat): 3460, 1750, and 1660 cm^{-1}; ^1H NMR ($CDCl_3$) δ: 2.12 (d, J=1.6 Hz, 3H), 3.59 (d, J=8 Hz, 1H), 3.79 (s, 3H), 4.12 (m, 1H), 4.44—4.85 (m, 2H and m, 1H), 6.65 (q, J=1.6 Hz, 1H), and 7.05—7.51 (m, 5H). Found: C, 50.19; H, 5.97%. Calcd for $C_{19}H_{17}O_8Br$: C, 50.35; H, 5.84%.

*Methyl 3-(2-Azido-4-methyl-3,6-dioxo-1,4-cyclohexadienyl)-2-hydroxypropionate (**4a**).* (General Procedure for Azidoquinone Formation). To a solution of **3a** (303 mg, 1 mmol) in methanol (10 ml) at 0 °C was added sodium azide (78 mg, 1.2 mmol) in water (2 ml). The resulting mixture gradually became red. After stirring for 1 h at room temperature, the solvent was removed under reduced pressure at a temperature below 40 °C, water (50 ml) was added and the mixture was extracted with chloroform (3×25 ml). The combined chloroform extracts were washed with water (3×25 ml), dried ($MgSO_4$), evaporated, and chromatographed (silica gel, chloroform solvent) to give **4a** (238 mg, 90%). IR (neat): 3460, 2120, 1735, and 1650 cm^{-1}; ^1H NMR ($CDCl_3$) δ: 2.07 (d, J=1.6 Hz, 3H), 2.87 (d, J=7 Hz, 2H), 2.96 (bs, 1H), 3.80 (s, 3H), 4.36 (t, J=7 Hz, 1H), and 6.61 (q, J=1.6 Hz, 1H). Anal.[13]

Compounds **4b**—**i** were prepared from the corresponding **3b**—**i** by the same procedure. The spectral data of these compounds are given below.

*Methyl 3-(2-Azido-4-methyl-3,6-dioxo-1,4-cyclohexadienyl)-2-hydroxybutyrate (**4b**).* (Oil, 90%); IR (neat): 3440, 2110, 1735, and 1650 cm^{-1}; ^1H NMR ($CDCl_3$) δ: 1.24 (d, J=7 Hz, 3H), 2.07 (d, J=1.6 Hz, 3H), 3.49 (m, 1H), 3.74 (s, 3H and m, 1H), 4.46 (d, J=8 Hz, 1H), and 6.55 (q, J=1.6 Hz, 1H). Anal.[13]

*Methyl 3-(2-Azido-4-methyl-3,6-dioxo-1,4-cyclohexadienyl)-2-hydroxypentanoate (**4c**).* (Oil, 98%); IR (neat): 3440, 2110, 1740, 1670, and 1655 cm^{-1}; ^1H NMR ($CDCl_3$) δ: 0.84 (t, J=7 Hz, 3H), 1.74 (m, 2H), 2.07 (d, J=1.6 Hz, 3H), 3.34 (dt, J=8 and 7.5 Hz, 1H), 3.72 (s, 3H), 3.94 (bs, 1H), 4.47 (t, J=8 Hz, 1H), and 6.60 (q, J=1.6 Hz, 1H). Anal.[13]

*Methyl 3-(2-Azido-4-methyl-3,6-dioxo-1,4-cyclohexadienyl)-2-hydroxyhexanoate (**4d**).* (88%); mp 93—94 °C (petroleum ether); IR (KBr): 3460, 2120, 2100, 1735, 1670, and 1650 cm^{-1}; ^1H NMR ($CDCl_3$) δ: 0.88 (t, J=7 Hz, 3H), 1.22 (m, 2H), 1.73 (m, 2H), 2.05 (d, J=1.6 Hz, 3H), 3.43 (m, 1H), 3.72 (s, 3H), 3.78 (d, J=9.5 Hz, 1H), 4.45 (dd, J=7 and 9.5 Hz, 1H), and 6.55 (q, J=1.6 Hz, 1H). Found: C, 54.60; H, 5.64%. Calcd for $C_{14}H_{17}O_5N_3$: C, 54.72; H, 5.58%.

*Dimethyl 3-(2-Azido-5-methyl-3,6-dioxo-1,4-cyclohexadienyl)-2-hydroxysuccinate (**4e**).* (Oil, 88%); IR (neat): 3460, 2120, 1735, and 1650 cm^{-1}; ^1H NMR ($CDCl_3$) δ: 2.10 (d, J=1.6 Hz, 3H), 3.38 (bd, J=7 Hz, 1H), 3.70 (s, 3H), 3.76 (s, 3H), 4.32 (d, J=5.5 Hz, 1H), 4.83 (dd, J=5.5 and 7 Hz, 1H), and 6.59 (q, J=1.6 Hz, 1H). Anal.[13]

*Dimethyl 3-(2-Azido-4-methyl-3,6-dioxo-1,4-cyclohexadienyl)-2-hydroxyhexanedioate (**4f**).* (Oil, 80%); IR (neat): 3440, 2110, 2095, 1745, 1730, 1670, and 1655 cm^{-1}; ^1H NMR ($CDCl_3$) δ: 2.13 (d, J=1.6 Hz, 3H), 2.13—2.46 (m, 4H), 3.64 (s, 3H), 3.75 (s, 3H and m, 2H), 4.57 (dd, J=8 and 10 Hz, 1H), and 6.64 (q, J=1.6 Hz, 1H). Found: C, 51.11; H, 4.75%. Calcd for $C_{15}H_{17}O_7N_3$: C, 51.28; H, 4.88%.

*Methyl 3-(2-Azido-4-methyl-3,6-dioxo-1,4-cyclohexadienyl)-2-hydroxy-6-phthalimidohexanoate (**4g**).* (71%); mp 117—120 °C (petroleum ether–dichloromethane); IR (KBr): 3460, 2110, 2100, 1770, 1735, 1705, and 1650 cm^{-1}; ^1H NMR ($CDCl_3$) δ: 1.30—2.07 (m, 4H), 2.07 (d, J=1.6 Hz, 3H), 3.32—3.80 (m, 2H and m, 2H), 3.70 (s, 3H), 4.44 (m, 1H), 6.51 (q, J=1.6 Hz, 1H), and 7.60—7.80 (m, 4H). Anal.[13]

*Methyl 3-(2-Azido-4-methyl-3,6-dioxo-1,4-cyclohexadienyl)-6-trifluoroacetamido-2-hydroxyhexanoate (**4h**).* (Oil, 85%); IR ($CHCl_3$): 3430, 2110, 1720, and 1650 cm^{-1}; ^1H NMR ($CDCl_3$) δ: 1.30—2.00 (m, 4H), 2.09 (d, J=1.6 Hz, 3H), 3.34 (m, 2H), 3.67 (m, 1H), 3.73 (s, 3H), 3.92 (bd, J=10 Hz, 1H), 4.45 (dd, J=7 and 10 Hz, 1H), 6.55 (q, J=1.6 Hz, 1H), and 6.95 (bs, 1H). Anal.[13]

*Methyl 3-(2-Azido-5-methyl-3,6-dioxo-1,4-cyclohexadienyl)-2-hydroxy-4-(phenoxycarbonyloxy)butyrate (**4i**).* (Oil, 68%); IR (neat): 3440, 2120, 1750, and 1660 cm^{-1}; ^1H NMR ($CDCl_3$) δ: 2.10 (d, J=1.6 Hz, 3H), 3.81 (s, 3H and m, 1H), 4.35—4.82 (m, 3H), 6.61 (q, J=1.6 Hz, 1H), and 7.09—7.53 (m, 5H). Anal.[13]

*Irradiation of **4a**.* (General Photochemical Procedure for 4,7-Indolequinone Formation). A solution of **4a** (265 mg, 1 mmol) in methanol (200 ml) was purged with nitrogen for 15 min and irradiated in a Pyrex tube for 5 h with a 300-W high pressure Hg lamp. After removal of the solvent, the crude residue was chromatographed on silica gel using chloroform to give methyl 6-methyl-4,7-dioxoindole-2-carboxylate (**5a**) (92 mg, 42%): Mp 249—250 °C (methanol–dichloromethane); IR (KBr): 3260, 1710, and 1660 cm^{-1}; ^1H NMR (DMSO-d_6) δ: 2.02 (d, J=1.6 Hz, 3H), 3.82 (s, 3H), 6.55 (q, J=1.6 Hz, 1H), 6.97 (s, 1H), and 13.49 (bs, 1H); MS, *m/e* (rel intensity), 219 (M^+, 92), 187 (82), 159 (78), 151 (48), and 131 (100). Found: C, 60.01; H, 4.32; N, 6.25%. Calcd for $C_{11}H_9O_4N$: C, 60.27; H, 4.14; N, 6.39%.

Physical properties of the other photoproducts **5b**—**i** are given below.

*Methyl 3,6-Dimethyl-4,7-dioxoindole-2-carboxylate (**5b**) from **4b**.* (62%); mp 275—277 °C (decomp); IR (KBr): 3250, 1700, and 1655 cm^{-1}; ^1H NMR (DMSO-d_6) δ: 2.01 (d, J=1.6 Hz, 3H), 2.47 (s, 3H), 3.81 (s, 3H), 6.50 (q, J=1.6 Hz, 1H), and 13.10 (bs, 1H). Found: C, 62.02; H, 4.77; N, 5.94%. Calcd for $C_{12}H_{11}O_4N$: C, 61.80; H, 4.75; N, 6.01%.

*Methyl 3-Ethyl-6-methyl-4,7-dioxoindole-2-carboxylate (**5c**) from **4c**.* (61%); mp 221—222 °C; IR (KBr): 3250, 1695, and 1650 cm^{-1}; ^1H NMR ($CDCl_3$) δ: 1.17 (t, J=7.5 Hz, 3H), 2.08 (d, J=1.6 Hz, 3H), 3.09 (q, J=7.5 Hz, 2H), 3.95 (s, 3H), 6.49 (q, J=1.6 Hz, 1H), and 9.97 (bs, 1H). Found: C, 63.30; H, 5.42; N, 5.64%. Calcd for $C_{13}H_{13}O_4N$: C, 63.15; H, 5.30; N, 5.67%.

*Methyl 6-Methyl-4,7-dioxo-3-propylindole-2-carboxylate (**5d**) from **4d**.* (60%); mp 183—184 °C; IR (KBr): 3260, 1695, and 1650 cm^{-1}; ^1H NMR ($CDCl_3$) δ: 0.95 (t, J=7.5 Hz, 3H), 1.61 (m, 2H), 2.08 (d, J=1.6 Hz, 3H), 3.07 (t, J=7.5 Hz, 2H), 3.94 (s, 3H), 6.47 (q, J=1.6 Hz, 1H), and 9.92 (bs, 1H); MS, *m/e* (rel intensity), 261 (M^+, 7), 260 (40), 229 (91), and 201 (100). Found: C, 64.45; H, 5.83; N, 5.26%. Calcd for $C_{14}H_{15}O_4N$: C, 64.36; H, 5.79; N, 5.36%.

*Dimethyl 6-Methyl-4,7-dioxoindole-2,3-dicarboxylate (**5e**) from **4e**.* (40%); mp 200—201 °C; IR (KBr): 3220, 1735, 1695, and 1660 cm^{-1}; ^1H NMR ($CDCl_3$) δ: 2.13 (d, J=1.6 Hz, 3H), 3.96 (s, 3H), 4.00 (s, 3H), 6.57 (q, J=1.6 Hz, 1H), and 8.70 (bs, 1H). Found: C, 56.54; H, 4.18; N, 4.91%. Calcd for $C_{13}H_{11}O_6N$: C, 56.32; H, 4.00; N, 5.05%.

*Methyl 3-[2-(Methoxycarbonyl)ethyl]-6-methyl-4,7-dioxoindole-2-carboxylate (**5f**) from **4f**.* (64%); mp 195—196 °C; IR (KBr): 3260, 1740, 1700, and 1660 cm^{-1}; ^1H NMR ($CDCl_3$) δ: 2.10 (d, J=1.6 Hz, 3H), 2.65 (t, J=7 Hz, 2H), 3.43 (t, J=7 Hz, 2H), 3.69 (s, 3H), 3.97 (s, 3H), 6.53 (q, J=1.6 Hz, 1H), and 10.15 (bs, 1H); MS, *m/e* (rel intensity),

305 (M^+, 8), 273 (35), 245 (94), and 213 (100). Found: C, 58.89; H, 4.77; N, 4.39%. Calcd for $C_{15}H_{15}O_6N$: C, 59.01; H, 4.95; N, 4.59%.

*Methyl 6-Methyl-4,7-dioxo-3-[3-(phthalimido)propyl]indole-2-carboxylate (**5g**) from **4g**.* (56%); mp 242—243 °C; IR (KBr): 3240, 1770, 1700, and 1650 cm $^{-1}$; H NMR (DMSO-d_6) δ: 1.90 (m, 2H), 1.99 (d, J=1.6 Hz, 3H), 3.03 (t, J=7 Hz, 2H), 3.61 (t, J=7 Hz, 2H), 3.76 (s, 3H), 6.48 (q, J=1.6 Hz, 1H), 7.83 (s, 4H), and 13.02 (bs, 1H); MS, *m/e* (rel intensity), 406 (M^+, 40), 373 (15), 329 (13), 233 (44), and 227 (100). Found: C, 64.93; H, 4.49; N, 6.85%. Calcd for $C_{22}H_{18}O_6N_2$: C, 65.02; H, 4.46; N, 6.89%.

*Methyl 6-Methyl-4,7-dioxo-3-[3-(trifluoroacetamido)propyl]indole-2-carboxylate (**5h**) from **4h**.* (42%); mp 241—242 °C; IR (KBr): 3240, 1700, and 1650 cm $^{-1}$; ^{1}H NMR (DMSO-d_6) δ: 1.79 (m, 2H), 2.04 (d, J=1.6 Hz, 3H), 3.13 (m, 4H), 3.86 (s, 3H), 6.43 (q, J=1.6 Hz, 1H), 8.85 (bs, 1H), and 12.74 (bs, 1H); MS, *m/e* (rel intensity), 372 (M^+, 5), 258 (75), 244 (19), and 227 (100). Found: C, 51.55; H, 4.28; N, 7.41%. Calcd for $C_{16}H_{15}O_5N_2F_3$: C, 51.16; H, 4.06; N, 7.53%.

*Methyl 6-Methyl-4,7-dioxo-3-(phenoxycarbonyloxymethyl)indole-2-carboxylate (**5i**) from **4i**.* (37%); mp 155—156 °C; IR (neat): 3240, 1760, 1700, and 1650 cm $^{-1}$; ^{1}H NMR ($CDCl_3$) δ: 2.10 (d, J=1.6 Hz, 3H), 3.98 (s, 3H), 5.70 (s, 2H), 6.53 (q, J=1.6 Hz, 1H), 7.10—7.40 (m, 5H), and 10.60 (bs, 1H). Found: C, 62.02; H, 4.18; N, 3.65%. Calcd for $C_{19}H_{15}O_7N$: C, 61.79; H, 4.09; N, 3.79%.

*Methyl 1,3,6-Trimethyl-4,7-dioxoindole-2-carboxylate (**6a**).* To a solution of **5b** (116 mg, 0.5 mmol) in dry DMSO (20 ml) at 20 °C was added under argon potassium *t*-butoxide (68 mg, 0.6 mmol). The resulting red solution was stirred for 10 min, and methyl iodide (156 μl, 2.5 mmol) was added. After stirring for 1 h at room temperature, the reaction mixture was poured into cold 0.1 M hydrochloric acid (100 ml) and the resulting suspension was extracted with chloroform (3×20 ml). The organic layer was washed with water and dried ($MgSO_4$). Removal of the solvent and chromatography gave **6a** (111 mg, 90%): Mp 141—143 °C; IR (KBr): 1705 and 1650 cm^{-1}; ^{1}H NMR ($CDCl_3$) δ: 2.08 (d, J=1.6 Hz, 3H), 2.58 (s, 3H), 3.92 (s, 3H), 4.25 (s, 3H), and 6.45 (q, J=1.6 Hz, 1H); MS, *m/e* (rel intensity), 247 (M^+, 100). Found: C, 63.00; H, 5.41; N, 5.50%. Calcd for $C_{13}H_{13}O_4N$: C, 63.15; H, 5.30; N, 5.67%.

*Methyl 1-Allyl-3,6-dimethyl-4,7-dioxoindole-2-carboxylate (**6b**).* Reaction of **5b** (116 mg, 0.5 mmol), potassium *t*-butoxide (75 mg, 0.67 mmol), and allyl bromide (0.5 ml, 5.76 mmol) in dry DMSO (20 ml) solution by the procedure described for the preparation of **6a** gave after chromatography **6b** (123 mg, 90%): Mp 144—145 °C; IR (KBr): 1700, 1650, and 1645 cm^{-1}; ^{1}H NMR ($CDCl_3$) δ: 2.05 (d, J=1.6 Hz, 3H), 2.59 (s, 3H) 3.91 (s, 3H), 4.91—6.19 (m, 5H), and 6.46 (q, J=1.6 Hz, 1H); MS, *m/e* (rel intensity), 273 (M^+, 26), 258 (63), 215 (65), and 71 (100). Found: C, 65.82; H, 5.49; H, 4.89%. Calcd for $C_{15}H_{15}O_4N$: C, 65.92; H, 5.53; N, 5.13%.

*Methyl 4,7-Diacetoxy-3-[2-(methoxycarbonyl)ethyl]-6-methylindole-2-carboxylate (**7**).* A solution of **5f** (153 mg, 0.5 mmol) in ether was reduced with excess aq sodium dithionite[10] to give methyl 4,7-dihydroxy-3-[2-(methoxycarbonyl)-ethyl]-6-methylindole-2-carboxylate, which was acetylated with acetic anhydride (2 ml) in the presence of pyridine (0.1 ml) to afford **7** (156 mg, 80%); mp 171—172 °C (methanol–petroleum ether); IR (KBr): 3340, 1750, 1720, and 1710 cm^{-1}; ^{1}H NMR ($CDCl_3$) δ: 2.24 (s, 3H), 2.40 (s, 6H), 2.58 (t, J=7 Hz, 2H), 3.38 (t, J=7 Hz, 2H), 3.68 (s, 3H), 3.92 (s, 3H), 6.70 (s, 1H), and 8.62 (bs, 1H). Found: C, 58.11; H, 5.38; N, 3.35%. Calcd for $C_{19}H_{21}O_8N$: C, 58.31; H, 5.41; N, 3.58%.

*Methyl 4,5,7-Triacetoxy-3-[2-(methoxycarbonyl)ethyl]-6-methylindole-2-carboxylate (**8**)* was prepared by the Thiele oxidation of **5f** (153 mg, 0.5 mmol) with acetic anhydride (5 ml) in the presence of conc H_2SO_4 (0.1 ml).[11] (79 mg, 35%); mp 238—239 °C (dichloromethane–petroleum ether); IR (KBr): 3350, 1770; 1750, 1735, and 1715 cm^{-1}; ^{1}H NMR ($CDCl_3$) δ: 2.07 (s, 3H), 2.32 (s, 3H), 2.42 (s, 6H), 2.56 (t, J=8 Hz, 2H), 3.34 (t, J=8 Hz, 2H), 3.70 (s, 3H), 3.94 (s, 3H), and 8.75 (bs, 1H); MS, *m/e* (rel intensity), 449 (M^+, 5), 409 (23), 366 (48), 334 (21), 324 (49), and 292 (100). Found: C, 55.90; H, 5.29; N, 3.23%. Calcd for $C_{21}H_{23}O_{10}N$: C, 56.12; H, 5.16; N, 3.12%.

During this investigation the author became particularly indebted to Professor Kazuhiro Maruyama for his invaluable suggestions and continuous encouragement.

References

1) T. Kozuka, *Bull. Chem. Soc. Jpn.*, **55**, 2415 (1982).

2) For excellent reviews of mitomycins and their chemistry see: R. H. Thomson, "Naturally Occurring Quinones," 2nd ed, Academic Press, New York (1971), pp. 653—660; T. Kametani and K. Takahashi, *Heterocycles*, **9**, 293 (1978); W. A. Remers, "The Chemistry of Antitumor Antibiotics," Wiley, New York (1979), Vol. 1, pp. 221—276; Y. Kishi, *J. Nat. Prod.*, **42**, 549 (1979).

3) B. Iddon, O. Meth-Cohn, E. F. V. Scriven, H. Suschitky, and P. T. Gallagher, *Angew. Chem., Int. Ed. Engl.*, **18**, 911 (1979).

4) H. W. Moore, H. R. Shelden, D. W. Deters, and R. J. Wikholm, *J. Am. Chem. Soc.*, **92**, 1675 (1970).

5) W. Weyler, Jr., D. S. Pearce, and H. W. Moore, *J. Am. Chem. Soc.*, **95**, 2603 (1973).

6) S. Patai, "Chemistry of Azide Groups," Wiley, New York (1971), pp. 581—585.

7) R. L. Hannan, R. B. Baeker, and H. Rapoport, *J. Org. Chem.*, **44**, 2153 (1979).

8) Ref. 4.

9) F. C. Chang and N. F. Wood, *Tetrahedron Lett.*, **1964**, 2969. Hydrolysis of **5b** did not occur under this reaction condition.

10) D. S. Pearce, M-S. Lee, and H. W. Moore, *J. Org. Chem.*, **39**, 1362, (1974).

11) T. R. Govindachari, K. Nagarajan, and P. C. Pathasarathly, *J. Chem. Soc.*, **1957**, 548.

12) *Via* Singlet nitrene: G. Smolinsky and B. I. Feuer, *J. Am. Chem. Soc.*, **86**, 3084 (1964); D. H. R. Barton, P. G. Sommers, and G. G. Weingarten, *J. Chem. Soc., C*, **1971**, 721; *Via* Triplet nitrene: Ref. 3.

13) Attempts to obtain a proper analysis failed since compound **4** was unstable when allowed to stand at room temperature for several hours; it was thus used in photochemical studies without further purification.

The Structure and Synthesis of Sudachiin A, a New Flavone Glucoside from *Citrus Sudachi*

Tokunaru HORIE,* Masao TSUKAYAMA,† and Mitsuru NAKAYAMA††

Department of Applied Chemistry, Technical College of Tokushima University, Minamijosanjima-cho, Tokushima 770

† *Department of Applied Chemistry, Faculty of Engineering, Tokushima University, Minamijosanjima-cho, Tokushima 770*

†† *Department of Chemistry, Faculty of Science, Hiroshima University, Higashisenda-machi, Naka-ku, Hiroshima 730*

(Received November 28, 1981)

Sudachiin A was isolated from the green peels of *Citrus sudachi* Hort. *ex* Shirai. This structure was deduced to be sudachitin 4′-β-D-glucoside by means of its spectra and degradation; this was confirmed by the synthesis of the one from sudachitin 7-benzyl ether and α-acetobromoglucose *via* several steps. 4′,5,7-Trihydroxy-3′,6,8-trimethoxyflavone 7-glucoside (sudachitin 7-β-D-glucoside), which was isolated from *Sideritis leucantha* Cavanilles, was also synthesized from sudachitin and α-acetobromoglucose in a similar manner.

In continuous investigations of the constituents in green peels of *Citrus sudachi* Hort. *ex* Shirai, we have already reported the isolation of several flavonoids, sudachitin (**1**),[1,2] demethoxysudachitin (**2**),[3] dinatin (**3**),[4] xanthomicrol (**4**),[4] 4′,5,7-trihydroxy-3′,6-dimethoxyflavone (**5**),[4] and 7-methylsudachitin (**6**).[4] In a recent preliminary communication[5] we reported the structure elucidation of sudachiin A (sudachitin 4′-β-D-glucoside) (**7**), a new flavone glucoside isolated from the same source. Recently, 4′,5,7-trihydroxy-3′,6,8-trimethoxyflavone 7-glucoside (sudachitin 7-β-D-glucoside) (**8**), one of the isomers of sudachiin A (**7**), was isolated from a whole plant of *Sideritis leucantha* Cavanilles by F. Tomas and E. Ferreres.[6] In the present paper we will describe the details of the structure elucidation of sudachiin A (**7**) and the synthesis of **7** and its isomer (**8**).

The methanol concentrate, obtained from fresh green peels, was washed with ether and then extracted with ethyl acetate. The extract, dissolved in methanol, was allowed to stand in a refrigerator to give precipitates, which were then removed by filtration. The resulting solution was concentrated and fractionated by column chromatography over polyamide. The yellow fraction eluted with methanol was subjected to repeated chromatography over polyamide to give a glycoside, named sudachiin A.

Sudachiin A, yellow needles (mp 211—213 °C, $[\alpha]_D$ −37.4° (0.5% aq NaOH)), was analyzed for $C_{24}H_{26}O_{13}$ (mol wt 522) by means of elemental analysis and CI-MS (*m/z* 523 (MH^+)).[7] The glycoside, which was easily converted into a hexaacetate (**9**; mp 212—213 °C), was hydrolyzed with 5% sulfuric acid to sudachitin (4′,5,7-trihydroxy-3′,6,8-trimethoxyflavone) (**1**)[1,2,8] and D-glucose. In the UV spectrum of the glucoside, Band I (λ_{max} 337 nm) was shifted to 385 nm in the presence of sodium acetate, and its intensity was markedly lower than that of Band II[9] (Table 1). On the other hand, the exhaustive methylation of sudachiin A with diazomethane, followed by the hydrolysis of the resultant methyl ether, gave 4′-hydroxy-3′,5,6,7,8-pentamethoxyflavone (sudachitin 5,7-dimethyl ether) (**10**; mp 145—146 °C).[10] Judging from the above results, sudachiin A seemed to be sudachitin 4′-D-glucoside (4′,5,7-trihydroxy-3′,6,8-trimethoxyflavone 4′-D-glucoside (**7**).

The ^1H NMR spectrum of the hexaacetate (**9**) showed the presence of two phenolic acetoxyl groups (δ 2.43 and 2.48) in the flavone nucleus and four acetoxyl groups (δ 2.04 and 2.08, each 6H) in the sugar moiety (Table 2). The proton signals attributable to the sugar moiety at δ 4.1—4.3 and 5.0—5.4 were superimposable on those of cirsilineol 4′-tetra-*O*-acetyl-β-D-glucopyranoside.[11] Consequently, sudachiin A (**7**) was shown to be sudachitin 4′-β-D-glucopyranoside; the structure of **7** was further confirmed by the following synthesis.

Sudachitin (**1**) was partially benzylated with benzyl chloride, potassium iodide, and aqueous potassium hydroxide in acetone-*N*,*N*-dimethylformamide (DMF) to give two monobenzyl ethers, **11** (mp 159—160 °C) and **12** (mp 177—178 °C), and 7,4′-dibenzyl ether (**13**; mp 126—127 °C) of **1** (Table 2), in yields of 40, 2, and 8% respectively. Each Band I of the UV spectra for the monobenzyl ethers in ethanol underwent a bathochromic shift upon the addition of aluminum chloride and sodium acetate (Table 1). In the UV spectra for **11** and **12** in the presence of sodium acetate, the magnitude (71 nm) of the Band I shift of **11** is much larger than that (40 nm) of **12**; furthermore, the intensity for the Band I of **11** is markedly greater than that for the Band II of **11**. These facts show that the two hydroxyl groups on **11** are located at the 5- and 4′-positions.[4,9] Therefore, the monobenzyl ethers, **11** and **12**, are the 7- and 4′-benzyl ethers of **1** respectively. Sudachitin 7-benzyl ether (**11**) was easily condensed with α-acetobromoglucose to give an *O*-acetylglucoside (**14**; mp 156—157 °C), which was subsequently debenzylated to sudachitin 4′-*O*-acetylglucoside (**15**; mp 196—197 °C; $[\alpha]_D$ −22.5° ($CHCl_3$)) with 10% palladium on charcoal. The hydrolysis of **15** with 5% aqueous sodium hydroxide gave the desired 4′-β-D-glucopyranoside (**7**; mp 211—213 °C; $[\alpha]_D$ −39.2° (0.5% aq NaOH)). The synthetic glucoside and its hexaacetate were found to be identical with natural sudachiin A and its hexaacetate respectively on the basis of a mixed-melting point determination and by IR, UV, and ^1H NMR spectral comparisons.

Sudachitin 7-β-D-glucopyranoside (**8**), one of the isomers of sudachiin A, was synthesized from sudachitin (**1**) and α-acetobromoglucose *via* the corresponding *O*-acetylglucoside by the same method as that described

Table 1. UV spectral data for sudachitin derivatives[a)]

Compd		λ_{max}/nm (log ε)					
		EtOH		EtOH–$AlCl_3$		EtOH–NaOAc	
7	(Nat.)	284 (4.34)	337 (4.29)	298 (4.33)	354 (4.35)	283 (4.43)	385 (4.13)
7	(Syn.)	283 (4.38)	337 (4.32)	298 (4.34)	354 (4.35)	283 (4.45)	383 (4.13)
1		283 (4.29)	350 (4.24)	292 (4.21)	364 (4.36)	331 (4.06)	400 (4.18)
10		268 (4.22)	339 (4.40)			337 (4.17)	407 (4.25)
11		278 (4.27)	349 (4.36)	290 (4.26)	365 (4.41)	267 (4.32)	420 (4.53)
12		283 (4.31)	342 (4.36)	298 (4.28)	360 (4.37)	284 (4.43)	314 (4.24) 382 (4.16)
13		283 (4.32)	343 (4.40)	292 (4.29)	358 (4.41)		
14		284 (4.44)	332 (4.33)	301 (4.39)	349 (4.36)		
15		285 (4.49)	327 (4.29)	307 (4.51)	345 (4.33)	282 (4.56)	383 (4.15)
16		277 (4.22)	349 (4.34)	286 (4.19) 304 (4.14)	363 (4.35)	266 (4.24)	422 (4.40)
8	(Syn.)	279 (4.21)	348 (4.33)	287 (4.19) 303sh (4.14)	364 (4.37)	266 (4.29)	422 (4.46)
8	(Nat.)[6)]	272	344	278 300 sh	360 390 sh	268	410

a) sh: Shoulder.

above. The direct condensation of **1** with α-acetobromoglucose gave sudachitin 7-β-D-tetra-*O*-acetylglucopyranoside (**16**; mp 156—157 °C; $[\alpha]_D$ +25.4° ($CHCl_3$)), which was then easily converted into a hexaacetate (**17**, mp 111—113 °C). The hydrolysis of **16** with 5% aqueous sodium hydroxide yielded the 7-β-D-glucopyranoside (**8**, mp 187—188 °C; $[\alpha]_D$ +58.9° (0.5% aq NaOH)). The spectral data of the synthetic 7-β-D-glucoside were superimposable on those of 4′,5,7-trihydroxy-3′,6,8-trimethoxyflavone 7-glucoside (**8**).[6)] The natural 7-glucoside (**8**) was shown to be sudachitin 7-β-D-glucopyranoside.

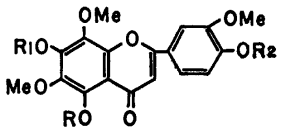

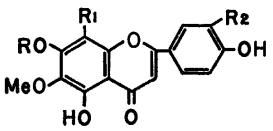

1 R=R_1=R_2=H
7 R=R_1=H, R_2=Glu.
8 R=R_2=H, R_1=Glu.
9 R=R_1=Ac, R_2=Tetra-*O*-acetylglu.
10 R=R_1=Me, R_2=H
11 R=R_2=H, R_1=$C_6H_5CH_2$
12 R=R_1=H, R_2=$C_6H_5CH_2$
13 R=H, R_1=R_2=$C_6H_5CH_2$
14 R=H, R_1=$C_6H_5CH_2$, R_2=Tetra-*O*-acetylglu.
15 R=R_1=H, R_2=Tetra-*O*-acetylglu.
16 R=R_2=H, R_1=Tetra-*O*-acetylglu.
17 R=R_2=Ac, R_1=Tetra-*O*-acetylglu.

2 R=R_2=H, R_1=OMe
3 R=R_1=R_2=H
4 R=Me, R_1=OMe, R_2=H
5 R=R_1=H, R_2=OMe
6 R=Me, R_1=R_2=OMe

Experimental

All the melting points are uncorrected. The UV spectra were measured in ethanol with a Hitachi 215 spectrophotometer, and the ^1H NMR spectra were measured in $CDCl_3$ with a JEOL PS-100 spectrometer (100 MHz), with tetramethylsilane as the internal standard. The mass spectra were obtained using a Shimadzu LKB-9000B mass spectrometer equipped with a chemical-ionization source. The operating conditions were as follows; ion source temp: 230—250 °C; electron energy: 140 eV; reactant gas pressure (isobutane): 0.3 Torr (1 Torr≈133.322Pa); emission current: 250 μA. Polyamide (Wako polyamide C-200) was used for the column.

Isolation of Sudachiin A (7). Fresh green peels (8 kg) of *C. sudachi* collected at Tokushima Prefecture in August were extracted with methanol (*ca.* 20 l) for several days. The methanol solution was concentrated to *ca.* 2.5 l under reduced pressure below 30 °C. The concentrate was treated with hexane and then ether. The resulting water-soluble layer was concentrated to 1.5 l and then extracted thoroughly with ethyl acetate. The extract added to a small amount of methanol was allowed to stand in a refrigerator to give precipitates, which were then removed by filtration. The methanol solution was subjected to chromatographic purification on polyamide, using methanol as the eluent. The yellow eluate was repeatedly chromatographed on polyamide to yield **7** (0.96 g: 0.012%; mp 211—213 °C (yellow needles from methanol); $[\alpha]_D$ −37.4° (0.5% aq NaOH, c=0.31). CI-MS (*i*-C_4H_{10}): *m/z* 523 (MH^+, 0.5), 417 (2), 403 (4.5), 363 (7), 362 (14), 361 (AGL·H, 100), 360 (14), 163 (4.5), 145 (30), 127 (5.5). Found: C, 52.72; H, 5.15%. Calcd for $C_{24}H_{26}O_{13}\cdot 1.5H_2O$: C, 52.46; H, 5.32%.

Sudachiin A Hexaacetate (9). The glycoside (**7**) was converted into a hexaacetate (**9**) by an acetic anhydride-pyridine method. **9**; mp 212—213 °C (colorless needles from ethanol); $[\alpha]_D$ −21.6° ($CHCl_3$, c=0.31). Found: C, 55.88; H, 4.66%. Calcd for $C_{36}H_{38}O_{19}$: C, 55.81; H, 4.94%.

Hydrolysis of Sudachiin A (7). A suspended mixture of **7** (101 mg) in 5% aq sulfuric acid (20 ml) was heated on a steam bath for 2 h under nitrogen. The precipitates thus separated were collected and recrystallized from aq ethanol to give an aglycone; mp 239—240 °C (yellow needles). Its acetate: mp 167—168 °C (colorless needles from ethanol). The aglycone and its acetate were identical with authentic sudachitin (4′,5,7-trihydroxy-3′,6,8-trimethoxyflavone) (**1**) and its acetate previously reported[1,2,8)] respectively.

The aqueous solution remaining after the separation of the aglycone was neutralized with barium carbonate, filtered, and concentrated. The resulting syrupy compound was found to be identical with D-glucose by silica gel TLC. Its osazone: mp and mmp 200—202 °C.

4′-Hydroxy-3′,5,6,7,8-pentamethoxyflavone (10) from Sudachiin

Table 2. ^{1}H NMR data for sudachitin derivatives[a)]

Compd	Solvent	Arom. H				OMe	OAc	Sugar moiety		$CH_2C_6H_5$	OH
		C_3-H	C_5'-H	C_2'-H	C_6'-H			OAc	Other H		
9	$CDCl_3$	6.60 s	7.22 d	7.43 s	7.48 q	3.85 s (3H) 3.91 s (3H) 4.02 s (3H)	2.43 s (3H) 2.48 s (3H)	2.04 s (6H) 2.08 s (6H)	3.8—4.3 m (3H) 5.0—5.4 m (4H)		
15	$CDCl_3$	6.59 s	7.20 d	7.43 s	7.48 q	3.90 s (3H) 3.98 s (3H) 4.01 s (3H)		2.05 s (6H) 2.09 s (6H)	3.7—4.3 m (3H) 5.0—5.4 m (4H)		6.4 b 12.67 bs
14	$CDCl_3$	6.61 s	7.21 d	*	*	3.90 s (9H)		2.04 s (6H) 2.08 s (6H)	3.7—4.3 m (3H) 5.0—5.4 m (4H)	5.29 s (2H) 7.3—7.6 m (7H)	12.49 b
17	$CDCl_3$	6.58 s	7.18 d	7.44 s	7.49 q	3.85 s (3H) 3.93 s (3H) 4.02 s (3H)	2.36 s (3H) 2.48 s (3H)	2.05 s (12H)	3.7—4.3 m (3H) 5.1—5.5 m (4H)		
16	$CDCl_3$	6.56 s	7.00 d	7.35 d′	7.48 q	3.89 s (3H) 3.92 s (3H) 3.97 s (3H)		2.03 s (6H) 2.07 s (6H)	3.6—4.3 m (3H) 5.0—5.5 m (4H)		7.4 b 12.65 bs
10	$CDCl_3$	6.60 s	7.06 d	7.43 d′	7.56 q	3.95 s (6H) 3.98 s (3H) 4.03 s (3H) 4.13 s (3H)					
11	DMSO	6.99 s	6.95 d	*	*	3.79 s (3H) 3.87 s (3H) 3.89 s (3H)				5.24 s (2H) 7.3—7.65 m (7H)	10.08 s 12.88 s
12	DMSO	6.96 s	7.20 d	7.57 s	7.61 q	3.75 s (3H) 3.86 s (6H)				5.16 s (2H) 7.3—7.5 m (5H)	12.85 s
13	DMSO	7.05 s	7.21 d	*	*	3.78 s (3H) 3.86 s (3H) 3.89 s (3H)				5.27 s (2H) 5.34 s (2H) 7.2—7.4 m (12H)	12.82 s

a) δ-Value: s, singlet; d, doublet (J=8.5 Hz); d′, doublet (J=2.5 Hz); q, quartet (J=8.5, 2.5 Hz).
* Overlapped with the benzyl aromatic protons.

A (7). A solution of **7** (206 mg) in ethanol was treated with an excess of diazomethane in ether. After standing at room temperature for 24 h, the mixture was evaporated under reduced pressure to dryness. The residue was heated at 100 °C with 5% sulfuric acid for 1 h, after which the mixture was worked up in the same manner as that described above to give precipitates, which were recrystallized from methanol as colorless needles **10** (83 mg); mp 145—146 °C. **10** was identical with the sample prepared by the method given in the literature.[10]

Partial Benzylation of Sudachitin (1). To a solution of **1** (1.5 g), benzyl chloride (0.8 g), and potassium iodide (0.83 g) in acetone–DMF (1:1) (60 ml), 1% aq potassium hydroxide (26 ml) was added. The reaction mixture was allowed to stand for 4 days at room temperature to give precipitates, which were then separated by filtration. Water was added to the filtrate, and the resulting precipitates were collected. The combined precipitates were recrystallized from methanol to recover sudachitin (**1**) (150 mg: 10%).

The mother liquor was evaporated, and the residue was chromatographed on silica gel with chloroform–ethyl acetate (5:1) to give three fractions. The first fraction was recrystallized from methanol–ethyl acetate to give sudachitin 4',7-dibenzyl ether as yellow needles (**13**) (188 mg: 8%); mp 126—127 °C. Found: C, 71.29; H, 5.45%. Calcd for $C_{32}H_{28}O_8$: C, 71.10; H, 5.22%.

The second fraction, which was a mixture of monobenzyl ethers, was separated into two components **11** and **12** by recrystallization from methanol–ethyl acetate and then by chromatography on silica gel with chloroform–ethyl acetate (5:1). Sudachitin 7-benzyl ether (**11**); yellow needles (755 mg: 40%), mp 159—160 °C. Found: C, 66.82; H, 4.99%. Calcd for $C_{25}H_{22}O_8$: C, 66.66; H, 4.92%.

Sudachitin 4'-benzyl ether (**12**); yellow needles (34 mg: 2%), mp 177—178 °C. Found: C, 66.46; H, 4.85%. Calcd for $C_{25}H_{22}O_8$: C, 66.66; H, 4.92%.

The third fraction was unchanged sudachitin (**1**) (250 mg: 17%).

7-Benzyloxy-4',5-dihydroxy-3',6,8-trimethoxyflavone 4'-Tetra-O-acetyl-β-D-glucopyranoside (14). To a solution of **11** (585 mg) and α-acetobromoglucose (1.1 g) in acetone–DMF (4:1) (25 ml), 2% aq potassium hydroxide (6 ml) was added. The mixture was allowed to stand in a refrigerator for 1 week to give an *O*-acetylglucoside as yellow crystals, which were separated by filtration. To the filtrate, water was added. The separated precipitates were collected and then chromatographed on silica gel, using chloroform–ethyl acetate (5:1), to give unchanged **11** (190 mg: 32%) and the *O*-acetylglucoside. The combined *O*-acetylglucoside was recrystallized from methanol to give **14** as pale yellow needles (450 mg: 44%); mp 156—157 °C. Found: C, 60.12; H, 5.23%. Calcd for $C_{39}H_{40}O_{17}$: C, 60.00; H, 5.16%.

Sudachitin 4'-Tetra-O-acetyl-β-D-glucopyranoside (15). *O*-Acetylglucoside (**14**) (241 mg) was hydrogenated over 10% palladium on charcoal (80 mg) in a mixture of ethyl acetate (15 ml) and methanol (7 ml) until the uptake of hydrogen ceased. The catalyst was filtered off, and then the solvent was removed under reduced pressure. The residue was recrystallized from aq ethanol to give **15** as pale yellow needles (190 mg: 90%); mp 196—197 °C; $[\alpha]_D$ −22.5° ($CHCl_3$, c=0.196). Found: C, 54.45; H, 4.99%. Calcd for $C_{32}H_{34}O_{17}\cdot H_2O$: C, 54.24; H, 5.12%.

Sudachitin 4'-β-D-Glucopyranoside Hexaacetate (Sudachiin A Hexaacetate) (9). Compound **15** was converted into the acetate **9** as colorless needles (mp 212—213 °C; undepressed on admixture with the natural sudachiin A hexaacetate.). The ^1H NMR spectrum of the acetate was also superimposable on that of the acetate of sudachiin A.

Sudachitin 4'-β-D-Glucopyranoside (Sudachiin A) (7). A solution of **15** (98 mg) in 5% aq sodium hydroxide was heated at 50—60 °C for 5 min. The reaction mixture was then cooled and acidified with acetic acid. The resulting precipitates were separated and recrystallized from aq methanol as pale yellow needles (67 mg: 85%); mp 211—213 °C; [α] −39.2° (0.5% aq NaOH, c=0.204). Found: C, 52.50; H, 5.50%. Calcd for $C_{24}H_{26}O_{13}\cdot 1.5H_2O$: C, 52.46; H, 5.32%.

The synthetic glucoside was identified with natural sudachiin A on the basis of a mixed-melting point determination and by IR and UV spectral comparisons.

Sudachitin 7-Tetra-O-acetyl-β-D-glucopyranoside (16). To a solution of **1** (1.035 g) and α-acetobromoglucose (2.0 g) in acetone–DMF (2:1) (50 ml), 2% aq potassium hydroxide (8.8 ml) was added. The mixture was allowed to stand in a refrigerator for 5 d, and then the solvent was removed under reduced pressure. The residue was diluted with water and extracted with ethyl acetate. The extract was washed with water and dried over sodium sulfate, and the solvent was evaporated under reduced pressure. The residue was chromatographed on polyamide (45 g), using methanol, to give **16** (710 mg: 36%), which was subsequently recrystallized from methanol; mp 156—157 °C (pale yellow needles); $[\alpha]_D$ +28.4° ($CHCl_3$, c=0.362). Found: C, 54.03; H, 5.42%. Calcd for $C_{32}H_{34}O_{17}\cdot H_2O$: C, 54.24; H, 5.12%.

Sudachitin 7-β-D-Glucopyranoside Hexaacetate (17). Compound **16** (70 mg) was acetylated by an acetic anhydride–pyridine method, and the acetate was chromatographed on silica gel with chloroform–ethyl acetate (5:1). The first fraction was dissolved in a small amount of methanol, and then water was added to give white precipitates (60 mg: 76%); mp 111—113 °C. Found: C, 55.52; H, 4.74%. Calcd for $C_{36}H_{38}O_{19}$: C, 55.81; H, 4.94%.

Sudachitin 7-β-D-Glucopyranoside (8). A solution of **16** (150 mg) in 5% aq sodium hydroxide was heated at 50—60 °C for 5 min. The reaction mixture was then cooled and acidified with acetic acid. The resulting semi-solids were separated and then chromatographed on silica gel, using ethyl methyl ketone (saturated water), to give **8** (91 mg: 80%), which was subsequently recrystallized from methanol; mp 187—188 °C (yellow needles, lit.[6] mp 185—187 °C); $[\alpha]_D$ +58.9 (0.5% aq NaOH, c=0.258). Found: C, 52.70; H, 5.53%. Calcd for $C_{24}H_{26}O_{13}\cdot 1.5H_2O$: C, 52.46; H, 5.32%.

The spectral data and mp of the synthetic glucoside were identical with those of natural 4',5,7-trihydroxy-3',6,8-trimethoxyflavone 7-glucoside.[6]

The authors wish to thank Professor Makoto Susuki, Meijo University, for the measurement of the CI-MS. The present work was partially supported by a Grant-in-Aid for Scientific Research from the Ministry of Education, Science and Culture.

References

1) T. Horie, M. Masumura, and S. Okumura, *Bull. Chem. Soc. Jpn.*, **34**, 1547 (1961).

2) T. Horie, M. Masumura, and S. Okumura, *Nippon Kagaku Zasshi*, **83**, 465, 468 (1962).

3) T. Horie, H. Shimoo, M. Masumura, and S. Okumura, *Nippon Kagaku Zasshi*, **83**, 602 (1962).

4) T. Horie and M. Nakayama, *Phytochemistry*, **20**, 337 (1981).

5) T. Horie, M. Nakayama, S. Hayashi, M. Tsukayama,

and M. Masumura, *Heterocycles*, **10**, 53 (1978).

6) F. Tomas and F. Ferreres, *Phytochemistry*, **19**, 2039 (1980).

7) M. Nakayama, S. Eguchi, S. Hayashi, T. Horie, M. Suzuki, K. Harada, N. Takeda, and A. Tatematsu, *Shitsuryo Bunseki*, **27**, 53 (1979).

8) T. Horie, M. Masumura, K. Kase, K. Fukui, and M. Nakayama, *Nippon Kagaku Kaishi*, **1974**, 2400.

9) T. J. Mabry, K. R. Markham, and M. B. Thomas, "The Systematic Identification of Flavonoids," Springer-Verlag, Heidelberg, New York (1970), p. 41; E. Rodriquerz, G. V. Velde, T. J. Mabry, S. S. Subramanian, and A. G. R. Nair, *Phytochemistry*, **11**, 2311 (1972).

10) H. Wagner, G. Maurer, L. Hörhammer, and L. Farkas, *Chem. Ber.*, **104**, 3357 (1971).

11) A. J. Kalra, M. Krishnamurti, and T. R. Seshadri, *Indian J. Chem.*, **12**, 1040 (1974). The synthesis of cirsilineol (4′,5-dihydroxy-3′,6,7-trimethoxyflavone) 4′-tetra-*O*-acetyl-*β*-D-glucopyranoside was achieved, and its ^{1}H NMR spectrum was measured in our laboratory.

Studies of the Selective *O*-Alkylation and Dealkylation of Flavonoids. V.[1] The Synthesis of 5,6-Dihydroxy-3,4′,8-trimethoxyflavone and a Revised Structure for the Flavone from *Conyza stricta*

Tokunaru Horie,* Hiroki Kourai, Hideaki Osaka and Mitsuru Nakayama†

Department of Applied Chemistry, Technical College of Tokushima University, Minamijosanjima-cho, Tokushima 770

† *Department of Chemistry, Faculty of Science, Hiroshima University, Higashisenda-machi, Naka-ku, Hiroshima 730*

(Received December 24, 1981)

5,6-Dihydroxy-3,4′,8-trimethoxyflavone, which was the proposed structure of the pigment occuring in *Conyza stricta*, was synthesized from 2,3,5,6-tetramethoxyacetophenone in six steps. The natural pigment was identical not with the synthesized flavone, but with 5,7-dihydroxy-3,4′,8-trimethoxyflavone, an isomer of the former.

Two new flavones (**A**) and (**B**) were isolated from *conyza stricta* by Sen *et al.*;[2] their structures were proposed to be 5,6-dihydroxy-3,4′,8-trimethoxyflavone (**1**) and 5,7-dihydroxy-3,3′,4′,5′,8-pentamethoxyflavone (**2**) on the basis of their spectroscopic data and degradation studies. The properties of natural flavone (**A**), however, did not agree with those of synthesized 5,6-dihydroxy-3,4′,8-trimethoxyflavone (**1**). A close inspection of the properties of natural flavone (**A**) and of the isomers of **1** indicated that those of the former were identical with those of 5,7-dihydroxy-3,4′,8-trimethoxyflavone (**3**),[3] an analogue of **2**. This paper will describe the synthesis of 5,6-dihydroxy-3,4′,8-trimethoxyflavone (**1**) and a revised structure, 5,7-dihydroxy-3,4′,8-trimethoxyflavone (**3**), for the natural flavone (**A**).

The outline of the synthesis was as follows. 2,3,5,6-Tetramethoxyacetophenone (**4**)[4] was brominated with copper(II) bromide, according to the method of Malik *et al.*;[5] then the resulting ω-bromo-2,3,5,6-tetramethoxyacetophenone (**5**) was converted into 2,3,5,6-tetramethoxy-ω-(*p*-methoxybenzoyloxy)acetophenone (**6**) with potassium *p*-methoxybenzoate in *N*,*N*-dimethylformamide. The benzoate (**6**) was demethylated with anhydrous aluminium chloride in acetonitrile to give 2-hydroxyacetophenone (**7**) in a good yield.

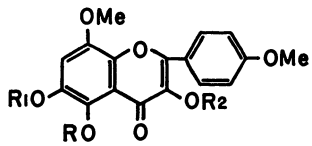

1 R=R$_1$=H, R$_2$=Me
8 R=R$_1$=Me, R$_2$=H
9 R=R$_1$=Me, R$_2$=Ac
10 R=R$_1$=R$_2$=Me
11 R=H, R$_1$=R$_2$=Me
12 R=Ac, R$_1$=R$_2$=Me
13 R=R$_1$=Ac, R$_2$=Me

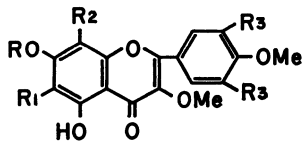

2 R=R$_1$=H, R$_2$=R$_3$=OMe
3 R=R$_1$=R$_3$=H, R$_2$=OMe
14 R=Me, R$_1$=OH, R$_2$=R$_3$=H

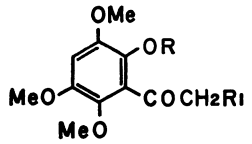

4 R=Me, R$_1$=H
5 R=Me, R$_1$=Br
6 R=Me, R$_1$=OCOC$_6$H$_4$OMe(*p*)
7 R=H, R$_1$=OCOC$_6$H$_4$OMe(*p*)

According to the Allan-Robinson method of flavone synthesis, the condensation of the 2-hydroxyacetophenone (**7**) with *p*-methoxybenzoic anhydride and potassium *p*-methoxybenzoate, followed by treatment with methanolic potassium hydroxide, gave 3-hydroxyflavone (**8**), which was easily converted into the acetate (**9**). The ^{1}H-NMR spectra for **8** and **9** showed a singlet peak corresponding to the C-7 proton at δ 6.87 and 6.90 respectively (Table 1). The methylation of the flavone (**8**) with dimethyl sulfate gave 3,4′,5,6,8-pentamethoxyflavone (**10**). The flavone (**10**) was demethylated with a 5—10%(w/v) anhydrous aluminium chloride–acetonitrile solution to give a 5-hydroxyflavone (**11**) in a quantitative yield. On the other hand, demethylation with an about 30%(w/v) anhydrous aluminium chloride–acetonitrile solution containing 0.5% (v/v) water at 70 °C for 48 h[1] gave the desired 5,6-dihydroxy-3,4′,8-trimethoxyflavone (**1**). The strontium chloride-coloration test of the flavone (**1**) indicated the presence of two hydroxyl groups adjacent to each other.[6] The ^{1}H-NMR data for the synthesized flavones are shown in Table 1. The chemical shifts of the C-7 proton on the flavones and their acetates appeared in the narrow range of δ 6.87—6.99, in contrast to those of the aromatic protons on the A ring of 5,7-dihydroxy-6- or 8-methoxyflavones and their acetates. The 3-methoxyflavone (**1**) and **11** showed also characteristic UV spectra, which failed to show Band II (Table 2).

The 5,6-dihydroxyflavone (**1**) and its diacetate (**13**) are not identical with the natural flavone (**A**) and its diacetate, which were sent us by Sen. However, the ^{1}H-NMR data of the natural flavone diacetate are similar to that of the synthesized (**13**), and the singlet peak at δ 6.89 can be attributed to the C-6 or C-8 proton on the acetate of 5,7-dihydroxy-3,4′,8-trimethoxyflavone (**3**)[3] or 5,6-dihydroxy-3,4′,7-trimethoxyflavone (**14**)[7] (Table 3). The results indicated that the structure of **A** is either **3** or **14**. Since the UV data of the natural flavone (**A**) are similar to those

TABLE 1. ^{1}H-NMR DATA OF 3,4′,5,6,8-PENTAHYDROXYFLAVONE DERIVATIVES (δ)[a]

Compd	Solvent	C_7–H	$C_{3',5'}$–H	$C_{2',6'}$H	OMe	OH	OAc
8	$CDCl_3$	6.87 s	7.00 d	8.22 d	3.86 s (3H), 3.91 s (6H) 3.98 s (3H)	6.85 b	
9	$CDCl_3$	6.90 s	6.97 d	7.88 d	3.86 s (3H), 3.89 s (3H) 3.91 s (3H), 3.95 s (3H)		2.35 s (3H)
10	$CDCl_3$	6.87 s	7.00 d	8.16 d	3.87 s (6H), 3.94 s (6H) 3.97 s (3H)		
11	$CDCl_3$	6.92 s	7.00 d	8.13 d	3.87 s (6H), 3.92 s (6H)	12.00 s	
12	$CDCl_3$	6.87 s	6.97 d	8.09 d	3.80 s (3H), 3.87 s (6H) 3.97 s (3H)		2.46 s (3H)
1	$CDCl_3$	6.91 s	6.99 d	8.13 d	3.88 s (6H), 3.90 s (3H)	11.77 s	
	DMSO	6.99 s	7.10 d	7.99 d	3.80 s (3H), 3.86 s (6H)	11.6 b	
13	$CDCl_3$	6.91 s	6.99 d	8.09 d	3.79 s (3H), 3.85 s (3H) 3.94 s (3H)		2.31 s (3H) 2.42 s (3H)

a) s: Singlet, b: broad, d: doublet(J=8.5 Hz).

TABLE 2. UV DATA OF 3,4′,5,6,8-PENTAHYDROXYFLAVONE DERIVATIVES[a]

Compd		λ_{max}/nm (log ε)			
1	EtOH		308 (4.29)	335sh (4.16)	
	EtOH–$AlCl_3$	289i (3.98)	328 (4.33)	360 (4.27)	
8	EtOH	272 (4.22)	292i (4.02)	345 (4.24)	375sh (4.16)
	EtOH–$AlCl_3$	261 (4.32)	282sh (4.23)	395i (4.25)	433 (4.33)
10	EtOH	273i (4.20)	295 (4.29)	329 (4.30)	
11	EtOH	280i (4.11)	308 (4.36)	338 (4.28)	
	EtOH–$AlCl_3$	290sh (4.04)	330 (4.36)	355 (4.35)	

a) sh: Shoulder, i: inflection point.

TABLE 3. COMPARISON BETWEEN ^{1}H-NMR DATA OF DIACETATES OF NATURAL AND ITS ISOMERIC FLAVONES IN $CDCl_3$ (δ)[a]

Compd	Arom. H			OMe			OAc	
13	6.91 s	6.99 d	8.09 d	3.79 s	3.85 s	3.94 s	2.31 s	2.42 s
Diacetate of **A**(Nat.)[2]	6.86 s	7.11 d	8.20 d	3.89 s	3.95 s	4.06 s	2.41 s	2.49 s
Diacetate of **3**[3]	6.75 s	7.00 d	7.08 d	3.80 s	3.88 s	3.98 s	2.36 s	2.43 s
Diacetate of **14**[b]	6.86 s	6.98 d	7.99 d	3.77 s	3.88 s	3.90 s	2.32 s	2.45 s

a) s: Singlet, d: doublet (J=8.5—9 Hz). b) Synthesized from 6-hydroxy-3,4′5,7-tetramethoxyflavone.[9]

of **13**, and not to those of **14**, the structure of **A** is preferable to that of **3** (Table 4). In conclusion, the natural flavone (**A**) is confirmed to be 5,7-dihydroxy-3,4′,8-trimethoxyflavone (**3**), analogous to **2**, on the basis of the following results: the melting points of the natural flavone (**A**) and its diacetate are undepressed on mixing with the synthesized (**3**) and its diacetate respectively (Table 5), and the UV and IR spectra of these natural flavones are also superimposable on each other.

These two substances, **2** and **3**, were also isolated from the same plant by Tandon *et al.* in 1977.[8]

Experimental

All the melting points were determined in glass capillaries and are uncorrected. The ^{1}H-NMR spectra were measured with a Hitachi R-24 spectrometer (60 MHz), using tetramethylsilane as the internal standard, and the chemical shifts are presented in terms of the δ values. The UV and IR spectra were taken on Hitachi 124 and 215 spectrophotometers.

*ω-Bromo-2,3,5,6-tetramethoxyacetophenone (**5**).* To a solution of 2,3,5,6-tetramethoxyacetophenone (**4**) (4 g) in chloroform–ethyl acetate (each 25 ml), copper(II) bromide (7.6 g) was added, after which the mixture was stirred for 24 h at room temperature. The precipitate was then filtered off, and the filtrate was concentrated under reduced pressure. The residue was dissolved in ether, washed with water, and dried. After the removal of the ether, the residue was recrystallized from ether–hexane to give pale yellow prisms; mp 91—93 °C; NMR ($CDCl_3$) δ 3.80, 3.88 (each 6H, s, OCH_3), 4.37 (2H, s, $-CH_2-$), 6.63 (1H, s, Arom. H); yield, 4 g (75%). Found: C, 45.28; H, 4.82%. Calcd for $C_{12}H_{15}O_5Br$: C, 45.16; H, 4.74%.

*2,3,5,6-Tetramethoxy-ω-(p-methoxybenzoyloxy)acetophenone (**6**).* A mixture of **5** (4 g) and potassium *p*-methoxybenzoate (5 g) in *N,N*-dimethylformamide (15—20 ml) was heated at 140—150 °C for 2 h. After the addition of water to the reaction mixture, the precipitate separated was collected, washed with water, and recrystallized from methanol to

Table 4. Comparison between UV spectral data of natural and its isomeric flavones[a)]

Compd		λ_{max}/nm (log ε)			
1	EtOH		308 (4.29)		335sh (4.16)
	EtOH-$AlCl_3$	289i (3.98)	328 (4.33)		360 (4.27)
	EtOH-AcONa	290i (4.18)	308 (4.20)		335i (4.12)
A(Nat.)	EtOH	276 (4.38)	304sh (4.23)		362 (4.07)
	EtOH-$AlCl_3$	284 (4.30)	311 (4.25)	345 (4.26)	412 (3.89)
	EtOH-AcONa	284 (4.50)	304i (4.29)		382 (4.00)
3	EtOH	276 (4.38)	304sh (4.23)		362 (4.08)
	EtOH-$AlCl_3$	284 (4.30)	311 (4.25)	344 (4.25)	408 (3.87)
	EtOH-AcONa	284 (4.50)	304i (4.30)		382 (4.00)
14	EtOH	283 (4.33)			339 (4.38)
	EtOH-$AlCl_3$	298 (4.36)			364 (4.42)
	EtOH-AcONa	285 (4.32)			339 (4.36)
13	EtOH	267 (4.21)	285i (4.08)		337 (4.35)
Acetate of **A**(Nat.)	EtOH	260 (4.22)			338 (4.29)
Acetate of **3**	EtOH	260 (4.23)			338 (4.30)

a) All the UV spectra were measured in our laboratory: i; inflection point, sh; shoulder.

Table 5. Melting points of dihydroxyflavones and their derivatives (°C)

Compd	Dihydroxyflavones		Diacetates	Monomethyl ether	Dimethyl ether
1	183.5—184.5	188.5—189.5[a)]	173—174	163—164	124—126
A(Nat.)	178—179[2)]	178—179[a)]	170—171[2)]	170—171[2)]	158—159[2)]
3	171—172[3)]	178—179[a)]	166.5—167.5[3)]	168—169[3)]	156—158[10)]
14	187—189	176—177[7)]	178—180 170—172[7)]	168—170[3)]	153—154[7)]

a) The melting points were measured with a Yanagimoto micro-melting apparatus.

give colorless prisms; mp 118—120 °C; NMR ($CDCl_3$) δ 3.80 (6H, s, OCH_3), 3.84 (9H, s, OCH_3), 5.22 (2H, s, $-CH_2-$), 6.61 (1H, s, Arom. H), 6.90, 8.04 (each 2H, d, J=9 Hz, Arom. H); yield, 3.69 g (81%). Found: C, 61.80; H, 5.83%. Calcd for $C_{20}H_{22}O_8$: C, 61.53; H, 5.68%.

2-Hydroxy-3,5,6-trimethoxy-ω-(p-methoxybenzoyloxy)acetophenone (7). To a solution of anhydrous aluminium chloride (12 g) in acetonitrile (40 ml), **6** (3.82 g) was added, and the mixture was heated at 60 °C for 3 h. The reaction mixture was then poured into a mixture of hydrochloric acid and ice under stirring. The precipitate was collected and recrystallized from methanol to give yellow prisms (2.50 g); mp 120—121 °C; NMR ($CDCl_3$) δ 3.86 (9H, s, OCH_3), 3.98 (3H, s, OCH_3), 5.49 (1H, s, Arom. H), 6.92, 8.08 (each 2H, d, J=9 Hz, Arom. H), 11.84 (1H, s, OH). The precipitate recovered (1 g) from the mother liquor of recrystallization was repeatedly demethylated by the above-described method; an additional 0.8 g of **7** was thus obtained; total yield, 3.3 g (90%). Found: C, 60.61; H, 5.42%. Calcd for $C_{19}H_{20}O_8$: C, 60.63; H, 5.36%.

3-Hydroxy-4',5,6,8-tetramethoxyflavone (8). A mixture of **7** (2.35 g), *p*-methoxybenzoic anhydride (10 g), and potassium *p*-methoxybenzoate (6.6 g) was heated at 170—180 °C under reduced pressure for 10 h. The mixture was then refluxed with a solution of potassium hydroxide (6.3 g) in 80% aqueous methanol (about 200 ml) under a nitrogen atmosphere for 30 min. The solvent was removed under reduced pressure, and water was added to the residue. The solution was saturated with carbon dioxide and then allowed to stand overnight in a refrigerator. The separated precipitate was collected and recrystallized from chloroform–methanol to give yellow prisms; mp 184—186 °C; yield, 0.67 g (30%). Found: C, 63.45; H, 5.04%. Calcd for $C_{19}H_{18}O_7$: C, 63.68; H, 5.06%.

Acetate (9): Colorless needles from methanol; mp 201—203 °C. Found: C, 62.74; H, 4.99%. Calcd for $C_{21}H_{20}O_8$: C, 62.99; H, 5.04%.

3,4',5,6,8-Pentamethoxyflavone (10). A mixture of **8** (500 mg), dimethyl sulfate (0.62 ml), and anhydrous potassium carbonate (1.2 g) in acetone (50 ml) was refluxed for 8 h. The reaction mixture was again refluxed for 30 min after the addition of water; then a part of the acetone was evaporated off. The resulting precipitate was recrystallized from methanol to give pale yellow needles; mp 124—126 °C; yield, 490 mg (94%). Found: C, 64.33; H, 5.41%. Calcd for $C_{20}H_{20}O_7$: C, 64.51; H, 5.41%.

5-Hydroxy-3,4',6,8-tetramethoxyflavone (11). To a solution of anhydrous aluminium chloride (0.52 g) in acetonitrile (10 ml), **10** (110 mg) was added, after which the mixture was heated at 60 °C for 1.5 h. After the addition of diluted hydrochloric acid, the mixture was heated on a steam-bath for 30 min and the acetonitrile was evaporated. The precipitate separated was recrystallized from methanol to give yellow needles; mp 163—164 °C; yield, 96 mg (91%). Found: C, 63.40; H, 5.01%. Calcd for $C_{19}H_{18}O_7$: C, 63.68; H, 5.06%.

Acetate (12): Colorless needles from methanol; mp 194—196 °C. Found: C, 62.68; H, 5.14%. Calcd for $C_{21}H_{20}O_8$: C, 62.99; H, 5.04%.

5,6-Dihydroxy-3,4',8-trimethoxyflavone (1). A mixture of **10** (180 mg) and anhydrous aluminium chloride (2 g) in 0.5% (v/v) aqueous acetonitrile (6 ml) was heated at 70

°C for 48 h, and after which the reaction mixture was treated by the method described for **11** to give a brownish-yellow precipitate. The precipitate was separated by preparative HPLC with a column packed with Hitachi gel #3019 using methanol, and then recrystallized from methanol to give orange-yellow needles; mp 183.5—184.5 °C; yield, 90 mg (54%). Found: C, 62.85; H, 4.72%. Calcd for $C_{18}H_{16}O_7$: C, 62.79; H, 4.68%.

*Diacetate (**13**)*: Colorless needles from methanol; mp 173—174 °C. Found: C, 61.45; H, 4.62%. Calcd for $C_{22}H_{20}O_9$: C, 61.68; H, 4.71%.

The authors are grateful to Dr. A. K. Sen, Indian Institute of Chemical Biology, for offering the samples of natural flavone and its acetate.

References

1) Part IV of this series; T. Horie, H. Kourai and H. Osaka, *Nippon Kagaku Kaishi*, **1982**, 1270.
2) A. K. Sen, S. B. Mahato, and N. L. Dutta, *Indian J. Chem.*, **14B**, 849 (1976).
3) T. Horie, *J. Sci. Hiroshima Univ., Series A-II*, **33**, 221 (1969).
4) T. Horie, M. Tsukayama, M. Masumura, M. Nakayama, and S. Hayashi, *Bull. Chem. Soc. Jpn.*, **52**, 2950 (1979).
5) M. L. Malik and S. K. Grover, *Indian J. Chem.*, **14B**, 513 (1976).
6) M. Shimizu and N. Morita, *Yakugaku Zasshi*, **88**, 1450 (1968).
7) A. C. Jain, T. R. Seshadri, and K. R. Sreenivasan, *J. Chem. Soc.*, **1955**, 3908.
8) S. Tandon and R. P. Rastogi, *Phytochemistry*, **16**, 1455 (1977).
9) L. R. Row and T. R. Seshadri, *Proc. Indian Acad. Sci.*, **23A**, 23 (1946).
10) M. Ahuja, M. Bandophdhyay, and T. R. Seshadri, *Indian J. Chem.*, **13**, 1134 (1975).

 © 1982 The Chemical Society of Japan Bull. Chem. Soc. Jpn., 55, 2937—2941 (1982)

Photoinduced Ring-opening Reaction of 1-(2-Naphthoyl)aziridine in Various Halogenated Hydrocarbons

Sei-ichi NISHIMOTO, Tsukuru IZUKAWA, and Tsutomu KAGIYA*

Department of Hydrocarbon Chemistry, Faculty of Engineering, Kyoto University, Sakyo-ku, Kyoto 606

(Received December 5, 1981)

The in-source photoreaction and the postreaction of 1-(2-naphthoyl)aziridine (NAz) in various halogenated hydrocarbons have been investigated at room temperature under deaerated conditions. Secondary amide such as *N*-(2-chloroethyl)-2-naphthamide (CENA) or *N*-(2-bromoethyl)-2-naphthamide (BENA) was obtained along with a rearranged product of 2-(2-naphthyl)-2-oxazoline (NOz). The initial rate of secondary amide formation increased with decreasing dissociation energy of the carbon–halogen bond of halogenated hydrocarbon. The yield of CENA in the postreaction was substantially equal to that of chloride ion formed *via* the photolyses of chlorinated hydrocarbons. The rearranged product of NOz was confirmed to undergo subsequently photochemical ring-opening reaction to afford CENA or BENA.

We previously reported the photoinduced ring-opening reaction of the aziridinyl group of 1-(2-naphthoyl)-aziridine (NAz) in deaerated solution to afford various secondary amides.[1] The structure of secondary amides obtained was dependent on solvent used for the photoreaction. In the case of chlorinated and brominated hydrocarbons, the formations of *N*-(2-chloroethyl)-2-naphthamide (CENA) and *N*-(2-bromoethyl)-2-naphthamide (BENA) were observed, respectively, accompanied by a rearranged product of 2-(2-naphthyl)-2-oxazoline (NOz).

In the present paper, the in-source photoreaction of NAz in a series of chlorinated and brominated hydrocarbons was investigated in further detail at room temperature under deaerated conditions. The dark reaction of NAz in preirradiated solvents was determined to clarify the influence of the photolysis of solvent. The behavior of NOz as an intermediate in the ring-opening of NAz to CENA or BENA is also described.

Experimental

IR spectra were recorded on a JASCO DS-403 spectrophotometer and ^{1}H NMR spectra on a JEOL PMX-60 spectrometer using tetramethylsilane as an internal standard, respectively. High speed liquid phase chromatography (HLPC) was carried out with a TOYO SODA HLC-802UR apparatus under the same column conditions as reported.[1] Colorimetry was performed with a Shimadzu UV-200S spectrophotometer.

Materials. 1-(2-Naphthoyl)aziridine (NAz) and 2-(2-naphthyl)-2-oxazoline (NOz) were prepared and purified as reported.[1] Dibromomethane was purified by distillation. *t*-Butyl chloride was passed through a silica-gel column, washed with ice water, dried with calcium chloride, and then fractionally distilled before use. The other halogenated hydrocarbons (spectroscopic or guaranteed grade) were used without further purification. Gaseous Cl_2 was prepared by the reaction of manganese dioxide (10 g) with concentrated hydrochloric acid (50 cm^3).[2]

Procedures. The in-source photoreaction of NAz in various halogenated hydrocarbons was carried out according to the same procedures as reported.[1]

In the postreaction of NAz, each halogenated hydrocarbon (2 cm^3) was irradiated in advance at room temperature under deaerated conditions in a Vycor or Pyrex glass tube, using a merry-go-round apparatus equipped with a high-pressure mercury lamp (EIKOSHA 400 W). NAz was dissolved in the resulting halogenated hydrocarbon and permitted to stand for a specified time at room temperature in the dark. The photolytic product such as HCl or Cl_2 was extracted with water (10 cm^3) from 1 cm^3 aliquots of chlorinated hydrocarbons after preirradiation. Chloride ion derived from HCl and Cl_2 in aqueous solution was determined by Volhard titration using silver nitrate.[3] Similarly, both HBr and Br_2 was extracted with water (100 cm^3) from 0.1 cm^3 aliquots of brominated hydrocarbons after preirradiation. From 5 cm^3 aliquots of the aqueous solution thus obtained Br_2 was extracted with CCl_4 (45 cm^3) and was determined colorimetrically with diphenylcarbazone.[4] Bromide ion due to HBr in aqueous solution was determined by Volhard titration and colorimetry with diphenylcarbazone.[5]

The structures of CENA, BENA, and NOz were identified by comparing their spectral data with those of the authentic sample.[1] The product afforded by the reaction of NOz with HCl in $CHCl_3$ was assigned to 2-(2-naphthyl)-2-oxazolinium hydrochloride from the IR spectral data; IR ($CHCl_3$): 2450 (=$\overset{+}{N}$H), 1947 (C=$\overset{+}{N}$H), 1640 (C=$\overset{+}{N}$), 1239 (C–O), and 895 (ring) cm^{-1}.[6]

The conversion of NAz and the product yield were determined by the same method as reported.[1]

Results and Discussion

In-source Photoreaction of NAz in Various Halogenated Hydrocarbons. Solutions of NAz in various halogenated hydrocarbons (see Table 1) were irradiated with the UV light through a Vycor (>215 nm) or a Pyrex (>286 nm) glass tube under deaerated conditions. Inspection of Table 1 provides a general feature that *N*-(2-chloroethyl)-2-naphthamide (CENA) is a common photoproduct in chlorinated hydrocarbons and *N*-(2-bromoethyl)-2-naphthamide (BENA) in brominated hydrocarbons, respectively, irrespective of the irradiation wavelength.

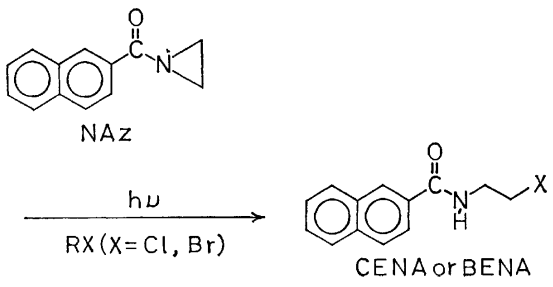

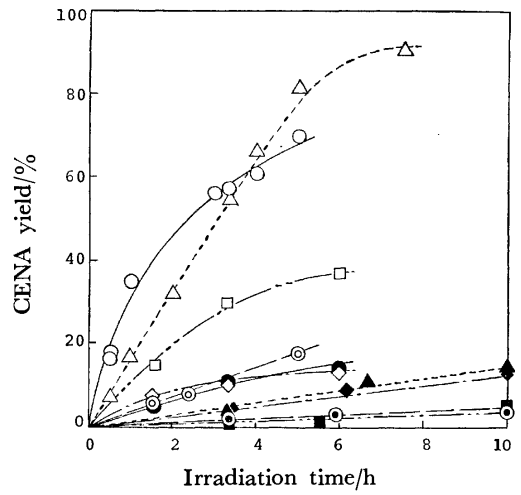

Fig. 1. Variation in CENA yield as a function of irradiation time in the in-source photoreaction of NAz. ——: CCl_4 (V:○, P:●), ----: $CHCl_3$ (V:△, P:▲), — —: CH_2Cl_2 (V:◎, P:⊙), ——: *t*-BuCl (V:◇, P:◆), ——: PhCl (V:□, P:■).

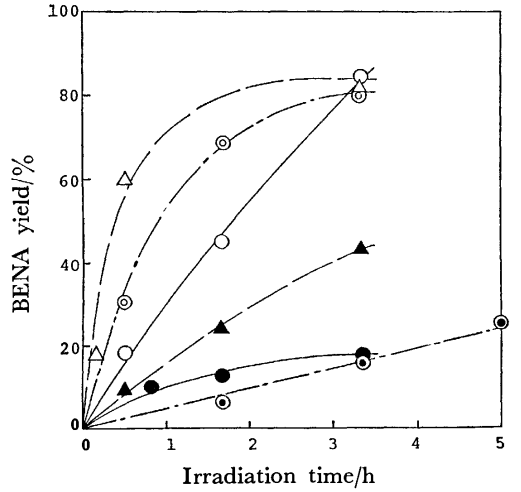

Fig. 2. Variation in BENA yield as a function of irradiation time in the in-source photoreaction of NAz. ——: CH_2Br_2 (V:○, P:●), — —: *n*-PrBr (V:△, P:▲), ——: PhBr (V:◎, P:⊙).

Variations in the CENA and BENA yields as a function of irradiation time are shown in Figs. 1 and 2, respectively. Table 1 summarizes the initial rate of the formation of halogen substituted secondary amide which was estimated from Figs. 1 and 2 by extrapolation. The initial rate in the Vycor system is larger than that in the Pyrex system by a factor of 3—76 in chlorinated hydrocarbons and 3—14 in brominated hydrocarbons, depending on the solvent structure. It can also be seen from Table 1 that the initial rate of CENA formation observed in a series of chloromethanes increases with increasing the number of substituted chlorine atom; $CCl_4 > CHCl_3 > CH_2Cl_2$. Comparing the initial rate of BENA formation with that of CENA formation observed in a couple of brominated and chlorinated hydrocarbons having mutually analogous structure, *e.g.*, CH_2Br_2/CH_2Cl_2 and PhBr/PhCl, the former was 6—33 times larger than the latter.

TABLE 1. IN-SOURCE PHOTOREACTION OF NAz IN VARIOUS HALOGENATED HYDROCARBONS[a]

Run	Solvent	Glass tube	$[NAz]_0$ / mmol dm^{-3}	Initial rate $\times 10^7$ / mol min^{-1}	
				CENA (BENA)[b]	NOz
1	CCl_4	V	91	5.8	0.041
2	CCl_4	P	91	0.52	0
3	$CHCl_3$	V	91	2.5	0.38
4	$CHCl_3$	P	91	0.23	0
5	CH_2Cl_2	V	90	0.52	0
6	CH_2Cl_2	P	90	0.056	0
7	*t*-BuCl	V	65	0.48	0
8	*t*-BuCl	P	65	0.15	0
9	PhCl	V	90	1.6	0
10	PhCl	P	90	0.021	0
11	CH_2Br_2	V	90	(4.9)	0
12	CH_2Br_2	P	90	(1.6)	3.8
13	*n*-PrBr	V	17	(4.6)	0
14	*n*-PrBr	P	17	(1.1)	0.27
15	PhBr	V	90	(9.3)	0
16	PhBr	P	90	(0.69)	0.75

a) Under the photoirradiation through a Vycor (V) or a Pyrex (P) glass tube at room temperature for 200 min. b) The value in parenthesis denotes the initial rate of BENA formation.

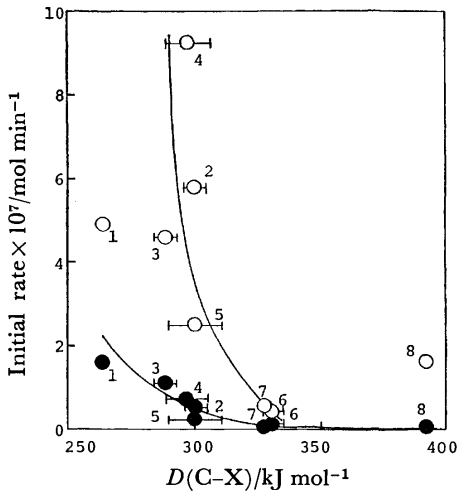

Fig. 3. Relationship between the initial rate of CENA or BENA formation and the carbon-halogen (C–X) bond-dissociation energy of halogenated hydrocarbon solvent for the Vycor (○) and Pyrex (●) systems. 1: CH_2Br_2, 2: CCl_4, 3: *n*-PrBr, 4: PhBr, 5: $CHCl_3$, 6: *t*-BuCl, 7: CH_2Cl_2, 8: PhCl.

As shown in Fig. 3, a fairly good correlation between the initial rate of secondary amide formation and the dissociation energy of the carbon-halogen bond D(C–X) of solvent[7] except for PhCl was obtained in each of the Vycor and Pyrex systems. Apparently, the decrease in the D(C–X) value tends to increase the initial rate of CENA or BENA formation. This seems to indicate that the photochemical ring-opening of NAz to CENA or BENA involves the radical decomposition of halogenated hydrocarbon solvent in its car-

Table 2. Postreaction of NAz in various halogenated hydrocarbons[a)]

Run	Solvent	Glass tube	$[NAz]_0$ / mmol dm^{-3}	Conversion / %	Product yield[b)]/%	
					CENA(BENA)[c)]	NOz
1	CCl_4	V	91	53	53	0
2	CCl_4	P	91	0	0	0
3	$CHCl_3$	V	91	52	52	0
4	$CHCl_3$	P	91	0	0	0
5	CH_2Cl_2	V	90	33	33	0
6	CH_2Cl_2	P	90	0	0	0
7	*t*-BuCl	V	65	9	9	0
8	*t*-BuCl	P	65	3	3	0
9	PhCl	V	90	39	39	0
10	PhCl	P	90	12	12	0
11	CH_2Br_2	V	90	49	(33)	14
12	CH_2Br_2	P	90	30	(18)	10
13	*n*-PrBr	V	17	17[d)]	(17)[d)]	0[d)]
14	*n*-PrBr	P	17	3	(3)	0
15	PhBr	V	90	54	(28)	26
16	PhBr	P	90	37	(11)	26

a) Under the photoirradiation through a Vycor (V) or a Pyrex (P) glass tube at room temperature for 200 min unless otherwise noted. b) Yield based on NAz. c) The value in parenthesis denotes the BENA yield. d) 30 min-irradiation.

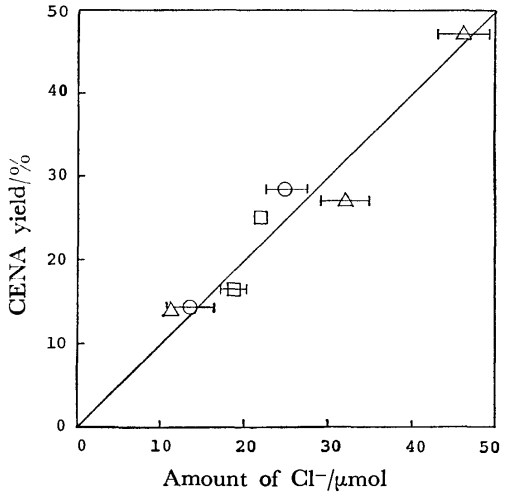

Fig. 4. A plot of CENA yield against the amount of chloride ion (Cl^-) in the Vycor postreaction system of NAz.
○: CCl_4, △: $CHCl_3$, □: CH_2Cl_2.

bon-halogen bond.

The previous paper suggested that both the CENA and BENA formations are due to the dark reaction of NAz with the photolytic product of a halogenated hydrocarbon.[1)] Supposing that the D(C–X) value of a given halogenated hydrocarbon provides a measure of the reactivity for photodecomposition, the previous account may be consistent with a correlation observed in Fig. 3. Nevertheless, in view of a fact that most of the incident light (not less than 90%) is absorbed by NAz under the present conditions except for the cases in PhCl and PhBr, it seems likely that the reaction of NAz in the electronically excited state with halogenated hydrocarbon solvents also affords CENA or BENA.

Postreaction of NAz in Various Halogenated Hydrocarbons. In order to estimate the contribution from the ring-opening of NAz arising from the photolysis of halogenated hydrocarbon, the dark reaction of NAz was carried out in various halogenated hydrocarbons pre-irradiated through a Vycor or Pyrex glass tube under deaerated conditions. The product yields are summarized in Table 2.

It can be seen from Table 2 that the postreaction of NAz in chlorinated hydrocarbons affords CENA as a sole product. Analogous to gaseous HCl,[1)] Cl_2 was confirmed to afford CENA exclusively when bubbled into a solution of NAz in CCl_4. Furthermore, as shown in Fig. 4, the CENA yield in the Vycor systems is in fair agreement with the amount of chloride ions produced *via* photolyses of chlorinated hydrocarbons. These results indicate that the photolytic products of both HCl and Cl_2 are responsible for the ionic ring-opening of NAz to afford CENA.

In the postreactions in CH_2Br_2 and PhBr, the yield of NOz is comparable to that of BENA (Table 2). This is in contrast to the postreaction in *n*-PrBr in which only BENA is obtained. On irradiation through a Pyrex glass for 1 h, both bromide ion (53.3 mmol dm^{-3}) and Br_2 (5.6 mmol dm^{-3}) were detected in CH_2Br_2, whereas only bromide ion (55.4 mmol dm^{-3}) was produced in *n*-PrBr. A separate experiment indicated that NAz is converted almost quantitatively to BENA (94%) in the presence of an equimolar amount of aqueous HBr in CH_2Br_2, accompanied by a minor product of NOz (6%). On the other hand, although the overall conversion decreased considerably, the yield of NOz (5%) was comparable to that of BENA (6%) in the presence of aqueous Br_2 in CH_2Br_2. It seems therefore that a photolytic product of Br_2 is a possible species being responsible for the rearrangement of NAz to NOz.

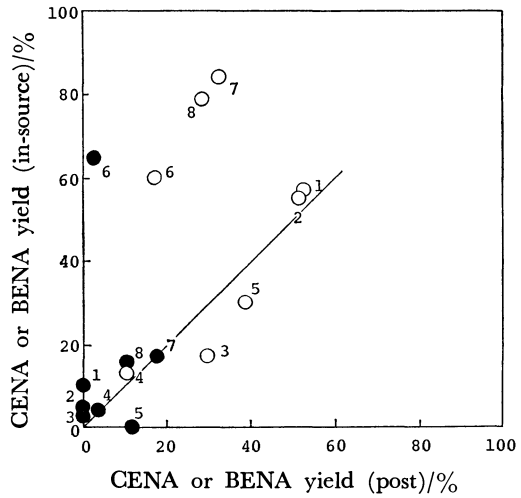

Fig. 5. Relationship between the CENA or BENA yield in the in-source photoreaction and that in the postreaction; (○) Vycor and (●) Pyrex systems.
1: CCl_4, 2: $CHCl_3$, 3: CH_2Cl_2, 4: *t*-BuCl, 5: PhCl, 6: *n*-PrBr, 7: CH_2Br_2, 8: PhBr.

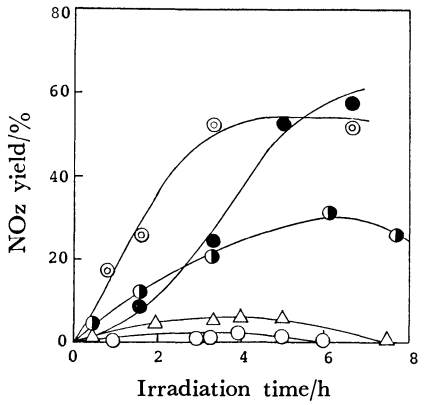

Fig. 6. Variation in NOz yield as a function of irradiation time in the in-soure photoreaction of NAz.
○: CCl_4 (V), △: $CHCl_3$ (V), ◎: CH_2Br_2 (P), ◑: *n*-PrBr (P), ●: PhBr (P).

In Fig. 5 the CENA or BENA yield at 200 min-irradiation in the in-source reaction system is plotted against that in the postreaction system. Under the irradiation through a Vycor glass tube, the stationary concentration of excited $CHCl_3$ in the absence of NAz (91 mmol dm^{-3}) was estimated to be at least 600-fold larger than that in the in-source photoreaction system because of the intense UV absorption by NAz. It follows that the apparent CENA yield in the postreaction system would provide a roughly 600-fold overestimation for the contribution from the photolysis of $CHCl_3$ to the CENA formation in the in-source photoreaction system. Taking into account such a circumstance, the apparent agreement between the CENA yields in the in-source photoreaction and postreaction in a series of chlorinated hydrocarbon solvents indicates that the photochemical CENA formation in source can be attributed almost exclusively to the reaction of excited NAz with solvent molecules. More explicitly, the BENA yield in the in-source photoreactions is seen to exceed considerably that in the postreactions

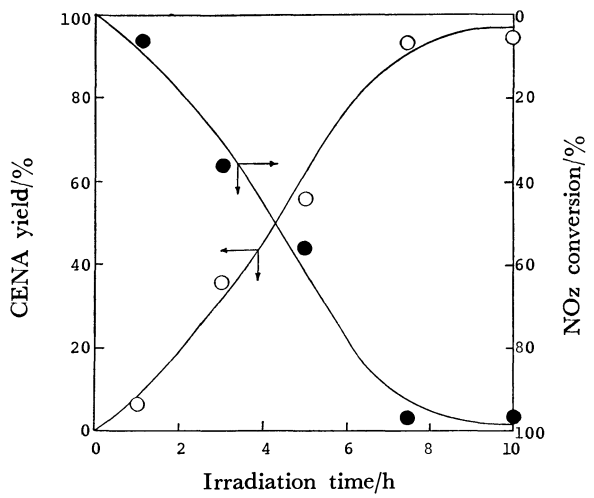

Fig. 7. Variation in NOz conversion (●) and CENA yield (○) as a function of irradiation time in the $CHCl_3$-Vycor in-source photoreaction system; $[NOz]_0$ = 91 mmol dm^{-3}.

(Fig. 5).

In this connection, it can be presumed from Fig. 3 that NAz undergoes radical cleavage of the aziridine ring moiety in the electronically excited state to abstract halogen atom from halogenated hydrocarbon solvents. Such a halogen abstraction would be a rate-determining step in the photochemical CENA and BENA formations in source.

Photochemical Formation and Decomposition of NOz in Various Halogenated Hydrocarbons. It is remarkable in Table 1 that although BENA is afforded exclusively on irradiation of NAz in brominated hydrocarbons through a Vycor glass tube, the rearrangement of NAz to NOz occurs simultaneously in the Pyrex system. Such a formation of NOz was also observed in CCl_4 and $CHCl_3$ even in the Vycor system.

Figure 6 shows the variation in NOz yield as a function of irradiation time. The yields of NOz exceed 50% in CH_2Br_2 and PhBr on irradiation for 200 and 300 min, respectively, and 30% in *n*-PrBr for 360 min. The NOz formation was nevertheless no more observed in these solvents by the prolonged irradiation for over 20 h under the same conditions. During the irradiation for over 300 min in CCl_4 and $CHCl_3$, an analogous variation in the NOz yield with its maximum value of <6% was observed.

As can be seen from Fig. 7, NOz undergoes ring-opening reaction to afford CENA as a sole product on irradiation of a deaerated solution in $CHCl_3$ through a Vycor glass tube. Apparently, the photochemical behavior of NOz is very similar to that of NAz. It is however remarkable that the reactivity of NOz toward HCl is quite different from that of NAz. Thus the slow formation of 2-(2-naphthyl)-2-oxazolinium hydrochloride salt[4] was observed when gaseous HCl was bubbled through a solution of NOz in $CHCl_3$, whereas NAz reacts rapidly with HCl to afford CENA under the same conditions.[1] It follows that the photochemical CENA formation shown in Fig. 7 may be attributed to the reaction of excited NOz with $CHCl_3$.

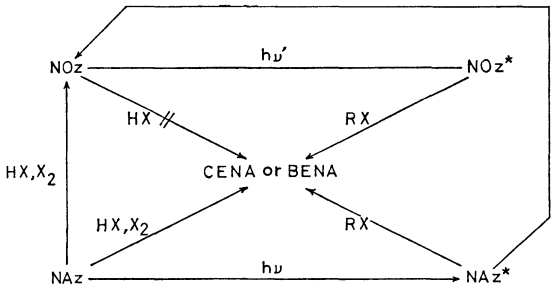

Scheme 1.

In view of the results presented above, the following scheme may be drawn for the photochemical ring-opening reaction of NAz in halogenated hydrocarbons (RX). Although hydrogen halide (HX) and halogen molecule (X_2) derived from the solvent photolysis are highly reactive to NAz, the formation of such species in the in-source photoreaction system would be minor under conditions investigated.

References

1) S. Nishimoto, T. Izukawa, and T. Kagiya, *Bull. Chem. Soc. Jpn.*, **55**, 1484 (1982).
2) M. Schmeisser, "Handbuch der Präparativen Anorganishen Chemie," ed by G. Brauer, Ferdinand Enke Verlag, Stuttgart (1960), p. 249.
3) M. A. Rosanoff and A. E. Hill, *J. Am. Chem. Soc.*, **29**, 269 (1907).
4) T. Okutani, *Nippon Kagaku Zasshi*, **88**, 737 (1967).
5) A. Tomonari, *Nippon Kagaku Zasshi*, **83**, 459 (1962).
6) T. Kagiya and T. Matsuda, *J. Macromol. Sci., Chem.*, **A-5**, 1277 (1971).
7) For CCl_4, *t*-BuCl, *n*-PrBr, and PhBr, J. A. Kerr, *Chem. Rev.*, **66**, 465 (1966); for $CHCl_3$ and CH_2Br_2, J. I. G. Cadogan, D. H. Hey, and P. G. Hibbert, *J. Chem. Soc.*, **1965**, 3939 and 3950; for PhCl, M. Fox, W. C. Nichols, Jr., and D. M. Lemal, *J. Am. Chem. Soc.*, **95**, 8164 (1973); and for CH_2Cl_2, standard bond energy of C–Cl bond is adopted (R. T. Sanderson, "Chemical Bonds and Bond Energy," Academic Press, Inc., New York (1971), p. 153).

Syntheses and Properties of Copolymers of Isopropenyl-1,3,5-triazines and Methacrylic Esters

Toshihiro SEO* and Toshio KAKURAI

Department of High Polymer Technology, Tokyo Institute of Technology, Ookayama, Meguro-ku, Tokyo 152

(Received December 28, 1981)

Copolymerizations of 2-amino-4-(substituted amino)-6-isopropenyl-1,3,5-triazines (methacryloguanamine) with alkyl methacrylates using redox initiator gave polymers with high molecular weights in satisfactory yields. The monomer reactivity ratios and *Q*-*e* values were also determined. Softening and glass transition temperatures rose and specific gravity increased with the increase in the content of triazine units. The copolymers were slightly soluble in nonpolar solvents and readily soluble in polar solvents with a solubility parameter (δ) = 11—13. This polymer with aminotriazine groups showed high viscosity in acid solution and can be utillized as polyelectrolyte.

Polymers containing amino-1,3,5-triazine groups have been investigated as industrial materials and heat-stable polymers. Furthermore, the polymers with aminotriazine groups in the side or main chain are expected to have a variety of other properties, such as rigidity, intermolecular interaction, thermal stability and basicity.[1-3]

The polymerization of several vinyl- and isopropenyl-1,3,5-triazines and the copolymerization with styrene,[4] acrylic or methacrylic acid[1] have been studied previously. Recently isopropenyl-1,3,5-triazines were readily prepared in high yields from methacrylic active esters and biguanides.[5]

This paper describes the determination of copolymerization parameters of 2-amino-4-(substituted amino)-6-isopropenyl-1,3,5-triazines with methacrylic esters and a survey for synthetic conditions to obtain the desired polymers with high molecular weights. Physical and thermal properties of the polymers, *e.g.*, softening and glass transition temperature, specific gravity, solubilities and solution viscosities are also reported.

Experimental

Materials. The mono- and disubstituted biguanides were prepared by the method of Kono and Odo[6] or Cohn[7] from dicyanodiamide and the corresponding amines. Methacrylic esters and *N*,*N*-dimethylaniline were purified by the usual methods.

The initiator, α,α′-azobisisobutyronitrile (AIBN) or benzoyl peroxide (BPO) was a commercial material.

Dioxane was purified by drying with anhydrous magnesium sulfate, refluxing with sodium, and fractionally distilling. Dimethyl sulfoxide (DMSO) was fractionally distilled under reduced pressure in the presence of nitrogen after drying with calcium hydride.

All the other reagents were commercially available and were used after purification, if necessary.

2,4-Diamino-6-isopropenyl-1,3,5-triazine (AIPT): 9.2 g (0.165 mol) of potassium hydroxide dissolved in 90 ml of methanol was added dropwise to the solution of 22.7 g (0.165 mol) biguanide hydrochloride dissolved in 200 ml of methanol at 5—10 °C under stirring. The resulting potassium chloride was filtered off, then the filtrate was concentrated using vacuum evaporator at 30—40 °C. To the concentrate, dissolved in 120 ml of DMSO, was added phenyl methacrylate 24.3 g (0.15 mol). After the temperature was kept at 30 °C for 3 d, the reaction mixture was poured into 2 l of water. The crude product obtained was recrystallyzed from methanol–Methyl Cellosolve to afford colorless crystals, mp 247—248 °C (lit, 247—248 °C)[4] in 81.6% yield.

Other 2,4-substituted amino-6-isopropenyl-1,3,5-triazines were prepared by the procedure described before.[5]

2-Amino-4-anilino-6-isopropenyl-1,3,5-triazine (AAIPT) was recrystallyzed from methanol, mp 174—175 °C (lit, 174—175.5 °C).[4]

2-Amino-4-(*N*-methylanilino)-6-isopropenyl-1,3,5-triazine (NMeAIPT) was recrystallyzed from benzene, mp 117—118 °C (lit, 118—119 °C).[4]

2-Amino-4-dimethylamino-6-isopropenyl-1,3,5-triazine (DMAIPT) was recrystallyzed from methanol, mp 191—192 °C (lit, 191—192 °C).[4]

Procedure. All the polymerization experiments were carried out in a glass tube sealed under a vacuum. Methanol was used as a precipitant. The composition of the polymer was calculated from the carbon and nitrogen contents.

Measurement. Reduced and intrinsic viscosities were determined using an Ostwald and an Ubbelode viscometer, respectively. Number average molecular weights (Mn) were measured by osmometry in a benzene or toluene solution (high speed membrane osmometer Mechrolab 501). Gel permeation chromatography (GPC) was done on a Toyo Soda Model HLC 801A with tetrahydrofuran as the solvent. Ultraviolet absorption spectra were obtained with a Hitachi Model 139 spectrometer.

The softening temperature was measured with a Shimadzu Type MM-2 micro softening point determination apparatus. The glass transition temperature was determined by the same heat-expansion measurement as was reported before.[8] The specific gravity of a polymer film was measured by the suspension method in concentrated sodium chloride or sucrose solution.

Results and Discussion

Homopolymerization. As shown in Table 1, 2-amino-4-anilino-6-isopropenyl-1,3,5-triazine (AAIPT), whose ceiling temperature was about 170 °C,[9] gave only polymers with reduced viscosities of 0.3—0.4 dl/g when polymerized at 60 °C using AIBN. However, poly(AAIPT) with high molecular weight (reduced viscosities of 2—3 dl/g) formed during a short reaction time in satisfactory yields when the polymerizations were attained at 30 °C using redox initiator.

Homopolymers of 2,4-diamino-6-isopropenyl-1,3,5-triazine (AIPT) precipitated from a solution, and their viscosities, obtained using both redox initiator

Table 1. Polymerization of isopropenyl-1,3,5-triazines

Monomer	Condition				Yield/%	η_{sp}[c]
	Initiator	T/°C	t/h	Solvent		
2-Amino-4-anilino-6-isopropenyl-1,3,5-triazine	AIBN[a]	60	4	DMSO	24.0	0.36
	AIBN[a]	60	18	DMSO	39.0	0.27
	AIBN[a]	60	12	Dioxane	31.5	0.29
	Redox[b]	30	1/2	Dioxane	38.9	1.93
	Redox[b]	30	2	Dioxane	47.1	2.75
2,4-Diamino-6-isopropenyl-1,3,5-triazine	AIBN[a]	60	5	Dioxane	32.5	11.9[d]
	Redox[b]	30	72	Dioxane	34.9	10.5[d]

a) Polymerization conditions: $[M]=0.20$ mol dm^{-3}, $[AIBN]=1.35\times10^{-3}$ mol dm^{-3}. b) Polymerization condition: $[M]=0.20$ mol dm^{-3}, [*N*,*N*-dimethylaniline]=[BPO]$=2.70\times10^{-3}$ mol dm^{-3}. c) $c=0.30$ g/dl, in DMSO at 30 °C. d) $c=0.30$ g/dl, in formic acid at 30 °C.

Taable 2. Copolymerization of 2-amino-4-anilino-6-isopropenyl-1,3,5-triazine(M_2) with methacrylic esters(M_1)

M_2 in monomer (mol%)	Reaction time[a] h	Yield %	M_2 in copolymer (mol%)	η_{sp}[c] in Dioxane	η_{sp}[c] in Formic acid
M_1: Butyl methacrylate					
20.01	3[b]	25.4	25.62	0.40	—
5.31	65	37.5	9.08	1.20	—
7.72	65	40.3	13.20	1.32	12.0
20.81	65	68.0	26.43	1.30	15.1
28.83	72	71.7	35.40	0.88	13.4
48.30	72	57.8	55.31	0.72	15.6
58.40	48	30.5	65.10	0.63[d]	—
M_1: Ethyl methacrylate					
5.04	48	32.3	7.27	1.67	—
8.01	48	40.5	10.92	2.08	—
11.02	48	52.4	13.40	1.03	—
12.10	48	25.6	15.60	1.02	—
17.14	48	20.4	20.31	1.40	—
M_1: Methyl methacrylate					
5.02	65	15.7	13.24	0.57	—
10.40	65	21.3	24.52	0.50	—
15.71	65	29.0	27.70	0.57	—
25.03	65	22.5	49.41	0.44[d]	—
40.00	65	20.6	54.33	—	—
50.04	65	19.8	68.14	—	—

a) Polymerization conditions: $[M_1]+[M_2]=0.20$—0.80 mol dm^{-3}, [*N*,*N*-dimethylaniline]=[BPO]$=(1.35$—$4.00)\times10^{-3}$ mol dm^{-3}, in dioxane at 30 °C. b) Polymerization conditions: $[M_1]+[M_2]=0.20$ mol dm^{-3}, $[AIBN]=1.35\times10^{-3}$ mol dm^{-3}, in DMSO at 60 °C. c) $c=0.30$ g/dl, at 30 °C. d) $c=0.30$ g/dl, in DMSO at 30 °C.

and AIBN, were nearly equal.

Redox polymerizations of other 2-amino-4-(substituted amino) derivatives gave high polymers in 70—90% yields in 1—2 h polymerization period.

Copolymerization. Copolymerizations of AAIPT or AIPT with methacrylic esters such as methyl, ethyl, or butyl methacrylate (MMA, EMA, or BMA) were carried out as shown in Tables 2 and 3 respectively.

Copolymerizations of AAIPT with alkyl methacrylates using redox initiator gave polymers with high molecular weights (viscosities of 0.5—1.7 dl/g), whereas the viscosity of the polymer prepared using AIBN was 0.4 dl/g. Similarly, the redox polymerizations of AIPT with alkyl methacrylates gave high polymers with viscosities of 0.9—1.5 dl/g.

Next, the monomer reactivity ratios were determined by the method of Finemann and Ross or Mayo and Lewis; Q-e values are summarized in Table 4.

The r_1r_2 values for copolymerization of AIPT or AAIPT with methacrylic esters are larger than those with styrene. This suggests that copolymerizations of isopropenyl-1,3,5-triazines with methacrylic esters give a lower alternating tendency than that with styrene. Q values were 0.9—1.2. The negative e values for AIPT and the positive e values for AAIPT may be due to the presence of a strong electron-donating effect of two amino groups and a weaker conjugation of anilino group with double bond.[4]

Table 3. Copolymerization of 2,4-diamino-6-isopropenyl-1,3,5-triazine(M_2) with methacrylic esters(M_1)

M_2 in monomer (mol%)	Reaction time[a] h	Yield %	M_2 in copolymer (mol%)	η_{sp}[c] in Dioxane	η_{sp}[c] in Formic acid
M_1: Butyl methacrylate					
20.01	4[b]	20.6	26.10	0.41	—
5.30	72	35.4	7.53	1.28	—
7.71	96	59.8	10.03	1.49	14.2
9.56	72	30.7	13.90	1.63	—
13.55	96	48.1	20.72	1.01	20.9
20.03	96	67.2	29.14	0.92	—
29.52	96	64.3	38.10	0.43[d]	8.4
38.50	96	49.6	48.30	0.67[e]	—
M_1: Ethyl methacrylate					
4.87	72	50.1	7.75	0.94	—
9.10	72	49.4	14.20	1.05	—
11.12	72	45.6	18.71	0.72	—
14.14	72	47.6	23.14	0.75[d]	—
19.80	72	64.0	28.81	0.94	—
M_1: Methyl methacrylate					
5.30	68	15.7	10.17	0.93	9.2
7.75	68	22.4	15.13	0.57	—
18.91	68	48.1	26.70	1.21[e]	15.2
41.30	68	61.3	43.21	0.28[e]	—
58.33	68	43.0	52.60	—	—

a) Polymerization conditions: $[M_1]+[M_2]=0.20$—1.00 mol dm^{-3}, $[N,N$-dimethylaniline$]=[BPO]=(1.35$—$4.00)\times 10^{-3}$ mol dm^{-3}, in dioxane at 30 °C. b) Polymerization conditions: $[M_1]+[M_2]=0.20$ mol dm^{-3}, $[AIBN]=1.35\times 10^{-3}$ mol dm^{-3}, in DMSO at 60 °C. c) $c=0.30$ g/dl, at 30 °C. d) $c=0.30$ g/dl, in Methyl Cellosolve at 30 °C. e $c=0.30$ g/dl, in DMSO at 30 °C.

Table 4. The copolymerization parameters of isopropenyl-1,3,5-triazine (M_2)

M_1[a]	r_1	r_2	r_1r_2	Q	e
M_2=2,4-Diamino-6-isopropenyl-1,3,5-triazine (AIPT)					
St	0.66	0.97	0.64	0.89	−0.13
BMA	0.51	1.42	0.72	1.07	−0.13
EMA	0.68	1.10	0.75	0.88	−0.15
MMA	0.47	1.50	0.71	1.24	−0.19
M_2=2-Amino-4-anilino-6-isopropenyl-1,3,5-triazine (AAIPT)					
St	0.39	0.78	0.30	1.07	0.29
BMA	0.68	1.25	0.85	1.15	0.05
EMA	0.63	1.39	0.88	1.02	0.03
MMA	0.42	2.10	0.86	1.50	0.02

a) St: Styrene ($Q_1=1.0$, $e_1=-0.8$), BMA: butyl methacrylate ($Q_1=0.74$, $e_1=0.39$), EMA: ethyl methacrylate ($Q_1=0.70$, $e_1=0.44$), MMA: methyl methacrylate ($Q_1=0.74$, $e_1=0.40$).

As shown in Table 5, viscosities in dioxane are different from those in benzene, and hence the affinities of triazine rings for solvent seem to influence to some extent the conformation of copolymers. $\bar{M}n$ of copolymers with viscosities of 1.6—1.7 dl/g and 0.6—1.0 dl/g were $(65$—$90)\times 10^4$ and $(10$—$40)\times 10^4$ respectively. The peak count number in GPC decreased with increasing $\bar{M}n$, as recognized generally.

In the UV spectra of copolymers given in Table 6, λ_{max} was assigned to triazine rings in analogy with the model compound; ε values decreased with increasing triazine content, which may show the presence of an interaction between aminotriazine groups.

The other absorption at about 259 nm for AAIPT–BMA copolymers probably indicates the existence of steric hindrance between triazine rings and butyl ester groups in side chain. This may be substantiated by the fact that λ_{max} of *o*-toluidino derivative shifted to a much lower wavelength compared with that of anilino derivative.

Properties. The previous reports[1,2] showed that various polymers containing vinyl-1,3,5-triazines (acryloguanamine) were prepared by the reaction of cyano groups in polymer side chain with dicyanodiamide and/or from polymers containing active ester groups as a pendant and biguanides; then their several properties were investigated. In this paper the thermal and physical properties of polymers containing isopropenyl-1,3,5-triazines (methacryloguanamine) were studied in detail.

As shown in Figs. 1—4, the glass transition temperature (T_g) of polymers was generally about 2/3—3/4 times the softening temperature (T_s). Ts of AIPT–BMA copolymers rose linearly with AIPT content and became above 300 °C at 60 mol% of triazine rings. Ts of AAIPT–BMA copolymers rose in proportion to AAIPT content, but became much lower

Table 5. The intrinsic viscosities and the number average molecular weights of copolymers of isopropenyl-1,3,5-triazines with methacrylic esters

Polymer[a)]	Content of isopropenyl-1,3,5-triazine	$[\eta]$ in Dioxane or (benzene) at 30 °C	$\overline{Mn} \times 10^{-4}$	Peak count number in GPC
Poly(BMA)	—	0.45 (0.50)	9.58	25.8
AIPT-BMA copolymer	12.9	1.07 (0.50)	47.5	23.5
AAIPT-BMA copolymer	11.0	0.55 (0.46)	15.9	25.6
NMeAIPT-BMA copolymer	19.0	0.99	37.5	
DMAIPT-BMA copolymer	20.5	0.55	24.3	
Poly(EMA)	—	1.61 (1.76)	87.9	23.0
AAIPT-EMA copolymer	7.3	1.67 (0.86)	65.0	23.1

a) BMA: Butyl methacrylate, EMA: ethyl methacrylate, AIPT: 2,4-diamino-6-isopropenyl-1,3,5-triazine, AAIPT: 2-amino-4-anilino-6-isopropenyl-1,3,5-triazine, NMeAIPT: 2-amino-4-(*N*-methylanilino)-6-isopropenyl-1,3,5-triazine, DMAIPT: 2-amino-4-dimethylamino-6-isopropenyl-1,3,5-triazine.

Table 6. The UV spectra of copolymers of 2,4-diamino-6-isopropenyl-1,3,5-triazine (AIPT) or 2-amino-4-anilino-6-isopropenyl-1,3,5-triazine (AAIPT) with butyl methacrylate

AIPT in AIPT-BMA copolymer (mol%)	λ_{max}/nm[a)] ($\varepsilon \times 10^{-3}$)	AAIPT in AAIPT-BMA copolymer (mol%)	λ_{max}/nm[a)] ($\varepsilon \times 10^{-3}$)
7.53	258 (3.96)	26.43	259 (18.8) 274 (17.7)
13.90	258 (3.46)	35.40	259 (17.8) 274 (16.8)
29.14	258 (3.32)	55.31	259 (16.8) 274 (16.0)
38.10	258 (2.84)	65.10	259 (10.6) 274 (10.2)
2,4-Diamino-6-methyl-1,3,5-triazine	256 (4·00)[b)]	2-Amino-4-anilino-6-ethyl-1,3,5-triazine	272 (18.7)[b)]
2,4-Diamino-6-ethyl-1,3,5-triazine	254 (3.00)	2-Amino-4-(*o*-toluidino)-6-isopropenyl-1,3,5-triazine	261 (12.8)[b)]

a) Measured in Methyl Cellosolve. b) Measured in ethanol.

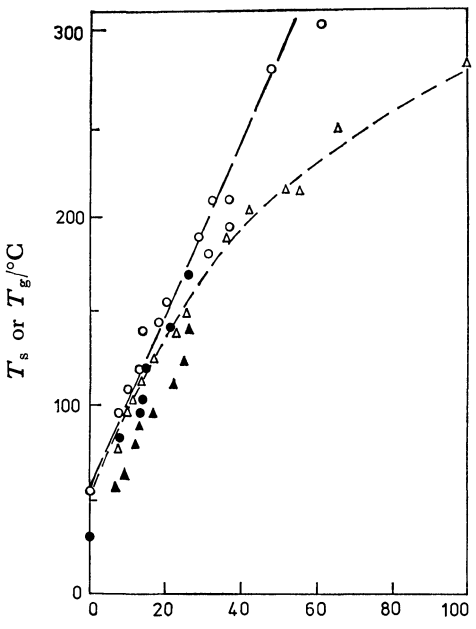

Fig. 1. The relationship between softening temperature (T_s) or glass transition temperature (T_g) and the composition of copolymer of 2,4-diamino-6-isopropenyl-1,3,5-triazine (AIPT) or 2-amino-4-anilino derivative (AAIPT) and butyl methacrylate (BMA).
T_s: ○; P(AIPT–BMA), △; P(AAIPT–BMA), T_g: ●; P(AIPT–BMA), ▲; P(AAIPT–BMA).

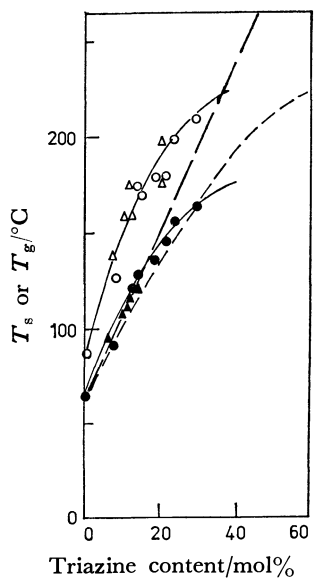

Fig. 2. The relationship between softening temperature (T_s) or glass transition temperature (T_g) and the composition of copolymer of 2,4-diamino-6-isopropenyl-1,3,5-triazine (AIPT) or 2-amino-4-anilino derivative (AAIPT) and ethyl methacrylate (EMA).
T_s: ○; P(AIPT–EMA), △; P(AAIPT–EMA), T_g: ●; P(AIPT–EMA), ▲: P(AAIPT–EMA), ——: T_s of P(AIPT–BMA), - - -: T_s of P(AAIPT–BMA).

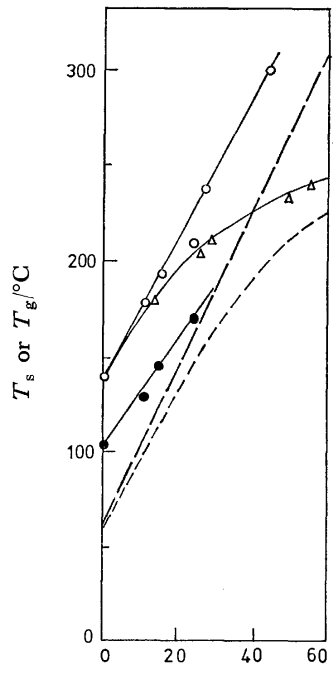

Fig. 3. The relationship between softening temperature (T_s) or glass transition temperature (T_g) and the composition of copolymer of 2,4-diamino-6-isopropenyl-1,3,5-triazine (AIPT) or 2-amino-4-anilino derivative (AAIPT) and methyl methacrylate (MMA).
T_s: ○; P(AIPT–MMA), △; P(AAIPT–MMA), T_g: ●; P(AIPT–MMA), ——: T_s of P(AIPT–BMA), – – –; T_s of P(AAIPT–BMA).

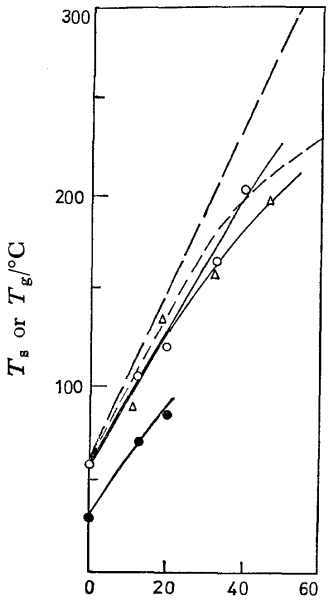

Fig. 4. The relationship between softening temperature (T_s) or glass transition temperature (T_g) and the composition of copolymer of 2-amino-4-dimethylamino-6-isopropenyl-1,3,5-triazine (DMAIPT) or 2-amino-4-(*N*-methylanilino) derivative (NMeAIPT) and butyl methacrylate (BMA).
T_s: ○; P(DMAIPT–BMA), △; P(NMeAIPT–BMA), T_g: ●; P(DMAIPT–BMA), ——; T_s of P(AIPT–BMA), – – –; T_s of P(AAIPT–BMA).

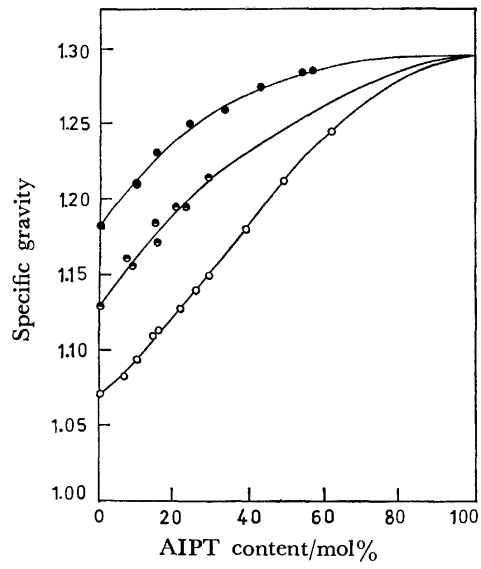

Fig. 5. The relationship between specific gravity and the composition of copolymer of 2,4-diamino-6-isopropenyl-1,3,5-triazine (AIPT) and methacrylic ester.
○: P(AIPT–BMA), ◓: P(AIPT–EMA), ●: P(AIPT–MMA).

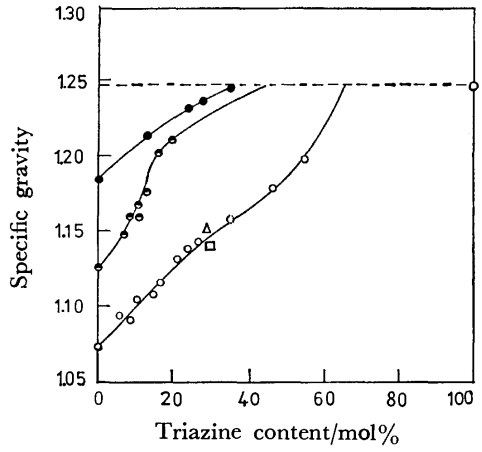

Fig. 6. The relationship between specific gravity and the composition of copolymer of 2-amino-4-anilino-6-isopropenyl-1,3,5-triazine (AAIPT) and methacrylic ester.
○: P(AAIPT–BMA), ◓: P(AAIPT–EMA), ●: P(AAIPT–MMA), □: P(DMAIPT–BMA), △: P(NMeAIPT–BMA).

than that of polymers containing AIPT beyond 40 mol% of triazine rings.

For copolymers of isopropenyl-1,3,5-triazines and EMA, the content of AIPT or AAIPT influenced significantly on T_s or T_g. In the introduction of AIPT to poly(methyl methacrylate), T_s or T_g rose more remarkably than that of AAIPT. The effect of DMAIPT or NMeAIPT on T_s or T_g was approximately equal to that of AAIPT, as given in Fig. 4.

As a result, the introduction of triazine rings to a polymer as a pendant decreased the flexibility of the polymer chain. Specifically, the softening and glass transition points rose considerably with the increase in the content of triazine units. And interac-

Table 7. Solubilities of copolymers of 2,4-diamino-6-isopropenyl-1,3,5-triazine (AIPT) and methacrylic or acrylic esters

Methacrylic or acrylic ester in copolymer	AIPT content in copolymer mol%	Solubilities[a] δ, 9.0 → 10.0 → 12.0 → 13.0								
		IPA	Bz	MEK	DOX	MCS	DMF	Ac.A	F.A	DMSO
Butyl methacrylate	7.53	+	++	++	++	++	++	+	−	−
	10.03	±	±	++	++	++	++	+	+	−
	20.72	−	−	−	++	++	++	+	+	+
	29.14	−	−	−	−	++	++	+	+	+
	38.10	−	−	−	−	+	−	+	+	+
Ethyl methacrylate	7.75	±	+	++	++	++	++	++	+	+
	14.20	±	−	+	++	++	++	++	+	+
	28.81	−	−	−	±	++	++	+	+	+
Methyl methacrylate	10.17	−	−	−	+	+	+	+	+	+
	26.70	−	−	−	−	±	±	++	++	+
	43.21	−	−	−	−	−	−	++	++	+
Methyl acrylate	2.27	−	±	+	±	++	+	++	++	+
	35.60	−	±	−	−	++	+	++	±	++
	57.84	−	−	−	−	±	−	++	+	+
Poly(AIPT)	100	−	−	−	−	−	−	±	+	−

a) ++: Readily soluble, +: soluble, ±: soluble on heating, −: insoluble, IPA: isopropyl alcohol, Bz: benzene, MEK: ethyl methyl ketone, DOX: dioxane, MCS: Methyl Cellosolve, DMF: *N*,*N*-dimethylformamide, Ac.A: acetic acid. F.A: formic acid, DMSO: dimethyl sulfoxide, δ: solubility parameter.

Table 8. Solubilities of copolymers of 2-amino-4-anilino-6-isopropenyl-1,3,5-triazine (AAIPT) and methacrylic esters

Methacrylic ester in copolymer	AAIPT content in copolymer mol%	Solubilities[a] δ, 9.0 → 10.0 → 12.0 → 13.0							
		IPA	Bz	MEK	DOX	MCS	DMF	Ac.A	F.A
Butyl methacrylate	9.08	±	++	+	++	++	++	+	−
	13.20	±	++	+	++	++	++	+	+
	26.43	−	−	+	++	++	++	+	+
	55.31	−	−	−	+	+	+	+	+
	65.10	−	−	−	−	−	+	+	+
Ethyl methacrylate	7.27	±	+	++	++	+	+	++	−
	13.40	±	−	++	++	+	+	++	+
	20.31	−	−	±	++	+	+	++	+
Methyl methacrylate	13.24	−	+	+	+	+	++	+	+
	24.52	−	−	−	+	+	++	+	+
	49.41	−	−	−	+	+	+	+	+
Poly(AAIPT)	100	−	−	−	±	±	+	±	±

a) ++: Readily soluble, +: soluble, ±: soluble on heating, −: insoluble, δ: solubility parameter.

tions between triazine rings with two amino groups were stronger than those between triazine rings with one amino or anilino group, and phenyl groups attached to the triazine rings may act as the external plasticizer.

Further, 40—60 °C rises in Ts occurred for each 10 mol% of introduction of methacryloguanamines to poly(methyl methacrylate), whereas about 100 °C rise occurred for that of acryloguanamines.[2] This suggests that the α-methyl group weakens the interaction between aminotriazine groups.

Next, as shown in Figs. 5 and 6, specific gravities of poly(AIPT) and poly(AAIPT) were 1.296 and 1.245 respectively, which were close to that of poly(vinyl alcohol)(1.2—1.3) and poly(vinyl chloride) (1.3—1.4).

The specific gravities of copolymers of AIPT and alkyl methacrylate increased from 1.07 to 1.30 with increasing AIPT content. Moreover, specific gravities of polymers containing AAIPT increased considerably with AAIPT content and came into agreement with that of poly(AAIPT) at 40—60 mol% of triazine rings. A similar relation may hold for the copolymer containing NMeAIPT or DMAIPT.

In addition, the polymer with less than 25 mol% of triazine rings formed a very transparent flexible hard film.

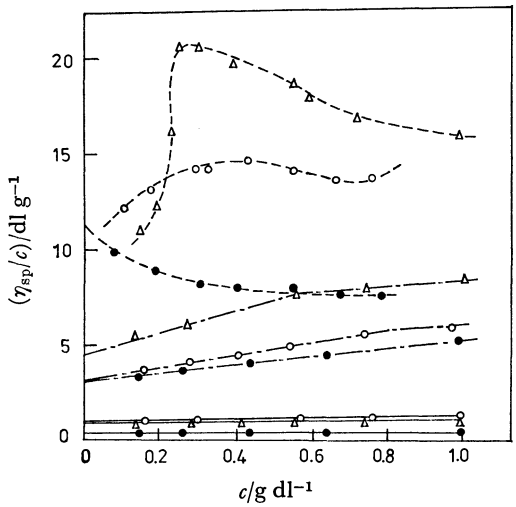

Fig. 7. The relationship between reduced viscosity and the concentration of copolymer of 2,4-diamino-6-isopropenyl-1,3,5-triazine (AIPT) and butyl methacrylate in various solvents.
Mole precent of AIPT in copolymer; ○: 7.53, △: 20.72, ●: 38.10, ——: in Methyl Cellosolve, —·—: in HCOOH+0.01 mol dm^{-3} HCOONa, — — —: in HCOOH.

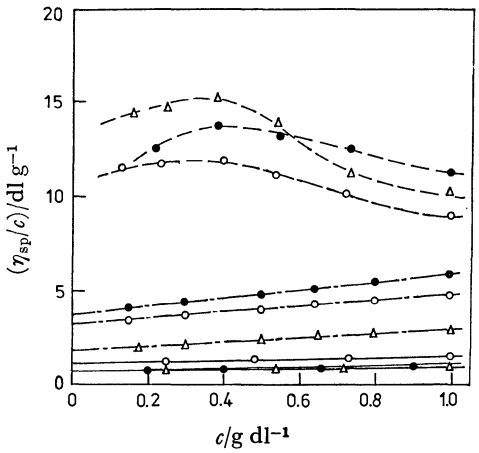

Fig. 8. The relationship between reduced viscosity and the concentration of copolymer of 2-amino-4-anilino-6-isopropenyl-1,3,5-triazine (AAIPT) and butyl methacrylate in various solvents.
Mole percent of AAIPT in copolymer; ○: 13.20, △: 26.43, ●: 35.40, ——: in dioxane, —·—: in HCOOH+0.1 mol dm^{-3} HCOONa, — — —: in HCOOH.

Since specific gravity is closely associated with index of refraction and dielectric constant, an introduction of aminotriazine rings to various polymers can be expected to improve their properties and produce materials useful industrially.

As given in Tables 7 and 8, the solubilities of copolymers of isopropenyl-1,3,5-triazines and alkyl methacrylates increased with increasing the number of carbon atoms of alkyl group.

Polymers containing below 20 mol% of AIPT were soluble in 2-propanol and polar solvents, but became insoluble in dioxane or DMF and soluble in only DMSO or organic acid at AIPT content of over 40 mol%. And even the introduction of 3 mol% of AIPT to poly(methyl acrylate) greatly decreased the solubilities, allowing effective interaction between aminotriazine groups in a very flexible polymer chain.

Further, polymers containing AAIPT were more readily soluble in organic solvents, with solubility parameter (δ)=10—13. Namely, polymers containing 40—50 mol% of AAIPT were soluble in dioxane and Methyl Cellosolve. Other polymers containing 4-(substituted amino) derivatives also exhibited similar solubilities as described above.

It was noteworthy that even copolymers with 10 mol% of triazine rings were soluble in organic acids. As shown in Figs. 7 and 8, the viscosities in formic acid were 10—20 times that in dioxane or Methyl Cellosolve; these increased with dilution and had a maximum value at a certain concentration. However, the viscosities decreased linearly in formic acid–sodium formate solution.

This result indicates that the basic aminotriazine rings have affinities for acid, and hence the protonation at the nitrogen atom of the triazine ring increased the intra- and intermolecular excluded volume effects in polymer solution. Thus, polymers having triazine rings as a pendant can be utilized as polyelectrolytes.[1]

In conclusion, the above-mentioned thermal and physical properties were markedly affected by the species and the number of substituted groups of triazine ring and the structure or composition of the polymer. Moreover, these effects were found to be based upon the rigidity of the basicity of triazine rings and their intra- and intermolecular interactions.

The knowledge obtained in this investigation can be available for the molecular design of polymer-containing heterocyclic rings with many nitrogen atoms.

The authors wish to thank Mr. T. Saito of Tokyo Institute of Technology for his elementary analyses. They are also grateful to Dr. Y. Yuki of Nagoya Institute of Technology for his helpful suggestions and are pleased to acknowledge the considerable assistance of Dr. T. Fukutomi of Tokyo Institute of Technology.

References

1) T. Seo, K. Abe, H. Honma, and T. Kakurai, ACS *Polym. Prepr.*, **20**, 661 (1979); Y. Yuki, H. Mutsujika, and K. Kito, *Kobunshi Ronbunshu*, **36**, 385 (1979); T. Seo, T. Kanai, and T. Kakurai, *Nippon Kagaku Kaishi*, **1981**, 1013; T. Seo, T. Hoga, and T. Kakurai, *ibid.*, **1982**, 485.

2) T. Seo, H. Ishiwata, and T. Kakurai, *Nippon Kagaku Kaishi*, **1980**, 87.

3) T. Seo, H. Ishiwata, and T. Kakurai, *Nippon Kagaku Kaishi*, **1974**, 2419; T. Seo, H. Okamoto, and T. Kakurai, *ibid.*, **1975**, 165.

4) Y. Yuki, N. Hiramatsu, T. Kakurai, and T. Noguchi, *Kobunshi Kagaku*, **26**, 134 (1969); Y. Yuki, T. Kakurai, and T. Noguchi, *Bull. Chem. Soc. Jpn.*, **43**, 2123 (1970).

5) T. Seo, Y. Aoki, and T. Kakurai, *Nippon Kagaku Kaishi*, **1980**, 342.

6) K. Kono and K. Odo, *Yukigosei Kagaku Kyokaishi*, **20**, 649 (1962).

7) G. Cohn, *J. Prakt. Chem.*, **84**, 394 (1911).

8) K. Ehara, *Kobunshi Kagaku*, **29**, 419 (1972).

9) Y. Yuki and M. Ootani, *Kobunshi Kagaku*, **30**, 275 (1973).

 © 1982 The Chemical Society of Japan Bull. Chem. Soc. Jpn., 55, 2949—2955 (1982)

Studies on Chemical Synthesis of mRNAs. I. Synthesis and Properties of N^2-Tritylguanosine Derivatives and Application to Synthesis of pGpUpU

Tsujiaki HATA,* Noboru GOKITA, Nobuo SAKAIRI,† Kazuo YAMAGUCHI, Mitsuo SEKINE, and Yoshiharu ISHIDO†

Department of Life Chemistry, Tokyo Institute of Technology, Nagatsuta, Midori-ku, Yokohama 227

† *Department of Chemistry, Tokyo Institute of Technology, Ookayama, Meguro-ku, Tokyo 152*

(Received January 5, 1982)

Trityl (Tr), 4-methoxytrityl (MMTr), and 4,4′-dimethoxytrityl (DMTr) groups were introduced into the 2-amino group of 2′,3′,5′-tri-*O*-acetylguanosine by treatment with the corresponding trityl chlorides in pyridine to afford the N^2-tritylated guanosine derivatives in high yields. Similarly, the N^6-tritylated adenosine derivatives were synthesized. The stability of the three kinds of trityl groups under acidic conditions were described. The MMTr and Tr groups were found to be suitable for the protection of the 2-amino group of guanosine in oligonucleotide synthesis. An appropriately protected N^2-tritylguanosine 5′-phosphorodithioate derivative was synthesized and utilized for the synthesis of pGpUpU.

In 1975, Miura[1] discovered the so-called "cap" structure in the 5′-terminal region of cytoplasmic polyhedrosis virus mRNA which was represented as m^{7}G$^{5'}$pppAmpGpU···. Since then, the cap structure has been found from several viruses, eukaryotic cells, and mammarian cells.[2] The cap structure is now well recognized as the common structure of eukaryotic mRNAs. Therefore, much attention has been paid to the correlation between the structure and functions of mRNAs in peptide synthesis.[3]

In connection with our study on the chemical synthesis of 5′-terminal structures of eukaryotic mRNAs, especially, the common sequence of mosaic viruses represented as m^{7}G$^{5'}$pppGpUpU···, we wish to report here a basic study on the protection of the 2-amino group of guanosine and also describe the synthesis of pGpUpU.

Results and Discussion

Since 7-methylguanosine (m^{7}G), contained in the cap structure, is quite unstable under alkaline conditions and decomposes to a ring-opening product,[4] the chemical synthesis of capped oligoribonucleotides should be designed to perform under neutral and mildly acidic conditions. In general,[5] the amino groups of nucleoside bases were masked with acyl groups. Only a few have been reported of the acid labile protecting groups for the amino groups. Among them, Holy[6] reported the dimethylaminomethylene group as the protecting group of the 2-amino function of guanine moiety. However, this group is unstable under both acidic and alkaline conditions. On the other hand, 4,4′-dimethoxytrityl (DMTr) group has been used as the acid labile protecting group of the 2-amino group of guanosine by Khorana[7] and Shimidzu.[8] In this study, we tried to use the latter type of protecting groups since introduction of trityl groups enhanced the lipophilicity of the product and the groups could serve as the markers which were easily detected by spraying 10% perchloric acid solution on a chromatogram.

First, the three kinds of trityl groups (Tr, MMTr, and DMTr), were introduced to the 2-amino group of 2′,3′,5′-tri-*O*-acetylguanosine (**1**). In a similar manner, 2′,3′,5′-tri-*O*-acetyladenosine (**2**) was also tritylated. The conditions and results are summarized in Table 1. It was found that the tritylations of **2** proceeded more readily than those of **1**. All the products **3** and **4** could be isolated in pure form as the stable compounds. The N^2-tritylguanosine derivatives **3a—c** were proved to be less polar than the N^6-trityladenosine derivatives **4a—c** from their R_f values.

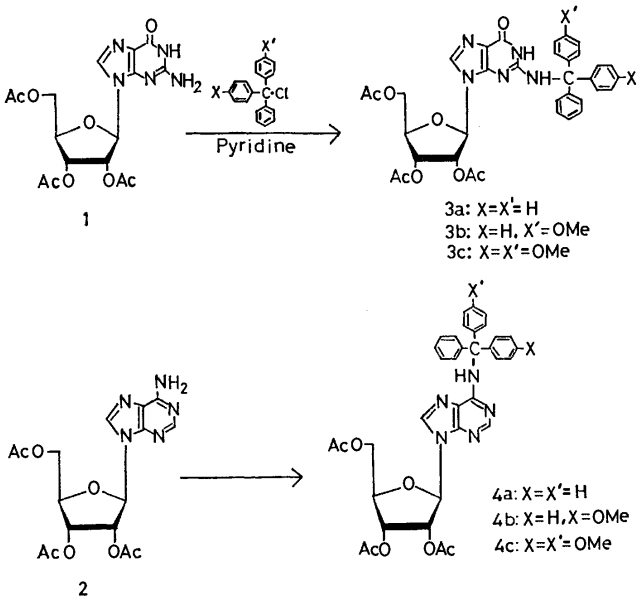

The stability of the Tr, MMTr, and DMTr groups introduced into **1** and **2** was examined. Compounds **3a—c** and **4a—c** were respectively stirred with silica gel (Wakogel C-200) in dichloromethane at room temperature for one day. The amounts of the detritylated compound **1** and **2** were estimated spectrophotometrically after thin layer chromatography. Table 4 shows that the adenosine derivatives are less stable than the guanosine derivatives on silica gel.

Similar results were obtained by treatment of **3a—c** and **4a—c** with 80% acetic acid as summarized in Table 5. Complete removal of each trityl group from **3** or **4** could be performed within one day at room

TABLE 1. CONDITIONS AND RESULTS OF N^2- AND N^6-TRITYLATION OF **1** AND **2**

Trityl chloride	(equiv.)	Temp/°C	Time/h	Product	Yields of **3** and **4**/%
TrCl	1.6	100	2	**3a**	91
MMTrCl	2.0	r. t.	24	**3b**	92
DMTrCl	1.6	r. t.	12	**3c**	96
TrCl	4.0	100	12	**4a**	80
MMTrCl	3.0	60	24	**4b**	91
DMTrCl	4.0	60	12	**4c**	95

TABLE 2. MELTING POINTS AND ELEMENTAL ANALYSES OF **3a—c** AND **4a—c**

Compound	Mp θ_m/°C	Formula	Found (%)			Calcd (%)		
			C	H	N	C	H	N
3a	155 (decomp)	$C_{35}H_{33}N_5O_8$	64.10	5.09	9.99	64.51	5.10	10.75
3b	156—157 (decomp)	$C_{36}H_{35}N_5O_9 \cdot 1/2H_2O$	63.27	5.24	9.77	63.52	5.33	10.29
3c	142—145	$C_{37}H_{37}N_5O_{10} \cdot H_2O$	61.21	5.29	9.36	60.90	5.39	9.60
4a	123—124	$C_{35}H_{33}N_5O_7$	66.11	5.34	10.53	66.13	5.43	10.78
4b	116—118	$C_{36}H_{35}N_5O_8$	64.48	5.34	10.12	64.95	5.30	10.52
4c	113—118	$C_{37}H_{37}N_5O_9$	63.20	5.48	9.40	63.06	5.43	9.94

TABLE 3. SPECTRAL DATA OF **3a—c** AND **4a—c**

Compound	UV (EtOH) $\lambda_{max}(\varepsilon \times 10^{-3})$	$\lambda_{min}(\varepsilon \times 10^{-3})$	$\lambda_{sh}(\varepsilon \times 10^{-3})$	^{1}H NMR($CDCl_3$) δ
3a	260 (17.4)	237 (10.8)	274 (14.4)	1.96(3H, s, $CH_3C(O)$), 2.06(6H, s, $CH_3C(O)$), 4.20(3H, s, H-4′ and 5′), 5.20(2H, m, H-2′ and 3′), 5.36(1H, d, $J_{1',2'}$=7.5 Hz, H-1′), 7.20(15H, m, Tr), 7.89(1H, s, H-8)
3b	260 (17.2)	247 (14.8)	277 (15.6)	1.96(3H, s, $CH_3C(O)$), 2.07(6H, s, $CH_3C(O)$), 3.64(3H, s, CH_3O), 4.20(3H, s, H-4′ and 5′), 5.24(2H, m, H-2′ and 3′), 5.40(1H, d, $J_{1',2'}$=7.5 Hz, H-1′), 6.68(2H, d, J=9 Hz, *m*-protons of MMTr), 7.20(13H, m, MMTr), 7.82(1H, s, H-8)
3c	262 (19.0)	249 (18.0)	277 (17.8)	1.96(3H, s, $CH_3C(O)$), 2.07(6H, s, $CH_3C(O)$), 3.68(6H, s, CH_3O), 4.20(3H, s, H-4′ and 5′), 5.32(2H, m, H-2′ and 3′), 5.46(1H, d, $J_{1',2'}$=7.5 Hz, H-1), 6.70(4H, d, J=9 Hz, *m*-protons of DMTr), 7.24(15H, m, DMTr), 7.55(1H, s, H-8)
4a	274 (17.8)	241 (5.2)	284 (12.0)	2.08(9H, m, $CH_3C(O)$), 4.39(3H, s, H-4′,5′), 5.68(1H, m, H-3′), 5.92(1H, t, $J_{1',2'}$=5 Hz, $J_{2',3'}$=5.5 Hz, H-2′), 6.14(1H, d, $J_{1',2'}$=5 Hz, H-1′), 6.98(1H, s, NH), 7.28 (15H, m, Tr), 7.91(1H, s, H-2), 8.04(1H, s, H-8)
4b	274 (18.4)	245 (8.0)	284 (12.0)	2.10(9H, m, $CH_3C(O)$), 3.78(3H, s, CH_3O), 4.40(3H, s, H-4′,5′), 5.70(1H, m, H-3′), 5.93(1H, t, $J_{1',2'}$=5 Hz, $J_{2',3'}$=5.5 Hz, H-2′), 6.15(1H, d, $J_{1',2'}$=5, H-1′), 6.78 (2H, d, J=9 Hz, *m*-protons of MMTr), 6.94(1H, s, NH), 7.30(13H, m, MMTr), 7.91(1H, s, H-2), 8.07(1H, s, H-8)
4c	274 (18.6)	248 (10.7)	284 (14.2)	2.08(9H, m, $CH_3C(O)$), 3.76(6H, s, CH_3O), 4.40(3H, s, H-4′,5′) 5.70(1H, m, H-3′), 5.93(1H, t, $J_{1',2'}$=5 Hz, $J_{2',3'}$=5.5 Hz, H-2′), 6.14(1H, d, $J_{1',2'}$=5 Hz, H-1′), 6.76 (4H, d, 9 Hz, *m*-protons of DMTr), 6.91(1H, s, NH), 7.30(1H, m, DMTr), 7.90(1H, s, H-2), 8.08(1H, s, H-8)

Table 4. Stability of trityl groups of **3** and **4** in CH_2Cl_2 in the presence of silica gel (Wakogel C-200)

Compound	**3a**	**3b**	**3c**	**4a**	**4b**	**4c**
Detritylation after 24 h (%)	3	26	75	17	64	84

Table 5. Deprotection of trityl groups from **3** and **4**

Conditions	Yield of **1**/%			Yield of **2**/%		
	3a	**3b**	**3c**	**4a**	**4b**	**4c**
R. t., 1 h	48	58	90	64	91	92
R. t., 6 h	70	94	95	94	96	96
R. t., 24 h	81	100	100	100	100	100
100 °C, 10 min	100	—	—	—	—	—

temperature except for **3a**. In the case of **3a**, the trityl group was removed completely at 100 °C for 10 min.

Recently, the 5′-terminal structure of brome mosaic virus mRNA has been determined by Kaesberg.[9] It was described as m^{7}G$^{5'}$ pppGpUpU···. From biological interest of the 5′-terminal structure of brome mosaic virus mRNA, we aimed to synthesize the terminal trimer pGpUpU utilizing the trityl group. In order to prepare a N^2-tritylguanosine derivative having the unmasked 2′-hydroxyl group as the starting material for the synthesis of pGpUpU, the selective deacetylation of **3a** by means of hydrazine hydrate was first examined to obtain 3′,5′-di-*O*-acetyl-N^2-tritylguanosine (**5**). However, **5** and the 2′,5′-diacetate (**6**) were not easily separated, and **5** could not be purified by recrystallization. Repeated chromatography was needed for the complete purification of **5**,[10] since the difference in R_f value between **5** and **6** was unappreciable. From the synthetic point of view this approach could not be applied to the preparation of **5** on a large scale. Therefore, the synthesis of a 2′-protected N^2-tritylguanosine derivative (**7**) was carried out by an alternative route outlined in Scheme 1.

We have chosen 4-methoxytetrahydropyranyl group[11] as the 2′-hydroxyl protecting group, since it could be removed under acidic conditions and had no chiral center in contrast with tetrahydropyranyl group. A convenient method for the synthesis of 3′,5′-di-*O*-acetyl-N^2-benzoylguanosine (**8**) has been reported recently.[12] The methoxytetrahydropyranylation of **8** gave the 2′-protected guanosine derivative (**9**) in 71% yield. Treatment of **9** with butylamine–methanol (1:1, v/v) gave 2′-(4-methoxytetrahydropyran-4-nyl)guanosine (**10**) in 76% yield. Acetylation of **10** with 20 equiv. of acetic anhydride in pyridine gave selectively the 3′,5′-di-*O*-acetylated derivative (**11**) in 90% yield. When more than 20 equiv. of acetic anhydride was used, N^2,$O^{3'}$,$O^{5'}$-triacetylated product (**12**) was formed to an appreciable extent. N^6-tritylation of **11** in pyridine at 100 °C for 1 h gave the fully protected guanosine derivative (**13**) in 87% yield. Deacylation of **13** by means of butylamine–methanol (1:1, v/v) gave **7** in 90% yield.

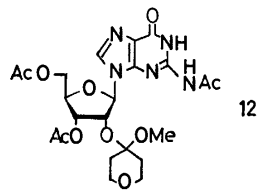

12

For the construction of the triphosphate bridge involved in the cap structure of the mRNA, a suitable protected phosphate group should be introduced into the 5′-hydroxyl group of **7**. In a previous paper,[13] we described the utility of 4-methoxyphenylthio group as the 5′-terminal phosphate protecting group in the synthesis of pTpTpT. Therefore, the phosphorylation of **7** with cyclohexylammonium *S*,*S*-bis(4-methoxyphenyl) phosphorodithioate (**14**)[13] was undertaken. Treatment of **7** with **14** in pyridine in the presence of TPS for 3 h gave **15** in 74% yield after chromatographic separation from **7**.

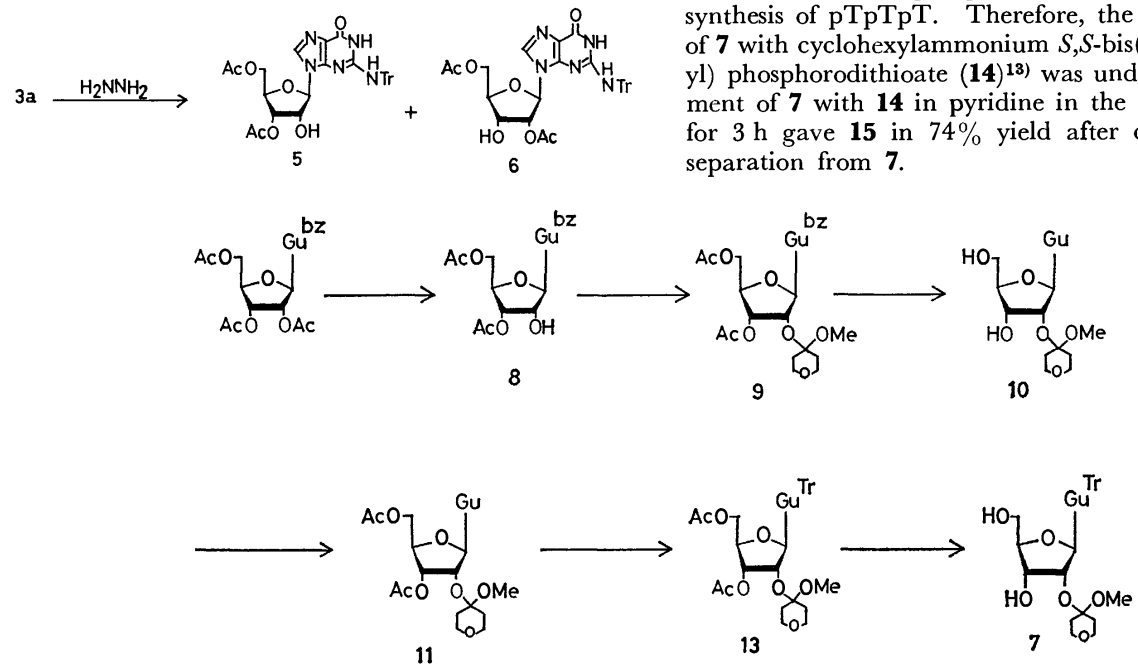

Scheme 1.

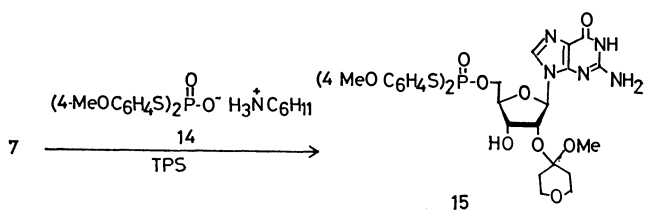

Next, the synthesis of the protected pGpUpU was performed according to Neilson's procedure.[14] Phosphorylation of **15** with 2,2,2-trichloroethyl dihydrogenphosphate was examined by using TPS, 1-(4-nitrophenylsulfonyl)-1*H*-1,2,4-triazole,[15] or dicyclohexylcarbodiimide (DCC). Among those condensing agents, TPS was found to be the most effective. When **15** was phosphorylated by using TPS, TLC of the reaction mixture showed more than 9 spots. However, the mixture was hydrolyzed with aqueous pyridine at room temperature for one day, the desired 3'-phosphorylated product (**16**) appeared as main spot on TLC. Subsequent coupling of **16** with 2',3'-di-*O*-benzoyluridine (**17**) in the presence of 1-(mesitylsulfonyl)-1*H*-1,2,4-triazole (MST)[15] gave the fully protected guanylyl(3'→5') uridine derivative (**18**) in 80% yield.

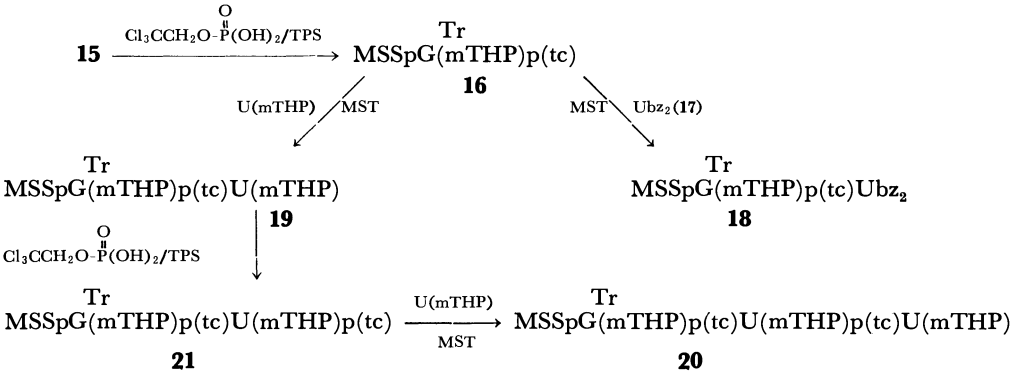

In a similar manner, the dinucleotide (**19**) was obtained in 60% yield from **16** and 2'-*O*-(4-methoxytetrahydropyranyl)uridine [U(mTHP)]. The trimer (**20**) was synthesized by a similar procedure: When a dinucleotide derivative obtained by the phosphorylation of **19** with 2,2,2-trichloroethyl phosphate in the presence of TPS was condensed with U(mTHP) by means of MST, the desired trinucleotide (**20**) was obtained in 54% yield.

During the coupling reactions by-products having blue fluorescence were detected on TLC. They appeared just on the desired products and decomposed to the starting material (**21**) and the desired product during workup. Since O^6-dialkoxyphosphinyl derivatives of **3a** has blue fluorescence,[16] the present by-products might be the O^6-phosphorylated derivatives concomitantly formed from the reaction of **18** or **20** with **16** or **21**.

Deprotection of the Protected Oligonucleotides. We first tested the deprotection of mononucleotide **15**. Treatment of **15** with silver acetate in pyridine–water (2:1, v/v) at room temperature for 24 h followed by chromatography on Whatman 3 MM papers gave 2'-*O*-(4-methoxytetrahydropyranyl)-N^2-tritylguanosine 5'-phosphate (**22**). Subsequent treatment of **22** with 0.01 M (1 M=1 mol dm^{-3}) HCl (pH 2.0) with vigorous stirring for 2 d gave guanosine 5'-phosphate (**23**). The overall yield of **23** from **15** was almost quantitative (99%).

The removal of the protecting groups from the dinucleotide **19** was carried out as follows. As described above, treatment of **19** with silver acetate[13] gave pG^{Tr}(mTHP)p(tc)U(mTHP) (**24**). The 2,2,2-trichloroethyl group was removed from **24** by treatment with zinc/acetylacetone according to the method reported by Adamiak.[17] Finally, the resulting product (**25**) was converted to pGpU in an overall yield of 50% by treatment with 0.01 M HCl for 2 d. Finally, in a similar manner, from the protected trinucleotide **20** pGpUpU was obtained in 41% yield. Both the dimer and the trimer were degraded by snake venom phosphodiesterase to give pG and pU in the theoretical ratios. Usually, 2,2,2-trichloroethyl group can also be removed by treatment with tetra-

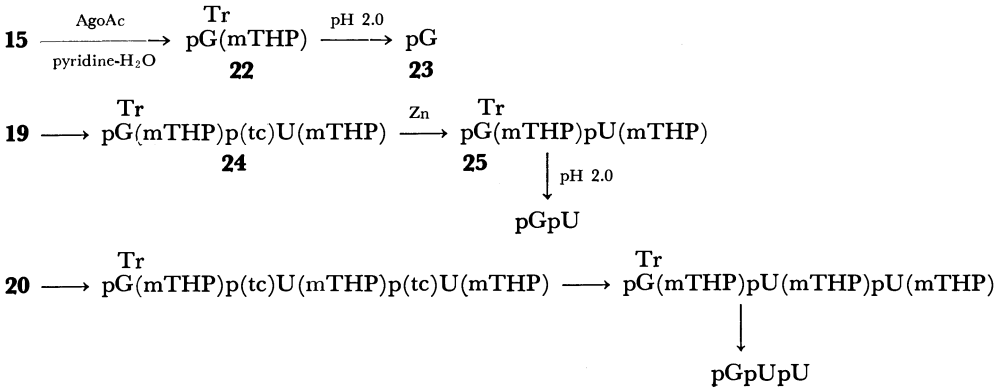

butylammonium fluoride (TBAF). However, attempts to remove the 2,2,2-trichloroethyl group from **24** by means of TBAF were unsuccessful. This result was consistent with that reported by Ogilvie[18] that the presence of a charged phosphate one unit removed from the triester phosphate was sufficient to prevent removal of the internucleotidic phenyl group by TBAF. On the other hand, treatment of **19** with TBAF gave the 5'-terminal phosphorofluoridate derivative, FpG^{Tr}-(mTHP)pU(mTHP), which remained unchanged upon treatment with silver acetate in aqueous pyridine. The decrease of the yields of the deprotected oligomers might be mainly due to side reactions or adsorption of the nucleotidic substances on the zinc surface on the removal of the 2,2,2-trichloroethyl group, although the latter group was rapidly deprotected. While improvement of the yields in the coupling and deblocking processes remained as a problem to be investigated, the present approach provides oligomers with the acid labile protecting groups, which may be useful for the joining with the 'cap' part. Further extention of this wark is now in progress.

Experimental

Melting points were determined on a Thomas-Hoover apparatus and are uncorrected. ^{1}H NMR spectra were recorded at 100 MHz on a JEOL ST-100 spectrometer. UV spectra were obtained on a Hitachi 124 spectrophotometer.

Paper chromatography was performed by descending technique using Toyo Roshi No. 51 and Whatman 3 MM papers. The solvent systems used were Solvent I: isopropyl alcohol–concentrated aqueous ammonia–water (7:1:2, v/v/v); Solvent II: isopropyl alcohol–concentrated aqueous ammonia–water (6:1:3, v/v/v). Paper electrophoresis was carried out with an apparatus similar to that described by Markham and Smith.[19] The buffer used were Buffer I: 0.05 M phosphate (pH 8.0); Buffer II: 0.873 M acetic acid (50 ml)–morpholine (3.3 ml) (pH 3.5) solution (1 l).

Pyridine was distilled from *p*-toluenesulfonyl chloride and stored over calcium hydride. Dichloromethane (CH_2Cl_2) was distilled after being kept over P_4O_{10} for 1 d, redistilled from potassium carbonate, and stored over molecular sievers (3A). Dioxane (1 l) was purified by passing nitrogen gas into the refluxing mixture which contained concentrated hydrochloric acid (13 ml) and water (10 ml) followed by neutralization with potassium hydroxide, extraction, and distillation over sodium. 2',3',5'-Tri-*O*-acetylguanosine (**1**) and 2',3',5'-tri-*O*-acetyladenosine (**2**) were prepared according to the literature method.[20]

Snake venom phosphodiesterase (1 mg/1 ml) was purchased from Boehringer Mannheim GmbH.

Typical Procedure for the Synthesis of **3** *and* **4**. Compound **1** (1.02 g, 2.5 mmol) was rendered anhydrous by repeated coevaporation with dry pyridine and dissolved in dry pyridine (25 ml) trityl chloride (1.12 g, 4 mmol) was added and the mixture was stirred at 100 °C for 2 h. The mixture was cooled to room temperature and ice (5 g) was added. After being kept for 30 min, the mixture was extracted with CH_2Cl_2 (3×30 ml). The combined organic extracts were dried over Na_2SO_4 and evaporated *in vacuo*. The residue was chromatographed on a column of silica gel using CH_2Cl_2–MeOH to give **3a** (1.49 g, 91%). The conditions and results are summarized in Table 1. Physical properties and elemental analysis of **3** and **4** are listed in Table 2.

3',5'-Di-O-acetyl-2'-O-(4-methoxytetrahydropyran-4-yl)-N^2-benzoylguanosine (**9**). To a solution of *p*-toluenesulfonic acid monohydrate (570 mg, 3 mmol) in dioxane (120 ml) was added **8** (5.64 g, 12 mmol). The mixture was stirred for 1 h, and then 5,6-dihydro-4-methoxy-2*H*-pyran (30 mmol)[11] was added. After 3 h, the resulting mixture was neutralized with 1 M methanolic sodium methoxide and evaporated to dryness. The residue was chromatographed on a column of silica gel (98:2—97:3 CH_2Cl_2–MeOH) to give **9** (5.61 g, 71%): Mp 129 °C; NMR ($CDCl_3$) δ 1.76 (4H, m, pyranyl ring protons), 2.06 (3H, s, $CH_3C(O)$), 2.16 (3H, s, $CH_3C(O)$), 2.56 (3H, s, CH_3–O), 3.63 (4H, m, pyranyl ring protons), 4.50 (3H, m, H-4' and 5'), 5.06 (1H, m, H-3'), 5.30 (1H, m, H-2'), 5.90 (1H, d, $J_{1',2'}$= 7.5 Hz, H-1'), 7.20—8.20 (6H, m, ArH and H-8). Found: C, 54.94; H, 5.35; N, 11.10%. Calcd for $C_{27}H_{31}O_{10}N_5 \cdot 1/2H_2O$: C, 54.56; H, 5.33; N, 11.78%.

2'-O-(4-Methoxytetrahydropyran-4-yl)guanosine (**10**). Compound **9** (7.51 g, 12.9 mmol) was dissolved in 1:1 butylamine–methanol (100 ml), and the solution was allowed to stand at room temperature. After 1 d, the solvent was evaporated *in vacuo*. The residue was washed with benzene and recrystallized from methanol to give **10** (3.91 g, 76%): Mp 226 °C (decomp); $UV^{H_2O}_{max}$ 252 nm (ε=14.4×10^3), $UV^{H_2O}_{min}$ 222 nm (ε=3×10^3), $UV^{H_2O}_{sh}$ 269 nm (ε=3×10^3); NMR ($CDCl_3$) δ 1.63 (4H, m, Pyranyl ring protons), 2.67 (3H, s, CH_3–O), 3.35 (4H, m, pyranyl ring protons), 3.58 (2H, m, H-5'), 3.94 (1H, m, H-4'), 4.07 (1H, m, H-3'), 4.70 (1H, dd, $J_{1',2'}$=7.4 Hz, $J_{2',3'}$=5 Hz, H-2'), 5.13 (2H, m, OH), 5.87 (1H, d, $J_{1',2'}$=7.4 Hz, H-1'), 6.45 (1H, br.s, NH_2), 7.98 (1H, s, H-8). Found: C, 48.05; H, 5.85; N, 17.68%. Calcd for $C_{16}H_{23}N_5O_7$: C, 48.36; H, 5.83; N, 17.62%.

3',5'-Di-O-acetyl-2'-O-(4-methoxytetrahydropyran-4-yl)guanosine (**11**). To a mixture of acetic anhydride (20 ml) and pyridine (23 ml) was added **10** (4.03 g, 10.2 mmol). The suspension was vigorously stirred at 60 °C for 2 h. The resulting homogeneous solution was cooled to room temperature. The crystalline precipitate was collected by filtration, washed with benzene, and recrystallized from methanol to give **11** (4.39 g, 90%): Mp 263 °C (decomp); $UV^{H_2O}_{max}$ 253 nm (ε=14.5×10^3), $UV^{H_2O}_{min}$ 222 nm (ε=2.9×10^3), $UV^{H_2O}_{sh}$ 270 nm (ε=10.4×10^3); NMR ($CDCl_3$) δ 2.06 (4H, m, pyranyl ring protons), 2.06 (3H, s, $CH_3C(O)$), 2.16 (3H, s, $CH_3C(O)$), 2.62 (3H, s, CH_3–O), 3.42 (4H, m, pyranyl ring protons), 4.30 (3H, br.s, H-4' and 5'), 5.11 (1H, dd, $J_{1',2'}$=7.6 Hz, $J_{2',3'}$=4.6 Hz, H-2'), 5.22 (1H, t, $J_{2',3'}$= 4.6 Hz, $J_{3',4'}$=4.6 Hz, H-3'), 5.90 (1H, d, $J_{1',2'}$=7.6 Hz, H-1'), 6.55 (1H, br.s, NH_2), 8.00 (1H, s, H-8). Found: C, 49.52; H, 5.74; N, 14.00%. Calcd for $C_{20}H_{27}N_5O_9$: C, 49.81; H, 5.65; N, 14.55%.

3',5'-Di-O-acetyl-2'-O-(4-methoxytetrahydropyran-4-yl)-N^2-tritylguanosine (**13**). To a solution of **11** (482 mg, 1 mmol) in pyridine (10 ml) was added trityl chloride (557 mg, 2 mmol) and the mixture was kept at 80 °C for 6 h. After being cooled to room temperature, the mixture was poured onto crushed ice. The resulting aqueous mixture was extracted with dichloromethane (4×10 ml). The combined organic extracts were dried over anhydrous Na_2SO_4 and evaporated *in vacuo*. The residue was chromatographed on a column of silica gel (99:1 CH_2Cl_2–MeOH) to give crude **7** (610 mg, 87%): NMR ($CDCl_3$) δ 1.55 (4H, m, pyranyl ring protons), 2.10 (3H, s, $CH_3C(O)$), 2.19 (3H, s, $CH_3C(O)$), 2.50 (3H, s, CH_3–O), 3.51 (4H, m, pyranyl ring protons), 4.18 (3H, br.s, H-4' and 5'), 4.52 (1H, dd, $J_{1',2'}$=7.6 Hz, $J_{2',3'}$=6.0 Hz, H-2'), 5.16 (1H, d, $J_{2',3'}$= 6 Hz, H-3'), 5.40 (1H, d, $J_{1',2'}$=7.6 Hz, H-1'), 7.04—7.60

(15H, m, Tr), 7.99 (1H, s, H-8). Since **11** could not be purified by recrystallization and repeated chromatography, the crude material was used for the next reaction.

2'-O-(4-Methoxytetrahydropyran-4-yl)-N²-tritylguanosine (7). The crude **11** (96 mg, 0.137 mmol) was dissolved in 1:1 butylamine–methanol (80 ml) and the mixture was kept at room temperature for one day. The solvent was removed *in vacuo* and the residue chromatographed on a column of silica gel (97:3, CH_2Cl_2–MeOH) to give **7** (79 mg, 90%): Mp 168 °C; UV_{max}^{EtOH} 261 nm ($\varepsilon=16.4\times10^3$), UV_{min}^{EtOH} 238 nm ($\varepsilon=10.8\times10^3$), UV_{sh}^{EtOH} 275 nm ($\varepsilon=14.5\times10^3$); NMR ($CDCl_3$) δ 1.62 (4H, m, pyranyl ring protons), 2.62 (3H, s, $3H_3$–O), 3.10—3.95 (6H, m, pyranyl ring protons and H-5'), 4.05—4.29 (2H, m, H-3',4'), 4.84 (1H, dd, $J_{1',2'}=7.5$ Hz, $J_{2',3'}=5.4$ Hz, H-2'), 5.54 (1H, d, $J_{1',2'}=7.5$ Hz, H-1'), 7.26 (15H, m, Tr), 7.76 (1H, s, H-8). Found: C, 62.57; H, 5.73; N, 10.23%. Calcd for $C_{35}H_{37}N_5O_7$: C, 62.21; H, 6.21; N, 10.36%.

S,S-Bis(4-methoxyphenyl)-2'-O-(4-methoxytetrahydropyran-4-yl)-N²-tritylguanosine-5'-phosphorodithioate (15). To a solution of **7** (303 mg, 0.47 mmol) in dry pyridine (1 ml) was added **14** (230 mg, 0.52 mmol) and TPS (171 mg, 0.56 mmol), successively. After the solution was stirred for 3 h, 1:1 pyridine–water (2 ml) was added. The mixture was extracted with dichloromethane (4×2 ml). The combined organic extracts were dried over anhydrous Na_2SO_4 and evaporated to dryness. The residue was chromatographed on a column of silica gel (99:1 CH_2Cl_2–MeOH) to give **15** (335 mg, 74%) as a foam: UV_{max}^{EtOH} 256 nm ($\varepsilon=33.0\times10^3$), UV_{min}^{EtOH} 227 nm ($\varepsilon=28.0\times10^3$), UV_{sh}^{EtOH} 242 nm ($\varepsilon=29.7\times10^3$); NMR ($CDCl_3$) δ 1.60 (4H, m, pyranyl ring protons), 2.71 (3H, s, CH_3–O), 3.58 (4H, m, pyranyl ring protons), 3.71 (6H, s, CH_3–O), 4.11 (2H, m, H-5'), 4.22—4.58 (3H, m, H-2',3' and 4'), 5.37 (1H, d, $J_{1',2'}=5.7$ Hz, H-1'), 6.78 (4H, d, $J=9$ Hz, *m*-protons of CH_3O–C_6H_4–S), 7.08—7.52 (19H, m, Tr and *o*-protons of CH_3O–C_6H_4–S). Found: C, 58.69: H, 5.20; N, 6.94%. Calcd for $C_{49}H_{50}N_5O_{10}PS_2\cdot2H_2O$: C, 58.85; H, 5.44; N, 7.00%.

Synthesis of 18. A mixture of **15** (34 mg, 0.035 mmol) and 2,2,2-trichloroethyl dihydrogenphosphate (16.1 mg, 0.07 mmol) was rendered anhydrous by repeated coevaporation with dry pyridine and finally dissolved in dry pyridine (0.5 ml). TPS (43 mg, 0.14 mmol) was added and the mixture was stirred at room temperature. After 1 d, the mixture was treated with 1:1 pyridine–water (10 ml) overnight. The main spot of R_f 0.1 (CH_2Cl_2:MeOH, 12:1, v/v) was observed on silica gel plate. The mixture was extracted with CH_2Cl_2 (4×5 ml). The organic exeracts were combined washed water (2×5 ml), and evaporated to dryness. The residue was mixed with **17** (48 mg, 0.105 mmol) and rendered anhydrous by repeated coevaporation with dry pyridine. The mixture was dissolved in dry pyridine (0.5 ml) and 1-(*p*-nitrobenzenesulfonyl)-1*H*-1,2,4-triazole (NBST) (53 mg, 0.21 mmol) was added. The mixture was stirred at room temperature for 3 d and then pyridine–water (1:1, v/v) (2 ml) was added. After being kept for 30 min, the mixture was extracted with CH_2Cl_2 (4×5 ml). The organic extracts were combined, dried over Na_2SO_4, evaporated to dryness, and chromatographed on a column of silica gel (99:1→99:2 CH_2Cl_2–MeOH) to give **18** (45 mg, 80%): UV_{max}^{EtOH} 256 nm ($\varepsilon=19200$), UV_{max}^{EtOH} 233 nm ($\varepsilon=21600$), UV_{min}^{EtOH} 247 nm ($\varepsilon=16000$), UV_{min}^{EtOH} 221 nm ($\varepsilon=19500$); NMR ($CDCl_3$) δ 1.68 (4H, m, pyranyl ring protons), 2.60 (3H, s, OCH_3), 3.60 (4H, m, pyranyl ring protons), 3.76 (6H, s, CH_3O–C_6H_4), 4.60 (6H, m, H-4',5', of Ura and Guo), 4.72 (2H, d, $J=7.8$ Hz, Cl_3CCH_2O), 5.12 (1H, m, H-2' of Guo), 5.80 (3H, m, H-2',3' of Ura and H-3' of Guo), 6.06 (1H, d, $J_{1',2'}=7.4$ Hz, H-1' of Guo), 6.22 (1H, d, $J_{1',2'}=8$ Hz, H-1' of Ura), 6.82 (4H, d, $J=9$ Hz, *m*-protons of CH_3O–C_6H_4–S), 7.28 (25H, m, Tr, *o*-protons of CH_3O–C_6H_4–S, *m,p*-protons of benzoyl), 7.96 (4H, m, *o*-protons of benzoyl). Found: C, 54.25; H, 4.44; N, 6.18%. Calcd for $C_{74}H_{70}Cl_3N_7O_{20}P_2S_2\cdot H_2O$: C, 54.60; H, 4.46; N, 6.18%.

Synthesis of 19. A mixture of **15** (70 mg, 0.073 mmol) and 2,2,2-trichloroethyl dihydrogenphosphate (33.5 mg, 0.146 mmol) was rendered anhydrous as described above and dissolved in dry pyridine (1 ml). TPS (88 mg, 0.292 mmol) was added and the mixture was stirred at room temperature in the dark for 1 d. Then, the mixture was treated with 1:1 pyridine–water (10 ml) and the resulting solution was kept overnight. Extraction with CH_2Cl_2 (4×10 ml) followed by evaporation gave **16**, which was mixed with 2'-*O*-(4-methoxytetrahydropyran-4-yl)uridine (52 mg, 0.146 mmol).

The mixture was rendered anhydrous by repeated coevaporation with dry pyridine and finally dissolved in dry pyridine (0.2 ml). 1-(Mesitylenesulfonyl)-1*H*-1,2,4-triazole (MST) (73 mg, 0.29 mmol) was added and the mixture was stirred continuously or 4 d. The usual workup gave **19** (66 mg, 60%): UV_{max}^{EtOH} 256 nm ($\varepsilon=45000$), UV_{min}^{EtOH} 227 nm ($\varepsilon=33000$), UV_{sh}^{EtOH} 243 nm ($\varepsilon=39000$); NMR ($CDCl_3$) δ 1.40—1.90 (8H, m, pyranyl ring protons), 2.59 (3H, s, CH_3O), 3.16 (3H, s, CH_3O), 3.60 (8H, m, pyranyl ring protons), 3.81 (6H, s, CH_3O–C_6H_4), 4.36 (8H, m, H-2', 3',4',5' of Ura and H-4',5' of Guo), 4.62 (2H, d, $J=7.8$ Hz, Cl_3CCH_2O), 4.76 (1H, m, H-2' of Guo), 5.00 (1H, m, H-3' of Guo), 5.41 (1H, d, $J_{1',2'}=8$ Hz, H-1' of Ura), 5.72 (1H, d, $J=8$ Hz, H-4 of Ura), 5.88 (1H, d, $J_{1',2'}=7.4$ Hz, H-1', of Guo), 6.88 (4H, d, $J=9$ Hz, *m*-protons of CH_3O–C_6H_4S–), 7.28 (20H, m, Tr, *o*-protons of CH_3O–C_6H_4S–, and H-5 of Ura). Found: C, 50.69; H, 4.86; N, 6.20. Calcd for $C_{66}H_{72}Cl_3N_7O_{20}P_2S_2\cdot2H_2O$: C, 51.08; H, 4.94; N, 6.32%.

Synthesis of 21. A mixture of **19** (104 mg, 0.069 mmol) and 2,2,2-trichloroethyl dihydrogenphosphate (31.4 mg, 0.137 mmol) was rendered anhydrous as described before and dissolved in dry pyridine (1 ml). TPS (83 mg, 0.274 mmol) was added and the mixture was stirred at room temperature for 1 d. The mixture was treated with 1:1 pyridine–water (10 ml) at room temperature overnight and then extracted with CH_2Cl_2 (4×5 ml). The organic extracts were combined, evaporated to dryness, and mixed with 2'-*O*-(4-methoxytetrahydropyran-4-yl)uridine (73.6 mg, 0.206 mmol). After being dried by coevaporation with dry pyridine several times, the mixture was treated with MST (103.4 mg, 0.412 mmol) in dry pyridine (0.2 ml) at room temperature for 5 d. The usual workup gave **21** (76 mg, 54%): UV_{max}^{EtOH} 257 nm ($\varepsilon=55000$); UV_{min}^{EtOH} 228 nm ($\varepsilon=33000$); NMR ($CDCl_3$) δ 1.40—1.98 (12H, m, pyranyl ring protons), 2.60 (3H, s, CH_3O of Guo), 3.10 (6H, s, CH_3O of Ura), 3.68 (12H, m, pyranyl ring protons), 3.80 (6H, s, CH_3O–C_6H_4), 4.40 (13H, m, H-2',3',4',5' of Guo), 4.64 (2H, d, $J=7.8$ Hz, Cl_3CCH_2O), 4.70 (2H, d, $J=7.8$ Hz, Cl_3CCH_2O), 5.04 (2H, m, H-2',3' of Guo), 5.48—6.12 (5H, m, H-1',4 of Ura and H-1' of Guo), 6.86 (4H, d, $J=9$ Hz, *m*-protons of $CH_3OC_6H_4S$–), 7.28 (20H, m, Tr *o*-protons of CH_3O–C_6H_4S–, and H-5 of the first Ura), 7.68 (1H, d, $J=8.2$ Hz, H-5 of the second Ura). Found: C, 47.15; H, 4.72, N, 6.25%. Calcd for $C_{83}H_{94}Cl_3N_9O_{30}P_3S_2\cdot2H_2O$: C, 47.39; H, 4.70; N, 6.00%.

Removal of Two 4-Methoxyphenylthio Groups from 15. To a solution of **15** (8.5 mg, 8.5 μmol) in 2:1 pyridine–water (1 ml) was added silver acetate (28 mg, 0.17 mmol). The solution was vigorously stirred at room temperature for 24 h. The resulting suspension was diluted with 2:1 pyridine–

water (10 ml) and bubbled by hydrogen sulfide at 0 °C until a clear supernatant solution had been obtained (*ca.* 5 min). The black precipitate was removed by centrifugation and the supernatant was passed through a column (1×2 cm) of Dowex 50 W×2 (pyridinium form). The column was washed with 1:5 pyridine–water (50 ml). The eluents were collected and concentrated to dryness. The residue was chromatographed on Whatman 3 MM papers (Solvent I). A band of R_f 0.44 was cut and eluted with 1:1 water–ethanol (200 ml) to give pG^{Tr}(mTHP) as ammonium salt (145 OD): UV_{max}^{EtOH} 256 nm, UV_{min}^{EtOH} 245 nm, UV_{sh}^{EtOH} 270 nm.

Complete Deprotection of pG^{Tr}(mTHP). The pG^{Tr}-(mTHP), (60 OD) obtained in the above experiment was concentrated to dryness and suspended in 0.01 M hydrochloric acid (pH 2.0) (5 ml). The heterogeneous mixture was vigorously stirred at room temperature for 2 d. The resulting emulsion was neutralized with pyridine (1 ml) and the solution was evaporated to dryness. The residue was analyzed by paper electrophoresis using Buffer I to give pG (48 OD) at 252.5 nm (λ_{max}), 99% from **15**, which was identified with the authentic sample.

*Removal of Bis(4-methoxyphenylthio) Group from **19**.* To a solution of **19** (9.3 mg, 6 μmol) in 2:1 pyridine–water (1 ml) was added silver acetate (20 mg, 0.12 mmol). The solution was worked up in the same manner as described in the case of **15**, which gave pG^{Tr}(mTHP)p(tc)U(mTHP) (**24**) (90 OD): R_f 0.4 (Solvent I); UV_{max}^{EtOH} 255 nm, UV_{min}^{EtOH} 228 nm.

*Removal of 2,2,2-Trichloroethyl Group from **24**.* The above-mentioned product (36 OD) was evaporated to dryness and dissolved in 1:2 *N,N*-dimethylformamide–water (0.6 ml). To the solution were added zinc power (3.1 mg, 48 μatom) and acetylacetone (0.06 ml). The resulting mixture was stirred vigorously at room temperature for 12 h. The mixture was diluted with 1:1 pyridine–water (10 ml) and passed through a column (1×3 cm) of Dowex 50 W×2 (pyridinium form). The column was washed with 1:1 pyridine–water (50 ml). The eluents were concentrated, applied to Whatman 3 MM papers, and chromatographed by using Solvent I. A band of R_f 0.27 was cut and eluted with 1:1 water–ethanol (200 ml) to give pG^{Tr}(mTHP)pU(mTHP) (**25**) (30 OD): $UV_{max}^{EtOH/H_2O\,(1:1)}$ 256 nm, $UV_{min}^{EtOH/H_2O\,(1:1)}$ 226 nm.

*Complete Deprotection of **25**.* Compound **25** (15 OD) obtained in the above experiment was evaporated to dryness and suspended in 0.01 M hydrochloric acid (pH 2.0) (2 ml). The suspension was stirred vigorously at room temperature for 2 d. The resulting emulsion was neutralized with pyridine (1 ml). The solution was concentrated, applied to Whatman 3 MM papers, and chromatographed (Solvent II) for 2 d to give pGpU (a band moved 2 cm from the origin, 12 OD) which was eluted with 0.05 M phosphate buffer (pH 7.0) (50 ml): $UV_{max}^{pH\,7.0*}$ 256 nm, $UV_{max}^{pH\,7.0*}$ 228 nm (*0.05 M phosphate buffer).

Enzyme Assay of pGpU. The dimer, pGpU (10 OD), obtained in the above experiment was incubated with snake venom phosphodiesterase (10 μg) in 0.1 M Tris–HCl buffer (pH 8.0, 0.12 ml) at 37 °C for 12 h. Then, the mixture was treated with pyridine (0.5 ml), applied to Toyo Roshi No. 51 A paper, and analyzed by paper electrophoresis (pH 3.5, 1500 **V**, 3 h), which showed the two bands of pG and pU eluted with water in the ratio of 0.89:1.00.

*Removal of Bis(4-methoxyphenylthio) Group from **20**.* To a solution of **20** (18.3 mg, 8.7 μmol) in 2:1 pyridine–water (0.5 ml) was added silver acetate (29 mg, 0.174 mmol). The solution was vigorously stirred at room temperature for 14 h. The same workup as described in the case of **15** gave pG^{Tr}(mTHP)p(tc)U(mTHP)p(tc)U(mTHP) (150 OD): R_f 0.41 (Solvent I) R_f 0.67 (Solvent D); UV_{max}^{EtOH} 250 nm.

Removal of 2,2,2-Trichloroethyl Group from pG^{Tr}(mTHP)p(tc)-U(mTHP)p(tc)U(mTHP). An aqueous ethanol solution of the product (60 OD) obtained above was evaporated and dissolved in 2:1 pyridine-*N,N*-dimethylacetamide (1 ml). To the solution was added zinc powder (9.2 mg, 0.14 mmol) and acetylacetone (0.1 ml). The resulting mixture was vigorously stirred at room temperature for 16 h. The same workup as described in the case of **24** gave a band of R_f 0.58 (Solvent II), which was eluted with 1:1 water–ethanol (100 ml) to give pG^{Tr}(mTHP)pU(mTHP)pU(mTHP) (30 OD): $UV_{max}^{EtOH\text{-}H_2O\,(1.1)}$ 252 nm.

Complete Deprotection of pG^{Tr}(mTHP)pU(mTHP)pU(mTHP). An aqueous ethanol solution of pG^{Tr}(mTHP)pU(mTHP) (30 OD) was evaporated to dryness and suspended in 0.01 M hydrochloric acid (3 ml). The suspension was vigorously stirred at room temperature for 4 d. The resulting emulsion was quenched with pyridine (1 ml). The solution was applied to Whatman 3 MM papers and chromatographed by using Solvent II to give pGpUpU (20 OD, *ca.* 40% from **20**): R_f 0.33 (Solvent II): $UV_{max}^{pH\,7.0}$ 255 nm, $UV_{max}^{pH\,7.0}$ 237 nm.

Enzyme Assay of pGpUpU. The trimer, pGpUpU (15 OD), was incubated with snake venom phosphodiestrase (15 μg) in 0.1 M Tris–HCl buffer (pH 8.0, 0.12 ml) at 37 °C for 12 h. Paper electrohoresis (Buffer II) showed the two bands corresponding to pG and pU, which was eluted in the ratio of 1.00:2.06.

References

1) Y. Furuichi and K. Miura, *Nature*, **253**, 374 (1975).
2) M. Kozak, *Cell*, **15**, 1109 (1978).
3) mRNA: the Relation of Structure to Function, "Progress in Nucleic Acid Research and Molecular Biology," ed by W. E. Cohn and E. Volkin, Academic Press, New York (1976), Vol. 19; K. Miura, *Adv. Biophys.*, **14**, 205 (1981).
4) J. A. Haines, C. B. Reese, and L. Todd, *J. Chem. Soc.*, **1962**, 5281; S. Hendler, E. Fürer, and P. R. Srinivasan, *Biochemistry*, **21**, 4141 (1970).
5) C. B. Reese, *Tetrahedron*, **34**, 3143 (1978).
6) J. Zemlicka and A. Holy, *Collect. Czech. Chem. Commun.*, **29**, 645 (1964).
7) H. Schaller, G. Weimann, B. Lerch, and H. G. Khorana, *J. Am. Chem. Soc.*, **85**, 3821 (1963).
8) T. Shimidzu and R. L. Letsinger, *J. Org. Chem.*, **33**, 708 (1968); *Bull. Chem. Soc. Jpn.*, **44**, 1673 (1971).
9) R. Dasgupta, D. S. Shih, C. Saris, and P. Kaesberg, *Nature*, **256**, 624 (1975).
10) The details of **5** and **6** will be reported elswhere.
11) C. B. Resse, R. Saffhill, J. E. Sulston, *J. Am. Chem. Soc.*, **89**, 3366 (1967); B. E. Griffin and C. B. Reese, *Tetrahedron*, **25**, 4057 (1969); C. B. Reese, R. Saffhill, J. E. Sulston, *ibid.*, **26**, 1023 (1970).
12) Y. Ishido, N. Nakazaki, and N. Sakairi, *J. Chem. Soc., Chem. Commun.*, **1976**, 832; *J. Chem. Soc., Perkin Trans. 1*, **1979**, 2088; N. Sakairi, K. Okazaki, and N. Nakazaki, *ibid.*, **1980**, 563.
13) M. Sekine, K. Hamaoki, and T. Hata, *J. Org. Chem.*, **44**, 2325 (1979).
14) T. Neilson and E. S. Werstiuk, *J. Am. Chem. Soc.*, **96**, 2295 (1974); **98**, 2689 (1976).
15) N. Katagiri, K. Itakura, and S. A. Narang, *J. Am. Chem. Soc.*, **97**, 7332 (1975).
16) H. P. Daskalov, M. Sekine, and T. Hata, *Tetrahedron Lett.*, **21**, 3899 (1980); *Bull. Chem. Soc. Jpn.*, **54**, 3076 (1981).
17) R. W. Adamiak, E. B. K. Grzeskowiak, R. Kierzek, A. Kraszewski, W. T. Markiewicz, J. Stawinski, and M. Wiewiorowski, *Nucleic Acids Res.*, **4**, 2321 (1977).
18) K. K. Ogilvie and S. L. Beaucage, *Nucleic Acids Res.*, **7**, 805 (1979).
19) R. Markham and J. D. Smith, *Biochem. J.*, **52**, 552 (1952).
20) H. Bredereck, *Chem. Ber.*, **80**, 401 (1947).

Reactions of Alkanoyl Fluorides with *F*-Isopropyl and *F*-1-Chloroethyl Anions

Nobuo Ishikawa,* Kazuhiko Iwamoto, Tatsumi Ishiwata, and Tomoya Kitazume
Department of Chemical Technology, Tokyo Institute of Technology, Ookayama, Meguro-ku, Tokyo 152
(Received January 13, 1982)

Reactions between alkanoyl chlorides and *F*-propene or *F*-chloroethene with fluoride ion were investigated. While alkyl (*F*-isopropyl) ketones and 1-(*F*-isopropyl)alkenol esters were formed in the former case, 1-(*F*-1-chloroethyl)alkenol esters were exclusively obtained in the latter case. Reaction mechanisms are discussed.

Some sorts of perfluoroalkenes are readily attacked by a fluoride ion affording perfluoroalkyl anions, which are used as a versatile nucleophile. A number of reactions of *F*-tert-butyl anion (**2**), the most stable perfluoroalkyl anion formed from *F*-2-methylpropene (**1**) and a fluoride ion, have been widely investigated by I. L. Knunyants and his coworkers.[1]

$$\underset{\mathbf{1}}{(CF_3)_2C{=}CF_2} + F^- \longrightarrow \underset{\mathbf{2}}{(CF_3)_3\bar{C}} \xrightarrow{RX} (CF_3)_3C\text{–}R$$

F-Propene (**3**), a monomer which is handled much more safely than *F*-isobutene, also gives *F*-isopropyl anion (**4**) by the action of a fluoride ion in an aprotic solvent. This carbanion is trapped readily by strong electrophiles such as 2,4-dinitrofluorobenzene[2] and aroyl fluorides,[3,4] giving organic molecules carrying *F*-isopropyl group.

$$\underset{\mathbf{3}}{CF_3CF{=}CF_2} \xrightarrow{F^-} \underset{\mathbf{4}}{(CF_3)_2\bar{C}F} \begin{cases} \xrightarrow{ArC(O)F} ArC(O)CF(CF_3)_2 \\ \xrightarrow{2,4\text{-DNFB}} 2,4\text{-}(NO_2)_2C_6H_3CF(CF_3)_2 \end{cases}$$

Alkanoyl fluorides as an electrophile, however, react with *F*-isopropyl anion not to give a single product. The reaction accompanies *O*-acylation and is more complicated than that of aroyl fluorides.

Although *F*-chloroethene (**5**), on the other hand, is less susceptible to the attack of a fluoride ion than *F*-propene, it is known to give *F*-1-chloroethyl anion (**6**) at higher temperatures. Some 1-chlorotetrafluoroethylated products such as triazine derivatives were reported to be formed.[5] We now wish to reveal

$$\underset{\mathbf{5}}{ClFC{=}CF_2} + F^- \longrightarrow \underset{\mathbf{6}}{ClF\bar{C}\text{–}CF_3} \xrightarrow{sym\text{-}C_3N_3F_3} C_3N_3F_2(CClFCF_3)\ \textit{etc.}$$

the details of the reactions of alkanoyl fluorides with *F*-isopropyl and *F*-chloroethyl anions.

Results and Discussion

Reactions of F-*Propene with Alkanoyl Chlorides in the Presence of Fluoride Ion.* An earlier report[6] revealed that *F*-propene reacts with perfluoroalkanoyl fluorides in the presence of cesium fluoride affording *F*-alkyl isopropyl ketones.

$$\mathbf{3} \xrightarrow{CsF} \mathbf{4} \xrightarrow{R_fC(O)F} R_f\text{–}\overset{O}{\overset{\|}{C}}\text{–}CF(CF_3)_2$$

In our previous paper, it was reported that *F*-propene and an aroyl chloride in the presence of potassium fluoride in *N,N*-dimethylformamide gave aryl (*F*-isopropyl) ketones in a good yield.[3]

$$\mathbf{3} + ArC(O)Cl \xrightarrow{KF/DMF} ArC(O)CF(CF_3)_2$$

However, alkanoyl chlorides and *F*-propene in potassium fluoride-*N,N*-dimethylformamide system gave alkanoyl fluorides and *F*-propene oligomers[7] as main products. When the reaction was carried out in potassium fluoride–diglyme system, a mixture of an *F*-isopropyl ketone (**7**) and an enol ester (**9**) were obtained. The reactions were carried out at 120—130 °C, and potassium fluoride was used in excess, so that the chloride had been converted to the fluoride prior to the reaction with *F*-isopropyl anion **4**.

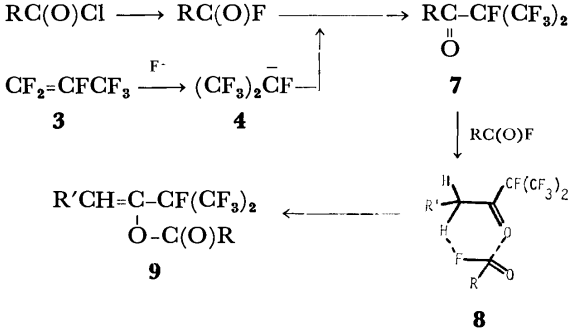

The enol ester **9** should be formed by the reaction of *F*-isopropyl ketone **7** with one more molecule of the alkanoyl fluoride. However, it was surprising to know that a nearly 1:1 mixture of **7** and **9** was always formed even by allowing a large excess amount of *F*-propene to react. This means that the formation of **9** from **5** undergoes as fast as the preceeding ketone formation. Another feature of this acylation was that the *O*-acylation giving **9** occurred exclusively and no *C*-acylated products were observed.

These facts can be explained by assuming a direct attack of acyl fluoride to the ketone **7**. Thus the α-hydrogen atoms of the alkyl group of **7** should be highly activated by the strong electron-withdrawing *F*-2-methylpropanoyl group, and they would readily accept the negative fluorine atom of the acyl fluoride. This H–F bond formation would assist the nucleophilic attack of the carbonyl oxygen of **7** to the carbonyl carbon of acyl fluoride to give *O*-acylated product **9**, through a six-membered cyclic transition state (**8**). The structures of enol esters **9** were elucidated from the ^1H and ^{19}F NMR spectral data (Table 1), though it was unable to determine whether these are in *E*-

Table 1. Physical properties of ketones, R-C(O)-CF(CF_3) (**7**)

Compd **7** R	Bp θ_b/°C (mmHg)**	IR C=O $\tilde{\nu}$/cm^{-1}	NMR $^{19}F(\delta)$[a] CF_3(J_{F-F})	NMR $^{19}F(\delta)$[a] CF	NMR $^1H(\delta)$ C(O)CH(J_{H-F})	NMR $^1H(\delta)$ C(O)-C-R'(H)	Found (Calcd)(%) C	Found (Calcd)(%) H
Me	53—54	1760	−3.0 d (5.6)	104m	2.47 d, 3H(5.9)	—	28.16(28.32)	1.52(1.43)
Et	66—69	1755	−2.4 d (6.0)	107m	2.90 m, 2H(3.0)	1.23 t, 3H	31.68(31.87)	2.36(2.23)
n-Pr	49—50(140)	1755	−3.0 d (5.6)	107m	2.75 m, 2H(3.9)	1.73 m, 2H; 1.0 t, 3H	35.32(35.01)	3.06(2.94)
i-Pr	89—90	1745	−3.8 d (6.2)	108m	3.28 m, 1H(2.9)	1.20 d, 6H	34.86(35.01)	2.78(2.94)
n-Bu	48—49(55)	1755	−2.5 d (6.2)	107m	2.72 m, 2H(3.6)	0.98 t, 3H; 1.1—1.85, 4H	37.96(37.81)	3.62(3.57)
t-Bu	49—51(130)	1730	−4.0 d (6.0)	105m	—	1.30 br, 9H	37.86(37.81)	3.62(3.57)
n-C_5H_{11}	75—77(90)	1755	−2.5 d (6.2)	111m	2.70 m, 2H(3.5)	0.90 t, 3H; 1.1—1.8, 6H	40.86(40.31)	4.24(4.13)

a) δ ppm from ext. CF_3CO_2H in CCl_4. ** 1 mmHg≈133.322 Pa.

Table 2. Physical properties of enol esters, R'CH=CCF(CF_3)$_2$ (**9**)
OC(O)R

Compd **9** R	R'	Bp θ_b/°C (mmHg)	IR $\tilde{\nu}$/cm^{-1} C=O	IR C=C	NMR $^{19}F(\delta)$[a] CF_3(J_{F-F})	NMR $^{19}F(\delta)$[a] CF	NMR $^1H(\delta)$ =C-H(J_{H-F})	Found (Calcd)(%) C	Found (Calcd)(%) H
Et	Me	58—60(25)	1785	1695	−2.5 d (6.4)	101m	6.03m (3.0)	38.53(38.31)	3.16(3.22)
n-Pr	Et	49—50(10)	1790	1690	−2.0 d (6.2)	101m	5.93m (3.3)	42.48(42.59)	4.42(4.22)
n-Bu	*n*-Pr	49—51(1.5)	1780	1685	−2.0 d (6.2)	101m	5.93m (3.0)	46.21(46.16)	5.11(5.07)
n-C_5H_{11}	*n*-Br	105—108(14)	1785	1690	−2.0 d (7.1)	102m	5.90m (3.0)	49.36(49.18)	5.56(5.78)

a) Table 1, footnote a).

Table 3. Physical properties of enol esters, R'-CH=C-CClF-CF_3 (**10**)
OC(O)R

Compd **10** R	R'	Bp θ_b/°C (mmHg)	Yield %	IR $\tilde{\nu}$/cm^{-1} C=O	IR C=C	NMR $^{19}F(\delta)$[a] CF_3(J_{F-F})	NMR $^{19}F(\delta)$[a] CFCl	NMR $^1H(\delta)$ =C-H(J_{H-F})	Found (Calcd)(%) C	Found (Calcd)(%) H
Et	Me	53—55(19)	83	1785	1690	3.0 d (6.6)	50.7m	6.07m (1.9)	39.23(38.65)	4.01(3.65)
n-Pr	Et	68—70(18)	90	1780	1675	3.5 d (6.6)	50.7m	5.97m (1.7)	43.88(43.42)	4.79(4.74)
n-Bu	*n*-Pr	57(1)	81	1780	1680	3.0 d (6.6)	50.5m	5.99m (1.8)	47.08(47.30)	5.48(5.62)
n-C_5H_{11}	*n*-Bu	69—72(2)	63	1780	1675	2.8 d (6.6)	50.5m	6.02m (1.8)	49.65(50.53)	5.88(6.36)

a) Table 1, footnote a).

or *Z*-form.

Reactions of F-*Chloroethene with Alkanoyl Chlorides in the Presence of Fluoride Ion.* The reaction of alkanoyl chlorides with *F*-chloroethene in the presence of potassium fluoride did not undergo smoothly as those with *F*-propene. This should be ascribed to the difficulty of formation of *F*-1-chloroethyl anion **6** compared with *F*-isopropyl anion **4**. Since the chlorine atom is less electronegative than trifluoromethyl group, the anion **6** should be less stable than **4**.

$$\underset{\mathbf{6}}{CF_3\bar{C}ClF} < \underset{\mathbf{4}}{CF_3\bar{C}FCF_3}$$

When cesium fluoride instead of potassium fluoride was used in the reaction, the corresponding enol esters (**10**) were obtained in good yields even at room temperatures (Table 2). Cesium fluoride is known as

$$\underset{\mathbf{5}}{RC(=O)Cl} + CF_2{=}CClF \xrightarrow[\text{r. t.}]{\text{CsF/diglyme}} \underset{\mathbf{10}}{R'\text{-}CH{=}C(OC(O)R)\text{-}CClF\text{-}CF_3}$$

a stronger source for fluoride ions than potassium fluoride in an aprotic solvent.[8] Hence CsF accelerated the formation of *F*-chloroethyl anion **6** which reacted with an alkanoyl fluoride in a similar manner as *F*-isopropyl anion **4**. In this case, however, no formation of the *F*-chloroethyl ketone (**11**) was ob-

$$\underset{\mathbf{6}}{R\text{-}C(=O)\text{-}F} + CF_3\bar{C}ClF \xrightarrow[\text{slow}]{} \underset{\mathbf{11}}{R\text{-}C(=O)\text{-}CClF\text{-}CF_3} \xrightarrow[\text{fast}]{\text{RC(O)F}} \mathbf{10}$$

served. This should be ascribed to the much slower first-step reaction of *F*-chloroethyl anion with alkanoyl fluoride compared with the following *O*-acylation.

When 2,2-dimethylbutanoyl chloride, which has no α-hydrogen atoms, was allowed to react with *F*-chloroethene, a kind of enol ester(**13**) carrying no chlorine atom was formed together with *F*-chloroethyl ketone (**12**). Although the formation of **13** seemed to be

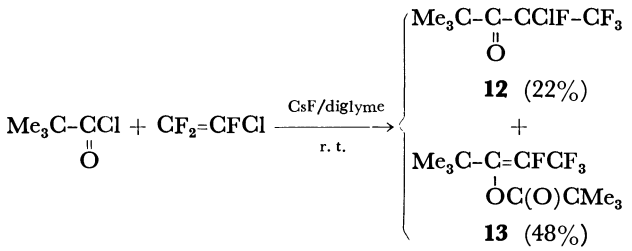

strange, it was rationalized by considering the formation of *F*-ethenyl anion(**15**) from *F*-chloroethene, followed by the addition of acyl fluoride.[5,9] Actually

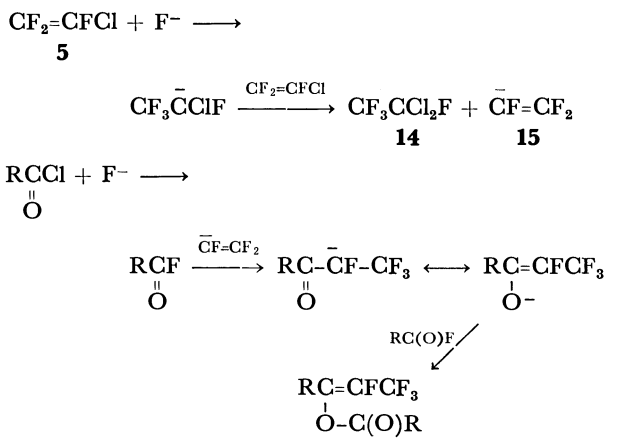

we observed the formation of 1,1-dichlorotetrafluoroethane **14** when *F*-chloroethene (**5**) was treated in cesium fluoride–diglyme system and no oligomerization of **5** occurred.

Experimental

*Heptyl (F-Isopropyl) Ketone (**7**, R=n-C_7H_{15}) and 1-(F-Isopropyl)-1-hexenyl Octanoate (**9**, R=n-C_7H_{15}, R′=n-C_6H_{13}).* Into a mixture of octanoyl chloride (1.63 g, 10 ml), calcine-dried potassium fluoride (3.50 g, 60 mmol) and freshly dried diglyme (10 ml) in a pressure-vessel, liquefied *F*-propene (3.0 g, 20 ml) was introduced at −70 °C. The vessel was brought to room temperature, and heated for 2 h in an oil bath kept at 120—130 °C with magnetic stirring. The reaction mixture was poured onto water and an oily material was extracted with diethyl ether. After the solvent was removed, the residue was subjected to vacuum distillation. **7** (R=*n*-C_7H_{15}), bp 59—62 °C/12 mmHg, and **9** (R=*n*-C_7H_{15}, R′=*n*-C_6H_{13}), bp 150—152 °C/11 mmHg, were obtained in yields of 48 and 20%, respectively.

Other *F*-isopropyl ketones (**7**) and enol esters (**9**) were prepared in a similar manner.

*1-(F-1-Chloroethyl)-1-propenyl Propionate (**10**, R=Et, R′=Me).* Propionyl chloride (1.85 g, 20 mmol), calcine-dried cesium fluoride (7.5 g, 50 mmol) and freshly dried diglyme (20 ml) were put in a pressure-vessel, and liquefied chlorotrifluoroethene (4.8 g, 40 mmol) was introduced at −70 °C. The mixture was stirred for 48 h at room temperature, and worked up as described above. The enol ester **10** (R=Et, R′=Me), bp 68—70 °C/18 mmHg, was obtained in 83% yield.

Other enol esters **10** were prepared in a similar manner.

Reaction between 2,2-Dimethylpropionyl Chloride and F-Chloroethene with a Fluoride Ion. When 2,2-dimethylpropionyl chloride and *F*-chloroethene were allowed to react in a similar manner, following two products were obtained.

*t-Butyl (F-1-Chloroethyl) Ketone (**12**):* Bp 45—46 °C/46 mmHg, 22%. IR: 1730, 1745 cm^{-1} (C=O). ^{19}F NMR: δ 2 (d, CF_3), 57 (br, CF) ppm; J_{F-F}=5.6 Hz. ^1H NMR: δ 1.34 (d); J_{H-F}=1.7 Hz. Too much volatile to be analyzed.

*1-t-Butyl-2,3,3,3-tetrafluoro-1-propenyl 2,2-Dimethylpropionate (**13**):* Bp 67—68 °C/13 mmHg, 48%. IR: 1765 (C=O), 1690 (C=C) cm^{-1}. ^{19}F NMR: δ −9 (d, CF_3), 71 (m, F) ppm, J_{F-F}=1.7 Hz. ^1H NMR: δ 1.29 (s, 9H), 1.25 (d, 9H), J_{H-F}=1.7 Hz. Found: C, 53.72; H, 6.47%. Calcd for $C_{12}H_{18}F_4O_2$: C, 53.33; H, 6.67%.

References

1) Review: B. L. Dyatkin, N. I. Delyagina, and S. R. Sterlin, *Usp. Khim.*, **45**, 205 (1976).
2) N. Ishikawa, Y. Inoue, and K. Kitagawa, *Nippon Kagaku Zasshi*, **91**, 742 (1970).
3) N. Ishikawa and S. Shin-ya, *Bull. Chem. Soc. Jpn.*, **48**, 1339 (1975).
4) N. Ishikawa and S. Shin-ya, *Chem. Lett.*, **1976**, 673.
5) R. D. Chambers and M. Y. Gribble, *J. Chem. Soc., Perkin Trans. 1*, **1973**, 1411.
6) R. D. Smith, F. S. Fawcett, and D. D. Coffman, *J. Am. Chem. Soc.*, **84**, 4285 (1962).
7) N. Ishikawa and M. Maruta, *Yuki Gosei Kagaku Kyokai Shi*, **39**, 51 (1981).
8) W. A. Sheppard and C. M. Sharts, "Organic Fluorine Chemistry," Benjamin, Inc., New York (1969), p. 83.
9) B. L. Dyatkin, N. G. Kizim, S. R. Sterlin, and L. A. Fedorov, *J. Organomet. Chem.*, **57**, 423 (1973).

 © 1982 The Chemical Society of Japan Bull. Chem. Soc. Jpn., 55, 2959—2964 (1982)

Mechanism of Dye-sensitized Photooxidation of Tryptophan, Tryptamine, and Their Derivatives. Singlet Oxygen Process in Competition with Type I Process

Kenzo INOUE,† Teruo MATSUURA, and Isao SAITO*

† *Department of Industrial Chemistry, Faculty of Engineering, Ehime University, Bunkyo-cho, Matsuyama 790*

Department of Synthetic Chemistry, Faculty of Engineering, Kyoto University, Sakyo-ku, Kyoto 606

(Received January 14, 1982)

Photosensitized oxidations of tryptophan (Trp), tryptamine, and their derivatives were investigated with a variety of sensitizers. Rose Bengal sensitized photooxidations proceed exclusively *via* Type II mechanism (singlet oxygen mechanism), whereas for thionine-sensitized photooxidations both Type I (nonsinglet oxygen mechanisms) and Type II mechanisms are operative under a given set of conditions. Rate constants of reaction, in units of 10^6 M^{-1} s^{-1}, were determined to be 3 for Trp, 4 for tryptophan methyl ester, 4 for N_b-acetyltryptophan methyl ester, 9 for tryptamine, and 7 for N_b-methoxycarbonyltryptamine in the Rose Bengal-sensitized photooxidations. These values are in good agreement with those obtained from reactions with chemically generated singlet oxygen. Quenching rate constants are somewhat larger than reaction rates constants, indicating that the quenching process is the major path for the interaction of singlet oxygen with these indolic substrates. Oxidation products in chemically generated singlet-oxygen reaction of Trp are compared with those obtained from dye-sensitized photooxidations.

Photooxidation of tryptophan (Trp) is of particular interest in connection with photodynamic degradation of Trp residues in proteins, and the possibility that the oxidation may represent a model for biological oxidation of Trp catalyzed dioxygenases. A number of reports on dye-sensitized photooxidation of Trp and related substrates have appeared in connection with photoproducts as well as mechanisms. The photooxidation of Trp gives many types of products, depending on experimental conditions such as wavelength of light, type and concentration of sensitizers, and solvents employed.[1] In earlier papers,[2] the photosensitized oxidation of Trp was shown to give a complex mixture of products, in which kynurenine and *N*-formylkynurenine (*N*-FK) were detected. Savige[3] reported that Methylene Bule (MB)-sensitized photooxidation of Trp in water gave *N*-FK and 3a-hydroxy-1,2,3,3a,8,8a-hexahydropyrrolo[2,3-*b*]indole-2-carboxylic acid (HPI). More recently, Nakagawa *et al.*[4] have reported isolation of 3a-hydroperoxy-1,2,3,3a,8,8a-hexahydropyrrole[2,3-*b*]indole-2-carboxylic acid (HPPI) as a primary product in Rose Bengal (RB)-sensitized photooxidation. This hydroperoxide (HPPI) decomposes to give *N*-FK and HPI under photolytic or thermolytic conditions.[4]

The mechanism of dye-sensitized photooxidation of Trp has long been a subject of controversy. Trp is reported to quench triplet states of sensitizers such as eosine and thionine under certain conditions.[5] A recent work[6] has demonstrated that the excited singlet states of RB and MB are also quenched by tryptamine and other indoles. These results may imply the importance of a nonsinglet oxygen (Type I[7]) mechanism involving interaction between photoexcited dyes and indoles in the sensitized photooxidation of Trp. In contrast to these reports, Nilsson *et al.*[8] pointed out that singlet oxygen ($^1O_2$) is involved in MB-sensitized photooxidation of Trp in aqueous methanol, and they have determined rate constants for the reaction (k_r) and quenching (k_q) of Trp with $^1O_2$. However, the rate constant of reaction, k_r, reported by Nilsson *et al.*[8] is approximately one order of magnitude smaller than the value obtained from the reaction of Trp with photophysically generated $^1O_2$ in D_2O (pD 8.4),[9] although the overall rate constant, k_r+k_q, has the same order of magnitude. Smith[10] showed that rate constants are highly dependent on the polarity of solvent. Furthermore, recent works[11,12] on photooxidations of Trp and tryptamine with hematoporphyrin sensitizer have shown that the reactions proceed *via* Type I mechanism, and that the singlet oxygen (Type II) mechanism is of minor importance even when reactions are carried out in the presence of micelles. These results apparently indicate that the dye-sensitized photooxidations of Trp and tryptamine are strongly dependent on reaction conditions, particularly on the type of sensitizer, solvent, and substrate concentration.

In this paper, the influence of conventional sensitizers such as RB and MB on the mechanism of sensitized photooxidation of Trp, tryptamine, and their derivatives has been examined as a model for photooxidation of Trp residues in a protein. Rate constants for the reaction and quenching of these substrates with $^1O_2$ in the RB-sensitized photooxidation have been compared with those obtained with chemically generated $^1O_2$. Oxidation products in both reactions were also examined.

Experimental

Materials. Rose Bengal (RB), Methylene Blue (MB), eosine, thionine, L-tryptophan (Trp, **1**), tryptophan methyl ester (**2**), and tryptamine (**4**) are commercially available. N_b-Acetyltryptophan methyl ester (**3**) and N_b-methoxycarbonyltryptamine (**5**) were prepared by the known methods. 3-(1,4-Epidioxy-4-methyl-1,4-dihydro-1-naphthyl)propionic acid (EP) was prepared by the published procedure.[13]

Procedure. A typical irradiation system consists of 10 ml of 1:1 MeOH–H_2O solution containing **1** (1.3×10^{-4} M) (1 M = 1 mol dm^{-3}), sensitizer (3.3×10^{-6} M), and varying amounts of sodium azide ($2—50\times10^{-3}$ M) in Pyrex reaction tubes. After the solutions were saturated with pure oxygen, the test tubes were sealed with jointed stoppers.

Table 1. Effects of azide ion and deuterated solvent on the rates of photooxidations of tryptophan derivatives with various sensitizers[a]

Sensitizer	1 (R = -C(H)(CO$_2$H)-NH$_2$)		2 (R = -C(H)(CO$_2$Me)-NH$_2$)		3 (R = -C(H)(CO$_2$Me)-NHCOMe)		4 (R = -CH$_2$NH$_2$)		5 (R = -CH$_2$NHCO$_2$Me)	
	I/%[b]	R_D/R_H[c]	I/%[b]	R_D/R_H[c]	I/%[b]	R_D/R_H[c]	I/%[b]	R_D/R_H[c]	I/%[b]	R_D/R_H[c]
Rose Bengal (RB)	100	9.6 (8.1)[d]	100	9.8 (8.7)[d]	100	10.2 (8.9)[d]	100	7.4	100	11.4 (9.5)[d]
Methylene Blue (MB)	90	9.0 (8.7)[d]	90	11.5 (9.1)[d]	90	9.5 (8.5)[d]	90	7.4	90	8.0 (6.5)[d]
Eosine	100	11.8	90	8.7	100	8.2	80	7.0	100	9.8
Thionine	60	7.5	80	8.3	80	8.3	40	4.0	40	4.7

a) In 1:1 MeOH-H_2O; [scns] = 3.3×10^{-6} M; [substrate] = 1.3×10^{-4} M. b) I denotes $(R_0-R_1)/R_0\times100$; R_0: the rate of photooxidation in the absence of NaN_3; R_1: the limiting rate of photooxidation in the presence of higher concentrations of NaN_3. c) The ratio of the photooxidation rates in 1:1 MeOD-D_2O *vs.* 1:1 MeOH-H_2O. d) The values in parentheses are for the higher concentrations of substrate; [substrate] = 3.7×10^{-3} M.

The samples were irradiated with a 500 W tungsten-bromine lamp operated at 40 V in a merry-go-round apparatus. Rates of photooxidation of **1** were followed by monitoring the decrease in the absorption maximum at 280 nm with a Nihon Bunko UV-1 spectrometer.

Measurement of Photooxidation Rates in MeOD-D_2O and in MeOH-H_2O. A comparison of photooxidation rates in 1:1 MeOD-D_2O and in 1:1 MeOH-H_2O was done in a merry-go-round apparatus under identical conditions. Rates of photooxidation were measured by the method described above.

Determination of Rate Constants. Rate constants for the reaction, k_r, and quenching, k_q, were measured by the direct disappearance method described by Foote and Ching[14] and by the competition technique. Solutions of various concentrations ($(0.3—3)\times10^{-4}$) of **1** containing RB (4×10^{-6} M) were irradiated. The concentrations of **1** before and after irradiation were determined from decrease in its absorption maximum. The relationship between the reciprocal of the amount of reacted **1** and the reciprocal of the initial concentration of **1** gives a straight line. From the slope and intercept, the sum, k_r+k_q, of reaction and quenching rate constants was obtained (within 10% error). Rate constants of the reactions were obtained from competition reactions. To a MeOH-H_2O solution of **1** containing RB was added a MeOH solution of diphenylisobenzofuran (DPBF), and the solution was irradiated as described above. Periodical change in concentration of **1** and DPBF was measured by decrease in the absorption maximum of **1** and in the fluorescence intensity of DPBF. Similar experiments were performed in order to determine in rate constant for **1** with $^1O_2$ generated from endoperoxide (EP). A solution of **1** (3.5 mM) and EP (25 mM) was warmed up to 35 °C with shaking. The rate constant was calculated from the disappearance of the peak area for **1** in high-performance liquid chromatography (HPLC, Waters, ALC/GPC 204, a Nucleosil $5C_{18}$ column, 90% aqueous methanol).

Quenching of Excited Singlet State of Dye. The fluorescence of dye was measured in the absence and presence of substrates **1**—**5** with a Nihon Bunko FP 550 at ambient temperature.

Results and Discussion

Participation of $^1O_2$ in the RB-sensitized photooxidation of **1**, **2**, **3**, **4**, and **5** was examined by the following experiments: (i) inhibition by azide ion, a well known singlet oxygen ($^1O_2$) quencher with a quenching rate constant of 10^8 M^{-1} s^{-1};[15] (ii) deuterium solvent effect on the rate of their photooxidations.[8]

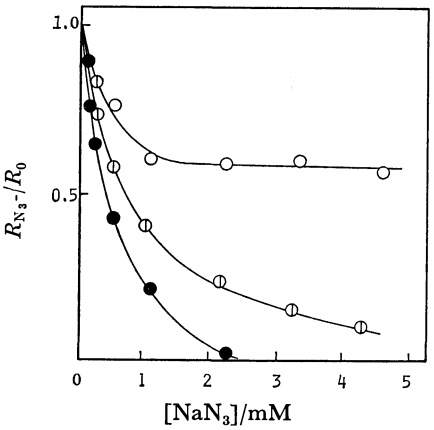

Fig. 1. Sodium azide inhibition of RB-(●), MB-(①), and thionine-(○) sensitized photooxidations of N_b-methoxycarbonyltryptamine (**5**) in methanol-water (1:1) at 25 °C as a function of sodium azide concentration.
[**5**] = 1.6×10^{-4} M; [sens] = 3.3×10^{-6} M.

Inhibition by Azide Ion. Reaction rate $R_{N_3^-}$ of RB-sensitized photooxidation of **5** in the presence of N_3^- was compared with that of control run, R_0. Ratio $R_{N_3^-}/R_0$ decreases with increasing concentration of N_3^- and the photooxidation was completely inhibited at concentration of 2.2 mM of N_3^-. In contrast, methylene blue (MB)- and thionine-sensitized photooxidations of **5** require much higher concentrations of N_3^- to exhibit the same extent of inhibition. In these cases, ratio $R_{N_3^-}/R_0$ decreases with increasing N_3^- concentration and reaches a constant value R_1 at higher concentrations of N_3^- (Fig. 1). By using this limiting value R_1, the extent I of contribution of $^1O_2$ process to overall reaction is calculated from the equation $I=(R_0-R_1)/R_0\times100$. Similar results have been obtained in the photooxidations of **1** and other indolic substrates **2**—**4** as summarized in Table 1. The data in Table 1 suggest that RB-sensitized photooxidations of

Table 2. Quenching of the fluorescence of dye sensitizers with tryptophan and tryptamine derivatives[a)]

Substrate	$k_q^s\tau/M^{-1}$ ($k_q^s/10^{-9}$ M^{-1} s^{-1})		
	Rose Bengal	Methylene Blue	Eosine
Tryptophan (**1**)	10.5 (16)	22	19 (0.59)
Tryptophan methyl ester (**2**)	7.5 (11)	19	21 (0.65)
N_b-Acetyltryptophan methyl ester (**3**)	15 (23)	23	24 (0.75)
Tryptamine (**4**)	13 (20)	32	23 (0.71)
N_b-Methoxycarbonyl-tryptamine (**5**)	10 (15)	13	25.5 (0.79)

a) Opitical density of dye sensitizer is adjusted to 0.1 at the excitation wavelength.

1—**5** proceed exclusively *via* the $^1O_2$ (Type II) mechanism, whereas the lack of complete inhibition by N_3^- in MB- and thionine-sensitized photooxidations indicated a significant contribution of Type I process and/or the quenching of the sensitizer triplets by N_3^-.

Azide ion is known to quench not only $^1O_2$ but also triplet states of certain dye sensitizers. Quenching rate constants $k_q(N_3^-)$ for sensitizer triplets have been determined previously, *e.g.*, $k_q(N_3^-)=5\times10^5$ M^{-1} s^{-1} for MB[16)] and $k_q(N_3^-)=8\times10^5$ M^{-1} s^{-1} for eosine.[16)] These rate constants are much smaller than those for quenching of the triplet states of MB and eosine by oxygen, $k_q(O_2)=3\times10^9$ M^{-1} s^{-1} and $k_q(O_2)=1.1\times10^9$ M^{-1} s^{-1},[17)] respectively. Therefore, the interaction between triplet sensitizers and N_3^- may be negligibly small in MB- and eosine-sensitized photooxidations. On the other hand, sensitizer triplets can interact with substrates to result in hydrogen abstraction or electron transfer (D-R mechanism).[18)] In fact, Trp is known to quench triplet states of sensitizers with the following rate constants: $k_q^t=2\times10^9$ M^{-1} s^{-1} for MB,[8)] $k_q^t=8.4\times10^8$ M^{-1} s^{-1} for eosine,[5)] and $k_q^t=3.9\times10^9$ M^{-1} s^{-1} for thionine.[5)] These rate constants are comparable to the rates of quenching of the respective sensitizer triplets by oxygen. Thus, it seems probable that MB-, eosine-, and thionine-sensitized photooxidations may involve Type I process in which sensitizer triplets react directly with indolic substrates. The inhibitory effect of N_3^- (Table 1) and the deuterium solvent effect on the rate of photooxidation (*vide infra*) indicate that in MB- or eosine-sensitized photooxidation direct reaction of triplet sensitizer with Trp is a minor process with the major process being $^1O_2$ reaction. In thionine-sensitized photooxidation, however, Type I reaction involving the thionine triplet cannot be neglected as judged from the inhibitory effect of N_3^- as shown in Table 1.

In order to get information on the interaction between singlet dye sensitizers and indolic substrates, quenching of the fluorescence of sensitizers by **1**—**5** was examined in MeOH–H_2O. The value $k_q^s\tau$, which is obtained from the slope of Stern-Volmer plots, may be taken as a rough measure for the interaction between singlet state of sensitizer and substrate. From $k_q^s\tau$ values apparent rate constants for the quenching of singlet state of sensitizers were calculated from the known lifetimes of singlet of sensitizers, $\tau=3.2\times10^{-9}$ s for eosine[19)] and $\tau=6.5\times10^{-10}$ s for RB.[19)] As shown in Table 2, the apparent rate constants are close to a diffusion controlled limit. This result may imply that the interaction between the excited singlet state of sensitizer and substrate becomes more important when higher concentrations of substrate and/or sensitizer are used, as pointed out by Davidson and Trethewey.[6)]

Deuterium Solvent Effect on the Rate of Photooxidation. The lifetime of $^1O_2$ is known to be approximately 10 times as long in MeOD–D_2O as in MeOH–H_2O.[8)] Therefore, about tenfold increase in the rate of photooxidation might be expected for a pure $^1O_2$ reaction in going from protonated to deuterated solvent.[20)] However, this increase would be smaller if Type I mechanism becomes predominant or if the acceptor concentration is high enough to quench $^1O_2$ significantly. The results are shown in Table 1. The rates of RB-sensitized photooxidation of Trp and its derivatives **2** and **3** increase approximately tenfold at lower concentrations of substrates in going from MeOH–H_2O to MeOD–D_2O. The R_D/R_H value for the photooxidation of **4** was somewhat smaller than that expected from the inhibitory effect by N_3^- (Table 1), the reason remaining unknown. However, as will be discussed below, a kinetic treatment indicates that the photooxidation of **4** occurs exclusively *via* the $^1O_2$ mechanism. The deuterium solvent effect together with inhibition experiments clearly demonstrates that RB-sensitized photooxidations of **1**—**5** proceed by the $^1O_2$ mechanism.

For the thionine-sensitized photooxidation, both Type I and $^1O_2$ (Type II) processes are operative under our experimental conditions. The ratio (I) of $^1O_2$ process to overall reaction as obtained from the inhibition experiment is consistent with the R_D/R_H value, suggesting that the lack of complete inhibition by N_3^- in thionine-sensitized photooxidation is mainly due to the contribution of Type I process. It seems probable that the thionine triplet tends to increase the ratio of a free radical process by reacting with indolic substrates directly.[21)] In every case, at higher concentrations of substrates R_D/R_H values become smaller, suggesting an increasing contribution of Type I process at higher substrate concentrations (Table 1).

Determination of Rate Constants. Kinetic scheme for the RB-sensitized photooxidation can be written as

$$^1O_2 + A \xrightarrow{k_r} AO_2,$$
$$^1O_2 + A \xrightarrow{k_q} A + O_2,$$
$$^1O_2 \xrightarrow{k_d} O_2,$$

Scheme 1.

where A denotes substrate. An application of the steady-state approximation to $^1O_2$ gives the following expression for the rate of disappearance of A:[14)]

$$\frac{d[A]}{dt} = K\left(\frac{k_r[A]}{(k_r+k_q)[A]+k_d}\right)$$

Table 3. Rate constants of tryptophan, tryptamine, and their derivatives with singlet oxygen in methanol-water

Substrate	$^1O_2$ Source	Rate constant/10^7 M^{-1} s^{-1}			Ref.
		k_r+k_q	k_r	k_q	
Tryptophan (**1**)	RB/*hν*/O_2	7.1	0.3	6.8	This work
	EP	2.1	0.5	1.6	This work
	MB/*hν*/O_2	4.4	0.4	4.0	Nilsson *et al.*[8]
	MB/*hν*/O_2	3.0			Smith[a),10]
	Flash photolysis technique	6.1			Rodgers *et al.*[b),24]
	Photophysical method	5.1	3.0	2.1	Matheson *et al.*[c),9]
Tryptophan methyl ester (**2**)	RB/*hν*/O_2	3.9	0.4	3.5	This work
N_b-Acetyltryptophan methyl ester (**3**)	RB/*hν*/O_2	6.3	0.4	5.9	This work
	EP	2.4	0.6	1.8	This work
Tryptamine (**4**)	RB/*hν*/O_2	5.5	0.9	4.6	This work
N_b-Methoxycarbonyl-tryptamine (**5**)	RB/*hν*/O_2	3.2	0.7	2.5	This work
	EP	3.2	1.3	1.9	This work

a) 1:1 MeOH-H_2O. b) In D_2O. c) In D_2O (pD 8.4).

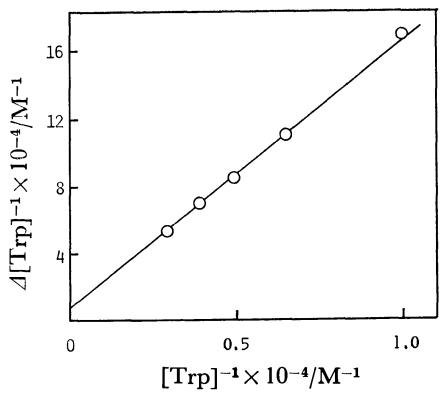

Fig. 2. Double reciprocal plot of tryptophan disappearance *vs.* tryptophan concentrations for the RB-sensitized photooxidation of tryptophan in methanol–water (1:1).
[sens]$=4\times10^{-6}$ M; [**1**]$=0.3$—3×10^{-4} M.

$$\Delta[A]^{-1} = (K\Delta t)^{-1}\left(\frac{k_r+k_q}{k_r}+\frac{k_d}{k_r}[A]^{-1}\right),$$

where K is the rate of $^1O_2$ formation. In fact, plots of $[Trp]^{-1}$ *vs.* $\Delta[Trp]^{-1}$ gave a linear relationship as shown in Fig. 2. For the RB-sensitized photooxidation of **4**, a straight line was also obtained, suggesting that only $^1O_2$ is participating in the reaction. From the slope and intercept, $k_d/(k_r+k_q)$ was obtained and the overall rate k_r+k_q was determined by using the literature k_d value[22] ($k_d=2.8\times10^5$ M^{-1} s^{-1}). In order to determine the absolute rate constants of k_r and k_q, a competition experiment between substrate and diphenylisobenzofuran (DPBF) was carried out. Disappearance rates of **1** and DPBF were determined from decrease in the absorption at 280 nm and in the fluoresence intensity at 477 nm, respectively. The kinetic equation for the competition reaction can be written as

$$\frac{k_r}{k_r^{DPBF}} = \frac{\log([A]_f/[A]_0)}{\log([DPBF]_f/[DPBF]_0)}.$$

The ratio k_r/k_r^{DPBF} obtained for **1** is 3.8×10^{-3}, and k_r was calculated to be 3×10^6 M^{-1} s^{-1} by using $k_r^{DPBF}=8\times10^8$ M^{-1} s^{-1} in 1:1 MeOH-H_2O.[8] The k_r value obtained is in fairly good agreement with that of Nilsson *et al.*[8] However, the rate constant k_r is approximately one order of magnitude smaller than that of Matheson and Lee,[9] although the quenching rate constants are comparable in both cases. The results together with the reported values are summarized in Table 3.

In view of the disagreement of our values with those obtained by Matheson and Lee,[9] we have performed a reaction with chemically generated $^1O_2$ from EP. It is noted that the thermolysis of EP results in nearly quantitative (>82%) production of $^1O_2$ at ambient

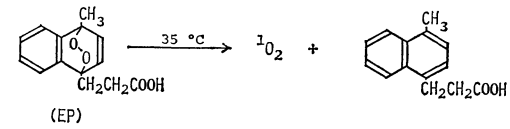

Scheme 2.

temperature.[13] The rate constant of reaction of **1** with chemically generated $^1O_2$ was in good agreement with the value obtained in the RB-sensitized photooxidation, whereas the quenching rate constant is somewhat larger than that obtained in the sensitized photooxidation (Table 3). A similar tendency was observed for **3** and **5**. The reason for this discrepancy is not clear. However, it is possible that the difference is due to difficulties in separating Type I and II processes kinetically. Thus substrates **1**—**5** quench $^1O_2$ with a somewhat higher rate than they react, as pointed out by Nilsson *et al.*[8] However, Matheson and Lee[9] reported a contradictory result, *i.e.*, that the main part of the interaction of $^1O_2$ with **1** is a chemical reaction.

Product Distribution. The dye-sensitized photooxidation of **1** is known to give (*N*-FK) and 3a-hydroxypyrrolidinoindole (HPI) *via* 3a-hydroperoxypyrro-

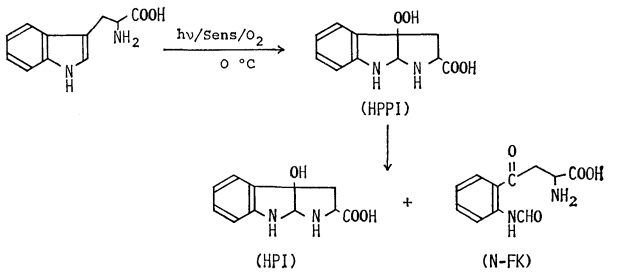

Scheme 3.

lidinoindole (HPPI)[4] (Scheme 3). The products of the reaction of chemically generated $^1O_2$ were compared with those for RB- and thionine-sensitized photooxidations. As already mentioned, the reaction mechanism is highly dependent on the type of sensitizer. The oxidation of **1** with RB proceeds exclusively by the $^1O_2$ mechanism, while with thionine it proceeds by a combination of $^1O_2$ and Type I mechanisms. Product ratio *N*-FK/HPI for the RB-sensitized photooxidation using a filter solution (aqueous $CaCl_2$–$CuCl_2$ solution, cutoff <550 nm) is the same as that obtained from the pure $^1O_2$ reaction (Table 4). However, when the photooxidation was carried out without filter, the yield of HPI decreased drastically. Savige[3] has reported that the photooxidation of **1** in water at 15—20 °C gives *N*-FK and HPI as the main product, while at temperatures above 20 °C it gives *N*-FK in improved yield but HPI in less yield, and that HPI is subjected to further photooxidation in the presence of MB. In fact, during the MB-sensitized photooxidation or direct irradiation (>290 nm) of HPI, at least 9 products were detected. Therefore, the low yield of HPI without filter solution may be due to its further photodecomposition by the action of shorter-wavelength light. Furthermore, the low yield of HPI in the thionine-sensitized photooxidation may be due to the co-occurrence of a free radical process (Type I mechanism). A similar result has been reported by Singh *et al.*,[23] who showed that product ratios *N*-FK/HPI in Sensitox II-sensitized photooxidation and in photophysically generated $^1O_2$ reaction are quite different from each other.

Although a number of interesting findings such as the formation of a tricyclic hydroperoxide like HPPI have been reported for the dye-sensitized photooxidation of indolic substrates including **1**,[1,4] the mechanism of the photooxidation has not yet be fully understood. The results described here demonstrate that the mechanisms of photooxidations of Trp, tryptamine, and their derivatives are strongly dependent on the type of sensitizers. The oxidation with RB sensitizer proceeds exclusively *via* the singlet oxygen process. However, if higher concentrations of substrates ($>10^{-3}$ M) were used, Type I process would become important. The oxidation with thionine sensitizer proceeds *via* a combination of Type I and II mechanisms even at lower concentrations of substrates. The rate constants of the reaction of $^1O_2$ with indolic substrates are somewhat smaller than those for the quenching reaction, indicating that the major part of the interaction of $^1O_2$ with Trp is the quenching process at least in aqueous methanol.

Table 4. Oxidation products of tryptophan under various conditions[a]

Reaction system	Experimental conditions	Product yield/%[b]	
		N-FK	HPI
EP	35 °C	23	42
Rose Bengal/O_2	>300 nm	30	1
	>550 nm[c]	23	44
Thionine/O_2	>300 nm	29	1
	>550 nm[c]	22	23

a) In 1:1 MeOH–H_2O. b) The yields were determined by HPLC analyses. c) Aqueous $CaCl_2$–$CuCl_2$ solution was used as a filter.

No variation in functional groups on side chains of Trp derivatives gives any significant effect on the rate of reaction with $^1O_2$ and on the extent of contribution of the $^1O_2$ mechanism under a given set of conditions. The product composition in the Rose Bengal-sensitized photooxidation of Trp under carefully controlled conditions is the same as that obtained in the reaction using chemically generated $^1O_2$. The present results suggest that the dye-sensitized photooxidation of tryptophan residues in a protein may porceed *via* a similar mechanism, and that the rate constant for the reaction of tryptophan residues with $^1O_2$ is of the same order of magnitude as that obtained for the present model compounds **1**—**5**.

References

1) J. D. Spikes and M. L. Macknight, *Ann. N.Y. Acad. Sci.*, **171**, 149 (1970); I. Saito, T. Matsuura, M. Nakagawa, and T. Hino, *Acc. Chem. Res.*, **10**, 346 (1977); M. Nakagawa, H. Watanabe, S. Kodato, H. Okajima, T. Hino, J. L. Flippen, and B. Witkop, *Proc. Natl. Acad. Sci., U.S.A.*, **74**, 4730 (1977); A. Fontana and C. Toniolo, *Prog. Chem. Org. Nat. Prod.*, **33**, 309 (1976) and references therein.

2) For example, R. S. Asquith and D. R. Rivett, *Biochim. Biophys. Acta*, **252**, 111 (1971); Z. Yoshida and M. Kato, *J. Am. Chem. Soc.*, **76**, 311 (1954).

3) W. E. Savige, *Int. Wool Text. Res. Conf., Vol. II*, **1975**, 570.

4) M. Nakagawa, S. Kato, S. Kataoka, and T. Hino, *J. Am. Chem. Soc.*, **101**, 3136 (1976).

5) I. Kralijic and I. Lindquist, *Photochem. Photobiol.*, **20**, 351 (1974).

6) R. S. Davidson and K. R. Trethewey, *J. Am. Chem. Soc.*, **98**, 4008 (1976).

7) K. Gollnick, *Adv. Photochem.*, **6**, 1 (1968).

8) R. Nilsson, P. B. Merkel, and D. R. Kearns, *Photochem. Photobiol.*, **16**, 117 (1972).

9) I. B. C. Matheson and J. Lee, *Photochem. Photobiol.*, **29**, 878 (1979).

10) G. J. Smith, *J. Chem. Soc., Faraday Trans. 2*, **74**, 1350 (1978).

11) C. Sconfienza, A. Van de Vorst, and G. Jori, *Photochem. Photobiol.*, **31**, 351 (1980).

12) E. Rossi, A. Van de Vorst, and G. Jori, *Photochem. Photobiol.*, **34**, 447 (1981).

13) I. Saito, T. Matsuura, and K. Inoue, *J. Am. Chem. Soc.*, **103**, 188 (1981).

14) C. S. Foote and T.-Y. Ching, *J. Am. Chem. Soc.*,

97, 6209 (1975).
15) N. Hasty, P. B. Merkel, P. Radlick, and D. R. Kearns, *Tetrahedron Lett.*, **1972**, 49.
16) R. Nilsson, P. B. Merkel, and D. R. Kearns, *Photochem. Photobiol.*, **16**, 109 (1972).
17) V. Kasche, *Photochem. Photobiol.*, **6**, 643 (1967).
18) Y. Usui and H. Koizumi, *Bull. Chem. Soc. Jpn.*, **40**, 440 (1967).
19) G. R. Fleming, A. W. E. Knight, J. M. Morris, R. J. S. Morrison, and G. W. Robinson, *J. Am. Chem. Soc.*, **99**, 4306 (1977).
20) P. R. Ogilby and C. S. Foote, *J. Am. Chem. Soc.*, **103**, 1219 (1981).
21) A. G. Kepka and L. I. Grossweiner, *Photochem. Photobiol.*, **16**, 305 (1972).
22) P. B. Merkel and D. R. Kearns, *J. Am. Chem. Soc.*, **94**, 7244 (1972).
23) A. Singh, M. J. Bell, G. W. Koroll, W. Kremers, and H. Singh, *Intl. Conf. on Oxygen and Oxy-radicals in Chem. and Biol., Austin*, 461 (1980).
24) B. A. Lindig and M. A. J. Rodgers, *Photochem. Photobiol.*, **33**, 627 (1981).

A New and Convenient Synthetic Method for Cyclopropyl Phenyl Sulfides

Kazuhiko TANAKA,* Hideki UNEME, Shuichi MATSUI, and Aritsune KAJI
Department of Chemistry, Faculty of Science, Kyoto University, Sakyo-ku, Kyoto 606
(Received January 20, 1982)

The reactions of a variety of 1,3-bis(phenylthio)propanes with butyllithium have been shown to produce cyclopropyl phenyl sulfides in good to high yields. A new and convenient *in situ* preparation of 1-lithiocyclopropyl phenyl sulfide can be readily carried out by treating 1,3-bis(phenylthio)propane with 2 equiv. of butyllithium at 0 °C in THF. The reaction with electrophiles proceeds in good yield. *O*-Aryl and *O*-alkyl *S*-cyclopropyl dithiocarbonates also can be prepared in good yields. 1,2-Bis(phenylthio)ethane was converted to phenyl vinyl sulfide on treatment with butyllithium, while 1,4-bis(phenylthio)butane was recovered unchanged by a similar treatment.

In 1973 Trost has reported that 1-lithiocyclopropyl phenyl sulfide, prepared by deprotonation of cyclopropyl phenyl sulfide is a useful reagent in the preparation of cyclobutanones and cyclobutenes.[1,2] Later, Miller and Cohen showed the transformations of 1-lithiocyclopropyl phenyl sulfide into useful synthetic intermediates such as γ-keto sulfides,[3] vinyl sulfides,[4] and 1-methoxycyclopropyl phenyl sulfide.[5] Cyclopropyl phenyl sulfide can be prepared by cyclization of 3-chloropropyl phenyl sulfide in liquid ammonia.[1a,6] Recently, Cohen has found the efficient method for conversion of 1,1,3-tris(phenylthio)propane into 1,1-bis(phenylthio)cyclopropane, which upon reductive lithiation with lithium naphthalenide affords lithiocyclopropane.[7a] In 1980 we reported preliminary results of one-step synthetic method for 1-lithiocyclopropyl phenyl sulfide utilizing readily available 1,3-bis(phenylthio)propane as the starting material.[8]

In this paper we investigated the scope and limitations of the new cyclization reaction as a viable route to various types of cyclopropyl phenyl sulfides.

Results and Discussion

Synthesis of Cyclopropyl Phenyl Sulfides. When 1 equiv. of butyllithium was added to THF solution of 1,3-bis(phenylthio)propane (**1**),[8,9] cyclopropyl phenyl sulfide (**2**)[1a] was obtained in 77% yield after quenching with aqueous ammonium chloride solution. The use of butyllithium in THF at −78 °C—0 °C for 3 h was found to be a convenient method for the synthesis of **2**. Additives such as hexamethylphosphoric triamide (HMPA) or *N,N,N′,N′*-tetramethylethylenediamine (TMEDA) were found to have a negligible effect on yield of **2**. The possibility that various types of substituted 1,3-bis(phenylthio)propanes may be converted to the corresponding cyclopropanes by this method was further investigated. A variety of the alkyl-substituted 1,3-bis(phenylthio)propanes used in this study were prepared by the reported procedures.[1a,10–13] The cyclization of sulfides was efficiently carried out in addition of 1 equiv. of butyllithium at −78 °C—0 °C in THF in the presence of HMPA. Results are summarized in Table 1. The structures and stereochemistry of the substituted cyclopropyl phenyl sulfides

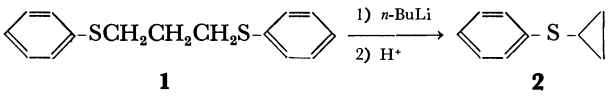

1 **2**

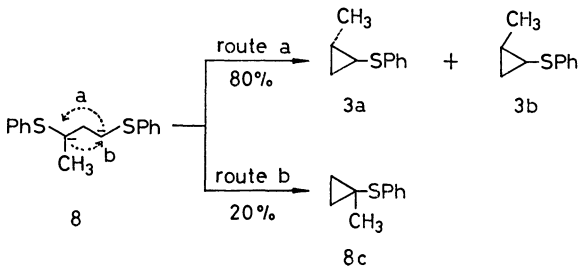

8 **3a** **3b** **8c**

Scheme 1.

were accomplished through the utilization of comparative spectroscopic data,[1] GLPC analyses, and authentic sample prepared from 1-lithiocyclopropyl phenyl sulfide. For example, GLPC analysis of cyclopropanes derived from sufide **3** showed a 9:1 mixture of **3a** and **3b** which was confirmed by comparison with the reported data.[1a] 1,3-Bis(phenylthio)butane (**8**) afforded three peaks, A, B, and C, in the ratio of 3:5:2. Peak A (retention time of 3.4 min) was shown to be 1-methylcyclopropyl phenyl sulfide (**8c**) by GLPC comparison with the authentic sample prepared from 1-lithiocyclopropyl phenyl sulfide and iodomethane.[1a,7c] Peak B (retention time of 4.3 min) and peak C (retention time of 5.7 min) were identified as trans-isomer (**3a**) and cis-isomer (**3b**) of 2-methylcyclopropyl phenyl sulfide by comparing the result from the reaction of sulfide **3**. These results clearly reflect the difference in acidity between C-1 hydrogen and C-3 hydrogen of sulfide **8** (Scheme 1).

Reaction of 2-methoxy-1,3-bis(phenylthio)propane (**12**) with 1 equiv. of butyllithium in THF gave only the elimination product **13**;[14] no cyclopropane could

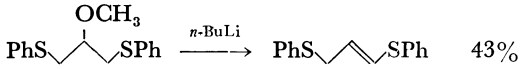

12 **13**

be detected. An interesting change was observed with 2-hydroxy analogue **14**. Thus, reaction of 1,3-bis(phenylthio)-2-propanol (**14**) with 2 equiv. of butyllithium gave cyclopropanol **16** in good yield, most probably through a dianion intermediate **15**. The protection of OH group was readily carried out by adding 1-chloromethoxy-2-methoxyethane[15] or chlorotrimethylsilane into the reaction mixture (Scheme 2).

The mechanism of this facile ring closure has not been studied in detail, but it may be pictured in terms of an initial formation of the sulfur-stabilized carbanion

Table 1. Preparation of cyclopropyl sulfides from 1,3-bis(phenylthio)propanes

1,3-Bis(phenylthio)propanes	Products	Ratio	Yield/%
$PhSCH_2CH(CH_3)CH_2SPh$ (3)	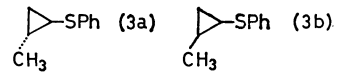 (3a) (3b)	9:1[a]	88
$PhSCH_2CH[(CH_2)_3CH_3]CH_2SPh$ (4)	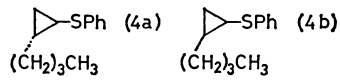 (4a) (4b)	4:1[a]	79
$PhSCH_2CH[(CH_2)_9CH_3]CH_2SPh$ (5)	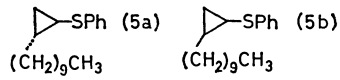 (5a) (5b)	7:1[a]	74
$PhSCH_2CH(C_6H_{11})CH_2SPh$ (6)	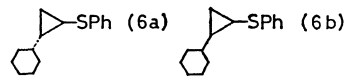 (6a) (6b)	>19:<1[a]	76
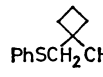 (7)	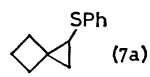 (7a)		61
$PhSCH_2CH_2CH(CH_3)SPh$ (8)	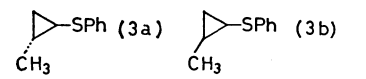 (3a) (3b) (8c)	5:2:3[b]	65
$PhSCH_2CH_2CH[(CH_2)_2CH_3]SPh$ (9)	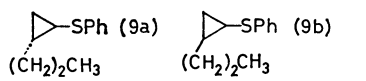 (9a) (9b) (9c)	2:4:5[b]	73
$PhSCH_2CH_2CH(CH_2CH_3)SPh$ (10)	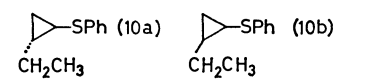 (10a) (10b) (10c)	2:2:1[b]	74
$PhSCH_2CH_2CH[(CH_2)_5CH_3]SPh$ (11)	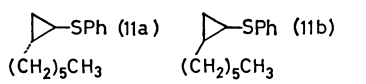 (11a) (11b) (11c)	1:2:2[b]	73

a) The trans/cis ratios of cyclopropyl sulfides were determined by ^{1}H-NMR and GLPC analyses. b) GLPC analyses showed three peaks. The first peak was presumed to be 1-alkylcyclopropyl phenyl sulfide by comparison of the data obtained from ^{1}H-NMR and GLPC.

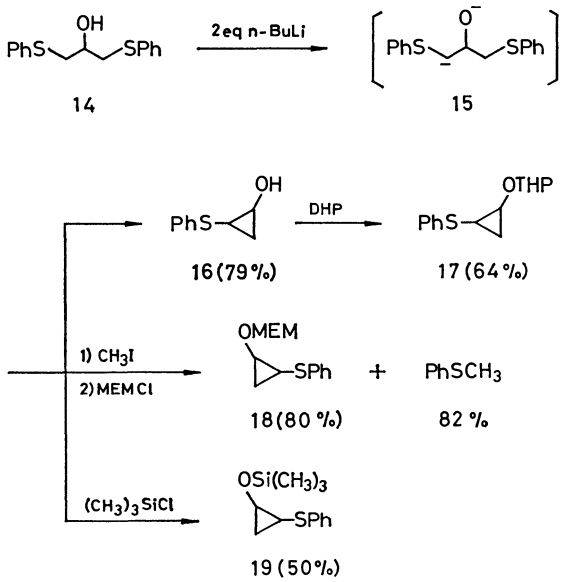

Scheme 2.

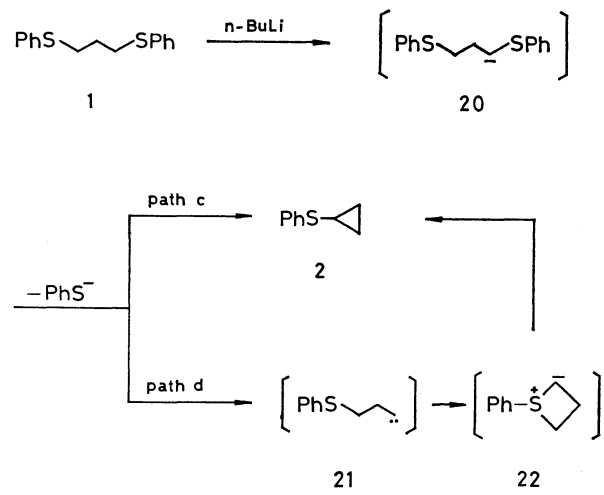

Scheme 3.

20 followed by an intramolecular nucleophilic displacement of benzenethiolate anion (path c, Scheme 3).[7e] Recently, Cohen proposed a similar cyclization in the reaction of 1,1,3-tris(phenylthio)propane with methyllithium in the presence of TMEDA in THF.[7a] An alternative mechanism to that proposed would involve a carbene intermediate **21** which rearranges to a ylide **22** to give **2** (path d).[16] This pathway (d) is considered unlikely, however, since the reaction of 1,3-bis(phenylthio)propane (**1**) with butyllithium in the presence of excess of cyclohexane gave none of the addition product derived from the carbene **21**. Cyclopropyl phenyl sulfide (**2**) was formed as the only isolable product (59%).

In investigating the scope and limitations of this

Table 2. Preparation of *S*-(3-chloropropyl) and *S*-cyclopropyl thiocarbonates

ROH (**34**)	CXS	Yield of **35**/%	Product **36**	Yield of **36**/%
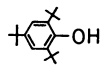	CS_2	75 (**35a**)	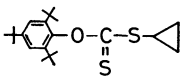	(**36a**) 77
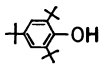	COS	85 (**35b**)	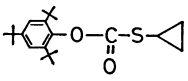	(**36b**) 94
	CS_2	80 (**35c**)	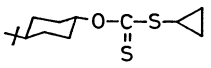	(**36c**) 86
	CS_2	76 (**35d**)	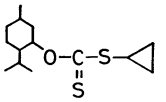	(**36d**) 80[a]
	CS_2	66 (**35e**)	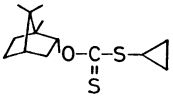	(**36e**) 82[b]

a) $[\alpha]_D^{25}$ −59.4° (*c* 1.47, $CHCl_3$). b) $[\alpha]_D^{23}$ −17.6° (*c* 1.61, $CHCl_3$).

new cyclization, it was found that when the sulfides contain *p*-methyl or *p*-chloro substituent on benzene ring, the yields of cyclopropanes were decreased under the same reaction conditions cited above, possibly due to insolubility of these sulfides **23** and **25** in THF at a lower temperature. The use of 1.5—2.5 equiv. of HMPA as a co-solvent gave satisfactory results.

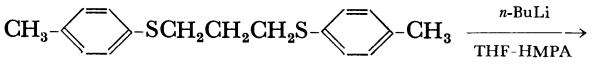

23

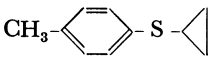

50%

24 (20% without HMPA)

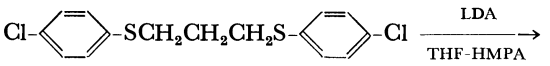

25

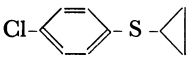

34%

26 (trace without HMPA)

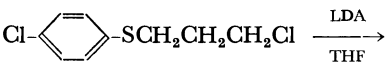

27

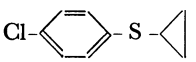

46%

26

Attempts to cyclize the sulfides **28**—**30** using lithium diisopropylamide (LDA) or butyllithium in the presence of HMPA, however, were not successful due to the decomposition of sulfides under these reaction conditions.

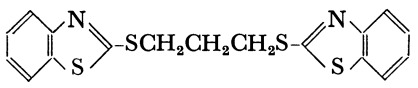

28

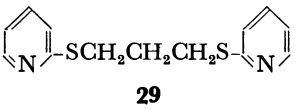

29

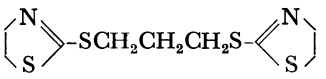

30

We briefly investigated the reaction of 1,2-bis(phenylthio)ethane (**31**)[17] or 1,4-bis(phenylthio)butane (**32**) with butyllithium in THF. Treatment of **31** in a mixture solvent of THF and HMPA afforded phenyl vinyl sulfide (**33**)[18] in 52% yield. However, the similar

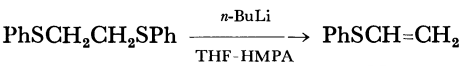

31 **33**

reaction of **31** in THF gave little of **33**; the Michael type addition of butyllithium to **33** took place. Treatment of **32** with butyllithium under various reaction conditions led to the recovery of the starting material **32**.

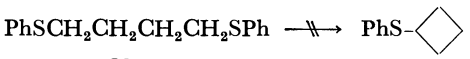

32

Next, we have developed a new method for the preparation of *S*-cyclopropyl thiocarbonate and dithiocarbonates. As outlined in Scheme 4, *S*-(3-chloropropyl) dithiocarbonates **35** were prepared from the corresponding alcohols and phenols **34**.[6,19] Treatment

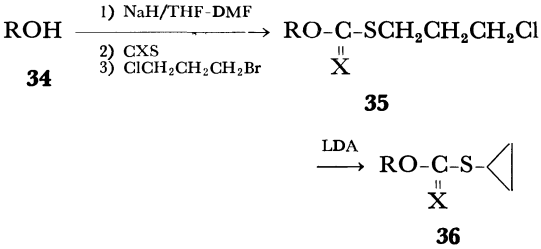

Scheme 4.

Table 3. Reactions of 1,3-bis(phenylthio)propane (**1**) and electrophiles in the presence of butyllithium

Electrophile[a]	Additive	Product (**38**)		Yield/%
4-Heptanone	—	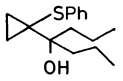	(**38a**)	71
Benzaldehyde	—	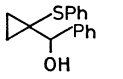	(**38b**)	67
Cyclohexanone	—	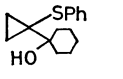	(**38c**)	60
Acetone	—	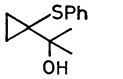	(**38d**)	34
3-Pentanone	—	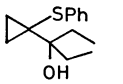	(**38e**)	69
3-Pentanone	CuI (10 mmol)	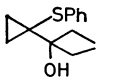	(**38e**)	85
Heptanal	CuI (10 mmol)	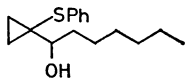	(**38f**)	59
2-Hexanone	CuI (10 mmol)	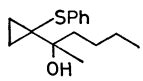	(**38g**)	65
D_2O	—	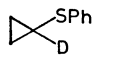	(**38h**)	65
CO_2	—	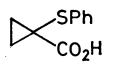	(**38i**)	55

a) The reaction was carried out by using 1,3-bis(phenylthio)propane (**1**) (10 mmol) and butyllithium (22 mmol) in THF.

of **35** in THF with 1.1 equiv. of LDA resulted in smooth cyclization to give *S*-cyclopropyl derivatives **36** in good to high yields as summarized in Table 2. The optically active *S*-cyclopropyl dithiocarbonates **36d** and **36e** could also be obtained by this procedure.

Direct Generation of 1-Lithiocyclopropyl Phenyl Sulfide. The finding that cyclopropyl phenyl sulfide (**2**) was formed on treatment of 1,3-bis(phenylthio)propane (**1**) with 1 equiv. of butyllithium suggested that it might be possible to trap 1-lithiocyclopropyl phenyl sulfide (**37**) with electrophiles in the reaction of **1** with 2 equiv. of butyllithium. Thus, treatment of sulfide **1** with 2 equiv. of butyllithium at 0 °C in THF gave a pale yellow solution of lithium reagent **37** after 3 h. Addition of 1 equiv. of 4-heptanone at −78 °C and allowing the reaction mixture to warm to room temperature resulted in the formation of the adduct **38a** in 51% yield. The yield of adduct was increased when 0.5 equiv. of 4-heptanone was added to the reaction mixture (71% yield). Results of one-pot reaction with a variety of electrophiles are summarized in Table 3. It was found that yields were improved when CuI was added to the reaction mixture to scavenge the thiolate anion as a copper(I) thiolate.

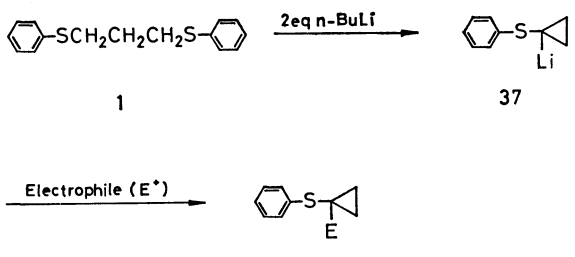

Experimental

General. All reactions involving organometallic species were run in flame-dried glasswares under an atmosphere of nitrogen or argon. ^{1}H-NMR spectra were determined in the indicated solvent on a JEOL Model PS-100 or a Hitachi Model R-24B spectrometer. Chemical shifts are expressed in parts per million downfield from internal tetramethylsilane. Infrared spectra were recorded on a Hitachi Model 215 spectrophotometer. GLPC analyses were performed on a Varian Aerograph Model 920 gas chromatograph using a 0.15 cm × 120 cm glass column (20% Silicone DC-550 on Celite 545). Mass spectra were recorded on a Hitachi Model M-52 mass spectrometer. Silica-gel columns for chromatography utilized Wakogel-200. Optical rotations were measured in 1-dm path length cell of 10 ml capacity using a JASCO Model DIP-181 polarimeter. Boiling points and melting points are uncorrected. All solvents and reagents were used as purchased unless otherwise specified. Aldehydes and ketones were purified by distillation. Tetrahydrofuran (THF) was dried by distillation from calcium hydride and subsequent distillation from lithium aluminium hydride under a nitrogen atmosphere, or distilled from sodium benzophenone ketyl under a nitrogen atmosphere. Diisopropylamine and *N,N,N',N'*-tetramethylethylenediamine were distilled from calcium hydride and stored over 4 Å molecular sieves. Hexamethylphosphoric triamide (HMPA) was distilled at 0.2—0.3 mmHg (1 mmHg ≈ 133.322 Pa) from calcium hydride and stored over 13 Å molecular sieves. Hexane and *N,N*-dimethyformamide were distilled from calcium hydride and stored over 4 Å molecular sieves. Elemental analyses were performed by the Microanalytical Laboratory, operated by the Institute for Chemical Research, Kyoto University.

1,3-Bis(phenylthio)propane (1). According to the method[8] previously described, sulfide **1** was prepared in 93% yield: bp 160—161 °C/0.2—0.3 mmHg; ^{1}H-NMR (CCl_4) δ 7.10 (m, 10H, C_6H_5S), 2.90 (t, J=7.5 Hz, 4H, CH_2S), 1.84 (q, J=7.5 Hz, 2H, CH_2).

Cyclopropyl Phenyl Sulfide (2). To a stirred solution of 2.60 g (10 mmol) of 1,3-bis(phenylthio)propane (**1**) in 20 ml of THF at −78 °C was added butyllithium (7.7 ml of a 1.5 M (1 M = 1 mol dm^{-3}) solution in hexane, 12 mmol). After it was stirred for 5 min, the cold bath was removed and the reaction mixture was stirred for 3 h in the ice bath. The reaction was quenched with saturated ammonium chloride solution (10 ml) and extracted four times with ether. The ether layers were combined, dried over anhydrous sodium sulfate, and evaporated to give a mixture of **2** and benzenethiol. Distillation under reduced pressure gave pure cyclopropyl phenyl sulfide (**2**):[1a,6] 1.15 g (77%); bp 89—90 °C/4.7 mmHg; IR (thin film) 3080, 3020, 1580, 1480, 1440, 1095, 1025 cm^{-1}; ^{1}H-NMR (CCl_4) δ 6.90—7.40 (m,

5H, SC_6H_5), 1.90—2.20 (m, 1H, CH), 0.80—1.00 (m, 2H), 0.50—0.80 (m, 2H). Found: C, 71.90; H, 6.83%. Calcd for $C_9H_{10}S$: C, 71.95; H, 6.71%. MS (20 eV) *m/e* 150 (M^+, 100).

Preparation of 1-(Phenylthio)-2-[(phenylthio)methyl]hexane (4): Diethyl 1,1-pentanedicarboxylate was prepared from diethyl malonate according to the literature.[10] Reduction of diethyl 1,1-pentanedicarboxylate (43.2 g, 0.2 mol) with lithium aluminium hydride (14.5 g, 0.38 mol) in dry ether under reflux gave 20.5 g (78%) of 2-(hydroxymethyl)-1-hexanol: bp 140—141 °C/18 mmHg. 1-Chloro-2-(chloromethyl)hexane was prepared from 2-(hydroxymethyl)-1-hexanol in 85% yield by the method of Trost:[1a] ^{1}H-NMR (CCl_4) δ 3.60 (m, 4H), 2.00 (m, 1H), 1.40 (m, 6H), 0.92 (m, 3H). To a stirred and cooled (ice-bath) solution prepared from Na (4.6 g, 0.2 mol) and methanol (150 ml) was added dropwise 22.1 g (0.2 mol) of benzenethiol. A solution of 12 g (0.07 mol) of 1-chloro-2-(chloromethyl)hexane in 10 ml of methanol was added dropwise. After being stirred at 0—5 °C for 1 h, the mixture was stirred at room temperature for 1 h, and then refluxed for 6 h. After evaporation of the solvent, the residue was diluted with ether, dried over anhydrous sodium sulfate, and concentrated. Distillation under reduced pressure gave 17.5 g (79%) of 1-(phenylthio)-2-[(phenylthio)methyl]hexane (**4**): bp 185—186 °C/0.8 mmHg; ^{1}H-NMR (CCl_4) δ 7.15 (m, 10H), 2.90 (m, 4H), 1.82 (m, 1H), 0.7—1.7 (m, 9H).

1-(Phenylthio)-2-[(phenylthio)methyl]dodecane (5): ^{1}H-NMR (CCl_4) δ 7.15 (m, 10H), 2.95 (m, 4H), 1.85 (m, 1H), 0.80—1.60 (m, 21H).

2-Cyclohexyl-1,3-bis(phenylthio)propane (6): ^{1}H-NMR (CCl_4) δ 7.10 (m, 10H), 2.95 (m, 4H), 0.60—2.00 (m, 12H).

1,3-Bis(phenylthio)butane (8): To a stirred and cooled (ice-bath) solution of 2.13 g (0.0926 mol) of Na in 300 ml of ethanol was added benzenethiol (10.2 g, 92.6 mmol) in 30 ml of ethanol. After an additional 30 min at 0 °C, a catalytic amount of sodium iodide was added, the cold bath was removed and the reaction mixture was refluxed for 10 h. Usual workup and distillation under reduced pressure gave pure sulfide **8** (8.42 g, 66%): bp 165—170 °C/0.6 mmHg; ^{1}H-NMR (CCl_4) δ 7.15 (m, 10H, C_6H_5S), 3.30 (q, J=7.1 Hz, 1H, CH), 3.00 (t, J=7.1 Hz, CH_2S), 1.80 (m, 2H, CH_2), 1.25 (d, J=7.1 Hz, 3H, CH_3).

Preparation of 1-(Phenylthio)-3-pentanol: According to Corey's procedure,[13] to a solution of 22 mmol of 1,4-diazabicyclo[2.2.2]octane (purified by sublimation) and 22 mmol of methyl phenyl sulfide in 40 ml of THF at 0 °C was added over 7 min 24 mmol of butyllithium. After stirring was continued at room temperature for 45 min, 20 mmol of 1,2-epoxybutane in 2 ml of THF was added dropwise at 0 °C. The reaction mixture was stirred for 45 h at room temperature and quenched with 20 ml of aqueous ammonium chloride solution. Usual workup gave 1-(phenylthio)-3-pentanol in 86% yield: bp 140—142 °C/3 mmHg; IR (thin film) 3370 (OH), 3050, 1575, 1480, 1435, 1020 cm^{-1}. ^{1}H-NMR (CCl_4) δ 6.90—7.30 (m, 5H, C_6H_5S), 3.40—3.70 (m, 1H, CH), 2.80—3.10 (m, 2H, SCH_2), 2.50—2.80 (m, 1H, OH), 1.20—1.80 (m, 4H), 0.88 (t, J=7 Hz, 3H, CH_3); MS (20 eV) *m/e* 196 (M^+, 85), 86 (100). Found: C, 67.26; H, 8.38%. Calcd for $C_{11}H_{16}OS$: C, 67.30; H, 8.22%.

In a similar way, 1-(phenylthio)-3-nonanol was obtained in 76% yield as white crystals after recrystallization from hexane: mp 45.0—45.7 °C; ^{1}H-NMR (CCl_4) δ 7.00—7.40 (m, 5H, C_6H_5S), 3.50—3.80 (m, 1H, CH), 2.90—3.10 (m, 2H, SCH_2), 1.98 (s, 1H, OH), 1.60—1.90 (m, 2H, CH_2), 1.24 (m, 10H), 0.86 (t, 3H, CH_3); MS (20 eV) *m/e* 252 (M^+, 45), 72 (100). Found: C, 71.17; H, 9.88%. Calcd for $C_{15}H_{24}OS$: C, 71.38; H, 9.58%.

1,3-Bis(phenylthio)pentane (**10**) was prepared from 1-(phenylthio)-3-pentanol: bp 184—187 °C/1.6 mmHg; ^{1}H-NMR (CCl_4) δ 7.00—7.40 (m, 10H, C_6H_5S), 2.90—3.20 (m, 3H), 1.40—1.90 (m, 4H, CH_2), 0.96 (t, J=7 Hz, 3H, CH_3); MS (20 eV) *m/e* 288 (M^+, 98), 123 (100).

1,3-Bis(phenylthio)nonane (**11**) was prepared from 1-(phenylthio)-3-nonanol: oil; ^{1}H-NMR (CCl_4) δ 7.00—7.40 (m, 10H, C_6H_5S), 2.90—3.30 (m, 3H), 1.10—2.00 (m, 12H), 0.85 (t, J=7 Hz, 3H, CH_3). MS (20 eV) *m/e* 344 (M^+, 100).

Reaction of 2-Methyl-1,3-bis(phenylthio)propane (3): To a solution of 10 mmol of sulfide **3** and 25 mmol of HMPA in 20 ml of THF at −78 °C was added over 10 min 12 mmol of butyllithium, and stirring was continued for 10 min. The cooling bath was removed, and the reaction mixture was stirred at 0 °C for 3 h. After quenching with 10 ml of saturated ammonium chloride solution, the mixture was acidified with 10% hydrochloric acid (50 ml) and extracted three times with ether. The combined extracts were washed twice with brine, dried over anhydrous sodium sulfate, and concentrated. Distillation under reduced pressure gave a mixture of cyclopropyl sulfides **3a** and **3b** of 9:1 ratio in 88% yield: bp 71—72 °C/0.8 mmHg; ^{1}H-NMR (CCl_4) δ 7.00—7.70 (m, 5H, C_6H_5S), 2.10—2.40 (m, 0.1H, SCH), 1.80—2.00 (m, 0.9H, SCH), 1.20—1.30 (m, 3H, CH_3), 0.20—1.20 (m, 3H); IR (thin film) 3060, 2950, 1580, 1480, 1440, 1090, 1025 cm^{-1}; MS (20 eV) *m/e* 164 (M^+, 100). Found: C, 73.50; H, 7.58%. Calcd for $C_{10}H_{12}S$: C, 73.12; H, 7.37%.

Reaction of 1-(Phenylthio)-2-[(phenylthio)methyl]hexane (4): Reaction of 10 mmol of sulfide **4** with 12 mmol of butyllithium in 20 ml of THF containing 20 mmol of HMPA gave a mixture of cyclopropyl sulfides **4a** and **4b**: bp 112—114 °C/1.7 mmHg; ^{1}H-NMR (CCl_4) δ 6.80—7.30 (m, 5H, C_6H_5S), 2.00—2.30 (m, 0.2H, CHS), 1.70—1.90 (m, 0.8H, SCH), 0.20—1.70 (m, 12H); IR (thin film) 3080, 2925, 1580, 1480, 1440, 1095, 1030 cm^{-1}; MS (20 eV) trans-isomer **4a** *m/e* 206 (M^+, 77), 55 (100); cis-isomer **4b** *m/e* 206 (M^+, 69), 142 (100). Found: C, 75.42; H, 9.02%. Calcd for $C_{13}H_{18}S$: C, 75.73; H, 8.74%.

Reaction of 1-(Phenylthio)-2-[(phenylthio)methyl]dodecane (5): Reaction of 10 mmol of sulfide **5** with 12 mmol of butyllithium in 20 ml of THF containing 20 mmol of HMPA gave a mixture of cyclopropyl sulfides **5a** and **5b**: bp 171—173 °C/1.6 mmHg; ^{1}H-NMR (CCl_4) δ 6.90—7.30 (m, 5H, C_6H_5S), 2.10—2.40 (m, 0.13H, SCH), 1.70—1.90 (m, 0.87H, SCH), 0.60—1.60 (m, 24H); IR (thin film) 3060, 2920, 1580, 1475, 1435, 1090, 1020 cm^{-1}; MS (20 eV) trans-isomer **5a** *m/e* 290 (M^+, 82), 82 (100); cis-isomer **5b** *m/e* 290 (M^+, 63), 82 (100). Found: C, 78.63; H, 10.51%. Calcd for $C_{19}H_{30}S$: C, 78.62; H, 10.27%.

Reaction of 2-Cyclohexyl-1,3-bis(phenylthio)propane (6): Reaction of 10 mmol of sulfide **6** with 12 mmol of butyllithium in 20 ml of THF containing 20 mmol of HMPA gave a mixture of cyclopropyl sulfides **6a** and **6b**: bp 136—136.5 °C/1.1 mmHg; ^{1}H-NMR (CCl_4) δ 6.90—7.40 (m, 5H, C_6H_5S), 0.50—2.00 (m, 15H); IR (thin film) 3070, 2920, 1580, 1480, 1450, 1440, 1090, 1025 cm^{-1}; MS (20 eV) trans-isomer *m/e* 232 (M^+, 81), 136 (100). Found: C, 77.81; H, 8.69%. Calcd for $C_{15}H_{20}S$: C, 77.59; H, 8.62%.

Reaction of 1,1-Bis[(phenylthio)methyl]cyclobutane (7): Reaction of 9.8 mmol of sulfide **7** with 12 mmol of butyllithium in 20 ml of THF containing 20 mmol of HMPA gave a 61% of 1-(phenylthio)spiro[2.3]hexane (**7a**): bp 83—84 °C/0.3 mmHg; IR (thin film) 3060, 2970, 1480, 1435, 1090, 1025 cm^{-1}; ^{1}H-NMR (CCl_4) δ 6.80—7.40 (m, 5H), 1.80—

2.50 (m, 6H), 0.78—1.80 (m, 2H), 0.50—0.78 (t, J=6 Hz, 1H). MS (20 eV) m/e 190 (M^+, 100). Found: C, 75.88; H, 7.67%. Calcd for $C_{12}H_{14}S$: C, 75.79; H, 7.37%.

Reaction of 1,3-Bis(phenylthio)butane (8): Reaction of sulfide **8** with 12 mmol of butyllithium in 20 ml of THF gave a mixture of cyclopropyl sulfides **3a**, **3b**, and **8c** (5:4:1) in 21% yield. A similar reaction of 10 mmol of sulfide **8** with 12 mmol of butyllithium in 20 ml of THF containing 25 mmol of HMPA gave a mixture of sulfides **3a**, **3b**, and **8c** (5:2:3) in 65% yield: bp 72—75 °C/2.2 mmHg; ^{1}H-NMR (CCl_4) δ 7.00—7.50 (m, 5H, C_6H_5S), 0.20—2.40 (m, 7H); IR (thin film) 3100, 1590, 1485, 1445, 1105, 1030 cm^{-1}; MS (20 eV) 1-methylcyclopropyl phenyl sulfide (**8c**): m/e 164 (M^+, 27), 131 (100); trans-isomer **3a**: m/e 164 (M^+, 100); cis-isomer **3b**: m/e 164 (M^+, 94), 110 (100). Found: C, 73.43; H, 7.60%. Calcd for $C_{10}H_{12}S$: C, 73.12; H, 7.37%.

Reaction of 1,3-Bis(phenylthio)hexane (9): Reaction of 10 mmol of sulfide **9** with 12 mmol of butyllithium in 20 ml of THF containing 20 mmol of HMPA gave a mixture of cyclopropyl sulfides **9a**, **9b**, and **9c**: bp 96—102.5 °C/2.8 mmHg; ^{1}H-NMR (CCl_4) δ 6.90—7.30 (m, 5H, C_6H_5S), 0.20—2.40 (m, 11H); IR (thin film) 3060, 2950, 1580, 1475, 1435, 1090, 1020 cm^{-1}; MS (20 eV) 1-propylcyclopropyl phenyl sulfide (**9c**): MS (20 eV) m/e 192 (M^+, 63), 159 (100); 2-propylcyclopropyl phenyl sulfides (**9a** and **9b**) m/e 192 (M^+, 94), 149 (100). Found: C, 75.09; H, 8.42%. Calcd for $C_{12}H_{16}S$: C, 75.00; H, 8.33%.

Reaction of 1,3-Bis(phenylthio)pentane (10): Reaction of 10 mmol of sulfide **10** with 12 mmol of butyllithium in 20 ml of THF containing 25 mmol of HMPA gave a mixture of cyclopropyl sulfides **10a**, **10b**, and **10c** in 74% yield: bp 100—106 °C/3.9 mmHg; ^{1}H-NMR (CCl_4) δ 6.90—7.40 (m, 5H, C_6H_5S), 0.30—2.40 (m, 9H); IR (thin film) 3070, 2960, 1580, 1480, 1435, 1090, 1025 cm^{-1}. Found: C, 74.23; H, 7.93%. Calcd for $C_{11}H_{14}S$: C, 74.10; H, 7.91%.

Reaction of 1,3-Bis(phenylthio)nonane (11): Reaction of 10 mmol of sulfide **11** with 12 mmol of butyllithium in 20 ml of THF containing 25 mmol of HMPA gave a mixture of cyclopropyl sulfides, **11a**, **11b**, and **11c**: bp 123—127 °C/0.9 mmHg; ^{1}H-NMR (CCl_4) δ 6.90—7.40 (m, 5H, C_6H_5S), 0.30—2.40 (m, 17H); IR (thin film) 3060, 2920, 1580, 1470, 1435, 1090, 1020 cm^{-1}. Found: C, 77.10; H, 9.60%. Calcd for $C_{15}H_{22}S$: C, 76.86; H, 9.46%.

Preparation of 2-Methoxy-1,3-bis(phenylthio)propane (12): According to Corey's procedure,[14] sulfide **12** was prepared from 1,3-bis(phenylthio)-2-propanol (**14**) (*vide infra*) and iodomethane in 91% yield: bp 180—182 °C/0.7 mmHg; ^{1}H-NMR (CCl_4) δ 6.90—7.40 (m, 10H, C_6H_5S), 3.20—3.50 (m, 1H, CH), 3.24 (s, 3H, OCH_3), 3.60 (d, J=6 Hz, 4H, CH_2); MS (20 eV) m/e 290 (M^+, 39), 135 (100).

Reaction of Sulfide 12 with Butyllithium: Reaction of 10 mmol of sulfide **12** with 12 mmol of butyllithium in THF containing 25 mmol of HMPA gave a mixture of 1,3-bis(phenylthio)propene (**13**) and sulfide **12**. Silica gel chromatography after distillation gave 1.12 g (43%) of **13** and 1.03 g (35%) of the starting material **12**. 1,3-Bis(phenylthio)propene (**13**): bp 192—198 °C/3.2 mmHg; ^{1}H-NMR (CCl_4) δ 6.90—7.40 (m, 10H, C_6H_5S), 5.60—6.20 (m, 2H, CH=CH), 3.40—3.70 (m, 2H, CH_2); MS (20 eV) m/e 258 (M^+, 14), 149 (100). This compound had properties (NMR, MS, TLC) with those of an authentic sample prepared by tosylation of 1,3-bis(phenylthio)-2-propanol (**14**), followed by elimination with LDA in THF.

Preparation of 1,3-Bis(ohenylthio)-2-propanol (14): According to Corey's procedure,[14] to a solution of 0.6 mol of sodium benzenethiolate in methanol was added 0.3 mol (27.8 g) of 1-chloro-2,3-epoxypropane at room temperature. After stirring was continued for 1 h, the mixture was heated at 50—60 °C for 1 h. Usual workup gave 77.3 g (93%) of **14**: bp 187—188 °C/0.3 mmHg; ^{1}H-NMR (CCl_4) δ 7.00—7.40 (m, 10H, C_6H_5S), 3.60—3.90 (m, 1H, CH), 2.80—3.20 (m, 5H, OH and CH_2); IR (thin film) 3420 (OH) cm^{-1}; MS (20 eV) m/e 276 (M^+, 23), 110 (100).

Synthesis of 2-(Phenylthio)cyclopropanol (16): To a solution of 40 mmol (11.06 g) of 1,3-bis(phenylthio)-2-propanol (**14**) in 80 ml of THF at −78 °C was added over 36 min 88 mmol of butyllithium, and stirring was continued for 10 min at −78 °C and for 3 h at 0 °C. The mixture was quenched with 10 ml of aqueous ammonium chloride and was extracted with ether three times. The combined extracts were washed once with brine, dried over anhydrous sodium sulfate, and concentrated to give a crude product. Distillation under reduced pressure gave 5.23 g (79%) of **16**: bp 114—119 °C/0.8—0.9 mmHg; ^{1}H-NMR (CCl_4) δ 7.10—7.50 (m, 5H, C_6H_5S), 4.25 (brs, 1H, OH), 3.40—3.70 (m, 1H, CH), 2.10—2.30 (m, 1H, CHS), 0.60—1.30 (m, 2H, CH_2); IR (thin film) 3330 (OH), 3000, 1580, 1480, 1435, 1325, 1200, 1090, 1025 cm^{-1}. Found: C, 65.24; H, 5.99%. Calcd for $C_9H_{10}OS$: C, 65.02; H, 6.06%.

2-[2-(Phenylthio)cyclopropyloxy]tetrahydropyran (17): A mixture of 5.9 mmol (0.98 g) of cyclopropanol **16**, 7.1 mmol (0.60 g) of 3,4-dihydro-2*H*-pyran and a catalytic amount of *p*-toluenesulfonic acid monohydrate in dry dichloromethane was stirred at 0 °C for 18 h. Workup and column chromatography on silica gel gave 0.94 g (64%) of **17**: bp 135—141 °C/0.8—0.9 mmHg; ^{1}H-NMR (CCl_4) δ 6.90—7.40 (m, 5H, C_6H_5S), 4.40—4.70 (m, 1H, OCH), 3.30—4.00 (m, 3H), 2.00—2.50 (m, 1H, SCH), 0.70—2.00 (m, 8H).

1-[(2-Methoxyethoxy)methoxy]-2-(phenylthio)cyclopropane (18): To a stirred solution of 40 mmol (11.04 g) of **14** in 120 ml of THF at −78 °C was added over 30 min 88 mmol of butyllithium. After completion of the addition, the reaction mixture was stirred at −78 °C for 10 min and at 0 °C for 3 h. The solution was then cooled to −78 °C, and treated with 60 mmol (8.50 g) of iodomethane and stirred at this temperature for 30 min and at 0 °C for 1 h. After the addition of 1-chloromethoxy-2-methoxyethane (5.48 g, 44 mmol), the reaction mixture was stirred at 0 °C for 15 h. Aqueous workup and distillation gave 4.08 g (82%) of methyl phenyl sulfide and 8.12 g (80%) of **18**: bp 146—151 °C/1.0—1.2 mmHg; ^{1}H-NMR (CCl_4) δ 6.90—7.40 (m, 5H, C_6H_5S), 4.62 (s, 2H, OCH_2), 3.30—3.90 (m, 4H, CH_2), 3.28 (s, 3H, CH_3O), 2.20—2.50 (m, 1H, CHO), 0.70—1.60 (m, 3H); MS (20 eV) m/e 254 (M^+, 4) 59 (100).

1,3-Bis(4-methylphenylthio)propane (23): According to the procedure for the preparation of **1**, sulfide **23** was prepared by adding a solution of 0.101 mol (20.3 g) of 1,3-dibromopropane in 50 ml of ethanol to a solution of sodium 4-methylbenzenethiolate (0.201 mol) in ethanol (200 ml). The crude sulfide was purified by distillation to yield 27.14 g (94%) of **23**: bp 167—168 °C/0.2—0.5 mmHg; ^{1}H-NMR (CCl_4) δ 7.12 (d, J=9.2 Hz, 4H), 6.93 (d, J=9.2 Hz, 4H), 2.88 (t, J=7.7 Hz, 4H, CH_2S), 1.80 (q, J=7.7 Hz, 2H, CH_2).

In a similar way, 1,3-bis(4-chlorophenylthio)propane (**25**) was prepared in 80% yield: mp 40—41 °C (ethanol–acetone); ^{1}H-NMR (CCl_4) δ 7.61 (s, 8H), 2.94 (t, 4H, CH_2S), 1.87 (q, J=6.6 Hz, 2H).

1-Chloro-3-(4-chlorophenylthio)propane (27): Reaction of 0.05 mol of sodium 4-chlorobenzenethiolate with 0.06 mol of 1-bromo-3-chloropropane in ethanol gave **27** in 90% yield: bp 109—112 °C/0.3—0.4 mmHg; ^{1}H-NMR (CCl_4) δ 7.20 (m, 4H), 3.60 (t, J=7.5 Hz, 2H, CH_2Cl), 3.00 (t, J=7.5 Hz, 2H, CH_2S), 2.00 (q, J=7.5 Hz, 2H, CH_2).

Reaction of 19.2 mmol of sulfide **23** with 23 mmol of butyllithium in 50 ml of THF containing 28.7 mmol of HMPA at −78 °C for 30 min and at 0 °C for 3 h gave cyclopropyl 4-methylphenyl sulfide (**24**) in 50% yield: bp 84—86 °C/1.5 mmHg (lit,[6] bp 87 °C/2.3 mmHg); ^{1}H-NMR (CCl_4) δ 6.90—7.20 (m, 4H, C_6H_5S), 2.27 (s, 3H, CH_3), 1.90—2.20 (m, 1H, CH), 0.50—1.10 (m, 4H); IR (thin film) 3080, 3010, 1490, 1280, 1090, 1025 cm^{-1}. Found: C, 73.29; H, 7.64%. Calcd for $C_{10}H_{12}S$: C, 73.12; H, 7.37%.

Reaction of 10 mmol of sulfide **25** with 11 mmol of LDA in 20 ml of THF containing 24.7 mmol of HMPA at −78—0 °C for 3 h gave 4-chlorophenyl cyclopropyl sulfide (**26**) in 34%: bp 79—81 °C/0.4 mmHg; ^{1}H-NMR (CCl_4) δ 7.16 (s, 4H, C_6H_5S), 2.08 (m, 1H), 1.00 (m, 2H), 0.65 (m, 2H); IR (thin film) 3080, 3000, 1470, 1090, 1010, 810 cm^{-1}. Found: C, 58.79; H, 5.00%. Calcd for C_9H_9ClS: C, 58.53; H, 4.91%.

Reaction of 30 mmol of sulfide **27** with 31 mmol of LDA in THF at −78 °C to room temperature gave the same sulfide **26** in 46% yield.

*1,2-Bis(phenylthio)ethane (**31**)*: Mp 68—69 °C (lit,[17] mp 69 °C); ^{1}H-NMR (CCl_4) δ 7.20 (m, 10H, C_6H_5S), 3.00 (s, 4H, CH_2).

Reaction of 10 mmol of sulfide **31** with 22 mmol of butyllithium in 20 ml of THF containing 25 mmol of HMPA at −78 °C for 3 h gave phenyl vinyl sulfide (**33**) in 52% yield: bp 80 °C/16 mmHg; ^{1}H-NMR was agreement with the literature.[18]

Preparation of O-*(2,4,6-Tri-*t*-butylphenyl)* S-*(3-Chloropropyl) dithiocarbonate (**35a**)*: To a stirred suspension of 1.83 g of sodium hydride (50% mineral oil; washed with hexane three times) in 40 ml of THF was added 2,4,6-tri-*t*-butylphenol (10 g, 0.0381 mol) with ice-bath cooling. After the addition, the bath was removed and the reaction mixture was stirred for 1 h. Carbon disulfide (4.64 g, 0.061 mol) was then added and the stirring was continued for 1 h. The above reaction mixture was added to the solution of 6.00 g (0.381 mol) of 1-bromo-3-chloropropane in 20 ml of dry DMF at 0 °C. After the mixture was stirred for 4 h at room temperature, aqueous workup and recrystallization from methanol gave 11.9 g (75%) of **35a**: mp 47—49 °C. ^{1}H-NMR (CCl_4) δ 7.25 (s, 2H), 3.65 (t, J=7 Hz, 2H), 3.40 (t, J=7 Hz, 2H), 2.30 (m, 2H), 1.40 (s, 27H).

Analogous procedures were followed for the preparation of **35b**, **35c**, **35d**, and **35e**.

O-*(2,4,6-Tri-*t*-butylphenyl)* S-*(3-Chloropropyl) Thiocarbonate (**35b**)*: Mp 75—77 °C (MeOH); ^{1}H-NMR (CCl_4) δ 7.24 (s, 2H), 3.60 (t, J=6.9 Hz, 2H), 3.04 (t, J=6.9 Hz, 2H), 2.12 (m, 2H), 1.36 (m, 27H, CH_3).

O-*(4-*t*-Butylcyclohexyl)* S-*(3-Chloropropyl) Dithiocarbonate (**35c**)*: A viscous oil; ^{1}H-NMR (CCl_4) δ 5.34 (m, 1H), 3.60 (t, J=6.9 Hz, 2H, CH_2), 3.25 (t, J=6.9 Hz, 2H, CH_2), 2.05—2.40 (m, 4H), 0.80—2.05 (m, 16H).

O-L-*Menthyl* S-*(3-Chloropropyl) Dithiocarbonate (**35d**)*: A viscous oil; ^{1}H-NMR (CCl_4) δ 5.83 (m, 1H), 3.55 (t, J=6.9 Hz, 2H, CH_2), 3.20 (t, J=6.9 Hz, 2H, CH_2), 2.00—2.40 (m, 3H), 1.60—2.00 (m, 17H).

O-L-*Bornyl* S-*(3-Chloropropyl) Dithiocarbonate (**35e**)*: Bp 163—165 °C/2—3 mmHg. ^{1}H-NMR ($CDCl_3$) δ 5.45 (m, 1H), 3.60 (t, J=7 Hz, 2H, CH_2Cl), 3.25 (t, J=7 Hz, CH_2S), 2.60—0.80 (m, 18H).

Synthesis of O-*(2,4,6-Tri-*t*-butylphenyl)* S-*Cyclopropyl Dithiocarbonate (**36a**)*: To a stirred solution of 30 mmol (4.2 ml) of diisopropylamine in 40 ml of THF was added at −78 °C over 20 min 30 mmol of butyllithium. The solution was stirred at this temperature for 20 min, and treated dropwise with 28.7 mmol of **35a** in 20 ml of THF. After 3 h, the reaction mixture was allowed to warm to room temperature with stirring (4 h) and then quenched with 10 ml of aqueous ammonium chloride solution. The mixture was poured onto 50 ml of 10% hydrochloric acid and extracted with ether (4×50 ml). The ethereal extracts were washed with saturated sodium chloride solution, dried over anhydrous sodium sulfate, and concentrated under reduced pressure to give pale yellow solid **36a**. The sample for analysis was prepared by repeated recrystallizations from methanol twice to give pale yellow crystals **36a** in 77% yield (8.40 g): mp 68—69 °C; ^{1}H-NMR (CCl_4) δ 7.20 (s, 2H), 2.40 (m, 1H), 1.35 (s, 27H, CH_3), 1.16 (m, 2H), 0.76 (m, 2H). Found: C, 69.62; H, 9.09%. Calcd for $C_{22}H_{34}OS_2$: C, 69.79; H, 9.05%.

Similar procedures to the above were used for cyclization.

O-*(2,4,6-Tri-*t*-butylphenyl)* S-*Cyclopropyl Thiocarbonate (**36b**)*: Mp 77—78 °C (MeOH); ^{1}H-NMR (CCl_4) δ 7.28 (s, 2H), 2.20 (m, 1H), 1.36 (m, 27H, CH_3), 1.04 (m, 2H), 0.68 (m, 2H). Found: C, 72.65; H, 9.57%. Calcd for $C_{22}H_{34}O_2S$: C, 72.88; H, 9.45%.

O-*(4-*t*-Butylcyclohexyl)* S-*Cyclopropyl Dithiocarbonate (**36c**)*: Mp 35—35.5 °C (EtOH); ^{1}H-NMR (CCl_4) δ 5.30 (m, 1H), 0.80—2.40 (m, 21H), 0.71 (m, 2H). Found: C, 61.65; H, 9.01%. Calcd for $C_{14}H_{24}OS_2$: C, 61.72; H, 8.88%.

O-L-*Menthyl* S-*Cyclopropyl Dithiocarbonate (**36d**)*: Mp 26—27 °C (EtOH); bp 117—120 °C/0.2 mmHg; ^{1}H-NMR (CCl_4) δ 5.40 (m, 1H), 2.30 (m, 2H), 0.50—2.10 (m, 21H); $[\alpha]_D^{25}$ −59.4° (*c* 1.47, $CHCl_3$). Found: C, 61.42; H, 9.08%. Calcd for $C_{14}H_{24}OS_2$: C, 61.72; H, 8.88%.

O-L-*Bornyl* S-*Cyclopropyl Dithiocarbonate (**36e**)*: Bp 119—125 °C/0.2 mmHg; ^{1}H-NMR ($CDCl_3$) δ 5.40 (m, 1H), 0.50—2.60 (m, 21H); $[\alpha]_D^{23}$ −17.6° (*c* 1.61, $CHCl_3$). Found: C, 62.51; H, 8.51%. Calcd for $C_{14}H_{22}OS_2$: C, 62.17; H, 8.20%.

*General Procedure for Addition of 1-Lithiocyclopropyl Phenyl Sulfide (**37**) to Carbonyl Compounds.* To a stirred solution of 1,3-bis(phenylthio)propane (**1**) (2.6 g, 10 mmol) in 20 ml of THF was added butyllithium (21 mmol) at −78 °C. After 5 min, the bath was removed and the mixture was stirred for 3 h at 0 °C. The resulting pale yellow solution was cooled to −78 °C, and the mixture of a carbonyl compound (10 mmol) in 3 ml of THF was added dropwise. After an additional 30 min at −78 °C, the solution was slowly warmed to room temperature. Saturated ammonium chloride solution (10 ml) was then added, and the reaction mixture was poured into 300 ml of water. The organic layer was removed, and the aqueous layer was extracted with ether (3×50 ml). The organics were combined, dried over anhydrous sodium sulfate and evaporated to give a crude adduct **38**. After chromatography on silica gel, eluted with hexane–benzene, a pure adduct **38** was obtained.

*Physical Properties of Adduct. 4-[1-(Phenylthio)cyclopropyl]-4-heptanol (**38a**)*: Bp 140 °C/0.9 mmHg; IR (thin film) 3530 (OH), 2970, 1585, 1480, 1440, 1025 cm^{-1}; ^{1}H-NMR (CCl_4) δ 7.10—7.50 (m, 5H, C_6H_5S), 0.70—1.80 (m, 19H); MS (20 eV) *m/e* 264 (M^+, 20), 117 (100). Found: C, 73.10; H, 9.49%. Calcd for $C_{16}H_{24}OS$: C, 72.68; H, 9.15%.

α-*[1-(Phenylthio)cyclopropyl]benzyl Alcohol (**38b**)*: IR (thin film) 3410 (OH), 2920, 1575, 1475, 1020 cm^{-1}; ^{1}H-NMR (CCl_4) δ 7.00—7.40 (m, 10H, C_6H_5), 4.63 (brs, 1H, CH), 2.64 (brs, 1H, OH), 0.80—1.21 (m, 4H); MS (20 eV) *m/e* 256 (M^+, 41), 150 (100). Found: C, 75.18; H, 6.50%. Calcd for $C_{16}H_{16}OS$: C, 74.96; H, 6.29%.

*1-[1-(Phenylthio)cyclopropyl]cyclohexanol (**38c**)*: IR (thin film) 3480 (OH), 2920, 1575, 1475, 1430, 1025 cm^{-1}; ^{1}H-NMR (CCl_4) δ 6.90—7.50 (m, 5H, C_6H_5S), 1.30—1.90 (m, 11H), 0.70—1.20 (m, 4H); MS (20 eV) *m/e* 248 (M^+, 20),

117 (100). Found: C, 72.62; H, 8.33%. Calcd for $C_{15}H_{20}OS$: C, 72.54; H, 8.12%.

2-[1-(Phenylthio)cyclopropyl]-2-propanol (38d): Bp 100 °C/0.9 mmHg; ^{1}H-NMR (CCl_4) δ 6.90—7.40 (m, 5H, C_6H_5S), 2.18 (brs, 1H, OH), 1.23 (s, 6H, CH_3), 0.80—1.20 (m, 4H); MS (20 eV) *m/e* 208 (M^+, 17), 59 (100). Found: C, 69.45; H, 8.05%. Calcd for $C_{12}H_{16}OS$: C, 69.19; H, 7.74%.

3-[1-(Phenylthio)cyclopropyl]-3-pentanol (38e): Bp 121 °C/0.6 mmHg; IR (thin film) 3490 (OH), 2960, 1580, 1475, 1430, 1025 cm^{-1}; ^{1}H-NMR (CCl_4) δ 7.10—7.60 (m, 5H, C_6H_5S), 1.40—1.90 (m, 4H), 0.70—1.40 (m, 11H); MS (20 eV) *m/e* 236 (M^+, 24), 117 (100). Found: C, 71.18; H, 8.82%. Calcd for $C_{14}H_{20}OS$: C, 71.14; H, 8.53%.

1-[1-(Phenthio)cyclopropyl]-1-heptanol (38f): Bp 151—152 °C/0.8 mmHg; IR (thin film) 3410 (OH), 2920, 1580, 1475, 1435, 1020 cm^{-1}; ^{1}H-NMR (CCl_4) δ 7.00—7.50 (m, 5H, C_6H_5S), 3.10—3.30 (m, 1H), 1.90—2.20 (m, 1H, OH), 0.70—1.80 (m, 17H); MS (20 eV) *m/e* 264 (M^+, 31), 117 (100). Found: C, 72.87; H, 9.30%. Calcd for $C_{16}H_{24}OS$: C, 72.68; H, 9.15%.

2-[1-(Phenylthio)cyclopropyl]-2-hexanol (38g): Bp 129 °C/0.6—0.7 mmHg; IR (thin film) 3495 (OH) cm^{-1}; ^{1}H-NMR (CCl_4) δ 6.90—7.40 (m, 5H, C_6H_5S), 0.70—1.80 (m, 17H); MS (20 eV) *m/e* 250 (M^+, 22), 117 (100). Found: C, 72.09; H, 9.19%. Calcd for $C_{15}H_{22}OS$: C, 71.95; H, 8.86%.

1-(Phenylthio)cyclopropanecarboxylic Acid (38i): ^{1}H-NMR (CCl_4) δ 9.80 (brs, 1H, COOH), 7.00—7.50 (m, 5H, C_6H_5S), 1.20—1.90 (m, 4H).[7c]

Support for this research through a grant from the Ministry of Education, Science and Culture (Grant No. 554145) is gratefully acknowledged.

References

1) a) B. M. Trost, D. E. Keely, H. C. Arndt, J. H. Rigby, and M. J. Bogdanowicz *J. Am. Chem. Soc.*, **99**, 3080 (1977); b) B. M. Trost, D. E. Keely, H. C. Arndt, and M. J. Bogdanowicz, *ibid.*, **99**, 3088 (1977); c) B. M. Trost, D. E. Keely, and M. J. Bogdanowicz, *ibid.*, **95**, 3068 (1973); d) B. M. Trost and L. N. Jungheim, *ibid.*, **102**, 7910 (1980); e) B. M. Trost and D. E. Keely, *ibid.*, **98**, 248 (1976); f) B. M. Trost and D. E. Keely, *ibid.*, **96**, 1252 (1974); g) B. M. Trost and J. H. Rigby, *J. Org. Chem.*, **43**, 2938 (1978); h) B. M. Trost and L. N. Jungheim, *J. Am. Chem. Soc.*, **102**, 7910 (1980).

2) B. M. Trost, *Acc. Chem. Res.*, **7**, 85 (1974).

3) R. D. Miller and D. R. McKean, *Tetrahedron Lett.*, **1979**, 583.

4) R. D. Miller, D. R. McKean, and D. Kaufmann, *Tetrahedron Lett.*, **1979**, 587.

5) T. Cohen and J. R. Matz, *J. Am. Chem. Soc.*, **102**, 6900 (1980); *Tetrahedron Lett.*, **22**, 2455 (1981); J. R. Matz and T. Cohen, *ibid.*, **22**, 2459 (1981).

6) W. E. Truce, K. R. Hollister, L. B. Lindy, and J. E. Parr, *J. Org. Chem.*, **33**, 43 (1968).

7) a) T. Cohen and W. M. Daniewski, *Tetrahedron Lett.*, **1978**, 2991; b) T. Cohen, R. B. Weisenfeld, and R. E. Gapinski, *J. Org. Chem.*, **44**, 4744 (1979); c) T. Cohen, W. M. Daniewski, and R. B. Weisenfeld, *Tetrahedron Lett.*, **1978**, 4665; d) J. E. Eisch and J. E. Galle, *J. Org. Chem.*, **44**, 3277 (1979); e) Y.-H. Chang and H. W. Pinnick, *ibid.*, **43**,373 (1978); f) C. L. Bumgardner, J. R. Lever, and S. T. Purrington, *ibid.*, **45**, 748 (1980); g) T. Shono, Y. Matsumura, S. Kashimura, and H. Kyotoku, *Tetrahedron Lett.*, **1978**, 1205; h) Y.-H. Chang, D. E. Campbell, and H. W. Pinnick, *ibid.*, **1977**, 3337; i) M. Braun and D. Seebach, *Chem. Ber.*, **109**, 669 (1976); j) J.-L. Burgot, J. Masson, P. Metzner, and J. Vialle, *Tetrahedron Lett.*, **1976**, 4297; k) J. Masson, P. Metzner, and J. Vialle, *Tetrahedron*, **33**, 3089 (1977); l) L. Brandsma, *Recl. Trav. Chim. Pays-Bus*, **89**, 593 (1970); m) C. Feugeas and J.-P. Galy, *C. R. Acad. Sci., Ser. C*, **270**, 2157 (1970); n) R. D. Little and J. R. Dawson, *J. Am. Chem. Soc.*, **100**, 4607 (1978). Preparation of cyclopropyl sulfides *via* a carbene intermediate, see: o) G. Boche and D. R. Schneider, *Tetrahedron Lett.*, **1975**, 4247; p) R. H. Rynbrand and F. E. Dutton, *ibid.*, **1972**, 1933; q) R. H. Rynbrand and F. E. Dutton, *J. Org. Chem.*, **40**, 2282 (1975); r) A. M. Van Leusen, and R. J. Mulder, and J. Starling, *Recl. Trav. Chim. Pays-Bas*, **86**, 225 (1967).

8) K. Tanaka, H. Uneme, S. Matsui, R. Tanikaga, and A. Kaji, *Chem. Lett.*, **1980**, 287.

9) F. G. Mann and D. Purdie, *J. Chem. Soc.*, **1935**, 1549.

10) C. Raha, *Org. Synth.*, Coll. Vol. IV, 263 (1963).

11) S. F. Normant and H. Deshayes, *Bull. Soc. Chim. Fr.*, **1972**, 2858.

12) A. P. Krapcho, *Synthesis*, **1974**, 383.

13) E. J. Corey and D. Seebach, *J. Org. Chem.*, **31**, 4097 (1966).

14) E. J. Corey, B. W. Erickson, and R. Noyori, *J. Am. Chem. Soc.*, **93**, 1724 (1971).

15) E. J. Corey, J.-L. Gras, and P. Ulrich, *Tetrahedron Lett.*, **1976**, 809.

16) T. Cohen, D. Quellette, and W. M. Daniewski, *Tetrahedron Lett.*, **1978**, 5063; D. Seebach, *Chem. Ber.*, **105**, 487 (1972); D. Seebach, *Angew. Chem.*, **79**, 469 (1967); P. Beak and J. W. Worley, *J. Am. Chem. Soc.*, **94**, 597 (1972); K. Kondo and I. Ojima, *Bull. Chem. Soc. Jpn.*, **48**, 1490 (1975).

17) E. V. Bell and G. M. Bennett, *J. Chem. Soc.*, **1928**, 3189.

18) H. J. Reich, W. W. Willis, Jr., and P. D. Clark, *J. Org. Chem.* **46**, 2775 (1981); W. E. Parham, F. D. Blake, and D. R. Theissen, *ibid.*, **27**, 2415 (1962); F. Cooke, R. Moerck, J. Schwindeman, and P. Magnus, *ibid.*, **45**, 1046 (1980); T. Okuyama, M. Masago, M. Nakada, and T. Fueno, *Tetrahedron* **33**, 2379 (1977); C. C. Price and H. Morita, *J. Am. Chem. Soc.*, **75**, 4747 (1953); W. Verboom, J. Meijer, and L. Brandsma, *Synthesis*, **1978**, 577; P. Bakuzis and M. L. F. Bakuzis, *J. Org. Chem.*, **46**, 235 (1981); P. B. Hopkin and P. L. Fuchs, *ibid.*, **43**, 1208 (1978).

19) H. W. Chen, J. P. Fackler, Jr., D. P. Schussler, and L. D. Thompson, *J. Am. Chem. Soc.*, **100**, 2370 (1978).

 © 1982 The Chemical Society of Japan Bull. Chem. Soc. Jpn., 55, 2973—2975 (1982)

Alcoholysis Equilibria of Triethylalkoxysilanes Catalyzed by Iodine or Iodine Monobromide

Katsuko Ito and Takeshi Ibaraki*

Department of Natural Science, Osaka Women's University, Daisen-cho, Sakai, Osaka 590

(Received January 23, 1982)

The equilibrium constants K of alcoholysis of triethylalkoxysilanes were determined at 20 °C and 40 °C. Iodine monobromide was used to promote the reactions associated with the tertiary alkoxyl groups, while the other reactions proceeded in the presence of iodine. The K values of the reaction systems with ethoxyl or propoxyl—primary, secondary, and tertiary alkoxyl pairs were 1 or above, about 0.5, and about 0.05, respectively. These values reflect the extent of the binding abilities of the alkoxyl groups to silicon, which is in the expected order of primary>secondary>tertiary alkoxyl groups. A mechanism is postulated for the reaction which involves participation by the iodine or iodine monobromide.

Alcoholysis of alkoxysilanes had been carried out previously in the absence of catalyst,[1] but it was noted that under anhydrous conditions alkoxysilanes were generally quite stable and that non-catalytic alcoholysis proceeded only slowly.[2,7] Various acids and bases have been employed to catalyze such reactions,[2-11] as well as alkali metals.[2-4,9,10] Reaction mechanisms have been proposed in some of these cases,[2,7-9] but quantitative data concerning the equilibria of such reactions cannot be found in the literature, although a few kinetic studies have been reported.[8,11]

Alkoxyl-alkoxyl exchange reactions are promoted by iodine or interhalogen compounds such as iodine monobromide, and the equilibrium compositions of such systems can be ascertained by gas chromatography as described in the previous paper.[12] Thus, the iodine- or iodine monobromide-catalyzed reactions of triethylalkoxysilanes with various alcohols were examined, and the equilibrium constants at two different temperatures were determined. For reactions with tertiary alcohols, iodine monobromide was employed because of its superior catalytic activity, while iodine was used in the other cases.

Results and Discussion

Alcoholysis Equilibria of Triethylalkoxysilanes. Thirteen reaction systems with different OR–OR′ pairs were studied at 20.0 °C and 40.0 °C in the presence of iodine or iodine monobromide.

$$Et_3SiOR + R'OH \rightleftharpoons Et_3SiOR' + ROH$$

The equilibria were established from both forward and reverse directions. In most cases the compositions of the reaction mixtures became constant within a few hours. Equilibrium constants, K, for these reactions are summarized in Table 1. The K values are close to unity when both alkoxyl groups have about the same binding ability to silicon and both alcohols have similar reactivity. The reaction systems with ethoxyl–methoxyl, propoxyl and butoxyl, and propoxyl–butoxyl pairs seem to correspond to such cases, as the K values are 1.00—1.12. (entries 1—3,13 in Table 1)

In the reaction systems with ethoxyl–isobutoxyl, pentyloxyl, and isopentyloxyl pairs, K values somewhat larger than unity were observed. (entries 4,7,8) Corresponding free-energy changes for these reactions are −0.62—−1.02 kJ, which suggest that the products are slightly more stable than reactants.

The K values of reaction systems associated with secondary alkoxyl groups are considerably less than unity (entries 5,9,10,12), so that the reverse reactions are spontaneous. Therefore, the alkoxyl groups with a side chain in the α-carbon appear to be attached more loosely to silicon than are the primary alkoxyl groups.

Since tertiary alcohols react slowly with triethylethoxysilane, iodine monobromide was used to accelerate the reactions. The K values observed for these reactions were small, about 0.05. (entries 6,11) These small values may be attributed to the steric hindrance of tertiary alkoxyl groups in the triethylalkoxysilanes.

The equilibrium constants determined at 20 °C and 40 °C were virtually the same, as shown in Table 1, so that the enthalpy changes in these reactions appear to be very small.

Proposed Reaction Mechanism. For the base-catalyzed alcoholysis of alkoxysilanes, some mechanisms with five- or six-coordinate intermediates have been proposed.[2,8,9] However, in the case of iodine- or iodine monobromide-catalyzed alcoholysis, a mechanism *via* a four-centered transition state as given below seems to be most suitable.

Iodine or iodine monobromide forms charge transfer complexes with alcohols,[13] and also with alkoxysilanes,[12] and hence the dative form of the complexes, *e.g.* $[R'OH\cdots I]^+I^-$ or $[Et_3SiOR\cdots I]^+I^-$, may be regarded as the reaction intermediate. In addition, alkoxysilane–alcohol complexing has been suggested,[14] so that the four-centered transition states are still more readily formed. The following mechanism may be derived.

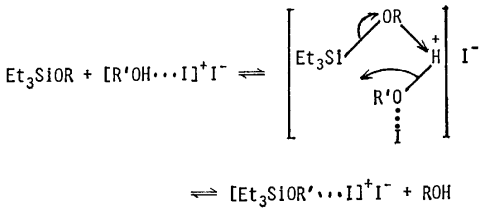

or

Table 1. Alcoholysis equilibrium constants of triethylalkoxysilanes

$Et_3SiOR + R'OH \rightleftharpoons Et_3SiOR' + ROH$

$K=\{[Et_3SiOR'][ROH]\}/\{[Et_3SiOR][R'OH]\}$

Entry	Substituent		Temp °C	Equilibrium constant K		
	OR	OR'		Forward reaction	Reverse reaction	Mean value[a]
1	OEt	OMe	20	1.08±0.03	1.08±0.02	1.08±0.03
			40	1.06±0.03	1.06±0.01	1.06±0.02
2	OEt	OPr^n	20	1.11±0.02	1.11±0.02	1.11±0.02
			40	1.09±0.02	1.10±0.02	1.09±0.02
3	OEt	OBu^n	20	1.12±0.03	1.13±0.03	1.12±0.03
			40	1.09±0.04	1.08±0.04	1.09±0.04
4	OEt	OBu^i	20	1.52±0.03	1.52±0.02	1.52±0.03
			40	1.48±0.03	1.48±0.04	1.48±0.03
5	OEt	OBu^s	20	0.51±0.01	0.50±0.01	0.51±0.01
			40	0.55±0.02	0.54±0.02	0.54±0.02
6	OEt	OBu^t	20	0.050±0.003	0.049±0.003	0.050±0.003
			40	0.053±0.002	0.052±0.003	0.053±0.002
7	OEt	$OC_5H_{11}{}^n$	20	1.31±0.02	1.32±0.03	1.32±0.03
			40	1.28±0.03	1.29±0.02	1.29±0.03
8	OEt	$OC_5H_{11}{}^i$	20	1.29±0.03	1.30±0.03	1.30±0.03
			40	1.27±0.04	1.27±0.03	1.27±0.03
9	OEt	$OCHMePr^n$	20	0.52±0.02	0.50±0.03	0.51±0.03
			40	0.53±0.01	0.53±0.03	0.53±0.02
10	OEt	$OCHEt_2$	20	0.43±0.03	0.42±0.01	0.43±0.02
			40	0.45±0.01	0.44±0.02	0.45±0.02
11	OEt	$OC_5H_{11}{}^t$	20	0.047±0.003	0.047±0.004	0.047±0.004
			40	0.050±0.002	0.050±0.005	0.050±0.003
12	OPr^n	OPr^i	20	0.40±0.01	0.40±0.01	0.40±0.01
13	OPr^n	OBu^n	20	0.99±0.01	1.00±0.02	1.00±0.03

a) Mean value of equilibrium constants of both forward and reverse reactions.

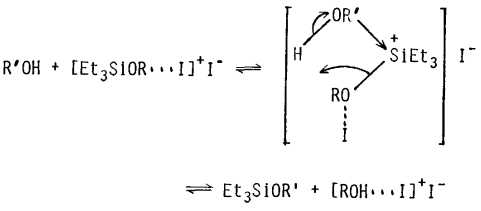

Experimental

General Procedure. In a reaction vessel (volume about 5 cm^3) with a sealing-cap, measured amounts of triethylalkoxysilane and alcohol were placed. Molar ratios of alkoxysilanes to alcohols in the reaction mixtures were in the range of 1:0.5 to 1:6. I_2 or IBr was added to the reaction mixtures as the solution in each alcohol. The reaction was promoted using about 0.001 (mole fraction) of catalyst.

Each reaction mixture thus prepared was divided into two or three parts and maintained in a thermostat set at (20.0±0.1) °C or (40.0±0.1) °C. One of them was used to monitor the time course of the reaction until the composition became constant. The others were then used to determine the equilibrium composition.

Analysis. Analyses were performed by means of GLPC using a Shimadzu model GC-4B gas chromatograph with a thermal conductivity detector. The stationary phases of the packings used in this investigation were as follows:

PEG 4000+SPAN 80 (entries 1,8 in Table 1), SPAN 80 (entries 2,4,5,7,13), PEG 1000+DOP-B (entry 3), PEG 4000 (entry 6), PEG 6000 (entries 9,10), PEG 1000 (entry 11), SPAN 80+PEG 6000 (entry 12).

Reagents. Triethylmethoxysilane and triethylethoxysilane were prepared by the reaction of tetramethoxysilane or tetraethoxysilane with ethylmagnesium bromide. The other triethylalkoxysilanes were prepared by iodine or iodine monobromide-catalyzed alcoholysis of triethylethoxysilane. After the resulting ethanol and excess alcohol had been removed by distillation, each triethylalkoxysilane was obtained by fractional distillation. These triethylalkoxysilanes were purified by repeated fractional distillation, and the following compounds were prepared.

Et_3SiOMe, Et_3SiOEt, Et_3SiOPr^n, Et_3SiOPr^i, Et_3SiOBu^n, Et_3SiOBu^i, Et_3SiOBu^s, Et_3SiOBu^t, $Et_3SiOC_5H_{11}{}^n$, $Et_3SiOC_5H_{11}{}^i$, $Et_3SiOC_5H_{11}{}^t$, $Et_3SiOCHMePr^n$: bp 205.1 °C; n_D^{20} 1.4243; ^{13}C NMR (neat) δ=4.78 (t, 3C), 6.22 (q, 3C), 13.58 (q), 18.48 (t), 23.31 (q), 41.96 (t), 67.63 (d). Found: C, 65.04; H, 13.25%. Calcd for $C_{11}H_{26}SiO$: C, 65.27; H, 12.95%. $Et_3SiOCHEt_2$: bp 206.2 °C; n_D^{20} 1.4272; ^{13}C NMR (neat) δ=4.88 (t, 3C), 6.27 (q, 3C), 8.83 (q, 2C), 28.94 (t, 2C), 74.12 (d). Found: C, 65.08; H, 13.25%. Calcd: C, 65.27; H, 12.95%.

The last two alkoxysilanes are unreported compounds, while the boiling points and refractive indices of the others were virtually identical with the reported values.[4]

The alcohols were purified by fractional distillation. Methanol, ethanol, 1- and 2-propanol were previously freed from water by refluxing with magnesium or magnesium activated with iodine. *t*-Butyl alcohol was repeatedly recrystallized after distillation.[15]

Iodine was purified by repeated sublimation with calcium oxide and potassium iodide. Iodine monobromide was prepared and purified by recrystallization.[12]

The authors wish to thank professor Makoto Kumada of Kyoto University and Dr. Kenzo Hirayama for their kind advice and encouragement. We also would

like to thank professor Toshiyuki Shono of Osaka University and his co-workers for the elemental analyses and for the NMR spectral data.

References

1) E. W. Abrahamson, I. Joffe, and H. W. Post, *J. Org. Chem.*, **13**, 275 (1948).
2) B. Helferich und W. Reimann, *Chem. Ber.*, **80**, 163 (1947).
3) E. Larsson, *Acta Chem. Scand.*, **8**, 898 (1954).
4) B. N. Dolgov, N. P. Kharitonov, and M. G. Voronkov, *J. Gen. Chem. USSR.*, **24**, 1169 (1954).
5) H. Gilman and G. N. R. Smart, *J. Org. Chem.*, **19**, 441 (1954).
6) M. G. Voronkov and B. N. Dolgov, *Bull. Acad. Sci. USSR., Div. Chem. Sci.*, **1957**, 1153.
7) M. G. Voronkov and L. A. Zhagata, *J. Gen. Chem. USSR.*, **37**, 2630 (1967).
8) R. L. Schowen and K. S. Latham, Jr., *J. Am. Chem. Soc.*, **89**, 4677 (1967).
9) L. H. Sommer and H. Fujimoto, *J. Am. Chem. Soc.*, **90**, 982 (1968).
10) H. G. Emblem and K. Hargreaves, *J. Inorg. Nucl. Chem.*, **30**, 721 (1968).
11) G. Tschernko und H. Hamann, *Z. Chem. (DDR)*, **18**, 64 (1978).
12) T. Ibaraki and K. Ito, *Bull. Chem. Soc. Jpn.*, **54**, 3235 (1981).
13) L. J. Andrews and R. M. Keefer, *Adv. Inorg. Chem. Radiochem.*, **3**, 91 (1961).
14) J. Nagy, S. Ferenczi-Gresz, R. Farkas, und T. Gábor, *Z. Anorg. Allg. Chem.*, **377**, 328 (1970).
15) J. A. Riddick and W. B. Bunger, "Organic Solvents, Techniques of Chemistry," 3rd ed, Wiley-Interscience, New York (1970), Vol. II, pp. 638—664.

Alkylation of Benzothiazolines and the Stevens Rearrangement of the Resulting 2,3,3-Trisubstituted Benzothiazolinium Salts

Kin-ya Akiba,† Yoshio Ohara, and Naoki Inamoto*
Department of Chemistry, Faculty of Science, The University of Tokyo, Hongo, Bunkyo-ku, Tokyo 113
(Received January 26, 1982)

Alkylation of 2-substituted 3-methyl- or 3-ethylbenzothiazolines with Meerwein reagents gave 2-substituted 3,3-dialkylbenzothiazolinium tetrafluoroborates (**3**). The configuration of two alkyl groups on the nitrogen was assigned by NMR spectra and NOE measurement. In the Stevens rearrangement of **3** with lithium diisopropylamide ethyl group showed a much larger migratory aptitude (Et:Me≧20:1) than methyl group irrespective of the configuration of **3**, and cyclic ammonium ylide with planar π-type carbanion was proposed as an intermediate. **3** suffered nucleophilic attack at the ring sulfur atom by butyllithium to afford a ring-opened ammonium ylide, which collapses to a radical pair to give unusual Stevens rearrangement product, where *o*-alkylthiophenyl group migrated selectively in preference to alkyl group, because of stabilization by participation of *o*-alkylthio group.

In an alkylation of a compound containing two hetero atoms such as sulfur and nitrogen, the position of alkylation is dependent on the structure of the compound and the kind of alkylating reagent.

For example, dimorpholino sulfide undergoes *S*-ethylation with triethyloxonium tetrafluoroborate, while it gives *N,N*-dimethylmorpholinium salt with methyl iodide.[1] 1-Pyrrolidinyl *p*-tolyl sulfoxide undergoes *O*-methylation with methyl trifluoromethanesulfonate,[2] and *S*-methyl-*S*-phenylsulfoximine[3] and 2-anilino-3-methylthio-1,4-naphthoquinone[4] *N*- and *S*-methylations with trimethyloxonium tetrafluoroborate, respectively.

In the benzothiazolines (**1**), it is also possible in their alkylation to give thionia (**2**) or azonia compound (**3**), but **3** was obtained in alkylation with Meerwein reagents.[5] Independently, Hori *et al.*[6] reported that **1** suffers *N*-methylation both with trimethyloxonium tetrafluoroborate (**4a**) and methyl iodide, but 2,2,3-trimethylbenzothiazoline *S*-methylation with methyl iodide.

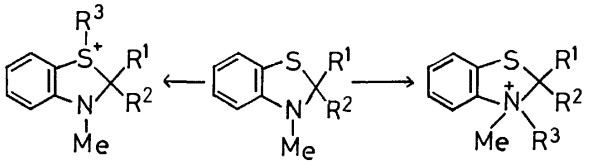

2 1 3

Moreover, it is well known that the quaternary ammonium salts undergo Stevens rearrangement[7] with bases *via* ammonium ylide[8] stereospecifically[9] in intramolecular manner.[10] Because of observation of CIDNP,[11] it is generally accepted that Stevens rearrangement involves a radical pair which recombines in a solvent cage. On the other hand, Dewar[12] have suggested that concerted S_Ni type mechanism, which is forbidden according to the Woodward-Hoffmann rule, is energetically not so unfavorable in gas phase based on the MINDO/3 calculation.

Therefore, we carried out the Stevens rearrangement of **3** (R^1=H, R^3≠Me) of a definite configuration with lithium diisopropylamide (LDA) or butyllithium in order to investigate the steric course and the migratory aptitude.[13]

This paper describes on alkylation of **1**, the structure of the resulting salts (**3**), and their Stevens rearrangement in detail.

Results and Discussion

Methylation of 3-Methylbenzothiazolines (1). Methylation of **1** with **4a** gave 3,3-dimethylbenzothiazolinium salts (**3**). The results are shown in Table 1.

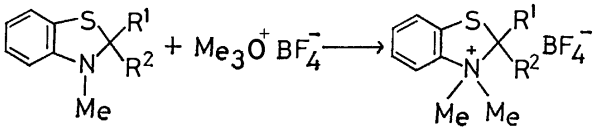

1 4a 3

The structure of **3** was easily determined by NMR. The salts (**3a—e**), where the 2-position is asymmetric, show two methyl signals with an equal intensity at δ 3.1 and 3.7 ppm region. Although these two signals may be assigned to *S*- and *N*-methyl groups of the thionia compound (**2**), they should be assigned to the dimethylammonio group because no spectral change could be observed by addition of excess trifluoroacetic acid (TFA) to **3c** and **3e**. The conclusion was confirmed by the fact that **3f** and **3g** which bear the same two substituents at 2-C show a single methyl peak and no spectral change could be also observed by addition of excess TFA.

The chemical shifts of the lower field methyl of **3a—e** are almost constant (δ 3.7). On the other hand, these of the higher field methyl are constant for **3a—d** (δ 3.12), but a distinct shift to lower field is observed for **3e** (R^2=Me). Hence, it can be concluded that the lower field methyl is assigned to lie *syn* to 2-C–H and the higher field methyl *syn* to 2-C–R. The assignement was supported by NOE measurement (*vide infra*).

From the filtrate in the recrystallization of **3c** obtained by the reaction of **1c** with **4a**, *N*-methyl-*o*-methylthioaniline (10%) and its hydrotetrafluoroborate

† Present address: Department of Chemistry, Faculty of Science, Hiroshima University, Higashisenda-machi, Hiroshima 730.

Table 1. Yields, mp, and chemical shifts (in DMSO-d_6) of **3**

3	R^1	R^2	Yield/%	Mp θ_m/°C	δ_{C_2-H}	δ_{N-Me}
3a	H	*p*-$MeOC_6H_4$	65	165—167	6.94	3.12, 3.65
3b	H	*p*-MeC_6H_4	59	195—197	6.94	3.10, 3.66
3c	H	C_6H_5	69	178.5—180.5	6.99	3.11, 3.71
3d	H	*p*-ClC_6H_4	58	196—197	7.00	3.17, 3.71
3e	H	Me	66	117.5—119	5.81	3.35, 3.73
3f	H	H	77	172—173.5	5.34	3.62
3g	Me	Me	72	177—178.5	—	3.53

(4.5%) were isolated. These products are probably due to decomposition of *S*-methylated product, because Hori *et al.*[6] have reported isolation of **X** type salt in the methylation of **1g** ($R^1=R^2=Me$) with methyl iodide.

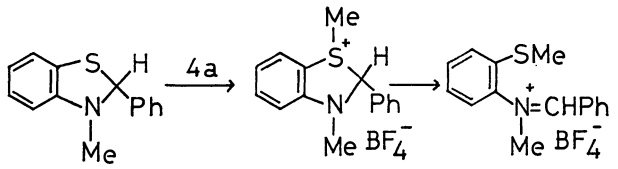

1c X

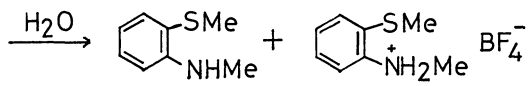

Alkylation of 3-Alkylbenzothiazolines. Ethylation of 2,3-dimethylbenzothiazoline (**1e**) with triethyloxonium tetrafluoroborate (**4b**) gave a diastereomeric mixture of **5A** and **5B** (**5A**/**5B**=*ca.* 10) in 61% yield, and methylation of 3-ethyl-2-methylbenzothiazoline (**1h**) with **4a** gave a mixture of the same salts (**5A**/**5B**=*ca.* 2) in 43% yield. The pure isomer **5A** could be isolated by repeated recrystallizations of the reaction mixture from **1e**.

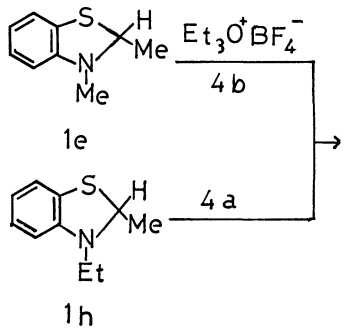

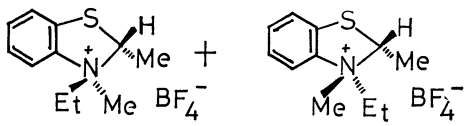

5A 5B

The salt (**6**) obtained by ethylation of 3-methylbenzothiazoline (**1f**) showed identical NMR spectrum with that obtained by methylation of 3-ethyl derivative (**1i**), confirming the structure **6**.

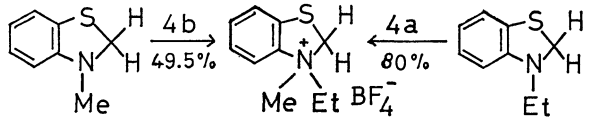

1f 6 1i

Ethylation of **1a—d** with **4b** gave a mixture of **7A** and **7B**. The results are summarized in Table 2.

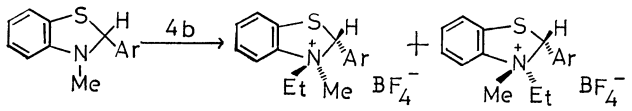

1a-d 7A 7B

Since in these cases purification of the salts by recrystallization was considerably difficult, the isolated yields were relatively low. But pure **A** type of isomers could be isolated in the cases of **7c** and **7d** by repeated recrystallizations.

Methylations of 3-ethyl-2-phenyl-(**1j**), 2,2-diethyl-3-methyl-(**1k**), 2,3-dimethyl-2-phenyl-(**1l**), and 2-t-butyl-3-phenylbenzothiazolines (**1m**) with **4a** gave only tarry materials which may be decomposition products *via* *S*-methylation, but further identification was not done.

On the other hand, reaction of **1c** with benzyl chloride in the presence of silver perchlorate gave 3-methyl-2-phenylbenzothiazolium perchlorate (**8**), which was also obtained in the reaction with only silver perchlorate.

Determination of Stereochemistry by NOE Measurement. In order to confirm the stereochemistry of **3** and **5**, the NOE measurement was performed. In the NMR spectra of **3c**, **3e**, and **5A**, the increase of intensities of 2-H was observed on irradiation of the alkyl groups on the nitrogen atom resonating at lower field, while little change was observed on irradiation of the substituent resonating at higher field as shown in Table 3, supporting the before-mentioned conclusion.

Reactions of 3a—d and 7 with LDA. Reactions of **3a—d** with LDA in ether or tetrahydrofuran (THF) at −50 °C gave 2-aryl-2,3-dimethylbenzothiazolines (**9a—d**) as product due to Stevens rearrangement through a cyclic ammonium ylide (**10**). The results are summarized in Table 4.

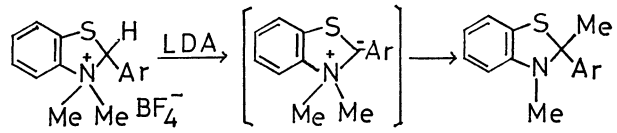

3a-d 10 9a-d

Table 2. Ethylation products (**7A** and **7B**) from **1a—d**

7	Ar	Yield/%	7A/7B	Mp θ_m/°C	δ_{N-Me} A	δ_{N-Me} B
7a	*p*-$MeOC_6H_4$	39	*ca.* 1	145.5—149.5	3.10	3.53
7b	*p*-MeC_6H_4	37	*ca.* 1	158—161	3.11	3.57
7c	C_6H_5	34	*ca.* 10	147—148.5	3.12	3.57
7d	*p*-ClC_6H_4	35	*ca.* 10	139—141	3.17	3.58

Table 3. NOE measurements of **3c**, **3e**, and **5A**

Salt	Irradiated group (δ)	Relative intensity of C_2-H/%
3c	3.71 (*N*-Me)	128±1
	3.11 (*N*-Me)	99±1
3e	3.73 (*N*-Me)	140±2
	3.35 (*N*-Me)	111±2
	1.86 (2-Me)	98±1
5A	3.8—4.3 (*N*-CH_2)	120±2
	3.41 (*N*-Me)	105±1
	1.78 (2-Me)	97±1

The salts (**3**) where the 2-substituent is an alkyl group was mostly recovered under the same conditions, probably because of much lower acidity of the 2-H.

The salts (**7A** and **7B**) should be very suitable models to study the stereochemical relation between the migratory group and the carbanion of the ylide, if the anion retains sp^3 type. If the migration occurs *via* concerted S_Ni type mechanism, **7A** and **7B** should give 2-aryl-2-ethyl-3-methyl-(**11**) and 2-aryl-3-ethyl-2-methylbenzothiazolines (**12**), respectively.

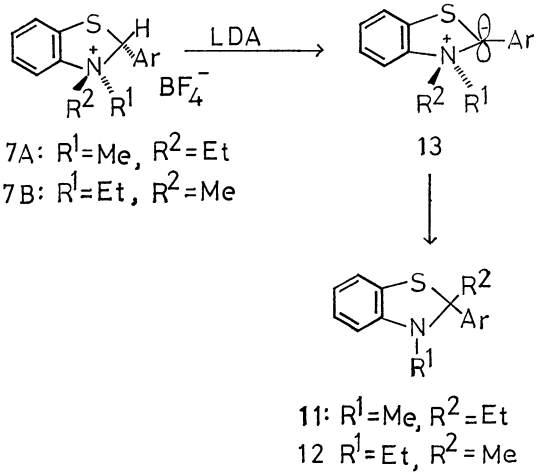

As was expected, reactions of pure **7cA** and **7dA** with LDA gave only **11** in 22 (in ether) and 33% (in THF) yields, respectively, and no **12** could be detected by NMR and GLC. However, a similar reaction of a 1:1 mixture of **7aA** and **7aB** or **7bA** and **7bB** in THF gave also only the corresponding **11** in 54 and 30% yields, respectively, being inconsistent with concerted S_Ni type mechanism. These facts indicate that ethyl group migrates exclusively irrespective of the stereochemistry of the starting salt.

In order to realize these phenomena, it is necessary to invoke not only a planar carbanion (**13**) conjugated with the aryl group as the intermediate, because inversion of sp^3 type carbanion is known to be slow enough to retain its configuration,[14] but also a preferential migration of ethyl group than methyl group.

Furthermore, in order to examine the difference of the migratory aptitudes of ethyl and methyl groups in general, benzylethylmethylphenylammonium tetrafluoroborate (**14**) was allowed to react with butyllithium to give **15**—**17** whose yields were estimated by GLC as shown below.

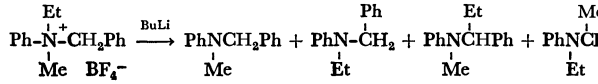

	14	**15**	**16**	**17**	**18**
in Et_2O		34%	6%	20%	—
in THF		35%	6%	12%	—

The compounds, **15** and **16**, are products due to decomposition of ylides resulting by deprotonation of the ethyl and the methyl groups, respectively, and **17** is the product resulting from the migration of the ethyl group. The product **18** due to methyl migration could not be detected.

Judged from the sensitivity of glc, the ratio of migratory aptitude of ethyl group to that of methyl group is estimated to be more than 20. This value is nearly consistent with that for Wittig rearrangement (Et/Me=39)[15] which is generally accepted to proceed by radical pair mechanism as in Stevens rearrangement. Therefore, the remarkable difference between the migratory aptitudes of the ethyl and the methyl groups

Table 4. Yields of Stevens rearrangement products

3	Ar	With LDA		With BuLi		
		9(in Et_2O)/%	**9**(in THF)/%	**19**/%	**20**/%	**21**/%
a	*p*-$MeOC_6H_4$	14	20	33	12	8
b	*p*-MeC_6H_4		47	27		
c	C_6H_5	45	41	38	14	6
d	*p*-ClC_6H_4	59	62	13		

should be attributed to the radical stability in the radical pair during Stevens rearrangement.[16]

Reactions of 3a—d with Butyllithium. Reactions of **3a—d** with butyllithium in ether at −50 °C followed quite different course and gave butyl *o*-(α-dimethylaminobenzyl)phenyl sulfide derivatives (**19**) together with butyl phenyl sulfide (**20**) and *o*-butylthio-*N,N*-dimethylaniline (**21**). The results were shown in Table 4. The structure of **19** was determined by unequivocal synthesis of **19c** (see Experimental).

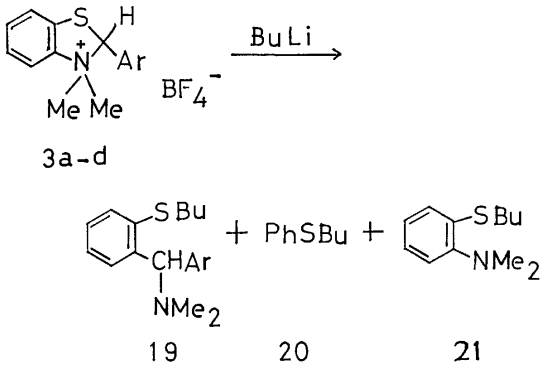

In the case of **3a**, *o*-[1-(*p*-methoxyphenyl)pentylthio]-*N,N*-dimethylaniline (**22**) (4%) was also obtained, and in the case of **3c**, *o*-butylthio-*N*-methylaniline (**23**) (6%) and benzyl phenyl ketone (3%) were also obtained.

A plausible reaction scheme is depicted as shown in Scheme 1.

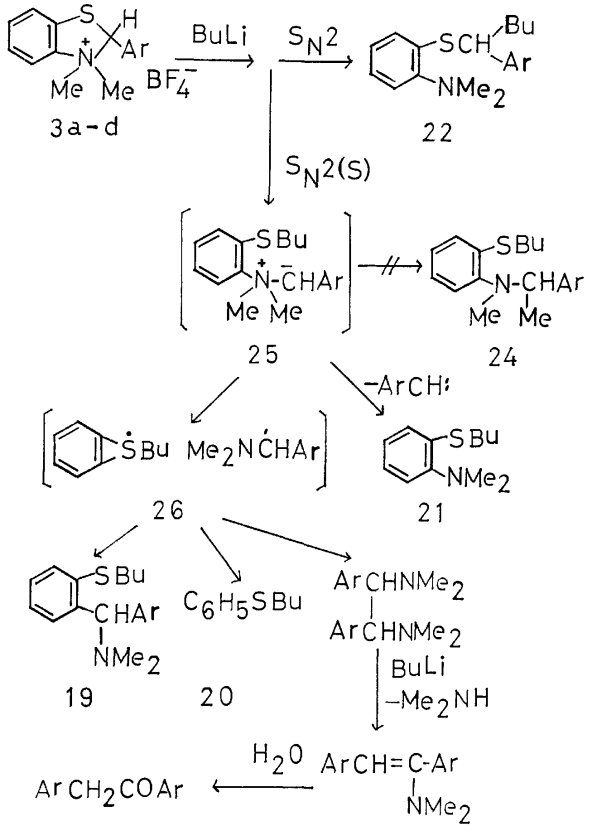

Scheme 1.

The normal product (**9**) derived from cyclic ammonium ylide (**10**) could not be obtained at all in contrast with the reaction with LDA. Formation of **19** can be rationalized by the formation of a ring-opened ammonium ylide (**25**) which then collapses to a radical pair (**26**) or decomposes to give **21** and arylcarbene. The radical pair (**26**) recombines to give **19** and also can afford **20** as an escape product. The starting salt (**3a—d**) is also attacked by butyllithium at the 2-position to a small extent to give **22**.

The most interesting point is that the product is not **24** but **19**, although an expected Stevens rearrangement product is **24**, because of higher migratory aptitude of alkyl groups than that of aryl groups in Stevens rearrangement.[7] However, **19** is the product due to migration of *o*-butylthiophenyl group.

The reason for this unusual aryl migration can be ascribed to participation of the adjacent sulfur atom in stabilizing the aryl radical as shown in **26**. This possibility was supported by reference reaction of trimethyl[*o*-(methylthio)phenyl]ammonium tetrafluoroborate (**27**) to give *N,N*-dimethyl-*o*-(methylthio)benzylamine (**28**) due to aryl migration as a major product (22%) under the same conditions, while *o*-methoxyphenyltrimethylammonium salt (**29**) did not give **30** under the same conditions.

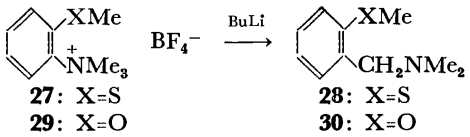

A similar attack on the divalent sulfur atom by butyllithium has been reported in the reactions of 1-methyl-2-nitrosoimino-1,2-dihydrobenzothiazole[17] and diphenylphosphinodithioate esters.[18]

A similar reaction of **7a** gave **31** as a mian product (11%).

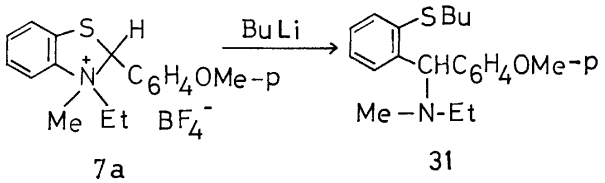

When there is no aryl group at 2-C, a similar reaction gave a complicated mixture and product such as **19** was not obtained.

Experimental

All the melting and boiling points are not corrected. IR spectra were measured with a Hitachi EPI-G2 spectrophotometer, ^{1}H NMR spectra with Hitachi R-24B and R-20B spectrometers using TMS as an internal standard, and MS and high-resolution MS (HMS) with Hitachi RMU-6L and JEOL D-300 mass spectrometers at 70 V, respectively.

Materials. Trimethyl-(**4a**)[19] and triethyloxonium tetrafluoroborates (**4b**),[20] 2,2,3-trimethyl-(**1g**),[21] 2,3-dimethyl-2-phenyl-(**1l**=**9c**),[22] and 2-*t*-butyl-3-phenylbenzothiazolines (**1m**)[23] were prepared according to the reported methods.

Syntheses of Benzothiazolines (1) by Grignard Reaction.[24] *General Procedure*: To a suspension of 3-methyl-(**32a**),[25] 3-ethyl-(**32b**),[21] or 3-methyl-2-methylthiobenzothiazolium io-

dide (**32c**)[22] (0.1 mmol) in ether (90—120 ml) was added dropwise an appropriate Grignard reagent (0.11—0.12 mmol) in ether (90—200 ml), filtered through a tube with glass wool, under nitrogen at −40 °C. The mixture was stirred at room temp for several hours and then refluxed for 0.5 h. The reaction mixture was washed with aq NH_4Cl and the ethereal layer was dried ($MgSO_4$). The solvent was evaporated *in vacuo* and the residue was recrystallized from ethanol, distilled, or purified by column chromatography (CC) (SiO_2, C_6H_6).

*2-(p-Methoxyphenyl)-3-methylbenzothiazoline (**1a**)*: 34% yield from **32a**, pale yellow crystals, mp 106.5—108.5 °C; NMR ($CDCl_3$): δ 2.58 (s, 3H), 3.79 (s, 3H), 5.94 (s, 1H), and 6.25—7.75 (m, 8H). Found: C, 69.87; H, 5.60; N, 5.52%. Calcd for $C_{15}H_{15}NOS$: C, 70.00; H, 5.87; N, 5.44%.

*3-Methyl-2-p-tolylbenzothiazoline (**1b**)*: 68% yield from **32a**, pale yellow crystals, mp 86—89 °C; NMR ($CDCl_3$) : δ 2.37 (s, 3H), 2.64 (s, 3H), 5.99 (s, 1H), and 6.3—7.6 (m, 8H). Found: C, 74.90; H, 6.11; N, 5.82%. Calcd for $C_{15}H_{15}NS$: C, 74.65; H, 6.26; N, 5.80%.

*3-Methyl-2-phenylbenzothiazoline (**1c**)*: 72% yield from **32a**, pale yellow crystals, mp 112—114 °C (lit,[25] 112—113 °C).

*2-(p-Chlorophenyl)-3-methylbenzothiazoline (**1d**)*: 55% yield from **32a**, colorless crystals, mp 77—79 °C; NMR ($CDCl_3$): δ 2.65 (s, 3H), 5.99 (s, 1H), and 6.35—7.7 (m, 8H). Found: C, 64.01; H, 4.80; N, 5.25%. Calcd for $C_{14}H_{12}NSCl$: C, 64.24; H, 4.62; N, 5.35%.

*2,3-Dimethylbenzothiazoline (**1e**)*: 67% yield from **32a**, pale yellow oil, bp 69 °C/0.2 mmHg (1 mmHg=133.322 Pa) (lit,[21] 120—121 °C/10 mmHg).

*3-Ethyl-2-methylbenzothiazoline (**1h**)*: 27% yield from **32b**, yellow oil, bp 95 °C/0.2 mmHg; NMR ($CDCl_3$): δ 1.15 (t, J=6 Hz, 3H), 1.53 (d, J=6 Hz, 3H), 3.21 (br q, J=7 Hz, 2H), 5.23 (q, J=6 Hz, 1H), and 6.2—7.2 (m, 4H). Found: C, 67.27; H, 7.25; N, 7.71%. Calcd for $C_{10}H_{13}NS$: C, 67.00; H, 7.31; N, 7.81%.

*3-Ethyl-2-phenylbenzothiazoline (**1j**)*: 33% yield from **32b**, yellow oil, bp 120 °C/0.25 mmHg; NMR ($CDCl_3$): δ 1.02 (t, J=7 Hz, 3H), 3.11 (m, 2H), 6.22 (s, 1H), and 6.3—7.7 (m, 9H). Found: C, 74.50; H, 6.42; N, 5.63%. Calcd for $C_{15}H_{15}NS$: C, 74.65; H, 6.26; N, 5.80%.

*2,2-Diethyl-3-methylbenzothiazoline (**1k**)*: 83% yield from **32c**, yellow oil;[26] NMR ($CDCl_3$): δ 0.95 (t, J=7 Hz, 6H), 1.82 (br q, J=7 Hz, 4H), 2.65 (s, 3H), and 6.0—7.1 (m, 4H).

*3-Methylbenzothiazoline (**1f**).* To **32a** (3.31 g, 11.9 mmol) in THF (80 ml), $NaBH_4$ (487 mg, 12.9 mmol) was added portionwise at −10 °C. The solution was stirred for 2 h at room temp, and usual work-up gave yellow oil (0.724 g, 40%); bp 90 °C/0.1 mmHg (lit,[25] 133 °C/11 mmHg).

*3-Ethylbenzothiazoline (**1i**)* was prepared from **32b** by a similar method to that of **1f** as pale yellow oil in 65% yield; bp 81 °C/0.1 mmHg; NMR ($CDCl_3$): δ 1.28 (t, J=7 Hz, 3H), 3.18 (q, J=7 Hz, 2H), 4.65 (s, 2H), and 6.3—7.1 (m, 4H). Found: C, 65.63; H, 6.60; N, 8.34%. Calcd for $C_9H_{11}NS$: C, 65.41; H, 6.60; N, 8.34%.

*Alkylations of **1** with Meerwein Reagents (**4**). General Procedure*: To **1** (7 mmol) in CH_2Cl_2 (20—30 ml) was added a slightly excess of **4a** or **4b**. After stirring at room temp for several hours, the reaction was quenched with a few ml of ethanol. The solvent was evaporated *in vacuo*, the residue was washed well with dry ether, and recrystallized to give colorless crystals unless otherwise noticed. The NMR spectra were determined in DMSO-d_6.

Methylation: **3a**: yield 69%, mp 165—167 °C (decomp) (from CH_2Cl_2–Et_2O); NMR: δ 3.12 (s, 3H), 3.65 (s, 3H), 3.87 (s, 3H), 6.94 (s, 1H), and 7.0—8.1 (m, 8H). Found: C, 53.31; H, 5.10; N, 3.73%. Calcd for $C_{16}H_{18}BF_4NOS$: C, 53.50; H, 5.05; N, 3.90%.

3b: pale yellow crystals, yield 59%, mp 195—197 °C (decomp) (from MeOH–Et_2O); NMR: δ 2.42 (s, 3H), 3.10 (s, 3H), 3.66 (s, 3H), 6.94 (s, 1H), and 7.2—8.1 (m, 8H). Found: C, 55.38; H, 5.16; N, 3.99%. Calcd for $C_{16}H_{18}BF_4NS$: C, 56.00; H, 5.29; N, 4.08%.

3c: yield 69%, mp 178.5—180.5 °C (decomp) (from MeOH–Et_2O); NMR: δ 3.11 (s, 3H), 3.71 (s, 3H), 6.99 (s, 1H), and 7.4—8.1 (m, 9H). Found: C, 54.50; H, 5.00; N, 4.11%. Calcd for $C_{15}H_{16}BF_4NS$: C, 54.73; H, 4.90; N, 4.26%. After collection of **3c**, the filtrate and washings were evaporated to be subjected to CC (SiO_2, CH_2Cl_2). *N*-Methyl-*o*-methylthioaniline[6] (IR (neat): 3360 cm^{-1} (NH); NMR ($CDCl_3$): δ 2.17 (s, 3H), 2.70 (s, 3H), 4.76 (br s, 1H), 6.3—6.8, and 6.95—7.45 (m, 4H)) and its hydrotetrafluoroborate (NMR: δ 2.47 (s, 3H), 2.97 (s, 3H), 7.0—7.7 (m, 4H), and 8.01 (br s, 2H)) were obtained in 10 and 4.5% yields, respectively. The NMR spectrum of the latter was in agreement with that of authentic sample obtained from *N*-methyl-*o*-methylthioaniline and tetrafluoroboric acid.

3d: yield 70%, mp 196—197 °C (decomp) (from EtOH–Et_2O); NMR: δ 3.17 (s, 3H), 3.71 (s, 3H), 7.00 (s, 1H), and 7.4—8.1 (m, 8H). Found: C, 49.65; H, 4.05; N, 3.59%. Calcd for $C_{15}H_{15}BClF_4NS$: C, 49.55; H, 4.16; N, 3.85%.

3e: yield 66%, mp 117.5—119.0 °C (decomp) (from CH_2Cl_2–Et_2O); NMR: δ 1.86 (d, J=7 Hz, 3H), 3.35 (s, 3H), 3.73 (s, 3H), 5.81 (q, J=7 Hz, 1H), and 7.3—8.0 (m, 4H). Found: C, 45.24; H, 5.42; N, 5.24%. Calcd for $C_{10}H_{14}BF_4NS$: C, 44.97; H, 5.28; N, 5.24%.

3f: yield 77%, mp 172—173.5 °C (decomp) (from EtOH–Et_2O); NMR: δ 3.62 (s, 6H), 5.34 (s, 2H), and 7.3—8.0 (m, 4H). Found: C, 42.55; H, 4.69; N, 5.71%. Calcd for $C_9H_{12}BF_4NS$: C, 42.72; H, 4.78; N, 5.53%.

3g: yield 71.5%, mp 177—178.5 °C (decomp) (from CH_2Cl_2); NMR: δ 1.95 (s, 6H), 3.55 (s, 6H), and 7.4—8.1 (m, 4H). Found: C, 47.22; H, 5.84; N, 5.27%. Calcd for $C_{11}H_{16}BF_4NS$: C, 47.00; H, 5.74; N, 4.98%.

5 (from **1h**): recryst from EtOH–Et_2O, yield 43% (**5A**/**5B**=*ca.* 2) (see below).

6 (from **1i**): recryst from EtOH–Et_2O, yield 80% (see below).

Ethylation: **5** (from **1e**): yield 61% (**5A**/**5B**=*ca.* 10); NMR: **5A**: δ 1.24 (t, J=7 Hz, 3H), 1.78 (d, J=7.5 Hz, 3H), 3.41 (s, 3H), 3.8—4.3 (m, 2H), 5.81 (q, J=7.5 Hz, 1H), and 7.3—8.0 (m, 4H); **5B**: δ 1.15 (t, J=7 Hz, 3H), 1.91 (d, J=7.5 Hz, 3H), 3.65 (s, 3H), 3.8—4.3 (m, 2H), *ca.* 5.9 (q, J=7.5 Hz, 1H), and 7.3—8.3 (m, 4H). Pure **5A**: mp 160—161.5 °C (decomp) (three times from CH_2Cl_2). Found: C, 47.12; H, 6.01; N, 5.25%. Calcd for $C_{11}H_{16}BF_4NS$: C, 47.00; H, 5.74; N, 4.98%.

6 (from **1f**): yield 49.5%, mp 93.5—95.0 °C (decomp) (from EtOH–Et_2O); NMR: δ 1.40 (t, J=7 Hz, 3H), 3.62 (s, 3H), 4.02 (dq, J=7 Hz and 2 Hz, 2H), 5.31 (s, 2H), and 7.2—7.9 (m, 4H). Found: C, 44.98; H, 5.23; N, 5.32%. Calcd for $C_{10}H_{14}BF_4NS$: C, 44.97; H, 5.28; N, 5.24%.

7aA+**7aB**: pale yellow crystals, yield 39%, mp 145.5—149.5 °C (from CH_2Cl_2–Et_2O) (**A**/**B**=*ca.* 1); NMR: **7aA**: δ 1.42 (t, J=7 Hz, 3H), 3.10 (s, 3H), 3.5—4.2 (m, 2H), 6.86 (s, 1H), and 6.95—8.0 (m, 8H); **7aB**: δ 1.09 (t, J=7 Hz, 3H), 3.53 (s, 3H), 3.5—4.5 (m, 2H), and 6.95—8.0 (m, 9H). Found (mixture): C, 54.65; H, 5.48; N, 3.71%. Calcd for $C_{17}H_{20}BF_4NOS$: C, 54.71; H, 5.40; N, 3.75%.

7bA+**7bB**: pale yellow crystals, yield 37%, mp 158—161 °C (**A**/**B**=*ca.* 1); NMR: **7bA**: δ 1.46 (t, J=7 Hz, 3H),

3.11 (s, 3H), 3.5—4.5 (m, 2H), 6.80 (s, 1H), and 7.2—8.0 (m, 8H); **7bB**: δ 1.13 (t, J=7 Hz, 3H), 3.57 (s, 3H), 3.5—4.5 (m, 2H), 7.07 (s, 1H), and 7.2—8.0 (m, 8H). Found (mixture): C, 57.43; H, 5.86; N, 4.09%. Calcd for $C_{17}H_{20}BF_4NS$: C, 57.16; H, 5.64; N, 3.92%.

7cA+**7cB**: yield 34% (**A**/**B**=*ca.* 10); NMR: **7cA**: δ 1.43 (t, J=7 Hz, 3H), 3.12 (s, 3H), 3.5—4.5 (m, 2H), 6.93 (s, 1H), and 7.4—8.0 (m, 9H); **7cB**: δ 1.08 (t, J=7 Hz, 3H), 3.57 (s, 3H), 3.5—4.5 (m, 2H), 7.17 (s, 1H), and 7.4—8.0 (m, 9H). Pure **7cA**: mp 144—145 °C (decomp) (three times from EtOH-Et_2O). Found: C, 55.76; H, 5.42; N, 3.91%. Calcd for $C_{16}H_{18}BF_4NS$: C, 56.00; H, 5.29; N, 4.08%.

7dA+**7dB**: pale yellow crystals (from CH_2Cl_2-Et_2O) (**A**/**B**=*ca.* 10), yield 35%; NMR: **7dA**: δ 1.42 (t, J=7 Hz, 3H), 3.17 (s, 3H), 3.7—4.6 (m, 2H), 6.89 (s, 1H), and 7.3—8.0 (m, 8H); **7dB**: δ 1.09 (t, J=7 Hz, 3H), 3.58 (s, 3H), 3.7—4.6 (m, 2H), 7.17 (s, 1H), and 7.3—8.0 (m, 8H). Pure **7dA**: mp 139—141 °C (three times from CH_2Cl_2-Et_2O). Found: C, 51.00; H, 4.38; N, 4.00%. Calcd for $C_{16}H_{17}BClF_4NS$: C, 50.89; H, 4.54; N, 3.71%.

Reaction of ***1c*** *with Silver Perchlorate.* 3-Methyl-2-phenylbenzothiazoline (**1c**) (1.1 g, 4.87 mmol) was subjected to the reaction with $AgClO_4$ (1.01 g, 4.89 mmol) in CH_2Cl_2 (20 ml) and $MeNO_2$ (10 ml). After usual work-up, recrystallization from MeOH gave **8** quantitatively, mp 219—223 °C (lit,[27] 219—220 °C).

Reactions of ***3a—d*** *and* ***7*** *with LDA. General Procedure*: To a suspension of the salt (**3a—d** and **7**) (1 mmol) in THF (5 ml) or ether (20 ml) at −40 °C was added LDA (1.1—2 mmol) in THF (5 ml) or ether (5 ml) under nitrogen. The mixture was stirred for 0.5 h at this temp, for 1.5 h at room temp, and then slightly heated. After removal of the solvent *in vacuo* and addition of water, the reaction mixture was extracted with ether. The ethereal layer was dried ($MgSO_4$) and evaporated to be subjected to dry column chromatography (DCC) (**9a**: SiO_2, CCl_4-CH_2Cl_2 (4:1); **9b**: SiO_2, CCl_4-CH_2Cl_2 (10:1); **9c**: SiO_2, CCl_4; **9d**: SiO_2, CCl_4-CH_2Cl_2 (3:1); **11a** and **11b**: SiO_2, hexane-Et_2O (3:1); **11c**: SiO_2, hexane-Et_2O (10:1); **11d**: SiO_2, CCl_4). The results were shown in Table 4 and in the text. These products were identified by a comparison of NMR spectra with authentic samples prepared independently (see below).

Independent Syntheses of ***9***, ***11***, *and* ***12***. *General Procedure*: To a suspension of 2-aryl-3-ethyl- or -3-methylbenzothiazolium perchlorate[27] (5 mmol) in ether (25—70 ml) at −40 °C was added an ethereal solution of Grignard reagent (8.5—10 mmol) under nitrogen. The mixture was stirred for several hours at room temp. After usual work-up, the residue was subjected to DCC (SiO_2, C_6H_6) to give **9** (as colorless crystals), **11** (as yellow viscous oil), and **12**.

9a: yield 68%, mp 58.5—59.5 °C (from EtOH); NMR ($CDCl_3$): δ 1.90 (s, 3H), 2.49 (s, 3H), 3.68 (s, 3H), and 6.1—7.6 (m, 8H). Found: C, 70.58; H, 6.47; N, 5.22%. Calcd for $C_{16}H_{17}NOS$: C, 70.81; H, 6.31; N, 5.16%.

9b: yield 61%, mp 104—105 °C (from EtOH); NMR ($CDCl_3$): δ 1.92 (s, 3H), 2.30 (s, 3H), 2.54 (s, 3H), and 6.1—7.6 (m, 8H). Found: C, 75.04; H, 6.65; N, 5.38%. Calcd for $C_{16}H_{17}NS$: C, 75.25; H, 6.71; N, 5.48%.

9d: yield 84%, mp 95.5—96.5 °C (from EtOH-hexane); NMR ($CDCl_3$): δ 1.95 (s, 3H), 2.55 (s, 3H), and 6.15—7.65 (m, 8H). Found: C, 65.27; H, 5.03; N, 5.25%. Calcd for $C_{15}H_{14}ClNS$: C, 65.32; H, 5.12; N, 5.08%.

11a: yield 68%; NMR ($CDCl_3$): δ 1.05 (t, J=7 Hz, 3H), 2.29 (q, J=7 Hz, 2H), 2.57 (s, 3H), 3.73 (s, 3H), and 6.1—7.6 (m, 8H); HMS: Found: *m/e* 285.1187. Calcd for $C_{17}H_{19}NOS$: 285.1187.

11b: yield 97%; NMR ($CDCl_3$): δ 1.08 (t, J=7 Hz, 3H), 2.32 (s, 3H), 2.33 (q, J=7 Hz, 2H), 2.62 (s, 3H), and 6.15—7.55 (m, 8H). Found: C, 75.73; H, 7.11; N, 5.28%. Calcd for $C_{17}H_{19}NS$: C, 75.79; H, 7.11; N, 5.20%.

11c: yield 77.5%; NMR ($CDCl_3$): δ 1.10 (t, J=7 Hz, 3H), 2.33 (q, J=7 Hz, 2H), 2.61 (s, 3H), and 6.1—7.65 (m, 9H). HMS: *m/e* 255.1109. Calcd for $C_{16}H_{17}NS$: 255.1082.

11d: yield 95%, bp 164 °C/0.1 mmHg; NMR ($CDCl_3$): δ 1.05 (t, J=7 Hz, 3H), 2.26 (q, J=7 Hz, 2H), and 6.1—7.6 (m, 8H). Found: C, 66.05; H, 5.42; N, 5.03%. Calcd for $C_{16}H_{16}ClNS$: C, 66.31; H, 5.56; N, 4.83%.

12a: colorless crystals, yield 92%, mp 78—79 °C (from EtOH-hexane); NMR ($CDCl_3$): δ 1.05 (t, J=7 Hz, 3H), 1.96 (s, 3H), 2.94 (q, J=7 Hz, 2H), 3.68 (s, 3H), and 6.1—7.7 (m, 8H). Found: C, 71.61; H, 7.00; N, 5.00%. Calcd for $C_{17}H_{19}NOS$: C, 71.54; H, 6.71; N, 4.91%.

12b: yellow viscous oil, yield 78%; NMR ($CDCl_3$): δ 1.11 (t, J=7 Hz, 3H), 2.04 (s, 3H), 3.04 (q, J=7 Hz, 2H), and 6.25—7.75 (m, 9H). Found: C, 75.12; H, 6.72; N, 5.46%. Calcd for $C_{16}H_{17}NS$: C, 75.25; H, 6.71; N, 5.48%.

Reactions of ***3a—d*** *and* ***7*** *with Butyllithium. General Procedure*: To a suspension of the salt (**3a—d** and **7**) (2 mmol) in ether (20 ml) under nitrogen at −60 °C was added butyllithium (2.2—2.4 mmol) and the mixture was stirred for 5 h at room temp. After usual work-up, the residue was subjected to DCC and/or TLC.

Reaction of ***3a***: DCC (SiO_2, CH_2Cl_2) afforded two fractions, R_f 0.1—0.2 and 0.5—0.9. TLC (SiO_2, Et_2O) of the former gave pale yellow viscous oil (**19a**) in 32% yield. TLC (SiO_2, hexane-C_6H_6 (1:1)) of the latter fraction gave **20** (12%), **21** (8%), and **22** (4%) as pale yellow oils. **19a**: NMR ($CDCl_3$): δ 0.91 (br t, J=7 Hz, 3H), 1.2—1.8 (m, 4H), 2.19 (s, 6H), 2.65—3.0 (br t, J=7 Hz, 2H), 3.70 (s, 3H), 4.72 (s, 1H), and 6.65—7.9 (m, 8H); MS: *m/e* 329 (M^+, 40%), 314 (M^+−Me, 100), 285 (M^+−NMe_2, 37), 272 (M^+−Bu, 49), and 164 ($Me_2\overset{+}{N}CH$–C_6H_4OMe, 77). **20**: NMR ($CDCl_3$): δ 0.90 (br t, J=7 Hz, 3H), 1.1—1.9 (m, 4H), 2.90 (br t, J=7 Hz, 2H), and 7.0—7.5 (m, 5H). **21**: NMR ($CDCl_3$): δ 0.91 (br t, J=7 Hz, 3H), 1.2—1.9 (m, 4H), 2.7—3.1 (br t, J=7 Hz, 2H), 2.76 (s, 6H), and 6.8—7.4 (m, 4H); MS: *m/e* 209 (M^+, 62%), 153 (M^+−Bu+H, 100), 152 (M^+−Bu, 46), 137 (56), 136 (54), and 120 (M^+−SBu, 32). **22**: NMR ($CDCl_3$): δ 0.83 (br t, J=7 Hz, 3H), 1.1—1.5 (m, 4H), 1.7—2.2 (m, 2H), 2.77 (s, 6H), 3.76 (s, 3H), 4.33 (t, J=7.5 Hz, 1H), and 6.7—7.4 (m, 8H); MS: *m/e* 329 (M^+, 4%), 209 (M^+−$Me_2NC_6H_4$, 58), 177 ($MeOC_6H_4\overset{+}{C}HBu$, 23), and 153 ($Me_2NC_6H_4SH^+$, 100).

Reaction of ***3b***: DCC (SiO_2, CH_2Cl_2) gave pale yellow viscous oil (**19b**) (27%); NMR ($CDCl_3$): δ 0.90 (br t, J=7 Hz, 3H), 1.1—1.9 (m, 4H), 2.18 (s, 6H), 2.23 (s, 3H), 2.7—3.0 (br t, J=7 Hz, 2H), 4.73 (s, 1H), and 6.9—7.9 (m, 8H).

Reaction of ***3c***: DCC (SiO_2, CCl_4-CH_2Cl_2 (2:1)) gave **19c** (38%), benzyl phenyl ketone (3%) (by IR and NMR), and a fraction of R_f 0.8—0.9, the latter of which was subjected again to TLC (SiO_2, C_6H_6-hexane (2:1)) to give **20** (14%), **21** (6%), and **23** (6%). **19c**: mp 42—43 °C; NMR ($CDCl_3$): δ 0.91 (br t, J=7 Hz, 3H), 1.2—1.9 (m, 4H), 2.22 (s, 6H), 2.86 (br t, J=7 Hz, 2H), 4.87 (s, 1H), and 7.0—8.0 (m, 9H); MS: *m/e* 299 (M^+, 74%), 284 (M^+−Me, 100), 242 (M^+−Bu, 54), and 211 (M^+−SBu+H, 55). Found: C, 76.49; H, 8.47; N, 4.65; S, 10.67%. Calcd for $C_{19}H_{25}NS$: C, 76.20; H, 8.41; N, 4.68; S, 10.71%. **23**: NMR ($CDCl_3$): δ 0.88 (br t, J=7 Hz, 3H), 1.1—1.8 (m, 4H), 2.6—3.0 (m, 2H), 2.89 (s, 3H), 5.1 (br s, 1H), and 6.5—7.6 (m, 4H); IR (neat): 3370 cm^{-1} (NH).

*Reaction of **3d***: DCC (SiO_2, CH_2Cl_2) gave **19d** (13%) as pale yellow viscous oil; NMR ($CDCl_3$): δ 0.75—1.1 (m, 3H), 1.2—1.8 (m, 4H), 2.19 (s, 6H), 2.7—3.0 (m, 2H), 4.79 (s, 1H), and 7.0—7.9 (m, 8H).

*Reaction of **7a***: TLC (SiO_2, CH_2Cl_2) gave **31** (11%) as pale yellow oil; NMR ($CDCl_3$): δ 0.96 (br t, J=7 Hz, 3H), 1.03 (t, J=7 Hz, 3H), 1.3—1.8 (m, 4H), 2.16 (s, 3H), 2.47 (q, J=7 Hz, 2H), 2.7—3.0 (m, 2H), 3.74 (s, 3H), 4.98 (s, 1H), and 6.7—7.9 (m, 8H). HMS: Found: *m/e* 343.1962. Calcd for $C_{21}H_{29}NOS$: 343.1968.

*Reaction of **14** with Butyllithium.* *N*-Benzyl-*N*-ethylaniline (5.70 g, 27.0 mmol) was methylated with **4a** (4.38 g, 29.6 mmol) in CH_2Cl_2 (30 ml). After addition of ether, the resulting precipitates were recrystallized from CH_2Cl_2–Et_2O to give **14** (5.82 g, 69%); NMR (DMSO-d_6): δ 1.09 (t, J=7 Hz, 3H), 3.37 (s, 3H), 4.08 (m, 2H), 5.00 (br d, J=2.5 Hz, 2H), and 6.8—7.8 (m, 10H). To **14** (1.06 g, 3.39 mmol) in THF (25 ml) was added BuLi (3.8 mmol) under nitrogen at −50 °C. The products extracted with ether was a mixture of **15** (35%), **16** (6%), and **17** (12%) by glc (column, OV-1, 170 °C). In ether (15 ml), the products were a mixture of **15** (34%), **16** (6%), and **17** (20%).

*Preparation of N-(α-Ethylbenzyl)-N-methylaniline (**17**).* *N*-Benzylideneaniline (5.31 g, 29.3 mmol) in ether (15 ml) was added to EtMgI (31.3 mmol) in ether (50 ml). The mixture was refluxed for 1.5 h and poured into ice and concd HCl (100 ml). After usual work-up, DCC (SiO_2, hexane–CH_2Cl_2 (1.7:1)) of the residue gave *N*-(α-ethylbenzyl)aniline (2.15 g, 35%). The product (2.05 g, 9.70 mmol) was methylated by **4a** (2.10 g, 14.2 mmol) in CH_2Cl_2 (20 ml) under reflux for 1 h. After addition of ether, the resulting precipitates were dissolved in CH_2Cl_2 followed by deprotonation with Et_3N (4.1 ml, 29 mmol). Usual work-up gave **17**, 1.76 g, 80.5% yield, bp 118 °C/0.05 mmHg; NMR ($CDCl_3$): δ 0.97 (t, J=7 Hz, 3H), 1.96 (m, 2H), 2.62 (s, 3H), 4.79 (br t, J=7 Hz, 1H), and 6.5—7.3 (m, 10H). Found: C, 85.20; H, 8.61; N, 6.31%. Calcd for $C_{16}H_{19}N$: C, 85.28; H, 8.50; N, 6.22%.

*Preparation of N-Ethyl-N-(α-methylbenzyl)aniline (**18**).* *N*-(α-Methylbenzyl)aniline (42% yield) was prepared from *N*-benzylideneaniline and MeMgI and ethylated with **4b** in a similar manner to that of **17** to afford **18** in 88% yield, bp 115 °C/0.07 mmHg; NMR ($CDCl_3$): δ 1.04 (t, J=7 Hz, 3H), 1.54 (d, J=7 Hz, 3H), 3.19 (q, J=7 Hz, 2H), 5.04 (br q, J=7 Hz, 1H), and 6.5—7.4 (m, 10H). Found: C, 85.17; H, 8.76; N, 6.03%. Calcd for $C_{16}H_{19}N$: C, 85.28; H, 8.50; N, 6.22%.

*Reaction of **27** with Butyllithium.* To trimethyl[*o*-(methylthio)phenyl]ammonium tetrafluoroborate (**27**)[28] (298 mg, 1.11 mmol) in ether (15 ml) was added BuLi (1.40 mmol). A similar treatment to that of **7** and submission to TLC (SiO_2, hexane–Et_2O (5:1)) gave **28**, 44.7 mg, 22% yield; NMR ($CDCl_3$): δ 2.25 (s, 6H), 2.42 (s, 3H), 3.45 (s, 2H), and 6.8—7.3 (m, 4H).

*Independent Synthesis of **19c**.* *o*-Butylthioaniline was prepared from sodium *o*-aminobenzenethiolate and BuBr in 82.5% yield, bp 87 °C/0.4 mmHg. The aniline was converted into *o*-bromophenyl butyl sulfide by Sandmeyer reaction in 40% yield. The sulfide (1.30 g, 5.32 mmol) was treated with BuLi (5.25 mmol) in ether (10 ml). Benzaldehyde (0.537 g, 5.06 mmol) in ether (10 ml) was added to this solution at −15 °C and the mixture was stirred for 14 h at room temp. After usual work-up, submission to DCC (SiO_2, CCl_4) gave α-(*o*-butylphenyl)benzyl alcohol, 1.26 g, 92% yield. This alcohol (1.17 g, 4.29 mmol) was treated with $SOCl_2$ (0.36 ml) in pyridine (0.39 ml) and ether (15 ml) by a similar method to that described in the literature.[29] Distillation gave butyl *o*-(α-chlorobenzyl)phenyl sulfide, 1.06 g, 85% yield; NMR ($CDCl_3$): δ 0.7—1.0 (m, 3H), 1.2—1.8 (m, 4H), 2.82 (br t, J=7 Hz, 2H), 6.78 (s, 1H), and 7.0—7.6 (m, 9H); MS: *m/e* 290 (M^+). Butyl *o*-(α-chlorobenzyl)-phenyl sulfide (0.85 g, 2.92 mmol) in ether (10 ml) was added at −60 °C to Me_2NLi (6.16 mmol) in ether (15 ml). After stirring for 2 h at room temp and then washing with water, the ethereal layer was subjected to DCC (SiO_2, CCl_4–CH_2Cl_2 (3:1)) to afford **19c** (671 mg, 77%); bp *ca.* 120 °C/0.1 mmHg. The spectral data were in agreement with those of reaction product.

References

1) J. L. Richards and D. S. Tarbell, *J. Org. Chem.*, **35**, 2079 (1970).
2) H. Minato, K. Yamaguchi, and M. Kobayashi, *Chem. Lett.*, **1975**, 991.
3) C. R. Johnson, E. R. Janiga, and M. Haake, *J. Am. Chem. Soc.*, **90**, 3890 (1968).
4) J. W. Masico, Jr., G. O. Morton, and L. Goldman, *J. Org. Chem.*, **42**, 2164 (1977).
5) K. Akiba, Y. Ohara, and N. Inamoto, *Heterocycles*, **6**, 13 (1977).
6) M. Hori, T. Kataoka, H. Shimizu, and Y. Imai, *Chem. Pharm. Bull. (Tokyo)*, **25**, 1482 (1977).
7) S. H. Pine, *Org. React.*, **18**, 403 (1970); *J. Chem. Educ.*, **48**, 99 (1971).
8) For review see: Y. Ohara and K. Akiba, *Kagaku No Ryoiki*, **33**, 843 (1979).
9) a) T. S. Johnstone and T. S. Stevens, *J. Chem. Soc.*, **1930**, 2107; b) J. H. Brewster and M. W. Kline, *J. Am. Chem. Soc.*, **74**, 5179 (1952); c) U. Schöllkopf, U. Ludwig, G. Ostermann, and M. Patsch, *Tetrahedron Lett.*, **1969**, 2619, 3415.
10) A. Campbell, A. H. J. Houston, and J. Kenyon, *J. Chem. Soc.*, **1949**, 93; B. J. Millard and T. S. Stevens, *ibid.*, **1963**, 3397.
11) U. E. Baldwin, W. F. Erickson, R. E. Hackler, and R. M. Scott, *Chem. Commun.*, **1970**, 576; A. R. Lepley, *ibid.*, **1969**, 1460.
12) M. J. S. Dewar and C. A. Ramsden, *J. Chem. Soc., Perkin Trans. 1*, **1974**, 1839.
13) Preliminary reports: K. Akiba, Y. Ohara, and N. Inamoto, *Heterocycles*, **11**, 231 (1978); Y. Ohara, K. Akiba, and N. Inamoto, *ibid.*, **13**, 289 (1979).
14) J. W. Henderson, *Chem. Soc. Rev.*, **2**, 397 (1973).
15) P. T. Lansbury, V. A. Pattison, J. D. Sidler, and J. B. Bieber, *J. Am. Chem. Soc.*, **88**, 78 (1966); H. Schäfer, U. Schöllkopf, and D. Walter, *Tetrahedron Lett.*, **1968**, 2809.
16) U. Schöllkopf, *Angew. Chem., Int. Ed. Engl.*, **9**, 763 (1970).
17) M. Hisaoka, K. Akiba, and Inamoto, *Bull. Chem. Soc. Jpn.*, **48**, 3274 (1975).
18) K. Goda, R. Okazaki, K. Akiba, and N. Inamoto, *Bull. Chem. Soc. Jpn.*, **51**, 260 (1978).
19) T. J. Curphey, *Org. Synth.*, **51**, 142 (1971).
20) H. Meerwein, *Org. Synth.*, Coll. Vol. **V**, 1080 (1973).
21) J. Metzger, H. Lanire, E. J. Vincent, and R. Dennilauler, *J. Chim. Phys.*, **60**, 944 (1963).
22) A. I. Kiprianov and V. A. Portnyagina, *Zh. Obshch. Khim.*, **25**, 2257 (1955); *Chem. Abstr.*, **50**, 9378[b] (1956).
23) K. Akiba, T. Kawamura, M. Hisaoka, and N. Inamoto, *Bull. Chem. Soc. Jpn.*, **48**, 3262 (1975).
24) Preliminary report: K. Akiba, Y. Ohara, M. Hisaoka, and N. Inamoto, *Heterocycles*, **3**, 567 (1975).

25) K. Baker and H. E. Fierz-David, *Helv. Chim. Acta*, **33**, 2011 (1950).
26) K. Akiba, H. Shiraishi, and N. Inamoto, *Bull. Chem. Soc. Jpn.*, **52**, 156 (1979).
27) A. I. Kiprianov and Ya. Shtets, *Zh. Obshch. Khim.*, **33**, 3519 (1963); *Chem. Abstr.*, **60**, 10839^{f} (1964).
28) Y. Ohara, K. Akiba, and N. Inamoto, unpublished result.
29) D. W. Meek, G. Dyer, and M. O. Workman, *Inorg. Synth.*, **16**, 168 (1976).

The Crystal and Molecular Structures of Tetronolide

Noriaki HIRAYAMA,* Masaji KASAI, Kunikatsu SHIRAHATA,
Yuji OHASHI,† and Yoshio SASADA†

Tokyo Research Laboratory, Kyowa Hakko Kogyo Co., Ltd., 3-6-6 Asahimachi, Machida-shi, Tokyo 194

† *Laboratory of Chemistry for Natural Products, Tokyo Institute of Technology, Nagatsuta, Midori-ku, Yokohama 227*

(Received February 4, 1982)

Tetronolide is an aglycone moiety of novel antitumor antibiotics tetrocarcins. The space group of the crystal is $P2_12_12_1$ with $a=20.138(3)$, $b=22.680(3)$, $c=7.848(1)$ Å and $Z=4$. The structure was solved by direct methods and refined by the block-diagonal least-squares using 3577 independent reflexions. The final R value was 0.085. It is established that tetronolide is [1R-(1R*,3R*,4R*,4aR*,6aR*,7E,10R*,11E,12aS*,13R*,16aR*,20aR*,20bS*)]-1,2,3,4,4a,6a,9,10,12a,13,16,20,20a,20b-tetradecahydro-4,10,13,21-tetrahydroxy-1,3,7,11,20a-pentamethyl-18,20-dioxo-18*H*-16a,19-metheno-16a*H*-benzo[*b*]naphth[2,1-*j*]oxacyclotetradecin-15-carbaldehyde or its enantiomer.

Tetronolide (**1**) is an aglycone moiety of novel antitumor antibiotics tetrocarcins,[1,2] which are produced by *Micromonospora chalcea KY11091*. The structure of tetronolide could not be determined by the ordinary spectroscopic and chemical methods.[3] Therefore X-ray analysis of tetronolide was undertaken. It has been revealed that the molecule contains a peculiar skeleton; chlorothricolide (**2**)[4] is the only compound which possesses the similar molecular skeleton.[5] The preliminary results have already been published.[6]

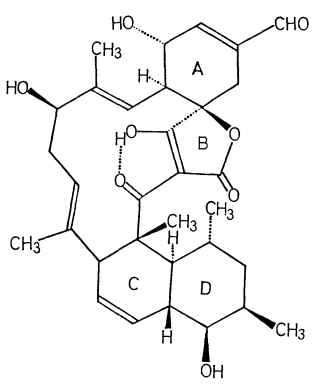

1

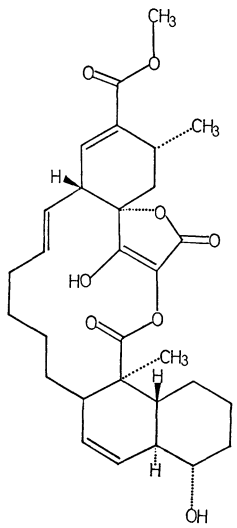

2

Experimental and Structure Determination

Prismatic crystals of the title compound were obtained from an ethyl acetate solution containing a trace amount of methanol. A $0.22\times0.22\times0.65$ mm^3 crystal was used for data collection on a Rigaku four-circle automated diffractometer with Mo $K\alpha$ radiation ($\lambda=0.71069$ Å). Preliminary unit cell dimensions and space group were obtained from photographs. The space group was assigned to be $P2_12_12_1$ from systematic absences ($h00$ for odd h, $0k0$ for odd k, $00l$ for odd l). Accurate cell dimensions were determined by the least-squares calculation with 2θ values of 16 high-angle reflexions measured on the diffractometer. Crystal data are as follows: $C_{32}H_{40}O_8$; M. W.=552.664; $P2_12_12_1$; $Z=4$; $a=20.138(3)$, $b=22.680(3)$, $c=7.848(1)$ Å; $D_x=1.19$ g cm^{-3}; μ(Mo $K\alpha$)$=3.65$ cm^{-1}. All independent reflexions within the range $2\theta\leqq55°$ were collected by use of the ω-2θ scan mode with a scanning rate $4°(2\theta)$ min^{-1}. Stationary background counts were accumulated for 10 s before and after each scan. Periodic checks of the intensity values of three standard reflexions showed no significant X-ray damage or crystal decay. Any corrections for absorption or extinction were not applied. A total of 3655 independent reflexions were obtained, of which 3577 ($|F_o|>3.0\sigma(|F_o|)$) were used for the structure determination.

The phases of 260 reflexions with $|E_o|\geqq1.67$ were assigned with MULTAN 78.[7] The best set of phases was employed to calculate an E map, which gave the appropriate peaks for all non-hydrogen atoms. The structural parameters were refined by the block-diagonal least-squares methods with the modified HBLS program. All of the hydrogen atoms were located from difference syntheses. In addition to the hydrogen atoms many peaks with height of about 0.3 eÅ^{-3} appeared on the difference map. Most of them were located between the molecules, of which six were regarded to correspond to solvent molecules of ethyl acetate, and their atomic parameters were successfully refined isotropically with the occupancy of 0.2. The weighting system applied was $w=1/(\sigma^2(F_o)+(0.015F_o)^2)$. The final R value is 0.085. Atomic scattering factors were taken from "International Tables for X-Ray Crystallography."[8] The final positional and thermal parameters are given in Table 1.**

Results and Discussion

Bond Lengths and Angles. The atomic numbering and ring names are shown in Fig. 1. The stereoscopic drawing of the tetronolide molecule is given in Fig. 2. Absolute configuration was not determined. Bond lengths and angles are tabulated in Table 2. The C–C bonds around the ring B are short, *i.e.*, C(30)–C(32)=1.48(1), C(2)–C(32)=1.42(1), C(1)–C(2)=1.49(1), and C(2)–C(3)=1.41(1) Å. This indicates that the π electrons are delocalized extensively through-

** The tables of the observed and calculated structure factors, the anisotropic thermal parameters of non-hydrogen atoms, the atomic parameters of hydrogen atoms and the solvent molecule, and torsional angles in the molecule are kept as Document No. 8241 at the Chemical Society of Japan.

Table 1. Final atomic parameters with their estimated standard deviations, multiplied by 10^4 for C and O atoms

Atom	x	y	z	B_{eq}/Å^2	Atom	x	y	z	B_{eq}/Å^2
O(1)	8837(2)	1182(2)	8546(6)	3.01	C(13)	10607(5)	1765(5)	4594(12)	5.54
O(2)	7990(2)	1783(2)	7979(7)	3.62	C(14)	10105(4)	2732(4)	5519(11)	4.05
O(3)	9437(2)	686(2)	4576(7)	3.45	C(15)	9604(4)	2831(4)	4050(12)	4.46
O(4)	9527(3)	837(2)	10050(9)	6.24	C(16)	8925(4)	2611(3)	4457(10)	3.45
O(5)	10816(2)	1449(2)	10138(7)	3.90	C(17)	8453(4)	2465(3)	3362(10)	3.03
O(6)	9908(3)	3032(3)	7023(9)	4.66	C(18)	8553(4)	2489(4)	1486(11)	4.38
O(7)	5785(2)	2288(2)	−178(7)	3.38	C(19)	7775(3)	2282(3)	4026(10)	2.84
O(8)	8520(2)	1128(2)	2783(6)	3.40	C(20)	7266(4)	2702(3)	3376(11)	3.22
C(1)	8374(3)	1428(3)	7441(9)	2.65	C(21)	6771(4)	2541(3)	2355(11)	3.44
C(2)	8513(3)	1212(3)	5685(10)	2.49	C(22)	6640(3)	1920(3)	1788(9)	2.38
C(3)	9122(3)	911(3)	5785(10)	2.50	C(23)	6362(3)	1901(3)	−39(10)	2.80
C(4)	9356(3)	879(3)	7631(10)	2.84	C(24)	6190(4)	1275(3)	−647(9)	2.70
C(5)	9397(4)	244(3)	8248(11)	4.08	C(25)	5527(4)	1052(3)	−233(10)	3.40
C(6)	9783(4)	176(3)	9850(10)	3.40	C(26)	6754(3)	858(3)	−233(10)	2.87
C(7)	10131(4)	617(3)	10549(10)	3.59	C(27)	6997(3)	874(3)	1639(10)	3.36
C(8)	10163(4)	1230(3)	9829(7)	2.82	C(28)	7456(4)	359(3)	1980(13)	4.02
C(9)	10000(4)	1231(3)	7923(9)	2.76	C(29)	7250(3)	1506(3)	2021(9)	2.15
C(10)	9786(5)	−413(4)	10641(13)	5.25	C(30)	7564(3)	1607(3)	3799(9)	2.31
C(11)	9940(3)	1859(3)	7293(10)	2.56	C(31)	7056(3)	1448(4)	5209(10)	3.62
C(12)	10199(4)	2086(3)	5894(10)	3.21	C(32)	8202(3)	1303(3)	4082(9)	2.36

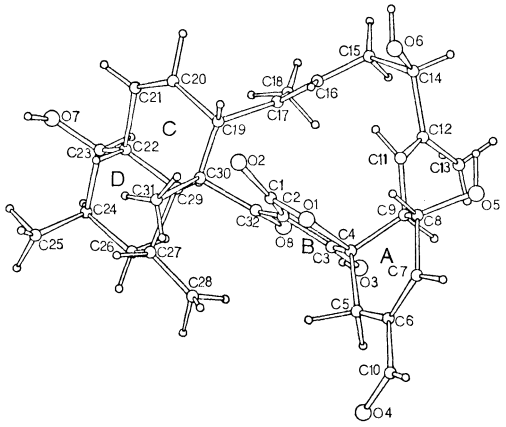

Fig. 1. The numbering system of tetronolide.

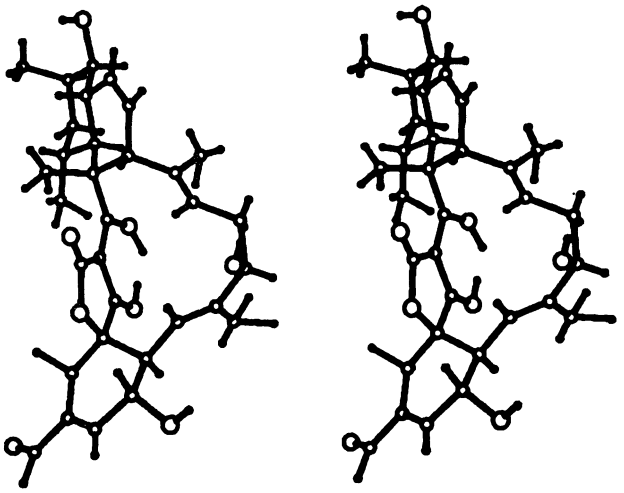

Fig. 2. Stereoscopic drawing of tetronolide.
The figure and Fig. 4 were drawn by TSD:XTAL, which is a computer-graphics interactive modeling program for a NOVA 3 computer.[9]

out this part. There is an intramolecular hydrogen bond between the O(3) and O(8) atoms. The bond lengths of C(3)–O(3) and C(32)–O(8) (1.250 and 1.267 Å, respectively) show that both of these bonds are intermediate of carbonyl and hydroxyl C–O bonds. Moreover the elctron density which corresponds to the two hydrogen atoms bonded to O(3) and O(8) atoms appeared on the difference map. These facts indicate that there are two tautomeric fomrs as $-\overset{\overset{O\cdots HO}{\|}}{C}-C=\overset{|}{C}-$ and $-\overset{|}{C}=C-\overset{\overset{OH\cdots O}{|}}{\underset{\|}{C}}-$. The geometry of the hydrogen bond is as follows: O(3)···O(8)=2.528(7), H(O(3))···O(8)=1.81(3), H(O(8))···O(3)=1.81(3) Å, ∠O(3)–H···O(8)=139(3), and ∠O(3)···H–O(8)=138(3)°.

In chlorothricolide (**2**) containing a closely related skeleton,[4] there is a similar but much weaker intramolecular C=O···H–O hydrogen bond; the O···O distance averaged over the two independent molecules of **2** in asymmetric unit is 2.95 Å.

The C(19)–C(30) distance is remarkably long (1.60 Å) and the corresponding C–C distance in **2** is also long (the average distance is 1.58 Å).

Of the two intramolecular short contacts, the contact between the C(28) atom and the O(8) atom is of perticular interest; the C(28)···O(8), HAC(28)···O(8) and HBC(28)···O(8) distances are 2.83(1), 2.35(7), and 2.56(9) Å, respectively. These values indicate that the C(28) methyl group is so sterically hindered by the O(8) atom that the rotation of the methyl group may be considerably restricted. On the other hand, the C(31) methyl group also contacts with the O(2) carbonyl oxygen atom. The geometry, the C-

TABLE 2. BOND LENGTHS AND ANGLES

Bond length	l/Å				
C(1)-C(2)	1.49(1)	C(19)-C(30)	1.60(1)	C(15)-C(14)-O(6)	111.5(7)
C(1)-O(1)	1.390(9)	C(27)-C(29)	1.55(1)	C(12)-C(14)-C(15)	111.6(7)
C(1)-O(2)	1.194(9)	C(29)-C(30)	1.55(1)	C(14)-C(15)-C(16)	112.9(8)
C(2)-C(3)	1.41(1)	C(30)-C(31)	1.55(1)	C(15)-C(16)-C(17)	127.1(8)
C(2)-C(32)	1.42(1)	C(30)-C(32)	1.48(1)	C(16)-C(17)-C(18)	122.5(8)
C(3)-C(4)	1.53(1)	C(32)-O(8)	1.267(9)	C(16)-C(17)-C(19)	119.4(7)
C(3)-O(3)	1.250(9)	C(10)-O(4)	1.19(1)	C(18)-C(17)-C(19)	118.1(7)
C(3)-C(4)	1.53(1)	Bond angle	ϕ/°	C(17)-C(19)-C(20)	109.0(6)
C(4)-C(5)	1.52(1)	C(2)-C(1)-O(1)	108.6(6)	C(17)-C(19)-C(30)	117.6(6)
C(4)-C(9)	1.54(1)	C(3)-C(2)-C(1)	105.7(6)	C(20)-C(19)-C(30)	112.9(6)
C(4)-O(1)	1.442(9)	O(1)-C(1)-O(2)	119.0(7)	C(19)-C(20)-C(21)	123.1(8)
C(5)-C(6)	1.49(1)	C(2)-C(1)-O(2)	132.1(7)	C(20)-C(21)-C(22)	124.6(8)
C(6)-C(10)	1.47(1)	C(1)-C(2)-C(32)	133.7(7)	C(21)-C(22)-C(29)	113.1(6)
C(6)-C(7)	1.34(1)	C(3)-C(2)-C(32)	120.3(7)	C(22)-C(29)-C(30)	109.8(6)
C(7)-C(8)	1.50(1)	C(2)-C(3)-O(3)	126.7(7)	C(29)-C(30)-C(19)	110.7(6)
C(8)-C(9)	1.53(1)	C(2)-C(3)-C(4)	110.3(6)	C(21)-C(22)-C(23)	111.5(6)
C(8)-O(5)	1.427(9)	C(4)-C(3)-O(3)	123.0(7)	C(29)-C(22)-C(23)	112.4(6)
C(9)-C(10)	1.51(1)	C(1)-O(1)-C(4)	111.5(5)	C(22)-C(23)-C(24)	113.4(6)
C(11)-C(12)	1.32(1)	C(3)-C(4)-O(1)	103.1(6)	C(22)-C(23)-O(7)	110.1(6)
C(12)-C(13)	1·50(1)	C(3)-C(4)-C(9)	112.1(6)	C(24)-C(23)-O(7)	110.7(6)
C(12)-C(14)	1.51(1)	O(1)-C(4)-C(5)	109.4(6)	C(23)-C(24)-C(26)	110.0(6)
C(14)-O(6)	1.42(1)	C(9)-C(4)-C(5)	113.5(6)	C(23)-C(24)-C(25)	113.0(6)
C(14)-C(15)	1.55(1)	C(4)-C(5)-C(6)	113.3(7)	C(26)-C(24)-C(25)	111.8(6)
C(15)-C(16)	1.49(1)	C(5)-C(6)-C(7)	122.9(8)	C(24)-C(26)-C(27)	115.2(6)
C(16)-C(17)	1.32(1)	C(5)-C(6)-C(10)	117.0(8)	C(26)-C(27)-C(28)	110.0(7)
C(17)-C(18)	1.49(1)	C(7)-C(6)-C(10)	120.2(8)	C(29)-C(27)-C(28)	118.6(7)
C(17)-C(19)	1.52(1)	C(6)-C(10)-O(4)	124.5(9)	C(26)-C(27)-C(29)	108.0(6)
C(19)-C(20)	1.49(1)	C(6)-C(7)-C(8)	124.0(7)	C(22)-C(29)-C(27)	106.0(6)
C(20)-C(21)	1.33(1)	C(7)-C(8)-C(9)	111.1(6)	C(19)-C(30)-C(32)	101.4(6)
C(21)-C(22)	1.50(1)	C(7)-C(8)-O(5)	107.3(6)	C(29)-C(30)-C(31)	109.9(6)
C(22)-C(29)	1.56(1)	C(9)-C(8)-O(5)	111.3(6)	C(31)-C(30)-C(32)	110.9(6)
C(22)-C(23)	1.54(1)	C(8)-C(9)-C(4)	108.9(6)	C(3)-C(4)-C(5)	111.3(6)
C(23)-C(24)	1.54(1)	C(8)-C(9)-C(11)	109.8(6)	C(9)-C(4)-O(1)	106.8(6)
C(23)-O(7)	1.460(9)	C(4)-C(9)-C(11)	111.9(6)	C(29)-C(30)-C(32)	115.0(6)
C(24)-C(25)	1.53(1)	C(9)-C(11)-C(12)	127.5(7)	C(19)-C(30)-C(31)	108.5(6)
C(24)-C(26)	1.51(1)	C(11)-C(12)-C(13)	126.4(8)	C(30)-C(32)-C(2)	125.9(7)
C(26)-C(27)	1.55(1)	C(11)-C(12)-C(14)	119.5(7)	C(30)-C(32)-O(8)	117.7(6)
C(27)-C(28)	1.51(1)	C(13)-C(12)-C(14)	114.1(7)	C(2)-C(32)-O(8)	116.4(7)
		C(12)-C(14)-O(6)	109.9(7)		

(31)···O(2) distance of 2.793 Å and the C(31)-H···O(2) angle of 145°, indicates that this contact is a hydrogen bond. Since a similar methyl group in **2** is trans to the carbonyl oxygen atom, there is no possibility for such an intramolecular hydrogen bond.

Some exo- and endocyclic bond angles of the γ-lactone ring are distorted. The C(1)-C(2)-C(32), O(2)-C(1)-C(2), and C(2)-C(3)-O(3) angles are 133.7, 132.1, and 126.7°, respectively. The corresponding bond angles in chlorothricolide are also large (the average values are 135.9, 126.8, and 133.0°). Such distortion of the bond angles may be explained by the planar geometry of ring B with O(3), C(32), and O(8) atoms caused by the extensive delocalization of the π electrons.

The O(1)-C(4)-C(3) angle of 101.1(6)° at the spiro group in tetronolide is small (the corresponding averaged value of 102.8° in **2** is also small).

Although the C(19)-C(30)-C(32) angle of 101.4(6)° is remarkably small in tetronolide, but the corresponding value 107.3° in **2** is within the expected region.

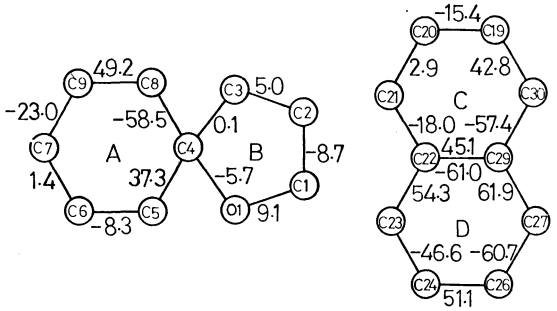

Fig. 3. Torsional angles in the rings, τ/°.

Other bond lengths and angles are normal.

Conformation. The thirteen-membered ring, two cyclohexene rings, and the cyclohexane ring take the crown, the half-chair, and the chair conformation, respectively. The γ-lactone ring is in the envelope con-

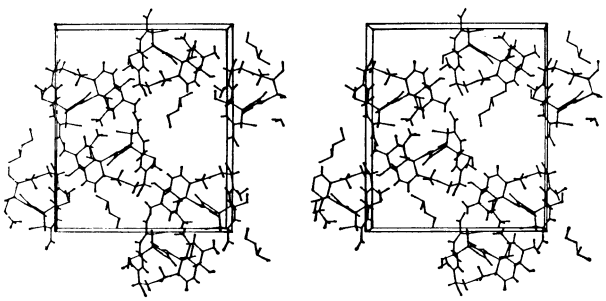

Fig. 4. Crystal structure viewed along the c axis. The vertical and holizontal axes denote b and a axes.

formation. The ring torsional angles in each ring are shown in Fig. 3. The conformational characteristics as a whole is similar to that of **2**. Ring A is more flattened than C. In the cyclohexane ring C(27) and C(29) are puckered, and C(23) and C(24) are flattened. Rings C and D are fused in the *trans*-decalin type.

Crystal Structure. The crystal structure viewed along the c axis is shown in Fig. 4. The molecules are connected by the two intermolecular hydrogen bonds and form the helical chain along the a axis. The geometry of the hydrogen bonds are $O(5)^{I}\cdots O(7)^{II}=2.865(8)$ Å, $\angle O(5)\text{-}H^{I}\cdots O(7)^{II}=172(3)°$; $O(7)^{II}\cdots O(6)^{I}=3.127(8)$ Å, $\angle O(7)\text{-}H^{II}\cdots O(6)^{I}=166(3)°$. Symmetry codes I and II denote (x,y,z) and $(0.5+x,\ 0.5-y,\ 1.0-z)$, respectively. The helical chains are stacked mainly by van der Waals interactions. There are large cavities between the helical chains, and the ethyl acetate molecule is located in the cavity. As mentioned in the experimental section many fragments corresponding to the low but significant electron density still remained at the final stage of the refinement. The fact indicates that much more solvent molecules must exist in the crystal.

References

1) F. Tomita and T. Tamaoki, *J. Antibiot.*, **33**, 940 (1980).
2) T. Tamaoki, M. Kasai, K. Shirahata, S. Ohkubo, M. Morimoto, K. Mineura, S. Ishii, and F. Tomita, *J. Antibiot.*, **33**, 946 (1980).
3) M. Kasai and K. Shirahata, *J. Antibiot.*, in press.
4) M. Brufani, S. Cerrini, W. Fedeli, F. Mazza, and R. Muntwyler, *Helv. Chim. Acta*, **55**, 2094 (1972).
5) A similar ring system is recently found in kijanimicin. A. K. Mallams, M. S. Puar, R. R. Rossman, A. T. McPhail, and R. D. Macfarlane, *J. Am. Chem. Soc.*, **103**, 3940 (1981).
6) N. Hirayama, M. Kasai, K. Shirahata, Y. Ohashi, and Y. Sasada, *Tetrahedron Lett.*, **1980**, 2559.
7) P. Main, S. E. Hull, L. Lessinger, G. Germain, J. P. Declercq, and M. M. Woolfson, MULTAN 78. A System of Computer Program for the Automatic Solution of Crystal Structures from X-Ray Diffraction Data, Univs. of York, England, and Louvain, Belgium (1978).
8) "International Tables for X-Ray Crystallography" Kynoch Press, Birmingham (1974), Vol. IV, pp. 72—102.
9) A. Takenaka and Y. Sasada, *J. Cryst. Soc. Jpn.*, **22**, 214 (1980).

Thermodynamic Properties for the Adduct Formation of Some Shift Reagents with Aniline

Hideo Kojima, Hiroshi Nonaka, and Minoru Hirota*
Department of Applied Chemistry, Faculty of Engineering, Yokohama National University, Hodogaya-ku, Yokohama 240
(Received February 6, 1982)

Equilibrium constants, enthalpies, and entropies of formation of the shift reagent-substrate adducts were determined by the measurement of infrared spectra. Aniline was employed as substrate in most cases since its NH stretching absorption bands (ν_{as}) does not overlap with those of the adducts and suitable to estimate the amount of its free species quantitatively. A series of $Ln(dpm)_3$ and $Ln(fod)_3$ (where Ln=Pr, Nd, Sm, Eu, Gd, Tb, Dy, Ho, and Yb) were used as shift reagents. The formation constants (K_1 and K_2), as well as ΔH, decrease in the increasing order of the atomic numbers of the central lanthanoid ions. The results were compared with those on some bis(β-diketonato) complexes of transition metal ions and discussed.

Since the discovery by Hinckley,[1] various lanthanoid shift reagents have been widely employed to expand the chemical shift range of NMR spectrum without remarkable broadening of the signals. Quite a few examples[2—5] of their application have been reported, and many new shift reagents, including Ag compounds[6] for aromatic substrates, have been prepared and used both to resolve the overlapping signals and to determine the stereochemistry of many complex organic compounds by use of the steric factor in the McConnell-Robertson equation.[7,8] However, the properties of the shift reagent-substrate complexes have not been known very thoroughly. Thus, the shift reagent-substrate complexes were studied quantitatively by the measurement of infrared spectra of the complexes in solution in order to determine their formation equilibrium constants and to estimate the enthalpies and the entropies of their formation.[9]

Theoretical

In general, 1:1 and 1:2 complexes RS and RS_2 are formed when the lanthanoid shift reagent (R) is added to the solution of the substrate (S). These reactions and their formation constants are expressed by the following equations. When the infrared X–H

$$R + S \rightleftharpoons RS \qquad K_1 = \frac{[RS]}{[R][S]} \tag{1}$$

$$RS + S \rightleftharpoons RS_2 \qquad K_2 = \frac{[RS_2]}{[RS][S]} \tag{2}$$

stretching bands are selected as key bands, addition of the shift reagent to the solution of substrate gives rise to new absorption band(s) in addition to the absorption band(s) due to the free species of the substrate, hereby accompanying a decrease in the intensity of the free band. The new bands are assigned to the complexed species RS and/or RS_2. If the measurements are carried out under conditions in which the Lambert-Beer law is valid, the concentration of the free substrate [S] is obtained from the intensity of the band assigned to the free substrate and its molar absorptivity ε_f, which can be determined easily by the measurement on the substrate alone in the same solvent. From the concentration of the free substrate [S] obtained by the infrared measurement, concentrations of the complexed substrate S_b and the free shift reagent [R] are derived by Eqs. 3 and 4, respectively.

$$S_b = (S_t - [S]) \tag{3}$$

$$[R] = R_t - (S_t - [S])/n \tag{4}$$

In these equations, S_t and R_t are stoichiometrical total concentrations of the substrate and the shift reagent, respectively, and n is the number of substrate molecules complexed to a shift reagent molecule.

When the second reaction to form 1:2 adduct is negligible, the first equilibrium constant K_1 is given by Eq. 5. Dissociation constant $K_D(=1/K)$ of the

$$K_1 = \frac{[S]\{nR_t - (S_t - [S])\}}{S_t - [S]} \tag{5}$$

shift reagent-substrate complex RS_n is then given by Eq. 6, by assuming that n molecules of substrate are coordinating to one molecule of the monomeric shift

$$\frac{S_t - [S]}{R_t \times [S]} = \frac{n}{K_D} - \frac{S_t - [S]}{K_D \times R_t} \tag{6}$$

reagent. Equation 6 is often called the Scatchard equation and is used to calculate K_D and n. When $(S_t - [S])/R_t[S]$ values are plotted against $(S_t - [S])/R_t$ values, both K_D and n are obtained from the slope and the intercept of the straight line calculated as the least squares of the plots. Another evidence for the stoichiometry of the complex is obtained when isosbestic points were observed with the concentration dependent spectra. The appearance of isosbestic points excludes the possibility of the coexistence of the 1:1 and 1:2 complexed species in the same solution. Thus the number of the coordinating substrate (n) can be determined by the Scatchard plot (Eq. 6).

When RS and RS_2 are present together in the same solution (apparently $1<n<2$), the following equation (Eq. 7), derived from Eqs. 1 and 2, is useful in evaluating the equilibrium constants K_1 and K_2.[10] The plot

$$\frac{[S]^3 + (2R_t - S_t)[S]^2}{S_t - [S]} = \frac{1}{K_2} \times \frac{(S_t - [S] + R_t)[S]}{S_t - [S]} + \frac{1}{K_1 K_2} \tag{7}$$

of $\{[S]^3 + (2R_t - S_t)[S]^2\}/(S_t - [S])$ (ordinate) *vs.* $(S_t - [S] - R_t)[S]/(S_t - [S])$ (abscissa) gives the K_1 and K_2 values from its slope and intercept.

In this way, the equilibrium constants are evaluated at various temperatures, the enthalpies and the entropies of formation of the complexes (RS and RS_2) being obtained from the $\log K$ *vs.* $1/T$ plots.

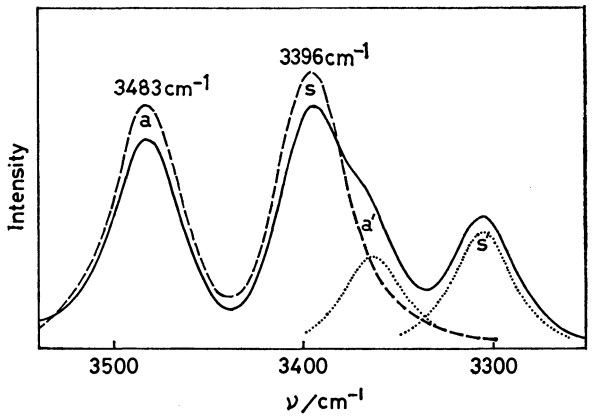

Fig. 1. NH Stretching bands of aniline in CCl_4 in the presence (——) and in the absence (----) of $Pr(dpm)_3$. Symmetric (s') and asymmetric (a') NH_2 stretching bands of the complexed species appear in the low frequency region. These bands are separated by the band shape analysis and illustrated by the dotted line (·····). The letters a and s denote asymmetric and symmetric stretching bands of the free species, respectively.

$$\ln K = -\frac{\Delta H}{R} \times \frac{1}{T} + \frac{\Delta S}{R} \qquad (8)$$

In this investigation, tris(dipivaloylmethanato)- or tris(6,6,7,7,8,8,8-heptafluoro-2,2-dimethyl-3,5-octanedionato)lanthanoid(III)'s were used as the shift reagents (R) and anilines as the substrates (S). The equilibrium constants were estimated by measuring the intensities of the N–H stretching absorption bands of the free species of aniline as a measure of [S].

Experimental

Materials. The shift reagents which had not been available commercially were prepared by reacting suitable 1,3-diones with lanthanoid nitrates in aqueous alcoholic solution at suitable pH (adjusted by adding sodium hydroxide).[11–13] Tris (dipivaloylmethanato) complexes of La, Nd, Sm, Gd, Tb, Dy, Ho, Er, and Yb ($Ln(dpm)_3$), tris(6,6,7,7,8,8,8-heptafluoro-2,2-dimethyl-3,5-octanedionato) complexes of La, Nd, Sm, Gd, Tb, Dy, Ho, Er, and Yb ($Ln(fod)_3$), tris(hexafluoroacetylacetonato) complexes of Eu, Pr, and Yb, and tris(1,1,1-trifluoroacetylacetonato) complexes of Eu, Pr, and Yb were prepared by this method. Two transition metal complexes $Co(dpm)_2$ and $Cu(dpm)_2$ were also prepared by the similar procedures. The hexafluoro- and trifluoroacetylacetonato complexes were sparingly soluble in carbon tetrachloride and, therefore, unsuitable for the measurement. These 1,3-diketonato complexes, together with commercially available ones, were purified by sublimation immediately before use. They were sublimed at temperatures about 10 °C lower than their melting points (100—220 °C for $Ln(fod)_3$ and 160—240 °C for $Ln(dpm)_3$). Then, they were dried for 2 d over phosphours pentaoxide at *ca.* 60 °C and used for the measurement. Commercially available spectro grade solvents were used. They were dried over phosphorus pentaoxide and distilled immediately before use.

Measurement of Infrared Spectra. Infrared spectra were recorded with a Hitachi 225 infrared spectrophotometer usually by use of a 2 cm cell. Temperature of the solution under measurement was controlled by circulating water, and other medium if needed, through the cell jacket from a thermostatic bath. The measurement was carried out with a concentration of *ca.* 3×10^{-3} mol l^{-1} for the shift reagent, changing the concentration of aniline from *ca.* 2×10^{-3} to *ca.* 8×10^{-3} mol l^{-1}. The concentration of the free substrate (aniline) [S] was determined by measuring the intensity of the asymmetric stretching band of NH_2 group appearing at 3483 cm^{-1} in carbon tetrachloride solution. As shown by an example of the spectrum in Fig. 1, the absorption band due to the asymmetric stretching mode of NH_2 vibration (located at the higher frequency) does not overlap with those of the complexed species, hence, being suitable for the determination of [S].

Measurement at a far higher concentration is necessary in order to determine the K_2 values for $Ln(dpm)_3$–aniline system. Thus, a variable cell whose length was adjusted to be 0.2 mm was used instead. Since the concentration of aniline can be increased about 100 times larger than that in a 2 cm cell, the equilibrium to form 1:1 adduct lies very far to the product and the second coordination forming 1:2 adduct occurs considerably. In this case, the variable temperature measurement was impossible and the measurement was carried out at 53 °C. Then the K_1's at 53 °C were calculated by assuming the ΔH and ΔS in Table 4. Calculated K_1's and [S]'s from ν_{as} intensities gave K_2 values.

Table 1. The coordination number (n) and the formation constant (K) values for some $Ln(dpm)_3$–aniline complexes in CCl_4

R	S	n	K	t/°C	Ref.
$Pr(dpm)_3$	$C_6H_5NH_2$	0.98	224	25	This work
$Eu(dpm)_3$	$C_6H_5NH_2$	0.90			16
$Dy(dpm)_3$	$C_6H_5NH_2$	0.95	128	25	This work
$Eu(dpm)_3$	t-C_4H_9OH	0.92	348	20	9

Results

Tris(dipivaloylmethanato)lanthanoid(III)–Aniline Complexes. In our previous report,[14] the composition and the thermodynamic properties of $Eu(dpm)_3$–t-butyl alcohol adduct were investigated by measuring the OH stretching absorption of the alcohol, giving n=0.92 from the Scatchard equation (Eq. 6).[15] The most probable coordination number (n) and the formation constant ($K(=1/K_D)$) were obtained similarly for the $Pr(dpm)_3$–aniline and $Dy(dpm)_3$–aniline complexes by the least squares calculations from the concentration data given in Table 2. The isosbestic points were also observed with the concentration dependent NH_2 absorption intensity data of $Eu(dpm)_3$–aniline in CCl_4.[16]

As expected from the results of the Scatchard plot, the K_1 values obtained by Eq. 1 was nearly constant when the concentrations of the substrate and the shift reagent were changed keeping the temperature constant. Two typical examples are given in Table 2.

Both the Scatchard plot and the constancy of the K_1 values from Eq. 2 show that only the formation of the 1:1 complex (RS) occurs considerably under the experimental conditions in a 2 cm cell. Since the complex formation of a fractional amount of aniline

Table 2. The formation constants (K_1) for $Pr(dpm)_3$-aniline and $Dy(dpm)_3$-aniline complexes at various concentrations of the substrate and the shift reagent (at 25 °C)

(a) $Pr(dpm)_3$-aniline complex.

Run	$S_t \times 10^3$/mol l^{-1}	$R_t \times 10^3$/mol l^{-1}	[S] $\times 10^3$/mol l^{-1}	K_1/l mol^{-1}
1	3.76	2.75	2.76	207
2	4.65	2.75	3.47	216
3	5.68	2.75	4.41	195
4	6.79	2.75	5.35	205
5	4.69	3.30	3.34	206
			Mean	206
			Standard Deviation	6.7

(b) $Dy(dpm)_3$-aniline complex.

Run	$S_t \times 10^3$/mol l^{-1}	$R_t \times 10^3$/mol l^{-1}	[S] $\times 10^3$/mol l^{-1}	K_1/l mol^{-1}
1	5.89	2.54	4.97	114
2	7.10	2.54	6.04	119
3	4.82	2.54	3.99	121
4	3.88	1.69	3.39	122
			Mean	119
			Standard Deviation	3.1

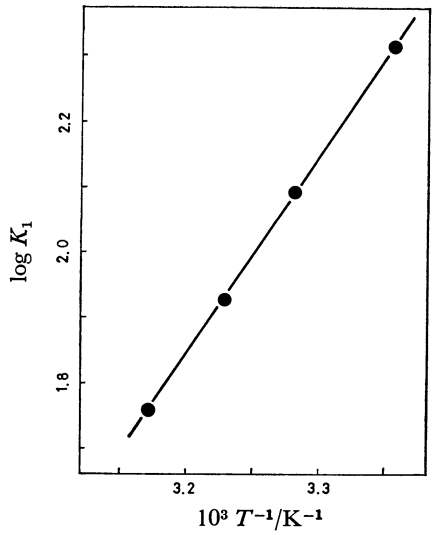

Fig. 2. The log K_1 *vs.* $1/T$ plot for the formation of $Pr(dpm)_3$–aniline adduct.

to the lanthanoid ion is not rationalized from the chemistry involved, the formation of 1:1 complex is supposed to occur actually in the aniline–$Ln(dpm)_3$–CCl_4 ternary system. In this case, the formation constants calculated from Eq. 2 should be better than those from the Scatchard plot (Eq. 6). Therefore, the equilibrum constants (K_1's) were estimated by Eq. 2 at various temperatures ranging from 18 to 47 °C. Results with $Pr(dpm)_3$–aniline complex in carbon tetrachloride solution is given in Table 3(a). The change in the K_1 values at varying temperatures is far larger than the variation among those observed at the same temperature (Table 2(a), standard deviation=6.7), which proves the meaningfulness of the temperature dependence measurement. The log K *vs.* $1/T$ plot (Fig. 2) shows a very good linear relation from which the enthalpy and entropy of the complex formation was estimated to be 58.6 kJ mol^{-1} and 152 J mol^{-1}K^{-1}, respectively. Quite similarly ,the enthalpies and the entropies of formation for a series of $Ln(dpm)_3$–aniline complexes were determined as given in Table 4 from the observed K_1's given in Table 3. In addition to the ΔH and ΔS values, the $\nu_s(NH_2)$ frequency shifts caused by the complex formation ($\Delta\nu_s$),[17] as well as ionic radii of trivalent lanthanoid cations (r)[18] are given in Table 4.

The second equilibrium constants, *i.e.* the formation constants of RS_2 from RS and S, were determined at 53 °C (Table 5). Since the formation of RS_2 proceeds consecutively following the formation of RS, considerably high concentration of the substrate becomes necessary in order to maintain the concentration of RS high enough to produce RS_2 measurably. Thus the measurement was carried out by using a thin cell (optical path length: 0.2 mm) so as to adjust the observed intensity of ν_{NH_2} band measurably. Under the conditions for the K_2 determination, more than 90% of $Ln(dpm)_3$ exists as the complexed species. As the K_2 value could not be determined as a function of temperature, the enthalpy and the entropy of formation of RS_2 from RS were not known. Under the conditions for the measurement with a 2 cm cell at 53 °C, only less than 1% of the shift reagent was estimated to form 1:2 adduct from the K_1 and K_2 values of $Pr(dpm)_3$–aniline system. The extent of the formation of 1:2 adduct becomes less as the atomic number of central lanthanoid ion increases, showing the assumption for K_1 determination is valid.

Tris(6,6,7,7,8,8,8-heptafluoro-2,2-dimethyl-3,5-octanedionato)lanthanoid–Aniline Adducts. The $Ln(fod)_3$ complexes are so hygroscopic that they absorb the moisture even during the infrared spectral measurement in carbon tetrachloride solutions. Free $Ln(fod)_3$'s are especially sensitive to the moisture, sometimes disturbing remarkably the measurement in use of their solu-

TABLE 3. TEMPERATURE DEPENDENCE OF THE FORMATION CONSTANTS K_1 OF VARIOUS Ln(dpm)$_3$–ANILINE 1 : 1 COMPLEXES IN CCl_4

T/°C	$S_t \times 10^3$/mol l^{-1}	$R_t \times 10^3$/mol l^{-1}	[S] $\times 10^3$/mol l^{-1}	K_1/l mol^{-1}
(a) Pr(dpm)$_3$–aniline				
25.0	4.69	3.30	3.34	206
31.8	3.10	3.12	2.39	124
36.7	3.10	3.12	2.55	84.1
42.3	3.10	3.12	2.68	57.1
(b) Nd(dpm)$_3$–aniline				
27.6	3.80	3.00	2.77	187
31.9	5.52	2.22	4.54	173
32.8	3.80	3.00	2.89	152
37.4	3.80	3.00	3.09	101
38.5	5.52	2.22	4.87	84.0
44.5	5.52	2.22	5.02	56.9
(c) Sm(dpm)$_3$–aniline				
24.0	3.36	3.09	2.38	197
28.6	3.36	3.09	2.50	155
32.6	3.36	3.09	2.63	118
36.5	3.36	3.09	2.77	84.9
40.9	3.36	3.09	2.96	40.8
(d) Eu(dpm)$_3$–aniline				
18.5	4.90	3.49	3.20	296
25.8	4.90	3.49	3.51	190
31.5	4.90	3.49	3.75	131
39.8	4.90	3.49	4.04	80.9
44.3	4.90	3.49	4.32	46.1
(e) Gd(dpm)$_3$–aniline				
21.8	5.77	3.65	3.85	284
27.7	5.77	3.65	4.11	203
31.2	5.77	3.65	4·25	167
45.4	5.77	3.65	4.87	64.8
(f) Tb(dpm)$_3$-aniline				
25.0	6.21	2.87	4.69	241
36.1	3.94	3.17	2.92	164
40.4	3.94	3.17	3.04	131
44.6	3·94	3.17	3.23	89.4
47.7	3.94	3.17	3.25	85.6
(g) Dy(dpm)$_3$–aniline				
19.8	3.33	3.22	2.45	154
25.3	3.33	3.22	2.57	119
30.0	3.33	3.22	2.73	83.8
36.2	3.33	3.22	2.85	61.9
41.6	3.33	3.22	3.01	37.3
(h) Ho(dpm)$_3$–aniline				
19.1	4.21	2.99	3.31	130
25.5	4.21	2.99	3.44	101
30.1	4.21	2.99	3.56	77.9
36.4	4.21	2.99	3.74	49.8
42.3	4.21	2.99	3.89	30.5
(i) Er(dpm)$_3$-aniline				
19.0	4.21	2.89	3.40	115
25.5	4.21	2.89	3.57	79.1
31.7	4.21	2.89	3.70	57.3
42.9	4.21	2.89	3.87	31.3
(j) Yb(dpm)$_3$-aniline				
19.3	3.66	3.09	3.10	71.7
26.2	3.66	3.09	3.24	48.4
33.4	3.66	3.09	3.39	29.1
38.3	3.66	3.09	3.43	24.0

Table 4. The enthalpies and the entropies of formation of Ln(dpm)$_3$-aniline complexes

Ln	Z[a]	K_1^{298}/l mol^{-1}	$-\Delta H$/kJ mol^{-1}	$-\Delta S$/J mol^{-1} K^{-1}	$r\times 10$/nm[b]	$\Delta\nu$/cm^{-1}
Pr	59	214	58.6±4.6	152±15	1.013	86
Nd	60	259	60.7±4.3	157±14	0.995	86.5
Sm	62	197	59.0±6.2	154±21	0.964	87
Eu	63	197	53.1±4.6	134±15	0.950	87
Gd	64	251	49.4±2.5	120± 8	0.938	89.5
Tb	65	263	49.8±4.7	119±16	0.923	90
Dy	66	116	49.0±3.0	125±10	0.908	87
Ho	67	96.3	48.5±4.7	123±16	0.894	89
Er	68	85.7	41.8±1.6	103± 5	0.881	91
Yb	70	54.1	45.2±4.6	118±15	0.858	89
Eu(*p*-toluidine)[c]		—	49.0±4.2	113±14		
En(*t*-C_4H_9OH)[d]		—	40.2±3.7	88±12		

a) Atomic numbers. b) See Ref. 18. c) The values for Eu(dpm)$_3$-*p*-toluidine complex. d) The values for Eu(dpm)$_3$-*t*-butyl alcohol complex.

Table 5. The second equilibrium constants (K_2) for Ln(dpm)$_3$-aniline at 53 °C in CCl_4

Ln	S_t/mol l^{-1}	R_t/mol l^{-1}	[S]/mol l^{-1}	K_1^{326}/l mol^{-1} [a]	K_2^{326}/l mol^{-1}
Pr	0.373	0.0892	0.211	38.3	29.7
Nd	0.578	0.0778	0.435	31.9	13.9
Sm	0.578	0.155	0.311	25.7	11.4
Eu	0.578	0.158	0.321	32.9	6.6
Gd	0.578	0.153	0.352	45.7	3.1
Tb	0.578	0.0695	0.472	56.1	2.6
Dy	0.578	0.181	0.365	21.4	1.1
Ho	0.578	0.148	0.398	21.3	1.2
Er	0.578	0.136	0.418	20.2	0.95
Yb	0.578	0.169	0.392	11.4	0.99

a) Calculated from ΔH and ΔS in Table 4.

Table 6. The enthalpies and the entropies of formation of Ln(fod)$_3$-aniline complexes

Ln	K_1^{298}/l mol^{-1}	$-\Delta H_1$/kJ mol^{-1}	$-\Delta S_1$/J mol^{-1} K^{-1}
Eu	4340	67.8±1.6	158± 6
Gd	1296	57.8±1.8	134± 6
Dy	1160	51.0±2.7	113± 9
Yb	1152	54.4±3.5	124±12

tions as references. Thus the measurement on Ln(fod)$_3$-aniline were repeated several times at a temperature, and only statistically meaningful data were used in the subsequent calculation of the enthalpies and the entropies of the adduct formation. Another difficulty arises from the fact that Ln(fod)$_3$ forms a considerable amount of the 1:2 adduct, in addition to the 1:1 adduct, at a low concentration. The K_1 and K_2 values can be estimated, in principle, from the concentration dependence data by use of Eq. 7. However, the $\{[S]^3+(2R_t-S_t)[S]^2\}/(S_t-[S])$ *vs.* $(S_t-[S]-R_t)/(S_t-[S])$ plot deviate remarkably from the regression line calculated statistically, giving only a fair linear relationship.[19] Rough estimation by Eq. 7 of the formation constants gave $K_1=124$ and $K_2=242$ for La(fod)$_3$-aniline (at 30.4 °C), $K_1=124$ and $K_2=56$ for Pr(fod)$_3$-aniline (at 27.5 °C), and $K_1=279$ and $K_2=45$ for Gd(fod)$_3$-aniline (at 30.2 °C).[20] As the formation of the 1:2 adduct is remarkable with the Ln(fod)$_3$ containing lower series of lanthanoid elements, the formation constant calculated by assuming that the 1:1 adduct is solely formed is somewhat less reliable with the complex of lower lanthanoid than with those of higher lanthanoid and also than that of corresponding Ln(dpm)$_3$. The K_1 values for some Ln(fod)$_3$-aniline adducts were given in Table 6. Except the case of the Pr(fod)$_3$ adduct, the effect of the second coordination was estimated to be rather unimportant (containing less than 5% of RS_2) under the conditions for measurement.

β-Diketonato Complexes of Some Transition Metal Ions. In order to compare the coordinational behavior of lanthanoid β-diketonato complexes with those of transition metal ions, some bis(β-diketonato) complexes of cobalt, nickel, and copper were prepared. The measurements similar to those on the lanthanoid shift reagents were carried out again on these complexes, the results being given in Table 7.

Discussion

As a whole, the formation constants of the 1:1 adducts (RS) and their enthalpies of formation (shown in Table 4) gradually decrease as the atomic number of the central lanthanoid ion increases. Evidently the entropic term also decreases accompanying the decrease in the enthalpy according to the general principle of

TABLE 7. THERMODYNAMIC PARAMETERS FOR THE FORMATION OF THE ANILINE ADDUCTS OF VARIOUS BIS(β-DIKETONATO) COMPLEXES OF SOME TRANSITION METAL IONS[a)]

	K_1^{298}/l mol^{-1}	$-\Delta H_1$/kJ mol^{-1}	$-\Delta S_1$/J mol^{-1} K^{-1}	K_2^{298}/l mol^{-1}	$-\Delta H_2$/kJ mol^{-1}	$-\Delta S_2$/J mol^{-1} K^{-1}
Co(acac)$_2$	290	59.8±6.3	154±21	88	46.0±5.0	117±17
Co(dpm)$_2$	15.1	63.6±5.1	191±17	—	—	—
Co(tfa)$_2$	54500	66.9±7.0	134±23	889	31.8±5.7	50±19
Ni(tfa)$_2$	9720	50.2±5.4	88±18	203	24.5±4.5	38±15
Cu(tfa)$_2$	19	20.7±4.1	45±14	—	—	—
Cu(hfa)$_2$	4870	41.0±6.2	67±20	31	34.7±4.8	88±16

a) acac=Acetylacetonato, tfa=1,1,1-trifluroacetylacetonato, and hfa=hexafluoroacetylacetonato.

"enthalpy-entropy compensation." There are some exceptions, however, in the decreasing sequence of the K_1 values. The K_1's for Gd(dpm)$_3$ and Tb(dpm)$_3$ are larger than expected even when the statistical error is taken into account. On the other hand, the enthalpies of formation decreases monotonously with the increase in atomic number, showing no indication of anomalous behavior. Thus the favorable formation of these two 1:1 adducts is due to the contribution of the entropic term, suggesting sterically favored arrangement of pivaloylmethanato ligands and the substrate in these adducts, though the details of their structure could not be clarified.

The atomic numbers of the central lanthanoid ions affect more pronouncely the formation constants of the 1:2 adducts than the case of the 1:1 adducts. For example, the K_2 of Yb(dpm)$_3$–aniline is *ca.* 30 times smaller than that of the similar adduct of Pr, while the difference among K_1's is less than 5 times at the largest. Since the Ln(dpm)$_3$ has a lanthanoid ion surrounded by bulky organic ligands as shown by means of X-ray crystal analyses,[21)] the coordination of the seventh and the eighth ligands, aniline in this case, might be hindered sterically. Important role of the steric effect relative to electronic and other effects has also been pointed out by one of the present authors by determining the coordinating abilities (relative equilibrium constants) towards Eu(dpm)$_3$ of various pyridinoid aza-aromatic compounds.[22)] The ionic radii of trivalent lanthanoid ions decrease with the increasing order of atomic number.[18)] The steric hindrance should become more serious with the lanthanoid complexes of higher atomic numbers because of the contraction of ionic radii. The arrangement of the ligands revealed by the X-ray studies[21)] has only C_2 symmetry, suggesting the remarkable bending of metal-ligand bonds. Therefore the steric effect in the first coordination process might be reduced by the bending of metal-ligand bonds towards the direction for minimizing the strain in the adduct molecule. For this reason, the crowdedness due to the contraction of ionic radii restricts more predominantly the approach of the second aniline molecule than that of the first one, which is in consequence with the fact that the K_2 values are more sensitive to the effect of atomic number. The coordination of the second aniline molecule is restricted more severely in Ln(dpm)$_3$ adducts than in Ln(fod)$_3$ adducts. This fact supports the above interpretation concerning the effect of atomic number.

The formation constants and the enthalpies of formation of bis(trifluoroacetylacetonato) complexes of Co, Ni, and Cu also decrease in the increasing order of atomic number. The decrease can be ascribed to the repulsive interaction between the d-electrons of the transition metal ion and the unshared electrons of aniline, since the ionic radii of these ions do not vary regularly with the change in atomic number (0.79 Å for Co^{2+}, 0.84 Å for Ni^{2+}, and 0.76 Å for Cu^{2+}).[23,24)] The similar effect can occur also in the series of the lanthanoid β-diketonato complexes due to the increasing f-electrons. However, the f-electrons occupy the inner electron shell and might interact considerably lesser extent with the unshared electrons of aniline. At present, we cannot conclude either of the effects plays more important role on the decrease of the formation constants and ΔH in the increasing order of atomic number of lanthanoids.

When compared the Eu(dpm)$_3$ adduct of aniline with that of *t*-butyl alcohol, the formation constant of the *t*-butyl alcohol adduct is somewhat larger than that of aniline adduct in spite of its lower enthalpy of formation even in the 1:1 adduct formation process. Since the alcoholic oxygen atom has two pairs of unshared electrons capable of forming the coordinate bond with the lanthanoid ion, the formation of the alcohol–Ln(dpm)$_3$ adduct should be statistically more favored than the formation of the aniline adduct.

The free shift reagents are supposed to exist as dimeric species under certain conditions.[25)] This possi-

$$2R \rightleftharpoons R_2 \qquad (9)$$

bility could not be excluded completely in our systems though which consisted of much lower concentrations of the shift reagents than the conditions for NMR measurements. However, the infrared spectra in CCl_4 of the shift reagents (in the C=O stretching region) were not dependent on the concentrations, giving no evidence for the equilibrium between monomeric and dimeric species (Eq. 9).

References

1 C. C. Hinckley, *J. Am. Chem. Soc.*, **91**, 5160 (1969).
2) J. Reuben, *Progr. Nucl. Magn. Reson. Spectrosc.*, **9**, 1 (1973).
3) A. F. Cockerill, G. L. O. Davies, R. C. Harden, and D. M. Rackham, *Chem. Rev.*, **73**, 553 (1973).
4) R. E. Sievers, "NMR Shift Reagent," Academic Press, New York (1973).
5) M. Kainosho, *Yukigosei Kagaku Kyokai Shi*, **31**, 12 (1973).

6) T. J. Wenzel, T. C. Bettes, J. E. Sadlowski, and R. E. Sievers, *J. Am. Chem. Soc.*, **102**, 5903 (1980).
7) H. M. McConnell and R. E. Robertson, *J. Chem. Phys.*, **28**, 749 (1958).
8) G. N. La Mair, W. D. Horrocks, Jr., and L. C. Allen, *J. Chem. Phys.*, **41**, 2126 (1964).
9) M. Hirota and S. Otsuka, *Chem. Lett.*, **1975**, 667.
10) Here, the total concentrations of the substrate and of the shift reagent are given by $S_t=[S]+[RS]+2[RS_2]$ and $R_t=[R]+[RS]+[RS_2]$, respectively. These equations were employed to derive Eq. 7.
11) C. C. Hinckley, *J. Org. Chem.*, **35**, 2834 (1970).
12) K. J. Eisentraut and R. E. Sievers, *J. Am. Chem. Soc.*, **87**, 5254 (1965).
13) C. S. Springer, Jr., D. W. Meek, and R. E. Sievers, *Inorg. Chem.*, **6**, 1105 (1967).
14) M. Hirota, S. Yoshida, Y. Nagawa, M. Ono, H. Endo, and H. Satonaka, *Bull. Chem. Soc. Jpn.*, **49**, 3200 (1976).
15) G. Scatchard, *Ann. N. Y. Acad. Sci.*, **51**, 660 (1949).
16) H. Nonaka, Unpublished data.
17) The complex formation shifts of the NH_2 stretching bands are evaluated by the frequency shifts of the symmetric stretching mode of vibration, since the asymmetric stretching absorption of the complexed species often overlap with the symmetric stretching absorption of the free species, which prevents the accurate determination of the absorption frequencies without the time-consuming band shape analyses in order to resolve them. The symmetric stretching absorptions of the complexes species did not overlap with any other bands when the measurements were carried out at low concentrations (*ca.* 2×10^{-3}—8×10^{-3} mol l^{-1} both with aniline and with $Ln(dpm)_3$).
18) a) D. H. Templeton and C. H. Dauben, *J. Am. Chem. Soc.*, **76**, 5237 (1954); b) F. A. Cotton and G. Wilkinson, "Advanced Inorganic Chemistry," 2nd ed, John Wiley & Sons, Inc., New York (1972), Chap. 31.
19) Both $\{[S]^3-(2R_t-S_t)[S]^2\}/(S_t-[S])$ and $\{S_t-[S]-R_t\}/(S_t-[S])$ are relatively small quantities obtained as differences of large quantities. Therefore the results are not very reliable since rather a small fluctuation of the data affects them remarkably.
20) H. Kojima, Unpublished data.
21) a) R. E. Cramer and K. Seff, *J. Chem. Soc., Chem. Commun.*, **1972**, 400; b) W. D. Horrocks, Jr., J. P. Sipe, III, and J. R. Luber, *J. Am. Chem. Soc.*, **93**, 5260 (1971).
22) Y. Nagawa, M. Ono, M. Hirota, Y. Hamada, and I. Takeuchi, *Bull. Chem. Soc. Jpn.*, **49**, 1322 (1976).
23) 1 Å$=10^{-1}$ nm.
24) "Kagaku Benran," 2nd ed, ed by the Chem. Soc. Jpn., Maruzen, Tokyo (1975), p. 1473.
25) J. K. M. Sanders, S. W. Hanson, and D. H. Williams, *J. Am. Chem. Soc.*, **94**, 5325 (1972).

Stereoselective α-Glucosylation with Tetra-*O*-benzyl-α-D-glucose and a Mixture of Trimethylsilyl Bromide, Cobalt(II) Bromide, Tetrabutylammonium Bromide, and a Molecular Sieve. A Synthesis of 3,6-Di-*O*-(α-D-glucopyranosyl)-D-glucose

Shinkiti Koto,* Naohiko Morishima, Chiharu Kusuhara, Shigeko Sekido, Toyosaku Yoshida, and Shonosuke Zen

School of Pharmaceutical Sciences, Kitasato University, Shirokane, Minato-ku, Tokyo 108

(Received February 6, 1981)

A mixture of trimethylsilyl bromide, cobalt(II) bromide, tetrabutylammonium bromide, and a molecular sieve (4A) is effective for the stereoselective, one-stage α-glucosylation of alcohol with 2,3,4,6-tetra-*O*-benzyl-α-D-glucopyranose in dichloromethane. Using this procedure, several disaccharide derivatives as well as *O*-α-D-glucopyranosyl-(1→3)-*O*-[α-D-glucopyranosyl-(1→6)]-D-glucopyranose are synthesized.

A variety of procedure for stereoselective α-glucosylation have recently been reported.[1] However, they all use moisture-sensitive compounds such as glycosyl halides.[1a,b] We are now developing a glycosylation procedure in which the anomeric center of 2,3,4,6-tetra-*O*-benzyl-α-D-gluopyranose (αGOH, **1**) is activated in the presence of an alcohol.[2] The treatment of the mixture of **1** and an alcohol (ROH) in CH_2Cl_2 containing methanesulfonic acid ($MeSO_3H$) and $CoBr_2$ has been found to give an anomeric mixture of the corresponding gucosides.[2c] In this reaction, HBr, generated *in situ* by the reaction of $MeSO_3H$ and $CoBr_2$, cooperates with $CoBr_2$ to convert **1** into the glucosyl bromide (**2**) in the presence of an alcohol, and **2** reacts with alcohol to afford the glucosides (Eq. 1, Q=H).[2c]

$$\alpha\text{GOH} + \text{ROH} \xrightarrow{\text{QBr/CoBr}_2} \alpha\text{GOR} + \beta\text{GOR} \qquad (1)$$

A glucosylation reaction (Eq. 1, $Q=Me_3Si$) was then provisionally set up by replacing the HBr acid with trimethylsilyl bromide (Me_3SiBr).[3a] This paper will report a handy stereoselective α-glucosylation procedure[4] developed by modifying this reaction and its use in the synthesis of several disaccharide derivatives and the first synthesis of *O*-α-D-glucopyranosyl-(1→3)-*O*-[α-D-glucopyranosyl-(1→6)]-D-glucopyranose (**23**), the trisaccharide constituting the branching poing of the dextrans from *Leuconostic mesenteroides*.[5]

Results and Discussion

α-Glucosylation of Simple Alcohols. Table 1 contains the results regarding the glucosylation of cyclohexylmethanol (Runs 1—9) (Eq. 1, $Q=Me_3Si$, R= cyclohexylmethyl). Compared to the previously used method, which uses $MeSO_3H$ and $CoBr_2$,[2c] the efficiency was greatly improved (Runs 2 and 3). The use of the molecular sieve, 4A (MS-4A), was essential (Runs 1 and 3), because it scavenges HBr, which causes an undesirable debenzylation reaction.[2c] The use of the mixture of Me_3SiCl[3b] and $CoBr_2$ also gave good results, but the efficiency was less satisfactory (Run 4).

It was found that the reaction of **1** with Me_3SiBr and $CoBr_2$ efficiently produced the glucosyl bromide **2**.[3c] However, trace amounts of the silylated compounds of **1** and alcohol were isolated from the product mixture of the glucosylation reaction. Hence, the silylation of the starting materials is considered to occur concurrently during the glucosylation reaction. Nevertheless, the experiments using 5α-cholestan-3β-ol as the alcohol confirmed that: (1) the trimethylsilyl compound (**3**) smoothly reacted with the mixture of Me_3SiBr and $CoBr_2$ to generate **2**,[3d] which then underwent the glucosylation of the alcohol in the presence of $CoBr_2$,[2c] and (2) the trimethylsilyl derivative of the alcohol readily reacted with **2** in the presence of $CoBr_2$ to furnish the corresponding glucosides. Therefore, the silylation reactions, if any, seem not to interfere with the glucosylation reaction (Eq. 1, $Q=Me_3Si$).

Because the glucosylation reaction proceeds *via* **2**, tetrabutylammonium bromide (*n*-Bu_4NBr) was then added to the reaction mixture, for the salt was expected to cause bromide ion-catalyzed stereoselective α-glucosylation (Eq. 2).[1b] Table 1 shows that the addition of *n*-Bu_4NBr gave rise to the predominant formation of the α-glucosides, though the reaction was slowed[2c] (Runs 3, 5—7). Slightly excess amounts (30%) of **1** and the reagent mixture in relation to the alcohol achieved a quantative glucosylation (Run 9). Other simple alcohols, such as cyclohexanol and 6-(2,4-dinitroanilino)-1-hexanol, furnished the corresponding α-glucosides in good yields (Runs 10 and 11). Thus, the replacement of HBr with Me_3SiBr and MS-4A makes it possible to carry out a longer glucosylation reaction (Runs 7—12) than before.[2c]

$$\alpha\text{GOH} + \text{ROH} \xrightarrow{\text{Me}_3\text{SiBr/CoBr}_2\text{/}n\text{-Bu}_4\text{NBr}} \alpha\text{GOR}\ (+\beta\text{GOR}) \qquad (2)$$

The Oligosaccharide Synthesis Using the Quarternary Mixture. The α-glucosylation procedure was then used for a systematized oligosaccharide synthesis using the benzyl as the persistent protecting group.[6] Table 1 shows that the reagent mixture was effective for the stereoselective α-glucosylation of the primary hydroxyl group of partially benzylated monosaccharides, such as **9**, **10**, and **11** (Runs 13—15). The reagent mixture performed the α-glucosylation of the secondary hydroxyl group of the xylopyranoside derivatives (**5** and **6**) with acceptable yields (Runs 16 and 17).

The reagent mixture was then applied to the step-by-step synthesis of the branched-chain trisaccharide (**23**) to establish the scope of the applicability of the present procedure, as is summarized in Fig. 1, the symbolism for monosaccharide derivatives exemplified in Table 5 is used. The first glucosylation step for

Table 1. Glucosylation with 2,3,4,6-tetra-*O*-benzyl-α-D-glucopyranose (αGOH, **1**) in CH_2Cl_2 at 25±3 °C[a]

Run	**1** (equiv.)	Alcohol[b]	Me_3SiX X	Me_3SiX (equiv.)	$CoBr_2$ (equiv.)	MS-4A w/w of **1**	*n*-Bu_4NBr (equiv.)	Time h	Yield[c] (α/β) %	Recov. of **1**/%
1	1.0	CmOH	Br	1.0	1.0	—	—	2	63 (55/45)	12
2	1.0	CmOH	Br	1.0	1.0	1.5	—	0.5	79 (41/59)	11
3	1.0	CmOH	Br	1.0	1.0	1.5	—	2	81 (40/60)	3
4	1.0	CmOH	Cl	1.0	1.0	1.5	—	2	59 (52/48)	37
5	1.0	CmOH	Br	1.0	1.0	1.5	1.0	2	54 (72/28)	40
6	1.0	CmOH	Br	1.0	1.0	1.5	1.0	6	65 (72/28)	34
7	1.0	CmOH	Br	1.0	1.0	1.5	1.0	16	82 (75/25)	4
8	1.3	CmOH	Br	1.0	1.0	1.5	1.0	16	94 (74/26)	—[d]
9	1.3	CmOH	Br	1.3	1.3	2.0	1.3	16	100 (76/24)	—[d]
10	1.3	ChOH	Br	1.3	1.3	2.0	1.3	16	90 (80/20)	—[d]
11	1.3	DhOH	Br	1.3	1.3	2.0	1.3	16	94 (73/27)	—[d]
12	1.3	CtOH	Br	1.3	1.3	2.0	1.3	24	87 (72/28)	—[d]
13	1.3	**9**	Br	1.3	1.3	2.0	1.3	16	69 (85/15)	—[d]
14	1.3	**10**	Br	1.3	1.3	2.0	1.3	18	61 (78/15)	—[d]
15	1.3	**11**	Br	1.3	1.3	2.0	1.3	20	73 (86/14)	—[d]
16	1.3	**5**[e]	Br	1.3	1.3	2.0	1.3	42	35 (82/18)	—[d]
17	1.3	**6**[e]	Br	1.3	1.3	2.0	1.3	42	49 (86/14)	—[d]
18	1.3	**7**	Br	1.3	1.3	2.0	1.3	42	32 (74/26)	—[d]
19	1.3	**17a**	Br	1.3	1.3	2.0	1.3	42	19 (86/14)	—[d]

a) Mole ratios are based on the amount of alcohol. b) CmOH=cyclohexylmethanol, ChOH=cyclohexanol, CtOH=5α-cholestan-3β-ol, DhOH=6-(2,4-dinitroanilino)-1-hexanol. The glucosides obtained are: Runs 1—9, αGOCm and βGOCm; Run 10, αGOCh and βGOCh; Run 11, αGODh and βGODh; Run 12, **4a** and **4b**; Run 13, **15a** and **15b**; Run 14, **14a** and **14b**; Run 15, **17a** and **17b** after de-*O*-acetylation; Run 16, **12a** and **12b**; Run 17, **13a** and **13b**; Run 18; **16a** and **16b**; Run 19, **22a** and **22b**. c) Yields are based on the amount of the alcohol charged. d) Not determined. e) N. Morishima, S. Koto, C. Kusuhara, and S. Zen, *Bull. Chem. Soc. Jpn.*, **55**, 631 (1982).

Table 2. ^{13}C NMR data of the anomeric carbons of the protected di- and trisaccharides[a]

Compound		C-1	C-1′→3	C-1″→6
Benzylates				
14a		95.1	97.3	
14b		95.1	102.5	
16a		94.9		97.5
16b		95.4		104.0
22a		95.2	97.4	97.4
22b		94.0	102.8	97.5
Acetates				
19	α	89.2	96.2	
	β	91.8	96.2	
21	α	89.1		96.0
	β	91.8		96.3
24	α	88.8	96.1	95.8
	β	91.7	96.1	95.8

a) The spectra were recorded by means of a JEOL-PS-100 spectrometer equipped with a JEOL-EC-100 computer and using a 8 mmϕ tube at 37 °C (noise decoupled; pulse width, 13 μs (45°), repetition, 2 s frequency range, 5000 Hz; 8 K data points).

the monosaccharide derivative (**11**) was carried out well (Table 1). After the deacetylation, however, the second glucosylation step for the disaccharide derivative (**17a**) (Run 19) was carried out only with difficulty to furnish the fully benzylated trisaccharide (**22a**). The chemical shift of the anomeric carbons of **22a** (Table 2) closely resembles that of the α(1→3), α(1→6)-trisaccharide derivatives.[7] The hydrogenolysis of **22a** gave **23**. The chemical shift of the anomeric and aglyconic carbons of **23** and its per-*O*-acetate (**24**) corresponds well with those of nigerose (**18**)[8] and isomaltose (**20**)[8] and their acetates (**19** and **21**). It should be noted, however, that the low yield of the glucosylation of the disaccharide derivative (**17a**) with **1** shows the limitations of the present method in a multistep glucosylation.

Experimental

General. The instruments used were identical with those described previously.[2,6] Such compounds as **1**, $CoBr_2$, *n*-Bu_4NBr, and solid glycosyl acceptors were stored *in vacuo* over P_2O_5. Me_3SiBr (PCR) was used without any pretreatments. MS-4A (Linde, 60—80 mesh) was dried at 450 °C in an electric furnace. Column chromatography was performed on silica gel (Kanto Kagaku, 100 mesh), using the gradient eluent system of benzene and 2-butanone (100:1→10:1), unless otherwise stated, each fraction was examined by TLC on silica gel (Merck, 7731).

The fully benzylated oligosaccharides (**14a**, **16a**, and **22a**) was hydrogenated twice over an equal amount of Pd on C (Kawaken, 10%) in AcOH (6 ml) containing H_2O (0.03 ml) at 410 kPa overnight. The oligosaccharides (**18**, **20**, and **23**) were acetylated with Ac_2O and AcONa at 100 °C.

The ^{13}C NMR data of di- and trisaccharides and their

Table 3. ^{13}C NMR data of 3,6-di-*O*-(α-D-glucopyranosyl)-D-glucopyranose and related disaccharides[a)]

Carbon	**18**	**20**	**23**	Carbon	**18**	**20**	**23**
1α	93.3 (93.1)	93.5 (93.8)	93.7	1′	100.1 (99.8)		100.6
1β	97.0 (97.0)	97.4 (97.7)	97.5	2′	72.8 (72.8)		73.1
2α	71.1 (71.3)	72.8 (73.3)	72.9	3′	74.0 (74.1)		74.4[b)]
2β	74.0 (74.1)	75.6 (75.9)	75.3	4′	71.1 (71.3)		70.9
3α	80.7 (80.8)	74.4 (75.0)	81.9	5′	72.8 (72.8)		73.1
3β	83.2 (83.2)	77.3 (77.7)	84.3	6′	61.5 (61.8)		61.8
4α	70.5 (70.6)	70.8 (71.3)	70.9	1″		99.3 (99.4)	99.4
4β	70.4 (70.6)	70.8 (71.3)	70.9	2″		72.8 (73.3)	73.1
5α	72.3 (72.2)	71.3 (71.3)	72.9	3″		74.4 (75.0)	74.2[b)]
5β	76.7 (76.6)	75.4 (75.9)	77.0	4″		70.8 (71.3)	70.9
6α	61.4 (61.8)	67.0 (67.4)	66.9	5″		73.1 (73.8)	73.1
6β	61.6 (61.8)	67.0 (67.4)	66.9	6″		61.7 (62.5)	61.8

a) The measurement conditions are described in Table 2. The values in parentheses are those reported previously (Ref. 8). b) Interexchangeable.

Table 4. Physical and analytical data of oligosaccharide derivatives

Compound	Mp θ_m/°C	$[\alpha]_D^{20}$/° (*c*, $CHCl_3$)	Found (%) C	Found (%) H	Formula	Calcd (%) C	Calcd (%) H
12a	—	+58 (1.0)	74.04	6.93	$C_{54}H_{58}O_{10}$	74.81	6.74
12b	—	+38 (1.5)	73.87	6.94			
13a	—	+40 (1.0)	74.79	6.94			
13b	91—92	+10 (1.0)	74.65	6.67			
14a	—	+72 (2.0)	76.88	6.70	$C_{68}H_{70}O_{11}$	76.81	6.64
14b	—	+57 (1.0)	76.18	6.79			
16a	102—105	+64 (0.6)	75.69	6.63			
16b	128—130	+39 (0.4)	75.99	6.60			
22a	—	+79 (1.0)	75.98	6.73	$C_{95}H_{98}O_{16}$	76.28	6.60
22b	—	+66 (0.7)	75.99	6.56			
24	—	+82 (0.3)	49.33	5.68	$C_{40}H_{54}O_{28}$	49.69	5.63
25	77—79	+97 (0.2)	49.85	5.69	$C_{42}H_{58}O_{28}$	49.90	5.78

Table 5. Symbolism of some monosaccharide derivatives[a)]

	1	**5**	**11**
Unprotected hydroxyl group[b)]	None	OH-3	OH-6
Temporary protecting group	None	None	Ac-3
Persistent protecting group	Bn	Bn	Bn
Anomeric configuration	α	α	α
Substituent at C-1	OH	OMe	OBn
Monosaccharide involved	D-Glc*p*	D-Xyl*p*	D-Glc*p*
Symbolism	DGlc*p*BnαOH	H3DXyl*p*BnαOMe	Ac 3 H6DGlc*p*BnαOBn

a) Ac=Acetyl, Bn=benzyl, Me=methyl. b) The hydroxyl group at C-1 is not taken into account.

derivatives are listed in Tables 2 and 3, while the physical and analytical data of new compounds are listed in Table 4.

Procedure for the Glucosylation Using the Benzylated Glucose (1). Me_3SiBr (22 μl, 0.17 mmol) was stirred into a mixture of **1** (90 mg, 0.17 mmol), the respective alcohol (0.13 mmol), $CoBr_2$ (37 mg, 0.17 mmol), *n*-Bu_4NBr (54 mg, 0.17 mmol), and MS-4A (180 mg) in CH_2Cl_2 (0.45 ml), and the resulting mixture was agitated at room temperature (22—28 °C). The filtrate of the reaction mixture was then evaporated and chromatographed. The glucosides thus obtained, the yields of which are listed in Table 1, were identified with those prepared before,[2,6)] except for ten compounds, **12a**, **12b**, **13a**, **13b**, **14a**, **14b**, **16a**, **16b**, **22a**, and **22b**.

*Benzyl 2,4,6-Tri-*O*-benzyl-α-D-glucopyranoside (7).* Benzyl α-D-glucopyranoside[6b,c)] (1.0 g, 3.7 mmol) was heated in $PhCH_2Cl$ (Tokyo Kasei, 10 ml) and powdered KOH (Wako, 0.95 g, 17 mmol) at 90—95 °C for 2 h under vigorous stirring. The filtrate of the reaction mixture was then evaporated and chromatographed. Benzyl 2,3,4,6-tetra-*O*-benzyl-α-D-glucopyranoside appeared first, and then the main fraction of **7** was obtained as a syrup (1.3 g). This was purified through acetylation with Ac_2O and pyridine, follow-

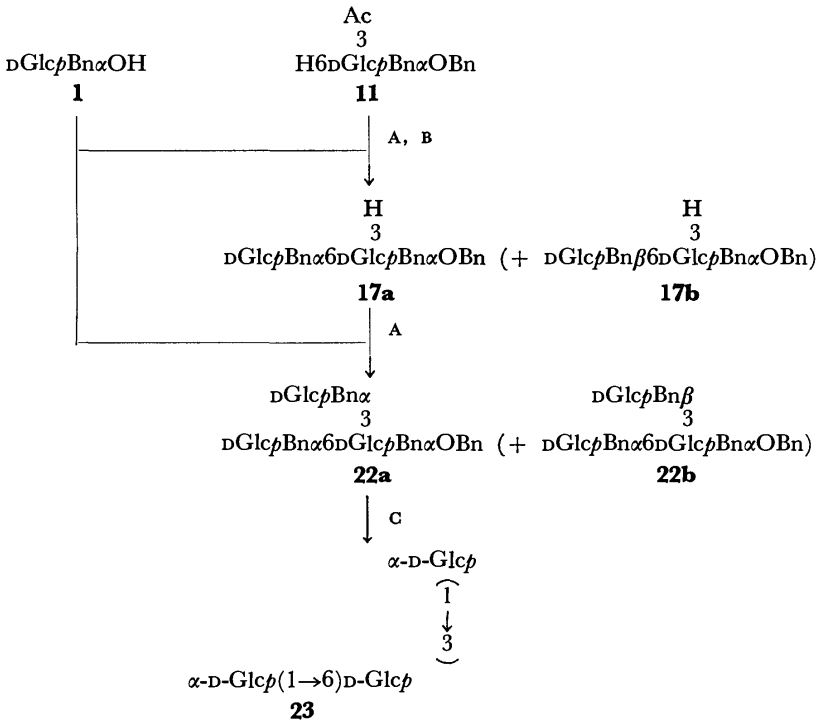

A : $Me_3SiBr/CoBr_2/n\text{-}Bu_4NBr/MS\text{-}4A/CH_2Cl_2$,
B : NaOMe/MeOH/1,4-dioxane, C : $H_2/Pd/C/AcOH$.

Fig. 1. Synthetic scheme of the glucotriose, **23**.

ed by chromatography of furnish the acetate (**8**) (1.1 g, 55%), mp 93—95 °C, $[\alpha]_D^{20}$ +81° (*c* 1.0, $CHCl_3$) (lit,[9] mp 76—78 °C, $[\alpha]_D^{20}$ +53.0 (*c* 1, $CHCl_3$)] (Found: C, 74.10, H, 6.63%).

The treatment of **8** with a dil. solution of NaOMe in MeOH gave **7** quantitatively; $[\alpha]_D^{20}$ +88° (*c* 2.3, $CHCl_3$). Found: C, 75.47, H, 6.58%. Calcd for $C_{34}H_{36}O_6$: C, 75.53; H, 6.71%.

Reaction of ***1*** *with* Me_3SiBr *and* $CoBr_2$. Me_3SiBr (11 μl, 0.083 mmol) was stirred into a mixture of **1** (45 mg, 0.083 mmol) and $CoBr_2$ (18.3 mg, 0.083 mmol) in CH_2Cl_2 (0.3 ml). After stirring for 0.5 h at room temperature, the mixture was filtered quickly. The ^1H NMR of the filtrate was essentially identical with that of 2,3,4,6-tetra-*O*-benzyl-α-D-glucopyranosyl bromide (**2**)[10] in CH_2Cl_2 (δ=6.59, J= 4 Hz).[2c]

*Reaction of 2,3,4,6-Tetra-*O*-benzyl-α-*D*-glucopyranosyloxytrimethylsilane (**3**) with* Me_3SiBr *and* $CoBr_2$. Compound **3**[11] (62.7 mg, 0.010 mmol) was treated with Me_3SiBr (13 μl, 0.010 mmol) and $CoBr_2$ (22.4 mg, 0.010 mmol) in CH_2Cl_2 for 15 min at room temperature. The filtrate showed a ^1H NMR spectrum almost identical with that of **2** in CH_2Cl_2.

Reaction of the Bromide **2** *with (5α-Cholestan-3β-yloxy)trimethylsilane in the Presence of* $CoBr_2$. A mixture of **2**[10] (42 mg, 0.07 mmol), and trimethylsilyl compound[12] (32 mg, 0.07 mmol), and $CoBr_2$ (15 mg, 0.07 mmol) in CH_2Cl_2 (0.4 ml) was stirred for 2 h at room temperature. The filtrate of the reaction mixture was then chromatographed[2b] to give **4a** (19 mg, 30%) and **4b** (11 mg, 17%).

Without $CoBr_2$, the glucosylation did not proceed.

Reaction of the Trimethylsilyl Glucose **3** *with 5α-Cholestan-3β-ol,* $CoBr_2$, Me_3SiBr, *and MS-4A.* A mixture of **2a** (55 mg, 0.090 mmol), the alcohol (26.3 mg, 0.068 mmol), $CoBr_2$ (21 mg, 0.095 mmol), MS-4A (72 mg), and Me_3SiBr (12 μl, 0.090 mmol) in CH_2Cl_2 (0.24 ml) was agitated for 6 h at room temperature. The subsequent chromatography of the mixture gave **4a** (15 mg, 24%) and **4b** (24 mg, 38%).

*Benzyl O-(2,3,4,6-Tetra-*O*-benzyl-α- and -β-*D*-glucopyranosyl)-(1→6)-2,4,6-tri-*O*-benzyl-α-*D*-glucopyranosides (**17a** and **17b**).* A mixture of **1** (570 mg, 1.06 mmol), **11** (400 mg, 0.81 mmol), $CoBr_2$ (232 mg, 1.06 mmol), n-Bu_4NBr (340 mg, 1.06 mmol), MS-4A (855 mg), and Me_3SiBr (138 μl, 1.06 mmol) in CH_2Cl_2 (2.45 ml) was stirred for 20 h at room temperature. The filtrate of the reaction mixture was then briefly chromatographed to give a sirupy mixture of the products (602 mg). This was de-*O*-acetylated and then chromatographed in the manner described before[6b] to give **17a** (475 mg, 60%) and **17b** (85 mg, 11%). They were identified with the respective samples synthesized previously.[6b]

*O-α-*D*-Glucopyranosyl-(1→3)-O-[α-*D*-glucopyranosyl-(1→6)]-*D*-glucopyranose (**29**).* Me_3SiBr (78 μl, 0.60 mmol) was stirred into a mixture of **1** (322 mg, 0.60 mmol), the disaccharide **17a** (445 mg, 0.46 mmol), $CoBr_2$ (1313 mg, 0.60 mmol), n-Bu_4NBr (191 mg, 0.60 mmol), and MS-4A (485 mg) in CH_2Cl_2 (1.6 ml), after which the stirring was continued for 40 h at room temperature. The filtrate of the reaction mixture was then evaporated and chromatographed to give a syrupy product mixture (266 mg) with three spots [R_f 0.58 (**22b**), 0.55 (**22a**), and 0.50 (the benzylate of α,α-trehalose[2a]), benzene–2-butanone (20:1)]. This was carefully separated through three chromatographies to give **22a** and **22b** (Table 1).

The hydrogenation of **22a** (90 mg) gave **23** (26 mg) as a foam, $[\alpha]_D^{20}$ +126° (*c* 0.4, H_2O) [lit,[5] $[\alpha]_D^{14}$ +133° (*c* 0.7, H_2O)]. Found: C, 40.37; 6.23%. Calcd for $C_{18}H_{32}O_{16}\cdot 1.5H_2O$: C, 40.67; H, 6.64%.

The reduction of **23** (10 mg, 0.010 mmol) with $NaBH_4$ (Wako, 30 mg) in H_2O (3 ml) for 48 h at room temperature, followed by the usual work-up and acetylation, furnished crystalline *O*-(2,3,4,6-tetra-*O*-acetyl-α-D-glucopyranosyl-(1→3)-*O*-[(2,3,4,6-tetra-*O*-acetyl-α-D-glucopyranosyl-(1→6)]-1,2,4,5-tetra-*O*-acetyl-D-glucitol (**25**) (8.4 mg, 42%).

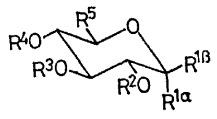

Bn = Benzyl,
Ct = 5α-cholestan-3β-yl,
G = 2,3,4,6-tetra-*O*-benzyl-D-glucopyranosyl,
AcG = 2,3,4,6-tetra-*O*-acetyl-D-glucopyranosyl,
Glc = D-glucopyranosyl.

Code	$R^{1\alpha}$	$R^{1\beta}$	R^2	R^3	R^4	R^5
1	OH	H	Bn	Bn	Bn	CH_2OBn
2	Br	H	Bn	Bn	Bn	CH_2OBn
3	$OSiMe_3$	H	Bn	Bn	Bn	CH_2OBn
4a	OCt	H	Bn	Bn	Bn	CH_2OBn
4b	H	OCt	Bn	Bn	Bn	CH_2OBn
5	OMe	H	Bn	H	Bn	H
6	OMe	H	Bn	Bn	H	H
7	OBn	H	Bn	H	Bn	CH_2OBn
8	OBn	H	Bn	Ac	Bn	CH_2OBn
9	OMe	H	Bn	Bn	Bn	CH_2OH
10	OBn	H	Bn	Bn	Bn	CH_2OH
11	OBn	H	Bn	Ac	Bn	CH_2OH
12a	OMe	H	Bn	αG	Bn	H
12b	OMe	H	Bn	βG	Bn	H
13a	OMe	H	Bn	Bn	αG	H
13b	OMe	H	Bn	Bn	βG	H
14a	OBn	H	Bn	αG	Bn	CH_2OBn
14b	OBn	H	Bn	βG	Bn	CH_2OBn
15a	OMe	H	Bn	Bn	Bn	$CH_2O\alpha G$
15b	OMe	H	Bn	Bn	Bn	$CH_2O\beta G$
16a	OBn	H	Bn	Bn	Bn	$CH_2O\alpha G$
16b	OBn	H	Bn	Bn	Bn	$CH_2O\beta G$
17a	OBn	H	Bn	H	Bn	$CH_2O\alpha G$
17b	OBn	H	Bn	H	Bn	$CH_2O\beta G$
18	H,	OH	H	αGlc	H	CH_2OH
19	H,	OAc	Ac	αAcG	Ac	CH_2OAc
20	H,	OH	H	H	H	$CH_2O\alpha Glc$
21	H,	OAc	Ac	Ac	Ac	$CH_2O\alpha AcG$
22a	OBn	H	Bn	αG	Bn	$CH_2O\alpha G$
22b	OBn	H	Bn	βG	Bn	$CH_2O\alpha G$
23	H,	OH	H	αGlc	H	$CH_2O\alpha Glc$
24	H,	OAc	Ac	αAcG	Ac	$CH_2O\alpha AcG$

References

1) a) R. Eby and C. Schuerch, *Carbohydr. Res.*, **34**, 79 (1974); P. A. Gent and R. Gigg, *J. Chem. Soc., Perkin Trans. 1*, **1974**, 1446; K. Igarashi, J. Irisawa, and T. Honma, *Carbohydr. Res.*, **39**, 341 (1975); R. Pougny, J. C. Jaquinet, M. Nassr, D. Duchet, M. L. Milat, and P. Sinaÿ, *J. Am. Chem. Soc.*, **99**, 6762 (1977); T. Mukaiyama, T. Nakatsuka, and S. Shoda, *Chem. Lett.*, **1979**, 487; T. Mukaiyama, Y. Murai, and S. Shoda, *ibid.*, **1981**, 431; b) R. U. Lemieux, K. B. Hendriks, R. V. Stick, and K. James, *J. Am. Chem. Soc.*, **97**, 4056 (1975); c) J. Leroux and A. S. Perlin, *Carbohydr. Res.*, **67**, 163 (1978); A. A. Pavia, J. -M. Rocheville, and S. N. Ung, *ibid.*, **79**, 79 (1980).

2) a) S. Koto, N. Morishima, and S. Zen, *Bull. Chem. Soc. Jpn.*, **52**, 784 (1979); b) S. Koto, T. Sato, N. Morishima, and S. Zen, *ibid.*, **53**, 1761 (1980); c) S. Koto, N. Morishima, and S. Zen, *Chem. Lett.*, **1976**, 1109; *Bull. Chem. Soc. Jpn.*, **55**, 1543 (1982).

3) a) M. E. Jung and G. L. Hatfield, *Tetrahedron Lett.*, **1978**, 4483; b) A. H. Schmidt and H. Russ, *Chem. Ber.*, **114**, 1099 (1981); c) H. Paulsen and Lockhoff, *Tetrahedron Lett.*, **1978**, 4027; J. Thiem and B. Meyer, *Chem. Ber.*, **113**, 3075 (1980); d) M. G. Voronkov, S. F. Pavlov, and E. I. Dubinskaya, *Dokl. Acad. Nauk SSR*, **227**, 607 (1976).

4) N. Morishima, S. Koto, C. Kusuhara, and S. Zen, *Chem. Lett.*, **1981**, 427.

5) F. Yamauchi and K. Matsuda, *Agric. Biol. Chem.*, **33**, 103 (1976).

6) a) S. Koto, T. Uchida, and S. Zen, *Bull. Chem. Soc. Jpn.*, **46**, 2520 (1973); b) S. Koto, S. Inada, T. Yoshida, M. Toyama, and S. Zen, *Can. J. Chem.*, **59**, 255 (1981); c) The gradient elution of a mixture of ethyl acetate and ethanol gave more reproducible results in the separation of the anomeric mixture of benzyl D-glucopyranosides obtained through the alcoholysis described in Ref. 6b.

7) R. Eby and C. Schuerch, *Carbohydr. Res.*, **79**, 53 (1980).

8) T. Usui, N. Yamaoka, K. Matsuda, K. Tuzimura, H. Sugiyama, and S. Sato, *J. Chem. Soc., Perkin Trans. 1*, **1973**, 2425.

9) T. Lakhanisky and H. P. Naveau, *Cellul. Chem. Technol.*, **6**, 127 (1972).

10) F. Weygand and H. Ziemann, *Justus Liebigs Ann. Chem.*, **657**, 179 (1962).

11) A. Klemer, E. Buhe, R. Kutz, S. Chahin, and L. Kleefeldt, *Justus Liebigs Ann. Chem.*, **739**, 185 (1970).

12) A. T. de B. Andrews, A. D. Boul, G. D. Meakins, and M. J. Sledge, *J. Chem. Soc., C*, **1970**, 1052.

Deoxygenation of Tertiary Amine Oxides with Carbon Disulfide

Toshiaki Yoshimura, Kaoru Asada, and Shigeru Oae*

Department of Chemistry, The University of Tsukuba, Niihari-gun, Sakura-mura, Ibaraki 305

(Received March 20, 1982)

Reduction of various tertiary amine oxides with carbon disulfide was examined and kinetic experiments were carried out. Trialkylamine oxides and *N,N*-dialkylarylamine *N*-oxides were readily reduced by CS_2 to give the corresponding tertiary amines in good yields, while heteroaromatic amine *N*-oxides such as picoline *N*-oxide were not affected. The oxygen atom in the *N*-oxide was found to be transferred to CO_2 upon mass spectral analysis of the gas evolved. The kinetic experiments were carried out following the UV spectra of *N,N*-dimethylaniline *N*-oxide in CH_3CN containing much excess of CS_2 and the rate was found to be of 2nd order in the *N*-oxide and CS_2. Activation parameters ($\Delta H^{\ddagger}=55.7$ kJ mol^{-1}, $\Delta S^{\ddagger}=-78.2$ J K^{-1} mol^{-1} at 20 °C) are characteristic of a normal bimolecular reaction. The logarithms of the rate constants for para-substituted *N,N*-dimethylaniline *N*-oxides are nicely correlated with Hammett σ values and a small negative ρ value ($\rho=-0.2$) was obtained. The rate of reaction was faster in polar aprotic solvents than in nonpolar or protic solvents. These observations seem to suggest that the reaction proceeds via an initial nucleophilic attack of the *N*-oxide oxygen at carbon disulfide followed by the rate-determining N–O bond fission to give the tertiary amine.

Tertiary amine oxides can be reduced back to the corresponding amines by various reducing agents such as trivalent phosphorus compounds, sulfur compounds, carbenes, hexachlorodisilane and metal hydride. These deoxygenation can roughly be classified into the following three types mechanistically.

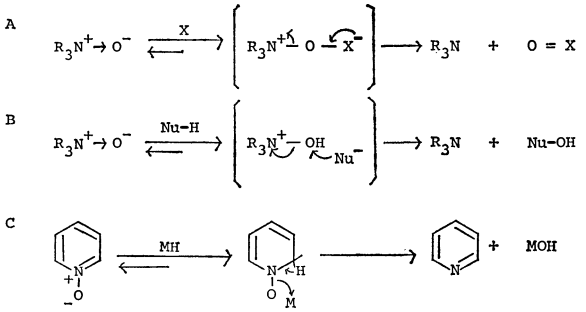

The mechanism A involves initial electrophilic attack of reagent such as trivalent phosphorus compound,[1] carbens,[2] sulfur dioxide[3] followed by back donation of an electron pair from the central atom of the reducing agent to cleave the N–O bond. Meanwhile, the mechanism B involves the initial coordination of electrophile on *N*-oxide oxygen followed by nucleophilic substitution at oxygen atom like in the reduction with thiols.[4] In the reduction of heteroaromatic *N*-oxides with metal hydride, the reaction proceeds *via* an initial addition of metal hydride to α-carbon and oxygen, followed by elimination of metal hydroxide (mechanism C).[5,6]

Tertiary amine oxides are mild nucleophilic oxidants which can oxidize both disulfides and sulfoxides,[7] whereas carbon disulfide is another dicoordinated sulfur compound which could function as a reducing agent.

Indeed, carbon disulfide is known to react with dialkylsulfilimine, which has also a semipolar S–N linkage, eventually affording dialkyl sulfide, the reduction product, and elemental sulfur.[8]

Meanwhile, Hamana *et al.*[9] reported that some tertiary amine oxides reacted with carbon disulfide affording the amines in very poor yields, however, they did not look into the mechanism.

Thus as a part of our systematic studies on the oxidation of organosulfur compounds, it is interesting to investigate the general scope of the reaction and the mechanism of this reduction, since the reaction is presumed to be classified into a modified A type. The reaction was found to be quite general for most aliphatic, aromatic tertiary amine oxides but not heteroaromatic *N*-oxides. This paper describes the scope of the reaction and the kinetic investigation of the reduction of *N,N*-dimethylaniline *N*-oxide (**1**) and substituted derivatives with carbon disulfide and the plausible mechanism based on both kinetic and product analyses.

Results and Discussion

Reaction of Amine Oxides and Carbon Disulfide. The addition of excess carbon disulfide to a stirred solution of a certain amine oxide in chloroform at 0 °C in the presence of anhydrous sodium sulfate[10] afforded the corresponding amine in a good yield. The yield was determined by gas chromatography after confirming by TLC that no amine *N*-oxide remained. As shown in Table 1, picoline *N*-oxide was not reduced at all upon the same treatment with CS_2. All these products were isolated by column chromatography and identified by IR and NMR. A small amount of elemental sulfur (25%) was also obtained when methanol was added to the reaction mixture. The reaction of (**1**) with an equimolar amount of CS_2 under the same conditions for two days also afforded the corresponding amine quantitatively.

When the reaction was carried out under reduced pressure, and gas evolved was analyzed by MS, CO_2 and a trace amount of COS were found. The following mechanism, Scheme, may be conceivable. The reaction is presumed to proceed through the initial nucleophilic attack of the *N*-oxide oxygen to carbon disulfide and subsequent N–O bond cleavage to form the amine and oxathiiranethione (**2**) or dithiiranone (**3**). The intermediate (**2**) is considered to decompose readily to elemental sulfur and COS which would then be hydrolyzed to CO_2 and H_2S. However, in a control experiment, hydrolysis of carbonyl sulfide was found to be very slow in the presence of *N,N*-dimethylaniline and water in acetonitrile. Meanwhile, only trace amounts of carbonyl sulfide and hydrogen sulfide were

Table 1. Reduction of tertiary amine oxides with carbon disulfide

$$RR'R''N{\rightarrow}O \xrightarrow{CS_2} RR'R''N$$

N-Oxide	Yield of amine/%	*N*-Oxide	Yield of amine/%
$(n\text{-Bu})_3N{\rightarrow}O$	69	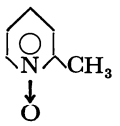	0
$PhN(CH_3)_2$ ↓ O	92		
$PhCH_2N(CH_3)_2$ ↓ O	80	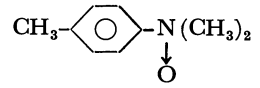	73
$PhN(CH_3)CH_2Ph$ ↓ O	79	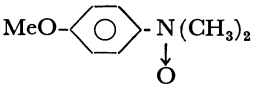	86
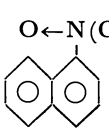	91	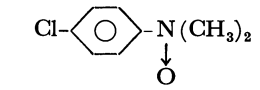	77

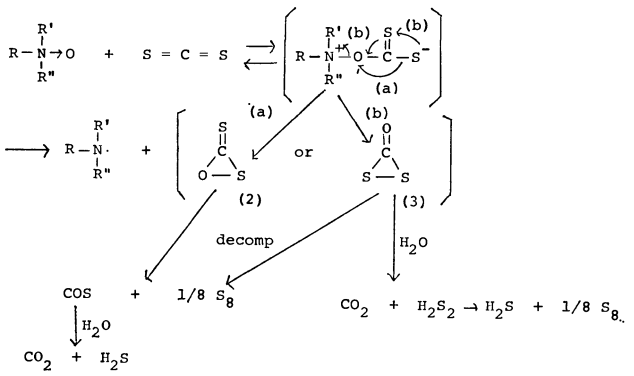

Scheme

formed in our system. This would suggest that formation of the intermediate (**2**) is quite unlikely. Meanwhile, the intermediate (**3**) might readily be hydrolyzed to CO_2 and H_2S_2 which is then decomposed to elemental sulfur and H_2S. Thus, a trapping experiment of H_2S_2 was carried out. The reduction of trimethylamine *N*-oxide with carbon disulfide in the presence of benzylidenacetophenone in chloroform at 0 °C afforded the Michael-type adduct of hydrogen disulfide (**4**) in 6% yield together with the usual reduction products. The disulfide (**4**) was identified by com-

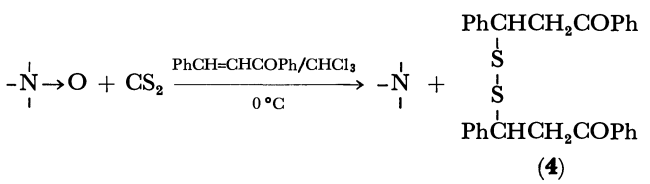

(**4**)

paring its mp, IR, NMR, and elemental analyses with those of the authentic sample.[11] In the reaction of **1** under similar conditions the disulfide was not obtained, however, in the presence of triethylamine as a base the same adduct was obtained in 6% yield. This observation alone may not be enough to suggest the reduction to involve the intermediate (**3**), since there are a few other possibilities for the formation of the adduct.

Table 2. Pseudo-first order rate constants of reduction of *N*,*N*-dimethylaniline *N*-oxide in various concentration of carbon disulfide

$[CS_2]$/M	$10^3\ k/s^{-1}$
0.166	9.97
0.133	8.17
0.0996	6.46
0.0830	5.23
0.0415	2.67

Hamana *et al.*[9] reported the formation of carbonyl sulfide and elemental sulfur in the reduction of nitrone with carbon disulfide based on their observation of the IR spectra. Meanwhile, the intermediate (**2**) was postulated by Neal *et al.*[12] in the formation of carbonyl sulfide during the oxygenation of carbon disulfide with cytochrome P-450. We have examined the gas evolved from the reaction of *N*-benzylideneaniline *N*-oxide with carbon disulfide. Carbonyl sulfide was found to be formed upon mass spectral analysis in agreement with the result of Hamana *et al.* Therefore, the mechanism for the reduction of *N*-oxide with carbon disulfide should be different from that of the nitrone. In order to clarify the mechanism of the reduction of *N*-oxides, kinetic experiments have been carried out.

Kinetics. Kinetics of the reaction of *N*,*N*-dimethylaniline *N*-oxide (**1**) with a large excess of carbon disulfide was carried out in acetonitrile at 20 °C by following the UV 250 nm absorption of *N*,*N*-dimethylaniline formed in the reaction. The rate of reaction was found to fit with the pseudo first order rate equation. However, it was rather difficult to obtain accurate rate constants in dry acetonitrile since a trace of water affects the rate of reaction. Therefore, acetonitrile containing 2% water was used as the choice solvent. Pseudo-first order rate constants shown in Table 2 were linearly correlated with the concentration of carbon disulfide. From these results, the rate was found to be of first order each with the *N*-oxide and CS_2 suggesting the mechanism to involve the transition state containing one molecule each of *N*-oxide

Table 3. Second order rate constants of the reduction of *p*-substituted *N,N*-dimethylaniline *N*-oxides with carbon disulfide

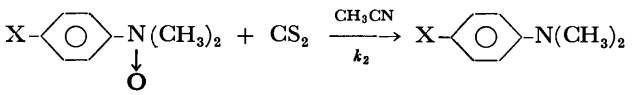

X	Temp/°C	$10^2 k_2$/l mol^{-1} s^{-1}	
H	15	4.28±0.11[a]	
H	20	6.01±0.05	
H	25	9.23±0.09	$\Delta H^* = 55.6 \pm 2.7$ kJ mo^{-1}
H	30	14.1 ±0.38	$\Delta S^* = -78.2 \pm 9.2$ J K mol^{-1}
CH_3O	20	6.49±0.02	at 20 °C for mol l^{-1} unit
CH_3	20	5.49±0.01	$\rho = -0.2$ ($\gamma = 0.979$)
Cl	20	4.96±0.01	
NO_2	20	4.14±0.01	

a) Errors shown in the table are standard deviation.

Table 4. Solvent effect on the rate of reduction of *N,N*-dimethyl-*p*-nitroaniline *N*-oxide with carbon disulfide

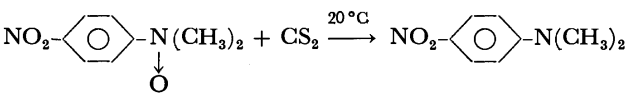

Solvent	k_2/l mol^{-1} s^{-1}
DMF	0.372
CH_3CN	0.253
CH_2Cl_2	0.121
$ClCH_2CH_2Cl$	0.0506
$CHCl_3$	1.687×10^{-3}

and carbon disulfide.

Activation parameters were obtained from Arrhenius plot of the second order rate constants at a temperature range of 15—30 °C as shown in Table 3. Activation parameters ($\Delta H^* = 55.6$ kJ^{-1} mol^{-1}, $\Delta S^* = -78.2$ J K^{-1} mol^{-1} at 20 °C for mol l^{-1} unit) reveal the characteristic feature of the normal bimolecular reaction.

The effect of substituent on the rate of the reactions of para-substituted *N,N*-dimethylaniline *N*-oxides and carbon disulfide was examined. The logarithms of these rate constants were nicely correlated with Hammett σ values and a small negative ρ value ($\rho = -0.2$) was obtained. The electron-releasing substituent accelerates the reaction, indicating the importance of the initial nucleophilic attack of the *N*-oxide oxygen to carbon disulfide. However, the ρ-value ($\rho = -0.2$) seems to be too small for the rate-determining initial attack. Perhaps the effect of polar substituent on the initial equilibrium formation of adduct is partially cancelled by the positive ρ-value on the subsequent rate-determining N–O bond cleavage.

The kinetic experiments in various anhydrous solvents using *N,N*-dimethyl-*p*-nitroaniline *N*-oxide were performed by following UV absorption at 390 nm. The results are shown in Table 4. When the reaction was carried out in methanol, the rate of reaction was too low to be measured. The reaction in dry CH_3CN is about six times faster than that in wet CH_3CN (2% H_2O). These results apparently show that hydrogen-bonding of the solvent such as methanol or chloroform to the *N*-oxide oxygen retards the reaction and the solvents, which have strong affinity for water, such as DMF and acetonitrile, accelerate the reaction. The water which hydrates the *N*-oxide is presumably removed partially from the *N*-oxide in DMF or acetonitrile.

Inspection of these experimental results has led us to postulate the mechanism involving the initial equilibrium attack of the *N*-oxide to carbon disulfide, followed by rate-determining N–O bond cleavage to form the corresponding amine and unstable dithiiranone (**3**) which is readily hydrolyzed to give CO_2 and H_2S_2. However, a question still remains, why the reaction of the nitrone with carbon disulfide did afford carbonyl sulfide instead of carbon dioxide.

The reaction of the nitrone is much slower than that of the *N*-oxide. When one compares the structures of the probable intermediates for both reactions, the leaving ability of a Schiff base from the adduct of nitrone is considered to be much poorer than that of the amine in the *N*-oxide, since the delocalization of positive charge on the nitrogen atom of the nitrone adduct would reduce the leaving ability of the Schiff base as compared to that of amine in the *N*-oxide which bears a full positive charge on the nitrogen atom. Therefore, the N–O bond cleavage in the adduct of the nitrone would require an anchimeric assistance of the neighboring thiocarbonate anion. Thus the direct nucleophilic attack of the neighboring thiolate group preferably occurs on the oxygen atom to form (**2**) rather than (**3**) in the reaction of nitrone with carbon disulfide. Whereas, the N–O bond in the adduct of tertiary amine oxide may be sufficiently polarized to allow the S–S bond formation, giving (**3**). Consequently the reduction of the tertiary amine oxide with carbon disulfide would proceed through a modified mechanism A while the reduction of the nitrone with CS_2 presumably proceeds through a modified mechanism B which involves internal nucleophilic attack as described in the introduction section.

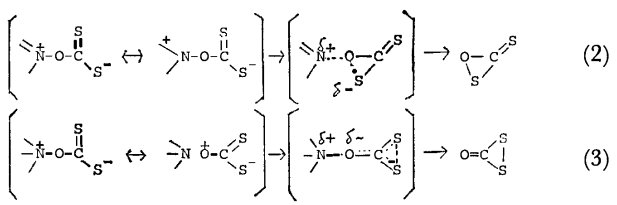

Experimental

Materials. Most of tertiary amine oxides used were prepared by oxidation of tertiary amines and *p*-substituted *N,N*-dimethylanilines[13] with hydrogen peroxide.[14] *N,N*-Dimethyl-*p*-nitroaniline *N*-oxide was prepared by oxidation with *m*-CPBA in $CHCl_3$ at room temperature for 1 week and purified by means of silica-gel column chromatography.

Gas Analysis. Carbon disulfide (1 ml) and acetonitrile (2 ml) were condensed in a 20 ml test tube reactor containing, (**1**) (100 mg) at −195 °C (liq. N_2) in a vaccum line. When the temperature was raised slowly to 0 °C, the reaction started evolving gas which was purified three times and subjected to mass spectroscopic analysis. A peak of CO_2 (m/e=44) was observed mainly and COS peak (m/e=60) was only 1% of that of CO_2.

Reaction of N-*Benzylideneaniline* N-*Oxide with Carbon Disulfide.* Carbon disulfide (1 ml) and acetonitrile (2 ml) were condensed in a 20 ml test tube reactor, connected to a vaccum line, containing *N*-benzylideneaniline *N*-oxide (100 mg) at −195 °C (liq. N_2). Then the temperature was raised to room temperature. The solution was kept standing at room temperature for 24 h. Gas evolved was purified three times and its mass spectrum was taken. m/e=44 (40%), 60 (60%).

Hydrolysis of Carbonyl Sulfide. Carbonyl sulfide (10 ml, 1 atom), prepared from NH_4SCN and H_2SO_4 and purified, was condensed in a 20 ml test tube reactor containing *N,N*-dimethylaniline (100 mg), H_2O (10 ml) in 2 ml of CH_3CN. The reaction was carried out at room temperature for 3 h. Analysis of the gas showed no CO_2 formation.

The Reaction of N-*Oxides and Carbon Disulfide.* To a stirred solution of an amine oxide (1.0—1.5 mmol) in 3 ml of $CHCl_3$ was added dropwise 3 ml of CS_2 over Na_2SO_4 at 0 °C. After 2 h, the solution was filtered and the filtrate was diluted with 3 ml of CH_3OH. Elemental sulfur was deposited. (Sulfur was confirmed by thin layer chromatography, melting point and liquid chromatography. Amines were identified by thin layer chromatography and gas chromatography). Isolation of amines was carried out with silica gel column chromatography.

Trapping Experiments of H_2S_2. *1)*: To a stirred solution of trimethylamine oxide (0.01 mole) and benzylidenacetophenone (0.01 mole) in 15 ml of $CHCl_3$ was added dropwise over Na_2SO_4 at 0 °C 15 ml of CS_2. White crystals were precipitated in 6% yield. The crystals were identified as bis(1,3-diphenyl-3-oxopropyl) disulfide by comparing its mp, IR, NMR, and elemental analyses with those of the authentic sample.[11]

2): To a stirred solution of (**1**) (1.5 g), chalcone (2.0 g) and triethylamine (2 ml) in 15 ml of $CHCl_3$ was added dropwise over *ca.* 1 g of anhydrous Na_2SO_4 at 0 °C in 15 ml of CS_2. After 2 h reaction, the solution was concentrated. The products were separated by silica-gel column chromatography. The disulfide (**4**) was obtained in 6% yield.

Kinetic Experiments. A solution of carbon disulfide (0.166 M) in CH_3CN–H_2O (2%) (2.5 ml) in a UV cell was incubated at a desired temperature for 30 min. To this was added 12 μl solution of (**1**) (8.23×10^{-5} M) in CH_3CN. UV absorption 250 nm (390 nm for *p*-nitro derivative) of *N,N*-dimethylaniline formed was then followed immediately. Pseudo first order rate constants were calculated from the following equation.

$$\ln\frac{A_\infty - A_0}{A_\infty - A_t} = kt \quad A\text{: UV absorption intensity}$$

Solvent Effect. The reaction of *N,N*-dimethyl-*p*-nitroaniline *N*-oxides with CS_2 in DMF, CH_2Cl_2, $ClCH_2CH_2Cl$, $CHCl_3$, and dry CH_3CN were followed with UV at 390 nm. All these solvents used were dried and freshly distilled.

References

1) E. Ochiai, *J. Org. Chem.*, **18**, 534 (1953); M. Hamana, *Yakugaku Zasshi*, **75**, 121 (1955); T. R. Emerson and C. W. Rees, *J. Chem. Soc.*, **1964**, 2319; E. Howard and W. F. Olszewski, *J. Am. Chem. Soc.*, **81**, 1483 (1959).

2) E. E. Schweizer, G. J. O'Neill, and J. N. Wemple, *J. Org. Chem.*, **29**, 1744 (1964); W. Kirmse, "Carbene Chemistry," Academic Press, N. Y. (1971), p. 437; E. E. Schiweizer and G. J. O'Neill, *J. Org. Chem.*, **28**, 2460 (1963).

3) P. A. Bather, J. R. Lindsay Smith, R. D. C. Norman, and J. S. Sadd, *J. Chem. Soc., Chem. Commun.*, **1969**, 1116. F. A. Daniher and B. E. Hackley, Jr., *J. Org. Chem.*, **31**, 4267 (1966).

4) D. I. Relyea, P. O. Tawney, and A. R. Williams, *J. Org. Chem.*, **27**, 477 (1962).

5) W. Traber, M. Hubmann, and P. Karrer, *Helv. Chim. Acta*, **43**, 265 (1960).

6) H. C. Brown and P. M. Weissman, *J. Am. Chem. Soc.*, **87**, 5614 (1965).

7) K. Ikura and S. Oae, *Tetrahedron Lett.*, **1968**, 3791; M. E. C. Biffin, J. Miller and D. B. Panl, *ibid.*, **1969**, 1015.

8) R. Appel and W. Buedmer, *Chem. Ber.*, **95**, 855 (1962).

9) M. Hamana, B. Umezawa and S. Nakashima, *Chem. Pharm. Bull.*, **10**, 969 (1962).

10) *N*-Oxides are usually hydrated and this reaction release the water. Thus without dehydrating agent, water was separated and much amount of *N*-oxides were extracted to the aqueous layer to prevent the reduction.

11) H. Tanaka and A. Yokoyama, *Chem. Pharm. Bull.*, **8**, 275 (1960).

12) R. R. Dalvi, R. E. Poore, and R. A. Neal, *Life Sci.*, **14**, 1785 (1974).

13) S. Hünig, H. Quast, W. Brenninger, and E. Frankenfeld, *Org. Synth.*, Coll. Vol. V, p.1018.

14) T. L. Kruger, W. N. White, H. White, S. L. Hartzell, J. W. Kress, and N. Walter, *J. Org. Chem.*, **40**, 77 (1975).

Catalytic Efficiency of Functionalized Vesicles in the Transamination of Pyridoxal-5′-phosphate with a Hydrophobic Amino Acid†

Yukito MURAKAMI,* Akio NAKANO, and Kazunari AKIYOSHI

Department of Organic Synthesis, Faculty of Engineering, Kyushu University, Hakozaki, Higashi-ku, Fukuoka 812

(Received April 13, 1982)

The transamination reaction of pyridoxal-5′-phosphate (PLP) with *N*-dodecyl-L-alaninamide ($AlaC_{12}$) was investigated in an aqueous phosphate–borate buffer at pH 7.0, μ 0.10 (KCl), and 30.0±0.1 °C in the presence of single-walled vesicles of *N,N*-ditetradecyl-N^{α}-(6-trimethylammoniohexanoyl)-L-histidinamide bromide ($N^+C_5His2C_{14}$). The electrostatic and hydrophobic interactions between the vesicles and the reactants resulted in incorporation of PLP and $AlaC_{12}$ into polar and hydrophobic domains of the vesicles, respectively, in the Schiff-base formation process. The isomerization of the aldimine Schiff-base to the corresponding ketimine Schiff-base was confirmed to be the rate-determining step in the transamination process. The reaction site in the vesicular system was found to be equivalent in polarity to dioxane–water (7:3 v/v). However, the overall reaction rate in the vesicles was enhanced 230-fold relative to that in dioxane–water (7:3 v/v). A hydrophobic and suitably polar microenvironment constructed at the reaction site is responsible for such a marked rate-enhancement. In addition, each vesicle of $N^+C_5His2C_{14}$ provided functional (imidazolyl) groups in its hydrogen-belt domain to catalyze the intramolecular prototropic shift to yield the ketimine Schiff-base. The microenvironmental effects of molecular assemblies of *N,N*-ditetradecyl-N^{α}-(6-trimethylammoniohexanoyl)-L-alaninamide bromide and CTAB on the overall transamination were also discussed.

Although the apoproteins in vitamin B_6-dependent enzymes play essential roles not only in rate enhancement but also in substrate-recognition and reaction specificity which leads to selective cleavage of the covalent bonds around the α-carbon atom of a substrate,[1] the mechanistic details as regards such functions have not been fully understood up to the present time. These functions may be characterized tentatively as follows: (1) each apoprotein provides a hydrophobic environment in its interior region in which pyridoxal-5′-phosphate is buried; (2) it catalyzes a specific reaction by its various functional groups such as the imidazolyl group of histidine and the ε-amino group of lysine; (3) it constructs a hydrophobic cavity, shape and size of which are specific to its substrate, so that the substrate-selectivity is exercised; (4) such a hydrophobic cavity fixes its specific substrate in space to carry out the desired reaction. On these grounds, micellar surfactants,[2,3] synthetic polymers,[4] and macrocyclic compounds[5,6] have been developed to simulate the functions of vitamin B_6-dependent enzymes.

We have recently reported that amphiphiles involving an amino acid residue interposed between a polar head group and an aliphatic double-chain form stable single-compartment vesicles in aqueous media due to formation of the hydrogen-belt region in the intramembrane region.[7] These amphiphiles were confirmed to construct three characteristic domains in their vesicular aggregates; a polar surface domain composed of charged head groups, semipolar barrier domain composed of amino acid residues (so-called hydrogen belt), and a hydrophobic interior domain composed of aliphatic double-chains. Thus, these various domains may be utilized as reaction site models of the apoenzymes, specific to the nature of reactants. In the present study, the transamination reaction of pyridoxal-5′-phosphate (PLP) with *N*-dodecyl-L-alaninamide ($AlaC_{12}$), a hydrophobic amino acid analogue, in the presence of single-walled vesicles of $N^+C_5His2C_{14}$ and $N^+C_5Ala2C_{14}$ as well as in the presence of CTAB micelles. The microenvironmental effects provided by these cationic amphiphiles on the transamination reaction have been characterized.

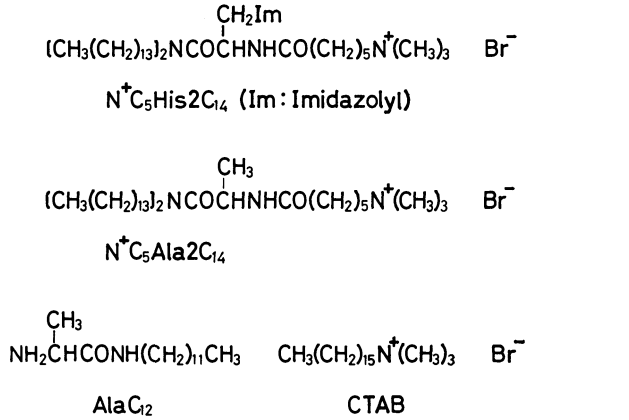

Experimental

Spectroscopic data were taken on a JASCO DS-403G grating IR spectrophotometer, a Hitachi Perkin-Elmer R-20 NMR spectrometer, a Union Giken SM-401 high-sensitivity UV-visible spectrophotometer, and a Hitachi 650—60 fluorescence spectrophotometer. pH-Measurements were carried out with a Beckman expandomatic SS-2 pH meter equipped with a Metrohm EA-125 combined electrode after calibration with a combination of appropriate standard aqueous buffers. Melting points were measured with a Yanagimoto MP-S1 apparatus (hot-plate type).

Hexadecyltrimethylammonium bromide (CTAB) of Nakarai Chemicals was recrystallized from ethanol, mp 237—239 °C (decomp). Dodecylamine of Nakarai Chemicals was distilled under reduced pressure, bp 95—98 °C/266 Pa. Pyridoxamine-5′-phosphate (PMP: Calbiochem, U.S.A.; A-grade), pyridoxal hydrochloride (PL: Mann Research Laboratories, U.S.A.), and pyridoxal-5′-phosphate (PLP: Nakarai Chemicals; bio-analytical grade) were used without further purification. *N*-Dodecyl-L-alaninamide ($AlaC_{12}$) was prepar-

† Contribution No. 661 from this Department.

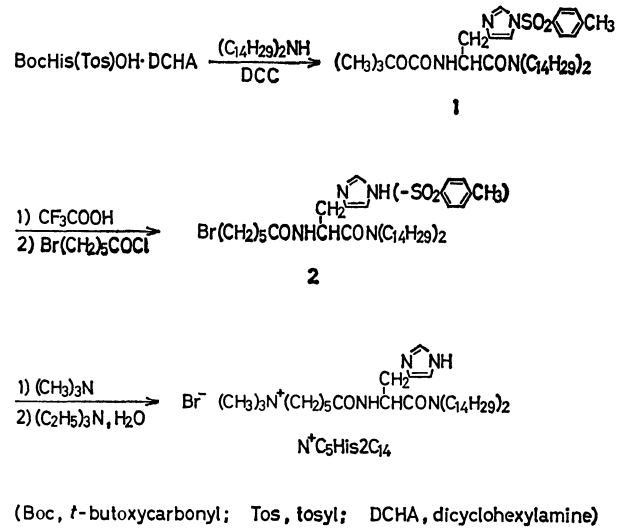

Scheme 1.

ed by condensation of *t*-butoxycarbonyl-L-alanine with dodecylamine in the presence of dicyclohexylcarbodiimide (DCC), followed by elimination of the *t*-butoxycarbonyl group with hydroformic acid. The product was recrystallized from diethyl ether to give a white solid, mp 51—52 °C. Found: C, 69.78; H, 12.38; N, 10.81%. Calcd for $C_{15}H_{32}N_2O$: C, 70.26; H, 12.58; N, 10.92%. *N,N*-Ditetradecyl-N^{α}-(6-trimethylammoniohexanoyl)-L-alaninamide bromide ($N^+C_5Ala2C_{14}$) was synthesized in a manner similar to that reported previously for the preparation of *N,N*-didodecyl-N^{α}-(6-trimethylammoniohexanoyl)-L-alaninamide bromide,[7d] and characterized as reported elsewhere.[7f]

The synthetic procedure for *N,N*-ditetradecyl-N^{α}-(6-trimethylammoniohexanoyl)-L-histidinamide bromide ($N^+C_5His2C_{14}$) is outlined in Scheme 1.

N,N-*Ditetradecyl*-N^{α}-t-*butoxycarbonyl*-N^{im}-*tosyl*-L-*histidinamide* (*1*). To a solution of the dicyclohexylamine adduct of N^{α}-*t*-butoxycarbonyl-N^{im}-tosyl-L-histidine (5.0 g, 8.5 mmol)[8] in dry dichloromethane (40 ml) was added *p*-toluenesulfonic acid (1.7 g, 8.8 mmol) in 5 min with stirring at room temperature. After *N,N*-ditetradecylamine (3.4 g, 8.8 mmol) and dicyclohexylcarbodiimide (1.85 g, 8.9 mmol) were added to the reaction mixture in this order at room temperature and 0 °C, respectively, the mixture was stirred for 3 h at 0 °C and for 12 h at room temperature. The resulting precipitates (*N,N'*-dicyclohexylurea) were removed by filtration, the solvent was evaporated *in vacuo*, and the residual oil was dissolved in ethyl acetate (150 ml). The solution was then washed with 10% aqueous citric acid, saturated aqueous sodium chloride, 4% aqueous sodium hydrogencarbonate, and saturated sodium chloride in this sequence. After being dried over Na_2SO_4, the mixture was evaporated *in vacuo* to afford an oil which was subsequently purified by centrifugal liquid chromatography with a combination of silica gel (Wako gel B-5) and chloroform; a pale yellow oil which was solidified in a refrigerator, yield 5.6 g (83%). IR (neat): 3200 (NH str.), 2840 and 2800 (CH str.), 1705 and 1625 (C=O str.) cm^{-1}. NMR ($CDCl_3$, TMS): δ 0.88 [6H, broad t, $C\underline{H}_3(CH_2)_{13}$–], 1.24 [48H, s, $CH_3(C\underline{H}_2)_{12}CH_2$–], 1.34 [9H, s, $(CH_3)_3COCO$–], 2.40 (3H, s, $-SO_2C_6H_4C\underline{H}_3$), 2.80 [2H, d, $-CH(C\underline{H}_2$Im-Tos)], 3.12 [4H, broad t, $CH_3(CH_2)_{12}C\underline{H}_2N$–], 4.75 (1H, broad q, –CH–), 5.20 (1H, d, NH), 6.98 (1H, s, Im-5H), 7.80 (1H, s, Im-2H), 7.23 (2H, d, tosyl's 3H and 5H), and 7.74 (2H, d, tosyl's 2H and 6H).

N,N-*Ditetradecyl*-N^{α}-*(6-bromohexanoyl)*-L-*histidinamide* (*2*). Trifluoroacetic acid (6 g, 53 mmol) was added to a dichloromethane solution (10 ml) of **1** (1.9 g, 2.4 mmol), and the mixture was stirred for 1.5 h at room temperature. Evaporation of an excess amount of trifluoroacetic acid *in vacuo* below 40 °C gave a pale brown oil (**1a**). Elimination of the *t*-butoxycarbonyl group was confirmed by NMR spectroscopy. The amine (**1a**) was dissolved in dry dichloromethane (5 ml) and the solution was cooled to 0 °C. Triethylamine (3.4 g, 34 mmol) was added dropwise to the solution, and then 6-bromohexanoyl chloride (1.0 g, 4.7 mmol) dissolved in dry dichloromethane (10 ml) was added dropwise to the mixture at 0 °C with stirring. The resulting mixture was stirred for 2.5 h at 0 °C and then washed with 4% aqueous citric acid, saturated aqueous sodium chloride, 4% aqueous sodium hydrogencarbonate, and saturated aqueous sodium chloride in this sequence. After being dried over Na_2SO_4, the solution was evaporated *in vacuo* to give a pale brown oil; yield 1.6 g (93%). A major fraction of the tosyl group was eliminated as confirmed by NMR spectroscopy. The product was used for the subsequent reaction without further purification. NMR ($CDCl_3$, TMS): δ 0.87 [6H, broad t, $C\underline{H}_3(CH_2)_{13}$–], 1.25 [48H, s, $CH_3(C\underline{H}_2)_{12}CH_2$–], ~2.00 [6H, m, $BrCH_2(C\underline{H}_2)_3CH_2CO$–], 2.35 [2H, broad t, $Br(CH_2)_4C\underline{H}_2CO$–], 2.80 (2H, d, $-CHC\underline{H}_2$Im–), 3.35 [2H, t, $BrC\underline{H}_2(CH_2)_4CO$–], 3.00—3.40 [4H, m, $CH_3(CH_2)_{12}C\underline{H}_2N$–], 5.05 (1H, broad q, –CH–), 6.45 (1H, d, NH), 7.15 (1H, s, Im-5H), and 7.94 (1H, s, Im-2H).

N,N-*Ditetradecyl*-N^{α}-*(6-trimethylammoniohexanoyl)*-L-*histidinamide Bromide* ($N^+C_5His2C_{14}$). Dry trimethylamine gas was introduced into a benzene solution (30 ml) of **2** (1.6 g, 2.2 mmol) for 1.5 h to reach the gas saturation level, and the solution was stirred at room temperature for 12 h. The solvent was evaporated off *in vacuo*, and the residual oil was dissolved in benzene–acetone (36 ml, 5:1 v/v). To the solution was added 30% aqueous triethylamine (2 ml) with stirring at room temperature to eliminate the tosyl group completely. After the resulting solution was stirred for 3.5 h, the solvent was evaporated off *in vacuo*. The crude product was purified by gel-filtration chromatography on columns of Sephadex LH-20 and Toyopearl HW-40 in this sequence with methanol as an eluant: a white glassy solid, yield 0.32 g (19%); mp 182 °C, $[\alpha]_D^{20}$ −14.2° (*c* 1.13, ethanol). IR (neat): 3280 (NH, OH str.) and 1630 (C=O str.) cm^{-1}. NMR ($CDCl_3$, TMS): δ 0.85 [6H, broad t, $C\underline{H}_3(CH_2)_{13}$–], 1.22 [48H, s, $CH_3(C\underline{H}_2)_{12}CH_2$–], ~1.90 [6H, m, $N^+CH_2(C\underline{H}_2)_3CH_2CO$–], 2.32 [2H, broad t, $N^+(CH_2)_4C\underline{H}_2CO$–], 2.80—3.62 [8H, m, $CH_3(CH_2)_{12}C\underline{H}_2N$–, $N^+C\underline{H}_2(CH_2)_4CO$–, and $-CHC\underline{H}_2$Im–], 3.35 [9H, s, $(CH_3)_3N^+$–], 5.05 (1H, broad q, NHC<u>H</u>CO–), 6.90 (1H, s, Im-5H), 7.62 (1H, d, NH), and 7.95 (1H, s, Im-2H). Found: C, 63.99; H, 10.58; N, 8.58%. Calcd for $C_{43}H_{84}N_5BrO_2\cdot(3/2)H_2O$: C, 63.75; H, 10.82; N, 8.65%.

Kinetic Measurements. An amount of pyridoxamine-5'-phosphate formed in the transamination reaction was determined by measuring a fluorescence intensity at the emission maximum of PMP excited at 328 nm. Each run was initiated by adding 50 μl of an aqueous solution of PLP (1.02×10^{-3} mol dm^{-3}) and 40 μl of an ethanol solution of *N*-dodecyl-L-alaninamide (1.99×10^{-2} mol dm^{-3}) to 2.00 ml of a reaction medium which was pre-equilibrated at 30.0±0.1 °C in a thermostated cell set in the fluorescence spectrophotometer. The reaction medium was prepared as follows; (1) an appropriate amount of the stock solution of an amphiphile in ethanol was placed in a glass vessel, ethanol was removed *in vacuo*, and 10 ml of the aqueous buffer (6.23 mmol dm^{-3} phosphate–1.88 mmol dm^{-3} borate, pH 7.0) containing 0.1

mol dm^{-3} potassium chloride was added to the residue; (2) the aqueous dispersion of an amphiphile thus prepared was sonicated for 4 min with a probe-type sonicator at 30-W power (W-220F, Heat Systems-Ultrasonics). The resulting vesicle solution was sufficiently clear without noticeable turbidity and gave good kinetic reproducibility. Kinetic measurements in aqueous dioxane were carried out under similar conditions. Light was emitted to an experimental solution only at the instant of each fluorescence intensity measurement.

Electron Microscopy. Both aqueous dispersion (A) and ultrasonicated aqueous solution (B) of $N^+C_5His2C_{14}$ were employed for the measurements. As sample A, 16 mg of $N^+C_5His2C_{14}$ was suspended in 2 ml of deionized and distilled water containing 2%(w/w) uranyl acetate and the dispersion was shaked occasionally and heated until the glassy solid disappeared completely to give slightly turbid dispersion. As sample B, an aqueous dispersion of $N^+C_5His2C_{14}$ (sample A) was sonicated for 4 min with a probe-type sonicator at 30-W power and allowed to stand for 10 min at 5 °C. A clear solution was then obtained. Samples A and B were applied on carbon grids and dried in a vacuum desiccator. A JEOL JEM-200B electron microscope, installed at the Research Laboratory of High Voltage Electron Microscope of our University, was used for the measurements. Electron micrographs for $N^+C_5His2C_{14}$ are shown in Fig. 1, while those for $N^+C_5Ala2C_{14}$ have been reported elsewhere.[7f] Both multiwalled vesicles and lamellae were observed in an electron micrograph of the aqueous dispersion as shown in Fig. 1. On the other hand, the sonicated aqueous solution showed exclusively the formation of single-walled vesicles. Similar patterns of electron micrographs have been observed for respective samples of $N^+C_5Ala2C_{14}$. The present amphiphiles were used in the state of single-walled vesicles for study.

Differential Scanning Calorimetry (DSC). Each 50-μl sample of an aqueous dispersion of the amphiphile [2.0% (w/w)] in an aqueous buffer of 6.23 mmol dm^{-3} phosphate–1.88 mmol dm^{-3} borate, containing 0.1 mol dm^{-3} potassium chloride, was sealed up in a silver sample cell. The measurements were made on a differential scanning calorimeter (Daini Seikosha SSC-560U): heating rate, 0.5 °C/min; sensitivity, 0.025 mcal/s/(full scale); chart speed, 0.5 cm/min. The obtained calorimetric parameters for the amphiphiles are as follows, where T_m represents a temperature at a peak maximum of DSC thermogram.

$N^+C_5Ala2C_{14}$: T_m, 2.0 °C; ΔH, 20.5 kJ mol^{-1}

$N^+C_5His2C_{14}$: T_m, 2.5 °C; ΔH, 19.2 kJ mol^{-1}

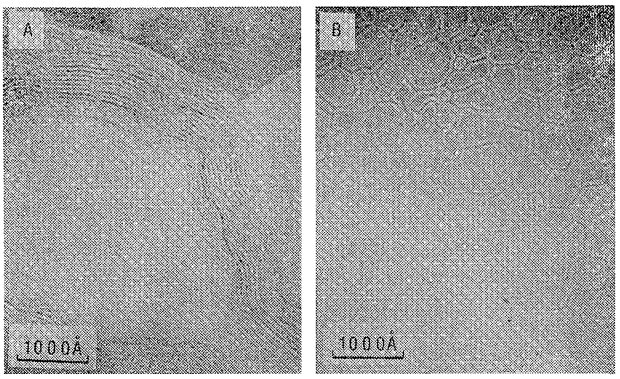

Fig. 1. Electron micrographs for $N^+C_5His2C_{14}$ negatively stained with uranyl acetate: A, 10 mmol dm^{-3} aqueous dispersion (magnification, ×92 000); B, 10 mmol dm^{-3} aqueous solution sonicated for 4 min at 30-W power and subsequently allowed to stand for 10 min at 5 °C (magnification, ×92 000).

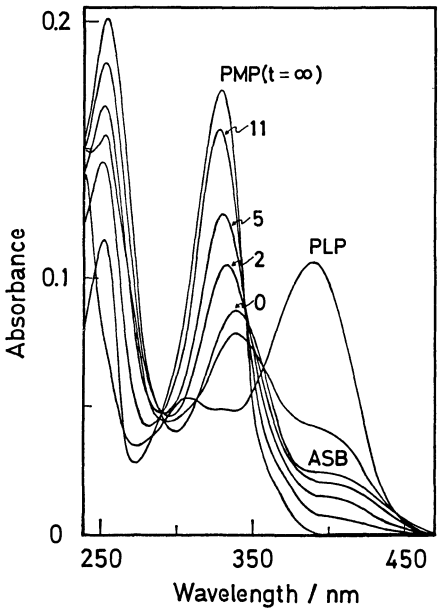

Fig. 2. Spectral change along the progress of reaction of PLP (2.44×10^{-5} mol dm^{-3}) with $AlaC_{12}$ (3.81×10^{-4} mol dm^{-3}) in the presence of $N^+C_5His2C_{14}$ (9.7×10^{-4} mol dm^{-3}) in aqueous phosphate (6.0 mmol dm^{-3}) –borate (1.8 mmol dm^{-3}), containing 1.9%(v/v) ethanol, at pH 7.0, μ 0.1 (KCl), and 30.0±0.1 °C. Numerals refer to reaction times (in h) for the second slow step.

Results and Discussion

The transamination reaction of pyridoxal-5′-phosphate (PLP) with $AlaC_{12}$ in the presence of an amphiphile was followed by electronic spectroscopy in an aqueous phosphate–borate buffer at pH 7.0, μ 0.10 (KCl), and 30.0±0.1 °C. Figure 2 shows the spectral change observed along the progress of transamination in the presence of $N^+C_5His2C_{14}$ vesicles. The spectral change shows that the reaction is consistent with a two-step mechanism. The first step, which reached an equilibrium stage within 4 min, was followed by a comparatively slow step. The isosbestic points associated with the respective steps are as follows: first, 312 and 357 nm; second, 292 and 345 nm. A half-life for the second slow step is several hours. Absorption spectra observed at the final stages of the respective steps showed that the first step is referred to the Schiff-base formation and the second one to the formation of pyridoxamine-5′-phosphate (PMP). The absorption spectrum observed at the final stage of the first step showed maxima at 338 and 415 nm, and is the typical one for a pyridoxylideneamino acid formed with PLP.[9] The absorption spectrum observed at the final stage of the second step, having maxima at 253 and 328 nm, is identical with that of PMP.[10] The absorption spectrum, which can be attributed to the corresponding ketimine Schiff-base (λ_{max} 310—330 nm),[9] was not detected in the course of the second step. A similar spectral behavior

Table 1. Equilibrium constants and spectral parameters for the Schiff-base formation between PLP and $AlaC_{12}$ in various media at 30.0±0.1 °C[a)]

Medium	Dioxane–Water (42:58 v/v)	Dioxane–Water (7:3 v/v)	CTAB	$N^+C_5Ala2C_{14}$	$N^+C_5His2C_{14}$
λ_{max}^{PLP}/nm	380	380[b)]	389	389	389
$\varepsilon_\lambda^{PLP}$	3.4×10^3	2.6×10^3 [b)]	4.4×10^3	4.4×10^3	4.4×10^3
$\varepsilon_\lambda^{ASB}$	1400	910	550	740	840
K_{SB}/mol^{-1} dm^3 [c)]	1.1×10^4	2.7×10^4	3.1×10^5	8.6×10^4	1.5×10^5

a) Cationic amphiphile systems: in aqueous phosphate (6.0 mmol dm^{-3})–borate (1.8 mmol dm^{-3}) containing 1.9% (v/v) ethanol at pH 7.0 and μ 0.1 (KCl); CTAB, 2.9×10^{-3} mol dm^{-3}; $N^+C_5Ala2C_{14}$, 9.7×10^{-4} mol dm^{-3}; $N^+C_5His2C_{14}$, 9.7×10^{-4} mol dm^{-3}. Dioxane–water (42:58 v/v): dioxane containing 58%(v/v) aqueous buffer (6.2 mmol dm^{-3} phosphate, 1.8 mmol dm^{-3} borate, and 0.1 mol dm^{-3} potassium chloride) and 1.9%(v/v) ethanol. Dioxane–water (7:3 v/v): dioxane containing 30%(v/v) aqueous buffer (6.2 mmol dm^{-3} phosphate, 1.8 mmol dm^{-3} borate, and 0.1 mol dm^{-3} potassium chloride) and 1.9%(v/v) ethanol. b) Wavelength and molar extinction coefficient of PLP employed for calculation of [ASB] in order to achieve accuracy of spectral analysis, while $\lambda_{max}=370$ nm and $\varepsilon^{PLP}(370\text{ nm})=4.1\times10^3$. c) Cationic amphiphile systems: PLP, 4.93×10^{-5} mol dm^{-3}; $AlaC_{12}$, 4.90×10^{-5} mol dm^{-3}. Dioxane–water (7:3 v/v): PLP, 4.90×10^{-5} mol dm^{-3}; $AlaC_{12}$, 9.80×10^{-5} mol dm^{-3}. Dioxane–water (42:58 v/v): PLP, 4.85×10^{-5} mol dm^{-3}; $AlaC_{12}$, 3.88×10^{-4} mol dm^{-3}.

along the progress of reaction was observed in other amphiphile systems. In the light of these observations, the overall reaction pathway is explicitly given by Eq. 1.

$$\text{PLP} + \text{AlaC}_{12} \underset{\text{fast}}{\overset{K_{SB}}{\rightleftharpoons}} \text{ASB} \underset{\text{slow}}{\overset{k_{AK}}{\rightleftharpoons}} \text{KSB} \xrightarrow[\text{very fast}]{} \text{PMP} + \text{PyC}_{12} \quad (1)$$

Here, ASB, KSB, and PyC_{12} refer to the aldimine Schiff-base, the ketimine Schiff-base, and *N*-dodecylpyruvinamide, respectively. Thus, the rate determining step for the present transamination reaction is the isomerization of the aldimine Schiff-base (ASB) to the corresponding ketimine Schiff-base (KSB). This finding is consistent with the results obtained in PLP-dependent transamination reactions both in an enzyme system[11)] and model systems.[12)] The present two reaction steps were treated separately since the respective rates were much different from each other.

Schiff-base Formation. In order to clarify microenvironmental effects on the aldimine Schiff-base formation, the equilibrium constants (K_{SB}) for the first step were determined in the presence and absence of the cationic amphiphiles. The equilibrium constant, as defined by Eq. 2, for the Schiff-base formation between PLP and $AlaC_{12}$ was evaluated as follows.

$$K_{SB} = \frac{[\text{ASB}]}{[\text{PLP}][\text{AlaC}_{12}]} \quad (2)$$

This is rearranged to give Eq. 3.

$$K_{SB} = \frac{[\text{ASB}]}{(T_P-[\text{ASB}])(T_A-[\text{ASB}])} \quad (3)$$

Here, T_P and T_A refer to total concentrations of PLP and $AlaC_{12}$, respectively. An absorbance (A_λ) at the absorption maximum of PLP (λ, 389 and 380 nm in molecular assemblies of the cationic amphiphiles and aqueous dioxane, respectively) is represented by Eq. 4.

$$A_\lambda = \varepsilon_\lambda^{PLP}(T_P-[\text{ASB}]) + \varepsilon_\lambda^{ASB}[\text{ASB}] \quad (4)$$

Here, $\varepsilon_\lambda^{PLP}$ and $\varepsilon_\lambda^{ASB}$ are molar extinction coefficients of PLP and ASB observed at the absorption maximum

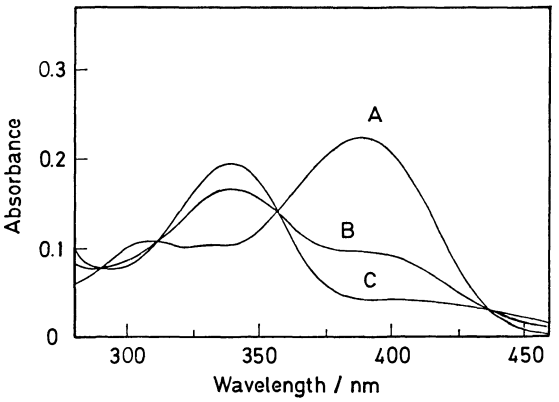

Fig. 3. Absorption spectra for the aldimine Schiff-base system of PLP (4.93×10^{-5} mol dm^{-3}) with varying amounts of $AlaC_{12}$ (A, 0; B, 4.90×10^{-5}; C, 3.86×10^{-4} mol dm^{-3}) in the presence of $N^+C_5His2C_{14}$ (9.7×10^{-4} mol dm^{-3}) in aqueous phosphate (6.0 mmol dm^{-3})–borate (1.8 mmol dm^{-3}), containing 1.9% (v/v) ethanol, at pH 7.0, μ 0.1 (KCl), and 30.0± 0.1 °C.

of PLP, respectively. Then, Eq. 4 is rearranged to Eq. 5. The value of $\varepsilon_\lambda^{ASB}$ was evaluated directly

$$[\text{ASB}] = \frac{\varepsilon_\lambda^{PLP}T_P - A_\lambda}{\varepsilon_\lambda^{PLP} - \varepsilon_\lambda^{ASB}} \quad (5)$$

from the spectrum observed in the presence of a large excess of $AlaC_{12}$; a complete conversion of PLP into the Schiff-base is assured under such conditions. Figure 3 shows the absorption spectra of the PLP–$AlaC_{12}$ system involving varying amounts of $AlaC_{12}$ in the presence of $N^+C_5His2C_{14}$. For a complete conversion of PLP into the aldimine Schiff-base, only a small excess of $AlaC_{12}$ (*ca.* 11 fold) over PLP was needed in the vesicular and micellar systems. On the other hand, over a 90-fold excess of $AlaC_{12}$ was required in aqueous dioxane to complete the conversion. The formation constants thus determined and the relevant spectral parameters in molecular assemblies of the cationic amphiphiles and in aqueous dioxane are listed in Table 1.

Table 2. Equilibrium constants and spectral parameters for two aldimine Schiff-bases (SB_1 and SB_2) in various media at 30.0±0.1 °C[a]

	Dioxane–Water[b]					CTAB	$N^+C_5Ala2C_{14}$	$N^+C_5His2C_{14}$
	10	20	30	39	48			
λ_{SB_1}/nm[c]	338	338	338	338	338	338	338	338
λ_{SB_2}/nm[d]	420	420	420	420	420	415	415	415
K_α	37.2	16.2	10.4	8.2	6.5	19.9	10.9	10.4

a) Cationic amphiphile systems: in aqueous phosphate (6.0 mmol dm^{-3})-borate (1.8 mmol dm^{-3}) containing 1.9% (v/v) ethanol at pH 7.0 and μ 0.1 (KCl); CTAB, 2.9×10^{-3} mol dm^{-3}; $N^+C_5Ala2C_{14}$, 9.7×10^{-4} mol dm^{-3}; $N^+C_5His2C_{14}$, 9.7×10^{-4} mol dm^{-3}; PLP, 4.93×10^{-5} mol dm^{-3}; $AlaC_{12}$, 3.86×10^{-4} mol dm^{-3}. Dioxane–water mixtures: each medium was prepared by mixing dioxane with aqueous buffer (6.2 mmol dm^{-3} phosphate, 1.8 mmol dm^{-3} borate, and 0.1 mol dm^{-3} potassium chloride); PLP, $(4.72—4.83)\times10^{-5}$ mol dm^{-3}; $AlaC_{12}$, $(2.42—4.72)\times10^{-3}$ mol dm^{-3}. b) Numerals refer to the content of aqueous buffer in %(v/v). c) ε_{SB_1}, 4.6×10^3. d) ε_{SB_2}, 9.4×10^3.

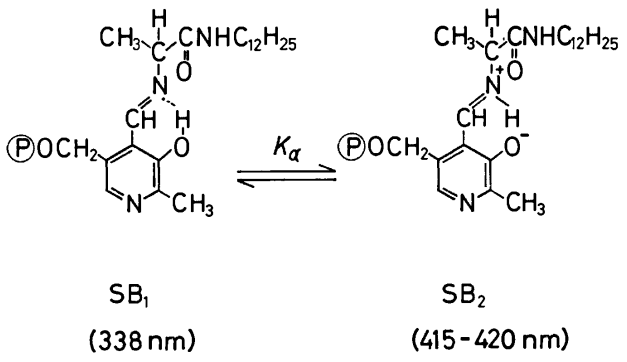

Ⓟ: A phosphate group.

Scheme 2.

The microenvironments constructed with the amphiphiles, into which the Schiff-base was incorporated, were characterized in terms of an equilibrium constant (K_α) defined by Eq. 6 on the following basis. An absorption spectrum of the aldimine Schiff-base showed the presence of two species in an equilibrium state (Fig. 3). They differ from each other in the protonation site as shown in Scheme 2. The neutral form (SB_1) with an ordinary amino acid was primarily observed in hydrophobic environments constructed with such components as organic solvents,[9] aqueous micelles,[13] reversed micelles,[3] and alkylamines bearing a long hydrocarbon chain.[14,15] The charged form (SB_2), on the other hand, was found exclusively in aqueous media.[16] These two species of the aldimine Schiff-base are in an equilibrium which is highly dependent on the microenvironmental polarity. The equilibrium constant between SB_1 and SB_2 is, therefore, referred to an efficient polarity parameter for characterization of the microenvironment to which the Schiff-base is bound.

$$K_\alpha = \frac{[SB_1]}{[SB_2]} = \frac{A_{SB_1}/\varepsilon_{SB_1}}{A_{SB_2}/\varepsilon_{SB_2}} \quad (6)$$

Here, A_{SB_1} and A_{SB_2} refer to absorbances observed at the absorption maxima of SB_1 and SB_2 species, respectively; ε_{SB_1} and ε_{SB_2} stand for molar extinction coefficients of SB_1 and SB_2 species at their absorption maxima, respectively. These values were determined according to the reported method employed for evaluation of those values for the Schiff-base of PLP with hexylamine.[15] Equation 7 can be derived on the basis of Scheme 2, where [ASB] refers to a total concentration of SB_1 and SB_2, and is equal to a PLP concentration employed under the conditions that PLP is completely converted into the Schiff-base ([PLP]≪[$AlaC_{12}$]).

$$A_{SB_1}/[ASB] = \varepsilon_{SB_1} - (\varepsilon_{SB_1}/\varepsilon_{SB_2})(A_{SB_2}/[ASB]) \quad (7)$$

The plot of $A_{SB_1}/[ASB]$ *vs.* $A_{SB_2}/[ASB]$ for the Schiff-base of PLP with $AlaC_{12}$ in aqueous dioxane resulted in a good linear relationship ($r>0.993$) as shown in Fig. 4. The data obtained in molecular assemblies of the cationic amphiphiles are also plotted in Fig. 4 and found along the correlation line for the dioxane–water system. The K_α-values thus obtained are summarized in Table 2, together with the relevant spectral parameters. Since the solvent-polarity parameter (Kosower's *Z*-value)[17] can be correlated with the standard Gibbs free energy ($\Delta G^0 = -RT\ln K_\alpha$),[15] we estimated the microenvironmental polarity of the reaction site for the Schiff-base formation in the light of a linear relation shown in Fig. 5. The result indi-

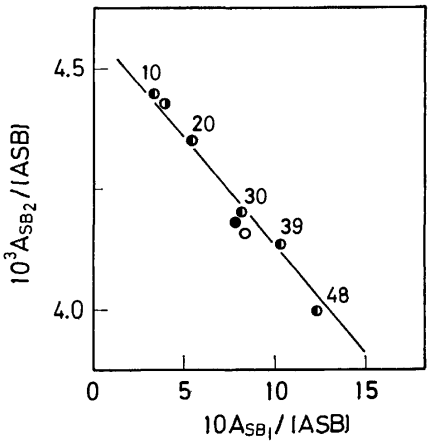

Fig. 4. Plot of $A_{SB_1}/[ASB]$ *vs.* $A_{SB_2}/[ASB]$ for equilibrium of aldimine Schiff-base species of PLP and $AlaC_{12}$ (SB_1 and SB_2) in dioxane–water mixtures (◐) and cationic amphiphile systems: $N^+C_5His2C_{14}$ (○), $N^+C_5Ala2C_{14}$ (●), and CTAB (◑). Numerals refer to the water contents in aqueous dioxane. See Table 2 for experimental conditions.

cates that the reaction sites in the vesicular and micellar systems are equivalent in polarity to dioxane–water (7:3 v/v) and dioxane–water (8:2 v/v), respectively. The reaction sites in the vesicular systems are more polar than that in the micellar system, most likely due to the presence of the hydrogen belt domain in the former. The hydrogen belt region divides the vesicular system into hydrophobic and polar domains,[7c] and PLP of hydrophilic nature is entrapped in the polar domain. The hydrophobic and less polar microenvironment provided by CTAB micelles is in favor of the Schiff-base formation relative to the polar reaction sites by the vesicular systems. The interaction modes of the reactants (PLP and $AlaC_{12}$) with the cationic aggregates were further examined on the basis of the following experimental facts. (1) The absorption maximum of PLP observed in the presence of the cationic aggregates (micelles and vesicles) was identical with that without those if $AlaC_{12}$ was absent. (2) The Schiff-base was not detected spectrophotometrically with a small excess of $AlaC_{12}$ over pyridoxal (PL), which has no phosphate group, in the cationic aggregates. (3) Formation of the Schiff-base of PLP with $AlaC_{12}$ was suppressed at higher ionic strength [μ=1.0 (KCl)]. (4) A large excess of an amino acid (L-alanine) was required to detect formation of the Schiff-base with PLP even in the presence of the cationic aggregates. (5) Without any cationic amphiphile, the content of dioxane in reaction media must exceed 40%(v/v) to investigate the Schiff-base formation between PLP and $AlaC_{12}$ because of the insolubility of $AlaC_{12}$ in water.

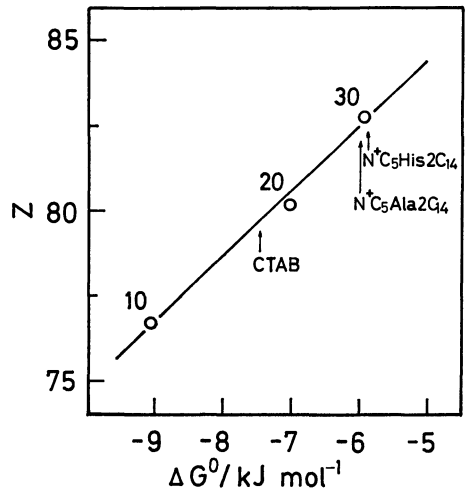

Fig. 5. Correlation of ΔG^0 with solvent polarity parameter (Z). Numerals refer to the water contents in aqueous dioxane. ΔG^0-Values for cationic amphiphile systems are shown by arrows.

These results indicate that PLP is concentrated at the surface area of the cationic aggregates due to the electrostatic interaction between the anionic phosphate group of PLP and the cationic head group of the amphiphile employed, while $AlaC_{12}$ is incorporated into the hydrophobic domain of the aggregates through mutual hydrophobic interaction. Consequently, both electrostatic and hydrophobic interactions play important roles in the Schiff-base formation in the presence of the amphiphile aggregates. The Schiff-base formation step in the present vesicular system is schematically shown in Fig. 6.

Transamination Reaction. The overall transamination reaction of PLP was followed by means of fluorescence spectroscopy at 30.0±0.1 °C in the presence and absence of cationic amphiphiles. The reaction was examined under the conditions of [$AlaC_{12}$]≫[PLP]; PLP was converted completely into the aldimine Schiff-base within 4 min. The reaction, for which the isomerization of the aldimine Schiff-base to the corresponding ketimine Schiff-base becomes rate-determining as mentioned above, was followed after complete formation of the aldimine Schiff-base. The fluorescence intensity at specified wavelengths (cationic aggregates, 393 nm; dioxane–water 405 nm) increased gradually along the progress of the reaction (Fig. 7). When a pseudo-substrate (1-dodecylamine) was used in place of $AlaC_{12}$, the fluorescence intensity remained unchanged. Table 3 summarizes the excitation wavelengths of PLP and PMP and the corresponding relative emission intensities in the presence and absence of the cationic amphiphiles. The fluorescence quantum yield of the Schiff-base was negligibly low compared with that of PMP.[14] The PMP concentration in the reaction system was determined on the basis

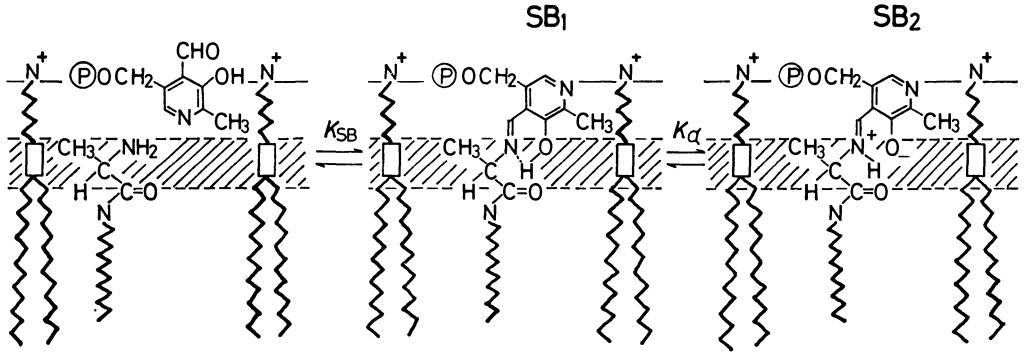

Fig. 6. Schematic representation of the Schiff-base formation step in vesicular phase: a rectangle, an amino acid residue; Ⓟ, a phosphate group. A shaded portion refers to the hydrogen belt region, which has some hydrophobic and polar nature, and to the reaction site for the overall transamination process.

Table 3. Fluorescence maxima (λ_F), relative emission intensities (I_{rel}), and excitation wavelengths (λ_E) for PLP and PMP in various media at 30.0±0.1 °C[a]

Medium	PLP			PMP		
	λ_F/nm	λ_E/nm	I_{rel}[b]	λ_F/nm	λ_E/nm	I_{rel}[b]
Aqueous buffer[c]	500	395	1.0	394	328	1250
Aqueous dioxane[d]	532	390	4.3	405	333	343
CTAB[e]	500	389	1.7	394	328	770
$N^+C_5Ala2C_{14}$[e]	504	389	2.0	393	328	687
$N^+C_5His2C_{14}$[e]	480	389	2.0	393	328	673

a) Fluorescence maxima in the absence of $AlaC_{12}$; concentrations of PLP and PMP, 2.44×10^{-5} mol dm^{-3}. b) Relative emission intensity with reference to the intensity for PLP in aqueous buffer. c) Aqueous phosphate (6.2 mmol dm^{-3})-borate (1.8 mmol dm^{-3}), containing 0.1 mol dm^{-3} potassium chloride (pH 7.0). d) Dioxane containing 30%(v/v) aqueous buffer (6.2 mmol dm^{-3} phosphate, 1.8 mmol dm^{-3} borate, and 0.1 mol dm^{-3} potassium chloride). e) In aqueous phosphate (6.1 mmol dm^{-3})-borate (1.8 mmol dm^{-3}) at pH 7.0 and μ 0.1 (KCl); CTAB, 2.9×10^{-3} mol dm^{-3}; $N^+C_5Ala2C_{14}$, 9.8×10^{-4} mol dm^{-3}; $N^+C_5His2C_{14}$, 9.8×10^{-4} mol dm^{-3}.

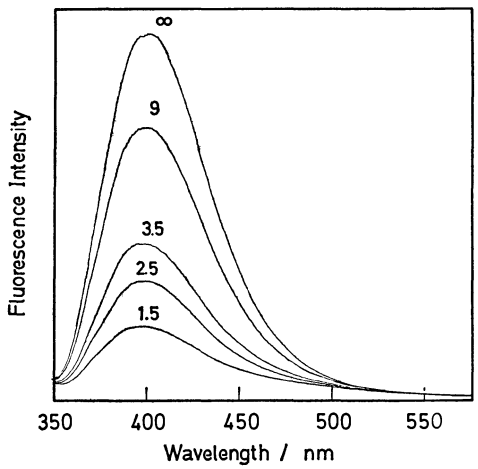

Fig. 7. Fluorescence-spectral change along the progress of reaction of PLP (2.44×10^{-5} mol dm^{-3}) with $AlaC_{12}$ (3.81×10^{-4} mol dm^{-3}) in the presence of $N^+C_5His2C_{14}$ (9.7×10^{-4} mol dm^{-3}) in aqueous phosphate (6.0 mmol dm^{-3})-borate (1.8 mmol dm^{-3}), containing 1.9%(v/v) ethanol, at pH 7.0, μ 0.1 (KCl), and 30.0±0.1 °C. Numerals refer to reaction times (in h) for the second slow step.

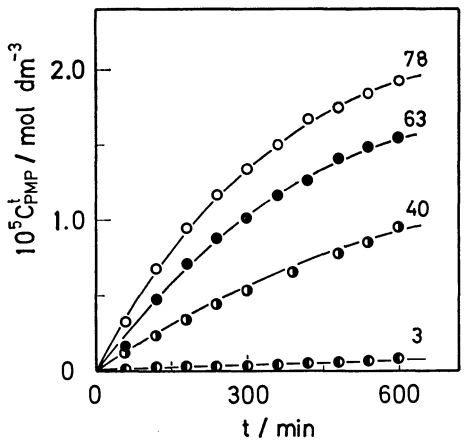

Fig. 8. Time-courses of PMP formation for transamination of PLP with $AlaC_{12}$ in aqueous dioxane (◐) and cationic amphiphile systems: $N^+C_5His2C_{14}$ (○), $N^+C_5Ala2C_{14}$ (●), and CTAB (◑). Numerals represent rates of conversion of PLP into PMP at t=600 min. See Table 4 for experimental conditions.

of Eq. 8 by measuring a fluorescence intensity (I_t) at appropriate time intervals.[18]

$$\frac{I_t}{I_0}=\frac{C^t_{PMP}}{C^0_{PMP}}\times10^{-0.5[(C^t_{PMP}-C^0_{PMP})\varepsilon_{PMP}+\varepsilon_{SB}C^t_{SB}]}. \quad (8)$$

Here, I_0 is a fluorescence intensity of PMP at its known concentration (C^0_{PMP}) in the absence of other reacting species; ε_{PMP} and ε_{SB} are molar extinction coefficients of PMP and the aldimine Schiff-base at a specified excitation wavelength, respectively; C^t_{PMP} and C^t_{SB} refer to concentrations of PMP and the aldimine Schiff-base observed at time t (s) after complete formation of the Schiff-base. C^t_{SB} is related with C^0_{SB} and C^t_{PMP} by Eq. 9, where C^0_{SB} refers to an initial concentration of the aldimine Schiff-base in the isomerization process and is equal to the PLP concentration used here (C^0_{PLP}).

$$C^t_{SB}=C^0_{SB}-C^t_{PMP} \quad (9)$$

The correlations between C^t_{PMP} and time are shown in Fig. 8. The rate equation for PMP formation is given by Eq. 10 in reference to Eq. 1, which is subsequently integrated to give Eq. 11.

$$\frac{dC_{PMP}}{dt}=-k_{AK}C^t_{SB}=-k_{AK}(C^0_{PLP}-C^t_{PMP}) \quad (10)$$

$$\ln\frac{C^0_{PLP}}{(C^0_{PLP}-C^t_{PMP})}=k_{AK}\cdot t \quad (11)$$

In each case, a good linear relationship between the left hand term of Eq. 11 and reaction time t was obtained as shown in Fig. 9 (r>0.998). The reaction was followed for 10 h and the first-order kinetics were found to hold in each kinetic run. The conversion rates of PLP to PMP at the ends of such kinetic runs (after 10 h) were determined as shown in Fig. 8. Under the conditions employed in this work, the reversed reaction from PMP to the aldimine Schiff-base was not detected. The rate constants for the isomerization process are summarized in Table 4, along with the overall second-order rate constants ($K_{SB}\cdot k_{AK}$) and relative effectiveness (k_{rel}) of the reac-

Table 4. Kinetic parameters for transamination in various media at 30.0±0.1 °C[a)]

Medium	Aqueous dioxane	CTAB	$N^+C_5Ala2C_{14}$	$N^+C_5His2C_{14}$
k_{AK}/s^{-1}	1.0×10^{-7}	1.3×10^{-6}	2.7×10^{-6}	4.2×10^{-6}
$K_{SB}\cdot k_{AK}/mol^{-1}\,dm^3\,s^{-1}$	2.7×10^{-3}	4.0×10^{-1}	2.3×10^{-1}	6.3×10^{-1}
k_{rel}[b)]	1	148	85	233

a) Cationic amphiphile systems: in aqueous phosphate (6.0 mmol dm^{-3})–borate (1.8 mmol dm^{-3}) containing 1.9% (v/v) ethanol at pH 7.0 and μ 0.1 (KCl); CTAB, 2.9×10^{-3} mol dm^{-3}; $N^+C_5Ala2C_{14}$, 9.7×10^{-4} mol dm^{-3}; $N^+C_5His2C_{14}$, 9.7×10^{-4} mol dm^{-3}; PLP, 2.44×10^{-5} mol dm^{-3}; $AlaC_{12}$, 3.81×10^{-4} mol dm^{-3}. Aqueous dioxane: dioxane containing 30%(v/v) aqueous buffer (6.2 mmol dm^{-3} phosphate, 1.8 mmol dm^{-3} borate, and 0.1 mol dm^{-3} potassium chloride) and 1.9%(v/v) ethanol; PLP, 2.44×10^{-5} mol dm^{-3}; $AlaC_{12}$, 1.23×10^{-3} mol dm^{-3}. b) Relative rate, taking $K_{SB}\cdot k_{AK}$ in aqueous dioxane as a reference.

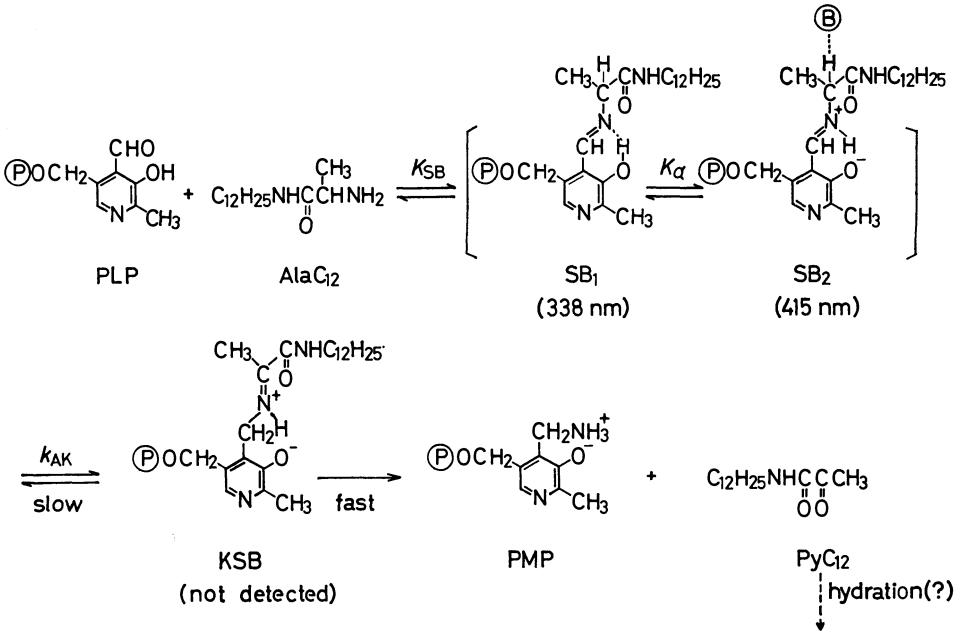

Ⓑ: A hydroxide ion and/or an imidazolyl group.
Ⓟ: A phosphate group.

Scheme 3.

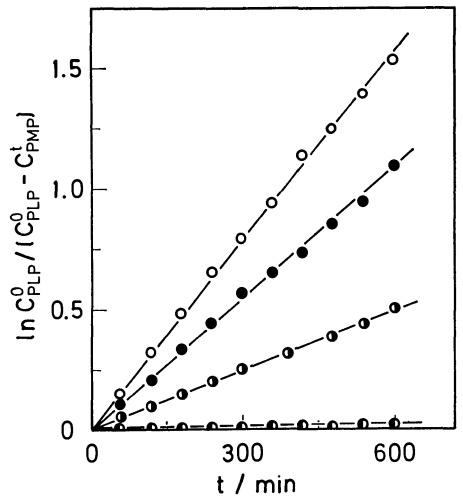

Fig. 9. Analysis of kinetic data (Fig. 8) on the basis of Eq. 11.

tion media.

The rate-determining step in the transamination reaction investigated here is referred to the isomerization of the aldimine Schiff-base to the ketimine one, since the accumulation of the latter was not detected spectrophotometrically in the course of the reaction. This means that the deprotonation from the α-carbon of the amino acid moiety is essential for the transamination, and such apparent intramolecular proton-transfer to afford the ketimine Schiff-base becomes rate-determining. The reaction was much accelerated in the cationic aggregate systems as compared with that in dioxane–water mixtures. This suggests that the concentration of hydroxide ion becomes efficient on the surface area of the cationic aggregates and is one of the important factors for rate enhancement as often observed in cationic micellar catalysis.[19] Secondly, the increase in a fraction of the active aldimine Schiff-base (SB_2), which is controlled by the microenvironmental property acted on the Schiff-base, is responsible for the rate acceleration. The fractions of the active SB_2 species in the whole aldimine Schiff-base were calculated with reference to K_α-values; 5 and 9% in the micellar and vesicular systems, respectively. Such difference reflects the microenvironmental property of reaction sites. Formation of the polar SB_2 species is favored in a polar microenvironment. Thirdly, the imidazolyl group placed at the

reaction site is in favor of the rate enhancement. The $N^+C_5His2C_{14}$ vesicles enhanced the reaction by more than 1.5 fold relative to the $N^+C_5Ala2C_{14}$ vesicles, even though the former may provide a microenvironment similar to that with the latter as mentioned above. The neutral imidazolyl group may act as a general-base catalyst which promotes the prototropic shift in a manner as observed for the imidazole-catalyzed transamination of α-aminophenylacetic acid.[12b] The overall transamination between PLP and $AlaC_{12}$ in the $N^+C_5His2C_{14}$ vesicles is now plausibly explained by Scheme 3.

In conclusion, a hydrophobic and polar microenvironment accelerates the overall transamination more than a hydrophobic but less polar one, even though the Schiff-base formation is more enhanced in the latter. The bilayer vesicles having an amino acid residue as a molecular component may provide better microenvironments for the transamination than ordinary micelles. This suggests that the hydrogen belt domain constructed in the vesicular assembly may be characterized as a suitable model for reaction sites in enzymes.[20] The vesicles formed with N^+C_5-$His2C_{14}$ provide functional groups in the hydrogen belt domain to catalyze the intramolecular prototropic shift and can be taken as a functionalized apoenzyme model for vitamin B_6-dependent enzymes

References

1) a) K. G. Scrimgeour, "Chemistry and Control of Enzyme Reactions" Academic Press, New York (1977), Chap. 8; b) H. C. Dunathan, *Adv. Enzymol.*, **35**, 79 (1971).

2) Y. Murakami and H. Kondo, *Bull. Chem. Soc. Jpn.*, **48**, 541 (1975).

3) H. Kondo, H. Yoshinaga, and J. Sunamoto, *Chem. Lett.*, **1980**, 973.

4) Y. N. Belokon', V. I. Tararov, T. F. Savel'eva, and V. M. Belikov, *Makromol. Chem.*, **181**, 2183 (1980).

5) R. Breslow, M. Hammond, and M. Lauer, *J. Am. Chem. Soc.*, **102**, 421 (1980).

6) H. Kuzuhara, T. Komatsu, and S. Emoto, *Tetrahedron Lett.*, **1978**, 3563.

7) a) Y. Murakami, A. Nakano, and K. Fukuya, *J. Am. Chem. Soc.*, **102**, 4253 (1980); b) Y. Murakami, A. Nakano, A. Yoshimatsu, and K. Fukuya, *ibid.*, **103**, 728 (1981); c) Y. Murakami, Y. Aoyama, A. Nakano, T. Tada, and K. Fukuya, *ibid.*, **103**, 3951 (1981); d) Y. Murakami, A. Nakano, and H. Ikeda, *J. Org. Chem.*, **47**, 2137 (1982); e) Y. Murakami, Y. Aoyama, J. Kikuchil K. Nishida, and A. Nakano, *J. Am. Chem. Soc.*, **104**, 2937 (1982); f) Y. Murakami, A. Nakano, and A. Yoshimatsu, *ibid.*, submitted for publication.

8) The dicyclohexylamine adduct of N^{α}-*t*-butoxycarbonyl-N^{1m}-tosyl-L-histidine was prepared in reference to the procedure reported by Fujii *et al*; mp 159—161 °C (lit, 160—162 °C): T. Fujii and S. Sakakibara, *Bull. Chem. Soc. Jpn.*, **47**, 3146 (1974).

9) Y. Matsushima and A. E. Martell, *J. Am. Chem. Soc.*, **89**, 1322 (1967).

10) The product analysis for the reaction of PLP (1.0×10^{-4} mol dm^{-3}) with $AlaC_{12}$ (1.0×10^{-4} mol dm^{-3}), which lasted 5 d at room temperature, was carried out by paper chromatography [Toyo filter paper No. 50, 1-propanol–aqueous ammonia (28%)–water (7:1:2 v/v) as an eluant, ninhydrin or iodide test for detection]. The result clearly indicated the disappearance of $AlaC_{12}$ along with the formation of PMP in the course of the reaction, while the formation of *N*-dodecylpyruvinamide was not detected.

11) G. G. Hammes and P. Fasella, *J. Am. Chem. Soc.*, **84**, 4644 (1962).

12) a) A. E. Braunstein, "The Enzymes," 2nd ed, ed by P. D. Boyer, H. Lardy, and K. Mirbäck, Academic Press, New York (1960), Vol. 2, pp. 113—181; b) T. C. Bruice and R. M. Topping, *J. Am. Chem. Soc.*, **85**, 1480 (1963).

13) V. Gani, A. Kupfer, and S. Shaltiel, *Biochemistry*, **17**, 1294 (1978).

14) K. O. Honikel and N. B. Madsen, *J. Biol. Chem.*, **247**, 1057 (1972).

15) J. Llor and M. Cortijo, *J. Chem. Soc., Perkin Trans. 2*, **1977**, 1111.

16) D. E. Metzler, *J. Am. Chem. Soc.*, **79**, 485 (1957).

17) E. M. Kosower, *J. Am. Chem. Soc.*, **80**, 3253 (1958).

18) T. Förster, "Fluoreszenz Organischer Verbindungen," Vandenhoeck & Ruprecht, Göttingen (1951).

19) J. H. Fendler and E. J. Fendler, "Catalysis in Micellar and Macromolecular Systems," Academic Press, New York (1975).

20) D. E. Metzler, *Adv. Enzymol.*, **50**, 1 (1979).

 © 1982 The Chemical Society of Japan Bull. Chem. Soc. Jpn., 55, 3013—3018 (1982)

Effect of Conformation on Ring Opening of Cis and Trans Dimers of Acenaphthylene in the Triplet State. Direct Detection of Hydrocarbon Biradical, 1,1′-Biacenaphthene-2,2′-diyl[1]

Harumichi Kobashi,* Hiroki Ikawa, Reiko Kondo, and Toshifumi Morita

Department of Chemistry, Faculty of Engineering, Gunma University, Kiryu, Gunma 376

(Received October 16, 1981)

Triplet sensitized photodecomposition of cis and trans dimers of acenaphthylene (c-D and t-D) has been studied in benzene by means of a nanosecond laser flash photolysis. An aromatic hydrocarbon biradical, 1,1′-biacenaphthene-2,2′-diyl (**1**) was found as an intermediate for the decomposition of triplet t-D to acenaphthylene monomers. The rate of bond opening was directly measured to be 8.3×10^6 s^{-1} at 20 °C. The temperature dependence of the rate yields the frequency factor 2.8×10^7 s^{-1} and activation energy 3.1 kJ mol^{-1}. The lifetime of **1** is 330 ns; this is insensitive to temperature changes (6—64 °C). Oxygen quenches **1** with the rate constant of 9×10^9 M^{-1} s^{-1} (1 M=1 mol dm^{-3}). On the other hand, the triplet state of c-D did not show any evidence of the presence of **1** as an intermediate. The difference of ring opening mechanisms between the two isomers is interpreted in terms of different steric hindrances between two acenaphthene rings. The triplet-triplet (T-T) absorption spectra of both dimers resemble each other. No characteristic absorption due to intramolecular triplet excimer of naphthalene was observed even for c-D.

Direct detection of unstable biradicals has been made in the Norrish type II reactions of alkyl phenyl ketones by means of laser photolysis methods.[2,3] Such studies are very important to elucidate reaction mechanisms, *i.e.*, to investigate channels of deactivation of a precursor in the excited state as well as behaviors in the biradical itself.[4]

Takamuku and Schnabel[5] reported the observation of biradical, **2**, produced through ring cleavage in the triplet state of r-1,c-2-bis(methoxycarbonyl)-t-3,t-4-di(1-naphthyl)cyclobutane. The spectrum of **2** drew our attention to the spectrum which had been observed in the triplet photosensitization of trans dimer of acenaphthylene during the course of our study about behavior of the triplet states containing acenaphthene units. We report here direct detection of a pure hydrocarbon biradical, **1**, formed through triplet sensitization of t-D and the influence of cis and trans conformations on the cleavage of a cyclobutane ring of acenaphthylene dimers, as studied by the laser flash photolysis. In addition, we show T-T absorption spectra of both dimers and compare them with the spectrum of acenaphthene.

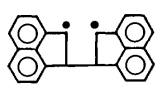

1

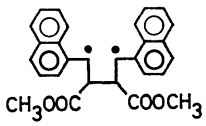

2

Experimental

Materials. The cis and trans dimers of acenaphthylene (c-D and t-D) were synthesized by photodimerization. Acenaphthylene monomer (M) as a starting material was purchased from Wako Pure Chemical Ind. and recrystallized once from ethanol. Procedures of synthesis and purification were essentially the same as the methods described by Nerbonne and Weiss[6] except for a slight modification noted below. A light source was a 450-W Hg-lamp (Ushio, UM-455) with a water-cooled quartz jacket. A few sealed glass tubes containing *ca.* 70 ml of acenaphthylene solution were immersed in a thermostated water bath at 25 °C and irradiated through a side window of the bath. The thick glass window and the tubes cut off the light less than 340 nm. In the preparation of c-D, cyclohexane was used as a solvent in the place of hexane in Ref. 6 and solutions of M were bubbled by oxygen before sealing. Purities of the dimers were checked by UV absorption[7,8a] and emission spectra[9] measured with a spectrophotometer (Hitachi Model 200-10) and a spectrophotofluorimeter (Hitachi Model MPF-2A), respectively.

Acenaphthene (ACN) as a reference to an unit chromophor of the dimers was purified by triple recrystallization from methanol. The zone-refined benzophenone (BP) or the G. R. grade acetophenone (AP) was used as a triplet sensitizer. Methylcyclohexane and isopentane for a mixed glass solvent at 77 K were purified by the usual methods. The spectrograde benzene (Dotite) was used as a solvent in steady illumination and fiash photolysis experiments.

The Nanosecond Flash Photolysis. The solutions of each dimer containing a sensitizer were degassed by several freeze-pump-thaw cycles. The nanosecond flash photolysis was done at 347 nm excitation using a ruby laser described elsewhere.[10] The laser beam excites the sensitizer but does not excite the dimers. Transient absorption spectra in the 340—600 nm range were measured at room temperature. For kinetic measurements, temperature control of a sample was carried out by circulating thermostated water in a quartz Dewar vessel equipped with a thermocouple.

Steady State Illumination. Both solutions of c-D and t-D containing BP were illuminated steadily with 365 nm light for isolation of decomposed products. The 365 nm light was obtained from a 100-W high-pressure Hg-lamp (Toshiba SHL-100UV) using a combination of glass lenses and a filter (Toshiba UV-D1C). After condensation of illuminated solutions with an evaporator, products were separated and identified by the aid of a TLC technique and a UV-VIS absorption measurement.

Results and Discussion

Steady State Illumination. Continuous irradiation with the 365 nm light gave rise to pale-yellow coloration of both dimer solutions. This coloration arises from gradual increase of the characteristic absorption band of M in the visible region. The relative rate of such change, as monitored at the absorption band, was faster for t-D than for c-D. Examination of the R_f

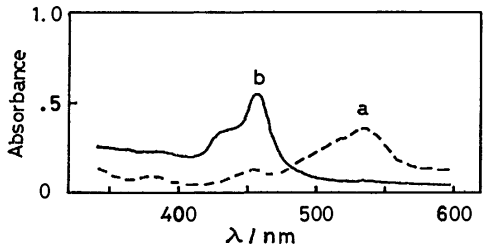

Fig. 1. Transient absorption spectra observed for cis dimer of acenaphthylene (5.0×10^{-3} M) in benzene containing benzophenone (4.0×10^{-3} M) as a sensitizer.
a: 30 and b: 130 ns after the start of laser oscillation.

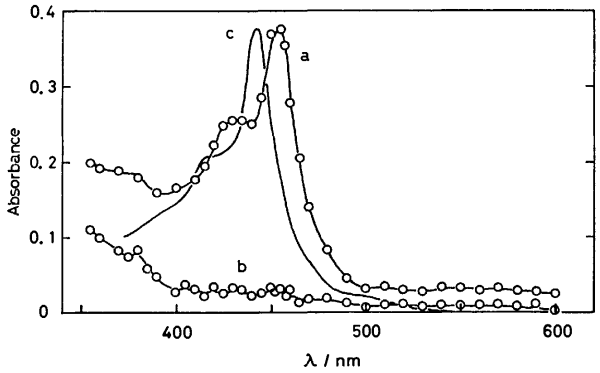

Fig. 2. Transient absorption spectra for cis dimer of acenaphthylene (5.0×10^{-3} M) [a and b] and for acenaphthene (1.0×10^{-2} M) [c] in benzene using acetophenone (1.0×10^{-2} M) as a sensitizer.
a: 250 ns, b: 3 μs, and c: 1 μs after the start of laser oscillation.

value of TLC and the UV absorption spectrum showed recovery of M for each solution. Products other than M, except for the starting materials, were unrecognized on a plate of TLC developed by the mixture of benzene and cyclohexane (1:3 in volume). It was thus confirmed that both of the dimers sensitized to the triplet state cause cycloreversion to acenaphthylene monomers.

Benzophenone (or Acetophenone)——Cis Dimer in Benzene. Figure 1 shows transient absorption spectra in the BP(4.0×10^{-3} M)-c-D (5.0×10^{-3} M) system obtained by the nanosecond flash photolysis. Similar spectra for the AP (1.0×10^{-2} M)-c-D (5.0×10^{-3} M) system is given in Fig. 2 together with the T-T absorption of ACN for the purpose of comparison. The absorption at 530 nm in Fig. 1a is attributable to triplet benzophenone (^{3}BP)[11] formed immediately after excitation. The ^{3}BP decays rapidly with the rate parameter of 1.7×10^7 s^{-1} under the present concentration of c-D. Since c-D has the lowest triplet state energy ($E_T^{(c)}=20.6\times10^3$ cm^{-1}), lower than that of BP ($E_T^{(BP)}=24.25\times10^3$ cm^{-1}),[12] the T-T energy transfer to c-D will dominate deactivation of ^{3}BP. The $E_T^{(c)}$ value was estimated from the 0-0 band of phosphorescence measured in methylcyclohexane–isopentane matrix at 77 K (Fig. 3a). A new band with maximum at 455 nm (Fig. 1b) grows up with a rate identical to the decay rate of ^{3}BP. After reaching its maximum intensity, this band disappears with a life of *ca.* 2 μs and no other specific absorption is observed. Decay time of this band was shortened by air saturation. The absorption spectrum is quite similar to that in Fig. 2a observed by replacing BP with AP ($E_T^{(AP)}=25.75\times10^3$ cm^{-1})[12] as a sensitizer. Namely, this transient is independent of a sensitizer. The band 1b is also similar in position and shape to the T-T absorption of ACN as a reference (Fig. 2c), although the maximum of the former band is slightly red-shifted, from 422 nm of the latter band to 455 nm. These observations allow us to assign both absorptions with the maxima at 455 nm (Figs. 1b and 2a) are to be attributed to the triplet state cis-dimer, ^{3}(c-D).

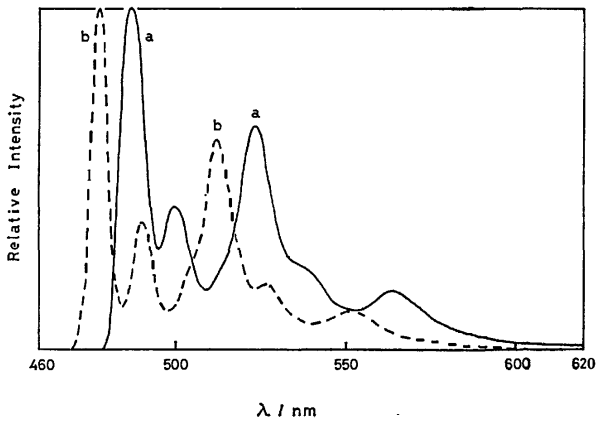

Fig. 3. Phosphorescence spectra measured for c-D [a] and ACN [b] in methylcyclohexane–isopentane matrix at 77 K (uncorrected for spectral response).

Decay rate of the band at 455 nm tends to become faster with each run. The sample solutions were also tinted with yellow by many shots of laser pulses. The UV-VIS absorption measurements confirmed the presence of M in these photolyzed solutions. This corresponds to recovery of M by the steady state illumination mentioned above. Therefore, it is considered that the acceleration of decay rate arises from quenching by M molecules accumulated gradually by each flash photolysis. The T-T energy transfer from ^{3}(c-D) to M by diffusional encounter may be responsible for the quenching, because the triplet energy of M, $E_T^{(M)}$, has been estimated to be 15000—16500 cm^{-1},[13] much lower than that of ^{3}(c-D). The plot of reciprocal lifetimes of ^{3}(c-D) against the number of experimental runs (25 points), in analogy to the Stern-Volmer plot, gave a good linear relation. Then, the intrinsic lifetime of ^{3}(c-D) was estimated, by the least square method, to be 2.2 μs at 20 °C from the extrapolation to the first experiment. An Arrhenius plot for the decay rate determined by this procedure as a function of temperature fits a straight line (Fig. 7c) yielding activation energy, $E_a^{(c)}=(25\pm3)$ kJ mol^{-1}, and the frequency factor, $A^{(c)}=(1.36\pm0.08)\times10^{10}$ s^{-1}, for 6 points between 9 and 58 °C.

Electronic Interaction between Naphthalene Rings of c-D. The electronic interaction between two naphthalene rings of c-D in the triplet state is important, because conformation of naphthalene rings of c-D (dihedral angle between the two rings≈60°)[9] is supposed to

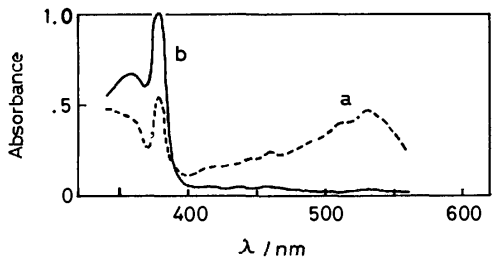

Fig. 4. Transient absorption spectra observed for trans dimer of acenaphthylene ($\approx 2\times10^{-3}$ M) in benzene containing benzophenone (4.0×10^{-3} M) as a sensitizer.
a: 40 and b: 230 ns after the start of laser oscillation.

be similar to that of 1,2-di-(1-naphthyl)ethane (DNE), which exhibits the phosphorescence and absorption of intramolecular triplet excimer of naphthalene.[14]

Let us first compare the phosphorescence spectrum of c-D with that of ACN in a rigid glass at 77 K (Fig. 3). The spectral shape of c-D (3a) is very similar to that of ACN (3b). No broad band characteristic of the triplet excimer[14,15] is observed around 520—500 nm. The 0-0 band of c-D is located at 486 nm, showing a red-shift compared with that of ACN. This red-shift and wavelength position are common to naphthalene dimers stable in the ground state such as an intramolecular sandwich dimer of 1,3-di(1-naphthyl)propane[16] and a dimer in poly(2-vinylnaphthalene).[17] They have the 0-0 bands at 485 nm and 482 nm, respectively. Phosphorescence features noted above indicate that at 77 K, c-D can not take a disposition similar to that of the triplet excimer, although some weak electronic interactions like those in the stable dimers are present between the naphthalene rings of ^{3}(c-D).

Next, we should notice the T-T absorption of c-D. The spectrum of ^{3}(c-D) is composed of the main band around 455 nm and a weak absorption tail in the longer wavelength region (530—600 nm). Since the two naphthalene rings in c-D and in DNE dispose in a similar manner, the transient absorption spectrum of c-D is expected at room temperature to involve a definite absorption band due to triplet excimer at 470 nm, like that observed in DNE.[14] However, the spectrum in Fig. 1b or 2a exhibits no additional absorption band around 470 nm other than the contribution of the red side slope of the main band. Kinetic measurements revealed further that both the main and the weak absorption band decay with approximately identical lifetimes up to 3 μs after excitation. Figures 2a and 2b represent this spectral change with time; the spectrum of ^{3}(c-D) decays monotonously without any spectral change. That is to say, the c-D does not show any distinct absorption around 470 nm due to the triplet excimer of naphthalene, although DNE does show such an absorption. Therefore, we consider that owing to structural rigidity, it is impossible for the two naphthalene rings of c-D, even at room temperature, to take a conformation favorable for exhibiting a distinguished absorption due to triplet excimer.

Benzophenone (or Acetophenone)——Trans Dimer in Benzene. Figure 4 shows time-dependent absorption spectra in the BP (4.0×10^{-3} M)-t-D ($\approx 2\times10^{-3}$ M) system. The spectrum at 40 ns (4a) consists of a band around 530 nm (^{3}BP), a weak band around 450 nm, and a sharp peak at 379 nm. The first and second bands decay rapidly in the initial time domain, but the band at 379 nm grows (4b). The rise time (120 ns) monitored at 379 nm was identical to the decay time observed at 450 nm. After reaching the maximum intensity, the 379 nm band decreases with the lapse of time, obeying the first-order decay kinetics. Its rate was not affected by photolysis numbers, in contrast to the decay of ^{3}(c-D). The decay time is 330 ns. Time dependences for 379 and 450 nm absorptions are illustrated in Fig. 5.

Intermediacy of the triplet t-D, ^{3}(t-D), is ambiguous in Fig. 4, since the expected absorption of ^{3}(t-D) is masked by the absorption of ^{3}BP in the 400—460 nm region. To clarify the spectrum of ^{3}(t-D), we chose AP as a sensitizer, because the extinction coefficient of ^{3}AP is rather low in the wavelength range

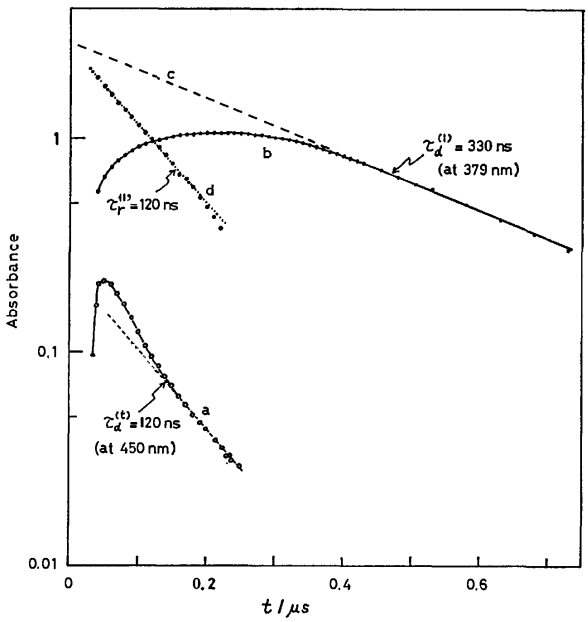

Fig. 5. Rise and decay profiles of transient absorptions monitored at 450 nm [a] and 379 nm [b].
Owing to overlap of ^{3}BP absorption, the linearity of [a] is wrong. [c]: the extrapolation of decay in Curve b. [d]: (Curve c—Curve b) *vs.* *t* plot. This slope derives the rise time of **1**.

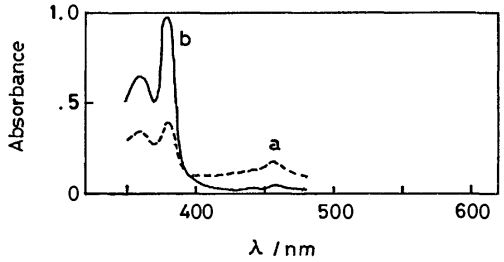

Fig. 6. Transient absorption spectra for the trans dimer (2.0×10^{-3} M) in benzene with acetophenone (1.0×10^{-2} M) as a sensitizer.
a: 40 and b: 170 ns after the start of laser oscillation.

greater than 400 nm.[18] Figure 6 represents transient spectra measured in such a system. A well-defined absorption band of ^{3}(t-D) is observed with maximum at 455 nm in the early time after excitation. It resembles well the spectra of ^{3}(c-D) in Figs. 1b and 2a, which demonstrates no large difference in the triplet electronic states of both dimers. Decay of this band is accompanied by remarkable growth of the 379 nm band, which is identical to the spectrum of Fig. 4b. It is thus clear that ^{3}(t-D) is a precursor generating the transient with the 379 nm absorption band.

Identification of Biradical **1** *and Its Properties.* We still have to assign the spectrum around 379 nm. The spectrum is quite similar to that of **2**[5] in both shape and position. The decay of this band obeys the first-order kinetics. Its lifetime (330 ns) is close to that of **2** (225 ns in acetonitrile).[5] As mentioned previously, t-D causes cycloreversion to the corresponding monomers, just like r-1,c-2-bis(methoxycarbonyl)-t-3,t-4-di(1-naphthyl)cyclobutane does. Since the biradical **2** is formed through one bond breaking of the cyclobutane ring of the latter, the present transient is supposed to be a transient formed in a similar fashion. Then, the species with 379 nm band is presumed to be biradical **1**. The similarity of the conjugate system of **1** and **2** is a reasonable way to interpret the similarity of their spectra. In fact, acenaphthene radical (**3**) corresponding to a half of **1** has been reported to possess an absorption in the identical wavelength region (320—400 nm)[19] and also 1-ethylnaphthalene-α-yl (**4**) shows an absorption spectrum similar to that of **1** in the near wavelength position.[20] Furthermore, the spectrum observed here differs from spectra of a group of hydrocarbon biradicals such as 2,3-dihydrophenalene-1,3-diyl (**5**) and 7,8,9,10-tetrahydrocyclohepta[*de*]naphthalene-7,10-diyl (**6**) measured by Muller *et al.*[21] and Gisin *et al.*,[22] respectively.

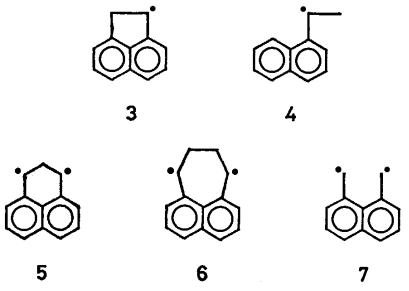

The above statement implys that the present intermediate keeps the acenaphthene structure but not 1,8-diethylnaphthalene-α,α′-diyl (**7**) structure in the bond scission of a cyclobutane ring; namely, the bond scission will occur between 1- and 1′-carbons, but not between 1- and 2-carbons. Hence, the spectrum in question can safely be assigned to be due to biradical **1**.

Dissolved oxygen quenches **1** with a bimolecular rate constant of 0.9×10^{10} M^{-1} s^{-1} in benzene at 19 °C.[23] This value is comparable with 2.1×10^{10} M^{-1} s^{-1} for **2** in acetonitrile[5] and 1.3×10^{10} M^{-1} s^{-1} for **6** in methanol.[22] This profound effect of oxygen has been known as a characteristic behavior for 1,4-biradicals in the triplet spin state produced from

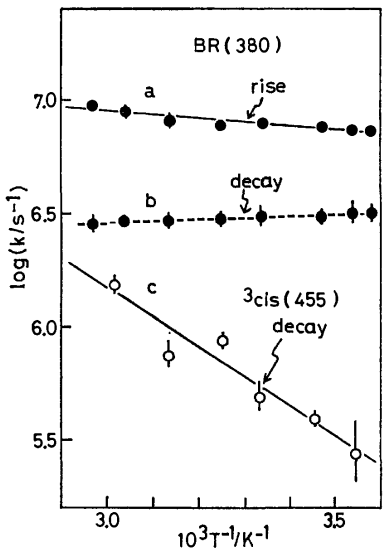

Fig. 7. Arrhenius plots for rise and decay rates of biradical **1** (BR) and for decay rate of triplet cis dimer (^{3}cis). Errors are indicated by bars. The numbers in parentheses denote the absorption wavelengths monitored.

TABLE 1. RISE (τ_r) AND DECAY (τ_d) TIMES OF TRANSIENT MONITORED AT EACH ABSORPTION MAXIMUM (λ_{max}) AT 20 °C

Transient	λ_{max}/nm	τ_r/ns	τ_d/ns
^{3}cis	455		2.2×10^3
^{3}trans	455		120
BR **1**	379	120	330
			65 (in air)

TABLE 2. ARRHENIUS PARAMETERS OBTAINED FOR THE DECAY RATE OF TRIPLET *cis* DIMER AND FOR THE RISE AND DECAY RATES OF BIRADICAL **1**
(temperature range: 6—60 °C)

	A/s^{-1}	E_a/kJ mol^{-1}
^{3}cis decay	1.36×10^{10}	25
1 rise	2.8×10^7	3.1
1 decay	1.9×10^6	−1.2

alkyl phenyl ketones by the type II reactions.[2,4] A preliminary result indicates that diethyl mercury, a compound involving a heavy atom, quenches **1** effectively with the rate constant of 3.7×10^7 M^{-1} s^{-1}. This finding would not contradict the assumption that **1** is a triplet biradical. The decay time of **1** was little influenced by temperature changes from 6 to 64 °C.[24] Inverse of the rise time of **1**[25] fits the Arrhenius equation of parameters, $E_a^{(t)}=3.1\pm0.2$ kJ mol^{-1} and $A^{(t)}=(2.8\pm0.4)\times10^7$ s^{-1}.

Arrhenius plots are shown in Fig. 7. Rate constants and Arrhenius parameters are collected in Tables 1 and 2, respectively.

Reaction Scheme. Reaction scheme of the triplet-sensitized ring opening of acenaphthylene dimers can be represented as Fig. 8.

The triplet-sensitized t-D causes a bond scission

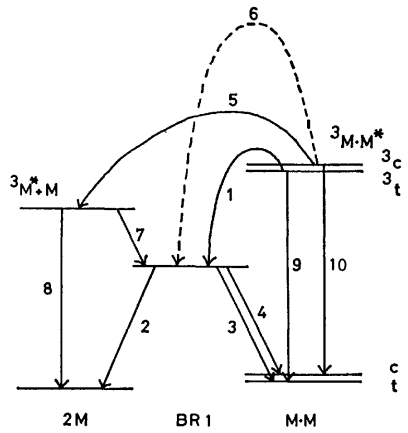

Fig. 8. Reaction scheme of cis and trans dimers of acenaphthylene sensitized to the triplet state.
BR **1** refers to biradical **1**, M acenaphthylene monomer, M-M the dimer of acenaphthylene, and c and t indicate the cis and the trans dimer, respectively. The process of direct decomposition from ^{3}c to 2M is omitted. Processes, 1, 5, and 6 are illustrated by curves to emphasize potential barriers.

(Process 1) to generate **1**, which subsequently undergoes the second bond cleavage leading to production of two acenaphthylene monomers, 2M (Process 2). Processes 3 and 4 going back to the ground states of t-D and c-D, respectively, should compete with Process 2, because **1** has been assumed as a common intermediate for the photodimerization of acenaphthylene (Process 7 followed by Processes 3 and 4).[8b,c] The rise time of **1**, $\tau_r^{(1)}$, corresponds to the decay time of ^{3}(t-D), $\tau_d^{(t)}$, which depends on the rates of both Processes 1 and 9. The deactivation to the ground state in ^{3}(t-D), Process 9, would not differ so much from the corresponding one in ^{3}ACN, for the electronic state of ^{3}(t-D) does not differ so much from that of ^{3}ACN. Since the decay time of ^{3}ACN, $\tau_d^{(ACN)}$ (>16 μs),[26] is considerably longer than $\tau_r^{(1)}$ (120 ns), contribution of Process 9 would be negligible to the decay of ^{3}(t-D). Namely, the inverse of $\tau_r^{(1)}$ gives the rate constant of primary bond opening (Process 1). Thus, the Arrhenius parameters, $E_a^{(t)}$ and $A^{(t)}$, obtained from Fig. 7a belong to this process of biradical formation. The small activation energy and moderate frequency factor reflect the ease of the reaction 1. Moreover, it is worth noting that the $E_a^{(t)}$ value (260 cm^{-1}) is very close to the frequency energy (280 cm^{-1}) of vibrational progression in $^1L_a \leftarrow {}^1A$ absorption spectrum and the frequency (269 cm^{-1}) in the Raman spectrum characteristic to t-D.[9] The bond opening of ^{3}(t-D) may be promoted by the thermal excitation of these modes.

On the other hand, the c-D sensitized to the triplet state dissociates to monomers with no production of **1** as an intermediate, *i.e.*, Process 6 was not found. Some possible mechanisms are as follows. Since $E_T^{(M)}$ is 15000—16500 cm^{-1},[13] $E_T^{(c)}$ 20600 cm^{-1}, and the ground state of c-D lies near the state of a pair of monomers (2M),[9] then the energy level of the state, ^{3}M*+M, is lower than that of ^{3}(c-D). Accordingly, two channels for decomposition are energetically possible: one is a pathway generating ^{3}M*+M (Process 5) and another a direct cycloreversion to 2M. According to the spin conservation rule, the spin-allowed Process 5 may be more favorable than the spin-forbidden direct decomposition to 2M. At the present stage of investigation, however, we can not decide clearly which process is dominant. Moreover, Process 10 (deactivation to the ground state) competing with the decomposition process is involved in the total decay of ^{3}(c-D), $\tau_d^{(c)}$. Its contribution to $\tau_d^{(c)}$ is larger than that of Process 9 to $\tau_d^{(t)}$, as judged from their lifetimes: $\tau_d^{(c)}$ 2.2 μs, $\tau_d^{(t)}$ 0.12 μs, and τ_d^{ACN} 16 μs, which is regarded as an approximate value to the reciprocal rates for Processes 9 and 10. Under these circumstances, temperature dependence of $\tau_d^{(c)}$ is swayed by relative contribution of the above competing processes. This suggests that the Arrhenius plot for the decay of ^{3}(c-D) would not become linear. Nevertheless, the present result showed that the plot becomes approximately linear (Fig. 7c). It is probably due to the narrowness of the temperature range. Therefore, the observed values of $E_a^{(c)}$ and $A^{(c)}$ do not directly reflect the temperature change of a certain ring opening reaction process. However, ^{3}(c-D) decays rather slowly compared with ^{3}(t-D); Process 5 proceeds more slowly than Process 1. If frequency factors for these two processes are nearly equal, an activation energy for Process 5 will be higher than $E_a^{(t)}$. This estimation relates to the next discussion.

Reactivity Difference between Cis and Trans Dimers. The striking difference in triplet reactivities between cis and trans dimers can be interpreted in terms of the difference in steric hindrances between two ACN rings, as follows. At least one bond of the cyclobutane ring of c-D or t-D must be stretched prior to bond scission. Stretching of C_1–C_1' bond in the directions

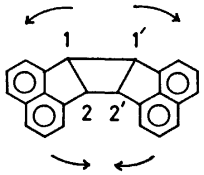

indicated by the arrows moves ACN rings in the directions indicated by arrows and gives rise to changes in the relative disposition of two ACN rings. In the case of c-D, the edges of the two ACN rings on the side of the C_2–C_2' bond are brought close to each other, whereas the other sides of the ACN rings separate. The very high potential barrier resulting from repulsion between two ACN rings should be overcome in order that the bond opening may proceed through such deformation. It seems impossible that c-D can cleave one bond in such a manner as to generate **1** (Process 6 in Fig. 8). It will be rather easy to break two bonds, C_1–C_1' and C_2–C_2', simultaneously, because such a high potential barrier is removed, although a fairly high potential barrier still remains for c-D to open the two bonds. In the case of t-D, the high potential barrier resulting from repulsion between ACN rings is absent and only one bond breaking is necessary to generate **1**. Therefore, it is considered that Process 1 proceeds very smoothly.

The authors wish to thank Prof. Haruo Shizuka for valuable discussion.

References

1) A preliminary report of this work was presented at 43rd National Meeting of the Chemical Society of Japan, Tokyo, April 1981, Abstr., No. I-3Y09, p. 563.

2) R. D. Small, Jr., and J. C. Scaiano, *Chem. Phys. Lett.*, **50**, 431 (1977); **59**, 246 (1978).

3) H. Hayashi and S. Nagakura, *Bull. Chem. Soc. Jpn.*, **53**, 1519 (1980); H. Hayashi, S. Nagakura, Y. Ito, Y. Umehara, and T. Matsuura, *Chem. Lett.*, **1980**, 939.

4) R. D. Small, Jr., and J. C. Scaiano, *J. Am. Chem. Soc.*, **100**, 4512 (1978); M. V. Encinas, P. J. Wagner, and J. C. Scaiano, *ibid.*, **102**, 1357 (1980).

5) S. Takamuku and W. Schnabel, *Chem. Phys. Lett.*, **69**, 399 (1980).

6) J. M. Nerbonne and R. G. Weiss, *J. Am. Chem. Soc.*, **101**, 402 (1979).

7) R. Livingston and K. S. Wei, *J. Phys. Chem.*, **71**, 541 (1967).

8) a) D. O. Cowan and J. C. Koziar, *J. Am. Chem. Soc.*, **97**, 249 (1975); b) D. O. Cowan and J. C. Koziar, *ibid.*, **92**, 6281; 6286 (1970); c) I. -M. Hartmann, W. Hartmann, and G. O. Schenck, *Chem. Ber.*, **100**, 3146 (1967).

9) N. Y. C. Chu and D. R. Kearns, *J. Phys. Chem.*, **74**, 1255 (1970).

10) H. Kobashi, H. Gyoda, and T. Morita, *Bull. Chem. Soc. Jpn.*, **50**, 1731 (1977); H. Kobashi, Y. Tomioka, and T. Morita, *ibid.*, **52**, 1568 (1979).

11) H. Tsubomura and S. Tanaka, *Chem. Phys. Lett.*, **1**, 309 (1967); T. S. Godfrey, J. W. Hilpern, and G. Porter, *Chem. Phys. Lett.*, **1**, 490 (1967); F. S. Dainton, T. J. Kemp, G. A. Salmon, and J. P. Keene, *Nature (London)*, **203**, 1050 (1964); S. Inbar, H. Linschitz, and S. G. Cohen, *J. Am. Chem. Soc.*, **103**, 1048 (1981).

12) V. L. Ermolaev, *Sov. Phys. Usp.*, **80**, 333 (1963).

13) E. W. Thulstrup and J. Michl, *J. Am. Chem. Soc.*, **98**, 4533 (1976).

14) P. C. Subdhi and E. C. Lim, *J. Chem. Phys.*, **63**, 5491 (1975); *Chem. Phys. Lett.*, **44**, 479 (1976); **56**, 59; **58**, 62 (1978); S. Okajima, P. C. Subdhi, and E. C. Lim, *J. Chem. Phys.*, **67**, 4611 (1977); D. Webster, J. F. Bangher, B. J. Lim, and E. C. Lim, *Chem. Phys. Lett.*, **77**, 294 (1981).

15) T. Takemura, H. Baba, and Y. Shindo, *Chem. Lett.*, **1974**, 1091; T. Takemura, M. Aikawa, H. Baba, and Y. Shindo, *J. Am. Chem. Soc.*, **98**, 2205 (1976).

16) E. A. Chandross and C. J. Dempster, *J. Am. Chem. Soc.*, **92**, 704 (1970).

17) M. Aikawa, T. Takemura, H. Baba, M. Irie, and K. Hayashi, *Bull. Chem. Soc. Jpn.*, **51**, 3643 (1978).

18) G. Porter and M. W. Windsor, *Proc. R. Soc. London, Ser. A*, **245**, 238 (1958); H. Lutz, E. Brehérét, and L. Lindqvist, *J. Phys. Chem.*, **77**, 1758 (1973).

19) Kh. I. Mamedov and S. G. Shukyurov, *Opt. Spektrosk.*, **33**, 608 (1972).

20) T. Shida and W. H. Hamill, *J. Am. Chem. Soc.*, **88**, 3689 (1966).

21) J. -F. Muller, D. Muller, H. J. Dewey, and J. Michl, *J. Am. Chem. Soc.*, **100**, 1629 (1978).

22) M. Gisin, E. Rommel, J. Wirz, M. N. Burnett, and R. M. Pagni, *J. Am. Chem. Soc.*, **101**, 2216 (1979).

23) The rate constant value was estimated by the Stern-Volmer equation $\tau^{-1}=\tau_0^{-1}+k_q[O_2]$, where $\tau=65$ ns, $\tau_0=330$ ns, and $[O_2]=1.4\times10^{-3}$ M. The concentration of dissolved oxygen was derived from data in the following reference; A. G. Loomis, "International Critical Tables of Numerical Data. Physics, Chemistry, and Technology," ed by E. W. Washburn *et al.*, McGraw-Hill, New York (1928), Vol. III, p. 261.

24) A least square fit to an Arrhenius plot gave a negative activation energy, $E_a=-1.2\pm0.2$ kJ mol^{-1} and a frequency factor, $A=(1.9\pm0.1)\times10^6$ s^{-1} with a relatively poor correlation factor, 0.91. In order to examine whether this small negative activation energy is meaningful or not, we are now investigating the effect of temperature over a wider range.

25) Uncorrected for small contribution of the decay rate of ^{3}BP.

26) Under the present experimental conditions, ^{3}ACN decayed according to the nearly complete second-order kinetics, probably due to T-T annihilation. Apparent decay time was *ca.* 4.4 μs in the initial stage of time and *ca.* 16 μs in the later stage. The latter value is given as $\tau_d^{(ACN)}$ in the text.

© 1982 The Chemical Society of Japan

NOTES

Bull. Chem. Soc. Jpn., 55, 3019—3020 (1982)

The Effect of Ultraviolet Radiation on the Wattability of Silicone Polymers

Kunio Esumi,* Kenjiro Meguro, Anthony M. Schwartz,† and Albert C. Zettlemoyer†

Department of Applied Chemistry, Science University of Tokyo, Kagurazaka, Shinjuku-ku, Tokyo 162

† *Center for Surface and Coating Research, Sinclair Laboratory, Lehigh University, Bethlehem, Pa 18015, U.S.A.*

(Received February 17, 1982)

Synopsis. The effect of UV radiation in air on the wettability of silicone polymers was studied by measuring the contact angles. From the contact-angle data, the surface energies were also calculated. As the irradiation progressed, the surface energy of the polar component increased, while the surface energy of the dispersive component remained constant, for all the samples. This increase in surface energy is attributable to a surface photooxidation of the silicone polymers. Especially, poly(diphenylsiloxane) showed a remarkable increase in the surface energy of the polar component after the irradiation.

The wettability of surfaces by liquids of known surface tensions has been determined by many investigators.[1,2] In particular, contact-angle measurements have been used to evaluate changes in surface composition.[3] We have ourselves previously reported that the water-contact angles on polystyrene and poly(methyl vinyl ketone) surfaces decreased dramatically as a function of the UV exposure time because of the photooxidation of the surfaces.[4] Generally, it is known that silicone polymers have relatively low surface-energy values. If the surface energy of a silicone polymer could be increased by UV radiation, the adhesion between liquids and the surface of the silicone polymer irradiated would be enhanced by an increase in the work of adhesion.

This report will describe the effect of UV radiation in air on the wettability of silicone polymers.

The silicone polymers used in this study were poly(methyl)3—7%(diphenyl)0.5—1.0%(methyl vinyl) siloxane, poly(diphenyl-siloxane), poly(dimethyl)1—2%-(methyl vinyl)siloxane, and poly(methyl vinyl)siloxane, all supplied by Petrarch System, Inc. (U.S.A.). A film of each polymer was cast from its benzene solution on an aluminum plate. Then, the plate was cured at 100 °C in an oven for 15 min. The plate was exposed in air with a low pressure mercury lamp (55.2 W, 1 W=1 J s^{-1}) supplied by the Oriel Co. (U.S.A.). The distance between the plate and the lamp was 5 cm.

The liquids used for contact-angle measurements were octane and diiodomethane. The contact angles were measured on the irradiated plate by using a goniometer at 20 °C. Three drops of the liquid were measured on both sides of the drops, and the six values were averaged. The overall variation in the contact-angle measurement was about ±3 degrees.

The free energy γ, of any interface can be regarded as the sum of two terms; one, designated γ^d, attributed to dispersion forces, and the other, γ^p, to polar forces. The value of γ_s^p can be calculated from the octane-water contact angle θ_{ows}, by means of Hamilton's[5] equations:

$$\cos\theta_{ows} = \frac{\gamma_w - \gamma_o - \gamma_{sw}}{\gamma_{ow}}$$

and:

$$I_{sw} = 2\sqrt{\gamma_s^p \gamma_w^p},$$

where γ_w and γ_o are the surface tensions of the mutually saturated water phase and octane phase respectively, where γ_{wo} is the interfacial tension of the two phases, where γ_w^p is the polar component of water-surface tension, and where I_{sw} is the term of polar interaction with water.

The value of γ_s^d can also be calculated from the diiodomethane-air contact angle, θ_m, using an equation developed by Fowkes:[6]

$$\gamma_s^d = \gamma_m \frac{(1+\cos\theta_m)^2}{4},$$

where γ_m is the surface tension of diiodomethane. Here, literature values[6,7] are applied in the surface-energy analysis:

$\gamma_w = 72.6$ erg/cm² **, $\gamma_o = 21.8$, $\gamma_{wo} = 50.8$, $\gamma_w^p = 50.8$, and $\gamma_m = 50.8$ at 20 °C.

Five different compositions have been made into plates, irradiated, and measured according to the above procedures. These compositions are:

1. Poly(dimethyl)3—7%(diphenyl)0.5—1.0%-(methyl vinyl)siloxane. This material is referred to as "PS 264".
2. Poly(diphenylsiloxane).
3. Poly(methyl)1—2%(methyl vinyl)siloxane.
4. PS 264+poly(diphenylsiloxane), 1:1 in weight.
5. PS 264+poly(methyl vinyl)siloxane, 5:1 in weight.

Tables 1—5 present the primary data and the derived results for compositions #1—#5. In each table, the last column, headed γ_s, is simply the sum of γ_s^p and γ_s^d. From these tables, it can be seen that the values of γ_s^p are increased as a function of the irradiation time for all the samples, while the values of γ_s^d remain almost constant. Two reasons for the increase in γ_s^p may be considered; a surface cracking due to UV irradiation and a surface photooxidation.

If a surface cracking has occurred during UV irradiation, the contact angle of octane-water might increase, for water can penetrate into such a crack and make the surface more hydrophilic. Also, if the silicone polymer surface is photooxidized during UV irradiation, the contact angle of octane-water is likely to be

** 1 erg=1×10⁻⁷ J.

Table 1. Composition #1. Poly(dimethyl)3—7%(diphenyl)0.5—1.0%(methyl vinyl)siloxane

UV irradiation time/min	Octane/Water contact angle θ/°	CH_2I_2 contact angle θ/°	γ_s^p erg cm^{-2}	γ_s^d erg cm^{-2}	γ_s erg cm^{-2}
0	21	73	0.1	21.2	21.3
10	24	68	0.1	24.0	24.1
20	42	65	0.8	25.7	26.5
30	60	61	3.2	28.0	31.2
40	70	59	5.5	29.1	34.6
50	77	59	7.6	29.1	36.7
60	79	58	8.3	29.7	38.0

Table 2. Composition #2. Poly(diphenylsiloxane)

UV irradiation time/min	Octane/Water contact angle θ/°	CH_2I_2 contact angle θ/°	γ_s^p erg cm^{-2}	γ_s^d erg cm^{-2}	γ_s erg cm^{-2}
0	34	24	0.4	46.5	46.9
10	89	50	12.3	34.3	46.6
20	98	57	16.5	30.3	46.8
30	115	40	25.7	39.6	65.3
40	117	44	26.9	37.5	64.4
50	119	39	28.0	40.1	68.1
60	119	38	28.0	40.6	68.6

Table 3. Composition #3. Poly(dimethyl)1—2%(methyl vinyl)siloxane

UV irradiation time/min	Octane/Water contact angle θ/°	CH_2I_2 contact angle θ/°	γ_s^p erg cm^{-2}	γ_s^d erg cm^{-2}	γ_s erg cm^{-2}
0	8	82	0.0	16.5	16.5
10	37	67	0.5	24.5	25.0
20	57	60	2.6	28.6	31.2
30	68	62	5.0	27.4	32.4
40	75	58	7.0	29.7	36.7
50	77	63	7.6	26.8	34.4
60	88	61	11.8	28.0	39.8

increased as a result of the formation of surface hydrophilic groups. To check whether or not cracks are formed after UV irradiation, SEM micrographs for the samples were obtained. No cracks were observed. Furthermore, all the samples irradiated *in vacuo* showed no changes in the octane–water contact angles after exposures of up to 1 h. Therefore, the increase in

Table 4. Composition #4. PS 264+poly(diphenylsiloxane), 1:1 in weight

UV irradiation time/min	Octane/Water contact angle θ/°	CH_2I_2 contact angle θ/°	γ_s^p erg cm^{-2}	γ_s^d erg cm^{-2}	γ_s erg cm^{-2}
0	8	68	0.0	24.0	24.0
10	39	62	0.6	27.4	28.0
20	61	62	3.4	27.4	30.8
30	80	60	8.7	28.6	37.3
40	82	59	9.4	29.1	38.5
50	87	59	11.4	29.1	40.5
60	87	59	11.4	29.1	40.5

Table 5. Composition #5. PS 264+poly(methyl vinyl)siloxane, 5:1 in weight

UV irradiation time/min	Octane/Water contact angle θ/°	CH_2I_2 contact angle θ/°	γ_s^p erg cm^{-2}	γ_s^d erg cm^{-2}	γ_s erg cm^{-2}
0	45	92	1.1	11.8	12.9
10	56	57	2.5	30.3	32.8
20	71	57	5.8	30.3	36.1
30	76	61	7.3	28.0	35.3
40	81	61	9.0	28.0	37.0
50	91	64	13.2	26.3	39.5
60	93	63	14.1	26.8	40.9

γ_s^p values after UV irradiation in air is attributed to the surface photooxidation of the silicone polymers. Especially, it is found that Composition #2 is easily photooxidized by UV irradiation.

Accordingly, it can be anticipated from the above results that the adhesion between liquids and irradiated silicone-polymer surfaces is enhanced by the increase in polar-polar interaction which is attributed to the work of adhesion.

References

1) W. A. Zisman, *Adv. Chem. Ser.*, **43**, 1 (1964).
2) J. R. Dann, *J. Colloid Sci.*, **32**, 302 (1970).
3) R. B. Fox, T. R. Price, and D. S. Cain, *Adv. Chem. Ser.*, **87**, 72 (1968).
4) K. Esumi, K. Meguro, A. M. Schwartz, and A. C. Zettlemoyer, *Bull. Chem. Soc. Jpn.*, **55**, 1649 (1982).
5) W. C. Hamilton, *J. Colloid Interface Sci.*, **40**, 219 (1972).
6) F. M. Fowkes, *Ind. Eng. Chem.*, **67**, 2538 (1963).
7) R. D. Bagnall and G. F. Green, *J. Colloid Interface Sci.*, **68**, 387 (1979).

Adsorption of Surface Active Agents on Coals

Kunio Esumi,* Kenjiro Meguro, and Hidemasa Honda
Department of Applied Chemistry, Faculty of Science, Science University of Tokyo, Kagurazaka, Shinjuku-ku, Tokyo 162
(Received April 13, 1982)

Synopsis. The interactions between surface active agents and coals with various carbon contents were studied by measuring adsorption isotherms and zeta potentials. A characteristic adsorption behavior was observed for the coals among three different surface active agents, but no correlation was found between the adsorption and the carbon content of the coal.

The surface properties of coal[1,2] have been investigated to understand the mechanisms of coal flotation, coal dust suppression, and coal–oil mixture behavior. Glanville and Wightman[3] studied the wetting rates of powdered coal by alkanol–water solutions; they found that a critical concentration of each alkanol was needed before any wetting occurred and that this critical wetting concentration was lower for alcohols with longer carbon chains. Recently, a coal–water mixture has been found attracting as a fuel source. Although it is important to elucidate the interactions between coal surfaces and surface active agents, there have been few reports on this subject.

In this paper, the interaction between coals of various carbon contents and surface active agents will be reported, using adsorption isotherm and zeta potential measurements.

The coals used in this study were Yallourn, Taiheiyo, Miike, Hon-gay, Tenpoku and Wandoan. They were dry sieved between 60 and 100 mesh screens. The pertinent properties of these coals are given in Table 1.

The surface active agents employed were sodium dodecylbenzenesulfonate (ABS), 1-dodecylpyridinium chloride (DPCl), and polyoxyethylene nonylphenyl ether (NP-7.5) which were supplied by Wako Pure Chemical, Industries, Ltd., Tokyo Kasei, Co. Ltd., and Nikko Chemical, Co., respectively. They were used without purification.

The water used was purified by passing through an ion exchange column followed by filtration from Milli-Q Water Purification System.

The amounts of surface active agents adsorbed on the coals were determined from the difference of the concentration of surface active agents before and after the adsorption by means of UV spectrophotometer (Hitachi ESP-3T). The zeta potentials of the coal surfaces were measured by mean of a Laser Zee Model 500 (Pen Kem Co.). The critical micelle concentration of the surface active agent was determined from the surface tension measurement.

Table 1. Pertinent properties of coals

	C[a] (wt%)	H[a]	H_2O[b]	Ash[b]	Specific surface area[c] $m^2 g^{-1}$
Yallourn	61.5	4.6	12.2	0.9	1.62
Tenpoku	68.1	5.5	14.3	22.9	4.19
Taiheiyo	74.8	6.0	6.6	8.4	0.68
Wandoan	80.2	6.6	9.3	8.0	2.30
Miike	85.2	6.5	1.2	7.8	0.53
Hon-gay	93.0	3.3	1.7	3.4	0.16

a) From JIS M 8813. b) From JIS M 8812, 60-100 mesh. c) From the nitrogen adsorption at 77 K.

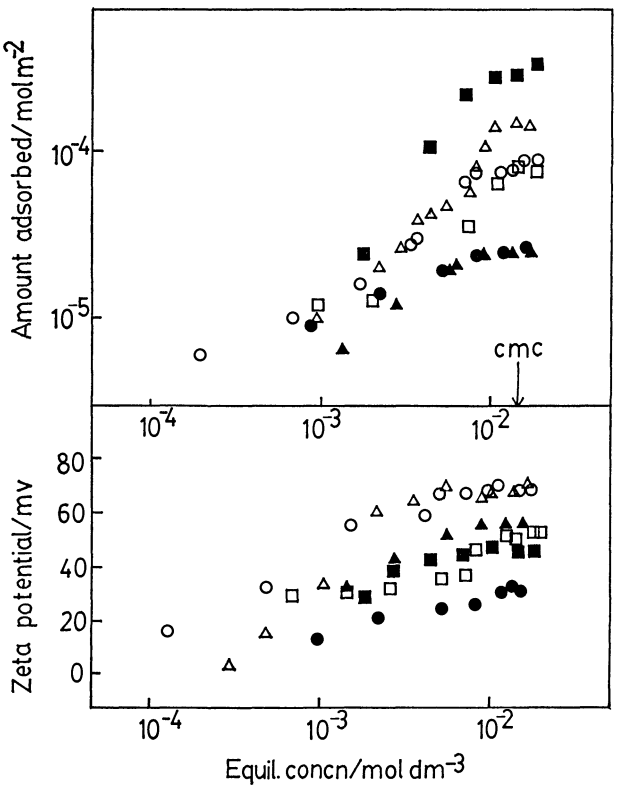

Fig. 1. Adsorption isotherms of DPCl on coals at 25 °C and the corresponding zeta potential result; (○) Yallourn, (●) Tenpoku, (△) Taiheiyo, (▲) Wandoan, (□) Miike, and (■) Hon-gay.

When the coals of various carbon contents shown in Table 1 were dispersed in water, they gave characteristic surface charges. All the coals except Hon-gay coal were found to be negatively charged in electrophoresis, while Hon-gay coal was positively charged. Generally the coal surface is more easily oxidized as the carbon content of the coal decreases. Such an oxidized coal surface would be expected to exhibit a negative charge in water due to dissociation of the carboxyl group. However, in this study, no relation between the carbon content of coal and the surface charge of the coal in water was obtained.

Adsorption isotherms of the surface active agents on coals from water and the corresponding surface charge of the coals are shown in Fig. 1. In Fig. 1, the amount of DPCl adsorbed increased with increasing the concentration of DPCl. Especially, in the case of Yallourn coal, the adsorption isotherm was similar to those which

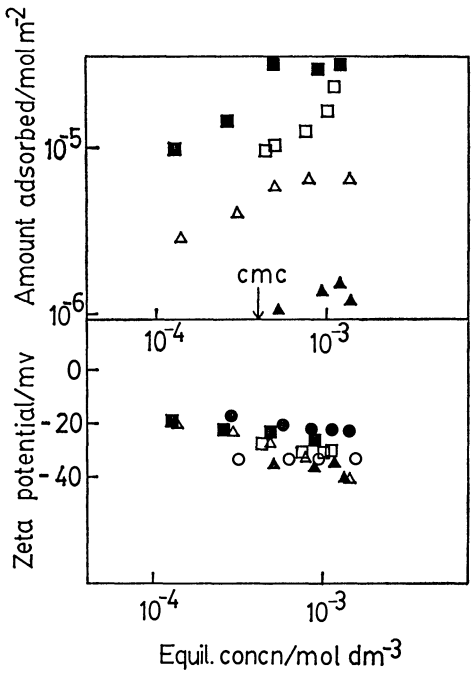

Fig. 2. Adsorption isotherms of ABS on coals at 25 °C and the corresponding zeta potential result; (○) Yallourn, (●) Tenpoku, (△) Taiheiyo, (▲) Wandoan, (□) Miike, and (■) Hon-gay.

Somasundaran and Fuerstenau[4] established in ionic surfactants–alumina system. That is, at low concentration, the adsorption obeyed Henry's law. The adsorption increased rapidly with the concentration of DPCl, but later increased more slowly. Finally, above the cmc, the adsorption reached a plateau. The zeta potential of coal by adsorption of DPCl increased positively on increasing the concentration. Two mechanisms are proposed for the orientation of DPCl on the coals. One is that DPCl molecules are adsorbed on the nonpolar surface of coal with the polar groups outward. The other is that the positively charged group of the DPCl molecule is oriented towards the negatively charged sites on the coal. Further, it is expected that near the cmc, a bimolecular layer of DPCl is formed on polar sites of the coal.

Figure 2 gives the adsorption isotherms of ABS on coals and the corresponding zeta potential measurements. In case of Yallourn and Tenpoku coals, the amount of ABS adsorbed was so small that it could hardly be estimated. The adsorption increased with increasing concentration of ABS and reached plateaus above the cmc for Hon-gay and Taiheiyo coals. On the other hand, the amount of ABS adsorbed on Wandoan and Miike coals increased even above the cmc. The zeta potential of the coals after the adsorption of ABS increased negatively with the concentration. This indicates that ABS molecules are adsorbed on nonpolar surface of coal with their polar groups outward.

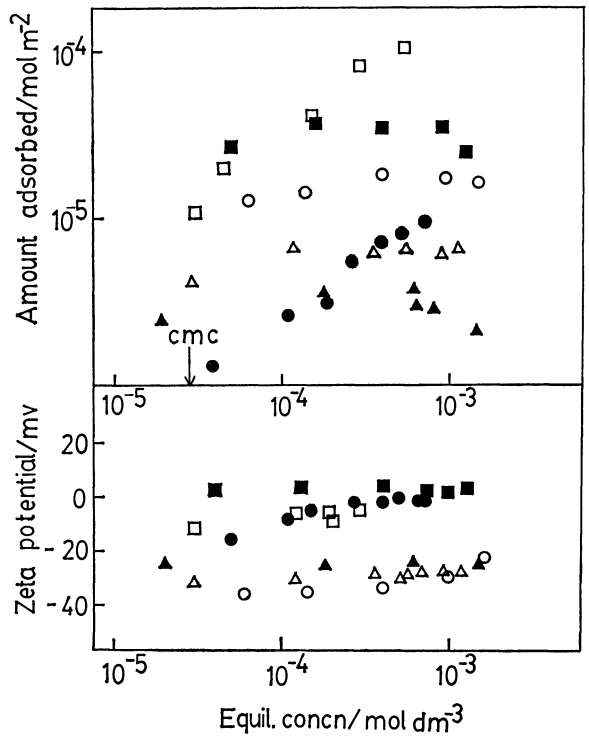

Fig. 3. Adsorption isotherms of NP-7.5 on coals at 25 °C and the corresponding zeta potential result; (○) Yallourn, (●) Tenpoku, (△) Taiheiyo, (▲) Wandoan, (□) Miike, and (■) Hon-gay.

Adsorption isotherms of NP-7.5 on coals and the corresponding zeta potential result are shown in Fig. 3. At above the cmc of NP-7.5, the adsorption increased with the concentration for Tenpoku and Miike coals, whereas for the other coals, the adsorption was almost constant. On the other hand, the zeta potential of the coals was almost constant in spite of different amounts adsorbed, because NP-7.5 is a nonionic surface active agent.

Comparing with the amount adsorbed of surface active agent on coals, the amount of DPCl adsorbed was much larger than that of ABS for all the coals. The amount of NP-7.5 adsorbed was intermediate between those of DPCl and ABS for all the coals. Furthermore, no correlation was observed among the amount of surface active agent adsorbed, the zeta potential of the coal after the adsorption, and the carbon content of the coal.

References

1) H. H. Huang, J. V. Calara, D. L. Bauer, and J. D. Miller, *Rec. Dev. Sep. Sci.*, **4**, 115 (1978).
2) J. W. Larsen, L. Kennard, and E. W. Kummerle, *Fuel*, **57**, 309 (1978).
3) J. O. Glanville and P. Wightman, *Fuel*, **59**, 557 (1980).
4) P. Somasundaran and D. W. Fuerstenau, *J. Phys. Chem.*, **70**, 90 (1966).

Preparation and Properties of Octahedral Nickel(II) Complexes with and Schiff Bases Derived from Substituted Salicylaldehydes and Bis(2-aminoethyl) Sulfide

Kiichi Hori* and Kazuko Takahashi

Department of Chemistry, Faculty of Science, Yamagata University, Yamagata 990

(Received December 18, 1981)

Synopsis The octahedral complexes listed in the title have been prepared. The magnetic and spectral properties of these complexes indicate that the non- and 5-substituted complexes have a structure bridged by the phenolic oxygen of the Schiff bases and the 3-substituted complexes probably are mononuclear.

The Schiff bases (H_2(X-saldaes), where X is a substituent on the benzene rings) derived from salicylaldehydes and bis(2-aminoethyl) sulfide form nickel(II) complexes which have electronic spectra characteristic of low spin five-coordinate structures and possess magnetic moments $\approx$1.1 BM in the solid state.[1] Under certain reaction conditions, three types of nickel(II) complexes with H_2(H-saldaes) were prepared: complexes of planar, octahedral, and polynuclear structures.[2] It is therefore of interest to investigate the effect of substituents on the benzene ring of the Schiff bases on the stereochemistry of the resulting complexes. In this paper, we report the syntheses and characterization of octahedral nickel(II) complexes with the substituted Schiff bases.

Experimental

Preparation. *Complexes* ***1*** *and* ***3*****—*****7***: The Schiff base, H_2(X-saldaes), (1 mmol) was dissolved in a minimum quantity of methanol (15—500 cm^3) under reflux. To this hot solution was added a solution of nickel(II) acetate tetrahydrate (1 mmol) in methanol (5 cm^3). The mixture was allowed to stand for 1—2 d at room temperature. For X= 3,5-Cl_2 and 3,5-Br_2, after the mixture had been concentrated to one-third of the volume under reduced pressure, the mixture was allowed to stand. The green crystals which precipitated were collected. The crystals were dissolved in a minimum quantity of methanol and recrystallized by concentrating the solution under reduced pressure.

Complex ***2***: Nickel(II) acetate tetrahydrate (1 mmol) was added to a solution of H_2(5-CH_3-saldaes) (1 mmol) in methanol (10 cm^3). The mixture was stirred, and water (5—10 cm^3) was added in order to facilitate the precipitation. The precipitate, which formed when the solution was cooled, was collected and redissolved in a minimum quantity of methanol. The resulting solution was allowed to stand for a long time (over 30 d) to concentrate very slowly. The green crystals thus precipitated were collected and washed with methanol.

Measurements. The magnetic susceptibilities were measured with a Shimadzu MB-2H magnetic balance over the temperature range of 80—300 K. The effective magnetic moments were calculated from the equation: $\mu_{eff}=2.83\sqrt{(\chi_A-N\alpha)T}$, where the temperature-independent paramagnetism, $N\alpha$, for nickel(II) ion was assumed to be 193×10^{-6} cgs emu.[3] The infrared spectra were measured with a JASCO DS-403 infrared spectrophotometer on Nujol mulls and KBr disks. The electronic spectra were measured with a Hitachi EPS-3T spectrophotometer.

Results and Discussion

The complexes obtained are listed in Table 1 with their analytical, spectral, and magnetic data. The Cl- or Br-substituted complexes were easily prepared, whereas the 5-CH_3-substituted complex was prepared with difficulty. Attempts to prepare the complexes with 3-CH_3 or 3-*i*-C_3H_7 substituents were unsuccessful.

The complexes are soluble only with difficulty in most nonpolar and semipolar solvents. They are soluble in solvents of high donor-ability such as pyridine and DMSO, but they decompose in these solvents. The reflectance spectra of the complexes possess two d-d bands (Table 1), indicating that the geometry around nickel(II) ions is octahedral.[4]

The complexes can be classified into two groups on the basis of the infrared spectral and magnetic data: (A) complexes **1**—**4** and (B) complexes **5**—**7**. The infrared spectra of complexes **1**—**4** show a broad weak band at 3300—3330 cm^{-1}, indicating the presence of a lattice water. The band near 1530 cm^{-1}, which characterizes the coordination mode of the phenolic oxygen in Schiff base complexes, was split into two bands separated by about 15 cm^{-1} (Table 1). This indicates that there are both the terminal and bridged coordination of the phenolic oxygens in complexes **1**—**4**.[5] For complexes **5**—**7** a relatively sharp weak band was observed at 3560—3570 cm^{-1}, which is assigned to the OH stretchings of a coordinated water from the position and shape of the band.

The magnetic moments of complexes **1**—**4** are 2.83—2.88 BM at 295 K and 2.10—2.25 BM at 80 K. The

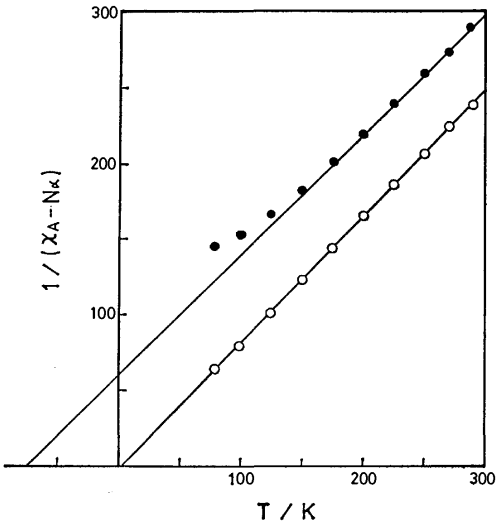

Fig. 1. Temperature dependence of magnetic susceptibility of (●) complex **1** and (○) complex **5**.

Table 1. Analytical, spectral, and magnetic data of the complexes

	Complex	Found (%)			Calcd (%)			Reflectance spectra[a]	IR spectra $\tilde{\nu}$/cm^{-1}		Magnetic data		
											μ_{eff}/BM		θ/K
		C	H	N	C	H	N	d-d Band $\tilde{\nu}$/10^3 cm^{-1}	Band near 1530 cm^{-1}		295 K	80 K	
1	Ni(H-saldaes)H_2O	53.53	5.18	6.80	53.63	5.00	6.95	8.62 16.08	1542	1525	2.87	2.20	−73
2	Ni(5-CH_3-saldaes)H_2O	55.41	5.80	6.42	55.71	5.61	6.50	8.55 15.43	1540	1527	2.83	2.15	−75
3	Ni(5-Cl-saldaes)H_2O	46.02	4.06	5.90	45.80	3.84	5.94	8.64 15.60	1535	1519	2.88	2.10	−98
4	Ni(5-Br-saldaes)H_2O	38.62	3.54	4.77	38.54	3.24	4.99	8.66 15.63	1530	1517	2.87	2.25	−75
5	Ni(3-Cl-saldaes)H_2O	45.60	4.07	5.92	45.80	3.84	5.94	9.01 16.95	1522		3.14	3.14	+3
6	Ni(3,5-Cl_2-saldaes)H_2O	39.94	2.86	5.19	39.97	2.98	5.18	9.09 17.0sh	1510		3.14	3.14	+2
7	Ni(3,5-Br_2-saldaes)H_2O	30.10	2.03	4.03	30.08	2.24	3.90	9.35 17.2sh	1500		3.15	3.15	0

a) sh = Shoulder.

value at 80 K is greatly less than the spin-only value, 2.83 BM. The temperature dependence of magnetic susceptibility of complex **1** is shown in Fig. 1 as a representative. The magnetic susceptibilities of complexes **1**—**4** obey the Curie-Weiss law over the temperature range of 150—300 K, but deviate in the temperature range of 80—100 K. The Weiss constants show negative large values (Table 1). It is likely that there is a strong antiferromagnetic interaction between nickel(II) ions in the complexes. These facts suggest that in the conformation around the bridging phenolic oxygen in the complexes, the phenolic C–O bond is coplanar with the two bridged nickel(II) ions.[6] The Schiff bases in the complexes seem to function as a quinquedentate ligand, because the analogous quadridentate Schiff bases[7] form nickel(II) complexes with a structure different from that of the present complexes. All the results shown above suggest that complexes **1**—**4** have a binuclear structure bridged by the phenolic oxygen.

On the other hand, complexes **5**—**7** show the magnetic moment value of 3.14—3.15 BM, which falls within the range usually found for octahedral mononuclear nickel(II) complexes. Their magnetic susceptibilities obey the Curie-Weiss law with very small values of the Weiss constant (θ=0—3 K) over the temperature range of 80—300 K. These results indicate that complexes **5**—**7** are magnetically diluted. It is thus probable that complexes **5**—**7** have an octahedral mononuclear structure in which the Schiff bases function as a quinquedentate ligand to form a six-coordination of the nickel(II) ion together with a molecule of water.

References

1) W. M. Coleman and L. T. Taylor, *J. Inorg. Nucl. Chem.*, **33**, 3049 (1971); L. T. Taylor and W. M. Coleman, *J. Am. Chem. Soc.*, **92**, 1449 (1970).

2) K. Hori and S. Misumi, *Nippon Kagaku Kaishi*, **1973**, 1451.

3) C. J. Ballhausen, "Introduction to Ligand Field Theory," McGraw-Hill, New York (1962), p. 142.

4) L. Sacconi, *Coord. Chem. Rev.*, **1**, 192 (1966), and reference therein.

5) S. J. Gruber, C. M. Harris, and E. Sinn, *J. Inorg. Nucl. Chem.*, **30**, 1805 (1968); E. Sinn and C. M. Harris, *Coord. Chem. Rev.*, **4**, 391 (1969).

6) M. Tanaka, M. Kitaoka, H. Okawa, and S. Kida, *Bull. Chem. Soc. Jpn.*, **49**, 2469 (1976); T. Tokii, S. Emori, and Y. Muto, *ibid.*, **52**, 2114 (1979).

7) W. C. Hoyt and C. W. Everett, Jr., *Inorg. Chem.*, **8**, 2013 (1969); G. H. Mockler, C. W. Chaffey, E. Sinn, and H. Wong, *ibid.*, **11**, 1308 (1972).

Ylide-Metal Complexes. VI.[1] The Preparation and Properties of IVA-group Metal (Ge, Sn, Pb) Complexes of Alkylidenetriphenylphosphoranes

Yoshihisa YAMAMOTO

Faculty of Pharmaceutical Sciences, Higashi Nippon Gakuen University, Ishikari-Tobetsu, Hokkaido 061-02

(Received December 26, 1981)

Synopsis. (Triphenylphosphonium alkylide)triphenylmetal chloride $[(C_6H_5)_3\overset{+}{P}CHR\text{-}M(C_6H_5)_3]Cl^-$ (R: H, Me, *i*-pr; M: Ge, Sn, Pb) and (triphenylphosphonium alkylide)metal chloride $[(C_6H_5)_3\overset{+}{P}CHR]_nMCl_n^-$, (M=Ge, n=4; M=Pb, n=2) have been isolated from a reaction mixture of alkylidenetriphenylphosphoranes and IVA-group metal compounds. The ylide in $[(C_6H_5)_3\overset{+}{P}CH_2\text{-}Pb(C_6H_5)_3]Cl^-$ is bonded to the lead atom through the carbanionic donor atom.

In this series, previous papers have been concerned with IB-group metal (Cu, Ag, Au) complexes[2,3] and IIB-group metal[4] (Zn, Cd, Hg) complexes of alkylidenetriphenylphosphoranes. The complexes of alkylidenetriphenylphosphorane $(C_6H_5)_3P{=}CH\text{-}R$ (R: H, Me, *i*-pr) and IVA-group metal (Ge, Sn, Pb) have, however, been the subject of little research, except for the germanium and tin complexes[5] with methylenetriphenylphosphorane (R=H). The present paper deals with the preparation and properties of IVA-group metal complexes of alkylidenetriphenylphosphoranes. Their properties are compared with those of IB-group metal[2,3] and IIB-group metal[4] complexes of those ylides.

Results and Discussion

(Triphenylphosphonium alkylide)triphenyl IVA-group metal complexes (**1a**, **2a**—**c**, and **3a**—**c**) have been isolated from a reaction mixture of alkylidenetriphenylphosphorane (methylene, **La**; ethylidene, **Lb**; and isobutylidene, **Lc**) and triphenylmetal chloride, $(C_6H_5)_3MCl$ (M: Ge, Sn, and Pb).

$$(C_6H_5)_3P{=}\overset{R}{\underset{|}{C}}H + (C_6H_5)_3MCl \longrightarrow [(C_6H_5)_3\overset{+}{P}\overset{R}{\underset{|}{C}}H\text{-}M(C_6H_5)_3]Cl^-$$

No	La	Lb	Lc
R	H	CH_3	$CH(CH_3)_2$
	Yellow	Orange	Red

No	1a	2a	2b	2c	3a	3b	3c
M	Ge	Sn	Sn	Sn	Pb	Pb	Pb
R	H	H	Me	*i*-pr	H	Me	*i*-pr

The **3a** is stable in dichloromethane, but it is unstable in chloroform.

The ^{1}H-NMR spectrum of the **3a** showed a doublet signal for CH_2P at 2.68 ppm and a multiplet signal for phenyl groups at around 7.5 ppm in a ratio of 2:15 at −60 °C in dichloromethane-d_2. The coupling constant (J_{HCP}) of the **3a** was 13.5 Hz, which was larger than that (7.5 Hz) of the **La**. The chemical shift of **3a** was at a lower field than that (δCH_2P: 0.13 ppm)[6] of **La**. These spectral properties were similar to those of the $[(C_6H_5)_3\overset{+}{P}\overset{R}{\underset{|}{C}}H\text{-}M\text{-}\overset{R}{\underset{|}{C}}H\overset{+}{P}(C_6H_5)_3]Cl_n$ (**4**) (M: IB-group metal,[2,3] IIB-group metal,[4] R: H; n=1, 2), so the ylide is bonded to the lead atom through the carbanionic donor atom.

Other complexes **1a**, **2a**—**c**, and **3b**—**c** are unstable in dichloromethane or chloroform at −60 °C, and ^{1}H NMR spectra of these complexes were not obtained. In both solvents, they are changed to the alkyltriphenylphosphonium chloride, $[(C_6H_5)_3\overset{+}{P}CH_2\text{-}R]Cl^-$ (**5**) (R: H (**5a**), Me (**5b**), *i*-pr (**5c**)). Their melting points or decomposition temperatures are not those of ylides, triphenylmetal chloride or salts **5**. Their color is white and they are thermally stable in the solid state. These properties resemble those of **4** (R: Me, *i*-pr),[2-4] and the ylides seem to be bonded to the metal atom in the solid state. The lability of **3b** and **3c** compared with **3a** complex can be ascribed to the difference in the carbanionic donor character of ylides.

Other types of ylide IVA-group metal chlorides (**6a**—**c** and **7a**—**b**) have been isolated from the reaction mixture of the $GeCl_4$ or $PbCl_2$ with the ylides (**La**—**c**). They are unstable in dichloromethane or chloroform at −60 °C and changed to the corresponding phosphonium salts (**5a**—**c**); therefore, their structures are still uncertain.

$$n(C_6H_5)_3P{=}\overset{R}{\underset{|}{C}}H \xrightarrow{MCl_{4(2)}} [(C_6H_5)_3\overset{+}{P}\overset{R}{\underset{|}{C}}H]_nMCl_{4(2)}$$
La—c

No	6a	6b	6c	7a	7b
M	Ge	Ge	Ge	Pb	Pb
R	H	Me	*i*-pr	H	Me

The **1a**, **2a**, **6a**, and **7a** complexes are unstable compared with **4** (R=H), *i.e.*, the Cu, Ag, Au, Zn and Cd complexes of **La** are stable at −60 °C. Germanium complexes of **1a** and **6a**—**c** are highly hygroscopic.

Experimental

Measurements. The ^{1}H NMR spectra were measured with an R-40 (Hitachi) spectrometer.

The reaction mole ratio of the ylides and the metal compounds, the melting point, the reaction time and analytical data of complexes are collected in Table 1. The precipitated white complexes are stable in dry THF at r.t. They are soluble in dichloromethane or chloroform and are insoluble in other common organic solvents.

Table 1. Reaction mole ratio, reaction time, yields, melting point, and analytical data of complexes

No	M	MCl_4(2) $(C_6H_5)_3MCl$ g (mmol)	R	$(C_6H_5)_3PCHR$ g (mmol)	Reaction temperature °C	Reaction time d	Yield g (%)	Mp θ_m/°C (Dp θ_d/°C)	Formula (Molecular weight)	Found (%) C	Found (%) H	Calcd (%) C	Calcd (%) H
1a	Ge	0.37 (1.09)	H	0.40 (1.45)	r.t.	1	0.35 (71.4)	—	$C_{37}H_{32}PGeCl$ (615.67)	71.49	5.51	72.18	5.24
2a	Sn	0.42 (1.09)	H	0.46 (1.66)	r.t.	2	0.61 (84.6)	(252)	$C_{37}H_{32}PSnCl$ (661.77)	67.18	5.20	67.15	4.87
2b	Sn	0.39 (1.01)	CH_3	0.36 (1.24)	r.t.	1	0.59 (86.3)	(310)	$C_{38}H_{34}PSnCl$ (675.80)	68.15	4.63	67.53	5.07
2c	Sn	0.35 (0.91)	i-C_3H_7	0.42 (1.32)	r.t.	0.5	0.52 (81.4)	(325)	$C_{40}H_{38}PSnCl$ (703.85)	68.21	5.25	68.26	5.44
3a	Pb	0.69 (1.46)	H	0.46 (1.66)	r.t.	0.5	0.80 (73.2)	162—165	$C_{37}H_{32}PPbCl$ (750.20)	58.92	4.33	59.24	4.30
3b	Pb	0.49 (1.03)	CH_3	0.34 (1.17)	r.t.	2	0.66 (83.5)	175—176	$C_{38}H_{34}PPbCl$ (764.23)	59.56	4.61	59.72	4.48
3c	Pb	0.29 (0.61)	i-C_3H_7	0.30 (0.94)	0	1.5	0.41 (84.6)	182—184	$C_{40}H_{38}PPbCl$ (792.28)	60.29	5.27	60.64	4.83
6a	Ge	0.066 (0.308)	H	0.34 (1.23)	r.t.	0.5	0.25 (61.5)	—	$C_{76}H_{68}P_4GeCl_4$ (1319.65)	69.51	6.03	69.17	5.20
6b	Ge	0.090 (0.42)	CH_3	0.26 (0.90)	r.t.	0.5	0.20 (77.0)	—	$C_{40}H_{38}P_2GeCl_4$ (795.07)	59.86	5.30	60.43	4.82
6c	Ge	0.136 (0.63)	i-C_3H_7	0.63 (1.978)	r.t.	0.5	0.45 (77.8)	—	$C_{66}H_{69}P_3GeCl_4$ (1169.58)	68.25	6.25	67.79	5.95
7a	Pb	0.11 (0.40)	H	0.28 (1.01)	r.t.	2	0.22 (66.7)	(195)	$C_{38}H_{34}P_2PbCl_2$ (830.65)	54.85	4.24	54.95	4.13
7b	Pb	0.17 (0.61)	CH_3	0.75 (2.58)	r.t.	1	0.31 (59.3)	(206)	$C_{40}H_{38}P_2PbCl_2$ (858.70)	54.26	4.59	55.95	4.46

Preparation of Complexes. *(Triphenylphosphonium methylide)triphenyllead Chloride (**3a**)*: Triphenyllead chloride (0.69 g, 1.46 mmol) was added to a dry THF (15 cm^3) solution of triphenylmethylenephosphorane (**La**) (0.46 g, 1.66 mmol) at r.t. under nitrogen. The mixture was stirred for 12 h; then the precipitated white complex was filtered under nitrogen, washed with dry ether and dried under vacuum.

*(Triphenylphosphonium alkylide)triphenylgermanium (**1a**), -tin (**2a**—**c**), and -lead (**3b**, **3c**) Chloride*: These complexes were prepared according to the procedure for **3a**.

*Tetra(triphenylphosphonium methylide)germanium Tetrachloride (**6a**)*: Tetrachlorogermanium (0.066 g, 0.308 mmol) was added to the dry THF (15 cm^3) solution of **La** (0.34 g, 1.23 mmol) at r.t. under nitrogen. The mixture was stirred, and the color of **La** changed from yellow to colorless, after 12 h, the white complex which precipitated was filtered under nitrogen, washed with dry ether, and dried under vaccum.

*Di(triphenylphosphonium ethylide)germanium Tetrachloride (**6b**), Tri(triphenylphosphonium isobutylide)germanium Tetrachloride (**6c**), Di(triphenylphosphonium methylide)lead Dichloride (**7a**), and Di(triphenylphosphonium ethylide)lead Dichloride (**7b**)*: These complexes were prepared according to the procedure for **6a**.

The present work was partially supported by a Grant-in-Aid for Scientific Research from the Ministry of Education, Science and Culture.

References

1) Part V, Y. Yamamoto, *Chem. Lett.*, **1980**, 311.
2) Y. Yamamoto and Z. Kanda, *Bull. Chem. Soc. Jpn.*, **52**, 2560 (1979).
3) Y. Yamamoto and H. Schmidbaur, *J. Organomet. Chem.*, **96**, 133 (1975); **97**, 479 (1975).
4) Y. Yamamoto and H. Sugimoto, *Bull. Chem. Soc. Jpn.*, **53**, 3176 (1980).
5) D. Seyferth and S. O. Grim, *J. Am. Chem. Soc.*, **83**, 1610 (1961).
6) H. Schmidbaur, H. Stuhler, and W. Vornberger, *Chem. Ber.*, **105**, 1084 (1972); R. Koster, D. Simic, and M. A. Grassberger, *Justus Liebigs Ann. Chem.*, **739**, 211 (1970).

Copper(II) Complexes of Schiff Bases Derived from Histamine or 2-(2-Aminoethyl)pyridine and 2,3-Butanedione or 4-Hydroxy-4-methyl-2-pentanone

Masahiro Abe, Yasuo Nakao,* Shinnichiro Suzuki,†
Masazo Kimura,† and Akitsugu Nakahara†

Chemical Laboratory, Faculty of Education, Okayama University, Okayama 700

† *Institute of Chemistry, College of General Education, Osaka University, Toyonaka, Osaka 560*

(Received January 26, 1982)

Synopsis. Copper(II) complexes of Schiff bases derived from histamine or 2-(2-aminoethyl)pyridine and 2,3-butanedione or 4-hydroxy-4-methyl-2-pentanone were prepared and characterized by elemental analyses, electronic and ESR spectra, and polarographic half-wave potentials. The relationship between structure of the chelates and the reduction potentials of copper(II) in these complexes was discussed in some detail.

A number of investigations have been carried out for the metal complexes with histidine, histamine, and their related ligands, since the histidine imidazole in metal-containing protein is one of the most important binding sites for metal ions in biological systems.[1] In connection with hemocyanin models, Simmons *et al.*[2] have synthesized copper(I) and copper(II) complexes of Schiff bases derived from 2,6-diacetylpyridine and histamine or 2-(2-aminoethyl)pyridine. We have also prepared four copper(II) complexes (**1**—**4**) of Schiff bases produced from histamine or 2-(2-aminoethyl)-pyridine and 2,3-butanedione or 4-hydroxy-4-methyl-2-pentanone, and studied electronic, ESR and electrochemical properties of these complexes for the purpose of elucidating the relationship between the structure of the chelates and the trends toward the formation of copper(I) species from the parent copper-(II) complexes, **1**—**4**.

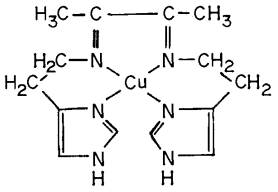

1

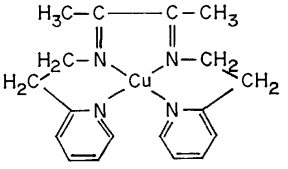

2

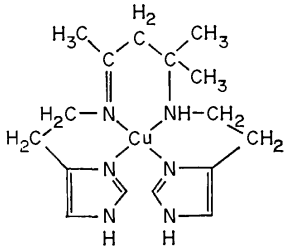

3

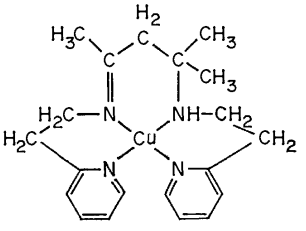

4

Experimental

Preparation of the Complexes. *[Cu(Hist=dia=Hist)](ClO$_4$)$_2$*,** ***1***: A mixture of 0.22 g (2.5 mmol) of 2,3-butanedione and 0.56 g (5.0 mmol) of histamine was dissolved in 40 cm^3 of methanol. The mixture was heated under reflux for 2 h. To this was added 0.96 g (2.5 mmol) of copper(II) perchlorate hexahydrate, and the resulting solution was refluxed again for 1 h. After it had been filtered, the filtrate was cooled to give dark violet crystals. Found: C, 30.29; H, 3.98; N, 14.47%. Calcd for [Cu($C_{14}H_{20}N_6$)]-(ClO_4)$_2$·1.5H_2O: C, 29.93; H, 4.13; N, 14.96%.

[Cu(2-Aep=dia=2-Aep)](ClO$_4$)$_2$,** ***2***: This complex was prepared by the same method as described for **1** using 2-(2-aminoethyl)pyridine instead of histamine. Found: C, 38.78; H, 3.91; N, 10.63%. Calcd for [Cu($C_{18}H_{22}N_4$)]-(ClO_4)$_2$: C, 38.82; H, 3.99; N, 10.06%.

[Cu(Hist=daa-Hist)](ClO$_4$)$_2$,*** ***3***: A mixture of 0.56 g (5.0 mmol) of histamine and 0.14 g (2.5 mmol) of sodium methoxide was dissolved in 50 cm^3 of acetone, being refluxed for 2 h. To this was added 0.96 g (2.5 mmol) of copper(II) perchlorate hexahydrate, and the resulting solution was heated again under reflux for 2 h. After it had been filtered, the filtrate was allowed to evaporate slowly. Dark blue crystalline products were deposited, being washed with acetone. Found: C, 32.19; H, 4.41; N, 14.13%. Calcd for [Cu($C_{16}H_{26}N_6$)](ClO_4)$_2$·1.5H_2O: C, 32.46; H, 4.95; N, 14.20%.

[Cu(2-Aep=daa-2-Aep)](ClO$_4$)$_2$,*** ***4***: This complex was prepared by the similar method as described for **3**. Found: C, 40.50; H, 4.74; N, 9.57%. Calcd for [Cu-($C_{20}H_{28}N_4$)](ClO_4)$_2$·0.5H_2O: C, 40.30; H, 4.91; N, 9.40%.

[Ni(Hist=dia=Hist)](ClO$_4$)$_2$. This was prepared by the same way as described for the corresponding copper(II) complex, **1**. Found: C, 31.08; H, 4.11; N, 15.56%. Calcd for [Ni($C_{14}H_{20}N_6$)](ClO_4)$_2$·0.5H_2O: C, 31.19; H, 3.93; N, 15.59%.

Measurements. IR spectra were recorded with a Hitachi EPI-2 Infrared spectrophotometer by employing the KBr-disk method, visible absorption spectra with a Hitachi 200—10 double beam spectrophotometer. Polarographic measurements were made with a Yanagimoto Polarograph P 8. Water was used as a solvent. Concentration of the copper(II) complexes used was 10^{-3} mol dm^{-3} and the supporting electrolyte used was 0.1 mol dm^{-3} KNO_3. Triton X-100 (0.002%) was employed as a maximum suppressor. The ESR spectra were measured at 77 K on a JEOL-FX-1 X-band ESR spectrometer modulated at 100 kHz. Water containing a small quantity of ethylene glycol was used as a solvent.

** Ligands, Hist=dia=Hist and 2-Aep=dia=2-Aep, represent Schiff bases derived from histamine and 2,3-butanedione, and 2-(2-aminoethyl)pyridine and 2,3-butanedione, respectively.

*** Ligands, Hist=daa-Hist and 2-Aep=daa-2-Aep, represent Schiff bases derived from histamine and 4-hydroxy-4-methyl-2-pentanone, and 2-(2-aminoethyl)pyridine and 4-hydroxy-4-methyl-2-pentanone, respectively.

Table 1. Physical properties of metal complexes

Complex No.	VIS[a]		$(E_{1/2})_1$ *vs.* SCE	$(E_{1/2})_2$ *vs.* SCE	ESR parameters	
	λ_{max}/nm	log ε	V	V	$g_{//}$	$A_{//}$/mT
1	612	2.11	−0.49	−0.83	2.22	19.3
2	613	2.13	−0.48	−0.70	2.22	19.6
3	626	2.14	−0.44	−0.78	2.27	18.6
4	641	2.19	−0.34	−0.68	2.28	16.6

a) Solvent: H_2O–DMSO (1:1).

Results and Discussion

Copper(II) complex **1** of the Schiff base derived from histamine and 2,3-butanedione had been obtained as greenish oily product by Kovacs and Shepherd.[3] In this work, we isolated the same complex as a dark violet crystal, to which the structural formula **1** was assigned on the basis of elemental analysis and IR spectral data (1620 cm^{-1} (C=N), $\approx$1100 cm^{-1} (ClO_4)). The corresponding complex **2** of the Schiff base containing 2-(2-aminoethyl)pyridine as amino compound and the complexes, **3** and **4** of Schiff bases derived from histamine or 2-(2-aminoethyl)pyridine and 4-hydroxy-4-methyl-2-pentanone were also isolated as blue-violet crystals. The absorption maxima for the d-d transition band, the half-wave potentials for the reduction of copper(II) at the dropping mercury electrode, and ESR parameters of these complexes are listed in Table 1. The ESR data clearly show that the $A_{//}$ values of complexes **1** and **2** are greater than those of complexes **3** and **4**, respectively, and that the $g_{//}$ values for these complexes decrease in the orders 3>1 and 4>2. The $A_{//}$ values for **1** and **2** with 6—5—6 fused ring structure are remarkably large, indicating that the coordination geometry around copper(II) ion is square-planar. On the other hand, complexes **3** and **4** with 6—6—6 fused-chelate-ring display the increasing trend towards the tetrahedral distortion.[4–6] The above conclusion is also supported by some other facts. The nickel(II) complex produced from histamine and 2,3-butanedione was isolated as yellowish brown crystals, whereas the attempts to obtain the nickel(II) complex of the Schiff base from histamine and 4-hydroxy-4-methyl-2-pentanone were unsuccessful. In the latter case the color of the reaction mixture did not even change from light green to yellowish brown which is characteristic of square-planar nickel(II) complexes. As shown in Table 1, the half-wave potential for the reduction of Cu(II) to Cu(I) is more negative in **1** than in **3**. In addition, the d-d absorption band of these complexes was observed at a shorter wavelength in **1** than in **3**. The geometrical difference between complexes **1** and **3** may be reflected by the differences observed in their λ_{max} and $(E_{1/2})_1$ values. The same trend is also observed in the comparison of **2** and **4**. It can be considered that the distortion towards a tetrahedral geometry is necessary for stabilizing the copper(I) state. Further the numerical data in Table 1 indicate that if the carbonyl moiety of the Schiff base is same, the half-wave potentials of the copper(II) complexes are more positive with 2-(2-aminoethyl)pyridine than with histamine. This is consistent with the result obtained through a comparison of $[Cu(pyep)]^{2+}$ and $[Cu(imep)]^{2+}$ as reported by Simmons *et al.*[2,7]

All attempts for preparing the copper(II) complexes of Schiff bases obtained from histamine or 2-(2-aminoethyl)pyridine with 2,5-hexanedione resulted in failure, producing only red-brown powder which could not be characterized as simple compound of definite composition. Further studies of these complexes are now under way.

We thank Mr. K. Hashimoto for technical assistance.

References

1) R. J. Sundberg and R. B. Martin, *Chem. Rev.*, **74**, 471 (1974).
2) M. G. Simmons, C. L. Merrill, L. J. Wilson, L. A. Bottomley, and K. M. Kadish, *J. Chem. Soc., Dalton Trans.*, **1980**, 1827.
3) D. Kovacs and R. E. Shepherd, *J. Inorg. Biochem.*, **10**, 67 (1979).
4) H. Yokoi, *Bull. Chem. Soc. Jpn.*, **47**, 3037 (1974).
5) H. Yokoi and A. W. Addison, *Inorg. Chem.*, **16**, 1341 (1977).
6) U. Sakaguchi and A. W. Addison, *J. Am. Chem. Soc.*, **99**, 5189 (1977).
7) The following abbreviations are used: imep=2,6-bis-[1-[2-(4-imidazolyl)ethylimino]ethyl]pyridine, pyep=2,6-bis-[1-[2-(2-pyridyl)ethylimino]ethyl]pyridine.

Apparent Extinction Coefficient for a Scanning Photosedimentometer

Junichi TAKAHASHI* and Akinori MUTA
Department of Inorganic Materials, Nagoya Institute of Technology, Gokiso-cho, Showa-ku, Nagoya 466
(Received February 6, 1982)

Synopsis. Particle-size distributions of subdivided samples were analyzed independently with electron microscopy and a scanning photosedimentometer. Apparent extinction coefficient for the optical scanning system was estimated by the comparative examination of the distributions.

In light transmission methods for particle-size distribution analysis, the effect of the extinction coefficient, which is defined as the effective particle cross section divided by its geometric cross section, must be taken into account when a sample under examination contains particles of a size comparable to the wavelength of the incident light. It has been confirmed by Rose[1] that, at any given particle diameter, an increasing solid angle was associated with a decreasing value of extinction coefficient, and for a solid angle of about 10°, deviations from unity in the value of the extinction coefficient were small at particle diameter larger than 3 μm. Therefore it was expected that significant errors as seen in the theoretical treatment of light-scanning properties of fine particles might be eliminated in the determination of particle-size distribution using an apparatus with white light and a large solid angle.

A scanning photosedimentometer has been developed by Muta and co-workers.[2,3] In this optical scanning system, a white light beam can be moved up and down by a specially-designed cam through the sedimentation tank in which steady-state settling conditions have been achieved. The cam has been designed so that the analyst can calculate the particle-size distribution of a sample from the graph of optical density versus square root of depth of the sedimentation tank, which can be easily converted to particle diameter using Stokes equation, in a simple manner. Thus a single quick continuous scan of the concentration gradient set up in the sedimentation tank gives enough information to enable the analyst to establish the particle-size distribution. This apparatus (*PSA*-2) is also characterized by a large solid angle subtended by the photo-sensitive receiver. Few data, however, are available on the examination of particle-size distribution by *PSA*-2 for a sample containing a number of fine particles.[4] Hence an attempt was made in this work to represent that the size distribution estimated using *PSA*-2 for a sample consisting of very small particles could be accepted without any special correction.

For particles with sizes ranging from d_1 to d_2, the energy removed from the forward beam by the particles is related to their cross-sectional area as follows:

$$S_m = \frac{1}{K_m C}(\log I_1 - \log I_2), \quad (1)$$

where S_m is the total cross-sectional area of the particles, I_1 and I_2 is the intensity of transmitted light for each particle of size d_1 and d_2, respectively, C is a constant, and K_m is the extinction coefficient for the particles. Thus the apparent extinction coefficient for *PSA*-2 could be evaluated by comparing the cross-sectional area analyzed independently with both *PSA*-2 and electron microscopy for subdivided samples. The solid material used in this study was Kanto loam JIS 11. Suspensions of the material were prepared by dispersing uniformly a definite amount of the powder in distilled water containing 0.1 wt% sodium *cyclo*-hexaphosphate as a dispersing agent. The original particle-size distribution of Kanto loam JIS 11 was evaluated by electron microscopy. The direct images of deposited particles on electron microscope grids covered with specimen support collodion film were observed with a transmission electrom microscope. The raw data obtained by examining about 3000 particles in electron micrographs were collected in the form of a number distribution and converted to a surface distribution. In Fig. 1 the percentage of particles per micrometer, $d\phi/dD$, is plotted against the projected area diameter which is the diameter of a circle having the same area as the particle. The distribution curve in Fig. 1 indicates that the sample is composed of fine particles smaller than 7 μm with a narrow-ranged size distribution. For the estimation of the apparent extinction coefficient for *PSA*-2, suspensions with the powder concentration of 0.05 vol% were subdivided into several portions, in which particle size ranged as narrow as possible, by a centrifugal withdrawal method described below.

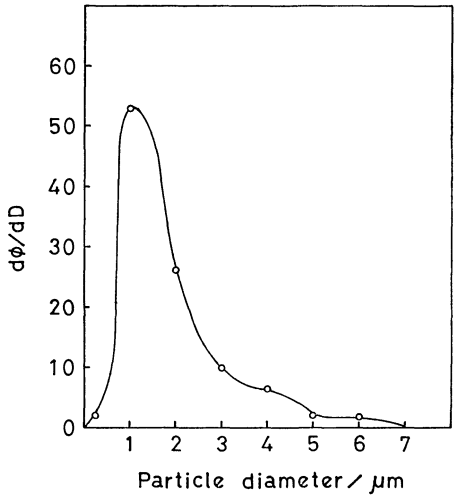

Fig. 1. The relative percentage frequency distribution of the original sample.

For a homogeneous suspension, a particle in a centrifugal field theoretically settles according to the equation,[5]

$$S = R\exp(-kD^2t) \quad k = \frac{\rho_s - \rho_f}{18\eta}\omega^2, \quad (2)$$

where t is the time for a particle of size D and density

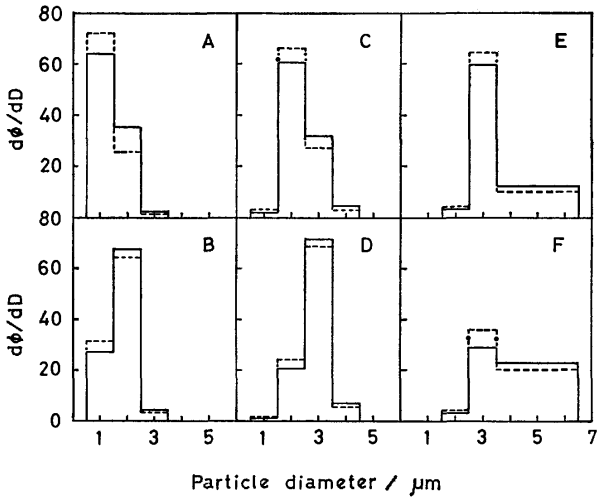

Fig. 2. The particle-size distribution of subdivided samples analyzed independently by *PSA*-2(——) and electron microscopy (----).

ρ_s to settle from the surface of the liquid with density ρ_f and viscosity η at distance S to the bottom of the tube at distance R, both S and R being distances from the axis of the centrifuge rotating at ω in radians per second. After t seconds, all particles greater than D will have settled out to the bottom of the tube with simultaneous partial sedimentation of all particles smaller than D. For each of these smaller sizes, Eq. 2 may be rewritten:

$$x_0 = R\exp(-kD^2t), \tag{3}$$

where x_0 is a starting point beyond which all the smaller particles will have reached R. The volume fraction of the suspension lying between R and x_0 for a cylindrical tube is equal to

$$\frac{R-x_0}{R-S} = \frac{R}{R-S}\{1-\exp(-kD^2t)\}. \tag{4}$$

Firstly, particles smaller than 0.5 μm were removed from the original samples because the presence of these particles yielded experimental errors due to the breakdown in the laws of geometric optics in the submicrometer particle-size range. This was carried out by repeated withdrawals of a definite amount of suspension from a cylindrical tube after centrifugal sedimentation. Electron microscopic observation of the residue after the operation indicated that it contained small amounts of submicron particles, which led to a negligible disturbance in the results obtained in the present study.

Experimental operations necessary for the subdivision of the sample into several portions with different size ranges were determined using Eqs. 2—4. To avoid an agglomeration of particles caused by centrifugal force, suspension of particles which remained at the bottom of the tube after a single withdrawal were placed in the ultrasonic bath prior to a subsequent centrifugal sedimentation. In the series of centrifugal withdrawal experiments, particle-size distribution of withdrawn portions or remaining portions was roughly checked with *PSA*-2, whenever required. Consequently, suspensions with the intended particle-size range, which were required for the estimation of the apparent extinction coefficient for *PSA*-2, were prepared by subdividing the original sample and mixing the subdivided samples up to a fixed particle concentration suitable for size distribution analysis.

Dristributions of the narrowly classified particles were measured using *PSA*-2 for the samples prepared by the procedure mentioned above. Fractional intensities of transmitted light for each sample are plotted against particle diameter in Fig. 2. An independent analysis by electron microscopy of the same sample was made and fractional projected areas of each sample are also included in Fig. 2. Now let the fractional intensity be dI_1, dI_2, dI_3, dI_5, fractional projected area dS_1, dS_2, dS_3, dS_5, and apparent extinction coefficient K_1, K_2, K_3, K_5, where each subscript indicates the corresponding particle diameter. Then from Eq. 1, both measured quantities can be correlated with each other using the apparent extinction coefficient. For instance, from sample A shown in Fig. 2,

$$dI_1 = \frac{K_1dS_1}{K_1dS_1+K_2dS_2+K_3dS_3}$$

$$dI_2 = \frac{K_2dS_2}{K_1dS_1+K_2dS_2+K_3dS_3},$$

and $K_1(dS_1/dI_1)=K_2(dS_2/dI_2)$, hence $K_1/K_2=(dI_1/dI_2\cdot dS_2/dS_1)$. In this way, the relative extinction coefficient of K_1/K_2, K_2/K_3, and K_3/K_5 was calculated from samples A and B, C and D, E and F, respectively, being $K_1/K_2=0.72$, $K_2/K_3=0.80$, and $K_3/K_5=0.75$.

On the basis of the result reported by Rose[1] for the solid angle subtended by the photo-cell of about 10° and that by Muta[2] on the comparative examination of particle-size distribution for several powders, the extinction coefficient for particles ranging from 4 to 6 μm, K_5, was assumed to be 1.3. Therefore the apparent extinction coefficients were evaluated, in turn, as $K_3=1.0$, $K_2=0.8$, and $K_1=0.6$. This result suggests that particle-size distribution of powder with a minimum size of about 1 μm could be accurately analyzed by the scanning photosedimentometer, *PSA*-2, without any substantial error.

References

1) H. E. Rose, *J. Appl. Chem.*, **2**, 80 (1952).
2) A. Muta, *Hitachi Rev.*, **14**, No. 11, 1 (1965).
3) A. Muta, N. Saito, and Y. Uehara, Presented at Symposium on Particle Size Analysis, Loughborough Univ., England, (1966).
4) A. Muta, *Hitachi Sci. Instrum. Tech. Data*, **1969**, 1.
5) T. Allen, "Particle Size Measurement," 2nd ed, Chapman and Hall, London (1975), p. 274.

Direct Preparation of θ-Zirconium Phosphate

Tsuyoshi KIJIMA

National Institute for Research in Inorganic Materials, Sakura-mura, Niihari-gun, Ibaraki 305

(Received February 17, 1982)

Synopsis The effects of temperature and Zr concentration in solution on the composition and degree of crystallinity of zirconium phosphate have been examined. Pure θ-zirconium phosphate with an interlayer spacing of 10.4 Å has been prepared by direct precipitation.

Cations having a large ionic radius, such as Cs^+, Ba^{2+}, hydrated Mg^{2+} *etc.*, are not, or only slowly, exchanged by α-zirconium phosphate (α-ZrP) $Zr(HPO_4)_2 \cdot H_2O$, owing to the small interlayer spacing (7.6 Å) of this exchanger.[1,2] These cations, however, can be easily exchanged by the highly hydrated form of α-ZrP with an interlayer spacing of 10.4 Å,[3] which was reported as $Zr(HPO_4)_2 \cdot 8H_2O$ and labeled θ-ZrP.[2,4] This ion exchange characteristics of θ-ZrP is noteworthy since it enlarges the practical use of crystalline zirconium phosphate as an ion exchanger. Conventionally, θ-ZrP is obtained by regenerating suitable salt forms of α-ZrP with HCl solution.[3] In this case the phase can be prepared in a pure form only when the starting α-ZrP has a good but not too high degree of crystallinity. A recent paper[5] reported that the methanol intercalate of α-ZrP obtained from the salt form of the exchanger is washed with water to give rise to θ-ZrP. However, both methods are not simple in procedure since they include ion exchange (or intercalation) and regeneration processes.

The composition and degree of crystallinity of solution-grown zirconium phosphate are strongly dependent on the preparation conditions, such as temperature, digestion time, concentrations of solutes, stirring time *etc.* In this study the effects of some of these factors were examined to prepare θ-ZrP directly from solution.

Experimental

Several ZrP samples were prepared as follows. In all runs, the concentration of phosphoric acid solution was held constant at 6 mol dm^{-3} since it was suggested by Clearfield *et al.*[6] that an excess of phosphoric acid as precipitant is available for the growth of ZrP crystals. One volume aliquots of $ZrOCl_2$ aqueous solution at various concentrations were added dropwise to one volume of the phosphate solution at different temperatures with stirring and the reaction mixtures were kept for 48 h at those temperatures while being stirred. The resulting precipitates were filtered and washed with distilled water. X-Ray diffraction patterns were taken on the wet samples obtained.

Results and Discussion

Table 1 shows the composition and degree of crystallinity of the various products obtained under different experimental conditions. The approximate phase composition was estimated by the relative intensity of the peaks at 10.4 and 7.6 Å as in a previous report.[3] When the concentration of the starting $ZrOCl_2$ solution is fixed at 2 mol dm^{-3}, the refluxed product is α-ZrP, while at 94 °C a mixture of the α and θ phases is precipitated. For samples prepared at 94 °C, as the concentration of the $ZrOCl_2$ solution is decreased, the percentage of θ-ZrP increases until at 0.05 mol dm^{-3} 100% of θ-ZrP with high degree of crystallinity is obtained. When 0.05 mol dm^{-3} $ZrOCl_2$ solution is used, the samples obtained at below 94 °C are formed of θ-ZrP, whose degree of crystallinity increases with an increase of the precipitation temperature, while at boiling temperature the θ and α phases are coprecipitated.

From these results the effects of concentration and temperature on the crystallization of θ-ZrP are summarized as follows. (1) The increase in solute concentration makes the θ phase unstable. (2) The crystallization of θ-ZrP is promoted by increasing the precipitation temperature but at near boiling temperature the θ phase is less stabilized. (3) The optimum Zr concentration and temperature for the preparation of pure and highly crystalline θ-ZrP are determined by a combination of these two effects. The Zr concentration of 0.05 mol dm^{-3} and digestion temperature of 94 °C for the use of 6 mol dm^{-3} H_3PO_4 solution and

Table 1. Preparation conditions of ZrP samples and their characterization[a]

Concentration of starting solution/mol dm^{-3}		Precipitation temperature/°C	Approximate phase/%		Crystallinity[b] (X-ray)
ZrOCl	H_3PO_4		θ-ZrP(10.4 Å)	α-ZrP(7.6 Å)	
2	6	*ca.* 105 (reflux)	0	100	H
2	6	94	54	46	L
0.4	6	94	84	16	M
0.2	6	94	93	7	H
0.05	6	*ca.* 105 (reflux)	85	15	H
0.05	6	94	100	0	H
0.05	6	80	100	0	M
0.05	6	60	100	0	L

a) Digestion time, 48 h. b) H, high; M, medium; L, low.

48-h digestion time can be taken to meet this optimum condition satisfactorily. Longer times for digestion will contribute to further increase in the degree of crystallinity of the θ-ZrP.

The preferred formation of θ-ZrP in dilute solution and/or at moderate but not too high temperatures could be explained in terms of the type of hydration in this phase. In the monohydrated phase, α-ZrP, the water molecules are located midway between any two POH sites on the interlayer surface and tightly held by bifurcated hydrogen bonds.[7] Therefore, this type of hydrate bonding is likely to be thermally stable and it also contributes to the increase of only 0.2 Å in the interlayer spacing over that of the anhydrous form of α-ZrP which is called ζ-ZrP.[8] The remaining moles of water in this phase, on the other hand, would be located within the interlayer space and weakly held by hydrogen bonding to free hydrogen atoms of the water molecules covering the layer surface. It is therefore apparent that only in very dilute and/or moderately hot solution θ-ZrP with such unstable interlayer water would be formed in preference to α-ZrP.

The interlayer spacing of θ-ZrP is increased by 2.8 Å over that of α-ZrP. By using a value of 24.3 Å^2 for the occupied area per POH site in α-ZrP[2,9] and about 14 Å^3 for the van der Waals volume of the water molecule,[10] the water content in a mole of θ-ZrP can be evaluated to be 1 plus $24.3 \times 2.8/14$ or 5.9. This value is less than the value of 8 water molecules earlier reported[2,4] but agrees well with a value of 6 ± 1 water molecules observed by Alberti *et al.*[3] It is therefore more reasonable to conclude that θ-ZrP is formed as a hexahydrate $Zr(HPO_4)_2 \cdot 6H_2O$. A similar calculation for another highly hydrated phase which has an interlayer spacing of 11.5 Å and composition $Zr(HPO_4)_2 \cdot 8 \pm 1H_2O$[3] yield a value of 7.8 water molecules, which is in good agreement with the observed value.

The author thanks Dr. M. Goto and Dr. S. Ueno for encouragement during this work.

References

1) G. Alberti, U. Costantino, and M. Pilliccioni, *J. Inorg. Nucl. Chem.*, **35**, 1327 (1973).
2) A. Clearfield, G. H. Nancollas, and R. H. Blessing, "Ion Exchange and Solvent Extraction," ed by J. A. Marinsky and Y. Marcus, Marcel Dekker, New York (1973), Vol. 5, Chap. 1.
3) G. Alberti, U. Costantino, and J. S. Gill, *J. Inorg. Nucl. Chem.*, **38**, 1733 (1976).
4) E. Torracca, G. Alberti, R. Platania, P. Scala, and P. Galli, "Ion Exchange in the Process Industries," Chemical Industry, London (1970), p. 315.
5) U. Costantino, *J. Chem. Soc., Dalton Trans.*, **1979**, 402.
6) A. Clearfield and J. A. Stynes, *J. Inorg. Nucl. Chem.*, **26**, 117 (1964).
7) J. Albertsson, Å. Oskarsson, R. Tellgren, and J. O. Thomas, *J. Phys. Chem.*, **81**, 1574 (1977).
8) A. Clearfield and S. A. Pack, *J. Inorg. Nucl. Chem.*, **37**, 1283 (1975).
9) T. Kijima, Y. Sekikawa, and S. Ueno, *J. Inorg. Nucl. Chem.*, **43**, 849 (1981).
10) K. Arakawa, "Structure and Physical Properties of Water (Kagaku No Ryoiki Extra No. 106, ed by M. Nakagaki)," Nankodo, Tokyo (1974), p. 15.

An Ultrasonic Nebulizer for Microliter Samples in Inductively Coupled Plasma Emission Spectrometry

Hiroshi KAWAGUCHI,* Tomokazu TANAKA, and Atsushi MIZUIKE
Faculty of Engineering, Nagoya University, Furo-cho, Chikusa-ku, Nagoya 464

(Received March 8, 1982)

Synopsis. A batch type ultrasonic nebulizer is constructed for 300-μl samples to produce an aerosol for more than 60 s. Desolvation facilities are not used. The internal standard method is employed to compensate for the instability of nebulization.

The most common method for introducing samples into an inductively coupled plasma (ICP) is the pneumatic nebulization of aqueous or organic solutions. Although ultrasonic nebulizers were extensively used in the early stage of the development of the ICP,[1,2] they were gradually replaced by pneumatic nebulizers mainly due to cumbersome operation procedures in conjunction with desolvation apparatus. Olson *et al.*[3] reported an ultrasonic nebulizer which provided rapid and convenient sample change capability and a long term stability but it is still not widely accepted.

Recently considerable attention has been paid to the microliter sample injection into the ICP by conventional pneumatic nebulization[4,5] or electrothermal vaporization.[6,7] Ultrasonic nebulizers are inherently suited for the nebulization of microliter samples because they can nebulize solutions quite efficiently. Though many types of ultrasonic nebulizers have been reported in the literature,[8–12] none of them were particularly intended to be used for microliter samples. Hoare and Mostyn[8] designed a multicell ultrasonic system in which each sample cell could be rotated in turn to locate in the focussed ultrasonic beam, but they did not mention explicitly the sample size required.

We have constructed a batch type ultrasonic nebulizer with easily exchangeable cells for microliter samples. Simultaneous multielement analysis can be performed with a conventional signal integrator without modification by using 300-μl sample solutions.

Experimental

Apparatus. A Shimadzu 1-m grating spectrometer (GE-100) equipped with a three-channel detector unit (M-4),[5] a three-channel integrator (ES-603) and a 27 MHz ICP generator (ICPS-2H) were used. The entrance and exit slitwidths of the spectrometer were set to 20 and 40 μm, respectively. The ICP was operated at a forward power of 1.2 kW and argon flow-rates of 10, 1.0 and 0.8 l min^{-1} were used for the outer, intermediate and carrier gas, respectively.

Ultrasonic Nebulizer (Fig. 1). An ultrasonic transducer for a household electronic humidifier (Mitsubishi Electric Co.) mounted at the bottom of the cooling water chamber was driven by a 1.72 MHz transistor oscillator. The sample cell was a glass tube (11.5 mm i.d., 25 mm long) with a thin bottom plate (0.15 mm thick microscope cover glass, stuck with an epoxy resin adhesive). Two sample cells were mounted in a sliding cell holder so that they were rapidly exchanged without disturbing the nebulization. A polyethylene buffle made of a sealing cap of a reagent bottle was placed on the top of the cell to prevent large aerosol droplets from reaching the fog chamber. Carrier gas was introduced tangentially at the top of the cell so that the aerosol produced was effectively mixed with the carrier gas. Both the top plate of the sliding cell holder and the cooling water chamber were made of Teflon to make the holder slide smoothly without a leak of cooling water. A 35-ml fog chamber was designed so that the condensed aerosol would not flow into the sample cell and contaminate a new sample. The aerosol was introduced into the ICP without any desolvation facilities.

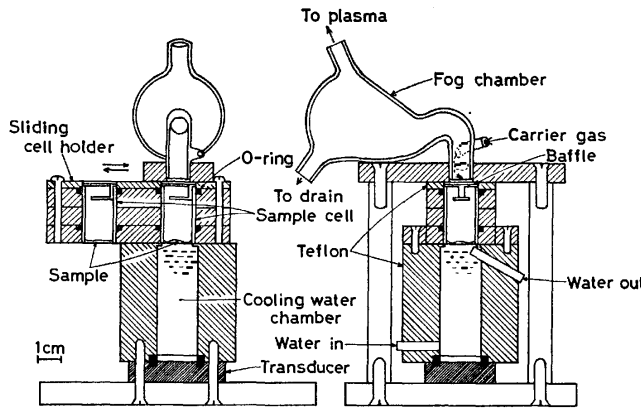

Fig. 1. Schematic diagram of the ultrasonic nebulizer for microliter samples.

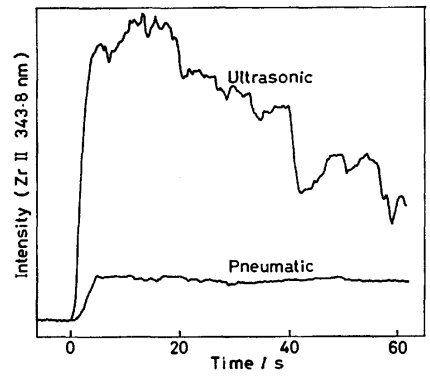

Fig. 2. Intensity-time curves for the Zr II 343.8 nm line.
The same intensity scale for the ultrasonic and pneumatic nebulizers. Zr: 1 μg ml^{-1}.

Solution. Standard solutions were prepared by dissolving reagent-grade salts or pure metals in appropriate mineral acids and diluting with water immediately before use.

Results and Discussion

Sample Volume. As the volume of the sample solutions in the cell was increased from 0 to 500 μl, the emission signals increased at first and then gradually decreased, with the maximum at about 300 μl, where the experiments hereafter were carried out.

Intensity-time Curves. Figure 2 shows intensity-time curves for the Zr II 343.8 nm line (1 μg Zr ml^{-1}) obtained with the present ultrasonic nebulizer and with a conventional pneumatic (concentric glass) nebulizer. In spite of the much smaller consumption of sample,

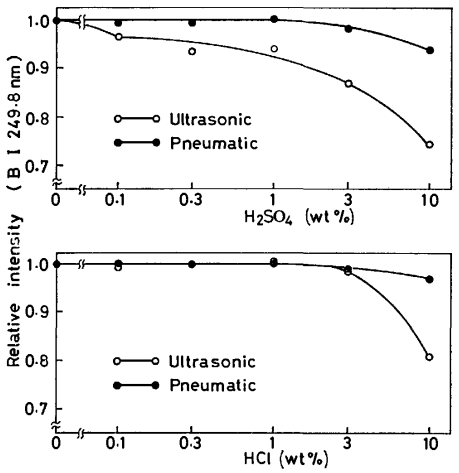

Fig. 3. Effects of acid concentrations on the intensity of the 249.8 nm line.
B: 10 μg ml^{-1}.

the signal intensity with the ultrasonic nebulizer is several times higher than that with the pneumatic nebulizer. The aerosol is produced for more than 60 s, so that a conventional signal integrator can be used without modification. Variation of the signal with time, however, is quite large as compared with that of the pneumatic nebulizer. Although various configurations of the fog chamber and sample cell were tried, the signal stability could not be improved.

Effect of Acid Concentrations. Generally the efficiency of the pneumatic nebulizer is known to be affected by acid concentrations[13] due to the variation of the viscosity of the solutions. The effects of sulfuric and hydrochloric acid concentrations on the emission intensity of the B I 249.8 nm line (10 μg B ml^{-1}) are shown in Fig. 3 for ultrasonic and pneumatic nebulizers. The efficiency of the ultrasonic nebulizer is affected more seriously than that of the pneumatic nebulizer by acid concentration.

Internal Standard Method. The instability of nebulization can be compensated to some extent by adopting the internal standard method. Though this method has not generally been applied in ICP emission spectrometry, it sometimes improves the precision of the analysis.[14] Yttrium was added as internal standard to the sample solutions and intensity-time curves of lines of various elements were compared with those of yttrium lines. The intensity-time curves of all the lines examined strikingly resembled each other irrespective of the excitation characteristics of the lines. Table 1 shows the relative standard deviations of intensities of various elements and those of ratios to the yttrium line intensities. In these experiments, each sample was nebulized for 10 s before the signal integration for 20 s. The determination was repeated 10 times for each sample. The use of the internal standard method reduced the relative standard deviation to less than 2%. The precision, however, is strongly dependent on the concentration level of the material being analyzed since the background fluctuation is not compensated by the internal standard method. Variation of the relative standard deviations with the change of titanium concentrations are shown in Table 2. The relative standard deviation of the intensity ratio increases rapidly below 0.1 μg ml^{-1} of titanium. Thus the detection limits cannot be improved.

Table 1. Relative standard deviations (RSD) of intensities and intensity ratios

Element	Wavelength nm	Concentration μg ml^{-1}	RSD (%) Intensity	RSD (%) Intensity ratio[a]
B I	249.77	5	6.6	1.8
Cd II	214.44	5	7.1	0.6
Co II	238.89	10	2.9	0.9
Cr II	205.55	10	6.0	1.1
Mn II	257.61	1	11.8	1.0
Ni II	232.00	10	10.6	1.6
P I	213.62	100	5.3	0.5
Zn I	213.86	10	12.2	1.5
Cu I	324.75	10	11.8	0.8
Ti II	334.94	10	9.2	1.3
Zr II	343.82	10	9.2	1.3

a) Internal standard: 10 μgY ml^{-1}, Y II 371.03 nm for Cu, Ti and Zr, and Y II 224.31 nm for other elements.

Table 2. Relative standard deviation of intensity ratios at different titanium concentrations

Ti (μg ml^{-1})	RSD (%) Intensity[a]	RSD (%) Intensity ratio[b]
0	2.22	14.0
0.01	1.89	13.9
0.1	2.16	6.98
1	9.04	1.59
10	11.8	0.19

a) Line+background. b) Internal standard: 10 μg Y ml^{-1}, Y II 371.03 nm.

Accuracy was tested by analyses of standard reference materials. Titanium (certified values 0.066, 0.098%) and chromium (certified values 0.011, 0.036%) in low alloy steels (Japan Standards of Iron and Steel, JSS 168-2 and 170-2) were determined by preparing solutions containing 10 mg of the sample and 10 μg of yttrium per ml with satisfactory results (0.065 and 0.098%Ti, and 0.012 and 0.038%Cr).

Although the proposed ultrasonic nebulizer is less stable and more susceptible to acid concentrations than the conventional pneumatic nebulizer, it may be quite useful for analyses of samples of limited volumes, *i.e.*, microliter samples.

References

1) G. W. Dickinson and V. A. Fassel, *Anal. Chem.*, **41**, 1021 (1969).
2) P. W. J. M. Boumans and F. J. De Bore, *Spectrochim. Acta, Part B*, **27**, 391 (1972).
3) K. W. Olson, W. J. Haas, Jr., and V. A. Fassel, *Anal. Chem.*, **49**, 632 (1977).
4) H. Uchida, Y. Nojiri, H. Haraguchi, and K. Fuwa, *Anal. Chim. Acta*, **123**, 57 (1981).
5) T. Ito, E. Nakagawa, H. Kawaguchi, and A. Mizuike, *Mikrochim. Acta*, **1982 I**, 423.
6) D. E. Nixon, V. A. Fassel, and R. N. Kniseley, *Anal. Chem.*, **46**, 210 (1974).
7) G. F. Kirkbright and R. D. Snook, *Anal. Chem.*, **51**, 1938 (1979).
8) H. C. Hoare and R. A. Mostyn, *Anal. Chem.*, **39**, 1153 (1967).
9) C. D. West, *Anal. Chem.*, **40**, 253 (1968).
10) M. Suzuki, *Bunseki Kagaku*, **19**, 207 (1970).
11) H. Kawaguchi, M. Hasegawa, and A. Mizuike, *Bunseki Kagaku*, **20**, 894 (1971).
12) M. B. Denton and H. V. Malmstadt, *Anal. Chem.*, **44**, 241 (1972).
13) S. Greenfield, H. McD. McGeachin, and P. B. Smith, *Anal. Chim. Acta*, **84**, 67 (1976).
14) Y. Endo and N. Sakao, *Bunseki Kagaku*, **30**, 433 (1981).

Oxidizing Action of Complex of *N,N*-Dimethylbenzylamine Oxide with $SbCl_5$

Jiro YAMAMOTO,* Yukio TANIOKA, and Masahiro UMEZU

Department of Industrial Chemistry, Faculty of Engineering, Tottori University, Tottori 680

(Received January 25, 1982)

Synopsis. A 1:1 complex of *N,N*-dimethylbenzylamine oxide–$SbCl_5$ (**1**) was prepared in carbon tetrachloride quantitatively. Complex **1** was found to be a better reagent for oxidation of benzoin, furoin, benzyl alchols and pinacols than the complexes pyridine *N*-oxide–$SbCl_5$ and trimethylamine oxide–$SbCl_5$. The reaction path in oxidation of benzhydrol with **1** is described.

In the previous paper,[1] we reported that 1:1 complexes of pyridine *N*-oxide (**2**) and trimethyamine oxide (**3**) with $SbCl_5$ behave as an oxidizing agent for some compounds. In this paper, we describe the oxidation of benzoin, furoin, benzhydrol and *o*- and *p*-nitrobenzyl alcohols using the complex formed *N,N*-dimethylbenzylamine oxide (**4**) with $SbCl_5$ [$PhCH_2(CH_3)_2N$–$OSbCl_5$, **1**].

Experimental

1:1 Complex of N,N-*Dimethylbenzylamine Oxide with* $SbCl_5$ *(1).* When a solution of **4** (9.50 g, 6.29 mmol) in CCl_4 (90 ml) was added to a solution of $SbCl_5$ (20.9 g, 62.9 mmol) in CCl_4, yellow crystalline complex **1** immediately deposited. The reaction mixture was filtered and washed with CCl_4 and then with petrolium ether. 30.1 g (99.0%), mp 206—208 °C (in a sealed capillary tube). ν_{max}^{KBr}; 1580 cm^{-1}, 1405 cm^{-1}, 1220 cm^{-1}, 1180 cm^{-1}, 1145 cm^{-1}, 975 cm^{-1}, 880 cm^{-1}, $\lambda_{max}^{CHCl_3}$; 268 nm (ε: 7120). Found: Cl, 39.40%. Calcd for $C_9H_{13}NOSbCl_5$: Cl, 40.10%.

Oxidation of Benzoin with **1**. A mixture of benzoin (0.50 g, 2.35 mmol) in nitromethane was kept for 5 h at 60 °C. The reaction mixture was poured into water and filtered. After filtrates were extracted with ether, the ether solution was washed with dil. HCl. The solution was dried, filtered and evaporated, and then benzil (0.48 g, 95%) was separated from the residue by column chromatography (benzene–silica gel). The same procedure was also applied in the oxidation of furoin, except that chloroform was used as a eluent in column chromatography.

Results and Discussion

The oxidation of *o*- and *p*-nitrobenzyl alcohols with **1** gave the corresponding aldehydes in low yield (Table 1). In the equimolar reaction of benzhydrol with **1** in nitromethane at room temperature, bis(diphenylmethyl)ether was obtained in a 58% yield. The yield of benzophenone and bis(biphenylmethyl)ether increased when the reaction was carried out at 40 °C (Table 1). On the other hand, the yield of benzophenone increased at high temperature (Fig. 1). These results indicate that bis(diphenylmethyl)ether changes to benzophenone promptly, but benzophenone does not. After treatment of bis(diphenylmethyl)ether with equimolar **1** in nitromethane, benzhydrol and benzophenone were obtained (Fig. 2). Therefore, it should be concluded that both benzhydrol and bis(diphenylmethyl)ether are in equilibrium in the presence of **1**. The

Table 1. Oxidation of benzhydrol and *o*- and *p*-nitrobenzyl alcohols with *N,N*-dimethylbenzyl amine oxide–$SbCl_5$ (1: 1) complex

Substrates[a] (mmol)	Oxidant	Reaction condition[b] Molar[e] ratio	Temp °C	Time h	Reaction products[c],[d] Yield/% [A]	[B]	Recovered starting materials (%)
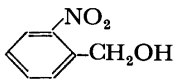 (3.3)	**1**	1.0	Reflux	1	9.3[f]	6.2[g]	68
		2.0	Reflux	10	17	5.8	58
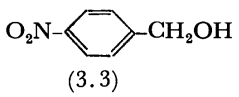 (3.3)		1.0	Reflux	1	15[h]	6.3	74
		2.0	Reflux	2	32	17	37
		1.0	r.t.	110	2.4[i]	58[j]	26
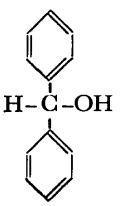 (2.7)	**4**	1.0	40	1	1.0	61	21
		1.0	40	2	2.4	65	16
		1.0	40	3	2.8	73	12
		2.0	40	1	14	33	24
		20	40	3	2.4	4	77

a) Starting materials(0.5 g) were used in each run. b) Nitromethane (10 ml) was used as a solvent in each run. c) Tarry products were formed. d) All products were separated by TLC (benzene-silica gel). e) Substrates/Oxidants. f) *o*-Nitrobenzaldehyde; mp 46—47 °C (lit,[2] 48 °C). g) They seem to be the corresponding bis(nitrobenzyl)ethers. h) *p*-Nitrobenzaldehyde; mp 104—105 °C (lit,[3] 106—107 °C). i) Benzophenone; mp 47—48 °C (lit,[4] 48 °C). j) Bis(diphenylmethyl)ether; mp 109 °C (lit,[5] 109 °C).

Table 2. Oxidation of benzoins and pinacohols with *N,N*-dimethylbenzylamine oxide–$SbCl_5$ (1:1) complex

Substrates[a] (mmol)	Oxidant	Reaction conditions[b] Molar[c] ratio	Temp °C	Time h	Products yield/%	Recovered starting materials (%)
CH_3 CH_3 CH_3-C—C-CH_3 OH OH	1	1.0	r.t.	30	60[d]	63
		1.0	40	1	62[e]	14
		2.0	40	1	43	7
(4.2)		1.0	80	1	36	8
Ph Ph Ph-C—C-Ph OH OH	1	1.0	r.t.	20	92	—
		1.0	50	5	81	—
		1.0	Reflux	5	80	—
(1.4)						
H Ph-C—C-Ph O OH	1	1.0	r.t.	24	92[f]	5.0
		1.0	40	5	91	3.4
		1.0	60	5	95	—
(2.5)	4	2.0	60	5	16	73
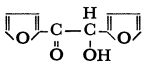	1	1.0	0	1	29[e],[g]	4.8
		1.0	5	1	30	4.6
		1.0	r.t.	1/6	38	10
(2.6)	4	2.0	30	20	—	87

a) Starting material (0.5 g) was used in each run. b) Nitromethane (10 ml) was used as a solvent in each run. c) Oxidants/substrates. d) The yield was determined as 2,4-dinitrophenylhydrazone. e) A lot of tarry products were formed. f) Benzil; 94—95 °C (lit,[6] 95 °C). g) Furil; 164—165 °C (lit,[7] 165 °C).

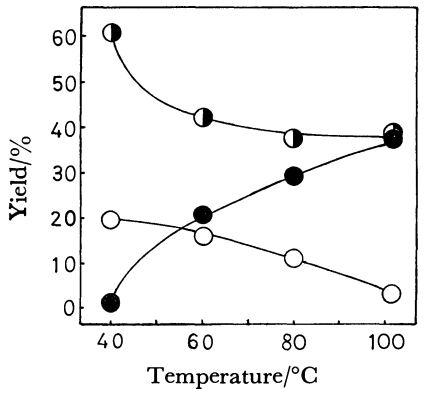

Fig. 1. The dependence of reaction temperature on the oxidation of benzhydrol with *N,N*-dimethylbenzylamine oxide–$SbCl_5$ (1:1) complex.
Reaction conditions: benzhydrol; 0.5 g (2.71 mmol), complex; 1.22 g (2.71 mmol), solvent; 10 ml of nitromethane, reaction time; 1 h. ●: Benzophenone, ◑: bis(diphenylmethyl)ether, ○: benbhydrol.

rate constants of each in the following equation depend

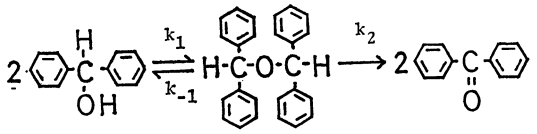

upon the reaction temperature, *i.e.* $k_2>k_1>k_{-1}$ near 40 °C, $k_1>k_2>k_{-1}$ from 60 °C to 70 °C and $K_2>k_1>k_{-1}\simeq 0$ near 100 °C (Fig. 1 and Fig. 2). In the first step of the reaction, a proton of benzhydrol is abstracted, as in the reaction of pyridine *N*-oxide with thiophenol.[8] After bis(diphenylmethyl)ether accumulates

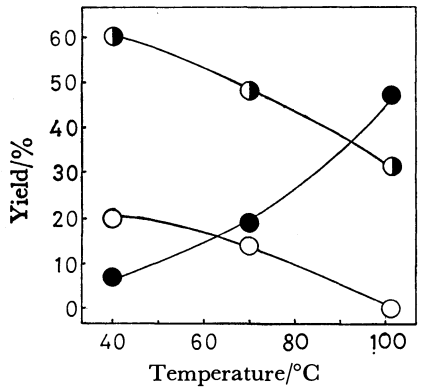

Fig. 2. The treatment of bis(diphenylmethyl)ether with *N,N*-dimethylbenzylamine oxide–$SbCl_5$ (1:1) complex. Reaction conditions: bis(diphenylmethyl)ether; 0.5 g (1.43 mmol), complex; 0.64 g (1.43 mmol), solvent; 10 ml of nitromethane, reaction time: 1 h. ●: Benzophenone, ◑: bis(diphenylmethyl)ether, ○: benzhydrol.

in the reaction system, it changes into both benzhydrol and benzophenone in accordance with the reaction temperature (Fig. 2). Compounds **4** seems to be less reactive than **1** in the reaction with benzhydrol (Table 1).

Although oxidation of benzoin with **1** under mild condition gave benzil in 95% that with **4** gave only 16.4%. A higher yield of benzoin was obtained in comparison with the case of using $SbCl_5$ as done for **2** and **3** reported before.[1] In the oxidation with furoin with **1**, moderate yields of furil were obtained (Table 2). Pinacolones were obtained in good yield in the oxidation of pinacols with **1** may be considered to be an effective catalyst for pinacol–pinacolone rearrangement.

The authors are grateful to Professors M. Tanaka and J. Kiji of Tottori University for their valuable advice.

References

1) J. Yamamoto, M. Murakami, N. Kameoka, N. Otani, M. Umezu, and T. Matsuura, *Bull. Chem. Soc. Jpn.*, **55**, 345 (1982).
2) W. Davey and J. R. Gewilt, *J. Chem. Soc.*, **1950**, 204.
3) S. W. Liebermann and R. Connor, *Org. Synth.*, Coll. Vol. II, 441 (1943).
4) L. Gattermann, "Die Praxis des Organischen Chemikers" Walter de Grytyer & Co., Berlin (1961), p. 297.
5) Demselben, *Ann. Chem.* **184**, 176 (1877).
6) T. G. Clarke and E. E. Dreger, *Org. Synth.*, Coll. Vol. I, 87 (1941).
7) W. W. Hartman and J. B. Dickey, *J. Am. Chem. Soc.*, **55**, 1228 (1933).
8) D. I. Relyea, P. O. Tawney, and A. R. Williams, *J. Org. Chem.*, **27**, 474 (1962).

Solvent Effect on Photooxidation of Triphenylphosphine Selenide Sensitized by Polymer-supported Rose Bengal

Seizo TAMAGAKI* and Ryuji AKATSUKA

Department of Applied Chemistry, Faculty of Engineering, Osaka City University, 3-138, Sugimoto 3-chome, Sumiyoshi-ku, Osaka 558

(Received October 22, 1981)

Synopsis. Solvent effect on the photooxygenation of triphenylphosphine selenide was examined by using crosslinked polystyrene- or silica gel-anchored Rose Bengal as sensitizers. Different types of solvent dependency of the product yields were observed in each case.

Recently, polymer-supported photosensitizers have been extensively utilized for synthetic photochemistry.[1] For instance, Rose Bengal anchored to 1%-crosslinked polystyrene beads have been successfully applied to the photogeneration of singlet oxygen.[2]

As part of our continuing interest in the photosensitized oxidation of thione compounds,[3] we have examined the photosensitized oxidation of triphenylphosphine selenide which has not yet been studied thus far, and shed light on the properties of Rose Bengal bound to different types of supports.

Results and Discussion

First, the efficiency of Rose Bengal itself as a sensitizer was examined in various solvents. Triphenylphosphine selenide was irradiated under oxygen bubbling for 5 h in the presence of Rose Bengal in Me_2C=O, MeCN, MeOH, and $CHCl_3$–MeOH (1:1 V/V) affording the corresponding oxide in 3, 11, 78, and 92% of isolated yields, respectively, but no product was obtained in nonpolar solvents such as benzene, $CHCl_3$, and CS_2, because Rose Bengal is not soluble in these solvents.

$$Ph_3P{=}Se + O_2 \xrightarrow[5\,h,\ \text{Rose Bengal}]{CHCl_3\text{-MeOH},\ h\nu} Ph_3P{=}O + Se$$
(92%) (75%)

Meanwhile, the effect of solvent on product yields for the reaction with styrene–1%-divinylbenzene copolymer-bound Rose Bengal (Ⓟ-RB: **1**) as a sensitizer was compared with that with silica gel-bound Rose Bengal (Ⓢ-RB: **2**).[4] Tables 1 and 2 list the yields for **1** and **2**, respectively. Inspection of these tables reveals that the yield is solvent dependent in both cases.

Ⓟ- -CH_2-RB (**1**) Ⓢ-$(CH_2)_3$-RB (**2**)

Ⓟ=Polystyrene copolymer; RB=Rose Bengal; Ⓢ=silica gel.

When **1** was employed, the yield of the product decreased in the order: CH_2Cl_2–MeOH (1:1)> $CHCl_3$ > CH_2Cl_2>benzene–MeOH (1:1)>CCl_4>benzene>MeCN>MeOH. Apparently, **1** did not act as a sensitizer in MeOH because of the hydrophobicity of the polystyrene copolymer bead. The lifetime of singlet oxygen in single component solvents was reported to decrease in the following order: CCl_4> $CHCl_3$>benzene≥MeCN>MeOH,[5] whereas the degree of swelling of the bead decreases in the order: benzene>$CHCl_3$>CH_2Cl_2>CCl_4>MeCN>MeOH. It is apparent, therefore, that neither the swelling index nor the lifetime of singlet oxygen alone can account for the observed order, but a combination thereof may be a possible explanation for that. The interesting finding is that the photooxidation is more efficient in MeOH-containing solvents such as $CHCl_3$–MeOH and benzene–MeOH than in $CHCl_3$ and benzene, respectively, although MeOH swells the polystyrene bead least and decreases the lifetime of singlet oxygen most of all the solvents examined.[6] This effect of MeOH is best explained if the reaction involves the intermediacy of the zwitterion having a structure like **4** (the peroxyselenide) depicted in Scheme 1 and if MeOH acts as the hydrogen-bonding donor toward **4**, thus promoting the nucleophilic attack on the negative oxygen by the second phosphine selenide. In aprotic solvents the intermediate **4** dissociates readily into the original selenide and ground-state dioxygen.

TABLE 1. SOLVENT EFFECT ON THE PHOTO-SENSITIZED OXYGENATION OF TRIPHENYLPHOSPHINE SELENIDE BY POLYSTYRENE-SUPPORTED ROSE BENGAL (**1**)[a]

Solvent	Ph_3P=O (%)	Ph_3P=Se (recovered) (%)	Swelling index[c]	Lifetime of $O_2{}^1$/μs
CH_2Cl_2-MeOH (1:1)	91	5	—	—
CH_2Cl_2-MeOH[b] (1:1)	32	61	—	—
$CHCl_3$	68	20	5.15	60
$CHCl_3$[b]	<1	95	—	—
CH_2Cl_2	55	31	4.46	—
Benzene-MeOH (1:1)	50	21	—	—
CCl_4	43	39	4.30	711
Benzene	5	90	5.54	24
MeCN	2	93	2.77	30
MeOH	<1	96	1.07	7

a) **1**: 100 mg; Ph_3P=Se: 0.5 mmol. Irradiated for 4 h. b) 1 mmol of DABCO was added. c) Swelling indices of 2%-crosslinked polystyrene bead: Swollen volume/dry volume.

Table 2. Solvent effect on the photosensitized oxygenation using silica gel-bound Rose Bengal (**2**)[a]

Sovent	$Ph_3P=O$ (%)	$Ph_3P=Se$ (%)
CCl_4	84	3
CH_2Cl_2	76	16
CH_2Cl_2[b]	28	c
$CHCl_3$	71	10
CH_2Cl_2–MeOH (1:1)	67	20
Benzene	43	43
MeCN	43	39
MeOH	39	34

a) **1**: 200 mg; $Ph_3P=Se$: 0.5 mmol: irradiated for 2 h. b) $Ph_3P=Se$: 0.167 mmol. c) Not determined.

A similar rate-enhancement due to hydrogen-bonding interaction between a zwitterion and MeOH was reported in the singlet oxygenation of sulfide in which the persulfoxide **3** is involved as a reactive intermediate.[7]

$$R_2S + O_2{}^1 \longrightarrow \underset{\mathbf{3}}{R_2\overset{+}{S}\text{-}O\text{-}O^-} \xrightarrow[MeOH]{R_2S} 2R_2S=O$$

Addition of 1,4-diazabicyclo[2.2.2]octane (DABCo), a typical singlet oxygen quencher, significantly inhibits the formation of the phosphine oxide especially in nonpolar solvents, implying that singlet oxygen is the only oxidizing species.[8] Thus, one of the tentative mechanisms of the oxidation may be visualized as follows: The initial pre-equilibrium formation of the peroxyselenide **4**, followed by attack of another selenide on it, yields the oxyselenide **5**, which rearranges and then eliminates selenium, eventually giving the phosphine oxide.

$$Ph_3P=Se + O_2{}^1 \longrightarrow \underset{\mathbf{4}}{Ph_3\overset{+}{P}\text{-}S\text{-}O\text{-}O^-} \xrightarrow{Ph_3P=Se} \underset{\mathbf{5}}{2Ph_3P=Se=O}$$

$$\mathbf{5} \longrightarrow Ph_3P\begin{matrix}\diagup Se \\ | \\ \diagdown O\end{matrix} \xrightarrow{-Se} Ph_3P=O$$

Scheme 1.

On the other hand, when Ⓢ-RB (**2**) was employed,[9] the sequence of the solvent effect on the yield was quite similar to that expected from the lifetime of singlet oxygen (Table 2). In contrast to the case with Ⓟ-RB (**1**) or Rose Bengal itself, no rate-enhancement by MeOH was observed. This is due to the fact that singlet oxygen, photogenerated in a silica particle, does not have sufficient lifetime to diffuse out of the particle with a diameter of 10^{-2} cm, since singlet oxygen has a short mean radius of diffusion of less than 10^{-4} cm during the lifetime.[10] The singlet oxygen would then react with triphenylphosphine selenide predominantly in the solvent channel of the same particle, giving **4**, which is then strongly adsorbed at the silica gel through hydrogen-bonding to react with another selenide. Even in MeOH solvent, **4** may hydrogen-bond effectively to silica rather than to MeOH. Accordingly, the main factor to determine the solvent effect is to be the lifetime or concentration of singlet oxygen in the solvent in question.

In conclusion, with Ⓟ-RB as a sensitizer, the yield of the phosphine oxide is remarkably increased by addition of MeOH, while with Ⓢ-RB, the solvent dependency of the yield just parallels the lifetime or concentration of singlet oxygen and thus the yield is the lowest in MeOH.

Experimental

Materials. Chloromethylated 1%-crosslinked polystyrene beads (0.75 meq CH_2Cl/g resin; 300 mesh) were purchased from Bio Rad Laboratories, Richmond, Cal. and Silica gel (Wakogel C-300) from Wako Pure Chemical Industry, Tokyo. Polystyrene-supported Rose Bengal (**1**: 2 mg of Rose Bengal per g of the polymer) was prepared according to the method of Blossey and Neckers.[2] Silica gel-supported Rose Bengal (**2**) was prepared by heating a DMF solution of Rose Bengal and silica gel modified with (3-chloropropyl)trichlorosilane at 120 °C for 20 h.[4] The resultant reddish silica gel was filtered and washed successively with H_2O, acetone, and $CHCl_3$ and then continuously extracted with $CHCl_3$–MeOH (1:1) until the color due to Rose Bengal did not come out into the eluent. The silica gel thus obtained (**2**: 0.3 mg of Rose Bengal per g of silica gel) was dried in a vacuum oven at 60 °C for 5 h.

Photooxidation of Triphenylphosphine Selenide Using Rose Bengal. Triphenylphosphine selenide (0.5 mmol) and 5 mg of Rose Bengal dissolved in 25 cm^3 of $CHCl_3$–MeOH (1:1) were placed in a Pyrex tube and irradiated with a tungsten-halogen lamp (500 W) under O_2 bubbling for 5 h until the selenide disappeared completely. The filtrate was concentrated to 0.5 cm^3 and the residue was chromatographed on TLC (Kieselgel 60, benzene) giving 92% of triphenylphosphine oxide.

General Procedure for Photooxygenation with Polymer-supported Rose Bengal. The selenide (0.5 mmol) and **1** (100 mg) or **2** (200 mg) in 25 cm^3 of a solvent were placed in a Pyrex tube with a magnetic stir bar and irradiated under O_2 bubbling with the tungsten lamp. After the irradiation, the polymer was filtered off and the filtrate was concentrated to 0.5 cm^3. The residue was subjected to TLC analysis. The results are summarized in Tables 1 and 2.

References

1) E. C. Blossey and D. C. Neckers, *Tetrahedron Lett.*, **1974**, 323.

2) A. P. Schaap, A. L. Tayer, E. C. Blossey, and D. C. Neckers, *J. Am. Chem. Soc.*, **97**, 3741 (1975).

3) S. Tamagaki, M. Nakamura, and S. Kozuka, *Tetrahedron Lett.*, **1979**, 3665; S. Tamagaki and K. Hotta, *J. Chem. Soc., Chem. Commun.*, **1980**, 598.

4) S. Tamagaki, C. Liesner, and D. C. Neckers, *J. Org. Chem.*, **45**, 1573 (1980).

5) P. B. Merkel and D. R. Kearns, *J. Am. Chem. Soc.*, **94**, 722 (1972).

6) In contrast, the oxidation of an olefin, 2,3-diphenyl-2,3-dihydro-1,4-dioxin, was reported to proceed by a cyclization mechanism where there was no special effect of MeOH on the rate. "Singlet Oxygen," ed by H. H. Wasserman and R. M. Murray, Academic Press, New York (1979), Chap. 6.

7) C. S. Foote and T. W. Peters, *J. Am. Chem. Soc.*, **93**, 3795 (1971).

8) DABCO suppressed the sensitized photooxidation incompletely in MeOH presumably because of interaction of DABCO with MeOH.

9) Silica gel does not swell out in any solvents.

10) S. Wolf, C. S. Foote, and J. Rebek, Jr., *J. Am. Chem. Soc.*, **100**, 7770 (1978).

Friedel-Crafts Reactions of Benzene with 1-Phenylpropanols. Effects of $CuCl_2$, Cu_2Cl_2, and Decalin

Katsuhiko Ichikawa, Keizo Chano, Masashi Inoue, and Toshio Sugita*

Department of Hydrocarbon Chemistry, Faculty of Engineering, Kyoto University, Sakyo-ku, Kyoto 606

(Received November 16, 1981)

Synopsis. Highly regioselective formation of 1,1-diphenylpropane was observed when copper(I) or (II) chlorides was added to the aluminium chloride-catalyzed reaction of benzene with 1-phenyl-1-propanol. In the reaction with 1-phenyl-2-propanol, the addition of copper salts increased the formation of 1,1-diphenylpropane. The addition of decalin diminished the alkylation reaction to give a reduction product.

In a previous paper, we reported that the Friedel-Crafts reaction of benzene with 2-phenyl-1-propanol, 1-phenyl-2-propanol (**1**), and the related compounds gave a mixture of 1-phenylpropane (**3**), 1,1-diphenylpropene (**4**), 1,1- (**5**) and 1,2-diphenylpropanes (**6**), and we also pointed out that the intermolecular hydride transfer from **5** to an intermediate, 1-methyl-2-phenylethyl or 1-phenylpropyl cation, played an important role in the reaction.[1] Schmerling and Vesely reported that an aromatic hydrocarbon was alkylated with a saturated hydrocarbon when it was treated with copper(II) and aluminium chlorides.[2] They suggested that the alkylation proceeded by an oxidative reaction involving copper(II) chloride. In order to investigate the effects of oxidizing reagents and hydride donors on the reaction, the aluminium chloride-catalyzed reactions of benzene with 1-phenyl-2- (**1**) and 1-propanols (**2**) were studied in the presence of copper(II) and (I) chlorides, and *trans*-decalin.

By the addition of copper(II) chloride as an oxidizing reagent, the yield of 1-phenylpropane (**3**) was diminished as expected, but the yield of 1,1-diphenylpropene (**4**) (an oxidized product) did not increase either in the case of **1** or of **2**. Furthermore, no distinct difference could be observed between the result obtained by the addition of copper(II) chloride and that by copper(I) chloride, in spite of the difference of their oxidizing ability. When the reaction of benzene with **2** was carried out in the presence of the copper salts, the yields of diphenylpropanes remarkably increased and the reaction regioselectively proceeded to afford 1,1-diphenylpropane (**5**). In the reaction with **1**, the addition of the copper salts also increased the yield of diphenylpropanes as well as the ratio of **5** in diphenylpropanes. In the reactions using copper(I) chloride, no distinct difference was observed between the results obtained under the ambient atmosphere and under argon. Nenitzescu and Cantuniari showed that the aluminium chloride-catalyzed hydride transfer reaction took place if the aluminium chloride contained water.[3] In the present case, the reaction mixture should contain water since the substrates were alcohols; thus hydride transfer was expected to occur. The present results, however, indicate that both copper(II) and (I) chlorides prevent the intermolecular hydride transfer reaction. Although the reason why the presence of each chloride gave similar results is still uncertain, it is suggested that the copper salts prevent the rearrangement of 1-phenylpropyl cation to a phenonium-type 1-methyl-2-

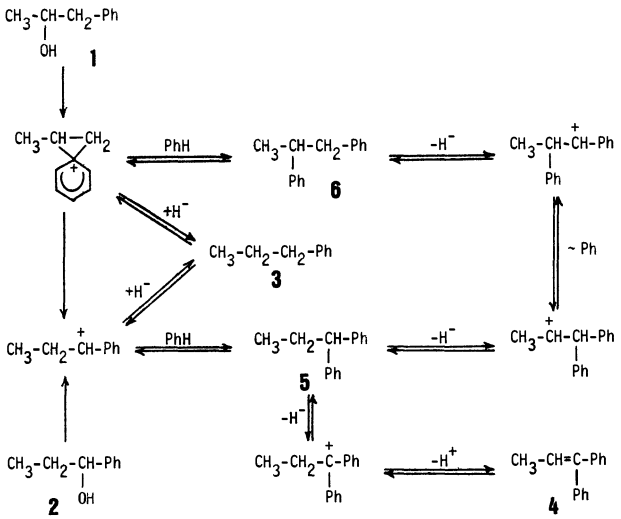

Scheme 1.

Table 1. Reaction of benzene with 1-phenylpropanols in the presence of additives

Substrate	Additive	Yield/%[a] 3	4	5+6	5 : 6[b]
$PhCH_2CHCH_3$ OH **1**	$CuCl_2$	2	0	85	21 : 79
	Cu_2Cl_2	0.5	0	75	19 : 81
	Decalin	80	0	trace	— : —
	None	9	3	67	7 : 93
$PhCHCH_2CH_3$ OH **2**	$CuCl_2$	3	0	97	100 : 0
	Cu_2Cl_2	1	0	99	100 : 0
	Decalin	62	0	trace	— : —
	None	17	4	79	54 : 46

a) Determined by GLPC. b) Determined by NMR.

phenylethyl cation; the rearrangement probably takes place *via* **5** and **6**, accompanied with hydride transfer and phenyl migration.

The addition of *trans*-decalin increased the yield of the reduction product (**3**), and gave a trace of the Friedel-Crafts alkylation products (**5** and **6**). It is thus indicated that the arylpropyl cations abstract a hydride ion from decalin easier than from **5** and other products, *i.e.*, decalin is very reactive as a hydride donor.

Experimental

The ^1H NMR spectra were taken on a JEOL PMX-60 (60 MHz) or a Varian HR-220 (220 MHz) apparatus in $CDCl_3$ with TMS as an internal standard.

Materials. Benzene was washed with conc H_2SO_4, and distilled over CaH_2. Commercial GR grade aluminium chloride was used without further purification. GR grade $CuCl_2$ was used after drying at 120 °C/3 mmHg (1 mmHg $\approx$133.322 Pa) for more than 3 h. White crystalline Cu_2Cl_2 was prepared from $CuCl_2$ and glycerol, washed with ethanol and dried under a reduced pressure.[4] **1**, **2** and *trans*-decalin were commercially available, and used without further purification.

The Reactions of Benzene with 1-Phenyl-1- and 2-propanols. A Typical Procedure: A solution of **2** (12 mmol) in benzene (10 ml) was added to a stirred mixture of $AlCl_3$ (22.5 mmol) and the additive ($CuCl_2$, 22.5 mmol) in benzene (20 ml) at 40 °C. The mixture was stirred at 40 °C for 2 h, and then poured into a mixture of saturated aqueous NH_4Cl solution (100 ml) and 30% aqueous ammonia (20 ml). *p*-Methoxytoluene was added as an internal standard, the organic layer was separated, the aqueous layer was extracted with ether, and the combined extracts were dried over $MgSO_4$. After removal of the solvents, the crude product was submitted to the GLPC analysis (PEG-20M 5% on Chromosorb W, 4 m). The crude product was distilled under a reduced pressure, and the diphenyl fraction (bp 109—111 °C/3 mmHg) was analyzed by means of the integral intensities of terminal methyl signals in its NMR spectrum: 1,1-diphenylpropane (**5**), δ=0.87 (t, J=8, 3H, CH_3), 2.04 (m, 2H, CH_2), 3.71 (t, J=10, 1H, CH), 7.13 (s, 10H, C_6H_5); 1,2-diphenylpropane (**6**), δ=1.20 (d, J=8, 3H, CH_3), 2.86 (m, 3H, $-CH_2-CH\langle$), 7.15 (10H, C_6H_5); 1,1-diphenylpropene (**4**), δ=1.73 (d, J=8, 3H, CH_3), 6.15 (q, 1H, =CH–), 7.19 (s, 10H, C_6H_5).

References

1) M. Inoue, N. Umaki, T. Sugita, and K. Ichikawa, *Nippon Kagaku, Kaishi*, **1978**, 775.

2) L. Schmerling and J. A. Vesely, *J. Org. Chem.*, **38**, 312 (1973).

3) C. D. Nenitzescu and I. P. Cantuniari, *Chem. Ber.*, **66**, 1097 (1933); C. D. Nenitzescu, "Carbonium Ions," ed by G. A. Olah and P. v. R. Schleyer, Wiley-Interscience, New York (1970), Vol. 2, p. 463.

4) "Handbuch der Präparativen Anorganischen Chemie," ed by G. Brauer, Ferdinand Enke Verlag, Stuttgart (1954), p. 751; B. K. Vaidya, *Nature (London)*, **123**, 414 (1928).

X-Ray Crystallographic Analysis of 3α,5-Epoxy-6β-iodo-3β-methyl-*A*-homo-4-oxa-5α-cholestane, a Major Product of Photo- and Thermally-induced Radical Rearrangements of Hypoiodites of 3α- and 3β-Methyl-5-cholesten-3-ols[1]

Akio FURUSAKI,* Chuji KATAYAMA,† and Hiroshi SUGINOME††

Department of Chemistry, Faculty of Science, Hokkaido University, Sapporo 060

† *Department of Chemistry, Faculty of Science, Nagoya University, Chikusa-ku, Nagoya 464*

†† *Department of Chemical Process Engineering, Faculty of Engineering, Hokkaido University, Sapporo 060*

(Received December 5, 1981)

Synopsis. The major product of photo- and thermally-induced radical rearrangements of hypoiodites of 3α- and 3β-methyl-5-cholesten-3-ols in the presence of iodine with mercury(II) or silver(II) oxide has been established as 3α,5-epoxy-6β-iodo-3β-methyl-*A*-homo-4-oxa-5α-cholestane by means of X-ray crystal structure analysis.

The photo- and thermally-induced rearrangements of hypoiodites of several 5-cholesten-3-ols in the presence of mercury(II) oxide and iodine generally lead to the formation of seven-membered oxabicyclics.[2-5] In a previous paper,[3] it was reported that hypoiodites of 3α- and 3β-methyl-5-cholesten-3-ols in benzene containing mercury(II) oxide and iodine gave virtually a single product. The **1** structure was proposed for this product on the basis of the spectroscopic data.[3] There was, however, some ambiguity in assigning the stereochemistry of its oxygen bridge. Therefore, in order to establish **1**, we have now undertaken an X-ray crystal structure analysis.

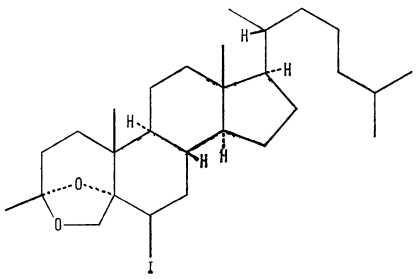

1

Experimental

A colorless single crystal with dimensions of about 0.2×0.2×0.5 mm³ was used for the X-ray measurement. The crystal data are as follows: $C_{28}H_{47}O_2I$, mol wt 542.6, orthorhombic, space group $P2_12_12_1$, $a=17.44(1)$, $b=21.27(2)$, $c=7.26(1)$ Å, $Z=4$, $D_c=1.338$ g cm^{-3}, μ(Mo $K\alpha$)$=11.9$ cm^{-1}. The cell dimensions and diffraction intensities were measured at about −80 °C on a Hilger & Watts four-circle diffractometer with Zr-filtered Mo $K\alpha$ radiation ($\lambda=0.71069$ Å). The ω-2θ step-scan technique was applied at an ω interval of 0.02°; the counting time at each step was 1 s. The background was measured for 25 s at each end of the scan range. The intensities thus obtained were corrected for the Lorentz and polarization factors, but not for the absorption or the extinction effect. In the range of 2θ values up to 48°, 1786 independent structure-factor amplitudes above the $3\sigma(F)$ level were selected for the structure determination.

Structure Determination

The structure was solved by the Monte Carlo direct method,[6] using the 20 strongest reflections as a starting set. In order to extend the tentative-phase set derived from random numbers, 12 cycles of the tangent procedure were carried out using 489 $|E|$ values above 1.30. Since the first random-phase set gave a low R_K value of 0.142 ($R_K=\Sigma||E_o|-k|E_c||/\Sigma|E_o|$), 6 additional cycles of the tangent procedure were performed by the use of 761 $|E|$ values above 1.10. An *E*-map based on 757 phases afforded all the 31 non-hydrogen atoms. The structure thus obtained was refined by the block-diagonal least-squares method with

Table 1. The final atomic parameters and estimated standard deviations

Atom	$x(\times10^4)$	$y(\times10^4)$	$z(\times10^3)$	B_{eq}[a]/Å²
I	4069.8(6)	3637.0(5)	130.6(2)	4.61
O(1)	1994(5)	4951(3)	−86(1)	3.34
O(2)	1658(4)	4067(3)	59(1)	2.54
C(1)	1834(8)	3889(5)	−318(2)	3.42
C(2)	1141(7)	4219(6)	−233(2)	3.25
C(3)	1349(7)	4547(5)	−56(2)	2.95
C(4)	2712(7)	4617(5)	−51(2)	3.81
C(5)	2434(7)	3936(6)	−9(2)	2.92
C(6)	2840(6)	3629(6)	157(2)	2.93
C(7)	2522(7)	2965(6)	199(2)	3.40
C(8)	2421(7)	2548(6)	27(2)	2.69
C(9)	2008(7)	2870(5)	−125(2)	2.64
C(10)	2390(7)	3499(5)	−188(2)	2.99
C(11)	1896(7)	2415(5)	−294(2)	2.87
C(12)	1486(8)	1805(6)	−235(2)	3.04
C(13)	1897(6)	1473(5)	−71(2)	2.45
C(14)	1994(6)	1957(5)	84(2)	2.34
C(15)	2268(8)	1568(6)	245(2)	3.53
C(16)	1797(7)	923(6)	221(2)	3.28
C(17)	1439(6)	935(5)	28(2)	1.99
C(18)	2723(6)	1194(5)	−136(2)	3.28
C(19)	3141(7)	3395(6)	−289(2)	3.36
C(20)	1406(7)	269(5)	−58(2)	2.67
C(21)	1143(8)	291(6)	−262(2)	3.43
C(22)	901(9)	−126(5)	57(2)	2.82
C(23)	875(8)	−845(5)	5(2)	2.78
C(24)	390(6)	−1224(5)	140(2)	3.70
C(25)	442(7)	−1954(5)	106(3)	4.70
C(26)	219(9)	−2160(6)	−75(2)	5.97
C(27)	−35(9)	−2257(7)	261(3)	7.51
C(28)	740(8)	4889(6)	39(2)	4.39

a) $B_{eq}=8\pi^2(u_1^2+u_2^2+u_3^2)/3$, where u_i is the root-mean-square deviation in the i-th principal axis of the thermal ellipsoid.

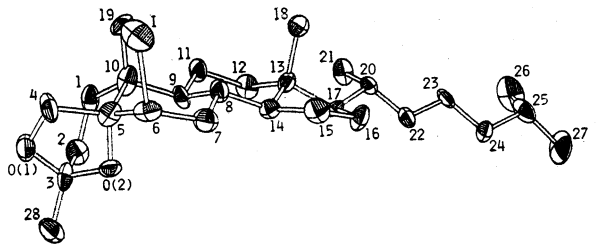

Fig. 1. A perspective view of the 3α,5-epoxy-6β-iodo-3β-methyl-*A*-homo-4-oxa-5α-cholestane molecule, and the numbering system of atoms.
Non-hydrogen atoms are represented as thermal ellipsoids enclosing 50% probabilities.

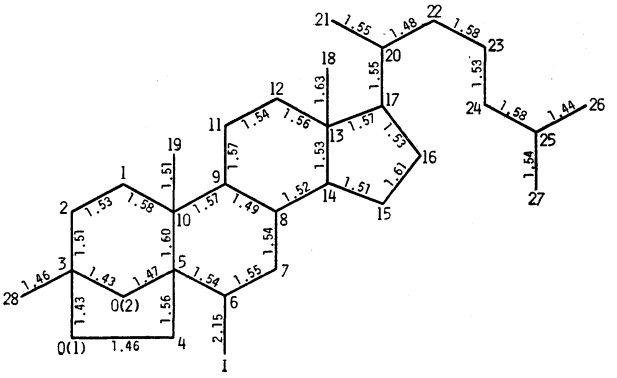

Fig. 2. The bond distances (*l*/Å).
The e.s.d.'s are 0.02—0.03 Å for C–C, 0.01—0.02 Å for C–O, and 0.01 Å for C–I.

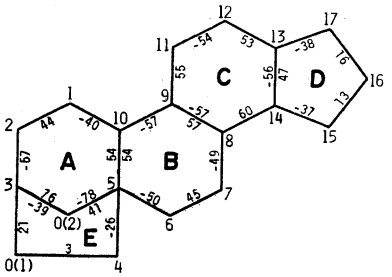

Fig. 3. The torsion angles (φ/°).
Only the torsion angles relevant to atoms which form the same ring are given in the ring.

anisotropic temperature factors. After 29 hydrogen atoms had been located in a difference Fourier map, further least-squares refinements were repeated including the hydrogen atoms with isotropic temperature factors. Since the absolute configuration of the present molecule was known,[3] the anomalous dispersion effects of the iodine atoms were included in these last refinements. The weighting scheme used was as follows:

$$w = 1/\{\sigma(F)^2 \exp(AX^2+BY^2+CXY+DX+EY)\},$$

where $X=|F_o|$ and $Y=\sin\theta/\lambda$. The *A*, *B*, *C*, *D*, and *E* coefficients are constants which were evaluated from the $(\Delta F)^2$ distribution in the (X,Y) space; $A=-0.1136\times10^{-5}$, $B=12.40$, $C=0.04025$, $D=-0.008957$, and $E=-12.24$. The final *R* value was 0.064. The final atomic parameters are listed in Table 1.[7]

The calculations were performed on a HITAC M-200H computer at the Hokkaido University Computing Center, using our own programs. The atomic scattering factors were taken from the International Tables.[8]

Results and Discussion

The molecular framework is shown in Fig. 1. It is concluded that the major product of the rearrangements of hypoiodites of 3α- and 3β-methyl-5-cholesten-3-ols has the **1** structure. The bond distances and torsion angles are given in Figs. 2 and 3, respectively. The A/B ring junction is cis. All the six-membered A-, B-, and C-rings take chair conformations, while the five-membered D- and E-rings adopt half-chair and envelope conformations respectively. The chair conformation of the A-ring is remarkably deformed by the bridging of the C(4)H_2–O(1) group so that the puckering of the C(3)–O(2)–C(5) part is great, whereas that of the C(2)–C(1)–C(10) part is small. Because of the occupation of the 1,3-diaxial positions on the B-ring, the C(19) and I atoms approach each other at a considerably shorter distance (3.49(1) Å) than the sum of their van der Waals radii, 4.15 Å. This severe steric hindrance results in an enlargement of the C(5)–C(10)–C(19) and C(9)–C(10)–C(19) bond angles (116-(1) and 113(1)° respectively) and a closing of the C(5)–C(6)–C(7)–C(8) torsion angle (45°). As Fig. 1 shows, the C(20)–C(22)–C(23)–C(24)–C(25)–C(27) side chain, together with the C(13) and C(17) ring atoms, takes a nearly-planar zigzag conformation.

We thank Professor Jiro Tanaka of Nagoya University for the generous permission to use a four-circle diffractometer.

References

1) Photo-induced Transformations. Part 64. Part 63: H. Suginome and A. Osada, *J. Chem. Soc., Perkin Trans. 1*, in press.
2) H. Suginome, A. Furusaki, K. Kato, N. Maeda, and F. Yonebayashi, *J. Chem. Soc., Perkin Trans. 1*, **1981**, 236.
3) H. Suginome and N. Maeda, *Bull. Chem. Soc. Jpn.*, **53**, 2621 (1980).
4) H. Suginome and N. Maeda, *Bull. Chem. Soc. Jpn.*, **53**, 2626 (1980).
5) H. Suginome, K. Kato, and T. Masamune, *Bull. Chem. Soc. Jpn.*, **54**, 3042 (1981).
6) A. Furusaki, *Acta Crystallogr., Sect. A*, **35**, 220 (1979).
7) The tables of the anisotropic temperature factors, hydrogen parameters, and bond angles, and the F_o-F_c table are kept at the Chemical Society of Japan (Document No. 8242).
8) "International Tables for X-Ray Crystallography," The Kynoch Press, Birmingham (1974), Vol. IV.

Regioselective Reaction of Allylic Carbanion Derived from 1-Phenylthio-2-octene with Conjugated Cyclopentenone Derivative and Synthesis of Prostaglandin E_1

Junzo NOKAMI,* Toshio ONO, Atsunori IWAO, and Shoji WAKABAYASHI
Okayama University of Science, Ridai, Okayama 700
(Received December 24, 1981)

Synopsis. The reaction of the allylic carbanion derived from 1-phenylthio-2-octene with conjugated cyclopentenone derivatives in the presence of hexamethylphosphoric triamide (HMPA) regioselectively gave the 1,4 adduct at the α carbon of the allylic sulfide. The reaction was employed for the synthesis of prostaglandin E_1.

There are many reports[1] on the regioselective reaction of allyl or allylic carbanions with electrophiles. Recently, Haynes *et al.*[2] reported HMPA-mediated conjugate addition of alkylthio(or phenylthio)allyl anion to cyclopentenone. We have also been interested in the reaction of the carbanion derived from 1-phenylthio(or 1-phenylsulfinyl)-2-octene with conjugated cycloalkenone,[3] because the phenylthio or phenylsulfinyl group shows versatility in functionalization associated with desulfurization.[4] In this report, we describe a synthesis of PG E_1 by using 1-phenylthio-2-octene (**1**) as an ω-side chain equivalent.

We have attempted to build the ω-side chain by the use of the sulfinyl carbanion derived from 1-phenylsulfinyl-2-octene (**2**). However, the reaction resulted in the formation of a mixture of 1,4-γ adduct **3a** (70%) and 1,2-α adduct **3b** (20%), and no additive effect of HMPA was observed.

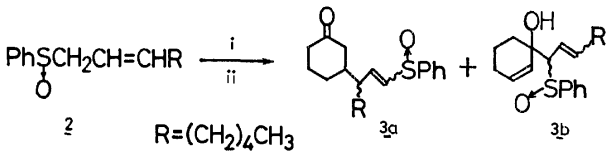

i) LDA, -78°C, THF; ii) cyclohexenone, -78°C, THF.

Fig. 1.

On the other hand, the reaction of the carbanion derived from **1** in the presence of HMPA gave 1,4 adduct as a sole product.[5] By applying this regioselective 1,4 addition of the carbanion to cyclopentenone derivative **4**, we have attempted the synthesis of PG E_1. The carbanion was prepared by the treatment of **1** with butyllithium at −45 °C. After a few minutes, HMPA and afterwards cyclopentenone derivative **4a** were added at −78 °C, and the mixture was kept for 5 min at that temperature. The reaction mixture was worked up to give the expected 1,4 adduct **5a** in 82% yield. The adduct **5a** was converted to allylic alcohol **7a** by a method similar to that reported.[6] Namely, **5a** was converted to sulfoxide **6a** by the oxidation using *m*-chloroperbenzoic acid at −10 °C in dichloromethane. After concentration, the residue was treated with trimethyl phosphite in methanol at 0 °C for 3 h to afford **7a** (*ca.* 1/1 mixture of 15-α/15-β) in 82% yield based on **5a**. Hydrolysis of **7a** in 1% acetonitrile solution of hydrofluoric acid at 0 °C gave methyl

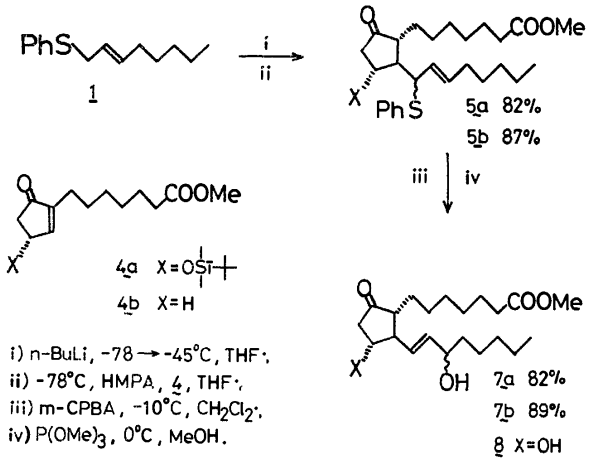

Fig. 2.

prostaglandin E_1 (**8**) (a mixture of 15-α and β) in 78% yield.

Experimental

Boiling points are uncorrected. IR spectra were determined with a Hitachi Model 260-30 spectrophotometer with a grating. ^{1}H NMR spectra were obtained with a Hitachi R-24B and/or a JEOL FX-100 spectrometers. Elemental analyses were carried out in this laboratory.

1-Phenylthio-2-octene (1). A mixture of 1-octene (28 ml, 0.179 mol), *N*-bromosuccinimide (22.7 g, 0.128 mol) and a catalytic amount of benzoyl peroxide was refluxed in carbon tetrachloride for 5 h under nitrogen. The reaction mixture was cooled and insoluble materials were filtered off. The concentrated filtrate was purified by column chromatography on alumina by elution with hexane to give a mixture of 1-bromo-2-octene and 3-bromo-1-octene (3:1) in 98% yield. The mixture of bromooctene (17.8 g, 0.093 mol) was treated with benzenethiol (6.75 ml, 0.066 mol) and sodium carbonate (14 g, 0.132 mol) in acetone with gentle heating. After 5 h, the reaction mixture was cooled and filtered. The filtrate was concentrated and washed with brine. Pure **1** was obtained by distillation in 80% yield, 101 °C/0.25 Torr†; NMR (CCl_4) δ 0.86 (m, 3H), 1.22 (m, 6H), 1.96 (m, 2H), 3.47 (m, 2H), 5.47 (m, 2H), 7.2 (m, 5H). The ratio of *E* and *Z* isomers was not determined.

1-Phenylsulfinyl-2-octene (2). Sulfide **1** was treated with sodium periodate (slight excess) in aqueous methanol at room temperature for 10 h. The reaction mixture was concentrated and extracted with chloroform. The extract was washed with brine, dried, and concentrated. The residue was chromatographed (SiO_2, hexane/ether, 1/1) to give **2** quantitatively; IR (neat) 1045 cm^{-1} (S–O); NMR ($CDCl_3$) δ 0.85 (m, 3H), 1.21 (m, 6H), 3.32 (m, 2H), 5.27 (m, 2H), 7.34 (broad s, 5H).

Reaction of Sulfinyl Carbanion with Cyclohexenone to 3a and 3b. 1-Phenylsulfinyl-2-octene (**2**) (0.1 ml, 0.47 mmol)

† 1 Torr ≈ 133.322 Pa.

was treated with lithium diisopropylamide (prepared from 0.6 mmol of diisopropylamine and 0.4 ml of butyllithium (1.56 mol dm^{-3} in hexane)) in THF at −78 °C for 30 min. 2-Cyclohexenone (0.05 ml, 0.5 mmol) was added to the reaction mixture, which was stirred for 5 min, poured into saturated aqueous ammonium chloride, and extracted with chloroform. After concentration of the extract, the residue was chromatographed on silica gel with hexane/ether (1/4) to give two major products. The less polar product could be assigned to **3b** (31 mg, containing *ca.* 10% non-isolated impurity); IR (neat) 3400 (O–H), 1010 (S–O) cm^{-1}; NMR ($CDCl_3$) δ 3.44 (m, 1H, S–CH–C=C), 4.80—6.20 (m, 4H, 2 CH=CH), 7.5 (m, 5H, phenyl). The polar product was assigned to **3a** (109 mg, 70%); IR (neat) 1705 (C=O), 1040 (S–O) cm^{-1}; NMR ($CDCl_3$) δ 0.84 (m, 3H), 1.0—2.4 (m, 18H), 6.30 (m, 2H, CH=CH–S), 7.51 (m, 5H, phenyl). Found: C, 72.33; H, 8.74%. Calcd for $C_{20}H_{28}O_2S$: C, 72.25; H, 8.49%.

Similar Reaction of the Sulfinyl Carbanion with ***4b*** gave 1,4-γ adduct **9** as the major product (*ca.* 60% yield); IR (neat) 2930, 1730 (C=O), 1040 (S–O), 1020 cm^{-1}; NMR ($CDCl_3$) δ 0.86 (m, 3H), 1.0—2.5 (m, 27H), 3.53 (s, 3H, $COOCH_3$), 6.10 (m, 2H, S–CH=CH), 7.36 (broad s, 5H, phenyl).

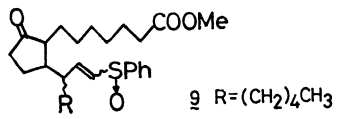

9 R=$(CH_2)_4CH_3$

Fig. 3.

Reaction of Sulfenyl Carbanion Derived from ***1*** *with* ***4a*** *to* ***5a***. Butyllithium (0.2 ml, 1.56 mol dm^{-3} in hexane) was added to a stirred solution of **1** (67 mg, 0.3 mmol) in THF (2 ml) at −78 °C. The reaction mixture was warmed to −45 °C during 40—50 min, and recooled to −78 °C. Then, HMPA (0.13 ml, 0.76 mmol) and afterward **4a** (90 mg, 0.25 mmol, 0.2 ml of THF solution) were added at −78 °C. After 5-min stirring at that temperature, water was added to the reaction mixture, which was extracted with ether immediately. The extract was washed with brine, dried, and concentrated. The residue was submitted to column chromatography on silica gel (hexane/ether, 1/1) to give a 1:1 diastereomeric mixture of **5a** (120 mg, 82%) as an oil; IR (neat) 2940, 2860, 1735 (C=O), 1460, 1250, 830 cm^{-1}; NMR ($CDCl_3$) δ 0.08 (m, 6H, $Si(CH_3)_2$), 0.84 (m, 3H, CH_3), 0.87 and 0.89 (each s, 9H, $SiC(CH_3)_3$), 1.0—2.7 (m, 24H), 3.65 (s, 3H, $COOCH_3$), 3.90 (m, 1H, S–CH–C=C), 4.40 (m, 1H, O–CH), 5.38 (m, 2H, CH=CH), 7.27 (m, 5H, phenyl). Found: C, 68.72; H, 9.51%. Calcd for $C_{33}H_{54}O_4SSi$: C, 68.94; H, 9.47%.

Similarly, **5b** was obtained from **4b**; IR (neat) 2950, 2870, 1735 (C=O), 1590, 1470, 1180, 1030 cm^{-1}; NMR ($CDCl_3$) δ 0.76 (m, 3H), 0.9—2.6 (m, 26H), 3.54 (s, 3H, $COOCH_3$), 3.56 (m, 1H, S–CH–C=C), 5.20 (m, 2H, CH=CH), 7.18 (m, 5H, phenyl).

Conversion of ***5a*** *to* ***7a***. The adduct **5a** (66 mg, 0.115 mmol) was treated with *m*-chloroperbenzoic acid (80%, 25 mg) in dichloromethane at −10 °C for 2 h. The reaction mixture was concentrated *in vacuo*. The residue was dissolved in methanol (1.5 ml), and treated with trimethyl phosphite (0.03 ml) at 0 °C for 3 h. After removal of the solvent, the residue was submitted to column chromatography on silica gel to yield *ca.* 1:1 of diastereomeric mixture of **7a** (45 mg, 82%); IR (neat) 3500 (O–H), 2860, 1735 (C=O), 1460, 1250, 1110, 830 cm^{-1}; NMR ($CDCl_3$) δ 0.08 (m, 6H, $Si(CH_3)_2$), 0.90 (m, 3H), 0.91 (s, 9H, $SiC(CH_3)_3$), 1.0—2.8 (m, 24H), 3.70 (s, 3H, $COOCH_3$), 4.10 (m, 2H, 2 O–CH), 5.64 (m, 2H, CH=CH). Found: C, 67.35; H, 10.54%. Calcd for $C_{27}H_{50}O_5Si$: C, 67.17; H, 10.44%.

Deprotection of ***7a*** *to* ***8***. To a solution of 28 mg of **7a** (diastereomeric mixture) in 2 ml of acetonitrile was added 0.5 ml of highly diluted hydrofluoric acid (5% acetonitrile solution of commercial HF (45%)) at 0 °C and the reaction mixture was stirred for 2 h to give **8** (78% yield) which was separated by column chromatography on silica gel (cyclohexane/ethyl acetate, 1/2) into two parts. The polar product (8.5 mg) was identified as PG E_1 by TLC comparison with an authentic sample and the less polar product (7 mg) was shown to be 15-epi PG E_1.

We thank Teijin Co. for the gift of an authentic sample. This research was supported by the Hattori Foundation.

References

1) M. Ono, *Yvki Gosei Kagaku Kyokai Shi*, **38**, 836, 923 (1980), and references cited therein; M. El-Bouz and L. Wartski, *Tetrahedron Lett.*, **21**, 2897 (1980); M. Hirama, *ibid.*, **22**, 1905 (1981).

2) M. R. Binns, R. K. Haynes, T. L. Houston, and W. R. Jackson, *Tetrahedron Lett.*, **21**, 573 (1980); M. R. Binns and R. K. Haynes, *J. Org. Chem.*, **46**, 3790 (1981).

3) J. Nokami, T. Ono, and S. Wakabayashi, the 44th National Meeting of the Chem. Soc. Jpn., Okayama, October 1981, Abstract II, 554.

4) B. M. Trost, *Acc. Chem. Res.*, **11**, 453 (1978); *Chem. Rev.*, **78**, 363 (1978).

5) Treatment of the carbanion with 2-cyclohexenone in the absence of HMPA gave a mixture of 1,4-α (37%), 1.2-γ (44%), and 1,2-α (18%) adducts.

6) K. Kondo, T. Umemoto, Y. Takahatake, and D. Tunemoto, *Tetrahedron Lett.*, **1977**, 113; K. Kondo, T. Umemoto, K. Yako, and D. Tunemoto, *ibid.*, **1978**, 3927.

A One Step Transformation of the Sodium Salt of α-*aci*-Nitrotoluene into 3,4,5-Triphenylisoxazole

Kimitoshi FUKUNAGA,* Akihiko OKAMOTO,† Keiji FURUMOTO,† and Makoto KIMURA

Faculty of Engineering, Yamaguchi University, Tokiwadai, Ube, Yamaguchi 755

† *Oshima National Mercantile Marine College, Komatsu, Oshima-cho, Yamaguchi 742-21*

(Received January 29, 1982)

Synopsis. 3,4,5-Triphenylisoxazole was produced by the reaction of the sodium salt of α-*aci*-nitrotoluene with the 1-cyano-1-methylethyl radical. The reaction was found to proceed *via* one electron transfer from α-*aci*-nitrotoluene anion to a 1-cyano-1-methylethyl radical.

Although a great number of works have been published on the reactivity of the 1-cyano-1-methylethyl radical,[1] little was known of their one electron transfer reactions.[2] We now report chemical evidence to support that one electron transfer is involved in the reaction of the 1-cyano-1-methylethyl radical generated by decomposition of 2,2'-azobisisobutyronitrile (AIBN) with the sodium salt of α-*aci*-nitrotoluene (**1**).

When a mixture of **1** and AIBN was heated in dimethyl sulfoxide (DMSO) at a bath temperature of 40—80 °C for 2—3 h, a crystalline product was obtained. The structure was confirmed to be 3,4,5-triphenylisoxazole (**2**) by the analysis of the spectra and a mixed melting point determination. From a number of experiments, it was found that the formation of **2** was accelerated with increasing of the reaction temperature (see Table 1). The kinetics of the decomposition of AIBN was studied in various solvents by Kulkarni *et al.*[3] They suggested that AIBN does not decompose to 1-cyano-1-methylethyl radical up to a temperature of 40 °C, that the formation of the radical from AIBN follows first order kinetics and that the rate constant is directly proportional to the reaction temperature. The dependence of the efficiency of this reaction on the reaction temperature correlates well with the dependence of the formation of 1-cyano-1-methylethyl radical on the reaction temperature. These facts imply that this reaction is initiated by thermal evolution of 1-cyano-1-methylethyl radical but not by one electron transfer from **1** to AIBN.

Analogous formation of 3,4,5-triphenyl-2-isoxazoline *N*-oxide (**3**) has been observed in the reaction of **1** with 2-bromo-2-nitropropane in DMSO at room temperature, for which a mechanism involving one electron transfer from **1** to 1-methyl-1-nitroethyl radical has been proposed.[4] In the reaction of **1** with 1-cyano-1-methylethyl radical, a similar mechanism should operate.

The above assumptions were strongly suggested by the fact that the reaction of **1** with 2-bromo-2-nitropropane under conditions similar to those employed for the reaction of **1** with AIBN resulted in the exclusive formation of **2** (see Experimental). It is surprising that relatively mild heating (70 °C, 2 h) of **3** in the reaction mixture afforded **2**, because it has been known that heating of **3** in a boiling ethanolic sodium hydroxide solution or without solvent under a reduced

Table 1. Reactions of sodium salt of α-*aci*-nitrotoluene (**1**) with AIBN[a]

Run	Amount of AIBN/mmol	Temp/°C	Time/h	Yield of **2**[b]/%
1	25	25	6	trace
2	5	40	6	4
3	15	40	3	12
4	25	40	3	16
5	25	70	2	25
6	25	80	2	26
7[c]	25	70	2	25

a) All the reactions were carried out using 3.95 g (25 mmol) of **1** in DMSO (25 ml). b) Pure isolated yield on **1**. c) The reaction was carried out under nitrogen.

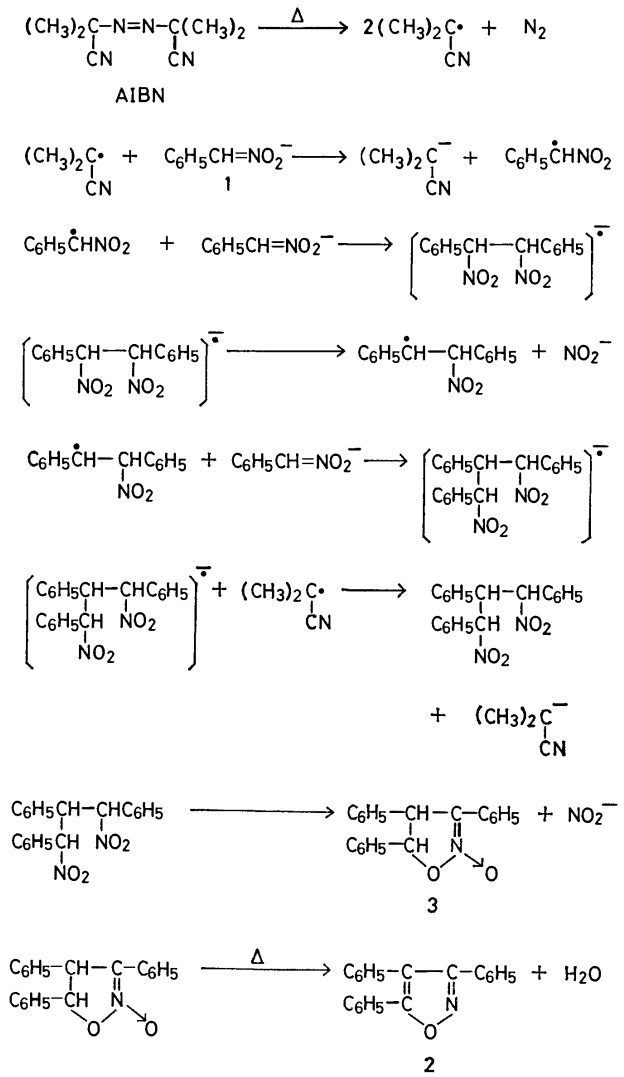

Scheme 1.

pressure above its melting point give rise to **2**.[5] Thus, reactions of 1-methyl-1-nitroethyl radical and 1-cyano-1-methylethyl radical with **1** give essentially the same product. The process outlined in Scheme 1 may explain the formation of **2**: here an intermolecular cyclization of the resulting 1,3-dinitro-1,2,3-triphenylpropane could lead to **3** which give **2** by thermal dehydration.

It is well known that the scope of the S_{RN} 1 reaction involving the 1-methyl-1-nitroethyl radical is limited by the competition between reaction (1) (leading to substitution) and reaction (2) (leading to the 2-nitropropane dimer) as shown in Scheme **2**.

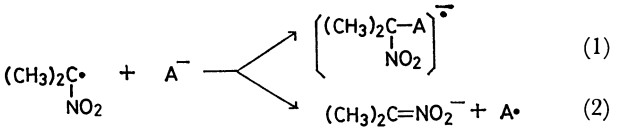

Scheme 2.

When the anion A^- contains a conjugated phenyl group which can lead to a substituted benzyl radical A, reaction (2) greatly predominates.[6] This may be the reason why 2-bromo-2-nitropropane fails to yield cross-coupling product with **1**.[4]

In order to generalize the preparative route for isoxazoles from nitroalkane, similar reactions of anions of *aci*-nitroalkanes, such as the lithium salt of *aci*-2-nitropropane or *aci*-nitrocyclohexane, with AIBN were studied. However, the reactions under comparable conditions were unsuccessful.

Apparently similar to 1-methyl-1-nitroethyl radical, the 1-cyano-1-methylethyl radical has a sufficiently high electron affinity that electron transfer take preference to the addition reaction. Thus, trapping of the radical A· by the anion A^- is greatly facilitated by the presence of phenyl and nitro groups which will stabilize the resulting radical anion $[A\text{–}A]^{\cdot-}$.

Experimental

General. Melting points were determined in capillary tubes in a liquid bath and are uncorrected. The IR spectra were recorded with a Hitachi 215 grating spectrophotometer. Mass spectra were determined with a Hitachi RMU-6C spectrometer.

Materials. Commercial DMSO was distilled prior to use. Commercial AIBN was recrystallized from methanol. The sodium salt of α-*aci*-nitrotoluene was prepared by addition of methanol solution of phenylnitromethane[7] to an equivalent amount of sodium methoxide in methanol. 2-Bromo-2-nitropropane was prepared as described previously.[4]

General Procedure for Reaction of 1 with AIBN: To a stirred suspension of **1** (3.95 g, 25 mmol) in DMSO (25 ml), AIBN (4.11 g, 25 mmol) was added in portions at 40 °C and the mixture was stirred at 70 °C for 2 h. The mixture was then poured into cold water to give a slightly yellow precipitate, which was collected by filtration, washed with water and dried. To the solid thus obtained methanol (30 ml) was added and the mixture was heated under reflux for 0.5 h, and then cooled to room temperature. The solid was again collected by filtration and recrystallized from ethanol to give **2** as colorless needles in 25% yield; mp 209—210 °C (lit,[8] mp 212 °C); MS 297.4 (M^+); IR (KBr) 1430, 1400, 920 cm^{-1} (C=C), 1210, 1010 cm^{-1} (–O–).

Reaction of 1 with 2-Bromo-2-nitropropane: To a stirred suspension of **1** (3.95 g, 25 mmol) in DMSO (25 ml), 2-bromo-2-nitropropane (2.10 g, 12.5 mmol) was added dropwise at room temperature. The resulting solution was stirred at 70 °C for 2 h, and then poured into cold water. The mixture was extracted with chloroform (100 ml). The extract was washed with water, dried over magnesium sulfate, and concentration gave a solid material. The crude material was twice recrystallized from ethanol to give **2** in 24% yield.

The authors wish to thank Dr. Hachiro Yamaguchi, Hiroshima University, for useful suggestions. The present work was supported by Grant-in-Aid for Scientific Research No. 575546 from the Ministry of Education, Science and Culture.

References

1) U. Schmidt and A. Muller, *Ann. Chem.*, **672**, 90 (1964); H. Iwamura, M. Iwamura, and K. Kushida, *Bull. Chem. Soc. Jpn.*, **44**, 876 (1971); T. Mitsuhashi and M. Ōki, *Chem. Lett.*, **1978**, 1089.

2) H. Fujihara, S. Fuke, M. Yoshida, and T. Maeshima, *Chem. Lett.*, **1981**, 1271.

3) M. G. Kulkarni, R. A. Mashelkar, and L. K. Doraiswamy, *Chem. Eng. Sci.*, **35**, 823 (1980).

4) K. Fukunaga, *Synthesis*, **1978**, 58; K. Fukunaga and M. Kimura, *Nippon Kagaku Kaishi*, **1982**, 1499.

5) E. P. Kohler and G. R. Barrett, *J. Am. Chem. Soc.*, **46**, 1733 (1924).

6) G. A. Russell, M. Jawdosiuk, and M. Makosza, *J. Am. Chem. Soc.*, **101**, 2355 (1979); G. A. Russell, B. Mudryk, and M. Jawdosiuk, *Synthesis*, **1981**, 62.

7) A. P. Black and F. H. Bakers, *Org. Synth.*, Coll. Vol. II, 512 (1943).

8) H. Wieland and E. Blümich, *Ann. Chem.*, **424**, 75 (1921).

A New Synthesis of (*Z*)-13-Eicosen-10-one and (*Z*)-12-Nonadecen-9-one, the Pheromones of Peach Fruit Moth

Takashi Yoshida* and Shojiro Saito

Department of Industrial Chemistry, Faculty of Engineering, Meiji University, Tama-ku, Kawasaki 214

(Received February 4, 1982)

Synopsis. (*Z*)-13-Eicosen-10-one and (*Z*)-12-nonadecen-9-one were easily synthesized from starting 1-(*p*-tolylsulfonyl)nonane and 1-(*p*-tolylsulfonyl)octane *via* 4 steps, respectively.

It is known that (*Z*)-13-eicosen-10-one (**5a**) and (*Z*)-12-nonadecen-9-one (**5b**) are the pheromones of Japanese peach fruit moth (*Carposia niponensis* Walshingham),[1] and that a mixture of **5a** and **5b** in the ratio of 20:1 has the strongest biological activity.[2] Three examples for the preparation of the pheromones have been reported: (i) the addition of 4-undecynal prepared from 3-bromo-1-propanol to nonylmagnesium bromide;[1] (ii) the addition of 3-decynenitrile to nonylmagnesium bromide;[3] (iii) the alkylation of diethyl 3-oxoglutarate.[4]

In previous papers, we reported the synthesis of the jasmonoids and 2,15-hexadecanedione using sulfones, such as *cis*-1-(*p*-tolylsulfonyl)-3-hexene,[5] 1-(*p*-tolylsulfonyl)hexane,[5] 1,1-ethylenedioxy-3-(*p*-tolylsulfonyl)cyclopentane,[6] and 1,6-bis(*p*-tolylsulfonyl)hexane.[7] In this paper, we wish to describe a new and simple synthesis of (*Z*)-13-eicosen-10-one (**5a**) and (*Z*)-12-nonadecen-9-one (**5b**) by the condensation of sulfones with ester,[8] followed by desulfonylation[9] and salt-free Wittig reaction.[10]

The synthesis of the title compounds, **5a** and **5b**, were carried out as follows.

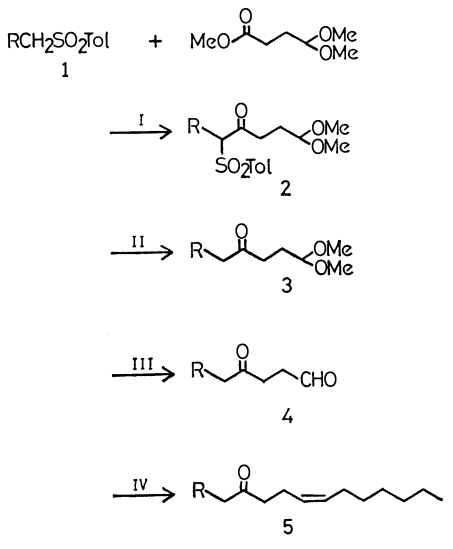

a: R = C_8H_{17}; b: R = C_7H_{15}

I: LDA, -78°C; II: Al(Hg), 10% aq THF; III; H_3O^+; IV: hepthyltriphenylphosphonium bromide

The condensation of the dianion of 1-(*p*-tolylsulfonyl)nonane (**1a**) generated with two equivalents of lithium diisopropylamide (LDA) with methyl 4,4-dimethoxybutanoate gave 1,1-dimethoxy-5-(*p*-tolylsulfonyl)-4-tridecanone (**2a**) in quantitative yield. The treatment of the sulfone **2a** with aluminium amalgam in 10% aqueous THF afforded 1,1-dimethoxy-4-tridecanone (**3a**) in 69% yield. The acetal **3a** was acidified with 5% hydrochloric acid to give 4-oxotridecanal (**4a**) in 81% yield. The salt-free Wittig reagent prepared from heptyltriphenylphosphonium bromide and sodium amide was added to a solution of **4a** in benzene to give (*Z*)-13-eicosen-10-one (**5a**) in 54% yield. (*Z*)-12-Nonadecen-9-one (**5b**) was synthesized from 1-(*p*-tolylsulfonyl)octane (**1b**) in the same procedure. The resulting products, **5a** and **5b**, had no infrared absorption band at 970 cm^{-1} region due to disubstituted trans-alkene. The structure of these products was identified by comparing their IR and NMR spectra with those of the reported data.[3,4] In conclusion, the method described above, compared with other methods, has various advantages: the starting sulfones are readily available, processes are short, simple, and easy, and the reaction proceeds smoothly to form the product in relatively good yield.

Experimental

Melting and boiling points are uncorrected. Melting points were taken on a Yanagimoto micro melting point apparatus. Infrared spectra were measured on a Shimazu IR-27G spectrophotometer. ^{1}H-NMR spectra were recorded on a Varian EM-390 spectrometer at 90 MHz, using TMS (δ=0.00 ppm) as an internal standard.

*1-(*p*-Tolylsulfonyl)nonane (**1a**) and 1-(*p*-Tolylsulfonyl)octane (**1b**).* 1-Bromononane (20 g, 0.097 mol) was added to a stirred solution of sodium *p*-toluenesulfinate tetrahydrate (30 g, 0.12 mol) in methanol (100 ml). The mixture was stirred under reflux for 6 h. After the removal of methanol, the residue was poured onto 300 ml of water. The organic layer was extracted with ethyl acetate. The extract was washed with water, dried over anhydrous sodium sulfate, and concentrated to give **1a** as a solid substance. Recrystallization from methanol–water afforded 26 g (95% yield) of **1a**, mp 51.4—51.5 °C. IR ($CHCl_3$): 2950, 1600, 1470, 1315, 1140 cm^{-1}. NMR (CCl_4): δ 0.75—1.05 (3H, br t, J=5.4 Hz), 1.1—1.5 (12H, br s), 1.5—1.8 (2H, br s), 2.47 (3H, s), 2.8—3.1 (2H, m), 7.38, 7.84 ppm (4H, an A_2B_2 pattern, J=7.5 Hz). Found: C, 68.37; H, 9.23%. Calcd for $C_{16}H_{26}O_2S$: C, 68.04; H, 9.26%. 1-(*p*-Tolylsulfonyl)-octane (**1b**) was obtained from 1-bromooctane (20 g, 0.10 mol) and sodium *p*-toluenesulfinate tetrahydrate (30 g, 0.12 mol) in methanol (100 ml) in the same procedure, mp 34.4—34.5 °C. IR ($CHCl_3$) 2950, 1600, 1470, 1320, 1150 cm^{-1}. NMR (CCl_4) δ 0.7—1.05 (3H, br t, J=5.4 Hz), 1.1—1.8 (12H, br s), 2.43 (3H, s), 2.8—3.1 (2H, m), 7.31, 7.75 ppm (4H, an A_2B_2 pattern, J=7.5 Hz). Found: C, 67.88; H, 8.82%. Calcd for $C_{15}H_{24}O_2S$: C, 67.12; H, 9.00%.

*1,1-Dimethoxy-5-(*p*-tolylsulfonyl)-4-tridecanone (**2a**) and 1,1-Dimethoxy-5-(*p*-tolylsulfonyl)-4-dodecanone (**2b**).* To lithium diisopropylamide (LDA) prepared from *n*-BuLi (15%

hexane solution, 6.0 g, 0.014 mol) and diisopropylamine (1.5 g, 0.015 mol) in dry THF (15 ml) was added a solution of **1a** (2.0 g, 0.007 mol) in dry THF (15 ml) at −78 °C under nitrogen. After the mixture was stirred for 1 h, methyl 4,4-dimethoxybutanoate (1.3 g, 0.008 mol) in dry THF (15 ml) was added. The mixture was stirred for 1 h at −78 °C and for an additional 3 h at room temperature. The mixture was poured onto cold 2% sulfuric acid. The organic layer was extracted with ethyl acetate. The extract was washed with water, dried over anhydrous sodium sulfate, and concentrated to give **2a** as a pale yellow viscous liquid in quantitative yield. The compound **2a** was purified by column chromatography over silica gel (60—80 mesh) with benzene as eluent to give white needles, mp 48.5—49.5 °C. IR (neat): 2900, 1720, 1600, 1470, 1320, 1150, 1080 cm^{-1}. NMR (CCl_4): δ 0.75—1.0 (3H, br t, J=5.4 Hz), 1.0—1.4 (12H, br s), 1.6—2.0 (4H, m), 2.35—3.15 (2H, m), 2.46 (3H, s), 3.35 (6H, s), 3.96 (1H, t, J=6.9 Hz), 4.33 (1H, t, J=6.0 Hz), 7.34, 7.66 ppm (4H, an A_2B_2 pattern, J=8.1 Hz). Found: C, 64.17; H, 8.73%. Calcd for $C_{22}H_{36}O_5S$: C, 64.05; H, 8.79%. 1,1-Dimethoxy-5-(*p*-tolylsulfonyl)-4-dodecanone (**2b**) was obtained from 1-(*p*-tolylsulfonyl)-octane (**1b**) (2.0 g, 0.007 mol) and methyl 4,4-dimethoxybutanoate (1.3 g, 0.008 mol) in quantitative yield, mp 41.5—42.5 °C. IR (neat): 2850, 1710, 1600, 1470, 1300, 1150, 1090 cm^{-1}. NMR (CCl_4): δ 0.75—1.0 (3H, br t, J=5.4 Hz), 1.0—1.4 (10H, br s), 1.6—2.0 (4H, m), 2.35—3.15 (2H, m), 2.45 (3H, s), 3.35 (6H, s), 3.96 (1H, t, J=6.9 Hz), 4.33 (1H, t, J=6.0 Hz), 7.34, 7.66 ppm (4H, an A_2B_2 pattern, J=8.1 Hz). Found: C 63.22; H 8.77%. Calcd for $C_{21}H_{34}O_5S$: C, 63.29; H, 8.60%.

*1,1-Dimethoxy-4-tridecanone (**3a**) and 1,1-Dimethoxy-4-dodecanone (**3b**).* To a stirred solution of **2a** (2.0 g, 4. 8mmol) in 10% aq. THF (60 ml) was added aluminium amalgam (1.5 g, 55.5 mmol). The mixture was stirred for 4 h at room temperature and then filtered. The filtrate was extracted with ethyl acetate. The extract was washed with water, dried over anhydrous sodium sulfate, and concentrated to give **3a** as a pale yellow liquid. The compound **3a** was purified by column chromatography over silica gel (60—80 mesh) with benzene–hexane (7:3) as eluent to give 0.86 g (69% yield) of **3a** as a colorless liquid. IR (neat): 2950, 1720, 1470, 1360, 1190, 1130, 1060 cm^{-1}. NMR (CCl_4): δ 0.8—1.05 (3H, br t, J=5.4 Hz), 1.1—1.9 (16H, m), 2.2—2.5 (4H, m), 3.25 (6H, s), 4.27 ppm (1H, t, J=6.0 Hz). 1,1-Dimethoxy-4-dodecanone (**3b**) was obtained from **2b** (2.0 g, 5.0 mmol) in the same procedure. IR (neat): 2900, 1720, 1460, 1360, 1190, 1120, 1060 cm^{-1}. NMR (CCl_4): δ 0.75—1.1 (3H, br t, J=5.4 Hz), 1.2—1.95 (14H, m), 2.3—2.55 (4H, m), 3.28 (6H, s), 4.33 ppm (1H, t, J=6.0 Hz).

*4-Oxotridecanal (**4a**) and 4-Oxododecanal (**4b**).* The acetal **3a** (0.6 g, 2.3 mmol) was added to 5% hydrochloric acid (5 ml) and the mixture was stirred for 5 h at 50 °C. The organic layer was extracted with ethyl acetate. The extract was washed with water, dried over anhydrous sodium sulfate, and concentrated to give **4a** as a pale yellow liquid. Compound **4a** was purified by column chromatography over silica gel (60—80 mesh) with benzene–hexane (5:5) as eluent to give 0.4 g (81% yield) of pure **4a** as a colorless liquid. IR (neat): 2900, 1730, 1710, 1470, 1410, 1090 cm^{-1}. NMR (CCl_4): δ 0.75—1.1 (3H, br t, J=5.4 Hz), 1.1—1.75 (14H, br s), 2.46 (2H, t, J=6.0 Hz), 2.73 (4H, s) 9.88 ppm (1H, s). 4-Oxododecanal (**4b**) was obtained from **3b** (1.0 g, 4.4 mmol) in the same procedure in 75% yield. IR (neat): 2900, 1730, 1710, 1470, 1400, 1090 cm^{-1}. NMR (CCl_4): δ 0.75—1.0 (3H, br t, J=5.4 Hz), 1.0—1.6 (12H, br s), 2.35 (2H, t, J=6.0 Hz), 3.60 (4H, s), 9.70 ppm (1H, s).

*(Z)-13-Eicosen-10-one (**5a**) and (Z)-12-Nonadecen-9-one (**5b**).* Sodium amide (0.1 g, 2.5 mmol) was added to a stirred solution of heptyltriphenylphosphonium bromide (0.4 g, 1.1 mmol) in dry benzene (50 ml) under nitrogen atmosphere. The temperature of the suspension was then slowly raised to the reflux temperature of benzene. The reaction mixture was stirred for 8 h under reflux. Stirring was discontinued and then the reaction mixture was cooled to room temperature. The upper layer (benzene phosphorane solution, Crystal Violet color) was separated by a syringe. The phosphorane was added to a stirred solution of (**4a**) (0.2 g, 0.87 mmol) in benzene (50 ml) over 0.5 h at room temperature. Stirring was continued for 15 h more at room temperature. Benzene was distilled under reduced pressure and hexane was poured onto the residue. The mixture was filtered and the filtrate was washed with 5% hydrochloric acid, brine, and dried over anhydrous sodium sulfate. Concentration of the hexane gave the crude product. This crude product was chromatographed over silica gel (60—80 mesh) with hexane–benzene (7:3) as eluent to give 0.14 g (54% yield) of **5a** as a pale yellow liquid. IR (neat): 2930, 1710, 1470, 1430, 1370, 1090 cm^{-1}. NMR (CCl_4): δ 0.7—1.0 (6H, br t, J=5.4 Hz), 1.1—1.7 (22H, br s), 1.9—2.15 (2H, m), 2.2—2.45 (6H, m), 5.2—5.45 ppm (2H, m). (*Z*)-12-Nonadecen-9-one (**5b**) was obtained from **4b** (0.2 g, 0.93 mmol) in the same procedure. IR (neat): 2950, 1710, 1460, 1370 cm^{-1}. NMR (CCl_4): δ 0.7—1.0 (6H, br t, J=5.4 Hz), 1.1—1.7 (20H, br s), 1.9—2.15 (2H, m), 2.2—2.45 (6H, m), 5.15—5.4 ppm (2H, m).

We wish to thank Dr. Tetsuo Miyakoshi and Mr. Hiroaki Omichi of Meiji University for their useful discussions and valuable suggestions.

References

1) Y. Tamaki, K. Honma, and K. Kawasaki, *Appl. Entmol. Zool.*, **12**, 60 (1977).
2) S. Shirasaki, M. Yamada, R. Saito, K. Yanaginuma, M. Kumakura, and Y. Tamaki, *Nippon Oyo Dobutsu Konchu Gakkai Shi*, **23**, 240 (1979).
3) S. Tamada, K. Mori, and M. Matsui, *Agric. Biol. Chem.*, **42**, 191 (1978).
4) Y. Naoshima, M. Kawakubo, S. Wakabayashi, and S. Hayashi, *Agric. Biol. Chem.*, **45**, 439 (1981).
5) T. Yoshida and S. Saito, submitted for publication in *Yukagaku*.
6) T. Yoshida, T. Miyakoshi, H. Omichi, and S. Saito, Preprint of Meeting Vol. II, 41st National Meeting of the Chemical Society of Japan, Osaka, April 1980, p. 1036.
7) T. Yoshida and S. Saito, submitted for publication in *Yukagaku*.
8) H. Stetter and R. Hesse, *Monatsh. Chem.*, **98**, 755 (1967).
9) E. J. Corey and M. Chaykovsky, *J. Am. Chem. Soc.*, **86**, 1639 (1964).
10) P. Teisseire and M. Rinaldi (Lab. Rech. Usine, Grasse, France), *Recherches (Paris)*, **13**, 4 (1963).

Studies on 2-Aziridinecarboxylic Acid. VI.[1] Synthesis of β-Alkoxy-α-Amino Acids *via* Ring-opening Reaction of Aziridine

Kiichiro NAKAJIMA, Masahiro NEYA, Shinichi YAMADA, and Kenji OKAWA*

Department of Chemistry, Faculty of Science, Kwansei Gakuin University, Nishinomiya 662

(Received February 12, 1982)

Synopsis. The reaction of aziridine derivatives having a urethane-type protecting group with several alcohols in the presence of boron trifluoride etherate afford the corresponding optically pure *O*-alkylserine and *O*-alkylthreonine derivatives *via* a ring-opening reaction of aziridine in good yield.

In 1976, we reported that *N*-aminoacyl 2-aziridinecarboxylic acid derivatives, *e.g.*, Z-Gly-(2*S*)-Azy-Gly-OBzl, were coverted into the corresponding *O*-alkylserine peptide by the reaction of several alcohols in the presence of boron trifluoride etherate.[2] The yields, however, were usually very poor.

In this communication, we describe the results of aziridine derivatives having a urethane-type protecting group, benzyl (2*S*)-1-benzyloxycarbonyl-2-aziridinecarboxylate[(2*S*)-Z-Azy-OBzl(**1**)] and methyl (2*S*,3*S*)-1-benzyloxycarbonyl-3-methyl-2-aziridinecarboxylate [(2*S*,3*S*)-Z-3-MeAzy-OMe(**2**)], with several alcohols. **1** and **2** were synthesized according to our previous report.[3,4]

(2*S*)-Z-Azy-OBzl(**1**) and (2*S*,3*S*)-Z-3-MeAzy-OMe (**2**) were very stable in alcoholic solution at a room temperature, even under heating and no ring-opening reaction of the aziridine residue with alcohols was observed. However, if a catalytic amount of boron trifluoride etherate was added to the alcoholic solution of the aziridine derivatives, the reaction occurred easily to give the corresponding *O*-alkylserine(**3**—**9**) and -threonine(**10**—**16**) derivatives in good yield as shown in Scheme 1 and Table 1.

The synthesized *O*-alkylserine and threonine derivatives were easily transformed into the corresponding L-*O*-alkyl serine(**17**, **18**, **19**) and L-*O*-alkylthreonine (**20**, **21**, **22**, **23**) by catalytic hydrogenolysis or the combination of catalytic hydrogenolysis and hydrolysis as shown in Scheme 1, giving the titled compounds.

This study showed that the ring-opening reaction of aziridine derivatives having the urethane-type protecting groups is an effective method for synthesizing optically active β-alkoxy-α-amino acids.

Experimental

The melting points given are uncorrected. Optical rotations were determined at the D line on a Perkin-Elmer 141 polarimeter. The NMR spectra were obtained with a Hitachi R-20 B high resolution spectrometer using TMS as the internal reference.

(2S)-Z-Azy-OBzl (1). To a solution of (2*S*)-H-Azy-OBzl[3] (1.2 g, 6.7 mmol) and Et_3N (0.76 ml, 5.4 mmol) in $CHCl_3$ was added benzyloxycarbonyl chloride (0.86 ml, 5.4 mmol) at 0 °C with stirring. After being stirred overnight, it was washed with 10% citric acid, 1 M (1 M=1 mol dm^{-3}) $NaHCO_3$, and water, then dried over Na_2SO_4 and concentrated *in vacuo*. The residue was purified by silica gel column chromatography and 1.61 g (96% from Z-Cl[1]) of **1** was obtained, $[\alpha]_D^{23}$ −18.1° (*c* 1.0, MeOH). NMR ($CDCl_3$) δ: 2.37 (1H q, *J*=1.5, 5 Hz), 3.08 (1H q, *J*=3.0, 5.0 Hz), 5.05, 5.07 (4H 2s), 2.54 (1H q, *J*=1.5, 3.0 Hz), 7.26 (10H s).

Found: C, 69.15; H, 5.53; N, 4.42%. Calcd for $C_{18}H_{17}O_4N$: C, 69.44; H, 5.50; N, 4.50%.

(2S,3S)-Z-3-MeAzy-OMe (2). To a solution of (2*S*,3*S*)-H-3-MeAzy-OMe[4] (11.3 g, 78 mmol) and Et_3N (10.9 ml, 78 mmol) in $CHCl_3$ (200 ml) was added 2-benzyloxycarbonyloximino-2-phenylacetonitrile (Z-ON) (19.7 g, 70 mmol) at room temperature with stirring. After the reaction mixture was worked up as described above, 14.8 g (85% from Z-ON) of **2** was isolated as syrup, $[\alpha]_D^{23}$ −66.2° (*c* 1.1, MeOH). NMR ($CDCl_3$) δ: 1.25 (3H d, *J*=6.0 Hz), 2.75 (1H m), 3.20 (1H d, *J*=6.5 Hz), 3.35 (3H s), 5.10 (2H s), 7.28 (5H s).

Found: C, 62.34; H, 6.15; N, 5.48%. Calcd for $C_{13}H_{15}O_4N$: C, 62.64; H, 6.07; N, 5.62%.

L-Z-Ser(OMe)-OBzl (3). General Method via *Ring-opening Reaction of Azy*: **1** (0.3 g, 0.96 mmol) was dissolved in $CHCl_3$ (3 ml) and MeOH (5 ml), then $BF_3 \cdot OEt_2$ (3 drops) was added at room temperature. The reaction mixture was left standing for 12 h, then washed with water, dried over Na_2SO_4, and concentrated *in vacuo*. The residue was subjected to silica gel column chromatography with elution by $CHCl_3$. The effluent was concentrated *in vacuo* and 0.21 g (64%) of **3** was obtained. NMR ($CDCl_3$) δ: 3.26 (3H s), 3.69 (2H m, β-proton), 4.52 (1H, α-proton), 5.74 (1H bd).

Found: C, 66.39; H, 6.21; N, 4.16%. Calcd for $C_{19}H_{21}O_5N$: C, 66.46; H, 6.16; N, 4.08%.

L-Z-Thr(OBu^t)-OMe (13). Via *Ring-opening Reaction of 3-MeAzy*: **2** (0.2 g, 0.8 mmol) was dissolved in $CHCl_3$ (2 ml) and *t*-BuOH (5 ml), then $BF_3 \cdot OEt_2$ (3 drops) was added at room temperature. The reaction mixture was left standing overnight at room temperature and was worked up as described above. 243 mg (94%) of **13** was obtained. NMR ($CDCl_3$) δ: 1.10 (9H s), 1.19 (3H d), 4.15 (1H m, β-proton), 4.25 (1H q, α-proton), 5.50 (1H b).

Found: C, 63.25; H, 7.94; N, 4.21%. Calcd for $C_{17}H_{25}O_5N$: C, 63.14; H, 7.79; N, 4.33%.

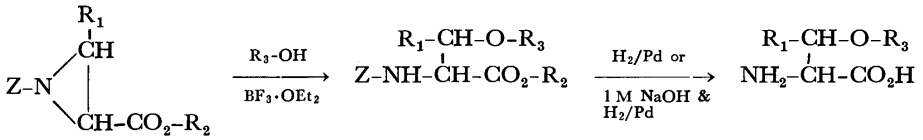

1: R_1=H, R_2=Bzl
2: R_1=Me, R_2=Me

3—**9**: R_1=H, R_2=Bzl
10—**16**: R_1=Me, R_2=Me

17—**19**: R_1=H
20—**23**: R_1=Me

Scheme 1.

Table 1. Properties and yields of *O*-alkyl-L-serine, L-threonine, and their derivatives

No.	Product[c] R_1	R_2	R_3	Yield/%	$[\alpha]_D^{24}$/°(MeOH)	Mp θ_m/°C
3	H	Bzl	Me	64	−19.1 (*c* 1.4)	syrup
4	H	Bzl	Pr^i	95	−19.5 (*c* 1.1)	syrup
5	H	Brl	Bu^s	73	−17.4 (*c* 0.9)	syrup
6	H	Bzl	Bu^t	58	−20.0 (*c* 1.1)	syrup
7	H	Bzl	Hex[c]	57	−20.1 (*c* 1.1)	57—58
8	H	Bzl	Bzl	100	−9.8 (*c* 1.1)	86—87
9	H	Bzl	Ph	27	−8.6 (*c* 1.1)	syrup
10	Me	Me	Me	98	−6.4 (*c* 1.1)	syrup
11	Me	Me	Pr^i	98	−10.7 (*c* 1.4)	syrup
12	Me	Me	Bu^s	92	−14.1 (*c* 1.2)	syrup
13	Me	Me	Bu^t	94	−3.1 (*c* 1.1)	syrup
14	Me	Me	Hex[c]	92	−9.1 (*c* 1.1)	syrup
15	Me	Me	Bzl	98	−6.9 (*c* 1.1)	72.5—73.0
16	Me	Me	Ph	57	+24.2 (*c* 1.1)	syrup
17	H	H	Pr^i	87	−11.8 (*c* 1.0)[a]	221 (d.)
18	H	H	Bu^t	100	−14.8 (*c* 1.0)[a]	209 (d.)
19	H	H	Hex[c]	82	−10.0 (*c* 1.0)[a]	193 (d.)
20	Me	H	Pr^i	86	−29.8 (*c* 1.1)[b]	212 (d.)
21	Me	H	Bu^s	75	−28.8 (*c* 1.0)[b]	198 (d.)
22	Me	H	Bu^t	82	−37.8 (*c* 1.0)[a]	207 (d.)
23	Me	H	Hex[c]	83	−35.5 (*c* 0.8)[a]	201 (d·)

a) Solvent: H_2O, b) solvent: 1 M HCl, c) Me: methyl, Bzl: benzyl, Pr^i: isopropyl, Bu^s: *s*-butyl, Bu^t: *t*-butyl, Ph: phenyl, Hex[c]: cyclohexyl.

Via t-*Butylation with Isobutylene of* L-*Z-Thr-OMe*: To a solution of L-Z-Thr-OMe (2.67 g, 10 mmol) and isobutylene (15 ml) in CH_2Cl_2 (15 ml) was added conc. H_2SO_4 (1 ml). The reaction mixture was left standing at room temperature for 3 d, and then washed with 1 M $NaHCO_3$ and water, dried over Na_2SO_4, and concentrated *in vacuo*. The residue was purified by silica gel column chromatography. 2.42 g (75%) of **13** was obtained, $[\alpha]_D^{24}$ +4.7° (*c* 2.0, DMF).

L-*Z-Ser(OBzl)-OH.* Via *Ring-opening Reaction of Azy*: **1** (0.2 g, 0.64 mmol) was dissolved in $CHCl_3$ (2 ml) and benzyl alcohol (5 ml), then $BF_3 \cdot OEt_2$ (3 drops) was added at room temperarure. The reaction mixture was left standing overnight and then worked up as described above. The obtained **8** (100% yield) was dissolved in MeOH (3 ml) and 2 M NaOH (5 ml) was added with stirring at room temperature for 2 h, then the solution was concentrated *in vacuo*. The residue was dissolved in water and adjusted to pH 2 with 3 M HCl, and the product was extracted with ethyl acetate. The solution was washed with water, dried over Na_2SO_4, and concentrated *in vacuo*. The residue was crystallized from CCl_4, 211 mg (100%), mp 99.5—100 °C, $[\alpha]_D^{24}$ +9.4° (*c* 1.3, MeOH). [mp 99—100 °C, $[\alpha]_D^{24}$ +9.5° (*c* 1.1, MeOH), prepared from Z-Cl and L-H-Ser(OBzl)-OH].

Found: 65.38; H, 5.85; N, 4.32%. Calcd for $C_{18}H_{19}O_5N$: C, 65.64; H, 5.81; N, 4.25%.

*O-Isopropyl-*L-*serine (18)*: H_2 gas was bubbled through a solution of **4** (218 mg, 0.59 mmol) in MeOH (10 ml) containing Pd black (100 mg) for 2 h. The catalyst removed by filtration and the filtrate was concentrated *in vacuo*. The residue was crystallized from water–acetone, and 75.5 mg (87%) of **18** was obtained.

O-*Isopropyl-*L-*threonine (20)*. **11** (224 mg, 0.72 mmol) was hydrolyzed with 1 M NaOH (2.5 ml) in MeOH (3 ml) at room temperature for 1 h. After L-Z-Thr(OPr^i) had been isolated by the usual procedure, the benzyloxycarbonyl group was removed by the catalytic hydrogenation described above. The product was crystallized from water-acetone, and 100 mg (85.7%) of **20** was obtained.

References

1) Part V. K. Okawa, K. Nakajima, T. Tanaka, and M. Neya, *Bull. Chem. Soc. Jpn.*, **55**, 174 (1982). Abbreviations of the IUPAC-IUB commission, *J. Biol. Chem.*, **247**, 977 (1972), are used. Z: benzyloxycarbonyl, OBzl: benzyl ester, OMe: methyl ester, Z-Cl: benzyloxycarbonyl chloride, Z-ON: 2-benzyloxycarbonyloximino-2-phenylacetonitrile. "Azyline" is used as the name of 2-aziridinecarboxylic acid, "Azy" being its abbreviation. 3-MeAzy: (2*S*,3*S*)-3-methyl-2-aziridinecarboxylic acid.

2) K. Okawa, K. Nakajima, T. Tanaka, and T. Maeda, "Peptide Chemistry 1976," ed by T. Nakajima, Protein Research Foundation, Osaka (1977) p. 13.

3) K. Nakajima, F. Takai, T. Tanaka, and K. Okawa, *Bull. Chem. Soc. Jpn.*, **51**, 1577 (1978).

4) K. Okawa and K. Nakajima, *Biopolymers*, **20**, 1811 (1891).

Chemical Studies on the Mistletoe. IV.[1] The Structure of Isoglucodistylin, a New Flavonoid Glycoside Isolated from *Taxillus kaempferi*

Atsushi SAKURAI,* Kyoji OKADA, and Yasuaki OKUMURA

Department of Chemistry, Faculty of Science, Shizuoka University, Ohya, Shizuoka 422

(Received March 23, 1982)

Synopsis. A new flavonoid glycoside, isoglucodistylin was isolated from *Taxillus kaempferi*, and (2*R*,3*S*)-taxifolin 3-β-D-glucopyranoside was assigned to this substance from studies on the hydrolysis products and on the isomerization products, and from analyses of the carbon-13 NMR spectra.

In our studies on the constituents of Japanese mistletoe, we reported the isolation and structure of taxillusin, a new flavonoid glycoside from *Taxillus kaempferi*, which was assigned to be (2*R*,3*R*)-taxifolin 3-β-D-glucopyranoside 6″-gallate (**1**).[2] During the course of the isolation of **1** by Sephadex LH-20 column chromatography, we found a presence of another new flavonoid glycoside and named it isoglucodistylin (**2**).

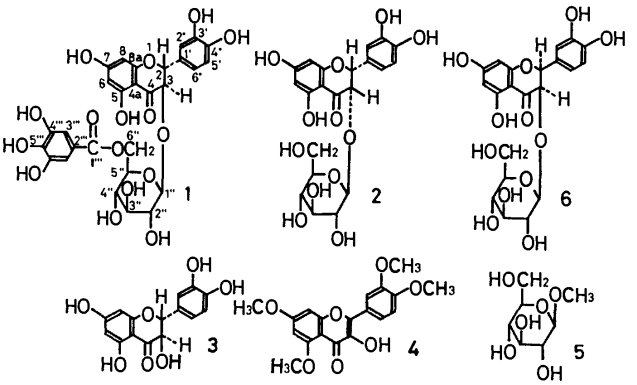

2 is amorphous white powder, mp 169—171 °C ($[\alpha]_D^{27}$ +25°), and the ultraviolet spectrum of **2** in ethanol shows the absorption maximum at 296 nm. Acid hydrolysis with hydrochloric acid gave (+)-taxifolin (**3**) ($[\alpha]_D^{27}$ +11°)[3] and glucose as the components. Methylation of **2** with dimethyl sulfate and potassium carbonate in acetone followed by acid hydrolysis and by air oxidation gave 3′,4′,5,7-tetra-*O*-methylquercetin (**4**).[4,5] This result indicates that glucose must be linked at the 3-position of taxifolin.

Taxifolin 3-glucoside (glucodistylin) had been isolated from the leaves of *Chamaecyparis obtusa* but this substance shows the ultraviolet absorption maximum at 292 nm in ethanol.[4] Both taxifolin 3-rhamnoside (astilbin) and aromadendrin 3-rhamnoside (engelitin) show their absorption maxima at 292 nm in ethanol and the configuration of the substituents at the 2- and 3-positions of both substances is *trans*.[6] While both the *cis* forms of astilbin and engelitin which have been prepared by isomerization of natural *trans* isomers show their absorption maxima at 296 nm in ethanol.[6] Therefore, glucodistylin must be a substance of *trans* form, and **2** might be 2,3-*cis*-taxifolin 3-glucoside.

The structure of **2** is supported by the carbon-13 NMR spectra of **1**, **2**, **3**, and methyl β-D-glucopyranoside (**5**) in DMSO-d_6 as shown in Table 1. The 3- and 4-carbons of taxifolin in **2** appear at a field

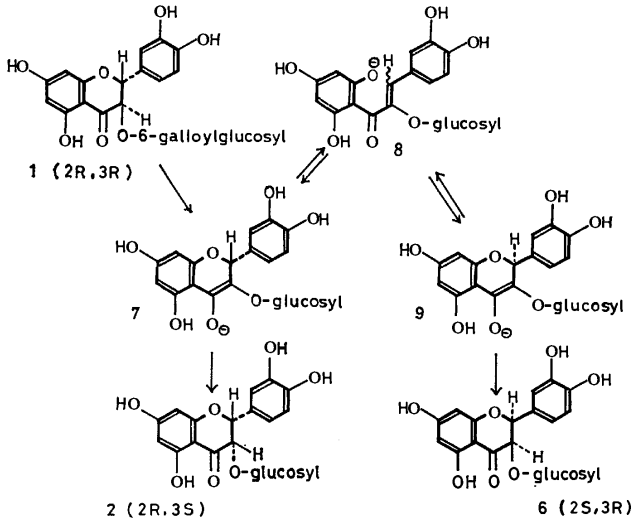

Scheme 1.

higher by 1.1 ppm and a field lower by 0.7 ppm respectively than those of **1**. This fact is the consequence of the difference in the configuration at the 3-position of taxifolin between **1** and **2**.

Acid hydrolysis of **2** gave (+)-taxifolin (**3**) of 2*R* and 3*R* configuration,[7] however, this result might be due to the isomerization at the 3-position from *cis* to *trans* form *via* enol. Therefore, the absolute configuration of **2** should be 2*R* and 3*S*.

The isomerization of **2** with aqueous sodium acetate in ethanol[6] gave a substance **6** but did not give 2,3-*trans*-taxifolin 3-β-glucoside. The ultraviolet spectrum of **6** in ethanol shows the absorption maximum at 295 nm. Acid hydrolysis of **6** with hydrochloric acid gave (−)-taxifolin ($[\alpha]_D^{28}$ −11°).[8] In the carbon-13 NMR spectra, the 1-carbon of glucose and the 2-carbon of taxifolin in **6** appear at fields lower by 1.8 and 0.7 ppm respectively than those of **2** as shown in Table 1. This fact is the consequence of the presence of less steric compression between the C-1 of glucose and the C-2 of taxifolin in **6**. These results indicate **6** to be (2*S*,3*R*)-taxifolin 3-β-D-glucopyranoside.

Hydrolysis of **1** with aqueous sodium carbonate gave **2**, **6**, and gallic acid, but did not give 2,3-*trans*-taxifolin 3-β-glucoside. The isomerization in the hydrolytic conditions was confirmed by high pressure liquid chromatography of recovered **1**. These results indicate that taxifolin glucosides in *cis* form might be more stable than those of *trans* in the conditions described above.

The formation of those **2** and **6** can be rationalized by the mechanistic sequence as shown in Scheme 1. During the base-catalyzed hydrolysis of the galloyl group, **1** is isomerized into **2** with inversion at the 3-position through an enolate **7**. When the C–O bond between the 1- and 2-positions of the enolate

Table 1. Carbon-13 NMR chemical shifts of **1**, **2**, **3**, **5**, and **6**, in DMSO-d_6

Compound		1	2	6	3	5
Taxifolin	2	80.5	80.6	81.3	82.9	—
	3	76.3	75.2	75.2	71.3	—
	4	191.9	192.6	192.7	197.5	—
	4a	101.0	101.0	100.9	100.2	—
	5	163.3	163.3	163.5	163.1	—
	6	95.9*	95.9*	95.9*	95.8*	—
	7	167.0	167.0	167.3	166.5	—
	8	95.0*	95.0*	95.1*	94.8*	—
	8a	161.3	161.6	161.7	162.3	—
	1'	126.3	126.5	126.4	127.8	—
	2'	114.4**	114.6**	114.8**	115.1	—
	3'	145.4***	145.5***	145.5***	145.5**	—
	4'	145.0***	145.0***	144.9***	144.7**	—
	5'	115.5**	115.4**	115.3**	115.1	—
	6'	118.3	118.7	118.6	119.2	—
Glucose	1	101.0	101.0	102.8	—	103.7
	2	73.5	73.4	73.4	—	73.2
	3	76.3	77.1	76.8	—	76.6
	4	69.3	69.8	69.9	—	69.9
	5	74.0	76.5	76.7	—	76.5
	6	63.2	61.0	61.2	—	60.9
Gallic acid	1	165.7	—	—	—	—
	2	119.4	—	—	—	—
	3	108.7	—	—	—	—
	4	145.4	—	—	—	—
	5	138.3	—	—	—	—
	CH_3	—	—	—	—	55.9

In parts per million downfield from tetramethylsilane. Asterisks indicate that assignments are not unambigous.

7 is cleaved to afford a phenolate **8**, the phenolate oxygen in **8** attacks at the 2-position from the opposite side to afford an enolate **9**, which then converted to **6** with inversion at the 3-position.

These carbon-13 NMR spectroscopic data and all experimental results described above support the structure of isoglucodistylin (**2**) to be (2*R*,3*S*)-taxifolin 3-*β*-D-glucopyranoside.

Experimental

All melting points are uncorrected. The carbon-13 NMR spectra were measured with a JEOL JNM-PFT-60 NMR spectrometer on sampling interval of 2.0 s. Chemical shifts were obtained by δ value (ppm) from TMS as internal standard at 15.04 MHz. The UV spectra were measured with a Hitachi EPS-3 recording spectrophotometer. HPLC apparatus used was JASCO TRI ROTAR high pressure liquid chromatography. Column used was 2.6 mm × 250 mm stainless steal peacked with LiCrosolb RP-8. Elution system was CH_3CN–H_2O (9:1) containing 0.02 M (1 M = 1 mol dm^{-3}) acetic acid.

Isolation of Isoglucodistylin (2). The fresh leaves and twigs of the mistletoe (2 kg) which occurred on *Pinus densiflora* were extracted with ethanol (6 L) and the extract was condensed to a syrup *in vacuo*. The syrup was triturated with water (2 L) and chloroform (2 L), and the undissolved material which accumulated between both layers was collected. The faintly yellowish powder (11.5 g) was subjected to chromatography on a column of Sephadex LH-20 (3.5 × 120 cm) eluting with ethanol. Concentrated to dryness of the fractions containing **2** and recrystallization from ethyl acetate gave **2** as colorless amorphous powder (mp 167—169 °C; yield, 100 mg (0.005% from wet plant); $[\alpha]_D^{27}$ +25° (*c* 0.3, EtOH); UV (EtOH): λ_{max} 296 nm (ε 17100)). Found: C, 51.98; H, 4.46%. Calcd for $C_{21}H_{22}O_{12}\cdot H_2O$: C, 52.07; H, 4.99%.

Acid Catalyzed Hydrolysis of 2. **2** was dissolved into 2 M hydrochloric acid and the mixture was refluxed for 2 h. Extraction with ethyl acetate and recrystallization from water gave **3** as faintly yellowish crystals (mp 240—242 °C; $[\alpha]_D^{27}$ +11° (*c* 1.0, EtOH); UV (EtOH): λ_{max} 291 nm (ε 19400)). Hydrolyzate free from **3** was subjected to TLC for detection of the sugar component. The sugar was proved to be identical with D-glucose.

Methylation of 2. According to Fukui, Nakadome, and Ariyoshi's method,[4] **2** was methylated with dimethyl sulfate and potassium carbonate in acetone followed by acid hydrolysis and then air oxidation. The product was identified with authentic 3′,4′,5,7-tetra-*O*-methylquercetin (**4**) which was prepared by methylation and acid hydrolysis of rutin in the same way.

Isomerization of 2 with Sodium Acetate. **2** was isomerized with ethanolic sodium acetate according to Tominaga and Yoshimura's method.[6] Separation of the isomerized mixture with a column of Sephadex LH-20 in the same way as described above gave **6** as colorless amorphous powder (mp 200—202 °C (decomp); yield, 15%; $[\alpha]_D^{27}$ +150° (*c* 0.1, EtOH); UV (EtOH): λ_{max} 295 nm (ε 18500)). Found: C, 52.16; H, 4.43%. Calcd for $C_{21}H_{22}O_{12}\cdot H_2O$: C, 52.07; H, 4.99%.

Acid Catalyzed Hydrolysis of 6. Acid hydrolysis of **6** with 2 M hydrochloric acid in the same way as described above gave (−)-taxifolin (mp 238—240 °C; $[\alpha]_D^{28}$ −11° (*c* 0.1, EtOH); UV (EtOH): λ_{max} 291 nm (ε 18800)).

Base Catalyzed Hydrolysis of 1. **1** (1.25 g) was dissolved into aqueous 0.5 M sodium carbonate (200 ml) and the mixture was stirred for 18 h at room temperature under nitrogen atmosphere. After having been acidified with hydrochloric acid, the reaction mixture was extracted with ethyl acetate. The extract was subjected to chromatography on a column of Sephadex LH-20 in the same way as described above gave **2** (75 mg), **6** (45 mg), and gallic acid (10 mg).

References

1) Part III: M. Taguchi, A. Sakurai, and Y. Okumura, *Reports of Faculty of Science, Shizuoka University*, **8**, 31 (1973).
2) A. Sakurai and Y. Okumura, *Chem. Lett.*, **1978**, 259.
3) J. C. Pew, *J. Am. Chem. Soc.*, **70**, 3031 (1948).
4) Y. Fukui, N. Nakadome, and H. Ariyoshi, *Yakugaku Zasshi*, **86**, 184 (1966).
5) T. Sasaki, *Yakugaku Zasshi*, **84**, 47 (1964).
6) T. Tominaga, *Yakugaku Zasshi*, **78**, 1077 (1958); T. Tominaga and K. Yoshimura, *ibid.*, **80**, 1332, 1337, 1340 (1960).
7) J. W. Clark-Lewis and W. Korytonyk, *J. Chem. Soc.*, **1958**, 2367.
8) M. Yamamoto, *Kumamoto Pharm. Bull.*, **5**, 54 (1962).

Ceroalbolinic Acid, a Common Body Pigment of Three *Ceroplastes* Scale Insects in Japan. Confirmation of Structure

Hajime KOMURA,* Kohsei MIZUKAWA, and Hiroyuki MINAKATA

Suntory Institute for Bioorganic Research, Wakayama-dai, Shimamoto-cho, Mishima-gun, Osaka 618

(Received March 26, 1982)

Synopsis. The structure of ceroalbolinic acid, a widely occurring insect pigment, a common body pigment of three Japanese *Ceroplastes* scale insects, has been confirmed as **2** by ^{13}C-NMR long-range selective proton decoupling (LSPD) experiments on its permethylated derivative **3**. Full assignments of skeletal carbons for **3** were also obtained.

The scale insects *Ceroplastes*(Coccidae) are pests which attack persimmon, citrus and other orchard trees and are widely distributed in Japan, Mexico, *etc.* The insect secretion has given rise to numerous new terpenoids[1,2] as well as waxes,[3] whereas one of the body pigments, the red carminic acid,[4] an anthraquinone *C*-glucoside isolated from *Dactylopius coccus*, is popularly used in food coloring and staining.

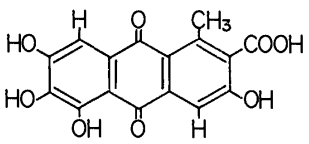

1

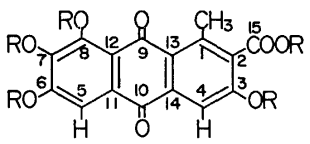

2, R=H; **3**, R=CH$_3$

The three Japanese species of *Ceroplastes*, *C. ceriferus*, *C. floridensis*, and *C. rubens* were treated with chloroform to extract the waxy coating, and then with methanol to extract the orange body pigment. Purification with Sephadex LH-20 and droplet counter-current chromatography(DCCC)[5] gave orange crystals. Yields of the pigment are 0.06, 0.15, and 0.21% respectively from *C. ceriferus*, *C. floridensis*, and *C. rubens* based on their fresh body weights. The ^{1}H-NMR in methanol-d_4 with only three singlets at 7.54, 7.16, and 2.78 ppm in 1:1:3 relative intensities showed the pigment to be identical with ceroalbolinic acid isolated from the Mexican species, *C. albolineatus*.[6-8] Structure **1** was ordiginally proposed,[6] but since a synthetic specimen of structure **1** did not coincide with ceroalbolinic acid, structure **2** was proposed instead without further evidence.[7] Thus, despite the relatively wide occurrence of this pigment, its structure was not settled[9] for long time. Full assignments of ^{13}C-NMR peaks of permethylated derivative **3** by long-range selective proton decoupling(LSPD) led unambiguously to structure **2**.

Permethylation[10] with dimethyl sulfate-potassium carbonate afforded the pentamethyl derivative **3** in quantitative yield. The ^{1}H-NMR peaks of 4-H and 5-H were based on the observation that the 4-H signal was sharpened upon decoupling of the 1-Me singlet. The ^{13}C-gated-^{1}H-decoupled spectrum with NOE show-

TABLE 1. ^{13}C-NMR T_1 AND LSPD EXPERIMENTS; ASSIGNMENTS AND COUPLING CONSTANTS FOR **3**(IN $CDCl_3$)

Carbons	δ	T_1/s	Off resonance	Non decoupled	LSPD of 5-H	LSPD of 4-H	LSPD of 1-Me	$^1J_{CH}$	$^2J_{CH}$	$^3J_{CH}$	$^4J_{CH}$
C-9	183.0	16.3	s	bs	bs	bs	*s*				
C-10	182.6	9.6	s	t	*d*	*d*	t			4.4(t)	
C-15	167.7	10.0	s	dq	dq	*q*	dq			4.4(q)	0.8(d)
C-3	158.5	7.6	s	dq	dq	*q*	dq		1.5(d)	4.4(q)	
C-6	156.8	8.5	s	dq	*q*	dp	dq		2.2(d)	4.4(q)	
C-8	154.3	15.4	s	dq	*q*	dq	dq			4.4(q)	0.8(d)
C-7	148.9	12.7	s	dq	*q*	dq	dq			4.4(q),7.3(d)	
C-1	139.9	8.2	s	q	q	q	*s*		5.9(q)		
C-14	136.1	9.1	s	d	d	*s*	d		1.5(d)		
C-2	131.0	13.3	s	dq	dq	*q*	*d*			5.1(q),5.1(d)	
C-11	129.6	10.0	s	d	*s*	d	d		2.2(d)		
C-13	127.4	16.2	s	dq	dq	*q*	*d*			3.7(q),6.6(d)	
C-12	123.2	15.5	s	d	*s*	d	d			6.6(d)	
C-4	106.4	0.6	d	d	d	d	d	166.5(d)			
C-5	105.6	0.6	d	d	d	d	d	165.6(d)			
OMe	61.7	2.4	q	q	q	q	q	146.2(q)			
OMe	61.2	3.7	q	q	q	q	q	146.2(q)			
OMe	56.3	1.3	q	q	q	q	q	145.5(q)			
OMe	56.3	1.3	q	q	q	q	q	145.5(q)			
OMe	52.5	1.7	q	q	q	q	q	148.9(q)			
1-Me	19.2	2.1	q	q	q	q	q	130.5(q)			

Italics denote change in multiplicity. s: Singlet, d: doublet, t: triplet, q: quartet, bs: broad singlet, dq: double quartet.

ed two skeletal carbonyl carbons at 183.0 and 182.6 ppm with broad singlet and triplet(J=4.4 Hz),[11] respectively. Selective irradiation of the 4- and 5-H signals both led to a collapse of the triplet to a doublet, whereas the broad singlet remained unchanged. The 182.6 ppm triplet is thus assigned to C-10 flanked by 4-H and 5-H in structure **3**; if the pentamethyl derivative were represented by the alternative structure, both carbonyls would have been doublets. Relaxation time(T_1) measurement also supported the structure **3**; the T_1 values of the skeletal carbons at lower-half part in the structure **3**, *i.e.* carbons 3,4,5,6, 10,11, and 14, are remarkably shorter compared with those of the upper-half (C-2,7,8,9,12, and 13) because of the presence of two protons in the same side of the ring.

LSPD of 4-H, 5-H, and 1-Me, which were carried out during the course of this study led to assignments of all ^{13}C-NMR peaks, as shown in the table, as well as to a full corroboration of structure **3** for pentamethylated ceroalbolinic acid. The present LSPD method is generally applicable in determining the substitution pattern of polysubstituted aromatic compounds, a problem frequently encountered and difficult to solve otherwise.

Interestingly, similar to the case of carminic acid reported by Eisner *et al.*,[12] ceroalbolinic acid also exhibited antifeedant activity against ants. This ceroalbolinic acid might therefore be working as one of the defense substances together with sticky waxy coating for *Ceroplastes* insects which cannot move anymore once after settled down on a tree, secreting so called honeydews without being attacked by ant or other carnivorous insects.

Experimental

All the melting points are uncorrected. ^{1}H- and ^{13}C-NMR were obtained on a JEOL FX-100 FT instrument at 25 °C, spectral width 2 (^{1}H) and 6 kHz (^{13}C), data points 16 kW, repetition time 5 (^{1}H) and 2.5—3.5 s (^{13}C), pulse width 17 (^{1}H) and 6 μs (^{13}C) (both 45° pulse), power level for LSPD 13 kHz, −50 dB with power attenuator. T_1 experiment was carried out with saturation-recovery method on an undegassed sample. Solvent peak was used as an internal standard for NMR, 7.24 (^{1}H, $CHCl_3$), 3.30 (^{1}H, CHD_2OD), 77.0 (^{13}C, $CDCl_3$), and 49.0 ppm (^{13}C, CD_3OD). EI- and FD-mass spectra were obtained on a JEOL JMS-01SG-2 mass spectrometer.

*Isolation of Ceroalbolinic Acid (**2**).* Crude methanol extracts of each insects were separately treated with almost equal volume of chloroform–water mixture (1:1 v/v) to remove lipophilic part. Aqueous layer of the mixture was then concentrated *in vacuo* to a thick syrup followed by column chromatography on a Sephadex LH-20 with 0.1% acetic acid in methanol to give pigment as a retarded band. After further purification on a DCCC (Tokyo Rika Kikai, Co.) with chloroform–methanol–0.02 mol/dm^3 aqueous hydrochloric acid (7:13:8 v/v) using aqueous layer as a mobile phase in ascending mode, ceroalbolinic acid crystallized out in the test tubes on a fraction collector. Mp>250 °C (lit,[6] 290 °C, decomp). FD-MS, m/z 331 ((M+1)$^+$, 100%), ^{13}C-NMR (methanol-d_4): 190.1 (C-9), 182.7 (C-10), 171.4 (C-15), and 20.4 (1-Me).

Methylation of Ceroalbolinic Acid. Ceroalbolinic acid was methylated for 5 h with excess amount of dimethyl sulfate and anhydrous potassium carbonate in refluxing acetone. The reaction was quenched by adding glacial acetic acid. After regular work-up of the mixture, yellow needles of pentamethyl derivative **3** were obtained in quantitative yield upon concentration and trituration with small amount of methanol. Crystals thus obtained were pure enough without further recrystallization. Mp 200.5—201.5 °C (lit,[6] 201—204 °C). ^{1}H-NMR ($CDCl_3$): 7.64 (4-H, br s, J<1 Hz), 7.57 (5-H, s), 4.05, 4.02, 4.00 4.00 3.92 (OMe ×5, s's), and 2.69 (1-Me, s). FD-MS, m/z 400 (M$^+$, 1005), EI-MS, m/z 400 (M$^+$, 97%), 385 ((M−CH_3)$^+$, 100%), 369 ((M−OMe)$^+$, 23%), and 367 ((M−33)$^+$, 53%).

References

1) Y. Naya, K. Yoshihara, T. Iwashita, H. Komura, K. Nakanishi, and Y. Hata, *J. Am. Chem. Soc.*, **103**, 7009 (1981).

2) L. Quijano, J. S. Calederón, and T. Ríos, *Chem. Lett.*, **1979**, 1387.

3) F. Miyamoto, H. Naoki, Y. Naya, and K. Nakanishi, *Tetrahedron*, **36**, 3481 (1980).

4) The Merck Index, 9th ed., 1844, p 235 (1976); the structure in the Merck Index was revised from an α- to a β-*C*-glucopyranoside: A. Fiecchi, M. Anastasia, G. Galli, and P. Gariboldi, *J. Org. Chem.*, **46**, 1511 (1981). We have also arrived at the same conclusion from ^{1}H-NMR (D_2O) data of carminic acid: 1′-H, 4.95 ppm, d, J=9.8 Hz. We are grateful to San-ei Kagaku Kogyo Co. for a gift of cochineal dye from which carminic acid was isolated.

5) For reviews, see: T. Tanimura, H. Otsuka, and Y. Ogihara, *Kagaku No Ryoiki*, **29**, 895 (1975); K. Hostettmann, *Planta Medica*, **39**, 1 (1980).

6) T. Ríos, *Tetrahedron*, **22**, 1507 (1966).

7) D. D. Gadgil, A. V. Rama Rao, and K. Venkataraman, *Tetrahedron Lett.*, **1968**, 2229.

8) Ceroalbolinic acid has been isolated previously from *C. rubens*: K. Doi, *Sci. Rep. Hirosaki Univ.*, **18**, 37 (1971).

9) Recently, Australian group has managed to synthesize ceroalbolinic acid with correct structure **2**: D. W. Cameron, C. Conn, and G. I. Feutrill, *Aust. J. Chem.*, **34**, 1945 (1981).

10) When smaller amount of dimethyl sulfate (*ca.* 8 mol equiv.) was used, less polar derivative, methyl ceroalbolinate 3,6,7-trimethyl ether, was obtained in addition to **3**. ^{1}H-NMR ($CDCl_3$): 13.12 (8-OH, s), 7.73 (4-H, br s), 7.39 (5-H, s), 4.03, 4.02, 4.02, 3.97 (OMe×4, s's), and 2.73 (1-Me, s). EI-MS, m/z 386 (M$^+$, 100%), 371 ((M−CH_3)$^+$, 50%), 355 ((M−OMe)$^+$, 21%), and 353 ((M−33)$^+$, 21%).

11) Höfle reported in his extensive studies on ^{13}C-NMR of some naphtho- and anthraquinones, a carbonyl carbon flanked with two protons at *peri*-positions appeared as triplet with $^3J_{CH}$=4.5 Hz for a simple anthraquinone derivative: G. Höfle, *Tetrahedron*, **33**, 1963 (1977).

12) T. Eisner, S. Nowicki, M. Goetz, and J. Meinwald, *Science*, **208**, 1039 (1980).

Radiation-induced Alkylation, Hydroxyalkylation, and Reduction of Pyridinecarboxamides in Acidic Alcoholic Solutions

Akira SUGIMORI,* Masayuki NISHIJIMA, and Hiroshi ITOH

Department of Chemistry, Faculty of Science and Technology, Sophia University, Kioi-cho 7-1, Chiyoda-ku, Tokyo 102

(Received March 27, 1982)

Synopsis. The γ-irradiation of pyridinecarboxamides in acidic methanol or ethanol brings about substitution of the ring hydrogen by alkyl or hydroxyalkyl groups derived from the solvent alcohols in relatively high G-values. In 2-propanol, little alkylation and hydroxyalkylation occur and reduction of $CONH_2$ to CH_2OH occurs in low G-values.

In spite of their biological importance, the radiation-induced reactions of pyridinecarboxamides have not yet been thoroughly studied, at least on the basis of product analyses. Concerning the radiation-induced reactions of model compounds for NAD (nicotinamide dinucleotide), hydroxylation in aqueous solutions[1] and dimer formation[2] have been reported. By means of pulse radiolysis technique, intermediates formed in the radiolysis of pyridinecarboxylic acid derivatives in aqueous alcohol were studied,[3,4] but the reports have not mentioned the structures of products. As an extension of our studies on photo- and radiation-induced reactions of pyridinecarboxylic acid derivatives,[5] we report here the radiation-induced reactions of pyridinecarboxamides, including biologically important 3-pyridinecarboxamide, in acidic alcohols. The radiation-induced reactions may furnish a useful synthetic method, owing to the specific type of reactions, which are different from those induced by a free radical initiator, and their relatively high G-values.

Results and Discussion

Gamma-irradiation of pyridinecarboxamides in acidic alcoholic solutions brings about substitution of the ring hydrogen by alkyl and hydroxyalkyl groups derived from the solvent alcohols and reduction of $CONH_2$ to CH_2OH.

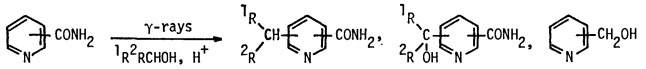

The radiation-induced reactions of pyridinecarboxamides are very similar to those of the corresponding carboxylic esters: 1) In acidic methanolic solutions, 2- and 3-pyridinecarboxamides give methylation products in relatively high G-values. The positions for methylation in carboxamides are similar to those of the corresponding carboxylic esters. 2) In acidic methanol, 4-pyridinecarboxamide undergoes hydroxymethylation rather than methylation. 3) In acidic 2-propanol little isopropylation occurs and, instead, reduction of $CONH_2$ at 2- and 4-positions to CH_2OH occurs.

The following differences between the radiation-induced reactions of pyridinecarboxamides and those of carboxylic esters should be noted: 1) Reduction of $CONH_2$ at 2- and 4-positions to CH_2OH is much less efficient than that of the esters. 2) During the irradiation of 3-pyridinecarboxamide in acidic 2-propanol, 6-ethyl-3-pyridinecarboxamide was obtained in higher yield than 6-isopropyl-3-pyridinecarboxamide.

The similarities of the reactions of amides and esters suggest that the mechanism for the radiation-induced reactions of pyridinecarboxamides should be parallel to that of pyridinecarboxylic esters:[5] for alkylation and reduction, hydroxyalkyl radicals and hydrogen atom play important roles. The fact that ethylation occurs more effectively than isopropylation in γ-irradiation of 3-pyridinecarboxamide in 2-propanol suggests that $CH_3\dot{C}HOH$ radical formed by C–C cleavage of 2-propanol is more efficient for alkylation than $(CH_3)_2\dot{C}OH$ radical which is formed predominantly during γ-irradiation of 2-propanol.[6] In the free radical reaction initiated by the thermal decomposition

TABLE 1. RADIATION-INDUCED REACTIONS OF PYRIDINECARBOXAMIDES IN ACIDIC ALCOHOLIC SOLUTIONS
[Pyridinecarboxamide] = 0.03 mol dm^{-3}; [H_2SO_4] = 0.05 mol dm^{-3}; dose rate, 5×10^5 rad h^{-1}; dose, 1.0×10^7 rad.

Substrate	Alcohol	Product (G-value)			
		Substitution product (Position and group introduced)		Reduction product	
2-Pyridinecarboxamide	MeOH	4-Methyl-	(0.55)		
		4-Methyl-6-hydroxymethyl	(0.28)		
	i-PrOH	—		2-Pyridylmethanol	(0.02)
3-Pyridinecarboxamide	MeOH	4-Methyl-	(0.26)		
		6-Methyl-	(0.97)		
	EtOH	6-Ethyl-	(1.04)		
	i-PrOH	6-Isopropyl-	(0.06)		
		6-Ethyl-	(0.14)		
4-Pyridinecarboxamide	MeOH	2-Hydroxymethyl-	(0.22)		
	i-PrOH	—		4-Pyridylmethanol	(0.13)

of ammonium peroxodisulfate,[7] 3-pyridinecarboxamide gives 2- and 4-hydroxymethyl-3-pyridinecarboxylic acid lactones (5,7-dihydrofuro[3,4-*b*]pyridin-5-one (**A**) and 1,3-dihydrofuro[3,4-*c*]pyridin-3-one (**B**)), which are the intramolecular alcoholysis products from 2- and 4-hydroxymethyl-3-pyridinecarboxamides in low yields.

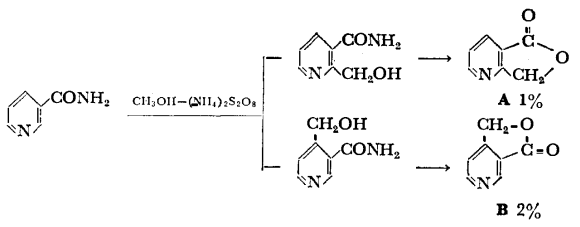

The γ-irradiation of pyridinecarboxamides and esters in methanol (and in the case of 3-pyridinecarboxamide in ethanol) gives methylation (and ethylation) products in rather high *G*-values and methylation by methanol can not be effected by an efficient free radical initiator $S_2O_8^{2-}$. Therefore, this type of radiation-induced alkylation should have synthetic utility for the introduction of alkyl groups to the pyridine nucleus.

Experimental

Materials. Commercial 2-, 3-, and 4-pyridinecarboxamides were used after the purification by recrystallization.

Gamma-irradiation. Solutions containing 0.03 mol dm^{-3} of pyridinecarboxamide and 0.05 mol dm^{-3} of H_2SO_4 were deaerated by bubbling Ar for 30 min. The solutions were irradiated at the ^{60}Co γ-facility of Japan Atomic Energy Research Institute in Takasaki (dose rate, 5×10^5 rad h^{-1}; dose, 1.0×10^7 rad).

$(NH_4)_2S_2O_8$-induced Reaction. A methanolic solution (50 cm^3) containing 3-pyridinecarboxamide (15 mmol), $(NH_4)_2S_2O_8$ (15 mmol), and H_2SO_4 (0.4 cm^3) was refluxed for 30 min.

Separation of Products. The irradiated solutions were concentrated under reduced pressure and neutralized with Na_2CO_3 and $NaHCO_3$. The products were separated by means of TLC (plate, Kieselgel 60 GF_{254} of E. Merck Co.; developing solvents; ethyl acetate, acetone, and their mixture).

Identification of Products. 4-Methyl-2-pyridinecarboxamide: mp 119—120 °C; IR (KBr disk) 3400, 3250, 1680 and 1360 cm^{-1}; ^1H NMR ($CDCl_3$) δ=8.40 (1H, d, J=4.4 Hz, H at 6-position), 8.02 (1H, d, J=1 Hz, H at 3-position), 7.23 (1H, dd, J=4.4 and 1 Hz, H at 5-position), and 2.44 (3H, s, CH_3); Found: C, 61.4; H, 6.2; N, 20.3%; Calcd for $C_7H_8N_2O$: C, 61.8; H, 5.9; N, 20.6%.

6-Ethyl-3-pyridinecarboxamide: mp 161—163 °C; IR (KBr disk) 3220, 1690, 1405, 1395, and 1375 cm^{-1}; ^1H NMR ($CDCl_3$) δ=8.84 (1H, d, J=2.0 Hz, H at 2-position), 8.09 (1H, dd, J=8.0 and 2.0 Hz, H at 4-position), 7.40 (1H, d, J=8.0 Hz, H at 5-position), 2.88 (2H, q, J=7.2 Hz, CH_2), and 1.30 (3H, t, J=7.2 Hz, CH_3); Found: C, 63.7; H, 6.7; N, 18.9%. Calcd for $C_8H_{10}N_2O$: C, 64.0; H, 6.7; N, 18.7%.

2-Hydroxymethyl-4-pyridinecarboxamide: mp 183—184.5 °C; IR (KBr disk) 3360, 3320, 1690, 1420, and 1040 cm^{-1}; ^1H NMR δ=8.56 (1H, d, J=5 Hz, H at 6-position), 7.74 (1H, d, J=1 Hz, H at 3-position), 7.56 (1H, dd, J=5 and 1 Hz, H at 5-position), and 4.80 (2H, s, CH_2); Found: C, 55.0; H, 5.6; N, 19.0%. Calcd for $C_7H_8N_2O_2$: C, 55.3; H, 5.3; N, 18.4%.

6-Isopropyl-3-pyridinecarboxamide (mp 135—136.5 °C) was identified only on the basis of ^1H NMR because of its low yield. ^1H NMR (D_2O) δ=8.80 (s), 8.05 (d, J=8 Hz), 7.35 (d, J=8 Hz), 3.00 (m, J=8 Hz), and 1.23 (d, J=8 Hz).

2-Hydroxymethyl-3-pyridinecarboxylic acid lactone: mp 108—111 °C; IR (KBr disk) 1760 cm^{-1} (γ-lactone C=O); ^1H NMR ($CDCl_3$) δ=8.85 (1H, dd, J=5.2 and 2.0 Hz, H at 6-position), 8.28 (1H, dd, J=7.6 and 2.0 Hz, H at 4-position), 7.45 (1H, dd, J=7.6 and 5.2 Hz, H at 5-position), and 5.33 (2H, s, CH_2); MS (70 eV) *m/e* (relative intensity) 135 (M^+; 58), 106 (100), 78 (38), 77 (22), and 51 (11); Found: *m/e* 135.0323. Calcd for $C_7H_5NO_2$: M, 135.0320.

4-Hydroxymethyl-3-pyridinecarboxylic acid lactone: mp 122—124 °C; IR (KBr disk) 1760 cm^{-1} (γ-lactone C=O); ^1H NMR ($CDCl_3$) δ=9.19 (1H, s, H at 2-position), 8.87 (1H, d, J=5 Hz, H at 6-position), 7.52 (1H, d, J=5 Hz, H at 5-position), and 5.38 (2H, s, CH_2); MS (70 eV) *m/e* (relative intensity) 135 (M^+; 100), 106 (66), 78 (37), and 51 (12); Found: *m/e* 135.0320. Calcd for $C_7H_5NO_2$: M, 135.0320.

4-Methyl-3-pyridinecarboxamide (mp 163.5—164.5 °C; lit, [8] 167—167.5 °C) and 6-methyl-3-pyridinecarboxamide (mp, 199—200 °C; lit,[9] 196—198 °C) were identified by means of melting point measurements and NMR and IR spectral analyses. Pyridylmethanols were identified by the accordance of the gas-chromatographic and spectral properties with the authentic ones.

References

1) L. Schachinger and B. Heindle, *Atomkernenergie*, **24**, 121 (1974).

2) A. J. Swallow, *Biochem. J.*, **61**, 197 (1955); G. Stein and A. J. Swallow, *J. Chem. Soc.*, **1958**, 306.

3) U. Brühlmann and E. Hayon, *J. Am. Chem. Soc.*, **96**, 6169 (1974).

4) M. Simić and M. Ebert, *Int. J. Radiat. Phys. Chem.*, **3**, 259 (1971).

5) K. Nakamura, Y. Morita, T. Suzuki, T. Sugiyama, and A. Sugimori, *Bull. Chem. Soc. Jpn.*, **52**, 488 (1979); K. Nakamura, T. Suzuki, and A. Sugimori, *Chem. Lett.*, **1977**, 1203.

6) The ratio of C–C/(C–H+O–H) cleavage in the initial decomposition of 2-propanol was estimated to be roughly 30/60; G. R. Freeman, "The Radiolysis of Alcohols," in "Actions Chimiques et Biologiques des Radiations," 14 ème serie ed by M. Haissinsky, Masson, Paris (1970), pp. 73—134.

7) F. Minisci, *Synthesis*, **1973**, 1; F. Minisci and O. Porta, *Adv. Heterocycl. Chem.*, **16**, 123.

8) J. M. Bobbitt and D. A. Scola, *J. Org. Chem.*, **25**, 560 (1960).

9) R. N. Castle and C. W. Whittle, *J. Org. Chem.*, **24**, 1189 (1959).

A Simple Synthesis of 7-*t*-Butyl-4-methyl-2,3-dihydrothiepin

Kagetoshi YAMAMOTO,* Shoko YAMAZAKI, and Ichiro MURATA*

Department of Chemistry, Faculty of Science, Osaka University, Toyonaka, Osaka 560

(Received April 16, 1982)

Synopsis The novel ring expansion reaction developed for the synthesis of 2,6-di-*t*-butylthiopyrans has been applied to the short path preparation of a dihydrothiepin derivative. Thus, 4-methyl-6-pivaloyl-3,6-dihydro-2*H*-thiopyran was converted into 7-*t*-butyl-4-methyl-2,3-dihydrothiepin in excellent yield by using chlorotrimethylsilane-zinc reagent in tetrahydrofuran.

Strategies for the synthesis of organic compounds using silicon-based reagents have been developed extensively, and their utility has been well documented.[1] However, one of these, chlorotrimethylsilane-zinc (or zinc amalgam) reagent induces formation of double bonds directly from ketones under mild conditions.[2] It provides some novel synthetic methods,[3] but has received little attention although it appears to occupy a prominent place in organic synthesis. In connection with our efforts directed toward the synthesis of stable monocyclic thiepins[4] we have recently demonstrated the novel and versatile synthesis of 2,6-di-*t*-butylthiopyrans from the corresponding acyldihydrothiophene using this reagent (see Scheme 1). Otherwise this substance is difficult to make.

This method appears to have promise as a tool for the synthesis of seven membered rings containing a sulfur atom such as thiepin derivatives directly from appropriate six-membered precursors. In this context, the synthesis of 7-*t*-butyl-4-methyl-2,3-dihydrothiepin (**5**) starting from readily available **1**[5] was examined (Scheme 2).

The desired precursor **4** was prepared starting from **1**; the anion **2**[5,6] generated from **1** with s-butyllithium in THF in the presence of TMEDA at −78 °C was

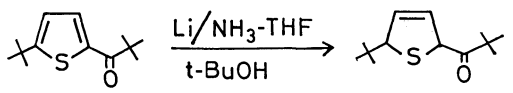

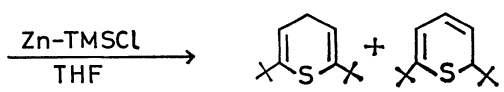

Scheme 1.

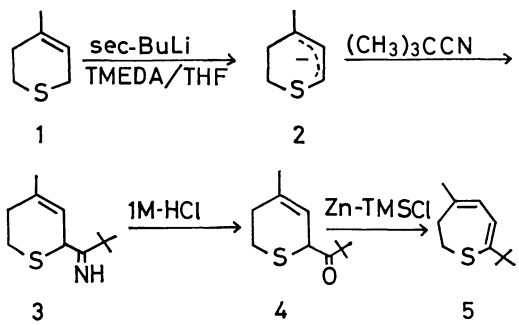

Scheme 2.

treated with pivalonitrile at −20 °C to give exclusively the crude imine **3** in high yield. Hydrolysis of **3** with 1 M (1 M=1 mol dm^{-3}) hydrochloric acid in THF–water formed **4**, whose structure was characterized unequivocally by a combination of elemental analysis and spectral data (^{1}H NMR, IR, and high resolution mass spectrum). It is interesting to note that the ambident anion **2** reacts exclusively at α-carbon of the sulfur atom with pivalonitrile.

The acylthiopyran **4** thus obtained led to the final product, dihydrothiepin (**5**) in excellent yield by treatment with chlorotrimethylsilane and activated zinc powder in THF at 0 °C. It was purified by column chromatography on alumina and elution with hexane. Its structure was confirmed by a full range of spectral data (see experimental section).

The successful conversion of **4** into **5** provides a new methodology for ring expansion reactions of sulfur heterocycles. Numerous applications will undoubtedly follow.

Experimental

^{1}H NMR (100 MHz) spectra were recorded on a Varian XL-100 spectrometer with TMS as the internal standard, IR spectra were recorded on a JASCO A-100 instrument, and mass spectra were obtained on a JEOL JMS-01SG-2 spectrometer.

*4-Methyl-6-pivaloyl-3,6-dihydro-2*H*-thiopyran (4).* To a solution of thiopyran (**1**; 0.31 g, 2.7 mmol) in 6 ml of tetrahydrofuran in the presence of 0.40 ml of TMEDA, was added 5.0 ml of 0.54 M s-butyllithium in hexane at −50 °C. After the solution was allowed to warm to −20 °C for 1 h, 0.28 ml (2.5 mmol) of pivalonitrile was added to the solution cooled to −50 °C with stirring, and the reaction mixture was stirred for an additional 3 h at −20 °C. After addition of water, the product was extracted with ether, and the ether solution dried over anhydrous sodium sulfate. Removal of the solvent gave the crude imine **3**; yield: 0.47 g (88.5%). IR (neat: ν=1620 cm^{-1}. ^{1}H NMR (CCl_4): δ=1.17 (s, 9H); 1.77 (s, 3H); 2.28 (m, 2H); 2.57 (m, 2H), 3.90 (d-like, 1H); 5.17 ppm (m, 1H). To 0.34 g (1.7 mmol) of crude imine **3** in 7 ml of THF was added 2 ml of 1 M hydrochloric acid at room temperature, the reaction mixture was stirred for 3 h. The product was extracted with hexane and the combined extracts dried over anhydrous sodium sulfate. Removal of the solvent gave crude acylthiopyran **4**, which was purified by short column chromatography (alumina) and elution with benzene to give pure **4**; yield: 0.336 g (98%). IR (neat): ν=1695 cm^{-1} (C=O). ^{1}H NMR ($CDCl_3$): δ=1.23 (s, 9H); 1.76 (bs, 3H); 2.22—3.00 (m, 4H); 4.30 (d, 1H, J=6.0 Hz); 5.33 ppm (m, 1H). Found: C, 66.95; H, 9.23; S, 15.72%. Calcd for $C_{11}H_{18}OS$: C, 66.62; H, 9.15; S, 16.17%. High Mass m/e=198.1070 (Calcd for $C_{11}H_{18}OS$; 198.1077).

7-t-Butyl-4-methyl-2,3-dihydrothiepin (5). To a suspension of 1.68 g of activated zinc powder in the solution of **4** (0.30 g, 1.5 mmol) in 15 ml of THF, 3.2 ml (25 mmol) of chlorotrimethylsilane was added dropwise at 0 °C with

stirring over 3 h. To the reaction mixture cooled to −20 °C, 1 ml of 1 M sodium hydroxide solution was added carefully. After removal of the zinc by decantation, the product was extracted with hexane, and the extracts were dried over anhydrous sodium sulfate. Evaporation of the solvent gave **5**, which was distilled at 50 °C/4 Torr. Yield: 270 mg (99%). ^{1}H NMR ($CDCl_3$): δ=1.16 (s, 9H); 1.86 (s, 3H); 2.66 (t-like, 2H); 2.87 (t, 2H, J=5.0 Hz); 5.73 (m, 1H); 5.87 ppm (d, 1H, J=8.0 Hz). Found: C, 72.56; H, 9.95; S, 17.36%. Calcd for $C_{11}H_{18}S$: C, 72.47; H, 9.95; S, 17.58. High Mass m/e=182.1122 (Calcd for $C_{11}H_{18}S$; 182.1127).

References

1) Recent reviews: W. C. Grouta, and D. Felker, *Synthesis*, **1980**, 861; E. W. Colvin, *Chem. Soc. Rev.*, **7**, 15 (1978); T. -H. Chan, *Acc. Chem. Res.*, **10**, 442 (1977); I. Kuwajima, *Yuki Gosei Kagaku Kyokai Shi*, **37**, 107 (1979); K. Tamao, J. Yoshida, and M. Kumada, *ibid.*, **38**, 41 (1980); S. Murai and N. Sonoda, *ibid.*, **39**, 301 (1981).

2) I. Elphimoff-Felkin and P. Sarda, *J. Chem. Soc., Chem. Commun.*, **1969**, 1065; W. B. Motherwell, *ibid.*, **1973**, 935; P. Hodge, M. N. Kham, *J. Chem. Soc., Perkin Trans. 1*, **1975**, 809.

3) Desulfurization: S. Kurozumi, T. Toru, M. Kobayashi, and S. Ishimoto, *Synth. Commun.*, **7**, 427 (1977); Preparation of silyl enol ethers from α-haloketones: G. C. Toshi and L. M. Pande, *Synthesis*, **1975**, 450; S. Hashimoto, A. Itoh, Y. Kitagawa, H. Yamamoto, and H. Nozaki, *J. Am. Chem. Soc.*, **99**, 4192 (1977), G. M. Rubottom, R. C. Mott, and D. S. Krueger, *Synth. Commun.*, **7**, 327 (1977); Preparation of ethyl trimethylsilylacetate (silylation reagent): R. J. Fessenden and J. S. Fessenden, *J. Org. Chem.*, **32**, 3535 (1967). E. Nakamura, T. Murofushi, M. Shimizu, and I. Kuwajima, *J. Am. Chem. Soc.*, **98**, 2346 (1976).

4) K. Nishino, S. Yano, Y. Kohashi, K. Yamamoto, and I. Murata, *J. Am. Chem. Soc.*, **101**, 5059 (1979); I. Murata, K. Nishino, S. Yano, Y. Kohashi, and K. Yamamoto, *Croat. Chem. Acta*, **53**, 615 (1980). The other derivatives (2-*t*-butylthiopyran and 2-*t*-butyl-6-isopropylthiopyran) were also prepared according to this procedure (unpublished work in these laboratories).

5) D. L. Stotter and R. E. Itornich, *J. Am. Chem. Soc.*, **95**, 4444 (1973).

6) K. Kondo, A. Negishi, K. Matsui, D. Tunemoto, and S. Masamune, *J. Chem. Soc., Chem. Commun.*, **1972**, 1311.

Origins and Spin Dependence of Near Infrared Magnetic Circular Dichroism of Iron(III) Hemoproteins

Takao YAMAMOTO,† Tsunenori NOZAWA, Nagao KOBAYASHI,†† and Masahiro HATANO*
Chemical Research Institute of Non-aqueous Solutions, Tohoku University, Sendai 980
(Received October 5, 1981)

Temperature variation experiments on near infrared magnetic circular dichroism spectra (700—2000 nm) have demonstrated that metmyoglobin (iron(III) myoglobin) cyanide and metmyoglobin fluoride derivatives which are typical low and high spin iron(III) heme complexes, respectively, exhibit the Faraday *C* term and the Faraday *C* and *A* terms, respectively. The results are consistent with theoretical predictions based on the assignment that the near infrared bands of the iron(III) heme complexes are attributable to the charge-transfer transitions from the occupied a_1 and a_2 π orbitals to the vacant iron $d\pi$ (d_{xz}, d_{yz}) orbitals in a C_{4v} notation.

The magnetic circular dichroism (MCD) spectra of heme for the ultraviolet and visible bands which consist mainly of porphyrin π to π^* transitions have reflected the electronic states of the heme iron.[1] The origins of the MCD have been explained in several ways.[1-10] Beyond the visible region, hemoproteins show several transitions ascribable to d-d transitions or to charge-transfer transitions associated with the d-electrons in the near infrared region,[11,12] so that these MCD bands should give more direct information of spin, oxidation, and ligand states of hemoproteins.

Cheng *et al.*[13] measured near infrared MCD spectra of methemoglobin (iron(III) hemoglobin) cyanide in the wavelength region from 800 to 2000 nm. Later, Stephens *et al.*[14] extended their studies to methemoglobin derivatives with fluoride, water, and azide. They explained all the MCD spectra as being composed of Faraday *C* terms in the charge-transfer transitions. Near infrared MCD spectra of various derivatives of metmyoglobin and myoglobin (iron(II) myoglobin) have been reported by Nozawa *et al.*[15] Near infrared MCD studies on cytochrome c′,[16] peroxidase,[17] P-450,[18] and cytochrome c[19] have appeared recently.

In this paper, assignment of Faraday parameters has been established experimentally by temperature variation studies on the typical low spin (metmyoglobin cyanide) and high spin (metmyoglobin fluoride) iron(III) hemoproteins. Further, the results are discussed in comparison with theoretical calculations.

Experimental

Horse heart myoglobin used was purchased from Sigma (type III). All chemicals were guaranteed grade reagents and used without further purification. ^2H_2O phosphate buffer (1/15 mol dm^{-3}, pH 6.98) and H_2O phosphate buffer (0.01 mol dm^{-3}, pH 7.0) were used to dissolve metmyoglobin cyanide and metmyoglobin fluoride, respectively. Potassium hexacyanoferrate(III) was used to oxidized myoglobin completely and excess hexacyanoferrate(III) was removed by passage through a column of Sephadex-G25 (medium). Metmyoglobin derivatives were prepared by adding respective solid salts to appropriate concentration (1 mol dm^{-3} KCN, 1.5 mol dm^{-3} NaF). Undissolved fraction was removed by low speed centrifugation (600 g). Amicon ultra filters (CF-25) were used to concentrate metmyoglobin solutions by the centrifugation.

Absorption spectra were recorded on a Hitachi EPS-3T spectrophotometer. MCD spectra from 800 to 1000 nm were obtained by use of a JASCO Model J-20A CD spectrometer with S-20 and S-1 type photomultipliers (Hamamatsu Television). The sensitivity of the J-20A is as high as 1×10^{-3} degree cm^{-1}. MCD spectra beyond 1000 nm were measured on a JASCO Model J-200 CD spectrometer with a CaF_2-photoelastic modulator (Morvue) incorporated. An S-1 type photomultiplier (Hamamatsu Television) and an InSb photovoltaic cell (Judson) were used as detectors for the wavelength regions from 800 to 1100 and beyond 1000 up to 2000 nm, respectively. The J-200 CD instrument has sensitivities of 2×10^{-3} and 5×10^{-3} degree cm^{-1} for the photomultiplier (800—1100 nm) and photovoltaic cell regions (1000—2000 nm), respectively. Electromagnets capable of producing magnetic fields up to 1.48 and 1.14 T were used for MCD measurements. The MCD magnitude is expressed by the molar ellipticity per Tesla ($[\theta]_M/10^4$ degree mol^{-1} dm^3 m^{-1} T^{-1} or 10 degree m^2 mol^{-1} T^{-1}).

Measurements at room temperature were carried out in 1/15 mol dm^{-3} ^2H_2O potassium phosphate buffer (pH 6.98). For low temperature measurements, mixtures of phosphate buffer and ethylene glycol-d_6 (50 : 50 in volume) and of phosphate buffer, potassium glycerophosphate, glycerol, and hydrochloric acid solution (4 : 20 : 10 : 5 in volume) were used in the regions from 1000 to 2000 (for metmyoglobin cyanide) and from 700 to 1000 nm (for metmyoglobin fluoride), respectively, to get transparent glass down to the liquid nitrogen temperature; the temperature was monitored with an alumel-chromel thermocouple inserted in the cell placed in a quartz Dewar vessel, and controlled by a stream of cold gaseous nitrogen evaporated from liquid nitrogen. Each scan was started 30 min after the temperature had reached a constant value. MCD measurements were repeated at least three times, results of a set being in good agreement with one another whithin experimental errors (±5%).

Results

Figure 1 demonstrates the effect of temperature on near infrared MCD and absorption spectra of metmyoglobin cyanide which is a typical low spin derivative. The MCD and absorption spectra at 0 °C show a good agreement with those previously reported by us.[15] The inset in Fig. 1 shows that the $[\theta]_M$ values of the MCD peaks at 6390 cm^{-1} (1560 nm), 7810 cm^{-1} (1280 nm),

† Present address: Kawamura Research Institute, 2-7-8, Kamikizaki, Urawa, Saitama 338.

†† Present address: Pharmaceutical Institute, Tohoku University, Aobayama, Sendai 980.

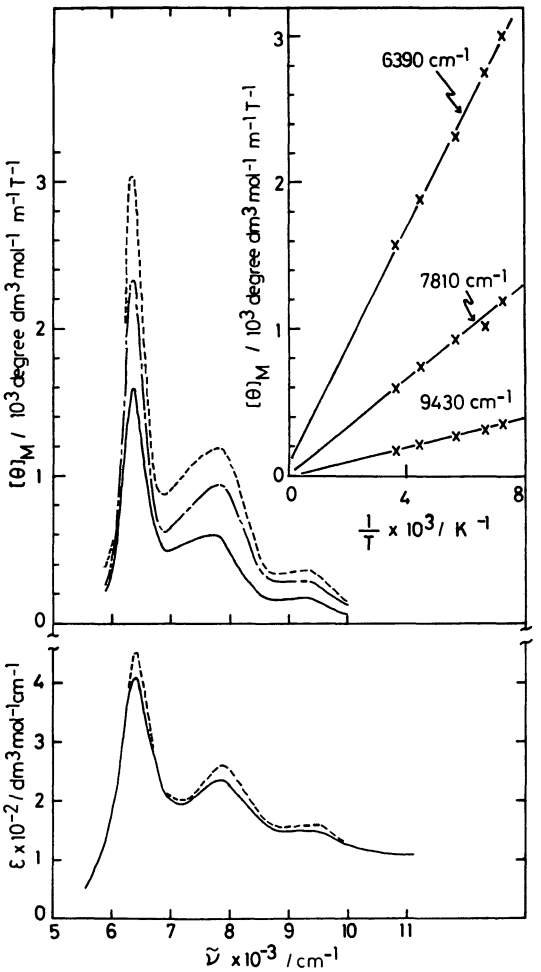

Fig. 1. Near infrared MCD and absorption spectra for metmyoglobin cyanide in the near infrared region at various temperatures(——; 273 K, —·—; 176 K, -----; 137 K). In the inset, the $[\theta]_M$ values are plotted against reciprocals of absolute temperatures. Metmyoglobin concentration, 3.83×10^{-3} mol dm^{-3} (on the heme basis), KCN concentration, 1×10^{-3} mol dm^{-3}, 1.48 T. Cell length, 3 mm. Other experimental conditions are described in the text.

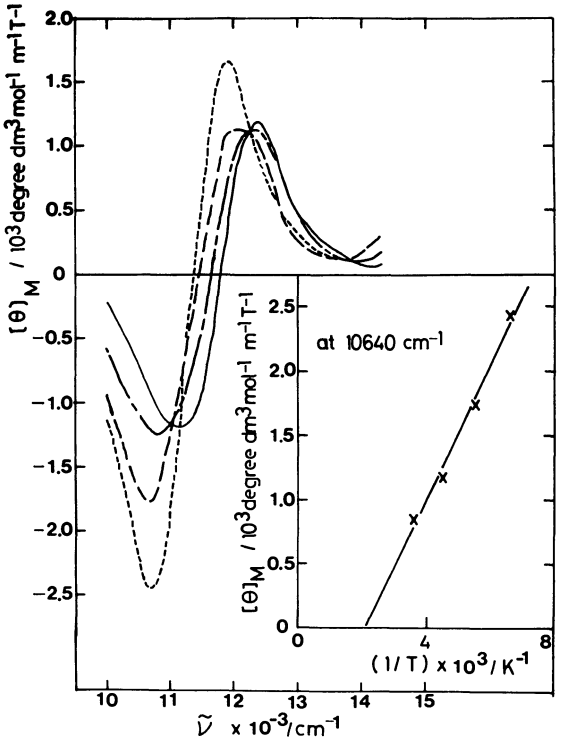

Fig. 2. MCD spectra for metmyoglobin fluoride in the near infrared region at various temperatures (——; 271 K, —·—; 219 K, ----; 179 K, and -----; 150 K). Metmyoglobin concentration, 6.04×10^{-3} mol dm^{-3}, NaF concentration, 1.5 mol dm^{-3}, cell length 2 mm, magnetic field 1.14 T. Other experimental conditions are described in the text.

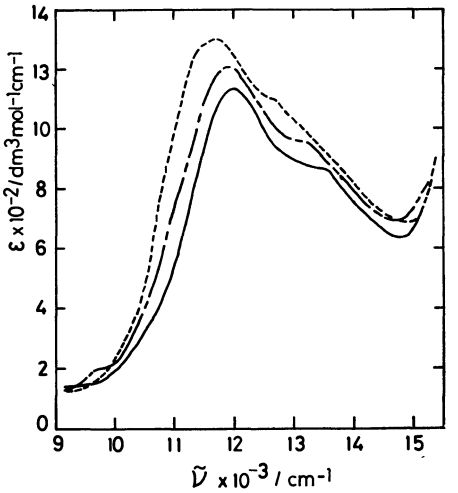

Fig. 3. Absorption spectra for metmyoglobin fluoride in the near infrared region at several temperatures (——; 293 K, —·—; 213 K, -----; 143 K). Other experimental conditions are the same as those for Fig. 2.

and 9430 cm^{-1} (1060 nm) increased in proportion to the reciprocal of absolute temperature ($1/T$). The extraporation of the lines gives zero intercepts at $1/T=0$. The absorption spectra exhibit only small increases in magnitude and band narrowing. These facts clearly indicate that the near infrared MCD spectra of metmyoglobin cyanide are composed of pure Faraday C terms. The intervals of the three peaks are 1420 and 1620 cm^{-1} and the intensity ratio among them is 93 : 35 : 1 at 0 °C.

Figure 2 illustrates the MCD spectra of metmyoglobin fluoride, a typical high spin iron(III) heme complex, at 271, 219, 179, and 150 K. Figure 3 shows the corresponding absorption spectra. The MCD and absorption spectra at 273 K agree with those previously reported by us.[15] The MCD peak around 12100 cm^{-1} (830 nm) exhibited only a small increase in intensity and a red shift by 400 cm^{-1} with temperature change from 271 and 150 K. The trough around 10600 cm^{-1} (940 nm) showed a red shift of 500 cm^{-1} and a 179% intensity increase. The absorption spectra also exhibited a 500 cm^{-1} red shift and an increase in magnitude around 11000 cm^{-1} by 80%. These complicated changes in the absorption and MCD spectra indicate that the near infrared MCD spectra are composed of a few Faraday

terms. The large temperature dependence of the MCD spectra suggests the presence of Faraday C term (around 10600 cm^{-1}). The temperature-independent Faraday A term with the S-shaped dispersion is also presumed to be present around 11500 cm^{-1}. Since the absorption spectra also increased in magnitude and exhibited a red shift, some changes in the MCD spectra should be due to that in the absorption spectra. Therefore it is concluded that the near infrared MCD spectra are composed of the large A term[20] around 11500 cm^{-1} and the C term around 10600 cm^{-1}.

Discussion

Electronic States of Heme. Actual heme chromophore has no C_{4v} symmetry rigorously. However, many studies have shown that it is a good approximation in the first order.[21] In this approximation the 3d iron has five orbitals with four different energies conventionally designated as b_2 (d_{xy} or ζ), e (d_{xz} or η, d_{yz} or ξ), a_1 (d_z^2 or u), and b_1 ($d_{x^2-y^2}$ or v) as shown in Fig. 4. The evidence from experiments and theories showed that the near infrared band in the Fe(III) hemoproteins should be the charge-transfer transition from the porphyrin highest occupied π orbitals (a_1 and a_2) to the iron vacant d-orbitals (e) in a C_{4v} approximation.[11,12]

Iron(III) Low Spin. Since a lower symmetry perturbation lifts the degeneracy in the e orbitals and the spin-orbit interaction mixes the t_{2g} (O_h) orbitals, the ground electronic states of the low spin iron(III) heme can be represented as the following Kramers' doublet:[22-25]

$$\begin{aligned}\phi_k^+ &= -A_k\phi_\xi^+ + iB_k\phi_\eta^+ + C_k\phi_\zeta^-,\\ \phi_k^- &= A_k\phi_\xi^- + iB_k\phi_\eta^- + C_k\phi_\zeta^+,\end{aligned} \quad (1)$$

where

$$\begin{aligned}\phi_\xi^+ &= |a_1\bar{a}_1a_2\bar{a}_2\xi\eta\bar{\eta}\zeta\bar{\zeta}|, \quad \phi_\xi^- = |a_1\bar{a}_1a_2\bar{a}_2\bar{\xi}\eta\bar{\eta}\zeta\bar{\zeta}|,\\ \phi_\eta^+ &= |a_1\bar{a}_1a_2\bar{a}_2\xi\bar{\xi}\eta\zeta\bar{\zeta}|, \quad \phi_\eta^- = |a_1\bar{a}_1a_2\bar{a}_2\xi\bar{\xi}\bar{\eta}\zeta\bar{\zeta}|,\\ \phi_\zeta^+ &= |a_1\bar{a}_1a_2\bar{a}_2\xi\bar{\xi}\eta\bar{\eta}\zeta|, \quad \phi_\zeta^- = |a_1\bar{a}_1a_2\bar{a}_2\xi\bar{\xi}\eta\bar{\eta}\bar{\zeta}|.\end{aligned} \quad (2)$$

In the Slater determinant, bar implies down spin and no bar stands for up spin. Similarly the charge-transfer state from the porphyrin a_1 (π) orbital to metal ξ, η (d_π) can be described as

$$\begin{aligned}\phi_4^+ &= -|a_1a_2\bar{a}_2\xi\bar{\xi}\eta\bar{\eta}\zeta\bar{\zeta}|,\\ \phi_4^- &= -|\bar{a}_1a_2\bar{a}_2\xi\bar{\xi}\eta\bar{\eta}\zeta\bar{\zeta}|.\end{aligned} \quad (3)$$

Electron paramagnetic resonance experiments for metmyoglobin cyanide give three g values as follows:[26]

$$g_x = 0.75,\ g_y = 1.88,\ g_z = 3.41.$$

Since these g values should arise from the Zeeman levels at the lowest Kramers' doublet, the relations expressed by

$$\begin{aligned}g_x &= 2|(B_1-C_1)^2 - A_1^2|,\\ g_y &= 2|(A_1-C_1)^2 - B_1^2|,\\ g_z &= 2|(A_1+B_1)^2 - C_1^2|,\end{aligned} \quad (4)$$

together with a normalization condition ($A_k^2+B_k^2+C_k^2=1$) give the A_k, B_k, and C_k values listed in Table 1, which also contains coefficients and relative energies for the second and third Kramers' doublets derived from a method similar to that of Griffith[23] and Kotani.[24]

Table 1. A set of coefficients and relative energies for respective Kramers' doublet

k	Relative energy	A_k	B_k	C_k
1	0	0.877	0.439	−0.188
2	1.417 λ[a]	0.463	−0.881	0.100
3	3.656 λ[a]	0.122	0.175	0.977

a) λ represents a spin-orbit coupling coefficient.

Iron(III) High Spin. The ground state of the iron(III) high spin heme belongs to the ^6A state described as follows for the state with $M=5/2$:

$$\phi_6 = |a_1\bar{a}_1a_2\bar{a}_2\xi\eta\zeta uv|, \quad (5)$$

and the other five wavefunctions for the ^6A state can be obtained by operating the shift operator $\mathbf{S}_-$ on Eq. 5. In high spin derivatives, the lowest charge-transfer transitions are from a_1, a_2, to b_2, e. These give rise to a

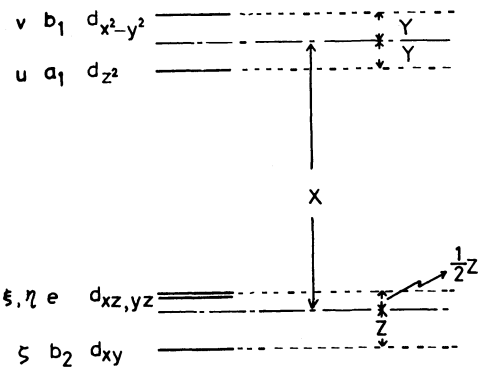

Fig. 4. Nomenclatures of 3d iron orbitals splitted in C_{4v} ligand field symmetry. X reperesents the octahedral (O_h) splitting energy of the 3d orbitals, Y and Z stand for those in the tetragonal field in the e_g and t_{2g} orbitals (O_h), respectively.

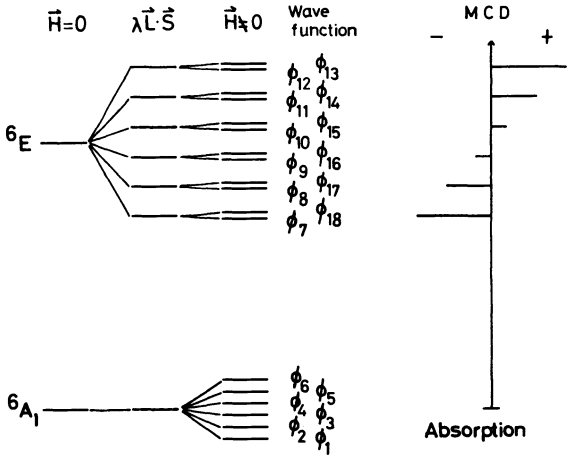

Fig. 5. The splitting pattern for the ground ($^6A_1$) and excited states (^6E) of the charge-transfer band in the high spin iron(III) heme derivatives by the effect of the spin-orbit coupling $\lambda\cdot\vec{L}\cdot\vec{S}$ and the magnetic field (H). The sign and relative magnitudes of Faraday C terms for the respective sublevels are also illustrated in the figure.

variety of states. However, to the first order in spin-orbit coupling only the states to which electric dipole transitions are allowed are the two ^{6}E states arising from e←a_1 and e←a_2, whose wavefunctions diagonalized in μ_z and $\lambda\vec{L}\cdot\vec{S}$ can be expressed for $M=5/2$ as follows:

$$\phi_{18} = -\frac{i}{\sqrt{2}}\left\{\left|\eta\frac{5}{2}\right\rangle + i\left|\xi\frac{5}{2}\right\rangle\right\},$$
$$\phi_{12} = -\frac{i}{\sqrt{2}}\left\{\left|\eta\frac{5}{2}\right\rangle - i\left|\xi\frac{5}{2}\right\rangle\right\}. \quad (6)$$

Similarly, the other diagonalized wavefunctions can be obtained as linear combinations of the two components with $M=-5/2$, $3/2$, $-3/2$, $1/2$, and $-1/2$. A schematic diagram for the iron(III) high spin ground and charge-transfer excited states are shown in Fig. 5 in the absence and presence of applied magnetic field.

Prediction of Faraday Parameters and Comparison with Experimental Results. Now we see how the MCD theory and the electronic states of the heme predict the kind and values of Faraday parameters for the charge-transfer transitions in the Fe(III) low and high spin heme complexes, and will compare calculated results with experimental data.

To calculate the Faraday parameters the following formulas[2-4] are used:

$$[\theta]_M = -24NH_z/\hbar c[f_1A + f_2(B+C/kT)], \quad (7)$$
$$A = (3/d_a)\sum_{a\to j}[\langle j|\mu_z|j\rangle - \langle a|\mu_z|a\rangle]\times \mathrm{Im}\{\langle a|m_x|j\rangle\langle j|m_y|a\rangle\}, \quad (8)$$
$$B = (3/d_a)\sum_{a\to j}\mathrm{Im}\{\sum_{k\neq a}[\langle k|\mu_z|a\rangle/(E_k-E_a)]\cdot[\langle a|m_x|j\rangle\langle j|m_y|k\rangle - \langle a|m_y|j\rangle\langle j|m_x|k\rangle] + \sum_{k\neq j}[\langle j|\mu_z|k\rangle/(E_k-E_j)]\cdot[\langle a|m_x|j\rangle\langle k|m_y|a\rangle - \langle a|m_y|j\rangle\langle k|m_x|a\rangle]\}, \quad (9)$$
$$C = (3/d_a)\sum_{a\to j}\langle a|\mu_z|a\rangle\mathrm{Im}\{\langle a|m_x|j\rangle\langle j|m_y|a\rangle\}, \quad (10)$$
$$f_1 = \frac{\pi^{1/2}\nu(\nu_{ja}-\nu)}{h\Delta_{ja}^3}\exp\left[-\frac{(\nu-\nu_{ja})^2}{\Delta_{ja}^2}\right], \quad (11)$$
$$f_2 = \frac{\pi^{1/2}\nu}{2\Delta_{ja}^2}\exp\left[-\frac{(\nu-\nu_{ja})^2}{\Delta_{ja}^2}\right]. \quad (12)$$

The symbol μ_z represents the z component of the magnetic moment operator and m_x and m_y stand for the x and y components of the electric moment operators. The number of degeneracies in the ground state is expressed by d_a. The summations are taken over all degenerate transitions for j←a.

Iron(III) Low Spin. According to the Boltzmann distribution and the energy separations among the three Kramers' doublets in Table 1, the populations in the lowest Kramers' doublets at 288 K were calculated to be 95 and 79% for the assumed spin-orbit coupling coefficient of 400 and 200 cm^{-1}, respectively. Hence in the following calculations, the contributions from the two higher Kramers' doublets were neglected.

By using the parameters A_1, B_1, and C_1 listed in Table 1 and Eqs. 1—3 and 7—11, one gets the Faraday A, B, and C terms as follows:

$$A = 0.81\langle a_1|m_x|\eta\rangle\langle\xi|m_y|a_1\rangle,$$
$$B = -1.84\times10^{-3}\langle a_1|m_x|\eta\rangle\langle\xi|m_y|a_1\rangle, \quad (13)$$
$$C = -1.96\langle a_1|m_x|\eta\rangle\langle\xi|m_y|a_1\rangle.$$

The extrema in the MCD spectra will be given as follows by assuming a Gaussian line shape:[27]

$$[\theta]_M^{max}(A) = (\pi^{1/2}e^{-1/2}\nu_{ja}/\sqrt{2}h\Delta_{ja}^2)A, \quad (14)$$
$$[\theta]_M^{max}(B+C/kT) = (\pi^{1/2}\nu_{ja}/2\Delta_{ja})(B+C/kT). \quad (15)$$

Here ν_{ja} is the frequency of transition and Δ_{ja} is the band width at $[\theta]_M=(1/e)[\theta]_M^{max}$. The ratios of the maximum values of the Faraday parameters given in Eqs. 14 and 15 can be estimated as follows:

$$[\theta]_M^{max}: \frac{C/kT}{B} = \frac{1}{kT}\cdot\frac{(-1.96)}{(-1.84\times10^{-3})} = 5.19, \quad (16)$$

$$[\theta]_M^{max}: \frac{C/kT}{A} = \frac{\sqrt{e}h\Delta_{ja}(-1.96)}{\sqrt{2}kT\ (0.81)} = -6.88, \quad (17)$$

where we adopted $\Delta_{ja}=500$ cm^{-1} and $kT=205$ cm^{-1}. These results predict that Faraday C terms will dominate in the MCD spectra of the Fe(III) low spin complexes even at 295 K. This agrees with the experimental result that the near infrared MCD spectra of the metmyoglobin cyanide are predominantly composed of Faraday C terms.

Iron(III) High Spin. In this case the spin-orbit interaction makes the excited states split into six sublevels as shown in Fig. 5. Hence Faraday parameters should be calculated for the six transitions to these six excited state sublevels. The calculated Faraday parameters A and C are:

$$A = (3/2)\langle a_1|m_x|\eta\rangle\langle\xi|m_y|a_1\rangle \text{ for all six transitions,}$$
$$C = (-15/2)\langle a_1|m_x|\eta\rangle\langle\xi|m_y|a_1\rangle \text{ for } (\Phi_{12}, \Phi_{13}) \longleftarrow (\Phi_1, \Phi_6),$$
$$(-9/2)\langle a_1|m_x|\eta\rangle\langle\xi|m_y|a_1\rangle \text{ for } (\Phi_{11}\ \Phi_{14}) \longleftarrow (\Phi_2, \Phi_5),$$
$$(-3/2)\langle a_1|m_x|\eta\rangle\langle\xi|m_y|a_1\rangle \text{ for } (\Phi_{10}, \Phi_{15}) \longleftarrow (\Phi_3, \Phi_4)$$
$$(3/2)\langle a_1|m_x|\eta\rangle\langle\xi|m_y|a_1\rangle \text{ for } (\Phi_9, \Phi_{16}) \longleftarrow (\Phi_3, \Phi_4),$$
$$(9/2)\langle a_1|m_x|\eta\rangle\langle\xi|m_y|a_1\rangle \text{ for } (\Phi_8, \Phi_{17}) \longleftarrow (\Phi_2, \Phi_5),$$
$$(15/2)\langle a_1|m_x|\eta\rangle\langle\xi|m_y|a_1\rangle \text{ for } (\Phi_7, \Phi_{18}) \longleftarrow (\Phi_1, \Phi_6). \quad (18)$$

Calculations indicate that so long as the sublevels of the ground and excited states are considered, the Faraday B term makes no contribution to the MCD spectra for this charge-transfer band. Since the signs of the six Faraday A terms are the same, the intensity of the Faraday A terms for the overall ^{6}E←^{6}A will be additive. On the other hand, the Faraday C terms for the transitions from (Φ_1, Φ_6) to (Φ_{12}, Φ_{13}) and (Φ_7, Φ_{18}) are of equal magnitude but of opposite signs, hence they partly cancel with one another. The effects of these addition and cancellations were calculated analytically by taking λ (spin-orbit coupling coefficient) to be equal to 200 cm^{-1} and $\Delta_{ja}=1000$ cm^{-1}. The calculated results indicated that the Faraday A term increased by a factor of about 6, but that the Faraday C term reduced to 1/4 of that of the largest component. Hence the ratio of the maximum intensity of the resultant Faraday terms will be

$$[\theta]_M^{max}: \frac{C/kT}{A} = \frac{f_2(15/2)\times(1/4)}{kTf_1(3/2)\times 6} = 1.24 \quad \text{at } T = 273\text{ K}, \qquad (19)$$
$$= 2.25 \quad \text{at } T = 150\text{ K}.$$

The values suggest that at 273 K the Faraday A term contribution is comparable to that of the Faraday C term, but that at 150 K the contribution from the Faraday C term becomes larger until at very low temperature the Faraday C term predominates in the near infrared MCD spectra. The contribution of the Faraday C terms extracted from the experimental results is rather small as compared with the values estimated above. Magnitudes of the estimated C terms are more sensitive to change in those of the band width (Δ_{ja}) and spin-orbit coupling constant (λ) than that of the A term, because the former is a difference and the latter is an addition of overlapping component bands. The magnitude of the estimated C term becomes smaller as Δ_{ja} increases and λ decreases. Although the set of parameters used in the calculation is one of reasonable sets, the difference between the estimated and experimental values may imply that Δ_{ja} is larger than 1000 cm^{-1} and that λ is smaller than 200 cm^{-1}.

In conclusion, the near infrared MCD bands for the typical low (metmyoglobin cyanide) and high (metmyoglobin fluoride) spin iron(III) heme complexes have experimentally been determined to be composed of Faraday C terms and Faraday C and A terms, respectively. The theoretical calculations of Faraday parameters are consistent with the experimental Faraday parameters.

The authors acknowledge the support from Grant-in-Aid for Scientific Research of the Japanese Government.

References

1) M. Hatano and T. Nozawa, "Advances in Biophysics," ed by M. Kotani, S. Yomosa, and M. Hatano, Japan Scientific Societies Press, Tokyo and University Park Press, Baltimore (1978), Vol. 11, p. 95.

2) A. D. Buckingham and P. J. Stephens, *Ann. Rev. Phys. Chem.*, **17**, 399 (1966).

3) P. N. Schatz and A. J. McCaffery, *Quart. Rev. Chem. Soc.*, **23**, 552 (1969).

4) P. J. Stephens, *Ann. Rev. Phys. Chem.*, **25**, 201 (1974).

5) A. Kaito and M. Hatano, *J. Am. Chem. Soc.*, **100**, 2034 and 4037 (1978) and references therein.

6) J. I. Treu and J. J. Hopfield, *J. Chem. Phys.*, **63**, 613 (1975).

7) M. A. Livshitz, A. M. Arutyunyan, and Yu. A. Sharonov, *J. Chem. Phys.*, **64**, 1276 (1976).

8) H. Kobayashi, T. Higuchi, and K. Eguchi, *Bull. Chem. Soc. Jpn.*, **48**, 457 (1976).

9) Y. Seno, N. Kameda, and J. Otsuka, *J. Chem. Phys.*, **72**, 6048, 6059 (1980).

10) Yu. A. Sharonov, A. P. Mineyev, M. A. Livshitz, N. A. Sharonova, V. B. Zhurkin, and Yu. P. Lysov, *Biophys. Struct. Mech.*, **4**, 139 (1978).

11) M. Zerner, M. Gouterman, and H. Kobayashi, *Theor. Chim. Acta*, **6**, 363 (1966).

12) D. W. Smith and R. J. P. Williams, *Struct. Bonding*, **7**, 1(1970).

13) J. C. Cheng, G. A. Osborne, P. J. Stephens, and W. A. Eaton, *Nature*, **241**, 193 (1973).

14) P. J. Stephens, J. C. Sutherland, J. C. Cheng, and W. A. Eaton, "Proceedings of the International Conference on Excited States of Biological Molecules, Leiden," ed by J. Birks, Wiley-Interscience, New York (1976), p. 434.

15) T. Nozawa, T. Yamamoto, and M. Hatano, *Biochim. Biophys. Acta*, **427**, 28 (1976).

16) J. Rawlings, P. J. Stephens, L. A. Nafie, and M. D. Kamen, *Biochemistry*, **16**, 1725 (1977).

17) N. Kobayashi, T. Nozawa, and M. Hatano, *Biochim. Biophys. Acta*, **493**, 340 (1977).

18) T. Nozawa, T. Shimizu, M. Hatano, H. Shimada, T. Iizuka, and Y. Ishimura, *Biochim. Biophys. Acta*, **534**, 285 (1978).

19) N. Kobayashi, T. Nozawa, and M. Hatano, *Bull. Chem. Soc. Jpn.*, **54**, 919 (1981).

20) Since heme b in myoglobin has not the true C_{4v} symmetry when all the substituents on the periphery of the porphyrin are taken into consideration, the porphyrin lowest unoccupied e orbitals (C_{4v}) are slightly split into two closely positioned orbitals in the actual symmetry lower than C_{4v}. Hence there can not be expected the true Faraday A term. However, as the calculation indicated (A. Kaito *et al.*, *Chem. Phys. Lett.*, **52**, 154 (1977)), the Faraday B terms predominantly mix among these two split orbitals to give an S-shaped MCD band which is a mimic Faraday A term. In this paper this apparent A term has been treated just like the true Faraday A term.

21) Y. Seno and J. Otsuka, "Advances in Biophysics," ed by M. Kotani, S. Yomosa, and M. Hatano, Japan Scientific Societies Press, Tokyo and University Park Press, Baltimore (1978), Vol. 11, p. 13.

22) M. Weissbluth, *Struct. Bonding*, **2**, 1 (1967).

23) J. S. Griffith, *Nature*, **180**, 30 (1957).

24) M. Kotani, *Suppl. Progr. Theor. Phys.*, **17**, 4 (1961).

25) H. Kobayashi, "Advances in Biophysics," ed by M. Kotani, University of Tokyo Press, Tokyo and University Park Press, Baltimore (1976), Vol. 8, p. 191.

26) G. Shulman, S. H. Glarum, and M. Karplus, *J. Mol. Biol.*, **57**, 93 (1971).

27) P. J. Stephens, W. Suetaka, and P. N. Schatz, *J. Chem. Phys.*, **44**, 4592 (1966).

On the Ratio of Zwitterion Form to Uncharged Form of Glycine at Equilibrium in Various Aqueous Media

Goro WADA,* Eiko TAMURA, Mitsuko OKINA, and Mariko NAKAMURA
Department of Chemistry, Nara Women's University, Nara 630

(Received November 19, 1981)

The ratios of the zwitterion form to the uncharged form of glycine, $K_D=[NH_3^+CH_2COO^-]/[NH_2CH_2COOH]$, were determined in mixtures of water with methanol, ethanol, *t*-butyl alcohol, dimethyl sulfoxide, acetonitrile, 1,4-dioxane, *N*,*N*-dimethylformamide, and tetrahydrofuran. The value of ln K_D decreases and, therefore, ΔG°_{298} increases, with the increase in the mole fractions of the organic solvents. The plots of ΔG° *vs.* reciprocal of the dielectric constants of the alcoholic mixtures are simply linear indifferent to the kind of alcohols, indicating that this relation obeys the Scatchard equation and that the free energy change of the process of the intramolecular protonation in glycine is controlled mainly by electrostatic interaction, especially by the entropy change associated with the preferential solvation around the charged amino and carboxyl groups.

In aqueous solution, glycine (aminoacetic acid) exists in various ionized or neutral forms depending upon the hydrogen-ion concentrations of the solution, as shown in the following scheme.[1]

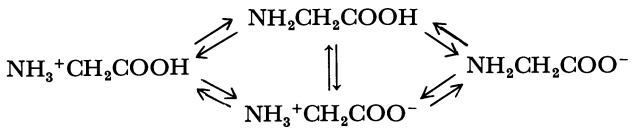

The formulas $NH_3^+CH_2COOH$ and $NH_2CH_2COO^-$ are cationic and anionic forms respectively, whereas NH_2CH_2COOH and $NH_3^+CH_2COO^-$ are both neutral, corresponding to the uncharged and zwitterion forms respectively, and establish a chemical equilibrium between themselves with a constant K_D:

$$K_D = \frac{[NH_3^+CH_2COO^-]}{[NH_2CH_2COOH]}. \quad (1)$$

These neutral forms are also at equilibria with other species with equilibrium constants, defined as follows.

$$K_1 = \frac{[NH_2CH_2COOH][H^+]}{[NH_3^+CH_2COOH]} \quad (2)$$

$$K_2 = \frac{[NH_3^+CH_2COO^-][H^+]}{[NH_3^+CH_2COOH]} \quad (3)$$

$$K_{12} = \frac{[NH_2CH_2COO^-][H^+]}{[NH_2CH_2COOH]} \quad (4)$$

$$K_{21} = \frac{[NH_2CH_2COO^-][H^+]}{[NH_3^+CH_2COO^-]} \quad (5)$$

According to the experimental method due to titration, the uncharged and the zwitterion forms can not be discriminated from each other, but only the sum of the concentrations of both species are determined. Thus, the apparent acidity constant of the acid form $NH_3^+CH_2COOH$ found experimentally, K, has a meaning as expressed by

$$K = \frac{([NH_2CH_2COOH] + [NH_3^+CH_2COO^-])[H^+]}{[NH_3^+CH_2COOH]}. \quad (6)$$

Then, the following relationships are derived from Eqs. 1, 2, 3, and 6.

$$K = K_1 + K_2 \quad (7)$$

$$K_D = \frac{K_2}{K_1} \quad (8)$$

Since $[NH_3^+CH_2COO^-]$ is much larger than $[NH_2CH_2COOH]$ in aqueous solution as will be seen later, K_2 is approximately equal to K, and therefore K_D can be considered to be equal to the ratio of K to K_1.

$$K \fallingdotseq K_2 \quad (7')$$

$$K_D \fallingdotseq \frac{K}{K_1} \quad (8')$$

For the determination of K_1, the ethyl ester of glycine, $NH_2CH_2COOC_2H_5$, was used in place of glycine, in order to mask the acidity of the carboxyl group, on the basis of an assumption that the basicity of amino group in glycine would not be greatly affected by the esterization of the carboxyl group, because the basicities of the methyl ester and ethyl ester of glycine have been known to be approximately identical.[2-4] Therefore,

$$K_1 = \frac{[NH_2CH_2COOC_2H_5][H^+]}{[NH_3^+CH_2COOC_2H_5]}. \quad (2')$$

In the present investigation, the values of K_D were determined in various aqueous solutions mixed with alcohols, such as methanol, ethanol, and *t*-butyl alcohol, and with other organic substances, such as acetonitrile, 1,4-dioxane, *N*,*N*-dimethylformamide (DMF), dimethyl sulfoxide (DMSO), and tetrahydrofuran (THF), at various mole fractions and various temperatures. The K_D values in water can be well compared with the data appearing in the literature.[4] Thus, the thermodynamic functions and the dielectric dependences of the equilibrium, the uncharged form⇄the zwitterion form, will be discussed.

Experimental

Materials. *Glycine*: Commercially obtained glycine of guaranteed reagent grade from Wako Pure Chemical Industries, Ltd. was recrystallized from water.

Glycine Ethyl Ester Hydrochloride: It was prepared by leading hydrogen chloride gas into the glycine suspended in ethanol. The crystals of the ester hydrochloride salt were purified by recrystallization from ethanol and its purity was checked by paper-chromatography.

Various Alcohols and Other Solvents: They were purified by ordinary methods.

Procedure and Calculations. Solutions of glycine which had been added by equimolar amount of hydrochloric acid or solutions of glycine ester hydrochloride were titrated with sodium hydroxide and the pH values of the solutions were

TABLE 1. VALUES OF K_1, K_2, AND K_D AT 25 °C IN MIXTURES OF WATER WITH ORGANIC SOLVENTS AT VARIOUS MOLE FRACTIONS x

Organic solvent	x	$\frac{K_1}{M}$	$\frac{K_2}{M}$	K_D
None	—	1.65×10^{-8}	3.90×10^{-3}	2.36×10^{5}
Methanol	0.051	1.86×10^{-8}	2.99×10^{-3}	1.61×10^{5}
	0.100	2.14×10^{-8}	3.28×10^{-3}	1.53×10^{5}
	0.199	2.57×10^{-8}	1.79×10^{-3}	6.96×10^{4}
	0.300	3.09×10^{-8}	1.19×10^{-3}	3.84×10^{4}
	0.400	4.17×10^{-8}	6.07×10^{-4}	1.45×10^{4}
	0.496	2.63×10^{-8}	9.95×10^{-5}	3.78×10^{3}
	0.601	3.31×10^{-8}	1.07×10^{-4}	3.23×10^{3}
	0.705	4.00×10^{-8}	3.93×10^{-5}	9.83×10^{2}
Ethanol	0.050	2.54×10^{-8}	2.06×10^{-3}	8.11×10^{4}
	0.098	2.62×10^{-8}	1.65×10^{-3}	6.30×10^{4}
	0.202	3.44×10^{-8}	1.05×10^{-3}	3.05×10^{4}
	0.299	4.32×10^{-8}	5.52×10^{-4}	1.28×10^{4}
	0.397	5.43×10^{-8}	1.63×10^{-4}	3.00×10^{3}
t-Butyl alcohol	0.050	2.97×10^{-8}	2.62×10^{-3}	8.83×10^{4}
	0.100	4.59×10^{-8}	2.29×10^{-3}	5.00×10^{4}
	0.300	9.07×10^{-8}	7.95×10^{-4}	8.77×10^{3}
DMSO	0.050	1.37×10^{-8}	1.51×10^{-3}	1.10×10^{5}
	0.100	1.14×10^{-8}	6.57×10^{-4}	5.76×10^{4}
Acetonitrile	0.300	5.49×10^{-8}	1.25×10^{-3}	2.28×10^{4}
1,4-Dioxane	0.300	7.01×10^{-8}	2.41×10^{-4}	3.44×10^{3}
DMF	0.300	1.53×10^{-8}	8.50×10^{-6}	5.56×10^{2}
THF	0.100	2.72×10^{-8}	1.05×10^{-3}	3.86×10^{4}

measured simultaneously by a pH-meter in a thermostat at given temperature. The hydrolysis of the ester was not observed appreciably during the course of titration. For the calculations of K and K_1, sets of pH values *vs.* volumes of sodium hydroxide solution at nearly middle points of the neutralization titration were used and averaged.

Results and Discussion

Equilibrium Constants and Related Thermodynamic Quantities. The values of K_1, K_2, and K_D at 25°C in mixtures of water with methanol, ethanol, *t*-butyl alcohol, DMSO, acetonitrile, 1,4-dioxane, DMF, and THF at various mole fractions are listed in Table 1. In the table, it is clearly seen that the zwitterion form is far more predominant than the uncharged one approximately by the order of magnitude 10^5 in water, but its ratio decreases with the increase in mole fraction of organic substances, especially in the case of DMF at $x=0.3$, the ratio being the smallest with the order of magnitude 10^2 among the data ever observed. Another feature is that K_D always decreases with temperature at any x in the all media, although the observed temperature dependences are not shown in Table 1.

In Fig. 1 are shown the variations of the free energies associated with the transformation of the uncharged form to the zwitterion form at various mole fractions of the organic solvents. The standard free energy change is calculated by the equation,

$$\Delta G^\circ = -RT \ln K_D. \quad (9)$$

The value of ΔG°_{298} in pure water is equal to −7.27 kcal mol^{-1} (1 cal=4.2 J), which agrees well with −7.3 kcal mol^{-1} obtained by Edsall and Blanchard.[4] Figure 1 indicates that ΔG°_{298} grows up gradually with the increase of x of alcohols, and is in a sequence at $x=0.3$, DMF> 1,4-dioxane> *t*-butyl alcohol> ethanol> acetonitrile>methanol.

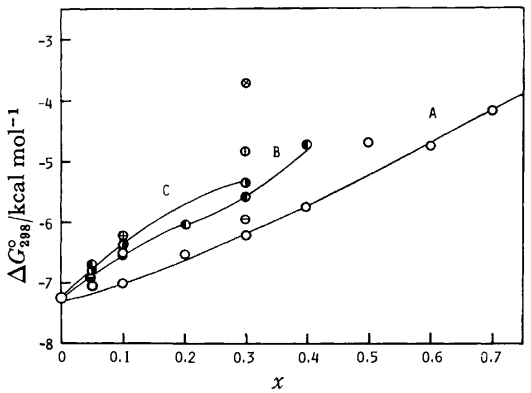

Fig. 1. The free energy ΔG°_{298} for the change of the uncharged form to the zwitterion form at 25 °C in mixtures of water and organic solvents at mole fractions x.
○: Methanol (A), ◐: ethanol (B), ◑: *t*-butyl alcohol (C), ◒: DMSO, ⊖: acetonitrile, ⓘ: 1,4-dioxane, ⊗: DMF, ⊕: THF.

Influence of Dielectric Constants of Media upon ΔG°. When ΔG°'s in various aqueous alcohols at diverse temperatures are plotted against reciprocals of the dielectric constants of the media, they come altogether on a single straight line with a positive slope indifferent to the kind of the alcohols, except for the case of *t*-butyl alcohol at $x=0.3$, as are drawn in Fig. 2. (Points for

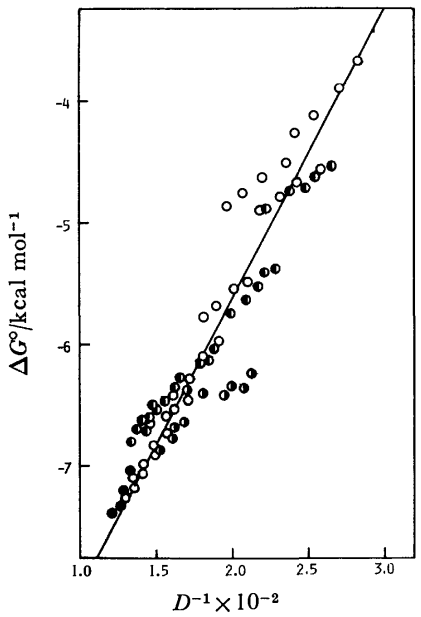

Fig. 2. Dependence of $\Delta G°$ in aqueous alcohols at various temperatures upon reciprocal of dielectric constants D^{-1}.
●: Water, ○: methanol, ◐: ethanol, ◑: *t*-butyl alcohol.

x=0.3 of *t*-butyl alcohol are omitted in the figure, which should appear towards the right out of the figure.) The dielectric constants of the media were calculated by numerical interpolations from the data observed by Åkerlöf.[5]

This linear relationship could be applied to the Scatchard equation,[6,7]

$$\Delta G° = \Delta G°_{\circ} - \frac{z_A z_B e^2 N_A}{rD}, \qquad (10)$$

where $\Delta G°$ originally implies a free energy change related to association of two ions, A and B, bearing electric charges $z_A e$ and $z_B e$ respectively at a distance r in media of various dielectric constants D and $\Delta G°_{\circ}$ and N_A are a constant and the Avogadro's number, respectively. In the present case, the change is not an approach between two separate ions, but an intramolecular prototropy resulting in occurrence of a zwitterion within an uncharged molecule. The zwitterion can be regarded as two ions which are combined with each other by a carbon chain behind. If the Scatchard's relationship could be valid in the zwitterion formation, the value of r may be estimated to be approximately 2 Å from the slope of the straight line in Fig. 2, assuming that the macroscopic value of D is roughly available in the very close vicinity around the polar groups. Since the value of r=2 Å looks like to be shorter than the expected value about 3.3 Å as the probable closest distance between N- and O-atoms ignoring the electric charges on respective atoms, it may be safely said that the positive electricity on the charged group $-NH_3^+$ is partly scattered on the three H-atoms and the centers of the electricities on both $-NH_3^+$ and $-C\overset{O}{\underset{O}{<}}(-)$ are forced to come closer to each other than the initial distance, although r may not be strictly equal to 2 Å, on account of certain theoretical inaccuracies involved in Eq. 10. Recently, these two functional groups were found to interact with each other at a fairly short distance in both gas phase[8] and solutions, from theoretical[9] and dilatometric[10] investigations.

Table 2. THERMODYNAMIC QUANTITIES FOR THE CHEMICAL CHANGE FROM THE UNCHARGED FORM TO THE ZWITTERION FORM, $\Delta G°_{298}$, $\Delta H°$, AND $\Delta S°$, IN AQUEOUS MIXTURES WITH VARIOUS ORGANIC SOLVENTS AT x=0.3
1 cal=4.2 J.

Organic solvent	$\Delta G°_{298}$ kcal mol^{-1}	$\Delta H°$ kcal mol^{-1}	$\Delta S°$ cal K^{-1} mol^{-1}
None(water)	−7.27	−10.3	−10.2
Methanol	−6.27	−10.7	−15.0
Ethanol	−5.60	−10.1	−15.0
t-Butyl alcohol	−5.38	−9.1	−11.5
Acetonitrile	−5.94	−9.1	−10.3
1,4-Dioxane	−4.82	−9.6	−15.8
DMF	−3.74	−11.7	−26.5

In the case of *t*-butyl alcohol, the plot of $\Delta G°$ *vs.* D^{-1} is supposed to deviate gradually from the common linearity in Fig. 2 as the mole fraction becomes larger than 0.1. Thus, the deviation found at x=0.3 might be only recognized by a consideration that the discrepancy between D values at a local spot around the ion and in the bulk of media can be no longer ignored and that the hydrophobicity of *t*-butyl group in the vicinity of the ion alters the structures not only of the zwitterion itself but also of the solvation sheaths surrounding the zwitterion strongly, in addition to the dielectric effect of the medium.

Thermodynamic Quantities, $\Delta G°_{298}$, $\Delta H°$, and $\Delta S°$ in Mixed Media. Table 2 shows the thermodynamic quantities, $\Delta G°_{298}$, $\Delta H°$, and $\Delta S°$, for the transformation of glycine from the uncharged form to the zwitterion form in pure water and in various mixed media at x=0.3. Values of $\Delta H°$ and $\Delta S°$ were obtained from the linear relationship of $\ln K_D$ *vs.* reciprocal of the absolute temperature. On general survey of the table, a trend is seen that the increase in $\Delta G°_{298}$ due to the addition of organic solvents is largely attributed to the decrease in $\Delta S°$, while $\Delta H°$ remains almost unchanged; namely this transformation is rather entropy-controlled.

This fact may indicate that the negative value of $\Delta H°$ is mainly caused by the change in the energy of chemical bondings related to protonation and deprotonation on amino and carboxyl groups respectively, while, on the other hand, the negative value of $\Delta S°$ depends upon the extent of solvation around the charged groups, the circumstances of the preferential solvation being different from solvent to solvent. The fact that $\Delta S°$ is more negative in the mixed solvents than in pure water, may suggest the possibility of the preferential solvation in the mixed solvents which is accompanied by a larger increment in the order than the simple hydration in pure water, in the vicinity of the zwitterions. After all, the gradual depression of K_D as x is increased may be mainly attributed to the growth of the degree of the preferential solvation in the mixed media with alcohols,

as shown in Fig. 1.

When the ionization constant K_a of various aliphatic carboxylic acids R–COOH or protonated amines $R'NH_3^+$ is empirically given by

$$-\log K_a = A_1T^{-1} - A_2 + A_3T, \quad (11)$$

where A_1, A_2, and A_3 are constants characteristic of the substance, ΔH° and ΔS° are expressed by the following equations.[11]

$$\Delta H^\circ = 2.303\,R(A_1 - A_3T^2) \quad (12)$$

$$\Delta S^\circ = 2.303\,R(A_2 - 2A_3T) \quad (13)$$

The transformation of glycine from the uncharged to zwitterion form consists of two processes; the protonation of amino group and the deprotonation of carboxyl group. If these two processes occur on separately different molecules, the total change is roughly expected as the sum of the following respective changes.

$$R'\text{-}NH_2 + H^+ \longrightarrow R'\text{-}NH_3^+ \quad (14)$$

$$R\text{-}COOH \longrightarrow R\text{-}COO^- + H^+ \quad (15)$$

$$R'\text{-}NH_2 + R\text{-}COOH \longrightarrow R'\text{-}NH_3^+ + R\text{-}COO^- \quad (16)$$

By using the values of A_1, A_2, and A_3,[11] the enthalpies and entropies at 25°C for several alkylamines (ammonium type) and aliphatic carboxylic acids can be calculated, and thus the final ΔH° and ΔS° for the Reaction 16 are readily estimated to be approximately -12 ± 2 kcal mol^{-1} and -15 ± 3 cal K^{-1} mol^{-1} respectively. These values are very close to those listed in Table 2, indicating that the thermodynamic quantities associated with a proton transfer in solution is almost unaffected whether it occurs intramolecularly or intermolecularly, although amino and carboxyl groups are located fairly close with each other in α-amino acids, like glycine. The value of ΔG° at $D=1$ (in gas phase) is assumed to be very large from the extrapolation in Eq. 10. This suggests that the value of K_D may be actually equal to zero in vacuum. In fact, it has been studied energetically and geometrically that the zwitterion is not expected to exist in gas-phase during at least an observable life time.[8,12]

Appendix

Examination of K_1 by Hammett-Taft Rule. For the determination of K_1, we have measured the basicity of ethyl ester of glycine in place of glycine, for the purpose of masking the acidic ionization of carboxyl group in glycine. Although the basicity of the ethyl ester has been found not to differ greatly from that of the methyl ester,[2-4] it is necessary to examine how much it differs from that of glycine itself. According to the Hammett–Taft rule for the substitution effect on pK_a, the pK_a of primary alkyl amines can be estimated by the following expression.[13]

$$pK_a = 13.23 - \Sigma\sigma^* \quad (17)$$

Since $\sigma^*(H)$, $\sigma^*(C_2H_5)$, and $\sigma^*(CH_2COOH)$ are $+0.49$, -0.10, and $+1.05$ respectively, $\sigma^*(CH_2COOC_2H_5)$ is supposed to be $+0.98$, taking into account that σ^* is reduced approximately half per every bond as the substitution group goes apart from N-atom. Therefore, the difference of $\log K_1$, $pK_a(NH_2CH_2COOC_2H_5) - pK_a(NH_2CH_2COOH)$ will be 0.22, which could be considered to have so small an effect upon the order of magnitude in K_D. Furthermore, the values of σ^* should be altered in mixed solvents, which are unknown at the present stage, in order to correct the observed data.

References

1) J. P. Greenstein and M. Winitz, "Chemistry of the Amino Acids," John Wiley & Sons, New York (1961), Vol. 1, Chap. 4, p. 445.
2) R. Wegscheider, *Monatsh.*, **16**, 153 (1895); **23**, 287 (1902).
3) L. Ebert, *Z. Phys. Chem.*, **121**, 385 (1926).
4) J. T. Edsall and M. H. Blanchard, *J. Am. Chem. Soc.*, **55**, 2337 (1933).
5) G. Åkerlöf, *J. Am. Chem. Soc.*, **54**, 4125 (1932).
6) G. Scatchard, *Chem. Rev.*, **10**, 229 (1932).
7) E. S. Amis, "Solvent Effects on Reaction Rates and Mechanisms," Academic Press, New York (1966), Chap. 1.
8) M. J. Locke, R. L. Hunter, and R. T. McIver, Jr., *J. Am. Chem. Soc.*, **101**, 272 (1979).
9) P. Palla, C. Petrongolo, and J. Tomasi, *J. Phys. Chem.*, **84**, 435 (1980).
10) L. Lepori and V. Mollica, *Z. Phys. Chem. Neue Folge*, **123**, 51 (1980).
11) R. A. Robinson and R. H. Stokes, "Electrolyte Solutions," Butterworth, London (1955), p. 496.
12) Y.-C. Tse, M. D. Newton, S. Vishveshwara, and J. A. Pople, *J. Am. Chem. Soc.*, **100**, 4329 (1978).
13) R. W. Taft, Jr., "Steric Effects in Organic Chemistry," ed by M. S. Newman, John Wiley & Sons, New York (1956), pp. 595 and 619.

Study on the Reaction of Monofunctional Fluorescent Reagents in Organic Solutions by Fluorometry

Akio Okamoto,* Katsumi Uchiyama, and Itaru Mita
Institute of Interdisciplinary Research, Faculty of Engineering, The University of Tokyo, 4-6-1, Komaba, Meguro-ku, Tokyo 153
(Received November 28, 1981)

Rections of some fluorescent reagents with substrates, used widely in biochemistry for quantitative analysis of some functional groups in aqueous media, have been studied in organic solutions with a view that they may be used also in the area of synthetic polymer science. Reactions studied by fluorometry were (i) 5-dimethylamino-1-naphthalensulfonyl chloride with butylamine, (ii) 2-naphthalenesulfonyl chloride with butylamine, and (iii) *N*-(1-naphthyl)maleimide with 1-pentanethiol. In polar solvents all the fluorescent probes studied are too labile and converted spontaneously into fluorescent compounds. In less polar solvents, however, such side reactions do not take place and the reaction of fluorescent reagents with substrates proceeds quantitatively with a simple second-order kinetics. The second-order rate constants for the three reactions are of the order of 10^{-3} to 10^{-1} M^{-1} s^{-1} in the range of about 30 to 50 °C, and they increase with the solvent polarity.

Fluorescent probes have been utilized widely in biochemistry either for analysing quantitatively functional groups in proteins or for probing the environment around the functional groups. In the former case, a component to be analyzed is converted by the reaction with a proper probe into a fluorescent derivative, and its quantity is determined from the emission intensity. In the later case, the details of the spectrum, lifetime, quantum yield, and depolarization provide information about the functional group and its surroundings. Two sorts of fluorescent probes have been used mainly.[1] The one is called fluorescent thiol reagent and comprises certain nonfluorescent *N*-substituted maleimides. They react with thiol compounds in aqueous solution to give fluorescent adducts.[2] The other is called fluorescent amine reagent and comprises nonfluorescent sulfonyl chlorides such as 5-dimethylamino-1-naphthalenesulfonyl chloride,[3] and nonfluorescent "fluorescamine."[4] They react almost quantitatively with primary amines in aqueous solution to give fluorescent products. Since these fluorescent reagents themselves are not soluble in water, it is a common practice to dissolve them first in an organic solvent such as acetone or dioxane then mix the solution with an aqueous solution of substrate.

A useful extension of the fluorescent probes is to make the probes react with substrates in organic solvents which are commonly used in studies on organic reactions or synthetic polymers. If it has become feasible to use the fluorescent probes in organic solutions in a similar manner to in aqueous solution, the fluorescent probes will be utilized more widely in organic chemistry or in polymer science. Only little has been reported, however, on the reaction kinetics of the fluorescent reagents, especially on the reaction in nonaqueous solvent.[5-7]

To advance the utilization of the fluorescent probes more widely, we investigated the reaction of monofunctional fluorescent amine reagents or sulfonyl chlorides with butylamine as well as of monofunctional thiol reagent with 1-pentanethiol in various solvents.

Experimental

Materials. *N*-(1-Naphthyl)maleimide (NMI) was prepared using a modified method of Tsou *et al.*[8] from 1-naphthylamine and maleic anhydride with acetic anhydride as dehydrating agent and sodium acetate and triethylamine as catalysts (51% yield). *N*-Butyl-5-dimethylamino-1-naphthalenesulfonamide (DNSBA) was prepared in a similar manner to the preparation of *N*-ethyl-5-dimethylamino-1-naphthalenesulfonamide.[8] A chloroform solution of 5-dimethylamino-1-naphthalensulfonyl chloride (dansyl chloride; DNSCl) (15 ml; 0.19 mol dm^{-3} (M†)) was mixed with a chloroform solution of butylamine (*n*-$BuNH_2$) (15 ml; 1.86 M) at room temperature. After 6 h the solution was washed with 0.1 M aqueous HCl solution and distilled water, dried over Na_2SO_4 overnight then the solvent was removed. The yellow residue was recrystallized from diethyl ether to give yellow-orange crystals which melted at 95—97 °C (40% yield). The structure was ascertained by NMR and IR. NMR ($CDCl_3$): δ 2.9 (N–C$\underline{H}_3$, –SO_2NH–C$\underline{H}_2$–), δ 5.3 (–SO_2N$\underline{H}$–), *etc.* IR: 3300 cm^{-1} (NH), 1320 and 1150 cm^{-1} (SO_2), *etc.* The purity was confirmed by TLC.

1-Pentanethiol (*n*-AmSH), 2-naphthalenesulfonyl chloride (NDSCl), DNSCl, and *n*-$BuNH_2$, all from Tokyo Kasei, were used without further purification. All the solvents (from Wako Pure Chemical Ind.) were of nonfluorescent "Dotite Luminasol" or "Dotite Spectrosol" grade except pyridine (Reagent grade) and used as received.

Apparatus. The NMR spectra were obtained on a 100-MHz JEOL MH-100 spectrometer. Infrared spectra were measured by using the KBr pellet technique with the aid of a JASCO IR-G spectrometer.

Kinetic studies by fluorometry were performed with a JASCO FP-550 spectrofluorometer using a 1 cm × 1 cm quartz cell with a cap without degassing. Fluorescence was measured using excitation waveloength at 290 nm for NMI, 280 nm for NDSCl, and 340 nm for DNSCl and observed in the range of 325—345 nm for NMI, 330—355 nm for NDSCI, and 480—505 nm for DNSCl, respectively. Fluorescence data are reported without spectral correction, except fluorescence spectra in the wavelength from 400 to 550 nm which were corrected by using the standard solution of quinine sulfate in 0.05 M H_2SO_4.

Results and Discussion

Reaction of 5-Dimethylamino-1-naphthalenesulfonyl Chloride with Butylamine. In the course of investigation of the reaction of 5-dimethylamino-1-naphthalenesulfon-

† 1 M = 1 mol dm^{-3}.

yl chloride (DNSCl) with butylamine (n-$BuNH_2$) in organic solvents, we found that the stability of DNSCl has to be taken into account. DNSCl is unstable at room temperature and even without amines it is converted by an unknown reaction to fluorescent products in polar solvents such as methanol (slow), acetonitrile, pyridine, DMF (rapid), and dimethyl sulfoxide (rapid). No further detailed study of the reaction was carried out in these solvents. One of the probable mechanisms of the solvolysis, however, may be analogous to that proposed for pyridine.[9]

$$RSO_2Cl + C_5H_5N \longrightarrow RSO_2N^+C_5H_5Cl^- \quad (1)$$

The reaction product in Eq. 1 is presumably fluorescent, since DNSCl is nonfluorescent probably because of the intramolecular heavy-atom effect of chlorine.[10]

On the other hand, DNSCl is stable in less polar solvents such as THF, chloroform, and ethyl acetate. So the reaction rate were measured in these solvents. The reaction mechanism is most reasonably formulated as a bimolecular nucleophilic substitution on sulfur, similar to that for the reaction of benzenesulfonyl chloride with aniline.[11]

$$RSO_2Cl + H_2NR' \longrightarrow RSO_2NHR' + HCl \quad (2)$$

In organic solvents, hydrogen chloride formed reacts immediately with amine.[12]

$$HCl + H_2NR' \longrightarrow H_3N^+R'Cl^- \quad (3)$$

Then the overall reaction is expressed as

$$RSO_2Cl + 2H_2NR' \longrightarrow RSO_2NHR' + H_3N^+R'Cl^-. \quad (4)$$

N-Butyl-5-dimethylamino-1-naphthalenesulfonamide (DNSBA), the reaction product of DNSCl with n-$BuNH_2$, was prepared and purified separately to examine its fluorescence prior to kinetic measurement. Figure 1 shows its absorption and fluorescence spectra in ethyl acetate. Although the absorption maxima are invariant with solvent polarity, the fluorescence maxima (λ_{max}) shift gradually to longer wavelength with increasing solvent polarity as is known for dansylamine.[13] The λ_{max} of DNSBA are 467, 487, 497, 499, 502, and 518 nm in cyclohexane, benzene, tetrahydrofuran, ethyl acetate, chloroform, and N,N-dimethylformamide, respectively. The plot of the energy of fluorescence maxima *vs.* solvent polarity parameter

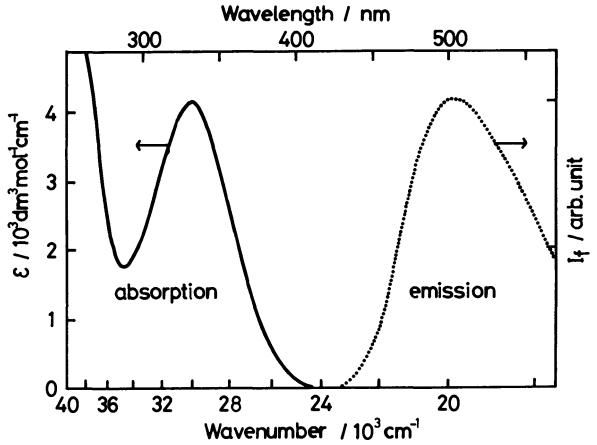

Fig. 1. Absorption and fluorescence spectra of DNSBA in EtAc.

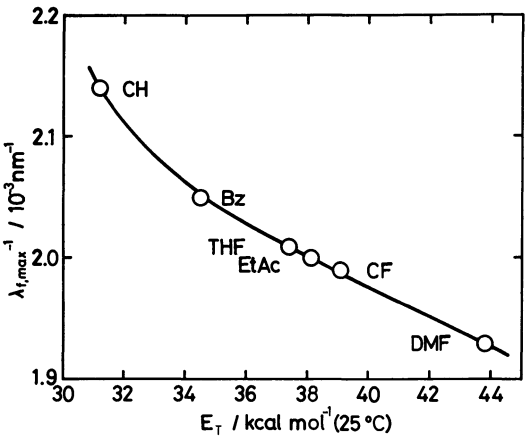

Fig. 2. Relationship between the energy of fluorescence maxima of DNSBA and the solvent-polarity parameter E_T in nonaqueous solents.

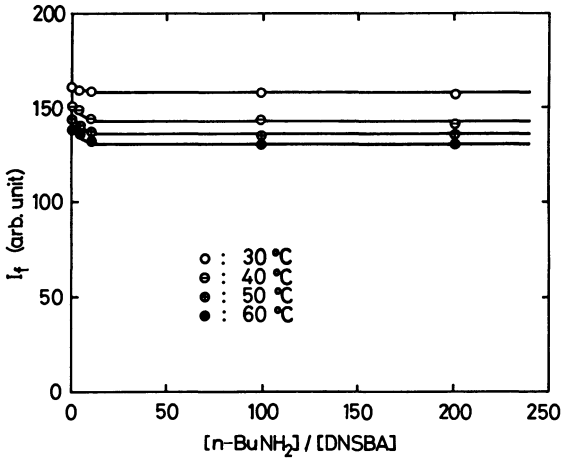

Fig. 3. The effect of addition of n-$BuNH_2$ on I_f of DNSBA in EtAc at several temperatures.

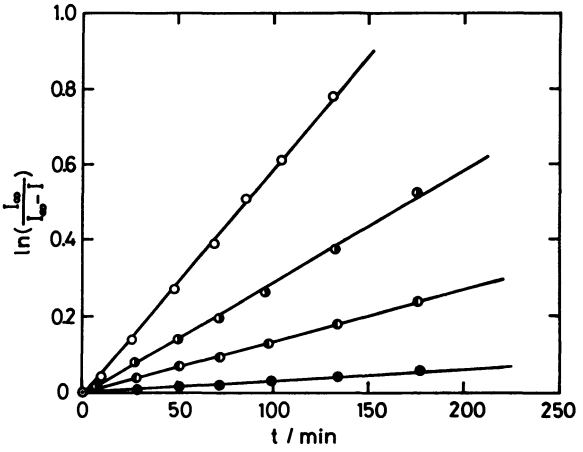

Fig. 4. Pseudo first-order plots of the reaction of DNSCl with n-$BuNH_2$ in THF at 50 °C: [DNSCl]=8.34×10^{-6} M; [n-$BuNH_2$]/[DNSCl]=40 (●), 200 (◐), 400 (◑), and 800 (○).

(Dimroth's E_T) for DNSBA in these solvents shows a satisfactory correlation as for dansylamine[13] (Fig. 2).

The proportionality between I_f and concentration of DNSBA holds for the concentration range [DNSBA]≦

1×10^{-5} mol dm^{-3} in all solvents used. The linearity does not hold at higher concentration of DNSBA. The temperature dependence of fluorescence intensity I_f of DNSBA in ethyl acetate is shown in Fig. 3, together with the effect of addition of n-$BuNH_2$ on I_f of the solution. The fluorescence intensity increases with a decrease in temperature and this may be a result of a decrease in the internal quenching of fluorescence.[14] The fluorescence intensity decreases by a few percent by the addition of n-$BuNH_2$ up to about ten fold excess to DNSBA in molality, but remains constant by further addition of n-$BuNH_2$. In any event, the effect of addition of n-$BuNH_2$ is not large and only a slight correction due to the effect is needed in the following kinetic studies.

Figure 4 shows the pseudo first-order plots of the reaction of DNSCl with excess n-$BuNH_2$ in THF at 50 °C. The second-order rate constants for the reaction in THF at 50 °C, calculated from the observed pseudo first-order rate constants and the concentration of n-$BuNH_2$ used, are entirely constant for widely different n-$BuNH_2$ concentrations as shown in Fig. 5. The second-order rate constants of the reaction in ethyl acetate (EtOAc) are also constant for different n-$BuNH_2$ concentrations. These facts show that the reaction is a simple bimolecular one in these conditions. The final fluorescence intensity of the reaction mixture was in fair agreement with that of the corresponding DNSBA solution as shown in Table 1. This confirms that the reaction proceeds quantitatively in these conditions.

Table 2 lists the second-order rate constants (k_2) of the reaction in various solvents mainly at 60 °C for the concentration of DNSCl ranging from 1×10^{-6} to 1×10^{-5} M. The correlation of k_2 to dielectric constant ε or $(\varepsilon-1)/(2\varepsilon-1)$ in various solvents is quite poor. On the contrary, the second-order rate constants are roughly proportional to the E_T values. This tendency may support the argument that the reaction of DNSCl with n-$BuNH_2$ is S_N2 type, because it is well known that the rate constant of a S_N2 reaction with solvated transition state becomes larger as the solvent becomes more dipolar aprotic in character.[15] The solvent effect of the present reaction may be different from that of the reaction of 2-thiophenesulfonyl chloride with anilines for which a linear correlation is found for the rate constants and the dielectric constants and a S_AN mechanism is proposed, bond-breaking being rate-determining step in aprotic solvents.[16]

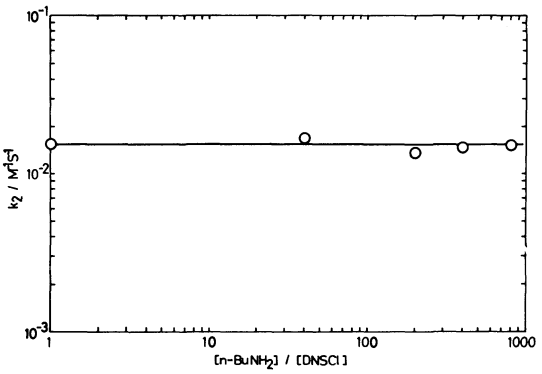

Fig. 5. Constancy of the second-order rate constants k_2 of the reaction of DNSCl with n-$BuNH_2$ in THF at 50 °C at different n-$BuNH_2$ concentration.

Table 1. Final fluorescence intensity of the reaction mixture of DNSCl with n-$BuNH_2$ in EtAc

[DNSCl] / 10^{-5} M	[n-$BuNH_2$] / 10^{-4} M	Temp/°C	I_f	$I_{f,model}$	$I_f/I_{f,model}$
1.15	2.85	40	134	133	1.01
1.15	2.85	50	130	126	1.03
1.15	2.85	60	116	122	0.95
0.98	2.48	70	95	99	0.96

Table 2. Second-order rate constants of the reaction of DNSCl with n-$BuNH_2$ in nonaqueous solvents

Solvents	ε	E_T / kcal mol^{-1}	Temperature / °C	k_2 / M^{-1} s^{-1}
Dichloromethane	8.9	41.1	30	2.2×10^{-1}
Chloroform	4.7	39.1	50	3.7×10^{-2}
Ethyl acetate	6.0	38.1	60	2.0×10^{-1}
1,2-Diethoxyethane	5.1	—	60	1.8×10^{-2}
Tetrahydrofuran	7.4	37.4	50	1.7×10^{-2}
1,4-Dioxane	2.2	36.0	60	4.3×10^{-2}
Benzene	2.3	34.5	50	1.6×10^{-3}
Toluene	2.4	33.9	60	1.1×10^{-3}
Cyclohexane	2.0	31.2	60	$\ll1\times10^{-3}$

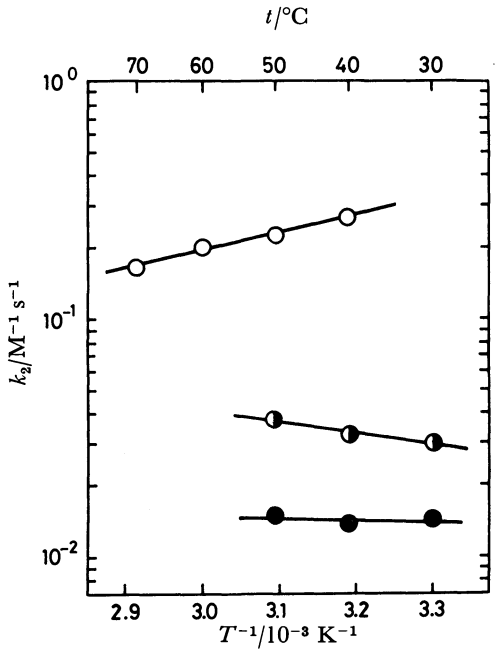

Fig. 6. Arrhenius plots of the second-order rate constants k_2 of the reaction of DNSCl with n-$BuNH_2$ in EtAc (○), chloroform (◑), and THF (●).

Arrhenius plots of the rate constants in ethyl acetate, chloroform, and tetrahydrofuran are shown in Fig. 6. The linear plot for the reaction in chloroform is normal but gives rather small activation energy (ΔE=2.1 kcal/mol). On the contrary, the reaction rate decreases with increasing temperature in ethyl acetate, and almost constant in tetrahydrofuran. In the case of the reaction of 2,4-dinitrobenzenesulfonyl chloride with n-$BuNH_2$ in

benzene, the amine is reported to act as a catalyst and the reaction is not of first-order with respect to amine.[12] In both ethyl acetate and tetrahydrofuran, however, the reaction of DNSCl with *n*-$BuNH_2$ is of first-order with respect to the amine as shown in Fig. 5. The anomalous temperature dependence of the reaction in these solvents may be explained as follows. In some S_N2 reactions, the degree of solvation of the reactants and the transition state are known to vary with solvent nature,[17] and the change in solvation is specified by the corresponding equilibrium constant which depends on the solvent nature as well as temperature. Accordingly, the cause of the anomaly may be ascribed to the temperature dependence of the equilibrium constant for the solvation. In this case, however, the reaction order is not affected and the reaction remains to be a simple bimolecular one.

The fluorescence of the reaction product of DNSCl with *n*-$BuNH_2$ can be excited at 350 nm or longer wavelength. Then DNSCl will be useful for a general fluorescent probe for studies in the field of polymer science and organic chemistry, because even the presence of chromophores such as phenyl groups and indole rings does not interfere the fluorescence measurement. This is the reason why we studied the reaction of DNSCl with *n*-$BuNH_2$ most thoroughly in various organic solvents as shown above. The situation is different for fluorescent probes such as 2-naphthalenesulfonyl chloride and *N*-(1-naphthyl)maleimide which are excited in the range of 270—280 nm. But these reagents are also useful in some cases as fluorescent probes to amino and mercapto groups. So the reaction of 2-naphthalenesulfonyl chloride with *n*-$BuNH_2$ and that of *N*-(1-naphthyl)maleimide with 1-pentanethiol were studied briefly in various organic solvents as shown below.

Reaction of 2-Naphthalenesulfonyl Chloride with Butylamine. 2-Naphthalenesulfonyl chloride (NDSCl) is also unstable at room temperature and converted by an unknown reaction to fluorescent products in such polar solvents as already listed in the preceding chapter. On the other hand, like DNSCl, NDSCl is stable in less polar solvents such as tetrahydrofuran and chloroform. So the reaction rate were measured in tetrahydrofuran (THF) and chloroform. The mechanism for the reaction of NDSCl with *n*-$BuNH_2$ may be similar to that of DNSCl with *n*-$BuNH_2$ as shown in Eq. 2 to 4. The first-order plots of the reaction in such solvents give straight lines, indicating that the reaction is first-order with respect to NDSCl and is a simple bimolecular one in these conditions. Second-order rate constants of the reaction were calculated from the observed pseudo first-order rate constants obtained for the reaction with *n*-$BuNH_2$ in large excess to NDSCl. The second-order rate constants of the reaction thus obtained are 4.6×10^{-2} $M^{-1}s^{-1}$ and 5.3×10^{-1} $M^{-1}s^{-1}$ in THF at 30 °C and in chloroform at 40 °C, respectively.

The emission spectrum of the product of the reaction of NDSCl with *n*-$BuNH_2$ in THF is shown in Fig. 7, together with that of naphthalene in THF. Figure 7 indicates that the emission spectrum is not much affected by the substitution of sulfamide group at β-position of the naphthalene ring.

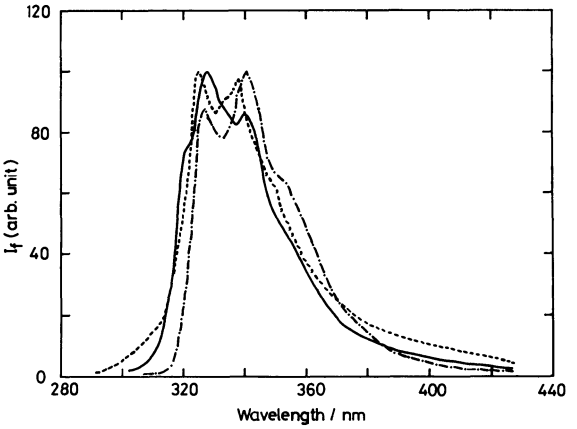

Fig. 7. Fluorescence spectra of naphthalene (——), the reaction product of NSCl with *n*-$BuNH_2$ (-·-·), and that of NMI with *n*-AmSH (------) in THF.

Reaction of N-(1-Naphthyl)maleimide with 1-Pentanethiol. Thiols and thiolate anions are known to add almost quantitatively to some nonfluorescent maleimides to give fluorescent adducts in aqueous solution.[6,18] So

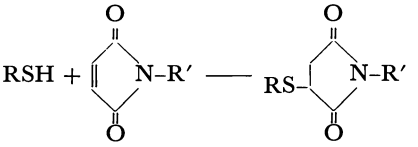

(5)

the reaction is widely used for quantitative analysis for mercapto groups in proteins and amino acids such as cysteine.

In the case of the reaction of *N*-(1-naphthyl)maleimide (NMI) with 1-pentanethiol (*n*-AmSH) in organic solvents, we also found that the stability of NMI has to be taken into account. The maleimide ring is known to be readily hydrolyzed to form the corresponding maleamic acid derivative in alkaline aqueous solution.[19] In addition, highly electrophilic maleimide double bond is easily susceptible to anionic polymerization by appropriate initiators in strongly polar media such as *N*,*N*-dimethylformamide (DMF).[20] In fact, NMI was not stable at room temperature in DMF and fluorescence developed even without thiols. Figure 8 shows the change in fluorescence intensity with time of NMI in

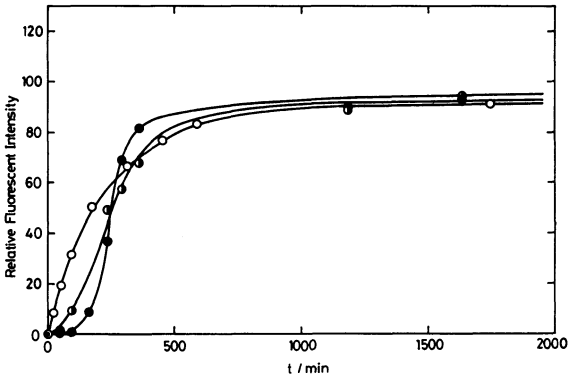

Fig. 8. Variation of the fluorescence intensity of NMI in DMF at 50 °C with time at volume fraction of acetic acid 0% (○), 9% (◑), and 33% (●).

DMF with various concentration of an acetic acid added to supress anionic polymerization. Although acetic acid seems to act as an inhibitor to any side reaction in the begining, its addition induces an autocatalytic reaction at a later stage. On the other hand, the first-order plots of the spontaneous deactivation reaction of NMI in DMF without acetic acid give straight lines. The first-order rate constant of the reaction is 6.5×10^{-5} s^{-1} at 50 °C and the value remains unaltered even when the equimolar amount of *n*-AmSH is added to the NMI solution. Although we did not study the detailed mechanism of the development of fluorescence of NMI in DMF, it is evident that the side reaction of NMI in DMF make impossible the kinetic study of the reaction of NMI with *n*-AmSH. Such a side reaction of maleimide ring is negligible for synthesis from bismaleimide compound and bisthiol in DMF, because the concentration of substrate is sufficiently high (10^{-1} to 10^{-2} M).[20] It should be noted, however, that the side reaction can not be ignored in the reaction of NMI as a fluorescent probe in DMF in which the concentration of substrate is limited (10^{-4} to 10^{-5} M).

NMI is stable in less polar solvents such as ethyl methyl ketone, benzene, and THF, and the fluorescence development of NMI in such less polar solvents is negligible for a few days at 50 °C. The reaction rate of NMI with *n*-AmSH in THF was followed by fluorometry. Since THF is miscible with water in all proportions, the effect of added H_2O is also studied. The pseudo first-order plots of the reaction of NMI with *n*-AmSH in THF at 50 °C with and without a small amount of H_2O give straight lines and the reaction proceeds quantitatively. The second-order rate constants of the reaction are evaluated as 4.3×10^{-2} M^{-1} s^{-1} in pure THF, 8.5×10^{-2} M^{-1} s^{-1} in THF with 0.3% H_2O, and 1.5×10^{-1} M^{-1} s^{-1} in THF with 3% H_2O. So the effect of the presence of H_2O is not very large.

The room temperature emission spectrum of the product of the reaction in THF is also shown in Fig. 7. The emission spectrum is not affected much by the substitution of thiol adduct of maleimide ring at α-position of naphthalene ring similarly to the case of NDSCl.

In conclusion, several reactions of some fluorescent reagents with substrates were confirmed to be simple second-order reactions as well as to proceed quantitatively in less polar solvents. Reaction rate of the fluorescent reagents studied here may be more rapid in polar aprotic solvents as is general for S_N2 type reactions. In polar solvents, however, all the fluorescent probes studied are too labile to study and converted spontaneously into fluorescent compounds. Application of the fluorescent probe to studies on organic reactions or synthetic polymers will be published elsewhere.[21]

References

1) Y. Kanaoka, *Angew. Chem.*, **89**, 142 (1977).
2) Y. Kanaoka, M. Machida, K. Ando, and T. Sekine, *Biochim. Biophys. Acta*, **207**, 269 (1970).
3) W. R. Gray, "Methods in Enzymology," ed by S. Colowick *et al.*, Academic Press, New York and London (1967), p. 139.
4) M. Weigle, S. L. DeBernardo, J. P. Tengi, and W. Leimgruber, *J. Am. Chem. Soc.*, **94**, 5927 (1972); S. Udenfriend, S. Sein, P. Bohlen, and W. Dairman, *Science*, **178**, 871 (1972).
5) Y. Eckstein and P. Dreyfuss, *Anal. Chem.*, **52**, 537 (1980).
6) T. Sekine, K. Ando, M. Machida, and Y. Kanaoka, *Anal. Biochem.*, **48**, 557 (1972).
7) L. K. Tan and R. A. Patsiga, *Anal. Lett.*, **10**, 437 (1977).
8) K. C. Tsou, R. J. Barret, and A. M. Seligwan, *J. Am. Chem. Soc.*, **77**, 4613 (1955).
9) O. Rogne, *J. Chem. Soc., B*, **1971**, 1334.
10) J. B. Birks, "Photophysics of Aromatic Molecules," John Wiley and Sons, New York (1970), p. 223.
11) O. Rogne, *J. Chem. Soc., Perkin Trans. 2*, **1975**, 1486.
12) L. M. Litibinenko and A. F. Popov, *Dokl. Acad. Nauk SSSR*, **160**, 1124 (1965).
13) Y-H. Li, L-M. Chan, L. Tyer, R. T. Moody, C. M. Himel, and D. M. Hercules, *J. Am. Chem. Soc.*, **97**, 3118 (1975).
14) p. 111 in Ref. 10.
15) A. J. Parker, *Chem. Rev.*, **69**, 1 (1969).
16) A. Arcoria, V. Librando, E. Maccarone, G. Musumarra, and G. A. Tomaselli, *Tetrahedron*, **33**, 105 (1977).
17) M. Tanaka, *Z. Phys. Chem. N. F.*, **96**, 239 (1975).
18) S. Simon and W. Konigsberg, *Proc. Natl. Acad. Sci. U. S. A.*, **56**, 749 (1966).
19) M. K. Hargreaves, J. G. Pritchard, and H. R. Dave, *Chem. Rev.*, **70**, 439 (1970).
20) J. V. Crivello, *J. Polym. Sci., Polym. Chem. Ed.*, **14**, 159 (1976).
21) A. Okamoto, A. Hayashi, K. Uchiyama, and I. Mita, to be submitted.

 © 1982 The Chemical Society of Japan Bull. Chem. Soc. Jpn., 55, 3073—3078 (1982)

Despretz Constants for Individual Ions

Toshiki WAKABAYASHI* and Katsuko TAKAIZUMI
The College of General Education, Tohoku University, Kawauchi, Sendai 980
(Received January 5, 1982)

The shifts (ΔT) in the temperature of maximum density (tmd) of water produced by electrolytes have been revised. It was found that the temperature dependences of S_V and/or b_V coefficients in the Redlich-Meyer equation should be taken into account, to obtain exactly the Despretz constants (K_D) or the standard partial molal expansibility ($\bar{E}°$) from tmd data. The K_D's for 1 : 1 electrolytes were divided into the ionic components ($K_{D,i}$), by applying the value for $\bar{E}_1^\circ$ (H^+, 4 °C). Of the familiar monovalent ions, the $K_{D,i}$ values are negative ($\Delta T>0$) only for H^+ and Li^+ ions and are positive for all the anions examined, including F^- ion. A further attempt was made to extract from $K_{D,i}$'s for organic ions the structural part $K_{st,i}$'s, based on a model. The $K_{st,i}$'s seem to reflect the structure-influencing ability of organic ions, but may not always be the case.

It has been recognized by many authors[1-7] that the shifts (ΔT) in the temperature of maximum density of water (tmd) produced by electrolytes as well as nonelectrolytes reflect the structural effects of ions on the solvent water. The shift produced by any solute at low concentrations is proportional to the solute concentration through the Despretz constant (K_D). Frank and Robinson[1] first noticed that K_D for alkali metal halides with a common anion increases in the order, $Li^+<K^+<Na^+$, in accordance with the effect of the cations on the relative partial molal entropy of water at 25 °C which were discussed in terms of the structural effect of ions. Darnell and Greyson[2] also noticed that with both alkali metal ions and halogenide ions, the ionic contributions to K_D seem to increase with increasing their structure-breaking ability with the exception of Na^+ ion.

With liquid nonelectrolytes as solutes, the observed ΔT's are usually divided into two parts, ΔT_V and ΔT_{st}, and hence K_D is also divided into K_D and K_{st}. The K_V is determined solely by the volumetric properties of the solute in its pure liquid state, while the K_{st}'s have been related qualitatively with the structural influences of the solutes on the solvent water,[8-14] that is, K_{st}'s have been confirmed to be positive for structure breakers ($\Delta T_{st}<0$) and negative for structure makers ($\Delta T_{st}>0$), though somewhat different approaches have been made by some authors.[15-17]

Some question has been recognized, however, with respect to tetraalkylammonium salts (R_4NX); the K_D increases with increasing alkyl-chain length.[2-4] This is contrary to the expectation that the hydrophobic nature of the alkyl radical would elevate the tmd of water similar to nonelectrolytes such as alcohols and some alkylamines.[7,8] Darnell and Greyson[2] inferred that the water structure-promoting characteristics of the species ordinarily found at room temperature would not be manifested in the neighbourhood of the tmd. They attributed the results to ion-size effects which would become important at temperatures approaching the tmd because of the enhanced structure of the solvent.

Estimating the K_{st}'s for R_4NBr, Wada and Miura[3] found that the K_{st} also increases with the alkyl-chain length. They proposed the idea that clathrate-like structures formed in the aqueous solution of $(n\text{-Bu})_4NBr$ contribute to the lowering of the tmd. Recently, Wada *et al.*[6] determined K_D's for twenty complex salts. They divided K_D's into ionic components ($K_{D,i}$) based on the assumption that $K_{D,i}(K^+)=K_{D,i}(Cl^-)$, and attempted further to extract the structural contributions of the complex ions from the $K_{D,i}$'s. They proposed that the hydrophobic ions may be divided into "iceberg" formations which elevate the tmd and "clathrate-like" formations which lower the tmd. In these estimations Wada and his coworkers employed the volumetric properties of the electrolytes in the solid state at 0 °C. As discussed later, the use of the volumetric properties of solutions in solid state seems questionable, particularly when the solutes are electrolytes.

In an earlier publication[7] we evaluated K_D's for some phosphonium halides, $(n\text{-Bu})_{4-n}Ph_nPX$ ($n=0$—4); the K_D for phosphonium chlorides increases with increasing the number of phenyl groups, indicating that in contrast to the conclusion obtained by other authors, the clathrate-like hydration would contribute toward elevating the tmd since the clathrate-like hydration supposed for the $(n\text{-Bu})_4P^+$ ion would successively disappear as the butyl groups are replaced by phenyl group since the K_V would decrease slightly with n.

Thus, the studies about the effects of electrolytes on the tmd may provide useful information about ionic hydration, however, there seems to be two problems; one is the way to divide K_D's for electrolytes into the ionic components; the other is to find a suitable procedure to extract the structural components ($K_{st,i}$) for organic ions from the $K_{D,i}$'s.

In the present work, we revise the procedure to determine the Despretz constants for electrolytes and then attempt to approach these subjects.

Principle

The Despretz Constant of an Electrolyte. The shift in the tmd of water produced by a solute can be derived as follows. The apparent molal volume ϕ_2 of solute is defined by

$$\phi_2 = \frac{1}{m}\left(\frac{1000+mM}{d} - \frac{1000}{d_\circ}\right), \quad (1)$$

where d is the density of solution, $d_\circ$ that of pure water, m the molality, and M the molecular weight of the solute. The molal volume of water, V_1, near the tmd can be expressed as

$$V_1 = V_1^*(1+\alpha_1(T-T_\circ^*)^2), \quad (2)$$

where V_1^* is the molal volume at the tmd ($T_\circ^*$) of pure

water, (namely 3.98 °C), and the value of α_1[8] is 7.8×10^{-6} deg^{-2}. Replacing d_0 in Eq. 1 by M_1/V_1, where M_1 is the molecular weight of water, differentiating with respect to temperature, and rearranging the result, we obtain

$$\Delta T = (T_m - T^*_\circ) = -\frac{d^*_\circ}{2000\,\alpha_1}\frac{\partial\phi_2}{\partial T}m, \qquad (3)$$

where the condition, $\partial d/\partial T=0$, at the tmd is considered; $d^*_\circ$ is the density of water at $T^*_\circ$.

For dilute aqueous solutions of electrolytes, ϕ_2 can be expressed as:

$$\phi_2 = \phi^\circ_2 + S_v m^{1/2} + b_v m, \qquad (4)$$

where ϕ°_2 is the partial molal volume of the electrolyte at infinite dilution and S_V, the Debye-Hückel limiting slope, for which the exact values have been given by Redlich and Meyer,[18] and b_V, the excess volume coefficient which includes all the effects arising from ion-solvent and ion-ion interactions. Insertion of Eq. 3 into Eq. 4 gives

$$\Delta T = -\frac{d^*_\circ}{2000\,\alpha_1}\left(\bar{E}^\circ - \frac{\partial S_v}{\partial T}m^{1/2} + \frac{\partial b_v}{\partial T}m\right)m, \qquad (5)$$

where $\bar{E}^\circ$ is the standard partial molal expansibility of electrolyte. The equation shows that, different from the case of nonelectrolyte solutes, for electrolytes the quantity that is directly proportional to concentration is not ΔT itself but a corrected one, and this is so even at low concentrations. Inserting the numerical values in Eq. 5, we obtain

$$\Delta T + 1.074\,m^{3/2} + 64.1\frac{\partial b_v}{\partial T}m^2 = -64.1\bar{E}^\circ m, \qquad (6)$$

where the value for $\partial S_V/\partial T$ at 3.98 °C was obtained from Eq. 20 in Ref. 19, as 1.675×10^{-2} cm^3 mol$^{-3/2}$ kg$^{1/2}$K.

Thus, it is reasonable to define the Despretz constant by

$$K_D = 64.1\,\bar{E}^\circ, \qquad (7)$$

where the dimensions for K_D and $\bar{E}^\circ$ are mol^{-1} kg K and cm^3 mol^{-1} K^{-1}, respectively. The Despretz constant is obtainable by Eq. 6 from the tmd data or by Eq. 7 from $\bar{E}^\circ$.

It may be a fact worth noting that the contributions from the temperature dependences of S_V and b_V have scarcely been considered, though the equations equivalent to Eqs. 3 and 7 have been treated by many authors. This subject will be discussed in a later section.

Since $\bar{E}^\circ$ can be split into the contributions from cation and anion, $\bar{E}^\circ_+$ and $\bar{E}^\circ_-$, K_D can also be split into the separate contributions, $K_{D,+}$ and $K_{D,-}$. Determination of the ionic Despretz constants is, therefore, a straightforward matter, if a reliable value for $\bar{E}^\circ_{ion}$ for any ion is available. Here the proton is chosen as the reference ion since for this $\bar{E}^\circ_+$ has been given as a function of temperature by Millero,[19]

$$\bar{E}^\circ_+(H^+) = -0.008 - 3.40\times10^{-4}t. \qquad (8)$$

Combining Eq. 7 with Eq. 8, we obtain the value, -0.60 K mol^{-1} kg for $K_D(H^+)$.

Separation of Structural Contribution from $K_{D,I}$ for Organic Ions. It is of interest to separate $K_{D,I}$ for large organic ions into two terms, a volumetric term, $K_{V,I}$, and a structural term, $K_{st,i}$. The latter term is considered to reflect the structural influence of the ion on the solvent water.

For nonelectrolyte solutes that are liquid at temperatures in the region of the tmd, Frank and Watson[9] have derived the following equation and confirmed its validity:

$$\Delta T = -\frac{x\alpha_2 V^\circ_2}{2(1-x)\alpha_1 V^*_1} - \frac{1}{2(1-x)\alpha_1 V^*_1}\frac{\partial\Delta V^M_x}{\partial T}, \qquad (9)$$

where x is the mole fraction of the solute, V°_2 and α_2 are the molar volume and the thermal expansion coefficient of the solute in pure liquid state at the tmd, and ΔV^M_x is the excess volume of mixing referred to a mixture of solute mole fraction x. The first term on the right hand side of the equation, first derived by Wada and Umeda,[8] is determined solely by the volumetric properties of the two pure liquids. This term expresses the shift in the tmd in an ideal mixture for which ΔV^M_x is 0 for all compositions, it is often referred to as the ideal term, and is always negative. The second term, on the other hand, expresses the effect arising from the solute-solvent interactions which induce the system to become nonideal.

Making an approximation, $\Delta V^M_x = bx(1-x)$,[20] and converting the mole fraction into molality, we can write the Despretz constant as:

$$K_D = K_v + K_{st}, \qquad (10)$$

where

$$K_v = d^*_\circ\alpha_2 V^\circ_2/(2000\,\alpha_1), \qquad (11a)$$

and

$$K_{st} = d^*_\circ(\partial b/\partial T)/(2000\alpha_1), \qquad (11b)$$

where in dilute solution $\partial\Delta V^M_x/\partial T$ and hence K_{st} are found to be negative for some organic compounds such as alcohols, alkylamines and tetrahydrofuran; most of these are known as the structure makers for the solvent water.

Equations 9—11 are valid for nonelectrolytes, but not for electrolytes. However, as shown by Wada and his coworkers,[3,6] we may consider that the $K_{D,I}$'s should also consist of two terms similar to the case of nonelectrolytes. The contribution of the volumetric term, $K_{V,i}$, may be significant for organic ions, since they are much larger in size than simple inorganic ions and their intrinsic expansibilities would be relatively large. In an ideal mixture, both the partial molal volume and the expansion coefficient are the same as those in the pure liquid for each component, and hence, the K_V does not contain any contribution from the structural changes of the solvent water induced by the solute. The thermal expansion coefficient of any substance is in general larger in the liquid state than in the solid state; therefore an excessively small value for K_V should be obtained if the solid expansibility is used in place of the liquid one. With electrolytes another factor should be taken into account; this is the electrostatic interactions between the ions in salt crystals. These result in much smaller expansibilities than those of molecular crystals, while in dilute electrolyte solutions the interactions are much weaker. Thus, it is obvious that to use the expansibilities for salt crystals in estimating K_V's would yield excessively

Table 1. The despretz constants, K_D/K mol^{-1} kg, for 1 : 1 electrolytes (Eq. 6)[a),b)]

	H^+	Li^+	Na^+	K^+	Rb^+	Cs^+	NH_4^+
Cl^-	5.9_5	5.1_8	12.4_8	11.0_3	11.0_9	11.5_9	6.5_1
	(5.9_5)	(5.0_0)	(12.6_6)	(11.0_3)	(11.3_2)	(11.5_8)	(6.5_9)
Br^-	6.5_5	6.4_7	14.0_1	12.2_8	12.8_8		7.8_2[c)]
	(7.3_5)	(6.4_0)	(14.0_6)	(12.4_3)	(12.7_2)	(12.9_8)	(7.9_9)
I^-	9.0_0	7.7_1	16.6_0	15.0_4	15.2_2		10.3_0[d)]
	(9.8_3)	(8.8_8)	(16.5_4)	(14.9_1)	(15.2_0)	(15.4_6)	(10.4_0)
NO_3^-	11.9_5	11.8_0	18.7_2	16.9_6	17.2_8	17.4_7	12.8_0
	(11.9_5)	(11.0_0)	(18.8_6)	(17.0_3)	(17.3_2)	(17.5_8)	(12.5_9)

a) Tmd data were, unless otherwise specified, taken from Ref. 21. The last term of the left hand side of Eq. 6 was ignored for all the salts. b) The bracketed values are reproduced from $K_{D,i}$. c) Ref. 3. d) Ref. 2.

small values which in turn would lead to excessively large values for K_{st}'s. This will at least be one of the reasons for finding unexpected values for K_{st}'s for hydrophobic salts.[3)]

Another approach may be possible: Consider a 1 : 1 electrolyte as the solute. Transfer of one ion pair from the solid phase to the solvent water produces two hydrated ions. For each ion we may divide this action into two processes. The first is the transfer of a hypothetical molecule (which is the same in the molecular structure as that of the ion but with no electric charge) from its hypothetical pure liquid to water; the second is the charging process of the molecule in water to yield the ion. The latter process should change the hydration state of the hypothetical molecule, other than possible volume change of the solute molecule itself by electrostriction effect. The changes in the hydration state would be significant for ions of small size while for large sized ions the changes would be comparatively minor due to their low electric fields, *i.e.*, the water structure around the hypothetical molecule will be less affected. In any case, the changes accompanied by the charging process are now all included in the $K_{st,i}$ term except for the volume change due to the electrostriction of the ion itself which should be included in $K_{v,i}$ term.

Thus, we can evaluate the $K_{st,i}$'s for ions by Eq. 11a, and hence, also the $K_{vt,i}$'s, if proper estimation is possible for V_2° and α_2 of hypothetical pure liquids.

Results and Discussion

Table 1 lists the Despretz constants for 1 : 1 electrolytes which were obtained by Eq. 6 from the tmd data found in the literature. For most of the simple electrolytes treated, Eq. 6, neglecting the second correaction term, gave reasonable results, as evidenced by the fact that the standard deviations (σ) between the observed tmd's and those reproduced from the K_D are reduced by one order or more by applying the first correction. As a whole, the contributions to K_D from the correction term amount to about 0.7 K mol^{-1} kg. The second correction term, $(\partial b_V/\partial T)m^2$, seems to be essential for the salts containing so-called hydrophobic ions. For instance, the tmd data for Bu_4NBr[3)] show that the K_D calculated from each tmd at each concentration increases successively with concentration from 782 K (referred to mole fraction scale) at mole fraction 2.3×10^{-4} to 1110 K at 3.42×10^{-3}. The reported value for K_D is 1086 K (σ=0.026 K), which was obtained without any corrections. Equation 6 gives 945 K with $\sigma=6.3\times10^{-3}$ K, where the value for $(\partial b_V/\partial T)$ was taken as 0.209 cm^3 mol^{-2} kg K^{-1}.[22)] On the other hand, $(\partial b_V/\partial T)$'s for Me_4NBr and Et_4NBr are slightly negative[22)] and the two correction terms partially set off each other.

Table 2 lists the ionic Despretz constants which are referred to the standard, $K_{D,+}(H^+)=-0.60$ K mol^{-1} kg. It is of interest to compare $K_{D,-}$'s for Cl^- and Br^- ions in the table with those obtained by extrapolation of the curve obtained by plotting K_D for R_4NX's *vs.* molecular weight of the cation, to zero molecular weight of the cation. Attempts of this kind have been made by other authors to determine the absolute partial molar volumes of halogenide ions[23)] or the absolute ionic molal expansibility for the Cl^- ion.[24)] As in the case of $\bar{E}^\circ$ (R_4NCl, 25 and 35 °C),[24)] the extrapolation was made by using only two lower members for both sets of salts, since the plots were not linear. The $K_{D,-}(Cl^-)$ found from tmd data for R_4NCl[2)] was 7.3 K mol^{-1} kg and $K_{D,-}(Br^-)$, from those for R_4NBr,[3)] 8.4. These are somewhat larger than those in Table 2. Although this may be one possible way to determine $K_{D,-}$, more reliable data are required to do this since disagreement among tmd data for R_4NX's are found (Table 2).

Table 2. The despretz constants for individual ions, $K_{D,i}$/K mol^{-1} kg[a)]

Ion	$K_{D,i}$	Ion	$K_{D,i}$		
H^+	−0.60	NH_4^+	-0.0_4[b)]	-0.1_3[c)]	
Li^+	-1.5_5	Me_4N^+	*2.0*$_6$[b)]	*1.8*$_5$[c)]	*0.8*$_5$[d)]
Na^+	6.1_1	Et_4N^+	*3.1*$_9$[b)]	*2.6*$_6$[c)]	*2.6*$_5$[d)]
K^+	4.4_8	Pr_4N^+	*3.7*$_6$[b)]		*3.8*$_2$[d)]
Rb^+	4.7_7	Bu_4N^+	*8.0*$_3$[b)]	*9.0*$_9$[c)]	*6.5*$_2$[d)]
Cs^+	5.0_3				
F^-	7.1[d)]	Bu_4P^+	*8.0*$_2$[e)]		
Cl^-	6.5_5	Bu_3PhP^+	*11.5*[e)]		
Br^-	7.9_5	$Bu_2Ph_2P^+$	*15.1*[e)]		
I^-	10.4[b)]	$BuPh_3P^+$	*18.5*[e)]		
OH^-	9.2_2	Ph_4P^+	*22.1*[e)]		
NO_3^-	12.5_5	$HCOO^-$	6.2_2		
SCN^-	13.1_7[c)]	CH_3COO^-	5.3_9		
BPh_4^-	17.9[f)]	$CH_3CH_2COO^-$	6.0_2		

a) The italicized values are obtained from K_D's which were determined by applying Eq. 6 with the two correction terms, and the others, from K_D's for which only the first correction was applied. The tmd data were taken from; b) Ref. 2, c) Ref. 3, d) Ref. 4, e) Ref. 7, and f) unpublished work.

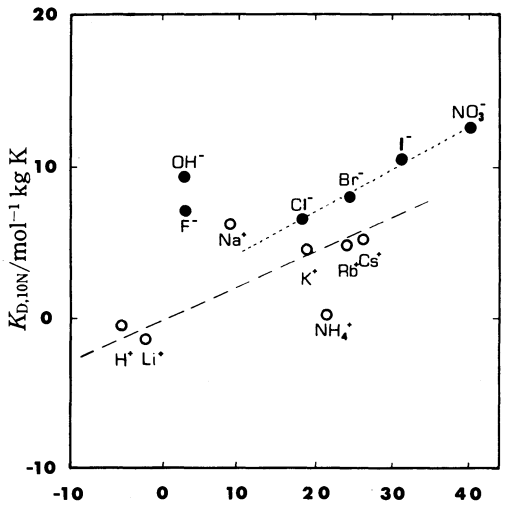

Fig. 1. Ionic Despretz Constants for monovalent ions plotted against the standard partial molal entropy of ion.

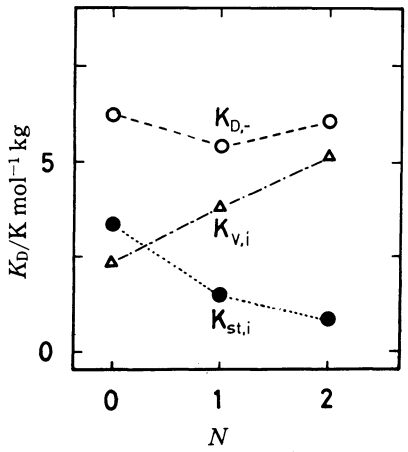

Fig. 2. $K_{D,-}$, $K_{V,i}$, and $K_{st,i}$ for carboxylate ions plotted against the number of carbon atoms (N) in alkyl groups.

The $K_{D,i}$'s for alkali metal ions are in the sequence, $Li^+ < K^+ < Rb^+ < Cs^+ < Na^+$ and those for halogenide ions, $Cl^- < F^- < Br^- < I^-$. These orders are, except for Na^+ and F^- ions, consistent with the sequences in the standard partial molal entropies, $\bar{S}_i^{\ominus}$,[25] for each set of the ions at 25 °C (Fig. 1). The $K_{D,-}$ values are somewhat higher than $K_{D,+}$ values when a comparison is made between cations and anions with the same ionic redius, in accordance with the similar trend found in $\bar{S}_i^{\ominus}$'s. The negative $K_{D,+}$ values for H^+ and Li^+ are notable since these ions are known as typical structure-making ions. The $K_{D,+}(NH_4^+)$ is considerably lower (probably negative) than for alkali metal ions (Table 2), suggesting that the ion would be capable of fitting into the partial water structure through hydrogen bonding. These seem to support an intuitive anticipation that the smaller the ionic Despretz constant, the greater is the structure-making ability of the ion.

However, necessity for reexamining in detail the content of $\bar{E}_{ion}^{\circ}$ and hence that of $K_{D,i}$ for simple ions comes from the disorder for Na^+, OH^-, and F^- ions in the seqiences in $K_{D,i}$. At 25 °C, $\bar{E}_{cation}^{\circ}$ for alkali metal ions[26] are in the sequence, $Na^+ > K^+ > Rb^+ > Cs^+ > Li^+$, which is almost reverse with that at 3.98°, while with anions, $F^- < Cl^- < Br^- < I^- (< NO_3^-)$, which is the same as that at 3.98° except for F^- ion. This fact is thought to reflect the difference in hydration between cation and anion.

The $\bar{E}_{ion}^{\circ}$ for simple ions can be decomposed into components corresponding to the decomposition of $\bar{V}_{ion}^{\circ}$. Applying a semiempirical equation, Millero[19,27] divided $\bar{V}_{ion}^{\circ}$ into three terms, the crystal partial molal volume $\bar{V}_{cryst}^{\circ}$, the electrostriction partial molal volume $\bar{V}_{elect}^{\circ}$, and the disordered or void-space partial molal volume $\bar{V}_{disord}^{\circ}$. Since $\bar{V}_{cryst}^{\circ}$ is hardly affected by temperature change, the corresponding expansibility can be ignored. He showed that $\bar{V}_{elect}^{\circ}$ goes through a minimum at a point near room temperature which depends on the ionic radius while $\bar{V}_{disord}^{\circ}$ increases with increasing temperature. The $\bar{E}_{elect}^{\circ}$, therefore, changes sign from positive to negative with rising temperature while the $\bar{E}_{disord}^{\circ}$ is always positive. The sign of the ionic charge would affect both the temperature at which the $\bar{E}_{elect}^{\circ}$ changes its sign and the magnitude of the $\bar{E}_{disord}^{\circ}$ through the effect of ionic charge on the orientation of water dipoles. This would be responsible for the difference between cation and anion in the ionic-radius dependence of the sequences in $\bar{E}_{ion}^{\circ}$ at the two temperatures.

More satisfactory knowledge is required to explain the irregularity for Na^+, OH^-, and F^- ions found in the magnitudes for $\bar{E}_{ion}^{\circ}$.

Organic Ions. Here, extraction of $K_{st,i}$ from $K_{D,i}$ for some organic ions is examined.

The first example is the carboxylate ion. The nitroalkanes RNO_2, having the same alkyl groups as those of carboxylate ions, may serve as model compounds in estimating $K_{v,i}$'s for the anions, which require expansibilities of the hypothetical liquids composed of hypothetical chargeless molecules, RCOO. The results for three carboxylate ions are shown in Fig. 2, where $K_{D,i}$, $K_{v,i}$, and $K_{st,i}$ are plotted against the number of carbon atoms in the alkyl groups. In the estimation for $K_{v,i}$ for the formate ion, V_2° and α_2 of formic acid were used, since no data are available for liquid HNO_2. This may be allowed as a first approximation, as expected from the following: The molal expansibility E° of nitromethane at 4 °C is 0.064 cm^3 mol^{-1} K^{-1}, comparable to that of super-cooled acetic acid, 0.060, which was estimated by extrapolation. E° of nitroethane, 0.079, is very close to E° of propionic acid, 0.078. These E°'s were calculated from volumetric data compiled by Riddick and Bunger.[28]

Although no regularity is found in $K_{D,i}$ with respect to the alkyl-chain length, a marked tendency is found in the order of $K_{st,i}$ which agrees with our anticipation that since alkyl groups would promote the water structures in their vicinity, the $K_{st,i}$ would decrease with increasing the alkyl-chain length. The results seem to indicate that the charged group, $-COO^-$, contributes positively to $K_{st,i}$ and hence may be regarded as a structure-breaking group.

Some alkanes of the type, R_4C, may permit us to

estimate $E°$'s for the hypothetical liquids corresponding to neutral compounds, R_4N's. The estimated value for $K_V(Me_4C)$ is 13.7 K mol^{-1} kg, with $a_2=1.8\times10^{-3}$ K^{-1} and $V°(4\ °C)=118.6$ cm^3 mol^{-1}.[28] Substitution of this value in Eq. 10 gives a large negative value for $K_{st,i}$, of about -11 K mol^{-1} kg. However, it may be reasonable to regard this value as the lower limit for $K_{st,i}(Me_4N^+)$, since no allowance was made for electrostriction of the ion itself which would lead to a lower $K_{v,i}$ value. Although no data are available for estimating $E°$'s of higher homologs, Pr_4C and $(n\text{-Bu})_4C$, $E°$'s of four *n*-alkanes, C_5, C_9, C_{13}, and C_{17}, are available, that is, 0.175, 0.189,[28] 0.24 and 0.28 cm^3 mol^{-1} K^{-1}, respectively. The last two were estimated by Gunn and Yamada's method,[29] which gives the values 0.169, and 0.195 for the first two members. Employing tentatively, in place of $K_{v,i}$'s, the K_V's calculated from these $E°$'s, 11.2, 12.1, 15.1, and 17.8 K mol^{-1} kg, we obtain large negative values, around -10 K mol^{-1} kg, for $K_{st,i}$ for all R_4N^+ ions.

It is impossible at this stage to judge whether or not the absolute values for "true" $K_{st,i}$ increase with lengthening the alkyl-chain length because any corrections have not been made for the electrostriction effect as already noted and the $K_{v,i}$'s used are tentative. We may at least state that the sign of $K_{st,i}$'s for the higher members of R_4N^+ ions would be negative. The negative sign assigned for lower members, Me_4N^+ and Et_4N^+, seems to be inconsistent with the view that Me_4N^+ ion is a structure breaker and that the Et_4N^+ ion hardly affects the water structure.

Generally it is assumed[25] that there are two contradictory factors that are responsible for the states of cosphere water around R_4N^+ ions, one is a weak electric field exerted by the ions which is important with Me_4N^+ ion and makes the ion a structure-breaker. The other is the structure-making ability of the alkyl groups. As the ion gets larger, from Me_4N^+ through Et_4N^+ and Pr_4N^+, the former effect becomes less important and the two effects balance near the Et_4N^+ ion. There are many criteria[25,30] indicating the Me_4N^+ ion to be a structure breaker, however, other facts have also been found. As revealed by the dielectric relaxation study by Haggis *et al.*,[31] the water relaxation time is lengthened by the presence of Me_4NBr, Me_4NI, and Et_4NCl, while it is shortened by the presence of inorganic salts. Pottel and Lossen[32] showed that the molal change of relaxation time of water in R_4NBr solutions with respect to the relaxation time of pure water is positive for all the R_4NBr examined. However the relative relaxation time change per mole of CH_2 group per kg water increases with the alkyl chain length from Me_4NBr to Et_4NBr and to Pr_4NBr. At this point it reaches a constant value equal to that for aliphatic hydrocarbons with an arbitrary number of CH_2 groups. On the other hand, a negative value was found for NH_4Br. Using the Samoilov equation, Uedaira[33] determined the activation energies of the exchange of the nearest water molecules next to an ion and found them to be positive for four R_4NBr's, from Me_4NBr to Bu_4NBr, *i.e.*, the water molecules close to the non-polar group are less mobile than in pure water. Wen and Hung[34] determined the standard molal free energy of transfer ($\Delta F°_{tr}$) of hydrocarbons (methane, ethane, propane, and butane) from water to 0.1 mol kg^{-1} solutions of R_4NBr at four temperatures. They found that the $\Delta F°_{tr}$ values are all negative except for methane in Me_4NBr solution at 5 °C and with NH_4Br solution they are positive. All these results seem to indicate that the Me_4N^+ ion is different from some simple ions known as structure breakers, such as Cs^+ and I^-. It displays, though weakly and partially, the effect on the water structure inherent to aliphatic hydrocarbons.

Comparison of K_D in D_2O for a given salt with that in H_2O seems to be of interest, since D_2O is known to possess more structure than H_2O and the structure-influencing ability of salt should be stronger in D_2O than in H_2O, while $K_{v,i}$ for any ion should be common to two solvents. The K_D's of R_4NBr's in D_2O were obtained by Conway and Laliberte[4] as well as those in H_2O. In spite of the anticipation that K_D for Me_4NBr would be larger in D_2O than in H_2O and the reverse would be true for Bu_4NBr, all the K_D's in D_2O are smaller by some 2 K mol^{-1} kg, including Me_4NBr, indicating that there would be some factor which is reflected in $K_{st,i}$ but not in other probes.[37] In this respect, Wen's comment[25] about the difference in volumetric property between two structure breakers, Cs^+ and Me_4N^+ ions, seems to be suggestive. The excess heats of mixing ($\Delta_m H^{ex}$) in the systems, Pr_4NBr–CsBr and Pr_4NBr–Me_4NBr, are negative whereas the excess volume of mixing ($\Delta_m V^{ex}$) in the Pr_4NBr–CsBr system is considerably larger than that in Pr_4NBr–KBr system, while $\Delta_m V^{ex}$ in Pr_4NBr–Me_4NBr system is comparable to that in Pr_4NBr–KBr system. He pointed out that $\Delta_m H^{ex}$ is largely a measure of change in the number of hydrogen bonds of water in the solution, whereas $\Delta_m V^{ex}$ is a measure of the change in the geometric arrangement of water and ions. This comment may be valid also in the present case, since K_D is essentially a volumetric property.

From the above, we may conclude that $K_{st,i}$ for the Me_4N^+ ion can be negative in spite of being a net structure breaker. This means that classification of ions into the structure maker and structure breaker based on the sign and magnitude of $K_{st,i}$ is not always consistent with that based on different probes. The situation may be more or less common to all classification criteria because our knowledge about the structures of water and the so-called hydrophobic hydration are far from complete.

For a series of phosphonin salts, $(n\text{-Bu})_{4-n}Ph_nPX$ ($n=0$—4), new values for K_D's are assigned in this work because the preceding values[7] had not been corrected for the temperature dependence of the b_v-coefficients. As seen from Table 2, the present conclusion is essentially the same as the preceding, the $K_{st,i}$ would increase with increase in the number of phenyl groups in agreement with information obtained from other probes[35,36] that the water structures around the cations decrease with *n*.

As a conclusive remark, it can be said that although $K_{D,i}$ for simple inorganic ions and $K_{st,i}$ for organic ions can be regarded as parameters indicating structure-

influencing ability of ions, it may not always be the case. Particularly, $K_{st,i}$'s for R_4N^+ ions are inconclusive, and more elaborate studies are required.

References

1) H. S. Frank and A. L. Robinson, *J. Chem. Phys.*, **8**, 933 (1940).
2) A. J. Darnell and J. Greyson, *J. Phys. Chem.*, **72**, 3021; 3032 (1968).
3) G. Wada and M. Miura, *Bull. Chem. Soc. Jpn.*, **42**, 2498 (1969).
4) B. E. Conway and L. H. Laliberte, *Trans. Faraday Soc.*, **66**, 3032 (1970).
5) J. R. Kuppers, *J. Phys. Chem.*, **78**, 1041 (1974).
6) G. Wada, E. Nagao, N. Kawamura, and K. Kinumoto, *Bull. Chem. Soc. Jpn.*, **51**, 1937 (1978).
7) K. Takaizumi and T. Wakabayashi, *Bull. Chem. Soc. Jpn.*, **55**, 2239 (1982).
8) G. Wada and S. Umeda, *Bull. Chem. Soc. Jpn.*, **35**, 646, 1797 (1962).
9) F. Franks and B. Watson, *Trans. Faraday Soc.*, **63**, 329 (1967).
10) D. A. Armitage, M. J. Blandamer, K. W. Morcom, and N. C. Treloar, *Nature*, **219**, 718 (1968).
11) D. D. MacDonald, M. D. Smith, and J. B. Hyne, *Can. J. Chem.*, **49**, 2815 (1971).
12) M. Sakurai, T. Komatsu, and T. Nakagawa, *Bull. Chem. Soc. Jpn.*, **45**, 1038 (1972).
13) S. V. Subrahmanyan and N. M. Moorthy, *Z. Phys. Chem. Neue Folge*, **88**, 116 (1974).
14) a) D. D. MacDonald and J. B. Hyne, *Can. J. Chem.*, **54**, 3073 (1976); b) D. D. Macdonald, *ibid.*, **55**, 800 (1977).
15) J. L. Neal and D. A. I. Goring, *J. Phys. Chem.*, **74**, 658 (1970).
16) J. R. Kuppers, *J. Phys. Chem.*, **79**, 2105 (1975).
17) J. R. Kuppers, *Can. J. Chem.*, **55**, 798 (1977).
18) O. Redlich and D. M. Meyer, *Chem. Rev.*, **64**, 221 (1964). The original equation is referred to the concentration scale, mol dm^{-3}, but in this study the difference between the scale and the molality scale is ignored for dilute solutions.
19) F. J. Millero, "The Partial Molal Volumes of Electrolytes in Aqueous Solutions," in "Water and Aqueous Solutions," ed by R. A. Horne, Wiley-Interscience, New York (1972), Chap. 13.
20) J. H. Hildebrand and R. L. Scott, "The Solubility of Nonelectrolytes," 3rd ed, Dover Publication, Inc., New York (1964), Chap. 8.
21) "International Critical Tables," ed by E. W. Washburn, McGraw Hill Book Co., Inc., New York (1933), Vol. 3.
22) G. Perron, N. Desrosiers, and J. E. Desnoyers, *Can. J. Chem.*, **54**, 2163 (1976).
23) B. E. Conway, R. E. Verrall, and J. E. Desnoyers, *Trans. Faraday Soc.*, **62**, 2738 (1966).
24) F. J. Millero and W. Drost-Hansen, *J. Phys. Chem.*, **72**, 1758 (1968).
25) H. L. Friedman and C. V. Krishnan, "Thermodynamics of Ion Hydration," in "Water," ed by F. Franks, Plenum Press, New York (1973), Vol. 3, Chap. 1.
26) F. J. Millero, *J. Phys. Chem.*, **72**, 4589 (1968).
27) F. J. Millero, *J. Phys. Chem.*, **73**, 2417 (1969).
28) J. A. Riddick and W. B. Bunger, "Organic Solvents," 3rd ed, Wiley-Interscience, New York (1970).
29) R. D. Gunn and T. Yamada, *AIChE J.*, **17**, 1341 (1971).
30) W. Y. Wen, "Aqueous Solutions of Symmetrical Tetraalkylammonium Salts," in "Water and Aqueous Solutions," ed by R. A. Horne, Wiley-Interscience, New York (1972), Chap. 15.
31) G. H. Haggis, J. B. Hasted, and T. J. Buchanan, *J. Chem. Phys.*, **20**, 1452 (1952).
32) R. Pottel and O. Lossen, *Ber. Bunsenges. Phys. Chem.*, **71**, 135 (1967).
33) H. Uedaira, *Zh. Fiz. Khim.*, **42**, 3024 (1968); *Chem. Abstr.*, **70**, 77184r (1969).
34) W.-Y. Wen and J. H. Hung, *J. Phys. Chem.*, **74**, 170 (1970).
35) K. Takaizumi and T. Wakabayashi, *J. Solution Chem.*, **9**, 809, 819 (1980).
36) T. Wakabayashi and K. Takaizumi, *J. Solution Chem.*, in press.
37) Some differences are found, as recognized by Perron *et al.*,[22] between $\phi_2°$'s for Pr_4NBr and Bu_4NBr in D_2O obtained by Conway and Laliberte[4] and those by Perron *et al.*,[22] and the K_D's in D_2O for the two salts might be inconclusive. Reexamination may be required.

 © 1982 The Chemical Society of Japan Bull. Chem. Soc. Jpn., 55, 3079—3084 (1982)

The Behavior of Carbon Black in a Detergent Solution

Yuji YONEYAMA* and Keizo OGINO

Department of Industrial and Engineering Chemistry, Faculty of Science and Technology, Science University of Tokyo, 2641, Yamazaki, Noda, Chiba 278

(Received January 11, 1982)

The behavior of carbon black (CB) in a detergent (sodium dodecyl sulfate (SDS): 20%, zeolite: 20%, sodium silicate: 5%, sodium carbonate: 3%, sodium (carboxylatomethyl)cellulose (CMC): 1%, sodium sulfate: 51%) solution is discussed in terms of the ζ-potential and potential energy of interaction. The ζ-potential of CB in each solution of SDS, various builders, and the detergent was measured by microelectrophoresis. The potential energies between CB and fabrics (nylon and cellulose), between CB and clay, and between CB and zeolite were calculated by the use of the theory of heterocoagulation. The potential energy between one CB particle and another CB particle was calculated by the use of D-L-V-O theory. The ζ-potential was increased by the addition of builders, except sodium sulfate. The high negative ζ-potential of CB in the detergent solution resulted from the effect of builders. From the potential energies, it became evident that 1) CB in the detergent solution deposits with difficulty onto fabrics; 2) The CB coagulates with zeolite only with difficulty; 3) The CB coagulates with clay or CB.

The builder for a detergent should have the following effects: (1) Sequestration for Ca^{2+} and Mg^{2+}; (2) Buffer for a detergent solution at pH 9.0—10.5; (3) Dispersion of soils. Sodium triphosphate has the above effects and had been used as the main builder in detergents. However, in recent years, the sodium triphosphate levels in detergents have been reduced significantly because it accelerates the eutrophication of lakes and rivers. In the many detergents which have no sodium triphosphate, sequestration for Ca^{2+} and Mg^{2+} is performed by zeolite, sodium carbonate, and sodium silicate. On the other hand, the detergent solution is buffered by sodium silicate and sodium carbonate. The question has been raised whether the dispersion of soils in the detergent solution is satisfied or not. In previous work,[1] it was shown that the deposition of the particle soil, clay (Kanto loam), onto fabrics can be depressed by the coagulation of the particle soil with zeolite. Generally, particle soil contains 1.5% carbon black. In this study, carbon black was used as another particle soil. The behavior of carbon black in the detergent solution was discussed in terms of the D-L-V-O theory and the heterocoagulation theory.

Experimental

Materials. Carbon black (DIABLACK-G, Mitsubishi Chemical Indiustries Ltd." were used as a particle soil model. The particle radii of carbon black are 24.5—30 nm.[2] In this study, the radius was assumed to be 27.5 nm. Sodium dodecyl sulfate (SDS) which was extracted with diethyl ether and recrystallized from ethanol was used for a surface active agent in a detergent. The other chemicals used for builders, such as sodium triphosphate, sodium slicate, sodium carbonate, sodium (carboxylatomethyl)cellulose (CMC), and sodium sulfate, were of reagent grade. The detergent composition is shown in Table 1. Doubly-distilled water was used.

TABLE 1. DETERGENT COMPOSITION

Materials	Compositional level wt%
SDS	20
Zeolite	20
Sodium silicate	5
Sodium carbonate	3
CMC	1
Sodium sulfate	51

Measurement of ζ-Potential. The ζ-potential was measured with an electrophoretic mass-transport analyzer in the previous work. The principle of this apparatus utilizes the difference between the density of particles and that of the solution. The surface of carbon black (CB) has many pores and is hydrophobic. The density was measured by a picnometer with hydrocarbon, methanol, or surfactant solution, and is about 1.8 g cm^{-3}.[2] The densities in aqueous solution used in this work seem to be lower than 1.8 g cm^{-3}, and to be changed by the kind of aqueous solution. Therefore, electrophoretic mass-transport analyzer is not well fitted for the measurement of the ζ-potential of CB. In this work, the ζ-potential of CB was measured with an LASER ZEE™ model 500 (PEN KEM Inc.). This apparatus uses microelectrophoresis, and is well fitted for the measurement of the ζ-potential of CB. The measurement was carried out with an applied potential gradient of 10 V cm^{-1} at 25 °C. The 0.0018 wt% suspension for ζ-potential measurement were prepared with an ultrasonic mixer for 10 min and allowed to stand for 12 h. The suspension were dispersed again with an ultrasonic mixer for 5 min before use. In some cases, the pH of the suspension was adjusted to the desired value by using dilute sodium hydroxide solution while stirring. The pH of the suspension was measured by a pH meter (HM-5A, TOA Electronics Ltd.).

Calculation of the Total Potential Energy. The potential energy for interaction between a spherical particle and a flat plate due to an electrical double layer is given by[3]

$$V_{E,S/P} = \frac{aD}{4kT}\left[(\psi_1^2+\psi_2^2)\ln\left\{\frac{\exp(2\kappa H_0)-1}{\exp(2\kappa H_0)}\right\} + 2\psi_1\psi_2 \ln\left\{\frac{\exp(\kappa H_0)+1}{\exp(\kappa H_0)-1}\right\}\right], \quad (1)$$

where a is the radius of the sperical particle, k is Boltzmann's constant, T is the absolute temperature, H_0 is the distance between the surfaces, ψ_1 and ψ_2 are the surface potentials of materials 1 and 2, κ is Debye-Hückel reciprocal length parameter,[4]

$$\kappa = \sqrt{\frac{4\pi e^2(n_+ Z_+^2 + n_- Z_-^2)}{DkT}}. \quad (2)$$

Z_{+or-} is the valence of the ionic species in solution, n_{+or-} is the concentration (ions cm^{-3}) of the same species in solution,

and e is the electronic charge.

The potential energy for interaction between a spherical particle and a flat plate due to van der Waals forces is given by[5,6]

$$V_{A,S/P} = -\frac{A_{12/3}}{6kT}\left[\frac{2a(H_0+a)}{H_0(H_0+2a)} - \ln\frac{H_0+2a}{H_0}\right], \quad (3)$$

$$A_{12/3} = \sqrt{A_{11/3}\cdot A_{22/3}}. \quad (4)$$

$A_{11/3}$ and $A_{22/3}$ are Hamaker's constants for interaction between materials 1, 1 and materials 2, 2 in the separating medium 3.

The total potential energy for interaction between a spherical particle and a flat plate is given by the sum of $V_{E,S/P}$ and $V_{A,S/P}$:

$$V_{T,S/P} = V_{E,S/P} + V_{A,S/P}. \quad (5)$$

The total potential energies for interaction between CB and nylon, between CB and cellulose were calculated from Eqs. 1—5.

It has been shown by Hogg *et al.*[7] that the potential energy for interaction between two spherical particles of radii a_1 and a_2 and surface potentials ψ_1 and ψ_2 is given by

$$V_{E,S/S} = \frac{a_1a_2D}{4(a_1+a_2)kT}\left[(\psi_1^2+\psi_2^2)\ln\left\{\frac{\exp(2\kappa H_0)-1}{\exp(2\kappa H_0)}\right\} + 2\psi_1\psi_2\ln\left\{\frac{\exp(\kappa H_0)+1}{\exp(\kappa H_0)-1}\right\}\right] \quad (6)$$

The potential energy for interaction between two spherical particles due to van der Waals forces is given by Hamaker[8]

$$V_{A,S/S} = -\frac{A_{12/3}}{12kT} \times \left\{\frac{y}{x^2+xy+x} + \frac{y}{x^2+xy+x+y} + 2\ln\frac{x^2+xy+x}{x^2+xy+x+y}\right\}, \quad (7)$$

where $x=H_0/2a_1$ and $y=a_2/a_1$. The total potential energies for interaction between CB and clay, and between CB and zeolite were calculated from Eqs. 6—7.

Verwey and Overbeek[9] have shown that the potential energies of interaction between two spherical particles are given by

$$V_E = \frac{aD\psi^2}{2kT}\ln[1+\exp(-\kappa H_0)], \quad (8)$$

$$V_A = -\frac{A}{6kT}\left(\frac{2}{S^2-4} + \frac{2}{S^2} + \ln\frac{S^2-4}{S^2}\right), \quad (9)$$

where $S=(2a+H_0)/a$. Equations 8 and 9 were used for calculation between one CB particle and another CB particle.

The above equations were expressed in kT units. Since the evaluation of surface potential involves some difficulties, the surface potentials were taken as the ζ-potentials. For the computation, the ζ-potentials of nylon, cellulose, clay, and zeolite in the previous paper were used. The Hamaker's constants for nylon and cellulose in water were estimated to be 5×10^{-14} erg from those for polyethylene and polystyrene.[10] The Hamaker's constants for zeolite and clay in water were estimated to be 4.4×10^{-13} erg from that for kaolinite.[11] The Hamaker's constant for CB in water was estimated to be 5×10^{-13} erg from that for graphite.[10] The radii of clay and zeolite were assumed to be 1×10^{-5} cm. The calculations of potential energies as a function of the distance between the surfaces were performed on an IBM 370 computer.

Results and Discussion

ζ-Potential of CB and the PH-Dependence. The water-soluble builders such as sodium triphosphate, sodium carbonate, and sodium silicate are added to water, and the pH of the solution is shifted to the alkali side. For this reason, the ζ-potentials of CB were measured in solutions of various pH (Fig. 1). The ζ-potential of CB is about −22 mV at pH 7, increased with increase of pH, and reached about −46 mV at pH 11. The structure of carbon black was reported by many investigators. Boehm[12] shows the surface structure model (Fig. 2). Murata and Imagawa[13] reported that the negative ζ-potential of carbon black results from the following mechanisms: (i) Ionization of -COOH and -OH or (ii) Adsorption of OH^- on the surface.

The Effect of Sodium Dodecyl Sulfate (SDS) on the ζ-Potential of CB and the Potential Energy. Figure 3 shows the effect of the concentration of SDS on the ζ-potential of CB. The negative ζ-potential of CB increased with increasing the concentration of SDS. The increase in the negative ζ-potential results from adsorption of dodecyl sulfate anion onto CB with some interactions such as van der Waals forces. Since the surface of CB is hydrophobic, the hydrophobic group of dodecyl sulfate anion are adsorbed directly to the surface of CB.

The ideal concentration of detergent is generally 0.2 wt% in washing process. Assuming the formulation of detergent shown in Table 1, the concentration of SDS in the 0.2 wt% detergent solution is 1.387×10^{-3} mol dm^{-3}. The ζ-potential of CB at this concentration was read from Fig. 3. The ζ-potentials of nylon, cellulose, zeolite, and clay in this concentration were −107,

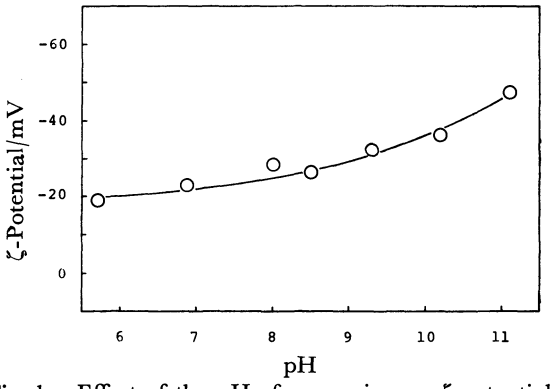

Fig. 1. Effect of the pH of suspension on ζ-potential of CB at 25 °C.

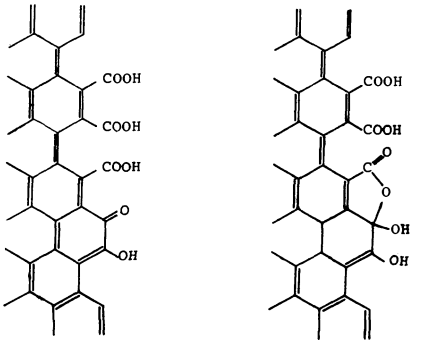

Fig. 2. Surface structure model of carbon black.

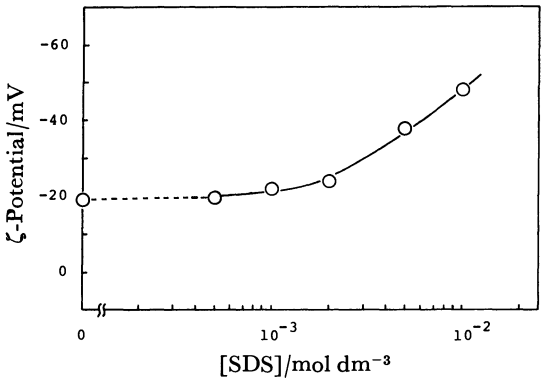

Fig. 3. Effect of the concentration of sodium dodecyl sulfate (SDS) on ζ-potential of CB at 25 °C.

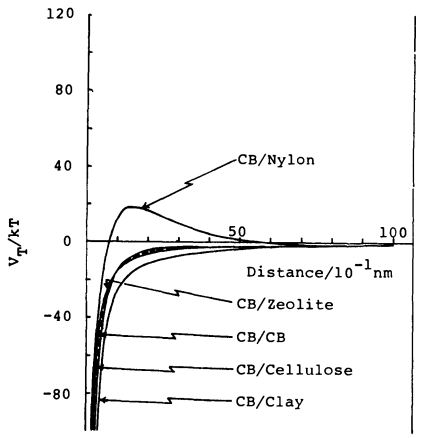

Fig. 4. Total potential energies, V_T, for the interactions between CB/nylon, CB/cellulose, CB/clay, CB/zeolite, and CB/CB in a 1.387×10^{-3} mol dm^{-3} sodium dodecyl sulfate solution at 30 °C. The Debye-Hückel reciprocal length parameter is assumed to be 7.115×10^6 cm^{-1}.

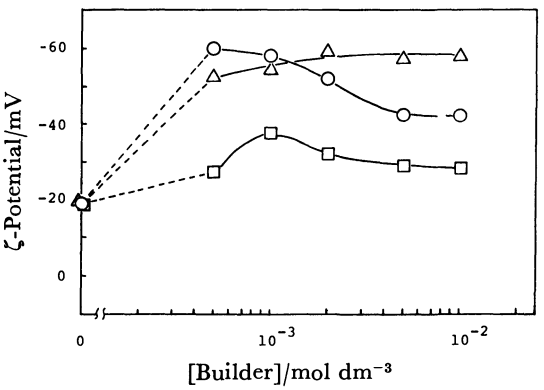

Fig. 5. Effect of the concentration of builder on ζ-potential of CB at 25 °C.
○: Sodium triphosphate, △: sodium carbonate, □: sodium sulfate.

−3, −53, and −17 mV respectively.[1] The total potential energies, V_T, for interactions between CB and nylon, between CB and cellulose, between CB and zeolite, between CB and clay, and between CB and CB were calculated using the ζ-potentials of nylon, cellulose, zeolite, and clay. The results are shown in Fig. 4. Assuming that the electrolyte added is completely ionized, the Debye-Hückel reciprocal length parameter in the 0.2 wt% detergent solution was calculated to be 7.115×10^6 cm^{-1}. Since the ζ-potential is related to the ionic strength, it is desirable that the ζ-potential be measured in the SDS solution in which κ is controlled to be 7.115×10^6 cm^{-1} by the addition of an electrolyte, for example potassium chloride. However, if κ in the SDS solution is controlled by the addition of an electrolyte, the solution is different from the detergent solution. Therefore, the ζ-potential obtained by such an operation seems not to be assigned a significance purely in terms of the effect of SDS in the detergent solution. For this reason, the addition of an electrolyte to control κ was not carried out. Thus we consider that the total potential energies, V_T, shown in Fig. 4 mean the behavior of CB under only the effect of SDS in the detergent solution.

A maximum total potential energy, $V_{T,max}$, suggests a repulsive force, and is related with the stability of the hydrophobic colloid. It is said that $V_{T,max}$ has to be about 15 kT to ensure a stability sufficient for all practical purposes.[9] If there is no maximum, rapid coagulation takes place. Similarly to the previous work, the coagulation or deposition was judged to take place with difficulty if $V_{T,max}$ is more than 15 kT, to take place easily if $V_{T,max}$ is less than 15 kT, and not to take place if $V_{T,max}$ is more than 100 kT.[14] On the basis of such criteria, it is clear from Fig. 4 that the deposition of CB onto nylon takes place with difficulty, and the deposition of CB onto cellulose and the coagulations between CB and clay, between CB and zeolite, and between CB and CB take place rapidly.

The Effect of Water-soluble Builder on the ζ-Potential of CB and the Potential Energy. The effects of sodium triphosphate, sodium silicate, sodium carbonate, sodium (carboxylatomethyl)cellulose(CMC), and sodium sulfate on the ζ-potential of CB are shown in Figs. 5—7.

As shown in Fig. 5, the negative ζ-potential of CB was increased with addition of sodium triphosphate. However, the negative ζ-potential decreased with increasing concentrations of sodium triphosphate. The ζ-potential of CB in sodium triphosphate solution was higher than the ζ-potential at the pH of suspension, pH 9.4—9.7. The increase of the negative ζ-potential results from the adsorption of triphosphate anion. The ζ-potential is

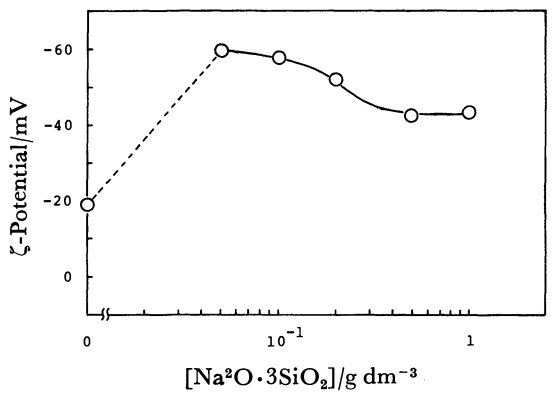

Fig. 6. Effect of the concentration of sodium silicate on ζ-potential of CB at 25 °C.

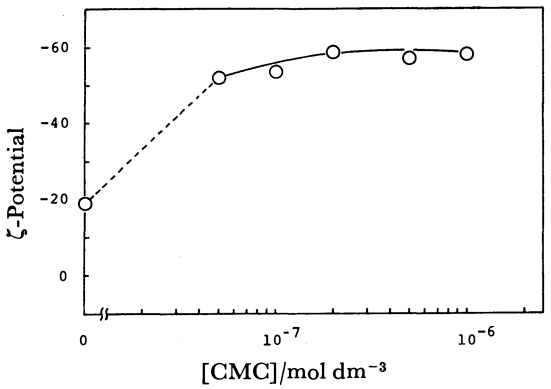

Fig. 7. Effect of the concentration of sodium (carboxylatomethyl)cellulose (CMC) on ζ-potential of CB at 25 °C.

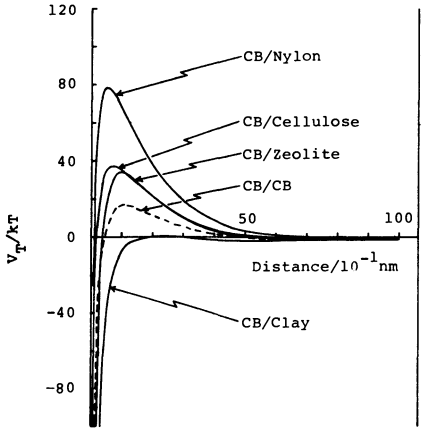

Fig. 8. Total potential energies, V_T, for the interactions between CB/nylon, CB/cellulose, CB/clay, CB/zeolite, and CB/CB in a 1.190×10^{-3} mol dm^{-3} sodium triphosphate solution at 30 °C. The Debye-Hückel reciprocal length parameter is assumed to be 7.115×10^6 cm^{-1}.

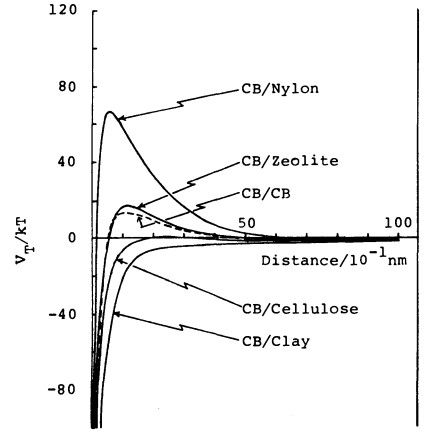

Fig. 9. Total potential energies, V_T, for the interactions between CB/nylon, CB/cellulose, CB/clay, CB/zeolite, and CB/CB in a 0.1 g dm^{-3} sodium silicate solution at 30 °C. The Debye-Hückel reciprocal length parammeter is assumed to be 7.115×10^6 cm^{-1}.

related to the ionic strength. The decrease of negative ζ-potential with increasing concentration of sodium triphosphate seems to result from the increase of the ionic strength.

In the addition of sodium silicate, the negative ζ-potential of CB increased significantly (Fig. 6). The increase was similar to that which occurred in the addition of sodium triphosphate. The ζ-potential was higher than that at the pH of suspension, pH 10.2—11.4. The increase was larger than that of clay.[1] Since the increase results from the adsorption of silicate anions, the adsorption of silicate anion on CB is more than that on clay.

In the addition of sodium carbonate, the negative ζ-potential increased (Fig. 5). The ζ-potential was higher than that at the pH of suspension, pH 10.3—11.4. As described above, the results are attributed to the effect of pH and/or the adsorption of carbonate anion.

The pH of the suspension did not increase due to the addition of CMC and sodium sulfate. Though the concentration of CMC was low, the negative ζ-potential increased significantly (Fig. 7). This suggests that CMC is useful to disperse CB. On the other hand, the increase of ζ-potential in the addition of sodium sulfate was slight (Fig. 5).

As done for SDS, the concentrations of these water-soluble builders in the 0.2 wt% detergent solution were calculated. These ζ-potentials at the concentrations were read from Figs. 5—7. The ζ-potentials of nylon, cellulose, zeolite, and clay and their concentrations are shown in Table 2. The V_T between each pair of materials were calculated with this ζ-potential. The results are shown in Figs. 8—12. The $V_{T,max}$ values in each solution are listed in Table 3. The V_T between CB and nylon in various builders' solutions have maxima: 78.3—14.4 kT. All of these values, except sodium sulfate, were more than the value in SDS solution, and more than 15 kT. CB deposits with difficulty onto nylon fabrics. Though the V_T between CB and cellulose in SDS solution was negative, the V_T in each solution of various builders had maxima. However, the $V_{T,max}$ in the solutions of sodium slicate, sodium carbonate, and sodium sulfate were less than 15 kT. Sodium triphosphate and CMC are useful for prevention of the

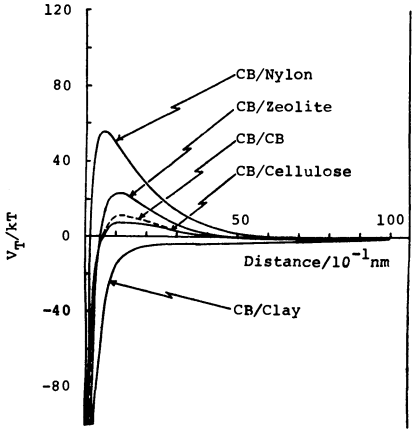

Fig. 10. Total potential energies, V_T, for the interactions between CB/nylon, CB/cellulose, CB/clay, CB/zeolite, and CB/CB in a 5.661×10^{-4} mol dm^{-3} sodium carbonate solution at 30 °C. The Debye-Hückel reciprocal length parameter is assumed to be 7.115×10^6 cm^{-1}.

Table 2. ζ-Potentials of nylon, cellulose, zeolite, and clay in the solutions of various builders at 30 °C[1)]

Builder	Concentration / mol dm^{-3}	ζ-Potential/mV			
		Nylon	Cellulose	Zeolite	Clay
$Na_5P_3O_{10}$	1.190×10^{-3}	−64	−40	−67	−28
$Na_2O\cdot3SiO_2$	0.1(g dm^{-3})	−59	−13	−52	−18
Na_2CO_3	5.661×10^{-4}	−55	−22	−61	−21
CMC	1.653×10^{-7}	−51	−32	−61	−17
Na_2SO_4	7.181×10^{-3}	−50	−23	−51	−29

Table 3. Maximum total potential energies, $V_{T,max}$, in the solution of SDS, various builders or detergent at 30 °C. The Debye-Hückel reciprocal length parameter is assumed to be 7.115×10^6 cm^{-1}

Electrolyte	Concentration / mol dm^{-3}	$V_{T,max}/kT$				
		CB/Nylon	CB/Cellulose	CB/Zeolite	CB/Clay	CB/CB
SDS	1.387×10^{-3}	18.8	*	*	*	*
$Na_5P_3O_{10}$	1.190×10^{-3}	78.3	37.4	34.1	*	16.4
$Na_2O\cdot3SiO_2$	0.1(g dm^{-3})	66.8	0.5	17.9	*	14.0
Na_2CO_3	5.661×10^{-4}	55.9	8.3	22.9	*	10.7
CMC	1.653×10^{-7}	56.7	24.1	28.2	*	16.4
Na_2SO_4	7.181×10^{-3}	14.4	1.1	*	*	*
Detergent	0.2 (wt%)	84.8	16.3	16.6	*	9.7

* The total potential energy was negative for every distance between two materials.

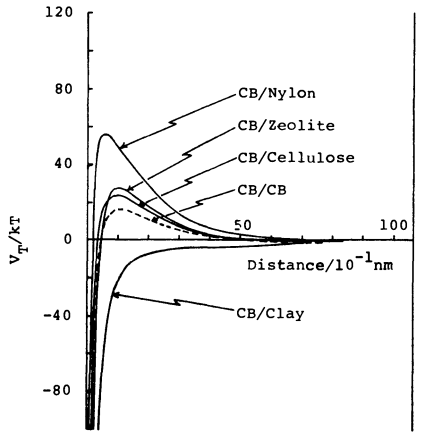

Fig. 11. Total potential energies, V_T, for the interactions between CB/nylon, CB/cellulose, CB/clay, CB/zeolite, and CB/CB in a 1.653×10^{-7} mol dm^{-3} sodium (carboxylatomethyl)cellulose solution at 30 °C. The Debye-Hückel reciprocal length parameter is assumed to be 7.115×10^6 cm^{-1}.

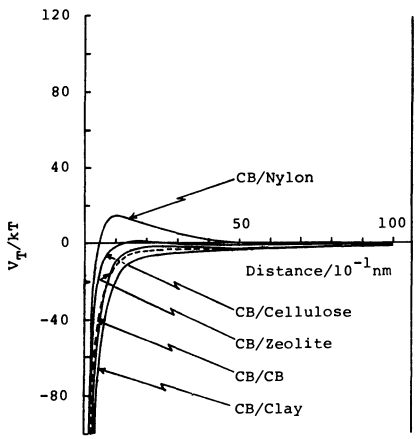

Fig. 12. Total potential energies, V_T, for the interactions between CB/nylon, CB/cellulose, CB/clay, CB/zeolite, and CB/CB in a 7.181×10^{-3} mol dm^{-3} sodium sulfate solution at 30 °C. The Debye-Hückel reciprocal length parameter is assumed to be 7.115×10^6 cm^{-1}.

deposition of CB onto cotton fabrics. The V_T between CB and zeolite in the solutions of various builders, except sodium sulfate, had large maxima of 34.1 − 17.9 kT. The coagulation between CB and zeolite in these builders takes place with difficulty. Though the V_T between CB and CB in the solutions of sodium triphosphate and CMC had maxima of $\geq15\ kT$, the V_T in the solution of the other builders were negative or had small maxima. The V_T values between CB and clay in the solutions of various builders were negative. The coagulation between CB and clay in the various builders' solutions also takes place easily.

The Behavior of CB in the Detergent Solution. The effect of the detergent concentration on the ζ-potential

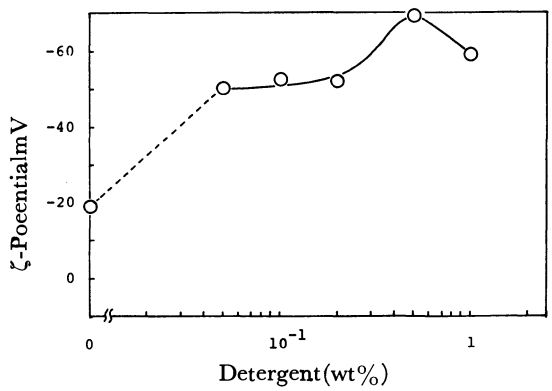

Fig. 13. Effect of the concentration of detergent on ζ-potential of CB at 25 °C.

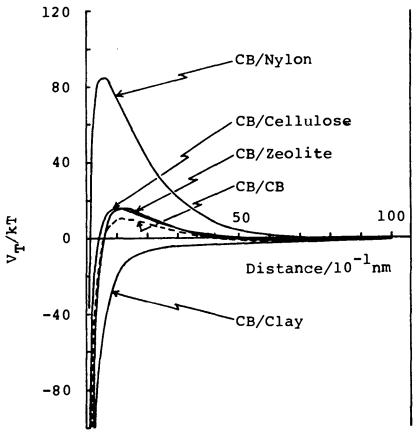

Fig. 14. Total potential energies, V_T, for the interactions between CB/nylon, CB/cellulose, CB/clay, CB/zeolite, and CB/CB in a 0.2 wt% detergent solution at 30 °C. The Debye-Hückel reciprocal length parameter is assumed to be 7.115×10^6 cm^{-1}.

of CB is shown in Fig. 13. The ζ-potential had a maximum at 0.5 wt%. The reason why the maximum existed at this concentration may be interesting; however, since the 0.5 wt% detergent solution is not for practical use, the discussion is excluded from this paper. The ζ-potential of CB at 0.2 wt% was read from Fig. 13. The ζ-potentials of nylon, cellulose, zeolite, and clay in 0.2 wt% detergent solution were −79.9, −28.7, −54.4, and −17.8 mV respectively.[1] The V_T values between each pair of materials in the 0.2 wt% detergent solution were calculated, and are shown in Fig. 14. The $V_{T,max}$ is shown in Table 3. From these results, we can see that CB in the detergent solution deposits with difficulty onto fabrics, coagulates with difficulty with zeolite, and coagulates easily with clay or CB. Consequently, when a detergent which is composed without sodium triphosphate is used, the ζ-potential of CB is increased by the effect of the builders, and the deposition of CB onto fabrics is prevented. Since CB in the detergent solution coagulates easily with clay, the behavior of this coagulated substance in the detergent solution will be discussed in the near future.

References

1) Y. Yoneyama and K. Ogino, *Tenside Deterg.*, **19**, 197 (1982).
2) J. B. Donnet and A. Voet, "Carbon Black," Marcel Dekker, Inc., New York (1976).
3) T. Imamura and F. Tokiwa, *Nippon Kagaku Kaishi*, **1972**, 2177.
4) A. L. Loeb, P. H. Wiersema, and J. Th. G. Overbeek, "The Electrical Double Layer Around Spherical Colloid Particles," The MIT Press, Cambridge, MA (1961), p. 7.
5) A. Kitahara, *Kagaku No Ryoiki*, **24**, 402 (1970).
6) S. Usui, "Kaimen Denki Gensho," ed by A. Kitahara and A. Watanabe, Kyoritsu, Tokyo (1978), p. 81.
7) R. Hogg, T. W. Healy, and D. W. Fuerstenau, *Trans. Faraday Soc.*, **62**, 1638 (1966).
8) H. C. Hamaker, *Physica*, **4**, 1058 (1937).
9) J. W. Verwey and J. Th. G. Overbeek, "Theory of the Stability of Lyophobic Colloids," Elsevier Publ. Co., Amsterdam (1948).
10) F. M. Fowkes, *Ind. Eng. Chem.*, **56**, 40 (1964).
11) A. W. Flegmann, J. W. Goodwin, and R. H. Ottewill, *Proc. Brit. Ceram.*, **13**, 31 (1969).
12) H. P. Boehm, *Angew. Chem.*, **78**, 617 (1966).
13) T. Murata and H. Imagawa, *Denki Kagaku*, **41**, 708 (1973).
14) T. Imamura and F. Tokiwa, *Nippon Kagaku Kaishi*, **1973**, 2051.

 © 1982 The Chemical Society of Japan Bull. Chem. Soc. Jpn., 55, 3085—3088 (1982)

Interaction between Hydrophilic Proteins and Nonionic Detergents Studied by Surface Tension Measurements

Nagamune NISHIKIDO,* Tomoyuki TAKAHARA, Hideki KOBAYASHI, and Mitsuru TANAKA
Department of Chemistry, Faculty of Science, Fukuoka University, Nanakuma, Jyōnan-ku, Fukuoka 814-01
(Received January 14, 1982)

The surface tensions of the systems of hexa(oxyethylene) dodecyl ether ($C_{12}E_6$) *vs.* lysozyme (Lyz) or bovine serum albumin (BSA) were measured for constructing the binding isotherms, since the surface tension method is more convenient for the systems of nonionic detergents and proteins than is equilibrium dialysis. The obtained binding isotherms depend on the protein concentration; this effect is much more remarkable for Lyz–$C_{12}E_6$ systems than for BSA–$C_{12}E_6$ ones. The binding isotherms of BSA–$C_{12}E_6$ systems obey the Scatchard equation, and the maximum number and estimated free energy for $C_{12}E_6$ binding to BSA are comparable to those for the system of Triton X-100 and BSA determined by equilibrium dialysis. The agreement suggests that the surface tension method is sound and has advantages over equilibrium dialysis for the estimation of the number of detergent molecules bound to protein. In the systems of Lyz–$C_{12}E_6$, the binding isotherms follow the Freundlich-type equation rather than the Scatchard equation. The remarkable protein concentration dependence of the binding isotherms and this result suggest the occurrence of protein aggregation.

Nonionic detergents such as Triton X-100 (poly-(oxyethylene) (9—10) *p*-(1,1,3,3-tetramethylbuthyl)-phenyl ether) have been widely used to solubilize membranes and to purify membrane proteins.[1,2] That is, they can often extract proteins from membranes without disruption of native conformation or loss of biological activity, in contrast to common synthetic ionic detergents, notably sodium dodecyl sulfate (SDS), which ordinarily solubilize lipid-associated proteins in a denatured and inactive form.

The interaction of proteins with ionic detergents has been a subject of intensive investigation. However, the interaction of nonionic detergents with proteins has not been investigated widely and the information so far gained is as follows.[1,3–5] The lipophilic proteins bind cooperatively large amounts of nonionic detergents at their critical micelle concentrations (cmc's), whereas a number of hydrophilic proteins bind few or no nonionic detergents. It seems that nonionic detergents can bind only to hydrophilic proteins possessing hydrophobic surface patch. For example, ovalbumin does not bind Triton X-100 at all within the concentration range studied (10^{-5}—10^{-4} mol dm^{-3}). Bovine serum albumin (BSA), possessing a hydrophobic surface patch, binds Triton X-100 by the maximum number of four per protein in a Langmuir-type binding, and no gross structural change occurs in BSA by binding of Triton X-100.

The interaction between detergents and proteins may be attributed to the binding of detergents to proteins, *i.e.*, to complex formation, and may be expressed directly and quantitatively by the binding isotherms. The amount of detergents bound to proteins is usually determined by means of equilibrium dialysis. However, nonionic detergents such as Triton X-100 do not penetrate the dialysis membrane fast enough for dialysis experiments.[1,3] On the contrary, the surface tension can be measured more easily and reflects sensitively the changes of dissolved state in bulk.

In this report, we have measured the surface tension of aqueous solutions of hexa (oxyethylene) dodecyl ether ($C_{12}E_6$) *vs.* lysozyme (Lyz) or bovine serum albumin (BSA), and constructed the binding isotherms by applying the surface tension data to the equations derived for determining the number of detergent molecules bound to a protein.

Experimental

Materials. Hen egg-white Lyz was supplied from Miles Biochemicals (six times recrystallized; activity: above 51000 units/mg; homogeneity: above 97%). BSA was also supplied from Miles Biochemicals (monomer standard protein powder; purity: above 99%). $C_{12}E_6$ was supplied from Nikkō Chemicals Co., Ltd. The high purity (above 99.5%) was confirmed by gas chromatography.

Surface Tension Measurements. The aqueous solutions of mixed BSA– or Lyz–$C_{12}E_6$ were free from buffer and salts. The pH's of the solutions were 5.6. The surface tension measurements for the solution were performed at 298.15±0.01 K by the Wilhelmy method with a 24 mm × 24 mm glass plate and a Kyowa CBVP Surface Tension-Meter A-3. Before the measurement the plate was cleaned by heating it in a "chromic acid mixture" for more than six hours and was washed thoroughly with three-times-distilled water.

Results and Discussion

In Figs. 1 and 2 are shown the plots of surface tension *vs.* detergent concentration at constant protein concentration for BAS– and Lyz–$C_{12}E_6$ systems, respectively. Each plot exhibits a sharp break at each cmc and the surface tension remains constant above the cmc. The values of the constant surface tensions for all the systems are identical regardless of the protein concentration. Next, we will derive the equations for determining the amount of nonionic detergents bound to proteins from these surface tension data.

It can be supposed that protein-nonionic detergent complexes are surface inactive, since the hydrophobic areas of protein and detergent are almost hidden by the complex formation. Then the following Langmuir equation may be valid for the adsorption equilibrium of nonionic detergent monomers at the air/water interface from the aqueous solution of protein and detergent, in the same way as in the case of the adsorption of detergent alone:[6–9]

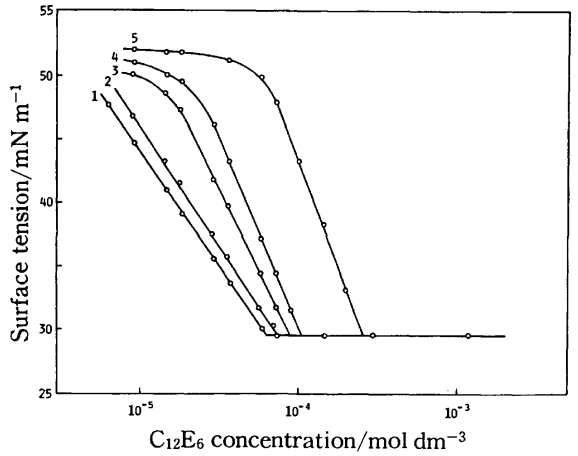

Fig. 1. Plots of surface tension *vs.* logarithm of $C_{12}E_6$ concentration at various BSA concentrations for BSA–$C_{12}E_6$ systems at 298.15 K.
BSA concentration: (1) $C_{12}E_6$ alone, (2) 1×10^{-6}, (3) 5×10^{-6}, (4) 1×10^{-5}, (5) 5×10^{-5} mol dm^{-3}.

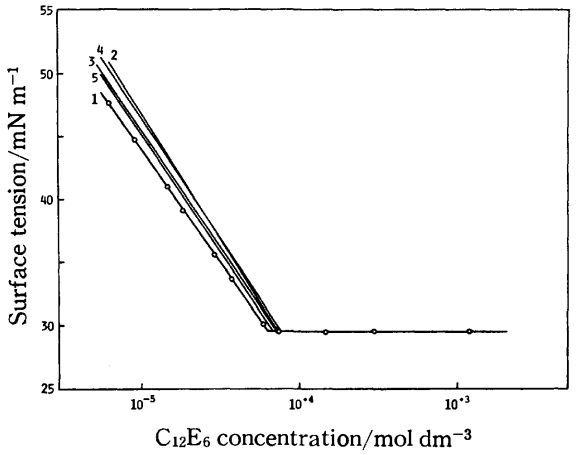

Fig. 2. Plots of surface tension *vs.* logarithm of $C_{12}E_6$ concentration at various Lyz concentrations for Lyz–$C_{12}E_6$ systems at 298.15 K.
Lyz concentration: (1) $C_{12}E_6$ alone, (2) 1×10^{-6}, (3) 2×10^{-6}, (4) 1.25×10^{-5}, (5) 1×10^{-4} mol dm^{-3}.

$$\Gamma_s = \frac{K_s(a-\Gamma_p f)C_s^f}{1+K_sC_s^f}, \tag{1}$$

where Γ_s: the amount of adsorbed detergent at the air/water interface,
Γ_p: the amount of adsorbed protein,
f: the factor for converting Γ_p to Γ_s-basis, defined as the ratio of the maximum adsorption of detergent to that of protein,
a: the maximum adsorption of detergent,
C_s^f: the concentration of detergent monomer,
K_s: the equilibrium constant.

It is also known that the Langmuir equation applies empirically to the adsorption of protein at the low concentration,[10,11] and thus we may write for the protein-component:

$$\Gamma_p f = \frac{K_p(a-\Gamma_s)C_p^f}{1+K_pC_p^f}, \quad \Gamma_p^\circ f = \frac{K_paC_p^\circ}{1+K_pC_p^\circ}, \tag{2a,2b}$$

where the subscript o denotes the quantity for the adsorption in the aqueous solutions of the protein alone, and the subscript p refers to protein. If the protein concentration is low enough so that $K_pC_p^f \approx K_pC_p^\circ \ll 1$ (Henry-type adsorption), we have from Eqs. 2a and 2b:

$$\Gamma_p f = \Gamma_p^\circ f + K_p(\Gamma_s-a)(C_p^\circ-C_p^f) - K_pC_p^\circ\Gamma_s. \tag{3}$$

In the case of the adsorption of nonionic detergent ($C_{12}E_6$) alone, the value of Γ_s is nearly equal to that of a in the concentration range greater than 1×10^{-5} mol dm^{-3}; this is the result of the direct measurement of the adsorption of $C_{12}E_6$ by a radiotracer technique.[12] Then, in the case of the adsorption from protein-detergent mixed solutions, the magnitude of the second term is expected to be much less than those of the others terms in Eq. 3 at the $C_{12}E_6$ concentration studied and we have:

$$\Gamma_p f \simeq \Gamma_p^\circ f - K_pC_p^\circ\Gamma_s = \Gamma_p^\circ f - \frac{\Gamma_p^\circ f}{a}\Gamma_s. \tag{4}$$

Irrespective of the concentration range where Eq. 4 is valid, Eq. 4 may be regarded as a working hypothesis for the mixed adsorption of detergent and protein. That is, Eq. 4 gives a relation between Γ_p and Γ_s, and means that the value of Γ_p decreases linearly with that of Γ_s. By introducing Eq. 4 into Eq. 1, we obtain

$$\Gamma_s = \frac{K_sa(a-\Gamma_p^\circ f)C_s^f}{a+K_s(a-\Gamma_p^\circ f)C_s^f}. \tag{5}$$

Next, we consider the Gibbs adsorption equation under the conditions of constant protein concentration, Eq. 6, since the concentrations of detergent and protein are low in the present case:[13]

$$\left(\frac{\partial\gamma}{\partial\mu_s}\right)_{T,\mu_p} \simeq \left(\frac{\partial\gamma}{\partial\ln C_s^f}\right)_{T,C_p} = -RT\Gamma_s, \tag{6}$$

where γ refers to the surface tension of the aqueous solution containing protein and detergent, and μ is the chemical potential. By integration of Eq. 6 after introduction of Eq. 5, we have

$$\gamma = -aRT\ln[a+K_s(a-\Gamma_p^\circ f)C_s^f] + \gamma_p + aRT\ln a, \tag{7}$$

where γ_p refers to the surface tension of the protein solution. In the case of detergent alone,

$$\gamma_s = -aRT\ln[1+K_sC_s^\circ] + \gamma_{H_2O}, \tag{8}$$

where γ_{H_2O} refers to the surface tension of pure water.

Now we assume: at the concentration (cmc′) where the surface tension γ begins to stay constant, detergent monomers begin to form micelles by themselves and the concentration of monomers is identical with the cmc of detergent alone (cmc°). In addition, as seen from Figs. 1 and 2, we take into account the experimental observation that the surface tensions at the cmc′ and cmc° are identical ($\gamma_{cmc'}=\gamma_{cmc^\circ}\equiv\gamma_{cmc}$). Then, we have by Eqs. 7 and 8:

$$\gamma_{cmc} = -aRT\ln[1+K_s\,cmc^\circ] + \gamma_{H_2O}, \tag{9}$$

$$\Gamma_p^\circ f = \frac{a(1+K_s\,cmc^\circ)\left\{1-\exp\left(-\frac{\gamma_{H_2O}-\gamma_p}{aRT}\right)\right\}}{K_s\,cmc^\circ}. \tag{10}$$

By applying Eqs. 7, 9, and 10 to the surface tension data shown in Figs. 1 and 2, we can obtain the mean number of detergent molecules bound to proteins, $\bar{\nu}$; $\bar{\nu}=$

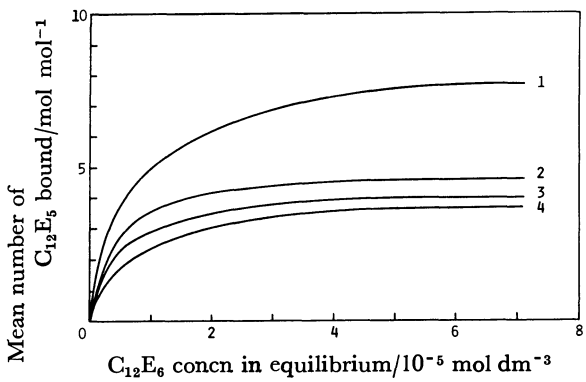

Fig. 3. Binding isotherms at various BSA concentrations for BSA–$C_{12}E_6$ systems at 298.15 K.
BSA concentration: (1) 1×10^{-6}, (2) 5×10^{-6}, (3) 1×10^{-5}, (4) 5×10^{-5} mol dm^{-3}.

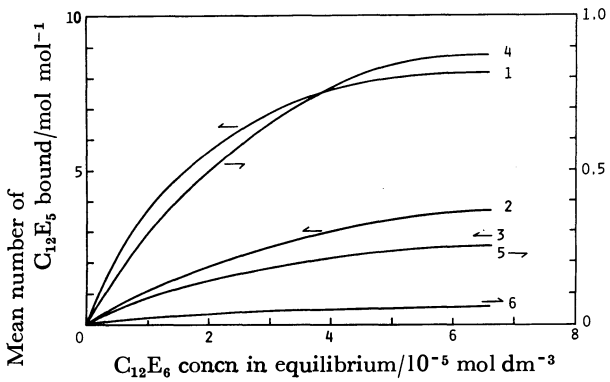

Fig. 4. Binding isotherms at various Lyz concentrations for Lyz–$C_{12}E_6$ systems at 298.15 K.
Lyz concentration: (1) 1×10^{-6}, (2) 2×10^{-6}, (3) 5×10^{-6}, (4) 1.25×10^{-5}, (5) 5×10^{-5}, (6) 1×10^{-4} mol dm^{-3}.

$(C_s-C_s^f)/C_p$, where C_s denotes the total detergent concentration. The process used to obtain the value of $\bar{\nu}$ is as follows. The value of a may be obtained from the slope of the surface tension *vs.* logarithm of concentration plot below the cmc of $C_{12}E_6$ solution (Fig. 1 or 2) by applying the Gibbs adsorption equation. Next, the value of K_s can be calculated by introducing the values of a, cmc° and γ_{H_2O} into Eq. 9 and then that of $\Gamma_p^\circ f$ can be calculated by the use of Eq. 10. Finally, it is possible to calculate the value of C_s^f by introducing the obtained values of K_s and $\Gamma_p^\circ f$ into Eq. 7 and thus we obtain the value of $\bar{\nu}$.

Figures 3 and 4 show the binding isotherms for BSA– and Lyz–$C_{12}E_6$ systems, respectively, at various protein concentrations. The confidence limit of protein concentration for estimating the value of $\bar{\nu}$ primarily depends on the value of cmc of detergent alone (cmc°) since the value of cmc° is the maximum concentration of detergent in unbound state. In this work, the confidence range of protein concentration is estimated to be from 10^{-6} to 10^{-4} mol dm^{-3}. It is realized from Figs. 3 and 4 that the bound number explicitly depends upon the protein concentration and decreases with the increase of concentration. The tendency of the concentration dependence is much more remarkable for Lyz–$C_{12}E_6$ than for BSA–$C_{12}E_6$ systems. In BSA–$C_{12}E_6$ systems, the bound number approaches a constant value with an increase in BSA concentration, in other words, the binding isotherms approximately coincide with one another at higher BSA concentrations. In this case, the maximum number of $C_{12}E_6$ bound is about four moles per mole of BSA, which agrees with that for Triton X-100 and BSA systems determined by equilibrium dialysis.[5] The dependence of the bound numbers on protein concentrations was also found for the systems of SDS *vs.* membrane protein, ferricytochrome *c*,[14] which exhibits a similar behavior to that of hydrophilic protein for the interaction with detergents.[15]

It is known that ionic detergents (at lower concentractions) and nonionic detergents bind to the hydrophobic regions of proteins primarily with hydrophobic bonds.[1,5,16] It may be anticipated that the hydrophobic regions of proteins, which are detergent-binding sites, come into contact and are effectively removed by protein-protein interactions within the protein aggregates; this aggregation effect may be enhanced by the increase in protein concentration.[1] In fact, Lyz is known to aggregate in solution, depending on the pH.[17] In addition, protein aggregation may also be favored sterically by detergent binding by way of the flexible hydrocarbon chain. The concentration dependence of the bound number is considered to be somehow due to the fact that detergent-binding sites become effectively hidden.

Just as the systems of BSA and Triton X-100, which were studied by equilibrium dialysis, the binding isotherms for BSA–$C_{12}E_6$ systems obey the Scatchard equation:[18]

$$\bar{\nu}/C_s^f = k_0 n - k_0\bar{\nu}, \qquad (11)$$

where k_0 denotes the intrinsic binding constant and n the maximum number of binding sites. The estimated values of k_0 and the free energies ΔG for $C_{12}E_6$ binding to BSA are listed in Table 1, with BSA concentrations. The mean value of ΔG, -7.2 ± 0.2 kcal mol^{-1}, can be made comparable to the value for the systems of Triton X-100 and BSA, -5.9 kcal mol^{-1}, by taking into account the difference of hydrophobic chain of $C_{12}E_6$ and of Triton X-100.[19] This agreement and the agreement of the maximum number of detergent molecules bound suggest that the surface tension method is not only sound but very advantageous for the estimation of the number of detergent molecules bound to proteins, since the surface tension measurements are more easily performed than the equilibrium dialysis

Table 1. Intrinsic binding constants k_0 and free energies ΔG for $C_{12}E_6$ binding to BSA

BSA concentration / mol dm^{-3}	k_0 / dm^3 mol^{-1}	ΔG / kcal mol^{-1} a)
1×10^{-5}	1.7×10^5	-7.2 ± 0.2
5×10^{-6}	2.3×10^5	-7.4 ± 0.2
1×10^{-5}	2.2×10^5	-7.3 ± 0.2
5×10^{-5}	1.6×10^5	-7.1 ± 0.2

a) 1 cal=4.184 J.

experiments. To establish the advantage of the surface tension method is one of the objectives of this work. The detergent binding for BSA–$C_{12}E_6$ systems means the statistical binding by hydrophobic bonding. However, the binding isotherms for Lyz–$C_{12}E_6$ systems obey the following Freundlich-type equation rather than the Scatchard equation:

$$\bar{\nu}/n = K(C_s^f)^a, \quad 0 \leq a \leq 1. \tag{12}$$

Equation 12 has been derived by assuming an exponential distribution of binding energies, *i.e.*, the heterogeneity of binding sites. This heterogeneity may be caused by the protein aggregation, which is more remarkable for Lyz. In the present case, the protein aggregate consists of several monomers at the most on the average. They may assume various arrangements, since the aggregating force including steric factors is rather weak compared to that for ordinary micelles of detergents. In addition, it is considered that the hydrophobic areas of protein are not completely hidden by the aggregation and thus the residual areas of the aggregate exhibit different geometries owing to the distribution of arrangements and sizes of aggregate. This may reflect the heterogeneity of binding sites. Thus, binding isotherms must be viewed with some caution, as it is probable that detergent-binding sites are effectively hidden by protein-protein interaction.

References

1) A. Helenius and K. Simons, *J. Biol. Chem.*, **247**, 3656 (1972).
2) A. Helenius and K. Simons, *Biochim. Biophys. Acta*, **415**, 29 (1975).
3) R. M. Dowben and W. R. Koehler, *Arch. Biochem. Biophys.*, **93**, 496 (1961).
4) W. R. Koehler and R. M. Dowben, *Arch. Biochem. Biophys.*, **93**, 501 (1961).
5) S. Makino, J. A. Reynolds, and C. Tanford, *J. Biol. Chem.*, **248**, 4926 (1973).
6) J.T. Davies and E. K. Rideal, "Interfacial Phenomena," Academic Press, New York (1961), p. 183.
7) H. Lange, *Kolloid Z. Z. Polym.*, **201**, 131 (1964).
8) H. Lange and K. H. Beck, *Kolloid Z. Z. Polym.*, **251**, 424 (1973).
9) M. Nakagaki, T. Handa, and S. Shimabayashi, *J. Colloid Interface Sci.*, **43**, 521 (1973).
10) M. C. Phillips, M. T. A. Evans, D. E. Graham, and D. Oldani, *Colloid Polym. Sci.*, **253**, 424 (1975).
11) D. E. Graham and M. C. Phillips, *J. Colloid Interface Sci.*, **70**, 415 (1979).
12) K. Tajima, M. Iwahashi, and T. Sasaki, *Bull. Chem. Soc. Jpn.*, **44**, 3251 (1971).
13) J. H. Buckingham, J. Lucassen, and F. Hollway, *J. Colloid Interface Sci.*, **67**, 423 (1978).
14) R. K. Burkhard and G. E. Stolzenberg, *Biochemistry*, **11**, 1672 (1972).
15) N. M. Shechter, M. Sharp, J. A. Reynolds, and C. Tanford, *Biochemistry*, **15**, 1897 (1976).
16) J. Steinhardt and J. A. Reynolds, "Multiple Eequilibria in Proteins," Academic Press, New York and London (1969), p. 239.
17) A. J. Sophoanopoulos and K. E. Van Holde, *J. Biol. Chem.*, **239**, 2516 (1964).
18) G. Scatchard, *Ann. N. Y. Acad. Sci.*, **51**, 660 (1949).
19) I. J. Lin, J. P. Friend, and Y. Zimmels, *J. Colloid Interface Sci.*, **45**, 378 (1973).
20) J. Steinhardt and J. A. Reynolds, "Multiple Equilibria in Proteins," p. 12.

The Isomerization of Butenes over KC_8

Susumu Tsuchiya,* Takatoshi Misumi, Noriyuki Ohuye, and Hayao Imamura
Department of Industrial Chemistry, Faculty of Engineering, Yamaguchi University, Tokiwadai, Ube 755
(Received February 15, 1982)

The isomerization of butenes over KC_8 has been investigated. The double-bond-migration and the cis-trans isomerization took place over KC_8, but the skeletal isomerization could not be observed. From the rates of reactions and the selectivity ratios, all six of the relative rate constants and the activation energies of reaction were determined. The reaction paths on the triangular graph calculated from the rates constants show the *cis*-convex-type profile, which suggests one of the catalytic characteristics of KC_8.

It is well known that graphite reacts with alkali metals to form a variety of intercalation compounds with a transition metal-like nature.[1] In these substances, the alkali metal atoms are not merely distributed randomly between the layers of the graphite structure, but have an ordered layer-lattice of their own. The corresponding intercalation compounds exhibit well-defined stoichiometric compounds, *e.g.*, KC_8.

Although the intercalation compounds of graphite have been known for at least fifty years, their catalytic and surface properties have only recently begun to be explored. In the present work, the interest has centered on the catalytic characteristics of KC_8, the isomerization of butenes being employed as a model reaction.

Experimental

Materials. The KC_8 samples used as catalysts were prepared *in vacuo* in the apparatus shown in Fig. 1. The graphite (1.25 g of Union Carbide Spectroscopic-grade powder) in the vessel, G, was first degassed for 3 h at 540 K. The bulb, K, containing potassium metal was then heated by applying a soft flame, so that the metal ran into the preparation vessel, P, the wall of which was covered with potassium film, leaving the dross behind. The weight ratio, potassium/graphite, was set as 0.60. K was then removed at the seal-off. After the stopcock, III, had been closed, this apparatus was removed from the vacuum line and inclined in order to transfer the graphite powder from the vessel, G, to P. After G had been removed from the seal-off, the apparatus was again connected to the vacuum line. P was heated in a electric heater for 24 h at 540 K to form KC_8, and then it was evacuated for 30 min. The excess potassium on KC_8 was separated by the evacuation. The intercalation compound thus formed was kept for another 24 h at the same temperature. The apparatus was then removed from the vacuum line at the seal-off point and inclined so as to transfer the KC_8 powder from P to the reactor, R. A capillary tube sampler connected to the apparatus was used for X-ray analysis *in vacuo* to identify the intercalation compound. The X-ray diffraction data of the KC_8 samples prepared thus agreed quite well with those reported by Rudroff and Schulze.[2] The color of the KC_8 obtained was gold.

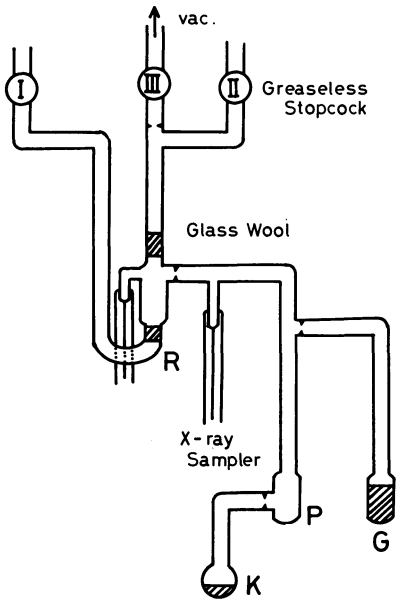

Fig. 1. Apparatus for preparation of KC_8.

The 1-butene, *cis*-2-, and *trans*-2-butene used as the reactants were obtained from the Tokyo Kasei Kogyo Co., Ltd., and were purified by repeated distillation *in vacuo*, the purity was confirmed by gas chromatography to be more than 99%.

Procedure. The apparatus used for the present study was essentially the same as that used previously.[3] A closed circulating system with a U-shaped reactor and with greaseless stopcocks, connected to a conventional vacuum line and a gas chromatograph, was used to follow the reaction. The volume of the reaction system corresponded to about 288 cm^3 at the reaction temperature of 373 K. The reaction mixtures were occasionally analyzed by means of the gas chromatograph with a column of dimethylsulfolane on Celite-545.

Before each run, the catalyst was evacuated for 2 h at 470 K, after which helium was introduced into the reactor. The reactor was then cooled to the reaction temperature and evacuated for a few minutes.

Results and Discussion

The double-bond-migration and the *cis-trans* isomerization of butenes took place over KC_8. The graphite does not show any catalytic activity for a reaction under the same experimental conditions. The skeletal isomerization could not be observed. No gaseous hydrocarbon other than butenes could be detected in the reaction mixtures under the present experimental conditions.

Figure 2 shows how the composition of the butenes changes with the time over KC_8 at 373 K when 1-butene is the reactant; *cis*-2-butene is predominantly formed. The ambient pressure of 1-butene at the initial state was 2.80×10^3 Pa in this reaction. When potassium metal was employed as the catalyst, *trans*-2-butene was predominantly formed as this temperature.[4] The results suggest that the KC_8 used as the catalyst is different in catalytic nature from potassium metal. The active sites of the catalyst are attributed to KC_8, and not to potassium atoms, which might be randomly present

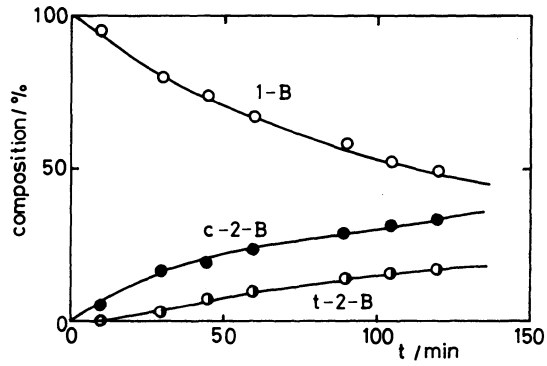

Fig. 2. Isomerization of 1-butene over KC_8 at 373 K.

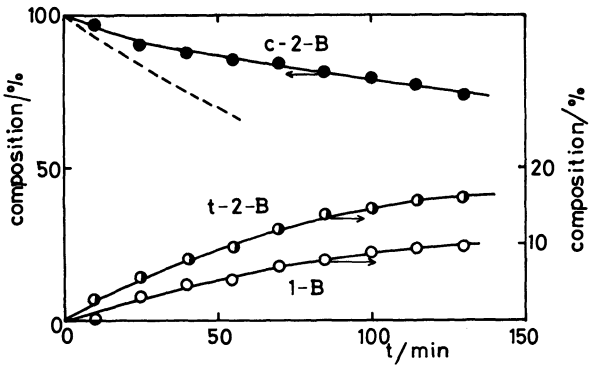

Fig. 3. Isomerization of *cis*-2-butene over KC_8 at 373 K.

between the layers of the graphite structure.

The equilibrium composition of butenes at 373 K, as calculated from the thermodynamical data,[5] is $x_{1e} : x_{ce} : x_{te} = 0.052 : 0.288 : 0.660$, where x_{1e}, x_{ce}, and x_{te} are the mole fractions of 1-butene, *cis*-2-butene, and *trans*-2-butene respectively at equilibrium. The amount of *cis*-2-butene formed at a later time becomes more than that at the equilibrium.

Figure 3 shows how composition of the butenes changes with the time at 373 K when *cis*-2-butene is the reactant. The ambient pressure of *cis*-2-butene at the initial state was 2.80×10^3 Pa in the reaction. The rate of the isomerization reaction of *cis*-2-butene is lower than that of 1-butene; the dotted line represents the time course of 1-butene shown in Fig. 2. The amount of 1-butene at the later time also exceeds that at equilibrium.

The isomerization reaction of butenes was almost first-order with respect to the pressure of reactants, ranging from 2.0×10^3 to 1.4×10^4 Pa. From the rates of reaction and the selectivity ratios, all six of the relative rate constants expressed by Scheme 1 and the activation energies of reaction were determined. The relative rate constants at 373 K and the activation energies (bracketed) are shown in Fig. 4.

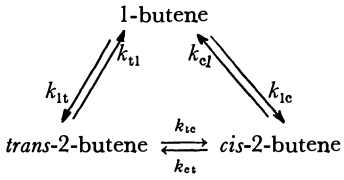

Scheme 1.

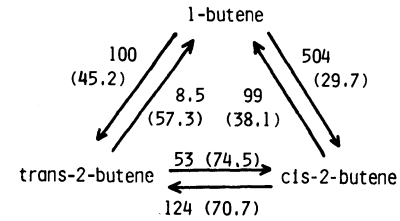

Fig. 4. Relative rate constants at 373 K and activation energies (kJ/mol) bracketed.

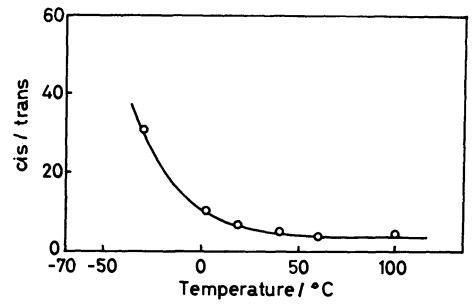

Fig. 5. Temperature dependence of selectivity ratio, *cis*/*trans*, for isomerization of 1-butene.

Figure 5 shows the temperature dependence of the *cis*/*trans* selectivity ratio, 1-butene being the reactant. The ratio became extremely high (more than 30) at a lower temperature.

Since the isomerization of butenes has been the subject of many detailed investigations, three mechanisms have been proposed for different catalytic systems:[6]

(a) A hydride-addition mechanism for metals and organometallic systems;

(b) a carbenium-ion mechanism for acid catalysts, and

(c) an allylic (carbanion) mechanism which is operative over basic catalysts. Each of these mechanisms has certain characteristic features. When the isomerization takes place with the allylic mechanism, the initial *cis*/*trans* ratio is more than unity and the initial 1/*trans* ratio is larger than the 1/*cis* ratio.[6,7]

The relative initial rates of isomerization are also similar to those for the carbanion mechanism; *i.e.*, the rate of the isomerization of 1-butene>that of *cis*-2>that of *trans*-2-butene. The data obtained in the present study are in agreement with an allylic mechanism. A further discussion of the reaction mechanism must await a new result which might be obtained from a rather sophisticated experiment.

Wei and Prater[8] developed an interesting method for evaluating the kinetic parameters of a monomolecular, or pseudomonomolecular, first-order multicomoponent system, triangular diagrams being employed. An extension of the Wei and Prater method was devised by Lombardo and Hall[9] to reduce the required work. Haag and Pines,[10] on the other hand, had proposed a method to estimate the relative values of six rate constants for the interconversion of butenes; they had shown that the reaction path could be calculated from the first-order rate equation by using the relative rate constants. The concentrations of 1- and of *cis*-2-butene were plotted

against that of *trans*-2-butene. Kagawa[11] kinetically analyzed the reaction path in a system consisting of a Langmuir-Hinshelwood-type reaction.

In the Haag and Pines analysis, mixtures of butenes were not used as the reactants; the differential equation employed was applied only for a pure reactant. In the present paper, the isomerization of butenes, is dealt with in a more general way.

Since there is no change in the total number of moles with the extent of reaction:

$$x_l + x_c + x_t = 1, \tag{1}$$

where x_l, x_c, and x_t are the mole fractions of 1-butene, *cis*-2-butene, and *trans*-2-butene respectively. The overall reaction rates can be accordingly expressed by Eq. 2:

$$\frac{dx_l}{dt} = -(k_{lc}+k_{lt})x_l + k_{cl}x_c + k_{tl}x_t \tag{2-l}$$

$$\frac{dx_c}{dt} = k_{lc}x_l - (k_{ct}+k_{cl})x_c + k_{tc}x_t \tag{2-c}$$

$$\frac{dx_t}{dt} = k_{lt}x_l + k_{ct}x_c - (k_{tl}+k_{tc})x_t \tag{2-t}$$

The particular solution of Eq. 2 satisfying the boundary conditions of the initial composition, x_{i0} (i=l, c, t), at $t=0$ and the equilibrium composition, x_{ie}, at $t=\infty$ is:

$$\begin{aligned} x_l = {} & (1/\sqrt{m^2-4n})[(k_{cl}-k_{tl})x_{c0} + k_{tl} \\ & - \{k_{lc}+k_{lt}+k_{tl}-(m+\sqrt{m^2-4n})/2\}x_{l0} \\ & - \{(m+\sqrt{m^2-4n})/2\}x_{le}]\exp[-\{(m-\sqrt{m^2-4n})/2\}t] \\ & - (1/\sqrt{m^2-4n})[(k_{cl}-k_{tl})x_{c0} + k_{tl} \\ & - \{k_{lc}+k_{lt}+k_{tl}-(m-\sqrt{m^2-4n})/2\}x_{l0} \\ & - \{(m-\sqrt{m^2-4n})/2\}x_{le}] \times \\ & \exp[-\{(m+\sqrt{m^2-4n})/2\}t] + x_{le}, \end{aligned} \tag{3-l}$$

$$\begin{aligned} x_c = {} & (1/\sqrt{m^2-4n})[(k_{lc}-k_{tc})x_{l0} + k_{tc} \\ & - \{k_{ct}+k_{cl}+k_{tc}-(m+\sqrt{m^2-4n})/2\}x_{c0} \\ & - \{(m+\sqrt{m^2-4n})/2\}x_{ce}]\exp[-\{(m-\sqrt{m^2-4n})/2\}t] \\ & - (1/\sqrt{m^2-4n})[(k_{lc}-k_{tc})x_{l0} + k_{tc} \\ & - \{k_{ct}+k_{cl}+k_{tc}-(m-\sqrt{m^2-4n})/2\}x_{c0} \\ & - \{(m-\sqrt{m^2-4n})/2\}x_{ce}] \times \\ & \exp[-\{(m+\sqrt{m^2-4n})/2\}t] + x_{ce}, \end{aligned} \tag{3-c}$$

$$\begin{aligned} x_t = {} & (1/\sqrt{m^2-4n})[\{k_{lt}+k_{tl}+k_{tc}-(m+\sqrt{m^2-4n})/2\}x_{l0} \\ & + \{k_{ct}+k_{tl}+k_{tc}-(m+\sqrt{m^2-4n})/2\}x_{c0} \\ & - \{k_{tl}+k_{tc}-(m+\sqrt{m^2-4n})/2+x_{te}(m+\sqrt{m^2-4n})/2\}] \times \\ & \exp[-\{(m-\sqrt{m^2-4n})/2\}t], \\ & - (1/\sqrt{m^2-4n})[\{k_{lt}+k_{tl}+k_{tc}-(m-\sqrt{m^2-4n})/2\}x_{l0} \\ & + \{k_{ct}+k_{tl}+k_{tc}-(m-\sqrt{m^2-4n})/2\}x_{c0} \\ & - \{k_{tl}+k_{tc}-(m-\sqrt{m^2-4n})/2 + x_{te}(m-\sqrt{m^2-4n})/2\}] \times \\ & \exp[-\{(m+\sqrt{m^2-4n})/2\}t] + x_{te}, \end{aligned} \tag{3-t}$$

where $$m = k_{lt} + k_{tc} + k_{cl} + k_{tl} + k_{lc} + k_{ct} \tag{4}$$

$$\begin{aligned} n = {} & k_{tl}k_{cl} + k_{lt}k_{tc} + k_{lt}k_{ct} + k_{tl}k_{lc} + k_{tl}k_{cl} \\ & + k_{tl}k_{ct} + k_{cl}k_{tc} + k_{lc}k_{ct} + k_{cl}k_{tc}. \end{aligned} \tag{5}$$

When the isomerization of butenes proceeds, the composition of butenes in the gas phase varies with the time. The values of x_l, x_c, and x_t corresponding to the reaction time, t, can be calculated from Eqs. 3, k_{ij}, x_{i0}, and x_{ie} being given. Figure 6 shows the reaction paths

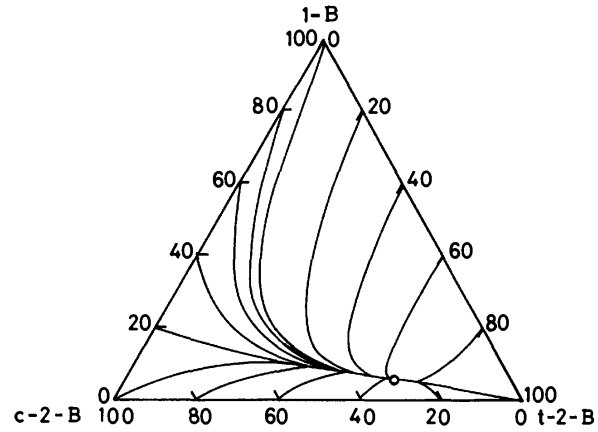

Fig. 6a. Reaction profile of isomerization of butenes over KC_8 at 373 K.

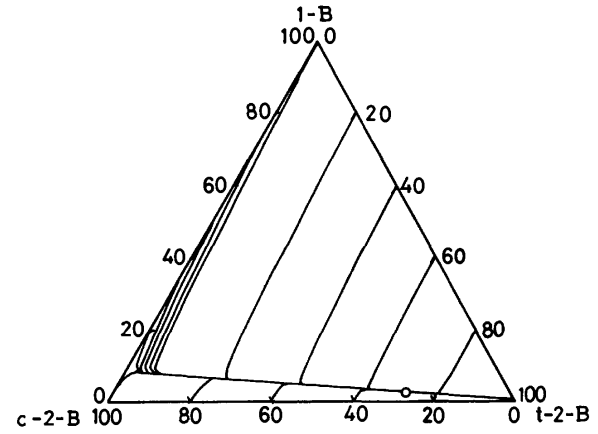

Fig. 6b. Reaction profile of isomerization of butenes over KC_8 at 292 K.

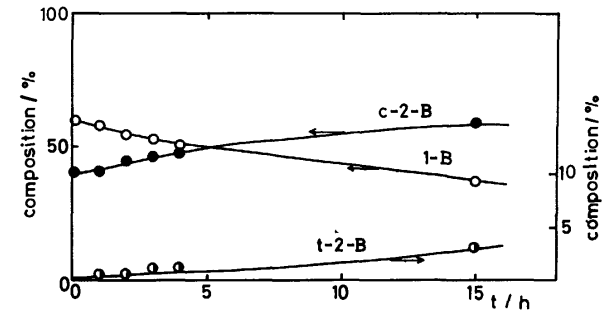

Fig. 7. Composition change with time, when the mixture of 0.6 1-butene/0.4 *cis*-2-butene reacted over KC_8 at 292 K.

calculated at 373 K and at 293 K respectively. These triangular graphs thus represent one of the catalytic characteristics of KC_8 for the isomerization of butenes. The curves, which originate from the left side of the triangle, bend convexly to the left. The profile may be named the *cis*-convex type. The *cis*-convexity became higher at a lower temperature, as is shown in Fig. 6b.

The mole fraction of *cis*-2-butene, x_c, seemingly increases with the time at the earlier period, as is shown in Fig. 6b, when mixtures of 1- and *cis*-2-butene are

employed as the reactants. The tendency is typically shown in Fig. 7; the time course of the 0.6/0.4 mixture is shown. The ambient pressures of 1-butene and of *cis*-2-butene at the initial state were 4.20×10^3 and 2.80×10^3 Pa respectively. The solid lines represent the curves calculated, while the points are the experimental results. The mole fraction of *cis*-2-butene, x_c, increased with the time and exceeded the equilibrium value, x_{ce} (0.288), although that at the initial state, x_{c0} (0.400), was higher than that at equilibrium. The curve of x_c, of course, will show its maximum and go downwards later. These results can be explained kinetically on the basis that k_{lc} (20.31) is much larger than k_{lt} (1.00) and k_{ct} (0.013) at 292 K.

Conclusion

The catalytic selectivity of KC_8 is different from that of potassium metal for the isomerization of butenes. The reaction may proceed by means of an allylic mechanism. One of the catalytic characteristics is thus shown in Fig. 6. The *cis*-convex type profile is due to the fact that the rate constant of the isomerization of 1-butene to *cis*-2-butene is higher than that to *trans*-2-butene and that of *cis*-2-butene to *trans*-2-butene.

The authors are grateful to Professor Tadato Mizota of the Department of Mining and Mineral Engineering of this faculty for his X-ray analysis. This work was supported by a Grant-in-Aid for Scientific Research, No. 56550575, from the Ministry of Education, Science and Culture, for which the authors' thanks are due.

References

1) M. A. Boersma, *Catal. Rev.*, **10**, 243 (1974).
2) W. Rudroff and E. Schulze, *Z. Anorg. Allg. Chem.*, **277**, 156 (1954).
3) S. Tsuchiya and T. Shiba, *Bull. Chem. Soc. Jpn.*, **38**, 1726 (1965).
4) Y. Ikefuji, N. Yoshioka, H. Noumi, and S. Tsuchiya, *Chem. Lett.*, **1975**, 805.
5) F. D. Rossini, K. S. Pitzer, R. L. Arnett, R. M. Braun, and G. C. Pimentel, "Selected Values of Physical and Thermodynamic Properties of Hydrocarbons and Related Compounds," Carnegie Press, Pittsburgh (1953).
6) J. Goldwasser and W. K. Hall, *J. Catal.*, **71**, 53 (1981).
7) H. Hattori, N. Yoshii, and K. Tanabe, *Proc. 5th Int. Congr. Catal. (Miami)*, **10**, 233 (1973).
8) J. Wei and C. D. Prater, "Adv. Catal.," ed by D. D. Eley, P. W. Selwood, and P. B. Weisz, Academic Press, New York (1962), Vol. 13, p. 203.
9) E. A. Lombardo and W. K. Hall, *AICHE J.*, **17** 1229 (1971).
10) W. O. Haag and H. Pines, *J. Am. Chem. Soc.*, **82**, 387, 2488 (1960).
11) S. Kagawa, *J. Catal.*, **37**, 182 (1975).

 © 1982 The Chemical Society of Japan Bull. Chem. Soc. Jpn., 55, 3093—3096 (1982)

Radiationless Transition between Randomly Fluctuating Levels. S_1-T_2-T_1 Intersystem Crossing in Condensed Phase

Nobuaki KANAMARU

Department of Chemistry, Faculty of Science, Nagoya University, Chikusa-ku, Nagoya 464

(Received February 17, 1982)

Radiationless transitions in aromatic molecules in condensed phase are examined for the case where sparse intermediate levels are involved. Effects of surrounding mediums on radiationless transitions are also discussed in which the random fluctuation of the vibrational manifolds in the solvent cages is shown to be important to meet the resonance conditions in the transitions. The theory is applied to explain the "unusually" fast S_1-T_2-T_1 intersystem crossing in the system such as anthracene derivatives.

The radiationless transitions in aromatic molecules have been studied quite extensively both theoretically and experimentally.[1] However, the quantitative interpretation of the experimental facts are not always in the stage of a good consensus. One of the examples is S_1-T_2-T_1 ISC of aromatic molecules (especially of anthracene derivatives) which may be the case where sparse intermediate levels are involved in the transitions.[2]

In this paper, brief but general discussion of the effect of solvent on the radiationless transitions will be presented. Particularly, the random fluctuations of the vibrational manifolds in the solvent cage is shown to be important to meet the resonance conditions[1b] in the transitions. This is closely related to the earlier discussion by the present author concerning the choice of basis sets in radiationless transitions.[3] Actually, several key features in this paper were already suggested in that paper. So, the present paper is intended to give more quantitative interpretation of S_1-T_2-T_1 ISC of some anthracene derivatives which was not the major subject of the previous paper, by taking the recent experimental data into account.[2,4-6] Thus, the "unusually" fast ISC of these compounds (even without heteroatoms), hardly explained by intramolecular mechanism (*e.g.*, the third triplet state had to be invoked),[2] is now interpreted by taking the effect of solvent cage into account.

Mechanism

Just like the presentation in the previous paper, we'll give kinetical arguments which could be converted into a quantum mechanical picture as a branched sequential decay in a system composed of both aromatic molecules and surrounding medium.[3]

However, before going into mechanism of ISC, we had better to discuss the effect of the medium on the radiationless transition in general which was discussed only implicitly in the previous paper.[3] Most recognized is the vibrational relaxation (VR) between vibrational levels in the same electronic state which allows for rapid communication (as fast as 10^{12} s^{-1}) within the vibrational manifolds generally accepted as a cause for the thermally activated processes of electronic relaxations.[1] In addition, VR works to give uncertainty widths to the initial and the final states of radiationless transitions allowing for transfer from the intermediate case to the statistical limit case as was actually discussed to explain the collisional effect in vapor phase[7] (*vide infra*). Another mechanism is a solvent effect on the location of energy levels (especially energy gap between the ground vibrational levels of the electronic states) which may partially explain the solvent effect on ER's. And thirdly, as was not widely recognized in spite of the earlier suggestions,[3] the location of energy levels are fluctuating with the change of the structure of solvent cages so that the resonance conditions towards the radiationless transition are sometimes met between some levels for every transient conformation of a system composed of a solute molecule plus surrounding solvent molecules. Actually, the interpretation of the collisional effects of S_1-T_1 ISC rates of naphthalene by Fung and Freed[8] and the theory of delayed fluorescences by van der Werf *et al.*[9] as well as that of electronic relaxation (ER) of small molecules in a densed medium by Nitzan and Jortner[10] are just like what to be supplemented by this scheme. The transition through this mechanism may be named as a nonadiabatic transition between randomly fluctuating levels[3] because the initial state and the final state represent different potential curves of the whole system (the solute molecule and the solvent molecules). In this quantum mechanical description, vibrational modes of solvent molecules (phonon modes) may be regarded to be working as accepting modes. However, semiclassical interpretation would be rather suitable to describe the real event, because the initial and final states can not be well defined in solution against the case in gaseous state (or in mixed crystal).[11] Uncertainty broadening of the energy levels due to vibrational relaxation might also give more probability for the resonance conditions to be met in such a way to

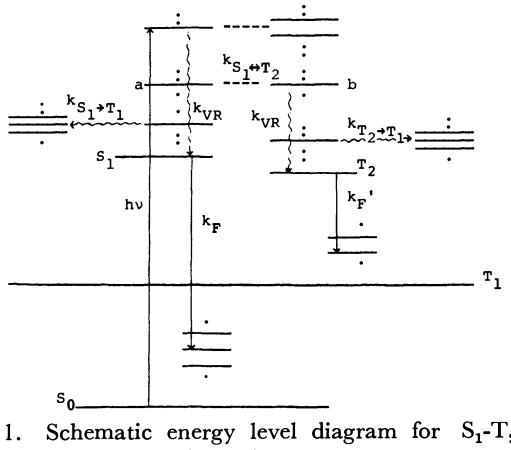

Fig. 1. Schematic energy level diagram for S_1-T_2-T_1 ISC in anthracene derivatives.

bring ER into the statistical limit[7,10] (*vide supra*). However, this VR effect appears to be minor compared to the preceding mechanisms. The most typical evidence to support this conjecture may be found in the "zeroth order" interpretation of the band shapes of radiative electronic transitions by the Franck-Condon intensity distribution of vibronic bands modified by broadening of the bands due to environmental (cage) effects[1,3] (inhomogeneous width), except for those in mixed crystal.[11],* A more quantitative account based on kinetics will be given later.

Now, let us discuss the mechanism of ISC. The energy level scheme suitable for the kinetical interpretation is given in Fig. 1 where only concerned evells and processes are indicated. This may appear to be practically the same as Fig. 2 of the previous paper which is purely intramolecular scheme.[3] However, it has to be noted that these levels are fluctuating under the influence of the medium, thus allowing for the resonance conditions to be met between some vibrational levels of S_1 and T_2. In fact, there always exist the coupled pairs (resonance states) as shown by a-b in the figure which can be populated by thermal activation and fluctuation of the levels. Thence, presentation of the mechanism for S_1-T_2-T_1 ISC would be straightforward:

(1) The first step is of course the optical preparation of an excited level, say, a higher vibrational level of S_1 indicated in the figure.

(2) It is immediately followed by vibrational relaxation ($k_{VR}\approx10^{12}$ s^{-1}) so that thermal equilibrium between vibrational manifolds may be reached unless subsequent processes are extremely fast.

(3) Thenceforth, radiative and radiationless transitions from this manifolds (S_1) to S_0 and T_1 (T_2) would start, if we apply the general picture presented in the previous paper (*e.g.* Fig. 1 therein[3]). However, this is not the case for the present system because of the resonance coupling between some S_1 and T_2 vibronic levels (to be represented by pure spin adiabatic Born-Oppenheimer basis[3]) assisted by the medium. The alternative explanation is based on the assumption of the near (not strictly) thermal equilibrium between S_1 and T_2 manifolds supported by the kinetical argument using the estimated numbers of the rates: *e.g.* for the case of anthracene molecule, $k_F\approx5\times10^7$ s^{-1}, $k_{S_1\to T_1}\lesssim10^5$ s^{-1}, $k_{T_2\to T_1}\approx10^{10}$ s^{-1}, $k_{VR}\approx10^{12}$ s^{-1} and $k_{S_1\leftrightarrow T_2}\lesssim10^{11}$ s^{-1} (H_{SO} matrix element including FC factor suitable for the coupling may be estimated to be $(\lesssim1)\times(\lesssim1)$ *i.e.* $\lesssim1$ cm^{-1}, indicates which the upper limit of the rates due to unknown effective Boltzmann factors[1,2]). In other words, the initial states for the following steps are not always represented by PS ABO basis (At least a-b level is a exactly spin contaminated level.[3]). This may be the reason why triplet-triplet fluorescence quantum yield corresponding to k_F' in the figure estimated from the intensity of T-T absorption (which may be that between PS ABO states) was much larger than the experimentally observed values[2a] (*vide infra*). Actually, possibility of thermal equilibration between S_1 and T_2 is already suggested by Campbell and Liu to account for sensitized chemical reactions from "T_2" states of anthracene derivatives.[12] Recent experimental results by Wilson and Halpern indicating fast T_2-S_1 ISC competing with T_2-T_1 internal conversion also conform to this. Thus, the observed decay rates of S_1 fluorescences should not be taken to be nearly equal to $k_{S_1\to T_1}$ plus $k_{S_1\to T_2\to T_1}$. For, S_1-T_2-T_1 and S_1-T_1 processes interfere with each other. In this respect, no "important" difference[2b] isseen between quantum mechanical and kinetical arguments, where kinetical scheme is represented by $S_1\rightleftarrows T_2\to T_1$ instead of $S_1\to T_2\to T_1$. The more quantum mechanical picture may be given as a behavior of a resonance state which arises from both S_1 and T_2 states with resonance conditions being satisfied and decays to either S_1 or T_2 state with probabilities proportional to the squares of their mixing coefficients.

Similar but different mechanisms were already proposed for slow internal conversions between excited states in strongly coupled systems *i.e.* between singlet excitonic states of multiple molecules and triplet $n\pi^*$ and $\pi\pi^*$ states of 1-indanone in EPA where energy gaps were in the range of 50 to 500 cm^{-1}.[3]

One of the experiments to prove this scheme might be to show the multiple exponential decay of S_1 fluorescence with the fast component corresponding to $k_{S_1\to T_2}$ and slow component corresponding to the weighed average of k_F's, $k_{S_1\to T_1}$, and $k_{T_2\to T_1}$, if a single level a in the figure could be excited by light absorption. This seems to be practically impossible, however, because the molecules are in condensed phase *i.e.* $k_{S_1\to T_2}$ decay process in some molecules would be cancelled out by k_{VR} rise process towards $k_{S_1\to T_2}$ in the other molecules under observation. In case a ground vibrational level of S_1 state is accidentally degenerate with any level in T_2 manifold, solvent fluctuation would rather lower the rate. Difference of collisional effects between vapor phase and condensed phase seems to be taken as one of the evidences (*vide infra*).

Another proof of this mechanism is to explain the observed decay rates of S_1 fluorescences by setting reasonable values of k's and location of a-b levels (Experimentally obtained temperature effect on the rates *i.e.* activation energies might give the rough estimate of the location.). In the case of anthracene where $k_{S_1\to T_2}(\gtrsim10^{11}$ s$^{-1})$ is not fast enough compared to k_{VR}, the upper limit of the decay rate of the fluorescence is approximately $k_{T_2\to T_1}\approx10^{10}$ s^{-1} (by taking account the effective Boltzmann factor suitable for near thermal equilibrium), only one order of magnitude larger than the experimental value,[1a] to be satisfactory. Therefore, the usual interpretation of the decay rate by thermally

---

* To make the contention of this sentence clearer according to referees' suggestions, we can make the following statements:

(1) The locations and the shapes of potential energy surfaces of a solute molecule are regulated by the arrangement (locations and orientations) of solvent molecules and are thermally fluctuating *i.e.* change from time to time.

(2) Therefore, resonance conditions are satisfied within a time scale of solvent relaxation.

These assumptions, though being slightly oversimplified, seem to be fair as long as the "intramolecular" radiationless transition is concerned *i.e.* in case where intermolecular modes are not important due to *e.g.* their lower frequencies compared to intramolecular modes.

activated S_1-T_2-T_1 process would apply for this system although thermal equilibrium between S_1 and T_2 is not well established. For anthracene derivatives such as 9-bromoanthracene,[2,4] however, $k_{S_1 \to T_2}$ would become orders of magnitude larger in spite of the possible reduction of FC factors by the increase of S_1-T_2 energy gaps. So thermal equilibrium between S_1 and T_2 is more reached by the heavey atom effect. Thus, the decay rates of T_2-T_1 fluorescences would not represent the rates ($k_{T_2 \to T_1}$'s) indicated in the figure but rather represent the weighed averages of the decay rates among the S_1 and T_2 levels. This explains "the small TTF quantum yields and apparent internal heavey atom effect"[2,4a] in these systems.

Finally, the kinetical discussion is made to show why the present mechanism is prediminant over the possible alternative based on the statistical limit descriptions in both S_1-T_2 and T_2-S_1 ISC's (*vide supra*) as was implicitly assumed in most of the experimental papers[4-6] though no quantitative verification was given so far. Actually, Gillispie and Lim's papers which showed the need of the third triplet state to explain the rates with a formula given *e.g.* by Nitzan *et al.*[7,10] can be taken to indicate inadequacy of the statistical limit assumption. Somehow, it is almost certain that broadening due to solvent fluctuation (inhomogeneous width) is much larger than the uncertainty broadening (homogeneous width). In actuality, since the rates involved in the observation is $< 10^{11}\ s^{-1}$ (according to the present interpretation), there is enough chance for solvent fluctuation to be involved in the mechanism.** Thus, the present mechanism can be taken as a sublation of the statistical limit picture and the previous mechanism.[2]

Concluding Remarks

Presentation of the mechanism is over. However, to seek other evidences than those presented above and in the previous paper[3] in different kinds of experiments to support this proposal would be desired to clear up some skepticisms. One of the key features in the mechanism is the importance of the resonance coupling. This may be actually evidenced in the recent experiments in isolated molecules.[1] For example, the steep rise of the decay rate of a single rotational level when it is brought into resonance with another by Stark field was suggested for H_2CO.[13] Recent results of Zeeman effect on the quenching rates of gaseous molecules[14] may also be related to this interpretation. Another important key feature is the existence of a possible two-step activation process of ER by a medium *i.e.* thermal activation and thermal fluctuation of energy levels. This may be related to the recent experimental facts of the temperature effect of T_1-S_0 ISC in anthracene and its deuterium substitute reported by Hung and Henry.[15]

Finally, it should be mentioned that this mechanism of ISC is not purely intramolecular, different from those of ordinary ER's in aromatic molecules in condensed phase which have been always assumed to be followed by fast vibrational relaxation.[1,7,10] In this respect, a recent paper by Hirayama on the ISC in cyanoanthracenes[6] is worthwhile subject to discuss. Although these systems do not belong to the case where "sparse" intermediate levels are involved but rather are described by conventional statistical limit picture as is consistent with their not-"unusual" lifetimes, the result indicates the difference of collisional effects in vapor phase from that in condensed phase (in nonpolar solvent). This seems to be an indication of the fact that solvent molecules work not only as vibrational relaxers but also as energy level fluctuators causing enhancement of the rate. As is mentioned before, weakening by solvent fluctuation is also possible, because of dilution of the effect by either more broadening or more rapid thermal equilibration (Thermal equilibration between vibrational levels can not be attained by a few collisions in vapor phase.). This is actually evidenced in Hirayama's data. It should also be noted that this kinds of mechanisms are expected to be playing crucial roles in the more complicated processes such as photoionization in solution[16] or phenomena to be named as solvent induced charge separation.[17] Somehow, the most desired experiments of the anthracene derivatives are high resolution observations in gas phase at collision free condition. Very recently, a preliminary experiment on this line was performed showing longer lifetime in the collision free condition.[18] This seems to conform to the present arguments.

The author is indebted to Prof. A. Nitzan for helpful comments.

** The author has seeked for the formalism which suitably represents the scheme illustrated by the figure but has merely come up with the kinetical interpretation. For, the other formalisms so far the author has tried *e.g.* using a density matrix has become more phenomenological than that of kinetics.

References

1) See, for example, a) J. B. Birks, "Photophysics of Aromatic Molecules," Wiley-Interscience, London (1970); b) "Radiationless Processes in Molecules and Condensed Phase," ed by F. K. Fong, Springer-Verlag, Berlin (1976).

2) a) G. D. Gillispie and E. C. Lim, *Chem. Phys. Lett.*, **63**, 355 (1979); b) *ibid.*, **70**, 532 (1980) and references therein.

3) N. Kanamaru, *Sci. Papers IPCR*, **71**, 85 (1977).

4) a) C. G. Morgante and W. S. Struve, *Chem. Phys. Lett.*, **68**, 272 (1979); b) K. Hamanoue, S. Hirayama, T. Nakayama, and H. Teranishi, *J. Phys. Chem.*, **84**, 2074 (1980) and references therein.

5) T. Wilson and A. M. Halpern, *J. Am. Chem. Soc.*, **102**, 7272, 7279 (1980).

6) S. Hirayama, *J. Am. Chem. Soc.*, **103**, 2934 (1981).

7) A. Nitzan, J. Jortner, and P. M. Renzepis, *Proc. R. Soc. London, Ser. A*, **327**, 367 (1972).

8) K. H. Fung and K. F. Freed, *Chem. Phys.*, **14**, 13 (1976).

9) R. van der Werf, D. Zevenhuijzen, and J. Jortner, *Chem. Phys.*, **27**, 319 (1978).

10) A. Nitzan and J. Jortner, *Theor. Chim. Acta*, **29**, 97 (1973).

11) See, for example, R. W. Olson and M. D. Fayer, *J. Phys. Chem.*, **84**, 2001 (1980).

12) R. O. Campbell and R. S. H. Liu, *J. Am. Chem. Soc.*, **95**, 6560 (1973).

13) J. C. Weisshaar and C. B. Moore, *J. Chem. Phys.*, **72**, 2875 (1980).

14) See, for example, K. Hashimoto, S. Nagakura, J. Nakamura, and S. Iwata, *Chem. Phys. Lett.*, **74**, 228 (1980).
15) I-F. Hung and B. R. Henry, *Chem. Phys.*, **27**, 263 (1978).
16) See, for example, H. Nakamura, J. Tanaka, N. Nakashima, and K. Yoshihara, *Chem. Phys. Lett.*, **77**, 419 (1981).
17) See, for example, a) N. Nakashima, M. Murakawa, and N. Mataga, *Bull. Chem. Soc. Jpn.*, **49**, 854 (1976); b) T. J. Meyer, *Acc. Chem. Res.*, **11**, 94 (1978); c) K. Rotkiewicz and W. Rubaszewska, *Chem. Phys. Lett.*, **70**, 444 (1980).
18) T. R. Hays, W. Herke, H. L. Selzle, and E. W. Schlag, *Chem. Phys. Lett.*, **77**, 19 (1981).

Two-photon Excitation Spectra of 1-Azabicyclo[2.2.2]octane and Trimethylamine

Hitoshi KUNO, Kazuo KASATANI, Masahiro KAWASAKI, and Hiroyasu SATO*
Chemistry Department of Resources, Faculty of Engineering, Mi'e University, Tsu 514
(Received February 24, 1982)

The two-photon fluorescence excitation spectra of 1-azabicyclo[2.2.2]octane (ABCO) and trimethylamine were measured in the excitation wavelength range of 410—520 nm. The effect of the polarization (linear or circular) indicates that the symmetries of the upper states are $\tilde{A}^1A_1$, $\tilde{B}^1A_1$, and $\tilde{C}^1E$ for ABCO while $\tilde{A}^1A_1$ and $\tilde{B}^1E$ for trimethylamine in C_{3v} point group approximation. Rotational envelopes for the sequence structures are calculated forcircularly and linearly polarized light excitation and are in good agreement with experiment.

The ultraviolet absorption bands of amines are considered as Rydberg transitions.[1] The polarization measurements in two-photon absorption have assigned the lowest excited state of the open amines, *e.g.*, trimethylamine as A_1 in C_{3v} point group.[2] In contrast to the open amine the caged one $N(C_2H_4)_3CH$ or ABCO has richly structured UV and multi-photon absorption spectra.[3] All of the observed transitions are considered as two-photon allowed ones to low-lying Rydberg states (3p, 3s←n).[1-3] Because the *ab initio* quantum chemical calculation predicts small core splitting for both trimethylamine and ABCO, the observed bands cannot be further classified as $^1E(3p_{xy})$, $^1A_1(3p_z)$ or the superposition of the two transitions.[4] In this report we have studied two-photon absorption of ABCO by linearly and circularly polarized light in order to assign the symmetries of the low lying Rydberg states and to compare them with those of trimethylamine.

Experimental

The apparatus for the UV fluorescence excitation spectra is similar to that previously reported, except for a dye laser.[2] Briefly, an 1 MW N_2 laser pumped dye laser light was focused into a quartz cell containing gases or solutions of amines with a lens (f=30 mm). The UV fluorescence was viewed through three UV transmitting filters (Toshiba UV-D33S) at 90° to the laser beam, and was detected by a solar blind photomultiplier (HTV-R166UH). The signal was averaged by a gated integrator. Linear polarization of the laser light was achieved by a polarizer which consists of ten quartz plates placed at Brewster's angle. Circularly polarized light was generated by passing the laser light through Fresnel rhombs.

The hydrochloride of ABCO was obtained from Tokyo Kasei Company. ABCO prepared from the hydrochloride solution was purified by sublimation through Molecular Sieves 13X. Trimethylamine was prepared from aq solution (30%, Nakarai Chemicals) with sodium hydroxide.

Results

ABCO. Figure 1 shows the two-photon fluorescence excitation spectra of ABCO in the vapor phase. Both the first and the second absorption bands show extensive progression and sequence structures. The origin of the first band was at 39097 cm^{-1} (511.55 nm). Since that of the second band was weak as has been reported by Parker and Avouris,[3b] the measured value (43940 cm^{-1}) would not be quite accurate. The reported values for the first absorption bands are 39080 cm^{-1} obtained in one-photon absorption by Halpern *et al.*,[3a] 39076 cm^{-1} and 39095 cm^{-1} reported in multi-photon ionization experiment by Halpern *et al.*[3d] and Gonohe *et al.*,[5] respectively.

The two-photon excitation spectrum of the pentane solution (10^{-3}—10^{-2} mol dm^{-3}) was also measured. The spectrum in solution appears blue shifted, compared to the spectrum in the vapor phase. The blue shift is expected for the Rydberg transitions.[1] Since the electronic transitions are Rydberg ones of the lone-pair electron on the nitrogen atom, the repulsion between lone-pair and bonding-pair electrons decreases upon excitation. Because the pyramidal NC_3 skeleton tends to flatten, the cage squashing mode $\nu'_{12}(a_1)$ with frequency 650±10 cm^{-1} is observed up to several quanta, along with many combination bands. These vibrational structures are also observed in one-photon absorption[3a] and multi-photon ionization[3b] spectra. The progression with 625 cm^{-1}/618 cm^{-1} was assigned to this ν_{12} mode in one-photon/multi-photon reports of Halpern *et al.*[3a,d] respectively. At wavelength longer than the 0-0 band, a hot band with frequency 603 cm^{-1} was identified as due to ν''_{12} observed in one-photon absorption (600 cm^{-1}),[3a] multi-photon ionization (602 cm^{-1}),[3d] and infrared spectra (604 cm^{-1}).[6]

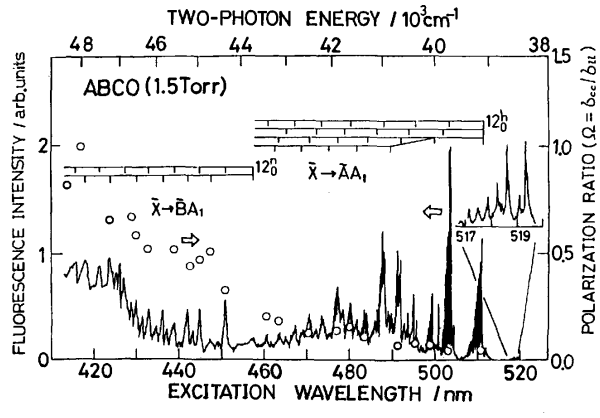

Fig. 1. Two-photon fluorescence excitation spectrum of ABCO in the vapor phase (recorded in linear polarization). The well resolved progressions are ν'_{12} (a_1) cage squashing mode built on the origin and on the ν'_{11} (a_1) and ν_{33}' (e) or ν_9' (a_1) modes after Halpern *et al.* (3a, d). Spectrum is corrected for the laser power. The pressure was a vapor pressure of ABCO at room temperature (1.5 Torr, 1 Torr ≈ 133.322 Pa).

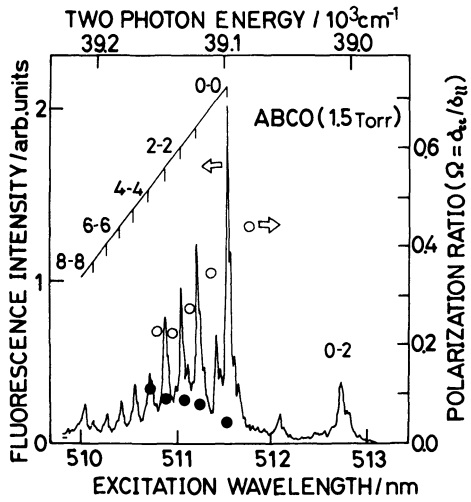

Fig. 2. The sequence structure of torsional motion built on the 0-0 band of ABCO ($\tilde{A}$–$\tilde{X}$) in the vapor phase (recorded in linear polarization) and polarization ratios (δ_{cc}/δ_{ll}) at the peaks (●) and the valleys (○). The origin (0-0) and the hot bands (v′-v″) are indicated in this figure.

The band structures were obtained at higher resolution. The detailed sequence structures of ν_{12} (0-0), (1-0), and (0-1) bands resemble each other (see Fig. 2 for example) while the spectral consequence of combination bands becomes highly conjunct and is different from that of the (0-0) bands. This is probably because of the different rovibronic selection rules *i.e.*, $\Delta K=0$ for A_1-A_1 (the 0-0 band) and $\Delta K=\pm1$, ±2 for E-A_1 transitions (the combination bands).[7]

Figure 2 shows the detailed structures of the first sequence bands. Similar sequence structures are observed in the multiphoton ionization spectrum of 1,4-diazabicyclo[2.2.2]octane.[8] They are assigned as due to the torsional motion about the z axis and the potential energy has a small hump at $\phi=0°$ and a double minimum around $\phi=10°$. Assuming a quartic-quadratic potential for the ground state of ABCO, Gonohe *et al.*[5] have assigned the strongest sequence structures to a cage torsional motion (ν_{19}) with low vibrational frequencies (54 cm^{-1} in the ground state). Actually, our studies show the increase of the hot bands in intensity with temperature from 20 °C to 90 °C.

The polarization ratio was measured to deduce the upper state symmetries (Figs. 1 and 2). According to McClain *et al.*[9] the intensity of two-photon absorption depends upon the polarizations of the two photons and so is different when using circularly and linearly polarized light sources. When the symmetry of the upper state is totally symmetric A_1 in C_{3v} point group, the ratios ($\Omega=\delta_{cc}/\delta_{ll}$) become less than 1.5 for the Q branches, where δ_{cc} is the absorptivity of two identical circularly polarized photons and δ_{ll} that by linearly polarized ones. For other cases, *i.e.*, O/P/R/S branches for A_1 and O/P/Q/R/S branches for E, the ratios are expected to be 1.5. The observed Ω values in Fig. 1 were less than 1.5 for all transitions, indicating two photon allowed A_1 symmetry of the excited states. Figure 2 shows the detailed excitation spectrum measured by the linearly polarized light and the polarization ratios. The Ω value for the peak at 511.55 nm is 0.04 which is in good agreement with $\Omega=0.030$—0.038 reported by Berg *et al.*[3c] The Ω values are larger at the positions between the peaks. This is because of the superposition of the branches other than the Q branches. These Ω values are well reproduced by calculation as will be discussed in the later section. The values at the peaks for the first absorption band were essentially constant while those increase with the excitation energy in the second absorption band (Fig. 1). In the second absorption band the Ω values at the peaks were not different from those for the valleys. The second band has a diffuse absorption structure compared to the first band. This diffuseness increases in the shorter wavelength region. Both the Ω values and the background intensity start increasing at $\lambda\simeq440$ nm. These results indicate the superposition of two state in this region; one is a totally symmetric state and the other one at the shorter wavelength region is a non-totally symmetric one.

Trimethylamine The two-photon excitation spectrum of trimethylamine and the polarization ratios were also measured in the vapor phase and the pentane solution as shown in Fig. 3. The Ω values were obtained in the vapor phase and not in the solution phase. In solution phase solvent induced mixing of electronic states would occur and the measured Ω value is an averaged one of the mixed states.[10] The excitation spectrum was measured in pentane solution in order to suppress the decomposition of trimethylamine at shorter wavelength region. Actually, the increase of the fluorescence quantum yield have been reported by addition of third-body or buffer gases in the vapor phase.[11,12] The shape of the spectrum in solution resembles that of the one-photon absorption spectrum in the ultraviolet region, while the excitation spectrum obtained in the vapor phase is quite different from that in the solution phase. The "structures" observed in the vapor phase are in good agreement with those reported by Halpern *et al.*[3d] The disparities of the excitation spectrum between vapor and solution phases may be due to the photo-decomposition[11,12] and the multiphoton ionization processes,[3d] because both processes quench the fluorescence. Since the Ω values are less than 1.5 for the first absorption band ($\lambda=500$—440 nm), the symmetry of the upper state is assigned to a totally symmetric one.

Although the two-photon fluorescence excitation spectrum in Fig. 3 and the reported one-photon absorption spectra cannot be clearly resolved spectroscopically, the polarization measurement can reveal these overlapped bands. At shorter wavelength ($\lambda<440$ nm) a non-totally symmetric upper state appears, as indicated by increase in the Ω values with decreasing wavelengths. This decomposition of the absorption spectrum into two parts is in good agreement with that reported by Cureton *et al.*[12] According to them, in the fluorescence decay of trimethylamine, one-photon excitation at longer wavelength region produces almost single exponential decay but at $\lambda<230$ nm this becomes dual exponential. This is explained on the basis that there are two strongly overlapping absorption bands, resulting

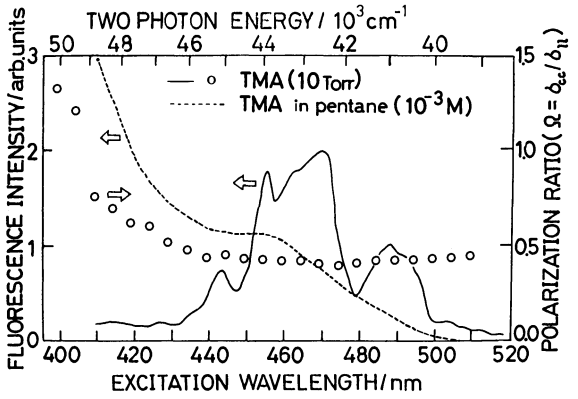

Fig. 3. Fluorescence excitation spectra of trimethylamine in pentane solution (1×10^{-3} mol dm^{-3}, broken line) and in the vapor phase (solid line: 10 Torr) recorded in linear polarization. Polarization ratios (δ_{cc}/δ_{ll}), were measured in the vapor phase (○). Spectrum is corrected for the laser power.

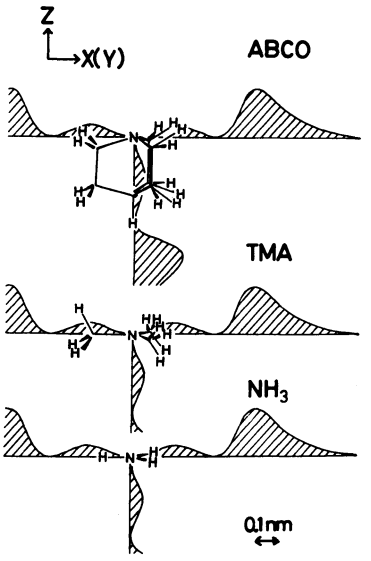

Fig. 4. Schematics for electron density ($r^2\psi(r)^2$) of 3p Rydberg orbitals and molecular structures of ABCO, trimethylamine (TMA), and ammonia.

inevitably in simultaneous excitation of both S_2 and S_1 states. They observed no significant improvement in fitting to three exponentials than was obtained for two, and thus there has been no evidence for multi-exponential fluorescence. This has been the case for other open amines, triethyl- and tripropylamine.

Discussion

Electronic States. Prior to considering the electronic states of ABCO and trimethylamine it is useful to review the states for ammonia. The first few excited states of ammonia result from excitation of an a_1 lone pair electron of the nitrogen atom,[13]

$$\cdots (e)^4(a_1)^2 \qquad \tilde{X}A_1$$
$$\cdots (e)^4(a_1)\,(3sa_1) \qquad \tilde{A}A_1$$
$$\cdots (e)^4(a_1)\,(3p_{xy}e) \qquad \tilde{B}E$$
$$\cdots (e)^4(a_1)\,(3p_za_1) \qquad \tilde{C}A_1.$$

Since alkyl substitution does not change the relative positions in energy of the ($3sa_1$) and ($3p_{xy}e$) orbitals, the first excited state of the open amines has A_1 symmetry, *i.e.* 3s←n. Actually, the Ω values for trimethylamine are less than 1.5 for λ=500—440 nm. Since the Ω values for trimethylamine increased from 0.5 to 1.4 with decreasing excitation wavelengths from 440 to 400 nm, the second absorption band can be assigned as E state.

The first absorption band of ABCO has A_1 symmetry as we saw from the polarization ratios. The observed Ω values in the region $\lambda<460$ nm increase from 0.2 to 1.0 with decreasing the wavelengths. Since the second band consists of two states, *i.e.*, totally and non-totally symmetric states, the second and third excited states have A_1 and E symmetries, respectively. The electronic states observed are $\tilde{A}A_1$, $\tilde{B}A_1$, and $\tilde{C}E$. The relative position of B and C states is reversed compared to ammonia and open amines. This may be explained by the variation of quantum defects caused by interaction between Rydberg orbitals and nuclei. The energy for the Rydberg orbitals is given by,

$$E_n = I_p - R/(n-\delta)^2,$$

where I_p is an ionization potential and R the Rydberg constant. The quantum defect δ will be large if the probability is high that the electron is near the nucleus, while δ will be small where the nuclei are situated on the nodal planes of the orbitals.[1,14] Actually for ammonia where the nuclei are three hydrogen atoms, δ_z for p_z is smaller than δ_{xy} for p_{xy}. The hydrogen atoms strongly interact with $3p_{xy}$ orbital, because ammonia has a planar structure in the excited state. For the $3p_z$ orbital this interaction is expected to be small. Schematics for these interactions are shown in Fig. 4, where radial populations ($r^2\psi(r)^2$) of 3p orbitals are illustrated along with molecular structures of ammonia and the amines. These interactions would be the case for trimethylamine *i.e.*, $\delta_z<\delta_{xy}$. For ABCO the skeletal CH_2 group may interact strongly with $3p_z$ as with $3p_{xy}$ orbitals, then $\delta_z\approx\delta_{xy}$. This difference may change the relative position of A_1 and E electronic states.

The energy difference between $A_1(3p_z)$ and $E(3p_{xy})$ for vertical excitation may be obtained from the threshold wavelength of each states in Fig. 1. It is rather small ($\approx$0.3 eV) as predicted by quantum chemical calculation[4] compared with that for ammonia ($\approx$0.5 eV).

Calculation of Rovibronic Profiles. As previously observed, the rotational profiles in the excitation spectra are strongly dependent upon the polarization of the absorbed photons. The theoretical explanation of this dependence is given by McClain *et al.*[9] and Wunsch *et al.*[15] They computed the polarization dependence of vibronic bands in benzene. In this section we apply this theory to the rovibronic bands in ABCO.

The probability for an identical two-photon absorption is described in detail by Wunsch *et al.*[15] In brief, it is given by two independent contributions, $C_0M_0R_0$ and $C_2M_2R_2$. Geometrical factors C_J, which depend on the polarization of the photons absorbed, are given by $C_0=1/3$, $C_2=2/15$ for linearly polarized photons and by $C_0=0$, $C_2=1/5$ for circularly polarized photons.

The molecular parameters M_J are obtained from the two-photon tensor elements. For the $A_1 \leftarrow A_1$ transition, $M_0=(M_{xx}+M_{yy}+M_{zz})^2/3$ and $M_2=(M_{xx}+M_{yy}-2M_{zz})^2/6$. The rotational factors R_2 are given by the Placzek-Teller factors[16] $b^{JK}_{J'K'}$ and contribute to all branches in the transition of $J \rightarrow J'$ and $K \rightarrow K'$;

for

$$J' = J,\ b^{JK}_{J'K'} = [J(J+1)-3K^2]^2/J(J+1)(2J-1)(2J+3)$$

$$J' = J+1,\ b^{JK}_{J'K'} = 3K^2[(J+1)^2-K^2]^2/J(J+1)(J+2)(2J+1)$$

$$J' = J+2,\ b^{JK}_{J'K'} = 3[(J+1)^2-K^2][(J+2)^2-K^2]/2(J+1)(J+2)(2J+1)(2J+3)$$

and $(2J+1)b^{JK}_{J'K'} = (2J'+1)b^{J'K'}_{JK}$.

Since R_0 is given by $R_0=\delta_{JJ'}\times\delta_{KK'}$ the $C_0M_0R_0$ contributes only to Q branches, where $\delta_{JJ'}$ and $\delta_{KK'}$ are delta functions. The selection rule is $\Delta K=0$ for the $A_1 \leftarrow A_1$ transition. By assuming the symmetric top molecule, rotational energies of ABCO were estimated by the formula,

$$E = BJ(J+1) + (C-B)K^2.$$

To compute a two-photon excitation spectrum, one must assume values for the rotational constants B and C. We took $B'=0.092\ cm^{-1}$, $B''=0.091\ cm^{-1}$, $C'=0.093\ cm^{-1}$, and $C''=0.095\ cm^{-1}$, which correspond to C-N-C angles 111.0° for $\tilde{A}$ and 109.5° for $\tilde{X}$, respectively. The CH_2 group was considered as a mass point in calculation of these constants. The angle 109.5° was taken from the structure of trimethylamine.[17] The shape of the calculated spectrum was very sensitive to these constants. Concerning the vibrational energy levels, the values for the ground state are obtained from Gonohe *et al.*,[5] while those for the excited state are taken from the experimental values in Fig. 2.

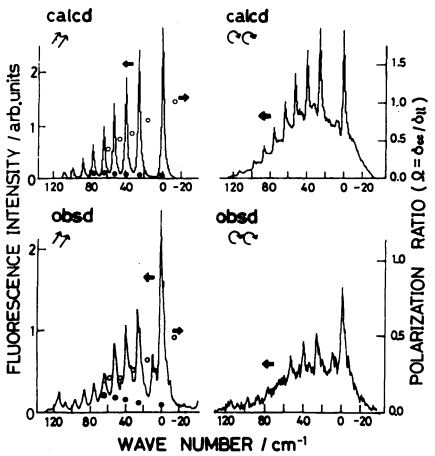

Fig. 5. The calculated and observed rovibronic structures of an A_1, $\Delta v=0$ transition in ABCO. ↑↑ and ↻↻ for linearly and circularly polarized light, respectively. The band in circularly polarized light is enlarged by a factor of 20 (calculation) and 14 (experimental). Circles are polarization ratios (δ_{cc}/δ_{ll}) (See Fig. 2).

Comparison of calculated profiles with experimental band shapes shows good agreement (Fig. 5). To reproduce the observed spectrum for circularly polarized light, the Q branch must include a small contribution from $C_0M_0R_0$ since the polarization of the laser light was not perfect. *Ca.* 1% of the linearly polarized light was included in the calculation. The molecular parameter M_0/M_2 is assumed to be 11.6, that corresponds to $M_{xx}=M_{yy}=0.56\ M_{zz}$. As shown in Fig. 5, this values reproduces experimental Ω values for the peaks and for the valley.

The authors thank Instrument Center, Institute for Molecular Science, Okazaki National Research Institute for the use of the laser.

References

1) M. B. Robin, "Higher Excited States of Polyatomic Molecules," Academic Press, New York (1974).
2) K. Kasatani, M. Kawasaki, H. Sato, Y. Murasawa, K. Obi, and I. Tanaka, *J. Chem. Phys.*, **74**, 3164 (1981).
3) a) A. M. Halpern, J. L. Roeber, and K. Weiss, *J. Chem. Phys.*, **49**, 1348 (1968); b) D. H. Parker and P. Avouris, *Chem. Phys. Lett.*, **53**, 515 (1978); c) J. O. Berg, D. H. Parker, and M. A. El-Sayed, *J. Chem. Phys.*, **68**, 566 (1978); d) A. M. Halpern, D. P. Gervity, L J. Rothberg and V. Vaida, *ibid.*, **76**, 102 (1982).
4) P. Avouris and A. R. Rossi, *J. Phys. Chem.*, **85**, 2340 (1981).
5) N. Gonohe, N. Mikami, and M. Ito, *Bull. Chem. Soc. Jpn.*, in press. We thank these authors for sending us the data prior to publication.
6) P. Brüesch and Hs. H. Günthard, *Spectrochim. Acta*, **22**, 877 (1966).
7) K. M. Chen and E. S. Yeung, *J. Chem. Phys.*, **69**, 43 (1978).
8) D. H. Parker and P. Avouris, *J. Chem. Phys.*, **71**, 1241 (1979).
9) W. M. McClain and R. A. Harris, "Excited States," ed by E. C. Lim, Academic Press, New York (1978), Vol. III.
10) D. M. Friedrich, J. van Alsten, and M. A. Walters, *Chem. Phys. Lett.*, **76**, 504 (1980).
11) a) Y. Matsumi and K. Obi, *Chem. Phys.*, **49**, 87 (1980); b) K. Obi and Y. Matsumi, *ibid.*, **49**, 95 (1980).
12) C. G. Cureton, K. Hara, D. V. O'Connor, and D. Phillips, *Chem. Phys.*, **63**, 31 (1981).
13) A. E. Douglas, *Discuss. Faraday Soc.*, **35**, 158 (1963).
14) E. Lindholm, *Ark. Fysik*, **40**, 97 (1970).
15) L. Wunsch, F. Metz, H. J. Neusser, and E. W. Schlag, *J. Chem. Phys.*, **66**, 386 (1977).
16) G.Placzek, "Handbuch der Radiologie," ed by E.Marx, Akademische Verlagsgesellschaft, Leipzig (1934), Vol. VI.
17) J. E. Wollrab and V. W. Laurie, *J. Chem. Phys.*, **51**, 1580 (1969).

 © 1982 The Chemical Society of Japan Bull. Chem. Soc. Jpn., 55, 3101—3103 (1982)

Viscosities of Aqueous Solutions of Sodium Alkanoates

Koichiro Miyajima,* Masahiro Sawada, and Masayuki Nakagaki
Faculty of Pharmaceutical Sciences, Kyoto University, Yoshida-shimoadachi-cho, Sakyo-ku, Kyoto 606
(Received February 26, 1982)

Viscosities of aqueous solutions of sodium salts of formic acid, acetic acid, propionic acid, and butyric acid were measured in the concentration range 0.01—0.1 mol dm^{-3} at 15, 25, and 35° C. For formate ion, values of B_{st}, the increment of viscosity B-coefficient arising from structural change of water, and of (dB_{ion}/dT), the temperature dependence of ionic B-coefficient, are both nearly zero, indicating that formate ion is neither a structure maker nor a structure breaker. For the alkanoate ions the signs of B_{st} and (dB_{ion}/dT) are positive and negative, respectively. From these facts, alkanoate ions may be concluded to be hydrophobic structure making ions.

It has long been recognized that the water structure around an ion plays an important role with respect to the interionic interactions in water.[1]

In a previous paper[2] concerning the mean activity coefficients ($\gamma_\pm$) of guanidinium salts with hydrophobic carboxylate ions, the order of $\gamma_\pm$ values among these salts was well interpreted by regarding acetate ion as a hydrophobic structure maker, which promotes the water structure by forming an ice-likeness in the vicinity of hydrophobic moiety.

In general, organic ions have more than one functional group besides the ionic residue, such as hydrophobic group and hydrophilic amino or hydroxyl group. These groups also play an important role in interionic interactions in water. In this connection, the simplest example is acetate ion which has the hydrophobic methyl group and the carboxylate ion residue. The structure around the hydrophobic methyl group would be different from that around the carboxylate ion. It has already been known by viscosity[3,4] and NMR measurements[5] that acetate ion is a structure maker. Gurney[3] postulated that the nature of structure promotion by acetate ion was based on the electrostriction of carboxylate ion, on the assumption that the valence electron of oxygen in carboxylate ion is localized. However, this assumption was denied by Spinner on the basis of IR and Raman studies.[6,7] Tamaki reached a similar conclusion from a viscosity study.[4] In the curve of B-coefficient *vs.* alkyl-carbon numbers (C_n) of carboxylate ions, the sign of the intercept at $C_n=0$ was positive. Unfortunately, formate ion was excluded in his study.

In order to elucidate the discrepancy between Gurney's and our views concerning the nature of structure promotion by acetate ion, we measured viscosities of aqueous solutions of some alkanoate ions including formate ion at various temperatures. The results indicate that the alkanoate ions studied are hydrophobic structure makers.

Experimental

Materials. Reagent grade sodium and potassium carboxylates obtained from Wako Chemical Co., Ltd. were used without further purification. Salts were dried *in vacuo* over P_2O_5 at room temperature. These salts were dissolved in redistilled and deionized water.

Methods. Viscosity measurements were made with an Ostwald type viscometer with an efflux time of *ca.* 360 s for water at 25 °C. Efflux time was measured with a Seiko stop watch 89 ST down to 0.01 s. At least five readings of efflux time with variation not exceeding ±0.05 s were taken for each solution. Viscosity η was calculated from average efflux time t and density d according to

$$\eta/d = \alpha t - \beta/t,$$

where α and β are the characteristic constants of the viscometer and are determined from the viscosities and densities of water at 15, 25, and 35 °C. The temperature of the thermostat bath was controlled to ±0.03 °C.

Results

Generally the relative viscosity (η_{rel}) of a dilute electrolyte solution can be expressed by the Jones-Dole equation

$$\eta/\eta_o = \eta_{rel} = 1 + A\sqrt{c} + Bc, \quad (1)$$

where η_o and η are the viscosities of solvent and solution, respectively, and c the molarity of electrolyte. The constant A relates to the interionic interaction of the Debye-Hückel type and is calculated by using molar conductivities of ions. The constant B is a so-called "viscosity B-coefficient" which is closely related to ion-solvent interaction. Equation 1 is valid for concentrations up to about 0.1 mol dm^{-3}. At higher concentrations than 0.1 mol dm^{-3}, an additional term, Dc^2 is required in the right hand side of Eq. 1. In the concentration range studied, the quantity $(\eta_{rel}-1)/\sqrt{c}$ was plotted against $\sqrt{c}$. The constants A and B were obtained from the intercept and slope, respectively. Figure 1 shows $(\eta_{rel}-1)/\sqrt{c}$ *vs.* $\sqrt{c}$ curves for some sodium alkanoates at 25 °C. The A values were found to be very small and agree with those calculated by using molar conductivity data reported by Falkenhagen and Vernon.[8]

The B-coefficient of an electrolyte is expressed by the sum of B-coefficients of each ion

$$B = \sum B_{ion}. \quad (2)$$

For the determination of B_{ion}, Eq. 2 was used by adopting the convention of Gurney[3] and Kaminsky[9] ($B_{K^+}=B_{Cl^-}$). Values of B_{ion} for Na^+ and K^+ at various temperatures were obtained from Kaminsky's data. B-coefficients of acetate ion obtained from aqueous solutions of sodium, potassium, and guanidinium acetate at 25 °C were 0.242, 0.229, and 0.231, respectively. The values of B_{ion} for the alkanoate ions at 25 °C were in fair agreement with those of Tamaki's work.[4] Table 1 shows the B-coefficients of the carboxylate ions at 15, 25, and 35 °C.

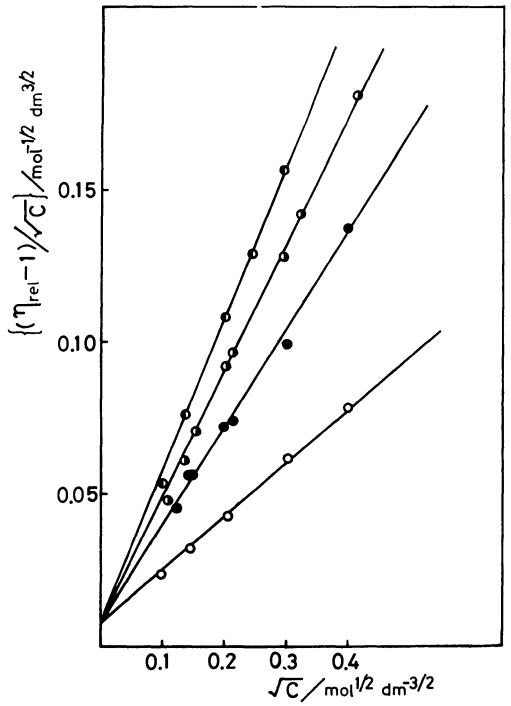

Fig. 1. Relationships between $(\eta_{rel}-1)/\sqrt{c}$ and $\sqrt{c}$ for sodium alkanoates at 25 °C.
○: Sodium formate, ●: sodium acetate, ◑: sodium propionate, ◐: sodium butylate.

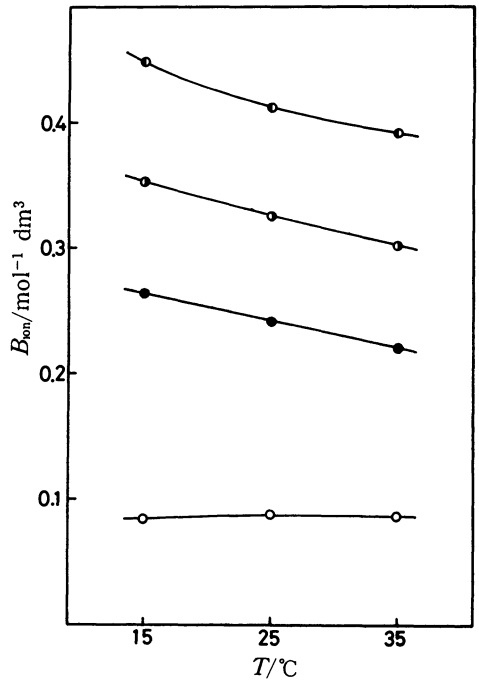

Fig. 2. Relationships between ionic B-coefficients of carboxylate ions and temperatures.
○: Sodium formate, ●: sodium acetate, ◑: sodium propionate, ◐: sodium butylate.

TABLE 1. B-COEFFICIENTS OF CARBOXYLATE IONS AT VARIOUS TEMPERATURES

Compound	B_{ion}/dm^3 mol^{-1}		
T/°C	15	25	35
$HCOO^-$	0.084	0.088	0.087
CH_3COO^-	0.264	0.242	0.221
$C_2H_5COO^-$	0.354	0.326	0.302
n-$C_3H_7COO^-$	0.450	0.413	0.393

TABLE 2. THE VALUES OF B_{st}, dB/dT, AND $\bar{V}_o$ OF CARBOXYLATE IONS AT 25 °C

Compound	B_{st}	dB_{ion}/dT	$\bar{V}_o$ [a]
	dm^3 mol^{-1}	dm^3 mol^{-1} K^{-1}	dm^3 mol^{-1}
$HCOO^-$	0.009	0.000	31.7
CH_3COO^-	0.127	−0.0022	45.9
$C_2H_5COO^-$	0.178	−0.0025	59.4
n-$C_3H_7COO^-$	0.223	−0.0028	75.9

a) "Water and Aqueous Solutions," ed by R. A. Horne, Wiley Interscience, New York (1972), p. 575.

B_{ion} is usually expressed by the sum of two contributions: 1) the hydrodynamic obstruction effect based on the size and shape of ion (B_{size}), and 2) the change of water structure induced by the addition of ion (B_{st}):

$$B_{ion} = B_{size} + B_{st}. \quad (3)$$

On the other hand, the viscosity of a dilute suspension of spherical colloid is represented by the Einstein equation

$$\eta_{rel} = 1 + 2.5\,\phi, \quad (4)$$

where ϕ is the volume fraction of colloidal particle. Equation 4 is an expression of the hydrodynamic effect of solute in a viscous flow. On the assumption that Eq. 4 is applicable to a solution of low molecular weight and ϕ is equal to the partial molar ionic volume at infinite dilution ($\bar{V}^\circ_{ion}$), B_{size} and B_{st} are expressed by

$$B_{size} = 0.0025\,\bar{V}^\circ_{ion}, \quad (5)$$

$$B_{st} = B_{ion} - 0.0025\,\bar{V}^\circ_{ion}. \quad (6)$$

As mentioned above, the sign and magnitude of B_{st} are regarded as a measure of ion-solvent interaction. Additional information on this interaction may be obtained from the sign and magnitude of the temperature dependence of B_{ion} (dB_{ion}/dT). Figure 2 shows the temperature dependence of B_{ion} for carboxylate ions. The values of (dB_{ion}/dT) obtained from the slope of B_{ion} *vs.* temperature curve are shown in Table 2 together with the values of B_{st} and $\bar{V}^\circ_{ion}$.

Discussion

The sign and magnitude of B_{st} are considered to reflect the structural change of water by the addition of ion. The ions associated with a large value of B_{st} with positive sign strongly promote the water structure, whereas the ions with a small value of B_{st} with negative sign break the water structure slightly.

As for the temperature dependence of B_{ion}, structure breaking ions should have a positive sign, since the structural water was already broken to a considerable extent by the thermal agitation at a high temperature. Therefore, the absolute value of B_{ion} decreases with temperature increase. From a consideration similar

to that for the case of structure breaking ions, the sign of (dB_{ion}/dT) of structure making ions should be negative. Consequently, the structure making ion has a positive sign of B_{st} and a negative sign of (dB_{ion}/dT), and *vice versa* for the structure breaking ion.

However, some ions of intermediate type between the structure maker and breaker do not obey this rule.[10] Judging from the ambiguity in the estimation of solute volume, the sign of (dB_{ion}/dT) would be more reliable than that of B_{st} for the determination of the structure making or breaking effect of the ion.[11,12]

As shown in Table 2, the values of B_{st} and (dB_{ion}/dT) for formate ion are both close to zero, indicating that formate ion is neither a structure maker nor a structure breaker, that is, formate ion hardly influences the water structure. This result is consistent with the conclusion that the valence electron of the carboxylate group is delocalized on the two oxygen atoms,[6,7] because the delocalization of the electron lowers the surface charge density of the carboxylate group and weakens the ionic hydration by the electrostriction.

The signs of B_{st} of the alkanoate ions are positive and their magnitudes increase with the alkyl-chain length. The signs of (dB_{ion}/dT) for the alkanoate ions are negative and their absolute values increase with the alkyl-chain length. These results indicate that the alkanoate ions are structure making ions. By taking into account the fact that formate ion is neither a structure maker nor a structure breaker, we conclude that the nature of the structure making action for these alkanoate ions originates from the alkyl groups which form the ice-like structure around themselves. In conclusion, alkanoate ions are not ionic or hydrophilic structure makers but hydrophobic structure makers.

References

1) J. E. Desnoyers, M. Arel, G. Perron, and C. Jolicoeur, *J. Phys. Chem.*, **73**, 3346 (1969).
2) K. Miyajima, H. Yoshida, and M. Nakagaki, *Bull. Chem. Soc. Jpn.*, **51**, 2506 (1978).
3) R. W. Gurney, "Ionic Process in Solution," translated by S. Kikuchi and S. Suzuki, Sangyo Tosho, Tokyo (1967), p. 165.
4) K. Tamaki, Y. Ohara, H. Kurachi, M. Akiyama, and H. Odaki, *Bull. Chem. Soc. Jpn.*, **47**, 384 (1974).
5) K. Miyajima, K. Kitamura, K. Inari, and M. Nakagaki, *Nippon Kagaku Kaishi*, **1975**, 2060.
6) E. Spinner, *J. Chem. Soc., B*, **1967**, 874.
7) E. Spinner, *J. Chem. Soc., B*, **1967**, 879.
8) H. Falkenhagen and E. L. Vernon, *Z. Phys.*, **33**, 140 (1932).
9) M. Kaminsky, *Discuss. Faraday Soc.*, **24**, 171 (1957).
10) E. R. Nightingale, Jr., "Chemical Physics of Ionic Solutions," ed by B. E. Conway and R. G. Barradas, John Wiley and Sons Inc., New York (1966), p. 93.
11) D. Feakins, D. J. Freemantle, and K. G. Lawrence, *J. Chem. Soc., Faraday Trans. 1*, **70**, 795 (1974).
12) B. S. Krumgals, *J. Phys. Chem.*, **83**, 763 (1979).

Spectroscopic Study of 10-Benzoyl-9-anthrol and Its Anion in Basic Media. An Estimation of Microscopic Polarity of PMMA

Kumao HAMANOUE,* Satoshi HIRAYAMA,† Masayuki AMANO, Kazuo NAKAJIMA, Toshihiro NAKAYAMA, and Hiroshi TERANISHI

Department of Chemistry, Faculty of Technology, Kyoto Institute of Technology, Matsugasaki, Sakyo-ku, Kyoto 606

†*Faculty of Textile Science, Kyoto Institute of Technology, Matsugasaki, Sakyo-ku, Kyoto 606*

(Received March 4, 1982)

The acid-base equilibrium of the title compound (BAOH) was studied in various media containing 4% triethylamine (TEA) by volume as a base. As the polarity of solvents increases, the equilibrium shifts toward the base form (BAO^-) and 100% yield of BAO^- is achieved in solvents with dielectric constant (ε) greater than 20. The equilibrium is also affected by temperature, favoring the base form at lower temperatures. The associated enthalpy change is estimated to be -14.6 kJ mol^{-1}. Of particular interest is the dominant existence of BAO^- in poly(methyl methacrylate) (PMMA), since the acid form (BAOH) dominates in a monomeric solvent (MMA). The microscopic effective dielectric constant of PMMA is estimated to correspond to that of a solvent with $\varepsilon=22$—30 by comparing spectral data in PMMA with those in various solvents. No base form is formed in polystyrene, indicating that not only rigidity but also polar groups in PMMA may be responsible for the anomalously large dielectric constant of PMMA.

In our study on photochemical reaction of nitroanthracenes (9-cyano- and 9-benzoyl-10-nitroanthracene) in various fluid solutions and poly (methyl methacrylate) (PMMA),[1] we have found that the form of the final photoproducts (10-cyano-9-anthrol (CAOH) or its anion (CAO^-) and 10-benzoyl-9-anthrol (BAOH) or its anion (BAO^-)) is very dependent on the basicity, polarity, and rigidity of medium as well as temperature. Of particular interest is the formation of BAO^- in basic PMMA, since in a basic monomeric medium the main photoproduct is BAOH.

According to the results of Kosower,[2] a solvent-environmental effect on a solute molecule is supported by a result of spectral shift which indicates that the molecular energy level is generally sensitive to the matrix. The primary polymer matrix effect is therefore manifested by changes in intermolecular interactions brought about by a decrease in the average separation between solute and solvent molecules and by an alteration of relative orientations of solvent molecules against solute molecule, all of which lead to a change in the coordination number of solvent shells. For this reason the effect of polymer matrix is frequently compared with solvent effects and discussed in the light of tsolven shift theories.[3-10]

Thus, our observation of the medium effect on the form of the final photoproducts of nitroanthracenes leads us to an extensive spectroscopic study on the interchange between BAOH and BAO^- in a wide variety of media. Detailed information on this acid-base equilibrium is not only interesting in itself but also valuable in understanding photochemical processes of the nitroanthracenes.[1]

We will also point out a possibility of utilizing the present acid-base pair of BAOH–BAO^- to estimate the microscopic polarity of polymers which is unaffected by the way of doping probe molecules.

Experimental

Chemicals. BAOH was synthesized from 9-benzoyl-10-nitroanthracene. The details of the methods of preparation of this material have been given in our previous paper.[1] Uvasol diethyl ether was purchased from E. Merck A. G. and used without further purification. Methyl methacrylate monomer (MMA) was of guaranteed grade (Wako Pure Chemical Industries, Ltd.) and was distilled by the method of Collins *et al.*[11] The purified monomer was stored in the dark in a refrigerator.

All the other chemicals used were of guaranteed grade (Wako Pure Chemical Industries, Ltd.) and were used without further purification, unless otherwise stated. In the following, "basic solvent" means a solvent which contains 4 vol% TEA.

To get a basic polymer sample, a solution of BAOH in 5 cm^3 of basic MMA and 0.5 mg of α,α'-azobisisobutyronitrile were poured into a 1 cm rectangular Pyrex cell, and degassed by seven freeze-pump-thaw cycles. After sealing the cell the sample solution was polymerized in bulk at 348 K for 24 h.

Measurements of Absorption Spectra and Z-Values. Using a Hitachi 200-20 spectrophotometer, absorption spectra were taken at room temperature and at low temperatures down to 143 K. To get a given low temperature a cold nitrogen gas, generated by heating liquid nitrogen in a metal Dewar vessel, was introduced into a quartz Dewar vessel in which a 1 cm rectangular sample cell made of Suprasil was mounted. The temperature was measured with a copper-constantan thermocouple which was inserted into a sample cell.

For the estimation of medium polarity, *Z*-values were determined with 1-methyl-4-(methoxycarbonyl)pyridinium iodide, which was recrystallized twice from methanol, yielding the melting point of 175—176 °C. The charge-transfer band of this salt was measured in a 1 cm rectangular quartz cell. (For a polymeric sample, 5 cm^3 of sample solution in MMA was polymerized by the same method as described before.)

Results and Discussion

Acid-base Equilibrium between BAOH and BAO^-. The pK_a value of BAOH has been determined to be 8.8 in water–ethanol mixed solvent by the ordinary spectroscopic method.[12] From this value it is expected that BAOH easily dissociates to BAO^- in slightly basic organic media.

In Fig. 1, we show the absorption spectral change of BAOH in ethanol caused by addition of triethylamine (TEA), which indicates that there exists an acid-base equilibrium between BAOH and BAO^-. The absorption

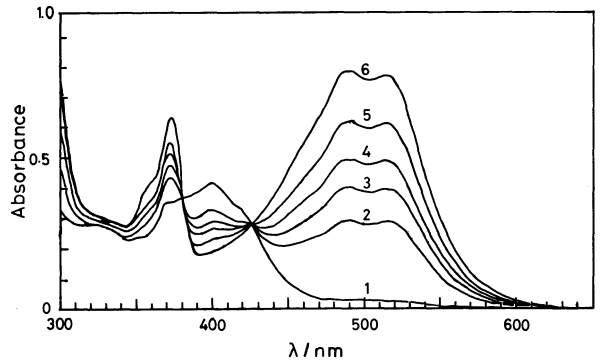

Fig. 1. Absorption spectral change of BAOH in ethanol (initial concentration 1.5×10^{-4} mol dm^{-3}) by the addition of different amount of TEA.
TEA volume ratio: 1; 0%, 2; 0.05%, 3; 0.1%, 4; 0.2%, 5; 0.5%, 6; 4%.

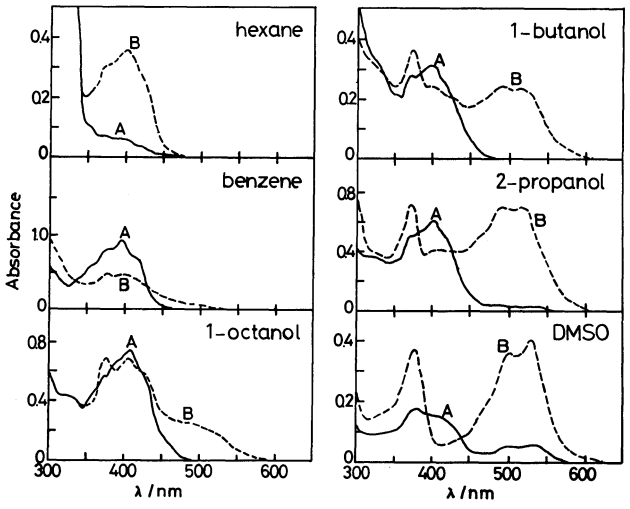

Fig. 2. Absorption spectra of BAOH in various solvents.
A: BAOH, B: BAOH+BAO$^-$ in basic solvent containing 4% TEA.

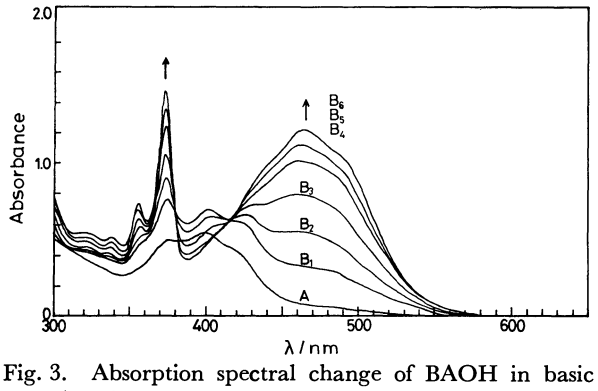

Fig. 3. Absorption spectral change of BAOH in basic EPA at low temperature.
A: At room temperature, B_1: 253 K, B_2: 233 K, B_3: 213 K, B_4: 193 K, B_5: 173 K, B_6: 143 K.

spectrum due to BAO$^-$ lies on the longer wavelength side and has two band maxima around 370 and 500 nm. Although the addition of 4% TEA to the ethanol solution is enough to dissociate BAOH into BAO$^-$ almost completely, which form of BAOH and BAO$^-$ dominates in other solvents depends on the nature of solvents even in the presence of TEA, as shown in Fig. 2. Since the standard free energy change associated with the equilibrium is a function of dielectric constant, it is fully expected that the acid-base equilibrium is affected by the polarity of solvents. However, instead of trying to formulate the general equation to give the standard free energy change, which would be extremely difficult, we measured absorption spectra of the acid-base pair in more than thirty organic solvents, whose dielectric constants range from 1.84 to 46.7, in order to find the threshold of dielectric constant above which BAO$^-$ dominates.

The obtained results indicate that the equilibrium between BAOH and BAO$^-$ is strongly dependent on the dielectric constant ε of solvents, that is, the amount of BAO$^-$ increases as the polarity of solvent increases and nearly 100% yield of BAO$^-$ is obtained in such basic solvents as acetone, ethanol, benzonitrile, methanol, *N*,*N*-dimethylformamide, acetonitrile, and dimethyl sulfoxide, all of which have dielectric constants greater than 20. No pure BAO$^-$ exists in neat TEA or in pure polar solvents even when their dielectric constants exceed 20.

The stability of BAO$^-$ is found to depend not only on the polarity and basicity of solvents but also on the temperature. A typical example is illustrated in Fig. 3. The spectra were taken for BAOH in basic EPA (ether: isopentane : ethanol=5 : 5 : 2 in volume ratio). At room temperature, one can see that the spectrum is mainly due to BAOH, being slightly superposed by that of BAO$^-$. This is because the polarity of EPA is much less than 20. As the temperature decreases, the absorbance of a new spectrum with a band maximum at 466 nm (Spectra B_1—B_6) increases, accompanied by two isosbestic points at 380 and 420 nm. The isosbestic point at 420 nm is not so clear. Spectra B_1—B_6 are similar to that of BAO$^-$ observed in basic ethanol at room temperature, but the former are appreciably blue-shifted compared with the latter. By changing the volume ratio of ethanol in basic EPA, the spectral shift of BAO$^-$ was examined at 196 K. The result shows that the absorption band maximum of BAO$^-$ which lies around 500 nm in basic ethanol shifts to the blue with decrease in the content of ethanol and gradually arrives at Spectrum B_4 in Fig. 3 as the ratio of ethanol approaches to that in EPA, *i.e.*, 5 : 5 : 2. Thus, it is concluded that Spectra B_1—B_6 are not due to new species but to BAO$^-$ (though blue-shifted because of the lower polarity of EPA), and that the spectral change of B_1 to B_6 with lowering temperature is due to a shift in equilibrium between BAOH and BAO$^-$.

Although the proton transfer in *p*-nitrophenol–TEA system has been studied quantitatively by Baba *et al.*,[13] we have roughly estimated the enthalpy change of BAOH into BAO$^-$ from the temperature dependence of the absorbance at 466 nm, by assuming that the absorbance at 143 K is due to BAO$^-$ alone. The estimated value is -14.6 kJ mol^{-1}. Since in basic EPA there is no spectral change in either BAOH or BAO$^-$ at various temperatures and since no change in Kosower's *Z*-value is observed for basic EPA, one can

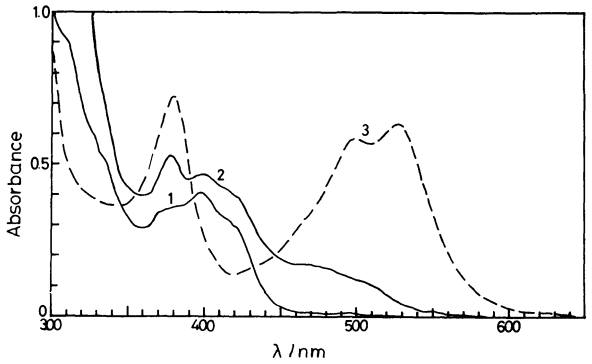

Fig. 4. Absorption spectral change of BAOH.
1: BAOH in MMA, 2: BAOH+BAO⁻ in basic MMA, 3: BAO⁻ in basic PMMA.

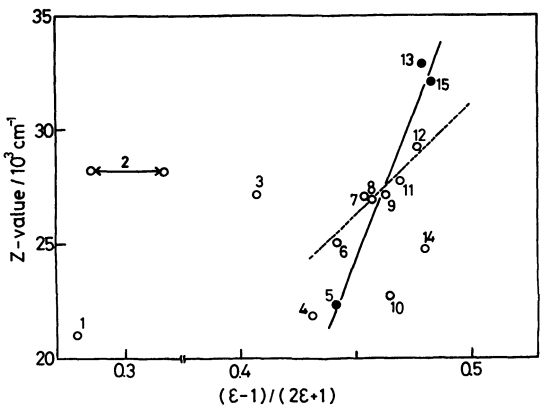

Fig. 5. Plot of Z-value against $(\varepsilon-1)/(2\varepsilon+1)$ for various solvents.
1: MMA, 2: PMMA, 3: tetrahydrofuran, 4: 1,2-dichloroethane, 5: pyridine, 6: 2-methyl-2-propanol, 7: 2-butanol, 8: 1-butanol, 9: 2-propanol, 10: acetone, 11: ethanol, 12: methanol, 13: *N*,*N*-dimethylformamide, 14: acetonitrile, 15: dimethyl sulfoxide.

say that the polarity of EPA is not affected by lowering temperature. Consequently, it can be said that in basic EPA, the observed temperature effect on the equilibrium emerges purely through an enthalpy change ΔH of constant negative value, but not through a change in the dielectric constant of EPA with temperature.

Spectral Shift in PMMA. In our study on the photochemistry of 9-cyano- or 9-benzoyl-10-nitroanthracene in basic PMMA, it was found that absorption spectra of photoproducts (CAO⁻ and BAO⁻) in polymeric media are more red-shifted and become more structured than those in the monomer solution (MMA).[1)]

Figure 4 shows the absorption spectral change of BAOH when the properties of medium (MMA) are modified. Only BAOH exists in MMA and it dissociates only slightly to BAO⁻ by the addition of TEA. After the polymerization of this basic sample solution at 348 K for 24 h, BAO⁻ is obtained in 100% yield. Of particular interest is the appearance of absorption spectra of BAO⁻ in a basic polymeric medium, since in a basic monomeric medium the observed absorption spectrum is dominated by BAOH, being superposed only slightly by that due to BAO⁻. Moreover, the absorption band of BAO⁻ obtained in basic PMMA is red-shifted compared with that in a basic monomeric medium and the spectral shape of the Franck-Condon envelope is rather similar to those in pyridine, 2-propanol, *N*,*N*-dimethylformamide, and dimethyl sulfoxide, each containing TEA.

In relation to this anomalous medium effect of PMMA, it is interesting to know the effect of the rigidity of basic PMMA on the dominant existence of BAO⁻. Upon polymerizing a basic MMA solution of BAOH gradually, a growth of the absorption of BAO⁻ was observed. Initially the almost colorless solutions became red as the medium became viscous and its color deepened upon further polymerization untill such a spectrum as given in Fig. 4 was obtained. This could be interpreted as follows: PMMA may not necessarily be extremely hard to favor the presence of BAO⁻ and even a soft rubber-like PMMA may exhibit a dielectric constant high enough for BAO⁻ to dominate it.

As described above, the equilibrium between BAOH and BAO⁻ is strongly dependent on the dielectric constant of solvents, giving 100% yield of BAO⁻ in basic solvents which have ε greater than 20. The dominant existence of BAO⁻ in basic PMMA can not be interpreted in terms of the formation of small cavities (filled with TEA) created in the polymeric medium in which most of the solute molecules might be located, because BAOH is the main form in both neat TEA and basic MMA.

It is obvious that the solvent molecules immediately around a solute molecule can no longer be described by the same parameters as those used for the bulk solvent. The more polar the solute, the greater would be the divergence between the properties of the solvent molecules near the solute and those of the bulk solvent. Since dielectric constants obtained by the usual macroscopic measurement reflect an average of solvent arrangements over macroscopic distances, they are inappropriate at the microscopic level to represent the solvent properties particularly when highly polar solute molecules are involved. Considering that the values of macroscopic dielectric constants are 2.9 for MMA[14)] and 3.0—3.6 for PMMA,[15)] one may envisage that the microscopic medium polarity in basic PMMA is much greater than that in basic MMA solution.

In order to scale the polarity of PMMA with another solvent-polarity parameter, we have measured the wave number of the longest wavelength charge-transfer absorption band of 1-methyl-4-(methoxycarbonyl)-pyridinium iodide in various solvents. It is obvious that the obtained values, when expressed in energy, should correspond to Kosower's Z-values. Thus we call them simply Z-values for convenience. The obtained Z-values are plotted in Fig. 5 against $(\varepsilon-1)/(2\varepsilon+1)$ for various solvents to see the correlation between Z-value and ε. (For PMMA, ε is the macroscopic dielectric constant, *i.e.*, 3.0—3.6.) As is well known, the points are scattered too much to draw a single correlation line, but two lines can be drawn if the data are restricted to those in akin solvents. The dotted line shows a correlation in basic alcohols and the solid line is drawn for the data in basic pyridine, *N*,*N*-dimethylformamide, and dimethyl sulfoxide. From these different lines, however, one can estimate similar effective dielectric constants 25.4

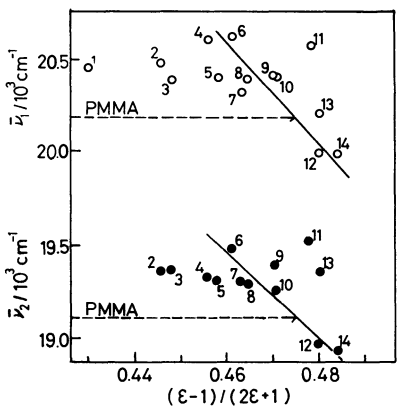

Fig. 6. Plot of two absorption peaks of BAO^- ($\bar{\nu}_1$, $\bar{\nu}_2$) against $(\varepsilon-1)/(2\varepsilon+1)$ for various solvents.
1: 1-Octanol, 2: 1-hexanol, 3: 1-pentanol, 4: 2-butanol, 5: 1-butanol, 6: 2-butanone, 7: 2-propanol, 8: acetone, 9: ethanol, 10: benzonitrile, 11: methanol, 12: *N,N*-dimethylformamide, 13: acetonitrile, 14: dimethyl sulfoxide.

(dotted line) and 21.6 (solid line) for that of PMMA and they are close to that which was estimated before, by comparing the spectral data of the acid-base pair of BAOH–BAO^- in PMMA with those in various solvents.

BAO^- provides a possibility of estimating the polarity of PMMA, since the solvent effect on the spectral shift of BAO^- is significant. Although solvent effects on absorption spectra have been studied for more than a century, it is difficult to understand these effects in terms of only one macroscopic physical solvent parameter. In general, most of the empirical solvent scales constitute a more comprehensive measure of solvent polarity than dielectric constant, and it can be said that only a multiparameter approach which includes terms corresponding to all possible solute-solvent interaction mechanisms is sufficient for the development of a quantitative model for medium effects of all kinds of solvents.[16] Since a large *Z*-value is obtained in PMMA, *i.e.*, 28.2×10^3 cm^{-1} in PMMA and 21.1×10^3 cm^{-1} in MMA, and since BAO^- is dominated in basic PMMA, it is evident that the microscopic medium polarity in PMMA is actually greater than that in MMA. Therefore, we have made a tentative plot of the wave number of two absorption peaks of BAO^- around 500 nm ($\bar{\nu}_1$,$\bar{\nu}_2$) against $(\varepsilon-1)/(2\varepsilon+1)$ for various solvents, and a good correlation is found for aprotic solvents as shown in Fig. 6. From this, one can estimate the effective dielectric constant of the basic PMMA to be 28.9—29.5.

All the values estimated so far for the effective dielectric constant of PMMA are much larger than the macroscopic dielectric constant of PMMA (ε=3.0—3.6) or MMA (ε=2.9), indicating the existence of a very polar microscopic region in PMMA. Thus there will be no doubt that the microscopic effective medium polarity of MMA will increase upon polymerization, resulting in the dominant existence of BAOH in basic MMA but of BAO^- in basic PMMA. Although the reason for this is not clear,[17] it may very well be related not only to the rigidity but also to the methoxycarbonyl group of PMMA, since it was confirmed that BAO^- could not exist in a basic polystyrene medium which was prepared similarly to PMMA. Further study on this problem is now in progress.

Finally, it would be worth mentioning that the present acid-base pair has an advantage as a probe to examine the microscopic dielectric constant of polymeric medium in the sense that it can be photochemically produced without modifying the microscopic environment. When a polar molecule is doped in a medium to probe its microscopic property, it is very likely that the molecules around the probe reorient to minimize the potential energy. This would make it impossible to know the "true face" of the polymer environment. Our "pre-probe" molecule, 9-benzoyl-10-nitroanthracene is, however, expected to behave as an inert molecule when doped in basic PMMA and upon irradiation it would generate BAO^- without modifying the environment; there will be an environment which is different from the polymer environment of BAO^- produced chemically from BAOH. Taking it into account that the two different ways of producing BAO^- yielded the same result, the anomalously high value of ε obtained for PMMA appears to reflect the true microscopic dielectric constant. Consequently, "photochemically producible probes" as described here will open a more reliable way for probing microscopic properties of polymeric media.

The initial part on this study was carried out in association with Messrs. Haruyo Ohya and Toshiharu Hidaka. We wish to express our sincere thanks for their help.

References

1) K. Hamanoue, S. Hirayama, T. Hidaka, H. Ohya, T. Nakayama, and H. Teranishi, *Polym. Photochem.*, **1**, 57 (1981).
2) E. M. Kosower, "An Introduction to Physical Organic Chemistry," John Wiley and Sons, New York (1968), p. 257.
3) N. S. Bayliss, *J. Chem. Phys.*, **18**, 292 (1950); N. S. Bayliss and E. G. McRae, *J. Phys. Chem.*, **58**, 1002 (1954).
4) W. Ooshika, *J. Phys. Soc. Jpn.*, **9**, 594 (1954).
5) N. Mataga, Y. Kaifu, and M. Koizumi, *Bull. Chem. Soc. Jpn.*, **29**, 465 (1956).
6) E. G. McRae, *J. Phys. Chem.*, **61**, 562 (1957).
7) B. S. Neporent and N. G. Bakhshiev, *Opt. Spectrosc.*, **5**, 634 (1958); N. G. Bakhshiev, *ibid.*, **7**, 29 (1959); *Bull. Acad. Sci. USSR, Phys. Ser.*, **26**, 1252 (1962).
8) E. Lippert, *Z. Elektrochem.*, **61**, 962 (1957); E. Lippert, W. Luder, F. Moll, W. Nagele, H. Boos, H. Prigge, and I. Seibold, *Z. Angew. Chem.*, **71**, 965 (1961).
9) S. Basu, *Adv. Quantum Chem.*, **1**, 145 (1964).
10) L. J. Bilot and A. Kawski, *Z. Naturforsch.*, *A*, **18**, 10, 256(1963).
11) E. A. Collins, J. Bares, and F. W. Billmeyer, Jr., "Experiments in Polymer Science," John Wiley and Sons, New York (1973), p. 333.
12) H. Hosoya, M. Koizumi, A. Ogura, and T. Nakamura, "Zoku Jikken Kagaku Koza," ed by the Chemical Society of Japan, Maruzen, Tokyo (1965), Vol. 11, p. 523.
13) H. Baba, A. Matsuyama, and H. Kokubun, *Spectrochim. Acta*, **25A**, 1709 (1969).
14) J. A. Riddick and W. B. Bunger, "Techniques of

Chemistry," 3rd ed, ed by A. Weissberger, Wiley-Interscience, New York (1970), Vol. II, p. 303.

15) J. Braundup and E. H. Immergut, "Polymer Handbook," 2nd ed, John Wiley and Sons, New York (1975), p. v-55.

16) M. J. Kamlet and R. W. Taft, *J. Am. Chem. Soc.*, **98**, 377, 2886 (1976); M. J. Kamlet, J. L. Abboud, and R. W. Taft, *ibid.*, **99**, 6027 (1977); J. L. Abboud and R. W. Taft, *J. Phys. Chem.*, **83**, 412 (1979).

17) One possibility might be the existence of a small amount of water in PMMA, which come together around a solute molecule as the polymerization proceeds. We have prepared a sample in a vacuum system, and MMA was dried using molecular sieves 3A (Wako Pure Chemical Industries, Ltd.) which was baked out at *ca.* 7×10^{-3} Pa and 500 °C for 20 h. However, we have obtained the same result.

 © 1982 The Chemical Society of Japan Bull. Chem. Soc. Jpn., 55, 3109—3112 (1982)

Macromolecular Ion Flotation of Fe^{3+}, Cu^{2+}, and Ni^{2+} Ions by Combined Use of Macromolecular Anions and Cationic Surfactant

Tsunetaka Sasaki,* Takashi Kudō, Ikuko Machida, and Satoshi Ishiwata
Department of Chemistry, Faculty of Science, Tokai University, 1117 Kitakaname, Hiratsuka 259-12
(Received March 8, 1982)

Macromolecular ion flotation of Fe^{3+}, Cu^{2+}, and Ni^{2+} ions was studied using macromolecular ions such as sodium metasilicate, sodium polyacrylate, sodium carboxymethylcellulose, sodium alginate, and sodium cyclo-hexaphosphate (SCHP) together with hexadecyltrimethylammonium chloride (HTAC). Diagrams of floatability *vs.* composition of macromolecular ion and HTAC, and floatability *vs.* pH at fixed composition of macromolecular ions and HTAC were constructed. Regions of optimum composition and pH for the flotation were determined and tabulated. Maximum floatabilities greater than 95%, some attaining nearly 100%, in the alkaline region were obtained for most of the systems, except for the system Fe^{3+}–SCHP–HTAC which showed its maximum floatability, 91.7%, in the acid region. Metallic ions are considered to be combined as hydroxides with macromolecules which are then floated.

In a previous paper,[1] we have reported the flotation of Fe^{3+} and MnO_4^- ions by sodium metasilicate and cationic surfactant and the flotation of MnO_4^- ions by many other macromolecular anions, including macroscopic or colloidal particles possessing ion exchange capacity and organic or inorganic polymer ions together with cationic surfactant.[2] The present paper reports the macormolecular ion flotation of Fe^{3+}, Cu^{2+}, and Ni^{2+} ions by various macromolecular anions, such as sodium polyacrylate (SPA), sodium alginate (SAlg), sodium carboxymethylcellulose (SCMC), sodium metasilicate (SMS), and sodium cyclo-hexaphosphate (SCHP) together with cationic surfactant, hexadecyltrimethylammonium chloride (HTAC).

Experimental

Materials. SPA was commercial pure product of polymerization degree 22000—66000. SAlg was a product of commercial pure grade. Its 0.3% aqueous solution showed relative viscosity to water of 12.5 at 30 °C. SMS, SCHP, and SCMC were commercial products of guaranteed grade. HTAC was a product of commercial pure grade. These reagents were kept in a desiccator and used without further purification. Iron(III) chloride, coppor(II) sulfate, and nickel(II) sulfate of guaranteed grade were used as cations to be floated.

Measurement. For the flotation measurement, 20 cm^3 of a solution containing ions to be floated, macromolecular ions, HTAC and HCl or NH_3 if necessary for controlling pH was introduced in a stoppered test tube of 16 mm in inner diameter and 290 mm in length equipped with a stopcock at the bottom. The test tube was slowly moved upside down for 2 min, then vigorously shaken 20 times by hand. After being kept for 10 min to complete flotation, concentrations of Fe^{3+}, Cu^{2+}, and Ni^{2+} ions in the underlying solution were measured and the floatability percent, F, was calculated by the following equation:

$$F = \frac{C_i - C_f}{C_i} \times 100\%,$$

where C_i and C_f denote concentrations of the ions to be floated in the solution before and after the flotation, respectively.

The concentrations of Fe^{3+}, Cu^{2+}, and Ni^{2+} ions were measured with a Hitachi Atomic Absorption Spectrometer 508 at wave lengths 248.3, 324.7, and 232 nm, respectively.

The measurement of flotation was carried out at room temperature, about 25 °C.

Results and Discussion

Flotation by SPA. Flotation of Fe^{3+} Ions: Figure 1 shows the floatability of Fe^{3+} ions as a function of total concentration of SPA+HTAC and weight fraction of SPA/(SPA+HTAC) at pH about 8.2. The concentra-

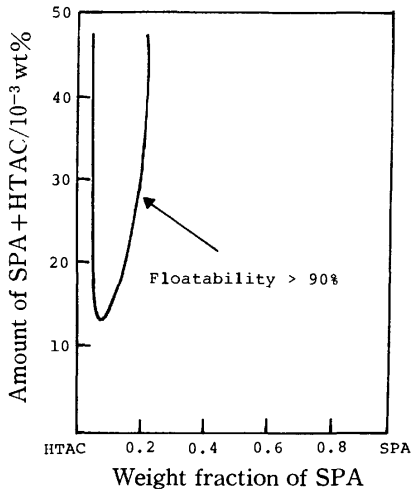

Fig. 1. Diagram of Fe^{3+} ion flotation by SPA and HTAC. F^{3+}: 1.98×10^{-4} mol dm^{-3}, pH: 8.2.

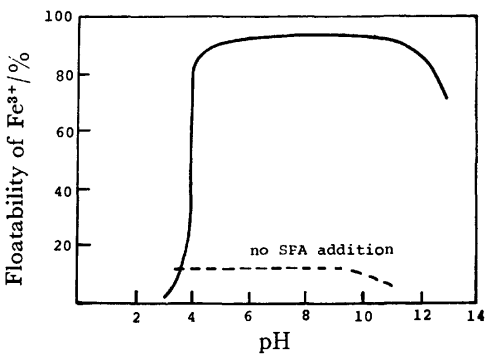

Fig. 2. Floatability of Fe^{3+} ion *vs.* initial pH for SPA+HTAC system.
Fe^{3+}: 1.93×10^{-4} mol dm^{-3}, SPA: 1.5×10^{-3} wt%, HTAC: 3.1×10^{-3} wt%.

tion of Fe^{3+} ions was kept constant at 1.92×10^{-4} mol dm^{-3}. The area inside the curve shows the optimum region of Fe^{3+} ion flotation, more than 90% floatability. Maximum floatability of 93.8% was obtained at 31×10^{-3} wt% SPA and 1.86×10^{-3} wt% HTAC.

Figure 2 shows the pH dependence of floatability of Fe^{3+} ions at the nearly maximum floatability condition of 1.9×10^{-4} mol dm^{-3} Fe^{3+}, 1.5×10^{-3} wt% SPA, and 28.8×10^{-3} wt% HTAC. As shown by the solid line, floatability became perceptible at about pH 3, sharply increased at pH 4, and gave a plateau of nearly 93% in pH range 5 to 11. Beyond pH 12, floatability sharply decreased. The beginning of the floatability increase at pH 3 is near the pH at which $Fe(OH)_3$ precipitation begins to form, as calculated from its solubility product and the concentration of Fe^{3+} ions used. It is confirmed that SPA effectively acts in the macromolecular ion flotation of Fe^{3+}, since the system without SPA exhibited only a slight floatability in this pH range as shown by the broken line in Fig. 2.

Flotation of Cu^{2+} Ions: Figures 3 and 4 show floatability *vs.* composition and floatability *vs.* pH relations for Cu^{2+}–SPA–HTAC system, corresponding to Figs. 1 and 2 for Fe^{3+} flotation, respectively. In Fig. 3, the concentration of Cu^{2+} ions was kept constant at 1.74×10^{-4} mol dm^{-3}, and pH at 9.8. The region of floatability more than 90% is indicated by a curve, the shape of which is different from that of Fig. 1 for Fe^{3+} ions; it forms a narrow vertical area resembling the case of the flotation of Fe^{3+} or MnO_4^- ions by SMS.[1]

The pH dependence of the floatability of Cu^{2+} ions is shown in Fig. 4, where concentrations of Cu^{2+} ions, SPA, and HTAC were 1.79×10^{-4} mol dm^{-3}, 4.1×10^{-3} wt%, and 15.5×10^{-3} wt%, respectively. Floatability sharply rose from about pH 6, showed a flat maximum of nearly 96% in pH range 7 to 9 and decreased to nearly zero beyond pH 10, as shown by the solid line. The sharp rise of floatability at pH 6 is close to the pH of the beginning of $Cu(OH)_2$ precipitate formation as calculated from its solubility product and Cu^{2+} ion concentration. Again, the addition of SPA is found effective for Cu^{2+} ion flotation, as is evident from the comparison of solid line with the floatability curve of the system without the addition of SPA, as shown by the broken line in Fig. 4.

Flotation by SAlg. Flotations of Fe^{3+} and Cu^{2+} Ions: Figures 5 and 6 show the floatability *vs.* composition and floatability *vs.* pH relations for the Fe^{3+}–SAlg–HTAC

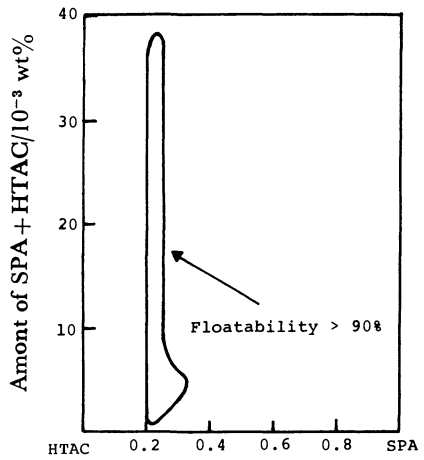

Fig. 3. Diagram of Cu^{2+} ion flotation by SPA and HTAC.
Cu^{2+}: 1.74×10^{-4} mol dm^{-3}, pH: 9.8.

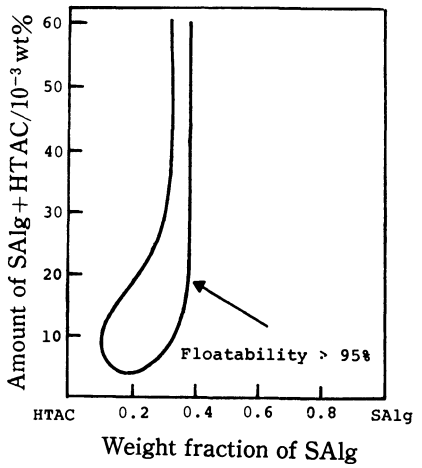

Fig. 5. Diagram of Fe^{3+} ion flotation by SAlg and HTAC.
Fe^{3+}: 1.80×10^{-4} mol dm^{-3}, pH: 9.0.

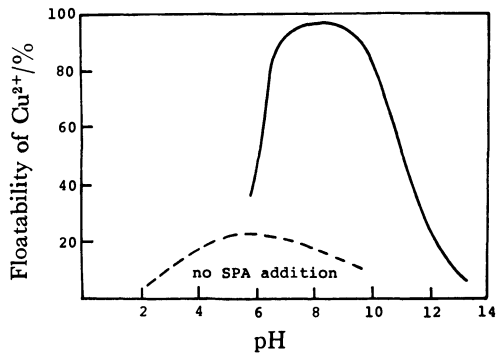

Fig. 4. Floatability of Cu^{2+} ion *vs.* initial pH for SPA+HTAC system.
Cu^{2+}: 1.79×10^{-4} mol dm^{-3}, SPA: 4.1×10^{-3} wt%, HTAC: 15.5×10^{-3} wt%.

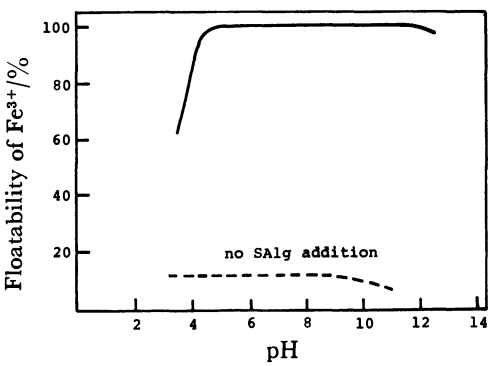

Fig. 6. Floatability of Fe^{3+} ion *vs.* initial pH for SAlg+HTAC system.
Fe^{3+}: 1.79×10^{-4} mol dm^{-3}, SAlg: 8.3×10^{-3} wt%, HTAC: 15.2×10^{-3} wt%.

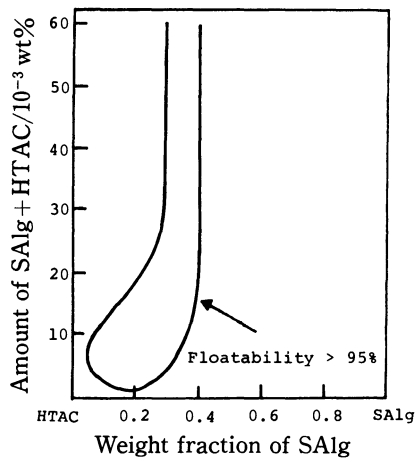

Fig. 7. Diagram of Cu^{2+} ion flotation by SAlg and HTAC.
Cu^{2+}: 1.81×10^{-4} mol dm^{-3}, pH: 9.1.

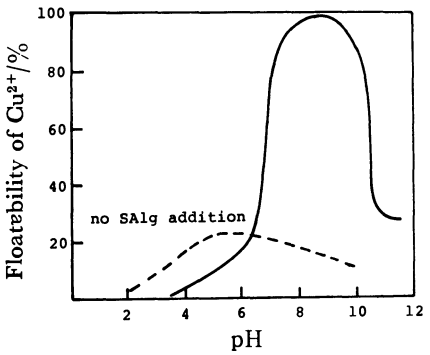

Fig. 8. Floatability of Cu^{2+} ion *vs.* initial pH.
Cu^{2+}: 1.74×10^{-4} mol dm^{-3}, SAlg: 8.2×10^{-3} wt%, HTAC: 15.6×10^{-3} wt%.

system. Figures 7 and 8 show similar relations for the Cu^{2+}–SAlg–HTAC system. Experimental conditions of Figs. 5 through 8 are listed in each figure caption. As shown in Figs. 5 and 7, and Figs. 6 and 8, the floatability behaviors of Fe^{3+} and Cu^{2+} ions for SAlg are similar as a whole to those for SPA. But in the former case, regions of optimum floatability more than 95% are shown in Figs. 5 and 7. The floatability of nearly 100% is seen in the pH region 5 to 12 for the Fe^{3+}–SAlg–HTAC system in Fig. 6. In the case of the Cu^{2+}–SAlg–HTAC system, a flat maximum of nearly 100% floatability is seen in the pH region 8 to 9 in Fig. 8. Figs. 6 and 8 also show the effectiveness of the addition of SAlg for the flotation of Fe^{3+} and Cu^{2+} ions as seen from the comparison of the solid line with the broken line in these figures.

Flotations of Fe^{3+}, Cu^{2+}, and Ni^{2+} Ions by Other Macromolecular Anions. Flotations of Fe^{3+}, Cu^{2+}, and Ni^{2+} were carried out using SMS, SCMC, and SHMP as macromolecular or polymer ions and HTAC as frother. Similar diagrams of floatability *vs.* composition and floatability *vs.* pH were obtained, which are not shown. Instead, the best conditions of flotation for these systems together with those for SPA and SAlg are shown in

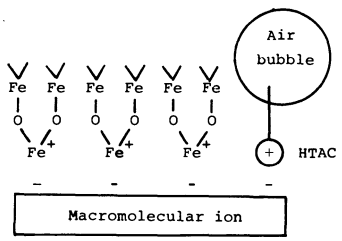

Fig. 9. Sublate structure consisting of macromolecular ion and Fe^{3+} ion.

Table 1. Macromolecular ion flotation of Fe^{3+}, Cu^{2+}, and Ni^{2+}

Ion	Concn of ion / 10^{-4} mol dm^{-3}	Concn of HTAC / wt%	Concn of SMS / wt%[a]	pH	F/%
Fe^{3+}	1.73	0.024	0.075	11.7	97.3
Cu^{2+}	1.82	0.0061	0.078	12.0	96.4
Ni^{2+}	1.72	0.0138	0.173	11.6	97.3
			Concn of SPA / wt%	pH[b]	
Fe^{3+}	1.93	0.0186	0.0031	8.2	93.8
Cu^{2+}	1.74	0.0153	0.0052	9.8	98.0
			Concn of SCMC / wt%	pH[b]	
Fe^{3+}	1.73	0.020	0.0139	9.1	98.4
Cu^{2+}	1.79	0.0153	0.0100	9.5	99.2
			Concn of SAlg / wt%	pH[b]	
Fe^{3+}	1.80	0.0182	0.0082	9.0	99.0
Cu^{2+}	1.81	0.0622	0.0005	9.1	98.6
			Concn of SCHP / wt%	pH[c]	
Fe^{3+}	1.77	0.0548	0.0327	1.8	91.7

a) Addition of 0.0008 wt% SPA. b) Addition of NH_3. c) Addition of HCl.

Table 1.

The floatabilities are 97 to 99% for most systems in the alkaline region, except for the Fe^{3+}–SCHP–HTAC system, which gave a maximum floatability of 91% at pH 1.7.

The tentative molecular model of the sublate containing metallic ions, for instance Fe^{3+} ions, is indicated in Fig. 9, except for the Fe^{3+}–SCHP–HTAC system. This model is the generalized reproduction of what has been proposed in the previous paper.[1] In Fig. 9, macromolecular anions take up both HTAC and metallic cations, and HTAC catches bubbles. The metallic ions are presumably in the state of large metallic hydroxide aggregates carrying a few residual positive charges. In the case of the Fe^{3+}–SCHP–HTAC system, simple Fe^{3+} ions are considered to combine with cyclo-hexaphosphate ions. Thus macromolecular ions or polymer ions in general are confirmed to be effective for the flotation of metallic cations such as Fe^{3+}, Cu^{2+}, and Ni^{2+} ions, as well as for the flotation of MnO_4^- ions already reported.[1]

The authors wish to thank the Ministry of Education, Science and culture for the financial support granted for this research.

References

1) I. Takayanagi, K. Kobayashi, K. Hachisuka, and T. Sasaki, *Bull. Chem. Soc. Jpn.*, **49**, 2419 (1976).

2) T. Sasaki, K. Matsubara, and I. Machida, *Bull. Chem. Soc. Jpn.*, **54**, 3153 (1981).

The Effect of Added NaCl on the Binding of Sodium Perfluorooctanoate to Lysozyme in Aqueous Solutions

Kohsuke FUKUSHIMA,* Gohsuke SUGIHARA, Yoshio MURATA, and Mitsuru TANAKA
Department of Chemistry, Faculty of Science, Fukuoka University, Fukuoka 814-01
(Received March 11, 1982)

The binding isotherms of sodium perfluorooctanoate (SPFO) to lysozyme have been investigated as a function of added NaCl by a potentiometric method utilizing a perfluorooctanoate ion selective electrode. The general feature of the binding of SPFO to lysozyme resembled that of sodium dodecyl sulfate. Although the lysozyme–SPFO system is different in detail from that of lysozyme–sodium dodecyl sulfate system, resulting from the mutual phobicity and the difference in hydrophobicity, the binding mechanism proposed for lysozyme–sodium dodecyl sulfate system can be true also for the binding of SPFO to lysozyme.

The investigations on the interaction of surfactants with proteins have so far been restricted to hydrocarbon surfactants. Fluorocarbon surfactants have been extensively investigated on their physicochemical properties in aqueous solutions,[1–6] and are interesting with respect to the nonideality in mixed micelles with hydrocarbon surfactants.[7–11] The surface activities of fluorocarbon surfactants are stronger than that of the hydrocarbon surfactant with corresponding carbon number. The binding of fluorocarbon surfactants to protein is expected to be the same as that of hydrocarbon surfactants. In the previous paper,[12] the effects of added NaCl on the initial binding ($\bar{\nu}<10$) and the subsequent binding ($\bar{\nu}\geq 10$) of sodium dodecyl sulfate (SDS) to lysozyme were discussed separately. It is interesting to know whether the binding mechanism proposed in the previous paper can be applied to the binding of a fluorocarbon surfactant to lysozyme.

In this work, the binding isotherms of SPFO to lysozyme were determined at different NaCl concentrations. The effect of added NaCl on the binding of SPFO was examined for comparison with that of SDS.

Experimental

Perfluorooctanoic acid (HPFO) was purchased from PCR Research Chemicals, Inc., Lot No. 4764. HPFO was recrystallized four times from distilled carbon tetrachloride. Solutions of the sodium salt (SPFO) were prepared by neutralization with sodium hydroxide. The purity of SPFO was checked by surface-tension measurements below and above the CMC. No minimum was observed. The solutions of hen egg-white lysozyme and other chemicals were the same as mentioned in previous papers.[12,13] The binding isotherms were made by means of potentiometry as described in the previous paper.[12] The carrier used in the SPFO-selective electrode was prepared by mixing equivalent amounts of SPFO and dimethyldioctadecylammonium chloride (Kaō Soap Co., Ltd.) in water. The resulting milky white precipitates (dimethyldioctadecylammonium perfluorooctanoate) were collected by centrifugation (3500 min^{-1} for 45 min) and resuspended in distilled water. Decantation was repeated twice and followed by recrystallization from acetone. The preparation of the poly(vinyl chloride) gel membrane is essentially the same as mentioned in the paper by Shirahama *et al.*[14]

All measurements were carried out at pH 5.8 and 25 °C. NaCl concentrations were 10, 20, 50, and 100×10^{-3} mol dm^{-3}. Every calibration curve of the electromotive force (emf) of SPFO in respective NaCl solutions showed good linearity in the concentration range 2×10^{-4} mol dm^{-3} to its CMC, and gave a slope close to the Nernstian response (56.2 ± 0.7 mV per decade change in perfluorooctanoate ion, PFO^-, at 25 °C).

In order to examine the accuracy of each emf value for the sample solution, emf's for several SPFO solutions of known concentration were also measured after measurments of the three sample solutions.

Results and Discussion

The equilibrium concentration of SPFO in the initial binding region ($\bar{\nu}<10$) increased with increasing NaCl concentration, as is shown in Fig. 1. On the other hand, the equilibrium SPFO concentration in the subsequent binding ($\bar{\nu}\geq 10$) decreased with increasing NaCl concentration. These tendencies were also seen in the binding of SDS in NaCl solutions. The flat region where $\bar{\nu}$ is kept at about 10 in Fig. 1 becomes narrower with increasing NaCl concentration as was seen in the case of SDS. It should be noted that the initial binding begins at a concentration higher than that of lysozyme–

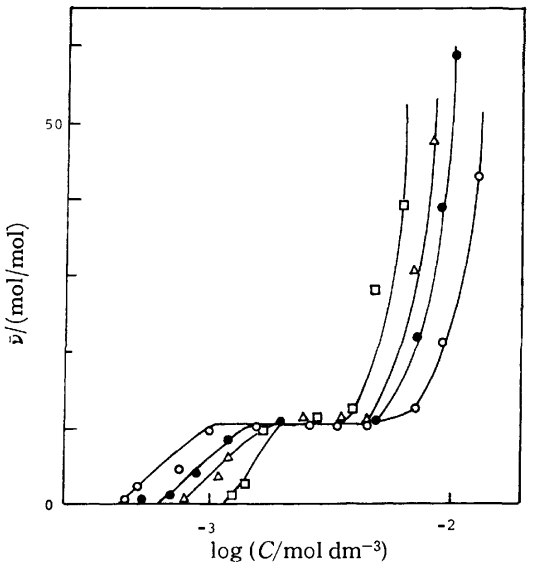

Fig. 1. Binding isotherms of lysozyme–SPFO system at 25 °C and pH 5.8.
$\bar{\nu}$: Binding number, C: equilibrium SPFO concentration, NaCl concentration; ○, 10, ● 20, △ 50, □100 mmol dm^{-3}.

SDS system. Hiramatsu *et al.* reported that the concentration of the initial binding depends on the hydrocarbon chain length of the surfactants for systems of bovine plasma albumin and cationic surfactants; the longer is the chain length, the lower the concentration of the initial binding.[15] Precipitation of lysozyme takes place when the binding begins, and it disappeares with further binding. The general feature of the binding of SPFO to lysozyme resembles that of SDS. So, the analysis of the binding isotherms can be made along a similar line to that discussed in the previous paper.[12]

The free energy difference of PFO^- ion between the states of the initial and final point of the flat region in Fig. 1, where $\bar{\nu}$ could be kept at 10, has been considered to be the free energy accumulation for the subsequent binding. This value (ΔG_{f-i}) is expressed as follows:

$$\Delta G_{f-i} = RT \ln \frac{a_f}{a_i} \simeq RT \ln \frac{C_f}{C_i}, \quad (1)$$

where a_i and a_f are the activities of the PFO^- ions in solution at the initial and final points of the region, respectively, and C_i and C_f are the respective equilibrium SPFO concentrations. The results obtained from Eq. 1 are shown in Fig. 2 together with the results obtained for lysozyme-SDS system. ΔG_{f-i}'s are larger than those of the lysozyme–SDS system in the concentration range of NaCl studied. It may be suggested that both the surface of the complex of lysozyme-PFO^- and singly dispersed PFO^- are less hydrophobic than that of the lysozyme-DS^- complex at a binding number just exceeding 10 and singly dispersed DS^- ion.

The plots of log $C_{\bar{\nu}}$ *vs.* log [Na^+] are given in Fig. 3. $C_{\bar{\nu}}$ and [Na^+] represent the equilibrium SPFO concentration where $\bar{\nu}$ ions of PFO^- are bound to a lysozyme molecule and total Na^+ ion concentration originating from NaCl and SPFO, respectively. The plot of log $C_{0.5}$ *vs.* log [Na^+] gives a straight line with positive slope o 0.3. At present, it is difficult to explain the meaning of the difference between 0.5 for SDS and 0.3 for SPFO. Nevertheless it is certain that the exchange between Cl^- and PFO^- ions and the binding of PFO^- ion to the positively charged sites take place simultaneously as in the case of SDS binding.[12]

According to the discussion in the previous paper,[12] the equilibrium surfactant concentration giving the binding number just exceeding 10 was considered to be the characteristic concentration of protein-ionic surfactant interaction. As is shown in Fig. 1, this concentration (C_{10}) seems to be independent of NaCl concentration. This result agrees with that of the lysozyme-SDS system discussed in the previous paper.[12] C_{10} for the lysozyme-SPFO system (4.8×10^{-3} mol dm^{-3}) is larger than that of the lysozyme–SDS system (2.9×10^{-4} mol dm^{-3}), corresponding to the large CMC in pure water (3.2×10^{-2} mol dm^{-3} at 25 °C) compared with that of SDS (8.2×10^{-3} mol dm^{-3} at 25 °C). Since the driving force for subsequent binding exceeding 10 is mainly hydrophobic interaction as described in the previous paper, C_{10} may be regarded as the concentration where SPFO molecule begins to form hemimicelles on the surface of the lysozyme. Thus there may exist a certain correlation between C_{10} and CMC. The differences between C_{10} and CMC of SPFO and of SDS are about 1 and 1.5 logarithmic units, respectively. The difference is a measure of the binding affinity, *i.e.*, the larger difference means easier binding to the complex compared with self-association (micelle formation) in bulk water. The smaller difference of SPFO means that the affinity between SPFO molecules and the lysozyme-PFO^- complex is smaller than that of the lysozyme-DS^- complex. PFO^- ions on the surface of lysozyme-PFO^- complex at C_{10} are more loosely interacting with each other and with hydrophobic part of lysozyme molecule than DS^- ions on the surface of lysozyme-DS^- complex at C_{10}, because of the shortness of hydrophobic part and mutual phobicity between fluorocarbon and hydrocarbon of lysozyme.[7-11] In other words, less hydrophobicity of lysozyme-PFO^- complex at C_{10} will be responsible for small difference between C_{10} and CMC, and large ΔG_{f-i}.

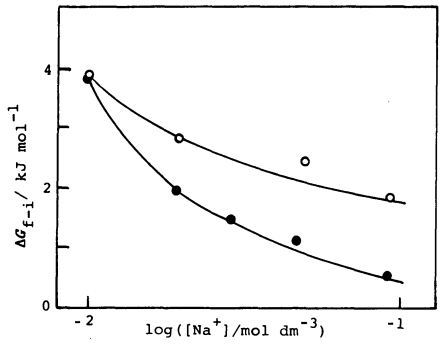

Fig. 2. ΔG_{f-i} *vs.* log [Na^+] plots evaluated from Eq. 1.
○: SPFO, ●: SDS.

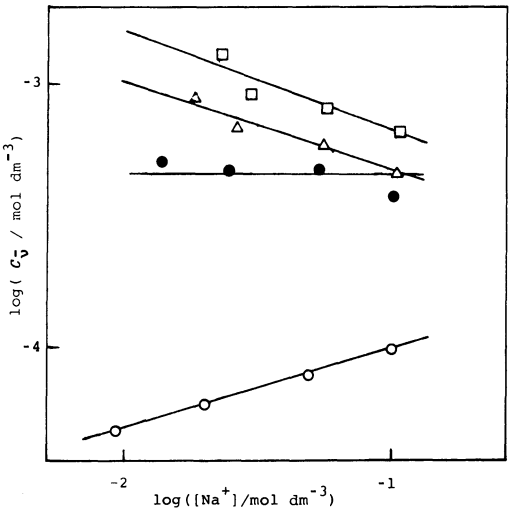

Fig. 3. log $C_{\bar{\nu}}$ *vs.* log [Na^+] plots.
$C_{\bar{\nu}}$: Equilibrium SPFO concentration at binding number $\bar{\nu}$, $\bar{\nu}$: ○0.5, ● 10, △17, □ 40.

Plots of log C_{17} and C_{40} *vs.* log [Na^+] give straight lines with negative slopes, as is shown in Fig. 3. The standard free energy change of the micelle formation from the phase separation model is expessed as

$$\Delta G^\circ/RT = \ln X_{CMC} + \beta \ln X_{Na^+}, \quad (2)$$

where X_{f-i} and X_{Na^+} are the mole fractions of the

surfactant and Na^+ ion in the intermiceller solution at CMC, respectively, and β is the binding number of Na^+ ions per surfactant molecule in micelle.[16] As discussed in the previous paper,[12] the intercept and slope of the straight line in the plot of ln $X_{\bar{\nu}}$ *vs.* ln X_{Na^+} will give $\Delta G^\circ_{\bar{\nu}}$ and β, where $\Delta G^\circ_{\bar{\nu}}$ is the difference between the standard Gibbs free energy of a mole of monomeric hydrated PFO^- ion with β counterion and that of a mole of PFO^- ion with β counterion bound to the complex, and $X_{\bar{\nu}}$ is the mole fraction of DS^- ion in solution at the binding number $\bar{\nu}$. Equation 2 can be applied to the plots of log $C_{\bar{\nu}}$ *vs.* log $[Na^+]$, if the common logarithmic concentration in mol dm^{-3} is converted into the natural logarithmic mole fraction. The results obtained by applying Eq. 2 to the plots in Fig. 3 are listed in Table 1 together with the data for the SPFO micelle itself. The β increases with increasing binding number and seems to approach the value of the micelle. $\Delta G^\circ_{\bar{\nu}}$'s are equal to ΔG° of SPFO micelle formation. These behaviors have also been seen in the lysozyme–SDS system. These suggest that the surface of lysozyme is also covered with PFO^- ions, likewise the lysozyme–DS^- complex, although the lysozyme–SPFO system is different in detail from that of lysozyme–SDS system, resulting from the mutual phobicity and the difference in hydrophobicity. The binding mechanism proposed for lysozyme–SDS system is also concluded to be true for the binding of SPFO to lysozyme.

Table 1. Thermodynamic parameters

$\bar{\nu}$	β	ΔG°/kJ mol^{-1}
17	0.35	−29
40	0.40	−29
Micelle[6]	0.55	−29

References

1) M. K. Bernett and W. A. Zisman, *J. Phys. Chem.*, **63**, 1911 (1959).
2) N. Muller and H. Simsohn, *J. Phys. Chem.*, **75**, 942 (1971).
3) K. Shinoda, M. Hatō, and T. Hayashi, *J. Phys. Chem.*, **76**, 909 (1972).
4) I. J. Lin, *J. Phys. Chem.*, **76**, 2019 (1972).
5) Th. F. Tadros, *J. Colloid Interface Sci.*, **74**, 196 (1980).
6) G. Sugihara and P. Mukerjee, *J. Phys. Chem.*, **85**, 1612 (1981).
7) P. Mukerjee and A.Y. S. Yang, *J. Phys. Chem.*, **80**, 1388 (1976).
8) K. J. Mysels, *J. Colloid Interface Sci.*, **66**, 331 (1978).
9) N. Funasaki and S. Hada, *J. Colloid Interface Sci.*, **72**, 425 (1980).
10) K. Shinoda and T. Nomura, *J. Phys. Chem.*, **84**, 365 (1980).
11) P. Mukerjee and T. Handa, *J. Phys. Chem.*, **85**, 2298 (1981).
12) K. Fukushima, Y. Murata, G. Sugihara, and M. Tanaka, *Bull. Chem. Soc. Jpn.*, **55**, 1376 (1982).
13) K. Fukushima, Y. Murata, N. Nishikido, G. Sugihara, and M. Tanaka, *Bull. Chem. Soc. Jpn.*, **54**, 3122 (1981).
14) K. Shirahama, H. Yasuda, and S. Sugimoto, *Bull. Chem. Soc. Jpn.*, **54**, 375 (1981).
15) K. Hiramatsu, C. Ueda, K. Iwata, K. Arikawa, and K. Aoki, *Bull. Chem. Soc. Jpn.*, **50**, 368 (1977).
16) M. Tanaka, "Ōyo Colloid Kagaku," ed by R. Matuura and T. Kondo, Hirokawa Publishing Co., Tokyo (1969), p. 205.

Motion of Methylammonium Ions in Solid $CH_3NH_3NO_3$ and CH_3NH_3SCN Studied by ^1H NMR

Hiroyuki Ishida, Ryuichi Ikeda,* and Daiyu Nakamura
Department of Chemistry, Faculty of Science, Nagoya University, Chikusa-ku, Nagoya 464
(Received April 2, 1982)

The proton spin-lattice relaxation time T_1 at 20 MHz and the second moment of ^1H NMR absorptions at 40 MHz were determined at various temperatures between 77 and 300 K for $CH_3NH_3NO_3$ and CH_3NH_3SCN, and their partially deuterated analogs, $CH_3ND_3NO_3$ and CH_3ND_3SCN. A phase transition was located at 242 K for CH_3NH_3SCN. The fully protonated compounds yielded two T_1 minima, the low- and high-temperature one of which could be attributed to the reorientation of the CH_3 and NH_3^+ groups, respectively, of the cation about the C–N bond axis. The activation energy was evaluated for these motional modes.

The motion of methylammonium (MA) ions in crystals has been extensively studied for methylammonium halides[1–7] and hexahalometallates(IV)[8,9] by means of ^1H NMR experiments. From these works, it became evident that the motional modes responsible for the ^1H nuclear spin-lattice relaxation time T_1 observed below room temperature are usually the reorientations of the cation about the C–N bond axis. Two kinds of such reorientations are considered to be possible. The first one is the correlated reorientation of the CH_3 and NH_3^+ groups in the cation, *i.e.*, the reorientation of the cation as a whole about its C_3 axis with keeping its rigid structure. We already observed this kind of motion in the crystals of $(MA)_2MX_6$ (M: Pt, Sn, Te; X: halogens)[8,9] where the interionic potential barrier experienced by the cation for the reorientation is smaller than the intraionic one. Another kind of the motion is the uncorrelated reorientation of the CH_3 and NH_3^+ groups. This was observed, *e.g.*, for (MA)Cl in which crystal the interionic potential barrier is known to exceed the intraionic one.[1–5]

From the size and shape of the anions, methylammonium nitrate and thiocyanate are thought to form crystals, in which the motion of the cations is expected to be hindered from an intermediate interionic potential barrier between those of the chloride and the hexahalometallates(IV). Accordingly, it is interesting to investigate the motion of the cation in these crystals by use of the ^1H NMR methods.

Experimental

Continuous wave ^1H NMR spectra were recorded by means of a JEOL JNM-MW-40S spectrometer operated at 40 MHz. A home-made pulsed NMR spectrometer described elsewhere[10] was employed to determine the T_1 values of ^1H nuclei at 20 MHz. The experiments of differential thermal analysis (DTA) were carried out in order to detect possible phase transition in the crystal of (MA)SCN by use of an apparatus reported previously.[11] Sample temperatures were determined by use of a copper-constantan thermocouple in each of these experiments.

Methylammonium nitrate was prepared by mixing an aqueous solution of methylamine and dilute nitric acid. Methylammonium thiocyanate was synthesized after the method described in the literature.[12] The crystals obtained were purified by repeated recrystallizations from absolute ethanol, twice for the nitrate and three times for the thiocyanate. Partially deuterated compounds, $CH_3ND_3NO_3$ and CH_3ND_3SCN were prepared by dissolving (MA)NO_3 and (MA)SCN, respectively, in heavy water. The extent of deuteration was estimated for both compounds to be more than 95% from the analysis of the infrared spectra. Since all the compounds studied are very hygroscopic, they were handled in a dry bag and placed in glass ampouls. Then, the ampouls filled with helium were sealed off after evacuating for 8 hours to remove a trace of water or solvent involved.

Results and Discussion

The second moment M_2 of ^1H NMR absorptions was determined at various temperatures between 77 and 300 K for (MA)NO_3 and (MA)SCN. The temperature dependences of the observed M_2 values are shown in Fig. 1.

Below 120 K, the almost constant M_2 values of 23 and 26 G^2 were obtained for (MA)NO_3 and (MA)SCN, respectively. With increasing temperature, a new plateau value of *ca.* 8 G^2 was reached for both compounds above 150 K and it continued up to room temperature. The theoretical M_2 values have been calculated for several motional modes of the cation[1,2] and reported to be 30, 19, and 8 G^2 for the rigid cation, for the C_3 reorienting CH_3 groups with rigid NH_3^+ ones, and for both groups reorienting about the C–N bond

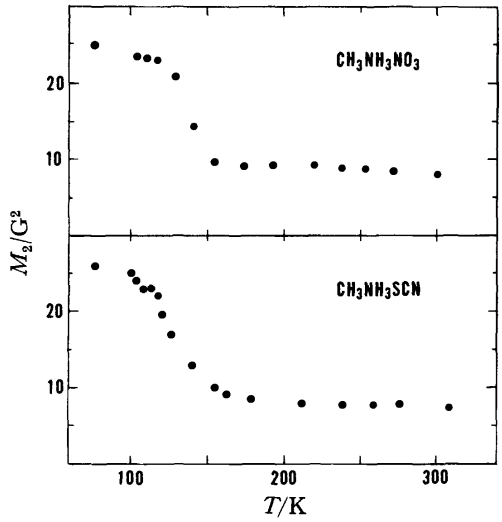

Fig. 1. Temperature dependences of the second moment M_2 of ^1H NMR absorptions for $CH_3NH_3NO_3$ and CH_3NH_3SCN.

axis, respectively. Although the exact interionic M_2 values of these compounds could not be calculated because of the lack of the crystal-structure data, they could be roughly estimated by referring to the data of (MA)Cl.[1] The resultant M_2 values including the interionic ones amount to 38, 23, and 9 G^2 for the three motional states described above in the same order. Comparing the observed and calculated values, the plateau value of M_2 obtained below 120 K for the two compounds can be interpreted in terms of the reorientation of the CH_3 groups alone, and the second plateau obtained above 150 K in terms of the reorientation of both CH_3 and NH_3^+ groups. These results indicate that the CH_3 group of the cation is quite free to reorient in the temperature range, 77—300 K. This is supported from the fact that the partially deuterated analog

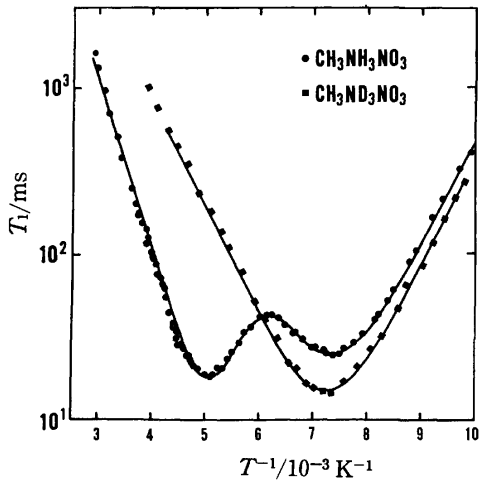

Fig. 2. Temperature dependences of T_1 values determined at 20 MHz for $CH_3NH_3NO_3$ and $CH_3ND_3NO_3$. The full lines are theoretical curves calculated in the manner described in the text.

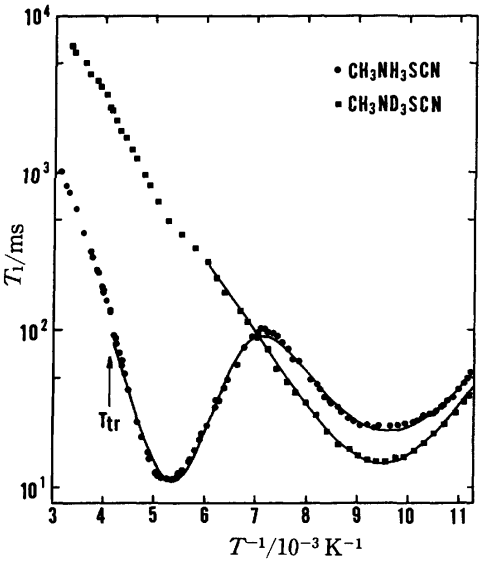

Fig. 3. Temperature dependences of T_1 values observed at 20 MHz for CH_3NH_3SCN and CH_3ND_3SCN. The full lines are theoretical curves calculated in the manner described in the text.

CH_3ND_3SCN yielded the M_2 value of 7.4 G^2 at 77 K. This value is very close to 6.3 G^2 which is calculated for the partially deuterated cation having the reorienting CH_3 group.[5]

The values of T_1 observed at various temperatures for the nitrates and the thiocyanates are shown in Figs. 2 and 3, respectively. The fully protonated nitrate exhibited two considerably well-separated T_1 minima, 24 and 18 ms at *ca.* 135 and 198 K, respectively. Its partially deuterated analog $CH_3ND_3NO_3$, on the other hand, yielded a single minimum of 14 ms at 137 K. Two well-separated T_1 minima, 24 and 11 ms were observed at *ca.* 105 and 192 K, respectively, for CH_3NH_3SCN, while a single minimum of 14.5 ms at *ca.* 105 K was obtained for CH_3ND_3SCN.

The observed T_1 curves can be analyzed by assuming the magnetic dipolar relaxation mechanism formulated by the following BPP equation[13]

$$T_1^{-1} = C[\tau/(1+\omega^2\tau^2) + 4\tau/(1+4\omega^2\tau^2)], \quad (1)$$

where C, τ, and ω denote a constant depending on a motional mode in question, the correlation time of the motion, and an angular resonance frequency, respectively. The correlation time can be related to the activation energy E_a for the motion by assuming the Arrhenius relationship,

$$\tau = \tau_\infty \exp(E_a/RT). \quad (2)$$

Here, τ_∞ and R denote the correlation time at the infinite temperature and the gas constant, respectively.

From the experimental results of T_1 and the foregoing discussion on the ^{1}H NMR second moment, it is evident that the T_1 minimum observed at the lower temperature in each of the fully protonated salts is attributable to the CH_3 reorientation about its C_3 axis, while that at the higher temperature to the NH_3^+ reorientation. The single T_1 minimum observed for the partially deuterated analogs can be naturally attributed to the CH_3 reorientation. For the T_1 curve of CH_3ND_3SCN, a shoulder appeared at *ca.* 200 K. This seems to be another minimum resulting from the incomplete deuteration of the NH_3^+ group in our experiments.

On the high-temperature side of each T_1 minimum, both of $CH_3NH_3NO_3$ and CH_3NH_3SCN showed somewhat nonexponential behavior on the free-induction decay signals plotted against the interval time between the 180° and 90° pulses. This seems to be explainable by the theory of symmetry-restricted spin diffusion by Emid *et al.*[14] When the nonexponential relaxation behavior was observed, the experimental T_1 values were evaluated from the initial linear portion of the recovery of the ^{1}H nuclear magnetization observed after the 90° pulse.

The temperature dependence of T_1 values determined for the thiocyanate showed a small T_1 jump at 242 K. The partially deuterated analog, CH_3ND_3SCN also exhibited a discontinuity in the temperature coefficient of the T_1 curve at 250 K. These experimental facts suggest the existence of a phase transition in these compounds. In fact, the measurements of DTA gave rise to a thermal anomaly for each compound at the same temperature as the T_1 anomaly was observed. Since no thermal hysteresis was observed, these anomalies

TABLE 1. THE ACTIVATION ENERGY E_a AND THE CORRELATION TIME τ_∞ FOR THE CH_3 AND NH_3^+ REORIENTATIONS OF METHYLAMMONIUM NITRATE AND THIOCYANATE

Compound	Reorientational mode	E_a/kJ mol^{-1}	τ_∞/s
$CH_3NH_3NO_3$	CH_3	11.7	1.5×10^{-13}
	NH_3^+	20.0	2.6×10^{-14}
$CH_3ND_3NO_3$	CH_3	12.2	1.2×10^{-13}
CH_3NH_3SCN			
High temp phase	NH_3^+	17.0	—
Low temp phase	CH_3	8.2	3.6×10^{-13}
Low temp phase	NH_3^+	19.9	1.3×10^{-14}
CH_3ND_3SCN			
High temp phase	CH_3	8.3	—
Low temp phase	CH_3	8.9	1.9×10^{-12}

are attributable to a second or higher-order phase transition. Because the transition temperature was observed to be shifted by as much as 8 K on the deuteration of the NH_3^+ group, it is anticipated that the NH_3^+ group plays an important role on the mechanism of the phase transition revealed.

When the reorientation of the CH_3 and NH_3^+ groups about the C–N bond axis is assumed to take place independently of each other, the resultant T_1 value arising from these two relaxation processes can be expressed by

$$T_1^{-1} = \frac{1}{2}[T_1^{-1}(CH_3) + T_1^{-1}(NH_3^+)], \quad (3)$$

where $T_1(CH_3)$ and $T_1(NH_3^+)$ are the relaxation times for the CH_3 and NH_3^+ reorientations, respectively, and are given by Eq. 1. The unknown parameters E_a, τ_∞, and C for the reorientations of these two groups were calculated by a least-squre fitting of Eq. 3 to the observed T_1 curves. The calculation was performed at the computation center of Nagoya University by used of the computer program SALS.[15] The values of E_a and τ_∞ thus calculated for the CH_3 and NH_3^+ reorientations are given in Table 1.

The E_a values obtained for both groups in the nitrate are greater than 8 kJ mol^{-1} which is the E_a value evaluated previously for the internal rotation of the methylammonium cation.[8,9] This means that not only the intraionic potential barrier but also the interionic one is responsible for the present E_a values. For the CH_3 reorientation, the fully and partially protonated thiocyanates yielded the E_a values of 8.2 and 8.9 kJ mol^{-1}, respectively. The fact that these E_a values are very close to that for the internal rotation of the cation, indicates that the barrier hindering the CH_3 reorientation originates almost from the intraionic interaction and the interionic contribution is quite small in this case. For the NH_3^+ reorientation, on the other hand, the thiocyanate gave rise to fairly large E_a values of 19.9 and 17.0 kJ mol^{-1} in the low- and the high-temperature phases, respectively, indicating the existence of interionic interaction, probably, considerably strong hydrogen bonding.

This work was supported by a Grant-in-Aid for Scientific Research No. 00543006 from the Ministry of Education, Science and Culture.

References

1) J. Tsau and D. F. R. Gilson, *Can. J. Chem.*, **48**, 717 (1970).
2) E. A. Andrew and P. C. Canepa, *J. Magn. Reson.*, **7**, 429 (1972).
3) J. Tegenfeldt and L. Ödberg, *J. Phys. Chem. Solids*, **33**, 215 (1972).
4) J. Tegenfeldt, T. Keowsim, and C. Säterkvist, *Acta Chem. Scand.*, **26**, 3524 (1972).
5) S. Albert and J. A. Ripmeester, *J. Chem. Phys.*, **58**, 541 (1973).
6) H. Ishida, R. Ikeda, and D. Nakamura, *Phys. Status Solidi A*, **60**, K115 (1980).
7) H. Ishida, R. Ikeda, and D. Nakamura, *J. Phys. Chem.*, **86**, 1003 (1982).
8) R. Ikeda, Y. Kume, D. Nakamura, Y. Furukawa, and H. Kiriyama, *J. Magn. Reson.*, **24**, 9 (1976).
9) Y. Furukawa, H. Kiriyama, and R. Ikeda, *Bull. Chem. Soc. Jpn.*, **54**, 103 (1981).
10) L. S. Prabhumirashi, R. Ikeda, and D. Nakamura, *Ber. Bunsenges. Phys. Chem.*, **85**, 1142 (1981).
11) Y. Kume, R. Ikeda, and D. Nakamura, *J. Magn. Reson.*, **33**, 331 (1979).
12) M. W. Partridge and W. F. Short, *J. Chem. Soc.*, **1947**, 390.
13) N. Bloembergen, E. M. Purcell, and R. V. Pound, *Phys. Rev.*, **73**, 679 (1948).
14) S. Emid, R. J. Baarda, J. Smidt, and R. A. Wind, *Physica*, **93B**, 327 (1978).
15) T. Nakagawa and Y. Koyanagi, Program library in the computation center of Nagoya University, code number 466.

 © 1982 The Chemical Society of Japan Bull. Chem. Soc. Jpn., 55, 3119—3122 (1982)

Multiatomic Ion Model for Interdiffusion in the System Na_2O-CaO-SiO_2

Masao NANBA, Yasumichi OISHI,* and Hajimu WAKABAYASHI†
Department of Nuclear Engineering, Kyushu University, Higashi-ku, Fukuoka 812
†*Government Industrial Research Institute, Osaka, Midorigaoka, Ikeda, Osaka 563*
(Received May 4, 1982)

Concentration distributions after interdiffusion at 1200 °C were analysed for the diffusion couple of average composition $16Na_2O \cdot 12CaO \cdot 72SiO_2$ (wt%) in terms of self-diffusion coefficients of constituent elements. Theoretical calculation was conducted using a multiatomic ion model assuming that Si migrates with oxygens as a silicate ion. The composition of the silicate ion was estimated by determining the parameters in the diffusion equation so as to provide the best fit of the theoretical calculations to the experimental concentration profiles.

In spite of its scientific and technological importance,[1,2] the interdiffusion mechanism of liquid silicates has not been thoroughly clarified because of the structural complexity of ionic solutions. Another reason is due to insufficient thermodynamic and self-diffusion data necessary for the analysis of interdiffusion. With respect to the diffusion data, a system CaO-Al_2O_3-SiO_2 is the only multioxide liquid for which tracer diffusion coefficients of all the constituent elements are known.[3] For the present system Na_2O-CaO-SiO_2, tracer diffusion coefficients of sodium,[4] calcium,[5,6] and oxygen[7] are known but that of silicon has not been determined as yet.

In Wakabayashi and Oishi's analysis of liquid-state interdiffusion in the system Na_2O-CaO-SiO_2,[8] simple application of the monoatomic diffusion model did not satisfactorily describe the concentration distribution but the assumption of two different oxygen species with different diffusivities gave theoretically calculated concentration distribution agreeable with the experimental results. They interpreted that the fast and slow oxygen species correspond to the non-bridging and bridging oxygens, respectively. A non-bridging-oxygen controlled mechanism was also discussed for dissolution of solid SiO_2 in liquid $Na_2O \cdot 3SiO_2$ by Barklage-Hilgefort and Frischat.[9] In these two papers, the diffusion coefficient of the fast, not the whole, oxygen is assumed to be equal to that obtained by the tracer technique. In the tracer technique, however, the oxygen diffusion coefficient was calculated on the assumption that all the oxygen atoms are equally capable of undergoing isotope exchange. This contradiction is dissolved in the present work by interpreting the tracer diffusion coefficient as the average of self-diffusion coefficients of the fast and slow oxygen species.[10] This interpretation implies that the constituent element N of compound M_mN_n diffuses not only as monoatomic ion N^{m-}, but also as neutral undissociated molecule M_mN_n or as ion pair $M^{n+}N^{m-}$; tracer diffusion coefficient D_N^* is expressed as the weighted average of the self-diffusion coefficients of those diffusing species, as described by Eq. 1,

$$D_N^* = y_1 D_{N_1} + y_2 D_{MN} + y_3 D_0, \quad (1)$$

where y_1, y_2, and y_3 represent the single-atomic fractions of element N, shared by N^{m-}, $M^{n+}N^{m-}$, and M_mN_n, respectively, and D_{N_1}, D_{MN}, and D_0 the self-diffusion coefficients of diffusing species N^{m-}, $M^{n+}N^{m-}$, and M_mN_n, respectively.

In the analysis[10] of the interdiffusion in liquid system CaO-Al_2O_3-SiO_2, theoretical calculation of the diffusion profiles showed good agreements with the experimental results in the case where the oxygen tracer diffusion coefficient defined as Eq. 1 was employed for a multiatomic ion model, in which the composition of the silicate ion was described in terms of unknown structure parameters. This analytical procedure was used in the present work to examine its applicability to the liquid interdiffusion of the system Na_2O-CaO-SiO_2. Since the Si self-diffusion coefficient in the system Na_2O-CaO-SiO_2 has not been determined, though those of three other elements are known, the self-diffusion coefficients of the fast and slow oxygens can not be determined only from the structure parameters of the silicate ion, as was the case in the system CaO-Al_2O_3-SiO_2. Consequently, the self-diffusion coefficient of the fast oxygen was also described with the aid of a new unknown parameter in the theoretical calculation of the diffusion profiles.

The flux density equation necessary for analysis of the present interdiffusion was derived in terms of self-diffusion coefficients of the constituent ions from Nernst-Haskel's equation modified with the mass flow term as defined by Darken.[11] The system Na_2O-CaO-SiO_2 is understood to be thermodynamically nonideal with respect to oxide components. However, instead of describing the non-ideality in terms of the thermodynamic factor, the present analysis of interdiffusion was conducted on the assumption that a nonideal system with respect to oxide components can be treated as an ideal system with respect to actually diffusing units.[10]

Theoretical

Multicomponent Diffusion Equation for Ionic Systems. The flux density of the ith ion can be described as Eq. 2 for chemical diffusion in a thermodynamically ideal ionic multicomponent system,

$$J_i = -D_i \frac{\partial C_i}{\partial x} + C_i v + D_i C_i Z_i \frac{F}{RT} \varepsilon, \quad (2)$$

where J_i is the diffusion flux density, D_i the self-diffusion coefficient, C_i the concentration, Z_i the valence of the ith diffusing species, x the diffusion distance, v the mass flow velocity, F the Faraday constant, R the gas constant, T the absolute temper-

ature, and ε the strength of the electric field resulted from differing diffusivities of various diffusing ions. The conditions of the volume-fixed frame and no electric current resulted are described by Eqs. 3 and 4, respectively,

$$\sum_{i=1}^{r} V_i J_i = 0 \tag{3}$$

$$\sum_{i=1}^{r} Z_i J_i = 0, \tag{4}$$

where V_i is the molar volume of diffusing species i, and r denotes the number of components. Conditions of the electrical neutrality and a constant molar volume of each component with Eqs. 3 and 4 allow to rewrite Eq. 2 in a general equation as Eq. 5,

$$J_i = -\sum_{i=1}^{r-2} M_{ij} \frac{\partial C_j}{\partial x} \qquad (i = 1,2,\cdots, r-2) \tag{5}$$

where the coefficient M_{ij} is given as Eq. 6 as a function of self-diffusion coefficients, concentrations, valences, and molar volumes of the components,

$$\begin{aligned} M_{ij} = {} & D_i\delta_{ij} - \frac{C_i}{(Z_{r-1}V_r - Z_rV_{r-1})\sum_{k=1}^{r} C_kZ_k^2D_k} \\ & \times \{(Z_{r-1}V_r - Z_rV_{r-1})[Z_iZ_jD_i \\ & + \sum_{k=1}^{r} C_kZ_kD_k(Z_kV_j - Z_jV_k)] \times D_j \\ & + (Z_rV_j - Z_jV_r)[Z_iZ_{r-1}D_i \\ & + \sum_{k=1}^{r} C_kZ_kD_k(Z_kV_{r-1} - Z_{r-1}V_k)] \times D_{r-1} \\ & + (Z_jV_{r-1} - Z_{r-1}V_j)[Z_iZ_rD_i \\ & + \sum_{k=1}^{r} C_kZ_kD_k(Z_kV_r - Z_rV_k)] \times D_r\}, \end{aligned} \tag{6}$$

where δ_{ij} is Kronecker's δ.

Diffusing Units and Their Self-diffusion Coefficients.

The self-diffusion coefficient of sodium[4] is greater than those of calcium[5] and oxygen,[7] in the system Na_2O–CaO–SiO_2, and the activation energy for sodium[4] is half of those for calcium[5] and oxygen.[7] These facts suggest that the diffusing unit of sodium is the single-atomic Na^+ ion. The self-diffusion coefficient of calcium is greater than that of oxygen in this system and similar to that of calcium[12] in the system CaO–Al_2O_3–SiO_2 in which the diffusing unit of calcium is interpreted to be the single-atomic Ca^{2+} ion.[10] Based on these facts, the diffusing unit of calcium in this system is assumed to be the single-atomic Ca^{2+} ion. For a simple demonstration of the present diffusion model, a single multiatomic silicate ion is assumed to be the diffusing unit of silicon as the average of various silicate ions which may actually exist in the liquid silicate.[13–15] Since the composition of the present system is rich in SiO_2, the structure model of the silicate ion is described as discrete ion as proposed by Bockris *et al.*[16] Table 1 summarizes the diffusing units and their self-diffusion coefficients assumed in this study. Here, the structure of the silicate ion is described as n-membered r-fold rings of SiO_4 tetrahedra joined at apices. The oxygens composing this silicate ion are the slower oxygen species and the remainders are the faster species, where the concentrations of the two kind of oxygens are given by Eqs. 7 and 8 from the requirement of the number conservation of the total oxygen atoms.

Table 1. DIFFUSING SPECIES AND THEIR SELF-DIFFUSION COEFFICIENTS

Diffusing species	Self-diffusion coefficient
Na^+	D_{Na}*
Ca^{2+}	D_{Ca}*
$Si_{nr}O_{n(2r+1)}^{2n-}$	D_S
O^{2-}	D_F

$$C_{Si} = C_{Si}\left(2+\frac{1}{r}\right) \tag{7}$$

$$C_F = C_O - C_{Si} \tag{8}$$

where C_{Si} represents the concentration of Si atoms and C_{Si}, C_F, and C_O represent concentrations of the slow, the fast, and the total oxygen atoms, respectively.

In Table 1 star-marked self-diffusion coefficients are those determined by the tracer technique, while the self-diffusion coefficients with no mark are defined as follows: The tracer diffusion coefficient of oxygen, D_O*, is the weighted average of self-diffusion coefficients of the slow and fast oxygen species, as described by Eq. 9,

$$D_O^* = \frac{C_{Si}}{C_O} D_S + \frac{C_F}{C_O} D_F \tag{9}$$

where D_S is the self-diffusion coefficient of the slow oxygen, which is the same as that of the silicate ion, and D_F is that of the fast oxygen.

Determination of Parameters for Diffusing Units.

The diffusion couples in the present work were designed with relatively small concentration differences (10 wt%) so that the self-diffusion coefficients of all the diffusing species may be regarded as composition-independent. Consequently, coefficient M_{ij} in Eq. 6 is also regarded as constant and calculated for the average composition of the diffusion couple where the valences of diffusing species are read from Table 1. The molar volumes are so defined that the volume of the system is determined only by the volume of the oxygen atoms, as described by Eq. 10,

$$\begin{cases} V_{Na^+} = V_{Ca^{2+}} = 0 \\ V(Si_{nr}O_{n(2r+1)})/V_{O^{2-}} = n(2r+1) \end{cases} \tag{10}$$

Self-diffusion coefficients of the constituent elements, D_{Na}*,[4] D_{Ca}*,[5] and D_O*[7] are taken from the literature.

Applying the continuity equation to Eq. 5, the analytical solution can be derived as Eq. 12 for the initial and boundary conditions described by Eqs. 11,

$$\begin{cases} C_i = C_{i,A} & x<0,\ t = 0 \\ C_i = C_{i,B} & x>0,\ t = 0 \\ C_i = C_{i,A} & x = -\infty,\ t>0 \\ C_i = C_{i,B} & x = +\infty,\ t>0 \end{cases} \tag{11}$$

where $C_{i,A}$ and $C_{i,B}$ denote the initial concentrations of diffusing species i in the left and right sides of the diffusion couple, respectively.

$$C_i = C_{i,B} + \frac{1}{2}\sum_{j=1}^{r-2}\sum_{k=1}^{r-2} S_{ik}R_{kj}(C_{j,A} - C_{j,B})\,erfc\left(\frac{x}{2\sqrt{\lambda_k t}}\right), \tag{12}$$

where S_{ij}, R_{ij}, and λ_i are the constants given by Eq. 13,[10]

$$\begin{aligned}
\lambda_1 &= \{(M_{11}+M_{22}) + Q\}/2 \\
\lambda_2 &= \{(M_{11}+M_{22}) - Q\}/2 \\
S_{11} &= (M_{11}-M_{22}) + Q \\
S_{12} &= (M_{11}-M_{22}) - Q \\
S_{21} &= S_{22} = 2M_{21} \\
R_{11} &= 1/2Q \\
R_{12} &= \{-(M_{11}-M_{22})+Q\}/4M_{12}Q \\
R_{21} &= -1/2Q \\
R_{22} &= \{(M_{11}-M_{22})+Q\}/4M_{12}Q \\
Q &= \{(M_{11}-M_{22})^2 + 4M_{12}M_{21}\}^{1/2}.
\end{aligned} \tag{13}$$

Theoretical concentration distributions were repeatedly calculated using Eq. 12 for various magnitudes of the parameters until the best fitting to the experimental distributions are attained. The best fitting was carried out by minimizing the objective function F given by Eq. 14,

$$F = [\sum_{i=1}^{3} \sum_{j=1}^{N_i} \{W_i^e(x_j) - W_i^c(x_j)\}^2/3N_i]^{1/2}, \tag{14}$$

where $W_i^e(x_i)$ and $W_i^c(x_j)$ represent the experimentally determined and calculated concentrations (in wt fraction) of oxide component i at diffusion distance x_j, respectively, and N_i denotes the number of the measurements for oxide component i. The experimental concentration distributions were taken from Wakabayashi and Oishi's paper.[8]

Results and Discussion

Figure 1 shows the theoretical concentration distributions (solid curves) calculated by Eq. 12 for the diffusion couple $16Na_2O \cdot 7CaO \cdot 77SiO_2$–$16Na_2O \cdot 17CaO \cdot 67SiO_2$ (wt%) at 1200 °C for diffusion time 4.00 h so as to best fit to the experimental results determined by Wakabayashi and Oishi[8] (plotted). The theoretical calculation is in good agreement with the experimental results. The experimentally determined "up-hill diffusion" of the component Na_2O which had no initial concentration difference has been satisfactorily described by the theoretical calculation of the present diffusion model. The solid curves for theoretical calculations in Fig. 1 were obtained for the self-diffusion coefficient of fast oxygen species, $D_F = 7.54 \times 10^{-8}$ cm²/s, which determined the self-diffusion coefficient of silicate ion as $D_S = 1.37 \times 10^{-8}$ cm²/s.

The theoretical calculation of the diffusion profiles was carried out also for the second diffusion couple $21Na_2O \cdot 7CaO \cdot 72SiO_2$–$11Na_2O \cdot 17CaO \cdot 72SiO_2$, for which Wakabayashi and Oishi determined the diffusion profiles experimentally at 1200 °C for diffusion time 2.00 h. The second diffusion couple was designed with no initial concentration difference in SiO_2 so as to have the same average composition as and a different compositional direction from the first diffusion couple.

The theoretical calculation for the second diffusion couple gave concentration distributions (solid curves) close to the experimental results (plotted), as shown in Fig. 2. However, with respect to the structure parammeter n, its magnitude could not be successfully optimized within the reasonable magnitude range. This

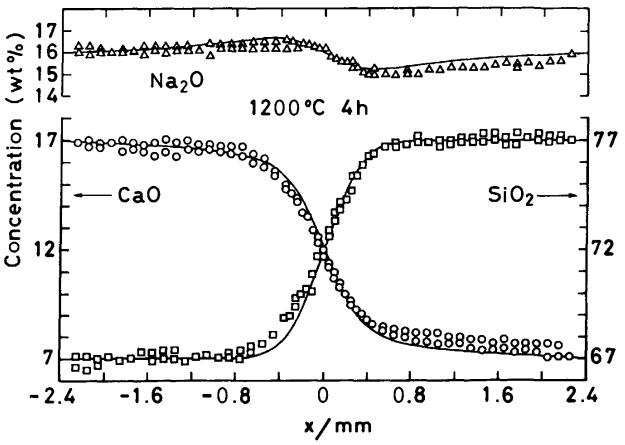

Fig. 1. Theoretical and experimental concentration distributions for the diffusion couple $16Na_2O \cdot 7CaO \cdot 77SiO_2$–$16Na_2O \cdot 17CaO \cdot 67SiO_2$ (wt%).

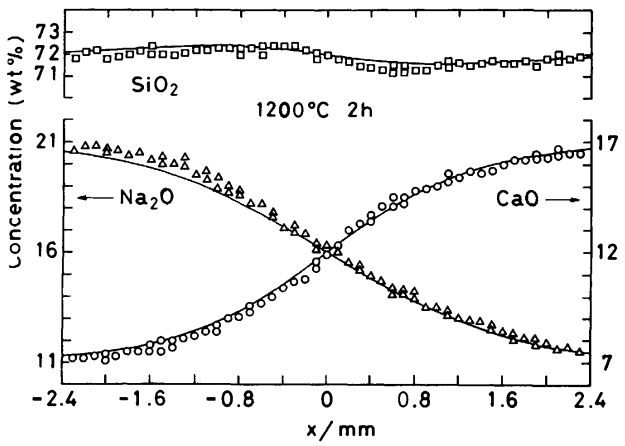

Fig. 2. Theoretical and experimental concentration distributions for the diffusion couple $21Na_2O \cdot 7CaO \cdot 72SiO_2$–$11Na_2O \cdot 17CaO \cdot 72SiO_2$ (wt%).

seems to be due to composition-dependences of the self-diffusion coefficients, the thermodynamical nonideality, or/and the size distribution of the silicate ions, which is suggested by the asymmetrical diffusion profiles.

The authors thank The Asahi Glass Foundation for the Contribution to Industrial Technology for financial support.

References

1) M. Kunugi, H. Jinno, and G. Kanbara, *Mem. Fac. Eng. Kyoto Univ.*, **31**, 356 (1969).
2) Y. Oishi, A. R. Cooper, Jr., and W. D. Kingery, *J. Am. Ceram. Soc.*, **48**, 88 (1965).
3) Y. Oishi, R. Terai, and H. Ueda, "Mass Transport Phenomena in Ceramics," ed by A. R. Cooper and A. H. Heuer, Plenum Press, New York (1974), p. 297.
4) J. R. Johnson, R. H. Bristow, and H. H. Blau, *J. Am. Ceram. Soc.*, **34**, 165 (1951).
5) H. Wakabayashi, *J. Non-Cryst. Solids*, **24**, 427 (1977).
6) R. Terai and E. Okawa, *Yogyo Kyokai Shi*, **85**, 294 (1977).
7) R. Terai and Y. Oishi, *Glastech. Ber.*, **50**, 68 (1977).
8) H. Wakabayashi and Y. Oishi, *J. Chem. Phys.*, **68**, 2046

(1978).
9) H. J. Barklage-Hilgefort and G. H. Frischat, *Phys. Chem. Glasses*, **21**, 212 (1980).
10) Y. Oishi, M. Nanba, and J. A. Pask, *J. Am. Ceram. Soc.*, **65**, 247 (1982).
11) L. S. Darken, *Trans. Metall. Soc. AIME*, **175**, 184 (1948).
12) H. Towers and J. Chipman, *Trans. Metall. Soc. AIME*, **209**, 769 (1957).
13) J. Götz, D. Hoebbel, and W. Wieker, *J. Non-Cryst. Solids*, **20**, 413 (1976).
14) T. Yanagase and Y. Suginohara, *J. Jpn. Inst. Met.*, **33**, 443 (1969).
15) H. Verveij and W. Konijnendijk, *J. Am. Ceram. Soc.*, **59**, 517 (1976).
16) J. O'M. Bockris, J. D. Mackenzie, and J. A. Kitchener, *Trans. Faraday Soc.*, **51**, 1734 (1955).

The Solubility of Ball-milled Amobarbital and the Stability of Its Amorphous State

Akiko IKEKAWA* and Sohachiro HAYAKAWA†

Faculty of Pharmaceutical Sciences, Showa University, Hatanodai, Shinagawa-ku, Tokyo 142

†*Department of Applied Physics, Faculty of Science, Tokyo Institute of Technology, Oh-okayama, Meguro-ku, Tokyo 152*

(Received February 18, 1982)

Amobarbital was ball-milled with methylcellulose (MC), microcrystalline cellulose, or dextran. The analysis of the IR spectra indicated that hydrogen bonds were formed between the C=O groups of amobarbital and the OH groups of the diluents upon ball-milling. It was also shown that formation of the bonds was more predominant with MC than with dextran. After suspensions of various kinds of samples in distilled water had been set aside for a week after the time of preparation, the solid state of the amobarbital remaining undissolved in the suspension was compared with the state before dissolution. There are three kinds of polymorphs for amobarbital: Crystals I, II, and III. Crystal I is given by heating Crystal II (at 150 °C), which has been recrystallized from a 25 v/v% aqueous ethanol solution. Crystal III is given by freeze-drying an aqueous solution. The above comparison suggests that Crystal III and the amorphous part are transformed into Crystal I in the absence of any diluent. It seems that the presence of dextran ball-milled with amobarbital prevents Crystal III from being transformed into Crystal I. The presence of MC ball-milled with amobarbital also seems to prevent both the amorphous part from crystallization and Crystal III from transformation into Crystal I. The solubility of amobarbital in distilled water increased remarkably upon ball-milling with diluents; this was attributed to the stabilization of the amorphous state by the interaction with diluents.

The solubility of amobarbital in distilled water increased upon ball-milling with such diluents as methylcellulose,[1] though the solubility increased only slightly without any diluent.[2] Previously, the effect of ball-milling, both with a diluent and without any diluent, on the solid state of amobarbital was investigated, and the relationship between the solid state and solubility was discussed.[1,2] Consequently, it was suggested that the interaction of amobarbital with diluents was one of the most important reasons for the increase in the solubility.[1] In this paper, the interaction of amobarbital with diluents resulting from ball-milling was investigated, and the influence of the interaction on the solid state was discussed.

Experimental

The materials used were amobarbital (5-ethyl-5-isopentylbarbituric acid), dextran 2000, microcrystalline cellulose (MCC), and methylcellulose (MC), all described in a previous paper.[3]

The following samples were ball-milled in the way described previously;[3] 10 g of commercial powders of amobarbital (AC) dextran or MCC; 5 g of MC; a mixture of 1 g of AC and 9 g of each of the diluents; a mixture of 3 g of AC and 7 g of dextran or MCC; a mixture of 2 g of AC and 3 g of MC. In this paper, the "mixture with dextran" contains 30 w/w% of amobarbital and the "mixture with MC" contains 40 w/w% of amobarbital, when no annotation is given.

Various kinds of samples were prepared as follows.

ACS: A suspension of 1 g of AC in 500 cm^3 of distilled water was stirred for 2 h, allowed to stand at 30 °C for a week, and then filtered. The residue was dried under reduced pressure at 70 °C.

AB: AC was ball-milled for 60 h.

ABS: ABS was prepared from AB in the same way as that used to obtain ACS from AC.

DexAB: A mixture with dextran was ball-milled for 200 h.

DexABS: A suspension of 3 g of DexAB in 500 cm^3 of distilled water was stirred for 2 h, allowed to stand at 30 °C for a week, and then filtered. The residue was washed with an aqueous saturated solution of amobarbital and dried under reduced pressure at 70 °C.

MCAB: A mixture with MC was ball-milled for 100 h.

MCABS: A suspension of 2 g of MCAB in 400 cm^3 of distilled water was stirred for 2 h, allowed to stand at 30 °C for a week, and then centrifuged. The precipitate was washed with an aqueous saturated solution of amobarbital and dried under reduced pressure at 70 °C.

The results of the elemental analysis for ACS, ABS, and DexABS were identical with the results for AC; this fact demonstrated that the amount of dextran contaminating DexABS was negligible. The nitrogen content in MCABS was a little smaller than the content in AC; this finding showed that MC mixed in MCABS because of the low solubility of MC in distilled water. The content of MC in MCABS was presumed to be 7.1 w/w% from the ratio of the content of nitrogen to that of carbon.

The IR spectra and X-ray diffraction diagrams were recorded in the way described previously.[3]

Results and Discussion

IR Spectra. Figures 1, 2, and 3 show the effect of ball-milling on the IR spectra of mixtures of amobarbital, as determined by a KBr method. The absorbances around the 3400, 1300—1450, and 1000—1120 cm^{-1} regions increased upon ball-milling. The bands from 1650—1800 cm^{-1}, corresponding to the stretching vibration of the C=O groups of amobarbital,[4] were also affected by ball-milling. The same trends were also found by a Nujol method. In the IR spectra of cellulose derivatives and dextran, the band around the 3400 cm^{-1} region was assigned to the stretching mode of hydrogen-bonded OH groups,[5] though this band was largely overlapped with the absorption of associated water.[6] Keighley *et al.* reported that the absorbance of the band at 2.92 μm (at 3420 cm^{-1}) was found to be higher by the use of a poly(tetrafluoroethylene) (PTFE) disk method than by the use of a KBr disk method or a nujol method. They suggested that this finding was associated with the formation of hydrogen bonds between the

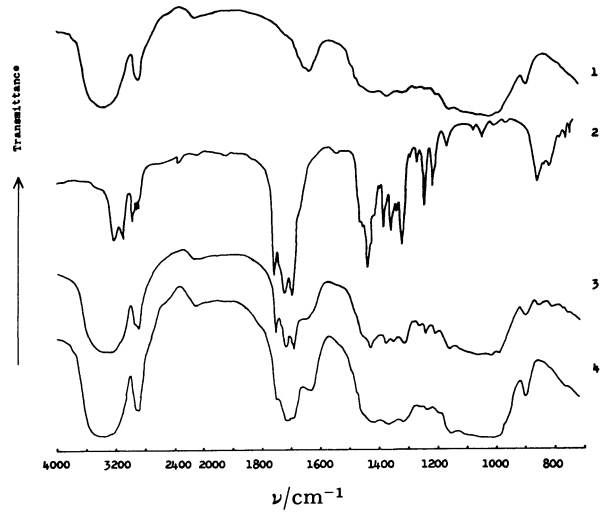

Fig. 1. Effect of ball-milling on IR spectra of the mixture of amobarbital and MCC.
1: MCC ball-milled for 200 h, 2: AB, 3: the mixture of "1" and "2" in the ratio of 9 : 1 by weight, 4: the mixture of 1 g of AC and 9 g of MCC ball-milled for 40 h. The spectra for the mixture ball-milled for 60 h were the same as those for the sample "4".

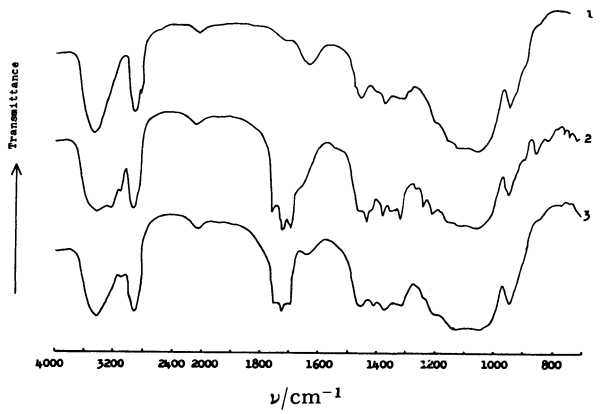

Fig. 2. Effect of ball-milling on IR spectra of the mixture of amobarbital and MC.
1: MC ball-milled for 100 h, 2: the mixture of AB and "1" in the ratio of 1 : 9 by weight, 3: the mixture of 1 g of AC and 9 g of MC ball-milled for 60 h.

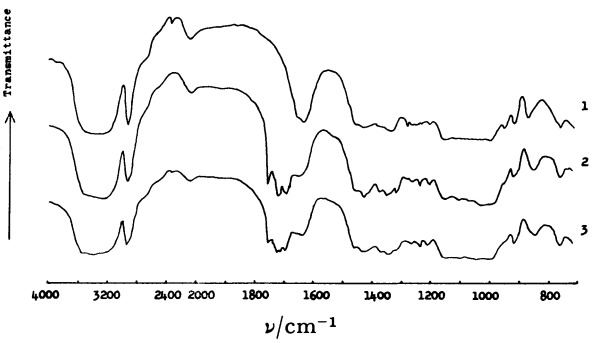

Fig. 3. Effect of ball-milling on IR spectra of the mixture of amobarbital and dextran.
1: Dextran ball-milled for 200 h, 2: the mixture of AB and "1" in the ratio of 1 : 9 by weight, 3: the mixture of 1 g of AC and 9 g of dextran ball-milled for 60 h.

cellulosic OH groups and the fluorine atoms of PTFE.[7] Marchessault *et al.* pointed out that the difference in a hydrogen-bonding system in various crystal-lattice types affected the intensities and frequencies of the bands in the OH stretching region.[8] The band at 1429 cm^{-1} was assigned to the CH_2 symmetric bending mode. The bands at 1315, 1335, and 1370 cm^{-1} were assigned to the CH_2 wagging mode, the C-O-H in-plane bending mode, and the CH bending mode respectively. The band at 1110 cm^{-1} was assigned to the C-O stretching mode, perhaps coupled to the C-C frequency. These bands were also reported to change with the variation in the crystal modifications or crystallinity; this was probably due to the change in the hydrogen-bonding system.[5,9] The above facts indicate that hydrogen bonds are formed between the C=O groups of amobarbital and the OH groups of the diluents.

The absorbance at each of the wave numbers, ν, was determined, assuming that the transmittance on the straight line passing through 3800 and 2000 cm^{-1}, or 2000 and 900 cm^{-1}, was 100%. Figure 4 represents the variations in $R_{\nu,\nu'}$ with ball-milling for the mixture with MCC containing 10 w/w% of amobarbital, where $R_{\nu,\nu'}$ is the ratio of the absorbance at the wave number of ν to the absorbance at ν'. $R_{1755,1690}$ was little influenced by ball-milling. $R_{1720,1690}$ increased in the first stage, while it stayed nearly constant after ball-milling for 15 h. $R_{1735,1690}$, $R_{1710,1690}$, and $R_{1700,1690}$ increased after ball-milling for 10 h. In the carbonyl absorptions of AB in Fig. 1, the absorption at 1755 cm^{-1} was considered to be due to the mode associated mainly with the C=O group in the 2-position, and the absorptions at 1720 and 1690 cm^{-1} bands, to be the antisymmetric and symmetric vibrations respectively, involving mainly the groups in the 4- and 6-positions.[4] It was previously reported that the 4- and 6-carbonyl groups formed hydrogen bonds with the NH groups, leaving the 2-carbonyl group unaffected in the solid state.[10] It was also noted that these bands showed a drop in frequency upon hydrogen bonding. The results in Fig. 4 support the following interpretations: (1) some part of the band at 1755 cm^{-1} shifts to a lower frequency upon the hydrogen bonding of the free C=O group in the 2-position, probably with the OH groups of MCC; (2) some part of the band at 1690 cm^{-1} shifts to a higher frequency upon the conversion of the bonds of the C=O group in the 4- or 6-position with the NH group of amobarbital to the bonds with the OH groups.

Figure 5 shows the variation in $R_{\nu,1690}$ (ν/cm^{-1} is between 1700 and 1755) with ball-milling for the mixture with MC. All of the $R_{\nu,1690}$ values in Fig. 5 increased in the first stage, while they stayed nearly constant after ball-milling for 10 h. The increase in $R_{1755,1690}$ indicates that the formation of hydrogen bonds of the C=O group in the 2-position with the OH groups of MC is not so predominant as the formation with those of MCC.

Table 1 presents the numerical values of $R_{\nu,1690}$ obtained by the use of a Nujol method. The band at 1640 cm^{-1} is the OH in-plane bending absorption of water adsorbed on diluents.[5,6] $R_{1640,1690}$ decreased upon ball-milling; this was probably a result of the squeezing

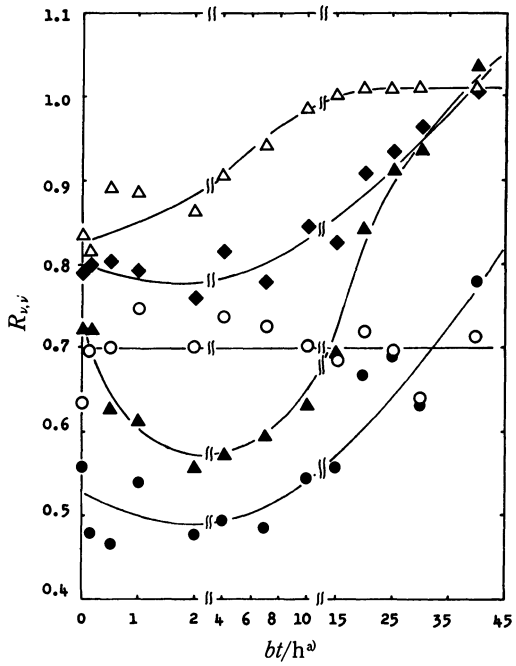

Fig. 4. Variation in $R_{\nu,\nu'}$ with ball-milling for the mixture with MCC containing 10 w/w % of amobarbital by a Nujol method.
ν'/cm^{-1}=1690, ν/cm^{-1}; ○: 1755, ●: 1735, △: 1720, ▲: 1710, ◆: 1700.
a) bt is the ball-milling time.

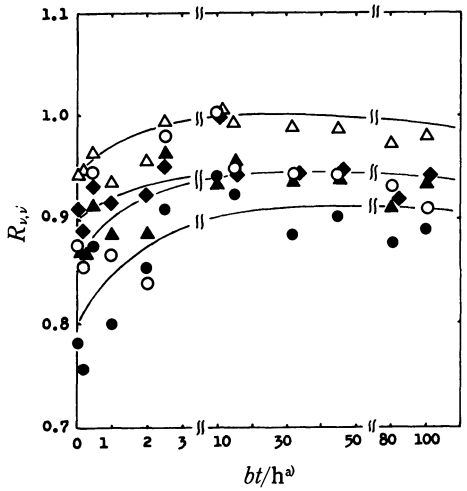

Fig. 5. Variation in $R_{\nu,\nu'}$ with ball-milling for the mixture with MC by a Nujol method.
ν'/cm^{-1}=1690, ν/cm^{-1}; ○: 1755, ●: 1735, △: 1720, ▲: 1710, ◆: 1700.
a) bt is the ball-milling time.

out of the adsorbed water caused by the formation of hydrogen bonds between the amobarbital and the diluents. It seemed probable from the change in $R_{1755,1690}$ that the absorbance at 1690 cm^{-1} after ball-milling was approximately 0.9 times as large as that before ball-milling for the mixture containing 30—40 w/w% of amobarbital. In this case, the $R_{3420,1690}$ value after ball-milling was 1.7—2.4 times as large as the value before ball-milling, though $R_{1640,1690}$ decreased upon ball-milling. The $R_{1110,1690}$ and $R_{1050,1690}$ values also doubled upon ball-milling. It is clear from these facts that the absorbances at 3420, 1110, and 1050 cm^{-1} increase upon ball-milling, though the variation in $R_{\nu,1690}$ for ν/cm^{-1} from 1450 to 1300 could not be discussed on the basis of a Nujol method. The band in the 1020—1060 cm^{-1} region has been suggested to be a skeletal vibration characteristic of the barbituric acid ring.[4] The skeletal vibration of amobarbital is probably affected by the change in the hydrogen bonds of the C=O groups. As is shown in Figs. 1, 2, 3, and Table 1, the absorbances of the NH stretching modes at 3200 and 3080 cm^{-1} and those of the NH out-of-plane deformation modes at 855 and 815 cm^{-1} decreased upon ball-milling, though the locations of these bands were not affected. The band of the stretching vibration of free NH has been reported to be observed in the 3300—3400 cm^{-1} region.[4] Probably, the increase in the absorbance at 3400 cm^{-1} is partly attributable to the free NH formed by the hydrogen bonding of the C=O groups with the OH groups of the diluents.

Effect of Dissolution on the Solid State of Amobarbital. A mixture with a water-soluble diluent containing approximately twice as much as the solubility of amobarbital was added to distilled water. After the suspension

Table 1. Numerical values of $R_{\nu,1690}$ for various kinds of mixtures (by a Nujol method)

Diluent	CA[a)] w/w%	bt[b)] h	ν/cm^{-1} 3420	1755	1735	1720	1710	1700	1640	1110	1050	850	815
Dextran	10	0[c)]	1.04	0.67	0.56	0.83	0.71	0.85	0.78	0.64	0.61		
Dextran	10	60	1.40	0.81	0.75	1.04	0.89	0.93	0.57	0.91	0.92		
MCC	10	0[c)]	1.16	0.67	0.56	0.85	0.72	0.81	0.81	0.74	0.73		
MCC	10	40	1.37	0.71	0.80	1.06	1.03	1.01	0.67	0.93	0.91		
MC	10	0[c)]	1.00	0.79	0.70	0.93	0.74	0.84	0.78	0.81	0.70		
MC	10	60	1.19	1.00	1.01	1.10	0.98	1.02	0.54	1.04	1.01		
Dextran	30	0[c)]	0.55	0.82	0.73	0.91	0.82	0.89	0.63	0.35	0.33	0.28	0.16
Dextran	30	203	0.95	0.92	0.82	0.98	0.86	0.91	0.45	0.61	0.65	0.27	0.13
MCC	30	0[c)]	0.40	0.80	0.65	0.91	0.77	0.87	0.50	0.30	0.31	0.26	0.16
MCC	30	203	0.94	0.88	0.74	0.99	0.84	0.92	0.39	0.69	0.83	0.16	0.08
MC	40	0[c)]	0.29	0.88	0.78	0.95	0.87	0.91	0.54	0.37	0.35	0.44	0.32
MC	40	101	0.70	0.91	0.89	0.98	0.93	0.94	0.33	0.73	0.75	0.33	0.23

a) CA is the content of amobarbital in the mixture. b) bt is the ball-milling time. c) A physical mixture of AB and the ball-milled diluent (Ten g of dextran or MCC was ball-milled for 200 h, and 5 g of MC was ball-milled for 100 h.)

had been allowed to stand for a week, the solid state of the amobarbital remaining undissolved was compared with the state before dissolution. As has been described previously, there are three polymorphs for amobarbital: Crystals I, II, and III. Crystal I was given by heating Crystal II (at 150 °C), which had been recrystallized from a 25 v/v% aqueous ethanol solution. Crystal III was given by freeze-drying an aqueous solution. It was also reported previously that AC and AB particles were composed of Crystal I, Crystal III and an amorphous part. The X-ray diffraction intensity at 12.7° of 2θ was lower than the intensity at 16.0° of 2θ in the diagram of Crystal I, while the opposite was observed in the diagram of Crystal III.[2] Figure 6 shows the X-ray-diffraction patterns of various kinds of amobarbital. Diffraction lines were not observed in the digram of dextran or MC. The crystallinity of amobarbital was determined by Ruland's method.[11] The ratio of the weight content of Crystal III to the content of Crystal I was determined from the ratio of the intensity of the diffraction line at 12.7° of 2θ to the intensity at 16.0° of 2θ.[2] The results of these determinations are shown in Table 2, where the MC content in MCABS was assumed to be 7.1 w/w% and where the contribution of MC to the scattering intensity was assumed to be identical with the contribution of the amorphous part of amobarbital. The contents of Crystal III in DexABS and MCABS were larger than those in ACS and ABS. It was noted previously that the $R_{3085,3020}$ and $R_{850,815}$ values for Crystal III were larger than those for Crystal I.[2] Table 3 presents the numerical values of $R_{\nu,\nu'}$ for various samples. The $R_{3085,3020}$ and $R_{850,815}$ values for DexABS and MCABS were larger than those for the other samples. This fact also shows that the content of Crystal III in DexABS and MCABS is larger than the content in the other samples. By the use of the solubility of amobarbital presented in Table 4, the solid state of the amobarbital remaining undissolved in the suspension was obtained on the basis of the following assumptions; (1) only a part of Crystal III or the amorphous part dissolved, and (2) no transformation occurred between Crystal I, Crystal III, and the amorphous state. A comparison of the results in Tables 2 and 4 demonstrates that Crystal III and the amorphous part are transformed into Crystal I by the dissolution of AB. The presence of dextran ball-milled with amobarbital is shown to prevent Crystal III from being transformed into Crystal I. The presence of MC ball-

TABLE 2. SOLID STATE OF AMOBARBITAL OBTAINED UPON VARIOUS KINDS OF PREPARATIONS

Sample	I[a] w/w%	III[b] w/w%	A_m[c] w/w%
AC	76±4[d]	11±1	13±3
ACS	74±3	14±1	12±4
AB	8±1	71±3	21±3
ABS	68±5	16±2	15±3
DexAB	6±1	34±6	60±5
DexABS	14±2	66±6	20±3
MCAB	3±1	25±5	73±12
MCABS	8±1	59±2	33±2

a) I: Crystal I. b) III: Crystal III .c) A_m: Amorphous part. d) The figure succeeding to ± is a standard deviation.

TABLE 3. NUMERICAL VALUES OF $R_{\nu,\nu'}$ FOR VARIOUS KINDS OF SAMPLES

Sample	ν/cm^{-1}	3085	1690	850
	ν'/cm^{-1}	3210	1750	815
ACS		1.07±0.01[a]	1.16±0.05	0.94±0.07
ABS		1.08±0.01	1.27±0.03	1.07±0.03
DexABS		1.13±0.02	1.26±0.01	1.11±0.02
MCABS		1.12±0.04	1.22±0.09	1.28±0.05

a) The figure succeeding to ± is a standard deviation.

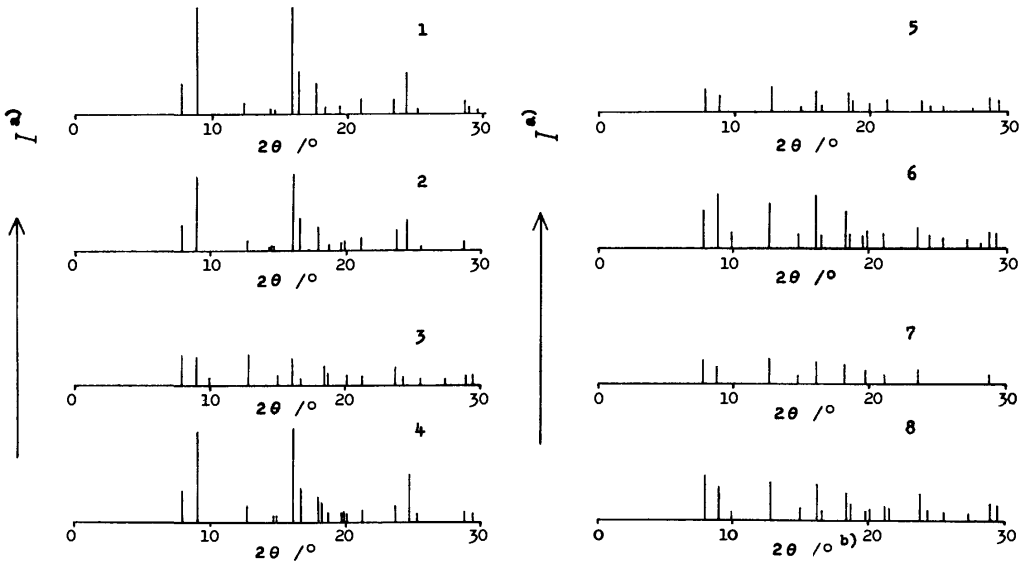

Fig. 6. X-Ray-diffraction patterns of various kinds of amobarbital.
1: AC, 2: ACS, 3: AB, 4: ABS, 5: DexAB, 6: DexABS, 7: MCAB, 8: MCABS.
a) I is the diffraction intensity. b) 2θ is the angle between the incident X-rays and the scattering X-rays.

Table 4. Solid state of amobarbital expected when only the part of crystal III or the amorphous part is assumed to be dissolved

Sample	Assumption		Expected crystal state		
	c[a] mg(100 cm^3)$^{-1}$	Dissolved part	I[b] w/w%	III[c] w/w%	A_m[d] w/w%
ABS	66	III	12	57	31
DexABS	66	A_m	9	54	37
MCABS	95	A_m	6	53	41

a) c is the solubility of amobarbital in distilled water. b) I: Crystal I. c) III: Crystal III. d) A_m: Amorphous part.

Table 5. Effect of ball-milling on the dissolution of amobarbital from various samples into a KH_2PO_4–Na_2HPO_4 buffer solution

Diluent	CA[a] w/w%	bt[b] h	c_{5min} mg(100 cm^3)$^{-1}$	c_{2h} mg(100 cm^3)$^{-1}$	c_e mg(100 cm^3)$^{-1}$
—	100	0		63.4±0.6[c]	61.5±1.2
—	100	60		65.7±1.1	63.0±1.3
Dextran	30	36	71.1±2.5		57.2±1.9
Dextran	30	200	62.8±2.5		58.3±1.9
MCC	10	20	87.4±2.6		59.6±1.7
MCC	10	40	76.1±2.3		62.9±1.7
MCC	30	200	80.0±2.1		59.7±2.2
MC	40	100		93.4±9.1	95.3±12.0

a) CA is the content of amobarbital in the mixture. b) bt is the ball-milling time. c) The figure succeeding to ± is a standard deviation.

milled with amobarbital is also shown to prevent the amorphous part from crystallization, as well as preventing Crystal III from being transformed into Crystal I.

Solubility of Amobarbital and the Stability of Its Amorphous State. Previously, a suspension of various kinds of samples containing amobarbital in a KH_2PO_4–Na_2HPO_4 buffer solution with a pH of 6.0 was shaken at 30 °C immediately after preparation, withdrawn from time to time, and filtered. Then the concentration of amobarbital in the filtrate was determined. In the case of amobarbital ball-milled with MC or without any diluent, the concentration increased with shaking and stayed nearly constant after 2 hs' shaking. The concentration of the mixture with dextran or MCC was at a maximum at the shaking time of 5 min. In Table 5 are summarized the results reported previously, where c_{5min} and c_{2h} are the concentrations after shaking for 5 min and for 2 h respectively, and where c_e is the concentration for the suspension allowed to stand at 30 °C for a week after shaking for 2 h. The concentrations increased more remarkably upon ball-milling with diluents than without any diluent. The c_{5min} values for the mixture with dextran were smaller than the values of c_{5min} or c_{2h} for the other mixtures. In the case of the mixture with MC, c_e was nearly identical with c_{2h}, while c_e was smaller than c_{5min} and approximately equal to the solubility of AC for the other mixtures. It was suggested that the increase in surface energy upon ball-milling was not the main reason for the increase in the solubility. Though the amorphous part seemed to control the solubility of amobarbital, the rate and extent of the increase in the amorphous part upon ball-milling were little influenced by the kind of diluent. After all, it was considered that the interaction of amobarbital with diluents resulting from ball-milling was one of the most important reasons for the increase in the solubility.[1,2]

In the case of the mixture with MCC containing 10 w/w% of amobarbital, c_{5min} was at its maximum around a ball-milling time of 20—25 h.[1] The decrease in c_{5min} after ball-milling for 25 h is probably to be attributed to the adsorption of amobarbital on MCC, as MCC is not soluble in distilled water. In the case of the mixture with MC, the variation in c_e with ball-milling was parallel to the variation in $R_{\nu,1690}$ in Fig. 5.[1] This fact shows that the large value of c_e is attributable to hydrogen bonding between amobarbital and MC. In Figs. 2 and 3, the variation in the carbonyl groups of amobarbital upon ball-milling with dextran was not so remarkable as the variation with MC; this fact shows that the interaction of amobarbital with dextran is weaker than the interaction with MC. The above results show that the solubilization of amobarbital upon ball-milling is attributable to the stabilization of the amorphous state caused by the interaction with diluents.

The authors are grateful to the members of the Analytical Center of Showa University for their measurements of the IR spectra and for the elemental analysis.

References

1) A. Ikekawa, and S. Hayakawa, *Bull. Chem. Soc. Jpn.*, **55**, 1261 (1982).
2) A. Ikekawa and S. Hayakawa, *Bull. Chem. Soc. Jpn.*, **54**, 2587 (1981).
3) N. Kaneniwa, A. Ikekawa, and M. Sumi, *Chem. Pharm. Bull.*, **26**, 2734, 2744 (1978).
4) R. J. Mesley, *Spectrochim. Acta, Part A*, **26**, 1427 (1970).

B. L. Chang, N. O. Neussle, and W. G. Honey, Jr., *J. Pharm. Sci.*, **64**, 1787 (1975).
5) H. G. Higgins, G. M. Stewart, and K. J. Harrington, *J. Polym. Sci.*, **51**, 59 (1961).
6) Anton N. J. Heyn, *Biopolymers*, **13**, 475 (1974).
7) J. H. Keighley and S. N. Pandey, *J. Text. Inst.*, **1**, 23 (1976).
8) R. H. Marchessault and C. Y. Liang, *J. Polym. Sci.*, **43**, 71 (1960).
9) M. L. Nelson and R. T. O'Connor, *J. Appl. Polym. Sci.*, **8**, 1311 (1964).
10) B. M. Craven and E. A. Vizzini, *Acta Crystallogr., Part B*, **25**, 1993 (1969); J. Caillet and P. Claverie, *ibid.*, **36**, 2642 (1980).
11) W. Ruland, *Acta Crystallogr.*, **14**, 1180 (1961).

 © 1982 The Chemical Society of Japan Bull. Chem. Soc. Jpn., 55, 3129—3134 (1982)

Vibration-rotation Spectrum of the Coriolis-interacting Band System ν_6 and ν_3 of Acetonitrile-d_3

Hiroatsu MATSUURA* and Hiromu MURATA

Department of Chemistry, Faculty of Science, Hiroshima University, Higashisenda-machi, Naka-ku, Hiroshima 730

(Received May 6, 1982)

The vibration-rotation infrared spectrum of the Coriolis-interacting band system ν_6 and ν_3 was measured with a resolution of 0.08 cm^{-1}. The analysis of the spectrum gave values, more precise than before, of the parameters for these bands along with the interaction parameters. A close examination of the observed spectrum revealed a weak Fermi resonance between ν_6 and $\nu_4+\nu_8$. The parameters determined, in cm^{-1}, include: $(\nu_0)_6$ 1046.659, α_6^A 0.01550, α_6^B −0.000443, $(\nu_0)_3$ 1110.46, α_3^A −0.0078, and α_3^B 0.00092, where α_6^B and α_3^B do not involve the contribution of the Coriolis interaction between ν_6 and ν_3.

The vibration-rotation infrared spectra of acetonitrile-d_3 or methyl-d_3 cyanide, CD_3CN, have been studied previously by several investigators.[1-4] The resolution of these spectra was, however, not high enough to provide precise values for molecular parameters. In order to improve the spectroscopic data for CD_3CN, Fourier transform infrared spectrum with a higher resolution was measured and analyzed in the present work. We report in this paper the spectral analysis of the ν_6 band (CD_3 degenerate deformation) which is strongly coupled with the ν_3 band (CD_3 symmetrical deformation) through an *xy*-type Coriolis interaction.

Experimental

The sample of acetonitrile-d_3 was a product of CEA, France, with a stated isotope purity of 99.7% and was used for the spectral measurements without further purification. The infrared spectrum was recorded on a JEOL JIR-40X Fourier transform infrared spectrometer. Sample pressures of 7—20 Torr† in a 1-m cell were utilized in the measurements. The effective spectral resolution was 0.08 cm^{-1}. The observed wavenumbers were calibrated by using the IUPAC wavenumber data.[5]

Spectral Analysis

The vibration-rotation spectrum in the whole ν_6 band region and the expanded spectra of the ^RR and ^PP branches are shown in Figs. 1 and 2, respectively. The spectra exhibit a number of P- and R-branch lines together with Q branches, in contrast with the previous spectra[1,3,4] in which only the Q branches were resolved. The assignment of the quantum number K to the Q branches and the associated P and R branches was made straightforwardly by examining the intensity alternation and the starting positions of series of P- and R-branch lines (Fig. 2). The K assignment established in this work agrees with that in the previous analyses.[1,3,4] The ^PP_K-branch lines with K=1—16 and the ^RR_K-branch lines with K=0—15 were finally identified and assigned for the ν_6 band. Vibration-rotation lines assignable definitely to the ν_3 band were not identified because of much weaker intensities than those for the ν_6 band.

Subband Analysis of ν_6. In advance of the analysis of the whole band system, the subbands in ν_6 were analyzed, and the effective rotational constant B'_{eff} was obtained for each subband by using a formula

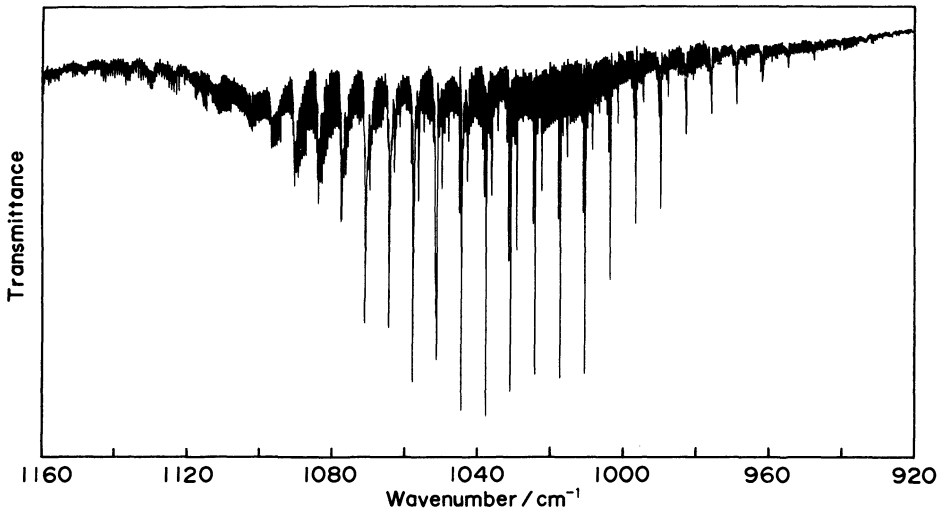

Fig. 1. Infrared spectrum of the ν_6 band region of gaseous CD_3CN.

† 1 Torr=133.322 Pa.

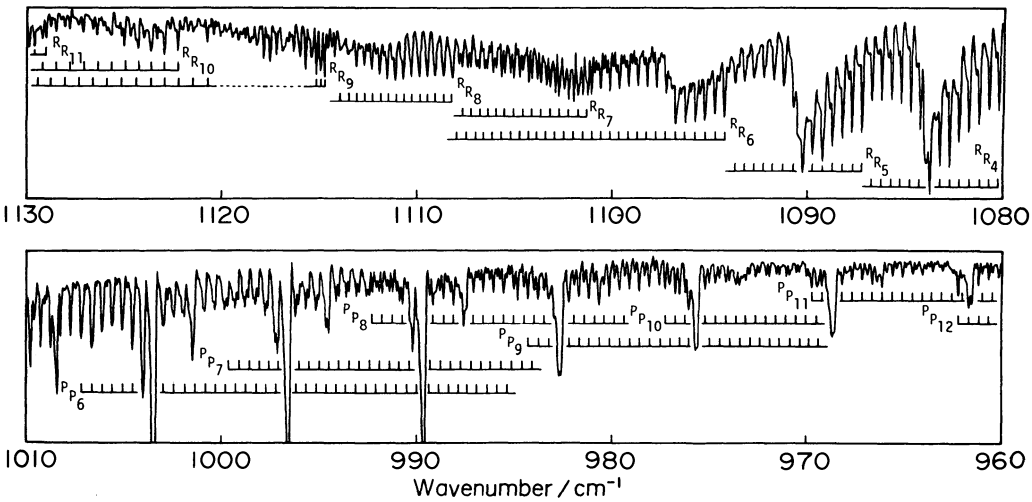

Fig. 2. Infrared spectra and assignments of the ^{R}R and ^{P}P branches of ν_6 of CD_3CN.

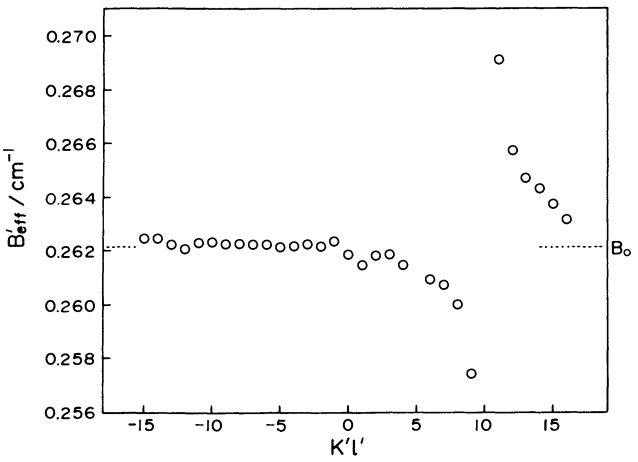

Fig. 3. Effective rotational constant B'_{eff} for ν_6 of CD_3CN. A value of B'_{eff} was not obtained for $K'l'=5$ because of severe overlapping of $^{R}R_4$-branch lines with stronger $^{R}R_3$-branch lines.

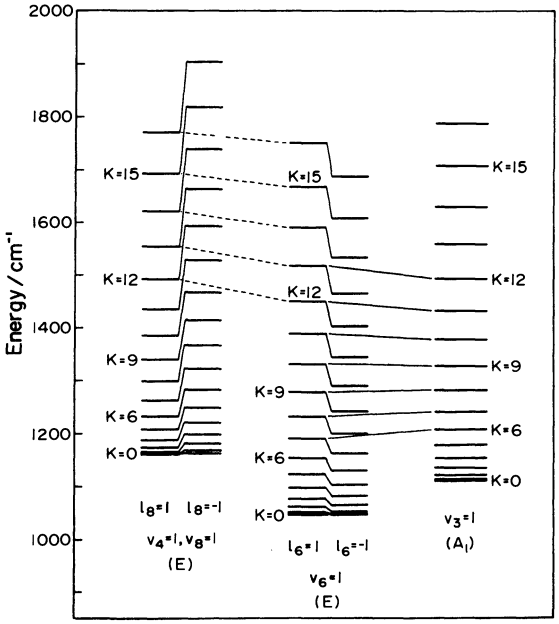

Fig. 4. Vibration-rotation energy levels for the ν_6 (E), ν_3 (A_1), and $\nu_4+\nu_8$ (E) states of CD_3CN and interactions coupling the levels (only significant interactions are shown). ——: Coriolis interaction between ν_6 and ν_3, and ----: Fermi resonance between ν_6 and $\nu_4+\nu_8$.

described previously.[6] The dependence of the B'_{eff} value on the upper-state quantum number $K'l'$ is shown in Fig. 3. If the ν_6 band was not perturbed by any interaction, the B'_{eff} value would be constant for all the subbands, namely for all the $K'l'$ values. Figure 3 shows, however, a striking variation of B'_{eff} between $K'l'=9$ and 11, indicating that an energy-level crossing with another state occurs around $K'l'=10$.

An examination of the energy levels for CD_3CN indicates that the perturbation observed in the ν_6 band is due to the xy-type Coriolis interaction between the $v_6=1$ state (to be denoted by the ν_6 state or simply ν_6) and the $v_3=1$ state (the ν_3 state), which has been noted previously by Masri *et al.*[3] The variation fashion of the B'_{eff} value indicates that the vibration-rotation levels of ν_6 for $K'l'\leq 9$ are lower than the coupling ν_3 levels and, beyond the level crossing, the ν_6 levels are higher than the ν_3 levels. The vibration-rotation energy levels, finally determined in this work, of ν_6 (E), ν_3 (A_1), and $\nu_4+\nu_8$ (E) and the interactions coupling the levels are shown in Fig. 4. The $\nu_4+\nu_8$ state interacts weakly with the ν_6 state through a Fermi resonance, as will be mentioned later.

Analysis of the Band System ν_6 and ν_3. In the band system ν_6 and ν_3, the vibration-rotation energies are strongly perturbed by the Coriolis resonance, so that the treatment of the Coriolis interaction based on the second-order perturbation theory, known as a Van Vleck transformation, which is usually employed in off-resonance systems, is no longer valid. Accordingly, this interaction was explicitly taken into account in the analysis. The non-zero matrix element of the Hamiltonian for the xy-type Coriolis interaction between ν_6 (E) and ν_3 (A_1) is given by[6-8]

$$\langle v_3=1; J,K|H_{Cor}/hc|v_6=1, l_6=\pm 1; J,K\pm 1\rangle = \pm \xi^{(y)}_{3,6} f(J,K\pm 1), \quad (1)$$

where

$$\xi^{(y)}_{3.6} = (1/\sqrt{2})[(\omega_6/\omega_3)^{1/2} + (\omega_3/\omega_6)^{1/2}](B\zeta^{(y)}_{3.6a}) \quad (2)$$

and

$$f(J,K\pm1) = [J(J+1) - K(K\pm1)]^{1/2}. \quad (3)$$

On the other hand, the vibration-rotation Hamiltonian gives the following unperturbed energy[9] with $|k|=K$:

$$\begin{aligned} E^0(v,l;J,k)/hc &= G(v,l) + B_v[J(J+1) - k^2] + A_v k^2 \\ &- \sum_t 2(A\zeta^{(z)}_{ta.tb})_v k l_t - (D_J)_v J^2(J+1)^2 \\ &- (D_{JK})_v J(J+1)k^2 - (D_K)_v k^4 \\ &+ \sum_t (\eta_{tJ})_v J(J+1)kl_t + \sum_t (\eta_{tk})_v k^3 l_t, \end{aligned} \quad (4)$$

where $G(v,l)$ is the vibrational term and the index t refers to the doubly-degenerate modes. The vibrational term $G(v,l)$, and accordingly the band origin $(\nu_0)_v$ to be derived from the spectral analysis, include a term $A(\zeta^{(z)}_{ta.tb})^2$ which originates from the non-vibrational Hamiltonian.

The vibration-rotation transition wavenumbers were calculated by solving the energy matrix with elements given by Eqs. 1 and 4. The ground-state constants B_0, $(D_J)_0$, and $(D_{JK})_0$ were constrained to the well-determined microwave data[10] and the constants A_0 and $(D_K)_0$ were fixed to the estimated values.[3,11] The least-squares calculation gave satisfactory agreement between the observed and calculated wavenumbers with the exception of those for the ${}^{R}R_K(J)$ lines with $K \gtrsim 12$.

The results of this preliminary calculation show that the perturbed ${}^{R}R_K(J)$ lines of ν_6 are shifted down more for larger K values, indicating that the perturbing vibration-rotation levels are higher than, but getting closer at higher levels to, those of the ν_6 levels. Possible interacting vibrational levels are $\nu_4+\nu_8$ and $\nu_7+\nu_8$ with estimated vibrational wavenumbers of about 1165 and 1180 cm^{-1}, respectively. Accordingly, the vibration-rotation energy levels for these combination bands were calculated by using the constants available. The results clarify that the levels of $\nu_4+\nu_8$ approach those of ν_6 within 40 cm^{-1} for $K'l' \geq 13$ but an expected interaction between ν_6 and $\nu_7+\nu_8$ should be much less significant than between ν_6 and $\nu_4+\nu_8$. The minor perturbation observed in ν_6 is thus found to be due to the Fermi resonance between ν_6 (E) and $\nu_4+\nu_8$ (E).

The whole band system was analyzed by taking account of the Coriolis interaction between ν_6 and ν_3 and the Fermi resonance between ν_6 and $\nu_4+\nu_8$, as well as the $q_t^{(+)}$-type l-doubling interaction[9] in the degenerate vibrational state. Thus, in order to obtain perturbed energies, the following 5×5 energy matrix was set up and solved for $K \geq 1$:

$$\begin{pmatrix} E^0(v_6=1,\, l_6=-1;J,\, K-1), & W_{468} & -\xi^{(y)}_{3.6} f(J,\, K-1) & -q_6^{(+)} f(J,\, K+1) f(J,\, K-1)/2 & 0 \\ & E^0(v_4=1,\, v_8=1,\, l_8=-1;J,\, K-1) & 0 & 0 & -q^{(+)}_{4.8} f(J,\, K+1) f(J,K-1)/2 \\ & & E^0(v_3=1;J,\, K) & \xi^{(y)}_{3.6} f(J,\, K+1) & 0 \\ & \text{(Hermitian)} & & E^0(v_6=1,\, l_6=1;J,\, K+1) & W_{468} \\ & & & & E^0(v_4=1, v_8=1,\, l_8=1;\, J,K+1) \end{pmatrix}, \quad (5)$$

where W_{468} is a parameter of the Fermi resonance between ν_6 and $\nu_4+\nu_8$ and is related to Mills' cubic force constant ϕ_{468} by $W_{468}=\phi_{468}/2\sqrt{2}$. For $K=0$, on the other hand, the matrix is reduced to 3×3 and 2×2 matrices; for A- species:††

$$\begin{pmatrix} E^0(v_3=1;J,\, K=0) & \sqrt{2}\,\xi^{(y)}_{3.6}[J(J+1)]^{1/2} & 0 \\ & E^0(v_6=1,\, l_6=1;\, J,\, K=1) + q_6^{(+)}J(J+1)/2 & W_{468} \\ \text{(Herimitian)} & & E^0(v_4=1,\, v_8=1,\, l_8=1;\, J,K=1) + q^{(+)}_{4.8}J(J+1)/2 \end{pmatrix}, \quad (6)$$

and for A+ species:

$$\begin{pmatrix} E^0(v_6=1,\, l_6=1;\, J,K=1) - q_6^{(+)}J(J+1)/2 & W_{468} \\ \text{(Hermitian)} & E^0(v_4=1,\, v_8=1,\, l_8=1;\, J,K=1) - q^{(+)}_{4.8}J(J+1)/2 \end{pmatrix}. \quad (7)$$

The ${}^{R}R_0(J)$ and ${}^{R}P_0(J)$ transitions go to the A- levels, while the ${}^{R}Q_0(J)$ transitions go to the A+ levels.[7,12]

Wavenumbers for the vibration-rotation transitions of CD_3CN were obtained as differences between the perturbed energies in the excited vibrational states and those in the ground vibrational state. These wavenumbers were fitted to the observed wavenumbers by the least-squares adjustment of the spectroscopic parameters. In the calculation, some of the parameters for ν_3 and $\nu_4+\nu_8$ were assumed or set equal to those in the ground state, since pertinent experimental data to fix them were not available in the present work. Approximate values for the band origin of $\nu_4+\nu_8$ and the Fermi resonance parameter W_{468} were predetermined, in advance of the principal calculation, so as to reproduce the observed data most satisfactorily.

The parameters for the ν_6 and ν_3 bands and the interaction parameters were finally determined, as listed in Table 1, from a total of 517 vibration-rotation transition wavenumbers of ${}^{P}P_K(J)$ with $K=1$—16, ${}^{R}R_K(J)$ with $K=0$—15, and ${}^{R}P_0(J)$. The transition lines which were badly overlapped with others were not adopted in the calculation. The parameters in Table 1 reproduce the observed wavenumbers with a root-mean-square error of 0.014 cm^{-1}. A list of the observed transition wavenumbers has been deposited with the Chemical Society of Japan (Document No. 8257).

Results and Discussion

In the present work, the parameters have been

†† In our earlier studies,[6,8] the different notation $A^{\pm}$ has been used; $A^{\pm}=A_{\mp}$.

TABLE 1. PARAMETERS FOR THE ν_6,ν_3, $\nu_4+\nu_8$ AND GROUND VIBRATIONAL STATES OF CD_3CN IN UNITS OF cm^{-1}

Parameter	ν_6	ν_3	$\nu_4+\nu_8$	Ground state
$(\nu_0)_v$	1046.659 (7) [a]	1110.46 (2)	1162 [b]	0
A_v	2.61450 (3)	2.6378 (3)	$=A_0$	2.630 [c]
B_v	0.262557 (8) [d]	0.26119 (4) [d]	0.26129 [e]	0.26211407 [f]
$(A\zeta^{(z)}_{ta.tb})_v$	−1.00068 (7)	—	2.104 [g]	—
$(D_J)_v$	$0.96\,(5)\times10^{-7}$	$=(D_J)_0$	$=(D_J)_0$	0.91567×10^{-7} [f]
$(D_{JK})_v$	$3.56\,(6)\times10^{-6}$	$=(D_{JK})_0$	$=(D_{JK})_0$	3.69125×10^{-6} [f]
$(D_K)_v$	$2.25\,(1)\times10^{-5}$	$=(D_K)_0$	$=(D_K)_0$	2.145×10^{-5} [h]
$(\eta_{tJ})_v$	$1.8\,(4)\times10^{-6}$	—	0	—
$(\eta_{tk})_v$	$-4.72\,(8)\times10^{-5}$	—	0	—
$q_t^{(+)}$	$1.3\,(2)\times10^{-4}$ [d]	—	0	—
$\xi^{(y)}_{3.6}$	−0.1901 (3)			
W_{468}	0.91 [b,i]			

a) Standard deviations of the parameters, given in parentheses, apply to the last significant figure. b) Predetermined. c) Ref. 3. d) The value does not involve the contribution of the Coriolis interaction between ν_6 and ν_3. e) Derived from α_4^B and α_8^B (Ref. 16). f) Ref. 10. g) Derived from $\zeta^{(z)}_{8a.8b}$ (Ref. 11). h) Ref. 11. i) This value gives the cubic force constant $\phi_{468}=2\sqrt{2}\,W_{468}=2.6\ cm^{-1}$.

derived for the ν_6 and ν_3 bands along with the parameter of the Coriolis interaction between these vibrational states. The errors in the band origins $(\nu_0)_v$ have been estimated from the uncertainty in the standard wavenumbers[5] used for the calibration, that in the least-squares fitting of the calibration wavenumbers, and that in the least-squares determination of $(\nu_0)_v$.

The values determined in the present analysis for the rotational constants $B_6\equiv B_{v_6=1}$ and $B_3\equiv B_{v_3=1}$ do not involve the contribution of the Coriolis interaction between ν_6 and ν_3, since the perturbed energies for ν_6 and ν_3 were obtained by solving the energy matrix with the off-diagonal terms representing this Coriolis interaction and the diagonal terms representing the unperturbed energies without the contribution of this interaction. The constants α_6^B and α_3^B defined by

$$B_v = B_e - \sum_r \alpha_r^B (v_r + d_r/2), \tag{8}$$

where d_r is the degeneracy of the normal modes, are derived from the values for B_6, B_3, and B_0. The derived values for α_6^B and α_3^B therefore lack the contribution of the above-mentioned Coriolis interaction, and accordingly correspond to the expression for α_r^B in the second-order perturbation theory[13,14]††† with the term containing $\zeta^{(y)}_{3.6a}$ being dropped.

The spectral analysis gave a value for $(A\zeta^{(z)}_{6a.6b})_{v_6=1}$ which shows a vibrational dependence given by[9,15]

$$(A\zeta^{(z)}_{ta.tb})_v = (A\zeta^{(z)}_{ta.tb})_e - \sum_r \alpha_r^{A\zeta_t}(v_r + d_r/2). \tag{9}$$

The constant in the equilibrium state, $(A\zeta^{(z)}_{ta.tb})_e$, is separable into A_e and $\zeta^{(z)}_{ta.tb}$, namely

$$(A\zeta^{(z)}_{ta.tb})_e = A_e\zeta^{(z)}_{ta.tb}. \tag{10}$$

A combination of Eqs. 9 and 10 and an equation for A_v, similar to that for B_v in Eq. 8, gives an explicit relation between the constant $\zeta^{(z)}_{ta.tb}$ and the observable $(A\zeta^{(z)}_{ta.tb})_v$

$$\begin{aligned}\zeta^{(z)}_{ta.tb} &= [(A\zeta^{(z)}_{ta.tb})_v + \sum_r \alpha_r^{A\zeta_t}(v_r+d_r/2)]/A_e \\ &= [(A\zeta^{(z)}_{ta.tb})_v + \sum_r \alpha_r^{A\zeta_t}(v_r+d_r/2)]/ \\ &\quad [A_v + \sum_r \alpha_r^{A}(v_r+d_r/2)].\end{aligned} \tag{11}$$

Since the determination of all of the constants $\alpha_r^{A\zeta_t}$ is practically impossible, a value for the Coriolis constant $\zeta^{(z)}_{ta.tb}$ with physical significance is never derived with a high precision.[9] In order to evaluate an effective value for $\zeta^{(z)}_{ta.tb}$, an approximation

$$(A\zeta^{(z)}_{ta.tb})_v \simeq A_v\zeta^{(z)}_{ta.tb} \tag{12}$$

has been conventionally used.[15] Physical meaning of the value thus derived is ambiguous and the resulting uncertainty in $\zeta^{(z)}_{ta.tb}$ is therefore unestimable. In the present analysis of ν_6 of CD_3CN, an effective value was derived for $\zeta^{(z)}_{6a.6b}$ by using Eq. 12. The value obtained is −0.3827 which may be compared with the value −0.374 calculated from the harmonic force constants.[11] These values agree with each other within 2.3%.

The parameter of the *xy*-type Coriolis interaction between ν_6 and ν_3, $\xi^{(y)}_{3.6}$ given by Eq. 2, involves the Coriolis constant $\zeta^{(y)}_{3.6a}$. This constant is, however, not separable from $\xi^{(y)}_{3.6}$, because the quantity $(B\zeta^{(y)}_{3.6a})$ shows a vibrational dependence as $(A\zeta^{(z)}_{ta.tb})_v$ does (Eq. 9). If an approximation

$$(B\zeta^{(y)}_{3.6a}) \simeq (B_3B_6)^{1/2}\zeta^{(y)}_{3.6a} \tag{13}$$

is made, an effective value for $\zeta^{(y)}_{3.6a}$ may be obtained from the $\xi^{(y)}_{3.6}$ value which was given by the spectral analysis. In doing this, the harmonic vibrational wavenumbers ω_6 and ω_3 are required, which are, in general, not easily derived. If, alternatively, the fundamental wavenumbers, not corrected for the vibrational anharmonicity, $(\nu_0)_6$ and $(\nu_0)_3$ are used for ω_6 and ω_3, possible errors may be involved in the derived value for $\zeta^{(y)}_{3.6a}$. To test the possibility of using the fundamental wavenumbers instead of the harmonic wavenumbers, calculations were made with Eq. 13 in two ways. The use of $(\nu_0)_6$ and $(\nu_0)_3$ determined in this work gave $|\zeta^{(y)}_{3.6a}|=0.505$, while the use of the harmonic wavenumbers,[11] $\omega_6=1061.7$ and $\omega_3=1128.0\ cm^{-1}$, ob-

††† In Ref. 14, there is a typographic error; for 4/3 in the second term of the right side of Eq. 5, read 3/4.

tained by correcting for the anharmonicity by Dennison's rule, gave $|\zeta^{(y)}_{3.6a}|=0.513$. The difference between the two values is 1.5%. These values may be compared with 0.493 calculated from the harmonic force constants.[11] The experimentally derived values (0.505 and 0.513) are larger than the calculated one by 2 and 4%, respectively.

The l-doubling constant $q_6^{(+)}$ determined by the present analysis method does not have, similarly to α_6^B and α_3^B, the contribution of the Coriolis interaction between ν_6 and ν_3. The value obtained is thus explained by the second-order perturbation expression[12,14] for $q_6^{(+)}$ less the term containing $\zeta^{(y)}_{3.6a}$. Strictly speaking, the constant $q_t^{(+)}$ should show a vibrational dependence.[9] However, an estimation of its effect is practically quite difficult.

As seen from Eqs. 6 and 7, the effective rotational constant, not perturbed by the Coriolis and the Fermi interactions, for the $Kl_6=1$ levels of ν_6 is given by

$$B^0_{eff} = B_6 + q_6^{(+)}/2 \text{ for } {}^{R}R_0(J) \text{ and } {}^{R}P_0(J) \text{ transitions} \quad (14a)$$

$$B^0_{eff} = B_6 - q_6^{(+)}/2 \text{ for } {}^{R}Q_0(J) \text{ transitions,} \quad (14b)$$

B^0_{eff} being the coefficient of $J(J+1)$ in the diagonal term of Eqs. 6 and 7 representing the $v_6=1$, $l_6=1$, $J,K=1$ state. The effective rotational constant B'_{eff} for $K'l'=1$, as given in Fig. 3, was derived from the ${}^{R}R_0(J)$ and ${}^{R}P_0(J)$ transitions. The value thus obtained involves the contributions of the l-doubling interaction mentioned above and the Coriolis interaction between ν_6 and ν_3. The smaller value for $K'l'=1$, as compared with those for the neighboring $K'l'$ values, is explained as follows. Although the l-doubling interaction with a positive $q_6^{(+)}$ value shifts up the energy levels associated with the ${}^{R}R_0(J)$ and ${}^{R}P_0(J)$ transitions (Eq. 14a), its effect is overwhelmed by the more dominant Coriolis interaction which shifts down the levels for $K'l'=1$ more largely than those for the neighboring $K'l'$ values (Eqs. 5 and 6). The constant B'_{eff}, if derived from the ${}^{R}Q_0(J)$ transitions, would be larger than that for the neighboring $K'l'$ values, since the levels associated with the ${}^{R}Q_0(J)$ transitions are completely free from the xy-type Coriolis interaction (Eq. 7), although the l-doubling interaction slightly shifts down the energy levels. The spectral observation in Fig. 1 that the contour of the ${}^{R}Q_0$ branch degrades to the higher wavenumber side, unlike the neighboring Q branches with sharper contours, is consistent with the expected B'_{eff} value.

The parameters $(\nu_0)_6 \equiv (\nu_0)_{v_6=1}$, $(\nu_0)_3 \equiv (\nu_0)_{v_3=1}$, α_6^A, α_3^A, α_6^B, α_3^B, $q_6^{(+)}$, $\zeta^{(z)}_{6a.6b}$, and $\zeta^{(y)}_{3.6a}$, determined explicitly or derived on assumptions in the present study are summarized in Table 2 in comparison with those reported previously. It is clearly shown that the precision of the parameters has been largely improved owing to the higher spectral resolution and the more legitimate procedure of the analysis in the present work. It should be noted, however, that the parameters for ν_3 were determined from the ν_6 transition lines through the Coriolis resonance between ν_3 ffnd ν_6. The transition lines associated intrinsically with ν_3 were not definitely identified because of their weak intensities.

The microwave spectra of CD_3CN in the excited vibrational states have been reported by Matsumura *et al.*[16] The observed spectral lines were complicated and they did not make definite assignments of the transitions for the ν_6 and ν_3 states. We therefore refrain from further discussion on their spectroscopic data.

Table 2. Comparison of the parameters for the ν_6 and ν_3 states[a]

Parameter	Present work	Previous works	
		Masri *et al.*[b]	Kondo and Person[c]
$(\nu_0)_6$	1046.659(7)[d]	1046.45	1047.0(1)
$(\nu_0)_3$	1110.46(2)	1110.0	1111.4(1)
α_6^A	0.01550(3)	0.0154	0.016(7)
α_3^A	−0.0078(3)	−0.0135[e]	0[e]
α_6^B	−0.000443(8)[f]	0[e]	0[e]
α_3^B	0.00092(4)[f]	0.0013[e]	0[e]
$q_6^{(+)}$	0.00013(2)[f]	0[e]	0[e]
$\zeta^{(z)}_{6a.6b}$	−0.3827[g]	−0.375[g]	−0.408[g]
$\lvert\zeta^{(y)}_{3.6a}\rvert$	0.513[h]	0.47	0.484[e]

a) The values are given in units of cm^{-1}, except for dimensionless $\zeta^{(z)}_{6a.6b}$ and $\zeta^{(y)}_{3.6a}$. b) Ref. 3. c) Ref. 4. d) Standard deviations of the parameters, given in parentheses, apply to the last significant figure. e) Assumed. f) The value does not involve the contribution of the Coriolis interaction between ν_6 and ν_3. g) Derived on the assumption that $(A\zeta^{(z)}_{6a.6b})_6 = A_6\zeta^{(z)}_{6a.6b}$. See text. h) Derived from $\xi^{(y)}_{3.6}$ by using the harmonic wavenumbers (Ref. 11), on the assumption that $(B\zeta^{(y)}_{3.6a}) = (B_3B_6)^{1/2}\zeta^{(y)}_{3.6a}$. See text.

The authors wish to thank Messrs. Noboru Kubota and Yuichi Shimooka for their assistance in the computational work. Numerical calculations were carried out with a HITAC M-200H computing system at Hiroshima University.

References

1) W. H. Fletcher and C. S. Shoup, *J. Mol. Spectrosc.*, **10**, 300 (1963).
2) R. Anttila, *J. Mol. Spectrosc.*, **41**, 487 (1972).
3) F. N. Masri, J. L. Duncan, and G. K. Speirs, *J. Mol. Spectrosc.*, **47**, 163 (1973).
4) S. Kondo and W. B. Person, *J. Mol. Spectrosc.*, **52**, 287 (1974).
5) IUPAC Commission on Molecular Structure and Spectroscopy, "Tables of Wavenumbers for the Calibration of Infrared Spectrometers," 2nd ed, compiled by A. R. H. Cole, Pergamon Press, Oxford (1977).
6) H. Matsuura and T. Shimanouchi, *J. Mol. Spectrosc.*, **60**, 93 (1976).
7) C. di Lauro and I. M. Mills, *J. Mol. Spectrosc.*, **21**, 386 (1966).
8) H. Matsuura, T. Nakagawa, and J. Overend, *J. Chem. Phys.*, **59**, 1449 (1973).
9) I. M. Mills, in "Molecular Spectroscopy: Modern Research," ed by K. N. Rao and C. W. Mathews, Academic Press, New York (1972), p. 115.
10) J. Demaison, A. Dubrulle, D. Boucher, and J. Burie, *J. Mol. Spectrosc.*, **76**, 1 (1979).
11) J. L. Duncan, D. C. McKean, F. Tullini, G. D. Nivellini, and J. P. Peña, *J. Mol. Spectrosc.*, **69**, 123 (1978).
12) G. J. Cartwright and I. M. Mills, *J. Mol. Spectrosc.*, **34**, 415 (1970).

13) K. Kuchitsu and S. J. Cyvin, "Molecular Structures and Vibrations," ed by S. J. Cyvin, Elsevier, Amsterdam (1972), p. 183.
14) H. Matsuura and J. Overend, *Bull. Chem. Soc. Jpn.*, **46**, 1102 (1973).
15) G. Herzberg, "Molecular Spectra and Molecular Structure, Infrared and Raman Spectra of Polyatomic Molecules," D. van Nostrand, Princeton (1945), Vol. II.
16) C. Matsumura, E. Hirota, T. Oka, and Y. Morino, *J. Mol. Spectrosc.*, **9**, 366 (1962).

The Structure of Dichloro(4-hydroxy-L-proline)cadmium(II)

Yasuhiko YUKAWA,* Yoshie INOMATA, Toshio TAKEUCHI,
Mamoru SHIMOI,† and Akira OUCHI†

Department of Chemistry, Faculty of Science and Technology, Sophia University, Kioi-cho, Chiyoda-ku, Tokyo 102
†*Department of Chemistry, College of General Education, The University of Tokyo, Komaba, Meguro-ku, Tokyo 153*

(Received November 4, 1981)

An X-ray diffraction study of the title complex has been carried out. The crystal is monoclinic, with the space group $P2_1$; $Z=2$; $a=8.196(4)$, $b=7.275(3)$, $c=7.740(4)$ Å, $\beta=103.73(4)°$. Full-matrix least-squares refinements have led to the final R value of 0.030. The structure consists of one-dimensional polymers bridged by chlorine atoms and a carboxyl group. Four chlorine atoms coordinate to a cadmium atom and form a square plane. The planes extend in the direction of the b axis like an infinite folding screen, sharing opposite edges. From the trough positions in the zigzag structure, the carboxyl oxygen atoms of 4-hydroxy-L-proline coordinate forkedly to two cadmium atoms. The ligand is a zwitter ion in the complex.

Amino acids such as 4-hydroxy-L-proline (Hhpro) and proline are important to biochemists who investigate the constitution and configuration of proteins. The crystal structure of Hhpro has been determined by Donohue and Trueblood[1] and by Koetzele *et al.*[2]

There are few studies, however, about metal complexes with Hhpro. In this work a cadmium complex with Hhpro was prepared. Its crystal and molecular structure was determined in order to investigate how Hhpro coordinates to the metal.

Experimental

Preparation of Dichloro(4-hydroxy-L-proline)cadmium(II); $CdCl_2$-(Hhpro). To an aqueous solution of 2.62 g (0.02 mol) of Hhpro, 4.57 g (0.02 mol) of $CdCl_2 \cdot 2.5H_2O$ was added. Then the solution (pH 3.7) was stirred for several hours on a water bath at 60—70 °C. Clear colorless prisms were obtained by standing at room temperature; they were dried *in vacuo* at 50 °C for several hours.

Found: C, 19.08; H, 2.86; N, 4.49; Cl, 22.40; Cd, 35.9%. Calcd for $CdCl_2(C_5H_9NO_3)$: C, 19.10; H, 2.88; N, 4.45; Cl, 22.55; Cd 35.75%.

X-Ray Measurements. The crystal data are given in Table 1.

The reflections were collected by the θ-2θ scan technique ($2\theta \leqq 70°$) on a Philips PW 1100 automated four-circle diffractometer. The 1990 independent reflections with $|F_o| \geqq 3\sigma(|F_o|)$ were used for the structure refinement. The intensities were corrected for Lorentz and polarization factors, but no correction was made for the absorption because of the low magnitude of $\mu r(=0.42)$. All the calculations were carried out on a HITAC M-200H computer at the Computer Center of the University of Tokyo, using the local versions of UNICS[3] and LINUS.[4] The atomic scattering factors were taken from tables.[5]

Structure Determination. The structure was solved by a heavy-atom method. The positions of the cadmium atom and chlorine atoms were obtained from a three-dimensional Patterson function, while the positions of all the other non-hydrogen atoms were successively located by Fourier syntheses. Since the positions of few hydrogen atoms were obtained by a difference Fourier syntheses, all of the positions were calculated and fixed. Their isotropic temperature factors were all assumed to be 5.0 Å^2. Since the absolute configuration of Hhpro was known, the structure analysis was based on the configuration.

Table 1. CRYSTAL DATA

$CdCl_2(C_5H_9NO_3)$	F.W.=314.44
Monoclinic	Space group $P2_1$
$a=8.196(4)$ Å	
$b=7.275(3)$ Å	$\beta=103.73(4)°$
$c=7.740(4)$ Å	
$Z=2$	$U=448.3(4)$Å^3
$D_m=2.35$ g cm^{-3}	$D_x=2.33$ g cm^{-3}
μ(Mo $K\alpha$)=29.7 cm^{-1}	

The crystal used for data collection showed quite severe extinction, and full-matrix least-squares refinements including an extinction correction were carried out, using LINUS. The weighting scheme was $W=1/[\{\sigma(|F_o|)\}^2+(0.06\times|F_o|)^2]$.

In the last cycle of the refinement with anisotropic temperature factors for all non-hydrogen atoms, all the parameter shifts were less than one-third of the corresponding standard deviations. The final R value ($R=\sum||F_o|-|F_c||/\sum|F_o|$) was 0.030.

IR Measurements. The infrared spectra of the samples were obtained by means of a Hitachi EPI-G2 type infrared spectrophotometer, using Nujol mull and KBr pellets.

Results and Discussion

The final atomic parameters are listed in Table 2,[6] the interatomic distances in Table 3, and the bond angles in Table 4. The perspective drawing of the complex and the numbering scheme of atoms are shown in Fig. 1.

The complex has the structure of a one-dimensional polymer bridged by chlorine atoms and carboxyl oxygen atoms as shown in Fig. 2. Four chlorine atoms coordinate to a cadmium atom and form a square plane within 0.002 Å. The cadmium atom deviates 0.04 Å from the plane. The planes extend zigzag in the direction of the b axis like an infinite folding screen, sharing opposite edges. The dihedral angle between adjacent planes is 142°. From the trough positions in the zigzag folding structure the carboxyl oxygen atoms of Hhpro coordinate forkedly to two cadmium atoms. Therefore the cadmium atom has octahedral coordination.

The bond distances of the coordinating Hhpro are not so different from those of the free molecule. The interatomic distance between N and O(2) is rather short, 2.62 Å. Koetzele *et al.*[2] carried out a neutron diffraction study of Hhpro. Their results also show

TABLE 2. FINAL POSITIONAL PARAMETERS ($\times 10^4$ FOR NON-HYDROGEN ATOMS; $\times 10^3$ FOR HYDROGEN ATOMS) AND EQUIVALENT ISOTROPIC TEMPERATURE FACTORS (B_{eq}/Å^2), WITH THE ESTIMATED STANDARD DEVIATIONS

Atom	x	y	z	B_{eq}/Å^2
Cd	23.7(5)	0	−38.8(5)	1.6
Cl(1)	2125(1)	−2494(4)	−502(1)	2.1
Cl(2)	2315(1)	2489(4)	1173(1)	1.8
O(1)	−273(4)	1025(5)	−2973(4)	2.1
O(2)	81(4)	4083(5)	−2780(4)	2.0
O(3)	5883(4)	1508(6)	−3728(5)	3.0
N	2705(4)	4107(6)	−4153(6)	2.5
C(1)	389(3)	2511(7)	−3292(3)	1.4
C(2)	1645(4)	2413(6)	−4484(4)	1.7
C(3)	2917(5)	842(7)	−4060(6)	2.3
C(4)	4530(5)	1645(6)	−2856(5)	2.0
C(5)	4119(5)	3659(7)	−2590(6)	2.5
H(21)	88	222	−581	
H(31)	317	29	−527	
H(32)	244	−27	−338	
H(41)	492	92	−160	
H(51)	374	383	−136	
H(52)	519	452	−257	
H(N1)	199	525	−386	
H(N2)	318	442	−530	

The numbering scheme of hydrogen atoms is based on the number of the atom attached to the hydrogen atom.

TABLE 3. INTERATOMIC DISTANCES WITH THE ESTIMATED STANDARD DEVIATIONS IN PARENTHESES

	l/Å		l/Å
Cd–Cd^{I}	3.638(1)	C(1)–C(2)	1.538(4)
		C(2)–N	1.494(6)
Cd–Cl(1)	2.585(2)	C(2)–C(3)	1.529(6)
Cd–Cl(2)	2.617(2)	C(3)–C(4)	1.540(5)
Cd–Cl(1)^{I}	2.636(2)	C(4)–O(3)	1.432(6)
Cd–Cl(2)^{II}	2.643(2)	C(4)–C(5)	1.529(6)
Cd–O(1)	2.347(3)	C(5)–N	1.499(5)
Cd–O(2)^{II}	2.303(3)	N···O(2)	2.615(5)
O(1)–C(1)	1.260(6)		
O(2)–C(1)	1.256(6)	N···O(3)^{III}	2.825(6)

Key to symmetry operations: I. $-x$, $0.5+y$, $-z$; II. $-x$, $-0.5+y$, $-z$; III. $1.0-x$, $0.5+y$, $-1.0-z$.

TABLE 4. BOND ANGLES, WITH THE ESTIMATED STANDARD DEVIATIONS IN PARENTHESES

	ϕ/°		ϕ/°
Cl(1)–Cd–Cl(2)	95.17(6)	C(3)–C(2)–N	103.9(3)
Cl(1)–Cd–O(1)	90.47(8)	C(2)–C(3)–C(4)	106.9(3)
Cl(1)–Cd–O(2)^{I}	95.97(9)	C(3)–C(4)–O(3)	109.8(3)
Cl(2)–Cd–O(1)	91.60(8)	C(3)–C(4)–C(5)	105.1(3)
Cl(2)–Cd–O(2)^{I}	92.61(9)	C(5)–C(4)–O(3)	110.5(4)
O(1)–C(1)–O(2)	126.3(3)	C(4)–C(5)–N	104.6(3)
O(1)–C(1)–C(2)	117.3(4)	C(5)–N–C(2)	105.4(3)
O(2)–C(1)–C(2)	116.4(4)		
C(1)–C(2)–C(3)	115.2(3)	C(4)–O(3)···N^{II}	141.9(3)
C(1)–C(2)–N	107.7(3)		

Key to symmetry operations: I. $-x$, $-0.5+y$, $-z$; II. $1.0-x$, $-0.5+y$, $-1.0-z$.

that the nitrogen atom in the pyrrolidine ring is close to the carboxyl oxygen atom. They have reported that

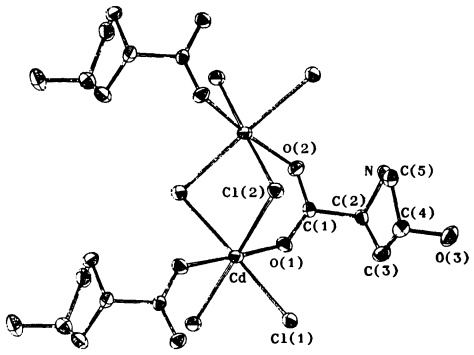

Fig. 1. The perspective drawing of $CdCl_2$(Hhpro) and the numbering scheme of non-hydrogen atoms.

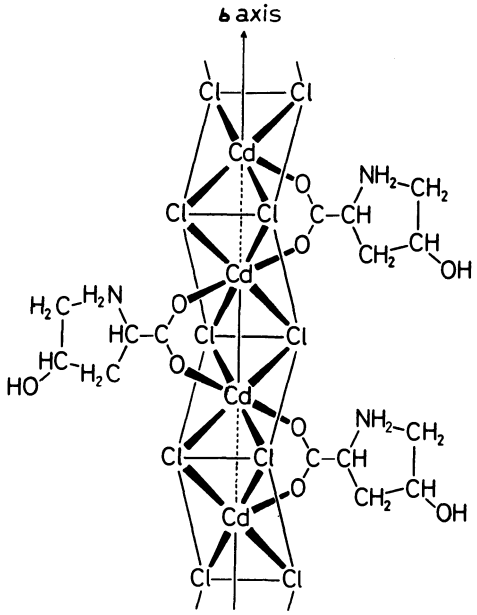

Fig. 2. The sketch of the structure.

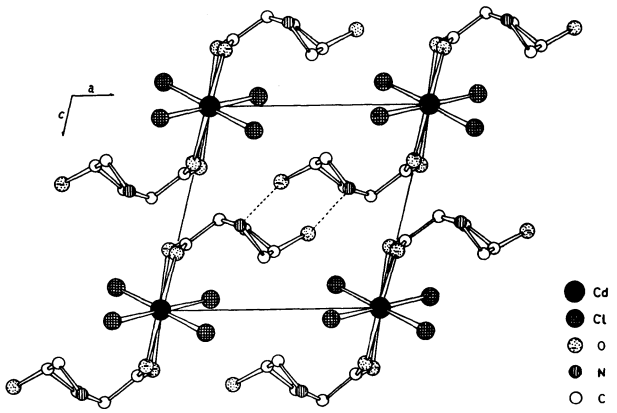

Fig. 3. The projection of the structure along the b axis. ------: Hydrogen bonding.

an unusual intramolecular hydrogen bond exists between these atoms: this intramolecular hydrogen bond remains after the coordination to cadmium atoms.

In the free molecule the four atoms of a pyrrolidine ring are nearly coplanar, except for the carbon atom carrying a hydroxyl group. On coordination, however, the pyrrolidine ring is bent on the line from N to C(3)

and C(4) and C(5) atoms deviate from the best-plane of the pyrrolidine ring. Some bond angles, N-C(2)-C(3), N-C(2)-C(1) and C(2)-N-C(5), are smaller than those of the free molecule, and other angles, C(1)-C(2)-C(3) and C(3)-C(4)-C(5), are larger.

The projection along the b axis is given in Fig. 3. The zigzag folding screen is parallel to the b axis with the cadmium atoms lying on the corners and on the middle of the b axis of the unit cell. It is connected with the neighboring one by hydrogen bonds between the nitrogen atom in the pyrrolidine ring and the hydroxyl oxygen atom, as indicated with broken lines in Fig. 3. Thus, a sheet forms parallel to the (101) plane. The whole structure is made up of these sheets, stacked together, only with van der Waals' contacts.

There are a few infinite folding screen structures: $CuCl_2$(1,2,4-triazole),[7] $Cu(benzoato)_2 \cdot 3H_2O$,[8] $CuCl_2$-(*N*-nitrosodimethylamine).[9] Each ligand of these complexes has two adjacent atoms which coordinate to form the structure favorably. In the case of Hhpro there is the nitrogen atom of pyrrolidine ring as a coordinating atom besides the carboxyl oxygen atoms. In general both of them coordinate to a metal, but only carboxyl group coordinates to cadmium atoms in $CdCl_2$(Hhpro). Since the preparation conditions of the complex were at rather low pH, the Hhpro behaves as a zwitter ion,

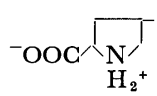

and the nitrogen atom will not be able to coordinate to a cadmium atom. This suggestion was confirmed by infrared spectra.

The infrared spectra of the free ligand, the deuterated ligand, $CdCl_2$(Hhpro), and the deuterated complex are shown in Fig. 4. The deuterated compounds were obtained by recrystallization from 99.75% D_2O. It has been established that the free ligand molecule is a zwitter ion, and the peaks in the region above 3000 cm^{-1} shift, by deuteration, from 2500 cm^{-1} to 2000 cm^{-1}. These peaks are assigned to an OH stretching vibration and to NH stretching vibrations.[10] The peaks at 1637 cm^{-1} and 1429 cm^{-1} shift to 1133 cm^{-1} and 993 cm^{-1}, respectively. In $CdCl_2$(Hhpro), similarly, the peaks in the region above 3000 cm^{-1} shift from 2500 cm^{-1} to 2250 cm^{-1} (the peak at 3475 cm^{-1} is assigned to an OH stretching vibration, and the others are NH stretching vibrations[11,12]), and the peaks at 1532 cm^{-1} and 1360 cm^{-1} shift to 1145 cm^{-1} and 1000 cm^{-1}, by deuteration respectively. If the ligand in $CdCl_2$(Hhpro) contained NH instead of NH_2^+, only one bending vibration should be observed. Since two corresponding peaks of NH bending vibrations are observed, the ligand can be regarded as a zwitter ion.

The characterization study of some metal complexes with Hhpro has been carried out in our group and will be published soon.

The authors wish to express their thanks to Professor Yoichi Iitaka for the X-ray diffractometer measurements, and to Dr. Shoichi Sato, The University of Tokyo for the helpful discussions. They would also like to thank Dr. F. S. Howell of Sophia University for correcting this manuscript. The present work was partially supported by a Grant-in-Aid for Scientific Research No. 547045 from the Ministry of Education, Science and Culture.

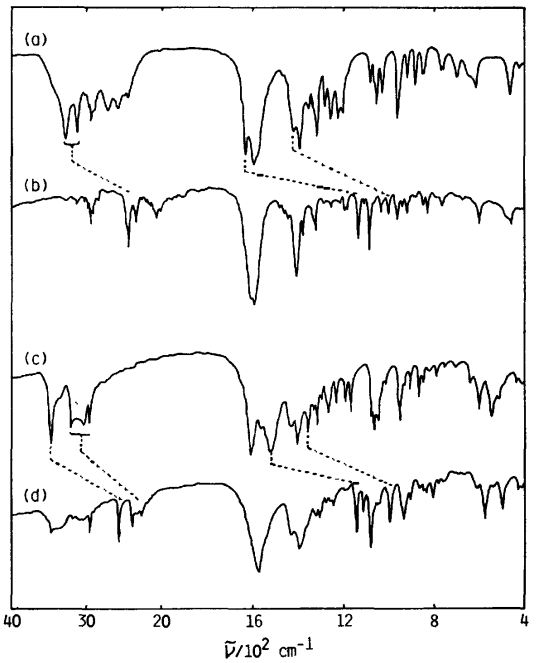

Fig. 4. Infrared spectra of (a) Hhpro, (b) the deuterated ligand, (c) $CdCl_2$(Hhpro), and (d) the deuterated complex. The shifts of the peaks by deuteration are indicated by the dotted lines.

References

1) J. Donohue and K. N. Trueblood, *Acta Crystallogr.*, **5**, 419 (1952).
2) T. F. Koetzele, M. S. Lehmann, and W. C. Hamilton, *Acta Crystallogr., Sect. B*, **29**, 231 (1973).
3) "The Universal Crystallographic Computation Program System (UNICS)," ed by T. Sakurai, Crystallographic Society of Japan, Tokyo (1967).
4) LINUS, H. Coppens and W. C. Hamilton, *Acta Crystallogr., Sect. A*, **26**, 71 (1970).
5) "International Tables for X-Ray Crystallography," Kynoch Press, Birmingham, U. K. (1974), Vol. IV.
6) The final thermal parameters and the final F_o-F_c table are deposited as Document No. 8246 at the Office of the Editor of the Bulletin of the Chemical Society of Japan.
7) J. A. J. Jarvis, *Acta Crysrtallogr.*, **15**, 964 (1962).
8) H. Koizumi, K. Osaki, and T. Watanabe, *J. Phys. Soc. Jpn.*, **18**, 117 (1963).
9) U. Klement, *Acta Crystallogr., Sect. B*, **25**, 2460 (1969).
10) M. J. Deveney, A. G. Walton, and J. L. Koenig, *Biopolymers*, **10**, 615 (1971).
11) L. J. Bellamy, "The Infrared Spectra of Complex Molecules," 3rd ed, Chapman and Hall, London (1975), pp. 107—128, 263—276.
12) K. Nakamoto, "Infrared and Raman Spectra of Inorganic and Coordination Compounds," John Wiley and Sons, Now York (1978), pp. 305—312.

Intercalation Compounds of FeOCl. Systematics of Amine Containing Lewis Base Intercalants

Yonezo MAEDA,* Miyako YAMASHITA, Hiroki OHSHIO,
Naoto TSUTSUMI, and Yoshimasa TAKASHIMA
Department of Chemistry, Faculty of Science, Kyushu University 33, Hakozaki, Higashi-ku, Fukuoka 812
(Received December 7, 1981)

New intercalated compounds of FeOCl and aniline derivatives were synthesized by soaking FeOCl in ethanol solution containing Lewis base intercalants. Only those Lewis base intercalants whose acid-dissociation constant is greater than 5 intercalate into the lattice of FeOCl. The acid-strength of the solvent is important for the formation of an intercalation compound. The intercalates of iron(III) chloride oxide $FeOCl(G)_{1/n}$ have been characterized by elemental analysis, powder pattern of X-ray diffraction, Fe-57 Mössbauer and infrared spectroscopies. The research on expansion of the b-axis of the unit cell and IR data confirm the location of the "guest" molecule within the van der Waals layer or the FeOCl lattice. Effective vibrating mass and lattice temperature derived from the Mössbauer spectra are affected by chemical bonding in the first coordination sphere of the iron atom.

Iron(III) chloride oxide (host matrix) is a layered compound whose crystal structure consists of a stack of double sheets of *cis*-$FeCl_2O_4$ octahedra, linked together with shared edges.[1] The length of the crystallographic b axis (c<a<b) perpendicular to the van der Waals plane (chlorine atom planes) increases along with the progress of intercalation. It has been shown recently that layered FeOCl reacts chemically with ammonia,[2] pyridine,[3,4] pyridine derivatives,[5] and phosphine[6] to give intercalated products.

It is not possible at present to predict whether a particular guest molecule will be able to intercalate or not into the FeOCl lattice. This is due to deficient knowledge of the intercalation of host lattice/guest species and of the influence of kinetics on solid state reactions. Lewis base (guest molecule) aniline does not intercalate into the layered plane of the van der Waals bonding. However, some derivatives of aniline have been found to intercalate into this plane in the present study. Our investigation indicates that a large number of layered compounds form intercalates when treated with Lewis bases of $pK_a>5$ and that the rate of the intercalation depends upon acid-strength of the solvent used.

The present study was also undertaken to examine the interlayer spacing and hence the molecular packing, the hyperfine interactions, lattice dynamics and vibrational spectra of the intercalate system.

Experimental

Sample Preparation. Iron(III) chloride oxide was prepared from Fe_2O_3 and $FeCl_3$ by the usual sealed tube technique discussed in the literature,[7] and was characterized by colorimetric iron determination and X-ray powder patterns. The intercalates listed in Table 1 were obtained by soaking FeOCl in the Lewis base or in the base dissolved in a dehydrated solvent. The experimental conditions for preparation of the compounds and analytical data are summarized in Tables 1 and 2. The stoichiometry was obtained by calculating iron and carbon contents. The progress of the intercalation was followed by X-ray observation of decay in the strongest (010) plane of FeOCl. At the end of the reaction period, the reaction mixture was filtered through sintered glass, the solid product was washed with absolute alcohol, dried *in vacuo*, and stored under nitrogen. The solvents used were dehydrated to avoid the influence of water. The reflection lines due to the (010) and (020) planes of the intercalates were used to calculate the length of the b-axis of the unit cell. The b-axis parameters are listed in Table 1.

Spectroscopy. Mössbauer measurements were carried out with an Austin Science Associates(ASA) spectrometer. The Iron-57 Mössbauer spectra of a powdered thin sample of the compound were recorded between 80 and 300 K using an ASA cryostat. A cobalt-57 source diffused into palladium foil was used. The isomer shift, δ_{Fe} was measured relative to the center of the spectrum of an iron foil enriched with iron-57 at 296 K, which was also used as a standard material for the velocity calibration. Calculation of Mössbauer spectroscopic

TABLE 1. PREPARATIVE CONDITIONS AND pK_a FOR $FeOCl(G)_{1/n}$ INTERCALATES

Intercalates	n[a]	Reaction time / d	Reaction temp / °C	Solvent	b[b] / Å	pK_a
8-Aminoquinoline	5	7	60	Et[c]	15.54	—
N,N-Dimethylaniline	9	1	29	—	13.91	5.10
p-Methoxyaniline	6	2	60	Et	14.39	5.30
p-Phenylenediamine	9	3	20	Et	13.61	6.16
					11.42	
p-Aminophenol	4	18	20	Et	13.78	5.50
p-Aminodiphenylamine	15	14	20	Et	13.35	—
p-Methylaniline	12	7	23	Et	13.68	5.10

a) $FeOCl(G)_{1/n}$. b) A b is the unit cell dimension of b-axis. The easy cleavage plane is perpendicular to the b direction.
c) Et: Ethanol.

Table 2. Analytical data for $FeOCl(G)_{1/n}$ intercalates

Intercalates	Calcd (%)				Found (%)			
	C	H	N	Fe	C	H	N	Fe
8-Aminoquinoline	17.07	1.58	3.98	39.67	17.14	1.74	3.90	39.90
N,N-Dimethylaniline	8.84	1.02	1.29	46.24	8.90	1.94	1.21	45.11
p-Methoxyaniline	10.96	1.18	1.83	43.68	11.59	1.73	1.77	44.89
p-Phenylenediamine	7.71	0.75	2.61	46.80	7.11	1.63	2.54	43.62
p-Aminophenol	13.44	1.32	2.61	41.65	12.05	1.89	2.30	41.01
p-Aminodiphenylamine	8.04	0.67	1.56	46.70	8.41	1.91	1.53	46.88
p-Methylaniline	6.03	0.65	1.00	48.05	5.62	2.25	0.95	47.63

data was effected using the least squares method at the Computer Center, Kyushu University. The infrared spectra of the samples in the potassium bromide region (650—4000 cm^{-1}) were obtained using a Hitachi Grating Infrared Spectrophotometer, type 215. X-Ray powder diffraction patterns of the samples were observed using a Rigakudenki Geigerflex Diffractrometer model DF.

Results and Discussion

Lattice Parameter of Intercalated FeOCl. The b-axis parameters of intercalated FeOCl are listed in Table 1 for compounds which attained a reproducible limiting composition. The X-ray powder pattern can be understood on the basis of an expansion of every layer ("stage 1" compound) in the direction of the b-axis of the unit cell. The powder X-ray diffraction patterns of the FeOCl intercalation compounds are usually dominated by (010) and (020) lines. The diffraction lines in a- and c-axis of the unit cell cannot be observed. However, they are assumed not to be significantly different from those in FeOCl pyridine intercalated compounds except that the b-axis parameter has variable values.[3,4] There are several possible orientations which a non-cubic symmetry guest molecule can adopt with respect to the van der Waals planes. In particular, it is interesting to ascertain the orientation of the nitrogen lone pair electrons with respect to the van der Waals plane. The b-axis parameter of 7.91 Å for FeOCl becomes about 13—14 Å for aniline derivatives and for *p*-aminodiphenylamine intercalates whose values are nearly equivalent to 13.27 Å for $FeOCl(pyridine)_{1/3}$. On the other hand, the b-axis parameter for 8-aminoquinoline intercalation is 15.54 Å. The value of 15.54 Å is the maximum in FeOCl intercalated compounds and the interlayer spacing of this compound is calculated to be 7.63 Å. Several structural models are proposed in Fig. 1 to account for the orientation of the Lewis bases, guest molecules in the FeOCl lattice. Substituting the hydrogen in the 4-position of a phenyl ring with a bulky group brings about lower content of the guest molecule with no increase in the b-axis parameter. This phenomena can be understood with model (a) of Fig. 1, which shows the orientation of Lewis bases in the FeOCl lattice.

The powder X-ray diffraction pattern for $FeOCl(p\text{-phenylenediamine})_{1/9}$ suggests that there are two orientations for the guest molecule in this sample, as shown in Fig. 1(b). The superhyperfine pattern could not be observed in the X-ray and electron diffraction patterns. However, it seems reasonable to infer that the presence of the two b-axis parameters is due to the superlattice structure as shown in Fig. 1(b), rather than due to a mixture of the 13.61 Å b-axis parameter sample with the 11.42 Å b-axis parameter sample, although we do not have any evidence for this. The larger b-axis parameter (13.61 Å) is in the same range as that for the FeOCl intercalation compound of aniline derivatives. The interlayer spacing parameter of 3.51 Å is calculated for the part with b-axis parameter of 11.42 Å. In the case of $FeOCl(NH_3)_{3/4}$ an increase of 3.42 Å in the direction of the b-axis of a unit cell has been observed.[2,4] The thickness of the plane of a phenyl ring is assumed to be about 2.0 Å. Accordingly the b-axis expansion of 3.51 Å in this compound would account for an orientation such that the phenyl plane of *p*-phenylenediamine is parallel to the van der Waals plane.

Acid-dissociation Constant and the Rate of Intercalation. All the values of the acid-dissociation constants, pK_a, of the guest molecule listed in Table 1 are larger than 5. The substituted aniline derivatives which could not

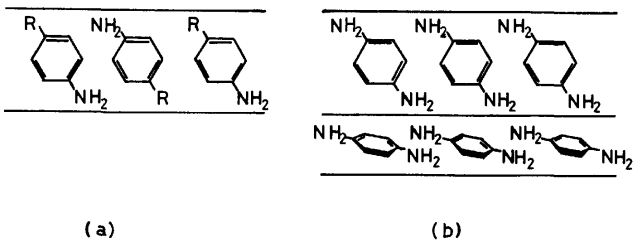

(a) (b)

Fig. 1. The orientations assumed for aniline derivatives (a) and for phenylenediamine (b) within the FeOCl layer lattice. The chlorine atom layers of the matrix are shown by straight lines.

Table 3. Chemical and physical properties of the solvents

Solvents	pK_a[a]	ε[b]	D[c]	η[d] (at 20 °C)	$\frac{t}{d}$[e]
Ethylene glycol	—	38	—	17.33	30
Methanol	16—18	33.2	11.7	0.61	3
Ethanol	18	24.3	1.69	1.19	7
2-Propanol	18	18.3	1.6	2.39	1/4

a) Acid dissociation constant. b) Dielectric constant. c) Dipole moment ($D=10^{-18}$ cgs). d) Viscocity (cP= 10^{-3} N s m^{-2}). e) Reaction time required to complete the intercalation.

intercalate into the FeOCl lattice are *p*-nitroaniline ($pK_a=1.0$), *p*-chloroaniline ($pK_a=4.0$), aniline-4-sulphonic acid ($pK_a=3.2$), and aniline ($pK_a=4.6$). It can be inferred that a neccesary (but not sufficient) condition for forming the FeOCl intercalation of these molecules under the conditions discussed above is that pK_a of guest molecule must be larger than 5. The analogous phenomena have been observed in pyridine intercalation of FeOCl[4] and TaS_2.[8] Table 3 shows the physical properties of various solvents and the relative rate of the intercalation when FeOCl(*p*-methylaniline)$_{1/12}$ is prepared in these solvents. The rate of the intercalation examined in this study depends upon the acid-strength of the solvents, as have been reported by Gerrard and Macklen.[9] The order of acid-strength is ethylene glycol≫methanol>water>ethanol >1-butanol>2-propanol. However, we must take into consideration the dielectric constant of the solvents because there are not such great differences in the pK_a values of the solvents examined; it is reasonable to consider that van der Waals bonding in liquid-solid systems may depend upon the dielectric constant of the solvent. Thus the Lewis base *p*-methylaniline could not intercalate into FeOCl lattice in a solvent of acetone, benzene, chloroform, dichloromethane, isopentyl alcohol, hexane, nitrobenzene, nitromethane, pentane, tetrahydrofuran, toluene, or trichloroethylene.

Mössbauer Spectra and Lattice Dynamics. The X-ray powder pattern can be understood as showing the formation of a "stage 1" compound in which every van der Waals layer includes an array of "guest" molecules. All the Mössbauer spectra were doublets, although the stoichiometry of the intercalation compounds examined in this study shows that not all of the iron atoms in FeOCl(G)$_{1/n}$ are structurally identical. The Mössbauer parameters for the FeOCl intercalates are summarized in Table 4. Full width at half-maximum (0.32—0.40 mm s^{-1}) is somewhat larger than natural line width. The full width at half-maximum of FeOCl(*p*-phenylenediamine)$_{1/9}$ is in the same range as that for other intercalates, which supports the view that all iron atoms of FeOCl(*p*-phenylenediamine)$_{1/9}$ are situated in the same coordination sphere, that is, in the structure of a mixed phase as shown in Fig. 1(b).

Mössbauer spectra for selected samples were measured at various temperatures to calculate the effective vibration mass and "lattice temperature" for the intercalation compounds. Using a Debye model for the solid, and assuming that the appropriate mass of the probe atom corresponds to the free-atom value, leads to a temperature dependence of the recoil-free fraction f, given by[10]

$$\mathrm{d}\ln f/\mathrm{d}T = -6E_R/k_B\theta_M^2 \quad (1)$$

in which E_R is the recoil energy after gamma ray emission and k_B is Boltzmann's constant. At temperatures well above the magnetic ordering temperature, the temperature dependence of the area under the resonance curve can be used to estimate a "lattice temperature," θ_M' based on the thermal motion of the Mössbauer active atom. In the case of ^{57}Fe Mössbauer data, two "lattice temperatures" can be calculated from the temperature dependence of the area under the resonance curve. In Eq. 1 $\mathrm{d}\ln f/\mathrm{d}T$ can be replaced for a thin absorber by the $\mathrm{d}\ln A/\mathrm{d}T$ (the temperature dependence of the area under the resonance curve) to yield the following relationship

$$\theta_M = \frac{E_\gamma}{C}\left[\frac{-3}{M_{eff}k_B\mathrm{d}\ln[A(T)/A(80)]/\mathrm{d}T}\right]^{1/2} = 11.659\left[\frac{-\mathrm{d}\ln(A(T)/A(80))}{\mathrm{d}T}\right]^{-1/2}. \quad (2)$$

A limitation of this approach is that when the Mössbauer active atom is incorporated in the solid by largely covalent bonding forces, the appropriate mass needed to describe its motion may be significantly larger than the atomic mass. The effective vibrating mass can frequently be estimated from the second order Doppler

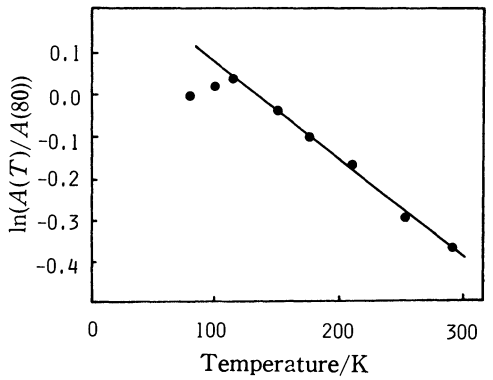

Fig. 2. Temperature dependence of the normalized ln (Area) parameter for FeOCl(8-aminoquinoline)$_{1/5}$.

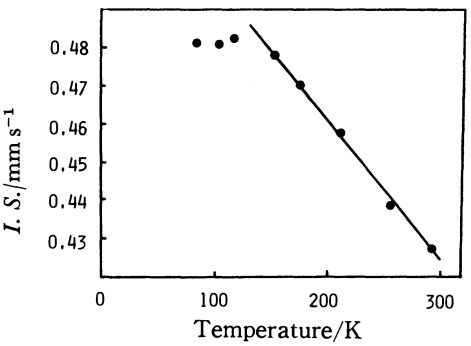

Fig. 3. Temperature dependence of the *I.S.* parameter for FeOCl(8-aminoquinoline)$_{1/5}$.

TABLE 4. MÖSSBAUER PARAMETERS OF FeOCl(G)$_{1/n}$ INTERCALATES

Intercalates	*I.S.*[a]		*Q.S.*[b]	
	80 K	297 K	80 K	297 K
8-Aminoquinoline	0.48	0.43	1.14	0.74
N,N-Dimethylaniline	0.47	0.39	1.11	0.69
p-Methoxyaniline	0.49	0.44	0.84	0.77
p-Phenylenediamine	0.51	0.41	1.01	0.72
p-Aminophenol	0.49	0.47	0.93	0.68
p-Aminodiphenylamine	0.37	0.38	0.93	0.74
p-Methylaniline	0.44	0.40	0.82	0.73

a) Isomer shift/mm s^{-1}. b) Quadrupole splitting/mm s^{-1}.

Table 5. Effective vibrating mass and lattice temperatures of $FeOCl(G)_{1/n}$ intercalates

Intercalates	M_{eff}/mass unit[a)]	θ_M/K[b)]	θ'_M/K[c)]	T_{range}/K
8-Aminoquinoline	115±1	240±5	169±7	150—297
N,N-Dimethylaniline	72±1	d)	d)	170—297
p-Aminodiphenylamine	85±1	270±6	222±8	225—297

a) Effective vibrating mass. b) Lattice temperature. c) Modified lattice temperature. d) This value is not calculated because plots of ln $(A(T)/A(80))$ show a linear curve only above 250 K.

shift, as follows:

$$M_{eff} = -4.168 \times 10^{-2}[d(IS)/dT]^{-1}. \quad (3)$$

Using this value for M_{eff} in Eq. 2, a modified "lattice temperature" θ'_M is calculated as follows:

$$\theta'_M = 4.3202 \times 10^2 \left[\frac{d(IS)/dT}{d\ln(A(T)/A(80))/dT}\right]^{1/2}. \quad (4)$$

Figures 2 and 3 show the temperature dependence of the ln $(A(T)/A(80))$ and isomer shift for FeOCl(8-aminoquinoline)$_{1/5}$, respectively. Linear regressions for both parameters were obtained above 150 K. The temperature ranges (T_{range}) for each sample in which a linear regression is maintained are listed in Table 5. The Mössbauer spectra become highly complex below 120 K because the magnetic ordering temperature of the intercalation compounds is about 120 K but is not sharply defined.

FeOCl (*N,N*-dimethylaniline)$_{1/9}$ does not give a linear curve for the temperature dependence of ln A because of the interference of the magnetic hyperfine structure at low temperature (<250 K). It is well known that a solution of *N,N*-dimethylaniline products triphenylmethane dye in the presence of an iron ion. A deep blue color appears in the process of preparing FeOCl-(*N,N*-dimethylaniline)$_{1/9}$ and letting the solution stand overnight brings about decomposition of the intercalation compound. This observation suggests that FeOCl-(*N,N*-dimethylaniline)$_{1/9}$ may not be pure material although no other peaks except those due to the intercalates are observed in X-ray powder pattern.

The fact that $\theta_M/\theta'_M > 1$, as understood from Table 5, leads to the conclusion that M_{eff} is substantially larger than the free-atom value in consonance with covalency of the iron atom bonding in the matrix. However, the concomitant b-axis expansion of the unit cell does not significantly affect the effective mass and "lattice temperature." Therefore, the significance of these data lies in the conclusion that M_{eff} and θ_M are significantly affected by the chemical bonding in the first coordination sphere of iron atoms.

The temperature dependence of the quadrupole splitting parameter for FeOCl (1.0×10^{-4} mm s^{-1} deg^{-1})[4)] is very small as shown in Fig. 4. However, most of the FeOCl intercalates examined in the present study show sigmoidal temperature dependence in the quadrupole hyperfine interaction. The value of the quadrupole hyperfine interaction in the intercalates is larger than that observed for FeOCl at low temperature and decreases at high temperatures, as listed in

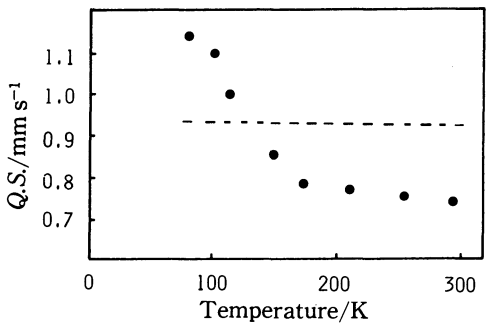

Fig. 4. Temperature dependence of the *Q.S.* parameter for FeOCl(8-aminoquinoline)$_{1/5}$. The dashed line represents the comparison data for unintercalated FeOCl over the same temperature range.

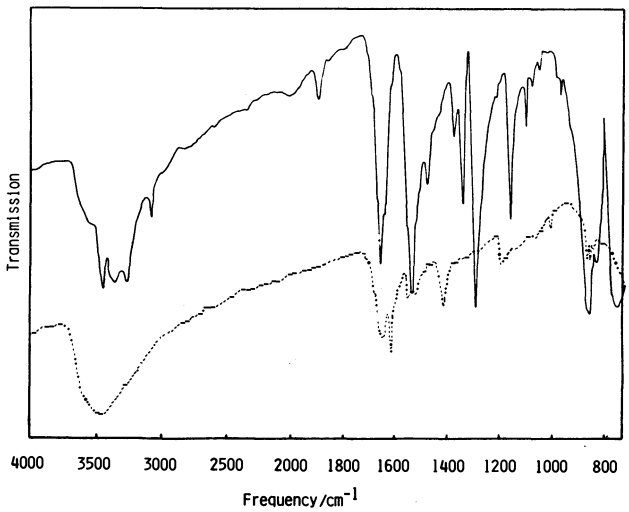

Fig. 5. Infrared spectra of FeOCl(*p*-phenylenediamine)$_{1/9}$ (dotted curve) and *p*-phenylenediamine (full curve).

Table 4.

Infrared Spectra. Some of the IR spectra of the FeOCl intercalates are shown in Figs. 5—8. The FeOCl matrix has absorptions at the bands 1640 (s) and 1400—1500(w) cm^{-1}. Most notable in a comparison between the FeOCl and the intercalation compounds are the facts that the out-of-plane bending modes of phenyl (700—800 cm^{-1}) are clearly noted in the intercalation compounds and that the ring expansion modes between 960—1200 cm^{-1} are strongly suppressed in the intercalate spectra. These observations indicate that the orientation of the aniline derivatives molecule is such that the plane of the aniline ring is perpendicular to the van der Waals layer, except in the case of FeOCl (*p*-phenylenediamine)$_{1/9}$.

In the IR spectrum of FeOCl (*p*-phenylenediamine)$_{1/9}$ the strong C–N stretching band at 1275 cm^{-1} (unintercalate base) is strongly suppressed as shown in Fig. 5. The bands at 1320 and 1352 cm^{-1} of phenyl origin are shifted to 1398 cm^{-1} or suppressed in the intercalation. The band at 1140 cm^{-1} is shifted to 1178 cm^{-1} in the intercalate. The ring expansion bands in plane (960—1200 cm^{-1}) are observed and a new sharp band appears at 1600 cm^{-1} in the intercalate. The IR

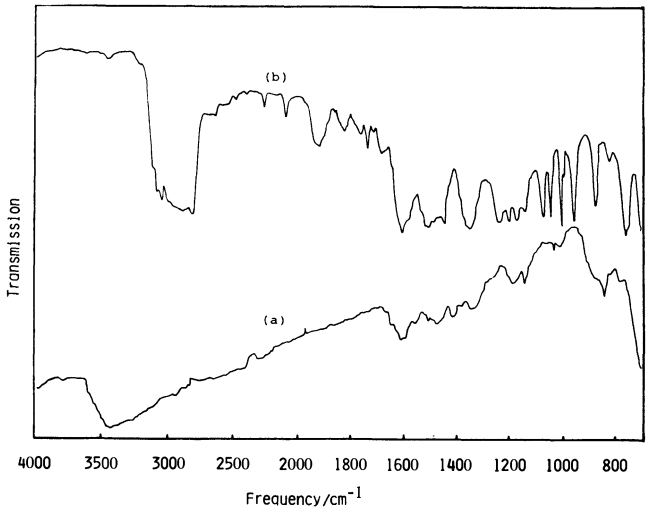

Fig. 6. Infrared spectra of FeOCl(N,N-dimethylaniline)$_{1/9}$ (a) N,N-dimethylaniline (b).

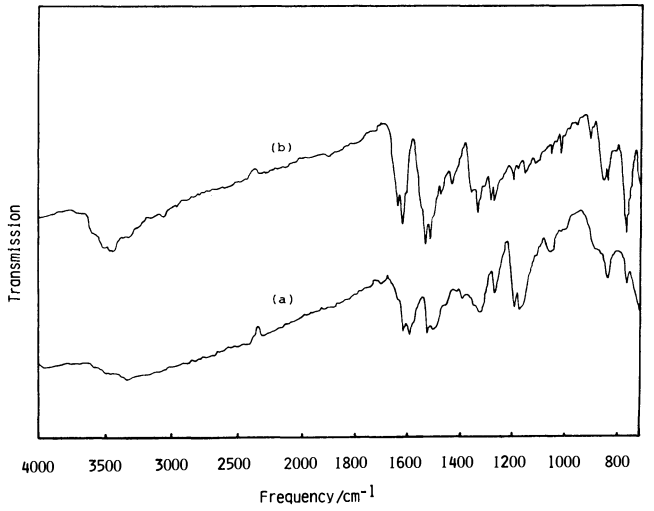

Fig. 7. Infrared spectra of FeOCl(p-aminodiphenylamine)$_{1/15}$ (a) and p-aminodiphenylamine (b).

spectrum of FeOCl (N,N-dimethylaniline)$_{1/9}$ in a KBr matrix is shown in Fig. 6. The symmetric stretching band of C–H in the methyl group at about 2814 cm^{-1} in the unintercalated base, the methyl group asymmetric deformation observed at 1459 cm^{-1} (liquid) and the ring expansion band in the plane between 1200 and 960 cm^{-1} (unintercalate) are not observed in the intercalate. Figure 7 shows the IR spectrum of FeOCl-(p-aminodiphenylamine)$_{1/15}$ in which new bands appear at 1580(s), 1180(s), 1160(s), and 1040(m) cm^{-1} The absorption due to tertiary amine at 1515 cm^{-1} (unintercalate base) is observed at the same position. Most of the bands of the base are observed in the intercalate, although the band at 750 cm^{-1} becomes weak in the intercalate. In the IR spectrum of FeOCl(p-aminophenol)$_{1/4}$ (Fig. 8) the ring expansion bands at 1100, and 983 cm^{-1} and the band at about 900 cm^{-1} (observed in unintercalate base) are not observed, and the phenyl band at 1490 cm^{-1} becomes weak in the intercalate.

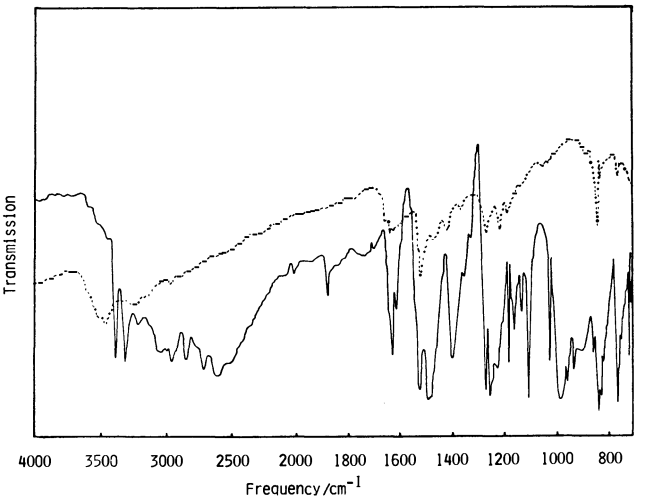

Fig. 8. Infrared spectra of FeOCl(p-aminophenol)$_{1/4}$ (dotted curve) and p-aminophenol (full curve).

It is notable that most of the absorptions observed in unintercalated base are observed in the IR spectrum of FeOCl(p-methoxyaniline)$_{1/6}$, except for the N–H stretching band at about 2900—3000 cm^{-1}. These data reflect a significant non-bonding (Coulomb) interaction between the base and van der Waals chlorine planes. The datum of FeOCl(p-methylaniline)$_{1/12}$ shows that the C–N stretching band of the methyl group is suppressed.

The molecular diameter of an aniline molecule is estimated to be about 4—5.3 Å on the ring plane and the ring thickness to be about 2.0 Å. The observed b-axis expansion of FeOCl intercalation is 5.4—6.5 Å and indicates that the orientation of aniline-derivatives molecule is perpendicular to the van der Waals layer. Within that restriction, two extreme orientations of the intercalant are still possible; an imaginary C_{2v} axis of aniline ring plane is either parallel to or perpendicular to the a direction of the FeOCl lattice. However, no clear-cut distinction between the two orientations can be drawn from the present data alone. The suppression of C–N stretching band supports the view that a lone-pair electron on the nitrogen atom coordinates to the iron atom, *viz.* the coordination structure drawn in Fig. 1.

References

1) M. D. Lind, *Acta Crystallogr., Sect. B*, **26**, 1058 (1970).
2) P. Hagenmuller, J. Portier, B. Barbe, and P. Bouclier, *Z. Anorg. Allg. Chem.*, **355**, 209 (1967).
3) S. Kikkawa, F. Kanamaru, and M. Koizumi, *Bull. Chem. Soc., Jpn.*, **52**, 963 (1979).
4) R. H. Herber and Y. Maeda, *Inorg. Chem.*, **20**, 1409 (1981).
5) R. H. Herber and Y. Maeda, "Proceedings of the Conference on Nuclear and Electron Resonance Spectroscopies Applied to Materials Science," ed by E. N. Kaufmann and G. K. Shenoy, North-Holland Publishing Co. Amsterdam (1981).
6) R. H. Herber and Y. Maeda, *Inorg. Chem.*, **19**, 3411

(1980).
7) F. Kanamaru, S. Yamanaka, M. Koizumi, and S. Nagai, *Chem. Lett.*, **1974**, 373.
8) F. R. Gamble, J. H. Osiecki, and F. J. Di Salvo, *J. Chem. Phys.*, **55**, 3525 (1971).
9) W. Gerrard and E. D. Macklen, *Chem. Rev.*, **59**, 1105 (1961).
10) Y. Hazony and R. H. Herber, "Mössbauer Effect Methodology," ed by I. J. Gruverman and C. W. Seidel, Plenum Press, New York (1969), Vol. 8, p. 107.

The Phase Relation of the Titanium-Sulfur System

Masanobu SAEKI* and Mitsuko ONODA
National Institute for Research in Inorganic Materials, 1-1, Namiki, Sakura-mura, Niihari-gun, Ibaraki 305
(Received December 19, 1981)

The phase relation of the titanium–sulfur system was studied in the range from $TiS_{1.38}$ through $TiS_{1.96}$ at 900 °C by the use of the thermobalance method under controlled sulfur pressure. It was found that four phases, (a) Ti_2S_3 (4H) with a short-range ordering of titanium vacancies, (b) the superstructure of Ti_2S_3 (4H) due to the ordering of titanium vacancies, (c) Ti_2S_3 (4H), and (d) TiS_2 (2H), exist in this composition range. The Ti_5S_8 phase of the 12R type reported previously was not detected for any composition.

Several phases have been reported in the TiS–TiS_2 range, namely, TiS (2H), Ti_8S_9 (9R), Ti_4S_5 (10H), Ti_3S_4 (21R), Ti_2S_3 (4H), Ti_5S_8 (12R), and TiS_2 (2H).[1] (The structure designations in the Ramsdell notation are given in the parentheses). The structures are based on close-packed sulfur layers; hexagonal close packing for TiS or TiS_2, and more complex stacking sequences for the intermediate phases. Titanium atoms occupy octahedral holes in the sulfur framework. Polytypism was observed by Tronc and Huber[2] in the composition around $TiS_{1.70}$.

In the composition range near $TiS_{1.5}$, the existence of the 4H-type has been reported by Jeannin[3] from his study of the phase relation in the Ti–S system. The structure of this 4H-type was also studied by Wadsley[4] and by Norrby and Franzen;[5] it was described as follows: the stacking sequences of sulfur layers are represented by chchch.., that is, there is alternating cubic and hexagonal close packing. Titanium atoms occupy the octahedral holes fully and partially in the alternating titanium layers. Recently, the existence of two superstructures related to the 4H-type was found, and the atomic arrangements were determined by means of X-ray diffractometry and high-resolution electron microscopy.[6-8] These superstructure arise from the ordered arrangement of titanium vacancies in partially occupied titanium layers and have been designated as the $(4H)_2$ type and the $(4H)_3$ type respectively.

The phase diagram of the Ti–S system has not been established because of the discrepancies between the experimental data reported by different investigators, as has been pointed out by Kjekshus and Pearson,[9] and Jeannin.[10] The reasons for these discrepancies may be as follows: (1) an equilibrium state is difficult to be attained because of the sluggishness of the transformation rate or the existence of an energy subminimum state, or (2) in the previous investigations, studies were performed for quenched specimens. The high-temperature states might not be held through the quenching processes.

In the present work the phase relation was examined by means of a thermobalance method, that is, an *in situ* observation, under a sulfur partial pressure controlled by H_2S–H_2 mixture gas. The aim is to give the phase relation including the superstructure, which has not yet been reported in any phase diagrams in the Ti–S system. Although the P_{S_2}-composition relation was reported by Abendroth and Schleton,[11] their data were not sufficiently accurate for determining the phase relation.

Experimental

The starting materials, Ti_2S_3 and TiS_2, were prepared by the following procedure. A mixture of titanium metal powder (purity 99.0%) and sulfur (purity 99.9999%) was sealed in an evacuated silica tube and heated in an electric furnace. Reaction was allowed to take place for a few days at 350 °C and subsequently at 900 °C. Quenching was made to water.

The chemical compositions of the starting materials were determined by oxidizing them to TiO_2 at 800 °C in air for several hours. The titanium content was calculated from the weight of TiO_2, while the sulfur content was determined by the weight change in converting sulfide to oxide within a reproducibility of $x=\pm0.004$ in TiS_x.

About 2 g of the starting materials, Ti_2S_3 or TiS_2, were placed in a silica crucible and suspended by means of a silica spring balance in an electric furnace, into the bottom of which H_2S–H_2 mixture gas was introduced at the rate of 5.0 $cm^3\ s^{-1}$. To attain an equilibrium at 900 °C, the sample weight was allowed to change as a result of the absoption or libration of sulfur gas. The equilibrium composition was determined by an *in situ* observation, that is, a measurement of the increase or decrease in the length of the silica spring using a cathetometer. The attainment of an equilibrium state was judged by the following conditions: (1) the sample weight does not change with time, and (2) the compositions determined through a sulfurization process of a sulfur-poor material and through a desulfurization of a sulfur-rich material agree with one another in the same atmosphere.

The oxygen and H_2O in the H_2 and H_2S had to be removed, as titanium sulfide is easily oxidized. The oxygen in the H_2 was allowed to react with hydrogen, while the H_2O was eliminated by passing the mixture gas over P_2O_5. If these procedures had not been performed, the TiO_2 would have occured as an impurity. Once produced, TiO_2 could not be sulfurized easily in the H_2S–H_2 atmosphere at 900 °C. In the present work, the production of titanium oxide could be ignored during the experiment, because an identical P_{S_2}-compoistion relation was obtained in repeated equilibrating experiments.

For identification, the powder samples were prepared by heating weighed quantities of titanium and sulfur at 900 °C in evacuated silica tubes, after which they were quenched. The powder X-ray diffraction patterns were taken by the counter-diffractometer method using Ni-filtered Cu $K\alpha$ ration. Electron-diffraction patterns were taken from the crushed particles by means of the 100 kV electron microscope.

Results

Phase Relation in the Composition Range of $TiS_{1.38}$—

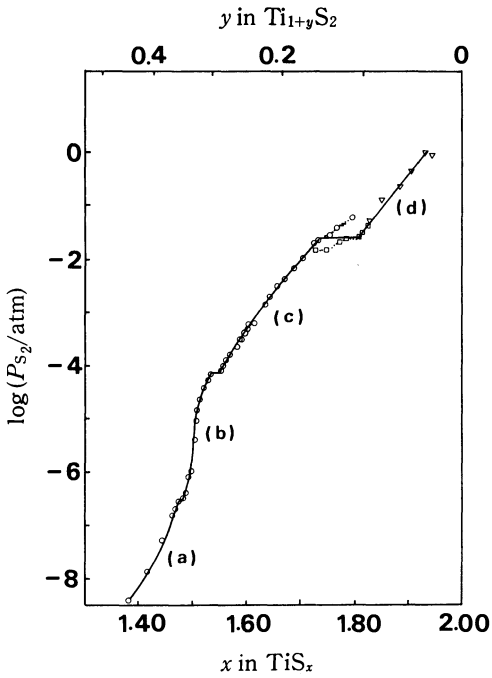

Fig. 1. P_{S_2}-composition relation of Ti–S system.
(a) is the range of Ti_2S_3 (4H) with short-range ordering of titanium vacancies, (b) the range of Ti_2S_3 $(4H)_{super}$, (c) the range of Ti_2S_3 (4H), and (d) the range of TiS_2 (2H).
○: Starting material; Ti_2S_3 (4H), method; H_2S–H_2 mixture gas, □: starting material; TiS_2 (2H), method; H_2S–H_2 mixture gas, ▽: starting material: TiS_2 (2H), method: quartz Bourdon gauge.

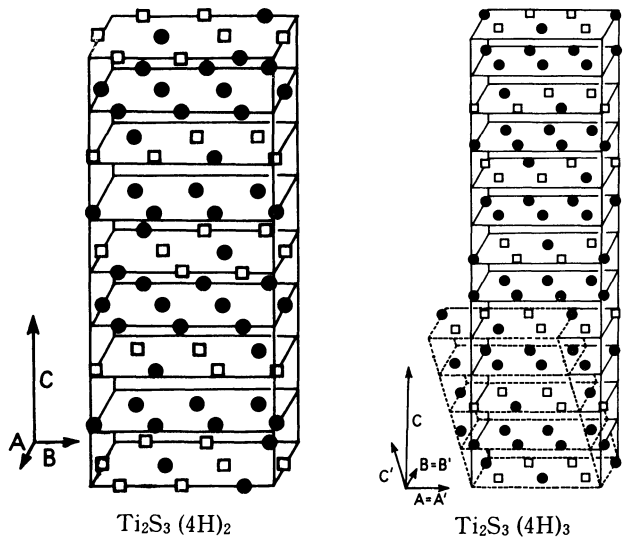

Fig. 2. Crystal structure of Ti_2S_3 $(4H)_2$ and Ti_2S_3 $(4H)_3$. For Ti_2S_3 $(4H)_2$ three axes of the monoclinic unit cell are represented by A, B, and C. For Ti_2S_3 $(4H)_3$, A, B, and C represent three axes of the rectangular unit cell, and A′, B′, and C′ represent them of the reduced monoclinic unit cell which is indecated by the dotted lines (see Ref. 5). Sulfur layers are eliminated.
●: Ti atoms, □: Ti vacancies.

$TiS_{1.96}$. The P_{S_2}-composition relation determined as described above is shown in Fig. 1. The P_{S_2} value was calculated from the gas-mixing ratio and the reaction temperature by the use of the thermodynamical data listed in the JANAF thermochemical tables.[12] Figure 1 shows that four ranges exist: (a)—$TiS_{1.475}$, (b) $TiS_{1.483}$—$TiS_{1.535}$, (c) $TiS_{1.550}$—$TiS_{1.730}$, and (d) $TiS_{1.810}$—. The details will be presented below.

(a) Phase up to the $TiS_{1.475}$ Composition: The powder X-ray diffraction pattern of the specimen quenched in the $TiS_{1.38}$—$TiS_{1.475}$ range was that of the Ti_2S_3 (4H) type. However, in the electron-diffraction pattern with an incident beam parallel to the c axis, super spots are observed. In order to assign the integral indices, the hexagonal cell constant, *a*, of the supercell was taken to be $\sqrt{3}$ times that of the 4H type. The diffuse-scattering distribution was observed along the super-spot rows in the pattern with an incident beam perpendicular to the c axis. These results suggest that titanium vacancies are in a long-range order state along the a and b axes and in a short-range order state along the c axis. A detailed analysis of the structure is now in progress.

(b) Phase in the $TiS_{1.483}$—$TiS_{1.535}$ Composition Range: The powder X-ray pattern of the quenched specimen at the composition of $TiS_{1.48}$—$TiS_{1.49}$ or $TiS_{1.51}$—$TiS_{1.53}$ was identical with that of the $(4H)_2$-type superstructure reported previously.[6] The quenched specimen at the composition close to $TiS_{1.50}$ exhibit a powder pattern of the $(4H)_3$ type superstructure whose data were also reported.[6] The superstructures, $(4H)_2$ and $(4H)_3$, arise from ordering of titanium atoms and vacancies in the partially occupied titanium layer and the piling up of the ordered-arrangement layers along the c axis. The titanium arrangements in $(4H)_2$ and $(4H)_3$ are shown in Fig. 2.

The P_{S_2}-composition curve in the (b) range in Fig. 1 does not indicate the boundary of the existence range of the two super-structures, $(4H)_2$ and $(4H)_3$. Either of the following two possibilities can be true; (1) Both the $(4H)_2$ and $(4H)_3$ types may appear at 900 °C within the (b) range; The phase boundary between $(4H)_2$ and $(4H)_3$ is not detected because the experimental procedure is insufficiently precise; or (2) only one of the two structures occurs at 900 °C, and the other appears through the quenching process. As it is difficult to decide which case occurs, the tentative designation "$(4H)_{super}$" is used for the phase in the $TiS_{1.483}$—$TiS_{1.535}$ range.

(c) Phase in $TiS_{1.550}$—$TiS_{1.730}$ Composition Range: Judging the result of X-ray and electron diffractometry, the structure of the quenched sample in this range is the same as that of Ti_2S_3 (4H).

(d) Phase in Compositions Richer in Sulfur than $TiS_{1.810}$: The sample richer in sulfur than $TiS_{1.810}$ gave powder patterns of the TiS_2 (2H) type. Because of the limitations in the sulfur partial pressure controlled by an H_2S–H_2 gas method, most of the P_{S_2} values of the TiS_2 phase shown in Fig. 1 were estimated from the total pressure measurement by means of a quartz Bourdon gauge. The details of the method and results were reported in a previous paper.[13]

Determination of the Phase Boundaries of Ti_2S_3 (4H) and TiS_2. The P_{S_2}-composition curve obtained by the sulfurization of Ti_2S_3 (4H) does not agree with that

obtained by the desulfurization of TiS_2 (2H) in the $TiS_{1.730}$—$TiS_{1.810}$ range, as is shown by the dotted lines in Fig. 1. The horizontal part, representing a two-phase region, does not emerge in this range, because the transformation process was so slow that the equilibrium state was not established. The quenched specimens gave the diffraction patterns of the mixture of TiS_2 (2H) and Ti_2S_3 (4H).

In order to estimate the length of time required to attain equilibrium in this range, powder specimens of Ti_2S_3 (4H) and TiS_2 (2H), put on different sides of an inverted U-type evacuated silica tube, were kept at 900 °C for a week. The quenched specimens on both sides differ from each other in composition and structure. Equilibrium was not established even after a week.

As has been described above, the phase boundary of Ti_2S_3 (4H) and TiS_2 (2H) could not be determined through the equilibration process. After the X-ray diffraction patterns were examined in detail, it was found that TiS_2 (2H) began to be formed at $P_{S_2}=0.023$ atm in the sulfurization process, while in the desulfurization process Ti_2S_3 (4H) began to be formed at the identical P_{S_2} value. This P_{S_2} value corresponds to that of the two-phase region, as is shown by the solid line in Fig. 1.

Discussion

The composition range corresponding to (a), (b), and (c) in Fig. 1 was regarded as a homogeneity range of the Ti_2S_3 (4H) phase by the previous researchers. In the present work, four phases, that is, (a) Ti_2S_3 (4H) with a short range order of titanium vacancies, (b) the superstructure of Ti_2S_3 (4H) due to the ordering of titanium vacancies, (c) Ti_2S_3 (4H), and TiS_2 (2H), were found by an *in situ* observation.

From the P_{S_2}-composition curve shown in Fig. 1, Gibbs free energies for the reactions at 900 °C were calculated:

$$TiS_{1.475}(4H) + ((1.483-1.475)/2)\ S_2(g) = TiS_{1.483}((4H)_{super})$$
$$\Delta G^\circ = (1/2)(1.483-1.475)RT \ln P_{S_2} = -600(J/mol)$$

$$Tis_{1.535}((4H)_{super}) + ((1.550-1.535)/2)\ S_2(g) = TiS_{1.550}(4H)$$
$$\Delta G^\circ = (1/2)(1.550-1.535)RT \ln P_{S_2} = -700(J/mol)$$

$$Tis_{1.730}(4H) + (1/2)(1.810-1.730)S_2(g) = TiS_{1.810}(2H)$$
$$\Delta G^\circ = (1/2)(1.810-1.730)RT \ln P_{S_2} = -1500(J/mol)$$

Although the existence of Ti_5S_8 (12R) has been reported in some papers,[3,14,15] it was not detected in the present experiments.

The authors wish to thank Professor Mitsuoki Nakahira of Okayama College of Science and Drs. Motohiko Ishii, Hiroshi Nozaki, and Isao Kawada of our Institute for their helpful discussions.

References

1) G. A. Wiegers and F. Jellinek, *J. Solid State Chem.*, **1**, 510 (1970).
2) E. Tronc and M. Huber, *J. Phys. Chem. Solids*, **34**, 2045 (1973).
3) Y. P. Jeannin, *Ann. Chim. (Paris)*, **7**, 57 (1962).
4) A. D. Wadsley, *Acta Crystallogr.*, **10**, 715 (1975).
5) I-J. Norrby and H. F. Franzen, *J. Solid State Chem.*, **2**, 36 (1970).
6) M. Onoda, M. Saeki, and I. Kawada, *Z. Anorg. Allg. Chem.*, **457** 62 (1979).
7) Y. Bando, M. Saeki, Y. Sekikawa, Y. Matsui, S. Horiuchi, and M. Nakahira, *Acta Crystallogr., Sect. A*, **35**, 564 (1979).
8) Y. Bando, M. Saeki, M. Onoda, I. Kawada, and M. Nakahira, *Acta Crystallogr., Sect. B*, **35**, 2522 (1979).
9) A. Kjekshus and W. B. Pearson, "Progress in Solid State Chemistry," ed by H. Reiss, Oxford (1964), Vol. 1, p. 83.
10) Y. P. Jeannin, "Problems of Nonstoichiometry," ed by A. Rabenau, North-Holland, Amsterdam (1970), p. 77.
11) R. P. Abendroth and A. W. Schlechten, *Trans. Met. Soc. AIME*, **215**, 145 (1959).
12) JANAF Thermochemical Tables, 2nd ed, U. S. Dept. of Commerce, Nat. But. Stand., Washington, D. C., 1971.
13) M. Saeki, *J. Cryst. Growth*, **36**, 77 (1976).
14) E. Flink, G. A. Wiegers, and F. Jellinek, *Recl. Trav. Chim. Pays-Bas*, **85**, 869 (1966).
15) M. Seaki and M. Onoda, *Bull. Chem. Soc. Jpn.*, **55**, 113 (1982).

 © 1982 The Chemical Society of Japan Bull. Chem. Soc. Jpn., 55, 3147—3150 (1982)

The Extraction-spectrophotometric Determination of Lead with Bismuthiol II

Kunihiro WATANABE,* Yoshitaka IMAEDA, and Kyōzō KAWAGAKI
Faculty of Science and Technology, Science University of Tokyo, Yamazaki, Noda, Chiba 278
(Received February 4, 1982)

The solvent extraction-spectrophotometric determination of lead(II) with bismuthiol II was conducted in the presence of 1,10-phenanthroline(phen). Lead(II) was quantitatively extracted as ternary complexes into the chloroform phase over the pH range of 3.0—7.0. The composition of the extracted ternary complexes were confirmed to be Pb: bismuthiol II: phen=1 : 2 : 2 or 1 : 2 : 1, depending on the concentration of bismuthiol II added to the aqueous solution. The absorption maximum of the ternary complex (1 : 2 : 2) in chloroform was found to be at 342 nm, with a molar extinction coefficient of 3.5×10^4 dm^3 mol^{-1} cm^{-1}. Under optimum conditions, the absorbance follows Beer's law up to 300 μg of lead in 10 ml of chloroform. The coefficient of the variation was 1.3% for 30 μg of lead. Many elements interfered with the determination of lead(II). However, the interfering ions, with the exception of the indium and bismuth ions, were masked with a potassium cyanide solution. The proposed method was then applied to the determination of lead in standard zinc metals. A good agreement was observed between the results obtained by the proposed method and the standard values of the samples.

Bismuthiol II (3-phenyl-5-mercapt-1,3,4-thiadiazole-2-thione) has been used for the gravimetric determination of various metal ions, and it is well-known to be chelating reagent which is useful for the sensitive colorimetric determination of selenium[1] and tellurium.[2] The determination of lead(II) with bismuthiol II was made by gravimetry.[3,4] The spectrophotometric determination of lead(II) has not, however, been studied because of the insolubility in water of the complexes formed and because it is impossible to extract them into organic solvents.[5] From experiments employing synergistic extraction, we found that the lead–bismuthiol II chelate was extracted into chloroform to form a ternary complex with 1,10-phenanthroline (phen). In the present study, the fundamental conditions for the extraction of lead(II) as the lead–bismuthiol II–phen in chloroform, the composition of the ternary complex, and its application to the determination of lead(II) are discussed. As a result, a highly selective method for the spectrophotometric determination of small amounts of lead(II) has been established and then applied to the determination of lead(II) in zinc metals.

Experimental

Reagents. *A Lead(II) Standard Stock Solution (1.00 mg/ml)*: 0.2500 g of lead metal (Wako Pure Chemicals, 99.99%) was dissolved in a small amount of dilute nitric acid, and the solution was diluted with water in a 250-ml volumetric flask (nitric acid was added to make the final acidity 0.01 mol dm^{-3}). The solution was then diluted as required.

0.1% Phen Solution: 0.1 g of phen (Wako Pure Chemicals) was dissolved with a small amount of ethanol, after which the mixture was diluted to 100 ml with water.

Buffer Solution: An acetate buffer solution was prepared by mixing 0.5 dm^3 of 2 mol dm^{-3} acetic acid with 0.5 dm^3 of 2 mol dm^{-3} sodium acetate.

The other reagents used were all of an analytical reagent grade.

Standard Procedure. An aliquot of a standard lead(II) solution was transferred to a 100-ml beaker, and then the buffer solution and the phen solution were added. After the solution had been diluted to 50 ml with water, the pH of the solution was adjusted with diluted hydrochloric acid or ammonia and a 0.1% bismuthiol II solution was added. The resulting aqueous solution was then transferred into a separatory funnel. The lead complex thus formed was extracted with 10 ml of chloroform by shaking it vigorously for 2 min. After the separation of the mixture into two phases, the organic phase was transferred into a 10-mm quartz cell and the absorbance of the extract at 342 nm or 370 nm wasmeasured against the reagent blank or chloroform.

Results and Discussion

Absorption Spectra. Bismuthiol II reacts with lead(II) to form a pale yellow complex. The absorption spectra of the Pb–bismuthiol II–phen complex and the Pb–bismuthiol II chelate extracted are shown in Fig. 1. The ternary complex has an apparent absorption maximum at 342 nm, whereas the Pb–bismuthiol II chelate gives hardly any absorbance because it is

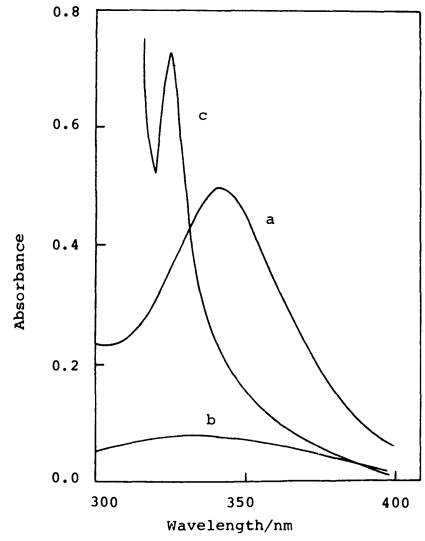

Fig. 1. Absorption spectra.
a): 0.1% phen 2 ml; Pb 30 μg, b): 0.1% phen none; Pb 30 μg, c): 0.1% phen 2 ml; Pb none. 0.1% bismuthiol II: 2 ml; pH: 4.0, reference: reagent blank (a, b); chloroform (c).

unextractable into chloroform.

Effect of pH. After the pH of solutions containing 30 μg of lead(II) and 2 ml of a 0.1% phen solution had been controlled to the desired values with aqueous ammonia and hydrochloric acid, 2 ml of a 0.1% bismuthiol II solution was added to the solution and the extraction was carried out by the above procedure. The results are shown in Fig. 2. Since the absorbance of the reagent blank increased remarkably below pH 2.5, the measurement of the absorbance at 342 nm became impossible below pH 2.5; therefore, the absorbance of the organic phase was measured at 370 nm, where the effect of absorption due to the reagent blank was less than at 342 nm. The extraction of the ternary complex starts at pH 0, reaches a maximum at pH 3.0, and thereafter remains constant over the range of pH 3.0—7.0. When a dilute reagent solution (0.2 ml of a 0.1% bismuthiol II solution) and 0.2 ml of 0.1% phen were used to examine the optimum pH over the range of 3.0—7.0, the absorbance of the extract showed a maximum at pH 3.5. All the extraction, however, was carried out at pH 4.0 in consideration of the effect of the reagent blank.

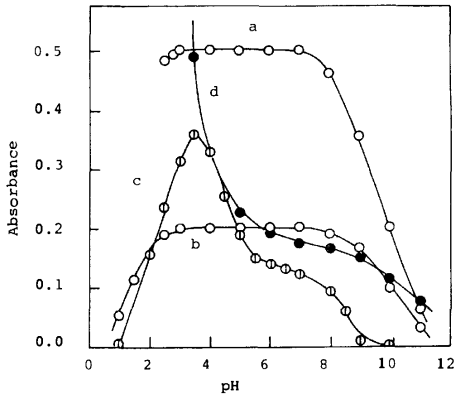

Fig. 2. Effect of pH on absorbance.
a, b): 0.1% bismuthiol II 2 ml; 0.1% phen 2 ml; Pb 30 μg, c): 0.1% bismuthiol II 0.2 ml; 0.1% phen 0.2 ml; Pb 30 μg, d): 0.1% bismuthiol II 2 ml; 0.1% phen 2 ml; Pb none, wavelength: 342 nm (a, c, d), 370 nm (b), reference: reagent blank (a, b, c); chloroform (d).

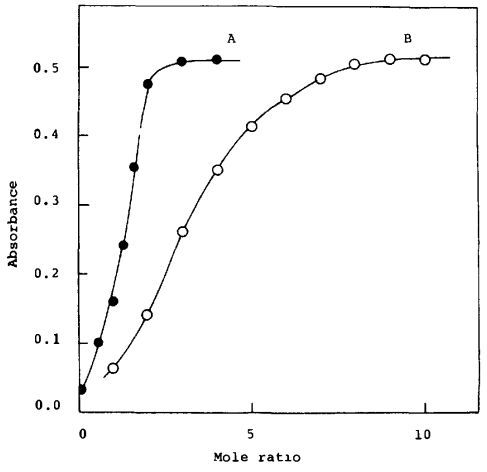

Fig. 3. Effect of amount of reagents.
A) Effect of amount of phen: 0.1% bismuthiol II 2 ml, B) effect of amount of bismuthiol II: 0.1% phen 2 ml, Pb: 30 μg, pH: 4.0, wavelength: 342 nm.

Effect of Bismuthiol II and Phen Concentrations. The extraction of lead(II) from aqueous solutions containing bismuthiol II in varying concentrations was examined, the phen concentration (2 ml of a 0.1% solution in 50 ml of an aqueous solution), the amount of lead (30 μg), and other variables being kept constant. The results are shown in Fig. 3. The absorbance of the extract was found to be constant above 2.9×10^{-5} mol dm^{-3} (mole ratio of lead : bismuthiol II = 1 : 10, Curve B). In the same way, the effect of the phen concentration is shown by Curve A, more than three-fold excess of phen over the lead concentration is necessary in order to obtain the maximum absorbance. The absorbance at a mole ratio of zero in Curve A corresponds to that of the binary Pb–bismuthiol II chelate.

Effect of Shaking Time. A 10 ml portion of chloroform was added to a solution containing the ternary complex, and the mixed solution was shaken vigorously. The ternary complex was completely extracted into chloroform by vigorous shaking for 30 s. Shaking for 1 min was found to be satisfactory for complete extraction.

Effect of Standing Time. The absorbance of the ternary complex in a closed quartz cell was measured at 5 min intervals. The absorbance was constant until 30 min, past which it decreased gradually. On the other hand, the absorbance of the ternary complex extracted from an aqueous solution containing 2 ml of 5% ascorbic acid remained unchanged, even after 2 h at room temperature.

Effect of Volume of Aqueous Phase. For the investigation of the effect of the volume of the aqueous solution, the volume of the aqueous phase was changed between 20 and 200 ml, the other factors being kept constant. The absorbance of the extract gradually increased in proportion to the volume of the aqueous phase.

Organic Solvents. Several kinds of organic solvents were tested in order to achieve a quantitative extraction of the lead complex. The ternary complex was extracted only in chloroform, not quantitatively in such solvents as benzene, toluene, xylene, carbon tetrachloride, isobutyl methyl ketone, ethyl acetate, and diisopropyl ether.

Calibration Curve and Molar Extinction Coefficient. A calibration curve for the determination of lead was made under optimum conditions. A good linear relationship was obtained over the concentration range from 3 μg to 300 μg of lead per 10 ml of chloroform. The molar extinction coefficients were 3.52×10^{4} dm^{3} mol^{-1} cm^{-1} (at 342 nm) and 3.72×10^{3} dm^{3} mol^{-1} cm^{-1} (at 400 nm), the sensitivity being 5.9×10^{-3} μg per cm^{2} for an absorbance of 0.001 (at 342 nm). Thirty replicate determinations of a sample solution containing 30 μg of lead(II) gave the coefficient of the variation of 1.3%. The extractability of the lead complex was larger than 99% under optimum conditions.

Composition of the Ternary Complexes. By the use of the equilibrium-shift method, lead: bismuthiol II

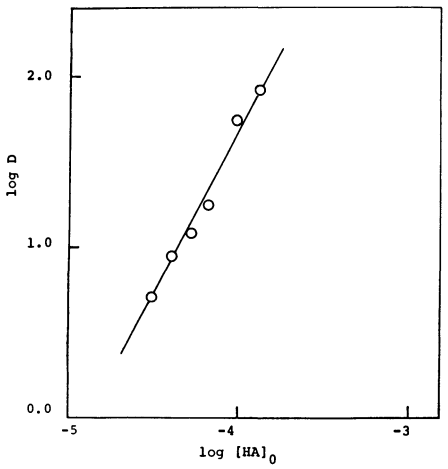

Fig. 4. Determination of the mole ratio of Pb: bismuthiol II in the ternary complex by equilibrium-shift method. Reference: reagent blank, 0.1% phen: 2 ml, Pb: 30 μg, pH: 4.0, aqueous phase: 50 ml, D: distribution ratio, $[HA]_0$: concentration of bismuthiol II in chloroform phase.

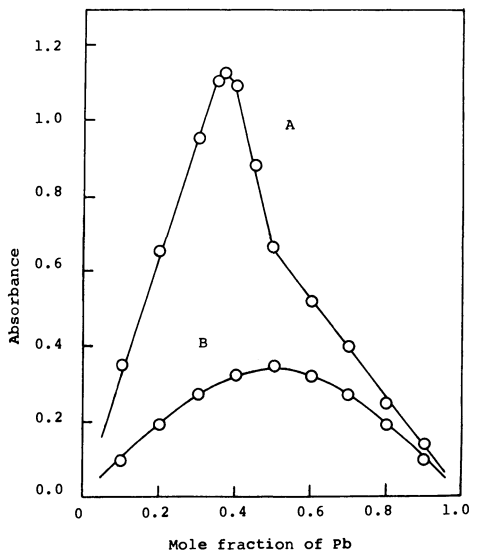

Fig. 5. Determination of the mole ratio of Pb: phen in the ternary complex by the continuous variation method.
Reference: reagent blank, pH: 4.0, 0.1% bismuthiol II: 2 ml (A), 0.2 ml (B), $[Pb]+[phen]=9.66\times10^{-6}$ mol dm^{-3} (50 ml).

Table 1. Effects of foreign ions

Ions	Amount μg	Added as	Pb found (μg)	Tolerance limits μg
Ag(I)	10	$AgNO_3$	36.7	0.4
Al(III)	1000	$Al(NO_3)_3\cdot9H_2O$	30.0	1000
As(III)	1000	As_2O_3+NaOH	30.0	1000
Au(III)	10	$HAuCl_4\cdot4H_2O$	38.2	0.3
Ba(II)	1000	$BaCl_2\cdot2H_2O$	30.0	1000
Bi(III)	10	Bi+HNO_3	37.8	0.3
Ca(II)	1000	$CaCl_2$	30.0	1000
Cd(II)	10	Cd+HNO_3	43.2	0.2
Co(II)	10	Co+HNO_3	92.3	0.1
Cr(III)	1000	$Cr(NO_3)_3\cdot9H_2O$	30.0	1000
Cu(II)	10	Cu+HNO_3	48.1	0.1
Fe(III)	10	Fe+HNO_3	62.4	0.1
Ga(III)	1000	Ga+HCl	30.0	1000
Hg(II)	10	$HgCl_2$	35.3	0.5
In(III)	10	In+HNO_3	59.1	0.1
Mg(II)	1000	MgO+HCl	30.0	1000
Ni(II)	10	Ni+HCl	52.5	0.1
Pd(II)	10	$PdCl_2$+HCl	44.2	0.2
Sb(III)	1000	Sb+H_2SO_4	30.0	1000
Sn(II)	1000	Sn+HCl	30.0	1000
Tl(I)	1000	$TlNO_3$	30.0	1000
V(V)	50	V+Aqua regia	39.1	5
W(VI)	100	$Na_2WO_4\cdot2H_2O$	28.0	15
Zn(II)	10	Zn+HCl	45.1	0.2

Pb taken: 30.0 μg. Wavelength: 342 nm.

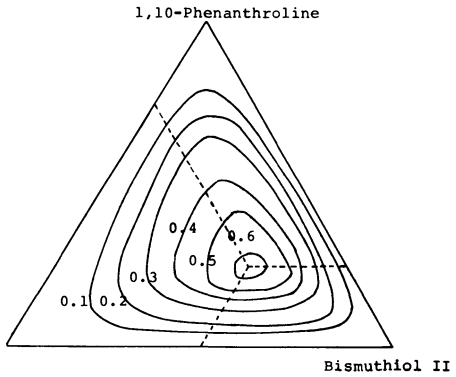

Fig. 6. Continuous variation method applied to three component system of Pb–bismuthiol II–phen complex. $[Pb]+[bismuthiol\ II]+[phen]=2.86\times10^{-5}$ mol dm^{-3}.

was found to be 1 : 2, as is shown in Fig. 4. On the other hand, lead : phen was obtained to be 1 : 1 or 1 : 2, depending on the concentration of bismuthiol II added to the aqueous solution. The 1 : 1 complex was formed in lower concentrations of bismuthiol II (6-fold of the Pb concentration), while the other complex was formed in a higher concentration of the reagent (60-fold) (Fig. 5). A triangular coordinate method extended to the three-component system of the continuous-variation plot was applied to the determination of the ternary complex. The results are shown in Fig. 6. The maximum absorbance is obtained at the mole ratio of lead: bismuthiol II: phen=1 : 2 : 1.

Effects of Diverse Ions and of Masking. The experimental results are summarized in Table 1. Each 10 μg of silver, gold, bismuth, cadmium, cobalt, copper, iron, mercury, indium, nickel, palladium, vanadium, and zinc interferes with the determination of lead. The interference of such ions as silver (up to 10 mg), gold (up to 8 mg), cadmium (up to 1 mg), cobalt (up to 100 μg), copper (up to 10 mg), mercury (up to 1 mg), nickel (up to 10 mg), vanadium (up to 10 mg), iron (up to 20 μg), and zinc (up to 10 mg) can be masked by the use of 20 ml of a 2% potassium cyanide solution. Zinc in the determination of lead in a metal was confirmed to be masked up to 0.5 g with 20 ml of 20%

TABLE 2. ANALYTICAL RESULTS OF ZINC-METAL STANDARD SAMPLES[a)]

Sample	Sample taken (mg)	Pb found (μg)	Pb found (%)
H-501	497.2	23.5	0.00473
Pb 0.0048%	497.2	24.3	0.00489
	497.2	24.1	0.00485
	497.2	24.5	0.00493
	497.2	24.0	0.00483
		Average	0.00485
H-502	15.43	31.1	0.202
Pb 0.21%	15.43	33.0	0.214
	15.43	31.4	0.203
	15.43	31.2	0.202
	15.43	31.9	0.207
		Average	0.206
H-503	2.969	32.3	1.088
Pb 1.11%	2.969	33.2	1.118
	2.969	32.5	1.095
	2.969	32.0	1.078
	2.969	32.9	1.108
		Average	1.097

a) Japanese standard samples (Kagaku Gijutusha Co.).

potassium cyanide. Indium and bismuth were not masked.

Determination of Lead in the Zinc Metal. The proposed method was applied to the analysis of lead in zinc metal. A sample solution was prepared as follows : Take less than 5 g of a sample in a beaker and dissolve the sample with 60 ml of nitric acid (2+1). Then dilute the solution to 100 ml in a volumetric flask.

A 10 ml aliquot (3—300 μg Pb) of this sample solution was taken for analysis, a 20 ml portion of a 20% potassium cyanide solution was used as a masking reagent in a draft chamber, and the pH of the sample solution was adjusted to pH 7. Two ml of a 0.1% phen solution and 2 ml of a 0.1% bismuthiol II solution were used as reagents.

The lead in standard samples of zinc metal was determined by the proposed method. The analytical results are shown in Table 2. Good agreement was observed between results obtained by the proposed method and the standard values of the samples. The present method is rapid and accurate enough for the determination of lead in zinc metal.

References

1) H. Yoshida, M. Taga, and S. Hikime, *Bunseki Kagaku*, **14**, 1109 (1965).
2) J. Jankovsky and O. Ksir, *Talanta*, **5**, 238 (1960).
3) A. K. Majumdar and B. R. Singh, *Z. Anal. Chem.*, **154**, 413 (1957).
4) A. K. Majumdar and B. R. Singh, *Z. Anal. Chem.*, **156**, 265 (1597).
5) H. Yoshida and S. Hikime, *Bunkoo Kenkyu*, **14**, 131 (1966).

 © 1982 The Chemical Society of Japan Bull. Chem. Soc. Jpn., 55, 3151—3154 (1982)

Synergistic Effect of Nitrogen Neutral Bases in the Solvent Extraction of Zinc(II) and Cadmium(II) Diphenylcarbazonates

Etsu YAMADA,* Eiichiro NAKAYAMA,† Tooru KUWAMOTO, and Taitiro FUJINAGA

Department of Chemistry, Faculty of Science, Kyoto University, Sakyo-ku, Kyoto 606

†Research Center for Instrumental Analysis, Faculty of Science, Kyoto University, Sakyo-ku, Kyoto 606

(Received February 9, 1982)

The extraction behavior of zinc and cadmium with diphenylcarbazone(DPC) into benzene and chloroform were studied in both the absence and presence of neutral bases(S). In the case of chloroform, all of the neutral bases gave rise to adduct complexes with the formula of $M(DPC)_2S$. On the other hand, in the case of benzene, the adduct complexes can be represented as $M(DPC)_2S$ for all neutral bases except for 1,10-phenanthroline(phen), in which the adduct complexes can be expressed as $M(DPC)_2(phen)_2$. The stability of the adduct complexes is related not only to the basicity of the bases, but also to the steric effect attributable to substitution. Furthermore, the adduct-formation constant increase in the following order against the normalized values of basicity: pyridine bases<2,2′-bipyridyl <1,10-phenanthroline derivatives. This order agrees with the increasing order of the coordinated ability as ligands. The basicity of the bases has a larger effect on the adduct-formation constants for Cd than on those for Zn. This may be attributed to the fact that Zn chelates have greater stability than the Cd chelates, as a result, the "residual Lewis acidity" of Zn is smaller than that of Cd, and therefore zinc chelates form less stable adducts.

In a previous paper by the present authors it has been shown that the cadmium complex of diphenylcarbazone is quantitatively extracted in the presence of 1,10-phenanthroline and that an extract has a higher molar absorptivity than that of diphenylthiocarbazone (dithizone).[1]

Several factors, such as the basicity of the bases and steric considerations, controlling the stability of the adduct complexes, have been investigated by a number of workers in connection with phosphorylated donors or pyridine bases.[2–5] In attempt to establish the relative importance of steric hindrance and other factors in the adduct formation, the present authors decided to study the effects of pyridine bases, and 2,2′-bipyridyl and 1,10-phenanthroline derivatives on the extraction of zinc and cadmium with DPC.

In addition, we investigated the extraction behavior of zinc and cadmium with mixtures of DPC and a neutral base in both solvents, benzene and chloroform, in order to check the solvent effect in this extraction system, which has lately been noted as an interesting problem.[6–8]

Experimental

Apparatus and Reagents. The apparatus and chemicals, such as cadmium, diphenylcarbazone, and 1,10-phenanthroline, used in the extraction have been previously described.[1]

The stock solution of zinc(II) [10^{-2} M (1 M=1 mol dm^{-3})] was prepared by dissolving weighed amounts of zinc chloride in dilute hydrochloric acid and then diluted with distilled water as required. The pyridine was purified by distillation under reduced pressure. All the other neutral bases, such as 2,2-bipyridyl, 2,9-dimethyl-1,10-phenanthroline, 4,7-diphenyl-1,10-phenanthroline, and 4,7-diphenyl-2,9-dimethyl-1,10-phenanthroline, were of an analytical-reagent grade and were used without further purification. All the other chemicals were also of an analytical-reagent grade.

Extraction Procedure. A 20 ml portion of a buffered cadmium or zinc solution (10^{-5} M) and a 20 ml portion of the reagent solution in chloroform or benzene were equilibrated at 25 °C by vigorously shaking for 30 min, a period which was adequate for equilibrium to be attained. The pH value of the aqueous phase after extraction was taken as the equilibrium pH value. After phase separation, the aqueous phase was immediately analyzed with the atomic-absorption spectrophotometer, whereas the organic phase was analyzed after back-extracting into a 0.2 M nitric acid solution.

Isolation of Cd/DPC/Phen Synergistic Complexes. Synergistic complexes were synthesized according to Healy's method.[9] A 250 ml portion of a buffered aqueous solution ($Na_2B_4O_7$–HCl) of 2.5×10^{-3} M cadmium chloride was added to a 250 ml of a chloroform solution of 5×10^{-3} M DPC and 2.5×10^{-3} M 1,10-phenanthroline. The mixture was shaken vigorously for about 20 min, the aqueous phase was removed, and the chloroform solution was dried by the use of anhydrous sodium sulfate and then evaporated with a rotary evaporator. After almost all the chloroform had been evaporated, a red-violet complex was precipitated by the addition of hexane. Further purification was brought about by recrystallization from chloroform. In the case of benzene, a 250 ml portion of a buffered aqueous solution of 2.5×10^{-3} M cadmium chloride was added to a 250 ml portion of a benzene solution of 5×10^{-3} M DPC and 5×10^{-3} M 1,10-phenanthroline. The procedure was also essentially the same as in the case of chloroform. These complexes were dried *in vacuo* at room temperature.

Results and Discussion

Relation of Stability Constants of Base Adducts to the Basicity of Neutral Bases. The equation of the extracted equilibrium of zinc and cadmium with DPC can be represented as follows.

$$M^{2+} + x\mathrm{HDPC}_{(o)} \overset{K_{ex,x}}{\rightleftarrows} M(DPC)_{x(o)} + xH^+, \quad (1)$$

where;

$$K_{ex,x} = \frac{[M(DPC)_x]_0[H^+]^x}{[M^{2+}][HDPC]_0^x} = \frac{D_0[H^+]^x}{[HDPC]_0^x}. \quad (2)$$

When neutral bases(S) are present, the extraction equation can be written as:

$$M^{2+} + x\mathrm{HDPC}_{(o)} + yS_{(o)} \overset{K_{ex,xy}}{\rightleftarrows} M(DPC)_xS_{y(o)} + xH^+. \quad (3)$$

The extraction constant, $K_{ex,xy}$ is given by:

$$K_{ex,xy} = \frac{[M(DPC)_xS_y]_0[H^+]^x}{[M^{2+}][HDPC]_x^0[S]_0^y} = \frac{D[H^+]^x}{[HDPC]_0^x[S]_0^y}. \quad (4)$$

The reaction of primary interest involves adduct formation in the organic phase. By the proper manipulation of the above equilibria, the expression for the adduct formation can be obtained as follows:

$$M(DPC)_{x(o)} + yS_{(o)} \overset{\beta_y}{\rightleftharpoons} M(DPC)_xS_{y(o)}, \quad (5)$$

where β_y is the adduct-formation constant. By introducing Eqs. 2 and 4 into Eq. 6, it can be shown that:

$$\beta_y = \frac{[M(DPC)_xS_y]_0}{[M(DCP)_x]_0[S]_0^y} = K_{ex,xy}/K_{ex,x}. \quad (6)$$

The extraction behavior of zinc and cadmium by DPC into benzene was studied in both the absence and presence of nitrogen neutral bases. The plots of log D *vs.* such variables as the pH of the aqueous phase and the logarithms of the concentrations of DPC and of neutral bases were obtained in order to determine the stoichiometry and equilibrium constants of the extraction.

In the absence of neutral bases, the slopes of log D *vs.* pH are 2; those of log D *vs.* log $[DPC]_0$ are also 2 for Zn and Cd. These results suggest that the extracted species are $Zn(DPC)_2$ and $Cd(DPC)_2$, which is in agreement with Balt's report.[10]

Extraction in the presence of neutral bases was also evaluated by slope analysis. The slopes of log D *vs.* pH are 2; those of log D *vs.* log $[DPC]_0$ are also 2. The plots of log D *vs.* log $[S]_0$ in the presence of pyridine bases, such as pyridine, 2-methylpyridine, 3-methylpyridine and 4-methylpyridine, exhibit a linear range of unit slopes. These results suggest that one pyridine base adducts to $Zn(DPC)_2$ or $Cd(DPC)_2$. In the presence of 1,10-phenanthroline, the plots of log D *vs.* log $[phen]_0$ are as shown in Fig. 1. The slope of log D *vs.* log $[phen]_0$ was 2, so it is suggested that two 1,10-phenanthroline adduct to $Cd(DPC)_2$, while a greater quantity of an additive causes the slope of the line to decrease gradually, become horizontal, and finally turn down in a negative slope, -2. The extraction behavior of zinc with DPC in the presence of 1,10-phenanthroline is similar to that of cadmium. Furthermore, extraction in the presence of 1,10-phenanthroline derivatives, such as 4,7-diphenyl-1,10-phenanthroline, 4,7-diphenyl-2,9-dimethyl-1,10-phenanthroline and 2,9-dimethyl-1,10-phenanthroline, was also examined. The slopes of log D *vs.* log $[S]_0$ are very close to unity. These results suggest that one 1,10-phenanthroline derivative adducts to $Zn(DPC)_2$ or $Cd(DPC)_2$.

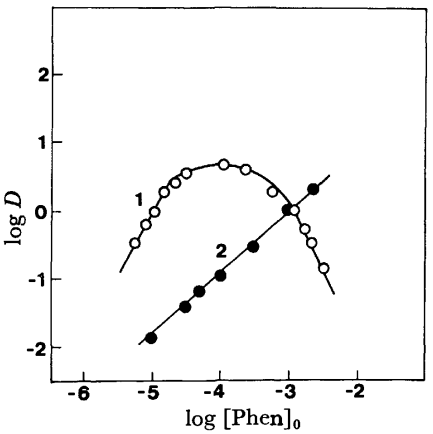

Fig. 1. Extraction of cadmium with mixtures of DPC and 1,10-phenanthroline into benzene and chloroform as a function of the phenanthroline concentration. $[DPC]_0 = 5 \times 10^{-4}$ M, pH 7.1. 1: Benzene, 2: chlofoform.

From these results, the adduct-formation constants were calculated. These values of Cd are listed in Table 1. In the case of pyridine bases, the adduct formation constants increase in the following order: 2-methylpyridine < pyridine < 3-methylpyridine < 4-methylpyridine. The increasing order of the adduct-formation constants corresponds with the increaseing basicity (K_{HB})[11,12] of the bases, except for 2-methylpyridine. The higher stability of 4-methylpyridine as compared with that of pyridine also reflects the increased donor power of the nitrogen atom due to the introduction of a methyl group. The much lower stability of 2-methylpyridine may be attributed to the steric interference of the 2-position methyl group. In the case of 1,10-phenanthroline derivatives, the adduct-formation constants increase in the following order: 2,9-dimethyl-1,10-phenanthroline < 4, 7-diphenyl-2, 9-dimethyl-1, 10-phenanthroline < 4, 7-diphenyl-1, 10-phenanthroline < 1,10-phenanthroline. The increasing order of the adduct-formation constants corresponds with the increasing basicity of the bases, except for 2,9-dimethyl-1,10-phenanthroline and 4,7-diphenyl-2,9-dimethyl-1,10-phenanthroline. The much lower stabilities of 2,9-dimethyl-1,10-phenanthroline and 4,7-diphenyl-2,9-dimethyl-1,10-phenanthroline may also be caused by the steric interference of 2,9-position methyl substituents.

Table 1. The effect of nitrogen bases on the synergistic extraction of cadmium and zinc diphenylcarbazonates into benzene

No.	Base	Cd			Zn			log K_{HB}
		log $K_{ex,x}$	log $K_{ex,xy}$	log β_y	log $K_{ex,x}$	log $K_{ex,xy}$	log β_y	
1	Pyridine	−10.43	−7.12	3.31	−8.36	−4.09	4.27	5.23
2	2-Methylpyridine	−10.43	−7.55	2.88	−8.36	−4.51	3.85	5.97
3	3-Methylpyridine	−10.43	−5.94	4.49	−8.36	—	—	5.68
4	4-Methylpyridne	−10.43	−5.61	4.82	−8.36	−3.56	4.80	6.02
5	2,2′-Bipyridyl	−10.43	−5.45	4.98	−8.36	—	—	4.33
6	1,10-Phenanthroline	−10.43	2.45	12.88	−8.36	1.60	9.96	4.92
7	4,7-Diphenyl-phen	−10.43	−0.58	9.85	−8.36	1.28	9.64	4.30
8	2,9-Dimethyl-phen	−10.43	−2.52	7.91	−8.36	−2.74	5.62	6.15
9	4,7-Diphenyl-2,9-dimethyl-phen	−10.43	−2.09	8.34	—	—	—	—

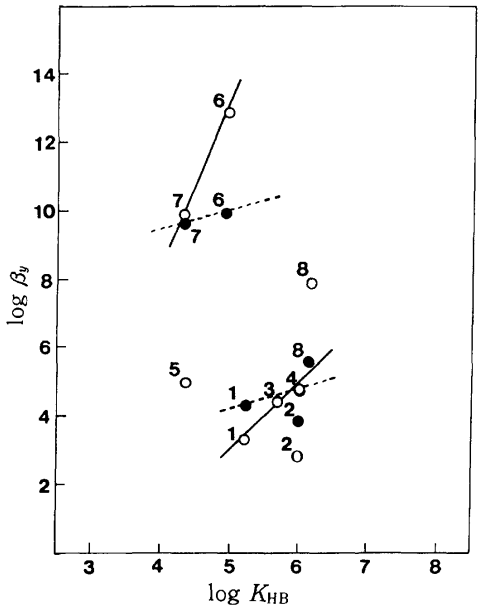

Fig. 2. Relationship of $\log \beta_y$ and $\log K_{HB}$ in the synergistic extraction of cadmium and zinc.
1: Pyridine, 2: 2-methylpyridine, 3: 3-methylpyridine, 4: 4-methylpyridine, 5: 2,2′-bipyridyl, 6: 1,10-phenanthroline, 7: 4,7-diphenyl-1,10-phenanthroline, 8: 2,9-dimethyl-1,10-phenanthroline, ○: cadmium, ●: zinc.

The adduct-formation constants of Zn are also listed in Table 1. The order is related not only to the basicity of the bases, but also to the steric effect due to substitution, in the same manner as in the case of Cd.

The relationship of $\log \beta_y$ and $\log K_{HB}$ in the synergistic extraction of Cd and Zn is shown in Fig. 2. A comparison of the adduct-formation constants of these bases against the normalized values of basicity shows that their values increase in the following order : pyridine bases$<$2,2′-bipyridyl$<$1,10-phenanthroline derivatives. This fact suggests that the stability of the adducts is related not only to the basicity of the bases, but also to the coordinated ability to act as ligands. The basicity of the bases has a larger effect on the adduct-formation constants of Cd than those of Zn. This may be attributed to the fact that zinc chelates have a greater stability than the cadmium chelates: as a result, the "residual Lewis acidity"[3] of Zn is smaller than that of Cd, and therefore zinc chelates form less stable adducts.

Effect of Organic Solvents. The behavior of the extraction of cadmium and zinc chelates into chloroform is similar to that into benzene, except for the case of 1,10-phenanthroline. In the absence of neutral bases, the extracted species are $Cd(DPC)_2$ and $Zn(DPC)_2$; the log D *vs.* pH plots and the log D *vs.* log $[DPC]_0$ plots, give the same slopes as in the case of benzene: the plots of log D *vs.* pH give a slope of 2, and the plots of log D *vs.* log $[DPC]_0$ give a slope 2, for both metals. In the presence of neutral bases, the plots of log D *vs.* pH exhibit a slope of 2, and the plots of log D *vs.* log $[DPC]_0$ exhibit a slope of 2, for both metals. In the case of Cd, the plots of log D *vs.* log $[S]_0$ all exhibit a linear range of unit slopes for pyridine, 2,2′-bipyridyl, and 1,10-phenanthroline. These results suggest that the extracted species are $Cd(DPC)_2S$. In the case of Zn, the plots of log D *vs.* log $[S]_0$ indicate a linear range of unit slopes for pyridine and 1,10-phenanthroline. These results suggest that the extracted species are $Zn(DPC)_2S$.

In the case of benzene, the extracted species of both metals are $M(DPC)_2S$ in all the neutral bases except 1,10-phenanthroline. In the presence of 1,10-phenanthroline, the extracted species of both metals are $M(DPC)_2(phen)_2$, different from those in chloroform. Furthermore, we carried out elementary analyses of the synthesized Cd–DPC–phen chelates and compared the results with those obtained from slope analysis. As is shown in Table 2, the results obtained from elementary analysis fit those obtained from slope analysis. Hence, the extracted species into chloroform can be expressed as $Cd(DPC)_2 \cdot phen$, and that into benzene, as $Cd(DPC)_2(phen)_2$.

Consequently, in the case of chloroform, one neutral base adducts to cadmium chelate and zinc chelate for all neutral bases, so the extraction can be expressed as:

$$M^{2+} + 2HDPC_{(o)} + S_{(o)} \rightleftarrows M(DPC)_2S_{(o)} + 2H^+. \quad (7)$$

On the other hand, in the case of benzene, the extraction can be represented as Eq. 7 for all neutral bases except for 1,10-phenanthroline. In the presence of 1,10-phenanthroline, the extraction stoichiometry can be expressed as:

$$M^{2+} + 2HDPC_{(o)} + 2phen_{(o)} \rightleftarrows M(DPC)_2(phen)_{2(o)} + 2H^+. \quad (8)$$

From these results, it would appear that the adduct stability is enhanced by an increase in the basicity of the adducting base, by an increase in the coordinated ability, and by an increase in the residual Lewis acidity of the metal atom, *i.e.*, after chelation. Furthermore, the composition of the extracted zinc and cadmium chelates with the mixtures of DPC and 1,10-phenanthroline is different depending on the solvent used in extraction.

References

1) E. Yamada, E. Nakayama, T. Kuwamoto, and T.

Table 2. Analytical data of Cd–DPC–phen complexes

Complex	Found (%)			Calcd (%)		
	C	H	N	C	H	N
$Cd(DPC)_2(phen)$ (from chloroform)	60.95	4.18	18.32	59.04	4.17	18.12
$Cd(DPC)_2(phen)_2$ (from benzene)	62.00	4.23	17.97	62.99	4.23	17.63

Fujinaga, *Anal. Chim. Acta*, **138**, 409 (1982).
2) H. M. N. H. Irving, "Solvent Extraction Chemistry," North-Holland, Amsterdam (1967), p. 91.
3) F-C. Chou and H. Freiser, *Anal. Chem.*, **40**, 34 (1968).
4) H. Kawamoto and H. Akaiwa, *J. Inorg. Nucl. Chem.*, **31**, 1141 (1969).
5) L. G. Gavrilova and Yu. A. Zolotov, *Zh. Anal. Khim.*, **25**, 1054 (1970).
6) G. W. Mason, N. L. Shofter, and D. F. Peppard, *J. Inorg. Nucl. Chem.*, **32**, 3899 (1970).
7) G. W. Mason, D. N. Metta, and D. F. Peppard, *J. Inorg. Nucl. Chem.*, **38**, 2077 (1976).
8) M. Niitsu and T. Sekine, *J. Inorg. Nucl. Chem.*, **38**, 1053 (1976).
9) T. V. Healy and J. R. Ferraro, *J. Inorg. Nucl. Chem.*, **24**, 1449 (1962).
10) S. Balt and E. V. Dalen, *Anal. Chim. Acta*, **27**, 188 (1962).
11) L. G. Sillen and A. E. Martell, "Stability Constants of Metal-Ion Complexes," The Chemical Society, London (1967).
12) L. G. Sillen and A. E. Martell, "Stability Constants of Metal-Ion Complexes," Supplement; the Chemical Society, London (1971).

A Thermodynamic Study of the Synergistic Solvent Extraction of a Series of Zinc(II) and Cadmium(II) Complexes

Etsu YAMADA,* Eiichiro NAKAYAMA,† Tooru KUWAMOTO, and Taitiro FUJINAGA
Department of Chemistry, Faculty of Science, Kyoto University, Sakyo-ku, Kyoto 606
†*Research Center for Instrumental Analysis, Faculty of Science, Kyoto University, Sakyo-ku, Kyoto 606*
(Received February 9, 1982)

The extraction of zinc and cadmium using chloroform and benzene solutions constaining diphenylcarbazone (DPC=Hdpc), either alone or combined with pyridine(py) or 1,10-phenanthroline(phen), was studied thermodynamically. The formation constants were measured as functions of the temperature in order to ascertain the free energy, enthalpy, and entropy changes. The thermodynamic parameters support a proposed mechanism for the synergism of zinc in which the coordination number of the zinc ion expands with formation of $Zn(dpc)_2S$, where S is pyridine or 1,10-phenanthroline. On the other hand, the thermodynamic values for the synergistic reaction of cadmium support a mechanism in which pyridine or 1,10-phenanthroline replaces the residual waters of hydration in the first coordination sphere of cadmium.

In recent years, synergistic extractions have been studied by a number of workers. Considerable attention has been given to the mechanism of synergistic solvent extraction. Three possible mechanisms to explain the data of synergistic solvent extraction of metal ions by the combined action of two specific solutes in the organic phase have been proposed:[1]

(i) The neutral additive replaces the residual waters of hydration in the first coordination sphere of the metal ion.

(ii) The neutral additive attaches the metal chelate, by means of a hydrogen bond, to the coordinated waters of the first hydration sphere.

(iii) The coordination number of the non-hydrated chelate expands to accommodate the direct coordination of the adduct to the metal.

Knowledge of the formation constants alone does not allow one to choose between the three mechanisms proposed. However, if the enthalpies and entropies of the extraction reactions are known, it is possible to evaluate the mechanism of synergistic solvent extraction. Accordingly several studies of the thermodynamics of synergistic solvent extraction have been reported.[2-8] Kandil *et al.* have concluded that the mechanisms of adduct formation by tributylphosphate and acetylacetone with tris-thenoyltrifluoroacetone (TTA=Htta) chelates of Eu and Tm involve the expansion of the coordination number of the central metal ions from 6 to 8. These studies have also shown that the third mechanism fits the experimental data best.

Nakayama[9,10] has studied the effect of the temperature on the extraction of several metal chelates of 8-quinolinol. In a previous paper by the present authors it has been shown that the cadmium complex of diphenylcarbazone is quantitatively extracted in the presence of 1,10-phenanthroline and that an extract has a higher molar absorptivity than that for diphenylthiocarbazone (dithizone).[11] In this study, the temperature effects on the distribution equilibraia of zinc and cadmium chelates with DPC alone or when combined with pyridine or 1,10-phenanthroline have been examined in order to explain the extraction mechanism in terms of thermodynamic data.

Experimental

Reagents and Apparatus. The chemicals, such as cadmium, diphenylcarbazone, and 1,10-phenanthroline, used in the extraction have been previously described.[11]

A stock solution of zinc(II)[10^{-2} M(1 M=1 mol dm^{-3})] was prepared by dissolving weighed amounts of zinc chloride in dilute hydrochloric acid and then diluted with distilled water as required. The pyridine was purified by distillation under reduced pressure. All the other chemicals were of an analytical-reagent grade.

Extraction was carried out in a cylindrical tube with a magnetic stirrer in a constant-temperature bath.[9] The temperature was controlled to ± 0.1 °C by means of a thermoregulator. A Komatsu-Yamato Coolnics Dip (CTR-1, CTR-3B) was used for cooling. For the pH measurement, a Hitachi-Horiba M-5 pH meter equipped with a glass-calomel electrode pair for high-temperature work was used. All the other equipment used was the same as has previously been described.

Extraction Procedure. A 30 ml portion of a buffered cadmium or zinc solution was stirred with a 10 ml portion of the reagent solution in a cylindrical tube standing in a constant temperature bath for 30 min, a time period which was found adequate for the attainment of equilibrium. The ionic strength was adjusted by adding sodium sulfate at 0.05. Sodium perchlorate was not used because cadmium and zinc complexes of 1,10-phenanthroline were extracted into the organic phase by forming ion-pair complexes with sodium perchlorate.

After stirring, the pH value of the aqueous phase was measured *in situ*. After phase-separation, the aqueous phase was immediately analyzed with the atomic absorption spectrophotometer, whereas the organic phase was analyzed after back-extracting into an aqueous nitric acid solution.

Results and Discussion

Extraction of Zinc and Cadmium with DPC in the Absence of Phenanthroline and Pyridine. The behavior of the extraction of zinc and cadmium with DPC alone into chloroform and benzene was studied at various temperatures.

For Zn, the plots of log D *vs.* pH when chloroform was used are shown in Fig. 1. The slopes of log D *vs.* pH are 2 at each temperature. The plots of log D *vs.* log $[DPC]_0$ at a constant pH are linear, with a slope of

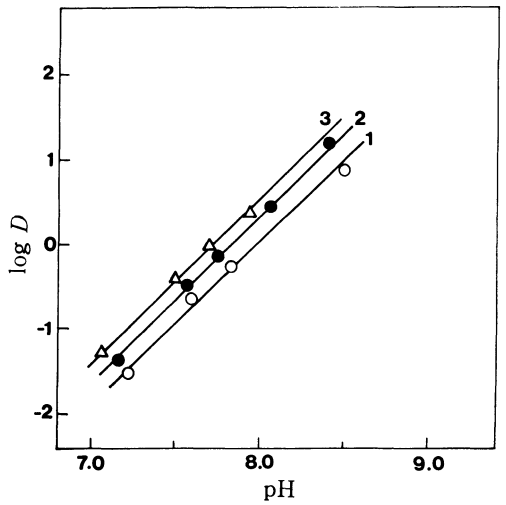

Fig. 1. Effect of pH on the distribution of zinc with DPC between chloroform and water.
$[DPC]_0 = 5 \times 10^{-4}$ M, $[Zn]_T = 10^{-5}$ M. 1: 25 °C, 2: 35 °C, 3: 45 °C.

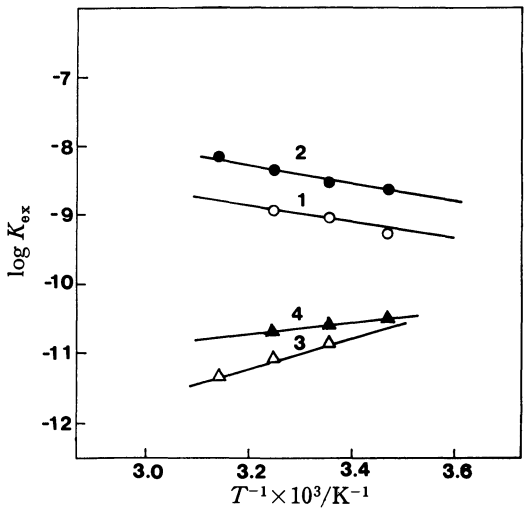

Fig. 2. Temperature effect on the distribution of zinc and cadmium between organic solvents and water.
1: Zinc into chloroform, 2: zinc into benzene, 3: cadmium into chloroform, 4: cadmium into benzene.

2. In the case of benzene, the slopes of log D *vs.* pH are 2 at each temperature, the same as those in chloroform. In this system, the slopes of log D *vs.* log $[DPC]_0$ at various temperatures are also 2. Thus, it can be concluded that only a single species, the simple 1 : 2 chelate, $Zn(dpc)_2$, is present in the organic phase. The overall reaction can be represented by Eq. 1:

$$Zn^{2+} + 2Hdpc_{(o)} \rightleftarrows Zn(dpc)_{2(o)} + 2H^+. \quad (1)$$

The extraction constant, K_{ex}, is a composite of the chelate formation constant, β_2, and its distribution constant, K_{DC}, as well as of the reagent acid-dissociation constant, K_a, and its distribution constant, K_{DR}:

$$K_{ex} = \beta_2 K_{DC} K_a^2 / K_{DR}^2. \quad (2)$$

The product, $\beta_2 K_{DC}$, corresponds to the heterogeneous equilibrium constant of the following reaction:

$$Zn^{2+} + 2dpc^- \overset{\beta_2 K_{DC}}{\rightleftarrows} Zn(dpc)_{2(o)}. \quad (3)$$

In the case of Cd, the plots of log D *vs.* pH in both solvents are linear and exhibit a slope of 2 at each temperature. The analogous log D *vs.* log $[DPC]_0$ plots are also linear, with a slope of 2. These results suggest that the extracted species of cadmium can also be expressed as a simple chelate, $Cd(dpc)_2$. Hence, the extraction constant of cadmium can be represented as:

$$K'_{ex} = \beta'_2 K'_{DC} K_a^2 / K_{DR}^2. \quad (4)$$

The plots of log K_{ex} *vs.* $1/T$ K are shown in Fig. 2. In the case of Zn, the distribution increases with an increase in the temperature. On the other hand, in the case of Cd, the distribution decreases with an increase in the temperature.

From these experimental data, the thermodynamic parameters, ΔG, ΔH, and ΔS, were calculated by using thermodynamic equations. These values are listed in Tables 1—3. The data in Table 1 show an endothermic

Table 1. Thermodynamic values for extraction of Zn^{2+} with dpc, dpc + phen, and dpc+py into chloroform and benzene at 25 °C

Species	log K_{ex}	ΔG kJ mol^{-1}	ΔH kJ mol^{-1}	ΔS J K^{-1} mol^{-1}
$Zn(dpc)_2$	−9.04	51.6	28.2	−79
$Zn(dpc)_2$·phen	−2.23	12.7	−28.1	−137
$Zn(dpc)_2$·py	−5.16	29.5	−18.3	−160
$Zn(dpc)_2$ [a]	−8.51	48.5	27.7	−70
	log β_{ad} [b]			
$Zn(dpc)_2$·phen	6.81	−38.9	−56.3	−58
$Zn(dpc)_2$·py	3.88	−22.1	−46.5	−81

a) Into benzene. b) β_{ad} is the adduct-formation constant which corresponds to $K_{ex,ad}/K_{ex}$.

Table 2. Thermodynamic values for extraction of Cd^{2+} with dpc, dpc+phen, and dpc+py into chloroform at 25 °C

Species	log K_{ex}	ΔG kJ mol^{-1}	ΔH kJ mol^{-1}	ΔS J K^{-1} mol^{-1}
$Cd(dpc)_2$	−10.85	61.9	−42.6	−351
$Cd(dpc)_2$·phen	−3.05	17.4	−42.6	−201
$Cd(dpc)_2$·py	−7.29	41.6	−34.9	−257
	log β_{ad}			
$Cd(dpc)_2$·phen	7.80	−44.5	0.0	150
$Cd(dpc)_2$·py	3.56	−20.3	7.7	94

Table 3. Thermodynamic values for extraction of Cd^{2+} with dpc, dpc+phen, and dpc+py into benzene at 25 °C

Species	log K_{ex}	ΔG kJ mol^{-1}	ΔH kJ mol^{-1}	ΔS J K^{-1} mol^{-1}
$Cd(dpc)_2$	−10.61	60.5	−16.2	−257
$Cd(dpc)_2$·2phen	2.08	−11.9	−44.8	−111
$Cd(dpc)_2$·py	−7.04	40.2	−38.0	−262
	log β_{ad}			
$Cd(dpc)_2$2phen	12.69	−72.4	−28.6	146
$Cd(dpc)_2$py	3.57	−20.3	−21.8	−5

Table 4. $\Delta(\Delta H)(=\Delta H_{Zn}-\Delta H_{Cd})$ and $\Delta(\Delta S)$ $(=\Delta S_{Zn}-\Delta S_{Cd})$ values for extraction between water and organic solvents

Solvents	$\Delta(H)$ / kJ mol^{-1}	$\Delta(\Delta S)$ / J K^{-1} mol^{-1}
Chloroform	70.8	272
Benzene	43.9	187

reaction for the formation of the Zn-DPC chelate. It has been reported that this behavior is quite characteristic of chelation reactions in which the waters of the inner-coordination sphere of the metal ion are displaced by the chelating reagent.[12] The extraction constants of the two metal chelates can be represented as Eqs. 3 and 4, but K_a and K_{DR} are independent of the metal. Therefore, by using the same solvent, the difference in the extraction constant between the two metal chelates can be related to the difference in the product, $\beta_2 K_{DC}$ $(\beta'_2 K'_{DC})$. Hence, $\Delta(\Delta H)$, which is the difference in enthalpy change calculated from the values of the extraction constant, can be represented as the sum of the difference in the enthalpy change of the chelate formation and of the distribution between the metal chelates. The calculated values of $\Delta(\Delta H)$ and $\Delta(\Delta S)$ are listed in Table 4. The values of $\Delta(\Delta H)$ are largely positive. If the extracted species of Zn had a composition like that of Cd, $\Delta(\Delta H)$ would be predicted to be fairly small, for the difference in enthalpy change of the chelate formation between Zn and Cd is generally small. Hence, it is conceivable that the extracted species of Zn is different from that of Cd. As for lanthanoids, ΔH, which is calculated from the extraction constant, has been reported to be 11.1 kcal/mol (46.4 kJ mol^{-1}) for $Eu(tta)_3$, 9.64 kcal/mol (40.3 kJ mol^{-1}) for $Tb(tta)_3$, and 12.4 kcal/mol (51.9 kJ mol^{-1}) for $Tm(tta)_3$.[3,5] The difference between the ΔH values of these lanthanoids is very small. The positive values of $\Delta(\Delta H)$ and $\Delta(\Delta S)$ would indicate that water molecules would be removed from Zn-DPC chelate in the process of extraction. Since hydrogen-bond energies are usually in the range of 10—25 kJ mol^{-1}, it would be expected to take ΔH values of 20—50 kJ mol^{-1} in order to remove two water molecules. The values of $\Delta(\Delta H)$ are 70.8 kJ mol^{-1} in the case of chloroform and 43.9 kJ mol^{-1} in the case of benzene. Therefore, these values are consistent with the postulate that the Zn-DPC chelate would be extracted as a non-hydrated chelate, $Zn(dpc)_2$, while the Cd-DPC chelate would be extracted as a hydrated species, $Cd(dpc)_2 \cdot 2H_2O$.

Furthermore, it became apparent from these results that the separation of zinc and cadmium may be further enhanced at high temperatures. For the purpose of enhancing the separation of zinc and cadmium, chloroform is better than benzene as the solvent for extraction. However, since chloroform has a low boiling point, for this purpose organic solvents whose boiling points are relatively high, such as 1,1,2,2-tetrachloroethane (TCE), are desirable. It was indicated that the separation of zinc and cadmium is further enhanced at high temperatures when both metals are extracted with 2-methyl-8-quinolinol into TCE.[13] Hence, it is conceivable that

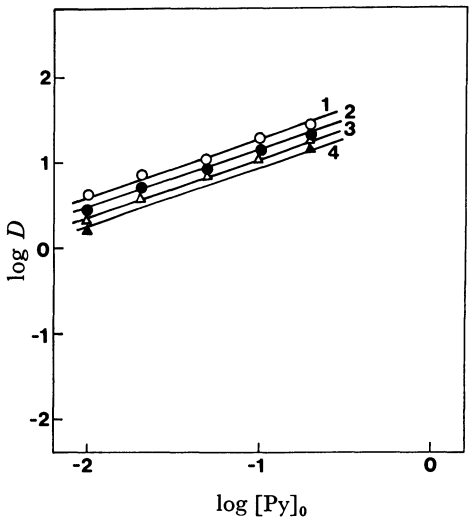

Fig. 3. Distribution of zinc with mixtures of DPC and pyridine into chloroform as a function of the pyridine concentration.
$[DPC]_0=5\times10^{-4}$ M, $[Zn]_T=10^{-5}$ M, pH 7.0. 1: 15 °C, 2: 25 °C, 3: 35 °C, 4: 45 °C.

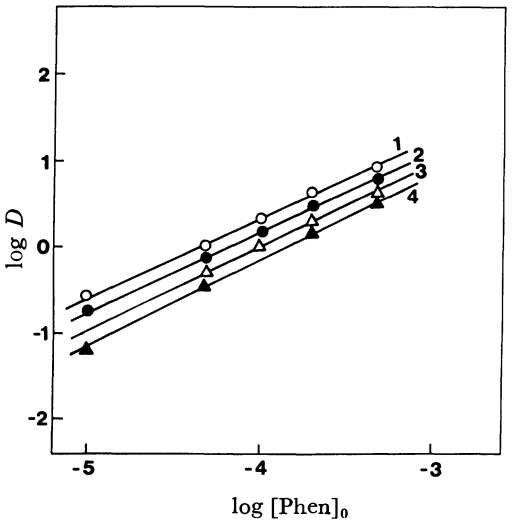

Fig. 4. Distribution of zinc with mixture of DPC and phenanthroline into chloroform as a function of the phenanthroline concentration.
$[DPC]_0=5\times10^{-4}$ M, $[Zn]_T=10^{-5}$ M, pH 6.5. 1: 15 °C, 2: 25 °C, 3: 35 °C, 4: 45 °C.

solvent extraction at high temperatures may be applied to the separation of metals of the same group by using the difference in extraction mechanism between those metals.

Extraction of Zinc with DPC in the Presence of 1,10-*Phenanthroline or Pyridine.* By slope analysis, the extraction of Zn with DPC into chloroform in the presence of 1,10-phenanthroline or pyridine was studied at various temperatures. The log D *vs.* pH plots are linear and exhibit a slope of 2 at each temperature. The plots of log D *vs.* log $[py]_0$ are shown in Fig. 3. The slopes of log D *vs.* log $[py]_0$ are unity, irrespective of the temperature. In Fig. 4, the plots of log D *vs.* log $[phen]_0$ are shown. The slopes of log D *vs.* log

$[phen]_0$ are also unity, irrespective of the temperature. These results indicate that the extracted species are $Zn(dpc)_2 \cdot py$ and $Zn(dpc)_2 \cdot phen$ respectively. These thermodynamic parameters are summarized in Table 1.

In the presence of pyridine, the value of ΔG, which is calculated from the adduct-formation constant, is negative, so it is obvious that the acceptor mother chelate is stabilized by the adduct-chelate formation. The rather large negative experimental enthalpy ($\Delta H = -46.5$ kJ mol^{-1}) clearly eliminates Mechanism (i), because in this system the enthalpy change would be small, since the number of bonds to zinc does not change. Furthermore, in the case of Mechanism (ii), the enthalpy change would be the energy of the hydrogen bond ($\approx$10 to 25 kJ mol^{-1}). Therefore, it may be concluded that the mechanism most likely to explain the experimental results is Mechanism (iii), in which the coordination number of zinc expands from four to five to accommodate the neutral pyridine molecule.

Hence, the synergistic reaction in the organic phase can be expressed as follows:

$$Zn(dpc)_{2(o)} + py_{(o)} \rightleftarrows Zn(dpc)_2 \cdot py_{(o)}. \quad (5)$$

In this case, the entropy change would be largely negative, consisting of the cratic part ($\Delta n = -1$), where Δn is the change in the number of species, and the unitary part of pyridine. The rather large negative experimental entropy change ($\Delta S = -81$ J K^{-1} mol^{-1}) fits Eq. 5. The experimental results for 1,10-phenanthroline are $\Delta H = -56.3$ kJ mol^{-1} and $\Delta S = -58$ J K^{-1} mol^{-1}, which fit only Mechanism (iii).

The synergistic reaction in the organic phase can be represented by Eq. 6:

$$Zn(dpc)_{2(o)} + phen_{(o)} \rightleftarrows Zn(dpc)_2 \cdot phen_{(o)}. \quad (6)$$

Since 1,10-phenanthroline is usually bidentate, in this case the coordination number of zinc increases from four to six. Compared with pyridine, both entropy and enthalpy favor adduct-chelate formation.

Extraction of Cadmium with DPC in the Presence of 1,10-Phenanthroline or Pyridine. The extraction of cadmium with DPC into chloroform and benzene in the presence of 1,10-phenanthroline or pyridine was studied at various temperatures.

In the case of chloroform, the slopes of log D *vs.* pH are 2 at each temperature in the presence of both pyridine and 1,10-phenanthroline, and the distribution ratio decreased with an increase in the temperature. The slopes of log D *vs.* log $[DPC]_0$ are also 2 at each temperature. In the presence of pyridine, the slopes of log D *vs.* log $[py]_0$ are unity. In the presence of 1,10-phenanthroline, the slopes of log D *vs.* log $[phen]_0$ are also unity. These results suggest that the extracted species are $Cd(dpc)_2 \cdot py$ and $Cd(dpc)_2 \cdot phen$. From these results, the thermodynamic parameters, ΔG, ΔH, and ΔS, which were calculated from the thermodynamic equations, are as listed in Table 2. The values of ΔG, which were calculated from the adduct-formation constant, are negative, so it is obvious that the acceptor mother chelates are stabilized by the adduct-chelate formation. In these cases, the ΔH values, which are 7.7 kJ mol^{-1} for pyridine and 0.0 kJ mol^{-1} for 1,10-phenanthroline, are quite small, or even close to zero.

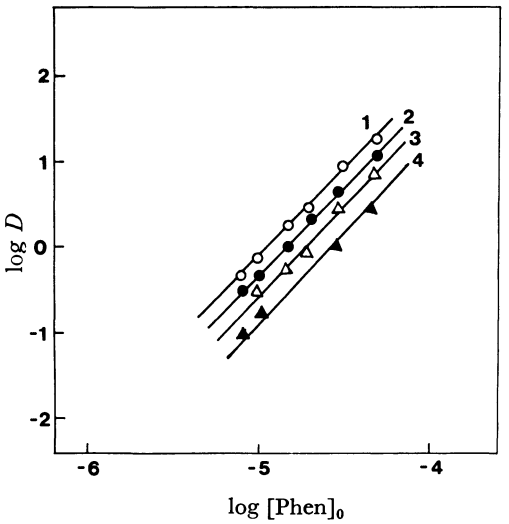

Fig. 5. Distribution of cadmium with mixtures of DPC and phenanthroline into benzene as a function of the phenanthroline concentration.
$[DPC]_0 = 5 \times 10^{-4}$ M, $[Cd]_T = 10^{-6}$ M, pH 7.1. 1: 15 °C, 2: 25 °C, 3: 35 °C, 4: 45 °C.

These relatively small experimental enthalpy changes clearly eliminate Mechanism (iii). These results fit the postulate that, in the absence of pyridine or 1,10-phenanthroline, the Cd-DPC chelate would be extracted as a hydrated species, $Cd(dpc)_2 \cdot 2H_2O$. In the case of Mechanism (ii), the entropy change would be largely negative, since Δn, the change in the number of species, decreases. However, the experimental entropy changes are positive, so these results do no fit Mechanism (ii). Consequently, we may conclude that the mechanism (ii). Consequently, we may conclude that the mechanism most likely to explain the experimental results is Mechanism (i), in which pyridine or 1,10-phenanthroline replaces the residual waters of hydration in the first coordination sphere of the cadmium ion.

Hence, the synergistic reaction in the organic phase can be expressed as follows:

$$Cd(dpc)_2 \cdot 2H_2O_{(o)} + S_{(o)} \rightleftarrows Cd(dpc)_2S_{(o)} + 2H_2O, \quad (7)$$

where S is pyridine or 1,10-phenanthroline.

Next, in the case of benzene, the slopes of log D *vs.* pH are 2 at each temperature in the presence of pyridine or 1,10-phenanthroline, and the distribution ratio decreases with an increase in the temperature. The slopes of log D *vs.* log $[DPC]_0$ are also 2. In the presence of pyridine, the slopes of log D *vs.* log $[py]_0$ are unity. In the presence of 1,10-phenanthroline, the plots of log D *vs.* log $[phen]_0$ are as shown in Fig. 5. The slopes of log D *vs.* log $[phen]_0$ are 2 at each temperature, unlike those with chloroform. These results suggest the idea that the extracted species are $Cd(dpc)_2 \cdot py$ and $Cd(dpc)_2 \cdot 2phen$. The thermodynamic parameters led to from these results are summarized in Table 3. The values of ΔG are largely negative, so the acceptor mother chelates are obviously stabilized by the adduct-chelate formation. In the absence of pyridine or 1,10-phenanthroline, the Cd-DPC chelate would be extracted into benzene as a hydrated species, $Cd(dpc)_2 \cdot 2H_2O$,

like that into chloroform, so it may be concluded that the mechanism most likely to explain the experimental results is Mechanism (i), in which pyridine or 1,10-phenanthroline replaces the residual waters of hydration in the first coordination sphere of the cadmium ion. Compared with the case of pyridine, in the case of 1,10-phenanthroline both entropy and enthalpy changes favor adduct-chelate formation : however, the contribution of the entropy change is larger than that of enthalpy. The difference in ΔS between pyridine and 1,10-phenanthroline in benzene is larger than that in chloroform. A large entropy change of this order reflects the steric hindrance caused by the first 1,10-phenanthroline molecule to the entrance of its second molecule. Furthermore, the steric effect may make it difficult for 1,10-phenanthroline to form a strong bond with the complex.

Thus, the thermodynamic results suggest that the mechanism for the synergism of zinc is different from that of cadmium.

References

1) Y. Marcus and A. S. Kertes, "Ion Exchange and Solvent Extraction of Metal Complexes," Wiley, New York (1969), p. 833.

2) M. S. Subrumanian and S. A. Pai, *J. Inorg. Nucl. Chem.*, **32**, 3677 (1970).

3) A. T. Kandil, H. F. Aly, M. Raieh, and G. R. Choppin, *J. Inorg. Nucl. Chem.*, **37**, 229 (1975).

4) K. L. Nash and G. R. Choppin, *J. Inorg. Nucl. Chem.*, **39**, 131 (1977).

5) A. T. Kandil and K. Farah, *J. Inorg. Nucl. Chem.*, **42**, 1491 (1980).

6) A. M. El-Atrash. A. T. Kandil, E. Souaya, and W. Georgy, *J. Radioanal. Chem.*, **43**, 73 (1978).

7) D. R. Dakternieks and D. P. Graddon, *Aust. J. Chem.*, **26**, 2537 (1973).

8) L. T. Ang and D. P. Graddon, *Aust. J. Chem.*, **29**, 1429 (1976).

9) E. Nakayama, *Memoirs of the Faculty of Science, Kyoto University, Series A of Physics, Astrophysics, and Chemistry*, **35**, 203 (1977).

10) E. Nakayama, *Memoirs of the Faculty of Science, Kyoto University, Series A of Physics, Astrophysics, and Chemistry*, **35**, 210 (1977).

11) E. Yamada, E. Nakayama, T. Kuwamoto, and T. Fujinaga, *Anal. Chim. Acta*, 38, 409 (1982).

12) G. R. Choppin and H. G. Friedman, *Inorg. Chem.*, **5** 1599 (1966).

13) T. Fujinaga, T. Kuwamoto, and E. Nakayama, *Abstr. Jpn. Soc. Anal. Chem.*, (1978), p. 268.

Coordination Structure of Cu^{2+} Ion in Highly Concentrated Aqueous $CuBr_2$ Solution, Determined by X-Ray Diffraction Analysis

Mitsuyoshi Ichihashi, Hisanobu Wakita,* Takeharu Mibuchi,† and Isao Masuda
Department of Chemistry, Faculty of Science, Fukuoka University, Nanakuma, Jonan-ku, Fukuoka 814-01
(Received February 26, 1982)

The solute structure of concentrated aqueous copper(II) bromide solutions was determined by the analysis of the radial distribution curves of X-ray diffraction measured on the solutions with varying concentrations, 4.364—1.016 mol dm^{-3}. The mixed-ligand aquabromocopper(II) complexes were found to be present in these solutions, and to have a distorted octahedral geometry. The Cu^{2+} ion was coordinated with Br^- ions at the equatorial sites whose bond lengths were shorter than the axial sites. The interatomic distances of the equatorial Cu–Br and Cu–OH_2 bonds were, respectively, 2.42—2.46 and 1.96—1.99 Å, and that of the axial Cu–OH_2 bond, 2.37—2.51 Å. The average coordination number of Br^- ions in the nearest neighbor of the Cu^{2+} ion increased from 0.33 to 1.31 as the concentration of $CuBr_2$ increased from 1.016 to 4.364 mol dm^{-3}. Even in the 4.364 mol dm^{-3} solution, which was nearly saturated, the coordination of the Br^- ion at the axial site was not evidenced. In the 1.474 mol dm^{-3} $CuBr_2$ solution dissolved in an aqueous 6.923 mol dm^{-3} HBr solution, the tetrabromocopper(II) complex species was proposed to exist in a flattened tetrahedral form, wherein the Cu–Br distance was 2.41 Å.

The octahedral structure of six-coordinate copper(II) complexes has been characterized by two kinds of coordination bonds, with different bond lengths, *i.e.*, a shorter one toward the equatorial site and a longer one toward the axial site; this has been interpreted as being related to the anisotropic electron-filling on the $d\gamma$ orbitals of Cu^{2+} ion in the octahedral ligand-field. The X-ray investigations have demonstrated that the mixed-ligand complexes $[Cu(en)_2(H_2O)_2]^{2+}$ and $[Cu(NH_3)_4(H_2O)_2]^{2+}$ in the aqueous solution have a structure wherein the two H_2O molecules are coordinated at the elongated axial sites, with a Cu–O bond distance of 2.92 Å in the former and of 2.33 Å in the latter.[1,2] On the other hand, Wertz *et al.* have determined the solute structure and the average coordination number around the Cu^{2+} ion with the concentrated aqueous $CuCl_2$ solutions of 3.18 and 4.35 mol dm^{-3}, and they have concluded that the coordination ability of the Cl^- ligand is $Cl^- \gg H_2O$ toward the axial coordination and $Cl^- > H_2O$ toward the equatorial coordination.[3,4] Judging from the spectrochemical series, Cl^- is expected to exert a weaker ligand-field than H_2O upon Cu^{2+}. The X-ray investigation by Golik *et al.* has shown that in the predominant complex species which are present in the aqueous 2.0 mol dm^{-3} $CuCl_2$ solution, two Cl^- ions are coordinated axially and four H_2O molecules are coordinated equatorially with Cu^{2+}.[5,6] From the UV- and visible-spectral investigations, Libuś has also supported the axial coordination of the Cl^- ligand in the complex $[CuCl(H_2O)_5]^+$ existing in the aqueous $CuCl_2$ solution.[7]

In contrast to the above results, Fontana *et al.* have reported the Raman spectrum of the aqueous 3.4 mol dm^{-3} $CuCl_2$ solution; it shows a pattern similar to that of crystal $(CH_3NH_3)_2CuCl_4$, which is composed of square-planar complex $[CuCl_4]^{2-}$.[8] Moreover, as for the aqueous 0.5 mol dm^{-3} $CuBr_2$ solution, the EXAFS measured by Fontaine *et al.* indicated that in the solution half of both the Cu^{2+} and the Br^- ions are linked each other with an interatomic distance of 2.35 ± 0.05 Å; this distance is rather closer to the equatorial Cu–Br than to the axial Cu–Br bond distances in crystal $CuBr_2$.[9–11] Hence, it is of interest to determine by X-ray investigation whether the coordination of the Br^- ion in the mixed-ligand aquabromocopper(II) complexes occurs at either the axial or the equatorial sites. Previously, we have reported that the X-ray scattering factor of the bromine is larger than that of the chlorine atom. This caused pronounced peak appearance in the X-ray radial distribution curve, which rendered a precise resolution of the solute structure of the aqueous $NiBr_2$ solution.[12] In the present paper, we attempt to elucidate the coordination structure of the mixed-ligand aquabromocopper(II) complexes in the aqueous solution by the X-ray investigation.

Experimental

Sample Solutions. The sample solutions A—D were prepared by dissolving copper(II) bromide obtained by the recrystallization of commercially available material from distilled water. The sample solutions E and F were prepared by dissolving recrystallized copper(II) bromide in an aqueous 47% hydrobromic acid solution, and then by diluting the solutions with distilled water. The copper and bromide ion concentrations of the solutions were determined by EDTA titration and the Volhard method, respectively. The composition of the sample solutions is shown in Table 1.

X-Ray Diffraction Measurements and Data Treatments. After the sample solutions had been left to stand at room temperature for 2—3 d, the diffraction intensities of the solutions were recorded, as previously reported.[12] The scatterd intensities were measured at every 0.1° between $\theta = 0.5°$ and 8°, 0.25° between $\theta = 8°$ and 30°, and 0.5° between $\theta = 30°$ and 65°; 2θ is the scattering angle. The time required for accumulating 40000 counts was recorded for the solutions A, B, C, E, and F; 80000 counts were taken for the solution D.

The measured intensity data were corrected for the air- and multiple-scatterings, and for the polarization and absorption due to the sample solutions, and then normalized to absolute intensities $I(\theta)$ according to the ordinary treatment.[13,14] Reduced intensities $i(\theta)$ were calculated by subtracting incoherent and independent coherent scatterings from $I(\theta)$.

The radial distribution function $D(r)$ employed is given in in Eq. 1:

† Present address: Idemitsu Kosan Co. Ltd., Sodegaura-machi, Kimitsu-gun, Chiba 292-01.

Table 1. Composition and parameter values of sample solutions

	Solution					
	A	B	C	D	E*	F*
Cu(mol dm^{-3})	1.016	2.006	3.262	4.364	2.101	1.474
Br (mol dm^{-3})	2.032	4.011	6.524	8.728	8.345	9.871
O (mol dm^{-3})	53.96	51.40	48.62	47.33	44.50	38.98
H (mol dm^{-3})	107.4	102.8	97.25	94.66	93.13	84.89
[Br]/[Cu]	2.00	2.00	2.00	2.00	3.97	6.70
V/Å^3	1634	827.7	509.0	380.5	790.3	1127
ρ/g cm^{-3}	1.199	1.374	1.605	1.827	1.606	1.592
μ/cm^{-1}	17.41	33.18	53.20	70.80	60.97	68.56

V, Stoichiometric volume containing one copper atom. This is used for diffraction data normalization; ρ, density; μ, linear absorption coefficient of the solution; *, hydrobromic acid solution.

$$D(r) = 4\pi r^2\rho_0 + \frac{2r}{\pi}\int_0^{15} s\cdot i(s)\cdot M(s)\cdot\sin(r\cdot s)\cdot ds, \quad (1)$$

where ρ_0 is the average scattering density of the sample solution, and is given in the electron units, and s is equal to $4\pi\sin\theta/\lambda$ (λ=0.7107 Å). The modification function $M(s)$ was that employed previously.[12]

As a first approximation to the structure, the theoretical peak shape was drawn by Fourier transformation of the theoretical intensities $i(s)_{calcd}$ given by Eq. 2:

$$i(s)_{calcd} = \sum_i^{i\neq j}\sum_j n_{ij}\cdot f_i(s)\cdot f_j(s)\,\frac{\sin(r_{ij}\cdot s)}{r_{ij}\cdot s}\exp(-b_{ij}\cdot s^2). \quad (2)$$

In Eq. 2, f_i(s) and f_j(s) are the atomic scattering factors of atoms i and j; and n_{ij}, r_{ij}, and b_{ij} are, respectively, the frequency factor, the distance and the temperature factor of the interactions between atom i and j.

In order to attain more precisely the structural parameter values, the above parameter values were refined so as to minimize the difference between $i(s)_{calcd}$ and observed $i(s)$, by means of a least-squares refinement.

Results

The radial distribution curves $D(r)$ and $D(r)-4\pi r^2\rho_0$ are shown in Figs. 1 and 2. For the solutions A—D, four peaks are seen in the $D(r)$ curves at *ca.* 1.0, 2.0, 2.5, and 3.3—3.5 Å; these would be closely concerned with the intra- and inter-molecular atomic interactions of the solute complex and the solvent H_2O molecules. The first broad peak around 1.0 Å is caused by the O–H interaction within the free and complexed H_2O molecules in the solution. The peak ascribable to these O–H interactions has been commonly observed in the $D(r)$ curves measured for the aqueous solution.[12,15]

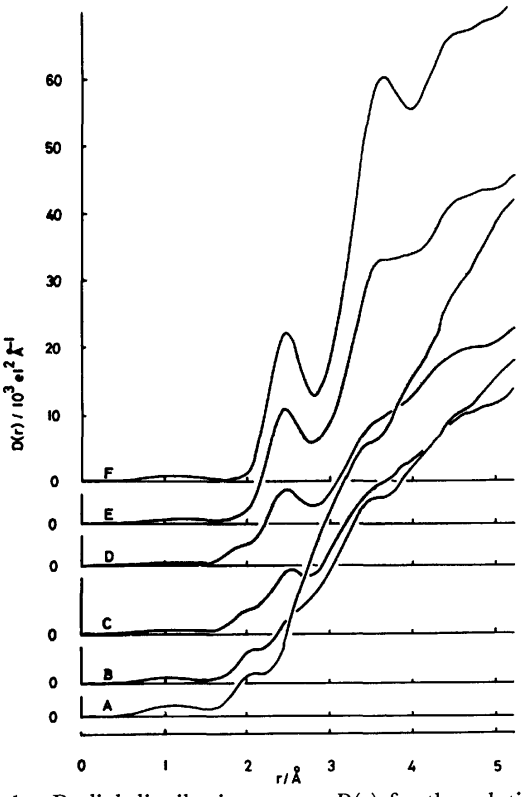

Fig. 1. Radial distribution curves $D(r)$ for the solutions A—F.

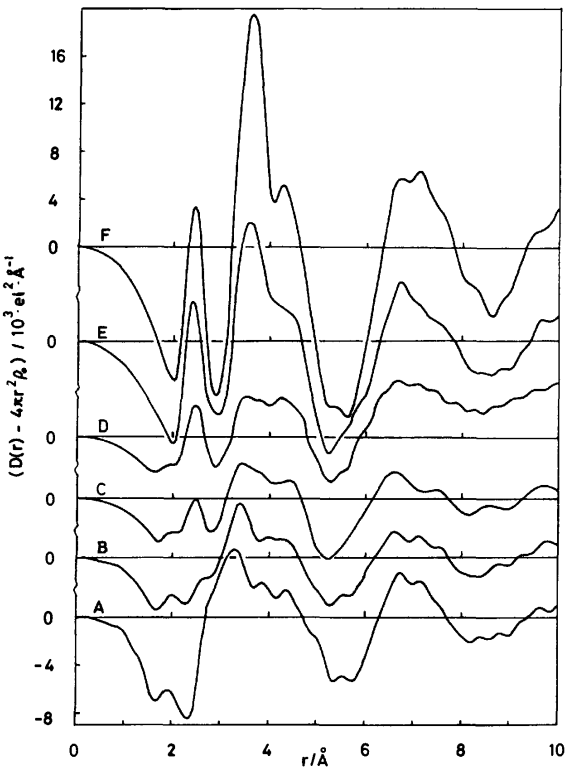

Fig. 2. $D(r)-4\pi r^2\rho_0$ curves for the solutions A—F.

The peak area around 2.0 Å decreases as the concentration of $CuBr_2$ increases, *i.e.*, the area becomes smaller in the order of the solutions, A>B>C>D; for the solution E the corresponding peak becomes very small and obscure; and for the solution F no peak is observed in this region. It has already been established that the hexaaquacopper(II) complex existing in the aqueous 3.550 mol dm^{-3} $Cu(ClO_4)_2$ solution holds a distorted octahedral form wherein the central Cu^{2+} ion binds four H_2O molecules at the equatorial sites with a distance of 1.94 Å and two H_2O molecules at the axial sites with a distance of 2.43 Å.[16] Thus, the above peak around 2.0 Å observed for the present $CuBr_2$ solutions may tentatively be ascribed to the Cu–OH_2 interaction at the equatorial position.

In contrast with the peak around 2.0 Å, the peak around 2.5 Å increases its peak area in the above mentioned order of solutions. The addition of the HBr causes the appearance of a quite distinct peak, as seen for the solutions E and F. In the crystal $CuBr_2$ the equatorial Cu–Br bond distance is 2.40 Å and the axial one, 3.18 Å.[11] Hence, the peak around 2.5 Å could be attributed to the interaction of the equatorial Cu–Br bond.

The broad peak located between 3.3—3.5 Å for the solutions A—D could be interpreted as being composed of the peaks due to the interaction between Br^- and OH_2 (both are free)[17] and those between Br^- and OH_2, and H_2O and OH_2 (these are bound at the *cis*-positions in an octahedral complex). An analogous peak due to these interactions was observed in the $D(r)$ curve of the highly concentrated aqueous $NiBr_2$ solution which contained predominantly $[NiBr(H_2O)_5]^+$ species.[12] In the cases of the solutions E and F that have HBr added, the comparable peak is seen at 3.6 Å, somewhat longer than 3.3—3.5 Å of the solutions A—D; this agrees with the expectation that the increased concentration of the Br^- ion aids the formation of the higher-order bromo-complexes, whereby the Br^-–Br^- interaction at the *cis*-position becomes prominent.

Then, in order to draw the structure of the predominant solute complex, the four possible geometries depicted in Fig. 3 were assumed: these are elongated octahedron (a), square pyramid (b), square plane (c), and tetrahedron (d). And the theoretical intensities $i(s)_{calcd}$ were calculated from Eq. 2, by substituting a set of the parameter values, n, r, and b that were tentatively taken for each of the assumptive models. The parameter n, the frequency factor which represents the number of the interactions between Cu^{2+} and any atom being on the axial position, was fixed at 2.0 with regard to model (a) and at 1.0 to model (b). The further refinements of these parameters were made by a least-squares method so that these gave an $s \cdot i(s)_{calcd}$ curve which was in good agreement with the observed $s \cdot i(s)$ curve in the region above $s>4$.

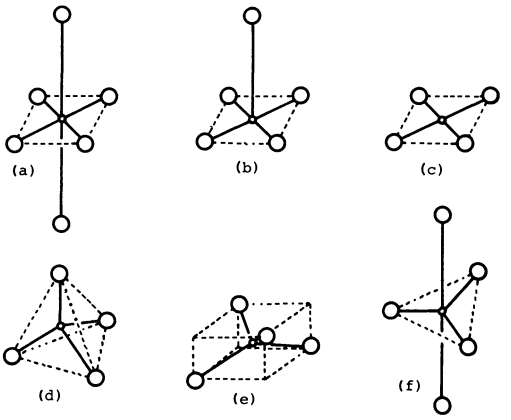

Fig. 3. Assumptive skeletal models.

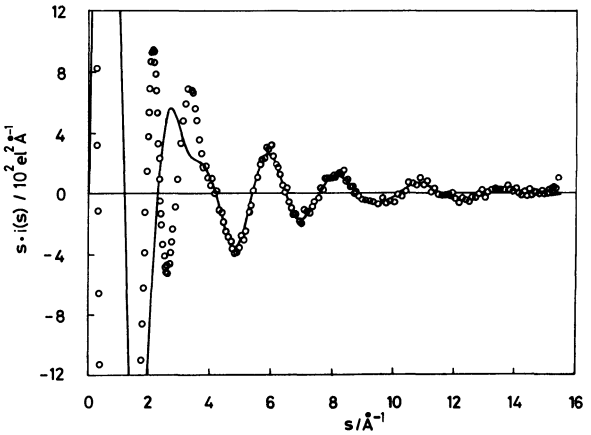

Fig. 4. Observed (○○) and calculated (——) $s \cdot i(s)$ curves for solution D.

Thus, the results indicated that the predominant complex species which existed in the solutions A—D can be most satisfactorily depicted by model (a). The

TABLE 2. REFINED PARAMETERS OBTAINED FROM THE REDUCED INTENSITY CURVE

Parameter		Solution					
		A	B	C	D	E	F
$Cu-O_{eq}$	r/Å	1.96	1.99	1.96	1.97	1.93[a]	—
	n	3.67	3.32	2.73	2.52	1.10[a]	—
$Cu-O_{ax}$	r/Å	2.50	2.51	2.41	2.37	2.42[a]	—
	n	2	2	2	2	2[a]	—
Cu–Br	r/Å	2.42	2.43	2.44	2.46	2.42[a]	2.41[b]
	n	0.33	0.60	1.10	1.31	2.91[a]	3.85[b]
$n(Cu-O_{eq})+n(Cu-Br)$		4.00	3.92	3.83	3.83	4.01[a]	—

r, Bond distance, n, frequency factor. a) The parameters obtained when model (a) was used. b) The parameters were evaluated only from the peak of the $D(r)$ curve at 2.4 Å.

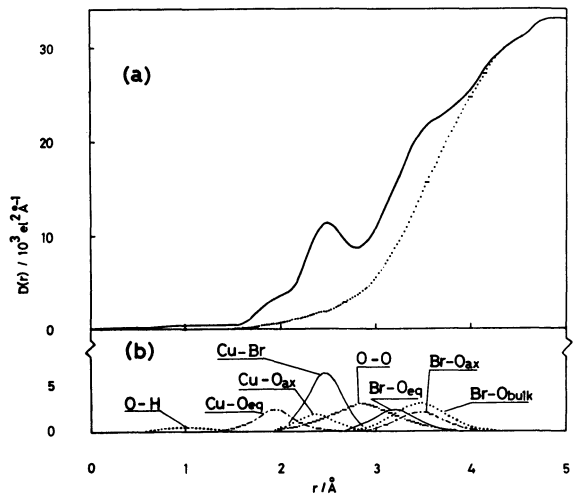

Fig. 5. (a); The $D(r)$ curve (——) and the residual distribution function (·····) for solution D. The residual distribution function is obtained by subtracting the calculated peak shapes shown in (b) from the $D(r)$ curve. (b); The peak shapes calculated by using the parameter values given in Table 2.

parameter values mostly fitted by the refinements are listed in Table 2. And the $s \cdot i(s)_{calcd}$ curve calculated from these data are in good agreement with the observed $s \cdot i(s)$ curve as is exemplified in Fig. 4 for the solution D. In Fig. 5, it is shown that the residual distribution function curve obtained by the subtraction of the $s \cdot i(s)_{calcd}$ curve from the observed $s \cdot i(s)$ curve gives a smooth curve, indicating a good reliability of these parameter values. With regard to the complex in the solution E, the structure model shown in Fig. 3-(d) could be discarded, but any of the three models (a), (b), and (c) could be accepted with the same margin of uncertainty. For the complex in the solution F, none of the above four models was satisfactorily consistent with the resultant data.

Discussion

On increasing $CuBr_2$ concentration in the aqueous solution, if the coordination of the Br^- ion occurred first at the axial and then at the equatorial sites, we think that the peak in the $D(r)$ curve owing to the axial Cu–Br interaction would appear at *ca.* 3.18 Å.[11] However, Figs. 1 and 2 show no appearance of such a peak, indicating no axial coordination of Br^- in the present solute complexes. And Table 2 shows that with increasing $CuBr_2$ concentration the mean frequency factor of the equatorial Cu–Br interaction increases and that of the equatorial Cu–O decreases, while the sum of the respective value is *ca.* 4, being invariable throughout the solutions A—D with different concentrations. These facts concur with the proposed structure-model (a) of the solute complex. The equatorial Cu–Br bond distance, 2.42—2.46 Å, is more close to the equatorial Cu–Br bond distance, 2.40 Å, than to the axial Cu–Br bond distance, 3.18 Å; these are known for the crystal $CuBr_2$.[11] Moreover, the distances of equatorial Cu–O, 1.96—1.99 Å, and of axial Cu–O, 2.37—2.51 Å, of the solute complex are, respectively, comparable to those of 1.943—1.976 and of 2.399—2.448 Å of crystal $CuSO_4 \cdot 3H_2O$.[18]

As has been pointed out, the mixed-ligand complexes $[Cu(NH_3)_4(H_2O)_2]^{2+}$ and $[Cu(en)_2(H_2O)_2]^{2+}$ hold H_2O, which is a weaker ligand than NH_3 or en, at the axial site; this structure of coordination is reasonably interpreted to be more stable than that which holds H_2O at the equatorial site. Thus, only judging from the spectrochemical series, it is predicted that in the mixed-ligand aquabromocopper(II) complexes the coordination of H_2O, which is a stronger ligand than Br^-, would occur at the equatorial site rather than at the axial site. On the contrary, the solute mixed-ligand complex in the aqueous $CuBr_2$ solution seems to have H_2O at the axial site. Though this work offers no kinetic datum of the complex-formation equilibrium, this structure implies a little difference in the apparent coordination abilities of H_2O and Br^- toward Cu^{2+} ion.

No satisfactory result of the data refinements was drawn for the solutions E and F. However, the peak at 2.4 Å on the $D(r)-4\pi r^2\rho_0$ curves might be attributed to the Cu–Br interaction. And in the aqueous solution, the presence of Cu^{2+} ions binding three, five, or six Br^- ions were not evidently indicated from the electronic spectral investigations.[19] By taking these results into consideration, the minimum amounts of Cu^{2+} existing in a tetrabromo complex species in solutions E and F were tentatively calculated from the peak areas in the

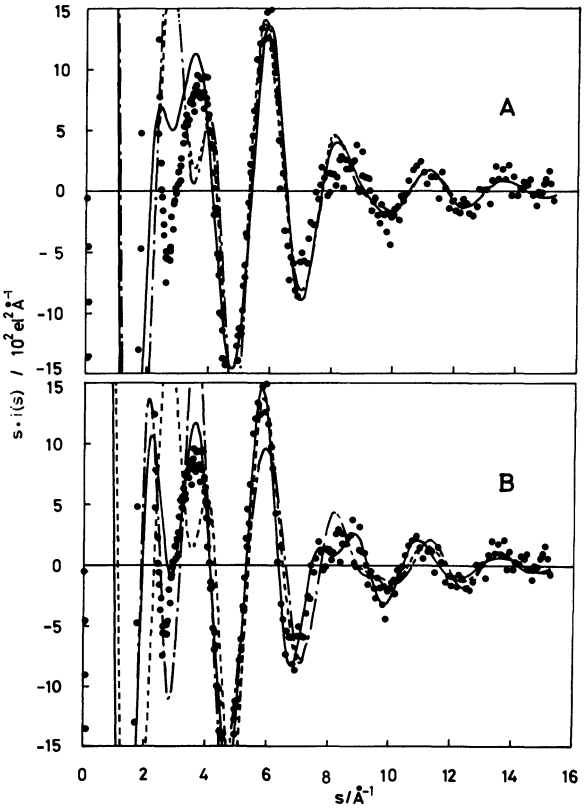

Fig. 6. Observed and calculated $s \cdot i(s)$ curves for solution F. A: Observed (●●); calculated for model (a) (– – –), for model (b) (——), for model (c) (------). B: Observed (●●), calculated for model (d) (– – –), for model (e) (——), for model (f) (------).

$D(r)$ curves: these are 92.5% of the total Cu^{2+} concentration in solution F, and 45.5% of that in solution E.[20] If the tetrabromo complex species had either a square-planar or tetrahedral structure, the Br^-–Br^- interactions within these complex molecules would give rise to the appearence of the peaks on the $D(r)$ and $D(r)-4\pi r^2\rho_0$ curves at around 3.41 and 4.82 Å for the former, or at around 3.94 Å for the latter. However, actually no peak is observed at these positions, but two peaks, a larger one at *ca.* 3.6 and a smaller one at *ca.* 4.35 Å, are observed. These facts led us to propose a flattened tetrahedral structure of the tetrabromo complex species, as shown in Fig. 3-(e). This structure is similar to that of $[CuBr_4]^{2-}$ in the Cs_2CuBr_4 crystal.[21] Then, for solution F, the observed $s\cdot i(s)$ curve is compared with the calculated ones using the refined parameter values which are taken for the assumptive models (a)—(f). In this case, a trigonal bipyramidal model (f) in Fig. 3, is also taken into consideration. As shown in Fig. 6, the curve calculated on model (e) is most like to the observed one.

References

1) T. Fujita and H. Ohtaki, 41st National Meeting of the Chemical Society of Japan, Osaka, April 1980, Abstr. No. 2L42.

2) T. Yamaguchi and H. Ohtaki, *Bull. Chem. Soc. Jpn.*, **52**, 415 (1979).

3) J. R. Bell, J. L. Tyvoll, and D. L. Wertz, *J. Am. Chem. Soc.*, **95**, 1456 (1973).

4) D. L. Wertz and J. L. Tyvoll, *J. Inorg. Nucl. Chem.*, **36**, 3713 (1974).

5) A. Z. Golik, A. K. Dorosh, A. F. Skryshevskii, and P. F. Cholpan, *Ukr. Fiz. Zh. (Russ. Ed.)*, **12**, 79 (1961).

6) Very recently, Magini has shown by X-ray diffraction method that in the aqueous 2.952 mol dm^{-3} $CuCl_2$ solution the coordination of *ca.* 1.2 Cl^- ions occurs at the equatorial sites of the Cu^{2+} ion. As to the coordination at the axial sites his investigation is inconclusive; M. Magini, *J. Chem. Phys.*, **74**, 2523 (1981).

7) Z. Libuś, *Inorg. Chem.*, **12**, 2972 (1973).

8) M. P. Fontana, G. Maisano, P. Migliardo, and F. Wanderlingh, *J. Chem. Phys.*, **69**, 676 (1978).

9) A. Fontaine, P. Lagarde, D. Raoux, M. P. Fontana, G. Maisano, P. Migliardo, and F. Wanderlingh, *Phys. Rev. Lett.*, **41**, 504 (1978).

10) P. Lagarde, A. Fontaine, D. Raoux, A. Sadoc, and P. Migliardo, *J. Chem. Phys.*, **72**, 3061 (1980).

11) L. Helmholz, *J. Am. Chem. Soc.*, **69**, 886 (1947).

12) H. Wakita, M. Ichihashi, T. Mibuchi, and I. Masuda, *Bull. Chem. Soc. Jpn.*, **55**, 817 (1982).

13) H. A. Levy, M. D. Danford, and A. H. Narten, ORNL-3960(1966).

14) B. E. Warren and R. L. Mozzi, *Acta Crystallogr.*, **21**, 459 (1966).

15) A. H. Narten, ORNL-4578 (1970).

16) H. Ohtaki and M. Maeda, *Bull. Chem. Soc. Jpn.*, **47**, 2197 (1974).

17) R. M. Lawrence and R. F. Kruh, *J. Chem. Phys.*, **47**, 4758(1967).

18) R. F. Zahrobsky and W. H. Baur, *Acta Crystallogr., Sect. B*, **24**, 508 (1968).

19) J. C. Barnes and D. N. Hume, *Inorg. Chem.*, **2**, 444 (1963).

20) The ratio, $x(\%)$, of the concentration of $[CuBr_4]^{2-}$ to the total concentration of Cu^{2+} was calculated by the relation,

$$4 \times \frac{x}{100} + 2 \times \frac{100-x}{100} = n,$$

where n is the frequency factor of Cu–Br interaction.

21) B. Morosin and E. C. Lingafelter, *Acta Crystallogr.*, **13**, 807 (1960).

 © 1982 The Chemical Society of Japan Bull. Chem. Soc. Jpn., 55, 3165—3169 (1982)

Synthesis and Characterization of Substituted Derivatives of (Tetraazacycloalkadienato)nickel(II) Complexes with Uninegative Ligands, and Crystal Structure of Parent Complex [Ni(Me$_2$[14]dienatoN$_4$)]Br·H$_2$O

Naohide MATSUMOTO,* Kenichiro WAKIZAKA, and Akira OHYOSHI
Department of Industrial Chemistry, Faculty of Engineering, Kumamoto University, Kurokami 2-39-1, Kumamoto 860
(Recieved February 18, 1982)

The (tetraazacycloalkadienato)nickel(II) complexes [Ni(Me$_2$[Z]dienatoN$_4$)]$^+$ (Z=13, 14), which have an unsaturated chelate ring containing nucleophilic center, react with electrophilic reagents such as benzoyl chloride, *p*-methylbenzoyl chloride, and *p*-nitrobenzoyl chloride to give the substituted derivatives [Ni(Me$_2$E[Z]dienatiN$_4$)]-PF$_6$. These complexes have been characterized by elemental analyses, ^{1}H NMR, infrared, and electronic spectra. One of the parent complexes [Ni(Me$_2$[14]dienatoN$_4$)]Br·H$_2$O has been subjected to the single-crystal X-ray diffraction technique and its structural data indicated that the average Ni–N bond distance is longer than that of the corresponding thirteen membered complex.

The γ-position of six-membered diiminato chelate rings[1–6] as well as that of the chelate rings of acetylacetonato complexes[7–9] have been found to be very reactive nucleophilic center. This reactivity has been employed to introduce a large number of substituents into macrocyclic ligands.[1–6] These substituent derivatives have been produced by what have been proposed to be electrophilic attacks on the γ-carbon in a manner similar to substitution in ordinary aromatic rings.

Recently, Busch and coworkers[10,11] reported the synthesis of a broad range of substituted derivatives [Ni(Me$_2$E$_2$[Z]tetraenatoN$_4$)](Z=14, 15, 16, E=acetyl, carbethoxyethyl, α-naphthylcarbamoyl, ethylcarbamoyl, benzoyl, *p*-methylbenzoyl, *p*-nitrobenzoyl, methylsuccinoyl, nitro) (**1**) by electrophilic substitution reaction at the γ-carbons of the parent complexes [Ni(Me$_2$[Z]-tetraenatoN$_4$)], where the parent complex has two nucleophilic centers, and elucidated that both the position of the d-d electronic band maxima and the half-wave potential for the Ni^{2+}/Ni^{3+} couple vary linearly with the Hammett substituent constants. This result indicates that the use of substituents affords a powerful technique for controlling the electronic character of the metal ion without altering the stereochemistry of the coordination sphere.

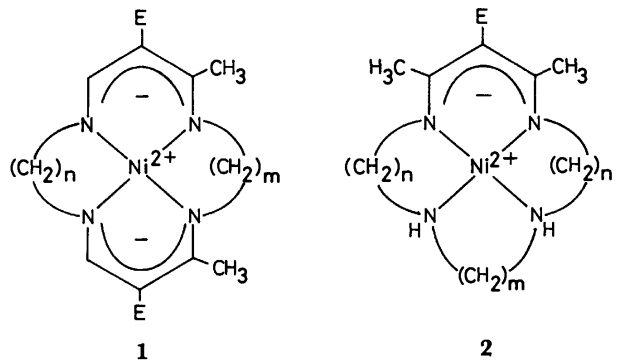

1 **2**

Fig. 1. Structures of [Ni(Me$_2$E$_2$[Z]tetraenatoN$_4$)] (**1**) and [Ni(Me$_2$E[Z]dienatoN$_4$)]$^+$ (**2**), where E and Z denote the substituent group and ring size, respectively. The abbreviation used in this report are based on Busch's modified scheme.[15,16]

In this study, the complexes [Ni(Me$_2$[Z]dienatoN$_4$)]$^+$ (**2**) firstly synthesized by Cummings and coworkers[12–14] were used as the parent complexes where each parent complex has only one nucleophilic center. The substituted derivatives [Ni(Me$_2$E[Z]dienatoN$_4$)]PF$_6$ have been prepared by electrophilic substitution reaction of the parent complex with *p*-substituted benzoyl chlorides and characterized by elemental analyses, infrared, ^{1}H NMR, and electronic spectra. The effects of the substituents on the properties of the central nickel ion as well as the macrocyclic ring-size effects were examined by the d-d band maxima of the electronic spectra. In addition, the crystal structure of one of the parent complexes [Ni(Me$_2$[14]dienatoN$_4$)]Br·H$_2$O has been determined by the single-crystal X-ray diffraction method in order to investigate the influence of ring-size on the molecular structure.

Experimental

Physical Measurements. Visible and ultraviolet spectra were obtained with a Hitachi recording spectrophotometer 323, while infrared spectra were recorded as KBr disks with a Shimadzu recording spectrophotometer IR-410. The 100 MHz ^{1}H NMR spectra were recorded on a JEOL MH 100 spectrometer. The solvent used was acetone-d_6 and in all cases shift measurements were made relative to tetramethylsilane. Elemental analysis was performed by Mr. S. Miyazaki at the Technical Service Center of Kumamoto University.

Syntheses. *3,7-Diazanonane-1,9-diamine ($H_2N(CH_2)_2NH(CH_2)_3NH(CH_2)_2NH_2$)* was prepared according to the method of Barefield *et al.*[17] The parent complexes [Ni(Me$_2$-[Z]dienatoN$_4$)]X (Z=13, 14 and X=Br, I, PF$_6$) were prepared by the method of Cummings[12] and identified by elemental analyses and infrared spectra.

(12-Benzoyl-11,13-dimethyl-1,4,7,10-tetraaza-10,12-cyclotrideca-dienato)nickel(II) Hexafluorophosphate, [Ni(Me$_2$Byzl[13]dienatoN$_4$)]-PF$_6$, 2(E=C$_6$H$_5$CO–, n=m=2): 0.224 g (1.6 mmol) of benzoyl chloride and 0.126 g (1.6 mmol) of pyridine were added to a solution of 0.357 g (1 mmol) of [Ni(Me$_2$[13]-dienatoN$_4$)]Br·1/2H$_2$O in 100 ml of chloroform. The solution was refluxed for 6 h and then evaporated to dryness under reduced pressure. The resultant orange-red viscous oil was dissolved in 50 ml of ethanol and addition of excess ammonium hexafluorophosphate in ethanol gave red-orange precipitates. This material was collected, recrystallized from ethanol and

dried *in vacuo*.

[12-(p-Methylbenzoyl)-11,13-dimethyl-1,4,7,10-tetraaza-10,12-cyclotridecadienato]nickel(II) Hexafluorophosphate, [Ni(Me$_2$MeBzyl[13]dienatoN$_4$)]PF$_6$, 2(E=p-CH$_3$C$_6$H$_4$CO–, n=m=2): *[12-(p-Nitrobenzoyl)-11,13-dimethyl-1,4,7,10-tetraaza-10,12-cyclotridecadienato]nickel(II) Hexafluorophosphate, [Ni(Me$_2$NitroBzyl[13]dienatoN$_4$)]PF$_6$, 2(E=p-NO$_2$C$_6$H$_4$CO–, n=m=2)*: These complexes were synthesized by a method similar to that for [Ni(Me$_2$Bzyl[13]dienatoN$_4$)]PF$_6$ except for using *p*-methylbenzoyl chloride and *p*-nitrobenzoyl chloride instead of benzoyl chloride, respectively.

(13-Benzoyl-12,14-dimethyl-1,4,8,11-tetraaza-11,13-cyclotetradienato)nickel(II) Hexafluorophosphate, [Ni(Me$_2$Bzyl[14]dienatoN$_4$)]PF$_6$, 2(E=C$_6$H$_5$CO–, n=2, m=3): 0.210 g (1.5 mmol) of benzoyl chloride and 0.151 g (1.5 mmol) of triethylamine were added to a solution of 0.380 g (1 mmol) of [Ni(Me$_2$[14]dienatoN$_4$)]Br·H$_2$O in 100 ml dichloromethane. The solution was refluxed for 6 h and then evaporated to dryness under reduced pressure. The resultant orange-red viscous oil was dissolved in 50 ml of ethanol and small ammount of dichloromethane. The saturated ammonium hexafluorophosphate solution in ethanol was slowly added to the solution to precipitate red-orange material. This material was collected, recrystallized from ethanol and small ammount of chloroform, and dried *in vacuo*.

[13-(p-Methylbenzoyl)-12,14-dimethyl-1,4,8,11-tetraaza-11,13-cyclotetradecadienato]nickel(II) Hexafluorophosphate, [Ni(Me$_2$MeBzyl[14]dienatoN$_4$)]PF$_6$, 2(E=p-CH$_3$C$_6$H$_4$CO–, n=2, m=3): *[13-(p-Nitrobenzoyl)-12,14-dimethyl-1,4,8,11-tetraaza-11,13-cyclotetradecadienato]nickel(II) Hexafluorophosphate, [Ni(Me$_2$NitroBzyl[14]dienatoN$_4$)]PF$_6$, 2(E=p-NO$_2$C$_6$H$_4$CO–, n=2, m=3)*: The above two complexes were synthesized by a method similar to that for [Ni(Me$_2$Bzyl[14]dienatoN$_4$)]PF$_6$ except for using *p*-methylbenzoyl chloride and *p*-nitrobenzoyl chloride, respectively, instead of benzoyl chloride.

X-Ray Diffraction. Red rhombic crystals of the complex [Ni(Me$_2$[14]dienatoN$_4$)]Br·H$_2$O, suitable for X-ray diffraction study, were prepared by slow evaporation from aqueous solution at room temperature. A crystal with dimensions of 0.4×0.3×0.4 mm was examined with a Rigaku AFC-5 four-circle automated diffractometer. The unit cell dimensions and their estimated standard deviations were obtained from a least-squares fit to 15 high angle reflections ($14°<2\theta<38°$) using Mo *Kα* graphite monochromatized radiation ($\lambda=0.71069$ Å) at 24±1 °C. Systematic absences $h0l$, $l=2n+1$ and $0k0$, $k=2n+1$, indicate the space group $P2_1/c$. The crystal data obtained were as follows: $NiC_{12}H_{25}N_4OBr$, F. W.=379.9, monoclinic system, space group=$P2_1/c$, $a=12.637(3)$, $b=11.090(3)$, $c=10.556(1)$ Å, $\beta=91.22(1)°$, $V=1596.1(6)$ Å^3, $Z=4$, $D_x=1.581$ g cm^{-3}.

The intensity data were collected by the 2θ-θ scan technique with a scan rate of 12°min^{-1}. For weak reflections the peak scan was repeated up to four times depending on their intensities. Three standard reflections were monitored every 100 reflections and their intensities showed a good stability. A total of 3130 reflections with $2\theta\leqq52°$ were collected. The ntensity data were corrected for the Lorentz and polarization effects, but not for the absorption, because of the crystal size and low absorption coefficient. Independent 2181 reflections with $|F_o|>3\sigma(|F_o|)$ were considered as "observed" and used for the structure determination.

Solution and Refinement of the Structure. The structure was solved by the conventional heavy-atom method and refined by the block-diagonal least-squares method. In the least-squares calculation, the function minimized was $\sum w(|F_o|-k|F_c|)^2$, where $w=1/\sigma(|F_o|)^2$ was adopted. The neutral atomic scattering factors for H, C_{COV}, N, O, Ni, and Br were taken from International Tables for X-ray Crystallography Vol. IV.[18] Anomalous dispersion corrections $\Delta f'$ and $\Delta f''$ for all the component atoms were also taken from the literature.[18] All the calculations were carried out on a FACOM M-200 computer in the Computer Center of Kyushu University by the use of a local version[19] of the UNICS II Crystallographic Computing System.[20,21]

The coordinates of the bromine and nickel atoms were obtained from a three-dimensional Patterson synthesis. Successive Fourier and difference Fourier syntheses revealed all the nonhydrogen atoms except for the water molecule of crystallization. Refinement with isotropic thermal parameters was carried out and the discrepancy indices $R_1=\sum||F_o|-|F_c||/\sum|F_o|$ and $R_w=[\sum w(|F_o|-|F_c|)^2/\sum w|F_o|^2]^{1/2}$ were 13.6 and 13.4%, respectively. After introducing anisotropic thermal parameters, a difference Fourier synthesis was calculated and revealed the missing water molecule. An occupancy factor of 1.0 was applied for the water, considering the peak height and the adjustment of the elemental analysis. Hydrogen atoms were inserted in their calculated positions and included in the refinement. Further refinement with anisotropic thermal parameters for nonhydrogen atoms and isotropic ones (4.0 Å^2) for hydrogen atoms gave the final values of 5.2 and 5.1% for R_1 and R_w, respectively. The final difference Fourier synthesis showed no significant feature, peaks being less than 0.5 eÅ^{-3}.

Final positional parameters of nonhydrogen atoms with their estimated standard deviations are given in Table 1. List of structure factors, anisotropic thermal parameters and atomic parameters of hydrogen atoms have been deposited at the Chemical Society of Japan as Document No. 8252.

Results and Discussion

Crystal Structure of Parent Complex [Ni(Me$_2$[14]dienatoN$_4$)]Br·H$_2$O. The crystal structure viewed along the b axis is shown in Fig. 2, where possible hydrogen bonds are drawn by dotted lines. A perspective drawing of the cation [Ni(Me$_2$[14]dienatoN$_4$)]$^+$ with the atom numbering scheme is shown in Fig. 3. The

Table 1. Atomic parameters for [Ni(Me$_2$[14]dienatoN$_4$)]Br·H$_2$O

Atom	x	y	z	B_{eq}/Å^2
Br	6576(1)	1700(1)	555(1)	5.0
Ni	2375(1)	3027(1)	2349(1)	2.8
N1	1309(5)	3134(6)	3427(6)	3.3
N2	2393(5)	4784(5)	2393(6)	3.4
N3	3536(4)	2933(5)	1340(5)	2.9
N4	2379(4)	1354(5)	2338(5)	3.2
C1	1086(7)	4391(8)	3814(8)	4.5
C2	1405(6)	5178(8)	2761(8)	4.7
C3	2709(6)	5467(8)	1262(7)	4.5
C4	3704(7)	5111(8)	872(8)	4.7
C5	3738(7)	3841(8)	345(8)	4.3
C6	3575(7)	1711(7)	756(7)	4.0
C7	3266(6)	805(8)	1734(7)	4.2
C8	1748(6)	622(7)	2880(7)	3.5
C9	989(6)	1024(7)	3616(8)	3.8
C10	818(6)	2239(8)	3914(8)	4.0
C11	17(7)	2497(9)	4882(9)	5.4
C12	1855(7)	−742(7)	2725(8)	4.7
Ow	5324(5)	3030(7)	2813(6)	6.7

TABLE 2. BOND LENGTHS AND ANGLES OF [Ni(Me_2[14]-dienatoN$_4$)]Br·H_2O WITH THEIR ESTIMATED STANDARD DEVIATIONS IN PARENTHESES

(a) Bond length	l/Å		l/Å
Ni–N(1)	1.869(6)	N(4)–C(7)	1.508(10)
Ni–N(2)	1.944(7)	N(4)–C(8)	1.322(10)
Ni–N(3)	1.930(6)	C(1)–C(2)	1.486(12)
Ni–N(4)	1.855(6)	C(3)–C(4)	1.480(13)
N(1)–C(1)	1.486(11)	C(4)–C(5)	1.516(13)
N(1)–C(10)	1.308(11)	C(6)–C(7)	1.508(12)
N(2)–C(2)	1.476(11)	C(8)–C(9)	1.381(12)
N(2)–C(3)	1.486(11)	C(8)–C(12)	1.529(12)
N(3)–C(5)	1.485(11)	C(9)–C(10)	1.405(12)
N(3)–C(6)	1.490(11)	C(10)–C(11)	1.538(13)
(b) Bond angle	θ/°		θ/°
N(1)–Ni–N(4)	94.0(2)	N(2)–C(3)–C(4)	117.7(7)
N(1)–Ni–N(2)	86.2(2)	C(3)–C(4)–C(5)	112.5(7)
N(2)–Ni–N(3)	93.2(2)	C(4)–C(5)–N(3)	111.2(7)
N(3)–Ni–N(4)	86.5(2)	C(5)–N(3)–C(6)	108.3(6)
Ni–N(1)–C(1)	113.1(5)	N(3)–C(6)–C(7)	108.0(6)
Ni–N(1)–C(10)	126.9(5)	C(6)–C(7)–N(4)	105.0(6)
Ni–N(2)–C(2)	106.9(5)	C(7)–N(4)–C(8)	118.0(6)
Ni–N(2)–C(3)	119.6(5)	N(4)–C(8)–C(9)	123.1(7)
Ni–N(3)–C(5)	121.3(4)	C(8)–C(9)–C(10)	124.4(7)
Ni–N(3)–N(6)	108.3(4)	C(10)–N(1)–C(1)	119.6(6)
Ni–N(4)–C(7)	114.1(4)	C(9)–C(10)–N(1)	123.4(7)
Ni–N(4)–N(8)	127.5(5)	N(4)–C(8)–C(12)	119.8(7)
N(1)–C(1)–C(2)	106.2(6)	C(12)–C(8)–C(9)	117.0(7)
C(1)–C(2)–N(2)	107.8(6)	N(1)–C(10)–C(11)	119.7(7)
C(2)–N(2)–C(3)	110.0(6)	C(11)–C(10)–C(9)	116.7(7)
(c) Intermolecular length		l/Å	
Br···Ow*	3.307(6)	*(x,y,z)	
Br···Ow*	3.341(8)	*($x,1/2-y,-1/2+z$)	
Ow···N(3)*	2.866(8)	*(x,y,z)	
Ow···HN3*	1.92(6)	*(x,y,z)	
Br···N(2)*	3.325(6)	*($1-x,-1/2+y,1/2-z$)	
Br···NH2*	2.46(6)	*($1-x,-1/2+y,1/2-z$)	

interatomic bond distances, angles and the intermolecular bond distances with their estimated standard deviations are given in Table 2.

As shown in Fig. 2 and Table 2, the atoms Br and Ow are hydrogen bonded to the secondary amine nitrogen atoms N(2) ($1-x$, $-1/2+y$, $1/2-z$) and N(3), respectively, and the evidence of the hydrogen bonds from this X-ray analysis confirmed the prediction of Cummings[12] based on the infrared and ^{1}H NMR spectra. The hydrogen bonds between the NH-proton and the electronegative anions have been studied for the complexes [Ni(Me_2[Z]dienatoN$_4$)]X (X=Br, I, SCN, BF_4, NO_3, PF_6; Z=13, 14) by the infrared and ^{1}H NMR spectra, in which the NH band shifts to higher energy with the change of the anion $Br^->I^->SCN^->NO_3^->BF_4^->PF_6^-$.[12]

As shown in Fig. 3, the macrocyclic cation exhibits nearly exactly Cs-m symmetry, although not required crystallographically. The pseudomirror plane containing Ni, C(4), and C(9) atoms is perpendicular to the coordination plane NiN_4. This molecular symmetry is also observed in the dicationic analogous compound with the same ring size [Co^{II}(Me_2[14]dieneN$_4$)·H_2O]-

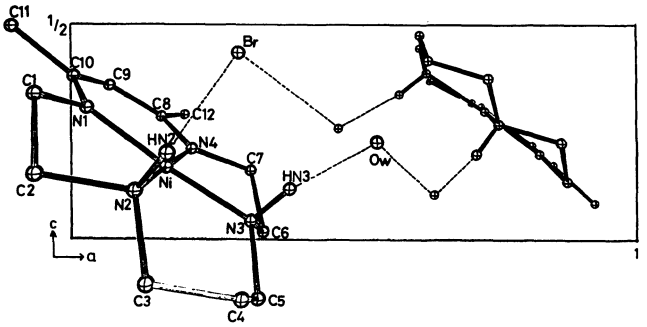

Fig. 2. Projection of the crystal structure [Ni(Me_2[14]-dienatoN$_4$)]Br·H_2O along the b axis.

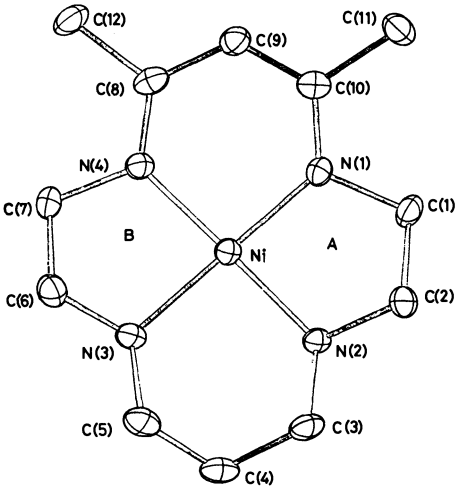

Fig. 3. ORTEP plot of [Ni(Me_2[14]dienatoN$_4$)]$^+$ Hydrogen atoms have been omitted for clarity.

$(PF_6)_2$,[22] while the analogous compound with thirteen ring size [Ni(Me_2[13]dienatoN$_4$)]ClO_4[23] exhibits C_2 symmetry.

The nickel ion has a square planar coordination geometry within the deviations of $\pm$0.03 Å and its four coordination sites are occupied by two iminate and two secondary amine nitrogen atoms. The four Ni–N bond distances fall into two groups, attributing to the difference between iminate and secondary amine nitrogen atoms. The average Ni–N (iminate) bond distance of 1.862(6) Å is shorter than the Ni–N (amine) of 1.937(7) Å. In addition, these two values are longer than the corresponding bond distances of Ni–N (iminate) (1.85(1) Å) and Ni–N (amine) (1.88(1) Å) in the case of [Ni(Me_2[13]dienatoN$_4$)]$^+$, respectively.[23]

For the unsaturated six-membered chelate ring, the planarity is preserved, in which the deviation from the least-squares plane defined by Ni, N(1), N(4), C(8), C(9), and C(10) is in the range from -0.03 to 0.03 Å. The C–C and C–N bond distances of the unsaturated chelate ring are intermediate between the corresponding single and double bond distances, respectively,[24] consistent with the conjugated chelate ring. The saturated six-membered chelate ring takes a chair conformation in which Ni and C(4) atoms displaced at -0.67 and 0.71 Å from the least-squares plane through N(3), N(2), C(3), and C(5), respectively. The

TABLE 3. ELEMENTAL ANALYSIS OF SUBSTITUTED COMPLEXES, $[Ni(Me_2E[Z]dienatoN_4)]PF_6$ [a]

Substituent(E)	Z	C(%)	H(%)	N(%)
C_6H_5CO	13	41.80(41.81)	4.65(4.87)	10.88(10.84)
p-$CH_3C_6H_4CO$	13	43.08(42.97)	5.27(5.12)	10.62(10.55)
p-$NO_2C_6H_4CO$	13	38.22(38.46)	4.29(4.30)	12.20(12.46)
C_6H_5CO	14	42.85(42.97)	5.16(5.12)	10.59(10.55)
p-CH_3CH_4CO	14	43.35(43.51)	5.46(5.20)	10.11(10.12)
p-$NO_2C_6H_4CO$ [b]	14	39.83(39.61)	4.61(4.55)	12.12(12.16)

a) Calculated values are given in parentheses. b) Calcd for $NiPF_6O_3N_5C_{19}H_{26}\cdot 1/2H_2O$.

TABLE 4. INFRARED SPECTRA FOR THE 13- AND 14-MEMBERED RING DERIVATIVES OF $[Ni(Me_2E[Z]\ dienatoN_4)]PF_6$ [a]

Substituent (E)	Ring size (Z)	$\bar{\nu}$/cm^{-1} Assignment ν_{NH}	$\nu_{C=O}$	Bzyl	$\nu_{C=C,C=N}$
H	13	3240	—	—	1560,1540,1524
C_6H_5CO	13	3240	1640	1590	1558,1550,1540
p-$CH_3C_6H_4CO$	13	3250	1643	1600	1560,1550,1540
p-$NO_2C_6H_4CO$	13	3220	1632	1598	1560,1540,1535
H	14	3220	—	—	1555,1550,1530
C_6H_5CO	14	3230	1635	1590	1560,1555,1540
p-$CH_3C_6H_4CO$	14	3230	1640	1600	1560,1555,1540
p-$NO_2C_6H_4CO$	14	3260	1636	1598	1560,1540,1525

a) Spectra were obtained by KBr method.

saturated five-membered chelate rings (A and B) are all found to occupy gauche conformation with absolute configuration $\lambda\delta$ or $\delta\lambda$ (C(1), 0.09, C(2) −0.52 Å from the plane of Ni, N(1), and N(2): C(6) −0.47, C(7) 0.14 Å from the plane of Ni, N(3), and N(4)), while the absolute configuration of the five-membered chelate rings of $[Ni(Me_2[13]dienatoN_4)]^+$ is $\lambda\lambda$ or $\delta\delta$, either.[23]

As a consequence of the planarity of the conjugated six-membered chelate rings, the combination of the absolute configuration of two five-membered chelate rings ($\lambda\delta$ or $\delta\lambda$) and the chair-conformation of the saturated six-membered chelate ring, the molecular symmetry of the complex should exhibit Cs-m symmetry and the two hydrogen atoms bonded to secondary amine nitrogens are placed on the same side from the coordination plane (NiN_4).

Synthesis and Characterization of the Substituted Derivatives. The parent complex $[Ni(Me_2[Z]dienatoN_4)]^+$ (Z=13, 14) which has an iminato chelate ring containing a nucleophilic center reacts with electrophilies to produce the derivatives that are substituted at the γ-position. The substituted derivatives $[Ni(Me_2E[Z]dienatoN_4)]PF_6$ where E denotes benzoyl, p-methylbenzoyl and p-nitrobenzoyl, and Z=13 and 14, were characterized by elemental analyses, infrared and ^1H NMR spectra. Elemental analyses for the substituted derivatives are given in Table 3. Some selected infrared and ^1H NMR spectral data with their assignments are given in Tables 4 and 5. Infrared spectra of the products differ from the parent complexes, most notably in the appearance of C=O stretch at *ca.* 1640 cm^{-1}. Two vibrations (*ca.* 1740 and 1770 cm^{-1}) due to C=O stretching vibrations of the starting material, benzoyl chlorides, are absent in the products, supporting the introduction of the substituent. These features are also observed in the substituent complexes $[Ni(Me_2E_2[Z]tetraenatoN_4)]$ (**1**) and their parent complexes, supporting the formation of the complex $[Ni(Me_2E[Z]dienatoN_4)]^+$ (**2**). As anticipated, the -CH reasonance at the γ-position has disappeared since the substituted group is introduced at the γ-position.

Electronic Spectra: Visible and ultraviolet spectra of the complexes were obtained on the 10^{-3}—10^{-4} M solution in methanol over the range from 14 to 48$\times 10^3$ cm^{-1} and the band maxima are given in Table 6. This type of complexes showed several band maxima in the ultraviolet region of the spectra with extinction coefficient in the range from 1500 to 10000 M^{-1} cm^{-1} which agree with assignment of the bands as representing charge-transfer transition. The spectra also exhibit a broad band in the visible region with an extinction coefficient in the range 100—200 M^{-1} cm^{-1} which is attributable to the d-d transition band.

As shown in Table 6, the energy of d-d band maxima increase, when the substituent group such as benzoyl group is attached to the γ-carbon of the conjugated six-membered chelate ring. This indicates that the electronic property of the central nickel ion is affected

TABLE 5. ^1H NMR SPECTRA OF $[Ni(Me_2E\ [Z]dienatoN_4)]PF_6$ [a]

Substituent	Z	CH [b]	CH [c]	NH [d]	CH_2 [e]	CH_3
H	13	—	4.77(s)	4.78	3.63—2.82	1.91
C_6H_5CO	13	7.69(q)	—	5.11	3.73—2.88	1.73
p-$CH_3C_6H_4CO$	13	7.61(q)	—	—	3.30—2.82	2.42*,1.75
p-$NO_2C_6H_4CO$	13	8.21(q)	—	5.13	3.75—2.87	1.77
H	14	—	4.80(s)	3.92	3.57—2.58	1.92
C_6H_5CO	14	7.73(q)	—	3.33	2.82(s)	1.80
p-$C_6H_3C_6H_4CO$	14	7.52(q)	—	—	2.81(s)	2.43*,1.82
p-$NO_2C_6H_4CO$	14	8.23(q)	—	4.11	3.53—2.81	1.80

a) Chemical shifts in ppm downfield from an internal TMS standard at 100 MHz in acetone-d_6. b) Signals for the benzoyl group. c) Signals for the γ-position proton. d) Center of broad signal. e) Boundaries of multiplet region. (s) Singlet. (q)Quartet. * Signals for the methyl proton of p-methylbenzoyl group.

Table 6. Electronic absorption bands for the 13- and 14-membered ring derivatives $[Ni(Me_2E[Z]dienato N_4)]PF_6$[a,b]

Substituent(E)	Z	d-d Transition $\tilde{\nu}/10^3\ cm^{-1}(\varepsilon)$	Other transitions $\tilde{\nu}/10^3\ cm^{-1}(\varepsilon)$
H	13	20.2(143)	28.2(8500) 29.4(5900) 36.1(4100) 39.3(6100)
C_6H_5CO	13	21.4(540)	28.3(7400) 35.6(1300) 39.6(5400)
p-$CH_3C_6H_4CO$	13	21.4(548)	28.2(8000) 38.4(25400)
p-$NO_2C_6H_4CO$	13	—	21.1(1400) 24.0(1600) 28.4(7200) 37.5(21200)
H	14	18.6(104)	27.8(4300) 28.9(3700) 35.5(2400) 39.2(4000)
C_6H_5CO	14	19.6(210)	27.8(7200) 35.6(4700) 39.4(21900)
p-$CH_3C_6H_4CO$	14	19.6(196)	27.8(7100) 38 0(22300)
p-$NO_2C_6H_4CO$	14	—	23.3(1800) 27.9(7200) 37.6(21500)

a) For details of structures refer to Fig. 1. b) Spectra were obtained in methanol.

through the conjugated π-system of the iminato chelate ring by the electronic property of the substituent group. The energy difference of the d-d band maxima of $[Ni(Me_2[Z]dienatoN_4)]^+$ and $[Ni(Me_2Bzyl[Z]dienato N_4)]^+$ (1.2 and $1.0\times10^3\ cm^{-1}$ for Z=13 and 14, respectively) is nearly half of that of $[Ni(Me_2[Z]tetraenatoN_4)]$ and $[Ni(Me_2Bzyl_2[Z]tetraenatoN_4)]$ (2.3, 2.1, and $2.8\times10^3\ cm^{-1}$ for Z=14, 15, and 16, respectively[11]). This result is consistent with the fact that the former (**2**) and latter (**1**) complexes have one and two substituent groups, respectively.

As seen in Table 6, the maximum wavenumber of the d-d transition band of $[Ni(Me_2E[13]dienatoN_4)]PF_6$ is greater than that of $[Ni(Me_2E[14]dienatoN_4)]PF_6$, indicating that the ligand field strength of the thirteen membered complex is greater than that of the fourteen membered complex. This is consistent with that the average Ni–N bond distance of the former complex is shorter than that of the latter, as being evidenced by the crystal structure determinations of $[Ni(Me_2[13]dienato N_4)]ClO_4$[23] and $[Ni(Me_2[14]dienatoN_4)]Br\cdot H_2O$.

The linear correlation between the d-d band maxima and the Hammett substituent constants of the *p*-substituted benzoyl derivatives has not been clearly observed in the present complexes (**2**), while it was observed in the complexes (**1**).[11] This might be the result of that the overall planarity between the conjugated chelate ring and the substituted π-system of benzoyl group is preserved for the complex (**1**), while the charge-delocalized chelate ring can be perpendicular to the benzoyl group for the complex (**2**), owing to the steric hindrance between the neighbouring two methyl groups and the substituent group at the γ-position.

The authors are grateful to Prof. S. Kida at the Faculty of Science, Kyushu University for allowing them to use the diffractometer.

References

1) K. Bowman, D. P. Riley, D. H. Busch, and P. W. R. Corfield, *J. Am. Chem. Soc.*, **97**, 5036 (1976).
2) C. J. Hipp and D. H. Busch, *Inorg. Chem.*, **12**, 894 (1973).
3) M. C. Weiss and V. L. Goedken, *J. Am. Chem. Soc.*, **98**, 3389 (1976).
4) B. Durham, T. J. Anderson, J. A. Switzer, J. F. Endicott, and M. D. Glick, *Inorg. Chem.*, **16**, 271 (1977).
5) F. V. Lovecchio, E. S. Gore, and D. H. Busch, *J. Am. Chem. Soc.*, **96**, 3110 (1974).
6) T. Tokumitsu and T. Hayashi, *Bull. Chem. Soc. Jpn.*, **54**, 2348 (1981).
7) J. P. Collman, R. A. Moss, H. Malz, and C. C. Heindel, *J. Am. Chem. Soc.*, **83**, 531 (1961).
8) K. Kasuga, M. Anami, and Y. Yamamoto, *Bull. Chem. Soc. Jpn.*, **51**, 476 (1978).
9) K. Kuroda, K. Yoshitani, K. Kunigita, Y. Kamiiba, and K. Watanabe, *Bull. Chem. Soc. Jpn.*, **49**, 2445 (1976).
10) D. G. Pillsbury and D. H. Busch, *J. Am. Chem. Soc.*, **98**, 7836 (1976).
11) J. A. Streeky, D. G. Pillsburry, and D. H. Busch, *Inorg. Chem.*, **19**, 3148 (1980).
12) S. C. Cummings and R. T. Sievers, *Inorg. Chem.*, **9**, 1131 (1970).
13) S. C. Cummings and R. T. Sievers, *J. Am. Chem. Soc.*, **92**, 215 (1970).
14) J. G. Martin and S. C. Cummings, *Inorg. Chem.*, **12**, 1477 (1973).
15) V. L. Goedken, P. H. Merrell, and D. H. Busch, *J. Am. Chem. Soc.*, **94**, 3397 (1972).
16) J. C. Dabrowiak, P. H. Merrell, and D. H. Busch, *Inorg. Chem.*, **11**, 1979 (1972).
17) E. K. Barefield, F. Wagner, A. W. Herlinger, and A. R. Dahl, *Inorg. Synth.*, **16**, 220 (1976).
18) "International Tables for X-Ray Crystallography," Kynoch Press, Birmingham (1974), Vol. IV.
19) S. Kawano, *Rep. Comp. Cent. Kyushu Univ.*, **13**, 39 (1980).
20) T. Sakurai, H. Iwasaki, Y. Watanabe, K. Kobayashi, Y. Bando, and Y. Nakamichi, *Rep. Inst. Phys. Chem. Res.*, **50**, 75 (1972).
21) C. K. Johnson, Report No. 3794, Oak Ridge National Laboratory, Oak Ridge, Tennessee (1965).
22) G. W. Roberts, S. C. Cummings, and J. A. Cunningham, *Inorg. Chem.*, **15**, 2503 (1976).
23) M. F. Richardson and R. E. Sievers, *J. Am. Chem. Soc.*, **94**, 4134 (1972).
24) D. Bruins and D. L. Weaver, *Inorg. Chem.*, **9**, 130 (1970).

Synthesis, Characterization, and Crystal Structure of Substituted Derivatives of (Tetraazacyclotetradecatetraenato)copper(II) Complexes

Naohide MATSUMOTO,* Masahiko IMAIZUMI, and Akira OHYOSHI
Department of Industrial Chemistry, Faculty of Engineering, Kumamoto University, Kurokami 2-39-1, Kumamoto 860
(Received March 1, 1982)

(Tetraazacyclotetradecatetraenato)copper(II) complexes with the general formula [Cu(Me_2E_2[14]tetraenatoN_4)], where E denotes the substituent group of acetyl, propionyl, isobutyryl, benzoyl, *p*-methylbenzoyl, or *p*-nitrobenzoyl, have been prepared *via* electrophilic substitution of the parent complex [Cu(Me_2[14]tetraenatoN_4)] with acid chlorides, and characterized by elemental analyses and infrared spectra. For the *p*-substituted benzoyl derivatives, both the position of d-d electronic band maxima and reduction potential assignable to $Cu^{2+}+e \rightarrow Cu^+$ vary linearly with the Hammett substituent constants. The crystal structure of one of the complexes [Cu(Me_2Acyl_2[14]tetraenatoN_4)]·H_2O has been determined by the single-crystal X-ray diffraction method. The copper atom assumes a square planar coordination geometry and the overall conformation of the complex assumes a chair-like shape, where the seat and the rests are formed by the coordination plane (CuN_4) and the two conjugated six-membered chelate rings respectively.

Kadish and Morrison[1-3] examined substituent effects in porphyrin complexes by substituting various groups at the para position of the phenyl rings of tetraphenylporphyrin. Busch and co-workers[4,5] reported syntheses of a broad range of substituted derivatives [Ni(Me_2E_2[Z]tetraenatoN_4)] (Z=14, 15, 16) by electrophilic substitution at the γ-carbon of the conjugated chelate rings (Fig. 1), and examined substituent effects on electronic spectral and electrochemical properties of the complexes. These studies elucidated that the use of substituents affords a powerful technique for controlling the electronic character of the metal ion without altering the stereochemistry of the coordination sphere.

In this study, we have prepared the substituted derivatives [Cu(Me_2E_2[14]tetraenatoN_4)] by electrophilic substitution of the parent complex [Cu(Me_2[14]-tetraenatoN_4)] with acid chlorides such as propionyl chloride, isobutyryl chloride, benzoyl chloride, *p*-methylbenzoyl chloride, and *p*-nitrobenzoyl chloride. These complexes were characterized by elemental analyses and infrared spectra. Substituent effects on the properties of the copper ion were examined by electronic spectra and cyclic voltamogram. In addition, the crystal structure of [Cu(Me_2Acyl_2[14]tetraenatoN_4)]·H_2O has been determined by the single-crystal X-ray diffraction method in order to confirm the basic structure for the series of complexes.

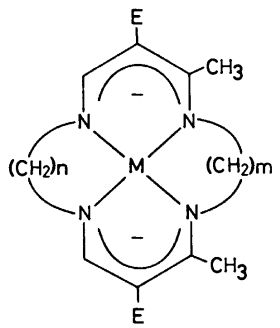

Fig. 1. Structure of [M^{2+}(Me_2E_2[Z]tetraenatoN_4)], where E and Z denote the substituted group and the macrocyclic ring size, respectively. (Z=14($n=m=2$), Z=15($n=2$, $m=3$), Z=16($n=m=3$)) The abbreviations used in this report are based on Busch's modified scheme.[6,7]

Experimental

Physical Measurements. Visible and ultraviolet spectra were recorded with a Hitachi recording spectrophotometer 323, while infrared spectra were recorded as KBr disk or nujol mull with a Shimadzu recording spectrophotometer IR-410. Elemental analyses were performed by Mr. Miyazaki at the Technical Service Center of Kumamoto University. Electrochemical measurements were performed with a Hokuto Denko Potentiostat/Galvanostat HA 101, a Hokuto Denko Function Generator HA 1074A, and a Rikadenki X-Y recorder BW-133. All measurements were made on acetonitrile solution containing 50 mM (1 M=1 mol dm^{-3}) tetrabutylammonium perchlorate as the supporting electrode. The working electrode was platinum disk electrode formed by sealing an 18—20 gauge platinum wire into soft glass. The reference electrode was a silver wire immersed in a 10 mM acetonitrile solution of silver perchlorate. Argon gas was bubbled into the solution for 30 min before measurement.

Syntheses. The acylated complex [Cu(Me_2Acyl_2[14]-tetraenatoN_4)]·H_2O was synthesized by the method of Jäger[8] or Riley and Busch.[9] Found: C, 50.09; H, 6.37; N, 14.59%. Calcd for $C_{16}H_{24}N_4O_3Cu$: C, 50.06, H, 6.30; N, 14.59%. IR (KBr): 1620 (C=O) and 1565 cm^{-1} (iminate ring).

(7,12-Dimethyl-1,4,8,11-tetraazacyclotetradeca-4,6,11,13-tetraenato)copper(II), [Cu(Me_2[14]tetraenatoN_4)]: This complex was first synthesized by Okawa and Busch[10] through a two-step procedure, in which the first step is removal of the acetyl groups along with the central nickel(II) ion and the second is reintroduction of the metal ion. In this work, this compound was synthesized through a one-step procedure by a similar method for the preparation of the corresponding nickel(II) complex.[5] In a 500 ml single-necked flask are combined 19.2 g (0.5 mol) of the complex [Cu(Me_2Acyl_2[14]tetraenatoN_4)]·H_2O, 9.5 g (0.5 mol) of *p*-toluenesulfonic acid monohydrate, and 150 ml of methanol. The mixture is refluxed under nitrogen for 30 min, during which time the solution becomes dark red. The solution is then cooled in a Dry Ice/acetone bath and a solution of 4 g (0.1 mol) of sodium hydroxide in 50 ml of methanol is added under nitrogen, during which time the solution becomes green. The solution is removed from the cold bath and maintained for 30 min at room temperature. The methanol is removed dy evaporation to dryness, and 50 ml of dry benzene is added. The resulting slurry is filtered quickly by a glass filter. The solution is

evaporated to dryness to give a greenish material. Found: C, 50.81; H, 6.50; N, 19.53%. Calcd for $C_{12}H_{18}N_4Cu$: C, 51.14; H, 6.44; N, 19.88%. The complex decomposes gradually even in the solid state under atmosphere, in which the color changes from green to black.

The synthesis of the substituted complexes is exemplified in detail by that of [Cu(Me_2Bzyl$_2$[14]tetraenatoN_4)], because the synthetic procedure is similar to one another.

(6,13-Dibenzoyl-5,14-dimethyl-1,4,8,11-tetraazacyclotetradeca-4,-6,11,13-tetraenato)copper(II), [Cu(Me_2Bzyl$_2$[14]tetraenatoN_4)]: Benzoyl chloride of 0.15 g (10.6 mmol) is added to a solution of 1 g (3.5 mmol) of the deacetylated complex and 1.45 g (14.4 mmol) of triethylamine in 40 ml of dichloromethane and 40 ml of benzene. The mixture is stirred and refluxed under nitrogen for 4 h. The solvent is removed by evaporation and the residue is dissolved in 50 ml of chloroform, and filtered. The volume of the solution is reduced and the solution is chromatographed on a column of Merck 60G ($\phi 2.0 \times 20$ cm^2) with chloroform as the eluent. The eluent of the first band is collected and the solvent is evaporated. Recrystallization is carried out in methanol to give red crystals. Found: C, 63.45; H, 5.27; N, 11.23%. Calcd for $C_{26}H_{26}N_4O_2Cu$: C, 63.72; H, 5.35; N, 11.43%. IR(KBr): 1618 (C=O), 1560 (iminate ring), and 1596 cm^{-1} (benzoyl group).

(6,13-Dipropionyl-5,14-dimethyl-1,4,8,11-tetraazacyclotetradeca-4,6,11,13-tetraenato)copper(II), [Cu(Me_2Propi$_2$[14]tetraenatoN_4)]: Propionyl chloride of 0.99 g (10.67 mmol) was used instead of benzoyl chloride. Found: C, 54.70; H, 6.37; N, 13.87%, Calcd for $C_{18}H_{26}N_4O_2Cu$: C, 54.87; H, 6.65; N, 14.22%. IR(KBr): 1618 (C=O) and 1560 cm^{-1} (iminate ring).

(6,13-Diisobutyryl-5,14-dimethyl-1,4,8,11-tetraazacyclotetradeca-4,6,11,13-tetraenato)copper(II), [Cu(Me_2iso-Butryl$_2$[14]tetraenato-N_4)]: Isobutyryl chloride of 1.14 g (10.67 mmol) was used instead of benzoyl chloride. Found: C, 56.80; H, 7.26; N, 13.19%. Calcd for $C_{20}H_{30}N_4O_2Cu$: C, 56.92; H, 7.16; N, 13.27%. IR(KBr): 1630 (C=O) and 1575 cm^{-1} (iminate ring).

(6,13-Bis(p-methylbenzoyl)-5,14-dimethyl-1,4,8,11-tetraazacyclotetradeca-4,6,11,13-tetraenato)copper(II), [Cu(Me_2p-MeBzyl$_2$-[14]tetraenatoN_4)]: *p*-Methylbenzoyl chloride of 1.65 g (10.67 mmol) was used instead of benzoyl chloride. Found: C, 64.72; H, 5.46; N, 10.34%. Calcd for $C_{28}H_{30}N_4O_2Cu$: C, 64.91; H, 5.83; N, 10.81%. IR(KBr): 1618 (C=O), 1550 (iminate ring), and 1600 cm^{-1} (benzoyl group).

(6,13-Bis(p-nitrobenzoyl)-5,14-dimethyl-1,4,8,11-tetraazacyclotetradeca-4,6,11,13-tetraenato)copper(II) Methanol, [Cu(Me_2p-NitroBzyl$_2$[14]tetraenatoN_4)]·CH_3OH: *p*-Nitrobenzoyl chloride of 1.98 g (10.67 mmol) was used instead of benzoyl chloride. Found: C, 52.76; H, 4.76; N, 14.04%. Calcd for $C_{26}H_{24}N_6O_6Cu\cdot(CH_3OH)$: C, 52.98; H, 4.61; N, 13.73%. IR(KBr): 1620 (C=O), 1560 (iminate ring), and 1595 cm^{-1} (benzoyl group).

X-Ray Diffraction. The crystals of [Cu(Me_2Acyl$_2$[14]-tetraenatoN_4)]·H_2O were grown from a 98% methanolic solution as red prismatic crystals. The cell dimensions were determined by a least-squares method based on the angular settings of 15 reflections measured on a Syntex P$\bar{1}$ automated four-circle diffractometer. Intensity data were also collected with the diffractometer by a θ-2θ scan technique with a variable scan rate from 4.0 to 24.0°min^{-1}. The crystal data obtained are as follows: $C_{16}H_{22}N_4O_2Cu\cdot H_2O$, F.W.=383.9, triclinic system, space group=P$\bar{1}$, a=10.641(5), b=10.649(4), c=7.548(3) Å, α=90.98(3), β=88.95(3), γ=87.59(3)°, V=854.3 Å^3, D_m=1.46 (in KI aqueous solution), D_x=1.48 g cm^{-3} for Z=2, and μ(Mo $K\alpha$)=13.0 cm^{-1}. A total of 1597 independent reflections with $2\theta \leqq 42°$ were collected and these data were corrected for Lorentz and polarization effects, but not for absorption.

Structure Determination. Structure was solved by the conventional heavy-atom method and refined by the block-diagonal least-squares method. The function minimized in the procedure of the least-squares method was $\sum w(|F_o|-k|F_c|)^2$, where w=1 was adopted. The atomic scattering factors for Cu, O, N, C_{cov}, and H were taken from the International Tables for X-ray Crystallography.[11] The anomalous dispersion corrections $\Delta f'$ and $\Delta f''$ for Cu were also taken from the literature.[11] All the calculation was carried out on a FACOM M-190 computer at the Computer Center of Kyushu University by the use of UNICS II program system.[12-14]

The coordinates of the copper atom were determined from a three-dimensional Patterson synthesis. Successive Fourier and difference Fourier syntheses revealed all the nonhydrogen atoms. Refinement was carried out by introducing initially isotropic thermal parameters and then anisotropic ones. At this stage, a difference Fourier synthesis was calculated and revealed all the hydrogen atoms except for those of water molecule. These hydrogen atoms were included in the refinement and gave the final value of 6.45% for $R=\sum||F_o|-|F_c||/\sum|F_o|$. The final difference Fourier synthesis showed four diffuse peaks (0.6 eÅ^{-3}) around the copper atom, but the other peaks are in the range -0.2 to 0.2 eÅ^{-3}. Final positional parameters with their estimated standard deviations are given in Table 1. Lists of structure factors, anisotropic thermal parameters, atomic parameters of hydrogen atoms, and selected least-squares planes have been deposited at the Chemical Society of Japan as Document No. 8245.

Results and Discussion

Crystal Structure of [Cu(Me_2Acyl$_2$[14]tetraenatoN_4)]·H_2O. Perspective drawings with the atom numbering scheme, bond distances, and angles are shown in Fig. 2. The

Table 1. Fractional atomic coordinates
All values have been multiplied by 10^4.

Atom	x/a	y/b	z/c
Cu	4344(1)	4343(1)	2498(2)
O(1)	7343(7)	213(7)	526(11)
O(2)	220(7)	7350(7)	4478(11)
N(1)	4312(7)	2539(7)	2386(11)
N(2)	6094(7)	4372(7)	2361(11)
N(3)	4415(7)	6116(7)	2622(11)
N(4)	2558(7)	4359(7)	2626(11)
C(1)	5345(9)	1735(9)	2113(13)
C(2)	6544(9)	2149(9)	1787(13)
C(3)	6888(9)	3428(9)	1955(13)
C(4)	6622(10)	5627(10)	2651(16)
C(5)	5615(10)	6607(10)	2313(16)
C(6)	3396(9)	6871(9)	3076(13)
C(7)	2170(9)	6569(9)	3219(13)
C(8)	1728(9)	5313(10)	2857(13)
C(9)	2098(10)	3093(10)	2228(15)
C(10)	3110(10)	2118(9)	2771(15)
C(11)	8902(10)	1659(11)	1041(16)
C(12)	7569(10)	1284(9)	1078(14)
C(13)	5118(12)	355(10)	2526(16)
C(14)	1650(11)	8908(10)	3957(16)
C(15)	1280(9)	7547(10)	3919(13)
C(16)	366(10)	5114(10)	2487(15)
O(3)	8104(9)	8117(9)	2517(18)

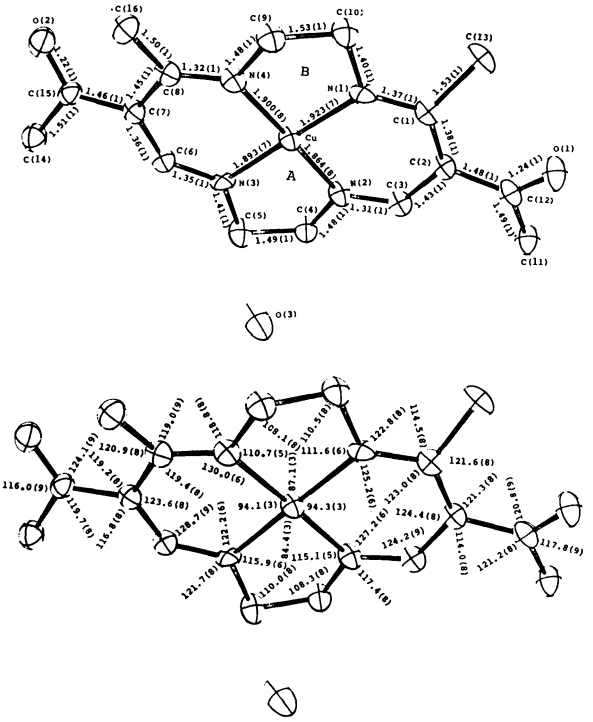

Fig. 2. ORTEP drawing of [Cu(Me$_2$Acyl$_2$[14]tetraenatoN$_4$)]·H$_2$O with the atom numbering scheme, bond distances and angles. The thermal ellipsoids are drawn at 25% probability level. The hydrogen atoms are omitted for clarity.

crystal structure consists of a discrete neutral complex [Cu(Me$_2$Acyl$_2$[14]tetraenatoN$_4$)] and a water molecule as crystal solvent. The copper atom is coordinated by four nitrogen atoms and the deviations of the component atoms from the coordination plane CuN$_4$ are in the range from −0.08 to +0.08 Å, showing a good planarity. The Cu–N bond distances are in the range expected for those of Cu–N(iminate)[15] and considerably shorter than those of the Cu–N (amine).[16]

For the two unsaturated six-membered chelate rings, the planarity for each chelate ring seems to be preserved, in which the deviations of the component atoms from the plane N$_2$C$_3$ are in the range from 0.05 to −0.03 Å. However, the C(13) of the methyl group bonded to C(1) deviates by 0.50 Å from the plane N$_2$C$_3$, due to the steric repulsion between the oxygen atom of the acyl group and itself. The C–C and C–N bond distances of the unsaturated chelate rings are intermediate between the corresponding single and double bond distances,[17] respectively, indicating that the chelate rings are π-electron conjugated systems. The saturated five-membered chelate rings (A and B) are all found to assume the gauche conformation with absolute configuration $\lambda\delta$ or $\delta\lambda$, where C(4) and C(5) deviate by 0.17 and −0.17 Å from the plane of CuN(2)N(3) and C(10) and C(9) deviate by 0.25 and −0.27 Å from the plane of CuN(1)N(4), respectively.

As a consequence of the planarities of the two conjugated chelate rings and the combination of the absolute configurations of the two saturated five-membered chelate rings, the overall conformation of the complex takes a chair-like shape, where the seat and the rests are formed by the coordination plane CuN$_4$ and the two unsaturated six-membered chelate rings, respectively. In other words, the two conjugated chelate rings are folded upward and downward on the CuN$_4$ plane with a gradient of 8°. This molecular conformation is apparently different from the so-called saddle shape conformation, which is observed in the analogous complexes with fifteen[18] and sixteen[19] membered ring sizes and in which the two unsaturated chelate rings are folded upward on the same side of the MN$_4$ plane.

Synthesis and Characterization. The complex [Cu(Me$_2$Acyl$_2$[14]tetraenatoN$_4$)] can be converted into a powerful nucleophile by removal of the acetyl groups. The unsubstituted complex [Cu(Me$_2$[14]tetraenatoN$_4$)] reacts with a variety of electrophiles to produce derivatives that are substituted at the γ and γ' positions. The complexes with substituted groups at the γ and γ' positions were characterized by elemental analyses and infrared spectra. Infrared spectra showed the C=O stretching band in *ca.* 1620 cm^{-1} and the band of the iminate rings in *ca.* 1550—1580 cm^{-1}. Two vibrations (*ca.* 1770 and 1740 cm^{-1}) due to the C=O stretching of the starting material, *i.e.*, acid chlorides, are absent in products, supporting the introduction of the substituent.

Electronic Spectra. Visible and ultraviolet spectra of the complexes were obtained on 10^{-4}—10^{-5} mol dm^{-3} solutions in chloroform over the range (14—48)×10^3 cm^{-1}, and the band maxima are given in Table 2. The complexes show band maxima in the ultraviolet region with extinction coefficients in the range from 20000 to 48000 dm^3 mol^{-1} cm^{-1} which agree with the assignment of the band as representing a charge-transfer transition. The spectrum also exhibits a broad band in the visible region with an extinction coefficient in the range 400—750 dm^3 mol^{-1} cm^{-1} which is attributable to the d-d transition band.

Effect of electronic properties of the substituent groups was observed in the d-d transition band rather than in the charge-transfer band. The energy of the d-d transition increases with an increase in electron-withdrawing strength of the substituent groups, which is consistent with the result of Busch and co-workers[4,5] reported for nickel(II) complexes with a broad range of substituent groups in the same ligand system. For the complexes with *p*-substituted benzoyl groups, the observed d-d band maxima are linearly correlated to the Hammett substituent constants of the *p*-substituted groups, as shown in Fig. 3. This may be a result of the

Table 2. Electronic absorption bands for the substituted derivatives [Cu(Me$_2$E$_2$[14]tetraenatoN$_4$)]

Substituent(E)	d-d Transition $\tilde{\nu}$/10^3 cm^{-1}(ε)	Other transition $\tilde{\nu}$/10^3 cm^{-1}(ε)
CH$_3$CO–	17.88(408)	31.87(47300)
C$_2$H$_5$CO–	17.79(395)	31.68(42600)
i-C$_3$H$_7$CO–	17.73(462)	31.74(39300)
p-NO$_2$C$_6$H$_4$CO–	18.52(757)	32.78(32600)
C$_6$H$_5$CO–	17.82(472)	30.90(32100)
p-CH$_3$C$_6$H$_4$CO–	17.73(429)	30.82(29900)

TABLE 3. ELECTROCHEMICAL DATA FOR THE SUBSTITUTED DERIVATIVES [Cu(Me$_2$E$_2$[14]TETRAENATON$_4$)]

Substituent(E)	Red V	Ox $\Delta Ep_{1/2}$ V	Red $\Delta Ep_{1/2}$ V	ΔEp mV	Ox $\Delta Ep_{1/2}$ V	Red $\Delta Ep_{1/2}$ V	ΔEp mV
CH_3CO-	−1.07	−0.22	−0.15	70	0.84	0.88	40
C_2H_5CO-	−0.95	−0.06	−0.02	40	0.98	1.03	50
i-C_3H_7CO-	−0.82	−0.15	−0.09	60	0.89	0.94	50
p-$NO_2C_6H_4CO$-	−0.98	−0.05	0.01	60	0.95	1.01	60
C_6H_5CO-	−0.88	−0.07	−0.02	50	0.91	0.95	40
p-$CH_3C_6H_4CO$-	−0.85	−0.23	−0.18	50	0.73	0.77	40

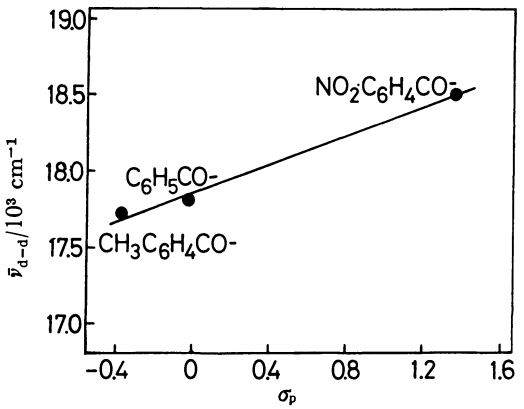

Fig. 3. Plot of d-d transitions energy of the substituted benzoyl derivatives *vs.* Hammett substituent constants of the *p*-substituent groups.

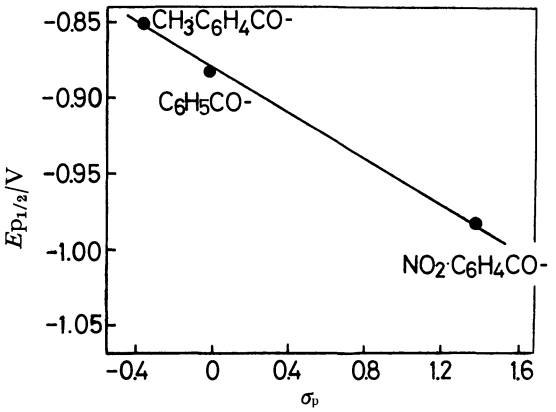

Fig. 4. Plot of reduction potentials of the substituted benzoyl derivatives *vs.* Hammett substituent constants of the *p*-substituent groups.

overall planarity between the charge-delocalized chelate ring and the substituted π-electron system of the benzoyl group. For the complexes with substituent groups CH_3CO-, C_2H_5CO-, and i-C_3H_7CO-, the tendency of their d-d transition band maxima is observed but not so large.

Electrochemistry. Electrochemical measurements were performed on 10^{-3} mol dm^{-3} solutions of the substituted complexes in acetonitrile. For the direct comparison of the values obtained, the conditions were kept as constant as possible with all the complexes. The cyclic voltamograms of these complexes were similar in shape and showed three electrode processes: (1) the irreversible reduction at a negative potential around −1 V, (2) the relatively well-behaved reduction at around 0 V, and (3) the relatively well-behaved oxidation at a positive potential around 1 V, as given in Table 3. Since Yokoi and Addison[20] reported that Cu^{2+}/Cu^{+} reduction potentials of square planar copper(II) complexes with imine or amine nitrogen atoms are in the range from −0.7 to −1.5 V, the reduction around −1 V of these complexes can be assigned to $Cu^{2+}+e\rightarrow Cu^{+}$, although it is irreversible. For the *p*-substituted benzoyl derivatives, only the reduction potential of the three electrode processes is linearly correlated to the Hammett substituent constants of the *p*-substituent groups, and the slope is −0.072, as shown in Fig. 4. For the corresponding nickel(II) complexes,[5] the linear correlation between the Hammett substituent constants and the oxidation potentials due to the Ni^{2+}/Ni^{3+} couple was also observed, the slopes being 0.035, 0.064, and 0.047 for the series of 14-, 15-, and 16-membered complexes, respectively.

The authors are grateful to Professor Sigeo Kida, Faculty of Science, Kyushu University, for guidance in the X-ray work.

References

1) K. M. Kadish and M. M. Morrison, *J. Am. Chem. Soc.*, **98**, 3326 (1976).
2) K. M. Kadish and M. M. Morrison, *Inorg. Chem.*, **15**, 980 (1976).
3) F. A. Walker, D. Beroiz and K. M. Kadish, *J. Am. Chem. Soc.*, **98**, 3484 (1976).
4) D. G. Pillsbury and D. H. Busch, *J. Am. Chem. Soc.*, **98**, 7836 (1976).
5) J. A. Streeky, D. G. Pillsburry, and D. H. Busch, *Inorg. Chem.*, **19**, 3148 (1980).
6) V. L. Goedken, P. H. Merrell, and D. H. Busch, *J. Am. Chem. Soc.*, **94**, 3397 (1972).
7) J. C. Dabrowiak, P. H. Merrell, and D. H. Busch, *Inorg. Chem.*, **11**, 1979 (1972).
8) E. Jäger, *Z. Anorg. Allg. Chem.*, **436**, 76 (1966).
9) D. P. Riley and D. H. Busch, *Inorg. Synth.*, **18**, 36 (1978).
10) H. Okawa and D. H. Busch, *Inorg. Chem.*, **18**, 1555 (1979).
11) "International Tables for X-Ray Crystallography," Kynoch Press, Birmingham (1974), Vol. IV.
12) T. Sakurai, H. Iwasaki, Y. Watanabe, K. Kobayashi, Y. Bando, and Y. Nakamichi, *Rep. Inst. Phys. Chem. Res.*, **50**, 75 (1972).
13) C. K. Johnson, Report No. 3794, Oak Ridge National

Laboratory, Oak Ridge, Tennessee (1965).
14) S. Kawano, *Rep. Comp. Cent. Kyushu University*, **13**, 39 (1980).
15) C. H. Wei, *Inorg. Chem.*, **11**, 2315 (1972).
16) R. G. Mirongiu, E. C. Lingafelter, and P. Paoletti, *Inorg. Chem.*, **8**, 2763 (1969).
17) D. Bruins and D. L. Weaver, *Inorg. Chem.*, **9**, 130 (1970).
18) C. J. Hipp, P. W. R. Corfield, J. D. Mokren, and D. H. Busch, *J. Am. Chem. Soc.*, **95**, 4465 (1973).
19) W. P. Schammel, K. B. Mertes, G. G. Christoph, and D. H. Busch, *J. Am. Chem. Soc.*, **101**, 1622 (1979); J. C. Stevens, P. J. Jackson, W. P. Schammel, G. G. Christoph, and D. H. Busch, *ibid.*, **102**, 3283 (1980).
20) H. Yokoi and A. W. Addison, *Inorg. Chem.*, **16**, 1341 (1977).

 © 1982 The Chemical Society of Japan Bull. Chem. Soc. Jpn., 55, 3175—3178 (1982)

Polarographic Behavior of Cobalt-1-Nitroso-2-naphthol Complex in Ammonium Citrate and Tartrate Solutions

Masao SUGAWARA, Toyoaki UCHIDA, and Tomihito KAMBARA*
Department of Chemistry, Faculty of Science, Hokkaido University, Kita-ku, Sapporo 060
(Received March 18, 1982)

The reduction behavior of cobalt(II) in ammonium citrate and tartrate solutions containing 1-nitroso-2-naphthol was investigated by means of d.c., a.c., normal and differential pulse polarography (n. p. p. and d. p. p.). When cobalt(II) is added to the supporting electrolyte of citrate or tartrate in the presence of the nitrosonaphthol, the reduction potential of 1-nitroso-2-naphthol shifts to a more negative value, the well-defined a. c. and d. p. p. peaks appearing. The drop time-potential curve indicated that adsorption of nitrosonaphthol as well as its reduction product at the mercury surface occurs. The analytical potentiality of the use of nitrosonaphthol for the microdetermination of cobalt(II) is also described.

The enhancement of current intensity of metal ions is often observed in solutions containing complex-forming molecules adsorbable at the electrode surface.[1-7] The phenomenon has been used for increasing the sensitivity of determination of metal ions.[2-5,8,9]

The well-known specific reagent for cobalt, 1-nitroso-2-naphthol, is reduced at the mercury electrode in four-electron step to the amine.[10-13] We found that the nitrosonaphthol is adsorbed on the mercury surface in a wide potential region, and by adding cobalt(II), the reduction of nitrosonaphthol shifts to a more negative potential, giving well-defined a.c. and d.p.p. peaks. In the present work, the behavior of cobalt–1-nitroso-2-naphthol complex in ammonium tartrate and citrate solutions is investigated with various methods of polarization of the dropping mercury electrode.

Experimental

Apparatus. D.c. and a.c. polarograms were obtained with a Yanagimoto polarograph model P-8. The dropping mercury electrode used had the characteristics: $m=2.53$ mg s^{-1} in deionized water and $t=3.87$ s in 0.1 M (1 M=1 mol dm^{-3}) ammonium citrate solution of pH 9.1 at open circuit and $h=39$ cm. A saturated calomel electrode was used as the reference electrode. For the a.c. polarography, the reference electrode was connected to a platinum coil counter electrode via a pool condenser of 3300 μF. Normal and differential pulse polarograms were recorded with a Princeton Applied Research model 174A polarographic analyzer, equipped with a Rika Denki X-Y recorder, model RW-11. A PAR 174/70 drop timer was used. The dropping mercury electrode used had the characteristics: $m=3.99$ mg s^{-1} in deionized water and $t=2.41$ s in 0.2 M ammonium tartrate solution of pH 8.7 at open circuit, when $h=71$ cm. A platinum wire served as the counter electrode and SCE as the reference electrode.

Electrolysis solutions were deaerated by bubbling pure nitrogen gas which had been passed through the supporting elcetrolyte of the same pH value. During electrolysis, nitrogen gas was passed over the solution. All polarograms were recorded at 25±0.1 °C. A Hitachi-Horiba glass electrode pH meter, F-5, was used for the pH measurements.

Reagents. Commercially available 1-nitroso-2-naphthol (Wako Chemicals Co.) was purified according to the literature.[14] A 0.01 mol dm^{-3} stock solution of the nitrosonaphthol was prepared by dissolving the purified reagent by weight in 10 cm^3 of 0.1 mol dm^{-3} sodium hydroxide solution and diluting to 50 cm^3 with deionized water. A 1.0×10^{-2} mol dm^{-3} stock solution of cobalt(II) was prepared from chloride and standardized chelatometrically. Other reagents used were all of the G. R. grade. Deionized water was used.

The electrolysis solution was prepared as follows. To a known portion of cobalt(II) solution in a 50-cm^3 volumetric flask are added in sequence 10 cm^3 of 1 mol dm^{-3} ammonium citrate or tartrate solution and 0.1 cm^3 of 0.01 mol dm^{-3} nitrosonaphthol solution, in order to prevent the appearance of precipitate. After standing for 30 min, the pH of solution is adjusted by adding an appropriate amount of 5 mol dm^{-3} ammonia solution and the mixture is diluted to the volume with deionized water. According to the procedure, the citrate or tartrate concentration in the electrolysis solution is always kept at 0.2 mol dm^{-3}.

Results and Discussion

D.c. and a.c. Polarographic Behavior. The cobalt–1-nitroso-2-naphthol complex is sparingly soluble in aqueous solutions and the precipitate once formed does not dissolve in the aqueous solution, but when the amount of cobalt(II) is low, a red-orange solution appears instead of the precipitate. D.c. and a.c. polarograms of cobalt(II) in an ammonium citrate solution of pH 9.1 containing an excess amount of 1-nitroso-2-naphthol are shown in Figs. 1 and 2, respectively. The d.c. first wave corresponds to the reduction of 1-nitroso-

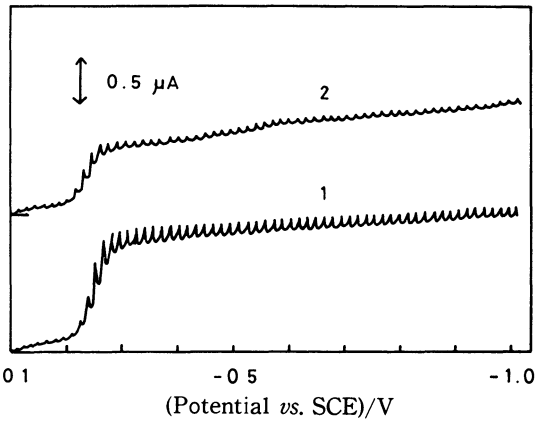

Fig. 1. D. c. polarograms of the cobalt–nitrosonaphthol system in 0.2 mol dm^{-3} diammonium hydrogencitrate-0.35 mol dm^{-3} ammonia buffer solution of pH 9.1.
(1) 60 μmol dm^{-3} R(NO)OH, (2) 1+10 μmol dm^{-3} cobalt(II).

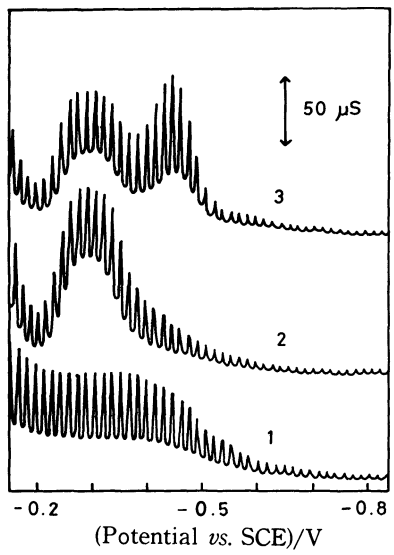

Fig. 2. A. c. polarograms of the cobalt-nitrosonaphthol system in the same supporting electrolyte as in Fig. 1. (1) Supporting electrolyte only, (2) 60 μmol dm^{-3} R(NO)OH, (3) 2+10 μmol dm^{-3} cobalt(II).

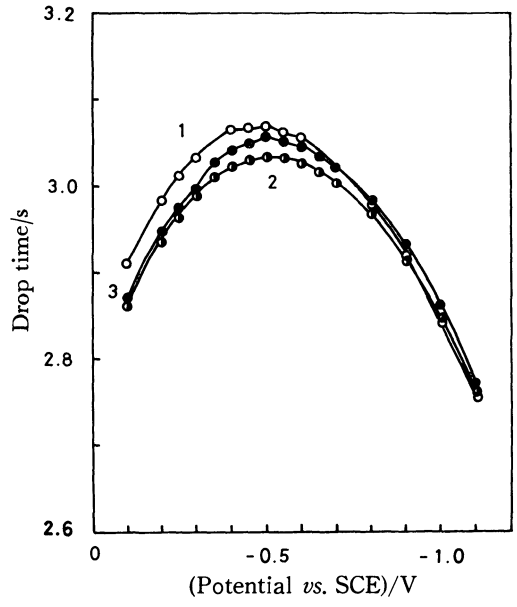

Fig. 3. Drop time *vs.* potential curves of the cobalt-nitrosonaphthol system in 0.2 mol dm^{-3} ammonium tartrate-0.05 mol dm^{-3} ammonia buffer solution of pH 8.7.
(1) Supporting electrolyte only, (2) 50 μmol dm^{-3} R(NO)OH, (3) 2+2 μmol dm^{-3} cobalt(II).

2-naphthol to the amine. When cobalt(II) is added to the solution, the first wave diminishes and an ill-defined second wave at about −0.52 V *vs.* SCE appears. The reduction of 1-nitroso-2-naphthol proceeds in a four-electron step involving four protons,[10,12] and is diffusion-controlled.[10,11] Tomes' method[15] applied to the first wave for evaluating the reversibility gave the difference of $E_{1/2}-E_{3/4}=25$ mV, which is fairly greater than 15 mV, expected from the reversible four-electron process. The d.c. second wave being ill-defined, the further analyses were impossible.

On the a.c. polarogram of cobalt ion, in the presence of an excess amount of 1-nitroso-2-naphthol, two well-developed peaks are observed. The first and second peaks correspond to the d.c. first and second steps, respectively, although the peak potential of the a.c. first peak is more negative by about 70 mV of the half-wave potential of the corresponding d.c. step. Compared with the a.c. polarogram of the supporting electrolyte alone, the depression of base current of the a.c. wave of nitrosonaphthol is observed. A plot of drop time *vs.* potential in the tartrate medium, as shown in Fig. 3, indicates that the nitrosonaphthol and its reduction product are adsorbed on the electrode surface. The similar results were obtained also in the citrate medium. The remarkably enhanced a.c. second peak, as compared with the d.c. second step, is ascribed to the adsorption of complex and its reduction product at the electrode surface, leading to the decrease in faradaic impedance.[1] In the citrate medium the peak height of the cobalt complex depends strongly on the solution pH, as shown in Fig. 4. The plot of peak potential *vs.* pH between 8.6 and 9.3 gave a straight line with a slope of −64 mV for the first and −76 mV for the second peak. The electrode process of nitrosonaphthol and its cobalt complex is seemingly not completely reversible in a.c. sense. The height of a.c. peak of the cobalt complex increases linearly with increasing concentration of cobalt(II) between 0.5 and 5 μmol dm^{-3}. At higher concentration of cobalt(II) above 5 μmol dm^{-3}, the linear relationship does not hold and the value of i_{AC}/C (μS mol^{-1} dm^3) increases with

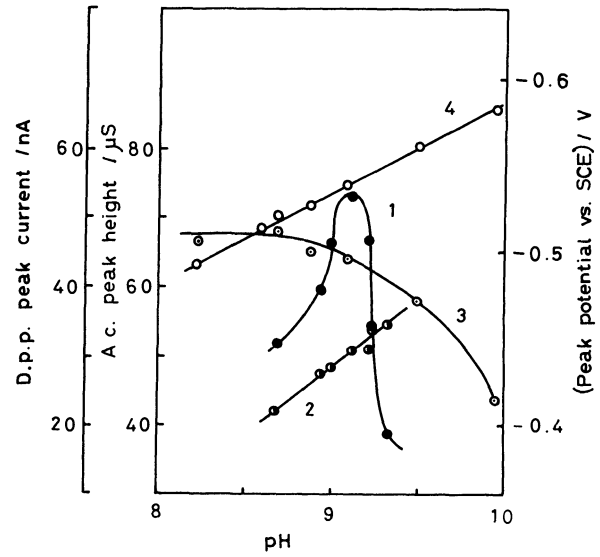

Fig. 4. Effect of pH on (1) a. c. peak height and (2) a. c. peak potential of the cobalt(II)-R(NO)OH complex in 0.2 mol dm^{-3} diammonium hydrogencitrate solution, (3) d. p. p. peak height and (4) d. p. p. peak potential of the cobalt-R(NO)OH complex in the 0.2 mol dm^{-3} ammonium tartrate solution.
(1) and (2): 10 μmol dm^{-3} cobalt(II)+184 μmol dm^{-3} R(NO)OH. (3) and (4): 0.5 μmol dm^{-3} cobalt(II)+10 μmol dm^{-3} R(NO)OH. D. p. p. condition: pulse amplitude $\Delta E=50$ mV; scan rate 5 mV s^{-1}; forced drop time $t_d=1$ s.

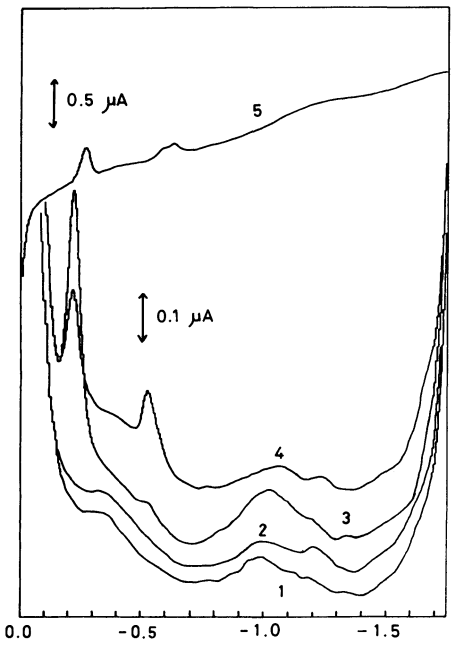

(Potential *vs.* SCE)/V

Fig. 5. D. p. and n. p. polarograms of the cobalt(II)–R(NO)OH system in the same supporting electrolyte as in Fig. 3. D. p. p. condition is the same as in Fig. 4. N. p. p. condition: scan rate 5 mV s^{-1}; initial potential E_i=0.0 V *vs.* SCE; t_d=1 s.
(1) Supporting electrolyte only, (2) 1+0.2 μmol dm^{-3} cobalt(II), (3) 1+1 μmol dm^{-3} R(NO)OH, (4) 2+1 μmol dm^{-3} R(NO)OH, (5) Normal pulse polarogram of solution (4).

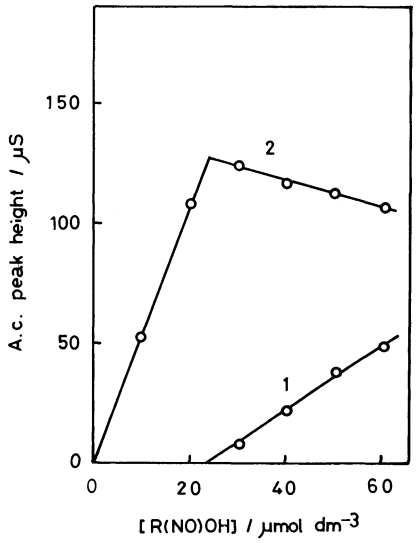

Fig. 6. Variation of a. c. peak height with R(NO)OH concentration in the same supporting electrolyte as in Fig. 1.
(1) First peak, (2) second peak, 9.8 μmol dm^{-3} cobalt(II).

increasing concentration C of cobalt(II).

Normal Pulse and Differential Pulse Polarographic Behavior. Normal and differential pulse polarograms of cobalt(II) in an ammonium tartrate solution containing an excess amount of nitrosonaphthol are shown in Fig. 5. On the normal pulse polarogram, a maximum, followed by a current suppression, is observed for the both waves at about −0.26 and −0.60 V. The phenomena are ascribed to Barker-Bolzan effect[1] indicating the rather strong adsorption of depolarizer at the electrode surface. On the differential pulse polarogram of the cobalt–nitrosonaphthol system three peaks are observed. The first peak at −0.21 V corresponds to the reduction of nitrosonaphthol and the second at −0.52 V to the reduction of nitrosonaphthol bound to cobalt(II). At a fairly negative potential (−1.20 V), an additional small peak appears, the potential of which coincides well with the potential of Co(II)/Co(Hg) system in the tartrate solution, as the polarograms 2 and 4 in Fig. 5 show. The height of the second peak was almost constant in the pH range from 8.2 to 8.9, and a plot of peak potential *vs.* pH gave a straight line having a slope of −52 mV, as shown in Fig. 4. The slope is in good accordance with the theoretical value of −59 mV for the reversible four-electron process involving four protons. The result indicates that the electrode reaction of cobalt complex is reversible in the d.p.p. sense. The peak height of cobalt complex increases with increasing concentration of cobalt(II) between 0.05 and 0.5 μmol dm^{-3}, but at the concentration of cobalt(II) above 0.6 μmol dm^{-3}, the increase in peak height becomes gradually saturated. The narrow concentration range, in which the calibration graph is linear, is one of the characteristic features indicating the adsorption of depolarizer. The calibration graph does not pass the origin, because a trace amount of cobalt(II) is present in the tartrate buffer solution as an impurity. The concentration of cobalt(II) impurity in the 0.2 mol dm^{-3} ammonium tartrate solution of pH 8.7 was found to be 0.11 μmol dm^{-3}.

The Composition of the Cobalt Complex and Electrode Reaction Mechanism. A plenty of data[10,11,16–20] on the composition of the cobalt-1-nitroso-2-naphthol complex indicate that the number of ligand bound to cobalt ion and the oxidation state of cobalt depend on the media employed. According to Kolthoff and Jacobsen,[11] bis(1-nitroso-2-naphtholato)cobalt(II) is formed in neutral and weakly alkaline solutions, and in an acidic solution, the cobalt(II) complex disproportionates rapidly, forming tris(1-nitroso-2-naphtholato)-cobalt(III). The similar disproportion process is suggested by Collahan *et al.*[18] based on the potentiometric titration in dioxane–water mixture. The formation of bis(1-nitroso-2-naphtholato)cobalt(II) in an ammonium citrate solution of pH 9.8 is also cited in the excellent monograph by Pyatnitskii.[20]

Dependence of a.c. peak height on various concentrations of 1-nitroso-2-naphthol in an ammonium citrate solution of pH 9.1 is shown in Fig. 6. The sharp increase in peak height of the cobalt complex is saturated at 2.3 of the molar ratio of nitrosonaphthol to cobalt(II). Further addition of the nitrosonaphthol decreases the peak height of the complex gradually, while the a.c. first peak of excess ligand appears. It seems that in the citrate solution bis(1-nitroso-2-naphtholato)cobalt(II) is predominantly formed according to

$$Co^{2+} + 2R(NO)OH \rightleftarrows Co[R(NO)O]_2 + 2H^+, \quad (1)$$

where R(NO)OH indicates the 1-nitroso-2-naphthol. The reduction of R(NO)OH at the mercury electrode[11,12] is given by

$$R(NO)OH + 4H^+ + 4e \rightleftarrows R(NH_2)OH + H_2O. \quad (2)$$

The nitrosonaphthol coordinated to cobalt(II) being stabilized, the reduction of the nitrosonaphthol in the complex shifts to a more negative potential. The overall electrode reaction is estimated to be

$$Co[R(NO)O]_2 + 8H^+ + 8e \rightleftarrows Co^{2+} + 2R(NH_2)O^- + 2H_2O. \quad (3)$$

In the ammonium tartrate solution of pH 8.7, the results of titration of 1 μmol dm^{-3} cobalt(II) with R(NO)OH gave the breaking point at around 2.6 of the molar ratio of the nitrosonaphthol to cobalt(II) for both the first and second waves. The results imply that a fraction of bis(1-nitroso-2-naphtholato)cobalt(II) in the tartrate solution differs slightly from that in the citrate medium. It should be noted that the decrease in a.c. and d.p.p. peak heights by adding excess amount of ligand is always observed and is due to the broadening of peaks. At 5 μmol dm^{-3} nitrosonaphthol, the half-width of d.p.p. peak of 1 μmol dm^{-3} cobalt(II) in the tartrate solution is 77 mV, however, it is 94 mV at 80 μmol dm^{-3} nitrosonaphthol. This is probably because the electrode reaction of the cobalt complex is hindered by the stronger adsorption of reduction product of nitrosonaphthol than the adsorption of the complex itself. The appearance of a small d.p.p. peak at −1.20 V in the tartrate solution, as described above, suggests that the cobalt(II) released by reduction is further reduced in the medium.

The adsorption of the cobalt complex at the mercury surface is not clear as judged from the drop time *vs.* potential plot, as shown in Fig. 3. However, the significantly enhanced response in a.c. polarography and also the narrow concentration range, for which the d.p.p. response is linear, imply that the cobalt complex is also adsorbed on the mercury surface.

TABLE 1. EFFECT OF FOREIGN METAL IONS ON THE d.p.p. DETERMINATION OF COBALT(II) IN 50 cm^3 OF 0.2 mol dm^{-3} AMMONIUM TARTRATE-0.05 mol dm^{-3} AMMONIA SOLUTION OF pH 8.7 CONTAINING 10 μmol dm^{-3} 1-NITROSO-2-NAPHTHOL

Metal	Metal added (μg)	Cobalt(II) found (μg)	Reovery %
Ni(II)	0.59	0.53	90
	2.94	0.49	83
Cd(II)	11.24	0.58	98
	22.48	0.31	53
Zn(II)	6.54	0.64	108
	13.08	0.66	112
	13.08	0.59	100 [a]
Fe(III)	5.58	0.62	105
	11.17	0.84	142
Cu(II)	0.64	0.93	158
	3.18	1.69	286

Cobalt(II) taken: 0.59 μg. a) Concentration of the nitrosonaphthol was increased by twice.

Analytical Potentiality. Although the remarkably enhanced a.c. response is obtained, the d.p.p. method is more sensitive, because of the inherent advantage to discriminate faradaic current from nonfaradaic one. In the alkaline solution of ammonium tartrate, cobalt at several ppb levels can be determined by differential pulse polarography. The slightly alkaline tartrate medium is preferable for the analytical purposes, because in this medium the interference by iron(III) is significantly suppressed. Effect of some metal ions on the d.p.p. determination of cobalt(II) is given in Table 1. Serious interference by copper(II) was found, which is due to the overlapping of the reduction peak of the copper(II)–nitrosonaphthol complex with the cobalt(II) peak. Improvement of selectivity of the method may be achieved by selective extraction of the cobalt complex in organic solvents. The extract may be directly subjected to polarographic measurements. Further study is under way.

References

1) G. C. Barker and J. A. Bolzan, *Fresenius' Z. Anal. Chem.*, **216**, 215 (1966).
2) D. Weiss, *Fresenius' Z. Anal. Chem.*, **185**, 273 (1963).
3) R. Kalvoda and J. Ai-chua, *J. Electroanal. Chem.*, **8**, 378 (1964).
4) G. Donoso N., M. A. Santa Ana V., and I. Chadwick W., *Anal. Chim. Acta*, **42**, 109 (1968).
5) R. Kalvoda, W. Anstine, and M. Heyrovsky, *Anal. Chim. Acta*, **50**, 93 (1970).
6) F. C. Anson and R. S. Rogers, *J. Electroanal. Chem.*, **47**, 287 (1973).
7) F. C. Anson, J. B. Flanagan, K. Takahashi, and A. Yamada, *J. Electroanal. Chem.*, **67**, 253 (1976).
8) C. J. Flora and E. Nieboer, *Anal. Chem.*, **52**, 1013 (1980).
9) J. Golmovsky, H. W. Nürnberg, and P. Valenta, *Z. Lebensm.-Unters. Forsch.*, **34**, 116 (1980).
10) I. M. Kolthoff and A. Langer, *J. Am. Chem. Soc.*, **62**, 3172 (1940).
11) I. M. Kolthoff and E. Jacobsen, *J. Am. Chem. Soc.*, **79**, 3677 (1957).
12) H. B. Mark, E. M. Smith, and C. N. Reilly, *J. Electroanal. Chem.*, **3**, 98 (1962).
13) P. Zuman and C. L. Perrin, "Organic Polarography," Interscience Publishers, New York (1969), p. 205.
14) O. G. Koch and G. A. Koch-Dedic, "Handbuch der Spurenanalyse," Zweite Auflage, Springer-Verlag, Berlin (1974), Teil 1, S. 588.
15) T. Tomes, *Collect. Czech. Chem. Commun.*, **9**, 12 (1937).
16) N. P. Komar and V. N. Talmacher, *Zh. Anal. Khim.*, **5**, 21 (1950).
17) M. Bobtelsky and E. Jungreis, *Anal. Chim. Acta*, **12**, 248 (1955).
18) C. L. Callahan, W. C. Fernelius, and B. P. Block, *Anal. Chim. Acta*, **16**, 101 (1957).
19) E. Casassas and L. Eek, *J. Chim. Phys.*, **64**, 971 (1967).
20) I. V. Pyatnitskii, "Analytical Chemistry of Cobalt," translated by N. Kaner, Ann Arbor-Humphery Science, Ann Arbor (1969), p. 24.

 © 1982 The Chemical Society of Japan Bull. Chem. Soc. Jpn., 55, 3179—3186 (1982)

Preparation, Resolution, and Spectroscopic Properties of Bis[(2-aminoethyl)-diphenylphosphine]- and (Ethylenediamine)[1,2-bis(diphenylphosphino)-ethane]-Cobalt(III) Complexes of Acetylacetonate, Malonate, Oxalate, and Carbonate Ions

Masamichi Atoh, Isamu Kinoshita†, Kazuo Kashiwabara, and Junnosuke Fujita*

Department of Chemistry, Faculty of Science, Nagoya University, Chikusa-ku, Nagoya 464

(Received April 1, 1982)

New complexes of the [Co(O–O)(edpp)$_2$]- and [Co(O–O)(en)(dppe)]- type were prepared from *trans*(Cl, Cl)-[$CoCl_2$(edpp)$_2$]ClO_4 and *trans*-[$CoCl_2$(en)(dppe)]$ClO_4\cdot H_2O$, respectively, where O–O is an acetylacetonate, malonate, oxalate, or carbonate ion, and en, edpp, and dppe denote ethylenediamine, (2-aminoethyl)diphenylphosphine, and 1,2-bis(diphenylphosphino)ethane, respectively. All the complexes of the former type gave two geometrical isomers of trans(P, P) and trans(P, N) configurations, which were assigned on the basis of the ^1H and ^{13}C NMR, and electronic absorption spectra. No trans(N, N) isomers were formed. The yields of the trans(P, N) isomers were always larger than those of the corresponding trans(P, P) isomers. With the decreasing ring members of the O–O chelates, the yield of the trans(P, P) isomer decreases, the trans(P, P)-carbonato complex being formed in trace amounts. The first absorption bands of the trans(P, P) isomers have very strong intensity as compared with those of the corresponding trans(P, N) and the dppe complexes. All the complexes except for [Co(O–O)(en)(dppe)]$^+$ (O–O=malonate and oxalate ions) were resolved by the chemical or SP-Sephadex C-25 column chromatographic method, and the circular dichroism spectra were recorded and compared with those of related complexes.

In previous papers, we have prepared bis(acetylacetonato)-[1] and bis(ethylenediamine)cobalt(III)[2] complexes of (2-aminoethyl)diphenylphosphine (edpp). Since the edpp chelate ligand has two bulky phenyl substituents on the phosphorus atom, inter- or intraligand interactions should be great in octahedral complexes. Stereochemical studies on bulky phosphine metal complexes would be significant in connection with stereoselectivity of transition metal phosphine complex catalysts in asymmetric syntheses. However, few octahedral complexes with bulky phosphine chelate ligands, in particular, those of cobalt(III) are known.[3] Cobalt(III) complexes with chelate phenylphosphine ligands so far known seem to be limited to those with 1,2-bis(diphenylphosphino)ethylene and *trans*-[$Co(CN)_2$(dppe)$_2$]$^+$ (dppe=1,2-bis(diphenylphosphino)ethane).[4] This paper reports the preparation, resolution, and spectroscopic properties of two geometrical isomers, trans(P,P) and trans(P,N), of the [Co(O–O)(edpp)$_2$]-type complexes (O–O=acetylacetonate, malonate, oxalate, or carbonate ion). The corresponding [Co(O–O)(en)(dppe)]-type complexes (en=ethylenediamine) were also prepared, and their properties were compared with those of the edpp complexes.

Experimental

(2-Aminoethyl)diphenylphosphine was prepared according to the literature method[5] and handled under nitrogen atmosphere until it formed cobalt(III) complexes. 1,2-Bis(diphenylphosphino)ethane was purchased from Strem Chemicals Inc. and used without further purification. Absorption, circular dichroism (CD), and ^1H and ^{13}C NMR spectra were recorded on a Hitachi 323 spectrophotometer, a JASCO J-40 spectropolarimeter, and Jeol JNM-PMX 60 and JNM-FX 100 spectrometers, respectively.

trans*(Cl, Cl)*-[$CoCl_2$*(edpp)*$_2$]ClO_4. To a methanol solution (100 cm^3) of $Co(ClO_4)_2\cdot 6H_2O$ (5.10 g, 13.9 mmol) was added edpp (6.36 g, 27.7 mmol) with stirring. A brown solid (probably [Co(edpp)$_2$] $(ClO_4)_2$) was obtained by evaporating the solution under reduced pressure. It was dissolved in dichloromethane, and chlorine gas was bubbled into the solution for 15 min to oxidize the Co(II) ions, giving a green solution. The excess chlorine was removed by bubbling nitrogen, and then the green solution was evaporated to dryness. The green residue was recrystallized by dissolving in hot methanol and by adding excess $NaClO_4$. Yield: *ca.* 50%. The complex is insoluble in water, but soluble in most polar organic solvents.

The perchlorate can be converted to chloride by using Dowex 1×8 (Cl^- form) in methanol. The methanol solution give green crystals by evaporating in a desiccator over P_2O_5. The chloride, *trans*(Cl,Cl)-[$CoCl_2$(edpp)$_2$]$Cl\cdot 2H_2O$ is also insoluble in water, but more soluble in organic solvents than the perchlorate is.

trans-[*$CoCl_2$(en)(dppe)*]$ClO_4\cdot H_2O$. To a solution of dppe (2.00 g, 5.02 mmol) in a mixture of ethanol (20 cm^3) and benzene (40 cm^3) were added ethylenediamine (0.34 g, 5.66 mmol) and $Co(ClO_4)_2\cdot 6H_2O$ (1.90 g, 5.19 mmol) with stirring. The resulting orange brown solution was evaporated to dryness under reduced pressure, and the residue was dissolved in dichloromethane. Chlorine gas was bubbled into the solution for 15 min and then nitrogen gas for 20 min to remove excess chlorine. The green solution obtained was filtered, and the filtrate was evaporated to dryness to give a green product. It was dissolved in methanol by heating at 70 °C for *ca.* 30 min, and the solution was filtered. The filtrate was mixed with excess $NaClO_4$ and allowed to stand at room temperature to yield green crystals. Yield: *ca.* 40%. The complex is insoluble in water, but soluble in most polar organic solvents.

trans*(P, P)*-[*Co(acac)(edpp)*$_2$]$Br_2\cdot 2CH_2Cl_2$ *and* trans*(P,N)*-[*Co(acac)(edpp)*$_2$]$Br_2\cdot 3H_2O$. An ethanol solution (200 cm^3) containing *trans*(Cl,Cl)-[$CoCl_2$(edpp)$_2$]ClO_4 (0.50 g, 0.73 mmol) and lithium acetylacetonate (0.08 g, 0.75 mmol) was stirred at room temperature for 1 h. The resulting red brown solution was diluted with water (1 dm^3) and passed through a column (ϕ 3 cm×50 cm) of SP-Sephadex C-25. The product adsorbed was first eluted with a 0.05 mol/dm^3 NaCl solution to remove a dark red by-product, [Co(acac)$_2$-

† Present address: Department of Chemistry, Faculty of Science, Osaka City University, Sumiyoshi-ku, Osaka 558.

(edpp)]$^{+}$,[1] and then with a 0.4 mol/dm^3 NaCl solution. The orange-red eluate of $[Co(acac)(edpp)_2]^{2+}$ was obtained, diluted twenty times with water, and poured again onto a column (ϕ 3 cm$\times$150 cm) of SP-Sephadex C-25. By elution with a 0.3 mol/dm^3 KBr solution, two orange-red bands (I and II) appeared. The eluate of the first band (I) was concentrated to a small volume under reduced pressure, and the complex was extracted with CH_2Cl_2. On addition of diethyl ether the extract gave red crystals of *trans*(P, P)$[Co(acac)(edpp)_2]Br_2\cdot 2CH_2Cl_2$ (I). Yield: *ca.* 10%. The presence of CH_2Cl_2 was confirmed by the ^{1}H NMR spectrum.

The second orange-red eluate was concentrated to a small volume under reduced pressure and allowed to stand to yield red crystals of *trans*(P, N)-$[Co(acac)(edpp)_2]Br_2\cdot 3H_2O$ (II). Yield: *ca.* 40%.

trans(P,P)-$[Co(O–O)(edpp)_2]^+$ (O–O=Oxalate (ox) and Malonate (mal) Ions), and trans(P,N)-$[Co(O–O)(edpp)_2]^+$ (O–O=CO_3^{2-}, ox, and mal Ions). These complexes were prepared by methods similar to those for the corresponding acetylacetonato complexes. A methanol solution (200 cm^3) containing *trans*(Cl,Cl)-$[CoCl_2(edpp)_2]ClO_4$ (0.50 g, 0.73 mmol), a slight excess of the ammonium salt of O–O (*e.g.*, $(NH_4)_2CO_3$), and a small amount of active charcoal was stirred at 50 °C for 1 h, and then filtered. The red filtrate was diluted with water (1 dm^3) and poured onto a column (ϕ 3 cm$\times$5 cm) of SP-Sephadex C-25. The SP-Sephadex adsorbed the product was placed on the top of the adsorbent layer of an SP-Sephadex column (ϕ 3 cm$\times$120 cm). By elution with a 0.05 mol/dm^3 NaCl or KBr solution, two bands, the first orange and the second red, were eluted. The choice of an eluent was made for better crystallization of the complex. In the case of the carbonato complex, the first orange band was too small in the amount to isolate the complex. Each eluate of the separated bands was concentrated under reduced pressure to a small volume. The concentrate gave crystals of the isomer on addition of NaCl or KBr and standing at a refrigerator. The complexes obtained from the first orange and the second red bands are trans(P, P) and trans(P, N) isomers, respectively. The total yields were *ca.* 30—50% for all the complexes. No formation of the trans(N, N) isomer was observed in all the complexes including the acac complex. The formation ratios, trans(P, N): trans(P, P), for the acac, mal, ox, and CO_3^{2-} complexes were 0.25 : 1, 0.08 : 1, 0.03 : 1, and 0 : 1, respectively.

$[Co(acac)(en)(dppe)]Br_2\cdot 2H_2O$. A methanol solution (250 cm^3) containing *trans*-$[CoCl_2(en)(dppe)]ClO_4\cdot H_2O$ (0.50 g, 0.71 mmol) and lithium acetylacetonate (0.08 g, 0.75 mmol) was stirred for 24 h at room temperature. The resulting red brown solution was diluted with water (2 dm^3) and poured onto a column (ϕ 3 cm$\times$50 cm) of SP-Sephadex C-25. The adsorbed red brown product was eluted with a 0.1 mol/dm^3 NaBr solution, giving first the brown-red band of $[Co(acac)_2(dppe)]^+$ [1] and then the red orange band of $[Co(acac)(en)(dppe)]^{2+}$. The eluate of the latter was concentrated to a small volume, and the complex was extracted with $CHCl_3$. The extract was evaporated to dryness, and the residue was dissolved in a small amount of methanol. On addition of diethyl ether the solution gave crystals of $[Co(acac)(en)(dppe)]Br_2\cdot 2H_2O$. Yield: *ca.* 8%.

$[Co(O–O)(en)(dppe)]^+$ (O–O=CO_3^{2-}, ox, and mal Ions). These complexes were prepared by methods similar to those for the corresponding bis(edpp) complexes, using *trans*-$[CoCl_2(en)(dppe)]ClO_4\cdot H_2O$ (0.50 g) instead of *trans*(Cl, Cl)-$[CoCl_2(edpp)_2]ClO_4$. Each of the resulting orange-red solutions was diluted with a water–methanol mixture (1 : 1, 1 dm^3), and the solution was poured onto a column (ϕ 3 cm$\times$50 cm) of SP-Sephadex C-25. After washing the column thoroughly with water and methanol, the product adsorbed was eluted with a 0.05 mol/dm^3 NaCl or KBr solution. One orange band was eluted. The oxalato complex was isolated as chloride by concentrating the eluate to a small volume and then by storeing in a refrigerator. In a similar manner the malonato complex was obtained as bromide. In the case of the carbonato complex, the eluate obtained with a NaCl solution was concentrated to a small volume, and the concentrate was mixed with $NaClO_4\cdot H_2O$ to give perchlorate of the complex. The yields of all the complexes were *ca.* 40%.

Optical Resolution. *trans(P, P)-* and *trans(P, N)-$[Co(acac)(edpp)_2]^{2+}$.* The racemic trans(P, P) isomer charged on the top of a column (ϕ 3 cm$\times$120 cm) of SP-Sephadex C-25 was eluted with an aqueous 0.1 mol/dm^3 sodium $(+)_{589}$-tartratoantimonate(III) solution, giving two bands of the enantiomers. Each eluate of the bands was concentrated to a small volume under reduced pressure. On addition of excess KBr the concentrate gave white precipitate of potassium $(+)_{589}$-tartratoantimonate(III), which was filtered off. The filtrate was mixed with CH_2Cl_2 to extract the complex. The red extract was evaporated to dryness under reduced pressure, and the residue was dissolved in water. The solution was poured again onto a small column of SP-Sephadex C-25, and the complex adsorbed was eluted with an aqueous 0.1 mol/dm^3 KBr solution. The eluate was concentrated to a small volume under reduced pressure, and the concentrate was stored in a refrigerator to yield dark red crystals of optically active bromide of the trans(P, P) isomer. The $(+)_{589}$-isomer was obtained from the first band.

The trans(P, N) isomer was resolved by the same column chromatographic method as that for the trans(P, P) isomer. The eluate of the complex resolved was poured on a small column of SP-Sephadex, and the complex was eluted with 0.1 mol/dm^3 NaCl. On addition of an aqueous $NaClO_4$ solution the eluate gave pink, crystalline precipitate of the active perchlorate. The $(+)_{589}$-isomer was eluted faster than its antipode.

trans(P, P)-$[Co(O–O)(edpp)_2]^+$ (O–O=ox and mal) and trans(P, N)-$[Co(O–O)(edpp)_2]^+$ (O–O=CO_3^{2+}, ox, and mal). These complexes were resolved by a similar column chromatographic method with an aqueous 0.03 mol/dm^3 NaCl solution. The band-separation of enantiomers was incomplete in all cases, and no better separation was resulted by using an eluent of sodium $(+)_{589}$-tartratoantimonate(III). However, the first several fractions showed an almost constant $\Delta\varepsilon/\varepsilon$ value. These fractions were collected and used for the measurement of CD spectra without isolating the active complex.

$[CoCO_3(en)(dppe)]^+$. The racemic $[CoCO_3(en)(dppe)]ClO_4\cdot 1/2(NaClO_4)\cdot 1.5H_2O$ complex (100 mg) was converted into chloride by stirring with an anion exchanger, Dowex 1$\times$8 in the chloride form in a mixture of methanol (50 cm^3) and water (50 cm^3) at 40 °C for 1 h. The exchanger was filtered off, and the filtrate was mixed with 90 mg of Ag(*d*-bcs)$\cdot H_2O$ (*d*-bcs denotes $(+)_{589}$-(1*R*, 3*S*, 4*S*, 7*R*)-3-bromo-9-camphorsulfonate ion).[6] The mixture was stirred at 40 °C for 20 min, and then white precipitate of AgCl was filtered off. The filtrate was slowly evaporated in a desiccator over silica gel to yield orange crystals of $(+)_{589}$-$[CoCO_3(en)(dppe)](d\text{-bcs})\cdot H_2O$ which were filtered and washed with water. The crystals which are hardly soluble in water were dissolved in methanol. The solution was diluted with about the same volume of water and poured onto a small column of SP-Sephadex C-25. The complex adsorbed was eluted with 0.25 mol/dm^3 NaCl. To the eluate was added an aqueous $NaClO_4$ solution to give orange crystals of $(+)_{589}$-$[CoCO_3(en)(dppe)]ClO_4\cdot 3.5(NaClO_4)\cdot H_2O$ which were filtered and washed with water.

[Co(acac)(en)(dppe)]$^{2+}$. This complex was resolved by SP-Sephadex column chromatography with an eluent of 0.2 mol/dm^3 sodium $(+)_{589}$-tartratoantimonate(III). Although no good separation of the bands of enantiomers was observed, the first several fractions showed an almost constant $\Delta\varepsilon/\varepsilon$ value. These fractions were collected, diluted with water, and poured onto a small column of SP-Sephadex C-25. The complex adsorbed was eluted with 0.5 mol/dm^3 NaCl, and the eluate was used for the measurement of CD spectra. This complex was not resolved by a chemical method with *d*-bcs similar to that for the corresponding carbonato complex.

Attempts to resolve $[Co(O–O)(en)(dppe)]^+$ (O–O=ox and mal) were unsuccessful.

Analytical data of all the new complexes are given in Table 1.

Results and Discussion

trans(Cl,Cl)-[CoCl$_2$(edpp)$_2$]ClO$_4$ and trans-[CoCl$_2$(en)-(dppe)]ClO$_4$·H$_2$O. A *trans*-dichlorobis(diamine)-cobalt(III) complex is known to be a good starting material for preparing various bis(diamine)cobalt(III) complexes. The $[CoCl_2(edpp)_2]ClO_4$ and $[CoCl_2(en)(dppe)]ClO_4\cdot H_2O$ complexes prepared in this study have the green color characteristic of a trans(Cl,Cl) configuration, and these chloride ions are easily replaced by the O–O chelate ligand such as an acetylacetonate or oxalate ion. Both dichloro complexes were prepared in fairly good yield from the corresponding cobalt(II) complexes, $Co(edpp)_2(ClO_4)_2$ and $Co(en)(dppe)(ClO_4)_2$ which had been prepared in methanol, by oxidizing with chlorine in dichloromethane. In the oxidation the presence of methanol lowered remarkably the yield of the cobalt(III) complexes, although the reason for this remains unknown. Attempts to prepare these Co(II)–phosphine complexes in dichloromethane were unsuccessful, because $Co(ClO_4)_2\cdot 6H_2O$ is insoluble in this solvent. The $[CoCl_2(edpp)_2]ClO_4$ complex can also be prepared by oxidizing $Co(edpp)_2(ClO_4)_2$ with air in methanol and by treating with hydrochloric acid, but the yield was very poor.

In Fig. 1 are compared absorption spectra of the two dichlorophosphine complexes with that of *trans*-$[CoCl_2(en)_2]^+$. The phosphine complexes exhibit a medium

Table 1. Analytical data of the new complexes

Complex		C(%) Found(Calcd)	H(%) Found(Calcd)	N(%) Found(Calcd)
trans(Cl,Cl)-[CoCl$_2$(edpp)$_2$]ClO$_4$	**1**	49.42(48.89)	4.72(4.69)	3.57(4.07)
trans(Cl,Cl)-[CoCl$_2$(edpp)$_2$]Cl·2H$_2$O	**2**	50.89(50.97)	5.11(5.50)	3.84(4.25)
trans-[CoCl$_2$(en)(dppe)]ClO$_4$·H$_2$O	**3**	47.64(47.65)	4.69(4.85)	3.85(3.97)
trans(P,P)-[Co(acac)(edpp)$_2$]Br$_2$·2CH$_2$Cl$_2$	**4**	43.82(44.43)	4.65(4.58)	3.06(2.96)
trans(P,N)-[Co(acac)(edpp)$_2$]Br$_2$·3H$_2$O	**5**	47.96(47.73)	5.00(5.46)	3.18(3.37)
$(+)_{589}$-*trans*(P,P)-[Co(acac)(edpp)$_2$]Br$_2$·2.5KBr·3H$_2$O	**6**	35.10(35.14)	3.54(4.02)	2.28(2.48)
$(+)_{589}$-*trans*(P,N)-[Co(acac)(edpp)$_2$](ClO$_4$)$_2$	**7**	46.38(46.55)	4.80(5.09)	3.04(3.29)
trans(P,N)-[Co(CO$_3$)(edpp)$_2$]Cl·3.5H$_2$O	**8**	51.76(51.53)	5.81(5.82)	3.82(4.14)
trans(P,P)-[Co(ox)(edpp)$_2$]Br·3H$_2$O	**9**	48.61(48.78)	4.78(5.17)	3.72(3.78)
trans(P,N)-[Co(ox)(edpp)$_2$]Cl·NaCl	**10**	51.49(51.52)	4.76(4.61)	3.59(4.00)
trans(P,P)-[Co(mal)(edpp)$_2$]Cl·0.5NaCl·H$_2$O	**11**	51.75(51.69)	5.31(5.31)	3.61(3.88)
trans(P,N)-[Co(mal)(edpp)$_2$]Br·0.5KBr·4H$_2$O	**12**	44.60(44.80)	5.62(5.69)	3.37(3.37)
[Co(acac)(en)(dppe)]Br$_2$·2H$_2$O	**13**	48.48(48.79)	5.10(5.33)	3.69(3.45)
[Co(CO$_3$)(en)(dppe)]ClO$_4$·0.5NaClO$_4$·1.5H$_2$O	**14**	45.47(45.52)	4.16(4.61)	3.22(3.66)
$(+)_{589}$-[Co(CO$_3$)(en)(dppe)](*d*-C$_{10}$H$_{14}$OBrSO$_3$)·1.5H$_2$O	**15**	51.53(51.21)	5.07(5.34)	2.31(3.06)
$(+)_{589}$-[Co(CO$_3$)(en)(dppe)]ClO$_4$·3.5NaClO$_4$·H$_2$O	**16**	31.92(32.01)	3.26(3.15)	2.49(2.57)
[Co(ox)(en)(dppe)]Cl·2H$_2$O	**17**	53.00(53.22)	5.45(5.35)	4.03(4.13)
[Co(mal)(en)(dppe)]Br·0.5KBr·H$_2$O	**18**	48.25(47.93)	4.94(4.67)	3.61(3.61)

Table 2. Absorption(AB) and CD spectral data in the visible to near ultraviolet region

Complex	AB $\tilde{\nu}/10^3$ cm^{-1} (log ε)	CD $\tilde{\nu}/10^3$ cm^{-1} ($\Delta\varepsilon$)
1,2	15.9 (2.03), 21.5(2.1)^{sh}, 27.5(3.7)^{sh}	
3	16.45(2.13), 22.5(2.6)^{sh}, 27.5(3.5)^{sh}	
6	19.3 (3.52), 24.6(3.91)	18.1(+6.93), 19.9(−1.23), 27.7(−25.3), 23.8(+3.80)
7	19.9 (2.81), 24 (2.9)^{sh}	18.9(+7.53), 22.3(+1.82), 25 (−4)^{sh}, 28.3(−44.1)
8	19.8 (2.55), 25 (2.5)^{sh}	18.7(+3.89), 21.2(−1.85), 24.8(+0.70), 27.3(+0.41)
9	20.4 (3.08), 28.3(4.40)	18.2(+2.14), 20.8(−2.72), 28.2(+6.72)
10	20.0 (2.54), 25 (2.5)^{sh}	18.8(+2.14), 21.6(−0.47), 25.1(+0.58)
11	20.4 (3.12), 27.8(4.49)	18.0(+2.72), 20.4(−4.18), 26.5(+5.65)
12	19.9 (2.56), 25 (2.7)^{sh}	18.7(+3.03), 21.7(−0.44), 25.0(+1.03),28.3(+1.35)
13	20.7 (2.96), 28.5(3.8)^{sh}	17.9(+0.21), 19.7(−2.21), 22.3(+4.89)
14	21.1 (2.90)	18.4(+0.94), 20.2(−1.73), 22.3(+1.81)
17	21.3 (2.91), 26 (2.7)^{sh}	
18	21.0 (2.91), 26 (2.7)^{sh}	

Solvent: CH_3OH except **13**(H_2O). sh: Shoulder.

Table 3. ^1H and ^{13}C NMR spectral data (δ from TMS)

Complex	^1H NMR[a] acac		^{13}C NMR[b] acac			edpp					
	CH_3	CH	CH_3	CH	CO	P-CH_2	N-CH_2	P-C_1	*o*-P	*m*-P	*p*-P
2						33.28t	41.64s	130.39t	135.51t	129.57t	132.54s
4	1.71	5.37	27.34s	98.50s	190.69s	24.71t	45.02s	125.00t 128.71t	132.66t 133.34t	129.63t 131.39t	131.98s 133.64s
5	1.83 2.27	5.17	27.77s 27.56d	100.30s	190.30s 190.66s	25.56d 34.55dd	41.59s 42.24s	122.18dd c	c	c	c
8						26.21d 31.17d	41.90s 42.85s	c	c	c	c
10						23.27d 35.04d	40.60s 41.58s	c	c	c	c
11						24.32t	45.83t	125.10t 128.17t	134.03t 134.42t	130.76t 131.73t	132.95s 134.37s

a) Solvent: $CDCl_3$. b) Solvent: $CDCl_3$ for **4**, **5**, **10**. CD_3OD for **2**, **8**, **11**. c) Not assigned. s: Singlet, d: doublet, dd: doublet of doublets, t: triplet.

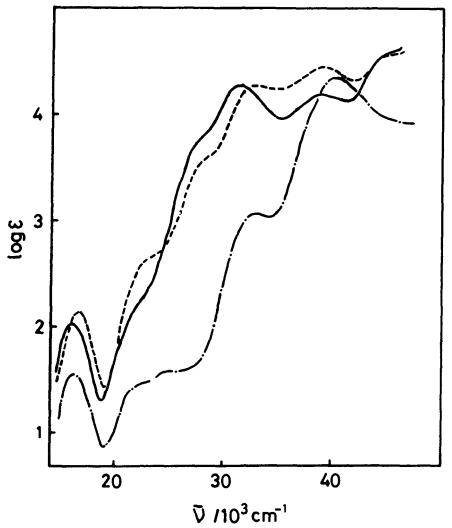

Fig. 1. Absorption spectra of *trans*(Cl,Cl)-$[CoCl_2(edpp)_2]^+$ (——), *trans*-$[CoCl_2(en)(dppe)]^+$ (------), and *trans*-$[CoCl_2(en)_2]^+$ (—·—) in methanol.

intensity band around 16000 cm^{-1} which should correspond to the split component (Ia) of the first absorption band of *trans*-$[CoCl_2(en)_2]^+$ [7] (Table 2). In the Ib and second band region only shoulder absorptions are observed. However, the spectral patterns of three complexes in Fig. 1 are similar to one another in the d-d transition region. Thus both phosphine complexes can be assigned to have the trans(Cl,Cl) configuration.

The *trans*(Cl,Cl)-$[CoCl_2(edpp)_2]^+$ complex has additional isomerism arising from the arrangement of nitrogen and phosphorus donor atoms, trans(P,P) and cis(P,P). In this study, only one isomer was obtained and no formation of the other was observed on column chromatography of Sephadex LH-20. The structure of the isomer obtained was recently determined to be the cis(P,P) configuration by X-ray analysis.[8] The preferential formation of the cis(P,P) isomer, in which steric interactions between the two diphenylphosphino groups should be larger than those in the trans(P,P) isomer, might result from a strong trans effect of the phosphine donor group. The absorption spectrum of *trans*(Cl,Cl),*cis*(P,P)-$[CoCl_2(edpp)_2]^+$ quite resembles that of $[CoCl_2(en)(dppe)]^+$ in which the three kinds of donor atoms are in the same geometrical arrangement. In the ^{13}C NMR spectrum, the edpp complex shows clear triplet signals for all the carbons except for the N-CH_2 and *p*-C of the phenyl group. Appearance of the triplet signals is attributable to the presence of coupling between the two phosphorus atoms in the cis positions (Table 3). Such virtual coupling has been observed for octahedral phosphine complexes of both trans(P,P) and cis(P,P) configurations, although it is observed for almost only a trans(P,P) complex in a four-coordinate, planar type.[1,3]

$[Co(O-O)(edpp)_2]^{n+}$ and $[Co(O-O)(en)(dppe)]^{n+}$ Complexes. The acac and other O-O chelate complexes of edpp were prepared from *trans*(Cl,Cl)-$[CoCl_2(edpp)_2]ClO_4$ and lithium acetylacetonate in ethanol in the absence of active charcoal, and ammonium salts of the O-O anions in methanol in the presence of active charcoal, respectively. The corresponding dppe complexes were prepared by similar methods from *trans*-$[CoCl_2(en)(dppe)]ClO_4 \cdot H_2O$. For the mal, ox, and CO_3^{2-} complexes, the use of the ammonium salts was necessary. No reactions took place with the sodium or potassium salts. All the complexes thus obtained are stable to air in the solid state, and soluble in water, alcohols, CH_2Cl_2, and $CHCl_3$. The complexes in solution, however, decompose gradually on heating above 60—70 °C to give Co(II) species, the acac complexes being the most stable. The CO_3^{2-} complexes regenerate the original *trans*-dichloro complexes by heating with hydrochloric acid.

Attempts to prepare $[Co(acac)(en)(dppe)]^{2+}$ by other methods were all unsuccessful. For example, reactions between $[Co(acac)_2(dppe)]^+$ [1] and en, and $[Co(acac)_2(en)]^+$ and dppe gave $[Co(acac)_2(en)]^+$ and $[Co(acac)(en)_2]^{2+}$, and $[Co(acac)_2(dppe)]^+$, respectively as main products, no desired complex being formed. In general, there is no convenient method for preparing cobalt(III) complexes consisting of three different chelate ligands. A good method for preparing such complexes is to derive from a *trans*-dichloro complex with two different chelate ligands, although preparative methods for which

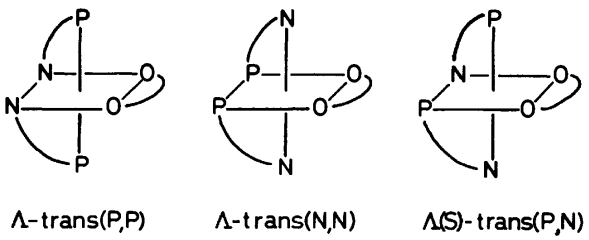

Fig. 2. Geometrical isomers of the $[Co(O–O)(edpp)_2]$-type complex.

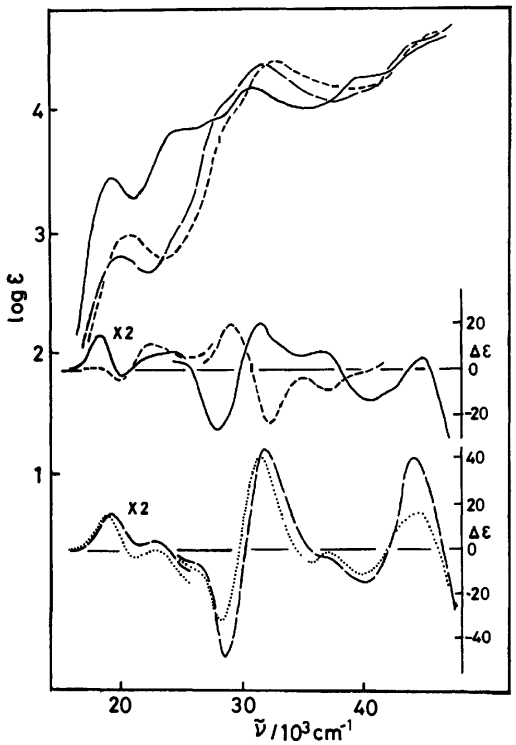

Fig. 3. Absorption and CD spectra of *trans*(P,P)-$[Co(acac)(edpp)_2]^{2+}$ (——), *trans*(P,N)-$[Co(acac)(edpp)_2]^{2+}$ (— —), and $[Co(acac)(en)(dppe)]^{2+}$ (------) in methanol. CD spectrum of *Δ-cis-β*-[Co(acac)(SS-PNNP)]$^{2+}$ (……) in methanol.[12] All of the enantiomers of edpp complexes given in Figs. 3, 6, 7, and 8 are those eluted faster in column chromatography.

are also undeveloped.[9]

The $[Co(O–O)(edpp)_2]$-type complex has three possible geometrical isomers, trans(P,P), trans(P,N), and trans(N,N) (Fig. 2). Except for the CO_3^{2-} complex, all the O–O complexes yielded two isomers. Only one isomer was obtained for the CO_3^{2-} complex, a trace of the other being formed. Isomers of I and II of $[Co(acac)(edpp)_2]^{2+}$ are red and orange-red in color, respectively, and show one and two kinds of the methyl signals for the acac part, respectively in the ^1H NMR spectra (Table 3). Thus I and II can be assigned to either trans(P,P)(C_2) or trans(N,N)(C_2), and trans-(P,N)(C_1) isomers, respectively from symmetry argument. Isomer I as well as isomer II gives the methine proton signal at a higher field than that of the $[Co(acac)(en)_2]^{2+}$ complex.[10] The methine proton signal should shift to the high field when the complex has the trans-

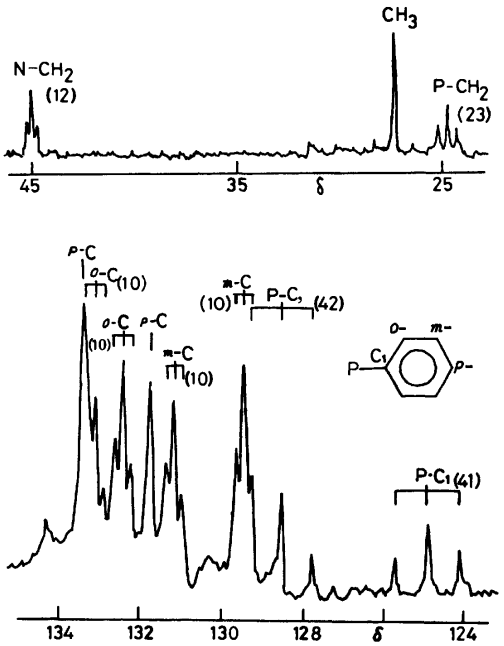

Fig. 4. ^{13}C NMR spectrum of *trans*(P,P)-$[Co(acac)(edpp)_2]^{2+}$. The number in parentheses is a coupling constant in Hz.

(P,P) configuration, since it is shielded by the phenyl group of the phosphine ligand disposed over the acac ring.[1] Thus isomer I can be assigned to the trans(P,P) isomer. The magnitude of the high field shift is fairly small as compared with those of bis(acac) complexes of a phenyl-substituted tertiary phosphine. However, the absorption spectrum confirms the trans(P,P) configuration for isomer I. Figure 3 shows absorption spectra of trans(P,P)(I) and trans(P,N)(II) isomers of $[Co(acac)(edpp)_2]^{2+}$. The former gives the very strong first absorption band and shows the remarkable red shift in the charge transfer bands as compared with the corresponding bands of the latter. Similar spectral differences have been observed between the trans(P,P) and cis(P,P) isomers of $[Co(acac)_2(PMe_2Ph)_2]^+$.[11] The absorption spectrum of the trans(P,N) isomer (II) resembles that of $[Co(acac)(en)(dppe)]^{2+}$ in which the donor atoms are arranged in the same manner, although the whole spectrum of the dppe complex shifts to the high energy side.

The ^{13}C NMR spectrum of the *trans*(P,P)-$[Co(acac)(edpp)_2]^{2+}$ isomer is shown in Fig. 4. Each carbon of the acac and of two methylenes of the edpp ligand is observed as one kind of signal. On the other hand, the signals of the phenyl carbons show two kinds of the phenyl group. The two phenyl groups on each phosphorus atom should be diastereotopic in a complex of chiral symmetry. The spectral assignment was made according to the previous work on bis(acac)cobalt(III) complexes of edpp and related ligands.[1] The chemical shifts and coupling constants are all similar among these complexes except one *m*-carbon of isomer I. Its chemical shift (131.4 ppm) is somewhat apart from those of other complexes (*ca.* 129 ppm). The P–CH_2 and all carbons of the phenyl groups except for the *p*-carbons show triplet signals owing to the couplings with the two

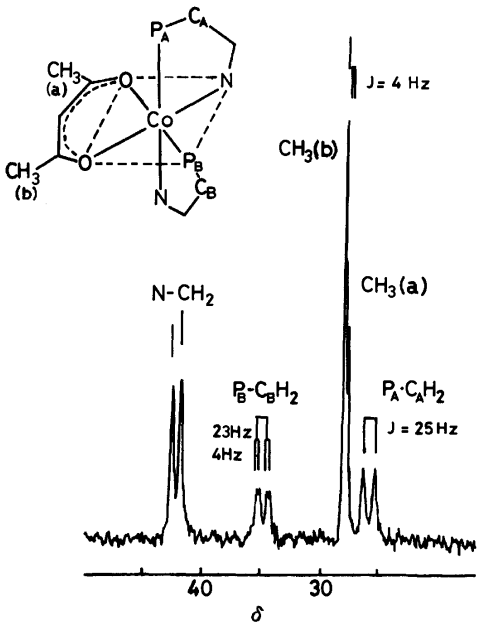

Fig. 5. ^{13}C NMR spectrum of *trans*(P,N)-[Co(acac)-(edpp)$_2$]$^{2+}$.

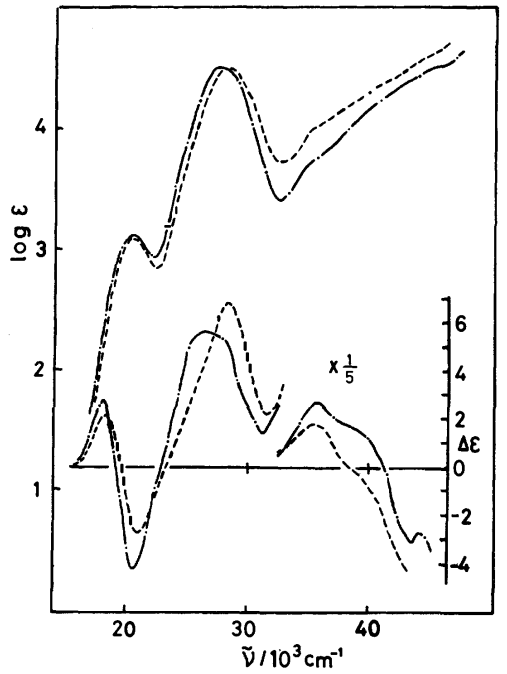

Fig. 6. Absorption and CD spectra of trans(P, P) isomers of [Co(ox)(edpp)$_2$]$^+$ (------) and [Co(mal)-(edpp)$_2$]$^+$ (•—•) in methanol.

phosphorus atoms in the trans positions.

Isomer II shows a complicated ^{13}C NMR spectrum, particularly in the phenyl region, because of C_1 symmetry of the complex. The singlet (27.77 ppm) and the doublet (27.56 ppm, $^4J(P_B,C)=4$ Hz) signals of the methyl groups can be assigned to the CH_3(b) and CH_3(a), respectively from a comparison of the spectrum of [Co(acac)$_2$(edpp)]$^+$ [1] (Fig. 5). The doublet (25.56 ppm, $^2J(P_A,C_A)=25$ Hz) and the doublet of doublets

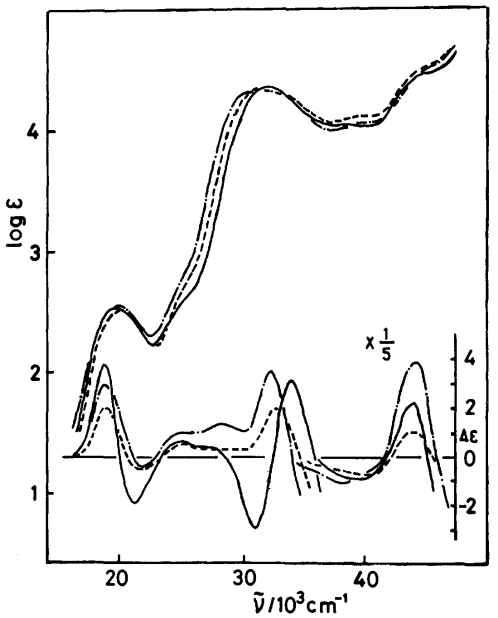

Fig. 7. Absorption and CD spectra of trans(P,N) isomers of [Co(CO_3)(edpp)$_2$]$^+$ (——), [Co(ox)(edpp)$_2$]$^+$ (------), and [Co(mal)(edpp)$_2$]$^+$ (•—•) in methanol.

(34.55 ppm, $^2J(P_B,C_B)=23$ Hz, $^4J(P_A,C_B)=4$ Hz) can be assigned to the C_A and C_B, respectively of the P–CH_2 groups. The coupling constant between the two phosphorus atoms in the cis positions seems to be practically zero. The two N–CH_2 groups show singlet signals with similar chemical shifts (41.59 and 42.24 ppm). The spectrum in the phenyl region is complicated because of the presence of four different phenyl groups, and was not assigned except for one doublet of doublets (122.18 ppm) which can be assigned to the P–C_1 bonded to the phosphorus atom.

The structures of other [Co(O–O)(edpp)$_2$]$^+$ (O–O= mal, ox, and CO_3^{2-}) complexes were also assigned on the basis of the absorption and ^{13}C NMR spectra. Two orange-red isomers of the mal and ox complexes show absorption spectra very similar to each other, and can be assigned to have the same geometrical configuration for the two edpp ligands (Fig. 6). The same conclusions can be given for three red isomers of the mal, ox, and CO_3^{2-} complexes (Fig. 7). The orange-red isomers have strong intensity in the first absorption bands and show a remarkable red shift in the charge transfer bands as compared with the corresponding bands of the red isomers. Such spectral differences between the isomers are the same as those observed for the acac complexes. Thus the orange-red and red isomers can be assigned to trans(P,P) and cis(P,P) (trans(P,N) or trans(N,N)) configurations, respectively. Further, the ^{13}C NMR spectra clearly indicate that the orange-red and red isomers have C_2 and C_1 symmetries, respectively (Table 3). Thus it is concluded that the orange-red and red isomers have trans(P,P) and trans(P,N) configurations, respectively for all the [Co(O–O)(edpp)$_2$]$^+$ complexes.

No trans(N,N) isomers were formed in the [Co(O–O)-(edpp)$_2$]-type complexes. Molecular models indicate

that steric hindrance between the two edpp ligands in the [Co(O–O)(edpp)$_2$]-type complex increases in the order of the trans(P,P)<trans(P,N)<trans(N,N) isomers. In particular, the trans(N,N) isomer involves considerable steric hindrance among the phenyl groups. The reason for this isomer being not formed is attributable to such steric hindrance. However, the yields of the more crowded trans(P,N) isomers are always much larger than those of the less crowded trans(P,P) isomers. The less stability of the trans(P,P) isomers should result from the strong trans effect of phosphine donor groups as seen in the *trans*(Cl,Cl),*cis*(P,P)-[CoCl$_2$(edpp)$_2$]$^+$ complex. The formation ratios of the trans(P,P) to trans(P,N) isomers increase with the increasing size of the O–O chelate ligands; trans(P,P): trans(P,N)=0.25 : 1, 0.08 : 1, 0.03 : 1, and 0 : 1 for the acac, mal, ox, and CO_3^{2-} complexes, respectively. When the O–O chelate ligand becomes larger, the more crowded trans(P,N) isomer will become further crowded to decrease the stability, while the less crowded trans-(P,P) isomer will be less affected. Thus the stability difference between the trans(P,N) and trans(P,P) isomers becomes smaller, and the relative yield of the latter increases. The CO_3^{2-} complex with the smallest O–O ligand forms almost only the trans(P,N) isomer.

Figure 3 shows CD spectra of trans(P,P) and trans-(P,N) isomers of [Co(acac)(edpp)$_2$]$^{2+}$, and [Co(acac)-(en)(dppe)]$^{2+}$, all of which are eluted faster on column chromatography. Both edpp complexes exhibit a similar spectral pattern and give a main CD band with the positive sign in the first absorption band region, suggesting Λ configuration. However, the CD spectrum of [Co(acac)(*SS*-PNNP)]$^{2+}$ (*SS*-PNNP=(*S*,*S*)-(C_6H_5)$_2$PCH$_2$CH(CH$_3$)NHCH$_2$CH$_2$NHCH(CH$_3$)CH$_2$P-(C_6H_5)$_2$), which forms only the Δ-*cis*-β isomer stereoselectively owing to the equatorial preference of the methyl group,[12] is quite similar to that of the trans-(P,N) isomer. In the *cis*-β-PNNP complex, the geometrical arrangement of N, P, and O donor atoms, and the distribution of chelate rings linking these donor atoms are the same as those in the trans(P,N) isomer when the central -NCH$_2$CH$_2$N- chelate ring is ignored. The presence of the central chelate ring would not play an important role in the CD spectrum of the Δ-*cis*-β-(*SS*-PNNP) complex, and the vicinal effect of the asymmetric nitrogen donor atoms would also be small. Thus the trans(P,N) isomer in Fig. 3 is assigned to Δ configuration. The trans(P,P) isomer which gives a CD pattern similar to that of the trans(P,N) isomer should also have the same Δ configuration. In addition to the chiral distribution of chelate rings, the Δ-trans(P,N) isomer as well as the Δ-*cis*-β-(*SS*-PNNP) complex involves another chirality of (*R*) configuration[13] arising from the arrangement of N, P, and O donor atoms. The Δ-trans-(P,P) isomer has no such chirality. However, the similarlity in the CD spectra of both isomers indicates that the optical activity arises mainly from the chiral distribution of chelate rings, the contribution of the chiral arrangement of donor atoms being small.

The CD spectrum of [Co(acac)(en)(dppe)]$^{2+}$ in Fig. 3 gives a pattern differing from those of the Δ-trans(P,N) and -trans(P,P) isomers in the first absorption band region, but nearly the opposite pattern in the higher energy region. The dppe complex has also chirality in the arrangement of the donor atoms, giving Δ(*S*) and Λ(*R*) configurations. The *trans*(P,N)-[Co(acac)-(edpp)$_2$]$^{2+}$ complex forms a different pair of enantiomers from those of the dppe complex, Δ(*R*) and Λ(*S*). Fujinami and Shibata[14] reported CD spectra of cobalt-(III) complexes of a similar type, Λ(*R*)-*cis*-[Co(CN)$_2$-(ox)(en)]$^-$ and Δ(*R*)-*cis*,*cis*,*cis*(C,N,O)-[Co(CN)$_2$(am)$_2$]$^-$ (am=glycinate or β-alaninate ion), and concluded that the CD pattern of the *cis*,*cis*,*cis*(C,N,O)-[CoC$_2$N$_2$O$_2$]-type complex in the first absorption band region depends mainly on the chiral arrangement of the donor atoms. It seems to be difficult to apply this conclusion to the CD spectrum of [Co(acac)(en)(dppe)]$^{2+}$ in Fig. 3, since it differs considerably from that of the *trans*(P,N)-edpp complex in the first absorption band region. However, the whole CD pattern of the dppe complex appears to be opposite to those of both Δ-isomers of the edpp complex. Thus we tentatively assign the dppe complex in Fig. 3 to Λ(*R*) configuration.

The trans(P,N) isomers of the mal, ox, and CO_3^{2-} complexes show CD spectra similar to one another over the whole region (Fig. 7). The spectrum of the CO_3^{2-} complex quite resemble that of Δ(*R*)-*cis*-β-[Co(CO_3)(*SS*-PNNP)]$^+$ prepared as an authentic complex for assigning the absolute configuration.[12] Thus all the isomers in Fig. 7 are assigned to Δ(*R*) configuration, although the CD spectra in the first absorption band region are the pattern characteristic of a Λ-tris(chelate) complex. The trans(P,P) isomers of the mal and ox complexes show CD spectra similar to each other (Fig. 6), and the pattern resembles that of Δ-trans(P,N) isomers. Since both Δ-trans(P,N) and -trans(P,P) isomers of the acac complex exhibit a similar CD spectra, these trans(P,P)

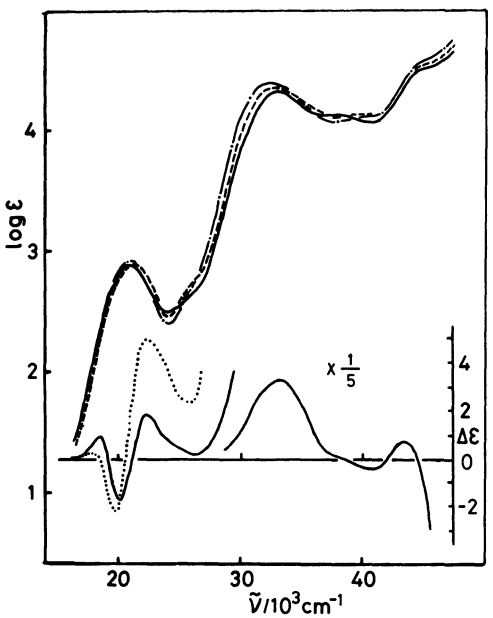

Fig. 8. Absorption spectra of [Co(CO_3)(en)(dppe)]$^+$ (——), [Co(ox)(en)(dppe)]$^+$ (------), and [Co(mal)(en)-(dppe)]$^+$ (—·—) in methanol. CD spectra of (+)$_{589}$-[Co(CO_3)(en)(dppe)]$^+$ and [Co(acac)(en)(dppe)]$^+$ (·····) in methanol.

isomers can be assigned to Δ configuration, although the spectra around 29000 cm^{-1} fairly differ from those of the trans(P,N) isomers. All the trans(P,N) and trans(P,P) isomers given in Figs. 6 and 7 are those eluted faster on column chromatography.

The CD spectrum of $[Co(CO_3)(en)(dppe)]^+$ which was obtained from the less soluble diastereomeric salt with *d*-bcs$^-$ is compared with that of $\Lambda(R)$-$[Co(acac)(en)(dppe)]^{2+}$ in Fig. 8. Both CD spectra are similar in shape in the first absorption band region, although their strength and the spectra in the higher energy region differ remarkably between these complexes. From the similarity in the CD patterns of both isomers in the first absorption band region, we tentatively assign the CO_3^{2-} complex to $\Lambda(R)$ configuration. In order to discuss the optical activity of mixed cobalt(III) complexes containing a phosphine ligand, more CD data will be needed.

References

1) K. Kashiwabara, I. Kinoshita, T. Ito, and J. Fujita, *Bull. Chem. Soc. Jpn.*, **54**, 725 (1981).

2) I. Kinoshita, K. Kashiwabara, J. Fujita, K. Matsumoto, and S. Ooi, *Bull. Chem. Soc. Jpn.*, **54**, 2683 (1981).

3) C. A. McAuliffe and W. Levason, "Phosphine, Arsine, and Stibine Complexes of Transition Elements," Elsevier, Amsterdam (1979).

4) a) V. M. Miskowski, J. L. Robbins, G. S. Hammond, and H. B. Gray, *J. Am. Chem. Soc.*, **98**, 2477 (1976); b) P. Rigo, B. Longato, and G. Favero, *Inorg. Chem.*, **11**, 300 (1972).

5) K. Issleib and D. Haferburg, *Z. Naturforsch., Teil B*, **20**, 916 (1965).

6) H. Regler and F. Heim, *J. Prakt. Chem.*, **148**, 1 (1937).

7) Y. Shimura and R. Tsuchida, *Bull. Chem. Soc. Jpn.*, **28**, 572 (1955).

8) I. Kinoshita, K. Matsumoto, S. Ooi, K. Kashiwabara, and J. Fujita, 31st Symposium on Coordination Chemistry, Japan (Sendai), 1981, Abstr. No. 3C06.

9) a) M. C. Couldwell, D. A. House, and H. K. J. Powell. *Inorg. Chem.*, **12**, 627 (1973); b) M. Kojima, H. Yamada, H. Ogino, and J. Fujita, *Bull. Chem. Soc. Jpn.*, **50**, 2325 (1977).

10) L. J. Boucher, E. J. Battis, and N. G. Paez, *J. Inorg. Nucl. Chem.*, **33**, 1373 (1971).

11) K. Kashiwabara, K. Katoh, T. Ohishi, J. Fujita, and M. Shibata, *Bull. Chem. Soc. Jpn.*, **55**, 149 (1982).

12) M. Atoh, K. Kashiwabara, and J. Fujita, to be published.

13) The nomenclature of the absolute configurations *R* and *S* follows the rule proposed by R. S. Cahn, C. K. Ingold, and V. Prelog, *Angew. Chem., Int. Ed. Engl.*, **5**, 385 (1966).

14) S. Fujinami and M. Shibata, *Bull. Chem. Soc. Jpn.*, **54**, 2939 (1981).

 © 1982 The Chemical Society of Japan Bull. Chem. Soc. Jpn., 55, 3187—3189 (1982)

Extraction of Titanium(IV)-Pyrocatechol Violet Complex with Tridodecylethylammonium Bromide

Yoshio Shijo,* Tokuo Shimizu, and Kaoru Sakai

Department of Environmental Chemistry, Faculty of Engineering, University of Utsunomiya, Ishii-machi, Utsunomiya 321

(Received April 2, 1982)

The extraction equilibria and the fundamental conditions for extracting the titanium(IV)–Pyrocatechol Volet complex anion in a form of an ionic associate with tridodecylethylammonium bromide into carbon tetrachloride is described. The absorption maxima of the extracted complex occurs at 586 nm, the molar absorptivity and the distribution ratio being 5.17×10^4 dm^3 mol^{-1} cm^{-1} and 2.82×10^2. The optimum pH range for the extraction is 5.1—6.4. The composition of the complex is estimated to be $Ti(PV)_2(R_3R'N)_2$. The extraction constant would be:

$$K_{ex}=\frac{[Ti(PV)_2(R_3R'N)_2]_0}{[Ti(PV)_2{}^{2-}][R_3R'N^+]^2},$$

log K_{ex} obtained is 13.5. The interference of foreign ions is discussed.

The lipophilic quaternary ammonium salts have played a very important role in the extraction of metal complex anions. Trioctylmethylammonium chloride (Aliquat 336 or Capliquat) has been in common use as an extracting reagent in this field. The chloride of several transition metals,[1] of vanadium,[2] of mercury,[3] thiocyanate of cadmium,[4] 2,2′-dihydroxyazobenzene complex of uranium,[5] chromate,[6] tetraboromopalladate,[7] 4,7-bis(*p*-sulfophenyl)-1,10-phenanthroline complex of iron,[8] dithizone complex of palladium,[9] 8-hydroxy-5-quinolinesulfonic acid complex of zinc,[10] and iodide of 18 elements in geochemical samples[11] were extracted with the foregoing reagent.

Tridodecylethylammonium bromide (TDEABr) synthesized in our laboratory which is more lipophilic than trioctylmethylammonium chloride has been used for extraction of the Pyrocatechol Violet (abbreviated to PV) complexes of copper,[12] tin,[13] aluminium,[14] zirconium,[15] niobium,[16] iron,[17] tungsten,[18] and vanadium.[19] The titanium(IV)–PV complex also can be extracted with TDEABr in carbon tetrachloride. The extraction equilibria and the fundamental conditions for extracting the titanium(IV)–PV complex with TDEABr will be discussed in this paper.

Experimental

Reagent. A 2.50×10^{-3} mol dm^{-3} titanium(IV) solution was prepared by following procedure. A definite amount of titanium oxide was fused with potassium disulfate and the melt was dissolved in 2 mol dm^{-3} sulfuric acid. The solution was diluted by 2 mol dm^{-3} sulfuric acid as required. A 5×10^{-4} mol dm^{-3} PV solution was prepared by dissolving the Dotite PV in deionized water without further purification. TDEABr was prepared by the method described in the previous work.[17] A 2×10^{-3} mol dm^{-3} TDEABr solution was prepared by dissolving TDEABr in carbon tetrachloride. A 2 mol dm^{-3} sodium acetate solution was used as a buffer solution. All the other chemicals used were of a guaranteed reagent quality.

Apparatus. A Hitachi 101 spectrophotometer, a Hitachi 200-20 UV-vis. recording spectrophotometer, and a Hitachi Horiba F-7 pH meter were used.

General Procedure. Mix, up to 5 μg of titanium(IV), a definite amount of 1 mol dm^{-3} sulfuric acid, and 2 cm^3 of 5×10^{-4} mol dm^{-3} PV solution in a 100-cm^3 polypropylene beaker. Adjust the pH of the solution to 5.6 by the addition of 2 cm^3 of 2 mol dm^{-3} sodium acetate solution, then dilute to 20 cm^3 with de-ionized water. Transfer the solution into a 35 cm^3 test tube, and extract with 5 cm^3 of 2×10^{-3} mol dm^{-3} TDEABr in carbon tetrachloride for 5 min. Separate the phases and centrifuge the organic phase for 2 min at 3000 min^{-1}. Measure the absorbance of the extract at 586 nm against the reagent blank.

Results and Discussion

Absorption Spectra. The absorption spectra of the titanium(IV)–PV–TDEA complex extracted into carbon tetrachloride and of the titanium(IV)–PV complex anion in an aqueous solution are shown in Fig. 1. The absorption maximum of the complex is slightly shifted toward longer wavelength, and the sensitivity is enhanced a little in an organic phase, as compared with in an aqueous phase.

Effect of pH. The aqueous solution containing titanium(IV) and PV was adjusted to various pH values with the sodium acetate buffer solution, and the extraction was carried out according to the foregoing procedure. As is indicated in Fig. 2, the maximum extraction of the complex is obtained in the pH range 5.1 to 6.4.

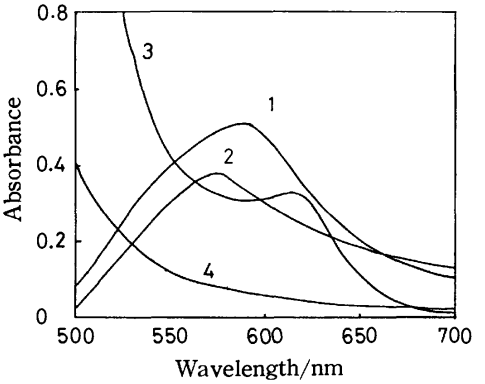

Fig. 1. Absorption spectra of the Ti–PV–TDEA complex in carbon tetrachloride and the Ti–PV complex in aqueous solution.
pH=5.6, $V_{aq}=20$ cm^3, $V_0=5$ cm^3, $[TDEABr]_0=2\times10^{-3}$ mol dm^{-3}. 1: Ti–PV–TDEA $[Ti]=2.5\times10^{-6}$ mol dm^{-3}, 2: Ti–PV $[Ti]=1\times10^{-5}$ mol dm^{-3}, 3: PV–EDEA $[PV]=5\times10^{-5}$ mol dm^{-3}, 4: PV $[PV]=1.25\times10^{-4}$ mol dm^{-3}.

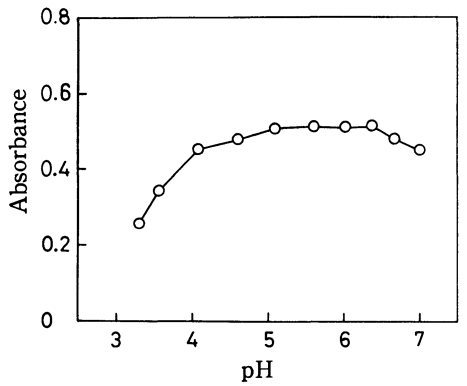

Fig. 2. Effect of pH on the extraction of the Ti-PV-TDEA complex.
[Ti]$=2.5\times10^{-6}$ mol dm^{-3}, [PV]$=5\times10^{-6}$ mol dm^{-3}, [TDEABr]$_0=2\times10^{-3}$ mol dm^{-3}, 586 nm.

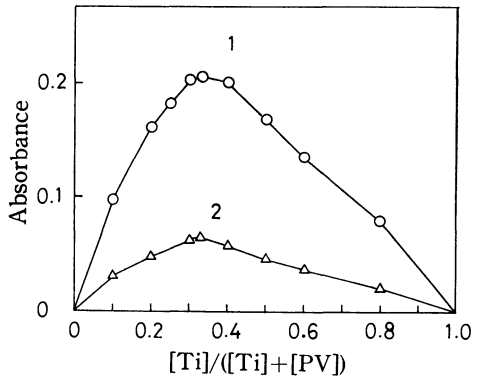

Fig. 3. Continuous variation method applied to the Ti-PV-TDEA and the Ti-PV complexes (Ti: PV).
pH=5.6, [Ti]+[PV]$=2.5\times10^{-5}$ mol dm^{-3}, 1: Ti-PV-TDEA, [TDEABr]$_0=2\times10^{-3}$ mol dm^{-3}, 586 nm, 2: Ti-PV, 572 nm.

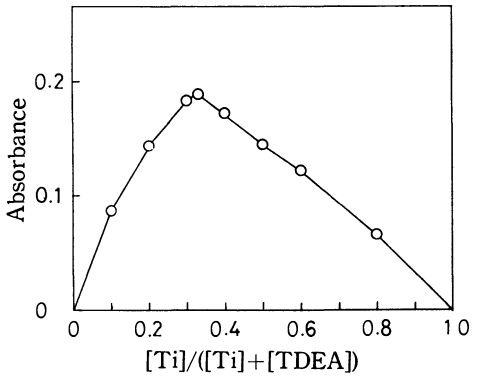

Fig. 4. Continuous variation method applied to the Ti-PV-TDEA complex (Ti: TDEA).
[Ti-PV]+[TDEA]$=5\times10^{-7}$ mol dm^{-3}, pH=5.6, 586 nm.

The absorbance of the extract increase gradually. The PV itself is also readily extracted with TDEABr.

Organic Solvents. Several kinds of organic solvents were tested in order to achieve a quantitative extraction of the complex with TDEABr. The complex is extracted in such solvents as carbon tetrachloride, benzene, toluene, xylene, butyl acetate, isobutyl methyl ketone, and chloroform. There are no serious differences among every solvent on the absorbance of the extract. The stability and the reproducibility of the absorbance, however, are better in the carbon tetrachloride.

Effect of the Reagent Concentration. The extraction of titanium(IV) from the aqueous solutions containing PV in various concentrations was examined. The optimum concentration of PV is in the range 4×10^{-5} mol dm^{-3} to 1×10^{-4} mol dm^{-3}. The concentration of TDEABr in carbon tetrachloride for the quantitative extraction is ranged from 1×10^{-4} mol dm^{-3} to 5×10^{-3} mol dm^{-3}.

Extractability and Molar Absorptivity. An aqueous solution of 20 cm^3 containing 2.40 μg of titanium(IV) and PV was shaken with 5 cm^3 of 5×10^{-3} mol dm^{-3} TDEABr in carbon tetrachloride under the optimum conditions. Extraction was repeated for the remaining aqueous phase after the separation of the extract. The extractability of the titanium(IV) was calculated from the absorbance of the extracts. It was found that 98.6% of the titanium(IV) was extracted by a single extraction. The distribution ratio and the molar absorptivity were 2.82×10^2 and 5.17×10^4 dm^3 mol^{-1} cm^{-1}, respectively. A calibration curve for the determination of the titanium(IV) was made under the optimum conditions. A good linear relationship was obtained over the concentration range from 0.3 μg to 5 μg of titanium(IV) per 5 cm^3 of carbon tetrachloride. The coefficient of the variation in ten measurements was 2.4%.

The Composition of the Complex. The composition of the complex was estimated by the continious-variation method. Figure 3 shows that the mole ratios of titanium(IV) : PV in the titanium(IV)-PV-TDEA complex and in the titanium(IV)-PV complex anion are found either to be 1 : 2. Figure 4 shows the mole ratio of titanium(IV) : TDEA to be 1 : 2. Thus, the composition of the associate complex is estimated to be $Ti(PV)_2(R_3R'N)_2$.

Extraction Constant. When the ionic associate of the titanium(IV)-PV complex anion with TDEA cation is extracted in the organic phase, the equation representing the extraction equilibria will be:

$$Ti(PV)_2^{2-} + 2R_3R'N^+ = Ti(PV)_2(R_3R'N)_{2(o)}. \quad (1)$$

The extraction constant, K_{ex}, is given by:

$$K_{ex} = \frac{[Ti(PV)_2(R_3R'N)_2]_o}{[Ti(PV)_2^{2-}][R_3R'N^+]^2}, \quad (2)$$

Table 1. Extraction constant for $Ti(PV)_2(R_3R'N)_2$ in carbon tetrachloride at 25 °C
pH=5.6 in an acetate buffer solution (2×10^{-2} mol dm^{-3}), [Ti]$=5\times10^{-6}$ mol dm^{-3}, [PV]$=7.5\times10^{-5}$ mol dm^{-3}, [TDEABr]$_0=5\times10^{-3}$ mol dm^{-3}, $V_{aq}=20$ cm^3, $V_0=10$ cm^3

[Br$^-$]/mol dm^{-3}	log K_{ex}
0.2	13.7
0.4	13.5
0.6	13.5
0.8	13.5
1.0	13.4
	av 13.5

All the concentrations in Table 1 indicate the initial concentrations.

where the subscript 0 denotes the organic phase. The extraction constant, K_{ex}, can be determined by the extraction data of the associate complex from various concentration of bromide in aqueous phase and the extraction constant of TDEABr. Table 1 shows the value of log K_{ex}. The average values of log K_{ex} is 13.5.

Effect of Foreign Ions. The masking reagents such as ethylenediaminetetraacetic acid, 1,2-cyclohexanediamine-*N*,*N*,*N*′,*N*′-tetraacetic acid, diethylenetriaminepentaacetic acid suppress thoroughly the extraction of the titanium(IV)-PV-TDEA complex. 3,6-Dioxaoctane-1,8-diamine-*N*,*N*,*N*′,*N*′-tetraacetic acid (GEDTA) is available as masking reagent in this extraction system, however the absorbance of the extract decreases about twenty percent by the addition of GEDTA. Beryllium, chromium(III), iron(III), bismuth, and thorium are masked by GEDTA, however aluminium, vanadium(V), molybdenum(VI), tungsten(VI), and Uranium(VI) interfere seriously. Iodide, thiocyanate, and perchlorate also interfere seriously, and give a negative error.

References

1) V. V. Bagreev, C. Fischer, L. M. Yudushkina, and Yu. A. Zolotov, *J. Inorg. Nucl. Chem.*, **40**, 553 (1978).
2) T. Sato, T. Nakamura, and S. Ikoma, *J. Inorg. Nucl. Chem.*, **41**, 223 (1979).
3) R. W. Cattral and H. Daud, *J. Inorg. Nucl. Chem.*, **41**, 1037 (1979).
4) D. Singh, D. V. Singh, and S. N. Tandon, *Chem. Anal. (Warsaw)*, **24**, 1055 (1979).
5) T. Taketatsu and A. Sato, *Bunseki Kagaku*, **29**, 78 (1980).
6) S. S. Chao and E. E. Pickett, *Anal. Chem.*, **52**, 335 (1980).
7) I. Tsukahara and M. Tanaka, *Anal. Chim. Acta*, **116**, 383 (1980).
8) K. Miyaishi, T. Imasaka, and N. Ishibashi, *Anal. Chim. Acta*, **124**, 381 (1981).
9) H. Akaiwa, H. Kawamoto, and E. Yoshimatsu, *Nippon Kagaku Kaishi*, **1981**, 79.
10) Y. Kondo, M. Kataoka, and T. Kambara, *Bunseki Kagaku*, **30**, 109 (1981).
11) J. R. Clark and J. G. Viets, *Anal. Chem.*, **53**, 61 (1981).
12) Y. Shijo. *Bull. Chem. Soc. Jpn.*, **47**, 1642 (1974).
13) Y. Shijo, *Nippon Kagaku Kaishi*, **1974**, 1658.
14) Y. Shijo, *Nippon Kagaku Kaishi*, **1974**, 1912.
15) Y. Shijo, *Bull. Chem. Soc. Jpn.*, **49**, 3029 (1976).
16) Y. Shijo, *Bull. Chem. Soc. Jpn.*, **50**, 1011 (1977).
17) Y. Shijo. *Bull. Chem. Soc. Jpn.*, **50**, 1013 (1977).
18) Y. Shijo, T. Shimizu, and K. Sakai, *Bull. Chem. Soc. Jpn.*, **54**, 143 (1981).
19) Y. Shijo, T. Shimizu, and K. Sakai, *Bull. Chem. Soc. Jpn.*, **54**, 700 (1981).

Effects of *N*-Methylated Diamine on Ion Pair Formation of Bis(2,4-pentanedionato)(diamine) Cobalt(III) Bromides in Nitrobenzene by Conductometry

Kazuaki Ito, Etsuro Iwamoto, and Yuroku Yamamoto*

Department of Chemistry, Faculty of Science, Hiroshima University, Naka-ku, Hiroshima 730

(Received April 2, 1982)

The conductometric study of bis(2,4-pentanedionato)(diamine) cobalt(III) bromides in nitrobenzene at 25 °C indicated that the ion association constant of the chelate salts increases in the order, $[Co(acac)_2(N,N,N',N'\text{-tmen})]Br < Bu_4NBr < [Co(acac)_2(N,N\text{-dmen})]Br < [Co(acac)_2(en)]Br < [Co(acac)_2(N,N'\text{-dmen})]Br$ (acac=2,4-pentanedione anion, diamine: en=ethylenediamine, *N,N*-dmen=*N,N*-dimethylethylenediamine, *N,N'*-dmen=*N,N'*-dimethylethylenediamine, *N,N,N',N'*-tmen=*N,N.N',N'*-tetramethylethylenediamine). The results were discussed from the view points of hydrogen bonds through the N–H protons of the chelate cations to the bromide anion and cation-solvent interactions.

The outer-sphere ion association of $[M(NH_3)_6]^{3+}$ and $[M(en)_3]^{3+}$ (M=Co and Cr) with some anions in aqueous[1-7] and nonaqueous solutions[8,9] has been determined by the conductometric and spectrophotometric methods. The results in aqueous solution indicated that the ion association of $[M(en)_3]^{3+}$ is promoted for the chloride ion,[1,5] but is reduced for the SO_4^{2-} and $C_2O_4^{2-}$ ions,[1-3,6] compared to that of $[M(NH_3)_6]^{3+}$. This result cannot be accounted for by the electrostatic theory of ionic association, suggesting the importance of the following ion-solvent interactions: hydration of the N–H protons of $[M(NH_3)_6]^{3+}$ and $[M(en)_3]^{3+}$, Cl^-, SO_4^{2-}, and $C_2O_4^{2-}$ and the dehydration accompanied by the ion pair formation. On the other hand, ion association of $[Co(en)_3]^{3+}$ salts in nonaqueous solvents such as DMSO is affected by the basicity of the solvents.[8,9]

The present study deals with the conductance of bis(2,4-pentanedionato)(diamine) cobalt(III) bromides([Co(acac)$_2$(diamine)]Br) in nitrobenzene at 25 °C to understand the effects of the replacement of the N–H protons by the CH_3 groups on ion pair formation. Nitrobenzene is dipolar aprotic (dielectric constant=34.82) and poorly basic (Gutmann's donor number=4.4). Thus, the ion pair formation of the chelate salts is affected by the ion-dipole interaction between the chelate cations and nitrobenzene molecules. The title compounds, which were confirmed to be stable in nitrobenzene by both spectrophotometry and conductometry, are 1 : 1 electrolytes and advantageous to elucidate the ligand and solvent effects on ion pair formation from conductance data.

Experimental

Four bis(2,4-pentanedionato)(diamine)cobalt(III) perchlorates were prepared by mixing $Na[Co(acac)_2(NO_2)_2]$ with equimolar amounts of the corresponding diamine, followed by addition of an aqueous solution of $NaClO_4$.[10] After triple recrystallizations, these samples were converted into the bromide salts by anion exchange resin in the Br^- form, and purified by recrystallizing twice from acetone (or ethanol)–ether. The purity of samples was checked by chemical analysis of C, H, and N, potentiometric titration of the bromide ion with silver nitrate, and the coulometric determination of water content by a Hiranuma AQ-3 aquacounter. Nitrobenzene was purified by shaking with sodium hydroxide, sulfuric acid, and distilled water, successively, and then by distillation under reduced pressure after drying over calcium chloride.

Conductances were measured at 1592 Hz by a LCR 10 type bridge (Ando Electric Co. Ltd.) which was calibrated with a standard resistance box(Shimadzu Seisakusho Co.). The cell was of the Kraus-Erlenmeyer type which was calibrated by fitting the conductance of KCl solutions (0.001—0.01 mol dm^{-3}) to the equation due to Lind, Zwolenik, and Fuoss.[11] The density and viscosity (0.01847 P) were measured with a digital density meter (Anton Paar Model DMA 02D) and Ubbelohde viscometer modified for use in a closed, dry atmosphere, respectively. All measurements were carried out in a water bath thermostated to 25±0.005 °C.

Results and Discussion

The measured equivalent conductances, Λ and

Table 1. Molar concentrations, C/mol dm^{-3}, and molar conductances, Λ/Ω^{-1} cm^2 mol^{-1} in nitrobenzene at 25 °C

[Co(acac)$_2$(en)]Br		[Co(acac)$_2$(*N,N'*-dmen)]Br	
$C\times10^4$	Λ	$C\times10^4$	Λ
17.662	21.207	15.383	19.348
13.757	22.441	11.946	20.604
9.7454	24.038	9.2914	21.847
6.9643	25.452	7.0486	23.170
4.6252	26.942	5.0765	24.610
3.3591	27.935	3.6338	26.008
2.4302	28.787	2.9198	26.842
1.4775	29.793	1.8535	28.319
0.6445	30.951	1.0947	29.704
[Co(acac)$_2$(*N,N*-dmen)]Br		[Co(acac)$_2$(*N,N,N',N'*-tmen)]Br	
$C\times10^4$	Λ	$C\times10^4$	Λ
23.391	21.253	25.104	30.074
18.277	22.492	15.491	30.812
14.116	23.740	12.177	31.102
10.347	25.130	7.5076	31.628
7.5084	26.440	3.1540	32.273
5.5730	27.496	1.6923	32.557
3.5078	28.887	0.8918	32.798
2.1521	30.007		
1.2072	30.941		
0.5627	31.797		

Table 2. Derived parameters

Electrolyte	Λ_o / Ω^{-1} cm^2 mol^{-1}	λ_o^+	K_a / dm^3 mol^{-1}	d / 10^{-1} nm	σ_Λ
[Co(acac)$_2$(en)]Br	32.23±0.03	10.6	449±7	18.1	0.026
[Co(acac)$_2$(*N*,*N*′-dmen)]Br	32.34±0.14	10.7	749±65	8.4	0.093
[Co(acac)$_2$(*N*,*N*-dmen)]Br	32.83±0.02	11.2	365±3	18.4	0.022
[Co(acac)$_2$(*N*,*N*,*N*′,*N*′-tmen)]Br	33.47±0.02	11.9	25±2	15.9	0.019
Bu_4NBr[a)]	33.27±0.03	11.7	74±2	12.5	0.008

a) From Ref. 15.

corresponding electrolyte concentrations in mol dm^{-3} are given in Table 1 for nitrobenzene solutions of [Co(acac)$_2$(diamine)]Br. The data were analyzed by using the Fuoss-Hsia equation[12a)] with Fernández-Prini coefficients[12b)] and $E=E_1\Lambda_0-2E_2$,[12c)]

$$\Lambda = \gamma[\Lambda_o - SC^{1/2}\gamma^{1/2} + EC\gamma\log C\gamma + J_1(\mathrm{d})C\gamma + J_2(\mathrm{d})C^{3/2}\gamma^{3/2}], \quad (1)$$

where the symbols have their usual meaning:[13)] S, E, J_1, and J_2 contain contributions from both the electrophoretic and the relaxation effects, and each depends on Λ_0, and γ is the fraction of free ions. The association constant K_a can be expressed as

$$K_a = (1-\gamma)/\gamma^2 C f_\pm^2, \quad (2)$$

The mean ionic activity coefficient $f_\pm$ is given by the extended Debye-Hückel equation

$$-\log f_\pm = A(C\gamma)^{1/2}/[1+Bd(C\gamma)^{1/2}]. \quad (3)$$

The method of fitting in terms of Λ_0, K_a and the ion-size parameter d is based on that of Hanna *et al.*[14)] The values of the standard deviation is defined as

$$\sigma_\Lambda = [\sum(\Lambda_{\mathrm{calcd}}-\Lambda_{\mathrm{obsd}})^2/(n-3)]^{1/2}, \quad (4)$$

where n is the number of experimental points. The results are given in Table 2.

The association constants of the chelate electrolytes show two features: (a) the chelate electrolytes associate more strongly than tetrabutylammonium bromide (Bu_4NBr) ($K_a=74$)[15)] except for [Co(acac)$_2$(*N*,*N*,*N*′,*N*′-tmen)]Br, and (b) the K_a value of [Co(acac)$_2$(*N*,*N*′-dmen)]Br is much larger than those of [Co(acac)$_2$(en)]Br and [Co(acac)$_2$(*N*,*N*-dmen)]Br.

Since the chelate electrolytes have approximately the same hydrodynamic size as Bu_4NBr, the electrostatic theory of ionic association predicts that they should have a similar association constant. However, en, *N*,*N*-dmen, and *N*,*N*′-dmen complexes have much larger association constants compared with that of Bu_4NBr. This increase in K_a should be attributed to the hydrogen bond between the N–H protons of the chelate cations and the bromide anion. This explains well that K_a of the *N*,*N*-dmen complex is smaller than that of the en complex due to the decrease in the number of the N–H protons by the introduction of the *N*-methyl groups. Furthermore, this effect was confirmed from the fact that the K_a value of the *N*,*N*,*N*′,*N*′-tmen complex without the N–H protons is much smaller than those of en, *N*,*N*-dmen, and *N*,*N*′-dmen complexes, and is further smaller than that of symmetrical Bu_4NBr in spite of the enhanced effect of the unsymmetrical charge distribution in the chelate cation on K_a. This suggests that when there is no hydrogen bonding, the pseudo aromaticity of the acac ligand reduces the ion pair formation, probably due to the repulsion between Br^- and the π electrons or solvation of the acac ligand by nitrobenzene through π-π interaction.

As to observation (b), it has been shown by the studies of the rate of H–D exchange[16)] and the acid ionization constant[17)] in aqueous solution that the alkyl substitution (CH_3NH– and $-CH_2NH_2$) in the coordinated amine results in stronger acidity of the residual N–H protons. Therefore, the result (b) suggests that the *N*-methyl groups of the *N*,*N*′-dmen complex activate the residual N–H protons to associate more strongly with the bromide anion.

As is clear from Table 2, the limiting ionic conductance (λ_o^+) of the chelate cations which was estimated using $\lambda_o^-(Br^-)=21.6$ in nitrobenzene[18)] is increased in spite of the increasing size with the introduction of CH_3 groups. Particularly, it is noteworthy that the mobility of the [Co(acac)$_2$(*N*,*N*,*N*′,*N*′-tmen)]$^+$ ion is much larger than that of the [Co(acac)$_2$(en)]$^+$ ion. This result conflicts with hydrodynamic theory, suggesting specific ion-solvent interactions. Since nitrobenzene is a dipolar aprotic and poorly basic solvent, the chelate cations are considered to be solvated mainly by cation-solvent dipole interaction. In this case, the N–H protons of the [Co(acac)$_2$(en)]$^+$ ion would be solvated and the introduction of the CH_3 groups promotes the desolvation, leading to the increase in mobility due to the decrease in its effective size. For the [Co(acac)$_2$(*N*,*N*′-dmen)]$^+$ ion, the methyl substitution (CH_3NH–) prevents the solvation of the residual N–H protons because of the steric hindrance by the nearest neighboring CH_3 groups, which corresponds to the activation of the N–H protons. This leads to the larger association of [Co(acac)$_2$(*N*,*N*′-dmen)]Br compared to [Co(acac)$_2$(en)]Br and [Co(acac)$_2$(*N*,*N*-dmen)]Br in which the methyl groups are too far from the residual N–H protons.

The above discussion explains well the data of [M(NH$_3$)$_6$]$^{3+}$ and [M(en)$_3$]$^{3+}$ salts: the larger K_a value of [M(en)$_3$]Cl^{2+} compared to that of [M(NH$_3$)$_6$]Cl^{2+}[1,5)] in spite of the increasing cation size is attributed to the stronger acidity of the N–H protons of [M(en)$_3$]$^{3+}$, which is considered as the result of the dehydration of the N–H protons by the hydrophobicity of the C_2H_4 groups. On the other hand, for SO_4^{2-} and $C_2O_4^{2-}$ salts,[1-3,6)] the hydrogen bonding of the N–H protons with SO_4^{2-} and $C_2O_4^{2-}$ is prevented by the strong hydration of divalent anions. This leads to the smaller

ionic association of SO_4^{2-} and $C_2O_4^{2-}$ with $[Co(en)_3]^{3+}$ than that with $[Co(NH_3)_6]^{3+}$.

A further study in other solvents is under way to ascertain the above concept.

This work was supported in part by a Grant-in-Aid for Scientific Research Nos. 443013 and 454183 from the Ministry of Education, Science and Culture.

References

1) I. L. Jenkins and C. B. Monk, *J. Chem. Soc.*, **1951**, 68.
2) N. Tanaka, Y. Kobayashi, and M. Kamada, *Bull. Chem. Soc. Jpn.*, **40**, 2939 (1967).
3) S. Katayama and R. Tamamushi, *Bull. Chem. Soc. Jpn.*, **41**, 606 (1968).
4) T. Takahashi, T. Koiso, and N. Tanaka, *Nippon Kagaku Kaishi*, **1974**, 65.
5) T. Takahashi and T. Koiso, *Bull. Chem. Soc. Jpn.*, **49**, 2784 (1976).
6) T. Takahashi and T. Koiso, *Bull. Chem. Soc. Jpn.*, **51**, 1307 (1978).
7) H. Kaneko and N. Wada, *J. Solution Chem.*, **7**, 19 (1978).
8) N. Tanaka and K. Harada, *Electrochim. Acta*, **21**, 615 (1976).
9) N. Tanaka and K. Harada, *Electrochim. Acta*, **22**, 815 (1977).
10) R. D. Archer and B. P. Cotsoradis, *Inorg, Chem.*, **4**, 1584 (1965).
11) J. E. Lind, J. J. Zwolenik, and R. M. Fuoss, *J. Am. Chem. Soc.*, **81**, 1559 (1959).
12) a) R.M. Fuoss and K-L. Hsia, *Proc. Natl. Acad. Sci. U. S. A.*, **57**, 1550 (1967); b) Fernández-Prini, *Trans. Faraday Soc.*, **65**, 3311 (1969); c) M. S. Chen, Dissertation, Yale University (1969).
13) R. M. Fuoss and F. Accascina, "Electrolytic Conductance," Interscience Publishers, Inc., New York (1959).
14) E. M. Hanna, A. D. Pethybridge, J. E. Prue, and D. J. Spiers, *J. Solution Chem.*, **3**, 563 (1974).
15) H. Sadek and R. M. Fuoss, *J. Am. Chem. Soc.*, **76**, 5905 (1954). The data were recalculated by using the Fuoss-Hsia equation (dielectric constant=34.82 and viscosity=0.01847 P).
16) a) D. A. Buckingham, B. M. Foxman, and A. M. Sargeson, *Inorg. Chem.*, **9**, 1790 (1970); b) D. A. Buckingham, C. R. Clark, and T. W. Lewis, *ibid.*, **18**, 2041 (1979).
17) F. Basolo and R. G. Pearson, "Mechanisms of Inorganic Reactions," 2nd ed, Wiley, New York (1967).
18) C. R. Witschonke and C. A. Kraus, *J. Am. Chem. Soc.*, **69**, 2472 (1947).

 © 1982 The Chemical Society of Japan Bull. Chem. Soc. Jpn., 55, 3193—3196 (1982)

Reaction Process of Titanium Tetrachloride with Ammonia in the Vapor Phase and Properties of the Titanium Nitride Formed

Yuzo Saeki,* Ryoko Matsuzaki, Akimasa Yajima, and Masayo Akiyama

Research Laboratory of Resources Utilization, Tokyo Institute of Technology, 4259, Nagatsuta-cho, Midori-ku, Yokohama 227

(Received March 13, 1982)

The reaction products of gaseous $TiCl_4$ with ammonia were $TiCl_4 \cdot 5NH_3$ at 200 °C, $TiCl_4 \cdot 5NH_3$, TiClN, and NH_4Cl at 250—400 °C, $TiCl_4 \cdot 5NH_3$, TiClN, TiN_x, and NH_4Cl at 450—650 °C, TiN_x and NH_4Cl at 700—1000 °C, and TiN_x, NH_4Cl, and HCl at 1100—1400 °C. The N/Ti atomic ratio, x, of the TiN_x formed was 1.21 at 700 °C, 1.16 at 800 °C, 1.13 at 900 °C, and 1.10 above 1000 °C. The lattice constants of the TiN_x formed are shown. The reaction process can be represented as follows: The reaction of gaseous $TiCl_4$ with ammonia occurs first to form $TiCl_4 \cdot 5NH_3$. Above *ca.* 220 °C, the $TiCl_4 \cdot 5NH_3$ decomposes to TiClN. Above *ca.* 430 °C, the TiClN reacts with ammonia to form TiN_x. Above *ca.* 1100 °C, in addition to these reactions, the reaction of $TiCl_2$, formed by the reduction of $TiCl_4$ with hydrogen resulting from the thermal dissociation of ammonia, with ammonia occurs to form TiN_x. On heating the TiN_x, formed by the vapor-phase reaction, at temperatures higher than 500 °C in an argon atmosphere, the value of x decreased and became close to that of the stoichiometric nitride, being 1.02 at 900—1100 °C.

The vapor-phase reaction of transition metal chlorides with ammonia has recently become important for the preparation of fine powders of transition metal nitrides; these are acquiring importance as new industrial materials. Concerning the formation of titanium nitride from titanium tetrachloride ($TiCl_4$) by a vapor-phase reaction, Kato *et al.*[1] have studied the preparation of fine titanium nitride powders by a vapor-phase reaction of the $TiCl_4$–NH_3–H_2–N_2 system at 700—1500 °C with emphasis on the effects of reaction conditions on the particle size and chemical composition. However, no information is at present available on the reaction process of $TiCl_4$ with ammonia in the vapor phase.

In this paper, the reaction products of gaseous $TiCl_4$ with ammonia at 200—1400 °C were examined in detail. The possible reactions which were considered to occur on the basis of the above experiments were examined. The N/Ti atomic ratios, lattice constants, and thermal stability of the titanium nitrides formed at various temperatures were examined. The titanium nitrides formed were also examined by electron microscopy.

Experimental

Materials. The $TiCl_4$ was prepared by the reaction of titanium sponge (Ti 99.7%) with chlorine at 500 °C and purified by fractional distillation. The chemical analysis gave Ti, 25.2; Cl, 74.7% (calcd for $TiCl_4$: Ti, 25.24; Cl, 74.76%). The ammonia was dried by passing it over sodium hydroxide granules.

Experimental Procedures. A transparent quartz or alumina reaction tube (1000 mm length) was used for examining the reaction products of gaseous $TiCl_4$ with ammonia. Gaseous $TiCl_4$ was formed by heating liquid $TiCl_4$ (17 g) at 105 °C and was carried by a stream of argon (50 cm³/min) into the reaction zone (28 mm i.d., 250 mm length) held at specified temperature. The $TiCl_4$ inlet tube consisted of two concentric tubes. Gaseous $TiCl_4$ carried by arogn was introduced through the inner tube and the outer tube was utilized for introducing argon (50 cm³/min) as a sheath gas to prevent formation of titanium nitride deposits at the chloride inlet tube. Ammonia was simultaneously introduced at a flow-rate of 100 cm³/min into the reaction zone through a separate tube. The mean flow-rate of gaseous $TiCl_4$ was 6.0 cm³/min. A quartz or alumina tube was inserted inside the reaction tube to make the removal of the reaction product easier. The reaction was allowed to proceed for 2 h.

The by-product NH_4Cl which deposited outside the reaction zone together with the titanium nitride formed was separated by heating the mixture in an argon stream at 400 °C (the sublimation point of NH_4Cl: 339 °C)[2] for 10—15 h.

Analytical. The chemical analysis of the reaction products was performed as follows: The titanium content was gravimetrically determined as TiO_2 using cupferron as a precipitating agent, after dissolving the sample in 3 M-nitric acid. The chlorine content was gravimetrically determined as AgCl from the filtrate. The ammonia content was determined by the Kjeldahl method from the nitric acid solution.

X-Ray analysis of the solid product was performed with an X-ray powder diffractometer equipped with a proporitonal counter using Ni filtered Cu radiation. The sample chamber of the diffractometer was maintained under a dry nitrogen atmosphere, if necessary, to prevent contamination of the sample by atmospheric moisture during the irradiation.

The sensitivity of the quartz helix used for thermogravimetry (TG) was approximately 94 mm/g. The sample (0.2 g) was heated at a rate of 2.5 °C/min and the flow-rate of ammonia was maintained at 50 cm³/min.

The N/Ti atomic ratio of the titanium nitride formed was evaluated as follows: The sample titanium nitride was oxidized to TiO_2 by heating in an oxygen atmosphere to 700 °C, using a Shimazu high-sensitive thermal balance Model TGA31. The titanium content of the sample was calculated from the amount of TiO_2 formed. The amount of nitrogen was determined as the difference between the amount of the initial sample and that of the titanium. The value of the N/Ti atomic ratio was evaluated with an accuracy within ± 0.01.

The lattice constant of the titanium nitride was calculated based on the X-ray diffraction data obtained by using silicon powders as an internal standard and under the scanning speed of 1/2—1/4°/min.

Throughout this work, the $TiCl_4$ and the reaction products were handled in an argon atmosphere to prevent contamination by atmospheric moisture.

Results and Discussion

Reaction Products of Gaseous Titanium Tetrachloride with Ammonia. The products formed by heating gaseous

Table 1. Reaction products of gaseous $TiCl_4$ with ammonia at various temperatures

Temp/°C	Products	
	In the reaction zone	Outside the reaction zone
200	$TiCl_4 \cdot 5NH_3$	$TiCl_4 \cdot 5NH_3$
250	$TiCl_4 \cdot 5NH_3 \gg TiClN$	$TiCl_4 \cdot 5NH_3$; NH_4Cl
300	$TiCl_4 \cdot 5NH_3 \gg TiClN$	$TiCl_4 \cdot 5NH_3$; NH_4Cl
350	$TiCl_4 \cdot 5NH_3 > TiClN$	$TiCl_4 \cdot 5NH_3$; NH_4Cl
400	TiClN	$TiCl_4 \cdot 5NH_3$; NH_4Cl
450	$TiClN > TiN_x$	$TiCl_4 \cdot 5NH_3$; NH_4Cl
500	TiClN, TiN_x	$TiCl_4 \cdot 5NH_3$; NH_4Cl
550	$TiN_x > TiClN$	$TiCl_4 \cdot 5NH_3$, TiN_x; NH_4Cl
600	$TiN_x > TiClN$	$TiN_x \gg TiCl_4 \cdot 5NH_3$; NH_4Cl
650	$TiN_x > TiClN$	$TiN_x \gg TiCl_4 \cdot 5NH_3$; NH_4Cl
700—900	TiN_x	TiN_x; NH_4Cl
1000	—	TiN_x; NH_4Cl
1100—1400	—	TiN_x; NH_4Cl, HCl

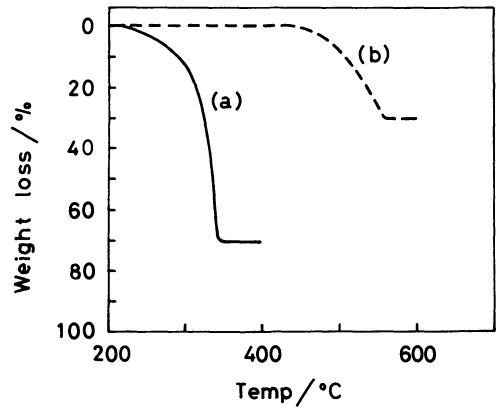

Fig. 1. TG curves of $TiCl_4 \cdot 5NH_3$ and TiClN in an ammonia stream.
(a): $TiCl_4 \cdot 5NH_3$, (b): TiClN.

$TiCl_4$ in an ammonia stream at various temperatures above 200 °C were examined both by X-ray analysis[3-5] and chemical analysis. The product formed at 200 °C showed a hitherto unknown X-ray diffraction pattern which was clearly different from those of known titanium compounds. The chemical analysis of the product gave Ti, 17.4; Cl, 51.6; NH_3, 30.8%. The ratio of Ti : Cl : NH_3 was calculated to be 1 : 4.00 : 4.98. This was considered to indicate that the product formed at 200 °C had a composition of $TiCl_4 \cdot 5NH_3$ (calcd for $TiCl_4 \cdot 5NH_3$: Ti, 17.42; Cl, 51.60; NH_3, 30.98%). The reaction products at various temperatures are shown in Table 1. Unreacted $TiCl_4$ was not observed throughout the temperature range of this work.

Reaction Process of Gaseous Titanium Tetrachloride with Ammonia. To elucidate the reaction process of gaseous $TiCl_4$ with ammonia, the behavior of the $TiCl_4 \cdot 5NH_3$ and the TiClN, which had been formed during the reaction process, on heating in an ammonia stream were examined. The thermal dissociation of ammonia[6] and the thermal decomposition of NH_4Cl[7] under the experimental conditions in this work were also examined.

Behavior of $TiCl_4 \cdot 5NH_3$ and TiClN on Heating in an Ammonia Stream: The TG curve of $TiCl_4 \cdot 5NH_3$ in an ammonia stream is shown in Fig. 1(a).

$TiCl_4 \cdot 5NH_3$ lost weight above 220 °C. The weight loss was accompanied by the vaporization of NH_4Cl and a small amount of $TiCl_4 \cdot 5NH_3$. The sample after heating to 400 °C was found to be TiClN by X-ray analysis.

In order to obtain more detailed information on the behavior of $TiCl_4 \cdot 5NH_3$ on heating in an ammonia stream, $TiCl_4 \cdot 5NH_3$ (1.0 g) in a quartz boat (70 mm length, 15 mm width, 7 mm depth) was placed in a straight reaction tube (28 mm i.d., 1000 mm length). Ammonia was introduced into the reaction tube at a flow-rate of 100 cm^3/min. The sample part was then placed in the centre of an electric furnace (300 mm heating length) maintained at a specified temperature for 1 h. The products obtained inside and outside the boat were examined by X-ray analysis and chemical analysis. The results are shown in Table 2.

From the results, it was found that $TiCl_4 \cdot 5NH_3$ decomposed to TiClN above about 220 °C and a part of $TiCl_4 \cdot 5NH_3$ vaporized above about 300 °C in an ammonia stream.

The TG curve of TiClN in an ammonia stream is shown in Fig. 1(b). The TiClN used was prepared by the reaction of gaseous $TiCl_4$ with ammonia at 400 °C. The chemical analysis gave Ti, 49.1; Cl, 36.4% (calcd for TiClN: Ti, 49.19; Cl, 36.42%). TiClN lost weight above 430 °C. The weight loss was accompanied by the vaporization of NH_4Cl alone. The sample after heating to 600 °C was found to be TiN_x. From these results, it was found that TiClN reacted with ammonia above about 430 °C to form TiN_x.

Table 2. Experimental results for $TiCl_4 \cdot 5NH_3$ on heating in an ammonia stream

Heating temp/°C	Products		Unreacted $TiCl_4 \cdot 5NH_3$ (%)
	In the boat	Outside the boat	
250	TiClN(4)	NH_4Cl	96
300	TiClN(41)	$TiCl_4 \cdot 5NH_3$(15), NH_4Cl	44
350	TiClN(71)	$TiCl_4 \cdot 5NH_3$(29), NH_4Cl	—

Note: the value in( ) is mole percentage of $TiCl_4 \cdot 5NH_3$ converted to the product.

Thermal Dissociation of Ammonia and Thermal Decomposition of NH_4Cl: Ammonia alone was introduced at a flow-rate of 100 cm^3/min into the reaction zone held at a specified temperature and the total volume of nitrogen and hydrogen, formed by the dissociation of ammonia, was measured. From the results, the percentage of the dissociated ammonia was found to be <1% at 800 °C, 1% at 900 °C, 2% at 1000 °C, 6% at 1100 °C, 23% at 1200 °C, 88% at 1300 °C, and 98% at 1400 °C.

Gaseous NH_4Cl was formed by heating solid NH_4Cl and was carried by a stream of argon at a flow-rate of 100 cm^3/min into the reaction zone held at a specified temperature for 2 h. The amount of NH_4Cl introduced, 6.5 g, was the same as that formed during the reaction of gaseous $TiCl_4$ with ammonia for 2 h at 700—1000 °C (Table 1). The percentages of the decomposed NH_4Cl at various temperatures were evaluated from the amount of HCl formed by the decomposition. From the results, the percentage of the decomposed NH_4Cl was found to be <1% at 1100 °C, 8% at 1200 °C, 29% at 1300 °C, and 65% at 1400 °C.

Based on the above experimental results, the reaction process of gaseous $TiCl_4$ with ammonia was discussed. As shown in Table 1, $TiCl_4 \cdot 5NH_3$ alone was formed at 200 °C. This fact indicates that the reaction of gaseous $TiCl_4$ with ammonia to form $TiCl_4 \cdot 5NH_3$ occurs first. The TiClN formed at 250—650 °C (Table 1) is considered to be due to the decomposition of $TiCl_4 \cdot 5NH_3$, because the $TiCl_4 \cdot 5NH_3$ decomposes above about 220 °C to TiClN, as described above. The TiN_x formed above 450 °C is considered to be due to the reaction of TiClN with ammonia, because the TiClN reacts with ammonia above about 430 °C to form TiN_x.

Above 1100 °C, HCl was formed in addition to TiN_x and NH_4Cl (Table 1). The percentage of HCl formed to the total amount of chlorine introduced as $TiCl_4$ was 36% at 1100 °C, 75% at 1200 °C, 92% at 1300 °C, and 93% at 1400 °C. This amount of HCl is considerably larger than the amount of HCl formed by the thermal decomposition of NH_4Cl at each temperature, as described above. Also, it has been reported that gaseous $TiCl_4$ reacts with hydrogen above about 800 °C to form gaseous titanium dichloride ($TiCl_2$) and HCl.[8] From these facts, it was considered that the reduction of gaseous $TiCl_4$ with hydrogen, formed by the thermal dissociation of ammonia, to $TiCl_2$ also occurred above 1100 °C and that the $TiCl_2$ reacted with ammonia to form TiN_x. Therefore, the reaction of gaseous $TiCl_2$ with ammonia was examined.

Table 3. N/Ti atomic ratio and lattice constant of the TiN_x formed

Formation temp/°C	x in TiN_x	a_0/Å
700	1.21	4.224
800	1.16	4.228
900	1.13	4.230
1000—1400	1.10	4.233

The $TiCl_2$ used was prepared by the disproportionation of commercial titanium trichloride ($TiCl_3$) *in vacuo* at 475 °C.[9] The chemical analysis gave Ti, 40.2; Cl, 59.7% (calcd for $TiCl_2$: Ti, 40.31; Cl, 59.69%). Gaseous $TiCl_2$ was formed by heating $TiCl_2$ at 800 °C and was carried by a stream of argon (50 cm^3/min) into the reaction zone held at a specified temperature. Ammonia was simultaneously introduced at a flow-rate of 100 cm^3/min through a separate tube into the reaction zone.

The products formed were TiN_x and NH_4Cl at 1000 °C and TiN_x, NH_4Cl, and a small amount of HCl at 1100 °C. The HCl formed at 1100 °C was considered to be formed by the reduction of $TiCl_4$, formed by the disproportionation of $TiCl_2$,[8,10] with hydrogen resulting from the thermal dissociation of ammonia. The results indicate that gaseous $TiCl_2$, formed by the reduction of gaseous $TiCl_4$ with hydrogen, reacts with ammonia to form TiN_x.

From these results, the reaction process of $TiCl_4$ with ammonia in the vapor phase can be represented as follows: The reaction of gaseous $TiCl_4$ with ammonia occurs first to form $TiCl_4 \cdot 5NH_3$. Above about 220 °C, the $TiCl_4 \cdot 5NH_3$ decomposes to TiClN. Above about 430 °C, the TiClN reacts with ammonia to form TiN_x. Above about 1100 °C, in addition to these reactions, the reaction of $TiCl_2$, formed by the reduction of $TiCl_4$ with hydrogen resulting from the thermal dissociation of ammonia, with ammonia occurs to form TiN_x.

Properties of the TiN_x Formed. The N/Ti atomic ratios of TiN_x formed at 700—1400 °C are shown in Table 3. Prior to this examination, the presence of residual NH_4Cl in the TiN_x, obtained after the removal of NH_4Cl at 400 °C in an argon stream, was checked by chemical analysis,[11] after the fusion of the TiN_x sample with sodium carbonate. From the results, the NH_4Cl content in the TiN_x was 6.9% for the TiN_x formed at 700 °C, 5.9% at 800 °C, 3.6% at 900 °C, 1.5% at

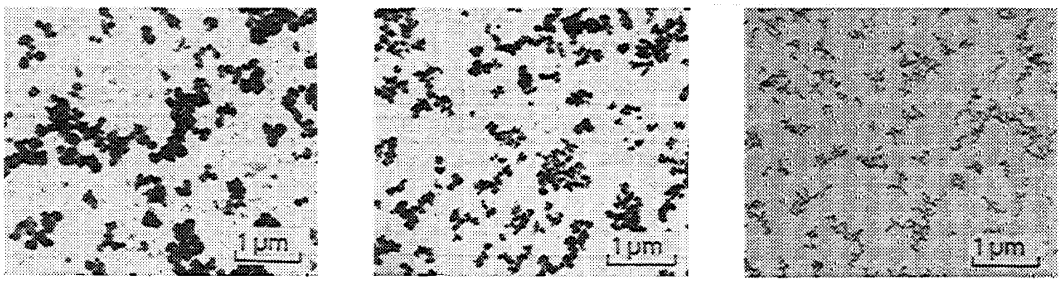

(a) 1200 °C (b) 1300 °C (c) 1400 °C

Flg. 2. Electoron micrographs of the $TiN_{x(x=1.10)}$ formd at various temperatures.

1000 °C, 1.0% at 1100 °C, 0.5% at 1200 °C, 0.2% at 1300 °C, and trace at 1400 °C. Further separation of the NH_4Cl at higher temperatures could not be carried out, by considering the thermal stability of the TiN_x formed, as described later. For the evaluation of the N/Ti atomic ratio of the TiN_x formed, the initial weight of the sample was corrected by subtracting the amount of NH_4Cl contained, because the NH_4Cl was vaporized during the oxidation.

Kato *et al.*[1] reported that the N/Ti atomic ratio of the TiN_x formed by a vapor-phase reaction of the $TiCl_4$–NH_3–H_2–N_2 system at 700—1500 °C was 1.1—1.4. Vorob'ev *et al.*[12] reported that the stoichiometric TiN was identified as a main component of the reaction products of gaseous $TiCl_4$ with ammonia at 800—1100 °C. But, the details of this study are not available.

It has been known that the TiN_x phase has a NaCl structure.[1,3] The lattice constant of TiN_x formed at each temperature is also shown in Table 3.

The TiN_x formed by the reaction of gaseous $TiCl_4$ with ammonia above 1000 °C were examined by electron microscopy. The typical micrographs of the TiN_x are shown in Fig. 2.

As seen from Fig. 2, the TiN_x formed at 1400 °C is uniform, ultrafine powders with the particle diameters of the order of 1/100 μm. The range of the particle sizes of the TiN_x formed at lower temperatures was found to be wide.

Finally, to obtain knowledge of the thermal stability of the TiN_x formed, the N/Ti atomic ratios of the samples obtained by heating $TiN_{1.21}$ at various temperatures in an argon atmosphere for 1 h were examined. The results are shown in Fig. 3. In addition, it was found that the residual NH_4Cl in the TiN_x was compeletely removed by the heating at 1100 °C.

The results indicated that when the TiN_x formed was heated in an argon atmosphere at temperatures higher than 500 °C, the N/Ti atomic ratio decreased and became close to that of the stoichiometric nitride; The value of x was 1.02 at the heating temperatures of 900—1100 °C.

The lattice constants of the TiN_x with various x values, obtained in this work, are shown in Fig. 4.

The N/Ti atomic ratio of TiN_x obtained after heating $TiN_{1.21}$ in an argon atmosphere at each temperature was found to be lower than that of the TiN_x formed by the vapor-phase reaction at the same temperature (Table 3). The facts are considered to be due to the presence of nitrogen during the reaction. This consideration was supported by the fact that no change in the N/Ti atomic ratio of the $TiN_{1.10}$ formed at 1000 °C by the vapor-phase reaction was observed after the heating at 1000 °C in an ammonia stream for 1 h.

The present work was partially supported by a Grant-in-Aid for Scientific Research No. 56470058 from the Ministry of Education, Science and Culture.

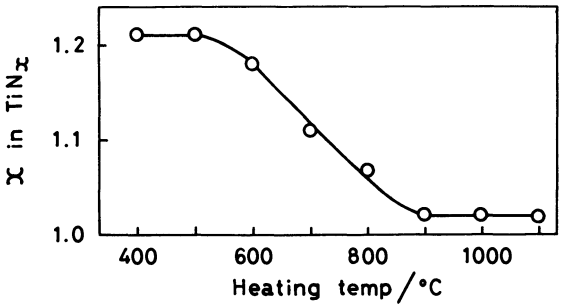

Fig. 3. N/Ti atomic ratios of TiN_x obtained after heating $TiN_{1.21}$ at various temperatures in an argon atmosphere.

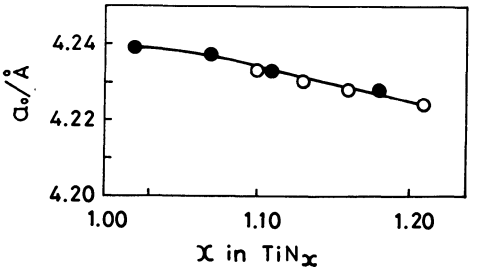

Fig. 4. Lattice constants of the TiN_x with various x values. ○: From TiN_x formed by the reaction of gaseous. $TiCl_4$ with ammonia, ●: from TiN_x obtained after the heating of $TiN_{1.21}$.

References

1) A. Kato, M. Iwata, J. Hojo, and M. Nagano, *Yogyo Kyokai Shi*, **83**, 453 (1975).
2) I. Barin and O. Knacke, "Thermochemical Properties of Inorganic Substances," Springer, Berlin, Heidelberg, New York (1973), p. 499.
3) ASTM, Powder Diffraction File 6-642.
4) JCPDS, Powder Diffraction File 18-1399.
5) ASTM, Powder Diffraction File 7-7.
6) "Gmelins Handbuch der Anorganischen Chemie, System Nummer 4, Stickstoff," Verlag Chemie, Weinheim (1955), p. 323.
7) "Gmelins Hanbuch der Anorganischen Chemie, System Nummer 23, Ammonium," Verlag Chemie, Weinheim (1955), p. 160.
8) K. Funaki and K. Uchimura, *Kogyo Kagaku Zasshi*, **59**, 14 (1956).
9) M. Nakahara and M. Shibata, "Mukikagōbutsu No Gōsei [II], Shin-Zikkenkagaku-Kōza 8," ed by the Chemical Society of Japan, Maruzen, Tokyo (1977), p. 780.
10) K. Funaki and K. Uchimura, *Kogyo Kagaku Zasshi*, **57**, 538 (1954).
11) JIS H 1615 (1973), p. 2.
12) N. I. Vorob'ev, D. I. Medvedev, N. V. Galitskii, Yu. M. Dmitriev, and L. G. Terekhova, *Deposited Doc.*, **VINITI 335-77** (1977); *Chem. Abstr.*, **90**, 139671w (1979).

 © 1982 The Chemical Society of Japan Bull. Chem. Soc. Jpn., 55, 3197—3199 (1982)

Preparation of Poly(dicarbon monofluoride) from Petroleum Coke

Nobuatsu WATANABE,* Yoshinori ASHIDA, and Tsuyoshi NAKAJIMA
Department of Industrial Chemistry, Faculty of Engineering, Kyoto University, Sakyo-ku, Kyoto 606
(Received March 31, 1982)

Graphite fluoride containing more than 60% poly(dicarbon monofluoride) $(C_2F)_n$ was prepared from petroleum coke heat-treated at 2700 °C at a temperature between 337 and 460 °C. The interlayer spacings and F/C ratios of these graphite fluorides were in the ranges of 0.82—0.74 nm and 0.58—0.68, respectively. The $(C_2F)_n$ content in graphite fluoride also increased with increasing fluorine pressure.

During the studies on the chemical composition and crystal structure of graphite fluoride,[1] a new compound, poly(dicarbon monofluoride) represented by the formula $(C_2F)_n$ has been found. The $(C_2F)_n$ is formed at a low temperature between 350 and 400 °C from a carbon material with high crystallinity such as natural graphite. Various kinds of artificial carbon materials are generally used in the industrial field. In most cases, these carbons are amorphous, having much smaller crystallites than natural graphite; however, the growing of small crystallites is attained by heat treatment at 2600—2800 °C. In this study, the preparation of $(C_2F)_n$ is attempted from petroleum coke heat-treated at high temperatures.

Experimental

The starting carbon material was petroleum coke (GL coke) of less than 46 μm, heated-treated at temperatures between 1500 and 2700 °C in a graphitization furnace. Structural parameters of these carbon materials are listed in Table 1. With increasing heat treatment temperature, the parameter indicating the interlayer spacing, C_0(004) decreased from 0.690 to 0.672 nm while those indicating the crystallite size, L_c and L_a, increased very much. Half of C_0 (004) length is the distance between two carbon network layers. Fluorination of petroleum coke was made at temperatures of 330—590 °C using an automatic thermobalance specially designed for fluorine atmosphere.[2] Fluorination reaction was continued until no weight increase was observed, and the products were analyzed by elemental analysis and X-ray diffractometry.

Results and Discussion

Figure 1 is an example of the change in (001) X-ray diffraction patterns of graphite fluoride prepared from petroleum coke heat-treated at 2700 °C. The peak position shifted from 14.5° to 10.8° in 2θ (by Cu $K\alpha$) with decreasing reaction temperature. It is known that $(C_2F)_n$ is preferentially formed at temperatures of 350—400 °C from a carbon material having a large crystallite size like natural graphite and its (001) diffraction line

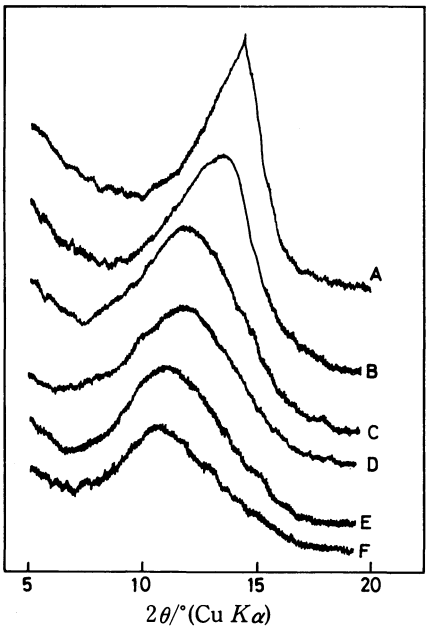

Fig. 1. (001) X-Ray diffraction patterns of graphite fluoride prepared from petroleum coke (PC 2700 °C). Reaction temperature: A: 590 °C, B: 550 °C, C: 467 °C; D: 426 °C; E: 370 °C, F: 337 °C.

appears at 10—11° in 2θ, whereas that for $(CF)_n$ is situated around 14—15°.[1] Figure 1 indicates that $(C_2F)_n$ is formed mainly below 400 °C, however, the peak profile of the product prepared at 337 °C is broader than that of the product prepared at 590 °C, probably because of the simultaneous formation of a small amount of $(CF)_n$. But only a slight change of the peak positions was observed for graphite fluoride prepared from the sample heat-treated at 1500 °C. Even in the reaction at low temperatures such as 330 °C, a product with the peak position much higher than 10° in 2θ was prepared, as shown in Fig. 2. This result shows no formation of $(C_2F)_n$ from this petroleum coke under any

Table 1. Structural parameters of heat-treated petroleum cokes (PC) used as starting materials

Materials	C_0(004)/nm	L_c(002)/nm	L_c(004)/nm	L_c(112)/nm	L_a(110)/nm
PC 2700°C[a)]	0.6722	>100	52	5.5	>100
PC 2300°C	0.6732	79	33	3.3	>100
PC 2100°C	0.6756	56	25	1.6	100
PC 1860°C	0.6770	39	22	1.2	74
PC 1500°C	0.6848	13	7	—	4.8
Original	0.6900	3.6	1.9	—	2.8

a) Heat treatment temperature.

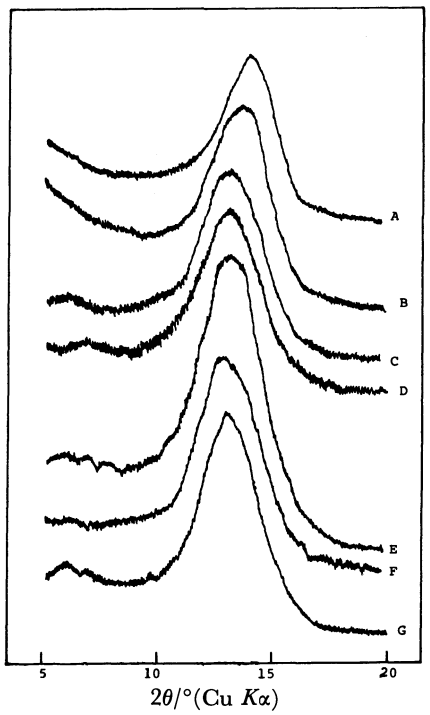

Fig. 2. X-Ray diffraction patterns of graphite fluoride prepared from petroleum coke (PC 1500 °C).
Reaction temperature: A: 590 °C, B: 550 °C, C: 460 °C, D: 410 °C, E: 370 °C, F: 350 °C, G: 330 °C.

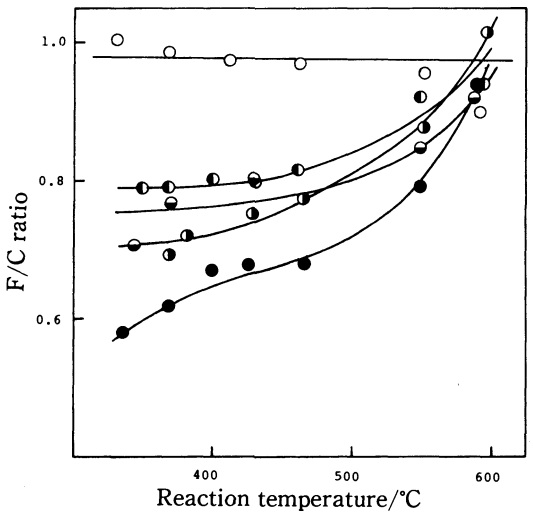

Fig 3. Dependence of F/C ratio of graphite fluoride on reaction temperature.
●: PC 2700 °C, ◑: PC 2300 °C, ◒: PC 2100 °C, ◐: PC 1860 °C, ○: PC 1500 °C.

conditions.

As already reported,[1] since $(CF)_n$ is formed even at low temperatures between 400 and 350 °C from a carbon material with low crystallinity or at a disordered place such as surface of a carbon particle, it is very difficult to obtain pure $(C_2F)_n$ from the artificial carbon materials. The $(C_2F)_n$ content in a product is estimated from the F/C ratio of the product by assuming only $(CF)_n$ as an impurity. By representing

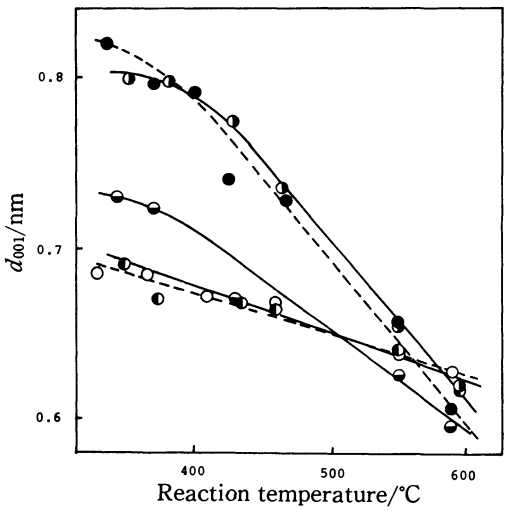

Fig. 4. Change in the interlayer spacings of graphite fluoride as a function of reaction temperature.
●: PC 2700 °C, ◑: PC 2300 °C, ◒: PC 2100 °C, ◐: PC 1860 °C, ○: PC 1500 °C.

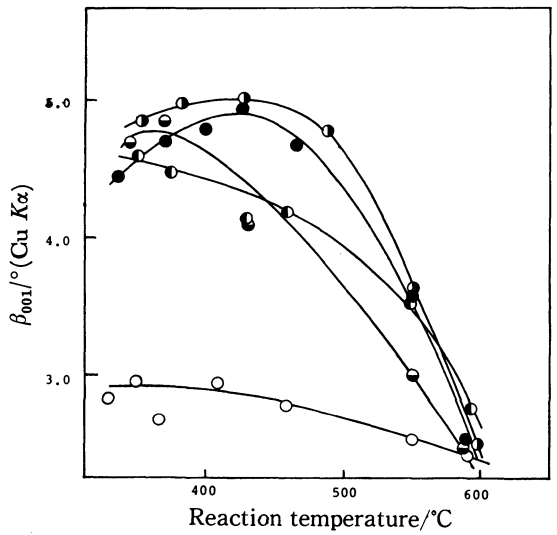

Fig. 5. Change in the half widths of (001) line of graphite fluoride as a function of reaction temperature.
●: PC 2700 °C, ◑: PC 2300 °C, ◒: PC 2100 °C, ◐: PC 1860 °C, ○: PC 1500 °C.

the amounts of $(C_2F)_n$ and $(CF)_n$ as X and 1-X, respectively, F/C ratio is related with X by the equation $F/C = 1 - 0.5X$. However, as graphite fluoride has CF_2 and CF_3 groups on the surface, the actual content is expected to become slightly higher than the value calculated by the above equation. From Fig. 3, graphite fluoride containing $(C_2F)_n$ by more than 60% is obtained from petroleum coke heat-treated at 2700 °C, that is: at 337—380 °C, $(C_2F)_n$: 70—80% and at 380—460 °C, $(C_2F)_n$: 60—70%. The sample heat-treated at 2300 °C gives graphite fluoride with $(C_2F)_n$ content of about 50% at 350—430 °C. Graphite fluorides prepared from petroleum coke heat-treated at 2100 and 1860 °C contain only about 40—50% $(C_2F)_n$ and only $(CF)_n$ is prepared at any temperature from

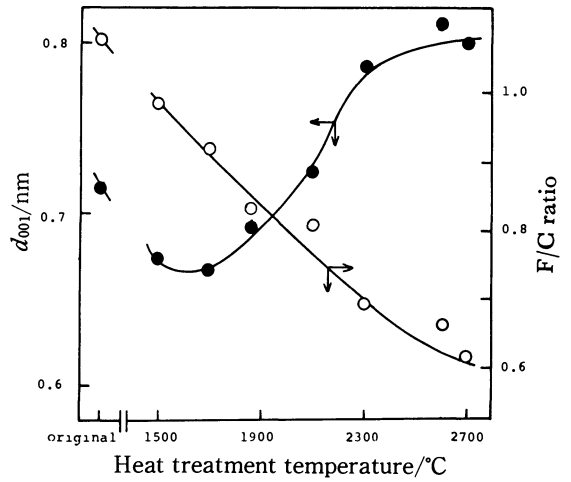

Fig. 6. Variation of the interlayer spacings and F/C of graphite fluoride as a function of heat treatment temperature.
Reaction conditions : 370 °C, F_2, 267×10^2 Pa.

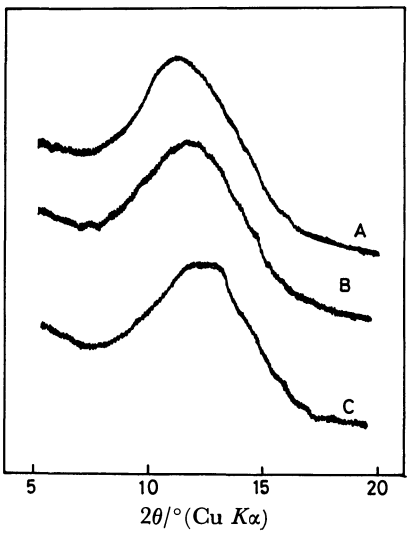

Fig. 7. Effect of fluorine pressure on (001) X-ray diffraction patterns of graphite fluoride prepared from petroleum coke (PC 2700 °C) at 430 °C.
A: 533×10^2 Pa, B: 267×10^2 Pa, C: 133×10^2 Pa.

petroleum coke heat-treated at 1500 °C. It is found by comparison of Fig. 3 with Table 1 that in order to obtain graphite fluoride with a $(C_2F)_n$ content of more than 60%, it is necessary to use petroleum coke with crystallite sizes, $L_c(002)$ and $L_a(110)$, of more than 100 nm.

The interlayer spacings d_{001} of graphite fluoride are *ca.* 0.9 nm for $(C_2F)_n$ and 0.6 nm for $(CF)_n$.[1] Figure 4 shows an increase of d_{001} values with increasing content of $(C_2F)_n$ in graphite fluoride as a function of reaction temperature. The d_{001} of graphite fluoride prepared below 400 °C is about 0.8 nm; this is smaller by 0.1 nm than the reported value 0.9 nm.[1] It is due to the overlapping of two diffraction peaks corresponding to $(C_2F)_n$ and $(CF)_n$. Such a tendency of d_{001} with decreasing temperature is also observed for graphite fluoride prepared from the sample treated at 1500 °C; however, in this case it would be attributable to the lower crystallinity of the prepared $(CF)_n$. Figure 5 shows more clearly the overlapping of two diffraction lines originating from $(C_2F)_n$ and $(CF)_n$. With increasing heat treatment temperature of petroleum coke, the half width of (001) diffraction line changes along more symmetric hyperbola as a function of temperature in accordance with increasing content of $(C_2F)_n$ in graphite fluoride. The hyperbola with a broad width has a maximum point at 430 °C, while in the case of graphite fluorides prepared from natural graphite, the maximum point of hyperbola with a narrow width is situated at 490 °C.[1] This indicates that $(C_2F)_n$ is preferencially formed from a carbon material with higher crystallinity. It is more distinctly shown in Fig. 6, which gives the change in the interlayer spacings d_{001} and F/C ratios of graphite fluoride as a function of crystallinity of a starting carbon material.

The dependence of $(C_2F)_n$ formation on fluorine pressure is given in Fig. 7, in which the peak position of (001) diffraction line shifts to lower angles with increasing fluorine pressure. That is, the interlayer spacing d_{001} increased from 0.72 to 0.80 nm and F/C ratio decreased from 0.67 to 0.64 with increase in the fluorine pressure from 133×10^2 to 533×10^2 Pa. These data mean that $(C_2F)_n$ is more easily formed under higher fluorine pressure. This is consistent with the previous result obtained for graphite fluoride prepared from natural graphite.[1]

References

1) Y. Kita, N. Watanabe, and Y. Fujii, *J. Am. Chem. Soc.*, **101**, 3832 (1979).
2) M. Takashima and N. Watanabe, *Nippon Kagaku Kaishi*, **1976**, 1222.

Direct Synthesis of Cyclic Carbonates in the Presence of Organometallic Compounds. Catalyses by Systems from IVA, VA, and VIA Group Compounds and Lewis Base

Ryoki NOMURA,* Masahiro KIMURA, Satoshi TESHIMA, Akira NINAGAWA, and Haruo MATSUDA
Department of Petroleum Chemistry, Faculty of Engineering, Osaka University, Yamada-oka, Suita, Osaka 565
(Received November 2, 1981)

In the cycloaddition of carbon dioxide to oxiranes to form cyclic carbonates in the presence of organometallic halides of group IVA, VA, and VIA, catalytic activities of organometallic halides are in the order Sb>Te>Sn≫Bi, Ge, and Si. An improvement of their catalytic activities is achieved by addition of an equimolar amount of Lewis base. In binary catalyst systems, the order of catalytic activities is in the order Sn>Te>Sb≫Bi, Ge, and Si. Organotin halide–base systems show the highest catalytic activity.

In our previous papers, we reported that pentavalent organoantimony halides such as Ph_4SbBr and Ph_3SbBr_2 are highly effective catalysts for the cycloaddition reaction of carbon dioxide (CO_2) to oxiranes to afford corresponding cyclic carbonates (1,3-dioxolan-2-ones).[1] The striking feature of organoantimony catalysts in the cycloaddition is attributable to the covalent nature of the antimony-halogen bonds[1] in contrast with ammonium halides such as tetraethylammonium chloride.[2]

In the present study, we carried out cycloadditions catalyzed by triphenyl derivatives of Sn^{IV}, Ge^{IV}, Si^{IV}, and Bi^{V} and by dimethyl and diphenyl derivatives of Te^{IV}, expecting a similar effect of metal-halogen bonds as in the pentavalent organoantimony halide-catalyzed cycloaddition. Further, an attempt was made to improve the catalytic activity of the organometallic halides by incorporation of an equimolar amount of Lewis base such as triethylamine (TEA), pyridine (Py), and triphenylphosphine (TPP) to the organometallic halides and it was found that the binary catalysts effectively enhance the catalytic activity, especially in the case of the organotin halides.

Some recent papers have claimed good catalytic activities of pairs of heavy metal halide and Lewis base[3] but do not explain the effect of added bases in detail. Therefore, we also attempted to discuss the effect of added bases.

Results and Disscussion

Catalytic Activities of Organometallic Halides of Groups IV, V, and VI. The cycloaddition of CO_2 to methyloxirane (propylene oxide, PO) was carried out in a stainless-steel autoclave at 100 °C under a fixed initial pressure of CO_2, 50 kg/cm², to compare catalytic activities of organometallic halides with one another,

TABLE 1. RELATIVE CATALYTIC ACTIVITIES OF THE ORGANOMETALLIC HALIDES–BASE SYSTEMS IN THE CYCLOADDITION REACTION OF CO_2 TO METHYLOXIRANE AT 100 °C

Catalyst	Relative rate constant[b]			
	No base	TEA[c]	Py[d]	TPP[e]
Ph_3SnCl	>0.01[f] (0.001)	0.22	0.20	0.20
Ph_3SnBr	>0.01[f] (0.01)	6.0	6.6	6.4
Ph_3SnI	>0.01[f] (0.09)	6.0	6.0	5.8
Ph_3GeBr	0[g]	>0.01[f] (0.16)	>0.01[f] (0.08)	>0.01[f] (0.16)
Ph_3SiBr	0[g]	>0.01[f] (0.26)	>0.01[f] (0.11)	>0.01[f] (0.22)
Ph_3SbBr_2	1.0[h]	1.1	1.4	0.74
Ph_4SbBr	5.0	—	—	—
Ph_3BiBr_2	0[g]	>0.01[f] (0.10)	>0.01[f] (0.07)	>0.01[f] (0.04)
Me_2TeCl_2	0[g]	—	—	—
Me_2TeBr_2	0.20	—	—	—
Me_2TeI_2	0.64	2.4	2.2	0.89
Tol_2TeCl_2[i]	0.02	0.08	0.08	0.02
—	—	>0.01[f] (9.7×10^{-4})	>0.01[f] (7.7×10^{-4})	>0.01[f] (7.6×10^{-4})

a) Methyloxirane: 50 mmol, base/organometallic halides: 1.0, initial pressure of CO_2: 50 kg/cm². b) Relative rate constant based on Ph_3SbBr_2; see h). c) TEA: Triethyl amine. d) Py: Pyridine. e) TPP: Triphenylphosphine. f) Relative rate constants measured at 120 °C are indicated in parentheses. g) No cycloaddition occurred even at 120 °C. h) 3.4×10^{-1} M^{-1} min^{-1} (1 M=1 mol dm^{-3}). i) Tol: p-$CH_3C_6H_4$–.

and relative rate constants are summarized in Table 1 for the catalysts employed. The catalytic activities of the organometallic halides are in the order

$$Sb > Te > Sn \gg Bi, Ge, Si. \quad (1)$$

Only the organotellurium compounds compare with the organoantimony catalysts in activity under the conditions examined. However, the reaction mixture became red-brown as reaction proceeded. Although organotin halides could not cause the cycloaddition at 100 °C, they gave 4-methyl-1,3-dioxolan-2-one (propylene carbonate, PC) at a significant rate, when reaction was carried out at 120 °C.[4]

The dependence of the catalytic activities of the organometallic halides on the polarity of the metal-halogen bonds may be expected, since the organometallic halides used in this study are considered to have relatively covalent metal-halogen bonds similarly to the organoantimony halides.[1] With regard to Sn, Sb, and Te compounds, the length of the metal-chlorine bond was reported to be in the order $Sb^{V}>Te^{IV}>Sn^{IV}$,[5,6] and it can be seen that the catalytic activity of the organometallic halides decreases with decrease in the bond length.

If the organometallic catalyst can be formed *in situ*, some simplification of the process for synthesis of the cyclic carbonate may be achieved. Among the organometallic halides examined, Me_2TeI_2 can be prepared by heating a mixture of tellurium powder and methyl iodide at 80 °C.[7] We attempted a cycloaddition reaction with a mixture of methyl iodide and tellurium which is expected to afford Me_2TeI_2 *in situ*. When methyl iodide and tellurium were added in a mole ratio of more than two, a quantitative yield of PC was obtained as shown in Table 2. However, the question whether Me_2TeI_2 is really formed *in situ*[8] and catalyzes the reaction remains to be solved. We also attempted the cycloaddition with combinations of tin metal-butyl[9] or -methyl iodide and antimony metal-methyl iodide, but they were not effective at all even at 120 °C.

Improvement of the Catalytic Activities of the Organometallic Halides by Addition of Lewis Bases. Generally, group IV organometallic halides are found to be less active for the cycloaddition reaction than organoantimony and organotellurium compounds. Thus, in order to improve the catalytic activity of the organometallic halides, an equimolar amount of Lewis base such as TEA, Py, and TPP was added to the organometallic compounds.[10] A marked rate enhancement was observed as shown in Table 1, *e.g.*, relative rate constants for Ph_3SnBr (or Ph_3SnI)–base systems are obviously larger than those for Ph_3SnBr (or Ph_3SnI) by a factor of $>10^2$. The order of the catalytic activities for the binary catalyst systems changed from (1) to

$$Sn > Te > Sb \gg Bi, Ge, Si. \quad (2)$$

The most active binary systems, such as Ph_3SnBr–TEA and Me_2TeI_2–TPP, surpassed Ph_4SbBr which is the most effective among the organoantimony compounds,[1] and could give the cyclic carbonate quantitatively even under atmospheric pressure of CO_2 at 60 °C, as shown in Fig. 1.

Effect of Added Bases. Tertiary amines or phosphines themselves have been known to show catalytic activity for the cycloaddition reaction,[11] but their catalytic activity is low as shown in Table 1 under the

Table 2. The cycloaddition reaction of CO_2 to PO in the presence of tellurium and methyl iodide[a]

Te(mmol)	MeI(mmol)	Temp/°C	Time/h	Yield/%
5	10	100	8	68
5	50	100	6	91
5	10	80	8	3
—	10	100	6	0
5	—	100	6	0

a) PO: 50 mmol, initial pressure of CO_2: 50 kg/cm.^{2}

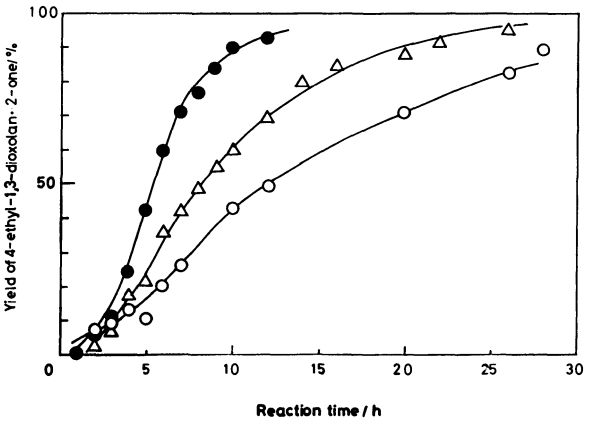

Fig. 1. Cycloaddition reaction under atmospheric pressure of CO_2 at 60 °C.
Ethyloxirane: 50 mmol, organometallic halides: 0.15 M (0.5 mmol). ○: Ph_4SbBr, ●: Ph_3SnBr–TEA (1/1), △: Me_2TeI_2–TPP (1/1), molar ratio in parentheses.

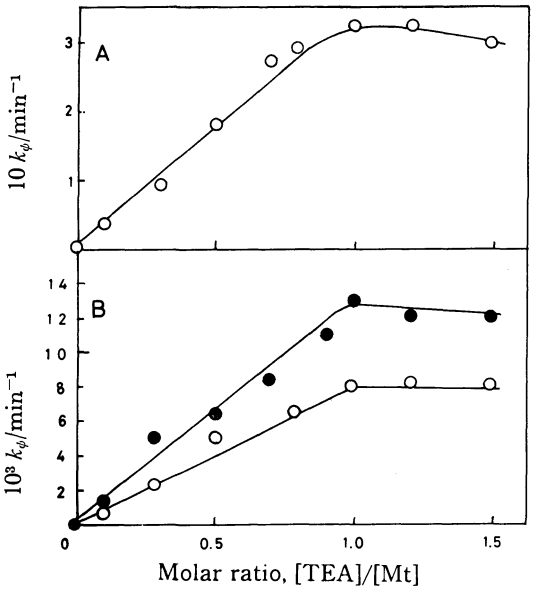

Fig. 2. Relation between k_ψ and molar ratio of [TEA]/[Mt].
Methyloxirane: 50 mmol, organometals [Mt]: 0.15 M, initial pressure of CO_2: 50 kg/cm^2. A: Ph_3SnBr–TEA at 100 °C. B: Ph_3SiBr–TEA (●) and Ph_3GeBr–TEA (○) at 120 °C.

relevant conditions. Consequently, the enhanced catalytic activity of the binary systems can be said to result from a cooperative effect of the organometallic halide with the base.

In order to understand the synergic effect of the organometallic compound with the base, the Ph_3SnBr–TEA system, showing a high rate enhancement, was examined in detail. Pseudo-first-order rate constant k_ϕ was plotted against the molar ratio of [TEA]/[Ph_3SnBr] as shown in Fig. 2. It can be seen from Fig. 2 that k_ϕ linearly increases with molar ratio, reaches a maximum value at molar ratio 1.0, and follows a gradual decrease. This characteristic curve indicates that the effective enhancement of the catalytic activity results from a 1 : 1 complexation between Ph_3SnBr and TEA.[5,12] Consequently, in the binary systems the pseudo-first-order rate constant k_ϕ may be divided into the respective contributions of organometallic halides alone, of bases alone, and of the organometallic halide–base complex and k_ϕ can be expressed as in Eq. 5 by using the equilibrium constant K shown in Eq. 3:

$$\text{Mt} + \text{base} \overset{K}{\rightleftharpoons} \text{Mt–base(complex)}, \quad (3)$$

$$k_\phi = k_{\phi\,\text{Mt}} + k_{\phi\,\text{base}} + k_{\phi\,\text{complex}} \quad (4)$$

$$= k_{\phi\,\text{Mt}} + k_{\phi\,\text{base}} + k_{\text{complex}} K[\text{Mt}][\text{base}], \quad (5)$$

$$k_{\phi\,\text{complex}} = k_{\text{complex}}[\text{complex}], \quad (6)$$

where Mt denotes the organometallic halide. From the results shown in Table 1, the contribution from base alone is negligible, and then Eqs. 7 and 8 can be introduced:

$$k_\phi = k_{\phi\,\text{Mt}} + k_{\text{complex}} K[\text{Mt}][\text{base}] \quad (7)$$

$$= k_{\phi\,\text{Mt}} + [\text{Mt}]^2 k_{\text{complex}} K([\text{base}]/[\text{Mt}]). \quad (8)$$

These equations indicate that the catalytic activity of the complex, $k_{\text{complex}}K$, can be calculated from the increment, $\Delta k_\phi/\Delta[\text{base}]$, in the linear part of the curve in Fig. 2.

Similar curves were also obtained for Ph_3GeBr– and Ph_3SiBr–TEA systems at 120 °C, as illustrated in Fig. 2, and for Ph_3SbBr_2–TEA and Me_2TeI_2–TPP systems at 100 °C. The calculated values of $k_{\text{complex}}K$ for each organometallic halide–base system are listed in Table 3. It is found that the value for Ph_3SnBr–TEA system is larger than those for the other binary systems, and that the value for Ph_3SbBr_2–TEA system is negligibly small.

Table 3. The catalytic activity of the complexes in the cycloaddition reaction of CO_2 to PO[a]

Binary system Mt–Base	$k_{\text{complex}}K/\text{M}^{-2}\,\text{min}^{-1}$ [b]
Ph_3SnBr–TEA	160[c]
Ph_3GrBr–TEA	0.38[d]
Ph_3SiBr–TEA	0.43[d]
Ph_3SbBr_2–TEA	0.24[c]
Ph_3BiBr_2–TEA	0.24[d]
Me_2TeI_2–TPP	4.3[c]

a) The catalytic activity of the complexes is defined in Eq. 8. b) The value of $k_{\text{complex}}K$ was calculated from the linear relation between k_ϕ and molar ratio (base/Mt) shown in Fig. 2. c) Obtained at 100 °C. d) Obtained at 120 °C.

Tetravalent organotin halides are known to react with bases such as amines or phosphines to give a pentacoordinated trigonal bipyramidal complex.[12,13] Such complexation would increase the polarity of the Sn-halogen bonds; in other words, it activates the Sn-halogen bonds. Further, there remains one active coordination site in the complexed tin atom because tin atom can generally uses six coordination sites.[12]

Pentavalent organoantimony compounds are also known to afford a hexacoordinated complex with bases.[10] However, their electron acceptability has been reported to be smaller than that of tetravalent tin compounds.[1,14] In addition, such a hexacoordination may result in a decrease of the polarity of the Sb-halogen bonds in contrast with pentacoordination.[5,12,15] Thus, the complexation is suggested to play a less significant role in the catalytic activity of the Ph_3SbBr_2–base systems than with the Ph_3SnBr–base systems.

On the basis of the results obtained, a reaction pathway as indicated by the set of Eq. 3 and the following two equations

$$CO_2 + PO \rightleftharpoons CO_2\text{–PO}, \quad (9)$$

$$CO_2\text{–PO} + \text{Mt(or Mt–base)} \longrightarrow \text{PC} + \text{Mt(or Mt–base)}, \quad (10)$$

is tentatively proposed. The intervention of the CO_2–PO complex has been deduced on the basis of appearance of a new absorption band in UV spectrum of the saturated solution of CO_2 in PO,[16] similarly to the CO_2–phenylaziridine systems.[19] A plausible intermediate is also shown in Scheme 1.

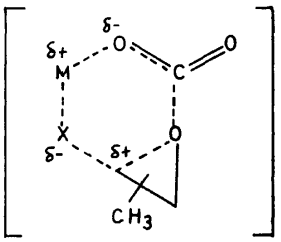

Scheme 1.

Experimental

Materials. The organometallic halides, Ph_3SnCl,[20] Ph_3SnBr,[21] Ph_3SnI,[21] Ph_3GeBr,[22] Ph_3SiBr,[23] Ph_3SbBr_2,[1] Ph_4SbBr,[1] Ph_3BiBr_2,[24] Me_2TeCl_2,[7] Me_2TeBr_2,[7] and $(p\text{-}CH_3C_6H_4)_2TeCl_2$[25] were prepared by the reported methods and checked by elemental analysis. Methyloxirane (PO) and ethyloxirane (1,2-butylene oxide, BO) was dried and stored over calcium hydride. The Lewis bases used as additive were distilled or recrystallized before use. The solvents were used after rectification.

Analysis. Analytical gas chromatography (GC) was performed on a Shimadzu GC-4BPTF gas chromatograph with an FID detector and on a GC-3BT with a TCD detector.

Reaction Procedures. Under a Pressure of CO_2: The cycloaddition reaction of CO_2 to PO was carried out in a 50 ml stainless-steel autoclave under the conditions as described previously.[1] The initial pressure of CO_2 was always 50 kg/cm^2.

Under Atmospheric Pressure of CO_2: The cycloaddition reaction of CO_2 to ethyloxirane was carried out under atmospheric pressure of CO_2 at 60 °C. The organometallic halides (0.5 mmol), the base (if solid (TPP)) and a magnetic stirring bar was placed in a 50 ml three-necked flask equipped with a condenser, a CO_2 inlet connected to a 1000 cm^3 balloon filled with CO_2, and a rubber septum (SGA Scientific Inc.) through which sample for GC analysis was taken. The flask was evacuated and flashed by CO_2 three times, and then 50 mmol of ethyloxirane and 0.5 mmol of the base (if liquid (TEA and Py)) was introduced through the septum by the syringe technique. The reaction was monitored by GC. The only detectable product was 4-ethyl-1,3-dioxolan-2-one (1,2-butylene carbonate).

The authors are greatly thankful to Messrs. Kiyoshi Ogawa and Hirohiko Katayama for their assistance in the preparation of the organotellurium and organogermanium compounds.

References

1) H. Matsuda, A. Ninagawa, and R. Nomura, *Chem. Lett.*, **1979**, 1261; R. Nomura, A. Ninagawa, and H. Matsuda, *J. Org. Chem.*, **45**, 3735 (1980).
2) A. L. Shapiro, I. S. Lyubovskii, and S. Z. Levin, *Zh. Org. Khim.*, **6**, 1366 (1970).
3) F. Ota and S. Tobita, Japan Patent 48-27314 (1973); *Chem. Abstr.*, **79**, 136527r (1973); M. Ratzenhofer and H. Kisch, *Angew. Chem.*, **92**, 303 (1980).
4) H. Matsuda, A. Ninagawa, R. Nomura, and T. Tsuchida, *Chem. Lett.*, **1979**, 573.
5) E. L. Muetterties and R. A. Schunn, *Quart. Rev.*, **20**, 245 (1966).
6) H. J. M. Bowen, "Tables of Interatomic Distances and Configuration in Molecules and Ions," The Chemical Society, London (1958).
7) R. H. Vernon, *J. Chem. Soc.*, **117**, 86 (1920).
8) R. H. Irgolic, "The Chemistry of Tellurium," Gordon and Breach, New York (1974), Chap. VII.
9) H. Matsuda and S. Matsuda, *Kogyo Kagaku Zasshi*, **63**, 114, 1958 (1960).
10) R. Nomura, H. Hisada, A. Ninagawa, and H. Matsuda, *Makromol. Chem.*, **183**, 1073 (1982).
11) For example, Montecatini, Ital. Patent 499185 (1954); *Chem. Abstr.*, **51**, 9681b (1957); Y. Fujita, T. Morimoto, and T. Nakanoichi, Japan Patent 48-22702 (1973); *Chem. Abstr.*, **79**, 146007 k (1973); C. Neri and G. Cipriani, Ger. Offen. 2 611 087 (1976); *Chem. Abstr.*, **86**, 29791v (1977).
12) G. P. Van der Kelen, E. V. Van den Berghe, and L. Verdonk, "Organotin Compounds," ed by A. K. Sawyer, Marcel Dekker, New York (1971), Vol. 1, Chap. 3.
13) J. E. Fergusson, D. K. Grant, R. H. Hickford, and C. J. Wilkins, *J. Chem. Soc.*, **1959**, 99; R. Hulme, *ibid.*, **1963**, 1524.
14) R. Nomura, H. Hisada, A. Ninagawa, and H. Matsuda, *Makromol. Chem., Rapid Commun.*, **1**, 135 (1980).
15) M. Webster, *Chem. Rev.*, **66**, 87 (1966).
16) In visible and near UV regions, neither CO_2[17] nor PO[18] has absorption band. On the other hand, a new absorption band at *ca.* 260 nm appeared when CO_2 was introduced into PO.
17) Y. Tanaka, A. S. Jursa, and F. J. LeBlanc, *J. Chem. Phys.*, **32**, 1199 (1960); J. W. Rabalais, J. M. McDonald, V. Scherr, and S. P. McGlynn, *Chem. Rev.*, **71**, 73 (1971).
18) G. Fleming, M. M. Anderson, A. J. Harrison, and L. W. Pickett, *J. Chem. Phys.*, **30**, 351 (1959).
19) T. Kagiya and T. Matsuda, *Polymer J.*, **2**, 398 (1971).
20) H. Gilman and H. W. Melvin, Jr., *J. Am. Chem. Soc.*, **71**, 4050 (1949).
21) R. F. Chambers and P. C. Scherer, *J. Am. Chem. Soc.*, **48**, 1054 (1926).
22) C. A. Kraus and L. S. Foster, *J. Am. Chem. Soc.*, **49**, 457 (1927).
23) C. Eaborn, *J. Chem. Soc.*, **1952**, 2846.
24) F. Challenger, *J. Chem. Soc.*, **105**, 2210 (1914).
25) J. Bergman, *Tetrahedron*, **28**, 3323 (1972).

Bromination of Methoxybiphenylenes

Hiroto KIDOKORO, Masaru SATO, and Seiji EBINE*
Department of Chemistry, Saitama University, Urawa, Saitama 338
(Received December 28, 1981)

Bromination of 2-methoxybiphenylene derivatives did not give biphenyl derivatives but benzocyclooctene derivatives. 1-Methoxybiphenylene, on the other hand, was brominated to give the benzobicyclo[4.2.0]octadienone derivatives.

Biphenylene is a condensed ring aromatic hydrocarbon of special interest, because its central four-membered ring is expected to have contribution of an antiaromatic cyclobutadiene structure. According to expectation, biphenylene has been evidenced to have some specific reactivity in addition to the reactivity common to other condensed ring aromatics.[1] For example, biphenylene was brominated in the presence of pyridine to give a monobromobiphenylene (substitution product) in 49% yield,[2] and in the absence of the catalyst to give benzocyclooctene derivatives (benzene ring-opened products) as the main products.[3] Photobromination of biphenylene gave also a benzobicyclo[4.2.0]octadienone derivative (addition product) besides two products described above.[4] On the other hand, a 2-substituted biphenylene was brominated at the 3-position regioselectively to give a 2-substituted 3-bromobiphenylene,[1] which was reported to be brominated further with the C_{4a}–C_{4b} bond fission to give biphenyl derivatives (four-membered-ring-opened products).[5,6] We here report the systematic reexamination on bromination of methoxybiphenylenes.[7]

2-Methoxybiphenylene was treated with 1.6 molar equivalents of bromine in carbon tetrachloride at 40 °C to give 3-bromo-2-methoxybiphenylene (**1**), tribromo compound **2**, and tribromo ketone **3** in 30, 14, and 6% yields, respectively. The structure of **3** was first assigned as 5,8,10-tribromo-7,(8*H*)-benzocyclooctenone by the following spectral data. IR (KBr): 1680 cm^{-1}. ^1H NMR ($CDCl_3$): δ 4.81 (d, 1H, J=9.6 Hz, H-8), 6.73 (d, 1H, J=9.6 Hz, H-9), 7.18 (s, 1H, H-6), and 7.2—8.0 (m, 4H, Ar-H). ^{13}C NMR ($CDCl_3$): δ 53.5 (C-8) and 185.2 (C-7). The isolation of **3** suggests an intermediate formation of 5,7,10-tribromo-8-methoxybenzocyclooctene (**2**) as its precursor. Monobromo compound **1** was further brominated in dichloromethane to give the same tribromo compound **2**, mp 118—119 °C in 70% yield. A tribromo compound having the same mp as that of **2** was previously prepared by bromination of **1** in acetic acid and assigned by McOmie and co-workers to 2′,4,6-tribromo-3-methoxybiphenyl (**4**) based on its IR and UV spectra.[5] We also reexamined the bromination of **1** under the same conditions described by the above authors[5] and obtained the same product as **2** in 43% yield, along with the starting biphenylene in 13% recovery. The ^1H NMR spectrum of **2** showed two olefinic doublets (J=1.2 Hz) at δ 6.53 and 6.66 in a similar magnetic field to the corresponding protons of 5,10-dibromobenzocyclooctene (δ 6.51, $J_{6,9}$=1.6 Hz).[3] The UV spectrum of **2** also resembles that of 5,10-dibromobenzocyclooctene rather than 2,2′-dibromobiphenyl (Fig. 1). In addition, **2** was converted with trifluoroacetic acid to tribromo ketone **3** in 63% yield, whose structure was conclusively determined by X-ray crystallographic analysis.[8] On the basis of these data the tribromo compound **2** should not be assigned to 2′,4,6-tribromo-3-methoxybiphenyl (**4**), but 5,7,10-tribromo-8-methoxybenzocyclooctene.

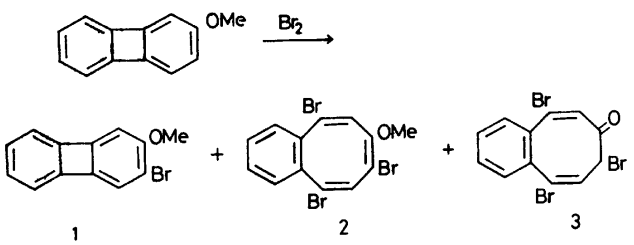

In order to generalize the fact that the further bromination of bromomethoxybiphenylenes gives brominated benzocyclooctenes, the bromination of other 2-methoxybiphenylenes was then examined. 2,7-Dimethoxybiphenylene was treated with 2 molar equivalents of bromine in dichloromethane to give 3-bromo-2,7-dimethoxybiphenylene (**5**) and 3,6-dibromo-2,7-dimethoxybiphenylene (**6**) in 30 and 20% yields, respectively, in partial agreement with McOmie *et al.*[6] who obtained only **6** in 46% yield under similar conditions. Compound **6** was further treated with 1.5 molar equivalents of bromine to give 2,5,8,10-tetrabromo-3,7-dimethoxybenzocyclooctene (**7**) in 89% yield. The ^1H NMR spectrum of **7**, like that of **2**, showed two olefinic doublets at δ 6.57 and 6.66 (J=1.2 Hz).

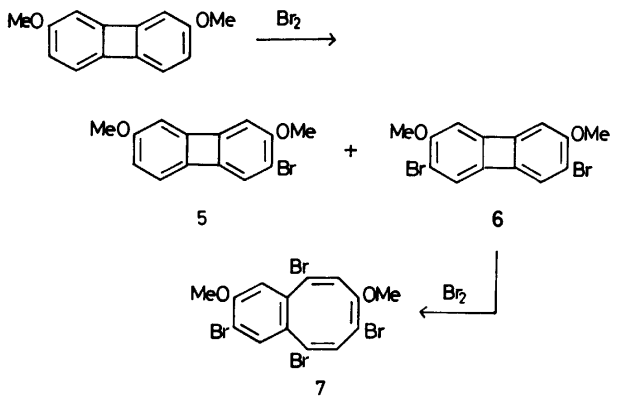

1,2-Dimethoxybiphenylene reacted with an excess of bromine to give 3-bromo-1,2-dimethoxybiphenylene (**8**) and 5,8,10-tribromo-6,7-dimethoxybenzocyclooctene (**9**) in 81 and 6% yields, respectively. Further bromina-

tion of **8** gave **9** in a low yield. The structure of **9** was assigned by the following ^{1}H NMR spectrum (CCl_4): δ 3.56 (s, 3H, OCH_3), 3.71 (s, 3H, OCH_3), 6.81 (s, 1H, H-9), and 7.44 (s, 4H, Ar–H). The UV spectra of **7** and **9** were closely similar to that of **2** (Fig. 2).

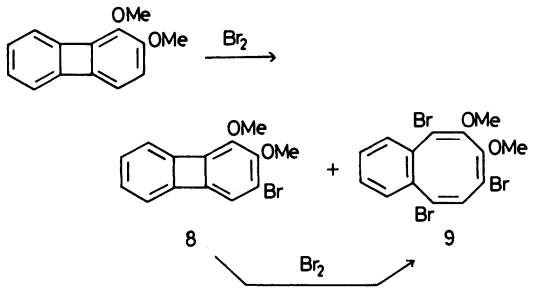

The bromination of biphenylene having one or two methoxyl groups at the 2- and other positions proceeds generally as follows. On treatment with bromine, biphenylene derivatives having an electron-releasing group at the 2-position give 3-substituted products predominantly.[1b] In agreement with this previous finding, 2-methoxy-, 1,2-dimethoxy- 2,7-dimethoxybiphenylenes undergo bromination at the 3- and 6-position to give 3-bromo and 3,6-dibromo derivatives **1**, **8**, and **6** respectively. On the other hand, biphenylene itself undergoes bromine addition followed by benzene ring-opening to give brominated benzocyclooctenes, because of latent antiaromatic character of the central four-membered ring. The above brominated methoxybiphenylenes (**1**, **6**, and **8**) are more electron-deficient than unbrominated methoxybiphenylenes and behave like biphenylene itself on further bromination: **1**, **6**, and **8** react with bromine to give first biphenylenium ions (**10**) and then dibromo adducts **11**, which undergo spontaneously ring-opening to give bromomethoxybenzocyclooctenes **2**, **7**, and **9** as shown in the following scheme. The bromide ion attacks **10** at the 4b-position and the subsequent C_{4a}–C_{4b} bond fission to **4** does not take place.

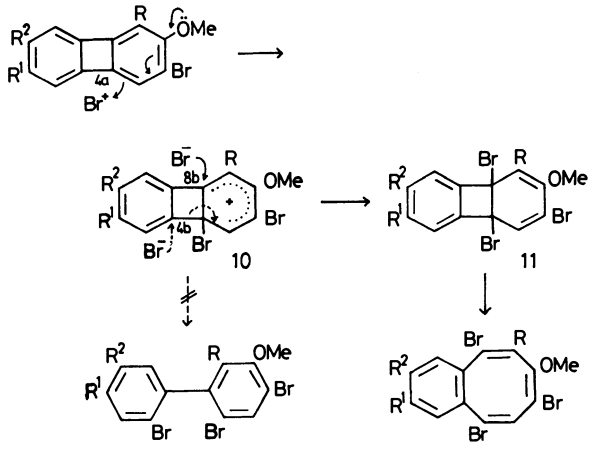

Bromination of 1-methoxybiphenylene proceeded in a somewhat different manner from that of 2-methoxybiphenylenes. Thus, 1-methoxybiphenylene was treated with an excess of bromine to give colorless crystals, mp

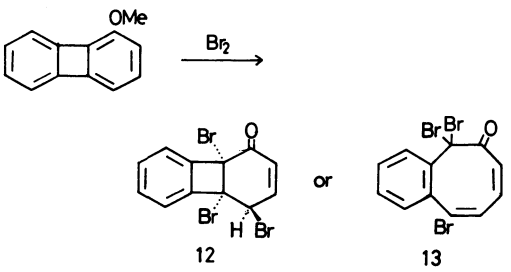

165—167 °C (decomp) in 25% yield, along with two kinds of unstable oils. The MS spectrum [M^+ *m/e* 404/406/408/410 (1.3/3.7/3.7/1.3%)] and IR spectrum (ν_{CO} 1683 cm^{-1}) suggest that the product is tribromo ketone **12** or **13**. The following ^{1}H NMR spectrum of the tribromo ketone is consistent with the structure **12**, rather than **13**: δ 5.35 (d, 1H, J=6.8 Hz), 5.93 (d, 1H, J=10.7 Hz), 6.98 (dd, J=10.7 and 6.5 Hz), and 7.1—7.8 (m, 4H, Ar–H). The ^{13}C NMR spectrum gave a further structual support showing the presence of three aliphatic carbon (47.7, 70.7, and 72.0 ppm) and two olefinic carbon signals (124.6 and 142.3 ppm). The stereochemistry of **12** was suggested by setting up the molecular model having a minimum steric strain. The formation of **12** on bromination of 1-methoxybiphenylene would be explained by the pathway described below.

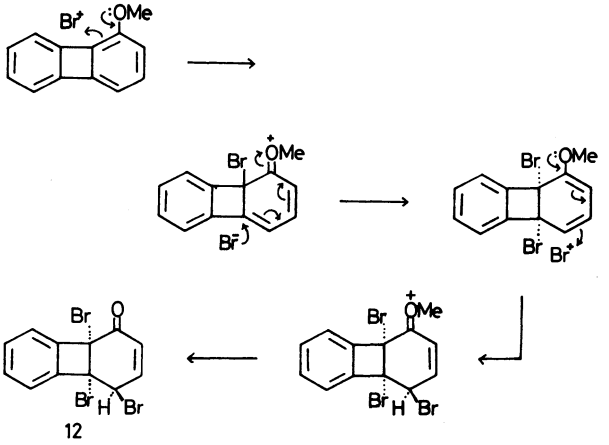

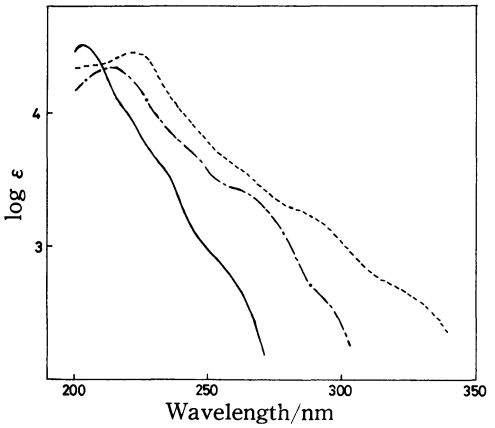

Fig. 1. UV spectra of 2,2′-dibromobiphenyl (——), 5,10-dibromobenzocyclooctene (– – –), and tribromo compound **2** (------).

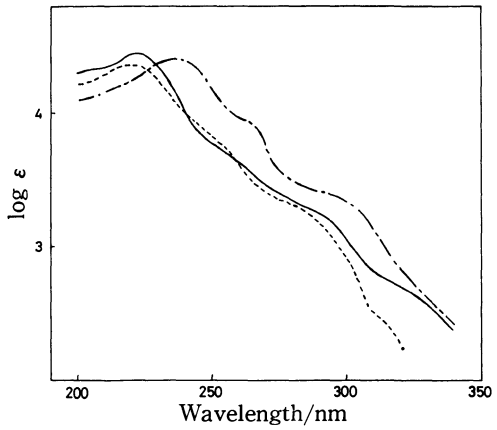

Fig. 2. UV spectra of **2** (——), **7** (– – –), and **9** (------).

The easy conversion of methoxybiphenylenes to methoxybenzocyclooctene derivatives stimulated the reexamination on bromination of 2,3-dimethoxybiphenylene, because the resulting bromodimethoxybenzocyclooctenes would be useful precursors to new benzocyclooctene-7,8-diones. It was previously reported that bromination of 2,3-dimethoxybiphenylene gave 1,4-dibromo-2,3-biphenylenedione.[6] The present reexamination on bromination of 2,3-dimethoxybiphenylene under various conditions, however, gave the same result as previously reported, no expected benzocyclooctene-7,8-dione being detected.

Experimental

Bromination of 2-Methoxybiphenylene in Carbon Tetrachloride. To a solution of 2-methoxybiphenylene (2.03 g, 11 mmol) in carbon tetrachloride (20 ml) was added a solution of bromine in carbon tetrachloride (37 g of 5% w/w solution, 11 mmol) under nitrogen. The mixture was stirred for 10 min at room-temperature and warmed at 40 °C for 50 min. A solution of bromine in carbon tetrachloride (10 g of 5% w/w solution, 6 mmol) was further added to the solution, whereupon the color of bromine was discharged almost instantaneously. The solution was washed with a saturated aq solution of sodium hydrogencarbonate and dried (anhyd $MgSO_4$). The yellow-brown oil which remained after evaporation was chromatographed on silica gel by elution with hexane–toluene (2 : 1). The following products were eluted successively. 3-Bromo-2-methoxybiphenylene (**1**) (860 mg, 30%): yellow needles, mp 100—101 °C (from cyclohexane–ethanol) (lit,[6] 102—103 °C). IR (KBr): 1420, 1254, 1233, and 746 cm^{-1}. ^1H NMR ($CDCl_3$): δ 3.92 (s, 3H, OCH_3), 6.3—6.9 (m, 6H). 5,7,10-Tribromo-8-methoxybenzocyclooctene (**2**) (538 mg, 14%): colorless needles, mp 118—119 °C (from ethanol–cyclohexane). Found: C, 37.01; H, 2.15%. Calcd for $C_{13}H_9Br_3O$: C, 37.09; H, 2.15%. UV (EtOH): 223 nm (log ε 4.46). IR (KBr): 1637, 1620, 1340, 1251, 1189, and 768 cm^{-1}. ^1H NMR ($CDCl_3$): δ 3.66 (s, 3H, OCH_3), 6.53 (d, 1H, J=1.2 Hz, H-6) 6.66 (d, 1H, $J_{6,9}$=1.2 Hz, H-9), 7.38 (s, 4H, Ar–H). ^{13}C NMR ($CDCl_3$): δ 57.2 (q), 98.8 (s), 122.7 (s), 126.2 (s), 128.3 (d), 128.6 (d), 128.9 (d), 129.1 (d), 129.5 (d), 133.1 (d), 136.7 (s), 137.4 (s), and 149.8 (s). MS (70 ev): M^+ [*m/e* 418/420/422/424 (3.5/8/8/3.5%)], M^+-Br [*m/e* 339/341/343 (52/100/49%)]. 5,8,10-Tribromo-7,(8*H*)-benzocyclooctenone (**3**) (274 mg, 6%): yellow cubes, mp 138—139 °C (from hexane–acetone). Found: C, 35.42; H, 1.77%. Calcd for $C_{12}H_7Br_3O$: C, 35.42; H, 1.73%. UV (CH_3CN): 213 (log ε 4.24) and 225sh nm (4.20). IR (KBr): 1683, 1595, 1138, 965, 860, and 765 cm^{-1}. ^1H NMR ($CDCl_3$): δ 4.81 (d, 1H, J=9.5 Hz, H-8), 6.73 (d, 1H, J=9.5 Hz, H-9), 7.18 (s, 1H, H-6), and 7.2—8.0 (m, 4H, Ar–H). ^{13}C NMR ($CDCl_3$): δ 53.6 (d, C-8), 120.7 (s), 128.3 (d), 129.6 (d), 130.3 (d), 131.0 (d), 132.5 (d), 133.5 (d), 134.3 (s), 137.0 (s), 137.9 (s), and 185.2 (s, C-7). MS (75 eV): M^+ [*m/e* 404/406/408/410 (0.02/0.04/0.04/0.02%)], M^+-2Br [*m/e* 246/248 (100/97%)].

5,7,10-Tribromo-8-methoxybenzocyclooctene (2). To a solution of **1** (0.25 g, 0.96 mmol) in dry dichloromethane (10 ml) was gradually added a solution of bromine (0.23 g, 2.8 mmol) in dry dichloromethane (7 ml) at 0 °C under nitrogen. The mixture was then kept for 1 h at a room-temperature. After evaporation, the residue was subjected to TLC on silica gel by elution with hexane–benzene. **2** (0.28 g, 70%) was obtained as colorless crystals, mp 118—120 °C.

5,8,10-Tribromo-7(8H)-benzocyclooctenone (3). To a solution of **2** (28 mg) in a small amount of chloroform-*d*, was added trifluoroacetic acid (0.5 ml). The solution was then warmed to 70—80 °C. After evaporation, the crystalline residue was recrystallized from hexane–acetone giving the tribromo ketone **3** (17 mg, 63%).

Bromination of 2,7-Dimethoxybiphenylene. To a solution of 2,7-dimethoxybiphenylene (0.25 g, 1.2 mmol) in dry dichloromethane (10 ml) was added a solution of bromine in dichloromethane (20 ml of 0.3% v/v solution, 1.2 mmol) at −50 °C under nitrogen. The solution was then stirred for 1 h at a room-temperature. After evaporation, the residue was passed through a short column packed with alumina in order to remove a tar. The yellow crystals obtained were purified by TLC on silica gel by elution with benzene, affording the following products, the unreacted starting material (28 mg, 11%) and 3-bromo-2,7-diemthoxybiphenylene (**5**) (102 mg, 30%), colorless crystals, mp 100—101 °C (from hexane–acetone). Found: C, 57.66; H, 3.72%. Calcd for $C_{14}H_{11}BrO_2$: C, 57.75; H, 3.82%. UV (CH_3CN): 250 (log ε 4.56), 258 (4.85), and 369 nm (3.67). IR (KBr): 1615, 1575, 1473, 1456, 1418, 1280, 1270, 1224, 1029, 1013, and 800 cm^{-1}. ^1H NMR ($CDCl_3$): δ 3.73 (s, 3H, OCH_3), 3.85 (s, 3H, OCH_3), 6.0—6.6 (m, 3H), 6.45 (s, 1H, H-8), and 6.72 (s, 1H, H-1). MS (70 eV): M^+ [*m/e* 290/292 (100/98%)], M^+-CH_3 [*m/e* 275/277 (70/68%)], and M^+-CH_3-CO [*m/e* 247/249 (44/43%)]. 3,6-Dibromo-2,7-dimethoxybiphenylene (**6**) (86 mg, 20%), colorless leaflets, mp 166—168 °C (lit,[6] 170—171 °C). ^1H NMR ($CDCl_3$): δ 3.84 (s, 6H, OCH_3), 6.47 (s, 2H, H-1,8), and 6.73 (s, 2H, H-4,5).

2,5,8,10-Tetrabromo-3,7-dimethoxybenzocyclooctene (7). To a solution of **6** (86 mg, 0.23 mmol) in dry dichloromethane (10 ml) was added a solution of bromine in dichloromethane (6 ml of 0.5% v/v solution, 0.58 mmol). The solution was stirred for 1 h at a room-temperature, then washed with water, and dried (anhyd $MgSO_4$). After evaporation, the residue was purified through TLC on silica gel by elution with toluene–hexane (1 : 1). The title compound (109 mg, 89%) was obtained as yellow cubes, mp 200—203 °C (decomp). Found: C, 31.96; H, 1.97%. Calcd for $C_{14}H_{10}Br_4O_2$: C, 31.73; H, 1.90%. UV (CH_3CN): 220sh (log ε 4.15) and 266 nm (4.41). IR (KBr): 2950, 1638 (w), 1620 (w), 1592, 1497, 1355, 1248, and 1049 cm^{-1}. ^1H NMR ($CDCl_3$): δ 3.65 (s, 3H, OCH_3), 3.90 (s, 3H, OCH_3), 6.57 (d, 1H, J=1.3 Hz, H-6), 6.66 (d, 1H, J=1.3 Hz, H-9), 6.80 (s, 1H, H-4), and 7.64 (s, 1H, H-1). MS (75 eV): M^+ [*m/e* 526/528/530/532/534 (0.8/3.0/5.5/3.0/0.8%)] and M^+-Br [*m/e* 447/449/451/453 (35/100/95/35%)].

Bromination of 1,2-Dimethoxybiphenylene. To a solution of 1,2-dimethoxybiphenylene (0.25 g, 1.2 mmol) in dry dichloromethane (40 ml) was slowly added a solution of

bromine in dichloromethane (27 ml of 0.5% v/v solution, 2.7 mmol) under ice-cooling. After being stirred for 1 h, the solution was washed with water and dried (anhyd $MgSO_4$). The solvent was evaporated and the resulting yellow oil was purified through TLC on silica gel by elution with hexane–benzene. 3-Bromo-1,2-dimethoxybiphenylene (**8**) (0.25 g, 81%), colorless crystals, mp 67—68 °C (from hexane–acetone). Found: C, 57.66; H, 3.72% . Calcd for $C_{14}H_{11}BrO_2$: C, 57.75; H, 3.81%. UV (CH_3CN): 257 (log ε 4.56), and 282 nm (4.09). IR (KBr): 2970, 1587, 1475, 1396, 1248, 1028, and 746 cm^{-1}. ^1H NMR ($CDCl_3$): δ 3.81 (s, 3H, OCH_3), 4.00 (s, 3H, OCH_3), 6.55 (s, 1H, H-4), and 7.44 (s, 4H, Ar–H). MS (75 eV): M^+ [*m/e* 290/292 (100/100%)] and M^+-CH_3 [*m/e* 275/277 (47/44%)]. 5,7,10-Tribromo-8,9-dimethoxybenzocyclooctene (**9**) (29 mg, 6%), yellow leaflets, mp 116—117 °C (from hexane–acetone). Found: C, 37.33; H, 2.51%. Calcd for $C_{14}H_{11}Br_3O_2$: C, 37.28; H, 2.46%. UV (EtOH): 220 nm (log ε 4.37). IR (KBr): 2970, 1307, 1294, and 1009 cm^{-1}. ^1H NMR (CCl_4): δ 3.59 (s, 3H, OCH_3), 3.71 (OCH_3), 6.81 (s, 1H, H-9), and 7.44 (s, 4H, Ar–H). MS (70 eV): M^+ [*m/e* 448/450/452/454 (3.2/9.2/9.2/3.2%)], M^+-Br [*m/e* 367/369/371 (37/76/38%)] and M^+-2Br [*m/e* 290/292 (96/100%)].

*5,7,10-Tribromo-8,9-dimethoxybenzocyclooctene (**9**).* To a solution of 3-bromo-1,2-dimethoxybiphenylene (30 mg, 0.1 mmol) was added a solution of bromine (25 mg, 0.16 mmol) in dichloromethane (1.6 ml) under stirring. The solution was stirred for 3 h at a room-temperature. After the usual work-up, followed by TLC on silica gel by elution with benzene–hexane, the oily product was separated into the title compound (9 mg, 19%) and the starting material (14 mg, 47%).

*4,4a,8b-Tribromo-1,4,4a,8b-tetrahydrobiphenylen-1-one (**12**).* To a solution of 1-methoxybiphenylene (0.10 g, 0.55 mmol) in dichloromethane (5 ml) was added under stirring a solution of bromine in dichloromethane (0.5%v/v solution) at 0 °C under nitrogen until the bromine-color of the reaction mixture remained unchanged (27 ml, 2.6 mmol). The solution was then stirred for 2 h at a room-temperature. After the usual work-up, an orange oil obtained was purified by measn of TLC by elution with toluene. In addition to an unstable red oil (55 mg) and an unstable orange oil (44 mg) [IR (Neat): 1697, 1668, and 757 cm^{-1}, ^1H NMR ($CDCl_3$): δ 6.34 (d, 1H, J= 10.3 Hz), 7.01 (d, 1H, J=10.4 Hz), 7.59 (s, 4H), and 7.1—7.6 (m)], the title compound (55 mg, 25%) was obtained as colorless crystals, mp 165—167 °C (decomp) from hexane). Found: C, 35.31; H, 1.77%. Calcd for $C_{12}H_7Br_3O$: C, 35.42; H, 1.74%. UV (CH_3CN): 257 (log ε 4.56) and 282 nm (4.09). IR (KBr): 1683, 1611, 1467, 800, and 750 cm^{-1}. ^1H NMR ($CDCl_3$): δ 5.35 (d, 1H, J=6.8 Hz, H-5), 5.93 (d, 1H, J= 10.7 Hz, H-3), 6.98 (dd, 1H, J=10.7 and 6.8 Hz, H-4), and 7.1—7.8 (m, 4H, Ar–H). ^{13}C NMR ($CDCl_3$): δ 47.7 (d), 70.7 (s), 72.0 (s), 121.3 (d), 123.0 (d), 124.6 (d), 131.9 (d), 132.0 (d), 141.6 (s), 142.3 (d), 143.3 (s), and 186.9 (s). MS (70 eV): M^+ [*m/e* 404/406/408/410 (0.4/1.0/1.0/0.4%)], M^+-Br [*m/e* 325/327/329 (18/38/18%)], $M^+-Br-CO$ [*m/e* 297/299/301 (13/26/13%)], and M^+-2Br [*m/e* 246/248 (40/38%)], and $M^+-3Br-CO$ [*m/e* 139 (100%)].

References

1) a) M. P. Cava and M. J. Mitchel, "Cyclobutadiene and Related Compounds," Academic Press, New York and London (1965), p. 255; b) J. W. Barton, "Nonbenzenoid Aromatics," ed by J. P. Snyder, Academic Press, New York and London (1969), p. 32.

2) W. Baker, J. W. Barton, and J. F. W. McOmie, *J. Chem. Soc.*, **1958**, 2666.

3) J. W. Barton, D. N. Henn, K. A. McLaughlan, and J. F. W. McOmie, *J. Chem. Soc.*, **1964**, 1622.

4) J. W. Barton and K. E. Whitaker, *J. Chem. Soc., C*, **1968**, 28.

5) W. Baker, J. F. W. McOmie, D. R. Preston, and V. Rogers, *J. Chem. Soc.*, **1958**, 414.

6) J. M. Blatchly, D. V. Gardner, J. F. W. McOmie, and M. L. Watts, *J. Chem. Soc., C*, **1968**, 1545.

7) A part of this work was published in a preliminary report: H. Kidokoro, M. Sato, and S. Ebine, *Chem. Lett.*, **1981**, 1269.

8) The details of the X-ray analysis of **3** will be published in the subsequent paper in this series.

Aldol Condensations Catalyzed by Co(II) Complexes of Pyridine-containing Copolymers

Ken-ichi WATANABE* and Atsushi IMAZAWA
Department of Chemistry, Faculty of Science, Tokyo Metropolitan University, Fukazawa, Setagaya-ku, Tokyo 158
(Received December 24, 1981)

The cross aldol condensations of aldehydes and ketones catalyzed by Co(II) complexes of pyridine-containing copolymers proceed under neutral conditions in DMF or DMSO to afford α,β-unsaturated ketones without any by-product. The solid complex catalysts are capable of repeated use. The reactions of aromatic aldehydes and ketones give good results but not those of aliphatic compounds. Effects of substituent groups in chalcone formation are observed. The catalytic reaction features with the polymer-complex catalysts are compared with that with Co(II)-pyridine complex. The polymer-complex-catalyzed aldol condensations are discussed briefly in relation to the enzymatic reaction of Class II aldolase (metalloenzyme).

Aldol condensation reactions are generally catalyzed by strong bases or acids. Recently, we have found that the condensation reactions are catalyzed by 2,2'-bipyridine complexes of the first-row transition metals[1] and Co(II) complexes of polymers[2] under neutral conditions. The reactions of aldehydes and ketones with these complex catalysts afford only cross condensation products, α,β-unsaturated ketones, in satisfactory yields. With regard to polymer-catalyzed aldol condensations, catalysis of ion exchange resins have been known, but the product yield of the reactions is low along with some by-products.[3] In this paper, the scope and limitation of the aldol condensation reactions promoted by the Co(II) complexes of pyridine-containing copolymers will be described in detail together with the catalytic behavior of the polymer complexes. Some consideration is also given to the catalysis of Class II aldolase.

Results and Discussion

Polymer Complex Catalysts. The polymers employed for the ligand are as follows:
Poly(4-vinylpyridine):[4] PVP, crosslinked poly(4-vinylpyridine):[4] VP, crosslinked 4-vinylpyridine-styrene copolymer:[5] VP–St (1 : 3), crosslinked 4-vinylpyridine-methyl methacrylate copolymer:[6] VP–MMA (1 : 3), crosslinked 4-vinylimidazol-methyl acrylate copolymer:[7] VIm–MA (1 : 10).

These polymers were prepared by conventional methods in the literature cited.[4-7] 1,4-Divinylbenzene was used as a crosslinking agent, 1 mol% to the polymers, and the crosslinked polymers were insoluble in the common organic solvents. The metal(II) complexes of these polymers were prepared by adding a solution of cobalt(II) acetate in *N,N*-dimethylformamide (DMF) to the swelled polymers in DMF and subsequent stirring at room temperature for 24 h. The cobalt(II) complexes thus obtained were reddish to light purple in color and the content of the Co(II) ion in the complexes was calculated from the difference of the initial amount to the residual untrapped amount of the Co(II) ion. The estimated ratio of the Co(II) ion to the pyridine or imidazol moiety in the complexes was about 1 : 1, which suggested the existence of vacant coordination sites for the ligand reactions (Table 1). In the IR spectra of the copolymer VP–St, absorption at 1600 cm^{-1} was observed and was attributed to the pyridine ring. This absorption shifted to 1620 cm^{-1} in the case of the Co(II) complex of the polymer.

Effects of Cross Linkage and Copolymer. In order to examine the activity of the Co(II)–polymer-complex catalysts thus prepared, aldol condensations of benzaldehyde with excess of acetophenone were carried out in the presence of the catalyst in DMF at 80 °C for 18 h. The amount of Co(II) ion in the polymer complex used was about 16 mol% of the aldehyde employed. After the reaction, the catalyst was removed from the reaction mixture by filtration. No change in appearance of the catalyst was observed. The filtrate was analyzed by means of GLC to determine the yield of the reaction product, 1,3-diphenyl-2-propen-1-one (chalcone). To isolate the chalcone, the filtrate was evaporated *in vacuo*

Table 1. Co(II)–polymer complexes

Ligand (crosslinked)	py-Unit (mmol/g)	Co(II) ion (mmol/g)	py-Unit to Co(II) ion
VP	6.0	4.0	1.5
VP–St	2.38	2.4[a]	0.99
VP–MMA	3.5	3.5	1.0
VIm–MA	1.4	1.55	0.9

a) $Ni(OAc)_2$ complex: 1.9 mmol/g.

Table 2. Aldol condensations with Co(II)–polymer complex catalysts

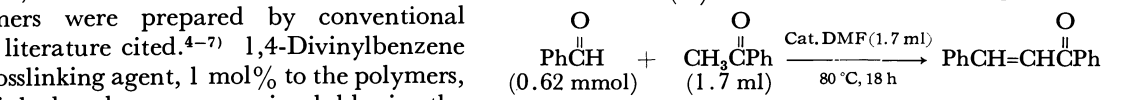

No.	Catalyst		Yield/%[a]
1	Co(II)–PVP	[Co(II) : py=1 : 1.5]	41
2	Co(II)–VP	[Co(II) : py=1 : 1.5]	53
3	Co(II)–VP–St	[Co(II) : py=1 : 1]	100 (84)
4	Co(II)–VP–MMA	[Co(II) : py=1 : 1]	(84)[b]
5	Co(II)–VIm–MA	[Co(II) : Im=1 : 0.9]	(64)[c]
6	Co(II)–py	[Co(II) : py=2 : 3]	80
7	Co(II)–Im	[Co(II) : Im=1 : 1]	(75)
8	$Co(OAc)_2 4H_2O$		31
9	Am. IR-120		36

a) By GLC analysis, based on benzaldehyde used. The values in parentheses are isolated yields. b) 84% in DMSO and 59% in MeOH (isolated). c) 83% in DMSO (isolated); 81% by reused catalyst in DMSO.

to give a yellow oil which was treated by preparative TLC, determined by means of mp, IR, and NMR. For example, in the reaction with the complex Co(II)–VP–St, the yield of chalcone by GLC was 100% and the isolated yield was 84%, mp 55—58 °C. The reaction conditions and the results are summarized in Table 2 together with some other data for comparison. The reaction did not proceed in the absence of the catalyst, and all the ligand polymers themselves without the Co(II) ion showed no catalytic activity. The reactions did not proceed at room temperature even over prolonged reaction periods in the presence of the polymer-complex catalyst. Only PVP was soluble in DMF and the Co(II)–PVP complex catalyst as a solution in DMF (Co(II) : pyridine unit=1 : 1.5) was used for the reaction No. 1 (homogeneous). The Co(II) ion itself showed some catalytic activity (No. 8). The PVP ligand seemed to enhance the reaction somewhat by co-ordination of the pyridine ring to Co(II) ions (No. 1). Crosslinking further enhanced the catalytic activity as observed in the reaction with Co(II)–VP (No. 2), affording higher product yield (53%) than that with Co(II)–PVP (41%) though it was not as good as that obtained with the Co(II)–py complex (No. 6, 80%). On the other hand, the crosslinked copolymer of 4-vinylpyridine and styrene Co(II)–VP–St showed a predominant result (No. 3, 100%). The reaction with the ion exchange resin Amberlite IR-120 (No. 9) afforded chalcone in low yield (36%) accompanying a considerable amount of the self-condensation product of acetophenone, 1,3-diphenyl-2-buten-1-one, and other by-products under similar reaction conditions (GLC). On the contrary, no side reactions were observed with the Co(II)–VP–St catalyst. The $Ni(OAc)_2$–VP–St copolymer was also prepared (Table 1, footnote), but, it showed almost no catalytic activity for chalcone formation under similar reaction conditions.

Various Aldol Condensations with Co(II)–VP–St Catalyst. It was proved above that the Co(II)–VP–St-copolymer-complex in DMF was the most effective catalyst system for the reaction. Therefore, various aldol condensations with this catalyst were subsequently investigated. The reaction conditions were similar to that of Table 2. The reaction products were isolated and identified as α,β-unsaturated ketones, and no side reactions were observed. The results of the reactions of *p*-substituted benzaldehyde or *p*-substituted acetophenones are shown in Table 3, and the reactions with some aliphatic carbonyl compounds are summarized in Table 4. The purity of the products thus obtained was consistently high, probably because the polymer-complex-catalyzed reactions took place under neutral conditions.

In general, reactions between aromatic aldehydes and ketones gave good results, but not those of aliphatic compounds. The reactions shown in Table 3 yielded the corresponding chalcones and the product yields were remarkably affected by the substituent groups of either aldehydes or ketones: reactants having electron-attractive substituents gave high yields (products: **a**, **b**, **g**, **h**) and those having electron-donative ones gave low yields (products: **e**, **f**, **i**). The reaction of 2-butanone with benzaldehyde gave only 1-phenyl-1-penten-3-one (Table 4, **k**), though the yield was low. This regioselectivity was the same for reactions catalyzed by Co(II)–bpy complex, namely base-catalyzed type.[1]

Table 3. Aldol condensations with Co(II)–VP–St catalyst(I)

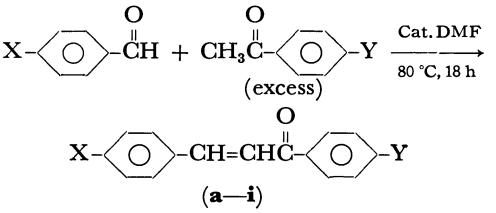

(**a**—**i**)

X	Y	Product	Yield/%	Mp θ_m/°C	(Lit)
CN	H	**a**	98	162—163	
NO_2	H	**b**	93[a]	164—165	(8)
Cl	H	**c**	81	117—118	(8)
H	H	**d**	84[b]	55—58	(9)
OCH_3	H	**e**	55	75—77	(9)
CH_3	H	**f**	44	97—98	(10)
H	CN	**g**	98	120—121	
H	NO_2	**h**	93	151—152	(11)
H	OCH_3	**i**	44	109—110	(12)

a) By reused catalyst(three times): 90—92%. b) By reused catalyst: 82%.

Table 4. Aldol condensations with Co(II)–VP–St catalyst(II)

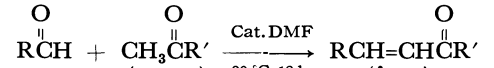

R	R′	Product	Yield/%	Mp θ_m/°C	(Lit)
Ph	CH_3	**j**	66[a]	41—42	(13)
Ph	C_2H_5	**k**	28[b]	39—40	(14)
PhCH=CH	Ph	**l**	50	103—106	(8)
$(CH_3)_2CH$	Ph	**m**	29	Oil	(15)
CH_3CH=CH	CH_3	**n**	6	Oil	(16)

a) Reflux 40 h. b) Co(II)–VP–MMA was used (in sealed tube, *in vacuo*).

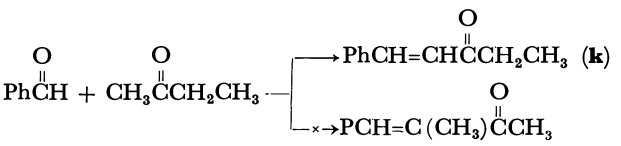

Catalysis of the Copolymer Complexes. On the basis of the above studies, the scope of the catalytic ability of the Co(II) copolymer complex is fairly wide, though it is limited for reactions with aliphatic carbonyl compounds. In order to examine this catalysis feature in detail, the polymer-complex-catalyzed reaction was compared with a pyridine-complex-catalyzed reaction under similar reaction conditions. As the polymer- and

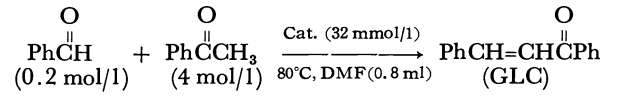

pyridine-complex catalysts, Co(II)–VP–St and Co(II)–4-isopropylpyridine complexes (1 : 1) were employed respectively. The yield of chalcone was determined by GLC analysis: the correlation of the yield with reaction

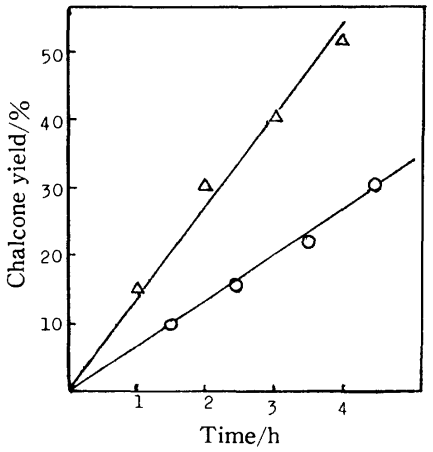

Fig. 1. Reaction profile of the aldol condensations of benzaldehyde and acetophenone catalyzed by polymer and monomer Co(II) complexes.
—○—: Co(II)–VP–St, —△—: Co(II)–*i*-Pr-py (1 : 1).

time is shown in Fig. 1. The catalytic activity of the polymer complex was lower than that of the pyridine complex for the initial stage of the reaction. However, Co(II)–VP–St is superior to Co(II)–py in the reactions for 18 h as shown in Table 2 (100% and 80%). Further, in an equimolar reaction, Co(II)–VP–St was also superior to Co(II)–py. When 0.62 mmol of benzaldehyde and acetophenone was used respectively under similar reaction conditions to that of Table 2 (18 h), the reaction with Co(II)–VP–St gave chalcone in a 70% yield (isolated), but Co(II)–py gave only 50% yield (isolated).

As mentioned above, the electron-attractive groups in the aromatic aldehydes or ketones enhance the reactivity of the substrates in these reactions (Table 3) as well as acid or base catalyzed aldol condensations.[17] On the contrary, no substituent effect was observed in the reactions with Co(II)–bpy complex (1 : 1) catalyst under similar reaction conditions, *e.g.* chalcone 81%, *p*-$NO_2C_6H_4CH$=CHCOPh 88%, *p*-ClC_6H_4CH=CHCOPh 72%, *p*-$CH_3OC_6H_4CH$=CHCOPh 88% *etc.*[1] Therefore, the fact that the substituent effect is observed in the aldol condensations with the polymer complex may be one of the unique features of the polymer complex catalyst though the reason of it is not clear.

Concerning the reaction solvent, an aprotic polar solvent such as DMF or DMSO was favorable (Table 2, footnote), and almost no reaction product was obtained in C_6H_6. Further, it was notable that no reaction took place in neat reaction. These facts suggest that an adequate solvent makes the polymer complex swell enough to ingest the substrates into the polymer and so helps good catalysis. A polymer complex catalyst has an advantage of being removed easily from the reaction mixture by filtration and so it can be used repeatedly. In our catalyst system, the polymer complex catalysts were also proved to be reusable with retention of almost the same catalytic activity (Tables 2 and 3, footnote).

Aldol condensations in biological systems are known to be catalyzed by aldolase enzymes, Class I and Class II;[18] the latter is a metalloenzyme containing zinc(II) ion in the active sites. In the reaction of Class II aldolase, however, catalysis of the enzyme has not been elucidated enough, although some models of the reaction mechanism have been proposed by biochemists.[19–21] We also prepared $Zn(OAc)_2$–VIm–MA (Zn : VIm= 1 : 1.35) complex by a procedure similar to that for Co(II) complex, and the yield of chalcone was 40% (isolated) under similar reaction conditions. The effect of a pyridine- or imidazol-containing copolymer as ligand may be important in the metalloenzyme if there is an interaction between metal(II) ion and imidazol ring of a histidine residue, since imidazol as well as pyridine can form π-bonding by coordination to the metall(II) ion.[22] The facts described in this paper might indicate the possibility that polymer complexes can be developed and applied to the aldolase model reaction system. Our catalyst system may present a new model for understanding the Zn(II) ion catalysis in the Class II aldolase.

Experimental

Instruments. The NMR and IR spectra were taken with a Hitachi Perkin-Elmer R-20A spectrophotometer (60 MHz) and a Hitachi 215 Grating Infrared spectrophotometer respectively. The GLC was carried out with a Hitachi K-53 gas chromatograph with a flame ionization detector, using a 1 m stainless steel tube column packed with 10% Carbowax 20 M on Diachrom A (career gas, N_2; temp 220—270 °C). The product yields were determined by GLC and NMR analysis using *p*-$CH_3OC_6H_4COCH_2Ph$ (or PhCOPh) and $Cl_2CHCHCl_2$ as the internal standard respectively. The atomic absorption spectra was taken with a Shimadzu Atomic Absorption-Flame Emission Spectrophotometer AA-640-13.

Preparation of Co(II) Complex of Copolymer VP–St. 4-Vinylpyridine (1.05 g, 10 mmol), styrene (4.17 g, 40 mmol), divinylbenzene (66 mg, 0.5 mmol), 2,2′-azobisisobutyronitrile (82 mg, 0.5 mmol), and benzene (10 ml, solvent) were mixed together in a 20 ml ampule. The contents were degassed by a vacuum system, and the ampule was sealed off under vacuum and heated at 70 °C for 40 h. The transparent copolymer thus obtained was washed with benzene in a Soxhlet extractor (10 h), dried under reduced pressure at 70 °C, yield 3.06 g. Found: C, 88.08; N, 3.06; H, 7.70%. Calcd (pyridine: benzene unit=1 : 3.2): C, 89.31; N, 3.02; H, 7.50%. The copolymer (1.043 g) was swelled in 16 ml of DMF and then added to a solution of $Co(OAc)_24H_2O$ (3 mmol, 1.5 × pyridine unit) in 5 ml DMF, and stirred for 24 h at room temperature. The reddish purple copolymer complex thus obtained was filtered off and washed with 179 ml of warm DMF. The filtrate and the washings were combined and the content of Co(II) ion in the solution was determined by atomic absorption spectrophotometry. The content of Co(II) ion in the polymer complex was calculated as 2.4 mmol; accordingly the pyridine unit co-ordinated to the Co(II) ion unit was 0.99 (Table 1). The polymer complex was washed with diethyl ether and dried under reduced pressure at 70 °C, yield 1.23 g.

General Procedure for Aldol Condensations. The complex catalyst, Co(II)–VP–St (51 mg) was kept in 0.5—1.7 ml DMF for swelling in 10 ml flask, then benzaldehyde (63 mg, 0.62 mmol) and excess acetophenone (1.7—2.5 ml) were added together into the flask and stirred at 80 °C for 18 h. The polymer catalyst was removed by filtration and the filtrate condensed to some extent under reduced pressure for GLC analysis. The yield of chalcone was calculated on the basis

of the benzaldehyde used (Table 2). In the reaction for Fig. 1, the reaction mixture was analyzed directly without filtration of the catalyst. To isolate the chalcone or its derivatives, the filtrate was evaporated *in vacuo* to expel the solvent, aldehyde and the excess ketone; the residue was then submitted to preparative TLC on silica gel (developed with hexane–ethyl acetate) and the reaction product extracted with ethyl acetate, dried and weighed (Tables 3 and 4).

Condensation Products (Tables 2, 3, and 4). **a**: 4-Cyanochalcone, mp 162—163 °C; IR 2210 cm^{-1} (CN), 1670 cm^{-1} (C=O); ^{1}H-NMR ($CDCl_3$): δ 7.50—8.15 (aromatic proton); Ms: *m/e*, 233 (M^+), 156 ($M^+-C_6H_5$), 128 ($M^+-C_6H_5CO$). **b**: 4-Nitrochalcone, mp 158—160 °C (lit,[8] 158—160 °C); IR 1670 cm^{-1}, 1520 cm^{-1} (NO_2); ^{1}H-NMR ($CDCl_3$): δ 7.50—8.50 (aromatic proton). **c**: 4-Chlorochalcone, mp 117—118 °C (lit,[8] 114 °C); IR 1670 cm^{-1}; ^{1}H-NMR ($CDCl_3$): 7.00—8.00 (aromatic proton). **d**: Chalcone, mp 57—58 °C (lit,[9] 57—58 °C); IR 1670 cm^{-1}; ^{1}H-NMR ($CDCl_3$): δ 6.98—7.98 (aromatic proton). **e**: 4-Methoxychalcone, mp 75—77 °C (lit,[9] 72—74 °C); IR 1660 cm^{-1}; ^{1}H-NMR ($CDCl_3$): δ 3.76 (3H, s, CH_3), 6.78—8.65 (aromatic proton). **f**: 4-Methylchalcone, mp 97—99 °C (lit,[10] 96 °C); IR 1650 cm^{-1}; ^{1}H-NMR ($CDCl_3$): δ 2.32 (3H, s, CH_3), 7.12—8.10 (aromatic proton). **g**: 4′-Cyanochalcone, mp 120—121 °C; IR 2230 cm^{-1} (-CN), 1660 cm^{-1} (C=O); ^{1}H-NMR ($CDCl_3$): δ 7.38—8.17 (aromatic proton). ***h***: 4′-Nitrochalcone, mp 151—152 °C; IR 1660 cm^{-1}, 1510 cm^{-1} (NO_2); ^{1}H-NMR ($CDCl_3$): δ 7.26—8.44 (aromatic proton). **i**: 4′-Methoxychalcone, mp 109—110 °C; IR 1660 cm^{-1}; ^{1}H-NMR ($CDCl_3$): δ 3.78 (3H, s, CH_3), 6.90 (2H, d, aromatic proton),7.20—7.67 (7H, aromatic proton). **j**: Benzylideneacetone, mp 41—42 °C (lit,[13] 41.5 °C); IR 1680 cm^{-1}; ^{1}H-NMR ($CDCl_3$): δ 2.39 (3H, s, CH_3), 6.75 (1H, d, -CH=), 7.35—7.72 (aromatic proton). **k**: 1-Penyl-1-penten-3-one, mp 39—40 °C (lit,[14] 38.5—39.5 °C); ^{1}H-NMR ($CDCl_3$): δ 1.18 (3H, t, CH_3), 2.7 (2H, q, $-CH_2-$), 6.84 (1H, d, -CH=), 7.38—7.78 (aromatic proton). **l**: Cinnamylidenacetophenone, mp 103—106 °C (lit,[8] 102—103 °C); IR 1655 cm^{-1}; ^{1}H-NMR ($CDCl_3$): δ, 6.95—8.10 (aromatic proton). **m**: 1-Phenyl-4-methyl-2-penten-1-one, IR 1680 cm^{-1}; ^{1}H-NMR ($CDCl_3$): δ 1.15 (6H, d, CH_3), 1.70 (1H, m, CH), 6.90—8.00 (aromatic proton); MS: *m/e*, 174 (M^+), 159 (M^+-CH_3), 144 (M^+-2CH_3), 131 ($M^+-CH(CH_3)_2$). **n**: 2,4-Heptadien-1-one, ^{1}H-NMR ($CDCl_3$): δ 1.84 (3H, d, CH_3), 2.20 (3H, s, CH_3).

References

1) K. Irie and K. Watanabe, *Bull. Chem. Soc. Jpn.*, **54**, 1195 (1981); **53**, 1366 (1980).
2) K. Irie, A. Imazawa, and K. Watanabe, *Chem. Lett.*, **1979**, 1401.
3) G. V. Austerweil and R. Pallaund, *J. Appl. Chem. (London)*, **5**, 213 (1955); M. J. Astle and M. L. Pinns, *J. Org. Chem.*, **24**, 56 (1959); A. T. Nielsen and W. J. Houlihan, *Org. React.*, **16**, 74 (1968).
4) M. Narita, *J. Polym. Sci., Polym. Chem. Ed.*, **15**, 353, (1977).
5) V. S. Pshezetsky, I. Massouh, and V. A. Kabanov, *J. Polym. Sci., C*, **22**, 309 (1968).
6) T. Tamikado, *J. Polym. Sci.*, **43**, 489 (1960).
7) C. G. Overberger and N. Vorchheimer, *J. Am. Chem. Soc.*, **85**, 951, (1963).
8) W. Davey and J. R. Gwilt, *J. Chem. Soc.*, **1957**, 1008.
9) F. G. Pond, O. P. Maxwell, and G. M. Norman, *J. Am. Chem. Soc.*, **21**, 955 (1899).
10) V. Hanzlik and A. Bianchi, *Ber.*, **32**, 2282 (1899).
11) E. A. Walker and J. R. Young, *J. Chem. Soc.*, **1975**, 2041.
12) W. Davey and D. J. Tivey, *J. Chem. Soc.*, **1958**, 1720.
13) N. L. Drake and P. Allen, *Org. Synth.* Coll. Vol. I, 77 (1941).
14) H. Haeussler and J. Dijkema, *Ber.*, **77**, 601 (1944).
15) R. Anet, *J. Org. Chem.*, **26**, 246 (1961).
16) V. V. Chelintsev and G. I. Kuznetsova, *Zh. Obshch. Khim.*, **9**, 1901 (1939); *Chem. Abstr.*, **34**, 4387 (1940).
17) A. T. Nielsen and W. J. Houlihan, *Org. React.*, **16**, 45 (1968).
18) B. L. Horecker, O. Tsales, and C. Y. Lai, "The Enzymes," 3rd ed, ed by P. D. Boyer, Academic Press, New York and London (1972), Vol. 7, pp. 213—258.
19) D. E. Morse and B. L. Horecker, *Adv. Enzymol.*, **31**, 125 (1968).
20) R. D. Kobes, R. T. Simpson, B. L. Vallee, and W. Rutter, *Biochemistry*, **8**, 585 (1969).
21) A. S. Mildvan, R. D. Kobes, and W. Rutter, *Biochemistry*, **10**, 1191 (1971).
22) H. Sigel and D. B. McCormick, *Acc. Chem. Res.*, **3**, 201 (1970); H. Sigel, "Metal Ions in Biological Systems," ed by H. Sigel, Marcel Dekker, Inc., New York (1973), Vol. 2, pp. 63—125.

Michael Additions Catalyzed by Metal(II) Complexes

Ken-ichi WATANABE,* Ken-ichi MIYAZU, and Kazuo IRIE
Department of Chemistry, Faculty of Science, Tokyo Metropolitan University, Fukazawa, Setagaya-ku, Tokyo 158
(Received January 22, 1982)

Michael-addition reactions have been found to proceed in the presence of the $Ni(OAc)_2$ or $Co(OAc)_2$–2,2′-bipyridine complex in DMF under neutral conditions at room temperature without any by-product. The reactions of chalcone and its derivatives with nitromethane generally gave good results. The effects of metal(II) ions, ligands, counter ions, and solvents on the catalysis were examined, and the features of the metal-complex-catalyzed Michael reactions were studied, with some considerations also being given to the catalysis mechanism.

Michael-addition reactions are generally carried out in the presence of strong base catalysts; reactions carried out under such drastic conditions have sometimes caused side reactions.[1] Recently, we have found that the reactions are catalyzed by the Ni(II) or Co(II)–2,2′-bipyridine(bpy) complex in DMF to afford addition products without any by-product; a brief note has already been reported.[2] With regard to Michael reactions catalyzed by metal complexes, Saegusa and his co-workers[3] employed the copper(I) isocyanate complex; however, acceptor compounds in the reactions were limited since the dimerization of olefins occurred. Nelson and his co-workers[4] employed the $Ni(acac)_2$ complex for the reaction of β-diketones with acceptor compounds, mainly α,β-unsaturated ketones. In this complex-catalyzed reaction, the complex catalyst and donor compounds are limited to $Ni(acac)_2$ and β-diketones, and the reactions are heterogeneous catalytic system in dioxane or dichloromethane. In our homogeneous catalytic system, for example, the reactions of α,β-unsaturated ketones with nitromethane proceed smoothly in the presence of the complex catalysts under neutral conditions at room temperature, without any by-product. The preparation of the complex catalysts is simple, the Michael reactions proceed under very mild conditions, and the reaction products are easily isolated in relatively pure form because there are no side reactions. The most important factors for the catalytic reactions are kinds of metal-ion species, ligands, counter ions of the complexes, and solvents. In this paper, the results of an examination of these factors and the scope and limitation of the complex-catalyzed Michael reactions will be described in detail; some considerations of the reaction mechanism will also be presented.

Results and Discussion

Effects of the Complex Catalysts. First of all, various kinds of metal complex catalysts were examined in the addition reaction of nitromethane to 1,3-diphenyl-2-propen-1-one(chalcone) in a DMF solvent. The reaction conditions are shown as follows:

$$\underset{(1\ \text{mmol})}{PhCH{=}CHC(=O)Ph} + \underset{(4\ \text{ml})}{CH_3NO_2} \xrightarrow[\text{DMF, rt, 42 h}\ (2\text{—}5\ \text{ml})]{\text{M(II)–L(1:1)}} PhCH(CH_2NO_2)-CH_2-C(=O)Ph$$

The metal-ion species (M(II)) employed for the reaction were Co(II), Ni(II), Cu(II), and Zn(II), while the ligands (L) were 2,2′-bipyridine (bpy), 4,4′-dimethyl-2,2′-bipyridine (dim-bpy), 1,10-phenanthroline (phen), 6-nitro-1,10-phenanthroline (6-NO_2-phen), and ethylenediamine (en). Equimolar amounts of the metal(II) salt and the ligand compound were added to DMF; then the complex formation was observed by means of the color changes. This complex solution was subsequently used as a catalyst for the reaction without the isolation of the complex as a crystal form. The amount of the complex catalyst used for the reaction was 16 mol% of chalcone. The homogeneous reaction mixture was stirred for 42 h at room temperature. No by-products were formed in the reactions (examined by TLC, GLC, and isolation), the amount of chalcone consumed after the reaction was determined by means of GLC analysis; the yield of the reaction product was then calculated. The product was 1,3-diphenyl-4-nitro-1-butanone, which was further isolated and determined by means of mp, IR, and NMR. For example, in the reaction with the Ni(II)–bpy (1 : 1) complex, the yield of the product, as determined by GLC, was 86%, and the isolated yield was 82% (mp 100—101 °C). The details of the method of GLC analysis and the isolation of the product will be described in the Experimental section.

The reaction did not proceed with only metal(II) ions, without the ligand, but the ligand compounds themselves showed a weak catalytic activity; *e.g.*, bpy itself without the metal(II) ion afforded the product in a 15% yield (GLC) under similar reaction conditions. The reaction also did not proceed without any solvent (heterogeneous). An aprotic and polar solvent, such

TABLE 1. MICHAEL ADDITION OF NITROMETHANE TO CHALCONE WITH COMPLEX CATALYSTS[a]

$M(II)X_2$[b]	Ligand[b]	Yield/%[c]
$Co(OAc)_2$	bpy	34
$Ni(OAc)_2$	bpy	86[d]
$Cu(OAc)_2$	bpy	2
$Zn(OAc)_2$	bpy	6
$CoCl_2 \cdot 6H_2O$	bpy	0
$Co(NO_3)_2 \cdot 6H_2O$	bpy	0
$NiCl_2 \cdot 6H_2O$	bpy	0
$Ni(NO_3)_2 \cdot 6H_2O$	bpy	0
$Ni(OAc)_2$	dim-bpy	65
$Ni(OAc)_2$	phen	37
$Ni(OAc)_2$	6-NO_2-phen	0
$Ni(OAc)_2$	en	21

a) Reaction conditions: rt, 42 h, DMF. b) Complex: M(II): L=1 : 1. c) Calculated from GLC analysis. d) In DMSO, 84%; HMPA, 78%; MeOH 6% (under similar reaction conditions).

as DMF or DMSO, was favorable for this catalytc! reaction, while an alcohol such as MeOH was entirely inadequate. However, when the amount of the solvent used was in a large excess (*e.g.*, 10 ml), the product yield decreased apparently. In all the reactions, a large excess of nitromethane (4 ml) was employed; otherwise, the product yield was very poor, as will be described below. The results of the reactions with various complex catalysts are summarized in Table 1. According to the results shown in Table 1, the catalysis of the $Ni(OAc)_2$–bpy (1 : 1) complex is best. On the contrary, the Cu(II) or Zn(II)–bpy (1 : 1) complex shows extremely poor catalytic activity under similar reaction conditions. It is also observed that the Cl^- or NO_3^- anion is unfavorable as the counter ion of the complex catalyst as far as Ni(II) or Co(II)–bpy is concerned. The ligands of dim-bpy and phen may exert a steric effect on the reactions, and 6-NO_2-phen has probably both steric and electronic effects (0%). Ethylenediamine is not effective as the ligand of the complex for this reaction (21%).

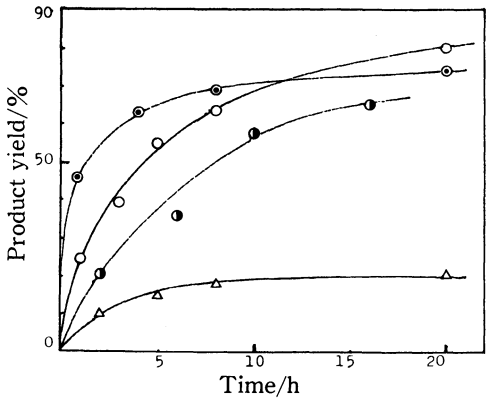

Fig. 1. Reaction profile of chalcone and nitromethane with Ni(II) complex catalysts (rt, in DMF).
○: Ni(II)–bpy(1 : 1); 16 mol% to chalcone, ⊙: (II)–$(bpy)_2$(1 : 2); 16 mol% to chalcone, △: Ni(II)–en(1 : 1); 16 mol% to chalcone, ◑: Ni(II)–bpy (1 : 1), 8 mol% to chalcone.

In order to examine this ligand effect further, the reactions of chalcone and nitromethane with some Ni(II) complex catalysts were followed over a period of 20 h by means of GLC analysis. The complexes employed were 16 mol% of $Ni(OAc)_2$–bpy, $Ni(OAc)_2$–$(bpy)_2$, $Ni(OAc)_2$–en, and 8 mol% of $Ni(OAc)_2$–bpy to chalcone. The reaction conditions were similar to those shown in Table 1. The correlations of the reaction time with the product yields are shown in Fig. 1. The figure displays a feature of the catalytic reactions reasonably well. The Ni(II)–$(bpy)_2$ complex, prepared by the addition of a two-fold mol quantity of bpy to the Ni(II) ion, accelerates the reaction in the first stage, but not in the later half. On the other hand, in the case of a low concentration of the Ni(II)–bpy (1 : 1) catalyst (8 mol%), the reaction is slow, but proceeds steadily throughout the reaction time. The reaction with Ni(II)–bpy (1 : 1) affords the product in an 80% yield for 20 h in Fig. 1 and in an 86% yield for 42 h (Table 1). In the reaction with Ni(II)–en (1 : 1), the yield of 20% is reached within just 20 h (Fig. 1), and a 21% yield within 42 h (Table 1). Therefore, the reaction time of 20 h seems to be generally enough for this complex-catalyzed Michael addition. It may be concluded that the $Ni(OAc)_2$–bpy–DMF system is the best combination for the complex-catalyzed Michael additions in this study. Some considerations of the enhanced effects of the bpy ligand and the OAc^- counter anion will be described below.

Various Michael Additions with the Ni(II) or Co(II)–bpy Complex. On the basis of the observations mntioned above, the reactions of various kinds of acceptor and donor compounds were carried out with the $Ni(OAc)_2$ or $Co(OAc)_2$–bpy (1 : 1) complex in DMF. The reaction conditions were similar to those shown in Table 1 except for the reaction time. In these experiments, all the reaction products were isolated and determined; they were found to be 1 : 1 adducts of the donor and acceptor compounds, except for one case. No by-product was observed in any of the reactions. The results are summarized in Table 2. In general, Ni(II) and Co(II) ion species each seem to display their own individual characteristics. For instance, the Co(II)–bpy complex is almost inactive in Reaction No. 1 (66 h, 50%) as compared with Ni(II)–bpy (18 h, 82%), but it shows almost the same activity in Reactions

Table 2. Various Michael additions with Ni(II) or Co(II)–bpy complex catalyst[a)]

No.	Acceptor (X–CH=CHCO–Y) X	Y	Donor (NM: CH_3NO_2)	Reaction time/h Ni(II)	Co(II)	Isolated yield/%[b)] Ni(II)	Co(II)
1	Ph	Ph	NM	18	66	82	50
2	Ph	*p*-$NO_2C_6H_4$	NM	18	15	87	88
3	Ph	*p*-ClC_6H_4	NM	20	42	86	86
4	*p*-$NO_2C_6H_4$	Ph	NM	45	23	73	57
5	*p*-ClC_6H_4	Ph	NM	18	69	78	48
6	PhCH=CH	Ph	NM	42	—	38	—
7	Ph	Me	NM	100	—	27[c)]	—
8	Ph	Ph	$PhNH_2$[d)]	23	—	72	—
9	CH_2=CHCOOMe		NM	—	18	—	70
10	CH_2=CHCN		$CH_2(CN)_2$	30	18	29	82[e)]

a) Reaction conditions: M(II)–bpy(1 : 1), rt, in DMF. b) Reaction product: 1 : 1 adduct except for in No. 10. c) In the case of 50 °C, 90 h: 20%. d) A large excess to the acceptor. e) Crude.

No. 2 and No. 3. The influence of the electron-attractive substituents of chalcone (NO_2, Cl) on the product yield are observed to some extent (Nos. 2 and 3). An inductive effect of the methyl group in the acceptor is observed in Reaction No. 7 (low reactivity). Reaction No. 9 with aniline did not proceed without the complex catalyst under these reaction conditions, although aniline itself might behave as a base catalyst. In the reaction of acrylonitrile with malononitrile, only 1,3,3,5-tetracyanopentane was obtained (No. 10). Besides the

$$CH_2{=}CHCN + CH_2(CN)_2 \longrightarrow NCCH_2CH_2{-}\overset{\overset{CN}{|}}{\underset{\underset{CN}{|}}{C}}{-}CH_2CH_2CN$$

reactions in the Table, the reactions of chalcone with acetophenone, *p*-nitroacetophenone, or dimethyl malonate were examined, but they did not proceed at all, not even at 80—100 °C. This complex-catalyzed Michael reaction seemed to be independent of the reaction temperature. When Reaction No. 7 was carried out at 50 °C for 90 h, the yield of the product was 20%, lower than that at room temperature, while Reaction No. 6 at 80 °C for 44 h gave a 37% yield (see Table 2).

Catalysis of the Metal(II) Complexes. With regard to the enhanced effect of the bpy ligand on the complex catalysis, several studies of other organic reactions have previously been reported.[5] According to their accounts, the net plus charge of the M(II) ion will increase upon the π-back donation of the M(II) ion to the bpy ligand in the complex; then, the resulting enhanced coordination force of the substrates to the M(II) ion will naturally accelerate the reactions. The ligand effects on the complex-catalyzed Michael reactions are also explainable by a similar π-back donation in the Ni(II) or Co(II)–bpy complexes. In the case of our study, no such reaction occurred with only the M(II) ion itself, but bpy complexes of the Ni(II) or Co(II) ion showed considerable catalytic activity. On the other hand, the ethylenediamine ligand with no π-back donation showed a very poor ligand effect on the complex catalysis.

In the course of the reaction, it is presumed that the substrates are activated by coordination to the M(II) ion of the complex catalysts. Therefore, the coordination of 4′-nitrochalcone to the Ni(II)–bpy complex was examined by means of the electronic absorption spectra, as is shown in Fig. 2. A solution of $Ni(OAc)_2$ in DMF showed an absorption maximum at 430 nm. When bpy was added to this solution (1 : 1), a new absorption maximum appeared at 630 nm which was attributed to the d-d band of Ni(II)–bpy chelation. When chalcone was added to this solution of the complex, the absorption maximum shifted to 620 nm. This fact might suggest that chalcone entered the first coordination sphere of the Ni(II) ion. Since no absorption shift was observed upon the addition of nitromethane to this complex solution, the interaction between the Ni(II) ion and nitromethane seemed to be extremely weak. Consequently, a high concentration of nitromethane (excess) might be required for satisfactory reactions. Therefore, in all the reactions shown in Tables 1 and 2, a large excess of nitromethane or other donors had to be employed. For example, in the reaction of chalcone and excess nitromethane (4 ml) with the Ni(II)–bpy complex, the yield of the product was 82% (Table 2, No. 1), but it decreased to 45% when an equimolar amount of nitromethane (1 mmol) was used under similar reaction conditions. On the other hand, if the coordination of chalcone is weakened or interrupted for some reason, the reaction will be very slow. According to the examination of some reaction solvents, MeOH was not suitable for the reaction (Table 1, footnote d). Therefore, the electronic absorption spectroscopy of this system was also carried out. A solution of the Ni(II)–bpy complex in MeOH showed an absorption maximum at 580 nm (Fig. 2). However, no shift of the absorption maximum was observed at all upon the addition of chalcone to this solution. This fact suggested that the coordination of chalcone to the Ni(II) ion was extremely weak or was interrupted by the stronger coordination of the methanol molecules. Actually, the yield of the reaction product in MeOH was only 6% for 42 h. The coordination of 4′-nitrochalcone was confirmed by the UV spectra, as above, and the yields in Reactions No. 2 and No. 3 (Table 2) were high. Therefore, it is presumed that the effects of electron-attractive groups in chalcone derivatives enhance their reactivity without any interruption of their coordination.

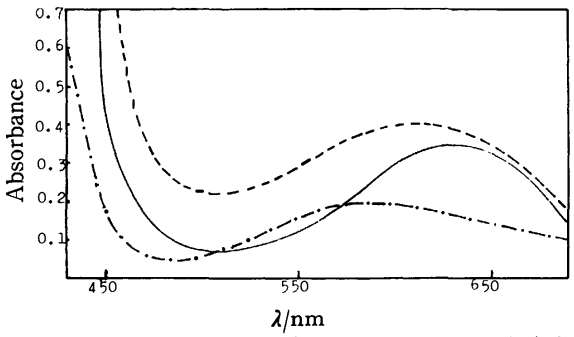

Fig. 2. Electronic absorption spectra of Ni(II)–bpy complexes in DMF or MeOH.
——: Ni(II)–bpy in DMF (λ_{max}=630 nm), ——: Ni(II)–bpy-4′-nitrochalcone (λ_{max}=620 nm), ·—·: Ni(II)–bpy in MeOH (λ_{max}=580 nm).

As for the behavior of the donor compound represented by nitromethane, it is considered that deprotonation occurs to form a donor anion in the first stage of the reaction; this process is also assisted by the metal complex. In our reaction system, the function of the M(II)–bpy complex catalyst as a base may be attributable not to the bpy ligand, but to the counter anion OAc^-, since bpy is not free because of the coordination in the complex. The IR spectra of $Ni(OAc)_2$ showed an absorption maximum of OAc^- at 1500 cm^{-1}, but it shifted to 1560 cm^{-1} in the spectra of the $Ni(OAc)_2$–bpy complex, which suggested the location of OAc^- at the outersphere of the complex, as in the case of [Ni(II)–bpy] $(OAc)_2$. Accordingly, both OAc^- and CH_3NO_2 are located considerably far from the central M(II) ion, although they have very weak interaction with the M(II) ion. In this situation, CH_3NO_2 may be catalyzed by OAc^- to form the $CH_2NO_2^-$ anion. Thus, the dual role of the complex catalyst, the simultaneous

activation of the acceptor by the M(II) ion and the donor by the OAc^- anion, should be emphasized.

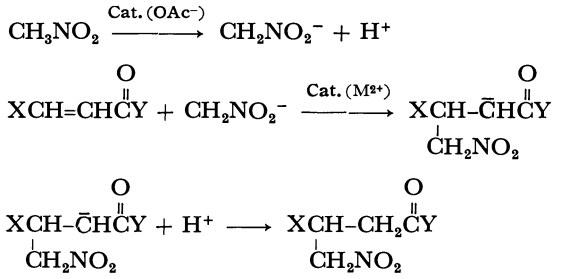

Experimental

Instruments. The GLC analysis was carried out with a Hitachi K-53 gas chromatograph with a flame ionization detector, using a 1.0 m stainless steel tube column packed with 10% Carbowax 20 M on Diachrom A (career gas, N_2; injection temp, 240 °C; oven temp, 220 °C). The NMR and IR spectra were taken with a Hitachi Perkin-Elmer R-20 A spectrophotometer (60 MHz) and a Hitachi 215 Grating Infrared spectrophotometer respectively, the UV spectra, with a Hitachi EPS-3 T spectrophotometer.

Materials. The anhydrous metal(II) acetates were provided by Kojundo Chemical Research, and the hydrous metal(II) salts, by Wako Pure Chemicals. All the ligand compounds were provided by the Tokyo Kasei Co. Chalcone and its derivatives were prepared by aldol condensations with the Co(II)-bpy complex catalyst in DMF, according to the methods described in our previous report.[6] The other compounds in Table 2 were all commercially available.

Reactions of Chalcone and Nitromethane with Metal(II)-complex Catalysts (Tables 1 and 2). To a solution of metal(II) salt (0.16 mmol) in 2 ml of DMF, equimolar amounts of the ligand compound were added (M^{2+} : L = 1 : 1). The color of the solution changed upon the complex formation. Then, 1 mmol of chalcone and 4 ml of nitromethane were added to the solution of the catalyst, after which the homogeneous reaction mixture was stirred for 42 h at room temperature. After the reaction, diethyl ether was added to the solution to precipitate the complex catalyst, and the supernatant was sampled for the GLC analysis (internal standard: α-(*p*-methoxyphenyl)acetophenone). Thus, the product yield was calculated from the quantity of chalcone unreacted, which was itself determined by comparing the relative peak area of chalcone *vs.* the internal standard with those shown in the calibration chart. The procedure for the isolation of the reaction product was that in which the reaction mixture was extracted with ethyl acetate, the organic layer was washed with water and then evaporated *in vacuo* to give a yellow oil. It was treated by the preparative TLC of silica gel (hexane–ethyl acetate), and the product was extracted with ethyl acetate and recrystallized with ethanol; 1,3-diphenyl-4-nitro-1-butanone, mp 100—101 °C (lit,[7] 101—102 °C), IR 1690 cm^{-1} (C=O), 1550 cm^{-1} (NO_2); ^{1}H-NMR ($CDCl_3$): δ 3.45 (d, 2H, CH_2–CO), 4.78 (d.d., 2H, CH_2–NO_2), 7.40—8.09 (m, aromatic).

Experiment for Fig. 1 (Reaction Profile). The reaction profile of chalcone and nitromethane with some complex catalysts was examined as follows: $Ni(OAc)_2$ and bpy (0.4 mmol each) were weighed in a volumetric flask (10 ml), DMF was added to the flask to dissolve the catalyst, and the solution was kept standing overnight at room temperature. Then, 2.5 mmol of chalcone and DMF were added to bring the flask up to the mark. The DMF solution (1 ml) was poured into each sample tube, and a further 1 ml of nitromethane was added to each sample tube. The reaction mixture was sampled from time to time, and a small quantity of methanol was added to a portion of the reaction mixture which was then stored in a freezer. The procedure of the GLC analysis of each sample was similar to that shown in Table 1.

UV Spectroscopy (Fig. 2). $Ni(OAc)_2$ (1.5 mmol) was dissolved in DMF (25 ml), and the UV spectra of this solution were measured. Then, to this solution 1.5 mmol of bpy was added and the UV spectra were measured again (absorption max., 630 nm). Next, 4′-nitrochalcone (0.6 mmol) was added to this complex solution, whereupon the absorption maximum was observed to shift to 620 nm. In the case of the methanol solvent, a similar procedure was carried out.

Reaction Products (Table 2). 1) As the forgoing. 2) Mp 98—99 °C; IR 1680 cm^{-1} (C=O), 1520 cm^{-1} (NO_2); ^{1}H-NMR ($CDCl_3$): δ 3.60 (d, 2H, CH_2–CO), 4.85 (d.d., 2H, CH_2–NO_2), 7.39—8.45 (m, aromatic). 3) Mp 82—84 °C (lit,[8] 80 °C); IR 1680 cm^{-1} (C=O), 1550 cm^{-1} (NO_2); ^{1}H-NMR ($CDCl_3$): δ 3.27 (d, 2H, CH_2–CO), 4.65 (d.d., 2H, CH_2–NO_2), 7.29—7.87 (m, aromatic). 4) Mp 105—106 °C; IR 1680 cm^{-1} (C=O), 1550 cm^{-1} (NO_2); ^{1}H-NMR ($CDCl_3$): δ 3.43 (d. 2H, CH_2–CO), 4.81 (d.d., 2H, CH_2–NO_2), 7.52—8.34 (m, aromatic). 5) Mp 97—98 °C; IR 1680 cm^{-1} (C=O), 1550 cm^{-1} (NO_2); ^{1}H-NMR ($CDCl_3$): δ 3.43 (d, 2H, CH_2–CO), 4.74 (d.d., 2H, CH_2–NO_2), 7.30—8.00 (m, aromatic). 6) Mp 85—87 °C (lit,[9] 83—84 °C); IR 1680 cm^{-1} (C=O), 1540 cm^{-1} (NO_2); ^{1}H-NMR ($CDCl_3$): δ 3.30 (d, 2H, CH_2–CO), 4.70 (d.d., 2H, CH_2–NO_2), 6.23 (d.d., 1H, =CH–), 6.73 (d, 1H, Ph–CH=), 7.40—8.18 (m, aromatic). 7) Mp 101—102 °C (lit,[10] 97—98 °C); IR 1720 cm^{-1} (C=O), 1550 cm^{-1} (NO_2); ^{1}H-NMR ($CDCl_3$): δ 2.11 (s, 3H, CH_3), 2.92 (d, 2H, CH_2–CO), 4.73 (d, 2H, CH_2–NO_2), 7.39 (s, aromatic). 8) Mp 175—176 °C (lit,[11] 171—172 °C). 9) Oil; IR (NaCl) 1730 cm^{-1} (COO), 1550 cm^{-1} (NO_2); ^{1}H-NMR ($CDCl_3$): δ 2.54 (4H, CH_2–CH_2), 3.76 (s, 3H, CH_3), 4.53 (t, 2H, CH_2–NO_2). 10) Mp 91—92 °C (lit,[12] 91 °C).

References

1) E. D. Bergann, K. Ginsberg, and R. Pappo, *Org. React.*, **10**, 179 (1959).

2) K. Irie, K. Miyazu, and K. Watanabe, *Chem. Lett.*, **1980**, 353.

3) T. Saegusa, Y. Ito, S. Tomita, and H. Kinoshita, *Bull. Chem. Soc. Jpn.*, **45**, 496 (1972).

4) J. H. Nelson, P. H. Howells, G. C. DeLullo, G. L. Landen, and R. A. Henry, *J. Org. Chem.*, **45**, 1246 (1980).

5) G. W. Watt and D. G. Upcharch, *J. Am. Chem. Soc.*, **90**, 914 (1968); H. Sigel and D. B. McCormick, *Acc. Chem. Res.*, **3**, 201 (1970); J. W. Jauregg, B. E. Hackley, T. A. Lies, O. O. Owens, and R. Proper, *J. Am. Chem. Soc.*, **77**, 922 (1955); R. W. Hay and K. N. Leong, *J. Chem. Soc., A*, **1971**, 3639.

6) K. Irie and K. Watanabe, *Bull. Chem. Soc. Jpn.*, **53**, 1366 (1980); *Chem. Lett.*, **1978**, 539.

7) W. Davey and D. J. Tivey, *J. Chem. Soc.*, **1958**, 2276.

8) E. P. Kohler and L. I. Smith, *J. Am. Chem. Soc.*, **44**, 624 (1922).

9) J. Struma and S. Altschuler, *Isr. J. Chem.*, **1**, 25 (1963); *Chem. Abstr.*, **60**, 1633a (1964).

10) L. M. Kozlov and E. F. Fink, *Tr. Kazan. Khim.-Tekhnol. Inst. im S. M. Kirova*, **1954—1955**, No. 19—20, 49 (1955); *Chem. Abstr.*, **51**, 11267h (1957).

11) N. S. Kozlov and I. A. Shur, *Zh. Obsch. Khim.*, **29**, 2706 (1959); *Chem. Abstr.*, **54**, 12045e (1960).

12) L. Belsky, *J. Chem. Soc., Chem. Commun.*, **1977**, 237.

Confirmation of the Sector Rule of the Benzenoid Chromophore

Sanji HAGISHITA* and Kaoru KURIYAMA
Shionogi Research Laboratories, Shionogi and Co., Ltd., Fukushima-ku, Osaka 553
(Received January 29, 1982)

1,2,3,4,4a,9,9a,10-Octahydroanthracene and tetralin derivatives with known absolute configurations were synthesized to estimate the contribution of a methyl substituent at the third sphere to the Cotton effect induced in the benzenoid transitions. The contributions were estimated from the CD spectra obtained based on the conformation of the skeleton deduced by Force Field Theory and the assumption that the contributions are additive. A large contribution was observed for the 1-*quasiequatorial*-methyl group in the ^1L_b benzenoid transition and for the 2-*axial*-methyl group in the ^1L_a benzenoid transition. The sign agreed well with the rule proposed by Snatzke except for the contribution of ring B in the ^1L_a benzenoid transition.

Snatzke *et al.* have proposed a refined sector rule for the benzene chromophore.[1,2] Although they described the sign of the contribution of the substituent in each section, the magnitude remained unclear. CD spectra of tetralin derivatives have been reported[3,4] but the data could not give the contribution of the substituent itself, owing to the ambiguity of the contribution of the tetralin skeleton. Further, the sign of the ^1L_b CD band could not be predicted in the molecule, which is complicated because of the presence of two rotational contributions of opposite signs, as in the case of (*S*)-(−)-anhalonine.[5] The present work studied the contributions of the chiral second and third spheres on the assumption that the contributions are additive. We chose substituted 1,2,3,4,4a,9,9a,10-octahydroanthracenes to find the contribution of 1-*quasiaxial*, 1-*quasiequatorial*, and 2-*axial* substituents,** since ring B would be fastened in the half chair conformation[6] due to ring C. Further, to find the contributions of the 2-*equatorial*-methyl group and the chiral second sphere, (+)-2,3-dimethyltetralin was synthesized and the CD spectrum was compared with that of (−)-2-methyltetralin.[4,7]

Synthesis

Wittig reaction of (4a*S*,9a*R*)-(+)-1,2,3,4,4a,9,9a,10-octahydro-9-anthracenone[1] [(+)-**1**] gave (+)-exo-olefin (+)-**2** in fairly good yield. Hydroboration of (+)-**2** gave three isomers: the first isomer (+)-**3** was isolated as the *p*-nitrobenzoate (+)-**6**; the second (+)-**5** was purified by preparative TLC and the third (+)-**4** was obtained as the (−)-ω-camphanic ester (−)-**7**.

Methyl derivatives (+)-**8**, (+)-**9**, and (+)-**10** were obtained by reduction of the tosylate of (+)-**3**, (+)-**4**, and (+)-**5**, respectively. The configuration of the methyl group and the ring juncture could be determined as follows.

Pyridinium chlorochromate oxidation of alcohol derivatives, (+)-**3**, (+)-**4**, and (+)-**5** gave the expected aldehyde (+)-**11**, (+)-**12**, and (+)-**13**, respectively. Further as a by-product, the *trans*-ketone (+)-**1** was obtained from (+)-**3** and (+)-**4**. The other isomer of the ketone (+)-**14** was isolated from (+)-**5**. The structure of (+)-**14** was assigned to be the *cis*-ring juncture by comparison with the physicochemical properties of (+)-**1**, since the C-9a position was only possible place to change. Then we could decide that (+)-**3** and (+)-**4** had the *trans*-ring juncture and (+)-**5** had the *cis*-ring juncture.

Further, the first isomer (+)-**3** was oxidized with the Jones' reagent giving the carboxylic acid (+)-**15** and (+)-**1**. From (+)-**15** the amino derivative (+)-**17** was obtained by the Curtius rearrangement. The coupling constant was 5 Hz between the protons at 9 and 9a of the carboxylic acid (+)-**15**. And the signal of the proton at 9 was observed as singlet in the amino derivative (+)-**17**. This small coupling constant led us to deter-

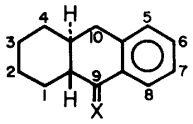

(+)-1, X=O
(+)-2, X=CH_2

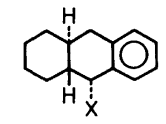

(+)-3, X=CH_2OH
(+)-6, X=CH_2OOC-C$_6H_4$-NO_2
(+)-8, X=CH_3
(+)-11, X=CHO
(+)-15, X=COOH
(+)-17, X=NH_2

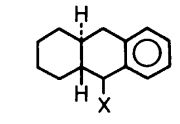

(+)-4, X=CH_2OH
(−)-7, X=CH_2OOC-
(+)-9, X=CH_3
(+)-12, X=CHO
(+)-16, X=OH
(+)-18, X=NH_2

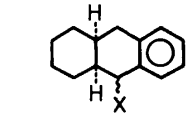

(+)-5, X=CH_2OH
(+)-10, X=CH_3
(+)-13, X=CHO

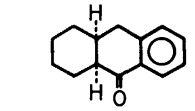

(+)-14

Scheme 1.

** Numbers 1 and 2 indicate the first and the second carbon atoms from the benzene ring.

Table 1. UV and CD spectra

Compd	Solvent	UV		CD		
		λ/nm	ε	λ/nm	Δε	$R\times 10^{42}$
(+)-**3**	MeOH	273	619	272	+0.406	+76.65
		266	556	265	+0.439	
		261.5	390			
		260	377			
		217^{sh}	7060			
		213	9010	210	+2.55	+200.96
		197	45600			
		195	46200			
(+)-**4**	MeOH	273	536	270	+0.0424	+5.37
		266	530	264	+0.0363	
		260^{sh}	388	255.5	+0.0272	
		217^{sh}	8330	222.5	+0.188	+16.30
		212	9600			
		196	45700			
		195	45300			
(+)-**8**	Hexane	273	735	273	+0.568	+96.0
		266	631	266	+0.558	
		261.5	431			
		259	412			
		217	7720	215^{sh}	+2.21	+296.3
		213	9240			
		209	9240			
		197	77600			
		194	77100			
(+)-**9**	Hexane	273	578	272.5	−0.0576	−3.37
		266	526	270	+0.0121	
		262	365	265	−0.0333	
		260	353	257.5	−0.0273	
		252^{sh}	207			
		217^{sh}	7780	214	+1.35	+206.2
		212.5	9050			
		197	46500			
		195	46500			
(+)-**25**	Isooctane	273.5	859	272.5	+0.303	+57.65
		266.5	704	265	+0.330	
		262	477			
		260	464			
		254^{sh}	243			
		217	8720	215	+2.142	+331.91
		213	10400			
		208	10500			
		197	58700			
		194	57700			
(+)-**30**	Hexane	273.5	703	272	+0.191	+45.2
		266	593	264.5	+0.248	
		262	413			
		260	396			
		216.5	7690	217	+1.43	+185.7
		212.5	9100			
		208	9020			
		196.5	51600			
		193	53000			
(+)-**33**$^{E)}$	Hexane	274	746	272	+0.161	+33.9
		266.5	595	265	+0.176	
		262	414			
		260	396			
		217	7980	217	+0.548	+78.3

TABLE 1. (Continued)

Compd	Solvent	UV λ/nm	UV ε	CD λ/nm	CD Δε	CD $R\times10^{42}$
		209	9120			
		197	50700			
		194	50400			
(+)-**34**	Isooctane	274	746	273	+0.267	+51.69
		267	611	265.5	+0.288	
		262	419			
		260	401			
		253[sh]	247			
		217	6930	215	+2.03	+318.5
		212.5	8140			
(−)-**35**[a)]	Hexane	273	289	272.5	+0.226	+37.64
		266	276	264.5	+0.233	
		262	202			
		260	193			
		217	7830	220	−0.604	−30.70
		213	9210			

sh: Shoulder. E): Enantiomer was measured. !: Lowest recorded value, not a maximum. a) The compound of 75.4% e.e. was measured and corrected to the optical purity.

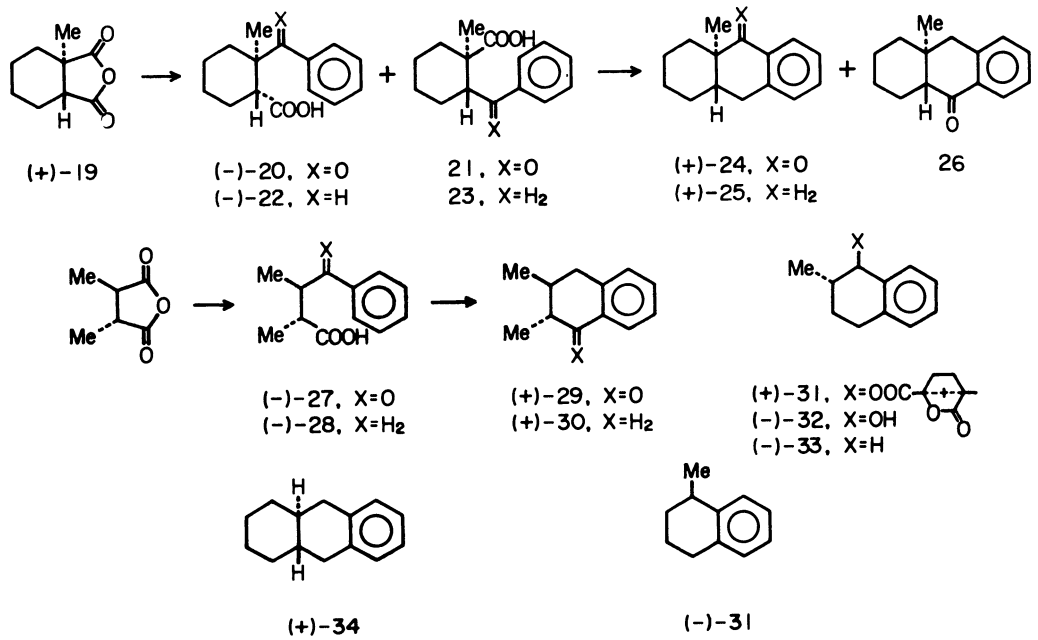

Scheme 2.

mine the configuration of the first isomer (+)-**3** to be 4a*S*, 9*R*, 9a*R* as shown in (+)-**3** of Scheme 1.

Reduction of the oxime of (+)-**1** gave almost selectively one *trans*-amino derivative (+)-**18**. The coupling constant was 8 Hz between the protons at **9** and **9a** and larger than that of the above amino isomer (+)-**17**. Further, reduction of (+)-**1** gave almost selectively one *trans*-isomer (+)-**16** of the alcohols with $NaBH_4$ or by the Meerwein-Pondorf-Verley method. The coupling constant was 6 Hz. Though the other *trans*-isomer could not be isolated, the signal of the proton at 9 was observed as singlet. Thus we can deduce that both major isomers have *quasiequatorial* substituent as (+)-**18** and (+)-**16**. The signals in a region of the methylene group of (+)-**17** and (+)-**18** showed quite similar pattern to those of (+)-**4**, (+)-**7** and (+)-**9**. This led us to determine their configuration to be 4a*S*, 9*S*, 9a*R*.

The second isomer (+)-**5** was deduced to have the *cis*-ring juncture as mentioned above and from the signals in a region of the methylene group in the NMR spectrum but the configuration of the substituent was remained unclear.

Friedel-Crafts reaction of benzene with (+)-(1*R*,2*R*)-*trans*-1-methyl-1,2-cyclohexanedicarboxylic anhydride[8)] [(+)-**19**] gave two isomers, **20** and **21** in a 10 : 1 ratio. Racemic **20** could be isolated by fractional recrystallization but not the optically active form. However, since both (−)-**20** and (−)-**21** lead to the same object compound **25**, the mixture of (−)-**20** and (−)-**21** was employed for further reaction without separation. Thus,

Table 2. Temperature-dependent CD spectra in methylcyclohexane–isopentane (85 : 15)

Compd	25 °C			−68 °C			−190 °C		
	λ/nm	Δε	$R\times10^{42}$	λ/nm	Δε	$R\times10^{42}$	λ/nm	Δε	$R\times10^{42}$
(+)-**8**	272.5	+0.491	+92.2	272.5	+0.479	+90.5	271.5	+0.436	+96.6
	265.5	+0.579		265	+0.633		265	+0.700	
(+)-**9**	273.5	−0.036		277	−0.006				
	269.5	+0.009		270	+0.061		270	+0.148	+26.95
	265	−0.047	−5.07	263	+0.027	+4.78	264.5	+0.175	
	259.5	−0.030		254.5	+0.015				
	253	−0.012		248.5	+0.009				
(−)-**35**	272.5	+0.217	+29.9	272.5	+0.177	+28.9	272.5	+0.117	+33.1
	265	+0.209		264.5	+0.197		264	+0.221	

the angular methyl compound (+)-**25** was obtained as shown in Scheme 2.

(+)-(2*S*,3*S*)-2,3-Dimethyltetralin (+)-**30** was prepared from (+)-(2*R*,3*R*)-dimethylsuccinic acid[9] according to the procedure cited for racemic **30**.[10] The synthesis of partially optical active (−)-(1*R*,2*S*)-2-methyl-1-tetralol (−)-**32** has been reported previously,[4,7] but we obtained optically pure (−)-**32** from the ω-camphanic ester (+)-**31** more easily.

Results and Discussion

CD and UV spectra of the prepared compounds are shown in Table 1 with the data for (+)-(4a*S*,9a*S*)-*trans*-1,2,3,4,4a,9,9a,10-octahydroanthracene[2] [(+)-**34**] and (−)-(1*R*)-1-methyltetralin [(−)-**35**],[4] which we also prepared. Four benzenoid transitions, ^1L_b, ^1L_a, ^1B_b, and ^1B_a, were found for the UV spectra and two, ^1L_b and ^1L_a, for the CD spectra. Assuming that the contributions of the substituent are additive, we can obtain the contributions, $\delta\Delta\varepsilon$ and δR, by subtracting the Δε values and rotational strengths, R, of (+)-**34** from the substituted 1,2,3,4,4a,9,9a,10-octahydroanthracenes. Further we can estimate the contribution of the 2-*equatorial*-methyl group by subtracting the Cotton effect of (+)-**33** from that of (+)-**30**. The contribution of ring B can be calculated by subtracting the contribution of the 2-*equatorial*-methyl group from the Cotton effect of (+)-**33**. However, *trans*-1,2,3,4,4a,9,9a,10-octahydroanthracene is not always rigid in conformation. Substituent groups often exert an influence on the conformation of ring B for deformation from a half-chair conformation. We deduced the stable conformation using the Force Field Theory, MMI,[11] with the results shown in Fig. 1. The 2-*equatorial*-methyl group in **30** and **33** does not cause the deformation of ring B from a half-chair form, and the *equatorial*-methyl forms **30a** and **33a** were more stable than the *axial*-methyl forms **30b** and **33b**, respectively. Also, the 2-*axial*-methyl group in compound **25** does not lead to as much deformation.

The 1-*quasiaxial*-methyl form **35a** was more stable than the 1-*quasiequatorial* **35b** as pointed out before[4,12] and the deformation from the half-chair form is smaller in the 1-*quasiaxial*-methyl **35a** than in 1-*quasiequatorial* **35b**. Further, ring B of **8a** is more twisted from the half-chair form than that of **35a** owing to an additional peri-effect.

The theory suggests that the 1-*quasiequatorial*-methyl compound **9** has a twist-boat conformation **9a** rather than a half-chair form.

We measured the temperature-dependent CD spectra of (+)-**8**, (+)-**9**, and (−)-**35**, which are shown in Table 2. The rotational strength of (+)-**8** and (−)-**35** were constant within experimental error with temperature changes, although the band at 272 nm became smaller at lower temperature in (−)-**35**. Next, (−)-**35** was

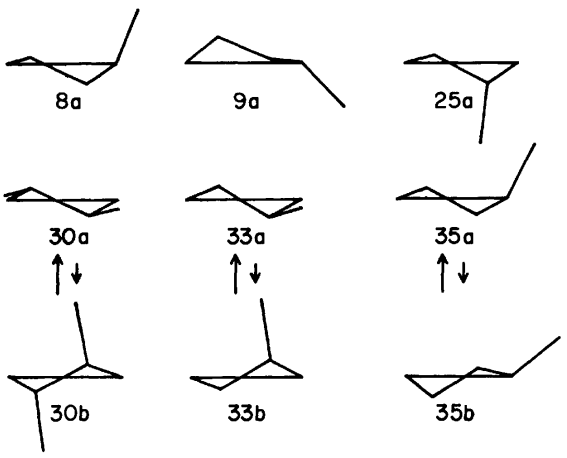

Fig. 1. Projection diagram of stable and metastable conformation obtained with Force Field Theory.

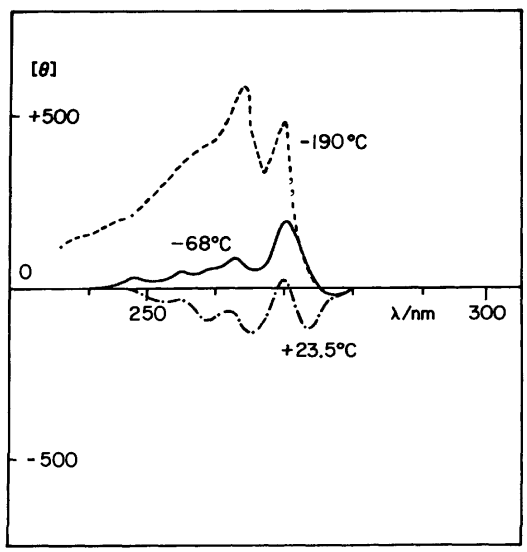

Fig. 2. Temperature-dependent CD spectra of (+)-**9**.

TABLE 3. CONTRIBUTION $\delta\Delta\varepsilon$ AND δR OF A METHYL GROUP TO TETRALIN

	^1L_b			^1L_a		
	λ/nm	$\delta\Delta\varepsilon$	$R\times10^{42}$ c.g.s.	λ/nm	$\delta\Delta\varepsilon$	$R\times10^{42}$ c.g.s.
1-Quasiaxial	272	−0.014	+10.5	215	+0.18[a)]	−22.2[a)]
	265	+0.117				
1-Quasiequatorial	272	$<$−0.325	$<$−55.1	215	—	—
	265	$<$−0.321				
2-Equatorial	272	+0.030	+11.3	215	+0.882	+107.4
	265	+0.042				
2-Axial	272	+0.036	+6.0	215	+0.112	+13.4
	265	+0.042				
Ring B	272	+0.131	+22.6	215	−0.334	−29.1
	265	+0.104				

a) These contributions were differences between the values of (+)-**8** and (+)-**34**.

considered to be fixed in the 1-*quasiaxial*-methyl form, which is a stable conformer, since the sign of the Cotton effect of (−)-**35** was the same as that of (+)-**8** in the region of the ^1L_b benzenoid transition. On the other hand, Cotton effects of (+)-**9** depended on the temperature and changed from negative at room temperature to positive at lower temperature as shown in Fig. 2. The analysis[12] showed that the conformational free-energy difference ($\Delta G°$) was 2.3 kJ/mol, assuming that (+)-**9** was composed of two conformers.

Since the introduction of the 2-*axial*- or the 2-*equatorial*-methyl group did not deform the half-chair conformation, we could obtain the contributions $\delta\Delta\varepsilon$ and δR of the 2-*axial*- and 2-*equatorial*-methyl groups and ring B, as mentioned above.

The contribution of the 1-*quasiaxial*-methyl group may be estimated either by subtracting the Cotton effects of (+)-**34** from those of (+)-**8** or by subtracting the contribution of ring B from the Cotton effect of (−)-**35**. The contribution obtained from both estimations had the same sign in δR in both regions of the benzenoid transitions, but the magnitudes differed and the $\delta\Delta\varepsilon$ values were ambiguous in sign. The chemical shift of the methyl group of (−)-**35** was lower than that of (+)-**8** and almost the same as that of (+)-**9**. This may suggest that compound (−)-**35** is composed of two conformers. But the Force Field Theory suggested that the more stable *quasiaxial*-methyl form **35a** showed less deformation from a half-chair form than that of **8a**. The proton at the C-1 position of (+)-**8** would cause more deformation of ring B owing to the *peri*-effect. Although the rotational strength of (−)-**35** was not influenced much by temperature, we adopted the difference of the Cotton effect of (−)-**35** at −190 °C from the contribution of ring B as the contribution of the 1-*quasiaxial*-methyl group.

As mentioned before, the Cotton effect of (+)-**9** depended on temperature. We estimated the stable conformer to be a twist-boat form from the Force Field Theory. Also, to estimate the conformation of (+)-**9**, we measured the CD spectra of 1,3,5(10)-estratriene,*** which was regarded as the 1-*quasiequatorial*-2-*equatorial*-dimethylene derivative with a half-chair conformation. The half-chair form of (+)-**9** can be regarded as the derivative with one 1-*quasiequatorial*-methyl and two 2-2-*equatorial*-methylene groups, in other words, it has one 2-*equatorial*-methylene group more than the steroid, if the methyl and the methylene groups in the 1-*quasiequatorial*-position make the same contribution to the Cotton effect. We estimated the contribution of the 2-*equatorial*-methylene group from the CD spectra of (+)-**34** to be small. We then compared the CD spectra of the steroid and (+)-**9**. The CD spectra of the steroid resembled that of (+)-**9** at room temperature rather than that at low temperature. This means that (+)-**9** is in equilibrium between the twist-boat and the half-chair forms, and the twist-boat form is the stable one. Therefore, we could not estimate the contribution of the 1-*quasiequatorial* group by direct comparison, but the negative Cotton effect was deduced for the unstable conformer from the Cotton effect at room temperature. The contributions of the 1-*quasiequatorial*-methyl group were larger than those obtained by subtracting the Cotton effects of (+)-**34** from those of (+)-**9** at room temperature. These results are summarized in Table 3. The sign of the contribution agreed well with Snatzke's sector rule except for ring B in the ^1L_a region, although the contribution of the 1-*quasiequatoria*-methyl group was not clear.

In the ^1L_b benzenoid transition, the 1-*quasiaxial*-, 2-*axial*- and 2-*equatorial*-methyl groups showed smaller contributions than the 1-*quasiequatorial* group. In the ^1L_a benzenoid transition, the 2-*equatorial*-methyl group contributed more than the 1-*quasiaxial* and 2-*axial*-methyl groups. Since ring B is not always in the complete half-chair conformation, the contribution is not directly attributable to the methyl group but contains the contribution of the deformation of ring B by the substituent. These apparent contributions should be useful for predicting the position and orientation of the substituent of the tetralin derivatives.****

*** In cyclohexane, 274 nm ($\Delta\varepsilon$ −0.124), 271 (+0.028), 266.5 (−0.085), 260 (−0.042).

**** We tried to analyze the contribution using the CNDO/S molecular orbital model[13] and the dipole velocity method[14] but have some doubt about the reliability and accuracy of the calculation owing to the quantitative instability with a number of configurations.

Experimental

Melting points are uncorrected. Optical rotations were determined with a Perkin-Elmer Model 141 polarimeter, using a 1.0-dm microcell. CD curves were obtained using a JASCO Model J-40 spectropolarimeter. Infrared spectra were recorded on a JASCO-DS-402G spectrophotometer. ^{1}H NMR spectra were measured with Varian A56/60D spectrometer using tetramethylsilane as the internal standard. UV spectra were obtained on a Hitachi Model 323 spectrometer.

*(4a*S, *9a*R*)-(+)-9-Methylene-1,2,3,4,4a,9,9a,10-octahydroanthracene, (+)-2.* Methyltriphenylphosphonium bromide (31 g) was added to a suspension of potassium *t*-butoxide (15 g) and the (+)-ketone (**1**, 5.8 g) in dry ether (400 ml) under a nitrogen atmosphere. The mixture was stirred overnight and poured onto ice water. The organic phase was separated and the aqueous phase was extracted with ether. The combined organic phases were washed with dimethyl sulfoxide–water (1 : 1) and then water, dried (Na_2SO_4) and concentrated *in vacuo*. The residue was crystallized from ether and the crystals were removed by filtration. The filtrate was chromatographed on thick silica gel plate (Merck Co., precoated, 2 mm) in hexane and then distilled at 121 °C at 0.9 mm Hg, 5.4 g (94.0%); $[\alpha]_D^{24.5}$ +140.3 ±1.7° (*c* 1.047, $CHCl_3$); IR (film) 888 cm^{-1}; NMR ($CDCl_3$) δ=0.9—2.5 (m, 10H), 2.5—3.1 (m, 2H), 4.97 (s, 1H), 5.49 (s, 1H), 7.0—7.3 (m, 3H), 7.4—7.8 (m, 1H); UV_{max} (hexane) 298^{sh} nm (ε 758), 288 (864), 281 (843), 250 (11300), 222^{sh} (10500), 211 (21700); CD (hexane) 283 nm ($\Delta\varepsilon$ +0.933), 243 (+4.88), 211.5 (+11.3), 190! (−7.24). Found: C, 91.00; H, 9.06%. Calcd for $C_{15}H_{18}$: C, 90.85; H, 9.15%.

Hydroboration of (+)-2. A solution of diborane in tetrahydrofuran, which was prepared from $NaBH_4$ (5.3 g), boron trifluoride etherate (44 g) and diglyme (130 ml), was added to a solution of the (+)-olefin (**2**, 5.40 g) in tetrahydrofuran (100 ml) with ice-cooling. The mixture was stirred at 0 °C for 2 h. Water was added dropwise carefully with ice-cooling. 3 mol dm^{-3} NaOH (22 ml) and then 30% hydrogen peroxide (25 ml) were added. The mixture was stirred for 4 h and allowed to stand for 2 d. Water (200 ml) was added. The mixture was extracted with ether. The solution was washed with water, dried (Na_2SO_4) and concentrated *in vacuo*. The small portion of residue was distilled at 160 °C (bath temperature) at 0.2 mmHg through a short-path distillation apparatus, $[\alpha]_D^{23.5}$ +73.0 ±0.8° (*c* 0.958, MeOH). Found: C, 83.69; H, 9.49%. Calcd for $C_{15}H_{20}O$: C, 83.28; H, 9.32%.

*(4a*S, *9*R, *9a*R*)-(+)-1,2,3,4,4a,9,9a,10-Octahydro-9-anthracenylmethyl* p-*Nitrobenzoate, (+)-6.* *p*-Nitrobenzoyl chloride (18 g) was added to a cold solution of the above (+)-alcohols (**3**, **4** and **5**, 5.6 g) in pyridine (80 ml). The mixture was allowed to stand at room temperature overnight, poured into water and extracted with ethyl acetate. The solution was washed with dilute HCl, aqueous $NaHCO_3$ and water, dried (Na_2SO_4) and concentrated *in vacuo*. The residue was crystallized from ether and recrystallized from ethyl acetate–ethanol, 0.432 g, mp 126—128 °C; $[\alpha]_D^{24}$ +136.1 ±2.1° (*c* 0.867, $CHCl_3$); IR ($CHCl_3$) 1724, 1530 cm^{-1}; UV_{max} (dioxan) 340^{sh} nm (ε 280), 261 (13300), 218^{sh} (12100), 207.5 (17100); CD (MeOH) 325 nm ($\Delta\varepsilon$ +0.018), 264.5 (+2.75), 259 (+2.58), 210 (+6.30). Found: C, 72.20; H, 6.39; N, 3.78%. Calcd for $C_{22}H_{23}NO_4$: C, 72.31; H, 6.34; N, 3.83%.

*(4a*S, *9*R, *9a*R*)-(+)-9-Hydroxymethyl-1,2,3,4,4a,9,9a,10-octahydroanthracene, (+)-3.* The (+)-ester (**6**, 2.6 g) was hydrolyzed with KOH (2 g) in water (10 ml) and methanol (20 ml) by heating under reflux for 2 h and treated as usual. The alcohol was crystallized from hexane, 1.5 g, mp 85—86 °C, $[\alpha]_D^{24}$ +105.5 ±1.4° (*c* 1.071, MeOH); IR (nujol) 3300, 1056 cm^{-1}; NMR ($CDCl_3$) δ=0.7—2.2 (m, 11H), 2.3—3.2 (m; 3H), 3.62 (dd, *J*=5, 11 Hz, 1H), 7.11 (s, 4H). Found: C, 83.28; H, 9.49%. Calcd for $C_{15}H_{20}O$: C, 83.28; H, 9.32%.

*(4a*S, *9*R, *9a*S*)-(+)-9-Hydroxymethyl-1,2,3,4,4a,9,9a,10-octahydroanthracene, (+)-5.* The mother liquor of the *p*-nitrobenzoate **6** was hydrolyzed as above. The oily residue (1.5 g) was chromatographed on thin silica gel plate (Merck Co., precoated, 0.5 mm) in hexane–ether (3 : 1). The fraction of the smaller R_f value was distilled at 160 °C at 0.2 mmHg through a short-path distillation apparatus, 300 mg; $[\alpha]_D^{24}$ +30.9 ±0.6° (*c* 0.941, MeOH); IR (film) 3350 cm^{-1}; NMR ($CDCl_3$) δ=0.8—2.4 (m, 10H), 2.6—3.3 (m, 3H), 3.87 (dd, *J*=7, 11 Hz, 1H), 4.22 (dd, *J*=6, 11 Hz, 1H), 6.9—7.5 (m, 4H); UV_{max} (MeOH) 274 nm (ε 600), 266 (566), 261^{sh} (405), 255^{sh} (278), 217^{sh} (8020), 213 (9140), 197.5 (44400), 195^{sh} (43000); CD (MeOH) 272.5 nm ($\Delta\varepsilon$ −0.215), 265.5 (−0.212), 259.5 (−0.136), 210 (−1.61). Found: C, 83.22; H, 9.40%. Calcd for $C_{15}H_{20}O$: C, 83.28; H, 9.32%.

*(−)-Camphanyl Ester of (4a*S, *9*S, *9a*R*)-(+)-9-Hydroxymethyl-1,2,3,4,4a,9,9a,10-octahydroanthracene, (−)-7.* A solution of the fraction with the larger R_f value (0.18 g) in pyridine (3 ml) was added to (−)-ω-camphanoyl chloride (0.362 g) in pyridine (3 ml). The mixture was allowed to stand at room temperature overnight, poured into water and extracted with ether. The solution was washed with ice-cold dilute HCl, aqueous $NaHCO_3$ and water, dried (Na_2SO_4) and concentrated *in vacuo*. The residue was chromatographed on thin silica gel plate (Merck Co., precoated, 0.5 mm) in hexane–ether (5 : 1). The development was repeated three times. The fraction of the smaller R_f value (−)-**7** was recrystallized from hexane, 181 mg, $[\alpha]_D^{22}$ 0°, $[\alpha]_{365}^{22}$ −5.9 ±0.3° (*c* 1.107, $CHCl_3$); mp 129.0—130.0; IR (Nujol) 1790, 1744 cm^{-1}; NMR ($CDCl_3$) δ=0.63 (s, 3H), 0.71 (s, 3H), 1.03 (s, 3H), 0.7—2.9 (m, 17H), 4.32 (dd, *J*=12, 3 Hz, 1H), 4.77 (dd, *J*=12, 4 Hz, 1H), 6.9—7.4 (m, 4H). Found: C, 75.33; H, 8.04%. Calcd for $C_{25}H_{32}O_4$: C, 75.73; H, 8.13%.

The fraction with the larger R_f value, the ω-camphanic ester of (+)-**3**, was recrystallized from hexane, 57.7 mg, mp 154 °C; $[\alpha]_D^{22}$ +76.9 ±1.0° (*c* 0.844, $CHCl_3$); IR (nujol) 1789, 1722 cm^{-1}; NMR ($CDCl_3$) δ=0.76 (s, 3H), 0.96 (s, 3H), 1.07 (s, 3H), 0.6—2.6 (m, 15H), 2.7—3.2 (m, 2H), 4.23 (dd, *J*=6, 12 Hz, 1H), 4.52 (dd, *J*=6, 12 Hz, 1H), 6.9—7.3 (m, 4H). Found: C, 74.90; H, 7.99%. Calcd for $C_{25}H_{32}O_4$: C, 75.73; H, 8.13%.

*(4a*S, *9*S, *9a*R*)-(+)-9-Hydroxymethyl-1,2,3,4,4a,9,9a,10-ocatahydroanthracene, (+)-4.* The ester [(−)-**7**, 400 mg] was hydrolyzed with 5% KOH in methanol (10 ml) by heating under reflux for 2 h. The residue was distilled at 160 °C (bath temperature) at 0.2 mmHg through a short-path distillation apparatus, 157 mg; $[\alpha]_D^{21}$ +76.4 ±0.8° (*c* 1.017, MeOH) IR (film) 3370, 1046 cm^{-1}; NMR ($CDCl_3$) δ=0.7—2.2 (m, 10H), 2.3—2.8 (m, 3H), 3.73 (dd, *J*=11, 3 Hz, 1H), 4.01 (dd, *J*=11, 3 Hz, 1H), 6.9—7.4 (m, 4H). Found: C, 82.63; H, 9.24%. Calcd for $C_{15}H_{20}O$: C, 83.28; H, 9.32%.

*(4a*S,*9*R,*9a*R*)-(+)-9-Methyl-1,2,3,4,4a,9,9a,10-octahydroanthracene, (+)-8.* A solution of *p*-toluenesulfonyl chloride (1.3 g) in pyridine (10 ml) was added to a solution of the (+)-alcohol (**3**, 30)1 mg in pyridine (3 ml) at −5——10 °C over a period of 1 h. The solution was allowed to stand at 4 °C overnight, poured into ice-cold dilute HCl and extracted with ether. The solution was washed with cold dilute HCl, aqueous $NaHCO_3$ and water, dried (Na_2SO_4) and concentrated *in vacuo*, 402 mg. The crystalline tosylate was used for the next preparation without further purification.

A solution of the optically active tosylate (400 mg) in dry

tetrahydrofuran (15 ml) was added to a slurry of $LiAlH_4$ (0.4 g) in tetrahydrofuran (5 ml) with ice-cooling. The mixture was then heated under reflux for 5 h. Excess $LiAlH_4$ was decomposed with a solution of methanol in ether and then dilute HCl. The mixture was chromatographed on thin silica gel plate (Merck Co., precoated, 0.5 mm) in hexane and distilled at 110 °C (bath temperature) at 0.2 mmHg giving a colorless oil, 141.5 mg; $[\alpha]_D^{23}$ +90.2 ±1.1° (*c* 1.282, hexane); IR (film) 755 cm^{-1}; NMR ($CDCl_3$) δ=1.08 (d, J=7 Hz, 3H), 0.9—3.2 (m, 10H), 7.05 (m, 4H). Found: C, 89.65; H, 10.15%. Calcd for $C_{15}H_{20}$: C, 89.94; H, 10.06%.

*(4a*S,*9*R,*9a*S*)-(+)-9-Methyl-1,2,3,4,4a,9,9a,10-octahydroanthracene, (+)-**10**.* The *cis*-alcohol [(+)-**5**] was treated as above. The oily residue was chromatographed on thin silica gel plate (Merck Co., precoated, 0.5 mm) in hexane and distilled at 110 °C at 0.2 mmHg; $[\alpha]_D^{22}$ +43.0 ±0.6° (*c* 1.146, hexane); CD 273.5 nm ($\Delta\varepsilon$ −0.158), 266.5 (−0.133), 260 (−0.064), 217 (+0.621); IR (film) 755 cm^{-1}; NMR ($CDCl_3$) δ=0.5—3.3 (m, 13H), 1.31 (d, J=7 Hz, 3H), 6.9—7.4 (m, 4H). Found: C, 89.13; H, 9.90%. Calcd for $C_{15}H_{20}$: C, 89.94; H, 10.06%.

*(4a*S, *9*S, *9a*R*)-(+)-9-Methyl-1,2,3,4,5a,9,9a,10-octahydroanthracene, (+)-**9**.* The *trans*-alcohol [(+)-**4**] was treated as above. The residue was chromatographed on thin silica gel plate (Merck Co., precoated, 0.5 mm) in hexane and distilled at 120 °C (bath temperature) at 0.2 mmHg through a short-path distillation apparatus. The distillate crystallized quickly, mp 65—68 °C; $[\alpha]_D^{22}$ +99.1 ±0.9° (*c* 1.018, hexane); IR (nujol) 763, 744 cm^{-1}; NMR ($CDCl_3$) δ=0.5—2.8 (m, 3H), 1.28 (d, J=7 Hz, 3H), 6.9—7.4 (m, 4H). Found: C, 89.66; H, 10.47%. Calcd for $C_{15}H_{20}$: C, 89.94; H, 10.06%.

*Oxidation of Alcohols (+)-**3**, (+)-**4**, and (+)-**5**.* *1)*: A solution of the (+)-*cis*-alcohol[(+)-**5**, 199 mg] in dichloromethane (6 ml) was added to a mixture of anhydrous sodium acetate (26 mg) and pyridinium chlorochromate (311 mg) in dichloromethane (5 ml) in one portion. The mixture was stirred at room temperature for 2 h. Ether was added. The mixture was chromatographed on florisil (20 g) in ether. The residue was chromatographed on thin silica gel plate (Merck Co., pre-coated plate) in benzene.

The fraction of the larger R_f value; oil (44.4 mg); IR (film) 1723 cm^{-1}; NMR ($CDCl_3$) δ=1.0—3.1 (m, 12H), 3.41 (dd, J=6, 2 Hz, 1H), 6.9—7.4 (m, 4H), 9.59 (d, J=2 Hz, 1H); This fraction was the aldehyde derivative **13**.

The fraction of smaller R_f value (42.4 mg) was recrystallized from pentane; mp 79—81 °C; $[\alpha]_D^{25}$ +40.8 ±0.6 (*c* 1.046, $CHCl_3$); IR (Nujol) 1677, 749, 738 cm^{-1}; NMR ($CDCl_3$) δ=1.2—2.9 (m, 10H), 2.99 (d, J=5 Hz, 1H), 7.1—7.6 (m, 3H), 8.15 (dd, J=8, 1 Hz, 1H); UV_{max} (heptane) 355 nm^{sh} (ε 118), 342 (174), 330 (192), 316 (209), 298 (1580), 288 (1650), 278^{sh} (1110), 251^{sh} (9620), 245 (12500), 204 (30400); CD (heptane) 374 nm ($\Delta\varepsilon$ +0.115), 357 (+0.348), 343.5 (+0.494), 330.5 (+0.424), 318 (+0.227), 307.5 (+0.064), 296 (−0.082), 286 (−0.109), 243 (+1.42), 222 (+0.594), 210.5 (−4.30), 193 (+7.79). Found: C, 83.70; H, 8.14%. Calcd for $C_{14}H_{16}O$: C, 83.96; H, 8.05%. This was the *cis*-ketone (+)-**14**.

2): The (+)-alcohol [(+)-**3**, 105 mg] was treated as above. The fraction of the larger R_f value (49.8 mg) could not be crystallized and was contaminated with other compounds but the following band and signal were observed; IR (film) 1720 cm^{-1}; NMR ($CDCl_3$) δ=9.61 (d, J=6 Hz). The fraction of the smaller R_f value (25.7 mg) was recrystallized from pentane and was identical with the authentic sample, (+)-**1**.

3): The alcohol [(+)-**4**, 117 mg] was treated as above. The fraction of the larger R_f value (64.3 mg) was recrystallized from pentane; mp 79—81 °C; $[\alpha]_D^{25}$ +15.2 ±0.4 (*c* 1.246, $CHCl_3$); IR (Nujol) 1728, 751 cm^{-1}; NMR ($CDCl_3$) δ=0.8—2.9 (m, 12H), 3.28 (dd, J=9, 6 Hz, 1H), 6.8—7.3 (m, 4H), 9.38 (d, J=5 Hz, 1H); UV_{max} (heptane) 296 nm (ε 103), 273 (400), 266 (408), 262^{sh} (325), 253 (266), 218^{sh} (8390); CD (heptane) 325 nm^{sh} ($\Delta\varepsilon$ −0.524), 313^{sh} (−1.15), 305 (−1.43), 296.5 (−1.38), 271.5 (−1.02), 265 (−0.709), 260 (−0.412), 225.5 (−1.02), 201.5 (+9.30). Found: C, 84.01; H, 8.54%. Calcd for $C_{15}H_{18}O$: C, 84.07; H, 8.47%.

The fraction of the smaller R_f value (9.5 mg) was recrystallized from pentane and was identical with the authentic sample, (+)-**1**.

*Reduction of (+)-**1**.* *a)*: $NaBH_4$ (0.3 g) was added in small portions to a suspension of (+)-**1** (0.317 g) in methanol (10 ml) at −10 °C. The mixture was stirred for 2 h. Dilute HCl was added. The crystals were collected by filtration, washed with water, dried and recrystallized from methanol, 0.212 g, mp 142—143 °C; $[\alpha]_D^{25}$ +119.4 ±1.0° (*c* 1.016, $CHCl_3$); IR (Nujol) 3380, 3350 cm^{-1}; NMR ($CDCl_3$) δ=0.8—3.2 (m, 12H), 4.26 (d, J=6 Hz, 1H), 6.8—7.3 (m, 3H), 7.3—7.7 (m, 1H); UV_{max} (MeOH) 273 nm (ε 407), 266 (395), 260^{sh} (294), 217^{sh} (7410), 212 (8530), 197.5 (36400); CD (MeOH) 274 nm ($\Delta\varepsilon$ +0.138), 268 (+0.155), 263 (+0.146), 215 (+2.88). Found: C, 82.80; H, 9.13%. Calcd for $C_{14}H_{18}O$: C, 83.12; H, 8.97%.

b): A mixture of (+)-**1** (0.570 g) and aluminum isopropoxide (0.60 g) in isopropyl alcohol (15 ml, freshly distilled over aluminum isopropoxide) was heated at refluxing 4 h. The rate of the distillation was about 5 to 10 drops a minute. Finally the solvent was distilled off *in vacuo*. Dilute HCl was added. The mixture was extracted with ether. The solution was washed with water, dried (Na_2SO_4) and concentrated *in vacuo*. The residue was chromatographed on thin silica gel plate (Merck Co., precoated) in benzene and recrystallized from methanol. This was identical with the above product.

From the mother liquor of procedures *a*) and *b*), the other isomer could not be isolated but a singlet was detected at δ=4.35 in $CDCl_3$.

*(4a*S, *9*R, *9a*R*)-(+)-1,2,3,4,4a,9,9a,10-Octahydroanthracene-9-carboxylic Acid, (+)-**15**.* Jones' reagent (0.5 ml) was added to a solution of the (+)-alcohol [(+)-**3**, 226 mg] in acetone (5 ml) with ice-cooling. Water was added. The mixture was extracted with ethyl acetate. The solution was washed with water, dried (Na_2SO_4), concentrated *in vacuo* and recrystallized from hexane; 112.4 mg, mp 182—183 °C; $[\alpha]_D^{24}$ +209.1 ±2.2° (*c* 0.657, MeOH); IR (Nujol) 1690 cm^{-1}; NMR ($CDCl_3$) δ=0.8—3.1 (m, 12H), 3.73 (d, J=5 Hz, 1H), 7.15 (s, 4H), 10.90 (s, 1H). Found: C, 77.56; H, 7.98%. Calcd for $C_{15}H_{18}O_2$: C, 78.23; H, 7.88%.

The mother liquor was chromatographed on thin silica gel plate (Merck Co., pre-coated plate) in benzene. The elute was recrystallized from hexane and was identical with the authentic sample, (+)-**1**.

*(4a*S, *9*R, *9a*R*)-(+)-9-Amino-1,2,3,4,4a,9,9a,9,10-octahydroanthracene, (+)-**17**.* A mixture of the (+)-carboxylic acid [(+)-**15**, 140 mg] and oxalyl chloride (1 ml) was stirred at room temperature for 3 h. The volatile materials were removed by distillation *in vacuo*.

A solution of the acid chloride in dry tetrahydrofuran (3 ml) was added to a cold solution of NaN_3 (0.25 g) in water (5 ml). The mixture was stirred at 0 °C for 3 h and extracted with ether. The solution was washed with water, dried (Na_2SO_4) and concentrated *in vacuo*.

Dry benzene (5 ml) was added. The solution was heated under reflux for 3 h and concentrated *in vacuo*.

A solution of the isocyanate in *t*-butanol and triethylamine (1 ml) was heated under reflux for 12 h and the volatile

materials were removed by distillation *in vacuo*.

Concentrated HCl (5 ml) was added. The mixture was heated at 100 °C for 18 h. After cooling, the mixture was washed with ether, treated with charcoal and concentrated *in vacuo*. The residue (57.5 mg) was recrystallized from ethyl acetate, mp 270—271 °C.

Dilute NH_4OH was added. The mixture was extracted with dichloromethane. The solution was washed with water, dried (Na_2SO_4) and concentrated *in vacuo*. The residue was distilled at 100 °C at 0.2 mmHg giving a colorless oil (28.7 mg). $[\alpha]_D^{23}$ +82.1 ±0.8° (*c* 1.092, $CHCl_3$); IR (film) 3370, 3290 cm^{-1}; NMR ($CDCl_3$) δ=0.7—2.3 (m, 12H), 2.6—3.2 (m, 2H), 3.76 (s, 1H), 7.0—7.4 (m, 4H); UV_{max} (MeOH) 272 nm (ε 411), 265 (424), 261^{sh} (347), 211^{sh} (9100), 195 (42200); CD (MeOH) 271.5 nm ($\Delta\varepsilon$ +0.409), 264 (+0.458), 216 (+2.45). Found: C, 83.20; H, 9.71; N, 6.69%. Calcd for $C_{14}H_{19}N$: C, 83.53; H, 9.51; N, 6.96%.

*(4a*S, *9*S, *9a*R*)-(+)-9-Amino-1,2,3,4,4a,9,9a,10-octahydroanthracene, (+)-**18**.* A mixture of the (+)-ketone [(+)-**1**, 507 mg], NH_2OH–HCl (411 mg), pyridine (4 ml) and ethanol (6 ml) was heated under reflux for 16 h, poured into water and extracted with ether. The solution was washed with water, dried (Na_2SO_4) and concentrated *in vacuo*.

A small amount of raney-Ni was added to a solution of the oxime in methanol (20 ml), a solution of Na_2HPO_2 (0.85 g) in water (5 ml), and 2 mol dm^{-3} NaOH (5 ml). After the bubbling had settled, the mixture was shaken under hydrogen atmosphere. The catalyst was filtered and washed with methanol. Dilute HCl was added. The crystals were collected by filtration, shaken with aqueous K_2CO_3 and extracted with dichloromethane. The solution was dried (Na_2SO_4) and concentrated *in vacuo*. The residue was recrystallized from hexane, 57.1 mg, mp 48—50 °C; $[\alpha]_D^{24}$ −96.3 ±0.9° (*c* 1.019, MeOH); IR (Nujol) 3390, 3300 cm^{-1}; NMR ($CDCl_3$) δ=0.7—2.8 (m, 12H), 3.49 (s, broad, 1H), 6.9—7.3 (m, 3H), 7.4—7.8 (m, 1H); CD (MeOH) 272 nm ($\Delta\varepsilon$ +0.199) 265 (+0.199), 217 (+2.41). Found: C, 83.52; H, 9.22; N, 6.87%. Calcd for $C_{14}H_{19}N$: C, 83.53; H, 9.51; N, 6.96%.

*Friedel-Crafts Reaction of (+)-**19** with Benzene.* Anhydrous $AlCl_3$ (8.5 g) was added in one portion to a solution of the anhydride[8] [(+)-**19**, 2.16 g] in benzene (20 ml). The mixture was heated under reflux with vigorous stirring for 3 h and poured into ice-cold HCl. The organic phase was separated and the aqueous phase was extracted with benzene. The combined organic phases were washed with water, dried (Na_2SO_4) and concentrated. The residue was chromatographed on silica gel (Merck Co., grade 1, 50 g) in ethyl acetate. The NMR spectrum showed it to be a mixture of *ca.* 10 : 1 of (−)-**20** and **21**. They could not be separated from each other by fractional recrystallization or TLC.

Racemic **20** was isolated by recrystallization twice from benzene–hexane; mp 138—139 °C; IR (Nujol) 1694, 1680 cm^{-1}; NMR ($CDCl_3$) δ=1.40 (s, 3H), 1.3—2.1 (m, 8H), 3.82 (m, 1H), 7.3—7.6 (m, 3H), 7.7—8.0 (m, 2H). Found: C, 72.22; H, 7.33%. Calcd for $C_{15}H_{18}O_3$: C, 73.15; H, 7.37%.

*(1*R, *2*S*)-(−)-2-Benzyl-2-methyl-1-cyclohexanecarboxylic Acid, (−)-**18**.* The (−)-ketone [(−)-**20**, 378 mg] was hydrogenolyzed by the same procedure cited for 2-benzoyl-1-cyclohexanecarboxylic acid.[1] The oily residue was distilled at 150 °C (bath temperature) at 0.2 mmHg through a short-path distillation apparatus. The NMR spectrum showed contamination by a small amount of **23**.

Racemic **22**: mp 133—135 °C; IR (Nujol) 1692 cm^{-1}; NMR ($CDCl_3$) δ=1.24 (s, 3H), 0.9—1.9 (m, 8H), 2.0—2.8 (m, 3H), 7.20 (s, 5H). Found: C, 77.54; H, 8.79%. Calcd for $C_{15}H_{20}O_2$: C, 77.55; H, 8.68%.

*(4a*R, *9a*S*)-(+)-4a-Methyl-1,2,3,4,4a,9,9a,10-octahydro-10-anthracenone, (+)-**24**.* The ring-forming reaction was carried out according to the procedure cited for 2-benzyl-1-cyclohexanecarboxylic acid.[1] The oily product, quantitative yield, was distilled at 140 °C at 0.5 mmHg through a short-path distillation apparatus and was contaminated with a small amount of **26**.

Racemic **24**: oil; IR (film) 1688 cm^{-1}; NMR ($CDCl_3$) δ=1.07 (s, 3H), 1.1—2.4 (m, 1H), 2.68 (s, 1H), 2.80 (d, *J*=5 Hz, 1H), 7.0—7.7 (m, 3H), 7.9—8.2 (m, 1H). Found: C, 83.62; H, 8.45%. Calcd for $C_{15}H_{18}O$: C, 84.07; H, 8.47%.

*(4a*S, *9a*S*)-(+)-4a-Methyl-1,2,3,4,4a,9,9a,10-octahydroanthracene, (+)-**25**.* The (+)-ketone [(+)-**24**] was hydrogenolyzed as above. The crude oily residue was chromatographed on thin silica gel plate (Merck Co., precoated, 0.5 mm) in hexane and distilled at 80 °C (bath temperature) at 0.2 mmHg through a short-path distillation apparatus, and crystallized then recrystallized from hexane mp 52—53 °C; $[\alpha]_D^{22}$ +81.5 ±0.4° (*c* 1.277, hexane); IR (film) 743 cm^{-1}; NMR ($CDCl_3$) δ=0.81 (s, 3H), 1.0—1.9 (m, 10H), 2.51 (br, s, 3H), 7.05 (s, 4H). Found: C, 89.99; H, 10.02%. Calcd for $C_{15}H_{20}$: C, 89.94; H, 10.06%.

*(2*R, *3*R*)-(−)-2,3-Dimethyl-4-phenyl-4-oxobutanoic Acid, (−)-**27**.* Mp 88—89 °C; $[\alpha]_D^{25}$ −1.22 ±0.20°, $[\alpha]_{365}^{25}$ −107.2 ±0.5° (*c* 2.035, MeOH).

*(2*R, *3*S*)-(−)-2,3-Dimethyl-4-phenylbutanoic Acid, (−)-**28**.* Bp 145 °C at 1.5 mmHg. $[\alpha]^{25}$ −28.8 ±0.4° (*c* 1.510, MeOH).

*(2*S, *3*S*)-(+)-2,3-Dimethyl-1,2,3,4-tetrahydro-1-naphthalenone, (+)-**29**.* Mp 34—36 °C; $[\alpha]^{25}$ +49.6 ±0.3° (*c* 2.353, hexane).

*(2*S, *3*S*)-(+)-2,3-Dimethyl-1,2,3,4-tetrahydronaphthalene, (+)-**30**.* The product was crystallized from hexane with cooling in a Dry Ice–acetone bath. The crystals were collected at that temperature. The crystals were recrystallized by the same method and then distilled, $[\alpha]_D^{25}$ +103.9 ±0.9° (*c* 1.139, hexane). The NMR spectrum did not show the signal attributable to *meso*-2,3-dimethyl-1,2,3,4-tetrahydronaphthalene.

*(+)-ω-Camphanic Ester of (1*R, *2*S*)-2-Methyl-1,2,3,4-tetrahydro-1-naphthol, (+)-**31**.* The (+)-alcohol (**32**) was treated according to the procedure cited for **4**. The ester was recrystallized five times from methanol; mp 128.5—129.5 °C; $[\alpha]_D^{25}$ +31.0 ±0.6° (*c* 1.020, $CHCl_3$); IR (Nujol) 1789, 1737 cm^{-1}; NMR ($CDCl_3$) δ=0.95 (s, 3H), 1.04 (d, *J*=6 Hz, 3H), 1.06 (s, 3H), 1.09 (s, 3H), 1.5—3.0 (m, 9H), 5.94 (d, *J*=6 Hz, 1H), 7.18 (s, 4H). Found: C, 73.40; H, 7.65%. Calcd for $C_{21}H_{26}O_4$: C, 73.66; H, 7.65%.

*(1*R, *2*S*)-(−)-2-Methyl-1,2,3,4-tetrahydro-1-naphthol, (−)-**32**.* Mp 55—56 °C; $[\alpha]_D^{24}$ −92.9 ±0.7° (*c* 1.375, benzene); (lit,[7] −91.6); CD 274.5 nm ($\Delta\varepsilon$ −0.030), 269 (−0.055), 261.5 (−0.045), 205! (−2.85).

*(2*S*)-(−)-2-Methyl-1,2,3,4-tetrahydronaphthalene, (−)-**33**.* $[\alpha]_D^{25}$ −103.4 ±1.3° (*c* 1.281, dioxan).

We thank Dr. Eiji Osawa and Dr. Masumi Yamakawa for allowing us to use a program of MMI and Mr. Tatsuo Iwata for assistance in performing the CD measurements.

References

1) G. Snatzke and P. C. Ho, *Tetrahedron*, **27**, 3645 (1971).
2) G. Snatzke, M. Kajtar, and F. Werner-Zamojska, *Tetrahedron*, **28**, 281 (1972).
3) R. Weidmann and J.-P. Guette, *C. R. Acad. Sci., Ser. C*, **268**, 2225 (1969).
4) J. Barry, H-B. Kagan, and G. Snatzke, *Tetrahedron*, **27**, 4737 (1971).
5) J. C. Craig, S.-Y. C. Lee, R. P. K. Chan, and I. Y.-F.

Wang, *J. Am. Chem. Soc.*, **99**, 7996 (1977).
6) P. B. Hulbert, W. Klyne, and P. M. Scopes, *J. Chem. Res. (M)*, **1981**, 401.
7) A. Schoofs, J. P. Guetté, and A. Horeau, *Bull. Soc. Chim. Fr.*, **1976**, 1215.
8) S. Hagishita and K. Kuriyama, *J. Chem. Soc., Perkin Trans. 2*, **1974**, 686.
9) G. E. McCasland and S. Proskow, *J. Am. Chem. Soc.*, **78**, 5636 (1956).
10) Y. Dozen and M. Hatta, *Bull. Chem. Soc. Jpn.*, **48**, 2842 (1975).
11) N. L. Allinger, *Adv. Phys. Org. Chem.*, **13**, 1 (1976).
12) K. M. Wellman, W. S. Briggs, and C. Djerassi, *J. Am. Chem. Soc.*, **87**, 73 (1965).
13) R. L. Ellis, G. Kuehlenz, and H. H. Jaffé, *Theor. Chim. Acta*, **26**, 131 (1972).
14) A. Imamura, T. Hirano, C. Nagata, and T. Tsuruta, *Bull. Chem. Soc. Jpn.*, **45**, 396 (1972).

Synthesis of 3-Acylfurans Using 3-(Phenylthio)propanal Dimethyl Acetal as a New Synthon. Syntheses of Ipomeanine and Isoegomaketone

Eiji WATANABE, Naohiro IMAI, Katsuhiko INOMATA, Hideki KINOSHITA,* and Hiroshi KOTAKE
Department of Chemistry, Faculty of Science, Kanazawa University, Kanazawa 920
(Received February 25, 1982)

It was found that 3-(phenylthio)propanal dimethyl acetal is a very useful starting material for the preparation of 3-acylfuranoterpenes. Syntheses of two naturally-occurring furans, isoegomaketone and ipomeanine were described.

In the past, a large number of 3-acylfurans have been found in nature.[1] A few methods of their syntheses have been reported[2] except those starting from 3-furyl type synthons,[3] however, a convenient and effective method of 3-acylfurans have not been reported yet.

In the previous paper,[4] it has been reported that the readily available 3-(phenylthio)propanal ethylene acetal (**2**) was proved to be very useful starting material for the preparation of 3-acylfurans. Syntheses of some 3-acylfurans were exemplified and one of naturally-occurring furanoterpenes, perillaketone (**1**) was synthesized in good yield starting from compound **2**.

In order to demonstrate more usefulness of this new method, its application to synthesis of more complex naturally-occurring furanoterpenes was investigated. The target compounds selected are isoegomaketone (**12b**) originally isolated from *Perilla furutescens* Brit.[5] and ipomeanine (**13**) which was produced by cerato-stomella.[6] In this paper, the syntheses of both furanoterpenes **12b** and **13** are described.

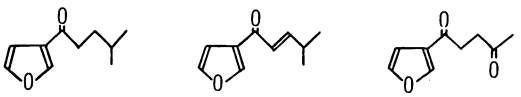

1 12b 13

The synthesis of ipomeanine (**13**) was examined according to Scheme 1. Acylation of compound **2** was performed by treatment of a lithiated **2** with acylaziridine **9c** at −78 °C to afford the desired product **3** in 65% yield. Compound **9c** was prepared by the reaction of commercially available levulinic acid with 1.2 equivalent of 1,2-ethanedithiol in the presence of boron trifluoride etherate followed by condensation reaction of the thiacetalized acid obtained with aziridine by 3-(5-nitro-2-oxo-1,2-dihydro-1-pyridyl)-1,2-benziso-thiazole 1,1-dioxide (BID-NPy)[7] in good yield as shown in the following scheme.

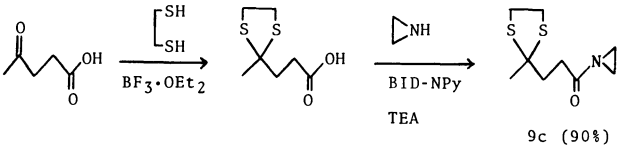

The 3-acyl-3-(phenylthio)propanal ethylene acetal **3** was treated with an equimolar amount of lithium diisopropylamide (LDA) in THF at −50 °C to room temperature followed by the passing of a large excess of gaseous formaldehyde into the reaction solution at room temperature. The resulting crude keto alcohol **4** was refluxed in benzene in the presence of a catalytic amount of *p*-toluenesulfonic acid (PTSA) for a couple of hours to give the desired product **12c** in only poor yield (36% based on **3**). All attempts to improve the yield of conversion of compound **4** to the furan derivative **12c** under various conditions were unsuccessful. The thioacetal group of **12c** was deprotected by treatment with $CuCl_2$ and CuO in refluxing wet acetone[8] to give the final product, ipomeanine, 1-(3-furyl)-1,4-pentanedione (**13**) in 89% yield.

Previously, we had reported that treatment of 2-alkyl-4,4-dimethoxy-2-phenylthio-1-butanol (**6**) easily derived from ethyl 4,4-dimethoxy-2-(phenylthio)butyrate (**5**), with PTSA in refluxing benzene gave 3-alkyl-furan (**7**)[9] in excellent yield as shown below. These findings

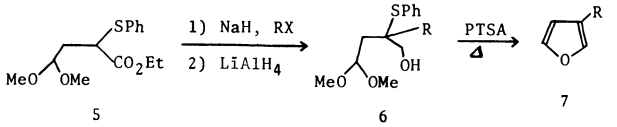

suggested that compound **6** was a more favorable starting material for the cyclization to furan ring. From this fact, we have thought that 3-(phenylthio)-propanal dimethyl acetal (**8**) was more effective synthon for the preparation of 3-acylfurans than compound **2** (Scheme 2). The starting material **8** was prepared by the reaction of 3-(phenylthio)propanal, which was easily obtained from equimolar quantities of acrylaldehyde and benzenethiol at 0 °C and used without further purification, with trimethyl orthoformate (1.1

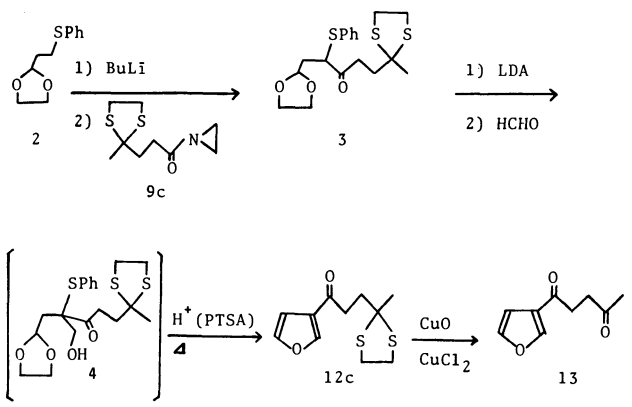

Scheme 1.

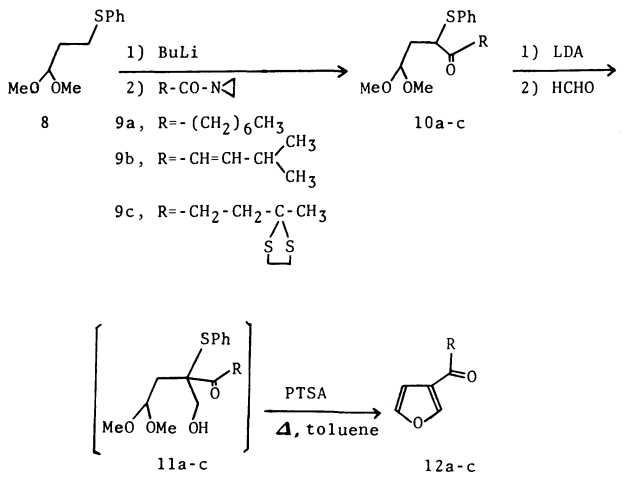

Scheme 2.

equiv.) in dry methanol in 85% yield. First of all, as a model experiment synthesis of 3-octanoylfuran (**12a**) was undertaken. Compound **8** was allowed to react with 1.1 equivalent of BuLi in THF at −78 °C followed by treatment with 1-octanoylaziridine (**9a**) to give the expected acyl compound **10a** in 64% yield. Compound **10a** was lithiated with 1.2 equivalent of LDA at −78 °C in THF followed by reaction with a large excess of formaldehyde to give the corresponding hydroxymethyl derivative **11a**, which was refluxed in toluene for 50 min in the presence of 6 mol percent of PTSA. The desired 3-octanoylfuran (**12a**) was obtained in 67% yield from **10a**. Many attempts to improve the yield of **12a** from **11a** were examined under various conditions. Subsequently, successive removal of the methanol formed *in situ* using Soxhlet's extractor where a large amount of boric acid was placed gave an outstanding result. Namely, the yield of **12a** was raised up to 84% yield under the same reaction conditions as used before. This good result prompted us to employ compound **8** as the starting material for the preparation of more complex furanoterpenes such as **12b** and **13**.

In a manner similar to the preparation of **12a**, treatment of **9b**—**c** gave the corresponding 3-acylfurans **10b**—**c** in 65% and 67% yields, respectively. Next, they were allowed to react with LDA at −78 °C and treated with formaldehyde as mentioned above to give the desired products **11b**—**c**. The resulting crude **11c** was transformed into the protected 3-acylfuran **12c** in 63% yield based on **10c**. This yield was greately raised compared with the result starting from compound **3**. Compound **12c** was converted to ipomeanine **13** according to the procedure as shown before.

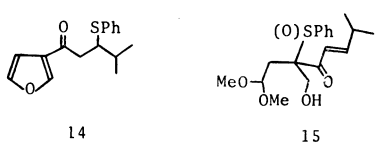

14 15

Similarly, when the crude material **11b** was refluxed in toluene including a small amount of PTSA, the reaction was accompanied by formation of 3-[4-methyl-3-(phenylthio)pentanoyl]furan (**14**) as by-product besides **12b**. In order to solve this problem, compound **11b** was converted into sulfoxide **15** with *m*-chloroperbenzoic acid, which was treated with PTSA in refluxing toluene. Unfortunately, the desired product was only produced in an unsatisfactory yield from **10b**. Next, the crude **11b** was refluxed for 17 min in toluene in the presence of 1.5 equivalent of iodine to oxidize the benzenethiol liberated in the reaction to the disulfide, 6 mol percent of PTSA, and boric acid. Eventually, isoegomaketone, 1-(3-furyl)-4-methyl-2-penten-1-one (**12b**) was obtained in 62% yield based on **10b**.

As mentioned above, it is evident that 3-(phenylthio)-propanal dimethyl acetal (**8**) is synthetically versatile starting material for more complex 3-acylfurans.

Experimental

The NMR spectra were recorded on a JEOL/MH-60, and a JEOL/PMX-60. The chemical shifts are reported on the δ scale relative to TMS as an internal standard. The IR spectra were measured with a JASCO IRA-1 diffraction grating infrared spectrometer.

Materials. All the solvents were distilled according to the usual methods and stored over a drying agent. Thin-layer chromatography (TLC) was performed on Merck's Silica gel 60 PF_{254} (Type 7749).

*Preparation of Acylaziridine Derivatives (**9a**—**c**).* *1-[4,4-(Ethylenedithio)pentanoyl]aziridine (**9c**)*: To a solution of BID-NPy (610 mg, 2 mmol) and 4,4-(ethylenedithio)-pentanoic acid (384 mg, 2 mmol)[10] in dry CH_2Cl_2 (5 ml) was added a solution of triethylamine (TEA) (222 mg, 2.2 mmol) in dry CH_2Cl_2 (5 ml) at 0 °C under N_2. The reaction mixture was stirred for 1.5 h at 0 °C and a solution of aziridine (220 mg, 2 mmol) in dry CH_2Cl_2 (5 ml) was added to the above solution at 0 °C. The reaction mixture was warmed to room temperature, stirred for 30 min, and treated with 10%-$NaHCO_3$ (10 ml). The mixture was extracted with ether several times and the combined extracts were washed with brine, dried over Na_2SO_4, concentrated *in vacuo* to give a residue which was subjected to preparative TLC (solvent; AcOEt: hexane=1 : 5 v/v). Compound **9c** was obtained in 90% yield as an oily product (365 mg); IR (neat) 1689, 1143, 1117, 1088 cm^{-1}; NMR ($CDCl_3$) δ 1.80 (s, 3H), 2.11—2.38 (m, 2H), 2.60—2.85 (m, 2H), 2.24 (s, 4H), 3.33 (s, 4H).

Other 1-acylaziridine compounds **9a**—**b** were obtained from aziridine and the corresponding acyl chlorides in 69% and 58% yields, respectively.

9a: Oil IR (neat) 1693, 1373, 1145, 996 cm^{-1}; NMR ($CDCl_3$) δ 0.86 (t, 3H, J=6.6 Hz), 1.03—2.00 (m, 10H), 2.17 (s, 4H), 2.41 (t, 2H, J=7.0 Hz).

9b: Oil bp 55—65 °C/0.4 Torr); IR (neat) 1670, 1630, 1107, 973 cm^{-1}; NMR ($CDCl_3$) δ 1.06 (d, 6H, J=6.0 Hz), 2.25 (s, 4H), 2.08—2.81 (m, 1H), 5.96 (dd, 1H, J=2.0, 16.0 Hz), 7.00 (dd, 1H, J=6.0, 16.0 Hz).

*7,7-Ethylenedithio-4-oxo-3-(phenylthio)octanal Dimethyl Acetal (**3**).* To a solution of **2** (344 mg, 1.64 mmol) in dry tetrahydrofuran (THF) (5 ml) was added 1.1 equiv. of BuLi at −78 °C under N_2. The solution was warmed from −78 °C to −20 °C in a period of 2 h and cooled down at −78 °C again. A solution of **9c** (364 mg, 1.80 mmol) in dry THF (5 ml) was added to it at −78 °C and the reaction mixture was gradually warmed to room temperature and allowed to stand overnight. After quenching with buffer solution of pH 7 and 1 M-HCl, the resulting solution was extracted with ether. The organic layer was dried over Na_2SO_4 and evaporated *in vacuo* to give a residual oil. Purification with preparative TLC in which development was repeated twice with solvent system of

benzene–hexane–EtOAc (5 : 5 : 1 v/v) gave the desired product in 65% yield (oil, 408 mg): IR (neat) 1702, 1580, 1130, 1012 cm^{-1}; NMR ($CDCl_3$) δ 1.70 (s, 3H), 1.92—2,33 (m, 4H), 2.58—3.07 (m, 2H), 3.23 (s, 4H), 3.63—4.00 (m, 5H), 4.93 (t, 1H, J=7.0 Hz), 7.03—7.50 (m, 5H).

*3-(Phenylthio)propanal Dimethyl Acetal (**8**).* A mixture of acryladehyde (5.482 g, 88.1 mmol) and benzenethiol (8.833 g, 80.3 mmol) was stirred for 2 h at 0 °C. The reaction mixture was diluted with dry methanol (30 ml). A solution of trimethyl orthoformate (9.359 g, 88.3 mmol) in dry methanol (10 ml) and a small amount of PTSA were added to it. The reaction solution was stirred for 2 h, treated with solid $NaHCO_3$, evaporated under reduced pressure to give a residue which was taken up into ether. The ether solution was washed with brine, dried over Na_2SO_4, and concentrated *in vacuo*. Distillation of the residual oil gave pure product as an oily material. Yield, 15.88 g (85%): Bp 89—91 °C/0.3 Torr. IR (neat) 1566, 1112, 869, 734 cm^{-1}; NMR ($CDCl_3$) δ 1.87 (m, 2H), 2.93 (q, 2H, J=5.8, 8.6 Hz), 3.28 s, (6H), 4.46 (t, 1H, J=5.8 Hz), 7.09—7.33 (m, 5H).

*Preparation of 3-Acyl-3-(phenylthio)propanal Dimethyl Acetal Derivatives (**10a—c**).* To a solution of **8** (157 mg, 0.74 mmol) in dry THF (5 ml) was added 1.1 equiv. of BuLi at −78 °C under N_2. The reaction solution was gradually warmed to room temperature and cooled down at −78 °C again. A solution of **9** (150 mg, 0.89 mmol) in dry THF (4 ml) was slowly added to it. The reaction mixture was kept at −78 °C for 2 h, warmed to room temperature, and quenched with buffer solution of pH 7 and 1 M-HCl. The resulting mixture was extracted with ether. The combined ether extracts were dried over Na_2SO_4. After removal of the solvent a residual oil was purified by TLC using hexane–ether (6 : 1 v/v) as solvent to give pure product **10a** in 68% yield (oil). IR (neat) 1700, 1580, 1120, 1065 cm^{-1}; NMR ($CDCl_3$) δ 1.73 (s, 3H), 1.94—2.33 (m, 4H), 2.73—3.03 (m, 2H), 3.27 (s, 4H), 3.30 (s, 6H), 3.78 (t, 1H, J=7.2 Hz), 4.46 (t, 1H, J=5.4 Hz), 7.16—7.42 (m, 5H).

In the same procedure as the preparation of **10a**, compounds **10b—c** were obtained from compound **8** and the corresponding 1-acylaziridines **9b—c** in 65% and 67% yields, respectively.

10b: Oil, IR (neat) 1680, 1655, 1618, 1118, 1070, 1048 cm^{-1}; NMR ($CDCl_3$) δ 1.05 (d, 6H, J=7.0 Hz), 1.67—2.78 (m, 2H), 2.31 (s, 3H), 3.34 (s, 3H), 3.93 (t, 6H, J=6.0 Hz), 4.55 (t, 1H, J=6.0 Hz), 6.36 (d, 1H, J=16.0 Hz), 6.90 (dd, 1H, J=6.0, 16.0 Hz), 7.26—7.63 (m, 5H).

10c: Oil, IR (neat) 1700, 1580, 1120, 1065 cm^{-1}; NMR ($CDCl_3$) δ 1.73 (s, 3H), 1.94—2.33 (m, 4H), 2.73—3.03 (m, 2H), 3.27 (s, 4H), 3.30 (s, 6H), 3.78 (t, 1H, J=7.2 Hz), 4.46 (t, 1H, J=5.4 Hz), 7.12—7.42 (m, 5H).

*Preparation of 3-Acyl-3-hydroxymethyl Derivatives (**11a—c**).* To a solution of 1.2 equiv. of LDA in dry THF (4 ml) was added slowly a solution of **10a** (172 mg, 0.51 mmol) in dry THF (4 ml) at −78 °C under N_2. The reaction solution was gradually warmed to room temperature in a period of about 3 h. A solution of formaldehyde in THF (20 ml) where it was generated from 25 equiv. of paraformaldehyde by heating and absorbed in dry THF containing molecular sieves, was added in one portion to the solution at room temperature. The solution was allowed to stand overnight and the insoluble materials were filtered off. The filtrate was treated with buffer solution of pH 7 and 1 M-HCl, and extracted with ether. The organic layer was washed with brine, dried over Na_2SO_4, and concentrated in vacuo to give a crude **11a** (197 mg). It was used in the subsequent reaction without further purification.

Crude compounds **11b—c** were obtained in the same way as described for the preparation of **11a**.

*1-(3-Furyl)-1-octanone (**12a**).* A solution of the crude material **11a** (197 mg) obtained above in dry toluene (30 ml) was added in one portion under N_2 to a flask containing PTSA (5.2 mg, 6 mol percent), equipped with a Soxhlet's extractor where 6 g of boric acid were placed. The toluene solution was refluxed for 45 min, then cooled down with a cold-bath, treated with 5 ml of 10%-$NaHCO_3$, and extracted with ether. The organic layer was dried over Na_2SO_4 and concentrated under reduced pressure. A crude residue was subjected to preparative TLC (hexane–ether=4 : 1 v/v) to give the desired furan in 84% yield based on **10a** (65 mg, oil). IR (neat) 3125, 1650, 1150, 869 cm^{-1}; NMR ($CDCl_3$) δ 0.90 (t, 3H, J=6.0 Hz), 0.77—1.82 (m, 10H), 2.70 (t, 3H, J=7.6 Hz), 6.75 (m, 1H), 7.40 (m, 1H), 7.96 (m, 1H).

*Isoegomaketone (**12b**).* Compound **12b** was obtained in 62% yield based on **10b** from a crude material **11b** in the presence of 1.5 equiv. of iodine in a manner silmiar to the preparation of **12a**. A crude product was purified by preparative TLC using hexane–benzene–AcOEt–ether (7 : 1 : 1 : 1 v/v) as solvent. Its IR and NMR spectra were in accord with the reported values.[3c] IR (neat) 3140, 1660, 1610, 1147, 865 cm^{-1}; NMR ($CDCl_3$) δ 1.10 (d, 6H, J=7.0 Hz), 2.13—2.70 (m, 1H), 6.40 (d, 1H, J=16.0 Hz), 6.67—7.00 (m, 2H), 7.35 (m, 1H), 7.98 (m, 1H).

*3-[4,4-(Ethylenedithio) pentanoyl]furan (**12c**).* *Method A*: The desired product was prepared in 63% yield based on **10c** from a crude material **11c** in the same manner as described for the preparation of **12a** (15 mol percent of PTSA, reflux for 1 h). IR (neat) 3130, 1559, 1306, 865 cm^{-1}; NMR ($CDCl_3$) δ 1.79 (s, 3H), 2.00—2.46 (m, 2H), 2.89—3.27 (m, 2H), 3.30 (s, 4H), 6.70 (m, 1H), 7.19—7.38 (m, 1H), 7.89 (m, 1H).

Method B: A crude material **4** which was prepared from **3** in the same way as described for the preparation of **11c** was dissolved in 20 ml of dry toluene and refluxed for 30 min in the presence of PTSA (4 mg) under N_2. The reaction mixture was neutralized with $NaHCO_3$, washed with brine, and extracted with ether. The combined extracts were dried over Na_2SO_4 and concentrated *in vacuo* to give a crude product, which was purified by preparative TLC (36 mg, 25%).

*Ipomeanine (**13**).* A solution of **12c** (31 mg, 0.128 mmol) in 99%-acetone (15 ml) was refluxed for 1 h in the presence of $CuCl_2 \cdot 2H_2O$ (46 mg, 0.27 mmol) and CuO (43 mg, 0.54 mmol). An insoluble material was filtered off and the filtrate was concentrated under reduced pressure to give a residue. The residual oil was purified by preparative TLC using ether–hexane (1 : 4 v/v) as solvent to afford compound **13** in 89% yield (23 mg). IR (neat) 1714, 1668, 1561, 1149, 866 cm^{-1}; NMR ($CDCl_3$) δ 2.20 (s, 3H), 2.67—3.61 (m, 4H), 6.74 (m, 1H), 7.43 (m, 1H), 8.05 (m, 1H).

The 2,4-dinitrophenylhydrazone was prepared as a red crystalline material, mp 231—233 °C (lit, mp 231—234 °C).[6]

References

1) "Dai Yuki-Kagaku," ed by M. Kotake, Asakura, Tokyo (1959), Vol. 14, pp. 21—25.

2) a) K. Kondo and M. Matsumoto, *Tetrahedron Lett.*, **1976**, 4363; b) A. Zamojski and T. Kozluk, *J. Org. Chem.*, **42**, 1089 (1977).

3) a) T. Matsuura, *Bull. Chem. Soc. Jpn.*, **30**, 430 (1957); b) R. F. Abdulla and K. H. Fuhr, *J. Org. Chem.*, **43**, 4248 (1978); c) R. A. Massay-Westropp and G. D. Reynolds, *Aust. J. Chem.*, **19**, 891 (1966).

4) K. Inomata, M. Sumita, and H. Kotake, *Chem. Lett.*, **1979**, 709.

5) H. Ito, *J. Pharm. Soc. Jpn.*, **84**, 1123 (1964). With

respect to previous synthesis of isoegomaketone, see Ref. 3c.
6) T. Kubota and N. Ichikawa, *Chem. Ind. (London)*, **1954**, 902.
7) A. Ahmed, H. Fukuda, K. Inomata, and H. Kotake, *Chem. Lett.*, **1980**, 1161.
8) K. Narasaka, T. Sakashita, and T. Mukaiyama, *Bull. Chem. Soc. Jpn.*, **45**, 3724 (1972).
9) H. Kotake, K. Inomata, S. Aoyama, and H. Kinoshita, *Chem. Lett.*, **1977**, 73.
10) M. Araki, S. Sakata, H. Takei, and T. Mukaiyama, *Bull. Chem. Soc. Jpn.*, **47**, 1777 (1974).

Vinyl Polymerization. 411. Experimental Supports for the Concept of Hard and Soft Hydrophobic Areas and Monomers in the So-called Uncatalyzed Polymerization

Tatsuro Ouchi,* Masaya Inaba, and Minoru Imoto
Department of Applied Chemistry, Faculty of Engineering, Kansai University, Senriyama, Suita, Osaka 564
(Received February 27, 1982)

We have proposed a concept of hard and soft hydrophobic areas (HA) and monomers. In order to verify such a concept, two series of experiments were carried out. Poly(styrene-alt-disodium maleate) (**1**) and poly(styrene-alt-sodium methyl maleate) (**2**) were used as initiating macromolecules for the copolymerizations of styrene/methyl methacrylate (MMA) and acrylonitrile/MMA. When **1** was used, MMA was more easily polymerized than styrene. Inversely, when **2** was used, styrene was more easily polymerized than MMA. Poly(styrene-co-sodium acrylate) (**3**) substances with various compositions were used as intiators for the copolymerizations. The produced copolymers of MMA and styrene were found to have a larger content of MMA as the mole ratio of acrylate in **3** became higher. Inversely, the produced copolymers of MMA and acrylonitrile had a larger content of acrylonitrile as the mole ratio of acrylate became higher. Those results could be reasonably explained by the concept of hard and soft hydrophobic areas and monomers.

Macromolecules having a hydrophilic group, such as starch, cellulose, polyamide and enzyme, can initiate the radical polymerization of vinyl monomers in water without any ordinary radical initiator. Such a simple and novel polymerization has been called an "uncatalyzed polymerization."[1-3] It has been clarified that the polymerization proceeds as follows: (i) the macromolecules form the hydophobic areas (HA) in a water phase, (ii) the vinyl monomer dissolves in the water phase and then is incorporated into HA, and (iii) in the HA, a radical polymerization proceeds.

Needless to say, the hydrophobicities of HA and monomers differ from each other. We called the more HA and hydrophobic monomers "hard," and the less HA and hydrophilic monomers "soft." The orders of hardness and softness of HA and monomers are expressed by Fig. 1.[2,4]

We have proposed "a concept of hard and soft HA and monomer," which means that the hard HA prefers to incorporate the hard monomer, while the soft HA prefers to incorporate the soft monomers.[2] This concept has been verified experimentally in several papers[2,4] by two methods, *i.e.*, by the coplymerization of styrene with methyl methacrylate (MMA) and by the selectivity of the monomer initiated with copolymers having different hydrophobicities.[5]

The present paper deals with the polymerizations of styrene, MMA, and acrylonitrile initiated by the water-soluble poly(styrene-alt-disodium maleate) (Copolymer **1**) or poly(styrene-alt-sodium methyl maleate) (Copolymer **2**), and with the copolymerizations of styrene with MMA and of MMA with acrylonitrile initiated with poly(styrene-co-sodium acrylate) (Copolymer **3**) substances with different compositions.

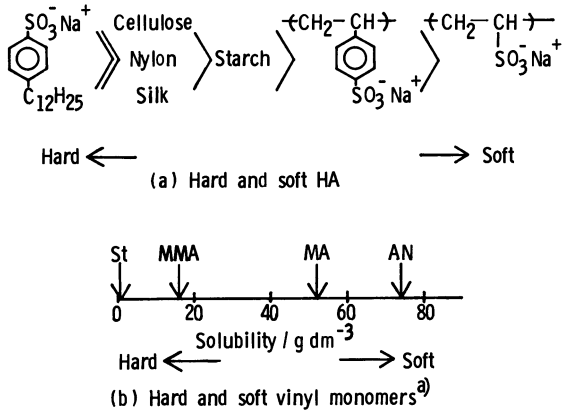

Fig. 1. Hard and soft HA and monomers.
St: Styrene, MMA: methyl methacrylate, MA: methyl acrylate, AN: acrylonitrile. a) The numbers indicate the solubilities into water at 20 °C.

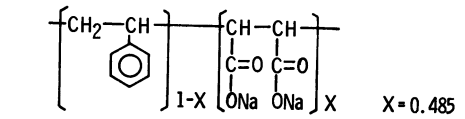

Copolymer 1, poly(styrene-alt-disodium maleate)

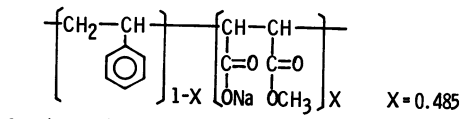

Copolymer 2, poly(styrene-alt-sodium methyl maleate)

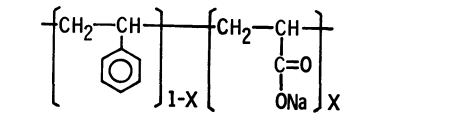

Copolymer 3, poly(styrene-co-sodium acrylate)

Experimental

Materials. The monomers were purified by the usual methods and distilled under a vacuum before use. Ion-exchanged and distilled water was used as the solvent.

Preparation of Poly(styrene-alt-disodium maleate) (Copolymer 1). Five cm^3 (43.3 mmol) of styrene and 4.25 g (43.3 mmol) of maleic anhydride (Manh) were dissolved in 5 cm^3 of benzene and then placed in a tube. The tube was sealed after thawing with nitrogen and heated at 60 °C for 100 h. After the reaction, the contents were poured into large amounts of hexane to precipitate the copolymer. The copolymer was twice

reprecipitated from acetone and benzene/hexane (1 : 2 by vol.). The yield was 99%. The mole fraction of Manh in the copolymer was determined by elemental analysis to be 0.485. Accordingly, the copolymer was mostly alternative. The molecular weight of the obtained poly(styrene-alt-Manh) was measured by the vapor-pressure osmometric method and found to be 1.79×10^4 in acetone at 37 °C. This copolymer was neutralized with calculated amount of a 1 mol dm^{-3} NaOH solution up to pH 10 and then freeze-dried.

Preparation of Poly(styrene-alt-sodium methyl maleate) (Copolymer 2). The poly(styrene-alt-Manh) described above was refluxed in dried methanol for 50 h and then poured into large amounts of water to precipitate the copolymer. By elemental analysis, the copolymer was found to be a monoester with the structure shown below. This acidic copolymer was changed into its sodium salt by neutralization with a 1 mol dm^{-3} NaOH solution at pH 10 and then freeze-dried.

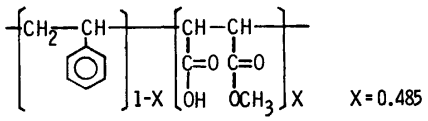

Poly(styrene-co-sodium acrylate) (Copolymer 3). Four kinds of Copolymer **3** (x=0.291, 0.537, 0.698, 0.782) and poly (sodium acrylate) (x=1.00) were prepared and purified by the method reported in a previous paper.[5] Here, x means the mole fraction of the sodium acrylate unit in Copolymer **3**.

Copolymers **1**, **2** and **3** were confirmed by the KI or ESR method to contain no peroxide moiety nor free radical.

Procedures of Polymerization. The vinyl monomers, Copolymer **1**, **2**, or **3** and water were placed in a tube. The tube was sealed under a vacuum after thawing with nitrogen and then incubated at 85 °C with or without shaking. After a certain time, the contents of the tube were poured into a large amount of methanol in order to precipitate the polymer produced. The conversion of the monomer was calculated from the weight of the polymer.

Results and Discussion

Polymerization of Vinyl Monomers Initiated by the Copolymer 1 or 2. An aqueous solution of Copolymer **1** or **2** was shaken with styrene, MMA, or acrylonitrile at 85 °C for 3 h. The results obtained are listed in Table 1.

The HA formed by Copolymer **1** is softer than the HA formed by Copolymer **2**; the hardness of the monomer is in order of: styrene>MMA>acrylonitrile. Accordingly, styrene was more easily incorporated in the HA formed by Copolymer **2** than in that formed by Copolymer **1** and more easily polymerized by Copolymer **2** than by Copolymer **1**, but MMA was, inversely, more easily polymerized by Copolymer **1** than by Copolymer **2**. Acrylonitrile is too soft to be easily incorporated into either Copolymer **1** or **2**.

Table 1. Polymerization of vinyl monomers with the copolymer 1 or 2[a]

Copolymer	Conversion[b]/%		
	Styrene	MMA	Acrylonitrile
1	3.30	5.59	0.14
2	5.44	5.04	0

a) Monomer, 3 cm^3; copolymer, 0.03 g; H_2O 10 cm; 85 °C; 3 h; with shaking. b) Each conversion contains the thermal conversion.

Copolymerization of MMA with Styrene or Acrylonitrile by Copolymer 3. The copolymerizations of MMA with styrene or acrylonitrile initiated by Copolymer **3** with various compositions were carried out.

The HA formed by Copolymer **3** having a higher x fraction are softer than those formed by Copolymer **3** having a lower x fraction.

First, a mixture of styrene and MMA and an aqueous solution of Copolymer **3** was allowed to stand at 85 °C for 3 h. The copolymers produced from the upper monomer layer and the lower aqueous layer were

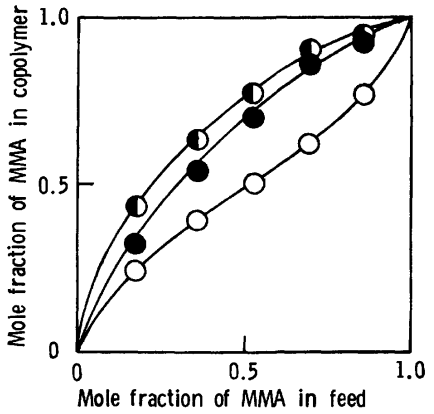

Fig. 2. Composition curves in the copolymerization of styrene and MMA on standing.
(MMA+styrene) 3 cm^3; Copolymer **3**, 0.03 g; H_2O 10 cm^3; 85 °C; 3 h.
—○—: Composition curve of the copolymers produced in monomer layer (x of Copolymer **3**=0.537), —●—: composition curve of the copolymers produced in water layer (x of Copolymer **3**=0.537), —◐—: composition curve of the copolymers produced in water layer (x of Copolymer **3**=0.782).

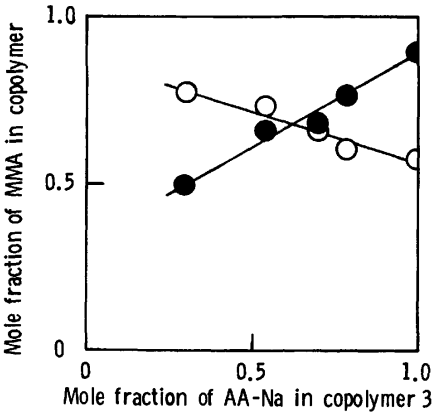

Fig. 3. Effects of the mole fraction of AA-Na in Copolymer **3** on the composition of copolymer produced in the water layer. Copolymer **3**, 0.03 g; H_2O, 10 cm^3; 85 °C; 8 h; on standing.
●: MMA, 1.5 cm^3; styrene, 1.5 cm^3 (mole ratio of MMA: styrene =0.48 : 0.52). ●: MMA, 1.5 cm^3; acrylonitrile, 1.5 cm^3 (mole ratio of acrylonitrile: MMA =0.38 : 0.62).

isolated separately. The conversions of the monomer mixture in the water phase were controlled as to be lower than 2.2%. The composition curves are shown in Fig. 2.

The curve of open circles indicates the composition curve of the copolymer produced in the monomer layer. Here, a usual thermal polymerization proceeds. Accordingly, the curve was very similar to that of an ordinary radical-copolymerization curve.

The black and half-black circles in Fig. 2 indicate the results obtained by Copolymer **3** having x values of 0.53 and 0.78 respectively. The latter copolymer forms a softer HA than the former copolymer. Accordingly, the copolymer of 0.78 of x is considered to incorporate MMA more easily than styrene. As is to be expected by the concept, the contents of MMA in the copolymer of MMA with styrene produced by Copolymer **3** of $x=0.78$ are larger than in those produced by Copolymer **3** of $x=0.53$.

A second support was given by the copolymerizations of MMA/styrene and MMA/acrylonitrile on standing, using Copolymers **3** with various compositions. The results obtained are shown in Fig. 3. In both copolymerizations, the mole ratios of the monomers in the feed were kept constant, while the composition of Copolymer **3** was varied. The abscissa of the figure indicates the x-value of Copolymer **3**. In the copolymerization of MMA and styrene, the curve shown by black circles was obtained. Clearly, the contents of MMA in the copolymer produced increased with the increase in the x-value.

Inversely, in the copolymerization of MMA and acrylonitrile, the contents of MMA in the copolymer produced decreased with the x-value.

These results can be explained by the difference in the incorporated amounts of the monomer into the HA formed by Copolymer **3** with various compositions. That is, they show the propriety of the concept of hard and soft HA and monomer.

References

1) S. Kimura, T. Takitani, and M. Imoto, *Bull. Chem. Soc. Jpn.*, **35**, 2012 (1962).

2) M. Imoto, T. Ouchi, M. Sakae, E. Morita, and T. Yamada, *Am. Chem. Soc. Symposium Ser.*, **121**, 103 (1980).

3) M. Imoto, E. Morita, and T. Ouchi, *J. Polym. Sci., Polym. Symp.*, **68**, 1 (1980).

4) M. Imoto, T. Ouchi, E. Morita, and T. Yamada, *Nippon Kagaku Kaishi*, **1980**, 333.

5) Part 410 of this series: T. Ouchi, M. Inaba, K. Tadano, and M. Imoto, *J.Polym. Sci., Polym. Chem. Ed.*, **20**, 2089 (1982).

Studies on 2-Aziridinecarboxylic Acid. VII.[1] Formation of Dehydroamino Acid Peptides *via* Isomerization of Peptides Containing 2-Aziridinecarboxylic Acid by Tertiary Amines

Kiichiro NAKAJIMA,* Hitomi ODA, and Kenji OKAWA
Department of Chemistry, Faculty of Science, Kwansei Gakuin University, Nishinomiya 662
(Received March 19, 1982)

Peptides containing 1-(α-aminoacyl)-2-aziridinecarboxylic acid were isomerized into the corresponding dehydroamino acid peptides by treatment with the tertiary amines, triethylamine or 1,4-diazabicyclo[2.2.2]octane (Dabco). Dehydrohydantoin derivatives were also prepared by treatment of benzyloxycarbonyl-2-aziridinecarboxylic acid derivatives with tertiary amines.

Recently many biologically active peptides containing dehydroamino acid (DHA) have been isolated and much attention has been directed to their synthesis. Literature concerning the synthesis of DHA peptides has mainly dealt with β-elimination of the O-leaving group of β-hydroxy α-amino acid derivatives,[2] and a more recent paper has reported Hofmann degradation reaction of 2,3-diaminopropionic acid derivatives.[3]

In the previous paper,[4] we reported the isomerization of peptides containing 2-aziridinecarboxylic acid (Azyline, Azy) and 3-methyl-2-aziridinecarboxylic acid (3-MeAzy) into the corresponding DHA peptides with NaI in an acetone solution. During our investigation on the reaction of Azy peptides with several amines, we found that they react with primary and secondary amines to form the corresponding amine adducts, α,β-diaminopropionic acid derivatives,[5] and the *trans*-acylation reaction occurs due to peptide bond cleavage.[5] Also, 1-acyl- and 1-(α-aminoacyl)-2-aziridinecarboxylic acid peptides are isomerized into the corresponding DHA peptides upon treatment with tertiary amines as in the reaction with NaI.

In the present study the reactions of Azy peptides with the tertiary amines, triethylamine and Dabco were observed in detail. The Azy and 3-MeAzy peptides used as the starting materials were synthesized by the mixed anhydride method from N-protected amino acid and Azy derivatives according to the procedure described

TABLE 1. YIELDS AND PROPERTIES OF AZY-PEPTIDES (**1**, **2**, **5**)

Azy peptide[a] ↓	Yield/%	Mp θ_m/°C	$[\alpha]_D^{23}$/°	Found (Calcd) (%) C	H	N
Z-Gly-Azy-$NHCH_3$ (**1a**)	70	193 (decomp)	−38.0 (*c* 0.8, MeOH)	57 84 (57.72	5 81 5.88	14.38 14 43)
Z-Gly-Azy-NHBzl (**1b**)	72	122.5—123.5	−90.0 (*c* 1.1, $CHCl_3$)	66.42 (66.48	5.53 5.58	11.11 11.08)
Z-Phe-Azy-$NHCH_3$ (**1c**)	56	170—171	−66.9 (*c* 1.1, $CHCl_3$)	66.08 (66.13	6.12 6.08	11.13 11.02)
Z-Ala-Azy-OBzl (**1d**)	83	58—61	−50.9 (*c* 1.0, DMSO)	65.91 (65.96	5.73 5.80	7.29 7.33)
Z-Phe-Azy-OBzl (**1e**)	72	68—69	−62.7 (*c* 1.0, DMSO)	70.69 (70.73	5.68 5.72	6.16 6.11)
Z-Gly-Azy-Gly-OBzl (**1f**)	92	118—119	−52.5 (*c* 1.0, MeOH)	62.23 (62.16	5.40 5.45	9.92 9.88)
Z-Phe-3-MeAzy-$NHCH_3$ (**2a**)	77	129—130	−25.3 (*c* 1.1,$CHCl_3$)	66.81 (66.82	6.27 6.37	10.69 10.63)
Z-Phe-3-MeAzy-NHBzl (**2b**)	62	157—157.5	−35.1 (*c* 0.23, $CHCl_3$)	71.28 (71.32	6.11 6.20	8.83 8.91)
Z-Phe-3-MeAzy-OBzl (**2c**)	80	95—97	−61.1 (*c* 1.0, MeOH)	71.26 (71.17	6.02 5.97	5.89 5.93)
Z-Gly-3-MeAzy-Gly-OBzl (**2d**)	90	123.5—124.5	−58.2 (*c* 1.0, AcOEt)	62.88 (62.86	5.70 5.73	9.68 9.56)
Z-Ala-3-MeAzy-Gly-OBzl (**2e**)	93	110—111	−59.7 (*c* 1.0, $CHCl_3$)	63.48 (63.50	5.98 6.00	9.30 9.27)
Z-Azy-Gly-OBzl (**5a**)	60	109—110	−50.6 (*c* 1.0, MeOH)	65.17 (65.21	5.50 5.47	7.71 7.60)
Boc-Azy-Gly-OBzl (**5b**)	61	71—71.5	−80.4 (*c* 1.0, MeOH)	61.22 (61.07	6.85 6.63	8.35 8.34)
Z-3-MeAzy-Gly-OBzl (**5c**)	73	62—64	−63.2 (*c* 1.0, MeOH)	65.95 (65.96	5.83 5.80	7.42 7.33)
Boc-3-MeAzy-Gly-OBzl (**5d**)	79	89.5—90	−70.0 (*c* 1.0, MeOH)	66.21 (66.06	7.24 7.34	8.01 8.04)

a) All Azy peptides were synthesized by the mixed anhydride method except **5a**—**d**. Arrow indicates final coupling position. Azy: (2*S*)-form, 3-MeAzy: (2*S*, 3*S*)-form.

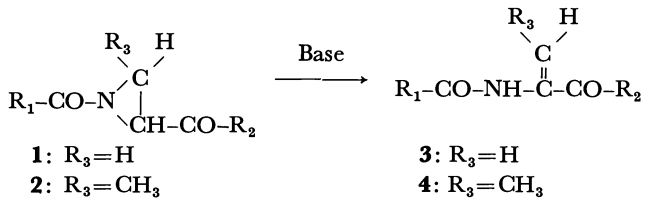

Scheme 1.

Table 2. Yields and properties of DHA-peptides (**3**, **4**)

Product (**3**, **4**)	Yield/%	Mp θ_m/°C	Base[a)]	Found (Calcd) (%) C	H	N	NH	NMR data of DHA δ, DMSO-d_6 =CH_2	CH_3
Z-Gly-⊿Ala-$NHCH_3$ (**3a**)	89	175 (decomp)	Et_3N(3)	57.84 57.72	5.81 5.88	14.38 14.43	9.01	5.58 6.20	—
Z-Gly-⊿Ala-NHBzl (**3b**)	84	117.5—118.5	Et_3N(3)	66.42 66.48	5.53 5.58	11.11 11.08	9.07	5.60 6.24	—
Z-Phe-⊿Ala-$NHCH_3$ (**3c**)	100	syrup	Et_3N(6)	66.08 66.13	6.12 6.08	11.13 11.02	8.58	6.30 6.60	—[b)]
Z-Ala-⊿Ala-OBzl (**3d**)	100	syrup	Et_3N(3)	65.91 65.96	5.73 5.80	7.29 7.33	8.34	5.92 6.56	—[b)]
Z-Phe-⊿Ala-OBzl (**3e**)	100	syrup	Et_3N(3)	70.69 70.73	5.68 5.72	6.16 6.11	8.12	5.92 6.60	—[b)]
Z-Gly-⊿Ala-Gly-OBzl (**3f**)	100	133—136	Et_3N(6)	62.23 62.16	5.40 5.45	9.92 9.88	8.99	5.57 6.31	—
Z-Phe-⊿Aba-$NHCH_3$ (**4a**)	77	165—167	Dabco(24)	66.81 66.82	6.27 6.37	10.69 10.63	9.05	— 6.36q	1.40d
Z-Phe-⊿Aba-NHBzl (**4b**)	88	162.5—163.5	Dabco(24)	71.28 71.32	6.11 6.20	8.83 8.91	9.15	— 6.44q	1.40d
Z-Phe-⊿Aba-OBzl (**4c**)	90	151—152	Dabco(6)	71.26 71.17	6.02 5.97	5.89 5.93	9.20	— 6.67q	1.68d
Z-Gly-⊿Aba-Gly-OBzl (**4d**)	87	101—102	Dabco(24)	62.88 62.86	5.70 5.73	9.68 9.56	9.01	— 6.55q	1.66d
Z-Ala-⊿Aba-Gly-OBzl (**4e**)	87	139—140.5	Dabco(24)	63.48 63.50	5.98 6.00	9.30 9.27	9.02	— 6.52q	1.65d

a) The reaction was carried out in a $CHCl_3$ solution at 35 °C and the base used was 2 equimolar against Azy peptide. The values in parenthesis are the reaction time/h. b) NMR spectrum in $CDCl_3$.

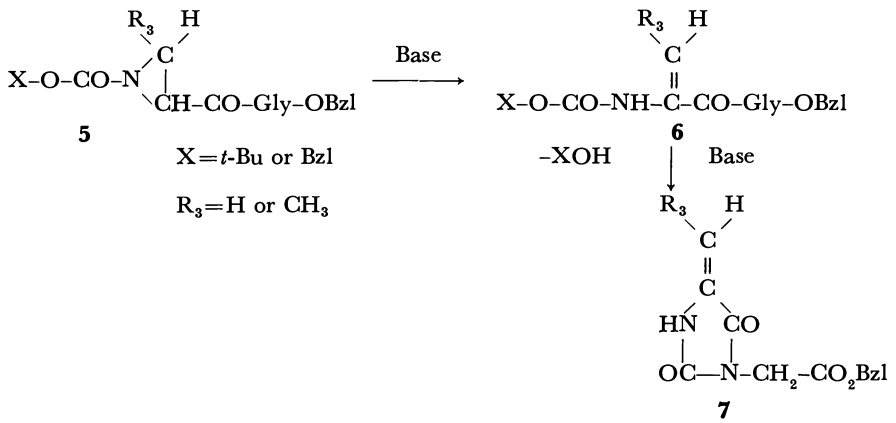

Scheme 2.

in our previous papers.[5-7)] Their properties and yields are summarized in Table 1 and the reaction procedure of the Azy peptides with amines is shown in Scheme 1.

Azy and 3-MeAzy peptides (**1a**—**f** and **2a**—**e**) were treated with 2 equimolar amount of tertiary amine (Et_3N or Dabco) in $CHCl_3$ solution at 35 °C for 3—24 h, and then the corresponding dehydroamino acid (DHA, ⊿AA) derivatives were isolated by silica-gel column chromatography. The DHA produced was identified by NMR.

In the NMR data, characteristic signals of the DHA structure appeared at δ 5.5—5.9 for the vinyl proton of dehydroalanine (⊿Ala), and at δ 1.4—1.7 as a doublet for the methyl proton and at δ 6.3—6.8 as a quartet for the β-proton of dehydro-α-aminobutyric acid (⊿Aba). ⊿Aba was of the (Z)-configuration. The product (**3**, **4**)

TABLE 3. Boc- AND Z-⊿AA-GLY-OBZL (**6**) AND DEHYDROHYDANTOIN (**7**)

Azy peptide (**5**)	Base	React time/h	Product yields/% DHA (**6**)	Product yields/% Hydantoin (**7**)
Z-Azy-Gly-OBzl (**5a**)	Et_3N	12	—	75
	Dabco	6	—	80
Boc-Azy-Gly-OBzl (**5b**)	Et_3N	24	95	—
	Dabco	6	100	—
Z-3-MeAzy-Gly-OBzl (**5c**)	Et_3N	7[a)]	—	—
	Dabco	3[a)]	68	28
Boc-3-MeAzy-Gly-OBzl (**5d**)	Et_3N	7[a)]	—	—
	Dabco	4[a)]	85	—

a) Reaction time/d.

of the isomerization of the Azy peptides are summarized in Table 2.

The reaction results show that 1-acyl-2-aziridinecarboxylic acid peptides (**1a**—**f**) were easily isomerized into the corresponding ⊿Ala peptides (**3a**—**f**) by the treatment of triethylamine, but contrary to our expectation, 1-acyl-3-methyl-2-aziridinecarboxylic acid peptides (**2a**—**e**) were not isomerized into the ⊿Aba peptides (**4a**—**e**), even after 7 d of treatment. Use of the more basic Dabco as an isomerizing reagent was necessary to obtaine ⊿Aba peptides (**4a**—**e**).

This isomerization reaction seems to be induced by a direct withdrawing of the α-proton of Azy or 3-MeAzy with base. The α-proton of unsubstituted Azy (**1a**—**f**) could be easily withdrawn by Et_3N treatment, but not that of the substituted 3-MeAzy (**2a**—**e**) because of the methyl group on the aziridine ring. Thus, the more basic Dabco was needed to withdraw the α-proton of 3-MeAzy for its isomerization.

We also examined the reaction of 1-benzyloxycarbonyl- and 1-*t*-butoxycarbonyl-2-aziridinecarboxylic acid peptides (**5a**—**d**) with amines. As shown in Scheme 2 and Table 3, the reaction of the Azy peptides blocked by urethane-type groups with tertiary amines afforeded not only the corresponding DHA peptides, but also dehydrohydantoin derivatives (**7a**, **7b**). Again, the 3-MeAzy peptides (**5c**, **5d**) were not isomerized with Et_3N and the benzyloxycarbonyl derivatives were more easily isomerized into the corresponding DHA peptides than the *t*-butoxycarbonyl peptides. The results of the dehydrohydantoin (**7**) formation reaction, which occurred *via* reaction of the DHA peptides produced by the reaction with tertiary amines, agreed very well with the results of the β-elimination reaction of O-activated Z-Ser- or Z-Thr- derivatives found by Campbell and Behr,[8)] us,[9)] and, Shin *et al.*[10)] Thus the benzyloxycarbonyl group of the aziridine is more labile than the *t*-butoxycarbonyl group in the basic conditions, that is, Z-Azy-Gly-OBzl (**5a**) and Z-3-MeAzy-Gly-OBzl (**5c**) isomerized more easily than Boc-Azy-Gly-OBzl (**5b**) and Boc-3-MeAzy-Gly-OBzl (**5d**) as shown in Table 3. The benzyloxycarbonyl group attached to the unsubstituted aziridinecarboxylic acid (**5a**) seemed to be very labile and Z-⊿Ala-Gly-OBzl could not be isolated after the reaction of **5a** with tertiary amine, even in Et_3N.

From the isomerization reaction of Azy and 3-MeAzy described above, it is concluded that Azy and 3-MeAzy has a distinctly different reactivity against tertiary amines and the isomerization by the tertiary amines, which can be used to the selective synthesis of DHA peptides, differs from that by NaI or the synthesis of DHA peptides *via* β-elimination of β-hydroxy α-amino acid.

Experimental

Uncorrected melting points are reported. The homogeneity of the products was checked by thin-layer chromatography on silica-gel plates. The optical rotations were determined at the D line on a Perkin-Elmer 141 polarimeter. The NMR spectra were obtained with a Hitachi R20B high-resolution NMR spectrometer, the chemical shifts being obtained using TMS as the internal reference. All the *N*-aminoacyl Azy and 3-MeAzy peptides used in this study were synthesized by the method described in literature,[6,7)] and their properties and yield are summarized in Table 1.

(2S)-Z-Azy-Gly-OBzl (5a). To a solution of (2*S*)-H-Azy-Gly-OBzl[11)] (1.63 g, 6.96 mmol) and Et_3N (0.97 ml, 6.96 mmol) in $CHCl_3$ (15 ml), was added Z-ON[1)] (1.95 g, 6.96 mmol) with stirring at 0 °C. After being stirred overnight at 25 °C, the solvent was removed *in vacuo* and the residue was dissolved in ethyl acetate. The ethyl acetate solution was washed with 10% citric acid, 1 M $NaHCO_3$ and water, and dried over Na_2SO_4, concentrated *in vacuo*. The residue was crystallized from ethyl acetate–hexane, 1.53 g (60%) of **5a** was obtained, mp 109—110 °C, $[\alpha]_D^{23}$ −50.6° (*c* 1.0, MeOH). NMR ($CDCl_3$) δ: 2.38 (1H q, J_{gem}=0.8 Hz, J_{trans}=3.5 Hz, Azy β-proton), 2.53 (1H q, J_{gem}=0.8 Hz, J_{cis}=6.3 Hz, Azy β-proton), 3.07 (1H q, J_{trans}=3.5 Hz, J_{cis}=6.3 Hz, Azy α-proton). Z-ON can be replaced with Z-Cl.[1)]

Found: C, 65.17; H, 5.50; N, 7.71%. Calcd for $C_{20}H_{20}O_5N_2$: C, 65.21; H, 5.47; N, 7.60%.

(2S)-Boc-Azy-Gly-OBzl (5b). To a solution of (2*S*)-H-Azy-Gly-OBzl[11)] (4.0 g, 17.1 mmol) and Et_3N (2.38 ml, 17.1 mmol) in $CHCl_3$ (50 ml), was added Boc-ON[1)] (4.63 g, 18.8 mmol) with stirring at 0 °C. After the reaction mixture had been worked up as described above, the product was crystallized from ethyl acetate–hexane, 3.51 g (61.3%) of **5b** was obtained. mp 71.0—72.5 °C, $[\alpha]_D^{23}$ −80.4° (*c* 1.0, MeOH). NMR ($CDCl_3$) δ: 2.30 (1H q, J_{gem}=0.8 Hz, J_{trans}=3.8 Hz, Azy β-proton), 2.49 (1H q, J_{gem}=0.8 Hz, J_{cis}=6.6 Hz, Azy β-proton), 3.03 (1H q, J_{trans}=3.8 Hz, J_{cis}=6.6 Hz, Azy α-proton).

Found: C, 61.22; H, 6.85; N, 8.35%. Calcd for $C_{17}H_{22}O_5N_2$: C, 61.07; H, 6.63; N, 8.34%.

(2S, 3S)-Z-3-MeAzy-Gly-OBzl (5c). To a solution of (2*S*, 3*S*)-H-3-MeAzy-Gly-OBzl[7)] (1.87 g, 7.54 mmol) and Et_3N (1.05 ml, 7.54 mmol) in $CHCl_3$ (15 ml), was added

Z–ON[1] (1.95 g, 7.54 mmol) with stirring at 0 °C. The reaction mixture was stirred overnight and worked up as described above. The product was crystallized from ethyl acetate–hexane, 2.10 g (72.8%) of **5c** was obtained, mp 62—64 °C, $[\alpha]_D^{23}$ −63.2° (*c* 1.0, MeOH). NMR ($CDCl_3$) δ: 1.28 (3H d, J=5.5 Hz, CH_3), 2.79 (1H m, 3-MeAzy, β-proton), 3.14 (1H d, J=7.0 Hz, 3-MeAzy, α-proton). Z–ON can be replaced with Z–Cl.

Found: C, 65.96; H, 5.83; N, 7.42%. Calcd for $C_{21}H_{22}O_5N_2$: C, 65.96; H, 5.80; N, 7.33%.

*(2S, 3S)-Boc-3-MeAzy-Gly-OBzl (**5d**).* To a solution of (2*S*, 3*S*)-H-3-MeAzy-Gly-OBzl[7] (1.25 g, 5.06 mmol) and Et_3N (0.70 ml, 5.06 mmol) in $CHCl_3$ (15 ml), was added Boc–ON[1] (1.40 g, 6.07 mmol) with stirring at 0 °C. The reaction mixture was stirred overnight and worked up as described above. The product was crystallized from ethyl acetate–hexane, 1.38 g (78.5%) of **5d** was obtained, mp 89.5—90.0 °C, $[\alpha]_D^{23}$ −70.0° (*c* 1.0, MeOH). NMR ($CDCl_3$) δ: 1.27 (3H d, J=5.5 Hz, CH_3), 2.74 (1H m, 3-MeAzy β-proton), 3.09 (1H d, J=6.4 Hz, 3-MeAzy α-proton).

Found: C, 62.21; H, 6.88; N, 8.01%. Calcd for $C_{18}H_{24}O_5N_2$: C, 62.06; H, 6.94; N, 8.04%.

*Z–Gly–ΔAla–NHBzl (**3b**). General Isomerization Procedure of Azy with Et_3N*: A solution of **1b** (100 mg, 0.27 mmol) and Et_3N (0.08 ml, 0.54 mmol) in $CHCl_3$ (5 ml) was stirred at 35 °C for 3 h. After the solvent had been removed *in vacuo*, the residue was dissolved in ethyl acetate. The ethyl acetate solution was washed with 10% citric acid and water, and then dried over Na_2SO_4, concentrated *in vacuo*. After the obtained residue was purified by the silica-gel column chromatography, the product was crystallized from $CHCl_3$–ether–hexane, 84.3 mg (84.3%) of **3b** was obtained, mp 117.5—118.5 °C.

*Z–Gly–ΔAba–Gly–OBzl (**4d**). General Isomerization Procedure of **3**-MeAzy with Dabco*: A solution of **2d** (200 mg, 0.45 mmol) and Dabco (102 mg, 0.91 mmol) in $CHCl_3$ (5 ml) was stirred at 35 °C for 24 h. After the reaction mixture had been worked up as described above, the residue was crystallized from ethyl acetate–hexane, 174 mg (87%) of **4d** was obtained, mp 101—102 °C [lit, mp 102—104 °C[4]].

*Benzyl 5-Methylenehydantoin-3-acetate (**7a**). Using Et_3N*: A solution of **5a** (200 mg, 0.54 mmol) snd Et_3N (0.15 ml, 1.09 mmol) in $CHCl_3$ (3 ml) was stirred at 35 °C for 12 h. After the reaction mixture had been worked up as described above, the residue was purified with silica-gel column chromatography and was crystallized from ethyl acetate–ether–hexane, 105 mg (75%) of **7a** was obtained, mp 171—172 °C. NMR ($CDCl_3$) δ: 4.32 (2H s), 4.92, (1H d, J=1.8 Hz), 5.15, 5.17 (4H 2s), 5.42 (1H d, J=1.8 Hz), 7.32 (5H s), 8.35 (1H bs).

Found: C, 60.05; H, 4.72; N, 10.72%. Calcd for $C_{13}H_{12}O_4N_2$: C, 59.99; H, 4.65; N, 10.77%.

*Z–ΔAla–Gly–OBzl (**6a**)* could not be prepared by this procedure.

Using Dabco: A solution of **5a** (200 mg, 0.54 mmol) and Dabco (121 mg, 1.08 mmol) in $CHCl_3$ (3 ml) was stirred at 35 °C for 6 h. After the reaction mixture had been worked up as described above, 112 mg (80%) of **7a** was obtained. **6a** could not be prepared.

*Boc–ΔAla–Gly–OBzl (**6b**). Using Et_3N*: A solution of **5b** (100 mg, 0.29 mmol) and Et_3N (0.08 ml, 0.58 mmol) in $CHCl_3$ (3 ml) was stirred at 35 °C for 24 h. After the reaction mixture had been worked up as described above, 95 mg (95%) of **6b** was obtained as an oily material. NMR ($CDCl_3$) δ: 1.48 (9H s), 4.12 (2H d, J=5.0 Hz) 5.15 (1H m) 5.18 (2H s), 6.00 (1H d, J=1.8 Hz), 6.78 (1H bt), 7.25 (1H bs), 7.32 (5H s).

Found: C, 61.15; H, 6.72; N, 8.28%. Calcd for $C_{17}H_{22}O_5N_2$: C, 61.07; H, 6.63; N, 8.34%. **7b** could not be prepared.

Using Dabco: A solution of **5b** (300 mg, 0.86 mmol) and Dabco (194 mg, 1.73 mmol) in $CHCl_3$ (5 ml) was stirred at 35 °C for 6 h. After the reaction mixture had been worked up as described above, 300 mg (100%) of **6b** was obtained as an oily material. **7b** could not be prepared.

*Z–ΔAba–Gly–OBzl (**6c**) and Benzyl 5-Ethylidenehydantoin-3-acetate (**7c**). Using Dabco*: A solution of **5c** (200 mg, 0.5 mmol) and Dabco (112 mg, 1 mmol) in $CHCl_3$ (3 ml) was stirred at 35 °C for 3 d. After the reaction mixture had been worked up as described above, the crude product of two components was subjected to silica-gel column chromatography developed by $CHCl_3$, yielding 136 mg (68%) of **6c**, mp 99—100 °C, and 38 mg (28%) of **7c**, mp 186—186.5 °C. **6c**: NMR ($CDCl_3$) δ: 1.70 (3H d, J=7.0 Hz), 4.16 (2H d, J=5.5 Hz), 5.12 (2H s), 5.20 (2H s), 6.52 (1H q, J=7.0 Hz), 6.76 (1H bs), 7.30 (10H s), 7.00 (1H bs), 7.15 (1H bs). **7c**: NMR ($CDCl_3$) δ: 1.83 (3H d, J=7.5 Hz), 4.35 (2H s), 5.19 (2H s), 5.98 (1H q. J=7.5 Hz), 7.32 (5H s), 9.05 (1H bs).

6c; Found: C, 66.02; H, 5.86; N, 7.23%. Calcd for $C_{21}H_{22}O_5N_2$: C, 65.96; H, 5.80; N, 7.33%.

7c; Found: C, 61.28; H, 5.20; N, 10.32%. Calcd for $C_{14}H_{14}O_4N_2$: C, 61.31; H, 5.15; N, 10.21%.

Using Et_3N: A solution of **5c** (200 mg, 0.5 mmol) and Et_3N (0.14 ml, 1 mmol) in $CHCl_3$ (3 ml) was stirred at 35 °C for 7 d. No reaction occurred and only **5c** was recovered.

*Boc–ΔAba–Gly–OBzl (**6d**). Using Dabco*: A solution of **5d** (200 mg, 0.57 mmol) and Dabco (128 mg, 1.14 mmol) in $CHCl_3$ (3 ml) was stirred at 35 °C for 4 d. After the reaction mixture had been worked up as described above, 170 mg (85%) of **6d** was obtained, mp 119.5—120.5 °C. NMR ($CDCl_3$) δ: 1.45 (9H s), 1.75 (3H d, J=7.0 Hz), 4.14 (2H d, J=5.5 Hz), 5.20 (2H s), 6.49 (1H q, J=7.0 Hz), 6.69 (1H bs), 7.34 (5H s), 7.28 (1H bs).

Found: C, 62.18; H, 6.81; N, 8.12%. Calcd for $C_{18}H_{24}O_5N_2$: C, 62.06; H, 6.94; N, 8.04%.

7d could not be prepared.

Using Et_3N: A solution of **5d** (100 mg, 0.29 mmol) and Et_3N (0.08 ml, 0.58 mmol) in $CHCl_3$ (3 ml) was stirred at 35 °C for 7 d. No reaction occurred and only **5d** was recovered.

References

1) Part VI: K. Nakajima, M. Neya, S. Yamada, and K. Okawa, *Bull. Chem. Soc. Jpn.*, **55**, 3049 (1982). The abbreviations of the IUPAC-IUB Commission (*J. Biol. Chem.*, **247**, 977 (1972)) are used. Z: benzyloxycarbonyl, OBzl: benzyl ester, Z–Cl: benzyloxycarbonyl chloride, Z–ON: 2-benzyloxycarbonyloxyimino-2-phenylacetonitrile. Boc–ON: 2-*t*-butoxycarbonyloxyimino-2-phenylacetonitrile. "Azyline" is used as the name of 2-aziridinecarboxylic acid, "Azy" being its abbreviation. 3-MeAzy: (2*S*, 3*S*)-3-methyl-2-aziridinecarboxylic acid. ΔAla: Dehydroalanine, ΔAba: dehydro-2-aminobutylic acid.

2) A. Srinivasan, R. W. Stephanson, and K. Olsen, *J. Org. Chem.*, **42**, 2253 (1977); D. H. Rich and J. P. Tam, *Tetrahedron Lett.*, **1975**, 211 (1975); C. Shin, Y. Yonezawa, M. Takahashi, and J. Yoshimura, *Bull. Chem. Soc. Jpn.*, **54**, 1132 (1981); D. H. Rich and J. P. Tam, *J. Org. Chem.*, **42**, 3815 (1977); S. Konno and C. H. Stammer, *Synthesis*, **1978**, 598 (1978).

3) S. Nomoto, A. Sano, and T. Shiba, *Tetrahedron Lett.*, **1979**, 521 (1979).

4) K. Okawa, K. Nakajima, T. Tanaka, and M. Neya, *Bull. Chem. Soc. Jpn.*, **55**, 174 (1982).

5) K. Nakajima, M. Iwai, and K. Okawa, "Peptide Chemistry 1980," ed by K. Okawa, Protein Research

Foundation, Osaka (1981), p. 5; K. Nakajima, T. Tanaka, K. Morita, and K. Okawa, *Bull. Chem. Soc. Jpn.*, **53**, 283 (1980).

6) K. Nakajima, F. Takai, T. Tanaka, and K. Okawa, *Bull. Chem. Soc. Jpn.*, **51**, 1577 (1978).

7) K. Okawa, K. Nakajima, T. Tanaka, and Y. Kawana, *Chem. Lett.*, **1975**, 591.

8) R. D. Campbell and F. E. Behr, *J. Org. Chem.*, **38**, 1183 (1973).

9) K. Nakajima, H. Kawai, M. Takai, and K. Okaw, *Bull. Chem. Soc. Jpn.*, **50**, 917 (1977).

10) C. Shin, Y. Yonezawa, T. Yamada, H. Hirano, and J. Yoshimura, 43rd National Meeting of the Chemical Society of Japan, Tokyo, April 1981, Abstr. No. 1G16.

11) K. Nakajima, K. Kanda, and Okawa, "Peptide Chemistry 1977," ed by T. Nakajima, Protein Research Foundation, Osaka (1977), p. 17.

Studies on 2-Aziridinecarboxylic Acid. VIII.[1] Total Synthesis of Actinomycin D and Its Serine Analogue *via* Ring-opening Reaction of 1-Benzyloxycarbonyl-2-aziridinecarboxylic Acid Moiety

Kiichiro NAKAJIMA,* Takumi TANAKA, Masahiro NEYA, and Kenji OKAWA
Department of Chemistry, Faculty of Science, Kwansei Gakuin University, Nishinomiya 662
(Received April 16, 1982)

Direct synthesis of peptides containing 1-benzyloxycarbonyl-2-aziridinecarboxylic acid were carried out by the reaction of β-hydroxy-α-amino acid peptides with DEAD–TPP reagents, and key *O*-peptide intermediates of actinomycin D synthesis were prepared *via* a ring-opening reaction of the aziridine with *N*-protected dipeptide. Peptide lactone was prepared by the DCC–HOBt method, and the subsequent debenzyl procedure and oxydation procedure gave the title compounds in good yields.

In a previous paper,[2] we reported the synthesis of *O*-peptides *via* the ring-opening reaction of 1-aminoacyl-2-aziridinecarboxylic acid peptides with some carboxylic acids. We used this reaction for the total synthesis of actinomycin D,[3] but some problems remain with respect to the yield and the generality in the synthesis of the peptides containing 2-aziridinecarboxylic acid (Azy) and *O*-peptides.

This paper reports the direct synthesis of 1-benzyloxycarbonyl-Azy peptides from the corresponding serine and threonine peptides. By an application of the ring-opening reaction to the above Azy peptides, total synthesis of actinomycin D and its analogue were successfully carried out.

1-Benzyloxycarbonyl-Azy peptides are usually prepared from *N*-terminus-free Azy peptides derived from *N*-trityl-β-hydroxy-α-amino acid or peptides. But this rocedure requires many steps to obtain 1-benzyloxycarbonyl- or 1-*t*-butoxycarbonyl-Azy peptides.[4] Recently, A. K. Bose and co-workers reported[5] that the reaction of Z–Ser–$NHC_6H_4CH_3$ with diethyl azodicarboxylate (DEAD)-triphenylphosphin (TPP) reagents gave the β-lactam derivative in 53% yield, while the corresponding threonine derivative gave only the 3-methyl-2-aziridinecarboxylic acid (3-MeAzy) in 53% yield. We applied this DEAD–TPP procedure to synthesize Azy peptides, which are the significant intermediates in *O*-peptide synthesis.

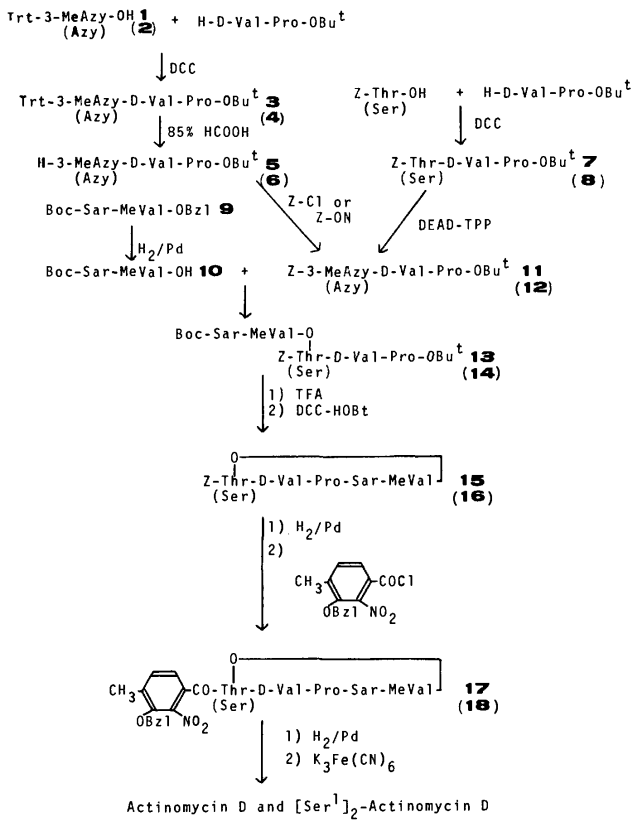

Scheme 1.

The synthetic routes used in this study of actinomycin D and its analogue are summarized in Scheme 1. In the usual procedure, the key intermediate (2*S*,3*S*)-Z-3-MeAzy-D-Val-Pro-OBu^t (**11**) and (2*S*)-Z-Azy-D-Val-Pro-OBu^t (**12**) were prepared from the corresponding 1-trityl-3-MeAzy and 1-trityl-Azy-tripeptides (**3**, **4**). **3** and **4** were prepared by the coupling of (2*S*,3*S*)-Trt-3-MeAzy-OH (**1**) or (2*S*)-Trt-Azy-OH (**2**) with D-Val-Pro-OBu^t by the DCC method, followed by detritylation and 1-benzyloxycarbonylation with Z-Cl[1] or Z-ON[1] to obtain **11** and **12**. In the direct synthetic procedure of **11** and **12** by using DEAD–TPP procedure, the reactions of both Z–Thr (**7**) and Z–Ser tripeptide (**8**) with DEAD–TPP reagents gave only the corresponding **11** and **12** without any β-lactam in good yield (*ca.* 80%). The products of each procedure were completely identified. Next, we carried out the ester formation reaction between Boc–Sar–MeVal–OH (**10**) and **11** or **12** in CH_2Cl_2 solution at 50 °C for 7 d without boron trifluoride etherate, which had been necessary for the ring-opening reaction of 1-aminoacyl- or 1-benzoyl-Azy peptides.[2,3] The desired pentapeptide esters (**13**, **14**) were obtained in about 80% yields. After the *t*-butoxycarbonyl and *t*-butyl ester had been removed by treatment with trifluoroacetic acid, cyclization (2 mmol in 1 L THF, at 25 °C for 7 d) was carried out with the aid of DCC-HOBt[1] (10 mmol each) to obtain the cyclic pentapeptide lactones (**15**, **16**) in 66.2% (Thr) and 42.9% (Ser) yields. The benzyloxycarbonyl group of **15** and **16** was removed by catalytic hydrogenolysis. The reaction of the resulting N-terminus free pentapeptide lactones with 3-benzyloxy-4-methyl-2-nitrobenzoyl chloride[6] gave the corresponding **17** and **18** in 90 and 95% yields. Subsequent debenzylation of **17** and **18** by catalytic hydrogenolysis, followed by oxydation with potassium hexacyanoferrate(III) in a mixture of

TABLE 1. PHYSICAL PROPERTIES AND BIOLOGICAL ACTIVITIES OF ACTINOMYCIN D AND [SER^1]$_2$-ACTINOMYCIN D

Characteristic	Synthetic actinomycin D	Natural actinomycin D[a)]	[Ser^1]$_2$-actinomycin D	[Ser^1]$_2$-actinomycin D[b)]
Melting point θ_m/°C	243—245	241—243	253—255	269—273
Optical rotation([α]$_D^{23}$/°)	−340.6[c)]	−323[d)]	−452[d)]	−435±15[d)]
UV absorption	24300(443)	24400(443)	24200(450)	24950(450)
[ε in methanol (λ/nm)]	33600(240)	34100(240)	37400(238)	36600(239)
IR absorption ($\tilde{\nu}$/cm^{-1}, KBr)	1745(lactone C=O)	1745	1740	
	1620—1670 (amide)	1620—1670	1610—1660	
	1580 (chromophore)	1580	1575	
	1195 (lactone COC)	1195	1195	
Antibacterial activity (MIC, g/ml)[e)]				
S. aureus JC-1 209P	0.78	0.78	3.13	—
B. subtilis ATCC-663	0.39	≦0.2	3.13	20% activity
E. coli NIHJ JC-2	>100	>50	>100	—
K. pmuno NCTC-418	>100	>50	>100	—
P. aeruginosa IAM-1095	100	50	100	—
P. vulgaris IAM-1025	>100	>50	>100	—

a) From the data of J. Meienhofer[9)]. b) From the data of H. Brockmann *et al.*[8)] c) In methanol at *c* 0.23. d) In methanol at *c* 0.25. e) Ref. 7.

methanol and 0.067 M phosphate buffer, pH 7.1, gave actinomycin D and [Ser^1]$_2$-actinomycin D in 74 and 51% yields, respectively.

The synthetic actinomycin D was indistinguishable from the natural substance as to physical properties and biological activity against some bacteria, although [Ser^1]$_2$-actinomycin D had only about 10% of the natural activity against gram-positive bacteria. The physical and biological data are summarized in Table 1. The CD curves of the synthetic products are shown in Fig. 1. The CD curve of the synthetic actinomycin D agreed with that of the natural product[7)] in methanol solution, and its serine analogue also showed a very similar pattern. Thus, the serine analogue seemed to have a very similar conformation in a methanol solution, although it had only 10% activity against gram-positive bacteria, which agrees with Brockmann's data.[8)] As the presence of the methyl group of threonine seems to be significant for the appearance of the antibacterial activity, we are now trying to synthesize a variety of actinomycin peptide analogues for a study of the biological activity-structure relationship.

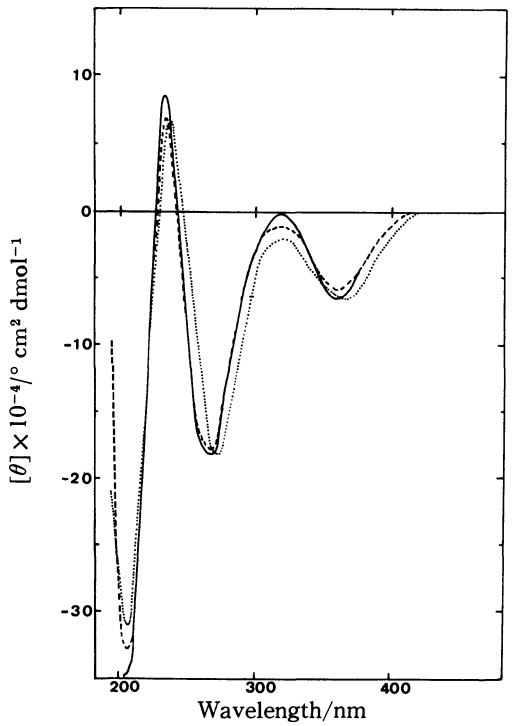

Fig. 1. CD spectra of natural actinomycin D (——), synthetic actinomycin D (----), and [Ser^1]$_2$-actinomycin D (·····) in methanol.

This study showed that the DEAD-TPP method for synthesizing Azy peptides is very convenient and shortens the step of the conventional Azy peptide synthetic procedure. Also, the method using the ring-opening reaction of aziridine is very useful for efficiently synthesizing peptide lactones.

Experimental

Melting points are uncorrected. Infrared spectra were obtained on a Hitachi EPI-G3 spectrometer, ultraviolet spectra on a Shimadzu UV-200 spectrophotometer. Optical rotations were determined at the D line on a Perkin-Elmer 141 polarimeter. The NMR spectra were obtained with a Hitachi R-20B High-resolution NMR Spectrometer, the chemical shifts being obtained using TMS as the internal reference. The homogeneity of the products was checked by thin-layer chromatography on silica-gel plates.

(2S)-1-Trityl-2-aziridinecarboxylic Acid (2). To a solution of (2*S*)-1-trityl-2-aziridinecarboxylic acid methyl ester[10)] (3.43 g, 10 mmol) in CH_3CN (40 ml), was added drop by drop a solution of 2 M LiOH (14.3 ml, 28.6 mmol) at 20 °C with stirring. After the solution was stirred for 24 h at 20 °C, the solvent was removed and the residue was dissolved in ethyl acetate. The solution was washed with 10% citric acid and water, dried over Na_2SO_4, and concentrated *in vacuo*. The obtained **2** was unstable and then was used immediately in the next coupling procedure.

[(2S)-1-Trityl-2-aziridinylcarbonyl]-D-valylproline t-Butyl Ester(4). Z-D-Valylproline *t*-butyl ester (4.05 g, 10 mmol) was hydrogenated over palladium in MeOH (50 ml) for 2 h to give N^a-free dipeptide. To a solution of 2 (3.17 g, 10 mmol) and N^a-free

dipeptide in CH_2Cl_2 (60 ml) was added a solution of DCC (2.06 g, 10 mmol) in CH_2Cl_2 (30 ml) at −10 °C with stirring. The reaction mixture was stirred for 3 h at −10 °C, and then overnight in a refrigerator. After *N,N'*-dicyclohexylurea (DCurea) was removed by filtration, the filtrate was concentrated *in vacuo*. The residue was dissolved in ethyl acetate, and the solution wss washed with 10% citric acid, 1 M $NaHCO_3$, and water, dried over Na_2SO_4, and concentrated *in vacuo*. 5.34 g (93.8%) of **4** was obtained as an amorphous powder, $[\alpha]_D^{23}$ −90.8° (*c* 1.0, MeOH).

Found: C, 73.53; H, 7.77; N, 7.38%. Calcd for $C_{35}H_{43}O_4N_3$: C, 73.79; H, 7.61; N, 7.38%.

N-*(Benzyloxycarbonyl)threonyl*-D-*valylproline* t-*Butyl Ester (7)*. *N*-(Benzyoxycarbonyl)-D-valylproline *t*-butyl ester (27 g, 66.7 mmol) was hydrogenated over palladium (10 g) in MeOH (200 ml) for 3 h to give N^{α}-free dipeptide. To a solution of *N*-(benzyloxycarbonyl)threonine (16.9 g, 66.7 mmol) and N^{α}-free dipeptide in CH_2Cl_2 (200 ml) was added a solution of DCC (13.8 g, 66.7 mmol) in CH_2Cl_2 (50 ml) at −10 °C. The reaction mixture was stirred at −10 °C for 3 h and was then kept overnight in a refirgerator. After removal of DCurea by filtration, the filtrate was concentrated *in vacuo*. The residue was dissolved in ethyl acetate, and the solution was washed with 10% citric acid, 1 M $NaHCO_3$, water, then dried over Na_2SO_4 and concentrated *in vacuo*. The residue was crystallized from ethyl acetate–hexane; 24 g (71%) of **7** was obtained: mp 91—92.5 °C, $[\alpha]_D^{23}$ −29.5° (*c* 1.1, MeOH).

Found: C, 61.85; H, 7.92; N, 8.21%. Calcd for $C_{26}H_{39}O_7N_3$: C, 61.76; H, 7.77; N, 8.31%.

N-*(Benzyloxycarbonyl)seryl*-D-*valylproline* t-*Butyl Ester (8)*. To a solution of *N*-(benzyloxycarbonyl)serine (957 mg, 4 mmol) and N^{α}-free dipeptide (from 1.62 g, 4 mmol of *N*-(benzyloxycarbonyl)-D-valylproline *t*-butyl ester) in CH_2Cl_2 (20 ml), was added a solution of DCC (825 mg, 4 mmol) in CH_2Cl_2 (20 ml) at −10 °C with stirring. After the reaction mixture was worked up as described in **7**, the residue was crystallized from ethyl acetate–hexane; 1.6 g (81.3%) of **8** was obtained: mp 141—142 °C, $[\alpha]_D^{23}$ −25.1° (*c* 1.0, MeOH).

Found: C, 60.90; H, 7.62; N, 8.45%. Calcd for $C_{25}H_{37}O_7N_3$: C, 61.08; H, 7.59; N, 8.55%.

N-*(t-Butoxycarbonyl)sarcosyl*-N-*methylvaline Benzyl Ester (9)*. To a solution of *t*-butoxycarbonylsarcosine (6.62 g, 35 mmol) and *N*-methylvaline benzyl ester (7.73 g, 35 mmol) in THF (100 ml) was added a solution of DCC (7.22 g, 35 mmol) in THF (80 ml) at −10 °C with stirring. After being stirred at 5 °C overnight, the DCurea was filtered off. The filtrate was concentrated *in vacuo* and the residue was dissolved in ethyl acetate, the solution was washed with 10% citric acid, 1 M $NaHCO_3$, water, then dried over Na_2SO_4 and concentrated *in vacuo*. The crude product was purified with silica-gel column chromatography (ethyl acetate–hexane, 1 : 5 v/v). 13.15 g (95.7%) of **9** was obtained as a syrup: $[\alpha]_D^{23}$ −81.6° (*c* 1.0, MeOH).

Found: C, 64.33; H, 8.19; N, 7.28%. Calcd for $C_{21}H_{32}O_5N_2$: C, 64.26; H, 8.22; N, 7.14%.

N-*(t-Butoxycarbonyl)sarcosyl*-N-*methylvaline (10)*. H_2 gas was bubbled through a solution of **9** (9 g, 23 mmol) in MeOH (80 ml) containing palladium (5 g) for 2 h with stirring. After the catalyst was filtered out, the filtrate was concentrated *in vacuo*. 6.95 g (100%) of **10** was obtained as a syrup: $[\alpha]_D^{23}$ −80.4° (*c* 1.0, MeOH).

Found: C, 55.49; H, 8.72; N, 9.35%. Calcd for $C_{14}H_{26}O_5N_2$: C, 55.61; H, 8.67; N, 9.27%.

[*(2S, 3S)-1-Benzyloxycarbonyl-3-methyl-2-aziridinylcarbonyl*]-D-*valylproline* t-*Butyl Ester (11)*. Via *Usual Procedure*: To a solution of **5**[3] (from 7.07 g, 12.1 mmol of **3**[3]) in $CHCl_3$ (40 ml) was added Et_3N (1.68 ml, 12.1 mmol) and Z–ON[1] (3.39 g, 12.1 mmol) at 25 °C with stirring. After the solution was stirred for 3 d, the solvent was removed *in vacuo*. The residue was worked up as described in **4**, and the crude product was purified by silica-gel column chromatography ($CHCl_3$) to give 4.91 g (83.1%) of **11** as a syrup: $[\alpha]_D^{23}$ −76.0° (*c* 0.9, MeOH). NMR ($CDCl_3$) δ: 1.28 (3H d, J=5.8 Hz, $=CHCH_3$), 2.83 (1H m, Azy; β-proton), 3.18 (1H d, J=6.6 Hz, Azy; α-proton). Z–ON can be replaced with Z–Cl.[1]

Found: C, 64.05; H, 7.65; N, 8.62%. Calcd for $C_{26}H_{37}O_6N_3$: C, 64.02; H, 7.83; N, 8.42%.

Via *DEAD–TPP Procedure*: To a solution of DEAD (174 mg, 1.0 mmol) and TPP (262 mg, 1.0 mmol) in an ice-cold dry THF (10 ml) was added **7** (200 mg, 0.4 mmol) at 0 °C with stirring. After being stirred for 1 h, the reaction was stopped by the addition of water (5 ml). The product was extracted with ethyl acetate and the solution was dried over Na_2SO_4 and concentrated *in vacuo*. The residue was dissolved in ether and the crystal which appeared, *N,N'*-bis(ethoxycarbonyl)hydrazine, were filtered off, then the filtrate was concentrated *in vacuo*. The residue was subjected to silica-gel column chromatography (AcOEt–hexane, 1 : 2 v/v). 169 mg (87.6%) of **11** was obtained as a syrup: $[\alpha]_D^{23}$ −74.9° (*c* 1.1, MeOH). The NMR spectrum of this product was identical with that from **11**.

[*(2S)-1-Benzyloxycarbonyl-2-aziridinylcarbonyl*]-D-*valylproline* t-*Butyl Ester (12)*. Via *Usual Procedure*: To a solution of **4** (2.34 g, 4.12 mmol) in abs. MeOH (30 ml) was added ice-cold 85% formic acid (15 ml). After this mixture was stirred for 3 h, the solvent was removed *in vacuo*. The residue was partitioned between ether and water. 1 M $NaHCO_3$ was added to the aqueous solution, producing an alkaline solution, and the isolated oil was extracted with ethyl acetate. After this solution was dried over Na_2SO_4, the solvent was removed *in vacuo* to give N^{α}-free tripeptide (**6**), which was used in the following reaction without further purification. To a solution of **6** in $CHCl_3$ (20 ml) was added Et_3N (0.55 ml, 3.91 mmol) and Z–Cl[1] (0.63 ml, 3.91 mmol) at −5 °C with stirring. After being stirred for 1 h, the reaction mixture was worked up as described in **11**; 1.62 g (83.3%) of **12** was obtained as syrup: $[\alpha]_D^{23}$ −26.0° (*c* 0.9, MeOH), NMR δ: 2.42 (1H q, J_{gem}=0.8 Hz, J_{trans}=3.0 Hz, Azy; β-proton), 2.53 (1H q, J_{gem}=0.8 Hz, J_{cis}=6.6 Hz, Azy; β-proton), 3.14 (1H q, J_{trans}=3.0 Hz, J_{cis}=6.6 Hz, Azy; α-proton).

Found: C, 63.15; H, 7.90; N, 8.59%. Calcd for $C_{25}H_{35}O_6N_3$: C, 63.41; H, 7.45; N, 8.87%.

Via *DEAD–TPP Procedure*: To a solution of DEAD (177 mg, 1.02 mmol) and TPP (267 mg, 1.02 mmol) in ice-cold dry THF (10 ml) was added **8** (200 mg, 0.407 mmol) at 0 °C with stirring. After the mixture was stirred for 1 h, the reaction was stopped by the addition of water (5 ml). The solution was worked up as described in **11**. The crude product was subjected to silica-gel column chromatography (AcOEt–hexane, 1 : 2 v/v). 161 mg (83.5%) of **12** was obtained as a syrup: $[\alpha]_D^{23}$ −25.4° (*c* 0.9, MeOH). The NMR spectrum of this product was identical with that of **12** given earlier.

[O-(t-*Butoxycarbonylsarcosyl*-N-*methylvalyl*)-N-*benzyloxycarbonylthreonly*]-D-*valylproline* t-*Butyl Ester (13)*. A solution of **11** (3.67 g, 7.53 mmol) and **9** (7.27 g, 24 mmol) in CH_2Cl_2 (60 ml) was refluxed for 7 d, and the solvent was removed *in vacuo*. The residue was dissolved in ethyl acetate and the solution was washed with 1 M $NaHCO_3$, and water, dried over Na_2SO_4, and then concentrated *in vacuo*. The residue was purified by silica-gel column chromatography ($CHCl_3$). 4.75 g (80%) of **13** was obtained as an amorphous powder: $[\alpha]_D^{23}$ −30.1° (*c* 1.0, MeOH).

Found: C, 60.92; H, 8.36; N, 8.81%. Calcd for $C_{40}H_{63}O_{11}N_5$: C, 60.82; H, 8.04; N, 8.87%.

[O-(t-*Butoxycarbonylsarcosyl*-N-*methylvalyl*)-N-*benzyloxycarbonylseryl*]-D-*valylproline* t-*Butyl Ester* (***14***). A solution of **12** (1.09 g, 2.3 mmol) and **9** (2.09 g, 6.9 mmol) in CH_2Cl_2 (20 ml) was refluxed for 7 d and the reaction mixture was worked up as described for **13**. 1.44 g (80.9%) of **14** was obtained as an amorphous powder: $[\alpha]_D^{23}$ −47.4° (*c* 1.0, MeOH).

Found: C, 60.16; H, 8.10; N, 9.13%. Calcd for $C_{39}H_{61}O_{11}N_5$: C, 60.37; H, 7.92; N, 9.03%.

N-(*Benzyloxycarbonyl*) *threonyl*-D-*valylprolysarcosyl*-N-*methylvaline Lactone* (***15***). A solution of **13** (1.51 g, 1.91 mmol) in TFA (20 ml) was stirred at 0 °C for 4 h; it was then concen trated *in vacuo*. The residue was dissolved in ethyl acetate and concentrated *in vacuo* (this procedure was repeated twotimes), and the residue was stored over KOH for 12 h in desiccator. The residue was dissolved in dry THF (100 ml), and Et_3N (0.27 ml, 1.91 mmol) was added at −5 °C; the mixture was diluted with THF (900 ml) and HOBt[1] (1.23 g, 9.53 mmol) was added. To a solution of the above mixture was added drop by drop a solution of DCC (1.97 g, 9.53 mmol) in THF (50 ml) at 0 °C for a period of 4 h with stirring. After the mixture was stirred for 5 d at 25 °C, the solvent was removed *in vacuo*. The residue was dissolved in ethyl acetate and the DCurea which appeared was filtered off. The filtrate was washed with 10% citric acid and 1 M $NaHCO_3$, and water, and then concentrat ed *in vacuo*. The residue was subjected to silica-gel column chromatography ($CHCl_3$–MeOH, 50 : 1 v/v). 0.78 g (66.2%) of **15** was obtained as an amorphous powder: $[\alpha]_D^{23}$ −25.4° (*c* 1.0, MeOH).

Found: C, 60.29; H, 7.68; N, 11.21%. Calcd for $C_{31}H_{45}O_8N_5$: C, 60.47; H, 7.37; N, 11.37%.

N-(*Benzyloxycarbonyl*) *seryl*-D-*valylprolylsarcosyl*-N-*methylvaline Lactone* (***16***). A solution of **14** (1.76 g, 2.27 mmol) in TFA (30 ml) was stirred at 0 °C for 4 h, and then was concentrated *in vacuo*. The residue was dissolved in ethyl acetate and concentrated *in vacuo* (this procedure was repeated two times), and the residue was stored over KOH for 12 h in desiccator. The residue was dissolved in dry THF (100 ml), and Et_3N (0.32 ml, 2.27 mmol) was added at −5 °C, this solution was diluted with THF (1.1 L), and HOBt (1.53 g, 11.35 mmol) was added. To a solution of this mixture, was added drop by drop a solution of DCC (2.34 g, 11.35 mmol) in THF (60 ml) at 0 °C for a period of 4 h with stirring. The reaction mixture was stirred at 25 °C for 5 d, and was worked up as described in **15**. The product was crystallized from ethyl acetate–hexane; 0.58 g (42.9%) of **16** was obtained: mp 228—231 °C, $[\alpha]_D^{23}$ −33.3° (*c* 1.0, MeOH).

Found: C, 60.01; H, 7.34; N, 11.92%. Calcd for $C_{30}H_{43}O_8N_5$: C, 59.89; H, 7.20; N, 11.64%.

(*3-Benzyloxy-4-methyl-2-nitrobenzoyl*) *threonyl*-D-*valylprolylsarcosyl*-N-*methylvaline Lactone* (***17***). A solution of **15** (342 mg, 0.56 mmol) in MeOH (15 ml) was hydrogenated over palladium black. After 2 h, the mixture was filtered and the filtrate was concentrated *in vacuo*. The residue was dissolved in $CHCl_3$ (10 ml) and then cooled to 0 °C. To the $CHCl_3$ solution was added Et_3N (0.093 ml, 0.67 mmol) and 3-benzyloxy-4-methyl-2-nitrobenzoyl chloride[6] (204 mg, 0.67 mmol) with stirring in the dark at 0 °C. After the reaction mixture was stirred for 1 h, the solvent was removed *in vacuo*. The residue was dissolved in ethyl acetate and the solution was washed with 10% citric acid, 1 M $NaHCO_3$ and water, dried over Na_2SO_4, and concentrated *in vacuo*. The crude product was purified with silica-gel column chromatography ($CHCl_3$) to give 375 mg (90.0%) of **17** as an amorphous powder: $[\alpha]_D^{23}$ −12.2° (*c* 0.5, MeOH).

Found: C, 60.70; H, 6.85; N, 11.32%. Calcd for $C_{38}H_{50}O_{10}N_6$: C, 60.79; H, 6.71; N, 11.19%.

(*3-Benzyloxy-4-methyl-2-nitrobenzoyl*) *seryl*-D-*valylprolylsarcosyl*-N-*methylvaline Lactone* (***18***). A solution of **16** (425 mg, 0.71 mmol) in MeOH (20 ml) was hydrogenated over palladium black. After 2 h, the mixture was filtered and the filtrate was concentrated *in vacuo*. The residue was dissolved in THF (10 ml) and then cooled to 0 °C. To the solution was added Et_3N (0.12 ml, 0.85 mmol) and 3-benzyloxy-4-methyl-2-nitrobenzoyl chloride[6] (259 mg, 0.85 mmol) with stirring in the dark at 0 °C. After being stirred for 1 h, the reaction mixture was worked up as described in **17**. 492 mg (95.0%) of **18** was obtained as an amorphous powder: $[\alpha]_D^{23}$ +19.9° (*c* 0.5, MeOH).

Found: C, 59.96; H, 6.54; N, 11.13%. Calcd for $C_{37}H_{48}O_{10}N_6$: C, 60.31; H, 6.57; N, 11.41%.

Actinomycin D. A solution of **17** (138 mg, 0.183 mmol) in MeOH (12 ml) was hydrogenated over palladium black in the dark. After 2 h, the mixture was filtered and the filtrate was added to an equal volume of stirred 0.067 M phosphate buffer pH 7.1 containing potassium hexacyanoferrate(III) (175 mg, 0.531 mmol). The mixture was stirred at 25 °C for 20 min. It was then partitioned between ethyl acetate and water, the aqueous layer being separated and extracted three times with ethyl acetate. The combined ethyl acetate layer was washed with 1 M $NaHCO_3$, 1 M HCl, and saturated NaCl, dried over Na_2SO_4, and concentrated *in vacuo* to afford a red crystalline residue, which was recrystallized from ethyl acetate–hexane to give actinomycin D, 84 mg (74%). Physical and spectral data are given in Table 1.

Found: C, 58.52; H, 6.94; N, 13.23%. Calcd for $C_{62}H_{86}O_{16}N_{12}\cdot H_2O$: C, 58.48; H, 6.97; N, 13.20%.

[*Ser*[1]]$_2$-*Actinomycin D.* A solution of **18** (184 mg, 0.25 mmol) in MeOH (15 ml) was hydrogenated over palladium black in the dark. After 2 h, the mixture was filtered and the filtrate was added to an equal volume of stirred 0.067 M phosphate buffer pH 7.1 containing potassium hexacyanoferrate(III) (238 mg, 0.724 mmol). The mixture was stirred at 25 °C for 20 min and worked up as described in actinomycin D. [Ser[1]]$_2$-actinomycin D was obtained 78 mg (51.0%) as a red crystalline substance from ethyl acetate–hexane. Physical and spectral data are given in Table 1.

Found: C, 61.09; H, 7.12; N, 14.27%. Calcd for $C_{60}H_{82}O_{16}N_{12}\cdot H_2O$: C, 61.00; H, 7.17; N, 14.23%.

Microbiological Assay. The results of the assay and the microorganisms employed are given in Table 1. The minimum amount of the compound necessary for the complete inhibition of growth was determined by the Stamp method using Mueller Hinton Ager.

References

1) Part VII. K. Nakajima, H. Oda, and K. Okawa, *Bull. Chem. Soc. Jpn.*, **55**, 3232 (1982). Abbreviations of the IUPAC-IUB commission, *J. Biol. Chem.*, **247**, 977 (1972), are used. Trt: trityl, Z: benzyloxycarbonyl, Bzl: benzyl, Z-Cl: benzyloxycarbonyl chloride, Z-ON: 2-benzyloxycarbonyloxyimino-2-phenylacetonitrile, HOBt: *N*-hydroxy benzotriazole. "Azyline" is used as the name of 2-aziridinecarboxylic acid, "Azy" being its abbreviation. 3-MeAzy: 3-methyl-2-aziridinecarboxylic acid.

2) T. Tanaka, K. Nakajima, T. Maeda, A. Nakamura, N. Hayashi, and K. Okawa, *Bull. Chem. Soc. Jpn.*, **52**, 3579 (1979).

3) T. Tanaka, K. Nakajima, and K. Okawa, *Bull. Chem. Soc. Jpn.*, **53**, 1352 (1979).

4) K. Okawa, K. Nakajima, T. Tanaka, and Y. Kawana, *Chem. Lett.*, **1975**, 591.

5) A. K. Bose, D. P. Sahu, and M. S. Manhas, *J. Org. Chem.*, **46**, 1229 (1981).

6) This compound was prepared by the reaction of the corresponding carboxylic acid and thionyl chloride. Recrystallized from benzene–heptane, mp 101—102 °C.

7) Natural actinomycin D for bioassay and CD curve measurement was purchased from Banyu Pharmaceutical Co., Ltd.

8) H. Brockmann and H. Lackner, *Chem. Ber.*, **101**, 1312 (1968).

9) J. Meienhofer, *J. Am. Chem. Soc.*, **92**, 3771 (1970).

10) This compound was prepared by the same prodceure as described by K. Okawa and K. Nakajima, *Biopolymers*, **20**, 1811 (1981), $[\alpha]_D^{23}$ −95.4° (*c* 1.1, MeOH).

Synthesis and Oxidative Cyclization of 3-(1-Cycloalkenyl)tropolones

Kimiaki IMAFUKU* and Kyoko INOUE

Department of Chemistry, Faculty of Science, Kumamoto University, Kurokami, Kumamoto 860

(Received March 29, 1982)

3-(1-Cyclopentenyl)-, 3-(1-cyclohexenyl)-, and 3-(1-cycloheptenyl)tropolones (**3a**, **3b**, and **3c**) were prepared by the hydrolysis of cycloadducts of dichloroketene to cyclopentylidene-, cyclohexylidene-, and cycloheptylidenecyclopentadiene, respectively. Compound **3a** was oxidized with performic acid to give 1,2,3,5-tetrahydrocyclohepta[*b*]cyclopenta[*d*]furan-5-one and 3-(2-oxocyclopentyl)tropolone. Oxidation of **3b** and **3c** gave 1,2,3,4-tetrahydro-6*H*-cyclohepta[*b*]benzofuran-6-one (**4b**) and 5,7,8,9,10,11-hexahydrodicyclohepta[*b*,*d*]furan-5-one, respectively. Dehydrogenation of **4b** with palladium catalyst gave 6*H*-cyclohepta[*b*]benzofuran-6-one.

Halogenated ketenes are versatile intermediates in organic synthesis.[1-3] In 1965, Stevens *et al.*[4,5] obtained tropolone in good yield by hydrolysis of the cyclopentadiene–dichloroketene adduct. This method is most interesting and useful synthetic method of tropolone and has been applied to synthesis of a variety of alkyl-substituted tropolones.[6-8] Hydrolysis of the fulvene–dichloroketene adducts also gave 3-alkenyltropolones.[9,10] These 3-alkenyltropolones were oxidized with peroxy acid or 2,3-dichloro-5,6-dicyano-1,4-benzoquinone to afford 8*H*-cyclohepta[*b*]furan-8-one.[10] On the other hand, hydrolysis of the spiro[2.4]hepta-4,6-diene–dichloroketene adduct gave 2,3-dihydro-8*H*-cyclohepta[*b*]furan-8-one.[11]

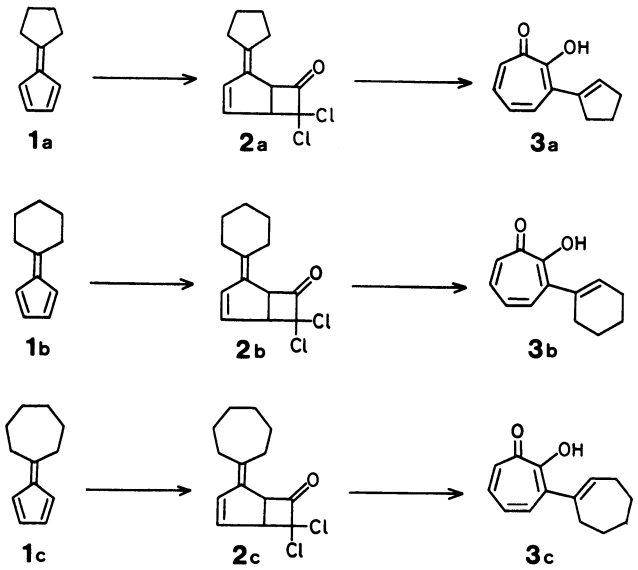

Scheme 1.

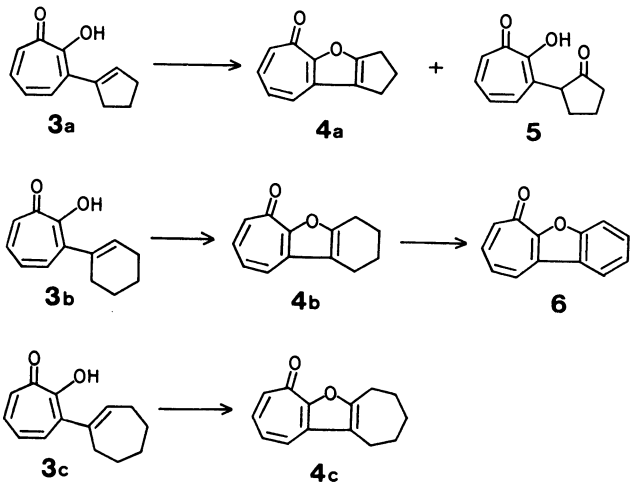

Scheme 2.

In this communication, we wish to report the synthesis of 3-(1-cycloalkenyl)tropolones by the hydrolysis of the cycloalkylidenecyclopentadiene–dichloroketene adducts and their oxidative cyclization with peroxy acid.

Results and Discussion

Synthesis of 3-(1-Cycloalkenyl)tropolones. The cycloaddition reaction of cyclopentylidenecyclopentadiene (**1a**)[12] with dichloroketene, produced *in situ* by the reaction of dichloroacetyl chloride with triethylamine, afforded a 1 : 1 adduct (**2a**) as a pale yellow oil. The IR spectrum shows a strong carbonyl absorption at 1800 cm^{-1}, which is reasonable for a cyclobutanone.[13] The assignment of the ^1H NMR spectrum was done in comparison with the spectra of 6,6-dimethyl-[9] and 6,6-diphenylfulvene–dichloroketene adducts.[14] The assignments are fit for the structure (**2a**): δ=1.5—2.0 (m, 4H, H-3′×2, H-4′×2), 2.1—2.6 (m, 4H, H-2′×2, H-5′×2), 3.95—4.20 (m, 1H, H-1), 4.62 (d, 1H, $J_{1,5}$=7.2 Hz, H-5), 5.8—6.0 (m, 1H, H-2), 6.49 (dd, 1H, $J_{2,3}$=6.0, $J_{1,3}$=1.8 Hz, H-3). Similarly, by the reactions of cyclohexylidenecyclopentadiene (**1b**)[12] and cycloheptylidenecyclopentadiene (**1c**) with dichloroketene, oily 1 : 1 adducts (**2b** and **2c**) were obtained, respectively. Their structures were also confirmed by the ^1H NMR spectral data.

Hydrolysis of the adduct (**2a**) with sodium hydroxide in aqueous acetic acid was carried out to give 3-(1-cyclopentenyl)tropolone (**3a**) in 26% yield. The ^1H NMR spectrum shows peaks at δ=1.7—2.3 (m, 2H, H-4′×2), 2.4—3.0 (m, 4H, H-3′×2, H-5′×2), 6.8—7.7 (m, 5H, H-2′,4,5,6,7), 9.50 (br, 1H, OH), supporting the structure. The elemental analysis also gave a satisfactory result. The adducts (**2b** and **2c**) were also hydrolyzed to afford 3-(1-cyclohexenyl)tropolone (**3b**) and 3-(1-cycloheptenyl)tropolone (**3c**) in 42 and 16% yields, respectively.

Oxidative Cyclization of 3-(1-Cycloalkenyl)tropolones with Peroxy Acid. Previously, we reported that the 3-alkenyltropolones were oxidized with peroxy acid or 2,3-dichloro-5,6-dicyano-1,4-benzoquinone to give 8*H*-cyclohepta[*b*]furan-8-one.[10]

3-(1-Cyclopentenyl)tropolone (**3a**) was oxidized with performic acid to give **4a** (mp 217—218 °C) and **5** (mp 97—99 °C) in 4.5 and 7.7% yields, respectively. From the elemental analysis and spectral data, the compound (**4a**) was assigned to 1,2,3,5-tetrahydrocyclohepta[*b*]cyclopenta[*d*]furan-5-one. This compound gave no coloration with iron(III) chloride. The IR spectrum shows a characteristic absorption at 1642 cm^{-1} for tropone carbonyl group. The ^1H NMR spectrum shows six protons at $\delta=2.3$—3.1 corresponding to three methylene groups in the five-membered ring and four protons for the aromatic seven-membered ring. On the other hand, the compound (**5**) was determined to be 3-(2-oxocyclopentyl)tropolone from its elemental analysis, spectral data, and coloration with iron(III) chloride. The IR spectrum shows a characteristic carbonyl absorption at 1745 cm^{-1} for a cyclopentanone. The ^1H NMR spectrum is also reasonable for the structure.

The 3-(1-cycloalkenyl)tropolones (**3b** and **3c**) were also oxidized with performic acid to afford 1,2,3,4-tetrahydro-6*H*-cyclohepta[*b*]benzofuran-6-one (**4b**) and 5,7,8,9,10,11-hexahydrodicyclohepta[*b*,*d*]furan-5-one(**4c**) in 38 and 26% yields, respectively. Their structures were determined by their elemental analysis and spectral data.

The compound (**4b**) was dehydrogenated with palladium catalyst to afford 6*H*-cyclohepta[*b*]benzofuran-6-one (**6**), which was confirmed by its elemental analysis and spectral data. The IR spectrum shows a tropone carbonyl absorption at 1635 cm^{-1}, the ^1H NMR spectrum showing aromatic protons as complex multiplet at $\delta=6.90$—8.05.

Experimental

The melting points were determined with a Yanagimoto MP-S2 melting-point measuring apparatus and are uncorrected. The IR spectra were taken on a JASCO IRA-1 spectrophotometer, the UV spectra on a Hitachi EPS-3T spectrophotometer. The ^1H NMR spectra were recorded with a Hitachi-Perkin-Elemer R-24 spectrometer (60 MHz).

*Cyclopentylidenecyclopentadiene (**1a**).* A mixture of cyclopentadiene (105 g, 1.6 mol) and cyclopentanone (143 g, 1.7 mol) was stirred overnight at room temperature in the presence of 40% methylamine solution (35 ml). The organic layer was washed with 1 M hydrochloric acid until the mixture was made slightly acidic. Then, the organic layer was washed with water and with saturated sodium chloride solution, dried over anhydrous sodium sulfate, and distilled under reduced pressure to give 77 g (36%) of cyclopentylidencyclopentadiene (**1a**) as an orange oil: bp 103—104 °C/18 Torr (lit,[12] 55—57 °C/2 Torr); NMR (CCl_4) $\delta=1.6$—1.9 (m, 4H), 2.5—2.9 (m, 4H), 6.20 (s, 4H).

*Cyclohexylidenecyclopentadiene (**1b**).* A mixture of cyclopentadiene (80 g, 1.2 mol) and cyclohexanone (127 g, 1.3 mol) was stirred overnight at room temperature in the presence of 40% methylamine solution (26 ml) and worked up, as mentioned above, to give 83 g (57%) of cyclohexylidenecyclopentadiene (**1b**) as an orange oil: bp 118—120 °C/17 Torr (lit,[12] 78—80 °C/2.5 Torr; NMR (CCl_4) $\delta=1.4$—1.9 (m, 6H), 2.3—2.8 (m, 4H), 6.36 (s, 4H).

*Cycloheptylidenecyclopentadiene (**1c**).* A mixture of cyclopentadiene (66 g, 1.0 mol) and cycloheptanone (134 g, 1.2 mol) was stirred overnight at room temperature in the presence of 40% methylamine (22 ml) and worked up, as mentioned above, to give 105 g (66%) of cycloheptylidenecyclopentadiene (**1c**) as an orange oil: bp 124—126 °C/18 Torr; NMR (CCl_4) $\delta=1.3$—1.9 (m, 8H), 2.2—2.9 (m, 4H), 6.2—6.5 (m, 4H).

*4-Cyclopentylidene-7,7-dichlorobicyclo[3.2.0]hept-2-en-6-one (**2a**).* A solution of triethylamine (56 g) in anhydrous hexane (500 ml) was added dropwise to a solution of **1a** (35 g) and dichloroacetyl chloride (41 g) in anhydrous hexane (700 ml) over a period of 3 h with stirring at room temperature. After additional stirring for 1 h, the mixture was allowed to stand overnight. The reaction mixture was washed with 1 M hydrochloric acid and with water, and dried over anhydrous sodium sulfate. After the evaporation of the solvent, the residue was distilled under reduced pressure to give 20 g (31%) of 4-cyclopentylidene-7,7-dichlorobicyclo[3.2.0]hept-2-en-6-one (**2a**) as a pale yellow oil: bp 125—127 °C/0.45 Torr; IR (neat) 1800 cm^{-1} (C=O); NMR (CCl_4) $\delta=1.5$—2.0 (m, 4H), 2.1—2.6 (m, 4H), 3.95—4.20 (m, 1H, H-1), 4.62 (d, 1H, $J_{1,5}=7.2$ Hz, H-5), 5.8—6.0 (m, 1H, H-2), 6.49 (dd, 1H, $J_{2,3}=6.0$, $J_{1,3}=1.8$ Hz, H-3).

*4-Cyclohexylidene-7,7-dichlorobicyclo[3.2.0]hept-2-en-6-one (**2b**).* A solution of triethylamine (40 g) in anhydrous hexane (250 ml) was added dropwise to a solution of **1b** (33 g) and dichloroacetyl chloride (32 g) in anhydrous hexane (250 ml) over a period of 3 h with stirring at room temperature. The reaction mixture was worked up, as mentioned above, to give 17 g (29%) of 4-cyclohexylidene-7,7-dichlorobicyclo[3.2.0]-hept-2-en-6-one (**2b**) as a pale yellow oil: bp 139—141 °C/0.45 Torr; IR (neat) 1800 cm^{-1} (C=O); NMR (CCl_4) $\delta=1.3$—1.9 (m, 6H), 2.0—2.7 (m, 4H), 3.95—4.15 (m, 1H, H-1), 4.74 (d, 1H, $J_{1,5}=6.6$ Hz, H-5), 5.92 (dd, 1H, $J_{2,3}=6.0$, $J_{1,2}=3.0$ Hz, H-2), 6.58 (dd, 1H, $J_{2,3}=6.0$, $J_{1,3}=1.8$ Hz, H-3).

*4-Cycloheptylidene-7,7-dichlorobicyclo[3.2.0]hept-2-en-6-one (**2c**).* A solution of triethylamine (46 g) in anhydrous hexane (500 ml) was added dropwise to a solution of **1c** (35 g) and dichloroacetyl chloride (34 g) in anhydrous hexane (700 ml) over a period of 3 h with stirring at room temperature. The reaction mixture was worked up, as mentioned above, to give 35 g (60%) of 4-cycloheptylidene-7,7-dichlorobicyclo[3.2.0]hept-2-en-6-one (**2c**) as a pale yellow oil: bp 151—152 °C/0.45 Torr; IR (neat) 1800 cm^{-1} (C=O); NMR (CCl_4) $\delta=1.3$—1.9 (m, 8H), 2.0—2.6 (m, 4H), 3.95—4.20 (m, 1H, H-1), 4.73 (d, 1H, $J_{1,5}=7.2$ Hz, H-5), 5.89 (dd, 1H, $J_{2,3}=6.0$, $J_{1,2}=2.4$ Hz, H-2), 6.57 (dd, 1H, $J_{2,3}=6.0$, $J_{1,3}=1.8$ Hz, H-3).

*3-(1-Cyclopentenyl)tropolone (**3a**).* A suspended solution of the cycloadduct (**2a**) (20 g) in acetic acid (99 g) and water (9 ml) containing sodium hydroxide (16 g) was refluxed for 10 h. The mixture was steam-distilled and the distillate was extracted with chloroform. The extract was washed with sodium hydrogencarbonate solution, water, and saturated sodium chloride solution. Evaporation of the solvent from the dried extract gave 4.0 g (26%) of 3-(1-cyclopentenyl)-tropolone (**3a**) as pale yellow needles (from hexane): mp 79—80 °C; IR ($CHCl_3$) 3140 (OH), 1616 cm^{-1} (C=O); NMR ($CDCl_3$) $\delta=1.7$—2.3 (m, 2H), 2.4—3.0 (m, 4H), 6.8—7.7 (m, 5H), 9.50 (br, 1H, OH). Found: C, 76.27: H, 6.45%. Calcd for $C_{12}H_{12}O_2$: C, 76.57; H, 6.43%.

*3-(1-Cyclohexenyl)tropolone (**3b**).* The cycloadduct (**2b**) (17 g) was hydrolyzed, as mentioned above, by refluxing for 10 h in acetic acid (71 g) and water (7 ml) containing sodium hydroxide (13 g) and steam-distilled to give 5.6 g (42%) of 3-(1-cyclohexenyl)tropolone (**3a**) as pale yellow needles (from hexane): mp 53—55 °C; IR ($CHCl_3$) 3140 (OH), 1615 cm^{-1} (C=O); NMR ($CDCl_3$) $\delta=1.4$—1.9 (m, 4H), 2.0—2.6 (m, 4H), 5.7—5.9 (m, 1H), 6.7—7.1 (m, 4H), 9.20 (br, 1H, OH).

Found: C, 77.21; H, 7.00%. Calcd for $C_{13}H_{14}O_2$: C, 77.20; H, 6.98%.

3-(1-Cycloheptenyl)tropolone (3c) The cycloadduct (**2c**) (35 g) was also hydrolyzed, as mentioned above, by refluxing for 10 h in acetic acid (157 g) and water (14 ml) containing sodium hydroxide (26 g) and steam-distilled to give 4.5 g (16%) of 3-(1-cycloheptenyl)tropolone (**3c**) as pale yellow needles (from hexane): mp 39—41 °C; IR ($CHCl_3$) 3120 (OH), 1614 cm^{-1} (C=O); NMR ($CDCl_3$) δ=1.5—2.0 (m, 6H), 2.1—2.6 (m, 4H), 5.65—5.95 (m, 1H, H-2'), 6.65—7.60 (m, 4H), 9.40 (br, 1H, OH). Found: C, 78.01; H, 7.27%. Calcd for $C_{14}H_{16}O_2$: C, 77.75; H, 7.46%.

Oxidation of 3-(1-Cyclopentenyl)tropolone (3a). 3-(1-Cyclopentenyl)tropolone (**3a**) (3.76 g) was added to a performic acid solution, prepared from 90% formic acid (50 ml) and 30% hydrogen peroxide (10 ml), and heated on a water bath for 2 h. The reaction mixture was alkalized with 20% sodium hydroxide solution and heated again on a water bath for 45 min. The mixture was slightly acidified with 3 M hydrochloric acid and extracted with chloroform. The extract was washed with water and dried over anhydrous sodium sulfate. After the evaporation of the solvent, the residue was chromatographed on four Wakogel B-10 plates (30×30 cm^2) with chloroform to afford two fractions. Crystals from the upper band were recrystallized from benzene to give 171 mg (4.5%) of 1,2,3,5-tetrahydrocyclohepta[*b*]cyclopenta[*d*]furan-5-one (**4a**): mp 217—218 °C; IR ($CHCl_3$) 1642 cm^{-1} (C=O); UV (CH_3OH) 227 (log ε 4.16), 286 (4.39), 313 nm (sh, 3.94); NMR ($CDCl_3$) δ=2.2—3.1 (m, 6H), 6.7—7.4 (m, 4H). Found: C, 77.24; H, 5.42%. Calcd for $C_{12}H_{10}O_2$: C, 77.40; H, 5.41%. Crystals from the lower band were also recrystallized from benzene to give 316 mg (7.7%) of 3-(2-oxocyclopentyl)tropolone (**5**): mp 97—99 °C; IR ($CHCl_3$) 3180 (OH), 1745 (C=O), 1618 cm^{-1} (C=O); NMR ($CDCl_3$) δ=1.5—2.8 (m, 6H), 3.42 (m, 1H, H-1'), 6.7—7.5 (m, 4H), 8.90 (br, 1H, OH). Found: C, 70.45; H, 5.93%. Calcd for $C_{12}H_{12}O_3$: C, 70.57; H, 5.92%.

Oxidation of 3-(1-Cyclohexenyl)tropolone (3b). 3-(1-Cyclohexenyl)tropolone (**3b**) (2.33 g) was added to a performic acid solution, prepared from 90% formic acid (25 ml) and 30% hydrogen peroxide (5 ml), and heated on a water bath for 2 h. The reaction mixture was alkalized with 20% sodium hydroxide solution and heated on a water bath for 45 min. The mixture was slightly acidified with 3 M hydrochloric acid and extracted with chloroform. The extract was washed with water and dried over anhydrous sodium sulfate. After the evaporation of the solvent, the residue was recrystallized from benzene to give 842 mg (38%) of 1,2,3,4-tetrahydro-6*H*-cyclohepta[*b*]benzofuran-6-one (**4b**): mp 174—176 °C; IR ($CHCl_3$) 1650 cm^{-1}; UV (CH_3OH) 229 (log ε 4.18), 284 (4.37), 313 nm (sh, 3.89); NMR ($CDCl_3$) δ=1.3—2.2 (m, 4H), 2.3—3.1 (m, 4H), 6.7—7.6 (m, 4H). Found: C, 77.69; H, 6.06%. Calcd for $C_{13}H_{12}O_2$: C, 77.98; H, 6.04%.

Dehydrogenation of 1,2,3,4-Tetrahydro-6H-cyclohepta[b]benzofuran-6-one (4b). A mixture of 1,2,3,4-tetrahydro-6*H*-cyclohepta[*b*]benzofuran-6-one (**4b**) (1.0 g) and 5% palladium-charcoal (2.0 g) in xylene (20 ml) was refluxed for 48 h. The catalyst was filtered off. The filtrate was chromatographed on three Wakogel B-10 plates (30×30 cm^2) with ethyl acetate. Crystals from the upper band gave 6*H*-cyclohepta[*b*]benzofura-6-one (**6**). Fraction from the lower band was a mixture of **4b** and **6**, and was rechromatographed. The fractions, corresponding to **6**, were combined and recrystallized from benzene to give 235 mg (24%) of **6**: mp 139—141 °C; IR ($CHCl_3$) 1635 cm^{-1} (C=O); UV (CH_3OH) 274 (log ε 4.40), 305 (4.18), 336 (sh, 3.89), 350 (sh, 3.78), 366 nm (sh, 3.61); NMR ($CDCl_3$) δ=6.90—8.05 (m). Found: C, 79.39; H, 4.07%. Calcd for $C_{13}H_8O_2$: C, 79.58; H, 4.11%.

Oxidation of 3-(1-Cycloheptenyl)tropolone (3c). 3-(1-Cycloheptenyl)tropolone (**3c**) (432 mg) was added to a performic acid solution, prepared from 90% formic acid (5 ml) and 30% hydrogen peroxide (1 ml), and heated on a water bath for 2 h. The reaction mixture was worked up, as mentioned above, and recrystalized from benzene to give 111 mg (26%) of 5,7,8,9,10,11-hexahydrodicyclohepta[*b*,*d*]furan-5-one (**4c**): mp 173—175 °C; IR ($CHCl_3$) 1648 cm^{-1} (C=O); UV (CH_3OH) 227 (log ε 4.18), 284 (4.37), 310 nm (sh, 3.91); NMR ($CDCl_3$) δ=1.6—2.2 (m, 6H), 2.4—3.1 (m, 4H), 6.7—7.4 (m, 4H). Found: C, 78.18; H, 6.79%. Calcd for $C_{14}H_{14}O_2$: C, 78.48; H, 6.59%.

References

1) W. T. Brady, *Synthesis*, **1971**, 415.
2) W. T. Brady, "The Chemistry of Ketenes, Allenes, and Related Compounds," ed by S. Patai, John Wiley and Sons, Inc., New York (1981), Part 1, p. 283.
3) W. T. Brady, *Tetrahedron*, **37**, 2949 (1981).
4) H. C. Stevens, D. A. Reich, D. R. Brandt, K. R. Fountain, and E. J. Gaughan, *J. Am. Chem. Soc.*, **87**, 5257 (1965).
5) H. C. Stevens, J. K. Rinehart, J. M. Lavanish, and G. M. Trents, *J. Org. Chem.*, **36**, 2780 (1971).
6) J.-H. Shin, *Daehan Hwahak Hwoejee* (*J. Korean Chem. Soc.*), **13**, 75 (1969).
7) J.-H. Shin, *Daehan Hwahak Hwoejee* (*J. Korean Chem. Soc.*), **13**, 83 (1969).
8) K. Tanaka and A. Yoshikoshi, *Tetrahedron*, **27**, 4889 (1971).
9) T. Asao, T. Machiguchi, T. Kitamura, and Y. Kitahara, *J. Chem. Soc., D*, **1970**, 89.
10) K. Imafuku, K. Yamaguchi, and H. Matsumura, *Bull. Chem. Soc. Jpn.*, **53**, 745 (1980).
11) J. Tsunetsugu, M. Asai, H. Uchiyama, Y. Kurata, A. Mori, M. Sato, and S. Ebine, 12nd Symposium on Non-benzenoid Aromatic Compounds, Matsumoto, 1979, No. 1N12.
12) E. P. Kohler and J. Kable, *J. Am. Chem. Soc.*, **57**, 917 (1935).
13) J. M. Conia and J. Ripoll, *Bull. Soc. Chim. Fr.*, **1963**, 768.
14) R. E. Harmon, W. D. Barta, S. K. Gupta, and G. Slomp, *J. Chem. Soc., C*, **1971**, 3645.

Noriceane (Tetracyclo[5.3.1.$0^{2,6}$.$0^{4,9}$]undecane) and 3,5-Dehydronoriceane (Pentacyclo[5.3.1.$0^{2,6}$.$0^{3,5}$.$0^{4,9}$]undecane)[1]

Takeo KATSUSHIMA, Ryohei YAMAGUCHI, and Mituyosi KAWANISI*
Department of Industrial Chemistry, Faculty of Engineering, Kyoto University, Yoshida, Sakyo-ku, Kyoto 606
(Received April 14, 1982)

Heating a mixture of *endo, exo-* and *endo, endo*-2,4-dibromohomoadamantanes at 180 °C in hexamethylphosphoric triamide (HMPT) brings about a novel skeletal rearrangement with concomitant dehydrobromination to give tricyclo[5.3.1.$0^{4,9}$]undeca-2,5-diene (**5**) in 88% yield. Direct photoexcitation of **5** in diethyl ether induces an intramolecular [2+2] cycloaddition to produce 3,5-dehydronoriceane (**2**). The bicyclo[2.1.0]pentane moiety constrained in the cage structure of **2** shows almost the same ^{13}C–H coupling constants as those of bicyclo[2.1.0]-pentane itself. Finally hydrogenation of **2** over PtO_2 easily proceeds to afford noriceane, which is named after the structure of iceane.

Among 2486 possible tetracyclic ring systems of empirical formula $C_{11}H_{16}$,[2] tetracyclo[5.3.1.$0^{2,6}$.$0^{4,9}$]-undecane (**1**) has a unique skeleton which is a nor-analogue of iceane (tetracyclo[5.3.1.$1^{2,6}$.$0^{4,9}$]dodecane) (**3**).[3] Iceane is named after the structure of crystalline water and, hence, we can term **1** as noriceane. In addition to its unique structure, **1** is a member of the tetracyclic $C_{11}H_{16}$ hydrocarbons which can be rearranged to the most stable isomer, 2,4-ethanonoradamantane by $AlBr_3$ catalyst.[2] In connection with our continuing interest in synthesis and reactions of strained cage molecules,[4] we could synthesize a highly strained compound, 3,5-dehydronoriceane (**2**), which has the partial bicyclo[2.1.0]pentane structure fixed in the rigid cage structure. Thus, taking account of its expected high chemical reactivity,[5] **2** can be a useful precursor of noriceane derivatives. We now describe here synthesis of noriceane (**1**) as well as 3,5-dehydronoriceane (**2**) in detail.[6]

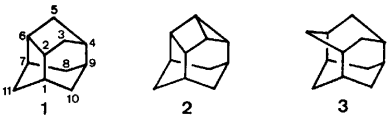

Scheme 1.

Results and Discussion

When a mixture of *endo,exo-*,and *endo,endo*-2,4-dibromo-homoadamantane (**4a** and **4b**)[4b] was heated at 180 °C in HMPT for 3 h, a novel skeletal rearrangement with concomitant dehydrobromination[7] took place to give a geometrically interesting diolefin, tricyclo[5.3.1.$0^{4,9}$]-undeca-2,5-diene (**5**) in 88% yield. The structure of **5** was confirmed by the following experimental results. Hydrogenation of **5** gave a saturated hydrocarbon, tricyclo[5.3.1.$0^{4,9}$]undecane (**6**). This hydrocarbon, **6**, was authentically prepared by reaction of protoadaman-tan-2-one (**7**)[8] with diazomethane under catalysis of $BF_3 \cdot OEt_2$ followed by Wolff-Kishner reduction of the resulting ring-enlarged ketone.[9]

On the other hand, *endo*-2-bromohomoadamant-4-ene (**8**), which was prepared by the elimination of one equivalent of hydrogen bromide under base-promoted reaction conditions,[4b] gave also **5** in 96% yield when heated at 180 °C in HMPT. Therefore, this novel skeletal rearrangement is supposed to proceed through a pathway such as shown in Scheme 3. Initially, the bromine atom on C_4 and its β-hydrogen were eliminated to give **8**. Subsequently, the loss of the remaining bromine atom on C_2 would lead to the homoallyl-cyclopropylcarbinyl rearrangement of carbocation inter-mediates (**9a**, **9b**, and **9c**) and only **9c** could release its β-hydrogen[10] to produce **5**. Although the mechanism of dehydrohalogenation with HMPT has not been estab-lished,[7] the degenerated homoallyl-cyclopropylcarbinyl rearrangement of **9a**, **9b**, and **9c** under stable ion conditions has been proposed.[11]

It can be expected from the geometry of **5** that the two

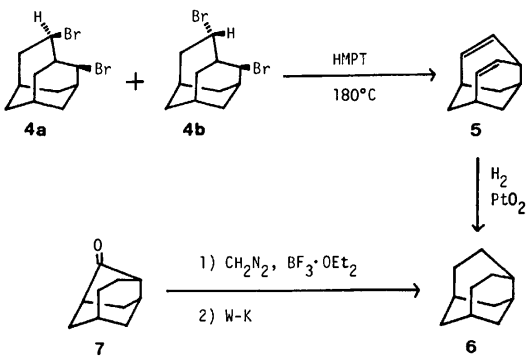

Scheme 2.

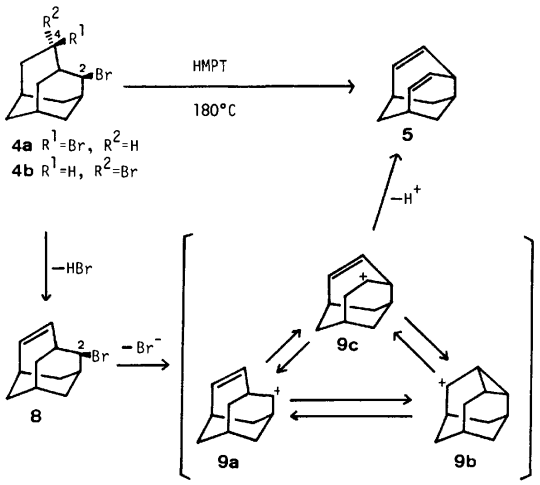

Scheme 3.

π-orbitals are juxtaposed to interact efficiently with each other. Indeed, the UV spectrum of **5** shows a π-π^* absorption at 231 nm (ε=1360 in EtOH) and indicates a homoconjugation between two olefinic moieties. Thus, direct irradiation of **5** in diethyl ether through quartz-filter by means of medium-pressure mercury lamp induced an efficient intramolecular [2+2] cycloaddition to afford 3,5-dehydronoriceane (**2**) in 87% yield. (Scheme 4) The IR spectrum of **2** showed an absorption band at 3100 cm^{-1} due to cyclopropane ring. In addition, the presence of C_{2v} symmetry was clearly indicated by the ^{13}C NMR spectrum which showed only 7 absorption signals.

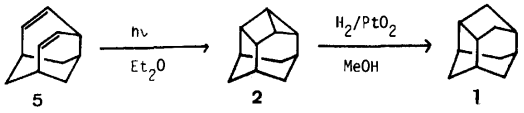

Scheme 4.

The compound (**2**) has partially a bicyclo[2.1.0]-pentane moiety within the rigid cage structure and is expected to possess significant chemical reactivity.[12] The observed ^{13}C–H coupling constants of **2** are almost the same as those of bicyclo[2.1.0]pentane[13] itself (Fig. 1) and strongly suggest the high strained nature of **2**. Thus, **2** was easily hydrogenated over PtO_2 in MeOH to afford noriceane (**1**). The C_{2v} symmetry of **1** was also clearly established by ^{13}C NMR spectroscopy. This hydrogenation is in good agreement with the well-known fact that cleavage of the central bond of bicyclo-[2.1.0]pentane ring system easily occurs in a number of reactions.[12]

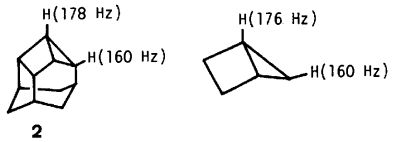

Fig. 1. ^{13}C–H coupling constants of **2** and bicyclo-[2.1.0]pentane.[13]

The fixed bicyclo[2.1.0]pentane ring in the cage structure of **2** is interesting in that any attacking species must approach the bicyclo[2.1.0]pentane unit from the *exo* side alone and, in addition, isomerization to cyclopentene derivatives is impeded on the stereochemical grounds.[10] Therefore, 3,5-dehydronoriceane (**2**) is expected to provide some information on reaction mechanism of bicyclo[2.1.0]pentane system which has been scarcely investigated.[5]

Experimental

All the temperatures were uncorrected. The melting points were measured in sealed capillaries. The IR spectra were obtained on a Shimadzu IR-27 spectrometer. The UV spectrum was recorded on a Hitachi ESP-spectrometer. The MS spectra were taken by using a Hitachi RMS-4 mass spectrometer. The exact mass spectrum was obtained on a Hitachi RMU-8GN mass spectrometer. The ^1H NMR spectra were obtained on a Varian EM-360 or EM-390 spectrometer and the ^{13}C NMR spectra were obtained on a Varian CFT-20 spectrometer, TMS being chosen as the inernal standard. ^{13}C–H coupling constants were measured by Gated decoupling method. Microanalyses were performed by Kyoto University Elemental Analysis Center.

Tricyclo[5.3.1.0^{4,9}]undeca-2,5-diene (5). A solution of a mixture of **4a** and **4b** (7.958 g; 25.8 mmol)[4b] in HMPT (100 ml) was heated at 180 °C for 3 h under nitrogen. To the cooled reaction mixture was then added hexane, and the organic layer was washed with water several times and dried (Na_2SO_4). The solvent was evaporated and the residue was chromatographed on alumina. Elution by hexane gave **5** (3.314 g, 88%): mp 155—158 °C. MS *m/e* (rel intensity): 146 (M^+, 84), 80 (100). IR (CCl_4): 3080, 2920, 1630, 1455, 1375, 910, 700 cm^{-1}. UV λ_{max} (EtOH): 231 nm (ε=1360). ^1H NMR δ (CCl_4): 6.00 (2H, d.d, J=9.0 and 5.4 Hz), 5.70 (2H, d.d, J=9.0 and 7.2 Hz), 2.93 (1H, d.t, J=8.7 and 5.1 Hz), 2.70—1.00 (9H, br complex m). ^{13}C NMR δ ($CDCl_3$): 137.0 (d), 132.8 (d), 39.4 (t), 38.2 (d), 32.2 (d), 26.9 (d), 24.0 (t). Found: C, 90.23; H, 9.66%. Calcd for $C_{11}H_{14}$: C, 90.35; H, 9.66%.

The same treatment of pure **4a** (622 mg; 2.02 mmol) in HMPT as above gave **5** (186 mg, 63%). Additionally the similar reaction of *endo*-2-bromotricyclo[4.3.1.1^{3,8}]undec-4-ene (**8**)[4b] (54 mg; 0.24 mmol) in HMPT (1 ml) to the above gave also **5** (33 mg, 96%).

Pentacyclo[5.3.1.0^{2,6}.0^{3,5}.0^{4,9}]undecane (2). A solution of **5** (201 mg; 1.39 mmol) in Et_2O (20 ml) was directly irradiated by 300-W medium pressure mercury lamp in a quartz vessel under nitrogen for 5 h. The solvent was evaporated and the residue was chromatographed on alumina. Elution by hexane gave **2** (175 mg, 87%): mp 183—186 °C. MS *m/e* (rel intensity): 146 (M^+, 52), 105 (67), 92 (89), 91 (60), 80 (100), 79 (93). IR (CCl_4): 3100, 2950, 1460, 1440, 1275, 1060, 895 cm^{-1}. ^1H NMR δ (CCl_4): 2.87—1.10 (14H, br complex m). ^{13}C NMR δ ($CDCl_3$): 43.3 (t), 38.3 (d), 33.1 (t), 30.3 (d), 22.5 (d), 20.0 (d), 7.3 (d). Found: C, 90.06; H, 9.81%. Calcd for $C_{11}H_{14}$: C, 90.35; H, 9.65%.

Tetracyclo[5.3.1.0^{2,6}.0^{4,9}]undecane (1). A solution of **2** (100 mg; 0.68 mmol) in MeOH (10 ml) was vigorously stirred in the presence of PtO_2 under hydrogen. After one equivalent of hydrogen was absorbed, the catalyst was removed by filtration. After removal of the solvent under reduced pressure the residue was chromatographed on alumina. Elution by pentane gave **1** (61 mg, 60%): mp 212—215 °C. MS *m/e* (rel intensity): 148 (M^+, 100), 119 (33), 92 (41), 91 (31), 80 (31), 79 (65). IR (CCl_4): 2910, 1465, 1065 cm^{-1}. ^1H NMR δ (CCl_4): 2.67—0.60 (16H, br complex m). ^{13}C NMR δ ($CDCl_3$): 41.9 (d), 40.9 (t), 38.1 (d), 33.7 (d), 30.9 (t), 30.5 (d), 29.5 (t). Found: C, 88.86; H, 11.04%. Calcd for $C_{11}H_{16}$: C, 89.12; H, 10.88%.

Tricyclo[5.3.1.0^{4,9}]undecane (6). A mixture of **5** (124 mg; 0.85 mmol) and a small amount of PtO_2 in MeOH (10 ml) was vigorously stirred under hydrogen. After two equivalents of hydrogen had been absorbed, the catalyst was removed by filtration and the solvent was evaporated. The residue was chromatographed on alumina. Elution by pentane gave **6** (85 mg, 66%): mp 242—246 °C. MS *m/e* (rel intensity): 150 (M^+, 100), 121 (43), 80 (43), 79 (50). IR (CCl_4): 2920, 1455 cm^{-1}. ^1H NMR δ (CCl_4): 3.10—0.90 (18H, br complex m). ^{13}C NMR δ ($CDCl_3$): 41.4 (t), 31.3 (t), 30.1 (t), 28.1 (t), 26.6 (d), 26.5 (d), 25.3 (d). Found: *m/e* 150.1382. Calcd for $C_{11}H_{18}$: M, 150.1408.

Preparation of 6 from Tricyclo[4.3.1.0^{3,8}]decan-2-one (7).[8] A solution of CH_2N_2 in Et_2O prepared from *N*-nitroso-*N*-methylurea (1.6 g) was added dropwise to a solution of **7**

(149 mg; 1.00 mmol) and a small amount of $BF_3 \cdot OEt_2$ in Et_2O (5 ml) under cooling with an ice–salt bath and then a small amount of acetic acid was added to the reaction mixture. The precipitates were removed by filtration and the filtrate was washed with aq $NaHCO_3$ and brine, and dried (Na_2SO_4). The solvent was evaporated and the residue was chromatographed on silica gel. Elution by hexane–Et_2O (9 : 1) gave the ring-enlarged ketone[9] (104 mg, 63%): MS *m/e* (rel intensity): 164 (M^+, 100). IR (nujol): 2930, 1710, 1460, 1375, 720 cm^{-1}. ^1H NMR δ ($CDCl_3$): 3.00—1.00 (16H, br complex m).

A mixture of the above ketone (41 mg; 0.25 mmol), KOH (200 mg; 3.56 mmol), 100% hydrazine hydrate (150 mg; 3.00 mmol) in diethylene glycol (0.6 ml) was stirred at 110 °C for 0.5 h and subsequently at 180 °C for 3 h. The sublimate on the condenser was collected and dissolved in pentane. The solution was washed with brine and dried (Na_2SO_4). Evaporation of the solvent gave crude **6** (30 mg, 80%). This compound was identical with **6** obtained by hydrogenation of **5** in every respect.

We thank Dr. Eiji Ōsawa for his valuable discussion and Dr. Ryusei Konaka of Shionogi Pharmaceutical Co. Ltd. for obtaining the exact mass spectrum of **6**. We are also indebted to Dr. David P. G. Hamon for providing IR and ^1H NMR spectra of tricyclo[5.3.1.$0^{4,9}$]-undecan-2-one. This work was partially supported by a Grant-in-Aid for Scientific Research from the Ministry of Education, Science and Culture (No. 434025).

References

1) Provided that there is no ambiguity, we have used trivial nomenclatures for simplicity. The IUPAC names are described in Experimental Section.

2) S. A. Godleski, P. v. R. Schleyer, and E. Ōsawa, *J. Chem. Soc., Chem. Commun.*, **1976**, 38; S. A. Godleski, P. v. R. Schleyer, E. Ōsawa, Y. Inamoto, and Y. Fujikura, *J. Org. Chem.*, **41**, 2596 (1976).

3) For synthesis of iceane; C. A. Cupas and L. Hodekowski, *J. Am. Chem. Soc.*, **96**, 4668 (1974); H. Tobler, R. O. Klaus, and C. Ganter, *Helv. Chim. Acta*, **58**, 1445 (1975); D. P. G. Hamon and G. F. Taylor, *Aust. J. Chem.*, **29**, 1721 (1976).

4) a) R. Yamaguchi, T. Katsushima, and M. Kawanishi, *Bull. Chem. Soc. Jpn.*, **47**, 2830 (1974); b) R. Yamaguchi, T. Katsushima, and M. Kawanishi, *ibid.*, **48**, 2328 (1975); c) R. Yamaguchi and M. Kawanishi, *Chem. Lett.*, **1975**, 649; d) T. Katsushima, R. Yamaguchi, and M. Kawanisi, *J. Chem. Soc., Chem. Commun.*, **1975**, 692; e) T. Katsushima, K. Maki, R. Yamaguchi, and M. Kawanisi, *Bull. Chem. Soc. Jpn.*, **53**, 2031 (1980); f) T. Katsushima, M. Yoshikawa, R. Yamaguchi, and M. Kawanisi, *ibid.*, **53**, 2618 (1980).

5) For reactions of **2**; T. Katsushima, R. Yamaguchi, M. Kawanisi, and E. Ōsawa, *J. Chem. Soc., Chem. Commun.*, **1976**, 40; *Bull. Chem. Soc. Jpn.*, **53**, 3313 (1980); T. Katsushima, R. Yamaguchi, S. Iemura, and M. Kawanisi, *ibid.*, **53**, 3318 (1980); *J. Chem. Soc., Chem. Commun.*, **1980**, 133; *Bull. Chem. Soc. Jpn.*, **53**, 3324 (1980).

6) A preliminary account appeatred in Ref. 4d.

7) For dehydrohalogenation with HMPT; R. Hana, *Tetrahedron Lett.*, **1968**, 2105; R. S. Monson, *J. Chem. Soc., D.* **1971**, 113.

8) C. A. Cupas, W. Schumann, and W. E. Heyd, *J. Am. Chem. Soc.*, **92**, 3237 (1970).

9) Although the position of the carbonyl function has not been determined, the regiochemistry of the ring-enlaged ketone does not matter to the present discussion. It can be added that IR and ^1H NMR spectra of this ketone are not identical with those of tricyclo[5.3.1.$0^{4,9}$]undecan-2-one: D. P. G. Hamon and G. F. Taylor, *Aust. J. Chem.*, **28**, 2255 (1975); R. K. Murray, Jr., K. A. Babiak, and T. K. Morgan, Jr., *J. Org. Chem.*, **40**, 2463 (1975).

10) For Bredt's Rule; G. Köbrich, *Angew. Chem.*, **85**, 494 (1973) and K. J. Shea, *Tetrahedron*, **36**, 1683 (1980).

11) G. A. Olah, G. Liang, K. A. Babiak, T. K. Morgan, Jr., and R. K. Murray, Jr., *J. Am. Chem. Soc.*, **98**, 576 (1976).

12) For reactions of bicyclo[2.1.0]pentane itself; R. M. Moriarty, "Topics in Stereochemistry," ed by E. L. Eliel and N. L. Allinger, Wiely, New York (1973), Vol. 8, p. 347; P. G. Gassman, *Acc. Chem. Res.*, **4**, 128 (1971); P. G. Gassman, T. J. Atkins, and J. T. Lumb, *J. Am. Chem. Soc.*, **94**, 7757 (1972); K. B. Wiberg and K. C. Bishop, III, *Tetrahedron Lett.*, **1973**, 2727; H. Takaya, T. Suzuki, M. Yamakawa, and R. Noyori, *J. Org. Chem.*, **46**, 2486 (1981), and references cited therein.

13) M. Christl, *Chem. Ber.*, **108**, 2781 (1975).

Total Synthesis of a Macrocyclic Lactone Antibiotic A26771B and Its Isomers Using Carbohydrates

Kuniaki TATSUTA,* Yoshiya AMEMIYA, Yoshinobu KANEMURA, and Mitsuhiro KINOSHITA
Department of Applied Chemistry, Faculty of Science and Technology, Keio University, Hiyoshi, Kohoku-ku, Yokohama 223
(Received April 7, 1982)

Total synthesis and antibacterial activities of a macrocyclic lactone antibiotic A26771B (**1**) and all its isomers (**2**, **3**, and **4**) are discussed. The starting 8,9,10,12-tetra-*O*-benzyl-2,3,4,5,11-pentadeoxy-*aldehydo*-D-*xylo*-(*E*)-6-dodecenose derived from D-glucose reacted with racemic Wittig reagent, (3-hydroxybutyl)triphenylphosphonium iodide to give 1,3,4,5-tetra-*O*-benzyl-2,8,9,10,11,14,16-heptadeoxy-DL-*glycero*-L-*xylo*-hexadeca-6,12-dienitol, which was in turn converted into methyl 15-*O*-acetyl-6,7,8,9,10,11,12,13,14,16-decadeoxy-4,5-*O*-isopropylidene-DL-*glycero*-L-*threo*-(*E*)-2-hexadecenonate (**13**) through effective oxidation and β-elimination. Saponification followed by Yamaguchi's lactonization of **13** afforded two diastereomeric 16-membered-ring lactones which were converted into (5*S*, 15*R*)-A26771B (**1**) and its (5*S*, 15*S*)-diastereomer (**2**) by successive deacetonation, selective succinylation and oxidation. The other starting 2,3,4,6-tetra-*O*-benzyl-5-deoxy-*aldehydo*-D-*lyxo*-hexose, which was prepared from 2-deoxy-D-glucose, reacted with a Wittig reagent to give 8,9,10,12-tetra-*O*-benzyl-2,3,4,5,11-pentadeoxy-*aldehydo*-D-*lyxo*-6-dodecenose (**20**) followed by hydrolysis. Similar reaction sequence from **20** with the aforesaid series for **1** and **2** afforded the (5*R*, 15*R*)-isomer (**3**) and (5*R*, 15*S*)-isomer (**4**).

A 16-membered macrocyclic lactone antibiotic A26771B (**1**), produced by *Penicillium turbatum*, possesses a novel structure and an interesting antibacterial activity.[1] The first stereospecific total synthesis and the absolute configuration of **1** were disclosed in our laboratories[2] and followed by the elegant synthesis of the racemate by Takei *et al.*[3] The previous stereospecific synthesis was based on a convergent scheme involving both optically pure C-1—C-12 and C-13—C-16 portions, which were derived from D-glucose. Herein we describe in detail, the total synthesis of the antibiotic A26771B [(5*S*,15*R*)-isomer (**1**)], its diastereomers [(5*S*,15*S*)-isomer (**2**) and (5*R*,15*R*)-isomer (**3**)] and enantiomer [(5*R*,15*S*)-isomer (**4**)] in order to further study their structure-activity relationships. The key step was effective separation of the (15*R*)- and (15*S*)-diastereomers after coupling a racemic C-13—C-16 portion (**8**) to an optically active C-1—C-12 portion (**7** or **20**). The latter portion was in turn prepared from D-glucose derivatives, because the C-5 positions of **1** (or **2**) and **3** (or **4**) were stereochemically corresponding to C-2 position of 5-deoxy-D-glucose and C-5 position of 2-deoxy-D-glucose, respectively.

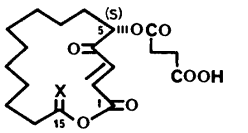

1: X = (R)-Me, H (A26771B)

2: X = (S)-H, Me

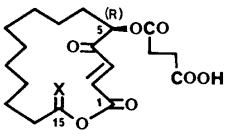

3: X = (R)-Me, H

4: X = (S)-H, Me

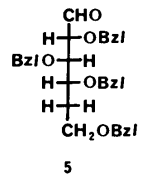

5

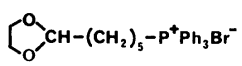

6

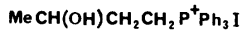

8

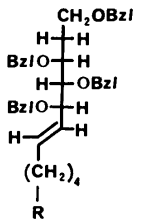

7: R = CHO

9: R = 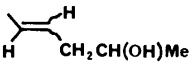

The synthesis of the antibiotic A26771B (**1**) and its (5*S*,15*S*)-diastereomer (**2**) was initiated from the C-1—C-12 portion (**7**), which was obtained from 2,3,4,6-tetra-*O*-benzyl-5-deoxy-*aldehydo*-D-*xylo*-hexose (**5**) and [5-(1,3-dioxolan-2-yl)pentyl]triphenylphosphonium bromide (**6**) by Wittig reaction and subsequent hydrolysis as described in the previous paper.[2] The second Wittig reagent **8** was prepared by a three-step sequence from 1,3-butanediol in a 72% yield. Reaction of **7** with the reactive ylide formed from **8** afforded a 1 : 1 mixture of the two diastereomeric 16-carbon products, 1,3,4,5-tetra-*O*-benzyl-2,8,9,10,11,14,16-heptadeoxy-DL-*glycero*-L-*xylo*-hexadeca-6,12-dienitol (**9**) in a 67% yield. The separation of the diastereomers was not overcome at this stage but done after lactonization as described later on. Catalytic reduction of **9** with hydrogen and palladium black gave the saturated alcohol **10**, which was selectively *t*-butyldimethylsilylated and then totally acetylated to afford the fully masked product **11**. Desilylation of **11** with difluoroacetic acid followed by successive catalytic oxidation of the resulting alcohol and esterification with diazomethane gave the methyl ester, methyl 3,4,5,15-tetra-*O*-acetyl-2,6,7,8,9,10,11,-12,13,14,16-undecadeoxy-DL-*glycero*-L-*xylo*-hexadeconate (**12**). Selective deacetylation of **12** accompanying the desired β-elimination with 4.5 equiv. of potassium *t*-butoxide and 2 equiv. of water followed by acetonation with 2,2-dimethoxypropane and *p*-toluenesulfonic acid in acetone gave the α,β-unsaturated ester, methyl 15-*O*-acetyl-6,7,8,9,10,11,12,13,14,16-decadeoxy-4,5-*O*-isopropylidene-DL-*glycero*-L-*threo*-(*E*)-2-hexadecenonate (**13**). Without water, the above-mentioned reaction gave a very low yield of the elimination product. The *E*-stereochemistry was defined by the 16 Hz coupling

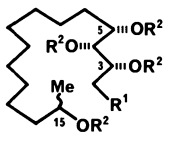

10 : $R^1 = CH_2OH$, $R^2 = H$

11 : $R^1 = CH_2OSiMe_2Bu^t$, $R^2 = Ac$

12 : $R^1 = COOMe$, $R^2 = Ac$

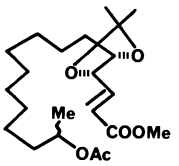

13

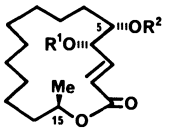

14 : $R^1, R^2 =$

16 : $R^1 = R^2 = H$

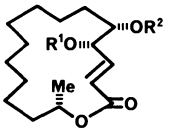

15 : $R^1, R^2 =$

17 : $R^1 = R^2 = H$

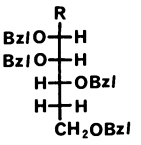

18 : $R = CH_2OTr$

19 : $R = CHO$

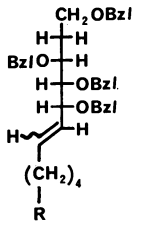

20 : $R = CHO$

21 : $R =$ 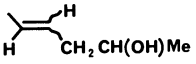

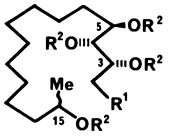

22 : $R^1 = CH_2OH$, $R^2 = H$

23 : $R^1 = CH_2OSiMe_2Bu^t$, $R^2 = Ac$

24 : $R^1 = COOMe$, $R^2 = Ac$

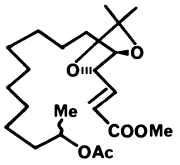

25

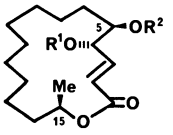

26 : $R^1, R^2 =$

28 : $R^1 = R^2 = H$

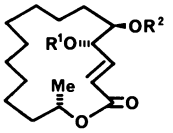

27 : $R^1, R^2 =$

29 : $R^1 = R^2 = H$

constant of the vinylic protons. When treated with lithium hydroxide in 50% aqueous THF, **13** quantitatively furnished the corresponding hydroxy acid, which was submitted to lactonization. Yamaguchi's method[4] among others gave the best yield of the desired lactones **14** and **15**. Namely, the hydroxy acid reacted with 2,4,6-trichlorobenzoyl chloride in the presence of triethylamine in THF to give the corresponding mixed anhydride, which was treated with 4-dimethylaminopyridine in toluene at 95 °C. The two diastereomeric 16-membered-ring lactones **14** and **15** were obtained and separated in 45% and 40% yields by silica gel column chromatography. The lactone **14** was identical in all respects with a sample of the same structure stereospecifically synthesized from D-glucose as previously described,[2] and convertible into the antibiotic A26771B (**1**). Therefore, **14** and **15** were found to be (4*S*,5*S*,15*R*)- and (4*S*,5*S*,15*S*)-isomers, respectively. Hydrolysis of **14** and **15** with difluoroacetic acid in aqueous MeOH gave the diols, 6,7,8,9,10,11,12,13,14,16-decadeoxy-D-*glycero*-L-*threo*-(*E*)-2-hexadecenono-1,15-lactone (**16**) and the L-*glycero*-L-*threo*-isomer (**17**) in 94% and 92% yields, respectively. Selective succinylation of **16** and **17** with succinic anhydride and *N*,*N*-diisopropylethylamine in CCl_4 gave predominantly 5-*O*-succinyl compounds, which were oxidized with acetic anhydride and DMSO to afford (5*S*,15*R*)-A26771B (**1**) and the (5*S*,15*S*)-isomer (**2**) in 70% and 73% yields, respectively. The synthetic product **1** thus obtained was identical both spectroscopically and chromatographically with an authentic sample of the natural antibiotic.

Subsequently, the (5*R*,15*R*)- and (5*R*,15*S*)-isomers (**3** and **4**) were synthesized by the similar strategy to the aforesaid. The starting 2,3,4,6-tetra-*O*-benzyl-1-*O*-trityl-5-deoxy-D-*lyxo*-hexose (**18**) was prepared from 2-deoxy-D-glucose successively by tritylation, $NaBH_4$ reduction and benzylation in a 65% yield. Detritylation of **18** with 90% trifluoroacetic acid followed by oxidation with trifluoroacetic anhydride and DMSO in dichloromethane gave 2,3,4,6-tetra-*O*-benzyl-5-deoxy-*aldehydo*-D-*lyxo*-hexose (**19**), in a 78% yield, which had the opposite configuration only at the C-2 position in comparison with **5**. The Wittig reaction of **19** with the ylide derived from **6**, followed by hydrolysis with 70% trifluoroacetic acid, gave the 12-carbon skeletal aldehyde **20** in an 82% yield. The second Wittig reaction of **20** with the ylide formed from **8** gave a 1 : 1 mixture of the two diastereomeric compounds, 1,3,4,5-tetra-*O*-benzyl-2,8,9,10,11,14,16-heptadeoxy-DL-*glycero*-D-*arabino*-hexadeca-6,12-dienitol (**21**). Reduction of **21** to give **22**, followed by successive silylation and acetylation, afforded **23**, which was in turn converted into the corresponding methyl ester **24** as efficiently as described in the preparation for **12**. Selective deacetylation with β-elimination of **24**, followed by acetonation gave methyl 15-*O*-acetyl-6, 7, 8, 9, 10, 11, 12, 13, 14, 16-decadeoxy-4,5-*O*-isopropylidene-DL-*glycero*-D-*erythro*-(*E*)-2-hexadecenonate (**25**) as described in the preparation for **13**. Saponification of **25** with LiOH gave the corresponding hydroxy acid, which was cyclized as described for the preparation of **14** and **15** to afford, after column chromatography, the two diastereomeric lactones **26** [(4*S*,5*R*,15*R*)-isomer] and **27** [(4*S*,5*R*,15*S*)-isomer] in 47% and 39% yields. The independent conversion of the diastereomers **26** and **27** into the optically pure (5*R*,15*R*)-isomer (**3**) and (5*R*,15*S*)-isomer (**4**) involved the same reagents and reaction conditions through **28** and **29** as mentioned in the scheme for the aforesaid compounds **1** and **2**, and gave similar yields. Conclusive evidence for the stereochemical assignments at the C-5

TABLE 1. MINIMAL INHIBITORY CONCENTRATION (mcg/ml) OF THE PRODUCTS

	A26771B	1	2	3	4
Staph. aureus 193	6.25	6.25	12.5	1.56	6.25
Staph. aureus 209P	6.25	6.25	12.5	3.12	6.25
Staph. aureus MS9610	6.25	6.25	12.5	3.12	3.12
Staph. aureus MS9351	6.25	6.25	12.5	3.12	6.25
Staph. aureus MS9861	6.25	6.25	12.5	1.56	6.25
Staph. aureus MS10225	6.25	6.25	12.5	3.12	6.25
Staph. aureus MS10246	6.25	6.25	12.5	3.12	6.25
Sarcina lutea PCI1001	6.25	6.25	12.5	6.25	12.5
B. subtilis B-558	50	50	50	50	50
E. coli NIHJ	>50	>50	>50	>50	>50

and C-15 positions was provided by identification of **4** with the natural antibiotic A26771B (**1**) in all respects except for the sign of the optical rotation.

Biological investigation of the natural antibiotic A26771B and synthetic products **1**, **2**, **3**, and **4** revealed (Table 1) that all products exhibited in vitro antibiotic activities against Gram-positive and macrolide-resistant Gram-positive bacteria and the (5*R*,15*R*)-isomer **3** was approximately twice as active as A26771B (**1**). This lack of the essential stereochemical requirement for the antibiotic activity of this class of novel compounds was the most striking aspect, suggesting pliable possibility in chemical modification of macrolide antibiotics.

Experimental

Melting points were determined on a micro hot-stage Yanaco MP-S3 and were uncorrected. IR and UV spectra were recorded on Hitachi Perkin-Elmer 225 and JASCO UV IDEC-1 spectrometers, respectively, and ^{1}H-NMR spectra in $CDCl_3$ with TMS as internal standard on a Varian EM-390 (90 MHz) or a Bruker WM 250 spectrometer (250 MHz). Optical rotations were measured on a Carl Zeiss photoelectric polarimeter. Silica gel TLC and column chromatography were performed on Merck TLC 60F-254 and Wakogel C-200, respectively. In general, evaporation was carried out under reduced pressure below 30 °C.

*(3-Hydroxybutyl)triphenylphosphonium Iodide (**8**).* To a stirred and ice-cooled solution of 1,3-butanediol (5.0 g, 55 mmol) in acetonitrile (75 ml) were added *p*-toleunesulfonyl chloride (10 g) and triethylamine (10 ml), and stirring at room temperature was continued for 2.5 h. The resulting solution was partitioned between ether and water, and the organic layer was washed successively with saturated aqueous $NaHCO_3$ and NaCl solutions, dried and evaporated to a residue, which was chromatographed on silica gel (250 g) with 3 : 2 hexane–ethyl acetate to give a syrup of the corresponding tosylate (11 g, 82%).

To a solution of the tosylate (11 g) in acetone (110 ml) was added NaI (12.7 g), and the solution was stirred at 60 °C for 1 h. The precipitated salt was filtered and the filtrate was evaporated to a residue, which was partitioned between benzene and water. The organic layer was dried and evaporated to give a syrup of the iodo compound.

A solution of the syrup in benzene (40 ml) was stirred with triphenylphosphine (14 g) at 80 °C for 20 h under argon. The precipitated product was filtered and recrystallized from methanol–ethyl acetate to give needles of **8** (18.2 g, 90%): mp 149—152 °C.

Found: C, 56.97; H, 5.20; I, 27.61%. Calcd for $C_{22}H_{24}$OIP: C, 57.16; H, 5.23; I, 27.45%.

*1,3,4,5-Tetra-O-benzyl-2,8,9,10,11,14,16-heptadeoxy-*DL*-glycero-*L*-xylo-hexadeca-6,12-dienitol (**9**).* To a suspension of **8** (5.4 g, 11.7 mmol) in dry THF (54 ml) were added with stirring at room temperature, under argon, 2M sodium methylsulfinylmethanide solution prepared *in situ* from NaH (199 mg, 8.29 mmol) and DMSO (4.14 ml), and then a 1.6 M butyllithium solution in hexane (6.23 ml, 10 mmol). After 5 min, to the resulting orange solution was added a solution of **7** (3.57 g, 5.88 mmol) in dry THF (18 ml) with stirring, and stirring at room temperature was continued for 0.5 h. The reaction solution was diluted with water and extracted with ether. The combined extracts were then evaporated, and the residue was chromatographed on silica gel (300 g) with 4 : 1 hexane–ethyl acetate to give a colorless syrup of **9** (2.57 g, 67%): R_f 0.20 (3 : 1 hexane–ethyl acetate); $[\alpha]_D^{15}$ +45° (*c* 1.0, $CHCl_3$); ^{1}H-NMR δ=1.13 and 1.18 (3H in total, each d, Me-15, $J_{15,Me}$=6 Hz), 3.50 (2H, t, H-1, $J_{1,2}$= 6 Hz), 3.53—4.05 (4H, m, H-3,4,5 and 15), 4.21—4.80 (8H, m, PhC$\underline{H_2}$O×4), 5.34—5.78 (4H, m, H-6,7,12 and 13), 7.33 (20H, s, Ph×4).

Found: C, 80.01; H, 8.17%. Calcd for $C_{44}H_{54}O_5$: C, 79.72; H, 8.21%.

*3,4,5,15-Tetra-O-acetyl-1-O-(*t*-butyldimethylsilyl)-2,6,7,8,9,10,-11,12,13,14,16-undecadeoxy-*DL*-glycero-*L*-xylo-hexadecitol (**11**).* A solution of **9** (547 mg) in methanol (8 ml) was shaken with palladium black and 3-atm hydrogen at room temperature for 15 h, filtered and evaporated to give a crude solid (250 mg) of **10**: R_f 0.25 (6 : 1 chloroform–methanol).

To a stirred solution of crude **10** (250 mg) in dry pyridine (2.5 ml) was added *t*-butyldimethylsilyl chlorde (150 mg), and the solution was kept at room temperature. After 3 h, TLC indicated the absence of starting material. Acetic anhydride (0.67 ml) was added and the mixture stirred overnight at room temperature. After addition of EtOH, the solution was evaporated and the residue was dissolved in ethyl acetate. The solution was washed successively with saturated aqueous $NaHCO_3$ and NaCl solutions, dried, and evaporated. The residue was chromatographed on silica gel (25 g) with 5 : 1 hexane–ethyl acetate to give a syrup of **11** (370 mg, 77% from **9**): R_f 0.37 (3 : 1 hexane–ethyl acetate); $[\alpha]_D^{17}$ 0° (*c* 1.0, $CHCl_3$); ^{1}H-NMR δ=0.05 (6H, s, Me_2Si), 0.88 (9H, s, *t*-BuSi), 1.20 (3H, d, Me-15, $J_{15,Me}$=6 Hz), 2.02, 2.05, and 2.08 (12H in total, each s, OAc×4), 3.62 (2H, t, H-1, $J_{1,2}$=6 Hz).

Found: C, 61.10; H, 9.32%. Calcd for $C_{30}H_{56}O_9Si$: C, 61.19; H, 9.59%.

*Methyl 3,4,5,15-Tetra-O-acetyl-2,6,7,8,9,10,11,12,13,14,16-undecadeoxy-*DL*-glycero-*L*-xylo-hexadeconate (**12**).* To a solution of **11** (340 mg, 0.577 mmol) in acetonitrile (10 ml) was added 0.08 M difluoroacetic acid solution in 50% aqueous acetonitrile (5.1 ml), and the solution was left at 50 °C for 5 h,

neutralized with a saturated aqueous $NaHCO_3$ solution and then extracted with ether. The combined extracts were washed with a saturated aqueous NaCl solution, dried, and evaporated to give a syrup of the crude alcohol (274 mg): R_f 0.13 (3 : 2 hexane–ethyl acetate).

Subsequently, gaseous oxygen (600 ml/min) was bubbled into a solution of the syrup (274 mg) in 75% aqueous dioxane at 85 °C for 5 h in the presence of platinum black (150 mg).

The mixture was filtered, and the filtrate was evaporated to give a residue of the carboxylic acid.

The residue was dissolved in ether (5 ml), and an excess of etheral diazomethane solution was added. The resulting yellowish solution was stirred for 0.5 h at room temperature and then evaporated to the residue, which was chromatographed on silica gel (20 g) with 2 : 1 hexane–ethyl acetate to give a syrup of **12** (250 mg, 86% from **11**): R_f 0.24 (3 : 2 hexane–ethyl acetate); $[\alpha]_D^{16}$ +15° (*c* 1.0, $CHCl_3$); ^{1}H-NMR δ=1.23 (3H, d, Me-15, $J_{15,Me}$=6 Hz), 2.02, 2.05 and 2.08 (12H in total, each s, OAc×4), 2.60 (2H, d, H-2, $J_{2,3}$=6 Hz), 3.68 (3H, s, COOMe).

Found: C, 59.71; H, 8.21%. Calcd for $C_{25}H_{42}O_{10}$: C, 59.74; H, 8.42%.

*Methyl 15-O-Acetyl-6,7,8,9,10,11,12,13,14,16-decadeoxy-4,5,-O-isopropylidene-*DL-glycero-L-threo-*(*E*)-2-hexadecenonate (**13**).* To a solution of **12** (330 mg) in *t*-butyl alcohol (9.9 ml) were added water (0.024 ml) and 0.5 M potassium *t*-butoxide solution in *t*-butyl alcohol (14.8 ml) at room temperature. After 2 min, the reaction solution was neutralized with Dowex 50WX8 (H type) and filtered. The filtrate was evaporated to a residue, which was chromatographed on silica gel (15 g) with 1 : 1 hexane–ethyl acetate to give a syrup of the (*E*)-unsaturated ester (115 mg, 49%).

A solution of the syrup (84 mg) in dry acetone (1.7 ml) was stirred with 2,2-dimethoxypropane (3.4 ml) in the presence of TsOH (4.2 mg) at room temperature for 1.5 h, neutralized with triethylamine and then evaporated to a residue. The residue was partitioned between chloroform and water, and the combined organic layers were evaporated to give a syrup, which was chromatographed on silica gel (10 g) with 5 : 1 hexane–ethyl acetate to give a syrup of **13** (77 mg, 82%): R_f 0.36 (5 : 1 hexane–ethyl acetate); $[\alpha]_D^{18}$ −13° (*c* 1.0, $CHCl_3$); UV_{max} (MeOH) 212 nm (ε 10200); ^{1}H-NMR δ=1.20 (3H, d, Me-15, $J_{15,Me}$=6 Hz), 1.41 and 1.44 (each 3H, s, Me_2C), 2.03 (3H, s, OAc), 3.72 (1H, m, H-5), 3.77 (3H, s, COOMe), 4.10—4.20 (1H, m, H-4), 4.80—4.95 (1H, m, H-15), 6.13 (1H, dd, H-2, $J_{2,3}$=16 Hz, $J_{2,4}$=1.5 Hz), 6.89 (1H, dd, H-3, $J_{2,3}$=16 Hz, $J_{3,4}$=6 Hz).

Found: C, 66.52; H, 9.49%. Calcd for $C_{22}H_{38}O_6$: C, 66.30; H, 9.61%.

*6,7,8,9,10,11,12,13,14,16-Decadeoxy-4,5-O-isopropylidene-*D-glycero-L-threo-(E)-*2-hexadecenono-1,15-lactone (**14**) and* L-glycero-L-threo-*isomer (**15**).* A solution of **13** (132 mg, 0.33 mmol) in 50% aqueous THF (5.0 ml) was stirred with a 0.2 M LiOH solution in 50% aqueous THF (5.8 ml) at 30° for 2 d. The resulting solution was neutralized with Dowex 50WX8 (H type) to pH 4, and then filtered. The filtrate was extracted with ether. The extracts were washed with a saturated aqueous NaCl solution, dried and evaporated to give quantitatively the corresponding hydroxy acid (120 mg): R_f 0.29 (3 : 2 hexane–acetone).

To a mixture of the hydroxy acid (120 mg) and triethylamine (0.108 ml) in dry THF (1.2 ml) was added a solution of 2,4,6-trichlorobenzoyl chloride[4] (172 mg) in dry THF (1.7 ml), and the mixture was stirred for 1 h at room temperature. After removal of triethylamine hydrochloride under argon, the filtrate was diluted with dry toluene (175 ml). The resulting solution was added dropwise to the refluxing solution of 4-dimethylaminopyridine (258 mg) in dry toluene (35 ml) at 95 °C over a 6-h period with stirring under argon, and stirring at this temperature was continued for another 40 min. The reaction solution diluted with ether (500 ml) was washed successively with satu rated aqueous citric acid and $NaHCO_3$ solutions, dried, and then evaporated to give a residue. The residue was chromatographed on silica gel (15 g) with 20 : 1 hexane–ethyl acetate. The eluates between 57—78 ml (R_f 0.30 with 10 : 1 hexane–ethyl acetate) were collected and evaporated to give a solid. Recrystallization from acetone–ethanol–water afforded colorless needles of **14** (52 mg, 45%): mp 74—75 °C (lit,[2] mp 74—75 °C); $[\alpha]_D^{13}$ +7.0° (*c* 1.0, $CHCl_3$); UV_{max} (MeOH) 212 nm (ε 10300); ^{1}H-NMR δ=1.27 (3H, d, Me-15, $J_{15,Me}$=6 Hz), 1.42 (6H, s, Me_2C), 3.73 (1H, m, H-5), 4.12 (1H, dt, H-4, $J_{3,4}$=6.0 Hz, $J_{2,4}$=1.5 Hz), 5.03 (1H, m, H-15), 6.11 (1H, dd, H-2, $J_{2,3}$=16 Hz, $J_{2,4}$=1.5 Hz), 6.88 (1H, dd, H-3, $J_{2,3}$=16 Hz, $J_{3,4}$=6.0 Hz).

Found: C, 70.55; H, 9.77%. Calcd for $C_{19}H_{32}O_4$: C, 70.33; H, 9.94%.

The other eluates between 80—105 ml (R_f 0.25 with 10 : 1 hexane–ethyl acetate) gave a colorless syrup of **15** (45 mg, 40%): $[\alpha]_D^{13}$ +52° (*c* 1.0, $CHCl_3$); UV_{max} (MeOH) 211 nm (ε 9800); ^{1}H-NMR δ=1.26 (3H, d, Me-15, $J_{15,Me}$=6 Hz), 1.46 (6H, s, Me_2C), 3.85 (1H, m, H-5), 4.05 (1H, dull t, H-4, *J*=8 Hz), 5.04 (1H, m, H-15), 6.07 (1H, dd, H-2, $J_{2,3}$=16 Hz, $J_{2,4}$=0.5 Hz), 6.76 (1H, dd, H-3, $J_{2,3}$=16 Hz, $J_{3,4}$=8 Hz).

Found: C, 70.63; H, 9.74%. Calcd for $C_{19}H_{32}O_4$: C, 70.33; H, 9.94%.

*6,7,8,9,10,11,12,13,14,16-Decadeoxy-*D-glycero-L-threo-(E)-*2-hexadecenono-1,15-lactone (**16**).* A sample of **14** (33 mg) was dissolved in a mixture (0.5 ml) of difluoroacetic acid, methanol and water (4 : 3 : 1). The solution was stirred for 1 h at room temperature and then evaporated to a residue, which was chromatograhed on silica gel (3 g) with 3 : 1 hexane–acetone to give needles of **16** (27 mg, 94%): R_f 0.51 (3 : 2 hexane–acetone): mp 86—87 °C (lit,[2] 86—87 °C): $[\alpha]_D^{15}$ −43° (*c* 1.0, $CHCl_3$); UV_{max} (MeOH) 214 nm (ε 10900).

Found: C, 67.55; H, 9.97%. Calcd for $C_{16}H_{28}O_4$: C, 67.57; H, 9.92%.

*6,7,8,9,10,11,12,13,14,16-Decadeoxy-*L-glycero-L-threo-(E)-*2-hexadecenono-1,15-lactone (**17**).* A sample of **15** (25 mg) was hydrolyzed by the procedure described in the preparation of **16** and then worked up to give a syrup of **17** (21 mg, 92%): R_f 0.49 (3 : 2 hexane–acetone); $[\alpha]_D^{15}$ +12.5° (*c* 1.0, $CHCl_3$); UV_{max} (MeOH) 213 nm (ε 10600).

Found: C, 67.69; H, 10.01%. Calcd for $C_{16}H_{28}O_4$: C, 67.57; H, 9.92%.

*A26771B: 5-O-(3-Carboxypropionyl)-4-oxo-4,6,7,8,9,10,11,12,-13,14,16-undecadeoxy-*D-glycero-L-glycero-(E)-*2-hexadecenono-1,15-lactone (**1**).* To a suspension of **16** (19 mg, 0.067 mmol) in dry CCl_4 (0.95 ml) were added succinic anhydride (10 mg) and *N,N*-diisopropylethylamine (0.024 ml) under argon, and the mixture was stirred for 2 h at 50 °C. After addition of ethyl acetate and water, the aqueous layer was acidified to pH 1 with 1 M HCl. The organic layer was dried and then evaporated to a residue, which was purified by PLC with 8 : 1 chloroform–ethanol to give crude crystals of the corresponding succinate (19 mg): R_f 0.55 (8 : 1 chloroform–ethanol); mp 120—122 °C (hexane–ethyl acetate).

The crystals (9.0 mg) was dissolved in a mixture of acetic anhydride (0.064 ml) and dry DMSO (0.22 ml), and the solution was kept at 30 °C for 20 h. The resulting solution diluted with ethyl acetate was washed with water, dried and evaporated to a residue, which was purified by PLC with 8 : 1 chloroform–ethanol to give, after recrystallization from ethyl acetate–hexane, needles (6.1 mg, 51% from **16**) of A26771B

(**1**): R_f 0.57 (8 : 1 chloroform-ethanol); mp and mmp 125—126 °C (lit,[2] mp 125—126 °C); $[\alpha]_D^{12}$ −13° (*c* 0.2, MeOH); UV_{max} (MeOH) 223 nm (ε 13300); IR (KBr) 1750, 1725, 1720, 1710, 1705 (succinyl ester, lactone) and ≈1645 (C=C) cm^{-1}; ^{1}H-NMR δ=1.30 (3H, d, Me-15, $J_{15,Me}$=6.5 Hz), 2.73 (4H, m, succinyl C$\underline{H}_2$–C$\underline{H}_2$), 5.15 (1H, m, H-15), 5.33 (1H, t, H-5, $J_{5,6}$=5.5 Hz). 6.75 and 7.22 (each 1H, AB-q, H-2 and 3, $J_{2,3}$=15.5 Hz). Its UV, IR, and ^{1}H-NMR spectra and TLC behavior were identical with those of an authentic sample of the natural product.

Found: C, 62.79; H, 8.05%. Calcd for $C_{20}H_{30}O_7$: C, 62.81; H, 7.91%.

5-O-(3-Carboxypropionyl)-4-oxo-4,6,7,8,9,10,11,12,13,14,16-undecadeoxy-L-glycero-L-glycero-(E)-*2-hexadecenono-1,15-lactone* (**2**). Following the procedure described for **1**, from **17**, a syrup of **2** (9.7 mg, 51% from **17**) was obtained: R_f 0.57 (8 : 1 chloroform–ethanol); $[\alpha]_D^{17}$ +25° (*c* 0.2, MeOH); UV_{max} (MeOH) 223 nm (ε 10100); IR ($CHCl_3$) 1740, 1735, 1720, 1710, 1700 (succinyl ester, lactone) and ≈1620 (C=C) cm^{-1}; ^{1}H-NMR δ=1.29 (3H, d, Me-15, $J_{15,Me}$=6.5 Hz), 2.76 (4H, m, succinyl C$\underline{H}_2$–C$\underline{H}_2$), 5.09 (1H, m, H-15), 5.35 (1H, t, H-5, $J_{5,6}$=6 Hz), 6.76 and 7.16 (each 1H, AB-q, H-2 and 3, $J_{2,3}$=16 Hz).

Found: C, 62.69; H, 8.11%. Calcd for $C_{20}H_{30}O_7$: C, 62.81; H, 7.91%.

2,3,4,6-Tetra-O-*benzyl-1*-O-*trityl-5-deoxy*-D-lyxo-*hexose* (**18**). To a stirred and ice-cooled solution of 2-deoxy-D-glucose (1.05 g, 6.4 mmol) in dry pyridine (10.5 ml) was added trityl chloride (1.96 g), and stirring was continued at room temperature for 15 h. After addition of a few drops of water, the resulting solution was evaporated to a residue, which was partitioned between ethyl acetate and a saturated aqueous NaCl solution. The organic layer was dried and evaporated to give quantitatively a crude solid of the *O*-trityl compound (2.7 g).

To a solution of this crude compound (24.7 g) in 80% aqueous ethanol (250 ml) was added $NaBH_4$ (2.3 g), and the solution was stirred for 1 h at room temperature. After neutralization with Dry Ice, the solution was evaporated to a residue, which was chromatographed twice on silica gel (400 g and 1 kg) with 5 : 1 and 10 : 1 chloroform–methanol, respectively, to give a pure syrup of the corresponding alcohol (22 g, 88%): $[\alpha]_D^{19}$ −2.5° (*c* 2.0, $CHCl_3$): ^{1}H-NMR δ=1.27—2.05 (2H, m, H-5), 2.93—4.20 (11H, m, H-1,2,3,4,6 and OH×4), 6.94—7.82 (15H, m, trityl).

Found: C, 73.70; H, 7.00%. Calcd for $C_{25}H_{28}O_5$: C, 73.51; H, 6.91%.

A solution of this alcohol (10 g) in dry THF (130 ml) was added to NaH (3 g), and the mixture was stirred at room temperature. After 1 h, benzyl bromide (14.6 ml) was added, and stirring at 50 °C was continued for another 2 h. The reaction mixture was partitioned between benzene and water, and the organic layer was washed with a saturated aqueous NaCl solution, dried and evaporated to a residue. The residue was chromatographed on silica gel (600 g) with 10 : 1 hexane-ethyl acetate to give a syrup of **18** (14 g, 65% from 2-deoxy-D-glucose): ^{1}H-NMR δ=1.75—1.95 (2H, m, H-5), 3.42 (2H, t, H-6, $J_{5,6}$=6.0 Hz), 3.47 (2H, d, H-1, $J_{1,2}$=6.0 Hz), 3.70—3.95 (3H, m, H-2,3 and 4), 4.28—4.79 (8H, m, PhC$\underline{H}_2$O×4), 6.95—7.55 (35H, m, Ph×7). Without further purification, the syrup was used for the next step.

2,3,4,6-Tetra-O-*benzyl-5-deoxy*-aldehydo-D-lyxo-*hexose* (**19**). An ice-cooled solution of **18** (11.5 g, 15 mmol) in 90% aqueous trifluoroacetic acid (50 ml) was stirred for 1 h, and then evaporated to a residue, which was partitioned between chloroform and a saturated aqueous $NaHCO_3$ solution. The organic layer was washed with a saturated aqueous NaCl solution, dried and evaporated to a residue, which was chromatographed on silica gel (600 g) with 10 : 1 benzene–ethyl acetate to give a syrup of the de-*O*-tritylated compound (7.50 g, 95%): R_f 0.11 (5 : 1 hexane–ethyl acetate); $[\alpha]_D^{19}$ +7.5° (*c* 1.0, $CHCl_3$); ^{1}H-NMR δ=1.76—2.10 (2H, m, H-5), 2.10—2.34 (1H, m, OH-1), 3.50 (2H, t, H-6, $J_{5,6}$=6 Hz), 3.61—4.00 (5H, m, H-1,2,3 and 4), 4.40—4.79 (8H, m, PhC$\underline{H}_2$O×4), 7.30 (20H, m, Ph×4).

Found: C, 77.26; H, 7.27%. Calcd for $C_{34}H_{38}O_5$: C, 77.54; H, 7.24%.

A solution of the syrup (7.50 g, 14.2 mmol) in CH_2Cl_2 (14 ml) was added to a mixture of DMSO (2.0 ml), trifluoroacetic anhydride (3.0 g) and CH_2Cl_2 (14 ml) at −76° over a period of 15 min with stirring, and stirring at −76 °C was continued for another 1 h. After addition of triethylamine (5.7 ml) at this temperature, the resulting solution was partitioned between ethyl acetate and water. The organic layer washed successively with a saturated aqueous $NaHCO_3$ solution and water, dried, and evaporated to a residue, which was chromatographed on silica gel (200 g) with 5 : 1 hexane–ethyl acetate to give a syrup of **19** (6.12 g, 82%): R_f 0.35 (5 : 1 hexane–ethyl acetate); ^{1}H-NMR δ=1.80—2.20 (2H, m, H-5), 3.47 (2H, t H-6, $J_{5,6}$=6.0 Hz), 3.71—4.12 (3H, m, H-2,3 and 4), 4.32—4.84 (8H, m, PhC$\underline{H}_2$O×4), 7.30 (20H, s, Ph×4), 9.69 (1H, d, CHO, $J_{1,2}$=2 Hz). As this compound was considerably labile, it was used for the next step without further purification.

8,9,10,12-Tetra-O-*benzyl-2,3,4,5,11-pentadeoxy*-aldehydo-D-lyxo-*6-dodecenose* (**20**) *and Its Ethylene Acetal.* To an ice-cooled solution of **6** (11.3 g, 23.3 mmol) in dry THF (110 ml) was added, under argon, 2 M sodium methylsulfinylmethanide solution prepared *in situ* from NaH (533 mg) and DMSO (11.1 ml). After the solution had been stirred at room temperature for 0.5 h, to the resulting deep red solution was added a solution of **19** (6.12 g, 11.7 mmol) in dry THF (61 ml), and stirring at room temperature was continued for another 0.5 h. The reaction mixture was partitioned between ether and a saturated aqueous NaCl solution. The organic layer was evaporated to a residue, which was chromatographed on silica gel (700 g) with 5 : 1 hexane–ethyl acetate to give the ethylene acetal of **20** as a colorless syrup (7.14 g, 94%): R_f 0.52 (2 : 14 : 1 : 2 benzene–chloroform–ethyl acetate–hexane); $[\alpha]_D^{15}$ +2.5° (*c* 2.0, $CHCl_3$); ^{1}H-NMR δ=3.50 (2H, t, H-12, $J_{11,12}$=6.0 Hz), 3.70—3.95 (4H, m, C$\underline{H}_2$ of ethylene acetal).

Found: C, 77.75; H, 7.76%. Calcd for $C_{42}H_{50}O_6$: C, 77.51; H, 7.74%.

The syrup (6.52 g) was dissolved in 70% aqueous trifluoroacetic acid (32.5 ml) at 5 °C and the solution was kept at this temperature overnight. The resulting solution was partitioned between chloroform and a saturated aqueous $NaHCO_3$ solution, and the organic layer was washed with a saturated aqueous NaCl solution ,dried, and evaporated to a residue. The residue was chromatographed on silica gel (200 g) with 5 : 1 hexane–ethyl acetate to give a syrup of **20** (5.28 g, 87%): R_f 0.59 (2 : 14 : 1 : 2 benzene–chloroform–ethyl acetate–hexane). As this compound **20** was considerably labile, it was used for the next step without further characterization.

1,3,4,5-Tetra-O-*benzyl-2,8,9,10,11,14,16-heptadeoxy*-DL-glycero-D-arabino-*hexadeca-6,12-dienitol* (**21**). A sample of **20** (4.39 g, 7.24 mmol) was treated by the procedure described in the preparation of **9** and then worked up to give a syrup of **21** (3.2 g, 66%): R_f 0.20 (3 : 1 hexane–ethyl acetate); $[\alpha]_D^{16}$ +5.0° (*c* 1.0, $CHCl_3$); ^{1}H-NMR δ=1.18 and 1.20 (3H in total, each d, Me-15, $J_{15,Me}$=6.5 Hz). 3.47 (2H, t, H-1, $J_{1,2}$=6 Hz), 3.50—3.92 (4H, m, H-3,4,5 and 15), 4.12—4.85 (8H, m, PhC$\underline{H}_2$O×4), 5.35—5.90 (4H, m, H-6,7,12 and 13), 7.30 (20H, s, Ph×4).

Found: C, 80.00; H, 8.26%. Calcd for $C_{44}H_{54}O_5$: C, 79.72; H, 8.21%.

3,4,5,15-Tetra-O-*acetyl-1*-O-(t-*butyldimethylsilyl*)-*2,6,7,8,9,10,-11,12,13,14,16-undecadeoxy*-DL-glycero-D-arabino-*hexadecitol* (**23**). A sample of **21** (3.13 g, 4.72 mmol) was treated by the procedure described in the preparation of **11** through **10** and then worked up to give, through **22**, a syrup of **23** (2.17 g, 78%): R_f 0.44 (3 : 1 hexane–ethyl acetate); $[\alpha]_D^{17}$ +30° (*c* 1.0. $CHCl_3$); ^{1}H-NMR δ=0.02 (6H, s, Me_2Si), 0.85 (9H, s, *t*-BuSi), 1.19 (3H, d, Me-15, $J_{15,Me}$=6.0 Hz), 2.02, 2.05 and 2.08 (12H in total, each s, OAc×4), 3.65 (2H, t, H-1, $J_{1,2}$=6 Hz).

Found: C, 61.22; H, 9.26%. Calcd for $C_{30}H_{56}O_9Si$: C, 61.19; H, 9.59%.

Methyl 3,4,5,15-Tetra-O-*acetyl-2,6,7,8,9,10,11,12,13,14,16-undecadeoxy*-DL-glycero-D-arabino-*hexadeconate* (**24**). A sample of **23** (291 mg, 0.50 mmol) was treated by the procedure described in the preparation of **12** and then worked up to give a syrup of **24** (208 mg, 84%): R_f 0.20 (3 : 2 hexane–ethyl acetate); $[\alpha]_D^{15}$ +47° (*c* 1.0. $CHCl_3$); ^{1}H-NMR δ=1.20 (3H, d, Me-15, $J_{15,Me}$=6.0 Hz), 2.00, 2·03 and 2.11 (12H in total, each s, OAc×4), 2.52 (2H, d, H-2, $J_{2,3}$=6.0 Hz), 3.65 (3H, s, COOMe).

Found: C, 59.56; H, 8.20%. Calcd for $C_{25}H_{42}O_{10}$: C, 59.74; H, 8.42%.

Methyl 15-O-*Acetyl-6,7,8,9,10,11,12,13,14,16-decadeoxy-4,5*-O-*isopropylidene*-DL-glycero-D-erythro-(E)-*2-hexadecenonate* (**25**). A sample of **24** (271 mg, 0.54 mmol) was treated by the procedure described in the preparation of **13** and then worked up to give a syrup of **25** (91 mg, 42%): R_f 0.29 (5 : 1 hexane-ethyl acetate); $[\alpha]_D^{15}$ −7.5° (*c* 1.0, $CHCl_3$); UV_{max} (MeOH) 212 nm (ε 10800); ^{1}H-NMR δ=1.20 (3H, d, Me-15, $J_{15,Me}$= 6 Hz), 1.39 and 1.51 (each 3H, each s, Me_2C), 2.04 (3H, s, OAc), 3.77 (3H, s, COOMe), 4.16—4.28 (1H, m, H-5), 4.64 (1H, m, H-4), 4.80—4.95 (1H, m, H-15), 6.09 (1H, dd, H-2, $J_{2,3}$=15.5 Hz, $J_{2,4}$=1.5 Hz), 6.85 (1H, dd, H-3, $J_{2,3}$=15.5 Hz, $J_{3,4}$=6 Hz).

Found: C, 66.25; H, 9.84%. Calcd for $C_{22}H_{38}O_6$: C, 66.30; H, 9.61%.

6,7,8,9,10,11,12,13,14,16-Decadeoxy-4,5-O-*isopropylidene*-D-glycero-D-erythro-(E)-*2-hexadecenono-1,15-lactone* (**26**) *and* L-glycero-D-erythro-*isomer* (**27**). A sample of **25** (97 mg, 0.243 mmol) was treated by the procedure described in the preparation of **14** and **15**, and then worked up to give **26** (37 mg, 47%) and **27** (32 mg, 39%) having the R_f -values of 0.24 and 0.18 (10 : 1 hexane–ethyl acetate) respectively.

26: Needles from ether–hexane; mp 57—58 °C; $[\alpha]_D^{17}$ −60° (*c* 2.0, $CHCl_3$); UV_{max} (MeOH) 212 nm (ε 11700); ^{1}H-NMR δ=1.27 (3H, d, Me-15, $J_{15,Me}$=6 Hz), 1.38 and 1.52 (each 3H, each s, Me_2C), 4.16—4.26 (1H, m, H-5), 4.64 (1H, dt, H-4, $J_{3,4}$=7 Hz, $J_{2,4}$=1 Hz), 5.08 (1H, m, H-15), 6.04 (1H, dd, H-2, $J_{2,3}$=16 Hz, $J_{2,4}$=1 Hz), 6.86 (1H, dd, H-3, $J_{2,3}$= 16 Hz, $J_{3,4}$=7 Hz).

Found: C, 70.42; H, 9.85%. Calcd for $C_{19}H_{32}O_4$: C, 70.33; H, 9.94%.

27: syrup; $[\alpha]_D^{17}$ +25° (*c* 2.0, $CHCl_3$); UV_{max} (MeOH) 212 nm (ε 11700); ^{1}H-NMR δ=1.27 (3H, d, Me-15, $J_{15,Me}$=6 Hz), 1.38 and 1.52 (each 3H, each s, Me_2C), 4.16—4.26 (1H, m, H-5), 4.61 (1H, dt, H-4, $J_{3,4}$=6.5 Hz, $J_{2,4}$=1 Hz), 5.07 (1H, m, H-15), 6.02 (1H, dd, H-2, $J_{2,3}$=16 Hz, $J_{2,4}$=1 Hz), 6.82 (1H, dd, H-3, $J_{2,3}$=16 Hz, $J_{3,4}$=6.5 Hz).

Found: C, 70.58; H, 9.76%. Calcd for $C_{19}H_{32}O_4$: C, 70.33; H, 9.94%.

6,7,8,9,10,11,12,13,14,16-Decadeoxy-D-glycero-D-erythro-(E)-*2-hexadecenono-1,15-lactone* (**28**). A sample of **26** (44.5 mg) was hydrolyzed by the procedure described in the preparation of **16** and then worked up to give needles of **28** (36 mg, 92%): R_f 0.48 (3 : 2 hexane–acetone); mp 118—119 °C; $[\alpha]_D^{16}$ −49° (*c* 2.0, $CHCl_3$); UV_{max} (MeOH) 214 nm (ε 11000).

Found: C, 67.70; H, 9.91%. Calcd for $C_{16}H_{28}O_4$: C, 67.57; H, 9.92%.

6,7,8,9,10,11,12,13,14,16-Decadeoxy-L-glycero-D-erythro-(E)-*2-hexadecenono-1,15-lactone* (**29**). A sample of **27** (35 mg) was hydrolyzed by the procedure described in the preparation of **16** and then worked up to give needles of **29** (29 mg, 93%); R_f 0.49 (3 : 2 hexane–acetone); mp 87—89 °C; $[\alpha]_D^{12}$ +12° (*c* 2.0, $CHCl_3$); UV_{max} (MeOH) 214 nm (ε 10800).

Found: C, 67.64; H, 9.94%. Calcd for $C_{16}H_{28}O_4$: C, 67.57; H, 9.92%.

5-O-*(3-Carboxypropionyl)-4-oxo-4,6,7,8,9,10,11,12,13,14,16-undecadeoxy*-D-glycero-D-glycero-(E)-*2-hexadecenono-1,15-lactone* (**3**). Following the procedure described for **1**, from **28**, a syrup of **3** (9.5 mg, 50% from **28**) was obtained: R_f 0.57 (8 : 1 chloroform–ethanol); $[\alpha]_D^{16}$ −25° (*c* 0.2, MeOH). The UV, IR and ^{1}H-NMR spectra were identical with those of **2**.

Found: C, 62.65; H, 8.04%. Calcd for $C_{20}H_{30}O_7$: C, 62.81; H, 7.91%.

5-O-*(3-Carboxypropionyl)-4-oxo-4,6,7,8,9,10,11,12,13,14,16-undecadeoxy*-L-glycero-D-glycero-(E)-*2-hexadecenono-1,15-lactone* (**4**). Following the procedure described for **1**, from **29**, needles of **4** (4.0 mg, 46% from **29**) were obtained: R_f 0.57 (8 : 1 chloroform–ethanol); $[\alpha]_D^{17}$ +13° (*c* 0.2, MeOH). The UV, IR, and ^{1}H-NMR spectra were identical with those of **1**.

Found: C, 62.74; H, 8.04%. Calcd for $C_{20}H_{30}O_7$: C, 62.81; H, 7.91%.

We are grateful to Prof. S. Umezawa, Institute of Bioorganic Chemistry, and Prof. H. Umezawa, Institute of Microbial Chemistry, for their generous support of our program. We also thank Dr. R. Nagarajan (Lilly Research Laboratories, Indianapolis) for a generous gift of natural A26771B, and Mr. S. Maniwa for his early contributions to this project, and Mr. S. Nakada for elemental analyses.

References

1) K. H. Michel, P. V. Demarco, and R. Nagarajan, *J. Antibiot.*, **30**, 571 (1977).

2) K. Tatsuta, A. Nakagawa, S. Maniwa, and M. Kinoshita, *Tetrahedron Lett.*, **21**, 1479 (1980); K. Tatsuta, A. Nakagawa, S. Maniwa, Y. Amemiya, and M. Kinoshita, *Nippon Kagaku Kaishi*, **1981**, 762.

3) M. Asaoka, N. Yanagida, and H. Takei, *Tetrahedron Lett.*, **21**, 4611 (1980); M. Asaoka, M. Abe, T. Mukuta, and H. Takei, *Chem. Lett.*, **1982**, 215.

4) J. Inanaga, K. Hirata, H. Saeki, T. Katsuki, and M. Yamaguchi, *Bull. Chem. Soc. Jpn.*, **52**, 1989 (1979).

A Novel Synthesis of a Branched-chain Amino Sugar, Methyl 2-Amino-2,3-dideoxy-3-*C*-formyl-α-D-xylofuranoside-3′*R*,5-hemiacetal

Kuniaki TATSUTA,* Satoru MIYASHITA, Kohji AKIMOTO, and Mitsuhiro KINOSHITA

Department of Applied Chemistry, Faculty of Science and Technology, Keio University, Hiyoshi, Kohoku-ku, Yokohama 223

(Received April 14, 1982)

Methyl 2-amino-2*N*,3*O*-(*o*-benzenedisulfonyl)-2-deoxy-α-D-glucopyranoside, which was prepared from methyl 2-amino-2-deoxy-α-D-glucopyranoside and *o*-benzenedisulfonyl dichloride, was treated with sodium methoxide to afford exclusively a branched-chain amino sugar, methyl 2,3-dideoxy-3-*C*-formyl-2-(*o*-sulfobenzenesulfonyl)amino-α-D-xylofuranoside-3′*R*,5-hemiacetal sodium salt (**6**). Some derivatives were synthesized from **6**.

A variety of carbohydrates have been used for stereospecific syntheses of natural products as chiral sources.[1] However, little has been reported using amino sugars,[2] because of their scanty derivatives.

We now report a novel synthesis of branched-chain amino sugar, which may be useful for a suitably functionalized skeleton of alkaloids and β-lactam antibiotics. A noteworthy feature of this synthesis is that it does not require the use of extrinsic protecting groups. The key step was a skeletal rearrangement of the *N*,*O*-*o*-benzenedisulfonyl derivative **3**, where the *o*-benzenedisulfonyl group played simultaneously two roles as an *N*-protecting group and a leaving sulfonyl group. The reagent *o*-benzenedisulfonyl dichloride (**2**) was prepared from dipotassium *o*-benzenedisulfonate and phosphorus pentachloride in an 81% yield.[3] Methyl 2-amino-2-deoxy-α-D-glucopyranoside[4] (**1**) reacted with **2** to give exclusively methyl 2-amino-2*N*,3*O*-(*o*-benzenedisulfonyl)-2-deoxy-α-D-glucopyranoside (**3**) in an 87% yield. Acetylation of **3** gave the corresponding diacetate **4**, which, on longer reaction time, was gradually converted into the triacetate **5**. The ^{1}H-NMR of **5** showed no signal due to the NH group, supporting the *o*-benzenedisulfonimido structure **5**. The ^{1}H-NMR of **3** showed $J_{1,2}$=3.5 Hz, $J_{2,3}$=11.0 Hz and $J_{3,4}$=8.5 Hz, indicating that the chair form existed in the C_1^4 conformation, where the migrating C-4—C-5 bond can be *trans* coplanar to the C-3-benzenesulfonyloxy bond. Therefore, the sequential skeletal rearrangement of **3** seems to be facilitated by the breaking of parallel bonds to give, stereospecifically, a ring-contracted branched-chain furanoside **6**, through the aldehydo structure **6′**.[5] Furthermore, the ring

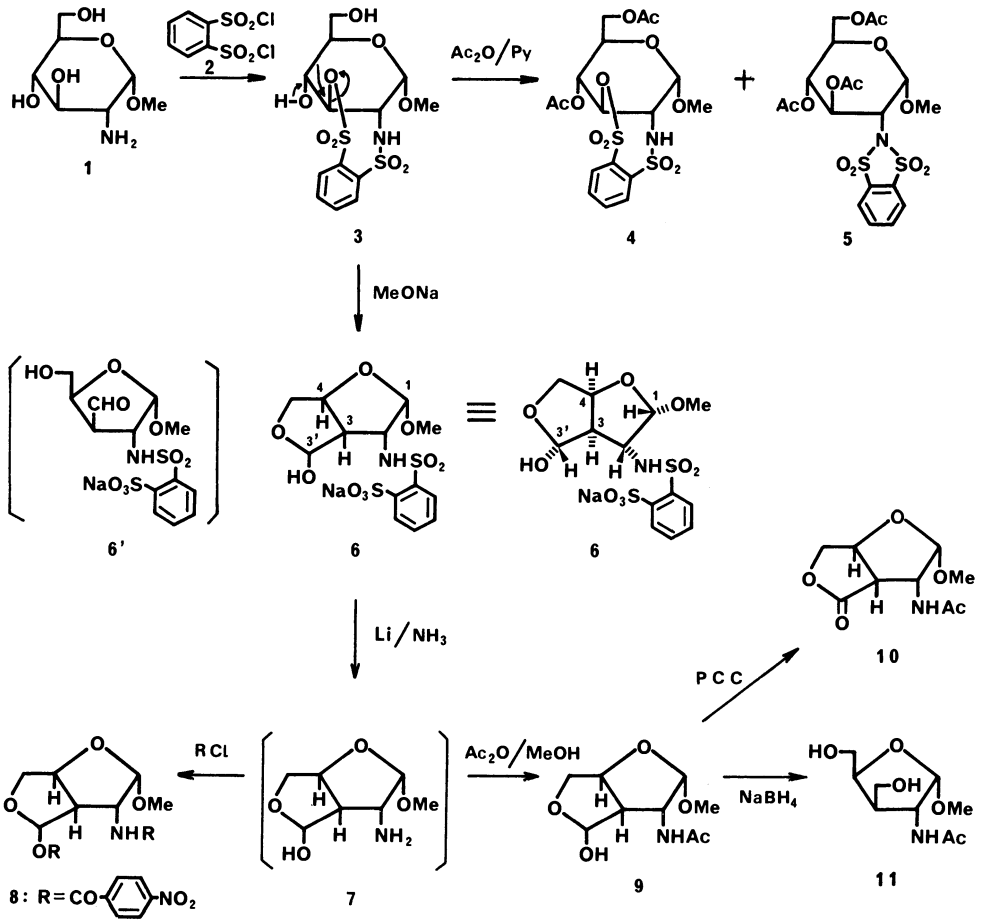

contraction of glycopyranosides through the possibly produced carbenium ion at their C-3 positions has been already reported to give stereospecifically 3-deoxy-3-*C*-formyl-xylo- or lyxo-furanosides.[5,6] When treated with sodium methoxide in methanol, **3** afforded a single product, methyl 2,3-dideoxy-3-*C*-formyl-2-(*o*-sulfobenzenesulfonyl)amino-*α*-D-xylofuranoside-3′*R*,5-hemiacetal sodium salt (**6**) in an 82% yield. Assignment of the absolute structure of **6** was based on the following aspects in addition to the aforesaid reaction mechanism: (i) the production of methyl 3-deoxy-3-*C*-formyl-*α*-D-xylofuranoside-3′,5-hemiacetal, for example, by solvolysis of methyl 3-*O*-(*p*-nitrobenzenesulfonyl)-*α*-D-glucopyranoside as reported by Austin *et al.*,[5] to support the stereochemistry at C-3 and C-4; (ii) the zero coupling constant between H-3 and H-3′ to show the dihedral angle to be approximately 90° supporting the *trans* configuration; (iii) the reasonable structure of the derivatives **7**—**11** as described later on. The characteristic signals (δ 101.72 ppm and 103.86 ppm) in the ^{13}C-NMR of **6** also supported the presence of two anomeric carbons. In the newly produced hemiacetal, however, an interconversion known as a mutarotation was not recognized at all even in H_2O or D_2O, indicating that the hydroxyl group at C-3′ was stereospecifically fixed in (*R*)-configuration.

Treatment of **6** with lithium in liquid ammonia afforded the crude amino furanoside (**7**), which was not purified because of its instability but characterized as the corresponding *p*-nitrobenzoyl derivative (**8**). Selective *N*-acetylation of the crude product **7** also gave crystalline methyl 2-acetamido-2,3-dideoxy-3-*C*-formyl-*α*-D-xylofuranoside-3′*R*,5-hemiacetal (**9**) in a 78% overall yield (from **6**). Compound **9** was oxidized with pyridinium chlorochromate to afford the *γ*-lactone, methyl 2-acetamido-2,3-dideoxy-3-*C*-carboxy-*α*-D-xylofuranoside-3′,5-lactone (**10**) in a 79% yield, and, on the other hand, reduced with sodium borohydride to yield the diol, methyl 2-acetamido-2,3-dideoxy-3-*C*-hydroxymethyl-*α*-D-xylofuranoside (**11**) in an 82% yield.

The application of these branched-chain derivatives to elaboration of *N*-containing natural products is an exciting prospect.

Experimental

Melting points were determined on a micro hot-stage Yanaco MP-S3 and were uncorrected. IR was recorded on a Hitachi Perkin-Elmer 225 spectrometer. ^{1}H-NMR spectra were recorded in $CDCl_3$ with TMS or D_2O with sodium 3-(trimethylsilyl)propionate-2,2,3,3-d_4 as internal standard on a Varian EM-390(90 MHz)or a Bruker WM 250 spectrometer (250 MHz), and ^{13}C-NMR spectra at 25.2 MHz or 62.9 MHz on a Varian XL 100 or a Bruker WM 250 spectrometer with TMS in $CDCl_3$ and dioxane in D_2O as internal standards. Optical rotations were measured on Carl Zeiss photoelectric polarimeter. Silica gel TLC and column chromatography were performed on Merck TLC 60F-254 and Wakogel C-200 or Kieselgel 60, respectively. In general, evaporation was carried out under reduced pressure below 30 °C.

Methyl 2-amino-2-deoxy-*α*-D-glucopyranoside[4b] (**1**) and *o*-benzenedisulfonyl dichloride[3] (**2**: mp 151—152 °C) were prepared according to the published procedures.

*Methyl 2-Amino-2*N,*3*O-*(*o*-benzenedisulfonyl)-2-deoxy-α*-D-*glucopyranoside (3).* To a stirred solution of **2** (10.0 g, 36 mmol) in pyridine (800 ml) was added dropwise a solution of monocarbonate of **1** (8.0 g, 31 mmol) in pyridine (80 ml) at room temperature over a period of 30 min, and stirring at this temperature was continued for another 30 min. After addition of ethanol (4.3 ml), the resulting solution was evaporated and co-evaporated with toluene to give a residue, which was chromatographed on silica gel (450 g) with 3 : 2 benzene–acetone to afford a solid. Recrystallization from ethyl acetate gave needles of **3** (10.7 g, 87%): R_f 0.37 (3 : 2 benzene–acetone); mp 131—132 °C; $[\alpha]_D^{18}$ +149° (*c* 1.0, acetone); IR (KBr): 1425, 1345, 1180, 1160 cm^{-1} (O–SO_2, N–SO_2); ^{1}H-NMR ($CDCl_3$): δ=3.44 (3H, s, OMe), 3.5—4.0 (5H, m, H-2,4,5 and 6), 4.88 (1H, d, H-1, $J_{1,2}$=3.5 Hz), 5.08 (1H, dd, H-3, $J_{2,3}$=11.0 Hz, $J_{3,4}$=8.5 Hz, *vice versa*), ≈5.7 (1H, a broad signal, NH), 7.6—7.9 (2H, m, aromatic), 8.2—8.3 (2H, m, aromatic).

Found: C, 39.84; H, 4.68; N, 3.23%. Calcd for $C_{13}H_{17}NO_9S_2$: C, 39.49; H, 4.33; N, 3.54%.

*Methyl 4,6-Di-*O*-acetyl-2-amino-2*N,*3*O-*(*o*-Benzenedisulfonyl)-2-deoxy-α*-D-*glucopyranoside (4) and Methyl 3,4,6-Tri-*O*-acetyl-2-amino-*N,N′-*(*o*-benzenedisulfonyl)-2-deoxy-α*-D-*glucopyranoside (5).* A solution of **3** (51.9 mg, 0.131 mmol) in pyridine (0.5 ml) was stirred with acetic anhydride (0.074 ml) at room temperature for 13 h. After addition of a few drops of ethanol, the resulting solution was evaporated to a residue, which was chromatographed on silica gel (5 g) with 3 : 1 benzene–ethyl acetate to give **4** (41 mg, 65%) and **5** (8.9 mg, 13%) having the R_f-values of 0.71 and 0.76 (3 : 2 benzene–acetone) respectively.

4: Cubics from ethyl acetate–hexane; mp 198—199 °C; $[\alpha]_D^{17}$ +135° (*c* 1.0, $CHCl_3$); IR (KBr) 1740, 1735, 1730 (OAc), 1425, 1360, 1345, 1185, 1175, 1145 cm^{-1} (O–SO_2, N–SO_2); ^{1}H-NMR ($CDCl_3$): δ=2.10 and 2.16 (each 3H, s, OAc), 3.49 (3H, s, OMe), 3.95—4.05 (2H, m, H-2 and 5), 4.15 (1H, dd, H-6, $J_{5,6}$=2.0 Hz, $J_{6,6'}$=12.5 Hz), 4.30 (1H, dd, H-6′, $J_{5,6'}$=4.5 Hz), 4.93 (1H, d, H-1, $J_{1,2}$=3.5 Hz), 5.21 (2H, m, H-3 and 4), 5.65 (1H, a broad signal, NH), 7.68 and 7.81 (each 1H, m, aromatic), 8.20 and 8.23 (each 1H, m, aromatic).

Found: C, 42.33; H, 4.41; N, 2.65; S. 13.19%. Calcd for $C_{17}H_{21}NO_{11}S_2$: C, 42.59; H, 4.41; N, 2.92; S, 13.37%.

5: Needles from benzene–hexane; mp 178—179 °C; $[\alpha]_D^{18}$ +118° (*c* 1.0, $CHCl_3$); IR (KBr): 1760, 1740, 1725, 1720 (OAc), 1430, 1365, 1190, 1180 cm^{-1} (N–SO_2); ^{1}H-NMR ($CDCl_3$): δ=2.09, 2.22 and 2.38 (each 3H, s, OAc), 3.50 (3H, s, OMe), 4.0—4.6 (3H, m, H-5 and 6), 4.84 (1H, dd, H-2, $J_{1,2}$=3.5 Hz, $J_{2,3}$=12 Hz), 5.02 (1H, d, H-1), 5.23 (1H, t, H-4, $J_{3,4}$=$J_{4,5}$=9.0 Hz), 6.38 (1H, dd, H-3), 7.9—8.1 (2H, m, aromatic), 8.5—8.7 (2H, m, aromatic).

Found: C, 43.65; H, 4.41; N, 2.84; S, 12.10%. Calcd for $C_{19}H_{23}NO_{12}S_2$: C, 43.76; H, 4.45; N, 2.69; S, 12.30%.

*Methyl 2,3-Dideoxy-3-*C*-formyl-2-(*o*-sulfobenzenesulfonyl)amino-α*-D-*xylofuranoside-3′*R,*5-hemiacetal Sodium Salt (6).* To a stirred and ice-cooled solution of **3** (5.76 g, 14.6 mmol) in dry methanol (115 ml) was added sodium methoxide (1.57 g, 29.2 mmol), and the solution was stirred at 50 °C overnight. After further addition of sodium methoxide (2.36 g, 43.7 mmol), stirring at 50 °C was continued for another 1 d. The resulting suspension was neutralized with Amberlite CG-50 (H type), filtered, and the filtrate evaporated to give a residue, which was chromatographed on silica gel (240 g) with 4 : 1 chloroform–methanol to give a solid of **6** (5.0 g, 82%): R_f 0.34 (4 : 1 chloroform–methanol); $[\alpha]_D^{19}$ +5° (*c* 1.0, MeOH); $[\alpha]_{365}^{19}$ −35° (*c* 1.0, MeOH); IR (KBr): 1340, 1170, 1140(N–SO_2, SO_3Na); ^{1}H-NMR (D_2O): δ=2.52 (1H, t, H-3, $J_{2,3}$=$J_{3,4}$≃7.5 Hz, $J_{3,3'}$=0 Hz), 3.08 (3H, s, OMe), 3.62 (1H, dd, H-2,

$J_{1,2}$=4.5 Hz), 3.84 (2H, broad s, H-5), 4.55 (1H, d, H-1), 4.77 (1H, m, H-4), 5.12 (1H, s, H-3′, $J_{3,3'}$=0 Hz), 7.55—7.80 (2H, m, aromatic), 8.05—8.20 (2H, m, aromatic); ^{13}C-NMR (62.9 MHz, D_2O) δ=55.24, 60.30 and 81.73 (C-2,3 and 4, *vice versa*), 55.70 (OMe), 71.61 (C-5), 101.72 and 103.86 (C-1 and 3′, *vice versa*), 130.97, 131.34, 132.94, 135.06, 136.37, and 141.69 (aromatic).

Found: C, 37.05; H, 3.89; N, 3.61%. Calcd for $C_{13}H_{16}NO_9S_2Na$: C, 37.41; H, 3.86; N, 3.36%.

Methyl 2-Amino-2,3-dideoxy-3-C-formyl-α-D-xylofuranoside-3′R,5-hemiacetal (7). A gaseous ammonia was introduced and trapped in a pre-cooled vessel containing **6** (2.17 g, 5.20 mmol) at −60 °C. To the resulting solution (about 60 ml) was added a piece of lithium metal (144 mg) by portions with stirring, and stirring at −50 °C was continued for 1 h. After careful addition of NH_4Cl (1.11 g), the mixture was allowed to evaporate to a residue, which was dried *in vacuo* to afford a crude solid (3.3 g) containing **7** with concomitant salts. As the product **7** was considerably labile, the solid was used for the next step without purification.

Methyl 2,3-Dideoxy-3-C-formyl-2-(p-nitrobenzoyl)amino-3′-C-(p-nitrobenzoyl)-α-D-xylofuranoside-3′R,5-hemiacetal (8). A crude solid of **7** (173 mg) was stirred with *p*-nitrobenzoyl chloride (400 mg) in pyridine (6.0 ml) at 70 °C overnight. After addition of ethanol, the resulting mixture was evaporated to give a residue, which was partitioned between ethyl acetate and a saturated aqueous $NaHCO_3$ solution. The combined organic layers were washed with a saturated aqueous NaCl solution, dried and evaporated to a residue, which was chromatographed on silica gel (15 g) with 4 : 1 benzene–ethyl acetate to afford, after recrystallization from ethyl acetate-hexane, needles of **8** (57 mg, 44% from **6**): mp 208—210 °C; $[\alpha]_D^{21}$ 0° (*c* 1.0, $CHCl_3$); $[\alpha]_{405}^{21}$ −35° (*c* 1.0, $CHCl_3$); IR (KBr): 1730 (ester), 1660 (amide I), 1600 (aromatic), 1525 (amide II), 1345 cm^{-1} (NO_2); ^{1}H-NMR ($CDCl_3$): δ=3.05 (1H, t, H-3, $J_{2,3}$=$J_{3,4}$=7.5 Hz, $J_{3,3'}$=0 Hz), 3.50 (3H, s, OMe), 4.19 (2H, broad s, H-5), 4.56 (1H, dt, H-2, $J_{1,2}$=4.5 Hz, $J_{2,NH}$=7.5 Hz), 5.0 (1H, m, H-4), 5.08 (1H, d, H-1), 6.82 (1H, d, NH), 6.93 (1H, s, H-3′), 7.9—8.4 (8H, m, aromatic); ^{13}C-NMR (25.2 MHz, $CDCl_3$): δ=54.71 (OMe), 56.03 and 56.65 (C-2 and 3), 73.20 (C-5), 80.68 (C-4), 103.21 and 103.41 (C-1 and 3′, *vice versa*), 123.16, 123.41, 128.00, 130.40, 134.88, 138.88, 149.32 and 150.22 (aromatic), 162.92, 164.92 (C=O).

Found: C, 53.12; H, 4.20; N, 8.63%. Calcd for $C_{21}H_{19}N_3O_{10}$: C, 53.28; H, 4.05; N, 8.88%.

Methyl 2-Acetamido-2,3-dideoxy-3-C-formyl-α-D-xylofuranoside-3′-R,5-hemiacetal (9). To a solution of a crude solid of **7** (1.0 g) in methanol (20 ml), were added triethylamine (0.22 ml) and, after 30 min, acetic anhydride (0.45 ml) with stirring at room temperature. After 1.5 h, the resulting solution was evaporated to a residue, which was chromatographed on silica gel (30 g) with 3 : 2 chloroform–acetone followed by recrystallization from acetone–hexane to give needles of **9** (267 mg, 78% from **6**): R_f 0.69 (3 : 1 ethyl acetate–methanol); mp 165 °C, $[\alpha]_D^{16}$ +58° (*c* 1.0, $CHCl_3$); IR (KBr): 1650 (amide I), 1550 cm^{-1} (amide II); ^{1}H-NMR ($CDCl_3$): δ=1.99 (3H, s, NAc), 2.55 (1H, t, H-3, $J_{2,3}$=$J_{3,4}$=7.5 Hz, $J_{3,3'}$=0 Hz); 3.48 (3H, s, OMe), 3.85—4.2 (3H, m, H-5 and OH), 4.21 (1H, dt, H-2, $J_{1,2}$=5.0 Hz, $J_{2,NH}$=7.5 Hz), 4.86 (1H, d, H-1), 4.7—4.9 (1H, m, H-4), 5.79 (1H, d, H-3′, $J_{3',OH}$=3.0 Hz, which collapsed to a singlet on addition of D_2O), 6.14 (1H, d, NH, which disappeared on addition of D_2O).

Found: C, 50.03; H, 6.87; N, 6.24%. Calcd for $C_9H_{15}NO_5$: C, 49.76; H, 6.96; N, 6.45%.

Methyl 2-Acetamido-2,3-dideoxy-3-C-carboxy-α-D-xylofuranoside-3′,5-lactone (10). To a vigorously stirred solution of **9** (1.75 g, 8.06 mmol) in dry $CHCl_3$ (35 ml) was added pyridinium chlorochromate (3.47 g, 16.1 mmol) by portions at room temperature, and stirring at this temperature was continued for 2 d. The turbid supernatant was pipetted off, and the precipitated mass was triturated several times with dichloromethane. The combined supernatants were evaporated to a residue, which was chromatographed on silica gel (150 g) with 2 : 1 chloroform–acetone followed by recrystallization from ethyl acetate-hexane to afford needles of **10** (1.37 g, 79%): R_f 0.29 (2 : 1 chloroform–acetone); mp 192 °C; $[\alpha]_D^{17}$ +100° (*c* 1.0, $CHCl_3$); IR (KBr): 1760 (lactone), 1650 (amide I), 1555 cm^{-1} (amide II); ^{1}H-NMR ($CDCl_3$ with a drop of D_2O): δ=2.02 (3H, s, NAc), 3.10 (1H, dd, H-3, $J_{2,3}$=5.0 Hz, $J_{3,4}$=6.0 Hz), 3.44 (3H, s, OMe), 4.40 (2H, d, H-5, $J_{4,5}$=3.0 Hz), 4.77 (1H, t, H-2, $J_{1,2}$=5.0 Hz), 4.90 (1H, dt, H-4), 5.08 (1H, d, H-1).

Found: C, 50.39; H, 6.14; N, 6.31%. Calcd for $C_9H_{13}NO_5$: C, 50.23; H, 6.09; N, 6.51%.

Methyl 2-Acetamido-2,3-dideoxy-3-C-hydroxymethyl-α-D-xylofuranoside (11). To a stirred solution of **9** (80 mg) in methanol (0.8 ml) was added $NaBH_4$ (28 mg) by portions at room temperature. After 30 min, the resulting solution was neutralized with Amberlite CG-50 (H type), filtered and then evaporated to a residue, which was chromatographed on silica gel (7.5 g) with 15 : 1 chloroform–methanol followed by recrystallization from benzene–hexane to afford needles of **11** (66 mg, 82%): R_f 0.13 (1 : 1 benzene–acetone); mp 113—114°; $[\alpha]_D^{19}$ +100° (*c* 1.0, $CHCl_3$); IR (KBr): —1650, 1610, 1555 cm^{-1} (amide); ^{1}H-NMR ($CDCl_3$): δ=2.04 (3H, s, NAc), 2.34 (1H, m, H-3), 3.43 (3H, s, OMe), 3.7—4.0 (5H, m, H-3′, 5 and OH), 4.20 (1H, dt, H-4, $J_{3,4}$=9.0 Hz, $J_{4,5}$=3.0 Hz), 4.42 (1H, ddd, H-2, $J_{1,2}$=5.0 Hz, $J_{2,NH}$=8.5 Hz, $J_{2,3}$=11.5 Hz), 4.71 (1H, t, OH, $J_{CH_2,OH}$=7.0 Hz, which disappeared on addition of D_2O), 4.95 (1H, d, H-1), 6.23 (1H, broad d, NH, which disappeared on addition of D_2O).

Found: C, 49.40; H, 7.59; N, 6.28%. Calcd for $C_9H_{17}NO_5$: C, 49.31; H, 7.82; N, 6.39%.

We are grateful to Prof. S. Umezawa, Institute of Bioorganic Chemistry, and Prof. H. Umezawa, Institute of Microbial Chemistry, for their generous support of our program. We also thank Mr. S. Nakada for elemental analyses and Miss Y. Suzuki for 250 MHz NMR analyses.

References

1) K. Tatsuta, Y. Amemiya, S. Maniwa, and M.Kinoshita, *Tetrahedron Lett.*, **21**, 2837 (1980); K. Tatsuta, Y. Amemiya, Y. Kanemura, and M. Kinoshita, *ibid.*, **22**, 3997 (1981); S. Hanessian, *Acc. Chem. Res.*, **12**, 159 (1979).

2) S. Kondo, S. Shibahara, S. Takahashi, K. Maeda, H. Umezawa, and M. Ohno, *J. Am. Chem. Soc.*, **93**, 6305 (1971).

3) W. R. H. Hurtley and S. Smiles, *J. Chem. Soc.*, **128**, 1821 (1926).

4) a) S. Umezawa, T. Tsuchiya, and K. Tatsuta, *Bull. Chem. Soc. Jpn.*, **39**, 1235 (1966); b) T. Tsuchiya, T. Usui, T. Kamiya, and S. Umezawa, *Carbohydr. Res.*, **77**, 267 (1979), and references cited therein.

5) P. W. Austin, J. G. Buchanan, and R. M. Saunders, *Chem. Commun.*, **1965**, 146; P. W. Austin, J. G. Buchanan, and R. M. Saunders, *J. Chem. Soc., C*, **1967**, 372.

6) N. M. K. Ng Ying Kin and J. M. Williams, *J. Chem. Soc., D*, **1971**, 1123; J. M. Williams, *Adv. Carbohydr. Chem. Biochem.*, **31**, 9 (1975).

 © 1982 The Chemical Society of Japan Bull. Chem. Soc. Jpn., 55, 3257—3261 (1982)

Syntheses and Properties of Di-, Tri-, and Tetracyclopropyltropylium and Di- and Tri-*t*-butyltropylium Ions

Koichi KOMATSU, Ken'ichi TAKEUCHI, Makoto ARIMA, Yoshinori WAKI, Shuzo SHIRAI, and Kunio OKAMOTO*

Department of Hydrocarbon Chemistry, Faculty of Engineering, Kyoto University, Sakyo-ku, Kyoto 606

(Received April 17, 1982)

The polysubstituted tropylium ions having cyclopropyl or *t*-butyl groups at the ring positions with the least steric hindrance, *i.e.* 1,3- and 1,4-dicyclopropyltropylium, 1,3- and 1,4-di-*t*-butyltropylium, 1,3,5-tricyclcpropyl- and 1,3,5-tri-*t*-butyltropylium and 1,2,4,6-tetracyclopropyltropylium ions (**4**), were synthesized, and their properties were compared with the known monosubstituted and unsubstituted cations. The ^{1}H and ^{13}C NMR spectra for the cyclopropyl derivatives and the ^{13}C NMR spectra for the *t*-butyl derivatives exhibited a gradual upfield shift for the seven-membered ring signals upon consecutive substitution. Accordingly, for the *t*-butyl derivatives, the pK_{R^+} values were found to linearly increase upon introduction of each substuent; for the cyclopropyl derivatives, a larger extent of the pK_{R^+} increase was observed with each substitution, and the pK_{R^+} of the tetrasubstituted derivative **4** amounted to 9.10 (50% aq MeCN, 25 °C), the highest value presently known for the hydrocarbon cations having the tropylium unit, although the cumulative substituent effect deviated from the linear additivity correlation as the substituent number increased. The substituent effects upon the reduction potential and the CT transition energy (pyrene as a donor) were also examined and shown to have the same tendency in general.

The stabilization of the carbocation by the cyclopropyl (c-Pr) group is now widely recognized.[1] Especially for the tropylium ion as the representative Hückel aromatic cation, our previous study on pK_{R^+} and one-electron reducibility indicated that the σ-conjugative stabilization by the c-Pr group is more than twice as effective as the stabilization by the *t*-butyl (*t*-Bu) group with its purely inductive electron donation, while the π-conjugative stabilization of the phenyl group was no more observable owing to the *ortho*-hydrogen repulsion.[2]

On the other hand, the detailed study on the reducibility of a series of polymethyltropylium ions revealed that the additivity of the substituent effect upon cation stability holds when no severe steric congestion is present around the tropylium ring, *i.e.* when the number of substituents does not exceed more than five.[3] Thus, we synthesized the tropylium ions substituted with two to four c-Pr groups and with two and three *t*-Bu groups at the ring positions where the effect of steric repulsion is minimized, and examined the additivity of the electronic effect of these substituents upon cation stability.

Syntheses. The 1,3- and 1,4-disubstituted (**2**) and 1,3,5-trisubstituted tropylium ions (**3**) each having the c-Pr (**2a**, **2b**, and **3a**) or *t*-Bu groups (**2c**, **2d**, and **3b**[4]) were synthesized as shown in Scheme 1, by the use of the conventional method involving the CuBr-catalyzed ring expansion of the substituted benzenes with diazomethane, followed by hydride abstraction.

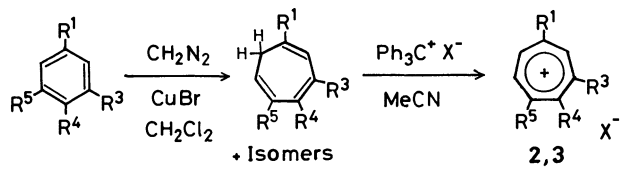

	R^1	R^3	R^4	R^5	X
2a·X⁻	c-Pr	c-Pr	H	H	BF_4
2b·X⁻	c-Pr	H	c-Pr	H	BF_4
2c·X⁻	*t*-Bu	*t*-Bu	H	H	ClO_4
2d·X⁻	*t*-Bu	H	*t*-Bu	H	ClO_4
3a·X⁻	c-Pr	c-Pr	H	c-Pr	BF_4
3b·X⁻	*t*-Bu	*t*-Bu	H	*t*-Bu	ClO_4

Scheme 1.

For the synthesis of the tetracyclopropyltropylium ion (**4**), we adopted a cation-anion combination reaction of the trisubstituted cation **3a** with cyclopropyllithium at −70 °C as shown in Scheme 2. 1,3,5,7-Tetracyclopropylcycloheptatriene (**5a**), which was isolated in 41% yield, was then treated with the trityl cation to give the 1,2,4,6-tetracyclopropyltropylium ion (**4**) in 85% yield. The 1,3,6,7-tetrasubstituted derivative **5b** with higher steric hindrance was isolated only in 8% yield.

Properties. The physical and spectral properties of the newly synthesized salts of the cations **2a—d**, **3a**, **b**, and **4** are shown in Table 1, together with the data for the unsubstituted (**6**) and monosubstituted cations (R–$C_7H_6^+$: R=c-Pr (**1a**), *t*-Bu (**1b**)) for the purpose of comparison.

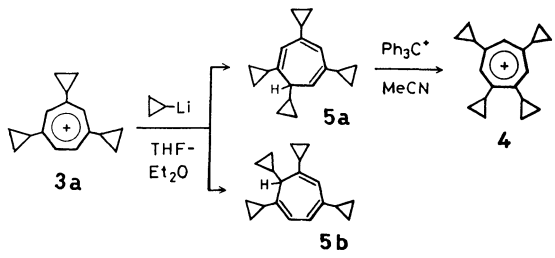

Scheme 2.

Among these data, it is to be noted that in the ^{1}H NMR spectra for a series of c-Pr-substituted cations the signal for the tropylium-ring protons, which appears as a somewhat broadened singlet except for the cation **4**, is gradually shifted upfield with higher substitution. This upfield shift is supposed to reflect mostly the electronic effect of the increasing number of c-Pr substituents delocalizing the positive charge away from the cationic ring, in addition to the anisotropic ring-current effect of the c-Pr ring.[5] A similar general trend

Table 1. Physical and spectral properties of the salts of unsubstituted (**6**) and substituted tropylium ions (**1**, **2**, **3**, and **4**)

Tropylium salt	Mp (decomp) θ_m/°C	UV (MeCN) λ_{max}/nm (log ε)	^{1}H NMR (CD_3CN) δ from Me_4Si
6·BF_4^-	≈200	219 (4.61)	9 29 (s)
		275 (3.65)	
c-Pr-substituted cations			
1a·BF_4^-[a]	58.2—60.0	247 (4.52)	8.83 (s, 6H, $-CH^+-$)
		328 (4.11)	2.85—2.45 (m, 1H, c-Pr-H_α)
			2.05—1.41 (m, 4H, c-Pr-H_β)
2a·BF_4^-	≈185[b]	230 (4.16)	8.38 (s, 5H, $-CH^+-$)
		274 (4.38)	2.76—2.30 (m, 2H, c-Pr-H_α)
		329 (4.11)	2.05—1.30 (m, 8H, c-Pr-H_β)
2b·BF_4^-	156.3—156.6	244 (4.49)	8.37 (s, 5H, $-CH^+-$)
		348 (4.35)	2.66—2.23 (m, 2H, c-Pr-H_α)
			1.90—1.21 (m, 8H, c-Pr-H_β)
3a·BF_4^-	189.5—191.0	279 (4.55)	7.96 (s, 4H, $-CH^+-$)
		343 (4.24)	2.68—2.16 (m, 3H, c-Pr-H_α)
			1.67—1.15 (m, 12H, c-Pr-H_β)
4·ClO_4^-	99.5—100.0	285 (4.81)	7.73 (d, J=1.3 Hz, 2H, $-CH^+-$)
		342 (4.38)	7.64 (t, 1H, $-CH^+-$)
			2.86—2.20 (m, 4H, c-Pr-H_α)
			1.63—1.04 (m, 16H, c-Pr-H_β)
t-Bu-substituted cations			
1b·ClO_4^-[c]	179.0—180.0	223 (4.50)[d]	9.4—9.1 (m, 6H, $-CH^+-$)[e]
		293 (3.69)	1.70 (s, 9H, *t*-Bu)
2c·ClO_4^-	204.0	234 (4.50)[d]	9.6—8.6 (m, 5H, $-CH^+-$)[e]
		291 (3.80)	1.66 (s, 18H, *t*-Bu)
2d·ClO_4^-	172.0—173.0	227 (4.60)[d]	9.3—8.6 (m, 5H, $-CH^+-$)[e]
		305 (3.90)	1.66 (s, 18H, *t*-Bu)
3b·ClO_4^-	195.5—196.0	240 (4.61)[d]	9.35 (s, 2H, $-CH^+-$)[e]
		299 (3.90)	9.13 (s, 2H, $-CH^+-$)
		307sh (3.84)	1.69 (s, 27H, *t*-Bu)

a) Ref. 2b. b) Charring without showing a clear mp. c) Ref. 2a. d) In 10% HCl. e) In CF_3CO_2H.

Table 2. ^{13}C NMR spectral data for the unsubstituted (**6**) and substituted tropylium ions (**1**, **2**, **3**, and **4**)

Cation[a]	^{13}C NMR chemical shift, δ (CD_3CN)					
	C-1	C-2	C-3	C-4	Substituent C-α	C-β
6	156.2	—	—	—	—	—
c-Pr-substituted cations						
1a	182.7	152.3[b]	152.5[b]	151.1	25.1	21.5
2a	147.6	177.3	147.5[b]	149.2[b]	24.5	19.5
2b	149.8	147.0[b]	177.3	148.6[b]	23.5	19.4
3a	173.4	143.9[b]	172.6	145.3[b]	24.3[c]	18.2[c]
					23.3[d]	17.6[d]
4	140.9	171.8	142.0	169.2	23.7[e]	17.5[e]
					21.6[f]	12.7[f]
t-Bu-substituted cations						
1b	184.0	153.9	154.1	154.3	42.2	31.5
2c	150.1	181.2	152.1	152.4	42.7	31.5
2d	152.3	151.9	181.4	151.3	41.5	31.2
3b	179.2	148.4	178.8	150.5	43.3[c]	31.7[c]
					42.1[d]	31.4[d]

a) The numbering systems are as follows:

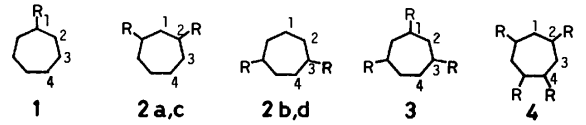

1 **2a,c** **2b,d** **3** **4**

b) These values may be interchangeable. c) At C-1. d) At C-3. e) At C-2. f) At C-4.

Table 3. Data of pK_{R^+}, reduction potential, and CT band with pyrene as a donor, for the unsubstituted (**6**) and substituted tropylium ions (**1**, **2**, **3**, and **4**)

Cation	pK_{R^+} [a]	Red potential *vs.* Ag/Ag$^+$ [b] / V	CT band [c] λ_{max}/nm	CT band [c] $\lambda/10^4$ cm^{-1}
6	3.88	−0.51	540[d]	1.85
c-Pr-substituted cations				
1a	5.76	−0.64	526[e]	1.90
2a	7.56	−0.76	500—510	2.00—1.96
2b	7.63	−0.76	495—505	2.02—1.98
3a	8.72	−0.86	485—495	2.06—2.02
4	9.10	−0.94	476—490	2.10—2.04
t-Bu-substituted cations				
1b	4.57	−0.61	508[d]	1.97
2c	4.90	−0.70	503	1.99
2d	5.42	−0.72	490—510	2.04—1.96
3b	6.26	−0.84	480—500	2.08—2.00

a) Determined spectrophotometrically in H_2O–MeCN (1 : 1 by volume); Ref. 7. b) Cathodic peak potential determined with CV in MeCN at a scan rate of 0.1 V/s; cation 1 mM; supporting electrolyte (Bu_4NClO_4), 0.1 M; Ref. 7. c) Observed in 1,2-dichloroethane; cation (acceptor), 1 mM; pyrene (donor), 0.1 M; Ref. 7. d) Ref. 2a. e) Ref. 2b.

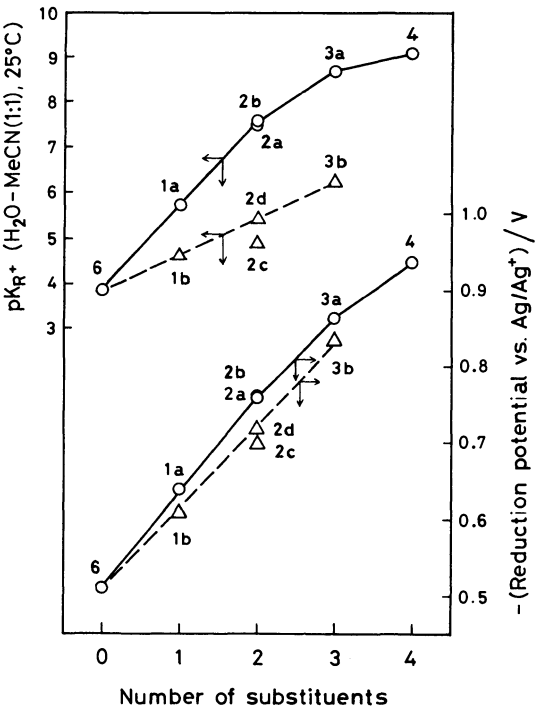

Fig. 1. Correlation of the pK_{R^+} and reduction potential with the number of substituent (○, c-Pr; △, *t*-Bu).

is observed for the ^{13}C NMR data shown in Table 2.

Compared with the case of c-Pr-substituted cations, the aromatic-ring proton signals in the ^1H NMR spectra of *t*-Bu derivatives do not exhibit any systematic upfield shift upon consecutive substitution, presumably due to the considerable steric compression effect of the bulky *t*-Bu groups. In the ^{13}C NMR spectra, however, the gradual upfield shift is again clearly observed for the ring-carbon signals, though the increment of the upfield shift upon each substitution is apparently smaller than that observed for a series of c-Pr derivatives.†

Based on these results of NMR measurements, it is now of particular interest to examine the additivity of the substituent effects of the c-Pr and *t*-Bu groups upon the cation stability expressed by the pK_{R^+} value. As shown in Table 3, the pK_{R^+} value increases upon consecutive c-Pr substitution and reaches the maximum value of 9.10 for the tetra-c-Pr derivative **4**. To our knowledge this is the highest pK_{R^+} value reported for the hydrocarbon cations having the tropylium unit.[6]

Also included in Table 3 are the data of reduction potentials determined by cyclic voltammetry (CV) and of charge-transfer (CT) band observed with pyrene as a π-donor. In our previous study,[2a,2b,3] the CT transition energy of various mono- and polysubstituted tropylium ions with pyrene as a donor was shown to exhibit a linear correlation with the one-electron reducibility of these cations in solution. For the present series of cations, a similar correlation seems to hold in general. However, for the highly substituted derivatives, the CT absorption bands become much too weak to allow the accurate determination of the absorption maxima, presumably due to the steric congestion between the donor and acceptor.

Thus, the more precisely measurable values of pK_{R^+} (limit of precision, $\pm$0.05) and reduction potential ($\pm$0.005 V) were plotted against the number of substituents to give the correlation shown in Fig. 1. From this plot is observed that, in contrast to the linear correlations obtained for the *t*-Bu derivatives, the pK_{R^+} of the c-Pr derivatives apparently deviates from the linear correlation line as the substituent number increases. This result seems to indicate that, for an aromatic cation like the tropylium ion, the additivity towards the cation stability holds for the substituents with the purely inductive electronic effect, whereas some saturation phenomenon exists for the cumulative effect of σ-conjugative substituents.†† The detailed discussion on the correlation between the pK_{R^+} and other indices corresponding to the electron affinity for a wider variety of stable cations will be made in a separate publication.[7]

† For the purpose of comparison, when we simply average the chemical shift values for the ring-carbons carrying no substituent, the following δ-values are obtained: **6**, 156.2; **1a**, 152.0; **2a**, 148.2; **2b**, 148.2; **3a**, 144.6; **4**, 141.6; **1b**, 154.1; **2c**, 151.8; **2d**, 151.7; **3b**, 149.5.

†† This phenomenon would be attributed to the decrease in population of the c-Pr groups taking the bisected conformation as the cationic ring becomes less electron-demanding with higher substitution. Especially in the case of the cation **4**, the parallel conformation rather than the bisected one may be sterically favored for the two neighboring c-Pr groups at C-1 and C-2. However, these groups are apparently not fixed in such geometry, as judged from the small chemical-shift difference (*ca.* 0.1 ppm) between H-3,7 and H-5; the c-Pr groups in hexacyclopropylbenzene, for example, have been reported to be freely rotating in solution though fixed in the parallel conformation in the crystalline state.[8]

Experimental

General. Melting points are uncorrected. The elemental analyses were performed by the Microanalytical Center, Kyoto University, Kyoto. The IR and UV spectra were recorded on Hitachi 215 snd Hitachi 200-10 spectrometers, respectively. The ^{1}H NMR spectra were taken with a Hitachi R-24 spectrometer with Me_4Si as the internal standard. The ^{13}C NMR spectra were recorded on a JEOL FX-100 spectrometer operated in the Fourier transform mode.

Materials. The di- and tricyclopropylbenzenes were prepared from the corresponding di- and trivinylbenzenes following the method of Effenberger and Kurtz.[9] The di- and tri-*t*-butylbenzenes were prepared by the Friedel-Crafts *t*-butylation of benzene with *t*-butyl chloride catalyzed by $FeCl_3$ or $AlCl_3$. Other materials used were of the reagent grade quality unless otherwise noted.

*1,3-Dicyclopropyltropylium Tetrafluoroborate (**2a**·BF_4^-).* A 0.43 M solution of diazomethane in CH_2Cl_2 (50 ml), prepared from *N*-methyl-*N*-nitrosourea,[10] was added dropwise to a stirred solution of 1,3-dicyclopropylbenzene (1.87 g; 11.8 mmol) in CH_2Cl_2 (10 ml) in the presence of CuBr (0.55 g; 3.9 mmol) at 40 °C over 30 min. After refluxing for 20 min, the mixture was filtered and evaporated to give 2.20 g of the crude product, which was found to contain about 20% of olefinic compounds by the ^{1}H NMR analysis. The hydride abstraction of the crude product with trityl tetrafluoroborate (1.00 g; 3.03 mmol) in MeCN (3 ml) and CH_2Cl_2 (3 ml), followed by precipitation with dry ether and recrystallization from MeCN, afforded 0.374 g (12.3% yield based on dicyclopropylbenzene) of the product, the ^{13}C NMR spectrum of which indicated the formation of both the 1,3- (**2a**) and 1,4-dicyclopropyltropylium (**2b**) ions in a ratio of 2 : 1. The fractional recrystallization from MeCN repeated twice yielded 0.050 g of **2a**·BF_4^- as white crystals. Found: C, 60.47; H, 6.01%. Calcd for $C_{13}H_{15}BF_4$: C, 60.50; H, 5.86%.

*1,4-Dicyclopropyltropylium Tetrafluoroborate (**2b**·BF_4^-).* In exctly the same way, 1,4-dicyclopropylbenzene was allowed to react with two-fold excess of diazomethane in CH_2Cl_2. The subsequent hydride abstraction and recrystallization from MeCN afforded **2b**·BF_4^- as white crystals in 10.6% yield. Found: C, 60.34; H, 5.77%. Calcd for $C_{13}H_{15}BF_4$: C, 60.50; H, 5.86%.

*1,3,5-Tricyclopropyltropylium Tetrafluoroborate (**3a**·BF_4^-).* Similarly, **3a**·BF_4^- was synthesized from 1,3,5-tricyclopropylbenzene in 10.0% yield as white crystals. Found: C, 64.73%; H, 6.57%. Calcd for $C_{16}H_{19}BF_4$: C, 64.46; H, 6.42%.

*1,3-Di-t-butyltropylium Perchlorate (**2c**·ClO_4^-).* In the same way, **2c**·ClO_4^- was synthesized through the ring-expansion of 1,3-di-*t*-butylbenzene with diazeomthane in heptane, followed by hydride abstraction with trityl perchlorate in 7.0% yield as white crystals. Found: C, 59.32; H, 7.72%. Calcd for $C_{15}H_{23}ClO_4$: C, 59.50; H, 7.66%.

*1,4-Di-t-butyltropylium Perchlorate (**2d**·ClO_4^-).* Similarly, **2d**·ClO_4^- was synthesized from 1,4-di-*t*-butylbenzene in 9.2% yield as white crystals. Found: C, 59.32; H, 7.72%. Calcd for $C_{15}H_{23}ClO_4$: C, 59.50; H, 7.66%.

*1,3,5-Tri-t-butyltropylium Perchlorate (**3b**·ClO_4^-).* Similarly, **3b**·ClO_4^- was synthesized from 1,3,5-tri-*t*-butylbenzene in 4.5% yield as white crystals. Found: C, 63.32; H, 8.72%. Calcd for $C_{19}H_{31}ClO_4$: C, 63.59; H, 8.71%.

*1,2,4,6-Tetracyclopropyltropylium Perchlorate (**4**·ClO_4^-).* An ethereal solution (5 ml) of 0.48 M cyclopropyllithium (2.4 mmol), prepared from cyclopropyl bromide and Li, was added dropwise to a stirred suspension of **3a**·BF_4^- (0.309 g; 1.04 mmol) in dry THF (4 ml) cooled at −70 °C over 5 min. After stirring at −70 °C for 10 min, the temperature was slowly raised to room temperature over 1 h. The mixture was hydrolyzed and worked up in the usual manner to give 0.30 g of the crude product, which exhibited three main spots at R_f 0.60, 0.49, and 0.34 on an analytical TLC plate developed with hexane–benzene (9 : 1) over SiO_2 (Merck, GF_{254}). From the fraction with R_f 0.60, we isolated, by the use of preparative TLC over SiO_2 (Merck, F_{254}, pre-coated), 1,3,5,7-tetracyclopropylcycloheptatriene (**5a**) (0.107 g; 40.9%) as a colorless oil: IR (neat) ν 3080 m, 3005 m, 1621 m, 1460 w, 1425 w, 1018 m cm^{-1}; ^{1}H NMR (CCl_4) δ 6.02 (br s, 1H, H-4), 5.45 (br s, 1H, H-2), 4.91 (br d, 1H, H-6), 1.93—0.95 (m, 5H, H-7+c-Pr-H$_\alpha$), 0.90—0.20 (m, 16H, c-Pr-H$_\beta$); ^{13}C NMR ($CDCl_3$) δ 144.7, 143.1, 136.8 (s×3, C-1,3,5), 123.7, 120.0, 117.5 (d×3, C-2,4,6), 47.2 (d, C-7), 18.2, 15.6, 14.9, 11.7 (d×4, c-Pr-C$_\alpha$), 8.6, 7.6, 7.1, 6.4, 5.4, 5.3, 4.0, 3.9 (t×8, c-Pr-C$_\beta$). From the fraction with R_f 0.49, we also obtained the colorless oil (0.0215 g; 8.2%), which was assigned as 1,3,6,7-tetracyclopropylcycloheptatriene (**5b**) on the basis of the following spectral data; IR (CCl_4) ν 3085 m, 3005 m, 1620 w, 1456 w, 1426 w, 1018 m cm^{-1}; ^{1}H NMR (CCl_4) δ 6.12 (br d, 1H, H-4), 5.82 (br d, 1H, H-5), 5.55 (br s, 1H, H-2), 2.00—1.10 (br m, 5H, H-7+c-Pr-H$_\alpha$), 1.00—0.30 (br m, 16H, c-Pr-H$_\beta$); ^{13}C NMR ($CDCl_3$) δ 141.4, 140.3. 140.0 (s×3, C-1,3,6), 122.1, 119.1, 118.5 (d×3, C-2,4,5), 50.4 (d, C-7), 19.5, 19.2, 18.1, 13.7 (d×4, c-Pr-C$_\alpha$), 8.7—3.8 (partially overlapped eight peaks, c-Pr-C$_\beta$).

To a stirred solution of **5a** (0.0965 g; 0.383 mmol) in MeCN (1 ml) was added trityl perchlorate (0.0800 g; 0.234 mmol) in one portion. After stirring at room temperature for 3 h, dry ether (20 ml) was added to cause the formation of precipitates, which were then filtered and purified by reprecipitation from MeCN–ether to give **4**·ClO_4^- (0.0684 g; 83.4%) as off-white crystals. Found: C, 64.24; H, 6.69%. Calcd for $C_{19}H_{23}ClO_4$: C, 65.04; H, 6.61%.

pK_{R^+} Measurements. The pK_{R^+} values were determined in H_2O–MeCN (1 : 1 by volume) at 25 °C according to the spectrophotometric method described in our previous paper in detail.[11] The buffer solutions were made up by mixing 0.1 M citric acid and 0.1 M Na_2HPO_4 in H_2O–MeCN (1 : 1) (pH 3.0—8.2), and 0.01 M Na_2HPO_4 and 0.01 M Na_3PO_4, with 0.02 M Na_2CO_3 added in H_2O–MeCN (1 : 1) (pH 8.0—11.0). The pH values were read on a Horiba H pH meter calibrated with standard buffers before use.

Cyclic Voltammetry. The measurements were carried out in MeCN by the instruments and method previously reported.[11] As the reduction potential, we took the value of the cathodic peak potential of the voltammogram obtained at the scan rate of 0.1 V/s. The potential was determined against the reference electrode, Ag/0.01 M $AgNO_3$ with 0.1 M Bu_4NClO_4 in MeCN, and calibrated with $E_{1/2}$ of ferrocene added as an internal standard immediately after each measurement.

Charge-transfer Spectra. The spectra were taken in exactly the same way as previously reported,[2b] for the solution of 1×10^{-3} M cation (acceptor) and 0.1 M pyrene (donor) in 1,2-dichloroethane.

References

1) For reviews, see H. G. Richey, Jr. (Chap. 25), and K. B. Wiberg, B. A. Hess, Jr., and A. J. Ashe, III (Chap. 26), "Carbonium Ions," ed by G. A. Olah and P. v. R. Schleyer, Wiley-Interscience, New York (1972), Vol. III.

2) a) K. Okamoto, K. Komatsu, O. Murai, O. Sakaguchi, and Y. Matsui, *Bull. Chem. Soc. Jpn.*, **46**, 1785 (1973); b) K.

Takeuchi, K. Komatsu, K. Yasuda, F. Mikuchi, and K. Okamoto, *J. Chem. Soc., Perkin Trans. 2*, **1979**, 1005; c) The pK_R^+ values measured in 23% EtOH for $R-C_7H_6^+$ were as follows: R=H, 4.3;[2a] R=c-Pr, 6.8 (K. Komatsu, K. Yasuda, and K. Okamoto; unpublished results); R=*t*-Bu, 5.0;[2a] R=Ph, 4.1.[2a]

3) K. Takeuchi, T. Kurosaki, Y. Yokomichi, Y. Kimura, Y. Kubota, H. Fujimoto, and K. Okamoto, *J. Chem. Soc., Perkin Trans. 2*, **1981**, 670.

4) The synthesis of the tetrafluoroborate salt of **3b** has already been reported: G. Vincow, M. L. Morrell, F. R. Hunter, and H. J. Dauben, Jr., *J. Chem. Phys.*, **48**, 2876 (1968).

5) A similar but smaller extent of upfield shift is observed for aromatic protons in a series of c-Pr-substituted benzenes, and has been ascribed to the ring current effect of the c-Pr group: P. Fischer, W. Kurtz, and F. Effenberger, *Chem. Ber.*, **106**, 549 (1973).

6) The highest pK_R^+ value so far reported for the hydrocarbon cations containing the tropylium ring is 8.7 determined for the cyclohept[*a*]acenaphthylenium ion in 20% aq MeCN: K. Yamamoto and I. Murata, *Angew. Chem.*, **88**, 262 (1976). The same value has also been observed for the 5,5a,6,11,11a,12-hexahydro-5,12-(1,2-benzeno)-6,11-(1,2-tropylio)naphthacene cation in 50% aq MeCN: K. Komatsu, K. Takahashi, and K. Okamoto, *Tetrahedron Lett.*, **1979**, 4747.

7) K. Okamoto, K. Takeuchi, K. Komatsu, Y. Kubota, R. Ohara, M. Arima, Y. Waki, and S. Shirai, *J. Chem. Soc., Perkin Trans. 2*, submitted for publication.

8) a) V. Usieli, R. Victor, and S. Sarel, *Tetrahedron Lett.*, **1976**, 2705; b) I. Bar, J. Bernstein, and A. Christensen, *Tetrahedron*, **33**, 3177 (1977).

9) F. Effenberger and W. Kurtz, *Chem. Ber.*, **106**, 511 (1973).

10) F. Arndt, *Org. Synth.*, Coll. Vol. II, 461 (1943).

11) K. Komatsu, K. Masumoto, Y. Waki, and K. Okamoto, *Bull. Chem. Soc. Jpn.*, **55**, 2470 (1982).

Acetolysis of [4.2.2]Propellan-7-ylmethyl Tosylates

Yoshito Tobe,* Tetsuo Yonezawa, Kiyomi Kakiuchi, and Yoshinobu Odaira
Department of Petroleum Chemistry, Faculty of Engineering, Osaka University, Suita, Osaka 565
(Received April 21, 1982)

The acetolysis rates and products of [4.2.2]propellan-7-ylmethyl tosylates were determined in order to clarify the effect of the central and external cyclobutane bonds on the modes of the ring expansion of the cyclobutylmethyl moiety. Since the products obtained from the *endo* tosylate were the olefin and the acetate having 1,7-tetramethylenenorbornane skeleton, it is deduced that the ring expansion occurs selectively to afford [4.3.2]propellan-7-yl cation which is stabilized by the external cyclobutane bond. In contrast, the *exo* tosylate gave the products derived from both [4.3.2]propellan-7-yl and -8-yl cations which are subject to the participation of the external and central cyclobutane bonds, respectively.

It has been documented that the solvolysis of cyclobutylmethyl derivatives proceeds with σ participation of the cyclobutane bond.[1] Since the ring expansion occurs so as to stabilize the ring-expanded cation, the specificity in the modes of the ring expansion is affected markedly by the geometry of the cyclobutylmethyl moieties, especially, involved in polycarbocyclic systems.[2] We have been interested in the solvolytic rearrangements of the propellane derivatives having one or two cyclobutane rings, [*m.n*.2]propellanes ($m \geq 3$, $n \geq 2$), such as [4.3.2]-propellan-7-yl tosylates (**1a**) and (**2a**),[3a,b] [3.3.2]-propellan-9-yl tosylate (**3**),[3c] [4.2.2]propellan-7-yl derivatives (**4a** and **5a**).[3d] In the above studies, it has been pointed out that the propellane derivatives undergo solvolysis with participation of the central (a) or external (b) bond of the cyclobutane ring depending on the ring size of the propellane framework and the stereochemistry of the leaving group. In this connection, we wish to report here the acetolysis of [4.2.2]propellan-7-ylmethyl tosylates (**4b** and **5b**) and emphasize that the central (a) and external (b) cyclobutane bonds which are remote from the cation center play an important role in the ring expansion of the cyclobutylmethyl moiety by 1,2-shift of the bond (c) or (d).

The tosylates **4b** and **5b** were prepared from the alcohols **4c** and **5c** which were obtained by the lithium aluminium hydride reduction of the corresponding methyl esters **4d** and **5d**.[4] In order to establish the *exo*/*endo* stereochemistry of **4b**—**d** and **5b**—**d** unambiguously, the unsaturated esters **6** and **7** were prepared by the ring contraction of the ketone **8**[5] in the manner similar to that of preparation of **4d** and **5d**.[4] The stereochemical assignment of **6** and **7** was based on the ^{1}H NMR spectra and the lanthanoide-induced shift in the ^{1}H NMR as follows: whereas the vinyl protons of **6** appeared as overlapping doublets (J=2 Hz) at δ 6.22 ($\Delta\delta$=0), those of **7** appeared at δ 6.03 (d, J=2 Hz) and 6.21 (d, J=2 Hz) ($\Delta\delta$=0.18). Moreover, in the lanthanoide-shifted NMR using Eu(dpm)$_3$, the S values[6] for the vinyl protons of **6** were 2.9 and 2.0 while those of **7** were 6.5 and 2.5. These results indicate clearly that the methoxycarbonyl group of **7** is located at exo direction which is nearer to the vinyl group. It is therefore deduced that **6** and **7** are the *endo* and *exo* isomers, respectively. Finally, catalytic hydrogenation of **6** and **7** with Pd/C gave the esters **4d** and **5d**, respectively, thus establishing the stereochemistry of **4b**—**d** and **5b**—**d**.

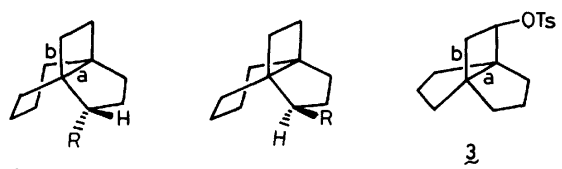

1a R = OTs
1b R = OAc
1c R = OH

2a R = OTs
2b R = OAc
2c R = OH

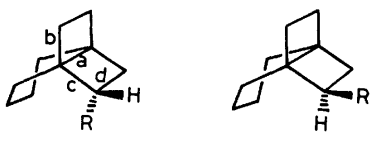

4a R = OTs
4b R = CH_2OTs
4c R = CH_2OH
4d R = CO_2Me
4e R = CH_2OAc

5a R = ODNB
5b R = CH_2OTs
5c R = CH_2OH
5d R = CO_2Me
5e R = CH_2OAc

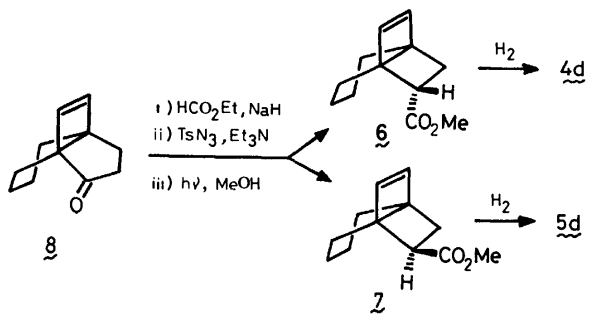

The kinetic data for the acetolysis of **4b** and **5b** were summarized in Table 1. As shown in Table 1, the *endo* tosylate **4b** undergoes acetolysis at a rate slightly greater than that of the *exo* one **5b**, but the difference is rather small.

The acetolysis products from **4b** and **5b** after 10 half-lives were separated by column chromatography on silica gel and the subsequent preparative GLC separation. The combined yields of the products were almost quantitative and the distribution of the products were listed in Table 2 together with that from [4.3.2]-propellan-7-yl tosylates (**1a** and **2a**). The structures of the acetates **1b** and **2b** were established by the identity in GLC, ^{1}H NMR, and IR spectra with authentic

Table 1. Kinetic data for acetolysis of **4b** and **5b**

Tosylate	Temp °C	k[a] s^{-1}	$\Delta H^{\neq}$ kcal mol^{-1}	$\Delta S^{\neq}$ e.u.	k_{rel}
4b	60.0	7.50×01^{-5}			
	70.0	2.24×10^{-4}	23.8	−6.1	6.2
	80.0	6.11×10^{-4}			
5b	70.0	3.62×10^{-5}	22.0	−5.2	1.0
	90.0	2.97×10^{-4}			

a) Average of at least duplicate measurements and the deviations are within 6%.

Table 2. Product distribution from acetolysis of **4b**, **5b**, **1a**, and **2a**

Tosylate	Products (%)								
	1b	**2b**	**9**	**10**	**11a**	**12a**	**13**	**A**[a]	**B**[a]
4b	8	—	6	62	20	—	—	4	—
5b	—	—	3	15	10	11	30	20	11
1a[b]	48	—	—	39	9	—	—	4	—
2a[b]	—	10	5	44	28	—	—	7	6

a) Unidentified tertiary acetate. b) Ref. 3a.

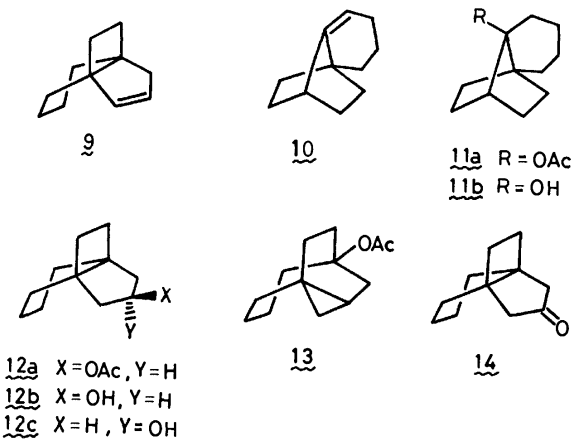

samples which were prepared by the acetylation of the alcohols **1c** and **2c**[3a] with acetic anhydride and pyridine. Similarly, [4.3.2]propell-7-ene (**9**) and tricyclo[5.2.2.$0^{1,6}$]undec-5-ene (**10**) were identified with the respective authentic materials.[3a] The structure of the acetate **11a** was confirmed by the lithium aluminium hydride reduction to the alcohol **11b**.[3a] The structure of [4.3.2]propellan-8-yl acetate **12a** was determined by the following chemical transformations: the lithium aluminium hydride reduction of **12a** followed by Jones' oxidation of the resulting alcohol **12b** gave propellan-8-one (**14**). The authentic sample of this ketone was obtained by the hydroboration-oxidation of the olefin **9** and the subsequent Jones' oxidation of the major alcohol **12c**.[7] The structure of the acetate **13** having tricyclo[4.3.2.$0^{1,8}$]undecane skeleton was elucidated on the basis of the spectroscopic data as well as mechanistic considerations. Although the two remaining acetates (unidentified **A** and **B**) were characterized to be tertiary acetates, the structures of them were not elucidated as yet.[9] In every case, the absence of unrearranged acetates **4e** and **5e** was checked by GLC and ^{1}H NMR spectra.

In contrast to the kinetic results, the product study of the acetolysis revealed clearly the effect of the cyclobutane bonds (a) and (b) on the modes of the ring expansion. As shown in Scheme 1, the ring expansion of the propellanylmethyl cations **15** and **16** would take place by 1,2-shift of the bond (c) or (d) to afford the [4.3.2]propellan-8-yl cations **17** and **20** or the [4.3.2]-propellan-7-yl cations **18** and **19**, respectively. It should be noted that one of each pair of the ring-expanded cations has boat conformation of the bicyclo[3.2.0]-heptane moiety (**17** and **19**) and the other has chair conformation (**18** and **20**). Since it has been shown that the magnitude of the long-range interaction of strained σ bond to carbonium ion centers is greatly dependent on the orientation of the participating bond and the p orbital of the cation center,[10] it is reasonable to consider that the cation **20** having chair conformation is subject to the long-range interaction (edge participation) of the central cyclobutane bond (a),[11] while the cation **17** having boat conformation is not stabilized by the participation of the bond (a). On the other hand, both [4.3.2]propellan-7-yl cations **18** and **19** are subject to the σ participation of the external cyclobutane bond (b).[3a] Moreover, the degree of the interaction may be almost independent of the conformation of the bicyclo-[3.2.0]heptane moiety, because it has been found that the σ participation is relatively insensitive to the chair/boat conformational change in bicyclo[3.2.0]hept-2-yl cations.[12]

As shown in Table 2, the *endo* tosylate **4b** gave the olefin **10** and the acetate **11a** having 1,7-tetramethylene-norbornane skeleton as the major products (total of **10** and **11a**; 82%) along with small amounts of [4.3.2]-propellane derivatives **1b** and **9** and unidentified **A**. Since these products except for **9** were obtained from the acetolysis of *endo*-[4.3.2]propellan-7-yl tosylate (**1a**), it is deduced that the ring expansion of the *endo* cation **15** occurs through 1,2-shift of the bond (d) selectively to afford the propellan-7-yl cation **18** which is stabilized by σ participation of the external cyclobutane bond (b). Interestingly, in the case of the *exo* tosylate **5b**, two new acetates **12a** and **13** derived from the propellan-8-yl cation **20** were formed in considerable amounts (total of **12a** and **13**; 41%) together with the products **9**, **10**, **11a**, unidentified **A**, and **B** which are derived from the propellan-7-yl cation **19**. Since while the cation **19** is stabilized by the σ participation of the external cyclobutane bond (b), the cation **20** is stabilized by the long-range interaction of the central cyclobutane bond (a), the ring expansion of the *exo* cation **16** occurs nonstereoselectively through 1,2-shift of the bond (c) as well as that of the bond (d).

It is thus deduced that the modes of the ring expansion of the propellan-7-ylmethyl cations (**15** and **16**) are critically governed by the *exo*/*endo* geometry of the cyclobutylmethyl moiety because the chair/boat conformation of the bicyclo[3.2.0]heptane moiety of the ring-expanded [4.3.2]propellan-7-yl and -8-yl cations (**17**—**20**) is dependent on the above geometry of **15** and **16**.

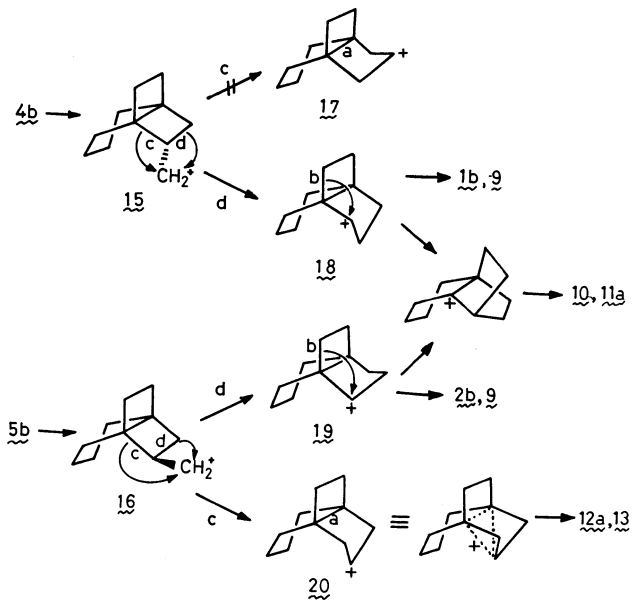

Scheme 1.

Experimental

All melting and boiling points are uncorrected. IR spectra were recorded on a JASCO IR-G spectrometer. Mass spectra were taken by using a Hitachi RMU-6E spectrometer. ^1H NMR spectra were obtained on a JEOL JNM-PS-100 spectrometer in CCl_4 solutions by using Me_4Si as an internal standard. Analytical GLC was carried out on a Hitachi 163 gas chromatograph (10% FFAP and 5% SE-30 columns) and preparative GLC separation was undertaken on a Varian Aerograph 920 gas chromatograph.

*Methyl [4.2.2]Propellane-7-carboxylates (**4d** and **5d**).* The esters **4d** and **5d** were prepared as described previpusly[4] and were separated by careful chromatography on silica gel with 2% ether–petroleum ether eluent.

4d: IR 1730, 1220, 1190, 1170, 1065 cm^{-1}; MS *m/e* (rel intensity) 194 (M^+, 55), 135 (84), 91 (100), 79 (94); NMR δ 1.12—2.58 (m, 14H), 3.20 (t, J=8 Hz, 1H), 3.64 (s, 3H). Found: C, 74.18; H, 9.41%. Calcd for $C_{12}H_{18}O_2$: C, 74.19; H, 9.34%.

5d: IR 1730, 1195, 1175, 1050 cm^{-1}; MS *m/e* (rel intensity) 194 (M^+, 60), 135 (100), 91 (90), 79 (90); NMR δ 1.10—2.72 (m, 14H), 3.08 (t, J=9 Hz, 1H), 3.64 (s, 3H). Found: C, 74.11; H, 9.29%. Calcd for $C_{12}H_{18}O_2$: C, 74.19; H, 9.34%.

*[4.2.2]Propellan-7-ylmethanols (**4c** and **5c**).* A solution of 3.0 g (15.5 mmol) of **4d** in 100 ml of ether was added dropwise to a suspension of 587 mg (15.5 mmol) of lithium aluminium hydride in 50 ml of ether and the mixture was stirred at room temperature for 1 h. Water was added carefully followed by 1 mol dm^{-3} HCl and the organic layer was separated. The aqueous layer was extracted with ether and the combined organic layer was washed with sodium hydrogencarbonate solution and water and then dried (Na_2SO_4). Evaporation of the solvent gave 2.4 g (93%) of **4c** as viscous oil, whose analytical sample was obtained by preparative GLC. In a similar manner, **5c** was prepared from **5d** in a 99% yield.

4c: IR 3300, 1010 cm^{-1}; MS *m/e* (rel intensity) 166 (M^+, 2), 93 (73), 91 (84), 79 (100); NMR δ 1.00—2.32 (m, 15H), 2.51 (quintet, J=8 Hz, 1H), 3.57, 3.60 (2d, J=6, 8 Hz, 2H). Found: C, 79.26; H, 11.01%. Calcd for $C_{11}H_{18}O$: C, 79.46; H, 10.92%.

5c: IR 3300, 1030, 1000 cm^{-1}; MS *m/e* (rel intensity) 166 (M^+, 5), 93 (77), 91 (80), 79 (100); NMR δ 1.10—2.64 (m, 16H), 3.64, 3.67 (2d, J=7, 8 Hz, 2H). Found: C, 79.37; H, 11.03%. Calcd for $C_{11}H_{18}O$: C, 79.46; H, 10.92%.

*[4.2.2]Propellan-7-ylmethyl Tosylates (**4b** and **5b**).* To a solution of 919 mg (5.54 mmol) of **4c** in 60 ml of pyridine cooled in an ice bath 2.11 g (11.1 mmol) of *p*-toluenesulfonyl chloride was added portionwise and the solution was allowed to stir for 1 h and then to stand in a refrigerator for 3 d. The mixture was poured onto water and extracted with ether. The extract was washed with 1 mol dm^{-3} HCl, sodium hydrogencarbonate solution, and water and then dried (Na_2SO_4). Evaporation of the solvent gave 1.66 g (94%) of **4b** as a white solid, which was purified by recrystallization from petroleum ether. Similarly, **5b** was prepared from **5c** in a 93% yield.

4b: Mp 68—69 °C; IR 1595, 1355, 1165, 935 cm^{-1}; NMR δ 1.08—1.64 (m, 9H), 1.76—2.22 (m, 5H), 2.42 (s, 3H), 2.63 (quintet, J=8 Hz, 1H), 3.96 (2d, J=7, 9 Hz, 2H), 7.25 (d, 2H), 7.68 (d, 2H). Found: C, 67.32; H, 7.53; S, 9.93%. Calcd for $C_{18}H_{24}O_3S$: C, 67.46; H, 7.55; S, 10.01%.

5b: Mp 34—35 °C; IR 1595, 1355, 1165, 940 cm^{-1}; NMR δ 1.10—2.32 (m, 14H), 2.40 (s, 3H), 2.58 (quintet, J=8 Hz, 1H), 3.99 (2d, J=6, 8 Hz, 2H), 7.20 (d, 2H), 7.60 (d, 2H). Found: C, 67.32; H, 7.54; S, 9.93%. Calcd for $C_{18}H_{24}O_3S$: C, 67.46; H, 7.55; S, 10.01%.

*Methyl [4.2.2]Propell-9-ene-7-carboxylates (**6** and **7**).* To an ice-cooled suspension of 480 mg of 50% sodium hydride (10 mmol) and 0.05 ml of ethanol in 20 ml of ether was added dropwise a mixture of 1.64 g (10.1 mmol) of the propellanone **8**[5] and 1.10 g (15 mmol) of ethyl formate and the mixture was stirred at room temperature for 3 h and then allowed to stand overnight. Water was added and the organic layer was separated which was washed once with water. The combined aqueous layer was washed with ether and then acidified with 1 mol dm^{-3} HCl. The oil separated was taken up in ether and the extract was washed with saturated sodium chloride solution. Evaporation of the solvent gave 1.5 g (78%) of the α-hydroxymethylene derivative of **8** as a pale yellow solid which was used without purification: IR 3040, 1690, 1600, 1200, 930, 780, 740 cm^{-1}.

p-Toluenesulfonyl azide (1.56 g, 7.9 mmol) was added dropwise to a solution of 1.5 g of the above hydroxymethylene ketone and 1.6 g (15.8 mmol) of triethylamine in 6 ml of dichloromethane cooled in an ice–salt bath (−5—−10 °C). The mixture was stirred at that temperature for 2 h. A solution of 530 mg (9.5 mmol) of potassium hydroxide in 6 ml of water was added and the mixture was stirred at room temperature for 15 min. The organic layer was separated and the aqueous layer was extracted with dichloromethane. The combined extract was washed with potassium hydroxide solution and water and then dried (Na_2SO_4). Evaporation of the solvent gave 1.5 g of the crude diazo ketone as a dark red oil (IR 3040, 2070, 1660, 1320, 780 cm^{-1}), which was dissolved in 100 ml of methanol and the solution was irradiated in a Pyrex vessel with a 500 W high-pressure mercury lamp for 22 h. Evaporation of the solvent followed by distillation at reduced pressure (bp 67—69 °C/133.3 Pa) gave 762 mg (50%) of a 1 : 2 mixture of **6** and **7** which were separated by chromatography on silica gel with 3% ether–petroleum ether eluent.

6: IR 3100, 3030, 1730, 1170, 760 cm^{-1}; MS *m/e* (rel intensity) 192 (M^+, 10), 133 (39), 105 (33), 91 (100); NMR δ 1.16—2.10 (m, 9H), 2.29 (dd, J=7, 12 Hz, 1H), 2.86 (dd, J=7, 8 Hz, 1H), 3.55 (s, 3H), 6.22 (d, J=2 Hz, 2H). Found: C, 74.70; H, 8.35. Calcd for $C_{12}H_{16}O_2$: C, 74.97; H, 8.39.

7: IR 3100, 3030, 1730, 1200, 790, 750 cm^{-1}; MS *m/e* (rel

intensity) 192 (M^+, 10), 133 (35), 105 (34), 91 (100); NMR δ 1.12—2.34 (m, 10H), 2.86 (dd, J=7, 10 Hz, 1H), 3.55 (s, 3H), 6.03 (d, J=2 Hz, 1H), 6.21 (d, J=2 Hz, 1H). Found: C, 75.16; H, 8.42%. Calcd for $C_{12}H_{16}O_2$: C, 74.97; H, 8.39%.

Hydrogenation of **6** *and* **7**. A sample of **6** (28 mg) and a catalytic amount of 5% Pd/C in 5 ml of ethanol was stirred under atmospheric hydrogen for 3 h. The catalyst was filtered off and the solvent evaporated to give 23 mg (82%) of **4b**. In a similar manner, hydrogenetion of **7** gave **5b** in a 96% yield.

Kinetic Measurements of Acetolysis of **4b** *and* **5b**. The rates of the acetolysis of **4b** and **5b** buffered with 2 equiv. of sodium acetate were measured by the titrimetric method as previously described.[3a] The results are summarized in Table 1.

Preparative Acetolysis of **4b** *and* **5b**. A solution of 1.47 g (4.59 mmol) of **4b** and 753 mg (9.18 mmol) of sodium acetate in 140 ml of acetic acid was heated at 80 °C for 23 h. The mixture was diluted with water and extracted with ether. The extract was washed with sodium hydrogencarbonate solution and water and then dried (Na_2SO_4). Evaporation of the solvent gave 751 mg (combined yield of the products; 98%) of a pale yellow oil. The products were analyzed by GLC (Table 2) and separated by chromatography on silica gel with ether–petroleum ether eluent followed by preparative GLC. Similarly, the acetolysis of 2.50 g (7.81 mmol) of **5b** gave 1.45 g of the products (combined yield; 94%) and the results are listed in Table 2.

1b: IR 1725, 1230, 1005, 955 cm^{-1}; MS *m/e* (rel intensity) 208 (M^+, trace), 148 (21), 120 (100); NMR δ 1.08—2.30 (m, 19H, s at 1.95), 4.86 (dd, J=4, 6 Hz, 1H). Found: C, 74.73; H, 9.97. Calcd for $C_{13}H_{20}O_2$: C, 74.96; H, 9.68.

2b: IR 1725, 1230, 1015 cm^{-1}; MS *m/e* (rel intensity) 208 (M^+, trace), 120 (100); NMR δ 1.10—2.24 (m, 19H, s at 1.96), 4.70 (t, J=8 Hz, 1H). Found: C, 74.58; H, 9.33. Calcd for $C_{13}H_{20}O_2$: C, 74.96; H, 9.68.

11a: IR 1725, 1230, 1160, 1125, 1000, 960 cm^{-1}; MS *m/e* (rel inrensity) 208 (M^+, 2), 148 (100), 120 (72); NMR δ 0.88—2.40 (m, 19H, s at 1.92), 3.65 (br t, J=3 Hz, 1H). Found: C, 75.01; H, 9.80. Calcd for $C_{13}H_{20}O_2$: C, 74.96; H, 9.68.

12a: IR 1730, 1225, 1005 cm^{-1}; MS *m/e* (rel intensity) 208 (M^+, trace), 120 (92), 92 (100), 91 (95); NMR δ 1.36—2.20 (m, 19H, s at 1.92), 5.30 (t, J=8 Hz, 1H). Found: C, 74.72: H, 9.79%. Calcd for $C_{13}H_{20}O_2$: C, 74.96; H, 9.68%.

13: IR 3040, 1720, 1230, 1025, 1005 cm^{-1}; MS *m/e* (rel intensity) 208 (M^+, trace), 120 (100); NMR δ 0.20 (t, J=4 Hz, 1H), 0.52—0.90 (m, 2H), 1.20—2.48 (m, 17H, s at 1.84). Found: C, 75.09; H, 9.78%. Calcd for $C_{13}H_{20}O_2$: C, 74.96; H, 9.68%.

Unidentified **A**: IR 1725, 1230, 1005, 955 cm^{-1}; MS *m/e* (rel intensity) 208 (M^+, trace), 148 (40), 123 (100); NMR δ 1.10—2.20 (m, s at 1.86). Found: C, 74.94; H, 9.64. Calcd for $C_{13}H_{20}O_2$: C, 74.96; H, 9.68.

Unidentified **B**: Mp 53—54 °C; IR 1715, 1240, 1220, 1030, 1000, 930 cm^{-1}; MS *m/e* (rel intensity) 208 (M^+, trace), 148 (69), 120 (100); NMR δ 1.20—2.52 (m, s at 1.84). Found: C, 74.65; H, 9.58%. Calcd for $C_{13}H_{20}O_2$: C, 74.96; H, 9.68%.

*[4.2.2]Propellan-7-ylmethyl Acetates (***4e** *and* **5e**). A solution of 100 mg (0.60 mmol) of **4c** in 2 ml of acetic anhydride and 5 ml of pyridine was stirred at room temperature for 5 h. Water was added and the solution was extracted with ether. The extract was washed successively with 1 mol dm^{-3} HCl, sodium hydrogencarbonate solution, and water and then dried (Na_2SO_4). Evaporation of the solvent gave 113 mg (91%) of **4e** as colorless oil. Similarly, **5e** was prepared from **5c** in a 88% yield.

4e: IR 1730, 1220, 1010 cm^{-1}; MS *m/e* (rel intensity) 208 (M^+, 3), 148 (100), 133 (100), 120 (67), 119 (73), 91 (77); NMR δ 1.20—1.74 (m, 9H), 1.84—2.25 (m, 8H, s at 1.92), 2.60 (quintet, J=8 Hz, 1H), 3.97 (d, J=8 Hz, 2H). Found: C, 74.90; H, 9.74%. Calcd for $C_{13}H_{20}O_2$: C, 74.96; H, 9.68%.

5e: IR 1730, 1220, 1020 cm^{-1}; MS *m/e* (rel intensity) 208 (M^+, 2), 148 (95), 133 (100), 120 (73), 119 (72), 91 (71); NMR δ 1.12—2.76 (m, 18H, s at 1.91), 4.06 (d, J=8 Hz, 2H). Found: C, 74.73; H, 9.67%. Calcd for $C_{13}H_{20}O_2$: C, 74.96; H, 9.68%.

Preparation of Authentic Sample of **1b** *and* **2b**. The acetates **1b** and **2b** were prepared from **1c** and **2c**[3a] in 90—95% yields in a manner similar to that described for **4e** and **5e**. The authentic samples thus prepared were identical in all respects (IR, NMR, and GLC) with the samples obtained from the acetolysis.

Lithium Aluminium Hydride Reduction of **11a**. The reduction of **11a** was carried out as described for the preparation of **4c** and **5c** to give the alcohol **11b** in a 92% yield which was identical with the authentic material.[3a]

Conversion of **12a** *to [4.3.2]Propellan-8-one (***14**). The reduction of **12a** was undertaken as described above to afford the alcohol **12b** (95%).

12b: IR 3300, 1060 cm^{-1}; MS *m/e* (rel intensity) 166 (M^+, trace), 138 (100), 120 (57), 109 (55); NMR δ 1.10—2.08 (m, 16H), 3.46 (br s, 1H), 4.33 (t, J=6 Hz, 1H). *p*-Nitrobenzoate of **12b** was prepared in a usual manner: mp 93—94 °C. Found: C, 68.46; H, 6.67; N, 4.45%. Calcd for $C_{18}H_{21}O_4N$: C, 68.55; H, 6.71; N, 4.44%.

A slightly excess of Jone's reagent was added dropwise to a solution of 46 mg (0.28 mmol) of **12b** in 2 ml of acetone and the mixture was allowed to stir at room temperature for 20 min. After evaporation of the solvent, the residue was dissolved in water and extracted with ether. The extract was washed with sodium hydrogencarbonate solution and water and then dried (Na_2SO_4). Evaporation of the solvent gave 44 mg (96%) of **14** which solidified on standing.

14: IR 1730, 1160 cm^{-1}; MS *m/e* (rel intensity) 164 (M^+, 13), 136 (82), 108 (100); NMR δ 1.20—2.16 (m, 12H), 2.20 (s, 4H). Semicarbazone: mp 209—211 °C. Found: C, 65.12; H, 8.60; N, 18.94%. Calcd for $C_{12}H_{19}ON_3$: C, 65.12; H, 8.65; N, 18.99%.

Preparation of Authentic Sample of **14**. To a suspension of 1.0 g (6.8 mmol) of the olefin **9** and 87 mg (2.3 mmol) of sodium borohydride in 10 ml of tetrahydrofuran was added dropwise under nitrogen 0.344 ml (2.72 mmol) of boron trifluoride etherate and the mixture was stirred at room temperature for 1 h. 0.2 ml of water, 0.75 ml of 3 mol dm^{-3} sodium hydroxide solution, and 0.75 ml of 30% hydrogen peroxide solution were added successively with caution and the mixture was allowed to stand overnight. The organic layer was separated and the aqueous layer was extracted with ether. The combined organic layer was washed with saturated sodium chloride solution and dried (Na_2SO_4). Evaporation of the solvent gave 1.1 g (97%) of a mixture of the alcohols **1c**, **2c**, and **12c** in a ratio of 2 : 1 : 10 (by GLC). **12c** was separated by silica-gel chromatography with 20% ether–pertoleum ether eluent.

12c: IR 3250, 1035 cm^{-1}; MS *m/e* (rel intensity) 166 (M^+, trace), 138 (100); NMR δ 1.28—2.04 (m, 16H), 3.23 (br s, 1H), 4.50 (t, J=7 Hz, 1H). *p*-Nitrobenzoate: Mp 113—115 °C. Found: C, 68.18; H, 6.57; N, 4.42%. Calcd for $C_{18}H_{21}O_4N$: C, 68.55; H, 6.71; N, 4.44%.

Jones' oxidation of 640 mg (3.86 mmol) of **12c** as described for the oxidation of **12b** gave 632 mg (100%) of the ketone **14** which was identical with the sample prepared from **12a**.

References

1) S. Winstein and N. J. Holness, *J. Am. Chem. Soc.*, **77**, 3054 (1955); J. J. Gajewski, R. L. Lyle, and R. P. Gajewski, *Tetrahedron Lett.*, **1970**, 1189; D. D. Roberts and C-H. Wu, *J. Org. Chem.*, **39**, 1570, 3937 (1974).

2) W. G. Dauben, J. L. Chitwood, and K. V. Scherer, *J. Am. Chem. Soc.*, **90**, 1014 (1968); W. G. Dauben and J. L. Chitwood, *ibid.*, **92**, 1624 (1970); P. G. Gassman and E. A. Armour, *ibid.*, **95**, 6129 (1973); P. G. Gassman and W. C. Pike, *ibid.*, **97**, 1250 (1975).

3) a) Y. Tobe, Y. Hayauchi, Y. Sakai, and Y. Odaira, *J. Org. Chem.*, **45**, 637 (1980); b) Y. Tobe, K. Terashima, Y. Sakai, and Y. Odaira, *J. Am. Chem. Soc.*, **103**, 2307 (1981); c) Y. Tobe, Y. Hayauchi, and Y. Odaira, *J. Org. Chem.*, **46**, 5219 (1981); d) Y. Tobe, M. Ohtani, and Y. Odaira, unpublished results.

4) Y. Sakai, S. Toyotani, Y. Tobe, and Y. Odaira, *Tetrahedron Lett.*, **1979**, 3855; Y. Sakai, S. Toyotani, M. Ohtani, M. Matsumoto, Y. Tobe, and Y. Odaira, *Bull. Chem. Soc. Jpn.*, **54**, 1474 (1981).

5) R. L. Cargill, D. M. Pond, and S. O. LeGrand, *J. Org. Chem.*, **35**, 359 (1970).

6) A. F. Cockerill and D. M. Rackham, *Tetrahedron Lett.*, **1970**, 5149.

7) Though the *exo*/*endo* stereochemistry of the acetate **12a** and the alcohols **12b** and **12c** was not determined, it may be reasonable to assume that **12a** and **12b** are *exo* isomers and **12c** is *endo* isomer on the basis of the following considerations: (i) The mechanistic consideration for the formation of **12a** shown in Scheme 1 suggests that the attack of an acetate anion from *exo* side is preferred. (ii) Since we have found out that the *endo* side of [4.3.2]propellane system is less hindered compared with the *exo* side,[8] the hydroboration of the olefin **9** would be expected to give the *endo* alcohol **12c** as a major product by the attack of diborane from the less hindered *endo* side.

8) Y. Tobe, A. Doi, K. Kimura, and Y. Odaira, *Bull. Chem. Soc. Jpn.*, **52**, 639 (1979).

9) Possibly, the unidentified acetates **A** and **B** may be tricyclo[4.3.2.$0^{1,7}$]undecane derivatives such as (**i**) and (**ii**) derived by 1,2-shift of the bond (a) and (e), respectively.

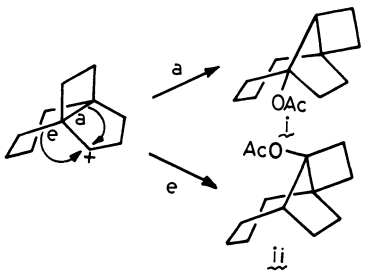

10) J. Haywood-Farmer, *Chem. Rev.*, **74**, 315 (1974).

11) For the long-range interaction of cyclobutane ring see Ref. 10.

12) K. Yano, M. Isobe, and K. Yoshida, *J. Am. Chem. Soc.*, **100**, 6166 (1978).

 © 1982 The Chemical Society of Japan Bull. Chem. Soc. Jpn., 55, 3267—3272 (1982)

Reactivities of Stable Rotamers. X. Reactions of 9-(2-Formyl-1-naphthyl)fluorene Rotamers and Related Compounds[1,2]

Ryo Saito and Michinori Ōki*

Department of Chemistry, Faculty of Science, The University of Tokyo, Bunkyo-ku, Tokyo 113

(Received April 30, 1982)

Rotational barrier (*ap*→*sp*) in 9-(2-formyl-1-naphthyl)fluorene was determined: $\Delta H^{\ddagger}$ 24.0 kcal/mol and $\Delta S^{\ddagger}$ −7.9 e.u. Oxidation of the aldehyde with chromium(VI) oxide was extremely slow in the *ap* form, whereas it proceeded smoothly in the *sp* form. As models of the 2 steps involved in the aldehyde oxidation, oxime formation of the aldehyde and oxidation of related alcohols were carried out to conclude that the second elimination step in the aldehyde oxidation is slow in the *ap* form because of the steric effect. Dehydration of the oxime of the aldehyde exhibited a large k_{sp}/k_{ap} value as well. Sodium tetrahydridoborate reduction and Grignard additions of the aldehyde were also carried out to show that the former gave a large k_{sp}/k_{ap} value whereas the latter exhibited rather a small k_{sp}/k_{ap}. The implication of the results is discussed.

Reactivity of rotational isomers is sometimes surprisingly different. We have demonstrated that deprotonation of 9-(2-methoxy-1-naphthyl)fluorene rotamers could differ by a factor of 1000.[3] Ionizing reactions of rotational isomers of 9-(2-bromomethyl-6-methylphenyl)-fluorene in ionizing-but-poorly-nucleophilic solvents exhibited striking difference: the *ap* form reacted to give a cyclized product, whereas the *sp* form was intact under the conditions.[4] Finding these differences, we were naturally interested in other reactions of rotamers and wished to extend to investigation to carbonyl compounds. This paper reports such an investigation on reactions of aldehydes and related compounds.

The synthesis of 9-(2-formyl-1-naphthyl)fluorene (**1**) rotamers was carried out in two ways. The first method is a Sommelet reaction[5] of 9-(2-bromomethyl-1-naphthyl)fluorene (**2**) which yielded a mixture of *ap*-**1** and *sp*-**1**. Chromatographic separation of the rotamers was found to be very difficult. However, as is discussed later, treatment of the rotameric mixture of **1** with chromium(VI) oxide oxidized the *sp*-form only, leaving the *ap*-

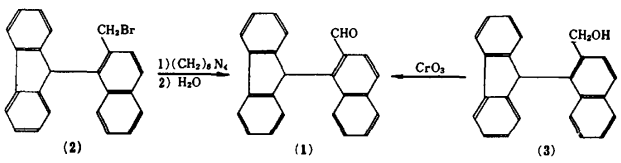

form intact. Thus this method is useful for the preparation of the *ap* isomer. The second method is oxidation of the corresponding alcohols (**3**). Since the separation of the rotamers of **1** was difficult, pure rotational isomers of **3**[6] were used. The high barrier to rotation in **3** enabled us to obtain *sp*-**1** and *ap*-**1** separately by this method.

Rotational Barriers and Populations of Rotamers. Conformations of the 9-arylfluorenes were determined by taking advantage of ^{1}H NMR spectral features. Due to the anisotropic effect of the fluorene ring, the proton in the 2-substituent of the naphthalene ring gives a high field signal if the conformation is *ap*, whereas it gives a signal at a low field if the conformation is *sp*. The chemical shift of the 8-proton of the naphthalene ring may also be used. It gives a low field signal in the *ap* conformation, whereas it gives a high field signal in the *sp*, due to the anisotropy effect of fluorene.

In order to discuss the reactivity of individual rotamers in a straightforward manner, it is necessary to establish that the conversion of one isomer to another is slow enough at a given temperature where a reaction is carried out. In this context, rotational barriers shall be discussed first together with populations of rotamers which can be obtained at the same time in the investigation of the barrier.

The rates of isomerization (*ap*→*sp*) of **1** are given in Table 1. From the results, $\Delta H^{\ddagger}$ 24.0±0.7 kcal/mol (1 cal=4.18 J) and $\Delta S^{\ddagger}$ −7.9±2.0 e.u. (1 e.u.=4.18 J/K mol) were obtained. Since the free energy of activation for rotation at ambient temperature is *ca.* 26.5 kcal/mol, we can claim that we look at the reactivities of individual rotamers if we run the reaction at ambient temperature within 24 h or at a lukewarm temperature for a shorter period. The equilibrium constant (*sp*/*ap*) is almost constant in the temperature range examined. The favoredness of the *sp* form may be ascribed to the steric effect including that for solvation, since the formyl group is polar and the oxygen in the formyl group can be larger than an sp^2 carbon.

Barrier to rotation of oximes (**5**) was not examined because they were sparingly soluble in nonpolar solvents. However, the height of the barrier may be assumed to be

Table 1. Rate constants for rotation and equilibrium constants of rotamers in 9-(2-formyl-1-naphthyl)fluorene (**1**)

Temperature/°C	$k(ap\rightarrow sp)/s^{-1}$	$K(sp/ap)$
55.6	1.28×10^{-5}	1.48
64.0	3.66×10^{-5}	1.49
73.2	9.58×10^{-4}	1.46
78.2	1.41×10^{-4}	1.49

Table 2. Rate constants for rotation and equilibrium constants of rotamers in 9-[2-(α-hydroxybenzyl)-1-naphthyl]fluorene (**7**)

Temperature/°C	$k(ap\rightarrow sp)/s^{-1}$	$K(sp/ap)$
96.4	1.28×10^{-5}	1.8
104.0	2.94×10^{-5}	1.8
114.0	9.37×10^{-5}	1.8
124.0	2.01×10^{-4}	1.8

almost equal to that of the aldehyde (**1**) because their steric structures are similar.

Barrier to rotation in 9-(2-cyano-1-naphthyl)fluorene (**6**) was determined at a temperature. At 77.0 °C in benzene-d_6, the nitrile gave a rate constant for rotation ($ap \rightarrow sp$) of 1.08×10^{-3} s^{-1}. From the value, the free energy of activation for rotation was calculated to be 25.4 kcal/mol. Thus we may neglect isomerization of the nitrile if reactions are carried out at room temperature for a few hours. The equilibrium constant (sp/ap) was 7.3 at the temperature. The reason for the favoredness of the *sp* form is not well understood at the moment. Molecular models suggest no significant congestion in the *ap* form.

The rate constant for rotation and equilibrium constants in 9-[2-(α-hydroxybenzyl)-1-naphthyl]fluorene (**7**) are given in Table 2. From the rate constants, $\Delta H^{\ddagger}$ 29.1 ± 1.1 kcal/mol and $\Delta S^{\ddagger}$ -2.7 ± 2.9 e.u. were obtained. The free energy of activation (*ca.* 30 kcal/mol) for rotation at ambient temperature assures again that conversion of a rotamer to another at temperature below 50 °C is negligible if the reaction is run during a reasonable period. Although $C_6H_5CH(OH)$ is a large group, the barrier to rotation and equilibrium constants are almost the same as those of **3** reported earlier.[6] The results will imply the followings. If, by rotation about the $C_6H_5CH(OH)$–naphthyl bond, a large group, either phenyl or hydroxyl, comes closely to the fluorene ring, the conformation will be extremely disfavored because of the steric effect. Therefore, this compound will take a conformation in which the hydrogen of the α-hydroxybenzyl group is close to the fluorenyl group, in the ground state. If this effect is operative, the *ap* form of compound **7** may be unfavorable relative to *ap*-**3** because of the decrease in entropy: this effect is ambiguous as far as the experimental data concern, because it is small. Infrared spectrum of *ap*-**7** as a 1.0×10^{-2} mol/L solution in carbon tetrachloride showed an absorption due to OH stretching at 3600 cm^{-1}, ε being 61.3. *sp*-**7** under similar conditions showed an absorption at 3620 cm^{-1} of ε 47.1. The absorption of *ap*-**7** at a relatively low frequency may indicate the presence of the OH···π bond as was the case of the primary alcohol (**3**).[6] The small *K* value implies that the *ap* form is stabilized relative to the *sp*: the cause is most probably the OH···π bond. The similar barrier height for rotation in **7** with that in **3** implies that the transition state energy is also similar. We may approximate the transition state for rotation by the interaction of the fluorene ring with the CH of the α-hydroxybenzyl group and the naphthalene ring.

Reactions. Reactions carried out in this work are summarized in the following scheme. Relative rates are given in Table 3.

Oxidation of a mixture of rotamers of **1** with chromium(VI) oxide in aqueous acetone yielded the corresponding *sp*-acid (**4**) within a few minutes but left *ap*-**1** intact. If the oxidizing mixture was left overnight, instead of the *ap*-carboxylic acid (**4**), a lactone (**8**) was obtained as a main product. The lactone can be formally formed by oxidation at the 9-position of fluorene and at the formyl group followed by lactonization. It is not clear which is the precedent reaction of the two oxidations, but we prefer the first oxidation at the 9-position of fluorene for the following reasons. Firstly there was no indication that the *ap*-**4** was produced. Secondly although the rotamers of **1** are stable in chloroform for at least 5 d at room temperature, their isomerization is detected if a pyridine solution is allowed to stand overnight. This is because the fluorene ring is proton donating. Although there is no strong base present in the system, water or acetone may act as a base to form a minute amount of the fluorenide anion which should be oxidized easily to form a 9-hydroxy compound. If the 9-hydroxyl group is introduced, the rotational barrier must be lowered, as are known in other cases,[7] to facilitate rotation at room temperature. Then the formyl group, in the *sp* conformation, must be easily oxidized.

Indeed, the lactone (**8**) could be better made by chromium(VI) oxide oxidation of the aldehyde (**1**) in the presence of pyridine. The lactone was formed by still another method. Air oxidation of the aldehyde in ethanol in the presence of potassium hydroxide afforded the lactone smoothly. Since oxidation of 9-alkylfluorenes with air in the presence of base to afford hydroperoxides is reported,[8] it will be natural to assume that the first step in the oxidation of **1** is the

Table 3. Relative rates of reactions of rotameric 9-(2-formyl-1-naphthyl)-fluorene and related compounds

Reaction	Compound	k_{sp}/k_{ap}
Oxidation with Cr(VI)	Aldehyde (**1**)	Very large
	Primary alcohol (**3**)	0.67
	Secondary alcohol (**7**)	*ca.* 34
	Secondary alcohol (**10**)	*ca.* 27
Oxime formation	Aldehyde (**1**)	3.7
Dehydration with $SOCl_2$	Oxime (**5**)	*ca.* 18
Reduction with $NaBH_4$	Aldehyde (**1**)	7.6
Addition of C_6H_5MgBr	Aldehyde (**1**)	1.8
Addition of CH_3MgI	Aldehyde (**1**)	1.7

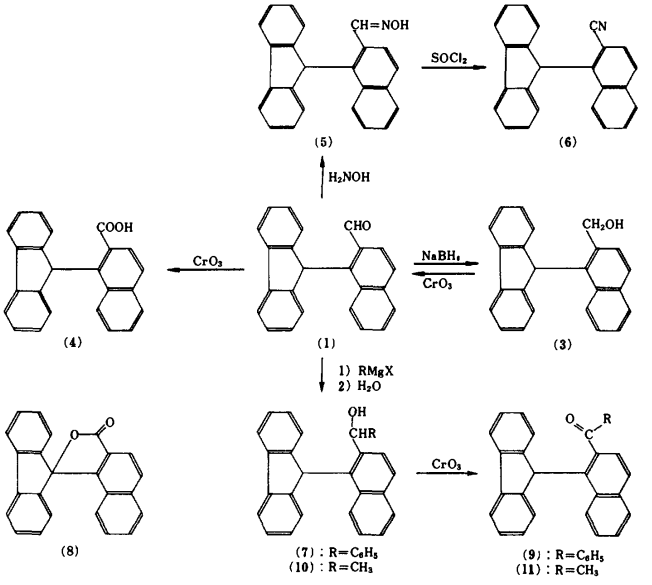

formation of a 9-hydroperoxy compound. Inversion at the anion formed as an intermediate or rotation about the C_9–C_{naph} bond in the hydroperoxide will make the formyl group vulnerable to further oxidation or an intramolecular redox reaction may take place to produce the lactone.

The lack of reactivity of *ap*-**1** was of interest. We wished to clarify an important factor which retards the oxidation of *ap*-**1**. Oxidation of an aldehyde is known to proceed *via* three steps:[9] coordination of the aldehyde oxygen to chromium, addition of water to the complex, forming a tetrahedral intermediate, and final E2 type elimination of chromate of a lower oxidation number. Therefore, we examine every step by using model reactions.

The first step, ligation of the aldehyde to chromium, does not seem to be significantly different of the two rotamers. A molecular model indicates that the aldehyde oxygen is exposed and is vulnerable to the chromium(VI) oxide attack even in the *ap* conformation. The ligation may be assumed to proceed without significant hindrance both in *sp* and *ap* forms.

As a model for the second step, we chose oxime formation under acidic conditions. Under the circumstances, the oximation is known to proceed *via* protonation of the aldehydic oxygen and addition of hydroxylamine to the protonated species,[10] the latter step being rate-determining. The results which are summarized in Table 3 together with others indicate that even *ap*-**1** was smoothly oximated and the relative rate (k_{sp}/k_{ap}) was 3.7. The reactivity of the *ap* form is indeed lower than that of the *sp* but the difference is not so large as is seen in oxidation of the aldehyde (**1**). Thus we may rule out the possibility that the addition step to the carbonyl of **1** is the key for the slow oxidation of *ap*-**1**.

As a model for the last step of oxidation, we chose chromium(VI) oxide oxidation of the corresponding alcohols, because the mechanism of the oxidation is similar with that of the last step in the aldehyde-oxidation.[11] Interestingly the primary alcohol (**3**) gave k_{sp}/k_{ap} 0.67, whereas 9-[2-(α-hydroxybenzyl-1-naphthyl]fluorene (**7**) gave the relative rate of *ca.* 30. Products were the aldehyde (**1**) and a ketone (**8**). Oxidation of 9-[2-(1-hydroxyethyl)-1-naphthyl]fluorene (**10**) gave also a large k_{sp}/k_{ap} value. The results indicate that the secondary alcohols (**7** and **10**) show similar reactivity ratio with the aldehyde (**1**), whereas the primary alcohol (**3**) shows about the same reactivity for the rotamers or even the *ap* form is slightly more reactive than the *sp*. This striking difference for the two types of compounds can be understood if one looks at the molecular models of the *ap* forms (Fig. 1). The models suggest that, for the primary alcohol, a proton to be removed after ligation of the oxygen to chromium is readily available because one of hydrogens in the α-position is exposed without significant hindrance. In contrast, in the secondary alcohol, the hydrogen to be removed as a proton is buried in a pocket made by phenyl (or methyl), naphthyl, and fluorenyl groups. Therefore, should the oxidation occur for the compound, additional energy is required to deform the molecule to make the attack to the proton possible. If the difference in reactivities of

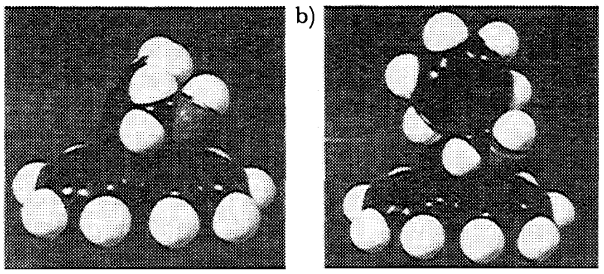

Fig. 1. CPK models of a) *ap*-9-[2-(hydroxymethyl-1-naphthyl)fluorene and b) *ap*-9-[2-(α-hydroxybenzyl)-1-naphthyl]fluorene.

ap-**3** and *sp*-**3** is significant, the cause may be the steric acceleration[12] because a tetrahedral carbon is larger than a trigonal carbon.

The situation of oxidation of aldehydes is close to that of the secondary alcohols, since it passes through a $RCH(OH)_2$ type intermediate. From the above results we conclude that oxidation of the *ap* form of the aldehyde (**1**) is very slow because of the steric effect in the last step relative to the *sp*. The key point of the last step in oxidation is that the transition state is space-demanding because of the concerted nature. Thus it becomes interesting to see whether other space-demanding reactions of the *ap* form are also slow relative to those of the *sp* form in this system.

As an example, we chose dehydration of oximes, since the reaction is known to be of E2 type if the conformation is anti (*Z*).[13] From the *ap* and *sp* aldehydes (**1**), only one form each of the oximes (**5**) was formed. Equilibration of the oxime by heating gave mixtures of the same composition of which components gave the identical NMR spectra with the starting material. This indicates that oximes are either both anti or both syn. There are various methods known for the determination of the stereochemistry of oximes. Of those, the NMR spectroscopic method is considered to be most reliable.[14] However, the chemical shifts in NMR spectroscopy may be affected by the ring current effect and the steric effect of the fluorene ring. Therefore, we prefered to use other methods, if available. Lanthanoid induced shifts (LIS) of syn and anti aldoximes are known.[15] However, attempted measurements of LIS of *sp* and *ap*-**5** failed because line-broadening occurred extensively when even a small amount of a shift reagent was added. In the preparation of aromatic aldoximes, the syn form is preferentially formed if the conditions are basic.[16] However, the syn oxime isomerizes to the anti form if acid is present. We therefore believe that we are dealing with the anti (*Z*) oximes. This assignment of stereochemistry is reasonable on the steric ground and is also consistent with the relative rates of dehydration discussed below.

Anti-oximes are easily dehydrated by acetic anhydride. However, heating was required for dehydration of oximes **5** with acetic anhydride. To avoid isomerization, more efficient dehydrating reagent is required. Dicyclohexylcarbodiimide is known to be an efficient dehydrating reagent.[17] However, to enhance the reactivity, triethylamine and copper ion are used in addition to the carbodiimide. As a result, the reaction

of *ap*-oxime afforded a mixture of various products. 1,1'-Carbonyldiimidazole is also known to be an efficient dehydrating reagent.[18] This reagent indeed dehydrated the oxime easily at room temperature. However, the product was found to be a mixture of *ap*- and *sp*-nitriles. We attribute the results to the basic property of imidazole which is formed by the reaction, although the basicity of imidazole is much lower than triethylamine. Thus it is necessary to carry out a reaction under non-basic conditions to avoid isomerization.

Finally we used thionyl chloride as a dehydrating reagent. It reacted smoothly to afford nitriles (**6**). The relative rate k_{sp}/k_{ap} is large 18 but not as large as that in oxidation of **1**, **7**, or **10**. We wish to attribute the results to the fact that the E2 type elimination takes place from a tetrahedral species in **1**, **7**, and **10**, whereas it occurs from a trigonal carbon in the oxime.

Sodium tetrahydridoborate reduction is claimed to take a four-membered ring transition state, carbonyl oxygen ligating to boron and hydride approaching the carbonyl carbon.[19] Therefore the transition state must be bulky in this reaction. It then is expected that *sp*-**1** will show a large reactivity relative to *ap*-**1**. The reduction proceeded smoothly from the both conformations to produce the primary alcohols (**3**). The relative rate k_{sp}/k_{ap} was 7.6. Although the difference is reduced somewhat from those in oxidation of the aldehyde (**1**) or the secondary alcohols (**7** and **10**) and dehydration of oximes (**5**), it is still significant. Space-demanding structure (transition state in this case) must be responsible to the result.

A Grignard addition reaction to a carbonyl compound is also cited very often that the transition state is a 4-membered ring and thus the reaction is concerted.[20] We have carried out the reaction of phenylmagnesium bromide with the aldehyde (**1**). Both conformations of **1** reacted smoothly to afford 9-[2-(α-hydroxybenzyl)-1-naphthyl]fluorene (**7**). However, the relative rate k_{sp}/k_{ap} was, to our surprise, low 1.8. Addition of methylmagnesium iodide also showed k_{sp}/k_{ap} of 1.7. Mechanism of Grignard addition to carbonyl compounds is complicated. A single-electron transfer process and a nucleophilic addition process are competing.[20] It may not be possible to exactly compare the reactivity of the aldehyde rotamers here, but it is at least clear that, in the reaction of *ap*-**1**, the process does not require much space. Ashby *et al.* depicted one of the Grignard reactions as it has coordination of oxygen to magnesium only.[21] The reaction of *ap*-**1** may be proceeding in this manner.

In conclusion, we wish to point out that, if a reaction passes through a bulky state, the relative rate k_{sp}/k_{ap} becomes very large in this system. Certain S_N2 type reactions of 9-(2-bromomethyl-6-methylphenyl)fluorene were also very slow in *ap* conformation relative to those in the *sp*.[4] Thus it is commonly noticed that the space-demanding reaction is slow in the *ap* of these systems. The technique may even be used for diagnosis whether a space-demanding transition state is really intervening in the reaction. If a reaction is not space-demanding, the k_{sp}/k_{ap} can be very close to unity in the system. Further study on other carbonyl compounds, which give a bulkier transition state, may exhibit even larger differences in reactivities.

Experimental

9-(2-Formyl-1-naphthyl)fluorene (1). a): To a solution of 1.00 g (3.1 mmol) of *ap*-9-(2-hydroxymethyl-1-naphthyl)-fluorene (**3**)[6] in 30 mL of acetone was added a little excess of the Jones reagent prepared from 2.7 g of chromium(VI) oxide, 4.6 mL of concentrated sulfuric acid, and 8 mL of water. The excessive chromium(VI) oxide was decomposed with methanol or ethanol. The precipitate was filtered off and the filtrate was poured into water. After the usual treatment, the product was chromatographed on silica gel (benzene eluent) to afford 0.98 g *ap*-**1**, mp 127—128.5 °C. Found: C, 89.73; H, 4.73%. Calcd for $C_{24}H_{16}O$: C, 89.97; H, 5.03%. ^{1}H NMR ($CDCl_3$, δ): 6.21 (1H, s), 7.07—8.10 (13H, m), 8.50—8.73 (1H, m), 8.95 (1H, s).

sp-**1**, mp 102.5—104 °C, was similarly prepared in 95% yield. Care was exercised to avoid further oxidation by limiting the amount of the Jones reagent. Found: C, 90.21; H, 4.73%. Calcd for $C_{24}H_{16}O$: C, 89.97; H, 5.03%. ^{1}H NMR ($CDCl_3$, δ): 6.03 (1H, d, J=8.1 Hz), *ca.* 6.70 (1H, s), 6.73—8.13 (13H, m), 10.85 (1H, s).

b): A mixture of 0.17 g (0.44 mmol) of a rotameric mixture of 9-(2-bromethyl-1-naphthyl)fluorene (**2**)[6] and 0.2 g (1.4 mmol) of hexamethylenetramine in 4 mL of chloroform was heated under reflux for 2 h with stirring. The precipitate was collected after cooling and was heated with 30 mL of 50% aqueous acetic acid at 100 °C for 1 h. The mixture was poured into water and extracted with ether. The ethereal extract was washed with aqueous sodium hydrogencarbonate and dried. After evaporation of the solvent, the residue was submitted to chromatography on silica gel but the separation was very tedious. The mixture was obtained as an oil in 78% yield. Pure *ap*-**1** could be obtained after oxidation as described below because the *ap* aldehyde resisted oxidtaion.

sp-*(2-Carboxy-1-naphthyl)fluorene (4).* To a solution of 1.00 g of *sp*-**1** in 30 mL of acetone, was added a little excess of the Jones reagent at room temperature. After 30 min, the reaction mixture was poured into water and was extracted with ether. After evaporation of the solvent, the residue was purified by chromatography on silica gel (dichloromethane solvent) to afford 80% *sp*-**4**, mp 228—230 °C. Found; C, 85.78; H, 4.59%. Calcd for $C_{24}H_{16}O_2$: C, 85.69; H, 4.79%. ^{1}H NMR ($CDCl_3$, δ): *ca.* 6.56 (1H, s), 6.62 (1H, d, J=8.0 Hz), 7.73—9.01 (13H, m).

Oxidation of a Rotameric Mixture of the Aldehyde (1). To a solution of 100 mg of a mixture (*ca.* 1 : 1) of *sp* and *ap* aldehydes (**1**) in 30 mL of acetone, was added the Jones reagent with stirring in small portions. The addition was terminated when the reddish-orange color persisted after 20 min. Methanol was added to destroy the excess of chromium(VI) oxide and the precipitate was removed by filtration. The filtrate was poured into water and the whole was extracted with ether. After washing and drying of the ether layer, the solvent was evaporated. The residue was submitted to chromatography on silica gel (benzene eluent) to give *ca.* 40 mg of *ap*-**1** and *ca.* 50 mg of *sp*-**4**. No *ap*-carboxylic acid was detected.

9-(2-Carboxy-1-naphthyl)-9-hydroxyfluorene Lactone (8).
a): A solution of 30 mg of a mixture of *ap* and *sp*-**1** in 10 mL of pyridine was mixed with 50 mg of chromium(VI) oxide and the mixture was allowed to stand for 10 h at room temperature. The excess of chromium(VI) oxide was decomposed with methanol and the product was taken up in ether. The

ethereal layer was washed with dilute hydrochloric acid and then with water. After evaporation of the solvent, the residue was recrystallized from benzene–hexane, mp 247.5—249 °C. The yield was almost quantitative. Found: C, 86.28; H, 4.12%. Calcd for $C_{24}H_{14}O_2$: C, 86.21; H, 4.12%. ^{1}H NMR ($CDCl_3$, δ): 6.83—8.13 (14H, m). IR (KBr): 1760 cm^{-1}. MS showed a molecular ion peak at *m/e* 334 while $C_{24}H_{14}O_2$ requires that at *m/e* 334.

b): A solution of 40 mg of a mixture of *sp*- and *ap*-**1** in 20 mL of ethanol was mixed with 0.1 mL of a solution made from 0.5 g of potassium hydroxide and 2 mL of water. The mixture was stirred for 1.5 h at room temperature and poured into water. The product was treated in the usual manner to give *ca.* 40 mg of the lactone.

*9-(2-Hydroxyiminomethyl-1-naphthyl)fluorene (**5**).* A solution of 0.150 g (0.47 mmol) of the *sp*-aldehyde (**1**) in 40 mL of ethanol was mixed with a solution of 0.1 g (1.2 mmol) of sodium acetate in 3 mL of water. A solution of 0.045 g (0.64 mmol) of hydroxylamine hydrochloride in 2 mL of water was added to the mixture and the whole was stirred at room temperature for 10 min. The mixture was concentrated *in vacuo* and was poured into water. The organic material was extracted with ether and the product was chromatographed on silica gel (benzene eluent). The *sp*-oxime, mp 170.5—171.5 °C, was obtained in 96% yield. Found: C, 85.96; H, 9.85; N, 4.08%. Calcd for $C_{24}H_{17}NO$: C, 85.94; H, 5.11; N, 4.18%. ^{1}H NMR ($CDCl_3$, δ): 5.89 (1H, s), 6.48 (1H, d, J=7.2 Hz), 6.67—8.00 (13H, m), 9.03 (1H, s). The OH proton was not detected in the spectrum.

The *ap*-oxime, mp 171.5—172.5 °C, was similarly prepared quantitatively. Found: C, 85.68; H, 4.88; N, 4.48%. ^{1}H NMR ($CDCl_3$, δ): 6.12 (1H, s), 6.94 (1H, s), 7.07—8.03 (13H, m), 8.45—8.63 (1H, m). The OH proton was not detected in the spectrum.

*9-[2-(α-Hydroxybenzyl)-1-naphthyl]fluorene (**7**).* A Grignard reagent was prepared from 0.25 g of magnesium, 1.13 mL of bromobenzene, and 10 mL of dry ether. A 1.4 mL portion of the Grignard reagent was added to 0.30 g of *ap*-**1** in 30 mL of ether and the mixture was decomposed after 10 min. After a usual manipulation, the product was chromatographed on silica gel (benzene eluent) to afford 0.36 g of *ap*-**7**, mp 176—177 °C. Found: C, 90.19; H, 5.37%. Calcd for $C_{30}H_{22}O$: C, 90.42; H, 5.56%. ^{1}H NMR ($CDCl_3$, δ): 4.88 (1H, s), 6.25 (1H, s), 6.50—8.00 (18H, m), 8.57 (1H, d, J=9.6 Hz). The OH proton was not detected in the spectrum.

sp-**7**, mp 175—177 °C, was similarly prepared in 97% yield. Found: C, 90.60; H, 5.33%. Calcd for $C_{30}H_{22}O$: C, 90.42; H, 5.56%. ^{1}H NMR ($CDCl_3$, δ): 5.87 (1H, s), 6.63 (1H, s), 6.40 (1H, d, J=9.0 Hz), 6.50—7.97 (18H, m). The OH proton was not detected in the spectrum.

*9-[2-(1-Hydroxyethyl)-1-naphthyl]fluorene (**10**)* was similarly prepared from the aldehyde (**1**) and methylmagnesium iodide almost quantitatively.

ap-**10**, oil. High resolution MS exhibited a molecular ion peak at *m/e* 336.1516, whereas $C_{25}H_{20}O$ requires 336.1514. ^{1}H NMR ($CDCl_3$, δ): 0.70 (3H, d, J=6.0 Hz), 3.82 (1H, q, J=6.0 Hz), 6.12 (1H, s), 7.03—8.03 (13H, m), 8.42—8.65 (1H, m). The OH proton was not detected in the spectrum.

sp-**10**, mp 120—124 °C. Found: C, 89.24; H, 5.88%. Calcd for $C_{25}H_{20}O$: C, 89.25; H, 5.99%. ^{1}H NMR ($CDCl_3$, δ): 1.79 (3H, d, J=6.6 Hz), 5.67 (1H, q, J=6.6 Hz), 6.12 (1H, s), 6.40 (1H, d, J=9.0 Hz), 6.76—8.00 (13H, m). The OH proton was not detected in the spectrum.

*9-(2-Benzoyl-1-naphthyl)fluorene (**9**).* A solution of 0.30 g of *ap*- or *sp*-**7** in 20 mL of acetone was oxidized with the Jones reagent as described in the preparation of the aldehyde (**1**). It took 30—60 min for the oxidation of the *ap*-isomer, whereas the oxidation of *sp*-**7** was over within several minutes.

ap-**9**, mp 123—124 °C. Found: C, 90.61; H, 4.94%. Calcd for $C_{30}H_{20}O$: C, 90.88; H, 5.08%. ^{1}H NMR ($CDCl_3$, δ): 6.08 (1H, s), 6.73—8.10 (18H, m), 8.68 (1H, d, J=9.0 Hz).

sp-**9**, mp 162.5—164 °C. Found: C, 91.10; H, 4.82%. Calcd for $C_{30}H_{20}O$: C, 90.88; H, 5.08%. ^{1}H NMR ($CDCl_3$, δ): 5.44 (1H, s), 6.57 (1H, d, J=9.0 Hz), 6.77—8.13 (18H, m).

*9-(2-Acetyl-1-naphthyl)fluorene (**11**)* was similarly prepared from the alcohol (**10**) by oxidation with chromium(VI) oxide. The *ap* form reacted much more slowly than the *sp* form.

ap-**11**, mp 108—109 °C. Found: C, 89.80; H, 5.21%. Calcd for $C_{25}H_{18}O$: C, 89.79; H, 5.43%. ^{1}H NMR ($CDCl_3$, δ): 1.60 (3H, s), 6.09 (1H, s), 7.07—8.07 (13H, m), 8.67 (1H, d, J=9.0 Hz).

sp-**11**, mp 103—105 °C. Found: C, 89.94; H, 5.23%. Calcd for $C_{25}H_{18}O$: C, 89.79; H, 5.43%. ^{1}H NMR ($CDCl_3$, δ): 2.77 (3H, s), 5.84 (1H, s), 6.56 (1H, d, J=8.4 Hz), 6.73—8.00 (13H, m).

*9-(2-Cyano-1-naphthyl)fluorene (**6**).* To a stirred solution of 0.15 g (0.45 mmol) of *ap*-**5** in 30 mL of dry ether was added 0.5 mL of thionyl chloride and the whole was stirred for 5 h at room temperature. The mixture was poured into water and extracted with ether. The extract was washed, dried, and evaporated. The residue was chromatographed on silica gel (benzene eluent) to afford 0.12 g of *ap*-**6**, mp 150.5—152 °C. Found: C, 90.75; H, 4.62; N, 4.44%. Calcd for $C_{24}H_{15}N$: C, 90.82; H, 4.76; N, 4.41%. ^{1}H NMR ($CDCl_3$, δ): 6.18 (1H, s), 7.07—8.07 (13H, m), 8.58—8.80 (1H, m).

The *sp* form, mp 165.5—167 °C, was prepared similarly in 71% yield. Since the dehydration of *sp*-**5** was much easier than that of the *ap* form, 0.1 mL of thionyl chloride and stirring for 2 h sufficed for the dehydration. Found: C, 91.08; H, 4.46%. Calcd for $C_{24}H_{15}N$: C, 90.82; H, 4.76%. ^{1}H NMR ($CDCl_3$, δ): 6.00 (1H, s), 6.58 (1H, d, J=9.0 Hz), 6.80—8.00 (13H, m).

Determination of Barriers to Rotation. A sample solution was prepared by dissolving 30 mg of the *ap* form of arylfluorenes in 0.4 mL of hexachlorobutadiene and was placed in an NMR sample tube. The tube was immersed in an appropriate boiling-solvent bath, the temperature of which was directly measured by a thermometer. The rate of isomerization was followed by ^{1}H NMR spectroscopy and was treated as a reversible first-order reaction. The rate constants thus obtained were put into the Eyring equation to obtain activation parameters. The following solvents were used for the bath (solvent and approximate boiling point given): acetone (55 °C), methanol (64 °C), 1,1,1-trichloroethane (73 °C), benzene (78 °C), dioxane (96 °C), toluene (104 °C), 1 : 1 chlorobenzene–toluene (114 °C), chlorobenzene (124 °C).

Determination of Spectra. Infrared spectra were recorded on a Hitachi EPI-G spectrophotometer. The wave numbers are not calibrated. The spectra of solid were obtained as KBr disks. The spectra of solution were obtained with a KBr cell of variable length. With solutions of *ca.* 0.2 M in carbon tetrachloride, the cell length was 0.25 mm and, with those of *ca.* 0.01 M, the cell length was 5 mm. ^{1}H NMR spectra were obtained with either a Hitachi R-20B or a Varian EM 390 spectrometer.

Competitive Reactions. Relative reactivities of rotamers were obtained by competitive reactions. Dehydration of oximes did not give clear results with this method. Thus the relative rate was checked by measuring the rates of reactions of individual rotamers. If one assumes that the rate expressions of the reactions of *sp* and *ap* rotamers are the same and that the rate is first order in the substrate, then

$$[\text{Relative reactivity}] = k_{sp}/k_{ap} = \frac{\log[sp]/[sp]_0}{\log[ap]/[ap]_0}$$

Competitive oximation of the aldehyde (**1**) was carried out by treating 30 mg each of *ap* and *sp* forms in 20 mL of ethanol with 0.5 mL of aqueous hydroxylamine hydrochloride, which was made by dissolving 130 mg of the salt in 10 mL of water, and 0.5 mL of aqueous sodium acetate, which was prepared by dissolving 300 mg of the salt in 5 mL of water. After 30 min at room temperature, the mixture was treated as described in the preparation of oximes and the unreacted starting materials were analyzed with the use of ^{1}H NMR spectra. The relative reactivity was obtained as an average of three runs.

Competitive oxidation of rotamers of 9-[2-(α-hydroxybenzyl)-1-naphthyl]fluorene (**7**) was carried out using 20 mg each of *sp*- and *ap*-**7** in 20 mL of acetone and 0.1 mL of the Jones reagent prepared as above. ^{1}H NMR showed the presence of 17.5% unreacted *sp* but at least 95% of the *ap* form was found unreacted.

Competitive oxidation of *ap*- and *sp*-9-[2-(1-hydroxyethyl)-1-naphthyl]fluorene (**10**) was carried out similarly. ^{1}H NMR showed the presence of 25.1% unreacted *sp* form whereas at least 95% of the *ap* form remained unreacted.

Competitive oxidation of 9-(2-hydroxymethyl-1-naphthyl)-fluorene (**5**) was carried out similarly. The relative reactivity is the average of three runs.

Competitive reduction of *sp*- and *ap*-9-(2-formyl-1-naphthyl)-fluorene (**1**) was carried out by treating a solution of 30 mg each of the rotamers in 20 mL of methanol with 1.0 mL of methanolic solution of sodium tetrahydridoborate, which was prepared by dissolving 20 mg of the hydride in 10 mL of methanol. After 10 min at room temperature, the mixture was manipulated in the usual manner and the unreacted materials were analyzed by ^{1}H NMR spectroscopy. The relative reactivity was obtained as an average of three runs.

Competitive Grignard reactions of *sp*- and *ap*-9-(2-formyl-1-naphthyl)fluorene (**1**) were carried out by treating 30 mg each of the aldehyde rotamers in 20 mL of ether with 0.1—0.2 mL of methylmagnesium iodide or phenylmagnesium bromide solution which was prepared as described for the preparation of **7** and **10**. After 10 min, the mixture was decomposed and the unreacted materials were analyzed by ^{1}H NMR spectroscopy. The relative reactivities are the averages of 2—3 runs.

Competitive dehydration of *ap*- and *sp*-9-(2-hydroxyiminomethyl-1-naphthyl)fluorene (**5**) was carried out by treating a solution of 20 mg each of the rotamers in 20 mL of dry ether with 0.1 mL of thionyl chloride at room temperature. After 1 h, the mixture was separated by TLC into oximes and nitriles. The unreacted oximes were analyzed by ^{1}H NMR spectroscopy. This operation gave 86.1% unreacted *ap* and less than 5% unreacted *sp*. This gave k_{sp}/k_{ap} of *ca.* 20.

*Relative Reactivity of 9-(2-Hydroxyiminomethyl-1-naphthyl)fluorene (**5**) toward Dehydration as Obtained by Individual Rate of Dehydration.* *ap*-**5** (20 mg) in 20 mL of ether was stirred with 0.1 mL of thionyl chloride at room temperature. The reaction was quenched at appropriate intervals. After 5 h, the conversion ratio was 48.4%. Under the same conditions the conversion ratio of the *sp* form was 82.3% after 40 min. If one assumes that the formation rate of the nitriles is expressed by the product of the concentrations of the reactants and the change in the concentration in thionyl chloride is neglected, the results give k_{sp}/k_{ap} of *c. a.* 16.

References

1) For Part IX, see S. Murata, S. Kanno, Y. Tanabe, M. Nakamura, and M. Ōki, *Bull. Chem. Soc. Jpn.*, **55**, 1522 (1982).
2) A part of the results was reported in a preliminary form: M. Ōki and R. Saito, *Chem. Lett.*, **1981**, 649.
3) M. Nakamura and M. Ōki, *Chem. Lett.*, **1975**, 671.
4) S. Murata, S. Kanno, Y. Tanabe, M. Nakamura, and M. Ōki, *Angew. Chem., Int. Ed. Engl.*, **20**, 606 (1981). See also Ref. 1.
5) S. Angyal, *Org. React.*, **8**, 197 (1954).
6) R. Saito and M. Ōki, *Bull. Chem. Soc. Jpn.*, **55**, 2508 (1982).
7) A. Rieker and H. Kessler, *Tetrahedron Lett.*, **1969**, 1227.
8) Y. Sprinzak, *J. Am. Chem. Soc.*, **80**, 5449 (1958).
9) J. Rocek, "Oxidation of Aldehydes by Transition Metals," in "The Chemistry of the Carbonyl Group," ed by S. Patai, John-Wiley & Sons, New York (1966), pp. 462—478.
10) L. P. Hammett, "Physical Organic Chemistry," McGraw-Hill, New York (1940), p. 333; W. P. Jencks, *J. Am. Chem. Soc.*, **81**, 475 (1959).
11) K. W. Wiberg, "Oxidation in Organic Chemistry," Academic Press, New York (1965), Part A, pp. 69—184.
12) H. C. Brown and R. S. Fletcher, *J. Am. Chem. Soc.*, **71**, 1845 (1949).
13) D.T. Mowry, *Chem. Rev.*, **42**, 189 (1948); T.Mukaiyama, K. Tonooka, and K. Inoue, *J. Org. Chem.*, **26**, 2202 (1961).
14) C. G. McCarty, "syn-anti Isomerisation and Rearrangements," in "The Chemistry of Carbon-Nitrogen Double Bond," ed by S. Patai, John-Wiley & Sons, New York (1970), pp. 363—464.
15) Z. W. Wolkowski, *Tetrahedron Lett.*, **1971**, 825.
16) H. Hjeds, K. P. Hansen, and B. Jerslev, *Acta Chem. Scand.*, **19**, 2166 (1965).
17) E. Vowinkel and J. Bartel, *Chem. Ber.*, **107**, 1221 (1974).
18) H. G. Foley and D. R. Dalton, *J. Chem. Soc., Chem. Commun.*, **1973**, 628.
19) D. C. Wigfield and F. W. Gowland, *Tetrahedron Lett.*, **1979**, 2209 and papers cited therein.
20) E. C. Ashby, J. Laemmle, and H. M. Neuman, *Acc. Chem. Res.*, **7**, 272 (1974); E. C. Ashby, *Pure Appl. Chem.*, **52**, 545 (1980).
21) E. C. Ashby and J. R. Bowers, Jr., *J. Am. Chem. Soc.*, **103**, 2242 (1981).

 © 1982 The Chemical Society of Japan Bull. Chem. Soc. Jpn., 55, 3273—3276 (1982)

Reactivities of Stable Rotamers. XI. Rotamer Distributions and Some Addition Reactions to the Carbonyl in 9-[2-(Substituted carbonyl)-1-naphthyl]fluorene Rotamers[1)]

Ryo Saito and Michinori Ōki*

Department of Chemistry, Faculty of Science, The University of Tokyo, Bunkyo-ku, Tokyo 113

(Received May 25, 1982)

Rotational isomers (*sp* and *ap*) of several 9-[2-(substituted carbonyl)-1-naphthyl]fluorenes where the substituent is methyl, phenyl, hydroxyl, methoxyl, 1-imidazolyl, or others have been obtained as stable entities. Barriers to rotation in these compounds were *ca.* 26.5 kcal for the process *sp*→*ap* but those for the reverse (*ap*→*sp*) were dependent on the substituent, ranging from 23.8 to 25.3 kcal/mol at 55 °C. The difference is reflected in the populations of rotamers: if the substituent is a hydroxyl, the *sp*/*ap* value becomes as large as *ca.* 20. The relative instability of the *ap* form was attributed to twisting of the carbonyl plane from that of naphthalene. Infrared spectra support the twisting. Addition reactions to the carbonyl occur smoothly in the *sp* conformation but they do not occur to a detectable extent in the *ap* conformation, if the substituent on the carbonyl is larger than hydrogen. The results are attributed to the steric effect of the fluorene ring.

In a previous paper,[1)] we have demonstrated that some reactions which take space-demanding transition states are very slow in an *ap* conformation, relative to the *sp*, of 9-(2-formyl-1-naphthyl)fluorene (**1a**). In contrast, an addition reaction of hydroxylamine to the carbonyl of *ap*-**1a** proceeded with a rate comparable with that of the *sp* form. The results imply that the transition state for the addition is not bulky: it may be assumed that, in the transition state for the addition where a tetrahedral carbon is developing from a trigonal, the hydrogen of the formyl group comes closely to the fluorene ring to minimize the transition state energy.

Then a question arises: what will happen when a bulkier substituent than hydrogen has to take a position which is close to the fluorene ring in the transition state of a reaction in the *ap* form? From our previous work, we collect that 9-(2-*t*-butylphenyl)fluorene exists as an *sp* conformation only.[2)] 9-(8-Methyl-1-naphthyl)-fluorene gives an equilibrium constant (*sp*/*ap*) of 25.[3)] These results suggest that, if a bulky group has to take a position which is close to the fluorene ring during a reaction in the *ap* form, the free energy of activation is different by 2 kcal/mol (1 cal=4.18 J) or more between *sp* and *ap* conformations. This should give a very large k_{sp}/k_{ap} value and may result in chemoselective reactions which occur in *sp* conformations only. To achieve this end, we carried out a series of addition reactions to carbonyls in ketones and acid derivatives. This paper reports results of such an investigation together with populations of rotamers and barriers to rotation in these compounds.

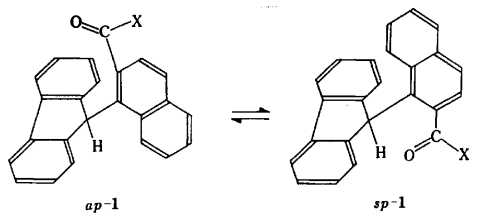

ap-1 ⇌ *sp*-1

a: X=H
b: X=CH_3
c: X=C_6H_5
d: X=OH
e: X=OCH_3
f: X=$OC_6H_4NO_2$-*p*
g: X=1-Imidazolyl
h: X=Cl

Barriers to Rotation and Populations of Rotamers. The assignment of the conformation of 9-[2-(substituted carbonyl)-1-naphthyl]fluorene (**1**) relies upon ^1H NMR spectral features as reported in previous papers. If the substituent has proton(s) not far from the carbonyl, the proton signal of the *ap* form appears in a high field relative to the *sp* form because of the ring current effect of fluorene. If there is no proton close to the carbonyl in the substituent, we use the method of preparation because barriers to rotation are high enough to retain the conformation when the reaction is carried out at room temperature. As an auxilary support, we may use the chemical shift of the 8-proton in the naphthalene ring: in the *ap* conformation, the proton is close to the plane of fluorene to give a signal at a very low field, whereas, in the *sp* conformation, the 8-proton is over the fluorene ring to exhibit a signal at a high field. It is interesting to note that the 8-H signal appears as an apparent doublet in the *sp* conformation, whereas it is often a multiplet in the *ap*.

Barriers to rotation were measured at one temperature. The measurement was carried out for the isomerization of *ap* forms because the *ap*'s are always minorities at equilibrium. The results are summarized in Table 1 together with those of the corresponding aldehyde (**1a**).[1)] Inspection of Table 1 reveals that the barriers to rotation for the process *sp*→*ap* are almost the same whereas those for the *ap*→*sp* processes vary to some extent. Although

Table 1. Barriers to rotation and equilibrium constants in 9-[2-(substituted carbonyl)-1-naphthyl]fluorene (**1**) in benzene-d_6 at 55 °C

Substituent	$k(ap\rightarrow sp)/s^{-1}$	$\Delta G^{\ddagger}$/kcal mol^{-1}		$K(sp/ap)$
		ap→*sp*	*sp*→*ap*	
H[a)]	1.28×10^{-5}	26.7	26.9	1.5
CH_3	2.64×10^{-4}	24.6	26.3	12
C_6H_5	1.86×10^{-4}	24.9	26.6	13
OH[b)]	0.98×10^{-3}	23.8	25.7	~20
OCH_3	9.45×10^{-5}	25.3	26.6	7

a) Hexachlorobutadiene solvent. b) Dimethyl-d_6 sulfoxide solvent.

solvents are different, at least we may compare the barriers including that for the carboxylic acid (**1d**). At any rate, reactivities of rotamers may be investigated without complication due to isomerization, if a reaction is carried out at room temperature, except for the *ap*-carboxylic acid (**1d**). Although not determined, other carbonyl compounds may be assumed to possess similar barriers to rotation.

The barriers of the carbonyl compounds are lower than the corresponding compounds carrying an sp^3-carbon substituent in the 2-position of the naphthalene ring.[4] This must be attributed to the relative size of the carbonyl group, since the van der Waals radius of a methyl group (2.0 Å) is known to be larger than the half-thickness of a π-system (1.8 Å), as discussed before.[1] The lowering of the transition state for rotation by introduction of a π-system, in place of a tetrahedral carbon, to the 2-position of naphthalene is more important than the effect in the ground state.

Similar barriers to rotation for the *sp*→*ap* process for all the compounds examined here mean that the energy difference between the ground state and the transition state for rotation is also similar. If we can assume that the main contribution to the transition state energy is the interaction of the carbonyl oxygen with the fluorene ring, then the ground state conformation will also have the carbonyl oxygen in similar situations. The barrier is highest when the substituent X is hydrogen. Similar barriers to rotation for all the compounds for the *sp*→*ap* process suggest that the lower barriers to rotation in **1b**, **1c**, and **1e** for the *ap*→*sp* process may be attributed to destabilization of the ground state in the *ap* form. Indeed, all the compounds, **1b**—**e**, have larger equilibrium constants (*sp*/*ap*) than **1a** in favor of the *sp* form.

Molecular models of these compounds suggest that, if the carbonyl group takes a planar conformation with the naphthalene ring, either the carbonyl-oxygen or the substituent X gives a severe interaction with the fluorene ring. Thus the carbonyl may not be coplanar with the naphthalene. In contrast, the formyl group can be coplanar with the naphthalene, if the hydrogen directs toward the fluorene ring. In order to get support for the suggestion by the model, infrared C=O stretching spectra were recorded. The results are given in Table 2.

Table 2. Infrared carbonyl stretching frequencies of 9-[2-(substituted carbonyl)-1-naphthyl]-fluorene (1)

Substituent	$\nu_{C=O}/cm^{-1}$			
	sp		*ap*	
	Solid	CCl_4 soln[a]	Solid	CCl_4 soln[a]
H	1672 1690 (sh)	1682 (329) 1700 (321)	1672	1692 (627)
CH_3	1688	1692 (378)	1700	1702 (279)
C_6H_5	1665	1688 (354)	1660	1665 (346)
OH	1680	1688 (934)	1700	1700 (374)
OCH_3	1708	1722 (560)	1720	1728 (459)

a) Numericals in parentheses are molecular extinction coefficients.

Although not observed for the benzoyl compound (**1c**), the carbonyl stretching frequencies for the *ap* forms are generally at higher wave numbers than those due to the *sp* forms. In contrast, the aldehydes (**1a**) show $\nu_{C=O}$ absorptions at about the same frequencies, though the *sp* form gives bifurcated bands probably due to the Fermi resonance. This suggests that the conjugation of the carbonyl with the naphthalene ring is diminished in these compounds and the two groups are not coplanar.[5] Benzophenone derivatives are insensitive to the steric environment because even the simplest example is not coplanar because of the steric effect.[6] Thus the population ratios and the relative barriers to rotation for the *ap*→*sp* process are explained by the destabilization of the *ap* forms.

Even though the above conclusion is reached, the instability of the *ap*-carboxylic acid (**1d**) relative to the *sp* form is unusual. We have tried to increase the population of the *ap* form by various methods, including solvent-change and acidification of a basic solution of **1d** in water, without success. Baeyer-Villiger oxidation of the aldehyde (**1a**) afforded formates instead of the corresponding acid probably due to the steric effect.[7] We suspect that extra stabilization is obtained by the dimeric hydrogen bonds in the *sp* conformation whereas the dimer is unfavorable in the *ap* conformation because of the steric effect.

Conformer distribution in 9-[2-(*p*-nitrophenoxycarbonyl)-1-naphthyl]fluorene (**1f**) is interesting because the *sp*/*ap* value is *ca.* 4 which is small relative to the corresponding methyl ester (**1e**). We wish to attribute the phenomenon to the charge-transfer interaction between the *p*-nitrophenyl group and the fluorene, which stabilizes the *ap* form of **1f**. Such a stabilization of the *ap* form in *p*-nitrobenzoate of 9-(2-hydroxy-1-naphthyl)-fluorene has been reported.[8]

Reactions. The reaction of carbonyl groups proceeds smoothly if the conformation is *sp*. Esterification of *sp*-carboxylic acid (**1d**) proceeded to give *sp* form of the methyl ester (**1e**). The *sp*-**1e** could be equilibrated by heating its solution. The conformational isomers (*ap* and *sp*) were separated. The attempted hydrolysis of the ester was too slow to be suitable for the comparative study of the reactivities of conformational isomers at room temperature. *p*-Nitrophenyl esters (**1f**), though they have been known to be hydrolyzed more easily than alkyl esters,[9] resisted hydrolysis as well. In an effort of searching more easily hydrolyzable acid derivatives, imidazolide (**1g**)[10] was prepared from the *sp*-acid. After equilibration, the rotational isomers (*ap* and *sp*) were isolated. Hydrolysis of the imidazolide in acidic aqueous acetone afforded *sp*-acid (**1d**) from the *sp*-imidazolide but the *ap* form resisted the hydrolysis at room temperature.

Addition of methylmagnesium iodide to *sp*-9-(2-acetyl-1-naphthyl)fluorene (**1b**) proceeds smoothly to afford *sp*-9-[2-(1-hydroxy-1-methylethyl)-1-naphthyl]-fluorene. Attempted isomerization of this compound failed to give any sign of the presence of its *ap* isomer: this type of rotamer distribution is known, if the aryl group in 9-arylfluorene carry a large group on one side.[2,3] In contrast, *ap*-**1b** did not show evidence that

he reaction occurred. Likewise, sodium tetrahydridoborate reduction of the acetyl compound (**1b**) proceeds smoothly if the conformation is *sp*, but does not proceed if the conformation is *ap*.

These reactivities of the substituted carbonyl compounds make a sharp contrast to those of the aldehyde (**1a**). In the aldehyde, the relative reactivities toward Grignard additions and sodium tetrahydridoborate reduction were 1.7 and 7.6, respectively.[1] Therefore, the addition reaction of the substituted carbonyl compounds (**1b** and **1g**) was definitely slow in the *ap* conformation. The reason for the difference must be of the steric origin. Molecular models suggest that, if it is the aldehyde, the change from the sp^2-carbon to the sp^3-carbon by addition is not too difficult because the hydrogen of the formyl group can direct toward the fluorene ring, the steric hindrance being not large. In contrast, if it is a ketone or an acid derivative, the formation of the tetrahedral carbon by addition is prohibitive, because either oxygen or carbon must become closely located to the fluorene ring. Thus the activation energy must be very high for the *ap* conformation, if the addition to the carbonyl is to occur.

From the stand point discussed above, it is interesting to note that the acid chloride (**1h**) is easily hydrolyzed to yield the corresponding carboxylic acid (**1d**) even in the *ap* conformation. It may be plausible to assume that the addition of water to the carbonyl moiety is also slow in *ap*-**1h**, although this is believed to be the initial step in the hydrolysis of acid chlorides.[11] It is possible that *ap*-**1h** dissociates to the acyl carbonium ion and the chloride ion, of which the former reacts with water to give the *ap*-carboxylic acid, although definitive support is lacking.

Experimental

*9-(2-Methoxycarbonyl-1-naphthyl)fluorene (**1e**).* A solution of 0.80 g *sp*-9-(2-carboxy-1-naphthyl)fluorene (**1d**)[1] in 70 mL of methanol was refluxed for 25 h with 2 mL of concentrated sulfuric acid. The mixture was concentrated and poured into water. After extraction with ether followed by washing and drying, the product was separated by silica gel chromatography (benzene eluent) to give 0.69 g of the *sp* ester and 0.09 g of the *ap*.

ap-**1e**, mp 130—131 °C. Found: C, 85.81; H, 5.11%. Calcd for $C_{25}H_{18}O_2$: C, 85.69; H, 5.18%. ^{1}H NMR ($CDCl_3$, δ): 2.83 (3H, s), 6.10 (1H, s), 7.10—8.10 (13H, m), 8.53—8.77 (1H, m).

sp-**1e**, mp 133—134 °C. Found: C, 85.73; H, 4.90%. Calcd for $C_{25}H_{18}O_2$: C, 85.69; H, 5.18%. ^{1}H NMR ($CDCl_3$, δ): 3.95 (3H, s), 6.20 (1H, s), 6.56 (1H, d, J=9.0 Hz), 6.70—7.96 (13H, m).

*9-[2-(1-Imidazolylcarbonyl)-1-naphthyl]fluorene (**1g**).* A mixture of 0.10 g of *sp*-**1d** and 5 mL of thionyl chloride was heated under reflux for 1 h and then excessive thionyl chloride was removed *in vacuo*. The residue was taken up in 20 mL of dichloromethane and was stirred with 0.1 g of imidazole for 30 min. The solvent was evaporated and the residue was purified by preparative TLC on silica gel (dichloromethane solvent) to give *sp*-**1g**, mp 133.5—138.0 °C (decomp), almost quantitatively. High resolution mass spectrum exhibited a molecular ion peak at *m/e* 386.1461, whereas the calculation for $C_{27}H_{18}N_2O$ requires 386.1420. ^{1}H NMR ($CDCl_3$, δ): 5.43 (1H, s), 6.62 (1H, d, J=9.0 Hz), 6.83—8.17 (16H, m).

When the reaction products taken up in dichloromethane was heated for 2 h, a *ca.* 5 : 1 mixture of *sp*- and *ap*-**1g** was obtained. This isomerization was probably catalyzed by imidazole. After evaporation of the solvent, the mixture was separated by preparative TLC as above to give pure *ap*-**1g**, mp 253—257 °C (decomp). High resolution mass spectrum exhibited a molecular ion peak at *m/e* 386.1462, whereas $C_{27}H_{18}N_2O$ requires 386.1420. ^{1}H NMR ($CDCl_3$, δ): 6.17 (1H, s), 6.60—8.20 (16H, m), 8.63—8.88 (1H, m).

*Acid Hydrolysis of Imidazolide (**1g**).* To a solution of 20 mg of *sp*-**1g** in 15 mL of acetone, 5 mL of water and 1 mL of concentrated hydrochloric acid were added and the mixture was allowed to stand overnight. The mixture was poured into water and extracted with ether. The ether extract gave *sp*-acid (**1d**) almost quantitatively.

A similar treatment of *ap*-**1g** gave no carboxylic acid but the imidazolide was recovered in good yield.

*9-[2-(p-Nitrophenoxycarbonyl)-1-naphthyl]fluorene (**1f**).* The acid chloride (**1h**) was prepared from 100 mg of the *sp*-acid (**1d**) and 5 mL of thionyl chloride as above. The chloride was dissolved in 20 mL of dichloromethane and stirred with 0.5 mL of pyridine and 100 mg (2.4 equiv.) of *p*-nitrophenol for 30 min at room temperature. After evaporation of the solvent, the residue was taken up in ether and washed with water. The ethereal layer was dried and evaporated. The residue was submitted to TLC on silica gel (2 : 1 benzene–hexane solvent) to give *ca.* 70 mg of *sp*-**1f**, mp 166—167 °C. Found: C, 78.65; H, 4.03; N, 3.06%. Calcd for $C_{30}H_{19}NO_4$: C, 78.76; H, 4.19; N, 3.06%. ^{1}H NMR ($CDCl_3$, δ): 6.38 (1H, s), 6.66 (1H, d, J=8.7 Hz), 6.7—8.3 (17H, m). IR (KBr disk): 1740, 1523, 1347 cm^{-1}.

The *sp* form of **1f** in benzene was refluxed overnight to give a 4 : 1 *sp* and *ap*-**1f**. The solvent was evaporated and the residue was submitted to TLC as above to give pure *ap*-**1f**, mp 162—163 °C. Found: C, 78.42; H, 3.96; N, 3.00%. Calcd for $C_{30}H_{19}NO_4$: C, 78.46; H, 4.19; N, 3.06%. ^{1}H NMR ($CDCl_3$, δ): 6.17 (1H, s), 6.33 (2H, d, J=9.0 Hz), 7.1—8.4 (15H, m), 8.57—8.85 (1H, m). IR (KBr disk): 1748, 1520, 1350 cm^{-1}.

Attempted Hydrolysis of p-*Nitrophenyl Ester (**1f**).* A solution of 30 mg of *sp*-**1f** in 5 mL of acetic acid was left to stand for a week at room temperature with 5 mL of water and 1 mL of concentrated sulfuric acid. No carboxylic acid (**1d**) was detected after this period and the ester was recovered almost quantitatively. Similarly *ap*-**1f** was recovered after attempted hydrolysis.

ap-*9-(2-Carboxy-1-naphthyl)fluorene* (ap-**1d**). The corresponding acid chloride (**1h**), prepared from 0.1 g of the *sp*-acid and 5 mL of thionyl chloride as described above, was dissolved in 20 mL of acetone and was treated with 5 mL of water at *ca.* 0 °C. After 1 h, the product was taken up in ether and evaporated. Preparative TLC on silica gel (ethyl acetate–dichloromethane 1 : 2) afforded *ca.* 5 mg of the *ap*-acid, mp 226—228 °C, and *ca.* 60 mg of *sp*-acid. High resolution MS showed a molecular ion peak at 336.1159, whereas the molecular formula $C_{24}H_{16}O_2$ requires 336.1151. ^{1}H NMR ($CDCl_3$, δ): 6.08 (1H, s), 7.07—8.07 (13H, m), 8.53—8.83 (1H, m).

*Addition of Methylmagnesium Iodide to 9-(2-Acetyl-1-naphthyl)-fluorene (**1b**).* A 2 mL portion of a Grignard reagent, which was prepared from 0.77 mL of methyl iodide, 0.25 g of magnesium, and 10 mL of ether, was added to 30 mg of *sp*-**1b**[1] and the mixture was allowed to stand for 1.5 h. The mixture was decomposed with 5% aqueous ammonium chloride and the product was treated in a usual manner. *sp*-9-[2-(1-Hydroxy-1-methylethyl)-1-naphthyl]fluorene, mp 133—134

°C was obtained almost quantitatively. Found: C, 89.20; H, 6.18%. Calcd for $C_{26}H_{22}O$: C, 89.11; H, 6.33%. ^{1}H NMR ($CDCl_3$, δ): 1.97 (6H, s), 6.81 (1H, s), 6.43 (1H, d, J=9.0 Hz), 6.63—8.00 (13H, m). The OH proton was not detected.

Similar treatment of *ap*-**1b** gave no sign of the reaction. The starting material was recovered almost quantitatively.

*Reduction of 9-(2-Acetyl-1-naphthyl)fluorene (**1b**) with Sodium Tetrahydridoborate.* A solution of 30 mg of *sp*-**1b** in 20 mL of methanol was mixed with 8 equivalents of sodium tetrahydridoborate. After 10 min, the mixture was poured into water and extracted with ether. The ethereal layer was washed and dried over magnesium sulfate. After evaporation of the solvent, the residue was found to be an almost pure *sp*-9-[2-(1-hydroxyethyl)-1-naphthyl]fluorene by its ^{1}H NMR spectrum.[1)]

The similar treatment of the *ap* form did not show any sign of the reduction. Although the same portions of sodium tetrahydridoborate were added three times to the mixture and the mixture was stirred for 80 more min at 0 °C and then for 1 h at room temperature, the *ap* form was recoved unreacted.

*Baeyer-Villiger Oxidation of 9-(2-Formyl-1-naphthyl)fluorene (**1a**).* To a solution of 20 mg of *ap*-**1a** in 20 mL of acetic acid was added 1 mL of a mixture prepared from 2 mL of 90% formic acid and 2 mL of 38% hydrogen peroxide. The whole was allowed to stand for 2 d and treated in a usual way. Purification of the product by chromatography on silica gel (benzene eluent) gave *ap*-9-(2-formyloxy-1-naphthyl)fluorene, mp 142—143 °C, almost quantitatively. Found: C, 85.73; H, 4.81%. Calcd for $C_{24}H_{16}O_2$: C, 85.69; H, 4.79%. ^{1}H-NMR ($CDCl_3$, δ): 5.90 (1H, s), 6.98 (1H, s), 6.90—8.07 (13H, m), 8.52 (1H, d, J=9.0 Hz). IR (KBr disk): 1740 cm^{-1}.

Similar treatment of *sp*-**1a** gave *sp*-(2-formyloxy-1-naphthyl)fluorene, oil, in *ca.* 50% yield. The *sp*-formate is relatively easily hydrolyzed and formation of *sp*-(2-hydroxy-1-naphthyl)fluorene was detected during silica gel TLC (benzene eluent). High resolution MS showed a molecular ion peak at *m/e* 336.1189, whereas calculation for $C_{24}H_{16}O_2$ requires 336.1151. ^{1}H NMR ($CDCl_3$, δ): 5.70 (1H, s), 6.45 (1H, d, J=9.0 Hz), 6.73—8.07 (13H, m), 8.47 (1H, s).

Barriers to Rotation. Pure *ap* isomer (30 mg) of the carbonyl compounds was dissolved in 0.4 mL of benzene-d_6 or dimethyl-d_6 sulfoxide and the solution was placed in an NMR sample tube. The tube was immersed in a boiling-acetone bath and the rate of isomerization was followed by ^{1}H NMR spectroscopy. The data were treated by assuming a reversible first order reaction to give a rate constant. The rate constant was put into the Eyring equation and the free energy of activation was obtained.

Spectral Measurement. Infrared spectra were obtained with a Hitachi EPI-G spectrophotometer. With solid samples, KBr discs were used. For the measurement of the spectra of solutions, the sample was dissolved in carbon tetrachloride to make up *ca.* 0.05 mol/L solution for the carbonyl region and a KBr cell of 0.25 mm length was used.

^{1}H NMR spectra were obtained with a Varian EM 390 spectrometer. The integration of peak areas was repeated several times and the average was used for the kinetic measurement.

References

1) Preceding paper: R. Saito and M. Ōki, *Bull. Chem. Soc. Jpn.*, **55**, 3267(1982).
2) M. Nakamura, N. Nakamura, and M. Ōki, *Bull. Chem. Soc. Jpn.*, **50**, 2986 (1977).
3) T. Mori and M. Ōki, *Bull. Chem. Soc. Jpn.*, **54**, 1199 (1981).
4) R. Saito and M. Ōki, *Bull. Chem. Soc. Jpn.*, **55**, 2508 (1982): S.Murata, T. Mori, and M. Ōki, *Chem. Lett.*, **1982**, 271.
5) L. J. Bellamy, "The Infra-Red Spectra of Complex Molecules," Methuen, London (1958), pp. 137—138.
6) G. M. Lobanova, *Kristallografiya*, **13**, 984 (1968); *Chem. Abstr.*, **70**, 41645c (1969); R. Hoffman and J. R. Swenson, *J. Phys. Chem.*, **74**, 415 (1970).
7) C. H. Hassall, *Org. React.*, **9**, 73 (1957).
8) J. Martinmaa and E. Tommila, *Suom. Kemistil.*, **40**, 222 (1967); *Chem. Abstr.*, **68**, 38909v (1968); M. L. Bender and B. W. Turnquest, *J. Am. Chem. Soc.*, **79**, 1652 (1957); R. L. VanEtten, J. F. Sebastian, G. A. Clowes, and M. L. Bender, *ibid.*, **89**, 3242 (1967). See also Ref. 10.
9) M. Nakamura and M. Ōki, *Chem. Lett.*, **1976**, 651.
10) J. Kerstein and W. F. Jencks, *J. Am. Chem. Soc.*, **86**, 4655 (1964).
11) C. A. Bunton and T. A. Lewis, *Chem. Ind. (London)*, **1956**, 180; E. R. A. Peeling, *J. Chem. Soc.*, **1959**, 2307.

 © 1982 The Chemical Society of Japan Bull. Chem. Soc. Jpn., 55, 3277—3282 (1982)

The Enantioselective Michael Addition of Thiols to Cycloalkenones by Using (2*S*, 4*S*)-2-Anilinomethyl-1-ethyl-4-hydroxypyrrolidine as Chiral Catalyst

Keisuke SUZUKI, Akihiko IKEGAWA, and Teruaki MUKAIYAMA*

Department of Chemistry, Faculty of Science, The University of Tokyo, Hongo, Bunkyo-ku, Tokyo 113

(Received May 24, 1982)

Catalytic asymmetric addition of thiols to 2-cycloalkenone was studied by using the chiral amino alcohols, derived from L-hydroxyproline or (*S*)-proline, as base catalysts. Detailed investigation was carried out on the effects of the structure of the catalyst, the reaction medium, the temperature, and the concentration on the enantioselectivity. Good optical yields (47—88%) were achieved by the reaction of arenethiols and 2-cyclohexen-1-one in toluene at −5 °C, by using the catalyst (2*S*, 4*S*)-2-anilinomethyl-1-ethyl-4-hydroxypyrrolidine.

Considerable attention has been focused on the asymmetric synthesis in the past decade, and a remarkable progress has made it one of the powerful tools in the preparation of chiral natural products.[1] Most of the fruitful cases to date are classified as "stoichiometric asymmetric synthesis," that is, a stoichiometric amount of chiral source is effectively used with the aid of the electronic and steric factors to obtain the desired chiral compound in high optical purity. However, from the synthetic point of view it suffers a fatal and inevitable disadvantage, namely, the separation of the chiral source from the reaction products. In this sense the development of "catalytic asymmetric synthesis" is very attractive and highly desirable in synthetic organic chemistry.

Concerning the catalytic asymmetric synthesis, there have been reported only limited successful examples, and most of them belong to the following two classes of reactions: i) The chiral transition-metal complex catalyzed reactions including the fruitful asymmetric hydrogenations—in this field, a rapid progress has been made recently; Sharpless' V catalyzed oxidation,[2a] Kumada's Ni catalyzed cross-coupling reaction,[2b] Otsuka's aymmetric isomerization,[2c] and so on. ii) The chiral base catalyzed reaction——although this type of reactions has been known for years, successful cases are rare; Wynberg has successfully employed cinchona alkaloids as chiral catalysts in the asymmetric Michael addition of thiols or β-keto esters,[3a,3b] and Cram reported the highly stereoselective Michael addition of β-keto esters using chiral crown ethers complexed to potassium base.[3c]

Recently we reported several types of successful asymmetric reactions based on the chiral pyrrolidine derivatives,[4] and this prompted us to undertake the exploration of the catalytic asymmetric synthesis using optically active pyrrolidine derivatives as chiral catalysts. It was found that (2*S*,4*S*)-2-anilinomethyl-1-ethyl-4-hydroxypyrrolidine (**5a**) is a quite efficient catalyst for the asymmetric addition of arenethiols to 2-cyclohexen-1-one and the optical yield as high as 88% was realized under the specified conditions as briefly reported in the previous communication.[5] Herein, we describe the results of the detailed investigation on the effects of the structure of the catalyst, the reaction medium, the temperature, and the concentration on the enantioselectivity.

Results

Chiral Catalysts. Chiral catalysts employed in the present study are derived from natural amino acids, L-hydroxyproline and (*S*)-proline. (2*S*,4*S*)-1-Benzyloxycarbonyl-4-hydroxyproline (Z-allohydroxyproline)[6] was treated with Ac_2O-pyridine to give the acetate **1**, which was condensed with several kinds of amines to afford the corresponding amides **2a**—**e**, respectively. Hydrogenation of **2a**—**e** on 10% Pd-C in MeOH gave the amines **3a**—**e**, which were successively acylated (**4a**—**f**), and reduced ($LiAlH_4$-THF) to give the chiral catalysts **5a**—**f**. The chiral catalysts **5g** and **5h** were also prepared by the similar procedure starting from (2*S*,4*R*)-1-benzyloxycarbonyl-4-hydroxyproline[6] (**1g**) and (*S*)-1-benzyloxycarbonylprolinanilide (**2h**).[4] The catalyst **5i** was prepared by the reduction of the

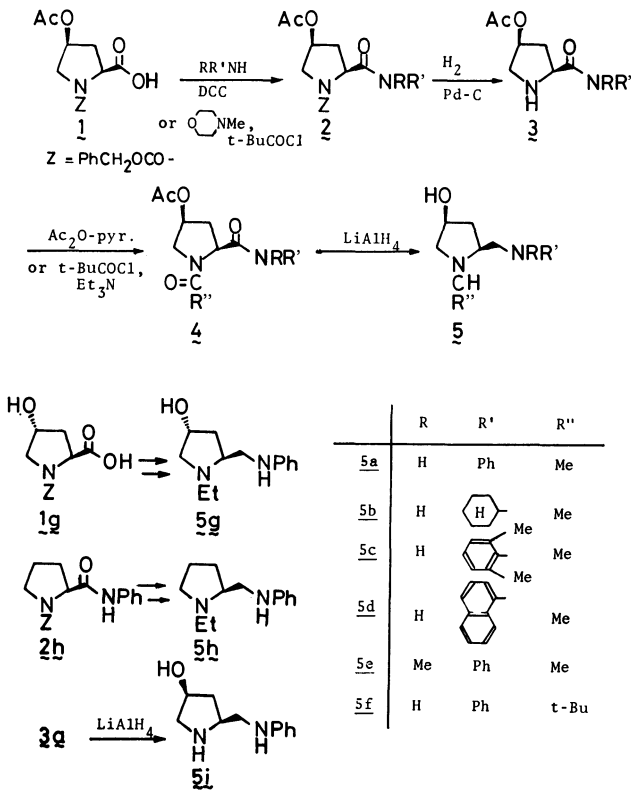

Fig. 1. Preparation of the catalysts.

Table 1. Effects of the structure of the catalysts in the asymmetric addition of benzenethiol to 2-cyclohexen-1-one

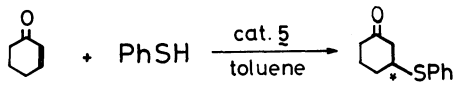

Entry	Catalyst	Yield/%	$[\alpha]_{577}^{21}$/°	Opt.yield/%[a]
1	**5a**	86	+48.7	67
2	**5b**	90	+24.6	34
3	**5c**	67	+50.1	69
4	**5d**	90	+52.5	72
5	**5e**	81	+41.6	57
6	**5f**	24	+19.0	26
7	**5g**	84	+ 7.1	10
8	**5h**	68	+ 0.9	3
9	**5i**	89	+15.4	21

a) Optical yields were calculated based on the reported value in Ref. 3a.

Table 2. Effects of the reaction medium

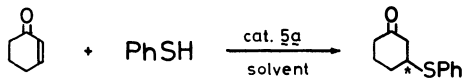

Entry	Solvent	Yield/%	Opt.yield/%
1	Petroleum ether	94	14
2	Cyclohexane	79	30
3	CH_2Cl_2	76	49
4	CCl_4	88	64
5	Benzene	87	65
6	Toluene	86	67
7	EtOH	91	0.1

amine **3a** with $LiAlH_4$ (Fig. 1).

The Structure of the Catalysts. Of the chiral bases **5a**—**i** thus prepared, the suitable structure of the catalyst for the asymmetric Michael addition of benzenethiol to 2-cyclohexen-1-one was pursued. The general reactions were carried out according to the following procedure: In the presence of 0.04 mmol of the catalyst (**5a**—**i**), 2-cyclohexen-1-one (5 mmol) in toluene (5 ml) and benzenethiol (4 mmol) in toluene (5 ml) were admixed and kept standing for 2 d. After the usual work-up (see Experimental section), the optical rotation of the resulting 3-phenylthio-1-cyclohexanone was measured in benzene at 21 °C.

The results are summarized in Table 1. The most noteworthy point is the pivotal role of the hydroxyl group in the enantioselection (entry 1, 7, 8). Obviously, the β-oriented hydroxyl group of the catalyst **5a** directs the stereochemical course of the present reaction, and either the absence or the difference of the orientation of the hydroxyl group of the pyrrolidine ring causes great diminution of the enantioselectivity. While the optical yields were fairly good in cases of the catalysts bearing an aromatic ring (**5a**, **5c**, **5d**), substantial decrease of the e.e. was observed when the catalyst (**5b**) lacked an aromatic ring. When the catalysts **5e**, **5i**, in which both of the amino groups are tertiary and secondary, respectively, were employed, the optical yields were reduced as compared with the case of the catalyst **5a** (entry 1, 5, 9). The poor chemical yield found for the entry 6 is attributable to the decrease of the basicity of the amine **5f** by virtue of the bulky substituent. Thus, it was noted that a slight change in the structure of the catalyst causes a great change in the optical yield in the present reaction and good results are obtained when the catalysts **5a**, **5c**, or **5d** were employed.

Table 3. Effects of the reaction temperature

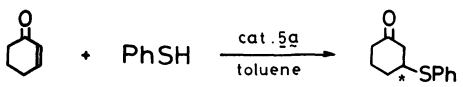

Entry	Temperature/°C	Yield/%	Opt.yield/%
1	50	88	58
2	25	86	67
3	−5	90	70
4	−20	72	69

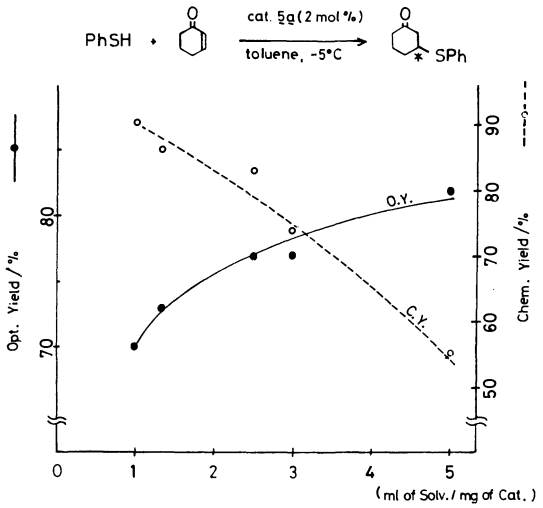

Fig. 2. Effect of the concentration.

Effect of the Reaction Medium. Next, we examined the effect of the reaction medium on the asymmetric induction. The addition of benzenethiol to 2-cyclohexen-1-one was performed in several kinds of solvents using **5a** as the chiral catalyst (Table 2).

It is noted that the optical yields were strongly dependent on the nature of the solvent used. Better results were obtained in nonpolar aromatic solvents (entry 5, 6) or carbon tetrachloride than the solvent like hydrocarbon or dichloromethane. In the case of ethanol, almost no enantioselection was observed.

Effect of the Reaction Temperature. In order to examine the influence of the reaction temperature on the optical yield, the aforementioned reaction was carried out in toluene at various temperatures ranging over −20 °C to 50 °C, and the results are shown in Table 3.

Although a slight decrease of the optical yield at a higher temperature (entry 1) was observed, the effect of the temperature is as a whole not so remarkable in

Table 4. Asymmetric Michael addition of various thiols to 2-cycloalkenones

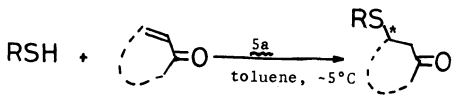

Entry	R	Enone	Yield/%	Opt.yield/%
1			83	77
2			75	73
3			84	47
4			75	83
5			74	88
6	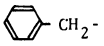		22	1
7			85	11
8			64	38
9			74	42

the present reaction.

Effect of Concentration. As the concentration of the reactants is considered to be a significant reaction parameter, the reaction was carried out at various concentration. With the molar ratio of each substrate held constant, the volume of the solvent employed was gradually increased. Figure 2 shows the chemical and optical yields dependence on the concentration.

An increase in the optical yield was observed under higher dilution condition at the expense of the reaction rate, and the concentration of 2 or 3 (ml toluene/mg catalyst) appears to strike the proper balance, producing the optically active adduct without suffering a significant decrease in the chemical yield.

Reaction with Various Thiols and Enones. Under the optimized conditions, the Michael additions of several other thiols to conjugated cycloalkenones were performed (Table 4).

The additions of aromatic thiols to 2-cyclohexen-1-one gave satisfactory results. Among them, the addition of *p-t*-butylbenzenethiol furnished the adduct in 88% optical purity where the *R* enantiomer was predominantly formed.[3a] On the other hand the alkanethiol (entry 6) gave a poor result, and this may be attributable to the difference of the pK_a values of the thiols. The addition of *p-t*-butylbenzenethiol to the other cycloalkenones gave the adducts in moderate optical yields.

Discussion

From the correlation between the structure of the catalyst and the enantioselectivity described above, we can now elucidate the mechanism of the enantioselection, briefly described in our previous paper.[5] Concerning this point, Wynberg *et al.* proposed a mechanism mainly based on the kinetic measurement and the structures of the substrates in their pioneering work on the cinchona alkaloid catalyzed asymmetric thiol addition.[3a] In our case, various sterically modified analogs of the base catalyst are readily available, and the elucidation of the mechanism depends mainly on the effects of the structure of the catalyst on the optical yields. From the experimental results, three notable points must be taken into consideration, namely, i) the role of the hydroxyl group of the catalyst, ii) the role of the aromatic ring, and iii) the absolute configuration of the predominantly formed enantiomer (*R*). With these in mind, and from the CPK model inspection, we propose the following mechanistic pathway (Fig. 3).

At the first stage of the reaction, the ammonium thiolate complex is formed, where the ammonium counterpart has a 5-5 fused rigid structure[4,5] by virtue of a hydrogen bonding as illustrated in **A**. This rigid structure is supposed to be a crucial factor in the enantioselection, because the enantioselectivity decreased when the substituent of the amine became more bulky, where the above structure is no longer a preferred one. Moreover, in a solvent like toluene, the thiolate anion is stabilized by π-π interaction, and the freedom of its location is further limited by the interaction with the aromatic ring of the catalyst. At the next stage, the approach of the cyclohexenone to the complex **A** takes place with a hydrogen-bond interaction between the carbonyl group and the hydroxyl group of the catalyst. In a protic solvent like ethanol, this interaction must be cancelled to result in no enantioselection. Finally, the attack of the thiolate anion to the enone occurs, where two pathways **B** and **C** are possible. In case of the pathway **C**, the steric congestion of the anilino

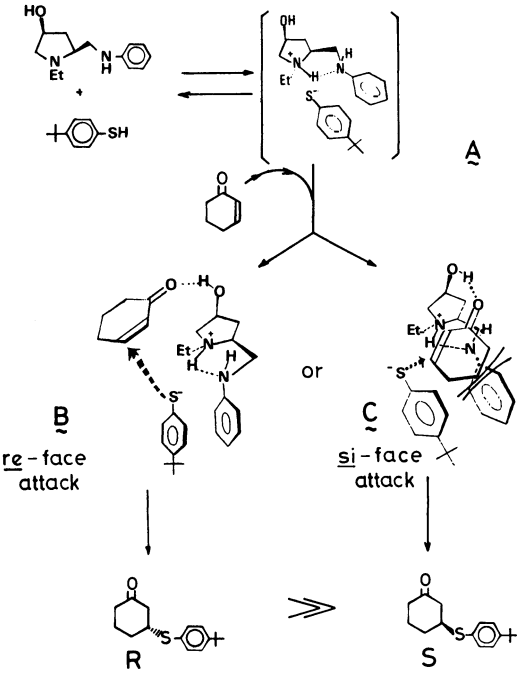

Fig. 3. Mechanism of the enantioselection.

group and the cyclohexenone ring may prevent the complex **A** and the enone from reaching the transition state, thus the preferential attack on the *re*-face of 2-cyclohexen-1-one, through the pathway **B**, takes place resulting in the predominant formation of the *R* enantiomer.

In conclusion, it is noted that the chiral amino alcohol **5a** is a highly efficient catalyst in the asymmetric Michael addition of aromatic thiols to 2-cyclohexen-1-one, and higher optical yields are realized in comparison with the earlier methods.

Experimental

General. Melting and boiling points are uncorrected. ^{1}H NMR spectra were recorded on a Varian EM-390 spectrometer with Me_4Si as an internal standard. IR spectra were taken on a Hitachi 260-30 spectrophotometer. MS data were obtained on a JEOL JMS-D 300 mass spectrometer at 70 eV. Optical rotations were measured on a JASCO DIP-181 polarimeter. All the solvents used were purified according to the standard procedure and stocked over molecular sieves 4A.

Materials. L-Hydroxyproline was kindly supplied from Ajinomoto Co., Inc., and was used without further purification. All the other reagents were commercially obtained and purified by distillation or recrystallization before use.

Preparation of (2S, 4S)-4-acetoxy-1-benzyloxycarbonylproline (1) To a suspension of (2*S*, 4*S*)-1-benzyloxycarbonyl-4-hydroxyproline[6] (10.8 g, 40.8 mmol) in CH_2Cl_2 (50 ml) was added acetic anhydride (6.50 g, 63.7 mmol), pyridine (13 ml) and catalytic amount of DMAP, and the resulting solution was stirred for 6 h at room temperature. The solvent was evaporated *in vacuo*, diluted with AcOEt, and washed with 2 mol dm^{-3} HCl saturated with NaCl. The organic layer was extracted with 4% aqueous $NaHCO_3$ solution, and the alkaline solution was washed with AcOEt, acidified with 6 mol dm^{-3} HCl and back-extracted with AcOEt (×3). The combined organic layer was washed with brine, dried over Na_2SO_4. Concentration under reduced pressure gave **1** as white crystals (9.39 g, 75%): mp 107—108 °C; $[\alpha]_D^{27}$ −58.7° (*c* 1.03, $CHCl_3$); IR (KBr disk) 1740, 1700, 1680, 1580, 1500, 770, and 700 cm^{-1}; NMR ($CDCl_3$) δ=1.9 (2H, s), 2.2—2.5 (2H, m), 3.6—3.7 (2H, m), 4.3—4.7 (1H, m), 5.1 (3H, s), and 10.5 (1H, s). Found: C, 58.76; H, 5.49; N, 4.47%. Calcd for $C_{15}H_{17}NO_6$: C, 58.63; H, 5.57; N, 4.56%.

(2S,4S)-2-Phenylcarbamoyl-1-benzyloxycarbonyl-4-pyrrolidinyl Acetate (2a). To a THF (40 ml) solution of the acetate **1** (9.10 g, 29.6 mmol) and *N*-methylmorpholine (3.00 g, 29.6 mmol) was slowly added a THF (5 ml) solution of pivaloyl chloride (3.31 g, 29.6 mmol) at −45 °C, and the mixture was gradually warmed to −15 °C during 30 min, stirred for further 30 min at the temperature, and cooled to −45 °C again. A THF (5 ml) solution of aniline (2.77 g, 29.7 mmol) was slowly added to this mixture, and the temperature was gradually raised to room temperature and kept for 4 h. Solvent was removed under reduced pressure, and the residue was taken up in AcOEt, washed successively with brine, ice-cold 1 mol dm^{-3} HCl, brine, ice-cold 4% $NaHCO_3$ solution, and dried over Na_2SO_4. After evaporation of the solvent, the residue was purified on a silica-gel column (AcOEt–hexane 3 : 2) to give white crystals in 75% (8.44 g) yield: mp 87—93 °C; $[\alpha]_D^{27}$ −65.4° (*c* 1.01, $CHCl_3$); IR (KBr disk) 3350, 1720, 1680, 1590, 1490, 750, and 690 cm^{-1}; NMR ($CDCl_3$) δ=1.9 (3H, s), 2.0—2.7 (2H, m), 3.4—3.7 (2H, m), 4.3—4.6 (1H, dd, J_1=3 Hz, J_2=9 Hz), 5.1 (3H, s), 6.9—7.5 (5H, m), and 7.2 (5H, m). Found: C, 66.16; H, 5.80; N, 7.30%. Calcd for $C_{21}H_{22}N_2O_5$: C, 65.96; H, 5.80; H, 7.33%.

(2S,4S)-1-Benzyloxycarbonyl-2-cyclohexylcarbamoyl-4-pyrrolidinyl Acetate (2b). A CH_2Cl_2 solution (2 ml) of the acetate **1** (152 mg, 0.50 mmol) was added at 0 °C to a solution of dicyclohexylcarbodiimide (107 mg, 0.52 mmol) in CH_2Cl_2 (1 ml) and the mixture was stirred for 20 min. Then a CH_2Cl_2 (1 ml) solution of cyclohexylamine (54 mg, 0.55 mmol) was added dropwise to the mixture, and the resulting mixture was stirred for 4 h, while gradually warmed up to room temperature, and stirred overnight. The reaction mixture was concentrated and the residue was suspended with AcOEt and filtered off. The filtrate was washed successively with 10% citric acid solution (5 ml×3), brine (5 ml×1), ice-cold 4% $NaHCO_3$ solution (5 ml×3), and brine (5 ml×1), dried over Na_2SO_4 and concentrated to afford crude crystals of the amide **2b** (220 mg), The crystals were further purified with SiO_2 TLC (AcOEt–hexane) to give white crystals in 95% (192 mg) yield. Mp 85—87 °C; $[\alpha]_D^{21}$ −37.6° (*c* 0.95, CH_2Cl_2); IR (KBr disk) 3330, 1740, 1700, 1660, and 730 cm^{-1}; NMR ($CDCl_3$) δ=0.7—2.1 (10H, m), 1.9 (3H, s), 2.1—2.9 (2H, m), 3.2—4.0 (3H, m), 4.4 (1H, dd, J_1=8 Hz, J_2=3 Hz), 5.1 (2H, s), 5.1—5.3 (1H, m), 6.0—6.4 (1H, broad), 7.5 (5H, s). Found: C, 65.19; H, 7.18; N, 7.47%. Calcd for $C_{21}H_{28}N_2O_5$: C, 64.93; H, 7.27; N, 7.21%.

(2S,4S)-1-Benzyloxycarbonyl-2-(2,6-xylylcarbamoyl)-4-pyrrolidinyl Acetate (2c): Yield 76%; mp 123—125 °C; $[\alpha]_D^{24}$ −54.9° (*c* 1.01, CH_2Cl_2); IR (KBr disk) 3260, 1740, 1710, 770, and 700 cm^{-1}; NMR ($CDCl_3$) δ=2.0 (3H, s), 2.2 (6H, s), 2.1—2.9 (2H, m), 3.5—4.1 (2H, m), 4.6 (1H, dd, J_1=9 Hz, J_2=3 Hz), 5.2 (2H, s), 5.1—5.4 (1H, m), 7.0 (3H, s), 7.3 (5H, s), and 7.8—8.3 (1H, broad). Found: C, 67.32; H, 6.52; N, 7.06%. Calcd for $C_{23}H_{26}N_2O_5$: C, 67.30; H, 6.39; N, 6.83%.

(2S,4S)-1-Benzyloxycarbonyl-2-(1-naphthylcarbamoyl)-4-pyrrolidinyl Acetate (2d): Yield 94%; $[\alpha]_D^{21}$ −26.1° (*c* 1.00, CH_2Cl_2); IR (KBr disk) 3300, 1740, 1700, 800, 780 and 700 cm^{-1}; NMR ($CDCl_3$) δ=1.9 (3H, s), 2.1—3.0 (2H, m), 3.8 (2H, d, J=6 Hz), 4.7 (1H, dd, J_1=9 Hz, J_2=2 Hz), 5.3 (2H, s), 5.2—5.4 (1H, m), 7.2—8.0 (12H, m), and 8.8—9.2 (1H, broad); MS, Found: *m/e* 432.1660. Calcd for $C_{25}H_{24}N_2O_5$: M, 432.1683.

(2S,4S)-1-Benzyloxycarbonyl-2-(methylphenylcarbamoyl)-4-pyrrolidinyl Acetate (2e): Yield 58%; $[\alpha]_D^{22}$ +81° (*c* 1.5, CH_2Cl_2); IR (neat) 3300, 1700, 1590, 1495, 770 and 700 cm^{-1}; NMR ($CDCl_3$) δ=2.0 (3H, s), 1.8—2.6 (2H, m), 3.1 (1.5H. s), 3.2 (1.5H, s), 3.4—4.5 (3H, m), 4.6—5.0 (1H, m), 5.0 (2H, s), and 6.9—7.3 (5H, m); MS, Found: *m/e* 396.1690. Calcd for $C_{22}H_{24}N_2O_5$: M, 396.1685.

(2S,4R)-1-Benzyloxycarbonyl-4-hydroxyprolinanilide(2g): Yield 47%; mp 146—147 °C; $[\alpha]_D^{26}$ −50° (*c* 1, MeOH); IR (KBr disk) 1700, 1685 cm^{-1}; NMR ($CDCl_3$–CD_3OD) δ=2.0—2.4 (2H, m), 2.95 (2H, s), 3.6 (2H, d, J=3 Hz), 4.35—4.55 (2H, m), 5.05 (2H, s), and 6.9—7.3 (10H, m). Found: C, 66.86; H, 5.81; N, 8.25%. Calcd for $C_{19}H_{20}N_2O_4$: C, 67.04; H, 5.92; N, 8.23%.

(2S,4S)-2-Phenylcarbamoyl-4-pyrrolidinyl Acetate (3a). The anilide **2a** (8.23 g, 21.7 mmol) and 10% Pd–C (800 mg) were stirred vigorously in MeOH (60 ml) under a H_2 atmosphere overnight. The reaction mixture was filtered through a Celite pad and the filtrate was concentrated to give **3a** in quantitative (5.33 g) yield: mp 64—72 °C; $[\alpha]_D^{22}$ −13.4° (*c* 1.06, EtOH); IR (KBr disk) 3350, 1720, 1660, 750, and 690 cm^{-1}; NMR ($CDCl_3$) δ=1.8 (3H, s), 2.3 (2H, dd, J_1=6 Hz, J_2=3 Hz), 2.6 (1H, broad), 3.0—3.4 (2H, m), 3.9 (1H, t, J=6 Hz), 5.1—5.3 (1H, m), 6.9—7.7 (5H,m), and 9.5—9.8 (1H, broad); Found C, 62.92; H, 6.65; N, 11.19%. Calcd for $C_{13}H_1N_2O_3$: C, 62.89; H, 6.50; N, 11.28%.

Similar treatment of **2b—e**, **2g**, and **2h** to that described

above gave the corresponding amines **3b**—**e**, **3g**, and **3h**, respectively. The yields and physical data are shown below.

(2S,4S)-2-Cyclohexylcarbamoyl-4-pyrrolidinyl Acetate (3b): Yield 100%; mp 122—123 °C (cyclohexane); $[\alpha]_D^{20}$ −11.4° (*c* 1.01, CH_2Cl_2); IR (KBr disk); 3300, 3200, 1730, and 1640 cm^{-1}; NMR ($CDCl_3$) δ=1.0—2.4 (13H, m), 1.95 (3H, s), 2.8—3.9 (4H, m), 5.0—5.3 (1H, m), and 7.2—7.5 (1H, m). Found: C, 61.18; H, 8.72; N, 10.91%. Calcd for $C_{13}H_{22}N_2O_3$: C, 61.39; H, 8.72; N, 11.02%.

(2S,4S)-(2,6-Xylylcarbamoyl)-4-pyrrolidinyl Acetate (3c): Yield 100%; $[\alpha]_D^{23}$ −38.3° (*c* 1.05, CH_2Cl_2); IR (KBr disk) 3330, 3225, 1720, 1640, and 785 cm^{-1}; NMR ($CDCl_3$) δ=2.0 (3H, s), 2.2 (6H, s), 2.3—2.5 (2H, m), 3.0—3.5 (3H, m), 3.8—4.0 (1H, dd, J_1=9 Hz, J_2=6 Hz), 5.1—5.4 (1H, m), 7.1 (3H, s), and 9.0—9.2 (1H, broad); MS, Found: *m/e* 276.1483. Calcd for $C_{15}H_{20}N_2O_3$: M, 276.1473.

(2S,4S)-2-(1-Naphthylcarbamoyl)-4-pyrrolidinyl Acetate (3d): Yield 100%; $[\alpha]_D^{21}$ +87° (*c* 1.0, CH_2Cl_2); IR (CH_2Cl_2) 3300, 1735, 1680, and 800 cm^{-1}; NMR ($CDCl_3$) δ=1.80 (3H, s), 2.1—2.6 (3H, m), 3.1—3.4 (2H, broad), 3.9—4.1 (1H, m), 5.1—5.4 (1H, m), and 7.1—8.3 (7H, m); MS, Found: *m/e* 298.1320. Calcd for $C_{17}H_{18}N_2O_3$: M, 298.1317.

(2S, 4S)-2-(Methylphenylcarbamoyl)-4-pyrrolidinyl Acetate (3e): Yield 95%; $[\alpha]_D^{23}$ −82.5° (*c* 1.0, CH_2Cl_2); IR (KBr disk) 3310, 1730, 1650, 1590, 1490, 780 cm^{-1}; NMR ($CDCl_3$) δ=1.7—2.2 (2H, m), 2.0 (3H, s), 2.5—3.9 (2H, m), 3.2 (3H, s), 4.3—4.6 (1H, broad), 4.8—5.1 (1H, m), and 7.0—7.5 (5H, m). Found: C, 63.69; H, 7.10; N, 10.29%. Calcd for $C_{14}H_{18}N_2O_3$: C, 64.10; H, 6.92; N, 10.68%.

(2S,4R)-4-Hydroxyprolinanilide (3g): Yield 100%; mp 149—150 °C (H_2O); $[\alpha]_D^{24}$ −38.5° (*c* 1, MeOH); IR (KBr disk) 3270, 1650, 1600, and 1500 cm^{-1}; NMR (CD_3OD) δ=1.7—2.2 (2H, m), 2.95 (2H, d, J=3 Hz), 3.95 (1H, t, J=8 Hz), 4.30 (1H, m), 4.65 (2H, s), and 6.8—7.5 (5H, m). Found: C, 63.32; H, 6.99; N, 13.28%. Calcd for $C_{11}H_{14}N_2O_2$: C, 64.06; H, 6.84; N, 13.58%.

(S)-Prolinanilide (3h): Yield 100%; mp 76—77 °C; $[\alpha]_D^{27}$ −71.0° (*c* 1.03, EtOH); IR (KBr disk) 3360, 3225, 1665, and 1600 cm^{-1}; NMR ($CDCl_3$) δ=1.1—2.2 (4H, m), 2.3—3.2 (3H, m), 3.5—3.9 (1H, m), 6.7—7.6 (5H, m); Found: C, 69.53; H, 7.58; N, 14.84%. Calcd for $C_{11}H_{14}N_2O$: C, 69.44; H, 7.42; N, 14.73%.

(2S,4S)-1-Acetyl-2-phenylcarbamoyl-4-pyrrolidinyl Acetate (4a). To a CH_2Cl_2 (5 ml) solution of **3a** was added a pyridine (9 ml) solution of acetic anhydride (1.12 g, 11.0 mmol) and a catalytic amount of 4-(dimethylamino)pyridine, and the solution was kept standing overnight at room temperature. The reaction mixture was diluted CH_2Cl_2, washed successively with 1 mol dm^{-3} HCl, brine, 4% aqueous $NaHCO_3$ solution and brine, and dried over Na_2SO_4. The solvent was removed under reduced pressure, and the purification of the residue with basic alumina thin layer chromatography (benzene–MeOH) gave **4a** as white crystals in 90% (2.55 g) yield. Mp 112—113.5 °C; $[\alpha]_D^{25}$ −115° (*c* 1.01, CH_2Cl_2); IR (CH_2Cl_2) 1730, 1680, 1590, 1490, 1220, and 1180 cm^{-1}; NMR ($CDCl_3$) δ=1.8—3.0 (2H, m), 1.8 (0.6H, s), 2.0 (2.4H, s), 2.1 (0.6H, s), 2.2 (2.4H, s), 3.5—3.9 (2H, m), 4.4—4.6 (0.2H, dd, J_1=9 Hz, J_2=3 Hz), 4.7—4.9 (0.8H, dd, J_1=9 Hz, J_2=3 Hz), 5.1—5.4 (1H, m), 6.9—7.7 (5H, m), 8.6—8.8 (0.2H, broad), and 9.3—9.6 (0.8H, broad); Found: C, 61.95; 6.41; N, 9.45%. Calcd for $C_{15}H_{18}N_2O_4$: C, 62.05; H, 6.25; N, 9.65%. The amides **4b**—**e**, **4g**, and **4h** were obtained according to essentially the same procedures as described above. The amide **4f** was obtained from **3a** by a similar procedure using pivaloyl chloride in place of acetic anhydride.

(2S,4S)-1-Acetyl-2-cyclohexylcarbamoyl-4-pyrrolidinyl Acetate (4b): Yield 79%; mp 107—109 °C (acetone–P.E.); IR (neat) 3300, 1740, 1660, and 1640 cm^{-1}; NMR ($CDCl_3$) δ=1.0—2.0 (10H, m), 2.0 (3H, s), 2.1 (3H, s), 2.1—2.9 (2H, m), 3.3—3.9 (4H, m), 4.1—4.6 (1H, m), 5.0—5.3 (1H, m), 6.5—6.8 (1H, broad); Found: C, 60.95; H, 8.10; N, 9.51%. Calcd for $C_{15}H_{24}N_2O_4$: C, 60.79; H, 8.16; N, 9.45%.

(2S,4S)-1-Acetyl-2-(2,6-xylylcarbamoyl)-4-pyrrolidinyl Acetate (4c): Yield 75%; mp 169—172 °C (THF-pentane); $[\alpha]_D^{21}$ −85° (*c* 1.1, CH_2Cl_2); IR (KBr disk) 3300, 1730, 1675, 1630, and 780 cm^{-1}; NMR ($CDCl_3$) δ=2.0 (3H, s), 2.1 (3H, s), 2.2 (6H, s), 2.0—3.0 (2H, m), 3.4—4.0 (2H, m), 4.8 (1H, dd, J_1=9 Hz, J_2=3 Hz), 5.1—5.4 (1H, m), 7.0 (3H, s), and 8.5—8.6 (1H, broad); Found: C, 64.16; H, 7.27; N, 8.72%. Calcd for $C_{17}H_{22}N_2O_4$: C, 64.13; H, 6.97; N, 8.80%.

(2S,4S)-1-Acetyl-2-(1-naphthylcarbamoyl)-4-pyrrolidinyl Acetate (4d): Yield 66%; mp 237—241 °C (EtOH); IR (KBr disk) 3320, 1730, 1670, 1630, and 800 cm^{-1}; NMR ($CDCl_3$) δ=1.6 (1.2H, s), 2.1 (2.8H, s), 2.2 (3H, s), 3.1—3.3 (1H, m), 3.6—4.0 (3H, m), 4.9—5.1 (1H, m), 5.3—5.5 (1H, m), 7.4—8.2 (7H, m), and 9.8—10.0 (1H, broad); Found: C, 66.87; H, 5.80; N, 8.05%. Calcd for $C_{19}H_{20}N_2O_4$: C, 67.04; H, 5.92; N, 8.23%.

(2S,4S)-1-Acetyl-2-methylphenylcarbamoyl-4-pyrrolidinyl Acetate (4e): Yield 91%; $[\alpha]_D^{23}$ +56° (*c* 0.51, EtOH); IR (neat) 1740, 1660, 1640, 780. and 700 cm^{-1}; NMR ($CDCl_3$) δ=1.9—2.5 (2H, m), 2.0 (6H, s), 3.2 (3H, s), 3.6 (1H, dd, J_1=12 Hz, J_2=4 Hz), 3.9 (1H, dd, J_1=12 Hz, J_2=2 Hz), 4.3 (1H, t, J=8 Hz), 4.9 (1H, m), 7.3 (5H, s); MS, Found: *m/e* 304.1422. Calcd for $C_{16}H_{20}N_2O_4$: M, 304.1422.

(2S, 4S)-2-Phenylcarbamoyl-1-pivaloyl-4-pyrrolidinyl Acetate(4f): Yield 72%; mp 134—135 °C; $[\alpha]_D^{24}$ −64.3° (*c* 1.02, CH_2Cl_2); IR (KBr disk) 3300,1740, 1700, 1600, 1500, 760, and 700, cm^{-1}; NMR ($CDCl_3$) δ=1.3 (9H, s), 2.0 (3H, s), 2.2—2.7 (2H, m), 3.7 (1H, dd, J_1=12 Hz, J_2=5 Hz), 4.2 (1H, dd, J_1=12 Hz, J_2=6 Hz), 4.8 (1H, dd, J_1=6 Hz, J_2=2 Hz), 5.1—5.3 (1H, m), 6.8—7.5 (5H, m), and 9.1—9.2 (1H, broad); Found: C, 64.89; H, 7.55; N, 8.28%. Calcd for $C_{18}H_{24}N_2O_4$: C, 65.04; H, 7.28; N, 8.43%.

(2S, 4R)-1-Acetyl-2-phenylcarbamoyl-4-pyrrolidinyl Acetate (4g): Yield 84%; $[\alpha]_D^{25}$ −43° (*c* 1.0, CH_2Cl_2); IR (neat) 3300, 1740, 1630, 1600, 1500, and 740 cm^{-1}; NMR ($CDCl_3$) δ=1.95 (3H, s), 2.00 (3H, s), 2.0—2.8 (2H, m), 3.4 (1H, dd, J_1=12 Hz, J_2=2 Hz), 3.9 (1H, dd, J_1=12 Hz, J_2=5 Hz), 4.7 (1H, t, J=7 Hz), 5.1—5.4 (1H, m), 6.8—7.6 (5H, m), and 9.5 (1H, broad); MS, Found; *m/e* 290.1236. Calcd for $C_{15}H_{18}N_2O_4$: M, 290.1266.

(S)-1-Acetylprolinanilide (4h): Yield 74%; $[\alpha]_D^{26}$−176° (*c* 1.1, CH_2Cl_2); IR (KBr disk) 3280, 1700, 1630, 1600, 1500, 760, and 700 cm^{-1}; NMR ($CDCl_3$) δ=1.6—2.7 (4H, m), 2.1 (3H, s), 3.3—3.6 (2H, m), 4.7 (1H, dd, J_1=8 Hz, J_2=2 Hz), 6.9—7.6 (5H, m), and 9.5—9.7 (1H, broad); MS, Found: *m/e* 232.1208. Calcd for $C_{13}H_{16}N_2O_2$: M, 232.1210.

(2S, 4S)-2-Anilinomethyl-1-ethyl-4-hydroxypyrrolidine (5a). Under an argon atmosphere, the acetate **4a** (500 mg, 1.73 mmol) in THF (30 ml) was added to a suspension of $LiAlH_4$ (520 mg, 13.7 mmol) in THF (5 ml) at 0 °C, and the mixture was refluxed for 18 h, and then quenched by the dropwise addition of saturated Na_2SO_4 solution at 0 °C. After removal of the inorganic material and concentration of the organic layer afforded an oil, which was further purified by basic alumina TLC (benzene–MeOH) and bulb-to-bulb distillation to give a colorless oil in 89% (338 mg) yield. Bp 150—170 °C/2 mmHg† (bath temp); $[\alpha]_D^{23}$ −58.1° (*c* 1.03, EtOH); IR (neat) 3375. 1600, 1500, 750, and 695 cm^{-1}; NMR ($CDCl_3$) δ=1.1 (3H, t, J=8 Hz), 1.5—1.9 (1H, m), 2.1—2.5 (3H, m), 2.5—3.0 (2H, m), 3.0—3.3 (4H, m), 4.1—4.5 (2H, m), and 6.5—7.3 (5H, m); Found: C, 70.90; H, 9.37; N, 12.54%.

† 1 mmHg ≈ 133.322 Pa.

Calcd for $C_{13}H_{20}N_2O$: C, 70.87; H, 9.15; N, 12.72%. Catalysts **5b**—**i** were also obtained by similar $LiAlH_4$ reductions.

(2S,4S)-2-(Cyclohexylaminomethyl)-1-ethyl-4-hydroxypyrrolidine (5b): Yield 81%; bp 140—155 °C/2 mmHg (bath temp); $[\alpha]_D^{21}$ −21° (*c* 1.7, MeOH); IR (neat) 3300 cm^{-1}; NMR ($CDCl_3$) δ=1.0 (3H, t, 6 Hz), 0.9—3.1 (21H, m), 3.3—4.4 (5H, m); MS, Found: *m/e* 227.2111 (M^++1). Calcd for $C_{13}H_{26}N_2O$: (M^+ +1), 227.2122.

(2S,4S)-1-Ethyl-4-hydroxy-2-(2,6-xylidinomethyl)pyrrolidine(5c): Yield 30%; bp 150—170 °C/0.2 mmHg (bath temp.); $[\alpha]_D^{21}$ −138° (*c* 0.9, CH_2Cl_2); IR (neat) 3350, 1470, and 765 cm^{-1}; NMR ($CDCl_3$) δ=1.2 (3H, t, J=8 Hz), 1.6—3.3 (9H, m), 4.0—4.3 (3H, m), and 6.8—7.0 (3H, m); MS, Found: *m/e* 248.1880. Calcd for $C_{15}H_{24}N_2O$: M, 248.1887.

(2S,4S)-1-Ethyl-4-hydroxy-2-(1-naphthylaminomethyl)pyrrolidine (5d): Yield 53%; $[\alpha]_D^{23}$ +1° (*c* 0.2, CH_2Cl_2); IR (neat) 3370, 1580, and 770 cm^{-1}; NMR ($CDCl_3$) δ=1.0 (3H, t, J=7 Hz), 1.5—3.8 (10H, m), 4.0—4.3 (1H, m), 5.0—5.6 (1H, broad), 6.4 (1H, dd, J_1=6 Hz, J_2=2 Hz), and 7.0—7.9 (6H, m); MS, Found: *m/e* 271.1747 (M^+ +1). Calcd for $C_{17}H_{23}N_2O$: (M^+ +1), 271.1809.

(2S,4S)-1-Ethyl-2-(N-methylanilinomethyl)-4-hydroxypyrrolidine (5e): Yield 82%; bp 150—160 °C/1 mmHg (bath temp); $[\alpha]_D^{23}$ −96° (*c* 0.94, EtOH); IR (neat) 3360, 1600, 1500, 750, and 695 cm^{-1}; NMR ($CDCl_3$) δ=1.1 (3H, t, J=6 Hz), 1.4—3.8 (10H, m), 2.9 (3H, s), 4.0—4.2 (1H, m), and 6.3—7.2 (5H, m); Found: C, 71.07; H, 9.76; N, 11.95%. Calcd for $C_{14}H_{22}N_2O$: C, 71.76; H, 9.46; N, 11.95%.

(2S,4S)-2-Anilinomethyl-4-hydroxy-1-(2,2-dimethylpropyl)pyrrolidine (5f): Yield 87%; bp 150—160 °C/0.4 mmHg (bath temp); $[\alpha]_D^{22}$ −56° (*c* 1.1, CH_2Cl_2); IR (neat) 3370, 1600, 1500, 750 and 690 cm^{-1}; NMR ($CDCl_3$) δ=0.8 (9H, s), 1.6—3.9 (10H, m), 4.0—4.3 (1H, m), and 6.3—7.1 (5H, m); Found: C, 73.42; H, 10.19; N, 10.90%. Calcd for $C_{16}H_{26}N_2O$: C, 73.24; H, 9.99; N, 10.68%.

(2S,4R)-2-Anilinomethyl-1-ethyl-4-hydroxypyrrolidine (5g): Yield 81%; bp 170—180 °C/5 mmHg (bath temp); $[\alpha]_D^{25}$ −39° (*c* 1.0, CH_2Cl_2); IR (KBr disk) 3380, 1600, 1520, 760, and 700 cm^{-1}; NMR ($CDCl_3$) δ=1.0 (3H, t, J=7 Hz), 1.4—4.4 (12H, m), and 6.3—7.3 (5H, m); MS, Found: *m/e* 220.1569. Calcd for $C_{13}H_{20}N_2O$: M, 220.1564.

(S)-2-Anilinomethyl-1-ethylpyrrolidine (5h): Yield 95%; bp 140—150 °C/3 mmHg (bath temp); $[\alpha]_D^{25}$ −53° (*c* 1.0, CH_2Cl_2); IR (neat) 3375, 1610, 1510, 755, and 700 cm^{-1}; NMR ($CDCl_3$) δ=1.1 (3H, t, J=8 Hz), 1.6—3.4 (11H, m), 3.9—4.4 (1H, broad), and 6.5—7.3 (5H, m); Found: C, 76.63; H, 9.91; N, 13.56%. Calcd for $C_{13}H_{20}N_2$: C, 76.42; H, 9.87; N, 13.71%.

(2S,4S)-2-Anilinomethyl-4-hydroxypyrrolidine (5i): Yield 93%; bp 170—180 °C/0.8 mmHg (bath temp); $[\alpha]_D^{25}$ +23.4° (*c* 1.02, $CHCl_3$); NMR ($CDCl_3$) δ=1.2—1.7 (1H, m), 1.9—2.5 (1H, m), 2.6—3.2 (8H, m), 4.1—4.4 (1H, m), and 6.4—7.2 (5H, m); Found: C, 67.86; H, 8.82; N, 14.10%. Calcd for $C_{11}H_{16}N_2O$: C, 68.72; H, 8.39; N, 14.57%.

General Procedure for the Michael Addition. Under an argon atmoshpere, a solution of the thiol (4 mmol) in the solvent (25 ml) and the cycloalkenone (5 mmol) containing the freshly distilled catalyst (0.08 mmol) in the solvent (25 ml) were mixed at the specified temperature and kept standing for two days at the temperature. The reaction mixture was washed successively with 1 mol dm^{-3} HCl (5 ml×3), brine (5 ml×1), 1 mol dm^{-3} NaOH (5 ml×3), brine (5 ml×1) and dried over anhydrous sodium sulfate. The solvent was evaporated under reduced pressure and the residue was chromatographed on silica-gel TLC (hexane–AcOEt). The adduct thus obtained was further purified by short path distillation using Kugelrohr apparatus.

The authors wish to thank Professor Hans Wynberg, the University of Groningen, for providing us valuable informations. Thanks are due to Mr. Masami Ishibashi for mass spectral measurements. Thanks are also due to the Ajinomoto Co., Inc. for the gift of L-hydroxyproline. The present work was supported by a Grant-in-Aid for Scientific Research No. 443006 from the Ministry of Education, Science and Culture.

References

1) J. D. Morrison and H. S. Mosher, "Asymmetric Organic Reactions," Prentice Hall Inc., (1971); D.Valentine, Jr., and J. W. Scott, *Synthesis*, **1978**, 329; J. W. ApSimon and R. P. Seguin, *Tetrahedron*, **35**, 2797 (1979).

2) a) K. B. Sharpless, *J. Am. Chem. Soc.*, **102**, 5974 (1980); b) T. Hayashi, M. Konishi, T. Hioki, M. Kumada, A. Ratajczad, and H. Niedbala, *Bull. Chem. Soc. Jpn.*, **54**, 3615 (1981); c) S. Otsuka, T. Yamagata, K. Tani, H. Takaya, A. Miyashita, R. Noyori, and S. Akutagawa, 44th National Meeting of the Chemical Society of Japan, Okayama, October 1981.

3) a) H. Hiemstra and H. Wynberg, *J. Am. Chem. Soc.*, **103**, 417 (1981); b) H. Wynberg and B. Greijdanus, *J. Chem. Soc., Chem. Commun.*, **1978**, 427; c) D. J. Cram and G. D. Y. Sogah, *ibid.*, **1981**, 625.

4) M. Asami, H. Ohno, S. Kobayashi, and T. Mukaiyama *Bull. Chem. Soc. Jpn.*, **51**, 1869 (1978); T. Mukaiyama, K. Soai, T. Sato, H. Shimizu, and K. Suzuki, *J. Am. Chem. Soc.*, **101**, 1455 (1979); T. Mukaiyama, Y. Sakito, and M. Asami, *Chem. Lett.*, **1978**, 1253; T. Mukaiyama, *Tetrahedron*, **37**, 4111 (1981).

5) T. Mukaiyama, A. Ikegawa, and K. Suzuki, *Chem. Lett.*, **1981**, 165.

6) A. A. Patchett and W. Witkop, *J. Am. Chem. Soc.*, **79**, 185 (1957).

Synthetic Studies of Rifamycins. V.[1] A Chiral Synthesis of an Ansa-chain Compound for the C-17—C-29 Portion of Rifamycin W†

Masaya NAKATA, Hiroyuki ENARI, and Mitsuhiro KINOSHITA*

Department of Applied Chemistry, Faculty of Science and Technology, Keio University, Hiyoshi, Kohoku-ku, Yokohama 223

(Received May 24, 1982)

The chiral synthesis of methyl 5,7,9-tri-*O*-acetyl-2-*C*-(acetoxymethyl)-2,4,6,8,10,11,12-heptadeoxy-4,6,8,10-tetra-*C*-methyl-*aldehydo*-L-*glycero*-L-*talo*-L-*manno*-(*E*)-11-tridecenuronate 1-(dimethyl acetal) (III), a useful synthetic segment for the C-17-C-29 portion of rifamycin W, is described. The key intermediate, 3-*O*-(*t*-butyldimethylsilyl)-2,4,7-trideoxy-5,6-*O*-isopropylidene-2,4-di-*C*-methyl-*aldehydo*-D-*glycero*-D-*talo*-heptose (**28**) was synthesized in 30% yield from methyl 4,6-*O*-benzylidene-3-deoxy-3-*C*-methyl-α-D-glucopyranoside in 15 steps. The synthesis involves key steps of highly stereoselective Grignard reaction and regiospecific *cis*-epoxide ring-opening reaction. The condensation of **28** with 3,3-diethoxy-2-lithio-1-propene afforded about 1.6: 1 excess of the "Cram" product (**30**, 56% yield). The desilylation of **30** followed by homogeneous hydrogenation with $(Ph_3P)_3RhCl$ gave only the *erythro* product **34**. 3,5-Di-*O*-benzyl-2,4,6-trideoxy-2,4,6-tri-*C*-methyl-L-*glycero*-L-*manno*-heptodialdose 1-(diethyl acetal) derived from **34**, condensed with the lithium reagent prepared (in ether at −95——90 °C) from butyllithium and 3-*C*-(benzyloxymethyl)-3,5,6-trideoxy-5-iodo-1,2-*O*-isopropylidene-α-D-hexenofuranose, derived from 3-deoxy-3-*C*-hydroxymethyl-1,2 : 5,6-di-*O*-isopropylidene-α-D-allofuranose, to afford a 4 : 1 mixture of the "Cram" product and its epimer in 80% yield. The homogeneous hydrogenation of the mixture followed by the debenzylation gave the diastereomerically pure major product, which could be transformed into III in 6 steps.

The first chiral synthesis of the ansa-chain portion of rifamycin S in the form of I was described in the preceding papers[1,2] from this laboratory. Recently, Nagaoka and Kishi[3] reported the highly stereocontroled synthesis of the optically active form of the ansa-chain compound II from (*S*)-(−)-3-*t*-butoxy-2-methyl-1-propanol. In this paper, we wish to report an improved convergent route for the chiral synthesis of the ansa-chain compound III, a useful synthetic segment for the C-17-C-29 portion of rifamycin W,[4] the biosynthetic progenitor of all the rifamycins.[5] Since the stereochemistry at C-28 of rifamycin W was unknown,[6] we assumed the configuration of the corresponding C-2 chiral center in III to be (*R*) by considering the facility of the synthesis. Naturally, when the opposite stereochemistry at C-2 of III was required, the chemical interchange of the acetoxymethyl and dimethoxymethyl groups at C-2 was considered feasible.

In keeping with the experimental results obtained in the synthesis of I,[1] our synthetic plan was made using the retrosynthetic analysis shown in Scheme 1. In the plan, it was expected that the starting symmetric dialdehyde **A** (a synthetic equivalent) is allowed to react successively with the lithium reagents, **B** and **E**, to afford predominantly the "Cram"[7] product **F** *via* the "Cram" product **C**, and the exo-methylene intermediates, **C** and **F**, are hydrogenated, under similar stereochemical control, to provide exclusively the *erythro*†† isomers, **D** and **G**, respectively. As the key intermediates corresponding to the synthetic equivalents, **A**, **B**, and **E**, in the planned convergence scheme, we chose the compounds, **28**, **29**, and **58**, respectively. The intermediates, **28** and **58** were obtainable by the chiral synthesis using appropriate sugar derivatives.

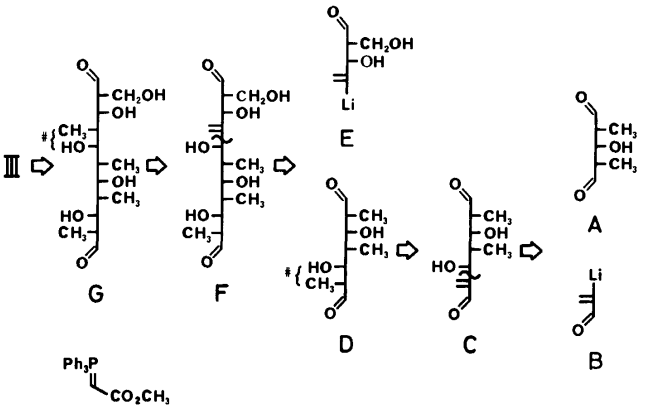

Scheme 1.

The key intermediate **28** was synthesized from 2-*O*-benzyl-3,6-dideoxy-3-*C*-methyl-D-glucopyranose (**6**) through the stereo- and regio-selective route. The compound **6** was prepared, through the route shown in Scheme 2, from methyl 4,6-*O*-benzylidene-3-deoxy-3-*C*-methyl-α-D-glucopyranoside (**2**),[8] which could be obtained on a large scale from methyl 4,6-*O*-benzylidene-3-deoxy-3-*C*-methyl-α-D-altropyranoside (**1**).[8,9]

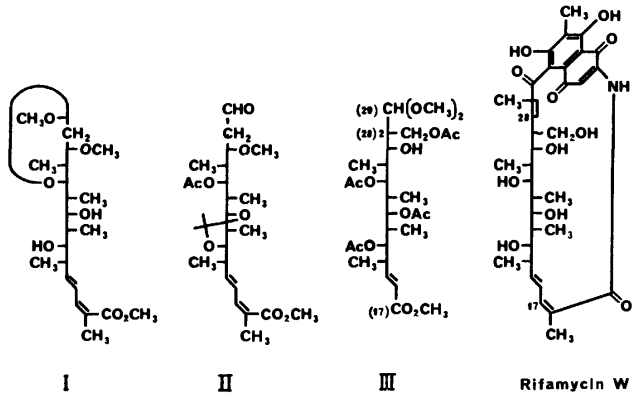

† Presented at the 45th National Meeting of Chemical Society of Japan, Tokyo, April 4, 1982.

†† In this article, the substituents on the same side of the chain in a Fischer projection of acyclic molecule are prefixed as *erythro*, while those on opposite sides are prefixed as *threo*.

The *O*-benzylation of **2** followed by the debenzylidenation of the resulting **3** with methanolic hydrogen chloride afforded crystalline **4**, which was selectively 6-*O*-mesylated with 1.14 equiv. of mesyl chloride in pyridine and subsequently reduced with lithium aluminium hydride to give **5**. The acetolysis of **5** with acetic anhydride containing 0.15 equimolar amounts of sulfuric acid, followed by the hydrolysis with sodium hydroxide yielded **6** in 75% overall yield based on **2**.

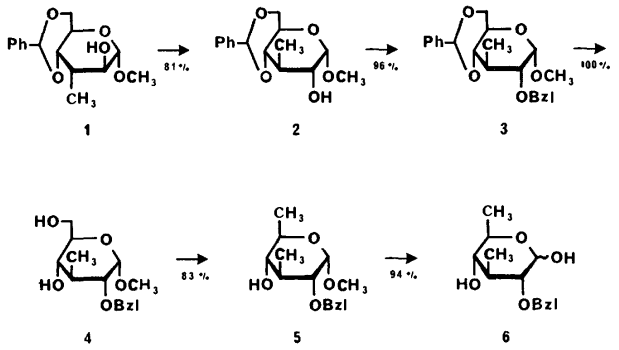

Scheme 2.

The Grignard reaction of **6** with 10 equimolar amounts of methylmagnesium iodide in ether afforded the product **7** (78%), its epimer **8** (1.5%), and the unchanged **6** (16%). The (6*R*)-configuration of the major product **7** was confirmed by the fact that **7** was transformed, through a sequence of reactions involving periodate-oxidation followed by successive debenzylation, acid hydrolysis, and bromine-oxidation, into the 1,4-lactone **9**, whose relative configuration was proved by ^{1}H-NMR analysis to be identical with that of (2*S*,3*S*,4*S*)-3-hydroxy-2-methyl-4-pentanolide[1] or its enantiomer.[10] The 2,3-acetonation of **7** with 1.5

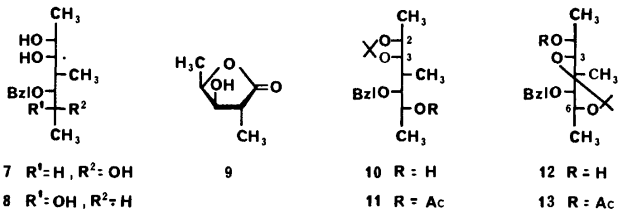

equimolar amounts of 2,2-dimethoxypropane (DMP) and 0.1 equimolar amounts of *p*-toluenesulfonic acid in DMF afforded, contrary to our expectation,[1] the mixture from which the two kinds of isomeric acetonides, **10** and **12** were isolated by column chromatography in 55% and 44% yields respectively. The structures of **10** (2,3-acetonide) and **12** (3,6-acetonide) were determined by the following facts: (i) **10** could be converted into the epoxide **16** through the sequence of reactions described later on, while **12** gave no epoxide in the same procedure as in the case of **10** and (ii) the debenzylated product obtained from **10** was cleaved with periodate reagent, while that from **12** was not affected by the same reagent. The ^{1}H-NMR spectra (250 MHz) of **10** and **12**, and of their acetates, **11** and **13**, showed signals in line with the structures as depicted. After many unsuccessful attempts, a 4.7 : 1 predominance of **10** was attained by the treatment of **7** with 2 equimolar amounts of DMP in acetone containing a catalytic amounts of concd sulfuric acid. Furthermore, **12** separated from **10** was treated with an equimolar amounts of zinc bromide in dichloromethane to give **10** in 94% isolated yield. The total yield of **10** thus amounted to 93%.

The acetylation of **10** with acetic anhydride and 4-(dimethylamino)pyridine (DMAP) in ethyl acetate afforded the 6-acetate **11** in 95% yield. The hydrogenolysis of **11** with hydrogen (palladium black) in ethanol followed by the immediate mesylation gave the 5-mesylate **14** in 92% yield after the chromatographic

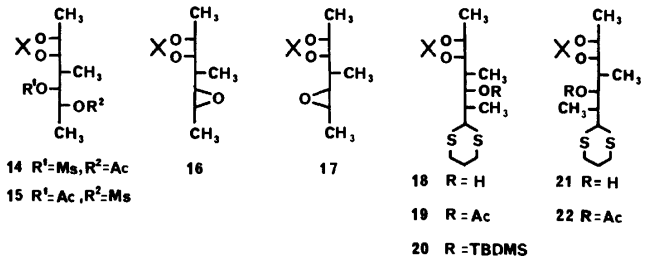

separation from the isomeric 6-mesylate **15** (5%), presumably resulted from the isomeric 5-acetate formed by the 6→5 *O*-acyl migration during the hydrogenolysis of **11**. The 5-mesylate **14** was then treated with sodium methoxide in chloroform to afford the *cis*-epoxide **16** in 81% yield after distillation. The 6-mesylate **15** also gave the diastereomeric *cis*-epoxide **17**. The reaction of **16** or **17** with 5 equiv. of 2-lithio-1,3-dithiane in THF at 5 °C afforded regiospecifically only the C-6-adduct **18** or **21** in 91% or 94% yield respectively. Since ring-opening of epoxides with nucleophiles is known to proceed with inversion at the center of addition,[11] the structures of **18** and **21** could be determined by the coupling features (double doublets) of the acetoxymethine protons in the ^{1}H-NMR spectra of their acetates, **19** and **22**.

The stereochemical control in this ring-opening process of *cis*-epoxide was truly remarkable. The analogous *cis*-epoxides, **23**,[12] **24**,[12] and **25**[13] also reacted with 2-lithio-1,3-dithiane to give only the corresponding

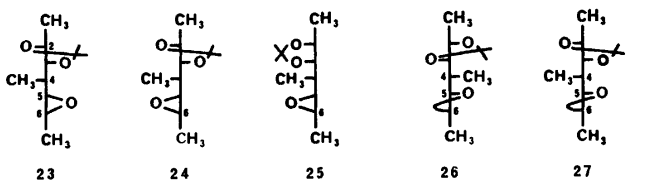

C-6-adducts in good yields. The high regioselectivity in ring-opening of these *cis*-epoxides was independent of the relative configurations at C-4 and C-5 and of the configurations of other chiral centers (C-2 and C-3). This result differed from the reported regioselectivities in the reactions of the *trans*-epoxides, **26** and **27**, with 2-lithio-1,3-dithiane. The epoxide **26** with *erythro*-configuration at C-4 and C-5 afforded a 3.1 : 1 mixture of C-6- and C-5-adducts,[1] while **27** with *threo*-configuration at C-4 and C-5 gave a 2.8 : 1 mixture of C-5- and

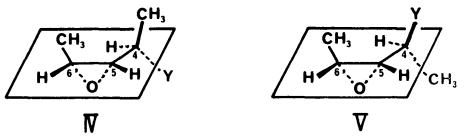

Scheme 3.

C-6-adducts.[10] Therefore, the regioselectivity of ring-opening in the *trans*-epoxides seemed to be affected by their C-4 configurations. The remarkable regioselectivity observed in the reactions of the *cis*-epoxides may be explained as follows. In the *cis* series, the free rotation of the ring-C-5-substituent ($CH(CH_3)Y$) about the C-4–C-5 bond axis should be restricted within narrow limits owing to larger nonbonding interaction of this group with the ring-methyl at C-6 than in the *trans* series. Therefore, each molecule of the *cis*-epoxides should have in the ground state a preferred conformation[14] which is rigidly held and resembles IV or V as depicted in Scheme 3. In this conformation, axial (β) attack at the C-5 position would involve the attacking group in an eclipsing interaction with the vicinal quasi axial 4-methyl group[15] or the 4-substituted Y, and addition will exclusively occur at the C-6-position, if the above-mentioned preferred reactant conformation is also favorable in the transition state of the reaction.

The *t*-butyldimethylsilylation of **18** provided, in 97% yield, the silyl ether **20**, whose dithioacetal group was cleaved with an 1 : 1 mixture of mercury(II)- and red mercury(II) oxide to generate the aldehyde **28** in 94% yield (or in 39.5% overall yield from **6**). The condensation of **28** with the lithium reagent **29** prepared from 3 equiv. of 2-bromo-3,3-diethoxy-1-propene[16] and 2.5 equiv. of butyllithium in THF at −110 °C was performed in THF at −110 °C to afford, after column chromatographic separation, **30** and **32** in 56 and 36% yields respectively based on **28**. The

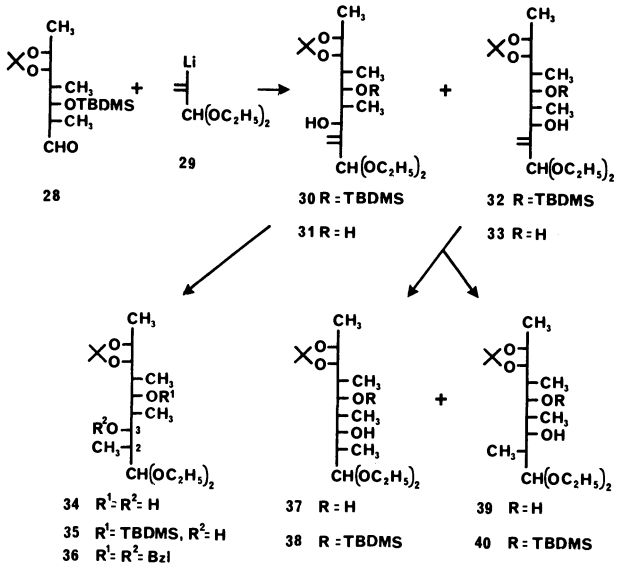

Scheme 4.

desilylation of **30** with tetrabutylammonium fluoride gave **31** in 98% yield. The homogeneous hydrogenation[1] of **31** with about 0.24 equimolar amounts of tris-(triphenylphosphine)chlororhodium (I)[17] in benzene under an atmospheric pressure of hydrogen yielded, in 93% yield, **34** as a sole hydrogenation product, whose diastereomeric homogeneity was confirmed by the TLC and 250 MHz ^{1}H-NMR analyses. The homogeneous hydrogenation of the silyl ether **30** proceeded more slowly and the reaction needed at least 1.5 equimolar amounts of the rhodium catalyst for its completion. The crude product **35** resulted in 79% yield was desilylated to afford the diastereomerically homogeneous **34**. In order to determine the configurations at C-2 and C-3 in **34**, **34** was transformed into the methyl L-heptopyranoside derivative **41** through the sequence of reactions involving deacetonation with pyridinium *p*-toluenesulfonate[18] (PPTS) in ethanol, followed by successive periodate-oxidation, sodium borohydride reduction, methanolysis with 0.5% methanolic hydrogen chloride, and acetylation. The structure shown for **41** was confirmed by the 250 MHz ^{1}H-NMR analysis

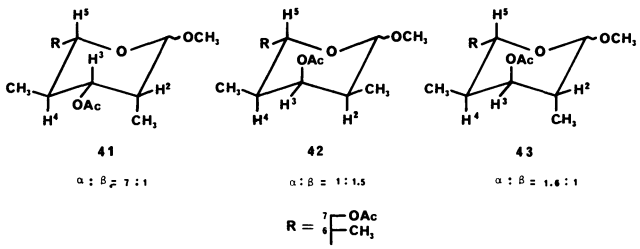

(using decoupling technique), indicating that the condensation of **28** with **29** yielded predominantly the "Cram" product **30**, which and whose desilylation product **31** were stereospecifically hydrogenated to afford the 2,3-*erythro* isomers, **35** and **34**, respectively. The minor methylene product **32** was shown to be the anti-"Cram" condensation product as follows. Unlike **31**, the desilylation product **33** from **32** afforded, on homogeneous hydrogenation, about 1 : 1 epimeric mixture of **37** and **39**, while the direct hydrogenation of **32** gave about 1 : 8 mixture of **37** and **39** *via* the corresponding mixture of **38** and **40**. The isolated **37** and **39** were transformed into the corresponding methyl L-heptopyranoside derivatives, **42** and **43**, by the procedure described in the transformation of **34** into **41**. The structures of **42** and **43** could also be well determined as depicted by the 250 MHz ^{1}H-NMR analyses.

The benzylation of **34** afforded **36** in 88% yield. The one stage deacetonation of **36** by the ethanolysis with ethanol (PPTS) or with ethanolic hydrogen chloride resulted in the low yield (≈55%) of **45**. Thus **36** was at first hydrolyzed with 75% dichloroacetic acid (DCA) and then the resulting aldehyde **44** was

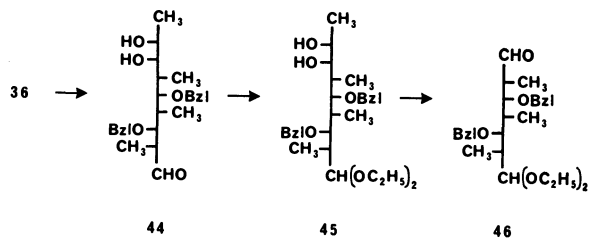

treated with ethanol in the presence of a catalytic amounts of *p*-toluenesulfonic acid to give **45** in 86% yield. The periodate-oxidation of **45** afforded the synthetic intermediate **46** in 81% yield. The lithium reagent **58** was prepared by the lithiation of the alkenyl halides, **54** and **56**, which were synthesized starting from 3-deoxy-3-*C*-hydroxymethyl-1,2:5,6-di-*O*-isopropylidene-α-D-allofuranose[19] (**47**) through the route shown in Scheme 5.

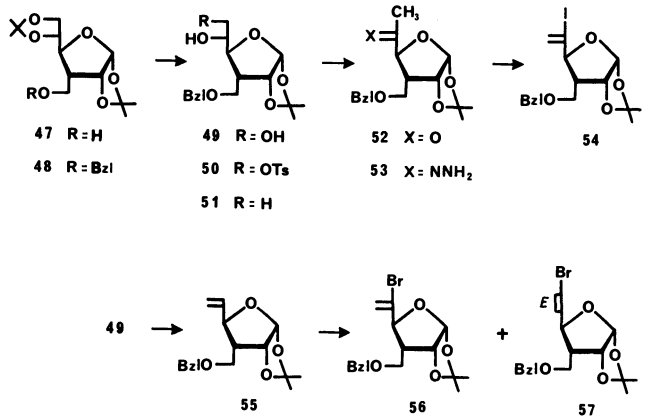

Scheme 5.

The benzylation of **47** followed by the selective hydrolysis of the resulting benzyl ether **48** with 75% acetic acid afforded the glycol **49** in 91% yield. The selective 6-*O*-tosylation of **49** followed by lithium aluminium hydride reduction gave **51** in 74% yield. The oxidation of **51** proceeded effectively with pyridinium chlorochromate (PCC) and molecular sieve 3A powder,[20] affording **52** in 92% yield. The methyl ketone **52** was converted into the alkenyl iodide **54** in 30% yield *via* the hydrazone **53**, according to the procedure of Barton *et al.*[21,8] The alkenyl bromide **56** was prepared from the 1,2-glycol **49**. The periodate-oxidation of **49** followed by the Wittig condensation with methylenetriphenylphosphorane in DMSO afforded **55** in 87% yield. The bromination of **55** with bromine in carbon tetrachloride followed by the elimination of hydrogen bromide with DBU in DMSO gave the isomeric alkenyl bromides, **56** and **57**, in 72 and 14% yields respectively after chromatographic separation.

The condensation of **46** with the lithium reagent **58**, prepared from 3.1 equiv. of alkenyl iodide **54** and 3.1 equiv. of butyllithium in ether at −95——90 °C, was carried out in ether at −95——90 °C to afford a 4 : 1 mixture of **59** and **60** in 80% yield. The isomeric ratio was estimated by the 250 MHz ^{1}H-NMR analysis. On the other hand, the lithiation of the alkenyl bromide **56** had to be performed in THF at −95 °C, because **56** was virtually unreactive to butyllithium in ether at −100 °C. Thus, **46** was allowed to react in THF at −95 °C with **58**, prepared from 3.0 equiv. of **56** and 2.5 equiv. of butyllithium, to yield a mixture of **59** and **60** in 52% yield, and unchanged **46** was recovered in 29% yield. As in the case of the condensation of **28** with **29**, the major epimer **59** was anticipated to be the "Cram" product, and its structure was confirmed in the later stage of this ansa-chain synthesis. Since the preparative separation of **59** from **60** by column chromatography was impracticable in this stage, the epimeric mixture was directly hydrogenated with 2 equimolar amounts of the rhodium catalyst to give, in 82% yield, a diastereomeric mixture (**61** and **62**), which was debenzylated with lithium in liquid ammonia to afford, after column chromatographic separation, the isomerically homogeneous **63** (in 77% yield) and a minor fraction containing the isomeric mixture (**65**). The acetylation of **63** with

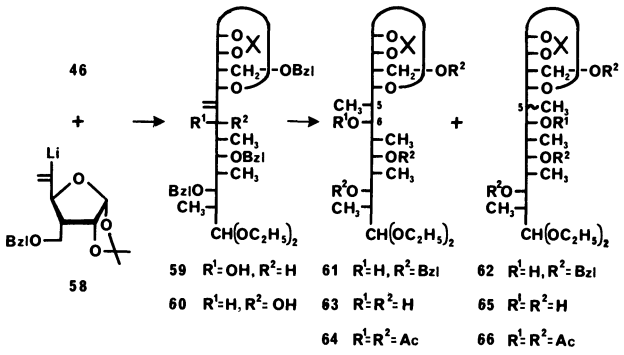

acetic anhydride and DMAP in ethyl acetate yielded the crystalline tetraacetate **64** in 91% yield. The acetylation product from the fraction of **65** was shown to be a 2 : 1 mixture of two C-5-epimeric acetates (**66**) by the TLC and ^{1}H-NMR analyses. The hydrolysis of **64** with 75% DCA followed by the Wittig condensation of the resulting aldehyde **67** with (methoxycarbonylmethylene)triphenylphosphorane gave **68** in 86% yield. The deacetonation of **68** with 80% trifluoroacetic acid (TFA) followed by the periodate-oxidation afforded the crystalline aldehyde **69**, which was treated with methanol containing a catalytic amounts of *p*-toluenesulfonic acid to give the target compound III in 43% yield based on **68**.

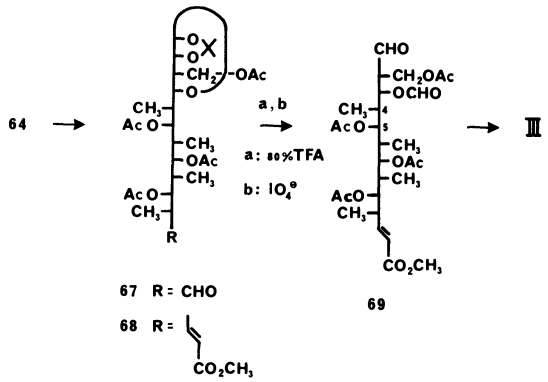

The configurations at C-4 and C-5 in **69** were determined by the following manner. The dimethyl acetal III was then reduced with a large excess of diisobutylaluminium hydride (DIBAL) in toluene at −78 °C. The methanolysis of resulting alylic alcohol with PPTS in methanol followed by the acetylation with acetic anhydride and DMAP afforded **70**, whose structure as depicted was confirmed by the 250 MHz ^{1}H-NMR analysis. Consequently, the structures shown for **64** and **59** were established. Furthermore, isomerically pure **59** and **61** were isolated by careful column

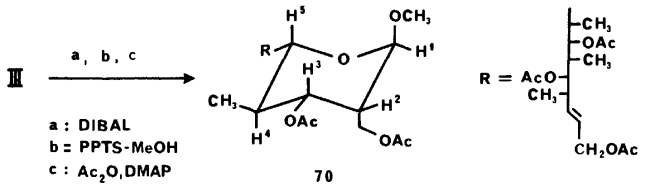

chromatography from the aforesaid condensation products and their hydrogenation products respectively, and it was confirmed that the "Cram" product **59**, as well as **30** and **31**, was stereospecifically hydrogenated to afford only the 5,6-*erythro* isomer **61**. It is interesting that, in the case of the anti-"Cram" products, **60**, **32**, and **33**, no remarkable stereoselectivity was observed.

Experimental

The melting points were determined on a micro hot-stage Yanaco MP-S3 and are uncorrected. The specific rotations were measured with a Carl Zeissphotoelectric polarimeter, using a 0.2-dm tube, in chloroform unless stated otherwise. The ^{1}H-NMR spectra were recorded with either a Varian EM-390 or a Bruker WM 250 spectrometer in $CDCl_3$ using TMS as the internal standard. The TLC was carried out on Merck TLC plates (60F-254, 0.25 mm). The column chromatography was performed on silica gel Wakogel C-200. In general, the evaporation of solvents was carried out under reduced pressure below 30 °C.

Methyl 2-O-Benzyl-4,6-O-benzylidene-3-deoxy-3-C-methyl-α-D-glucopyranoside (3). Sodium hydride (15.9 g, 55% emulsion in mineral oil) was washed free from the mineral oil with hexane and evaporated until the last traces of hexane were removed from the sodium hydride. The powdered residue was added to an ice-cooled solution of **2** (51.0 g, 0.182 mol) in dry DMF (360 ml). The mixture was stirred at room temperature for 0.5 h and then ice-cooled. Benzyl bromide (43.2 ml, 0.364 mol) was added dropwise to the stirred mixture over a period of 25 min. After the mixture had been stirred for 1.5 h at room temperature, it was poured into ice water (150 ml) and the new mixture was extracted with chloroform (200 ml × 3). The extracts were washed with a saturated aqueous NaCl solution, dried, and evaporated to a crystalline solid (102.8 g), which was chromatographed on silica gel (1.5 kg) with 15 : 1 benzene–ethyl acetate to afford a practically pure sample of **3** (64.4 g, 96%); mp 121—122.8 °C. Recrystallization from hexane gave an analytical sample as colorless needles: mp 121.7—122.1 °C; $[\alpha]_D^{27}$ +46° (c 2.14); ^{1}H-NMR δ=1.13 (3H, d, 3-Me, J=6.3 Hz), 2.0—2.5 (1H, m, H-3), 2.9—3.3 (2H, m, H-2 and 4), 3.37 (3H, s, OMe), 3.5—3.85 (2H, m, H-6 and 6′), 4.1—4.3 (1H, m, H-5), 4.5—4.6 (3H, sharp m, H-1 and OC<u>H</u>$_2$Ph), 5.41 (1H, s, C<u>H</u>Ph), and 7.2—7.5 (10H, m, 2 × Ph),

Found: C, 71.61; H, 7.11%. Calcd for $C_{22}H_{26}O_5$: C, 71.33; H, 7.08%.

Methyl 2-O-Benzyl-3-deoxy-3-C-methyl-α-D-glucopyranoside (4). A suspension of **3** (69.4 g) in dry methanol (700 ml) was stirred in an ice bath. 3.68 M HCl††† in methanol (102 ml) was then added to the suspension over a period of 10 min. After the mixture had been stirred at room temperature for 40 min, the reaction mixture was ice-cooled, neutralized (pH 6) with $NaHCO_3$ (43.5 g), and evaporated to a crystalline solid. The residue was repeatedly extracted with acetone (*ca.* 1 l) to remove insoluble matter. The acetone extracts were evaporated to afford **4** (50.0 g, 100%) as colorless crystals; mp 143.5—147 °C. Recrystallization from acetone gave a pure sample: Colorless needles, mp 143.8—144.6 °C; $[\alpha]_D^{27}$ +106° (c 1.20); ^{1}H-NMR δ=1.13 (3H, d, 3-Me, J=6.3 Hz), 1.8—2.2 (1H, m, H-3), 2.3—2.6 (1H, br, OH), 2.6—2.8 (1H, br, OH), 3.07 (1H, dd, H-2, $J_{1,2}$=3.3 Hz, $J_{2,3}$=9.6 Hz), 3.36 (3H, s, 1-OMe), 3.2—3.6 (2H, m, H-4 and 5), 3.6—3.8 (2H, m, H-6 and 6′), 4.5—4.6 (3H, sharp m, H-1 and OC<u>H</u>$_2$Ph), and 7.30 (5H, s, Ph).

Found: C, 63.64; H, 7.69%. Calcd for $C_{15}H_{22}O_5$: C, 63.81; H, 7.85%.

Methyl 2-O-Benzyl-3,6-dideoxy-3-C-methyl-α-D-glucopyranoside (5). To an ice-cooled solution of the crude sample of **4** (25.4 g, mp 143.5—147 °C) in dry pyridine was added mesyl chloride (8.00 ml, 0.1035 mol) over a period of 0.5 h and stirred under ice-cooling for 3 h. The reaction mixture was then poured into a cold saturated aqueous $NaHCO_3$ solution (250 ml) and the mixture was extracted with ethyl acetate (300 ml × 3). The extracts were combined, washed successively with a saturated aqueous $KHSO_4$ solution (300 ml × 5) and a saturated aqueous NaCl solution (300 ml × 2), dried, and evaporated. The residual pale yellow crude syrup (31.9 g) of the 6-mesylate was dissolved in dry ether (480 ml), and $LiAlH_4$ (7.5 g, 0.198 mol) was added portionwise to the solution under ice-cooling over a period of 10 min. After being stirred at room temperature for 3 h, $Na_2SO_4 \cdot 10H_2O$ (62.7 g, 0.195 mol) was added to the reaction mixture, and resulting insoluble matter was filtered and washed with chloroform (80 ml × 5). The filtrate and washings were combined and evaporated to a pale yellow syrup (33.5 g), which was chromatographed on silica gel (1 kg) with 2 : 1 benzene–ethyl acetate to afford a colorless syrup of **5** (20.0 g, 83%): $[\alpha]_D^{16}$ +101° (c 1.41); ^{1}H-NMR δ=1.11 and 1.22 (each 3H, each d, 3-Me and H-6, J=6.3 Hz), 1.7—1.9 (1H, br, 4-OH), 1.7—2.15 (1H, m, H-3), 2.79 (1H, m, H-4, $J_{3,4}$=$J_{4,5}$=9.3 Hz), 3.07 (1H, dd, H-2, $J_{1,2}$=3.3 Hz, $J_{2,3}$=10.5 Hz), 3.35 (3H, s, 1-OMe), 3.52 (1H, dq, H-5), 4.5—4.6 (3H, sharp m, H-1 and OC<u>H</u>$_2$Ph), and 7.30 (5H, s, Ph).

Found: C, 67.42; H, 8.34%. Calcd for $C_{15}H_{22}O_4$: C, 67.64; H, 8.33%.

2-O-Benzyl-3,6-dideoxy-3-C-methyl-D-glucopyranose (6). To a solution of **5** (14.8 g, 0.0556 mol) in acetic anhydride (440 ml), concd H_2SO_4 (0.46 ml) was added dropwise under ice-cooling over a period of 15 min. After being stirred at 0 °C for 15 min, the reaction mixture was poured into a cold saturated aqueous $NaHCO_3$ solution (400 ml), and then extracted with ethyl acetate (300 ml × 3). The extracts were combined, washed successively with a saturated aqueous $NaHCO_3$ (400 ml × 2) and a saturated aqueous NaCl solution (400 ml × 2), dried, and evaporated to a yellow-brown syrup (18.7 g). To a solution of this syrup in dioxane (167 ml) was added dropwise 1 M aqueous NaOH solution (167 ml) and the mixture was kept at room temperature for 5.5 h. The reaction mixture was then neutralized (pH 7) with CO_2 gas and evaporated. The residue was triturated with acetone (600 ml) and the insoluble matter was removed by filtration. The filtrate was evaporated to afford crude **6** (13.2 g, 94% from **5**); colorless crystals, mp 141—145 °C. Recrystallization from benzene gave a pure sample of **6** as colorless needles; mp 148—150 °C; $[\alpha]_D^{17}$ +55° (c 1.18, EtOH, after 24 h); ^{1}H-NMR δ=1.14, 1.23, and 1.29 (6H, each d, 3-Me and 3 × H-6, J=6.3 Hz), 1.4—2.2 (2H, m, H-3 and OH), 2.7—3.4 (3H, m, H-2,4, and OH), 3.80 (1H, dq, H-5, $J_{4,5}$= 9.0 Hz), 4.4—4.7 (2H, m, OC<u>H</u>$_2$Ph), 4.95 and 5.17 (1H, each d, β and α anomeric H-1, $J_{1\alpha,2}$=3.3 Hz, $J_{1\beta,2}$=11.4 Hz), and 7.36 (5H, s, Ph); α/β=5/6.

Found: C, 66.47; H, 7.97%. Calcd for $C_{14}H_{20}O_4$: C, 66.64; H, 7.99%.

††† 1 M = 1 mol dm^{-3}.

5-O-Benzyl-1,4,7-trideoxy-4-C-methyl-D-glycero-L-gulo-heptitol (7) and L-glycero Epimer (8). A solution of **6** (18.8 g, 0.0741 mol) in dry THF (56.0 ml) was added dropwise to a stirred ice-cooled ether solution of methylmagnesium iodide [prepared from magnesium turnings (18.0 g, 0.740 mol) and methyl iodide (46.1 ml, 0.74 mol) in dry ether (360 ml)] over a period of 15 min under argon. After being stirred at room temperature for 20 h, 1 M HCl (770 ml) was carefully added under ice-cooling, after which the mixture was extracted with chloroform (700 ml × 1, 300 ml × 2). The extracts were combined, dried and evaporated to a syrup (26.5 g), which was chromatographed on silica gel (1.6 kg) with 1 : 5 benzene–ethyl acetate to afford **7** (14.9 g, 75%), **8** (53 mg, 0.26%), a mixture of **7** and **8** (0.86 g, 4.3%), and unchanged **6** (2.9 g, 16%). The epimeric mixture (0.86 g) was again chromatographed on silica gel (130 g) with the same solvent system to give **7** (0.60 g) and **8** (0.24 g). The total isolated yields of **7** and **8** amounted to 78% and 1.5% respectively. **7** (R_f=0.34 in 1 : 5 benzene–ethyl acetate), colorless syrup; $[\alpha]_D^{21}$ −65° (*c* 1.00); ^{1}H-NMR δ=0.95 and 1.25 (3H and 6H, each d, 3 × Me, J=6.7 and 6.0 Hz), 2.0—2.6 (2H, m, H-4 and OH), 3.18 (1H, dd, H-5, J=2.1 and 4.5 Hz), 3.5—4.2 (4H, m, H-2,3,6, and OH), 4.59 (2H, ABq, OC$\underline{H}_2$Ph, J_{gem}=11.2 Hz), and 7.37 (5H, s, Ph).

Found: C, 67.02; H, 8.89%. Calcd for $C_{15}H_{24}O_4$: C, 67.13; H, 9.02%.

8 (R_f=0.29 in 1 : 5 benzene–ethyl acetate), colorless syrup; ^{1}H-NMR δ=1.08 (3H, d, 4-Me, J=7.2 Hz), 1.24 and 1.28 (each 3H, each d, 2 × Me, J=6.0 Hz), 2.1—2.5 (1H, m, H-4), 3.33 (1H, dd, H-5, $J_{4,5}$=3.0 Hz, $J_{5,6}$=5.8 Hz), 3.55 (1H, dd, H-3, $J_{3,4}$=2.4 Hz, $J_{2,3}$=6.7 Hz), 3.74 (1H, dq, H-2), 4.01 (1H, dq, H-6), 4.59 (2H, s, OC$\underline{H}_2$Ph), and 7.36 (5H, s, Ph).

(2R,3R,4R)-3-Hydroxy-2-methyl-4-pentanolide (9). A solution of $NaIO_4$ (90 mg) in water (0.9 ml) was added to a solution of **7** (37.5 mg) in acetone (0.75 ml) under ice-cooling. After being stirred for 20 min, the resulting insoluble matter was filtered and washed with acetone. The filtrate and washings were combined, neutralized (pH 7) with $NaHCO_3$ and then evaporated. Chloroform (2 ml) was added to the residue and the solution washed with a saturated aqueous NaCl solution, dried, and evaporated. The residual syrup (29.7 mg) was hydrogenolyzed in methanol (0.6 ml) with palladium black at room temperature for 16 min under bubbling with H_2 gas to afford methyl 2,5-dideoxy-2-*C*-methylpentofuranoside (16.2 mg, 83%) after chromatographic purification (silica gel 1.5 g, 1 : 2 benzene–ethyl acetate). The methyl furanoside (16.2 mg) was hydrolyzed with 1 : 1 mixture of 1 M hydrochloric acid and 1,4-dioxane (0.16 ml) at room temperature for 18.5 h and the acid neutralized with $NaHCO_3$. The solution was treated with bromine (7.4×10^{-6} l) for 24 h at room temperature. The reaction mixture was extracted with ethyl acetate, and the extract was washed successively with saturated aqueous $Na_2S_2O_3$ and NaCl solutions, dried, and evaporated to a pale yellow liquid, which was purified by column chromatography (silica gel 0.7 g, 1 : 3 benzene–ethyl acetate) to give the lactone **9** (7.0 mg, 42% from **7**). The ^{1}H-NMR data (90 MHz) of **9** [δ=4.10 (1H, dd, H-3, $J_{2,3}$=$J_{3,4}$=4.8 Hz) and 4.62 (1H, dq, H-4, $J_{4,Me}$=6.6 Hz)] were very similar to the reported data.[1,10]

2,3- and 3,6-O-Acetonides (10 and 12). To an ice-cooled solution of **7** (24.8 g, 0.0924 mol) and DMP (22.7 ml, 0.185 mol) in dry acetone (500 ml) was added dropwise concd H_2SO_4 (25.0×10^{-6} l) over a period of 2 min. After being kept at 0 °C for 0.5 h, the reaction mixture was neutralized with solid Na_2CO_3. The insoluble matter was filtered and washed with acetone (10 ml × 5). The combined filtrate and washings were evaporated to a pale yellow syrup (38.2 g), which was chromatographed on silica gel (1.6 kg) with 20 : 1 chloroform–acetone to afford **10** (21.9 g, 77%) and **12** (4.8 g, 17%): **10** (R_f=0.43 in 20 : 1 chloroform–acetone), colorless syrup; $[\alpha]_D^{17}$ 0°, $[\alpha]_{365}^{17}$ −68° (*c* 1.10); ^{1}H-NMR (250 MHz) δ=1.04, 1.16, and 1.19 (each 3H, each d, 3 × Me, J=6.3, 6.3, and 7.0 Hz), 1.30 and 1.45 (each 3H, each s, CMe_2), 1.85—2.0 (1H, m, H-4), 2.95—3.0 (1H, br, 6-OH), 3.07 (1H, dd, H-5, $J_{4,5}$=2.8 Hz, $J_{5,6}$=5.3 Hz), 3.91 (1H, dq, H-6, $J_{6,7}$=6.3 Hz), 4.15—4.25 (2H, m, H-2 and 3), 4.65 (2H, s, OC$\underline{H}_2$Ph), and 7.3—7.4 (5H, m, Ph).

Found: C, 69.82; H, 8.92%. Calcd for $C_{18}H_{28}O_4$: C, 70.10; H, 9.15%.

12 (R_f=0.23 in 20 : 1 chloroform–acetone), colorless needles; mp 114.8—115.4 °C (benzene); $[\alpha]_D^{17}$ −39° (*c* 1.17); ^{1}H-NMR (250 MHz) δ=0.89, 1.15, and 1.22 (each 3H, each d, 3 × Me, J=7.3 Hz), 1.31 and 1.34 (each 3H, each, s, CMe_2), 1.6—1.7 (1H, br, 2-OH), 2.35—2.45 (1H, m, H-4), 2.94 (1H, d, H-5, $J_{4,5}$=2.3 Hz, $J_{5,6}$=0 Hz), 3.73 (1H, dq, H-2, $J_{2,3}$=7.8 Hz), 3.84 (1H, dd, H-3, $J_{3,4}$=1.3 Hz), 3.98 (1H, q, H-6), 4.60 (2H, ABq, OC$\underline{H}_2$Ph, J_{gem}=12.5 Hz), and 7.25—7.45 (5H, m, Ph).

Found: C, 70.22; H, 8.97%. Calcd for $C_{18}H_{28}O_4$: C, 70.10; H, 9.15%.

A mixture of **12** (4.8 g, 15.6 mmol), $ZnBr_2$ (3.5 g, 15.6 mmol), and dichloromethane (48 ml) was stirred at 0 °C for 4 h, and then neutralized (pH 7) with Na_2CO_3. The insoluble matter was filtered and washed with dichloromethane. The combined filtrate and washings were evaporated to a yellow syrup (5.8 g), which was chromatographed on silica gel (300 g) with 20 : 1 chloroform–acetone to give **10** (4.5 g, 94%) and **12** (0.2 g, 4%).

6-O-Acetyl-5-O-benzyl-1,4,7-trideoxy-2,3-O-isopropylidene-4-C-methyl-D-glycero-L-gulo-heptitol (11). To a solution of **10** (21.8 g, 70.7 mmol) in ethyl acetate (220 ml) was added acetic anhydride (13.4 ml, 141 mmol) and DMAP (8.6 g, 70.7 mmol). After being kept at room temperature for 15 min, the reaction mixture was poured into a cold saturated aqueous $NaHCO_3$ solution (300 ml) and the new mixture was extracted with ethyl acetate (250 ml × 2). The extracts were washed with water (300 ml × 2) and a saturated aqueous NaCl solution (300 ml × 2), dried, and evaporated to a yellow syrup (24.6 g), which was chromatographed on silica gel (1 kg) with 10 : 1 benzene–ethyl acetate to afford **11** (23.6 g, 95%). R_f=0.48 (10 : 1 benzene–ethyl acetate), colorless syrup; $[\alpha]_D^{16}$ +15° (*c* 1.34); ^{1}H-NMR δ=1.10 and 1.11 (each 3H, each d, 4-Me and 3 × H-1, J=6.7 and 5.2 Hz), 1.18 (3H, d, H-7, J=7.3 Hz), 1.25 and 1.40 (each 3H, each s, CMe_2), 1.6—2.1 (1H, m, H-4), 1.96 (3H, s, 6-OAc), 3.27 (1H, dd, H-5, $J_{4,5}$=2.9 Hz, $J_{5,6}$=7.3 Hz), 3.8—4.1 (2H, m, H-2 and 3), 4.62 (2H, ABq, OC$\underline{H}_2$Ph, J_{gem}=11.8 Hz), 5.15 (1H, dq, H-6), and 7.32 (5H, s, Ph).

Found: C, 68.78; H, 8.58%. Calcd for $C_{20}H_{30}O_5$: C, 68.54; H, 8.63%.

2-O-Acetyl Derivative (13) of 12. By the procedure described in the preparation of **11**, a sample of **12** (101 mg) was acetylated to afford **13** (111 mg, 96%): R_f=0.52 (10 : 1 benzene-ethyl acetate), colorless syrup; ^{1}H-NMR δ=0.81 (3H, d, 4-Me or H-7, J=7.5 Hz), 1.16 (3H, d, H-7 or 4-Me, J=7.1 Hz), 1.24 (3H, d, H-1, J=6.3 Hz), 1.30 and 1.33 (each 3H, each s, CMe_2), 1.8—2.2 (1H, m, H-4), 1.99 (3H, s, 2-OAc), 2.90 (1H, dd, H-5, J=0 and 2.3 Hz), 3.8—4.1 (2H, m, H-3 and 6), 4.50 (2H, ABq, OC$\underline{H}_2$Ph, J_{gem}=12.0 Hz), 4.82 (1H, dq, H-2, $J_{2,3}$=9.5 Hz), and 7.27 (5H, s, Ph).

6-O-Acetyl-1,4,7-trideoxy-2,3-O-isopropylidene-5-O-mesyl-4-C-methyl-D-glycero-L-gulo-heptitol (14) and 5-O-Acetyl-1,4,7-trideoxy-2,3-O-isopropylidene-6-O-mesyl-4-C-methyl-D-glycero-L-gulo-heptitol (15). A mixture of **11** (5.50 g, 15.7 mmol), pal-

ladium black (*ca.* 3 g), and ethanol (110 ml) was vigorously stirred at room temperature for 20 min under bubbling with H_2 gas, and the suspension filtered. The filtrate was evaporated to a colorless syrup (4.43 g), which was coevaporated with benzene (4 ml×5). The final residue (4.11 g) was immediately dissolved in dry pyridine (41 ml) and ice-cooled. Mesyl chloride (2.4 ml, 31.4 mmol) was added dropwise to the solution over a period of 10 min and the mixture was kept at room temperature for 2 h. The reaction mixture was poured into a cold saturated aqueous $NaHCO_3$ solution (50 ml), and extracted with ethyl acetate (70 ml×3). The extracts were combined, washed successively with saturated aqueous $KHSO_4$ (50 ml×5) and NaCl (50 ml×3) solution, dried, and evaporated to a crystalline residue (5.62 g). The residue was chromatographed on silica gel (560 g) with 5 : 1 benzene–ethyl acetate to afford **14** (4.89 g, 92%) and **15** (0.266 g, 5%): **14** (R_f=0.48 in 3 : 1 benzene–ethyl acetate), colorless needles; mp 78—83 °C; ^{1}H-NMR δ=1.13, 1.23, and 1.32 (each 3H, each d, 3×Me, J=6.6, 6.2, and 6.2 Hz), 1.36 and 1.47 (each 3H, each s, CMe_2), 1.8—2.2 (1H, m, H-4), 2.11 (3H, s, 6-OAc), 3.08 (3H, s, 5-OMs), 4.04 (1H, dd, H-3, $J_{2,3}$=6.0 Hz, $J_{3,4}$=7.4 Hz), 4.40 (1H, dq, H-2, $J_{1,2}$=6.2 Hz), 4.60 (1H, dd, H-5, $J_{4,5}$=2.7 Hz, $J_{5,6}$=7.8 Hz), and 5.16 (1H, dq, H-6, $J_{6,7}$=6.2 Hz): **15** (R_f=0.42 in 3 : 1 benzene–ethyl acetate), colorless syrup; ^{1}H-NMR δ=1.08, 1.23, and 1.39 (each 3H, each d, 3×Me, J=6.0, 6.4, and 6.0 Hz), 1.31 and 1.44 (each 3H, each s, CMe_2), 1.8—2.2 (1H, m, H-4), 2.13 (3H, s, 5-OAc), 2.96 (3H, s, 6-OMs), 3.72 (1H, dd, H-3, $J_{2,3}$=6.4 Hz, $J_{3,4}$=7.7 Hz), 4.26 (1H, dq, H-2, $J_{1,2}$=6.4 Hz), and 4.7—5.0 (2H, m, H-5 and 6).

*5,6-Anhydro-1,4,7-trideoxy-2,3-*O*-isopropylidene-4-*C*-methyl-*D*-glycero-*D*-manno-heptitol (**16**).* To an ice-cooled solution of **14** (4.86 g, 14.4 mmol) in chloroform (48 ml) was added 3.6 M sodium methoxide in methanol (1.0 ml) over a period of 5 min. After being stirred under ice-cooling for 45 min the mixture was neutralized with CO_2 gas, poured into cold water (30 ml), and then extracted with dichloromethane (20 ml×3). The extracts were washed with a saturated aqueous NaCl solution (30 ml×3), dried, and evaporated to a colorless oil (2.94 g). The oil was subsequently chromatographed on silica gel (88 g) with 5 : 1 benzene–ethyl acetate to afford oily **16** (2.69 g, 93%), which was subjected to bulb-to-bulb distillation to give a pure sample of **16** (2.34 g, 81%): R_f=0.50 (5 : 1 benzene–ethyl acetate); bp 45—56 °C (bath temp)/6 Torr††††; $[\alpha]_D^{20}$ +8° (*c* 1.49); ^{1}H-NMR δ=1.08 (3H, d, 4-Me, J=6.8 Hz), 1.21 (3H, d, H-1, J=6.0 Hz), 1.30 (3H, d, H-7, J=5.7 Hz), 1.36 and 1.47 (each 3H, each s, CMe_2), 2.72 (1H, dd, H-5, $J_{5,6}$=4.2 Hz, $J_{4,5}$=9.0 Hz), 3.06 (1H, dq, H-6), 4.02 (1H, dd, H-3, $J_{2,3}$=6.0 Hz, $J_{3,4}$=7.5 Hz), and 4.34 (1H, dq, H-2).

Found: C, 65.04; H, 9.69%. Calcd for $C_{11}H_{20}O_3$: C, 65.97; H, 10.07%.

*2,3-Anhydro-1,4,7-trideoxy-5,6-*O*-isopropylidene-4-*C*-methyl-*D*-glycero-*D*-gulo-heptitol (**17**).* By the procedure described in the preparation of **16**, a sample of **15** (0.865 g) afforded, after silica gel column chromatography, **17** (0.240 g, 47%) as a colorless oil: R_f=0.44 (5 : 1 benzene–ethyl acetate); bp 78—84 °C (bath temp)/6 Torr; $[\alpha]_D^{24}$ −49° (*c* 0.92); ^{1}H-NMR δ=1.13 (3H, d, H-7, J=6.3 Hz), 1.20 (3H, d, 4-Me, J=6.0 Hz), 1.25 (3H, d, H-1, J=5.4 Hz), 1.32 and 1.45 (each 3H, each s, CMe_2), 1.4—1.8 (1H, m, H-4), 2.77 (1H, dd, H-3, $J_{2,3}$=3.8 Hz, $J_{3,4}$=8.1 Hz), 3.05 (1H, dq, H-2), 3.91 (1H, dd, H-5, $J_{5,6}$=6.3 Hz, $J_{4,5}$=5.1 Hz), and 4.26 (1H, dq, H-6).

Found: C, 65.41; H, 9.74%. Calcd for $C_{11}H_{20}O_3$: C, 65.97; H, 10.07%.

†††† 1 Torr ≈ 133.322 Pa.

*2,4,7-Trideoxy-5,6-*O*-isopropylidene-2,4-di-*C*-methyl-*D*-glycero-*D*-talo-heptose Trimethylene Dithioacetal (**18**).* A solution of 1,3-dithiane 97%, (3.95 g, 31.9 mmol) in dry THF (40 ml) was cooled to −40 °C under argon, and 1.57 M butyllithium in hexane (20.3 ml) was added dropwise. After being stirred for 2 h at −20 °C, the mixture was recooled to −40 °C. A solution of **16** (1.28 g, 6.38 mmol) in dry THF (2.6 ml) was added dropwise to this stirred solution, and stirring was continued at −20 °C for 2 h and at 5 °C for 66 h. The mixture was now poured into cold water (30 ml), and extracted with chloroform (40 ml×3). The extracts were combined, successively washed with water (50 ml×3) and a saturated aqueous NaCl solution (40 ml×2), dried, and evaporated to a crystalline solid (4.80 g), which was chromatographed on silica gel (340 g) with 5 : 1 benzene–ethyl acetate to afford **18** (1.87 g, 91%) as colorless crystals. Recrystallization of the sample (35 mg) from hexane gave a pure sample of **18** (22 mg) as plates: R_f=0.43 (5 : 1 benzene–ethyl acetate), mp 104—105 °C; $[\alpha]_D^{28}$ −40° (*c* 1.38); ^{1}H-NMR δ=1.04, 1.11, and 1.29 (each 3H, each d, 3×Me, J=6.6, 6.0, and 6.9 Hz), 1.33 and 1.48 (each 3H, each s, CMe_2), 1.7—2.2 (4H, m, H-2,4, 2×Ha), 2.7—3.1 (5H, m, 4×Hb, 3-OH), 3.41 (1H, ddd, H-3, $J_{3,OH}$=8.1 Hz, J=8.1 and 3.6 Hz), 4.1—4.5 (2H, m, H-5 and 6), and 4.66 (1H, d, H-1, $J_{1,2}$=2.4 Hz).

Found: C, 56.10; H, 8.59; S, 19.93%. Calcd for $C_{15}H_{28}O_3S_2$: C, 56.21; H, 8.81; S, 20.00%.

*Acetyl Derivative (**19**)*: Colorless syrup, R_f=0.31 (5 : 1 hexane–acetone); ^{1}H-NMR δ=4.90 (1H, dd, H-3, J=5.9 and 7.1 Hz).

*2,4,7-Trideoxy-5,6-*O*-isopropylidene-2,4-di-*C*-methyl-*D*-glycero-*D*-gulo-heptose Trimethylene Dithioacetal (**21**).* By the procedure described in the preparation of **18**, **17** (62 mg) was allowed to react with 5 equiv. of 2-lithio-1,3-dithiane in THF to afford, after silica gel column chromatography, **21** (94 mg, 94%) as a colorless crystals. A part of this sample (29 mg) was recrystallized from hexane to give a pure sample of **21** as colorless needles: R_f=0.33 (5 : 1 benzene–ethyl acetate), mp 104—105 °C; $[\alpha]_D^{28}$ −31° (*c* 1.32); ^{1}H-NMR δ=0.93, 0.94, and 1.18 (each 3H, each d, 2- and 4-Me, and 3×H-7, J=7.5, 6.9, and 6.0 Hz), 1.28 and 1.43 (each 3H, each s, CMe_2), 1.5—2.2 (4H, m, H-2,4, 2×Ha), 2.6—3.1 (5H, m, 4×Hb, 3-OH), 3.62 (1H, broad d, H-3, J=1.8 and 9.3 Hz†††††), 4.0—4.2 (1H, m, H-5), 4.27 (1H, dq, H-6, $J_{5,6}$=$J_{6,7}$=6.0 Hz), and 4.57 (1H, d, H-1, $J_{1,2}$=2.1 Hz).

Found: C, 56.44; H, 8.60; S, 20.04%. Calcd for $C_{15}H_{28}O_3S_2$: C, 56.21; H, 8.81; S; 20.00%.

*Acetyl Derivative (**22**)*: colorless syrup, R_f=0.55 (5 : 1 benzene–ethyl acetate); ^{1}H-NMR δ=5.16 (1H, dd, H-3, J=0 and 11.4 Hz).

*3-O-(t-Butyldimethylsilyl)-2,4,7-trideoxy-5,6-O-isopropylidene-2,4-di-C-methyl-D-glycero-D-talo-heptose Trimethylene Dithioacetal (**20**).* To a solution of **18** (907 mg, 2.83 mmol) and imidazole (936 mg, 14.2 mmol) in dry DMF (4.5 ml) at room temperature was added *t*-butyldimethylchlorosilane (2.13 g, 14.2 mmol). The resulting homogeneous solution was stirred at 60 °C for 18.5 h, after which time the reaction mixture was poured into cold water (12 ml) and extracted with ethyl acetate (15 ml×3). The extracts were successively washed with water (20 ml×3) and a saturated aqueous NaCl solution (20 ml×2), dried, and evaporated to a colorless crystalline mass (1.92 g). The solid was then chromatographed on silica gel (60 g) with 50 : 1 benzene–ethyl acetate to afford **20** (1.19 g, 97%) as colorless needles, mp 62—67 °C. Recrystallization of a portion of this product from hexane gave a pure sample: mp 65—67 °C; $[\alpha]_D^{28}$ +20° (*c* 1.48); ^{1}H-NMR

††††† Measured in $CDCl_3+D_2O$.

δ=0.83 (9H, s, *t*-Bu), 0.91, 0.97, and 1.07 (each 3H, each d, Me×3, J=6.6, 6.6, and 6.0 Hz), 1.16 and 1.30 (each 3H, each s, CMe_2), 1.6—2.1 (4H, m, 2×Ha, H-2,4), 2.55—2.9 (4H, m, 4×Hb), 3.55 (1H, dd, H-3, J=4.5 and 6.8 Hz), 3.8—4.2 (2H, m, H-5, 6), and 4.22 (1H, d, H-1, $J_{1,2}$=4.1 Hz).

Found: C, 58.15; H, 9.47; S, 14.46%. Calcd for $C_{21}H_{42}O_3S_2Si$: C, 58.01; H, 9.74; S, 14.75%.

3-O-(t-Butyldimethylsilyl)-2,4,7-trideoxy-5,6-O-isopropylidene-2,4-di-C-methyl-aldehydo-D-glycero-D-talo-*heptose(**28**).* To a mixture of **20** (1.06 g, 2.44 mmol) and mercury(II) oxide (2.34 g, 10.7 mmol) in 80% aqueous acetone (74 ml) was added mercury(II) chloride (2.93 g, 10.7 mmol) at room temperature with efficient stirring. The mixture was stirred at 60 °C for 15 min under argon, cooled, and filtered through Celite 545. The filter cake was washed with acetone (60 ml), and then the filtrate and the washings were combined. After the subsequent removal of the acetone by concentration, an aqueous 10% KI solution (50 ml) was added to the red aqueous residue. The resulting colorless solution was extracted with chloroform (30 ml×3) and the extracts were washed with a 10% aqueous KI solution (40 ml) and a saturated aqueous NaCl solution (40 ml×2), dried, and evaporated. The residual colorless syrup (0.88 g) was chromatographed rapidly on silica gel (41 g) with 40 : 1 benzene–ethyl acetate to afford **28** (0.788 g, 94%) as a colorless syrup: R_f=0.30 (40 : 1 benzene–ethyl acetate); $[\alpha]_D^{23}$ −6°, $[\alpha]_{546}^{23}$ 0°, $[\alpha]_{405}^{23}$ +15°, and $[\alpha]_{365}^{23}$ +36° (*c* 1.19); IR ($CHCl_3$, 0.15 M) 1710 cm^{-1}; ^{1}H-NMR δ=0.8—1.2 (12H, m, *t*-Bu and 1×Me), 1.14 and 1.21 (each 3H, each d, 2×Me, J=7.0 and 6.0 Hz), 1.30—1.42 (each 3H, each s, CMe_2), 1.7—2.0 (1H, m, H-4), 2.4—2.7 (1H, m, H-2), 3.78 (1H, dd, H-3, J=2.3 and 7.5 Hz), 4.00 (1H, dd, H-5, $J_{4,5}$=4.8 Hz, $J_{5,6}$=6.3 Hz), 4.22 (1H, dq, H-6, J=6.3 Hz), and 9.71 (1H, d, H-1, $J_{1,2}$=1.8 Hz).

Found: C, 62.50; H, 10.28%. Calcd for $C_{18}H_{36}O_4Si$: C, 62.74; H, 10.53%.

5-O-(t-Butyldimethylsilyl)-2,4,6,9-tetradeoxy-7,8-O-isopropylidene-4,6-di-C-methyl-2-methylene-D-erthro-L-altro-*nonose Diethyl Acetal (**30**) and* L-allo *Epimer (**32**).* To a solution of 2-bromo-3,3-diethoxy-1-propene[16] (0.925 g, 4.42 mmol) in dry THF (6.4 ml)cooled at −108—−110 °C (ether and liquid nitrogen) was added 1.51 M butyllithium in hexane (2.4 ml, 3.62 mmol) over a period of 5 min under argon. After being stirred at the same temperature for 15 min, a solution of **28** (0.508 g, 1.47 mmol) in dry THF (0.5 ml) was added to the mixture over a period of 5 min, and stirring was continued at the same temperature for 15 min. The reaction mixture was quenched by adding a saturated aqueous NH_4Cl solution (3 ml) and then it was extracted with ether (4 ml×3) at room temperature. The organic layer were washed with a saturated aqueous NaCl solution, dried, and evaporated to a yellow syrup (1.08 g). The crude product was immediately chromatographed on silica gel** (110 g) with 12 : 1 benzene–ethyl acetate over a period of 5.5 h*** to afford **30** (0.394 g, 56%) and **32** (0.250 g, 36%) as colorless syrups: **30**, R_f=0.34 (15 : 1 benzene–ethyl acetate); $[\alpha]_D^{23}$ −35° (*c* 1.00); ^{1}H-NMR (250 MHz) δ=0.15 and 0.16 (each 3H, each s, $SiMe_2$), 0.92 (3H, d, 4-Me, J=7.5 Hz), 0.93 (9H, s, *t*-Bu), 1.04 (3H, d, 6-Me, J=7.3 Hz), 1.17 and 1.21 [each 3H, each t, $CH(OCH_2Me)_2$, J=7.0 Hz], 1.27 (3H, d, H-9, J=6.5 Hz), 1.33 and 1.46 (each 3H, each s, CMe_2), 1.97 (1H, ddq, H-6, $J_{5,6}$=8.0 Hz, $J_{6,7}$=3.8 Hz), 2.10 (1H, dq, H-4, $J_{3,4}\approx$0 Hz, $J_{4,5}$=2.0 Hz), 3.35—3.7 [4H, m, $CH(OCH_2Me)_2$], 3.72 (1H, dd, H-5), 3.92 (1H, s, 3-OH), 4.28 (1H, dd, H-7, $J_{7,8}$=6.5 Hz), 4.34 (1H, dq, H-8), 4.75 (1H, s, H-1), 4.80 (1H, s like, H-3), 5.35 and 5.44 (each 1H, each s like, $=CH_2$).

Found: C, 63.19; H, 10.39%. Calcd for $C_{25}H_{50}O_6Si$: C, 63.25; H, 10.61%.

32, R_f=0.26 (15 : 1 benzene–ethyl acetate); $[\alpha]_D^{24}$ −23° (*c* 1.08); ^{1}H-NMR (250 MHz) δ=0.13 and 0.14 (each 3H, each s, $SiMe_2$), 0.83 (3H, d, 4-Me, J=7.3 Hz), 0.93 (9H, s, *t*-Bu), 1.03 (3H, d, 6-Me, J=7.0 Hz), 1.22 (3H, d, H-9, J=6.8 Hz), 1.22 and 1.23 [each 3H, each t, $CH(OCH_2Me)_2$, J=7.5 Hz], 1.31 and 1.45 (each 3H, each s, CMe_2), 1.97 (1H, ddq, H-6, $J_{5,6}$=7.5 Hz, $J_{6,7}$=4.8 Hz), 2.13 (1H, ddq, H-4, $J_{3,4}$=10.0 Hz, $J_{4,5}$=2.8 Hz), 3.52 (1H, d, 3-OH, J=4.8 Hz), 3.51 and 3.69 [each 2H, each dq, $CH(OCH_2Me)_2$, J_{gem}=11.5 Hz), 3.79 (1H, dd, H-5), 4.11 (1H, dd, H-3), 4.16 (1H, dd, H-7, $J_{7,8}$=6.8 Hz), 4.34 (1H, dq, H-8), 4.95 (1H, s, H-1), 5.22 and 5.40 (each 1H, each s like, $=CH_2$).

Found: C, 63.65; H, 10.31%. Calcd for $C_{25}H_{50}O_6Si$: C, 63.25; H, 10.61%.

2,4,6,9-Tetradeoxy-7,8-O-isopropylidene-4,6-di-C-methyl-2-methylene-D-erythro-L-altro-*nonose Diethyl Acetal (**31**) and* L-allo *Epimer (**33**).* An 1.0 M *n*-Bu_4NF in THF (1.6 ml, 1.6 mmol) was added to an ice-cooled solution of **30** (0.391 g, 0.823 mmol) in dry THF (3.9 ml), and the mixture was stirred at 0 °C for 15 min. Ice water (3 ml) was then added to the reaction mixture and it was extracted with chloroform (8 ml×3). The extracts were washed with water (5 ml×3) and a saturated aqueous NaCl solution, dried, and evaporated to a yellow syrup (0.408 g). The syrup was chromatograohed on silica gel (20 g) with 6 : 1 benzene–acetone to afford **31** (0.290 g, 98%) as a colorless syrup: R_f=0.35 (6 : 1 benzene–acetone); $[\alpha]_D^{23}$ −29° (*c* 1.02); ^{1}H-NMR (250 MHz) δ=0.97 (3H, d, 4-Me, J=7.5 Hz), 1.00 (3H, d, 6-Me, J=6.8 Hz). 1.20 and 1.22 [each 3H, each t, $CH(OCH_2Me)_2$, J=7.5 Hz], 1.26 (3H, d, H-9, J=6.3 Hz), 1.34 and 1.47 (each 3H, each s CMe_2), 2.00 (1H, ddq, H-6, $J_{5,6}$=8.5 Hz, $J_{6,7}$=5.0 Hz), 2.11 (1H, ddq, H-4, $J_{3,4}$=1.6 Hz, $J_{4,5}$=3.0 Hz), 2.98 (1H, d, 3-OH, J=2.5 Hz), 3.33 (1H, d, 5-OH, J=7.8 Hz), 3.4—3.5 (1H, m, H-5), 3.4—3.75 [4H, m, $CH(OCH_2Me)_2$], 4.32 (1H, dd, H-7, $J_{7,8}$=6.3 Hz), 4.46 (1H, dq, H-8), 4.79 (2H, s, like, H-1 and 3), 5.34 and 5.37 (each 1H, each s like, $=CH_2$).

Found: C, 63.54; H, 9.78%. Calcd for $C_{19}H_{36}O_6$: C, 63.31; H, 10.07%. By the procedure described for the preparation of **31**, **32** (0.417 g) provided **33** (0.293 g, 93%) as a colorless syrup: R_f=0.23 (6 : 1 benzene–acetone); $[\alpha]_D^{24}$ −91° (*c* 1.10); ^{1}H-NMR (250 MHz) δ=0.75 (3H, d, 4-Me, J=7.3 Hz), 1.10 (3H, d, 6-Me, J=7.3 Hz), 1.23 and 1.24 [each 3H, each t, $CH(OCH_2Me)_2$, J=7.5 Hz], 1.28 (3H, d, H-9, J=6.8 Hz), 1.35 and 1.49 (each 3H, each s, CMe_2), 1.99 (1H, ddq, H-6, $J_{5,6}$=4.0 Hz, $J_{6,7}$=2.8 Hz), 2.10 (1H, ddq, H-4, $J_{3,4}$=9.3 Hz, $J_{4,5}$=7.5 Hz), 3.4—3.8 [5H, m, H-5, and $CH(OCH_2Me)_2$], 3.80 (1H, d like, 5-OH, J=6.3 Hz), 4.20 (1H, d like, H-3, $J_{3,OH}$=0 Hz), 4.33 (1H, dd, H-7, $J_{7,8}$=6.8 Hz), 4.43 (1H, dq, H-8), 4.60 (1H, s like, 3-OH), 4.99 (1H, s, H-1), 5.25 and 5.41 (each 1H, each s like, $=CH_2$).

Found: C, 63.07; H, 9.88%. Calcd for $C_{19}H_{36}O_6$: C, 63.31; H, 10.01%.

2,4,6,9-Tetradeoxy-7,8-O-isopropylidene-2,4,6-tri-C-methyl-D-arabino-L-manno-*nonose Diethyl Acetal (**34**).* *(a)*: A solution of **31** (0.290 g, 0.803 mmol) and tris(triphenylphosphine)chlororhodium(I)[17] (0.174 g, 0.188 mmol) in benzene (14.5 ml) was stirred under an atmospheric pressure of hydrogen at room temperature for 14 h. The reaction mixture was then evaporated and the residue was passed through Florisil (100—200 mesh, 20 g)with ether and again evaporated to afford a practically pure sample of **34** (0.270 g, 93%) as a pale

** The use of Merck Kieselgel 60 instead of Wakogel C-200 resulted in decomposition of the product in large extent.

*** The elution speed was desired to be as fast as possible.

yellow syrup, which was shown to be isomerically homogeneous by TLC and ^{1}H-NMR analyses. A portion of this sample (15 mg) was chromatographed on silica gel (1 g) with 3 : 1 benzene–ethyl acetate to give a pure sample of **34** (14.4 mg): colorless syrup, R_f=0.31 (3 : 1 benzene–ethyl acetate); $[\alpha]_D^{24}$ +24° (*c* 0.72); ^{1}H-NMR (250 MHz) δ=0.82, 0.92, and 1.07 (each 3H, each d, 2,4,6-Me, J=7.0 Hz), 1.24 (3H, d, H-9, J=6.3 Hz), 1.23 and 1.25 [each 3H, each t, CH(OC$\underline{H}_2$Me)$_2$, J=7.0 Hz], 1.34 and 1.46 (each 3H, each s, CMe$_2$), 1.8—2.05 (3H, m, H-2,4 and H-6), 3.31 (1H, ddd, H-5, J=3.3 and 9.0 Hz, $J_{5.OH}$=9.0 Hz), 3.5—3.9 [4H, m, CH(OC$\underline{H}_2$Me)$_2$], 3.91 (1H, d, 5-OH), 4.02 (1H, dd, H-3, J=1.5 and 9.5 Hz, $J_{3,OH}$= 0 Hz), 4.25 (1H, dd, H-7, $J_{6,7}$=$J_{7.8}$=6.3 Hz), 4.44 (1H, d, H-1, $J_{1,2}$=6.0 Hz), 4.47 (1H, dq, H-8), and 4.59 (1H, s, 3-OH).

Found: C, 63.19; H, 10.27%. Calcd for $C_{19}H_{38}O_6$: C, 62.96; H, 10.57%.

(b): A sample of **30** (57.6 mg, 0.121 mmol) was hydrogenated in benzene (2.9 ml) with $(Ph_3P)_3RhCl$ (169 mg, 0.182 mmol) under atmospheric pressure of H_2 at room temperature for 20 h. The reaction product was treated with Florisil (13 g) and ether to afford crude **35** (45.7 mg, 79%) as a yellow syrup. This syrup was desilylated with 2 equimolar amounts of Bu_4NF in THF at 0 °C for 15 min and then worked up by the usual way to give a yellow syup (44.7 mg). This was chromatographed on silica gel (2.3 g) with 2 : 1 hexane–ethyl acetate to afford **34** (32.4 mg, 93% from **35**), which was isomerically homogeneous and identical with the sample of **34** obtained in (*a*).

*2,4,6,9-Tetradeoxy-7,8-O-isopropylidene-2,4,6-tri-C-methyl-*D-arabino-L-allo-*nonose Diethyl Acetal (37) and* L-altro *Epimer (39).* *(a)*: By the procedure described in the case of the homogeneous hydrogenation of **31**, **33** (0.473 g, 1.31 mmol) was treated with $(Ph_3P)_3RhCl$ (0.284 g, 0.307 mmol) in benzene for 17 h, and the reaction mixture was worked up to afford a yellow syrup (0.475 g). The syrup was chromatographed on silica gel (50 g) with 2 : 1 hexane–ethyl acetate to give **37** (0.179 g, 38%) as colorless needles, **39** (0.173 g, 37%) as colorless syrup, and a mixture of **37** and **39** (40 mg, 8.5%): **37**, R_f=0.40 (2 : 1 hexane–ethyl acetate); mp 69.5—72 °C (from hexane); $[\alpha]_D^{24}$ −19° (*c* 1.29); ^{1}H-NMR (250 MHz) δ=0.96 (3H, d, 4-Me, J=7.0 Hz), 1.03 (3H, d, 2-Me, J=7.0 Hz), 1.07 (3H, d, 6-Me, J=6.8 Hz), 1.22 and 1.24 [each 3H, each t, CH(OCH$_2$-$\underline{Me}$)$_2$, J=7.0 Hz], 1.26 (3H, d, H-9, J=6.3 Hz), 1.34 and 1.47 (each 3H, each s, CMe$_2$), 1.99 (1H, ddq, H-6, $J_{5,6}$=6.8 Hz, $J_{6,7}$=4.2 Hz), 2.04 (1H, ddq, H-4, $J_{3,4}$=7.0 Hz, $J_{4.5}$=7.0 Hz), 2.23 (1H, ddq, H-2, $J_{1,2}$=5.5 Hz, $J_{2,3}$=6.5 Hz), 3.44 (1H, ddd, H-5, $J_{5.OH}$=6.8 Hz), 3.53, 3.55, 3.70, and 3.76 [each 1H, each dq, CH(OC$\underline{H}_2$Me)$_2$, J_{gem}=10.0 Hz], 3.60 (1H, ddd, H-3, $J_{3.OH}$=3.5 Hz), 3.87 (1H, d, 5-OH), 4.25 (1H, dd, H-7, $J_{7,8}$=6.3 Hz), 4.43 (1H, dq, H-8), 4.50 (1H, d, H-1), and 4.61 (1H, d, 3-OH).

Found: C, 62.87; H, 10.32%. Calcd for $C_{19}H_{38}O_6$: C, 62.96; H, 10.57%.

39, R_f=0.33 (2 : 1 hexane–ethyl acetate); $[\alpha]_D^{23}$ −22° (*c* 1.12); ^{1}H-NMR (250 MHz) δ=0.75 (3H, d, 4-Me, J=7.0 Hz), 0.96 (3H, d, 2-Me, J=7.0 Hz), 1.09 (3H, d, 6-Me, J= 7.0 Hz), 1.22 and 1.23 [each 3H, each t, CH(OCH$_2$$\underline{Me}$)$_2$, J= 7.0 Hz), 1.27 (3H, d, H-9, J=6.7 Hz), 1.35 and 1.47 (each 3H, each s, CMe$_2$), 1.80 (1H, ddq, H-4, $J_{3,4}$=9.0 Hz, $J_{4.5}$=7.0 Hz), 1.88 (1H, ddq, H-2, $J_{1,2}$=6.0 Hz, $J_{2,3}$=1.0 Hz), 1.98 (1H, ddq, H-6, $J_{5,6}$=4.1 Hz, $J_{6,7}$=3.0 Hz), 3.42 (1H, ddd, H-5, $J_{5.OH}$=7.0 Hz), 3.45—3.80 [4H, m, CH(OC$\underline{H}_2$Me)$_2$] 3.73 (1H, d, 5-OH), 3.95 (1H, dd, H-3, $J_{3,OH}$=0 Hz), 4.31 (1H, dd, H-7, $J_{7,8}$=6.7 Hz), 4.38 (1H, s like, 3-OH), 4.42 (1H, dq, H-8), and 4.47 (1H, d, H-1).

Found: C, 62.82; H, 10.29%. Calcd for $C_{19}H_{38}O_6$: C, 62.96; H, 10.57%.

(b): By the procedure described in the case of the hydrogenation of **30**, **32** (41 mg, 0.86 mmol) was treated with the rhodium catalyst (120 mg, 0.129 mmol) for 22 h, and the reaction mixture was worked up to afford a yellow syrup (a mixture of **38** and **40**). A solution of this syrup in THF (0.34 ml) was treated with 1.0 M *n*-Bu_4NF in THF (0.14 ml) at 0 °C for 15 min and then worked up to give a syrup, which was chromatographed on silica gel (4 g) with 2 : 1 hexane–ethyl acetate to afford **37** (1.7 mg, 6.6%), **39** (12.8 mg, 50%), and a mixture of **37** and **39** (2.3 mg).

Transformation of 34 into 41. To a solution of **34** (9.5 mg, 0.026 mmol) in dry ethanol (0.23 ml) was added a 0.026 M ethanolic PPTS solution (0.1 ml), and the mixture was stirred at 55 °C for 4 h. The reaction mixture was then neutralized with triethylamine and evaporated. The residue was chromatographed on silica gel (0.5 g) with 2 : 1 benzene–acetone to afford a colorless syrup (6.5 mg). To a solution of this syrup in acetone (0.065 ml) was added a solution of $NaIO_4$ (6.5 mg, 0.03 mmol) in water (0.065 ml) under ice-cooling. After being stirred for 20 min, the mixture was diluted with water and then extracted with ether. The extract was washed with a saturated aqueous NaCl solution, dried, and evaporated to a colorless syrup (5.4 mg). To a solution of this syrup in 95% ethanol (0.054 ml) was added $NaBH_4$ (1.8 mg, 0.048 mmol), and the mixture was stirred at room temperature for 30 min. The resulting mixture was neiutralzed with solid CO_2, concentrated, and extracted with chloroform. The extract was evaporated to a colorless syrup (5.5 mg,) which was dissolved in a 0.5% methanolic hydrogen chloride (0.055 ml). The resulting solution was kept at room temperature for 1 h, and the reaction mixture was neutralized with solid $NaHCO_4$ and evaporated. The residue was partitioned between ethyl acetate and water. The aqueous layer was saturated with NaCl and extracted with ethyl acetate. The combined organic layers were dried and evaporated to a colorless syrup (4.7 mg), which was dissolved in ethyl acetate (0.047 ml). To this solution was added acetic anhydride (0.01 ml) and DMAP (13.4 mg) and stirred at room temperature for 20 min. The reaction mixture was then diluted with ethyl acetate, and washed with a saturated aqueous NaCl solution, dried, and evaporated. The residue was chromatographed on silica gel (0.6 g) with 10 : 1 benzene–ethyl acetate to afford **41** (4.0 mg, 51% from **34**) as a colorless syrup: ^{1}H-NMR (250 MHz) δ= 0.84 and 0.86 (3H, each d, β- and α-4-Me, J=7.0 Hz), 0.90 and 0.97 (3H, each d, β- and α-2-Me, J=7.0 Hz), 1.09 and 1.12 (3H, each d, α- and β-6-Me, J=7.0 Hz), 1.95—2.05 (1H, m, H-4), 2.05 and 2.09 (0.75H, each s, 2×β-OAc), 2.06 and 2.07 (5.25H, each s, 2×α-OAc), 2.10—2.25 (2H, m, H-2 and 6), 2.98 and 3.41 (1H, each dd, β- and α-H-5, $J_{4,\beta\text{-}5}$=$J_{4,\alpha\text{-}5}$= 11.3 Hz, $J_{\beta\text{-}5.6}$=$J_{\alpha\text{-}5.6}$=2.0 Hz), 3.31 and 3.46 (3H, each s, α- and β-OMe), 3.96 and 3.99 (1H, each dd, α- and β-H-7, $J_{6,7}$= 7.5 Hz, $J_{7,7'}$=10.8 Hz), 4.31 (1H, dd, H-7′, $J_{6,7'}$=5.0 Hz), 4.29 (overlapped one of the double doublets of H-7′ proton, H-1β), 4.49 (d, H-1α, $J_{\alpha\text{-}1.2}$=1.5 Hz), and 4.59—4.93 (1H, each dd, β- and α-H-3, $J_{2,\beta\text{-}3}$=$J_{2,\alpha\text{-}3}$=5.3 Hz, $J_{\beta\text{-}3.4}$=$J_{\alpha\text{-}3,4}$= 10.5 Hz).

Transformation of 37 and 39 into 42 and 43. By the procedure described in the preceding paragraph, **37** (22.3 mg) and **39** (18.4 mg) were coverted into **42** (12.8 mg, 69% yield based on **37**) and **43** (9.7 mg, 63% yield based on **39**) respectively: **42**, ^{1}H-NMR (250 MHz) δ=0.83 and 0.84 (3H, each d, β- and α-4-Me, J=7.0 Hz), 0.86 (3H, d, 2-Me, J=7.0 Hz), 1.11 (3H, d, 6-Me, J=7.0 Hz), 1.73 (0.6H, ddq, β-H-2), 1.85 —2.05 (1.4H, m, α-H-2, α- and β-H-4), 2.0—2.15 (1H, m, H-6), 2.04, 2.05, 2.10, and 2.11 (6H, each s, 2×OAc), 3.33 and 3.47 (3H, each s, α- and β-OMe), 3.42 and 3.67 (1H, each dd, β- and α-H-5, $J_{4,\beta\text{-}5}$=11.0 Hz, $J_{\beta\text{-}5.6}$=2.1 Hz,

$J_{4,\alpha\text{-}5}=11.0$ Hz, $J_{\alpha\text{-}5,6}=1.9$ Hz), 3.93 and 3.98 (1H, each dd, H,α- and β-H-7, $J_{6,7}=8.0$ Hz, $J_{7,7'}=11.0$ Hz), 4.26 and 4.27 (1 each dd, α- and β-H-7', $J_{6,7'}=6.0$ Hz), 4.23 and 4.46 (1H, each d, β- and α-H-1, $J_{\beta\text{-}1,2}=9.0$ Hz, $J_{\alpha\text{-}1,2}=3.9$ Hz), and 5.12 and 5.22 (1H, each dd, α- and β-H-3, $J_{2,\alpha\text{-}3}=J_{\alpha\text{-}3,4}=3.1$ Hz, $J_{2,\beta\text{-}3}=J_{\beta\text{-}3,4}=3.0$ Hz); **43**, ^{1}H-NMR (250 MHz) $\delta=0.83$ and 0.88 (3H, each d, β- and α-4-Me, $J=7.0$ Hz), 0.98 and 1.04 (3H, each d, β- and α-2-Me, $J=7.0$ Hz), 1.10 and 1.12 (3H, each d, α- and β-6-Me, $J=7.0$ Hz), 1.9—2.2 (3H, m, H-2,4, and 6), 2.05, 2.06, 2.07, and 2.09 (6H, each s, 2×OAc), 3.34 and 3.47 (3H, each s, α- and β-OMe), 3.43 and 3.70 (1H, each dd, β- and α-H-5, $J_{4,\beta\text{-}5}=11.0$ Hz, $J_{\beta\text{-}5,6}=2.0$ Hz, $J_{4,\alpha\text{-}5}=10.0$ Hz, and $J_{\alpha\text{-}5,6}=3.0$ Hz), 3.96 and 4.00 (1H, each dd, α- and β-H-7, $J_{6,7}=8.0$ Hz, $J_{7,7'}=11.0$ Hz), 4.31 (1H, dd, H-7', $J_{6,7'}=5.2$ Hz), 4.38 and 4.55 (1H, each d, α- and β-H-1, $J_{\alpha\text{-}1,2}=1.8$ Hz, $J_{\beta\text{-}1,2}=2.5$ Hz). and 4.67 and 4.90 (1H, each dd, α- and β-H-3, $J_{2,\alpha\text{-}3}=J_{\alpha\text{-}3,4}=4.0$ Hz, $J_{2,\beta\text{-}3}=J_{\beta\text{-}3,4}=2.7$ Hz).

*3,5-Di-*O*-benzyl-2,4,6,9-tetradeoxy-7,8-*O*-isopropylidene-2,4,6-tri-*C*-methyl-*D*-arabino-*L*-manno-nonose Diethyl Acetal (**36**).* After a mixture of the crude **34** (0.353 g), NaH (0.119 g, 0.496 mmol) and dry DMF (3.6 ml) had been stirred at room temperature for 0.5 h, benzyl bromide (0.47 ml, 0.395 mmol) was added to the resulting solution over a period of 2 min under ice-cooling, and the mixture was stirred at 45 °C for 2 h. The reaction mixture was then poured into ice water (5 ml) and the new mixture was extracted with chloroform (8 ml×3). The extracts were washed with a saturated aqueous NaCl solution (10 ml×2), dried, and evaporated. The residual syrup (0.746 g) was chromatographed on silica gel (37 g) with 15 : 1 benzene–ethyl acetate to afford a practically pure sample of **36** (0.472 g, 88%). A part of this sample (14 mg) was chromatographed twice by using silica gel (1 g) with the same solvent system to give an analytical sample (12.5 mg) as a colorless syrup: $R_f=0.38$ (15 : 1 benzene–ethyl acetate); $[\alpha]_D^{24}=[\alpha]_{365}^{24}=0°$ (*c* 1.10); ^{1}H-NMR $\delta=0.9$—1.3 [18H, m, 2,4,6-Me, H-9, and CH(OCH$_2$Me)$_2$], 1.34 and 1.47 (each 3H, each s, CMe$_2$), 1.85—2.25 (3H, m, H-2,4, and 6), 3.2—4.0 [6H, m, H-3,5, and CH(OCH$_2$Me)$_2$], 4.2—4.8 (7H, m, H-1, 7, 8 and 2×OCH$_2$Ph), and 7.43 (10H, s, 2×Ph).

Found: C, 71.91; H, 9.02%. Calcd for $C_{33}H_{50}O_6$: C, 71.68; H, 9.22%.

*3,5-Di-*O*-benzyl-2,4,6,9-tetradeoxy-2,4,6-tri-*C*-methyl-*D*-arabino-*L*-manno-nonose Diethyl Acetal (**45**).* A mixture of crude **36** (0.390 g) and 75% DCA (11.7 ml) was stirred at 0 °C for 20 min. The resulting solution was poured into an ice-cooled saturated aqueous NaHCO$_3$ solution (60 ml). The mixture was then extracted with ethyl acetate (40 ml×3), and the extracts were washed with a saturated aqueous NaCl solution (50 ml×2), dried, and evaporated to a yellow brown syrup of **44** (0.32 g, 95%). The syrup was thoroughly dried under reduced pressure for 18 h and dissolved in dry ethanol (2.4 ml). To this solution was added dried *p*-toluenesulfonic acid (2.4 mg, 0.0139 mmol). After being kept at room temperature for 3 h, the reaction mixture was neutralized (pH 7) with triethylamine and evaporated to a yellow-brown syrup (0.42 g), which was chromatographed on silica gel (20 g) with 3 : 1 benzene–ethyl acetate to afford **45** (0.312 g, 86% based on **36**) as a colorless syrup: $R_f=0.50$ (2 : 1 benzene–ethyl acetate); $[\alpha]_D^{31}$ +26° (*c* 1.36); ^{1}H-NMR $\delta=0.98$ (6H, d, 2×Me, $J=7.3$ Hz), 1.1—1.3 (12H, m, 2×Me and 2×OCH$_2$Me), 1.5—1.65 (2H, br, 2×OH), 2.0—2.45 (3H, m, H-2,4, and 6), 3.35—4.05 (8H, m, H-3,5,7,8, and 2×OCH$_2$-Me), 4.55—4.85 (5H, m, H-1 and 2×OCH$_2$Ph), 7.34 and 7.37 (each 5H, each s, 2×Ph).

Found: C, 71.41; H, 9.09%. Calcd for $C_{30}H_{46}O_6$: C, 71.68; H, 9.22%.

*3,5-Di-*O*-benzyl-2,4,6-trideoxy-2,4,6-tri-*C*-methyl-*L*-glycero-*L*-manno-heptodialdose 1-(Diethyl acetal) (**46**).* To an ice-cooled solution of **45** (0.172 g, 0.342 mmol) in acetone (1.7 ml) was slowly added a solution of NaIO$_4$ (0.183 g, 0.856 mmol) in water (1.8 ml). After being stirred at room temperature for 2 h, the mixture was diluted with water (2 ml) and extracted with ether (5 ml×3). The combined extracts were washed with a saturated aqueous NaCl solution (5 ml×2) dried and evaporated. The residual syrup (0.16 g) was chromatographed on silica gel (8 g) with 15 : 1 benzene–ethyl acetate to afford a pure sample of **46** (0.127 g, 81%): colorless syrup, $R_f=0.41$ (15 : 1 benzene–ethyl acetate): IR (CHCl$_3$, 0.15 M) 1719 cm^{-1}; ^{1}H-NMR $\delta=0.87$ and 0.92 (each 3H, each d, 2×Me, $J=7.2$ and 7.5 Hz), 1.1—1.3 (9H, m, Me and 2×OCH$_2$Me), 1.8—2.2 (2H, m, H-2 and 4), 2.5—3.0 (1H, m, H-6), 3.1—3.9 (6H, m, H-3,5, and 2×OCH$_2$Me), 4.25—4.55 (5H, m, 2×OCH$_2$Ph and H-1), 7.23 (10H, s, 2×Ph), and 9.72 (1H, s like, H-7, $J_{6,7}=0$ Hz).

*3-C-(Benzyloxymethyl)-3-deoxy-1,2:5,6-Di-*O*-isopropylidene-α-*D*-allofuranose (**48**).* By the procedure described in the benzylation of **2**, **47** (2.08 g, 7.57 mmol) was benzylated with NaH (22.7 mmol) and benzyl bromide (1.78 ml, 15.2 mmol) in DMF (21 ml). The crude product (3.73 g) was chromatographed on silica gel (138 g) with 20 : 1 toluene–ethyl acetate to afford **48** (2.58 g, 94%) as a pale yellow syrup: $[\alpha]_D^{15}$ +6°, $[\alpha]_{365}^{15}$ +15° (*c* 1.02); ^{1}H-NMR $\delta=1.32$, 1.34, and 1.48 (total 12H, each s, 2×CMe$_2$), 2.0—2.3 (1H, m, H-3), 3.5—4.1 (6H, m, H-4,5,6, and CH$_2$OBzl), 4.51 (2H, s, OCH$_2$Ph), 4.73 (1H, dd, H-2, $J_{1,2}=J_{2,3}=3.8$ Hz), 5.75 (1H, d, H-1), and 7.34 (5H, s, Ph).

Found: C, 66.12; H, 7.77%. Calcd for $C_{20}H_{28}H_6$: C, 65.91; H, 7.74%.

*3-C-(Benzyloxymethyl)-3-deoxy-1,2-*O*-isopropylidene-α-*D*-allofuranose (**49**).* A solution of **48** (2.55 g) in 75% acetic acid (26 ml) was stirred at 33 °C for 5 h and then evaporated to a yellow syrup (3.00 g), which was subsequently chromatographed on silica gel (68 g) with 1 : 2 toluene–ethyl acetate to afford **49** (2.19 g, 97%) as a pale yellow syrup: $[\alpha]_D^{17}$ +6°, $[\alpha]_{365}^{17}$ +10° (*c* 1.76); ^{1}H-NMR $\delta=1.29$ and 1.48 (each 3H, each s, CMe$_2$), 2.0—2.4 (1H, m, H-3), 3.4—4.0 (6H, m, H-4, 5,6, and CH$_2$OBzl), 4.54 (2H, s, OCH$_2$Ph), 4.64 (1H, dd, H-2, $J_{1,2}=J_{2,3}=3.7$ Hz), 5.75 (1H, d, H-1), and 7.38 (5H, s, Ph).

Found: C, 62.67; H, 7.31%. Calcd for $C_{17}H_{24}O_6$: C, 62.95; H, 7.46%.

*3-C-(Benzyloxymethyl)-3-deoxy-1,2-*O*-isopropylidene-6-*O*-tosyl-α-*D*-allofuranose (**50**).* To a solution of **49** (3.40 g, 10.5 mmol) in dry pyridine (17 ml) was added a solution of tosyl chloride (2.40 g, 12.6 mmol) in dry pyridine (4.8 ml) under ice-cooling. After being kept at room temperature for 3 h, the reaction mixture was poured into ice water (65 ml) and the mixture was extracted with ethyl acetate. The extract was washed successively with saturated aqueous KHSO$_4$, NaHCO$_3$, and NaCl solutions, dried, and evaporated to afford acrude sample of **50** (5.02 g) as a pale yellow syrup, which was suitable for the next synthesis. A pure sample of **50** was obtained by silica gel column chromatography with 9 : 1 benzene–ethyl acetate: $R_f=0.35$ (9 : 1 benzene–ethyl acetate); $[\alpha]_D^{15}$ +3°, $[\alpha]_{365}^{15}$ +8° (*c* 0.63); IR (CHCl$_3$) 1177 and 1365 cm^{-1}.

Found: C, 60.20; H, 6.27; S, 6.52%. Calcd for $C_{24}H_{30}O_8S$: C, 60.24; H, 6.32; S, 6.70%.

*3-C-(Benzyloxymethyl)-3,6-dideoxy-1,2-*O*-isopropylidene-α-*D*-allofuranose (**51**).* To an ice-cooled solution of the crude sample of **50** (5.02 g) in dry ether (50 ml) was slowly added powdered LiAlH$_4$ (0.796 g, 21.0 mmol) under stirring. The stirring was continued for 3 h under ice-cooling, and to the reaction mixture were added dropwise water (0.8 ml), 15% NaOH solution (0.8 ml), and water (2.4 ml) successively. The

resulting mixture was then filtered, and the filter cake was washed with ether. The filtrate and washings were combined, and evaporated to a syrup (3.1 g), which was chromatographed on silica gel (160 g) with 3 : 1 toluene–ethyl acetate to afford a pure sample of **51** (2.39 g, 74% based on **49**): colorless syrup, R_f=0.32 (3 : 1 toluene–ethyl acetate); $[\alpha]_D^{16}$ +7°, $[\alpha]_{365}^{16}$ +11° (*c* 2.35); ^{1}H-NMR δ=1.26 (3H, d. H-6, $J_{5,6}$=6.0 Hz), 1.28 and 1.48 (each 3H, each s, CMe_2), 1.9—2.25 (1H, m, H-3), 3.5—3.9 (4H, m, H-4,5, and $C\underline{H}_2OBzl$), 3.96 (1H, broad s, 5-OH), 4.53 (2H, ABq, $OC\underline{H}_2Ph$, J_{gem}=11.1 Hz), 4.66 (1H, dd, H-2, $J_{1,2}=J_{2,3}$=3.9 Hz), 5.74 (1H. d, H-1), and 7.35 (5H' s, Ph).

Found: C, 66.10; H, 7.70%. Calcd for $C_{17}H_{24}O_5$: C, 66.21; H, 7.85%.

*3-C-(Benzyloxymethyl)-3,6-dideoxy-1,2-O-isopropylidene-α-D-allofuranos-5-ulose (**52**).* To a stirred mixture of PCC (4.80 g, 22.3 mmol), molecular sieve 3A powder (5.57 g), and dry dichloromethane (19 ml) was added a solution of **51** (2.29 g, 7.43 mmol) in dichloromethane (4.6 ml) at room temperature. After being stirred at room temperature for 2.5 h, the reaction mixture was diluted with ether (25 ml) and filtered through a column filled with silica gel (60 g). Removal of the solvent gave almost pure sample of **52** (2.10 g, 92%) as a colorless syrup. A portion of this sample was chromatographed on silica gel with 10 : 1 benzene–ethyl acetate to afford an analytical sample of **52**: R_f=0.56 (3 : 1 toluene–ethyl acetate); $[\alpha]_D^{15}$ +3°, $[\alpha]_{436}^{15}$ +4°, and $[\alpha]_{365}^{15}$ 0° (*c* 2.09); IR ($CHCl_3$) 1720 cm^{-1}; ^{1}H-NMR δ=1.35 and 1.49 (each 3H, each s, CMe_2), 2.1—2.5 (1H, m, H-3), 2.20 (3H, s, H-6), 3.61 (1H, dd, one of the $C\underline{H}_2OBzl$, J_{gem}=9.1 Hz, J=4.6 Hz), 3.79 (1H, dd, one of the $C\underline{H}_2OBzl$, J=9.1 Hz), 4.11 (1H, d, H-4, $J_{3,4}$=9.7 Hz), 4.49 (2H, s, $OC\underline{H}_2Ph$), 4.73 (1H, dd, H-2, $J_{1,2}=J_{2,3}$=3.9 Hz), 5.90 (1H, d, H-1), and 7.34 (5H, m, Ph).

Found: C, 66.31; H, 7.12%. Calcd for $C_{17}H_{22}O_5$: C, 66.65; H, 7.24%.

*3-C-(Benzyloxymethyl)-3,5,6-trideoxy-5-iodo-1,2-O-isopropylidene-α-D-ribo-5-hexenofuranose (**54**).* A mixture of **52** (1.02 g, 3.33 mmol), ethanol (10 ml), triethylamine (3.93 ml, 28.2 mmol), and 100% hydrazine hydrate (0.645 ml, 13.3 mmol) was refluxed for 10 min. The cooled reaction mixture was diluted with chloroform (33 ml), and the mixture was washed with water (20 ml). The aqueous layer was extracted with chloroform. The combined organic layers were washed with a saturated aqueous NaCl solution, dried, and evaporated to afford the hydrazone **53** (1.06 g, 100%) as a pale yellow syrup. To an ice-cooled mixture of **53** (1.06 g), dry THF (37 ml), and triethylamine (23.1 ml, 166 mmol) was added dropwise a solution of iodine (1.85 g, 7.30 mmol) in dry THF (18.5 ml). After being stirred at 0 °C for 5 min, the reaction mixture was diluted with ether (110 ml) and washed successively with 10% aqueous citric acid, saturated aqueous $Na_2S_2O_3$, and NaCl solutions, dried, and evaporated. The residual dark brown syrup (1.56 g) was chromatographed on silica gel (207 g) with 30 : 1 toluene–ethyl acetate to give colorless needles of **54** (0.407 g, 30%). Recrystallization from hexane afforded an analytical sample: R_f=0.34 (30 : 1 toluene–ethyl acetate); mp 67—67.5 °C; $[\alpha]_D^{15}$ +50° (*c* 1.25); IR (KBr) 1612 cm^{-1}; ^{1}H-NMR δ=1.35 and 1.50 (each 3H, each s, CMe_2), 2.1—2.45 (1H, m, H-3), 3.42 (1H, dd, one of the $C\underline{H}_2OBzl$, J_{gem}=9.4 Hz, J=5.5 Hz), 3.62 (1H, d, H-4, $J_{3,4}$=9.4 Hz), 3.76 (1H, dd, one of the $C\underline{H}_2OBzl$, J=9.4 Hz), 4.50 (2H, s, $OC\underline{H}_2Ph$), 4.73 (1H, dd, H-2, $J_{1,2}=J_{2,3}$=3.8 Hz), 5.88 (1H, d, H-1), 5.95 and 6.39 (each 1H, each d, $C=CH_2$, J=1.5 Hz), and 7.37 (5H, s, Ph).

Found: C, 48.76; H, 5.03; I, 30.66%. Calcd for $C_{17}H_{21}O_4I$: C, 49.05; H, 5.08; I, 30.49%.

*3-C-(Benzyloxymethyl)-3,5,6-trideoxy-1,2-O-isopropylidene-α-D-ribo-5-hexenofuranose (**55**).* To an ice-cooled solution of **49** (0.703 g, 2.17 mmol) in acetone (7 ml) was added a solution of $NaIO_4$ (0.695 g, 3.25 mmol) in water (7 ml). After being stirred under ice-cooling for 10 min, the mixture was diluted with water (7 ml) and extracted with ehter (7 ml×4). The combined extracts were washed with a saturated aqueous NaCl solution (7 ml), dried, and evaporated to afford a syrup of the crude aldehyde (0.614 g, 97%). A suspension of 55% NaH (0.275 g, 6.30 mmol) in dry DMSO (19 ml) was stirred at 75 °C for 45 min under argon and then cooled to room temperature. To this solution was added methyltriphenylphosphonium bromide (2.25 g, 6.30 mmol) and the mixture was stirred at room temperature for 0.5 h. A solution of the aforesaid crude aldehyde (614 mg) in dry DMSO (3.1 ml) was added dropwise to the ice-cooled resulting organge-yellow solution of the ylide over a period of 10 min. After the mixture had been stirred at room temperature for 0.5 h, it was poured into ice water (80 ml), and new mixture was extracted with ether. The extract was successively washed with water, a saturated aqueous NaCl solution, dried, and evaporated. The residue (1.55 g) was chromatographed on silica gel (31 g) with 20 : 1 benzene–ethyl acetate to afford **55** (0.544 g, 87% based on **49**) as a colorless syrup: $[\alpha]_D^{25}$ +16° (*c* 0.64); ^{1}H-NMR δ=1.33 and 1.51 (each 3H, each s, CMe_2), 1.9—2.3 (1H, m, H-3), 3.47 (1H, dd, one of the $C\underline{H}_2OBzl$, J_{gem}=9.3 Hz, J=5.3 Hz), 3.78 (1H, dd, one of the $C\underline{H}_2OBzl$, J=9.3 Hz), 4.19 (1H, dd, H-4, $J_{3,4}$=6.8 Hz, $J_{4,5}$=10.4 Hz), 4.50 (2H, s, $OC\underline{H}_2Ph$), 4.71 (1H, dd, H-2, $J_{1,2}=J_{2,3}$=3.8 Hz), 5.15 (1H, dd, H-6(*E*), $J_{5,6}$=10.3 Hz, J_{gem}=*ca.* 1 Hz), 5.26 (1H, dd, H-6(*Z*), $J_{5,6}$=16.5 Hz), 5.38 (2H, d and ddd, H-1 and H-5), and 7.36 (5H, s, Ph).

Found: C, 70.19; H, 7.54%. Calcd for $C_{17}H_{22}O_4$: C, 70.32; H, 7.64%.

*3-C-(Benzyloxymethyl)-5-bromo-3,5,6-trideoxy-1,2-O-isopropylidene-α-D-ribo-5-hexenofuranose (**56**) and 3-C-(Benzyloxymethyl)-6-bromo-3,5,6-trideoxy-1,2-O-isopropylidene-α-D-ribo-(E)-5-hexenofuranose (**57**).* To a stirred cooled (−10 °C) solution of **55** (0.541 g, 1.86 mmol) in carbon tetrachloride (5.4 ml) was added dropwise a solution of bromine (0.298 g, 1.86 mmol) in carbon tetrachloride (0.96 ml) over a period of 20 min. After being at −10 °C for 5 min, a saturated aqueous $NaHCO_3$ solution was added to the reaction mixture. The organic layer was separated and the aqueous layer was extracted with chloroform. The combined organic layers were washed with a saturated aqueous NaCl solution, dried, and evaporated. The residue was chromatographed on silica gel (25 g) with 40 : 1 toluene–ethyl acetate to afford dibromide (0.675 g, 81%) as a pale yellow syrup. The TLC (40 : 1 toluene–ethyl acetate) of this sample revealed it to be a mixture of two diastereomers with R_f=0.31 and 0.27. To a solution of the dibromide (0.674 g) in dry DMSO (4.7 ml) was added a solution of DBU (0.457 g, 3.00 mmol) in dry DMSO (2.0 ml), and the mixture was stirred at room temperature for 2 h. The reaction mixture was then diluted with water (35 ml) and extracted with ether (20 ml×4). The extracts were combined, successively washed with water and a saturated aqueous NaCl solution, dried, and evaporated. The residue (0.56 g) was chromatographed on silica gel (28 g) with 30 : 1 toluene–ethyl acetate to afford a mixture of **56** and **57**(0.496g, 90 %)and the starting dibromide (43 mg, 6.4%). The mixture of **56** and **57** was again chromatographed on silica gel (74 g) with 8 : 1 hexane–ethyl acetate to give **56** (0.401 g, 72%) and **57** (80 mg, 14%): **56** (colorless needles), R_f=0.29 (8 : 1 hexane–ethyl acetate), mp 71—72 °C (heptane); $[\alpha]_D^{17}$ +53° (*c* 1.13); IR ($CHCl_3$) 1630 cm^{-1}; ^{1}H-NMR δ=1.33 and 1.49 (each 3H, each s, CMe_2), 2.3—2.7 (1H, m, H-3), 3.47 (1H, dd, one of the $C\underline{H}_2OBzl$, J_{gem}=9.3 Hz, J=5.3 Hz), 3.77 (1H, dd, one of the

$C\underline{H}_2OBzl$, J=9.3 Hz), 4.20 (1H, d, H-4, $J_{3,4}$=10.5 Hz), 4.50 (2H, s, $OC\underline{H}_2Ph$), 4.73 (1H, dd, H-2, $J_{1,2}=J_{2,3}$=3.5 Hz), 5.64 and 5.91 (each 1H, each d, C=CH_2, J=2.1 Hz), 5.88 (1H, d, H-1), and 7.35 (5H, s, Ph).

Found: C, 55.42; H, 5.69; Br, 21.42%. Calcd for $C_{17}H_{21}O_4Br$: C, 55.30; H, 5.73; Br, 21.64%.

57 (colroless syrup), R_f=0.25 (8 : 1 hexane–ethyl acetate); $[\alpha]_D^{30}$ +30° (c 1.24); IR ($CHCl_3$) 1623 cm^{-1}; ^{1}H-NMR δ=1.32 and 1.49 (each 3H, each s, CMe_2), 2.1—2.2 (1H, m, H-3), 3.49 (1H, dd, one of the $C\underline{H}_2OBzl$, J_{gem}=9.0 Hz, J=6.3 Hz), 3.78 (1H, dd, one of the $C\underline{H}_2OBzl$, J=7.8 Hz), 4.26 (1H, dd, H-4, $J_{3,4}$=10.3 Hz, $J_{4,5}$=6.8 Hz), 4.52 and 4.53 (each 1H, each d, $OC\underline{H}_2Ph$, J_{gem}=12.5 Hz), 4.72 (1H, dd, H-2, $J_{1,2}=J=J_{2,3}$=4.0 Hz), 5.82 (1H, d, H-1), 6.24 (1H, dd, H-5, $J_{5,6}$=14.3 Hz), 6.42 (1H, d, H-6), and 7.34 (5H, s, Ph).

Found: C, 55.18; H, 5.75; Br; 21.41%. Calcd for $C_{17}H_{21}O_4Br$: C, 55.30; H, 5.73; Br, 21.64%.

*A Mixture of 8,10-Di-O-benzyl-3-C-(benzyloxymethyl)-3,5,7,9,11-pentadeoxy-1,2-O-isopropylidene-7,9,11-tri-C-methyl-5-methylene-*L*-erythro-*D*-altro-α-*D*-ribo-dodecodialdofuranose-(1,4)12-(Diethyl acetal) (**59**) and* L-erythro-D-allo-α-D-ribo *Epimer (**60**).* To a cooled (−90—−94 °C) solution of **54** (0.588 g, 1.41 mmol) in dry ether (13 ml) was added 1.28 M butyllithium in hexane (1.1 ml, 1.41 mmol) over a period of 3 min under argon. After being stirred at the same temperature for 45 min, a solution of **46** (0.209 g, 0.458 mmol) in dry ether (0.42 ml) was added to the mixture over a period of 2 min, and stirring was continued at the same temperature for 0.5 h. To the reaction mixture was added a saturated aqueous NH_4Cl solution (3 ml), and the separated aqueous layer was extracted with ether (6 ml×2). The organic layers were combined, washed with a saturated aqueous NaCl solution, dried, and evaporated. The residual yellow syrup (0.673 g) was chromatographed on silica gel (70 g) with 20 : 1 toluene–acetone to afford the following fractions: Fr-1, a mixture of **46**, **55**, and **54**(95.7 mg); Fr-2, **55**(0.152 g); Fr-3, *ca.* 4: 1 mixture of **59** and **60** (0.272 g, 80%). The Fr-3 showed on the TLC (20 : 1 toluene–acetone) the major spot (**59**, R_f=0.29) and the minor one (**60**, R_f=0.31); ^{1}H-NMR (250 MHz) δ=0.90, 0.93, and 1.08 (each 0.6H, each d, 7,9,11-Me, J=7.0 Hz), 0.96, 1.00, and 1.02 (each 2.4H, each d, 7,9,11-Me, J=7.0 Hz), 1.15 (3H, t, $OCH_2\underline{Me}$, J=7.0 Hz), 1.18 (2.4H, t, $OCH_2\underline{Me}$, J=7.0 Hz), 1.20 (0.6H, t, $OCH_2\underline{Me}$, J=7.0 Hz), 1.34 (3H, s, CMe_2), 1.46 (2.4H, s, CMe_2), 1.50 (0.6H, s, CMe_2), 2.0—2.4 (4H, m, H-3, 7,9, and 11), 3.3—3.95 (10H, m, H-6,8,10, and 2×$OC\underline{H}_2Me$, and $C\underline{H}_2OBzl$, 6-OH), 4.04 (0.8H, d, H-4, $J_{3,4}$=10.5 Hz), 4.15 (0.2H, d, H-4, $J_{3,4}$=10.5 Hz), 4.35—4.85 (7H, m, 3×$C\underline{H}_2Ph$, and H-12), 4.77 (1H, dd, H-2, $J_{1,2}=J_{2,3}$=4.0 Hz), 5.28 and 5.29 (each 0.2H, each s, C=$C\underline{H}_2$), 5.32 and 5.44 (each 0.8H, each s, C=$C\underline{H}_2$), 5.82 (1H, d, H-1), 7.32 and 7.33 (15H, each s, 3×Ph).

*3,5,7,9,11-Pentadeoxy-3-*C*-(hydroxymethyl)-1,2-*O*-isopropylidene-5,7,9,11-tetra-*C*-methyl-*L*-erythro-*D*-altro-β-*L*-talo-dodecodialdofuranose-(1,4) 12-(Diethyl acetal) (**63**) and Its Isomeric Mixture (**65**).* A sample (0.231 g, 0.310 mmol) of the epimeric mixture (**59** and **60**) obtained in the preceding experiment was dissolved in dry benzene (12 ml). To this solution was added $(Ph_3P)_3RhCl$ (0.573 g, 0.619 mmol), and the solution stirred under an atmospheric pressure of H_2 at room temperature for 1 d. The reaction mixture was then evaporated and the residue was passed through Florisil (100—200 mesh, 40 g) with ether. The effluent was evaporated to afford a pale yellow syrup of the crude hydrogenation product (0.189 g, 82%). To a solution of this product in dry ether (3.8 ml) was added liquid ammonia (19 ml), and then lithium (0.070 g, 10 mmol) was added under cooling (−78 °C). After the mixture had been stirred at the same temperature for 50 min, the excess lithium was destroyed by addition of solid NH_4Cl. The mixture was then diluted with ether (10 ml) and allowed to concentrate spontaneously. The residue was taken with ether (10 ml), and the solution washed with a saturated aqueous NaCl solution (3 ml×2), dried, and evaporated. The residual syrup was chromatographed on silica gel (10 g) with 2 : 1 benzene–acetone to afford **63** (colorless syrup, R_f=0.25 (2 : 1 benzene–acetone), 93 mg, 77%) and a colorless syrup [R_f=0.51 (2 : 1 benzene–acetone), 17 mg] containing **65**.

*8,10-Di-O-benzyl-3-C-(benzyloxymethyl)-3,5,7,9,11-pentadeoxy-1,2-O-isopropylidene-5,7,9,11-tetra-C-methyl-*L*-erythro-*D*-altro-β-*L*-talo-dodecodialdofuranose-(1, 4) 12-(Diethyl acetatal) (**61**).*

(a): A sample (60 mg) of the aforesaid crude hydrogenation product from a mixture of **59** and **60** was at first chromatographed on silica gel (6 g) with 35 : 1 chroloform–acetone to afford a pale-yellow syrup (42 mg). This was again chromatographed on silica gel (8.4 g) with 7 : 1 *s*-BuCl–ethyl acetate to give **61** (31 mg) and a product (8.4 mg) shown to be **62** by ^{1}H-NMR analysis: **61**, colorless syrup, R_f=0.31 (7 : 1 *s*-BuCl–ethyl acetate); $[\alpha]_D^{17}$ +16° (c 0.92); ^{1}H-NMR (250 mHz) δ=0.76, 0.92, 0.97, and 1.08 (each 3H, each d, 5,7,9,11-Me, J=7.0 Hz), 1.17 and 1.19 (each 3H, each t, 2×$OCH_2\underline{Me}$, J=7.0 Hz), 1.32 and 1.50 (each 3H, each s, CMe_2), 1.65—1.80, 1.90—2.05, and 2.05—2.30 (each 1H, 1H, and 3H, each m, H-3,5,7,9, and 11), 3.3—4.0 (10H, m, H-6,8,10, 2×OCH_2Me, $C\underline{H}_2OBzl$, and 6-OH), 4.4—4.75 (9H, m, H-2,4,12, and 3×$OC\underline{H}_2Ph$), 5.77 (1H,d, H-1, $J_{1,2}$=3.5 Hz), 7.32 and 7.34 (15H, each s, 3×Ph).

Found: C, 72.06; H, 8.43%. Calcd for $C_{45}H_{64}O_9$: C, 72.16; H, 8.61%.

62, colorless syrup, R_f=0.38 (7 : 1 *s*-BuCl–ethyl acetate); ^{1}H-NMR (250 MHz) δ=0.90, 0.92, 0.93, and 1.04 (each 3H, each d, 5,7,9,11-Me, J=7.0 Hz), 1.17 and 1.20 (each 3H, each t, 2×$OCH_2\underline{Me}$, J=7.0 Hz), 1.32 and 1.50 (each 3H, each s, CMe_2), 1.90—2.00 (1H, m, H-5), 1.95—2.25 (3H, m, H-7,9, and 11), 2.25—2.40 (1H, m, H-3), 3.15 (1H, d, 6-OH, $J_{6,OH}$=1.0 Hz), 3.3—3.65 (4H, m, one of the CH_2OBzl, and three of the 2×$OC\underline{H}_2Me$), 3.7—3.9 (2H, m, one of the $C\underline{H}_2OBzl$, and one of the 2×$OC\underline{H}_2Me$), 3.74 (1H, dd, H-6 or 8, J=2.3 and 11.0 Hz), 3.85 (1H, dd, H-6 or 8, J=0 and 9.5 Hz), 3.95 (1H, dd, H-10, $J_{9,10}$=0 Hz, $J_{10,11}$=9.0 Hz), 4.01 (1H, dd, H-4, $J_{3,4}$=10.3 Hz, $J_{4,5}$=2.3 Hz), 4.35—4.7 (6H, m, 3×$OC\underline{H}_2Ph$), 4.56 (1H, d, H-12, $J_{11,12}$=3.5 Hz), 4.69 (1H, dd, H-2, $J_{1,2}=J_{2,3}$=3.8 Hz), 5.79 (1H, d, H-1), and 7.2—7.4 (15H, m, 3×Ph).

(b): By the procedure described in the preparation of the mixture of **59** and **60**, a crude condensation product (213 mg) was obtained from **54** (155 mg) and **46** (66.1 mg). This sample was chromatographed on silica gel (32 g) with 20 : 1 toluene–acetone to afford the six fractions: Fr-1, **54** (30.1 mg); Fr-2, **54**+**46** (5.9 mg); Fr-3, **46**+**55** (11.5 mg); Fr-4, **55** (38.3 mg); Fr-5, **60** (major)+**59** (minor) (18.6 mg, 17.2% yield); Fr-6, **59** (63.5 mg, 58.7% yield). Thus obtained chromatographically pure sample (10 mg, 0.013 mmol) of **59** was hydrogenated in dry benzene (0.5 ml) with $(Ph_3P)_3RhCl$ (24.8 mg, 0.0268 mmol) at room temperature under an atmospheric pressure of H_2 for 14 h. The reaction mixture was evaporated and the residue was passed through Florisil (1 g) with ether and evaporated to a syrup whose TLC showed only one spot of **61**. The chromatographic purification (silica gel, 1 g, 3.5 : 1 hexane–ethyl acetate) gave a colorless syrup of **61** (8.6 mg, 86%).

*6,8,10-Tri-O-acetyl-3-C-(acetoxymethyl)-3,5,7,9,11-pentadeoxy-1,2-O-isopropylidene-5,7,9,11-tetra-C-methyl-*L*-erythro-*D*-altro-β-*L*-talo-dodecodialdofuranose-(1, 4) 12-(Diethyl acetal) (**64**).*

To a mixture of **63** (81 mg, 0.169 mmol), DMAP (99 mg, 0.810 mmol), and ethyl acetate (0.81 ml) was added acetic anhydride (0.096 ml, 1.02 mmol). The mixture was stirred at room temperature for 23.5 h and then poured into a cold saturated aqueous $NaHCO_3$ solution (2 ml). The mixture was extracted with ethyl acetate (3 ml×3) and the extracts were washed with a saturated aqueous NaCl solution, dried, and evaporated. The residue was chromatographed on silica gel (10 g) with 10 : 1 benzene–acetone to afford **64** (99 mg, 91%) as colorless needles: R_f=0.38 (6 : 1 benzene–acetone); mp 100—102 °C; $[\alpha]_D^{19}$ 0°, $[\alpha]_{365}^{19}$ +60° (*c* 1.09); IR ($CHCl_3$, 0.15M) 1732 cm^{-1}; ^{1}H-NMR δ=0.9—1.3 (18H, m, 5,7,9,11-Me, and 2×$OCH_2\underline{Me}$), 1.33 and 1.46 (each 3H, each s, CMe_2), 2.00, 2.02, 2.03, and 2.08 (12H, each s, 4×OAc), 1.9—2.6 (5H, m, H-3,5,7,9,11), 3.3—4.25 (8H, m, H-4,12, $C\underline{H}_2OAc$ and 2×$OC\underline{H}_2Me$), 4.5—5.2 (4H, m, H-2,6,8, and 10), and 5.72 (1H, d, H-1, $J_{1,2}$=2.3 Hz).

Found: C, 59.12; H, 8.17%. Calcd for $C_{32}H_{54}O_{13}$: C, 59.42; H, 8.42%.

*C-5-Epimeric Actates (**66**).* The syrup (17 mg), R_f=0.51) obtained in the preparation of **63** was acetylated by the procedure described in the preparation of **64**. The crude product was purified by silica gel column chromatography with 2 : 1 toluene–ethyl acetate to afford a sample of **66** (16 mg): colorless syrup, R_f=0.50, 0.45 (1 : 1 hexane–ethyl acetate); ^{1}H-NMR (250 MHz) δ=0.9—1.05 (12H, m, 4×Me), 1.19 and 1.20 (2H and 4H, each t, 2×$OCH_2\underline{Me}$, J=6.8 Hz), 1.32 and 1.50 (each 1H, each s, CMe_2), 1.34 and 1.49 (each 2H, each s, CMe_2), 2.00, 2.05, 2.05, and 2.06 (each 1H, each s, 4×OAc), 2.01, 2.03, 2.09, and 2.10 (each 2H, each s, 4×OAc), 1.9—2.5 (5H, m, H-3,5,7,9, and 11), 3.35—3.80 (4H, m, 2×$OC\underline{H}_2Me$), 3.96 (2H/3, dd, H-4, J=5.0 and 10.0 Hz), 4.03 (1H/3, dd, H-4, J=1.0 and 10.0 Hz), 4.1—4.2 (2H, m, H-12 and one of $C\underline{H}_2OAc$), 4.29 (1H/3, dd, one of $C\underline{H}_2OAc$, J=7.8 and 10.8 Hz), 4.39 (2H/3, dd, one of $C\underline{H}_2OAc$, J=4.8 and 10.8 Hz), 4.55—4.7 (2H, m, H-2 and $C\underline{H}OAc$), 4.89 (2H/3, dd, $C\underline{H}OAc$, J=4.8 and 7.5 Hz), 5.0—5.15 (4H/3, m, 2×$C\underline{H}OAc$), 5.72 and 5.75 (1H/3 and 2H/3, each d, H-1, J=3.8 Hz).

*Methyl 6,8,10-Tri-O-acetyl-3-C-(acetoxymethyl)-3,5,7,9,11,12,-13-heptadeoxy-1,2-O-isopropylidene-5,7,9,11-tetra-C-methyl-*L*-erythro-*D*-altro-β-*L*-talo-(E)-12-tetradecenofuranuronate-(1,4)(**68**).* A mixture of **64** (86 mg, 0.133 mmol) and 75% DCA (1.7 ml) was stirred at 0 °C for 40 min. The resulting solution was poured into a cold saturated aqueous $NaHCO_3$ solution (20 ml) containing solid $NaHCO_3$. The mixture was then extracted with ethyl acetate (20 ml×2, 10 ml×1), and the extracts were washed with a saturated aqueous NaCl solution (20 ml×2), dried, and evaporated to afford colorless needles of **67** (74 mg, 97%): mp 97—102 °C. To a solution of this crystals (74 mg) in dry toluene (2.2 ml) was added (methoxycarbonylmethylene) triphenylphosphorane (90 mg, 0.27 mmol), and the mixture was stirred at 95—98 °C for 4 h under argon. The reaction mixture was concentrated to a yellow syrup which was chromatographed on silica gel (13 g) with 3 : 2 *s*-BuCl–ethyl acetate to give **68** (73 mg, 89%) as a pale yellow syrup: R_f=0.34 (3 : 2 *s*-BuCl–ethyl acetate); $[\alpha]_D^{18}$ +5°, $[\alpha]_{365}^{18}$ +15° (*c* 1.02); IR ($CHCl_3$, 0.1 M), 1725, 1650, 1220, and 984 cm^{-1}; ^{1}H-NMR (250 MHz) δ=0.90 (3H, d, 5-Me, J=7.0 Hz), 0.95 (3H, d, 7-Me, J=7.0 Hz), 0.96 (3H, d, 9-Me, J=7.0 Hz), 1.09 (3H, d, 11-Me, J=7.0 Hz), 1.32, and 1.45 (each 3H, each s, CMe_2), 1.8—2.0 (1H, m, H-5), 1.94, 2.01, 2.03, and 2.09 (each 3H, each s, 4×OAc), 2.1—2.3 (2H, m, H-3,7), 2.4—2.6 (2H, m, H-9,11), 3.71 (3H, s, COOMe), 3.84 (1H, dd, H-4, $J_{3,4}$=10.2 Hz, $J_{4,5}$=1.3 Hz), 4.13 and 4.24 (each 1H, each dd, $C\underline{H}_2OAc$, J_{gem}=11.0 Hz, J=6.1 and 8.1 Hz), 4.64 (1H, dd, H-2, $J_{1,2}$=$J_{2,3}$=3.8 Hz), 4.82 (1H, dd, H-8, $J_{7,8}$=5.3 Hz, $J_{8,9}$=8.5 Hz), 4.90 (1H, dd, H-10, $J_{9,10}$=2.0 Hz, $J_{10,11}$=9.2 Hz), 5.18 (1H, dd, H-6, $J_{5,6}$=9.9 Hz, $J_{6,7}$=0.9 Hz), 5.77 (1H, d, H-13, $J_{12,13}$=15.0 Hz), 5.77 (1H, d, H-1), and 6.75 (1H, dd, H-12, $J_{11,12}$=9.0 Hz).

Found: C, 59.43; H, 7.63%. Calcd for $C_{31}H_{48}O_3$: C, 59.22; H, 7.69%.

*Methyl 5,7,9-Tri-O-acetyl-2-C-(acetoxymethyl)-2,4,6,8,10,11,-12-heptadeoxy-4,6,8,10-tetra-C-methyl-*aldehydo-L-glycero-L-talo-L-manno-(E)-11-tridecenuronate 1-(Dimethyl acetal) (III).* A mixture of **68** (30.0 mg, 0.0477 mmol) and 75% TFA (0.3 ml) was kept in a refrigerator for 24 h. The reaction mixture was poured in to a cold saturated aqueous $NaHCO_3$ solution, and the mixture was extracted with ethyl acetate. The extract was washed with a saturated aqueous NaCl solution, dried, and evaporated toa colorless syrup, which was dissolved in acetone (0.56 ml) and ice-cooled. To this solution was added a solution of $NaIO_4$ (40.8 mg, 0.191 mmol) in water (0.5 ml), and the mixture was stirred at room temperature for 2.5 h. The reaction mixture was diluted with water, and extracted with ethyl acetate. The extract was washed with a saturated aqueous NaCl solution, dried, and evaporated to give the crude crystalline aldehyde **69**. The crude **69** was dissolved in dry methanol (0.56 ml) and to this, a 0.095 M methanolic *p*-toluenesulfonic acid (0.01 ml) was added. After being stirred at room temperature for 24 h, the reaction mixture was neutralized with triethylamine and evaporated. The residue was then chromatographed on silica gel (Kieselgel 60, 3 g) with 1 : 1 toluene–ethyl acetate to afford III (12.3 mg, 43% based on **68**) as a colorless syrup: $[\alpha]_D^{16}$ −8° (*c* 0.98); IR ($CHCl_3$), 1726 and 1652 cm^{-1}; ^{1}H-NMR (250 MHz) δ=0.89 (3H, d, 4-Me, J=7.0 Hz), 0.92 and 0.97 (each 3H, each d, 6- and 8-Me, J=7.3 and 7.0 Hz), 1.07 (3H, d, 10-Me, J=6.4 Hz), 1.65—1.85 (1H, m, H-4), 1.96, 2.00, 2.04, and 2.07 (each 3H, each s, 4×OAc), 2.1—2.2 (1H, m, H-2), 2.2—2.4 (2H, m, H-6 and 8), 2.45—2.65 (1H, m, H-10), 3.30 (1H, d, 3-OH, J=3.9 Hz), 3.41 and 3.44 (each 3H, each s, 2×OMe), 3.51 (1H, ddd, H-3, $J_{2,3}$=10.0 Hz, $J_{3,4}$=1.0 Hz), 3.71 (3H, s, COOMe), 3.98 and 4.24 (each 1H, each dd, $C\underline{H}_2OAc$, J=6.0 and 3.8 Hz, J_{gem}=11.6 Hz), 4.62 (1H, d, H-1, $J_{1,2}$=4.0 Hz), 4.85 (1H, dd, H-7, $J_{6,7}$=$J_{7,8}$=7.0 Hz), 4.98 (1H, dd, H-9, $J_{8,9}$=2.0 Hz, $J_{9,10}$=9.8 Hz), 5.02 (1H, dd, H-5, $J_{4,5}$=10.0 Hz, $J_{5,6}$=1.3 Hz), 5.79 (1H, dd, H-12, $J_{10,12}$=0.7 Hz, $J_{11,12}$=16.0 Hz), and 6.76 (1H, dd, H-11, $J_{10,11}$=9.3 Hz).

Found: C, 57.31; H, 7.72%. Calcd for $C_{29}H_{48}O_{13}$: C, 57.60; H, 8.00%.

*Transformation of III into **70**.* A solution of III (10.2 mg, 0.0169 mmol) in dry toluene (1 ml) was cooled at −78 °C and to this was added portionwise 1.76 M DIBAL in hexane (0.258 ml, 0.454 mmol) over a period of 9 h under argon. After being stirred for additional 1 h, the mixture was warmed up to room temperature and was added 50% acetic acid (0.05 ml). The precipitates formed was filtered and washed with acetone. The filtrate and washings were combined and evaporated to afford a colorless syrup (4.6 mg). To a solution of this syrup in dry methanol (0.16 ml) was added 0.022 M methanolic PPTS solution (0.05 ml), and the mixture was stirred at 55 °C for 24 h. The reaction mixture was then neutralized with triethylamine and evaporated to a colorless syrup (4.2 mg) of cyclic methyl acetal derivative. A solution of the acetal in ethyl acetate (0.1 ml) was treated with acetic anhydride (0.008 ml, 0.08 mmol), DMAP (8.2 mg, 0.067 mmol) at 24 °C for 2 h. The reaction mixture was worked up by the usual way. The crude product was chromatographed on silica gel (1 g) with 3 : 2 toluene–ethyl acetate to afford **70** (2.7 mg, 27% from III) as a colorless syrup: R_f=0.38 (3 : 2 toluene–ethyl acetate); ^{1}H-NMR (250 MHz) δ=0.82 (3H, d, 4-Me,

J=6.3 Hz), 0.93 and 0.99 (each 3H, each d, 6- and 8-Me, J= 7.5 and 7.5 Hz), 1.02 (3H, d, 10-Me, J=7.3 Hz), 1.65 —1.85 (1H, m, H-4), 1.97, 2.03, 2.05, 2.05, and 2.09 (each 3H, each s, 5×OAc), 2.05—2.25 (2H, m, H-6 and 8), 2.25—2.40 (1H, m, H-2), 2.35—2.50 (1H, m, H-10), 3.36 (3H, s, OMe), 3.49 (1H, d, H-5, $J_{4,5}$=10.0 Hz, $J_{5,6}$=0 Hz), 4.06 and 4.28 (each 1H, each dd, 2-C$\underline{H}_2$OAc, J_{gem}=11.0 Hz, J=10.0 and 83. Hz), 4.35—4.55 (2H, m, 2×H-13), 4.69 (1H, d, H-1, $J_{1,2}$= 2.0 Hz), 4.95—5.05 (2H, m, H-7 and 9), 5.05 (1H, dd, H-3, $J_{2,3}$=5.0 Hz, $J_{3,4}$=11.0 Hz), and 5.55—5.60 (2H, m, H-11 and 12).

We wish to thank Mr. Saburo Nakada for carrying out the elemental analyses. We also would like to thank Miss Yukiko Suzuki of the Institute of Bio-organic Chemistry for the measurements of the 250 MHz ^{1}H-NMR spectra, and Miss Shioko Kurihara for her technical assistance. This research was supported by a Grant-in-Aid for Scientific Research No. 56550595 from the Ministry of Education, Science and Culture, Japan and the Institute of Microbial Chemistry.

References

1) Part IV: N. Nakata, H. Takao, Y. Ikeyama, T. Sakai, K. Tatsuta, and M. Kinoshita, *Bull. Chem. Soc. Jpn.*, **54**, 1749 (1981).

2) M. Nakata, T. Sakai, K. Tatsuta, and M. Kinoshita, *Bull. Chem. Soc. Jpn.*, **54**, 1743 (1981).

3) H. Nagaoka and Y. Kishi, *Tetrahedron*, **37**, 3873 (1981).

4) R. J. White, E. Martinelli, and G. Lancini, *Proc. Natl. Acad. Sci. U. S. A.*, **71**, 3260 (1974); E. Martinelli, G. G. Gallo, P. Antonini, and R. J. White, *Tetrahedron*, **30**, 3087 (1974); R. J. White, E. Martinelli, G. G. Gallo, G. Lancini, and P. Beynone, *Nature*, **243**, 273 (1973).

5) O. Ghisalba, P. Traxler, and J. Nüesch, *J. Antibiot.*, **31**, 1124 (1978); O. Ghisalba, P. Traxler, H. Fuhrer, and W. Richter, *ibid.*, **32**, 1267 (1979); O. Ghisalba, P. Traxler, H. Fhurer, and W. Richter, *ibid.*, **33**, 847 (1980).

6) See the paper cited under Ref. 4.

7) D. J. Cram and F. A. A. Elhafez, *J. Am. Chem. Soc.*, **74**, 5828 (1952).

8) M. Nakata, Y. Ikeyama, H. Takao, and M. Kinoshita, *Bull. Chem. Soc. Jpn.*, **53**, 3252 (1980).

9) T. D. Inch and G. J. Lewis, *Carbohydr. Res.*, **15**, 1 (1970).

10) M. Kinoshita, N. Ohsawa, and S. Gomi, *Carbohydr. Res.*, **105**, 000 (1982).

11) J. G. Buchanan and H. Z. Sable, ed by "Selective Organic Transformations," B. S. Thyagarajan, Wiley-Interscience, New York (1972), Vol. 2, p. 1.

12) M. Kinoshita and S. Gomi, unpublished results.

13) M. Kinoshita and S. Sato, Unpublished results.

14) The large coupling constants ($J_{4,5}$=8—9 Hz) observed in the *cis*-epoxides may suport the conformations, IV and V.

15) Kishi *et al.* have suggested that high regioselectivity of the reaction of 3,4-*erthro*-5-benzyloxy-*cis*-2,3-epoxy-4-methyl-1-pentanol with $LiCuMe_2$ was ascribed to a steric hindrance of the 4-methyl group (M. R. Johonson, T. Nakata, and Y. Kishi, *Tetrahedron Lett.*, **1979**, 4343).

16) J. Ficini and J.-C. Depezy, *Tetrahedron Lett.*, **1969**, 4797; A. B. Smith, III, P. A. Levenberg, P. J. Jerris, R. M. Scarborough, Jr., and P. M. Wovkulich, *J. Am. Chem. Soc.*, **103**, 1501 (1981).

17) J. H. Osborn and G. Wilkinson, *Inorg. Synth.*, **10**, 67 (1967).

18) N. Miyashita, A. Yoshikoshi, and P. A. Grieco, *J. Org. Chem.*, **42**, 3772 (1977).

19) A. Rosental and M. Sprinzl, *Can. J. Chem.*, **47**, 4477 (1969); K. Tatsuta, Y. Amemiya, Y. Kanemura, and M. Kinoshita, *Tetrahedron Lett.*, **22**, 3997 (1981).

20) J. Herscovici and K. Antonakis, *J. Chem. Soc., Chem. Commun.*, **1980**, 561.

21) P. H. D. Barton, R. E. O'Brien, and S. Strenhell, *J. Chem. Soc.*, **1962**, 470.

Study of Ion Transport across Amphoteric Ion Exchange Membrane. I. Electroconductive Membrane Permeability

Akira YAMAUCHI,* Shigeru TSURUYAMA, Harumi MASUMORI, Yoshihiko NAGATA, Kozue KAIBARA, and Hideo KIMIZUKA

Department of Chemistry, Faculty of Science, Kyushu University, Hakozaki, Higashi-ku, Fukuoka 812

(Received January 13, 1982)

Basic ion transport characteristics of a homogeneous amphoteric ion exchange membrane (Kanegafuchi Chem. Ind. 1.0-PA-29) were studied by measuring the membrane potentials and conductances. Concentration cell systems of NaCl, KCl, $CaCl_2$, and $SrCl_2$ with a concentration range of 10^{-1}—10^{-3} mol dm^{-3} were studied and the electroconductive membrane permeabilities were estimated from the electrochemical data. Generally, Cl^- is slightly more permeable than cations under the present experimental conditions, except the result that K^+ is more permeable at low concentrations. Unlike the usual uniform cation exchange membrane of which transport characteristics to ions strongly depend upon the number of ionic charges, a "1.0-PA-29" amphoteric membrane exhibits different transport properties for the NaCl and KCl systems. In the NaCl system, the membrane was constantly anionic selective, while in the KCl system, biphasic ion selectivities were observed depending upon the external KCl concentration. Fundamental electrochemical properties of the membrane systems were discussed by examining the dependencies of membrane permeability on external electrolyte concentrations and on differences in ionic species. The present result suggests that the ionic size is one of the critical factors determining the transport characteristics across amphoteric ion exchange membrane.

Amphoteric membranes are specified upon a fact that both cationic and anionic sites are attached as ion exchange groups to polymeric substances which build up membrane phase. Since the early work on mosaic membranes by Sollner,[1] many studies on the amphoteric membranes were carried out with the charge-mosaic membrane systems.[2-4] In these investigations, unusual properties of the mosaic system, which cannot be observed in uniform ion exchange membranes, such as the piezodialysis and circulating electric current were found out. On the other hand, the layered type membrane systems in which the cation and anion exchange membranes form a contiguous layers were also studied.[5-7] Especially, the interesting current-voltage characteristics of the layered membrane have been extensively investigated.

These two types of amphoteric membranes or composite membranes have been investigated with several interests. From the theoretical point of views, Kedem and Katchalsky treated generally the transport phenomena observed in these systems on the basis of nonequilibrium thermodynamics in their series of papers.[8-10] Weinstein *et al.* also developed the theoretical model for the charge-mosaic membrane based on nonequilibrium thermodynamics[11] and the experimental verification of their model was carried out.[12] Practical applications of these membranes have been also extensively discussed. Large salt fluxes resulted from the structure of charge-mosaic membrane were paid an attention to utilize for the water conditioning processes. The layered membrane was also considered to be a generalized model involving the surface adsorption phenomena; therefore, the layered model was employed to solve the fouling phenomena which are serious problems in the electrodialysis processes. Many investigators have also taken a great interest in the biological membrane as an amphoteric ion exchange membrane and made an attempt to explain the mechanisms of bioelectrical phenomena in relation to the amphoteric properties of cell membranes.

Experimental studies on amphoteric ion exchange membranes were hitherto performed with the system where the cationic and anionic sites are macroscopically separated each other (see *e.g.*, Refs. 7 and 12). The physicochemical properties of amphoteric membranes should be examined on the system where the cationic and anionic sites are dispersed homogeneously within membrane phase.[13] However, investigations for the basic characteristics of the homogeneous type amphoteric membrane have not been systematically carried out yet. In the present and following papers of this communication series, the basic transport properties of amphoteric ion exchange membranes will be discussed from the theoretical and experimental points of views using the homogeneous type membrane recently developed by a Kanegafuchi Chemical Industry Co., Ltd.[14]

Experimental

The amphoteric ion exchange membrane used in the present experiments is coded as a "1.0-PA-29," which was developed by a Central Research Laboratory of Kanegafuchi Chemical Industry Co., Ltd. and kindly supplied for our experiments. This membrane was developed for the membrane treatment to separate organic substances having a low molecular weight from inorganic salt mixture. A brief sketch of the membrane preparation is as follows.[14] Support membranes were prepared on a glass surface from a dope containing poly(vinyl chloride) (degree of polymerization: 1000) of 11 wt% dissolved in a tetrahydrofuran/*N*,*N*-dimethylformamide (1/1.6 in weight) mixture. On this support membrane, partially chloromethylated polystyrene of 0.5 wt% dissolved in a chloroform/ethanol (1/2 in weight) mixture were applied as a functioning membrane base; chloromethyl groups in polymer were partially treated with trimethylamine. After this step, crosslinking and sulfonation processes were performed by sulfuric acid. Concentration of sulfuric acid and reaction time were controlled to realize the minimum salt rejection rate, which is known to be minimized under the conditions where anionic to cationic exchange capacity ratio approaches to unity.[13,14] All the membrane preparation processes described above were carried out by means of the dip coating techniques. Primary permeation test of the membrane showed that the rejection rates, [(feed

concentration—permeate concentration)/feed concentration] × 100%, under the operating pressure of 20 kg cm^{-2} were about 30% for 0.2% NaCl solution and over 93% for 2% sucrose solution, respectively. The ion exchange capacity estimated by ordinary titration method and by elementary analysis was 1 mequiv. (g-wet membrane)$^{-1}$ and the cationic/anionic exchange capacity ratio was ranged 1.0 ± 0.2. The thickness of membrane was 0.1 mm when the membrane was immersed in electrolyte solutions used in the present study. The closest distance between cationic and anionic exchange sites can be roughly estimated to be *ca.* 0.75 nm when the total ion exchange capacity is 2 mequiv. and the degree of swelling is 0.5. Then Eguchi *et al.* suggested that the mosaic membrane model [11] is unsuitable for the analysis of transport characteristics in the present membrane.[14]

In the present preliminary experiments, the electrochemical properties were studied on the concentration cell systems using NaCl, KCl, $CaCl_2$, and $SrCl_2$ as electrolytes. Experimental setup was the same as that reported elsewhere.[15,16] The amphoteric membrane was placed in the measurement cell to separate solution phases I and II, and the electrolyte concentration of phase I was varied from 10^{-1} to 10^{-3} mol dm^{-3}, while that of phase II was kept constant at 10^{-2} mol dm^{-3}. In this study, the membrane potentials and conductances were measured by a Takeda Riken TR 6856 high input impedance voltmeter and a Yokogawa-Hewlett-Packard 4255A (connected with 4440B) impedance bridge circuit, respectively. All experiments were carried out at the regulated room temperature (25 ± 1 °C).

Results and Discussion

Before the measurements were carried out, the sample membrane was checked on locally uniform properties of electrochemical data in the NaCl system and both sides of the membrane showed the identical electrochemical properties. The volume flow was also checked in the NaCl system; under the present experimental conditions, effects of solvent flow cause about 5% changes in transport parameters at most, which were within experimental errors.[17] More complete treatment involving the effects of solvent flow will be presented elsewhere based on nonequilibrium thermodynamics.

Membrane potential data as a function of the mean electrolyte activity of phase I are summarized in Fig. 1. In general, a 1.0-PA-29 amphoteric ion exchange membrane was more permselective to chloride ions than to metal cations under the present experimental conditions and this tendency became evident with increasing electrolyte concentration of phase I. Apparent transport numbers of Na^+ are nearly constant at 0.4, but those of Ca^{2+} and Sr^{2+} decrease from 0.45 to 0.29 and from 0.42 to 0.29, respectively, when the electrolyte concentrations of phase I are varied from 10^{-3} to 10^{-1} mol dm^{-3}. On the other hand, the KCl system exhibits biphasic ion selectivity behavior above and below the concentration of 10^{-2} mol dm^{-3} as illustrated in Fig. 1; apparent transport numbers of K^+ ranged from 0.42 to 0.46 and from 0.51 to 0.54 at lower and higher concentration ranges, respectively. In case of the usual cationic or anionic ion exchange membrane, the selectivity to ions is monophasic and the number of ionic charge is a dominant factor determining the ionic

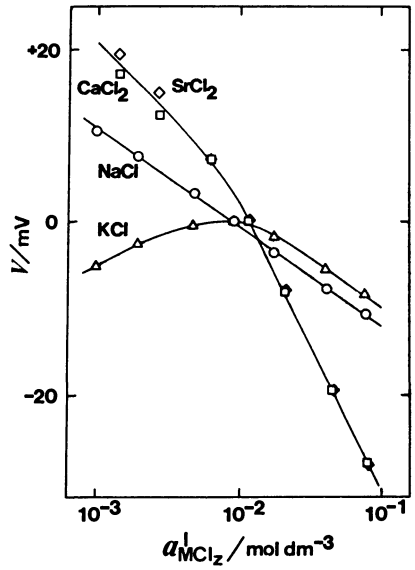

Fig. 1. Membrane potential data as a function of mean electrolyte activity of phase I.
○: NaCl, △: KCl, □: $CaCl_2$, ◇: $SrCl_2$.

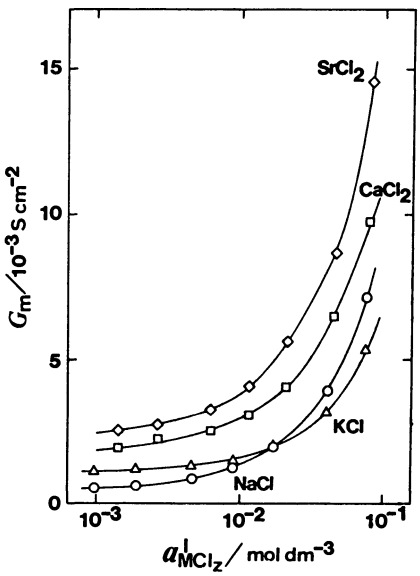

Fig. 2. Membrane conductance data as a function of mean electrolyte activity of phase I.
Symbols are the same as in Fig. 1.

permselectivity, so the membrane potential responses to univalent cations are almost the same irrespective of ionic species. On the basis of present results, there seems to be a possibility to discriminate Na^+ from K^+ by means of the amphoteric type ion exchange membrane.

The membrane conductance data are given in Fig. 2. Conductances continuously increase with increasing electrolyte concentrations of phase I in all the systems. It should be noted that the membrane conductances of 2-1 electrolyte systems are twice as high as those of 1-1 electrolyte systems.

According to the previous theory,[18] the present systems are described by the following modified phenomenological equation:

$$\begin{bmatrix} J_M \\ J_{Cl} \end{bmatrix} = - \begin{bmatrix} P_{M\cdot M} & P_{M\cdot Cl} \\ P_{Cl\cdot M} & P_{Cl\cdot Cl} \end{bmatrix} \times \begin{bmatrix} a_M^{II} \exp(ZFV/2RT) - a_M^{I} \exp(-ZFV/2RT) \\ a_{Cl}^{II} \exp(-FV/2RT) - a_{Cl}^{I} \exp(FV/2RT) \end{bmatrix}, \quad (1)$$

where J is the ionic flux, a is the activity, Z is the charge of metal cation M, and V is the transmembrane potential; F, R, and T indicate the usual physical meanings; the subscripts M and Cl refer to metal cations, Na^+, K^+, Ca^{2+}, and Sr^{2+}, and to anion, Cl^-; the superscripts I and II indicate the solution phases separated by the membrane phase, respectively. $P_{M\cdot M}$, $P_{M\cdot Cl}$, $P_{Cl\cdot M}$, and $P_{Cl\cdot Cl}$ are the membrane permeability matrix elements representing the partial contributions to the membrane transport processes due to the inter-ionic correlations indicated by the subscripts. In the present study, the electroconductive membrane permeabilities, defined by the following equations as a function of the permeability matrix elements, were estimated from the electrochemical measurements:

$$P_M = P_{M\cdot M} - P_{Cl\cdot M}/Z, \quad P_{Cl} = -ZP_{M\cdot Cl} + P_{Cl\cdot Cl}, \quad (2)$$

where P_M and P_{Cl} are the electroconductive permeabilities to metal cation and chloride ion, respectively. Electrochemical properties of the membrane system are described by use of the electroconductive membrane permeability:

$$\begin{aligned} I &= -ZFP_M[a_M^{II} \exp(ZFV/2RT) - a_M^{I} \exp(-ZFV/2RT)] \\ &\quad + FP_{Cl}[a_{Cl}^{II} \exp(-FV/2RT) - a_{Cl}^{I} \exp(FV/2RT)] \\ &= -t_M G_m(V - V_M) - t_{Cl} G_m(V - V_{Cl}) \quad (3) \\ &= -G_m(V - V_0) \end{aligned}$$

$$V_0 = t_M V_M + t_{Cl} V_{Cl}, \quad (4)$$

where I is the electric current across membrane, G_m is the membrane conductance, t is the transport number, and V_0 is the membrane potential in absence of membrane current; V_M and V_{Cl} are the Nernst equilibrium potentials for metal cation and chloride ion, respectively. Therefore, the electroconductive membrane permeabilities, P_M and P_{Cl}, are calculated by the next equations with the membrane potential and conductance data:

$$P_M = \frac{t_M G_m RT}{Z^2F^2(a_M^{I}a_M^{II})^{1/2}} \frac{ZF(V - V_M)/2RT}{\sinh[ZF(V - V_M)/2RT]}$$

$$P_{Cl} = \frac{t_{Cl} G_m RT}{F^2(a_{Cl}^{I}a_{Cl}^{II})^{1/2}} \frac{-F(V - V_{Cl})/2RT}{\sinh[-F(V - V_{Cl})/2RT]}. \quad (5)$$

The electroconductive permeability having a dimension of cm s^{-1} represents an electrically migrating speed of ions across the membrane phase and indicates a measure of the membrane permselectivity to ions.

Calculated results of these conductive permeabilities to metal cations and chloride ions are given in Figs. 3 and 4. In Fig. 5, the metal cation to chloride ion permeability ratios are plotted as a function of electrolyte activity in phase I. As expected from the membrane potential data, the conductive membrane permeabilities to chloride ions, P_{Cl}, exceeded those of cations, P_M. In the present study, the order of conductive membrane permeabilities to ions are as follows: $P_{Cl}(Ca^{2+},Sr^{2+}) > P_{Cl}(Na^+,K^+) \geq P_K > P_{Na} > P_{Ca},P_{Sr}$. These results may not be caused by unbalanced distribution of cationic and anionic exchange groups, since the membrane preparation processes are controlled to minimize the salt rejection rate and, accordingly, the capacity ratio is close to unity (see experimental section and Refs. 13 and 14). Furthermore, P_{Cl} also exceeded P_M even in 2-1 electrolyte systems in which cations seem to interact more strongly with fixed charges. Physical meanings of the electroconductive membrane permeabilities, P_M and P_{Cl}, are expressed as:[16,18,19]

$$P_M = \frac{RT\bar{U}_M}{\delta} \frac{\bar{C}_M}{(a_M^{I}a_M^{II})^{1/2}}, \quad P_{Cl} = \frac{RT\bar{U}_{Cl}}{\delta} \frac{\bar{C}_{Cl}}{(a_{Cl}^{I}a_M^{II})^{1/2}}, \quad (6)$$

where $\bar{U}$ and $\bar{C}$ are the integral average values of ionic mobility and concentration within membrane of thickness of δ. Membrane potential is expressed as a function of the permeability ratio[18] and the biphasic response observed in the KCl system seems to be due to the concentration dependent change in $\bar{U}_K$ and $\bar{U}_{Cl}$, since it is reasonable to consider $\bar{C}_K$ is nearly equal to $\bar{C}_{Cl}$. The permeability ratios, namely the relative membrane permeabilities, seem to decrease with the

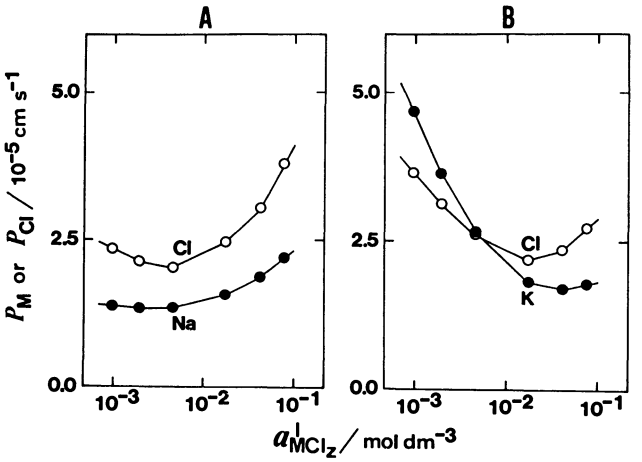

Fig. 3. Electroconductive membrane permeabilities for NaCl (A) and KCl (B) systems.
Closed and open circles indicate metal cation and chloride ion, respectively.

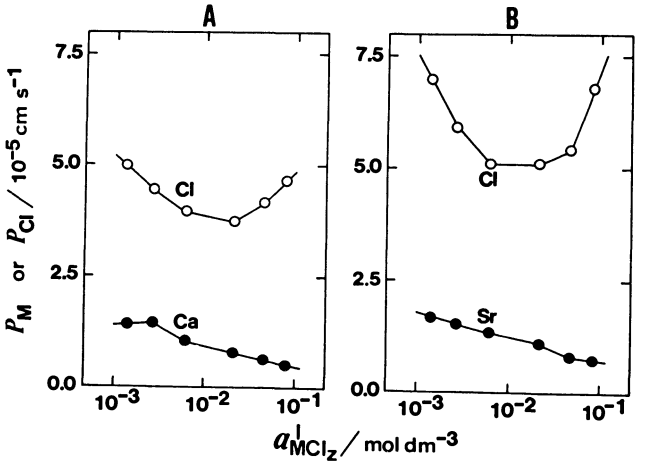

Fig. 4. Electroconductive membrane permeabilities for $CaCl_2$ (A) and $SrCl_2$ (B) systems. Symbols are the same as in Fig. 3.

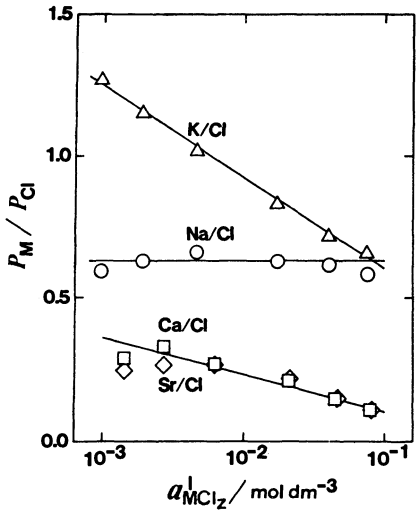

Fig. 5. Membrane permeability ratios as a function of mean electrolyte activity of phase I.
○: P_{Na}/P_{Cl}, △: P_K/P_{Cl}, □: P_{Ca}/P_{Cl}, ◇: P_{Sr}/P_{Cl}.

increasing cationic size. The ratios of hydrated ionic radii of metal cations to chloride ion are as follows: Na^+/Cl^-, 1.08; K^+/Cl^-, 1.00; Ca^{2+}/Cl^- and Sr^{2+}/Cl^-, 1.24. Thus it is suggested that the ionic size plays an important role to determine the ionic transport characteristics of amphoteric membrane.

Ion exchange membranes capable to separate ions of opposite charges have been practically used in various fields. It is also possible to exclude multivalent ion permeations by means of the membrane surface finishing with polyionic substances as in the case of ion exchange membranes selective to univalent ions used for the desalination processes. Further studies to improve the ionic selectivity of membranes and to aim at the perfect separation of two ions have been extensively continued. One possible way to realize the higher ionic selectivity is to introduce the exchange groups which can interact with specific ions, and the other is to apply the sieve effects to discriminate ionic sizes. The sieve effects are typically illustrated in the membrane systems having antibiotics and crown compounds as ionophores.[20,21] Even in case of the usual uniform ion exchange membrane, there exists indeed a difference in permeability to ions of the same charge determined by ionic mobility and concentration within membrane (see Eq. 6); however, the uniform ion exchange membrane is not so selective to generate the different membrane potential responses to each ionic species. It is the most noticeable difference between uniform and amphoteric ion exchange membranes with high charge densities that potential responses of the former are expressed by the Nernst relation characterized by the number of ionic charges, while those of latter are strongly affected by ionic size effects.

The transport mechanisms of amphoteric ion exchange membrane in which both cationic and anionic exchange groups are homogeneously dispersed within membrane phase seem to differ from those of mosaic membrane in which both the exchange groups form blocks of respective charges. Eguchi *et al.* suggested that salt permeation processes across the 1.0-PA-29 membrane are not controlled by coupling flow mechanisms which are remarkable features of the charge-mosaic membrane and they concluded that the analysis based on the mosaic model cannot be applicable to the present membrane.[14]

The present results indicate that the number of ionic charge is not a dominant factor to determine the ionic transport characteristics across the amphoteric ion exchange membrane. On the other hand, the membrane potentials, as a fundamental transport property, of usual polymeric ion exchange membrane with the same fixed charges, either the cationic or anionic exchange type, depend completely upon the number of ionic charge of permeant ions, and accordingly it is very difficult to endow a permselectivity to ions with the same charge. The 1.0-PA-29 amphoteric ion exchange membrane exhibits a possibility to discriminate Na^+ from K^+ as indicated in the membrane potential data and the permeability values. The origin of these permselectivities of amphoteric ion exchange membrane would be based on the discrimination of the hydrated radius of permeant ion. The effects of ionic size on transport characteristics, namely the sieve effect, across amphoteric ion exchange membrane are more clearly illustrated by the experimental results using symmetric tetraalkylammonium salts, which will be reported in the following communication. These transport characteristics of amphoteric membrane may be partly involved in the functions of biological membrane having a steep ionic selectivity, although the specific proteinic substances are known to control the complex and delicate ion transport mechanism.

We thank members of Central Research Laboratory of Kanegafuchi Chemical Industry Co., Ltd., especially Dr. Tamiyuki Eguchi for preparing and supplying the amphoteric membrane used in this work. This work was supported in part by a Grant-in-Aid for Scientific Research from the Ministry of Education, Science and Culture.

References

1) K. Sollner, *Biochem. Z.*, **244**, 370 (1932).
2) R. Neihof and K. Sollner, *J. Phys. Colloid Chem.*, **54**, 157 (1950).
3) R. Neihof and K. Sollner, *J. Gen. Physiol.*, **38**, 613 (1955).
4) J. N. Weinstein and S. R. Caplan, *Science*, **161**, 70 (1968).
5) V. Frilette, *J. Phys. Chem.*, **60**, 435 (1956).
6) N. Ishibashi and K. Hirano, *J. Electrochem. Soc. Jpn.*, **26**, E8 (1958).
7) A. A. Sonin and G. Grossman, *J. Phys. Chem.*, **76**, 3996 (1972).
8) O. Kedem and A. Katchalsky, *Trans. Faraday Soc.*, **59**, 1918 (1963).
9) O. Kedem and A. Katchalsky, *Trans. Faraday Soc.*, **59**, 1931 (1963).
10) O. Kedem and A. Katchalsky, *Trans. Faraday Soc.*, **59**, 1941 (1963).
11) J. N. Weinstein, B. J. Bunow, and S. R. Caplan, *Desalination*, **11**, 341 (1972).
12) J. N. Weinstein, B. M. Misra, D. Kalif, and S. R.

Caplan, *Desalination*, **12**, 1 (1973).
13) T. Yamabe, K. Umezawa, S. Yoshida, and N. Takai, *Desalination*, **15**, 127 (1974).
14) T. Eguchi, S. Mori, and M. Shimokawa, *Membrane*, **3**, 289 (1978).
15) K. Kaibara, H. Ito, N. Inoue, and H. Kimizuka, *Mem. Fac. Sci., Kyushu Univ. Ser. C*, **12**, 125 (1980).
16) K. Kaibara and H. Kimizuka, *Bull. Chem. Soc. Jpn.*, **55**, 1743 (1982).
17) Y. Nagata, M. Sc. Thesis, Kyushu University, Fukuoka, Japan, 1981.
18) H. Kimizuka and K. Kaibara, *J. Colloid Interface Sci.*, **52**, 516 (1975).
19) H. Kimizuka, K. Kaibara, E. Kumamoto, and M. Shirōzu, *J. Membr. Sci.*, **4**, 81 (1978).
20) "Membranes, A Series of Advances Vol. 2, Lipid Bilayers and Antibiotics," ed by G. Eisenman, Marcel Dekker Inc., New York (1973).
21) S. Kopolow, T. E. Hogen Esch, and J. Smid, *Macromolecules*, **6**, 133 (1973).

The Photoreduction and Photosensitized Reduction of Dyes Bound to a Surfactant Micellar Surface

Yoshiharu Usui* and Kazuhiko Saga
Department of Chemistry, Faculty of Sciences, Ibaraki University, Bunkyo, Mito 310
(Received January 26, 1982)

The photochemical reduction of thionine(Th) and Methylene Blue(MB) bound to anionic sodium dodecyl sulfate(SDS) micelles in an aqueous solution was inhibited at the lower concentration range of a reductant anion, EDTA, because of the electrostatic repulsion between the micelles and the reductant. The concentration dependence of EDTA on the quantum yield of photoreduction has shown to be, anomalously a sigmoidal type: this is explained by mechanistic interpretation based on the cooperative effects of the ionic strength and the essential concentration of EDTA. The enhancement effect for the quantum yield of the photoreduction of eosine bound to a cationic micelle by the EDTA anion was conversely observed, because of the electrostatic attraction. When 10-dodecyl) (Acridine Orange) was incorporated into SDS micelles in water containing EDTA and ascorbic acid, and the mixture was excited, the photosensitized reduction of MB bound to the micelles occurred. It was found that the quantum yield of the sensitized reduction depended on the concentration of MB and was larger than the yield on the direct excitation of MB.

Mechanistic investigations of photooxidation, photoreduction, and photosensitization in a heterogeneous system such as micelles, vesicles and emulsions, are important from the several points of view regarding photobiological phenomena (photoreception, photodynamic action, *etc.*) and solar-energy utilization, as modefied by the photosynthetic phenomenon. In recent years, an increasing number of such studies have focused on the photochemical and photophysical properties of molecular assembly systems. For example, some specific micellar effects on the properties of the excited state have been investigated and reported for cases of excimer and exciplex formation,[1-4] excitation-energy transfer,[3-6] and electron-transfer phenomena.[3,4,7-9] However, the mechanistic study of the photochemical reaction between the micellar surface and the bulky phase has been rather insufficient in contrast to the many studies at the interior site of a micelle.

Previously, we attempted to study the effect of an anionic reductant, EDTA, on the photoreduction of Methylene Blue bound to sodium dodecyl sulfate micelles, semiquantitatively.[10] The photoreduction was considerably inhibited because of the electrostatic repulsion between the anionic reductant and the micelles. Further, the concentration dependence of EDTA on the quantum yield was shown as a sigmoidal type——a so-called micellar effect. In the present work, we have performed a detailed mechanistic investigation of the micellar effect which was observed on the photoreduction and the photosensitized reduction of organic dyes bound on the surface of ionic surfactant micelles from the standpoint of reaction kinetics.

Experimental

Materials. The thionine ($C_{12}H_{10}ClN_3S$; Th), Methylene Blue ($C_{16}H_{18}ClN_3S$; MB), and Eosine Yellowish ($C_{20}H_6O_5Br_4Na_2$; E) were recrystallized twice from methanol, 1-butanol, and ethanol respectively. The 10-dodecyl (Acridine Orange) ($C_{29}H_{44}N_3Br$; DAO) was prepared as previously described and was purified by means of alumina-column chromatography and recrystallization from a 1 : 1 ether and ethanol mixed solution.[11] The sodium dodecyl sulfate (SDS) was recrystallized twice from methanol. The ethylenediaminetetraacetic acid disodium salt (EDTA) was used without further purification.

Apparatus and Procedure. A degassed sample in a $1\times1\times4$ cm^3 cell was irradiated by means of a steady illumination apparatus with a 300W tungsten lamp at 25 °C. The experimental procedure used to determine the quantum yield of dye-photoreduction was similar to that described previously.[12] Flash-photolysis experiments were carried out by using a pulsed dye laser (Phase-R: 2100B, Dye: G4, FWHM of pulse: $\approx$500 ns) and a monitoring system composed of a monochromator, a transient recorder, and a spectral data-analyser (Union Giken, RA-415).

Results and Discussion

Preliminary investigations of the photoreduction rate of Methylene Blue bound to anionic SDS micelles (MB/S) by EDTA trianion (HY^{3-}) were carried out at pH=8.0. The photoreduction of MB/S by HY^{3-} at a higher concentration proceeded at a rate which was proportional to the light quantities absorbed by the dye with a stationary irradiation. Then, in a way similar to that used for the reaction in an aqueous homogeneous solution, the quantum yield (Φ_{MB}) was determined from the slope of the linear relationship between $\ln(e^A-1)$ and time (A is the absorbance of the dye).[10,13] The reaction was significantly inhibited in a lower concentration range of the reductant, and the concentration dependence of HY^{3-} on Φ_{MB} was shown as a sigmoidal curve (Fig. 1). This inhibition may be supposed to be due to the environmental effect on the micellar periphery, *i.e.*, the so-called micellar effect.[10] In order to check the phenomenon as the electrostatic effect between the ionic micelle and the reductant, a kinetical investigation of the anomalous concentration effect on the photoreduction must be considered in the cases of several combinations of dyes, surfactants, and reductants.

Effect of the HY^{3-} Concentration on the Quantum Yield of Dye Photoreduction. As is shown in Fig. 1, we have observed that the rate of Th by HY^{3-} under the lower concentration at pH=8.0 was considerably retarded by the addition of SDS; *i.e.*, the photoreduction of thionine

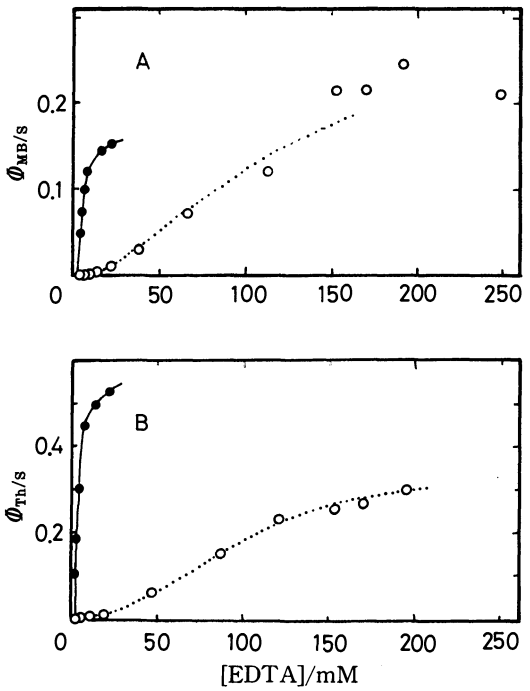

Fig. 1. Micellar charge effect on the photoreduction of Methylene Blue (A) and thionine (B).
(A) ○: In deaerated micellar solution, [MB]=10 μM, [SDS]=10 mM, pH=7.0, ●: in deaerated aqueous solution. [MB]=10 μM, pH=6.7, $\Phi_{MB}=3.6\times10^{6}$ [EDTA]/$(1.2\times10^{4}+2.5\times10^{7}$[EDTA]). (B) ○: In deaerated micellar solution, [Th]=10 μM, [SDS]=20 mM, pH=8.0, ●: in deaerated aqueous solution, [Th]=10 μM, pH=8.0, $\Phi_{Th}=1.3\times10^{8}$[EDTA]/$(8.0\times10^{4}+2.8\times10^{8}$[EDTA]). Dotted lines show EDTA concentration effect on $\Phi_{Th/S}$ ($\Phi_{MB/S}$) calculated from Eq. 9, where the copperative effect of the concentration and the ionic strength on the photoreduction is considered (see text and Table 1).

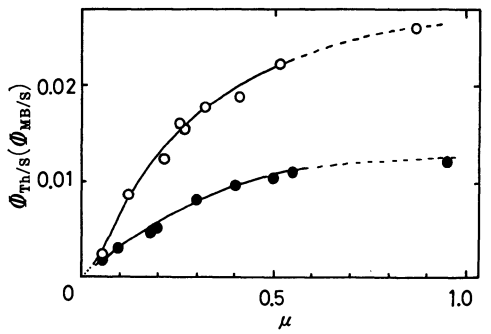

Fig. 2. Ionic strength effect on the photoreduction yields of Th/S and MB/S at a constant concentration of EDTA (5 mM).
●: [MB]=10 μM, [SDS]=10 mM, pH=7.0, ○: [Th]=10 μM, [SDS]=20 mM, pH=8.0. (Several inorganic neutral salt of NaCl, $NaNO_3$, and Na_2SO_4 were used for adjustment of μ.)

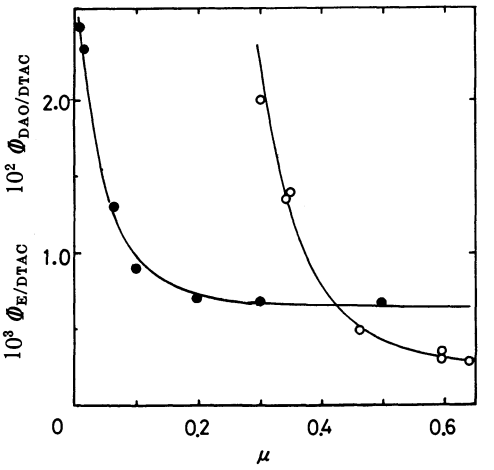

Fig. 3. Ionic strength effect on the photoreduction yield of E/DTAC and DAO/DTAC at a constant concentration of EDTA.
●: [E]=10 μM, [DTAC]=20 mM, $[HY^{3-}]$=10 mM, ○: [DAO]=5 μM, [DTAC]=25 mM, $[HY^{3-}]$=10 mM. (NaCl was used for adjustment of μ.)

bound to SDS micelles (Th/S+HY^{3-} system) is inhibited just as the case of the MB/S+HY^{3-} system.[10] On the contrary, the photoreduction of Eosine Y (E) by HY^{3-} was enhanced by binding to an oppositely charged cationic micelle of dodecyltrimethylammonium chloride (DTAC) at the lower concentration of HY^{3-} of 1.0×10^{-4}M (1 M=1 mol dm^{-3}): *i.e.*, the quantum yield for E/DTAC photoreduction was 5.5×10^{-3} at [DTAC]=30 mM and pH=8.0, and five times larger than the value without DTAC. Although the photoreduction occurs *via* electron transfer between a bound triplet dye and HY^{3-} because there is no fluorescence quenching of the bound MB/S by HY^{3-}, the observed decay constant (1.2×10^{5} s^{-1}) of the triplet dye bound to the micelles of 2×10^{-4} M was scarcely affected by the addition of HY^{3-} in the lower-concentration range, thus exhibiting the inhibition of photoreduction shown in Fig. 1. The fluorescence of Methylene Blue and thionine bound to anionic SDS micelles is scarcely quenched by adding 0.36 M of $S_2O_3^{2-}$ or 0.1 M of SCN^- anion, which quench these dyes efficiently in an aqueous solution.[10] Judging from the above results, it seems that the reaction of triplet dyes with HY^{3-} was inhibited because of the electrostatic repulsion between the anionic SDS micelles and the reductant anion, HY^{3-}.

Effect of the Ionic Strength on the Photoreduction Yield. With the concentration of dye and HY^{3-} fixed at 10 μM and 5 mM respectively, the effect of the ionic strength (μ) on the quantum yield of the photoreduction of dye was investigated over the wide range of $0\lesssim\mu\lesssim1$. Figure 2 shows that $\Phi_{Th/S}$ or $\Phi_{MB/S}$ tends to the constant value of a maximum yield with μ : *i.e.*, there is a positive μ-effect. In order to confirm that a neutral salt effect for the electrostatic repulsion between HY^{3-} and triplet Methylene Blue or thionine bound on an anionic SDS micelle is responsible for the positive μ-effect, we tried to produce a μ-effect on the system of E/DTAC+HY^{3-}. Interference with the electrostatic attraction force between HY^{3-} and a cationic DTAC micelle fixing triplet eosine, *i.e.*, a negative μ-effect was observed during the reaction (Fig. 3). A comparison of the results shown in Figs. 2 and 3 shows that these remarkable opposite effects support the idea that the μ-effect on the electrostatic interaction between the micelle ion and

the HY^{3-} anion is very sensitive to the yield of photoreduction.

$\Phi_{Th/S}$ value around $\mu=0.8$ at $[HY^{3-}]=5$ mM in Fig. 2 is smaller by a factor of ten than the yield of thionine reduction obtained in an aqueous homogeneous solution at $\mu=0.8$, and also smaller than the yield at the concentration of HY^{3-} of 0.16 M in a micellar solution where the calculated ionic strength relative to EDTA is 0.80. Thus, it may be supposed that both the HY^{3-} concentration and ionic strength of the reductant affect the yield of photoreduction in a Th/S+HY^{3-} or MB/S+HY^{3-} system. Also, the μ-effect on the photoreduction of 10-dodecyl (Acridine Orange) (DAO) dissolved in cationic DTAC micelles with HY^{3-} was performed where the DAO was anchored in the micelles. As is shown in Fig. 3, a μ-effect on the yield similar to that in the case of E/DTAC+HY^{3-} system was observed, but the effective values of μ were larger than the case of the photoreduction occurring on the micellar surface (the E/DTAC+HY^{3-} system).

Effect of the HY^{3-} Concentration on the $\Phi_{Th/S}$ under a Constant Ionic Strength. In a degassed aqueous solution of Th and HY^{3-}, the effect of the HY^{3-} concentration on the yield of the photoreduction was checked. The Φ_{Th} increased with the HY^{3-} concentration and tended to constant saturation value. A fairly linear relationship of $1/\Phi_{Th}$ against $1/[HY^{3-}]$ was obtained. Judging from the kinetical results and the results of an investigation previously reported,[10,13,14] the following scheme and equation of Φ_{Th} can be obtained:

$$Th \xrightarrow{h\nu} {}^1Th^* \xrightarrow{\phi_{st}} {}^3Th + EDTA \longrightarrow \begin{cases} Th^- + EDTA^+ \ (k_e^r) \\ Th + EDTA \ (HY^{3-}) \end{cases} k_e^s$$

$$\Phi_{Th} = \frac{\phi_{st} k_e^r [HY^{3-}]}{k_d' + k_e^s [HY^{3-}]} \qquad (1)$$

The k_e^r and k_e^s values were obtained from the plot of Φ_{Th}^{-1} *vs.* $[HY^{3-}]^{-1}$ to be 2.3×10^8 mol^{-1} dm^3 s^{-1} and 2.8×10^8 mol^{-1} dm^3 s^{-1} respectively, using ϕ_{st} (0.55) and k_d' (8.0×10^4 s^{-1}) values.[14,15]

In the case of the Th/S+HY^{3-} system, at a constant ionic strength of 0.1 or 0.8, the dependence of $\Phi_{Th/S}$ on the concentration of HY^{3-} shows not the sigmoidal curve, but the usual saturation-type one as was checked in an aqueous solution. The results are expressed as a linear relationship between $1/\Phi_{Th/S}$ and $1/[HY^{3-}]$ in Fig. 4. By analogy with the kinetical treatment for the data obtained in the MB/S+HY^{3-} system,[10] $\Phi_{Th/S}$ can be tentatively expressed at a constant μ as follows:

$$\Phi_{Th/S} = \frac{\phi_{st} k^r [HY^{3-}]_s}{k_d + k^s [HY^{3-}]_s} = \frac{\phi_{st} k^r A(\mu) [HY^{3-}]}{k_d + k^s A(\mu) [HY^{3-}]}, \qquad (2)$$

where the HY^{3-} concentration on the surface of a micelle, $[HY^{3-}]_s$, is assumed to be proportional to the concentration of HY^{3-} added, *i.e.*, $[HY^{3-}]_s = A(\mu)[HY^{3-}]$. $A(\mu)$ is a constant, depending on the ionic strength of the solution. The intersystem crossing probability, ϕ_{st}, of Th/S is assumed to be the same (0.55) as that in an aqueous solution referring in the case of MB/S photoreduction.[10] k_d is the decay constant of the bound triplet dye. k^r and k^s are the reaction and quenching-rate parameters respectively for the reaction of triplet dye with HY^{3-} on the surface of a micelle. From the values of an intercept of the line in Fig. 4 and the ϕ_{st} value of Th, the reactivity ratio, k^r/k^s for Th bound with HY^{3-} was obtained as 0.06 at a constant μ value of 0.1; this is smaller than the value (0.83) in an aqueous solution. At a constant μ value of 0.8, k^r/k^s equals 0.7—1.0, which is comparable to the value obtained in an aqueous solution. Judging from the finding that the value of the degree of the fluorescence depolarization, P (0.24) of thionine at $\mu=0.8$ was almost the same as the value at $\mu=0.1$, it was supposed that the molecular rotation of the dye was still restricted and that the dye was bound to the micelles even at such a high ionic strength as 0.80 ($P=0.095$ in an aqueous solution). Therefore, the micellar effect of the inhibition for the photoreduction might be responsible for the decrement in the k^r/k^s value as a parameter for the reactivity ratio of the bound dye. Incidentally, the concentration effect of HY^{3-} on $\Phi_{Th/S}$ did not obey any relationship such as Eq. 2 at a given concentration of electrolytes.

Kinetic Analysis for $\Phi_{Th/S}$ Values from the Ionic-strength Effect. As for the kinetic treatment of the intramicellar photochemical processes, several theoretical considerations have been given.[9,16–21] Mostly, these studies have dealt with the reaction between molecules

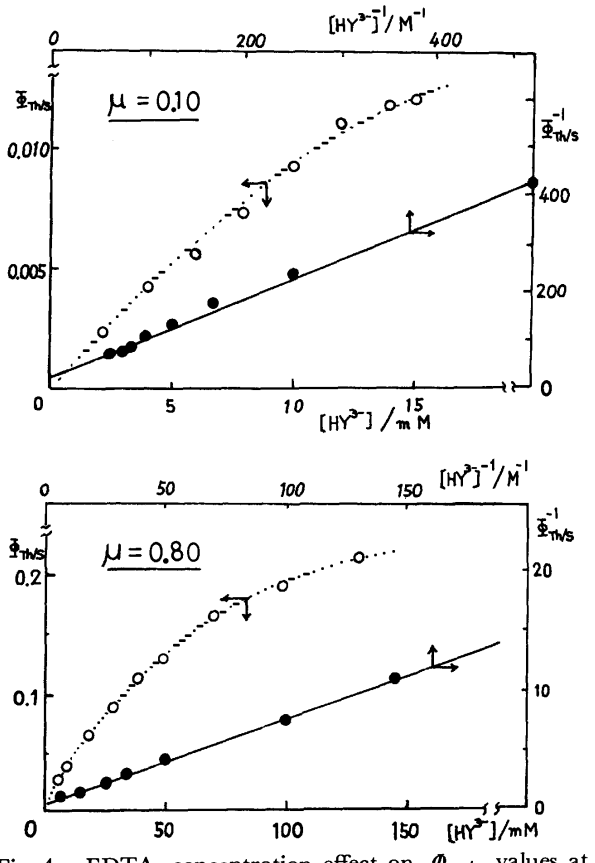

Fig. 4. EDTA concentration effect on $\Phi_{Th/S}$ values at constant μ of 0.1 and 0.8. [Th]=10 μM, [SDS]=20 mM, pH=8.0.

or ions which are located on a micellar surface or at the micellar interior. In our systems, the treatment for the positional situation should be considered as that of the reaction of excited dye bound on the Stern layer or the outer layer (Gouy-Chapman layer) of an ionic micelle with HY^{3-} located in the aqueous bulk phase. Further, from the standpoint of the quantitative explanation of the anomalous effects on the photoreduction yield, it can not yet be decided how much these theoretical models suggested for the reactions on the micelle are applicable to the present situation of the systems.

Thus, for the reaction molecules far from a micellar surface, we attempted to use the well-known model of the electrostatic interaction introduced by Debye and Hückel. Since a spherical micelle is held at $\mu \lesssim 0.4$ at the dilute solution of SDS ($\approx$10 mM. CMC is 8.1 mM), let us assume approximately that such a deformation of the micelle occuring at $\mu > 0.4$ does not affect on the following kinetic treatment.[22] Then, the distribution of HY^{3-} at a distance, r, apart from a center of the charged micelle under a given ionic strength, μ, is denoted as $n_Y(r,\mu)$, which means the number of molecules per cm^3, and it is expressed by the Boltzmann equation, using the Debye-Hückel's theory. At an infinite ionic strength, $n_Y(r,\mu)$ is denoted as $n_Y(r,\infty)$, in which the value of the number on HY^{3-} ions in the bulk phase, n_{Yb}, can be taken as approximately equal, because the electrostatic repulsion is negligible at an infinite ionic strength when a large amount of electrolytes is added, *i.e.*, this is the neutral salt effect. This means that $n_Y(r,\mu)$ converges to n_{Yb} according to the following Boltzmann equation upon an increase in r or μ to infinity:

$$n_Y(r,\mu) = n_{Yb} \exp(-eZ\Psi/kT), \tag{3}$$

where Z indicates the charge number and where the following potential, Ψ, obeys the well-known Poisson-Boltzmann equation:

$$\Psi = \frac{Ze}{4\pi\varepsilon r} \exp(-\sqrt{\beta} r) \tag{4}$$

$$\beta = 2 \times 10^3 N_A e^2 \mu / \varepsilon kT.$$

[Abbreviations: Ze-central charge, ε-dielectric constant, N_A-Avogadro number, k-Boltzmann constant, T-absolute temperature] Denoting the HY^{3-} concentration at the distance (r_{Th}) of the Th binding site on the surrounding micelle as $[HY^{3-}]_{Th}$, the relation of $[HY^{3-}]_{Th}$ with $A(\mu)$ in Eq. 2 can be written as:

$$[HY^{3-}]_{Th} = \left(\frac{n_Y(r_{Th},\mu)}{n_{Yb}}\right)[HY^{3-}] \equiv A(\mu)[HY^{3-}]. \tag{5}$$

Using Eq. 5, $\Phi_{Th/S}$ can be expressed approximately as Eq. 6 at a lower concentration of HY^{3-} from Eq. 2;

$$\Phi_{Th/S} \approx \frac{\phi_{st} k^r}{k_d}[HY^{3-}]_{Th} = \frac{\phi_{st} k^r A(\mu)}{k_d}[HY^{3-}]. \tag{6}$$

When the electrostatic potential, Ψ, on the surrounding micelles becomes small at a long distance of r, the treatment by the Debye-Hückel theory can be performed for the following evaluation.[23,24] When $eZ\Psi < kT$, the Ψ of Eq. 3 satisfies the Poisson-Boltzmann equation; a similar treatment is also possible for the cases on an ionic sphere of macromolecules. Using Ψ in the $n_Y(r,\mu)$-Boltzmann equation, the correlation of $n_Y(r,\mu)$ with μ is given as follows:

$$n_Y(r,\mu) = n_{Yb} \exp(-Ae^{-\alpha\sqrt{\mu}}), \tag{7}$$

where $A = Ze^2/4\pi\varepsilon rkT$ and $\alpha = r\sqrt{2\times 10^3 N_A e^2/\varepsilon kT}$.

The charge number of micelles was estimated from the product of the aggregation number of SDS (62) and the fraction of charge (0.17).[25] Putting the charge numbers of HY^{3-} and micelles as $-3e$ and $-10e$ respectively, the numerical values of A and α are $210r^{-1}$ and $0.325r$ at a given parameter of the distance, r. $A(\mu)$ defined in Eq. 5 can be calculated as the function of μ from the $n_Y(r,\mu)/n_{Yb}$ ratio in Eq. 7. Further, for the observed ionic strength effect on $\Phi_{Th/S}$, the dependence of $\Phi_{Th/S}$ on μ can be compared with that of $A(\mu)$ on μ, normalizing the $A(\mu)$ value to $\Phi_{Th/S}$ at a given parameter, r, because $\Phi_{Th/S}$ is proportional to $A(\mu)$, as is shown in Eq. 6. The correlation of the μ-effects on both $A(\mu)$ and $\Phi_{Th/S}$ is investigated in the region of r=10—30 Å; the degree of coincidence is shown in Fig. 5. The figure shows that the correlation is fairly good around r=18—20 Å, about three times of the micellar radius;[25] *i.e.*, it is shown to be the thionine binding position where the bound triplet dye will react with HY^{3-}. For the case of MB/S+HY^{3-}, the similar results are obtained, as is shown in Fig. 5.

In the plots of $\Phi_{Th/S}$ against μ in Fig. 5, $\Phi_{Th/S}$ is taken as a function of μ at a given concentration of HY^{3-}, *i.e.*, $\Phi_{Th/S}(\mu)$. Putting the ratio of $\Phi_{Th/S}(\mu)$ to the normalized quantum yield, $\Phi_{Th/S}(\mu)_N$, as $\gamma(\mu)$, *i.e.*, $\gamma(\mu) = \Phi_{Th/S}(\mu)/\Phi_{Th/S}(\mu)_N = A(\mu)/A(\mu)_N$, the relation of $[HY^{3-}]_S = A(\mu)[HY^{3-}] = \gamma(\mu)A(\mu)_N[HY^{3-}]$ can be obtained. Thus, the quantum yield given in Eq. 2 can be written as:

$$\Phi(\mu) = \frac{\phi_{st} k^r \gamma(\mu)[HY^{3-}]}{(k_d/A(\mu)) + k^s \gamma(\mu)[HY^{3-}]}. \tag{8}$$

The $\gamma(\mu)$ factor indicates a correction for the ionic strength by the HY^{3-} anion itself. Now, estimating the $\gamma(\mu)$ value from Fig. 2 at the ionic strength corresponding

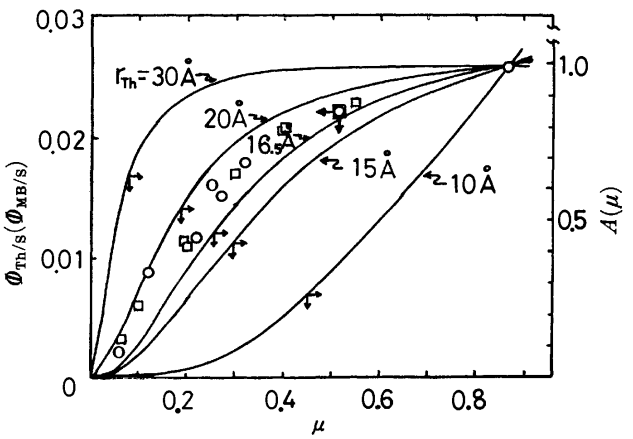

Fig. 5. Comparison of the effects of $\Phi_{Th/S}$ on μ and of $A(\mu)$ on μ.
○: [Th]=10 μM, [SDS]=20 mM, [HY^{3-}]=5 mM, pH=8.0. □: [MB]=10 μM, [SDS]=10 mM, [HY^{3-}] =5 mM, pH=7.0. (The curves of $A(\mu)$ *vs.* μ are drawn with a parameter of r_{Th} or r_{MB} normalizing at μ=0.88.)

Table 1. Comparison of observed quantum yields with that corrected for the μ-effect of the HY^{3-} ion

$[HY^{3-}]/M^{a)}$	$\gamma(\mu)[HY^{3-}]/M^{b)}$	$\Phi_{Th/S}$	
		Obsd[c)]	Calcd[d)]
0.19	0.19	0.257	0.271
0.17	0.167	0.256	0.253
0.15	0.143	0.241	0.232
0.13	0.124	0.213	0.213
0.085	0.0635	0.141	0.142
0.045	0.0261	0.0583	0.0641
0.018	0.00575	0.0213	0.0155
0.0094	0.00158	0.0048	0.0044
0.0050	0.00034	0.0026	(0.001)

a) Concentrations of HY^{3-} examined in Fig. 1. b) $\gamma(\mu)$ was estimated from the μ-effect in Fig. 2 at the μ-values corresponding to the HY^{3-} concentrations in column a). c) Quantum yields observed in Fig. 1 at the concentration in column a). d) Calculated quatum yields from Eq. 9 (see text).

to the HY^{3-} concentration which were examined in the experiment on the HY^{3-}-concentration effect on $\Phi_{Th/S}$, and calculating the vaue of $\gamma(\mu)[HY^{3-}]$, we can plot $1/\Phi(\mu)$ against the $1/\gamma(\mu)[HY^{3-}]$ values. Since the linear relationship was observed for the double reciprocal plots, the following numerical equation can be written by using the values of the slope and intercept:

$$\Phi(\mu) = \frac{\gamma(\mu)[HY^{3-}]}{0.36+1.8\gamma(\mu)[HY^{3-}]}. \quad (9)$$

On the other hand, by multiplying the correction factor $\gamma(\mu)$ by the values of $[HY^{3-}]$, which are examined in Fig. 1, we can compare the values of the quantum yield with that observed for the HY^{3-} concentration effect, as is shown in Table 1, where a fair coincidence of both the numerical equation 9 and the observed yield is obtained. Thus, since the quantum yields were quantitatively evaluated by the correction of the ionic strength upon the concentration effect of HY^{3-}, the relationship between the calculated $\Phi_{Th/S}$ values in Table 1 and the concentration of HY^{3-} can be shown as the sigmoidal curve in Fig. 1 (dotted line), and the cooperative effect of the HY^{3-} concentration and the ionic strength on the photoreduction for the micellar system can be considered to hold, judging from the agreement between the calculated curve and the observed values shown in Fig. 1.

Photoreduction of 10-Dodecyl (Acridine Orange), DAO in Micelles by HY^{3-}. DAO is a little soluble in water and is likely to be incorporated into SDS micelles. From an eye to comparing a micellar effect on the photoreduction with the different binding situation of dyes, the effects of HY^{3-} concentration and ionic strength were investigated in the cases of the DAO/S or DAO/DTAC+HY^{3-} systems.

The photoreduction of DAO/S by HY^{3-} was not observed either at a high ionic strength (0.6) or at a high concentration of the reductant (200 mM). For the DAO/DTAC+HY^{3-} system, the photoreduction yield (Φ_{DAO}) in the micellar solution was found to be about 5 times larger than that in a mixture of 30% ethanol and water ($[HY^{3-}]=10$ mM). Such an enhancement was also observed to a considerable extent in the case of the E/DTAC+HY^{3-} system because the electrostatic attraction between the cationic micelles and the HY^{3-} anion was more effective on the surface. Since the DAO/DTAC fluorescence quenching by added bromide ions increased about thirty times over that for the mixture of 30% methanol and water, the Acridine Orange chromophore must be located near the surface in a micellar particle. It was considered that the efficient quenching was due to the electrostatic attraction between the micelle and the bromide ion.

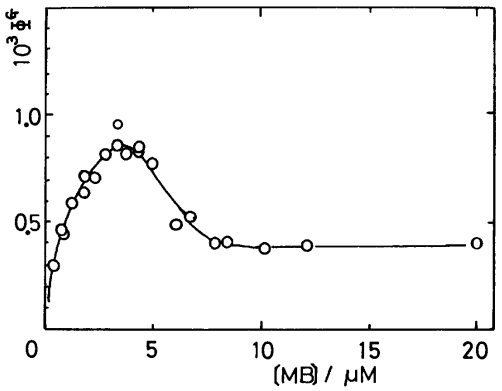

Fig. 6. Concentration effect of Methylene Blue on 10-dodecyl (Acridine Orange)-sensitized reduction yield Φ^G. [DAO]=8 μM, [SDS]=8 mM, $[HY^{3-}]=10$ mM.

When the ionic strength effect on Φ_{DAO} was compared to that in the case of the E/DTAC+HY^{3-} system, as is shown in Fig. 3, a decreasing effect on Φ_{DAO} by μ was observed in the higher region of 0.3—0.5, where the effect reached saturation in the case of the E/DTAC+HY^{3-} system. This result might be caused by the different position of the binding site of these dyes. At a constant μ, the effect of the HY^{3-} concentration on Φ_{DAO} was analysed by holding the linear relationship between $1/\Phi_{DAO}$ and $1/[HY^{3-}]$. Thus, it was confirmed that the results could also be explained by Eq. 8 in the case of the DAO/DTAC+HY^{3-} system.

Photosensitized Reduction of Methylene Blue by 10-Dodecyl (Acridine Orange) in SDS Micellar Solution. When DAO was incorporated into MB/S micelles (DAO/S/MB) and was excited, the photosensitized reduction of the MB bound at the surface by HY^{3-} occurred. The quantum yield of the sensitized reaction, Φ^G, depends on the MB concentration and is larger than that of the direct excitation of MB, Φ_R at the optimal concentration region, as is shown in Fig. 6. At the higher concentrations of MB over 10 μM, the quenching of DAO fluorescence by MB becomes considerable, involving the phenomenon of the DAO-sensitized fluorescence of MB *via* the dipole-dipole interaction (Förster mechanism), as has been reported previously.[5] If triplet MB can be formed from the singlet-excited state of MB produced by the singlet energy transfer on the micelles, the quantum yield of the photoreduction, Φ^G, must be smaller that that by the direct excitation of MB as a part of the

efficiency of the energy transfer. When the decrement at a higher concentration of MB in Fig. 6 is due to the contribution of the singlet energy transfer, the sensitized reaction mechanism can be discussed from the stand-points of both singlet and triplet energy transfer between DAO and MB on the micelles. The DAO-sensitized reduction of MB by ascorbic acid as a reductant also occurred in a homogeneous solution and more efficiently in a DAO/S/MB micellar solution ($\Phi^{G}_{max} \simeq 0.1$, pH=3.0). Similarly, the quantum yield of the sensitized reduction of DAO/S/MB depended on the concentration of MB and was larger than that of the direct excitation of MB bound in micelles. By laser-flash photolysis it was found that triplet DAO was rapidly quenched by the MB on the micelles. The observed decay constant of triplet DAO in micelles is $9.5 \times 10^2\ s^{-1}$ without MB and $1.4 \times 10^4\ s^{-1}$ with MB (5 μM), at pH=6.2. This may suggest that the increase in the yield Φ^{G} in the lower-concentration region of MB is responsible for the triplet energy transfer from DAO to MB. Further mechanistic investigations are required to elucide the reason why the value of Φ^{G} is larger than that of Φ^{R} in the micellar system.

The present work was partially supported by a Grant-in-Aid for Scientific Research No. 00547002 from the Ministry of Education, Science, and Culture. The authors wish to express their thanks to Miss Yoshiko Iijima, Mr. Yasuo Tazawa, and Mr. Masami Shichinohe for their contributions to this work.

References

1) H. Masuhara, K. Kaji, and N. Mataga, *Bull. Chem. Soc. Jpn.*, **50**, 2084 (1977).
2) Y. Waka, K. Hamamoto, and N. Mataga, *Photochem. Photobiol.*, **32**, 27 (1980).
3) B. A. Lindig and M. A. J. Rodgers, *Photochem. Photobiol.*, **31**, 617 (1980).
4) K. Kalyanasundaram, *Chem. Soc. Rev.*, **7**, 453 (1978).
5) Y. Usui and A. Gotou, *Photochem. Photobiol.*, **29**, 165 (1979).
6) J. R. Escabi-Perez, F. Nome, and J. H. Fendler, *J. Am. Chem. Soc.*, **99**, 7749 (1977).
7) K. Kano, K. Takuma, T. Ikeda, D. Nakajima, Y. Tsutsui, and T. Matsuo, *Photochem. Photobiol.*, **27**, 695 (1978).
8) P-A. Brugger and M. Grätzel, *J. Am. Chem. Soc.*, **102**, 2461 (1980).
9) Y. Waka, K. Hamamoto, and N. Mataga, *Chem. Phys. Lett.*, **62**, 364 (1979).
10) Y. Usui, S. Kodera, and N. Nishida, *Chem. Lett.*, **1976**, 1329.
11) E. Miethke and V. Zanker, *Z. Phys. Chem., N. F.*, **18**, 375 (1958).
12) Y. Usui, *Bull. Chem. Soc. Jpn.*, **38**, 206 (1965).
13) N. Kosui, K. Uchida, and M. Koizumi, *Bull. Chem. Soc. Jpn.*, **38**, 1958 (1965).
14) R. Bonneau, P. Fornier de Violet, and J. Joussot-Dubien, *Photochem. Photobiol.*, **19**, 129 (1974).
15) M. Nemoto, K. Kikuchi, and H. Kokubun, *Bull. Chem. Soc. Jpn.*, **42**, 264 (1969).
16) P. P. Infelta, M. Grätzel, and J. K. Thomas, *J. Phys. Chem.*, **78**, 190 (1974).
17) A. M. Tachiya, *Chem. Phys. Lett.*, **33**, 289 (1975).
18) M. Maestri, P. P. Infelta, and M. Gräztel, *J. Chem. Phys.*, **69**, 1522 (1978).
19) M. Van der Auweraer, J. C. Dederen, E. Gelade, and F. C. DeSchryver, *J. Chem. Phys.*, **74**, 1140 (1981).
20) H. Sano and M. Tachiya, *J. Chem. Phys.*, **75**, 2870 (1981).
21) A. Yekta, M. Aikawa, and N. J. Turro, *Chem. Phys. Lett.*, **63**, 543 (1979).
22) F. M. Menger, *Acc. Chem. Res.*, **12**, 111 (1979).
23) S. L. Brenner and R. E. Roberts, *J. Phys. Chem.*, **77**, 2367 (1973).
24) The distributions can be calculated by the solution of a Poisson-Boltzmann equation generalized to take into account the probable change in the microscopic dielectric constant in the vicinity of the micellar interface. (R. A. Goldstein and J. J. Kozak, *J. Chem. Phys.*, **62**, 279 (1975); R. A. Goldstein, P. F. Hay, and J. J. Kozak, *J. Phys. Chem.*, **77**, 2367 (1975).)
25) J. H. Fendler and E. J. Fendler, "Catalysis in Micellar and Macromolecular Systems," Academic Press, N. Y. (1975), p. 31.

Glass Formation in the HI + Water System

Yoshifumi AKAMA and Hitoshi KANNO*
Department of Chemistry, Meisei University, Hino, Tokyo 191
(Received February 12, 1982)

Glass transition temperature (T_g) of aqueous HI solution was measured as a function of HI concentration. The T_g data of aqueous HI solution suggest an anomalously low T_g value for glassy bulk pure water. Double-glass-transition phenomenon is observed at the water-rich edge of glass-forming composition range.

Recent papers of Angell *et al.*[1,2] and of Lesikar[3-5] have shown that the glass transition temperature (T_g) can be a useful diagnostic tool for clarifying various thermodynamic properties of solutions. In addition, there is gathering evidence[6-8] that spectroscopic and structural studies of aqueous solutions in the glassy state can give unique information unobtainable from investigations at ordinary temperatures, *e.g.*, Kanno and Hiraishi[8] have recently showed that unambiguous detection of low frequency Raman bands, which are hidden or obscured by the strong Rayleigh scattering wing in a Raman spectrum for the liquid state, becomes possible in a Raman spectrum for the glassy state. Therefore, accumulation of glass formation data for various aqueous solutions should be worthwhile as the first step for adding aqueous solutions in the glassy state to our objectives of solution chemistry.

In this study, the glass formation of the HI+water system was investigated as a function of HI concentration. As iodide ion is a typical structure breaker and HI is a structurally simple acid, glass formation data of this system will be useful to see effects of various factors (*e.g.*, ionic radius, structure making or breaking properties of ions) on the glass-forming ability of aqueous solutions.

Experimental

Sample of hydriodic acid with various concentrations were prepared from an encapsulated 57 wt% HI aqueous solution and distilled water by simple mixing of the required amounts of them. Sample solutions got colored with pale yellow due to slight decomposition of HI soon after the mixing. T_g measurements were usually made within an hour after sample preparation. As the sample solution left standing for 2 d gave the same T_g value as the one obtained immediately after the preparation, we concluded that the trace of HI decomposition has a negligible effect on the glass formation and T_g value to the sample.

A sample solution (*ca.* 0.05 ml) in a 2 mm diameter Pyrex glass tube, in which an alumel-chromel thermocouple junction was inserted, was vitrified in liquid nitrogen. The overall cooling rate was about 1000 K/min. A simple differential thermal analysis technique was used to measure T_g.[1] Benzene was used as the reference material, and the temperature difference between the vitrified sample and the reference was recorded together with the temperature of the quenched sample. T_g and T_c (crystallization temperature) values were taken to represent the onset of transition as shown in Fig. 2. DTA measurements were carried out at a heating rate of about 5 K/min in the glass transition temperature region. T_g values were found to be reproducible in this study to within 0.5 K and the accuracy of temperature reading is estimated to be ± 1 K from a determination of melting points of several guaranteed grade reagents (absolute ethanol, acetone, and chloroform). Quenched samples were checked for crystallinity by visual inspection. Any incompletely vitrified samples were associated with loss of transparency. Visual inspection showed that the glass-forming composition region of HI+water system ranges from *ca.* 40 to 57% (wt% HI). The upper limit of the glass-forming composition range was not well established because of the non-availability of higher HI concentrations (>57%) in this study. The glass transition was also observed for incompletely vitrified samples, and this arises from the fact that the residual portion which remains uncrystallized in the quenching process becomes a glassy state.

Results and Discussion

The results of T_g and T_c are shown in Fig. 1 together with the phase diagram of the HI+H_2O system as an inset. It is clearly seen that the solution near the first eutectic composition is prone to supercooling to a vitreous state. This tendency is in accordance with many other binary systems.[1,9-11] In fact, most liquid mixtures which have glass-forming composition regions are usually glass-forming at the first eutectic composition.

In the glass-forming composition region of aqueous HI solution, T_g increases almost linearly with increase in HI concentration, ranging from -140 ± 1 °C at 40 wt% HI to -124 ± 1 °C at 57 wt% HI. Simple linear composition dependence of T_g is usually observed for a nearly ideal solution.[6] With this system, we may regard the solution as an ideal or quasi-ideal solution of water and $HI\cdot4H_2O$. A simple least-square curve fitting yields the following formula for the concentration dependence of T_g:

$$T_g = 0.91X - 177, \quad (1)$$

where X is concentration of HI in wt% and T_g in °C.

The estimation of T_g for a pure non-glass-forming liquid from T_g data of binary mixtures by extrapolation is now well established and the T_g values estimated give concordant results.[2,4] Rasmussen and MacKenzie[12] measured glass transition temperatures of several binary aqueous solutions: water+methanol, water+glycerol, and water+ethylene glycol. The extrapolation of the obtained T_g data to pure water gives -137 ± 2 °C as the T_g of glassy bulk water. Angell and Sare[1] also gave a similar value from studies of a large number of aqueous electrolyte solutions. This value is almost identical with the glass transition temperature (−139 °C) obtained[13] for an amorphous solid water made by the vapor deposition method. All these data, therefore, suggest that T_g of bulk pure water will be very close to −138 °C if a glassy bulk water is successfully formed

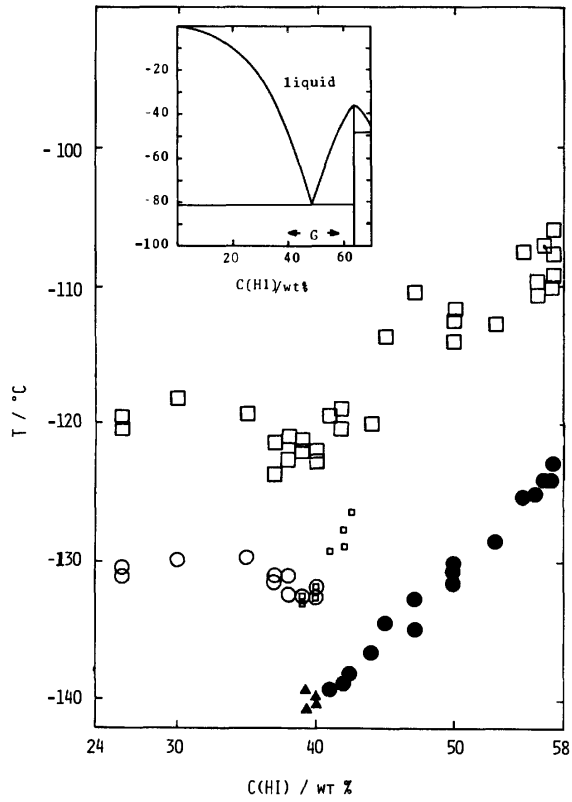

Fig. 1. Variation of T_g and T_c as a function of HI concentration (C). The inset shows the phase diagram of the HI+H_2O system [from: J. Timmermans, "Physico Chemical Constants of Binary Systems," Interscience Publishers, Inc., New York (1960), Vol. 4, p. 466].
●: T_g in the glass-forming composition region, ○: T_g of the portion remained uncrystallized in the non-glass-forming composition region, or the second glass transition temperature (T_{g_2}) in the double glass transition region, ▲: the first glass transition temperature (T_{g_1}) in the double glass transition region, □ : the first crystallization temperature (T_{c_1}), □: crystallization temperature (T_c) or the second crystallization temperature (T_{c_2}).
The -G- mark in the inset shows the glass forming composition range.

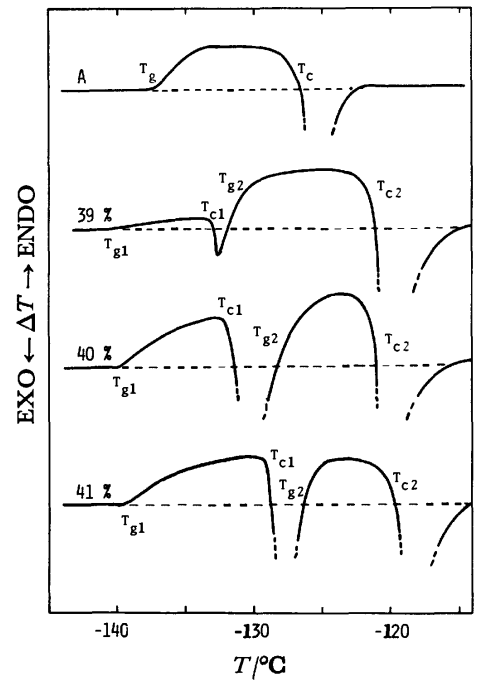

Fig. 2. DTA traces of glassy aqueous HI solutions.
The A trace shows a typical DTA trace of a glassy sample.

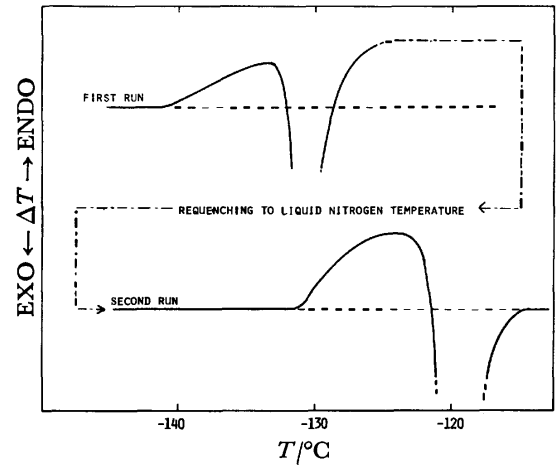

Fig. 3. Confirmation of the second glass transition in the glassy HI solution (HI=40 wt%).

and subjected to T_g measurement. However, it is interesting to note that Eq. 1 predicts T_g of glassy bulk pure water to be −177 °C, far below the T_g value (−138 °C) expected from other data.[1,12,13]

There have been a few interesting observations[14,15] which might offer a clue to clarifying this anomalously low T_g value. In a recent positron annihilation study of a γ-irradiated ice, Eldrup[14] reported that mono-vacancies produced by γ-irradiation become mobile at −175±5 °C. Another suggestive coincidence, though it might be merely accidental, is that the glass transition in a glassy crystal ice, which is claimed to be associated with proton disorder in the ice crystal,[15] occurs at −173 °C. In addition, the T_g values so far reported for the vapor deposited amorphous ice and glassy bulk water scatter from −170 to −120 °C,[15] although recent data are clustering around −138±2 °C. We cannot, at present, give any clear-cut explanation to this low T_g (−177 °C) expected from a simple extrapolation based on Eq. 1 for the glassy bulk water. However, we conjecture, though rather intuitively, that hydronium ions stabilized in the glassy HI solution may be responsible for this low T_g. In fact, the T_g data of HX solutions (X=F, Cl, and Br)[16] also predict that the glass transition of a glassy bulk water should be lower than −139 °C. Furthermore, a recent finding of polymorphism of amorphous ice[17] adds a new possibility and complication to a clear-cut explanation. The T_g measurement on a high density amorphous ice will be very valuable in clarifying this situation.

Another interesting feature in the glass formation of the HI+water system is the observation of the double glass transition phenomenon at both boundaries of the

glass-forming composition range. In the water-rich side of the glass-forming boundary, thermal effect of the first glass transition grows with increase in HI concentration and the two glass transitions gradually merge into a single large glass transition around 42 wt% HI (see (b), (c), and (d) DTA curves in Fig. 2).

As it is difficult to see clearly the second glass transition in the DTA traces shown in Fig. 2, we carried out the following additional experiment to confirm that there are really two glass transitions in these DTA traces: just after recording the first T_g and T_c curves as usual in the first run, the sample was requenched to the liquid nitrogen temperature and then a DTA trace was recorded again. The schematic DTA traces thus obtained are shown in Fig. 3, where we clearly see the second glass transition in the second warm-up DTA trace. This phenomenon reflects the phase separation in the supercooled solution. However, it is difficult at present to determine whether the observed double glass transition is a reflection of a "real" liquid-liquid immiscibility or of a simple pseudo-phase separation produced in the process of vitrification.

The first phase-separated portion, which is very unstable in the liquid state as evidenced by its immediate crystallization after the first glass transition in the warm-up DTA trace, is considered to be a water-rich phase because the T_g and T_c values of the other phase-separated portion are very close to those of the solution with the eutectic composition. Therefore, the phase separation must be described as: the solution → a water-rich phase+a phase of eutectic composition. The closeness of T_g of the water-rich phase to that of a vapor-deposited amorphous ice indicates that the composition of the water-rich phase should be very close to pure water.

The fact that the double glass transition phenomenon in aqueous solution has been observed only at the edge of the glass-forming composition region, seems to suggest that the phenomenon is associated with a metastable immiscibility. Two mechanisms have been postulated for the phase separation in supercooled solutions and glasses.[18,19] The invariance of the concentration of one phase (the phase of eutectic composition) in the phase-separated glasses in this study indicates that the observed phase separation in the $HI+H_2O$ system is due to the nucleation and growth mechanism.

It is to be noted here that there have been several attempts to detect a possible liquid-liquid immiscibility in the $LiCl+H_2O$ system at low temperatures and normal pressure.[20-22] Despite of two positive reports,[20,21] recent works have given rather a negative view for phase separation in the $LiCl+H_2O$ system.[22]

In contrast to the good reproducibility of the two-glass-transition phenomenon in the water-rich side of the glass-forming composition range, the double glass transition phenomenon in the vicinity of *ca.* 57 wt% HI solution is not good in reproducibility; even the sample which has shown two glass transitions in the first run does not necessarily give two glass transitions in the second run. Therefore, this "seemingly two" glass transition may not be due to phase separation. As the quenched sample is translucent, we come to conclude that it is in an incomplete glassy state and is not a phase-separated glass. It may be considered that the rearrangement motion of micro-crystals in the quenched sample is the cause for the second T_g-like heat anomaly in the DTA trace though no detailed mechanism is known.

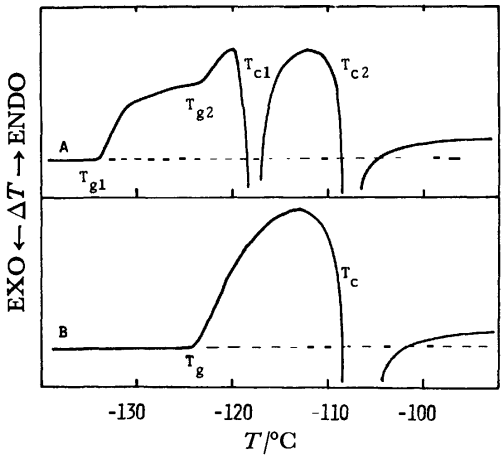

Fig. 4. DTA traces of the glassy aqueous HI solution (HI≈57 wt%).
(A): There are two glass transitions, (B): there is only one glass transition.

Lastly we point out the importance of crystallization temperature, to which little attention has been paid, as an auxiliary diagnostic parameter in the study of glass-forming properties of aqueous solutions. In fact, two crystallization peaks are observed in the concentration range where two glass transitions are observed. It can be seen in Fig. 1 that the solution at HI concentrations less than 40 wt% will divide into two phases (one is ice and the other the solution of eutectic composition) in the crystallization process, the latter phase being glass-forming in the rapid cooling. This is supported by the observation that the T_g value of the portion uncrystallized is very close to the T_g of the solution at HI=48 wt% (the eutectic composition). The invariance of T_c in this non-glass-forming composition range is also an additional support for the conclusion.

We are thankful to Professor C. A. Angell at Purdue University for his criticism on the first draft. This work was in part assisted by a Grant-in-Aid for Scientific Research from the Ministry of Education, Science and Culture.

References

1) C. A. Angell and E. J. Sare, *J. Chem. Phys.*, **52**, 1058 (1970).
2) C. A. Angell, J. M. Sare, and E. J. Sare, *J. Phys. Chem.*, **82**, 2622 (1978); C. A. Angell and J. C. Tucker, *ibid.*, **84**, 268 (1980).
3) A. V. Lesikar, *Phys. Chem. Glasses*, **16**, 83 (1975).
4) A. V. Lasikar, *J. Chem. Phys.*, **63**, 2297 (1975); **66**, 4263 (1977); **68**, 3323 (1978).
5) A. V. Lesikar, *J. Solution Chem.*, **6**, 81, 839 (1977).
6) M. H. Herzog-Cance, J. Potier, A. Potier, P. Dhamelincourt, B. Sombret, and F. Wallart, *J. Raman Spec-*

trosc., **7**, 303 (1978).
7) H. Kanno and Y. Akama, *Chem. Phys. Lett.*, **72**, 181 (1980).
8) H. Kanno and J. Hiraishi, *Chem. Phys. Lett.*, **62**, 82 (1979); **72**, 541 (1980); *J. Raman Spectrosc.*, **9**, 85 (1980).
9) E. Thillo, C. Wiecker, and W. Wiecker, *Silikattechnik*, **15**, 109 (1964).
10) M. Imaoka, "Advances in Glass Technology," Plenum Press, New York (1962), Part 1, p. 149.
11) L. C. Shepley and A. B. Bestul, *J. Chem. Phys.*, **39**, 680 (1963).
12) D. H. Rasmussen and A. P. MacKenzie, *J. Phys. Chem.*, **75**, 967 (1971).
13) M. Sugisaki, H. Suga, and S. Seki, *Bull. Chem. Soc. Jpn.*, **41**, 2591 (1968).
14) M. Eldrup, *J. Chem. Phys.*, **64**, 5283 (1976).
15) H. Suga and S. Seki, *J. Non-Cryst. Solids*, **16**, 171 (1974).
16) H. Kanno and K. Satoh, to be published.
17) S. A. Rice, *Topics Current Chem.*, **60**, 109 (1975); A. H. Narten, C. G. Venkatesh, and S. A. Rice, *J. Chem. Phys.*, **64**, 1106 (1976).
18) J. W. Cahn, *J. Chem. Phys.*, **42**, 93 (1965); J. W. Cahn and R. J. Charles, *Phys. Chem. Glasses*, **6**, 181 (1965).
19) H. Rawson, "Inorganic Glass Forming System," Academic Press, London (1967), Chaps. 7 and 8.
20) C. A. Angell and E. J. Sare, *J. Chem. Phys.*, **49**, 4713 (1968).
21) S. Y. Hsich, R. W. Gammon, P. B. Macedo, and C. J. Montrose, *J. Chem. Phys.*, **56**, 1663 (1972).
22) J. Dupuy, J. F. Jal, C. Fierador, P. Chieux, A. Wright, R. Caleczuk, and C. A. Angell, *Nature*, **296**, 138 (1982).

The Reactions of Singlet NH Radicals with Methyl and Ethyl Alcohols in the Liquid Phase

Jun KAWAI, Shigeru TSUNASHIMA,* and Shin SATO†

Department of Applied Physics, Tokyo Institute of Technology, Ookayama, Meguro-ku, Tokyo 152

† *Research Laboratory for Nuclear Reactors, Tokyo Institute of Technology, Ookayama, Meguro-ku, Tokyo 152*

(Received March 4, 1982)

The reactions of the singlet NH($a^1\Delta$) radicals with alcohols were studied by the photolyses of hydrogen azide in liquid methyl and ethyl alcohols at the temperature of Dry Ice–methyl alcohol and at 0 °C. The main products were nitrogen, ammonia, and oxime ethers; acetaldehyde oxime *O*-ethyl ether from ethyl alcohol and formaldehyde oxime *O*-methyl ether from methyl alcohol. The relative yields of the products were independent of the changes in the reaction temperature and in the concentration of the hydrogen azide examined. Methoxyamine or ethoxyamine, a possible insertion product of the singlet NH into the O–H bond of alcohol, was detected as a form of oxime ether by the reactions with the aldehyde eventually formed. It was concluded that the singlet NH radicals can effectively insert into the O–H bond of the alcohol.

Recently, it was shown that the singlet NH radicals, NH($a^1\Delta$), inserted into the C–H bonds of hydrocarbons and carboxylic acids to form amines and amino acids respectively and added to the double bond of olefins to form aziridines.[1–7] These reactions are essentially the same as those observed in the reactions of O(^{1}D) and $CH_2(^1A_1)$.[8,9] An insertion reaction into the O–H bond of an alcohol may be expected to occur; however, the reaction has not been examined in the case of NH.

In order to investigate the reactions of methylene with alcohol, Ogoshi and Takezaki photolyzed ketene in the presence of methyl alcohol vapor at 40 °C. The main products were dimethyl ether and ethyl alcohol. If these products were formed by the insertion into the C–H and O–H bonds of methyl alcohol, the efficiencies of these two processes should be almost equal.[10] Using diazomethane as the source of methylene, Kerr *et al.* found that the insertion of methylene into the O–H bond of alcohol was more efficient than that into the primary C–H bond and reported the values of the relative efficiencies as follows: 21.8 (methyl alcohol), 21.2 (ethyl alcohol), 14.9 (isopropyl alcohol), and 10.9 (*t*-butyl alcohol).[11]

The present paper reports the results obtained in the photolyses of hydrogen azide in liquid methyl and ethyl alcohols at the temperature of Dry Ice–methyl alcohol and at 0 °C.

Experimental

The experimental methods and the apparatus used were essentially the same as those described in the previous papers.[1–3]

Ethyl alcohol (Amakasu Kagaku Sangyo Co., 99.5%) and methyl alcohol (Tokyo Kasei Co., 99.5%) were used after having been degassed at −60 °C and −80 °C respectively and distilled at room temperature *in vacuo*. Further purified ethyl alcohol was also used to check the possibility of interference by acetaldehyde, *i. e.*, ethyl alcohol was treated with Ag_2O for several days and distilled from NaOH solution. The alcohols were stored under vacuum after purification. Hydrogen azide was prepared and purified by the method described in the previous papers.[1–3] Methyl alcohol-d_4 (Merck Sharp and Dohme, Canada Ltd.) was used without further purification except for low temperature distillation *in vacuo*. 2-Amino-1-ethanol and methoxyamine hydrochloride were purchased from the Tokyo Kasei Co. and used as supplied.

A Pyrex tube of 10 mm o.d. was used as a reaction cell. About 1 ml of a methyl or ethyl alcohol solution of hydrogen azide was irradiated with a medium pressure mercury lamp (Toshiba H400-P) at 0 °C or at the temperature of Dry Ice–methyl alcohol. Uncondensable products at −196 °C were analyzed with a combination of a Toepler pump, a gas buret, and a CuO furnace at 300 °C. The volatile products at room temperature were transferred in a trap containing NaOH coated glass wool *in vacuo* together with the reactants. After the treatment with NaOH, the products uncondensable at −40 °C (ethyl alcohol) or −60 °C (methyl alcohol) were analyzed by GLC using a column packed with Amine 220 on NaOH coated Celite 545 (Gasukuro Kogyo Co., 5 m in length). For the analysis of less volatile products, a KOH solution of methyl alcohol was added to the reaction mixture and directly injected into a gas chromatograph equipped with FID (Hitachi 023). A column packed with Tenax GC (Gasukuro Kogyo Co., 1 m in length) was used. *s*-Butyl alcohol was used as the standard. For the identification of the products, a GC-mass spectrometer (Nichiden Varian, TE 600) and an NMR (Varian 390) were used.

Results

The products obtained in the photolysis of hydrogen azide in liquid methyl or ethyl alcohol were fractionated into three parts; uncondensable products at −196 °C, products more volatile than the solvent, and the less volatile products than the reactants. The uncondensable product at −196 °C was nitrogen for both methyl and ethyl alcohols. A negligibly small amount of hydrogen was also formed. The yield was less than 2% of that of nitrogen. No methane formation was detected by the mass spectrometric analysis. Ammonia formation was observed in the second fraction both for methyl and ethyl alcohols. From this fraction, formaldehyde oxime *O*-methyl ether and methoxyamine were detected in the case of methyl alcohol. The yield of the latter was about 1/100 of that of the former. No formaldehyde was detected. The identification of formaldehyde oxime *O*-methyl ether was based on the following results:

a) The molecular weight of the product was 59. The mass spectrum is shown in Table 1.

b) The product did not form a salt with hydrogen azide as well as with hydrogen chloride.

c) This product was also obtained without treat-

Table 1. Mass spectra of formaldehy de oxime *O*-methyl ether and acetaldehyde oxime *O*-ethyl ether

m/e	Formaldehyde oxime *O*-methyl ether			Acetaldehyde oxime *O*-ethyl ether
	$NH+CH_3OH$	$CH_2O+CH_3ONH_2$	$NH+CD_3OD$	$NH+C_2H_5OH$
15	15	13		74
18			16	10
26				15
27	28	22		46
28	100	100	34	38
29	66	65		93
30	22	26	100	30
31	72	65		13
32			11	
34			43	
40				13
41				63
42				100
43				13
44	53	53	16	23
46			35	
59	85	83		79
62			20	
64			46	
72				10
87				18

Table 2. The yields of ammonia and formaldehyde oxime *O*-methyl ether relative to that of nitrogen obtained in the photolysis of hydrogen azide in liquid methyl alcohol

$[HN_3]$ / mol dm^{-3}	Photolysis time / min	NH_3/N_2	FM/N_2[a]
0.033[b]	60	0.28	0.24
0.036[b]	60	0.24	0.16
0.073[b]	60	0.34	0.28
0.105[b]	60	0.24	0.19
0.143[c]	60	0.34	0.22
0.147[b]	15	0.29	0.26
0.145[b]	30	0.29	0.22
0.152[b]	60	0.34	0.30
0.154[b]	60	0.41	0.20
0.152[b]	90	0.40	0.24
0.144[b]	120	0.25	0.30
0.210[b]	60	0.37	0.26
	Average	0.32±0.06	0.24±0.05

a) FM=Formaldehyde oxime *O*-methyl ether. b) Experiments at the temperature of Dry Ice–methyl alcohol. c) Experiments at 0 °C.

Table 3. The yields of ammonia and acetaldehyde oxime *O*-ethyl ether relative to that of nitrogen obtained in the photolysis of hydrogen azide in liquid ethyl alcohol

$[HN_3]$ / mol dm^{-3}	Photolysis time / min	NH_3/N_2	AE/N_2[a]
0.054[b]	60	0.32	0.25
0.099[b]	30	0.30	0.21
0.091[c]	60	0.31	0.21
0.097[b]	60	0.41	0.18
0.102[b,d]	60	n.d.[e]	0.21
0.103[b]	60	n.d.[e]	0.21
0.106[b]	90	0.30	0.23
0.153[b]	60	0.36	n.d.[e]
	Average	0.33±0.04	0.22±0.02

a) AE: Acetaldehyde oxime *O*-ethyl ether. b) Experiments at the temperature of Dry Ice–methyl alcohol. c) Experiments at 0 °C. d) Further purified ethyl alcohol was used. e) n.d.: Not determined.

ment with NaOH.

d) When methyl alcohol-d_4 was used, the molecular weight of the product increased to 64. This result suggested that the product had five hydrogen atoms.

e) The mass spectrum and the retention time of GLC of this compound agreed with those of the product obtained by the reaction of methoxyamine hydrochloride with KOH and formaldehyde. (see Table 1).

In the case of ethyl alcohol, a similar product, having a molecular weight of 87, was found to be formed in the second fraction along with ammonia. From the mass spectrum shown in Table 1, this product was identified to be acetaldehyde oxime *O*-ethyl ether. In the case of the mixture of methyl and ethyl alcohols, two new products were observed to be formed along with ammonia, formaldehyde oxime *O*-ethyl ether, and acetaldehyde oxime *O*-methyl ether. Their molecular weights were both 73. One of the new products gave the same mass spectrum and the retention time as those obtained

TABLE 4. THE YIELD OF 2-AMINO-1-ETHANOL RELATIVE TO THAT OF NITROGEN OBTAINED IN THE PHOTOLYSIS OF HYDROGEN AZIDE IN LIQUID ETHYL ALCOHOL[a)]

$[HN_3]$ / mol dm^{-3}	$[NH_2CH_2CH_2OH]/[N_2]$
0.099	0.16
0.101	0.06
0.102	0.07
0.150	0.13
Average	0.10±0.05

a) Obtained at the temperature of Dry Ice–methyl alcohol with photolysis time of 60 min.

from the product formed by the reaction of methoxyamine hydrochloride with KOH and acetaldehyde. This product was identified to be acetaldehyde oxime *O*-methyl ether. The other was concomitantly identified to be formaldehyde oxime *O*-ethyl ether. No acetaldehyde was detected in the case of ethyl alcohol.

From the less volatile fraction, no retrievable products were obtained in the case of methyl alcohol. In the case of ethyl alcohol, 2-amino-1-ethanol was observed to be formed. The assignment was based on comparisons of its mass spectrum and retention time with those of the authentic sample. $CH_3CH{=}NCH_2CH_2OH$, a possible product formed by the reaction of 2-amino-1-ethanol with acetaldehyde, could not be observed. The yield of this product should be less than 1/10 of that of 2-amino-1-ethanol, if any.

Tables 2, 3, and 4 show the yields of the products relative to that of nitrogen obtained under various experimental conditions. The relative yields were almost constant for the changes in the concentration of hydrogen azide and in the reaction temperature examined.

Discussion

As shown in Tables 2, 3, and 4, the relative yields of the products were independent of the changes in the concentration of hydrogen azide. This trend is similar to those obtained in the cases of olefin and carboxylic acid.[5–7)] The following reaction mechanism can be considered to explain the results obtained in the case of ethyl alcohol:

$$HN_3 + h\nu \longrightarrow {}^1NH + N_2 \quad (1)$$

$${}^1NH + C_2H_5OH \longrightarrow NH_2CH_2CH_2OH \quad (2a)$$

$$\longrightarrow [CH_3CH(NH_2)OH]$$

$$\longrightarrow NH_3 + CH_3CHO \quad (2b)$$

$$\longrightarrow C_2H_5ONH_2 \quad (2c)$$

$$\longrightarrow {}^3NH + C_2H_5OH \quad (2d)$$

$$C_2H_5ONH_2 + CH_3CHO \longrightarrow CH_3CH{=}NOC_2H_5 + H_2O \quad (3)$$

$$C_2H_5ONH_2 \longrightarrow CH_3CHO + NH_3 \quad (4)$$

$${}^3NH + HN_3 \longrightarrow NH_2 + N_3 \quad (5)$$

$$NH_2 + HN_3 \longrightarrow NH_3 + N_3 \quad (6)$$

$$2N_3 \longrightarrow 3N_2 \quad (7)$$

Here, ^1NH and ^3NH represent the NH radicals in the singlet state ($a^1\Delta$) and the triplet state ($X^3\Sigma^-$) respectively.

The insertion of a singlet NH radical into the C–H bond at the β position will give 2-amino-1-ethanol (Reaction 2a). 1-Amino-1-ethanol may be formed by the insertion into the C–H bond at the α position; however, this compound is known to be unstable and to decompose to acetaldehyde and ammonia (Reaction 2b). Ethoxyamine may be formed by the insertion into the O–H bond of alcohol (Reaction 2c). Neither ethoxyamine nor acetaldehyde formation was detected in this study. Instead of these products, acetaldehyde oxime *O*-ethyl ether was found to be one of main products. This product may be formed by the condensation reactions of alkoxyamine and aldehyde (Reaction 3).[12)] Reaction 4 is included in the mechanism in order to take into account the possibility that ethoxyamine is unstable and also k_{2b} is smaller than k_{2c}. This point will be discussed later. Although ethoxyamine was not detected in the case of ethyl alcohol, methoxyamine, a possible insertion product into the O–H bond of methyl alcohol, was detected as a minor product. This difference might be explained by the difference in the stability of the alkoxyamine.

Reaction 2d is included in the mechanism to explain the fact that the amount of ammonia formed was more than that of acetaldehyde oxime *O*-ethyl ether or formaldehyde oxime *O*-methyl ether. The deactivation process has been considered in the cases of hydrocarbons and carboxylic acids.[1–7)] The reaction of the triplet NH radicals is assumed to be a hydrogen-atom abstraction from hydrogen azide (Reaction 5). The triplet NH radicals might also abstract a hydrogen atom from ethyl alcohol;

$${}^3NH + CH_3CH_2OH \longrightarrow NH_2 + CH_3CHOH$$

$$\Delta H = 10\ \text{kJ/mol}^{13)} \quad (8)$$

although the reaction is slightly endothermic. If CH_3CHOH radicals abstract a hydrogen atom from hydrogen azide;

$$CH_3CHOH + HN_3 \longrightarrow CH_3CH_2OH + N_3 \quad (9)$$

Reaction 8 followed by Reaction 9 would be indistinguishable from Reaction 5.

In the above reaction mechanism, a hydrogen atom abstraction by the singlet NH radicals was neglected:

$${}^1NH + CH_3CH_2OH \longrightarrow NH_2 + CH_2CH_2OH \quad (10a)$$

$$\longrightarrow NH_2 + CH_3CHOH \quad (10b)$$

$$\longrightarrow NH_2 + CH_3CH_2O \quad (10c)$$

All these reactions are energetically possible. If resultant alcohol radicals abstracted a hydrogen atom from hydrogen azide, Reactions 10's would be indistinguishable from Reaction 2d. If all these radicals recombined with NH_2, Reactions 10a—c would be hard to discriminate from Reactions 2a—c, respectively. If one of these assumptions were the case, it would be difficult to estimate the extent of the participation of the abstraction reactions. In the intermediate case, that is, if some of the alcohol radicals abstracted a hydrogen atom and the rest recombined with NH_2

radicals, the relative yields of the products should depend on the concentration of hydrogen azide. This case is most probable if the singlet NH radicals abstracted a hydrogen atom from alcohol. The concentration dependence observed, however, was different from that expected. Similar reaction mechanism may be considered in the case of methyl alcohol except for Reaction 2a.

Assuming the above reaction mechanism, the following relations can be expected to hold:
for the case of ethyl alcohol,

$$([NH_2CH_2CH_2OH] + 4[NH_3] - 2[CH_3CH{=}NOC_2H_5])/[N_2] = 1.0 \quad (11)$$

for the case of methyl alcohol,

$$(4[NH_3] - 2[CH_2{=}NOCH_3])/[N_2] = 1.0 \quad (12)$$

Using the values shown in Tables 2, 3, and 4, the left-hand-sides of Eqs. 11 and 12 were calculated to be 1.0 ± 0.1 and 0.81 ± 0.13 respectively; *i.e.*, the total yields of the products observed were successfully explained by the above mechanism.

Similar to alkoxyamine, 2-amino-1-ethanol may react with acetaldehyde:

$$NH_2CH_2CH_2OH + CH_3CHO \longrightarrow CH_3CH{=}NCH_2CH_2OH + H_2O \quad (13)$$

Reaction 13, however, should be unimportant under the present experimental conditions, since the material balance was good and no $CH_3CH{=}NCH_2CH_2OH$ formation was observed in the ethyl alcohol solution.

In the case of propionic acid, the singlet NH radicals inserted into the C–H bonds of α and β positions with almost equal rates.[6,7] For the insertion into the C–H bonds of paraffin, however, the relative rates of the insertion into the primary, secondary, and tertiary C–H bonds were 1.0, 1.9, and 2.3 respectively.[3] That is, the insertion rate slightly depends on the strength of the C–H bond. If this relation held in the case of ethyl alcohol, k_{2b} would be equal or slightly larger than $(2/3)k_{2c}$. The amount of acetaldehyde formed by Reaction 2b should be almost equal to that of 2-amino-1-ethanol. The yield of 2-amino-1-ethanol was about a half of that of acetaldehyde oxime *O*-ethyl ether. This was the main reason why Reaction 4 was included in the mechanism. The validity of Reaction 4 is unknown at present. Another possible assumption is that the singlet NH radicals can abstract two hydrogen atoms at once from ethyl alcohol to form ammonia and acetaldehyde:

$$^1NH + C_2H_5OH \longrightarrow NH_3 + CH_3CHO \quad (14)$$

Reaction 14 is indistinguishable from Reaction 2b. Similar reactions which involve the abstraction of two hydrogen atoms have been considered in the case of the reactions of $O(^1D)$ with ethane or ethylene. The extent of the reaction is about 3% of the total $O(^1D)$ reactions in the liquid Ar.[14] For the case of the singlet NH, the concentration dependence of the ammonia formation could also be explained by the presence of the similar reaction in the case of the olefin, but not in the case of the paraffin. If Reaction 14 were included in the mechanism instead of Reaction 4, k_{2c} should be equal to $k_{2b}+k_{14}$ to explain the observed material balance.

In the above discussions, acetaldehyde was assumed to be formed by Reactions 2b and 4. Since acetaldehyde is known as a possible impurity in ethyl alcohol, it is possible to consider that the impurity affects Reaction 3. This possibility was, however, dismissed because of the following facts:

a) No aldehyde was detected in this study, although this result does not conclusively eliminate the possibility of the presence of aldehyde, because of possible condensation reactions of aldehyde in the present analytical system.

b) The amount of acetaldehyde oxime *O*-methyl ether did not decrease when more highly purified ethyl alcohol was used. (see Table 3).

c) When the acetaldehyde was assumed to be an impurity, Eq. 11 should be changed to Eq. 15:

$$([NH_2CH_2CH_2OH] + [CH_3CH{=}NOC_2H_5] + 4[NH_3] - 3[NH_3]_{2b})/[N_2] = 1.0 \quad (15)$$

Here, $[NH_3]_{2b}$ represents the amount of ammonia formed by Reaction 2b. If $[NH_3]_{2b}$ is assumed to be equal to $[NH_2CH_2CH_2OH]$, the left-hand-side of Eq. 15 becomes 1.3.

Assuming Reaction 4 and $k_{2a}=k_{2b}$, the relative efficiencies of Reactions 2a—d can be estimated to be 0.1_6, 0.1_6, 0.5_0, and 0.1_8 respectively. That is, the main reaction of the singlet NH with ethyl alcohol is the insertion into the O–H bond. For the case of methyl alcohol, the insertion into the C–H or O–H bond was calculated to be 85% of the reaction of NH radicals. The efficiencies could not be estimated seperately, because of the presence of Reaction 4. The insertion into the O–H bond, however, may be more important than the C–H bond of methyl alcohol.

The authors are much obliged to Professors Takeshi Nakai and Yoshihiko Morooka for the NMR measurements and helpful discussions.

References

1) S. Tsunashima, M. Hotta, and S. Sato, *Chem. Phys. Lett.*, **64**, 435 (1979).
2) S. Tsunashima, J. Hamada, M. Hotta, and S. Sato, *Bull. Chem. Soc. Jpn.*, **53**, 2443 (1980).
3) J. Hamada, S. Tsunashiaa, and S. Sato, *Bull. Chem. Soc. Jpn.*, **55**, 1739 (1982).
4) O. Kajimoto and T. Fueno, *Chem. Phys. Lett.*, **80**, 484 (1981).
5) T. Kitamura, S. Tsunashima, and S. Sato, *Bull. Chem. Soc. Jpn.*, **54**, 55 (1981).
6) S. Sato, T. Kitamura, and S. Tsunashima, *Chem. Lett.*, **1980**, 687.
7) S. Tsunashima, T. Kitamura, and S. Sato, *Bull. Chem. Soc. Jpn.*, **54**, 2869 (1981).
8) R. J. Cvetanović, *Adv. Photochem.*, **1**, 115 (1963).
9) R. A. Moss and M. Jones, Jr., "Carbenes," John Wiley and Sons, New York (1973), I and (1975), II.

10) H. Ogoshi and Y. Takezaki, *Bull. Inst. Chem. Res., Kyoto University*, **38**, 299 (1960).
11) J. A. Kerr, B. V. O'Grady, and A. F. Trotman-Dickenson, *J. Chem. Soc., A*, **1967**, 897.
12) L. F. Fieser and M. Fieser, "Textbook of Organic Chemistry," Maruzen, Tokyo (1952), p. 207.
13) J. A. Kerr, M. J. Parsonage, and A. F. Trotman-Dickenson, "CRC Handbook of Chemistry and Physics," **55**, F219 (1974—1975).
14) W. B. DeMore, *J. Phys. Chem.*, **73**, 391 (1969).

 © 1982 The Chemical Society of Japan Bull. Chem. Soc. Jpn., 55, 3317—3320 (1982)

Preparation and Electrical Properties of $Eu(II)_xNb(IV)O_{2+x}$

Kenji Ishikawa, Gin-ya Adachi,* and Jiro Shiokawa
Department of Applied Chemistry, Faculty of Engineering, Osaka University, Yamadaoka, Suita, Osaka 565
(Received March 17, 1982)

Nonstoichiometric compounds, Eu_xNbO_{2+x}, were prepared. A cubic tungsten bronze type structure was found in the single phase region of Eu_xNbO_{2+x} ($0.5 \leqq x \leqq 1.0$). Magnetic susceptibility measurements showed that the oxidation state of europium in the bronzes was bivalent. The Eu_xNbO_{2+x} was a metallic conductor in the temperature range 4.2—300 K. Thermoelectromotive force measurements (100—350 K) indicated that the charge carriers were electrons and that the effective mass of the electrons increased with decreasing x in Eu_xNbO_{2+x}.

Europium niobium bronzes, Eu_xNbO_{2+x}, where x lies between 0.50 and 1.00 are tungsten bronze type compounds. At values of x greater than 0.65, the niobium bronzes crystallize in the cubic tungsten bronze type structure and exhibit the metallic properties of bluish luster and electronic conduction.[1,2] At values of x less than 0.65, the structure is the tetragonal tungsten bronze type and the bronzes are nonmetallic.[1-5] In the bronzes, Nb^{4+} ions co-exist with Nb^{5+} ions and the number of Nb^{4+} ions, which is equal to the number of conduction electrons for the cubic bronzes, is controlled simply by controlling the europium concentration, since the bronzes are expressed by a formula $Eu^{2+}Nb^{4+}_{2x-1}Nb^{5+}_{2-2x}O^{2-}_3$. However, the number of Nb^{4+} ions is also controlled by removing lattice oxygens from the bronzes, and the lattice oxygen should be removed until all the Nb^{5+} ions is reduced to Nb^{4+}, *i.e.*, $Eu^{2+}_x Nb^{4+}O^{2-}_{2+x}$. In this paper chemical and physical properties of Eu_xNbO_{2+x} are discussed and compared with those of Eu_xNbO_3.

Experimental

Preparative. A fully mixed powder of Eu_2O_3 (purity 99.9%: Shin-etsu Chemical Co.,), Nb_2O_5 (purity 99.9%: Wako Chemical Industries, Ltd.,), and Nb (purity 99.9%: Wako Chemical Industries, Ltd.,) was pressed into pellets. The pellets were packed into a Mo box and sealed in a silica tube under vacuum. The pellets were degassed under vacuum at 450 K for 3 h before the sealing procedure. The silica tube was set up in a vertical furnace and heated at 1423—1473 K for 6 h. The sample was ground in an agate mortar, re-pressed into pellets, degassed, sealed in a silica tube under vacuum, and heated again at 1423—1473 K for 30 h. The reaction was completed during the procedure described above and assumed to proceed as follows.

$$0.5xEu_2O_3 + (0.4-0.1x)Nb_2O_5 + (0.2+0.2x)Nb \longrightarrow Eu_xNbO_{2+x} \quad (1)$$

However, in practice a small excess of niobium metal was used to compensate for a slight oxidation of the samples during the synthetic procedure.

Analyses. The phase purity and the structure type of the samples were analyzed by X-ray powder diffraction with a Rigaku Denki "Rotor-flex diffractometer."

The Eu/Nb ratios, namely x in Eu_xNbO_{2+x}, were determined by fluorescence X-ray analysis with a Rigaku Denki "Ultra Trace unit," and the O/Nb ratios were obtained by weighing the samples before and after complete oxidation and assuming the following oxidation reaction,

$$Eu_xNbO_{2+x} + 0.25(x+1)O_2 \longrightarrow 0.5xEu_2O_3 + 0.5Nb_2O_5. \quad (2)$$

Magnetic and Electrical Measurements. The magnetic moments of the samples were obtained from magnetic susceptibility measurements with a Shimadzu magnetic balance "MB-11" under a He atmosphere in the temperature range 4.2 to 300 K.

Electrical resistivity measurements were done for the polycrystalline sintered bars with a simple four-probe d.c. method in a helium atmosphere from 4.2 to 300 K. The heating rate of each measurement was below 1 K/min. The dc currents was produced with a Takeda Riken dc generator "TR-6141," and the potential difference between the two potential leads was recorded with a Yokogawa Denki "Type 3036 X-Y recorder;" the resistivity measurements were carried out in the ohmic region of the current. Since the measured voltage included a thermally generated emf, the dc current was stopped at regular time intervals and the emf was separated. The shape and size of the samples and the attachment of electrical leads used were the same as those described in the previous paper.[1]

Thermoelectric Power Measurements. Thermoelectric powers of the rectangular samples of about 2 mm^2 in cross section and about 4 mm long were measured under a He atmosphere in the range 100—373 K. The temperature difference between both side of the sample was adjusted to fall within 10 K. The absolute Seebeck coefficient was obtained after compensating the emf of copper action as the electrode of our apparatus and given according to the following equation:

$$S = S_{Cu} - \Delta V/\Delta T, \quad (3)$$

where S_{Cu} was the absolute Seebeck coefficient of Copper,[6] ΔV was the thermoelectric voltage of the sample, and ΔT was the temperature difference between both sides of the samples.

Results and Discussion

The phases and analytical data for Eu_xNbO_{2+x} and Eu_xNbO_3 obtained are listed in Table 1, which shows that the single phase region of Eu_xNbO_{2+x} is from $x=0.5$ to $x=1.0$. The niobium bronze Eu_xNbO_3 of $x=0.50$—0.65 has a tetragonal form[1-5] and for $x=0.65$—1.00 has a cubic form,[1,2] while Eu_xNbO_{2+x} has a cubic form in the single phase region.

Lattice constants of the cubic phased Eu_xNbO_{2+x} and Eu_xNbO_3 are plotted in Fig. 1 as a function of the europium concentration x. The lattice constants of Eu_xNbO_3 increases almost linearly with an increase in x.[2] The least-squares fitting generates the following equation:

$$a(\text{cubic}) = 3.874 + 0.1515x(\text{Å}). \quad (4)$$

Lattice constants of Eu_xNbO_{2+x} also increase with an increase in x in the range from $x=0.5$ to $x=1.0$, but

Table 1. Analytical and crystal data for Eu_xNbO_3 and Eu_xNbO_{2+x}

Exptl No.	Eu_xNbO_y (nominal) x	y	Eu_xNbO_y (analytical) x	y	Phase	a(cubic) Å	a(tetragonal) Å	c(tetragonal) Å
Eu_xNbO_3								
A	1.00	3.00	1.01	3.01	Cubic	4.026		
B	0.90	3.00	0.90	3.00	Cubic	4.010		
C	0.85	3.00	0.88	3.03	Cubic	4.009		
D	0.80	3.00	0.82	3.03	Cubic	4.002		
E	0.75	3.00	0.76	3.03	Cubic	3.985		
F	0.70	3.00	0.70	3.09	Cubic	3.980		
G	0.65	3.00	0.68	3.05	Cubic	3.978		
H	0.60	3.00	0.60	3.03	Tetragonal	—	12.361	3.885
I	0.55	3.00	0.58	3.02	Tetragonal	—	12.363	3.892
J	0.50	3.00	0.51	3.02	Tetragonal	—	12.355	3.901
Eu_xNbO_{2+x}								
A	1.00	3.00	1.01	3.01	Cubic	4.026		
K	0.90	2.90	0.90	2.94	Cubic	4.013		
L	0.80	2.80	0.79	2.93	Cubic	3.993		
M	0.70	2.70	0.71	2.82	Cubic	3.992		
N	0.60	2.60	0.62	2.70	Cubic	3.983		
O	0.50	2.50	0.52	2.66	Cubic	3.977		
P	0.50	2.50	0.51	2.47	Cubic+u[a)]	3.988		
Q	0.45	2.45	0.47	2.38	Cubic+u	3.990		
R	0.40	2.40	0.42	2.39	Cubic+u	3.982		
S	0.30	2.30	0.30	2.16	Cubic+u	3.982		

a) u: Unknown phase.

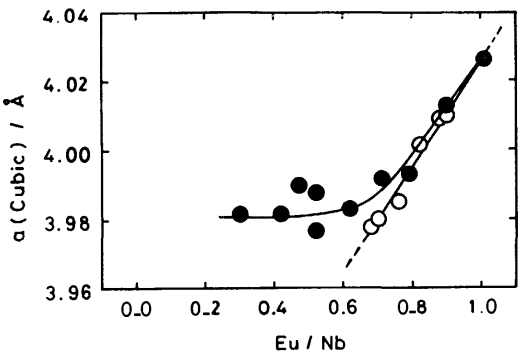

Fig. 1. Lattice constants *vs.* Eu concentration for Eu_xNbO_3 (○) and Eu_xNbO_{2+x} (●).

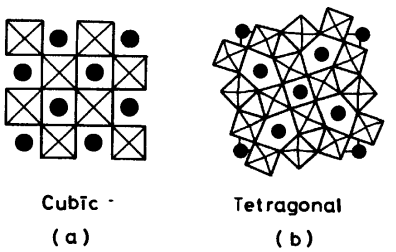

Fig. 2. Schematic diagram for the cubic and the tetragonal Eu_xNbO_3.
The bivalent europium cation can occupy the positions expressed by the black circles.

the change is not linear and the constants of Eu_xNbO_{2+x} are greater than those of Eu_xNbO_3 on a fixed composition especially below $x=0.7$. Below $x=0.5$, an unknown phase appeared in addition to a cubic phase of $a=3.982$ Å, and the tetragonal phase which was found in the Eu_xNbO_3 of $x=0.5$—0.65 was not observed.

The phase change of Eu_xNbO_3 from a cubic to a tetragonal form is explained as follows. The crystal structure of the cubic and the tetragonal niobates are revealed in Figs. 2 (a) and (b). A bivalent europium cation occupies a body-centered site of the cubic lattice (Fig. 2 (a)) and the site expressed by the black circle in the tetragonal cell (Fig. 2 (b)). Since the lattice constant decreases with a decrease in the europium concentration for the cubic Eu_xNbO_3, the maximum ionic radius to be able to occupy the body-centered site of the perovskite structure also decreases with decreasing the europium concentration, and at $x=0.65$ the maximum ionic radius becomes equal to the ionic radius of Eu^{2+}. At $x=0.65$, the lattice constant "a" is 3.987 ± 3 Å and the tolerance factor[7] "t" is 1.01. The tolerance factor is defined by the following equation:

$$t = (r(Eu^{2+}) + r(O_2^-))/\sqrt{2}\,a, \qquad (5)$$

where $r(Eu^{2+})$ (1.45 Å: 6th coordination) and $r(O^{2-})$ (1.40 Å: 6th coordination) are ionic radii[8] of Eu^{2+} and O^{2-} and a (3.987 Å for $Eu_{0.65}NbO_3$) is a cubic lattice constant. Below $x=0.65$ $t>1$, the body-centered site of the cubic Eu_xNbO_3 can no longer accomodate a bivalent europium cation, and the cubic phase transforms to the tetragonal phase. This can provide room for a bivalent europium cation in the limited range from $x=0.5$ to $x=0.65$.[1-5]

The above discussion is also applicable to Eu_xNbO_{2+x}. The lower limit of the lattice constant for the cubic Eu_xNbO_{2+x} seems to be almost the same as the lattice size of $Eu_{0.65}NbO_3$. However, the tetragonal phase,

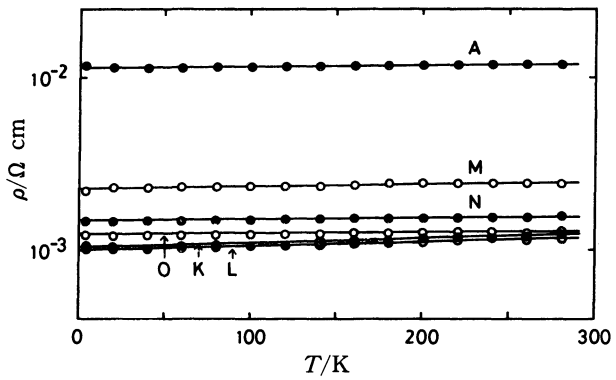

Fig. 3. Temperature dependence of resistivity for Eu_xNbO_{2+x}.
A—O are experimental number in Tables 1 and 2.

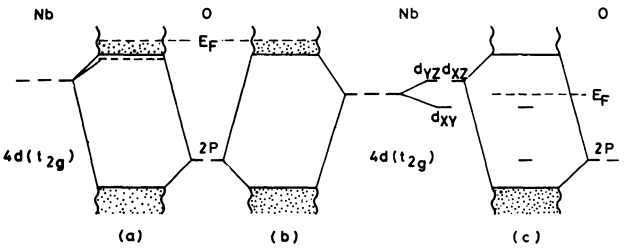

Fig. 4. Energy-level diagram for Eu_xNbO_{2+x} and Eu_xNbO_3.

which was found for Eu_xNbO_3 at x=0.5—0.65, was not found and an unknown phase was detected in the Eu_xNbO_{2+x} below x=0.5.

The electrical resistivity measurements for Eu_xNbO_{2+x} (Fig. 3) show that the cubic Eu_xNbO_{2+x} is a metallic conductor at x=0.5—1.0. These results are different from those of Eu_xNbO_3 in a low x region. In the case of Eu_xNbO_3, semiconduction was observed for the cubic samples at x=0.5—0.65[1-5] and metallic conduction was observed for the cubic samples at x=0.65—1.0.[1,2]

The difference in the electrical conduction between Eu_xNbO_{2+x} and Eu_xNbO_3 at x=0.5—0.65 is related to the distinction in their crystal structure. The difference on conduction manner owing to the structural difference was already discussed for Eu_xNbO_3 with a band model in the previous paper.[1]

An energy level diagram for Eu_xNbO_{2+x} is proposed in Fig. 4, which is assembled on the basis of Goodenough's model for Na_xWO_3.[9] The conduction band is composed of $4d(t_{2g})$ orbitals of niobium and 2p orbitals of oxygen. The $4d(t_{2g})$ levels of niobium, which are composed of $4d(t_{2g})$ orbitals around oxygen vacancies, are located below the conduction band.

The number of conduction electrons is equal to the number of Nb^{4+} as for Eu_xNbO_3,[1] and there is a Nb^{4+} per one formula of Eu_xNbO_{2+x}. Therefore, Eu_xNbO_{2+x} exhibits a metallic conduction (Fig. 3) as the cubic Eu_xNbO_3. However the mobility of an electron and an effective mass of electron for Eu_xNbO_{2+x} should be

Table 2. Magnetic and electrical data for Eu_xNbO_3 and Eu_xNbO_{2+x}

Exptl No.	Eu_xNbO_y (analytical) x	y	Magnetic moments μ_{eff} (μ_B) (Obsd)	μ_{eff}[a] (μ_B) (Calcd)	μ_{eff}[b] (μ_B) (Calcd)	Conduction	S[c] $\mu V K^{-1}$	S_0[d] $\mu V K^{-1}$	m^*/m_0[e]
Eu_xNbO_3									
A	1.01	3.01	7.92	8.16	7.98	m[f]	−7.0	−3.26	2.1
B	0.90	3.00	7.61	7.68	7.52	m	−6.2	−3.77	1.6
C	0.88	3.03	7.36	7.58	7.45	m	−8.2	−4.10	2.0
D	0.82	3.03	7.16	7.31	7.19	m	−11.1	−4.63	2.4
E	0.76	3.03	6.80	7.03	6.92	m	−14.7	−5.36	2.7
F	0.70	3.09	6.34	6.69	6.64	m	−17.2	−8.74	2.0
G	0.68	3.05	6.46	6.61	6.54	m	−22.2	−7.81	2.8
H	0.60	3.03	6.04	6.18	6.15	s[g]	−182	—	—
I	0.58	3.02	5.89	6.07	6.05	s	−152	—	—
J	0.51	3.02	5.47	5.67	5.67	s	—	—	—
Eu_xNbO_{2+x}									
A	1.01	3.01	7.92	8.16	7.98	m	−7.0	−3.26	2.1
K	0.90	2.94	7.70	7.71	7.53	m	−6.2	−3.42	1.8
L	0.79	2.93	7.15	7.21	7.06	m	−8.3	−3.99	2.1
M	0.71	2.82	6.69	6.87	6.70	m	−12.9	−3.77	3.4
N	0.62	2.70	6.29	6.47	6.27	m	−12.8	−3.56	3.6
O	0.52	2.66	5.70	5.89	5.70	m	−18.8	−3.99	4.7
P	0.51	2.47	5.74	5.94	5.66	—	—	—	—
Q	0.47	2.38	5.50	5.73	5.41	—	—	—	—
R	0.42	2.39	5.22	5.47	5.18	—	—	—	—
S	0.30	2.16	4.36	4.77	4.35	—	—	—	—

a) μ_{eff} (calcd)$=\sqrt{x\mu^2(Eu^{2+})+(Nb^{4+}/Nb)\mu^2(Nb^{4+})}$; μ (Eu^{2+})=7.94μ_B; μ (Nb^{4+})=1.73 μ_B. b) μ_{eff} (calcd)$=\sqrt{x}\mu(Eu^{2+})$. c) S: Observed absolute Seebeck coefficient at 300 K. d) S_0: Calculated absolute Seebeck coefficient at 300 K. e) m^*: Effective mass of electron; m_0: rest mass of electron. f) m: Metallic. g) s: Semiconductive.

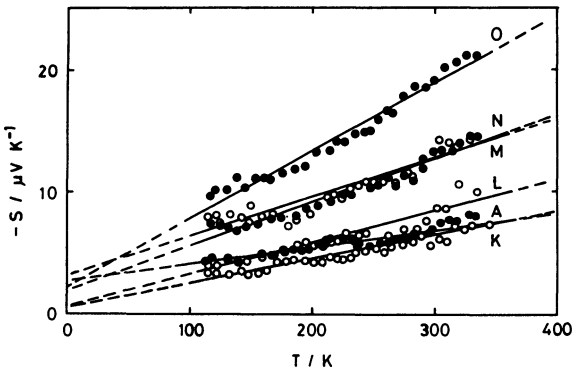

Fig. 5. Temperature dependence of the Seebeck coefficient for Eu_xNbO_{2+x}.
A—O are experimental number in Tables 1 and 2.

different from those for Eu_xNbO_3, since positive charged oxygen vacancies are considered to attract the conduction electrons around the vacancies electrostatically.

The effective masses of electrons for metallic Eu_xNbO_{2+x} are roughly evaluated by a thermoelectric power measurement, assuming that all the 4d electrons of niobium are concerned to the electrical conduction. For the free-electron approximation, the Seebeck coefficient is given by the relation:[10]

$$S = \frac{2}{3}\left(\frac{\pi}{3}\right)^{2/3} \frac{m^* k^2 T}{e(h/2\pi)^2} N^{-2/3}. \quad (6)$$

The effective mass is obtained by comparison of the observed Seebeck coefficient with the calculated value ($m^* = m_0$). Figure 5 shows that the Seebeck coefficient of Eu_xNbO_{2+x} at various temperatures. Temperature dependence of the Seebeck coefficient for each Eu_xNbO_{2+x} is almost linear and this fact suggests that the behavior of the conduction electrons resemble that of the free electrons. The Seebeck coefficient of Eu_xNbO_{2+x} increases with decreasing x at each temperature (Fig. 5). The increase in the Seebeck coefficient means that the effective mass of the electrons of Eu_xNbO_{2+x} increases with decreasing x. In Table 2, effective electric masses of Eu_xNbO_{2+x} and Eu_xNbO_3 are listed. The effective electric mass for Eu_xNbO_{2+x} increases with decreasing x from $2m_0$ to $5m_0$. However, the effective mass for Eu_xNbO_3 is independent of x and about $2m_0$ for any sample obtained. An interpretation for the disagreement in masses of Eu_xNbO_{2+x} and Eu_xNbO_3 is as follows. The host lattice of Eu_xNbO_3, namely NbO_3, where the conduction electrons go through, is not changed with x, and the effective mass is not affected by x. On the other hand, Eu_xNbO_{2+x} has oxygen vacancies, and the lattice of Eu_xNbO_{2+x} is fairly different from that of Eu_xNbO_3 at low x. The conduction electrons are trapped near the oxygen vacancies through the electrostatic force; the electrostatic interaction of the electrons with the vacancies is strong at low x, because there exist many vacancies at low x. This is the reason why the effective mass of the electrons for Eu_xNbO_{2+x} increases with decreasing x.

References

1) K. Ishikawa, G. Adachi, M. Hasegawa, K. Sato, and J. Shiokawa, *J. Electrochem. Soc.*, **128**, 1374 (1981).
2) G. V. Bazuev, O. V. Makarova, and G. P. Shveikin, *Dokl. Akad. Nauk SSSR*, **223**, 358 (1975).
3) F. Studer, J. P. Fayolle, and B. Raveau, *Mater. Res. Bull.*, **11**, 1125 (1976).
4) F. Studer, G. Allais, and B. Raveau, *J. Phys. Chem. Solids*, **41**, 1187 (1980).
5) F. Studer, G. Allais, and B. Raveau, *J. Phys. Chem. Solids*, **41**, 1199 (1980).
6) N. Cusack and P. Kendall, *Proc. Phys. Soc.*, **72**, 898 (1958).
7) J. B. Goodenough and J. A. Kafalas, *J. Solid State Chem.*, **6**, 493 (1973).
8) R. D. Shannon, *Acta Crystallogr., Sect. A*, **32**, 751 (1976).
9) J. B. Goodenough, "Metallic Oxide," in "Progress in Solid State Chemistry," ed by H. Reiss, Pergamon, Oxford New York (1972), Vol. 5.
10) B. L. Crowder and M. J. Sienko, *J. Chem. Phys.*, **38**, 1576 (1963).

Time-resolved Emission Spectra of 2-Acetylanthracene/Methanol/Hexane System. Evidence for the Photoassociation of a 1 : 2 Hydrogen Bonded Complex

Takashi TAMAKI
Research Institute for Polymers and Textiles, Yatabe-Higashi 1-1-4, Tsukuba, Ibaraki 305

(Received March 30, 1982)

Synopsis. The deconvolved time-resolved emission spectra of 2-acetylanthracene in hexane containing 0.1 mol dm^{-3} of methanol revealed a considerable time-dependent spectral shift associated with the photoassociation of the hydrogen-bonded complex which includes two methanol molecules.

The photodynamics of solvent-solute interaction have been extensively investigated. It is of particular interest that the fluorescence spectra of aromatic compounds, such as heterocycles, amines, and ketones, in nonpolar solvents are significantly perturbed by the addition of small amounts of polar solvents (<1% by volume).[1-8] This fluorescence perturbation is due to a specific solvent-solute interaction giving rise to a hydrogen-bonded (H-bonded) complex and/or an exciplex. Acylanthracenes are suitable for the purpose of this investigation, because their fluorescence characteristics (intensity, lifetime, and emission maximum) are very sensitive to the addition of alcohols to the nonpolar solutions.[9,10] This communication describes the time-resolved emission spectra (TRES) of 2-acetylanthracene (**2A**) in hexane containing 0.1 mol dm^{-3} of methanol at 20 °C under an air atmosphere. The results obtained are in excellent consistence with a photostationary study which indicated that at least two methanol molecules participate in the complex formation in the excited singlet state.[10b]

Experimental

2A was the same as that used previously.[10] The hexane and methanol were Spectro- and GR-grade reagents, respectively. To a 3 cm^3 hexane solution of **2A** (3×10^{-5} mol dm^{-3}) was added 1.4×10^{-2} cm^3 of methanol. The nanosecond decay curves and corrected steady-state fluorescence spectra were obtained similarly to those described previously.[11] The fluorescence decay curves collected at every 5 nm from $\lambda=400$ to 520 nm were subjected to deconvolution analysis by an iterative nonlinear least squares method.[11] The decay function, $i(\lambda, t)$, was chosen to be a sum of three exponential terms,

$$i(\lambda,t)=\sum_j^3 C_j(\lambda)\cdot\exp\{-t/\tau_j(\lambda)\}$$

where $C_j(\lambda)$ and $\tau_j(\lambda)$ were treated as free parameters. This decay function gave a good fit between the observed and simulated decay curves at every wavelength and the three decay times were found to be 11 ± 1.6, 4.9 ± 0.1, and 2.1 ± 0.9 ns. The value of $C(\lambda)$ associated with the shortest decay time was negative at wavelengths above 490 nm and at the red end, $i(\lambda, t)$ showed a typical rise and decay, indicating that a large portion of the long wavelength emission results from an excited-state reaction. The deconvolved TRES were constructed by multiplying $i(\lambda, t)/\sum_j^3 C_j(\lambda)\tau_j(\lambda)$ by the corrected total fluorescence spectrum at the corresponding wavelength.[12,13]

Results and Discussion

Figure 1 shows the deconvolved TRES obtained at four delay times. These spectra are normalized at the maximum intensity. Time-dependent spectral shifts are clearly evident, whereas little spectral shift could be detected by convolved spectroscopy.[10b] The TRES in Fig. 1 can be compared with the spectra of the fluorescence origins which have been assigned to the system concerned, as shown in the following reaction scheme;[10b]

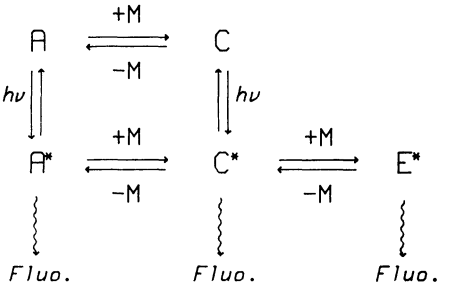

where M, A, C, and E are methanol, an uncomplexed **2A**, a 1 : 1, and a 1 : 2 complex respectively. Figure 2 shows the normalized steady-state fluorescence spectra of C and E obtained from the photostationary study, together with that of A, which is assumed to be the same as in pure hexane.

The spectrum at 24.3 ns shown in Fig. 1 has a remarkable resemblance to spectrum E shown in Fig. 2. In fact, this component spectrum is dominant even at 6—7 ns delay times. On the other hand, the TRES at shorter delay times can not be matched identically with

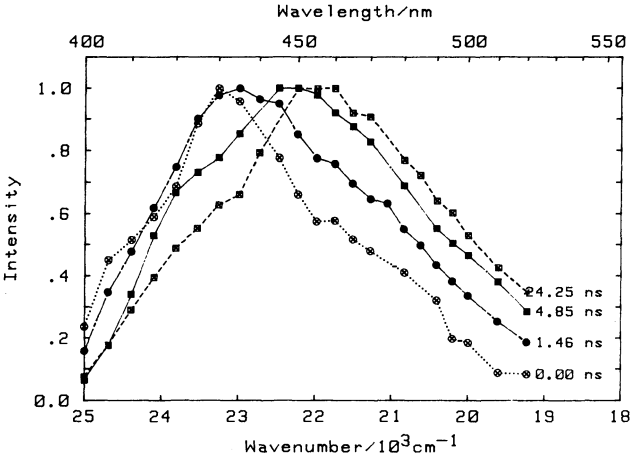

Fig. 1. Time-resolved emission spectra of 2-acetylanthracene in hexane containing 0.1 mol dm^{-3} of methanol at 20 °C. Normalized at the maximum intensity.

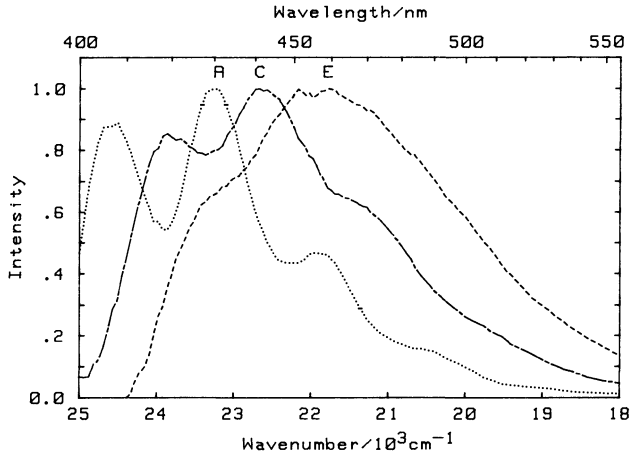

Fig. 2. Fluorescence spectra of three component origins involved in a 2-acetylanthracene/methanol/hexane system; A) an uncomplexed, C) a 1 : 1 complex, and E) a 1 : 2 complex. Normalized at the maximum intensity.

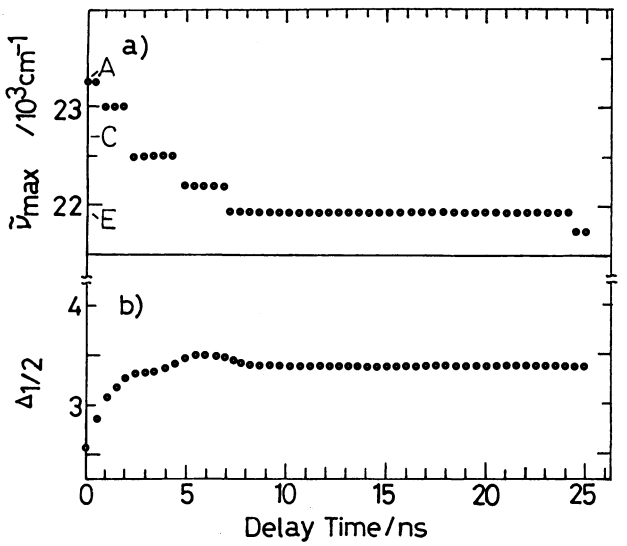

Fig. 3. Time-dependent changes in a) emission maxima ($\tilde{\nu}_{max}$) and b) half bandwidths ($\Delta_{1/2}$) of the TRES observed.

the individual component spectrum, but they can be simulated by superimposing the spectra from selected component sources with a variety of their contributions which depend on the delay time. Indeed, the TRES at 4.85 and 1.46 ns are approximately identical with the spectrum of C plus E (the relative fluorescence intensity of E to C, $F_{E/C} \simeq 1$) and of A plus C ($F_{C/A} \simeq 3.5$), respectively. It can be safely said that the contribution from E* is negligible for the TRES at delay times <2 ns. The spectrum at t_0 itself contains a considerable contribution from C* as well as from A* ($F_{C/A} \simeq 2$). This may result from the static formation of C prior to the pulse excitation.[14] About 1.7 times increase in the relative contribution from C* at 1.46 ns suggests that the dynamic formation of this component is important in this time region. It is also probable that at the longer delay times, the formation of E* prevails at the expense of C*.

The emission maxima, $\tilde{\nu}_{max}(t)$, and half bandwidths, $\Delta_{1/2}(t)$, of the observed TRES are shown in Figs. 3a and 3b, respectively. The emission maxima of the three components (A, C, and E) are also shown in Fig. 3a. From this figure, it is clear that the spectral relaxation of the TRES is substantially complete in 10 ns with the relaxed $\tilde{\nu}_{max}$ reaching the energy level of E. As is shown in Fig. 3b, $\Delta_{1/2}(t)$ first increases rapidly, then more slowly to a maximum value; later it decreases to a plateau value corresponding to the half bandwidth of the spectrum of E (*ca.* 3900 cm^{-1}), This variance of $\Delta_{1/2}(t)$ occurs just in the time period at which the spectral relaxation is occuring. These facts indicate that the observed TRES reflect the photodynamics of the specific H-bond interaction.

In conclusion, the excellent agreement between the photostationary and photodynamic studies strongly supports the validity of the reaction scheme postulated, which describes a step-wise photoassociation of the H-bonded complexes. It appears likely that the photoassociation of C occurs during the first 2 ns, followed by the formation of E. Finally, it should be mentioned that little effect on the fluorescence of **2A** could be detected when the methanol was replaced by acetonitrile. This confirms that H-bonding is responsible for the interaction. In pure methanol, the photostationary fluorescence of **2A** showed a large red-shift due to the combination of the specific H-bonding and nonspecific solvent relaxation.[10] However, the latter effect may be negligible for the present system and if any, the ultra fast relaxation of the surrounding solvent ($\approx 10^{-11}$ s) could not be associated with the TRES observed in the ns domain.

References

1) N. Mataga and T. Kubota, "Molecular Interactions and Electronic Spectra," Marcel Dekker, New York (1970).
2) M. S. Walker, T. W. Bender, and R. Lumry, *J. Chem. Phys.*, **47**, 1020 (1967); M. V. Hershberger, R. Lumry, and R. Verrall, *Photochem. Photobiol.*, **33**, 609 (1981).
3) E. A. Chandross, "The Exciplex," ed by M. Gordon and W. R. Ware, Academic Press Inc., New York (1975), p. 187.
4) H. Kokubun, *Z. Phys. Chem. N. F.*, **17**, 281 (1958); **101**, 137 (1976).
5) M. Kitamura and H. Baba, *Bull. Chem. Soc. Jpn.*, **48**, 1191 (1975).
6) W. R. Ware, S. K. Lee, G. J. Brant, and P. P. Chow, *J. Chem. Phys.*, **54**, 4729 (1971).
7) R. P. DeToma and L. Brand, *Chem. Phys. Lett.*, **47**, 231 (1977).
8) Y. Tanimoto, K. Inoue, Y. Furukawa, Y. Segawa, and M. Itoh, *Bull. Chem. Soc. Jpn.*, **52**, 1601 (1979).
9) A. S. Cherkasov, *Opt. Spectrosc.*, **9**, 285 (1960).
10) a) T. Tamaki, *Bull. Chem. Soc. Jpn.*, **53**, 577 (1980); b) T. Tamaki, *ibid.*, **55**, 1761 (1982).
11) T. Tamaki, *Bull. Chem. Soc. Jpn.*, **55**, 1756 (1982).
12) J. H. Easter, R. P. DeToma, and L. Brand, *Biophys. J.*, **16**, 571 (1976).
13) S. R. Meech, D. V. O'Connor, A. J. Roberts, and D. Phillips, *Photochem. Photobiol.*, **33**, 159 (1981).
14) From absorption measurements, the static formation of C amounts to *ca.* 20% (*i.e.*, $[C]/[A] \simeq 0.27$) under the experimental conditions, indicating that the fluorescence efficiency of C is about 7 times greater than that of A. This fluorescence enhancement is the result of the inhibition of the intersystem crossing due to the displacement of the singlet energy level.[10,11]

The Evaluation of the Association Degree of Sodium Counterinos by Complexes between Sodium Dodecyl Sulfate and Bovine Serum Albumin, Mainly on the Basis of a Conductivity Measurement

Kunio TAKEDA

Department of Applied Chemistry, Faculty of Science, Okayama University of Science, 1-1 Ridai, Okayama 700

(Received January 20, 1982)

Synopsis. Bovine serum albumin was titrated conductometrically with sodium dodecyl sulfate (SDS). Plots of the specific conductance *versus* the SDS concentration revealed four inflections. The association degrees of sodium counterions by the complexes were evaluated from the changes in the increment of the specific conductance of SDS with the complex growth.

The interactions of proteins with surfactants have received extensive attentions.[1] More recently, the present author and others have demonstrated the usefulness of the conductivity method for detecting protein–surfactant complex formation,[2] while this method has also been frequently used to determine the critical micelle concentration (CMC) of ionic surfactants. In the process of the complex formation between sodium dodecyl sulfate (SDS) and bovine serum albumin (BSA), four inflection points appeared in the plot of the specific conductance versus the SDS concentration at a constant BSA concentration. It is confirmed that these inflections appear with an intimate correlation with the formation of the SDS–BSA complex and the subsequent conformational changes of the protein.[2] It can generally be expected that these critical conductance changes mainly reflect the degree of association of sodium counterions.[3-6] The behavior of the counterions, despite their intrinsic interest, is still a matter of uncertainty.

The aim of this paper is the evaluation of the association degree of the sodium counterions by the complex, mainly on the basis of the conductance change with the complex formation.

Experimental

The crystalline BSA was obtained from Miles Laboratories Inc., and its concentration was determined spectrophotometrically using $E_{1cm}^{1\%}=6.8$ at 282 nm.[7] The crystalline SDS was purchased from BDH Chemicals Ltd., and recrystallized twice from 1-butanol and once from pure water. The conductivity measurements were carried out with a Universal Bridge 4265B of Yokogawa-Hewlett-Packard.[2] All the measurements were made at 25.000±0.005 °C in buffer solutions (pH 7.0; ionic strength, 0.014) containing 3.33 mM of NaH_2PO_4 and 3.56 mM of Na_2HPO_4 (1 M=1 mol/dm^3 was used as the concentration unit).

Results and Discussion

The conductance change with the complex formation was reexamined in order to evaluate the association degree of the sodium counterions by the complexes. The slope of each linear part between the inflections is presented in the second column of Table 1. The slope becomes milder, step by step, as seen in Table 1. The four linear parts below the CMC are considered to be correlated with the same number of types of complexes depending on the surfactant concentration ranges. These types of complexes are considered to be identical with the four observed previously under other experimental conditions.[8-10] When the specific conductance due to the species composing the buffer is subtracted from the total of the system, the residual conductance, κ, can be expected just for the behavior of the surfactant and the protein. Here, it is important that the contribution of the protein to the conductance is negligibly

Table 1. Association degree of sodium counterions and other parameters of SDS–BSA complexes

Type of complex (Concentration ranges of total SDS)[a]	$d\kappa/dC_{DS}^{total}$ / $10^{-5}\ \Omega^{-1}\ M^{-1}$	$\mu_{complex}$ / $10^{-4}\ cm^2\ s^{-1}\ V^{-1}$	μ_{Na} / $10^{-4}\ cm^2\ s^{-1}\ v^{-1}$	γ_{Na}	α	$(1-\alpha)$
Complex 1	5.6	1.6[b]	4.2	0.86	1.01	−0.01
(below 1.9 mM)		1.2[c]			1.06	−0.06
		1.7[d]			1.00	0
Complex 2	5.2	2.5[b]	4.1	0.86	0.82	0.18
(between 1.9 and 4.6 mM)		2.0[c]			0.88	0.12
Complex 3	4.4	2.8[b]	4.1	0.84	0.67	0.33
(between 4.6 and 6 6 mM)		2.4[c]			0.71	0.29
Complex 4	3.6	3.6[b]	4.0	0.80	0.50	0.50
(between 6.6 and 8.0 mM)						
SDS micelle	2.3	4.3[e]	4.0	0.80	0.29[f]	0.71
(above 8.0 mM)						

a) The total SDS concentrations where the inflections appeared in the plot of the specific conductance *versus* the total SDS in the presence of 1.0×10^{-5} M BSA (see Ref. 2). b), c), and d) Calculated by means of Eq. 4 on the basis of the data in Refs. 8, 9, and 10 respectively. e) This is the $\mu_{micelle}$ value obtained through the use of Eq. 4 on the basis of the reference values.[8,12] f) Calculated by substituting $\mu_{micelle}$ in place of $\mu_{complex}$ in Eq. 3.

small compared with that of the surfactant.[2] If we define the degree of the dissociation of sodium counterions from the complexes, α, the conductance, κ, may be expressed as follows:

$$\kappa = \frac{F}{1000}(\mu_{Na}\gamma_{Na}C_{Na} + \mu_{DS}^{free}\gamma_{DS}^{free}C_{DS}^{free} + \alpha\mu_{complex}C_{DS}^{bound}), \quad (1)$$

where F: Faraday's constant, μ: mobility, γ: activity coefficient, C: concentration (M), Na: sodium ion, free DS: free dodecyl sulfate ion, and bound DS: bound dodecyl sulfate ion. If we introduce the relation: $C_{DS}^{bound}=C_{DS}^{total}-C_{DS}^{free}$ where C_{DS}^{total} is the total concentration of SDS, as is often done in binding studies of these systems, we can adopt the following relation: $C_{Na}=C_{DS}^{free}+\alpha(C_{DS}^{total}-C_{DS}^{free})$. Then, Eq. 1 can be rewritten as:

$$\kappa = \frac{F}{1000}\{(\mu_{Na}\gamma_{Na}+\mu_{complex})\alpha C_{DS}^{total} + [(1-\alpha)\mu_{Na}\gamma_{Na}+\mu_{DS}^{free}\gamma_{DS}^{free}-\alpha\mu_{complex}]C_{DS}^{free}\}. \quad (2)$$

The slope, $d\kappa/dC_{DS}^{total}$, in the plot of the specific conductance *versus* the total SDS concentration is given by:

$$d\kappa/dC_{DS}^{total} = \frac{F}{1000}(\mu_{Na}\gamma_{Na}+\mu_{complex})\alpha. \quad (3)$$

If we know μ_{Na}, γ_{Na}, and $\mu_{complex}$, we can determine the α-values.

Aoki has found step-by-step changes in the complex mobilities with the complex formation between SDS and horse serum albumin and has reported four types of their mobilities.[8] Decker and Foster have also obtained three types of mobilities of the complexes between BSA and sodium dodecylbenzenesulfonate in the low concentration range of the surfactant.[9] These mobilities are 10—20% slower than those found by Aoki in a similar concentration range of SDS. Pallansch and Briggs have reported the mobility of the smallest SDS–BSA complex;[10] it is consistent with the corresponding value reported by Aoki when the difference in ionic strength is corrected by Eq. 4. These data would indicate what magnitudes of mobilities the complexes have. According to these data, the mobilities of the present SDS–BSA complexes were obtained through the correction of only the difference in ionic strength by applying the following relation:[11,12]

$$\log\mu = -A\log I_S + B, \quad (4)$$

where A and B are constants and I_s is the ionic strength. The constant, A, was determined to be 0.095 according to the dependence of the mobility of the SDS micelle on the ionic strength obtained by Stigter and Mysels;[11] it was then used in the calculation. The value of μ_{Na} was obtained from the equivalent conductivity of the sodium ion reported by Mukerjee *et al.*[4] and by the subsequent interpolation of the log-log plot of μ_{Na} *versus* the ionic strength, such as in Eq. 4. The activity coefficient, γ_{Na}, of 0.80 was adopted in the vicinity of the CMC, on the basis of the results of Botre *et al.*[3] Its value in an infinite dilution of SDS was computed to be 0.89 under the present conditions (I_s=0.014) by the application of the usual Debye-Hückel approximation.[13] The values of γ_{Na} between 0.80 and 0.89 were determined using this relationship: $-\log\gamma = S\sqrt{C_{DS}^{total}}$ (S: constant), given by Shedlovsky *et al.*[14] All the parameters used are listed in Table 1.[15] This table also shows the values of α and the association degree of counterions by each complex, $(1-\alpha)$, calculated by means of Eq. 3 using these parameters. The value of α for the SDS micelle obtained by this treatment is in good agreement with the literature values (0.22—0.29).[11,14] This would suggest the rationality of the above calculation.

The association degrees $(1-\alpha)$ of the counterions by the complexes are quite small compared with that of the SDS micelle. As may be seen in Table 1, the value of $(1-\alpha)$ increases with the complex formation. The association degree is considered to give a measure of the interactions between SDS and BSA. The increase of surfactants bound to the protein needs low electrostatic field on the surface of the complex and must lead to an increase in $(1-\alpha)$. In spite of the increase in the association degree of the counterions, the polyelectrolytic nature of the complex is expected to be strengthened because of the acquisition of a high net charge introduced by the bound dodecyl sulfate ions. It should be noted that a similarity of the complex to the micelle also appears in the behavior of the counterions, although other such similar properties between them have previously been discussed.[5,6,16]

References

1) J. Steinhardt and J. A. Reynolds, "Multiple Equilibria in Protein," Academic Press, N. Y. (1969), pp. 239—302.

2) K. Takeda, M. Miura, and T. Takagi, *J. Colloid Interface Sci.*, **82**, 38 (1981).

3) C. Botre, V. L. Crescenzi, and M. B. Epstein, *J. Phys. Chem.*, **63**, 650 (1959).

4) P. Mukerjee, K. J. Mysels, and P. Kapauan, *J. Phys. Chem.*, **71**, 4166 (1967).

5) M. N. Jones, *J. Colloid Interface Sci.*, **23**, 36 (1967).

6) N. Murai, S. Makino, and S. Sugai, *J. Colloid Interface Sci.*, **41**, 399 (1972).

7) "Handbook of Biochemistry (Selected Data for Molecular Biology)," 2nd ed, ed by H. A. Sober and R. A. Harte, CRC Press, Cleveland, Ohio (1973), p. C-71.

8) K. Aoki, *J. Am. Chem. Soc.*, **80**, 4904 (1958).

9) R. V. Decker and J. F. Foster, *Biochemistry*, **5**, 1242 (1966).

10) M. J. Pallansch and D. R. Briggs, *J. Am. Chem. Soc.*, **76**, 1396 (1954).

11) D. Stigter and K. J. Mysels, *J. Phys. Chem.*, **59**, 45 (1955).

12) H. W. Hoyer and A. Greenfield, *J. Phys. Chem.*, **61**, 735 (1957).

13) W. J. Moore, "Physical Chemistry," 3rd ed, Prentice-Hall, Englewood Cliffs, N. J. (1962), pp. 351—357.

14) L. Shedlovsky, W. Jakob, and M. B. Epstein, *J. Phys. Chem.*, **67**, 2075 (1963). The middle concentration of SDS in each step was used as C_{DS}^{total}.

15) The binding ratios of SDS for Complex 1 under the present conditions[2] are in good agreement with those of the smallest complex in Ref. 10, while the value of $\mu_{micelle}$ as calculated by Eq. 4 on the basis of Ref. 8 agrees fairly with those obtained in different ways.[12] The evaluation of the mobilities at both ends in this table seems to be reliable; therefore, other mobilities between them might also be reasonable in relation to the corresponding complexes.

16) J. Steinhardt, N. Stocker, D. Carrol, and K. Birdi, *Biochemistry*, **13**, 4461 (1974).

Effect of Temperature and Solvent on the 1,3-Dipolar Cycloaddition of Diazodiphenylmethane with Several Dipolarophiles

Yosuke Yoshimura, Jiro Osugi, and Masaru Nakahara*

Department of Chemistry, Faculty of Science, Kyoto University, Oiwake-cho, Kitashirakawa, Sakyo-ku, Kyoto 606

(Received March 27, 1982)

Synopsis. The title reaction is studied with a series of CN- or $COOCH_3$-substituted dipolarophiles. All the reactions obey the second-order rate law. The activation enthalpies and entropies are 44—52 kJ mol^{-1} and −(129—166) J K^{-1} mol^{-1}, respectively. The rate constants are insensitive to solvent. The reactivity and product of dimethyl maleate are anomalous.

In previous papers,[1,2] effects of temperature and solvent on the 1,4-cycloaddition reaction between tetracyanoethylene (TCNE) and styrenes have been investigated to shed light on the reaction mechanism. It is of considerable interest to compare the mechanism between 1,3-dipolar cycloaddition and 1,4-cycloaddition reactions. The cycloaddition reaction of diazodiphenylmethane (Ph_2CN_2) with some olefins has long been known,[3] and the first kinetic study of this reaction as a kind of 1,3-dipolar cycloaddition appeared two decades ago.[4] The reaction provides such adducts as 1-pyrazoline (**1**), 2-pyrazoline (**2**), and cyclopropane (**3**) depending on dipolarophiles used. The variety of these products is understood so far according to the following scheme:[5]

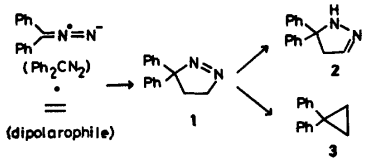

Scheme 1.

where **2** and **3** are formed from **1** by the H shift and the N_2 elimination, respectively. Until now there has been no thorough kinetic study where dipolarophiles are varied systematically so as to cover the product variety. It is worthwhile to examine the credibility of the Scheme 1 because some different scheme is proposed in a recent report on the 1,3-dipolar cycloaddition reaction of Ph_2CN_2 with TCNE in which the final product is of type **3**.[6]

Experimental

Materials. Ph_2CN_2 was obtained by the oxidation of benzophenone hydrazone with mercury(II) oxide (yellow).[3] Crude Ph_2CN_2 was recrystallized from petroleum ether in the form of needles, the melting point being 29 °C as reported;[3] crystals from methanol were of the form of flake with mp 22 °C. Dimethyl fumarate (DMF), dimethyl maleate (DMM), methyl acrylate (MA), fumaronitrile (FN), and acrylonitrile (AN) were supplied by Nakarai Chemicals, Ltd. and purified by the usual method. Maleonitrile (MN) was synthesized in a reported manner.[7] All solvents used were purified by the standard method.

Products. The adduct of each dipolarophile was identified by means of elemental analysis and by using the melting point, ^1H NMR, and IR data available in the literature: see Refs. 3, 8, and 9 for DMF, DMM, and MA and AN, respectively. FN and MN, which were studied here for the first time, gave 3,4-dicyano-5,5-diphenyl-2-pyrazoline, and unfortunately, the adduct could not be crystallized: NMR ($CDCl_3$) δ= 7.4, 7.2 (m 11H) and 4.81 (s 1H); IR (neat) 3300 (νNH) and 2220 cm^{-1} (νCN).

Kinetic Measurements. The disappearance of Ph_2CN_2 was followed around 525 nm by using a Hitachi Perkin-Elmer 139 UV visible spectrophotometer. Temperature was controlled to ±0.05 °C at 20, 25, 30, and 35 °C. Although Ph_2CN_2 is known to decompose (first-order reaction) at ambient temperature, the decomposition is so slow (1% in toluene at 25 °C for a period of 3.5 d) that it is negligible in the present work (each run finished within 6 h). All reactions studied obey the second-order rate law shown by

$$-\frac{d[Ph_2CN_2]}{dt} = k[Ph_2CN_2][\text{dipolhrophile}]$$

where [ ], t, and k denote the concentration, the time ,and the rate constant, respectively. The rate constants were determined from the second-order plots, *i.e.*, log $[Ph_2CN_2]/[\text{dipolarophile}]$ *vs.* t. Their uncertainty is about 1%.

Results and Discussion

In the temperature (T) range studied here, the values of $\ln(k/T)$ are linear against $1/T$. According to the Eyring equation[10] these linear relations lead to determination of the activation enthalpies (ΔH^*) and entropies (ΔS^*) listed in Table 1. In broad terms, ΔH^* and ΔS^* differ little from one dipolarophile to another in spite of the product diversity; there exist some differences which will be discussed later in relation to the molecular structure of the dipolarophile. Thus, all reactions studied can be classified into the same kind of 1,3-dipolar cycloaddition from the kinetic point of view. The similarity of the transition state in these reactions strongly suggest that not only DMM but also other dipolarophiles once produce the adduct of type **1** just

Table 1. Kinetic parameters for 1,3-dipolar cycloaddition of Ph_2CN_2 with various dipolarophiles in toluene at 25 °C

Dipolarophile[a]		A[b]	10^4k[c]	ΔH^*[d]	ΔS^*[e]
X(H)C=C(H)X	(DMM)	1	2.77	44±1	−166±1
X(H)C=C(X)H	(DMF)	2	53.3	44±1	−141±1
H(H)C=C(X)H	(MA)	3	19.8	44±3	−150±3
NC(H)C=C(H)CN	(MN)	2	25.0	47±1	−136±2
NC(H)C=C(CN)H	(FN)	2	9.97	51±1	−130±1
H(H)C=C(CN)H	(AN)	3	9.72	52±2	−129±2

a) X=$COOCH_3$. b) Adduct of Ph_2CN_2; see Scheme 1. c) mol^{-1} dm^3 s^{-1}. d) kJ mol^{-1}. e) J K^{-1} mol^{-1}.

Table 2. Rate constants (k) for 1,3-dipolar cycloaddition reactions of Ph_2CN_2 with DMM, DMF, and MA in several solvents at 25 °C

Solvent	$10^4\ k/mol^{-1}\ dm^3\ s^{-1}$		
	DMM	DMF	MA
PhMe	2.77	53.3	19.8
PhCl	2.57	62.3	21.5
$(ClCH_2)_2$	2.28	65.5	20.3
Me_2NCHO	3.36	96.3	31.0
MeCN	3.02	103.5	27.4

as illustrated by Scheme 1; when the adduct is of type **2** or **3**, type **1** exists only as an unstable intermediate. In the present work, low temperature (≈0 °C) experiments were carried out to find such an intermediate in the reaction mixture but not successful. Further consideration as to why the stability of type **1** depends so much on the substituents in the dipolarophile will be given later in this note.

These reactions seem to proceed by a concerted mechanism for the following reasons: 1) the values of ΔH^* and ΔS^* in Table 1 are in the ranges of the corresponding ones for some other 1,3-dipolar cycloadditions for which a concerted mechanism is concluded[11] and 2) the rate constants are insensitive to solvent polarity as seen in Table 2. The latter fact shows unlikelihood of a two-step machanism involving a zwitterionic intermediate; if the transition state has zwitterionic character to a significant extent, a rate factor of over 10^4 (*cf.* smaller than two in Table 2) would be expected in the range of solvent polarity covered in Table 2.[1,12]

Although differences in the kinetic parameters in Table 1 are relatively small, some of them are important. In the case of $COOCH_3$ substituted dipolarophiles, the *cis* form is less reactive than the *trans* form, while the former is more reactive than the latter in the case of CN-substituted ones. DMM is unique also with respect to the type of adduct. DMM is lower in reactivity than MN in spite of its lower ΔH^*, the reactivity difference being controlled by the entropy term. The anomalous behavior of DMM would be ascribed to the steric hindrance between the bulky $COOCH_3$ groups. Since such a steric hindrance prevents conjugation due to coplanarity between the pyrazoline ring and $COOCH_3$ group in the adduct of DMM (type **1** and *cis* form[13]), the H shift does not occur, and thus, the *cis* form of type **1** (produced by DMM) which is thermodynamically less stable than the *trans* form (produced by DMF) is isolated. With heat or a catalyst,[8] the adduct can be isomerized to type **2** which is the same as the adduct of DMF. The above consideration is supported by the fact that MN and FN give the same adduct (type **2**); the steric hindrance by a CN group is negligible compared with that by a $COOCH_3$ group.

References

1) Y. Uosaki, M. Nakahara, and J. Osugi, *Bull. Chem. Soc. Jpn.*, **55**, 41 (1982).

2) Y. Uosaki, M. Nakahara, and J. Osugi, *Int. J. Chem. Kinet.*, (1982), in press.

3) H. Staudinger, E. Anthes, and F. Pfenninger, *Ber.*, **49**, 1928 (1916).

4) R. Huisgen, H. Stangl, H. J. Sturm, and H. Wagenhofer *Angew. Chem.*, **73**, 170 (1961).

5) For a review see G. W. Cowell and A. Ledwith, *Q. Rev., Chem. Soc.*, **24**, 119 (1970).

6) T. Oshima, A. Yoshioka, and T. Nagai, *J. Chem. Soc., Perkin Trans. 2*, **1978**, 1283.

7) R. P. Linstead and M. Whalley, *J. Chem. Soc.*, **1952**, 4839.

8) M. Yu. Kornilov and F. N. Tolstukha, *Khim. Geterotsikl. Soedin.*, **1977**, 271.

9) H. M. Walborsky and F. N. Hornyak, *J. Am. Chem. Soc.*, **77**, 6026 (1955).

10) S. Glasstone, K. J. Laidler, and H. Eyring, "The Theory of Rate Processes," McGraw-Hill, New York (1941).

11) R. Huisgen, *Angew. Chem.*, **75**, 742 (1963).

12) E. M. Kosower, "An Introduction to Physical Organic Chemistry," John Wiley and Sons, Inc., New York (1968), p. 213.

13) It is widely accepted that the 1,3-dipolar cycloaddition is stereospecific. Although the product is described as the *trans* form without evidence in Ref. 8, the coupling constant $J_{3,4}$ is 7.5 Hz, which does not necessarily indicate the *trans* form.

Comment on Momentum Distributions of Valence Electrons of Atoms and Simple Molecules

Isao H. SUZUKI* and C. E. BRION†
Electrotechnical Laboratory, Sakura-mura, Niihari-gun, Ibaraki 305
†*Department of Chemistry, University of British Columbia, Vancouver, B.C., V6T 1Y6, Canada*
(Received April 23, 1982)

Synopsis. The relationship between vertical ionization potentials and experimental electron momentum distributions of individual valence orbitals has been examined in some series of orbitals with the same characteristics of atoms and simple molecules. It has been found that effectively pure s- and p-orbitals show trends consistent with the predicitions of the virial theorem.

The symmetric noncoplanar configuration of the binary (e,2e) method is powerful for studies of molecular electronic structure. This technique provides not only binding energy spectra of valence electrons of atoms and molecules but also their orbital momentum distributions (MD).[1–20] The relative (e,2e) cross-section is essentially given by the square of the Fourier transform of the wave function of the struck electron, in the plane wave impulse approximation including the target Hartree-Fock state.[1–3]

$$\sigma(q) \propto \left| \int \psi(r) \times e^{iqr} d^3r \right|^2.$$

In this expression ψ means the one-electron wave function describing the orbital of the struck electron prior to the (e,2e) reaction.

Most of the MD measured so far can be classified into s-type and p-type.[1–20] The former is for orbitals with isotropic spatial distributions, *e.g.*, atomic s-orbitals. The s-type MD shows a maximum at $q=0$ a_o^{-1}. The latter (*i.e.*, p-type) is for those with antisymmetric spatial distributions, *e.g.*, atomic p-orbitals. The p-type MD shows zero intensity at $q=0$ a_o^{-1} and exhibits a maximum at $q \cong 0.4$—1.0 a_o^{-1}.

The virial theorem predicts a relationship between total energy of a molecule and total kinetic energy of the bound electrons. This theorem does not apply to individual orbitals, but some relationship may exist between orbital energy and the kinetic energy of its orbital electron in a series of orbitals with similar characteristics.[21,22] It is interesting to examine the qualitative applicability of the virial theorem to individual orbitals. For this purpose the MD's observed by the binary (e,2e) method can be used as a measure of the kinetic energy of the orbital electron.

The aim of the present study is to discuss and to clarify the relationship between the measured MD and the orbital energy. The MD data used here are those for valence orbitals of rare gas atoms and of molecules which consist of one or two central atoms with or without a few hydrogen atoms: Ne, Ar, Kr, Xe (atoms), HF, HCl, HBr, HI, H_2O, NH_3, CH_4, H_2S, PH_3 (pseudo-atoms), N_2, CO, O_2, (diatomic molecules), and C_2H_2, C_2H_4, C_2H_6 (pseudo-diatomic molecules).[1–20]

Figure 1 shows the degree of correlation between q_{hw} and the square root of the vertical ionization potential

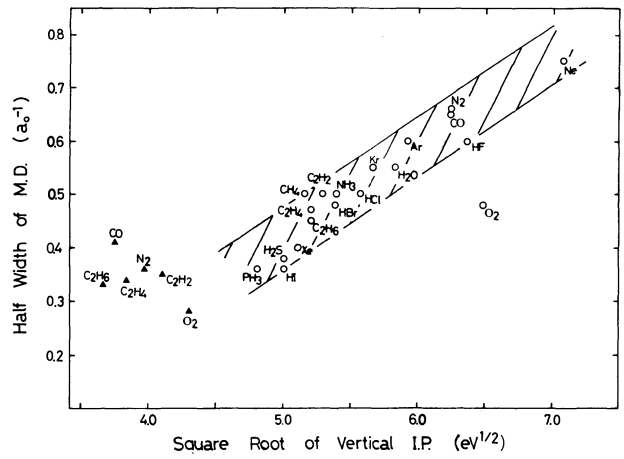

Fig. 1. Correlation between half width (q_{hw}) of s-type momentum distributions and vertical ionization potentials (IP) for valence orbitals. See text for definition of q_{hw} and for data marks (○ and ▲). The chemical formula of atoms and molecules are added to the data marks but the orbitals' symbols are omitted for clarity.

(IP). The q_{hw} means the momentum at which the s-type MD becomes a half of its maximum intensity. The vertical IP means the centroid of main and all satellite peaks belonging to the same hole state, if satellite peaks are observed in the ionizing process.[1,2] In this case accuracy of the IP is ± 1—2 eV. This centroid IP corresponds to the orbital energy when the ground state of the target atom or molecule is well described with a single configuration.[1,2] The open circles (○) indicate the data for the orbitals mainly composed of atomic 2s, 3s, 4s, and 5s-orbitals.[1–20] The solid triangles (▲) indicate the data for the orbitals mainly consisting of bonding combination of atomic 2p-orbitals.[13–20] The error in the estimation of q_{hw} is about five times the sizes of the circles or triangles shown.

The data shown with the open circles represent a linear relationship between the q_{hw} and the square root of the vertical IP. This feature means that a high q_{hw} corresponds to a high IP (a large negative orbital energy in Koopmans' theorem). Thus, the orbital showing a higher q_{hw} has a spatial distribution which tends to be contracted to regions of larger potential energy, *i.e.*, nearer to the nuclei. The orbital with a lower q_{hw} is distributed more in regions of lower potential energy. This fact shows that the virial theorem qualitatively holds for individual orbitals at least in the series of the orbitals studied here which have the s-type MD and consist mainly of atomic s-orbitals. An exception is $O_2 2\sigma_g$ orbital. This is probably due to correlation effects in the neutral ground state as well as in the ionic state.

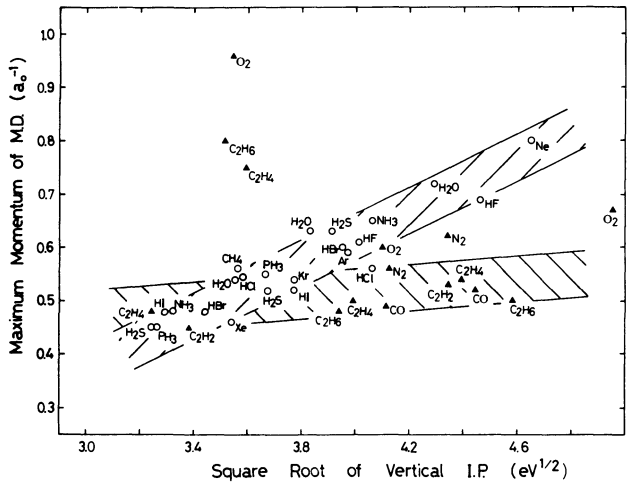

Fig. 2. Correlation between maximum momentum (q_m) of p-type momentum distributions and vertical ionization potentials (IP) for valence orbitals. See text for definition of q_m and for data marks (○ and ▲).

The relation between the solid triangles' data and the IP is complicated. The virial theorem can not be applied to this type of the orbitals.

Figure 2 shows correlation between q_m and the square root of the vertical IP. The q_m indicates the momentum at which the p-type MD is a maximum. The open circles (○) are data for the orbitals of the atoms and the pseudo-atoms. The solid triangles (▲) are data for the orbitals of the diatomic and seudo-diatomic molecules. The errors in estimation of q_m are about four times the sizes of the circles or the triangles shown.

From Fig. 2, it is seen that the q_m for the atoms and the pseudo-atoms has nearly a linear dependence on the square root of the vertical IP. One of the open circles (datum for HCl 5σ orbital) is slightly lower than the hatched area for the atoms and the pseudo-atoms' data. However, the datum point marginally overlaps with the area if the error of q_m is taken into account. This near linear dependence suggests that the virial theorem can qualitatively be applied to individual orbitals in the series of the orbitals of the atoms and the pseudo-atoms showing the p-type MD's which have been examined in the present study.

The orbitals of the diatomic and pseudo-diatomic molecules showing p-type MD's are classified into two groups, antibonding orbitals and others. The former have two nodal planes bisecting the molecular axis and parallel to the axis. Then their wave functions rapidly vary in coordinate space, and the antibonding orbitals are expected to have considerably higher MD's. These orbitals here considered are O_2 $1\pi_g$, C_2H_4 $1b_{1g}$ and C_2H_6 $1e_g$ orbitals; q_m=0.96, 0.75, and 0.8 a_o^{-1}, respectively. The three data points of interest are plotted quite high above the hatched area for the atoms and the pseudo-atoms' data.

The second group of the orbital consist of the antibonding combination of atomic 2s-orbitals and π-bonding orbitals. Both have one nodal plane, bisecting the molecular axis or parallel to this axis. The q_m for these orbitals is slightly dependent on the IP. The π-bonding orbital is diffuse and has much weight of spatial distribution in the intermediate region of atoms. The orbitals of 2s antibonding combination is spatially distributed to the opposite regions to the molecular center. These characteristics are assumed to bring about the weak dependent feature of the q_m on the IP. The three data, O_2, $2\sigma_u$, O_2 $1\pi_u$, and N_2 $2\sigma_u$ orbitals, deviate slightly to higher q_m from the hatched area for this group of the orbitals.

References

1) I. E. McCarthy and E. Weigold, *Phys. Reports*, **27**, 275 (1976).
2) E. Weigold and I. E. McCarthy, *Adv. Atom. Mol. Phys.*, **14**, 127 (1978).
3) S. T. Hood, A. Hamnett, and C. E. Brion, *J. Electron Spectrosc. Relat. Phenom.*, **11**, 205 (1977).
4) S. T. Hood, A. Hamnett, and C. E. Brion, *Chem. Phys. Lett.*, **39**, 252 (1976).
5) A. J. Dixon, S. Dey, I. E. McCarthy, E. Weigold, and G. R. J. Williams, *Chem. Phys.*, **21**, 81 (1977).
6) G. R. J. Williams, I. E. McCarthy, and E. Weigold, *Chem. Phys.*, **22**, 281 (1977).
7) C. E. Brion, S. T. Hood, I. H. Suzuki, E. Weigold, and G. R. J. Williams, *J. Electron Spectrosc. Relat. Phenom.*, **21**, 71 (1980).
8) E. Weigold, S. T. Hood, and I. E. McCarthy, *Phys. Rev. A*, **11**, 566 (1975).
9) J. F. Williams, *J. Phys. B*, **11**, 2015 (1978).
10) I. H. Suzuki, C. E. Brion, E. Weigold, and G. R. J. Williams, *Abstr. 9th ICAS/XXII CSI (Tokyo)*, **1981**, 469.
11) J. P. D. Cook, C. E. Brion, and A. Hamnett, *Chem. Phys.*, **45**, 1 (1980).
12) A. Hamnett, S. T. Hood, and C. E. Brion, *J. Electron Spectrosc. Relat. Phenom.*, **11**, 263 (1977).
13) E. Weigold, S. Dey, A. J. Dixon, I. E. McCarthy, K. R. Lassey, and P. J. O. Teubner, *J. Electron Spectrosc. Relat. Phenom.*, **10**, 177 (1977).
14) S. Dey, A. J. Dixon, K. R. Lassey, I. E. McCarthy, P. J. O. Teubner, E. Weigold, P. S. Bagus, and E. D. Viinikka, *Phys. Rev. A*, **15**, 102 (1977).
15) I. H. Suzuki, E. Weigold, and C. E. Brion, *J. Electron Spectrosc. Relat. Phenom.*, **20**, 289 (1980).
16) A. J. Dixon, I. E. McCarthy, E. Weigold, and G. R. J. Williams, *J. Electron Spectrosc. Relat. Phenom.*, **12**, 239 (1977).
17) M. A. Coplan, J. H. Moore, and J. A. Tossell, *J. Chem. Phys.*, **68**, 329 (1978).
18) A. J. Dixon, S. T. Hood, E. Weigold, and G. R. J. Williams, *J. Electron Spectrosc. Relat. Phenom.*, **14**, 267 (1978).
19) M. A. Coplan, A. L. Migdall, J. H. Moore, and J. A. Tossell, *J. Am. Chem. Soc.*, **100**, 5008 (1978).
20) S. Dey, A. J. Dixon, I. E. McCarthy, and E. Weigold, *J. Electron Spectrosc. Relat. Phenom.*, **9**, 397 (1976).
21) I. R. Epstein and A. C. Tanner, "Compton Scattering," ed by B. Williams, McGraw-Hill, New York (1977), p. 209.
22) M. A. Coplan, J. H. Moore, J. A. Tossell, and A. Gupta, *J. Chem. Phys.*, **71**, 4005 (1979).

Standard Enthalpies of Combustion and Vaporization of *N,N*-Dimethylaniline**

Jun-ichi Furukawa,†† Minoru Sakiyama,* Syûzô Seki,†††
Yoshihiro Saito,† and Kazuhito Kusano†

Chemical Thermodynamics Laboratory and Department of Chemistry, Faculty of Science, Osaka University, Toyonaka 560
†Department of Industrial Chemistry, Faculty of Engineering, Miyazaki University, Miyazaki 880

(Received May 4, 1982)

Synopsis. Standard energy of combustion and standard enthalpy of vaporization of *N,N*-dimethylaniline have been determined by oxygen bomb combustion calorimetry and vaporization calorimetry, respectively. Derived standard enthalpies at 298.15 K are as follows: $\Delta H_c^\circ(1) = -(4767.8 \pm 3.2)$, $\Delta H_f^\circ(1) = (47.7 \pm 3.4)$, $\Delta H_v^\circ = (52.83 \pm 0.03)$, and $\Delta H_f^\circ(g) = (100.5 \pm 3.4)$ kJ mol^{-1}, respectively.

Despite the fact that *N,N*-dimethylaniline is one of the representative tertiary amines, literature data of standard thermodynamic quantities are meager. We have determined standard energy of combustion and standard enthalpy of vaporization, both at 298.15 K, by calorimetric methods. Results of these measurements are briefly reported in this note.

Experimental

Materials. Commercial *N,N*-dimethylaniline (Wako, Special Grade) was purified by treatment with acetic anhydride, hydrochloric acid, tin(II) chloride, and aqueous sodium hydroxide, followed by extraction with diethyl ether, drying with sodium hydroxide, fractional distillation at reduced pressure (twice) and drying with calcium hydride. Gas-liquid chromatographic analysis using PEG 20M as liquid phase gave the purity of 99.96 mass per cent.

Combustion Calorimetry. An isoperibol rotating bomb calorimeter with a platinum-lined bomb of Osaka University, described elsewhere,[1,2] was used without rotating the bomb. The calorimeter was calibrated by burnig thermochemical standard benzoic acid (U. S. National Bureau of Standards, SRM 39i) under certificate conditions. Mean and standard deviation of the mean (sdm) for the energy equivalent of the empty calorimetric system ε(calor)[5] was determined to be (15161.67 ± 0.74) J K^{-1} from eleven calibration experiments.

N,N-Dimethylaniline, which had been placed in a glass vacuum system together with activated molecular sieve 4A, was transfered into a vessel, where inverted soft glass ampoules with a thin tubular stem had been located, by vacuum distillation, and then charged into the ampoules under the pressure of dry nitrogen. The fine neck of the ampoule was fused at the outside of the vacuum system with a small city-gas flame to seal the ampoule. The ampoule filled with a sample was placed in an open platinum crucible together with a small amount of paraffin oil which acted as a promoter, and combustion was started by igniting the oil at 3 MPa of oxygen pressure.

Complete combustion was achieved by reducing the mass of *N,N*-dimethylaniline to below 0.26 g, while adjusting the mass of the paraffin oil so that the resultant corrected temperature rise would be similar to that of the calibration experiments (1.84 K). Otherwise, the formation of soot in the crucibles or the formation of yellow colored bomb solution with irritating odor resulted. Only four experiments were successful.

Vaporization Calorimetry. A carrier-gas type vaporization calorimeter of Miyazaki University[3] was used. The calorimetric system was tested by measuring ΔH_v° of cyclohexane and decane. Mean and sdm of each of five determinations were (33.03 ± 0.04) and (51.36 ± 0.06) kJ mol^{-1} for cyclohexane and normal decane, respectively, while the recommended values[4] are (33.03 ± 0.04) and (51.35 ± 0.04) kJ mol^{-1}, respectively.

Auxiliary Quantities. Relative atomic masses were taken from the recommendation of the IUPAC Commission on Atomic Weights (1977). Densities, specific heat capacities, $(\partial U/\partial p)_T$ values, and specific energies of combustion of the paraffin oil and cotton fuse, are collected in Table 1. Internal volume of the bomb was 0.3469 dm^3.

Results and Discussion

Results of combustion calorimetric experiments on *N,N*-dimethylaniline are presented in Table 2. Molar standard energy of combustion given in this table refer to the following idealized combustion reaction at 298.15 K: $C_8H_{11}N(1) + (43/4)O_2(g) = 8CO_2(g) + (11/2) \cdot H_2O(1) + (1/2)N_2(g)$. Most of the symbols used in Table 2 are essentially similar to those used by Hubbard *et al.*[5] ΔU_Σ denotes the sum of contributions from items 81—85 and 87—94 as defined in Ref. 5. The mean and sdm of observed molar standard energies of combustion were $-(4762.2 \pm 1.3)$ kJ mol^{-1}.

Results of vaporization calorimetric experiments are summarized in Table 3. Molar enthalpy of vaporization ΔH_v was calculated with the equation: $\Delta H_v =$

Table 1. Auxiliary quantities

Substance	Formula	ρ / g cm^{-3}	c_p / J K^{-1} g^{-1}	$-(\partial U/\partial p)_T$ / J MPa^{-1} g^{-1}	$-\{\Delta U_c^\circ/M\}$ / J g^{-1}
N,N-Dimethylaniline	$C_8H_{11}N$	0.9522	1.791	0.275	—
Liquid paraffin	$CH_{1.885}$	0.8824	2.22	0.257	45909.3±4.1[a]
Cotton fuse	$CH_{1.86}O_{0.93}$	1.5	1.70	0.29	16507

a) Uncertainty is the estimated sdm.

** Contribution No. 33 from Chemical Thermodynamics Laboratory, Faculty of Science, Osaka University.

†† Present address: Sakamoto Works, Kanegafuchi Chemical Industry Co., Ltd., Otsu 520-01.

††† Present address: Department of Chemistry, School of Science, Kwansei Gakuin University, Nishinomiya 662.

Table 2. Combustion calorimetric results on *N,N*-dimethylaniline

Exptl	1	2	3	4
m'(compd)/g	0.23033	0.25878	0.24377	0.23743
m''(auxil)/g	0.41121	0.38376	0.40034	0.40886
m'''(fuse)/g	0.00156	0.00154	0.00150	0.00149
$m^{i}(H_2O)$/g	3.141	3.048	3.100	3.059
p^{i}(gas)/MPa	3.046	3.038	3.037	3.037
θ_i/°C	23.12339	23.12896	23.14412	23.12653
θ_f/°C	24.98875	24.98488	25.00985	25.00199
$\Delta\theta_{corr}$/°C	0.02196	0.02186	0.02012	0.02147
$n^{f}(HNO_3)$/mmol	0.402	0.436	0.415	0.387
ΔU_{ign}/J	6.3	4.1	5.2	4.2
ε^{i}(cont)/J K^{-1}	26.3	25.9	26.1	25.9
ε^{f}(cont)/J K^{-1}	27.9	27.4	27.7	27.5
ΔU_{Σ}	11.5	11.4	11.5	11.5
$-\Delta U_{IBP}$	27991.0	27850.8	28025.1	28153.2
$-\{\Delta U_c^\circ/M\}$/kJ g^{-1}	39.299	39.300	39.322	39.271
$-\Delta U_c^\circ$/kJ mol^{-1}	4762.4	4762.5	4765.1	4759.0

Table 3. Vaporization calorimetric results on *N,N*-dimethylaniline at 298.15 K

Exptl	m/mg	t/s	I[1)]/mA	ΔH_v/kJ mol^{-1}
1	31.55	1197.8	15.059	52.80
2	31.51	1197.4	15.059	52.85
3	31.62	1202.0	15.058	52.86
4	31.62	1200.9	15.053	52.78
5	31.60	1200.4	15.053	52.79
6	31.70	1205.1	15.060	52.88
7	31.64	1202.9	15.060	52.88
8	41.20	1797.5	15.050	52.82
9	41.34	1803.2	15.050	52.81

a) R(heater)=50.608 Ω.

$I^2Rt(M/m)$, where I is the current made to flow through the heater with the resistance R of 50.608 Ω at 298.15 K for the duration t, and, m and M are the mass and the molar mass, respectively, of the material vaporized during the experiment. Mean and sdm for the nine experiments were $(52.83\pm0.01_3)$ kJ mol^{-1}. Since the vapor pressure of *N,N*-dimethylaniline is much lower than 10^4 Pa at 298.15 K, ΔH_v, thus derived, may be taken to be ΔH_v°.

Derived standard thermodynamic quantities at 298.15 K are as follows: $\Delta U_c^\circ(1)=-(4762.2\pm3.2)$, $\Delta H_c^\circ(1)=-(4767.8\pm3.2)$, $\Delta H_f^\circ(1)=(47.7\pm3.4)$, $\Delta H_v^\circ=(52.83\pm0.03)$, and $\Delta H_f^\circ(g)=(100.5\pm3.4)$ kJ mol^{-1}, respectively, where uncertainties are the overall values. The overall standard deviation of mean for $\Delta U_c^\circ(1)$ and $\Delta H_c^\circ(1)$, $s(\bar{U})_\Sigma$, was calculated with the equation: $s(\bar{U})_\Sigma=\Delta U_c^\circ(1)[\sum_{i=1}^{4}\{f_i s_r(i)\}^2]^{1/2}$, where $s_r(i)$ and f_i are the relative standard deviation of mean and the weight, respectively, of the i-th contribution, which follows: (1) The experimental value of $\Delta U_c^\circ(1)$; (2) the energy equivalent; (3) the certified specific energy of combustion of the thermochemical standard benzoic acid; and (4) the specific standard energy of combustion of the paraffine oil. By letting $f_1=f_2=f_3=1$, $f_4=2$, $s_r(1)=2.7\times10^{-4}$, $s_r(2)=0.5\times10^{-4}$, $s_r(3)=0.4\times10^{-4}$, and $s_r(4)=0.9\times10^{-4}$, $s(\bar{U})_\Sigma$ was calculated to be 1.6 kJ mol^{-1}. The overall uncertainties for $\Delta U_c^\circ(1)$ and $\Delta H_c^\circ(1)$ are $\{2s(\bar{U})_\Sigma\}$. The following CODATA key values for thermodynamics[6)] were used to calculate $\Delta H_f^\circ(1)$: $\Delta H_f^\circ(CO_2, g)=-(393.51\pm0.13)$ and $\Delta H_f^\circ(H_2O, 1)=-(285.830\pm0.042)$ kJ mol^{-1}, respectively, where uncertainties are those at the 95 per cent confidence level. The overall uncertainty for ΔH_v° is twice the sdm, $\{2s(\Delta H_v)\}$. The overall uncertainties for $\Delta H_f^\circ(1)$ and $\Delta H_f^\circ(g)$ are $[\{2s(\bar{U})_\Sigma\}^2+\{8\times0.13\}^2+\{5.5\times0.042\}^2]^{1/2}$ and $[\{2s(\bar{U})_\Sigma\}^2+\{8\times0.13\}^2+\{5.5\times0.042\}^2+\{2s(\Delta H_v)\}^2]^{1/2}$, respectively.

The large uncertainty assigned to $\Delta U_c^\circ(1)$ originates mainly from the relatively small masses of *N,N*-dimethylaniline used in the combustion experiments.

The only experimental value of $\Delta H_c^\circ(1)$ reported so far is the old value of Stohmann (-4782.4 kJ mol^{-1}),[7)] while estimated values, *e.g.* -4754.3[8,9)] and -4753.6[10)] kJ mol^{-1}, respectively, are less negative than the old experimental value.[7)] The present value is intermediate between the two groups. No other calorimetric value has been reported for ΔH_v°. The present value is higher than the value derived from the analysis of vapor pressure data, 49.8 kJ mol^{-1},[9)] by 3.0 kJ mol^{-1}.

References

1) M. Sakiyama, T. Nakano, and S. Seki, *Bull. Chem. Soc. Jpn.*, **48**, 1705 (1975).
2) K. Nishiyama, M. Sakiyama, S. Seki, H. Horita, T. Otsubo, and S. Misumi, *Bull. Chem. Soc. Jpn.*, **53**, 869 (1980).
3) K. Kusano and Y. Saito, *Bull. Fac. Eng. Miyazaki Univ.*, **23**, 1 (1977).
4) H. S. Osborn and D. C. Ginnings, *J. Res. Natl. Bur. Stand.*, **39**, 453 (1947).
5) W. N. Hubbard, D. W. Scott, and G. Waddington, "Experimental Thermochemistry," ed by F. D. Rossini, Interscience, New York (1956), Vol. 1, Chap. 5.
6) CODATA Task Group on Key Values for Thermodynamics, *CODATA Bulletin*, **1977**, 28; *J. Chem. Thermodyn.*, **10**, 903 (1978).
7) F. Stohmann, *Z. Phys. Chem.*, **6**, 334 (1890).
8) M. S. Kharasch, *J. Natl. Bur. Stand.*, **2**, 359 (1929).
9) G. N. Vriens and A. G. Hill, *Ind. Eng. Chem.*, **44**, 2732 (1952).
10) J. B. Pedley and J. Rylance, "Sussex-N. P. L. Computer Analysed Thermochemical Data: Organic and Organometallic Compounds," Univ. of Sussex, Brighton (1977).

Chemical Reaction Following Electroreduction of Benzophenones. 2. Relationship between the Rate Constant of Disproportionation and Spin Density

Naoyoshi EGASHIRA,* Yusaku TAKITA, and Fumiaki HORI
Department of Environmental Chemistry and Engineering, Faculty of Engineering, Oita University, 700 Dannoharu, Oita 870-11

(Received August 17, 1981)

Synopsis. Electroreduction of benzophenones in DMF in the presence of Li^+ was investigated by cyclic voltammetry. Most of these radical anions underwent disproportionation reactions. The relationship between the logarithm of the rate constant of the reaction and the spin density of the carbon atom at the carbonyl group was found to be linear.

In recent years there have been numerous investigations dealing with the behavior of radical anions generated in various ways.[1-3] Generally the radical anions undergo a dimerization[4,5] or a disproportionation reaction[6] in the presence of cations.

The authors reported in the previous paper[7] that the disproportionation of the electrogenerated radical anions of several substituted benzophenones **1** were accelerated by the addition of lithium iodide, and that a linear relationship was found between the logarithms of the rate constants of the disproportionation, ln k_{obsd}, evaluated from cyclic voltammetry (CV). This was confirmed by the digital simulation and the spin density, ρ_s, of the carbon atom at the carbonyl group of benzophenones. In this paper, we report that the above relationship is valid for the other benzophenones, **2** and **3**. Furthermore, a linear relationship between ln k_{obsd} and the electron density, q, of the oxygen atom at the carbonyl group was found for benzophenones **1**, **2**, and **3**.

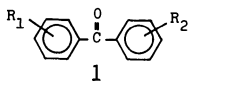

1

a R_1=H, R_2=H
b R_1=*o*-CH_3, R_2=H
c R_1=*m*-CH_3, R_2=H
d R_1=*p*-CH_3, R_2=H
e R_1=*p*-CH_3, R_2=*p'*-CH_3
f R_1=*p*-OCH_3, R_2=H
g R_1=*p*-OCH_3, R_2=*p'*-OCH_3

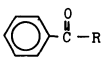

2

a R= 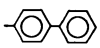
b R=
c R=
d R=
e R=
f R=

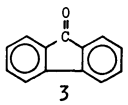

3

Experimental

Chemicals. All the substituted benzophenones (**1a**, **1d**, **1e**, **2c**, **2d**, **2e**: Waco, **1b**, **1c**, **2a**: Aldrich, **1f**, **1g**, **2b**, **2f**, **3**: Tokyo Kasei) were purified by recrystallization. Benzyl alcohols used as authentic samples for a high performances liquid chromatography (HPLC) were prepared with the method of Meerwein-Pondorf: α-(4-biphenyl)benzyl alcohol **4**: mp 97.0—97.5 °C (lit,[8] 96 °C), IR(KBr) 3260 cm^{-1} (OH); α-(2-thienyl)benzyl alcohol **5**: mp 56.5 °C (lit,[9] 57—58 °C); IR (KBr) 3260 cm^{-1} (OH), α-(*p*-methoxyphenyl)benzyl alcohol **6**: mp 66—67 °C (lit,[10] 59—60 °C), IR (KBr) 3270 cm^{-1} (OH).

CV. CV was carried out in the same way as described in the previous paper.[7] The differecne between cathodic peak and the switching potentials was 0.1V. The sweep rate was 0.1V/s.

Controlled Potential Electrolysis. Reduction of 2.0 g of **2a** in 100 ml of DMF containing 3.0 g of LiI was carried out at the potential of the first wave, −1.80 V *vs.* SCE. After passing $2F$** of electricity, the catholyte was analyzed by HPLC.

Results and Discussion

The first wave of the voltammogram for **2a** is a reversible one-electron transfer: $i_{pa}/i_{pc}=1$ and $|E_{pc}-E_{pa}|=70$ mV. By the addition of LiI, i_{pa} decreases and i_{pc} increases slightly. Controlled potential electrolysis at −1.80 V *vs.* SCE in the presence of Li^+ gave **4**, a two-electron reduction product in 70% yield. All the remainder except the product was the starting material. These results show that the following disproportionation occurs:

$$R + e \rightleftharpoons R^{\cdot}$$
$$2R^{\cdot} \longrightarrow R^{=} + R,$$

where R is a reactant, $R^{\cdot}$ a radical anion and $R^{=}$ a dianion of a reactant.

The profile of the voltammogram for other benzophenones examined was similar to that of **2a**. The electrolysis of **2f** and **1f** gave **5** and **6** in 30% and 62% yield, respectively. In both cases, the remainder was mostly the starting material. From the above results we concluded that the following chemical reaction was disproportionation for all the benzophenones tested. The rate constants of disproportionation, k_{obsd}, were estimated from the voltammetric data of these compounds by using digital simulation (Table 1). The plots of ln k_{obsd} against ρ_s gave a straight line as shown in Fig. 1. It was confirmed that the k_{obsd} was predictable from the ρ_s.

The reaction rate of benzophenones having an electron-attracting substituent (**2a**, **2b**) and having a hetero atom (**2c**, **2d**) would tend to be slower than that of **1a**. **1b** and **3** exhibited reversible cyclic voltammograms even in the presence of 16-fold concentration excess of Li^+. This does not promote the reaction. The behavior of **1b** can be attributed to the 2-methyl group which inhibits mutual access to the carbon atom in the carbonyl group, and that of **3** to both steric hindrance (corresponding to the 2 and 2′ positions of

** F=96487 C mol^{-1}.

Table 1. Experimental data and calculated parameter for benzophenones

Compd	$-E_{pc}$[a] / V	$k_{obsd}\times10^{3}$ [a,b] / $M^{-1}s^{-1}$	ρ_s[d]	q[e]	Ref.
1a	1.79	0.39	0.3437	1.7374	7
1b	1.85	—	0.3467	1.7465	7
1c	1.80	0.50	0.3462	1.7379	7
1d	1.83	0.70	0.3589	1.7486	7
1e	1.90	1.90	0.3810	1.7605	7
1f	1.86	3.89	0.3510	1.7446	7
1g	1.98	0.57[c]	0.3597	1.7518	7
2a	1.71	0.23	0.3111	1.7308	
2b	1.70	0.93	0.3121	1.7295	
2c	1.56	0.32	0.3294	1.7270	
2d	1.64	0.90[c]	0.3403	1.7363	
2e	1.48	0.21	0.3198	1.7242	
2f	1.65	0.62	0.3526	1.7554	
3	1.30	—	0.2827	1.6963	

a) Determined with a hanging mercury drop electrode. b) The rate constant of the disproportionation in the presence of 4 mM (1 M=1 mol dm^{-3}) LiI. c) 0.4 mM LiI. d) Calcd by employing McLachlan's procedure; $\lambda=1.2$. e) Calcd by employing the Hückel MO theory.

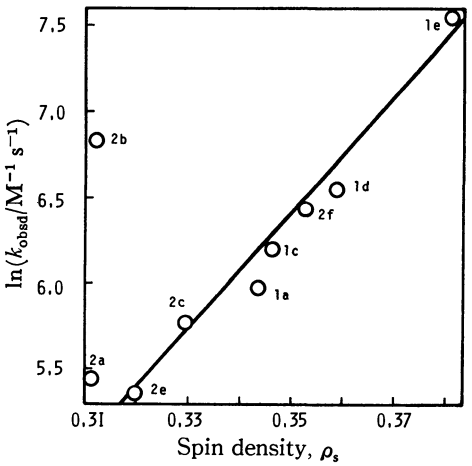

Fig. 1. Correlation between the rate constant of the disproportionation, k_{obsd}, and the spin density, ρ_s, for benzophenones.

1a) and the lowering of ρ_s.

Furthermore the plots of ln k_{obsd} against q were found to be linear. This suggested that ρ_s and q may bear a linear relationship to each other. Thus, the change in k_{obsd} with ρ_s and/or q is probably based on the change in association constants for the ion-pair formation between radical anions and Li^+. At present, unfortunately, no association constants of the ion-pairs have been obtained; and the contribution of ρ_s and q to k_{obsd} cannot be discussed separately.

References

1) M. Szwarc and J. Jagur-Grodzinski, "Ion and Ion Pairs in Organic Reactions," ed by M. Szwarc, Wiley-Interscience, New York, N. Y. (1974), Vol. 2, pp. 90—106.
2) B. Lundgren, G. Levin, S. Claesson, and M. Szwarc, *J. Am. Chem. Soc.*, **97**, 262 (1975).
3) T. L. Staples, J. Jagur-Grodzinski, and M. Szwarc, *J. Am. Chem. Soc.*, **91**, 3721 (1969).
4) M. J. Hazerlrigg and A. J. Bard, *J. Electrochem. Soc.*, **122**, 211 (1975).
5) A. Lasia, *J. Electroanal. Chem. Interfacial Electrochem.*, **42**, 253 (1973).
6) A. Kapturkiewicz and M. K. Kalinowski, *J. Phys. Chem.*, **82**, 1141 (1978).
7) N. Egashira, Y. Takita, and F. Hori, *Denki Kagaku*, **49**, 217 (1981).
8) M. P. J. Montagne, *Recl. Trav. Chim. Pays-Bas*, **27**, 358 (1908).
9) W. Minnis, *J. Am. Chem. Soc.*, **51**, 2143 (1929).
10) J. F. Norris and J. T. Blake, *J. Am. Chem. Soc.*, **50**, 1808 (1928).

Redox Reaction of the Central Metal Ions Coordinated to Tetra(*p*-sulfophenyl)porphine (TPPS). II. Photoreduction of [Fe(III)TPPS]$_2$O by Ethanol

Keiichiro HATANO* and Yoshitaka ISHIDA
Department of Pharmaceutical Sciences, Nagoya City University, Mizuho-ku, Nagoya 467
(Received November 26, 1981)

Synopsis. Iron(III) ion coordinated to TPPS was reduced to the divalent ion by ethanol on illumination of light. The reaction rates appear to obey the half-order kinetic of the metalloporphyrin in the buffered solutions of pH 7 to 11. A possible reaction mechanism is discussed.

The photochemical redox behavior of metalloporphyrins is of continuing interest due to their biomimetic functions as chlorophylls in photosynthesis and their possibilities as photosensitizers for solar energy conversion. Besides our study of the photoreduction of Co(III)-TPPS,[1] some recent work that is relevant to our present kinetic investigation of iron porphyrin photochemistry may be cited as follows: the photoreduction of Mn(III)-TPyP[2] and the Mn(IV) derivatives by ethanol or water studied extensively by Harriman and Porter,[3] and the photoreduction of hemin in ethanol–pyridine–water mixed solvents by Bartocci *et al.*[4]

Dimer formation for Fe(III), Mn(III), or Mn(IV) porphyrin in basic solutions is certain,[5] or at least suggested by the X-ray moleculer structures.[6,7] The coordination of water or alcohols to these metalloporphyrins is certain from the crystal structures.[8–10] This note describes some details of earlier data[11] of the photoreduction of Fe(III)TPPS, here we treat the μ-oxo dimer formation and the axial ligation of ethanol.

Figure 1 shows typical spectral changes of Fe(III)-TPPS in the deaerated aqueous ethanol during the photolysis in two separate experiments. The changes can be ascribed to the photoreduction of the central iron(III) ion of FeTPPS to the iron(II) ion, judging from the spectral characteristic of the product Fe(II)-TPPS, and the reoxidation of it to the original Fe(III)-TPPS by air introduction. Fe(III)TPPS restored by a cycle of the redox reactions is, though dependent on the irradiation time and other conditions, almost quantitative (>95%) in regular experiments. Furthermore, acetaldehyde detected in the irradiated solution as the oxidation product of ethanol confirms that the overall reaction is an autoxidation reaction of ethanol catalyzed by the Fe(III)⇌Fe(II) couple of FeTPPS. Some apparent isosbestic points are found in the spectral changes, but close inspection in the spectra reveals that the photochemical reaction is not a simple interconversion of Fe(II)- and Fe(III)TPPS but that some other minor species also take part. In particular, the spectrum of μ-oxo dimer in alkaline solution resembles closely that of the ethanol coordinated iron(III)-porphyrin species which are expected to be formed in the neutral aqueous solution with the addition of ethanol. Thus, several species having a similar absorption spectrum or very small abundance in the solution are considered to overlap into a spectrum represented by that of μ-oxo dimer. This situation does not allow the strict and accurate analysis of the reaction rates. However, the distinct absorption of Fe(II)TPPS in the Soret region and the known optical density can permit the plausible reaction mechanism elucidation unless the trace of spectra goes severely off from the quasi-isosbestic points in the spectral changes. The observed rates of the photoreduction fit approximately the following equation under the conditions of the constant photon flux and pH:

$$d[\text{Fe(II)TPPS}]/dt = k'[(\text{FeTPPS})_2\text{O}]^{1/2}[\text{ethanol}].$$

Figure 2 demonstrates the half-order rate dependence in the metalloporphyrin kinetics. The half-order kinetic is also confirmed by the experiments varying the initial concentrations of Fe(III)TPPS. Fleischer *et al.*[5] have studied the kinetics of the monomer-dimer equilibrium reaction of Fe(III)TPPS in aqueous

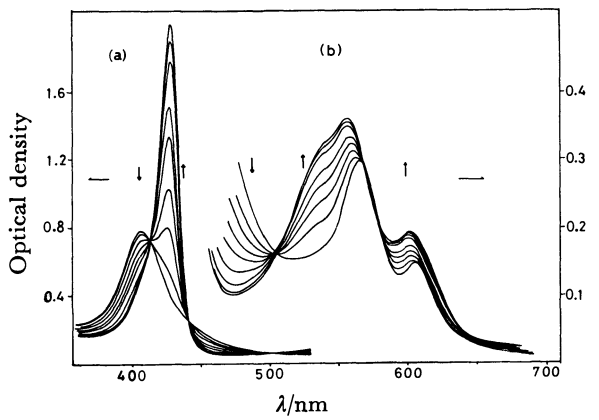

Fig. 1. Spectral changes of FeTPPS during photolysis. Experimental conditions and reaction times shown in the order of arrows are: (a) 3.8×10^{-6} M $(\text{FeTPPS})_2\text{O}$, 2.5 M ethanol, at pH 8.0, and 0, 10, 20, 30, 45, 60, 90, 120, and 210 min. (b) 4.5×10^{-5} M $(\text{FeTPPS})_2\text{O}$, 4.0 M ethanol, at pH 8.4, and 0, 10, 20, 30, 40, 55, 70, 90, 120 min. 1 M=1 mol dm^{-3}.

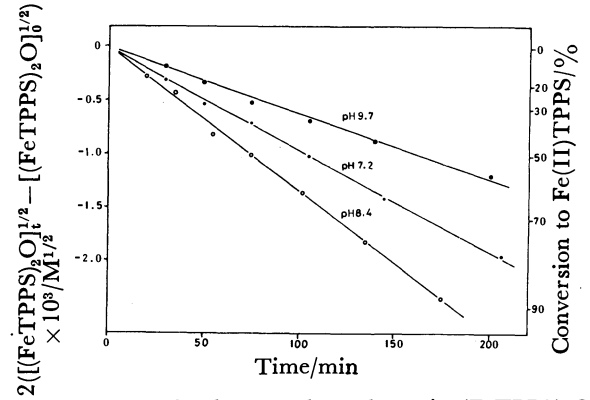

Fig. 2. The half-order rate dependence in $(\text{FeTPPS})_2\text{O}$ kinetics at various pH. The right hand scale shows % conversion of $(\text{FeTPPS})_2\text{O}$ to Fe(II)TPPS.

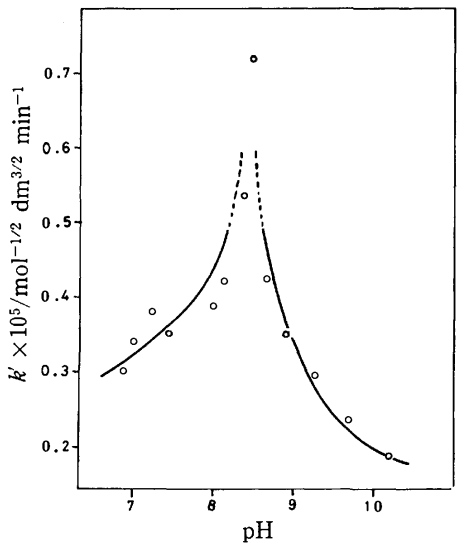

Fig. 3. The pH profile of the rate constants, k'. [Ethanol] $=2.5$ M.

solutions; the rate of the reaction is reported to be faster than that of the present photoreaction. Therefore, the rate-determining step of the photoreduction should not be the dissociation of dimer into monomer. The initial stage of the linkage chain hydrogen-bromine reaction has been classically analyzed as the half-order kinetic approximation in bromine concentration.[12] A similar interpretation can apply for the present reaction mechanism. Thus, a photoinduced electron transfer reaction is considered to be the rate-determining step involving a monomeric photosensitive species. The plausible representation of the reaction scheme to elucidate the kinetics is written as:

$$(\mathrm{FeTPPS})_2\mathrm{O} + \mathrm{H_2O} \rightleftharpoons 2\mathrm{Fe(III)TPPS(OH)}$$

$$\mathrm{Fe(III)TPPS(OH)} + \mathrm{C_2H_5OH} \rightleftharpoons \mathrm{Fe(III)TPPS(OH)(C_2H_5OH)}$$

$$\mathrm{Fe(III)TPPS(OH)(C_2H_5OH)} \xrightarrow{h\nu} \mathrm{Fe(II)TPPS} + \mathrm{CH_3\dot{C}HOH} + \mathrm{H_2O}.$$

The first-order kinetic in ethanol concentrations substantiates the coordination of one ethanol molecule to a photosensitive ferric species. The mechanistic representation is principally identical to the photoreduction of Co(III)TPPS.[1] The entity of the particular ternary complex coordinating an OH ion as the photosensitive species is supported by the kinetic studies in solutions of varying pH. As shown in Fig. 3, the volcano-shape profile of the rate constants, k', against pH indicates that there is an optimal concentration of hydroxide ion to stabilize the photosensitive species.

The overall quantum yield depends on the quantity of the photosensitive species in solutions. The highest observed quantum yield (*ca.* 0.01) is achieved at high ethanol concentration (5.2 M), optimal pH (8.5), and relatively low concentration of FeTPPS (1.6×10^{-6} M). The pursuit of higher values is hampered by the low solubility of FeTPPS in ethanol.

The reoxidation reaction occurs. The rate is too rapid to be followed by the traditional spectromeric device. This suggests that the reducing potential of Fe(II)TPPS is higher than that of Co(II)TPPS, toward the dioxygen molecule.

Experimental

FeTPPS was prepared as described.[5] Dark green powder was obtained by treatment of crude material in methanolic solutions with sodium methoxide several times. Found: C, 43.19; H, 3.04; N, 4.86; S, 10.57%. Calcd for $(\mathrm{FeTPPS\,Na_4})_2\mathrm{O}\ 16\mathrm{H_2O}$, $\mathrm{C_{88}H_{80}N_8S_8O_{41}Fe_2Na_8}$: C, 43.01; H, 3.29; N, 4.56; S, 10.44%.

Procedures and instruments employed in the experiments were the same as reported previously[1] except that a Wacom XD-501S xenon lamp was also used. The quantum yield was determined by comparison of spectrometric measurements to the CoTPPS case. Acetaldehyde was analyzed in the sample distilled in vacuo from the FeTPPS solution photolyzed for 45 h using a qualitative *p*-phenylenediamine–$\mathrm{H_2O_2}$ method[13] and a nitroprusside method[13] as a quantitative detection. Although both methods are not specific for acetaldehyde, the negligible amount of the porphyrin decomposition and the normal quantum yield (10^{-3} order) for alcohol oxidation support this assignment.

We thank Kuniko Uchiyama for experimental assistance.

References

1) K. Hatano, K. Usui, and Y. Ishida, *Bull. Chem. Soc. Jpn.*, **54**, 413 (1981).
2) Abbreviation: TPyP=the dianion of meso-tetrapyridylporphine.
3) A. Harriman and G. Porter, *J. Chem. Soc., Faraday Trans. 2*, **75**, 1543 (1979); **76**, 1415 (1980).
4) C. Bartocci, F. Scandola, A. Ferri, and V. Carassiti, *J. Am. Chem. Soc.*, **102**, 7067 (1980).
5) E. B. Fleischer, J. M. Palmer, T. S. Srivastava, and A. Chatterjee, *J. Am. Chem. Soc.*, **93**, 3162 (1971).
6) A. B. Hoffman, D. M. Collins, V. W. Day, E. B. Fleischer, T. S. Srivastava, and J. L. Hoard, *J. Am. Chem. Soc.*, **94**, 3620 (1972).
7) B. C. Schardt, F. J. Hollander, and C. L. Hill, *J. Chem. Soc., Chem. Commun.*, **1981**, 765.
8) F. W. B. Einstein and A. C. Willis, *Inorg. Chem.*, **17**, 3040 (1978).
9) W. R. Scheidt, I. A. Cohen, and M. E. Kastner, *Biochemistry.*, **18**, 3546 (1979).
10) K. Hatano, K. Anzai, and Y. Iitaka, submitted.
11) The preliminary results of this work were presented in the Annual Meeting of the Pharmaceutical Society of Japan at Nagoya, 1976, Preprint Vol. IV, p. 116.
12) Keith J. Laidler, "Reaction Kinetics," Pergamon Press, London (1963), Vol. 1, translated into Japanese by T. Takaishi, 1965.
13) Morizo Ishidate, "Biryo Teisei Bunseki (Qualitative Analysis)," Nanzando, Tokyo (1966).

Application of Coagulated Ion-exchanger Colorimetry to the Determination of Trace Amounts of Phosphate in Water

Kiichi Matsuhisa,† Kunio Ohzeki,* and Tomihito Kambara
Department of Chemistry, Faculty of Science, Hokkaido University, Sapporo 060
†*Division of Environmental Conservation, Graduate School of Environmental Science, Hokkaido University, Sapporo 060*
(Received March 30, 1982)

Synopsis. The combined use of finely divided anion and cation exchange resins reported previously[1] was partly modified and applied to the determination of trace amounts of phosphate in some environmental water samples, such as rain, snow, lake water and seawater. Both orthophosphate and total phosphate were determined and satisfactory results were obtained.

The ion-exchanger colorimetry developed by Yoshimura *et al.*[2] is an excellent method for trace analysis, in which a colored metal complex with negative or positive charge is concentrated on the corresponding ion-exchanger and determined spectrophotometrically in a 1-mm cell.

On the other hand, we reported a new type of ion-exchanger colorimetry,[3] in which a combination of finely divided anion and cation exchange resins was used. One of the characteristics of fine particle ion-exchangers is the coagulation. The coagulated resins are collected on a filter paper as a disk of thin layer, which is directly subjected to spectrophotometric analysis, no cell being required. Therefore, hereafter, we call the method the coagulated ion-exchanger colorimetry.

Experimental

Reagents. Phosphate, molybdate, antimony tartrate, and ascorbic acid solutions were prepared according to the previous report.[1]

Mixed Reagent: A 100-ml portion of 2.5 M (1 M=1 mol dm^{-3}) sulfuric acid was mixed with 30 ml of the ammonium molybdate solution and 10 ml of the potassium antimony tartrate solution. When a considerable amount of sulfuric acid was already contained in the sample solution, as in the case of hydrolyzable phosphate sample, the acid amount in the mixed reagent was reduced, so that a constant acidity in the final test solution was kept to 0.18 M.

Dipping Solution: The composition was the same as in the previous report.[1]

Mixed reagent and dipping solution were prepared fresh daily and stored in a thermostat kept at 25±1 °C.

Ion-Exchange Resin Suspension. The cation exchange resin suspension (CRS) and anion exchange resin suspension (ARS) were freshly prepared according to the method reported.[4] The exchange capacities were 11.8 μequiv. ml^{-1} for CRS and 7.0 μequiv. ml^{-1} for ARS, respectively. Both suspensions were kept at 25±1 °C.

Apparatus. A Shimadzu UV 140-01 spectrophotometer was used. A Toyo KG 25 filter holder was used with filter papers of No. 5B (Toyo Roshi). A vacuum gauge used was a NRK product, type STV-75. Decomposition vessels of 70-ml capacity (Uniseal) were used.

Procedure. A 50-ml aliquot of the test solution containing less than 0.3 μg of phosphorus as phosphate was taken into a 100-ml beaker and the solution was kept at 25±1 °C in a water bath. A 6.0-ml portion of the mixed reagent and 2.0 ml of the ascorbic acid solutions were added and the solution was stirred by means of a magnetic stirrer for 5 min. Finally, 4.0 ml of ARS and 2.0 ml of CRS were added and the mixture was stirred for 10 min. The coagulated resins were collected on a filter paper strip placed on the holder with suction under *ca.* 160 mmHg by running water. A disk of colored resin, 17 mm in diameter and about 0.3 mm in thickness, was formed. The filter strip was soaked in the dipping solution for 15 min. It was then fixed on a glass plate fitted on the one side of cell holder, which is nearer to the light source, *i.e.*, the light beam goes successively through the thin layer, filter paper, and finally glass plate. The absorbance of the resin phase was measured at 700 nm against a dry filter paper or another white paper.

Another disk of resin was prepared without addition of phosphate. The absorbance corresponding to the reagent blank including the resins was also measured. The net absorbance of the complex on the resin phase was obtained as the difference.

The main differences of the proposed procedure from the previous one[1] were in the following respects: firstly, 5 min were allowed for the development of the molybdenum blue complex (in the previous procedure, ARS and CRS were successively added immediately after the color developing reagents); secondly, resin suspensions with higher exchange capacities were used, namely, the total exchange capacities were 23.6 μequiv. for cation exchanger and 28.0 μequiv. for anion exchanger (in the previous procedure, the values were 10.4 and 15.2, respectively); thirdly, the suction pressure of *ca.* 4 times higher than that in the previous procedure was applied to collect the mixed resins.

Sample Preparation for Dissolved Orthophosphate (P-D, ortho). The sample water was filtered through No. 5C filter paper.

Sample Pretreatment for Total Phosphate (P, total). A 50-ml portion of sample water was used without filtration. According to the JIS method,[5] it was digested with hot sulfuric and nitric acids, neutralized, and finally diluted to 50 ml with water. In the case of seawater, a 10-ml portion of sample was digested. A large amount of precipitate was formed, which was removed by filtration. The filtrate together with washings were neutralized and diluted to 100 ml with water. The solution for the blank test was prepared according to the same procedure with deionized water, instead of sample solution.

Pretreatment of Seawater for Hydrolyzable Phosphate (P, hydro). Familiar Harvey's method[6] being partly modified, a 10-ml portion of seawater was taken into a Teflon crucible and 1.0 ml of 9 M sulfuric acid was added. The crucible was set in the jacket previously kept at 125 °C in an air-bath, and then allowed to stand for ca. 40 min at a room temperature. The sample solution was transferred into a 50-ml volumetric flask and diluted to the mark with water. The 5-ml portions of the solution were subjected to the standard addition method.

Results and Discussion

Stirring Time for Color Development. The thin layer with a constant coloration was obtained by

Table 1. Determination of phosphate

Sample	Date 1981	Amount ml	P-D, ortho ppb[a)]	P, total ppb[a)]
Snow, fresh (Sapporo C.)	Mar. 16	50.0	$3.0_5\pm0.1_7$	
		10.0		$3.7_8\pm0.2_1$
Snow, old (Asari-dake)	May 01	50.0	$4.1_4\pm0.0_9$	
		10.0		$7.6_3\pm0.5_6$
Lake water (Shikotsu-ko)	Jun. 04	50.0	$5.1_8\pm0.2_3$	
		10.0		$8.3_0\pm1.0_0$
Rain (Ebetsu C.)	Jul. 07	50.0	$3.7_6\pm0.6_4$	
		25.0		$4.7_0\pm1.7_1$
Rain (Sapporo C.)	Jul. 10	50.0	$5.3_7\pm0.6_3$	
		25.0		$7.5_4\pm1.4_5$

a) The 95% confidence limits ($n=3$).

Table 2. Determination of phosphate in seawater[a)]

Date 1981	Sample amount ml	P-D, ortho ppb[b)]	P, total ppb[b)]	Sum of (P, hydro) and (P, ortho) ppb[b)]
Jun. 25	4.0	26.2 ± 1.2		
	2.0		31.1 ± 9.5	
Jun. 29	4.0	24.8 ± 5.8		
	2.0		37.0 ± 13.0	
Aug. 10	4.0	23.3 ± 2.7		
Aug. 15	4.0	21.5 ± 5.0		
Sep. 08	4.0	17.4 ± 5.0		
	1.0			41.1 ± 6.7[c)]
	1.0			41.8 ± 6.0[d)]
Sep. 16	2.0	17.7 ± 1.1		
	1.0			40.0 ± 1.1[c)]

a) Surface seawater at Ishikari bay. b) The standard addition method was applied and the 90% confidence limits ($n=4$) were calculated. c) 90-min heating. d) 250-min heating.

stirring the test solution in the range 5—30 min before the addition of CRS and ARS. When the resins were added immediately after the addition of the mixed reagent and ascorbic acid solution, a lower absorbance was observed.

Calibration Graph. The calibration graph was linear over the concentration range 1.0—6.0 ng P ml^{-1}. The mean absorbance with the standard deviation was 0.148 ± 0.005 ($n=3$) for 1.0 ppb P and 0.833 ± 0.012 ($n=5$) for 6.0 ppb P. The modified procedure having an improved sensitivity was advantageous in comparison with the previous one.[1)]

Determination of Phosphate. The results are summarized in Tables 1 and 2. The amount of orthophosphate is determined much more precisely than that of total phosphate, since no pretreatment except filtration is required. The application of the JIS method[5)] to the determination of total phosphate has been reported to be difficult.[7)] A large amount of precipitate formed in the course of acid digestion will cause the loss of phosphorus and poor reproducibility (Table 2).

On the other hand, the sum of hydrolyzable phosphate and orthophosphate (P, ortho)[8)] in seawater is fairly precisely determined (Table 2). Sample seawater was heated in the presence of sulfuric acid at 125 °C in a Uniseal decomposition vessel. A 90-min heating was enough to hydrolyze any phosphate present in seawater. The combined use of sulfuric acid and potassium peroxodisulfate for the determination of total phosphate was also examined, but no reliable result was obtained.

References

1) K. Matsuhisa, K. Ohzeki, and T. Kambara, *Bull. Chem Soc. Jpn.*, **54**, 2675 (1981).
2) K. Yoshimura, H. Waki, and S. Ohashi, *Kagaku Zokan*, **78**, 95 (1978).
3) K. Ohzeki, T. Sakuma, and T. Kambara, *Bull. Chem. Soc. Jpn.*, **53**, 2878 (1980).
4) M. Abe, K. Ohzeki, and T. Kambara, *Bull. Chem. Soc. Jpn.*, **51**, 1090 (1978).
5) JIS K 0102 (1981), "Testing Methods for Industrial Wastewater."
6) H. W. Harvey, *J. Mar. Biol. Ass. U. K.*, **27**, 337 (1948).
7) K. Hiiro, *Bunseki Kagaku*, **30**, T 45 (1981).
8) APHA, AWWA, WPCF; "Standard Methods for the Examination of Water and Wastewater," 14th ed, (1975), p. 466.

Reactions of 3-Acetyltropolone and Its Methyl Ethers with *o*-Aminophenol

Kimiaki IMAFUKU,* Akihiro SHIGENOBU, and Makoto OGURA
Department of Chemistry, Faculty of Science, Kumamoto University, Kurokami, Kumamoto 860
(Received April 3, 1982)

Synopsis. 3-Acetyltropolone (**1**) and 2-acetyl-7-methoxytropone (**2a**) reacted with *o*-aminophenol in ethanol to afford 2-acetyl-7-(*o*-hydroxyanilino)tropone (**3**). The reaction of 3-acetyl-2-methoxytropone (**2b**) gave 3-acetyl-2-(*o*-hydroxyanilino)tropone (**5**). The compounds **3** and **5** were cyclized to 6-acetyl- and 10-acetylcyclohepta[*b*][1,4]benzoxazines (**4** and **6**), respectively, by heating their acetic acid solutions in the presence of a trace amount of concentrated sulfuric acid. The compounds **4** and **6** were also obtained directly from **1** (or **2a**) and **2b**, respectively, by the reaction with *o*-aminophenol in acetic acid. The compound **5** exists as a tautomeric mixture with **5'**.

It is well known that the reactions of so-called ractive troponoids——2-methoxytropones or 2-chlorotropones ——with *o*-phenylenediamine,[1,2] *o*-aminophenol,[3] and *o*-aminobenzenethiol[4] afford 6*H*-cyclohepta[*b*]quinoxaline, cyclohepta[*b*][1,4]benzoxazine, and cyclohepta-[*b*][1,4]benzothiazine, respectively. These products are heterocyclic compounds containing two hetero-atoms with a 6,6,7-ring system. Previously, in a series of chemistry of 3-acetyltropolone, we reported the formation of a benzodiazaheptalene derivative with a 6,7,7-ring system, besides 5*H*- and 6*H*-cyclohepta[*b*]quinoxalines with a 6,6,7-ring system, by the reactions of 3-acetyltropolone methyl ethers with *o*-phenylenediamine.[5]

In the present work, the reactions of 3-acetyltropolone (**1**) and its methyl ethers (**2a** and **2b**) with *o*-aminophenol were carried out in expectation of the formation of an oxazepine ring—a 6,7,7-ring system. However, the reactions gave no oxazepine ring but gave acetyl-substituted (*o*-hydroxyanilino)tropones (**3** and **5**) and cyclohepta[*b*][1,4]benzoxazines (**4** and **6**).

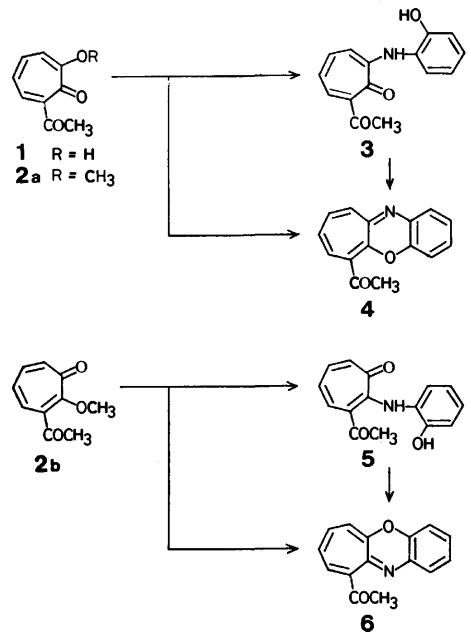

Scheme 1.

Results and Discussion

In general, tropolones do not show any indication to react with nucleophilic reagents as well as phenols. However, tropolones bearing a strong electron-withdrawing group, such as nitro or nitroso group, react with nucleophiles to give 2-substituted tropones.[6] Recently, we found that 3-acetyltropolone (**1**) reacts with amines to afford 2-acetyl-7-aminotropones.[7] The refluxing of 3-acetyltropolone (**1**) with *o*-aminophenol in ethanol gave 2-acetyl-7-(*o*-hydroxyanilino)tropone (**3**) in 15% yield. The reactivity of **1** would be based on the electron-withdrawing effect of the acetyl group. The same reaction was carried out in acetic acid containing a trace amount of concentrated sulfuric acid to afford a cyclized product——6-acetylcyclohepta[*b*][1,4]benzoxazine (**4**)——in 3% yield. The compound (**3**) in acetic acid was refluxed in the presence of concentrated sulfuric acid to cyclize to **4**.

The refluxing of 2-acetyl-7-methoxytropone (**2a**) with *o*-aminophenol in ethanol gave **3** in 44% yield, the same reaction in acetic acid giving **4** in 33% yield. Similarly, the reaction of 3-acetyl-2-methoxytropone (**2b**) with *o*-aminophenol in ethanol gave 3-acetyl-2-(*o*-hydroxyanilino)tropone (**5**) in 31% yield, the reaction in acetic acid giving 10-acetylcyclohepta[*b*][1,4]benzoxazine (**6**) in 27% yield. The compound (**5**) was also converted to **6** in 55% yield by heating its acetic acid solution. The structures of all the products were determined by their elemental analyses and spectral data (see: Experimental part).

As shown in Fig. 1, the ^{1}H NMR spectrum of **5** in chloroform-d_1 shows two singlet peaks at δ 2.03 and 2.50 for =C(OH)–CH_3 and –C(=O)–CH_3 protons, respectively. These two singlet peaks indicate that **5** exists as a tautomeric mixture with **5'**. The spectrum in more polar solvent—methanol-d_4—shows only one singlet peak at δ 2.02 and the signal near δ 2.50, which

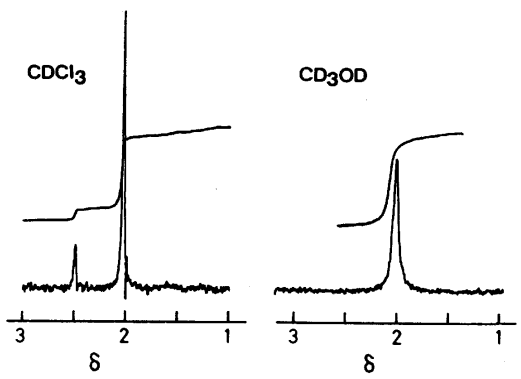

Fig. 1. The ^{1}H NMR spectra of **5** in chloroform-d_1 and methanol-d_4.

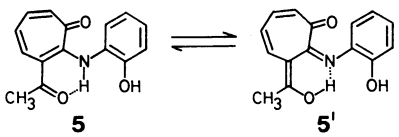

Scheme 2.

appeared in chloroform-d_1, is not observed. A similar keto-enol tautomerism of the acetyl group was observed in the spectrum of 6-acetyl-5*H*-cyclohepta[*b*]quinoxaline.[5]

The ^{1}H NMR spectrum of **4** measured in trifluoroacetic acid shows shift of the seven-membered ring protons by *ca.* 1.0 ppm and that of the benzene ring protons by *ca.* 0.1 ppm towards lower magnetic field than those in chloroform-d_1. Similar phenomena were observed in a parent compound——cyclohepta[*b*][1,4]benzoxazine,[3] and 6*H*-cyclohepta[*b*]quinoxaline.[2] These observations indicate that the positive charge is delocalized over both the seven-membered ring and the heterocycle but little over t he benzene ring. The spectrum of **6** also shows a similar tendency.

In this work, the expected 6,7,7-ring system, which is produced by the reaction at the acetyl group, was not isolated. This might be due to the instability of the oxazepine ring.

Experimental

The melting points were determined with a Yanagimoto MP-S2 melting-point measuring apparatus and are uncorrected. The IR spectra were taken on a JASCO IRA-1 spectrophotometer, and the UV spectra on a Hitachi EPS-3T spectrophotometer. The spectra in acidic medium were measured by adding three drops of 1M hydrochloric acid to the sample solution. The ^{1}H NMR spectra were recorded with a Hitachi-Perkin-Elmer R-24 spectrometer (60 MHz).

*Reaction of 3-Acetyltropolone (**1**) with* o*-Aminophenol. a)*: A mixture of 3-acetyltropolone (**1**) (200 mg, 1.2 mmol) and *o*-aminophenol (250 mg, 2.3 mmol) in absolute ethanol (15 ml) was refluxed for 6 h. After removal of the solvent, the residue was twice chromatographed on a Wakogel B-10 plate (30×30 cm²) with chloroform to afford 47 mg (15%) of 2-acetyl-7-(*o*-hydroxyanilino)tropone (**3**) as reddish orange plates (from benzene–hexane); mp 109—110 °C; IR ($CHCl_3$) 3380, 3260 1700, 1595 cm^{-1}; UV (CH_3OH) 232 (log ε 4.36), 360 (3.90), 433 nm (4.33); UV (CH_3OH+HCl) 236 (log ε 4.36), 359 (3.89), 433 nm (4.31); NMR ($CDCl_3$) δ=2.50 (s, 3H,$COCH_3$), 6.5—7.6 (m, 9H), 8.85 (br, 1H). Found: C, 70.45; H, 5.14; N, 5.44%. Calcd for $C_{15}H_{13}NO_3$: C, 70.58; H, 5.13; N, 5.49%.

b): Concentrated sulfuric acid (3 drops) was added to a solution of **1** (216 mg, 1.3 mmol) and *o*-aminophenol (287 mg, 2.6 mmol) in acetic acid (5 ml). The mixture was refluxed for 3 h. After removal of the acetic acid under reduced pressure, the residue was dissolved in chloroform, washed with saturated sodium hydrogencarbonate solution and twice with water, and dried over anhydrous sodium sulfate. The chloroform was evaporated off and the residue was chromatographed on two Wakogel B-10 plates (30×30 cm²) with chloroform to afford 10 mg (3%) of 6-acetylcyclohepta[*b*][1,4]benzoxazine (**4**) as dark brown plates (from benzene–hexane); mp 97—99 °C; IR ($CHCl_3$) 1705 cm^{-1}; UV (CH_3OH) 265 (log ε 4.38), 432 nm (4.31); UV (CH_3OH+HCl) 229 (log ε 4.39), 274 (4.36), 325 (3.85), 461 nm (3.92); NMR ($CDCl_3$) δ=2.38 (s, 3H, $COCH_3$), 5.7—6.2 (m, 4H, H-7,8,9,10), 6.4—7.3 (m, 4H, H-1,2,3,4). Found: C, 75.90; H, 4.77; N, 5.92%. Calcd for $C_{15}H_{11}NO_2$: C, 75.93; H, 4.67; N, 5.90%.

*Cyclization of 2-Acetyl-7-(*o*-hydroxyanilino)tropone (**3**).* A solution of **3** (178 mg) in acetic acid (5 ml) containing concentrated sulfuric acid (3 drops) was refluxed for 2 h. The reaction mixture was worked up, as mentioned above, to give 87 mg (53%) of **4**.

*Reaction of 2-Acetyl-7-methoxytropone (**2a**) with* o*-Aminophenol. a)*: A mixture of 2-acetyl-7-methoxytropone (**2a**) (206 mg, 1.2 mmol) and *o*-aminophenol (234 mg, 2.1 mmol) in absolute ethanol (15 ml) was refluxed for 4 h. The reaction mixture was worked up, as mentioned above, to give 135 mg (44%) of **3**.

b): A solution of **2a** (181 mg, 1.1 mmol) and *o*-aminophenol (217 mg, 1.9 mmol) in acetic acid (5 ml) containing concentrated sulfuric acid (3 drops) was refluxed for 4 h. The reaction mixture was worked up, as mentioned above, to give 79 mg (33%) of **4**.

*Reaction of 3-Acetyl-2-methoxytropone (**2b**) with* o*-Aminophenol. a)*: A mixture of 3-acetyl-2-methoxytropone (**2b**) (275 mg, 1.5 mmol) and *o*-aminophenol (328 mg, 3.0 mmol) in absolute ethanol (15 ml) was refluxed for 5 h. After removal of the solvent, the residue was twice chromatographed on two Wakogel B-10 plates (30×30 cm²) with chloroform to afford 122 mg (31%) of 3-acetyl-2-(*o*-hydroxyanilino)tropone (**5**) as reddish brown needles (from benzene–hexane); mp 149—150 °C; IR ($CHCl_3$) 3370, 3200, 1720, 1600 cm^{-1}; UV (CH_3OH) 252 (log ε 4.30), 425 nm (4.18); UV (CH_3OH+HCl) 396 nm (log ε 3.96); NMR ($CDCl_3$) δ=2.03 (s, =C(OH)-CH_3), 2.50 (s, -C(=O)-CH_3), 6.5—7.5 (m, 9H), 9.62 (br, 1H); NMR (CD_3OD) δ=2.02 (s, 3H, =C(OH)-CH_3), 6.5—7.5 (m, 9H). Found: C, 70.56; H, 5.22; N, 5.27%. Calcd for $C_{15}H_{13}NO_3$: C, 70.58; H, 5.13; N, 5.49%.

b): A solution of **2b** (178 mg, 1.0 mmol) and *o*-aminophenol (217 mg, 2.0 mmol) in acetic acid (5 ml) containing concentrated sulfuric acid (3 drops) was refluxed for 5 h. The acetic acid was evaporated off under reduced pressure and the residue was worked up, as mentioned above, to give 65 mg (27%) of 10-acetylcyclohepta[*b*][1,4]benzoxazine (**6**) as dark brown plates; mp 124—125 °C; IR ($CHCl_3$) 1700 cm^{-1}; UV (CH_3OH) 263 (log ε 4.28), 425 nm (3.95); UV (CH_3OH+HCl) 236 (log ε 4.27), 267 (4.15), 275 (4.13), 336 (3.80), 406 (3.78), 452 nm (sh, 3.73); NMR ($CDCl_3$) δ=2.40 (s, 3H, $COCH_3$), 5.5—6.5 (m, 4H, H-6,7,8,9), 6.6—7.0 (m, 4H, H-1,2,3,4). Found: C, 75.92; H, 4.83; N, 5.74%. Calcd for $C_{15}H_{11}NO_2$: C, 75.93; H, 4.67; N, 5.90%.

*Cyclization of 3-Acetyl-2-(*o*-hydroxyanilino)tropone (**5**).* A solution of **5** (106 mg) in acetic acid (5 ml) containing concentrated sulfuric acid (3 drops) was refluxed for 1.5 h. The reaction mixture was worked up, as mentioned above, to give 54 mg (55%) of **6**.

The present work was supported in part by a Grant-in-Aid for Scientific Research No. 56540308 from the Ministry of Education, Science and Culture.

References

1) T. Nozoe, Y. Kitahara, K. Takase, and M. Sasaki, *Proc. Jpn. Acad.*, **32**, 349 (1956).

2) T. Fukunaga, 23rd IUPAC Congress, Boston, 1971.

3) T. Nozoe, H. Okai, and T. Someya, *Bull. Chem. Soc. Jpn.*, **51**, 2185 (1978).

4) T. Nozoe, T. Asao, and K. Takahashi, *Bull. Chem. Soc. Jpn.*, **34**, 146 (1961).

5) K. Imafuku, A. Yamane, and H. Matsumura, *J. Heterocycl. Chem.*, **18**, 335 (1981).

6) T. Nozoe, Y. Kitahara, K. Doi, and T. Arai, *Tohoku Daigaku Hisui-yoeki Kagaku Kenkyusho Hokoku*, **7**, 13 (1957).

7) K. Imafuku and A. Shimazu, *Synthesis*, **1982**, in press.

Hydrogen Peroxide-catalyzed Ozonation of Refractory Organics. I. Hydroxyl Radical Formation

Keisuke NAMBA* and Shigeki NAKAYAMA
Product Development Laboratory, Mitsubishi Electric Corporation, Amagasaki, Hyogo 661
(Recieved November 30, 1981)

Synopsis. The kinetics of hydrogen peroxide-catalyzed ozonation was studied in aqueous solutions of various lower alcohols containing ethanol as a reference. The relative rates of degradation of alcohols obtained support the initiation of the reaction by hydroxyl radicals formed in the reaction between ozone and hydrogen peroxide.

The use of ozone for water treatments has been growing steadily in responce both to increasing requirement for environmental protection and to recent improvement in the efficiency of ozone generator.[1] Ozone is known to be efficient in decolorization of effluents containing organics, but believed generally to be ineffective toward removal of COD (Chemical Oxygen Demand) and TOC (Total Organic Carbon). This may be ascribed to the characteristics of ozone which reacts very rapidly with unsaturated compounds but slowly with saturated ones.

The authors have been studying catalytic ozonation to remove COD and TOC in effluents containing refractory organics, and developed several ozonation methods, *i.e.*, high-pH ozonation,[2] UV-irradiated ozonation[3] and hydrogen peroxide (H_2O_2)-catalyzed ozonation.[4] Of these methods, H_2O_2-catalyzed ozonation is the most practical because of its simplicity and economic advantage, and was commercialized to remove COD in the effluent from an electrodeposition process.

In a series of investigations on the reaction mechanism of H_2O_2-catalyzed ozonation, the authors found that hydroxyl radical is formed and acts as an initiator for the oxidation of refractory organics. The present paper reports an experimental result supporting the OH radical formation.

Experimental

Ozonation was carried out at room temperatures (22—27 °C) by using an apparatus shown in Fig. 1. Ozone was generated from oxygen (99.98%) in a Mitsubishi OS-1 ozonizer (max. capacity, 2 g-O_3/h). The stream of ozonized oxygen from the ozonizer, containing 20 g/m³ ozone, was passed at a constant flow rate of 1000 cm³/min through a 1000 cm³ gas absorption bottle (6.5 cm I.D.) filled with various solutions for ozonation. An ozone monitor was set up for measuring ozone concentration in the inlet and outlet gas stream.

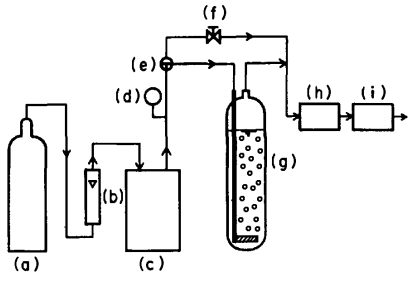

Fig. 1. Apparatus. (a): O_2-cylinder, (b): flow meter, (c): ozonizer, (d): pressure gauge, (e): three-way cock, (f): needle valve, (g): gas absorption bottle (reactor), (h): ozone monitor, (i): activated carbon column.

Aqueous solutions (*ca.* 1—10^{-1} mol/m³) of methanol, ethanol, 1-propanol, 2-propanol, 1-butanol, 2-methyl-1-propanol, 2-butanol, and 2-methyl-2-propanol were used for the ozonation. All chemicals were of commercially available reagent grade. H_2O_2 was added to the solution just before the ozonation. The pH of the solution was kept 7.5 during the ozonation by dosing sodium hydroxide; otherwise, the pH decreased gradually with the reaction time.

The concentrations of alcohols and the reaction products were measured by a gas chromatograph with a flame ionization detector and 2 m packed columns of PORAPAK-Q, -N and TENAX-GC. H_2O_2 concentration was measured by means of iodometry using ammonium molybdate.

Results and Discussion

The degradation of ethanol by ozone (feeding rate, 20 mg/min) in the presence of H_2O_2 (initial concentration, 5×10^{-1} mol/m³) is shown in Fig. 2. The effect of H_2O_2 on enhancement of the degradation of alcohols is remarkable. Figure 3 shows a typical reaction profile of H_2O_2-catalyzed ozonation: ethanol disappeared rapidly in the early stage of the reaction consuming about equimolar amount of ozone and acetaldehyde and acetic acid were formed in the later stage. TOC was also decreased after an induction period. The molar ratio of consumed H_2O_2 to consumed ozone was about 1/20. The amount of organics fleeing from the bottle during the ozonation was confirmed to be negligible. These results indicate clearly that H_2O_2 accelerates ozone

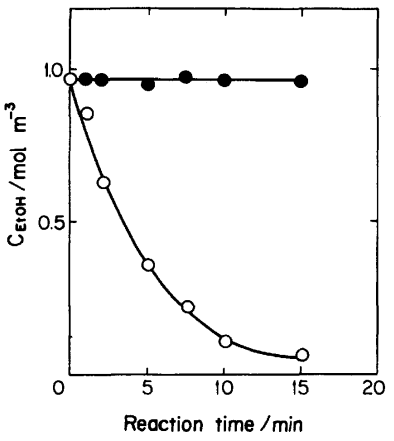

Fig. 2. Effect of H_2O_2 on the degradation of ethanol in water.
Temp: 25 °C, pH: 7.5, —○—: $[H_2O_2]_i=5\times10^{-1}$ mol/m³, —●—: $[H_2O_2]_i=0$ mol/m³.

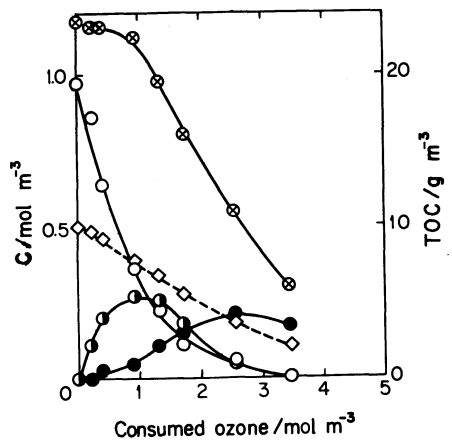

Fig. 3. H_2O_2-catalyzed ozonation of ethanol in water.
Temp: 25 °C, pH: 7.5, —○—: ethanol, —◑—: acetaldehyde, —●—: acetic acid, —⊗—: TOC, --◇--: H_2O_2.

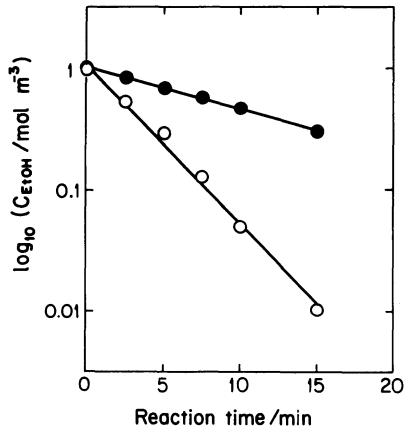

Fig. 4. Competitive degradation of ethanol and 2-methyl-2-propanol in water by H_2O_2-catalyzed ozonation.
Temp: 25 °C, pH: 7.5, —○—: ethanol, —●—: 2-methyl-2-propanol.

oxidation of ethanol.

The mechanism of the acceleration may be attributed to HO radical formation by the reaction of H_2O_2 with ozone, as was suggested by Taube and Bray.[5] In order to comfirm the assumption, the relative rate constants for the degradation of several lower alcohols were determined by competition kinetic measurements, and compared with the literature values.[6] Solutions containing two kinds of alcohols, with ethanol being the reference, were ozonized in the presence of H_2O_2, and relative rate constants were obtained, by assuming first order reaction rate with respect to concentration of alcohol, from the following equation:

$$k_{rel} = \frac{\ln([C_1]_f/[C_1]_i)}{\ln([C_2]_f/[C_2]_i)},$$

where C_1 and C_2 are the concentrations of objective alcohol and ethanol, respectively, the subscripts i and f denoting the conditions before and after the reaction, respectively. Figure 4 shows a typical profile of competitive degradation obtained with a mixed solution of ethanol and 2-methyl-2-propanol. The values of k_{rel} obtained are shown in Table 1 together with those obtained for the reactions between alcohols and HO radical.[6] It should be noted that both values agree quite well with each other, which means that the oxidation of alcohols is initiated by HO radical in the H_2O_2-catalyzed ozonation.

Table 1. Relative degradation rate constants of lower alcohols in water by H_2O_2-catalyzed ozonation and HO radical

Compound	k_{rel}	k_{ROH}/k_{EtOH} [a)]
Methanol	0.40	0.46
Ethanol	1	1
1-Propanol	1.51	1.48
2-Propanol	1.17	1.10
1-Butanol	2.12	2.19
2-Methyl-1-propanol	1.93	1.80—1.91
2-Butanol	1.53	1.31—1.69
2-Methyl-2-propanol	0.28	0.28

a) Calculated value from Ref. 6.

References

1) N. Tabata, "2nd International Symposium on Ozone Technology," International Ozone Institute, (1976), pp. 120—131.

2) S. Nakayama and I. Yoshiyasu, 31st National Meeting of Chemical Society of Japan, Sendai, October, 1974.

3) S. Nakayama and K. Esaki, *Mizu Shori Gijutsu*, **19**, 241 (1978).

4) S. Nakayama, Y. Taniguchi, K. Namba, and N. Tabata, *Ozone; Sci. Engr.*, **1**, 119 (1979).

5) H. Taube and W. C. Bray, *J. Am. Chem. Soc.*, **62**, 3357 (1940).

6) Leon M. Dorfman and Gerald E. Adams, "Reactivity of the Hydroxyl Radical in Aqueous Solutions," NSRDS-National Bureau of Standards-46, U. S. Government Printing Office, Washington, D. C. (1973).

Synthesis of Polymethyl Crown Ethers. A New Class of Lipophilic Crown Ethers

Isao IKEDA, Shingo YAMAMURA, and Mitsuo OKAHARA*

Department of Applied Chemistry, Faculty of Engineering, Osaka University, Yamadaoka 2-1, Suita, Osaka 565

(Received February 15, 1982)

Synopsis. A new class of lipophilic polymethyl crown ethers were synthesized from oligopropylene glycols *via* the intramolecular cyclization, and the stability constants of some complexes in methanol were determined.

Crown ethers show a superior ability as catalyst in nucleophilic substitution reaction of solid-liquid phase-transfer systems. In the case of liquid-liquid systems, however, quaternary onium salts usually show a better performance than ordinary crown ethers. The differences in effectiveness as phase transfer catalysts between crown ethers and quaternary salts may be attributed to the difference of lipophilicity between crown complexed cations and quaternary onium cations.

To overcome this unsatisfactory ability of crown ethers, some investigators[1-4] introduced a lipophilic group, such as an alkyl group or an acyl group, into the crown ether molecule. Although these lipophilic crown ethers also show excellent performance in the extraction and the transportation of salts, their preparation is tedious and require the use of uncommon reagents.

Previously we reported a new method for the preparation of crown ethers by the intramolecular cyclization of substituted and unsubstituted oligoethylene glycols.[5-7] Now we have found that the intramolecular cyclization method could be successfully applied to the preparation of polymethyl crown ethers which have not been prepared previously except for tetramethyl-12-crown-4,[8] from oligopropylene glycols. Introduction of polymethyl groups on the crown ring endows an additional lipophilicity in a different way from the known substituents and may improve the function of the crown ethers. The raw materials, penta-, hexa-, and heptapropylene glycol, were isolated from polypropylene glycol #400 by fractional distillations.

In the cyclization reaction of oligopropylene glycols, three kinds of condensations may generally take place, since the glycols are made up of three combinations of primary and secondary hydroxyl groups, depending on the origin of the oligopropylene glycols. Among these three kinds of condensations, there should be differences in reactivity and selectivity. Therefore, it is necessary to determine the ratio of the primary to secondary hydroxyl groups in the glycols. ^{1}H-NMR of acetylated hexapropylene glycol, examined as an example, showed a sextet signal at δ=4.91 and no signal at around δ=4.0—4.6, indicating the absence of primary hydroxyl group at least in the extent of NMR precision [CCl_4, δ; 1.0—1.3 (two d, 18H), 1.96 (s, 6H), 3.2—3.7 (m, 16H), 4.91 (sxt, 2H)]. Good yields of the polymethyl crown ethers prove the successful application of the intramolecular cyclization method to glycols which have two secondary hydroxyl groups.

The yields of polymethyl crown ethers seemed to be somewhat low compared with those of the cyclization of oligoethylene glycols in which two primary hydroxyl groups were concerned. This depended on the production of allyl ethers as by-product *via* elimination reaction.

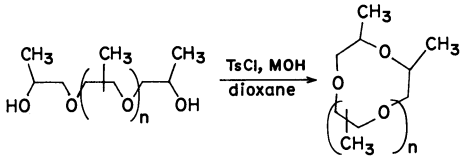

1a-c 2a-c

a; n=3, M=Na **b**; n=4, M=K **c**; n=5 M=K

Scheme

To inspect the influences of polymethyl substitution on the complexation with metal cation, stability constants with sodium and potassium cations in methanol were determined and compared with those of unsubstituted crown ethers (Table 2). Polymethyl groups

Table 1. Preparation of polymethyl crown ethers

Crown ether	Yield[a] %	Bp θ_b/°C (Torr)
Pentamethyl-15-crown-5 (**2a**)	30	100 (0.1)
Hexamethyl-18-crown-6 (**2b**)	37	105 (0.05)
Heptamethyl-21-crown-7 (**2c**)	27	115 (0.05)

a) Yield of pure, isolated product; not optimized. b) Kugelrohr distillation. c) Satisfactory microanalyses obtained (C±0.34, H±0.06). The ^{1}H-NMR spectra (CCl_4) of **2** showed two signals at δ=1.04 (d, 3(n+2)H, CH_3) and at δ=3.0—4.0 (m, 3 (n+2)H, OCH_2CHO). The mass spectra showed the parent peak, m/e=117 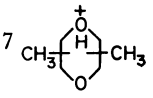 and m/e=59 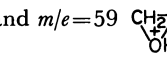 respectively.

Table 2. Stability constants of polymethyl crown ethers with metal cations

Crown ether	log K'[a]	
	Na^+	K^+
Pentamethyl-15-crown-5 (**2a**)	3.34	2.85
15-Crown-5	3.31	(3.34—3.55)[b]
Hexamethyl- 18-crown-6 (**2b**)	2.94	3.86
18-Crown-6	4.32[c]	6.10[c]
Heptamethyl-21-crown-7 (**2c**)	2.34	3.27
21-Crown-7	2.46	4.41[c]

a) In methanol, 25 °C. b) This value depends on the ratio of K^+ cation and the ligand. Considering the formation of 2 : 1 complex, log K'_1=3.36 and log K'_2=2.62 were obtained. c) Values reported in Ref.[9]

somewhat inhibit the complexation of crown ring with metal cations, probably due to the steric effect, and thence the rigidity of the crown rings. The stability constants of complexes, however, remained still high especially for hexamethyl-18-crown-6 with potassium cation, log $K'=3.86$, and for pentamethyl-15-crown-5 with sodium cation, 3.34. The catalytic activity and extraction activity of the polymethyl crown ethers are under investigation.

Experimental

The ^{1}H-NMR spectra were taken at 100 MHz on a JEOL JNM-PS-100 spectrometer using the tetramethylsilane internal standard. The infrared spectra were obtained on a Hitachi 260-10 spectrometer. The mass spectra were taken at an ionization potential of 70 eV on a Hitachi RMU-6E mass spectrometer.

Isolation of Oligopropylene Glycol. Commercial polypropylene glyco ♯400 were fractionally distilled to separate penta-, hexa-, and heptapropylene glycol (95—97 °C/0.05 Torr (1 Torr≈133.3 Pa), 116—118 °C/0.005 Torr and 155—158 °C/0.005 Torr, respectively). They showed a single peak in each gas liquid chromatogram (silicone gum SE30 10%, 270 °C).

Polymethyl Crown Ethers. General Procedure: A mixture of hexapropylene glycol (3.6 g, 0.01 mol), tosyl chloride (2.0 g, 0.01 mol) and dioxane (30 ml) was added to a suspension of pulverized potassium hydroxide (2.7 g, 0.04 mol) in dioxane (50 ml) over a period of 2 h under stirring at 60 °C, and stirred for an additional 4 h at the same temperature. The precipitate was separated off by filtration and washed twice with dioxane. After evaporation of the dioxane from the combined solution of filtrate and washings, the resulting viscous pale yellow liquid (4.2 g) was chromatographed on silica gel, and eluted with a mixture of hexane and acetone (95 : 5) to give a colorless liquid (**2b**, 1.3 g, 37%). The yields of the crown ethers are summarized in Table 1. Mutual relations of methyl groups on a macrocycle can not be resolved, because the raw oligopropylene glycols do not have regular structures, which are prepared by addition of propylene oxide to propylene glycol in alkaline conditions.

Isolation of Allyl Ethers. By-product allyl ethers were isolated from the crude product on a silica-gel column (hexane–acetone, 90 : 10), as a following fraction of the objective polymethyl crown ethers, IR (neat film); 3090, 1645, 1000, and 920 cm^{-1}, ^{1}H-NMR (CCl_4, δ); 3.98 (d+m, 2H), 5.02 (d+d, 1H), 5.18 (d+d, 1H), and 5.8 (m, 1H).

References

1) D. Landini, F. Montanari, and F. M. Pirisi, *J. Chem. Soc., Chem. Commun.*, **1974**, 879.
2) M. Cinquini and P. Tundo, *Synthesis*, **1976**, 516.
3) W. W. Parish, P. E. Stott, C. W. McCausland, and J. S. Bradshaw *J. Org. Chem.*, **43**, 4577 (1978).
4) P. E. Stott, J. S. Bradshaw, and W. W. Parish, *J. Am. Chem. Soc.*, **102**, 4810 (1980).
5) P.-L. Kuo, M. Miki, and M. Okahara, *J. Chem. Soc., Chem. Commun.*, **1978**, 504.
6) N. Kawamura, M. Miki, I. Ikeda, and M. Okahara, *Tetrahedron Lett.*, **1979**, 535.
7) I. Ikeda, S. Yamamura, Y. Nakatsuji, and M. Okahara, *J. Org. Chem.*, **34**, 5355 (1980).
8) J. L. Down, J. Lewis, B. Moore, and G. Wilkinson, *J. Chem. Soc.*, **1959**, 3767.
9) H. K. Frensdorff, *J. Am. Chem. Soc.*, **93**, 600 (1971).

Reaction between Enamines and Schiff Basess.[1] Evidence for the Thermal [2+2] Cycloaddition Reaction

Yujiro NOMURA,* Muneaki KIMURA, Tomoyuki SHIBATA,
Yoshito TAKEUCHI, and Shuji TOMODA
Department of Chemistry, College of General Education, The University of Tokyo, Komaba, Meguro-ku, Tokyo 153
(Received February 25, 1982)

Synopsis. Reaction between 4-(1-phenyl-1-propenyl)morpholine and *N*-benzylideneanilines provided *N*-(3-aryl-2-methyl-1-phenylallylidene)anilines in 60—65% yields, which unequivocally established the initial [2+2] cycloaddition reaction between enamines and Schiff bases.

Thermal [2+2] cycloaddition reactions are generally prohibited by the Woodward-Hoffmann rule.[2] Several exceptions involving Schiff bases include reactions with electron-deficient double bonds, such as heterocumulenes, N=O bond, and C=C bond carrying highly electronegative substituents.[3] More recently, titanium(IV) chloride-mediated [2+2] cycloadditions between Schiff bases and ketene acetals, representative electron-rich olefins, have been reported.[4]

In our previous communications, we postulated thermal [2+2] cycloaddition reaction between *N*-benzylideneanilines and enamines, another class of highly nucleophilic olefins, as the most reasonable explanation for the formation of decahydroacridines[5] and hexahydro-4-azaindacenes[6] in acetic acid as the solvent. We wish to present herein direct evidence for the intermediacy of the [2+2] cycloadduct in the reaction between the enamine (**1**) and the Schiff bases (**2**) in acetic acid.

The reactions between *N*-benzylideneanilines (**2**) and 4-(1-phenyl-1-propenyl)morpholine (**1**) were performed at room temperature under nitrogen using acetic acid as the solvent. The products, *N*-(3-aryl-2-methyl-1-phenylallylidene)anilines (**3**), were obtained in 60—65% yield after recrystallization from methanol (Table 1).

Structural assignments of these products were based on elemental analysis, spectroscopic methods and independent synthesis of their hydrolyzed products. For example, **3a**, which had a sharp melting point (mp 108—109 °C), showed strong IR absorption bands at 1605 and 1590 cm^{-1}, one of which can be assigned to the conjugated imine moiety. On the other hand, the ^1H NMR spectrum, obtained as a solution in deuteriochloroform, exhibited two methyl doublets (in each case, $J=1$ Hz; assigned to allylic coupling with the olefinic proton) due to *syn-anti* isomerism about the C=N double bond (Table 2). The relatively large difference in the chemical shifts of the methyl group between the *syn* and *anti* isomers of **3a** ($\Delta\delta=0.58$) can be attributed to the strong shielding effect of the *N*-aryl ring (Ar^2) on the methyl protons in the *syn* isomer[7] which may most probably exist as the *s-trans* conformational isomer by steric reasons.

Since these spectral and analytical informations alone may not be sufficient to prove the structure **3a**, we hydrolyzed it with MeOH–HCl to obtain the α,β-unsaturated ketone (**4a**) virtually quantitatively (98% yield). The ^1H NMR spectrum of **4a** indicated one methyl doublet ($J=1$ Hz) in accord with nearly complete stereospecificity of the reaction leading to **3a**. This was also in agreement with the experimental observation that the stereoisomerism observed for **3** by ^1H NMR is due to *syn-anti* isomerism rather than *cis-trans* isomerism involving the olefinic C=C double bond. The structure of **4a** was confirmed by spectral (IR and ^1H NMR) comparison with an authentic sample prepared by the aldol condensation between *p*-chlorobenzaldehyde and propiophenone.[8]

The present reaction can be rationalized by the mechanism illustrated in Scheme 1. Reaction between **1** and **2** would produce the azetidine intermediate (**5**) either by concerted [2+2] cycloaddition or by stepwise cycloaddition *via* zwitterionic intermediate as **6**. The azetidine intermediate **5** would rapidly undergo deamination in the acid medium to afford 2-azetine derivative

TABLE 1. SYNTHESIS AND PROPERTIES OF **3**

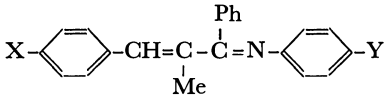

3

Compd	X	Y	Mp θ_m/°C[a]	Yield/%[b]	M+(*m/e*)	Mol. Formula	Found (Calcd) (%) C	H	N	Cl
3a	Cl	H	108—109	62	331	$C_{22}H_{18}NCl$	79.83 (79.63	5.24 5.47	4.31 4.22	10.95 10.68)
3b	Cl	Cl	112—113	60	365	$C_{22}H_{17}NCl_2$	71.86 (72.14	4.53 4.68	4.07 3.82	19.52 19.36)
3c	Cl	CH_3O	132—133	63	361	$C_{23}H_{20}NOCl$	76.26 (76.34	5.43 5.57	3.86 3.87	9.83 9.80)
3d	NO_2	H	140—141	65	342	$C_{22}H_{18}N_2O_2$	77.34 (77.17	5.24 5.30	8.04 8.18)	— —

a) Uncorrected. b) Isolated yield (recrystallized from methanol). c) Measured at 70 eV.

Table 2. ^{1}H NMR spectra of *syn* and *anti* isomers of **3**[a]

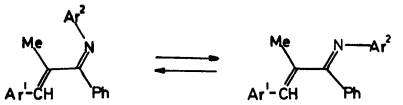

syn-**3** *anti*-**3**

Compd	δ (Me)[b] *syn*	δ (Me)[b] *anti*	δ(sp²-protons)[c]	*syn* : *anti*[d]
3a	1.78	2.36	6.3—7.9	32 : 68
3b	1.82	2.35	6.1—8.1	34 : 66
3c	1.84	2.38	6.4—8.0	31 : 69
3d	1.88	2.40	6.4—8.1	35 : 65

a) 100 MHz NMR spectra obtained in $CDCl_3$ with tetramethylsilane as internal standard. Assignments of these isomers were based on Ref. 7. b) Each peak shows up as a finely-split doublet with a coupling constant of about 1 Hz. c) Benzylidene and aromatic protons (multiplet). d) Determined by ^{1}H NMR integration of the methyl groups.

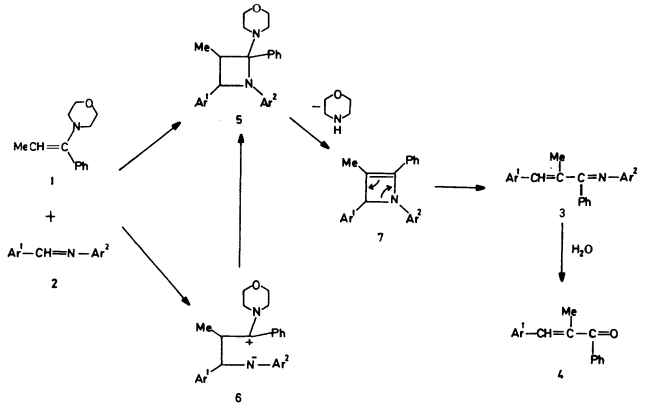

Scheme 1. Mechanism for the formation of **3**.

7, which would then collapse into the conjugated imine **3** by ring-opening process. Whether the [2+2] cycloaddition route is concerted or stepwise, it is intriguing that this route appears to be operative only in acetic acid.[9]

Experimental

Enamine (**1**) was prepared according to the procedure previously described.[10] *N*-Benzylideneanilines (**2**) were prepared by the known method.[11] Acetic acid was distilled over phosphorus pentaoxide under nitrogen. Melting points were uncorrected. IR spectra were recorded as nujol paste with a HITACHI EPS-3T Recording Spectrometer. ^{1}H NMR spectra were obtained on a JEOL JNM-MH-100 Spectrometer operated at 100 MHz. Elemental analyses were performed by Organic Analysis Laboratory of the University of Tokyo.

General Procedure for the Reaction between ***1*** *and* ***2***: A solution of **2** (41 mmol) in anhydrous acetic acid (100 ml) was slowly added to enamine (**1**) (10.4 g, 51 mmol) with stirring at room temperature under nitrogen. The resulting yellow precipitates, obtained after 7 h stirring, were collected by filtration and recrystallized from methanol to give product **3** in 60—65% yields (see Tables 1 and 2 for pertinent data of **3**).

References

1) Enamines X of this series: Enamines IX, Ref. 6.
2) R. B. Woodward and R. Hoffmann, "The Conservation of Orbital Symmetry," Academic Press, New York (1970).
3) J.-P. Anselme, "Chemistry of the Carbon-Nitrogen Double Bond," ed by S. Patai, Interscience, New York (1970).
4) I. Ojima, S. Inaba, and K. Yoshida, *Tetrahedron Lett.*, **1977**, 3643.
5) Y. Nomura, S. Tomoda, and Y. Takeuchi, *Chem. Lett.*, **1972**, 79.
6) Y. Nomura, M. Kimura, Y. Takeuchi, and S. Tomoda, *Chem. Lett.*, **1978**, 427.
7) D. Y. Curtin and J. W. Hausser, *J. Am. Chem. Soc.*, **83**, 3474 (1961).
8) E. P. Kohler, *Am. Chem. J.*, **31**, 655 (1904).
9) Reactions between enamines and Schiff bases in neutral solvent, such as methanol, afford Stork products: see, S. Tomoda, Y. Takeuchi, and Y. Nomura, *Tetrahedron Lett.*, **40**, 3549 (1969).
10) R. W. Layer, *Chem. Rev.*, **63**, 489 (1963).
11) S. Hünig, E. Lücke, and W. Brenninger, *Org. Synth.*, **41**, 65 (1961).

α-Pentafluoropropionylation of Ketones and Aldehydes Using Hexafluoropropene Oxide. A Facile Synthesis of Fluorinated 1,3-Diketones

Takashi ISHIHARA,* Toshio SEKI, and Teiichi ANDO
Department of Industrial Chemistry, Faculty of Engineering, Kyoto University, Sakyo-ku, Kyoto 606
(Received March 29, 1982)

Synopsis. Hexafluoropropene oxide reacts smoothly with morpholine enamines from ketones and aldehydes at 0 °C to room temperature in anhydrous THF to give pentafluorinated 1,3-diketones in good yields. The keto-enol equilibrium in the products is generally in favor of their enol form.

Fluorinated 1,3-dicarbonyl compounds have proved to be of much value as intermediates in a variety of organic transformations and as extracting agents in inorganic syntheses.[1] Two types of methods have hitherto been used for preparing these compounds; (i) the base-promoted condensation of an ester with a ketone or an aldehyde, and (ii) the Lewis acid-catalyzed acylation of a fluorine-containing ketone with an acid anhydride. These reactions are, however, often accompanied by side reactions[1a,b,2] such as self-condensation or cleavage reaction, resulting in reduced yields of the desired fluorinated 1,3-dicarbonyl compounds. In our continuing studies to extend the utilities of hexafluoropropene and its oxide to organic syntheses, we have now found that hexafluoropropene oxide (HFPO) reacts smoothly with enamines from ketones and aldehydes under mild, neutral conditions.

This paper describes the α-pentafluoropropionylation of ketones and aldehydes using HFPO, which provides a convenient method for the synthesis of fluorinated 1,3-diketones.

Results and Discussion

In the present study the morpholine enamines from ketones and aldehydes were chosen as the starting enamine. The reaction of the enamines with HFPO took place exothermically, requiring the use of a solvent. Among the solvents examined, freshly distilled, anhydrous THF gave the best results. The reactions cleanly proceeded under the conditions described in the Experimental to afford the corresponding pentafluoro 1,3-diketones (**1**—**6**) in good yields. Table 1 summarizes the results of the reactions, together with the keto : enol ratios in the products. The use of anhydrous ether as solvent strikingly decreased the yields of the products. Thus, the reactions of the morpholine enamines from cyclohexanone, 3-pentanone, and acetophenone with HFPO in ether gave the corresponding 1,3-diketones in yields of no more than 25%. These results must be due to much less solubility of HFPO in ether than in THF.[3]

The IR and ^{1}H NMR analyses of the pentafluoropropionylated compounds (**1**—**6**) thus obtained revealed that, except for **5**, they possess an extremely high enolic character. The keto : enol ratios, listed in Table 1, were determined by comparing the integrated intensity of the vinylic hydrogen or of the enolic hydrogen in the enol form with that of the α-methylene or methyl group in the keto form (Table 2). Compounds **1**, **2**, **4**, and **6** exist nearly exclusively as enols and compound **3** exists as a nearly equimolar mixture of the two tautomers, whereas **5** exhibits only the keto character.

To be noted is that the resonance peaks due to the enolic hydrogens are sharp (half-height width *ca.* 3—6 Hz) and appear at very low fields, *i.e.*, at 13—17 ppm, as shown in Table 2. These absorptions can be inter-

Table 1. Preparation of fluorinated 1,3-diketones

Enamine[a]	Product		Yield/% (keto : enol ratio)[b]
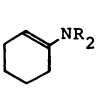	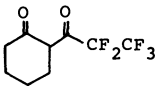	(**1**)	80 (0 : 100)
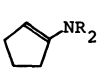	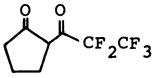	(**2**)	69 (0 : 100)
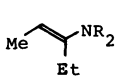	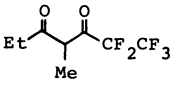	(**3**)	66 (50 : 50)
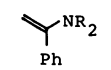	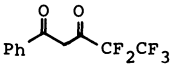	(**4**)	73 (0 : 100)
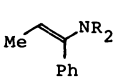	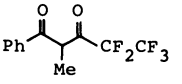	(**5**)	74 (100 : 0)
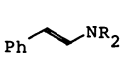	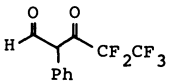	(**6**)	71 (0 : 100)

a) The NR_2 denotes the morpholino group. b) Determined by ^{1}H NMR analyses in CCl_4 solutions (15%).

Table 2. ^{1}H NMR parameters of the products

Compd	Chemical shifts and *J*/Hz
1	1.7 (m, 4H), 2.5 (m, 4H), 15.29 (s, 1H)
2	2.0 (m, 2H), 2.4 (m, 2H), 2.8 (m, 2H), 13.26 (s, 1H)
3	1.15 (t, 3H, 7.5), 1.94 (t, 3H, 2.9), 2.56 (q, 2H, 7.5), 16.10 (t, 1H, 1.8) 1.06 (t, 3H, 7.5), 1.34 (d, 3H, 6.9), 2.48 (q, 2H, 7.5), 4.01 (q, 1H, 6.9)
4	6.55 (s, 1H), 7.5 (m, 3H), 7.9 (m, 2H), 15.24 (s, 1H)
5	1.48 (d, 3H, 7.2), 4.88 (q, 1H, 7.2), 7.7 (m, 5H)
6	7.3 (m, 5H), 8.20 (s, 1H), 14.37 (s, 1H)

preted as characteristic of 1,3-dicarbonyl compounds containing electron-withdrawing substituent groups, on the basis of the generalization suggested by Lintvedt and Holtzclaw[4] and of the observations made by Engel and Chappelow.[5]

The strong and broad absorptions in the regions of 1690—1560 and 3500—2200 cm^{-1} in the IR spectra of these fluoro 1,3-diketones also reveal the presence of the intramolecularly hydrogen-bonded enolic structure. The former absorption can be ascribed to the conjugate chelation[6] of the keto groups in the molecule.

In the reactions of the morpholine enamines from acetophenone, propiophenone, and phenylacetaldehyde with HFPO, pentafluoropropionylated enamines[7] were obtained when the reaction was quenched with a 5% $NaHCO_3$ aqueous solution, instead of an acid. Successive acid treatment of them gave the corresponding 1,3-diketones (**4**—**6**). These facts strongly suggest that the initial step of the reaction is the isomerization of HFPO[8] to pentafluoropropionyl fluoride by an enamine, followed by the acylation of the enamine with the acid fluoride to give the products.

Experimental

Infrared spectra were recorded with a Shimadzu IR-400 infrared spectrometer. A Varian EM-390 spectrometer was used to measure ^1H and ^{19}F NMR spectra, in solutions of CCl_4 with internal Me_4Si and external trifluoroacetic acid as a reference, respectively. Mass spectra were obtained with a Hitachi RMS-4 spectrometer.

The morpholine enamines from ketones and aldehydes were prepared according to the literature procedure.[9]

General Procedure for the Reaction of HFPO with Morpholine Enamines. Into a stirred solution of a morpholine enamine (25 mmol) in anhydrous THF (25 ml), which had been cooled to −20 to −15 °C, was introduced HFPO (16 mmol) under nitrogen at such a rate that the reaction temperature should not rise over 0 °C. After the introduction of HFPO was over, the whole mixture was stirred at room temperature for 20 h. In the case of the morpholine enamine from 3-pentanone, the temperature was maintained at −50 to −40 °C for 10 h and then at room temperature for 10 h. To the mixture was added 5% HCl (20 ml) dropwise under cooling with an ice–water bath. After stirred at room temperature for 2 h, the reaction mixture was poured into water (70 ml). The organic layer was separated and the aqueous layer was extracted with ether. The combined extracts were washed with water, dried (Na_2SO_4), and concentrated under reduced pressure. The residual oil was chromatographed on silica gel with hexane or benzene and, if necessary, the product was distilled *in vacuo* to give a pure 1,3-diketone.

When the reaction was quenched with a 5% $NaHCO_3$ aqueous solution, β-pentafluoropropionylated morpholine enamines were obtained as the product.

*2-(Pentafluoropropionyl)cyclohexanone (**1**)*: Bp 77—78 °C/20 mmHg (1 mmHg = 133.3 Pa) (lit,[10] bp 104.5 °C/42 mmHg); IR (film) 3300—2400, 1620—1560, 1260—1100, 1036, 922, 725 cm^{-1}; ^{19}F NMR δ −3.34 (s, 3F), −39.86 (s, 2F); MS *m/e* (%) 244 (M^+, 35), 125 (100).

*2-(Pentafluoropropionyl)cyclopentanone (**2**)*: Bp 83—84 °C/35 mmHg (lit,[10] bp 82 °C/30 mmHg); IR (film) 3400—2250, 1690, 1633, 1330, 1288, 1205, 1098, 1029, 1016, 815, 744 cm^{-1}; ^{19}F NMR δ −4.65 (t, J = 1.7 Hz, 3F), −43.08 (q, J = 1.7 Hz, 2F); MS *m/e* (%) 230 (M^+, 42), 111 (100).

*1,1,1,2,2-Pentafluoro-4-methyl-3,5-heptanedione (**3**)*: Bp 82—84 °C/54 mmHg; IR (film) 3500—2300, 1758, 1717, 1632, 1328, 1200, 1120, 1084, 1072, 972 cm^{-1}; ^{19}F NMR δ −3.35 (s, 3F), −43.60 and −43.70 (two s, 2F) for the keto form, −3.95 (t, J = 1.7 Hz, 3F), −38.02 (m, 2F) for the enol form; MS *m/e* (%) 232 (M^+, 4), 57 (100).

Found: C, 41.60; H, 3.78%. Calcd for $C_8H_9F_5O_2$: C, 41.39; H, 3.91%.

*4,4,5,5,5-Pentafluoro-1-phenyl-1,3-pentanedione (**4**)*: Bp 75.5—76.5 °C/4 mmHg (lit,[10] bp 128.5 °C/28 mmHg); IR (film) 3200—2300, 1606, 1576, 1330, 1203, 1126, 1028, 1010, 998, 768, 690 cm^{-1}; ^{19}F NMR δ −4.05 (s, 3F), −45.00 (s, 2F); MS *m/e* (%) 266 (M^+, 43), 69 (100).

*4,4,5,5,5-Pentafluoro-2-methyl-1-phenyl-1,3-pentanedione (**5**)*: Bp 75—75.5 °C/1 mmHg; IR (film) 1762, 1682, 1452, 1335, 1278, 1210, 1110, 970, 718, 704 cm^{-1}; ^{19}F NMR δ −3.63 (s, 3F), −43.30 and −43.57 (two s, 2F); MS *m/e* (%) 280 (M^+, 2), 105 (100).

Found: C, 51.32; H, 3.11%. Calcd for $C_{12}H_9F_5O_2$: C, 51.44; H, 3.24%.

*4,4,5,5,5-Pentafluoro-2-phenyl-1,3-pentanedione (**6**)*: Mp 73.5—74.5 °C; IR (KBr) 3500—2300, 1608, 1592, 1377, 1230, 1183, 1133, 1119, 1035, 1020, 830, 716 cm^{-1}; ^{19}F NMR δ −3.17 (s, 3F), −37.53 (s, 2F).

Found: C, 49.77; H, 2.54%. Calcd for $C_{11}H_7F_5O_2$: C, 49.63; H, 2.65%.

This work was partially supported by a Grant-in-Aid for Scientific Research No. 56750596 from the Ministry of Education, Science and Culture. The authors wish to thank Daikin Kogyo Co. Ltd. for supplying the sample of HFPO.

References

1) a) P. Mushak, M. T. Glenn, and J. Savory, "Fluoro-β-diketones and Metal Fluoro-β-diketonates," in "Fluorine Chemistry Reviews," ed by P. Tarrant, Marcel Dekker, New York (1973), Vol. 6, p. 43; b) M. Hudlicky, "Chemistry of Organic Fluorine Compounds," 2nd ed, Wiley, New York (1976); c) W. H. Pirkle and P. L. Rinaldi, *J. Org. Chem.*, **43**, 4475 (1978) and references cited therein; d) T. J. Wenzel and R. E. Sievers, *Anal. Chem.*, **53**, 393 (1981).

2) R. Filler, Y. S. Rao, A. Biezais, F. N. Miller, and V. D. Beaucaire, *J. Org. Chem.*, **35**, 930 (1970).

3) N. Ishikawa, *Yuki Gosei Kagaku Kyokai Shi*, **35**, 131 (1977).

4) R. L. Lintvedt and H. F. Holtzclaw, Jr., *Inorg. Chem.*, **5**, 239 (1966).

5) J. F. Engel and C. C. Chappelow, Jr., *J. Chem. Eng. Data*, **16**, 381 (1971).

6) L. J. Bellamy, "The Infra-red Spectra of Complex Molecules," 2nd ed, Wiley, New York (1958), p. 184.

7) The spectroscopic (IR, MS, ^1H and ^{19}F NMR) and analytical data of the 4,4,5,5,5-pentafluoro-1-morpholino-1-penten-3-one derivatives obtained were in good agreement with the assigned structures.

8) N. Ishikawa and S. Sasaki, *Nippon Kagaku Kaishi*, **1976**, 1954; R. D. Chambers, "Fluorine in Organic Chemistry," Wiley, New York (1973), p. 229.

9) G. Stork, A. Brizzolara, H. Landesman, J. Szmuszkovicz, and R. Terrell, *J. Am. Chem. Soc.*, **85**, 207 (1963).

10) R. A. Moore and R. Levine, *J. Org. Chem.*, **29**, 1439 (1964).

Acid Catalysis of the Transformation of 1-Methoxycarbonyl-2-imidazoline to 1-Methoxycarbonyl-2-imidazolidinone, a Carboxybiotin Model

Hiroki KONDO,* Katsuhito MIURA, and Junzo SUNAMOTO
Department of Industrial Chemistry, Faculty of Engineering, Nagasaki University, Nagasaki 852
(Received April 26, 1982)

Synopsis. The transformation of 1-methoxycarbonyl-2-ethoxy-2-imidazoline into 1-methoxycarbonyl-2-imidazolidinone a 1-carboxybiotin model, is facilitated by acid.

Activation of biotin (**3**) through enolization of its urea moiety to form an isourea structure is an attractive hypothesis to account for the much higher reactivity of the coenzyme in enzymatic carboxylation reactions.[1] The putative enolbiotin may be generated by a variety of means, *e.g.*, phosphorylation by ATP of the urea moiety.[2] 2-Methoxy-2-imidazoline (**4**), a model for

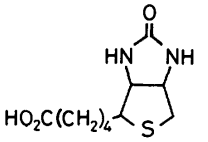

3

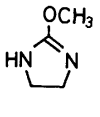

4

enolbiotin, shows a much higher nucleophilicity than the corresponding keto compound toward carboxylic esters.[3] The problem is that the enol form is regarded much less stable thermodynamically, and hence is unlikely to be present in a significant amount.[4] In addition, the isolated intermediate of biotin carboxylation is always 1-carboxybiotin (in its methyl ester form) and it serves as a carboxyl donor in the subsequent transcarboxylase reaction.[5] Therefore, if the enolbiotin hypothesis is correct, the question how the carboxylated enolbiotin is converted to the keto form should be answered unequivocally. We found that 1-methoxycarbonyl-2-imidazoline (**1**) is readily converted to 1-methoxycarbonyl-2-imidazolidinone (**2**) in the presence of acid such as hydrochloric acid and trifluoroacetic acid.

Results and Discussion

1 is a stable, isolable 2-alkylisourea derivative, just like 1,3-diisopropyl-2-ethylisourea.[6] It was established that 2-alkylisoureas undergo an S_N2 reaction with a nucleophile such as phenol to give alkyl phenyl ether and urea.[7] Reaction of **1** under acidic conditions apparently follows a similar pathway. Thus, treatment of **1** with hydrochloric acid in chloroform at 30 °C converts **1** into **2** quantitatively (Eq. 1). Since the pK_a value of **4** in water is 9.1,[3] **1** should be present in the protonated form at 3-N position under the present conditions. The

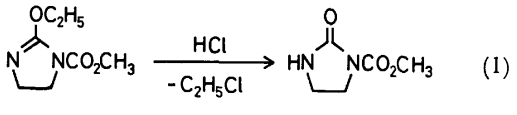

1 2 (1)

Table 1. Effect of acid strength on the rate of transformation of **1** into **2**

Acid	Solvent	pK_a[a]	Temp/°C	k_{obsd}/s^{-1}
HCl[b]	$CDCl_3$	−6.1	30	5×10^{-4}
Picric Acid[b]	DMSO-d_6	−0.2	25	2×10^{-4}
CF_3CO_2H	—	0.25	70	6.2×10^{-5}
CF_3CO_2H[c]	—		70	1.1×10^{-3}
$(CH_3O)_2PO(OH)$[b]	$CDCl_3$	1.29	60	0

a) Value in water. b) Equimolar to **1**. c) Thiophenol was added in 15-fold excess over **1**.

reaction can be carried out also in trifluoroacetic acid at 70 °C to produce **2** and ethyl trifluoroacetate (Table 1). Addition of 15-fold molar excess of thiophenol enhances the conversion rate by 18-fold, the reaction product being solely ethyl phenyl sulfide besides **2**. On the other hand, dimethyl hydrogenphosphate was found to be without effect under comparable conditions. These data indicate that the transformation reaction is highly dependent upon the acidity of the catalyst employed and the presence of a nucleophile as the ethyl acceptor (Table 1).[8] Picric acid is an exception. It has a pK_a value comparable to that of trifluoroacetic acid, but is by far the more effective than the latter. Thus, the rate constant for the transformation in DMSO-d_6 is 2×10^{-4} s^{-1} in the presence of equimolar picric acid at 25 °C. It should be noted that neither the reaction rate nor the reaction product (1-ethoxy-2,4,6-trinitrobenzene) is altered by the addition of excess thiophenol. This anomalous behavior of picric acid may be explicable in terms of formation of a picrate or the like with substrate prior to the transformation. This is reminiscent of a fact that in model as well as in enzymatic systems prior formation of a complex between substrate and catalyst is one of the driving forces for the efficient catalysis to occur.[9]

A similar acid catalysis of acyl transfer was observed for *O*-benzoyl-*N*,*N*-dimethyl-*N*′-(*N*-methyl-2,4-dinitroanilino)isourea, an isolable *O*-acylisourea derivative.[10] This reaction was accompanied by an intramolecular acyl migration to the imine nitrogen, though at low pH values such as 1 the proportion of the side reaction was suppressed to such an extent that the intermolecular reaction predominates by a large margin. It is noted that an analogous intramolecular alkyl migration has not been observed for **1** under the present conditions. The thermodynamic instability of 2-alkyl- or 2-acylisourea relative to the urea must be primarily responsible for the ready transformation of **1** into **2**,[4,11] and acid facilitates the reaction.[12] It would not be unrealistic to assume that the putative 1-carboxy-*O*-phosphoenolbiotin might be converted analogously to 1-carboxybiotin at the enzyme active site, possibly by general acid catalysis.

Experimental

2-Imidazolidinone (**5**) was obtained from Wako Pure Chemical Ind. 2-Ethoxy-2-imidazoline (**6**) was prepared according to a literature.[13] 1-Methoxycarbonyl-2-imidazolidinone (**2**) was synthesized by reaction of **5** with methyl chloroformate:[14] mp 179—181 °C (lit,[14] mp 180 °C). 1-Methoxycarbonyl-2-ethoxy-2-imidazoline (**1**) was prepared either by reaction of **6** with methyl chloroformate or by reaction of **2** with triethyloxonium tetrafluoroborate:[15] mp 67—69 °C (lit,[15] mp 67—70 °C). Reaction rates for the transformation of **1** into **2** were determined by ^{1}H NMR spectroscopy on a JEOL JNM-MH-100 spectrometer under conditions given in Table 1.

The authors thank the Ministry of Education, Science and Culture for financial support through Grants-in-Aid for Special Project Research 521325 and 56109007.

References

1) H. G. Wood and R. E. Barden, *Annu. Rev. Biochem.*, **46**, 385 (1977).
2) R. Kluger and P. D. Adawadkar, *J. Am. Chem. Soc.*, **98**, 3741 (1976).
3) A. F. Hegarty, T. C. Bruice, and S. J. Benkovic, *J. Chem. Soc., Chem. Commun.*, **1969**, 1173.
4) G. M. Maggiora, *J. Theor. Biol.*, **43**, 51 (1974).
5) R. B. Guchhait, S. E. Polakis, D. Hollis, C. Fenselau, and M. D. Lane, *J. Biol. Chem.*, **249**, 6646 (1974).
6) E. Schmidt and W. Carl, *Justus Liebigs Ann. Chem.*, **639**, 24 (1961).
7) F. L. Bach, *J. Org. Chem.*, **30**, 1300 (1965).
8) It does not appear feasible to correlate rates with acid strength in a quantitative manner, because pK_a values in water were used for the reaction in organic media and reactions were carried out in various solvents. Nevertheless, the rate difference among acids is large enough to offset this solvent effect.
9) W. P. Jencks, "Catalysis in Chemistry and Enzymology," McGraw-Hill, New York (1969), Chap. 1.
10) A. F. Hegarty, M. T. McCormack, G. Fergason, and P. J. Roberts, *J. Am. Chem. Soc.*, **99**, 2015 (1977).
11) M. J. Cravey and H. Kohn, *J. Am. Chem. Soc.*, **102**, 3928 (1980).
12) Similar treatment of 2-ethoxy-2-imidazoline (**6**) with acid did not provide 2-imidazolidinone (**5**) without serious side reactions, which were not identified yet.
13) R. N. Boyd and M. Meadow, *Anal. Chem.*, **32**, 551 (1960).
14) H. J. Schaeffer and P. S. Bhargava, *J. Pharm. Sci.*, **53**, 137 (1964).
15) H. Kohn, M. J. Cravey, J. H. Arceneaux, R. L. Cravey, and M. R. Willcott, *J. Org. Chem.*, **42**, 941 (1977).

Photochemical Reactions in Polyethylene Glycol. 2.[1] Photo-induced Nucleophilic Substitution of Dimethoxybenzenes in the Presence of Polyethylene Glycol

Nobutaka SUZUKI,* Yasuo AYAGUCHI, and Yasuji IZAWA
Department of Industrial Chemistry, Faculty of Engineering, Mie University, Tsu, Mie 514
(Received February 4, 1982)

Synopsis. Polyethylene glycol can replace crown ether as co-solvent for photochemical substitution reactions of dimethoxybenzenes with KCN in CH_2Cl_2 in either the presence or the absence of terephthalonitrile.

The chemistry of cyclic polyethers (crown ethers) is attracting keen interests of many investigators[2] because of the high selectivity of reaction by activated anion species in their circumstances. Many interesting photochemical reactions have been found to proceed in crown ether.[2]

In a previous report,[1] we described the first example of photochemical reaction that a much higher selectivity is obtained in PEG employed in place of crown ether in a photochemical nucleophilic substitution of anisole to give *o*- and *p*-methoxybenzonitriles (**3**). There have been known a few photochemical reactions in PEG or acyclic polyethers,[3,4] though photochemical nucleophilic substitutions of aromatic systems in protic solvents have been well documented.[1,5-8]

When a crown ether is present, photocyanation proceeds in aprotic solvents more easily than in protic solvents,[9] while addition of electron acceptor, such as terephthalonitrile (**2**), improves both the yield of photocyanation products and the specificity of substitution.[10] This report is concerned with photochemical cyanation of *o*- and *p*-dimethoxybenzenes (**1a** and **1b**) with KCN in an aprotic solvent, in the presence and absence of **2** when PEG is used as co-solvent (Scheme 1).

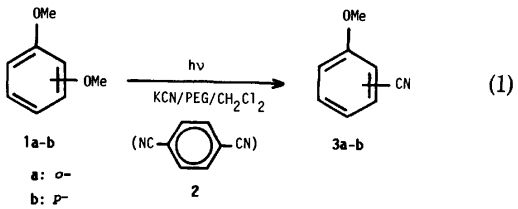

Scheme 1.

Results and Discussion

Photoreaction in a Quartz Cell in the Absence of **2**. Consumption of **1** in the presence of PEG was slightly slower than in the presence of crown ether. However, conversion yields[11] of **3** with PEG were comparable to that for **3a** and superior to those with crown ether for **3b** (see runs #1, 5, 7, and 12 in Table 1).

In comparison with the results obtained by Heijer *et al.*[8] in *t*-BuOH–H_2O, both the consumption and the conversion yield were worse for **1a** with PEG, but those for **1b** were much better.

Both the conversion of **1** and the formation of **3** were neither quenched by 1,3-pentadiene (≈50 mM) (1 M= 1 mol/dm^3) nor sensitized by acetone (≈50 mM) whose E_T (≈78 kcal/mol)[12] is high enough for sensitizing **1** to their triplet states. Fluorescence of **1** was not affected by either 1,3-pentadiene or acetone. These data suggest that the cyanations proceed through comparatively short-lived intermediates (probably S_1 state).[12]

Photoreaction in the Presence of **2**. Both the consumption of **1a** and conversion yield of **3a** with PEG were half as much as those with crown ether. However, those with PEG for the reaction of **1a** were similar to these with crown ether. Photolyses of **1b** with PEG were superior to those with crown ether and could be used for the preparation of **3b**. Both the conversion of **1** and the formation of **3** were quenched by 1,3-pentadiene[12] ($k_q\tau_0$/dm^3 mol^{-1}: 11 for **1a** and 6 for **1b**; 6 for **3a** and 16 for **3b**) and slightly sensitized with acetone.[12] These data suggest that the cyanations in the presence of **2** proceed through comparatively long-lived intermediates[12] (probably the T_1 state of **1** and/or of a charge transfer complex of **1** and **2** like **4**).[8]

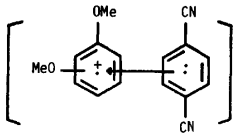

4

Photoreactions in the Presence/Absence of **2**. Substitution of KCN with NaCN did not affect the consumption of **1** but did the conversion yields of **3a** (increased) and **3b** (decreased). This reflects the tolerance of PEG for the size of the cationic guests incorporated in it compared with crown ether.

Prolonged irradiation caused a slight decrease in the conversion yield of **3**. This implies that further reactions, *e.g.*, the cyanation of **3**,[13] may be faster than cyanations of **1**.[8]

Although, in Pyrex cells with PEG, consumption of **1** was much slower than in quartz cells, conversion yields of **3** increased remarkably, especially for **1b** (see runs #1 through 4 and 8 through 11 in Table 1). This phenomenon may result from a further photocyanation of **3**[8] in a quartz cell (see Table 2).

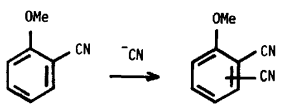

Scheme 2.

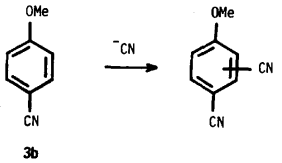

Scheme 3.

Table 1. Photosubstitution of dimethoxybenzenes (**1a** and **1b**) with CN^-

Run	1	Cell[a]	Co-solv.[b]	MCN[c]	2 used (mM)	Yield[d] & C.Y.[e] of 3/%		
1	**1a**	Q	PEG	K	—	20.2	31.7	(63.8)
2		Q			150	7.6	28.5	(26.6)
3		P			—	7.2	45.9	(15.7)
4		P			150	5.5	67.9	(8.1)
5		Q	CE		—	35.5	39.6	(89.7)
6		Q			150	33.4	57.5	(58.1)
7		Q	PEG	Na	—	22.8	37.2	(61.3)
		Q[f]	BH		—		73.2	(30.2) g)
8	**1b**	Q		K	—	29.1	32.5	(89.7)
9		Q			150	63.5	72.6	(87.5)
10		P		P	—	27.1	41.6	(65.1)
11		P		P	150	71.5	96.6	(74.0)
12		Q	CE		—	26.5	28.4	(93.3)
13		Q			150	57.9	73.9	(78.3)
14		Q	PEG	Na	—	23.6	27.7	(85.0)
		Q[f]	BH		—		22.2	(61.6) g)

a) Q: Quartz cell; P: Pyrex cell. b) PEG: PEG #200/CH_2Cl_2; CE: 18-Crown-6/CH_2Cl_2; BH: *t*-BuOH/H_2O (3 : 1). c) K: KCN; Na: NaCN. d) Yield of **3** based on initial amount of **1**. e) Yield based on **1** consumed.[11] Consumption of **1** is given in parentheses. f) Filter: 1 cm of a solution of **5** in water (100 mg dm^{-3}). g) See Ref. 8.

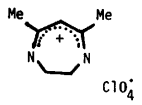

5

Table 2. Photodegradation of methoxybenzonitriles (**3a** and **3b**) in pyrex cells

Run	3	2 used (mM)	Conv. of 3/%		
			2 h	4 h	6 h
1	**3a**	—	10.7	12.3	19.9
2		150	41.0	59.7	69.2
3	**3b**	—	0	0.3	0
4		150	10.4	13.0	13.3

The photochemical decay rate of **3a** was much higher than that of **3b** in Pyrex cells and this tendency is more marked in quartz cells, especially in the presence of **2** (Schemes 2 and 3).

Suspected transformation of **1** and **2** to yield the corresponding **3** was excluded for these photocyanation reactions (Scheme 4).

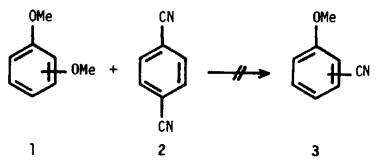

1 2 3 (4)

Scheme 4.

Experimental

Instrumentation. All mps were taken with a microscope hot stage and are uncorrected. UV-visible spectra were recorded on a Shimadzu UV-200, fluorescence/phosphorescense spectra on a Hitachi MPF-2A, and GLC on a Yanagimoto Yanaco G-80F (FID). The GLC conditions used: Column A (5.0 mm×2.0 m, 5% PEG-20M on 60—80 mesh Gasport in a stainless steel column) was used for product analyses; column B (3.8 mm×3.0 m, 25% Apiezon L on 30—60 mesh fire brick in a glass column) was used to analyse the degradation of **1**.

Materials. Dimethoxybenzenes (**1a** and **1b**), terephthalonitrile (**2**), 18-crown-6, and KCN were purchased. CH_2Cl_2 was distilled from CaH_2. PEG #200 (Nakarai Chem. Co.) was dried azeotropically by toluene. Methoxybenzonitrile (**3a**[14] and **3b**[14]) were prepared according to the literature methods. 1,3-Pentadiene (bp 42—44 °C) and acetone were distilled before use.

General Experimental Procedures. A solution of **1** (10 mM), KCN (30 mM), and PEG (1 M) or 18-crown-6 in CH_2Cl_2 (10 cm^3) in the presence or absence of **2** (150 mM) was irradiated externally with a high-pressure mercury lamp (Eikosha P1H-300, 300 W) through a water-cooled quartz or Pyrex cell. The irradiated solution was analysed by GLC after washing with water to remove PEG and KCN. The results are given in Table 1.

Degradation of 3. Photodegradation of **3a** and **3b** (10 mM) was observed under conditions similar to those used for **1** (see Table 2).

Attempt of Photochemical Transformation of 1 and 2 to 3. A solution of **1** (10 mM) and **2** (10 mM) was irradiated and the mixture was analysed by GLC. No formation of cyanoanisoles (**3**) was observed.

References

1) Part 1. N. Suzuki, K. Shimazu, T. Ito, and Y. Izawa, *J. Chem. Soc., Chem. Commun.*, **1980**, 1253 and references cited therein.

2) "Chemistry of Crown Ethers," ed by R. Oda, T. Shono, and I. Tabushi, as "Kagaku Zokan," Kagaku Dojin, Kyoto (1978), Vol. 74, (in Japanese).

3) S. Yanagida and M. Okahara, Ref. 2, p. 149,

4) For dark reactions using PEG: W. P. Weber and G. W. Gokel, "Phase Transfer Catalysis in Org. Synth.," Springer-Verlag, Berlin (1978), p. 3; E. Santaniello, A. Manzocchi, and P. Sozzani, *Tetrahedron Lett.*, **1979**, 4581; V. N. R. Pillai, M. Mutter, E. Baeyer, and I. Gatfield, *J. Org. Chem.*, **45**, 5364 (1980); K. Sukata, *J. Synth. Org. Chem. Jpn.*, **39**, 86 (1981); *ibid.*, **39**, 443 and 1131 (1981).

5) J. A. Barltrop, N. J. Bunce, and A. Thomson, *J. Chem. Soc., C*, **1967**, 1142.

6) S. Nilsson, *Acta Chem. Scand.*, **27**, 329 (1973).

7) J. A. J. Vink, C. M. Lok, J. Cornelisse, and E. Havinga, *J. Chem. Soc., Chem. Commun.*, **1972**, 710; J. A. J. Vink, P. L. Verheijdt, J. Cornelisse, and E. Havinga, *Tetrahedron*, **28**, 5081 (1972).

8) J. D. Heijer, O. B. Shadid, J. Cornelisse, and E. Havinga, *Tetrahedron*, **33**, 779 (1977).

9) R. Beugelmans, H. Ginsburg, A. Lecas, M.-T. LeGoff, J. Pusset, and G. Roussi, *J. Chem. Soc., Chem. Commun.*, **1977**, 885; R. Beugelmans, M.-T. LeGoff, J. Pusset, and G. Roussi, *ibid.*, **1976**, 377.

10) K. Mizuno, C. Pac, and H. Sakurai, *J. Chem. Soc., Chem. Commun.*, **1975**, 553; M. Yasuda, C. Pac, and H. Sakurai, *J. Chem. Soc., Perkin Trans. I*, **1981**, 747.

11) Conversion yields: Yields based on the starting material consumed.

12) N. J. Turro, "Modern Molecular Photochemistry," Benjamin/Cummings, Menlo Park, CA. (1978), pp. 351—354.

13) J. Cornelisse and E. Havinga, *Chem. Rev.*, **75**, 353 (1975); J. Cornelisse, *Pure Appl. Chem.*, **41**, 433 (1975); G. Lodder and E. Havinga, *Tetrahedron*, **28**, 5583 (1972).

14) H. H. Hodgson and F. Heyworth, *J. Chem. Soc.*, **1949**, 1131.

Photosensitized Desulfurization of Heterocyclic Thioketones and Its Accompanied Chemiluminescence[1)]

Nobutaka SUZUKI,* Kaniti SANO, Satoshi WAKATSUKI, Noriyuki TANI, and Yasuji IZAWA
Department of Industrial Chemistry, Faculty of Engineering, Mie University, Tsu, Mie 514
(Received April 30, 1982)

Synopsis. Photosensitized oxygenation of 10-methyl-9(10*H*)-acridinethione, 9*H*-xanthene-9-thione, and 9*H*-thioxanthene-9-thione at −78 °C gave the corresponding ketones, 10-methyl-9(10*H*)-acridinone, 9*H*-xanthen-9-one, and 9*H*-thioxanthen-9-one quantitatively in a 3—10 min-irradiation. Weak chemiluminescence was observed from the irradiated solution upon warming-up.

For photooxygenation of thiocarbonyl compounds, two alternative mechanisms have been proposed, *i.e.*, the 1,2,3-dioxathietane[2-6)] (path a) and the sulfine mechanisms[7-8)] (path b). Chemiluminescence (CL) has been expected to be accompanied with the decomposition of 1,2,3-dioxathietane (**2**)[9)] which is generated on sensitized photooxygenation of C=S compounds. The intermediate (**2**) is supposed to have a large energy enough for exciting the produced ketone (**3**) or added fluorescers to their S_1 excited states.[10)]

Since the first report by Schönberg and Mostafa,[2)] on photooxidation of thiobenzophenones and 4*H*-thiopyran-4-ones in sunlight, a number of reports on photooxidative desulfurization of C=S compounds (**1**) appeared:[2-8,11)] Sensitized photooxygenation of 4*H*-pyran-4-thiones and 4*H*-thiopyran-4-thiones by Ishibe *et al.*;[3)] of 2,2,4,4-tetramethyl-3-thioxo-1-cyclobutanone and dibenzyl thioketone by Worman *et al.*;[4)] of 9*H*-xanthene-9-thione, 9*H*-fluorene-9-thione, and alicyclic thioketones by Ramamurthy *et al.*[5)] Through the corresponding 1,2,3-dioxathietane intermediates (**2**) the reactions were supposed to proceed. Photooxygenation of sulfines (**4**)[11)] and O-alkyl thiocarboxylates[6)] was also claimed to proceed through the similar intermediates (path a).

Photooxygenation of di-*t*-butyl thioketone[7)] and 1,2-benzodithiole-3-thione[8)] was found by Tamagaki *et al.* to give the corresponding sulfines (**4**) and ketones (**3**), and hence, an alternative sulfine mechanism (path b) was proposed for the oxidation. On the other hand, Tamagaki *et al.* also reported that di-*t*-butyl sulfine was inert to singlet oxygen.[7)] Theoretical calculation of molecular orbitals suggests that the oxidation of thioketones proceeds stepwisely through the 1,2,3-dioxathietane (**2**) and its successive, radical decomposition to the ketone (**3**) and S=O.[9)] Energy liberated on the decomposition of **2** was calculated as *ca.* 92.1 kcal/mol[1,10)] which is large enough for exciting the ketones (**3**) produced or the added fluorescers to their S_1 excited state [67.3,[12)] 68.8,[13)] 67.2[14)] for **3a**, **3b**, and **3c** and 66.0,[14)] 64.9,[14)] and 50.2 kcal/mol[14)] for 9,10-diphenylanthracene (DPA), 9,10-dibromoanthracene (DBA), and rubrene, resp.].

For finding out such chemiluminescent intermediates (**2**) and for clarification of the oxygenation mechanism, namely, the 1,2,3-dioxathietane or the sulfine mechanism, investigation was carried out for the sensitized photooxygenation of aromatic thioketones, **1a**, **1b**, and **1c**, which would give fluorescent ketones, **3a**, **3b**, and **3c** resp. In the present paper, photosensitized oxygenation of 10-methyl-9(10*H*)-acridinethione (**1a**),[15)] 9*H*-xanthene-9-thione (**1b**),[16)] and 9*H*-thioxanthene-9-thione (**1c**)[17)] is described to give the corresponding ketones (**3a**—**c**) in quantitative yields with 3—10 min-irradiation.

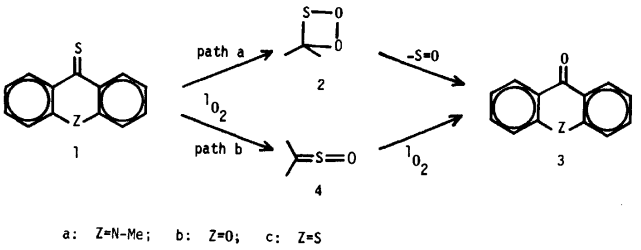

Scheme 1.

Each solution of the heterocyclic thioketones (**1a**—**c**) with Methylene Blue as a sensitizer in CH_2Cl_2 was irradiated under flushing O_2 gas at −78 °C for 60 min with a tungsten-halogen lamp through an optical glass filter (<510 nm cut off) cooling with a Pyrex/water filter in a Pyrex or quartz cell. Samples taken during irradiation were analysed by GLC after standing at room temperature for 30 min. The results are shown in Table 1. These results show that the present oxygenation reactions yield the corresponding ketones (**3a**—**c**) in quantitative yields[18)] in a short time-irradiation. According to Zwanenburg *et al.*,[11)] photooxygenation of aromatic sulfine compounds needs fairly long time-irradiation (2.5—6 h/5—20 mM), and hence, we speculate in spite of Tamagaki's report[8)] that the present photooxygenation proceed predominantly through path a.

For detection of the expected chemiluminescence at the spontaneous decomposition of the 1,2,3-dioxathietane (**2**), efforts were made, when the intact irradiated solution (10^{-2}—10^{-4} M) or the solutions added into several fluorescers (rubrene, DPA, and DBA at 10^{-2}—10^{-4} M) were warmed up to room temperature. Weak chemiluminescence (*ca.* 10^{-8} einstein/mol) was detected (Table 2). Since it was so weak, the emission spectra could not be measured. Although they were very weak, these were the first examples of the detection of the chemiluminescence for the supposed 1,2,3-dioxathietane. The weakness of the light emitted may result from further photochemical decomposition of **2** once produced during irradiation.[19)]

Table 1. Photooxygenation of thioketones (**1a**—**c**)

1	Concn mM	MB (mM)	Irrad. time min	Product yield (3)[a)] %
1a;	10.1	1.0	3	85
1b:	11.4	1.1	10	100
1c:	10.9	1.2	5	100

a) Yields based on the starting materials used.

Table 2. Relative quantum yields of chemiluminescence of **1**

Additive [A]	[A]/[**1**]	Φ_{CL}(rel)		
		1a[a]	**1b**[a]	**1c**[a]
none	—	5	8	100
DBA[b]	1—10	17	25	17
DPA[b]	1—10	8	5	100
Rubrene	1—10	—	17	100

a) 10^{-2}—10^{-4} M. b) DBA: 9,10-Dibromoanthracene; DPA: 9,10-diphenylanthracene.

Table 3. Effect of inhibitors on photooxygenation of **1**

Inhibitors [I]	[I]/[**1**]	Φ_{CL}(rel)		
		1a[a]	**1b**[a]	**1c**[a]
DABCO[b]	25	Q[c]	Q	Q
β-Carotene	5	Q	Q	—
TBP[b]	25	—	N[d]	N

a) 10^{-2}—10^{-4} M. b) DABCO: 1,4-diazabicyclo[2.2.2]octane; TBP: 2,4,6-tri-*t*-butylphenol. c) Q: Quenched. d) N: No effect.

Influence of $^1O_2$-quenchers (DABCO[20] and β-carotene[20]) and a radical scavenger (2,4,6-tri-*t*-butylphenol)[20] on the oxygenation (see Table 3) suggests that the reactions proceed with $^1O_2$ non-radically.

Experimental

The thioketones (**1a—c**) were prepared by the reaction of the corresponding ketones (**3a—c**) (Nakarai Chem. Co.) with P_2S_5 according to the usual procedure: *10-Methyl-9(10H)-acridinethione* (**1a**), mp 268—273 °C (lit,[15] mp >260 °C); ν_{max} (KBr) 1580, 1500, 1220, 1180, 1000, and 740 cm^{-1}; δ_{ppm} (DMSO-d_6) 3.96 (s, 3H), 7.28 (m, 3H), 7.78 (m, 3H), and 8.88 (m, 2H); *m/z* 225 (M^+); *9H-xanthene-8-thione* (**1b**), mp 156—158 °C (lit,[16] mp 155—156 °C); ν_{max} (KBr) 1590, 1450, 1320, 1100, 770, and 740 cm^{-1}; *m/z* 212 (M^+); *9H-thioxanthene-9-thione* (**1c**), mp 193—205 °C (decomp) (lit,[17] mp 180—215 °C); ν_{max} (KBr) 1590, 1450, 1320, 1060, 740 cm^{-1}; *m/z* 228 (M^+).

Photosensitized Oxygenation. Each solution of the thioketones (**1a—c**) (*ca.* 10 mM) with Methylene Blue (*ca.* 1 mM: Nakarai Chem. Co.) in CH_2Cl_2 (distilled from CaH_2 before use) was irradiated under O_2 atmosphere at −78 °C for 60 min with a projector lamp (Silvania/Kondo tungsten-halogen lamp ELH 120 V/300 W at 100 V) through an optical glass filter (Toshiba Y-52, <510 nm cut off) and a Pyrex/water filter in a Pyrex or quartz cell (φ 10 mm). Aliquots were taken during irradiation and analysed by glc and tlc after standing at room temperature for 30 min. The conditions of GLC used were as follows: For **1a** and **3a**: Yanagimoto Yanaco G-80F with FID, 10% Silicone GE-SE-30 on Diasolid L (60—80 mesh) in a stainless steel column, 0.93 m × φ 4 mm, col. temp 250 °C, inj. temp 280 °C, carrier gas (N_2), 75.0 ml/min, internal standard, 9*H*-xanthene-9-thione. For **1b** and **3b**: Yanagimoto Yanaco G-1800F with FID, the same column as above; col. temp 250 °C, inj. temp 264 °C, carrier gas (N_2), 42.9 ml/min, internal standard, 9-benzylidene-9*H*-xanthene. For **1c** and **3c**: G-1800F, the same column as above, col. temp 250 °C, inj. temp 275 °C, carrier gas (N_2), 54.5 ml/min, internal standard, 9*H*-xanthen-9-one. The results are shown in Table 1.

Observation of the Chemiluminescence. Each irradiated cold solution as above (**1** : 10^{-2}—10^{-4} M) was poured into a quartz fluorescence cubette (1 cm) placed in front of photomultiplier tube (Hamamatsu R-105UH) and the integrated light intensity *vs.* time was recorded while the temperature of the solution rose to room temp (20 °C). The same cubette containing a fluorescer (DBA, DPA, or rubrene, 10^{-2}—10^{-4} M) was also used for the measurement. Quartz tubes were also applied for the irradiation instead of Pyrex cells in order to detect emission directly through it at ultraviolet range, with being warmed-up gradually from −78 °C. (See Table 2). The amounts of light emission are relative to CL of luminol in an aqueous solution.[24]

References

1) Preliminary Commun.: N. Suzuki, K. Sano, N. Tani, and Y. Izawa, *Heterocycles*, **16**, 1133 (1981).

2) A. Schönberg and A. Mostafa, *J. Chem. Soc.*, **1943**, 275.

3) N. Ishibe, M. Odani, and M. Sunami, *J. Chem. Soc., Chem. Commun.*, **1971**, 118.

4) J. J. Worman, M. Shen, and P. C. Nichols, *Can. J. Chem.*, **50**, 3923 (1972).

5) R. Rajee and V. Ramamurthy, *Tetrahedron Lett.*, **1978**, 5127.

6) J. E. Gano and S. Atik, *Tetrahedron Lett.*, **1979**, 4635.

7) S. Tamagaki, R. Akatsuka, M. Nakamura, and S. Kozuka, *Tetrahedron Lett.*, **1979**, 3665.

8) S. Tamagaki and K. Hotta, *J. Chem. Soc., Chem. Commun.*, **1980**, 598.

9) L. Carlsen, *J. Chem. Soc., Perkin Trans. 2*, **1980**, 188.

10) Heat of decomposition (ΔH) of **2** to a C=O and a S=O compounds was calculated as follows[1] assuming that the ring strain of **2** is not much different from that of ordinary 1,2-dioxetanes (26 kcal/mol);[23] C–C–O–O→C=O+C=O; C–S–O–O→C=O+S=O: a) 1 C–C⇝1 C–S (ΔHa), b) 1 C–O⇝1 S–O (ΔHb), c) 1 C=O⇝1 S=O (ΔHc), where $\Delta Ha = 82.6^{21} - 65^{21} = +17.6$; $\Delta Hb = 85.5^{21} - 83^{22} = +2.5$; and $\Delta Hc = 179^{21} - 151^{22} = +28$: therefore, $\Delta H' = -(\Delta Ha + \Delta Hb) + \Delta Hc = +7.9$ (kcal/mol); and $\Delta H = \Delta H$ (dioxetane)[23] $- \Delta H' = -(ca.\ 100—7.9) = ca.\ -92.1$ (kcal/mol).

11) B. Zwanenburg, A. Wagenaar, and J. Strating, *Tetrahedron Lett.*, **1970**, 4683.

12) E. H. White, N. Suzuki, and W. H. Hendrickson, *Chem. Lett.*, **1979**, 1491.

13) S. L. Murov, "Handbook of Photochemistry," Dekker, New York, N. Y. (1973).

14) Calculated from λ_{max} of the fluorescence spectra measured in CH_2Cl_2 at room temp. (19 °C).

15) J. Jaeken, M. A. de Ramaix, Ger. Patent, 1146751, Apr. 4 (1963); *Chem. Abstr.*, **59**, 15422 (1963).

16) E. G. Davis and S. Smiles, *J. Chem. Soc.*, **1910**, 1296.

17) A. Schönberg and M. M. Sidky, *J. Am. Chem. Soc.*, **81**, 2259 (1959); R. Meyer, *Chem. Ber.*, **33**, 2570 (1900).

18) No other organic products than **3** were detected by TLC and GLC.

19) *Photolyses of 1,2-dioxetanes*: P. D. Bartlett and A. P. Schaap, *J. Am. Chem. Soc.*, **92**, 3223 (1970); T. Wilson and A. P. Schaap, *ibid.*, **93**, 4126 (1971); N. J. Turro, P. Lechtken, A. Lyons, R. R. Hautala, E. Carnaham, and T. J. Katz, *ibid.*, **95**, 2035 (1973); N. J. Turro, H.-C. Steinmetzer, and A. Yekta, *ibid.*, **95**, 6468 (1973). Prolonged irradiation of the ordinary 1,2-dioxetanes resulted in the similar decomposition even by the light of >510 nm (See also Ref. 12). This might be caused by the reabsorption of the CL as suggested by one of the referees.

20) M. E. Landis and D. C. Madoux, *J. Am. Chem. Soc.*, **101**, 5106 (1979).

21) J. D. Roberts and M. C. Caserio, "Basic Principles of Organic Chemistry," Benjamin, New York, N. Y. (1964).

22) J. G. Calvert and J. N. Pitts, Jr., "Photochemistry," Wiley, New York, N. Y. (1966), p. 824.

23) L. J. Bollyky, *J. Am. Chem. Soc.*, **92**, 3230 (1970); P. Lechtken and G. Höhne, *Angew. Chem., Int. Ed. Engl.*, **12**, 772 (1973); T. Wilson, D. E. Golan, M. S. Harris, and A. L. Baumstark, *J. Am. Chem. Soc.*, **98**, 1086 (1976); W. Adam, *Adv. Heterocycl. Chem.*, **21**, 437 (1977).

24) J. Lee and H. H. Seliger, *Photochem. Photobiol.*, **4**, 1015 (1965); **15**, 227 (1972).

A Method for the Determination of Mutual Diffusion Coefficients of Electrolytes in Water by Means of Conductivity Measurements

Katsuyoshi KAMAKURA

Department of Industrial Chemistry, Toyama Technical College, Hongo-cho, Toyama 930-11

(Received July 18, 1981)

A method for determining diffusion coefficients of electrolytes was studied by the use of a conductance cell made of a Pyrex glass tube (4—7 cm in diameter and 6.5 cm in length). A pair of platinized platinum electrodes are sealed into the tube at a position 10 mm below the top of the glass tube. The diffusion was carried out from solution in the cell to an outer solvent, and the rate was measured from the decrease in conductance at a fixed position in the cell. In the graphical relation between the measured diffusion coefficient and the time, the differential diffusion coefficient at the initial concentration of the diffusing solution was estimated by extrapolation of the linear portion of the plot to time→0. The differential diffusion coefficients obtained in 0.1 mol dm^{-3} solutions at 25 °C were as follows: HCl, $(3.12\pm0.08)\times10^{-5}$; KI, $(1.909\pm0.020)\times10^{-5}$; NaCl, $(1.520\pm0.016)\times10^{-5}$; $\frac{1}{2}Na_2SO_4$, $(1.059\pm0.028)\times10^{-5}$; $CuSO_4$, $(0.610\pm0.033)\times10^{-5}$ $cm^2\ s^{-1}$.

The diffusion coefficients of electrolytes have been measured by a number of different methods. For example, the rate of diffusion from solution to solvent through a porous plate is measured.[1] The widely used methods such as the schlieren or the capillary method[2] were carried out on a system with a sharp boundary between the solution and solvent at the start of diffusion. A method for the determination of the diffusion coefficient of electrolytes by means of conductance measurements was already reported by H. S. Harned *et al.*[3] The apparatus is complicated because it has two electrode couples and also a shearing mechanism for the formation of the boundary between solution and solvent. Further, the measurement must be extended over several days. The capillary method is applied to the measurement of self-diffusion coefficients of various ions or molecules in water by means of isotopic tracers; the inner diameter of the cell should be very small in order to avoid random flow in systems with very small density-gradients. It was shown in a previous paper[4] that the system of sharp density-gradient is resistant to convection or to random flow. If the capillary method is applied to the measurement of mutual-diffusion coefficients, the inner diameter may be larger than that of the capillary used for measuring the self-diffusion coefficient.

The diffusion coefficient of an electrolyte in agar or gelatin gel had been measured by means of a glass tube cell, which is a type of conductance cell, developed in this laboratory.[5,6] The diffusion cell will be applied to the measurement of the mutual-diffusion coefficient of an electrolyte in water. This apparatus has a couple of electrodes, and the boundary between solution and solvent is formed by pouring solvent into a test tube outside the cell filled with solution. Consequently, the apparatus or the mechanism is simple, and the measurement is carried out within ten hours. In the present paper, we deal with cells of different inner diameters and apply them to the measurement of diffusion coefficients in water. In addition, the differential diffusion coefficient will be obtained by extrapolating the measured diffusion coefficients to time $t\rightarrow0$.

Principle of the Method

The diffusion cell is a conductance cell which is made of a glass tube equipped with platinized platinum wires. If the cell is filled with a solution and placed vertically in water, the solute diffuses into the outer water with the elapse of time. The diffusing solution in the cell gradually acquires a concentration gradient with time. The decrease in conductance at a fixed position in the cell can then be measured with the electrodes. The measured conductance is converted to concentration by a calibration curve. Under these conditions, the equation for diffusion in one dimension is

$$\frac{\partial c}{\partial t} = D\frac{\partial^2 c}{\partial x^2}, \tag{1}$$

where c is the concentration of the electrolyte at time t, D the diffusion coefficient, x the coordinate along which diffusion takes place. For this diffusion experiment, it may be assumed that (1) the concentration outside the cell is infinitely low during the diffusion experiment, and (2) the cell is infinite in length. Then the following equation is obtained by solving Eq. 1.

$$\frac{c_e}{2c_0} = \frac{1}{\sqrt{2\pi}}\int_0^{x/\sqrt{2Dt}} \exp(\xi^2/2)d\xi, \tag{2}$$

where c_e is the concentration of the diffusing solution at the electrodes, c_0 the initial concentration at the electrodes, and x the distance between the electrodes and the open end of the cell.

Next we will discuss the stability of the concentration gradient in the cell. The stability is related to the following factors: (1) the inner diameter of cell, (2) the density gradient in the cell, (3) the temperature variation, and (4) the vibration of the apparatus. As the inner diameter is reduced, the concentration gradient becomes stable independently of other factors. The density gradient is related to the concentration of diffusing solution or the kind of solute. In a previous paper it was shown that the intermediate layer between the upper and the lower convection keeps sharp stable density-gradient, when a two-layer system which consists of water (upper layer) and an aqueous solution (lower layer) is heated from one side and cooled from the opposite side.[4] The small temperature-variation during the diffusion experiment may not deform the concentration gradient, because this method is especially applied to the

system of a sharp density-gradient in the cell of small inner-diameter. The effect of vibration of the apparatus will also become small for a cell of small inner-diameter and for a system of sharp density-gradient. In spite of the above discussion, there will be turbulence of the concentration gradient in the vicinity of the top of the cell, especially during the pouring of the solvent. Therefore, the distance x_m measured by use of vernier calipers may not be appropriate for calculating the diffusion coefficient; then the effective distance x_e should be applied to Eq. 2. When c_e $(2c_o)^{-1}$ at time t is measured, the value of $x/(2Dt)^{0.5}$ is calculated from Eq. 1, and then the distance x is proportional to the square root of diffusion coefficient D. Then the effective x_e can be evaluated from

$$X_e = x_m(D/D_m)^{0.5}. \quad (3)$$

Here, D_m is the diffusion coefficient calculated from Eq. 2 by the use of x_m, and D is the true value of the diffusion coefficient.

Experimental

Materials. All the chemicals were of reagent grade, and were used without further purification. Anhydrides were dried at the following temperatures: KCl, 150 °C; NaCl, 250 °C; KI and Na_2SO_4, 110 °C. The salts were weighed out to give the solutions of indicated concentrations. The HCl solution was prepared by dilution after the determination of concentration by alkalimetry. Water used was distilled after passage through an ion-exchange column. Just prior to use, the water was boiled to remove dissolved gas. The solution was heated near to the boiling point in an Erlenmeyer flask with a glass tube (2 mm × 140 cm) through a rubber stopper, and then the solvent loss was within 0.1%.

Apparatus and Procedure. The diffusion cell is similar to that described previously.[6] The apparatus is shown in Fig. 1. The diffusion cell is made of a Pyrex glass tube (6.5 cm in length) equipped with platinized platinum electrodes at a position 10 mm below the top of the glass tube. The electrodes are wires 0.3 mm in diameter, 1 mm in length and 1.5 mm in distance between the wires.

A solution was poured into the cell, and the cell was set in the test tube (100 mm × 27 mm) in which water was previously placed so as to reach slightly below the top of the cell. The test tube was immersed vertically in a thermostat (Yamato BKR-41) at 25±0.05 °C. After about 20 min, water thermostated at 25 °C was poured into the test tube up to about 15 mm above the top of cell at a flow rate of 1.5 cm^3 min^{-1}, and the diffusion started.

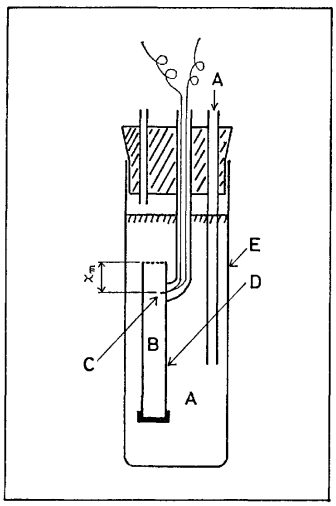

Fig. 1. Apparatus for measuring diffusion.
A: Water, B: diffusing solution, C: electrodes, D: conductance cell, E: test tube.

Measurement of Conductance. The conductance was measured with a universal bridge (Yokogawa-Hewlett Packard 4255A) equipped with a variable condenser (0—1 μF).

Results and Discussion

Determination of Effective Distance. The diffusion experiment was carried out for 0.1 mol dm^{-3} KCl, and the apparent diffusion coefficient was calculated from Eq. 2 by the use of the measured distance, x_m, between the electrodes and the top of the cell. The apparent differential diffusion coefficient, D_m, at 0.1 mol dm^{-3} KCl was obtained by means of an extrapolation method which is described later. The effective distance, x_e, was determined by substituting x_m, D_m, and D (the value in the literature[7,8] instead of the true value) into Eq. 3, as is shown in Table 1. The ratios x_e/x_m were almost constant for cells of 4 mm in inner diameter, and the mean value was 104.5%. This fact may be taken to indicate that a small limited-amount of the solution is present on top of the cell, and that the concentration gradient is stable.

Differential Diffusion Coefficient. The diffusion coefficient was measured for different electrolytes. The typical relation between the diffusion coefficient D and the time t is shown in Fig. 2. The D values change slightly with time. The increase in D for Na_2SO_4 or $CuSO_4$ may be due to the dependence of diffusion coefficient on the concentration or due to the error caused by the vibration of apparatus or by the temperature variation. The decrease for KCl or NaCl seems to be caused by the increase of the concentration in the test tube in spite of assumption (1) for Eq. 2 or by the obstruction of electrodes (platinum wires) to the diffusion. The D with no such effects may be obtained by extrapolation of the linear portion of the plot to $t \to 0$. The diffusion coefficient D_e esti-

Table 1. Apparent diffusion coefficients (D_m) and effective distances (x_e) for different cells[a]

Cell No.	x_m / cm	Inner diameter / mm	$D_m \times 10^5$ [b] / cm^2 s^{-1}	x_e/x_m [c] / %
1	1.073	4	1.712±0.010	103.8
2	1.105	4	1.683±0.025	104.7
3	1.028	4	1.663±0.021	105.3
4	1.085	4	1.689±0.014	104.5
5	1.069	4	1.695±0.019	104.3
6	1.005	6	1.688±0.022	104.5
7	1.094	7	1.754±0.031	102.5
8	1.099	7	1.802±0.030	101.2

a) Measurements were carried out for KCl in 1.000 × 10^{-1} mol dm^{-3} soln at 25 °C. b) Average and standard deviation σ_{n-1} of three measurements. c) Calculated from Eq. 3 by substituting $D = 1.844 \times 10^{-5}$ cm^2 s^{-1}.

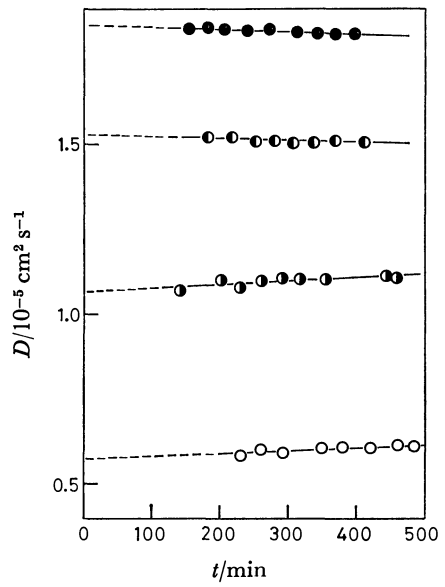

Fig. 2. Plots of D *vs.* t.
The measurements were carried out for the electrolytes in 1.000×10^{-1} mol dm^{-3} solns at 25 °C. ●: KCl, ◐: NaCl, ◑: $\frac{1}{2}Na_2SO_4$, ○: $CuSO_4$.

mated by extrapolation is regarded as the differential diffusion coefficient at the initial concentration of the diffusing solution.

Inner Diameter of Cell. Diffusion experiments were carried out for cells of different inner diameters, and the results are listed in Table 1. The standard deviations of D_e estimated for the cells of large inner diameter (7 mm) are large, compared with the values obtained for the cells of small inner diameters (6 and 4 mm). Therefore, other experiments were carried out for the cells of 4 mm in inner diameter.

Accuracy of the Method. The diffusion coefficient, D_e, estimated by the extrapolation and the diffusion coefficient, D_r, taken from other literature are given in Table 2. If the diffusion coefficient is small, the decrease in concentration at the electrodes during the diffusion experiment is also small, and the error in D_e may become large. For example, the c_e/c_o was 0.95 after 300 min for the diffusion of $CuSO_4$. The deviations of the D_e values from each D_r were within 2.5% except for $CuSO_4$.

Table 2. Diffusion coefficients (D_e) of different electrolytes in 1.000×10^{-1} mol dm^{-3} solns at 25 °C

Electrolyte	$D_e\times10^5$ [a] / cm^2 s^{-1}	$D_r\times10^5$ / cm^2 s^{-1}	D_e/D_r / %
HCl	3.12 ±0.08	3.05[b]	102.2
KI	1.909±0.020	1.865[b]	102.4
NaCl	1.520±0.016	1.483[b]	102.5
$\frac{1}{2}Na_2SO_4$	1.059±0.028		
$CuSO_4$	0.610±0.033	0.580[c]	105.2

a) Average and standard deviation σ_{n-1} of four measurements. b) Ref. 7. c) Interpolated from the data in Ref. 9.

References

1) J. W. McBain and T. H. Liu, *J. Am. Chem. Soc.*, **53**, 59 (1931).
2) J. H. Wang and J. W. Kennedy, *J. Am. Chem. Soc.*, **72**, 2080 (1950); J. H. Wang, *ibid.*, **73**, 510 (1951).
3) H. S. Harned and R. L. Nuttall, *J. Am. Chem. Soc.*, **69**, 736 (1947).
4) K. Kamakura, *Denki Kagaku*, **49**, 330 (1981).
5) K. Kamakura, A. Yanagihara, and Y. Nagai, *Nippon Kagaku Kaishi*, **1976**, 1641.
6) K. Kamakura and T. Kishikawa, *Nippon Kagaku Kaishi*, **1977**, 1261.
7) "Kagakubinran (Handbook of Chemistry)," ed by the Chemical Society of Japan, Maruzen, Tokyo (1975), p. 1194.
8) H. S. Harned and R. L. Nuttall, *J. Am. Chem. Soc.*, **71**, 1460 (1949).
9) L. A. Woolf and A. W. Hoveling, *J. Phys. Chem.*, **74**, 2406 (1970).

An Evaluation of the Effective HLB of Surface-active Crown Compounds

Ping-Lin Kuo, Isao Ikeda, and Mitsuo Okahara*

Department of Applied Chemistry, Faculty of Engineering, Osaka University, Yamadaoka 2-1, Suita, Osaka 565

(Received March 1, 1982)

The hydrophilicity of surface-active crown compounds and their change upon the addition of electrolytes were investigated by measuring the phase-inversion temperature (PIT), the phenol index, and the cloud point. Sodium chloride and potassium chloride were observed to raise the hydrophilicity of 15-crowns and 18-crowns respectively, in contrast with their lowering effect on the hydrophilicity of usual poly(oxyethylene)-type nonionics. The effective HLBs of dodecyl crown ethers, estimated from both the PIT and the phenol index, were compared with those of poly(oxyethylene) dodecyl ethers, and the hydrophilicity of the crown rings were discussed in conjunction with that of the poly(oxyethylene) chain.

Although some studies of surface-active crown compounds have recently been made,[1–4] and a little fragmental information on the hydrophilicity of the crown ring have been given,[2–4] the function of this new type of hydrophilic group has not yet been fully clarified.

We have previously prepared long-chain alkyl crown ethers (**1**) and long-chain *N*-alkyl monoaza crown ethers (**2**),[5,6] which are the most typical surface-active crown compounds, and their surface-active properties[7,8] and the selective increase in the cloud points of their aqueous solutions upon the addition of electrolytes[9] have been reported.

In this paper, the effective HLBs of crown compounds and their changes upon the addition of electrolytes are evaluated by measuring the phase-inversion temperature (PIT), reported by Shinoda,[10–12] and the phenol index, proposed by Marszall;[13–16] they are also compared with those estimated from the cloud points in order to get information about the hydrophilicity of a crown ring.

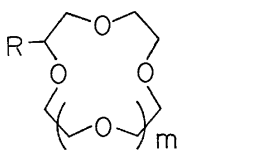

1

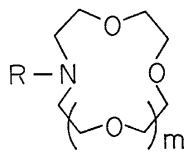

2

$R = C_8H_{17}, C_{12}H_{25}$ $m = 2, 3$

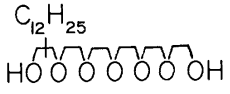

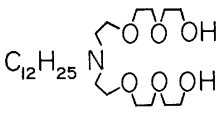

Experimental

Materials. Surface-active crown compounds (octyl-15-crown-5 (C_8O15C), octyl-18-crown-6 (C_8O18C), dodecyl-18-crown-6 ($C_{12}O18C$), *N*-octylmonoaza-18-crown-6 (C_8N18C), and *N*-dodecylmonoaza-18-crown-6 ($C_{12}N18C$)) were synthesized according to the reported method of intramolecular cyclization from the corresponding open-chain compounds (dodecyl-substituted hexaethylene glycol ($C_{12}O18H$), *N,N*-bis(8-hydroxy-3,6-dioxaoctyl)dodecylamine ($C_{12}N18H$)),[5,6] and their purity was ascertained by means of GLC. The monodispersed poly(oxyethylene) dodecyl ethers ($C_{12}H_{25}O(EO)_nH$, $n=4,5,6,7,8$) were supplied by the Nikko Chemical Co. The KCl, NaCl, and dodecane ($n_D^{25}=1.4195$) were commercial guaranteed-grade reagents.

Phenol Index. Because of the low hydrophilicity of crown compounds, the method reported by Marszall[13] was modified and a dilute phenol solution was used. Thus, a 0.5% aqueous phenol solution was added, drop by drop, to a 5-ml portion of a 0.025 M (mol dm^{-3}) aqueous solution of surface-active compounds at a constant temperature (5, 10, 15, 25 °C). The end point was determined as the aqueous solution became distinctly turbid. The number of milliliters of the phenol solution used to reach the end point of titration is given as its phenol index. Crown ethers, C_8O15C and $C_{12}O18C$, which have low cloud points were measured at 5, 10, and 15 °C, while other crown compounds were all titrated at 25 °C.

Phase-inversion Temperature (PIT).[11] A 4 wt%/system amount of surface-active crown compounds ($C_{12}O18C$, $C_{12}N18C$) or the corresponding open-chain compounds ($C_{12}O18H$, $C_{12}N18H$) were added to a dodecane/water mixture (1:1 by volume) to make an emulsion. The emulsion was heated under stirring while the temperature was being raised. The inversion of O/W into W/O on heating (about 1 °C/2 min) or of W/O into O/W on cooling was visually observed. The differences between these two inversion temperatures were within about 3 °C. Also, the temperature at which the electric conductivity of the emulsion dropped abruptly on heating was measured. The temperatures obtained by these two methods showed almost the same value; the average values were marked as PIT.

Results and Discussion

As for the hydrophilicity of the crown ring, Kuwamura[2,3] reported, from his study of the cloud point, that the acetal-type crown ring obtained from hexaethylene glycol and aldehyde is almost equivalent to 4 oxyethylene units in poly(oxyethylene) monoalkyl ether, and that the crown ring made of hexaethylene glycol and a triazine subunit exhibits almost the same performance as monoaza-18-crown-6 and 1,10-diaza-18-crown-6. Moroi[4] concluded, from a comparison of the CMCs, that a diaza-18-crown-6 ring is equivalent to 20 oxyethylene units in a polyoxyethylene-type nonionic surfactant with an identical alkyl-chain length.

As the properties of surfactants are considered to be changed under the application conditions, the concept of effective HLB has been proposed[13,15,16] in

order to compare the hydrophilicity of surfactants under different conditions. The HLB of the usual nonionics with the poly(oxyethylene) group as hydrophile can be estimated by Griffin's equation[17] or other similar equations.[18] However, because of the lack of a hydroxyl group in the hydrophilic group, and because of the specific cyclic structure, the HLB values of crown compounds are considered to be different from those of the usual poly(oxyethylene) nonionics; they can not be estimated by the equations mentioned above.

The interaction of phenol with polyethylene glycols or nonionic surfactants in water has recently been studied in detail.[19–24] Though the phenol added to an aqueous solution of a nonionic surfactant increases the water-structuring, a major portion of it complexes with the poly(oxyethylene) chain[19] and is included in the micelle.[22] The phenol-micelle binding increases the micelle aggregation number and lowers the cloud point.[23,24] After a certain amount of a phenol solution is added, the solution of nonionics becomes turbid. Therefore, the nonionics having a higher hydration ability requires a greater volume of a phenol solution to induce turbidity.[13–16,19–21] Marszall utilized the correlation between the required amount of phenol and the hydrophilicity of a nonionics to estimate the effective HLB of the nonionics in the presence of additives.[13–16] Thus, it is reasonable to expect that the hydration ability of crown compounds and its change upon the addition of an electrolyte can be evaluated from an investigation of the interaction of the crown compound with phenol.

The phenol-index values of alkyl crown ether and *N*-alkyl monoaza crown ether were measured; the results are shown in Table 1. It was found that the phenol-index values of crown compounds increased with an increase in ring size and with a decrease in alkyl-chain length, and decreased with an increase in the temperature.

The phenomenon that the addition of alkali metal salts to an aqueous solution of nonionics reduces the phenol index has been reported[15,21] and interpreted to indicate that the presence of an electrolyte increases the micellar binding with phenol, probably as a result of lowering the solubility of phenol and surfactant and increasing the aggregation number of surfactant.[21] This means that the effective HLB of a nonionics decreases as a result of the salting-out effect of electrolytes. The phenol indices of crown compounds, however, increased upon the addition of KCl or NaCl to the aqueous solutions. Thus, the phenol index of crown compounds which have the hydrophilic group of the 18-crown ring (C_8O18C, C_8N18C) was significantly increased (by 14.80 and 4.18) with KCl, but by only 1.27 and 0.70 with NaCl. Conversely, the phenol index of C_8O15C, which has the 15-crown ring as the hydrophilic group, increased slightly (by 0.10) with KCl, but remarkably (by 0.86) with NaCl. The finding that the effective HLB of a crown compound in water selectively increased depending on the kind of salt and the ring size of the crown compound can be explained by the formation of the cationic complexes of crown compound shown in Eq. 1, and hence the increase in the hydration of surface-active species. These phenomena are in line with the tendency for salts selectively to increase the cloud point of an aqueous solution of crown compounds.[9]

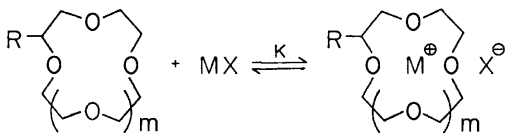

(1)

Marszall reported that the nonionics with a given lipophilic group showing the same phenol-index value have the same effective HLB, and that the effective HLB of a nonionics in the presence of additives can be obtained from the plot of the phenol index versus HLB.[13–16]

In order to evaluate the effective HLB of crown compounds in the absence or presence of salt, the phenol-index values of $C_{12}H_{25}O(EO)_nH$ (n=4,5,6,7,8) at 5, 10, 15, and 25 °C versus their Griffin HLB values were plotted (Fig. 1). The effective HLBs of crown compounds were estimated from the phenol index using these plots; it was thus found that the effective HLB of *N*-dodecyl monoaza crown ether ($C_{12}N18C$) is 0.6 higher than that of dodecyl crown ether ($C_{12}O18C$). Under the conditions shown in Table 1, the extent of the effective HLB increase (1.8, 0.7) of 18-crowns ($C_{12}O18C$, $C_{12}N18C$) by KCl was larger than that by NaCl (0.3, 0.2). These salts increased the effective HLB of alkyl crown ether ($C_{12}O18C$)

Table 1. The phenol indices of alkyl-substituted crown and monoaza crown ethers in the absence and presence of K(Na)Cl[a]

Crown ether	t/°C	—	KCl	NaCl
C_8O15C	10	0.42	0.52	1.28
C_8O18C	25	1.28	16.08	2.55
C_8N18C	25	4.52	8.70	5.22
$C_{12}O18C$	25	—	16.22 (12.3)[b]	0.48 (10.6)[b]
	15	0.60 (−)	31.60 (12.1)[b]	1.95 (10.7)[b]
	5	2.44 (10.4)[b]	60.80 (—)	4.26 (10.7)[b]
$C_{12}N18C$	25	0.82 (10.9)[b]	5.00 (11.7)[b]	1.82 (11.2)[b]
	15	3.10 (11.0)[b]	7.78 (11.5)[b]	3.90 (11.1)[b]

a) The concentrations of KCl and NaCl are 0.5 M, while those of crown compounds are 0.025 M. b) The data in the parentheses are effective HLBs evaluated from phenol index using the plots shown in Fig. 1.

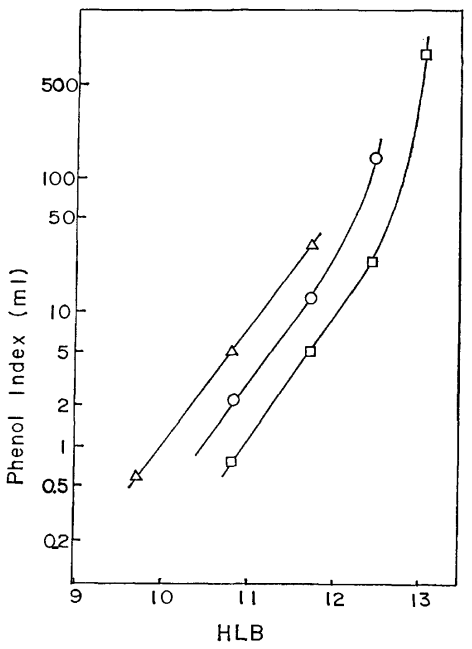

Fig. 1. The relationship between the phenol index and the HLB calculated by Griffin's method for $C_{12}H_{25}O$-$(EO)_nH$ (n=4,5,6,7,8) at 5 °C (—△—), 15 °C (—○—), and 25 °C (—□—).

more than that of *N*-alkyl monoaza crown ether ($C_{12}N18C$), much as with the tendency of the alkali-salt effect on the cloud point of these two kinds of crown compounds.

The O/W-type emulsion produced by using a proper nonionic surfactant as an emulsifier becomes unstable on heating and is inverted into a W/O-type emulsion. The temperature at which phase inversion occurs is called the PIT. The higher the HLB of the emusifier is, the higher PIT the emulsion exhibits. The PITs of $C_{12}O18C$ and $C_{12}N18C$ acting as the emulsifier for the dodecane/water system were 12 °C and 25 °C respectively, but those of the corresponding open-chain compounds, $C_{12}O18H$ and $C_{12}N18H$, were 82 °C and 83 °C respectively (Table 2). By adding KCl to the emulsion under the conditions described in Table 2, the PITs of two crown compounds, $C_{12}O18C$ and $C_{12}N18C$, increased by 27 °C, and 13 °C. Those of open-chain compounds, $C_{12}O18H$ and $C_{12}N18H$, decreased by 8 °C and 7 °C respectively in the same way as the PIT was observed to decrease in usual poly(oxyethylene) nonionics.[12] The fact that the PIT of the emulsion prepared by the use of a crown-compound emulsifier increased upon the addition of salts can also be explained by postulating that the salt enables alkyl crown ethers (**1**) or monoaza crown ethers (**2**) to form cationic complexes and to enhance their hydrophilicity, as has been described in the case of the phenol index.

The HLB of an emulsifier can be estimated from the PIT of the emulsion.[10,12] Using the plot of the PIT of 1:1 dodecane/water system emulsified with poly(oxyethylene) dodecyl ether[25] versus its Griffin HLB value, the effective HLB values of crown compounds were estimated from the PIT obtained under

Table 2. The PITs and effective HLBs of crown compounds and the corresponding open-chain compounds[a]

Compound	PIT(°C)		Effective HLB	
	—	KCl	—	KCl
$C_{12}O18C$	12	39	9.2	10.6
$C_{12}O18H$	82	75	12.8	12.4
$C_{12}N18C$	25	38	9.8	10.5
$C_{12}N18H$	83	75	12.9	12.4

a) The mole ratio of KCl to the surfactant is 3:1, and the concentration of surfactants is 4 wt%/system.

the same conditions; *i.e.*, the effective HLB values of $C_{12}O18C$ and $C_{12}N18C$ are 9.2 and 9.8, while those of $C_{12}O18H$ and $C_{12}N18H$ are 12.8 and 12.9 repectively. Upon the addition of KCl, the effective HLB values of $C_{12}O18C$ and $C_{12}N18C$ increased by 1.4 and 0.7 respectively, but those of the corresponding open-chain compounds, $C_{12}O18H$ and $C_{12}N18H$, decreased to almost the same extent, 0.4 and 0.5 respectively. Furthermore, KCl raised the effective HLB of $C_{12}O18C$ more than that of $C_{12}N18C$. This fact can be explained by the same reason that KCl raised the phenol index and cloud point of 18-crown ethers more than those of monoaza 18-crown ethers. Because of the restriction of emulsion stability, the amount of KCl added is limited to a triple mole of surfactant for PIT measurements. For the phenol-titration method, however, the concentration of KCl is 0.5 M, which corresponds to twenty times the molar amount of the surfactant. Therefore, in the presence of KCl, the extent of the increase in the effective HLB obtained by the phenol-titration method may be larger than that obtained by the PIT method.

Furthermore, it is well known that HLB also has a linear relationship with the cloud point below 100 °C.[13,26] The plot of the cloud point versus HLB for oligoethylene glycol dodecyl ether[18] was used to estimate the hydrophilicity of the crown ring, and it was found that the HLB values of $C_{12}O18C$ and $C_{12}N18C$ were 10.3 and 10.6 respectively, resembling the values obtained by the phenol-titration method, which is essentially similar to the cloud point method. Also, the fact that the effective HLB values of $C_{12}O18C$ and $C_{12}N18C$ obtained by the phenol-titration method were 0.9 and 1.2 larger than those obtained by the PIT method, is attributed to the deviation caused by different evaluating methods.

From the evaluations described above, the hydrophilicity of 18-crown-6 and monoaza-18-crown-6 rings with a dodecyl group can be concluded to be approximately equivalent to that of 4.0 and 4.5 units of oxyethylene chains respectively.

References

1) J. Le Moigne, Ph. Gramain, and J. Simon, *J. Colloid Interface Sci.*, **60**, 565 (1977).

2) T. Kuwamura and T. Kawachi, *Yukagaku*, **28**, 195 (1979).

3) T. Kuwamura and S. Yoshida, *Nippon Kagaku Kaishi*,

1980, 472.
4) Y. Moroi, E. Pramauro, M. Grätzel, E. Pelizzetti, and P. Tundo, *J. Colloid Interface Sci.*, **69**, 341 (1979).
5) I. Ikeda, S. Yamamura, Y. Nakatsuji, and M. Okahara, *J. Org. Chem.*, **45**, 5355 (1980).
6) P.-L. Kuo, M. Miki, I. Ikeda, and M. Okahara, *J. Am. Oil Chem. Soc.*, **57**, 227 (1980).
7) P.-L. Kuo, I. Ikeda, and M. Okahara, *Tenside Deterg.* **19**, 4 (1982).
8) P.-L. Kuo, I. Ikeda, and M. Okahara, *Tenside Deterg.* **19**, 204 (1982).
9) M. Okahara, P. -L. Kuo, S. Yamamura, and I. Ikeda, *J. Chem. Soc., Chem. Commun.*, **1980**, 586.
10) K. Shinoda, *Nippon Kagaku Zasshi*, **89**, 435 (1968).
11) K. Shinoda and H. Arai, *J. Phy. Chem.*, **68**, 3485 (1964).
12) K. Shinoda and H. Takeda, *J. Colloid Interface Sci.*, **32**, 642 (1970).
13) L. Marszall, *Fette Seifen Anstrichm.*, **82**, 40 (1980).
14) L. Marszall, *J. Colloid Interface Sci.*, **65**, 589 (1978).
15) L. Marszall, *Tenside Deterg.*, **18**, 26 (1981).
16) L. Marszall and J. W. V. Valkenburg, *Ind. Eng. Chem. Prod. Res. Dev.*, **20**, 708 (1981).
17) W. C. Griffin, *J. Soc. Cosmet. Chem.*, **1**, 311 (1949).
18) H. Schott, *J. Pharmac. Sci.*, **58**, 1443 (1969).
19) D. Guttman and T. Higuchi, *J. Am. Pharm. Assoc., Sci. Ed.*, **45**, 659 (1966).
20) B. N. Kabadi and E. Roy Hammarlund, *J. Pharm. Sci.*, **55**, 1069 (1966).
21) M. Donbrow and E. Azaz, *J. Colloid Interface Sci.*, **57**, 20 (1976).
22) E. Azaz and M. Donbrow, *J. Colloid Interface Sci.*, **57**, 11 (1976).
23) H. Saito and K. Shinoda, *J. Colloid Interface Sci.*, **24**, 10 (1967).
24) T. Nakagawa and K. Tori, *Kolloid Z.*, **168**, 132 (1960).
25) T. Mitsui, Y. Machida, and F. Harusawa, *Bull. Chem. Soc. Jpn.*, **43**, 3044 (1970).
26) A. T. Florence, F. Madsen, and F. Puisieux, *J. Pharm. Pharmacol.*, **27**, 385 (1978).

Effect of Adsorption by Cellulose Acetate Membrane on Reverse Osmosis of Some Monoamino Monocarboxylic and Monoamino Dicarboxylic Acids in Aqueous Solutions

Osami Tozawa* and Danji Nomura

Department of Food Science and Technology, Faculty of Agriculture, Kyushu University, Hakozaki, Higashi-ku, Fukuoka 812

(Received March 4, 1982)

Taft's polar and steric parameters, $\Sigma\sigma^*$, ΣE_s, and nonpolar parameter, ΣS^* governing the reverse osmosis of nonionized polar aliphatic and alicyclic organic compounds using a cellulose acetate membrane were also applicable to aliphatic monoamino monocarboxylic acids having zwitter ion structure. These three parameters were further extended so as to include the cases of sulfur-containing amino acids, hydroxy-substituted, and aromatic type amino acids. Reverse osmosis of monoamino monocarboxylic acids in binary aqueous solution systems containing L-alanine was carried out. As a result, added amino acids were adsorbed by the membrane when added in low concentration (<0.001 mol dm^{-3}), and the permeation of L-alanine was governed by the difference of Taft's polar parameter between L-alanine and the added amino acid. Reverse osmosis of monoamino dicarboxylic acids indicated that hydrogen ions were adsorbed by the membrane, and the adsorption isotherms of hydrogen ions were approximately represented by the Langmuir formula for each amino acid. The electrostatic repulsion between R^- ionic species in monoamino dicarboxylic acid and the negatively dissociated groups of the membrane was weakened by neutralization of the membrane by hydrogen ion adsorption, resulting in decreased amino acid rejection. It was noted that the ultraviolet spectrum and the titration curve of permeate of amino acids were different from those of the feed solution; relationship between this phenomenon and adsorption of hydrogen ions was investigated.

Reverse osmosis and ultrafiltration methods have been used for the concentration of protein solutions, purification of enzymes, *etc.* When enzymatic processes are conducted in an ultrafiltration reactor however, pretreatment of the membrane with deposition of inert proteinic gel onto the membrane surface is necessary because the enzyme is inactivated when adsorbed on the surface of a membrane.[1-3] It is further reported that the adsorption of solutes at a membrane-solution interface results in the formation of a gel layer; this causes difficulty in washing the membrane.[4] These studies indicate that adsorption of solutes by a membrane is one of the major problems in reverse osmosis and ultrafiltration processes.

It has been reported that a variety of substances can be adsorbed on cellulosic materials, *i.e.*, adsorption of *m*-aminobenzoic acid on cellulose acetate powder,[5] cellulose-triacetate and cellulose-acetate-butyrate on porous adsorbents (calcium silicate or aluminum silicate),[6] sulfobromophthalein sodium on regenerated cellulose membrane which immobilizes activated charcoal.[7] Literature further reports that surface flow of *p*-chlorophenol[8] and cumene[9] is caused by their adsorption on a cellulose acetate membrane. Little work has been done so far to explain the mechanism of ionic permeation through a membrane on which adsorption layer is formed.

The purpose of this study is to explain, on the basis of preferential sorption-capillary flow mechanism,[10] the effect of adsorption of ions at the membrane-solution interface during permeation of amino acids through a cellulose acetate membrane.

In the previous papers,[11-14] a number of the following facts were elucidated: (a) Factors governing the reverse osmosis of monoamino monocarboxylic acids in a single system; (b) effect of adsorption of an added amino acid on reverse osmosis of monoamino monocarboxylic acids in binary aq. solutions systems containing L-alanine and (c) the effect of adsorption of hydrogen ions on reverse osmosis of monoamino dicarboxylic acids in single system.

In this paper, the effects of adsorption of hydrogen ions is explained by measuring the UV spectrum and the titration curve of the permeate, are summarized along with previous work.

Transport Equations

Rejection, η is defined as follows:

$$\eta \equiv \frac{C_2-C_3}{C_2}, \tag{1}$$

where C_2 and C_3 refer to the concentration at the membrane-solution interface and in the permeate, respectively. Generally, C_2 differs from the concentration in the feed solution, C_1. C_2 can be expressed as[15]

$$C_2 = C_3 + (C_1-C_3)\exp\left(\frac{N_w+N_s}{c_1 k}\right), \tag{2}$$

where c_1 is the molar density of the feed solution, k is the mass transfer coefficient, and N_w and N_s refer to the molar flux of water and solute, respectively. k depends on the shape of the reverse osmosis cell and the streaming state of solution in the cell. On the cell used in this study, k can be represented as follows:[11]

$$k = 7.586\left(\frac{D}{l}\right)R_e^{0.420}S_c^{1/3}, \tag{3}$$

where D is the diffusivity, l is the inside diameter of the cell, R_e is the Reynolds number, and S_c is the Schmidt number. The solute transport parameter, $D/K\delta$ is defined as[15]

$$D/K\delta \equiv \frac{N_s}{C_2-C_3} = \frac{JC_3}{C_2-C_3} = J\left(\frac{1}{\eta}-1\right), \tag{4}$$

where J is the volume flux of permeate.

Experimental

Amino Acids and Membranes. Reagent grade amino acids were used. DDS-600, 800, 870, and 880 cellulose acetate membranes (Loeb type, De Danske Sukkerfabrikker, Denmark) were used. Cellulose acetate (Eastman 398-3) membranes were also prepared according to the method developed by Manjikian.[16]

Analysis and Procedures. The concentration of amino acid in single aq solution was measured with ninhydrin method using a Hitachi spectrophotometer, model 100-30. Amino acids in binary aq solution were analyzed by paper or thin-layer chromatography, using a DMU-33C densitometer (Toyo Kagaku Sangyo, Inc.). The concn of sodium chloride was measured with a MS conductivity bridge CD-35MII. Hydrogen ion concn was determined by using a Hitachi-Horiba F-7Lc pH meter. UV spectra were recorded with a UV-300 spectrophotometer (Shimadzu Seisakusho, Inc.). The titration curve was determined with a UCB-7 automatic titrator (Hiranuma Sangyo, Inc.). Experiments were conducted in a batch using a stirred reverse osmosis cell (Bio Engineering RO-3). The volume and effective membrane area were 200 cm^3 and 32.2 cm^2, respectively. The stirrer was rotated at 300 min^{-1} by magnetic force. When constant permeation of the membrane was achieved, a 2500 cm^3 volume reservoir was attached to the cell. The cell was immersed in a water bath kept at 30 °C. The operating pressure was 1.96 MPa. Figure 1 shows the relationship between η of 0.085 mol dm^{-3} of sodium chloride aq solution and the pure water permeability, A obtained by using a cellulose acetate membrane. Figure 1 shows that the property of a DDS-membrane is the same as that of a laboratory-made membrane. Before the experiments, membranes were always tested with distilled water and 0.085 mol dm^{-3} of sodium chloride aq solution, and the relationship shown in Fig. 1 was confirmed.

Results and Discussion

Factors Governing Permeation of Monoamino Monocarboxylic Acids in a Single System. A monoamino monocarboxylic acid existing as zwitter ion in aq solution posesses zero net charge. Therefore, Eq. 5 proposed by Matsuura *et al.*[17] for the solute transport parameter, $D/K\delta$ of nonionized polar aliphatic and alicyclic compounds is employed to determine the factors governing the reverse osmosis of monoamino monocarboxylic acids (0.001 mol dm^{-3}):[11,12]

$$\ln (D/K\delta) = \ln C^* + \rho^*\Sigma\sigma^* + \delta^*\Sigma E_s + \omega^*\Sigma S^*. \quad (5)$$

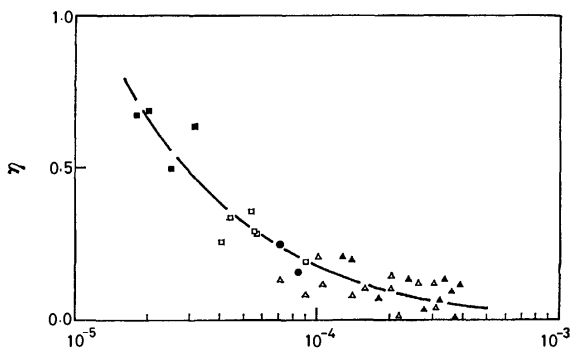

Fig. 1. Relation between η and A for 0.085 mol dm^{-3} of NaCl aq soln.
△: DDS-600, ▲: DDS-800, □: DDS-870, ■: DDS-880, ●: laboratory-made.

D is the diffusivity, δ is the effective thickness of the membrane, K is the reciprocal of the distribution coefficient, and $\ln C^*$ is constant, depending on the porous structure of the membrane surface, the chemical nature of the membrane material, and the nature of the functional group in the solute molecule; $\rho^*\Sigma\sigma^*$, $\delta^*\Sigma E_s$, and $\omega^*\Sigma S^*$ refer to polar, steric, and nonpolar effects, respectively; $\Sigma\sigma^*$, Taft's polar parameter; ΣE_s, Taft's steric parameter; ΣS^*, nonpolar parameter (modified Small's number); and ρ^*, δ^*, and ω^* are the characteristic proportionality constants associated with $\Sigma\sigma^*$, ΣE_s, and ΣS^*, respectively. ρ^* and ω^* do not depend on the porous structure of the membrane surface, whereas δ^* depends on the porosity of the membrane. $\Sigma\sigma^*$ and ΣE_s for a variety of substituents are tabulated in Taft's table,[18] however, the number of substituents listed is not enough, on the other hand, ΣS^* is applicable to substituents composed of hydrocarbons only.[9] Therefore, in order to apply Eq. 5 to sulfur-containing, hydroxy-substituted, and aromatic type amino acids, it is necessary to correlate the characteristic parameters ($\Sigma\sigma^*$, ΣE_s, and ΣS^*) with other physical quantities. The proportion of the ionic bond in an optional substituent can be calculated by measuring the polarity between diverse atoms.[19] $\Sigma\sigma^*$ was a correlation on the basis of the ionic bond proportion. Steric effects depend on the size and shape of the solute molecule. Hence, ΣE_s was correlated on the basis of the molecular weight of the substituent. On the other hand, a nonpolar effect would depend on a hydrophobic interaction energy between the membrane and solute, called an interaction energy of London-van der Waals dispersion force. ΣS^* was a correlationship of interaction energy. The values of the parameters obtained are tabulated in Table 1. The nonpolar effect is considered negligible if the molecular structure of the solute contains a straight chain involving no more than three carbon atoms not associated with a polar functional group.[17] For glycine and L-alanine, Eq. 5 can be reduced to

$$\ln (D/K\delta) = \ln C^* + \rho^*\Sigma\sigma^* + \delta^*\Sigma E_s. \quad (6)$$

As $\Sigma\sigma^*$ and ΣE_s in L-alanine are zero, $\ln C^*$ can be expressed as

$$\ln C^* = \ln (D/K\delta)_{\text{L-alanine}}. \quad (7)$$

From Eqs. 6 and 7, we have

$$\delta^* = \frac{\ln (D/K\delta)_{\text{glycine}} - \ln (D/K\delta)_{\text{L-alanine}} - \rho^*(\Sigma\sigma^*)_{\text{glycine}}}{(\Sigma E_s)_{\text{glycine}}}, \quad (8)$$

where the reaction constant in the hydrolysis reaction of the ester (=1.465)[18] was employed as a numerical value of ρ^*. From Eq. 5, ω^* can be expressed as follows:

$$\omega^* = \frac{\ln (D/K\delta) - \ln C^* - \rho^*\Sigma\sigma^* - \delta^*\Sigma E_s}{\Sigma S^*}. \quad (9)$$

ω^* is correlated with the number of carbon atoms in

Table 1. Summary of physicochemical properties of some amino acids

Number	Amino acid	ΣE_s	$\Sigma\sigma^*$	ΣS^* / $J^{0.5}\,cm^{1.5}\,mol^{-1}$	$k\times10^4$ / $cm\,s^{-1}$
1	Glycine	1.24	0.490	184	78
2	L-Alanine	0.00	0.000	438	70
3	L-Valine	−0.47	−0.190	933	61
4	L-Leucine	−0.93	−0.125	1205	57
5	L-Isoleucine	−1.13	−0.210	1205	57
6	DL-Norvaline	−0.36	−0.115	982	61
7	DL-Norleucine	−0.39	−0.130	1254	57
8	D-Phenylglycine	−2.55	0.600	685	57
9	L-Phenylalanine	−0.38	0.215	957	55
10	DL-2-Aminobutyric acid	−0.07	−0.100	710	65
11	L-Serine	−0.18	0.555	415	67
12	L-Threonine	−0.30	0.530	696	62
13	L-Homoserine	−0.30	0.530	696	62
14	L-Tyrosine	−0.38	0.800	980	53
15	Dopa	−0.46	0.600	1066	52
16	L-Cysteine	−0.32	−0.400	661	64
17	L-Methionine	−0.46	−0.290	1236	57
18	DL-Homocysteine	−0.40	−0.360	939	59
19	DL-Ethionine	−0.50	−0.250	1530	54

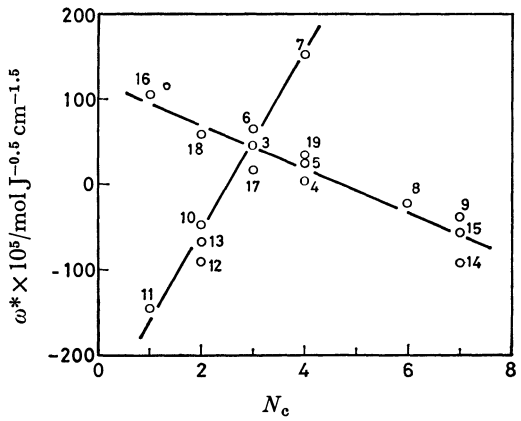

Fig. 2. Relation between ω^* and N_c.
Number is solute number of amino acid, membrane: DDS ($A=8.16\times10^{-5}$ mol cm^{-2} s^{-1} MPa^{-1}).

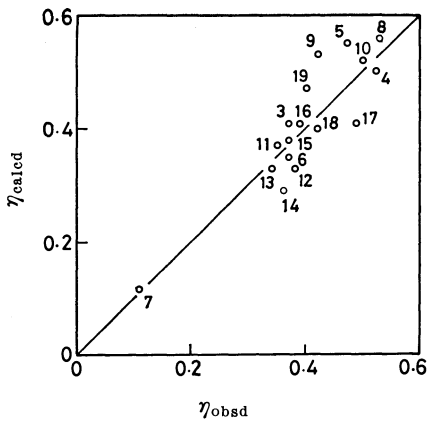

Fig. 3. Calculation of rejection of amino acid.
Number is solute number of amino acid, membrane: DDS ($A=8.16\times10^{-5}$ mol cm^{-2} s^{-1} MPa^{-1}).

a substituent, N_c, as shown in Fig. 2. ω^* of aliphatic amino acids having straight chain and hydroxy-substituted amino acids varies as the number of carbon atoms, but ω^* of aliphatic amino acids having branched chain, sulfur-containing amino acids and aromatic amino acids varies inversely with the number of carbon atoms. These relations are approximated by a first-order equation as follows:
for the former,

$$\omega^* = -2.66\times10^{-3} + (1.05\times10^{-3})(N_c), \quad (10)$$

for the latter,

$$\omega^* = 1.19\times10^{-3} - (2.54\times10^{-4})(N_c). \quad (11)$$

By using Eqs. 4, 5, 7, 8, 10, and 11, rejection values of each amino acid are calculated, and compared with the real values, as is shown in Fig. 3. The calculated values are in fair agreement with the real values, which shows that polar, steric, and nonpolar effects all play some role in the reverse osmosis of monoamino monocarboxylic acids. It is further noted that the order of rejection of amino acids is nearly consistent with Matsuura and Sourirajan's data[20] (Laboratory-made Batch 316 (10/30)-type cellulose acetate membrane).

Interaction between Two Monoamino Monocarboxylic Acids on a Membrane-solution Interface. The reverse osmosis of fourteen kinds of solution consisting of L-alanine (0.001 mol dm^{-3}) and added amino acids (0.00025—0.004 mol dm^{-3}) of aliphatic, hydroxy-substituted, sulfur-containing, and aromatic types has been reported in a previous paper.[13] The results show that the rejection of L-alanine is almost constant in the concentration range (0.001—0.004 mol dm^{-3}) in all the systems, except when the concentration of the acids is decreased to 0.00025 mol dm^{-3}, the rejection of L-alanine increases considerably. Rejection of the added amino acids is almost constant through out the con-

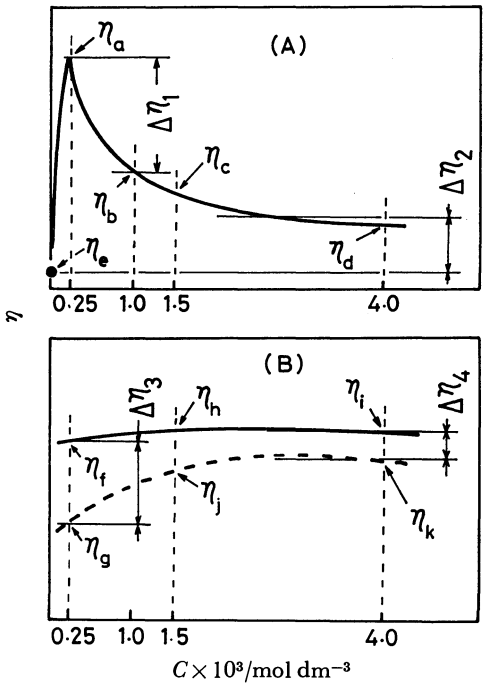

Fig. 4. Schematic diagram of reverse osmosis.
(A): L-Alanine, (B): added amino acid, solid line: binary system, broken line: single system.

centration range of 0.00025—0.004 mol dm^{-3} in most of the systems. On the other hand, in a single system, rejection of amino acids is almost constant in the concentration range of 0.001 to 0.004 mol dm^{-3}, but decreases when the concentration of the amino acid decreases below 0.001 mol dm^{-3}. Figure 4 shows the schematic diagram of the reverse osmosis systems mentioned above. The four equations shown below represent the change in the rejection pattern of these amino acids:

$$\Delta\eta_1 \equiv \eta_a - \eta_b, \quad (12)$$

$$\Delta\eta_2 \equiv (\eta_c+\eta_d)/2 - \eta_e, \quad (13)$$

$$\Delta\eta_3 \equiv \eta_f - \eta_g, \quad (14)$$

$$\Delta\eta_4 \equiv (\eta_h+\eta_i)/2 - (\eta_j+\eta_k)/2, \quad (15)$$

where η_a, η_b,$\cdots\eta_j$, and η_k are shown in Fig. 4. $\Delta\eta_1$, $\Delta\eta_2$, $\Delta\eta_3$, and $\Delta\eta_4$ are used in order to summarize experimental data of rejection in many systems. $\Delta\eta_1$, $\Delta\eta_2$, $\Delta\eta_3$, and $\Delta\eta_4$ in each system are tabulated in Table 2. A glance at Table 2 shows that $\Delta\eta_1$, $\Delta\eta_2$, $\Delta\eta_3$, and $\Delta\eta_4$ are positive in most of the systems. Therefore, the rejection of both L-alanine and the added amino acids is higher in a binary system than in a single system. On the other hand, $\Delta\eta_1$ is greater in systems consisting of L-alanine and aliphatic amino acid than in the other systems. $\Delta\eta_1$ is correlated by $\Sigma\sigma^*$ of each added amino acid, as shown in Fig. 5. When $\Sigma\sigma^*$ of the added amino acid and that of L-alanine are close to each other, rejection of L-alanine increases considerably, but when they are further apart, rejection of L-alanine is not much effected. In the single systems shown in Fig. 6, rejection of some amino acids, (especially aliphatic amino acids) shifts from positive to negative as the concn. of feed solution decreases from 0.001 to 0.00025 mol dm^{-3}. It has been reported

Table 2. Difference between amino acid rejection in binary and single systems[a)]

Added amino acid	$\Delta\eta_1$	$\Delta\eta_2$	$\Delta\eta_3$	$\Delta\eta_4$
L-Serine	0.02	0.10	0.15	0.15
L-Threonine	0.08	0.11	0.09	−0.09
DL-2-Aminobutyric acid	0.21	0.11	0.89	0.05
DL-Norleucine	0.52	0.23	0.46	0.00
DL-Norvaline	0.26	0.03	−0.17	0.15
L-Leucine	0.30	0.23	0.44	0.03
L-Valine	0.34	0.11	0.90	0.21
L-Isoleucine	0.16	0.06	0.08	−0.11
L-Methionine	0.03	0.21	0.35	0.02
DL-Ethionine	0.06	0.27	0.48	0.28
DL-Homocysteine	0.04	0.35	—	—
L-Phenylalanine	0.09	0.09	0.12	0.14
D-Phenylglycine	0.02	0.10	0.14	−0.12
L-Tyrosine	0.14	0.00	0.13	0.24

a) The membrane is DDS membrane (A=8.16×10^{-5} mol cm^{-2} s^{-1} MPa^{-1}).

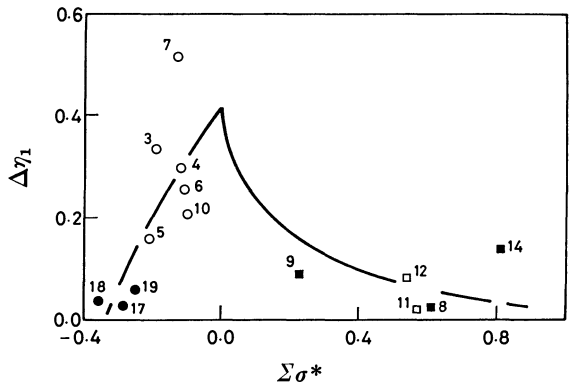

Fig. 5. Effect of Taft's polar parameter on $\Delta\eta_1$.
Number is solute number of amino acid, ○: aliphatic type, ●: sulfur-containing type, □: hydroxy-substituted type, ■: aromatic type, membrane : DDS (A= 8.16×10^{-5} mol cm^{-2} s^{-1} MPa^{-1}).

in the literature that the molar surface tension increment of aliphatic amino acids decreases as the length of the hydrocarbon side chain increases. For example, the molar increment of surface tension is positive for glycine and alanine, but negative for 2-aminobutyric acid, valine, and 2-aminohexanoic acid, showing that 2-aminobutyric acid, valine, and 2-aminohexanoic acid are positively adsorbed at the liquid surface in accordance with Gibbs' theorem.[21,22] These facts reflect that the typical behavior of amino acids is attributed to the surface flow of amino acids caused by the formation of an adsorption layer of amino acids on a surface of the membrane near 0.00025 mol dm^{-3}. On the basis of the assumption mentioned above, the relation between $\Delta\eta_1$ and $\Sigma\sigma^*$ of added amino acids shown in Fig. 5 is explained below. In the first place, for systems consisting of L-alanine and aliphatic amino acids, L-alanine interacts with the adsorption layer of the aliphatic amino acid. But, L-alanine does not have

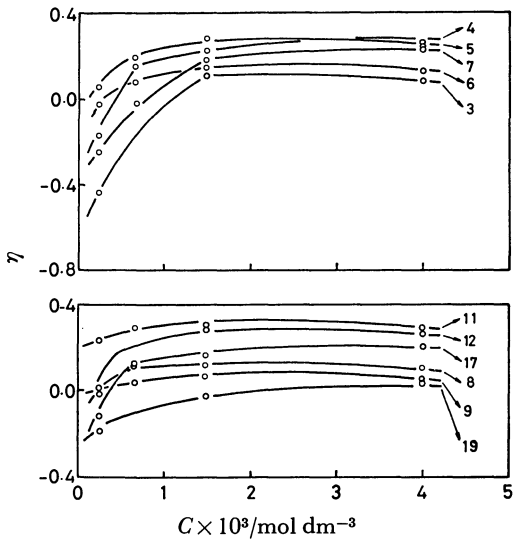

Fig. 6. Effect of concentration on rejection for single system.
Number is solute number of amino acid, membrane : DDS-600.

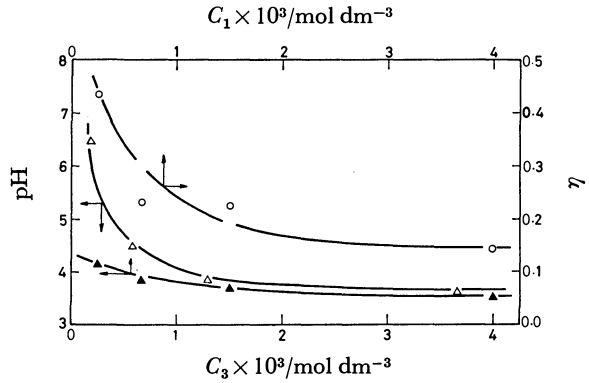

Fig. 7. pH change in reverse osmosis of L-glutamic acid in aq soln.
○: Rejection of L-glutamic acid, ▲: pH of feed soln, △: pH of permeate (16 cm³ of initial product), membrane : DDS-600.

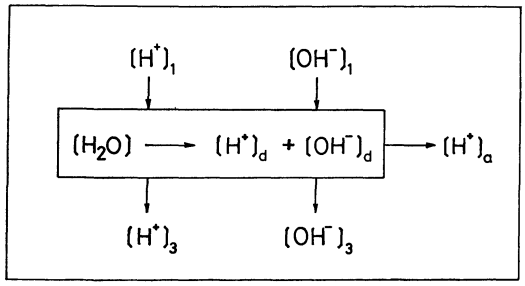

Fig. 8. Adsorption model of hydrogen ion.
Subscript 1: feed soln, 3: permeate, a: adsorption, d: dissociation, □: membrane.

a strong affinity for the adsorption layer because the Taft's polar parameter of the aliphatic amino acid and that of L-alanine are close to each other, *i.e.*, the acidity of the aliphatic amino acid is approximately equal to that of L-alanine. Therefore, rejection of L-alanine increases at the concn of the added amino acids (0.00025 mol dm^{-3}). In the case of systems consisting of L-alanine and added amino acids of hydroxy-substituted, sulfur-containing, and aromatic types, the adsorption layer is formed, but, L-alanine has a strong affinity for the adsorption layer according to Taft's polar parameter, hence, rejection of L-alanine is uneffected.

Hydrogen Ion Adsorption during Permeation of Monoamino Dicarboxylic Acids. The results of the reverse osmosis of monoamino dicarboxylic acids in aq solution have been reported in a previous paper in order to study the adsorption of hydrogen ions on the membrane.[14] Figure 7 shows the result of reverse osmosis of L-glutamic acid. The high pH of the L-glutamic acid permeate solution (16 cm^3 of initial permeate) as compared to that of feed solution is prominent in the low concentration range. This can be explained on the basis that a cellulose acetate membrane is slightly negatively charged,[23] therefore, hydrogen ions become adsorbed on its surface. In the case of the initial permeate, rejection increases as the concentration of the feed solution decreases. This behavior is considered to be due to the higher electrostatic repulsion force between the membrane and the R^- ion of L-glutamic acid. An electrostatic repulsion force is also reported in case of lower organic acids,[24] however, these authors considered the cellulose acetate membrane to be a non charged membrane, and they used a dielectric exclusion force to explain the above phenomenon. To confirm this fact that a cellulose acetate membrane has a weak ion-exchange character, an experiment on the adsorption of Methylene Blue and erioglaucine A on the membrane was carried out. As a result, positively charged oxidation type ions were more abundantly adsorbed than non charged reduction type ions. The adsorption model is shown in Fig. 8 in order to describe quantitatively the adsorption of hydrogen ions under the reverse somosis. Hydrogen ions produced from a monoamino dicarboxylic acid and hydroxide ions enter the membrane, whereas, only hydrogen ions are adsorbed, resulting in the dissociation of a part of the water within the membrane. We assume the dissociation of water to explain this phenomenon because the ionic product of water represented by Eq. 16 has to be applied to the permeate:

$$K_w = [H^+][OH^-]. \quad (16)$$

Applying a material balance of hydrogen and hydroxide ions to a unit volume of solution which permeate through the membrane, we obtain

$$[H^+]_3 = [H^+]_1 - [H^+]_a + [H^+]_d, \quad (17)$$

$$[OH^-]_3 = [OH^-]_1 + [OH^-]_d, \quad (18)$$

where subscripts 1, 3, a, and d refer to the feed solution, permeate, adsorption, and dissociation, respectively. $[H^+]_1$ is essentially the hydrogen ion concentration in the amino acid solution not permeated through the membrane whose amino acid concentration is the same as that of the permeate. However, in this study we consider it as the hydrogen ion concentration in the feed solution because the rejection is low; in other words, C_1 is approximately equal to C_3. Assuming that the hydrogen ion and hydroxide ion concentrations in the pores of membrane are iden-

tical with those in the permeate, the electrical neutrality condition can be expressed as follows:

$$[H^+]_3 + [R^+] = [R^-] + 2[R^{2-}] + [OH^-]_3 + [X^-], \quad (19)$$

where $[R^+]$, $[R^-]$, and $[R^{2-}]$ are the concentrations of each ionic species in the monoamino dicarboxylic acid, and $[X^-]$ is the concentration of the negatively dissociated group not adsorbed by hydrogen ions. Inserting Eqs. 17 and 18 in Eq. 19, we have

$$[H^+]_1 - [H^+]_a + [H^+]_d + [R^+] = [R^-] + 2[R^{2-}] + [OH^-]_1 + [OH^-]_d + [X^-]. \quad (20)$$

Here, we have

$$[H^+]_d = [OH^-]_d. \quad (21)$$

From Eqs. 20 and 21, the electrical neutrality condition in the pores can be represented also as follows:

$$[H^+]_a = [H^+]_1 - [OH^-]_1 + [R^+] - [R^-] - 2[R^{2-}] - [X^-]. \quad (22)$$

Using Eqs. 16, 17, 18, and 21, amount of adsorbed hydrogen ion, M can be derived as follows:

$$M = \int_0^V [H^+]_a dV = \int_0^V \left[K_w\left(\frac{1}{[H^+]_3} - \frac{1}{[H^+]_1}\right) + [H^+]_1 - [H^+]_3\right] dV, \quad (23)$$

where V is permeate volume. When the permeation proceeds to the permeate volume where $[H^+]_a$ is zero, *i.e.*, $[H^+]_1$ is equal to $[H^+]_3$, the adsorption of hydrogen ions stop. Then $[H^+]_1$ is in equilibrium with an equilibrium amount of adsorbed hydrogen ions, M_e. Figure 9 shows the adsorption isotherm of hydrogen ions of each amino acid. The adsorption isotherm may be represented by the Langmuir formula given by

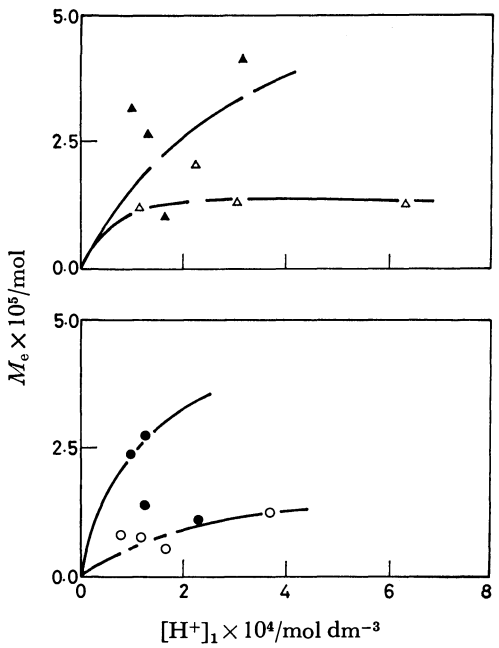

Fig. 9. Adsorption isotherm of the hydrogen ion.
○: L-Glutamic acid, △: L-aspartic acid, ▲: DL-2-aminoadipic acid, ●: DL-2-aminopimelic acid, membrane : DDS-600.

$$M_e = \frac{ab[H^+]_1}{1 + a[H^+]_1}, \quad (24)$$

where a and b are constants. Figure 9 shows some variation because the data were taken from the permeate solution, whereas, in the case of the sorption method, the adsorption of hydrogen ions could hardly be noted. The amount required to saturate the unit volume of the membrane is about 0.03 mol dm^{-3} for L-glutamic acid and L-aspartic acid. This value is in fair agreement with the fixed-charge concentration, 0.010 mol dm^{-3} reported by Igawa *et al.*[25] The effect of the adsorption of hydrogen ions in the case of monoamino dicarboxylic acids permeation is shown in Fig. 10. In the case when the membrane approaches equilibrium quickly, an electrostatic repulsion force between the ionic species R^- and the dissociated groups of the membrane is weakened by the neutralization of the membrane with hydrogen ions, resulting in a decrease of the rejection and approaches a constant value as permeation proceeds. On the other hand, when the amount of adsorbed approaches equilibrium slowly, rejection is almost constant because the charge density of the membrane is not changed so much with adsorption of hydrogen ions.

Ultraviolet Spectrum and Titration Curve of Permeate of Amino Acids. UV spectra of the permeate of each monoamino dicarboxylic acid are shown in Fig. 11. The initial permeates exhibit their absorption maxima at a wavelength of 255 nm, however, the absorption maxima disappear as the permeation proceeds. When the concentration of the feed solution is high, the above maxima are smaller. The permeate volume of each amino acid where the absorption maxima vanish, is roughly the same as that in which $[H^+]_a$ is zero, as mentioned earlier. As a general rule, the absorption of the carboxyl group is obscured by the amino auxochrome whose absorption is very strong, therefore, the absorption maxima do not appear in α type of amino acids. But as mentioned above, the absorption maxima appear in amino acid solutions permeated through the

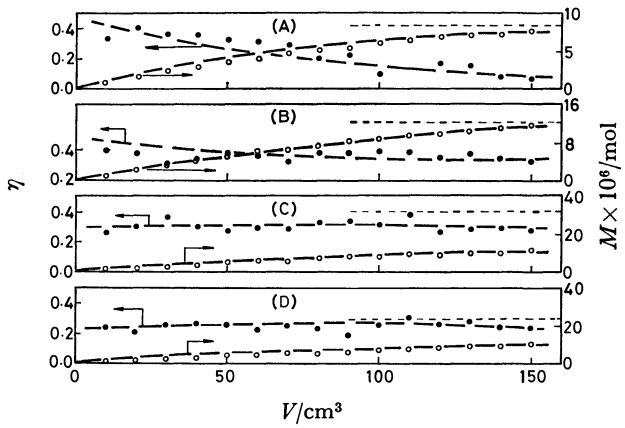

Fig.10. Relation between rejection and permeate volume.
C_1: 0.00025 mol dm^{-3}, ----: equilibrium amount adsorbed, M_e, (A): L-glutamic acid, (B): L-aspartic acid, (C): DL-2-aminoadipic acid, (D): DL-2-aminopimelic acid, membrane : DDS-600.

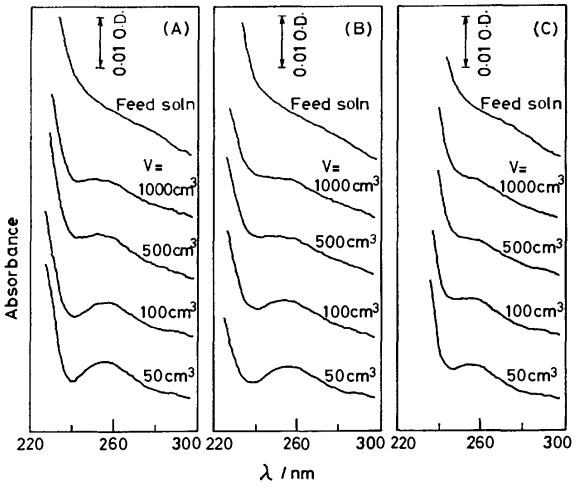

Fig.11. UV spectra of permeate of amino acids. (A): L-Glutamic acid (C_1=0.001 mol dm^{-3}, pH_1=3.72), (B): L-aspartic acid (C_1=0.001 mol dm^{-3}, pH_1=3.53), (C): L-glutamic acid (C_1=0.01 mol dm^{-3}, pH_1=3.37), membrane : laboratory-made.

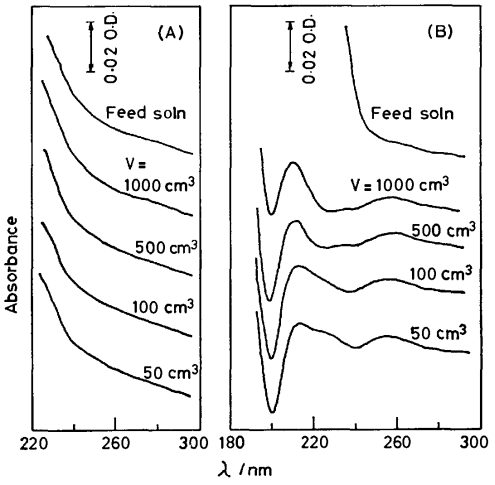

Fig.12. UV spectra of permeate of amino acids. (A): L-Glutamic acid (C_1=0.001 mol dm^{-3}, pH_1=7.0 by NaOH), (B): L-glutamic acid (C_1=0.01 mol dm^{-3}, pH_1=3.37), membrane; (A): laboratory-made, (B): DDS-990 ($A=4.2\times10^{-5}$ mol cm^{-2} s^{-1} MPa^{-1}, η_{NaCl}=0.89).

membrane. This happens because the absorption strength of the amino auxochrome is weakened with the decrease of the hydrogen ion concentration in solution by adsorption of hydrogen ions. When the pH of a monoamino dicarboxylic acid aq solution is adjusted to 7 with sodium hydroxide, the hydrogen ions in the solution disappear; as a result, the adsorption does not occur. Therefore, the absorption maxima do not appear in the permeate, as shown in Fig. 12-A. Monoamino dicarboxylic acid permeates, through high-rejection membrane exhibit their absorption maxima in wavelength 212 nm and 255 nm, as shown in Fig. 12-B. Also, the maxima are not inclined to disappear as the permeation proceeds. This is because 1000 cm^3 of the permeate volume is not high enough to attain equilibrium. On the other hand,

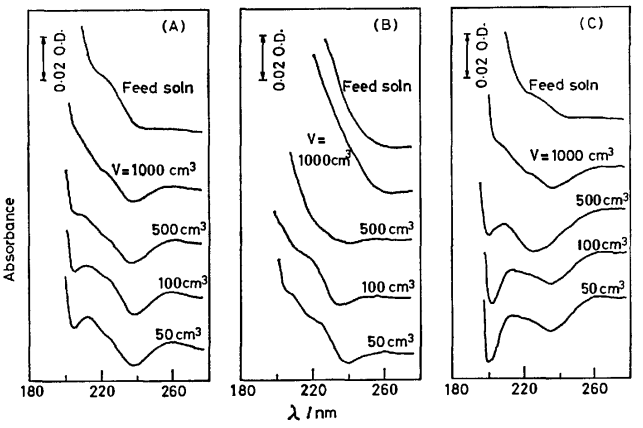

Fig.13. UV spectra of permeate of amino acids. (A): Glycine (C_1=0.001 mol dm^{-3}, pH_1=5.85), (B): L-alanine (C_1=0.001 mol dm^{-3}, pH_1=5.71), (C): L-alanine (C_1=0.001 mol dm^{-3}, pH_1=3.80 by HCl), membrane : laboratory-made.

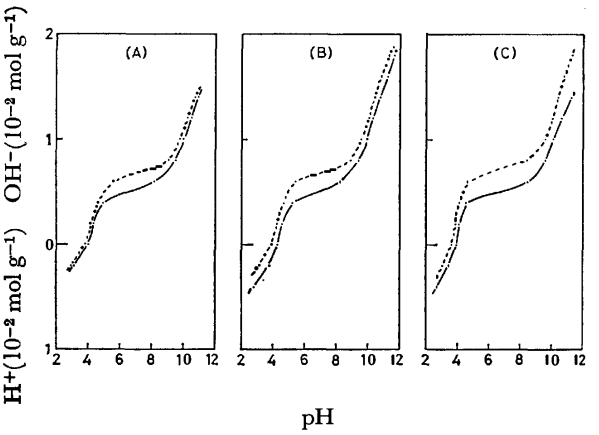

Fig.14. Titration curve of amino acids. (A): L-Glutamic acid (C=0.00075 mol dm^{-3}), (B): L-glutamic acid (C=0.00044 mol dm^{-3}), (C): L-aspartic acid (C=0.00061 mol dm^{-3}), ——: permeate, ----: standard soln, membrane; (A): DDS-600, (B),(C): laboratory-made.

the UV spectra of the permeate of some monoamino monocarboxylic acids are shown in Fig. 13. Glycine exhibits an absorption maximum at 211 nm and 260 nm, and L-alanine at 260 nm, but acquires the UV spectrum of the feed solution as the permeation proceeds. In the case of a monoamino monocarboxylic acid, hydrogen ions in zwitter form are adsorbed; as a result, the above maximum appears. When the L-alanine aq solution is acidified with hydrochloric acid, the permeate exhibits its strong absorption maximum at 211 nm and 260 nm. Figure 14 shows the titration curve of monoamino dicarboxylic acids. Here, the amino acid concentration of the permeate is the same as that of a standard solution. The titration curve of the permeate is located below that of the standard solution because the hydrogen ion concentration of the permeate is lower than that of the standard solution. From Fig. 14, it can be seen that the dissociation constants of the amino acids in the permeate is the same as that in the standard solution.

References

1) G. Greco, Jr., *Biotechnol. Bioeng.*, **22**, 215 (1980).
2) G. Greco, Jr., D. Albanesi, M. Cantarella, L. Gianfreda, R. Palescandolo, and V. Scardi, *Appl. Microbiol.*, **8**, 249 (1979).
3) D. E. Kohlwey and M. Cheryan, *Enzyme Microb. Technol.*, **3**, 64 (1981).
4) Y. Kiso, T. Kitao, M. Sugihara, and Y. Terashima, *Nippon Kagaku Kaishi*, **1981**, 1805.
5) C. Kamizawa, H. Masuda, and S. Ishizaka, *Bull. Chem. Soc. Jpn.*, **45**, 2964 (1972).
6) P. R. M. Nair, K. C. Patel, and R. D. Patel, *Angew. Makromol. Chem.*, **78**, 109 (1979).
7) M. Tamura, T. Uragami, and M. Sugihara, *Kobunshi*, **36**, 241 (1979).
8) T. Matsuura and S. Sourirajan, *J. Appl. Polym. Sci.*, **16**, 2531 (1972).
9) T. Matsuura and S. Sourirajan, *J. Appl. Polym. Sci.*, **17**, 3683 (1973).
10) S. Sourirajan, *Ind. Eng. Chem., Fundam.*, **2**, 51 (1963).
11) D. Nomura and O. Tozawa, *Maku* (Membrane, in Japanese), **2**, 469 (1977).
12) O. Tozawa and D. Nomura, *Nippon Kagaku Kaishi*, **1978**, 1291.
13) O. Tozawa and D. Nomura, *Nippon Kagaku Kaishi*, **1980**, 127.
14) O. Tozawa and D. Nomura, *Nippon Kagaku Kaishi*, **1981**, 270.
15) S. Kimura and S. Sourirajan, *AIChE J.*, **13**, 497 (1967).
16) S. Manjikian, *Ind. Eng. Chem., Prod. Res. Dev.*, **6**, 23 (1967).
17) T. Matsuura, J. M. Dickson, and S. Sourirajan, *Ind. Eng. Chem., Process Des. Dev.*, **15**, 149 (1976).
18) R. W. Taft, Jr., "Steric Effects in Organic Chemistry," ed by M. S. Newman, Wiley, N. Y. (1956), pp. 598, 608, 619.
19) H. Azumi, "Ryōshi Kagaku," Baifukan, Tokyo (1969), p. 116.
20) T. Matsuura and S. Sourirajan, *J. Appl. Polym. Sci.*, **18**, 3593 (1974).
21) J. R. Pappenheimer, M. P. Lepie, and J. Wyman, Jr., *J. Am. Chem. Soc.*, **58**, 1851 (1936).
22) J. W. Belton, *Trans. Faraday Soc.*, **35**, 1293 (1939).
23) M. E. Heyde, C. R. Peters, and J. E. Anderson, *J. Colloid Interface Sci.*, **50**, 467 (1975).
24) T. Matsuura and S. Sourirajan, *J. Appl. Polym. Sci.*, **17**, 3661 (1973).
25) M. Igawa, S. Yoshida, and T. Yamabe, *Nippon Kagaku Kaishi*, **1975**, 1713.

Estimation of Parameters, G_{11}, G_{22}, and G_{12} in the Kirkwood-Buff Solution Theory on the Basis of the Concentration Fluctuation Data Obtained from Rayleigh Scattering

Tadashi KATO, (the late) Tsunetake FUJIYAMA, and Hiroyasu NOMURA*,†

Institute for Molecular Science, Myodaiji, Okazaki 444

†*Department of Chemical Engineering, Faculty of Engineering, Nagoya University, Chikusa-ku, Nagoya 464*

(Received March 8, 1982)

A concentration fluctuation value obtained from Rayleigh scattering intensity was confirmed to give a thermodynamic quantity of an equilibrium system. An observation of concentration fluctuation by a light scattering method was found to be the most direct and useful way of determining a concentration derivative of a chemical potential. For methanol, ethanol, and 1-propanol–carbon tetrachloride systems, the Kirkwood-Buff parameters, G_{11}, G_{22}, and G_{12}, were determined by the use of concentration fluctuation data. The structure of these systems was discussed on the basis of the calculated Kirkwood-Buff parameters.

The solution theory of Kirkwood and Buff is only one theory so far reported which can describe a thermodynamic properties of a solution for the whole concentration range.[1–4] This theory relates thermodynamic quantities of a system to the radial distribution function $g(r)$ through a "concentration fluctuation." In this theory, a parameter G_{ij} plays an important role, which is defined as,

$$G_{ij} = \int_0^\infty \{g_{ij}(r) - 1\} 4r^2 dr, \tag{1}$$

where $g_{ij}(r)$ is the radial distribution function between species i and j. It is important to notice that $g_{ij}(r)$ is a microscopic expression of the structure of a solution. In the case of a binary solution, the parameters G_{11}, G_{22}, and G_{12} appear in this theory. As $g_{ij}(r)$ is an observable quantity by an X-ray or a neutron diffraction method, G_{ij} is also an observable by these methods in principle. In practice, however, these measurements can not give separately each value of $g_{ij}(r)$. Therefore, it is of much importance to determine the G_{11}, G_{22}, and G_{12} values experimentally from macroscopic quantities such as molar volume, compressibility, concentration dependences of chemical potential, and other thermodynamic quantities. Because of the difficulty of obtaining the $(\partial\mu_2/\partial x_2)_{P,T}$ value experimentally with high accuracy, however, such attempts have been reported in only a few papers.

Ben-Naim estimated the concentration dependence of G_{ij} in binary solutions of ethanol and water based on the concentration dependence of the vapor pressure.[5] Similarly, Donkersloot[6] has determined G_{ij}'s for binary solutions of cyclohexane–2,3-dimethylbutane, methanol–water, and ethanol–water. He also calculated the zero-angle X-ray scattering intensities from the G_{ij} values so obtained and compared them with the experimental data.[6,7]

Kato and Fujiyama have discussed the local structures in various solutions on the basis of the quantitative analysis of the concentration fluctuation, $V^*\langle(\Delta x_2)^2\rangle$, obtained from the Rayleigh scattering intensities[8–14] where V^* refers to the volume of the region in which concentration fluctuation is considered. If V^* is large enough to permit the application of statistical mechanics, $V^*\langle(\Delta x_2)^2\rangle$ can be directly related to the concentration derivative of the chemical potential.

In the present work, we will evaluate the Kirkwood-Buff parameters G_{11}, G_{22}, and G_{12}, for binary solutions of methanol–carbon tetrachloride, ethanol–carbon tetrachloride, and 1-propanol–carbon tetrachloride by the use of the concentration fluctuation data obtained from the Rayleigh scattering intensity measurement.[14] We will emphasize the usefulness and reliability of the concentration fluctuation data obtained from the light scattering experiment. At the same time, the structure of the carbon tetrachloride–alcohol systems will be discussed on the basis of the calculated Kirkwood-Buff parameters.

Concentration Fluctuation Obtained from Rayleigh Scattering Intensity and Thermodynamic Property

We first examine the concentration fluctuation values obtained from a light scattering experiment. The concentration fluctuation of a solution can be expressed in terms of the excess chemical potential μ_2^{E} [14] or of the excess free energy G^E as

$$N\langle(\Delta x_2)^2\rangle = \frac{x_1 x_2}{1 + \frac{x_2}{RT}\left(\frac{\partial\mu_2^{E}}{\partial x_2}\right)_{P,T}} \tag{2}$$

or

$$N\langle(\Delta x_2)^2\rangle = \frac{x_1 x_2}{1 + \frac{x_1 x_2}{RT}\left(\frac{\partial^2 G^E}{\partial {x_2}^2}\right)_{P,T}} \tag{3}$$

$$G^E = x_1\mu_1^{E} + x_2\mu_2^{E}, \tag{4}$$

where x_1 and x_2 are the mole fractions of 1 and 2, respectively, μ_1^{E} and μ_2^{E}, the excess chemical potentials of 1 and 2, respectively, R the gas constant, P the pressure, and T the temperature. N of the left of Eq. 1 or 2 is the total number of molecules in the volume V^* ($N=\rho V^*$, ρ: the number density of the solution). Equation 2 enables us to calculate the $(\partial\mu_2^{E}/\partial x_2)_{P,T}$ values using the $N\langle(\Delta x_2)^2\rangle$ values obtained from the light scattering experiment[14] and compare them with those obtained from the vapor-liquid equilibrium experiments.[15] In these calculations, μ_2^{E} was calculated from the vapor pressure data, and was plotted against the concentration. The $(\partial\mu_2/\partial x_2)_{P,T}$ value was derived graphically. The Gibbs-Duhem relation, $x_1(\partial\mu_1/\partial x_2) + x_2(\partial\mu_2/\partial x_2) = 0$, was carefully taken

into account in this process. The results are illustrated in Fig. 1. As shown in Fig. 1, the $-(\partial\mu_2^E/\partial x_2)_{P,T}$ values obtained from these two different procedures agree with each other satisfactorily within their experimental errors. In other words, V^* is ascertained to be large enough to permit the application of statistical mechanics.

In most reports on solution chemistry, G^E is given by a polynomial formula. For example, the excess Gibbs' free energy for the methanol–carbon tetrachloride is given by two relations, one proposed by Scatchard *et al.*[16] and the other by Moelwyn-Hughes *et al.*[17] These empirical formulae give almost the same G^E values. However, if we calculate the concentration fluctuation values $N\langle(\Delta x_2)^2\rangle$, using these two empirical formulae through Eq. 3, the results are completely different with each other. Of course they don't agree with those obtained from the light scattering data shown in Ref. 14. These situations are illustrated in Fig. 2. The results indicate that the given polynomial formulae of G^E do not well express their second derivative, *e.g.*, $(\partial^2 G^E/\partial x_2^2)_{P,T}$ with sufficient accuracy. In other words, it is not easy to predict the concentration fluctuation values from the observed free energy data, although it is possible in principle. By the same reason, it is also difficult to predict the chemical potential values from the concentration fluctuation values obtained by light scattering experiments.[18]

Thus, we can conclude as follows:

(1) A concentration fluctuation value obtained from Rayleigh scattering intensity is a thermodynamic quantity of an equilibrium system.

(2) An observation of concentration fluctuation by a light scattering method is the most direct and useful way of determining a concentration derivative of a chemical potential.

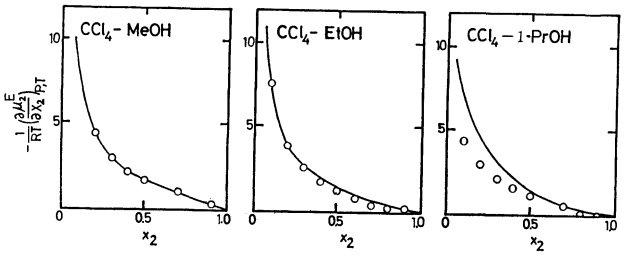

Fig. 1. Plots of $-(1/RT)(\partial\mu_2^E/\partial x_2)_{P,T}$ *vs.* x_2 (suffix 2 refers to alcohol).
○: Calculated from concentration fluctuation data by light scattering, ——: calculated from vapor-liquid equilibrium data.

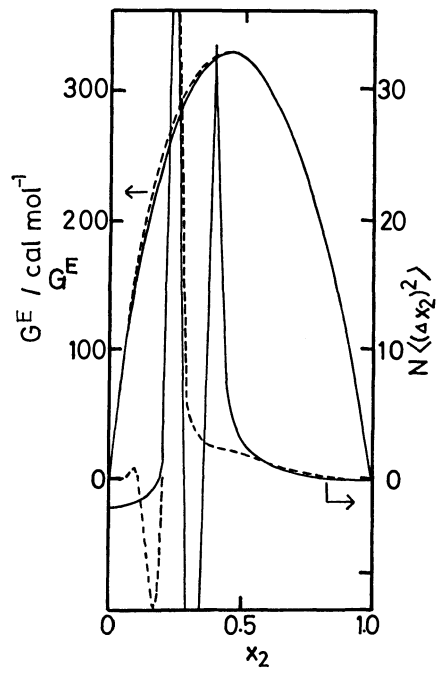

Fig. 2. Excess Gibbs' free energy calculated by empirical formulae proposed by Scatchard *et al.*[16] (——) and Moelwyn-Hughes *et al.*[17] (……) and concentration fluctuation values $N\langle(\Delta x_2)^2\rangle$ calculated from Eq. 3 for carbon tetrachloride–methanol system at 35 °C.

Determination of the Kirkwood-Buff Parameters, G_{11}, G_{22}, and G_{12}, for CCl_4–Methanol, CCl_4–Ethanol, and CCl_4–1-Propanol Systems

According to the Kirkwood-Buff theory, the partial molar volumes v_1, v_2, the isothermal compressibility, κ_T, and the concentration derivative of the chemical potential, $(\partial\mu_2/\partial x_2)_{P,T}$ can be expressed as functions of G_{11}, G_{22}, G_{12}, ρ_1, and ρ_2 where ρ_1 and ρ_2 are the number densities of 1 and 2, respectively. Therefore, G_{11}, G_{22}, and G_{12} can be obtained from these thermodynamic quantities.[5] For numerical calculations, the following data were used.

The concentration derivative of the chemical potential, $(\partial\mu_2/\partial x_2)_{P,T}$ was calculated from the data on the concentration fluctuation obtained from Rayleigh scattering.[14]

Density data for carbon tetrachloride–methanol,[16,19,20] carbon tetrachloride–ethanol,[21] and carbon tetrachloride–1-propanol[20] systems are found in the literature. From these data, the partial molar volumes of each system are calculated.

The isothemal compressibility can be expressed in terms of the adiabatic compressibility, κ_s, the thermal expansion coefficient, α, and the isobaric heat content, C_P, as

$$\kappa_T = \kappa_s + \frac{TV\alpha^2}{C} \qquad \alpha \equiv \frac{1}{v}\left(\frac{\partial v}{\partial T}\right)_P. \tag{5}$$

The isobaric heat content for the solution was calculated from that of the pure component and the temperature dependence of the mixing enthalpy.[22] The expansion coefficent for the carbon tetrachloride–methanol system was calculated from the temperature dependence of the density.[23] For the carbon tetrachloride–ethanol and carbon tetrachloride–1-propanol systems, the data of the temperature dependence of the density can not be found in the literature. So, we evaluated α values from those for the pure alcohol and carbon tetrachloride taking into account the concentration dependence of α for the carbon tetrachloride–methanol system.

The adiabatic compressibility is related to the sound velocity, u_s, by the Laplace equation:

$$\kappa_s = \frac{1}{du_s^2}, \tag{6}$$

where d is the density. The sound velocities for the carbon tetrachloride–ethanol and carbon tetrachloride–1-propanol systems were measured using an ultrasonic interferometer which was operated at a fixed frequency of 5.000 MHz. For the carbon tetrachloride–methanol system, the data of Nomura *et al.*[23] were used.

Discussion

Limiting Values of G_{11}, G_{22}, and G_{12}. Figures 3—5 show the concentration dependences of G_{11}, G_{22}, and G_{12}. For the pure liquids, 1 and 2, G_{11} and G_{22} are expressed as

$$G_{11}^{\circ} = -\frac{1}{\rho_1} + \kappa_{T_1} kT$$

$$G_{22}^{\circ} = -\frac{1}{\rho_2} + \kappa_{T_2} kT.$$

It can be seen from Fig. 3 that the limiting value of G_{11} at $x_2 \to 0$ coincides with G_{11}° value for pure carbon tetrachloride which is $G_{11}^{\circ} = -94.3$ cm^3 mol^{-1}. At the same time, each limiting value of G_{22} at $x_1 \to 0$ coincides with the G_{22}° value for each alcohol ($G_{22}^{\circ} = -37.6$ cm^3 mol^{-1} for methanol, -55.8 cm^3 mol^{-1} for ethanol, and -72.6 cm^3 mol^{-1} for 1-propanol).

The limiting value of G_{12} at $x_1 \to 0$ and $x_2 \to 0$ are expressed as

$$\lim_{x_1 \to 0} G_{12} = \frac{1}{\rho_2} - \bar{v}_1^{\circ} + G_{22}^{\circ}$$

$$= -93.4 \text{ cm}^3 \text{ mol}^{-1} \text{ (MeOH–CCl}_4\text{)}$$

$$= -92.8 \text{ cm}^3 \text{ mol}^{-1} \text{ (EtOH–CCl}_4\text{)}$$

$$= -92.8 \text{ cm}^3 \text{ mol}^{-1} \text{ (1-PrOH–CCl}_4\text{)},$$

$$\lim_{x_2 \to 0} G_{12} = \frac{1}{\rho_1} - \bar{v}_2^{\circ} + G_{11}^{\circ}$$

$$= -38.4 \text{ cm}^3 \text{ mol}^{-1} \text{ (MeOH–CCl}_4\text{)}$$

$$= -57.0 \text{ cm}^3 \text{ mol}^{-1} \text{ (EtOH–CCl}_4\text{)}$$

$$= -84.8 \text{ cm}^3 \text{ mol}^{-1} \text{ (1-PrOH–CCl}_4\text{)},$$

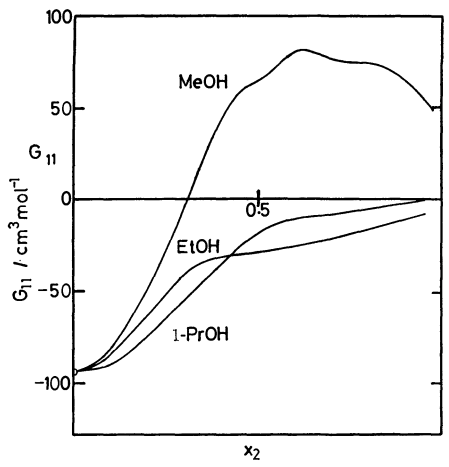

Fig. 3. Concentration dependence of G_{11}.

where $\bar{v}_1^{\circ}$ and $\bar{v}_2^{\circ}$ are the partial molar volumes at infinite dilution. Figure 5 shows that the values of G_{12} tend smoothly to these limiting values. The behavior of these limiting values of G_{11}, G_{22}, and G_{12}, on each side, indicates that the estimation of these value

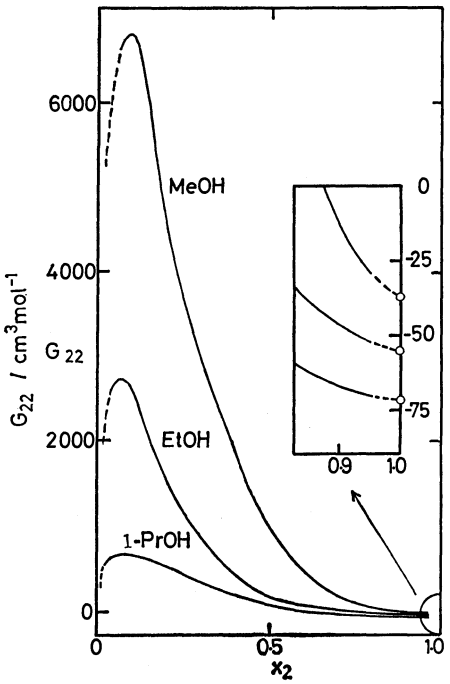

Fig. 4. Concentration dependence of G_{22}.

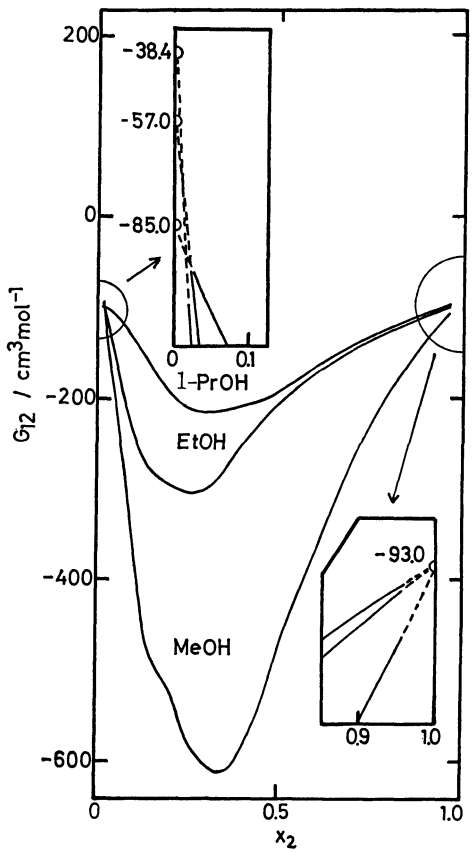

Fig. 5. Concentration dependence of G_{12}.

is reasonable.

Concentration Dependences of G_{11}, G_{22}, and G_{12}. The results shown in Figs. 3—5 may be summarized as follows:

(1) G_{11} is only slightly dependent on the concentration at $x_2<0.1$ especially for the 1-propanol system.

(2) The concentration dependence of G_{11} is similar to that for ordinary binary solutions such as cyclohexane–2,3-dimethylbutane obtained by Dunkersloot.[6]

(3) The magnitudes of G_{22} are much larger than those for ordinary solutions especially in the low concentration range of alcohol and are in the order methanol>ethanol>1-propanol. The magnitude of G_{22} rapidly decreases as the alcohol concentration increases.

(4) G_{12} acquires a minimum value. The magnitudes of the minimum values are in the order 1-propanol>ethanol>methanol.

Interpretation of G_{11}, G_{22}, and G_{12}. Evaluation of the parameters G_{11}, G_{22}, and G_{12} enables us to discuss the solute-solute, solvent-solvent, and solute solvent interactions independently. G_{ij} should be related to the intermolecular interactions and local structures formed in a solution.

It is preferable to discuss the quantity $g_{ij}(r)$ included in G_{ij}, but it cannot be done easily at this stage. Therefore, we will discuss G_{ij} from the standpoint of fluctuations. The parameters G_{11}, G_{22}, and G_{12} can be expressed in terms of the mean numbers of molecules in the volume V, N_1, and N_2, as[24]

$$G_{11} \equiv \int \{g_{11}(r)-1\}\mathrm{d}^3r = v\frac{\overline{N_1^2}-(\overline{N}_1)^2}{(\overline{N}_1)^2} - v_1$$

$$G_{22} \equiv \int \{g_{22}(r)-1\}\mathrm{d}^3r = v\frac{\overline{N_2^2}-(\overline{N}_2)^2}{(\overline{N}_2)^2} - v_2 \qquad (7)$$

$$G_{12} \equiv \int \{g_{12}(r)-1\}\mathrm{d}^3r = v\frac{\overline{N_1N_2}-\overline{N}_1\overline{N}_2}{\overline{N}_1\overline{N}_2}.$$

Equation 7 corresponds to the following relations;

$G_{11}+\bar{v}_1$: number fluctuation of solvent molecules,

$G_{22}+\bar{v}_2$: number fluctuation of solute molecules,

G_{12} : correlation of number fluctuation between solute and solvent molecules.

The large negative value of G_{12} for the alcohol–carbon tetrachloride system indicates the large negative correlation of the number fluctuation between solute and solvent molecules. Similarly, the abrupt increase of G_{22} in the low alcohol concentration range suggests a sudden increase of the correlation between alcohols in the solution. The magnitude of the correlations are in the order methanol>ethanol>1-propanol. On the other hand, G_{11} is slightly dependent on the concentration at $x_2<0.1$. This shows that the structure existing in carbon tetrachloride is held in the solution at the low concentration of alcohol, especially in the case of 1-propanol. These results correspond to the fact that the intermolecular interaction between alcohols is much stronger than that between carbon tetrachlorides in the binary solution of alcohol and carbon tetrachloride.

Concluding Discussion. From the discussion of the preceeding paragraphs the properties of the binary solution of alcohol and carbon tetrachloride may be summarized as follows.

1) The behavior of carbon tetrachloride molecules is not singular but quite normal.

2) All the peculiar properties of the solution come not from the intermolecular interaction between alcohol and carbon tetrachloride, but from the strong interaction between the alcohol molecules as can be seen from the magnitudes of G_{22} and G_{12}.

3) The magnitude of the interactions between the alcohol molecules is in the order methanol>ethanol>1-propanol. For the 1-propanol system, the interaction between the alcohol molecules is weaker.

4) The singular behavior of the alcohol molecules arises from the fact that the alcohol molecules are surrounded by carbon tetrachloride molecules as can be seen from the sharp maximum of G_{22} at low concentrations of alcohol. The above conclusions strongly suggest the formation of a local structure composed of alcohol molecules in the carbon tetrachloride solution. The detailed discussion concerning the local structure formation can be made only when each $g_{ij}(r)$ included in G_{ij} can be quantitatively related to the specific intermolecular interactions in a solution. Work along this line is in progress.

References

1) J. G. Kirkwood and F. P. Buff, *J. Chem. Phys.*, **19**, 774 (1951).

2) F. P. Buff and R. Brout, *J. Chem. Phys.*, **23**, 458 (1955).

3) F. P. Buff and G. M. Schindler, *J. Chem. Phys.*, **29**, 1075 (1958).

4) F. P. Buff and R. Brout, *J. Chem. Phys.*, **33**, 1417 (1960).

5) A. Ben-Naim, *J. Chem. Phys.*, **67**, 4884 (1977).

6) M. C. A. Dunkersloot, *J. Solution Chem.*, **8**, 293 (1979).

7) M. C. A. Dunkersloot, *Chem. Phys. Lett.*, **60**, 435 (1979).

8) T. Kato and T. Fujiyama, *J. Phys. Chem.*, **80**, 2771 (1976).

9) T. Kato and T. Fujiyama, *Bull. Chem. Soc. Jpn.*, **51**, 3128 (1978).

10) T. Kato, S. Hyodo, and T. Fujiyama, *J. Phys. Chem.*, **82**, 1010 (1978).

11) K. Iwasaki, M. Tanaka, and T. Fujiyama, *Bull. Chem. Soc. Jpn.*, **49**, 2719 (1976).

12) K. Iwasaki and T. Fujiyama, *J. Phys. Chem.*, **81**, 1908 (1977), **83**, 463 (1979).

13) T. Kato, **K.** Yano, and T. Fujiyama, *Bull. Chem. Soc. Jpn.*, **53**, 53 (1980).

14) T. Kato, T. Nakanishi, and T. Fujiyama, *Bull. Chem. Soc. Jpn.*, **53**, 2173 (1980).

15) G. Scatchard, S. E. Wood, and J. M. Mochel, *J. Am. Chem. Soc.*, **68**, 1960 (1946) (the methanol–carbon tetrachloride system at 35 °C and 55 °C). J. A. Barker, I. Brown, and F. Smith, *Discuss. Faraday Soc.*, **15**, 142 (1953) (the ethanol–carbon tetrachloride system at 45 °C and 65 °C). G. C. Paraskevopulos and R. W. Missen, *Trans. Faraday Soc.*, **58**, 869 (1962) (the 1-propanol–carbon tetrachloride system at 35 °C). The $(1/RT)\ (\partial\mu_2/\partial x_2)_{P,T}$ values obtained at various temperatures agree with each other within the experimental errors. Therefore, the temperature dependence of $(1/RT)(\partial\mu_2/\partial x_2)_{P,T}$ values is small near room temperature.

16) G. Scatchard, S. E. Wood, and J. M. Mochel, *J.*

Am. Chem. Soc., **68**, 1960 (1946).
17) E. A. Moelwyn-Hughes and R. W. Missen, *J. Phys. Chem.*, **61**, 518 (1957).
18) Therefore, the method of Millar *et al.* is not generally available. See G. A. Millar, *J. Phys. Chem.*, **71**, 2305 (1967).
19) G. Scatchard and L. B. Ticknor, *J. Am. Chem. Soc.*, **74**, 3724 (1952).
20) G. C. Paraskevopulos and R. W. Missen, *Trans. Faraday Soc.*, **58**, 869 (1962).
21) J. A. Barker, I. Brown, and F. Smith, *Discuss. Faraday Soc.*, **15**, 142 (1953).
22) J.-E. A. Otterstedt and R. W. Missen, *Trans. Faraday Soc.*, **58**, 879 (1962).
23) H. Nomura, T. Banba, and Y. Miyahara, *Nippon Onkyō Gakkaishi*, **30**, 228 (1974).
24) See for example, "Kagaku Tōkeirikigaku (Statistical Thermodynamics)," Asakura-Shoten, Tokyo (1966), p. 110.

 © 1982 The Chemical Society of Japan Bull. Chem. Soc. Jpn., 55, 3373—3376 (1982)

The Investigation of Energy Efficiency of the ZnO Semiconductor Photoelectrode by Photothermal Measurement

Yasuhisa MAEDA, Akira FUJISHIMA,* and Kenichi HONDA

Department of Synthetic Chemistry, Faculty of Engineering, The University of Tokyo, Bunkyo-ku, Tokyo 113

(Received March 11, 1982)

The energy efficiency of a polycrystalline ZnO photoanode in an electrolyte solution containing redox agents was investigated by measuring the temperature change of the electrode surface. The results of photothermal measurements show that the energy efficiency depends on the kind of redox agents used. Reducing agents with more positive potentials gave larger energy efficiencies, but the potential must be negative enough to decrease ZnO dissolution.

A number of photoelectrochemical cells using semiconductor electrodes have been reported for the photodecomposition of water and the conversion of solar energy into electricity.[1-17] The energy conversion and quantum efficiencies of photoelectrochemical cells are needed for effective utilization of solar energy. However, during the course of a photoelectrochemical reaction only a portion of the photons absorbed by the semiconductor can be utilized by the electrode reaction, while the remaining portion is converted to heat. Thus, photothermal measurements of a semiconductor electrode during the course of electrolysis can be used to determine the energy efficiency (*i.e.* the ratio of the chemical or electrical power output to the radiant power input).

We have developed a new method to determine the quantum efficiency and the energy efficiency by measuring the temperature change of the surface of a semiconductor electrode with a thermistor.[18-21] When a semiconductor is illuminated with a pulse of monochromatic light having a photon energy E and an average absorbed intensity I for a period of time t, the relationship between the temperature change and the applied potential is represented by Eq. 1, which applies in a limited photocurrent region

$$E\frac{\Delta T}{\Delta T^\circ} = \frac{Q_{s.c.} + T\Delta S}{It} + \eta e(V - V_{FB}), \qquad (1)$$

where ΔT is the temperature change of the semiconductor surface with an applied potential V (*vs.* a reference electrode), ΔT° is the temperature change of the semiconductor surface for an open circuit, ΔS is the entropy change of the semiconductor electrode reaction, $Q_{s.c.}$ is the heat evolved in the semiconductor due to radiationless processes, η is the quantum efficiency of the photoelectrode reaction, and V_{FB} is the flatband potential (*vs.* a reference electrode).

Under constant illumination conditions, *i.e.* EIt= constant, a plot of $E(\Delta T/\Delta T^\circ)$ *vs.* $(V-V_{FB})$ yields a straight line, whose slope is the quantum efficiency, η and whose intercept gives the quantity $(Q_{s.c.}+T\Delta S)/It$ and also $E(\Delta T/\Delta T^\circ)$ when $V=V_{FB}$.

The energy conversion efficiency, therefore, can be obtained when we know the value of the entropy change $T\Delta S$ associated with the electrode reaction.

In previous papers,[18-21] we investigated only the quantum efficiency of photoelectrode reactions from the slope of the linear plot of $E(\Delta T/\Delta T^\circ)$ *vs.* $(V-V_{FB})$, but we had not made a detailed analysis of the energy efficiency.

In this paper, during the course of photoelectrochemical reactions at a ZnO polycrystalline electrode in an electrolyte solution containing redox agents, we determined both the quantum and energy efficiencies. The significance of the intercept and the value of energy efficiency are discussed from the point of view of redox potential.

Experimental

The semiconductor electrode used was a sintered polycrystalline ZnO prepared by pressing reagent-grade ZnO powder at a pressure of 150 kgf/cm²† and then heating at 1300 °C for 3 h in air. After making an ohmic contact with an In–Ga alloy, a copper wire was attached with silver epoxy resin. All surfaces except one were covered with epoxy resin. The exposed polycrystalline face of ZnO was etched in concentrated HCl for 10 s, and then washed with water. The procedure for the photothermal measurement was described in previous papers.[18-21] A platinum electrode was used as the counter electrode and a saturated calomel electrode (SCE) was the reference electrode. A potentiostat (Nikko Keisoku) was used to control the potential of the ZnO electrode with respect to SCE. The supporting electrolyte was 0.2 M Na_2SO_4 (1 M=1 mol dm^{-3}) and all the redox agents used were of reagent-grade.

Results and Discussion

Figure 1 shows the plots of $E(\Delta T/\Delta T^\circ)$ *vs.* V during the course of photoelectrochemical reactions of the ZnO polycrystalline electrode in the electrolyte solution containing one of four different kinds of reducing agents. The electrode was irradiated for 10 s with monochromatic light provided by a 340 nm interference filter. The values of $E(\Delta T/\Delta T^\circ)$ were different for each reducing agent at a given potential. The slopes of the linear plots of $E\ \Delta T/\Delta T^\circ$ *vs.* V, *i.e.* the quantum efficiencies of the photoelectrode reactions, were 0.90 for each reducing agent except S^{2-} for which the slope was 0.80. In the case of S^{2-} the smaller value might be due to the optical absorption of sulfur generated by the oxidation of sulfur ion at the electrode/electrolyte interface. The values obtained by extrapolating the linear portion of $E(\Delta T/\Delta T^\circ)$ *vs.* V to the flatband potentials which were obtained from the onset potentials of the photocurrents depended on the kind of reducing agent. The onset potential was the lowest potential at which a photo-

† 1 kgf=9.80665 N.

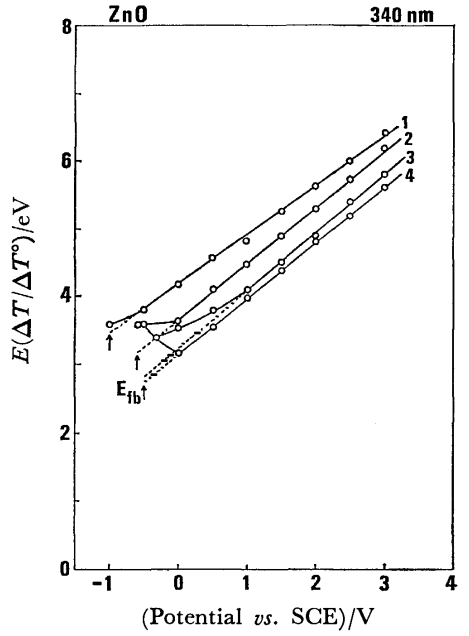

Fig. 1. Normalized temperature change *vs.* potential of a ZnO polycrystal electrode.
Curve 1: 0.5 M Na_2S, curve 2: 0.5 M $Na_2S_2O_3$, curve 3: 0.5 M H_2Q, curve 4: 0.5 M KBr in 0.2 M Na_2SO_4.

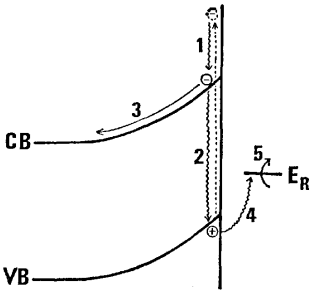

Fig. 2. The state of heat generating during the course of photoelectrode reaction.

current was measurable. As shown in Fig. 1, the onset potentials in the case of S^{2-}, $S_2O_3^{2-}$, H_2Q, and Br^- were -1.0, -0.60, -0.50, and -0.50 V *vs.* SCE, respectively. That of S^{2-} was more negative relative to others because of the higher pH value of this electrolyte.

The heat generated during the course of the photoelectrode reaction consists of five components evolved in the processes shown in Fig. 2, namely (1) radiationless transition within the conduction band (*i.e.* when the photon energy absorbed is in excess of the band gap energy), (2) electron-hole recombination, (3) electron transport from the surface to the bulk through the space charge layer in the conduction band, (4) charge transfer reaction between the hole in the valence band and the redox species in the electrolyte solution, and (5) entropy change of the redox reaction. The Joule heat in the solution due to the current flow is very small and can be neglected.

When one photon with energy E is absorbed by the electrode surface, the photoelectrochemical reaction proceeds with a quantum efficiency η at an applied electrode potential V, and the heat generated by the five processes discussed above are as follows: (1) $E-E_g$ (E_g: the band gap of the semiconductor), (2) $E_g(1-\eta)$ (if the semiconductor is not a fluorescent or phosphorescent material), (3) $\eta e(V-V_{FB})$, (4) $\eta(E_v-E_R)$ (E_R: redox potential, E_v: energy position of the valence band), and (5) $\eta T\Delta S$.

In the supporting Na_2SO_4 electrolyte solution, the photoelectrode reaction results in the dissolution of the ZnO electrode,[22]

$$ZnO + 2p^+ \longrightarrow Zn^{2+} + \frac{1}{2}O_2.$$

However, when electrolyte solution contains a redox agent, the oxidation of the reducing agent and the dissolution reaction proceed competitively. It is probable that $\eta e(E_v-E_R)$ and $T\Delta S$ represent the heat due to these two photoelectrode reactions. Therefore, by using the competitive oxidation ratio[23] of a reducing agent $\alpha(0\leqq\alpha\leqq1)$ and the five types of heat losses, Eq. 1 can be as follows;

$$\begin{aligned} ITE(\Delta T/\Delta T°) = {} & (E-E_g) + E_g(1-\eta) + \eta\alpha(E_v-E_R) \\ & + \eta(1-\alpha)(E_v-E_D) + \eta\alpha T\Delta S \\ & + \eta(1-\alpha)T\Delta S' + \eta e(V-V_{FB}), \end{aligned} \quad (2)$$

where E_D is the decomposition potential of ZnO (the value thermodynamically calculated[24] is $+0.65$ V *vs.* SCE), ΔS is the entropy change of the oxidation reaction of a reducing agent, and $\Delta S'$ is the entropy change of the dissolution reaction of ZnO.

From the measurement of reaction heat (Peltier heat) by using a platinum electrode,[25] the values of $T\Delta S$ for the redox reaction employed were found to be a fairly small fraction of $E(\Delta T/\Delta T°)$. For example, the Peltier heat for the oxidation of S^{2-} and H_2Q was below one fifth of that for the oxidation of $Fe(CN)_6^{4-}$ which was the biggest value, 0.4 eV, we observed. However, it was difficult to determine the accurate value of the Peltier heat for each electrode reaction by a metal electrode. Therefore, we could not say the exact values for the Peltier heat, but we thought that $T\Delta S$ and $T\Delta S'$ in these cases might be negligible.

When the quantum efficiencies of photoelectrode reactions are the same in different electrolyte solutions, the value of the intercept at the flatband potential,

$$\begin{aligned} Q = {} & (E-E_g) + E_g(1-\eta) \\ & + \eta\alpha(E_v-E_R) + (1-\alpha)(E_v-E_D), \end{aligned} \quad (3)$$

is expected to depend on the competition ratio α, and the redox potential E_R. Q was plotted against redox potential in Fig. 3 for H_2Q, $S_2O_3^{2-}$, SO_3^{2-}, and S^{2-} all which have more negative redox potentials than the decomposition potential of ZnO, 0.65 V *vs.* SCE. As shown in this figure, Q was smaller as the redox potential was more positive. The nearly linear relationship between the redox potential and Q is evident. The slope of this line $\eta\alpha$ is about 0.85, a value almost the same as the quantum efficiency in each electrolyte solution which was 0.90. Therefore the competitive ratio was close to 1, and we conclude that the main photoelectrode reactions in these solutions are as follows:

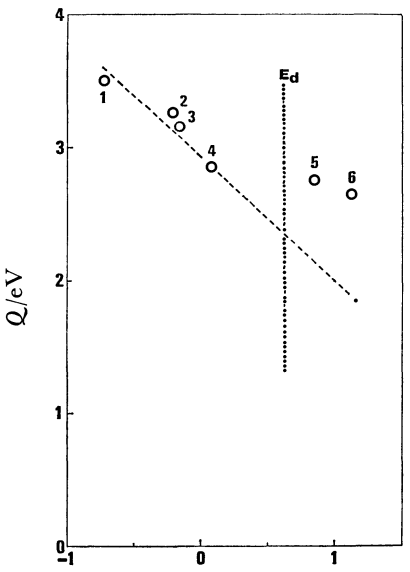

Fig. 3. Relationship between Q and redox potential. No. 1: 0.5 M Na_2S, No. 2: 0.5 Na_2SO_3, No. 3: 0.5 M $Na_2S_2O_3$, No. 4: 0.5 M H_2Q, No. 5: 0.5 M KBr, No. 6: 0.5 M KCl in 0.2 M Na_2SO_4.

$$H_2Q + 2p^+ \longrightarrow Q + 2H^+$$
$$2S_2O_3^{2-} + 2p^+ \longrightarrow S_4O_6^{2-},$$
$$2SO_3^{2-} + 2p^+ \longrightarrow S_2O_6^{2-},$$
$$S^{2-} + 2p^+ \longrightarrow S.$$

In case of Br^- and Cl^- which have a more positive oxidation potential than the decomposition potential of ZnO, +0.65 V *vs.* SCE, Q was smaller as the redox potential was more positive, but the degree of the decrease in Q was smaller in comparison to that for H_2Q, $S_2O_3^{2-}$, SO_3^{2-}, and S^{2-} which have more negative redox potentials. This suggests that the competitive ratios of Cl^- and Br^- are small, and that in these solutions the dissolution reaction of ZnO is faster than the oxidation of Cl^- and Br^-. In this figure, it is evident that Q depends on the competition ratio and redox potential of the reducing agents.

From the point of view of thermodynamics[24,26] a reducing agent with a redox potential more negative than the decomposition potential of a semiconductor can decrease photoelectrocorrosion of the semiconductor. In fact using the rotating ring-disk electrode technique, we reported that a reducing agent with a more negative redox potential has a larger competition ratio and can better stabilize the ZnO electrode.[27] The present measurements confirm this relationship for the stabilization of the ZnO electrode.

The electrochemical photocell in which a photosemiconductor works with a counter electrode in a redox couple solution is called as the regenerative photocell. In the photocell absorbed light energy is converted to electrical energy. The ideal maximum energy conversion efficiency ϕ_v is represented as follows,

$$\phi_v = \frac{|E_{FB} - E_R|}{E} \times 100 \ (\%), \tag{4}$$

where E_{FB} is the flatband potential, E is absorbed light energy. $|E_{FB} - E_R|$ means the maximum photovoltage in the regenerative cell.

Table 1. Energy efficiencies for the photooxidation of each reducing agent on ZnO polycrystal electrode

Redox agent	(E_r *vs.* SCE)/V	Q/eV	ϕ_T/%	ϕ_V/%
S^{2-}	−0.72	3.50	2.8	7.9
SO_3^{2-}	−0.22	3.25	10.8	10.7
$S_2O_3^{2-}$	−0.16	3.15	12.5	12.2
H_2Q	+0.08	2.85	20.8	16.1

$$\phi_T = \frac{3.6 - Q}{3.6} \times 100 \ (\%), \quad \phi_V = \frac{|E_{FB} - E_r|}{3.6} \times 100 \ (\%)$$

On the other hand, from the photothermal data the energy conversion efficiency ϕ_T can be obtained by using the value of Q,

$$\phi_T = \frac{E - Q}{E} \times 100 \ (\%). \tag{5}$$

The energy efficiencies for the reducing agents S^{2-}, SO_3^{2-}, $S_2O_3^{2-}$, and H_2Q under irradiation of monochromatic light 340 nm (3.6 eV) were given from the values of Q as shown in Table 1.

The meaning of ϕ_T can be considered as follows. When the competitive oxidation ratio α is 1.0, the value of Q is expressed from Eq. 3 as below,

$$Q = \eta(E_v - E_R) + E - E_g\eta. \tag{6}$$

Therefore

$$\frac{E - Q}{E} = \frac{\eta\{E_g - (E_v - F_R)\}}{E}. \tag{7}$$

Since $|E_g - E_v|$ equals almost to the flatband potential, the next equation is given,

$$\frac{E - Q}{E} = \frac{\eta|E_{FB} - E_R|}{E}. \tag{8}$$

Therefore, from Eq. 8 the energy efficiency ϕ_T can be derived as the product of the quantum efficiency (which is obtained from the slope of the photothermal measurement) and the maximum photovoltage under monochromatic light irradiation. In the case of ZnO, the value of quantum efficiency is near 1, so ϕ_T is expected to equal to ϕ_v. In Table 1 energy efficiencies ϕ_v are also shown.

The values of ϕ_T and ϕ_v are similar in the case of each reducing agent. It was ascertained that a reducing agent with a more positive redox potential gave larger energy efficiency.

We conclude that the photothermal measurement technique provides information on the energy efficiency and the stabilization of a semiconductor electrode by redox agents.

References

1) A. Fujishima and K. Honda, *Nature*, **238**, 37 (1972).
2) T. Ohnishi, Y. Nakato, and H. Tsubomura, *Ber. Bunsenges. Phys. Chem.*, **79**, 523 (1975).
3) J. H. Carey and B. G. Oliver, *Nature*, **259**, 554 (1976).
4) M. S. Wrighton, A. B. Ellis, P. T. Wolczanski, D. L. Morse, H. B. Abrahamson, and D. S. Ginley, *J. Am. Chem. Soc.*, **98**, 2774 (1976).

5) H. Gerischer and J. Gobrecht, *Ber. Bunsenges. Phys. Chem.*, **80**, 1635 (1976).
6) A. B. Ellis, S. W. Kaiser, and M. S. Wrighton, *J. Am. Chem. Soc.*, **98**, 6855 (1976).
7) D. Laser and A. J. Bard, *J. Electrochem. Soc.* **123**, 1027 (1976).
8) A. B. Ellis, S. W. Kaiser, J. M. Bolts, and M. S. Wrighton, *J. Am. Chem. Soc.*, **99**, 2839 (1977).
9) A. B. Ellis, J. M. Bolts, S. W. Kaiser, and M. S. Wrighton, *J. Am. Chem. Soc.*, **99**, 2848 (1977).
10) A. Heller, K. C. Chang, and B. Miller, *J. Am. Chem. Soc.*, **100**, 684 (1978).
11) R. N. Noufi, P. K. Kohl, and A. J. Bard, *J. Electrochem. Soc.*, **125**, 375 (1978).
12) H. Tributsch, *Ber. Bunsenges. Phys. Chem.*, **82**, 169 (1978).
13) B. A. Parkinson, A. Heller, and B. Miller, *J. Electrochem. Soc.*, **126**, 954 (1979).
14) P. A. Kohl and A. J. Bard, *J. Electrochem. Soc.*, **126**, 603 (1979).
15) R. N. Noufi, D. Tench, and L. F. Warren, *J. Electrochem. Soc.*, **127**, 2709 (1980).
16) L. F. Schneemeyer and M. S. Wrighton, *J. Am. Chem. Soc.*, **102**, 6964 (1980).
17) H. S. White, F. F. Fan, and A. J. Bard, *J. Electrochem. Soc.*, **128**, 1045 (1981).
18) A. Fujishima, Y. Maeda, K. Honda, G. H. Brilmyer, and A. J. Bard, *J. Electrochem. Soc.*, **127**, 840 (1980).
19) Y. Maeda, A. Fujishima, and K. Honda, *Chem. Lett.*, **1980**, 271.
20) A. Fujishima, Y. Maeda, and K. Honda, *Bull. Chem. Soc. Jpn.*, **53**, 2735 (1980).
21) Y. Maeda, A. Fujishima, and K. Honda, *Nippon Kagaku Kaishi*, **1981**, 349.
22) H. Gerischer, *J. Electrochem. Soc.*, **113**, 1174 (1966).
23) T. Inoue, T. Watanabe, A. Fujishima, K. Honda, and K. Kohayakawa, *J. Electrochem. Soc.*, **124**, 719 (1977).
24) H. Gerischer, *J. Electrochem. Soc.*, **82**, 133 (1977).
25) R. Tamamushi, *J. Electroanal. Chem. Interfacial Electrochem.*, **45**, 500 (1973); **65**, 263 (1975).
26) A. J. Bard and M. S. Wrighton, *J. Electrochem. Soc.*, **124**, 1706 (1977).
27) T. Inoue, A. Fujishima, and K. Honda, *Bull. Chem. Soc. Jpn.*, **52**, 3217 (1979).

 © 1982 The Chemical Society of Japan Bull. Chem. Soc. Jpn., 55, 3377—3380 (1982)

Resonance Raman Spectra and Inter-radical Vibrations of Chloranil Anion Radical Dimers

Susumu MATSUZAKI, Tetsuya MITSUISHI, and Koichi TOYODA*

Department of Chemistry, Faculty of Science, Kumamoto University, Kumamoto 860

(Received March 15, 1982)

Resonance Raman spectra of chloranil anion radical dimers were measured in ethanol at 140 K by an exciting radiation within the CT band, and all the Raman lines observed were shown to be totally symmetric. Two strong Raman lines at 114 cm^{-1} and 168 cm^{-1} have been assigned to inter-radical stretching vibrations of the dimer. The relative intensity of these lines changed depending on the counter ion species. Formation of two dimers has been supposed to explain the spectral behavior. Influence of 18-crown-6 on the spectra was investigated. The result strongly suggests that one dimer gives two inter-radical Raman lines. Two interpretations are proposed for the simultaneous resonance enhancement of these Raman lines: mechanical coupling of the inter- and intra-radical vibrations or distorsion of the D_{2h} eclipsed dimer structure. Other five lines at higher frequencies have been assigned to intra-radical vibrations of the dimer.

A number of organic ion radicals are known to form dimers in the solution under appropriate conditions of temperature and concentration, and the monomer-dimer equilibrium has been studied by electronic absorption spectra.[1-3] Recently resonance Raman spectra of some ion radical dimers have been measured by exciting radiations close to the CT band, and new broad Raman lines have been observed at lower frequencies.[4-6] The Raman lines are assigned to the stretching vibrations of the inter-radical bond of the dimer because of the remarkable resonance enhancement by the CT transition of the dimer. In the case of tetracyanoethylene anion radical dimer, $(TCNE^{\cdot-})_2$, in 2-methyltetrahydrofuran (MTHF),[6] two inter-radical Raman lines were observed at *ca.* 150 cm^{-1} and 180 cm^{-1}, which showed obvious change of the relative intensity depending on the counter ions (Na^+, K^+, Rb^+, and Cs^+). Formation of two different dimers has been proposed as the most probable interpretation of the spectral behavior.

Structure of organic ion radicals in the solution has been investigated by ESR spectra, but the dimer has the singlet ground state so that no ESR signals are observed. Electronic spectra have also given little information about the detailed structure of the dimer because the absorption bands are broad and structureless. Vibrational spectroscopy will be, at present, the most suitable tool for the structural investigation of the dimer in the solution. Resonance Raman spectra particularly have the advantage that the inter-radical vibrations are observed directly. The spectra will give information about the structure of the ground state as well as the excited state when the nature of the resonance Raman effect in the dimer is elucidated by accumulation of the data.

In this paper, we present the resonance Raman spectra of chloranil anion radical dimer, $(CA^{\cdot-})_2$, in ethanol and discuss the result from the standpoint of the dimer structure.

Experimental

Commercially available chloranil (CA) was crystallized twice from dry benzene and sublimed twice *in vacuo*. Commercially available alkaline iodide (M·I) was dried *in vacuo* at 110 °C for 12 h to avoid the decomposition of radicals by moisture in the salts. Alkaline metal salts of chloranil (M·CA) were prepared from CA and M·I by the method of Torrey and Hunter in dry acetone or acetonitrile:[7] M= Li, Na, K, Rb, and Cs. It is well known that M·CA usually contains the solvent in preparation.[8] The salts, therefore, were dried over P_2O_5 in an evacuated desiccator for a week. IR spectra of the salts agreed well with those reported in the literature.[9] The salt was dissolved in dry ethanol of spectroscopic grade *in vacuo* to give the sample solution (*ca.* 10^{-3} mol/dm^3).

A glass cryostat with quartz windows was used for both Raman and electronic absorption measurements. The cryostat was cooled by flowing cold N_2 gas. Raman spectra were recorded on a JASCO R-800 Raman spectrometer equipped with a NEC GLG-108 He–Ne laser and GLG-3200 Ar^+ laser. Electronic spectra were recorded on a Hitachi 200-20 spectrophotometer.

Results and Discussion

Observed Spectra. In the visible spectra of Na·CA (Fig. 1), only an absorption band of $CA^{\cdot-}$ is observed at room temperature, but another new peak appears at 670 nm when the solution is cooled to 140 K. This peak is assigned to the CT band of $(CA^{\cdot-})_2$.[3]

Time-dependence of the Raman spectra observed at room temperature showed that $CA^{\cdot-}$ in ethanol was gradually decomposed even in oxgen-free atmosphere. The spectra of the monomer, therefore, were measured at 200 K because the radical was practically

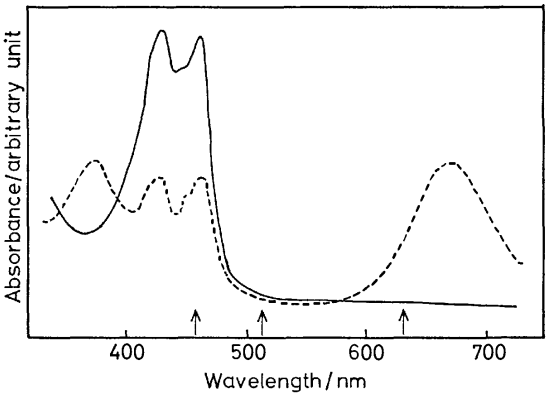

Fig. 1. Electronic absorption spectra of Na·CA in ethanol.
——: Room temperature, ----: 140 K.

stable and the dimer formation was still negligible at this temperature. Several Raman lines of $CA^{\cdot-}$ were observed with 457.9 nm excitation within the first absorption band of the radical. The frequencies are given in Table 1 together with the frequencies and assignment reported by Girlando, *et al.*[9] The table shows that the frequency of ν_1 in ethanol differs remarkably from that in acetone and in the powder sample.[10] This mode is C=O stretching, and the difference probably arises from the hydrogen bond formation between the radical and the solvent.

Figure 2 shows the temperature-dependence of the Raman spectra of Na·CA by 632.8 nm excitation within the CT band of the dimer. No Raman lines of the sample are observed at 200 K because very few dimers are formed at this temperature and the monomer Raman lines show no practical resonance enhancement by this exciting radiation. When the solution is cooled to 140 K, seven new lines appear.[11] This spectral change is reversible and reproducible. None of these Raman lines, on the other hand, are observed at 140 K when excited with the Ar^+ 514.5 nm line which is far from the CT band. These Raman lines, therefore, are undoubtedly resonance enhanced by the CT transition of the dimer. All of them were found to be totally symmetric by the depolarization ratios (*ca.* 1/3). The result shows that the resonance enhancement originates from the Franck-Condon type term of the scattering tensor.[12] The Raman frequencies of the dimer are given in Table 2 together with the corresponding frequencies of the monomer. Raman lines at 114 cm^{-1} and 168 cm^{-1} are much broader than those at higher frequencies and will be assigned to inter-radical vibrations by comparison with those observed in other dimers.[4-6] The relative intensity of 114 cm^{-1} line to 168 cm^{-1} line is dependent on the counter ions in the order, $Li^+ \simeq Na^+ > K^+ > Rb^+$ (Fig. 3).[13] The result shows that a kind of association of the dimer and the cations is present in ethanol because it is not expected that the spectra of free dimers are affected by the counter ion. Ethanol has a large dielectric constant, so that the association should be very weak. The spectral change is similar to that observed in $(TCNE^{\cdot-})_2$ in MTHF[6] except that the magnitude of the change is rather small in the present case. Therefore, in the preliminary report of the present investigation,[14] we gave the same interpretation as the case of $(TCNE^{\cdot-})_2$; *i.e.*, two different

TABLE 1. RAMAN FREQUENCY OF CHLORANIL ANION RADICAL[a]

Acetone solution[b] ν/cm^{-1}	Ethanol solution[c] ν/cm^{-1}	Assignment[b]
334 s	335 m	$a_g \nu_5$
501[d]	512 s	$a_g \nu_4$
	846 w	$a_g \nu_4 + \nu_5$
1016 w	1026 w	$a_g \nu_3$
1521 m	1562 m	$a_g \nu_1$
1584 m	1585 vs	$a_g \nu_2$

a) 457.9 nm excitation. b) Ref. 9 in the text. c) This work. d) Solution in dimethyl sulfoxide. See Ref. 9.

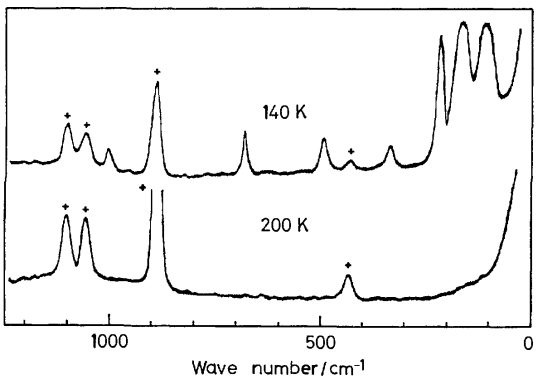

Fig. 2. Resonance Raman spectra of Na·CA in ethanol with 632.8 nm excitation.
+: Solvent Raman lines.

TABLE 2. RAMAN FREQUENCY OF CHLORANIL ANION RADICAL DIMER

Observed dimer line[a] ν/cm^{-1}	Assignment[b]	Corresponding monomer vibration ν/cm^{-1}	Assignment[c]
114 s	a_g R-R stretch.[d]		
168 s	a_g R-R stretch.		
217 s	a_g	220[e]	$b_{3u} \nu_{29}$
335 w	a_g Intra-radical vibration	335	$a_g \nu_5$
493 m	a_g	512	$a_g \nu_4$
683 m	a_g	695[e]	$b_{3u} \nu_{28}$
1000 w	a_g	1026	$a_g \nu_3$

a) 632.8 nm excitation. b) This work. c) Ref. 9 in the text. d) R-R stretch. represents inter-radical stretching vibration. e) IR frequency of the solid radical salt. From Ref. 9.

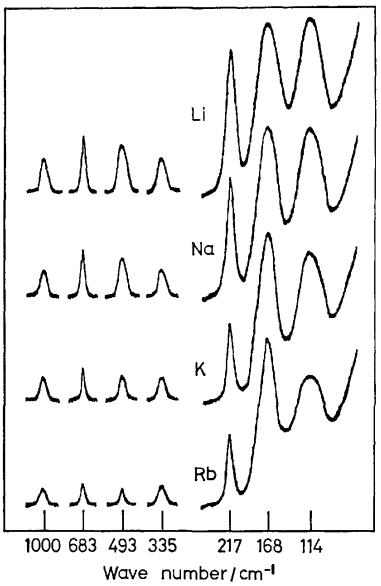

Fig. 3. Counter ion dependence of the resonance Raman spectra of $(CA^{\cdot-})_2$ in ethanol.
Raman intensities of the dimers are normalized by that of 168 cm^{-1} line.

dimers were present in the solution and the ratio of the equilibrium concentrations was dependent on the counter ions. If this is the case, it is most probable that the difference in the dimers arises from that in the pairing mode of the dimer and the counter ion, *i.e.*, solvent-separated ion pairs and free ions: contact ion pairs are probably excluded because of the large dielectric constant of ethanol. It was also implicitly assumed in the report that the respective Raman lines corresponded to the same inter-radical vibrational mode of the different dimers. However, the large frequency difference ($>50\ cm^{-1}$) in the two Raman lines seems to be unexplainable from this standpoint because the structures of the free dimer and the loosely ion-paired dimer are not expected to be so different from one another. Furthermore, strength of the association between the component cation and anion in the ion-paired dimers probably decreases continuously to the state of the free dimer in such a polar solvent as ethanol, and the dimers are not expected to be present as two distinct species. It is, therefore, necessary to examine the possibility that one dimer gives two inter-radical Raman lines.

For the purpose of this examination, spectral change by the addition of crown ether (18-crown-6) was investigated for K·CA in ethanol. It is well known that the crown ether forms very stable complexes with K^+; therefore, practically all of the cations are expected to be complexed by the crown ether. It has been reported that crown ethers inhibit the dimer formation of K·TCNE in MTHF, where ion pair formation is indicated by ESR.[15] Also in the present case, crown ether was expected to affect strongly the Raman spectra if the solution contained the ion-paired dimers of distinct structures. However, no drastic changes were observed when 18-crown-6 was added in large excess, but only a minor change occurred in the relative intensity of the two Raman lines (Fig. 4). The resulting spectrum is quite similar to that of Li·CA which is expected to have the strongest tendency to give free dimers because of the largest solvation energy of Li^+ among all the alkali metal cations. The change occurred probably because the crown ether weakened the interaction between the component cation and anion of the ion-paired dimer and allowed the dimer to be in the state of practically free dimers: this is also supported by the fact that the solubility of K·CA considerably increased by addition of the crown ether. The result shows that both of the two Raman lines are attributable to one dimer, *i.e.*, they correspond to the different vibrational modes of the dimer: mechanism of the simultaneous resonance enhancement of two inter-radical Raman lines will be discussed in the next section. The spectral change by the counter ion or the crown ether will be interpreted as follows. Observed Raman spectra correspond to the statistical average over the many dimers of various interaction strengths between the component cation and anion. If the average deviates by the counter ion or the crown ether and if the relative intensity of the Raman lines is different from each other in the respective dimers, spectral changes probably occur as observed in this investigation. Temperature dependences of the spectra were investigated in the range, 140 K—160 K, but practically no dependences were observed. The result may also be an evidence against the assumption of the presence of two dimers because the equilibrium of the dimers should be dependent on the temperature.

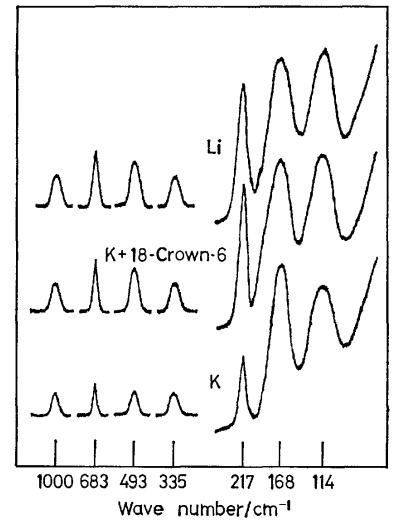

Fig. 4. Spectral change of K·CA by addition of 18-crown-6.

Normal Vibrations and Resonance Raman Effect. When two N-atomic radicals form a dimer, six of the 12 translational and rotational degrees of freedom of the radicals are frozen to produce six inter-radical vibrations of the dimer, because the resulting dimer only possesses six translational and rotational degrees of freedom. The inter-radical vibrational modes are easily obtained for the case of dimers of D_{2h} eclipsed structure by the *out-of-phase* combination of the corresponding translational and rotational motions of the component radicals: *e.g.*, the combination of the rotational motions around y-axis gives a librational mode of b_{1u} symmetry. The normal vibrations thus obtained are shown in Fig. 5: Q_1 (a_g), out-of-plane stretching mode; Q_2 (b_{1g}) and Q_3 (b_{2g}), in-plane slipping modes; Q_4 (a_u), in-plane twisting mode; Q_5 (b_{1u}) and Q_6 (b_{2u}), out-of-plane librational modes. The totally symmetric stretching mode, Q_1, is expected to show remarkable resonance enhancement by the Franck-Condon type term of the scattering tensor,[12] because the potential curves along this normal coordinate are probably much different from one another in the ground and CT excited states: the dimer is stabilized by the CT interaction in the ground state whereas in the CT excited state the component radicals should merely contact with each other in the solvent cage.[16] The two low frequency Raman lines will be assigned to this normal mode, but there is one totally symmetric vibration in the case of the eclipsed dimer structure. Two interpretations are possible for the simultaneous resonance enhancement of the two inter-radical Raman lines as discussed in the following.

The first interpretation is given on the basis of the intensity borrowing by the mechanical coupling of

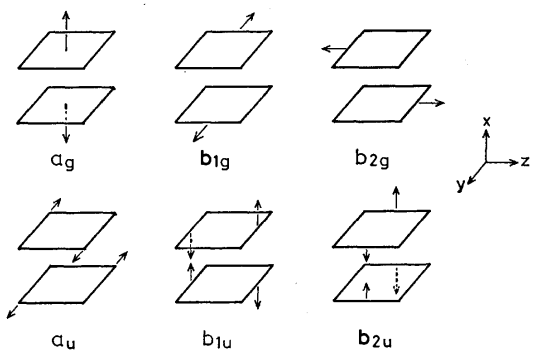

Fig. 5. Inter-radical vibrations of dimer of D_{2h} eclipsed structure.
Rectangles represent planer radicals, and arrows show the displacements: y- and z-axes are parallel to the molecular short and long axes respectively, and x-axis is perpendicular to the molecular plane.

the inter- and intra-radical vibrations. The number of the normal vibrations of the N-atomic radical is 3N−6, so that the resulting dimer possesses 2(3N−6) intra-radical vibrations. The i-th normal coordinates (Q_A^i and Q_B^i) of radicals A and B are combined with one another to produce new normal coordinates ($Q_\pm^i$): $Q_\pm^i=(1/\sqrt{2})(Q_A^i\pm Q_B^i)$. The combination gives totally symmetric vibrations only for the following two cases. When Q_A^i and Q_B^i are a_g modes, the *in-phase* combination (Q_+^i) remains totally symmetric and *out-of-phase* combination (Q_-^i) gives an IR-active mode of b_{3u} symmetry.[17] Q_+^i may couple with Q_1, but such a coupling is expected to be small because the former is the in-plane vibration whereas the latter is the out-of-plane one. When Q_A^i and Q_B^i are out-of-plane bending modes of b_{3u} symmetry, on the other hand, the *out-of-phase* combination gives totally symmetric vibrations. Such out-of-plane a_g modes are expected to couple considerably with Q_1 and to show resonance enhancement through the intensity borrowing by the mechanical coupling. Chloranil has three b_{3u} modes (ν_{28}, ν_{29}, and ν_{30}),[9] and the frequencies of ν_{28} and ν_{29} have been reported to be 695 cm^{-1} and 220 cm^{-1} respectively. The Raman lines at 683 cm^{-1} and 217 cm^{-1} will be reasonably assigned to the *out-of-phase* combination modes of ν_{28} and ν_{29} respectively. The third b_{3u} mode, ν_{30}, has not yet been observed for $CA^{\cdot-}$, but the frequency of the neutral molecule has been reported to be 88 cm^{-1}.[9] This mode may, therefore, have a frequency around 100 cm^{-1} also in the case of the radical. If Q_1 and the *out-of-phase* combination mode of ν_{30} strongly couple with each other, two Raman lines of comparable intensities will be observed in the low frequency region as in the present case. It is well known that, in general, the extent of the mechanical coupling of vibrational modes increases with a decrease in the difference of their frequencies. It is, therefore, expected that Raman line at 217 cm^{-1} has stronger intensity than that at 685 cm^{-1}: this expectation agrees well with the result obtained (Fig. 3).

The second interpretation is given on the basis of the distorsion of the dimer from the D_{2h} eclipsed structure. If the component radicals slip along y- or z-axis, the dimer has the slipped structure of C_{2h} symmetry; therefore, the dimer has two totally symmetric inter-radical modes. The slipped structure is occasionally met in the crystal structure of organic ion radical salts,[18] and the dimer in the solution may possess this structure. At this stage, it is not clear which interpretation is valid. The experiment of isotopic shifts may give conclusive information but $(CA^{\cdot-})_2$ seems to be unsuitable for this purpose because the inter-radical Raman lines are broad and the molecular weight is heavy: TCNE is a probable candidate for the purpose.

The remaining three Raman lines at 1000 cm^{-1}, 493 cm^{-1}, and 335 cm^{-1} will be assigned to ν_3, ν_4, and ν_5, respectively, as shown in Table 2. The mechanism for the resonance enhancement of these lines is not elucidated at present: measurements of the excitation profile may give some information. No distinct features have been observed in the region of ν_1 and ν_2. This result is probably attributed to the low sensitivity of our instrument in this region.

References

1) R. H. Boyd and W. D. Phyllips, *J. Chem. Phys.*, **43**, 2927 (1965).
2) M. Itoh, *Bull. Chem. Soc. Jpn.*, **45**, 1947 (1972).
3) N. Sakai, I. Shirotani, and S. Minomura, *Bull. Chem. Soc. Jpn.*, **44**, 675 (1971).
4) K. Yokoyama and S. Maeda, *Chem. Phys. Lett.*, **48**, 59 (1977).
5) S. Yamaguchi, K. Yokoyama, and S. Maeda, *Bull. Chem. Soc. Jpn.*, **51**, 3193 (1978).
6) K. Yokoyama, S. Maeda, C. Etoh, S. Matsuzaki, and K. Toyoda, *Bull. Chem. Soc. Jpn.*, **53**, 36 (1980).
7) H. A. Torrey and W. H. Hunter, *J. Am. Chem. Soc.*, **34**, 702 (1912).
8) S. Hiroma and H. Kuroda, *Bull. Chem. Soc. Jpn.*, **47**, 3014 (1974).
9) A. Girlando, I. Zanon, R. Bozio, and C. Pecile, *J. Chem. Phys.*, **68**, 22 (1978).
10) The Raman spectra measured for the aceton solution and the powder sample agreed with those in Ref. 9.
11) It is estimated that *ca.* 50% of the radicals dimerize at this temperature from the formation constant reported in Ref. 3.
12) J. Tang and A. C. Albrecht, "Raman Spectroscopy," ed by H. A. Szymanski, Plenum Press, New York (1970), Vol. 2, p. 33.
13) No Raman data of Cs·CA were obtained because of the poor solubility in ethanol.
14) S. Matsuzaki, T. Mitsuishi, C. Etoh, and K. Toyoda, *Chem. Lett.*, **1979**, 1417.
15) M. T. Watts, M. L. Lu, R. C. Chen, and M. P. Eastman, *J. Phys. Chem.*, **77**, 2959 (1973).
16) N. Mataga and T. Kubota, "Molecular Interactions and Electronic Spectra," Marcel Dekker Inc., New York (1970), p. 275.
17) R. Bozio, A. Girlando, and C. Pecile, *Chem. Phys.*, **21**, 257 (1977).
18) M. Konno, H. Kobayashi, F. Marumo, and Y. Saito, *Bull. Chem. Soc. Jpn.*, **46**, 1987 (1973).

 © 1982 The Chemical Society of Japan Bull. Chem. Soc. Jpn., 55, 3381—3385 (1982)

Penetration of Leucine and Norleucine into Lecithin Monolayers from Underlying Aqueous Solutions

Masayuki NAKAGAKI and Emiko OKAMURA*

Faculty of Pharmaceutical Sciences, Kyoto University, Yoshida-Shimoadachicho, Sakyo-ku, Kyoto 606

(Received March 20, 1982)

The surface pressure of the monolayers of dimyristoyl phosphatidylcholine(DMPC) on leucine and norleucine solutions was measured and the amounts of these amino acids which had penetrated into the DMPC monolayer were calculated by means of a successive approximation. Although the amounts of leucine and norleucine adsorbed onto the solution surface were nearly equal and were larger than that of lysine, the amount of leucine which had penetrated into the DMPC monolayer was remarkably small. That of norleucine was not so small, but was still smaller than that of lysine except for the region where the molecular area of DMPC is large. The partial molecular areas of amino acid, $\overline{A}_2$, and DMPC, $\overline{A}_3$, were calculated in each case. The value of $\overline{A}_2$, was the largest in the case of leucine and the smallest in the case of lysine, which means that the area occupied by lysine is smaller than that of norleucine because the interaction of ε-amino group with DMPC contracts the mixed monolayer. The change in the value of $\overline{A}_3$ due to the interaction with amino acid, however, was not large, which means that the change in the state of DMPC itself is not large and rather independent of the kind of amino acid.

It has been widely accepted that biomembranes such as protoplasmic membranes essentially consist of bimolecular lipid layers in which some proteins are dissolved.[1] The study of the penetration of proteins into lipid monolayers is, therefore, considered to be one of the useful techniques for the investigation of the structure and functions of biomembranes.[2,3] In order to discuss the interaction between lipids and proteins from this point of view, the penetration of L-lysine into lecithin monolayers was studied in our previous work.[4]

L-Leucine and L-norleucine have four carbon atoms in the side chains, which is the same as in the case of L-lysine. Leucine has a branched carbon chain, whereas norleucine does not. The side chain of lysine has an amino group at the end of the carbon side chain of norleucine. The effect of the ε-amino group of lysine and that of the branched carbon chain are, therefore, expected to become clear by the comparison of the features of the penetration of these amino acids into lecithin monolayers. In this work, the surface tension of aqueous solutions as well as the surface pressure of the solutions has been measured, and the amounts of these amino acids adsorbed onto the surface and penetrated into the monolayers, respectively, have been calculated. This will facilitate discussion of the interaction between these amino acids and lecithin.

Experimental

Materials. L-Leucine and L-norleucine from Nakarai Chemicals, Ltd., were dissolved in redistilled water. L-α-Dimyristoyl phosphatidylcholine (DMPC) from Sigma Company was used as lecithin; it was dissolved in distilled chloroform and preserved in a refrigerator until use. The stock solution was prepared every few days in order to avoid disintegration.

Surface-tension Measurement. Surface tension of amino acid solution, γ, was measured by the capillary-height method. The surface pressure of amino acid, F, was obtained by Eq. 1:

$$F = \gamma_0 - \gamma, \quad (1)$$

where γ_0 is the surface tension of pure water. The temperature of the solution was kept at 25±0.5 °C.

Surface-pressure Measurement. The surface pressure of the DMPC monolayer was measured by Wilhelmy's plate method. The details of this method were described in our previous paper.[4] The temperature of the solution was kept at 25±0.5 °C.

Results

Surface Tension of Amino Acid Solution. Figure 1 shows the surface tension of leucine or norleucine solution. The surface tension of lysine solution (Fig. 1 in Ref. 4) is also shown by a broken line. It is seen that the surface tension of the solution decreases slightly with the increase in the concentration of amino acid, C_2, both in the case of leucine and of norleucine. The extent of decrease was a little larger than that of lysine, but there were no differences between leucine and norleucine.

Surface Pressure-Area Curves of the DMPC Monolayers. Figure 2 shows the surface pressure-area curves of the DMPC monolayers spread on leucine solutions of various concentrations. The curve shifted only at the low surface pressure region when the concentration, C_2, was high. On the other hand, the surface pressure increased with increase in C_2, when norleucine solution was used, as shown in Fig. 3.

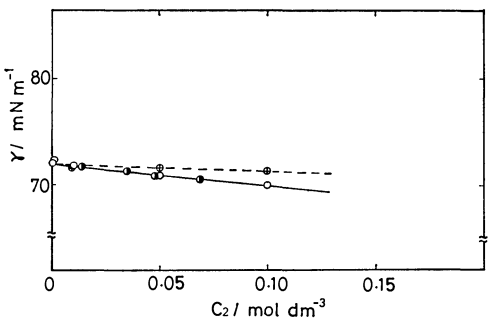

Fig. 1. The relation of surface tension, γ, and the concentration of solution, C_2.
○: L-Leucine, ◑: L-norleucine, ⊕: L-lysine. Temp: 25+0.5 °C.

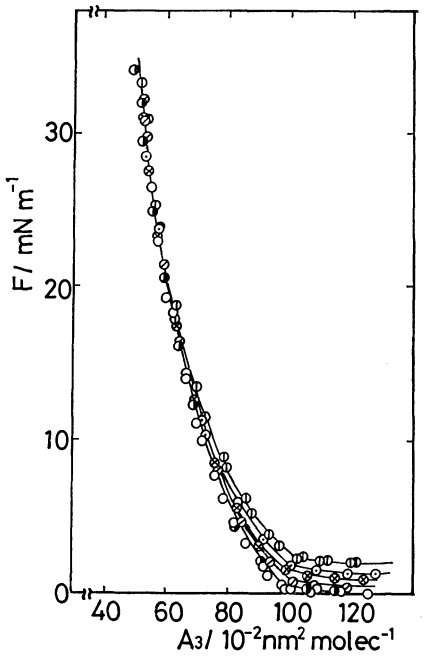

Fig. 2. F-A_3 curves of the DMPC monolayers on the leucine solutions.
C_2/mol dm^{-3}: ○; 0, ◑; 0.01, ⊘; 0.02, ⊗; 0.05, ⊙; 0.07, ⓘ; 0.10.

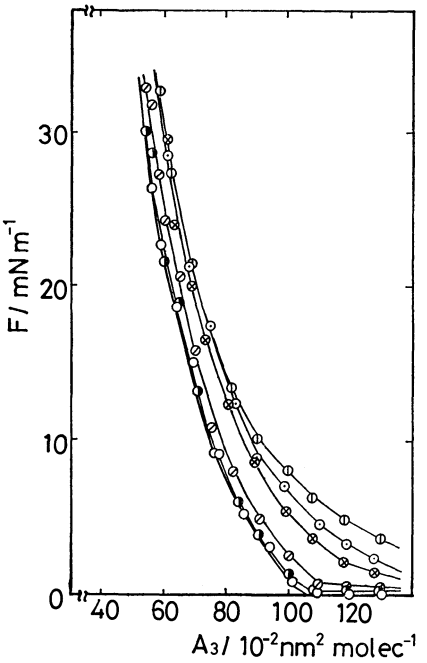

Fig. 3. F-A_3 curves of the DMPC monolayers on the norleucine solutions.
C_2/mol dm^{-3}: ○; 0, ◑; 0.01, ⊘; 0.02, ⊗; 0.05, ⊙; 0.07, ⓘ; 0.10.

The Amount Which Had Been Adsorbed onto the Solution Surface or Which Had Penetrated into a DMPC Monolayer. The change of the surface pressure against the concentration of solution was obtained from the surface pressure-area curves (Figs. 2 and 3); this change is shown in Fig. 4 for leucine or in Fig. 5 for norleucine. The closed circles represent the values when no monolayer exists at the interface, as obtained from Fig. 1. It is seen from these two figures (Figs. 4 and 5), that the change of the surface pressure is very small in the case of leucine, and that in the case of norleucine the surface pressure increases with the increase in the concentration, C_2.

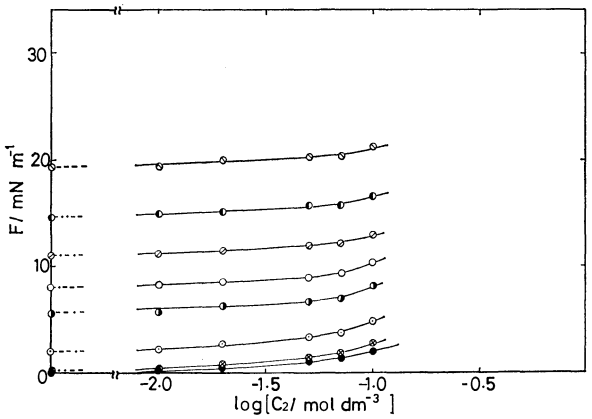

Fig. 4. The relation of the surface pressure, F, and the concentration of leucine solution, C_2, at various areas per molecule of DMPC, A_3.
$A_3/10^{-2}$ nm^2 molecule^{-1}: ●; no insoluble monolayer, ⊗; 100, ⊙; 90, ◑; 80, ○; 75, ⊘; 70, ◐; 65, ⊘; 60.

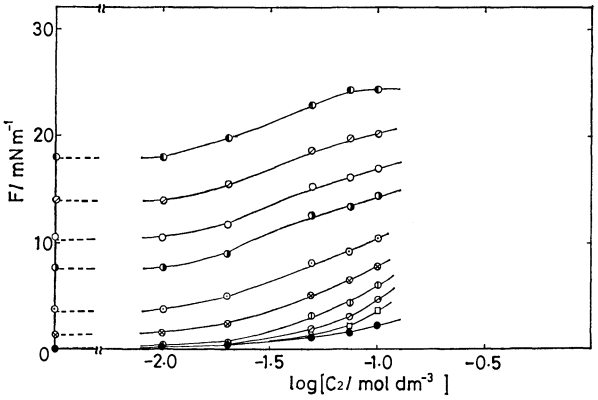

Fig. 5. The relation of the surface pressure, F, and the concentration of norleucine solution, C_2, at various areas per molecule of DMPC, A_3.
$A_3/10^{-2}$ nm^2 molecule^{-1}: ●; no insoluble monolayer, □; 130, ⊖; 120, ⓘ; 110, ⊗; 100, ⊙; 90, ◑; 80, ○; 75, ⊘; 70, ◐; 65.

The amount which had been adsorbed onto the liquid-air interface or which had penetrated into a DMPC monolayer, Γ_2, was calculated by the following equation:

$$\Gamma_2 = (1/RT)(1-\overline{A_3}/A_3)(\partial F/\partial \ln C_2)_{A_3}, \quad (2)$$

where R, T are the gas constant and the absolute temperature, respectively, $\overline{A_3}$ is the partial molecular area of DMPC which was approximated by the molecular area of DMPC on pure water, $A_3°$, by Pethica.[5] This equation, proposed by Pethica, has been used in order to calculated the amount of solute molecules penetrated into lipid monolayers.[6,7] Values of Γ_2 thus calculated are shown in Figs. 6 (a) and (b). It is seen that the amounts adsorbed onto the liquid-air

interface of leucine and norleucine are nearly equal and are larger than that of lysine, whereas the amount of leucine penetrated into the DMPC monolayer is remarkably small and that of norleucine is not so small but is still smaller than that of lysine.

On the other hand, both the amount of leucine and of norleucine penetrated into a monolayer vary with the area per molecule of lecithin at constant C_2, as is shown in Figs. 7 (a) and (b). It is seen that the amount which penetrated is larger at the higher concentrations, and it is smaller at the smaller areas per molecule of lecithin, the latter suggesting that the molecules which have penetrated are excluded by the compression of the monolayer. It is also found that the amount of leucine which penetrated is always smaller than that of lysine, but the amount of norleucine which penetrated becomes larger than that of lysine when the area per molecule of lecithin is large.

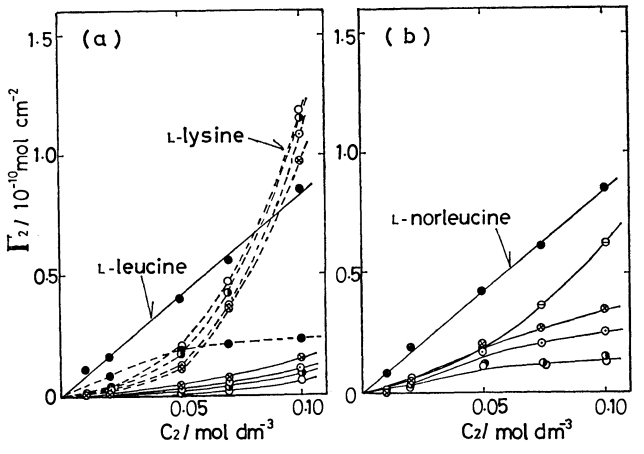

Fig. 6. The amount of amino acid penetrated into DMPC monolayer, Γ_2, *vs.* C_2.
(a): Leucine, (b): norleucine. The broken lines show the amounts of lysine in Ref. 4. A_3/10^{-2} nm^2 molecule^{-1}: ●; no insoluble monolayer, ⊖; 120, ⊗; 100, ⊙; 90, ◑; 80, ○; 75.

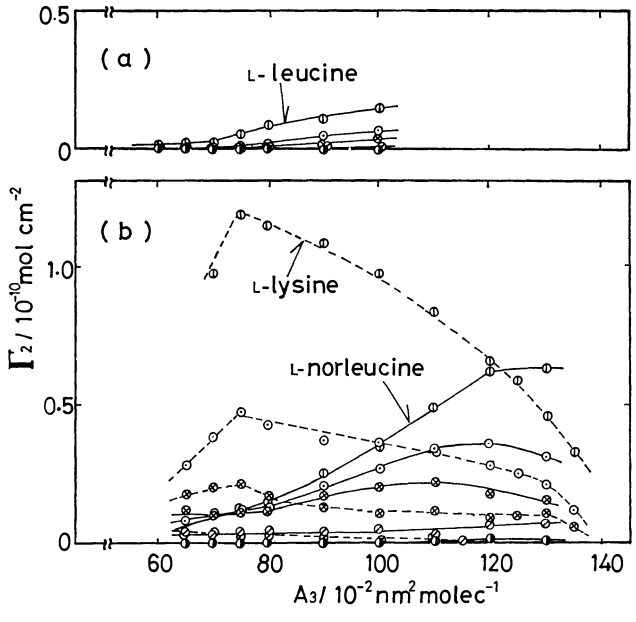

Fig. 7. The relation of the amount of amino acid penetrated, Γ_2, and the area per molecule of DMPC, A_3.
(a): Leucine, (b): norleucine. The broken lines show the amounts of lysine in Ref. 4. C_2/mol dm^{-3}: ◑; 0.01, ⊘; 0.02, ⊗; 0.05, ⊙; 0.07, ⊕; 0.10.

Discussion

The Mixed Monolayers of DMPC and Leucine or Norleucine. It may be considered that a mixed monolayer of DMPC and leucine or norleucine is formed as the result of the penetration of these amino acids into a DMPC monolayer. The mole fraction of leucine or norleucine in this mixed monolayer, X_2, and the average area per molecule of the monolayer, A_{23}, are given by:

$$X_2 = \frac{\Gamma_2}{\Gamma_2+\Gamma_3} \tag{3}$$

and

$$A_{23} = \frac{1}{(\Gamma_2+\Gamma_3)N_A} \tag{4}$$

respectively, where Γ_3 is the moles of DMPC per unit area ($=1/(A_3\times N_A)$), and N_A is the Avogadro number. The relation between X_2 and A_{23} is shown in Fig. 8 (a) in the case of leucine and in Fig. 8 (b) in the case of norleucine. The values of A_{23} vary with the surface pressure and with the mole fraction. The value of A_{23} increases with the increase in X_2 at each surface pressure in the case of leucine, and also in the case of norleucine, although the values of A_{23} stop increasing and start decreasing at a large X_2, as is shown for norleucine at the surface pressure of 5 mN m^{-1}. The curve with a maximum point is of the same shape as lysine,[4] although the slope of this curve is not so sharp as in the case of lysine.

The partial molecular area of DMPC on the solution, $\overline{A}_3$, obtained from Fig. 8, was not equal to that on pure water, $A_3°$, in the cases of both leucine and norleucine. The amount which penetrated, Γ_2, was,

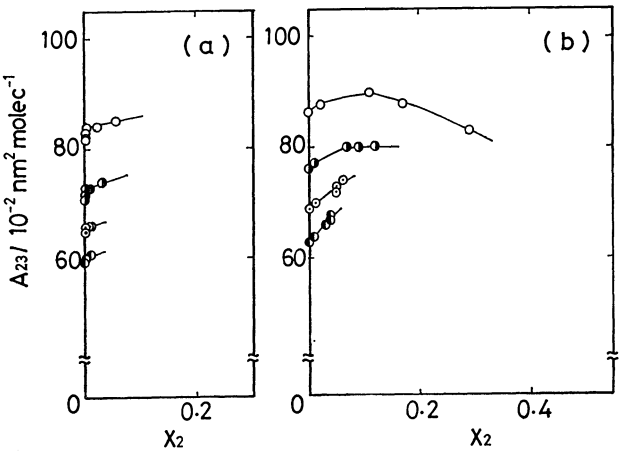

Fig. 8. The relation of the average area per molecule of an amino acid–DMPC monolayer, A_{23}, and the mole fraction of amino acid, X_2.
Obtained from Fig. 7. (a): Leucine, (b): norleucine. F/mN m^{-1}: ○; 5, ◑; 10, ⊙; 15, ◐; 20.

therefore, recalculated by substituting in Eq. 2 the value of $\overline{A}_3$ instead of $A_3°$, as described in Ref. 4. The amount thus obtained is shown in Figs. 9 (a) and (b). The features of the curve of Γ_2 as a function of A_3 did not vary, although the value of Γ_2 was a little smaller than that in Figs. 7 (a) and (b).

The Interaction between Leucine or Norleucine and DMPC. The mole fraction of leucine or norleucine, X_2, and the average area per molecule of the monolayer, A_{23}, were calculated again, by using recalculated values of Γ_2. The recalculated relation between X_2 and A_{23} is shown in Figs. 10 (a) and (b) in the cases of leucine and norleucine, respectively. From this figure, the relation between X_2 and A_{23} can be described as follows:

(1) for leucine,

$$A_{23} = A_3° + 1.7 + 38.4X_2 \quad (5)$$

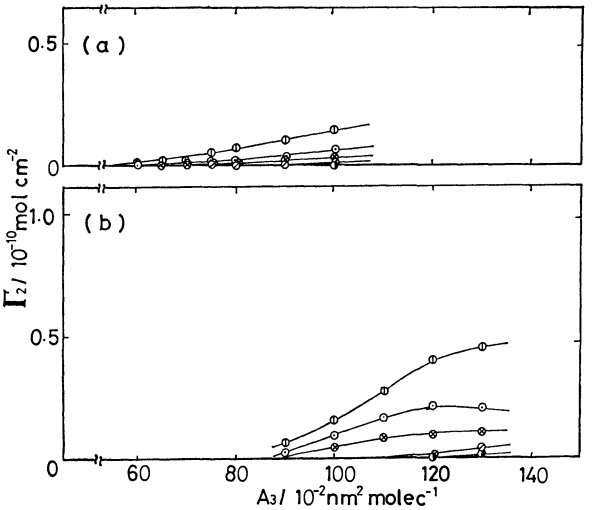

Fig. 9. The relation of the amount of amino acid penetrated, Γ_2, obtained by using the corrected value of $\overline{A}_3$, and the area per molecule of DMPC, A_3.
(a): Leucine, (b): norleucine. C_2/mol dm^{-3}: ◑; 0.01, ⊘; 0.02, ⊗; 0.05, ⊙; 0.07, ⓘ; 0.10.

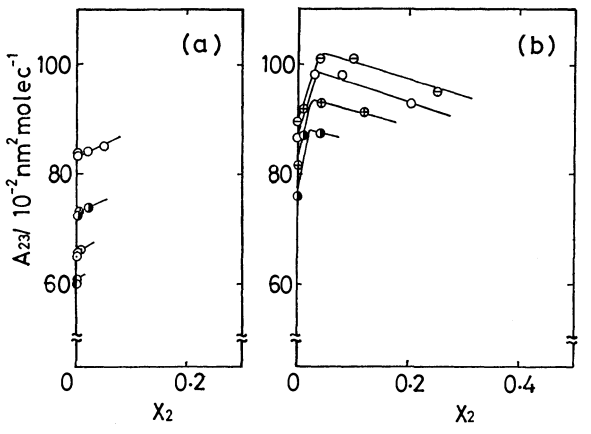

Fig.10. The relation of the average area per molecule of an amino acid-DMPC monolayer, A_{23}, and the mole fraction of amino acid, X_2.
Obtained from Fig. 9. (a): Leucine, (b): norleucine. F/mN m^{-1}: ⊖; 4, ○; 5, ⊕; 7, ◑; 10, ⊙; 15, ◐; 20.

at each surface pressure, F, when the values of X_2 are smaller than 0.10, and

(2) for norleucine,

$$A_{23} = A_3° + 13.0 - 27.0X_2 \quad (6)$$

in the region where F is smaller than 10 mN m^{-1} and the values of X_2 are from 0.04 to 0.30.

From these equations, the partial molecular area of amino acid, $\overline{A}_2$, and that of DMPC, $\overline{A}_3$, are written as follows:

$$\begin{cases} \overline{A}_2 = A_3° + 40.1 \\ \overline{A}_3 = A_3° + 1.7 \end{cases} \quad \text{(for leucine)} \quad (5a)$$

$$\begin{cases} \overline{A}_2 = A_3° - 14.0 \\ \overline{A}_3 = A_3° + 13.0 \end{cases} \quad \text{(for norleucine).} \quad (6a)$$

These are shown in Fig. 11. The values of $\overline{A}_2$ and $\overline{A}_3$ in the case of lysine as well as the molecular area of DMPC on pure water $A_3°$ (▲) are also shown in this figure. It is concluded from Fig. 11 that the interaction between leucine or norleucine and DMPC can be compared with that of lysine and DMPC as follows:

(1) The partial molecular area of amino acid, $\overline{A}_2$, is the largest in the case of leucine, and the smallest in the case of lysine. This would mean that the area occupied by lysine is smaller than that of norleucine, because the interaction of ε-amino group with DMPC contracts the mixed monolayer, while leucine occupies a larger area because of the branching of the carbon chain.

(2) The increase in the partial molecular area of DMPC, $\overline{A}_3$, due to the interaction with amino acid, is not large in comparison with the change in $\overline{A}_2$. This means that the change in the state of DMPC itself is not large, irrespective of the kind of amino acid.

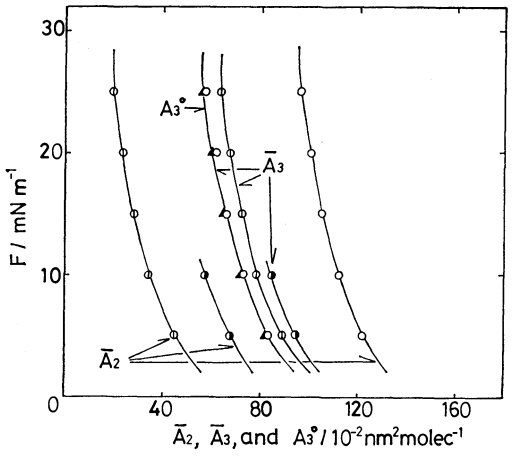

Fig.11. The relation of the surface pressure, F, and the partial molecular areas of amino acid, $\overline{A}_2$; DMPC on solution, $\overline{A}_3$; and DMPC on water, $A_3°$.
○: Leucine, ◑: norleucine, ⓘ: lysine. Symbols(▲) designate the values of $A_3°$.

References

1) S. J. Singer and G. L. Nicolson, *Science*, **175**, 720 (1972).
2) T. Yamashita, "Seitai Hyōmen," ed by M. Nakagaki and S. Iwata, Nankōdō, Tokyo (1975), p. 66.
3) M. Nakagaki and H. Ichihashi, *Yakugaku Zasshi*, **99**, 999 (1979).
4) M. Nakagaki and E. Okamura, *Bull. Chem. Soc. Jpn.*, **55**, 1352 (1982).
5) B. A. Pethica, *Trans. Faraday Soc.*, **51**, 1402 (1955).
6) M. Nakagaki and T. Handa, *Bull. Chem. Soc. Jpn.*, **49**, 2934 (1976).
7) M. A. McGregor and G. T. Barnes, *J. Colloid Interface Sci.*, **54**, 439 (1976).

The structure of the Cyclodextrin Complex. XIV. Crystal Structure of Hexakis(2,3,6-tri-*O*-methyl)-α-cyclodextrin–Benzaldehyde (1 : 1) Complex

Kazuaki HARATA,* Kaneto UEKAMA,† Masaki OTAGIRI,†
Fumitoshi HIRAYAMA,† and Yukio SUGIYAMA††

Research Institute for Polymers and Textiles, 1-1-4, Yatabe-Higashi, Tsukuba, Ibaraki 305
†*Faculty of Pharmaceutical Sciences, Kumamoto University, 5-1, Oe-honmachi, Kumamoto 862*
††*Kaken Chemical Co., Ltd., Honkomagome, Bunkyo-ku, Tokyo 113*

(Received March 26, 1982)

The crystal structure of the hexakis(2,3,6-tri-*O*-methyl)-α-cyclodextrin (abbreviated to methyl-α-CDx)–benzaldehyde (1:1) complex, $C_{54}H_{96}O_{30}\cdot C_7H_6O$, was investigated by the X-ray method. The crystal is monoclinic with the space group $P2_1$ and $Z=2$; the cell dimensions are $a=11.604(1)$, $b=23.832(3)$, $c=13.539(1)$ Å, and $\beta=106.11(1)°$. The structure was determined by inspection of a Patterson map and a trial-and-error method combined with the rigid-body least-squares technique, and refined by the block-diagonal least-squares method to the final *R*-value of 0.10 for 3597 reflections ($\sin\theta/\lambda \leqq 0.49$). The methyl-α-CDx molecule is in the shape of a distorted and truncated hexagonal cone. The guest benzaldehyde molecule is fully included within the host cavity. The carbonyl group is located at the center of the cavity, while the phenyl group is located at the base-side of the host cone. Methyl-α-CDx molecules, of which *pseudo* hexagonal axis is inclined by an angle of 17.0° against the crystallographic a axis, are stacked along the a axis to form a head-to-tail channel-type structure.

The complex formation of many compounds, especially pharmaceuticals, with cyclodextrins and their derivatives has been intensively investigated as the cyclodextrins increase solubility and chemical stability of guest compounds.[1,2] These effects of cyclodextrins have been interpreted on the basis of the inclusion phenomena of various guest compounds into cyclodextrins. Previously, we reported on the crystal structure of the α-cyclodextrin–benzaldehyde complex,[3] in which the benzaldehyde molecule is included in the column formed by the stack of α-cyclodextrin rings. Permethylated α-cyclodextrin (hexakis(2,3,6-tri-*O*-methyl)-α-cyclodextrin, abbreviated to methyl-α-CDx) also forms a crystalline complex with benzaldehyde. In this paper, we deal with the crystal structure of the methyl-α-CDx–benzaldehyde (1:1) complex, which will be discussed mainly in comparison with the structure of the α-cyclodextrin–benzaldehyde complex and the methyl-α-CDx–*p*-iodoaniline complex.[4]

Experimental

Crystals of the methyl-α-CDx–benzaldehyde (1:1) complex were obtained by standing an aqueous solution at 40 °C, which contains methyl-α-CDx and benzaldehyde in a 1:1 molar ratio. Measurements of lattice parameters and reflection intensities were carried out on a Nicolet P3/F diffractometer with graphite-monochromated Cu $K\alpha$ radiation. By using the θ-2θ scan technique, 3597 independent reflections with $|F_o| \geqq 3\sigma(F)$ were collected up to 100° in 2θ. No corrections were made for absorption or extinction effects.

Crystal Data: $C_{54}H_{96}O_{30}\cdot C_7H_6O$, F.W.=1331.7, monoclinic, space group $P2_1$, $Z=2$, $a=11.604(1)$, $b=23.832(3)$, $c=13.593(1)$ Å, $\beta=106.11(1)°$, $V=3597.1$ Å^3, $D_x=1.229$, $D_m=1.22$ g cm^{-3}.

Determination and Refinement of the Structure

The orientation of the *pseudo* hexagonal axis of methyl-α-CDx was deduced by inspection of a Patterson map. The rotational parameter around the molecular axis and the translational parameters along the crystallographic a and c axes were determined by the trial-and-error method. After the correction of the position and orientation of each 2,3,6-tri-*O*-methylglucose residue by the rigid-body least-squares technique, atomic parameters of methyl-α-CDx were refined by the block-diagonal least-squares method. At this stage, the benzaldehyde molecule was found on a Fourier map. Successive block-diagonal least-squares refinement of the structure converged the *R*-value to 0.10. The quantity minimized was $\Sigma w(|F_o|-|F_c|)^2$ with $w=1.0$ for all the reflections. The atomic scattering factors were taken from the "International Tables for X-Ray Crystallography."[5] The final atomic coordinates and B_{eq} values are given in Table 1. Tables of anisotropic temperature factors, observed and calculated structure factors, bond distances and angles, and conformation angles in methyl-α-CDx are on file with The Chemical Society of Japan (Document No. 8259). The computation was carried out on a FACOM M-200 computer at the RIPS Center, Tsukuba.

Description and Discussion of the Structure

Outline of the Structure. The structure and numbering scheme of the complex is shown in Fig. 1. Methyl-α-CDx is in the shape of a distorted and truncated hexagonal cone. The guest benzaldehyde molecule is included in the cavity of methyl-α-CDx. The carbonyl group is located at the center of the cavity, while the phenyl group is located at the O(2), O(3) side. Methyl-α-CDx molecules are stacked along the a axis to form a head-to-tail channel-type structure as shown in Fig. 3.

Conformation of Methyl-α-CDx. Average bond distances and angles over six 2,3,6-tri-*O*-methylglucose residues are shown in Fig. 2. Geometrical data of the methyl-α-CDx ring are given in Tables 2 and 3. The C(6)–O(6) bonds in the G4 and G5 residues are in a *gauche-gauche* conformation, while the others have a *gauche-trans* conformation. All O(2)–C(7) bonds are

TABLE 1. FRACTIONAL COORDINATES ($\times 10^4$) AND B_{eq} OF THE METHYL-α-CDx–BENZALDEHYDE COMPLEX

	x	y	z	B_{eq}/Å^2
C(1,G1)	1224(13)	4789(-)	3473(11)	8.0
C(2,G1)	2185(14)	4888(7)	4527(13)	9.3
C(3,G1)	2551(14)	4326(7)	5115(11)	8.3
C(4,G1)	1412(15)	4037(6)	5239(12)	8.6
C(5,G1)	436(13)	3990(6)	4233(12)	8.0
C(6,G1)	-852(14)	3837(8)	4384(15)	10.2
C(7,G1)	3327(19)	5708(7)	4418(16)	12.1
C(8,G1)	4594(16)	4404(15)	6320(21)	19.6
C(9,G1)	-2368(32)	3343(21)	3257(32)	40.9
O(2,G1)	3252(10)	5132(5)	4330(9)	10.2
O(3,G1)	3310(15)	4455(6)	6158(9)	14.5
O(4,G1)	1775(8)	3482(4)	5589(7)	7.5
O(5,G1)	245(8)	4543(4)	3725(8)	8.2
O(6,G1)	-1592(11)	3689(7)	3456(10)	13.6
C(1,G2)	1369(12)	3856(7)	-100(11)	7.8
C(2,G2)	2346(14)	4314(7)	332(12)	8.4
C(3,G2)	2619(13)	4310(7)	1576(11)	8.2
C(4,G2)	1434(11)	4460(7)	1803(10)	7.2
C(5,G2)	411(13)	4057(6)	1239(10)	7.1
C(6,G2)	-823(11)	4322(7)	1266(12)	8.2
C(7,G2)	3777(23)	4517(13)	-571(20)	18.7
C(8,G2)	4593(15)	4592(11)	2633(15)	13.3
C(9,G2)	-2893(14)	4114(9)	795(18)	12.8
O(2,G2)	3433(9)	4167(5)	102(9)	9.7
O(3,G2)	3425(9)	4781(5)	1898(8)	9.3
O(4,G2)	1716(8)	4365(4)	2900(6)	7.0
O(5,G2)	326(8)	4046(4)	185(7)	7.0
O(6,G2)	-1674(10)	3909(6)	839(10)	11.1
C(1,G3)	1427(13)	1612(7)	-460(10)	7.6
C(2,G3)	2627(12)	1930(7)	-378(11)	7.6
C(3,G3)	2725(12)	2473(7)	206(10)	7.2
C(4,G3)	1636(12)	2854(6)	-275(11)	7.0
C(5,G3)	483(13)	2514(6)	-269(11)	7.7
C(6,G3)	-618(13)	2859(7)	-892(13)	8.9
C(7,G3)	4508(19)	1499(9)	-415(18)	13.4
C(8,G3)	4660(16)	2900(10)	1055(15)	12.6
C(9,G3)	-2501(27)	2770(11)	-505(39)	33.1
O(2,G3)	3545(10)	1565(15)	107(9)	9.9
O(3,G3)	3767(9)	2761(5)	59(9)	9.5
O(4,G3)	1749(8)	3330(4)	387(6)	6.4
O(5,G3)	477(8)	2011(4)	-882(7)	7.4
O(6,G3)	-1704(10)	2537(5)	-847(11)	13.0
C(1,G4)	232(15)	259(7)	2203(12)	9.0
C(2,G4)	1197(13)	55(6)	1689(12)	8.2
C(3,G4)	1753(14)	539(6)	1325(11)	7.8
C(4,G4)	798(11)	910(6)	617(11)	6.4
C(5,G4)	-275(12)	1051(6)	1063(10)	7.2
C(6,G4)	-1346(13)	1266(6)	211(12)	8.4
C(7,G4)	1831(19)	-840(7)	2538(16)	12.5
C(8,G4)	3788(17)	363(11)	1256(16)	13.6
C(9,G4)	-2738(20)	1075(11)	-1462(16)	16.5
O(2,G4)	2101(9)	-262(4)	2397(8)	9.2
O(3,G4)	2508(9)	355(5)	722(9)	9.6
O(4,G4)	1375(7)	1450(4)	535(6)	6.5
O(5,G4)	-672(8)	549(4)	1420(7)	7.3
O(6,G4)	-1682(10)	860(5)	-601(9)	10.4
C(1,G5)	601(13)	1219(8)	5851(12)	9.1
C(2,G5)	1311(14)	660(7)	5860(11)	8.7
C(3,G5)	1567(13)	590(7)	4791(11)	8.4
C(4,G5)	405(13)	619(7)	3976(10)	7.4
C(5,G5)	-265(12)	1166(7)	4024(10)	7.8
C(6,G5)	-1548(19)	1248(9)	3241(15)	13.1
C(7,G5)	2460(18)	451(10)	7562(12)	12.7
C(8,G5)	3455(19)	55(13)	4908(19)	15.7
C(9,G5)	-3340(22)	706(15)	2518(18)	19.1
O(2,G5)	2427(10)	695(5)	6604(8)	10.1
O(3,G5)	2069(12)	58(5)	4786(9)	10.7
O(4,G5)	783(8)	639(4)	3001(7)	7.2
O(5,G5)	-471(8)	1169(5)	5011(7)	8.3
O(6,G5)	-2132(14)	745(10)	3326(12)	17.8
C(1,G6)	1813(13)	3329(8)	6612(11)	8.5
C(2,G6)	2808(13)	2936(6)	7093(12)	8.1
C(3,G6)	2635(13)	2378(7)	6435(11)	7.7
C(4,G6)	1399(13)	2141(6)	6404(11)	7.4
C(5,G6)	387(13)	2572(7)	5962(12)	9.0
C(6,G6)	-783(15)	2296(8)	6345(19)	13.5
C(7,G6)	4802(20)	3215(14)	7934(18)	18.5
C(8,G6)	4276(17)	1766(10)	6434(17)	13.1
C(9,G6)	-2663(33)	2374(22)	6294(27)	29.6
O(2,G6)	3933(10)	3181(5)	7053(8)	10.2
O(3,G6)	3527(9)	2002(5)	7028(8)	9.4
O(4,G6)	1266(8)	1687(4)	5691(7)	7.8
O(5,G6)	677(9)	3077(5)	6609(8)	8.8
O(6,G6)	-1563(19)	2705(11)	5940(18)	25.0
C(1,BA)	2389(24)	2403(24)	3262(22)	30.5
C(2,BA)	3069(24)	1883(11)	3244(16)	15.8
C(3,BA)	4302(35)	1853(18)	3531(20)	26.6
C(4,BA)	4992(44)	2269(28)	3963(26)	40.3
C(5,BA)	4360(30)	2685(18)	3765(20)	23.9
C(6,BA)	3237(27)	2811(19)	3615(21)	22.9
C(7,BA)	1323(37)	2562(21)	2968(24)	26.6
O(1,BA)	475(30)	2317(15)	2597(21)	34.1

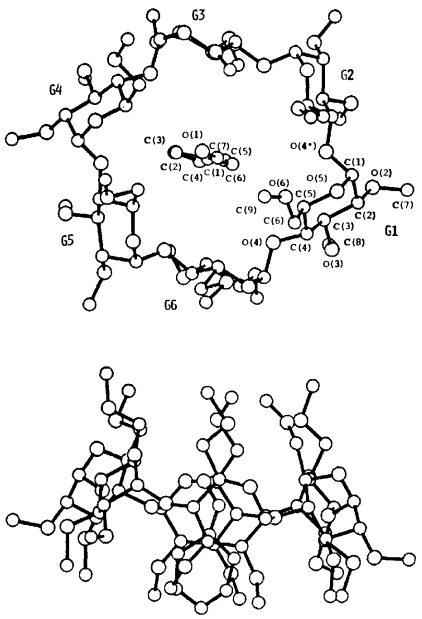

Fig. 1. Structure and numbering scheme of the methyl-α-CDx–benzaldehyde complex.

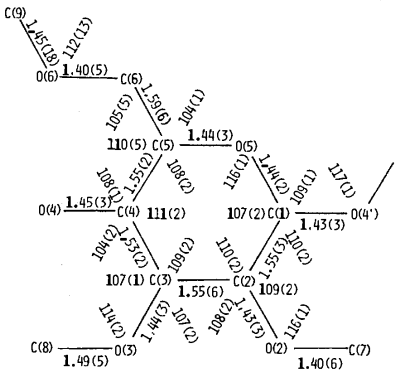

Fig. 2. Average bond distances (l/Å) and angles (ϕ/°) over six 2,3,6-tri-*O*-methylglucose residues. Standard deviations in parentheses were estimated according to the equation:

$$\sigma = [\sum_{i=1}^{6}(x_i - \bar{x})^2/5]^{1/2},$$

where x_i refers to the bond distance or angle in the i-th residue, and $\bar{x}$ is the average value.

directed outside the methyl-α-CDx ring. The O(3)–C(8) and O(6)–C(9) bonds are oriented along the molecular axis of methyl-α-CDx. Six O(4) atoms form a distorted hexagon. The longest diagonal distance (8.95 Å) is found between O(4,G2) and O(4,G5), the shortest one (8.29 Å) being found between O(4,G1) and O(4,G4). The O(4)···O(4) distances between ad-

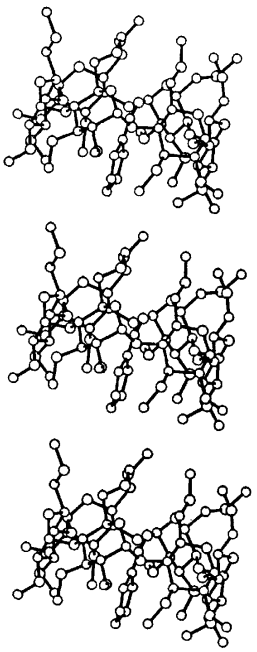

Fig. 3. Stacking feature of the methyl-α-CDx–benzaldehyde complex.

TABLE 2. GEOMETRICAL DATA FOR METHYL-α-CDx

I. O(4)···O(4) distances

Distance	*l*/Å	Distance	*l*/Å
O(4,G1)···O(4,G2)	4.19	O(4,G5)···O(4,G6)	4.32
O(4,G1)···O(4,G6)	4.19	O(4,G1)···O(4,G4)	8.29
O(4,G2)···O(4,G3)	4.21	O(4,G2)···O(4,G5)	8.95
O(4,G3)···O(4,G4)	4.51	O(4,G3)···O(4,G6)	8.33
O(4,G4)···O(4,G5)	4.08		

II. O(2)···O(3) and O(2)···C(8) distances

Distance	*l*/Å	Distance	*l*/Å
O(2,G1)···O(3,G2)	3.46	O(2,G4)···C(8,G4)	3.18
O(2,G2)···O(3,G3)	3.38	O(2,G5)···C(8,G5)	3.25
O(2,G3)···O(3,G4)	3.32	O(2,G6)···C(8,G6)	3.53
O(2,G4)···O(3,G5)	3.33	O(2,G1)···C(8,G2)	3.37
O(2,G5)···O(3,G6)	3.35	O(2,G2)···C(8,G3)	3.43
O(2,G6)···O(3,G1)	3.27	O(2,G3)···C(8,G4)	3.23
O(2,G1)···C(8,G1)	3.22	O(2,G4)···C(8,G5)	3.41
O(2,G2)···C(8,G2)	3.47	O(2,G5)···C(8,G6)	3.38
O(2,G3)···C(8,G3)	3.54	O(2,G6)···C(8,G1)	3.24

III. Tilt-angles[a)]

Residue	ϕ/°	Residue	ϕ/°
G1	27.9	G4	22.9
G2	23.7	G5	26.1
G3	1.7	G6	3.8

a) The tilt-angle is defined as the angle made by the plane through the six O(4) atoms and the plane through O(4′), C(1), C(4), and O(4) of each residue.

jacent residues vary in the range 4.08—4.32 Å. These O(4) atoms are roughly coplanar with a maximum deviation of 0.23 Å. The O(2)···O(3) distances (3.27—3.46 Å) between adjacent residues are significantly larger than those found in α-cyclodextrin complexes.[3)] This may be ascribed to the large tilt of the four residues (G1, G2, G4, and G5), which results from the repulsive interaction between the C(8) methyl group and the O(2) atoms of the adjacent residue. The C(8) methyl group is located at a position nearly equidistant from the two vicinal O(2) atoms; 3.18—3.53 Å between C(8) and O(2), and 3.23—3.43 Å between C(8) and O(2) of the adjacent residue.

TABLE 3. LEAST-SQUARES PLANE THROUGH SIX O(4) ATOMS AND DEVIATIONS FROM THE PLANE

The plane equation is of the $AX+BY+CZ=D$ form where X, Y, and Z are the coordinates in Å units along the a, b, and c* axes, respectively.

$0.9506X-0.1139Y+0.2889Z=0.9720$

Deviations of atoms from the plane

	l/Å		*l*/Å
O(4,G1)	0.14	O(4,G4)	0.16
O(4,G2)	−0.21	O(4,G5)	−0.23
O(4,G3)	0.06	O(4,G6)	0.06

TABLE 4. INTERMOLECULAR DISTANCES BETWEEN METHYL-α-CDx AND BENZALDEHYDE

Distance	*l*/Å	Distance	*l*/Å
O(4,G1)···C(6,BA)	3.89	C(5,G5)···O(1,BA)	3.59
C(5,G3)···O(1,BA)	3.91	O(4,G5)···C(2,BA)	3.93
C(5,G4)···O(1,BA)	3.63	C(8,G6)···C(4,BA)	3.86
O(4,G4)···C(2,BA)	3.79	C(8,G6)···C(3,BA)	3.94
C(5,G5)···O(1,BA)	3.82	C(6,G5)···O(1,BA)	3.73

The macrocyclic conformation of α-cyclodextrin and methyl-α-CDx has been discussed previously on the basis of the tilt-angle of each residue as well as the geometry of the O(4) hexagon.[3,4)] The tilt-angles (Table 2) were calculated as the angle made by the O(4) plane and the plane through C(1), C(4), O(4), and O(4′). The G3 and G6 residues are nearly perpendicular to the O(4) plane, while the other four residues are sharply inclined with the O(6) side nearer to the molecular axis of methyl-α-CDx. Although the average tilt-angle (17.7°) is somewhat larger than that of the *p*-iodoaniline complex (16.5°), the conformational feature of methyl-α-CDx is quite similar in both complexes.

Methyl-α-CDx-Guest Interaction. The guest benzaldehyde molecule is included within the methyl-α-CDx cavity. The carbonyl group is located at the center of the cavity, while the phenyl group is located at the O(2), O(3) side. The benzaldehyde molecule is sandwiched between the G3 and G6 residues, and the plane through benzaldehyde is nearly parallel to the longest diagonal of the methyl-α-CDx ring. The C(7,BA)–O(1,BA) bond of benzaldehyde is oriented toward the C(5,G4) atom. This inclusion geometry is similar to that of the iodophenyl group,[4)] in which iodine atom is located at the center of the cavity. Intermolecular distances between methyl-α-CDx and benzaldehyde are given in Table 4. The shortest distance of 3.59 Å is found between C(5,G5) and O(1, BA). The comparison of the inclusion geometry between the α-cyclodextrin complex[3)] and the present

complex shows that the permethylation of α-cyclodextrin remarkably affects the position and orientation of the guest molecule as well as the macrocyclic conformation of methyl-α-CDx. In the α-cyclodextrin–benzaldehyde complex, the benzaldehyde molecule is turned upside down in the cavity. Although the phenyl group is also located at the similar position, the carbonyl group protrudes from the cavity and is in contact with the next α-cyclodextrin molecule. Such orientation of the benzaldehyde molecule may be unfavorable in the methyl-α-CDx cavity. The protrusion of the carbonyl group from the O(2), O(3), side may be obstructed by the next methyl-α-CDx molecule, which partly blocks the O(2), O(3) side of the methyl-α-CDx ring. The introduction of methyl groups into the α-cyclodextrin ring enlarges the O(2), O(3) side of the cavity as indicated by the O(2)···O(3) distances, so that the guest molecule seems to be more loosely bound in the methyl-α-CDx cavity.

Molecular Packing. Methyl-α-CDx molecules are stacked along the a axis to form an endless column as shown in Fig. 3. This packing feature resembles that found in the *p*-iodoaniline complex.[4] But, the molecular axis of methyl-α-CDx, which is defined as the axis through the center of gravity of six O(4) atoms and perpendicular to the O(4) plane, is more inclined against the column axis: 3.7° in the *p*-iodoaniline complex and 17.0° in the benzaldehyde complex. Adjacent methyl-α-CDx rings along the column are shifted laterally with respect to each other within the molecular plane. Such a shift reduces the region of overlap of the molecule, and as a result, enables the close packing along the column axis. The distance between the O(4) planes of neighboring methyl-α-CDx molecules in the benzaldehyde complex is 0.32 Å shorter

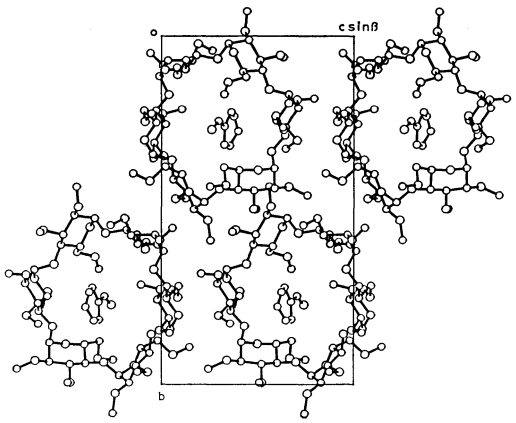

Fig. 4. Crystal structure viewed down along the a axis.

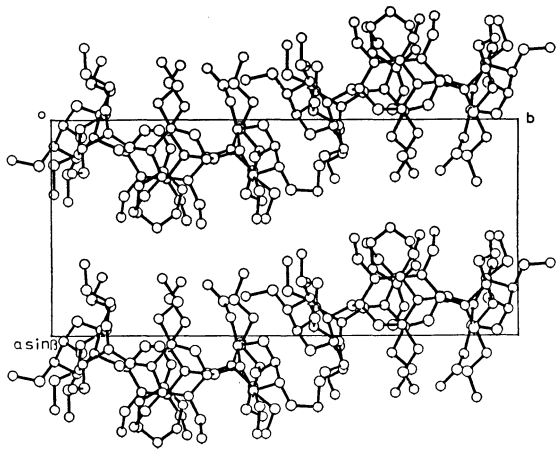

Fig. 5. Crystal structure viewed down along the c axis.

Table 5. Intermolecular distances less than 3.7 Å

Distance	*l*/Å		Distance	*l*/Å	
C(2,G1)–O(6,G5)	3.57	(f)	C(8,G2)–C(8,G5)	3.64	(g)
C(6,G1)–O(3,G5)	3.55	(f)	O(3,G2)–O(6,G4)	3.44	(e)
C(7,G1)–O(6,G5)	3.69	(f)	O(3,G2)–C(9,G4)	3.20	(e)
C(8,G1)–C(8,G5)	3.52	(g)	O(5,G2)–C(2,G4)	3.59	(e)
O(2,G1)–C(8,G5)	3.68	(g)	C(9,G3)–C(7,G6)	3.42	(d)
O(3,G1)–C(9,G5)	3.48	(f)	O(3,G3)–C(7,G6)	3.58	(c)
O(3,G1)–O(6,G5)	3.51	(f)	C(8,G4)–C(9,G5)	3.40	(a)
O(5,G1)–C(2,G5)	3.35	(f)	C(9,G6)–C(4,BA)	3.56	(b)

Code	Symmetry operator		
a	$1+x$,	y,	z
b	$-1+x$,	y,	z
c	x,	y,	$-1+z$
d	$-1+x$,	y,	$-1+z$
e	$-x$,	$1/2+y$,	$-z$
f	$-x$,	$1/2+y$,	$1-z$
g	$1-x$,	$1/2+y$,	$1-z$

than the corresponding distance in the *p*-iodoaniline complex, although the repetition unit along the column differs by only 0.16 Å. In the α-cyclodextrin–benzaldehyde complex,[3] the α-cyclodextrin molecules stacked along the column axis are linked to one another *via* direct and water-mediated hydrogen bonds. Owing to the methylation of all hydroxyl groups, methyl-α-CDx forms no intermolecular hydrogen bonds, but instead, forms van der Waals contacts, most of which involve methyl groups as shown in Figs. 4 and 5.

References

1) W. Saenger, *Angew. Chem., Int. Ed. Engl.*, **19**, 344 (1980).
2) K. Uekama, *Yakugaku Zasshi*, **101**, 857 (1981).
3) K. Harata, K. Uekama, M. Otagiri, F. Hirayama, and H. Ogino, *Bull. Chem. Soc. Jpn.*, **54**, 1954 (1981).
4) K. Harata, K. Uekama, M. Otagiri, and F. Hirayama, *Bull. Chem. Soc. Jpn.*, **55**, 407 (1982).
5) "International Tables for X-Ray Crystallography," Kynoch Press, Birmingham (1974), Vol. IV, pp. 72—75.

Further Studies of Electroluminescence Spectra of the *n*-GaP Semiconductor Electrode in Relation with the Surface-trapped Holes

Yoshihiro NAKATO, Akira TSUMURA, and Hiroshi TSUBOMURA*

Department of Chemistry, Faculty of Engineering Science, Osaka University, Toyonaka, Osaka 560

(Received April 7, 1982)

Electroluminescence spectra of an *n*-type gallium phosphide (*n*-GaP) electrode caused in the presence of oxidants such as $[Fe(CN)_6]^{3-}$ and $S_2O_8^{2-}$ were measured as functions of the electrode potential, the solution pH, and the kind of crystal faces. The electroluminescence spectra consisted of two bands; one was assigned to arise from electronic transitions in the bulk and the other from those at the surface. It was found that the position and the spectral shape of the luminescence band arising from the surface were quite independent of various experimental conditions, while its intensity was strongly dependent on them. These results were explained well by the view that the luminescence band is caused by "surface-trapped holes" acting as a precursor of anodic dissolution reaction of the electrode, as proposed previously. The physicochemical model of the surface-trapped hole was discussed on the basis of the above results.

Extensive work has been done on the semiconductor photoelectrochemical cells in relation with solar energy conversion.[1-4] The main difficulty in this method arises from the fact that most of the available semiconductors with moderate bandgaps are more or less photocorrosive in electrolyte solutions.

The photoelectrochemical stability of semiconductor electrodes was first discussed on the basis of the thermodynamic decomposition potentials,[5-8] and later, much attention has been paid to the kinetic stability of the electrodes.[1,3-5,8] It is very important to understand the physicochemical nature of holes and electrons at the surface, which act as precursors or intermediates of the electrode reactions. Many workers have often pointed out the importance of surface states as arising from surface defects or impurities,[3,4] but the detailed nature of them on a molecular level has still been quite obscure.

We studied electrochemical and luminescent properties of an *n*-type gallium phosphide (*n*-GaP) electrode, and proposed a concept of "surface-trapped holes" as a precursor of various anodic reactions of the electrode.[9] We also studied electro- and photoluminescence spectra of other *n*-type semiconductors such as *n*-CdS, *n*-ZnO, and *n*-TiO_2, and reported that some of the luminescence bands were interpreted as arising from the surface-trapped holes similar to those of *n*-GaP.[10] In the present paper we will report the results of further detailed studies on the electroluminescence spectra of the *n*-GaP electrode.

Experimental

Electrodes were prepared by using single crystal wafers of *n*-GaP, cut perpendicular to the (111)-axis of the crystal, in a similar way to reported before.[9a] They were etched in hot aqua regia for about 20 s before use. The (111)-face (Ga-face) and the $(\bar{1}\bar{1}\bar{1})$-face (P-face) were distinguishable by microscopic inspection of the etched surface.[9a]

Electroluminescence was emitted when the *n*-GaP electrode was kept at cathodic potentials by use of a potentiostat in aqueous solutions containing an oxidant such as $S_2O_8^{2-}$ or $[Fe(CN)_6]^{3-}$. In general the luminescence arises *via* radiative recombination between holes injected by the oxidant in solution and electrons in the conduction band. The luminescence spectra were measured by using a Jobin-Yvon H20 monochromator and an HTV R316 photomultiplier cooled at −20 °C. The observed spectra were corrected with reference to the spectral sensitivity of the photomultiplier, which was measured by use of an Eppley thermopile. The peak wavelengths of the corrected spectra agreed well with those reported by other workers.[11,12]

Luminescence (or photoluminescence) was also emitted when the electrode in an electrolyte solution without oxidants was illuminated at the 365 nm band by use of a 500 W high pressure mercury lamp combined with a Shimadzu-Bosch-Lomb monochromator and appropriate light filters. The luminescence spectra were measured with the same detector system as used for the electroluminescence spectra.

The current-potential curves were obtained with a Nikko-Keisoku NPGS-301 potentiostat. Solutions were prepared by use of deionized water and reagent grade chemicals. They were stirred magnetically and deaerated by bubbling nitrogen during experiments. The pH of the solutions in the range of 3 to 11 was controlled by using an appropriate buffer mixture; acetate, phosphate, borate, or carbonate. The concentration unit, mol/dm^3, is abbreviated as M in the present paper.

Results

In Fig. 1, electroluminescence spectra from the Ga-face (——) and the P-face (—·—) of an *n*-GaP electrode caused by an oxidant, $[Fe(CN)_6]^{3-}$, and that from the Ga-face (----) caused by an oxidant, $S_2O_8^{2-}$, are shown, together with a photoluminescence spectrum (·····). The electroluminescence spectra from the Ga- and the P-face caused by $[Fe(CN)_6]^{3-}$ almost agree with each other except for a slight difference in a swelling near 1.4 eV. The position and the spectral shape of the photoluminescence spectrum were nearly independent of the electrode potential, the solution pH, and the kind of the crystal face.

In Fig. 2, the potential dependence of the electroluminescence spectra from the Ga-face caused by $[Fe(CN)_6]^{3-}$ at pH 5.5 is shown. It is seen that the spectra hardly change with the electrode potential except for slight differences in the extent of the swelling near 1.4 eV. Similar results were observed in solutions of other pH values, and also for the spectra from the P-face. The electroluminescence spectra caused by $[Fe(CN)_6]^{3-}$ also hardly depended on the solution pH except for the slight difference in the swelling near 1.4 eV, as seen from a comparison of Figs. 1 and 2.

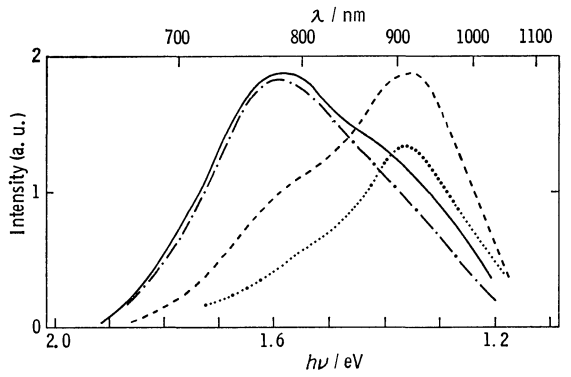

Fig. 1. Electro- and photo-luminescence spectra of an *n*-GaP electrode: Spectra from the Ga-face (——) and the P-face (—·—) generated at −2.2 V *vs.* SCE in a 0.1 M NaOH aqueous solution containing 0.1 M $K_3[Fe(CN)_6]$ and 0.1 M $K_4[Fe(CN)_6]$; that from the Ga-face (----) generated at −1.9 V *vs.* SCE in a 0.1 M NaOH solution containing 0.5 M $Na_2S_2O_8$; and that from the Ga-face (·····) generated by illumination in a 0.1 M NaOH solution.

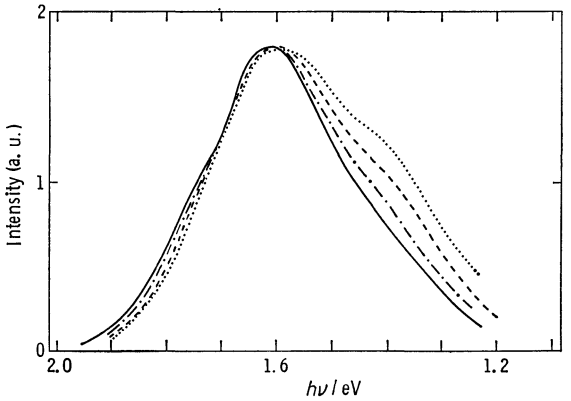

Fig. 2. Electroluminescence spectra from the Ga-face of an *n*-GaP electrode in a solution containing 0.1 M $K_3[Fe(CN)_6]$ and 0.1 M $K_4[Fe(CN)_6]$ at pH 5.5. The spectra were measured at −1.75 V *vs.* SCE (—·—), −1.60 V (——), −1.40 V (----), and −1.35 V (·····).

In Fig. 3, the potential dependence of the peak intensity (I) of the electroluminescence spectra in a $[Fe(CN)_6]^{3-}/[Fe(CN)_6]^{4-}$ solution at pH 4.4 is compared with that of the dark cathodic current (j). These results were obtained by scanning the potential cyclically in a limited range of the potential. The luminescence intensity *vs.* potential curves depended on both the scanning rate and the scanned range of the potential, though the general patterns were rather similar to each other.

Similar experiments were made in solutions of various pH. The results at pH 12.8 are shown in Fig. 4.

Discussion

In a previous letter,[10] it has been concluded that the photoluminescence spectrum of the *n*-GaP electrode arises mainly from electronic transitions in the bulk of the semiconductor, while the electroluminescence spectra caused by $[Fe(CN)_6]^{3-}$ arise mostly from electronic transitions at the surface. It has also been concluded[10] that the swelling of the electroluminescence spectra caused by $[Fe(CN)_6]^{3-}$ appearing at 1.4 eV (Figs. 1 and 2), where the photoluminescence peak just lies, is due to a small contribution of the luminescence band arising from the bulk.

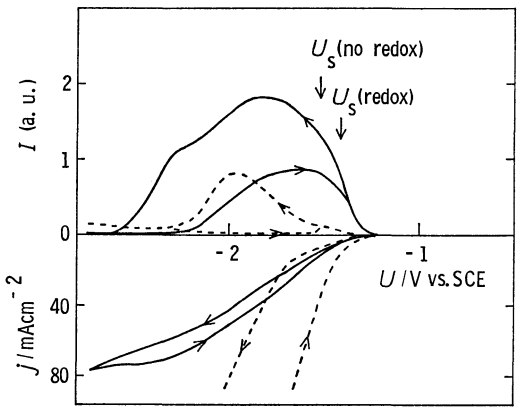

Fig. 3. Potential dependences of the peak intensity of the electroluminescence spectra (I) and the cathodic current (j) for the Ga-face (——) and the P-face (----) in a solution containing 0.1 M $K_3[Fe(CN)_6]$ and 0.1 M $K_4[Fe(CN)_6]$ at pH 4.4. The scan rate is 200 s/V. The U_s values indicated by arrows are for the Ga-face. The U_s (no redox) for the P-face is almost the same as that for the Ga-face.[9b]

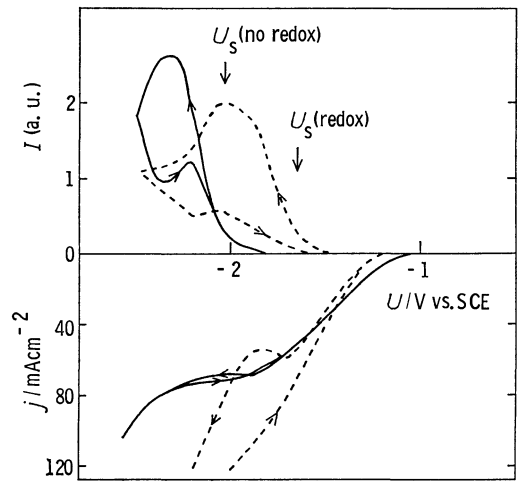

Fig. 4. Potential dependences of the peak intensity of the electroluminescence spectra (I) and the cathodic current (j) for the Ga-face (——) and the P-face (----) in a 0.1 M NaOH solution (pH 12.8). Other conditions are the same as in Fig. 3.

The electroluminescence spectrum caused by $S_2O_8^{2-}$ (a broken line in Fig. 1) shows a strong peak at 1.36 eV and a shoulder near 1.6 eV, suggesting that the luminescence spectrum arises mostly from the bulk, contrary to the spectrum caused by $[Fe(CN)_6]^{3-}$. According to the literature,[11,12] the $S_2O_8^{2-}$ ions are first reduced by electrons in the conduction band, and the resulting radical, $SO_4^{-}\cdot$, acts as a very strong oxidant. The above result can therefore be explained by assuming that holes injected by the $SO_4^{-}\cdot$ radicals are quite hot and a large part of them can diffuse into

the bulk.

As mentioned in the preceding section, the electroluminescence spectra caused by $[Fe(CN)_6]^{3-}$ hardly change with the electrode potential, the solution pH, and the kind of the crystal face, except for the differences in the extent of the swelling near 1.4 eV, *i.e.*, the extent of the contribution of the luminescence band arising from the bulk. This means that the position and the spectral shape of the luminescence band arising from the surface are quite independent of these experimental conditions. The changes of the contribution of the luminescence band arising from the bulk with the electrode potential and the pH can be explained qualitatively by taking account of the changes of the surface density of the electrons in the conduction band as well as those of the initial energy of the injected holes.

The intensity of the electroluminescence spectra at *ca.* 1.6 eV (*i.e.*, the intensity of the luminescence band arising from the surface), on the contrary, depends strongly on the electrode potential, the pH, and the kind of the crystal face, as seen in Figs. 3 and 4. In these figures U_s(redox) is a potential which was determined previously from the intercept of a Mott-Schottky plot with the abscissa,[9b] and thus $-eU_s$(redox) approximately indicates the energy of the conduction band edge at the electrode surface in contact with the $[Fe(CN)_6]^{3-}/[Fe(CN)_6]^{4-}$ solution under anodic bias.[9a] The U_s value in the absence of the redox couple, designated as U_s(no redox), is also included in Figs. 3 and 4. Since the deviation of U_s(redox) from U_s(no redox) was attributed to the accumulated surface-trapped holes and/or oxidative surface intermediates produced during the reaction of the holes with the solution,[9b,c] U_s(redox) is thought to approach U_s(no redox) as the electrode potential is shifted to the negative and the surface density of the electrons in the conduction band increases. Accordingly, we can roughly estimate that the flatband potential of *n*-GaP lies around U_s(no redox) even in the presence of the redox couple.

Based on this argument on the U_s and the previously reported assignment of the electroluminescence spectra peaked at 1.6 eV as being a recombination luminescence between the surface-trapped holes and the electrons in the conduction band,[9b,c] the main features of the results shown in Figs. 3 and 4 can be explained qualitatively as follows.

As seen in Fig. 3, when the electrode potential is swept from positive to negative in an acidic solution, the electroluminescence spectra from the Ga-face start to appear at a potential slightly less negative than U_s(no redox), and reach the maximum at a potential slightly more negative than the U_s(no redox), then decrease rather rapidly at more cathodic potentials. The slight shift of U_s(redox) from U_s(no redox) shown in Fig. 3 suggests that the surface-trapped holes and/or oxidative surface intermediates are accumulated under anodic bias only to a small extent in this case.[9b] Since the surface density of the electrons in the conduction band at anodic potentials are negligibly small, most of the surface-trapped holes formed through the hole injection by the oxidant, $[Fe(CN)_6]^{3-}$, should only be reduced again by the reductant, $[Fe(CN)_6]^{4-}$, at such potentials.[9b] The initial increase of the luminescence intensity when the electrode potential is swept from positive to negative can then be attributed to the increase of the surface density of the electrons in the conduction band. The decrease of the intensity at the more cathodic potentials can be explained by assuming that when the surface density of the electrons in the conduction band becomes very high, the electrode is covered with chemically reduced surface species, with which the injected holes or the oxidant in solution react effectively, not forming the surface-trapped holes.

The onset potential of the cathodic current at the Ga-face in an acidic solution lies very close to a potential at which the electroluminescence starts to appear (Fig. 3). Therefore, the cathodic current near the onset potential can be explained as due mostly to the electron transfer from the conduction band into the $[Fe(CN)_6]^{3-}$ ions *via* the injected holes. The direct electron transfer from the conduction band to the oxidant may partly contribute to the current. At potentials more negative than *ca.* −2.0 V *vs.* SCE, evolution of gas, most probably, hydrogen gas, was observed at the electrode surface. Since the hydrogen evolution is thought to proceed with adsorbed hydrogen atoms (or a kind of surface hydrides) as a reaction intermediate, the above fact means that a kind of surface hydrides is formed at highly negative potentials. This is in harmony with the above argument that the decrease in the electroluminescence intensity at highly negative potentials is due to the formation of certain chemically reduced surface species. The formation of surface hydrides at cathodic potentials was also discussed in the literature.[13–15]

The electroluminescence intensity *vs.* potential curve for the Ga-face shows hysteresis as seen in Fig. 3. From the discussions made so far, it is very plausible that the chemical structure of the electrode surface changes with the electrode potential from the more or less oxidative structures in an anodic region to the reductive ones in a cathodic region. The hysteresis can then be explained as being due to that the sweep rate of the electrode potential is faster than the rate of the chemical change at the electrode surface. This explanation is supported by a fact that the hysteresis becomes more prominent as the sweep rate becomes high.

The electroluminescence intensity *vs.* potential curve for the P-face in an acidic solution is rather similar in its essential pattern to that for the Ga-face (Fig. 3), and therefore can be explained similarly. The minor differences may be attributable to the differences in the quantity and the reactivity of the oxidative or reductive surface intermediates between the two faces.

The onset potential of the cathodic current at the Ga-face in a high pH solution lies considerably more positive than U_s(no redox) (Fig. 4). As reported in a previous paper[9b] and also seen from the large shift of U_s(redox) from U_s(no redox) shown in Fig. 4, the surface-trapped holes and, especially, the oxidative surface intermediates produced *via* the reaction of the holes with the solution are thought to be accumulated

in a large amount at the electrode surface under anodic bias in the case where it is in contact with the $[Fe(CN_6)]^{3-}/[Fe(CN)_6]^{4-}$ solution of high pH. The above-mentioned cathodic current can then be explained by assuming that some of the accumulated oxidative surface intermediates (possibly certain surface radicals[9a]) act as effective mediators for the electron transfer from the conduction band to the oxidant in solution.

The electroluminescence spectra from the Ga-face in a high pH solution start to appear at a potential only slightly more positive than U_s(no redox), contrary to the cathodic current (Fig. 4). Since the oxidative surface intermediates are accumulated much at the electrode surface in this case, as mentioned above, some of the $[Fe(CN)_6]^{3-}$ ions coming to the surface may be reduced by the conduction band electrons trapped at the accumulated surface intermediates, not causing the hole injection. The holes injected by the $[Fe(CN)_6]^{3-}$ ions may also be reduced by the electrons trapped at the surface intermediates. These considerations imply that the surface-trapped holes are not effectively formed in the presence of largely accumulated surface intermediates. Accordingly, the electroluminescence is thought to become detectable only when the surface density of the electrons in the conduction band becomes considerably high, *i.e.*, the electrode potential approaches U_s(no redox).

The onset potential of the cathodic current at the P-face lies less positive than that at the Ga-face (Fig. 4). The potential at which the electroluminescence starts to appear at the P-face also lies more positive than that at the Ga-face (Fig. 4). These results can be explained, according to the above arguments on the results for the Ga-face, by assuming that the density of the accumulated surface intermediates at the P-face is less than that at the Ga-face. This explanation is in agreement with a reported result[9b] that the shift of U_s(redox) from U_s(no redox) at the P-face is smaller than that at the Ga-face.

It is interesting to note in Fig. 4 that when the electrode potential is swept from positive to negative, the cathodic current at the P-face once decreases in the potential range where the electroluminescence just becomes strong. This can be explained by assuming that when the radiative recombination between the surface-trapped holes and the electrons in the conduction band becomes appreciable, the density of the surface intermediates (*i.e.*, the mediators of electron transfer, which are produced *via* the surface-trapped holes) decreases. Similar behavior was generally observed for both the Ga- and P-face in solutions of pH 6 to 11, *i.e.*, in cases where the density of the accumulated surface intermediates is estimated to be moderate. The large cathodic currents at the P-face on potential sweeps from negative to positive in Fig. 4 might be mediated by reductive surface species produced at cathodic potentials.

It is finally noted that the large differences in the dependence of the luminescence intensity on the potential between the Ga- and the P-face observed at any pH (Figs. 3 and 4) are in a sharp contrast to the similarities of the position and the spectral shape of the luminescence spectra (Fig. 1). The difference in the dependence of the luminescence intensity on the potential should imply that the luminescence spectra from the Ga- and the P-face arise from the surface of different chemical structures. The spectral similarity therefore shows that the luminescent species (*i.e.*, the surface-trapped holes) exist in such a way that their energy is almost independent of detailed differences in surface chemical structures between the Ga- and the P-face. This is difficult to explain if the surface-trapped holes are assumed to be holes trapped at certain surface sites such as kinks, steps, *etc.* The above result might rather be reasonably explained by a previously proposed model for the surface-trapped hole[9b,c] that it is an electron deficiency delocalized over a relatively wide range of the crystal lattice inside the surface. The energy of such an electron deficiency should not be affected much by the surface chemical structure.[16] The slight deviation of its energy from the valence band edge at the surface ($\approx$0.6 eV[9b,c]) is thought to be mainly attributable to the distortion of the crystal lattice at the surface.

References

1) H. Gerischer, *Topics Appl. Phys.*, **31**, 115 (1979).
2) A. J. Bard, *J. Photochem.*, **10**, 59 (1979); *Science*, **207**, 139 (1980).
3) "Photoeffects at Semiconductor-Electrolyte Interfaces" ed by A. J. Nozik, (1981), ACS Symposium Series No. 146.
4) *Faraday Discuss. Chem. Soc.*, No. 70, "Photoelectrochemistry" (1980).
5) H. Gerischer, *J. Electroanal. Chem.*, **82**, 133 (1977); *J. Vac. Sci. Technol.*, **15**, 1422 (1978).
6) A. J. Bard and M. S. Wrighton, *J. Electrochem. Soc.*, **124**, 1706 (1977).
7) A. Fujishima, T. Inoue, T. Watanabe, and K. Honda, *Chem. Lett.*, **1978**, 357.
8) R. Memming, *J. Electrochem. Soc.*, **125**, 117 (1978).
9) a) Y. Nakato, A. Tsumura, and H. Tsubomura, *J. Electrochem. Soc.*, **127**, 1502 (1980); b) **128**, 1300 (1981); c) *Chem. Lett.*, **1981**, 127; d) **1981**, 383; e) Ref. 3, p. 145.
10) Y. Nakato, A. Tsumura, and H. Tsubomura, *Chem. Phys. Lett.*, **85**, 387 (1982).
11) K. H. Beckmann and R. Memming, *J. Electrochem. Soc.*, **116**, 368 (1969).
12) B. Pettinger, H.-R. Schoeppel, and H. Gerischer, *Ber. Bunsenges. Phys. Chem.*, **80**, 849 (1976).
13) Y. Nakato, S. Tonomura, and H. Tsubomura, *Ber. Bunsenges. Phys. Chem.*, **80**, 1289 (1976).
14) H. Yoneyama, S. Mayumi, and H. Tamura, *J. Electrochem. Soc.*, **125**, 68 (1978).
15) H. Gerischer, *Adv. Electrochem. Electrochem. Eng.*, **1**, 139 (1961).
16) If the surface of the *n*-GaP electrode is assumed to be covered with a very thin hydroxide or oxide layer,[9a] the energies of the valence electrons in the surface Ga–P bonds should lie relatively deep due to the stabilization (or the inductive effect) by adjacent, electronegative oxygen atoms. This implies that the electron deficiency (hole) is little distributed on the Ga–P bonds just at the surface and its energy is hardly affected by the surface chemical structure.

Asymmetric Adsorption of Alanine by Quartz Powder from Ethanol Solution

Shozo FURUYAMA,* Michio SAWADA, Kinji HACHIYA, and Tetsuo MORIMOTO
Department of Chemistry, Faculty of Science, Okayama University, Tsushima, Okayama 700
(Received March 25, 1982)

The asymmetric adsorption of the racemic alanine by the optically active quartz from ethanol solution at 8 °C was studied by the ^{14}C-tracer method and the newly developed ^{14}C-tracer·ninhydrin-colorimetry combination method. The preferential adsorption of L-alanine by levorotatory quartz (*l*-quartz) and D-alanine by dextrorotatory quartz (*d*-quartz) was confirmed. The asymmetric adsorptivity (A_s) falls in the range of 1.1—1.3, which is comparable with the value determined at −80 °C in the previous paper. The effects of water content in the ethanol solution and of the adsorption temperature upon the adsorption affinity of alanine to quartz were also measured. The cause for the asymmetric adsorption is discussed from the crystallographic point of view.

It has been a great concern of many workers whether quartz surface adsorbs racemic adsorbates asymmetrically, because this phenomenon may relate to the genesis of the first optically active molecules in nature.[1] Various results showing the asymmetric adsorption had been reported. However, their reliability was recently questioned.[2] In 1974, Bonner *et al.* reported that they had succeeded in obtaining the unambiguous evidence for the occurrence of this phenomenon by using the radioactive alanine hydrochloride in rigorously dehydrated *N,N*-dimethylformamide (DMF) solution.[3,4] In the previous work, we also confirmed the occurrence of the asymmetric adsorption of alanine and alanine hydrochloride from an ordinary or a rigorously dehydrated ethanol solution at −80 °C by using the ninhydrin-colorimetry technique.[5]

In the present study, we checked the effects of water content in solution and of adsorption temperature upon the adsorption affinity of alanine. The value of asymmetric adsorptivity, A_s, for alanine by quartz powder at 8 °C was determined by the ^{14}C-tracer method and the newly developed ^{14}C-tracer·ninhydrin-colorimetry combination (TN) method. The TN method has the advantage that it can determine the value of A_s by one adsorption experiment, as will be demonstrated later. The cause of the asymmetric adsorption by quartz is also discussed from the crystallographic point of view.

Experimental

Materials. Dextrorotatory (*d*-) and levorotatory (*l*-) quartzs ($[\alpha]_D=22°$) were purchased from Toyo Communication Equipment Co. Ltd. They were ground by an agate-motor into powders of two uniform sizes. Sample A has 105—53 μm of average particle size and 0.08 $m^2 g^{-1}$ of the BET surface area. The values for sample B are <53 μm and 0.38 $m^2 g^{-1}$ respectively. D- and L-(U-^{14}C)-alanine (20—40 and 150 mC_i $mmol^{-1}$ respectively) were supplied from Radiochemical Center Amersham. Reagent grade racemic alanine was dissolved in a 99.8% ethanol to obtain DL-alanine solutions of various concentrations. D- or L-(U-^{14}C)-alanine was then added to them to prepare the *DL- and D*L-alanine stock solutions, whose radioactivity ranged from 4000 to 6000 cpm (asterisk denotes ^{14}C). The rigorously deoxygenated ninhydrin-hydrindantin reagent was prepared as follows.[6] 20 cm^3 of lithium acetate buffer solution (pH=5.2±0.5) was added to 60 cm^3 of dimethyl sulfoxide. After 15 min agitation, 1.6 g of ninhydrin and 0.12 g of hydrindantin were dissolved successively in the solution (all these treatments were carried out under a highly deoxygenated nitrogen stream).

Procedure for ^{14}C-Tracer Method. 5 g of the *d*- or *l*-quartz powder was degassed in a Pyrex sample tube for 1 h at 150 °C under a vacuum of 10^{-3} Pa. After cooling in a dry box, the powder was transferred into a polyethylene bottle containing 5 cm^3 of *DL- or D*L-alanine solution. After a vigorous agitation, the sample was equilibrated for 2 h. Then its supernatant solution was centrifuged for 10 min and three aliquots (0.5 cm^3) of it were transferred into a glass bottle containing 2.0 cm^3 of PCS scintillant. The decrease in the radioactivity due to the adsorption was determined by an Aloka LSC-651 Scintillation Counter. The deviation in nine countings (three countings for each aliquot) was within 2%.

Procedure for ^{14}C-Tracer·Ninhydrin-Colorimetry Combination (TN) Method. 8 g of the *l*-quartz B was treated as above and placed in 20 cm^3 of *DL- and D*L-alanine solution. After the measurement of the decrease in the radioactivity, 5 cm^3 of the solution was transferred into a test tube and dried on a water bath. Then 5 cm^3 of the deoxygenated water and 3 cm^3 of the deoxygenated ninhydrin-hydrindantin reagent were successively added into the test tube. After being sealed, the test tube was heated at 100 °C for 15 min. The magnitude of the absorption at 570 nm ($\varepsilon=(2.22\pm0.04)\times10^5$ M^{-1} cm^{-1}) for the colored solution was measured to determine the decrease in the total alanine concentration due to the adsorption.

Results and Discussion

The amount of D-alanine adsorbed by the *d*-quartz B from 0.94×10^{-5} M *DL-alanine solution was measured by the ^{14}C-tracer method at 8 °C as a function of water content. The plot in Fig. 1 shows that the amount of D-alanine adsorbed decreases almost linearly with the increase in water content up to 10% and becomes negligible at 20%. However, this test showed that a rigorous dehydration of ethanol (for example to less than 100 ppm as in the previous work[5]) is not indispensable for the present purpose.

The adsorption isotherm for D-alanine by the *d*-quartz B was measured at 8 °C and −80 °C using various concentrations of *DL-alanine solutions. Figure 2 shows that D-alanine is more strongly adsorbed at −80 °C than at 8 °C, although the difference is not as prominent as expected from the large difference in the adsorption temperature. The small temperature dependence of the adsorption affinity of D-alanine to *d*-quartz means that the magnitude of the

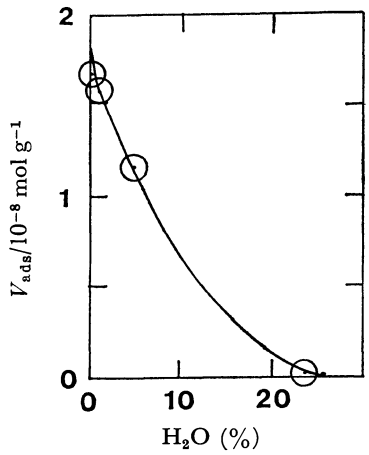

Fig. 1. Effect of water content in ethanol upon the amount of *D-alanine adsorbed (V_{ads}).
2 g of the *d*-quartz B was contacted with 10 cm^3 of (0.94×10^{-5} M) *DL-alanine solution for 2 h.

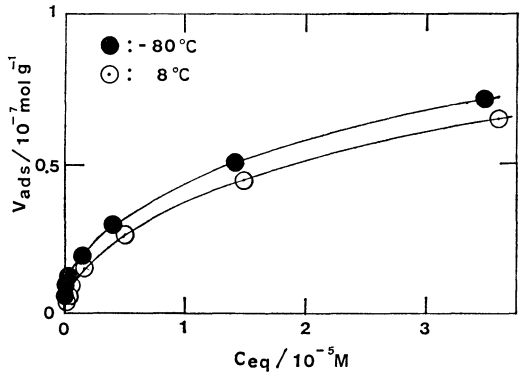

Fig. 2. Adsorption isotherm of *D-alanine on *d*-quartz B at 8 and −80 °C.
2 g of the *d*-quartz B was contacted with 10 cm^3 of ($(0.094-9.4)\times10^{-5}$ M) *DL-alanine solution for 2 h. The values for V_{ads} and C_{eq} are for the *D-alanine only.

isosteric heat of adsorption, q_{st}, for D-alanine is almost comparable with that for ethanol. However, since the concentration of D-alanine is almost 10^{-6} times as small as that of ethanol, it is certain that the adsorption affinity to *d*-quartz of D-alanine is much larger than that of ethanol. The entropy of adsorption for D-alanine, therefore, must be much larger than that for ethanol. The reason can be well explained if one borrows the term "chelate effect" which is frequently used in coordination chemistry.[7] As will be discussed later, a D-alanine molecule forms three hydrogen bonds with three surface hydroxyl groups when it is adsorbed by the *d*-quartz (two by the carboxyl group and one by the amino group). However, since these two groups are attached to the same molecule, the loss of the translational freedom by the adsorption is three per one molecule. On the other hand, nine translational freedoms are lost when the corresponding three ethanol molecules are adsorbed. This smaller number of losses of the translational degrees of freedom may be the principal cause for the larger entropy of adsorption, and thus the larger adsorption affinity, of D-alanine than those of ethanol. (That the number of losses in the rotational freedom for a D-alanine molecule is smaller than that for three corresponding ethanol molecules (three *vs.* nine) may partially contribute to the larger entropy of adsorption of D-alanine. The vibrational term, however, is essentially unrelated to the entropy of adsorption.) However, since the strengths of the hydrogen bonds of O-H---O and O-H---N are almost equal,[8] the magnitude of q_{st} for D-alanine (precisely speaking, the q_{st} per hydrogen bond in D-alanine) becomes nearly equal to that for ethanol.

By applying the Langmuir equation to the isotherm in Fig. 2, the monolayer capacity for DL-alanine is obtained as 1.8×10^{-7} mol g^{-1}. This, when combined with the value of the BET surface area (0.38 m^2 g^{-1}), yields a value of 3.5 nm^2 molecule^{-1} for the adsorption cross section for DL-alanine.

The asymmetric adsorptivity (A_s) is defined as follows:

$$A_s = \left(\frac{V_{ads}}{C_{eq}}\right)_{L(\text{or D})} \Big/ \left(\frac{V_{ads}}{C_{eq}}\right)_{D(\text{or L})} . \quad (1)$$

Here V_{ads} and C_{eq} denote the amount of alanine adsorbed and the equilibrium concentration respectively. The value of A_s for alanine by quartz was determined at 8 °C with the ^{14}C-tracer method. The result is summarized in Table 1. Table 1 shows that the *d*-quartz preferentially adsorbs D-alanine and the *l*-quartz adsorbs L-alanine, as found in the preceding experiments.[3-5] The value of A_s for alanine falls in the range of 1.1—1.3 at the higher alanine concentrations. This is almost the same as the value (1.2) determined at −80 °C by the ninhydrin-colorimetry in the previous paper,[5] but slightly lower than the value for alanine hydrochloride (1.4—1.7) from the rigorously dehydrated DMF solution determined by Bonner *et al.*[4] The present value is also apparently lower than the value ($\approx$2) determined by the present authors at −80 °C using the rigorously dehydrated ethanol solution.[5] The value determined at the lowest concentration is apparently small, although we do not know the reason.

To determine the A_s value by the tracer method or the ninhydrin-colorimetry alone, two separate adsorption experiments are necessary. For example, the A_s value obtained from the data of Bonner *et al.* is determined by the combination of the values of the amounts for the labeled enantiomer adsorbed by the *d*- and *l*-quartzs separately.[4] In the present study, the A_s value was obtained from the difference between the amounts of the two enantiomers adsorbed by the *d*- or *l*-quartz. However, since there is no guarantee that the surface properties of the two quartzs or the water content in the two alanine solutions are identical, it was feared that the A_s value might contain a large error. To eliminate this fear, we have developed the TN method by which the A_s value can be determined from one adsorption experiment. According to this method, the values of V_{ads} and C_{eq} of the labeled enantiomer are determined by the tracer method, while the values for the total alanine are obtained by the ninhydrin-colorimetry. The difference between the two measurements yields the values for the nonlabeled enantiomer. The results obtained by the TN method

Table 1. The data for the asymmetric adsorption of alanine at 8 °C determined by the ^{14}C-tracer method

Quartz[a]	*DL			D*L			A_s
		$\left(\frac{10^8 V_{ads}}{\text{mol g}^{-1}}\right)_D$	$\left(\frac{10^5 C_{eq}}{\text{M}}\right)_D$		$\left(\frac{10^8 V_{ads}}{\text{mol g}^{-1}}\right)_L$	$\left(\frac{10^5 C_{eq}}{\text{M}}\right)_L$	
d	b)	3.22	20.28	c)	2.89	20.61	1.13
l	d)	5.10	18.40	e)	6.02	17.48	1.24
d	f)	2.43	6.97	g)	2.29	7.11	1.08
l	h)	3.65	5.75	i)	4.01	5.39	1.17
d	j)	1.88	2.82	k)	1.57	3.13	1.33
l	l)	2.56	2.14	m)	2.66	2.04	1.09
l	n)	0.813	0.127	o)	0.817	0.123	1.04

a) 5 g of the powder A was placed in 5 cm^3 of DL-alanine solution. Radioactivity (count per 5 min) of the alanine solution measured before and after the adsorption was; b) 37185 and 32091. c) 27388 and 24019. d) 37185 and 29119. e) 27388 and 20382. f) 33321 and 24721. g) 28653 and 21656. h) 33321 and 20385. i) 28653 and 16415. j) 33378 and 20053. k) 28662 and 19063. l) 33378 and 15209. m) 28662 and 12398. n) 33556 and 4535. o) 28523 and 3743.

Table 2. The data for the asymmetric adsorption of alanine at 8 °C determined by the TN method

Quartz[a]	Alanine[b]	$(10^9 V_{ads}/\text{mol g}^{-1})/(10^5 C_{eq}/\text{M})$			A_s
		D+L	D	L	
l	*DL	$\frac{33.2}{3.37}$	$\frac{15.2}{1.74}$	$\left(\frac{18.0}{1.63}\right)$[c,d]	1.26
l	D*L	$\frac{29.6}{3.52}$	$\left(\frac{13.2}{1.82}\right)$[c,e]	$\frac{16.4}{1.70}$	1.33

a) 8 g of the *l*-quartz B. b) 20 cm^3. The initial concentration of DL-alanine solution is 4.70×10^{-5} M. c) Calculated value. The radioactivity (counts per 5 min) of the alanine solution measured before and after the adsorption was; d) 37149 and 27403 e) 27403 and 19748.

are summarized in Table 2. The value of A_s (≈ 1.3) accords well with the value determined by the tracer method.

Now it becomes unambiguous that the *d*-quartz preferentially adsorbs D-alanine and the *l*-quartz adsorbs L-alanine. Our next step is to solve the question "on what plane does the asymmetric adsorption occur?" According to an electron-microscopic observation, the powdered sample seems to contain various planes randomly. Therefore the A_s value obtained on the powdered sample is not helpful to solve this question. We are obliged to discuss this matter solely from the crystallographic point of view.

The projections of silicon and oxygen atoms on the (0001) and (10$\bar{1}$0) planes of quartz are schematically represented in Figs. 3 and 4. As can be seen in Fig. 3, silicon and oxygen atoms locate in nearly the same level on the (10$\bar{1}$0) plane. However, it is shown in Fig. 4 that the configuration of silicon atoms on the (10$\bar{1}$0) plane of *l*- and *d*-quartz is identical, while that of oxygen atoms is mirror-symmetrical to each other. The (10$\bar{1}$0) plane is a chiral plane where the asymmetric adsorption of alanine may occur.

Many workers have shown that the surface of the

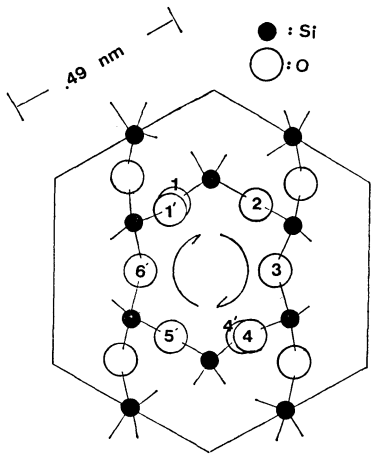

Fig. 3. A schematic representation of the (0001) plane of quartz.
Pairs of 1 and 4′, 2 and 5′, 3 and 6′, and 4 and 1′ oxygen atoms exist in the same plane.
If the helix of oxygen atoms (1–2–3–4) is clockwise, the quartz is *l*-quatz.

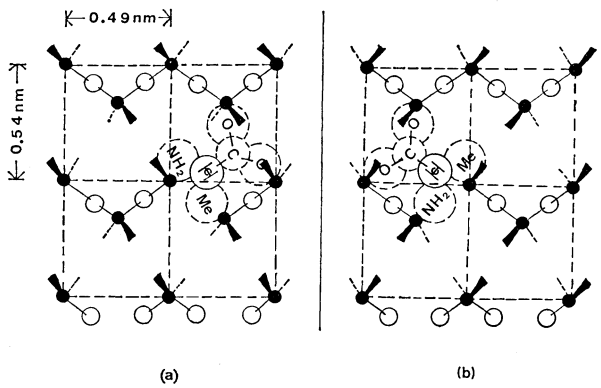

Fig. 4. Schematic representations of the (10$\bar{1}$0) plane of *l*-and *d*-quartzs, and of the configuration of the adsorbed L-alanine molecule.
(a): *l*-Quartz, (b): *d*-quartz, ●: silicon atom, ○: frame oxygen atom, ◄: surface hydroxyl group.

powdered quartz is covered by hydroxyl groups which can not be removed even by heating up to 150 °C.[9] If this is the case, the $(10\bar{1}0)$ planes of the present *l*- and *d*-quartz samples have the hydroxyl groups which are disposed mirror-symmetrically to each other, as shown in Fig. 4. The carboxyl, amino, and even methyl groups of the alanine molecule, when the molecule is adsorbed on the $(10\bar{1}0)$ plane, interact (*i.e.*, form the hydrogen bond) with the surface hydroxyl group. However, it may be the carboxyl group which interacts with the hydroxyl group most strongly and, therefore, principally determines the adsorbed structure of the alanine molecule. The pairs of the hydroxyl groups which can interact satisfactorily with the carboxyl group are limited. If an L-alanine molecule is put on the $(10\bar{1}0)$ plane of the *l*-quartz, as shown in Fig. 4, we notice that not only the carboxyl group but also the amino group can interact with the surface hydroxyl group very well, although the methyl group can not. However, if an L-alanine molecule is put on the *d*-quartz surface so that the carboxyl group preferably interacts with a pair of the hydroxyl groups, the amino group can not interact with the hydroxyl group well. Instead, the methyl group interacts with the hydroxyl group preferably. It is well known that the hydrogen bond between an amino group and a hydroxyl group is stronger than that between a methyl group and a hydroxyl group (16—29 kJ mol^{-1} against 11 kJ mol^{-1}).[8] It may not be unreasonable to conclude that the larger interaction between NH_2 and OH groups than that between CH_3 and OH groups is the principal cause (or at least one of the principal causes) for the preferential adsorption of L-alanine by the *l*-quartz than by the *d*-quartz. The same may be true for the preferential adsorption of D-alanine by the *d*-quartz rather than by the *l*-quartz.

The explanation above seems to work well. However, two questions are raised to the adsorption model. (1) If the asymmetric adsorption results from the different heat of formation for NH_2–OH hydrogen bond and for CH_3–OH hydrogen bond, the A_s value must be temperature dependent. Is the fact that the A_s value at 8 °C is apparently comparable with the value at −80 °C obtained in the previous study inconsistent with the above model?[5] (2) Does the present model work well even in aqueous solution where the alanine molecule dissociate to the dipolar ion $CH_3(H)C(COO^-)NH_3^+$? We can not answer the first question definitely, partly because the techniques and conditions adopted in the two experiments are quite different and, therefore, the certainty of the data can not bear the quantitative discussion. We should establish the experimental technique and condition to solve this question. As to the second question, we assert that the model works well even in the aqueous solution. However, if the strength of the NH_3^+–OH bond is weaker than the CH_3–OH bond, the asymmetric adsorptivity becomes opposite (*i.e.*, the *d*-quartz adsorbs preferentially the L-alanine and the *l*-quartz adsorbs the D-alanine). However, since the adsorption affinity of alanine falls drastically in the aqueous solution and the amount adsorbed of it by quartz is extremely low, as shown in Fig. 1, the experimental determination of the A_s value must be very difficult. The lateral electrostatic interaction between the adsorbed dipolar alanine ions can be neglected if the concentration of the adsorbed species is quite low.

The present authors thank Professor Emeritus Takao Kwan (The University of Tokyo) who first stimulated our interest in this study.

References

1) G. Karagunis and G. Coumoulos, *Nature*, **142**, 162 (1938).
2) A. Amariglio, H. Amariglio, and X. Duval, *Helv. Chim. Acta*, **51**, 2110 (1968).
3) W. A. Bonner, P. R. Kavasmaneck, and F. S. Martin, *Science*, **186**, 143 (1974); *Origins of Life*, **6**, 367 (1975).
4) W. A. Bonner and P. R. Kavasmaneck, *J. Org. Chem.*, **41**, 2225 (1976).
5) S. Furuyama, H. Kimura, M. Sawada, and T. Morimoto, *Chem. Lett.*, **1978**, 381.
6) S. Moor, *J. Biol. Chem.*, **243**, 6281 (1968).
7) F. A. Cotton and G. Wilkinson, "Basic Inorganic Chemistry," John Wiley and Sons, Inc., New York (1976), Chap. 6.
8) C. A. Coulson, "Valence," 2nd ed, The Clarendon Press, Oxford (1961), Chap. 13.
9) G. S. Moore and H. E. Rose, *Nature*, **242**, 187 (1973).

The Crystal and Molecular Structure of 7,8-Epoxyhalochamigrene

Akio Furusaki,* Chuji Katayama,† Takeshi Matsumoto, Minoru Suzuki, Teruaki Suzuki, Hajime Kikuchi, and Etsuro Kurosawa

Department of Chemistry, Faculty of Science, Hokkaido University, Kita-ku, Sapporo 060

†*Department of Chemistry, Faculty of Science, Nagoya University, Chikusa-ku, Nagoya 464*

(Received April 21, 1982)

The molecular structure of 7,8-epoxyhalochamigrene, $C_{15}H_{23}OBr_2Cl$, has been confirmed by means of X-ray crystallographic analysis. The crystals are orthorhombic, with sixteen molecules in a unit cell with dimensions of $a=10.303$, $b=71.31$, and $c=9.061$ Å; the space group is $P2_12_12_1$. 4241 independent intensity data were collected on a four-circle diffractometer with graphite-monochromated Cu $K\alpha$ radiation. The structure was solved by the Monte Carlo direct method, using 20 reflections as a starting set, and was refined by the block-diagonal least-squares method. The final R value was 0.072. The molecular structure thus obtained corresponds to that proposed by Howard and Fenical on the basis of chemical and spectroscopic evidence. The four crystallographically-independent molecules have almost the same geometries. Of the two spiro-linked six-membered rings, the one having the epoxy group takes a half-chair conformation, while the other adopts a chair conformation. The crystal consists of alternating single and triple molecular layers parallel to the (010) plane; the latter layer has a molecular arrangement approximately of $P2_12_12_1$ symmetry.

A number of halogenated chamigrene derivatives[1] such as halochamigrene[2] have been isolated from the red algae of the genus *Laurencia*. 7,8-Epoxyhalochamigrene, which had already been obtained by oxidation of halochamigrene,[2a] was recently reported to exist also in nature, *e.g.*, in the red algae *L. nipponica*[3] and *L. okamurai*.[4] On the basis of the chemical and spectroscopic evidence, the **1** and **2** structures were proposed for halochamigrene and 7,8-epoxyhalochamigrene respectively;[2] however, there was no conclusive proof as to these structures. Therefore, in order to establish **1** and **2**, we have now undertaken an X-ray crystallographic study of 7,8-epoxyhalochamigrene.

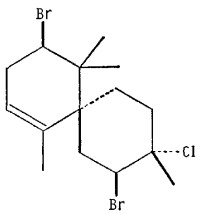

1

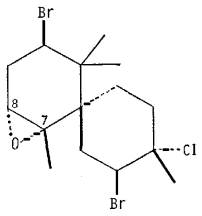

2

Experimental

A colorless single crystal cut into a cube with an edge of about 0.2 mm was used for the X-ray experiment. The crystal data are summarized in Table 1. The unit-cell dimensions and diffraction intensities were measured on a Rigaku four-circle diffractometer with graphite-monochromated Cu $K\alpha$ radiation ($\lambda=1.54178$ Å). Because of the long b unit-cell edge, it was necessary to obtain high resolution of the diffraction peaks. For this purpose, a Rigaku RU-200 X-ray tube with a focal size of 0.3×0.3 mm^2 was employed (50 kV, 60 mA). The θ-2θ continuous-scan technique was applied at a θ scan rate of 10° min^{-1}; the scan width in θ was $(0.6+0.142\tan\theta)$°. The background was measured for 5 s at each end of the scan range. Three standard reflections, measured at intervals of every 200 reflections, showed no significant decrease in intensity during the course of the data collection. The intensities were corrected for the Lorentz and polarization factors, but not for absorption or extinction effect. In the range of 2θ values up to 120°, 4241 independent structure factors above the $3\sigma(F)$ level were selected for the structure determination.

Table 1. The crystal data

$C_{15}H_{23}OBr_2Cl$	Mol wt 414.61
Crystal system	Orthorhombic
Space group	$P2_12_12_1$
Cell dimensions	$a=10.303\,(2)$ Å
	$b=71.31\,(1)$ Å
	$c=9.061\,(8)$ Å
V	6658 Å^3
Z	16
D_c	1.655 g cm^{-3}
μ(Cu $K\alpha$)	76.8 cm^{-1}

Structure Determination

Because of the presence of eight independent bromine atoms, the heavy-atom method seemed somewhat troublesome to apply to the present structure; hence, the Monte Carlo direct method[5] was tried. The 20 reflections with the greatest $|E|$ values were chosen as a starting set. In order to extend each of the tentative-phase sets derived from random numbers, 12 cycles of the tangent procedure were performed using 1111 $|E|$ values above 1.30. Since the phase set extended from the 66thly-generated random set showed a low R_K value of 0.258 ($R_K=\Sigma||E_o|-k|E_c||/\Sigma|E_o|$), 10 additional cycles of the tangent procedure were carried out by the use of 1347 $|E|$ values above 1.20; the R_K value became 0.268. An E-map based on 1286 phases afforded all the 76 non-hydrogen atoms.

After the structure had been refined by the block-diagonal least-squares method with anisotropic temperature factors, the absolute configuration was determined by taking account of the anomalous dispersion of bromine and chlorine atoms for Cu $K\alpha$ radiation. The R ratio for the two enantiomeric structures, 1.018, rejected one of them at the 99.5% confidence level.[6] A difference Fourier map revealed all the 92 hydrogen atoms. Further least-squares refinements were performed including the hydrogen atoms and the anomalous dispersion effects. The weighting scheme used

was as follows:

$$w = 1/\{\sigma(F)^2 \exp(c_1X^2+c_2Y^2+c_3XY+c_4X+c_5Y)\},$$

where $X=|F_o|$ and $Y=\sin\theta/\lambda$. The c_1, c_2, c_3, c_4, and c_5 coefficients were evaluated from the $(\Delta F)^2$ distribution; $c_1=0.7702\times10^{-6}$, $c_2=8.060$, $c_3=0.01900$, $c_4=-0.4314\times10^{-2}$, and $c_5=-8.129$. In this manner, the R value reached 0.072. The final atomic parameters are listed in Table 2.[7]

The calculations were done on a HITAC M-200H computer at the Hokkaido University Computing Center, using our own programs. The atomic scattering factors and dispersion corrections were taken from the International Tables for X-Ray Crystallography.[8]

Results and Discussion

Molecular Structure. The molecular skeleton obtained is shown in Fig. 1, while the bond distances and angles and the torsion angles for the spiro[5.5]-undecane systems are given in Tables 3 and 4 respectively. From these results, it is concluded that the structure of 7,8-epoxyhalochamigrene, including the absolute configuration, corresponds to **2**; consequently the structure of halochamigrene is **1**. The four crystallographically-independent molecules have almost the same geometries. The average bond distances and angles for these four molecules are given in the last column of Table 3.

Table 2. The final atomic parameters and estimated standard deviations

The e.s.d.'s given in the parentheses refer to the last decimal position.

Atom	$x\times10^3$	$y\times10^4$	$z\times10^3$	B_{eq}[a]/Å^2	Atom	$x\times10^3$	$y\times10^4$	$z\times10^3$	B_{eq}[a]/Å^2
Br(A1)	340.3(3)	581.3(2)	213.1(2)	6.14	Br(C1)	249.7(2)	923.6(2)	920.9(2)	5.23
Br(A2)	756.7(3)	−374.1(4)	382.0(3)	9.76	Br(C2)	466.4(3)	1976.4(2)	643.3(3)	7.14
Cl(A)	287.6(5)	620.9(5)	588.0(6)	5.56	Cl(C)	574.0(6)	797.6(6)	909.3(6)	6.87
O(A)	348(1)	−176(1)	576(1)	5.12	O(C)	598(1)	1362(1)	477(1)	5.31
C(A1)	430(2)	222(2)	302(2)	4.04	C(C1)	350(2)	1248(2)	774(2)	3.75
C(A2)	351(2)	387(2)	371(2)	4.59	C(C2)	390(2)	1046(2)	816(2)	4.22
C(A3)	409(2)	463(2)	508(2)	4.22	C(C3)	516(2)	1042(2)	897(2)	4.56
C(A4)	416(2)	296(2)	617(1)	4.18	C(C4)	623(2)	1147(2)	809(2)	4.63
C(A5)	511(2)	143(2)	557(2)	4.15	C(C5)	584(2)	1354(2)	783(2)	3.93
C(A6)	467(2)	63(2)	409(2)	3.69	C(C6)	453(2)	1374(2)	699(2)	4.04
C(A7)	346(2)	−72(2)	432(2)	4.08	C(C7)	468(2)	1319(2)	539(2)	3.85
C(A8)	354(2)	−278(2)	437(2)	4.63	C(C8)	487(2)	1463(2)	416(2)	5.17
C(A9)	490(3)	−375(2)	417(2)	6.91	C(C9)	485(2)	1671(2)	453(2)	5.98
C(A10)	592(2)	−239(2)	430(2)	5.89	C(C10)	496(2)	1704(2)	614(2)	4.82
C(A11)	585(2)	−54(2)	336(2)	5.10	C(C11)	403(2)	1583(2)	711(2)	4.67
C(A12)	708(2)	58(2)	333(2)	5.63	C(C12)	406(2)	1654(2)	872(2)	5.55
C(A13)	550(2)	−110(2)	177(2)	5.21	C(C13)	266(2)	1600(2)	651(2)	5.34
C(A14)	209(2)	−1(2)	402(2)	5.17	C(C14)	426(2)	1128(2)	480(2)	3.73
C(A15)	531(2)	567(2)	499(3)	6.11	C(C15)	509(2)	1113(2)	1058(2)	5.43
Br(B1)	−230.8(3)	1570.0(2)	153.5(2)	6.06	Br(D1)	596.9(3)	2165.2(2)	134.8(3)	6.51
Br(B2)	−53.4(3)	470.3(2)	338.2(3)	6.87	Br(D2)	377.5(3)	3253.4(2)	307.2(4)	9.18
Cl(B)	92.3(7)	1678.0(6)	194.4(9)	9.58	Cl(D)	275.8(7)	2046.1(6)	149.7(8)	8.98
O(B)	92(1)	1039(2)	569(1)	5.20	O(D)	240(1)	2672(2)	526(1)	5.68
C(B1)	−144(2)	1223(2)	274(1)	3.73	C(D1)	500(2)	2508(2)	250(2)	3.64
C(B2)	−97(2)	1426(2)	255(2)	4.19	C(D2)	454(2)	2303(2)	228(2)	4.58
C(B3)	37(2)	1436(2)	172(2)	6.88	C(D3)	329(2)	2291(2)	140(2)	5.47
C(B4)	131(2)	1319(2)	261(2)	4.83	C(D4)	227(2)	2403(2)	222(2)	5.33
C(B5)	84(2)	1113(2)	265(2)	4.37	C(D5)	269(2)	2614(2)	226(2)	4.44
C(B6)	−45(2)	1083(2)	342(2)	3.54	C(D6)	393(2)	2647(2)	308(2)	4.71
C(B7)	−33(2)	1106(2)	508(2)	4.39	C(D7)	374(2)	2615(2)	480(2)	4.12
C(B8)	−25(2)	943(2)	611(2)	4.94	C(D8)	347(2)	2783(2)	579(2)	5.39
C(B9)	−38(2)	753(2)	561(2)	5.57	C(D9)	357(2)	2976(2)	524(2)	5.91
C(B10)	−16(2)	740(2)	391(2)	4.45	C(D10)	352(2)	2989(2)	356(2)	5.90
C(B11)	−102(2)	876(2)	306(2)	4.45	C(D11)	445(2)	2857(2)	279(2)	4.56
C(B12)	−93(2)	828(2)	140(2)	5.08	C(D12)	446(2)	2899(2)	113(2)	6.55
C(B13)	−244(2)	859(2)	350(2)	5.37	C(D13)	583(2)	2875(2)	339(2)	5.20
C(B14)	−69(2)	1283(2)	590(2)	5.80	C(D14)	414(2)	2442(2)	556(2)	5.91
C(B15)	24(2)	1389(2)	11(2)	5.68	C(D15)	347(3)	2335(3)	−26(2)	6.98

a) $B_{eq}=8\pi^2(u_1^2+u_2^2+u_3^2)/3$, where u_i is the root-mean-square deviation in the ith principal axis of the thermal ellipsoid.

Table 3. The bond distances and angles, with their standard deviations

	Mol. A	Mol. B	Mol. C	Mol. D	Mean
Bond distance	l/Å	l/Å	l/Å	l/Å	l/Å
C(1)-C(2)	1.56(2)	1.53(2)	1.55(2)	1.55(2)	1.55
C(1)-C(6)	1.54(2)	1.55(2)	1.54(2)	1.58(2)	1.55
C(2)-C(3)	1.48(2)	1.58(3)	1.49(3)	1.52(3)	1.52
C(2)-Br(1)	2.00(1)	1.95(2)	1.94(2)	1.96(2)	1.96
C(3)-C(4)	1.55(2)	1.51(3)	1.55(3)	1.51(3)	1.53
C(3)-C(15)	1.46(3)	1.51(3)	1.55(2)	1.55(3)	1.52
C(3)-Cl	1.83(2)	1.83(2)	1.85(2)	1.83(2)	1.84
C(4)-C(5)	1.56(2)	1.54(2)	1.55(2)	1.56(2)	1.55
C(5)-C(6)	1.52(2)	1.52(2)	1.56(3)	1.50(3)	1.53
C(6)-C(7)	1.59(2)	1.52(2)	1.51(2)	1.58(2)	1.55
C(6)-C(11)	1.62(3)	1.61(2)	1.58(2)	1.62(2)	1.61
C(7)-C(8)	1.47(2)	1.50(2)	1.52(2)	1.52(2)	1.50
C(7)-C(14)	1.52(3)	1.51(2)	1.52(2)	1.48(2)	1.51
C(7)-O	1.50(2)	1.48(2)	1.49(2)	1.49(2)	1.49
C(8)-C(9)	1.57(3)	1.43(2)	1.52(2)	1.46(2)	1.50
C(8)-O	1.46(2)	1.44(2)	1.46(2)	1.44(2)	1.45
C(9)-C(10)	1.44(3)	1.56(3)	1.48(3)	1.53(3)	1.50
C(10)-C(11)	1.57(2)	1.52(2)	1.56(2)	1.51(3)	1.54
C(10)-Br(2)	2.00(2)	2.02(1)	1.98(1)	1.96(1)	1.99
C(11)-C(12)	1.50(3)	1.54(2)	1.54(2)	1.53(3)	1.53
C(11)-C(13)	1.53(2)	1.52(3)	1.52(3)	1.53(3)	1.53
C-H					1.03
Bond angle	ϕ/°	ϕ/°	ϕ/°	ϕ/°	ϕ/°
C(2)-C(1)-C(6)	115(1)	117(1)	118(1)	115(1)	116
C(1)-C(2)-C(3)	114(1)	112(1)	112(1)	113(1)	113
C(1)-C(2)-Br(1)	105(1)	109(1)	110(1)	107(1)	108
C(3)-C(2)-Br(1)	112(1)	112(1)	113(1)	113(1)	113
C(2)-C(3)-C(4)	106(1)	106(2)	111(1)	107(1)	108
C(2)-C(3)-C(15)	119(2)	112(2)	115(2)	113(2)	115
C(2)-C(3)-Cl	106(1)	105(1)	109(1)	106(1)	107
C(4)-C(3)-C(15)	113(2)	117(2)	111(1)	117(2)	115
C(4)-C(3)-Cl	105(1)	106(1)	105(1)	106(1)	106
C(15)-C(3)-Cl	107(1)	110(1)	106(1)	106(1)	107
C(3)-C(4)-C(5)	110(1)	110(2)	110(1)	110(2)	110
C(4)-C(5)-C(6)	113(1)	115(1)	113(1)	113(1)	114
C(1)-C(6)-C(5)	111(1)	108(1)	109(1)	109(1)	109
C(1)-C(6)-C(7)	109(1)	112(1)	110(1)	109(1)	110
C(1)-C(6)-C(11)	108(1)	106(1)	107(1)	107(1)	107
C(5)-C(6)-C(7)	110(1)	111(1)	111(1)	111(1)	111
C(5)-C(6)-C(11)	109(1)	111(1)	109(1)	110(1)	110
C(7)-C(6)-C(11)	109(1)	109(1)	110(1)	110(1)	110
C(6)-C(7)-C(8)	124(2)	123(1)	122(1)	119(1)	122
C(6)-C(7)-C(14)	120(1)	124(1)	123(1)	123(1)	123
C(6)-C(7)-O	113(1)	114(1)	113(1)	111(1)	113
C(8)-C(7)-C(14)	113(1)	111(1)	113(1)	116(1)	113
C(8)-C(7)-O	59(1)	58(1)	58(1)	57(1)	58
C(14)-C(7)-O	109(1)	107(1)	108(1)	111(1)	109
C(7)-C(8)-C(9)	119(2)	122(1)	120(1)	122(2)	121
C(7)-C(8)-O	62(1)	61(1)	60(1)	61(1)	61
C(9)-C(8)-O	111(1)	116(2)	114(2)	118(2)	115
C(8)-C(9)-C(10)	110(1)	111(1)	112(1)	113(1)	112
C(9)-C(10)-C(11)	120(2)	112(1)	115(1)	114(2)	115
C(9)-C(10)-Br(2)	106(1)	105(1)	106(1)	106(1)	106
C(11)-C(10)-Br(2)	109(1)	112(1)	112(1)	114(1)	112
C(6)-C(11)-C(10)	104(1)	106(1)	107(1)	107(1)	106
C(6)-C(11)-C(12)	112(1)	112(1)	112(1)	110(1)	112
C(6)-C(11)-C(13)	110(2)	112(1)	111(1)	109(1)	111
C(10)-C(11)-C(12)	115(2)	109(1)	110(1)	109(1)	111
C(10)-C(11)-C(13)	107(1)	112(1)	109(1)	112(1)	110
C(12)-C(11)-C(13)	109(1)	107(2)	109(2)	109(2)	109
C(7)-O-C(8)	59(1)	62(1)	62(1)	63(1)	62

Table 4. The torsion angles for the six-membered rings

	Mol. A	Mol. B	Mol. C	Mol. D
	ϕ/°	ϕ/°	ϕ/°	ϕ/°
C(6)-C(1)-C(2)-C(3)	50	51	49	50
C(1)-C(2)-C(3)-C(4)	−59	−57	−54	−58
C(2)-C(3)-C(4)-C(5)	64	62	60	64
C(3)-C(4)-C(5)-C(6)	−61	−63	−58	−63
C(4)-C(5)-C(6)-C(1)	47	51	50	50
C(5)-C(6)-C(1)-C(2)	−41	−45	−45	−44
C(11)-C(6)-C(7)-C(8)	20	21	23	26
C(6)-C(7)-C(8)-C(9)	−1	−5	−3	−9
C(7)-C(8)-C(9)-C(10)	13	19	15	19
C(8)-C(9)-C(10)-C(11)	−51	−53	−48	−50
C(9)-C(10)-C(11)-C(6)	70	70	69	68
C(10)-C(11)-C(6)-C(7)	−47	−51	−52	−53

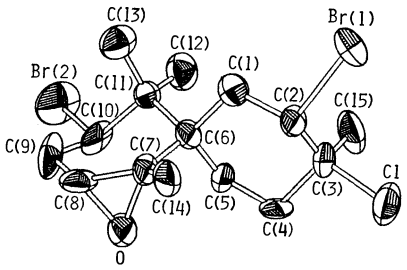

Fig. 1. A perspective view of the 7,8-epoxyhalochamigrene A-molecule, and the crystallographic numbering system.
Non-hydrogen atoms are represented as thermal ellipsoids enclosing 50% probabilities.

Of the two spiro-linked six-membered rings, the cyclohexane ring having the epoxy group takes a half-chair conformation; the Br(2), C(1), and C(12) atoms are equatorially or pseudoequatorially bonded to this ring, while the C(5) and C(13) atoms are axially or pseudoaxially oriented. On the other hand, the remaining six-membered ring has a somewhat deformed chair conformation; the Br(1), Cl, and C(11) atoms take the equatorial orientations, while the C(7) and C(15) atoms occupy the axial positions. Such a conformation of the spiro[5.5]undecane system brings the C(2)H and C(14)H_3 groups very close to each other; the C(2)···C(14) distances for the four molecules are 3.11—3.21 Å. The severe steric repulsion between these groups results in a considerable flattening of the C(5)-C(6)-C(1)-C(2) moiety (see Table 4).

In all four molecules, the C(6)-C(11) bond distance (1.58—1.62 Å) is appreciably longer than the standard C-C single-bond distance.[9] This bond lengthening is probably due to the strong steric repulsions between the bulky groups attached to the C(6) and C(11) atoms. The fact that the C(3)-C(2)-Br(1) bond angle is greater than the C(1)-C(2)-Br(1) angle on the average by 5° indicates that the Cl atom and C(15)H_3 group repel the Br(1) atom to a considerable extent. The Br(2) atom also suffers a similar steric hindrance from the C(12)H_3 and C(13)H_3 *gem*-dimethyl groups; the average difference between the C(9)-C(10)-Br(2) and C(11)-C(10)-Br(2) bond angles is 6°.

As to the valence angles at the C(3) atom, an interesting fact is found: the sum of the average C(2)-C(3)-C(4), C(2)-C(3)-C(15), and C(4)-C(3)-C(15) bond angles, 338°, is considerably larger than three times the tetrahedral angle, while all the average C(2)-C(3)-Cl, C(4)-C(3)-Cl, and C(15)-C(3)-Cl bond angles are smaller than the tetrahedral angle. This suggests that the C(3) atomic orbital used for the C(3)-Cl bond may involve a greater amount of p-character than the pure sp^3 hybrid orbital, and that, as the result, the C(3)-Cl bond may be somewhat lengthened. In fact, the average C(3)-Cl bond distance of 1.84 Å is significantly longer than the usual C-Cl distance, 1.77 Å.[9]

Crystal Structure. The most interesting point in the present structure is how the four crystallographically-independent A-, B-, C-, and D-molecules are arranged. As Fig. 2 shows, the crystal may be taken as composed of the following three kinds of molecular layers parallel to the (010) plane: (1) A layers consisting of only A-molecules and placed at $y=0$ or 1/2; (2) D layers made up of only D-molecules and situated at $y=1/4$ or 3/4; (3) BC layers containing both B- and C-molecules and lying between the A and D layers. The structure has the sequence of layers, A, BC, D, BC, A, ..., repeating after four layers.

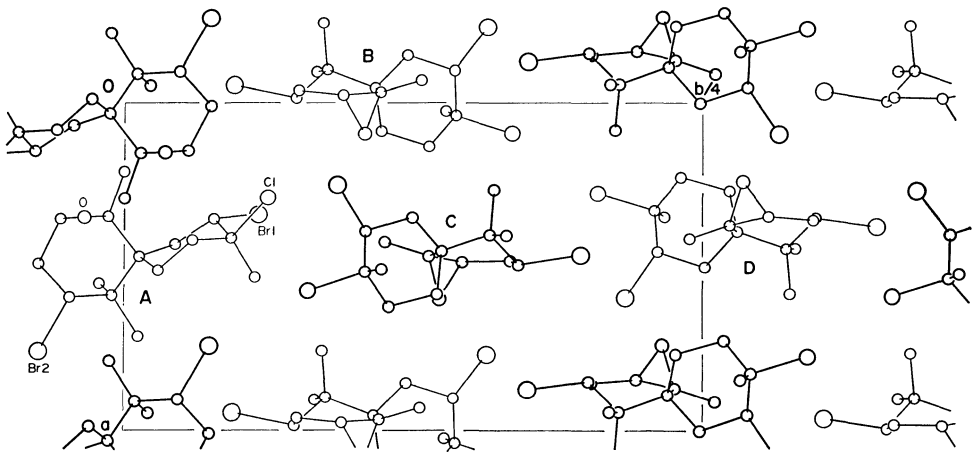

Fig. 2. The molecular arrangement viewed along the c axis.

Although the B- and C-molecules are independent, they are related to each other by an approximate two-fold screw axis along the a axis. These molecules are also related to the D-molecule by an approximate two-fold screw axis (with a translation of $b/8$) along the b axis or by an approximate two-fold rotation axis along the c axis. Consequently, the molecular arrangement in the triple molecular layer formed by adjacent BC, D, and BC layers looks as if it were part of a structure having the $P2_12_12$ space group and unit-cell dimensions of $a'=a$, $b'=b/4$, and $c'=c$. These triple molecular layers and the monomolecular A layers are alternately stacked. The orientation of the A-molecule is substantially different from those of the other three molecules; *e.g.*, the two molecules marked with A and B in Fig. 2 do not take the same orientation until either of them rotates by about 90° around a special axis lying nearly in the [$\bar{8}$10] direction.

The molecules are bonded mainly by the van der Waals interactions. The halogen atoms are arranged near either surface of the molecular layer to which they belong. The intermolecular halogen-halogen distances, which are shorter than the usual van der Waals distances, are given in Table 5. Of these, the closest Br(A1)···Br(C1), Br(A2)···Cl(C), and Cl(B)···Cl(D) contacts correspond to the apparent reductions, about 0.17 and 0.09 Å respectively, of the chlorine and bromine van der Waals radii.

Table 5. The intermolecular halogen-halogen distances shorter than the usual van der Waals distances

		l/Å
Br(A1)	Br(C1)[a]	3.720(3)
Br(A2)	Cl(C)[b]	3.497(5)
Br(C1)	Cl(A)[c]	3.729(5)
Cl(B)	Cl(D)[c]	3.260(8)

The symmetry codes are as follows: a) x, y, $-1+z$; b) $3/2-x$, $-y$, $-1/2+z$; c) x, y, z.

References

1) a) D. J. Faulkner, *Tetrahedron*, **33**, 1421 (1977); b) J. D. Martin and J. Darias, "Marine Natural Products," ed by P. J. Scheuer, Academic Press Inc., New York (1978), Vol. I, p. 125.

2) a) B. M. Howard and W. Fenical, *Tetrahedron Lett.*, **1975**, 1687; b) B. M. Howard and W. Fenical, *ibid.*, **1976**, 2519; c) M. Suzuki, A. Furusaki, and E. Kurosawa, *Tetrahedron*, **35**, 823 (1979).

3) T. Suzuki, H. Kikuchi, and E. Kurosawa, *Bull. Chem. Soc. Jpn.*, in press.

4) M. Ojika, Y. Shizuri, and K. Yamada, 43rd National Meeting of the Chemical Society of Japan, Tokyo, April 1981, Abstr. No. 2F34.

5) A. Furusaki, *Acta Crystallogr., Sect. A*, **35**, 220 (1979).

6) W. C. Hamilton, *Acta Crystallogr.*, **18**, 502 (1965).

7) The tables of the anisotropic temperature factors and hydrogen parameters and the F_o-F_c table are kept at the Chemical Society of Japan (Document No. 8249).

8) "International Tables for X-Ray Crystallography," The Kynoch Press, Birmingham (1974), Vol. IV, p. 72.

9) "Tables of Interatomic Distances and Configuration in Molecules and Ions, Supplement," ed by L. E. Sutton, The Chemical Society, London (1965).

 © 1982 The Chemical Society of Japan Bull. Chem. Soc. Jpn., 55, 3403—3406 (1982)

Kinetic Studies of the Micelle System of Octylammonium Alkanoates in Hexane Solution by the Ultrasonic Absorption Method

Teruyo YAMASHITA, Hiroshige YANO,* Shoji HARADA,† and Tatsuya YASUNAGA†

Daiichi College of Pharmaceutical Science, Tamagawa-cho 22-1, Minami-ku, Fukuoka 815

†*Department of Chemistry, Faculty of Science, Hiroshima University, Higashisenda-machi 1-1-89, Naka-ku, Hiroshima 730*

(Received April 21, 1982)

Ultrasonic absorption was measured in hexane solutions of octylammonium alkanoates (nonanoate, decanoate, dodecanoate, and tetradecanoate). The value of critical micelle concentration (CMC) was determined to be 0.02 M (1 M = 1 mol dm^{-3}) for all the surfactants. The excess ultrasonic absorption, observed in the solutions above the CMC, was ascribed to the association-dissociation of the monomer to and from the micelle. From the concentration dependences of the ultrasonic parameters, the mean aggregation number of the micelle, the rate constants, and the enthalpy change of the above reaction were obtained. These results were discussed in relation to the shape of the reversed micelle and the solute-solvent interactions.

A large amount of experimental information has been provided for the physicochemical properties of micelles in aqueous solution. In the field of the kinetics, two distinct reaction processes of micelle formation have been observed in different time regions:[1-4] one is a micelle formation and decomposition and the other is an association-dissociation of the monomer to and from the micelle. On the other hand, relatively little is known with regard to the micelles in organic solvents[5-8] in spite of their important roles as catalysis, solubilizing agents, and model systems for the membranes and molecular aggregations. Especially, their kinetics have rarely been studied.[8,9] The difficulty of this study seems to be due to the following reasons: (i) since the aggregation number of the micelle is very low, an abrupt and large change of the physicochemical properties of the solution cannot be expected at the CMC, and (ii) micelle formation and monomer exchange reactions are too rapid to be observed by conventional techniques. To overcome these difficulties, the ultrasonic absorption method is a very valuable technique for the study of the dynamic features of the micelle in organic solution. In the present work we applied the technique to the hexane solution of octylammonium alkanoates of different chain lengths: *i.e.*, octylammonium nonanoate (OAN), decanoate (OADe), dodecanoate (OAD), and tetradecanoate (OAT).

The purposes of this work are to decide the reaction responsible for the relaxation absorption. to obtain the kinetic parameters concerning the reaction, and to see the effect of the chain length of the detergents.

Experimental

Octylammonium alkanoates were prepared by the method already reported,[10] and dried at room temperature under reduced pressure until the weight became constant. The melting points of the detergents were satisfactorily consistent with the corresponding literature values.[11] Hexane was dried on P_2O_5 and distilled.

Ultrasonic absorption was measured by the pulse technique in the frequency range 5—95 MHz for the solutions of the concentrations from 0.05 to 0.35 M at intervals of 0.05 M at 30 °C. Details of the apparatus have been described elsewhere.[12] The sing-around method was employed for the measurement of sound velocity. The density was measured by a pycnometer.

Results and Discussion

Since many physicochemical properties of the detergent solution change at the CMC, a number of methods have been applied for the determination of the CMC. The velocity of sound, which is used in this work, is one of them: the CMC is determined from the break point of the velocity *vs.* concentration plot. As an example, the concentration dependence of the sound velocity of OAN is shown in Fig. 1, where the CMC was determined to be 0.02 M. In the same way, the value of the CMC was obtained to be 0.02 M for OADe, OAD, and OAT. Consequently, we could not observe any difference in the CMC's of the four detergents. The relationship between the alkyl chain length and the CMC is not clear in organic solution, in contrast to that in aqueous solution. Generally, the CMC increases with increase of the lipophilic part of the detergent in organic solution.[13] But the relationship is not always straightforward. In some cases, no effect was observed, *e.g.*, octylammonium alkanoates in CCl_4;[13] the present result, constant CMC irrespective to the chain length, is another example.

Ultrasonic relaxation absorptions were observed in

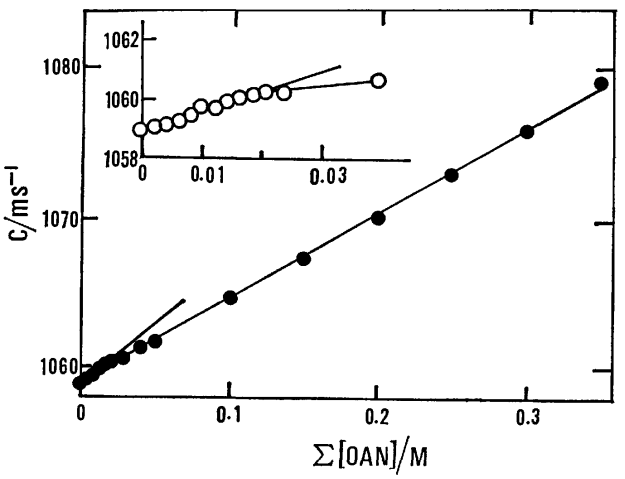

Fig. 1. Concentration dependence of the sound velocity of OAN in hexane at 30 °C.

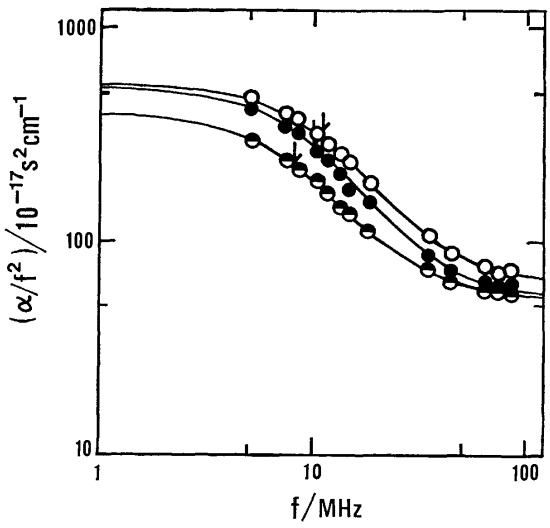

Fig. 2. Ultrasonic absorption spectra of OAT in hexane at 30 °C.
The solid lines are theoretical curves calculated by Eq. 1 with f_r, A, and B in Table 1. The arrows indicate the relaxation frequency: ◓: 0.15 M, ●: 0.25 M, ○: 0.35 M.

all the detergent solutions in the concentration range above the CMC. Representative absorption spectra of OAT are shown in Fig. 2. Similar absorption spectra were obtained in other detergent solutions. All of the spectra were represented by the single relaxation equation:

$$\alpha/f^2 = A/\{1+(f/f_r)^2\} + B, \quad (1)$$

where α is the absorption coefficient, f the frequency, f_r the relaxation frequency, A and B are the relaxing and nonrelaxing absorptions, respectively. The absorption parameters, f_r, A, and B, were determined by a computor so as to give the best fit of the experimental data to Eq. 1 and are listed in Table 1.

Since the relaxation absorption is observed only in the solutions above the CMC, it is clear that the present absorption is related to the micelle. As plausible reactions responsible for the present absorption, micelle formation and decomposition and association-dissociation of the monomer to and from the micelle were investigated. However, the micelle formation reaction,

$$nS \rightleftharpoons S_n, \quad (2)$$

(S=detergent monomer and S_n=micelle composed of n detergent molecules) could not give any satisfactory interpretations to the present data.

The association-dissociation of the monomer to and from the micelle,

$$S_n + S \underset{k_{-1}}{\overset{k_1}{\rightleftharpoons}} S_{n+1}, \quad (3)$$

was examined as follows. By assuming that $[S_n]=[S_{n+1}]$, the equilibrium constant is given by

$$K = \frac{k_1}{k_{-1}} = \frac{1}{[S]}. \quad (4)$$

For Reaction 3, the reciprocal relaxation time, τ^{-1} is expressed by

$$\tau^{-1}(=2\pi f_r) = k_1([S]+[S_n]) + k_{-1}, \quad (5)$$

Table 1. Ultrasonic parameters of octylammonium alkanoates in hexane

C / M	A / 10^{-17} s^2 cm^{-1}	B / 10^{-17} s^2 cm^{-1}	f_r / MHz
	OAN		
0.05	299	54.6	5.3
0.10	303	58.6	5.9
0.15	422	55.6	6.7
0.20	485	56.6	7.1
0.25	503	58.5	7.8
0.30	519	58.1	8.7
0.35	536	60.7	9.1
	OADe		
0.05	264	50.5	5.9
0.10	354	55.6	6.6
0.15	407	60.3	7.1
0.20	485	60.6	7.6
0.25	520	61.3	8.1
0.30	537	64.1	9.1
0.35	598	64.1	9.4
	OAD		
0.05	305	54.7	6.3
0.10	304	54.7	6.9
0.15	388	62.7	7.5
0.20	432	62.7	8.3
0.25	458	60.3	9.2
0.30	511	64.7	9.7
0.35	486	61.3	10.6
	OAT		
0.05	282	48.1	6.7
0.10	331	54.6	7.5
0.15	349	54.7	8.1
0.20	443	58.5	9.0
0.25	483	54.5	9.6
0.30	468	60.3	10.1
0.35	492	64.1	10.9

and, furthermore, rewritten by Eq. 4 to be

$$\tau^{-1} = k_{-1}([S_n]/[S]+2). \quad (6)$$

With the relationship between the micelle concentration, $[S_n]$, and the overall concentration, C, of detergent,

$$[S_n] = \frac{C-[S]}{2n}, \quad (7)$$

Eq. 6 is rewritten as follows:

$$\tau^{-1} = k_{-1}\left\{\frac{C}{2n[S]}+\left(2-\frac{1}{2n}\right)\right\}. \quad (8)$$

The plots of the experimental data, τ^{-1} *vs.* C, are shown in Fig. 3. The fact that these points form a straight line indicates that the present absorption is based on Reaction 3. The values of k_{-1} and n were determined from the slope and the intercept of the straight line, respectively, and k_1 was calculated from k_{-1} and the equilibrium constant by Eq. 4. The values obtained are listed in Table 2.

Attribution of the absorption to Reaction 3 was further examined from the standpoint of absorption am-

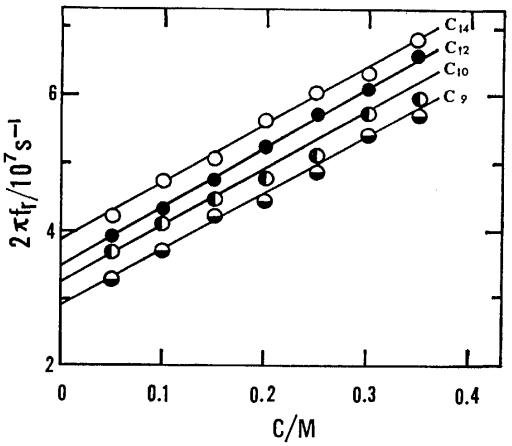

Fig. 3. Concentration dependence of the relaxation frequencies of detergent in hexane at 30 °C.

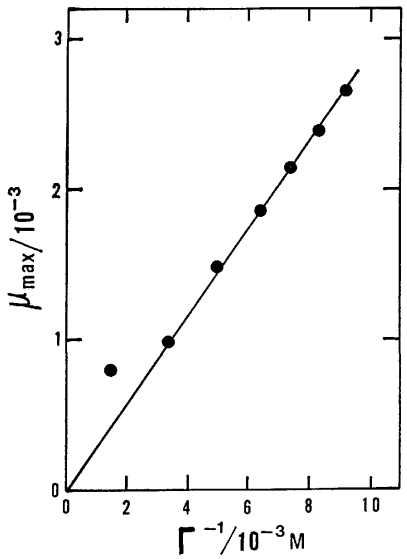

Fig. 4. The plot of μ_{max} *vs.* Γ^{-1} for OAN in hexane at 30 °C.
The solid line represents the theoretical curve calculated by Eq. 9 using the parameters in Table 2.

plitude. The relaxation absorption per wavelength, μ_{max}, is expressed by

$$\mu_{max} = \frac{\pi\rho C^2}{2RT}\left(\Delta V - \frac{\alpha}{\rho C_p}\Delta H\right)^2 \Gamma^{-1}, \quad (9)$$

with

$$\Gamma = \frac{1}{[S]} + \frac{1}{[S_n]} + \frac{1}{[S_{n+1}]}, \quad (10)$$

where ρ is the density, C the sound velocity, α the thermal expansion coefficient, C_p the specific heat at constant pressure and ΔV and ΔH are the standard volume change and the enthalpy change of the reaction, respectively. Since the values in the parentheses are constant for a reaction, the plot of μ_{max} *vs.* Γ^{-1} will give a straight line which goes through the origin of the coordinates. The plots for OAN are shown in Fig. 4. Similar plots were obtained for OADe, OAD, and OAT. These results are in agreement with the above prediction, and suggest that the

Table 2. Physicochemical parameters of the micelle and the association-dissociation of the monomer to and from the micelle

Detergent	CMC / M	n	k_1 / 10^8 M^{-1} s^{-1}	k_{-1} / 10^7 s^{-1}	ΔH / kcal M^{-1}
OAN	0.02	4.8	7.6	1.5	−4.9
OADe	0.02	5.3	8.6	1.7	−5.1
OAD	0.02	5.4	9.2	1.8	−5.2
OAT	0.02	5.9	10.1	2.0	−5.4

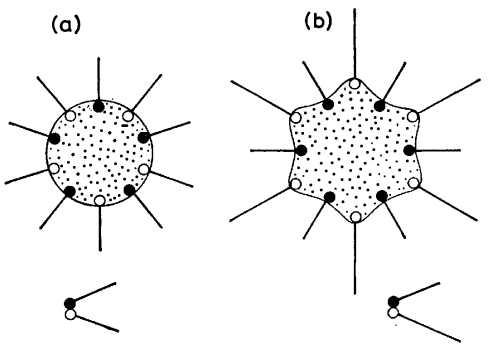

Fig. 5. Schematic representations of the reversed micelles and the monomers in hexane: (a) OAN, (b) OAT, (●——) octylammonium, and (○——) alkanoate.
The dotted region means the polar core.

present relaxation absorption is based on the association-dissociation of the monomer to and from the micelle. Additional support of this assignment of the relaxation absorption will be given by the fact that the time constant of the present system falls in the range of the reported lifetime of the detergent monomers in the presence of the higher aggregates in nonpolar solvents: *i.e.*, 10^{-5}—10^{-8} s.[14]

For the reactions in organic solutions, the ΔV term is usually much smaller than the ΔH term because of the small value of ΔV and the large value of $\alpha/\rho C_p$ in the ΔH term.[15] Therefore, neglecting the ΔV term, ΔH value was obtained from the slope of the plot in Fig. 4 and is listed in Table 2.

As is well known, detergents in nonpolar solvents aggregate to form a reversed micelle, where the polar head groups locate around a polar solvent core which is often called the polar core, with the hydrocarbon chains directed outside to the solvent. Schematic second-order models of the reversed micelles of the present systems are shown in Fig. 5. In the case of OAN, since the alkyl chain length of alkanoate is about the same as that of ammonium, the lipophilic effects on them are of the same magnitude. Consequently, the surfaces of the micelle and the polar core will be as shown in Fig. 5 (a). On the other hand, in the case of OAT, the lipophilic effect on carboxylate is larger than that on ammonium. This fact will result in pulling the carboxylate out a little and enlarging the sizes of the polar core and the micelle, as shown in Fig. 5 (b). If we accept these pictures, we can attribute the increase of the aggregation number with increase of the chain length of the alkanoate, seen in Table

2, to the enlargement, or the variation of the shape, of the micelle.

Kinetics of the association-dissociation of the monomer to and from the micelle have been studied only in the aqueous solution.[16] The result indicated that there is a progressive decrease in both rate constants, k_1 and k_{-1}, with increasing the chain length of the detergent. The reason of the decrease of k_1 has been ascribed to the degree of packing, *i.e.*, how closely the monomer units are distributed on the surface of the micelle; that of k_{-1} has been thought to be due to the increase of cohesive forces between the hydrophobic ends.

These ideas were applied to the present system. With increase of the chain length of the alkanoate, the degree of packing in the micelle will decrease, in spite of the increase of the aggregation number, and therefore the detergent monomer can move into micelle more easily, *i.e.*, k_1 will increase. The increase of k_{-1} will be ascribed to the decrease of the electrostatic cohesive force between the polar head groups, which are packed less closely with increase of the chain length.

The chain length dependence of $|\Delta H|$ seems to be too small to develop a meaningful discussion now; we will attempt this after gathering the data for other surfactants in organic solvents.

References

1) E. Aniansson, S. Wail, M. Almgren, H. Hoffmann, I. Kielmann, W. Ulbricht, R. Zana, J. Lang, and C. Tondre, *J. Phys. Chem.*, **80**, 905 (1976).
2) T. Inoue, Y. Shibuya, and R. Shimozawa, *J. Colloid Interface Sci.*, **65**, 370 (1978).
3) S. Diekmann, *Ber. Bunsenges. Phys. Chem.*, **83**, 528 (1979).
4) J. Gettins, P. Jobling, M. Walsh, and E. Wyn-Jones, *J. Chem. Soc., Faraday Trans. 2*, **76**, 794 (1980).
5) A. Kitahara, "Cationic Surfactants," ed by E. Jungermann, Dekker, New York (1970).
6) J. Fendler and E. Fendler, "Catalysis in Micellar and Macromolecular Systems," Academic Press, New York (1975).
7) A. S. Kertes and H. Gutmann, "Surface and Colloid Science," ed by E. Matijevic, Wiley, New York (1976), Vol. 8, Chap. 3.
8) "Micellization, Solubilization, and Microemulsions," ed by K. Mittal, Plenum Press, New York and London (1977), Vols. 1 and 2.
9) K. Tamura and Z. Schelly, *J. Am. Chem. Soc.*, **103**, 1018 (1981).
10) A. Kitahara, *Bull. Chem. Soc. Jpn.*, **28**, 234 (1955).
11) E. Fendler, J. Fendler, R. Medary, and O. El Seoud, *J. Phys. Chem.*, **77**, 1432 (1973).
12) N. Tatsumoto, *J. Chem. Phys.*, **47**, 4561 (1967).
13) J. Fendler, E. Fendler, R. Medary, and O. El Seoud, *J. Chem. Soc., Faraday Trans. 1*, **69**, 280 (1973).
14) J. Fendler, *Acc. Chem. Res.*, **9**, 153 (1976).
15) M. Eigen and L. DeMayer, "Technique of Organic Chemistry," 2nd ed, ed by S. Friess, E. Lewis, and A. Weissberger, Interscience, New York (1963), Vol. 8, Part 2, Chap. 18.
16) J. Rassing, P. Sams, and E. Wyn-Jones, *J. Chem. Soc., Faraday Trans. 2*, **70**, 1247 (1974).

 © 1982 The Chemical Society of Japan Bull. Chem. Soc. Jpn., 55, 3407—3412 (1982)

Polarized Absorption Spectra of Aromatic Radicals in Stretched Polymer Film. IV. Radical Ions of 9-Substituted Anthracenes

Hiroshi HIRATSUKA,* Hitoshi NAKAMURA, Yoshie TANIZAKI,† and Keihachiro NAKAJIMA

Department of Chemistry, Faculty of Science, Tokyo Institute of Technology, Ohokayama, Meguro-ku, Tokyo 152

(Received April 22, 1982)

Radical ions of some 9-substituted anthracene derivatives have been prepared in polymer film by γ-irradiation at 77 K. By use of the polarized absorption spectra of these radical ions, the absorption spectra have been resolved into two components (resolved spectra), the transition moments of which are polarized parallel to the molecular long and short axes, respectively. Correlation of the characteristic absorption bands is discussed briefly.

In previous papers we have shown that the stretched film technique combined with γ-irradiation is available for the polarization measurement of the radical ions of anthracene and pyrene,[1] and acridine and phenazine.[2] By qualitative analysis of the polarized absorption spectra, the polarization direction of the electronic transition band was determined and the assignments of the bands were carried out for these radical ions.

We note here the efficient preparation method for the radical ions in the films. Radical anions are produced by γ-irradiation of the poly(vinyl alcohol) film containing the solvent *s*-butylamine and the solute aromatic molecule (PVA–BuA system). For the preparation of the cation, a poly(vinyl chloride) film containing *s*-butyl chloride and aromatic molecule is irradiated (PVC–BuCl system). In order to remove the absorption due to solvated electron or positive hole, it is essential to dope the film with enough solute ($\approx 10^{-2}$ mol dm^{-3}).

In this paper we apply this method to 9-substituted anthracenes and examine the applicability of the method. Furthermore, stretched films were used and the polarized absorption spectra of the radical ions were determined and analyzed quantitatively. The resultant resolved spectra are used to discuss the correlation of the electronic transition bands in the visible region.

Experimental

Commercially available reagents, 9-methylanthracene (G.R. grade of Tokyo Kasei Co. Ltd.) and 9-bromo-, 9-nitro-, and 9-cyanoanthracene (Aldrich Chemical Co., Inc.), were used. 9-Aminoanthracene was synthesized according to the literature.[3] Poly(vinyl alcohol) film (PVA), 0.2 mm thick, and poly(vinyl chloride) film (PVC), 0.18 mm thick, were employed as before.[1] Parent compounds were doped into PVA film with the aid of a solvent, *s*-butylamine (G.R. grade of Tokyo Kasei Co. Ltd.), and into PVC film by use of *s*-butyl chloride (G.R. grade of Tokyo Kasei Co. Ltd.). For the measurement of the polarized absorption spectra, sample films PVA and PVC were stretched 3 and 4 times, respectively. These films were irradiated by ^{60}Co γ-rays for 2 h at 77 K with a dose rate of 1.0×10^{6} rad/h. Absorption spectra were measured in the range from 300 to 850 nm with a JASCO SS-50 spectrophotometer equipped with a Rochon polarizer. MO calculations were carried out for the radical ions after Zahradník and Čársky.[4] Parameters used were taken from Ishitani and Nagakura.[5]

† Present address: The Department of Materials Science and Technology, Technological University of Nagaoka, Nagaoka, Niigata 949-54.

Results and Discussion

Identification of the Absorption Spectra. 9-Methylanthracene: Figures 1a and 1b show the absorption spectra of the γ-irradiated PVA–BuA and PVC–BuCl systems of 9-methylanthracene, respectively. Dodd has reported that the characteristic absorption maxima of the 9-methylanthracene radical anion and the cation are respectively at 13750 cm^{-1} in tetrahydrofuran and at 14050 cm^{-1} in boric acid glass.[6] These maxima are well correspondent to the absorption peak at 13.7×10^{3} cm^{-1} in Fig. 1a and that at 14.2×10^{3} cm^{-1} in Fig. 1b. In addition to this, these spectra resemble strongly those of the anthracene radical anion ($A^{-\cdot}$) and the cation ($A^{+\cdot}$) in the same systems.[1] Therefore the spectra of Figs. 1a and 1b are attributed to the 9-methylanthracene radical anion ($MA^{-\cdot}$) and the cation ($MA^{+\cdot}$), respectively.

9-Bromoanthracene: Figures 1c and 1d show the absorption spectra of the γ-irradiated PVA–BuA and the PVC–BuCl systems of 9-bromoanthracene, respectively. These spectra are similar to those of the 9-bromoanthracene radical anion ($BA^{-\cdot}$) in an organic glass[7]

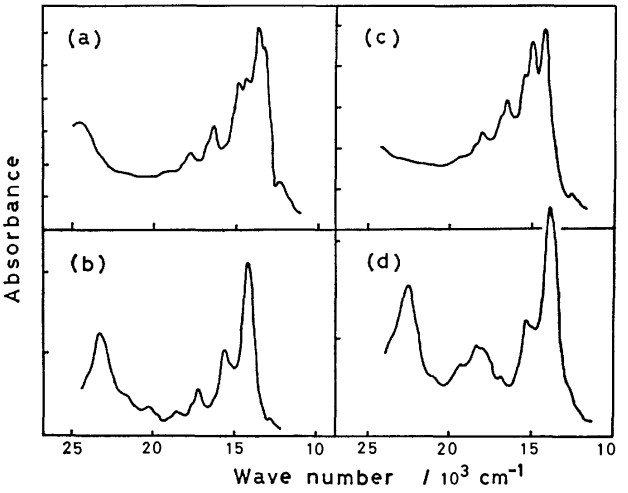

Fig. 1. Absorption spectra of 9-methylanthracene in the γ-irradiated PVA (a) and PVC (b) films, and 9-bromoanthracene in the irradiated PVA (c) and PVC (d) films, respectively.

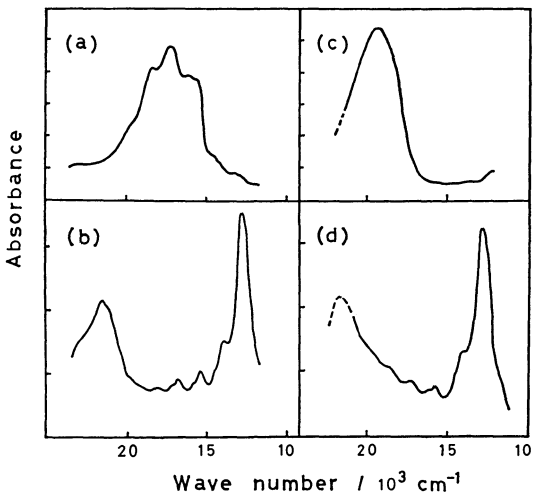

Fig. 2. Absorption spectra of 9-cyanoanthracene in the γ-irradiated PVA (a) and PVC (b) films, and 9-nitroanthracene in the irradiated PVA (c) and PVC (d) films, respectively.

and of the cation ($BA^{+\cdot}$) in a glass of 1:4 butyl chloride–methylcyclohexane.[8] Therefore, the absorption spectra of the PVA–BuA and PVC–BuCl systems are ascribed to $BA^{-\cdot}$ and $BA^{+\cdot}$, respectively.

9-Cyano-, 9-Nitro-, and 9-Aminoanthracene: Figures 2a and 2c show the absorption spectra of 9-cyano- and 9-nitroanthracene in the γ-irradiated PVA–BuA system, respectively. The spectrum of Fig. 2a resembles that of the 9-cyanoanthracene radical anion ($CA^{-\cdot}$) in dimethoxyethane, reported by Panayotov and Tsvetanov,[9] and is attributed to $CA^{-\cdot}$. The spectrum of Fig. 2c is quite different from those of $A^{-\cdot}$, $MA^{-\cdot}$, $BA^{-\cdot}$, and $CA^{-\cdot}$. As is shown in the following section, however, the resolved spectra (Fig. 5) are reasonably explained by the result calculated for the 9-nitroanthracene radical anion ($NA^{-\cdot}$). Therefore this spectrum is attributed to $NA^{-\cdot}$.

Figures 2b, 2d, and 6a show the resultant absorption spectra of 9-cyano-, 9-nitro-, and 9-aminoanthracene in the γ-irradiated PVC–BuCl systems, respectively. The former two spectra are similar to each other and also to those of $A^{+\cdot}$ and $MA^{+\cdot}$. These spectra are explained by MO calculations on the corresponding radical cations and are ascribed to their radical cations, $CA^{+\cdot}$ and $NA^{+\cdot}$. The spectrum of Fig. 6a is different from those of the other 9-substituted anthracene cations. The MO calculation for the 9-aminoanthracene radical cation ($AA^{+\cdot}$), however, explains this spectrum. Hence, this is attributed to $AA^{+\cdot}$.

Resolved Spectra. According to the symmetry of the 9-substituted anthracenes, the $\pi^*\leftarrow\pi$ electronic transition should be polarized parallel to the long or short axis in the molecular plane. By use of the polarized absorption spectra, the absorption spectrum can be resolved into two components (resolved spectra), the transition moments of which are polarized along the long and short axes.

The absorption spectrum of the symmetric and stable molecule in the PVA film can be resolved by the so-called one-parameter method developed by one of us (Y. Tanizaki).[10] This method requires the values of the stretch ratio (Rs) of the film and the dichroic ratio ($Rd:=A_{//}/A_{\perp}$). In our experiment, however, we could not determine the Rs value in the same manner as for the stable molecule because a considerable amount of the solvent, *s*-butylamine or *s*-butyl chloride, is reserved in the film for efficient preparation of the radical ions. Therefore the one-parameter method is not applicable to our case. Instead, the two-parameter method proposed by Margulies and Yogev is applied.[11] This method requires two extreme Rd values of the pure long and short axis polarized transition bands. This may be considered to be a special case of the method given by Thulstrup *et al.*[12]

The resolved spectra, A_l and A_s, are obtained by resolving the absorption spectrum A according to the following equations:

$$A_l = \frac{Rd-Rd^s}{Rd^l-Rd^s}\cdot\frac{Rd^l+2}{Rd+2}\cdot A$$

$$A_s = \frac{Rd^l-Rd}{Rd^l-Rd^s}\cdot\frac{Rd^s+2}{Rd+2}\cdot A,$$

where Rd^l and Rd^s are two extreme Rd values of the pure long and short axis polarized bands, respectively. These equations are equivalent to Eqs. 42 and 43 of Ref. 11.

In the case of the anthracenes discussed here, the long and short axes are respectively the Y and Z axes, and A_l and A_s are written as A_Y and A_Z. In the following discussion the resultant resolved spectra (A_Y and A_Z) are shown without showing the polarized absorption spectra.

As shown in Figs. 1 and 2, the absorption spectra of 9-substituted anthracenes resemble each other, except for $CA^{-\cdot}$, $NA^{-\cdot}$, and $AA^{+\cdot}$. There are characteristic bands in the region $(13—14)\times10^3$ cm^{-1} and $(22—24)\times10^3$ cm^{-1}. Considering the Rd curve behavior and the results of MO calculations, these bands are respectively assigned to Y and Z axis polarized transitions.[1] These absorption bands, however, are overlapped with other weak transition bands and are not considered to be "pure electronic transition bands." In order to calculate the resolved spectra, several sets of parameters (Rd^l and Rd^s) have been chosen by reference to the Rd values of these bands. A similar procedure has been taken for the cases of $CA^{-\cdot}$, $NA^{-\cdot}$ and $AA^{+\cdot}$. For these parameter sets, no marked changes were seen in the characteristics of the resolved spectra. Therefore one of the representative results is presented for each radical ion. These are shown in Figs. 3—6.

Anthracene: Figures 3a and 3b show the resolved spectra of $A^{-\cdot}$ and $A^{+\cdot}$. These are obtained by use of the polarized absorption spectra reported previously (Figs. 3 and 4 in Ref. 1). These resemble each other and are well explained by the calculated results shown at the bottom. For example, the intense A_Y band at 13.7×10^3 cm^{-1} and A_Z band at 24.7×10^3 cm^{-1} of $A^{-\cdot}$ are assigned to $^2B_{1g}\leftarrow{}^2B_{3u}$ and $^2B_{2g}\leftarrow{}^2B_{3u}$ transitions, respectively. The very weak absorption below 13.0×10^3 cm^{-1} is ascribed to the forbidden transition ($^2A_u\leftarrow{}^2B_{3u}$). In addition to these bands, a relatively weak

A_z band is clearly distinguished in the region (15—20) $\times 10^3$ cm^{-1}. This is assigned to the first $^2B_{2g} \leftarrow {}^2B_{3u}$ transition, as has been predicted in the previous paper.[1] Similar assignments are carried out for $A^{+\cdot}$ and these results are summarized in Table 1.

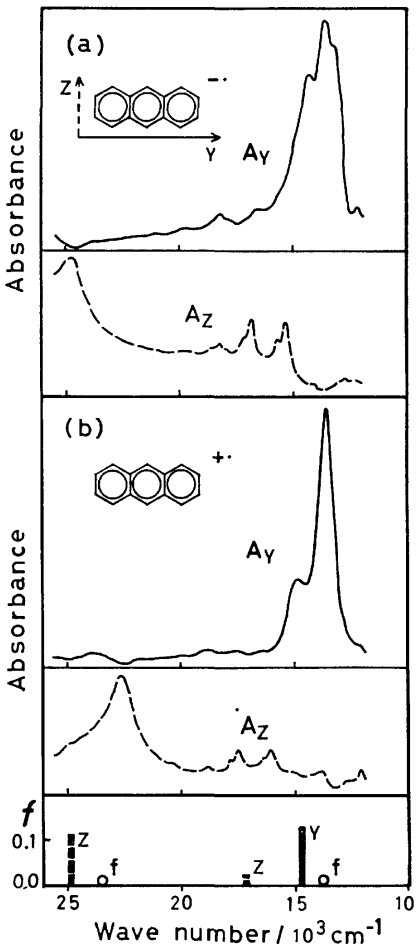

Fig. 3. Resolved spectra of anthracene radical anion (a) and cation (b).
Rd^l and Rd^s values used are 2.85 and 0.89 for (a), and 1.75 and 0.89 for (b), respectively. A_Y and A_Z represent the components polarized parallel to the long and short axes, respectively. Calculated results are shown in the bottom, where f means forbidden transition.

9-Methyl- and 9-Bromoanthracene: Figures 4a and 4b show the resolved spectra of $MA^{-\cdot}$ and $MA^{+\cdot}$. These spectra are very similar to those of $A^{-\cdot}$ and $A^{+\cdot}$. In the A_Z spectrum of $MA^{+\cdot}$, a weak band is found in the region (20—22) $\times 10^3$ cm^{-1} in addition to the characteristic bands. This is related to the second forbidden transition of $A^{+\cdot}$.

Figures 4c and 4d show the resolved spectra of $BA^{-\cdot}$ and $BA^{+\cdot}$. These spectra are also similar to those of $A^{-\cdot}$ and $A^{+\cdot}$, respectively. In A_Z spectrum of $BA^{+\cdot}$, an extra absorption appears in the region (17—21) $\times 10^3$ cm^{-1}. But we are not yet able to assign this band.

9-Cyano- and 9-Nitroanthracene: Figures 5a and 5b show the resolved spectra of $CA^{-\cdot}$ and $CA^{+\cdot}$. The calculated results for these ions are also shown at the bottom. Spectra of $CA^{+\cdot}$ resemble those of $A^{+\cdot}$, while those of $CA^{-\cdot}$ are rather different from those of $A^{-\cdot}$. The latter spectra are explained by the calculated result as follows. The first weak A_Y band below 15 $\times 10^3$ cm^{-1} is assigned to the first Y-polarized transition.

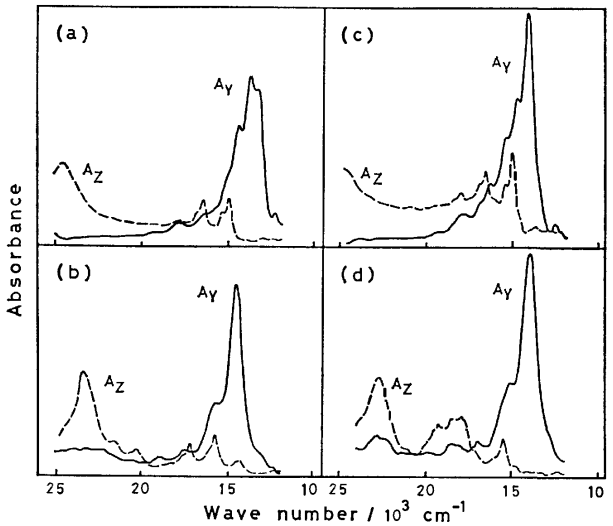

Fig. 4. Resolved spectra of 9-methylanthracene radical anion (a) (Rd^l=1.95, Rd^s=0.95) and cation (b) (1.65, 0.99), and 9-bromoanthracene anion (c) (2.10, 0.98) and cation (d) (1.41, 0.99).

Table 1. Calculated and experimental results for anthracene radical ions[a]

	Transition energy ($\times 10^3$ cm^{-1})			Polarization[b]			Symmetry		Oscillator strength (Calcd)
	Calcd	Obsd		Calcd	Obsd				
		Anion[c]	Cation[d]		Anion	Cation	Anion	Cation	
1	13.7	<13.0	<13.0	f			Au	B_{1g}	0.000
2	14.7	13.7	13.6	Y	Y	Y	B_{1g}	A_u	0.131
3	17.1	15.4	16.0	Z	Z	Z	B_{2g}	B_{3u}	0.023
4	23.5			f			B_{3u}	B_{2g}	0.000
5	24.8	24.7	22.6	Z	Z	Z	B_{2g}	B_{3u}	0.114
6	26.7			f			A_u	B_{1g}	0.000

a) Calculated result is available for the radical anion and cation. b) Y and Z are molecular long and short axes, respectively; f means that the transition is forbidden. c) In γ-irradiated poly(vinyl alcohol) film. d) In γ-irradiated poly(vinyl chloride) film.

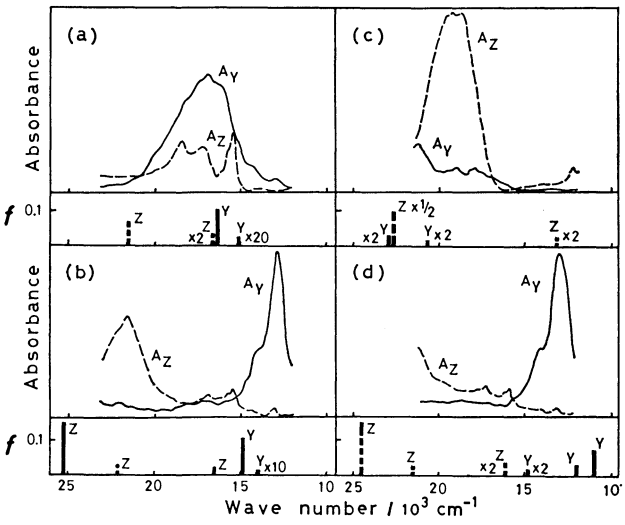

Fig. 5. Resolved spectra of 9-cyanoanthracene radical anion (a) ($Rd^l=1.68$, $Rd^s=0.99$) and cation (b) (1.51, 0.99), and 9-nitroanthracene anion (c) (1.20, 0.88) and cation (d) (1.44, 0.99). Calculated results are shown in the bottom.

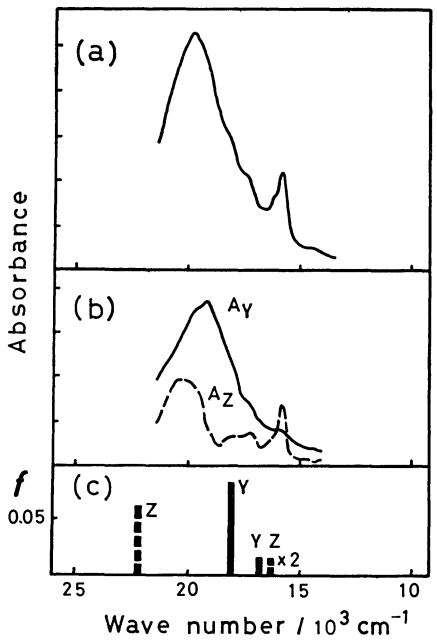

Fig. 6. Absorption spectrum of 9-aminoanthracene in the γ-irradiated PVC film (a) and its resolved spectra (b) ($Rd^l=1.42$, $Rd^s=0.90$).
Calculated results are shown in the bottom.

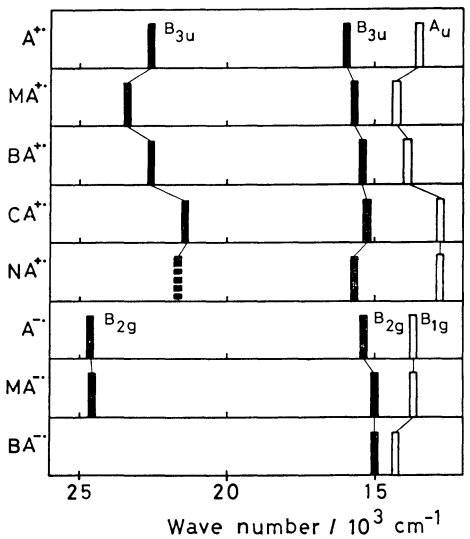

Fig. 7. Correlation diagram of the characteristic absorption bands of 9-substituted anthracenes in the visible region.
Full and open columns represent the short axis- and long axis-polarized transition bands, respectively.

The sharp A_Z peak at 15.5×10^3 cm^{-1} should be assigned to the first Z-polarized transition. The broad intense A_Y band in the region $(15—20)\times10^3$ cm^{-1} is ascribed to the second Y-polarized transition. The A_Z peak at about 18.5×10^3 cm^{-1} is tentatively assigned to the second Z-polarized transition.

Figures 5c and 5d show the resolved spectra of NA$^{-\cdot}$ and NA$^{+\cdot}$. Spectral characteristics of NA$^{+\cdot}$ are similar to those of A$^{+\cdot}$, while those of NA$^{-\cdot}$ are quite different from those of other anions. The NA$^{-\cdot}$ spectra are, however, analyzed based on the result calculated for NA$^{-\cdot}$ as follows. The A_Z band below 15×10^3 cm^{-1} and the intense A_Z band in the region $(17—21)\times10^3$ cm^{-1} are assigned to the first and the second Z-polarized transitions. The A_Y band in the region $(16—20)\times10^3$ cm^{-1} and that above 20×10^3 cm^{-1} are assigned to the first and the second Y-polarized transitions. Thus the spectrum of Fig. 2c is reasonably attributed to NA$^{-\cdot}$.

9-Aminoanthracene: Figure 6b shows the resolved spectra of AA$^{+\cdot}$. These spectra are quite different from those of other cations. These are explained by the calculated result as follows. The A_Y band below 17×10^3 cm^{-1} and the intense A_Y band in the region $(17—21)\times10^3$ cm^{-1} are ascribed to the first and the second Y-polarized transitions. A_Z bands in the region $(15.5—18)\times10^3$ cm^{-1} and at about 20×10^3 cm^{-1} are attributed to the first and the second Z-polarized transitions.

Correlation of Electronic Transition Bands. As is discussed in the section about the resolved spectra, the three characteristic absorption bands of anthracene radical ions are correlated respectively to those of the substituted anthracene ions. This situation is shown in Fig. 7, where full and open columns represent the A_Y and A_Z bands, respectively. Their positions show the absorption maximum or first peak of the bands. The spectra of CA$^{-\cdot}$, NA$^{-\cdot}$, and AA$^{+\cdot}$ have a different appearance than those of other ions. Therefore the electronic transitions of these ions are discussed qualitatively by making reference to SCF MO's of A$^{-\cdot}$ and A$^{+\cdot}$.

SCF MO's related to the visible absorptions of CA$^{-\cdot}$ and NA$^{-\cdot}$ are shown in Fig. 8, and are correlated with those of A$^{-\cdot}$. The correlation of MO's of CA$^{-\cdot}$ (or NA$^{-\cdot}$) with those of A$^{-\cdot}$ is obtained by expanding the wavefunctions of CA$^{-\cdot}$ (or NA$^{-\cdot}$) by those of A$^{-\cdot}$ and substituent group, as follows:

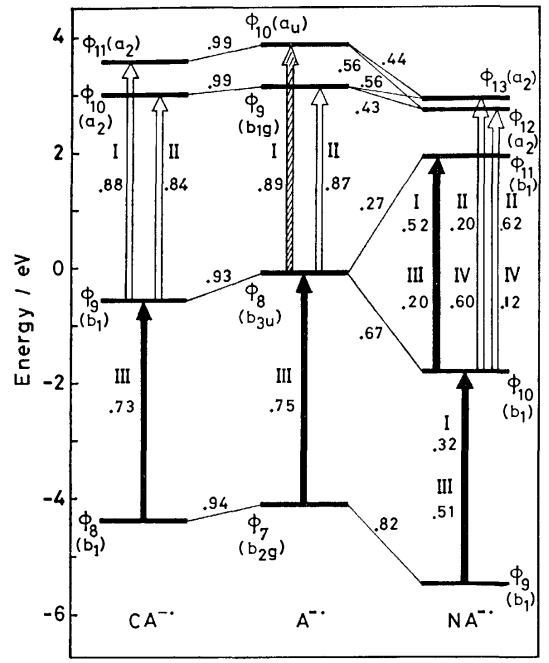

Fig. 8. Correlation diagram of MO's of 9-cyano and 9-nitroanthracene radical anions ($CA^{-\cdot}$ and $NA^{-\cdot}$) with those of anthracene radical anion ($A^{-\cdot}$). The figures along the joining fine lines are contribution weight from the MO's of $A^{-\cdot}$ to those of $CA^{-\cdot}$ and $NA^{-\cdot}$. The figures along the vertical arrows are contribution weight from the configuration to each transition. See text.

$$\phi_1(CA^{-\cdot} \text{ or } NA^{-\cdot}) = \sum_m C_m^1 \phi_m(A^{-\cdot}) + \sum_n C_n^1 \phi_n(CN \text{ or } NO_2).$$

Contribution of ϕ_m ($A^{-\cdot}$) to $\phi_1(CA^{-\cdot}$ or $NA^{-\cdot})$ is given by the square of the coefficient, $(C_m^1)^2$. These values are shown along the correlating lines between MO's.

It is found that ϕ_8, ϕ_9, ϕ_{10}, and ϕ_{11} of $CA^{-\cdot}$ are well correlated to ϕ_7, ϕ_8, ϕ_9, and ϕ_{10} of $A^{-\cdot}$, respectively. The contribution of CN group-MO is less than 7% for these MO's. These MO's are related to the main configurations of the visible transitions of $CA^{-\cdot}$ and $A^{-\cdot}$ as follows:

$$\Psi_I(A^{-\cdot}) = (0.89)^{1/2}\Phi_{8-10} + \cdots \quad (^2A_u \leftarrow {}^2B_{3u})$$
$$\Psi_{II}(A^{-\cdot}) = (0.87)^{1/2}\Phi_{8-9} + \cdots \quad (^2B_{1g} \leftarrow {}^2B_{3u})$$
$$\Psi_{III}(A^{-\cdot}) = (0.75)^{1/2}\Phi_{7-8} + \cdots \quad (^2B_{2g} \leftarrow {}^2B_{3u})$$
$$\Psi_I(CA^{-\cdot}) = (0.88)^{1/2}\Phi_{9-11} + \cdots$$
$$\Psi_{II}(CA^{-\cdot}) = (0.84)^{1/2}\Phi_{9-10} + \cdots$$
$$\Psi_{III}(CA^{-\cdot}) = (0.73)^{1/2}\Phi_{8-9} + \cdots .$$

Contributions of these configurations (squares of the coefficient) are also shown along the vertical transition arrows. Considering these contributions and correlation of MO's, it is understood that the first three transitions of $CA^{-\cdot}$ are well correlated with those of $A^{-\cdot}$. But it should be noticed here that the energy depression of $\phi_8(A^{-\cdot})$ is larger than those of the other MO's($A^{-\cdot}$) on CN group substitution. Therefore the transition energies of I and II transitions increase, while that of III decreases. As a result these transition bands overlap one another

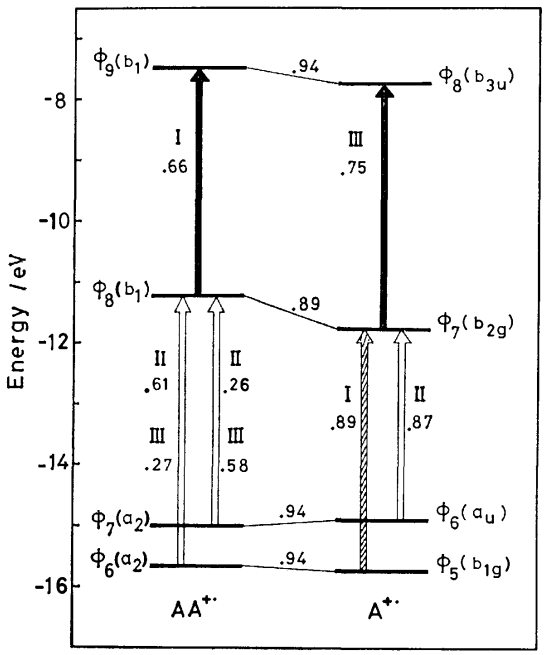

Fig. 9. Correlation diagram of MO's of 9-aminoanthracene ($AA^{+\cdot}$) and anthracene radical cations ($A^{+\cdot}$). See the captions of Fig. 8.

and the appearance of the $CA^{-\cdot}$ spectrum is different from those of other anions.

In the case of $NA^{-\cdot}$, the situation is quite different. The most characteristic point is the great participation of the vacant orbital of NO_2 in the visible transitions. Contributions from NO_2 vacant orbital to $\phi_9(NA^{-\cdot})$ and $\phi_{10}(NA^{-\cdot})$ are 12 and 17%, while that to $\phi_{11}(NA^{-\cdot})$ is 46%. This is caused by a strong coupling of the vacant NO_2 orbital with $\phi_8(A^{-\cdot})$. As a result, transition bands with quite different character appear in the spectrum of $NA^{-\cdot}$. The first four transitions are represented as follows:

$$\Psi_I(NA^{-\cdot}) = (0.52)^{1/2}\Phi_{10-11} + (0.32)^{1/2}\Phi_{9-11} + \cdots$$
$$\Psi_{II}(NA^{-\cdot}) = (0.62)^{1/2}\Phi_{10-12} + (0.20)^{1/2}\Phi_{10-13} + \cdots$$
$$\Psi_{III}(NA^{-\cdot}) = (0.51)^{1/2}\Phi_{9-10} + (0.20)^{1/2}\Phi_{10-11} + \cdots$$
$$\Psi_{IV}(NA^{-\cdot}) = (0.60)^{1/2}\Phi_{10-13} + (0.12)^{1/2}\Phi_{10-12} + \cdots .$$

Therefore I and III transition bands have the character of charge transfer state from anthracene to the nitro group.

The SCF MO diagram of $AA^{+\cdot}$ and $A^{+\cdot}$ is shown in Fig. 9. As in the case of $CA^{-\cdot}$, MO's of $AA^{+\cdot}$ are well correlated with those of $A^{+\cdot}$. Contributions of amino group to MO's of $AA^{+\cdot}$, ϕ_6—ϕ_9, are less than 11%. It should be noticed that the energy increase of $\phi_7(A^{+\cdot})$ is larger than those of other MO's($A^{+\cdot}$). Therefore, to a first approximation, energies of configurations $\Phi_{5-7}(A^{+\cdot})$ and $\Phi_{6-7}(A^{+\cdot})$ increase while that of $\Phi_{7-8}(A^{+\cdot})$ decreases. The MO's shown in Fig. 9 are related to first three transitions of $AA^{+\cdot}$ and $A^{+\cdot}$ as follows:

$$\Psi_I(A^{+\cdot}) = (0.89)^{1/2}\Phi_{5-7} + \cdots \quad (^2B_{1g} \leftarrow {}^2B_{2g})$$
$$\Psi_{II}(A^{+\cdot}) = (0.87)^{1/2}\Phi_{6-7} + \cdots \quad (^2A_u \leftarrow {}^2B_{2g})$$
$$\Psi_{III}(A^{+\cdot}) = (0.75)^{1/2}\Phi_{7-8} + \cdots \quad (^2B_{3u} \leftarrow {}^2B_{2g})$$

$$\Psi_{I}(AA^{+\cdot}) = (0.66)^{1/2}\Phi_{8-9} + \cdots$$

$$\Psi_{II}(AA^{+\cdot}) = (0.61)^{1/2}\Phi_{6-8} - (0.26)^{1/2}\Phi_{7-8} + \cdots$$

$$\Psi_{III}(AA^{+\cdot}) = (0.58)^{1/2}\Phi_{7-8} + (0.27)^{1/2}\Phi_{6-8} + \cdots.$$

Therefore I and II transition bands of $A^{+\cdot}$ shift to blue while III to red on amino group substitution. As a result these transition bands overlap one another. This situation can be understood by the resolved spectra of $AA^{+\cdot}$.

Conclusion

Radical anions and cations of 9-methyl-, 9-bromo-, 9-cyano-, and 9-nitroanthracene have been prepared by γ-irradiation of the PVA–BuA and PVC–BuCl systems of their parent compounds. Cations of 9-aminoanthracene have also been prepared in the PVC–BuCl system. The stretched film technique combined with γ-irradiation has been applied to these radical ions. Resolved spectra have been obtained by analyzing the polarized absorption spectra quantitatively.

The authors would like to thank Prof. Yuji Mori and Prof. Yoshihiko Hatano of Tokyo Institute of Technology, and Prof. Tadamasa Shida of Kyoto University for their valuable suggestions. This work was partially supported by a Grant-in-Aid for Scientific Research from the Ministry of Education, Science and Culture (No. 474215).

References

1) H. Hiratsuka and Y. Tanizaki, *J. Phys. Chem.*, **83**, 2501 (1979).
2) K. Sekiguchi, H. Hiratsuka, Y. Hatano, and Y. Tanizaki, *J. Phys. Chem.*, **84**, 452 (1980).
3) J. Meisenheimer and E. Connerade, *Ann. Chem.*, **330**, 165 (1903).
4) R. Zahradnik and P. Carsky, *J. Phys. Chem.*, **74**, 1235 (1970).
5) A. Ishitani and S. Nagakura, *Theor. Chim. Acta*, **4**, 236 (1966).
6) J. W. Dodd, *J. Chem. Soc., B*, **1971**, 2427.
7) T. Matsuyama and H. Yamaoka, *Annu. Rep. Res. React. Inst. Kyoto Univ.*, **7**, 29 (1974).
8) B. Badger and B. Brocklehurst, *Trans. Faraday Soc.*, **65**, 2588 (1969).
9) I. M. Panayotov and Ch. B. Tsvetanov, *Monatsh. Chem.*, **101**, 1672 (1970).
10) Y. Tanizaki and S. Kubodera, *J. Mol. Spectrosc.*, **24**, 1 (1967); Y. Tanizaki, T. Yoshinaga, and H. Hiratsuka, *Spectrochim. Acta, Part A*, **34**, 205 (1978).
11) L. Margulies and A. Yogev, *Chem. Phys.*, **27**, 89 (1978).
12) E. W. Thulstrup, J. Michl, and J. H. Eggars, *J. Phys. Chem.*, **74**, 3808 (1970).

 © 1982 The Chemical Society of Japan Bull. Chem. Soc. Jpn., 55, 3413—3416 (1982)

A Kinetic Study of Poly(acrylic acid)–Copper(II) Interactions in Aqueous Solutions

Ryuichi YAMADA, Kiyoshi TAMURA, Shoji HARADA,† and Tatsuya YASUNAGA†,*

Department of Chemistry, National Defense Academy, Hashirimizu 1-10-20, Yokosuka 239

†*Department of Chemistry, Faculty of Science, Hiroshima University, Higashisenda-machi 1-1-89, Naka-ku, Hiroshima 730*

(Received April 30, 1982)

Concentration-jump kinetic studies of the aqueous poly(acrylic acid)–copper(II) system reveal the presence of a relaxation phenomenon in the time range of 10^2 ms. Kinetic data under various pH's and compositions, together with the potentiometric results, indicate that this relaxation effect is due to the following complex-formation reaction:

$$CuL_2 + L_2^{2-} \underset{k_{-2}}{\overset{k_2}{\rightleftharpoons}} Cu(L_2)_2^{2-},$$

where L_2^{2-} is a coordination unit consisting of two adjacent carboxylato side groups on the polymer chain. The specific features of the pH dependence of the τ^{-1} value are discussed in relation to the degree of dissociation of the carboxyl groups. The rate and stability constants of the reaction are determined to be: $k_2 = 5.6 \times 10^3$ M^{-1} s^{-1} (1 M = 1 mol dm^{-3}), $k_{-2} = 0.7$ s^{-1}, and K_2 $(= k_2/k_{-2}) = 7.9 \times 10^3$, at pH 7.0, $I \approx 0$, and 25 °C. The overall complex-formation mechanism, involving the very rapid formation of CuL_2, is discussed.

The metal–polymer complex has been the subject of increasing interest recently[1–3] in the fields of the coordination chemistry, biochemistry, and industrial applications. Although there has been a considerable accumulation of experimental results available about metal–polymer systems, most of them have been limited to the equilibrium properties of the systems (based on the measurements by spectrophotometry, potentiometry, ESR, viscosity, and so on) or their catalytic effects. Only a few kinetic studies[4,5] of metal–polymer interactions have been done up to the present.

In the present work, we studied the kinetics of the poly(acrylic acid)–copper(II) system, since the polymer is one of the simplest polyelectrolytes consisting of a uniform arrangement of carboxyl groups and since the nature of the system has been comparatively well known.[6–11] The stopped-flow experiments on this system revealed the presence of a relaxation effect in the time range of 10^2 ms; this is slower by almost three orders of magnitude than the temperature-jump relaxation phenomenon reported in the same system.[4] The relaxation effect is also unusually slow compared with those for the complex formation of copper(II) with simple ligands.[12] The apparent slowness may reflect the restriction of the movement of the side groups on the polymer as well as electrostatic repulsions between the polymer chains. It is the purpose of this work to elucidate the metal–polymer interactions through the kinetic treatment of the relaxation process. The kinetic information obtained will be helpful in understanding the dynamic behavior of metal–polymer systems.

Experimental

Materials. Poly(sodium acrylate), abbreviated as NaPAA, was synthesized[13] from acrylic acid of a reagent grade (Wako Pure Chem., Ltd.), dialized against deionized-distilled water, lyophilized, and finally vacuum-dried at 60 °C for 12 h. The degree of polymerization was determined to be 1400 from the intrinsic viscosity in 2 M NaOH solution.[14] All the other chemicals were of a reagent grade and were used without further purification.

Sample solutions were prepared from aqueous stock solutions of 0.1 M $CuSO_4$ and 0.1 M NaPAA. Here and hereafter, the concentration of NaPAA (or PAA) will be expressed by the residue mole. The pH of the solutions was controlled with NaOH. No neutral salt was added to the solutions; thus, all the experiments were carried out under an approximately zero ionic strength ($I \approx 0$). Bromophenol Blue, Bromocresol Green, Methyl Red, and Bromocresol Purple were used as colorimetric pH-indicators for the kinetic measurements covering the pH range of 4—7. All the solutions were prepared by using deionized-distilled water.

Equilibrium Measurements. The absorption spectra in the UV range of 190—360 nm were recorded on an Union Giken SM-401 spectrophotometer equipped with a data-processing unit. Quartz cells with a path length of 10 mm were used. The concentration of free copper ions in PAA–copper solutions was potentiometrically determined by using a Hitachi-Horiba M-5 pH-meter equipped with a copper-ion electrode (Model 8006-05T).

Kinetic Measurement. The stopped-flow apparatus was a modification of the Union Giken gas pressure-driven type.[15] It was constructed by assembling a mixing unit (Union Giken UO-001) and an optical detection system. The optical path length of the observation cell, equipped with quartz windows, was 10 mm. The reaction signal (transmittance against the time) was stored in a digital memory and then recorded on an X-Y recorder. The dead time of the apparatus was 1.7 ms at a driving pressure of 5 atm and a mixing volume ratio of 1:1. The flow system was thermostatted at 25.0±0.5 °C.

Results and Discussion

The concentration-jump experiments were carried out by mixing the $CuSO_4$ solution (containing a pH-indicator) and the NaPAA solution. The pH's of both solutions were adjusted to appropriate values to give a definite pH value after mixing. The observed signal curves exhibited a single exponential time-dependence and enabled us to adopt the usual relaxation treatment. All the relaxation times, τ, quoted in this study are the means of several measurements; the maximum errors are about ±15%. A representative relaxation

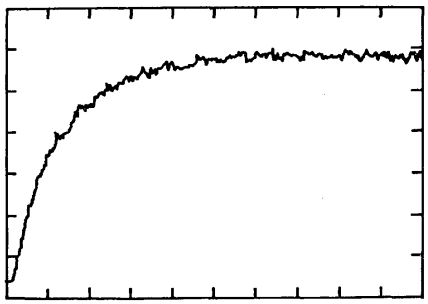

Fig. 1. Relaxation effect in the PAA–copper(II) system; ΣPAA$=1.25\times10^{-3}$ M, ΣCu$=1.25\times10^{-4}$ M, pH 7.0, and $I\approx0$, with 1.0×10^{-5} M Bromocresol Purple as an indicator.
The observation wavelength is 592 nm. The abscissa scale is 200 ms per division, and the vertical scale is in arbitrary unit of absorbance. The relaxation curve corresponds to a decrease in absorbance with time.

effect is shown in Fig. 1. Here, ΣPAA and ΣCu indicate the total concentrations of PAA and copper, respectively. The relaxation curve shows a decrease in the absorbance with the time, indicating a pH decrease due to the deprotonation from carboxyl groups on PAA. The deprotonation can be ascribed to the perturbation of the dissociation equilibrium of the acid groups induced by the complex formation of copper with PAA. Blank experiments of mixing solutions of PAA and an indicator or of diluting a copper-indicator solution with water showed no relaxation effect in the same time range. Therefore, the relaxation phenomenon observed is really to be associated with the PAA–copper interactions.

Additional concentration-jump experiments were carried out without using an indicator. The observation wavelength was 257 nm, at which the PAA–copper(II) system showed an absorption maximum due to complexation, while neither PAA nor copper exhibited any significant absorbance. The relaxation time measured was similar to the τ obtained for the sample with an indicator, but the signal amplitude was much smaller than that in the latter experiment. The relaxation curve showed an increase in the absorbance with the time, indicating the formation of PAA–copper complexes. The above results exhibit that the same phenomenon was observed by the two-type experiments. The presence of another reaction process, which is too fast to be observed by the stopped-flow apparatus, can be conjectured by a comparison of the observed signal amplitude with the total absorption change on mixing the PAA and copper solutions; the faster process contributes most of the absorbance change, while the slower observed process contributes only a small part of it.

Taking into account the results of the earlier equilibrium studies,[6–11] the PAA–copper complexation may proceed *via* the following reaction scheme:

$$\mathrm{Cu} + \mathrm{L_2} \underset{k_{-1}}{\overset{k_1}{\rightleftharpoons}} \mathrm{CuL_2}, \quad (1)$$

$$\mathrm{CuL_2} + \mathrm{L_2} \underset{k_{-2}}{\overset{k_2}{\rightleftharpoons}} \mathrm{Cu(L_2)_2}, \quad (2)$$

where the charges are omitted for the sake of simplicity and where L_2 denotes a coordination unit consisting of two adjacent carboxylato groups on a polymer chain. In the above reaction scheme, Eq. 1 is a very fast complex-formation reaction to which the temperature-jump relaxation effect has been ascribed.[4] Therefore, it may be reasonable to ascribe the rapid absorption change, which occurred within the dead time of the present concentration-jump experiments, to the CuL_2 complex formation through Eq. 1.

The result of the potentiometric measurements showed that almost all copper ions bind to PAA and that no free Cu^{2+} remains in the mixed solutions at the pH values higher than 4.5. Therefore, the observed relaxation effect is very likely attributable to the interactions involving uncomplexed carboxylato groups on PAA and copper ions already bound to the polymer sites, *i.e.*, Eq. 2. This assignment was supported by the pH dependence of the reciprocal relaxation time, τ^{-1}, for the solutions of 2.5×10^{-3} M ΣPAA and 2.5×10^{-4} M ΣCu (after mixing). Figure 2 shows the experimental results. In the low pH-region, the τ^{-1} increases with an increase in the pH. With a further increase in pH, the value of τ^{-1} attains its maximum at pH 5.3 and then finally decreases. If we ascribe the observed relaxation effect to Eq. 2, we can easily explain the above features of the pH dependence of τ^{-1}. When the pH increases, the deprotonation of the carboxyl group, HL, on PAA increases the concentration of the uncomplexed carboxylato group, L, resulting in an increase in the L_2 concentration. This effect causes an increase in the τ^{-1} in the lower pH-region. With a further increase in pH, the electrostatic repulsion caused by the high population of the uncomplexed carboxylato groups on PAA prevents the approach of the second coordination unit to form the $Cu(L_2)_2$ complex. This effect explains the decrease in

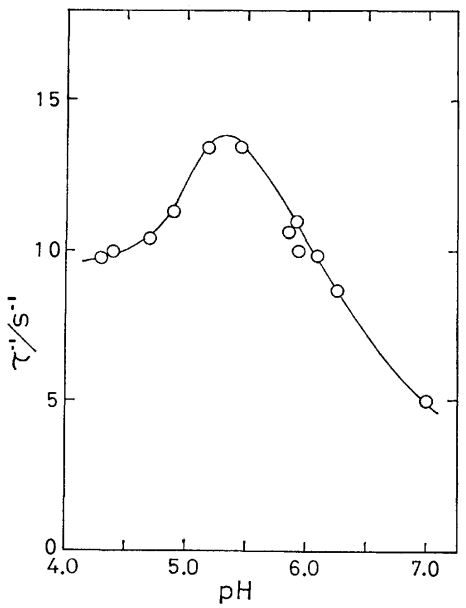

Fig. 2. The pH dependence of the relaxation time for the PAA–copper(II) system; ΣPAA$=2.50\times10^{-3}$ M and ΣCu$=2.50\times10^{-4}$ M, at 25 °C and $I\approx0$.

Table 1. Kinetic data for the PAA–copper(II) system[a] at 25 °C, $I \approx 0$, and pH 7.0

ΣPAA	ΣCu	R	τ^{-1}
10^{-3} M			s^{-1}
1.25	0.125	10	3.34
2.00	0.200	10	4.12
2.00	0.250	8	4.98
2.50	0.125	20	6.02
2.50	0.250	10	4.79
2.50	0.313	8	4.36
4.00	0.250	16	10.1
4.00	0.400	10	7.30
5.00	0.250	20	12.3
5.00	0.500	10	10.4

a) Solutions contain 1.0×10^{-5} M Bromocresol Purple as an indicator.

τ^{-1} observed in the higher pH-region.

Since the kinetic behavior of PAA varies so much with the pH, as has been described above, the kinetic experiments should be carried out at a constant pH for a quantitative analysis to be made. Thus, the concentration-jump experiments were carried out at pH 7.0 by varying the concentrations of both ΣPAA and ΣCu. The values of τ^{-1} thus obtained are listed in Table 1. The experimental data in Table 1 exhibit the following kinetic features: i) when the concentrations of the polymer (ΣPAA) and copper(II) (ΣCu) simultaneously increase under a constant mixing ratio R ($=\Sigma$PAA/ΣCu), the τ^{-1} value increases; ii) the value of τ^{-1} increases with an increase in the polymer concentration at a constant copper(II) concentration, and iii) it decreases with an increase in the copper(II) concentration at a constant polymer concentration.

Below, we will perform a relaxation analysis of the kinetic data in Table 1. From Eq. 2, the rate equation is given by;

$$d[Cu(L_2)_2]/dt = k_2[CuL_2][L_2] - k_{-2}[Cu(L_2)_2], \quad (3)$$

where the square brackets denote the molar concentrations. By assuming that the carboxyl group, HL, the uncomplexed carboxylato group, L, and the coordinated ligand-unit are randomly distributed over a polymer chain, the concentration of the uncoordinated ligand-unit, L_2, may be expressed in terms of the concentration [L] multiplied by the probability for one definite L to find another L at its adjacent position on the polymer:[16]

$$[L_2] = \frac{[L]^2}{[L]+[HL]+[CuL_2]+2[Cu(L_2)_2]}. \quad (4)$$

The protolytic reactions of acid groups on PAA and of the pH-indicator reach equilibrium much faster than the metal-complex reactions, and they can be assumed to be in equilibrium at all times of the relaxation process. Thus, we may use the equilibrium relations:

$$K_a = ([H][L]/[HL])z^{n-1}, \quad (5)$$

$$K_{In} = [H][In]/[HIn], \quad (6)$$

where In denotes the anionic form of the indicator; K_a and K_{In} are the dissociation constant of HL and that of the indicator, respectively. The quantity z in Eq. 5 is the ratio of the populations of charged to uncharged groups on the polymer.[7] Taking into account the metal complexation, it is given by:

$$z = \{[L]+2[Cu(L_2)_2]\}/\{[HL]+2[CuL_2]+2[Cu(L_2)_2]\}. \quad (7)$$

For the relaxation treatment of Eq. 2, the coupling effect of Eq. 1 can be ruled out, since the potentiometric results indicate that the concentration of the free copper(II) ion is negligibly small in the final equilibrium solutions. Thus, we have the conservation relations:

$$\Sigma Cu = [CuL_2] + [Cu(L_2)_2], \quad (8)$$

$$\Sigma PAA = [L] + [HL] + 2[CuL_2] + 4[Cu(L_2)_2]. \quad (9)$$

By expanding Eq. 3 in the vicinity of the equilibrium concentrations and by using Eqs. 4—9 together with the electroneutrality condition, the relaxation time is found to be:

$$1/\tau = k_2 B,$$

$$B = [CuL_2]\left(\frac{[L_2]}{[L]}\right)\left(\frac{4}{1+\alpha} - \frac{[L_2]}{[L]}\right) + [L_2] + \frac{1}{K_2}, \quad (10)$$

where K_2 ($=k_2/k_{-2}$) is the equilibrium constant of Eq. 2 and where:

$$\alpha = \frac{[H]}{\gamma[L]+K_a z^{1-n}+(n-1)(1+z)\beta},$$

$$\beta = \frac{[H][L]}{[L]+2[Cu(L_2)_2]}, \quad (11)$$

$$\gamma = \frac{K_{In}+[H]}{K_{In}+[H]+[In]}.$$

The quantity α expresses the contributions from the rapid protolytic reactions to the relaxation time. However, under the present experimental conditions, the values of α were less than 3×10^{-3}, too small to be significant in Eq. 1.

The experimental data in Table 1 were fitted to Eq. 10 by optimizing the adjustable parameters, K_2 and k_2, so as to minimize the root-mean-square percentage deviation between the calculated and observed values of τ^{-1}. The calculations were carried out using an iterative computer routine. As is shown in Fig. 3, the calculated τ^{-1} values agree fairly well with the experimental values (the r.m.s. % deviation=9.5). The K_2, k_2, and k_{-2} values thus determined are shown in Table 2, together with the equilibrium parameters used.

In relation to the $Cu(L_2)_2$ formation through Eq. 2, the following two possibilities may be considered.[10,11] One is the $Cu(L_2)_2$ complex formation *via* the intra-polymer reaction; the reacting CuL_2 and L_2 units lie on the same polymer chain, and the complex formation proceeds by means of the bending of the polymer chain. The other is the inter-polymer complex formation; the reacting CuL_2 and L_2 units lie on different polymer chains, and the reaction occurs by the approach of the two polymer chains. In the present kinetic treatment, we assumed, as a first approximation, the random distribution of the reacting units (*i.e.*, CuL_2 and L_2) in solution; thus, we could not discriminate the contributions from the two types of com-

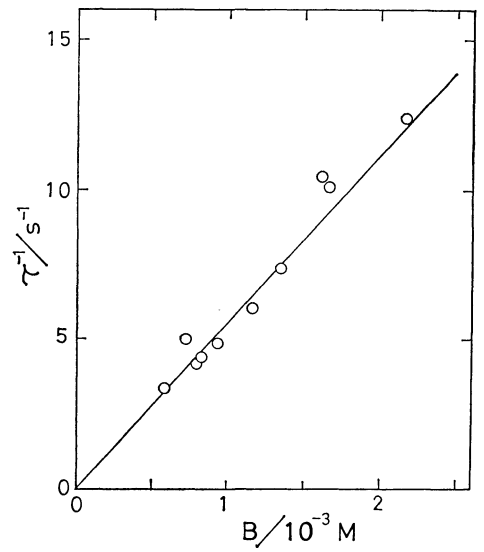

Fig. 3. τ^{-1} *vs.* B plot of the PAA-copper(II) system at 25 °C, $I \approx 0$, and pH 7.0.
The straight line expresses the τ^{-1} value calculated by Eq. 10 using the parameters in Table 2.

TABLE 2. EQUILIBRIUM PARAMETERS USED AND KINETIC RESULTS OBTAINED FOR THE PAA-COPPER(II) SYSTEM AT 25 °C, $I \approx 0$, AND pH 7.0

Formation constant of the $Cu(L_2)_2$ complex	$K_2=(7.9\pm3.3)\times10^3$ a)
Dissociation parameters of carboxyl group on PAA	$pK_a=6.17$ b) $n=2.0$ b)
Dissociation constant of Bromocresol Purple	$pK_{In}=6.42$ c)
Rate constants of the $Cu(L_2)_2$ complex formation	$k_2=(5.6\pm0.6)\times10^3\ M^{-1}\ s^{-1}$ a) $k_{-2}=0.7\pm0.3\ s^{-1}$ a)

a) This work. b) Ref. 7. c) Ref. 17.

plex formation. For a detailed treatment of the reaction mechanism, we need knowledge of the local distribution of the polymer sites in solution. Therefore, we must be satisfied at present with the determination of the overall rate constants, as given in Table 2.

The rate constant of the $Cu(L_2)_2$ formation (k_2 in Table 2) is by three to four orders of magnitude smaller than the formation-rate constant of CuL_2,[4] *i.e.*, $k_1=(0.93-1.7)\times10^8\ M^{-1}\ s^{-1}$, and also than those of the copper(II) complexes of simple ligands.[12] The unusually small value of k_2 may reflect the electrostatic repulsion between the negatively charged polymer chains, which prohibits the approach of the reacting units in either intra- or the inter-polymer complex formation. Here, it may be worthwhile to consider the reactivity of the polymer from another point of view. According to the Eigen mechanism,[12] the rate constant of the metal-complex formation is described in terms of the association constant, K_o, of the ion-pair formation and the first-order rate constant, k_o, of the water release from the inner-coordination sphere of the metal. Thus, by applying this idea to the present case, we obtain: $k_2=K_ok_o$. An oxygen-17 NMR study of the hexaaquacopper(II) ion[18] gave the rate constant of water exchange as: $k_o=2\times10^8\ s^{-1}$ (at 25 °C). A comparison of this value with that of k_2 obtained in this study gives an estimate for K_o of the extremely small value of 10^{-5}. This result also supports the strong hindrance of the approach of the reaction partners of CuL_2 and L_2.

References

1) S. L. Davydova and N. A. Plate, *Coord. Chem. Rev.*, **16**, 195 (1975).
2) "Kobunshi Kinzoku Sakutai," ed by T. Saegusa, E. Tsuchida, and H. Hirai, Kagakudojin, Tokyo (1978).
3) "Biological Systems as Viewed from Coordination Chemistry and Their Models," ed by the Chem. Soc. Jpn., Japan Scientific Societies Press, Tokyo (1978).
4) H. Nishikawa and E. Tsuchida, *Bull. Chem. Soc. Jpn.*, **49**, 1545 (1976).
5) E. Tsuchida and H. Nishikawa, *J. Polym. Sci., Polym. Chem. Ed.*, **14**, 1557 (1976).
6) F. T. Wall and S. J. Gill, *J. Phys. Chem.*, **58**, 1128 (1954).
7) H. P. Gregor, L. B. Luttinger, and E. M. Loebl, *J. Phys. Chem.*, **59**, 34, 366 (1955).
8) A. M. Kotliar and H. Morawetz, *J. Am. Chem. Soc.*, **77**, 3692 (1955).
9) J. V. McLaren, J. D. Watts, and A. Gilbert, *J. Polym. Sci., Part C*, **16**, 1903 (1967).
10) K. Yamaoka and T. Masujima, *Bull. Chem. Soc. Jpn.*, **52**, 1819 (1979).
11) S. Noji and K. Yamaoka, *Macromolecules*, **12**, 1110 (1979).
12) M. Eigen and R. G. Wilkins, *Adv. Chem. Ser.*, **49**, 55 (1964); D. J. Hewkin and R. H. Prince, *Coord. Chem. Rev.*, **5**, 45 (1970).
13) H. Ito and S. Suzuki, *Kogyo Kagaku Zasshi*, **59**, 717, (1956).
14) A. Takahashi, S. Hayashi, and I. Kagawa, *Kogyo Kagaku Zasshi*, **60**, 1059 (1957).
15) K. Hiromi, "Kinetics of Fast Enzyme Reactions," Kodansha Ltd., Tokyo (1979), Chap. 2.
16) Nishikawa and Tsuchida (Ref. 4) expressed the concentration of L_2 by: $[L_2]=[L]^2/([L]+[HL])$. However, Eq. 4 may be more appropriate for the present system, in which the population of the coordinated carboxylato is comparatively high.
17) I. M. Kolthoff, *J. Phys. Chem.*, **34**, 1466 (1930).
18) T. J. Swift and R. E. Connick, *J. Chem. Phys.*, **37**, 307 (1962); **41**, 2553 (1964).

 © 1982 The Chemical Society of Japan Bull. Chem. Soc. Jpn., 55, 3417—3421 (1982)

Electronic Structure of $V_2(CO)_8(\mu\text{-}PPh_2)_2$ and $Mn_2(CO)_8(\mu\text{-}AsPh_2)_2$ by Electron Spin Resonance Study of Their Ion Radicals

Takashi KAWAMURA,* Sachio ENOKI, Shigeru HAYASHIDA, and Teijiro YONEZAWA

Department of Hydrocarbon Chemistry, Faculty of Engineering, Kyoto University, Sakyo-ku, Kyoto 606

(Received May 12, 1982)

The anion radical of $V_2(CO)_8(\mu\text{-}PPh_2)_2$ and the cation radical of $Mn_2(CO)_8(\mu\text{-}AsPh_2)_2$ are generated by chemical reduction of the vanadium complex with $LiBHEt_3$ or potassium naphthalenide and by radiochemical oxidation of the manganese complex in frozen Freon mixture, respectively. Their anisotropic ESR spectra show that the V_2P_2 and the Mn_2As_2 rhomboids are planar. Their g and hyperfine splitting tensors are analyzed on the basis of a qualitative molecular orbital scheme for metal-metal bonds developed from a hypothesis that metal-ligand interactions are larger than metal-metal interactions. The odd electron orbital of $V_2(CO)_8(\mu\text{-}PPh_2)_2^{-\cdot}$ is assigned to the metal-metal π^* MO and the odd electron density on the vanadium d AO is estimated as 0.21. The odd electron of $Mn_2(CO)_8(\mu\text{-}AsPh_2)_2^{+\cdot}$ is concluded to be accomodated in the metal-metal σ^* MO and odd electron densities on manganese and arsenic atoms are evaluated as $\rho(\text{Mn d})=0.25$ and $\rho(\text{As p})=0.08$ or 0.16, respectively. Order of magnitude estimates of orbital energy differences between metal-metal MO's are obtained from analyses of g tensors as $\varepsilon(\pi^*)-\varepsilon(\sigma)\simeq 0.4$ and $\varepsilon(\pi^*)-\varepsilon(\delta)\simeq 0.9$ eV for the anionic divanadium complex and $\varepsilon(\sigma^*)-\varepsilon(\delta^*)\simeq 1.1$ and $\varepsilon(\sigma^*)-\varepsilon(\pi)\simeq 1.4$ eV for the cationic dimanganese complex.

There has been considerable recent interest in electronic structures of complexes of $M_2(CO)_8(\mu\text{-}PR_2)_2$ with D_{2h} geometries where M is vanadium, chromium or manganese. Metal-metal bond lengths are shown by Vahrenkamp[1] to be consistent with formal bond orders of 2, 1 and 0 deduced from the 18 electron rule for the vanadium, the chromium and the manganese complexes, respectively. Molecular orbital (MO) calculations by Teo, *et al.*[2] and Shaik, *et al.*[3] gave $\pi^2\delta^2\sigma^2\delta^{*2}$ double bond, $\pi^2\delta^2\delta^{*2}\sigma^2\pi^{*2}$ single bond and $\pi^2\delta^2\delta^{*2}\pi^{*2}\sigma^2\sigma^{*2}$ no bond configurations for metal-metal bonds of the vanadium, the chromium and the manganese complexes, respectively.

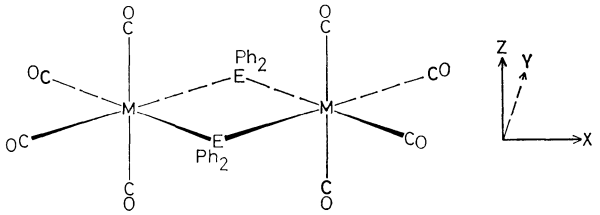

A preliminary ESR study of $Mn_2(CO)_8(\mu\text{-}AsPh_2)_2^{+\cdot}$ has been reported from this laboratory,[4] and its odd electron orbital has been assigned to the b_{3u} MO with a metal-metal σ^* character and consisting mainly of the Mn $d_{x^2-y^2}$ and As p_x atomic orbitals (AO), with which calculated MO schemes[2,3] are consistent. We have been trying to extend the study to ion radicals of bioctahedral molybdenum, which is located in the same column as chromium in the periodic table, and vanadium complexes. Meanwhile, Madach and Vahrenkamp[5] reported that $V_2(CO)_8(\mu\text{-}PMe_2)_2$ can be reduced chemically into a stable anion radical and that its solution ESR spectrum shows hyperfine splittings due to pairs of vanadium and phosphorus nuclei. The extended Huckel MO calculation[3] predicted that its odd electron will occupy the metal-metal π^* MO, into which the phosphorus valence shell AO's are symmetry-forbidden to mix. The phosphorus splitting in the solution ESR spectrum was thus mentioned as somewhat confusing.[5] Since metal d AO's play dominant roles in the formation of metal-metal bond rather than metal s AO's, anisotropic spectra are more informative for the study of electronic structure of the anion radical. We report here a study of anisotropic ESR spectra of frozen solutions of $V_2(CO)_8(\mu\text{-}PPh_2)_2^{-\cdot}$ and $Mn_2(CO)_8(\mu\text{-}AsPh_2)_2^{+\cdot}$ in order to obtain quantitative informations about their electronic structures.

Results

$V_2(CO)_8(\mu\text{-}PPh_2)_2^{-\cdot}$. When a dilute benzene solution of $V_2(CO)_8(\mu\text{-}PPh_2)_2$ is mixed with an equimolar amount of potassium naphthalenide at room temperature, a paramagnetic vanadium complex is formed immediately after the mixing. The solution exhibits an isotropic ESR spectrum split into a 15-fold multiplet of 23.4×10^{-4} cm^{-1} due to a pair of equivalent vanadium nuclei (99.8% natural abundance, $I=7/2$) split further into triplets of 6.0×10^{-4} cm^{-1} due to a pair of equivalent phosphorus nuclei (100%, $I=1/2$) at $g=2.019$. The spectrum is quite similar to that of $V_2(CO)_8(\mu\text{-}PMe_2)_2^{-\cdot}$[5] and is attributed to $V_2(CO)_8(\mu\text{-}PPh_2)_2^{-\cdot}$.

The same anion radical is formed gradually in 0.5—1 h when the parent complex is reacted in benzene with 2—3 equivalents of $LiBHEt_3$. This slow formation of the anion radical suggests that this radical may be generated by electron transfer from an intermediate(s) formed in a foregoing step(s) rather than by direct electron transfer from the hydroborate to the parent neutral complex. The anisotropic spectra of the anion radical in benzene solutions frozen at 77 K are obtained at X-, K-, and Q-bands (Fig. 1). These anisotropic spectra fit a rhombic spin Hamiltonian in which two vanadium nuclei are magnetically equivalent and three principal directions of the g tensor and those of the vanadium hyperfine splitting tensor are parallel to each other. This spin Hamiltonian shows that the V_2P_2 rhomboid of the anion radical is planar corresponding to a D_{2h} geometry of the anion radical, otherwise even the two vanadium nuclei can not be magnetically equivalent in the anisotropic spectra.[6] The principal values of the g tensor are:

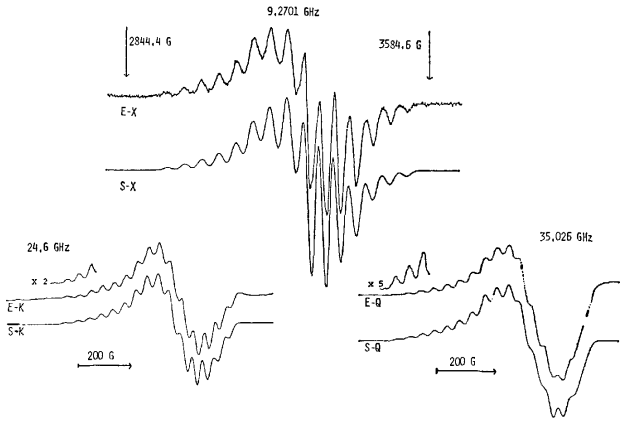

Fig. 1. Experimental (E-) and simulated (S-) ESR spectra of frozen benzene solutions of $V_2(CO)_8(\mu\text{-}PPh_2)_2^{-\cdot}$ observed at X- (X), K- (K), and Q-bands (Q) at 77 K.

$$g_{\alpha\alpha} = 2.001,$$
$$g_{\beta\beta} = 2.018,$$
$$g_{\gamma\gamma} = 2.038,$$

and those for the vanadium splitting tensor are:

$$|A_{\alpha\alpha}(V)|/hc = |A_{\beta\beta}(V)|/hc = (15\pm2)\times10^{-4}\ cm^{-1},$$
$$|A_{\gamma\gamma}(V)|/hc = 39.2\times10^{-4}\ cm^{-1},$$

where α, β, and γ designate the rectangular axes for the spin Hamiltonian. It should be pointed out that the vanadium splitting tensor is axially symmetric. Hyperfine splittings due to the phosphorus nuclei are unfortunately hidden behind the line width in the anisotropic spectra.

$Mn_2(CO)_8(\mu\text{-}AsPh_2)_2^{+\cdot}$. The analysis of the ESR spectra of $Mn_2(CO)_8(\mu\text{-}AsPh_2)_2^{+\cdot}$ has been reported in the preliminary report.[4] The principal values of the g tensor are:

$$g_{\alpha\alpha} = 2.031,$$
$$g_{\beta\beta} = 2.025,$$
$$g_{\gamma\gamma} = 2.001,$$

and those for the manganese and arsenic hyperfine splitting tensors are:

$$|A_{\alpha\alpha}(Mn)|/hc = |A_{\beta\beta}(Mn)|/hc \leqq 3\times10^{-4}\ cm^{-1},$$
$$|A_{\gamma\gamma}(Mn)|/hc = 43.0\times10^{-4}\ cm^{-1},$$
$$|A_{\alpha\alpha}(As)|/hc = 14.4\times10^{-4}\ cm^{-1},$$
$$|A_{\beta\beta}(As)|/hc = 41.5\times10^{-4}\ cm^{-1},$$
$$|A_{\gamma\gamma}(As)|/hc = 39.9\times10^{-4}\ cm^{-1}.[4]$$

Discussion

Qualitative Molecular Orbital Scheme for Metal-Metal Bond. The results of molecular orbital calculations of $M_2(CO)_8(\mu\text{-}PH_2)_2$[2,3] can be reproduced qualitatively from a hypothesis that metal-ligand interactions are larger than metal-metal interactions (Fig. 2). Larger interactions are considered first and weaker ones are taken into account thereafter. The present qualitative molecular orbital scheme starts from an electronic structure for a mononuclear fragment with a pseudoctahedral geometry, then two mononuclear

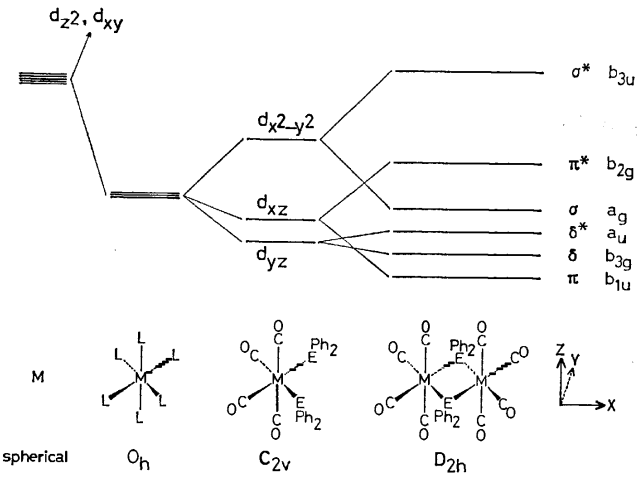

Fig. 2. Construction of qualitative metal-metal MO's for $M_2(CO)_8(\mu\text{-}EPh_2)_2$.
The σ^* MO is the odd electron orbital of $Mn_2(CO)_8(\mu\text{-}AsPh_2)_2^{+\cdot}$ with eleven d electrons. The π^* MO is the odd electron orbital of $V_2(CO)_8(\mu\text{-}PPh_2)_2^{-\cdot}$ which has nine d electrons. Relative orbital energy levels of δ^* and π MO's for the divanadium anion and those between σ and δ MO's for the dimanganese cation do not have much significances.

fragments are combined together through weak metal-metal interactions into the bioctahedral complex, $M_2(CO)_8(\mu\text{-}ER_2)_2$.

When the mononuclear fragment is octahedral (O_h), the e_g d orbitals (d_{z^2} and d_{xy}) are located above the t_{2g} d orbitals ($d_{x^2-y^2}$, d_{xz}, and d_{yz}) in the energy diagram. When the symmetry of the fragment is lowered to the pseudoctahedral one (C_{2v}), the degeneracy of the t_{2g} orbitals is broken and the orbital energy sequence is expected to be $d_{x^2-y^2} > d_{xz} > d_{yz}$. The orbital energy of the d_{yz} is the lowest because this orbital interacts with vacant π^* MO's of three carbonyl ligands and its interaction with lone pair orbitals of the ligands is symmetry-forbidden. The $d_{x^2-y^2}$ orbital has the highest energy, since this orbital interacts with π^* MO's of only two carbonyls and with lone pair orbitals of six ligands whereas the d_{xz} orbital interacts with vacant π^* MO's of three carbonyls and lone pair orbitals of the two axial carbonyls.

When a pair of pseudoctahedral fragments are joined together to from a bioctahedral (D_{2h}) dimetallic complex, bonding and antibonding pairs of MO's with metal-metal σ, π, and δ symmetries are formed from the t_{2g} d orbitals through relatively weak metal-metal interactions. Among these six MO's, the σ^* MO has been calculated to have the highest orbital energy, and the π^* MO has the second highest energy.[2,3] The energies of the metal-metal MO's derived from the e_g d orbitals (d_{xy} and d_{z^2}) are far higher than those of the metal-metal MO's arising from the t_{2g} d orbitals ($d_{x^2-y^2}$, d_{xz}, and d_{yz}). This is because of the aforementioned hypothesis.

In $V_2(CO)_8(\mu\text{-}PR_2)_2$, eight "d electrons" from a pair of V(I) ions occupy the lowest four metal-metal MO's giving a double bond configuration of $\pi^2\delta^2\delta^{*2}\sigma^2$. Upon one electron reduction of this complex, the odd

electron enters into the metal-metal π^* MO. The formal metal-metal bond order of the resulted anion radical is 1.5. In $Mn_2(CO)_8(\mu\text{-}AsR_2)_2$, twelve "d electrons" from a pair of Mn(I) ions occupy the six metal-metal MO's derived from the t_{2g} d orbitals, resulting in an electronic configuration of $\pi^2\delta^2\delta^{*2}\sigma^2\pi^{*2}\sigma^{*2}$ with a formal metal-metal bond order of zero. Upon one electron oxidation of this dimanganese complex, the odd electron remains in the σ^* MO. The formal metal-metal bond order of the resulted cation is 0.5.

The purposes of the present study are (i) examination of the validity of the present qualitative MO scheme in interpretations of ESR spectra, (ii) experimental estimation of the weight of d AO's in metal-metal MO's, and (iii) experimental estimation of differences between energies of metal-metal MO's.

Symmetry of Odd Electron Orbital of $V_2(CO)_8(\mu\text{-}PPh_2)_2^{-\cdot}$. A shift of a principal value of a g tensor, g_{xx} for example, from the free electron value of $g_e=2.0023$ has the following form:[7]

$$\Delta g_{xx} \equiv g_{xx} - g_e = 2\sum_n^{*p} \langle\psi_p|\sum_k \zeta_k l_{kx}|\psi_n\rangle \times \langle\psi_n|\sum_k l_{kx}|\psi_p\rangle/(\varepsilon_p-\varepsilon_n), \quad (1)$$

where ψ and ε are the MO and its orbital energy with the subscripts of p and n standing for the odd electron orbital and for the other MO's, respectively, l_{kx} is the x component of the orbital angular momentum of an electron on the k-th atom, and ζ_k is its one-electron spin-orbit coupling constant. The y or z principal value can be expressed by changing x in this equation into y or z.

The large anisotropy in the vanadium hyperfine splitting tensor indicates that odd electron densities on vanadium 3d AO's are large. Orbital energy differences between the odd electron orbital and MO's with dominant metal characters, which appear as the denominator in Eq. 1, are smaller than those for ligand MO's in the present MO scheme. Thus the sign of the g shift in Eq. 1 can be predicted by taking only l-s couplings in vanadium atoms into account, although the l-s coupling constant for 3d AO's of V(I) (136 cm^{-1})[8] is not distinguishably large in comparison with those for phosphorus 3p (231 cm^{-1}),[9] oxygen 2p (152 cm^{-1})[9] and carbon 2p (28 cm^{-1})[9] AO's.[10] In this approximation, all the numerators in Eq. 1 are zero or positive and signs of g shifts can be correlated directly with those of denominators in Eq. 1. A vacant ψ_n induces a negative g shift and a doubly occupied ψ_n results in a positive g shift as long as the ψ_n and the odd electron orbital share a non-zero matric element of l-s couplings in the metals.

In the present qualitative MO scheme, the odd electron of $V_2(CO)_8(\mu\text{-}PPh_2)_2^{-\cdot}$ is accomodated in the π^* (b_{2g}, d_{xz}*) MO. The unique axis of the axially symmetric vanadium splitting tensor should be the molecular y axis. Table 1 summerizes the shifts of the principal values of the g tensor from g_e predicted by Eq. 1 and the qualitative MO scheme in Fig. 2. For example, the shift of g_{yy} from g_e, Δg_{yy}, arises from the doubly occupied σ (a_g, $d_{x^2-y^2}$) MO and an unoccupied a_g MO consisting mainly of d_{z^2} AO's. Since

Table 1. g Shift of $V_2(CO)_8(\mu\text{-}PPh_2)_2^{-\cdot}$ with electronic configuration of $(\pi b_{1u})^2(\delta b_{3g})^2$-$(\delta^* a_u)^2(\sigma a_g)^2(\pi^* b_{2g})^1$ based on Eq. 1

$\Delta g_{\alpha\alpha}$	l_α[a]	ψ_n[b]	Occptn. of ψ_n	Sign of $\Delta g_{\alpha\alpha}$
Δg_{xx}	$l_x(b_{3g})$	b_{1g}, d_{xy}	unocc.	+
Δg_{yy}	$l_y(b_{2g})$	a_g, $d_{x^2-y^2}$, σ / a_g, d_{z^2}	unocc. / occ.	+
Δg_{zz}	$l_z(b_{1g})$	b_{3g}, d_{yz}, δ	occ.	+

a) Component of l and its symmetry in D_{2h}. b) MO's which share non-zero matrix elements of l_α with the odd electron orbital, $\psi_p=\pi^*$. The notation of [b_{3g}, d_{yz}, δ], for exsample, indicates that ψ_n is the b_{3g} MO constructed from V d_{yz} AO's and that ψ_n is the metal-metal δ MO.

metal-metal electronic interactions are assumed to be smaller than metal-ligand interactions, the σ MO contribution is expected to dominate and a positive value of Δg_{yy} is expected.

These theoretical expectations deduced from the qualitative MO scheme in Fig. 2 are consistent with the experimental results under the assignment of the spin Hamiltonian axes of α, β, and γ to the molecular axes of x, z, and y, respectively.

Odd Electron Distribution in $V_2(CO)_8(\mu\text{-}PPh_2)_2^{-\cdot}$. The odd electron density on the vanadium d_{xz} AO, $\rho(V\,xz)$, can be correlated with the vanadium hyperfine splitting tensor with corrections for second order effects of unquenched orbital angular momenta of electrons as follows:[11,12]

$$\left.\begin{aligned} A_{xx}(V) &= a(V) - B(V\,xz)\rho(V\,xz) \\ &\quad - (7/4)B(V\,xz)\Delta g_{xx} \\ &\quad - (3/8)B(V\,xz)(\Delta g_{yy}-\Delta g_{zz}) \\ A_{yy}(V) &= a(V) + 2B(V\,xz)\rho(V\,xz) \\ &\quad - (7/4)B(V\,xz)\Delta g_{yy} \\ &\quad - (3/8)B(V\,xz)(\Delta g_{xx}+\Delta g_{zz}) \\ A_{zz}(V) &= a(V) - B(V\,xz)\rho(V\,xz) \\ &\quad - (7/4)B(V\,xz)\Delta g_{zz} \\ &\quad + (3/8)B(V\,xz)(\Delta g_{xx}+\Delta g_{yy}) \end{aligned}\right\} \quad (2)$$

$$a(V) = Q_V(V)\rho(V\,s) + Q_I(V)\rho(V\,xz), \quad (3)$$

where $2B(V\,xz)$ is the parallel splitting constant of a vanadium nucleus with a unit odd electron density on its d_{xz} AO and $a(V)$ is the vanadium Fermi contact term arising from the odd electron density on the vanadium 4s AO, $\rho(V\,s)$, and from the spin polarization of the inner shell s electrons which is proportional to $\rho(V\,xz)$. The coefficient, $Q_V(V)$ or $Q_I(V)$, is the Fermi contact term of a vanadium nucleus with a unit odd electron density on its 4s AO or on its 3d AO. The valence orbital parameters of $Q_V(V)$ and $2B(V\,xz)$ have been evaluated as 1390×10^{-4} and -83.4×10^{-4} cm^{-1}, respectively.[13] The inner shell parameter, $Q_I(V)$, can be estimated as $-(100\pm20)\times10^{-4}$ cm^{-1} from theoretical and experimental studies on ESR of mononuclear vanadium complexes.[14]

The isotropic vanadium splitting of 23.4×10^{-4} cm^{-1}, observed in the solution ESR spectrum, indicates that all the signs of the principal values of the vanadium

splitting tensor are identical. Since the odd electron in the metal-metal π^* MO is symmetry-forbidden to delocalize onto vanadium 4s AO's, the Fermi contact term of the vanadium nuclei, $a(V)$, arises only from the inner shell spin polarization and should be negative due to the negative value of $Q_I(V)$. These analyses result in the assignment of negative signs to all the principal values of the vanadium splitting tensor. By using Eq. 2, the Fermi contact term and the odd electron density on the vanadium d_{xz} AO are estimated as $a(V)/hc=-24.3\times10^{-4}$ cm^{-1} and $\rho(V\ xz)=0.21$ respectively. Since $\rho(V\ s)=0$, Eq. 3 and the estimate of $\rho(V\ xz)=0.21$ give $a(V)/hc=(-16.8--25.2)\times10^{-4}$ cm^{-1}, which is consistent with the above estimation of $a(V)/hc=-24.3\times10^{-4}$ cm^{-1} deduced from the analysis with Eq. 2. Present analyses are self-consistent. The relatively small odd electron density on the vanadium $3d_{xz}$ AO implies a rather extensive π back donation from metals to carbonyl π^* MO's and/or mixing of vanadium $4p_z$ AO's into the metal-metal π^* MO. Since vanadium 4p AO's are rather diffuse, the odd electron densities on these AO's do not give much influences on g and hyperfine splitting tensors.

Orbital Energy Differences. Since the odd electron orbital is the metal-metal π^* MO and the odd electron density on the vanadium d_{xz} AO is 0.21, this orbital can be expressed as follows:

$$\pi^* = \sqrt{0.21}d_{xz}(V_1) + \sqrt{0.21}d_{xz}(V_2) + \cdots, \quad (4)$$

where the subscripts for V are numberings for the vanadium atoms. By assuming that the other MO's with dominant metal characters are localized on the metals and taking l-s couplings only in the metals into account, Eq. 1 correlates experimental g shifts with orbital energy differences as following:

$$\Delta g_{\beta\beta} = \Delta g_{zz} = 2\langle\pi^*|\zeta(l_{1z}+l_{2z})|\delta\rangle\langle\delta|l_{1z}+l_{2z}|\pi^*\rangle / [\varepsilon(\pi^*)-\varepsilon(\delta)] \quad (5)$$

$$\Delta g_{\gamma\gamma} = \Delta g_{yy} = 2\langle\pi^*|\zeta(l_{1y}+l_{2y})|\sigma\rangle\langle\sigma|l_{1y}+l_{2y}|\pi^*\rangle / [\varepsilon(\pi^*)-\varepsilon(\sigma)], \quad (6)$$

where ζ is the l-s coupling constant of d AO's of V(I) (136 cm^{-1})[8] and l_{1z} is the z component of the orbital angular momentum around the vanadium atom 1 and so on. We have neglected the contribution to Δg_{yy} from the unoccupied a_g MO consisting of vanadium d_{z^2} AO's in Eq. 6 (*vide supra*). Analyses of the g shifts with Eqs. 5 and 6 give estimates of orbital energy differences as $\varepsilon(\pi^*)-\varepsilon(\delta)\simeq0.9$ and $\varepsilon(\pi^*)-\varepsilon(\sigma)\simeq0.4$ eV. Because of approximations adopted here, these differences should be regarded as estimates of order of magnitudes. These values are in fair agreement with values of $\varepsilon(\pi^*)-\varepsilon(\delta)\simeq0.5$ and $\varepsilon(\pi^*)-\varepsilon(\sigma)\simeq0.6$ eV obtained by an extended Huckel calculation of $V_2(CO)_8(\mu\text{-}PH_2)_2$.[15]

$Mn_2(CO)_8(\mu\text{-}AsPh_2)_2^{+\cdot}$. Analyses of ESR parameters of $Mn_2(CO)_8(\mu\text{-}AsPh_2)_2^{+\cdot}$ have led to conclusions that the odd electron occupies the metal-metal σ^* MO and that its densities on the 4s and $3d_{x^2-y^2}$ AO's of the manganese atoms and the arsenic $4p_x$ AO's are $\rho(Mn\ s)=0.004$, $\rho(Mn\ x^2-y^2)=0.25$ and $\rho(As\ x)=0.08$ or 0.16, respectively.[4] The ambiguity in the estimate of $\rho(As\ x)$ is due to the uncertainty of the signs of the experimental principal values of the arsenic splitting tensor.

Orbital energy differences can be estimated from g shifts by using the following equations:

$$\Delta g_{xx} = 2\langle\sigma^*|\zeta(l_{1x}+l_{2x})|\delta^*\rangle\langle\delta^*|l_{1x}+l_{2x}|\sigma^*\rangle / [\varepsilon(\sigma^*)-\varepsilon(\delta^*)] \quad (7)$$

$$\Delta g_{yy} = 2\langle\sigma^*|\zeta(l_{1y}+l_{2y})|\pi\rangle\langle\pi|l_{1y}+l_{2y}|\sigma^*\rangle / [\varepsilon(\sigma^*)-\varepsilon(\pi)], \quad (8)$$

where ζ is the l-s coupling constant of Mn(I) 3d AO's (254 cm^{-1})[8] and the other notations have similar significances as in Eqs. 5 and 6. The experimental g shifts of $\Delta g_{xx}=0.029$ and $\Delta g_{yy}=0.023$ lead to order of magnitude estimates of the orbital energy differences of $\varepsilon(\sigma^*)-\varepsilon(\delta^*)\simeq1.1$ and $\varepsilon(\sigma^*)-\varepsilon(\pi)\simeq1.4$ eV. These estimates are comparable with energy differences of $\varepsilon(\sigma^*)-\varepsilon(\delta^*)\simeq1.2$ and $\varepsilon(\sigma^*)-\varepsilon(\pi)\simeq1.3$ eV calculated for $Mn_2(CO)_8(\mu\text{-}PH_2)_2^{+\cdot}$ with the nonparameterized MO method by Teo and his coworkers.[2]

Concluding Remarks. Magnitudes of negative shifts of Δg_{zz} of $Mn_2(CO)_8(\mu\text{-}AsPh_2)_2^{+\cdot}$ (−0.001) and of Δg_{xx} of $V_2(CO)_8(\mu\text{-}PPh_2)_2^{-\cdot}$ (−0.001) are far smaller than shifts of the other principal values of g tensors of both radicals. These results indicate that the energy separation between e_g and t_{2g} d orbitals in the mononuclear fragment is far larger than those among the six metal-metal MO's derived from t_{2g} d orbitals upon the formation of the dinuclear complex.

The analyses of the hyperfine splitting tensors of arsenic and manganese nuclei of $Mn_2(CO)_8(\mu\text{-}AsPh_2)_2^{+\cdot}$ have indicated that the metal-metal σ^* MO consists of 50% of the manganese $d_{x^2-y^2}$ components and 16 or 32% of arsenic p_x components. The proposal that the Mn $d_{x^2-y^2}$ orbital in the C_{2v} mononuclear fragment has the highest orbital energy among the t_{2g} d orbitals is based on this relatively large mixing between the arsenide lone pair orbitals and the manganese $d_{x^2-y^2}$ orbitals. The weight of the vanadium d_{xz} AO's in the metal-metal π^* MO of $V_2(CO)_8(\mu\text{-}PPh_2)_2^{-\cdot}$ is 42% which is not very large. Since vanadium is electropositive and the carbonyl ligand is a good π accepter, most of the remaining part of the π^* MO would be carbonyl π^* MO's.

Finally, we discuss on the isotropic splitting by phosphorus nuclei resolved in the solution ESR spectrum of $V_2(CO)_8(\mu\text{-}PPh_2)_2^{-\cdot}$. The odd electron in the metal-metal π^* MO is symmetry forbidden to delocalize onto the valence shell AO'S of the phosphorus atoms. The odd electron density on the vanadium d_{xz} AO's would induce spin polarization of electrons in σ bonds between the vanadium and phosphorus atoms, which should result in negative spin densities on the phosphorus 3s AO's. The observed isotropic phosphorus splitting constant of 6.0×10^{-4} cm^{-1} corresponds to the phosphorus 3s spin density of (−)0.0014. This spin density is not an unacceptable value as induced by spin polarization. This explanation predicts that the sign of the isotropic splitting constant of the phosphorus nucleus should be negative.

Experimental

$V_2(CO)_8(\mu\text{-}PPh_2)_2^{-\cdot}$. $V_2(CO)_8(\mu\text{-}PPh_2)_2$[16] (1 mg, 2 μmol) was dissolved in dry benzene (0.8 ml) in a quartz

ESR sample tube under argon. When a tetrahydrofuran solution of potassium naphthalenide (0.05 mol dm^{-3}, 50 μl, 2.5 μmol) was added to this solution, a strong ESR signal of $V_2(CO)_8(\mu\text{-}PPh_2)_2^{-\cdot}$ appeared immediately and lasted for days at room temperature. When a tetrahydrofuran solution of $LiBHEt_3$ (Aldrich Super-Hydride, 1 mol dm^{-3}, 5 μl, 5 μmol) was added to the benzene solution of the neutral divanadium complex, an ESR signal of the divanadium anion radical grew slowly in 0.5—1 h.

$Mn_2(CO)_8(\mu\text{-}AsPh_2)_2^{+\cdot}$. $Mn_2(CO)_8(\mu\text{-}AsPh_2)_2$[17] (*ca.* 0.4 mg) was dissolved in Freon mixture ($CFCl_3$: CF_2Br-CF_2Br=1:1 volume ratio)[18] (0.7 ml) under vacuum and irradiated with 2 Mrad of ^{60}Co γ-rays at 77 K. ESR spectra of $Mn_2(CO)_8(\mu\text{-}AsPh_2)_2^{+\cdot}$ were measured at low microwave powers (0.1—0.5 mW) after appropriate annealings of irradiated samples. A competitive positive hole capture between $Mn_2(CO)_8(\mu\text{-}AsPh_2)_2$ and isoquinoline was performed by γ-irradiations of Freon mixture solutions (0.7 ml) containing $Mn_2(CO)_8(\mu\text{-}AsPh_2)_2$ (0.05 mg, 0.06 μmol) and isoquinoline (7 μl, 0.05 μmol or 70 μl, 0.5 μmol). The irradiated sample containing the smaller amount of isoquinoline gave a superimposed ESR spectrum of signals due to $Mn_2(CO)_8(\mu\text{-}AsPh_2)_2^{+\cdot}$ and the isoquinoline cation radical,[19] and the other sample gave signals arising only from the isoquinoline cation radical.

ESR Measurements. The spectrometer and monitoring of microwave frequencies and field sweeps for measurements of X-band ESR spectra have been mentioned earlier.[11] K- and Q-band spectra were obtained on JEOL PE-2K and PE-3Q spectrometers, respectively. Q-band microwave frequencies were measured with a Shimada Rika 2A550 resonant cavity wavemeter. The K-band microwave frequency appearing in Fig. 1 is a nominal one. Field sweeps in K- and Q-band spectra were calibrated with hydrogen atom signals in irradiated samples (g=2.0022, a_H/hc=471.7×10^{-4} cm^{-1}) after higher order corrections for the hyperfine interaction.

Simulations. ESR spectra were simulated on a FACOM M200 computer with a FORTRAN program prepared according to a second order perturbation solution[20] for a rhombic spin Hamiltonian.

We thank Mr. M. Kohno (JEOL) for his measurements of Q-band ESR spectra, and Professor N. Hirota and Dr. H. Ohya-Nishiguchi (Kyoto University) for giving us a chance to use a Q-band ESR spectrometer. Samples were exposed to γ-rays at the Research Laboratory of Radioisotopes of Kyoto University. Spectrum simulations were performed on a FACOM M200 computer at the Data Processing Center of Kyoto University.

References

1) H. Vahrenkamp, *Chem. Ber.*, **111**, 3472 (1978).
2) B. K. Teo, M. B. Hall, R. F. Fenske, and L. F. Dahl, *J. Organomet. Chem.*, **70**, 413 (1974).
3) S. Shaik, R. Hoffmann, R. Fisel, and R. H. Summerville, *J. Am. Chem. Soc.*, **102**, 4555 (1974).
4) S. Hayashida, T. Kawamura, and T. Yonezawa, *Chem. Lett.*, **1981**, 985.
5) T. Madach and H. Vahrenkamp, *Chem. Ber.*, **114**, 513 (1981).
6) For such an example, see: B. M. Peake, P. H. Rieger, B. H. Robinson, and J. Simpson, *J. Am. Chem. Soc.*, **102**, 156 (1980).
7) A. J. Stone, *Proc. R. Soc. London, Ser. A*, **271**, 424 (1963).
8) T. M. Dunn, *Trans. Faraday Soc.*, **57**, 1441 (1961).
9) D. S. McClure, *J. Chem. Phys.*, **17**, 905 (1949).
10) a) The values of $g_{\beta\beta}-g_e$ and $g_{\gamma\gamma}-g_e$ of the present divanadium anion radical are far larger than the shifts of the principal values of the g tensor of $\cdot PPh_2$[10b] and the shift of the isotropic g factor of formaldehyde anion radical,[10c] showing that g shifts of the divanadium anion originate mainly from the *l-s* couplings on the metals; b) B. W. Fullam, S. P. Mishra, and M. C. R. Symons, *J. Chem. Soc., Dalton Trans.*, **1974**, 2145; c) K. Eiben and R. W. Fessenden, *J. Phys. Chem.*, **75**, 1186 (1971).
11) T. Kawamura, K. Fukamachi, T. Sowa, S. Hayashida, and T. Yonezawa, *J. Am. Chem. Soc.*, **103**, 364 (1981).
12) Corrections for second order effects of unquenched orbital angular momenta of electrons (the third and the fourth terms in Eq. 2 are based on the following assumptions: (i) the MO's with dominant metal characters, except the odd electron orbital, are localized on the metals; (ii) the *l-s* coupling takes place only in the metal atoms; and (iii) the mixing of d_{z^2} AO's into the odd electron orbital through *l-s* couplings is neglected because this mixing is dominated by the mixing of the metal-metal σ^* MO into the odd electron orbital.
13) J. R. Morton and K. F. Preston, *J. Magn. Reson.*, **30**, 577 (1978).
14) R. E. Watson and A. J. Freeman, *Phys. Rev.*, **123**, 2027 (1961); B. A. Goodman and J. B. Raynor, *Adv. Inorg. Chem. Radiochem.*, **13**, 135 (1970).
15) Read from Fig. 2 in Ref. 4. Note that extended Huckel values are for the neutral complex with a metal-metal formal bond order of 2 whereas the present "experimental" orbital energy differences are obtained from data of the anionic complex which has a metal-metal formal bond order of 1.5.
16) W. Hieber and E. Winter, *Chem. Ber.*, **97**, 1037 (1964).
17) R. F. Lambert, *Chem. Ind. (London)*, **1961**, 830.
18) a) A. Grimson and G. A. Simpson, *J. Phys. Chem.*, **72**, 1776 (1968); b) T. Shida and S. Iwata, *J. Am. Chem. Soc.*, **95**, 3473 (1973).
19) T. Kato and T. Shida, *J. Am. Chem. Soc.*, **101**, 6869 (1979).
20) A. Rockenbauer and P. Simon, *J. Magn. Reson.*, **11**, 217 (1973).

Multiphoton Ionization Spectrum of *p*-Terphenyl in a Supersonic Free Jet

Jun-ichi MURAKAMI,† Katsuhiko OKUYAMA, and Mitsuo ITO*
Department of Chemistry, Faculty of Science, Tohoku University, Sendai 980
(Received May 24, 1982)

The one-photon absorption spectrum of *p*-terphenyl vapor was observed in a supersonic free jet by using multiphoton ionization spectroscopy. In the spectrum were observed the progressions of the in-phase and out-of-phase torsional vibrations of the benzene rings. It was concluded that *p*-terphenyl has a planar structure in the first excited singlet state, whereas it is twisted in the ground state.

It has long been predicted that there exist low-lying hidden electronic excited states in polyphenyls[1,2] and their identifications have been of continuing interest for the spectroscopists. However, the electronic absorption spectra of polyphenyls in vapor are completely diffuse at room temperature due to excitation of low-frequency vibrations, which prevents conclusive assignment of the excited states. It was recently demonstrated for biphenyl, however, that the diffuseness can be removed in a supersonic free jet.[3] In the jet spectrum the well-resolved vibrational structure was observed and its analysis led us definite assignment of the S_1 and S_2 states and revealed the planar structure in the excited states. The success for biphenyl seems to promise that the systematic study of the electronic spectra of polyphenyls is possible by using a supersonic free jet. In this paper we report the one-photon electronic absorption spectrum of *p*-terphenyl in a supersonic free jet. In the case of *p*-terphenyl, the molecule has two torsional vibrations of the in-phase and the out-of-phase mode and the conjugation between the benzene rings is expected to be stronger than in biphenyl. It seems interesting to study how these effects are reflected in the electronic spectrum.

Experimental

The spectrum was observed by multiphoton ionization spectroscopy. Because of the high sensitivity, this method is quite suitable for observing the spectrum of a molecule with very low vapor pressure such as *p*-terphenyl. The ionization potential of *p*-terphenyl is 7.8 eV and the lowest excited state lies at about 4 eV. Hence in the excitation with the second harmonic of the visible dye laser ($\approx$300 nm), one can obtain the one-photon resonant two-photon ionization spectrum of the molecule. *p*-Terphenyl vapor obtained by heating the sample at 400 K was seeded in 3 atm He gas and the mixed gas was expanded from a pulsed nozzle (400 μm diameter) which is synchronized with a N_2 laser pumped scanning dye laser (Rhodamine B). The experimental setup is the same as reported in our previous works.[4,5] *p*-Terphenyl was zone-refined and was free from impurities, which was confirmed by their layer chromatography and gas chromatography with several developing solvents.

Results and Discussion

In Fig. 1 is shown a part of the observed one-photon resonant two-photon ionization spectrum of *p*-terphenyl in a supersonic free jet. The frequencies of the observed bands and their assignments are listed in Table 1. As is seen from the figure and table, the simple vibrational structure appears in the cold spectrum in contrast to the broad spectrum at room temperature. The observed spectrum consists of the two progressions A and B (see Fig. 1) and their combinations (see Table 1). Since both A and B progressions start from the same band at 32460 cm^{-1} and no prominent vibrational structure was observed to the red of the band, we assign it to be the 0-0 band of the first singlet excited state (S_1).

The frequency intervals of the A and B progressions are 62 and 89 cm^{-1}, respectively, and the spacings are almost constant for the two progressions (see Table 1). In the case of biphenyl,[3] the observed low-frequency vibration ($\approx$60 cm^{-1}) was assigned to the torsional mode of the benzene rings from the isotopic

Table 1. Vibronic bands of *p*-terphenyl in the MPI spectrum in a supersonic free jet

$\tilde{\nu}$/cm^{-1}	$\Delta\tilde{\nu}$/cm^{-1}	Analysis	Assignment[a]
32460	0		0-0
32522	62	0+62	A_0^1
32549	89	0+89	B_0^1
32583	123	0+2×62	A_0^2
32612	152	0+62+89	$A_0^1B_0^1$
32639	179	0+2×89	B_0^2
32645	185	0+3×62	A_0^3
32673	213	0+2×62+89	$A_0^2B_0^1$
32699	239	0+62+2×89	$A_0^1B_0^2$
32705	245	0+4×62	A_0^4
32725	265	0+3×89	B_0^3
32733	273	0+3×62+89	$A_0^3B_0^1$
32760	300	0+2×62+2×89	$A_0^2B_0^2$
32768	308	0+5×62	A_0^5
32790	330	0+62+3×89	$A_0^1B_0^3$
32798	338	0+4×62+89	$A_0^4B_0^1$
32824	364	0+3×62+2×89	$A_0^3B_0^2$
32830	370	0+6×62	A_0^6
32850	390	0+2×62+3×89	$A_0^2B_0^3$
32853	392		
32864	404	0+5×62+89	$A_0^5B_0^1$
32870	410		
32887	426	0+4×62+2×89	$A_0^4B_0^2$
32891	431	0+7×62	A_0^7
32913	453	0+3×62+3×89	$A_0^3B_0^3$
32921	461	0+6×62+89	$A_0^6B_0^1$
32947	487	0+5×62+2×89	$A_0^5B_0^2$
32950	490	0+8×62	A_0^8

a) A and B represent the out-of-phase and in-phase torsional vibrations, respectively.

† Present address: Research Institute for Scientific Measurements, Tohoku University, Sendai 980.

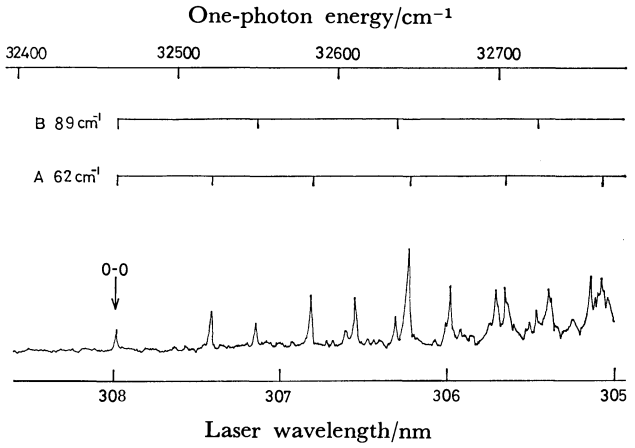

Fig. 1. The one-photon resonant two-photon ionization spectrum of *p*-terphenyl in a supersonic free jet.

ratio of the vibrational frequency. The low-frequency vibrations of *p*-terphenyl are also considered to be the torsional ones. In the case of *p*-terphenyl, however, there exist two torsional vibrations of the in-phase and the out-of-phase mode. Hence it seems quite reasonable to assign 62 and 89 cm^{-1} of the A and B progressions to the in-phase and out-of-phase torsional vibrations. In order to establish the assignment, the **GF** matrix calculation was made with the simplified force field of $V=(1/2)K\{(\Delta\tau_1)^2+(\Delta\tau_2)^2\}+K_{12}(\Delta\tau_1)(\Delta\tau_2)$, where $\Delta\tau$ is internal coordinate of the torsion of the interphenyl bond. It was found that a reasonable set of the force constants is obtained only when 62 and 89 cm^{-1} are assigned to the out-of-phase and in-phase modes, respectively. The force constants obtained are $K=1.7\times10^{-12}$ dyn cm/rad† and $K_{12}=-0.3\times10^{-12}$ dyn cm/rad. It is interesting to note that the value of K is ≈1.4 times larger than the corresponding force constant of biphenyl ($K=1.2\times10^{-12}$ dyn cm/rad). This is consistent with the expectation that conjugation between the benzene rings is stronger in *p*-terphenyl than in biphenyl.

Another interesting information obtained from the observed spectrum is the molecular geometry of *p*-terphenyl in the S_1 state. The harmonic torsional progressions of A and B suggest that *p*-terphenyl has a planar or a perpendicular form in the S_1 state. The fact that the S_1 state of *p*-terphenyl (33000 cm^{-1}) lies much lower in energy than that of biphenyl[4] implies the more extensive conjugation between the benzene rings in the former molecule than in the latter. The biphenyl molecule in the S_1 state has the planar structure owing to the predominance of the conjugation over the repulsion between the ortho-hydrogens.[4] We therefore can conclude that *p*-terphenyl also has a planar structure in the S_1 state.

Although the geometry of *p*-terphenyl vapor in the electronic ground state is not known yet, the molecule is considered to have a twisted structure as in the solution.[6] The twisted structure of the S_0 state is also consistent with the observed progression of torsional vibrations in the S_0-S_1 absorption spectrum, since the final state S_1 is planar as discussed above. The facts that only several members of the torsional progression were observed and that the 0-0 band appeared strongly are in contrast with the case of biphenyl where the torsional progressions with more than 20 quanta were observed and the 0-0 band was too weak to be observed. This strongly indicates from the Franck-Condon principle that although both biphenyl and *p*-terphenyl in vapor have a planar structure in the excited states, the dihedral angle of the latter is smaller than that of the former ($\approx42°$) in the ground states. The smaller dihedral angle for *p*-terphenyl is consistent with the result that in solution the angle is 10° compared with 20° in biphenyl.[6]

The authors wish to thank Prof. N. Mikami for his valuable discussions.

† 1 dyn=10^{-5} N.

References

1) Anneliese Wenzel, *J. Chem. Phys.*, **21**, 403 (1953).
2) N. I. Wakayama, S. Matsuzaki, and M. Mizuno, *Chem. Phys. Lett.*, **74**, 37 (1980).
3) J. Murakami, M. Ito, and K. Kaya, *J. Chem. Phys.*, **74**, 6505 (1981).
4) J. Murakami, K. Kaya, and M. Ito, *J. Chem. Phys.*, **72**, 3263 (1980).
5) J. Murakami, M. Ito, and K. Kaya, *Chem. Phys. Lett.*, **80**, 203 (1981).
6) H. Suzuki, *Bull. Chem. Soc. Jpn.*, **33**, 109 (1960).

 © 1982 The Chemical Society of Japan Bull. Chem. Soc. Jpn., 55, 3424—3428 (1982) [Vol. 55, No. 11

Conformation of Condensed Polycyclic Aromatic Hydrocarbons. I. The Molecular and Crystal Structure of Anthra[2,1,9,8-*hijkl*]-benzo[*de*]naphtho[2,1,8,7-*stuv*]pentacene

Shoji FUJISAWA, Isao OONISHI,* Junji AOKI, Yuji OHASHI,† and Yoshio SASADA†

Department of Chemistry, Faculty of Science, Toho University, Funabashi, Chiba 274

†*Laboratory of Chemistry for Natural Products, Tokyo Institute of Technology, Nagatsuta, Midori-ku, Yokohama 227*

(Received December 17, 1981)

The crystal structure of the title compound, $C_{38}H_{18}$, has been determined by X-ray analysis. The space group is Pa, with unit cell dimensions $a=31.276(4)$, $b=3.7818(4)$, $c=21.663(3)$ Å, $\beta=124.22(1)°$ and $Z=4$. The structure was solved by the direct method and refined by full-matrix least-squares methods to an R value of 0.073 for 2619 reflections. Two crystallographically independent molecules are largely distorted from a planar structure due to the repulsions between the crowded hydrogen atoms, with different conformations to each other. The molecules are stacked face-to-face by van der Waals forces to form column structures along the b axis.

On treating naphthanthrone(6*H*-benzo[*cd*]pyren-6-one, hereafter abbreviated as NT) with copper powder, three condensed polycyclic aromatic hydrocarbons, diphenanthro[5,4,3-*abcd*:5′,4′,3′-*jklm*]perylene(DPP) (**1**), anthra[2,1,9,8-*ijklm*]benzo[*uv*]naphto[*defg*]pentaphene (**2**), and anthra[2,1,9,8-*hijkl*]benzo[*de*]naphtho[2,1,8,7-*stuv*]pentaphene (**3**) have been obtained.[1] All of these

1

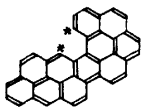

2

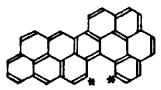

3

have eleven benzene rings. These hydrocarbons are stereochemically interesting, because they exhibit great steric hindrance between hydrogen atoms attached to carbon atoms indicated by asterisks, which is usually known as 1···7 interaction. They are also very important in the field of organic semiconductors due to their high photoconductivity.[2] However, the deficiency of information on their structures does not permit a detailed explanation of physical properties. The X-ray analysis was undertaken in order to elucidate the structure of anthra[2,1,9,8-*hijkl*]benzo[*de*]-naphtho[2,1,8,7-*stuv*]pentaphene (**3**) and to compare its conformation with those of the related molecules.

Experimental

The compound was prepared by the method described in the previous paper,[1] and purified by recrystallization from chlorobenzene, chromatography on activated alumina, and sublimation in vacuum. The crystal used for X-ray work was grown from an *o*-dichlorobenzene solution. Preliminary unit cell dimensions and space group ($P2_1/a$) were obtained from oscillation and Weissenberg photographs. However, a careful reexamination of the Weissenberg photographs of b and c axes exposed for a long time (about 200 h) revealed that the 030 reflection had weak but significant intensity. Therefore, the true space group should be Pa. The unit cell dimensions were refined by the least-squares method on the basis of 2θ values measured on a Rigaku automated four-circle diffractometer (16 reflections, $2\theta \leqq 25°$). The crystal data are listed in Table 1. Intensity data up to $2\theta \leqq 125°$ were collected on the diffractometer with Ni-filtered Cu $K\alpha$ radiation ($\lambda=1.5418$ Å). An $\omega/2\theta$ scan technique was employed with a scan rate of 4° min^{-1} in 2θ. Three standard reflections were monitored after every 50 measurements; the net counts of these reflections did not change significantly over the period of data collection. A total of 2619 independent reflections, ($|F_o| \geqq 3\sigma(|F_o|)$), was used for the structure determination. Corrections for Lorentz and polarization factors were made, but not for absorption.

Structure Determination

The first trial structure was obtained by the MULTAN 78 program,[3] on the assumption of the space group $P2_1/a$. As the ten peaks occupying the centers of the benzene rings on the E-maps could be interpreted not to be false but true ones, we assumed that the crystal was disordered and molecules took alternative positions randomly. Refinement by the least-squares methods reduced the R value to 0.23. But further refinement was impossible on this model.

A new model with space group Pa was constructed from the old model with $P2_1/a$ by removing the crystallographic center of symmetry. The refinement was carried out by the block-diagonal least-squares method. After the R value converged to 0.133, the full-matrix least-squares program SHELX 76[4] was applied, where some rigid groups and bond lengths were under constraint. When the R value deduced to 0.102, the usual refinement without constraint were carried out by the block-diagonal least-squares method. The final R was 0.073 for 2619 observed reflections. No peaks higher than 0.4 eÅ^{-3} was found on the final difference map. The atomic scattering factors were taken from the International Tables for X-ray Crystallography.[5] The final atomic parameters and their estimated standard deviations are listed in Table 2. Lists of the ob-

Table 1. Crystal data

$C_{38}H_{18}$, *M.W.* 474.6, mp 362 °C	
$\lambda_{max}^{benzene}=533$ nm	
Space group: Pa	
$a=31.276(4)$ Å	$U=2118.7(5)$ Å^3
$b=3.7818(4)$ Å	$Z=4$
$c=21.663(3)$ Å	$D_x=1.488$ g/cm^3
$\beta=124.22(1)°$	μ(Cu $K\alpha$)$=26.4$ cm^{-1}

TABLE 2. FINAL ATOMIC COORDINATES WITH THEIR ESTIMATED STANDARD DEVIATIONS, MULTIPLIED BY 10^4

Atom	x	y	z	B or B_{eq}/Å^2	Atom	x	y	z	B or B_{eq}/Å^2
C(1A)	−281(2)	1440(17)	3090(3)	2.8	C(1B)	5051(2)	−3561(20)	7161(4)	3.8
C(2A)	−482(2)	1338(18)	3530(4)	3.3	C(2B)	5234(3)	−3619(20)	6722(4)	4.2
C(3A)	−182(3)	2524(19)	4273(4)	4.0	C(3B)	4946(2)	−2349(20)	5991(4)	4.0
C(4A)	320(3)	3810(20)	4578(4)	4.0	C(4B)	4465(2)	−935(19)	5698(4)	3.5
C(5A)	524(3)	3914(20)	4143(4)	4.0	C(5B)	4252(2)	−821(16)	6127(3)	2.4
C(6A)	1019(2)	5357(17)	4439(3)	2.7	C(6B)	3740(2)	443(18)	5849(3)	3.4
C(7A)	1245(2)	5619(15)	4032(3)	1.7	C(7B)	3571(3)	526(22)	6307(4)	4.6
C(8A)	1743(2)	6947(17)	4313(3)	2.5	C(8B)	3073(3)	2141(19)	6022(4)	4.0
C(9A)	1928(2)	7061(16)	3856(3)	2.8	C(9B)	2864(2)	2214(18)	6422(3)	3.2
C(10A)	1618(3)	5835(19)	3112(4)	3.9	C(10B)	3134(2)	744(15)	7174(3)	1.8
C(11A)	1847(2)	5755(15)	2689(3)	1.8	C(11B)	2945(2)	745(20)	7631(4)	3.9
C(12A)	2407(3)	5903(21)	2970(4)	4.8	C(12B)	2395(2)	1343(13)	7312(3)	1.6
C(13A)	2790(2)	5273(16)	3729(3)	2.5	C(13B)	2004(2)	557(19)	6575(4)	3.6
C(14A)	3310(2)	6048(16)	4023(3)	2.5	C(14B)	1489(2)	1248(22)	6296(4)	4.6
C(15A)	3450(3)	7456(26)	3561(5)	6.0	C(15B)	1350(2)	2763(15)	6737(3)	2.1
C(16A)	3071(2)	8056(15)	2801(3)	1.8	C(16B)	1727(3)	3429(22)	7495(4)	5.2
C(17A)	3226(3)	9114(23)	2338(5)	5.4	C(17B)	1598(2)	4639(17)	8005(3)	2.8
C(18A)	2868(3)	9499(20)	1593(4)	4.1	C(18B)	1957(3)	4708(19)	8756(4)	3.9
C(19A)	2345(3)	8510(18)	1253(4)	3.3	C(19B)	2480(3)	3644(19)	9063(4)	3.8
C(20A)	1969(3)	8459(20)	484(4)	4.0	C(20B)	2835(3)	3440(20)	9849(4)	4.1
C(21A)	1486(3)	7026(20)	182(4)	4.2	C(21B)	3331(3)	2398(19)	10158(3)	3.5
C(22A)	1329(3)	5893(20)	652(4)	4.0	C(22B)	3492(2)	1237(17)	9683(3)	2.7
C(23A)	819(2)	4729(18)	331(3)	3.4	C(23B)	4003(2)	−16(20)	9986(3)	3.9
C(24A)	649(2)	3850(17)	788(3)	2.8	C(24B)	4150(3)	−1013(22)	9533(4)	4.6
C(25A)	987(2)	4127(20)	1570(4)	3.7	C(25B)	3810(2)	−715(15)	8739(3)	2.4
C(26A)	808(2)	3464(14)	2047(3)	1.9	C(26B)	3989(3)	−1388(20)	8263(4)	4.3
C(27A)	310(3)	2254(20)	1766(4)	4.4	C(27B)	4477(2)	−3028(15)	8530(3)	2.0
C(28A)	132(2)	1681(16)	2214(3)	2.8	C(28B)	4665(2)	−3108(18)	8079(3)	3.1
C(29A)	−375(3)	367(21)	1935(4)	4.3	C(29B)	5171(2)	−4688(17)	8380(3)	2.8
C(30A)	−581(2)	223(19)	2345(4)	3.9	C(30B)	5348(2)	−4781(18)	7937(4)	3.6
C(31A)	223(2)	2724(16)	3396(3)	2.7	C(31B)	4548(2)	−2107(17)	6867(3)	3.1
C(32A)	428(2)	2979(14)	2963(3)	1.7	C(32B)	4353(2)	−1990(19)	7332(4)	4.0
C(33A)	932(2)	4423(18)	3287(4)	3.7	C(33B)	3859(2)	−714(15)	7066(3)	2.0
C(34A)	1117(2)	4547(16)	2827(3)	2.4	C(34B)	3651(2)	−522(17)	7505(3)	2.8
C(35A)	1499(2)	5281(14)	1893(3)	1.8	C(35B)	3293(3)	435(19)	8417(4)	4.1
C(36A)	1670(2)	6158(17)	1435(3)	3.1	C(36B)	3135(2)	1377(17)	8905(3)	2.8
C(37A)	2181(2)	7468(18)	1721(4)	3.4	C(37B)	2621(2)	2474(16)	8585(3)	2.9
C(38A)	2549(2)	7273(13)	2505(3)	1.5	C(38B)	2255(3)	2594(22)	7786(4)	4.9

served and calculated structure factors, parameters of hydrogen atoms and thermal parameters for non-hydrogen atoms are kept in the office of the chemical society of Japan (Document No. 8250). The computation was done on the M-180 computer at Tokyo Institute of Technology and on the M-200H computer at the Computer Center of the University of Tokyo.

Results

Figure 1 illustrates the crystal structure viewed along the b axis. There exist two crystallographically independent molecules, A and B, in an asymmetric unit. Figure 2 shows the perspective drawing of the A molecule. A similar figure has been obtained for the B molecule. Molecules are largely distorted from a planar structure due to the repulsions between crowded hydrogen atoms. The numbering scheme is indicated in Fig. 3, together with the average values of the two corresponding bond lengths in the A and B molecules. Individual bond lengths and angles for each molecule are listed in Tables 3 and 4, respectively. The average C–C length of 1.413(10) Å is similar to 1.41(1) Å in NT,[6] 1.407(6) Å in 7*H*-benzo[*hi*]chrysen-7-one,[7] and 1.409(9) Å in tetrabenzo[*a,cd,j,lm*]perylene (TBP).[8] Although the values of the bond lengths and angles are not so reliable due to the pseudo symmetry described above, a similar distortion of the NT moiety is observed; the bond lengths of C(20)–C(21), C(36)–C(37), and C(11)–C(12) increases in that order (1.37→1.42→1.48 Å). They correspond to the sequences observed in TBP (1.348→1.418→1.474 Å) and DPP (1.37→1.43→1.49 Å).[9]

Although the C–C–C bond angles range from 115°

to 129°, the three bonds around each carbon atom are nearly coplanar. The large difference in the bond angle C(10)-C(11)-C(12), 128.7° in A and 120.9° in B, will be discussed in the next section.

The molecules are stacked face-to-face by van der Waals forces to make column structures along the b axis. Figure 4 shows the overlapping mode of the A molecules; the situation for the B molecule is close to this. A list of the equations of several planes and their dihedral angles is deposited in the office of the Chemical Society of Japan. The deviations of the atoms from the mean plane of the whole molecule range from 0.92 to −0.60 Å. The interplanar spacings are 3.67 Å in A and 3.66 Å in B, which are

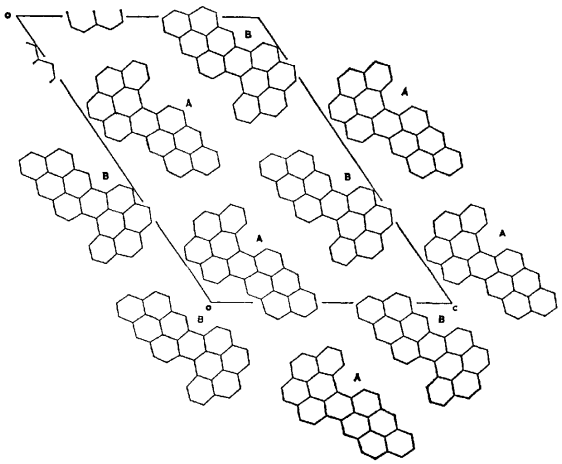

Fig. 1. A projection of the crystal structure along the b axis.

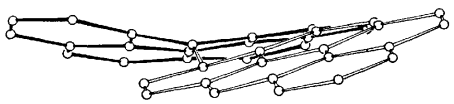

Fig. 2. A perspective drawing of the A molecule.

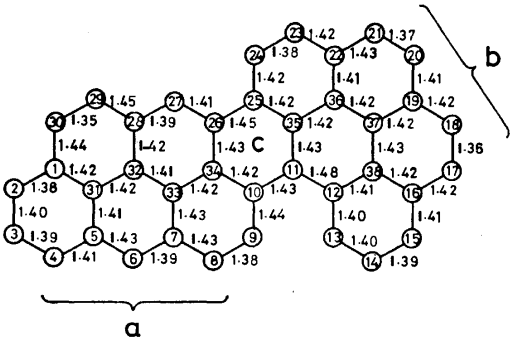

Fig. 3. The numbering scheme and mean values (l/Å) of bond lengths in the A and B molecules.

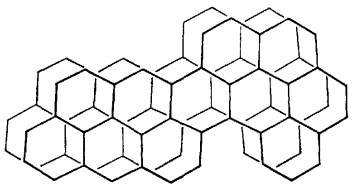

Fig. 4. Overlapping mode of the A molecules.

Table 3. Bond lengths

	A	B		A	B
	l/Å	l/Å		l/Å	l/Å
C(1)—C(2)	1.405	1.358	C(17)—C(18)	1.359	1.363
C(1)—C(30)	1.414	1.466	C(18)—C(19)	1.414	1.434
C(1)—C(31)	1.409	1.434	C(19)—C(20)	1.398	1.418
C(2)—C(3)	1.406	1.394	C(19)—C(37)	1.425	1.407
C(3)—C(4)	1.405	1.371	C(20)—C(21)	1.377	1.357
C(4)—C(5)	1.405	1.416	C(21)—C(22)	1.422	1.443
C(5)—C(6)	1.409	1.439	C(22)—C(23)	1.407	1.424
C(5)—C(31)	1.413	1.414	C(22)—C(36)	1.410	1.406
C(6)—C(7)	1.409	1.364	C(23)—C(24)	1.401	1.351
C(7)—C(8)	1.410	1.447	C(24)—C(25)	1.410	1.430
C(7)—C(33)	1.412	1.438	C(25)—C(26)	1.446	1.447
C(8)—C(9)	1.400	1.349	C(25)—C(35)	1.408	1.423
C(9)—C(10)	1.413	1.459	C(26)—C(27)	1.394	1.432
C(10)—C(11)	1.448	1.413	C(26)—C(34)	1.457	1.403
C(10)—C(34)	1.409	1.433	C(27)—C(28)	1.380	1.397
C(11)—C(12)	1.497	1.464	C(28)—C(29)	1.432	1.458
C(11)—C(35)	1.443	1.420	C(28)—C(32)	1.429	1.405
C(12)—C(13)	1.407	1.392	C(29)—C(30)	1.357	1.350
C(13)—C(38)	1.409	1.407	C(31)—C(32)	1.407	1.440
C(12)—C(14)	1.404	1.389	C(32)—C(33)	1.424	1.398
C(14)—C(15)	1.404	1.378	C(33)—C(34)	1.407	1.429
C(15)—C(16)	1.407	1.405	C(35)—C(36)	1.408	1.439
C(16)—C(17)	1.396	1.446	C(36)—C(37)	1.439	1.408
C(16)—C(38)	1.408	1.432	C(37)—C(38)	1.421	1.442

The e.s.d.'s range from 0.009 to 0.012 Å.

Table 4. Bond angles

	A	B		A	B
	ϕ/°	ϕ/°		ϕ/°	ϕ/°
C(2)--C(1)--C(30)	120.3	123.6	C(23)-C(22)-C(36)	119.8	119.5
C(2)--C(1)--C(31)	119.9	119.0	C(22)-C(23)-C(24)	120.1	120.7
C(30)-C(1)--C(31)	119.7	117.4	C(23)-C(24)-C(25)	120.4	121.7
C(1)--C(2)--C(3)	120.2	122.2	C(24)-C(25)-C(26)	121.1	121.3
C(2)--C(3)--C(4)	119.9	120.0	C(24)-C(25)-C(35)	119.6	119.0
C(3)--C(4)--C(5)	120.2	120.4	C(26)-C(25)-C(35)	119.2	119.6
C(4)--C(5)--C(6)	120.1	123.9	C(25)-C(26)-C(27)	122.1	122.7
C(4)--C(5)--C(31)	119.9	119.1	C(25)-C(26)-C(34)	120.7	117.0
C(6)--C(5)--C(31)	120.0	117.0	C(27)-C(26)-C(34)	116.6	120.3
C(5)--C(6)--C(7)	123.4	119.9	C(26)-C(27)-C(28)	122.7	120.0
C(6)--C(7)--C(8)	125.2	117.6	C(27)-C(28)-C(29)	123.2	118.4
C(6)--C(7)--C(33)	115.1	125.1	C(27)-C(28)-C(32)	118.9	120.4
C(8)--C(7)--C(33)	119.7	117.3	C(29)-C(28)-C(32)	117.1	120.9
C(7)--C(8)--C(9)	120.1	121.9	C(28)-C(29)-C(30)	123.9	117.9
C(8)--C(9)--C(10)	120.3	121.5	C(1)--C(30)-C(29)	118.8	123.9
C(9)--C(10)-C(11)	117.6	125.0	C(1)--C(31)-C(5)	119.9	119.3
C(9)--C(10)-C(34)	119.6	118.0	C(1)--C(31)-C(32)	121.3	119.4
C(11)-C(10)-C(34)	122.7	116.7	C(5)--C(31)-C(32)	118.8	121.3
C(10)-C(11)-C(12)	128.7	120.9	C(28)-C(32)-C(31)	119.1	120.2
C(10)-C(11)-C(35)	116.7	120.0	C(28)-C(32)-C(33)	121.6	118.1
C(12)-C(11)-C(35)	114.6	118.9	C(31)-C(32)-C(33)	119.3	121.7
C(11)-C(12)-C(13)	120.0	123.4	C(7)--C(33)-C(32)	123.4	115.0
C(11)-C(12)-C(38)	119.4	118.2	C(7)--C(33)-C(34)	120.1	121.3
C(13)-C(12)-C(38)	119.7	118.3	C(32)-C(33)-C(34)	116.4	123.7
C(12)-C(13)-C(14)	120.2	121.1	C(10)-C(34)-C(26)	117.0	124.1
C(13)-C(14)-C(15)	120.1	121.0	C(10)-C(34)-C(33)	120.0	119.5
C(14)-C(15)-C(16)	120.0	120.1	C(26)-C(34)-C(33)	123.0	116.4
C(15)-C(16)-C(17)	118.9	122.6	C(11)-C(35)-C(25)	121.1	120.5
C(15)-C(16)-C(38)	119.8	118.5	C(11)-C(35)-C(36)	118.8	120.8
C(17)-C(16)-C(38)	121.1	118.7	C(25)-C(35)-C(36)	120.1	118.7
C(16)-C(17)-C(18)	119.7	121.5	C(22)-C(36)-C(35)	120.3	120.2
C(17)-C(18)-C(19)	122.0	120.5	C(22)-C(36)-C(37)	116.7	121.2
C(18)-C(19)-C(20)	125.2	119.4	C(35)-C(36)-C(37)	123.3	118.6
C(18)-C(19)-C(37)	118.4	119.6	C(19)-C(37)-C(36)	123.0	118.2
C(20)-C(19)-C(37)	116.5	120.7	C(19)-C(37)-C(38)	119.5	120.5
C(19)-C(20)-C(21)	122.4	120.9	C(36)-C(37)-C(38)	117.0	121.1
C(20)-C(21)-C(22)	120.4	119.8	C(12)-C(38)-C(16)	120.2	120.6
C(21)-C(22)-C(23)	119.5	121.6	C(12)-C(38)-C(37)	120.3	120.1
C(21)-C(22)-C(36)	120.5	118.9	C(16)-C(38)-C(37)	119.0	118.5

The e.s.d.'s range from 0.6 to 0.8°.

comparable to 3.84 Å in DPP.[9]

The molecules can also be regarded as two nearly planar NT skeletons connected by the central benzene ring. The deviations from the mean planes of the NT skeletons a, b are shown in Fig. 5. In both molecules, the planarity of (a) is better than that of (b). This brings about a wider interplanar spacing between (b)'s than that between (a)'s. Their values are 3.48 and 3.57 Å in A and 3.46 and 3.57 Å in B for (a) and (b) stackings, respectively. Each pair of NT skeletons in the A and B molecules makes an angle of 22.3° and an angle of 23.0°, respectively. The mean plane of the central benzene ring makes an angle of 5.7° with (a) and of 17.0° with (b) in A. The corresponding ones are 9.2° and 14.3° in B. Both central benzene rings take conformations of twisted

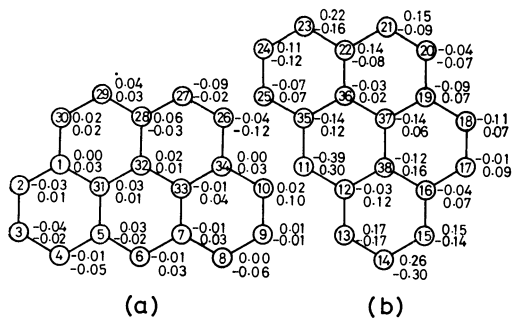

Fig. 5. Distances (l/Å) of atoms from the mean planes of (a) and (b) skeletons; upper and lower values of each pair refer to those in the A and B molecules, respectively.

boat form.

Discussion

The present study has established the structure of 3 and a large distortion from a planar structure occuring from the 1···7 interaction. Relief of such repulsion can be achieved by two modes of distortion as shown in Fig. 6; one is the enlargement of the C(3)–C(4)–C(5) angle, an angle-expansion mode, and the other is the twisting of the two C–C bonds opposite to each other, a twist mode. We define the values α and β to estimate the degree of the distortion as shown in Fig. 6. They are closely related to each other to avoid the 1···7 repulsion; β decreases with the increase of $(\alpha-120°)$.

In the present molecules, α and β of A are 128.7° and 30.1°, wheareas those of B are 120.9° and 37.6°, respectively. These values are significantly different for the two molecules. The repulsion has been relieved to equal extent, since the distance of C(9)···C(13) is 2.94 Å in A and 2.96 Å in B.

Four related molecules have been reported, as shown in Fig. 7, where the asterisks indicate the 1···7 interaction. The values of α and β, and the non-bonded distances between 2 and 6 carbon atoms are listed in Table 5. The four molecules are divided into two classes; an approximate two-fold axis exists perpendicular to the molecular plane in (1)—(3), whereas it lies in the molecular plane in (4). In each molecule of the former class, the two 1···7 repulsions may prevent the enlargement of α from 120° and should bring about the twisting mode. For the molecule of the latter class, on the other hand, only a repulsion may allow the angle-expansion mode to be taken.

Considering the values of α and β, the A and B molecules in the present crystal belong to the former and latter classes, respectively. The molecule has only a 1···7 repulsion between H(C9) and H(C13), but it has a fairly strong 1···6 repulsion between H(C24) and H(C27) opposite to the 1···7 repulsion. The distances between H(C24) and H(C27) are nearly the same as those of H(C9)···H(C13) for both molecules; 1.87(9) and 1.91(9) Å for A and 2.01(9) and 2.00(9) Å for B.†† The present molecule may be described as an intermediate between the two classes. Consequently, both modes of distortion characteristic of the two classes can occur and the two molecular conformations will probably be observed in solution.

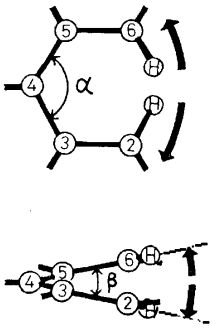

Fig. 6. Relief modes of 1···7 interaction.

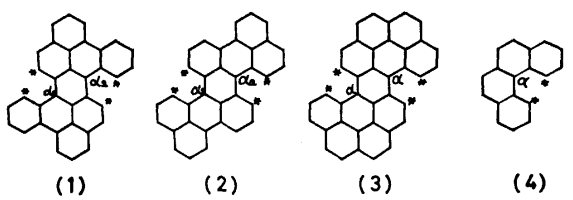

Fig. 7. (1): Tetrabenzo[*a,cd,j,lm*]perylene,[8] (2): tetrabenzo[*de,hi,op,st*]pentacene,[10] (3): diphenanthro[5,4,3-*abcd*:5′,4′,3′-*jklm*]perylene,[9] (4): benzo[*c*]phenanthrene.[11]

Table 5. Comparison of steric hindrances

Molecule	R		α/°	β/°	d(C···C)/Å
(1)[a]	0.056	α_1)	123.5	41.0	2.971
		α_2)	122.7	41.5	2.944
(2)	0.28 (*hk*0)	α_1)	130	25	2.84
	0.28 (0*kl*)	α_2)	126	37	3.08
(3)[b]	0.103 A)		119	39	3.01
	B)		121	30	2.87
This crystal	0.073 A)		128.7	30.1	2.94
	B)		120.9	37.6	2.96
(4)	0.23 (*hk*0)		131	32	3.01
	0.25 (0*kl*)				
	0.27 (*h*0*l*)				

a) The number of each molecule refers to that in Fig. 7. b) A and B indicate the crystallographically independent molecules which have symmetry C_2 perpendicular to molecular plane.

References

1) S. Fujisawa, J. Aoki, M. Takekawa, and S. Iwashima, *Bull. Chem. Soc. Jpn.*, **52**, 2159 (1979).
2) Y. Kamura, H. Inokuchi, J. Aoki, and S. Fujisawa, *Chem. Phys. Lett.*, **46**, 356 (1977).
3) P. Main, L. Lessinger, M. M. Woolfson, G. Germain, and J. P. Declercq, MULTAN78. A System of Computer Programs for the Automatic Solution of Crystal Structure from X-Ray Diffraction Data. Univs. of York, England, and Louvain, Belgium (1978).
4) G. M. Sheldrick, SHELX. A program for crystal structure determination. Univ. of Cambridge, England (1976).
5) "International Tables for X-Ray Crystallography," Birmingham, Kynoch Press (1974), Vol. IV.
6) S. Fujisawa, I. Oonishi, J. Aoki, and S. Iwashima, *Bull. Chem. Soc. Jpn.*, **49**, 3454 (1976).
7) S. Fujisawa, S. Sato, and Y. Saito, *Acta Crystallogr., Sect. B*, **37**, 2194 (1981).
8) Y. Kohno, M. Konno, Y. Saito, and H. Inokuchi, *Acta Crystallogr., Sect. B*, **31**, 2076 (1975).
9) I. Oonishi, S. Fujisawa, J. Aoki, and T. Danno, *Bull. Chem. Soc. Jpn.*, **51**, 2259 (1978).
10) M. G. Rossmann, *J. Chem. Soc.*, **1959**, 2607.
11) F. H. Herbstein and G. M. J. Schmidt, *J. Chem. Soc.*, **1954**, 3302.

†† The distances of H···H based on the coordinates derived from an idealized geometry are 1.87 (H(C9)···H(C13)) and 1.87 Å (H(C24)···H(C27)) in A, and those of B are 1.96 and 2.02 Å. These agree with the observed values within the estimated standard deviations.

The Crystal and Molecular Structure of 3-(1,4-Epoxy-2-hydroxy-2,6,6-trimethylcyclohexyl)-1-methyl-2-propyl *p*-Nitrobenzoate

Yukishige KITANO,* Tetsuya KATO,† Hisao KONDO,† and Tamaichi ASHIDA††

Toray Research Center Inc., Sonoyama, Ohtsu 520

†*Basic Research Laboratories, Toray Industries, Inc., Tebiro, Kamakura 248*

††*Faculty of Engineering, Nagoya University, Chikusa-ku, Nagoya 464*

(Received January 11, 1982)

The relative configuration of natural 3,6-epoxy-5-hydroxy-5,6-dihydro-β-ionol, $C_{13}H_{22}O_3$, a principal tobacco constituent, has been established by an X-ray crystal structure analysis of its *p*-nitrobenzoate, $C_{20}H_{25}NO_6$, as (±)-(1*R*,2*R*,5*S*)-2,5-epoxy-2-[(1*E*,3*S*)-3-hydroxy-1-butenyl]-1,3,3-trimethyl-1-cyclohexanol. The derivative crystallizes in space group $P\bar{1}$ with $a=11.618(1)$, $b=12.373(2)$, $c=7.934(1)$ Å, $\alpha=108.43(1)$, $\beta=108.89(1)$, $\gamma=95.95(1)°$ and $Z=2$. The crystal structure was solved by the direct phasing method and refined by the block-diagonal least-squares method to the final *R* index of 0.073 for 2550 reflections. The hydrogen bondings linking the two molecules placed in pairs around a crystallographic center of symmetry are disordered over two sites in the crystal.

A novel flavor substance, (−)-3,6-epoxy-5-hydroxy-5,6-dihydro-β-ionol (**1**), was initially found in the volatile fraction of air-cured Japanese Suifu tobacco.[1] Enzell *et al.* also isolated the compound **1** from sun-cured Greek tobacco and established the relative configurations at C-3, C-5, and C-6, but the configuration at the remaining asymmetric center, C-9, remained unsettled.[2] In order to establish this relative configuration at C-9, the crystalline *p*-nitrobenzoate derivative **2** was synthesized and subjected to a single crystal X-ray diffraction analysis. A brief account on this work has appeared previously.[3]

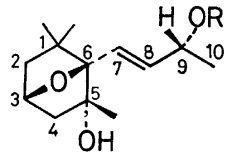

1 R=H

2 R=*p*-Nitrobenzoyl

Experimental

The title compound was crystallized from a hexane solution as colorless plates elongated along the b direction. A well-shaped crystal of dimensions $0.05\times0.3\times0.2$ mm³ was mounted with the b axis coincident with the goniometer ϕ axis and used for the X-ray measurements. Preliminary unit cell dimensions and space group information were obtained from oscillation and Weissenberg photographs. Accurate cell dimensions were obtained by a least-squares fit of the 2θ values of 25 reflections measured on a Rigaku automated four-circle diffractometer. Intensity data were also collected on this instrument using graphite-monochromated Cu $K\alpha$ radiation and 2θ-ω scanning mode at a rate of $10°(\omega)$/min with a scan range of $(0.8+0.142\tan\theta)°(\omega)$. As a check on the crystal and electronic stability, three representative reflections were measured after every 50 measurements. The intensities of these standards decreased gradually during the data collection. A total of 2550 unique reflection intensities were collected up to $2\theta=120°$ with the criterion $F\geqq3\sigma(F)$; these were corrected for crystal deterioration and for Lorentz and polarization effects, but not for absorption.

Crystal Data. $C_{20}H_{25}NO_6$, M.W.=375.41, triclinic, space group $P\bar{1}$, $a=11.618(1)$, $b=12.373(2)$, $c=7.934(1)$ Å, $\alpha=108.43(1)$, $\beta=108.89(1)$, $\gamma=95.95(1)°$, $V=996.51$ Å³, $D_m=1.24$, and $D_x=1.252$ Mg m^{-3} for $Z=2$, μ(Cu $K\alpha$)=7.76 cm^{-1}.

Structure Determination and Refinement

The structure was solved by the multiple-solution tangent formula program MULTAN 78.[4] The phase set with the highest combined figure of merit gave a reasonable structure containing all the atoms except one. Successive Fourier and difference Fourier maps revealed all the remaining atoms including hydrogen atoms. The parameters were refined by the block-diagonal least-squares program HBLS V.[5] The final refinement in which anisotropic temperature factors were assumed for the non-hydrogen atoms and isotropic ones for the hydrogen atoms gave $R=0.073$ for 2550 reflections. In the refinement the function minimized was $\Sigma\omega(|F_o|-|F_c|)^2$ with $\omega=(\sigma^2(F_o)+a|F_o|+b|F_o|^2)^{-1}$ where $\sigma(F_o)$ is the standard deviation based on counting statistics. The final values of *a* and *b* were −0.1262 and 0.0029 respectively. The atomic scattering factors were taken from International Tables for X-Ray Crystallography.[6] Final positional and thermal parameters of the atoms are listed in Tables 1 and 2.[7]

Discussion

A stereodrawing of the molecule is shown in Fig. 1. Figure 2 shows the atomic labelling and the bond lengths and angles for non-hydrogen atoms. Bond lengths and angles involving hydrogen atoms are shown in Table 3. The conformations around the C(6)–C(1) and C(6)–C(5) bonds are shown in Fig. 3 as the Newmann projections. Further details of the molecular geometry are given in Table 4. The estimated standard deviations of the bond lengths for non-hydrogen atoms are 0.006—0.009 Å, while those of the bond angles are 0.4—0.6°.

Since the atoms C(3) and C(6) are bridged by an epoxyl O(1) atom, the cyclohexane ring adopts a boat conformation. The epoxyl bridge plane C(3)–O(1)–C(6) bisects the cyclohexane ring at the dihedral angles of 124.8° and 118.2° to the C(6)–C(1)–C(2)–C(3) plane and C(3)–C(4)–C(5)–C(6) planes respectively. The O(2)H and C(12)H_3 groups are axially attached to the cyclohexane ring; this severe 1,3-

TABLE 1. POSITIONAL($\times 10^4$) AND THERMAL ($\times 10$) PARAMETERS FOR THE NON-HYDROGEN ATOMS

Atom	x	y	z	B_{eq}/Å^2 a)
C(1)	5139(4)	2822(4)	7067(7)	53
C(2)	5121(5)	1533(4)	5946(8)	68
C(3)	6240(6)	1692(4)	5406(8)	69
C(4)	5935(6)	2151(4)	3717(8)	73
C(5)	6062(4)	3450(4)	4789(7)	51
C(6)	6277(4)	3496(3)	6896(6)	45
C(7)	6856(4)	4680(4)	8395(6)	45
C(8)	8034(4)	5070(4)	9625(6)	48
C(9)	8521(4)	6282(4)	11063(6)	51
C(10)	9272(6)	6347(6)	13054(8)	82
C(11)	5495(6)	2997(4)	9220(7)	67
C(12)	3873(5)	3160(4)	6329(8)	65
C(13)	7185(5)	4206(5)	4799(8)	68
C(14)	8888(4)	7529(4)	9454(8)	64
C(15)	9823(5)	8178(4)	9001(7)	58
C(16)	11094(4)	8268(4)	9887(7)	60
C(17)	11943(5)	8935(4)	9532(8)	65
C(18)	11507(5)	9506(4)	8278(8)	63
C(19)	10239(5)	9421(4)	7358(7)	62
C(20)	9404(5)	8760(4)	7743(7)	62
N	12411(4)	10223(4)	7910(7)	76
O(1)	7115(3)	2723(2)	6999(4)	55
O(2)	4990(3)	3850(3)	3933(5)	60
O(3)	9379(3)	6939(3)	10560(5)	59
O(4)	7782(3)	7530(3)	8833(6)	78
O(5)	13523(4)	10358(3)	8820(7)	86
O(6)	12013(5)	10641(4)	6667(7)	106

a) The equivalent isotropic temperature factor defined by W. C. Hamilton (*Acta Crystallogr.*, **12**, 609 (1959)).

TABLE 2. POSITIONAL($\times 10^3$) AND ISOTROPIC THERMAL ($\times 10$) PARAMETERS FOR THE HYDROGEN ATOMS

Atom	x	y	z	B/Å^2
H1(C2)	512(5)	104(5)	689(8)	67(15)
H2(C2)	416(5)	102(4)	483(7)	64(14)
H(C3)	675(4)	107(4)	525(6)	39(11)
H1(C4)	656(4)	211(3)	332(5)	26(9)
H2(C4)	503(5)	158(5)	254(8)	66(14)
H(C7)	638(4)	530(3)	830(6)	28(9)
H(C8)	859(4)	436(3)	966(6)	32(10)
H(C9)	792(3)	678(3)	1110(5)	22(9)
H1(C10)	975(4)	585(3)	1301(6)	31(10)
H2(C10)	865(4)	572(4)	1339(6)	40(11)
H3(C10)	963(5)	732(5)	1387(7)	65(14)
H1(C11)	554(4)	382(4)	996(7)	48(12)
H2(C11)	493(5)	235(4)	930(7)	57(13)
H3(C11)	637(5)	278(5)	957(7)	66(15)
H1(C12)	395(4)	395(3)	691(6)	27(9)
H2(C12)	333(4)	276(4)	655(7)	52(13)
H3(C12)	371(5)	279(4)	475(7)	61(14)
H1(C13)	789(4)	414(4)	538(6)	36(10)
H2(C13)	715(5)	511(5)	551(7)	65(14)
H3(C13)	723(4)	413(4)	361(6)	36(10)
H(C16)	1124(5)	768(4)	1077(7)	60(14)
H(C17)	1291(4)	897(4)	1004(7)	53(13)
H(C19)	979(6)	1007(6)	653(9)	92(18)
H(C20)	852(5)	893(4)	756(7)	65(14)
H1(O2)a)	507(10)	468(7)	466(14)	35(22)
H2(O2)a)	434(10)	292(10)	319(15)	71(31)

a) Occupancy factor 0.5.

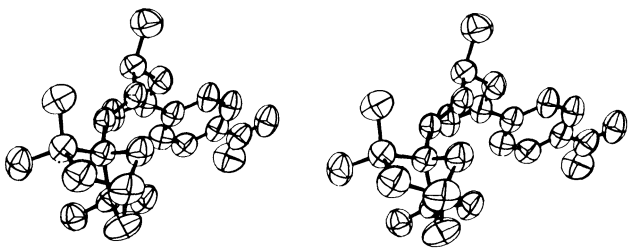

Fig. 1. A stereodrawing of the molecule viewed along the b axis.
The thermal ellipsoids correspond to 50% probability.

diaxial interaction results in an enlargement of the C(6)-C(5)-O(2), C(1)-C(6)-C(5), and C(6)-C(1)-C(12) bond angles (114.5, 114.4, and 116.8° respectively). In the side chain, the atoms C(6), C(7), C(8), and C(9) make a plane, the C(8) and O(1) atoms being synperiplanar about the C(6)-C(7) bond, while the atoms C(10) and O(3) deviate significantly from this plane onto the opposite sides; the torsion angles C(7)-C(8)-C(9)-C(10) and C(7)-C(8)-C(9)-O(3) are 132.9° and −110.0° respectively. The mean C–C length of 1.549 Å in the cyclohexane ring agrees well with the expected value and the three methyl carbons also have a reasonable mean bond length of 1.543 Å. The epoxyl O(1)-C(3) and O(1)-C(6)

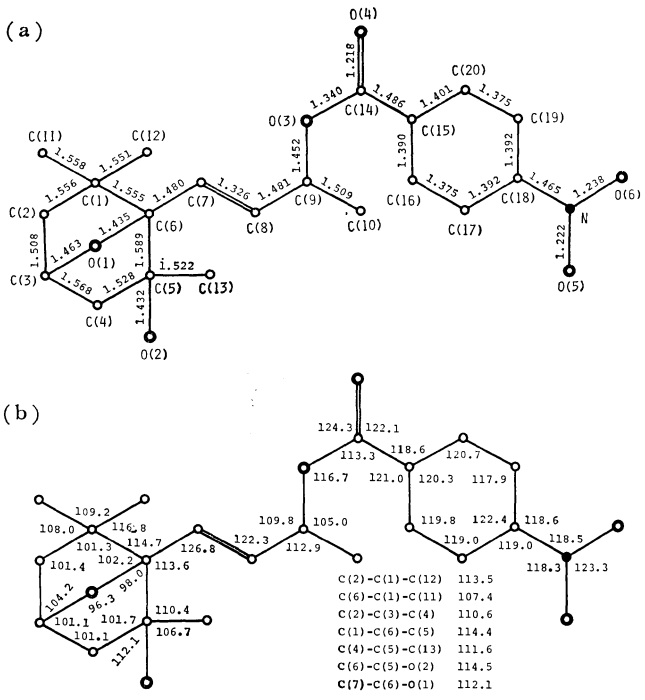

Fig. 2. A schematic drawing of the molecule showing (a) the bond lengths (l/Å) and (b) the bond angles (ϕ/°), together with atomic numbering.

TABLE 3. BOND LENGTHS AND ANGLES INVOLVING THE HYDROGEN ATOMS

Bond length	l/Å		l/Å
C(2)-H1(C2)	1.11(6)	C(2)-H2(C2)	1.13(6)
C(3)-H(C3)	1.02(5)	C(4)-H1(C4)	0.89(4)
C(4)-H2(C4)	1.13(6)	C(7)-H(C7)	1.00(4)
C(8)-H(C8)	1.15(5)	C(9)-H(C9)	0.98(4)
C(10)-H1(C10)	0.87(5)	C(10)-H2(C10)	1.15(5)
C(10)-H3(C10)	1.13(6)	C(11)-H1(C11)	0.99(5)
C(11)-H2(C11)	1.02(6)	C(11)-H3(C11)	1.05(6)
C(12)-H1(C12)	0.92(5)	C(12)-H2(C12)	0.85(5)
C(12)-H3(C12)	1.13(6)	C(13)-H1(C13)	0.83(5)
C(13)-H2(C13)	1.09(6)	C(13)-H3(C13)	0.94(5)
C(16)-H(C16)	1.15(6)	C(17)-H(C17)	1.06(5)
C(19)-H(C19)	1.24(7)	C(20)-H(C20)	1.05(6)
O(2)-H1(O2)	0.99(11)	O(2)-H2(O2)	0.78(12)
Bond angle	ϕ/°		ϕ/°
C(1)-C(2)-H1(C2)	108(3)	C(3)-C(2)-H1(C2)	119(3)
C(1)-C(2)-H2(C2)	113(3)	C(3)-C(2)-H2(C2)	122(3)
C(2)-C(3)-H(C3)	121(3)	C(4)-C(3)-H(C3)	112(3)
C(3)-C(4)-H1(C4)	107(3)	C(5)-C(4)-H1(C4)	106(3)
C(3)-C(4)-H2(C4)	109(3)	C(5)-C(4)-H2(C4)	122(3)
C(6)-C(7)-H(C7)	117(3)	C(8)-C(7)-H(C7)	115(3)
C(7)-C(8)-H(C8)	115(2)	C(9)-C(8)-H(C8)	122(3)
C(8)-C(9)-H(C9)	117(2)	C(10)-C(9)-H(C9)	111(2)
C(9)-C(10)-H1(C10)	111(3)	C(9)-C(10)-H2(C10)	106(3)
C(9)-C(10)-H3(C10)	102(3)	C(1)-C(11)-H1(C11)	109(3)
C(1)-C(11)-H2(C11)	108(3)	C(1)-C(11)-H3(C11)	102(3)
C(1)-C(12)-H1(C12)	111(3)	C(1)-C(12)-H2(C12)	108(4)
C(1)-C(12)-H3(C12)	97(3)	C(5)-C(13)-H1(C13)	118(3)
C(5)-C(13)-H2(C13)	105(3)	C(5)-C(13)-H3(C13)	117(3)
C(15)-C(16)-H(C16)	109(3)	C(17)-C(16)-H(C16)	130(3)
C(16)-C(17)-H(C17)	124(3)	C(18)-C(17)-H(C17)	117(3)
C(18)-C(19)-H(C19)	126(3)	C(20)-C(19)-H(C19)	115(3)
C(19)-C(20)-H(C20)	120(3)	C(15)-C(20)-H(C20)	115(3)
C(5)-O(2)-H1(O2)	111(7)	C(5)-O(2)-H2(O2)	120(8)

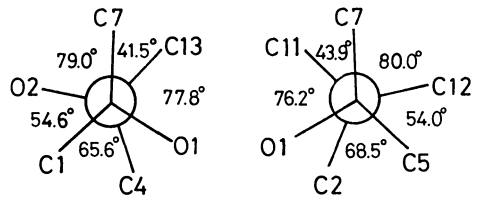

(a) (b)

Fig. 3. Newmann projections showing the conformations about (a) the C(6)-C(5) and (b) C(6)-C(1) bonds.

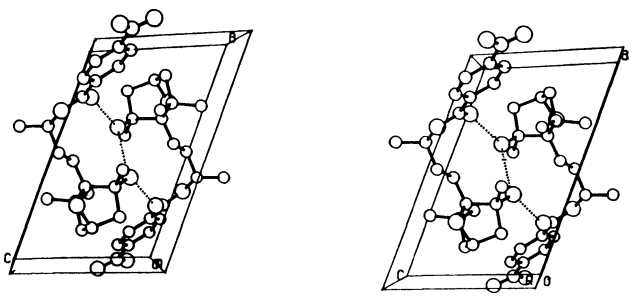

Fig. 4. A stereodrawing of the molecular packing viewed along the a axis.
Hydrogen bondings are shown by dotted lines.

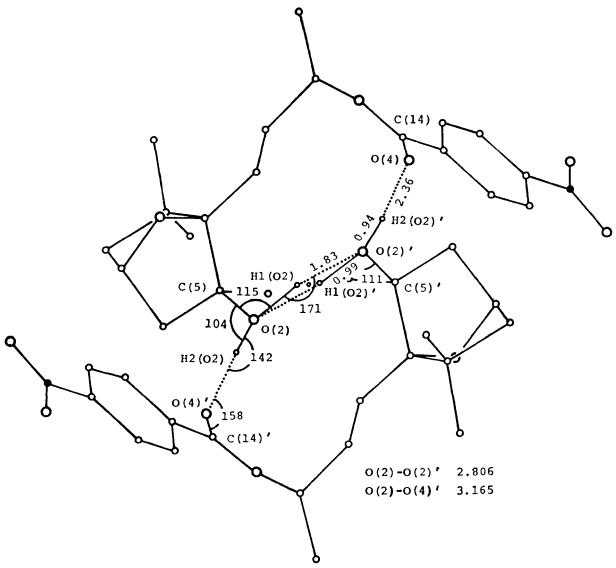

Fig. 5. Interatomic distances and angles associated with the hydrogen bondings.

TABLE 4. MOLECULAR GEOMETRY

(1) Least-squares planes defined by atomic positions and deviations (d/Å) of the atoms[a)]

Plane (1): C(1), C(2), C(3), and C(6)

$-0.3384X+0.3931Y-0.8550Z+4.895=0$

C(1) −0.009(17) C(2) 0.012(17) C(3) −0.010(17) C(6) 0.005(16) O(1)[b)] 0.80(2)

Plane (2): C(3), O(1), and C(6)

$-0.5501X-0.5404Y+0.6366Z+1.017=0$

C(1)[b)] 1.25(4) C(2)[b)] 1.21(4) C(4)[b)] −1.32(4) C(5)[b)] −1.39(4)

Plane (3): C(3), C(4), C(5), and C(6)

$0.9635X+0.1519Y+0.2203Z-6.324=0$

C(3) 0.031(12) C(4) −0.051(12) C(5) 0.027(11) C(6) −0.017(11) O(1)[b)] 0.86(1)

Plane (4): C(6), C(7), C(8), and C(9)

$-0.4797X-0.5867Y+0.6525Z+0.690=0$

C(6) −0.003(30) C(7) 0.004(30) C(8) 0.003(30) C(9) −0.003(30) C(3)[b)] 0.10(3)
C(10)[b)] 1.01(3) O(1)[b)] 0.12(3)

Plane (5): C(15), C(16), C(17), C(18), C(19), and C(20)

$-0.3228X+0.5584Y+0.7642Z-6.412=0$

C(15) 0.001(32) C(16) −0.003(32) C(17) 0.001(32) C(18) 0.004(32)
C(19) −0.005(32) C(20) 0.003(32) C(14)[b)] 0.09(3) O(3)[b)] −0.02(3)
O(4)[b)] 0.22(3) N[b)] 0.02(3) O(5)[b)] 0.12(3) O(6)[b)] −0.10(3)

(2) Dihedral angles (ϕ/°) between the planes

(1) and (2) 124.8(4) (1) and (3) 117.0(3) (1) and (4) 128.8(4) (2) and (3) 118.2(4)
(2) and (4) 4.9(6) (4) and (5) 71.1(3) (3) and (4) 114.0(4)

(3) Torsion angles

	ϕ/°		ϕ/°
C(6)-C(1)-C(2)-C(3)	1.7(6)	C(1)-C(2)-C(3)-C(4)	−75.4(6)
C(2)-C(3)-C(4)-C(5)	79.0(6)	C(3)-C(4)-C(5)-C(6)	−5.9(6)
C(4)-C(5)-C(6)-C(1)	−65.6(5)	C(5)-C(6)-C(1)-C(2)	68.8(5)
C(3)-O(1)-C(6)-C(1)	55.5(4)	C(3)-O(1)-C(6)-C(5)	−61.6(4)
C(3)-O(1)-C(6)-C(7)	178.8(4)	C(8)-C(9)-O(3)-C(14)	91.3(5)
C(10)-C(9)-O(3)-C(14)	−146.5(5)	C(8)-C(7)-C(6)-O(1)	5.5(7)
C(8)-C(7)-C(6)-C(1)	121.4(6)	C(8)-C(7)-C(6)-C(5)	−104.4(6)
C(7)-C(6)-C(1)-C(11)	−44.2(6)	C(7)-C(6)-C(1)-C(12)	78.8(6)
C(7)-C(6)-C(5)-C(13)	41.5(6)	C(7)-C(6)-C(5)-O(2)	−78.8(6)
C(6)-O(1)-C(3)-C(2)	−55.7(5)	C(6)-O(1)-C(3)-C(4)	59.1(5)
C(6)-C(7)-C(8)-C(9)	179.4(4)	C(7)-C(8)-C(9)-C(10)	132.9(5)
C(7)-C(8)-C(9)-O(3)	−110.0(5)	C(9)-O(3)-C(14)-O(4)	−1.2(9)
C(16)-C(15)-C(14)-O(3)	−8.2(8)	C(20)-C(15)-C(14)-O(4)	−3.2(9)
C(17)-C(18)-N-O(5)	−4.8(9)	C(19)-C(18)-N-O(6)	−6.4(9)

a) X, Y, and Z are coordinates expressed by the following equation

$$\begin{pmatrix} X \\ Y \\ Z \end{pmatrix} = \begin{pmatrix} a & b\cos\gamma & c\cos\beta \\ 0 & b\sin\gamma & -c\cos\alpha^{*}\sin\beta \\ 0 & 0 & c\sin\alpha^{*}\sin\beta \end{pmatrix} \begin{pmatrix} x \\ y \\ z \end{pmatrix}.$$

b) Atoms not included in the calculation of the plane.

distances (1.463 Å and 1.435 Å) and C(3)-O(1)-C(6) angle (96.3°) compare well with the values 1.443 Å, 1.452 Å and 96.2° for a toxisterol epoxide[8)] and the values 1.448 Å, 1.459 Å and 97.0° for triterpenoid baccharis oxide.[9)] The C(7)-C(8) double bond length of 1.326 Å and the two neighboring C(sp^2)-C(sp^3) bond lengths of 1.480 Å and 1.481 Å are also reasonable. All bond lengths and angles in the *p*-nitrobenzoate moiety are normal.

The molecular arrangement of the crystal is shown in Fig. 4. The molecules are placed in pairs around a center of symmetry, connected by two kinds of hydrogen bonds. As shown in Fig. 5, the final difference Fourier synthesis phased by all the atoms except H(O2) atom gave two peaks (H1(O2) and H2(O2)) at the positions expected for the H(O2) atom. From the facts that the electron density map shows heights of 0.4 and 0.3 e/Å^3 at the H1(O2) and H2(O2) peaks respectively and that the both O(2)-H1(O2) and O(2)-H2(O2) directions are favorable for hydrogen-bond formation, it was concluded that the two kinds of hydrogen bond exist at random; *i.e.*, when the O(2)H hydroxyl group donates its proton to the O(2)′ atom of the molecule connected by the crystallographic center of symmetry at (1/2, 1/2, 1/2), the hydrogen bond O(2)′-H2(O2)′···O(4) is formed, while when the O(2)H group donates its proton to the O(4)′ atom, the O(2)′-H1(O2)′···O(2) hydrogen bond is formed. As a result of the random distribution of these hydrogen bonds, the crystal is kept centrosym-

Table 5. Intermolecular distances shorter than 3.5 Å

From the unit (x, y, z) to the unit $(-x, -y, -z)$

From	To	Distance	Translation
C(7)	O(2)	3.418(6)	(1, 1, 1)
O(2)	O(2)	2.806(7)	(1, 1, 1) a)
O(2)	O(4)	3.165(6)	(1, 1, 1) a)
O(4)	O(5)	3.371(9)	(2, 1, 1)
O(19)	O(6)	3.383(8)	(2, 2, 1)
C(16)	O(1)	3.326(7)	(2, 1, 2)
C(15)	C(19)	3.453(8)	(2, 2, 2)
C(18)	O(4)	3.496(8)	(2, 2, 2)
O(4)	O(5)	3.489(7)	(2, 2, 2)
O(4)	O(6)	3.486(7)	(2, 2, 2)
N	O(4)	3.228(7)	(2, 2, 2)

a) Hydrogen bonding.

metric. The intermolecular distances less than 3.5 Å are listed in Table 5. Excepting the hydrogen-bond interactions, there are no closer intermolecular contacts than van der Waals contacts.

This X-ray crystallographic study showed the relative configuration of **1** to be (±)-(1*R*,2*R*,5*S*)-2,5-epoxy-2-[(1*E*,3*S*)-3-hydroxy-1-butenyl]-1,3,3-trimethyl-1-cyclohexanol.

References

1) Y. Takagi, T. Fujimoto, H. Kaneko, T. Fukuzumi, and M. Noguchi, 22nd Symposium on the Chemistry of Terpenes, Essential Oils and Aromatics, Yokohama, 1978, Abstr. No. A23.

2) D. Behr, I. Wahlberg, T. Nishida, and C. R. Enzell, *Acta Chem. Scand., Sect. B*, **33**, 701 (1979).

3) T. Kato, H. Kondo, Y. Kitano, G. Hata, and Y. Takagi, *Chem. Lett.*, **1980**, 757 and 8th International Congress on Essential Oils, Paris, Oct., 1980.

4) P. Main, S. E. Hull, L. Lessinger, G. Germain, J. P. Declercq, and M. M. Woolfson, "MULTAN 78, A System of Computer Programmes for The Automatic Solution of Crystal Structure from X-Ray Diffraction Data," Univ. of York, England, and Louvain, Belgium (1978).

5) T. Ashida, "The Universal Crystallographic Computing System-Osaka," The Computation Center, Osaka University (1973).

6) "International Tables for X-Ray Crystallography," Kynoch Press, Birmingham (1974), Vol. IV, p. 72.

7) The lists of structure factors and anisotropic thermal parameters for the non-hydrogen atoms are deposited at the office of this Bulletin as Document No. 8256.

8) P. F. Lindley and M. M. Mahmoud, *Acta Crystallogr., Sect. B*, **34**, 445 (1978).

9) F. Mo, *Acta Crystallogr., Sect. B*, **29**, 1769 (1973).

The Complex Formation of Poly(*N*-vinylpyrrolidone) with Manganese Dodecyl Sulfate in Water Studied by ESR

Masayuki AIZAWA,* Tsuyoshi KOMATSU, and Tsurutaro NAKAGAWA
Department of Polymer Science, Faculty of Science, Hokkaido University, Sapporo 060
(Received February 4, 1982)

ESR measurements of Mn^{2+} ions in aqueous manganese dodecyl sulfate ($Mn(DS)_2$) solutions with or without 0.05% poly(*N*-vinylpyrrolidone)(PVP) were carried out at 30 °C. The dependences of linewidths and of absorption intensities on the $Mn(DS)_2$ concentration in ($Mn(DS)_2$+0.05% PVP) solutions changed abruptly at a concentration where a PVP–$Mn(DS)_2$ complex begins to form. The same dependence in $Mn(DS)_2$ solutions was found around the CMC of $Mn(DS)_2$ in water. From the quantitative analysis of the data obtained, it was concluded that the $Mn(DS)_2$ molecules in the complex form a nearly micelle-like aggregate, and that most of Mn^{2+} ions bound onto the micelle-like aggregate or the $Mn(DS)_2$ micelle exist in the Stern layer. In addition, the PVP concentration dependence of the similar quantities in ($Mn(DS)_2$+PVP) solutions with a constant $Mn(DS)_2$ concentration suggested that the polymer–surfactant complex changes its structure at higher PVP concentrations.

In the past three decades, many investigators have been engaged in the study of the interaction between nonionic polymers and surfactants in water.[1] By applying various types of measurements (viscosity,[2–5] surface tension,[4,6,7] solubilization,[5–8] electric conductivity,[3–5] ionic activity,[5,9] *etc.*[10,11]) details of the interaction and its mechanism have become increasingly clear. One of the important observations reported so far is that a type of complex formation occurs between some polymers and surfactants; this was first suggested by the fact that the viscosity curve of some polymer solutions with surfactants resembles that of polyelectrolyte solutions.[12]

Since the complex can solubilize hydrophobic compounds,[1,8] its structure was presumed to have a hydrophobic region. The most acceptable structural model at present[1,7,9,10] has surfactants bound onto a polymer to form a micelle-like structure. The full description of the structure, however, has not yet been achieved completely. Several problems remain to be solved: the number of surfactant ions in one micelle-like aggregate;[10] the degree of dissociation of the counterions from the complex;[5] the binding mode of the polymer to the surfactants which constitute the micelle-like aggregate.[11]

Recently, magnetic resonance methods have been widely applied to study micellar solutions.[23] For example, the binding manner of ions to a micellar surface has been studied by the ESR measurement of manganese(II) ions (Mn^{2+} ions) introduced as counterions[13–15] or probe-ions[16] into micellar solutions. This method can yield information on the hydrophilic region of micelles in contrast with the spin-probe or spin-label method with nitroxide radicals which gives mainly information on the hydrophobic region of the micelles. If one uses surfactants which contain Mn^{2+} ions as counterions, this method is free from disturbing the system under investigation. In addition, ESR measurements by this method can easily be applied to systems with lower sample concentrations. In contrast, the NMR method requires a higher concentration owing to its lower sensitivity.[11]

The aim of the present paper is to investigate the behavior of Mn^{2+} ions in (polymer+surfactant) solutions by the ESR method to clarify the binding state of Mn^{2+} ions in the polymer–surfactant complex in comparison with the behavior of Mn^{2+} ions in $Mn(DS)_2$ solutions. In order to obtain the degree of dissociation of Mn^{2+} ions from the complex, absorption intensities of ESR signals will be measured. Linewidths of ESR signals will also be measured so as to establish the binding state of Mn^{2+} ions in the complex.

Experimental

Manganese dodecyl sulfate ($Mn(DS)_2$) was synthesized from commercial sodium dodecyl sulfate of specially prepared reagent grade and manganese chloride of guaranteed reagent grade according to Miyamoto's method.[17] The $Mn(DS)_2$ was purified by several recrystallization from water.

Poly(*N*-vinylpyrrolidone)(PVP) which was purchased from Nakarai Chemicals Ltd. was purified by dialysis using cellophane tubing.

Surface tension measurements by a capillary rise method were carried out at 25±0.05 °C to ascertain the purity of $Mn(DS)_2$ and the existence of the interaction between PVP and $Mn(DS)_2$ in water.

The ESR spectra were recorded at 30±0.5 °C on a JEOL model FEIX spectrometer equipped with a variable temperature accessory.

The ESR signal of solid DPPH was used as an external reference in the calculation of the absorption intensities of Mn^{2+} ions in a series of sample solutions.

Results and Discussion

In Fig. 1, the values of the surface tension of aqueous $Mn(DS)_2$ solutions are plotted against the molar concentration of $Mn(DS)_2$, *m*. Obviously there is no minimum in the resultant curve. From the break point on its curve, the value of the CMC of $Mn(DS)_2$ in water was estimated to be 1.4 mmol kg^{-1} which is slightly higher than that reported in the literature.[18]

A similar plot of aqueous ($Mn(DS)_2$+0.05% PVP) solutions is also illustrated in Fig. 1; in this case, *m* is the number of moles of $Mn(DS)_2$ per kilogram of a 0.05% aqueous PVP solution. This plot is evidently different from that of aqueous $Mn(DS)_2$ solutions. It has two break points whose concentrations do not coincide with the CMC of $Mn(DS)_2$ in water. This fact indicates that $Mn(DS)_2$ interacts with PVP

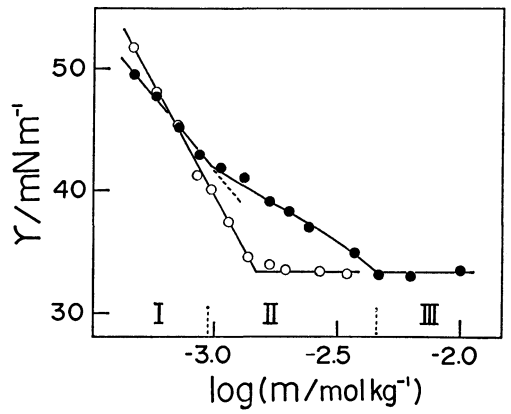

Fig. 1. Surface tension *vs.* log(m/mol kg^{-1}).
○: $Mn(DS)_2$ solutions, ●: ($Mn(DS)_2$+0.05% PVP) solutions.

in some manner.

If one interprets the two break points according to the previous studies on the interaction between sodium dodecyl sulfate and some nonionic polymers,[4,7] a kind of complex formation between $Mn(DS)_2$ and PVP starts at the concentration of the lower break point, m_1, and continues to the concentration of the higher one, m_2. Above m_2, micelles of $Mn(DS)_2$ are produced in the solution without further complex formation. Thus, chemical species in the solution vary with m in the following way: in region I ($m<m_1$), Mn^{2+} ions and dodecyl sulfate ions (DS^- ions); in region II ($m_1 \leqq m<m_2$), Mn^{2+} ions, DS^- ions, and complexes formed between PVP and $Mn(DS)_2$ (P-S complexes); in region III ($m_2<m$), Mn^{2+} ions, DS^- ions, P-S complexes, and $Mn(DS)_2$ micelles. These three concentration regions are indicated by roman numerals above the abscissa in the figure.

ESR spectra of Mn^{2+} ions ($S=5/2$ and $I=5/2$) obtained in the present study were composed of six unequivalent lines; each of which contains five unresolved lines. Since the fourth line from the low field side is nearly Lorentzian, its linewidths and absorption intensities were measured as a function of m.

Figure 2(a) shows the dependence of the peak-to-peak linewidth, W_{pp}, on m in two systems; the one is aqueous $Mn(DS)_2$ solutions, and the other is aqueous ($Mn(DS)_2$+0.05% PVP) solutions. In appearance, there is little difference between the two systems; W_{pp} is nearly constant to $m = ca.$ 1 mmol kg^{-1}, and then increases with m. Since this concentration approximately corresponds to the CMC of $Mn(DS)_2$ in water or to the concentration, m_1, at which the P-S complex begins to form in the ($Mn(DS)_2$+0.05% PVP) solutions, the increase in W_{pp} reflects the formation of micelles or P-S complexes.

According to Garrett and Morgan,[19] the broadening of W_{pp} of Mn^{2+} complexes in solutions is caused by the decrease in perturbational correlation time and/or by the alteration in the time-dependent spin Hamiltonian of Mn^{2+} ions. When Mn^{2+} ions are bound onto the surface of the micelle-like region, both effects can be expected to occur.

The similarity of the W_{pp}-m plot between the two

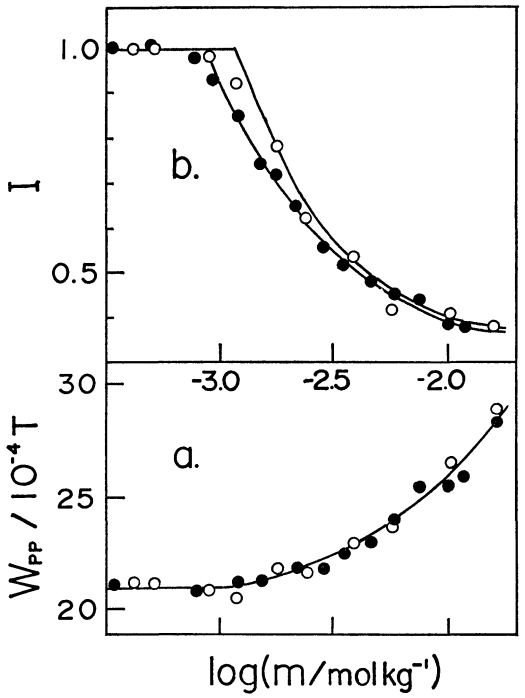

Fig. 2. (a) Linewidth *vs.* log(m/mol kg^{-1}). (b) Normalized intensity *vs.* log(m/mol kg^{-1}). ○: $Mn(DS)_2$ solutions, ●: ($Mn(DS)_2$+0.05% PVP) solutions.

systems, therefore, may imply that there is little difference in the binding state of Mn^{2+} ions; it suggests that $Mn(DS)_2$ molecules bound onto the PVP aggregate to form a micelle-like structure.

Normalized absorption intensities, I, of Mn^{2+} ions in the two systems are shown as a function of m in Fig. 2(b); here, I was obtained by the normalization of values which resulted from dividing absorption intensities, I_A, by m. The I_A was calculated through the following relation which holds for Lorentzian line shapes:

$$I_A \propto h_{pp} \times W_{pp}^2, \quad (1)$$

where h_{pp} is the peak-to-peak height.

A small difference in the behavior of the I-m curve can be seen between the two systems owing to the rate of change in I being greater than that in W_{pp}. In the case of $Mn(DS)_2$ solutions, I takes a constant value (=1.0) below m=1.1 mmol kg^{-1} which is nearly equal to the CMC, and then decreases steeply to a saturation value ($\approx$0.35). On the other hand, in the case of ($Mn(DS)_2$+0.05% PVP) solutions, the steep decrease in I begins at $m=0.9_4$ mmol kg^{-1} which is approximately equal to m_1 in Fig. 1. At higher concentrations, the I-m curve approaches gradually to that of $Mn(DS)_2$ solutions.

According to the previous ESR studies on Mn^{2+} complexes in solutions,[20,21] the loss of signal intensity of Mn^{2+} ions is attributed to the extreme broadening of the linewidths beyond detection. This broadening is caused by a large distortion from the octahedral symmetry of $Mn(H_2O)_6^{2+}$ on the formation of unsymmetrical inner-sphere complexes.

If one considers, on the basis of a simple micellar model, that Mn^{2+} ions in $Mn(DS)_2$ micellar solutions

exist in three regions; the Stern layer, the diffuse layer, and the bulk water, Mn^{2+} ions "bound" onto the micelles are those in the two layers. Since Mn^{2+} ions in the Stern layer form inner-sphere complexes with DS^- ions constituting micelles, they are responsible for the intensity loss. On the other hand, those in the diffuse layer which form outer-sphere complexes with the DS^- ions contribute to the broadening of linewidths in Fig. 2(a).

By analyzing the intensity loss in Fig. 2(b) on the basis of the simple idea, one can proceed to a quantitative discussion.

Denoting the degree of dissociation of Mn^{2+} ions from $Mn(DS)_2$ micelles by α, and the fraction of Mn^{2+} ions in the diffuse layer in total Mn^{2+} ions bound onto micelles by β, I_A is combined with α and β by the following relation;

$$I_A \propto m_f + \alpha(m-m_f) + \beta(1-\alpha)(m-m_f), \quad (2)$$

where m_f is the concentration of free $Mn(DS)_2$ being in equilibrium with the $Mn(DS)_2$ in a micellar state. The second and the third term represent the contribution from Mn^{2+} ions dissociating from micelles and those in the diffuse layer, respectively.

Dividing the right hand side of Eq. 2 by m, I is derived as follows:

$$I = \frac{m_f}{m} + \alpha\left(1-\frac{m_f}{m}\right) + \beta(1-\alpha)\left(1-\frac{m_f}{m}\right)$$

$$= (1-\alpha-\beta+\alpha\beta)\frac{m_f}{m} + \alpha + \beta - \alpha\beta. \quad (3)$$

Moreover, by simple transformation of Eq. 3, the following equation is obtained;

$$m(1-I) = (\alpha\beta+1-\alpha-\beta)(m-m_f). \quad (4)$$

Supposing that $Mn(DS)_2$ molecules bound onto PVP form a micelle-like aggregate, in the case of ($Mn(DS)_2$+0.05% PVP) solutions, the equations similar to Eqs. 3 and 4 can be described as follows:

$$I = (1-\alpha^p-\beta^p+\alpha^p\beta^p)\frac{m_f^p}{m} + \alpha^p + \beta^p - \alpha^p\beta^p, \quad (5)$$

$$m(1-I) = (\alpha^p\beta^p+1-\alpha^p-\beta^p)(m-m_f^p), \quad (6)$$

where α^p, β^p, and m_f^p are the corresponding quantities to α, β, and m_f in Eqs. 3 and 4.

Plots of I *vs.* m_f/m and I *vs.* m_f^p/m based on Eqs. 3 and 5 respectively are shown in Fig. 3. Here, the concentrations at the break points in Fig. 2(b) were used as the constant values of m_f and m_f^p; that is, m_f=1.1 mmol kg^{-1} and m_f^p=0.9$_4$ mmol kg^{-1}. In the strict sense, m_f^p varies from 0.9$_4$ mmol kg^{-1} to 1.1 mmol kg^{-1} in region II with an increase in m. The present assumption that m_f^p takes a constant value of 0.9$_4$ mmol kg^{-1}, however, does not introduce serious errors in the calculation of m_f^p/m in Eq. 5 and ($m-m_f^p$) in Eq. 6, since the difference between the two values of m_f^p (=0.1$_6$ mmol kg^{-1}) is much smaller than the value of m_2 (=4.6 mmol kg^{-1}); the errors become largest at m_2. Roman numerals above the abscissa indicate the regions corresponding to the three concentration regions in Fig. 1. The two plots in the figure are depicted by the same straight line in regions II and III; in the plot of I *vs.* m_f^p/m, there is no inflection at the boundary between region II and region III.

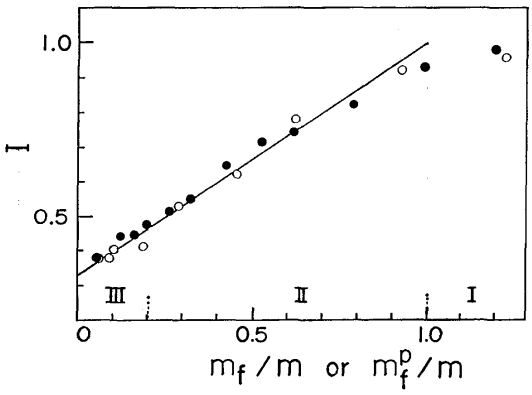

Fig. 3. Plots of I in $Mn(DS)_2$ solutions *vs.* m_f/m: (○), and I in ($Mn(DS)_2$+0.05% PVP) solutions *vs.* m_f^p/m: (●).

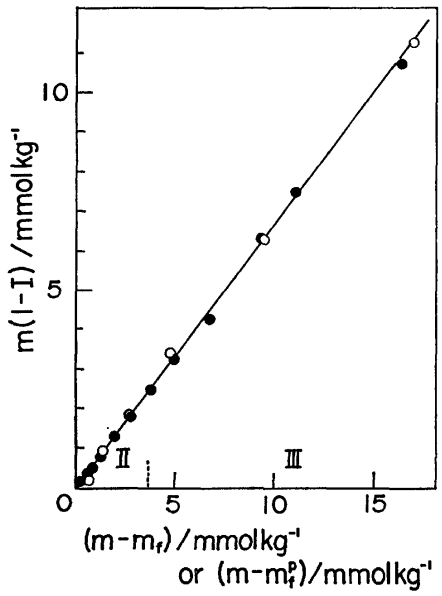

Fig. 4. Plots of $m(1-I)$ in $Mn(DS)_2$ solutions *vs.* ($m-m_f$): (○), and $m(1-I)$ in ($Mn(DS)_2$+0.05% PVP) solutions *vs.* ($m-m_f^p$): (●).

Similarly, plots of $m(1-I)$ *vs.* ($m-m_f$) and $m(1-I)$ *vs.* ($m-m_f^p$) based on Eqs. 4 and 6 respectively are shown in Fig. 4. The two plots are evidently on the same line with no inflection in regions II and III as well as in Fig. 3.

Thus, the results obtained in Figs. 3 and 4 indicate that $\alpha \approx \alpha^p$ and $\beta \approx \beta^p$; in other words, the binding manner of Mn^{2+} ions onto the micelle-like aggregate is similar to that of Mn^{2+} ions onto the $Mn(DS)_2$ micelles.

From the dependence of m_1 or CMC on the hydrocarbon chain length of surfactants, Arai and coworkers[7] have reported that the free energy of transferring a CH_2 from aqueous solution to the micelle-like aggregate in the P-S complex agrees with the result in the simple micellar solutions without added polymers. It can, therefore, be supposed that the structure of this micelle-like aggregate is almost identical with that

of an ordinary micelle.

It is clear from Eqs. 3 and 4, that the simultaneous determination of α and β from the y-intercept and the slope of the straight lines (Figs. 3 and 4) is impossible; the value of β was therefore estimated by the use of a value for α reported by Satake and coworkers.[22] From electric conductivity data, they estimated α of magnesium dodecyl sulfate ($Mg(DS)_2$) micelles to be 0.21 in a 0.1 mol dm^{-3} $MgSO_4$ solution.

The use of this value for $Mn(DS)_2$ micelles in the present study is permissible for the following two reasons; one is the similar chemical character of Mn^{2+} ions and Mg^{2+} ions,[24] and the other is the weak effect of added electrolytes on the aggregation number of dodecyl sulfate ions in micelles of bivalent metal dodecyl sulfates.[22]

Substituting this value (=0.21) for α in the following equation which is obtained by analysis of the lines in Figs. 3 and 4:

$$\alpha + \beta - \alpha\beta = 0.32, \quad (7)$$

the value of β is estimated to be 0.14.

The magnitude of this β value implies that most of Mn^{2+} ions bound onto micelles exist in the Stern layer as inner-sphere complexes with DS^- ions. Since β^p is nearly equal to β, the same conclusion can also be derived in the case of the micelle-like aggregate in P–S complexes.

In order to investigate whether the structures of P–S complexes change or not with an increase in the PVP concentration, the linewidths and relative intensities of the ESR signal of Mn^{2+} ions in ($Mn(DS)_2$+PVP) solutions with various amounts of PVP were measured at a constant $Mn(DS)_2$ concentration.

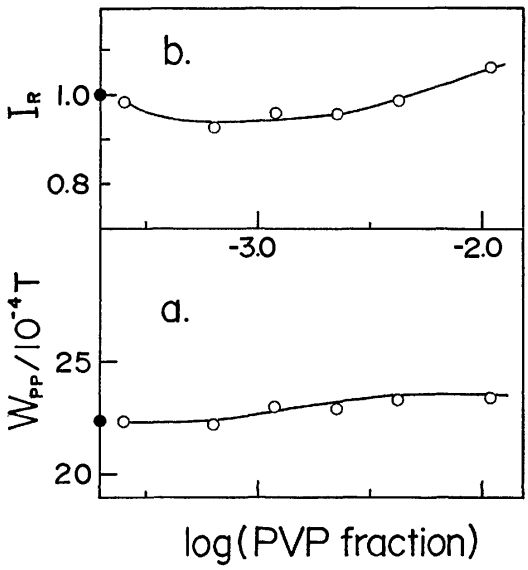

Fig. 5. (a) Linewidth *vs.* log(weight fraction of PVP). (b) Relative intensity *vs.* log(weight fraction of PVP). $Mn(DS)_2$ concentration=3.21 mmol kg^{-1}. Closed circles represent the values of the $Mn(DS)_2$ solution without PVP.

If the structure assumed for the complexes in the above discussion remains unchanged with increase in the PVP concentration, W_{pp} will increase slightly, whereas I will decrease asymptotically, for the concentration m_1 gradually decreases with the increase in the PVP concentration.[11]

The results where m=3.21 mmol kg^{-1} are shown as a function of the weight fraction of PVP in Fig. 5; the relative intensity, I_R, means the ratio of I_A in ($Mn(DS)_2$+PVP) solutions to that in the $Mn(DS)_2$ solutions without PVP. Obviously, the curves depicted in the figure are not the predicted ones. W_{pp} in Fig. 5(a) is nearly constant below 0.2%, and then increases slightly, while I_R decreases asymptotically to 0.2%, but above that concentration it increases evidently.

This behavior may suggest a structural change of the P–S complex at higher PVP concentrations; the structure may transform into one with a weak binding potential for Mn^{2+} ions.

References

1) S. Saito, *Yukagaku*, **12**, 133 (1963).
2) T. Isemura and A. Imanishi, *J. Polym. Sci.*, **33**, 337 (1958).
3) S. Harada, T. Komatsu, and T. Nakagawa, *Nippon Kagaku Kaishi*, **1974**, 622.
4) M. N. Jones, *J. Colloid Interface Sci.*, **23**, 36 (1967).
5) N. Murai, S. Makino, and S. Sugai, *J. Colloid Interface Sci.*, **41**, 399 (1972).
6) M. J. Schwuger, *J. Colloid Interface Sci.*, **43**, 491 (1973).
7) H. Arai, M. Murata, and K. Shinoda, *J. Colloid Interface Sci.*, **37**, 223 (1971).
8) F. Tokiwa and K. Tsujii, *Bull. Chem. Soc. Jpn.*, **46**, 2684 (1973).
9) M. Nakagaki and S. Shimabayashi, *Nippon Kagaku Kaishi*, **1972**, 989.
10) K. Shirahama, *Colloid Polym. Sci.*, **252**, 978 (1974).
11) B. Cabane, *J. Phys. Chem.*, **81**, 1639 (1977).
12) S. Saito, *Kolloid-Z.*, **133**, 12 (1953).
13) J. Oakes, *J. Chem. Soc., Faraday Trans. 2*, **69**, 1321 (1973).
14) A. Kitahara, O. Ohashi, and K. Kon-no, *J. Colloid Interface Sci.*, **49**, 108 (1974).
15) M. Ueki and Y. Uzu, *Bull. Chem. Soc. Jpn.*, **53**, 1445 (1980).
16) A. Hasegawa, Y. Michihara, and M. Miura, *Bull. Chem. Soc. Jpn.*, **43**, 3116 (1970).
17) S. Miyamoto, *Bull. Chem. Soc. Jpn.*, **33**, 371 (1960).
18) S. Miyamoto, *Bull. Chem. Soc. Jpn.*, **33**, 375 (1960).
19) B. B. Garrett and L. O. Morgan, *J. Chem. Phys.*, **44**, 890 (1966).
20) L. Burlamacchi and E. Tiezzi, *J. Phys. Chem.*, **73**, 1588 (1969).
21) L. Burlamacchi, G. Martini, and M. Romanelli, *J. Chem. Phys.*, **59**, 3008 (1973).
22) I. Satake, I. Iwamatsu, S. Hosokawa, and R. Matuura, *Bull. Chem. Soc. Jpn.*, **36**, 204 (1963).
23) H. Wennerström and B. Lindman, *Phys. Rep.*, **52**, 33 (1979).
24) G. Anderegg, *Helv. Chim. Acta*, **43**, 414 (1960).

The Solvent Extraction of Silver and Thallium(I) Picrates by Crown Ethers

Yasuyuki TAKEDA,* Masashi NEMOTO, and Shizuo FUJIWARA
Department of Chemistry, Faculty of Science, Chiba University, Yayoi-chō, Chiba 260

(Received March 16, 1982)

Extraction constants of silver and thallium(I) picrates and those of 12-crown-4 (12C4) and benzo-15-crown-5 (B15C5) with silver and thallium(I) picrates have been determined between benzene and water at 25 °C. Ion-pair complex-formation constants ($K_{MLA,o}$) of 12C4 and B15C5 with silver and thallium picrates in the benzene solution have been calculated and compared with those of 15-crown-5 (15C5), 18-crown-6 (18C6), dibenzo-18-crown-6 (DB18C6), and dibenzo-24-crown-8 (DB24C8). The $K_{MLA,o}$ sequences of the crown ethers with Ag^+ and Tl^+ are 15C5, 18C6>DB18C6>B15C5>DB24C8≫12C4 and 18C6≫DB18C6>DB24C8>15C5>B15C5≫12C4, respectively. For both Ag^+ and Tl^+ systems, the relative sizes of the cation and the crown ether cavity, the number of donor oxygen atoms in the crown ether ring, the basicity of donor oxygen atom, and the flexibility of the crown ether are important factors in determining stabilities of the complexes with these crown ethers in the benzene solution.

Crown ethers form stable stoichiometric complexes with Ag^+ and Tl^+ as well as with alkali metal ions. The complexing-power of crown ethers for Ag^+ and Tl^+ has been investigated by solvent extraction.[1-5]

In the present study, the extraction constants of silver and thallium(I) picrates and those of 12-crown-4 (12C4) and benzo-15-crown-5 (B15C5) with silver and thallium(I) picrates have been determined between benzene and water at 25 °C. Ion-pair complex-formation constants of 12C4 and B15C5 with silver and thallium picrates in the benzene solution have been calculated and compared with those of 15-crown-5 (15C5),[1] 18-crown-6 (18C6),[1] dibenzo-18-crown-6 (DB18C6),[2,4] and dibenzo-24-crown-8 (DB24C8)[5] in order to study the factors governing the stabilities of these complexes.

Experimental

The 12C4 (Wako-Pure Chemicals, Ltd.) was used without further purification. The method of purification of the B15C5 (Merck Japan Ltd.) has been described in the literature.[6] The purity of $AgNO_3$ and $TlNO_3$, and the concentrations of the picric acid solutions were determined by KCl, EDTA, and alkaline titrations, respectively. Analytical-grade benzene was washed twice with distilled water. All the experiments were conducted at 25±0.2 °C. Most of the experimental procedures were similar to those in the previous papers.[1,2] The concentrations of $AgNO_3$, $TlNO_3$, picric acid, 12C4, and B15C5 were $(2—6)\times10^{-3}$, $(1—9)\times10^{-3}$, $1\times10^{-3}—1.5\times10^{-2}$, $6\times10^{-3}—3.9\times10^{-1}$, and $5.9\times10^{-5}—3.9\times10^{-2}$ mol dm^{-3}, respectively. All the extractions were carried out in the pH range of 2.0—2.7.

Results

In an equilibrium between an aqueous solution of a univalent metal ion (M^+) and a picrate ion (A^-), and benzene, and its solution of a crown ether (L), the following equilibrium constants may be defined:

$$K_{ex}(MA) = [MA]_o[H^+]/[M^+][HA]_o \quad (1)$$

$$K_{ex}(MLA) = [MLA]_o[H^+]/[M^+][L]_o[HA]_o \quad (2)$$

$$K_{D,L} = [L]_o/[L] \quad (3)$$

$$K_{ex}(HA) = [HA]_o/[H^+][A^-] \quad (4)$$

$$K_{ML} = [ML^+]/[M^+][L] \quad (5)$$

$$K'_{ex} = [MLA]_o/[ML^+][A^-], \quad (6)$$

where the subscript "o" and the lack of subscript denote the organic and the aqueous phase, respectively; square brackets indicate the molar concentrations. Thus, $K_{ex}(MLA)$ can be written as follows:

$$K_{ex}(MLA) = K_{D,L}^{-1}K_{ex}(HA)^{-1}K_{ML}K'_{ex}. \quad (7)$$

In the absence of the crown ether, the distribution ratio of the metal may be written as

$$D = [MA]_o/[M^+]. \quad (8)$$

The substitution of Eqs. 1 and 4 into Eq. 8 gives:

$$D = K_{ex}(MA)K_{ex}(HA)[A^-]. \quad (9)$$

The log D *vs.* log[A^-] plot in Fig. 1 shows a straight line with a slope of 1. This indicates that the K_{ex}(MA) can be represented by Eq. 1. The value of [A^-] in Eq. 9 was calculated from Eq. 10:

$$[A^-] = ([HA]_t-[MA]_o)/\{1+(K_{HA}+K_{ex}(HA))[H^+]\}, \quad (10)$$

where $K_{HA}=1.9_5$,[7] $K_{ex}(HA)=247$,[8] and the subscript "t" denotes the total concentration. When the extraction system contains a crown ether, D may be represented by:

$$D = [MLA]_o/([M^+]+[ML^+]). \quad (11)$$

In the case of $[M^+]\gg[ML^+]$, Eq. 11 becomes:

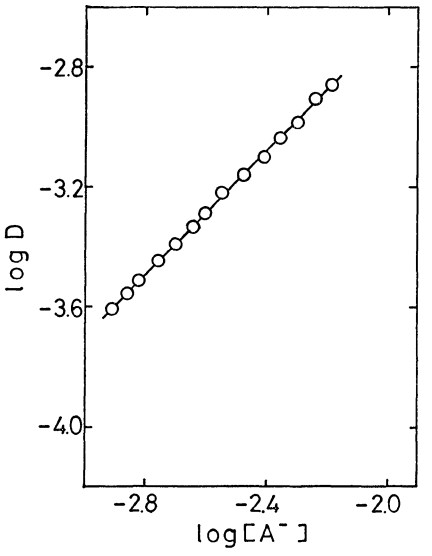

Fig. 1. Plot of log D *vs.* log[A^-] for the Tl^+ system.

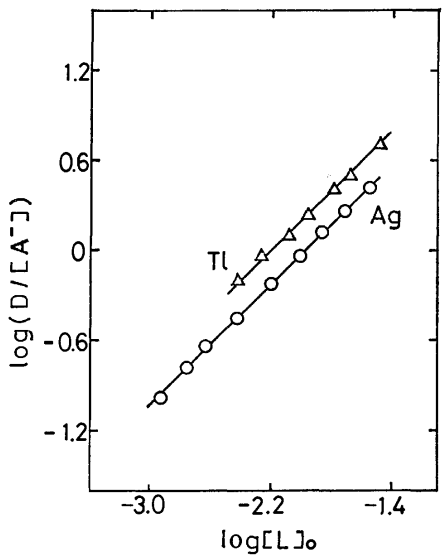

Fig. 2. Plot of $\log(D/[A^-])$ *vs.* $\log[L]_o$ for the 12C4–Ag^+ and Tl^+ systems.

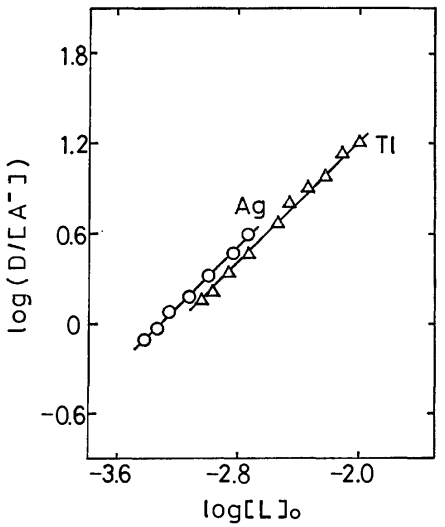

Fig. 3. Plot of $\log(D/[A^-])$ *vs.* $\log[L]_o$ for the B15C5–Ag^+ and Tl^+ systems.

$$D = K_{ex}(MLA)K_{ex}(HA)[A^-][L]_o. \quad (12)$$

The $\log(D/[A^-])$ *vs.* $\log[L]_o$ plots in Figs. 2 and 3 show a linear relationship with a slope of 1 in every case, indicating that 12C4 and B15C5 form 1:1 complexes with Ag^+ and Tl^+. The values of $[A^-]$ and $[L]_o$ in Eq. 12 were calculated from Eqs. 13 and 14 respectively:

$$[A^-] = ([HA]_t - [MLA]_o)/\{1 + (K_{HA} + K_{ex}(HA))[H^+]\} \quad (13)$$

$$[L]_o = ([L]_t - [MLA]_o)/(1 + K_{D,L}^{-1}). \quad (14)$$

The equilibrium constants obtained from these data are listed in Table 1.

Table 1. Equilibrium constants at 25 °C

	$\log\{K_{ex}(MA)K_{ex}(HA)\}$	
	Benzene	Chloroform[3]
Ag^+	−0.26[2]	−1.33
Tl^+	−0.68	−1.33
	$\log K_{ex}(MLA)$ for benzene system	
	Ag^+	Tl^+
12C4	−0.43	−0.17
15C5[1]	2.06	1.41
B15C5	0.94	0.84
18C6[1]	2.05	3.91
DB18C6	1.17[2]	2.10[4]
DB24C8[5]	0.70	1.67
	$\log(K_{ML}K'_{ex})$ for benzene system	
	Ag^+	Tl^+
12C4	1.14	1.40
15C5[1]	3.65	3.00
B15C5	4.63	4.53

Discussion

Although a Ag^+ ion is much more strongly hydrated than a Tl^+ ion, for the benzene system, silver picrate is more extractable than thallium picrate and, for the chloroform system, the extractability of the former is equal to that of the latter (Table 1). In the cases of both Ag^+ and Tl^+, the picrate is more extractable by benzene than by chloroform. The reason why the Ag^+ ion is more extractable than the Tl^+ ion for the benzene system and the Ag^+ ion is more extractable by benzene than by chloroform may be due to the strong interaction of the Ag^+ ion with the π-electrons of a benzene molecule.

The crystal ionic radius of Ag^+ (1.26 Å[9]) is nearly equal to that of K^+ (1.33 Å[9]) and that of Tl^+ (1.40 Å[9]) is almost identical with those of K^+ and Rb^+ (1.48 Å[9]). However, in the cases of both 12C4 and B15C5, the $\log K_{ex}(MLA)$ value of Ag^+ is much larger than that of K^+ (12C4: −1.82,[10] B15C5: −0.46[6]) and that of Tl^+ is much greater than those of K^+ and Rb^+ (12C4: −2.10,[10] B15C5: −0.95[6]). The covalent bond[11] of Ag^+ and Tl^+ ions with oxygen atoms of the crown ether is one of the reasons for the above phenomena.

The $\log(K_{ML}K'_{ex})$ value sequences of 12C4, 15C5, and B15C5 with Ag^+ and Tl^+ are B15C5>15C5≫12C4 and B15C5≫15C5≫12C4, respectively (Table 1). Since both 12C4 and 15C5 are rigid and the sizes of Ag^+ and Tl^+ are larger than the cavity sizes of 12C4 (1.0—1.3 Å[12]) and 15C5 (1.7—2.2 Å[12]), the magnitude of the $\log K_{ML}$ value may largely depend on the number of donor oxygen atoms of the crown ether. Thus, for both Ag^+ and Tl^+, the $\log K_{ML}$ value for 15C5 is larger than that for 12C4. The size of the 15C5 complex with the same metal ion (Ag^+ and Tl^+) is larger than that of the 12C4 complex. Moreover, 15C5 may more effectively screen the surface charge of the metal ion trapped in its cavity than 12C4 because of its larger size. Consequently, for both Ag^+ and Tl^+, the $\log K'_{ex}$ value of 15C5 is larger than that of 12C4. The fact that the $\log(K_{ML}K'_{ex})$ value of 15C5 is greater than that of 12C4 is in agreement with the above discussion. In an aqueous solution, B15C5 complexes with Ag^+ and Tl^+ may be more unstable than 15C5 complexes

owing to the two aromatic ether oxygen atoms. Since the B15C5 complex with the same metal ion has a larger molar volume than the 15C5 complex, the former may be more extractable by benzene than the latter. It thus appears that, in the case of both Ag^+ and Tl^+, the $\log(K_{ML}K'_{ex})$ sequences of B15C5 and 15C5 depend completely on the $\log K'_{ex}$ sequences.

$K_{ex}(MLA)/K_{ex}(MA)$ $(=K_{MLA,o})$ represents the ion-pair complex-formation constant of the crown ether with silver or thallium picrate in a benzene solution. Since the complex-formation reaction is an ion-pair complex-formation reaction, the anion has a large influence on the stability of the complex compared with the reaction between a free metal ion and a crown ether. The $\log K_{MLA,o}$ sequences of the crown ethers with Ag^+ and Tl^+ are 15C5, 18C6>DB18C6> B15C5 > DB24C8 ≫ 12C4 and 18C6 ≫ DB18C6 > DB24C8>15C5>B15C5≫12C4, respectively (Table 2). This indicates that, for both the Ag^+ and Tl^+ systems, the relative sizes of the cation and crown ether cavity; the number of donor oxygen atoms in crown ether ring; the basicity of donor oxygen atom; and the flexibility of the crown ether are important factors in determining the stabilities of the complexes.

TABLE 2. $\log(K_{MLA,o}/mol^{-1}\,dm^3)$ VALUES IN BENZENE AT 25 °C

	Ag^+	Tl^+
12C4	2.22	2.90
15C5	4.71[2)]	4.48
B15C5	3.59	3.91
18C6	4.70[2)]	6.98
DB18C6	3.82[2)]	5.17
DB24C8	3.35[2)]	4.74

Although Ag^+ fits more closely into the 12C4 and B15C5 cavities than Tl^+, the $\log K_{MLA,o}$ value of Tl^+ is larger than that of Ag^+. This may be attributed to the fact that silver picrate is strongly solvated by benzene. However, in the case of 15C5, the Ag^+ complex is more stable than the Tl^+ complex. This can be considered to reflect the increase in basicity of the two donor oxygen atoms on going from B15C5 to 15C5. The reason why, in the cases of 18C6, DB18C6, and DB24C8, the Tl^+ complex is much more stable than the Ag^+ complex may be attributed to the strong solvation of silver picrate by benzene and the more optimal size of Tl^+ for each of the cavities of these crown ethers than Ag^+.

References

1) Y. Takeda and H. Gotō, *Bull. Chem. Soc. Jpn.*, **52**, 1920 (1979).
2) Y. Takeda and F. Takahashi, *Bull. Chem. Soc. Jpn.*, **53**, 1167 (1980).
3) T. Maeda, K. Kimura, and T. Shono, *Fresenius' Z. Anal. Chem.*, **298**, 363 (1979).
4) T. Sekine, H. Wakabayashi, and Y. Hasegawa, *Bull. Chem. Soc. Jpn.*, **51**, 645 (1978).
5) Y. Takeda, *Bull. Chem. Soc. Jpn.*, **52**, 2501 (1979).
6) Y. Takeda, M. Wado, and S. Fujiwara, *Bull. Chem. Soc. Jpn.*, **54**, 3727 (1981).
7) "Dissociation Constants of Organic Acids in an Aqueous Solution," ed by G. Kortün, W. Vogel, and K. Andrussov, Butterworths, London (1961).
8) Y. Takeda and H. Katō, *Bull. Chem. Soc. Jpn.*, **52**, 1027 (1979).
9) L. Pauling, "The Nature of the Chemical Bond," 3rd ed, Cornell University Press (1960).
10) Y. Takeda, *Bull. Chem. Soc. Jpn.*, **53**, 2393 (1980).
11) J. M. Lehn, *Struct. Bonding (Berlin)*, **16**, 1 (1973).
12) C. J. Pedersen and H. K. Frensdorff, *Angew. Chem., Int. Ed. Engl.*, **11**, 16 (1972).

 © 1982 The Chemical Society of Japan Bull. Chem. Soc. Jpn., 55, 3441—3445 (1982)

Kinetic Studies of the Electron Transfer Reactions in Iron(II) and Iron(III) Systems. XII. The Ratios of the Reaction Rates of the Outer-sphere *vs.* Inner-sphere Electron Transfer Mechanisms in the Presence of X^- ($X^-=Cl^-$, SCN^-, and N_3^-) in Aqueous Solutions, as Judged from the Kinetics of the Dissociation Reactions of FeX^{2+}

Goro WADA,* Tomiko INATANI, and Sachiko ICHIMURA

Department of Chemistry, Faculty of Science, Nara Women's University, Nara 630

(Received February 3, 1982)

The electron transfer reactions between Fe^{2+} and FeX^{2+} ($X^-=Cl^-$, SCN^-, or N_3^-) may take place through the inner- or outer-sphere mechanism or through both in parallel. The process of the outer-sphere mechanism is just equivalent to the process of dissociation of FeX^{2+} catalyzed by Fe^{2+} in appearance. When the overall rate constant of the electron transfer reaction and the rate constant of Fe^{2+}-assisted dissociation reaction of FeX^{2+} are denoted by k_E and k_o respectively, the fraction r of the outer-sphere mechanism to the total is given in terms of $r=2k_o/k_E$. Thus, the r values were determined with the results that $r(Cl^-)=44\%$ at $I=1.5$ M (1 M=1 mol dm^{-3}) and 25 °C, $r(SCN^-)=100\%$ at $I=0.5$ M and 25 °C, and $r(N_3^-)=0\%$ at $I=0.55$ M and 10 °C. These facts suggest that r depends considerably upon the bridging ability of X^-; formation of binuclear intermediate may be favored by the symmetrical structure and the size of X^-, which make the inner-sphere mechanism easier with the stronger coordinate bond and the weaker electric repulsion between the two reactants beyond the bridging ligand.

The electron transfer reactions between iron(II) and iron(III), $Fe^{II}+Fe^{III}\rightarrow Fe^{II}+Fe^{II}$, have been known to be accelerated by the presence of some anions, X^-, in aqueous perchloric acid media.[1-8] In such catalytic actions, X^- usually coordinates to iron(III) to form a precursor complex, FeX^{2+}, which participates in the electron transfer reaction *via* either of the two paths shown as follows:

$$FeX^{2+} + F^{2+} \quad \text{(Path-I)}$$

$$Fe^{2+} + FeX^{2+} \rightleftharpoons Fe^{3+} + FeX^{+} \quad \text{(Path-O)}$$

The former of the two paths is called the inner-sphere mechanism, in which X^- bridges the two reacting ions and is transferred from Fe(III) to Fe(II) as an atom or radical (X) transfer, leaving an electron of X^- on Fe(III), while the latter path is the outer-sphere mechanism, in which an electron of Fe(II) is directly transferred to Fe(III) without accompanying any ligand substitution in the first coordination spheres of both ions. Generally, the two reaction mechanisms may compete with each other, with a certain ratio, the outer-sphere *vs.* inner-sphere mechanism, depending upon the properties of the bridging anion ligand X^- in aqueous solution.

Since the chemical species appearing as the reactants or products in the Path-I are identical in both sides, the rate constants of the forward and reverse reactions are equally k_1, while the Path-O is not a symmetric reaction with the product species different from the reactant ones, so that the rate constant of the forward reaction k_o should be unequal to that of the reverse reaction k_o'.

Now, let us consider an aqueous solution containing Fe(II), Fe(III), and X^-; all of the probable chemical species being at equilibrium. If the electron transfer reactions, both Path-I and Path-O, are simultaneously occurring in this system, the overall reaction rate, R, can be expressed by the sum of the three individual rates.

$$R = k_i[Fe^{2+}][FeX^{2+}] + k_o[Fe^{2+}][FeX^{2+}] + k_o'[Fe^{3+}][FeX^{+}] \quad (1)$$

Since the reaction system is at equilibrium, the concentrations of all the species in it must be individually kept constant. Although FeX^+ produced is very labile and is going soon to decompose, any probable side-reaction is quite indifferent to the reverse process of Path-O. Generally, the reverse process has the same mechanism as that of the forward process. Therefore, the rate of the forward reaction in Path-O should be equal to that of the reverse one at equilibrium.

$$k_o[Fe^{2+}][FeX^{2+}] = k_o'[Fe^{3+}][FeX^{+}] \quad (2)$$

By using the relationship of Eq. 2, Eq. 1 then becomes[8]

$$R = (k_1+2k_o)[Fe^{2+}][FeX^{2+}] \quad (3)$$

and the apparent overall rate constant k_E of the electron transfer reaction is expressed as follows:

$$k_E = k_1 + 2k_o. \quad (4)$$

If both k_E and k_o are separately determined for a reaction system in the presence of X^-, we can define the fraction r of the outer-sphere mechanism to the overall reaction rate.

$$r = \frac{2k_o}{k_E} \quad (5)$$

In order to determine k_E, the radioactive isotope ^{59}Fe has been frequently used as a tracer by several workers since the first investigation by Silverman and Dodson.[1] For the determination of k_o, on the other hand, an idea is useful as described below.

When the dissociation reaction of FeX^{2+}, $FeX^{2+}\rightarrow Fe^{3+}+X^-$, is accelerated by the presence of Fe^{2+}, it looks like that Fe^{2+} acts as a catalyst for the dissociation reaction:

$$FeX^{2+} + Fe^{2+} \xrightarrow{k_d} Fe^{3+} + FeX^{+} \quad \text{(Path-D)}$$

Reaction Path-D is seemingly a ligand exchange reaction of X^-, but it is just the same reaction with Path-O in appearance. Consequently, the observed k_d is equivalent to k_o of the outer-sphere electron transfer in Path-O.

In the present investigation, the kinetics of the catalytic dissociation of FeX^{2+} was studied, and the values of r were determined in the cases of Cl^-, SCN^-, and N_3^- and were interpreted by virtue of the nature of these anions. For the case of Cl^-, Sutin and his coworkers[8] estimated the r value earlier, which will be compared with the present results.

Experimental

Materials. *$Fe(ClO_4)_2$*: The preparative method was described elsewhere.[9]

$Fe(ClO_4)_3$: Aqueous perchloric acid solution of $Fe(ClO_4)_2$ was oxidized to $Fe(ClO_4)_3$ by adding approximately equivalent amount of H_2O_2. The precipitated crystals of $Fe(ClO_4)_3$ were filtered, washed by chloroform, and dried in vacuum.

NaCl, KSCN, NaN_3, and $NaClO_4$: Commercial reagents of the purest grade were recrystalized from their aqueous solutions, respectively.

Water: Tap water was purified by double distillation after being deionized through ion-exchange resin.

Procedure. Kinetic measurements were carried out by use of a Yanako stopped-flow spectrophotometer Model SPS-1 connected with an Iwatsu memoriscope MS-5019A. The reaction compartment was thermostated at a given reaction temperature. The dissociation reaction of FeX^{2+} in the presence or absence of Fe^{2+} was initiated by mixing two solutions A and B, containing Fe^{3+}, X^-, $HClO_4$, and $NaClO_4$ in A and Fe^{2+} or none, $HClO_4$, and $NaClO_4$ in B, respectively. Sodium perchlorate was used for adjusting the ionic strength of the reaction media. The reaction rate was followed by the decrement in absorbance due to the disappearance of FeX^{2+}, at wavelengths 370 nm for $FeCl^{2+}$, 460 nm for $FeSCN^{2+}$ and FeN_3^{2+}, respectively.

The apparent dissociation rate constant k_{app} was obtained from the linearity of $\ln([FeX^{2+}]-[FeX^{2+}]_e)$ *vs.* time t by the following relationship:

$$\ln\frac{[FeX^{2+}]-[FeX^{2+}]_e}{[FeX^{2+}]_o-[FeX^{2+}]_e} = -k_{app}t. \quad (6)$$

Since FeX^{2+} in solution A was in equilibrium with free Fe^{3+} and X^- before mixing with solution B, the equilibrium was suddenly perturbed and forced to shift towards a new equilibrium by dilution, with the forward (dissociation) rate constant k and the reverse (recombination) one k'. If the formation constant of FeX^{2+} is denoted by K_x ($=[FeX^{2+}]/[Fe^{3+}][X^-]$), K_x is equal to k'/k and, thus, k is given by the following equation:

$$k = \frac{k_{app}}{1+K_x([Fe^{3+}]_e+[X^-]_e)}. \quad (7)$$

The notations [ ]$_o$ and [ ]$_e$ in Eqs. 6 and 7 denote the concentrations at the initial time and at the equilibrium, respectively.

Results and Discussion

An example of a plot of $\ln([FeN_3^{2+}]-[FeN_3^{2+}]_e)$ against reaction time t is shown in Fig. 1. The observed straight line represents Eq. 6 very well, from

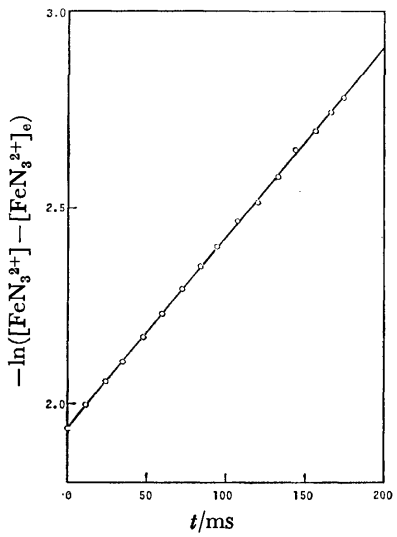

Fig. 1. Linear relationship of $-\ln([FeN_3^{2+}]-[FeN_3^{2+}]_o)$ *vs.* t at $[Fe(ClO_4)_3]_t=[NaN_3]_t=1.96\times10^{-3}$ M, $[Fe(ClO_4)_2]_t=0$, $[HClO_4]_t=0.01$ M, $I=0.55$ M at 10 °C.

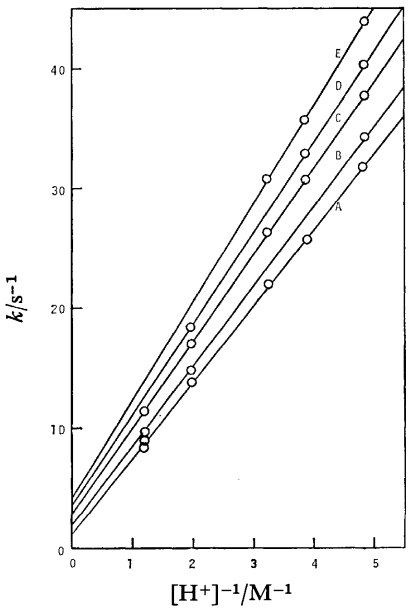

Fig. 2. Linear relationship of k *vs.* $[H^+]^{-1}$, at $[Fe^{3+}]_t=4.63\times10^{-3}$ M, $[Cl^-]_t=4.58\times10^{-3}$ M, $[H^+]=0.2$—0.8 M, $I=1.5$ M at 25 °C.
A: $[Fe^{2+}]_t=0$, B: $[Fe^{2+}]_t=0.05$ M, C: $[Fe^{2+}]_t=0.01$ M, D: $[Fe^{2+}]_t=0.15$ M, E: $[Fe^{2+}]_t=0.20$ M.

the slope of which k_{app} can be calculated. On account of the relatively low value of the formation constants, $K_{Cl}=3.0\times10^{10}$) and $K_{SCN}=4.2\times10^2$,[11] both at $I=0$ and 25 °C, k is considered to be approximately equal to k_{app} from Eq. 7 for $X^-=Cl^-$ or SCN^-. In the case of N_3^-, however, the situation is more complicated as will be described below.

Dissociation of $FeCl^{2+}$ and $FeNCS^{2+}$ Catalyzed by Fe^{2+}. The reaction rate was found to be dependent upon the concentration of perchloric acid, either in the absence or presence of Fe^{2+}. Since the rate constant k is in linear relationship with the reciprocal of hydrogen

ion concentration at $[Fe^{2+}]_t=0$—0.2 M ($[\ ]_t$ represents the total concentration), as shown in Fig. 2, the reaction scheme and the rate equation are given as follows:

$$\begin{array}{ccc} & \xrightarrow{k_1} Fe^{3+} + X^- & \text{(i)} \\ FeX^{2+} & \\ & + Fe^{2+} \xrightarrow{k_3} Fe^{3+} + FeX^+ & \text{(iii)} \\ H^+ \uparrow\downarrow -H^+ & & \\ & \xrightarrow{k_2} Fe(OH)^{2+} + X^- & \text{(ii)} \\ Fe(OH)X^+ & \\ & + Fe^{2+} \xrightarrow{k_4} Fe(OH)^{2+} + FeX^+ & \text{(iv)} \end{array}$$

$$k = k_1 + \frac{k_2K_H}{[H^+]} + \left(k_3 + \frac{k_4K_H}{[H^+]}\right)[Fe^{2+}], \quad (8)$$

where the individual rate constants are denoted by k_1, k_3, k_2, and k_4 respectively, and the hydrolysis constant of FeX^{2+} is expressed as $K_H=[Fe(OH)X^+][H^+]/[FeX^{2+}]$. In the absence of Fe^{2+}, k_1 and k_2K_H are determined from the intercept and the slope of the straight line obtained by plotting the observed k against $[H^+]^{-1}$, respectively. In the presence of Fe^{2+}, the linear relationship of $\{k-(k_1+k_2K_H/[H^+])\}/[Fe^{2+}]$ against $[H^+]^{-1}$ gives k_3 and k_4K_H from the intercept and the slope of the straight line, respectively, the linearity being shown in Fig. 3.

The experimental results thus obtained are listed in Table 1 for both $X^-=Cl^-$ and SCN^-. From the table, it is clear that Fe^{2+} catalyzes the dissociation

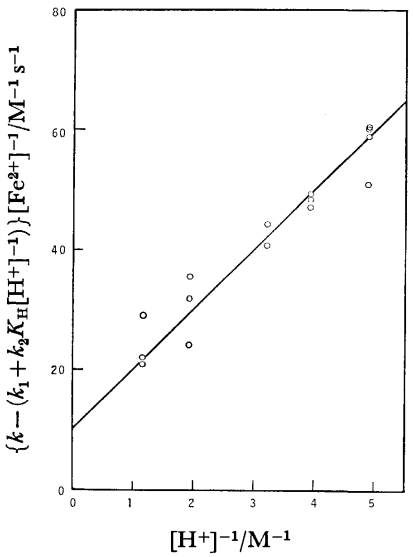

Fig. 3. Linear relationship of $\{k-(k_1+k_2K_H[H^+]^{-1})\}[Fe^{2+}]^{-1}$ *vs.* $[H^+]^{-1}$, the conditions being the same as in Fig. 2.

reaction of FeX^{2+} in both systems, and that the reaction is more accelerated by Fe^{2+} in the $FeNCS^{2+}$ system than in the $FeCl^{2+}$ system, according to the value of k_3/k_1. Further, the unhydrolyzed species, FeX^{2+}, is more easily accelerated to dissociate that the hydrolyzed one, $Fe(OH)X^+$, because k_3/k_1 is larger than k_4/k_2. Anyway, the rate constant k_3 for Reaction iii coincides with the rate constant k_o in the electron transfer reaction through the outer-sphere mechanism, Path-O, which is really the rate constant aimed in the present study.

Dissociation of FeN_3^{2+} Catalyzed by Fe^{2+}. In the reaction system containing N_3^-, the equilibrium, $H^+ + N_3^- \rightleftarrows HN_3$, has to be taken into account, in addition to the equilibria of the complex formation between Fe^{3+} and N_3^-, and of the hydrolysis of Fe^{3+}, in order to calculate the concentrations of free Fe^{3+}, N_3^-, and other relevant species. The equilibrium constants used are as follows: $K_{N_3}=[FeN_3^{2+}]/[Fe^{3+}][N_3^-]=2.7\times10^4$ M^{-1},[5,12] $K_a=[H^+][N_3^-]/[HN_3]=3.0\times10^{-5}$ M,[5] and $K_h=[Fe(OH)^{2+}][H^+]/[Fe^{3+}]=6.7\times10^{-3}$ M[6] at $I=0.55$ M and 10 °C. The reaction temperature chosen was 10 °C, because of the fact that the rate-determining step in the electron transfer reaction between Fe^{2+} and FeN_3^{2+} is the first stage among the successively occurring elementary processes below 13 °C, above which temperature the reaction mechanism would be more complicated.[5]

The rate measurements were performed at $[Fe(ClO_4)_3]_t=[NaN_3]_t=1.96\times10^{-3}$ M, $[HClO_4]_t=0.01$—0.5 M, $[Fe(ClO_4)_2]_t=0$—0.08 M, $I=0.55$ M and 10 °C. The observed k_{app} was transformed into k according to Eq. 7, since the values of the denominator on the right-hand side in Eq. 7 are no longer regarded to be nearly equal to unity for $X^-=N_3^-$, under the present conditions. When all the observed k's are plotted against $[H^+]$, k first decreases rapidly with the increase in $[H^+]$ in its low concentration range, and then k grows up almost linearly with a mild slope at higher $[H^+]$ range. Moreover, another linear relationship is also seen between k and $[H^+]^{-1}$ only within the lower $[H^+]$ range, $[H^+]=0.01$—0.075 M, namely $[H^+]^{-1}=13$—100 M^{-1}, as is shown in Fig. 4. Many observed points appear within the limited range as shown in the figure, independently of $[Fe^{2+}]$. Accordingly, the rate constant k can be expressed by Eq. 9, in which a term proportional to $[H^+]$ is supplemented to Eq. 8. This supplemented term may correspond to Reaction v, as shown below.

$$k = k_1 + \frac{k_2K_H}{[H^+]} + \left(k_3 + \frac{k_4K_H}{[H^+]}\right)[Fe^{2+}] + k_5[H^+], \quad (9)$$

Table 1. The individual rate constants for the dissociation reactions of $FeCl^{2+}$, $FeNCS^{2+}$, and FeN_3^{2+} catalyzed by Fe^{2+}

X^-	I / M	Temp / °C	k_1 / s^{-1}	k_2K_H / M s^{-1}	k_3 / M^{-1} s^{-1}	k_4K_H / s^{-1}	k_5 / M^{-1} s^{-1}	k_3/k_1 / M^{-1}	k_4/k_2 / M^{-1}
Cl^-	1.5	25	1.3	6.3	10.0	9.9	—	7.7	1.6
SCN^-	0.5	25	0.80	0.21	23	1.1	—	29	5.2
SCN^-	1.5	25	0.39	0.16	30	2	—	77	13
N_3^-	0.55	10	5.3×10^{-2}	1.4×10^{-2}	≈0	≈0	8.5×10^{-2}	0	0

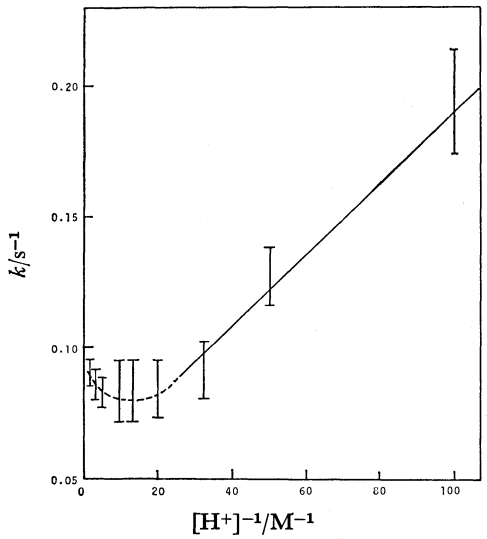

Fig. 4. Linear relationship of k *vs.* $[H^+]^{-1}$, at $[Fe^{3+}]_t = [N_3^-]_t = 1.96\times10^{-3}$ M, $[H^+]=0.01$—0.05 M ($[H^+]^{-1}=100$—20 M^{-1}), $I=0.55$ M, and 10 °C.
About 20 observed points scattering randomly between the two limiting values indifferent to the concentrations of existing Fe^{2+}, $[Fe^{2+}]_t=0.025$, 0.050, or 0.075 M, at each $[H^+]^{-1}$ values.

$$FeN_3^{2+} + H^+ \xrightarrow{k_5} Fe^{3+} + HN_3. \qquad (v)$$

Reaction v is a hydrogen ion-assisted dissociation of FeN_3^{2+}, where H^+ acts similarly as a catalyst in place of Fe^{2+} in Reaction iii.

Figure 4 looks like indicating that the rate constant k is probably unaffected by the concentration of Fe^{2+} within the experimental errors. The least squares method based on 128 observations give the most probable individual rate constants as follows:

$$k_1 = (5.34\pm0.22)\times10^{-2}\ s^{-1}$$
$$k_2K_H = (1.37\pm0.05)\times10^{-2}\ s^{-1}$$
$$k_3 = (0.00\pm0.43)\times10^{-1}\ M^{-1}\ s^{-1}$$
$$k_4K_H = (0.02\pm0.09)\times10^{-2}\ s^{-1}$$
$$k_5 = (8.52\pm0.72)\times10^{-2}\ M^{-1}\ s^{-1}.$$

With fairly large errors, k_3 and k_4K_H should be regarded as zero, suggesting that the FeN_3^{2+} dissociation is not catalyzed by Fe^{2+}. These rate constants are listed in Table 1, along with those for $X^-=Cl^-$ and SCN^-.

The Ratio of Outer-sphere Mechanism in the Electron Transfer Reaction. As has been described above, the electron transfer reaction between Fe^{2+} and FeX^{2+} proceeds through either the inner-sphere or the outer-sphere mechanism or through both. The observed k_3 gives directly the rate constant k_o in the outer-sphere path. In Table 2, the overall rate constant k_E reported by previous workers, the outer-sphere rate constants k_o, and their ratios r defined by Eq. 5 are listed. According to the table, the electron transfer between Fe^{2+} and $FeNCS^{2+}$ occurs wholly through the outer-sphere path. On the contrary, the electron transfer between Fe^{2+} and FeN_3^{2+} occurs wholly through the inner-sphere path, while that between Fe^{2+} and $FeCl^{2+}$ undergoes both paths competitively.

TABLE 2. THE TOTAL AND THE OUTER-SPHERE RATE CONSTANTS, k_E AND k_o, AND THEIR RATIO r OF THE ELECTRON TRANSFER REACTION

X^-	I / M	Temp / °C	k_o / $M^{-1}\ s^{-1}$	k_E[a] / $M^{-1}\ s^{-1}$	r / %
Cl^-	1.5	25	10	45[6,8]	44
SCN^-	0.5	25	23	41.5[3]	≈100
N_3^-	0.55	10	≈0	4.75×10^3 [5]	≈0

a) Corrected to the given temperatures and ionic strengths.

To compare the two redox mechanisms, N_3^- and SCN^- have been frequently used, on the basis that the former ion is capable of bridging two reactants, resulting in the inner-sphere mechanism, whereas the latter ion is not.[13,14] The assumed intermediate complex in the inner-sphere mechanism bridged by N_3^- may be $[Fe\text{-}N\text{-}N\text{-}N\text{-}Fe]^{4+}$ with a linear and symmetric structure. On the other hand, SCN^- is linear, but not symmetric having a larger S atom on one end than an N atom on the other end. Thus, the coordination of S with Fe^{2+} in the binuclear structure, $[Fe^{III}\text{-}N\text{-}C\text{-}S\text{-}Fe^{II}]$, will be sterically unfavorable as a bridging ligand.

An additional condition is required for the inner-sphere mechanism that at least one of the two reactants should be substitution-labile, and this is fully satisfied in Fe^{2+}. Since the rate constant for the solvent water exchange reaction on Fe^{3+}_{aq} has been known to be $1.6\times10^2\ s^{-1}$ at 25 °C, that on Fe^{2+}_{aq} may be larger than this value.[15] In this connection, the large value of $k_E(N_3^-)/k_E(SCN^-)$ ratio is usually believed to give a firm indication of the inner-sphere mechanism for $CoX(NH_3)_5^{2+}/Fe^{2+}_{aq}$,[16] $CoX(NH_3)_5^{2+}/Eu^{2+}_{aq}$,[17] *etc.*

For Cl^-, both mechanisms are probable. Chloride ion has more than two lone electron-pairs which may be favorable to bridge the two reactants, leading to the inner-sphere path, so-called "chlorine atom transfer." But in the Cl^--bridged binuclear intermediate, $[Fe\text{-}Cl\text{-}Fe]^{4+}$, the nuclear distance between the two metal ions is too short to overcome the Coulombic repulsion between electric charges of the same sign, as compared with the case of N_3^- with the longer nuclear distance between the two iron ions, this fact being unfavorable to the inner-sphere mechanism. After all, the two mechanisms compete with each other in the Cl^- system. Sutin and his co-workers[8] carried out similar experiments, and concluded that the electron transfer between Fe^{2+} and $FeCl^{2+}$ proceeded mainly by a chloride-bridged inner-sphere activated intermediate at $I=3.0$ M and 25 °C, ignoring the process between Fe^{2+} and $Fe(OH)Cl^+$, namely the fourth term $(k_4K_H/[H^+])[Fe^{2+}]$ in Eq. 8, in the dissociation reaction of $FeCl^{2+}$. The forward and reverse reactions for the systems Co^{II}(chelate) and $Fe^{III}(CN)_5X$ are also considered to have trends of taking place through both mechanisms.[18] This is probably due to the fact that the bridging ligand, CN^-, is not only unsymmetric but also still too small to separate the electric charges on two reacting ions in its binuclear intermediate, inspite of its strong coordinating ability.

If the activation energies of the electron transfer reaction differed to a considerable extent between the two mechanisms, the ratio r would vary with temperature, and finally the reaction would go almost 100% *via* one of the two mechanisms at appropriately elevated or lowered temperatures. The systems of SCN^- and N_3^- observed above are just instances of such two limiting cases, respectively, while the Cl^- system may probably be transient between the two.

In conclusion, the symmetry and the length or size of the bridging ligand may be important factors to decide an inner-sphere mechanism or an outer-sphere one, or both in parallel.

Difference between Reaction Mechanisms of Outer-sphere Electron Transfer and Ligand Exchange. In the above descriptions, the electron transfer reaction through the outer-sphere mechanism (Path-O, k_o) and the dissociation reaction catalyzed by Fe^{2+} (Path-iii, k_3) are expressed by an identical equation.

$$Fe^{2+} + FeX^{2+} \longrightarrow Fe^{3+} + FeX^{+}$$

When one of the iron species is labeled by the isotopic tracer ^{59}Fe (represented by *Fe), however, two distinctly different reactions will become possible. If only one electron is really transferred from Fe^{2+} to FeX^{2+} with no change in chemical bondings (the outer-sphere electron transfer), the reaction is expressed as follows:

$$Fe^{2+} + {}^*FeX^{2+} \longrightarrow Fe^{3+} + {}^*FeX^{+}. \qquad (E)$$

On the other hand, if X^- is transferred from FeX^{2-} to Fe^{2+} without altering their oxidation states (the ligand exchange), the labeled Fe(III) remains still as Fe(III).

$$Fe^{2+} + {}^*FeX^{2+} \longrightarrow FeX^{+} + {}^*Fe^{3+} \qquad (S)$$

These two chemical reactions, E and S, involve quite different elementary processes with each other, but in the present experimental method, we cannot distinguish between them explicitly.

Since the unimolecular dissociation reaction of FeX^{2+}, $FeX^{2+} \rightarrow Fe^{3+} + X^-$ (k_1), has been revealed to be very slow as shown in Table 1,[19] Reaction S might be reasonably supposed to occur in a way that Fe^{2+} encounters directly with FeX^{2+} before the spontaneous decomposition of FeX^{2+}, forming an inner-sphere intermediate. If so, N_3^- may be considered to be most favorable for Reaction S due to its largest bridging ability among three ligand anions. This expectation, however, is denied by the results in Table 1 which informs us that k_3 is almost zero in the case of N_3^-. Therefore, Reaction S may be impossible, and the acceleration of the FeX^{2+} dissociation by Fe^{2+} proceeds probably through the outer-sphere electron transfer due to Path-O, with the rate constant k_3 which is essentially the same with k_o.

When Mg^{2+}, Co^{2+}, Ni^{2+}, or Mn^{2+} was used in place of Fe^{2+} in the $FeCl^{2+}$ dissociation reaction, the reaction was found to be little affected by the presence of these ions.[8] This fact indicates that these metal ions except Fe^{2+} work neither as Cl^- acceptor (Reaction S) nor as electron donor (Reaction E). Only Fe^{2+} can catalyze the dissociation reaction of $FeCl^{2+}$ *via* the electron transfer process of the outer-sphere mechanism.

References

1) J. Silverman and R. W. Dodson, *J. Phys. Chem.*, **56**, 846 (1952).
2) J. Hudis and A. C. Wahl, *J. Am. Chem. Soc.*, **75**, 4153 (1953).
3) G. S. Laurence, *Trans. Faraday Soc.*, **53**, 1326 (1957).
4) R. A. Horne, *J. Phys. Chem.*, **64**, 1512 (1960).
5) D. Bunn, F. S. Dainton, and S. Duckworth, *Trans. Faraday Soc.*, **57**, 1131 (1961).
6) N. Sutin, J. K. Rowley, and R. W. Dodson, *J. Phys. Chem.*, **65**, 1248 (1961).
7) N. Sutin, *Ann. Rev. Nucl. Sci.*, **12**, 285 (1962).
8) R. J. Campion, T. J. Conocchioli, and N. Sutin, *J. Am. Chem. Soc.*, **86**, 4591 (1964).
9) G. Wada, K. Takahashi, and M. Isobe, *Bull. Chem. Soc. Jpn.*, **54**, 3739 (1981).
10) E. Rabinowitch and W. H. Stockmayer, *J. Am. Chem. Soc.*, **64**, 335 (1942).
11) S. K. K. Jatkar and B. N. Mattoo, *J. Indian Chem. Soc.*, **31**, 299 (1954).
12) S. Ahrland and E. Avsar, *Acta Chem. Scand., Ser. A*, **30**, 15 (1976); E. Avsar, *ibid.*, **34**, 405 (1980).
13) F. Basolo and R. G. Pearson, "Mechanisms of Inorganic Reactions," John Wiley & Sons, New York (1967), p. 483.
14) J. Burgess, "Metal Ions in Solution," John Wiley & Sons, New York (1978), p. 430.
15) M. Grant and R. B. Jordan, *Inorg. Chem.*, **20**, 55 (1981).
16) J. H. Espenson, *Inorg. Chem.*, **4**, 121 (1965).
17) J. P. Candlin, J. Halpern, and D. L. Trimm, *J. Am. Chem. Soc.*, **86**, 1019 (1964).
18) D. H. Huchital and J. Lepore, *Inorg. Chem.*, **17**, 1134 (1978).
19) G. Wada and Y. Kobayashi, *Bull. Chem. Soc. Jpn.*, **48**, 2451 (1975).

Reaction Process of Vanadium Tetrachloride with Ammonia in the Vapor Phase and Properties of the Vanadium Nitride Formed

Yuzo Saeki,* Takashi Shimizu, Akimasa Yajima, and Ryoko Matsuzaki

Research Laboratory of Resources Utilization, Tokyo Institute of Technology, 4259, Nagatsuta-cho, Midori-ku, Yokohama 227

(Received February 19, 1982)

The reaction products of gaseous VCl_4 with ammonia were $VCl_4 \cdot 4NH_3$ at 200 °C, $VCl_4 \cdot 4NH_3$, VN_x, and NH_4Cl at 250—550 °C, and VN_x and NH_4Cl at 600—1000 °C. At 1100 °C, small amounts of VCl_2 and HCl were formed in addition to VN_x and NH_4Cl. The N/V atomic ratio, x, of the VN_x formed was 1.20 at 600 °C, 1.15 at 700 °C, 1.14 at 800 °C, and 1.13 at 900 and 1000 °C. The lattice constants of the VN_x formed were shown. The reaction process of gaseous VCl_4 with ammonia can be represented as follows: The reaction of gaseous VCl_4 with ammonia first occurs to form $VCl_4 \cdot 4NH_3$. Above about 215 °C, the reaction of $VCl_4 \cdot 4NH_3$ with ammonia also occurs to form VN_x. At 1100 °C, in addition to these reactions, the reaction of gaseous VCl_4 with hydrogen formed by the thermal dissociation of ammonia occurs to form VCl_2. On heating the VN_x, formed by the vapor-phase reaction, at temperatures higher than 500 °C in an argon atmosphere, the value of x decreased with the increase in the heating temperature to 1.03 at 900—1000 °C.

The vapor-phase reaction of transition metal chlorides with ammonia has recently become important for the preparation of fine powders of transition metal nitrides, which are acquiring importance as new industrial materials. Concerning the formation of vanadium nitride powders by the vapor-phase reaction of vanadium tetrachloride (VCl_4) with ammonia, Hojo *et al.*[1] have studied the preparation of fine vanadium nitride powders by a vapor-phase reaction of the VCl_4–NH_3–H_2–N_2 system at 700—1200 °C with emphasis on the effects of reaction conditions on particle size and chemical composition. However, no information is at present available on the reaction process of VCl_4 with ammonia in the vapor phase.

In this paper, the reaction products of gaseous VCl_4 with ammonia at 200—1100 °C were examined in detail. In order to elucidate the reaction process of gaseous VCl_4 with ammonia, the behavior of $VCl_4 \cdot 4NH_3$, which was newly-found during the reaction process, on heating in an ammonia stream and the thermal dissociation of ammonia under the experimental conditions in this work were examined. The N/V atomic ratios, lattice constants, and thermal stability in an argon atmosphere of the vanadium nitrides formed at various temperatures were examined. The vanadium nitrides formed were also examined by electron microscopy.

Experimental

Materials. The VCl_4 used was prepared by the reaction of vanadium (V>99.8%, Atomergic Chemetals Corp., U.S.A.) with chlorine at 500 °C.[2] The chemical analysis gave V, 26.4; Cl, 73.5% (calcd for VCl_4:V, 26.43; Cl, 73.57%). The Ammonia was dried by passing it over sodium hydroxide granules.

Experimental Procedures. A transparent quartz reaction tube (1000 mm length) was used for examining the reaction products of gaseous VCl_4 with ammonia at various temperatures. Gaseous VCl_4 was formed by heating liquid VCl_4 (22 g) at 125 °C and carried by a stream of argon (50 cm³/min) into the reaction zone (28 mm i.d., 250 mm length) held at a specified temperature. The VCl_4 inlet tube consisted of two concentric tubes. Gaseous VCl_4 carried by argon was introduced through the inner tube and the outer tube was used for introducing argon (50 cm³/min) as a sheath gas to prevent formation of vanadium nitride deposits at the chloride inlet tube. Ammonia was simultaneously introduced at a flow-rate of 100 cm³/min into the reaction zone through a separate tube. The mean flow-rate of gaseous VCl_4 was 6.0 cm³/min. A quartz tube was inserted inside the reaction tube to make the removal of the reaction product easier. The reaction was allowed to proceed for 2 h.

The by-product ammonium chloride (NH_4Cl) which deposited outside the reaction zone together with the vanadium nitride formed was separated by heating the mixture in an argon stream at 400 °C (the sublimation point of NH_4Cl: 339 °C)[3] for 10—15 h.

Analytical. The vanadium, chlorine and ammonia contents of the product formed were determined by chelatometric titration,[4] gravimetric method as AgCl, and the Kjeldahl method, respectively, after dissolving the sample in dilute nitric acid.

X-Ray analysis of the solid product was performed with an X-ray powder diffractometer equipped with a proportional counter using Ni filtered Cu radiation. The sample chamber of the diffractometer was maintained under a dry nitrogen atmosphere, if necessary, to prevent any contamination of the sample with atmospheric moisture during the irradiation. The lattice constant of the vanadium nitride was calculated based on the X-ray diffraction data obtained by using silicon powders as an internal standard under a scanning speed of 1/2—1/4°/min.

The sensitivity of the quartz helix used for thermogravimetry (TG) was approximately 72 mm/g. The sample (0.2 g) was heated at a rate of 2.5 °C/min and the flow-rate of ammonia was maintained at 50 cm³/min.

The N/V atomic ratio of the vanadium nitride formed was evaluated as follows: The sample vanadium nitride was oxidized to V_2O_5 by heating in an oxygen atmosphere up to 550 °C, using a Shimazu high-sensitive thermal balance Model TGA31. The amount of vanadium in the sample was calculated from the amount of V_2O_5 formed. The amount of nitrogen was determined as the difference between the amount of initial sample and that of the vanadium. The value of the N/V atomic ratio was evaluated with an accuracy within ± 0.01.

Throughout this work, the VCl_4 and the reaction products were handled in an argon atmosphere to prevent any contamination with atmospheric moisture.

Results and Discussion

Reaction Products of Gaseous Vanadium Tetrachloride with Ammonia. The products formed by heating gaseous VCl_4 in an ammonia stream at various temperatures were examined by X-ray analysis[5-7] and chemical analysis. Reaction temperatures above 200 °C were employed, because gaseous VCl_4 was generated at 125 °C. The results are shown in Table 1. Unreacted VCl_4 was not observed throughout the temperature range in this work. The products were obtained inside and outside the reaction zone below 550 °C. The portion of the product obtained outside the reaction zone increased with the increase in the reaction temperature and above 600 °C all the products were obtained outside the reaction zone.

The product formed at 200 °C showed a hitherto unknown X-ray diffraction pattern which was different from those of known vanadium compounds. The chemical analysis of the product gave V, 19.3; Cl, 54.5; NH_3, 26.2%. The ratio of V:Cl:NH_3 was calculated to be 1:4.06:4.06. This result was considered to indicate that the product formed at 200 °C had a composition of $VCl_4 \cdot 4NH_3$ (calcd for $VCl_4 \cdot 4NH_3$: V, 19.53; Cl, 54.36; NH_3, 26.11%). But the observed values for chlorine and ammonia were slightly higher than the calculated values. The evaporation of VCl_4 on heating liquid VCl_4 is accompanied by the decomposition of liquid VCl_4, $VCl_4(l) \rightarrow VCl_3(s) + 1/2Cl_2(g)$.[8] The resulting chlorine was considered to react with ammonia to form NH_4Cl. Accordingly, the amount of chlorine formed by heating liquid VCl_4 at 125 °C for 2 h was examined. The result showed that 0.07 g of chlorine was formed during the heating. From this result, the product formed at 200 °C was considered to be $VCl_4 \cdot 4NH_3$ containing a small amount of NH_4Cl. The chemical analysis of the sample obtained after the removal of the NH_4Cl from the product at 190 °C in an ammonia atmosphere gave V, 19.5; Cl, 54.3; NH_3, 26.0%. From the results, the product formed at 200 °C was confirmed to have the composition of $VCl_4 \cdot 4NH_3$.

The products formed at 250 and 300 °C were identified by X-ray analysis as a mixture of $VCl_4 \cdot 4NH_3$ and a small amount of NH_4Cl. However, it was found that when the products were treated with 1 M hydrochloric acid, $VCl_4 \cdot 4NH_3$ and NH_4Cl were dissolved leaving a small residue of black powder which was identified as vanadium nitride (VN_x) by X-ray and chemical analyses. These results indicated that a small amount of VN_x was formed in addition to $VCl_4 \cdot 4NH_3$ and NH_4Cl at 250 and 300 °C. The products formed at 500 and 550 °C were identified as a mixture of VN_x and NH_4Cl by X-ray analysis. But, the formation of a small amount of $VCl_4 \cdot 4NH_3$ in addition to these products was found by chemical analysis. Contrary to the experimental results obtained for the reaction products at temperatures below 1000 °C, a small amount of VCl_2 was formed in addition to VN_x and NH_4Cl at 1100 °C. It was also found that hydrogen chloride (HCl) was formed.

Table 1. Reaction products of gaseous VCl_4 with ammonia at various temperatures

Temp/°C	Products
200	$VCl_4 \cdot 4NH_3$
250	$VCl_4 \cdot 4NH_3 \gg VN_x$; NH_4Cl
300	$VCl_4 \cdot 4NH_3 \gg VN_x$; NH_4Cl
350	$VCl_4 \cdot 4NH_3 > VN_x$; NH_4Cl
400	$VCl_4 \cdot 4NH_3 > VN_x$; NH_4Cl
450	$VN_x > VCl_4 \cdot 4NH_3$; NH_4Cl
500	$VN_x \gg VCl_4 \cdot 4NH_3$; NH_4Cl
550	$VN_x \gg VCl_4 \cdot 4NH_3$; NH_4Cl
600—1000	VN_x; NH_4Cl
1100	$VN_x > VCl_2$; NH_4Cl, HCl

Reaction Process of Gaseous Vanadium Tetrachloride with Ammonia. To elucidate the reaction process of gaseous VCl_4 with ammonia, the behavior of $VCl_4 \cdot 4NH_3$, formed during the reaction process, on heating in an ammonia stream and the thermal dissociation of ammonia[9] under the experimental conditions in this work were examined.

Behavior of $VCl_4 \cdot 4NH_3$ on Heating in an Ammonia Stream: TG of $VCl_4 \cdot 4NH_3$ (0.2 g) in an ammonia stream (50 cm^3/min) was carried out. When ammonia was introduced at room temperature, the sample gained weight gradually and reached a constant value after 6 h, showing about 10% increase in weight. After the weight increase, the sample gave the same X-ray diffraction pattern with the initial sample. When the heating of the sample was started, the sample lost weight gradually and reached the initial weight at 190 °C. The TG curve of $VCl_4 \cdot 4NH_3$ in an ammonia stream above 200 °C is shown in Fig. 1.

$VCl_4 \cdot 4NH_3$ lost weight above 215 °C. The weight loss was accompanied by the vaporization of NH_4Cl and a small amount of $VCl_4 \cdot 4NH_3$. The sample after heating up to 450 °C was found to be VN_x by X-ray analysis.

In order to obtain more detailed information on the behavior of $VCl_4 \cdot 4NH_3$ on heating in an ammonia stream, $VCl_4 \cdot 4NH_3$ (1.0 g) in a quartz boat (70 mm length, 15 mm width, 7 mm depth) was placed in a straight reaction tube (28 mm i.d., 1000 mm length). Ammonia was introduced into the reaction

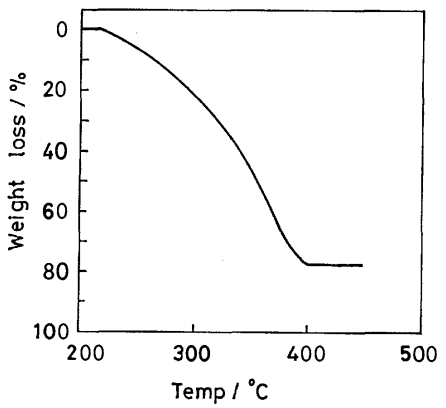

Fig. 1. TG curve of $VCl_4 \cdot 4NH_3$ in an ammonia stream.

Table 2. Experimental results for $VCl_4 \cdot 4NH_3$ on heating in an ammonia stream

Heating temp/°C	Products		Unreacted $VCl_4 \cdot 4NH_3$/%
	In the boat	Outside the boat	
250	$VN_x(<1)$	$VCl_4 \cdot 4NH_3(1)$, NH_4Cl	98
300	$VN_x(7)$	$VCl_4 \cdot 4NH_3(7)$, NH_4Cl	86
350	$VN_x(86)$	$VCl_4 \cdot 4NH_3(10)$, $VN_x(<1)$, NH_4Cl	3
400	$VN_x(92)$	$VCl_4 \cdot 4NH_3(5)$, $VN_x(2)$, NH_4Cl	<1
450	$VN_x(95)$	$VCl_4 \cdot 4NH_3(3)$, $VN_x(2)$, NH_4Cl	—

Note: the value in parentheses is mole percentage of $VCl_4 \cdot 4NH_3$ converted to the product.

tube at a flow-rate of 100 cm³/min. The sample part was then placed in the centre of an electric furnace (300 mm heating length) maintained at a specified temperature for 1 h. The products obtained inside and outside the boat were examined by X-ray and chemical analyses. The results are shown in Table 2.

The results showed that $VCl_4 \cdot 4NH_3$ reacted with ammonia to form VN_x above about 215 °C and a part of the $VCl_4 \cdot 4NH_3$ vaporized. The formation of a small amount of VN_x outside the boat was considered to indicate that the reaction of gaseous $VCl_4 \cdot 4NH_3$ with ammonia also occurred above about 350 °C.

Thermal Dissociation of Ammonia: Ammonia alone was introduced at a flow-rate of 100 cm³/min into the reaction zone held at a specified temperature and the total volume of nitrogen and hydrogen, formed by the dissociation of ammonia, was measured. From the results, the percentage of the dissociated ammonia was found to be <1% at 800 °C, 1% at 900 °C, 2% at 1000 °C, and 6% at 1100 °C.

Based on the experimental results mentioned above, the reaction process of gaseous VCl_4 with ammonia was discussed. As shown in Table 1, $VCl_4 \cdot 4NH_3$ alone was formed at 200 °C. This fact indicates that the reaction of gaseous VCl_4 with ammonia first occurs to form $VCl_4 \cdot 4NH_3$. The VN_x formed by the vapor-phase reaction above 250 °C (Table 1) are considered to be due to the reaction of $VCl_4 \cdot 4NH_3$ with ammonia, because the $VCl_4 \cdot 4NH_3$ reacts with ammonia above about 215 °C to form VN_x. The formation of VCl_2 at 1100 °C (Table 1) is considered to be due to the reaction of gaseous VCl_4 with hydrogen[2] formed by the thermal dissociation of ammonia.

Properties of the Vanadium Nitride Formed. The N/V atomic ratios of VN_x formed by the vapor-phase reaction at 600—1000 °C are shown in Table 3. Prior to this examination, the VN_x obtained after the removal of by-product NH_4Cl at 400 °C in an argon stream was dissolved in dilute nitric acid and the presence of residual NH_4Cl was checked by chemical analysis.[10] From the results, the VN_x formed at 1000 °C was found to contain no residual NH_4Cl. The VN_x formed at 600—900 °C was found to contain a small amount of residual NH_4Cl; The NH_4Cl content was 0.3% for the VN_x formed at 900 °C, 2.4% at 800 °C, 2.6% at 700 °C, and 3.6% at 600 °C. But, further separation of the NH_4Cl was not possible as the N/V atomic ratio of VN_x decreased on heating at temperatures higher than 500 °C in an argon atmosphere, as described later. So, for the evaluation of the N/V atomic ratios of the VN_x formed below 900 °C, the initial weight of the sample was corrected by subtracting the amount of NH_4Cl contained, because the NH_4Cl was vaporized during the oxidation.

Table 3. N/V atomic ratio and lattice constant of the VN_x formed by the reaction of gaseous VCl_4 with ammonia

Formation temp/°C	x in VN_x	a_0/Å
600	1.20	Not determined
700	1.15	4.115
800	1.14	4.126
900	1.13	4.133
1000	1.13	4.133

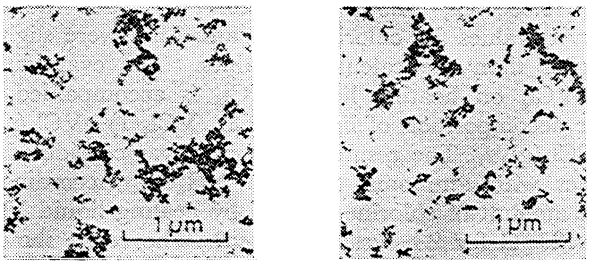

(a) 900 °C (b) 1000 °C

Fig. 2. Electron micrographs of $VN_{x(x=1.13)}$ formed at 900 and 1000 °C.

It has been known that VN_x phase has a NaCl structure.[7] The lattice constant of VN_x formed at each temperature is also shown in Table 3. As X-ray diffraction lines of the $VN_{1.20}$ formed at 600 °C were relatively weak and diffuse, the exact value of the lattice constant was not calculated.

The VN_x formed by the vapor-phase reaction at 600—1000 °C was examined by electron microscopy. The typical micrographs of the VN_x are shown in Fig. 2. The VN_x formed is relatively uniform, ultrafine powders with particle diameters of the order of 1/100 μm.

Finally, to obtain knowledge of the thermal stability of the VN_x formed by the vapor-phase reaction, the N/V atomic ratio of the sample obtained by heating $VN_{1.20}$ formed at 600 °C, which had the largest N/V atomic ratio in the VN_x formed in this work, at various temperatures in an argon atmosphere was examined. The results are shown in Fig. 3. In addition,

it was found that the residual NH_4Cl in the VN_x was completely removed by the heating above 900 °C.

The results indicated that when the VN_x formed by the vapor-phase reaction was heated in an argon atmosphere at temperatures higher than 500 °C, the N/V atomic ratio decreased and became close to that of the stoichiometric nitride; The value of x was 1.03 at the heating temperatures of 900 and 1000 °C. Hojo *et al.*[1] reported that when the VN_x with $x>1$ was heated *in vacuo* up to 1150 °C, the x value reduced to 1.02.

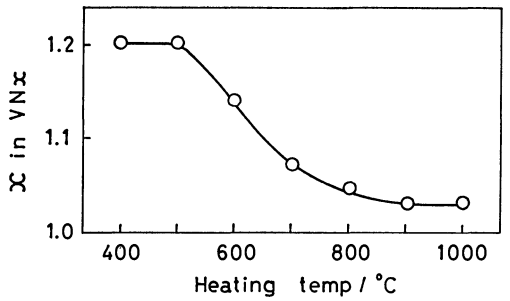

Fig. 3. N/V atomic ratio of VN_x obtained after heating $VN_{1.20}$ at various temperatures in an argon atmosphere for 1 h.

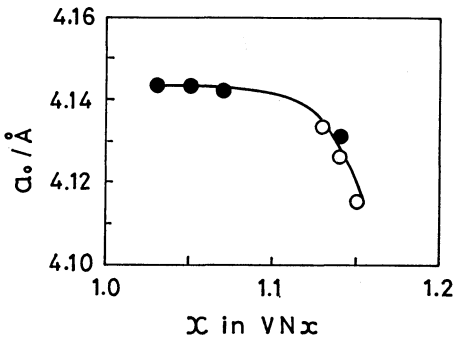

Fig. 4. Lattice constants (a_0) of VN_x with various x values.
●: From VN_x obtained after the heating of $VN_{1.20}$,
○: from VN_x formed by the reaction of gaseous VCl_4 with ammonia (Table 3).

The lattice constants of the VN_x with various x values, obtained in this work, are shown in Fig. 4.

The N/V atomic ratio of VN_x obtained after heating $VN_{1.20}$ in an argon atmosphere at each temperature was found to be lower than that of the VN_x formed by the vapor-phase reaction at the same temperature (Table 3). The difference in the N/V atomic ratio became larger with the increase in the temperature. These facts are considered to be due to the presence of nitrogen during the reaction, because the dissociation pressure of ammonia is relatively high even at low temperatures and markedly increases with the increase in the temperature.[9] This consideration was supported by the fact that no change in the N/V atomic ratio of the $VN_{1.13}$ formed at 1000 °C by the vapor-phase reaction was observed after heating at 1000 °C in an ammonia stream for 1 h.

The present work was partially supported by a Grant-in-Aid for Scientific Research No. 56470058 from the Ministry of Education, Science and Culture.

References

1) J. Hojo, O. Iwamoto, and A. Kato, *Nippon Kagaku Kaishi*, **1975**, 820.
2) A. Yajima, R. Matsuzaki, and Y. Saeki, *Bull. Chem. Soc. Jpn.*, **53**, 2843 (1980).
3) I. Barin and O. Knacke, "Thermochemical Properties of Inorganic Substances," Springer-Verlag, Berlin, Heiderberg, New York (1973), p. 499.
4) J. Kritil, *Z. Anal. Chem.*, **219**, 412 (1965).
5) JCPDS, Powder Diffraction Data Card, 25-1252.
6) JCPDS, Powder Diffraction File, 15-215.
7) ASTM, Powder Diffraction File, 7-7.
8) H. Lamprey and P. F. Forsyth, *Talanta*, **7**, 264 (1961); J. H. Simons and M. G. Powell, *J. Am. Chem. Soc.*, **67**, 75 (1945).
9) "Gmelins Handbuch der Anorganischen Chemie, System Nummer 4, Stickstoff," Verlag Chemie, Weinheim (1955), p. 323.
10) JIS H-1615 (1973), p. 2.

Pyrolytic Sulfurization Gas Chromatography. XII. The Simultaneous Determination of the Atomic Ratio between C, H, O, and N in an Organic Compound at the Centimilligram Level

Tadashi HARA* and Fujio OKUI

Department of Chemical Engineering, Faculty of Engineering, Doshisha University, Karasuma Imadegawa, Kamigyo-ku, Kyoto 602

(Received February 25, 1982)

The atomic ratio between C, H, O, and N in an ordinary organic compound and a metal organic chelate compound could be simultaneously and satisfactorily determined by the use of 30—130 μg of a sample which cannot be accurately weighed by a microbalance or an ultramicrobalance. This was done by adopting the following modifications: 1) The amount of S was reduced to 0.5 mg from the 5 mg used in the previous studies; 2) the stainless steel column in the gas chromatograph was replaced by a Teflon column; 3) the poly(vinyl chloride) and silicone rubber tubes were replaced by stainless steel and copper tubes; and 4) a correction procedure was established for the analysis of a small amount of a sample.

With the objective of establishing a new elemental analysis method by which several elements can be simultaneously determined, pyrolytic sulfurization gas chromatography(PSGC) was originated and has been investigated fundamentally by the present authors. It has been successfully applied to the simultaneous determination of the atomic ratio between C, H, O, and N in an ordinary organic compound,[1,2] a metal organic chelate compound,[3] a polymer,[4] and an organic halogen compound.[5,6]

In conventional organic elemental analysis, the atomic ratio between C, H, O, and N is determined by combining the content of C, H, and N obtained by a CHN analyzer with the content of O obtained by an oxygen analyzer. To obtain the exact atomic ratio between C, H, O, and N, a sample of more than either 1 mg or 100 μg must be weighed by a microbalance(sensitivity 1 μg) or an ultramicrobalance(sensitivity 0.1 μg) respectively. On the other hand, since one of the most remarkable characteristics of PSGC is that the atomic ratio between C, H, O, and N can be simultaneously determined without weighing the sample, the amount of sample necessary for an analysis by PSGC can be decreased to a minimum so long as the products can be detected by gas chromatography. The present study has been carried out for the purpose of decreasing the amount of sample necessary for an analysis by PSGC.

When about 50 μg of a sample, which is one tenth of the amount of a sample in the ordinary PSGC method, was analyzed by the conventional PSGC method, the carbon content was found to be less than the theoretical value. This was attributed to the partial dissolution of carbon disulfide(CS_2) into residual sulfur. Therefore, the amount of S was reduced to 0.5 mg from the 5 mg used in the conventional PSGC method. Thus, the atomic ratio between C, H, O, and N could be simultaneously determined by the use of 30—130 μg of a sample and 0.5 mg of S. In addition to ordinary compounds, metal organic chelate compounds, which are difficult to analyze even by mass spectrometry, could be analyzed with satisfactory results.

Experimental

Reagents. All the reagents used as the analytical samples were of a reagent grade for elemental analysis except for cyanoguanidine, which was of a reagent grade for the melting-point standard.

Apparatus. The displacement apparatus,[1] which had been used for the preparation of the ampule containing a sample and S, was modified as follows: As the charging tube of He, a stainless steel tube (1 mm i.d., 1.5 mm o.d.) was used instead of a poly(vinyl chloride) tube, and as the exhaust tube of air, a copper tube (4 mm i.d., 5 mm o.d.) was used instead of a silicone rubber tube. To improve the precision and accuracy of the gas-chromatographic analysis, Teflon columns were used instead of the stainless steel columns used in the previous studies.

The other equipment used in the experiment was the same as that previously reported.

Procedure. A definite volume of a powdered sample was placed in a reaction tube by the use of the sampler[1]-I, which was composed of a glass capillary tube and a plunger (13%Rh–Pt alloy, 0.2 mm diam.) used to push the sample into the reaction tube. About 0.5 mg of S was added to it by the use of the sampler-II, which was also composed of a glass capillary tube and a plunger (Ni–Cr alloy, 0.4 mm diam.). According to this procedure, S could be taken in the range from about 0.45 mg to 0.55 mg. The reaction tube containing the sample and S thus obtained was treated by the same procedure as in the previous study.[7]

Results and Discussion

Amounts of Sample and S. In order to minimize the amount of sample necessary for the PSGC analysis, the effect of the amount of the sample on the analytical values was examined by the use of alanine as a standard sample in the following manner. A known amount of a sample was made to react with 5 mg of S in an ampule, and the reaction products were analyzed by the ordinary PSGC method. The peak areas of the products were then plotted against the weight of the sample (Fig. 1). Figure 1 shows that the calibration curves of all products pass through the point of origin of the coordinate axis except for that of CS_2. Since the peak-area ratio of each product to hydrogen sulfide(H_2S) is required to be a definite value in PSGC, these ratios were also calculated

Table 1. Effect of column material on the fluctuation of the peak-area ratios[a)]

Column material	Sulfur (mg)	Sample (μg)	C.V.(%)[b)]				
			N_2	CO_2	H_2S	COS	CS_2
Stainless steel	5	500	0.897	2.73	0.614	0.736	0.924
Stainless steel	0.5	50	3.39	10.2	0.793	3.29	3.16
Teflon	5	500	0.451	0.942	0.230	0.484	1.06
Teflon	0.5	50	2.51	4.27	0.714	1.24	1.02

a) The ratios of the peak area of each product to the sum of the peak area of each product. b) Average of 10 runs for alanine.

and plotted against the weight of the sample (Fig. 2). As can be seen from Fig. 2, the peak-area ratio of CS_2 to H_2S decreases with a decrease in the weight of the sample. These results could be explained by the fact that CS_2 as a reaction product partly remained in the residual sulfur because of its dissolution. Therefore, it was necessary to reduce the amount of S with a decrease in the amount of the sample. Almost entirely satisfactory results for 30—130 μg of the sample were obtained by the use of about 0.5 mg of S, as will be shown later.

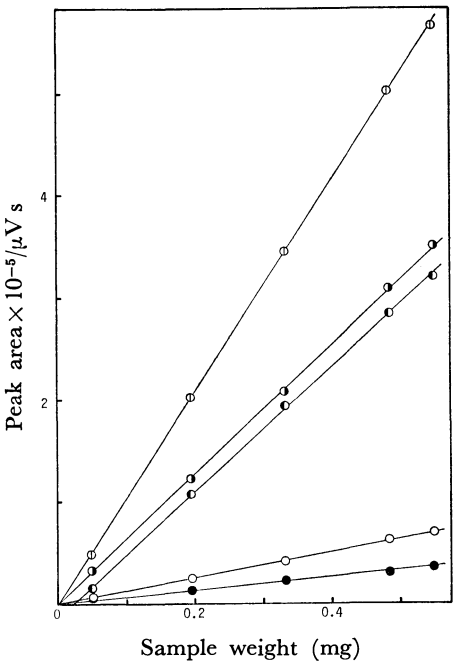

Fig. 1. Relationship between sample weight and peak area of the product.
○: N_2, ●: CO_2, ⓘ: H_2S, ◑: COS, ◐: CS_2.

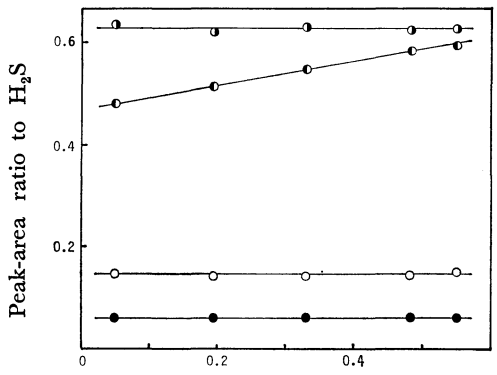

Fig. 2. Relationship between sample weight and peak-area ratio of the product to H_2S (5 mg of S was used).
○: N_2/H_2S, ●: CO_2/H_2S, ◑: COS/H_2S, ◐: CS_2/H_2S.

Improvement of the Apparatus. The analytical value obtained under the experimental conditions of the conventional PSGC method gave an error increasing with a decrease in the amount of sample. In order to improve the precision and accuracy of the analytical data, 1) the column material in a gas chromatograph and 2) the displacement apparatus were modified in the following way. 1) The stainless steel columns used in the previous studies were replaced by Teflon columns under the same gas-chromatographic conditions. The present column material was compared with the previous one by analyzing *ca.* 0.5 mg and *ca.* 50 μg of alanine samples (Table 1). Judging from the results shown in Table 1, the Teflon column is superior to the stainless steel column. 2) To minimize the fluctuation in the analytical value of nitrogen (N_2)(Table 1) which seemed to be due to the contamination of air passing through the tubes of poly(vinyl chloride) and silicone rubber, the displacement apparatus was modified in the following manner. As the charging tube of He, a stainless steel tube(1 mm i.d., 1.5 mm o.d.) was used instead of a poly(vinyl chloride)tube, and as the exhaust tube of air, a copper tube(4 mm i.d., 5 mm o.d.) was used instead of a silicone rubber tube. The present displacement apparatus was compared with the previous one by analyzing *ca.* 50 μg of alanine (Table 2). Table 2 shows that the present apparatus is superior to the previous one with regard to the fluctuation of the analytical data of N_2. As a result of the above-mentioned improvements, it is suggested that the atomic ratio between C, H, O, and N for centimilligrams of a sample can be simultaneously determined with the same pre-

Table 2. Effect of the displacement apparatus on the fluctuation of the peak-area ratios

	C.V.(%)[a)]				
	N_2	CO_2	H_2S	COS	CS_2
Present	0.987	3.39	0.767	0.853	1.29
Previous	2.51	4.27	0.714	1.24	1.02

a) Average of 10 runs for alanine.

cision and accuracy as in the ordinary PSGC method. The following investigations were undertaken by the use of the modified apparatus.

Sampling Amounts. Since it was difficult to weigh centimilligrams of a sample accurately by means of a microbalance, the weight of a sample was calculated approximately by the use of Eq. 1 from the analytical data:

$$W(\mathrm{mg}) = \frac{1}{F}\Sigma M(\mathrm{X})K(\mathrm{X})A(X), \quad (1)$$

where W is the weight of a sample, X is the reaction product, $M(\mathrm{X})$ is the value obtained by subtracting the amount of S from the formula weight of X, $K(\mathrm{X})$ is the calculation factor of X, $A(\mathrm{X})$ is the peak area of X, and F is the conversion factor obtained by the use of Eq. 2 from the calibration curve of H_2S in Fig. 1:

$$F = \frac{M_t}{3.50w}A(\mathrm{H_2S}), \quad (2)$$

where w is the weight of alanine, M_t is the molecular weight of alanine, and 3.50 indicates the mole number of H_2S produced from 1 mol of alanine. By the use of Eq. 1, the weight of a sample could be calculated within a relative error of about $\pm 10\%$. Sulfur in the range from about 0.45 mg to 0.55 mg was conveniently sampled by means of the sampler-II.

Effect of the Sample Amount on the Peak-area Ratio. Centimilligrams of alanine as a standard sample was made to react with *ca.* 0.5 mg of S in an ampule and then analyzed by PSGC. The peak-area ratios of the products to H_2S were plotted against the calculated weight of a sample (Fig. 3). It is apparent from Fig. 3 that the atomic ratio between C, H, O, and N in a sample can be determined by the use of a sample in the range from about 50 μg to 130 μg, for the peak-area ratios of all the products to H_2S indicated definite values.

Correction of Blank Values. As can be seen from Fig. 3, the peak-area ratio of carbonyl sulfide(COS) to H_2S increased with a decrease in the amount of a sample to less than 50 μg, while the peak-area ratio of CS_2 to H_2S decreased with a decrease in the amount of a sample to less than 30 μg. Then, the following investigation was made with regard to 1) the blank value of COS and 2) the blank value of CS_2. 1) In the ordinary PSGC, a small peak of COS was still detected in the analysis of a sample consisting of either C and H or C, H, and N, but it was neglected in the calculation of the atomic ratio because it was negligibly small. In the present study, however, a smaller amount of a sample is used, and the peak area of COS is presumed to be influenced by the peak area of COS as a blank value. Then, a 30—100 μg of cyanoguanidine, which consists of C, H, and N, was analyzed by the present method, and the value of the peak area of COS was examined. The peak area of COS as a blank value was approximately a definite value, regardless of the amount of the sample. Therefore, the peak-area ratio of COS to H_2S was calculated from the value which was obtained by subtracting the value of COS as a blank one from the analytical value of alanine as a standard sample; it was then plotted against the sample amount (Fig. 4). Figure 4 shows that the peak-area ratio of COS to H_2S comes to a definite value when the blank value is corrected. 2) The peak-area ratio of CS_2 to H_2S decreased with a decrease in the amount of the sample to less than 30 μg (Fig. 3). It was presumed that a part of the CS_2 remained in the residual sulfur in the ampule. Therefore, the effect of the amount of residual sulfur on the peak area of CS_2 was investigated by the use of the analytical data in Fig. 3 in the following manner. The amount of S(W_c) consumed by pyrolytic sulfurization reaction was calculated by means of Eq. 3:

$$W_c(\mathrm{mg}) = \frac{M_s}{F}(A(\mathrm{H_2S}) + K(\mathrm{COS})A(\mathrm{COS}) + 2K(\mathrm{CS_2})A(\mathrm{CS_2})), \quad (3)$$

where M_s is the atomic weight of S, F is the same factor as in Eq. 1, X is the reaction product, $A(\mathrm{X})$ is the peak area of X, and $K(\mathrm{X})$ is the calculation factor of X. Therefore, the amount of residual sulfur (W_r) was found approximately by Eq. 4:

$$W_r(\mathrm{mg}) = 0.5 - W_c. \quad (4)$$

The relationship between W_r and the deficient amount of CS_2, calculated from the data in Fig. 3, was plotted in Fig. 5. Figure 5 shows that the amount of CS_2 dis-

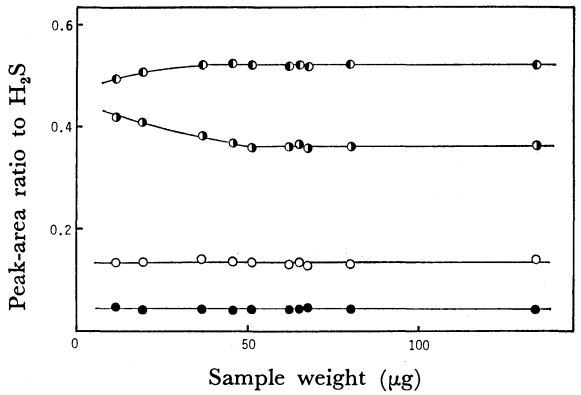

Fig. 3. Relationship between sample weight and peak-area ratio of the product to H_2S.
○: N_2/H_2S, ●: CO_2/H_2S, ◑: COS/H_2S, ◐: CS_2/H_2S.

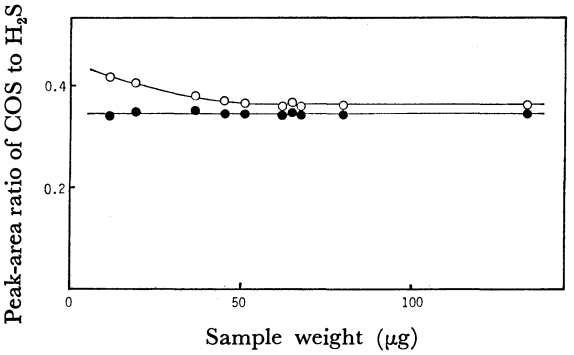

Fig. 4. Relationship between sample weight and peak-area ratio of COS to H_2S.
○: Uncorrected peak-area ratio, ●: corrected peak-area ratio.

Table 3. Corrections for COS and CS_2

Sample	Sample weight (μg)	Correction	C (wt%)			H (wt%)			O (wt%)		
			Calcd	Found	Error	Calcd	Found	Error	Calcd	Found	Error
Cholesterol	62	N[a]	83.87	83.66	−0.21	11.99	11.79	−0.20	4.14	4.55	+0.41
		A[b]	83.87	83.85	−0.02	11.99	11.84	−0.15	4.14	4.31	+0.17
Sucrose	27	N	42.11	41.57	−0.54	6.48	6.23	−0.25	51.41	52.20	+0.79
		B[c]	42.11	42.06	−0.05	6.48	6.31	−0.17	51.41	51.63	+0.22

a) Not corrected, b) corrected for COS, c) corrected for both COS and CS_2.

Table 4. Analytical results of various organic compounds

Sample	Calculated weight (μg)	C (wt%)			H (wt%)			O (wt%)			N (wt%)		
		Calcd	Found	Error	Calcd	Found	Error	Calcd	Found	Error	Calcd	Found	Error
Anthracene	55	94.34	94.37	+0.03	5.66	5.63	−0.03						
Acetanilide	48	71.09	71.30	+0.21	6.71	6.61	−0.10	11.84	11.88	+0.04	10.36	10.21	−0.15
Phenacetin	60	67.02	66.99	−0.03	7.31	7.18	−0.13	17.85	18.06	+0.21	7.82	7.77	−0.05
Nicotinic acid	65	58.54	58.64	+0.10	4.09	3.98	−0.11	25.99	26.19	+0.20	11.38	11.19	−0.19
p-Nitroaniline	53	52.17	52.01	−0.16	4.38	4.30	−0.08	23.17	23.36	+0.19	20.28	20.33	+0.05
Caffeine	61	49.48	49.75	+0.27	5.19	5.00	−0.19	16.48	16.37	−0.11	28.85	28.88	+0.03
Alanine	45	40.44	40.43	−0.01	7.92	7.93	+0.01	35.92	36.03	+0.11	15.72	15.61	−0.11
Triphenylphosphine	70	93.46	93.55	+0.09	6.54	6.45	−0.09						
Phenylmercury(II) acetate	65[a]	70.58	70.39	−0.19	5.92	5.96	+0.04	23.50	23.65	+0.15			
Tris(2,4-pentanedionato)iron(III)	58[a]	60.59	60.78	+0.19	7.12	7.14	+0.02	32.29	32.08	−0.21			
Bis(2,4-pentanedionato) magnesium(II)	67[a]	51.27	51.18	−0.09	7.75	7.84	+0.09	40.98	40.98	0.00			

a) Includes the weight of the metal.

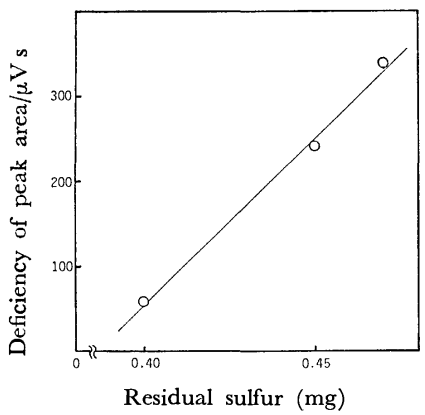

Fig. 5. Relationship between residual sulfur and deficiency of peak area of CS_2.

solved in the residual sulfur is approximately proportional to the amount of the residual sulfur. Therefore, the deficient amount of CS_2 was calculated by the use of Eq. 5, obtained from the calibration curve in Fig. 5:

$$\alpha(\mu V\,s) = 3.8\times10^{3}W_r - 1.5\times10^{3}, \quad (5)$$

where α is the deficient amount of CS_2. Judging from the results shown in Fig. 5, Eq. 5 can be applied when W_r is in the range from 0.39 mg to 0.5 mg. Thus, the atomic ratio between C, H, O, and N should be estimated by calculating α by means of Eqs. 3, 4, and 5 and by correcting the apparent peak area of CS_2. Examples of these corrections are shown in Table 3. As can be seen from Table 3, the atomic ratio between C, H, and O was markedly improved by applying the above-mentioned corrections. Both the oxygen content in cholesterol and the amount of COS produced from 62 μg of cholesterol were small, but a satisfactory result was obtained.

Analysis of Various Organic Compounds. Various organic compounds and metal organic chelate compounds were analyzed by the present procedure; the results are shown in Table 4. Table 4 indicates that the atomic ratio between C, H, O, and N can be simultaneously and satisfactorily determined by the use of centimilligrams of a sample.

The present study is expected to be especially significant for the organic elemental analysis of micro amounts of a sample which cannot be accurately weighed by a microbalance or an ultramicrobalance.

This study was supported by a Grant-in-Aid for the Special Research Project on "Trace Characterization" given by the Ministry of Education, Science and Culture.

References

1) K. Tsuji, K. Fujinaga, and T. Hara, *Bull. Chem. Soc. Jpn.*, **50**, 2292 (1977).

2) T. Hara, K. Fujinaga, and K. Tsuji, *Bull. Chem. Soc. Jpn.*, **51**, 1110 (1978).
3) T. Hara, K. Fujinaga, and K. Tsuji, *Bull. Chem. Soc. Jpn.*, **51**, 2951 (1978).
4) T. Hara, K. Fujinaga, F. Okui, and K. Negayama, *Sci. Eng. Rev. Doshisha Univ.*, **21**, 241 (1981).
5) T. Hara, K. Fujinaga, and F. Okui, *Bull. Chem. Soc. Jpn.*, **53**, 1308 (1980).
6) T. Hara, K. Fujinaga, and F. Okui, *Bull. Chem. Soc. Jpn.*, **54**, 2956 (1981).
7) T. Hara and F. Okui, *Bull. Chem. Soc. Jpn.*, **55**, 2127 (1982).

Spectrophotometric Determination of Palladium(II) by Extraction of Its 1-Pyrrolidinecarbodithioate into Molten Naphthalene

Avadesh KUMAR, M. F. HUSSAIN, Masatada SATAKE,*,† and B. K. PURI

Department of Chemistry, Indian Institute of Technology, Hauz Khas, New Delhi-110 016, India
†*Faculty of Engineering, Fukui University, Fukui 910*

(Received February 1, 1982)

A new spectrophotometric method for the determination of palladium after extraction of its 1-pyrrolidinecarbodithioate into molten naphthalene has been developed. Palladium forms a water-insoluble, thermally stable 1:2 complex with 1-pyrrolidinecarbodithioate which is easily extracted into molten naphthalene in the pH range of 3.0—6.0. At room temperature, solid naphthalene containing the metal-complex is dissolved in chloroform (10 ml). It has an absorption maximum in the range of 336—342 nm. Beer's law holds in the concentration range of 2.5—90.0 μg of palladium in 10 ml of chloroform solution. The molar absorptivity(1 mol^{-1} cm^{-1}) and sensitivity(μg/cm^2) are found to be 6.4×10^3 and 0.0166, respectively. Samples containing 30 μg of palladium gives a mean absorbance of 0.18 with a standard deviation of 0.0025. Other factors such as amount of reagent and naphthalene, pH, aqueous phase volume and diverse ions have been examined. The method has been applied to the analysis of some alloys.

Ammonium 1-pyrrolidinecarbodithioate has been used as an analytical reagent in the determination of various metal ions spectrophotometrically and atomic absorption spectrophotometrically after extracting their metal complexes into suitable solvents.[1-3] Recently it has been utilized in the spectrophotometric determination of copper, bismuth and cobalt after extracting their complexes into molten naphthalene.[4] The main advantages of this method are that the equilibrium distribution in the two phases is achieved in a few seconds and the metal chelates are dissolved merely by contact with the molten naphthalene. A very small amount (2 g) of the organic phase is required for the complete extraction which enhances the sensitivity as the whole of the organic phase may be taken for the analysis. This technique is especially useful for the extraction of those metal ions which form complexes with the complexing agent at high tempera ture.[5] The present communication describes conditions for the extraction of palladium with potassium 1-pyrrolidinecarbodithioate (PPDC) into molten naphthalene and its subsequent determination by spectrophotometric method after dissolution of naphthalene extract in chloroform. The interference of the various ions has been studied and the conditions have been developed for the determination of palladium in some alloys.

Experimental

Reagents. Palladium nitrate solution was prepared in redistilled water and standardized gravimetrically.[6]

PPDC solution, 0.2% was prepared by dissolving 0.2 g of PPDC in 100 ml of water.

Naphthalene and chloroform(analytical grade) were checked spectrophotometrically before use.

Alkali salt(1%) and metal salt(0.2%) solutions were prepared to study interference.

Dilute solution of perchloric acid, ammonia or acetate buffer prepared from 1 M(1 M=1 mol dm^{-3}) acetic acid and 1 M ammonium acetate were used to adjust pH.

Apparatus. An Elico pH meter and a SP-700 spectrophotometer were used.

General Procedure. An aliquot of palladium solution was taken in a beaker, to this was added 3.0 ml of reagent solution. The pH was adjusted to 4.2 with 2.0 ml of buffer solution. This solution was transferred to a 100-ml round bottomed flask and warmed on a water bath at about 60 °C and naphthalene (2 g) was added to it. The flask was stoppered and heating was continued till naphthalene melted and formed a separate liquid-layer. The flask was taken off from the water bath and stirred vigorously till the naphthalene separated out as a solid mass. Once more the naphthalene was melted, shaken vigorously and allowed to stand. The naphthalene was filtered off, dried on a filter paper and dissolved in chloroform in a 10 ml standard flask. This solution was dried by adding anhydrous sodium sulfate (2 g), and the absorbance was measured in a 1-cm cell at 340 nm against a reagent blank. A calibration curve was prepared under similar conditions.

Results and Discussion

Absorption Spectra. The absorption spectra of potassium 1-pyrrolidinecarbodithioate and palladium(II) 1-pyrrolidinecarbodithioate in naphthalene and chloroform solution were measured against water and reagent blank, respectively and are shown in Fig. 1. The palladium complex absorbs strongly in the region 336—342 nm where the reagent absorbs very little. All absorbance measurements were made at 340 nm.

Effect of pH. Extraction was carried out at different pH, other conditions as described in the general procedure being kept constant. The characteristics of all spectral curves were the same, indicating the presence of only one complex. The results are shown in Fig. 2. Optimum pH corresponds to 3.0—6.0.

Effect of Reagent Concentration. Extractions were carried out at a fixed pH but at varying reagent concentrations and it was observed that the extractions were quantitative for 1.5—6.0 ml of 0.2% of potassium 1-pyrrolidinecarbodithioate (Fig. 3). Consequently, 2.0 ml of the reagent was used in each case.

Effect of Buffer Solution. Sample solutions containing 30 μg of palladium, 3.0 ml of 0.2% PPDC solution and various amounts of the acetate buffer solution (pH 4.2) were added and the extractions were carried out by the general procedure. The absorbance remained constant for 0.5—6.5 ml of the buffer used In all the cases, 2.0 ml of the buffer was used.

Effect of Amount of Naphthalene. At fixed pH and reagent concentration, the extractions were car-

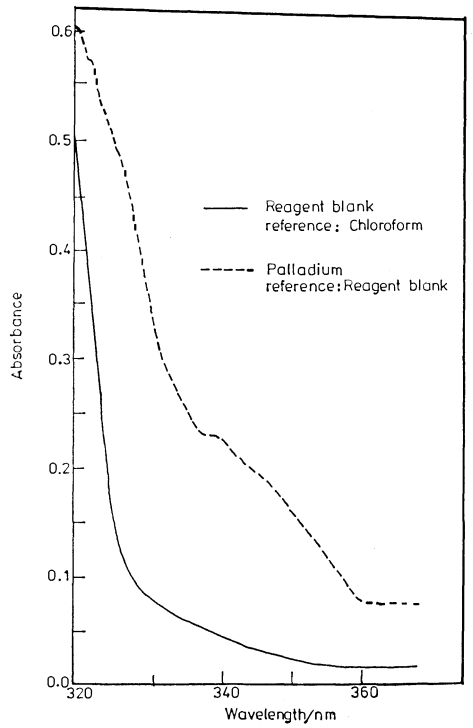

Fig. 1. Absorption spectra of 1-pyrrolidinecarbodithioate and palladium complex in naphthalene–chloroform solution.
Reagent blank: 1-pyrrolidinecarbodithioate: 3.0 ml (0.2%), naphthalene: 2.0 g, pH: 5.0, reference: water; palladium: 40 μg, rest of the conditions were the same as above, reference: reagent blank.

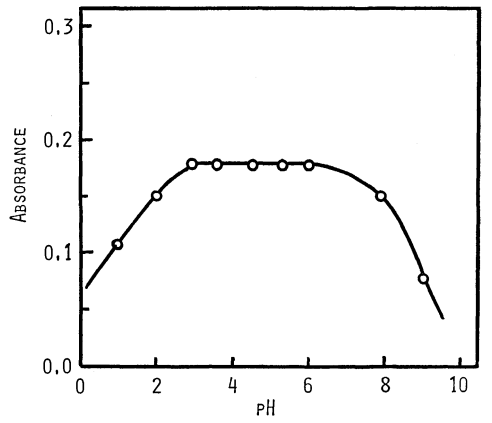

Fig. 2. Effect of pH on absorbance.
Palladium: 30 μg, wavelength: 340 nm, 1-pyrrolidinecarbodithioate: 3.0 ml (0.2%), naphthalene: 2 g, reference: reagent blank.

ried out by taking 0.5—3.5 g of naphthalene in different steps. It was observed that the absorbance remained constant for 1.0—3.0 g of naphthalene and thus 2.0 g of naphthalene was used throughout the experiment. Below 1.0 g, the extraction was incomplete while above 3.0 g of the naphthalene, it was difficult to dissolve it in a limited quantity of chloroform (10 ml).

Effect of Aqueous Phase Volume. Since the organic phase is very small (2 g) as compared to the aqueous phase (40 ml), it was essential to study the

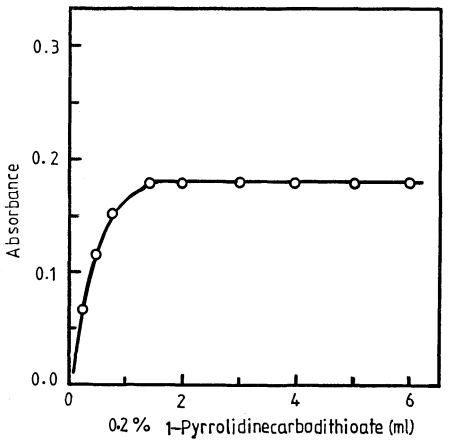

Fig. 3. Effect of reagent concentration on absorbance.
Palladium: 30 μg, rest of the conditions were the same as in Fig. 2.

TABLE 1. EFFECT OF DIVERSE SALTS

Alkali salt added	Anion added (mg)	Absorbance 340 nm
—	—	0.180
Potassium chloride	23.80	0.180
Potassium bromide	33.60	0.178
Potassium iodide	38.25	0.181
Potassium thiocyanate	29.85	0.182
Sodium acetate	40.00	0.180
Sodium sulfate	40.00	0.180
Sodium oxalate	33.60	0.177
Potassium sodium tartrate	39.40	0.178
Sodium citrate	31.45	0.177
Sodium orthophosphate	25.60	0.178
Sodium thiosulfate	21.00	0.182
Disodium EDTA	40.00	0.178
Sodium fluoride	22.60	0.178

Pd: 30.0 μg, pH: 4.2, 0.2% PPDC: 3.0 ml, buffer: 2.0 ml.

effect of the volume of the aqueous phase on the extraction. It was observed that the absorbance remained constant upto 50 ml of the aqueous phase. Above this volume of the aqueous phase, the extraction was not quantitative.

Effect of Digestion Time. The palladium(II) 1-pyrrolidinecarbodithioate in the solution was warmed on a water-bath at 60 °C and the effect of digestion time on the absorbance was investigated between 1—20 min. It was found that the absorbance remained constant during this period. Therefore, 10 min of digestion time was selected for all measurements.

Effect of Shaking Time. The sample solution containing palladium(II) 1-pyrrolidinecarbodithioate and 2.0 g of naphthalene was warmed on a water-bath for 10 min at the temperature 60 °C and the extraction was carried out by vigorous shaking of the contents upto 30 min. It was observed that the shaking time of 1 min was sufficient for the complete extraction.

Effect of Standing Time of Chloroform Solution. The absorbance of the complex in naphthalene–chloroform was noted at an interval of 20 min and it was noted that the absorbance remained constant for more than 24 h indicating that the complex is quite stable in the extract.

Effect of Electrolytes. Various electrolytes such as sodium perchlorate, sodium nitrate, sodium sulfate, and sodium acetate (0.01—1.0 M) caused no improvement in the extraction indicating that the extraction was complete.

Composition of the Complex. The composition of palladium(II) 1-pyrrolidinecarbodithioate was established by Job's method of continuous variation and the mole ratio method. A sharp peak at 0.33 mole fraction in Job's curve and a clear break at 1:2 metal: carbodithioate ratio in the mole ratio plot suggest the extraction of $Pd(C_4H_8NCS_2)_2$ under these conditions.

Calibration Curve. With the optimum conditions described above a calibration curve was constructed for palladium complex at 340 nm. It was observed that Beer's law was obeyed over the concentration

Table 2. Effect of diverse cations

Metal ion	Metal ion added(mg)	Absorbance	Remarks
—	—	0.180	
Ag^{+}	1.500	0.150	
Ag^{+}	1.125	0.178	
Al^{3+}	0.900	0.184	
Al^{3+}	0.625	0.182	
As^{3+}	0.740	0.182	
As^{3+}	0.555	0.180	
Be^{2+}	0.404	0.176	
Be^{2+}	0.303	0.178	
Bi^{3+}	0.860	0.192	
Bi^{3+}	0.645	0.182	
Cd^{2+}	1.200	0.184	
Cd^{2+}	0.900	0.181	
Co^{2+}	0.666	0.340	
Co^{2+}		0.186	* After masking with 5 ml of 1% EDTA solution
Co^{2+}	0.500	0.330	
Co^{2+}		0.184	* After masking with 5 ml of 1% EDTA solution
Cr^{3+}	0.520	0.183	
Cr^{3+}	0.390	0.181	
Cu^{2+}	0.431	0.334	
Cu^{2+}		0.183	* After masking with 5 ml of 1% EDTA solution
Cu^{2+}	0.323	0.295	
Cu^{2+}		0.180	* After masking with 5 ml of 1% EDTA solution
Fe^{3+}	0.332	0.280	
Fe^{3+}		0.184	* After masking with 10 ml of 1% EDTA solution
Fe^{3+}	0.240	0.220	
Fe^{3+}		0.182	* After masking with 10 ml of 1% EDTA solution
Hg^{2+}	0.294	0.242	
Hg^{2+}		0.188	* After masking with 10 ml of 1% EDTA solution
Hg^{2+}	0.220	0.210	
Hg^{2+}		0.184	* After masking with 10 ml of 1% EDTA solution
Ir^{3+}	0.520	0.186	
Ir^{3+}	0.390	0.180	
Mn^{2+}	0.960	0.182	
Mn^{2+}	0.720	0.180	
Mo^{6+}	1.088	0.183	
Mo^{6+}	0.816	0.180	
Ni^{2+}	0.500	0.780	
Ni^{2+}		0.210	* After masking with 5 ml of 1% EDTA solution
Ni^{2+}	0.375	0.480	
Ni^{2+}		0.183	* After masking with 5 ml of 1% EDTA solution
Os^{8+}	1.080	0.185	
Os^{8+}	0.810	0.182	
Pb^{2+}	0.616	0.180	
Pb^{2+}	0.462	0.180	
Pt^{4+}	0.240	0.188	
Pt^{4+}	0.180	0.182	
Rh^{3+}	0.202	0.188	
Rh^{3+}	0.156	0.183	
Ru^{3+}	0.387	0.184	
Ru^{3+}	0.289	0.182	
Sb^{3+}	0.640	0.182	
Sb^{3+}	0.480	0.180	
Te^{4+}	0.200	0.178	
Te^{4+}	0.150	0.178	
Th^{4+}	0.320	0.184	
Th^{4+}	0.240	0.182	
Tl^{+}	0.204	0.184	
Tl^{+}	0.152	0.182	
U^{6+}	0.560	0.184	
U^{6+}	0.420	0.181	
V^{5+}	0.870	0.182	
V^{5+}	0.652	0.180	
W^{6+}	1.114	0.182	
W^{6+}	0.834	0.180	
Zn^{2+}	0.596	0.178	
Zn^{2+}	0.427	0.180	
Zr^{4+}	0.916	0.182	
Zr^{4+}	0.687	0.181	

Pd: 30.0 μg, pH: 4.2, 0.2% PPDC: 3.0 ml, buffer: 2.0 ml.

Table 3. Determination of palladium in alloys

Alloy	Composition of alloy (%)	Amount of palladium taken/μg	Amount of palladium found/μg	Average μg	Other method[a]
Oakay	Ni:60, Pt:20, V:9.5, Pd:10.5	31.5	31.4 31.6 31.6 31.8 31.6	31.6	31.1
Platinum-Iridium	Pt:55, Ir:28, Rh:7, Cu:3, Fe:3.5, Pd:3.5	39.2	39.3 39.5 39.3 39.0 39.4	39.3	39.5

a) Average of the five determinations.

range of 2.5—90.0 μg in 10 ml of the final solution. Ten samples containing 30 μg of palladium were prepared by the general procedure gave a mean absorbance of 0.18 when measured in a 1-cm cell with a relative standard deviation of 0.0025. The molar absorptivity was calculated to be 6.4×10^3 l mol^{-1} cm^{-1} at 340 nm, and the sensitivity 0.0166 μg of palladium per cm^2 for the absorbance of 0.001.

Interference. The interference of various ions was studied in detail. Generally, 50 mg of alkali salt and 2 mg of metal ion were added individually to the aliquots containing 30 μg of palladium. Among the anions examined (Table 1) none interfered. This non-interference of the various anions may be attributed to their low stability constants as compared to palladium 1-pyrrolidinecarbodithioate.[7] Among the metal ions studied (Table 2) only Fe(III), Ni(II), Co(II), Hg(II), and Cu(II) interfered but their interference was eliminated by using suitable masking agents (Table 2). Obviously, the method is quite selective for the extraction of palladium.

Analysis of Alloy. 25—50 mg of the alloy of known composition, and 20—40 ml of aqua regia were added and the solution evaporated to about 5 ml. Concentrated hydrochloric acid (10 ml) was added, the solution was warmed, transferred to a 500 ml standard flask and made upto the mark with distilled water.[8] An aliquot was taken, 5 ml of 1% EDTA, and 3.0 ml of the reagent solutions were added. The pH of this solution was adjusted to 4.2 with 2 ml of the buffer solution and the palladium complex was extracted into molten naphthalene according to the general procedure. The results are given in Table 3 and are compared with a recent method.[9]

In conclusion, this simple and inexpensive procedure for palladium can be successfully applied to the alloy sample analysis.

The extraction with molten naphthalene is useful for the strongly hydrated oxinates of zinc,[10] magnesium[11] and cadmium,[12] and for the nioxime complexes[13] of nickel and palladium and bismuth 2-mercaptobenzothiazole complex[14] that offer a low solubility in nonaqueous solvents.

Sincere thanks of the authors are due to C. S. I. R., Delhi for the award of a fellowship to one of them (M. F. H.).

References

1) C. H. McMaster, *Anal. Chem.*, **41**, 1489 (1969).
2) K. A. Uvarova and Yu. I. Usatenko, *Zavod. Lab.*, **38**, 1431 (1972).
3) W. Crump, J. Hans, and W. C. Purdy, *Talanta*, **16**, 124 (1969).
4) M. Shimizu, K. Taniguchi, and M. Satake, *Fukui Daigaku Kogakubu Kenkyu Hokoku Jpn.*, **24**, 337 (1976).
5) B. K. Puri and M. Gautam, *Talanta*, **25**, 484 (1978).
6) F. E. Beamish, J. J. Russel, and J. Seath, *Ind. Eng. Chem., Anal. Ed.*, 174 (1937).
7) D. D. Perrin, "Masking and Demasking of Chemical Reactions," Wiley-Interscience, New York (1970).
8) N. H. Furman, "Scott's Standard Methods of Chemical Analysis," 5th ed, D. Van Nostrand Company, Inc., New York (1959), Vol. 1, p. 722.
9) B. K. Deshmukh and R. B. Kharat, *J. Indian Chem. Soc.*, **58**, 131 (1981).
10) T. Fujinaga, M. Satake, and T. Yonekubo, *Jpn. Analyst*, **19**, 216 (1969).
11) M. Satake, *Memoirs Fac. Eng., Fukui Univ.*, **18**, 225 (1970).
12) T. Fujinaga, M. Satake, and T. Yonekubo, *Bull. Chem. Soc. Jpn.*, **46**, 2090 (1973).
13) M. Satake, *Anal. Chim. Acta*, **92**, 423 (1977).
14) M. Satake and T. Yamauchi, *Memoirs Fac. Eng., Fukui Univ.*, **25**, 107 (1977).

Studies on Dissolved Metalloenzymes in Lake Water. I. Identification of Alkaline Phosphatase

Kensei Kobayashi, Kimikazu Iwase, Masahiro Matsui, Masami Watanabe, Hirotaka Ueda, Kitao Fujiwara, Hiroki Haraguchi, and Keiichiro Fuwa*

Department of Chemistry, Faculty of Science, The University of Tokyo, Hongo, Bunkyo-ku, Tokyo 113

(Received March 6, 1982)

Metalloenzyme (alkaline phosphatase) dissolved in lake water has been identified by means of high performance liquid chromatography (HPLC). Water samples were collected from Lake Kasumigaura in Ibaraki, and filtered with a 0.2—0.45 μm membrane filter immediately after sampling. Filtered water was concentrated to 100—2000 fold by ultrafiltration membrane which could concentrate the components of molecular weight larger than 10000. The enzymatic activity of alkaline phosphatase was measured using *p*-nitrophenyl dihydrogenphosphate as a substrate. Chelating agents added to the concentrated lake water inhibited the appearance of enzymatic activity, while the enzymatic activity was recovered with addition of zinc ion. The HPLC chromatograms of the concentrated lake water were examined, where an aqueous porous gel column was used for separation. The effluent at molecular weight of *ca.* 90000 showed specific activity of alkaline phosphatase. Zinc was also found in the same fraction. These facts suggest that alkaline phosphatase with the nature similar to procaryotes was present in the lake water.

Recently, the present authors reported that alkaline phosphatase existed as a dissolved form in sea water.[1,2] In these studies the identification of alkaline phosphatase was made by measuring the high performance liquid chromatogram as well as enzymatic activity and zinc content, and also biological significances of dissolved metalloenzymes in natural water were discussed along with the natural cycles of nutrient and trace elements. As is well known, alkaline phosphatase is one of the typical metalloenzymes containing four zinc atoms in one molecule,[3] and concerns with the phosphorus cycle in animals and microorganisms. Thus, further study on dissolved metalloenzymes in natural water may help to elucidate not only biological activities, but also elemental cycles. In addition, the identification of the chemical forms of trace metals in water has also been receiving great attention in the fields of bioinorganic and analytical chemistry.[4] In this sense, the dissolved metalloenzymes can be considered as one of the chemical forms of trace metals in water.

As was suggested in the previous papers,[1,2] alkaline phosphatase is also one of the most significant enzymes in limnology, because it may concern with the phosphorus cycles in natural water. Free dissolved phosphatase activity in pond water was first reported by Overbeck and Babenzien in 1963.[5] Reichardt *et al.* did consider the ecological importance of free phosphatase in lake water.[6] Since then, a number of investigations on phosphatase activity and its role in freshwater have been done. Furthermore, several reports on other types of enzymatic activities have been also given in terms of natural water. For example, Morrison *et al.* determined cellulase activity,[7] and Little *et al.* determined proteolytic enzymes in lake water.[8]

In this paper, the study on dissolved alkaline phosphatase has been extended to lake water. Lake Kasumigaura was chosen as the target, since it is one of the typical eutrophic lakes in Japan. The dissolved alkaline phosphatase activity was measured and identification of the enzyme was discussed along with the enzymatic properties.

Experimental

Chemicals. *E. coli* alkaline phosphatase (Boehringer-Mannheim, No. 15429) whose specific activity was 20 U mg^{-1} was used as a standard enzyme. *p*-Nitrophenyl dihydrogenphosphate was dissolved in 0.6 M tris(hydroxymethyl)-methanamine hydrochloride (pH 8.0; abbreviated as Tris buffer) (1 M=1 mol dm^{-3}). Chloride salts were used as metal(II) ion standards. Calibration proteins for the molecular weight (M. W.) standard of HPLC are as follows: Urease (Jack bean; M. W.: 480000);[9] aldolase (rabbit muscle; M. W.: 161000);[10] alkaline phosphatase (*E. coli*; M. W.: 89000);[11] carbonic anhydrase (Bovine erythrocytes; M. W.: 31000);[12] and ribonuclease (Bovine pancreas; M. W.: 13700).[13]

Instruments. A Shimadzu UV-210A spectrophotometer with a SFU-6 semi-auto flow cell unit was used for the measurements of enzymatic activity. The optical path of the absorption cell was 10 mm. A Shimadzu LC-3A high performance liquid chromatography with a SPD-2A spectrophotometric detector was used for HPLC-separation. Zinc concentration was determined by a Jarrell-Ash Model 975 Plasma Atom Comp. Ultrafiltration and incubation for activity measurements were all performed under the controlled temperature by a thermostatic bath circulator (Model TRL-111SP; Thomas Scientific Co., Ltd.).

Sampling and Filtration of Lake Water. The sampling stations in Lake Kasumigaura are located as shown in Fig. 1. In Stations 4 and 9, water samples were collected from depths of 0.5, 1.5, and 5.0 m; in the other stations, only from a depth of 0.5 m. Samples were taken once a month starting in April, 1980.

Water samples were also collected from the Shinobazu pond in Tokyo.

The water was filtered through a glass-fiber membrane filter (pore size: 1.0 μm) and then a Toyo Kagaku UK-4 membrane filter (pore size: 0.2 μm) as soon as possible after collection, in order to remove microorganisms. Enzymes in thus filtered water are hereafter called *dissolved enzymes.*

Concentration of Lake Water Samples. As enzyme levels in lake water are too low to be analyzed by the chromatographic technique, the filtered water samples were concentrated using the ultrafiltration technique. An Amicon YM-10 or UM-10 type membrane, or a Toyo Kagaku UK-10 type membrane, through which only molecules with a mo-

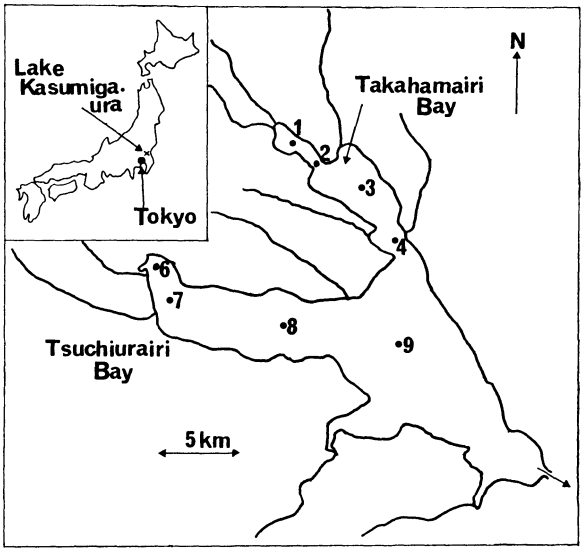

Fig. 1. Sampling stations in Lake Kasumigaura.

lecular weight over 10000 can be concentrated, was attached to an Amicon ultrafiltration cell (Model 202), in which samples were concentrated to 1/100—1/2000 of their original volumes. Samples were kept at about 4 °C throughout the operation.

Measurements of Phosphatase Activity. The enzymatic reaction of alkaline phosphatase for the substrate *p*-nitrophenyl dihydrogenphosphate proceeds as follows:

$$O_2N\text{-}C_6H_4\text{-}OPO_3H_2 + H_2O \longrightarrow O_2N\text{-}C_6H_4\text{-}OH + H_3PO_4. \quad (1)$$

The absorbance of the product, *p*-nitrophenol, was measured at 410 nm.[14] Assay procedures were as follows: The substrate solution (volume: V_1) and either a water sample or distilled water (blank) (volume: V_2) were mixed and then kept at 25 °C. After an interval of time, t, the absorbance of the mixture at 410 nm was measured using spectrophotometer equipped with a 10-mm long light path cuvette. When the absorbance of the sample-mixture and the blank-mixture, and the absorption coefficients of the substrate (S) and the product (P) at 410 nm are A, A_0, ε_S, ε_P, respectively, the enzymatic activity of the water sample, α, is given in Eq. 2:

$$\alpha = \frac{(A-A_0)(V_1+V_2)}{(\varepsilon_P-\varepsilon_S)V_2 t}. \quad (2)$$

When V_1, V_2, and t were taken as 4 cm^3, 1 cm^3, and 1440 min, respectively, in measuring unconcentrated samples, and $(\varepsilon_P-\varepsilon_S)$ is determined as 16200 mol^{-1} dm^3, the value of α is shown in Eq. 2′:

$$\alpha = 2.1 \times 10^{-7} (A-A_0) \text{ mol dm}^{-3} \text{ min}^{-1}. \quad (2')$$

Separation and Detection Using High Performance Liquid Chromatography (HPLC). The HPLC separation was performed using a Shimadzu W-71 aqueous porous gel column (7.9 mm i.d.×50 cm), with which molecules can be separated according to their molecular weight (range 10000—500000). Two types of the carriers were used, *i.e.*, a) 0.2% KH_2PO_4-KOH buffer (pH 7.3) for general separation, and b) 0.01 M Tris·HCl buffer (pH 8.0) for the distribution measurement of phosphatase activity, since phosphate inhibits phosphatase activity. The flow rate of the carrier was 1.0 cm^3 min^{-1}, and the solutes in the effluent were detected with the absorbance at 210 nm (general) and 280 nm (for protein). Chromatography was carried out at room temperature. Chromatographic effluents were collected by a fraction collector every 0.3—0.5 min.

Results and Discussion

Phosphatase Activity in Lake Waters. Table 1 shows the phosphatase activity of the water in Lake Kasumigaura. All the activity measurements were performed for the untreated samples. Activity values varied with sampling seasons and sampling points from less than 0.4 to 9.0 nmol dm^{-3} min^{-1}. The average value of activity, 1.4 nmol dm^{-3} min^{-1}, is comparable to the value in Lake Kinneret reported by Berman[15] and the value in the Shinobazu pond, Tokyo, measured by the present authors, and higher than the level in sea water samples.[16]

Characterization of Phosphatase Activity in Lake Water. Phosphatase activity in the lake water was inhibited

Table 1. Dissolved phosphatase activity in lake water

Station	Depth / m	Dissolved phosphatase activity/nmol dm^{-3} min^{-1}								
		Apr.	May	Jun.	Jul.	Aug.	Sep.	Oct.	Nov.	Dec.
Lake Kasumigaura										
1	0.5	1.3	1.9	0.9	3.9	7.4	1.8	1.7	2.5	<0.4
2	0.5	2.6	2.1	1.1	9.0	2.9	2.4	0.9	1.2	0.4
3	0.5	2.4	0.9	0.9	4.9	1.2	2.0	<0.4	0.7	0.4
4	0.5	1.7	1.7	1.5	1.1	<0.4	1.9	<0.4	0.8	0.6
	1.5	1.5	0.9	0.4	1.3	0.6	1.5	<0.4	1.2	0.6
	5.0	1.3	0.9	2.8	1.1	0.6	1.7	1.5	1.6	0.6
6	0.5	1.1	2.1	<0.4	2.6	3.6	2.9	1.7	4.6	0.4
7	0.5	1.7	1.7	<0.4	1.9	1.8	1.0	0.6	3.9	0.7
8	0.5	1.7	2.1	1.5	0.9	1.0	0.5	<0.4	1.6	0.6
9	0.5	1.3	1.3	1.3	0.4	<0.4	0.9	<0.4	1.3	0.4
	1.5	1.5	0.9	1.5	1.5	1.5	1.2	<0.4	1.2	0.5
	5.0	1.5	0.9	0.5	1.1	<0.4	0.8	<0.4	1.0	0.5
The Shinobazu Pond										
H	0.1	—	1.0	—	—	—	—	0.8	—	—

by treating with chelating agents such as ethylendiaminetetraacetic acid (EDTA) or 2,6-pyridinedicarboxylic acid (PDA). However, it is well known that such inhibited activity may be recovered by adding metal ions, such as zinc(II) and cobalt(II). The recovery effect of metal ions added to *apo-lake water* (the sample treated with chelating agents) is summarized in Table 2. Phosphatase activity was completely recovered when zinc(II) was added, and partly when cobalt(II) or manganese(II) was added. When heated over 80 °C, the sample completely lost activity. These results suggest that phosphatase activity in lake water originates from the zinc-metalloenzyme *alkaline phosphatase.*

In Fig. 2, the pH dependence of dissolved alkaline phosphatase activity in Lake Kasumigaura is shown. The maximum activity of *lake water* alkaline phosphatase was obtained at pH 8.9, which was a little higher than that of *E. coli* alkaline phosphatase (8.0).

The variations of phosphatase activity of *lake water* alkaline phosphatase, and of *E. coli*, with temperature and substrate concentration were also examined. The apparent activation energy (E_a) and the Michaelis constant (K_m) were estimated from the Arrhenius and the Michaelis plots.[6] The results are summarized in Table 3. Both the E_a and K_m of *lake water* alkaline phosphatase were different from those of *E. coli* alkaline phosphatase. This may indicate that *lake water* alkaline phosphatase is similar to that of *E. coli*, but exactly not the same.

Separation by HPLC. The HPLC chromatogram of concentrated lake water using 0.2% phosphate buffer

Table 2. Recovery ratio of phosphatase activity in lake water

Apo-sample(mm^3)[a]	Metal ion[b]	Relative activity %
50	None	0
50	Manganese(II)	41
50	Cobalt(II)	32
50	Nickel(II)	4
50	Copper(II)	9
50	Zinc(II)	100
50	Cadmium(II)	4

a) Concentrated (×400) lake water dialyzed against 0.01 M 2,6-pyridinedicarboxylic acid (pH 7.0). Lake water was sampled in Lake Kasumigaura in August, 1980. b) 50 μg of each metal ion was added in the form of chloride salt.

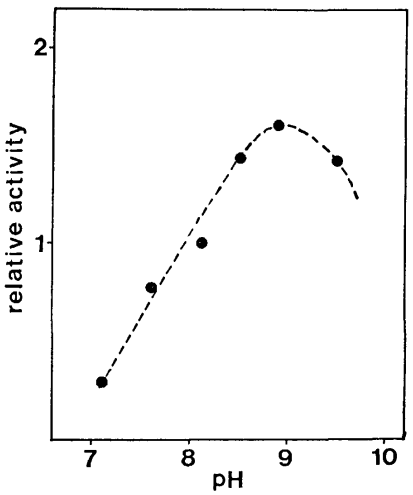

Fig. 2. pH dependence of dissolved alkaline phosphatase activity in lake water.
Activity was measured using 1 mM *p*-nitrophenyl dihydrogenphosphate in 0.1 M Tris–HCl buffer at various pH, at 30 °C. The sample was collected in Lake Kasumigaura (Sta. 2) on November 20, 1980.

Table 3. Apparent activation energies and Michaelis constants of alkaline phosphatases

Source of alkaline phosphatase	Apparent activation energy[b] E_a/kcal mol^{-1}	Michaelis constant[c] K_m/μM
Lake water[a]	6.93	1.0
E. coli	8.73	1.5

a) Concentrated lake water collected in Lake Kasumigaura (Sta. 2) on November 20, 1980. b) Obtained with the Arrhenius plot. Activities were measured using 1 mM *p*-nitrophenyl phosphate in 0.1 M Tris·HCl buffer (pH 8.1), at various temperatures (0—30 °C). c) Obtained with the Michaelis plot. Activities were measured using *p*-nitrophenyl dihydrogenphosphate of various concentrations (1 μM—1 mM) in 0.1 M Tris·HCl buffer (pH 8.1) at 30 °C.

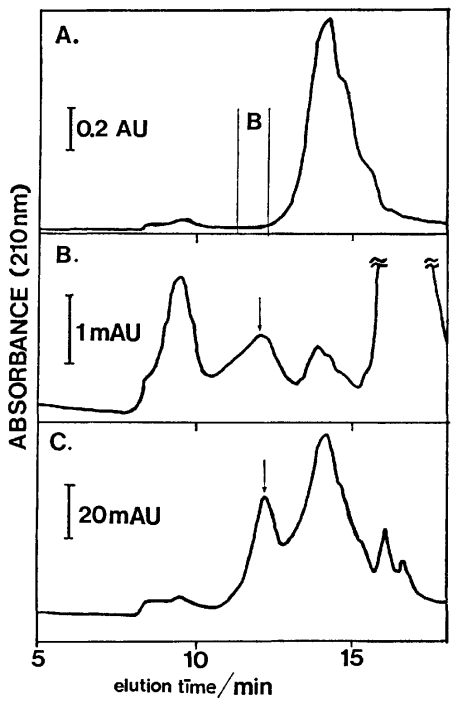

Fig. 3. Chromatograms of lake water.
Column: Shimadzu W-71 (7.9 mm i.d. × 50 cm), flow rate: 1.0 mL min^{-1}, carrier: 0.2% KH_2PO_4–KOH (pH 7.3), sample: concentrated (×500) lake water from Lake Kasumigaura sampled in February, 1980, temperature: at room temperature. (A): Lake water only, 100 μL; (B): fraction of (A) between 11.3 and 12.3 min; (C): (A) +20 μg of *E. coli* alkaline phosphatase.

(pH 7.3) as a carrier is shown in Fig. 3(A). As has been reported in the previous papers,[1,2] the chromatogram peak of alkaline phosphatase is located near 12 min. However, no marked peak could be noticed near the elution time of alkaline phosphatase in the chromatogram (A). Then, the effluent between 11.3 and 12.3 min of A was collected and concentrated. The chromatograph of the fractionated effluent was again examined under the same conditions, and the chromatogram B was obtained. In the chromatogram B, some apparent peak can be observed at the elution time at *ca.* 12 min. The chromatogram C is that of concentrated lake water spiked with *E. coli* alkaline phosphatase, which provided the elution peak at 12 min. From the comparison between the chromatograms B and C, the peak near 12 min in the chromatogram B corresponds to the distinct peak at the elution time of *E. coli* alkaline phosphatase. Fig. 4 shows the chromatograms of concentrated lake water detected both by absorbance and phosphatase activity, using 0.01 M Tris buffer (pH 8.0) as the carrier. There is a sharp peak of activity, and its elution time is the same as that of *E. coli* alkaline phosphatase. Zinc could also be found in this fraction. These results suggest that phosphatase activity in lake water originates from the alkaline phosphatase, whose molecular weight is close to that of *E. coli* alkaline phosphatase.

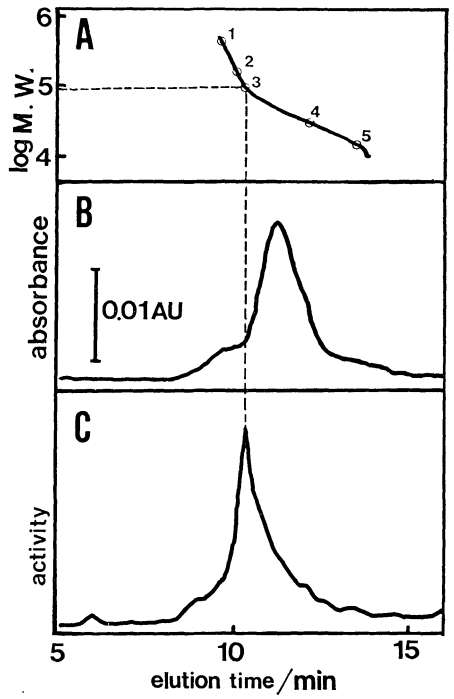

Fig. 4. Distribution of phosphatase activity of lake water.
Column: Shimadzu W-71 (7.9 mm i.d. × 50 cm), flow rate: 1.0 mL min^{-1}, carrier: 10 mM Tris buffer (pH 8.0), sample: concentrated (×2,300) lake water from Lake Kasumigaura sampled in August, 1980, 100 μL, temperature: 25 °C. (A) Calibration curve by standard enzymes [1, Urease (Jack bean; M. W.: 480000); 2, aldolase (rabbit muscle; M. W.: 161000); 3, alkaline phosphatase (*E. coli*; M. W.: 89000); 4, carbonic anhydrase (Bovine erythrocytes; M. W.: 31000); 5, ribonuclease (Bovine pancreas; M. W.: 13700)]; (B) chromatogram detected in absorbance at 280 nm; (C) distribution of phosphatase activity.

Conclusion

The results described above lead us to the conclusion that dissolved zinc-metalloenzyme alkaline phosphatase, which may be provided by procaryotes, is present in Lake Kasumigaura. It has been known that alkaline phosphatase of eucaryotes (molecular weight around 150000) is usually larger than the alkaline phosphatase of procaryotes (molecular weight around 90000).[17] As Lake Kasumigaura is known to be an algae-rich lake, a large portion of the alkaline phosphatase in the lake would be provided by algae, such as *Microcystis*. Further work to identify the isozymes using electrophoresis, *etc.* is in progress.

In Lake Kasumigaura, the concentration of alkaline phosphatase-formed zinc has been calculated as about 0.2 ng dm^{-3} (0.2 ppt), using the value of standard *E. coli* alkaline phosphatase, that is, almost one ten-thousandth of the total zinc in the lake water.

In consequence, the existence of active dissolved alkaline phosphatase may be related to the phosphorus cycles in the lake water, as has been discussed in other lakes.[15,18–20] The study on the correlation between the dissolved alkaline phosphatase and phosphorus concentration/cycle in the eutrophic lake including Lake Kasumigaura should be biochemically and ecologically important and interesting.

The present authors thank Dr. Akira Otsuki, Division of Chemistry and Physics, the National Institute for Environmental Studies, for his kind advice in limnology and for the sampling arrangement in Lake Kasumigaura.

This research has been supported by Grant-in-Aid for Special Project on Trace Characterization under Grant No. 510804 from the Ministry of Education, Science and Culture.

References

1) H. Haraguchi, K. Kobayashi, M. Matsui, and K. Fuwa, *Chem. Lett.*, **1982**, 175.
2) K. Kobayashi, M. Matsui, H. Haraguchi, and K. Fuwa, *J. Inorg. Biochem.*, in press.
3) J. E. Coleman and J. F. Chlebowski, "Advances in Inorganic Biochemistry," ed by G. L. Eichhorn and L. G. Marzilli, Elsevier, New York (1979), Vol. 1, Chap. 1.
4) T. M. Florence and G. E. Batley, *Talanta*, **24**, 151 (1977).
5) J. Overbeck and H. D. Babenzien, *Naturwissenschaften*, **50**, 571 (1963).
6) W. Reichardt, J. Overbeck, and L. Steubing, *Nature*, **216**, 1345 (1967).
7) S. J. Morrison, J. D. King, R. J. Bobbie, R. E. Bechtold, and D. C. White, *Mar. Biol. (Berlin)*, **41**, 229 (1977).
8) J. E. Little, R. E. Sjogren, and G. R. Carson, *Appl. Environ. Microbiol.*, **37**, 900 (1979).
9) W. N. Fishwein and P. P. Carbone, *Proc. Soc. Exp.*

Biol. Med., **134**, 1083 (1970).
10) C. L. Siam and B. L. Horecker, *Arch. Biochim. Biophys.*, **123**, 186 (1968).
11) R. T. Simpson, B. L. Vallee, and G. H. Tait, *Biochemistry*, **7**, 4336 (1968).
12) J. E. Coleman, "Inorganic Biochemistry," ed by G. L. Eichhorn, Elsevier, Amsterdam (1973), Vol. 1, Chap. 16.
13) C. H. W. Hirs, S. Moore, and W. H. Stein, *J. Biol. Chem.*, **219**, 623 (1956).
14) A. Garen and C. Levinthal, *Biochim. Biophys. Acta*, **38**, 470 (1960).
15) T. Berman and G. Moses, *Hydrobiologia*, **40**, 487 (1972).
16) H. Kobori and N. Taga, *J. Exp. Mar. Biol. Ecol.*, **36**, 23 (1979).
17) J. F. Chlebowski and J. E. Coleman, "Metal Ions in Biological Systems," ed by H. Sigel, Marcel Dekker, New York (1976), Vol. 6, Chap. 1.
18) T. Berman, *Limnol. Oceanogr.*, **5**, 663 (1970).
19) R. J. Stevens and M. P. Parr, *Freshwater Biol.*, **7**, 351 (1977).
20) S. Niewolak, *Rocz. Nauk. Roln., Ser. H*, **98**, 147 (1978).

Selective Determination of Histamine in Urine by Solvent Extraction with Tetrabromophenolphthalein Ethyl Ester and Atomic Absorption Spectrophotometry

Tadao SAKAI,* Noriko OHNO, Takashi WAKISAKA, and Yoshinori KIDANI†

Department of Chemistry, Gifu College of Dentistry, Takano 1851, Hozumi-cho, Gifu 501-02

†*Faculty of Pharmaceutical Sciences, Nagoya City University, 3-1, Tanabedori, Mizuho-ku, Nagoya, Aichi 467*

(Received March 8, 1982)

A simple determination method of histamine in urine by solvent extraction and atomic absorption spectrophotometry has been established. The method is based on the formation of histamine–Cu(II) chelate cation, followed by the extraction of ion-associates with tetrabromophenolphthalein ethyl ester into 1,2-dichloroethane. Histamine in urine can be successfully determined without separation and purification from other histamine derivatives and amines. A linearity is obtained in the concentration range $(0.4—4)\times10^{-5}$ M (1 M=1 mol dm^{-3}) histamine in aqueous solutions. The relative deviation is *ca.* 1.8%.

It is well known that histamine is produced from histidine in the presence of histidine decarboxylase and stored in the mast cells. The activity is considerably noted because histamine in mammalian tissues shows an important physiological action in the central nervous system. Therefore, the measurements of histamine in urine, tissues and brain are of great importance in clinical chemistry.

Fluorimetry with column chromatography,[1] high-performance liquid chromatography,[2] high-performance liquid chromatography with fluoresence detection[3] and radioisotope technique using ^{14}C-histamine for the assay and activity measurements of histamine and its derivatives in urine and tissues were reported. However, these procedures were somewhat complicated for the separation and purification.

The present paper describes a simple and selective atomic absorption spectrophotometric method without separation and purification of other biogenic amines and histamine derivatives for the assay of histamine in urine. The method is based on the formation of chelate compounds between Cu(II) and histamine and solvent extraction with hydrophobic tetrabromophenolphthalein ethyl ester (TBPE) into 1,2-dichloroethane. Acetylcholine and serotonine at the concentration of $(3—6)\times10^{-4}$ M do not cause errors. Catecholamines such as adrenaline and noradrenaline at the concentrations less than 6×10^{-5} M do not interfere, either.

Experimental

Reagents. Reagent solutions were prepared from reagent grade chemicals and distilled water, and they are stored in polyethylene bottles. Histamine standard solution of 1×10^{-2} M was prepared by dissolving 1.8407 g of histamine dihydrochloride (M.W. 184.07) to make the solution 1 L with distilled water. A 5×10^{-3} M copper(II) chloride solution was prepared by dissolving 0.8524 g of copper(II) chloride dihydrate in distilled water to make it 1 L. A 4×10^{-3} M TBPE ethanol solution was prepared by dissolving 0.2800 g of tetrabromophenolphthalein ethyl ester potassium salt in hot ethanol to make it 100 ml. A borate-phosphate buffer solution(pH 9.0) was prepared by adding 1 M NaOH to a 0.3 M potassium dihydrogenphosphate solution containing 0.1 M sodium borate. 1,2-Dichloroethane was used as an extractant.

Apparatus. A Nippon Jarrell-Ash, Model AA-780, atomic absorption spectrophotometer equipped with 10-cm slit burner and a cupric hollow-cathode lamp(Hamamatsu TV Co., Ltd.) was used and peak hights were recorded with a Yanako Model YR-110 chart recorder. Hitachi-Horiba, Model F-7II, pH meter was used for pH measurements. An Iwaki shaker, Model KM, was used for the solvent extraction.

Recommended Procedure. Take 2 ml of sample solutions containing about 90 μg/ml of histamine, 1.5 ml of 5×10^{-3} M copper(II) chloride solution, 5 ml of a buffer solution (pH 9.0) and 2 ml of a TBPE solution into a 50 ml calibrated flask, and dilute the mixture to 50 ml with water. Transfer the aqueous solution into a 100 ml separatory funnel and shake it for 5 min with 10 ml of 1,2-dichloroethane. Keep the funnel standing for 15 min and then separate the organic layer. Run off the extract into a glass tube through a filter paper to remove water droplets. Add 4 ml of ethanol to 1 ml of the extracts. Record the absorption signal at 3247 Å after mixing the solution. Take the peak height as the analytical signal. Run a reagent blank at the same instrumental settings and subtract it from the analytical values. Linear relationship between the absorbance of the extract and the concentration of histamine was held for the concentration range of $(0.4—4)\times10^{-5}$ M histamine in aqueous solutions.

Results and Discussion

Analytical Conditions for Copper Determination. The operating conditions used for copper determination were as follows: lamp current, 9 mA; wavelength, 3247 Å; flow-rate of acetylene, 1.75 l/min; flow-rate of air, 8.5 l/min; burner height, 23 mm; absorption-sens, 0.1 and burner length, 10 cm.

Effect of pH on Extraction. It was reported[5] that histamine formed the complexes with transition metal ions such as copper, zinc, cobalt, nickel, and iron. Of these metals, however, it was found that the height of the absorption peak given by the extract was considerably increased when copper(II) was present in the aqueous solution. Therefore, the effect of pH on the extraction in the presence of copper(II) was studied by extracting Cu(II)–histamine chelate cations with TBPE anion from a series of aqueous buffer solution of various pH. Figure 1 shows that the atomic absorption of copper(II) in the extracts was maximum and constant over the pH range of 8.5—10, whereas in the absence of histamine, copper(II) was not ex-

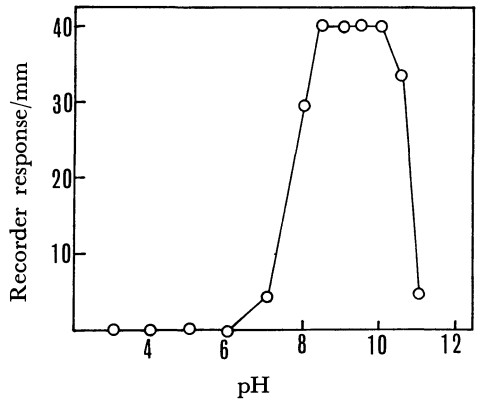

Fig. 1. Effect of pH on extraction.
Histamine: 3×10^{-5} M, Cu(II): 1.5×10^{-4} M, TBPE: 1.6×10^{-4} M.

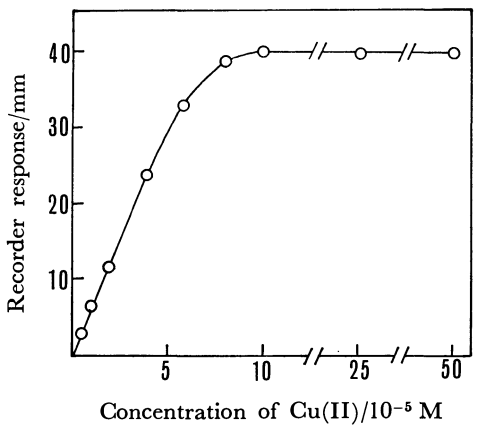

Fig. 2. Effect of copper(II) concentration.
Histamine: 3×10^{-5} M, TBPE: 1.6×10^{-4} M, pH: 9.0.

tracted with TBPE. In both acidic and alkaline media, the atomic absorption of copper(II) was markedly decreased. This may be caused by the decrease of Cu(II)–histamine complex formation in the acidic medium (pK_a for histamine, 5.1[6]), as well as copper(II) hydroxide precipitation in the alkaline medium. Extraction is recommended to carry out at pH 9.0.

Effect of Copper(II) Concentration. Various amounts of copper(II) were added to aqueous solutions of histamine and the extraction was carried out as described above. Figure 2 shows that 3-fold molar ratio of Cu(II) to histamine is enough to obtain maximum and constant atomic absorption. A copper(II) concentration of 1.5×10^{-4} M is recommended when histamine concentration is 3×10^{-5} M.

Effect of Counter Ions for the Extraction. Hydrophobic anions such as perchlorate, tetraphenylborate (TPB), picrate and TBPE were studied as a counter ion for the extraction of hydrophilic Cu(II)–histamine cations. The ion-associates with perchlorate and picrate anions were not extractable into nitrobenzene, though it has a higher dielectric constant. On the other hand, the addition of TPB showed a high atomic absorption, but the peak height was remarkably decreased when TPB concentration was maintained more than 1×10^{-4} M, because the concentrated TPB and histamine produce white precipitates in the aqueous

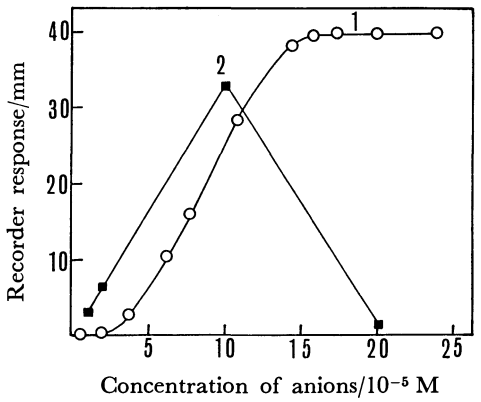

Fig. 3. Effect of TBPE and TPB concentrations on extraction.
1: TBPE, 2: TPB, histamine: 3×10^{-5} M, Cu(II): 1.5×10^{-4} M, pH: 9.0.

phase. Figure 3 shows that the extraction of Cu(II)–histamine–TBPE ion-associates was maximum and constant, when TBPE used was more than 1.5×10^{-4} M (5-fold molar ratio to histamine). Excess amounts of phosphate buffer did not give any influence on the atomic absorption, but separation of two layers became incomplete when the addition of the buffer solution was less than 1 ml. The previous papers[7] described that ion-associates with TBPE was the most extractable species into 1,2-dichloroethane.

Effect of Shaking Time and Stability of the Extract. Extraction was completed quantitatively within 30 s, and shaking for up to 15 min did not produced any further change in absorption signal, and which was remained almost constant for at least 5 h after extraction.

Calibration Curve and Precision. Under the optimum conditions, the calibration curve was made with a histamine standard solution containing 1.5×10^{-4} M copper(II) chloride solution. It shows a good linearity over the range of $(0.4—4)\times10^{-5}$ M (0.736—7.36 μg/ml) histamine with an aqueous/organic solvent volume ratio of 5. The relative standard deviation (ten determinations) was estimated to be 1.8% for 3×10^{-5} M histamine.

Interferences of Diverse Substances. To the solution containing 3×10^{-5} M histamine and 1.5×10^{-4} M copper(II) chloride solutions, various amounts of foreign compounds were added and their influences were examined. The results are summarized in Table 1. Inorganic substances, such as sodium chloride, potassium chloride, sodium nitrate, sodium carbonate, and sodium sulfate did not show any interference. Furthermore, calcium, magnesium, cobalt, lead, nickel, zinc, iron, and iodide ions of 5-fold molar excess over 3×10^{-5} M histamine did neither show any influence. Though citrate ion interfered considerably with the determination, it was minimized by addition of calcium ions at a concentration almost equal to that of citrate ion.

Histidine, serotonine, acetylcholine and imidazole-4-acetic acid, being analogous to histamine and giving a strong influence on other measurements,[1,3] did not interfere with histamine in 10—20 fold ratio. Of bio-

TABLE 1. EFFECT OF VARIOUS SUBSTANCES ON DETERMINATION OF HISTAMINE

Substances	Mole ratio [Ion]/[HA]	Mole ratio [Ion]/[Cu(II)]	Recovery of histamine %
Sodium chloride	500	100	100
Potassium chloride	500	100	100
Sodium nitrate	50	10	100
Sodium carbonate	50	10	102
Sodium sulfate	50	10	101
Calcium chloride	5	1	103
Magnesium chloride	5	1	105
Cobalt(III) chloride	5	1	105
Lead(II) chloride	5	1	103
Nickel sulfate	5	1	100
Zinc acetate	5	1	101
Iron(III) nitrate	5	1	102
Ammonium chloride	5	1	102
Potassium chromate	5	1	100
Potassium iodide	5	1	100
Histidine	10	2	100
Acetylcholine	20	4	98
Serotonine	10	2	102
Imidazole-4-acetic acid	10	2	99
Adrenaline	2	0.4	95
	1	0.2	100
Noradrenaline	2	0.4	97
	1	0.2	99
Dopa	1	0.2	100
(Dihydroxyphenyl-alanine)	2	0.4	100
Dopamine	2	0.4	98
	1	0.2	100

Histamine taken: 3×10^{-5} M, Cu(II) taken: 1.5×10^{-4} M, TBPE: 1.6×10^{-4} M, pH on extraction: 9.0, solvent: 1,2-dichloroethane

genic amines, catecholamines such as adrenaline, noradrenaline and dopamine which coexist with histamine in biological materials did not interfere less than 1—2 fold ratios to 3×10^{-5} M histamine. Histamine is a major component in biological materials and the content ratio for [Adrenaline]/[Histamine(HA)] is 0.03; for [Noradrenaline]/[HA], 0.2; [Dopamine]/[HA], 0.02 in heart and the corresponding ratios are 0.06, 0.4, 0.02 in spleen.[8] Consequently, about 5 μg/ml levels of histamine in tissues and urine can be selectively determined by this method.

Composition of the Extracted Species. In order to clarify the composition of the extracted species, continuous variation plots were made. The results shown in Figs. 4 and 5 reveal that a 1:1 chelate cation is formed between Cu(II) and histamine, and that in the organic phase a 1:3 ion-associate is formed between Cu(II)–histamine cations and TBPE anions. Moreover, an ion-associate was dried at reduced pressure for 48 h and the powdery precipitates obtained was analyzed. Found: C, 39.7; H, 2.4; N, 2.0; O, 8.6; Br, 46.6; Cu, 1.0%. Calcd for Cu(II)–histamine–TBPE associate: C, 39.7; H, 2.2; N, 1.3; O, 9.1; Br, 45.8; Cu, 1.9%. Thus the results obtained by the

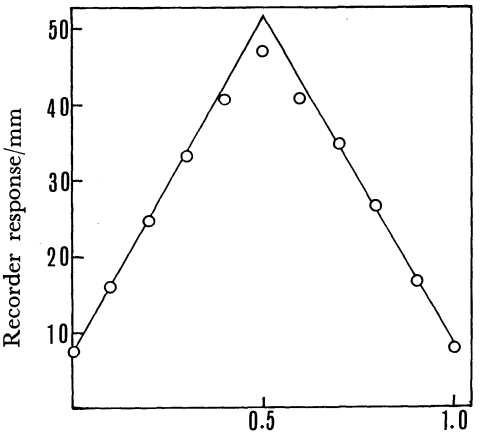

Fig. 4. Continuous variation plots.
[HA]+[Cu(II)]=1×10^{-4} M, TBPE: 1.6×10^{-4} M, pH: 9.0.

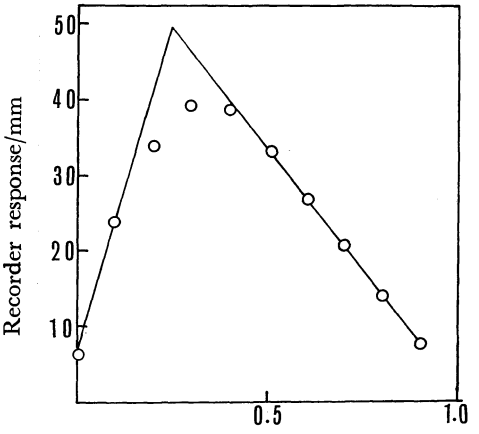

Fig. 5. Continuous variation plots.
[HA]+[TBPE]=2×10^{-4} M, Cu(II): 2×10^{-4} M, pH: 9.0.

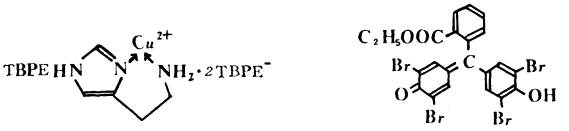

Ion-associate with TBPE TBPE molecule

Chart 1.

two methods suggest that the chemical formula of the extracted species may be formulated as [Cu(II)–histamine]·$(TBPE)_3$. The ion-associate produced is assumed to show its structure in Chart 1 because the absorption spectrum of the associate with TBPE showed the charge transfer complex type in our previous paper,[7] being a maximum wavelength at 515 nm.

Application to Histamine Determination. Known amounts of histamine standard solution were added in human urine. Sample solutions containing 92 μg of histamine were analyzed by the proposed method. The results obtained were 81 μg and 79 μg histamine for two samples (3 determinations) and the recoveries were 88 and 86%, respectively. On the other hand,

5 mg/ml of histidine dihydrochloride was injected intravenously to two rats (about 150 g, ♂). Urine was withdrawn after 24 h and histamine in urine was determined by this method. 58 μg histamine could consequently be found in 50 ml of the recovered urine.

The recovery of histamine by the proposed method is not high enough as we expected. However, the procedure is very simple and this is available for the practical determination of histamine in biogenic amines, as the selective method.

References

1) A. Yamatodani, *Medical J. Osaka University*, **30**, 421 (1978).
2) M. Goto, T. Nakamura, Y. Shibata, and D. Ishii, *J. Chromatogr.*, **226**, 33 (1981).
3) Y. Tsuruta, K. Kohashi, and Y. Ohkura, *J. Chromatogr.*, **224**, 105 (1981).
4) D. D. Brown, R. Tomchick, and J. Axelrod, *J. Biol. Chem.*, **243**, 2948 (1959).
5) "Kagaku Daiziten," Kyoritsu Publishing Co., Tokyo (1971), p. 375.
6) "Prespectives in Clinical Pharmacy," (Translation by S. Naito), Hirokawa Publishing Co., Tokyo (1979), p. 228.
7) T. Sakai, I. Hara, and M. Tsubouchi, *Chem. Pharm. Bull.*, **24**, 1254 (1976); T. Sakai and M. Tsubouchi, *ibid.*, **24**, 2883 (1976).
8) A. Yamatodani and H. Wada, *Bunseki*, **1978**, 842.

Preparation and Electrochemical Behaviors of Phenoxide-coordinated Iron(III) Porphyrins

Hiroshi Sugimoto,* Nobuhiro Ueda, and Masayasu Mori

Department of Chemistry, Faculty of Science, Osaka City University, Sugimoto, Sumiyoshi-ku, Osaka 558

(Received March 23, 1982)

A new series of iron(III) porphyrins having various phenoxide anions as the axial ligand, [Fe^{III}(porphyrin)-(4-X-$C_6H_4O^-$)] (porphyrin=octaethylporphyrin and tetraphenylporphyrin; X=OCH_3, CH_3, H, C_6H_5, Cl, Br, $COCH_3$, CN, CHO, and NO_2) were synthesized. All these complexes are five-coordinated high-spin complexes ($S=5/2$). Their electrochemical behaviors were investigated by the cyclic voltammetry and the controlled potential coulometry. The complexes showed significantly negative potentials for the Fe^{II}/Fe^{III} redox couple (−0.4——0.8 V). A good linear relationship was found between the half-wave potentials of the Fe^{II}/Fe^{III} redox couple and the Hammett σ-values of the substituent X. A new characteristic feature is the appearance of the redox peaks of the coordinated phenoxide anions near the redox couple of the porphyrin ring oxidoreduction. The role of the tyrosine-67 in the enzymatic mechanism for cytochrome c is discussed.

As to the biological functions of cytochrome c such as its electron transferring activities, some hypotheses were presented on the basis of the crystallographic data of its several variant forms.[1,2] All of these hypotheses point out the importance of the interaction between the heme (iron porphyrin) and the tyrosine-67 residue, where the phenol group or its anionic form may act as the one-electron donor to the ferric porphyrin through the ionic interaction (tyr-67)$^-$..... (heme)$^+$ to give ferrous porphyrin and tyrosine radical.[2] It, therefore, seemed to be considerable interest to evaluate qualitatively the strength of the ionic interaction by use of model complexes.

For this purpose, we systematically prepared a series of iron(III) porphyrin complexes having phenoxide anions substituted at the 4-position (*para*-position), and investigated their basic physicochemical properties, particularly electrochemical behaviors.

Experimental

Syntheses of Complexes, General Procedures. To a dichloromethane solution of (octaethylporphyrinato)iron(III) acetate,[3] [Fe^{III}(oep)(OAc)] or (tetraphenylporphyrinato)iron-(III) acetate, [Fe^{III}(tpp)(OAc)] (100 mg) was added a dichloromethane solution of phenol derivatives (100 mg). Due to the low solubility in dichloromethane, *p*-hydroxybenzaldehyde and methyl *p*-hydroxybenzoate were dissolved in methanol, and biphenyl-4-ol was dissolved in acetone. After stirring for about 3—4 h, the solvent was removed to dryness. The residual solid was washed with acetonitrile and recrystallized from dichloromethane–methanol (1:1 vol/vol) or dichloromethane–acetonitrile (1:1 vol/vol) to give purple crystals in about 60—80% yields. The elemental analyses, and the spectral data of UV-VIS and IR are summarized in Tables 1, 2, and 3, respectively.

Cyclic Voltammetry and Controlled Potential Coulometry. Dichloromethane was dried and distilled over CaH_2 before use. As a supporting electrolyte, tetrabutylammonium per-

Table 1. Elemental analyses

	Compound	C (%) Found(Calcd)	H (%) Found(Calcd)	N (%) Found(Calcd)
1	[Fe^{III}(oep)(4-CH_3O-$C_6H_4O^-$)]·$(H_2O)_{1/2}$	71.72(71.65)	7.21(7.27)	8.32(7.77)
2	[Fe^{III}(oep)(4-CH_3-$C_6H_4O^-$)]·$(H_2O)_{1/2}$	73.17(73.28)	7.32(7.43)	8.47(7.95)
3	[Fe^{III}(oep)(4-C_6H_5-$C_6H_4O^-$)]·$(H_2O)_{1/2}$	75.47(75.18)	7.00(7.10)	7.45(7.31)
4	[Fe^{III}(oep)($C_6H_5O^-$)]·$(H_2O)_{1/2}$	72.93(73.03)	7.21(7.30)	8.66(8.11)
5	[Fe^{III}(oep)(4-Cl-$C_6H_4O^-$)]·$(H_2O)_{1/2}$	69.52(69.57)	6.64(6.67)	7.57(7.73)
6	[Fe^{III}(oep)(4-Br-$C_6H_4O^-$)]·(H_2O)	64.97(64.79)	6.21(6.47)	7.09(7.20)
7	[Fe^{III}(oep)(4-CH_3CO-$C_6H_4O^-$)]·$(H_2O)_{1/2}$	71.91(72.12)	7.71(7.65)	7.08(7.15)
8	[Fe^{III}(oep)(4-CN-$C_6H_4O^-$)]·(H_2O)	71.54(71.26)	6.76(6.67)	9.69(9.67)
9	[Fe^{III}(oep)(4-CHO-$C_6H_4O^-$)]·$(H_2O)_{3/2}$	70.38(70.10)	7.92(7.61)	7.04(7.12)
10	[Fe^{III}(oep)(4-NO_2-$C_6H_4O^-$)]·$(H_2O)_{1/2}$	68.80(68.47)	6.66(6.70)	9.61(9.51)
11	[Fe^{III}(tpp)(4-CH_3O-$C_6H_4O^-$)]·(H_2O)	75.55(75.65)	4.38(4.61)	7.17(6.92)
12	[Fe^{III}(tpp)(4-CH_3-$C_6H_4O^-$)]·$(H_2O)_{1/2}$	77.85(78.06)	4.88(4.62)	6.80(7.14)
13	[Fe^{III}(tpp)(4-C_6H_5-$C_6H_4O^-$)]·$(H_2O)_2$	76.38(76.97)	4.32(4.73)	6.29(6.41)
14	[Fe^{III}(tpp)($C_6H_5O^-$)]·$(H_2O)_{1/2}$	77.95(77.92)	4.53(4.45)	7.37(7.27)
15	[Fe^{III}(tpp)(4-Cl-$C_6H_4O^-$)]·(H_2O)	74.15(73.76)	4.07(4.21)	6.84(6.88)
16	[Fe^{III}(tpp)(4-Br-$C_6H_4O^-$)]·(H_2O)	69.52(69.94)	3.86(3.99)	6.35(6.52)
17	[Fe^{III}(tpp)(4-CH_3CO-$C_6H_4O^-$)]·$(H_2O)_{1/2}$	76.72(76.85)	6.94(6.89)	4.42(4.47)
18	[Fe^{III}(tpp)(4-CN-$C_6H_4O^-$)]·$(H_2O)_{1/2}$	73.62(76.98)	3.99(4.05)	8.71(8.80)
19	[Fe^{III}(tpp)(4-CHO-$C_6H_4O^-$)]·(H_2O)	75.62(75.84)	4.16(4.24)	6.96(6.94)
20	[Fe^{III}(tpp)(4-NO_2-$C_6H_4O^-$)]·$(C_6H_6)_{1/2}$	74.95(75.27)	4.30(4.17)	8.14(8.28)

Table 2. UV-VIS spectral data for phenoxide complexes of iron(III) porphyrins in CH_2Cl_2

Compound	λ_{max}/nm (log ε)						
1		392 (4.63)	489 (3.71)	510 sh (3.66)	600 (3.55)		
2		391 (4.51)	488 (3.56)	513 sh (3.51)	600 (3.38)		
3		392 (4.87)	491 (3.93)	515 sh (3.87)	604 (3.75)		
4		391 (4.45)	488 (3.52)	515 sh (3.47)	602 (3.35)		
5		390 (4.40)	491 (3.49)	515 (3.46)	606 (3.32)		
6		391 (4.57)	491 (3.67)	515 (3.63)	607 (3.49)		
7	370 sh (4.70)	393 (4.74)	495 (3.87)	520 sh (3.85)	612 (3.63)		
8	370 sh (4.72)	393 (4.75)	496 (3.86)	522 (3.84)	615 (3.61)		
9	370 sh (4.73)	394 (4.75)	496 (3.85)	520 sh (3.82)	613 (3.57)		
10	365 sh (4.34)	394 (4.43)	490 (3.81)	522 (3.76)	615 (3.53)		
[Fe^{III}(oep)(OAc)]		381 (5.01)	460 (3.88)	508 (3.97)	537 (3.99)	584 (3.46)	640 (3.65)
[Fe^{III}(oep)F]		395 (4.96)	481 (3.95)	514 (3.86)	599 (3.80)		
[Fe^{III}(oep)Cl]		381 (4.93)	461 (3.76)	508 (3.87)	536 (3.89)	584 (3.33)	640 (3.58)
11		414 (4.81)		566 sh (3.57)	620 sh (3.49)		
12		413 (4.64)	484 sh (3.75)	540 sh (3.46)	620 (3.33)		
13		414 (4.99)	487 sh (4.06)	561 (3.76)	610 sh (3.64)		
14		415 (4.64)		571 (3.41)	614 sh (3.31)		
15		414 (5.15)	485 sh (4.27)	548 sh (3.97)	629 (3.83)		
16		414 (5.48)	486 sh (4.60)	550 sh (4.30)	631 (4.16)		
17	340 (4.40)	415 (4.84)	495 (3.96)	555 sh (3.66)	632 (3.50)	655 (3.49)	
18	342 (4.55)	415 (4.94)	498 (4.04)	555 sh (3.70)	636 (3.86)	661 (3.86)	
19	346 (4.42)	415 (4.73)	496 (3.79)	555 sh (3.46)	636 (3.28)	662 (3.27)	
20	359 (4.54)	405 (4.93)	499 (4.03)	560 sh (3.66)	640 (3.49)	685 (3.50)	

sh: Shoulder.

Table 3. Characteristic IR bands for coordinated phenoxide anions of phenoxide compllexes of iron(III) porphyrins

Compound	$\nu_{C=C}$/cm^{-1}	$\nu_{C=C}$/cm^{-1}	ν_{C-O}/cm^{-1}	Others
1		1486	1224	
2		1492	1262, 1254	
3	1590	1477	1253, 1260	
4	1584	1484	1267, 1280	
5	1577	1475	1261	
6	1571	1472	1255	
7	1584	1492	1267	1664 ($\nu_{C=O}$)
8	1588	1498, 1485	1298	2208 ($\nu_{C\equiv N}$)
9	1581	1495	1282	1670 ($\nu_{C=O}$)
10		1482	1276	1575, 1328 (nitro group)
11	1594	1491	1226	
12	1594	1493	1246	
13	1592	1476	1255	
14	1594, 1581	1482, 1474	1257	
15	1594	1475	1262	
16	1594, 1571	1473	1259	
17	1581	1492	1266	1661 ($\nu_{C=O}$)
18	1589	1484	1281	2212 ($\nu_{C\equiv N}$)
19	1581	1490	1273, 1281	1683 ($\nu_{C=O}$)
20		1481	1274	1574, 1328 (nitro group)

chlorate (TBAP) was used after being subjected twice to recrystallization from benzene. Cyclic voltammograms were obtained on a HA-104 potentiostat (Hokuto Denko) in combination with a HB-107A function generator (Hokuto Denko). A three-electrode system was used which consisted of platinum working and counter electrodes and a commercial saturated calomel electrode (SCE) separated from the bulk of solution by a bridge filled with the solvent containing supporting electrolyte. The bridge had its solution changed periodically to avoid aqueous contaminants from entering the cell *via* SCE. All solutions were purged of oxygen by passing purified nitrogen through them for 10 min just before

taking cyclic voltammograms. After the degassing a blanket of nitrogen was kept over the solution. The half-wave potential $E_{1/2}$ was taken as that potential lying midway between the oxidation and reduction peaks for a given couple. All experiments were carried out at room temperature (15 °C) and the potentials reported refer to the SCE. The scan rate was constantly 100 mV/s. The controlled potential coulometry was carried out on a HA-104 potentiostat with a HF-201 coulomb-amperehour meter (Hokuto Denko). The number of electron was obtained as the mean value of three experiments.

Results and Discussion

The acetate ion of the starting complexes could be easily replaced by various types of phenoxide anions.

$$[Fe^{III}(porphyrin)(OAc)] + HO\text{-}C_6H_4\text{-}X \longrightarrow [Fe^{III}(porphyrin)(4\text{-}X\text{-}C_6H_4O^-)]$$

The substituents X were varied from the most electron donating OCH_3 to the most electron-withdrawing NO_2.

The coordinated phenoxide anions could be easily confirmed by the characteristic IR bands[4] as summarized in Table 3. These complexes showed UV-VIS spectra (Fig. 1) similar to those of the typical iron(III) high-spin complexes.[5] Compared with the acetate complex, the Soret band of these complexes shifted toward longer wavelength region by about 10 nm, and the so-called charge-transfer band around 600—650 nm shifted toward shorter wavelength region by about 20—30 nm. These absorption maxima are similar to those of fluoro complex, $[Fe^{III}(oep)F]$.

All of these complexes showed magnetic susceptibilities of about 5.9 BM at room temperature, indicating that these phenoxide complexes are of five-coordinated high-spin ($S=5/2$) type.

Although the absorption maxima of the charge-transfer band were expected to be a good indicator of the strength of the interaction between iron(III) porphyrin-phenoxide anion, the effect of substituent X was found to be small. Since the redox potential of the cobalt(III)[6] or iron(III) porphyrins[7] are also known to be sensitive to the nature of the counter anions, such quantities of the phenoxide complexes were measured by the cyclic voltammetry. The half-wave potentials thus obtained are summarized in Table 4. In order to eliminate the complication by the coordination of polar solvent molecules,[7] the cyclic voltammograms were obtained in dichloromethane. As in the case of usual iron(III) porphyrins,[7] two quasi-reversible redox couples were observed at −0.5——0.8 V and +1.1—+1.2 V. From the electrospectrochemistry and the controlled potential coulometry, these couples could be assigned to the Fe^{II}/Fe^{III} and Fe^{III}/Fe^{IV} or porphyrin ring oxidoreduction as shown in Fig. 2, reflecting the effect of the substituents on the porphyrin ligand. The values of octaethylporphyrin derivatives were more negative by about 0.1 V than those of tetraphenylporphyrin derivatives. The Fe^{II}/Fe^{III} redox values were found to be significantly dependent on the kind of substituent X in the phenoxide anion and ranged over −0.8——0.4 V. These values are much negative compared with usual iron(III) complexes,[7] in particular the values of 4-methoxyphenoxide complexes are probably the most negative ones reported so far in iron(III) porphyrins. As shown in Fig. 3, there are good linear correlation between the half-wave potentials and the Hammett σ-values of substituent X.

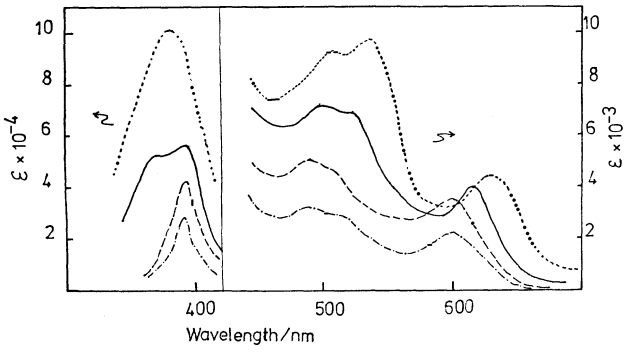

Fig. 1. UV-VIS spectra of (— — —) $[Fe^{III}(oep)(4\text{-}CH_3O\text{-}C_6H_4O^-)]$, (—·—·—) $[Fe^{III}(oep)(C_6H_5O^-)]$, (——) $[Fe^{III}(oep)(4\text{-}CN\text{-}C_6H_4O^-)]$, and (·····) $[Fe^{III}(oep)(OAc)]$ in CH_2Cl_2.

Table 4. The half-wave potentials of the Fe^{II}/Fe^{III}, porphyrin ring oxidoreduction, and the oxidation peaks of phenoxide anions for phenoxide complexes of iron(III) porphyrins in CH_2Cl_2

Compound	Fe^{II}/Fe^{III}	Oxidation peak of phenoxide anion	Porphyrin ring oxidation
1	−0.80	+0.92	+1.06
2	−0.83	+0.98	+1.10
3	−0.71	+0.99	+1.10
4	−0.75	+1.05[a]	+1.07
5	−0.66	+1.02[a]	+1.09
6	−0.65	+1.01[a]	+1.09
7	−0.66	b)	+1.04
8	−0.58	b)	+1.06
9	−0.60	b)	+1.11
10	−0.50	b)	+1.06
11	−0.66	+0.98	+1.19
12	−0.65	+1.14	+1.19
13	−0.62	+1.10[a]	+1.16
14	−0.63	b)	+1.18
15	−0.58	b)	+1.18
16	−0.56	b)	+1.12
17	−0.50	b)	+1.17
18	−0.50	b)	+1.19
19	−0.46	b)	+1.16
20	−0.43	b)	+1.19
$[Fe^{III}(tpp)ClO_4]$	+0.22		+1.10[c]
$[Fe^{III}(tpp)Br]$	−0.21		+1.18[c]
$[Fe^{III}(tpp)Cl]$	−0.29		+1.14[c]
$[Fe^{III}(tpp)N_3]$	−0.42		+1.08[c]
$[Fe^{III}(tpp)F]$	−0.50		+1.14[c]

a) Inflection. b) Not observed. c) Ref. 7.

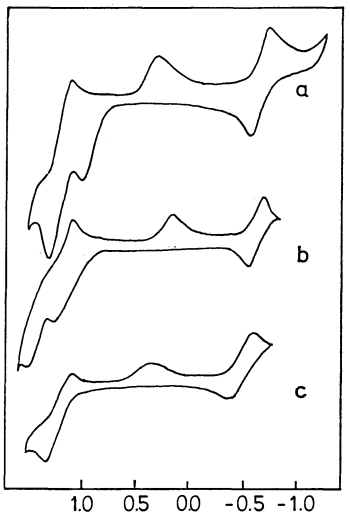

Fig. 2. Cyclic voltammograms of (a) [Fe^{III}(tpp)(4-CH_3O-$C_6H_4O^-$)], (b) [Fe^{III}(tpp)(4-C_6H_5-$C_6H_4O^-$)], and (c) [Fe^{III}(tpp)(4-CN-$C_6H_4O^-$)] in CH_2Cl_2.

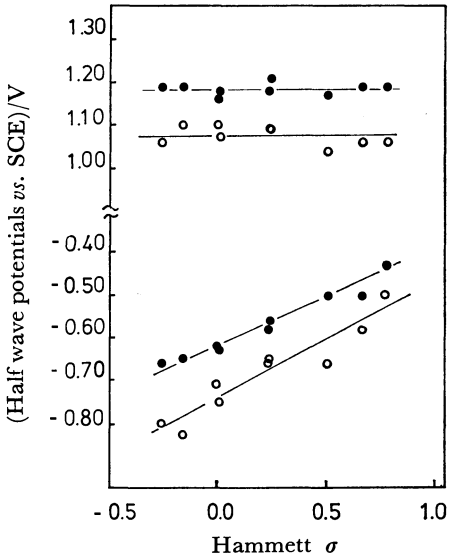

Fig. 3. The correlation between the half-wave potentials of [Fe^{III}(porphyrin)(4-X-$C_6H_4O^-$)] and the Hammett σ-values of substituent X; (○) octaethylporphyrin derivatives and (●) tetraphenylporphyrin derivatives.
The σ-values adopted are follows; X=CH_3O(−0.268), CH_3(−0.170), H(0.00), C_6H_5(−0.01), Cl(+0.227), Br(+0.232), CN(+0.660), CH_3CO(+0.502), NO_2-(+0.778).

On the other hand, the redox couple at +1.1—+1.2 V showed no correlation with Hammett σ-values of X. This probably means that the redox couple is assignable to the redox process on the porphyrin ring rather than on metal.[7]

A new characteristic feature in these phenoxide complexes is the appearance of an additive oxidation and corresponding reduction peaks near the redox potential of porphyrin ring. These new oxidation peaks are remarkably dependent on the kind of substituent X. In 4-methoxyphenoxide complexes, the peaks could be clearly observed as a separated peak at about +0.9 V (Fig. 2a). These peaks were proved to be a one-electron process by the controlled potential coulometry and could be unambiguously assigned to the oxidation of coordinated phenoxide anions. The peak positions are consistent with those of the corresponding free phenols or phenoxide anions found in the literatures.[8] Such additive peaks have never been observed in iron(III) porphyrins, because the electrochemical studies so far dealt with iron(III) porphyrins with electrochemically inert halide ions or another inorganic anions. Very recently we reported that the catecholate complexes of iron(III) porphyrins had similar oxidoreduction peaks of coordinated catecholate anions.[9] As the electron-donating character of the substituent X decreases, the peak shifted to a more positive region finally to overlap the peak of porphyrin ring oxidation (Fig. 2b) and give a single peak (Fig. 2c). The overlapped peak at about +1.1—+1.2 V had doubled in current.

Very negative values of the Fe^{II}/Fe^{III} redox couple of these phenoxide complexes suggest that the strong electron donation, *i.e.*, the charge-transfer occurs from the phenoxide anions to iron(III) ion.

$$Fe^{3+} \leftarrow L^- \longleftrightarrow Fe^{2+}\text{----}L\cdot$$

Moreover, the coordinated phenoxide anions are subjected to the one-electron oxidation at more negative voltage than that of the porphyrin ring oxidation. These facts suggest the important catalytic role of the phenoxide anions (tyrosine-67) as a deliverer of electrons in enzymatic mechanism.[2] It is reasonably sup-

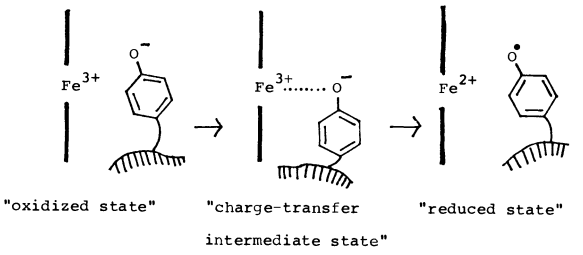

posed that phenoxide group of tyr-67 in the enzyme can be brought so close to the ferric heme moiety probably due to the conformation change of the peptide chain that the electron transfer smoothly proceeds resulting ferrous heme and phenoxide radical as illustrated above.

The present work was partially supported by a Grant-in-Aid for Scientific Research from the Ministry of Education, Science and Culture.

References

1) a) T. Takano, O. B. Kallai, R. Swanson, and R. E. Dickerson, *J. Biol. Chem.*, **248**, 5234 (1973); b) F. R. Salemme, J. Kraut, and M. D. Kamen, *ibid.*, **248**, 7701 (1973); c) R. Swanson, B. L. Trus, N. Mandel, G. Mandel, O. B. Kallai, and R. E. Dickerson, *ibid.*, **252**, 759 (1977); d) T. Ashida, N. Tanaka, T. Yamane, T. Sukihara, and M. Kakudo, *J. Biochem. (Tokyo)*, **73**, 463 (1973).

2) N. Tanaka, T. Yamane, T. Tsukihara, T. Ashida, and M. Kakudo, *J. Biochem. (Tokyo)*, **77**, 147 (1975).
3) a) J. W. Buchler and H. H. Schneehage, *Z. Naturforsh., Teil B*, **28**, 433 (1973); b) H. Ogoshi, E. Watanabe, Z. Yoshida, J. Kincaid, and K. Nakamoto, *J. Am. Chem. Soc.*, **95**, 2845 (1973).
4) J. W. Buchler, L. Puppe, K. Rohbock, and H. H. Schneehage, *Chem. Ber.*, **106**, 2710 (1973).
5) "The Porphyrins," ed by D. Dolphin, Academic Press, New York (1978), Vol. III, Chap. 2.
6) a) "The Porphyrins," ed by D. Dolphin, Academic Press, New York (1978), Vol. V, Chap. 3; b) L. A. Truxillo and D. Davis, *Anal. Chem.*, **47**, 2260 (1975); c) H. Sugimoto, N. Ueda, and M. Mori, *Bull. Chem. Soc. Jpn.*, **54**, 3425 (1981).
7) L. A. Bottomley and K. M. Kadish, *Inorg. Chem.*, **20**, 1348 (1981).
8) "Encyclopedia of Electrochemistry of the Element," ed by A. J. Band, H. Lund, V. D. Parker, G. Sundholm, U. Svanholm, and A. Ronlān, Marcel Dekker, Inc., New York and Basel (1978), Vol. XI.
9) H. Sugimoto, N. Ueda, and M. Mori, *Chem. Lett.*, **1982**, 449.

Characterization of Cobalt(III) Complexes with L-Penicillaminate. Crystal Structure of (Diethylenetriamine)(L-penicillaminato)-cobalt(III) Chloride Monohydrate

Ken-ichi Okamoto,* Katsuhiko Wakayama, Hisahiko Einaga,† Masaaki Ohmasa,† and Jinsai Hidaka

Department of Chemistry, University of Tsukuba, Ibaraki 305

†*Institute of Materials Science, University of Tsukuba, Ibaraki 305*

(Received April 7, 1982)

The crystal structure of the title complex, which was chromatographically obtained as the first eluted isomer, has been determined by the X-ray diffraction method. The dark-brown needle crystal was hexagonal, space group $P6_1$, $a=21.035(5)$, $c=6.459(3)$ Å, $Z=6$, and the final R value was 0.076 for 1504 non-zero reflections. Of three possible isomers for the (diethylenetriamine)(L-penicillaminato)cobalt(III) complex, the complex isolated has *trans*(N_1N) configuration. The average Co–N distance for the nitrogen atoms bonded cis to the sulfur atom is 1.961 Å, whereas the trans Co–N length is 2.007 Å.

Some cobalt(III) complexes with thiolato ligands such as penicillamine and cysteine have been investigated for their stereochemical and biochemical interests.[1–3] It appears that the presence of a thiolato donor atom in the coordination sphere induces an extreme specificity concerned with the formation of possible isomers.[2,3] This work deals with the stereochemistry of the mixed cobalt(III) complex with the L-penicillaminate (L-pen) and diethylenetriamine (dien) ligands, where L-pen functions as a tripod-like terdentate ligand and has a similar framework to the L-cysteinate ion. For the [Co(L-pen)(dien)]$^+$ complex having a thiolato donor atom, three geometrical isomers are possible. They are designated as *trans*(N_1N), *trans*(N_1O), and *trans*(N_1S) with respect to the coordinated atoms as shown in Fig. 1. These isomers belong to a *cis*(*SO*)-[Co(N)$_4$(S)(O)] type and it is difficult to assign spectrochemically their geometrical configurations.

The present paper deals with the crystal and molecular structure of [Co(L-pen)(dien)]Cl·H_2O which was isolated from the first eluate by means of a column chromatographic separation. The trans effect due to the coordinated thiolato donor atom in the L-pen ligand is also discussed. A preliminary report has been presented.[4]

Experimental

(Diethylenetriamine)(L-penicillaminato)cobalt(III) chloride was prepared by a modification of a method in the literatures.[5] To a suspension containing 5.4 g of [$CoCl_3$(dien)][6] in 100 cm^3 of water was added a solution containing 5.1 g of silver nitrate in 20 cm^3 of water. The precipitated silver chloride was filtered off. After nitrogen gas was vigorously bubbled into the filtrate for 30 min, an aqueous solution containing 3.0 g of L-penicillamine was added to it. The nitrogen gas was constantly bubbled into the mixture at room temperature for about 20 h. The reaction mixture was poured onto a column (30 mm × 1000 mm) containing cation exchange resin (Dowex 50W-X8, 200—400 mesh, Na^+ form). After the column had been swept with water, the adsorbed band was eluted with 0.075 mol dm^{-3} aqueous solution of NaCl. Three brown bands were eluted in succession. The first eluate was concentrated to a small volume with a rotary evaporator below 15 °C. The deposited NaCl was filtered off and a large amount of ethanol–acetone (1:2) mixture added to the filtrate. The solution was kept in a refrigerator overnight. The crude crystals were collected by filtration. The dark-brown needle crystals were obtained by recrystallization from a small amount of water by adding acetone.

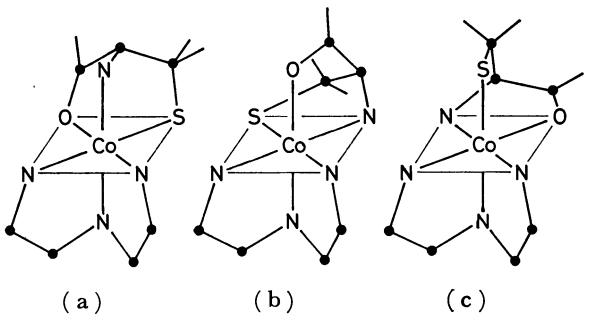

Fig. 1. Three possible isomers of [Co(L-pen)(dien)]$^+$; (a) *trans*(N_1N), (b) *trans*(N_1O), and (c) *trans*(N_1S).

Preliminary photographic examination established a hexagonal unit cell containing six chemical units of [Co(L-pen)(dien)]Cl·H_2O. The systematic absence led to the space group $P6_1$. The least-squares refinement of setting angles of 41 reflections, measured on a Rigaku Denki automatic four circle diffractometer (AFC-5) using Mo $K\alpha$ radiation monochromatized by a graphite plate, led to the cell constants: $a=21.035$ (5) Å, $c=6.459$ (3) Å. The calculated density of 1.46 g cm^{-3} agrees with the observed density of 1.49 g cm^{-3} by the flotation method.

The intensity data up to $2\theta<55°$ were collected by use of ω-2θ scanning technique, the scanning rate being 4° in ω per minute. During the course of the data collection, three reflections were monitored every 100 reflections. The intensity data were converted to the F_o data in the usual manner. Absorption corrections were not applied. The standard deviations were estimated by counting statistics. A total of 1504 independent reflections with $F_o>3\sigma(F_o)$ were retained as observed, and employed in solving and refining the structure.

The electronic absorption spectra were recorded with a JASCO UVIDEC-1 spectrophotometer, and the CD spectra, with a JASCO J-20 spectropolarimeter. All measurements were carried out in aqueous solution at room temperature.

Determination of Crystal Structure

The position of the cobalt atom was obtained from the three-dimentional Patterson function. Fourier and

Table 1. The atomic positional parameters, with their e.s.d.'s in parentheses

Atom	x	y	z	B_{eq}/Å^2 a)
Co	0.4304(1)	0.1098(1)	0.1250	2.56
S	0.8796(2)	0.2085(2)	0.4666(7)	3.42
Cl	0.4363(2)	−0.0881(2)	0.0755(6)	4.03
O(1)	0.5903(5)	−0.0792(6)	0.3399(14)	3.48
O(2)	0.6732(6)	0.0167(6)	0.1524(16)	4.25
O(3)	0.6012(7)	0.7669(7)	0.2468(20)	6.66
N(1)	0.3610(6)	0.0064(6)	0.1855(17)	2.87
N(2)	0.4965(6)	0.2120(6)	0.0394(18)	3.21
N(3)	0.4534(7)	0.1441(7)	0.4117(17)	3.79
N(4)	0.5183(6)	0.0968(6)	0.0978(17)	3.25
C(1)	0.2611(8)	0.0242(8)	0.0665(25)	3.84
C(2)	0.1943(10)	0.2145(10)	0.0430(27)	5.30
C(3)	0.2109(8)	−0.0137(9)	0.2536(27)	4.79
C(4)	0.3062(7)	−0.0146(7)	0.0207(21)	3.08
C(5)	0.6514(8)	−0.0149(8)	0.3215(21)	3.54
C(6)	0.5068(11)	0.2594(9)	0.2205(25)	5.36
C(7)	0.7118(10)	0.4891(10)	0.0842(23)	5.60
C(8)	0.4343(8)	−0.2182(8)	0.4498(27)	4.08
C(9)	0.5870(7)	0.1689(8)	0.0675(24)	3.47

a) B_{eq} is the equivalent isotropic temperature factors defined by Hamilton.[17]

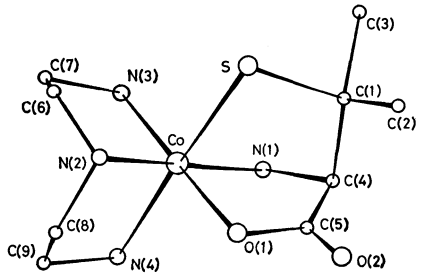

Fig. 2. A perspective drawing of *trans(N$_1$N)*-[Co(L-pen)(dien)]$^+$ with the numbering scheme of atoms.

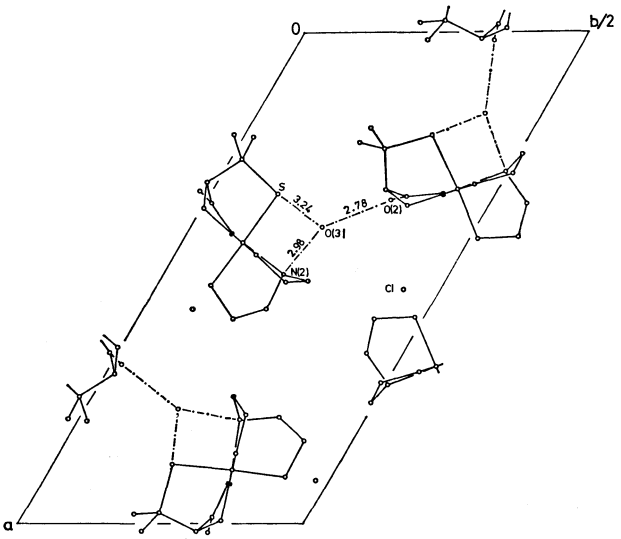

Fig. 3. A projection of the crystal packing viewed along the c axis.

difference-Fourier maps based on the cobalt atom revealed the rest of the structure. The structure was refined by a full-matrix least-squares refinement of the positional and anisotropic thermal parameters (program RFINE by L. W. Finger, which was modified by H. Horiuchi (1979), was used). The final R values in the space groups $P6_1$ and $P6_5$ converged 0.076 and 0.077, respectively, using the anomalous scattering factors. Taking the known absolute configuration of the L-penicillaminate in the complex into consideration, the space group must be $P6_1$. The atomic scattering factors were taken from the International Tables for X-Ray Crystallography.[7] The calculations were carried out on a FACOM M-200 computer at the University of Tsukuba. The final atomic parameters and their standard deviations are given in Table 1. A list of the anisotropic thermal parameters and a table of the observed and calculated structure factors are kept at the Chemical Society of Japan (Document No. 8248).

Results and Discussion

Description of the Structure. A perspective drawing of the complex cations obtained is given in Fig. 2 and their packing mode is illustrated in Fig. 3. The atomic numbering scheme is given in Figs. 2 and 3. The bond lengths and angles with their estimated standard deviations in the complex ions are listed in Table 2. The coordination geometry around the cobalt atom is approximately octahedral. The L-penicillaminate and diethylenetriamine coordinate facially to the cobalt atom as terdentate ligands. The nitrogen atom of the L-pen ligand occupies the trans position to the imino nitrogen atom of the dien ligand. Therefore, this cation is determined to have a *trans(N$_1$N)* configuration as shown in Fig. 1 (a).

The bond lengths and angles are similar to those for the cobalt(III) complexes with diethylenetriamine and/or sulfur-containing amino carboxylates.[2,8-12] The averages of the cobalt-ligand bond lengths are 2.255 (5) Å for Co–S, 1.926 (9) Å for Co–O, and 1.972 (11) Å for Co–N. The Co–N distance involving the nitrogen atom bonded trans to the sulfur atom is 2.007 Å and the average cis Co–N distance is 1.961 Å, giving a difference between trans and cis distances of 0.046 Å. This fact suggests that the trans effect due to the coordinated sulfur atom and the difference (0.046 Å) corresponds with those of the cobalt(III) complexes with the thiolato ligands such as 2-aminoethanethiolate.[13]

The crystal structure consists of the complex cations, chloride anions, and water molecules. As shown in Fig. 3, a water molecule O(3) atom is surrounded by the three atoms: *e.g.*, the oxygen O(2) atom of the complex cation and the sulfur S and nitrogen N(2) atoms of the other complex cation. The O(3)–O(2) or O(3)–N(2) distance is mostly less than 3 Å and O(3)–S one is 3.24 Å. These distances suggest that those are hydrogen bonds.

In order to examine the conformations of chelate rings, the displacements of relevant atoms from the chelate ring plane, which is defined by the central

Table 2. Intermolecular distances and bond angles (with e.s.d.'s) for *trans(N$_1$N)*-[Co(L-pen)(dien)]Cl·H$_2$O

Bond distance	*l*/Å	Bond distance	*l*/Å
Co-S	2.255(5)	N(4)-C(9)	1.494(14)
Co-O(1)	1.926(9)	O(1)-C(5)	1.326(14)
Co-N(1)	1.959(10)	O(2)-C(5)	1.240(17)
Co-N(2)	1.967(10)	C(1)-C(2)	1.546(26)
Co-N(3)	1.957(11)	C(1)-C(3)	1.538(22)
Co-N(4)	2.007(15)	C(1)-C(4)	1.558(27)
S-C(1)	1.852(13)	C(4)-C(5)	1.509(19)
N(1)-C(4)	1.465(18)	C(6)-C(7)	1.512(26)
N(2)-C(6)	1.480(21)	C(8)-C(9)	1.523(26)
N(3)-C(7)	1.482(19)		
Bond angle	*φ*/°	Bond angle	*φ*/°
S-Co-N(1)	83.6(4)	S-N(3)-C(7)	111.0(11)
S-Co-N(2)	94.8(5)	Co-N(4)-C(9)	111.3(11)
S-Co-N(3)	90.7(5)	Co-O(1)-C(5)	111.6(8)
S-Co-N(4)	175.9(3)	S-C(1)-C(2)	111.4(12)
S-Co-O(1)	89.4(4)	S-C(1)-C(3)	109.8(11)
N(1)-Co-N(2)	174.9(5)	S-C(1)-C(4)	106.2(9)
N(1)-Co-N(3)	97.5(5)	C(2)-C(1)-C(3)	110.0(13)
N(1)-Co-N(4)	95.3(5)	C(2)-C(1)-C(4)	110.9(14)
N(1)-Co-O(1)	84.3(4)	C(3)-C(1)-C(4)	108.5(14)
N(2)-Co-N(3)	87.3(5)	N(1)-C(4)-C(1)	107.3(12)
N(2)-Co-N(4)	85.9(5)	N(1)-C(4)-C(5)	106.3(11)
N(2)-Co-O(1)	90.9(4)	C(1)-C(4)-C(5)	109.6(14)
N(3)-Co-N(4)	93.3(6)	O(1)-C(5)-O(2)	122.4(12)
N(3)-Co-O(1)	178.2(4)	O(1)-C(5)-C(4)	114.6(11)
N(4)-Co-O(1)	86.6(5)	O(2)-C(5)-C(4)	123.0(11)
Co-S-C(1)	97.9(6)	N(2)-C(6)-C(7)	110.3(16)
Co-N(1)-C(4)	103.2(8)	N(3)-C(7)-C(6)	109.0(12)
Co-N(2)-C(6)	107.5(8)	N(2)-C(8)-C(9)	110.5(12)
Co-N(2)-C(8)	109.0(10)	N(4)-C(9)-C(8)	106.9(12)

Table 3. Displacements of atoms from the least-squeares plane (*d*/Å)

Diamine chelate ring:			
Plane 1;	$-0.9856X+0.1689Y+0.0085Z+7.4323=0$		
Co	0.0001	C(6)	0.4312
N(2)	0.0000	C(7)	−0.1352
N(3)	0.0000		
Plane 2;	$-0.1161X-0.2647Y-0.9573Z+2.2171=0$		
Co	0.0000	C(8)	0.3621
N(2)	0.0000	C(9)	−0.2393
N(4)	0.0000		
S-N chelate ring			
	$-0.0401X-0.1954Y-0.9799Z+1.4969=0$		
Co	0.0000	C(1)	0.7804
S	0.0000	C(4)	1.1540
N(1)	0.0001		
O-N chelate ring			
	$-0.9810X+0.1942Y+0.0012Z+7.3511=0$		
Co	0.0000	C(4)	0.8379
O(1)	0.0000	C(5)	0.3712
N(1)	0.0000		

The *X*, *Y*, and *Z* coordinates in Å are referred to the crystallographic axes.

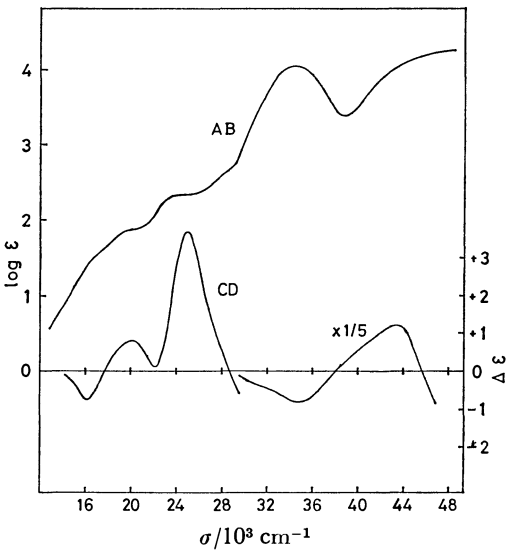

Fig. 4. Absorption and CD spectra of *trans(N$_1$N)*-[Co(L-pen)(dien)]+.

cobalt atom and the two coordinated atoms in the chelate ring, were calculated. The results are given in Table 3. The diamine chelate rings in the dien ligand take reasonable conformations,[8] *δ* form for N(2)-C(8)-C(9)-N(4) and *λ* one for N(2)-C(6)-C(7)-N(3). The N-S chelate ring in the L-pen ligand has a similar conformation to that of the *trans(O)*-[Co(*R*,*R*-ebsmc)]+ complex, where *R*,*R*-ebsmc denotes *N*,*N'*-ethylenebis(*S*-methyl-L-cysteinate) which has the same frame-work as the L-pen ligand.[9]

Electronic Absorption and CD Spectra. The electronic absorption and CD spectra of the *trans(N$_1$N)*-[Co(L-pen)(dien)]+ complex are shown in Fig. 4. The sulfur-to-metal charge transfer band of this complex is observed at 34.5×10^3 cm^{-1}, as in the case of the cobalt(III) complexes with thiolato and thioether ligands.[3,9,14] In the first absorption band region, the complex shows an explicit shoulder (*ca.* 16.7×10^3 cm^{-1}) on the lower energy side of the major peak (20.0×10^3 cm^{-1}) and the lower energy component is characteristic of thiolato coordination.[3,15] The absorption spectrum of this complex shows comparatively intense humps in the region from 23×10^3 cm^{-1} to 28×10^3 cm^{-1} and an intense positive CD band ($\Delta\varepsilon$ +3.75 at 25.0×10^3 cm^{-1}) in appearance corresponds to the humps. The absorption and CD spectral behavior in this region are common to those of the *trans(N$_1$O)*- and *trans(N$_1$S)*-[Co(L-pen)(dien)]+ complexes.[4,16] Similar spectral patterns are observed for the [Co(L-pen)(NH$_3$)$_3$]+ complex, which belongs to the *cis(SO)*-[Co(N)$_4$(S)(O)] type. It does not have chirality arising from the skew pair of chelate rings because of the coordination of three ammonia molecules instead of dien.[16] Taking these facts into account, it can be considered that the absorption and CD bands in this region are characteristic of the coordinated thiolato donor atom of the ligand.

References

1) G. Gorin, J. E. Spessard, G. A. Wessler, and J. P. Oliver, *J. Am. Chem. Soc.*, **81**, 3193 (1959); W. G. Jackson and A. M. Sargeson, *Inorg. Chem.*, **17**, 2165 (1978); H. C. Freeman, C. J. Moore, W. G. Jackson, and A. M. Sargeson, *ibid.*, **17**, 3513 (1978).

2) P. de Meester and D. J. Hodgson, *J. Am. Chem. Soc.*, **99**, 101 (1977); H. M. Helis, P. de Meester, and D. J. Hodgson, *ibid.*, **99**, 3309 (1977).

3) K. Yamanari, N. Takeshita, T. Komorita, and Y. Shimura, *Chem. Lett.*, **1981**, 861.

4) K. Okamoto, K. Wakayama, M. Ohmasa, and J. Hidaka, *Chem. Lett.*, **1981**, 453.

5) J. L. Legg and D. W. Cooke, *Inorg. Chem.*, **5**, 594 (1966); K. Okamoto, J. Hidaka, and Y. Shimura, *Bull. Chem. Soc. Jpn.*, **48**, 2425 (1975).

6) P. H. Crayton, *Inorg. Synth.*, **7**, 207 (1963).

7) "International Tables for X-Ray Crystallography," The Kynoch Press, Birmingham (1974), Vol. IV.

8) M. Konno, F. Marumo, and Y. Saito, *Acta Crystallogr., Sect. B*, **29**, 739 (1973).

9) K. Okamoto, T. Isago, M. Ohmasa, and J. Hidaka, *Bull. Chem. Soc. Jpn.*, **55**, 1077 (1982).

10) P. de Meester and D. J. Hodgson, *J. Chem. Soc., Dalton Trans.*, **1976**, 618.

11) R. C. Elder, G. J. Kennard, M. D. Payne, and E. Deutsch, *Inorg. Chem.*, **17**, 1296 (1978).

12) R. J. Magee, W. Mazurek, M. J. O'Connor, and A. T. Phillip, *Aust. J. Chem.*, **27**, 1629 (1974).

13) R. C. Elder, L. R. Florian, R. E. Lake, and A. M. Yacynych, *Inorg. Chem.*, **13**, 2360 (1974); B. A. Lange, K. Libson, E. Deutsch, and R. C. Elder, *ibid.*, **15**, 2985 (1976); R. C. Elder, M. J. Heeg, M. D. Payne, M. Trkula, and E. Deutsch, *ibid.*, **17**, 431 (1978).

14) T. Isago, K. Igi, and J. Hidaka, *Bull. Chem. Soc. Jpn.*, **52**, 407 (1979); K. Yamanari, J. Hidaka, and Y. Shimura, *ibid.*, **50**, 2299 (1977).

15) V. H. Houlding, H. Mäcke, and A. W. Adamson, *Inorg. Chem.*, **20**, 4279 (1981).

16) The present authors, to be published.

17) W. C. Hamilton, *Acta Crystallogr.*, **12**, 609 (1959).

 © 1982 The Chemical Society of Japan Bull. Chem. Soc. Jpn., 55, 3477—3481 (1982)

Spectrophotometric Determination of Silicic Acid by Flow Injection Analysis

Takushi Yokoyama,* Yukio Hirai, Norimasa Yoza, Toshikazu Tarutani, and Shigeru Ohashi

Department of Chemistry, Faculty of Science, Kyushu University 33, Hakozaki, Higashi-ku, Fukuoka 812

(Received April 10, 1982)

Flow injection analysis (FIA) was developed for the spectrophotometric determination of silicic acid based on the formation of a yellow molybdosilicic acid (yellow method) and a heteropoly blue complex (blue method). In the yellow method, silicic acid in the concentration range of 2 to 100 ppm (SiO_2) could be determined at a sampling rate of 60 samples/h. The FIA system was modified to determine silicic acid in the presence of orthophosphate. Oxalic acid was used for the decomposition of molybdophosphoric acid. The modified system was employed for the rapid and selective determination of silicic acid in well and river waters. In the blue method, ascorbic acid was used to reduce the yellow molybdosilicic acid to a heteropoly blue complex. Silicic acid in the concentration range of 0.02 to 1.0 ppm (SiO_2) could be determined at a sampling rate of 40 samples/h. The FIA system was also modified to determine silicic acid in the presence of orthophosphate. The reducing agent was introduced after molybdophosphoric acid had been completely decomposed by adding oxalic acid. The modified system was employed for the determination of silicic acid in sea water.

The silicic acid content of natural waters is of particular interest in geochemistry inasmuch as it is related to the weathering of rocks and the formation of clay minerals. Recently, interest in the study of the behavior of silicic acid in natural waters has increased, because silicic acid as well as orthophosphate is one of the major inorganic nutrients for planktons and microorganisms. Since it is necessary to analyze a large number of samples, rapid and automatic method of analysis for silicic acid is increasingly becoming important.

Silicic acid is usually determined by spectrophotometric method based on the formation of a yellow molybdosilicic acid (yellow method). Often, to enhance the sensitivity of the analysis, the molybdosilicic acid is reduced to yield a heteropoly blue complex (blue method).

An air-segmented method has been applied to the determination of silicic acid.[1] The method is satisfactory with respect to reproducibility and sensitivity, but the disadvantages are that the instrument is expensive and that the procedure is somewhat time-consuming. Recently a flow-coulometric method has been developed for the rapid determination of silicic acid.[2] The method is convenient but less sensitive than the conventional spectrophotometric method.

Flow injection analysis (FIA) is a simple and convenient approach to rapid chemical analysis.[3] The present authors have already reported successful applications of FIA to the determination of phosphorus compounds.[4,5] One of the most advantages of FIA is that reaction conditions, *e.g.*, reaction time, reaction temperature, reagent concentration, *etc*, can easily be kept constant with a simple apparatus. The formation of molybdosilicic acid is susceptible to such conditions as described above. Therefore the application of FIA is effective to achieve a rapid and precise analysis for silicic acid.

In a previous paper,[6] we have briefly reported a successful application of FIA to the determination of silicic acid based on the formation of a molybdosilicic acid. The present work was carried out to attain two purposes. One is to determine silicic acid rapidly and precisely in the wide range of concentration. The other is to modify the FIA system for the determination of silicic acid in the presence of orthophosphate. The FIA system was found to be useful for the determination of silicic acid in natural waters such as well, river and sea waters.

Experimental

Samples and Reagents. All reagents used were of analytical reagent grade. Unless otherwise stated deionized distilled water was used. A monosilicic acid stock solution (100 ppm SiO_2) was prepared by dissolving silica gel (Mallinckrodt Chemical Works) in a boiling water. The concentration of this stock solution was standardized spectrophotometrically. Working standard solutions were prepared by diluting the stock solution with water. A molybdenum(VI) reagent was prepared by dissolving 8.83 g of hexaammonium heptamolybdate ($(NH_4)_6Mo_7O_{24}\cdot 4H_2O$) in *ca.* 0.9 dm^3 of water. After 7.5 cm^3 of concentrated sulfuric acid had been added, the solution was diluted to 1 dm^3 with water. The reagent was composed of 0.05 mol dm^{-3} Mo^{VI} and 0.135 mol dm^{-3} H_2SO_4. A 0.5 mol dm^{-3} oxalic acid solution was prepared by dissolving oxalic acid ($H_2C_2O_4\cdot 2H_2O$). Orthophosphate solution was prepared by dissolving potassium dihydrogenorthophosphate (KH_2PO_4), which had been dried for 1 h at 110 °C. L-Ascorbic acid solutions (0.02 mol dm^{-3}) containing various amounts of sulfuric acid were prepared under cooling with ice. Artificial sea water as a carrier solution for the analysis of sea water was prepared by dissolving 24.7 g of sodium chloride, 13 g of magnesium chloride ($MgCl_2\cdot 6H_2O$) and 4 g of anhydrous sodium sulfate in water, and then the volume was made up to 1 dm^3. Natural water was filtered just after sampling by membrane filter (0.45 μm pore size) and stored in a 50-cm^3 polyethylene bottle. The determination of silicic acid in natural water samples was carried out within 24 h after sampling.

Apparatus, Manifold, and Procedure. Four kinds of manifolds (systems I—IV) were designed (Fig. 1). Two reciprocating pumps (Kyowa KHU-W-104 (P_1) and Kyowa KHU-W-52 (P_2)) with double plungers were used to introduce carrier solutions into analytical lines. A sample (S) was injected into a carrier stream *via* a loop-valve in-

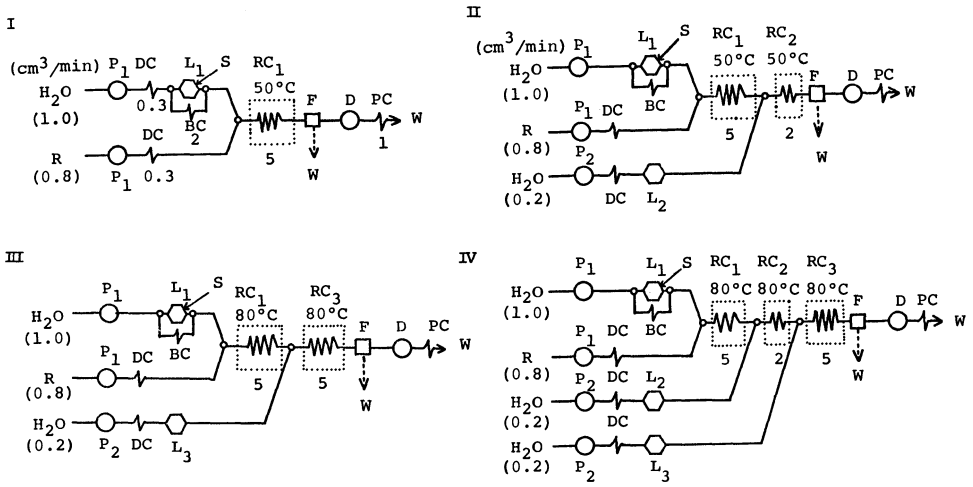

Fig. 1. FIA systems I—IV for the determination of silicic acid based on the yellow method (I and II) and the blue method (III and IV). FIA systems II and IV were designed to determine silicic acid in the presence of orthophosphate. R: molybdenum(VI) reagent, P_1 and P_2: reciprocating pump, DC: damper coil, BC: bypass coil, RC_1, RC_2, and RC_3: reaction coil, PC: back pressure coil, L_1, L_2, and L_3: loop valve injector, F: three way valve, D: detector and W: waste. The numerals under the coils refer to their lengths in meter. The numerals under the pump indicate the flow rate of solutions. The dotted lines show the manifolds immersed in the thermostated silicone oil-bath.

jector (L_1, Seishin VMU-6). The injected sample was then transported through reaction coils (RC_1, RC_2, and RC_3, PTFE 0.5 mm ID). To accelerate chemical reaction the reaction coils were heated in a silicone-oil bath (Thomas-T-201). Color complexes formed in the reaction coils were monitored using a spectrophotometer (D, Hitachi 200—10) with a flow-through cell (8 mm light path, 8 μl volume).

An elastic precoil (DC, Technicon Part No. 065-116-0536-13, 30 cm) was applied to dampen the pressure pulse caused by the reciprocating pumps. A bypass coil (BC, PTFE 0.3 mm i.d., 2 m) was also applied to minimize the injection shock. A three way valve (F, Kyowa KMM-4V) was located just before the detector to observe the variation in absorbance of a sample zone in the flow-through cell (Stopped-flow method). A back pressure coil (PC, PTFE 0.3 mm i.d., 1 m) was attached at the exit of the flow-through detector to eliminate a noise due to gas-bubbling. Both an oxalic acid and an ascorbic acid solutions were introduced *via* loop-valve injectors L_2 and L_3, (Kyowa KMM-4V-2) respectively. The function of these valves was precisely described in a previous paper.[5] This method makes it possible to put in, cut off or exchange a reagent without any reconditioning of a pump.

In FIA system I, a sample was mixed with a molybdenum (VI) reagent (R). A molybdosilicic acid formed in the reaction coil (RC_1) was directly monitored at 400 nm. FIA system II was designed to determine silicic acid in the presence of orthophosphate. The oxalic acid solution was added from another line using the loop-valve injector (L_2) to decompose molybdophosphoric acid formed in the first reaction coil (RC_1). The remaining molybdosilicic acid was monitored at 400 nm. In FIA system III, the ascorbic acid solution was introduced using the loop-valve injector (L_3) to reduce the molybdosilicic acid in the reaction coil (RC_3). The resultant blue complex was monitored at 820 nm. FIA system IV was designed to determine silicic acid in the presence of orthophosphate. After decomposition of molybdophosphoric acid, the remaining molybdosilicic acid was reduced with ascorbic acid to a heteropoly blue complex.

Results and Discussion

Flow Injection Analysis for Silicic Acid Based on the Formation of a Molybdosilicic Acid. Flow rates of carrier solutions through the pump (P_1) and a length of the reaction coil (RC_1) of the FIA system I were designed to determine silicic acid at 60 samples/h. Taking the composition of a molybdosilicic acid (Si:Mo= 1:12) and the flow rate of each carrier solution into account, 0.05 mol dm^{-3} molybdenum(VI) reagent solution was used to determine silicic acid up to 100 ppm (SiO_2). The acid concentration of the molybdenum(VI) reagent was adjusted to 0.135 mol dm^{-3} in H_2SO_4.[7] The temperature of the heating bath was kept at 50 °C to accelerate the chemical reaction. The residence time of a sample in the reaction coil was about 1 min.

Figure 2 shows a normal FIA signal and a stopped-flow signal. The same sample was injected twice. At the top of the second signal, the valve F was switched to hold the sample zone in the flow-through cell.

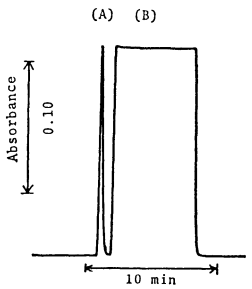

Fig. 2. FIA profile (A) and stopped flow signal (B) for silicic acid obtained by FIA system I.
Sample: 50 ppm (SiO_2), 0.10 cm^3.

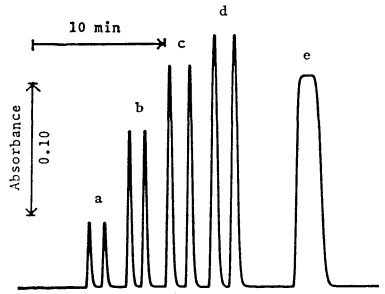

Fig. 3. Effect of the length of sample loop on the FIA signal.
Sample: 10 ppm (SiO_2), a; 0.08, b; 0.50, c; 1.0, d; 1.5, and e; 5.0 m. FIA system I was used.

There was no remarkable change in absorbance. This suggests the completion of the color forming reaction.

Figure 3 shows the effect of the sample volume on the FIA signal. The injection volume of a sample was varied by using the sampling loops (PTFE, 0.5 mm i.d.) with different length. The peak height of the FIA signal increased with lengthening the sampling loop up to 1.5 m and decreased at 5.0 m.[8] Therefore, sampling loops of 0.08 and 1.5 m, corresponding to *ca.* 0.10 and 0.50 cm^3, were used.

To demonstrate the reproducibility, the samples (2, 20, and 100 ppm (SiO_2)) were injected ten times. The precisions (C.V.) were 1.7, 0.2, and 0.07% for silicic acid of 2, 20, and 100 ppm (SiO_2), respectively. The standard sample of silicic acid could be measured in the concentration range of 2 to 100 ppm. The sampling rate was 60 samples/h. The detection limit (S/N=2) was 0.3 ppm.

Orthophosphate reacts with molybdenum(VI) reagent to form a yellow molybdophosphoric acid and the complex interferes with the determination of silicic acid. In order to eliminate the interference, decomposing agents have been employed for the decomposition of molybdophosphoric acid. In Japanese Industrial Standard (JIS) method,[9] oxalic acid is used as the decomposing agent. As it is necessary to add an excessive amount of the decomposing agent compared with that of molybdenum(VI),[10] 0.5 mol dm^{-3} oxalic acid solution was used.

The FIA system II was designed to determine silicic acid in the presence of orthophosphate. Oxalic acid solution was introduced from another line using a loop-valve injector (L_2). As the decomposition of molybdophosphoric acid proceeds rapidly even at room temperature,[10] a short reaction coil (RC_2, 2 m) was applied. The heating bath was kept at 50 °C. The remaining molybdosilicic acid was monitored at 400 nm.

The efficiency of the decomposition effect of oxalic acid was examined. The results are shown in Fig. 4. From the FIA signals (a—c), it is clear that both molybdosilicic acid and molybdophosphoric acid form independently in the absence of oxalic acid. From the FIA signals (d—k), the interference due to orthophosphate up to 100 ppm (PO_4^{3-}) could be eliminated by the addition of oxalic acid. Further increase in the concentration of phosphate caused a decrease in peak height. At 300 and 400 ppm (PO_4^{3-}), the FIA signals became double peak. The decrease in peak height and the appearance of double peak may be caused by the deficiency of molybdenum(VI) to be required for the formation of molybdosilicic acid, because molybdenum(VI) is consumed by the formation of molybdophosphoric acid.

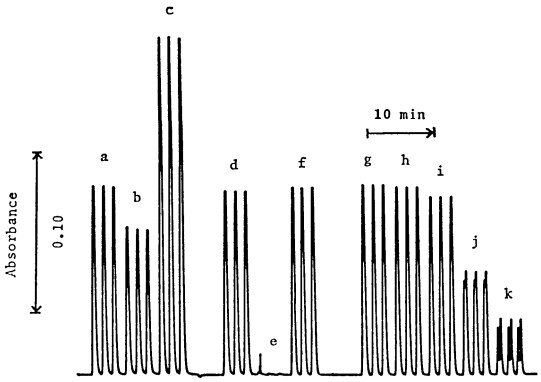

Fig. 4. Detection peaks for silicic acid samples containing various amounts of orthophosphate in the absence (a—c) and presence (d—k) of oxalic acid.
Sample: a; 10 ppm (SiO_2)+0 ppm (PO_4^{3-}), b; 0 ppm (SiO_2)+20 ppm (PO_4^{3-}), c; 10 ppm (SiO_2)+20 ppm (PO_4^{3-}), d; 10 ppm (SiO_2)+0 ppm (PO_4^{3-}), e; 0 ppm (SiO_2)+20 ppm (PO_4^{3-}), f; 10 ppm (SiO_2)+20 ppm (PO_4^{3-}), g; 10 ppm (SiO_2)+50 ppm (PO_4^{3-}), h; 10 ppm (SiO_2)+100 ppm (PO_4^{3-}), i; 10 ppm (SiO_2)+200 ppm (PO_4^{3-}), j; 10 ppm (SiO_2)+300 ppm (PO_4^{3-}), and k; 10 ppm (SiO_2)+400 ppm (PO_4^{3-}), 0.50 cm^3. Each sample was injected in triplicate.

Table 1. Silicic acid concentration in well and river water samples obtained by the FIA and JIS method

Sample	FIA(SiO_2 ppm)	JIS(SiO_2 ppm)
Well water		
(A)	17.8	17.4
(B)	20.0	19.3
(C)	20.9	20.3
River water		
(D)	9.9	9.5
(E)	12.6	12.1
(F)	12.5	12.1
(G)	12.4	12.1
(H)	12.6	12.3
(I)	11.8	11.5
(J)	13.4	13.1
(K)	13.7	13.3
(L)	14.2	14.0

Determination of Silicic Acid in Well and River Waters. The FIA system II was employed for the determination of silicic acid in well and river waters. Routine runs for the determination are illustrated in Fig. 5, together with that for a series of standard silicic acid. The sampling rate was 40 samples/h. The analytical values obtained by FIA are shown in Table 1, together with those obtained by JIS method. Both results coincide satisfactorily with a correlation coefficient of 0.998.

Flow Injection Analysis for Silicic Acid Based on the Formation of a Heteropoly Blue Complex. To get higher sensitivity and avoid the interference due to absorption by foreign compounds at 400 nm, a method was examined for the determination of silicic acid based on the formation of a heteropoly blue complex. Among many reducing agents,[11] ascorbic acid was used to reduce a yellow molybdosilicic acid to a blue compound because of its simple preparation. The reducing agent was composed of 0.02 mol dm^{-3} ascorbic acid and 2 mol dm^{-3} sulfuric acid. The reducing agent was added after the formation of molybdosilicic acid.[11]

In the FIA system III, the ascorbic acid solution was introduced from the another line using a loop-valve injector (L_3). A five meter reaction coil (RC_3) was applied to reduce a molybdosilicic acid to a heteropoly blue complex. Figure 6 shows that FIA signal and stopped-flow signal greatly depended on the temperature of the heating bath. The stopped-flow signal at 60 °C showed a steep increase in absorbance followed by a steady state. The signal was quite different from the signal observed in Fig. 2. There was no remarkable increase in the base line level when the carrier reagent was stopped in the flow-through cell (Fig. 6(IV)). This indicates that the formation of blue isopolymolybdic acid during the stopping period is negligible. Therefore the difference in height between the FIA signal and the top of the stopped flow signal is regarded as an unreduced portion of the molybdosilicic acid. At 80 °C, more than 90% of molybdosilicic acid was reduced. The determination of silicic acid hereafter was carried out at 80 °C.

The standard sample of silicic acid could be measured in the concentration ranges of 0.02 to 0.1 and 0.2 to 1.0 ppm (SiO_2). The samples were injected successively at the sampling rate of 40 samples/h. The detection limit (S/N=2) was 0.01 ppm (SiO_2). The precision (C.V.) was 0.5% for 0.6 ppm silicic acid.

The formation of a heteropoly blue complex of silicon and molybdenum and blue isopolymolybdic acid is susceptible to acid concentration, temperature and addition of decomposing agent of molybdophosphoric acid.[7] The effect of acid concentration on the FIA signal and the base line level was examined by using FIA system IV. The effect was examined under two conditions. Figure 7 shows the effect of the acid con-

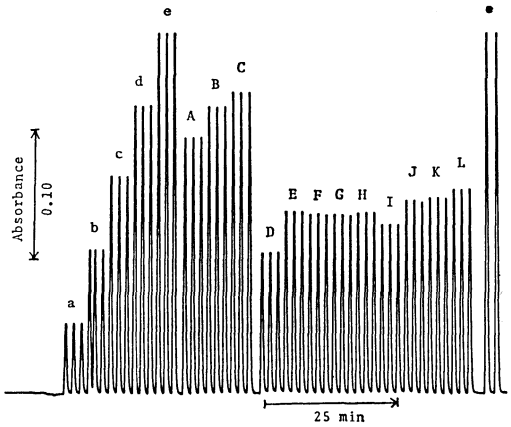

Fig. 5. Determination of silicic acid in well and river waters using FIA system II.
The first fifteen peaks on the left and the last two peaks on the right were obtained by injecting standard samples of silicic acid. Sample: a; 5, b; 10, c; 15, d; 20, and e; 25 ppm (SiO_2), A—C; well waters, D—L; river waters. Sample volume: 0.50 cm^3.

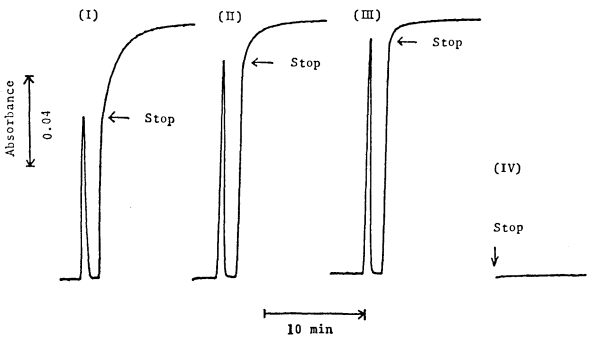

Fig. 6. FIA profiles and stopped flow signals for silicic acid of 1 ppm (SiO_2), 0.50 cm^3.
Temperature of the heating bath: (I); 60 °C, (II); 70 °C, and (III); 80 °C. The signal (IV) shows a stopped flow signal of a base line level at 80 °C. FIA system III was used.

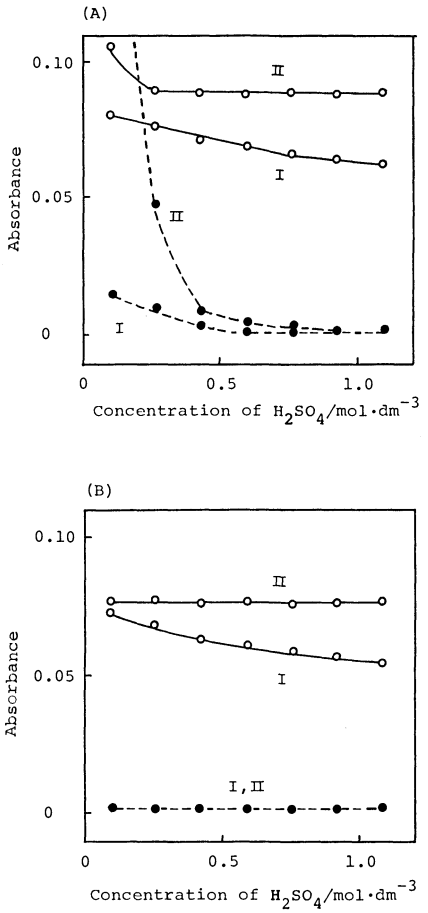

Fig. 7. Effect of acid concentration in the reaction coil (RC_3) and temperature of the heating bath on the FIA peak height and base-line level in the absence (A) and presence (B) of oxalic acid.
FIA system IV was used. ○: Peak height, ●: base line level. I: 50 °C and II: 80 °C. Sample: 1 ppm (SiO_2), 0.50 cm^3.

centration on the FIA signal and the base line in the absence and the presence of oxalic acid, respectively. Oxalic acid and ascorbic acid solutions were introduced with the loop-valve injectors (L_2) and (L_3), respectively. Figure 7(A) shows the results obtained by introducing water in place of oxalic acid solution. The abscissa of Fig. 7 indicates the acid concentration in the reaction coil (RC_3). The acid concentration was controlled by adding various amounts of sulfuric acid to the ascorbic acid solution.

It is clear from Fig. 7(A) that the rate of the formation of both a heteropoly blue complex and blue isopolymolybdic acid increases at higher temperature and at lower acid concentration. Therefore a suitable amount of sulfuric acid must be added to avoid the formation of the blue isopolymolybdic acid in the absence of oxalic acid. It is also necessary to increase the temperature of the heating bath to accelerate the formation of the heteropoly blue complex.

From Fig. 7(B), it is seen that blue isopolymolybdic acid does not form in the presence of oxalic acid. This fact also indicates that oxalic acid reacts with molybdenum(VI). The absorbance of the plateau region of the heteropoly blue complex at 80 °C obtained in the presence of oxalic acid is somewhat lower than that obtained in the absence of oxalic acid, because oxalic acid decomposes a part of molybdosilicic acid at such a high temperature as 80 °C.

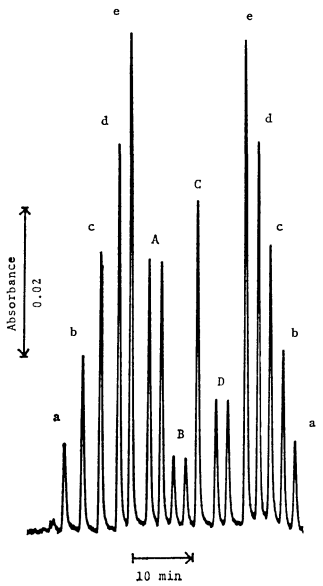

Fig. 8. Determination of silicic acid in sea waters using FIA system IV.
The first five peaks on the left and last five peaks on the right were obtained by injecting standard samples of silicic acid. Sample: a; 0.2, b; 0.4, c; 0.6, d; 0.8, and e; 1.0 ppm (SiO_2), A—D; sea waters, 0.50 cm^3. Each sample was injected in duplicate except C.

It must be noted that there is no need to add sulfuric acid to the ascorbic acid solution, when oxalic acid is used. This fact is favorable for the preparation of ascorbic acid solution, because ascorbic acid is easily oxidized in the presence of sulfuric acid.

Determination of Silicic Acid in Sea Water. The FIA system IV was employed for the determination of silicic acid in sea water. Artificial sea water was introduced as a carrier solution of a sample. Figure 8 shows routine runs for the analysis of sea water. A reducing agent, ascorbic acid solution, was composed of 0.02 mol dm^{-3} L-ascorbic acid and 2 mol dm^{-3} sulfuric acid. The silicic acid concentration of the four samples were (A) 0.57, (B) 0.15, (C) 0.69, and (D) 0.30 ppm (SiO_2), respectively.

The present work was partially supported by a Grant-in-Aid for Scientific Research No. 56030024 from the Ministry of Education, Science and Culture.

References

1) Techicon Autoanalyzer Methodology, Industrial Method No. 174-72WM/Preliminary.
2) T. Hori, T. Itoh, S. Okazaki, and T. Fujinaga, *Bunseki Kagaku*, **30**, 582 (1981).
3) J. Ruzicka and E. H. Hansen, "Flow Injection Analysis," John Wiley and Sons, New York (1981).
4) Y. Hirai, N. Yoza, and S. Ohashi, *Anal. Chim. Acta*, **115**, 269 (1980).
5) Y. Hirai, N. Yoza, and S. Ohashi, *J. Chromatogr.*, **206**, 501 (1981).
6) Y. Hirai, T. Yokoyama, N. Yoza, T. Tarutani, and S. Ohashi, *Bunseki Kagaku*, **30**, 350 (1981).
7) I. Iwasaki, *Bunseki Kagaku*, **9**, 185 (1960).
8) Y. Hirai, N. Yoza, and S. Ohashi, *Bunseki Kagaku*, **30**, 465 (1981).
9) JIS K 0101 (1979).
10) S. Misumi and T. Tarutani, *Bunseki Kagaku*, **10**, 1113 (1961).
11) Y. Umezaki, *Nippon Kagaku Zasshi*, **82**, 1353 (1961).

Electron Transfer from Tetrakis(isocyanide)rhodium(I) Monomers, and the Oligomers to Iron(III) and Cobalt(III) Complexes. Enhancement of the Reactivity by the Oligomerization

Shunichi Fukuzumi, Nobuaki Nishizawa, and Toshio Tanaka*

Department of Applied Chemistry, Faculty of Engineering, Osaka University, Suita, Osaka 565

(Received April 17, 1982)

Electron transfer reactions from tetrakis(isocyanide)rhodium(I) ($[RhL_4]^+$ to iron(III) complexes of the $[Fe(N\text{–}N)_3]^{3+}$ type (N–N=1,10-phenanthroline, 2,2′-bipyridine) proceed through precursor complexes formed between $[RhL_4]^+$ and $[Fe(N\text{–}N)_3]^{3+}$ with 1:1, 1:2, and 2:1 stoichiometry. A similar scheme is suggested for the reaction of bis(isocyanide)bis(triphenylphosphine)rhodium(I) with the same oxidants. The intramolecular electron transfer rate constants k_1 in the 1:1 precursor complexes have been determined in MeCN at 298 K. In accordance with Marcus theory, the log k_1 values are linearly related with the reduction potentials of oxidants with the theoretical slope of 8.5. The $[RhL_4]^+$ cations form oligomers in MeCN; $[RhL_4^+]_n$ (n=2,3), and the equilibrium constants for oligomerization have been determined. For a given oxidant $[Co(bpy)_3]^{3+}$ (bpy= 2,2′-bipyridine), the log k_1 value of $[RhL_4^+]_n$ increases in parallel with the HOMO energy of $[RhL_4^+]_n$; monomer<dimer<trimer.

Considerable interest exists in transition metal complex oligomers from the view point of their potential role in solar energy storage reaction,[1] as well as the understanding of the fundamental nature associated with the metal-metal interaction.[2] The redox properties of such metal complex oligomers, however, have scarcely been known especially in the comparison between the oligomers and the monomer. Thus, there has been no report yet on electron transfer reactions of rhodium(I) complex monomers and the oligomers, although extensive studies have been carried out on the oxidative addition reactions to rhodium(I) complexes, as well as the catalytic reactions.[3,4]

In the present study, we report kinetics of electron transfer reactions of tetrakis(isocyanide)rhodium(I) and the oligomers, $[RhL_4^+]_n$ (n=1—3) with some oxidants, $[Fe(N\text{–}N)_3]^{3+}$ (N–N=2,2′-bipyridine, substituted 1,10-phenanthrolines) and $[Co(bpy)_3]^{3+}$ (bpy=2,2′-bipyridine), as well as the effects of the ligand (L) on the oligomerization of $[RhL_4]^+$. Mechanisms for the electron transfer reactions of $[RhL_4^+]_n$ which forms highly associative precursor complexes with oxidants prior to electron transfer are discussed based on the kinetics. The intramolecular electron transfer rate constants in the precursor complexes have been obtained for both the $[RhL_4]^+$ monomers and the oligomers, and are compared in the context of the Marcus theory.[5]

Results and Discussion

Oligomerization of $[RhL_4]^+$. The $[Rh(PhNC)_4]^+$ cation has been reported to oligomerize in MeCN, yielding the dimer, $[Rh_2(PhNC)_8]^{2+}$, and the trimer, $[Rh_3(PhNC)_{12}]^{3+}$, which involve face to face contact of the $[Rh(PhNC)_4]^+$ units with weak, but direct Rh(I)–Rh(I) bonds.[2e] The formation of oligomers is characterized from the electronic spectra which show absorption bands in longer wavelengths than those due to the monomer.[2e] The electronic transition energies of the monomers, the dimers, and the trimers of a series of $[RhL_4]^+$ were determined as listed in Table 1. The equilibrium constants K_D and K_T for oligomerization defined by Eqs. 1 and 2 were determined by Eqs. 3 and 4, respectively,[2e]

$$2[RhL_4]^+ \overset{K_D}{\rightleftharpoons} [Rh_2L_8]^{2+} \quad (1)$$

$$[Rh_2L_8]^{2+} + [RhL_4]^+ \overset{K_T}{\rightleftharpoons} [Rh_3L_{12}]^{3+} \quad (2)$$

$$[Rh]/A_D^{1/2} = 1/(\varepsilon_D K_D)^{1/2} + 2A_D^{1/2}/\varepsilon_D \quad (3)$$

$$A_T = (\varepsilon_T K_T A_D^{3/2})/(\varepsilon_D^{3/2} K_D^{1/2}), \quad (4)$$

where [Rh] is the total Rh concentration in terms of the monomer, A_D and A_T are the absorbances due to dimers and trimers, respectively, and ε_D and ε_T are the corresponding molar extinction coefficients. According to Eq. 3, there is a linear relation between $[Rh]/A_D^{1/2}$ and $A_D^{1/2}$; the values of ε_D and K_T are obtained from the slope and the intercept, respectively. The K_T value is evaluated from a proportional relation between A_T and $A_D^{3/2}$ in Eq. 4, using the values of ε_D and K_D obtained from Eq. 3 as well as ε_T evaluated from the relation $\varepsilon_T = 1.5\ \varepsilon_D$.[2e] Application of Eqs. 3 and 4 to $[Rh(p\text{-}MeOC_6H_4NC)_4]^+$ and $[Rh(p\text{-}MeC_6H_4NC)_4]^+$ in MeCN containing 0.1 mol dm^{-3} n-Bu_4NClO_4 at 298 K is shown in Figs. 1a and 1b, respectively. The K_D and K_T values also are listed in Table 1. Plots of Eqs. 3 and 4 require the presence of a large amount of the oligomers within limited solubilities of $[RhL_4]^+$. Thus, when the K_D and K_T values are small (<2 mol^{-1} dm^3), Eqs. 5 and 6 are

$$A_D = \varepsilon_D K_D [Rh]^2 \quad (5)$$

$$A_T = \varepsilon_T K_D K_T [Rh]^3 \quad (6)$$

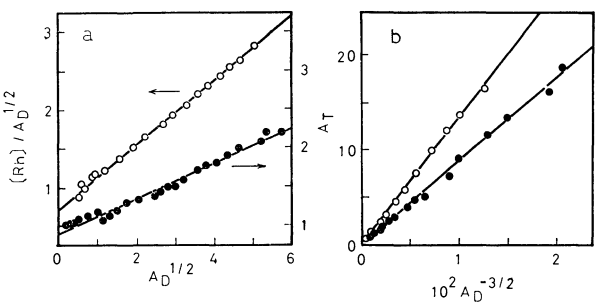

Fig. 1. Plots for the determination of (a) K_D and (b) K_T in MeCN containing 0.1 mol dm^{-3} n-Bu_4NClO_4 at 298 K; ○ $[Rh(p\text{-}MeOC_6H_4NC)_4]^+$, A_D at 564 nm and A_T at 710 nm, ● $[Rh(p\text{-}MeC_6H_4NC)_4]^+$, A_T at 563 nm and A_T at 705 nm. See Eqs. 3 and 4 in text.

used instead of Eqs. 3 and 4, respectively. By using the relations, $\varepsilon_D=2\,\varepsilon_M$ and $\varepsilon_T=3\,\varepsilon_M$,[2e] the K_D or K_T value for $[Rh(PhCH_2NC)_4]^+$ was estimated from the slope in Fig. 2a or 2b. Similarly, the K_D values for $[Rh(2,4,6\text{-}Me_3C_6H_2NC)_4]^+$ (Fig. 2a), $[Rh(t\text{-}BuNC)_4]^+$, and $[Rh(cyclo\text{-}C_6H_{11}NC)_4]^+$ were obtained from the plots of Eq. 5. No appreciable oligomer formation was observed for $[Rh(p\text{-}ClC_6H_4NC)_4]^+$, $[Rh(2,6\text{-}Me_2C_6H_3NC)_4]^+$, $[Rh(p\text{-}MeOC_6H_4NC)_2(PPh_3)_2]^+$, and $[Rh(2,4,6\text{-}Me_3C_6H_2NC)_2(PPh_3)_2]^+$.

For tetrakis(*p*-substituted phenyl isocyanide)rhodium(I), $[Rh(p\text{-}RC_6H_4NC)_4]^+$, the K_D and K_T values increase in the order R=Cl<H<Me<MeO, which is compatible with the donor ability of the para-substituents. In addition, the rhodium(I) complexes with *t*-BuNC and *cyclo*-$C_6H_{11}NC$ as ligands (Nos. 9 and 10), whose donor ability is less than PhNC,[6] oligomerize in less extents than $[Rh(PhNC)_4]^+$. On the other hand, methyl substitution on the 2,6 positions of PhNC (Nos. 5 and 6) causes substantial decrease of the K_D and K_T values compared with the corresponding rhodium(I) complexes without substituents at these positions (Nos. 2 and 3). Such a steric effect on the 2,6 positions is consistent with a staggered configration of the ligands in the crystal structure of dimeric $[Rh(PhNC)_4^+]_2$.[2e] No appreciable oligomerization in MeCN was observed also in the rhodium(I) complexes with bulky triphenylphosphine (Nos. 7 and 8). Thus, the K_D and K_T values seem to be determined by the balance between the electronic and the steric effects of the ligands.

Kinetics and Reaction Scheme for Electron Transfer Reactions between $[RhL_4]^+$ *and* $[Fe(N\text{–}N)_3]^{3+}$. Upon mixing $[Rh(p\text{-}MeC_6H_4NC)_4]^+$ and $[Fe(phen)_3]^{3+}$ in MeCN containing 0.1 mol dm^{-3} *n*-Bu_4NClO_4 at 298 K, an intense absorption band due to the reduced iron(II) species, $[Fe(phen)_3]^{2+}$, appears at 507 nm without delay. The stoichiometry of the reaction has been established as 1:1 by the spectral titration of the iron(II) species using $[Fe(phen)_3]^{2+}$ prepared independently as a reference, as shown in Fig. 3. All the rhodium(I) complexes studied here also were readily oxidized by various iron(III) complexes, $[Fe(N\text{–}N)_3]^{3+}$, as oxidants in MeCN (Eq. 7). The oxidized rhodium-

$$[RhL_4]^+ + [Fe(N\text{–}N)_3]^{3+} \longrightarrow [RhL_4]^{2+} + [Fe(N\text{–}N)_3]^{2+} \quad (7)$$

(II) species has well been regarded as radicals,[7] and dimerizes rapidly as shown in Eq. 8.[8] Thus, electron

$$2[RhL_4]^{2+} \xrightarrow{\text{fast}} [Rh_2L_8]^{4+} \quad (8)$$

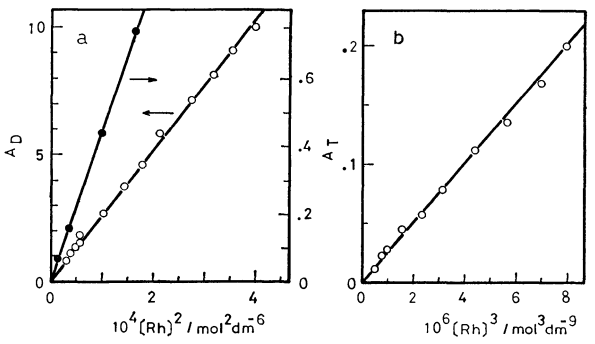

Fig. 2. Plots of (a) A_D *vs.* $[Rh]^2$ and (b) A_T *vs.* $[Rh]^3$; ● $[Rh(2,4,6\text{-}Me_3C_6H_2NC)_4]^+$, A_D at 526 nm, ○ $[Rh(PhCH_2NC)_4]^+$, A_D at 530 nm and A_T at 670 nm.

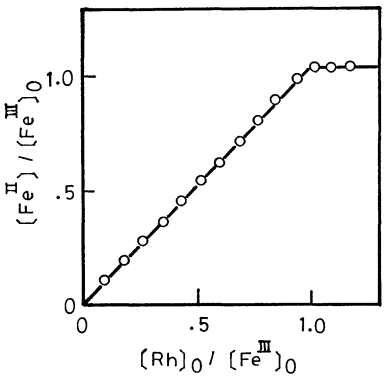

Fig. 3. Stoichiometry of the reaction between $[Rh(p\text{-}MeC_6H_4NC)_4]^+$ and $[Fe(phen)_3]^{3+}$ (1.06×10^{-4} mol dm^{-3}) in MeCN.

Table 1. Electronic transition energies of $[RhL_4^+]_n$ (n=1—3) and the equilibrium constants for the oligomer formation[a]

No.	$[RhL_4]^+$	Monomer[b]	Dimer		Trimer	
		$h\nu_M$ / eV	$h\nu_D$ / eV	K_D / mol^{-1} dm^3	$h\nu_T$ / eV	K_T / mol^{-1} dm^3
1	$[Rh(p\text{-}MeOC_6H_4NC)_4]^+$	3.08	2.20	4.3×10^2	1.75	1.3×10^2
2	$[Rh(p\text{-}MeC_6H_4NC)_4]^+$	3.05	2.20		1.76	6.2×10
3[c]	$[Rh(PhNC)_4]^+$	3.02	2.18		1.71	1.0×10
4	$[Rh(p\text{-}ClC_6H_4NC)_4]^+$	3.00	d)		d)	
5	$[Rh(2,6\text{-}Me_2C_6H_3NC)_4]^+$	3.03	d)		d)	
6	$[Rh(2,4,6\text{-}Me_3C_6H_2NC)_4]^+$	3.06	2.36	4.2×10^{-1}	d)	
7	$[Rh(p\text{-}MeOC_6H_4NC)_2(PPh_3)_2]^+$	2.97	d)		d)	
8	$[Rh(2,4,6\text{-}Me_3C_6H_2NC)_2(PPh_3)_2]^+$	3.02	d)		d)	
9	$[Rh(t\text{-}BuNC)_4]^+$	3.24	2.43	2.2×10^{-2}	d)	
10	$[Rh(cyclo\text{-}C_6H_{11}NC)_4]^+$	3.22	2.39	1.5	d)	
11	$[Rh(PhCH_2NC)_4]^+$	3.20	2.34	1.2	1.85	7.5×10^{-1}

a) In MeCN with 0.1 mol dm^{-3} *n*-Bu_4NClO_4. b) The $^1A_{1g}\rightarrow{}^1A_{2u}$ transition. c) From Ref. 2e. d) Not observed.

transfer from $[RhL_4]^+$ to $[Fe(N\text{-}N)_3]^{3+}$ is irreversible and no back electron transfer may occur.

Rates of the electron transfer reactions between $[RhL_4]^+$ and $[Fe(N\text{-}N)_3]^{3+}$ were followed by monitoring the rise of the absorbance due to $[Fe(N\text{-}N)_3]^{2+}$ in MeCN at 298 K, using a stopped flow spectrophotometer. The ionic strength was maintained constant with n-Bu_4NClO_4 (0.1 mol dm^{-3} in most cases). The reactions of $[Rh(2,4,6\text{-}Me_3C_6H_2NC)_4]^+$ and $[Rh(t\text{-}BuNC)_4]^+$ which do not oligomerize appreciably obeyed pseudo-first-order kinetics with excess amounts of either $[Fe(N\text{-}N)_3]^{3+}$ or $[RhL_4]^+$; the kinetic plots were linear over several half-lives. As typical examples, the dependences of the pseudo-first-order rate constants k_{Fe} and k_{Rh} on the concentrations of $[Fe(N\text{-}N)_3]^{3+}$ and $[Rh(2,4,6\text{-}Me_3C_6H_2NC)_4]^+$, respectively, are shown in Fig. 4. The rate constants k_{Fe} and k_{Rh} are different from each other at the same concentrations of reactants used in a large excess. In additon, k_{Rh} exhibits "saturation kinetics" with increasing the concentration of $[Rh(2,4,6\text{-}Me_3C_6H_2NC)_4]^+$, while k_{Fe} is linear against the concentration of $[Fe(N\text{-}N)_3]^{3+}$. However, the intercepts of k_{Fe} and k_{Rh} on extrapolation to [Fe]=0 and [Rh]=0, respectively, are identical, irrespective of the reactant used in excess and the ionic strength (μ=0.1 and 0.05) (Fig. 4). Such a complicated kinetics is quite different from other electron transfer reactions of transition metal complexes which show simple second-order kinetics (first-order on each reactant).[9] Furthermore, the intercept and the curveture found in Fig. 4 cannot be attributed to the reversibility of Eq. 7 in competition with the reaction in Eq. 8 since the electron transfer reaction proceeds to completion and the pseudo-first-order kinetics holds precisely under the experimental conditions in Fig. 4.

The pseudo-first-order kinetics and the complicated kinetic behavior of the pseudo-first-order rate constants in Fig. 4 may be best interpreted by assuming the following scheme for the electron transfer reaction (Eq. 7) as the rate-determining step,

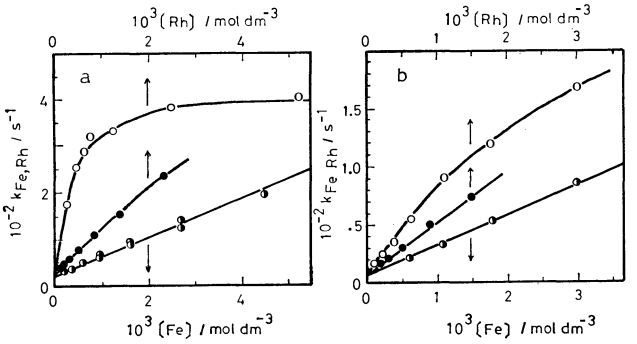

Fig. 4. Kinetics of the oxidation of $[RhL_4]^+$ (L=2,4,6-$Me_3C_6H_2NC$) with $[Fe(N\text{-}N)_3]^{3+}$; the pseudo-first-order rate constant as a function of large excess $[Fe(N\text{-}N)_3]^{3+}$ or $[RhL_4]^+$ in MeCN at 298 K; (a) N-N=phen, (b) N-N=bpy; ○ excess $[RhL_4]^+$ with 0.1 mol dm^{-3} n-Bu_4NClO_4, ● excess $[RhL_4]^+$ with 0.05 mol dm^{-3} n-Bu_4NClO_4, ◑ excess $[Fe(N\text{-}N)_3]^{3+}$ with 0.1 mol dm^{-3} n-Bu_4NClO_4.

$$[RhL_4]^+ + [Fe(N\text{-}N)_3]^{3+} \overset{K_1}{\rightleftharpoons} ([RhL_4]^+[Fe(N\text{-}N)_3]^{3+}) \xrightarrow[\text{e.t.}]{k_1} \quad (9)$$

$$([RhL_4]^+[Fe(N\text{-}N)_3]^{3+}) + [Fe(N\text{-}N)_3]^{3+} \overset{K_2}{\rightleftharpoons} ([RhL_4]^+2[Fe(N\text{-}N)_3]^{3+}) \xrightarrow[\text{e.t.}]{k_2} \quad (10)$$

$$([RhL_4]^+[Fe(N\text{-}N)_3]^{3+}) + [RhL_4]^+ \overset{K_3}{\rightleftharpoons} (2[RhL_4]^+[Fe(N\text{-}N)_3]^{3+}) \xrightarrow[\text{e.t.}]{k_3} \quad (11)$$

Scheme 1.

where e. t. represents the intramolecular electron transfer. Combination of Eq. 9 with Eqs. 10 and 11 gives the kinetic expressions of Eqs. 12 and 13, respectively,

$$k_{Fe} = \frac{k_1K_1[Fe] + k_2K_1K_2[Fe]^2}{1 + K_1[Fe] + K_1K_2[Fe]^2} \quad (12)$$

$$k_{Rh} = \frac{k_1K_1[Rh] + k_3K_1K_3[Rh]^2}{1 + K_1[Rh] + K_1K_3[Rh]^2} \quad (13)$$

for the oxidation of $[RhL_4]^+$ with $[Fe(N\text{-}N)_3]^{3+}$. When $K_1[Fe]$, $K_1[Rh] \gg 1$, Eqs. 12 and 13 are reduced to Eqs. 14 and 15, respectively.

$$k_{Fe} = \frac{k_1 + k_2K_2[Fe]}{1 + K_2[Fe]} \quad (14)$$

$$k_{Rh} = \frac{k_1 + k_3K_3[Rh]}{1 + K_3[Rh]} \quad (15)$$

The dependences of k_{Fe} and k_{Rh} on [Fe] and [Rh] in Fig. 4 are well reproduced by Eqs. 14 and 15, respectively, with the rate and the equilibrium constants listed in Table 2. The k_2, K_2, k_3, and K_3 in Eqs. 14 and 15 will be vanished at the intercepts of k_{Fe} and k_{Rh} (extrapolation to [Fe], [Rh]=0 in Fig. 4), which yield the same intramolecular electron transfer rate constant k_1 in Scheme 1. Such an intramolecular rate constant k_1 should be independent of the ionic strength of the media,[10] in accordance with the results in Fig. 4. On the other hand, the equilibrium constants K_1, K_2, and K_3 depended on the ionic strength of the media. At the ionic strength μ=0.1, the equilibrium constant K_1 was too high to be determined ($K_1[Fe]$, $K_1[Rh] \gg 1$; $K_1 \gg 1 \times 10^4$ mol^{-1} dm^3), and Eqs. 14 and 15 were applied to the results in Fig. 4. When the ionic strength μ was reduced from 0.1 to 0.05, however, the k_{Fe} values decreased to reach zero with decreasing [Fe] in the lower concentrations ($>4.0 \times 10^{-4}$ mol dm^{-3}) in contrast with the results at μ=0.1 in Fig. 4. The K_1 values at μ=0.05 were determined by fitting the data to Eq. 12,[11] and also listed in Table 2. The rate and the equilibrium constants were evaluated also for the reaction of $[Rh(t\text{-}BuNC)_4]^+$ with $[Fe(phen)_3]^{3+}$ (Table 2).

The large equilibrium constants K_1, K_2, and K_3 (Table 2) indicate the exceptionally high affinity of the cationic oxidants towards the cationic reductants in MeCN. Such cation-cation interactions are supported by the salt effects on the equilibrium constants since if the ions are of the same sign, decreasing the ionic strength makes the equilibrium constants de-

TABLE 2. RATE AND EQUILIBRIUM CONSTANTS FOR THE ELECTRON TRANSFER REACTIONS BETWEEN $[RhL_4]^+$ AND $[Fe(N\text{–}N)_3]^{3+}$ IN MeCN AT 298 K[a]

$[RhL_4]^+ + [Fe(N\text{–}N)_3]^{3+}$							
L	N-N	k_1 / s^{-1}	K_1[b] / $mol^{-1}\,dm^3$	k_2 / s^{-1}	K_2 / $mol^{-1}\,dm^3$	k_3 / s^{-1}	K_3 / $mol^{-1}\,dm^3$
2,4,6-$Me_3C_6H_2NC$	bpy	2.7	7.8×10^3	d)		2.7×10^2	3.5×10^2
2,4,6-$Me_3C_6H_2NC$	phen	2.0×10	1.6×10^4	e)		4.6×10^2	2.2×10^3
t-BuNC	phen	4.0×10	c)	6.2×10^2	1.3×10^3	9.7×10^2	2.9×10^3

a) With 0.1 mol dm^{-3} *n*-Bu_4NClO_4 unless otherwise noted. b) With 0.05 mol dm^{-3} *n*-Bu_4NClO_4. With 0.1 mol dm^{-3} *n*-Bu_4NClO_4, $K \gg 1\times10^4$ $mol^{-1}\,dm^3$ (see text). c) Not determined. d) $k_2K_2 = 2.8\times10^4$ $mol^{-1}\,dm^3\,s^{-1}$. e) $k_2K_2 = 4.3\times10^4$ $mol^{-1}\,dm^3\,s^{-1}$.

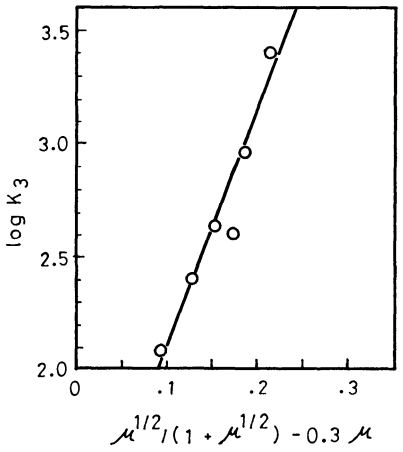

Fig. 5. Salt effect on the equilibrium constant K_3 for the oxidation of $[Rh(2,4,6\text{-}Me_3C_6H_2NC)_4]^+$ with $[Fe(phen)_3]^{3+}$; the solid line is drawn with the theoretical slope, $8A = 11$ in Eq. 16, see text.[14]

crease,[12] as observed for K_1 (Table 2). To confirm this quantitatively, the salt effect on K_3 was examined in detail for the reaction of $[Rh(2,4,6\text{-}Me_3C_6H_2NC)_4]^+$ with $[Fe(phen)_3]^{3+}$ in MeCN at various ionic strengths adjusted by *n*-Bu_4NClO_4. The theoretical salt effect on K_3 may be given by Eq. 16 when the activity coefficients of ions are evaluated from the Davies equation,[13]

$$\log K_3 = \log K_3^0 + 2z_Az_BA(\mu^{1/2}/(1+\mu^{1/2}) - 0.3\,\mu) \qquad (16)$$

where K_3^0 is the equilibrium constant at $\mu=0$, z_A and z_B are the charges of $([RhL_4]^+[Fe(phen)_3]^{3+})$ and $[RhL_4]^+$, respectively; $z_A=4$, $z_B=1$, and A is the Debye-Hückel coefficient.[14] The experimental salt effect on K_3 shows reasonable agreement with the theoretical slope of Eq. 16 ($2z_Az_BA=11$) as shown in Fig. 5. Thus, Scheme 1 can account for the pseudo-first-order kinetics, the complex dependences of k_{Fe} and k_{Rh} on [Fe] and [Rh], respectively (Fig. 4), and the salt effects, which otherwise would be impossible to be explained together. The high affinity between the cationic oxidants and the cationic reductants (Table 2) is unprecedented,[15] and at present the origin of the interaction is not clear. However, the similar affinity of $[RhL_4]^+$ towards 2,2′-bipyridine (bpy) observed in the ligand substitution reactions of $[RhL_4]^+$ with bpy[16] suggests that the interaction between $[RhL_4]^+$ and $[Fe(N\text{–}N)_3]^{3+}$ could be mediated by the N–N ligand of $[Fe(N\text{–}N)_3]^{3+}$.

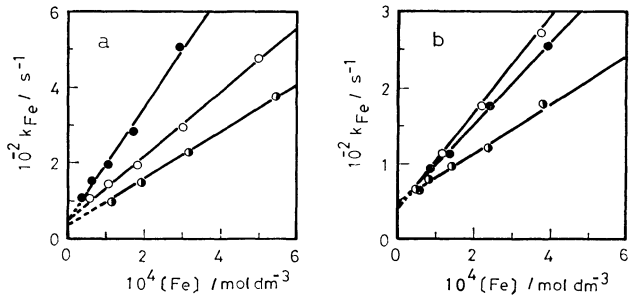

Fig. 6. Plots of the pseudo-first-order rate constant k_{Fe} for the reactions of $[RhL_4]^+$ with (a) large excess $[Fe(phen)_3]^{3+}$ and (b) $[Fe(bpy)_3]^{3+}$ in MeCN containing 0.1 mol dm^{-3} *n*-Bu_4NClO_4 at 298 K; ○ $[Rh(p\text{-}MeC_6H_4NC)_4]^+$, ● $[Rh(PhCH_2NC)_4]^+$, ◑ $[Rh(PhNC)_4]^+$.

Electron Transfer Rate Constants in the $[RhL_4]^+$ Monomer–$[Fe(N\text{–}N)_3]^{3+}$ System. Under the conditions of $K_2[Fe] \ll 1$, Eq. 14 can be reduced to Eq. 17, which predicts a linear relation between k_{Fe} and [Fe]. Plots

$$k_{Fe} = k_1 + k_2K_2[Fe] \qquad (17)$$

of the pseudo-first-order rate constant k_{Fe} against the concentrations of $[Fe(phen)_3]^{3+}$ and $[Fe(bpy)_3]^{3+}$ are illustrated in Figs. 6a and 6b, respectively. The concentrations of the Rh^I complexes used in the reactions were between 3.0×10^{-6} and 3.2×10^{-4} mol dm^{-3}, except for $[Rh(p\text{-}MeOC_6H_4NC)_4]^+$, $[Rh(p\text{-}MeC_6H_4NC)_4]^+$, and $[Rh(PhNC)_4]^+$ whose concentrations were less than 1×10^{-5} mol dm^{-3} in order to avoid the appreciable oligomerization in the higher concentrations. Under such concentrations, only monomeric $[RhL_4]^+$ may be involved in the electron transfer reactions with $[Fe(N\text{–}N)_3]^{3+}$. The electron transfer rate constants of k_1 and k_2K_2 for the $[RhL_4]^+$–$[Fe(N\text{–}N)_3]^{3+}$ system, obtained from the intercept and the slope of the plots of Eq. 17, respectively, are listed in Table 3. The k_3 and K_3 values have not been determined except for the Rh^I complexes in Table 2, because the reactions of the other Rh^I complexes in a large excess ($>1\times10^{-3}$ mol dm^{-3}) were too fast to follow by the stopped flow technique.

It is noteworthy that the k_1 value is rather independent of the ligands except for the sterically hindered 2,4,6-$Me_3C_6H_2NC$, *t*-BuNC, and PPh_3, and that the k_2K_2 value is more or less in parallel with the k_1 value. Such an insensitive dependence of k_1 as well as k_2K_2 on the diversed type ligands agrees with the

Table 3. Rate constants of electron transfer reactions between a series of rhodium(I) isocyanide complexes and $[Fe(N-N)_3]^{3+}$ in MeCN[a]

$[RhL_4]^+$	$[Fe(bpy)_3]^{3+}$		$[Fe(phen)_3]^{3+}$	
	k_1 / s^{-1}	k_2K_2 / $mol^{-1}\,dm^3\,s^{-1}$	k_1 / s^{-1}	k_2K_2 / $mol^{-1}\,dm^3\,s^{-1}$
$[Rh(p\text{-}MeOC_6H_4NC)_4]^+$	1.2×10^2	9.0×10^4	—	—
$[Rh(p\text{-}MeC_6H_4NC)_4]^+$	3.4×10	6.5×10^5	4.6×10	8.5×10^5
$[Rh(PhNC)_4]^+$	5.0×10	3.2×10^5	3.2×10	6.1×10^5
$[Rh(p\text{-}ClC_6H_4NC)_4]^+$	5.3×10	2.1×10^5	1.5×10^2	1.7×10^5
$[Rh(2,6\text{-}Me_2C_6H_3NC)_4]^+$	8.6×10	7.4×10^5	9.4×10	5.5×10^5
$[Rh(2,4,6\text{-}Me_3C_6H_2NC)_4]^+$	2.7	2.8×10^4	2.0×10	4.3×10^5
$[Rh(p\text{-}MeOC_6H_4NC)_2(PPh_3)_2]^+$	4.0×10	2.0×10^5	4.0×10	3.5×10^5
$[Rh(2,4,6\text{-}Me_3C_6H_2NC)_2(PPh_3)_2]^+$	3.7	8.7×10^4	6.5	1.4×10^5
$[Rh(t\text{-}BuNC)_4]^+$	5.0	5.3×10^5	4.0×10	8.0×10^5
$[Rh(cyclo\text{-}C_6H_{11}NC)_4]^+$	3.7×10	3.0×10^5	7.2×10	8.1×10^5
$[Rh(PhCH_2NC)_4]^+$	4.3×10	5.4×10^5	4.6×10	1.5×10^6

a) With 0.1 mol dm^{-3} n-Bu_4NClO_4 at 298 K.

Table 4. Rate constants of electron transfer reactions between the $[RhL_4]^+$ monomer and several oxidants and reduction potentials of the oxidants[a]

No.	Oxidants	E^0_{red} *vs.* SCE / V	$[Rh(t\text{-}BuNC)_4]^+$		$[Rh(2,4,6\text{-}Me_3C_6H_2NC)_4]^+$	
			k_1 / s^{-1}	k_2K_2 / $mol^{-1}\,dm^3\,s^{-1}$	k_1 / s^{-1}	k_2K_2 / $mol^{-1}\,dm^3\,s^{-1}$
1′	$[Fe(5\text{-}NO_2phen)_3]^{3+}$	1.27	3.8×10	8.1×10^4	1.1×10^2	4.0×10^4
2′	$[Fe(5\text{-}Clphen)_3]^{3+}$	1.17	3.8×10	3.8×10^5	1.3×10	2.1×10^5
3′	$[Fe(phen)_3]^{3+}$	1.07	4.0×10	3.6×10^5	2.0×10	4.3×10^4
4′	$[Fe(bpy)_3]^{3+}$	1.06	5.0	5.3×10^4	2.7	2.8×10^4
5′	$[Fe(4,7\text{-}Ph_2phen)_3]^{3+}$	1.01	3.5	7.5×10^4	4.6	1.3×10^4
6′	$[Co(bpy)_3]^{3+}$	0.31	1.5×10^{-6}	1.9×10^{-4}	1.0×10^{-6}	1.9×10^{-4}

a) In MeCN containing 0.1 mol dm^{-3} n-Bu_4NClO_4 at 298 K.

HOMO energy of the nearly nonbonding d_{z^2} level of the Rh^I complexes which may be insensitive to the difference of ligands.[17]

Kinetic studies were performed also for the oxidation of fixed $[RhL_4]^+$ (L=*t*-BuNC, 2,4,6-$Me_3C_6H_2NC$) with various oxidants; $[Fe(5\text{-}NO_2phen)_3]^{3+}$, $[Fe(5\text{-}Clphen)_3]^{3+}$, $[Fe(phen)_3]^{3+}$, $[Fe(bpy)_3]^{3+}$, $[Fe(4,7\text{-}Ph_2phen)_3]^{3+}$, and $[Co(bpy)_3]^{3+}$. The electron transfer rates were measured as described above, except for the oxidation with $[Co(bpy)_3]^{3+}$ which was followed by the decay of the 440 nm and 459 nm bands of $[Rh(t\text{-}BuNC)_4]^+$ and $[Rh(2,4,6\text{-}Me_3C_6H_2NC)_4]^+$, respectively ($^1A_{1g}\rightarrow{}^3A_{2u}$ transition), in the presence of excess $[Co(bpy)_3]^{3+}$ (8.9×10^{-4}—1.0×10^{-2} mol dm^{-3}) using a conventional spectrophotometer; the reaction rate was much slower than that with $[Fe(N-N)_3]^{3+}$. The pseudo-first-order rate constant k_{Co} in the presence of excess $[Co(bpy)_3]^{3+}$ also showed a linear relation with the Co concentration. The rate constants k_1 and k_2K_2 determined from the intercept and the slope of the linear plots of k_{Fe} *vs.* [Fe] and k_{Co} *vs.* [Co] are listed in Table 4. The reduction potentials of the oxidants determined by cyclic voltammetry in MeCN also are listed in Table 4 for comparison. There can be seen a trend that the electron transfer rate constants k_1 and k_2K_2 decrease with decreasing the reduction potentials of the oxidants; this is particularly the case in $[Co(bpy)_3]^{3+}$.

Electron Transfer Rate Constants in the $[RhL_4]^+$ Oligomer–$[Co(bpy)_3]^{3+}$ System. As described in the foregoing section, high concentration solutions of $[Rh(PhNC)_4]^+$ ($>1\times10^{-3}$ mol dm^{-3}) exhibit an absorption band attributable to the dimer, $[Rh_2(PhNC)_8]^{2+}$. The rate of reaction of $[Rh(PhNC)_4]^+$ with excess $[Co(bpy)_3]^{3+}$ under such conditions was measured by monitoring the decay of an absorbance due to the dimer at 600 nm, as shown by the open circles in Fig. 7. This decay curve can be expressed by Eq. 18 as plotted by the closed circles (Fig. 7),

$$A_D^{-1/2} = at + b \qquad (18)$$

where a and b are constants as 6.4×10^{-4} s^{-1} and 1.21, respectively. On the other hand, the absorbance A_D is proportional to the square of the total amount of Rh under the experimental conditions stated in Fig. 7; A_D (at 600 nm) $=1.20\times10^5$ $[Rh]^2$. Thus, Eq. 18 may alternatively be formulated as the pseudo-second-order rate law shown in Eq. 19. It was confirmed that the decay of the absorbance due to monomeric $[Rh(PhNC)_4]^+$ at 462 nm with time also followed Eq. 19, yielding the same value of k_{Co}. Moreover, the kinetics of the oxidation of $[Rh(p\text{-}MeC_6H_4NC)_4]^+$ (4.0×10^{-4} mol dm^{-3})[18] with $[Co(bpy)_3]^{3+}$ also followed Eq. 19, which reveals that the oxidation of the Rh^I

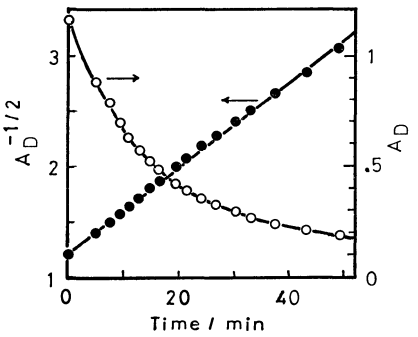

Fig. 7. Decay of the absorbance at 600 nm with time in the reaction of $[Rh_2(PhNC)_8]^{2+}$ (2.5×10^{-3} mol dm^{-3} as $[Rh(PhNC)_4]^+$) with large excess $[Co(bpy)_3]^{3+}$ (2.0×10^{-2} mol dm^{-3}) in MeCN containing 0.1 mol dm^{-3} n-Bu_4NClO_4 at 298 K (○), and the second-order plot as $A_D^{-1/2}$ *vs.* time (●), see text.

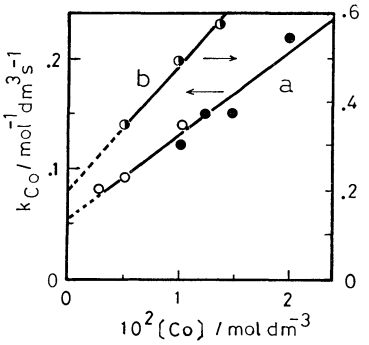

Fig. 8. Dependence of the pseudo-second-order rate constant k_{Co} on the concentration of $[Co(bpy)_3]^{3+}$ for the oxidation of (a) $[Rh(PhNC)_4]^+$ and (b) $[Rh(p\text{-}MeC_6H_4NC)_4]^+$ (4.0×10^{-4} mol dm^{-3}) in MeCN containing 0.1 mol dm^{-3} n-Bu_4NClO_4 at 298 K; ●,◑ determined from the decay of the dimer band at 600 nm, ○ determined from the decay of the monomer band at 459 nm.
The ratio of [Co]/[Rh]=10 for $[Rh(PhNC)_4]^+$.

$$-d[Rh]/dt = k_{Co}[Rh]^2 \quad (19)$$

complexes proceeds through the dimers present in solution.

The pseudo-second-order rate constants, k_{Co}/mol^{-1} dm^3 s^{-1}, obtained for the oxidation of $[Rh(PhNC)_4]^+$ and $[Rh(p\text{-}MeC_6H_4NC)_4]^+$ show linear dependences on the concentration of $[Co(bpy)_3]^{3+}$, as shown in Fig. 8. Thus, the rate constant k_{Co} is written by Eq. 20. The kinetic formulation of Eq. 20 for the dimer oxidation is analogous to that for the monomer oxidation in Eq. 17. Then, the reaction scheme for the oxidation of $[Rh(PhNC)_4]^+$ and $[Rh(p\text{-}MeC_6H_4NC)_4]^+$ with $[Co(bpy)_3]^{3+}$ may be given by combining the scheme for the monomer oxidation (Scheme 1) with the corresponding scheme for the dimer oxidation as follows.

$$k_{Co}/\text{mol}^{-1}\,\text{dm}^3\,\text{s}^{-1} = k_a + k_b[Co] \quad (20)$$

$$[RhL_4]^+ + [RhL_4]^+ \overset{K_D}{\rightleftharpoons} [Rh_2L_8]^{2+} \quad (21)$$

$$[RhL_4]^+ + [Co(bpy)_3]^{3+} \overset{K_{1M}}{\rightleftharpoons} ([RhL_4]^+[Co(bpy)_3]^{3+}) \xrightarrow[\text{e.t.}]{k_{1M}} \quad (22)$$

$$([RhL_4]^+[Co(bpy)_3]^{3+}) + [Co(bpy)_3]^{3+} \overset{K_{2M}}{\rightleftharpoons} ([RhL_4]^+2[Co(bpy)_3]^{3+} \xrightarrow[\text{e.t.}]{k_{2M}} \quad (23)$$

$$[Rh_2L_8]^{2+} + [Co(bpy)_3]^{3+} \overset{K_{1D}}{\rightleftharpoons} ([Rh_2L_8]^{2+}[Co(bpy)_3]^{3+}) \xrightarrow[\text{e.t.}]{k_{1D}} \quad (24)$$

$$([Rh_2L_8]^{2+}[Co(bpy)_3]^{3+}) + [Co(bpy)_3]^{3+} \overset{K_{2D}}{\rightleftharpoons} ([Rh_2L_8]^{2+}2[Co(bpy)_3]^{3+}) \xrightarrow[\text{e.t.}]{k_{2D}} \quad (25)$$

Scheme 2.

The second and the third steps in Scheme 2 are the same as Eqs. 9 and 10 in Scheme 1 for the monomer oxidation, respectively. The observed pseudo-second-order kinetics in excess $[Co(bpy)_3]^{3+}$ shows that the dimer oxidation (Eqs. 24 and 25) is much faster than the corresponding monomer oxidation (Eqs. 22 and 23); $k_{1D}\gg k_{1M}$, $k_{2D}\gg k_{2M}$. According to Scheme 2, the pseudo-second-order rate constant, k_{Co}/mol^{-1} dm^3 s^{-1}, is given by Eq. 26 under the conditions of $[Rh_2L_8]^{2+}\ll[RhL_4]^+$. When the equilibrium constants for the complex formation with $[Co(bpy)_3]^{3+}$ are assumed to be the same between the monomer and the dimer, *i.e.*, $K_{1D}=K_{1M}$ and $K_{2D}=K_{2M}$, Eq. 26 has an equivalent form to Eq. 12 derived from Scheme 1. Then, Eq. 26 is reduced to Eq. 27 which is analogous to Eq. 17 for the oxidation of monomeric $[RhL_4]^+$ with excess $[Fe(N\text{–}N)_3]^{3+}$. The electron transfer rate constants for the dimer, k_{1D} and $k_{2D}K_{2D}$, were thus obtained from the relations $k_a=k_{1D}K_D$ and $k_b=k_{2D}K_{2D}K_D$, respectively, using the k_a and k_b values in Eq. 20 as well as the K_D values (Table 1), and listed in Table 5. In spite of the apparant difference in the reactivity between $[Rh(PhNC)_4]^+$ and $[Rh(p\text{-}MeC_6H_4NC)_4]^+$ as seen in Fig. 8, the rate constants k_{1D} and $k_{2D}K_{2D}$ are almost the same for both dimers. This is analogous result to the oxidation of the corresponding monomers (Table 3).

$$k_{Co}/\text{mol}^{-1}\,\text{dm}^3\,\text{s}^{-1} = \frac{k_{1D}K_DK_{1D}[Co]+k_{2D}K_DK_{1D}K_{2D}[Co]^2}{1+K_{1M}[Co]+K_{1M}K_{2M}[Co]^2} \quad (26)$$

$$k_{Co}/\text{mol}^{-1}\,\text{dm}^3\,\text{s}^{-1} = K_D(k_{1D}+k_{2D}K_{2D}[Co]) \quad (27)$$

Table 5. Electron transfer rate constants for the oxidation of $[RhL_4^+]_n$ (n=2 and 3) with $[Co(bpy)_3]^{3+}$ a)

	k_{1D} / s^{-1}	$k_{2D}K_{2D}$ / mol^{-1} dm^3 s^{-1}
$[Rh_2(PhNC)_8]^{2+}$	1.6×10^{-3}	2.2×10^{-1}
$[Rh_2(p\text{-}MeC_6H_4NC)_8]^{2+}$	1.5×10^{-3}	2.2×10^{-1}
	k_{1T}/s^{-1}	
$[Rh_3(p\text{-}MeOC_6H_4NC)_{12}]^{3+}$	5.4×10^{-1}	—

a) In MeCN with 0.1 mol dm^{-3} n-Bu_4NClO_4 at 298 K.

The kinetics of the oxidation of $[Rh(p\text{-}MeOC_6H_4NC)_4]^+$ with excess $[Co(bpy)_3]^{3+}$ was third-order in the range of the Rh concentration 1.5×10^{-4}—4.8×10^{-4} mol dm^{-3}, as expressed by Eq. 28; the third-order plots were obtained as a linear relation between A_D^{-1} *vs.* time, since $A_D=\varepsilon_D K_D[Rh]^2$. This indicates that

$$-d[Rh]/dt = k_{Co}[Rh]^3 \quad (28)$$

the oxidation occurs through trimeric $[Rh_3(p\text{-}MeOC_6H_4NC)_{12}]^{3+}$, the concentration of which is proportional to $[Rh]^3$. The pseudo-third-order rate constant k_{Co}/mol^{-2} dm^6 s^{-1} was constant irrespective of the concentration of $[Co(bpy)_3]^{3+}$ in the range of 1.4×10^{-3}—3.0×10^{-3} mol dm^{-3}, and thus k_{Co}/mol^{-2} dm^6 s^{-1}=$k_{1T}K_DK_T$. Using the K_D and K_T values in Table 1, the intramolecular electron transfer rate constant of the trimer, k_{1T}, is determined as 5.4×10^{-1} (Table 5).

Comparison of Intramolecular Electron Transfer Rate Constants between the $[RhL_4]^+$ Monomers and the Oligomers. For a particular $[RhL_4]^+$, the logarithm of the intramolecular electron transfer rate constant, $\log k_1$, varies with the reduction potentials of the oxidants (Table 4), as illustrated in Fig. 9a. Although the number of the oxidants used in this study is limited, the slope of the correlation can be expressed by Eq. 29 which is equivalent to the Marcus relation expressed by Eq. 30.[5,19]

$$\log k_1 = 8.5E^0_{red} + \text{Const} \quad (29)$$

$$\Delta G_1^* = 0.5\Delta G^0 + \text{Const} \quad (30)$$

For a given oxidant, $[Co(bpy)_3]^{3+}$, the intramolecular electron transfer rate constant k_1 of $[RhL_4^+]_n$ (n=1—3) increases in the order monomer<dimer<trimer (Tables 4 and 5). This order is in parallel with the HOMO energy level from which electron is removed; monomer<dimer<trimer, as illustrated in Fig. 10. The energy difference between the monomer and the dimer (ΔE_D) as well as the trimer (ΔE_T)

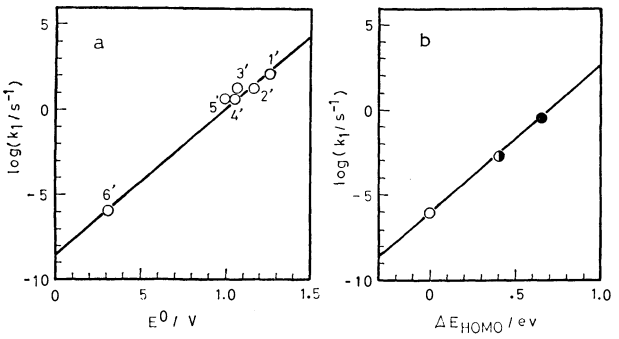

Fig. 9. Marcus plot for the intramolecular electron transfer rate constant k_1 of $[RhL_4^+]_n$ (n=1—3).
(a) Plot of log k_1 for the oxidation of $[Rh(2,4,6\text{-}Me_3C_6H_2NC)_4]^+$ *vs.* the reduction potentials of the oxidants, E^0_{red}, numbers refer to the oxidants in Table 4. (b) Plot of log k_1 for the oxidation of $[RhL_4^+]_n$ with $[Co(bpy)_3]^{3+}$ *vs.* the difference in the HOMO energies, ΔE_{HOMO}, between the $[RhL_4]^+$ oligomers and the monomer; ○ $[RhL_4]^+$ (L=2,4,6-$Me_3C_6H_2NC$, *t*-BuNC), ◑ $[RhL_4^+]_2$ (L=PhNC, *p*-MeC_6H_4NC), ● $[RhL_4^+]_3$ (L=*p*-$MeOC_6H_4NC$). The lines are arbitrarily drawn with the Marcus slope of 8.5 to show the agreement,[19] see text.

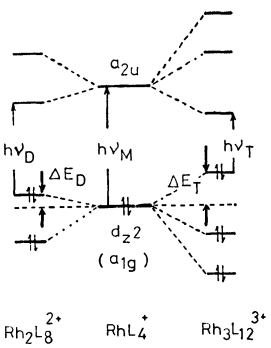

Fig. 10. Energy diagram for the $[RhL_4]^+$ monomer, the dimer, and the trimer.[2e]

is estimated from the electronic transition energies listed in Table 1, using Eq. 31. A plot of $\log k_1$ *vs.*

$$\Delta E_D = (h\nu_M - h\nu_D)/2, \quad \Delta E_T = (h\nu_M - h\nu_T)/2 \quad (31)$$

ΔE_{HOMO} thus obtained shows a linear relation as shown in Fig. 9b, from which the following equation is obtained. Thus, the Marcus slope in Eq. 29 can be

$$\log k_1 = 8.5\Delta E_{HOMO} + \text{Const} \quad (32)$$

applied also to the difference of the reactivity among the $[RhL_4]^+$ monomer, the dimer, and the trimer. The constancy of k_1 for the $[RhL_4]^+$ monomers with different ligands also accords with Eq. 32, since the HOMO energies are constant irrespective of the ligands.[17]

Summary and Conclusions. Square-planar rhodium(I) isocyanide complexes can interact with one another through the d_{z^2} HOMO orbital, yielding the dimer and the trimer. The strength of the rhodium-rhodium interaction which reflects the magnitude of the equilibrium constants for the oligomer formation is determined by the balance between electronic and steric effects of the ligands. Such availability of the interacting HOMO gives a novel feature in the electron transfer reactions. A series of $[RhL_4]^+$ forms strongly associative precursor complexes with oxidants, $[Fe(N\text{-}N)_3]^{3+}$ and $[Co(bpy)_3]^{3+}$, prior to the electron transfer. Since the oxidant or the $[RhL_4]^+$ cation can interact from both sides of the square-planar $[RhL_4]^+$, not only the 1:1 complex but also the 1:2 and the 2:1 complexes are formed between the $[RhL_4]^+$ and the oxidants. The rate constants of the intramolecular electron transfer in the precursor complexes are readily separated from the observed rate constants and largely depend on the energy difference between the HOMO of the $[RhL_4^+]_n$ (n=1—3) and the LUMO of the oxidants represented by the reduction potentials, following the Marcus relation. As such, the rate constants of intramolecular electron transfer of $[RhL_4^+]_n$ increase in the order monomer<dimer<trimer with increasing the HOMO energy.

Experimental

Materials. A series of tetrakis(isocyanide)- and bis(isocyanide)bis(triphenylphosphine)rhodium(I) perchlorates used in this study was prepared as described elsewhere.[20] 2, 2′-Bipyridine (bpy), 1,10-phenanthroline monohydrate

Table 6. Absorption spectral data for $[RhL_4^+]_n$ (n=1—3) in MeCN[a]

No.	$^1A_{1g}\rightarrow{}^1E_u$	$^1A_{1g}\rightarrow{}^3E_u$	$^1A_{1g}\rightarrow{}^1A_{2u}$	$^1A_{1g}\rightarrow{}^3A_{2u}$	Dimer	Trimer
1	327(25.0)	c)	403(3.15)	459(0.87)	564(4.77)	710(7.16)[e]
2	340(111)	c)	407(5.83)	462(0.85)	563(8.93)	705(13.4)[e]
3[b]	335(49.1)	c)	411(5.94)	466(0.65)	568(10.5)	c)
4	337(29.8)	c)	413(2.94)	460(0.65)	c)	c)
5	336(49.3)	c)	409(4.90)	459(0.92)	c)	c)
6	342(51.0)	c)	405(5.13)	478(0.45)	526(10.3)[d]	c)
7	345(21.9)	c)	418(3.87)	472(0.32)	c)	c)
8	330(20.5)	c)	411(4.77)	440(0.35)	c)	c)
9	309(25.3)	336(4.03)	383(10.4)	441(0.34)	510(20.8)[d]	c)
10	312(27.8)	340(3.40)	385(9.33)	443(0.40)	518(18.7)[d]	c)
11	311(35.0)	338(4.22)	387(11.0)		530(22.0)[d]	670(33.0)[e]

a) Band positions are given in nm; $\varepsilon\times10^{-3}$ values in parentheses; the number of compounds are listed in Table 1. b) Taken from Ref. 2e. c) Not observed. d) Estimated from the relation $\varepsilon_T=1.5\varepsilon_D$.

(phen), and substituted 1,10-phenanthroline (5-NO_2phen, 5-Clphen, 4,7-Ph_2phen) were obtained from Wako Pure Chemicals. The $[Fe(N\text{–}N)_3]X_2$ complexes (X=ClO_4 or PF_6; N–N=bpy, phen, 5-NO_2phen, 5-Clphen, and 4,7-Ph_2phen) were obtained according to the literature method.[21] The iron(III) complexes were synthesized as the sulfate by oxidation of the corresponding iron(II) complexes with ceric ammonium sulfate in concentrated sulfic acid. Of those, $[Fe(5\text{-}NO_2phen)_3](ClO_4)_3$ was obtained by the careful addition of 0.1 mol dm^{-3} perchloric acid to the oxidized solution, and the hexafluorophosphate salts, $[Fe(phen)_3](PF_6)_3$ and $[Fe(bpy)_3](PF_6)_3$, and the other perchlorate salts were obtained by the addition of NH_4PF_6 and $NaClO_4$, respectively. The $[Co(bpy)_3](PF_6)_3$ complex was prepared by refluxing a 30% methanol solution containing pentaamminechlorocobalt(III) chloride, $[Co(NH_3)_5Cl]Cl_2$,[22] and 2,2′-bipyridine, followed by the addition of NH_4PF_6 as described elsewhere.[23] Recrystallization was performed from hot water two times. Reagent grade acetonitrile (Wako Pure Chemicals) was purified by the standard procedure,[24] followed by redistillation from diphosphorous pentaoxide.

Oligomer Formation of $[RhL_4]^+$. Electronic absorption spectra were measured with a Union SM-401 spectrophotometer, using a 10 or 1 mm cell placed in a compartment thermostated at 298 K. Absorption maxima observed for the $[RhL_4]^+$ monomers and oligomers as well as their assignment are listed in Table 6. Equilibrium constants for the oligomer formation were determined from the change of absorbances of the $[RhL_4]^+$ oligomers as a function of the total concentration in MeCN (1×10^{-4}—1×10^{-2} mol dm^{-3}) containing 0.1 mol dm^{-3} n-Bu_4NClO_4 at 298 K. The oligomer formation of $[Rh(p\text{-}ClC_6H_4NC)_4]^+$ has not been observed in the electronic spectra because of the limited solubility in MeCN ($<2\times10^{-4}$ mol dm^{-3}). There has been found no evidence also for oligomerization of the mixed ligands rhodium(I) complexes, $[RhL_2(PPh_3)_2]^+$ (L=p-$MeOC_6H_4NC$ and 2,4,6-$Me_3C_6H_2NC$), even in nearly saturated solutions.

Electron Transfer Reactions. Acetonitrile solutions of the $[RhL_4]^+$ complexes as well as oxidants ($[Fe(N\text{–}N)_3]^{3+}$ and $[Co(bpy)_3]^{3+}$) were freshly prepared before use. The reactions were carried out at 298 K under the conditions with either the rhodium(I) complex or the oxidant in a large excess. Rates of the reactions between $[RhL_4]^+$ and $[Fe(N\text{–}N)_3]^{3+}$ were measured by monitoring the rise of absorbances due to $[Fe(N\text{–}N)_3]^{2+}$ (λ_{max}: 520 nm for $[Fe(bpy)_3]^{2+}$, 507 nm for $[Fe(phen)_3]^{2+}$, 510 nm for $[Fe(5\text{-}NO_2phen)_3]^{2+}$ and $[Fe(5\text{-}Clphen)_3]^{2+}$, and 530 nm for $[Fe(4,7\text{-}Ph_2phen)_3]^{2+}$),[25] by using a Union RA-103 stopped flow spectrophotometer. The ionic strength of the reaction medium was adjusted to 0.1 with n-Bu_4NClO_4 other than the cases to examine the effect of ionic strengths on the reaction. Rates of the reactions between $[RhL_4]^+$ and $[Co(bpy)_3]^{3+}$ were measured by monitoring the decay of the absorption band ($^1A_{1g}\rightarrow{}^3A_{2u}$) of $[RhL_4]^+$ listed in Table 6 by using a Union SM-401 spectrophotometer.

Cyclic Voltammetry. The standard reduction potentials of $[Fe(N\text{–}N)_3]^{3+}$ and $[Co(bpy)_3]^{3+}$ were measured by cyclic voltammetry on a Hokuto Denko Model HA-301 potentiostat/galvanostat. The experiments were carried out in MeCN containing 0.1 mol dm^{-3} n-Bu_4NClO_4 as a supporting electrolyte, using a platinum working electrode and a saturated NaCl calomel reference electrode. The scan rates were varied in the 20—500 mV s^{-1} range. The separation of cathodic and anodic peaks was 62 mV at the scan rate of 20 mV s^{-1} which is very close to the theoretical separation of 59 mV s^{-1} for a reversible one-electron process.[26] Attempts to measure the E^0 values for the $[RhL_4]^{+/2+}$ couple in MeCN by cyclic voltammetry have been unsuccessful; the anodic oxidation of the $[RhL_4]^+$ complexes was irreversible and no cathodic wave on the reverse scan was observed at various sweep rate between 100 and 900 mV s^{-1}.[8]

References

1) A. W. Maverick and H. B. Gray, *Pure Appl. Chem.*, **52**, 2339 (1980); H. B. Gray, K. R. Mann, N. S. Lewis, J. A. Thich, and R. M. Richma, *Adv. Chem. Ser.*, **168**, 44 (1978); I. S. Sigal, K. R. Mann, and H. B. Gray, *J. Am. Chem. Soc.*, **102**, 7252 (1980); A. W. Maverick and H. B. Gray, *ibid.*, **103**, 1298 (1981); K. R. Mann and H. B. Gray, *Adv. Chem. Ser.*, **173**, 225 (1979).

2) a) K. R. Mann, J. G. Gordon II, and H. B. Gray, *J. Am. Chem. Soc.*, **97**, 3553 (1975); b) N. S. Lewis, K. R. Mann, J. G. Gordon II, and H. B. Gray, *ibid.*, **98**, 7461 (1976); K. Kawakami, M. Haga, and T. Tanaka, *J. Organomet. Chem.*, **60**, 363 (1973); d) A. L. Balch, *J. Am. Chem. Soc.*, **98**, 8049 (1976); e) K. R. Mann, N. S. Lewis, R. M. Williams, H. B. Gray, and J. G. Gordon II, *Inorg. Chem.*, **17**, 828 (1978); f) K. Kawakami, M. Okajima, and T. Tanaka, *Bull. Chem. Soc. Jpn.*, **51**, 2327 (1978).

3) M. Haga, K. Kawakami, and T. Tanaka, *Inorg. Chim. Acta*, **12**, 93 (1975), **15**, 1946 (1976); Y. Ohtani, M. Fujimoto, and A. Yamagishi, *Bull. Chem. Soc. Jpn.*, **50**, 1453 (1977); S. Carra and R. Ugo, *Inorg. Chim. Acta Rev.*, **1**, 49 (1967); J. P. Collman and W. R. Ropper, *Adv. Organomet. Chem.*,

7, 53 (1968); A. J. Hart-Davis and W. A. G. Graham, *Inorg. Chem.*, **9**, 2658 (1970); S. Otsuka and K. Ataka, *Bull. Chem. Soc. Jpn.*, **50**, 1118 (1977); R. Kuwae, T. Tanaka, and K. Kawakami, *ibid.*, **52**, 437 (1979).

4) F. A. Cotton and G. Wilkinson, "Advanced Inorganic Chemistry," 4th ed, John Wiley & Sons Inc., New York, (1980), Chap. 30, and references cited therein.

5) R. A. Marcus, *Ann. Rev. Phys. Chem.*, **15**, 155 (1964); *J. Phys. Chem.*, **72**, 891 (1968); **67**, 853 (1963).

6) The ionization potential of alkyl isocyanide (*cyclo*-$C_6H_{11}NC$=11.0 eV, *n*-BuNC=11.1 eV) is generally higher than that of phenyl isocyanide (PhNC=9.50 eV); V. Y. Young and K. L. Cheng, *J. Elect. Spect. Relat. Phenom.*, **9**, 317 (1976).

7) T. L. Kelly and J. F. Endicott, *J. Am. Chem. Soc.*, **94**, 1797 (1972); B. B. Wayland and A. R. Newman, *ibid.*, **101**, 6472 (1979); H. Ogoshi, J. Setsune, and Z. Yoshida, *ibid.*, **99**, 3869 (1977).

8) The instability of the oxidized rhodium(II) species is shown by the cyclic voltammetry which reveals the irreversible anodic oxidation of rhodium(I) complexes; S. Fukuzumi, N. Nishizawa, and T. Tanaka, *Bull. Chem. Soc. Jpn.*, **55**, 2892 (1982).

9) M. Chou, C. Creutz, and N. Sutin, *J. Am. Chem. Soc.*, **99**, 5615 (1977); H. Taube, "Electron Transfer Reactions of Complex Ions in Solution," Academic Press, New York, (1970); W. L. Reynolds and R. W. Lummy, "Mechanisms of Electron Transfer," Ronald Press, New York, (1966).

10) J. H. Espenson, "Chemical Kinetics and Reaction Mechanisms," McGraw-Hill Inc., New York, (1981), p. 175.

11) Under the condition of $K_2[Fe] \ll 1$, Eq, 12 is reduced to the equation, $k_{Fe}=(k_1K_1[Fe]+k_2K_1K_2[Fe]^2)/(1+K_1[Fe])$, which is rewritten as the relation, $(k_{Fe}-k_2K_2[Fe])^{-1}=(k_1K_1-k_2K_2)^{-1}[Fe]^{-1}+K_1(k_1K_1-k_2K_2)^{-1}$. The equilibrium constant K_1 was determined from a linear plot of $(k_{Fe}-k_2K_2[Fe])^{-1}$ *vs.* $[Fe]^{-1}$. The k_2K_2 value was estimated from Eq. 17 for the higher concentration of Fe.

12) P. W. Atkins, "Physical Chemistry," W. H. Freeman and Comp, San Francisco, (1978), p. 914.

13) C. Davies, "Ion Association," Butterworths, London, (1962).

14) The Debye-Hückel coefficient is given by $1.825\times 10^6\ (\rho/\varepsilon^3T^3)^{1/2}$ from which A is evaluated as 1.37 in MeCN at 298 K. Then 8 A gives the slope of 11 in Fig. 5.

15) For highly charged reactants with opposite signs the interaction in the precursor complex is enhanced by the electrostatic force; A. Haim and N. Sutin, *Inorg. Chem.*, **15**, 476 (1976); A. J. Miralles, R. E. Armstrong, and A. Haim, *J. Am. Chem. Soc.*, **99**, 1416 (1977); A. P. Szecsy and A. Haim, *ibid.*, **103**, 1679 (1981); S. Kondo, Y. Sasaki, and K. Saito, *Inorg. Chem.*, **20**, 429 (1981).

16) S. Fukuzumi and T. Tanaka, unpublished data.

17) H. Isci and W. R. Mason, *Inorg. Chem.*, **14**, 913 (1975).

18) For the higher concentrations of $[Rh(p\text{-}MeOC_6H_4\text{-}NC)_4]^+$, the contribution of the trimer to the rate was not neglected.

19) Since $\Delta G^*=-2.3\,RT\log(Nhk_1/RT)$, the slope of 0.5 in Eq. 30 yields $(0.5\,F)/(2.3\,RT)=8.5$ in Eq. 29 where F is Faraday constant.

20) T. Iinuma and T. Tanaka, *Inorg. Chim. Acta*, **49**, 79 (1981).

21) M. H. Ford-Smith and N. Sutin, *J. Am. Chem. Soc.*, **83**, 1830 (1961).

22) W. A. Hyes, L. K. Yanowski, and M. Schiller, *J. Am. Chem. Soc.*, **60**, 3053 (1938).

23) P. Ellis, R. G. Wilkins, and M. T. G. Williams, *J. Chem. Soc.*, **1957**, 4456.

24) D. D. Perrin, W. L. F. Armarego, and D. R. Perrin, "Purification of Laboratory Chemicals," Pergamon Press, New York, (1966).

25) R. S. Nicholson and I. Shain, *Anal. Chem.*, **36**, 706 (1964).

26) S. Fukuzumi, C. L. Wong, and J. K. Kochi, *J. Am. Chem. Soc.*, **102**, 2298 (1980).

Spectroscopic Studies of Copper(I) Complexes of 1,8-Di(2-pyridyl)-3,6-dithiaoctane in a Nonaqueous Solvent. The Halide-ion Effect on Their Structure

Susumu KITAGAWA,* Megumu MUNAKATA, and Shoji OKADA

Department of Chemistry, Faculty of Science and Technology, Kinki University, Kowakae, Higashi-Osaka 577

(Received May 4, 1982)

The complexes of 1,8-di(2-pyridyl)-3,6-dithiaoctane(pdto) with CuX(X=Cl and Br) and $[Cu(CH_3CN)_4]ClO_4$ have been synthesized in chloroform, methanol, ethanol, and acetone. Their absorption spectra show an intense metal-to-ligand charge-transfer band at 307 nm: This band is assigned to pyridyl nitrogen←Cu. $[Cu(pdto)]^+$ (**1**) has been prepared from $[Cu(CH_3CN)_4]ClO_4$, its pdto acting as a four-coordinate ligand. CuX reacts with pdto to yield two complexes: One is **1**, and the other is [CuX(pdto)] (**2**). Both complexes are four-coordinate, but in the **2** one of the two pyridyl groups is dissociated. The complex **2** is unstable and is oxidized by oxygen. Neither complex reacts with CO, indicating the tight binding of pdto with Cu(I). The **1** and **2** are equilibrated in solution. The ^1H NMR spectra well demonstrate that **2** is dominant in chloroform and that **1** is the principal form in alcohol, while the **1**/**2** ratio is 3/7. This solvent-dependence is ascribed to the coordination ability and/or polarity of the solvent.

Recent interest in copper proteins has been focused on the copper(I) complexes containing several types of donor atoms. In addition to ligands having N and O donor atoms, copper(I) complexes with ligands containing sulfur have been synthesized and characterized.[1-7] 1,8-Di(2-pyridyl)-3,6-dithiaoctane (pdto), which is a quadridentate N_2S_2-type ligand, gives both copper(I) and copper(II) complexes. The crystal structure of their perchlorate and hexafluorophosphate have been determined by X-ray crystallography.[7] The geometry of this copper(I) complex is tetrahedral, characteristic of usual four-coordinate copper(I) complexes. This suggests that the Cu(I) complex of pdto is four-coordinate, the set of donor atoms being of the N_2S_2-type. However, in the presence of a halide ion(X^-), all the donor atoms of pdto do not necessarily bind the Cu(I) ion in a nonaqueous solvent. We have previously pointed out[8,9] that copper(I) complexes prepared from CuX in a nonaqueous solvent are accompanied by halide ion-bindings, and sometimes their bridging, leading to a binuclear structure. In this sense, both the copper(I) starting material and the solvent used play an important role in the formation of the copper(I) complexes. It is of significance to substantiate the coordination chemistry of CuX–pdto systems in various solvents. The purpose of this work is to elucidate the structure of copper(I) complexes prepared from CuX and pdto, and their equilibria in solution, with the aid of absorption and ^1H NMR spectroscopy.

Experimental

Materials. Reagent-grade copper(I) chloride and bromide were purified according to the literature.[11] All the materials were dried *in vacuo* (75—100 °C). The $[Cu(CH_3CN)_4]ClO_4$ was prepared in the usual way,[12] and recrystallized from ether under nitrogen. The $AgClO_4$ was purchased from Wako LTD., and was used without further purification. 1,8-Di(2-pyridyl)-3,6-dithiaoctane(pdto) was prepared by the methods of Goodwin and Lions.[13]

The acetone, chloroform, methanol, and ethanol were all dried and distilled before use.

Preparation of $[Cu(pdto)]ClO_4$. A 50-cm^3 portion of a 2.5×10^{-5} mol pdto chloroform solution was added to 7.6 mg (2.5×10^{-5} mol) of $[Cu(CH_3CN)_4]ClO_4$ under nitrogen, and this mixture was stirred for 1 h. A colorless solution of $[Cu(pdto)]ClO_4$ was thus formed. This solution was transferred anaerobically into a cuvette (1 cm path length) with a stop cock, and the absorption spectrum was measured by means of a Hitachi 200-10 spectrometer. The complex in the other solvent was prepared in a similar way.

Preparation of [*CuX(pdto)*]. A 50-cm^3 portion of a 2.5×10^{-5} mol pdto chloroform solution was added to 2.5×10^{-5} mol of CuX under nitrogen, and this mixture was stirred for 3 h. In other solvents, the copper complexes were prepared in a similar way. A 10.4 mg (5.0×10^{-5} mol) of $AgClO_4$ was added to the resultant solution. The solution was stirred for 0.5 h and filtered off under nitrogen, and the filtrate was transferred anaerobically into a cuvette for the measurement of the absorption spectra.

Physical Measurements. The ^1H NMR spectra were measured on a JEOL FX200 FT NMR spectrometer. Between 256 and 320 transients were accumulated with the use of a 13-μs pulse (90°). 4 K data points were collected over the band-width of 2500 kHz. The temperature was set at -90 ± 2 °C (acetone-d_6 and methanol-d_4) and -59 ± 1 °C (chloroform-*d*).

The conductances were measured at 25 °C with a Kyoto Elec. Co. Model CM-05, and a cell with two platinum electrodes.

Cyclic voltammetric measurements were made with a Hokuto Model HA104 potentiostat/galvanostat driven by a model HB107A function generator. A Pt wire served as the working electrode, while a Pt coil was used as the counter electrode. A commercial saturated calomel electrode (SCE) was utilized as the reference electrode. Tetrabutylammonium perchlorate (TBAP) was used as the supporting electrolyte.

Results and Discussion

[Cu(pdto)]ClO$_4$. Figure 1(1) shows the absorption spectrum of $[Cu(pdto)]ClO_4$ in the region of 300—500 nm. Only a single band appears at 307 nm when 1 equivalent of pdto is added to $[Cu(CH_3CN)_4]ClO_4$ in $CHCl_3$. The intensities of this band did not increase further upon the addition of an excess of pdto, indicating that pdto has a high

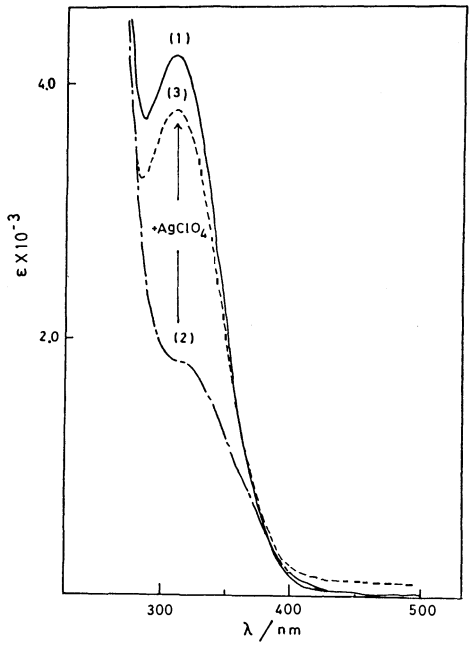

Fig. 1. Absorption spectra of a $CHCl_3$ solution. (1): 5.0×10^{-4} M† of $[Cu(pdto)]ClO_4$, (2): 5.0×10^{-4} M of [CuCl(pdto)], (3): the addition of 1.0×10^{-3} M of $AgClO_4$ to a solution of (2).

affinity for the Cu(I) ion and yields a $[Cu(pdto)]ClO_4$ quantitatively. The pdto itself has no absorption band in this region. The dithioether–Cu(I) complexes, such as $[Cu(2,5\text{-dithiahexane})_2]BF_4$ and $[Cu(3,6\text{-dithiaoctane})_2]BF_4$, have no absorption bands in this region.[2] This leads to the conclusion that there is no charge-transfer band between thioether S and Cu(I) in the region of 300—800 nm.[14] We have elsewhere demonstrated that $[Cu(py)_4]ClO_4$ reveals, at 330 nm an intense band, which is assigned to the metal-to-ligand charge transfer(MLCT) band as py←Cu(I).[9] Consequently, the band at 307 nm of $[Cu(pdto)]ClO_4$ is also ascribed to the MLCT band of py(pdto)←Cu(I).

$[Cu(pdto)]ClO_4$ was also prepared in several solvents, such as methanol, ethanol, and acetone. The values of λ_{max} and ε_{max} are listed in Table 1, together with the molar conductivities (Λ_M) of the solution of $[Cu(pdto)]ClO_4$. In the case of acetone, the MLCT band is covered with the absorption peak of acetone itself. As is shown in Table 1, the λ_{max} value of the MLCT band is unaffected by the solvent used, while the ε_{max} value shows a solvent-dependence which falls within $4.0—4.5\times10^3$ M^{-1} cm^{-1}. A solution of $[Cu(pdto)]ClO_4$ gives molar conductivities of 1.1, 104, 46, and 160 for $CHCl_3$, CH_3OH, C_2H_5OH, and $(CH_3)_2CO$ respectively, which are characteristic of a typical 1:1 electrolyte.[10] This strongly supports the dissociation of the ClO_4^- ion and the coordination of the four donor atoms(N_2S_2) of pdto. Hence, $[Cu(pdto)]ClO_4$ prepared from $[Cu(CH_3CN)_4]ClO_4$ and pdto in the above solvents is a four-coordinate monomer, just as in the solid state.[7]

The ^1H NMR spectra were measured for $[Cu(pdto)]ClO_4$ in several solvents. All the ^1H NMR spectra at room temperature are influenced by the chemical-exchange effect to give unresolved broad signals for each proton of pdto. At a low temperature, the chamical exchange is depressed and the ^1H NMR spectra exhibit well-resolved signals of 2-pyridyl group of pdto, but the methylene protons still show unresolved signals because of collapsing to each other. Figures 2(1) and (4) show the aromatic region of the ^1H NMR spectra in the acetone solution, indicating the unbound and bound 2-pyridyl groups of pdto respectively. The unbound 2-pyridyl group gives four signals which can be readily assigned to 6,4,3,5-H(from downfield to upfield) with the aid of the double-resonance technique. When pdto is coordinated to Cu(I), the 2-pyridyl group signals shift downfield. The protons in the 3 and 5 positions are almost collapsing, but the 3-H signal has a slight bias toward downfield. The assignments of these signals were done with the aid of the double-resonance technique; the signals of 8.73, 8.14, 7.69, and 7.67 ppm are 6, 4, 3, and 5-H respectively. Four similar signals with the same intensity are also observed in the cases of methanol (Fig. 4) and chloroform.

Halide Ion-binding. Absorption Spectra: The pdto also reacts with CuX(X=Cl and Br) in $CHCl_3$, CH_3OH, C_2H_5OH, and $(CH_3)_2CO$ to yield clear solutions. Both methanol and ethanol solutions give the MLCT band at 307 nm with an ε_{max} value of *ca.* 4×10^3 M^{-1} cm^{-1}, which is in good agreement with that of $[Cu(pdto)]ClO_4$. It is worth noting that the MLCT band of the $CHCl_3$ solution has a λ_{max} value of 314 nm and an ε_{max} value of 1.9×10^3 M^{-1} cm^{-1}, both different from those of $[Cu(pdto)]ClO_4$ in $CHCl_3$. The ε_{max} is anomalously small. The large excess of pdto did not increase the absorbance, indicating that the ε_{max} of 1.9×10^3 M^{-1} cm^{-1} is characteristic of [CuCl(pdto)]. The difference in both ε_{max} and λ_{max}

Table 1. Absorption maxima, extinction coefficients of the MLCT band, and molar conductivities of [Cu(pdto)]X and [CuX(pdto)]

Solvent	X	λ_{max} nm[a]	ε_{max} M^{-1} cm^{-1} [b]	Λ_M Ω^{-1} cm^2 mol^{-1}
$CHCl_3$	Cl	314[d]	1.9×10^3	—[e]
	Br	314[d]	1.9×10^3	—[e]
	ClO_4	309	4.1×10^3	1.1
CH_3OH	Cl	307	4.5×10^3	85
	ClO_4	307	4.5×10^3	104
C_2H_5OH	Cl	307	4.0×10^3	33
	Br	307	4.0×10^3	34
	ClO_4	307	4.0×10^3	46
$(CH_3)_2CO$	Cl	—[f]	—[f]	71
	Br	—[f]	—[f]	61
	ClO_4	—[f]	—[f]	160

a) Error limit, ±2 nm. b) Error limit, $\pm0.1\times10^3$ M^{-1} cm^{-1}. c) The standard Λ_M values of a typical 1:1 electrolyte are 95(CH_3OH), 41(C_2H_5OH), and 120($(CH_3)_2CO$) Ω^{-1} cm^2 mol^{-1}. Ref. 10. d) The absorption peak appears as a shoulder. e) The Λ_M value is very small (<1 Ω^{-1} cm^2 mol^{-1}). f) The absorption peak is covered by that of acetone.

† 1 M = 1 mol dm^{-3}.

is associated with the halide ion-binding to Cu(I).

In order to demonstrate the halide ion-binding, we use a comparable amount of $AgClO_4$,[8] which will break down the Cu–Cl bond if it exists. The white precipitate of AgCl appeared rapidly upon the addition of $AgClO_4$ to the solution of CuX and pdto, resulting in a spectrum similar to that of $[Cu(pdto)]ClO_4$ (Fig. 1). This drastic change in the MLCT band would not occur without halide ion-binding to Cu(I). This reaction, thus, follows Eq. 1;

$$[CuX(pdto)] + AgClO_4 \longrightarrow [Cu(pdto)]ClO_4 + AgClO_4 \quad (1)$$

If the precursor complex, [CuX(pdto)], is a four-coordinate, one of the donor atoms(N_2S_2) of pdto should be dissociated; in this sense, a N_2S or NS_2 donor set may be considered. The coordination of two N and one S atoms is unfavorable, because the complex contains a very unstable chelate ring of eight members. The NS_2 is most feasible for explaining the spectral change; the rupture of the Cu–X bond by Ag^+ is followed by the formation of the bonding of Cu–py, and, consequently, the absorbance of the MLCT band increases. The alcohol solution undergoes a minor change in absorbance upon the addition of $AgClO_4$.

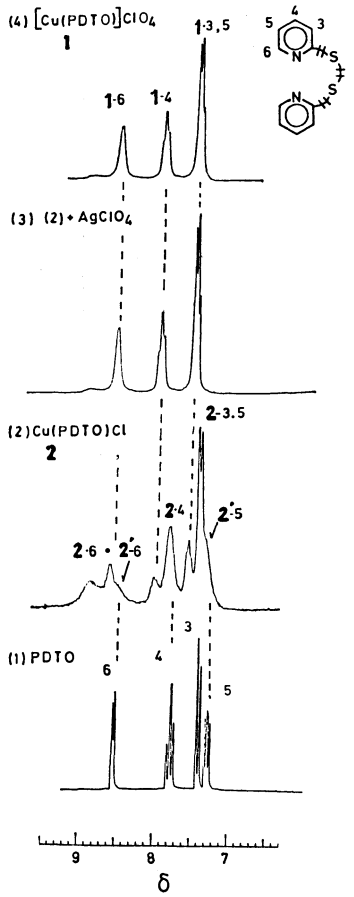

Fig. 2. ^1H NMR spectra at −90 °C of an acetone-d_6 solution.
(1): 5.0×10^{-3} M of pdto, (2): equimolar quantities (5.0×10^{-3} M) of CuCl and pdto, (3): the addition of 1.0×10^{-2} M $AgClO_4$ to a solution of (2), (4): 5.0×10^{-3} M of $[Cu(pdto)]ClO_4$.

Molar Conductivities: The molar conductivities, $\Lambda_M(X)$ (or $\Lambda_M(ClO_4)$), of a solution containing equimolar amounts of CuX and pdto(or $[Cu(CH_3CN)_4]ClO_4$ and pdto) have been measured (Table 1). Table 1 shows that the $\Lambda_M(X)$ of the acetone solution is much smaller than the $\Lambda_M(ClO_4)$, indicative of the presence of halide ion-binding. On the other hand, the alcohol solution also gives a $\Lambda_M(X)$ smaller than the $\Lambda_M(ClO_4)$. This difference is possibly attributable to the difference in the mobilities of ClO_4^- and Cl^- in alcohol. This trend has been found in the systems containing *n*-Bu_4NClO_4 or *n*-Bu_4NCl in *n*-propanol.[15] Otherwise, the difference in Λ_M might arise from the presence of species having a coordinated halide ion, of which minute quantities are demonstrated by the ^1H NMR spectra to be considered below. The $\Lambda_M(ClO_4)$ of the $CHCl_3$ solution is quite small (1.1 Ω^{-1} cm^2 mol^{-1}). Unfortunately, the value $\Lambda_M(X)$ is less than 1 Ω^{-1} cm^2 mol^{-1}, undetectable with our instrument, also implying the presence of a coordinated halide ion.

^1H NMR Spectra: The ^1H NMR spectra were measured in order to elucidate the species in solution. Figure 2(2) shows the ^1H NMR spectra at −90 °C of [CuCl(pdto)] in acetone. This spectrum is quite different from that of $[Cu(pdto)]ClO_4$ (Fig. 2(4)); three types of 2-pyridyl signals were observed. Type-1 signals have the same chemical shifts as those of Fig. 2(4), indicating the formation of [Cu(pdto)]Cl. Type-2 signals are ascribed to coordinated 2-pyridyl of [CuCl(pdto)]. The last Type-2′ corresponds to

Table 2. Observed ^1H NMR shifts[a] of $[Cu(pdto)]ClO_4$ and [CuCl(pdto)]

Complex	Solvent	6-H	5-H	4-H	3-H
pdto	$CDCl_3$[b]	8.58	7.23	7.76	7.25
	CD_3OD[c]	8.46	7.34	7.85	7.47
	$(CD_3)_2CO$[c]	8.57	7.35	7.85	7.47
$[Cu(pdto)]ClO_4$	$CDCl_3$[b]	8.51	7.47	7.92	7.49
	CD_3OD[c]	8.57	7.51	7.97	7.53
	$(CD_3)_2CO$[c]	8.73	7.67	8.14	7.69
[CuCl(pdto)]	$CDCl_3$[b]	8.83[d]	7·39[d]	7.83[d]	7.44[d]
	$(CD_3)_2CO$[c]	8.98[d]	7.51[d]	7.92[d]	7.53[d]
[CuBr(pdto)]	$(CD_3)_2CO$[c]	9.02[d]	7.56[d]	7.94[d]	7.46[d]

a) In ppm from TMS. b) Measured at −59 °C. c) Measured at −90 °C. b) The shifts of a bound py are presented; the shifts of an unbound py are similar to those of metal-free py.

TABLE 3. CONCENTRATION RATIO[a)]

Solvent		I	II
CuCl[b)]	$CDCl_3$	0	100
	CD_3OD	100	0
	$(CD_3)_2CO$	30	70
CuBr[c)]	$(CD_3)_2CO$	6	94

a) Obtained from the ^1H NMR spectra, in percentages.
b) [CuCl]/[pdto]=1. c) [CuBr]/[pdto]=1.

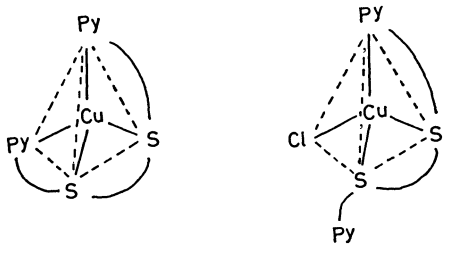

Fig. 3. Proposed structure of $[Cu(pdto)]^+$ (**1**) and [CuX(pdto)] (**2**).

the signals of which shifts are similar to those of a metal-free 2-pyridyl. The computer simulation of the three types of signals gives the ratios of intensities of the Type 1, 2, and 2′ signals; thus, $r_{1/2}=3/7$ and $r_{2/2'}=1$ are obtained. The equal intensities of Type-2 and Type-2′ signals indicate the coordination of pdto as a NS_2 donor set; one 2-pyridyl of pdto is dissociated, as has been discussed in the previous section, and of course, a five-coordinate species is avoided. Upon the addition of $AgClO_4$ as well as in the case of absorption spectra, the Type-2 and Type-2′ signals disappear and the intensity of the Type-1 signals increases. The final spectrum well corresponds to that of $[Cu(pdto)]ClO_4$ (Figs. 2(3) and (4)). These ^1H NMR spectra excellently illustrate the halide ion-binding to Cu(I) and the formation of Cu-2-pyridyl bonding after the removal of the halide ion by Ag^+. We are now in a position to present a structure which best explains the spectral properties obtained here: The proposed structure of [CuX(pdto)] is Structure **2** in Fig. 3, where one 2-pyridyl group of pdto is coordinated to Cu(I), while the other is dissociated. $[Cu(pdto)]^+$ is also presented as Structure **1** in Fig. 3. The ^1H NMR spectrum of a $CDCl_3$ solution exhibits the signals of [CuCl(pdto)], but no signals of [Cu(pdto)]Cl, indicating the formation of [CuCl(pdto)] to a great extent. In this case, $AgClO_4$ also influences this spectrum and provides a spectrum similar to that of $[Cu(pdto)]ClO_4$ in $CDCl_3$. The observed ^1H NMR shifts are listed in Table 2. On the other hand, the ^1H NMR spectrum of CD_3OD solution with CuCl and pdto is just the same as that of $[Cu(pdto)]ClO_4$ (Fig. 4). Hence, CuCl reacts with pdto in alcohols, mostly yielding [Cu(pdto)]Cl. This is also suggested by the same values of λ_{max} and ε_{max} between CuCl and $[Cu(CH_3CN)_4]ClO_4$.

Solution Equilibria: The absorption, ^1H NMR spectra, and molar conductivities characterize the reaction of CuX with pdto, comprising a part of Scheme 1. The equilibrium between Complex **1** and **2** is dependent

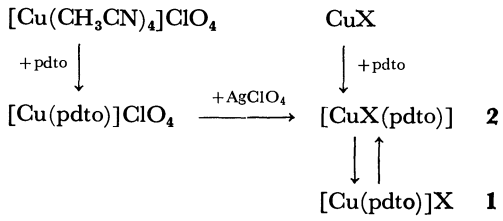

Scheme 1.

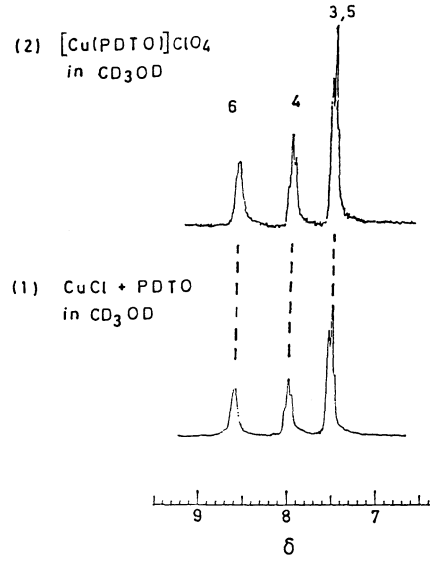

Fig. 4. ^1H NMR spectra at −90 °C of a methanol-d_4 solution.
(1): Equimolar quantities (5.0×10^{-3} M) of CuCl and pdto, (2): 5.0×10^{-3} M of $[Cu(pdto)]ClO_4$.

on the solvent used. Complex **2** dominantly forms in $CHCl_3$, while Complex **1** selectively forms in alcohol. In acetone, Complex **2** is in equilibrium with Complex **1**. The ^1H NMR spectra (Fig. 2) provides a **1**/**2** ratio of 3/7. Chloroform has a lower polarity than acetone, as has been characterized by the dielectric constant, ε. Methanol has the greatest ε value among the four solvents used. The order is 32.7 (methanol) > 24.6(ethanol) > 20.7(acetone) > 4.8(chloroform).[15)] This order is also considered to be that of the coordination ability of the solvents. On this basis, the step of Cu–X bond fission is likely to be significant in the complex formation. In alcohol, its bulk properties and/or its coordination ability allow the Cu–X bond fission to occur readily and promote the coordination of the four donor atoms (N_2S_2) of pdto. On the other hand, in a non-polar solvent such as chloroform, halide ion-binding to Cu(I) appears to be tight: Hence, it is not broken even by the 2-pyridyl of pdto. The similar halide ion-binding has also been found in the acetone solution of CuX and 2,2′-bipyridine(bpy);[8)] a binuclear $[CuX(bpy)]_2$ preferably forms in acetone, while a monomer $[Cu(bpy)_2]^+$ principally forms in alcohol. Consequently, alcohol is available for the breakdown of the Cu–X bond.

It is to be noted in Table 3 that **1**/**2** ratio is smaller in the case of Br^- than in the case of Cl^-. This indicates that Complex **2** prefers Br^- to Cl^-, the Cu–Br bond being stronger than the Cu–Cl bond. This is reasonable, for CuCl itself is rather more unstable

than CuBr upon exposure to air.

The oxidation-reduction potentials of the copper of [CuCl(pdto)] and [Cu(pdto)]ClO_4 in acetone at 25 °C have been measured by means of cyclic voltammetry(CV). [Cu(pdto)]ClO_4 gave a single pair of waves corresponding to the electrode reaction of Cu^I/Cu^{II}, the half-wave potential of which is 0.60 V *vs.* SCE. In the case of an acetone solution containing equimolar quantities of CuCl and pdto, two pairs of waves were observed. The first pair, in the cathodic region, has an $E_{1/2}$ value of 0.60 V *vs.* SCE, indicative of the Cu^I/Cu^{II} reaction of [Cu(pdto)]Cl, while the second, with an $E_{1/2}$ value of 0.49 V, is attributable to the Cu^I/Cu^{II} reaction of [CuCl(pdto)]. Hence, copper(I) states are more stable in [Cu(pdto)]Cl than in [CuCl(pdto)].

Neither [Cu(pdto)]ClO_4 nor [CuCl(pdto)] reacts with CO, as is demonstrated by monitoring the absorption and ^1H NMR spectra. This indicates that pdto in both complexes tightly binds the Cu(I) atom, which prevents the substitution reaction, and that they keep the structure, presumably a tetrahedral environment, around the Cu(I) atom, the rigidity of which inhibits the addition reaction and accompanying conformational change.

[Cu(pdto)]ClO_4 is quite stable against oxygen, while [CuCl(pdto)] is gradually oxidized upon exposure to air. This is accounted for by their redox properties obtained from CV. Hence, pdto stabilizes the copper (I) ion when all four donor atoms of pdto bind the Cu(I) ion.

This work was supported in part by a grant from the Ministry of Education, Science and Culture.

References

1) P. S. K. Chia, S. E. Livingstone, and T. N. Lockyer, *Aust. J. Chem.*, **19**, 1835 (1966).
2) E. W. Ainscough, A. M. Brodie, and K. C. Palmer, *J. Chem. Soc., Dalton Trans.*, **1979**, 2375.
3) E. N. Baker and G. E. Norris, *J. Chem. Soc., Dalton Trans.*, **1977**, 877.
4) E. N. Baker and P. M. Garrick, *J. Chem. Soc., Dalton Trans.*, **1978**, 416.
5) K. D. Karlin, P. L. Dahlstrom, J. R. Hyde, and J. Zubieta, *J. Chem. Soc., Chem. Commun.*, **1980**, 906.
6) E. W. Ainscough, E. N. Baker, A. M. Brodie, N. G. Larsen, and K. L. Brown, *J. Chem. Soc., Dalton Trans.*, **1981**, 1746.
7) G. R. Brubaker, J. N. Brown, N. K. Yoo, R. A. Kinsey, T. M. Kutchan, and E. A. Mottel, *Inorg. Chem.*, **18**, 299 (1979).
8) S. Kitagawa and M. Munakata, *Inorg. Chem.*, **20**, 2261 (1981).
9) S. Kitagawa, M. Munakata, and A. Higashic, *Inorg. Chim. Acta*, **59**, 219 (1982).
10) W. J. Geary, *Coord. Chem. Rev.*, **7**, 181 (1971).
11) L. F. Andrieth, J. C. Bailar, W. C. Fernelius, W. C. Johonson, and R. E. Kirk, *Inorg. Synth.*, **2**, 1 (1946).
12) P. Hemmerich and C. Sigwart, *Experientia*, **19**, 488 (1963).
13) H. A. Goodwin and F. Lions, *J. Am. Chem. Soc.*, **82**, 5013 (1960).
14) V. M. Miskowski, J. A. Thich, R. Solomon, and H. J. Schugar, *J. Am. Chem. Soc.*, **98**, 8344 (1976).
15) D. F. Evans, J. Thomas, J. A. Nades, and S. M. A. Matesich, *J. Phys. Chem.*, **75**, 1714 (1971).
16) J. A. Riddick and W. B. Bunger, "Technique of Chemistry. II," Wiley-Interscience, New York (1970).

Argon Plasma Treatment of Packing Materials for Gas Chromatography and Comparison with Acid Wash and Dimethyldichlorosilane Treatment of Support

Seiji Oka, Yukio Yamamoto,* and Koichiro Hayashi

The Institute of Scientific and Industrial Research, Osaka University, 8-1 Mihogaoka, Ibaraki, Osaka 567

(Received May 6, 1982)

Argon plasma treatment of column packings for gas chromatography was examined with commercially obtained diatomaceous earth coated with several kinds of stationary liquid phases, such as squalane, Apiezon L, dioctyl phthalate, Silicone DC, and polyethylene glycol. It was found that the plasma treatment improves chromatographic properties of all the packings examined except those with polyethylene glycol. The effect of the plasma treatment is attributable to the reduction of support adsorptivity by the formation of an inert coating on the support surface. The plasma treatment of Chromosorb W coated with 5% squalane was compared with dimethyldichlorosilane (DMCS) treatment of the acid-washed (AW) support, the so-called AW-DMCS-treatment of support. Although the AW-DMCS-treatment is superior to the plasma treatment for the reduction of support adsorptivity, a complete elimination of the adsorptivity was attained by the plasma treatment of the packing having the AW-DMCS-treated support.

Preceding papers have illustrated the effect of argon plasma treatment of diatomaceous earth coated with squalane or Apiezon L on gas chromatograms of hydrocarbons.[1,2] By the plasma treatment, the chromatographic resolution was improved and the retention times were decreased. The effect has been attributed to the reduction of support adsorptivity by the formation of an inert coating on the support surface, based on the following results. (1) By the plasma treatment, the tailings of aromatic hydrocarbon peaks were reduced, and their retention times were decreased more than those of saturated aliphatic hydrocarbons. (2) The weight loss of the packing treated which occurred by the extracting the stationary liquid phase decreased with increasing treatment time, indicating the formation of an insoluble component on the support surface. (3) The ESCA spectrum of the support recovered from the treated packing by extracting the liquid phase indicated that the support surface is covered with an organic component. (4) NMR spectrometry showed that the soluble fraction of liquid phase of the treated packing remains unchanged.

The experiments described here were undertaken to enhance the utility of argon plasma treatment for the improvement of chromatographic properties of column packings. The plasma treatment of various kinds of familiar packings was examined. A comparison was made with dimethyldichlorosilane (DMCS) treatment of acid-washed (AW) support, the so-called AW-DMCS-treatment of support, which is usually used to reduce the support adsorptivity.

Experimental

Column packings (60/80 mesh) were obtained from Wako Pure Chemical Industry. The apparatus and experimental details of the plasma treatment were described previously.[2] The gas chromatographic test of the treated packing was also carried out as described previously; the packing was packed into a 1 m×3 mm i.d. stainless steel tube, and the nitrogen flow rate was 30 ml/min. Before its use, the packing was conditioned longer than overnight at a temperature 10 °C below the maximum temperature of the packing.

Results and Discussion

Figure 1 shows the effect of argon plasma treatment of Chromosorb W (non-acid washed (NAW)) coated with 5% squalane (max. temp, 140 °C) on the gas chromatogram of aromatic ketones. The retention times and tailings of the peaks are reduced by the plasma treatment. On the 60 min treated packing, sharp peaks with improved separations are obtained. A similar effect was also observed on the gas chromatogram of aliphatic ketones such as 5-nonanone and 6-undecanone. The results suggest that the plasma treatment enables the packing to be used for the

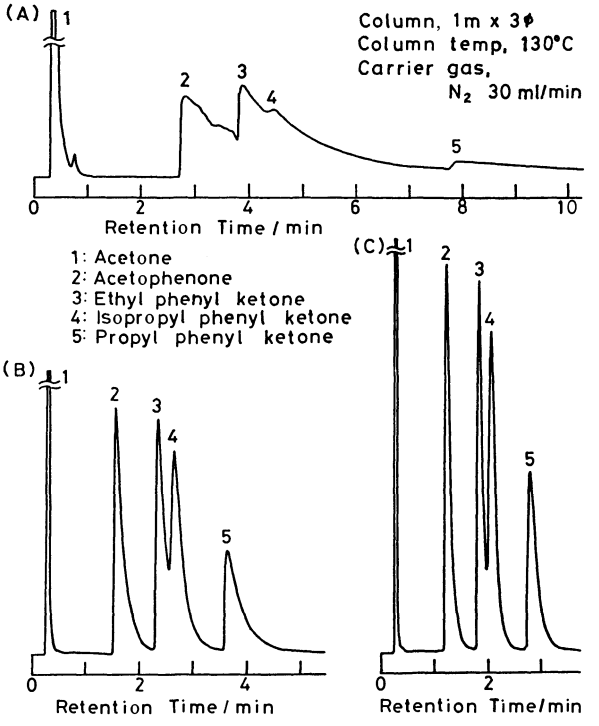

Fig. 1. Gas chromatograms on Chromosorb W (NAW) coated with 5% squalane: (A) untreated; (B) 30 min plasma treated; (C) 60 min plasma treated.

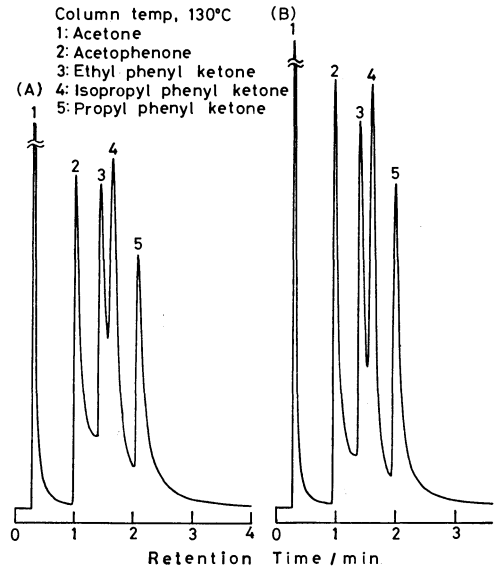

Fig. 2. Gas chromatograms on Chromosorb W (NAW) coated with 5% Silicone DC 200: (A) untreated; (B) 60 min plasma treated.

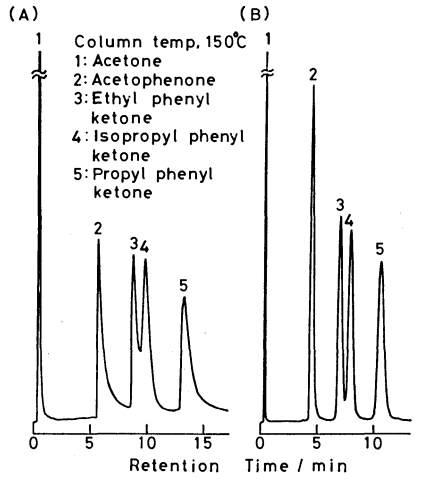

Fig. 3. Gas chromatograms on Shimalite (NAW) coated with 25% Silicone DC 702: (A) untreated; (B) 90 min plasma treated.

analysis of ketones as well as hydrocarbons.

Figures 2 and 3 show the gas chromatograms of the aromatic ketones on untreated and treated packings, Chromosorb W (NAW) coated with 5% Silicone DC 200 (max. temp, 200 °C) and Shimalite (NAW) coated with 25% Silicone DC 702 (max. temp, 200 °C), respectively. The decrease in the retention times and the improvement of peak separations by the plasma treatment are also observed with these packings.

Similar results were obtained by the plasma treatment of other kinds of packings: Chromosorb W (NAW) coated with 20% Apiezon L and 10% KOH (max. temp, 180 °C) and Chromosorb W (NAW) coated with 10% dioctyl phthalate (max. temp, 140 °C). The former packing is used for the analysis of amines, and the latter for the analysis of alcohols and esters. Examples of the gas chromatograms on these packings are shown in Figs. 4 and 5, illustrating

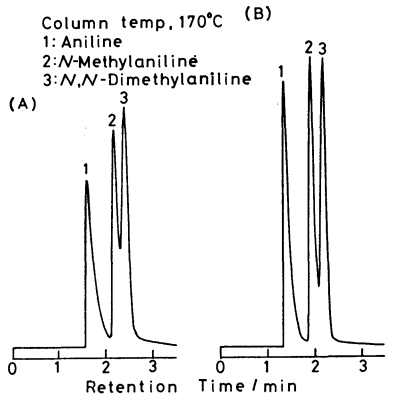

Fig. 4. Gas chromatograms on Chromosorb W (NAW) coated with 20% Apiezon L and 10% KOH: (A) untreated; (B) 10 min plasma treated.

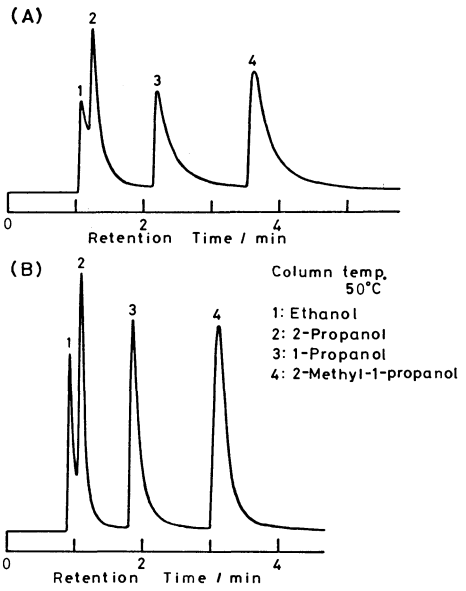

Fig. 5. Gas chromatograms on Chromosorb W (NAW) coated with 10% dioctyl phthalate: (A) untreated; (B) 60 min plasma treated.

the improvement of their chromatographic properties by the plasma treatment.

By the plasma treatment the retention times and tailings of chromatographic peaks were reduced in all the cases of the packings described above, although the treatment times needed for an appreciable effect to occur on the gas chromatograms differ from one another. The prolonged plasma treatment resulted in further decrease in the retention times accompanying a decrease in the peak separations. According to the previous studies,[1,2] it is reasonable to assume that the effect of the plasma treatment of these packings is due to the reduction of support adsorptivity.

The surface of the diatomite supports is covered with reactive silanol groups, which cause tailings of chromatographic peaks,[3] and the AW-DMCS-treated supports are usually used to avoid the adsorption on the support surface. Thus, it is interesting to compare the effect of the plasma treatment of packing with that of the AW-DMCS-treatment of support,

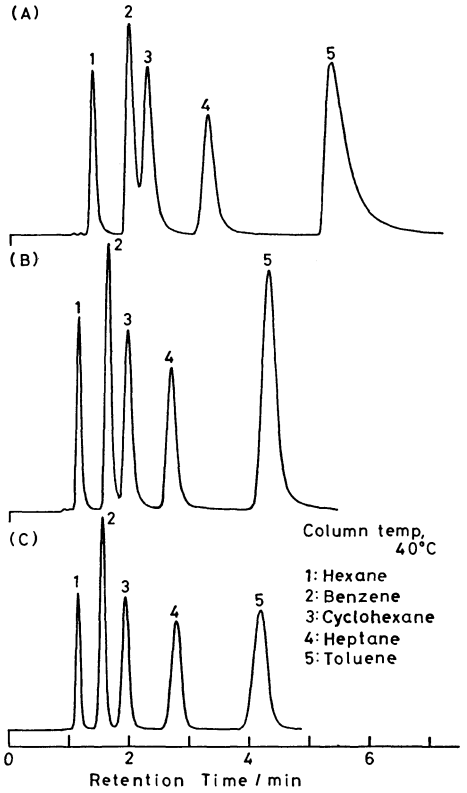

Fig. 6. Gas chromatograms on Chromosorb W coated with 5% squalane: (A) untreated packing, AW support; (B) 30 min plasma treated packing, AW support; (C) untreated packing, AW-DMCS treated support.

Figure 6 illustrates the gas chromatograms of a hydrocarbon mixture on Chromosorb W (NAW) coated with 5% squalane, in order to compare the effect of the plasma treatment of the packing having the AW support with that of the AW-DMCS-treatment. These chromatograms should also be compared with those on the untreated and treated packings having the NAW support, which have previously been shown in Ref. 1 (Fig. 3). A comparison of the figures shows that the chromatograms on the 30 min plasma treated packings having the NAW and AW supports (Fig. 3(b) in Ref. 1 and Fig. 6(B), respectively) are almost identical with that on the untreated packing having the AW-DMCS-treated support (Fig. 6(C)). On these packings, benzene and cyclohexane are well separated and the tailing of the peak of toluene is completely suppressed in contrast to the untreated packings having the NAW and AW supports (Fig. 3(a) in Ref. 1 and Fig. 6(A), respectively). That is to say, the effect of the plasma treatment of the packings having the NAW and AW supports on the gas chromatograms of the hydrocarbon mixture is almost the same as that of the AW-DMCS-treatment of support. It is also shown that, on the untreated packings, the AW support is better for the separation of benzene and cyclohexane than the NAW support (Fig. 6(A) compared with Fig. 3(a) in Ref. 1).

Since polar compounds are sensitive to the support adsorptivity and are expected to give more detailed information about it than the hydrocarbons, the gas

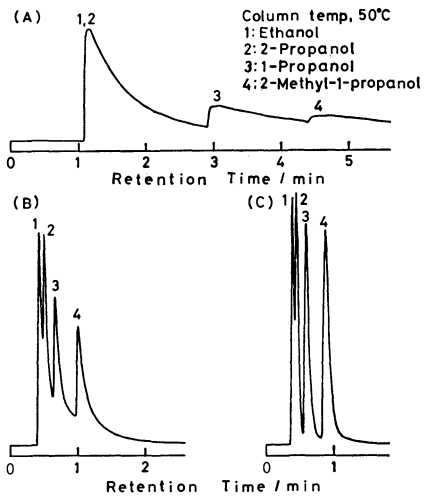

Fig. 7. Gas chromatograms on Chromosorb W coated with 5% squalane: (A) 60 min plasma treated packing, NAW support; (B) untreated packing, AW-DMCS treated support; (C) 30 min plasma treated packing, AW-DMCS treated support.

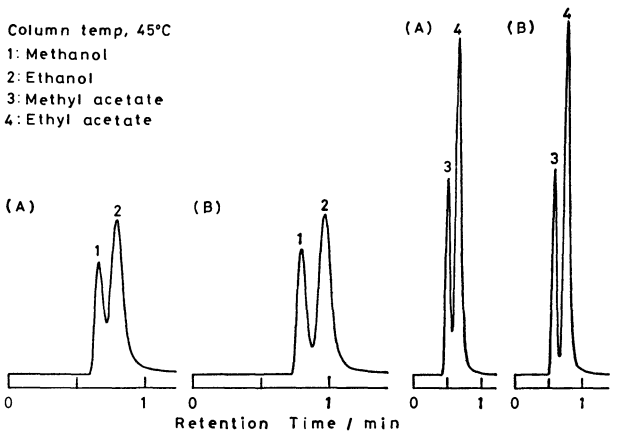

Fig. 8. Gas chromatograms on Chromosorb W (NAW) coated with 10% polyethylene glycol 20M: (A) untreated; (B) 20 min plasma treated.

chromatograms of alcohols on the packings with 5% squalane are compared in Fig. 7. On the 60 min treated packing having the NAW support, the peaks are very broad with extensive tailings. The tailings are appreciably reduced on the untreated packing having the AW-DMCS-treated support, indicating that the AW-DMCS-treatment of support is superior to the plasma treatment of the packing for the reduction of the support adsorptivity. However, a complete suppression of the tailings is attained by the 30 min plasma treatment of the packing having the AW-DMCS treated support, as is shown by Fig. 7(C). Thus, the plasma treatment is useful for the complete suppression of the adsorption on the support surface when used together with the AW-DMCS-treatment of support.

The effect of the plasma treatment of diatomaceous earth coated with polyethylene glycol was different from that of the other packings described above; the plasma treatment tends to increase the retention times

on the packings. Figure 8 shows the gas chromatograms of alcohols and esters on the untreated and treated Chromosorb W (NAW) coated with 10% polyethylene glycol 20 M (max. temp, 200 °C), demonstrating that both the retention times and the peak separations are increased by the plasma treatment. The plasma treatment of Shimalite (base-treated) coated with 25% polyethylene glycol 6000 (max. temp, 200 °C) was also examined, but the observed effect on the gas chromatograms was only a slight increase in the retention times. Such exceptional results can be ascribed to the high polarity of the liquid phase; the adsorption on support surface is not important on the packings with the polar liquid phase. In practice, tailings of the peaks are not observed even on the untreated packings. The increase in the retention times by the plasma treatment is probably due to some modification of the liquid phase.

This work was supported in part by Shimadzu Co.

References

1) Y. Yamamoto, S. Oka, and K. Hayashi, *Chem. Lett.*, **1981**, 221.
2) Y. Yamamoto, S. Oka, and K. Hayashi, *Bull. Chem. Soc. Jpn.*, **55**, 441 (1982).
3) O. E. Schupp, III, "Gas Chromatography," ed by E. S. Perry and A. Weissberger, Interscience, New York, N. Y. (1968), p. 173.

Mössbauer Emission Spectroscopic Study of Some Spin Crossover Cobalt(II) Complexes

Yonezo MAEDA,* Hiroki OHSHIO, and Yoshimasa TAKASHIMA

Department of Chemistry, Faculty of Science, Kyushu University 33, Higashi-ku, Fukuoka 812

(Received October 8, 1981)

The Mössbauer emission spectra of $[^{57}Co(terpy)_2]X_2$ (X=Cl and ClO_4), $[^{57}Co(snn)_2](ClO_4)_2$, and $[^{57}Co(snnme)_2](ClO_4)_2$ (terpy=2,2′: 6′2″-terpyridine, snn=*N*-(2-pyridylmethylene)-2-(methylthio)aniline, and snnme=*N*-(6-methyl-2-pyridylmethylene)-2-(methylthio)aniline) were examined. These cobalt complexes show thermally induced spin crossover behavior and the temperature dependence of their magnetic moment varies with the counter anion, although the corresponding iron complexes are in a low-spin state. The high-spin iron(II) species ascribed to a metastable form are observed in the emission spectra of $[^{57}Co(terpy)_2](ClO_4)_2\cdot 2H_2O$ and $[^{57}Co(snnme)_2](ClO_4)_2$, and their spectral areas increase with decreasing source temperature. The effective vibrating mass for the iron complex observed in the emission spectra of $[^{57}Co(snnme)_2](ClO_4)_2$ was calculated from the temperature dependence of the isomer shift value, and was used to distinguish whether the iron complex formed by EC-decay of a cobalt-57 atom is stable or metastable.

The Mössbauer emission spectroscopic method provides for studying the after-effects attended by EC-decay of a cobalt-57 atom in a solid state. The chemical after-effects in solids, reflected in the Mössbauer spectra, are categorized as follows: (i) The oxidation state of the iron atom formed in the EC-decay of a cobalt-57 atom in the lattice of the labeled cobalt complexes is different from that of the parent cobalt atom (formation of foreign-charge state). (ii) An iron atom after EC-decay does not have the same spin state as the corresponding iron complexes but the same oxidation state (formation of anomalous spin state). (iii) An iron atom after EC-decay is stabilized in a coordination atmosphere different from that of a cobalt atom because of the radiolysis of the ligands, although it does have the same spin and oxidation state as the corresponding iron complex. These phenomena have been explained by various mechanisms as described below:

Friedt and Danon reported on the behavior of $^{57}CoX_2$ in terms of the lattice energy.[1] Friedt *et al.* reported that iron(III) appearing in the emission spectra of $^{57}CoSO_4\cdot nH_2O$ was due to the radiolysis of hydrated water.[2-4] The role of the radicals resulting from autoradiolysis of ligands due to photoelectrons and X-rays have been extensively examined, and Sano *et al.* concluded that the redox properties of radicals affect the final oxidation state of the daughter atom, and that these effects are due to the radiolytic self-decomposition of the molecular environment of the decaying atoms.[5-8] These mechanisms have been supported by performing an external irradiation experiment using electrons and X-rays.

On the other hand, Nath *et al.* suggested that the multiple charged iron atom after Auger cascade was rapidly neutralized by electron transfer from ligands, and the coulomb repulsion between the iron and ligands resulted in the fragmentation of molecules; the fragmentation was highly dependent on the degree of bonding conjugation in the molecule.[9,10]

The Mössbauer emission spectra of some cobalt complexes with imines or their derivatives were measured by Gütlich *et al.*[11-15] They proposed that the anomalous spin states appearing in these emission spectra had lifetimes of the order of 100—400 ns and were the immediate precursors of the stable states. Several studies were performed from the view point of the spin state of the daughter iron atom.[16-19]

In this study we measured the Mössbauer emission spectra of spin crossover cobalt complexes in order to investigate how the difference in the spin state of a parent cobalt atom affects the lifetime of a metastable state of a daughter iron atom. The effective vibrating mass calculated using the method proposed by Herber[20] was used to distinguish between the metastable and the stable state.

Experimental

The cobalt complexes used in this study were prepared described in the literature. $[Co(terpy)_2]X_2$ (X=Cl and ClO_4),[21] $[Co(snn)_2](ClO_4)_2$,[22] and $[Co(snnme)_2](ClO_4)_2$:[23] terpy; 2,2′: 6′,2″-terpyridine, snn; *N*-(2-pyridylmethylene)-2-(methylthio)aniline, and snnme; *N*-(6-methyl-2-pyridylmethylene-2-(methylthio)aniline. Iron complexes were prepared by methods similar to those of the cobalt complexes. The elemental analysis was performed with unlabeled samples and the values found for carbon, nitrogen, and hydrogen deviated by less than 0.3% from the calculated values. The compounds for the Mössbauer emission spectroscopic measurement were all labeled with 1 mCi of cobalt-57. The magnetic susceptibilities at 297 K and 80 K were measured on polycrystalline samples by the Faraday method. $HgCo(NCS)_4$ was used as the calibration substance. The effective magnetic moment was calculated using the formula $\mu_{eff}=2.84\sqrt{\chi_M T}$, where χ_M is the molar susceptibility after dia-

TABLE 1. EFFECTIVE MAGNETIC MOMENT OF COBALT AND IRON COMPLEXES

Complex	μ_{eff}/BM	
	297 K	80 K
$[Co(terpy)_2]Cl_2\cdot 5H_2O$	2.53	2.10
$[Co(terpy)_2](ClO_4)_2\cdot 2H_2O$	3.70	3.10
$[Co(snn)_2](ClO_4)_2$	2.59	2.02
$[Co(snnme)_2](ClO_4)_2$	5.10	3.85
$[Fe(snn)_2](ClO_4)_2$	dia.	dia.
$[Fe(snnme)_2](ClO_4)_2\cdot 2H_2O$	2.60	1.19

magnetic corrections. These data are listed in Table 1.

The external irradiation experiments with γ-ray for [Fe(snn)$_2$](ClO$_4$)$_2$ and [Fe(snnme)$_2$](ClO$_4$)$_2\cdot$2H$_2$O were performed as described elsewhere.[24]

Mössbauer spectra were measured with a constant acceleration spectrometer(Austin Science Associate). The data are stored in a 1024 channel analyzer, type 5200 (Inotech, Inc). Temperature was monitored with a calibrated copper *vs.* constantan thermocouple in a variable temperature cryostat, type ASD-4V(Austin Science Associate) and maintained with a temperature controller, type S-8(Austin Science Associate). In the emission spectroscopy, potassium hexacyanoferrate(III) enriched with iron-57 was used as a standard absorber and was maintained at room temperature. A cobalt-57 source of 10 mCi diffused into palladium foil was used for the absorption experiment. All the spectra were fitted by Lorentzian line shapes using the least-square method at the Computer Center, Kyushu University; the velocity scale was normalized with respect to the center of the spectrum of an iron foil at 297 K. The geometry effect on the spectra(dimensions of source and absorber in relation to the distance between them) were taken into consideration in the fitting procedure. The experimental errors for Mössbauer parameters(isomer shift, quadrupole splitting, and full width at half-maximum) are estimated to be about $\pm$0.01 mm s^{-1} or less.

Results and Discussion

Figures 1—4 show the Mössbauer emission spectra recorded for [^{57}Co(terpy)$_2$]Cl$_2\cdot$5H$_2$O, [^{57}Co(terpy)$_2$](ClO$_4$)$_2\cdot$2H$_2$O, [^{57}Co(snn)$_2$](ClO$_4$)$_2$, and [^{57}Co(snnme)$_2$](ClO$_4$)$_2$, respectively. The values for the Mössbauer parameters are listed in Tables 2—4 together with those for the absorption spectra of the analogous iron complexes and those for the corresponding iron-57 doped cobalt complexes. It was found that the iron atoms in the iron complexes and in the matrices of the cobalt complexes were in a low-spin state, while the corresponding cobalt complexes exhibited thermally induced spin crossover behavior.

The emission spectrum of [^{57}Co(terpy)$_2$]Cl$_2\cdot$5H$_2$O recorded at 80 K is very similar to that at 297 K; both spectra are characterized by two quadrupole doublets(A and B) assigned to low-spin iron(II). An additional resonance line C ascribed to low-spin iron (III) is observed at 80 K. The disappearance of the species C at 297 K is due to the decrease of the recoil free fraction of this species. The values of the isomer shift and the quadrupole splitting of A are similar to those for the absorption spectra of the corresponding iron complex. The similarity between their parameters indicates that A is attributable to an iron atom stabilized without undergoing any after-effect, and that the electronic ground state of A, which is formed in the lattice of the paramagnetic cobalt compound by nuclear disintegration, is not influenced by the high-spin character of the surrounding cobalt ions at room temperature. The doublet B is attributable to a species stabilized in a coordination atmosphere different from that of A. This stabilization occurs

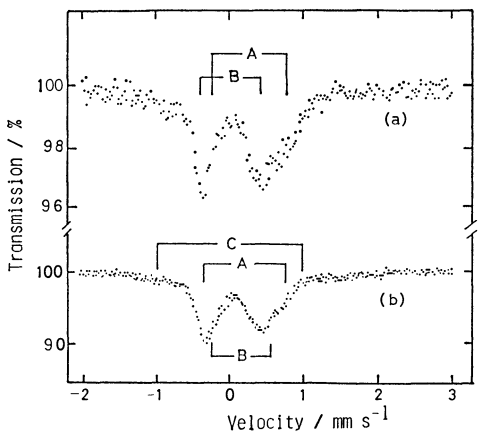

Fig. 1. Mössbauer emission spectra of [^{57}Co(terpy)$_2$]Cl$_2\cdot$5H$_2$O at (a) 297 K and (b) 80 K.

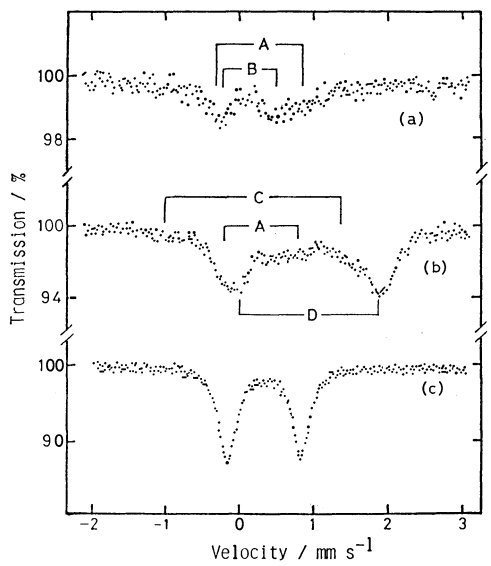

Fig. 2. Mössbauer emission spectra of [^{57}Co(terpy)$_2$](ClO$_4$)$_2\cdot$2H$_2$O at (a) 297 K and (b) 80 K, and Mössbauer absorption spectrum (c) of [^{57}Fe$_{0.1}$Co$_{0.9}$(terpy)$_2$](ClO$_4$)$_2\cdot$2H$_2$O at 80 K.

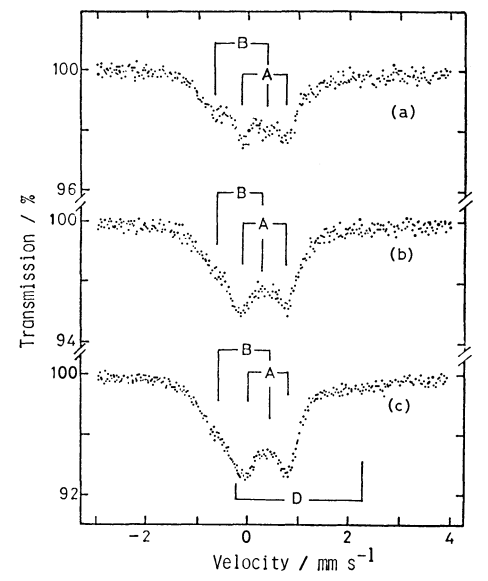

Fig. 3. Mössbauer emission spectra of [^{57}Co(snn)$_2$](ClO$_4$)$_2$ at (a) 297 K, (b) 200 K, and (c) 80 K.

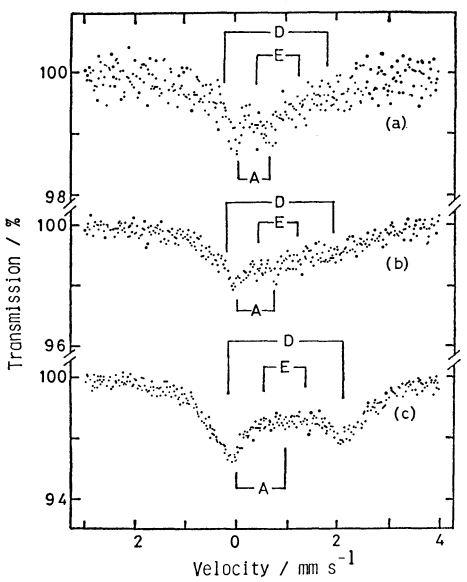

Fig. 4. Mössbauer emission spectra of $[^{57}Co(snnme)_2](ClO_4)_2$ at (a) 297 K, (b) 200 K, and (c) 80 K.

within the lifetimes of iron-57 m (10^{-7} s) through a secondary process after EC-decay. The coordination structure around B is distorted from the original coordination atmosphere by after-effects of nuclear disintegration.

The Mössbauer emission spectrum recorded at 80 K for $[^{57}Co(terpy)_2](ClO_4)_2\cdot 2H_2O$ is quite different from that at 297 K. The spectrum at 297 K is fitted to doublet A and B. However, when the source temperature was lowered, two additional resonance lines, D ascribed to high-spin iron(II) and C to low-spin iron(III) appeared in the emission spectra. These C and D lines are obviously attributable to a new chemical species because their chemical states are different from that of iron-57 doped in the host matrix $[Co(terpy)_2](ClO_4)_2\cdot 2H_2O$ as shown in Fig. 2. The decrease in the recoil free fraction with increasing temperature have resulted in the disappearance of C in the Mössbauer spectra at 297 K; C is a minor absorption peak even at 80 K. There is a possibility that the high-spin species D is in the stable state produced by the radiolytic reaction between the ligands and ClO_4^-. However we ascribe D to a metastable species leading to stable low-spin iron(II) for the following reasons:[15,25] It is assumed that the average ligand field strength experienced by the iron-57 daughter atom on the Mössbauer time scale of *ca.* 10^{-7}—10^{-8} s tends to decrease effectively because of coulomb repulsion between central iron-57 atom and ligands after Auger cascade. The absence of D in other emission spectra is caused by rapid relaxation of energy produced by EC-decay. Berlin and Schmand[26] have concluded that the existence of a metastable state is proved in the emission spectra of $^{57}CoSO_4\cdot 7H_2O$ because the metastable state has a long relaxation time of energy deposited on an iron atom after EC-decay; and they determined the lifetime of high-spin iron (II) species as a function of temperature.

The chemical structure of ligands snn and snnme are the same except for the methyl group located at the 6-position of pyridine. Therefore, the effects of autoradiolysis on both ligands by photoelectron and X-rays emitted following EC-decay are assumed to be similar. However, the methyl group of $[Co(snnme)_2](ClO_4)_2$ causes magnetic behavior different from that of $[Co(snn)_2](ClO_4)_2$.

The Mössbauer emission spectra of $[^{57}Co(snn)_2](ClO_4)_2$ at various temperatures are mainly composed of two kinds of quadrupole doublets A and B, and the ratios of the absorption areas of A and B to the total absorption area are almost the same in the range of the source temperature(80 K—297 K). This indicates that these species are in a stable state. The Mössbauer parameter of A appearing in the emission spectra is in good agreement with that obtained for the Mössbauer absorption spectra of $[^{57}Fe_{0.1}Co_{0.9}$-

Table 2. The Mössbauer parameters of the emission and absorption spectra of $[^{57}Co(terpy)_2]X_2$ and related iron compounds

Complex	T / K	δ [a] / mm s^{-1}	ΔE_Q [b] / mm s^{-1}	Γ [c] / mm s^{-1}	A [d] / %	Assignment[e]
$[^{57}Co(terpy)_2]Cl_2\cdot 5H_2O$	297	0.21	0.99	0.44	44	A
		0	0.82	0.28	56	B
	80	0.07	1.97	0.40	11	C
		0.24	1.11	0.24	21	A
		0.14	0.73	0.43	68	B
$[^{57}Co(terpy)_2](ClO_4)_2\cdot 2H_2O$	297	0.22	1.18	0.30	34	A
		0.06	0.74	0.33	66	B
	80	0.16	2.50	0.41	9	C
		0.24	0.99	0.32	13	A
		0.93	1.92	0.60	78	D
$[^{57}Fe_{0.1}Co_{0.9}(terpy)_2](ClO_4)_2\cdot 2H_2O$	297	0.23	1.05			
	80	0.34	1.00			
$[Fe(terpy)_2](ClO_4)_2$ [f]	300	0.21	1.06			
	4.2	0.29	1.06			

a) Isomer shift. b) Quadrupole splitting. c) Full width at half-maximum. d) Relative peak area. e) A: Low-spin Fe(II), B: low-spin Fe(II), C: low-spin Fe(III), and D: high-spin Fe(II)(metastable). f) Data from Ref. 27.

Table 3. The Mössbauer parameters of the emission and absorption spectra of $[^{57}Co(snn)_2](ClO_4)_2$ and related iron compounds

Complex	T / K	δ / mm s^{-1}	ΔE_Q / mm s^{-1}	Γ / mm s^{-1}	A / %	Assignment
$[^{57}Co(snn)_2](ClO_4)_2$	297	0.33	0.90	0.55	68	A
		−0.17	1.08	0.49	32	B
	200	0.32	0.93	0.60	71	A
		−0.19	0.99	0.66	29	B
	80	0.37	0.89	0.55	56	A
		−0.12	1.04	0.71	31	B
		1.01	2.61	1.19	13	D
$[^{57}Fe_{0.1}Co_{0.9}(snn)_2](ClO_4)_2$	297	0.31	0.73	0.23		
	80	0.39	0.72	0.27		
$[Fe(snn)_2](ClO_4)_2$	297	0.29	0.75	0.31		
	80	0.37	0.72	0.36		
$[Fe(snn)_2](ClO_4)_2$ irrad.[a]	80	0.39	0.74	0.31		

a) Total exposure dose is 5.2×10^8 R.

Table 4. The Mössbauer parameters of the emission and absorption spectra of $[^{57}Co(snnme)_2](ClO_4)_2$ and related iron compounds

Complex	T / K	δ / mm s^{-1}	ΔE_Q / mm s^{-1}	Γ / mm s^{-1}	A / %	Assignment
$[^{57}Co(snnme)_2](ClO_4)_2$	297	0.33	0.68	0.32	31	A
		0.78	0.78	0.29	13	E[a]
		0.72	2.07	1.38	56	D
	200	0.35	0.77	0.35	18	A
		0.76	0.82	0.43	15	E
		0.84	2.11	1.29	67	D
	80	0.44	0.99	0.47	13	A
		0.93	0.91	0.38	7	E
		0.95	2.33	1.22	80	D
$[^{57}Fe_{0.1}Co_{0.9}(snnme)_2](ClO_4)_2$	297	0.38	0.88	0.28		
	80	0.47	0.87	0.29		
$[Fe(snnme)_2](ClO_4)_2\cdot2H_2O$	297	0.35	0.83	0.34		
	80	0.41	0.80	0.36		
$[Fe(snnme)_2](ClO_4)_2\cdot2H_2O$ irrad.[b]	80	0.45	0.81	0.33		

a) E: high-spin Fe(II). b) Total exposure dose is 5.2×10^8 R.

$(snn)_2](ClO_4)_2$. The high-spin chemical species D appearing in the emission spectrum recorded at 80 K for $[^{57}Co(snn)_2](ClO_4)_2$ disappeared as the source temperature was increased due to the decrease of the recoil free fraction.

The high-spin character of $[Co(snnme)_2](ClO_4)_2$ is enhanced in comparison with $[Co(snn)_2](ClO_4)_2$ as indicated by the effective magnetic moments. The emission spectra of $[^{57}Co(snnme)_2](ClO_4)_2$ at various temperatures are composed of three species (A, D, and E). It is worthy of note that high-spin iron(II) D appearing in the emission spectra of $[^{57}Co(snnme)_2](ClO_4)_2$ can be ascribed to a metastable state, because the ratio of the peak area of D to the total absorption area increases as the source temperature decreases, and this phenomenon is in good accord with that of $[^{57}Co(terpy)_2](ClO_4)_2\cdot2H_2O$. The three emission spectra of $[^{57}Co(snnme)_2](ClO_4)_2$ consist of two kinds of high-spin iron(II) (D and E) and low-spin iron(II) A. The species E ascribed to high-spin iron(II) is in a stable state with the ligands partly decomposed by autoradiolysis. The assumption that E is in a stable state is supported by the temperature independent ratio of the peak area of E to the total absorption area, and by the high value (>57) of the effective vibrating mass(EVM) as described later.

The absence of E in $[^{57}Co(snn)_2](ClO_4)_2$ or of B in $[^{57}Co(snnme)_2](ClO_4)_2$ can account for the fact that snn makes a stronger ligand field around the center atom than snnme; that is, the iron atom after EC-decay in the former complex is still in a low-spin state even if snn is exposed to secondary process following EC-decay because of its strong ligand field. On the other hand, the high-spin species is believed to be produced easily in the latter complex because the slight increase of the bond length between the iron atom and the coordination atom brings about a predominance of high-spin character.

External irradiation experiments with γ-rays were performed for $[Fe(snn)_2](ClO_4)_2$ and $[Fe(snnme)_2]$-

$(ClO_4)_2 \cdot 2H_2O$ and no chemical effect was observed in the irradiated samples.

Next we discuss the difference in the EVM for each chemical species of $[^{57}Co(snnme)_2](ClO_4)_2$, cobalt(II) complexes reported by other authors, and the corresponding iron complexes. The EVM can frequently be estimated from the second order Doppler shift, and is given by

$$M_{eff} = -\frac{3}{2} \times \frac{E_\gamma K}{c^2} \left(\frac{dIS}{dT} \right)^{-1}, \quad (1)$$

where E is the energy of the Mössbauer transition. The calculated data are listed in Table 5. The values of EVM obtained from the Mössbauer emission spectra is less than that from the absorption spectra for the corresponding iron compounds. The values for the metastable species D are smaller than the free-atom value 56.95 amu. On the other hand, it is interesting that the value obtained for E is larger than 56.95 amu. These results can reasonably be accounted for as follows. Equation 1 is based on a harmonic system. It is reasonable to conclude that the iron atom emerging in the emission spectra is in a excited state after EC-decay. Thus the local lattice vibrating behavior is no longer expressed in a harmonic system if anharmonicity remains on the time scale of 10^{-7}—10^{-8} s after EC-decay. It is reasonable to rewrite EVM as follows by considering the anharmonicity of the lattice vibration in order to supplement this model.

$$M_{eff} = -\frac{3}{2} \times \frac{E_\gamma K}{c^2} \left(\frac{dIS}{dT} \right)^{-1} (1 + 2\alpha KT) \quad (2)$$

where α is a positive coefficient derived from Thirring expansion.[27] This equation is useful for evaluating the EVM value for the chemical species in a metastable state. Namely, the value of EVM will exceed 56.95 amu if the second term in the parentheses (Eq. 2) is taken into account. The vibrational motion of the molecular moiety containing a daughter iron atom in a metastable state is disturbed by the "hot process" defined as all those processes occuring after EC-decay. Unfortunately, we cannot estimate the coefficient α because we cannot know the absolute value of EVM for a species in the metastable state. The value for E is calculated to be larger than 56.95 amu from Eq. 1, and this implies that E, rather than D, is in a stable state. The data for the other cobalt complexes listed in Table 5 are also interpreted in a similar manner. In this way, the daughter atoms in a metastable state can be distinguished from those in a stable state by evaluating the EVM value.

Table 5. Effective vibrating mass of each species appearing in absorption and emission Mössbauer spectra

Complex	l.s.	h.s.	h.s.[d]
$[Fe(snn)_2](ClO_4)_2$	128		
$[Fe(snnme)_2](ClO_4)_2 \cdot 2H_2O$	129		
$[Fe(phen)_2(NCS)_2]$	300		
$[Fe(phen)_2(CN)_2]$	134		
$[^{57}Co(snnme)_2](ClO_4)_2$	80	58	39
$[^{57}Co(pmi)_3](ClO_4)_2$[a]	90	73	27
$[^{57}Co(phen)_2(CN)_2]$[a]	115		44
$[^{57}Co(2\text{-}CH_3\text{-}phen)_3](ClO_4)_2$[b]	154±15		41±2
$[^{57}Co(phen)_2(NCS)_2]$[c]		56±3	

a—c) Data for the isomer shifts are quoted from Refs. 14, 12, and 11, respectively. d) Metastable state.

The origin of a metastable state is believed to be as follows in connection with bonding between an iron and a coordination atom.

(i) The bonds between the metal and the ligands are excited by the photoelectrons and X-rays emitted after Auger cascade.

(ii) Auger cascade produces a highly charged iron atom. The coulomb repulsion occurs between the highly-positive charged iron atom and the positively charged ligands; these arise from electron transfer from ligands to an iron atom in order to neutralize the positive charge on the iron atom, and the coulomb repulsion changes the bond length.

At the same time, inter- or intramolecular vibration modes are excited through the secondary process and the energy deposited on a daughter atom is released to this vibrational system. This relaxation time would be dependent on the temperature of the lattice system. The decrease and disappearance of D as the source temperature rises in the emission spectra of $[^{57}Co(terpy)_2](ClO_4)_2 \cdot 2H_2O$ and $[^{57}Co(snnme)_2](ClO_4)_2$, respectively, suggest that the energy deposited by EC-decay is easily transferred to the lattice system as phonons. In these cases the spin-orbit coupling of the iron atoms is presumed to play an important role in the rapid relaxation of the energy to the lattice system.

It is concluded that the stronger the low-spin character of the cobalt complexes and the lower the source temperature, the longer the lifetime of a metastable state. At low temperatures, several parts of the decayed atoms become observable in the metastable state because of the greater lifetime of this state.

References

1) J. M. Friedt and J. Danon, *Radiochem. Radioanal. Lett.*, **3**, 147 (1970).
2) J. M. Friedt and J. P. Adloff, *Inorg. Nucl. Chem. Lett.*, **5**, 163 (1969).
3) J. M. Friedt and Y. Llabador, *Radiochem. Radioanal. Lett.*, **9**, 237 (1972).
4) E. Baggio-Saitovitch, J. M. Friedt, and J. Dannon, *J. Chem. Phys.*, **56**, 1269 (1972).
5) H. Sano and F. Hashimoto, *Bull. Chem. Soc. Jpn.*, **38**, 1565 (1965).
6) H. Sano, K. Sato, and H. Iwagami, *Bull. Chem. Soc. Jpn.*, **44**, 2570 (1971).
7) H. Sano and H. Iwagami, *J. Chem. Soc., Chem. Commun.*, **1971**, 1637.
8) H. Sano and T. Ohnuma, *Chem. Phys. Lett.*, **26**, 348 (1974).
9) A. Nath, M. P. Klein, W. Kundig, and D. Lichtenstein, *Radiat. Eff.*, **2**, 211 (1970).
10) M. B. Miscroch, C. J. Schramm, Jr., and A. Nath, *J. Chem. Phys.*, **65**, 1982 (1976).
11) J. Ensling, P. Gütlich, and K. M. Hasselbach, *Chem. Phys. Lett.*, **42**, 232 (1976).

12) J. Fleish and P. Gutlich, *Chem. Phys. Lett.*, **42**, 237 (1976).
13) J. Fleish and P. Gütlich, *Chem. Phys. Lett.*, **45**, 29 (1977).
14) J. Ensling, J. Fleish, and P. Gütlich, *Chem. Phys. Lett.*, **45**, 22 (1977).
15) J. Fleish, P. Gütlich, and H. Koppen, *Radiochem. Radioanal. Lett.*, **42**, 279 (1980).
16) A. G. Maddock and J. J. Schleifer, *J. Chem. Soc., Dalton Trans.*, **1977**, 617.
17) J. Akashi, K. Endo, and H. Sano, *Radiochem. Radioanal. Lett.*, **43**, 129 (1980).
18) K. Endo, A. Amano, and H. Sano, *Radioisotope*, **28**, 215 (1979).
19) N. Ikeda, J. Akashi, and R. Seki, *Radiochem. Radioanal. Lett.*, **42**, 235 (1980).
20) Y. Hazony and R. H. Herber, *J. Phys. (Paris)*, **66**, 131 (1974).
21) J. G. Schmidt, W. S. Brey, and R. C. Staufer, *Inorg. Chem.*, **6**, 268 (1967).
22) P. S. K. Chia and S. E. Livingstone, *Aust. J. Chem.*, **22**, 1825 (1969).
23) P. S. K. Chia and S. E. Livingstone, *Aust. J. Chem.*, **22**, 1613 (1969).
24) Y. Maeda, H. Ohshio, and Y. Takashima, *Bull. Chem. Soc. Jpn.*, **53**, 1312 (1980).
25) Y. Maeda, H. Ohshio, and Y. Takashima, *Chem. Lett.*, **1980**, 1359.
26) H. Berlin and J. Schmand, *J. Phys. (Paris)*, Cl-135 (1980).
27) R. A. Sack, A. A. Maradudin, and G. H. Weiss, *Phys. Rev.*, **124**, 717 (1961).

Solvent Extraction of Alkali Metal Picrates with Poly- and Bis(benzo-12-crown-4)s

Takumi MAEDA, Keiichi KIMURA,* and Toshiyuki SHONO*

Department of Applied Chemistry, Faculty of Engineering, Osaka University, Yamadaoka, Suita, Osaka 565

(Received October 9, 1981)

Solvent extractions of alkali metal picrates were carried out using newly synthesized poly- and bis(crown ether)s containing benzo-12-crown-4 moieties in a water–chloroform system. The extraction equilibrium constants(K_e) and the complexation constants (K_c) in the chloroform phase were determined at 25 °C. The K_e values for the alkali metal cations decreases as follows: $Na^+ > K^+ > Rb^+ \geq Cs^+$ with the poly(benzo-12-crown-4) and K^+, Rb^+, $Cs^+ > Na^+$ with the bis(benzo-12-crown-4). The poly(benzo-12-crown-4) improved the sodium-ion selectivity of the corresponding monocyclic analog because of the easy formation of 2:1 crown ether unit-cation complexes assisted by the cooperative action of two adjacent crown ether units, while the bis(benzo-12-crown-4) did not. A separate extraction experiment was also undertaken in a water–dichloromethane system in order to compare the extractability of these benzo-12-crown-4 derivatives with that of 12-crown-4.

It is known that 12-crown-4 has a relatively small cavity, which seems to be suitable for forming stable complexes with Li^+ or Na^+. However, only a few papers have been published on the solvent extraction of metal cations using 12-crown-4 and its derivatives.[1,2] On the other hand, our previous work concerning the cation-binding ability of benzo-15-crown-5 and benzo-18-crown-6 derivatives has made it clear that poly- and bis(crown ether)s have much greater extractabilities and selectivities than their monocyclic analogs, especially for the cations which form 2:1 crown ether unit-cation complexes with them.[3–6] Some cooperative effects of adjacent crown ether units of the crown ethers were thought to bring about these results. This observation induced us to synthesize poly- and bis(crown ether)s containing benzo-12-crown-4 moieties and then to investigate their binding properties for alkali metal cations.

In this paper, we will consider the solvent extraction of alkali metal picrates with newly synthesized poly- and bis(crown ether)s **2**($n=1$), **3** and their monocyclic analogs **1**($n=1$), **4** in water–chloroform and water–dichloromethane systems.

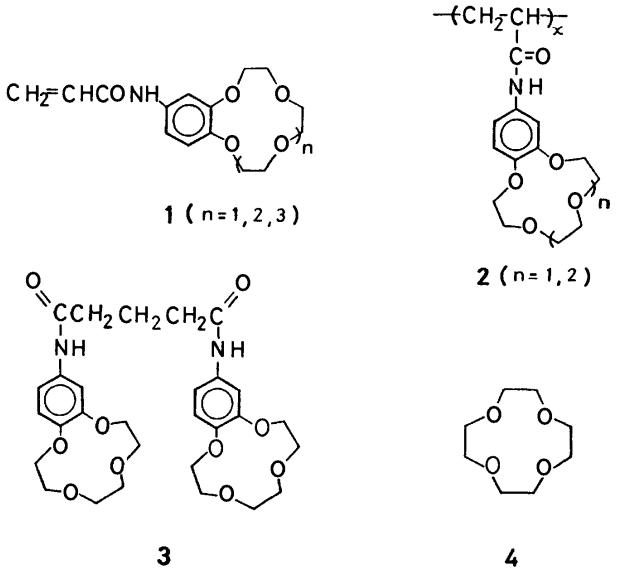

Fig. 1. Crown ether derivatives used in this study.

Experimental

Materials. 12-Crown-4 was obtained from Wako Pure Chemical Industries, Ltd., and used without further purification. Benzo-12-crown-4 was prepared according to Liotta's method.[7] The monocyclic crown ether **1**($n=1$) and poly- and bis(crown ether)s **2**($n=1$) and **3** were derived from benzo-12-crown-4 in the manner described elsewhere.[3] The analytical data of **1**($n=1$) and **3** are as follows: **1**($n=1$): mp 105.0—106.5 °C; M^+ 293. Found: C, 61.18; H, 6.70; N, 4.34%. Calcd for $C_{15}H_{19}O_5N$: C, 61.42; H, 6.53; N, 4.78%. **3**: Mp 170.0—171.0 °C; M^+ 574. Found: C, 60.20; H, 6.85; N, 4.88%. Calcd for $C_{29}H_{38}O_{10}N_2$: C, 60.62 H, 6.67; N, 4.88%. Poly(crown ether) **2**($n=1$) was purified by reprecipitation in chloroform–diethyl ether system. The alkali metal picrates were synthesized according to Fuoss' method.[8] Tetrahydrofuran (THF) was dried over sodium. Chloroform and dichloromethane were purified by distillation just before use.

Optical Spectra. Optical spectral changes in the above crown ether–cation complexes were measured by adding the crown ethers to 2.5×10^{-5} M(1 M = 1 mol dm^{-3}) THF solutions of alkali metal picrates. Measurements were carried out with a Hitachi 340 recording spectrophotometer.

Extraction. Equal volumes (10 ml) of organic and aqueous solutions were shaken in a stoppered flask for 40 min at 25±0.1 °C.

Chloroform was chosen primarily as the organic phase for extraction. However, in order to compare the extractabilities and cation selectivities of the crown ethers **1**, **2** ($n=1$), and **3** with those of **4**, solvent extractions were also carried out with a dichloromethane solution of the crown ethers (1.4×10^{-2} M or 3.5×10^{-3} M for crown ether units) and an aqueous solution of alkali metal hydroxide (1.0×10^{-2} M) and picric acid(7.0×10^{-4} M), because the chloroform solution containing **4** often became turbid.

Extraction equilibrium constants with **1**, **2**($n=1$), and **3** were calculated in a water–chloroform system. In this system, the concentrations of the crown ether in the organic phase were $(1.0—5.0)\times10^{-4}$ M for **2** ($n=1$) and $(1.0—5.0)\times10^{-3}$ M for **1** ($n=1$) and **3**, while that of the alkali metal picrate in the aqueous phase was 1.0×10^{-2} M. After the complete phase separation, a 2-ml portion of acetonitrile was added to 2 ml of the chloroform phase, and the concentration of the picrate was determined spectrophotomerically[$\lambda_{max}=374$ nm, ε: Na^+ 1.86, K^+ 1.87, Rb^+ 1.88, Cs^+ 1.86 ($\times10^4$ M^{-1} cm^{-1})]. The distribution constants of

the picrates in the absence of crown ethers, K_d, have been obtained previously [Na^+ 1.20, K^+ 2.67 Rb^+ 3.66, Cs^+ 6.66 ($\times 10^{-3}$ M^{-1})].[4]

Extraction Equilibrium Constant and Complexation Constant for the Organic Phase. The overall extraction equilibrium may be written as:

$$M^+ + Pi^- + n\text{Cr}^* \rightleftharpoons M(\text{Cr})_n\text{Pi}^*$$

$$K_e = [M(\text{Cr})_n\text{Pi}^*]/[M^+][Pi^-][\text{Cr}^*]^n \quad (1)$$

where M^+, Pi^-, and Cr denote an alkali metal cation, a picrate anion, and a crown ether unit, respectively. The asterisk refers to the species in the organic phase.[9] This equilibrium consists of the following equilibria:[10]

$$M^+ + Pi^- \rightleftharpoons \text{MPi}^*$$

$$K_d = [\text{MPi}^*]/[M^+][Pi^-], \quad (2)$$

$$\text{MPi}^* + n\text{Cr}^* \rightleftharpoons M(\text{Cr})_n\text{Pi}^*$$

$$K_c = [M(\text{Cr})_n\text{Pi}^*]/[\text{MPi}^*][\text{Cr}^*]^n. \quad (3)$$

K_c represents the complexation constant in the organic phase, which can be calculated with Eq. 4;

$$K_c = K_e/K_d. \quad (4)$$

In the same way as has been described in the previous paper, the following relations can be derived;[4,11]

$$D = K_e(M^\circ - A)(Cr^\circ - A), \quad (5)$$

$$D = K_e(M^\circ - A)(Cr^\circ - 2A)^2, \quad (6)$$

$$D = K_e(M^\circ - A)(Cr^\circ - 2A), \quad (7)$$

where D is the distribution ratio of the metal between the two phases. M°, Cr°, and A denote the initial concentrations of metal cations and crown ether units, and the concentrations of the picrates extracted into the organic phase as the counter anions, respectively. Equation 5 is applied when 1:1 crown ether unit-cation complexes are formed. When 2:1 crown ether unit-cation complexes are formed by monomeric crown ethers, Eq. 6 is used. However, in the system of poly- and bis(crown ether)s, which may be thought to form intramolecular 2:1 crown ether unit-cation complexes, Eq. 7 can be applied.

Results and Discussion

Optical Spectra of Alkali Metal Picrates and Their Crown Ether Complexes. Optical spectral changes of alkali metal picrates in THF accompanying an increase in the concentration of crown ether units suggest the stoichiometry of the crown ether unit-cation complexes qualitatively.[6,12] The maxima of the main absorption band, λ_{max}, for alkali metal picrates are found to be at 351 nm (Na^+), 358 nm (K^+), 359 nm (Rb^+), and 361 nm (Cs^+). In their complexes with crown ethers, the increase in the distance between cations and counter anions causes bathochromic shifts of the spectrum. When 1:1 crown ether unit-cation complexes are formed, cations and their counter anions are close to each other, forming tight ion-pairs. In this case, the bathochromic shift is not very large. On the other hand, in 2:1 crown ether unit-cation complexes, cations are forced to separate from their counter anions, which results in the large spectral shift to nearly 380 nm. Figure 2 shows some typical optical spectra for the 1:1 and 2:1 crown ether unit-cation complexes. In the **3**–Na^+ system, the addition of a large excess of crown ethers (the molar ratio of crown ether unit to picrate salt is 100) causes a spectral shift to only 353 nm, which suggests that 1:1 crown ether unit-cation complexes are formed. On the contrary, in the system of **2**(n=1)–Na^+, the absorption maximum shifts to 378 nm, showing the formation of 2:1 crown ether unit-cation complexes. However, a much higher concentration of crown ether units is needed for the pronounced bathochromic shift of the spectrum in the **2**(n=1)–Na^+ system than for that in the system of **2**(n=2)–K^+, which suggests that the complexation constant of the **2**(n=1)–Na^+ complex is quite small. From the results of similar experiments for other systems, the stoichiometry of these complexes was determined to be as follows: for Na^+ through Cs^+, only **2**(n=1) forms 2:1 crown ether unit-cation complexes; **1**(n=1) and **3** form 1:1 complexes.

Extraction Equilibria. Table 1 shows a considerable difference in the extractability for Na^+ between **1**(n=1) and **4**, although they have the same number of oxygen atoms. For the system of **4**, the extractability apparently depends on the relation between the cation size and the cavity size of **4**. For the sys-

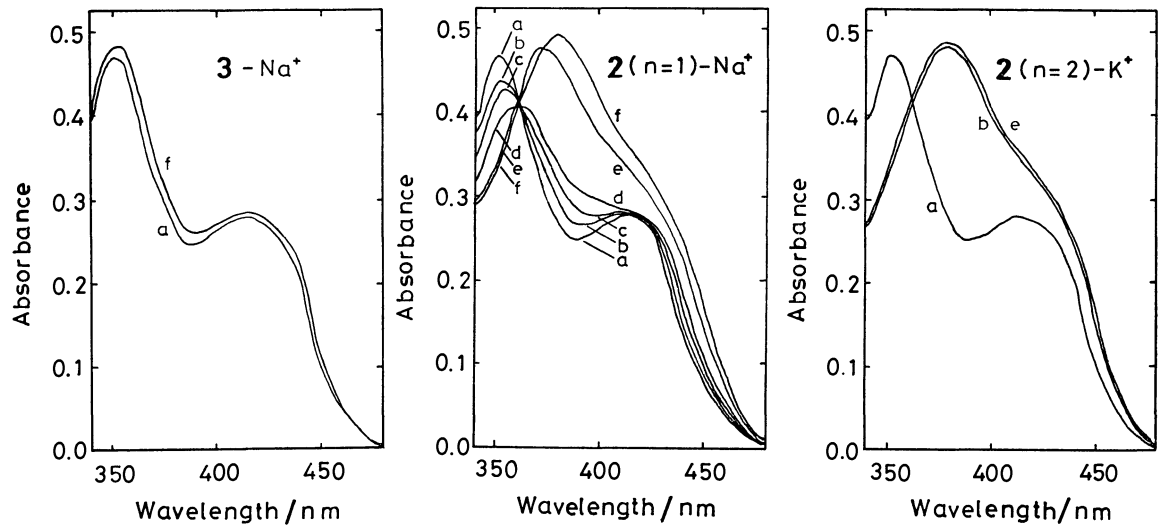

Fig. 2. Optical spectra of picrate solutions in THF in the presence of various amounts of crown ethers. [Metal picrates]=2.5×10^{-5} M, [crown ether unit]/[metal picrate]: a; 0, b; 3, c; 5, d; 10, e; 50, f; 100.

TABLE 1. EXTRACTION OF ALKALI METAL PICRATES WITH 12-CROWN-4 DERIVATIVES IN H_2O-CH_2Cl_2 SYSTEM[a]

Crown	Picrate salt extracted (%)			
	Na^+	K^+	Rb^+	Cs^+
1(n=1)	5.81	9.10	10.1	10.3
2(n=1)	78.3 (36.1)	63.3 (25.3)	53.6 (20.5)	50.6 (18.7)
3	17.2	19.4	18.8	19.4
4	18.6	6.90	4.30	3.50

a) [Picric acid]=7×10^{-4} M, [metal hydroxide]=1×10^{-2} M, [crown ether unit]=1.4×10^{-2} M(3.5×10^{-3} M in parentheses).

TABLE 2. DISTRIBUTION RATIOS OF ALKALI METAL CATIONS IN H_2O-$CHCl_3$ SYSTEM[a]

Crown	D ($\times10^{-3}$)			
	Na^+	K^+	Rb^+	Cs^+
1(n=1)	(0.670)	(1.85)	(2.20)	(2.55)
2(n=1)	7.15	6.67	4.68	4.43
3	(5.03)	(6.19)	(5.76)	(5.44)
1(n=2)	5.26[b]	16.7	9.72	0.708[b]
1(n=3)	6.16[b]	53.2	47.3	46.9

a) [Picrate]=1×10^{-2} M, [crown ether unit]=5×10^{-4} M (5×10^{-3} M in parentheses). b) Taken from Ref. 4.

tem of **1**(n=1), the distribution of picrate itself from the aqueous phase to the dichloromethane phase, the order of which can be expected to be the same as that in chloroform ($Cs^+>Rb^+>K^+>Na^+$, see Experimental), might contribute significantly to the extractability compared to the complexing ability, probably because the benzene ring decreases the basicity of the oxygen atoms adjacent to aromatic carbons,[13] which seems to lower the complexing ability. Poly(crown ether) **2**(n=1) has a much greater extractability for Na^+ than the others. Because of the extremely strong hydration, very little Li^+ was extracted [*e.g.*, <1% for **1**(n=1)], so no further investigation was made with respect to Li^+. Values of distribution ratios, D, are useful for comparing the extractability of the crown ethers for these cations. Since **1**(n=1) and **3** have much smaller extractabilities than **2**(n=1) and **1**(n=2, 3), the concentrations of **1**(n=1) and **3** in extractions were ten times higher than those of **2**(n=1) and **1**(n=2, 3). It should be noted that poly(crown ether) **2**(n=1) has a larger extractability and selectivity for Na^+ than **1**(n=2, 3) does.

The plots of logarithms of both sides in Eqs. 5—7 gave straight lines with a slope of 1, indicating that the stoichiometry of the complexes and the assumptions used for the derivation of these equations are reasonable. Figure 3 shows the plots for the **2**(n=1) systems as the examples. The values of log K_e, which are obtained from the intercepts of the lines, and those of log K_c, which are calculated from Eq. 4, are listed in Tables 3 and 4. There is a close correlation between the D and K_e values. **1**(n=1) and **3** have very small log K_e values for all the cations. The order of log K_e

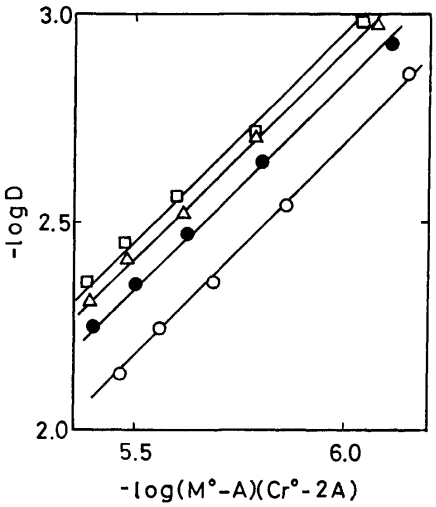

Fig. 3. Plots of $-\log D$ *vs.* $-\log(M°-A)(Cr°-2A)$ for poly(crown ether) **2**(n=1) systems.
○: Na^+, ●: K^+, △: Rb^+, □: Cs^+.

TABLE 3. EXTRACTION EQUILIBRIUM CONSTANTS IN H_2O-$CHCl_3$ SYSTEM AT 25 °C

Crown	log K_e[a]			
	Na^+	K^+	Rb^+	Cs^+
1(n=1)	1.12	1.56	1.64	1.70
2(n=1)	3.30	3.16	3.08	3.04
3	2.00	2.10	2.07	2.05
1(n=2)[b]	3.10	(7.10)	(6.54)	(5.59)
1(n=3)[b]	3.16	5.22	4.64	4.24

a) The unit of K_e is M^{-2} (M^{-3} in parentheses). b) Taken from Ref. 4.

TABLE 4. COMPLEXATION CONSTANTS IN CHLOROFORM PHASE AT 25 °C

Crown	log K_c[a]			
	Na^+	K^+	Rb^+	Cs^+
1(n=1)	4.04	4.13	4.08	3.88
2(n=1)	6.22	5.73	5.52	5.22
3	4.92	4.67	4.51	4.23
1(n=2)[b]	6.02	(9.67)	(8.98)	(7.77)
1(n=3)[b]	6.08	7.79	7.08	6.42

a) The unit of K_c is M^{-1} (M^{-2} in parentheses). b) Taken from Ref. 4.

values for alkali metal ions with **1**(n=1) and **3** are $Cs^+>Rb^+>K^+>Na^+$ and K^+, Rb^+, $Cs^+>Na^+$, respectively. On the other hand, a relatively high selectivity for Na^+ was observed with poly(crown ether) **2**(n=1).

The stoichiometry of the crown ether unit-cation complexes is likely to have a correlation with these results. When we compare the relative size of the cavity of 12-crown-4 and alkali metal cations (cavity radius: 12-crown-4 0.5—0.65 Å[1], ionic radius: Na^+ 0.95 Å, K^+ 1.33 Å, Rb^+ 1.48 Å, Cs^+ 1.69 Å[14]), **1**, **2**(n=1), and **3** may be anticipated to form 2:1 crown ether unit-cation complexes. Nevertheless, the formation of the 2:1 crown ether unit-cation complexes was ob-

served only with **2**(n=1) (see the optical measurement section). For the systems of **1**(n=1) and **3**, the comparison of the values of log K_e and log K_c shows a large difference in the sequence between them, which suggests that the extractability for the cations depends mainly on the value of K_d and not on that of K_c. However, poly(crown ether) **2**(n=1), which may be thought to have a close proximity of adjacent crown ether moieties induced by the rigidity of its comformation, may be able to form 2:1 crown ether unit-cation complexes more easily than **1**(n=1) and **3**. Therefore, the suitable structure of the crown ether to form the 2:1 crown ether unit-cation complex with Na^+ may result in the selective binding of **2**(n=1) for Na^+. Moreover, the large lipophilicity of **2**(n=1) may also be thought to bring about its high extractability for Na^+, which is comparable to that of **1**(n=2,3). In this case, the values of log K_e reflect those of log K_c. That is to say, the extractability of **2**(n=1) for the cations depends mainly on the values of K_c and not on those of K_d, as was observed in our previous work with benzo-15-crown-5 and benzo-18-crown-6 derivatives.[4,5]

In conclusion, the newly synthesized poly(crown ether) **2**(n=1) forms 2:1 crown ether unit-cation complexes with alkali metal cations, and the cooperative effect of two adjacent crown ether units of **2**(n=1) in forming the 2:1 complexes brings about the selectivity and the large extractability for Na^+.

References

1) Y. Takeda, *Bull. Chem. Soc. Jpn.*, **53**, 2393 (1980).
2) Y. Takeda, *Bull. Chem. Soc. Jpn.*, **54**, 526 (1981).
3) K. Kimura, T. Maeda, and T. Shono, *Anal. Lett.*, **A11** 821 (1978).
4) K. Kimura, T. Maeda, and T. Shono, *Talanta*, **26**, 945 (1979).
5) T. Maeda, K. Kimura, and T. Shono, *Fresenius' Z. Anal. Chem.*, **298**, 363 (1979).
6) K. Kimura, T. Tsuchida, T. Maeda, and T. Shono, *Talanta*, **27**, 801 (1980).
7) F. L. Cook, T. C. Caruso, M. P. Byrne, C. W. Bowers, D. H. Spec, and C. L. Liotta, *Tetrahedron Lett.*, **1974**, 4029.
8) M. A. Coplan and R. M. Fuoss, *J. Phys. Chem.*, **68**, 1177 (1964).
9) K. H. Wong, K. Yagi, and J. Smid, *J. Membr. Biol.*, **18**, 379 (1979).
10) J. M. Timko, S. S. Moore, D. M. Walba, P. C. Hiberty, and D. J. Cram, *J. Am. Chem. Soc.*, **99**, 4207 (1977).
11) A. Sadakane, T. Iwachido, and K. Toei, *Bull. Chem. Soc. Jpn.*, **48**, 60 (1975).
12) M. Bourgoin, K. H. Wong, J. Y. Hui, and J. Smid, *J. Am. Chem. Soc.*, **97**, 3462 (1975).
13) C. J. Pedersen, *J. Am. Chem. Soc.*, **89**, 7017 (1967).
14) L. Pauling, "The Nature of the Chemical Bond," 3rd ed, Cornell Univ. Press, Ithaca, New York (1960).

Graphite Furnace Atomic Absorption Spectrometry with a Tantalum Boat for the Determination of Yttrium, Samarium, and Dysprodium in a Mish Metal

Hidehiro DAIDOJI* and Shohei TAMURA

The Institute for Solid State Physics, The University of Tokyo, Roppongi, Minato-ku, Tokyo 106

(Received January 12, 1982)

The determination of yttrium, samarium, and dysprodium by means of graphite-furnace atomic absorption spectrometry (AAS) was studied by a tantalum boat inserted into a graphite tube atomizer. These elements could not be determined by the use of a commercial graphite tube. In the atomization from a tantalum boat, better analytical sensitivities and negligible memory effects for these rare earths are obtained. The analytical sensitivities of yttrium, samarium, and dysprodium with the tantalum boat were 0.60 ng, 0.86 ng, and 0.17 ng respectively. This method was applied for the determination of yttrium, samarium, and dysprodium in a mish metal. The measurements were performed with slightly acidified solutions (0.01 mol dm^{-3} HCl or HNO_3). The sensitivities and the precisions for these elements decreased with increasing acid concentration. An enhancement in the sensitivities of yttrium and dysprodium upon the addition of a large excess of lanthanum, neodymium, and praseodymium salts were observed. The yttrium, samarium, and dysprodium in a mish metal were determined with both analytical curves of standard solutions containing an excess of lanthanum, cerium, and neodymium ions and of the standard addition. The precisions for this work were in the 3—9.3% range.

Atomic absorption analysis in an electrically heated graphite atomizer has a number of disadvantages. The graphite itself has been improved to overcome these problems. Particularly, a graphite-tube atomizer pyrocoated with a hydrocarbon such as methane has recently been used. Attempts have also been made to use a pre-coated graphite tube with salts of tantalum,[1,2,6] zirconium,[3,4] tungsten,[5] or lanthanum.[3,6] Other attempts have been to use a tantalum or tungsten liner, collar or wire inserted inside the graphite furnace.[7–15] Enhancements in the sensitivity of many elements were obtained with a metal liner, collar, or wire, because metal carbide formation in these causes is impossible. There have been few studies for the determination of rare earths by means of graphite-furnace atomic absorption spectrometry (AAS). Dittrich[16] determined traces of rare earths by means of electrothermal atomization with a carbon rod, a graphite furnace, and a tantalum ribbon. Kuga[17] and Grobenski[18] measured rare earth by the use of a pyrolitic graphite-coated tube. Sastry[6] repoated the determination of rare earth in uranium by the use of a pyrolitic carbon-coated tube pre-coates with lanthanum, tantalum, or yttrium. Moreover, Wahab[14,15] studied the atomization of yttrium using a pyrocoated graphite tube, a carbidized graphite tube, and tantalum or tungsten foil.

In this work, we determined yttrium, samarium, and dysprodium in a mish metal by the use of a laboratory-made tantalum boat inserted inside a graphite tube.

Experimental

Instrumentation. A Nippon Jarrel-Ash atomic absorption spectrophotometer, AA-1E, fitted with a flameless atomizer, FLA 100, A Hamamatsu TV deuterium Arc lamp, and hollow cathode lamps, was used.

Reagents. Stock solutions of 1000 or 2000 μg ml^{-1} of yttrium, samarium, dysprodium, praseodymium, neodymium, and lanthanum were prepared from oxides of these elements dissolved in hydrochloric acid and nitric acid respectively. Stock solutions of 1000 μg ml^{-1} aluminum and iron were prepared from high-purity metals dissolved in hydrochloric acid and nitric acid respectively. A stock solution of 5000 μg ml^{-1} cerium was prepared from cerium nitrate dissolved in distilled water. The acidities of these solutions were 0.1—0.5 mol dm^{-3}. Analytical solutions were prepared from stock solutions by dilution with distilled water. Distilled water was prepared by the distillation of Milli-Q water.

Tantalum Boat. The tantalum boat was made by cutting pure tantalum foil (99.95%) 0.1 mm thick and exerting pressure on it. This boat was then fitted in a commercial graphite tube with an inner diameter of 3.2 mm, as is shown in Fig. 1.

Procedure. A comparison of the situation with and without the tantalum boat was achieved by the injection of volumes (10 μl) of standard solutions and by the subsequent measurement of the peak absorbance. The hollow cathode lamps were used at 14 mA for yttrium, at 10 mA for samarium, and at 12 mA for dysprodium. The argon flow rate through the graphite furnace was 2.0 l min^{-1}.

Results and Discussion

The ashing and atomizing conditions in the use of the tantalum boat for yttrium, dysprodium, and samarium are shown in Figs. 2—4. The dotted lines in each figure show the relationship between the absorbances (as the peak height) and the ashing temperature. The full lines show the relationship between the absorbances and the atomizing temperature. The operating conditions selected from these results are shown in Table 1. When yttrium, samarium, and dysprodium are determined under these operating conditions, the absolute sensitivities are obtained as 0.60 ng for yttrium, 0.86 ng for samarium, and 0.17 ng for dysprodium. These sensitivities are similar to the values in previous reports.[6,13,17,18] The sensitivity of samarium by the use of a commercial graphite tube is obtained as 20 ng. In this determination, a strong memory effect of carbide formation is observed. The determinations of yttrium and dysprodium by the use

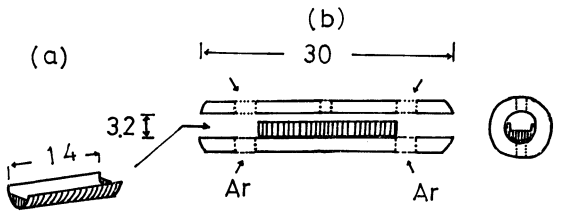

Fig. 1. Design of tantalum boat (a) and commercial graphite tube (b) used in this study.

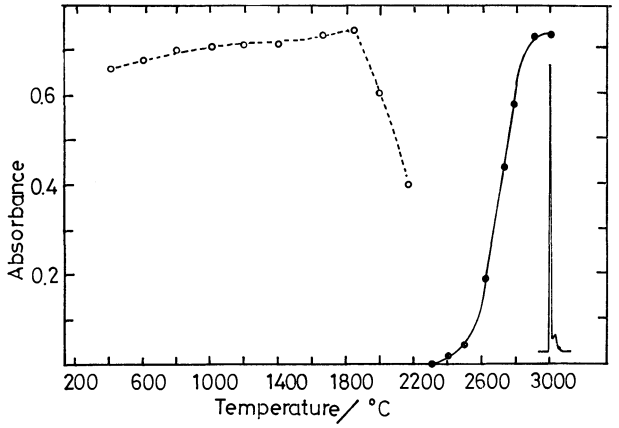

Fig. 2. Ashing and atomizing conditions for yttrium of 100 ng at 410.2 nm.
Dry: 120 °C, --O-- ashing: 40 s, atomizing-3000 °C-7 s, —●— atomizing: ashing-1600 °C-40 s.

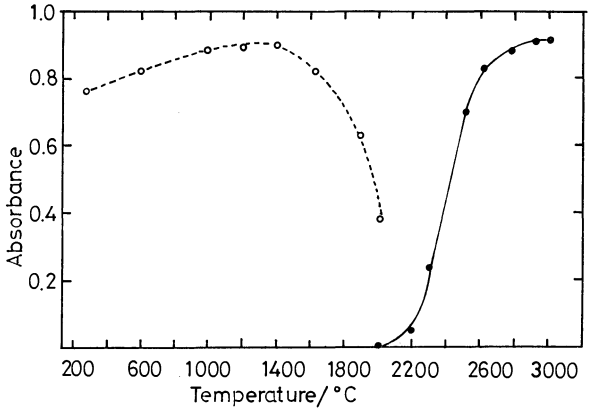

Fig. 3. Ashing and atomising conditions for dysprodium of 43 ng at 421.1 nm.
Dry: 120 °C, --O-- ashing: 40 s, atomizing-2900 °C-7 s, —●— atomizing: ashing-1400 °C-40 s.

of the graphite tube were impossible, because the memory effects by the formation of the refractory carbides of these elements are too great.

Wavelength and Sensitivity. Tables 2—4 show several atom lines of yttrium, dysprodium, and samarium, the relative intensities emitted by the hollow cathode lamps, the *gf* values,[21] and the absorbances of 50 ng of yttrium, 43 ng of dysprodium, and 100 ng of samarium by the use of the tantalum boat. Wahab[13,14] and Manning[19] used 407.7 nm in the determination of yttrium. In this work, the atom line at 410.2 nm shows the highest intensity and the maximum absorption of all the atom lines of yttrium. For dysprodium,

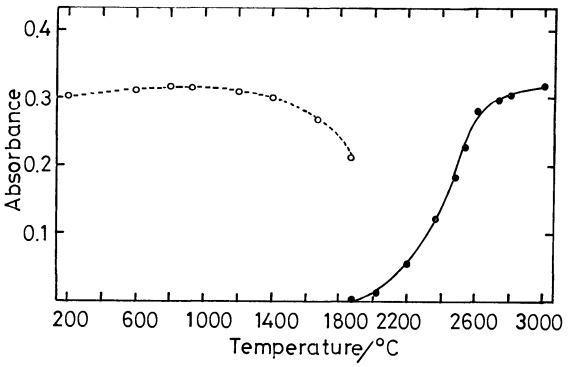

Fig. 4. Ashing and atomizing conditions for samarium of 100 ng at 429.7 nm.
--O-- Ashing: 40 s, atomizing-2900 °C, —●— atomizing: 10 s, ashing-900 °C.

Table 1. Operating conditions for the determination of Y, Dy, and Sm with a tantalum boat inserted inside a graphite tube

Wavelength nm		Temperature/°C (Time/s) Drying	Ashing	Atomizing
Y	410.2	120 (30)	1600 (40)	3000 (10)
Dy	421.1	120 (30)	1400 (40)	2900 (10)
Sm	429.7	120 (30)	900 (40)	2900 (10)

Table 2. Relative intensity and absorbance for yttrium at various wavelengths

Wavelength/nm	Relative intensity	*gf*[a]	Absorbance[b]
410.2	100	1.3	0.375
407.7	78	1.1	0.270
414.3	52	0.8	0.222
412.8	78	1.1	0.155
417.4	22	0.24	0.098
464.3	83	0.12	0.082
416.8	13	0.29	0.045

a) C. H. Corliss and W. R. Bozman, NBS Monograph 53. b) 50 ng of yttrium.

the most sensitive lines are observed at 421.1 nm and 419.4 nm. The sensitivity at 419.4 nm is high in comparison with the results obtained by the use of a nitrous oxide–acetylene flame.[19,20] For samarium, absorbances are obtained at various atom lines.

Effect of Acids and Matrix Elements. The effects of acids for the determined elements are shown in Figs. 5—7. The sensitivities and precisions for these elements decrease with increasing acid concentration. Therefore, the acidity for the determination of these elements is selected as 0.01 mol dm^{-3} HCl for yttrium and dysprodium and as 0.01 mol dm^{-3} HNO_3 for samarium. The effect of acids for samarium differ from those in the previous report using pyrolitic-coated graphite tube.[18]

Graphite-furnace AAS, with the tantalum boat inserted inside the graphite tube, was used for the determination of yttrium, dysprodium, and samarium in a mish metal. The composition of a mish metal con-

TABLE 3. RELATIVE INTENSITY AND ABSORBANCE FOR DYSPRODIUM AT VARIOUS WAVELENGTHS

Wavelength/nm	Relative intensity	Absorbance[a)]
421.1	100	0.910
419.4	52	0.905
418.6	67	0.855
404.6	70	0.820
422.1	15	0.175
416.8	33	0.140
421.5	12	0.110
422.5	7	0.050

a) 43 ng of dysprodium.

TABLE 4. RELATIVE INTENSITY AND ABSORBANCE FOR SAMARIUM AT VARIOUS WAVELENGTHS

Wavelength/nm	Relative intensity	gf[a)]	Absorbance[b)]
429.7	52	5.7	0.310
444.2	50	0.56	0.262
476.0	60	1.1	0.248
472.8	42	1.5	0.248
478.3	51	0.77	0.248
511.7	75	?	0.248
464.9	37	0.42	0.244
458.2	43	0.34	0.236
459.6	27	?	0.230
520.0	100	0.49	0.228
471.7	52	0.35	0.200
436.3	25	0.48	0.200
527.1	56	0.63	0.194
464.5	25	0.28	0.180
484.1	37	3.6	0.174
488.4	100	0.27	0.168
428.2	54	2.0	0.142
468.9	24	0.91	0.142
433.6	38	0.12	0.142
478.5	41	0.54	0.142
440.3	32	1.0	0.138
467.1	44	0.62	0.136
491.8	29	0.73	0.120
484.8	23	0.61	0.088
438.0	12	0.86	0.086
504.4	29	2.2	0.086
497.6	12	0.25	0.080
540.4	100	0.17	0.054
534.1	67	0.15	0.052
551.6	47	0.50	0.050

a) NBS Monograph 53. b) 100 ng of samarium.

sists of 45% cerium, 30% lanthanum, 15% neodymium, 4% praseodymium, and small percentage of iron, aluminum, and silicon. The interferences of these matrix elements with the determinations of yttrium, dysprodium, and samarium are shown in Figs. 8—10. Enhancements in the absorption sensitivity of yttrium are observed with increasing lanthanum, praseodymium, and neodymium concentrations. With increasing samarium concentration, the absorption of yttrium decreases. The sensitivity of dysprodium is

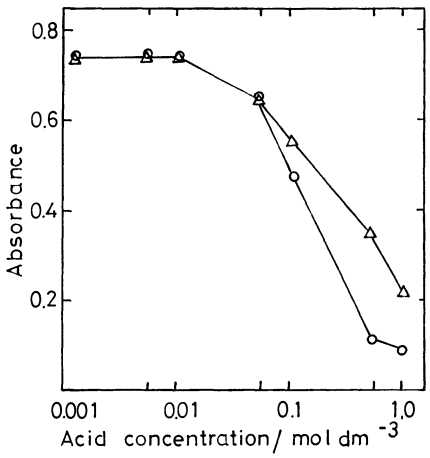

Fig. 5. Effect of acids on absorbance of yttrium of 100 ng.
○: HCl, △: HNO_3.

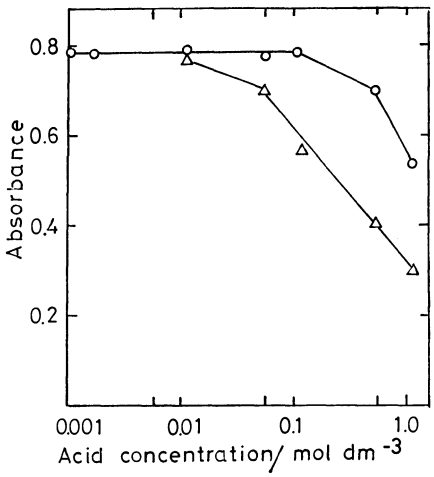

Fig. 6. Effect of acids on absorbance of dysprodium of 43 ng.
○: HCl, △: HNO_3.

enhances by increasing lanthanum, praseodymium, cerium and neodymium concentrations. The effects of other elements are negligible. In the determination of samarium, the effect of iron is important. The existence of 100 μg ml^{-1} of iron causes a remarkable decrease in the absorbance of samarium. However, the effect of iron in this sample is slight, for the concentration of iron in this sample is below 50 μg ml^{-1}. The sensitivity of samarium is slightly decreased by the presence of lanthanum and neodymium. The effects of the other elements on samarium are negligible.

Two samples of about 0.5 g were dissolved in hydrochloric acid and in nitric acid. The sample solution containing hydrochloric acid was used to analyze the yttrium and dysprodium, while the other solution was used to analyze the samarium. The determinations of these elements were done by the following two methods. One method used the analytical curves in the range of 1.0—6.0 μg ml^{-1} of yttrium and in the range of 0.5—3.0 μg ml^{-1} of dysprodium. To these standard solutions of yttrium and dysprodium we added 500 μg ml^{-1} of lanthanum, 600 μg ml^{-1} of cerium,

Table 5. Comparison between determinations of Y, Dy, and Sm by graphite-furnace AAS with a tantalum boat and by flame AAS

	Graphite-furnace AAS				Flame AAS	
	Standard[a]		Standard addition		Standard addition	
	Found(wt%)	RSD(%)	Found(wt%)	RSD(%)	Found(wt%)	RSD(%)
Y	0.70_2	3.1	0.69_4	9.3	0.69	2.5
Dy	0.20_2	5.5	0.19_0	2.6	0.19	1.6
Sm	0.82_4	8.2	0.81_7	3.6	0.80	1.8

a) Standard method (1.0—6.0 μg ml^{-1} of Y+0.5—3.0 μg ml^{-1} of Dy)+500 μg ml^{-1} of La+600 μg ml^{-1} of Ce+300 μg ml^{-1} of Nd, (1.0—6.0 μg ml^{-1} of Sm)+500 μg ml^{-1} of La+600 μg ml^{-1} of Ce+100 μg ml^{-1} of Nd. b) RSD: relative standard deviation, $n=10$.

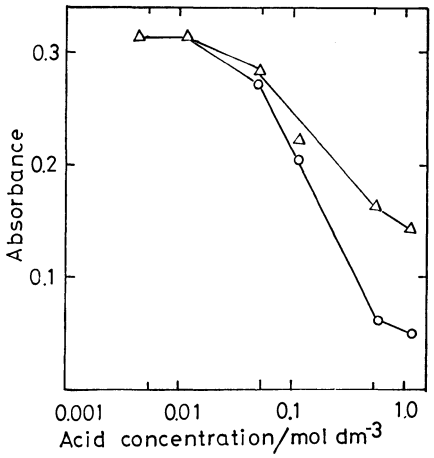

Fig. 7. Effect of acids on absorbance of samarium of 100 ng.
○: HCl, △: HNO_3.

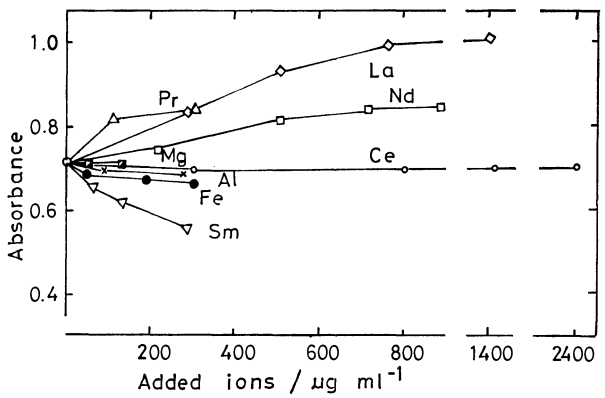

Fig. 8. Effect of matrix elements on absorbance of yttrium of 10 μg ml^{-1}.

and 300 μg ml^{-1} of neodymium. To the other solutions containing 1.0—6.0 μg ml^{-1} of samarium, we added 500 μg ml^{-1} of lanthanum, 600 μg ml^{-1} of cerium, and 100 μg ml^{-1} of neodymium. The other method used the analytical curves obtained by standard addition. Both analytical curves for each element gave identical slopes. These results are shown in Table 5. The precision of these determinations was in the range of 3—9.3%. It was found that the concentrations of these elements in a mish metal was 0.70% for yttrium, 0.20% for dysprodium, and 0.82% for

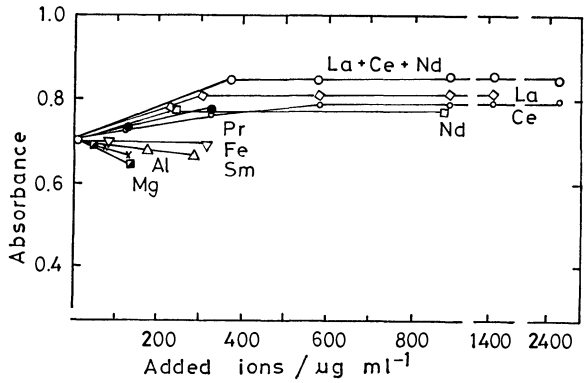

Fig. 9. Effect of matrix elements on absorbance of dysprodium of 4.3 μg ml^{-1}.

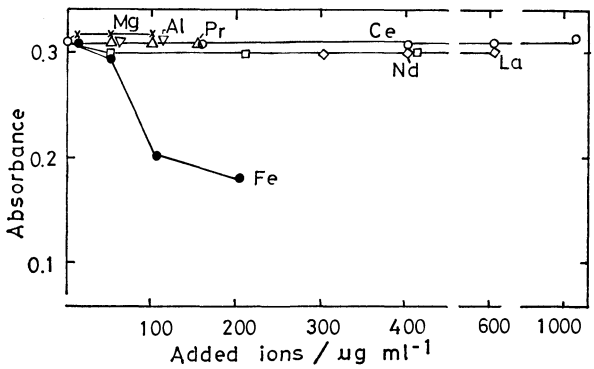

Fig. 10. Effect of matrix elements on absorbance of samarium of 10 μg ml^{-1}.

samarium. It was also estimated by flame AAS; these results are shown in Table 5.

Conclusion

Yttrium, dysprodium, and samarium are determined by the means of graphite-furnace AAS with a tantalum boat inserted inside a graphie tube. In this method, the memory effect of carbide formation is negligible and the analytical sensitivities of these elements suffice for the determination of this sample.

References

1) V. J. Zatk, *Anal. Chem.*, **50**, 538 (1978).
2) J. Takahashi, T. Kitahara, N. Hirabayashi, K. Sato,

K. Yoshida, H. Haraguchi, and K. Fuwa, *Bunseki Kagaku*, **30**, 90 (1981).
3) J. H. Runnels, R. Merryfield, and H. B. Fisher, *Anal. Chem.*, **47**, 1258 (1975).
4) K. Kuga, *Bunseki Kagaku*, **30**, 529 (1981).
5) E. Norval, H. G. C. Human, and R. P. Butler, *Anal. Chem.*, **51**, 2046 (1979).
6) M. D. Sastry, M. K. Bhide, K. Savitri, Y. Babu, and B. D. Joshi, *Fresenius' Z. Anal. Chem.*, **298**, 367 (1979).
7) C. D. Wall, *Talanta*, **24**, 755 (1977).
8) C. W. Fuller, *Analyst*, **99**, 739 (1974).
9) R. B. Baird and S. M. Gabrielian, *Appl. Spectrosc.*, **28**, 273 (1974).
10) C. D. Renshaw, *At. Absorp. Newsl.*, **12**, 158 (1973).
11) J. Aggett and A. J. Sprott, *Anal. Chim. Acta*, **72**, 49 (1974).
12) D. C. Manning, W. Slavin, and S. Mayers, *Anal. Chem.*, **51**, 2375 (1979).
13) D. C. Manning and W. Slavin, *Anal. Chim. Acta*, **118**, 301 (1980).
14) H. S. Wahab and C. L. Chakrabariti, *Spectrochim. Acta, Part B*, **30**, 463 (1981).
15) H. S. Wahab and C. L. Chakrabariti, *Spectrochim. Acta, Part B*, **30**, 477 (1981).
16) K. Dittrich, E. John, and I. Rohde, *Anal. Chim. Acta*, **94**, 75 (1977).
17) K. Kuga and K. Tuji, *Bunseki Kagaku*, **27**, 441 (1978).
18) Z. Grobenski, *Fresenious' Z. Anal. Chem.*, **289**, 337 (1978).
19) D. C. Manning, *At. Absorp. Newsl.*, **5**, 131 (1966).
20) K. Fuwa, S. Shimomura, and S. Toda, "Atomic absorption Spectrometry," Hirokawa Publishing Co., Tokyo (1980), pp. 630, 637.
21) C. H. Corliss and W. R. Bozman, NBS Monograph 53, "Experimental Transition Probabilities for Spectral Lines of Seventy Elements," NBS, Washington, D.C. (1962).

Spectrophotometric and Electrochemical Investigations of [Tetrakis(1-methylpyridinium-4-yl)porphine]iron(III) Ion in Aqueous Solution

Hirondo KURIHARA,* Fumihiro ARIFUKU, Isao ANDO, Minoru SAITA, Rika NISHINO, and Kikujiro UJIMOTO

Department of Chemistry, Faculty of Science, Fukuoka University, Nanakuma 11, Jonan-ku, Fukuoka 814-01

(Received February 4, 1982)

The equilibria among the species of [tetrakis(1-methylpyridinium-4-yl)porphine]iron(III) ion (Fe(III)-TMPyP) in aqueous solution and the redox reactions of their central metals were investigated by means of spectrophotometric, electrochemical and spectroelectrochemical methods. Two acid-dissociation equilibria involving three monomeric species of Fe(III)-TMPyP were found: one with a pK_a of 5.5 and the other with a pK_a of *ca.* 12. After electrochemical reduction, an equilibrium between two monomeric species of Fe(II)-TMPyP with a pK_a of 11 was observed. In the Fe(III)-TMPyP solution at relatively high concentration, two additional different species, probably dimeric, were found in the pH regions of 5—8 and 9—13, respectively. The consistency of specification of the species with the scheme of redox reactions is discussed.

Since water-soluble metalloporphyrins were synthesized by introducing hydrophilic groups into the meso-positions of porphine rings, they have attracted the increasing interest of many chemists and biochemists as model substances for studies on biological processes.[1] Considerable information that is attractive to chemists has become available: *e.g.* the reaction mechanisms of complex formation,[2,3] the specification of species,[4-8] the substitution of axial ligands[9-12] and the mechanisms of redox reactions.[13,14]

Among water-soluble porphyrins, [tetrakis(1-methyl pyridinium-4-yl)porphine]iron(III) ion (Fe(III)-TMPyP) has often been studied because of its stability and relatively high solubility over a wide pH region. Nevertheless, the specification of species is very complicated and has not yet been clarified completely, owing to simultaneous acid-dissociation and dimerization equilibria depending on pH and/or concentration.

Therefore, this work was undertaken in order to specify the species of Fe(III)-TMPyP in aqueous solution and to clarify the mechanism of electrochemical redox reaction of the central metal of each species. In the course of the work, a paper concerning the same subject was published by Forshey and Kuwana.[15] However, our spectrophotometric, electrochemical and spectroelectrochemical investigations gave results which were significantly different from those reported,[15] especially in the pH region of 5—10. In addition, at pH 11 we newly confirmed monomeric iron(II) and iron(III) species. In this paper, we provide an overall scheme for the acid-dissociation equilibria among the Fe(III)-TMPyP species in aqueous solution at pH 1—13 and for the redox reactions of the species involved.

Experimental

Materials and Sample Solutions. Fe(III)-TMPyP perchlorate was prepared according to the method of Hambright and Fleischer[2] with a slight modification and stored in aqueous solution because of its explosiveness. The concentration of the Fe(III)-TMPyP stock solution was determined spectrophotometrically at 403 nm by the use of a molar absorption coefficient of 1.02×10^5 mol^{-1} dm^3 cm^{-1} at pH 2 and at an ionic strength of 0.1 mol dm^{-3}.[7] All other chemicals of guaranteed reagent grade were used without further purification.

Sample solutions were prepared by diluting the stock solution appropriately with deionized-distilled water. The pH values of the sample solutions were adjusted with sulfuric acid or sodium hydroxide solution and the ionic strength with sodium sulfate solution at 0.1 mol dm^{-3}, except for the highly acidic ($pH\leqslant1$) and basic ($pH\geqslant13$) solutions. In case buffered solutions were required, the following buffers were used: acetate buffer at pH 3—6, phosphate at pH 4.5—7.2, and phosphate-borate at 5.8—9.

Spectrophotometric, Electrochemical, and Spectroelectrochemical Measurements. A Shimadzu UV-300 and a Hitachi 100-30 spectrophotometer were used for the spectrophotometric investigation over a wide pH range. The pH values of the solutions were measured with a TOA HM-5B pH meter.

The cyclic voltammograms of Fe(III)-TMPyP in the same pH region were obtained by means of an NF FG-121B function generator and a Yanaco P8-CV potentiostat equipped with a conventional three-electrode system. A glassy carbon rod (GC-30, Tokai Carbon) plugged into a Teflon tube was used as the working electrode. The carbon surface exposed to a solution was a circle 0.196 cm^2 in area. The electrode surface was polished with diamond lapping paste (6×10^4 meshes) until a mirrorlike finish was obtained. Then it was wiped with a chamois skin dampened with carbon tetrachloride and rinsed with methanol and then with water. A platinum plate ($0.1\times5\times5$ mm^3) and a saturated calomel electrode (SCE) were employed as the counter and reference electrodes, respectively. Prior to both the electrochemical and spectroelectrochemical measurements, the sample solution was deoxygenated by bubbling a high-purity nitrogen gas through the solution for about 15 min, and the measurements were carried out under an atmosphere of nitrogen.

The spectroelectrochemical examination was achieved with an optically transparent thin layer electrode (OTTLE)[16] constructed with a gold minigrid (500 wires per inch, Buckbee Mears) which was sandwiched between two micro-slide glasses. The distance between two plates was controlled with Teflon spacers (*ca.* 0.1 mm thick, Delectrix DF-1200). The assembled OTTLE system had a thickness of an absorbing medium of *ca.* 0.22 mm and a transmittance of *ca.* 53%. While the Soret-band spectra of Fe(III)- and/or Fe(II)-TMPyP were measured with a Hitachi 100-30 spectrophotometer, the potential at the gold minigrid as the working electrode was controlled by a Yanaco P8-DP potentiostat using an SCE both as the counter and as the ref-

erence electrode.

All the measurements were performed at 25 °C.

Results and Discussion

Spectrophotometry. Figure 1 shows the typical UV- and visible spectra of Fe(III)–TMPyP aqueous solutions at various pH values. Since the spectra at pH above 10 changed gradually, they were obtained within 0.5 h after the preparation of each sample solution, except for spectrum e′. Three different species, corresponding to spectra a, c, and e in Fig. 1, were observed in turn with two sets of isosbestic points with increasing pH of the solution.

Insofar as we know, spectrum e at pH above 13 was observed for the first time, although spectra a and c were in fair agreement with those in the literature.[6,8] The e spectrum faded out depending on the time after the preparation of the sample solution and then altered to spectrum e′ after 48 h. This suggests that decomposition and/or transformation of species e to other formes should occur in such a strongly basic solution.

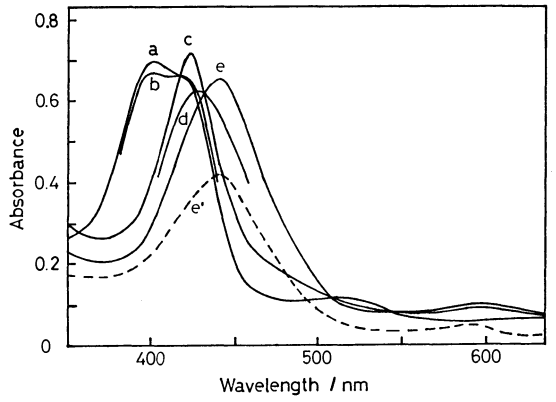

Fig. 1. Absorption spectra of Fe(III)-TMPy Paqueous solution at various pH.
Concentration: 7.06×10^{-6} mol dm^{-3}; pH of solutions: a 1.4, b 4.2, c 7.6, d 11.9, e 13.1, e′ 13.1 after 48 h.

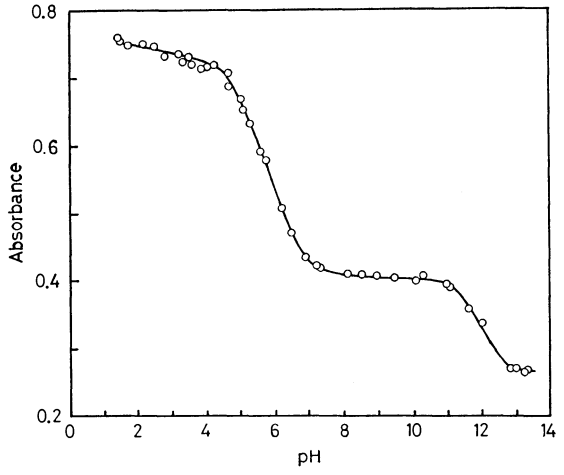

Fig. 2. Spectrophotometric pH titration curve of Fe(III)-TMPyP solution.
Concentration: 7.08×10^{-6} mol dm^{-3}; λ: 403 nm.

In order to examine the equilibria involving the new species e, spectrophotometric pH titrations were performed at the wavelengths of absorption maxima in spectra a, c, and e (403, 424, 440, and 596 nm). In the region of pH above 10, the absorbance at the time immediately after preparation was employed to remove any effect due to the decomposition and/or transformation of the species included. Figure 2 shows the pH titration curve obtained with 7.6×10^{-6} mol dm^{-3} Fe(III)-TMPyP solution at 403 nm. Since the phosphate buffer appreciably depressed the absorbance at pH below 6, the acetate buffer was used in that pH region.

A set of two inflection points was observed in each instance, and their positions were the same irrespective of the wavelength examined. This indicates the existence of two equilibria accompanying proton transfer: the one at pH 4—8 includes species a and c, and the other at pH 11—13 includes species c and e. We also examined the relationship between the absorbance and the concentration of Fe(III)–TMPyP solutions (Beer's law test) over the concentration range of 2.5×10^{-7}—1×10^{-5} and 5×10^{-7}—1×10^{-5} mol dm^{-3} at pH 2 and 13.6, respectively, at the wavelengths of absorption maxima (403 and 440 nm). The absorbance immediately after the preparation of sample solutions was employed at pH 13.6. The excellent proportionality obtained in the Beer's law test gave no evidence for any dimeric species in concentrations lower than 1×10^{-5} mol dm^{-3}. Therefore, at least species a and e should be monomeric, and the former in acidic solution is probably $[Fe(III)\text{–}TMPyP(H_2O)]^{5+}$ as proposed in the literature,[7,15] or diaqua-monomer.

Consequently, the equilibrium between species a and c may be represented by one of the following equations:

$$\text{Monomer} \rightleftharpoons \text{Monomer}' + n\,H^+, \quad (1)$$

$$2\ \text{Monomer} \rightleftharpoons \text{Dimer} + n\,H^+. \quad (2)$$

The number of transferred protons, n, and the equilibrium constant, K_a, were evaluated from the data of the pH titration experiments according to Eqs. 1 and 2 (Table 1). As can be seen in Table 1, the equilibrium in the region of pH 4—8 should include the reaction accompanying one proton transfer between different monomers under the experimental conditions employed, because the n and pK_a values according to Eq. 1 are close to an integer and to the pH value corresponding to the inflection point, respectively.

Table 1. The number of transferred protons (n) and the equilibrium constant (K_a) obtained from pH titration curves

pH	λ / nm	M⇌M′		2M⇌D	
		n	pK_a	n	pK_a
4—8	403	0.9	5.1	1.4	2.9
	424	0.9	5.3	1.2	2.2
	596	1.0	5.9	1.8	5.5
10—14	424	1.0	11.4	1.5	16.6
	440	1.1	13.2	1.6	13.9

M: Monomer, M′: monomer′, D: dimer.

This fact leads to the specification of species c to be $[Fe(III)-TMPyP(H_2O)(OH)]^{4+}$. Similary, species e can also be specified to be $[Fe(III)-TMPyP(OH)_2]^{3+}$ from the values of n and pK_a in Table 1. Only one equilibrium with a pK_a of 5.5 in the region of pH 4—8 is inconsistent with the two equilibria with pK_a values of 4.7 and 6.5 reported by Pasternack *et al.*[7] However, the specification of the three monomeric species is well consistent with the results obtained by the present electrochemical and spectroelectrochemical investigations, as described in the last section.

Electrochemistry. Figure 3 illustrates typical cyclic voltammograms of 1.4×10^{-4} mol dm^{-3} Fe(III)-TMPyP solutions at different pH values obtained at a scan rate of 0.1 V s^{-1}. Peak A accompanied by a corresponding oxidation wave was assigned to the reduction peak of monomeric species. The potential of peak A was independent of the pH of the solution, in acidic solution at pH below 5.5. On the other hand, at pH above 5.5 peak A shifted to become more negative with increasing pH and an additional reduction peak B appeared at a more negative potential than that of peak A with no corresponding oxidation wave. Multicycle or slow (0.01 V s^{-1}) scanning diminished peak B. The number of transferred electrons in the redox reactions was confirmed to be unity from the results of electrochemical and spectroelectrochemical measurements. These phenomena are fundamentally similar to those reported already.[15]

However, we found that in the region of pH 5.5—9 the reduction potential, $(E_p)_R$, of peak A in buffered solutions differs significantly from that in solutions free from the buffer, as shown in Fig. 4. In order to clarify the reason, nonbuffered sample solutions in

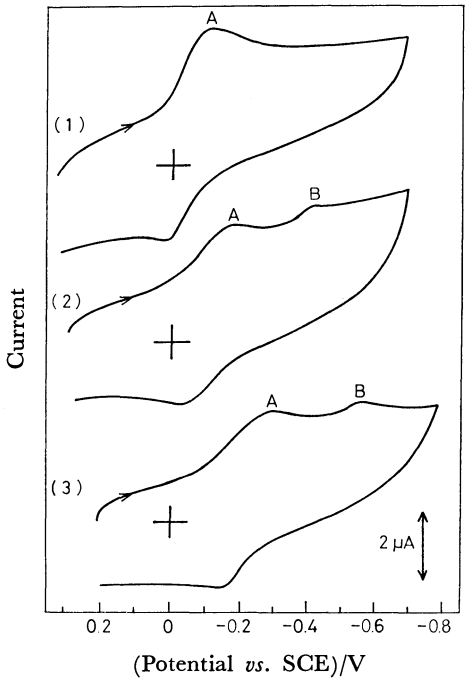

Fig. 3. Cyclic voltammograms of Fe(III)-TMPyP solution.
Concentration: 1.4×10^{-4} mol dm^{-3}; scan rate: 0.1 V s^{-1}; pH: (1) 4.6, (2) 6.5, (3) 9.4.

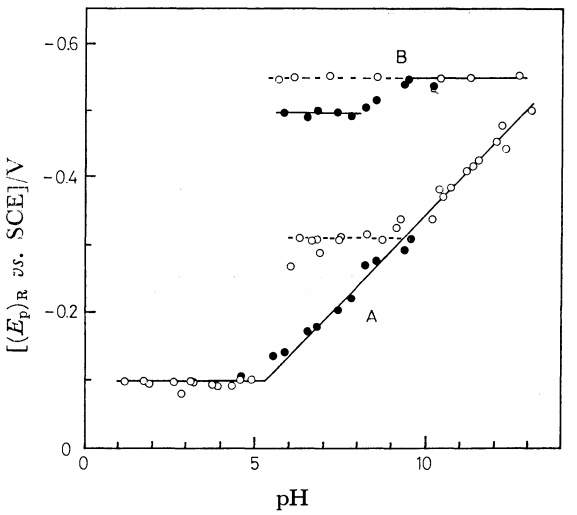

Fig. 4. Plot of $(E_p)_R$ *vs.* pH for Fe(III)-TMPyP solution.
○: In nonbuffered solution, ●: in buffered solution. Others are the same as in Fig. 3. $(E_p)_R$: see text.

the neutral pH region were reduced in an H-shaped cell which was separated into two compartments by a sintered glass. The pH of the solution in the compartment in which the working electrode was immersed increased beyond 9 as the electrolytic reduction progressed, indicating that the reduction of Fe(III)-TMPyP consumes hydrogen ions. This fact suggests that near the surface of the working electrode the pH value of the nonbuffered solutions in the pH range of 5.5—9 varied to higher pH than that of the bulk during the cathodic potential scanning.

As can be seen in Fig. 4, $(E_p)_R$ of peak A shifts by *ca.* −60 mV/pH at pH higher than 5.5, while it is independent of pH below 5.5. This finding indicates that the reduction yielding peak A accompanies only one-electron transfer in the region of pH below 5.5, and both one-electron and one-proton additions in the region of pH above 5.5.

Peak B may be assigned to that arising from the reduction of dimeric species as proposed by Forshey and Kuwana.[15] There is a probability of dimerization, because the electrochemical data were obtained on a concentrated solution, 10^{-4} mol dm^{-3}. In preliminary experiments, the value of the peak-current ratio of B to A increased with increasing the concentration beyond 10^{-5} mol dm^{-3}. The $(E_p)_R$ value of peak B in the buffered solution was appreciably different from that in the nonbuffered solution over the pH range of 5.5—9. This may also be ascribed to the variation in pH due to the reduction which consumes hydrogen ions.

The decomposition and/or transformation of the monomeric species at very high pH, mentioned in the preceding section, was investigated by following the time-course of $I-E$ curves of peak A by means of linear sweep voltammetry. The reduction current of peak A decreased with an increase in time at pH above 11.5. Figure 5 demonstrates a typical example of the time dependence of the $I-E$ curve at pH 12.5. In Fig. 6 is shown the time-dependent variation of

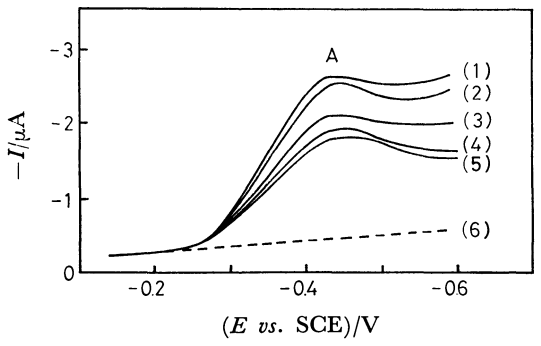

Fig. 5. $I-E$ curves of Fe(III)-TMPyP solution at various time after sample preparation.
Concentration: 1.0×10^{-4} mol dm^{-3}; pH: 12.5; time: (1) 0.5 h, (2) 2 h, (3) 7 h, (4) 24 h, (5) 7 d; (6): base line.

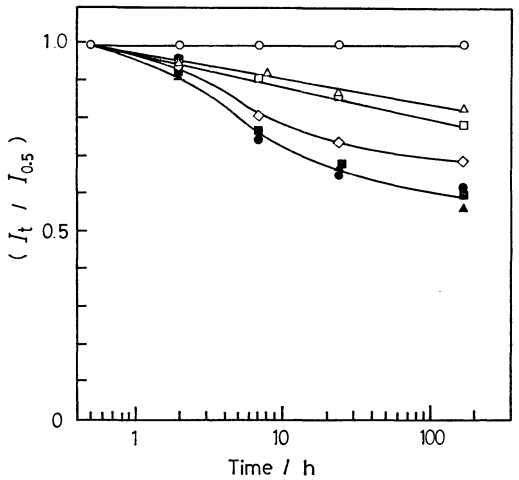

Fig. 6. $(I_t/I_{0.5})$ *vs.* time after sample preparation.
pH: ○ 11.30, △ 11.50, □ 11.80, ◇ 12.15, ● 12.49, ▲ 12.79, ■ 13.25.

$(I_t/I_{0.5})$ values, which are the ratios of the reduction currents of peak A at various times after the sample preparation to that obtained within 0.5 h. The $(I_t/I_{0.5})$ value decreases with increasing time after preparation at different rates depending on the pH of the solution, and finally it seems to approach a limiting value. This phenomenon corresponds well with the fade-out of spectrum e at pH 13.1, suggesting the fact that the monomeric species in highly basic solution transformes gradually into other forms which are inert to both the spectrophotometric and electrochemical detection.

Spectroelectrochemistry. The Soret-band spectra of 1.7×10^{-4} mol dm^{-3} Fe(III)-TMPyP aqueous solutions at various pH values were obtained before and after the electrochemical reduction by the use of an OTTLE. Figure 7 shows the wavelengths of Soret-band maxima, λ_{max}, of both iron(II) and iron(III) species plotted as a function of pH. The spectra before reduction, of course, were identical with those obtained at corresponding pH values in.

Spectrophotometry. The variation in Soret-band spectrum during incremental charge addition at pH below 10.5 was the same as that reported by Forshey

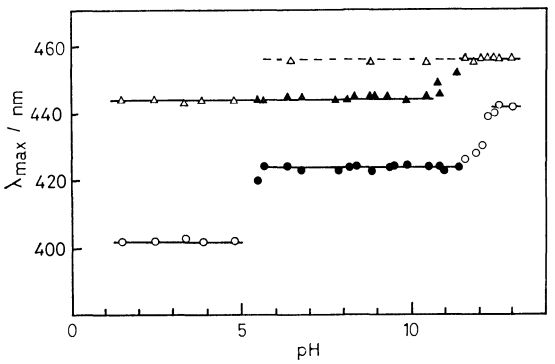

Fig. 7. Wavelength of Soret-band maxima (λ_{max}) *vs.* pH of Fe(III)-TMPyP solution before and after the reduction on OTTLE.
Concentration: 1.7×10^{-4} mol dm^{-3}. ○,●: Before the reduction in non-buffered and buffered solutions; △,▲: after the reduction in nonbuffered and buffered solutions, respectively.

and Kuwana.[15] At pH above 10.5, a new spectrum with an absorption maximum of 456 nm was observed as an iron(II) species. The λ_{max} values of iron(II) species in nonbuffered solutions at pH 6—10.5 were also different from those in buffered solutions, owing to the cause mentioned in *Electrochemistry.*

Consequently, three iron(III) species were observed predominantly in respective pH regions before the reduction. After the reduction, however, only two iron(II) species were recognized as the predominants in the regions of pH above and below 11, although Forshey and Kuwana proposed two different iron(II) species at pH values below 11.[15]

Equilibria among Species and Schemes of Their Redox Reactions. The spectrophotometric investigation revealed two acid-dissociation equilibria with pK_a values of 5.5 and 12 in dilute Fe(III)-TMPyP solutions over the pH range of 1—13. The equilibria involve three monomeric species which were specified to be those given in Scheme 1. Each equilibrium undergoes the transfer process of one proton. After the reduction with the OTTLE, an equilibrium with a pK_a of *ca.* 11 was found between two iron(II) species, probably both monomeric, which were also assigned to be those in Scheme 1 according to the results of this work. Cyclic voltammetric examination showed that the reduction of the monomeric species accompanies additions of only one electron at pH below 5.5, and of both one electron and one proton at pH above 5.5. At pH above 11.5, the monomeric species transforms gradually into other forms, inert for the detection methods employed in this study.

Preliminary ESR experiments provided additional information for the specification of the monomeric species. Namely, only a high-spin signal with a g-value of 5.5[4] was observed in acidic solution, and the signal height decreased with increasing pH. At pH values above 11 low-spin signals appeared with g-values of 1.9, 2.1, and 2.5;[4] these signals grew markedly with increasing pH. This phenomenon suggests the successive replacement of the axial ligands from a water molecule to a hydroxide ion, as shown in Scheme 1.

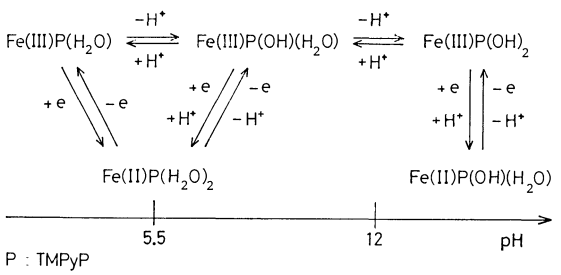

Scheme 1.

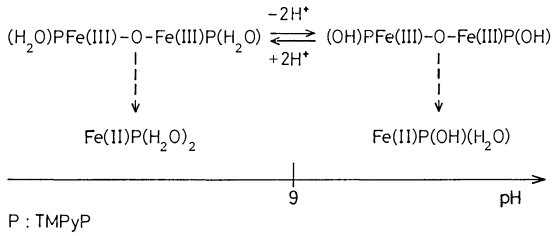

Scheme 2.

Two different dimeric species, probably μ-oxo-iron(III) dimer,[7,15] were found over the pH range of 5.5—9 and 9—13 in the electrochemical experiments. The reduction peaks of the dimeric species were not accompanied by any corresponding oxidation wave and diminished by the repetition of a cyclic potential sweep regardless of the pH range. These phenomena probably mean that the reduction of dimer gives iron(II) monomers and the dimerization of iron(III) monomers is a very slow process. These results lead to Scheme 2, which indicates that the reduction of both two iron(III) dimers results in formation of the iron(II) monomers with different combinations of the axial ligands depending on the pH of the solution. The specification of the dimeric species and the investigation of their reduction mechanism are in progress.

The authors wish to thank Messrs. Ikuhiro Tokuda, Ryuji Kikuchi, Hiroshi Kohama, and Toshihiro Takuma for technical collaboration. The present work was partially supported by a grant from the Central Research Institute of Fukuoka University.

References

1) K. M. Smith, "Porphyrins and Metalloporphyrins," Elsevier Sci. Pub. Co., Amsterdam (1975).
2) P. Hambright and E. B. Fleischer, *Inorg. Chem.*, **9**, 1757 (1970).
3) P. Hambright and P. B. Chock, *J. Am. Chem. Soc.*, **96**, 3123 (1974).
4) E. B. Fleischer, J. M. Palmer, T. S. Srivastava, and A. Chatterjee, *J. Am. Chem. Soc.*, **93**, 3162 (1971).
5) H. Baker, P. Hambright, and L. Wagner, *J. Am. Chem. Soc.*, **95**, 5942 (1973).
6) R. F. Pasternack, L. Francesconi, D. Raff, and E. Spiro, *Inorg. Chem.*, **12**, 2606 (1973).
7) R. F. Pasternack, H. Lee, P. Malek, and C. Spencer, *J. Inorg. Nucl. Chem.*, **39**, 1865 (1977).
8) F. L. Harris and D. L. Toppen, *Inorg. Chem.*, **17**, 71 (1978).
9) E. B. Fleischer, S. Jacobs, and L. Mestichelli, *J. Am. Chem. Soc.*, **90**, 2527 (1968).
10) E. B. Fleischer and M. Krishnamurthy, *J. Coord. Chem.*, **2**, 89 (1972).
11) R. F. Pasternack and M. A. Cobb, *J. Inorg. Nucl. Chem.*, **35**, 4327 (1973).
12) F. L. Harris and D. L. Toppen, *Inorg. Chem.*, **17**, 74 (1978).
13) R. F. Pasternack and N. Sutin, *Inorg. Chem.*, **13**, 1956 (1974).
14) R. F. Pasternack, M. A. Cobb, and N. Sutin, *Inorg. Chem.*, **14**, 866 (1975).
15) P. A. Forshey and T. Kuwana, *Inorg. Chem.*, **20**, 693 (1981).
16) R. W. Murray, W. R. Heineman, and G. W. O'Dom, *Anal. Chem.*, **39**, 1666 (1967).

 © 1982 The Chemical Society of Japan Bull. Chem. Soc. Jpn., 55, 3520—3522 (1982) [Vol. 55, No. 11

The Spectrofluorometric Determination of 9,10-Phenanthrenequinone

Masaki TACHIBANA,* Makoto HAYAKAWA,† and Motohisa FURUSAWA

Faculty of Engineering, Yamanashi University, Takeda, Kofu 400

(Received April 12, 1982)

9,10-Phenanthrenequinone (9,10-PQ) reacts with guanidine in an alkaline medium to form 2-amino-1*H*-phenanthro[9,10-*d*]imidazole. The reaction can be used for the fluorometric determination of 9,10-PQ, since the reaction product is fluorescent in an acidic solution. A dimethyl sulfoxide-methanol mixture is suitable as the solvent. A sample solution was allowed to stand for 15 min at room temperature after the additions of guanidine hydrochloride and sodium methoxide solutions, followed by the addition of hydrochloric acid. After the solution had been allowed to stand for 20 min, the fluorescence intensity of the solution was measured at 403 nm with excitation at 363 nm. The fluorescence intensity was stable for at least 8 h. The determination limit of 9,10-PQ was 50 ng.

For the determination of small amounts of 9,10-phenanthrenequinone (9,10-PQ), spectrophotometric methods[1-2] have been developed. In these methods, however, the determination limit of 9,10-PQ is approximately 1 μg.

In the present paper, a spectrofluorometric determination of 9,10-PQ will be described for the determination of minute amounts of 9,10-PQ. In order to convert 9,10-PQ into a fluorescent substance, the reaction of 9,10-PQ with guanidine[3] is useful. 9,10-PQ forms 2-amino-1*H*-phenanthro[9,10-*d*]imidazole with guanidine in an alkaline medium, and the product is fluorescent in an acidic solution.

Experimental

Reagents. Dimethyl sulfoxide (DMSO) was purified by using active aluminium oxide and a molecular sieve. To 500 g of commercial DMSO, 50 g of active aluminium oxide was added. The mixture was sufficiently shaken and then allowed to stand for several hours. After the DMSO had been separated by decantation, this process was repeated by using the molecular sieve instead of the aluminium oxide. Finally, the molecular sieve was filtered off.

9,10-PQ was purified by zone melting. Guanidine hydrochloride used was of a special-use reagent grade purchased from Tokyo Kasei Kogyo Co., Ltd. Methanol used was of a guaranteed reagent grade. Sodium methoxide was purchased from Kanto Chemicals Co., Inc.

Solutions. The guanidine solution was prepared by dissolving 50 mg of the hydrochloride in 100 ml of DMSO. The sodium methoxide solution was prepared by dissolving 1.00 g of the solid in 100 ml of a mixture of DMSO and methanol (4:1).

Apparatus. All the fluorometric measurements were carried out using a Hitachi 650-10S fluorescence spectrophotometer. A 150-W xenon lamp was used as the exciting source. A 10 mm × 10 mm × 45 mm quartz cell was used.

Procedure. Five milliliters of a sample solution containing less than about 1 μg of 9,10-PQ in a mixture of DMSO and methanol (4:1) was transferred into a 10-ml volumetric flask (amber). Then, 1 ml of the guanidine solution and 1 ml of the sodium methoxide solution were added. After the mixture had been allowed to stand for 15 min at room temperature, it was diluted to 10 ml with a 0.1 M (1 M = 1 mol dm^{-3}) solution of hydrochloric acid dissolved in DMSO. The resultant solution was allowed to stand for 20 min. The 9,10-PQ was determined by measuring the fluorescence intensity of the solution at 403 nm, with excitation at 363 nm. A solution containing 1.00 μg of 9,10-PQ was treated under the same conditions and at the same time; the resultant fluorescence was used as the standard.

Results and Discussion

Fluorescence Spectra. The fluorescence spectra of the reaction product of 9,10-PQ with guanidine are shown in Fig. 1. The excitation spectrum has maxima at 266 nm, 313 nm, and 363 nm. The emission spectrum exhibits a maximum at 403 nm. As the excitation wavelength, 363 nm was selected for the determination in order to minimize the interference of diverse substances. The fluorescence intensity of the reagent blank was negligibly small.

Effects of Sodium Methoxide and Methanol. DMSO was selected as the solvent considering the solubility of polynuclear aromatic compounds including 9,10-PQ. For the reaction of 9,10-PQ with guanidine, it is necessary to alkalify the solution. For this purpose, sodium methoxide was useful. To dissolve sodium methoxide in DMSO, the presence of methanol is necessary. The effect of sodium methoxide on the fluorescence intensity was studied by varying the amounts of sodium methoxide. The fluorescence intensities were almost constant over the range of 8—20 mg of

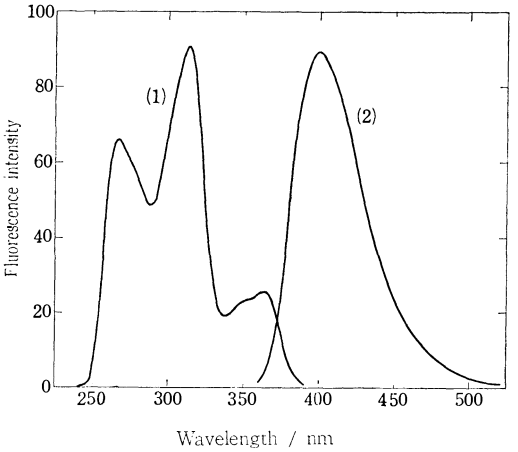

Fig. 1. Fluorescence spectra of the reaction product of 9,10-phenanthrenequinone (9,10-PQ) with guanidine. (1): Excitation spectrum, uncorrected; (2): emission spectrum, uncorrected.

† Present address: Risu Pack Co., 9-25, Kanda-machi, Gifu 500.

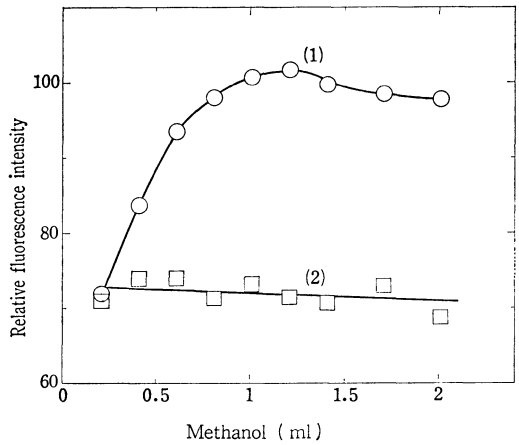

Fig. 2. Effect of the amounts of methanol on the fluorescence intensity.
Standard: fluorescence intensity of anthracene solution (40 ng/ml) in CH_3OH–DMSO (1:4) was taken as 100 div.; 9,10-PQ: 1.00 μg; (1): methanol was added before the reaction; (2): methanol was added after acidifying the solution of the reaction product (0.2 ml of methanol exists during the reaction).

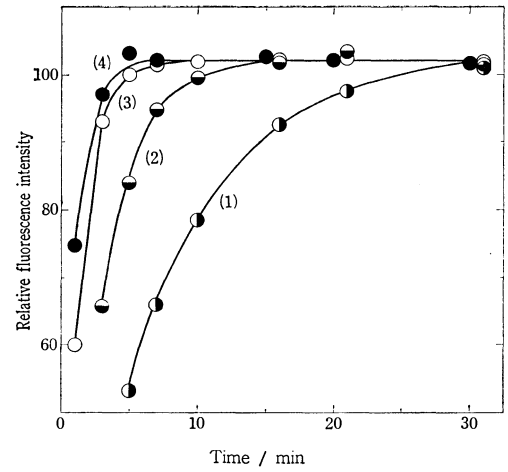

Fig. 3. Effect of reaction time on the fluorescence intensity in the presence of various amounts of guanidine hydrochloride.
Standard: fluorescence intensity of anthracene solution (40 ng/ml) in CH_3OH–DMSO (1:4) was taken as 100 div.; (1): 0.05 mg; (2): 0.15 mg; (3): 0.5 mg; (4): 1.5 mg; temp: 20 °C.

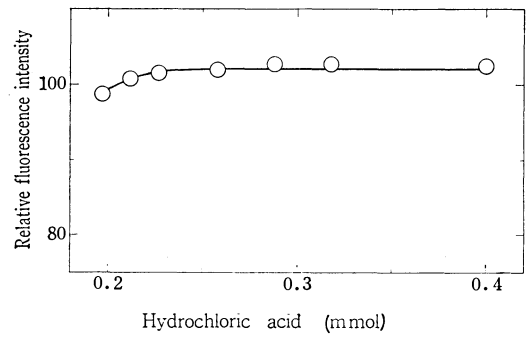

Fig. 4. Effect of the amounts of hydrochloric acid. 9,10-PQ: 1.00 μg; standard: fluorescence intensity of anthracene solution (40 ng/ml) in CH_3OH–DMSO (1:4) was taken as 100 div.

sodium methoxide. It is recommended, therefore, that 10 mg of sodium methoxide is added for the determination.

The reaction of 9,10-PQ with guanidine was carried out in the presence of various amounts of methanol. The fluorescence intensities measured are illustrated in Fig. 2 (1). For comparison, the effect of methanol was also studied in the case in which methanol was added after the solution of the reaction product had been acidified. These experimental results are shown in Fig. 2 (2). Figure 2 indicates that the reaction of 9,10-PQ with guanidine is influenced by the presence of methanol and that the maximum intensity is obtained when 1.2 ml of methanol exists during the reaction. Therefore, a mixture of DMSO and methanol (4:1) is suitable as the solvent for dissolving the sample and sodium methoxide.

Effects of Guanidine and Reaction Time. The hydrochloride of guanidine was used because of its high solubility in DMSO. The sulfate dissolves only slightly in DMSO. The amounts of guanidine and the reaction time are important variables for the determination. The effect of the reaction time on the fluorescence intensity was investigated at 20 °C in the presence of 0.05—1.5 mg of guanidine hydrochloride. The results of these experiments are shown in Fig. 3. Figure 3 indicates that the reaction of 9,10-PQ with guanidine is completed within 10 min at 20 °C when more than 0.5 mg of guanidine hydrochloride has been added. It is recommended, therefore, that the solution is allowed to stand for 15 min at room temperature in the presence of 0.5 mg of guanidine hydrochloride.

Effect of Hydrochloric Acid. The reaction product of 9,10-PQ with guanidine is not fluorescent in an alkaline solution, whereas it is fluorescent in an acidic solution. To acidify the solution, hydrochloric acid dissolved in DMSO was employed. The effect of the amounts of hydrochloric acid on the fluorescence intensity is illustrated in Fig. 4. The amounts of hydrochloric acid were varied from 0.20 to 0.40 mmol, because 0.19 mmol of hydrochloric acid was required to neutralize 10 mg of sodium methoxide. From the results in Fig. 4, the intensities are almost constant over the range from 0.23 to 0.40 mmol. In the determination procedure, about 3 ml of 0.1 M hydrochloric acid was used.

Stability of Fluorescence. In order to investigate the stability of the fluorescence intensity of the reaction product, a solution containing 1.00 μg of 9,10-PQ was operated according to the procedure. The fluorescence intensity was measured by varying the standing time from 2 min to 8 h. The intensity increased for a while after the solution had been acidified. The fluorescence intensity, however, remained highly constant for at least 8 h after 15 min. An amber volumetric flask was used in the procedure to shield it from light in some degree, since the intensity was relatively unstable under scattered sunlight.

Calibration Curve and Reproducibility. A calibration curve was prepared from 9,10-PQ solutions con-

TABLE 1. EFFECTS OF DIVERSE SUBSTANCES

Substances added (μg)		Relative fluorescence intensity[a)]	Difference
None		100.0	
Biphenyl	103	103.3	+0.3
Naphthalene	105	99.3	−0.7
Acenaphthene	104	100.0	±0.0
Dibenzofuran	106	99.4	−0.6
Dibenzothiophene	104	100.4	+0.4
Fluorene	5.3	99.2	−0.8
	21	96.6	−3.4
Carbazole	1.0	100.4	+0.4
	2.1	103.3	+3.3
Phenanthrene	21	100.9	+0.9
	103	102.1	+2.1
Anthracene	0.005	100.4	+0.4
	0.020	103.8	+3.8
Acridine	2.2	99.3	−0.7
	5.5	97.7	−2.3
Fluoranthene	0.11	100.8	+0.8
	0.21	102.6	+2.6
9-Fluorenone	20	99.3	−0.7
	102	96.2	−3.8
Acenaphthenequinone	107	99.2	−0.8
Anthraquinone	10	99.7	−0.3
	51	96.6	−3.4

a) The fluorescence intensity of the solution of the reaction product (1.00 μg 9,10-PQ per 10 ml) was taken as 100 div.

taining 0—1.00 μg per 5 ml according to the procedure. As the standard, the solution obtained by operating 1.00 μg of 9,10-PQ was used. The calibration curve thus prepared was linear between the fluorescence intensity and the concentration of 9,10-PQ. The coefficient of variation obtained in 10 measurements was 1.3% at 1.00 μg of 9,10-PQ. In these measurements, an anthracene solution was used as the standard.

Effect of Diverse Substances. The effects of 14 substances on the determination are summarized in Table 1. The determination of 9,10-PQ is not interfered with the presence of 100-fold amounts of biphenyl, naphthalene, acenaphthene, dibenzofuran, dibenzothiophene, and acenaphthenequinone and 20-fold amounts of phenanthrene, 9-fluorenone, and anthraquinone. Fluorene and acridine reduce the fluorescence intensity. Carbazole gives a positive error. Anthracene and fluoranthene give serious interferences

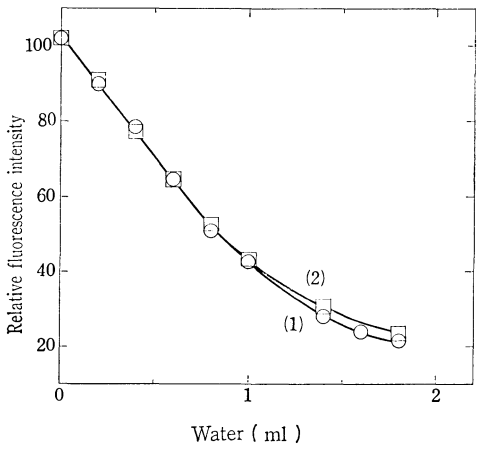

Fig. 5. Effect of water on the fluorescence intensity. 9,10-PQ: 1.00 μg; standard: fluorescence intensity of anthracene solution (40 ng/ml) in CH_3OH–DMSO (1:4) was taken as 100 div.; (1): water was added before the reaction; (2): water was added after acidifying the solution of the reaction product.

because they are fluorescent at the characteristic wavelength of the reaction product of 9,10-PQ.

Effect of Water. The effect of water on the fluorescence intensity was studied by varying the water content in the solvent. The fluorescence intensities measured are shown in Fig. 5 (1). For comparison, the additions of water were performed after the solution of the reaction product had been acidified. As is shown in Fig. 5 (2), these results are identical with that in Fig. 5 (1). Figure 5 indicates that the fluorescence intensity greatly decreases in the presence of water. Therefore, a nonaqueous solvent is desirable for a highly sensitive determination of 9,10-PQ. The identical solvent must be used during the determination to avoid the influence of water, which is contained in the solvent as an impurity.

The authors are indebted to Miss Sumiko Yamada for her technical assistance. The present work was partially supported by a Grant-in-Aid for Scientific Research from the Ministry of Education, Science and Culture.

References

1) E. Sawicki and W. Elbert, *Anal. Chim. Acta*, **22**, 448 (1960).
2) I. A. Zolotarevskaya and A. I. Kamneva, *Zh. Anal. Khim.*, **27**, 1227 (1972).
3) S. Yamada and H. A. Itano, *Biochim. Biophys. Acta*, **130**, 538 (1966).

The Stereochemistry of the Photochemical Rearrangement of 1-Substituted 1a,7b-Dihydro-1*H*-cyclopropa[*a*]naphthalenes under Sensitized Conditions[1)]

Masahiko KATO,* Hisako KOBAYASHI, Hiroyuki YAMAMOTO,
Koji SETO, Satoru ITO, and Toshio MIWA

Faculty of Science, Osaka City University, Sugimoto-3, Sumiyoshi-ku, Osaka 558

(Received December 21, 1981)

The photolysis of 1-substituted 1a,7b-dihydro-1*H*-cyclopropa[*a*]naphthalenes in the presence of Michler's ketone leads principally to 5-substituted 5*H*-benzocycloheptenes as primary products *via* a stepwise mechanism. The reaction proceeds smoothly with inversion of the migrating carbon if there is no steric hindrance, but it proceeds predominantly with retention if the inversion course is severely suppressed by steric hindrance. The marked difference in the *exo-endo* ratio of the secondary photocyclization products depending on the irradiation conditions was also recognized for 1-methoxycarbonylmethyl derivative.

The stereochemical course of the photochemical Berson-Willcott rearrangements had been reported by us for 1-methoxycarbonylmethyl-1a,7b-dihydro-1*H*-cyclopropa[*a*]naphthalene (**1a**) under direct irradiation[2)] and by Klärner for 7-cyano- and 7-methoxycarbonyl-2,7-dimethyl-1,3,5-cycloheptatriene (**2**) under sensitized irradiation.[3)] In both cases, the rearrangements proceeded principally by way of inversion at the migrating carbon center. In the former case, in parallel with a result for the 4-*t*-butyl derivative of **1a**,[4)] we suggested a concerted mechanism controlled by the Woodward-Hoffmann rule, while in the latter, Klärner proposed a biradical pathway.

In the course of a photochemical study of 1-*exo*-methoxycarbonyl derivative (**1b**) in the presence of several sensitizers, 5-methoxycarbonyl-5*H*-benzocycloheptene (**3b**)[5)] was obtained as a primary product but 7-methoxycarbonyl-7*H*-benzocycloheptene or the secondary photo-products derived from it were not detected. This and the results by Klärner[3)] suggest that the reaction course and the stereochemistry under such photolytic conditions might be different from the results of direct irradiation. Interest has also been focused on the effect of a substituent on C-1, *i.e.*, electron-attracting or releasing, which would affect the bond strength of the three-membered rings not only in their ground state[6)] but also in the excited states.[6)] In order to clarify these points, we studied the stereochemical course of sensitized reactions of a series of 1-substituted 1a,7b-dihydro-1*H*-cyclopropa[*a*]naphthalenes (**1**) using their racemic and optically active forms. The substituents chosen were methoxycarbonylmethyl as an electron-releasing group, and methoxycarbonyl and cyano as electron-attracting groups with large and small steric requirement, respectively.

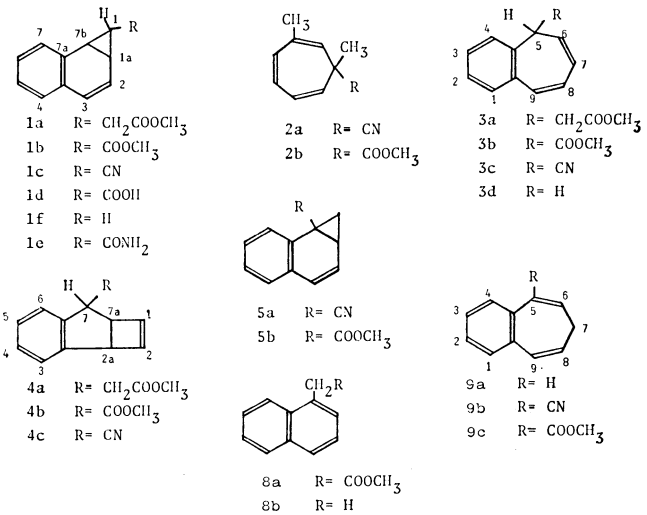

Scheme 1.

*Photochemistry of 1-exo-Methoxycarbonyl Derivative (**1b**). Irradiation in the Presence of Michler's Ketone*: Irradiation of **1b** in benzene with 4,4'-bis(dimethylamino)benzophenone (Michler's ketone) for 2.5 h gave a recovery of material corresponding to 75% of the initial weight of **1b**, from which **1b** (30%), **3b** (30%), and **8a** (10%) were separated. Under these conditions, the cyclization products from **3b** were negligible but prolonged irradiation gave a small amount of an *exo-endo* mixture of 7-methoxycarbonyl-2a,7a-dihydro-7*H*-cyclobut[*a*]-indene (**4b**), which was not detected under direct irradiation.

When we used **1b**-1-d_1 for photolysis, we obtained only **3b**-5-d_1 as new products; this result supports the regiospecific rearrangement at C-1.

In the same experiment, (+)-**1b** ($[\alpha]_D$ +124°) gave **3b** ($[\alpha]_D$ −2.82°) in addition to a recovery of **1b** ($[\alpha]_D$ +114°).

Identification of the Products: **3b** was identical with a sample obtained by alcoholysis of the corresponding nitrile (**3c**) reported previously.[5)] An *exo-endo* mixture of **4b** was separated by VPC. The mass spectra of the two components showed very similar fragmentation patterns except for their relative intensities: peaks at *m/e* 200 (M^+), 174 ($M^+-C_2H_2$), 141 (base peak, $M^+-COOCH_3$), 115 ($M^+-CHCHCOOCH_3$).

The UV spectra of *exo*-**4b** and *endo*-**4b** are very similar and are characteristic of benzocyclopentenes.[7)] The NMR spectra of both compounds could be accounted for by structure **4b** (Aromatic H: aliphatic H: olefinic H: OCH_3=4:3:2:3) and the coupling patterns between the olefinic protons and H_{7b}'s of *exo*- and *endo*-**4b** were quite similar to those of known *exo*- and *endo*-**4a**, respectively.[8,9)]

*Irradiation of Optically Active 1-Methoxycarbonylmethyl Derivative (**1a**)*: Because of its facile double epimerization above room temperature, the *exo*-ester (**1a**), carefully obtained below 3 °C from the known (+)-(1*R*)-**1d**[1)] ($[\alpha]_D$ +147°, >95% optically pure), was irradiated in dichloromethane in the presence of Michler's ketone below 0 °C for 5 min. After chromatographic

separation of the products from the sensitizer, they were identified and estimated to consist of **1a** (53%), **3a** (38%),[2] and **4a** (*endo* (6%)+*exo* (1.5%)).[8] Repeated chromatography on silica gel of the mixture gave **3a** and *endo*-**4a** in optically active forms (**3a**, $[\alpha]_D$ +65° (76% enantiomer excess (e.e.); *endo*-**4a**, $[\alpha]_D$ +81° (76% e.e.)).

In a separate experiment, (+)-(5S)-**3a** ($[\alpha]_D$ +86°, >95% optically pure) was similarly photolyzed in benzene to give a product (30%) consisting of *exo*- and *endo*-**4a** (1:5) which retained their optical activities [*endo*-**4a**, $[\alpha]_D$ −107° (>95% optically pure); *exo*-**4a**, $[\alpha]_D$ +180°]; these determined the (7*S*)-configuration for both (+)-*exo*-**4a** and (−)-*endo*-**4a**.

Therefore, the stereochemistry of the rearrangement of *exo*-**1a** to **3a** under the above conditions is deduced to be 88% retention of the C-1 configuration; this result is opposite to the one for the same rearrangement under direct irradiation.[2,5] When we use (+)-**1a** (*exo*:*endo*=2:1; $[\alpha]_D$ +24.7°) after thermal equilibration as the starting material, we obtain (+)-**3a** in 16% e.e. (58% retention) after 20% conversion. In this case, if a rearrangement starting from *exo*-**1a**, which forms 67% of the starting ester, proceeds with 88% retention as observed above, the calculated percentage of retention originating from *exo*-**1a** will be 59% in the total rearrangement, which is well coincident with the observed value (58%). Therefore, the *endo*-**1a**, composing 33% of the starting material, is supposed to rearrange solely to (−)-**3a** through inversion of the C-1 configuration. The longer irradiation time (72% conversion) using an *exo-endo* mixture of optically active **1a** (2:1) gave *endo*-**4a**, instead of **3a**, as the main product with the same enantiomer excess within the experimental error (19% e.e.; 59% retention).

*Photochemistry of 1-Cyano Derivative (**1c**). Synthesis of (1*R*)-(−)-1-endo-Cyano Derivative (1-endo-**1c**)*: Because of the double epimerization of *exo*-**1a**, *endo*-**1a**, and *endo*-**1b**,[5] we could not make clear the stereochemistry of the photochemical *exo-endo* isomerization for these compounds under the above conditions. In hopes of obtaining a thermally stable and optically active **1c**, we synthesized it from an optically active acid **1d** under mild conditions. Thus, from (+)-**1d** ($[\alpha]_D$ +143°) we obtained (+)-**1c** as colorless crystals ($[\alpha]_D$ +103°, mp 76 °C) by dehydration with trifluoroacetic anhydride[10] *via* the amide,[11] **1e** ($[\alpha]_D$ +201°, mp 261—262 °C). The obtained nitrile **1c** showed a characteristic 1-*endo* proton triplet (J=4.3 Hz) at δ 0.69 ppm. Upon heating this nitrile **1c** at 130 °C for 20 min, an *exo-endo* (2:3) mixture of **1c** was obtained, from which *endo*-**1c** was isolated as colorless crystals, mp 153 °C, $[\alpha]_D$ −579°. In the NMR spectrum, the latter showed a triplet of C-1 proton at δ 2.19 ppm with a *cis* vicinal proton coupling (J=8.3 Hz) characteristic to the cyclopropane ring.[5,12] The UV spectrum was very similar in shape to that of *exo*-**1c**, but the maximum (270 nm (log ε 3.89)) appeared at a shorter wavelength than that of *exo*-**1c** (273 nm (log ε 3.89)). From the absolute configuration of the starting (+)-**1d**, the absolute configuration of (+)-*exo*-**1c** must be (1*R*). Therefore, the configuration of (−)-*endo*-**1c** corresponds to (1*R*), because the latter should be formed *via* a symmetry-allowed double Cope rearrangement from the former.[13,14] The minus sign in *endo*-**1c** is coincident with the existence of an enantiomeric benzonorcaradiene moiety against (1*R*)-(+)-*exo*-**1c**.[15]

*Irradiation of **1c***: Solutions of racemic *exo*- and of *endo*-**1c** in benzene were irradiated for 15 min in the presence of Michler's ketone to give 68% and 88% recovery of the initial amount of the starting material, respectively. The products were *exo*-**1c**, *endo*-**1c**, and 7b-cyano-1a,7b-dihydro-1*H*-cyclopropa[*a*]naphthalene (**5a**)[16] in 34.9%, 6.2%, and 25.4%, respectively from *exo*-**1c** and 44.8%, 15.7%, and 25.0%, respectively from *endo*-**1c**.

In an independent experiment, we observed that 5-cyano-5*H*-benzocycloheptene (**3c**) rearranged readily to **5a** under the same conditions. Therefore, both isomers of **1c** interconvert with each other and probably rearrange to **5a** *via* **3c**.

In order to test the possibility of trapping **3c**, if it were formed from **1c**, an authentic sample of **3c** was irradiated with Michler's ketone in furan as a solvent instead of benzene; we obtained, in addition to **5a** (25%), a 1:1 adduct (*adduct*-1; 23%) composed of furan and **3c** as expected. In the direct irradiation of **3c** in furan, we obtained two kinds of 1:1 adducts (40%): one was identical with the above *adduct*-1 and the other was an isomer (*adduct*-2).

The Structures of Adduct-1 and -2: The NMR spectra of these two adducts showed quite similar coupling patterns over all the region; therefore, it is reasonable to suppose that they have the same molecular framework. The confirmation of the existence of vicinal couplings by the stepwise decoupling experiment on the NMR signals of the *adduct*-1 revealed a carbon skeleton (**A**) and a 2,3-dihydrofuran moiety (**B**)[17] in *adduct*-1. As the two fragments contain all of the carbons and hydrogens in the molecule, we can obtain the structures **6** and **7** from their spectral analysis. Of **6** and **7**, the latter, in which the proton H_{10} is located in proximity to the oxygen of the furan ring, was chosen for the adduct by considering its NMR spectrum. The *syn* structures, **7a** and **7c**, rather than the *anti*, **7b** and **7d**, were selected because their NMR spectra, taken with a shift reagent, showed an extraordinary lower field shift of H_{10} and the least shifts of H_{12} and H_5 signals. The larger lower field shifts of H_{11} as well as H_{10} signals in *adduct*-1 compared

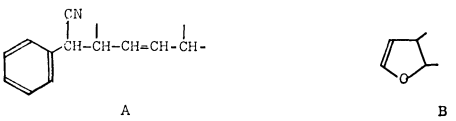

A B

Scheme 2.

7 6

Scheme 3.

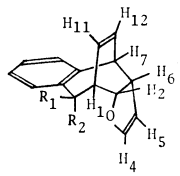

7a R_1= CN, R_2= H
7c R_1= H, R_2= CN
10a R_1= CH_2COOCH_3, R_2= H
10b R_1= R_2= H

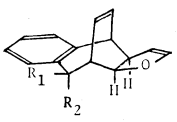

7b R_1= CN, R_2= H
7d R_1= H, R_2= CN

Scheme 4.

Table 1. The induced shifts in NMR signals of the furan adduct-1 and -2 observed by the addition of $Eu(fod)_3$

Added $Eu(fod)_3$	Observed proton chemical shifts (δ)					
	H_2	H_4	H_5	H_{10}	H_{11}	H_{12}
Adduct-1 (2.2 mg/0.4 mL $CDCl_3$)						
0.0 mg	4.98	6.20	4.43	4.55	6.07	6.71
3.5 mg	5.17	6.31	4.50	4.81	6.20	6.77
$\Delta\delta H_i/\Delta\delta H_{12}$	3.17	1.83	1.16	4.33	2.17	1.00
Adduct-2 (1.2 mg/0.4 mL $CDCl_3$)						
0.0 mg	5.04	6.15	4.45	4.22	6.08	6.57
3.0 mg	5.26	6.43	4.58	4.58	6.21	6.71
$\Delta\delta H_i/\Delta\delta H_{12}$	1.57	2.00	0.98	2.57	0.93	1.00

with those of the same proton signals in *adduct*-2 suggested the structure **7a** for *adduct*-1 and **7c** for *adduct*-2.

*Irradiation of (1*R)-exo-*(+)-**1c** in Furan*: Irradiation of *exo*-(+)-**1c**, $[\alpha]_D$ +103°, in furan in the presence of Michler's ketone was performed as mentioned above. The isolated products were, in addition to *exo*-(+)-**1c** ($[\alpha]_D$ +110°; 56%), *endo*-(+)-**1c** ($[\alpha]_D$ +572°; 19%), **5a** (13%), and *adduct*-1 ($[\alpha]_D$ −0.8°; 12%).

*Photochemistry of **1f**-1,1-*d_2. *Synthesis of **1f**-1,1-*d_2: In all the above-mentioned examples of the sensitized irradiation of 1-substituted **1**, the products detected were only the ones derived from the rearrangement of C-1 toward C-7a. This fact was quite different from the results obtained under direct irradiation. In order to test whether such regioselectivity of rearrangement under sensitized conditions is available in the simplest case, we studied the rearrangement of **1f**-1,1-d_2. Though **1f**-1,1-d_2 was previously prepared from naphthalene with dideuteriocarbene,[18] the yield and deuterium content were unsatisfactory. So we prepared it starting from 1,2-dihydronaphthalene as follows: addition of dibromocarbene, reduction with tributyltin deuteride,[19,20] and NBS bromination followed by dehydrobromination with calcium hydrogen phosphate in DMF.[21] The deuterium content of C-1 of **1f**-1,1-d_2 was estimated to be 97% by H NMR spectrum.

*Irradiation of **1f**-1,1-*d_2: **1f**-1,1-d_2 dissolved in benzene was irradiated with Michler's ketone for 15 min to give a mixture of **1f**-d_2[18] (**C**), 5*H*-benzocycloheptene-d_2 (mainly **3d**-5,5-d_2)[18] (**D**), and 1-(methyl-d_2)naphthalene (**11b**-d_2) in a ratio of 11.2:9.0:1.0; this was estimated by a combination of VPC and NMR measurements. A longer irradiation time did not increase the amount of **3d**, because the latter was found to be transformed back to **1f** under the same conditions in an independent experiment.

The deuterium distribution in compound **C** was studied carefully with use of the FT-NMR spectrum. Thus the integrated area of the signal of the proton bound to C-1a did not change compared with that of the olefinic proton signals (2H). On the other hand, the area due to the proton bound to C-7b decreases, in compensation for the increase of those due to the *exo*- and *endo*-protons on C-1. The results allowed us to estimate that compound **C** contained **1f**-1,1-d_2 and **1f**-1,7b-d_2 in a ratio of 3.2:1.

Similar irradiation of 7*H*-benzocycloheptene (**12a**) gave a mixture of **9a**, **1f**, **3d**, and **8b** in a ratio of 73.5:20:6.5:trace, respectively. From this experiment, it is clear that **9a**-7,7-d_2, if it were formed from **1f**-1,1-d_2 in the above experiment, should partly survive and partly give **1f**-1,1a-d_2 by [1,7]D-shift from C-7 to C-6 and simultaneous bond formation between C-5 and C-7.

The fact that no deuterium incorporation was found in C-1a of compound **C** shows that the rearrangement proceeds through one direction, similar to other cases mentioned above. It is noteworthy that, while 1-methylnaphthalene was identified, neither naphthalene nor 2-methylnaphthalene was detected in the sensitized reaction.

*Formation of the Furan Adducts of **1a** and **1f**.* Irradiation of **1a** and **1f** in furan in the presence of Michler's ketone gave *adduct*-3 and -4, respectively. Their similarities in the proton NMR spectral pattern to those of *adduct*-1, except for the signals due to substituent and/or H_1, determined the structures: **10a** and **10b**, respectively. *Adduct*-3 was obtained in 44% yield from the irradiation of **3a** in furan in the presence of the sensitizer.

Discussion

The photochemical Berson-Willcott rearrangement of benzonorcaradiene was initially reported by Ciganek on 1,1-dicyano-1a,7b-dihydro-1*H*-cyclopropa[*a*]naphthalene in 1968.[22] The stereochemical course of the photochemical rearrangement of tropilidenes was studied by Klärner[3] under benzophenone sensitized conditions on 1,3-dimethyl-2,4,6-cycloheptatriene-1-carboxylic ester and nitrile (**2a** and **2b**), which proceed mainly with inversion at the migrating carbon center of their norcaradiene tautomers. They proposed a stepwise mechanism through the biradical intermediates keeping the substituents *exo* in order to relieve the repulsion between π-electrons to predict inversion and partial racemization.

In the above experiment, we found that the stereochemical course of the rearrangement of **1a** under Michler's ketone-sensitized irradiation was quite different in nature from that under direct irradiation. Fukui deduced as follows: "In a triplet-state reaction each bond, which is to be newly formed through the overlapping of AO's of the two parts where the orbital interaction is considered, should be formed so as to result in a structure having two unpaired electrons not in conjugation with each other by virtue of that

bond. Excited singlet-state reactions are not necessarily subject to such a limitation."[23]

There are many examples in which different products are produced under sensitized irradiation from those under the direct type,[24] but little is known concerning the case which gives the same products with different stereochemistry depending on the irradiation conditions. Mariano reported that the di-π-methane rearrangement of **11** gives stereospecifically *cis* product (**12c**) from its excited singlet but mainly *trans* (**12t**) on sensitized irradiation.[25] Swenton described the different behavior of **13** under direct irradiation and under 2-acetonaphthone sensitization.[26] These examples are not similar to our case precisely in the sense of whether the migrating carbon changes the stereochemistry or not. Our results obtained on *exo*-**1a** are unique because of its completely opposite stereochemistry toward **3a** depending on the irradiation conditions. It is noteworthy that the optical purities of the products from direct irradiation are the same within the experimental error and hence stereochemistry is not altered whether we use *exo*-**1a**, obtained below 3 °C from pure (1*R*)-(+)-**1d**, or an thermally equilibrated *exo*-*endo* mixture (2:1) of **1a** obtained from the same acid.[27] This means that, under the direct irradiation, the *exo*-**1a** and *endo*-**1a** follow the same stereochemistry, 80% inversion and 20% retention of the configuration at the migrating center. These facts suggest the presence of different mechanisms for the two modes of irradiation; under direct irradiation, both *exo*- and *endo*-**1a** follow mainly the same symmetry-allowed suprafacial [1,5]sigmatropic shift with inversion at the migrating center, but under sensitized conditions, they follow a stepwise process with either the stereochemistry governed by the principle of the least motion or that of releasing the steric hindrance in the process. Thus, under the sensitized irradiation, the rearrangement of *endo*-**1a** proceeds with inversion at the migrating center in accordance with the principle of least motion[28] with little change in spatial environment, while that of the *exo*-**1a** proceeds mainly with retention at the center, avoiding the steric hindrance caused by the substituent on C-1 and a hydrogen on C-7 in the least motion movement. Borden reported such a least motion pathway for the thermal [1,5]sigmatropic shift of **16**, contrary to the prediction of the Woodward-Hoffmann rule. Direct irradiation of **16** also affords **17** with high stereoselectivity.[29]

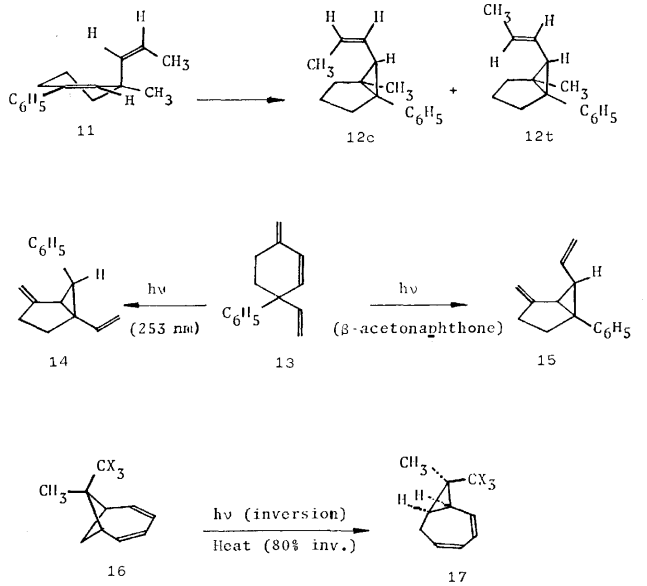

Scheme 5.

The suppression of the reaction by steric repulsion was recognized in the case of a kinetic study on the rearrangement of 3-isopropyl derivative of *exo*-**1a** compared with that of *endo*-**1a** under direct irradiation.[30] Swenton found, in addition to the path ii products, the presence of path i products in the case of direct irradiation of **5b**. He attributed this to the steric hindrance between a peri-hydrogen and the methoxycarbonyl group present in the intermediate (**18**). Such obstruction to path ii is not seen in the case of photolysis of **5a**.[16]

In the study of **1a**, it was difficult to recover *exo*-**1a** without contamination of *endo*-**1a** owing to its thermal instability; even so, the stepwise mechanism under sensitized conditions was supported by the findings that (1*R*)-*exo*-**1c** was recovered from the reaction mixture without racemization and at the same time (1*S*)-*endo*-**1c** was obtained with high optical rotation[31] when (1*R*)-*exo*-**1c** was irradiated in furan. Simple Hückel calculations predict the resonance energy of 1-phenylallyl radical (**19**) composed of a part of **20** to be larger than that of *o*-vinylbenzyl radical (**21**) composed of a part of **22**. Thus the cleavage of a bond C-1 to C-1a in **1** is expected to be easier than that of C-1 to C-7b.[32]

The adduct of (1*R*)-(+)-**1c** to furan was found to be optically inactive. We could not detect any of **9b** in the reaction mixture, so the possibility of racemization of an initially formed optically active **3c** under reaction conditions is rather low. The fact that the absolute configuration of C-7b on *exo*-**1c** is conserved in *endo*-**1c** obtained by the sensitized irradiation shows the existence of diradical intermediates **23c** and **24c**[33,34] during the epimerization. But it is difficult to explain why the *endo*-**1c** rearranges to *exo*-**1c** much faster than the *exo*-**1c** does to *endo*-**1c** in the comparative study.[35]

The occurrence of biradical intermediates **23c** and **24c** clarifies the production of **3c** in an optically in-

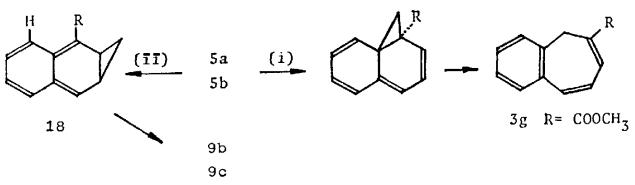

Scheme 6.

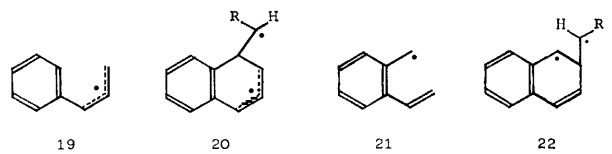

$RE(\mathbf{19}) - RE(\mathbf{21}) = -0.09\beta$ (RE=Resonance energy)

Scheme 7.

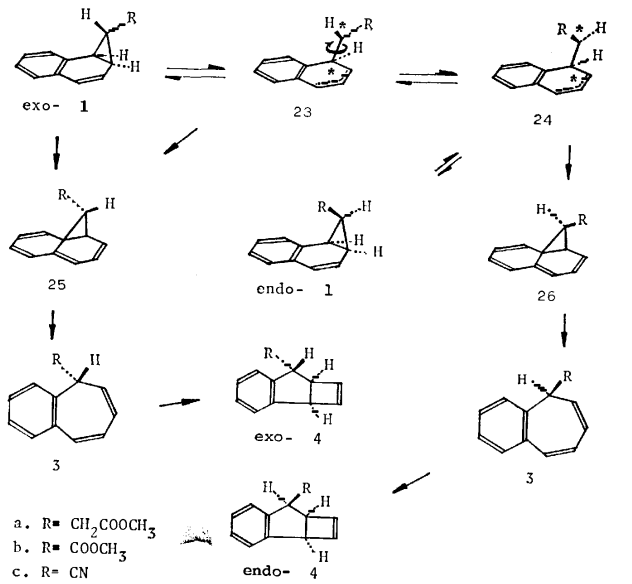

Scheme 8.

active form.

The stereochemical results of the rearrangement of (+)-**1b** are explained as follows. In this case, as is expected from the fact that **1b** exists solely in its *exo* form and *endo*-**1b**, when it is prepared by photolysis of **3b**,[5] isomerizes readily at room temperature, the steric repulsion between methoxycarbonyl group and π-electrons in the ring **24b** is too large to get close enough to *endo*-**1b**; therefore, the loss of the optical activity of (+)-**1b** is found to be quite small (8%) during irradiation. For the rearrangement to **3b**, the closure of **23b** and **24b** to position C-7a is expected to have the same order of large steric repulsion, because the steric requirement of methoxycarbonyl group is larger than that of cyano group. Therefore, we may obtain **3b** at a rate rather slower than those of **3a** or **3c** and in almost racemic form. However, another explanation for the occurrence of racemic **3b** from (1*R*)-**1b** is possible: that is the racemization of initially formed optically active **3b** under the reaction conditions. This possibility has not been investigated yet.

Next, we must deal with the mechanism of cycloaddition of **1c**, **1a**, and **1f** to furan. Generally, the photochemical [4πs+2πs]-addition is not allowed under the control imposed by the orbital symmetry rule. Two mechanistic alternate pathways may serve to predict the adducts. One is the successive photochemically allowed processes, [2πs+2πs] or [4πs+4πs] cycloaddition, as observed in the photochemical addition of furan to benzene,[36] followed by [1,3]sigmatropic shift to give products. The other is a stepwise biradical or the equivalent process. As the latter cannot explain the regioselectivity of the adduct, the former mechanism assisted by the overlap of the secondary orbitals may satisfactorily predict the selectivity. The stereoselective formation of *exo*-adducts shows that a steric factor is playing an important role as the controlling factor.

Finally, the fact that the *exo-endo* ratio of the cyclization products **4a** formed from **3a** is quite different depending on the irradiation conditions is also interesting. Under direct irradiation, **3a** gives mainly *exo*-**4a** (*exo*:*endo*=95:5) in various solvents, but under sensitized conditions, it gives **4a** in variable ratios of 10:90 to 40:60 (*exo*:*endo*) depending mainly on the reaction temperature. These facts suggest the existence of two different cyclization mechanisms depending on the conditions used. It was reported that, under direct irradiation, such cyclization often proceeds by the concerted disrotatory mode[37] but under the sensitized conditions and/or from easily attained excited triplets, the reaction proceeds with initial *cis-trans* isomerization followed by the thermally allowed conrotatory ring closure.[38,39] It is possible to assume that these two modes of mechanisms might have played a role in the above case, and from each of their favored conformations, they will give the *exo-endo* mixture of **4a** in different ratios following the "accordant rule" discussed by Dauben.[40]

Experimental

General Procedure. UV, IR, H-NMR, and Mass spectra were recorded according to the methods given in the previous paper.[4] C-13 NMR spectra were recorded on a JNM FX-100 spectrometer (25.05 MHz) in $CDCl_3$ and the chemical shifts are expressed in ppm to the middle peak of the solvent-carbon as a standard (δ 77.1 ppm). A Varian Aerograph model 90P was used for the preparative VPC (helium flow rate; 30—40 mL/min) and a Shimazu Gas Chromatograph GC-4BM was used for the analytical purposes (Hydrogen flame ionization detector). The columns used for separation are ϕ 3.2 mm×1.8 m columns charged with: A, 10% Silicone DC QF-1; B, 5% Silicone OV-17; C, 3% Silicone OV-17; D, 5% Silicone SE-30, on Chromosorb WAW.

For irradiation of more than 100 mL volume, a solution charged in a vessel fitted with a quartz cooling jacket was purged with dry nitrogen for 5 min and internally irradiated with an Ushio High Pressure mercury arc (UM-452) through a Pyrex filter. For small scale irradiation (less than 15 mL), unless otherwise described, a solution charged in a drum-shaped Pyrex vessel with a ground glass joint fitted with a three-way cock, was purged with dry nitrogen for 5 min and dipped in ice water in a quartz Dewar bottle with a flat quartz window. The solution was then irradiated externally with an Ushio lamp (USH-500D) through a Toshiba filter (UV-31). After irradiation, the solvent was evaporated under reduced pressure and the residue taken in chloroform was chromatographed on silica gel to remove the sensitizer. The product mixture was then purified by the appropriate method.

Photolysis of ***1b***. A solution of **1b** (233 mg, 1.2 mmol) and Michler's ketone (1.31 g, 4.9 mmol) dissolved in benzene (400 mL) was irradiated for 2.5 h. The usual work-up gave a mixture (175 mg, 75% of the starting material) mainly composed of **1b** and **3b**. They were purified by chromatography on silica gel (5 g) using hexane–ether (95:5 *v/v*) as an eluent. A mixture (139 mg, 60%) composed of **1b** and **3b** (1:1), in addition to **8a** (23 mg, 10%), was separated and each was identified by direct comparison with the authentic samples.[5] For further identification, the mixture in ethyl acetate was hydrogenated over 10% palladium on carbon at room temperature to give two products (1:1): one was identified with known 2,3-dihydro-**1b**[41] and the other was tetrahydro-**3b**. They were separated by VPC

TABLE 2. PRODUCT DISTRIBUTIONS FOR THE PHOTOLYSIS OF **1b** IN THE PRESENCE OF SEVERAL SENSITIZERS

Sensitizer	E_T / kJ mol^{-1}	Products' ratio				
		1b	**3b**	**8a**	*exo*-**4b**	*endo*-**4b**
Acetophenone	308.3	54.5	Trace	37.0	2.2	6.3
Benzophenone	287.0	84.1	6.9	4.9	2	2
Michler's ketone	259.4	45	30	15	5	5
β-Acetonaphthone	248.5	79	4.7	4.7	3.1	8.2
α-Acetonaphthone	248.5	50	Trace	3.6	3	10.1
Benzil	223.4	100	0	0	0	0
Pyrene	201.2	100	0	0	0	0

(column A, 152 °C: *retention time*; 23.1 min, 14.2 min, respectively). **3b** NMR ($CDCl_3$) δ: 3.62 (1H, d, J=5 Hz), 3.74 (3H, s), 5.9—6.2 (2H, m), 6.38—6.6 (2H, m), 6.9—7.4 (4H, m). Mass *m/e* (rel intensity, %): 200 (M^+, 15), 141 (100), 115 (25). Tetrahydro-**3b** NMR (CCl_4) δ: 2.77 (2H, m), 3.67 (3H, s), 3.78 (1H, d,d, J=2.2, 6.4 Hz), 1.48—2.13 (6H, m), 6.84—7.13 (4H, m). UV (CH_3OH) λ_{max}: 256.5 (sh), 264, 272 nm. Mass *m/e* (%): 204 (M^+, 18), 172 (10), 145 (100), 117 (20), 91 (16). Found: C, 76.41; H, 7.87%. Calcd for $C_{13}H_{16}O_2$: C, 76.44, H, 7.90%.

Photolysis of **1b**-1-d_1. A solution of **1b**-1-d_1 (198 mg, 0.99 mmol) and Michler's ketone (1.01 g, 3.8 mmol) dissolved in benzene (400 mL) was irradiated for 3 h at 0—5 °C. After work-up as above, a product mixture (182 mg) was chromatographed on silica gel (6 g, 5% ether–hexane) to give a mixture (151 mg) of **1b**-d_1 and **3b**-d_1 (1.1:1.0). Careful examination of the proton NMR spectrum and comparisons with those of **1b** and **3b** revealed that (1) the area ratio of proton signals for H_1 (δ: 0.74 ppm), H_{1a} (δ: 2.49 ppm, d,d, J=8.2, 4.2 Hz), and H_{7b} (δ: 2.92 ppm, d, J=8.2 Hz) on **1b**-d_1 is equal to 7:100:98, which corresponds to the ratio observed in the starting **1b**-1-d_1 within the experimental error, and that (2) the signal due to H_5 for **3b**-d_1 was very feeble compared with those of olefinic protons (δ: 5.9—6.2 ppm, 2H; δ: 6.38—6.6 ppm, 1H), which fits those for **3b**-5-d_1.

Photolysis of **1b** *in Benzene with Several Sensitizers.* The irradiation was carried out in benzene solution (150 mg, 0.75 mmol/300 mL) in the presence of 4 equiv. mol of sensitizer for 2 h. The yields of the products were assayed by VPC (column A, 162 °C; *exo*-**4b** (*retention time*, 9.6 min), *endo*-**4b** (*r.t.*, 12 min), **1b**+**3b** (*r.t.*, 20.8 min), **8a** (*r.t.*, 24.4 min)) and NMR spectroscopy (Table 2).

Characterization of **4b**: After evaporation of the solvent, the residue taken in methanol was treated with sodium borohydride (4 equiv. mol) to make separation of the products from ketonic sensitizer easier. The usual work-up followed by chromatography (silica gel/10% ether–hexane) gave *exo*- and *endo*-**4b** together with **8a**. They were further purified by preparative VPC (column A, 162 °C) as mentioned above. *exo*-**4b** NMR (CCl_4) δ: 3.65 (3H, s), 3.78—3.95 (2H, m), 4.31—4.40 (1H, m), 6.12 and 6.31 (2H, AB type d, J=2.8 Hz), 7.07—7.38 (4H, m). UV (cyclohexane) λ_{max} (log ε): 255.5 (2.71), 262 (2.89), 268 (3.06), 275 (3.11) nm. IR (liq. film) ν_{max}: 1731, 1486, 1442, 1251, 1178, 772, 747 cm^{-1}. Mass *m/e* (rel intensity, %): 200 (M^+, 12), 185 (11), 174 (7), 141 (100), 115 (10). Found: C, 77.91; H, 6.15%. Calcd for $C_{13}H_{12}O_2$: C, 77.98; H, 6.04%. *endo*-**4b** NMR (CCl_4) δ: 3.73 (3H, s), 3.89, 4.04 (AB part of ABX, J_{ab}=10, J_{ax}=3.6 Hz), 4.24 (1H, X part of ABX, J_{ax}=3.6 Hz), 6.04 and 6.38 (2H, AB type, J=2.8 Hz), 7.08—7.36 (4H, m). UV (cyclohexane) λ_{max}: 263, 268, 275.5 nm. Found: C, 77.96; H, 6.12%. Calcd for $C_{13}H_{12}O_2$: C, 77.98; H, 6.04%.

*Photolysis of (1R)-***1b**. A solution of (1*R*)-**1b** ($[\alpha]_D^{14}$ +124° (*c* 1.16, CH_3OH); 228 mg, 1.14 mmol), prepared from (1*R*)-**1d** ($[\alpha]_D$ +143°), and Michler's ketone (1.84 g, 6.84 mmol) dissolved in benzene (120 mL) was irradiated under ice-cooling for 2 h. The usual work-up gave a mixture (102 mg, 45%) composed of mainly **3b** and **1b**, in addition to small amounts of *exo*- and *endo*-**4b** and **8a** (VPC, column C, 165 °C). The mixture was separated by medium pressure liquid chromatography (Kieselgel 60, 23 g/5% ether–hexane) into 60 fractions of 5 ml each. Fractions 20—23 contained **3b** (22.7 mg, $[\alpha]_D^{14}$ −2.82° (*c* 1.13, 95% C_2H_5OH)) and fractions 27—30 contained recovered **1b** (23.3 mg, $[\alpha]_D^{15}$ +114° (*c* 1.16, CH_3OH)).

Synthesis of Optically Active **1a**. (1*R*)-**1d** (522 mg, $[\alpha]_D$ +143°, optical purity >95%) was transformed to the corresponding diazo ketone (yellow silky crystals, 578 mg, 98%; ν_{max}: 2120, 1600 cm^{-1}), *via* the acid chloride (solid, 599 mg; $\nu_{C=O}$ 1760 cm^{-1}) by the usual method.[8] The diazo ketone dissolved in anhydrous methanol was irradiated at *ca.* 2 °C until 80% of the theoretical amount of nitrogen had evolved (22 min) and then concentrated below 3 °C under reduced pressure. The residue taken in cold chloroform was chromatographed on silica gel below 5 °C to give an optically active 1-*exo*-(+)-**1a** (300 mg; no contaminants other than **1a**, by TLC).

For the synthesis of *exo-endo* mixture (2:1) of (1*R*)-**1a**, the above photolysate was purified by chromatography on silica gel at room temperature with 10% ether–hexane as an eluent. Then the product (393 mg, 65% of the theoretical amount) was thermally equilibrated by heating it at 95 °C for 5 min ($[\alpha]_D^{31}$ +24.7° (*c* 1.2, CH_3OH)).

Photolysis of exo-endo *Mixture of (1R)-***1a**. A solution of (1*R*)-**1a** ($[\alpha]_D$ +24.7°; 118 mg, 0.55 mmol) and Michler's ketone (888 mg, 3.31 mmol) dissolved in dichloromethane (130 mL) was irradiated under nitrogen below 5 °C for 30 min. After the usual work-up, the product was rechromatographed on silica gel (12 g/benzene) to give an *exo-endo* mixture of **4a** (43.6 mg). VPC separation (column B, 150 °C) of it gave (−)-*endo*-**4a** ($[\alpha]_D^{25.5}$ −28° (*c* 0.35, $CHCl_3$) 19% enantiomer excess) and (+)-*exo*-**4a** ($[\alpha]_D^{23}$ +56° (*c* 0.35, $CHCl_3$)).[8]

Similarly, a solution of (1*R*)-**1a** (228 mg, 1.07 mmol) and Michler's ketone (1.72 g, 6.42 mmol) in benzene (110 mL) was irradiated at 40±1 °C for 5 min. The usual work-up and repeated chromatography gave a mixture (182 mg, 80%), which was estimated to be composed of **1a** (80%) and **3a** (20%), in addition to a minor amount of **4a**. A pure sample (3.5 mg) of **3a** was isolated by medium pressure liquid chromatography (Kieselgel 60, 23 g) and estimated to be 16% enantiomer excess by NMR measurement in the presence of tris[3-(2,2,3,3,4,4,4-heptafluoro-1-hydroxybutylidene)-*d*-camphorato]europium (III).

Photolysis of (1R)-exo-***1a***.* (1*R*)-*exo*-**1a**, obtained above, was photolyzed in dichloromethane (5 min) below 3 °C as described in the case of (1*R*)-**1a** (*exo-endo* mixture) and gave (+)-**3a**[1] ($[\alpha]_D^{18}$ +65° (*c* 0.63, 95% C_2H_5OH); 76% enantiomer excess (chiral NMR shift reagent)) and *endo*-**4a**[1] ($[\alpha]_D^{18}$ −81° (*c* 0.21, $CHCl_3$); 76% enantiomer excess) in addition to a recovery of **1a** ($[\alpha]_D^{23}$ −3.1° (*c* 1.04, CH_3OH).

Synthesis of Optically Active ***3a***. (5*S*)-(+)-**3a** ($[\alpha]_D^{17}$ +86° (*c* 0.88, 95% C_2H_5OH)) was prepared from benzotropylium tetrafluoroborate as described previously.[2]

*Photolysis of (+)-****3a***. A solution of (+)-**3a** (128 mg, 0.60 mmol; $[\alpha]_D$ +86°, 95% optically pure) and Michler's ketone (802 mg, 2.99 mmol) dissolved in benzene (110 mL) was irradiated under nitrogen for 40 min at 40 °C. After the usual work-up, an *exo-endo* mixture (1:4.8; 39 mg) of **4a** was obtained. VPC separation (column B, 150 °C) of the mixture gave (−)-*endo*-**4a** ($[\alpha]_D^{27}$ −107° (*c* 0.38, $CHCl_3$)) and (+)-*exo*-**4a** ($[\alpha]_D^{27}$ +180° (*c* 0.08, $CHCl_3$)).

Synthesis of Optically Active ***1e***. Into the acid chloride, obtained from (1*R*)-(+)-**1d** ($[\alpha]_D$ +143°, optical purity >95%; 1.16 g, 6.24 mmol) and dissolved in anhydrous ether (170 mL), was passed gaseous ammonia at 0 °C for 25 min until the pH of the solution reached 10 against a wet test paper. After stirring for 1 h at room temperature, water (150 mL) was added to the solution. The aqueous solution was separated and extracted three times with dichloromethane and the combined organic layer was washed successively with water and saturated brine, and then dried. The crude amide (1.11 g, 96%) was recrystallized from methanol. **1e** colorless crystals (775 mg, 67%), mp 261—262 °C; $[\alpha]_D^{15}$ +201° (*c* 0.51, dioxane). IR (Nujol mull) ν_{max}: 3420, 3230, 1645, 1605, 775, 735 cm^{-1}. NMR (DMSO-d_6) δ: 0.72 (1H, t, J=4.0 Hz), 2.5 (H_{1a}, m), 2.83 (1H, d,d, J=8.3, 4.0 Hz), 6.2—6.5 (2H, m) 7.0—7.5 (4H, m). Found: C, 77.76; H, 5.99; N, 7.52%. Calcd for $C_{12}H_{11}NO$: C, 77.81; H, 5.99; N, 7.56%.

Synthesis of Optically Active ***1c***. To a solution of the amide ($[\alpha]_D$ +201°; 519 mg, 2.81 mmol) and anhydrous pyridine (445 mg, 5.62 mmol) in anhydrous dioxane (12 mL) was added dropwise a solution of trifluoroacetic anhydride (649 mg, 3.1 mmol) in dioxane (5 mL) in a period of 25 min. After stirring for 3 h at room temperature, chloroform (50 mL) was added to the mixture. The organic layer was then washed successively with water (three times), and with saturated brine and dried. Evaporation of the solvent gave a crude nitrile (487 mg, 100%). Chromatographic separation (silica gel (12 g)/10% ether–hexane), followed by recrystallization from hexane gave **1c** as colorless crystals (280 mg, mp 76.5 °C; $[\alpha]_D^{15}$ +103° (*c* 0.95, CH_3OH)). *exo*-**1c** IR (Nujol mull) ν_{max}: 2225, 770, 730 cm^{-1}. UV (CH_3OH) λ_{max} (log ε): 273 nm (3.89): (cyclohexane) λ_{max}: 273 nm (3.89). H-NMR ($CDCl_3$) δ: 0.69 (1H, t, J=4.3 Hz), 2.69 (1H, d,d,d, J=8.3, 4.3, 4.2 Hz), 3.10 (1H, d,d,d, J=8.3, 4.3, 0.7 Hz), 6.25 (1H, d,d,d, J=9.8, 4.2, 0.7 Hz), 6.39 (1H, d, J=9.8 Hz), 7.0—7.5 (4H, m). C-13 NMR ($CDCl_3$) δ: 130.5 (s), 130.0 (s), 129.0 (d), 128.4 (d), 128.1 (d), 127.7 (d), 126.8 (d), 123.9 (d), 121.5 (s), 28.8 (d, J=168 Hz), 25.7 (d, J=171 Hz), 7.6 (d, J=178 Hz). Found: C, 86.32; H, 5.48; N, 8.36%. Calcd for $C_{12}H_9N$: C, 86.20; H, 5.43; N, 8.38%.

*Thermal Conversion of (+)-*exo-***1c*** to* endo-***1c***. (+)-*exo*-**1c** ($[\alpha]_D^{18}$ +103°; 16.6 mg) dissolved in DMSO-d_6 (0.4 mL) was heated in an NMR tube at 130 °C for 20 min. The mixture (*exo*:*endo*=2:3) was separated by chromatography on silica gel (10 g) and 37 fractions (fr. 1—30; 10% ether–hexane: fr. 31—37; CH_2Cl_2) of 8 mL each were collected. Fractions 6—10 contained 8 mg of (+)-*exo*-**1c**, mp 76.5 °C, $[\alpha]_D^{18}$ +103° (*c* 0.21, CH_3OH), and fraction 35, (−)-*endo*-**1c**, mp 153 °C, $[\alpha]_D^{16}$ −579° (*c* 0.17, CH_3OH). IR (Nujol mull) ν_{max}: 2217 cm^{-1}. UV (CH_3OH) λ_{max} (log ε): 270 nm (3.89): (cyclohexane) λ_{max} 270 nm (3.88). NMR ($CDCl_3$) δ: 2.19 (H_1, t, J=8.3 Hz), 2.63 (H_{1a}, d,t, J=8.3, 5.1 Hz), 3.03 (H_{7b}, t,d, J=8.3, 0.7 Hz), 6.12 (H_2, d,d,d, J=9.7, 5.1, 0.7 Hz), 6.70 (H_3, d, J=9.7 Hz), 7.2—7.4 (4H, m).

*Photolysis of 1-*exo-***1c*** in Benzene.* A solution of *exo*-**1c** (64.5 mg, 0.39 mmol) and Michler's ketone (486 mg, 1.81 mmol) in benzene (40 mL) was irradiated with HPL (100 W) through a Pyrex filter under ice cooling for 15 min. The usual work-up gave a mixture (44.0 mg, 68.2%), which was separated by column chromatography into *endo*-**1c** (4.0 mg, 6.2%) and a mixture (7:5) of *exo*-**1c** and **5a** (39 mg, 60%). The latter was estimated by VPC (column C, 165 °C: *retention time*; **5a**, 3.5 min; **1c** 5.7 min).

Photolysis of endo-***1c*** *in Benzene.* The same experiment as that of *exo*-**1c** was carried out using *endo*-**1c** (63.6 mg, 0.38 mmol). We obtained a mixture of products (55.7 mg, 88%) which was revealed by VPC and NMR spectroscopy to contain *endo*-**1c** (10 mg, 15.7%), *exo*-**1c** (28.5 mg, 44.8%), and **5a** (15.9 mg, 25.0%).

Photolysis of Optically Active exo-***1c*** *in Furan.* A solution of (+)-*exo*-***1c*** ($[\alpha]_D$ +103°, 133 mg, 0.80 mmol) and Michler's ketone (1.28 g, 4.77 mmol) dissolved in furan (110 mL) was irradiated below 5 °C under nitrogen for 15 min. After furan was recovered by distillation, the residue was chromatographed on silica gel (90 g/chloroform) to give an *adduct*-1 (12.1 mg), (−)-*endo*-**1c** (17.2 mg), and **5a** (10.8 mg) in addition to the recovered (+)-*exo*-**1c** (50.9 mg, $[\alpha]_D^{20}$ +110°, mp 74.5 °C). (−)-*endo*-**1c** Colorless needles, mp 153 °C; $[\alpha]_D^{16}$ +572° (*c* 0.8, CH_3OH). NMR ($CDCl_3$) δ: 2.19 (1H, t, J=8.3 Hz), 2.63 (1H, t,d, J=8.3, 5.1 Hz), 3.03 (1H, t,d, J=8.3, 0.7 Hz), 6.12 (1H, d,d,d, J=9.7, 5.1, 0.7 Hz), 6.70 (1H, d, J=9.7 Hz), 7.4—7.21 (4H, m). *Adduct*-1 Colorless needles, mp 107—109 °C; $[\alpha]_D^{15}$ −0.8° (*c* 0.25, $CHCl_3$). IR (Nujol mull) ν_{max}: 2230, 1615, 1140, 1070, 1015 cm^{-1}. NMR ($CDCl_3$) δ: 3.42 (1H, d,d, J=6.8, 2.9 Hz), 3.51 (1H, broad d, J=2.4 Hz), 3.62 (1H, m), 4.43 (1H, t, J=2.3 Hz), 4.56 (1H, d, J=3.2 Hz), 5.00 (1H, d,d, J=11.7, 6.8 Hz), 6.08 (1H, d,d, J=2.9, 2.0 Hz), 6.21 (1H, d, J=7.1 Hz), 6.72 (1H, m), 7.35—6.9 (4H, m). Found: C, 81.66; H, 5.53; N, 5.88%. Calcd for $C_{16}H_{13}NO$: C, 81.68; H, 5.57; N, 5.95%. Mass *m/e* (rel intensity): 235 (M^+, 0.38), 206 (2.73), 168 (46.9), 167 (100). **5a** IR (liq. film) ν_{max}: 3030, 2920, 2235, 1490, 1455, 1215, 1045, 955, 900, 855, 778, 740 cm^{-1}.

Photolysis of ***3c***. A solution of **3c** (58 mg, 0.35 mmol) and Michler's ketone (465 mg, 1.73 mmol) in benzene (13 mL) was irradiated externally for 3 h under ice-cooling to give, in addition to **3c** (7.5 mg, 13%), **5a** (19.5 mg, 34%) after chromatographic separation followed by preparative VPC (column A, 150 °C: *retention time*; **3c**, 10.3 min; **5a**, 11.4 min).

Photolysis of ***3c*** *in Furan.* A solution of **3c** (17 mg, 0.1 mmol) and Michler's ketone (136 mg, 0.81 mmol) dissolved in furan (13 mL) was irradiated externally for 2 h. The solution was concentrated and the residue taken in benzene was chromatographed on silica gel to give 10 mg of material composed of **5a** (52%) and *adduct*-1 (48%) estimated by VPC (column D, 169 °C: *retention time*; **5a**, 2.4 min; *adduct*-1, 9.6 min).

*Synthesis of 1a,2,3,7b-Tetrahydro-1*H*-cyclopropa*[a]*naphthalene-1,1-*d_2. To a stirred solution of 1,2-dihydronaphthalene containing 20% of naphthalene (12 g, 92 mmol) dissolved

in tribromomethane (60 g, 0.24 mol) was added dropwise 50% aq sodium hydroxide (20 mL) in the presence of tetrabutylammonium iodide (0.35 g, 0.95 mmol) under ice-cooling in a period of 10 min. Then the solution was vigorously stirred for 0.5 h. Then it was gradually warmed and stirred for 24 h at 40 °C. After cooling, water was added to the mixture and the aqueous layer was extracted with chloroform. The combined organic layer was washed with water and dried. Separation by chromatography (silica gel/hexane) of the product gave 1,1-dibromo-1a,2,3,7b-tetrahydro-1*H*-cyclopropa[*a*]naphthalene (17.3 g, 63%) as a yellow oil. A mixture of the bromide (5.8 g, 19 mmol), 40% tributyltin deuteride (32 g; contaminated by tributyltin chloride) and a catalytic amount of 2,2′-azobis(2-methylpropionitrile) (60 mg) was stirred at 95±5 °C for 26 h. The mixture was separated by column chromatography (Woelm neutral aluminium oxide, 300 g/hexane) to give 2,3-dihydro-**1f**-1,1-d_2 (2.5 g, 17 mmol, 89%). For analysis, it was purified by preparative VPC (column A, 99 °C; *retention time*, 12 min). Found: C, 90.36; H, 8.44% (H_2O as D_2O). Calcd for $C_{11}H_{14}$: C, 90.35; H, 9.65%: for $C_{11}H_{10}D_2$: C, 90.35; H, 8.27%. NMR (CCl_4) δ: 1.7—2.85 (6H, m), 6.85—7.5 (4H, m).

Synthesis of ***1f***-1,1-d_2. A solution of 2,3-dihydro-**1f**-1,1-d_2 (1.1 g, 7.7 mmol) and *N*-bromosuccinimide (1.4 g, 7.9 mmol) in carbon tetrachloride (70 mL) was refluxed in the presence of 2,2′-azobis-(2-methylpropionitrile) (60 mg) for 2.5 h. The solution was filtered and the filtrate was concentrated to dryness to give a yellow liquid, which was taken in *N*,*N*-dimethylformamide (40 mL). The solution was stirred with calcium hydrogen phosphate (1.38 g, 10.1 mmol) at 80—90 °C for 16 h. After cooling, the solution was diluted with water (100 mL) and extracted with ether. The combined ether solution was washed with water and dried. Evaporation of the solvent in vacuo left a crude product, which was purified by column chromatography (silica gel, 15 g/hexane). **1f**-1,1-d_2 (626 mg, 44%) was obtained as a colorless liquid. For photolysis, it was further purified by preparative VPC (column A, 100 °C; *retention time*, 14 min). NMR (CCl_4) δ: 1.93 (1H, broad; when irradiated on 6.18 ppm it becomes a broad doublet, J=8 Hz), 2.36 (1H, broad d, J=8 Hz), 6.18 (2H, two sharp signals), 6.9—7.35 (4H, m). The proton area ratio of *exo*-H_1 to olefinic 2H is 2:167=1:83.5 (purity 97%).

The same experiments as above were carried out using 1,1-dibromo-1a,2,3,7b-tetrahydro-1*H*-cyclopropa[*a*]naphthalene and tributyltin hydride in place of tributyltin deuteride. We obtained **1f** as a colorless liquid. UV (95% C_2H_5OH) λmax (log ε): 274.5 (3.87), 306 (3.11). H-NMR (CCl_4) δ: −0.3 (1H, d,t, J=3.8, 5 Hz), 1.50 (1H, d,t, J=3.8, 9 Hz), 1.96 (1H, m), 2.40 (1H, d,d,d, J=9, 7, 5 Hz), 6.20 (2H, m), 6.9—7.4 (4H, m). C-13 NMR ($CDCl_3$) δ: 9.45 (t, J_{CH}=164 Hz), 17.7 (d, J_{CH}=165 Hz), 20.6 (d, J_{CH}=163 Hz), 123.6, 125.7, 127.1, 127.7, 128.2, 129.0, 130.7, 135.5.

Photolysis of ***1f***. A solution of **1f** (34 mg, 0.24 mmol) and Michler's ketone (318 mg, 1.9 mmol) dissolved in benzene (130 mL) was irradiated under ice-cooling for 30 min. The usual work-up and VPC separation left a mixture of products (6 mg). Careful examination of the NMR spectrum revealed that the mixture contained mainly 5*H*-benzocycloheptene (**3f**) in addition to a minor amount of **1f**. **3f** NMR (CCl_4) δ: 3.02 (2H, d, J=6.5 Hz), 5.73 (1H, m), 6.03 (1H, m), 6.43 (1H, d,d, J=11, 6 Hz), 7.04 (1H, d, J=11 Hz).

Photolysis of ***1f***-1,1-d_2. A solution of **1f**-1,1-d_2 (23 mg, 0.16 mmol) and Michler's ketone (230 mg, 0.86 mmol) dissolved in benzene (100 mL) was irradiated for 15 min. The NMR spectrum of the isolated mixture (12 mg) was compared with that of the products from **1f**. They were quite similar, but in the former, the signal due to H_5 of **3f** were very weak and that of H_6 appeared as a broad doublet at 5.8 ppm. Further, the signal due to H_1 of **1f** appeared as weak as that of H_5 on **3f**. VPC (column A, 100 °C) of the mixture showed 4 peaks: peak-1 (unknown; *retention time*, 18.4 min; 7.1%), peak-2 (**3f**; 21.6 min; 39.4%), peak-3 (**1f**; 25.6 min; 49.1%), and peak-4 (**8b**-d_2; 33.2 min; 4.4%). In the NMR spectrum of peak-3, the peak area ratio for H_{7b}:H_{1a}:*endo*-H_1:H_2+H_3 is equal to 32:42:5:83. These results define unambiguously that **1f**-d_2 is composed of **1f**-1,1- and 1,7b-d_2 in a ratio of 3.2:1.

Photolysis of ***9a***. A solution of **9a** (33.5 mg, 0.24 mmol) and Michler's ketone (31.9 mg, 1.18 mmol) dissolved in benzene (100 mL) was irradiated for 30 min. The product (9 mg), isolated as above, showed 5 peaks in the VPC (column A, 100 °C) with a area ratio for an unknown, naphthalene, a mixture (1:2) of **3d** and **9a**, **1f**, and **8b** was 1:6:125:96:2, respectively. The NMR spectrum of the mixture also supports these assignments.

Photolysis of ***1a*** *in Furan*. A solution of **1a** (15 mg) and Michler's ketone (80 mg) dissolved in furan (12 mL) was irradiated externally for 3 h. The product was separated as above by chromatography (silica gel 5 g/benzene followed by benzene–ethyl acetate (9:1 v/v)) to give a product mixture (6.5 mg). This was estimated by VPC (column B, 165 °C) to contain the *adduct*-3 (30%).

Photolysis of ***3a*** *in Furan*. A solution of **3a** (40 mg, 0.19 mmol) and Michler's ketone (450 mg, 1.68 mmol) dissolved in furan (75 mL) was irradiated with a medium pressure mercury lamp (500 watts) for 0.5 h in a Pyrex jacket. After separation of the mixture by the usual method, the products were purified by preparative TLC (silica gel/20% ether–hexane) to give *adduct*-3 (23 mg, 43%). *Adduct*-3 IR (liq. film) ν_{max}: 3050, 2925, 1735, 1616, 1250, 1140, 1075, 760, 740, 725 cm^{-1}. UV (95% C_2H_5OH) λ_{max} (ε): 220 (end absorp., 9990), 260 (648), 267 (678), 275 (617) nm. NMR ($CDCl_3$) δ: 2.5—2.9 (2H, m), 3.0—3.56 (3H, m), 3.82 (3H, s), 4.47 (1H, t, J=2.5 Hz), 5.10 (1H, d,d, J=7, 11 Hz), 6.1—6.3 (2H, m), 6.78 (1H, d,d, J=7, 8 Hz), 6.9—7.4 (4H, m). C-13 NMR ($CDCl_3$) δ: 36.7 (d), 38.6 (d), 41.9 (t), 45.6 (d), 49.3 (d), 51.8 (q), 82.5 (d), 101.4 (d), 125.9 (d), 126.6 (d), 128.3 (d), 129.6 (d), 131.0 (d), 138.4 (d), 138.6 (s), 140.8 (s), 146.6 (d), 173.0 (s). Mass *m/e* (rel intensity): 250 (1.78, M^+-OCH_4), 215 (11.3), 214 (64.3, M^+−furan), 155 (14.9), 154 (59.5), 142 (12.5), 141 (100). Found: C, 77.04; H, 6.52%. Calcd for $C_{18}H_{18}O_3$: C, 76.57; H, 6.43%.

Photolysis of ***1f*** *in Furan*. Irradiation of **1f** (94 mg, 0.67 mmol) and Michler's ketone (888 mg, 3.3 mmol) in furan (80 mL) for 45 min gave a product (76 mg) after chromatography (silica gel, 20 g/hexane). VPC separation (column D, 170 °C) of the product gave **1f** (23.5 mg; *retention time*, 1 min) and *adduct*-4 (5.2 mg; *r.t.*, 4.8 min). *Adduct*-4 UV (95% C_2H_5OH) λ_{max} (ε): 220 (end absorp. 8900), 260 (599), 267 (751), 275 (723) nm. IR (liq. film) ν_{max}: 3050, 2925, 1616, 1140, 1075, 1017, 745, 720, 710 cm^{-1}. NMR ($CDCl_3$) δ: 2.83 (*exo*-H_{10}, d,d, J=4, 20 Hz), 2.9—3.15 (H_6, m), 3.3—3.8 (*endo*-H_{10}, H_7, H_1, m), 4.27 (H_5, t, J=2.5 Hz), 5.0 (H_2, d,d, J=6.5, 10.5 Hz), 6.10 (H_{11}, d,d, J=6, 8 Hz), 6.22 (H_4, t, J=2.5 Hz), 6.6 (H_{12}, d,d, J=6, 8 Hz), 6.86—7.2 (4H, m). Mass *m/e* (rel intensity): 210 (M^+, 0.55), 165 (3.1), 142 (100, M^+−furan). Found: C, 86.00; H, 6.78%. Calcd for $C_{15}H_{14}O$: C, 85.68; H, 6.71%.

The authors wish to thank Mr. Jun-Ichi Goda of our University for the elementary analyses and Mr. Tadasu Tahara of the Nitto Kasei Chemical Co. for a generous supply of tributyltin chloride.

References

1) This paper is dedicated to Emeritus Professor Takeo Sakan on the occasion of his 70th birthday.

2) M. Kato, M. Funakura, M. Tsuji, and T. Miwa, *J. Chem. Soc., Chem. Commun.*, **1976**, 63.

3) F. -G. Klārner and S. Yaslak, *Chem. Ber.*, **112**, 2286 (1979).

4) M. Kato, K. Takatoku, S. Ito, M. Funakura, and T. Miwa, *Bull. Chem. Soc. Jpn.*, **53**, 3648 (1980).

5) M. Kato, K. Takatoku, S. Ito, and Mīwa, *Tetrahedron Lett.*, **1979**, 867.

6) H. Günther, *Tetrahedron Lett.*, **1970**, 5173; S. W. Stayley, M. A. Fox, and A. Cairncross, *J. Am. Chem. Soc.*, **99**, 4524 (1977).

7) H. Meier, J. Heiss, H. Suhr, and E. Muller, *Tetrahedron*, **24**, 2307 (1968).

8) M. Kato, M. Kawamura, Y. Okamoto, and T. Miwa, *Tetrahedron Lett.*, **1972**, 1171.

9) D. Wendisch and W. Metzner, *Chem. Ber.*, **101**, 4106 (1968).

10) F. Campagna, A. Carotti, and G. Casini, *Tetrahedron Lett.*, **1977**, 1813.

11) J. S. Swenton, K. A. Burdett, D. M. Madigan, and P. D. Rosso, *J. Org. Chem.*, **40**, 1280 (1975).

12) N. F. Chamberlain, "The Practice of NMR Spectroscopy," Plenum Press, New York and London (1974), p. 299.

13) O. L. Chapman, M. Kane, J. D. Lassila, R. L. Loeschen, and H. E. Wright, *J. Am. Chem. Soc.*, **91**, 6856 (1969).

14) A. S. Kende, Z. Goldschmidt, and P. T. Izzo, *J. Am. Chem. Soc.*, **91**, 6858 (1969).

15) D. I. Schuster, R. H. Brown, and B. M. Rosnick, *J. Am. Chem. Soc.*, **100**, 4504 (1978).

16) J. S. Swenton, K. A. Burdett, D. M. Madigan, T. Johnson, and P. D. Rosso, *J. Am. Chem. Soc.*, **97**, 3428 (1975).

17) A. G. Anastassiou, E. Reichmanis, S. J. Girgenti, and M. Schaefer-Ridder, *J. Org. Chem.*, **43**, 315 (1978).

18) G. W. Gruber and M. Pomerantz, *J. Am. Chem. Soc.*, **91**, 4004 (1969); *J. Org. Chem.*, **33**, 4501 (1968).

19) H. G. Kuivila, L. W. Menapace, and C. R. Warner, *J. Am. Chem. Soc.*, **84**, 3584 (1962); H. G. Kuivila, *Acc. Chem. Res.*, **1**, 299 (1968); E. J. Corey and J. W. Suggs, *J. Org. Chem.*, **40**, 2554 (1975).

20) D. E. Applequist, M. R. Johnston, and F. Fisher, *J. Am. Chem. Soc.*, **92**, 4614 (1970).

21) K. A. Burdett, F. L. Shenton, D. H. Yates, and J. S. Swenton, *Tetrahedron*, **30**, 2057 (1974).

22) E. Ciganek, *J. Am. Chem. Soc.*, **89**, 1458 (1968).

23) K. Fukui, *Acc. Chem. Res.*, **4**, 57 (1971).

24) J. Eriksen, K. Krogh-Jespersen, M. A. Ratner, and D. I. Schuster, *J. Am. Chem. Soc.*, **97**, 5596 (1975).

25) P. S. Mariano and J. -K. Ko, *J. Am. Chem. Soc.*, **95**, 8670 (1973).

26) J. S. Swenton, R. M. Blankenship, and R. Sanitra, *J. Am. Chem. Soc.*, **97**, 4941 (1975).

27) We confirmed the optical yields for the rearrangement under direct irradiation[8] as follows: **1a** obtained from **1d** ($[\alpha]_D$ +143°) below 5 °C gave *exo*-**4a** ($[\alpha]_D$ −122° (*c* 0.65, $CHCl_3$)) and the thermally equilibrated *exo-endo* mixture (2:1) of **1a** ($[\alpha]_D$ +29° (*c* 0.98, $CHCl_3$)) obtained from the same acid gave *exo*-**4a** ($[\alpha]_D$ −120° (*c* 0.65, $CHCl_3$)). The enantiomer excesses of both *exo*-**4a** were found to be 60% by NMR measurements using tris[3-(2,2,3,3,4,4,4-heptafluoro-1-hydroxybutylidene)-*d*-camphorato]europium-(III) as a chiral shift reagent.

28) J. Hine, *J. Am. Chem. Soc.*, **88**, 5525 (1966); O. S. Tee and Y. Yates, *ibid.*, **94**, 3074 (1972).

29) W. T. Borden, J. G. Lee, and S. D. Young, *J. Am. Chem. Soc.*, **102**, 4841 (1980).

30) M. Kato, M. Tsuji, and T. Miwa, *Bull. Chem. Soc. Jpn.*, **51**, 1450 (1978).

31) The determination of optical purity with chiral NMR shift reagent was unsuccessful but the absolute value of the specific rotation was the same as the one thermally obtained from (1*R*)-*exo*-**1c**.

32) These facts are parallel with the thermal behavior of **1a**. When **1a** was heated above 250 °C for 1.5 h, it gave, in addition to a trace amount of naphthalene, methyl 3-(1-naphthyl)acrylate (29%) and methyl 3-(1-naphthyl)propanoate (53%). The latter was identified by direct comparison with an authentic sample and the former was confirmed by the spectral data (NMR ($CDCl_3$) olefinic protons δ: 8.2 (1H, d, J=16 Hz), 6.2 (1H, d, J=16 Hz): UV λ_{max}: 330 nm. IR ν_{max}: 1710, 1635 cm^{-1}) and by quantitative transformation to the latter under catalytic hydrogenation (H_2 (10% Pd–C, CH_3OH)).

33) N. H. Fischer and H.-N. Lin, *J. Org. Chem.*, **38**, 3073 (1973).

34) M. P. Schneider and R. J. Crawford, *Can. J. Chem.*, **48**, 628 (1970); M. J. Jorgenson, *J. Am. Chem. Soc.*, **91**, 6432 (1969).

35) In a rough approximation, the rotamer relationships about the sp^2–sp^3 bond of **23** or **24** (C_{7b}–C_1) are similar to those of substituted acetaldehydes or 3-substituted propenes.[42] Karabatsos described that, of the two minimum energy-tautomers, **27a** has an advantage over **28a** by 250 cal/mol when two ethyl groups are attached to the α-carbon of acetaldehyde. Further, **27a** increases its stability about 350 cal/mol by the phenyl substitution in place of ethyl group in butanal.[42] Therefore, in 2-phenylbutanal, **27a** might be estimated to be more stable (250—600 cal/mol) than **28a**. Similar trends are seen in the substituted propenes (**27b** and **28b**). In the conformers, **23c** and **24c**, because the substituents are regarded as a phenyl and a vinylmethinyl group (**29** and **30**), the steric requirement is supposed to be of the same order as the one substituted with a phenyl and an ethyl group. If we assume the conformer **23c** related to **29** is more stable and hence more populated than **24c** related to **30** and that there is little difference in steric requirement for reconversion processes of **23c** to *exo*-**1c** and of **24c** to *endo*-**1c**, the rates of ring closure might be governed mainly by the population of **23c** against that of **24c**.

36) J. C. Berridge, D. Bryce-Smith, A. Gilvert, and T.

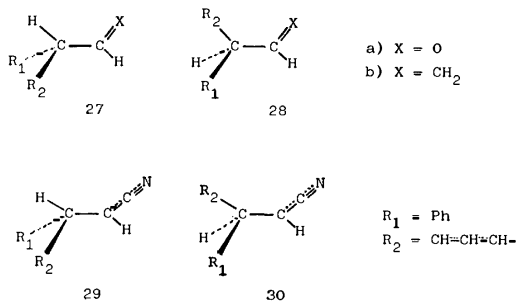

27 28 29 30

Scheme 9,

S. Cantrell, *J. Chem. Soc., Chem. Commun.*, **1975**, 611.
37) R. S. Lie, *J. Am. Chem. Soc.*, **89**, 112 (1967).
38) K. Schafner and M. Demuth, "Rearrangements in Ground and Excited States," ed by P. de Mayo, Academic Press, New York (1980), Vol. 3, p. 334.
39) D. I. Schuster and D. J. Blythin, *J. Org. Chem.*, **35**, 3190 (1970).
40) W. G. Dauben and M. S. Kellog, *J. Am. Chem. Soc.*, **102**, 4456 (1980).
41) R. Huisgen and G. Juppe, *Chem. Ber.*, **94**, 2332 (1961).
42) G. J. Karabatsos and D. J. Fenoglio, "Topics in Stereochemistry," ed by E. L. Eliel and N. L. Allinger, Wiley-Interscience, New York (1970), Vol. 5, p. 167.

Photochemical Reaction of 4-Hydroxy-diphenylamine with Polychloromethane

Tadao HINOHARA* and Kazuo AMANO

Department of Chemistry, Faculty of Engineering, Toyo University, Kuzirai, Kawagoe, Saitama 350

(Received January 16, 1982)

The main photochemical reaction of 4-hydroxy-diphenylamine (R) in the aerated cyclohexane was photocyclization. In the presence of polychloromethane (Q), however, photooxidation to *N*-phenyl-*p*-benzoquinone monoimine (PBQI) took place instead of the photocyclization. The formation of PBQI was in parallel with the quenching of fluorescence by Q, and it was proposed that both PBQI formation and fluorescence quenching by Q proceed *via* exciplex, $(R^+Q^-)^*$, which is nonfluorescent. The kinetic analysis based on this reaction mechanism gives the fluorescence quenching constant, which is in good agreement with the value obtained directly from the fluorescence quenching study. This agreement strongly supports the validity of the proposed reaction mechanism.

The electron donor and acceptor system involves the electron transfer as the deactivation process of the electronically excited state of the donor or acceptor and forms a resultant pair of radical cation and anion which participates in various types of reactions.[1] The aromatic amine and polychloromethane (Q) system can be regarded as one electron donor–acceptor system. Latowsky and Zelent have made systematic studies on the photochemistry of monophenylamines–Q systems and have pointed out that the primary process may be an electron transfer from the excited amine to Q, however, the final products were not simple enough to allow them to analyze the over-all reaction completely.[2] Diphenylamine and its *N*-substituted derivatives have been known to photocyclize to give carbazoles.[3,4] This photocyclization has been proposed to proceed *via* triplet state.[5] In the presence of Q, however, photolysis of diphenylamines furnishes a variety of products which are quite different from the photocyclization product.[6–9] These new products are considered to arise from the electron transfer from the excited amine to Q. The present authors extended the treatment to 4-substituted diphenylamines because the effect of substituent in the benzene nucleus on the photochemical path ways of diphenylamine has rarely been reported.

In this paper, the identification of the photolysis product from 4-hydroxy-diphenylamine and Q system together with the discussion on the mechanism of the reaction will be presented.

Experimental

Materials. 4-Hydroxy-diphenylamine was obtained commercially and purified by repeated recrystallization. Polychloromethanes and solvents were the spectroscopic grade reagents and were used without further purification.

Light Source and Actinometry. The high pressure mercury lamp was used with an interference filter for 313 nm light source. The intensity of the incident light was measured by the method of potassium trioxalatoferrate(III) actinometer.

Analysis. Measurement of the quantum yield of the reaction was carried out spectroscopically by monitoring the increase in characteristic absorption of the reaction product. The absorption spectra were measured by Hitachi EPS-2-model spectrophotometer and emission spectra were taken with a Hitachi MPE-3-model fluorescence spectrophotometer.

Results and Discussion

The progressive spectral changes of 4-hydroxy-diphenylamine (AH_2) in aerated cyclohexane solution caused by irradiation of 313 nm light in the absence and presence of Q are given in Fig. 1 (a) and Fig. 1 (b), respectively. The spectral changes under the absence of Q are characteristic for the well-known photocyclization. The final spectrum obtained under the presence of Q shown in Fig. 1 (b), however, is quite different from that shown in Fig. 1 (a), and is identical with that of *N*-phenyl-*p*-benzoquinone monoimine (PBQI) reported by Teuber.[10] Further confirmation of the reaction product was carried out as follows: The crude product separated from the irradiated solution was submitted to the alumina chromatography using benzene as a solvent. The red fine crystal was separated from benzene. The melting point of this crystal coincided with that reported for PBQI,[11] and the mixed melting point with the synthesized PBQI showed no depression. Since the irradiation of *p*-aminophenol in the presence of Q gave complicated reaction products other than *p*-benzoqui-

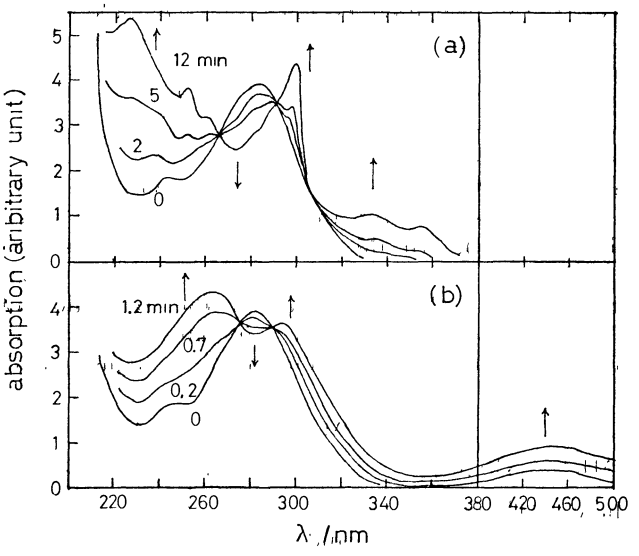

Fig. 1. Spectral changes of 4-hydroxy-diphenylamine in aerated cyclohexane caused by irradiation of 313 nm light in the absence (a), and in the presence (b) of $CHCl_3$.

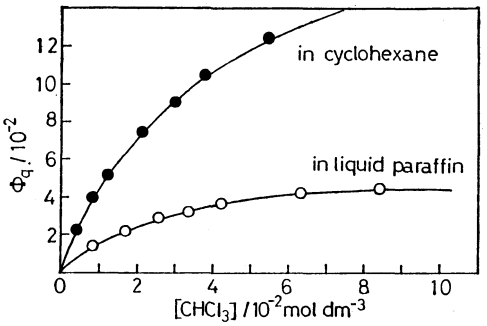

Fig. 2. Dependence of the quantum yield on the concentration of $CHCl_3$ in cyclohexane and in liquid paraffin.

TABLE 1. QUANTUM YIELDS (Φ_q) AND FLUORESCENCE QUENCHING CONSTANTS (k_Q)

	CH_2Cl_2	$CHCl_3$	CCl_4
Φ_q	0.01	0.04	0.43
k_Q[a)]	6.0	23.5	79.2
k_Q[b)]	7.3	20	75
$1/(k_0k_1\tau)$	0.91	0.20	0.013
$k_Q/(k_0k_1\tau)$	6.6	4.0	1.0

a) Obtained from the fluorescence quenching experiment. b) Obtained from the reaction kinetics.

none monoimine, the photooxidation by Q giving benzoquinone monoimine-type product is the characteristic reaction for AH_2.

The quantum yield of PBQI formation (Φ_q) in cyclohexane increased with increasing the concentration of Q, as shown in Fig. 2. Polychloromethane acts as a quencher on the fluorescence of AH_2 and the Stern-Volmer plots give a straight line. Values of Φ_q, obtained under the condition where the concentration of Q is 0.01 mol dm^{-3}, and values of the fluorescence quenching constant (k_Q) are listed in Table 1. It may be seen in the Table that the effect of Q on PBQI formation becomes more notable as the fluorescence quenching ability of Q increases. This result suggests that the process of fluorescence quenching by Q leads to the formation of PBQI. To make sure of this assumption, the mechanism of the reaction and fluorescence quenching by Q were studied. The photochemical reaction of aromatic amine with Q has been known to result in the formation of hydrogen chloride (HCl). In the present case, the formation of HCl was confirmed from the increase in the concentration of hydrogen ion under the irradiation of AH_2–Q–ethanol–water system. Similar to the case of aniline derivatives,[2)] the following mechanism may be presented:

$$AH_2^* + CH_nCl_{4-n} \longrightarrow AH_2^+ + (CH_nCl_{4-n})^-, \quad (1)$$

$$AH_2^+ + (CH_nCl_{4-n})^- \longrightarrow A + CH_{n+1}Cl_{3-n} + HCl, \quad (2)$$

where AH_2^* and A are the excited AH_2 and PBQI, respectively. CH_nCl_{4-n} and $CH_{n+1}Cl_{3-n}$ denote polychloromethane, where $n=0$, 1, 2.

It has been reported that the aromatic amine forms a stable complex with Q in their ground state.[12,13)] On the other hand, Sharpe[14)] reported that the amine forms a complex with Q only in the excited state. The fluorescence spectrum of AH_2 was sensitively affected by the addition of Q, while the absorption spectrum was almost unchanged. The quantum yield (Φ_q) was found to be markedly reduced in liquid paraffin compared with that in cyclohexane, as shown in Fig. 2. These results clearly indicate that the diffusion controlled encounter process is involved in the reaction between the excited amine and Q and the role of the stable complex is not important.

The results described above can be accounted for by the following reaction scheme. Polychloromethane

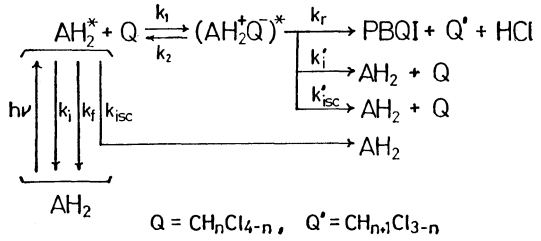

Reaction scheme.

forms a exciplex, $(AH_2^+Q^-)^*$, *via* the encounter complex with the excited amine. As for the relaxation process of the exciplex, the reaction leading to PBQI (rate constant: k_r), nonradiative relaxation (k_i'), and intersystem crossing (k'_{isc}) are taken into account. The stability of the exciplex depends on the nature of Q. Using the steady state approximation, the following equations are obtained for Φ_q and Φ_f°/Φ_f:

$$\Phi_q = \frac{k_0k_1\tau[Q]}{1+k_Q[Q]}, \quad (3)$$

$$\Phi_f^\circ/\Phi_f = 1 + k_Q[Q], \quad (4)$$

where

$$k_Q = k_1\tau/(1+k_2\tau), \quad \tau = 1/(k_i+k_f+k_{isc}),$$
$$\tau' = 1/(k_i'+k_r+k'_{isc}),$$

and

$$k_0 = k_r\tau'/(1+k_2\tau).$$

Equation 3 is rewritten as follows:

$$\Phi_q^{-1} = k_Q/k_0k_1\tau + (1/k_0k_1\tau)[Q]^{-1}.$$

Then, the reciprocal of the quantum yield is expected to have a linear relation with the reciprocal of the concentration of Q. The experimental results meet with this expectation, and the value of k_Q is obtained from the intercept ($k_Q/k_0k_1\tau$) and slope ($1/k_0k_1\tau$) of the straight line. This value of k_Q can be compared with that obtained directly from the fluorescence quenching and these are summarized in Table 1. The good agreement of the values obtained by reaction kinetic analysis and by the fluorescence quenching experiment strongly supports the validity of the proposed reaction scheme.

A part of this work was carried out at Gunma University. The authors wish to thank Professor Kohji Matsui of Gunma University and Professor Ikuzo Tanaka of Tokyo Institute of Technology for their helpful discussions.

References

1) B. Stevens, "Advances in Photochemistry," ed by J. N. Pitts, G. S. Hammond, and W. A. Noyes, Wiley-Interscience, New York (1971), Vol. 8, pp. 161—227.
2) T. Latowski and B. Zelent, *Rocz. Chem.*, **51**, 1709 (1977) and references cited therein.
3) E. J. Bowen and J. H. D. Eland, *Proc. Chem. Soc.*, **1963**, 202.
4) K. H. Grellmann, G. H. Shermann, and H. Linshitz, *J. Am. Chem. Soc.*, **85**, 1881 (1963); H. Linschitz and K. H. Grellmann, *ibid.*, **86**, 303 (1964).
5) E. W. Forster, K. H. Grellmann, and H. Linschitz, *J. Am. Chem. Soc.*, **95**, 3180 (1973) and references cited therein.
6) T. Iwasaki, T. Sawada, M. Okuyama, and H. Kamada, *Photogr. Sci. Eng.*, **22**, 312 (1978).
7) T. Iwasaki, T. Sawada, and M. Okuyama, *J. Phys. Chem.*, **82**, 371 (1978).
8) Y. Wada, T. Goto, M. Yamamoto, and Y. Nishizima, 1980 Symposium on photochemistry, Mie, October 1980.
9) K. Wyrzykowska, M. Grodowski, K. Weis, and T. Latowski, *Photochem. Photobiol.*, **28**, 311 (1978).
10) H. H. Teuber and W. Schmidt, *Ber.*, **93**, 1258 (1960).
11) R. Willstater and C. W. Moore, *Ber.*, **40**, **II**, 2675 (1907).
12) K. M. C. Davis and M. F. Farmer, *J. Chem. Soc., (B)*, **1976**, 28.
13) K. M. Morcom and D. N. Travers, *Trans. Faraday Soc.*, **62**, 2063 (1966).
14) A. N. Sharpe and S. Walker, *J. Chem. Soc.*, **1961**, 2974.

Studies on Catalytic Activity of Chelating Resins. I. The Catalytic Activity of Resin–Metal Chelates for the Oxidation of 2,6-Dihydroxyphenylacetic Acid and Hydroquinone

Hiroaki EGAWA,* Takamasa NONAKA, and Noboru KOZAKURA

Department of Industrial Chemistry, Faculty of Engineering, Kumamoto University, Kurokami, Kumamoto 860

(Received January 29, 1982)

Some crosslinked chelating resins were prepared and the catalytic activity of the resin–metal chelates for the oxidation of 2,6-dihydroxyphenylacetic acid(homogentisic acid) and hydroquinone was investigated. The resin–Cu(II), resin–Au(III), and resin–Ag(I) chelates had a high catalytic activity. Especially resin–Cu(II) chelate had the highest catalytic activity for these oxidation reactions, and its activity did not decrease even after repeated use. The chelating resins having hydrazide or polyethylenepolyamine side chains had a high catalytic activity. In order to have a high catalytic activity, the resin–metal chelates must leave coordination places open for the substrate to coordinate to metal in the chelates. In the oxidation of homogentisic acid, the catalytic activity of gel type resin increased with the increase of crosslinking degree in the range from 0.5% to 7.5%. However, the catalytic activity of the macroreticular chelating reins was scarcely affected by the degree of crosslinking. The oxidation reaction of homogentisic acid showed a kinetic behavior of a typical Michaelis-Menten type.

It is known that Cu(II) ion acts as a catalyst for the oxidation of organic substrates by molecular oxygen.[1,2] Pecht and coworkers reported that the binding of Cu(II) to polyhistidine enhanced the catalytic activity of Cu(II) for the oxidation of homogentisic acid and hydroquinone.[3] However, the catalytic activity of crosslinked chelating resin–metal complexes(resin–metal chelates) for the oxidation of the substrate mentioned above have never been investigated. The use of resin–metal chelates as catalysts have apparently the following advantages:

1) The resin–metal chelates can easily be separated by filtration from the products after use.

2) The resin–metal chelates can be used repeatedly many times. Therefore, if the resin–metal chelates have a high catalytic activity for the various reactions, they will be applicable to an industrial use. Many kinds of the chelating resins having thiol group, hydrazino carbonyl group, and polyethylenepolyamine side chain have been prepared in our laboratory. In this report the oxidation of homogentisic acid and hydroquinone catalyzed by resin–metal chelates was investigated.

Experimental

Preparation of Crosslinked Chelating Resins. Seven chelating ion exchange resins were used for this research. Each resin was prepared as follows, and the estimated structures of functional groups in these chelating ion exchange resins with the abbreviated symbols are shown below.

RST: The macroreticular styrene–divinylbenzene (7 mol%) copolymer beads were prepared by suspension polymerization in the presence of 2,2,4-trimethylpentane (100 vol%). The gel type syrene–divinylbenzene copolymer beads were also prepared by suspension polymerization. Abovementioned styrene–divinylbenzene copolymer beads and commercial macroreticular copolymer beads were chloromethylated with chloromethylether at 0—5 °C. The chloromethylated copolymer beads were treated with triethylenetetramine.[4]

RMH: The macroreticular methyl methacrylate–divinylbenzene copolymer beads (RM) were prepared by suspension polymerization in the presence of 2,2,4-trimethylpentane. The copolymer beads were treated with hydrazine hydrate.[5]

RMT: The macroreticular copolymer beads (RM) were treated with triethylenetetramine.[6]

RGT: The macroreticular poly(glycidyl methacrylate) beads (RG) were prepared by suspension polymerization in the presence of 2,2,4-trimethylpentane (50 vol%). The polymer beads were treated with triethylenetetramine.[7]

RGS: The macroreticular polymer beads (RG) were treated with ammonium thiocyanate, and then followed by the reaction with ethanolic potassium hydrogensulfide.[8]

The cationic exchange resin WK-11 and the chelating resin CR-10 were kindly supplied from Mitsubishi Kasei

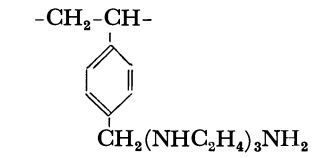

RST

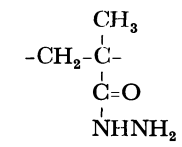

RMH

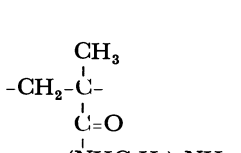

RMT

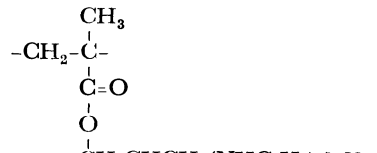

RGT

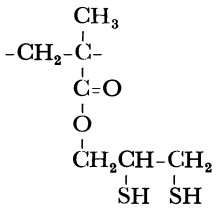

RGS

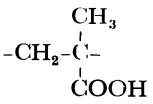

WK-11

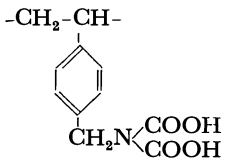

CR-10

Table 1. Characterization of the macroreticular chelating resins used in this research

Resin	Specific surface area $m^2\ g^{-1}$	Pore volume $ml\ g^{-1}$	Average pore radius Å	Anion exchange capacity mequiv. g^{-1}	Cu^{2+} adsorbed (mmol/g)
RST-L[a)]	16.1	1.02	700	9.04	2.56
RST-I[a)]	302	0.70	215	4.28	1.35
RST-II[a)]	242	0.49	230	4.21	1.27
RST-III[a)]	94	0.88	680	3.60	0.93
RST-IV	38	0.83	290	6.96	1.69
RMH 3-50[b)]	5.0	0.59	2400	3.83	2.23
RMH 5-50	12.2	0.46	750	3.55	2.32
RMH 10-50	16.9	0.45	530	3.08	1.86
RMT 5-10	0	0	—	5.94	0.35
RMT 5-30	1.0	0.07	395	7.81	1.26
RMT 5-50	4.6	0.28	775	7.15	1.98
RMT 5-90	0.4	1.01	39000	7.36	0.87
RGT	0.7	0.65	10000	7.05	1.99
RGS	0.6	0.52	9400	—	0.78
WK-11	—	—	—	—	1.00
CR-10	—	—	—	—	1.64

a) RST-L, -I, -II, and -III were prepared from commercial copolymer beads. b) The former and latter numbers represent the volume percentage of divinylbenzene in the monomer mixture and the volume percentage of 2,2,4-trimethylpentane to the monomer mixture, respectively.

Kogyo Co. Ltd. The resins used in this research were macroreticular chelating resins except the resins described as gel type resin. The characterization of the resins used in this research is shown in Table 1.

Adsorption of Metal Ion on the Chelating Resins. The chelating resin (0.25 g) was weighed accurately and immersed in 50 cm^3 of an aqueous metal solution at room temperature for 96 h. The amount of metal ion adsorbed on the resins was calculated by chelatometric determination of the metal ion concentration in the supernatant.

Measurement of Anionic Exchange Capacity of Resins. The resin (OH type) (0.5 g) was weighed accurately and immersed in 100 cm^3 of a 0.1 mol dm^{-3} HCl–1 mol dm^{-3} KCl aqueous solution at room temperature for 24 h with occasional shaking. The aniohic exchange capacity was determined by titrating the concentration of hydrochloric acid in the supernatant with a 0.1 mol dm^{-3} NaOH solution.

Measurement of the Catalytic Activity. A mixture containing homogentisic acid (or hydroquinone), phosphate buffer solution (pH 7), and resin–metal chelates was placed in a 500 cm^3 three-neck flask and stirred at a revolution rate of 300 rpm at 40 °C (or 50 °C for hydroquinone). The catalytic reactions were carried out under air except the experiments described as under nitrogen. The initial concentrations of homogentisic acid and hydroquinone were controlled to 4×10^{-4} mol dm^{-3}. The rate of their oxidation was measured by the titration with ammonium cerium nitrate or spectrophotometrically at 290 nm.

Results and Discussion

Effect of the Kind of Metal Ion on the Catalytic Activity. The effect of adsorbed metal ions on the catalytic activity was investigated by use of macroreticular chelating resins at 40 °C. The amount of metal added to the reaction system was kept constant (4×10^{-4} g atom). The amounts of the resin–metal chelates added to the reaction system were different in each oxidation reaction, since the amounts of metal ions adsorbed on the resins were different. The oxidation rates of homogentisic acid are shown in Fig. 1, in which the catalytic activity decreased in the following order; RST-Cu(II) > RST-Au(III) > RST-Ag(I) > RST-Hg(II) > RST-Fe(III). RST-Ni(II) and RST-Zn(II) chelates showed scarcely the catalytic activity for the oxidation of homogentisic acid.

In the oxidation of hydroquinone, the catalytic activity decreased in the following order: RST-Au(III) > RST-Ag(I) > RST-Cu(II) > RST-Hg(II).

The RST–metal chelates which showed a high catalytic activity were used repeatedly three times. The results are shown in Fig. 2. The chelates were dried at 50 °C for 12 h after they were once used. Then they were used repeatedly as catalysts. Figure 2 shows that the catalytic activity of RST-Cu(II) chelates did not decrease, even when the chelates were used repeatedly, whereas those of RST-Au(III), RST-Ag(I), and RST-Hg(II) chelates decreased gradually, as the chelates were used repeatedly. Especially, the

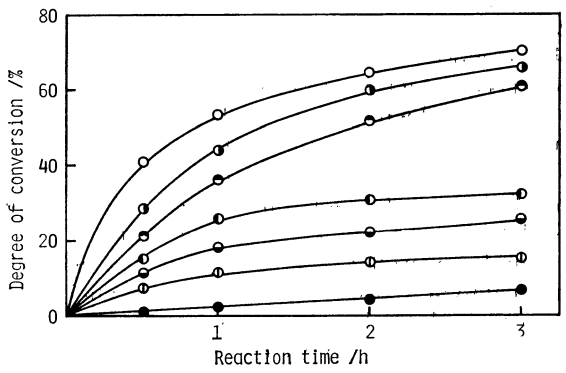

Fig. 1. Effect of the kind of metal ions on the oxidation of homogentisic acid.
Metal content: 4×10^{-4} g atom, catalyst: RST-L–metal chelate. Metal ion; ○: Cu(II), ◑: Au(III), ◓: Ag(I), ◐: Hg(II), ◒: Fe(III), ⓘ: adsorption of substrate, ●: autoxidation.

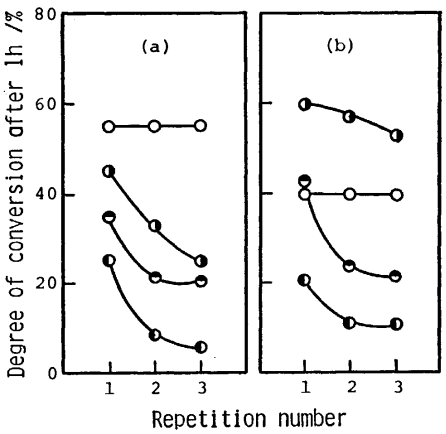

Fig. 2. The catalytic activity of RST–metal chelates for the oxidation of homogentisic acid and hydroquinone after repeated use.
Metal content: 4×10^{-4} g atom, catalyst: RST-L–metal chelate, (a): homogentisic acid, (b): hydroquinone. Metal ion; ○: Cu(II), ◑: Au(III), ◓: Ag(I), ◐: Hg(II).

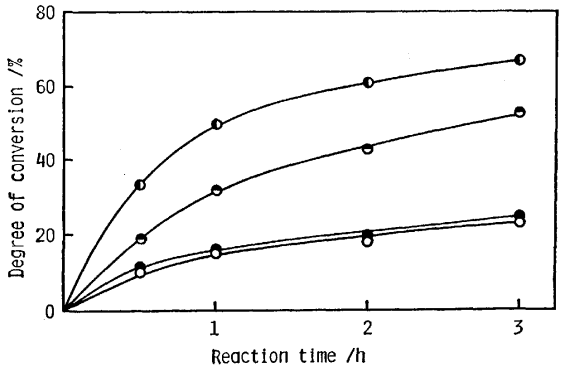

Fig. 3. Effect of the mole ratio of Cu(II) to the ligand on the oxidation of homogentisic acid.
Cu(II) content: 1.25×10^{-4} g atom, catalyst: RST-L–Cu chelate. Cu(II)/N(mole ratio); ◐: 0.28; ◓: 0.22, ●: 0.11, ○: 0.06.

extent of the decrease of the catalytic activity of RST–Ag(I) and RST–Hg(II) chelates is larger than that of RST–Au(III) chelate. During the oxidation reaction Ag(I) and Hg(II) were eluted from the chelates into the reaction solution.

Copper(II), gold(III), and mercury(II) in the resin–metal chelates which showed high catalytic activities have the coordination number of 4, while the coordination number of 2 in the reduced states. This change of the coordination number is responsible for the catalytic activity. The fact that Cu(I) forms a stable complex as well as Cu(II) is probably the reason why the catalytic activity of RST–Cu(II) chelate did not decrease, when the chelate was used repeatedly. The reason of a high catalytic activity of the RST–Ag(I) chelate is not clear yet.

Effect of the Mole Ratio of Cu(II) Adsorbed to the Ligand in Resins(Cu(II)/N) on the Catalytic Activity. Figure 3 shows the oxidation rate of homogentisic acid catalyzed by the RST–Cu(II) chelates with various Cu(II)/N ratios. The catalytic activity increased with

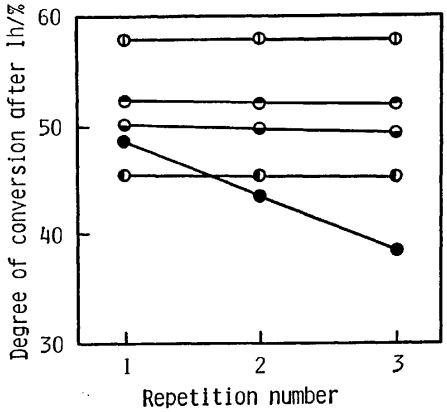

Fig. 4. The catalytic activity of various resin–Cu(II) chelates for the oxidation of homogentisic acid after repeated use.

	◐	◓	◒	●	◐
Resin	RMH 5-50	RST-I	WK-11	RGS	CR-10
Cu(II) content / 10^{-4} g atom	3.0	3.0	3.0	1.0	4.0

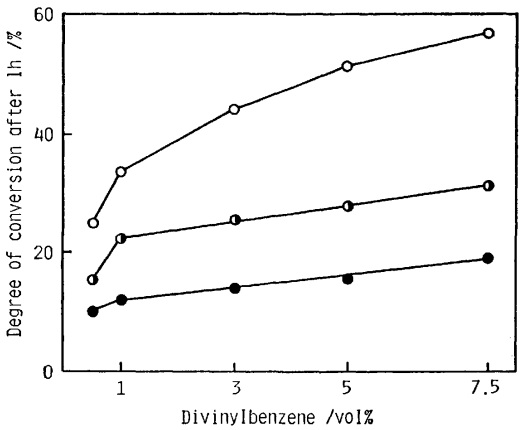

Fig. 5. Effect of the degree of crosslinking of the resins on the oxidation of homogentisic acid(I).
Cu(II) content: 2×10^{-4} g atom, catalyst: RST(gel type)–Cu(II) chelate. Repetition number; ○: 1, ◑: 2, ●: 3.

an increase in the Cu(II)/N ratios in the resin–metal chelates. These results suggest that, in order to have a high catalytic activity, the resin–metal chelates must leave coordination places open for the substrate to coordinate to the metal. The same results were also observed for RMT–Cu(II) and RGT–Cu(II) chelates. These results agree with those obtained by Sigel,[9] and Hatano *et al.*[10]

Effect of the Kind of Chelating Resins on the Catalytic Activity. The catalytic activity of various resin–Cu(II) chelates for the oxidation of homogentisic acid was investigated. The amounts of Cu(II) added into the reaction system are listed below Fig. 4 which revealed the highest catalytic activity of RMH–Cu(II) chelate. These resin–Cu(II) chelates were used three times. The catalytic activities of RMH–Cu(II), RST–Cu(II), WK-11–Cu(II), and CR-10–Cu(II)chelates scarcely decreased, whereas that of RGS–Cu(II) chelate decreased gradually, as these chelates were

used repeatedly. The decrease of catalytic activity of RGS-Cu(II) chelate is ascribed to the elution of Cu(II) ion from the resin-metal chelate during the oxidation reaction.

Effect of the Degree of Crosslinking of Chelating Resins on the Catalytic Activity. Firstly, the effect of the degree of crosslinking of resins on the oxidation of homogentisic acid was investigated by use of gel type resins with different degrees of crosslinking. Figure 5 shows that the catalytic activity of gel type resin-Cu(II) chelates increased with an increase in the degree of crosslinking in the range from 0.5% to 7.5%, and the catalytic activity decreased gradually, as the resin-Cu(II) chelates were used repeatedly. The anion exchange capacity and the adsorption capacity for Cu(II) ion of these resins are listed in Table 2, which shows that both these capacities decreased with an increase of the crosslinking degree, and the decrease of the adsorption capacity is larger than that of the anion exchange capacity. The adsorption capacity of highly crosslinked resins for metal ions seems to be limited by steric hindrance. From the results mentioned above, the catalytic activity increase with an increase of crosslinking degree of resins is ascribed to the fact that metals in the higher crosslinked resin-metal chelates have a larger number of coordination places for substrate than those in the lower crosslinked resin-metal chelates. Figure 6 shows the oxidation rate of homogentisic acid catalyzed by RMH-Cu(II)

Table 2. Anion exchange capacity of gel type resins and the amount of Cu(II) adsorbed with the resins

Crosslinking of gel type resins (DVB[a] %)	Anion exchange capacity / mequiv. g-resin^{-1}	Cu(II) adsorbed (mmol/g-resin)
0.5	7.85	1.71
1.0	7.70	1.59
3.0	6.81	0.82
5.0	6.34	0.48
7.5	5.81	0.10

a) Divinylbenzene (volume percent) in the monomer mixture.

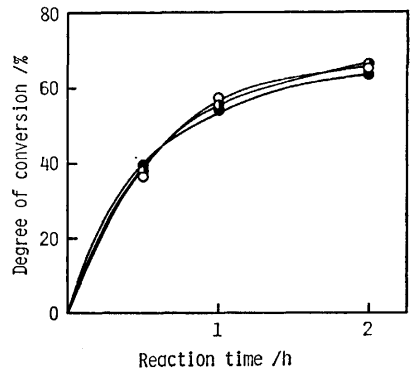

Fig. 6. Effect of the degree of crosslinking of the resins on the oxidation of homogentisic acid (II).
Cu(II) content: 4×10^{-4} g atom, catalyst: RMH-Cu(II) chelate. Resin; ◑: RMH 3-50, ○: RMH 5-50, ●: RMH 10-50 (See Table 1).

chelates with different degrees of crosslinking. In this case, the catalytic activity did not decrease with an increase in the degree of crosslinking, and the catalytic activity did not decrease after repeated use. The decrease of the catalytic activity of gel type resin-Cu(II) chelates is ascribed to the elution of Cu(II) ion from the chelates to the reaction system during the oxidation reaction. The results suggest that the macroreticular chelating resins are suitable as catalysts for the oxidation reaction.

The Effect of the Porosity of Macroreticular Chelating Resins on the Catalytic Activity. The catalytic activity of resin-Cu(II) chelates for the oxidation of homogentisic acid was investigated by use of the macroreticular chelating resin(RMT) with different porosities. The results are shown in Fig. 7. RMT with different porosities were prepared by the amination of macroreticular copolymer beads which were polymerized by varying the amount of 2,2,4-trimethylpentane in the suspension polymerization. The chelating resin prepared by use of 2,2,4-trimethylpentane (50 vol% on monomer) had the specific surface area of 4.6 m^2/g, the pore volume of 0.28 cm^3 and the average pore radius of 775 Å (Table 1), and this resin had the maximum adsorption capacity for Cu(II) ion (Fig. 7). These results suggest that the resin which was prepared under the conditions mentioned above had the most suitable pore structures for the adsorption of Cu(II) ion. The catalytic activity of this resin did not decrease, when the resin was used repeatedly. However, the catalytic activity of all other resins decreased gradually after repeated use. The reason is also ascribed to the elution of Cu(II) adsorbed because of the instability of these resin-Cu(II) chelates. Figure 8 shows the oxidation rate of homogentisic acid catalyzed by RST-Cu(II) chelates. These RST have different porosities, especially, specific surface areas (Table 1). The catalytic activity increased

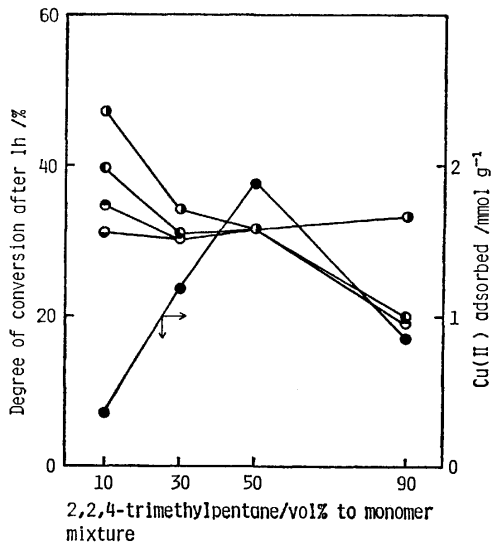

Fig. 7. Effect of the porosity of macroreticular resins on the oxidation of homogentisic acid (I).
Cu(II) content: 2×10^{-4} g atom, catalyst: RMT-Cu(II) chelate. Repetition number; ◑: 1, ◐: 2, ◓: 3, ◒: 4. ●: The amount of Cu(II) adsorbed.

TABLE 3. KINETIC PARAMETERS FOR THE OXIDATION OF HOMOGENTISIC ACID CATALYZED BY RESIN–Cu(II) CHELATES

No.	Catalyst [a] (Resin–Metal chelate)	V_{max} / 10^{-5} mol min^{-1}	K_m / 10^{-4} mol	k_3 / 10^{-2} min^{-1}
1	RST-L-Cu(II)	2.00	7.83	5.01
2	RGT-Cu(II)	1.46	6.16	3.61
3	RMH 5-50-Cu(II)	1.45	6.07	3.62
4	RMT 5-50-Cu(II)	1.49	8.21	3.71
5	Cu^{2+}	2.67	9.05	265.5

a) In the catalytic reaction by resin–Cu(II) chelates, Cu(II) content in the reaction system was 2×10^{-4} g atom, whereas in the catalytic reaction by Cu^{2+} only, Cu(II) content was 5×10^{-6} g atom.

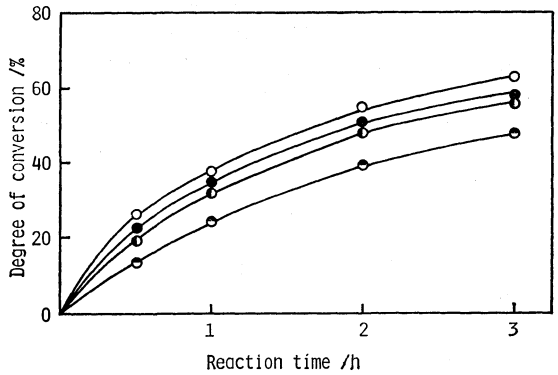

Fig. 8. Effect of the porosity of macroreticular chelating resins on the oxidation of homogentisic acid (II). Cu(II) content: 2×10^{-4} g atom, catalyst: RST–Cu(II) chelate. ○: RST-I, ●: RST-II, ◐: RST-III, ◓: RST-IV.

with an increase in the specific surface area of the resins and was little affected by the pore volume and average pore radius.

Kinetic Behavior of the Oxidation of Homogentisic Acid Catalyzed by Resin–Cu(II) Chelates. The catalytic activity of the RST–Cu(II) chelate for the oxidation of homogentisic acid was investigated under nitrogen, but it was not recognized. The result shows that molecular oxygen is necessary for this reaction.

The oxidation rate of homogentisic acid was observed at its various concentrations. The rate is proportional to the concentration of homogentisic acid in the lower concentrations and becomes independent of it in the higher concentrations. This is the kinetic behavior of a typical Michaelis-Menten type, which indicates the presence of a catalyst-substrate complex. These results suggest that the oxidation of homogentisic acid catalyzed by resin–Cu(II) chelates proceeds through the following mechanism which is similar to that of the oxidation of ascorbic acid catalyzed by ascorbic acid oxidase or lactose.

The plots of the reciprocal of the rate *vs.* the reciprocal of the substrate concentration gave straight lines in this oxidation reaction catalyzed by resin–Cu(II) chelates. From the intercept of each line and its slope, the specific rate for the decomposition of the reaction intermediate (k_3) and Michaelis-Menten constant (K_m) can be calculated. The data are listed in Table 3. For comparison, the results observed for Cu(II) ion are also listed in Table 3. The highest V_{max} value was observed for RST–Cu(II) chelate except the value observed for Cu(II) ion only. The lowest K_m value was observed for RMH–Cu(II) chelates. These results suggest that the oxidation rate of homogentisic acid catalyzed by RST–Cu(II) chelate is larger than that catalyzed by other resin–Cu(II) chelates and the affinity of RMH–Cu(II) chelate to the substrate is larger than that of other resin–Cu(II) chelates.

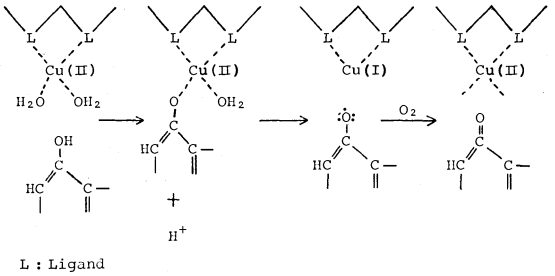

From the results mentioned above, the macroreticular resin–Cu(II) chelates were found to be suitable as catalysts for the oxidation of substrates such as homogentisic acid, hydroquinone, *etc.* and the catalytic activity of the resin–Cu(II) chelates was affected by the porosity of the resins. The macroreticular resin–Cu(II) chelates can be used repeatedly for these catalytic reactions.

The present work was partially supported by a Grant-in-Aid for Scientific Research No. 010405 from the Ministry of Education, Science and Culture.

References

1) M. M. Taqui Khan and A. E. Martell, *J. Am. Chem. Soc.*, **89**, 4176 (1967).
2) M. M. Taqui Khan and A. E. Martell, *J. Am. Chem. Soc.*, **89**, 7104 (1967).
3) I. Pecht, A. Levitzki, and M. Anbar, *J. Am. Chem. Soc.*, **89**, 1587 (1967).
4) H. Egawa and H. Saeki, *Kogyo Kagaku Zasshi*, **74**, 772 (1971).
5) H. Egawa, T. Nonaka, and Y. Hujiyama, *Nippon Kagaku Kaishi*, **1977**, 888.
6) H. Egawa and M. Takahara, *Nippon Kagaku Kaishi*, **1973**, 1786.
7) H. Egawa, T. Nonaka, and H. Maeda, *Nippon Kagaku Kaishi*, **1979**, 1756.
8) H. Egawa, Y. Jogo, and H. Maeda, *Nippon Kagaku Kaishi*, **1979**, 1760.
9) H. Sigel, *Angew. Chem.*, **81**, 161 (1969).
10) M. Hatano, T. Nozawa, T. Yamamoto, and S. Kambara, *Makromol. Chem.*, **115**, 10 (1968).

Carbon Black as an Electron-transfer Catalyst. The Two-phase Dehydrogenation of Hydrazo Nitriles by an Aqueous Solution of Potassium Hexacyanoferrate(III), Using Carbon Black as the Catalyst

Norio Tsubokawa,* Naoki Takeda, and Yasuo Sone

Department of Applied Chemistry, Faculty of Engineering, Niigata University, Ikarashi, Niigata, Niigata 950-21

(Received February 5, 1982)

The two-phase(aqueous and organic phase) dehydrogenation of hydrazo nitriles by an aqueous solution of potassium hexacyanoferrate(III), using carbon black as the catalyst, was carried out at 40 °C with shaking. In the presence of carbon black, the two-phase dehydrogenation of hydrazo nitriles was accelerated, and the corresponding azo nitriles were obtained in good yields. The catalytic activity of channel blacks was larger than that of furnace blacks. Moreover, the increasing content of phenolic hydroxyl groups tended to increase the catalytic activity of carbon blacks. It became apparent that phenolic hydroxyl groups on the surface of carbon black act as an electron-transfer catalyst in the two-phase dehydrogenation. The reaction scheme was considered to be as follows. In the aqueous phase, phenolic hydroxyl groups on the surface are oxidized by an aqueous solution of $K_3[Fe(CN)_6]$ to give phenoxyl radicals, and then the carbon black with phenoxyl radicals is transferred into the organic phase, which contains hydrazo nitriles. Subsequently, in the organic phase, the phenoxyl radicals oxidize the hydrazo nitriles to give the corresponding azo nitriles, by which phenolic hydroxyl groups are regenerated. Thus, it was concluded that phenolic hydroxyl groups on the surface are recycled and that carbon black mediates the redox reaction occurring between aqueous and organic phases.

Recently, oxidation-reduction polymers containing 1,4-dihydronicotinamide(NAH), 2,4,5,6(1*H*,3*H*)-pyrimidinetetrone (alloxan), and 1,1'-dialkyl-4,4'-bipyridinium(viologen) moieties have been prepared, and their behavior as polymeric electron carriers has been investigated.[1] For instance, it has been reported that a polymer containing alloxan moieties mediates the redox reaction occurring between aqueous and organic phases (two-phase reaction).[1] Furthermore, it has been proved that the redox reaction between insoluble solids—two polymer beads, one containing NAH moietics and the other containing *p*-benzoquinone, was feasibly mediated by alloxan as an electron-transfer catalyst.[1,2]

On the other hand, using hindered phenols (*e.g.*, 2,4,6-triphenylphenol) as electron-transfer catalysts, the two-phase dehydrogenation of 1,2-disubstituted hydrazines in an organic solvent by means of an aqueous solution of potassium hexacyanoferrate(III) has been reported by Dimroth and Tüncher.[3]

The presence of phenolic hydroxyl groups on the surface of carbon black has been supported in the literature.[4,5] It is well known that phenolic hydroxyl groups are easily oxidized to quinonic oxygen groups or phenoxyl radicals (so-called "quinone radicals").[5,6]

In the present paper, we wish to report that, as well as hindered phenols, phenolic hydroxyl groups on the surface of carbon black act as electron-transfer catalysts in the two-phase dehydrogenation of hydrazo nitriles by means of an aqueous solution of $K_3[Fe(CN)_6]$:

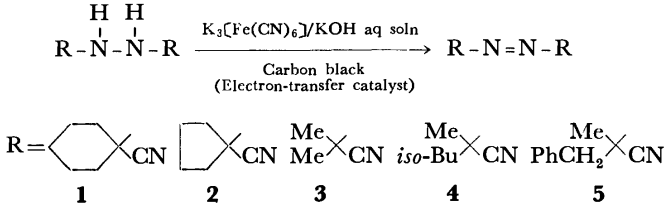

1 **2** **3** **4** **5**

Experimental

Materials and Reagents. The carbon black used was of two types: furnace black and color-channel black. The furnace blacks, Philblack O (BET specific surface area; 79.6 $m^2 g^{-1}$) and Philblack I (116.8 $m^2 g^{-1}$), were dried *in vacuo* after Soxhlet extraction with benzene to remove the resinous substances present on the surface. The color-channel blacks, Carbolac 1 (839.2 $m^2 g^{-1}$), FW 200 (460 $m^2 g^{-1}$), and Neospectra II (906 $m^2 g^{-1}$), were dried *in vacuo* without extraction, because it was known that channel blacks contain no resinous substances.

The hydrazo nitriles (**1**, **2**, **3**, **4**, and **5**) were prepared by the reaction of the corresponding ketones with sodium cyanide and hydrazine sulfate according to the method of Overberger *et al.*[7-9] All of these compounds were identified by means of mp, IR, NMR, and elemental analysis.

The benzene and dichloromethane used as solvents were purified and distilled by a general method.

Guaranteed-reagent-grade $K_3[Fe(CN)_6]$ from the Tokyo Kasei Kogyo Co., Ltd., was used without further purification.

Procedure of Two-phase Dehydrogenation. A typical example was as follows.[10] A solution of 2.0 g (6.0 mmol) of $K_3[Fe(CN)_6]$ in 10.0 cm^3 of aqueous potassium hydroxide (2.0 mol dm^3) was added to a mixture of 0.5 g of carbon black and 0.5 g (2.0 mmol) of **1** in 10.0 cm^3 of benzene. The reaction mixture was then shaken at 40 °C for 6 h. After the reaction, the carbon black was filtered with suction and washed with benzene. The benzene layer was separated from the filtrate, washed with 5 times with water, and dried over sodium sulfate. The solvent was removed under reduced pressure, and the residue was recrystallized from ethanol. The yield of the corresponding azo nitriles was determined by measuring the absorbance of the adsorption maximum at 350 nm (95% ethanol) due to the azo nitriles.

Treatment of Carbon Black with Sodium Tetrahydroborate. The treatment of carbon black with $NaBH_4$ was carried out according to the method of Studebaker.[11] For instance, 2.0 g of carbon black was stirred into 50 cm^3 of an aqueous solution containing 0.2 g of $NaBH_4$ and 0.6 g of sodium

hydroxide under a nitrogen atmosphere. After reacting for 2 h at room temperature, the solution was made acidic with dilute sulfuric acid. The carbon black was subsequently filtered, washed with degassed hot water until the filtrate was neutral, and then dried *in vacuo*.

Treatment of Carbon Black with Hydrogen Peroxide. Into a mixture of 5.0 cm^3 of concentrated sulfuric acid, 50 cm^3 of glacial acetic acid, and 2.0 g of carbon black, 50 cm^3 of H_2O_2 (*ca.* 35%) was stirred drop by drop.[12,13] After the reaction for 24 h at room temperature, the carbon black was filtered, washed with water until the filtrate was neutral, and then dried *in vacuo*.

Treatment of Carbon Black with Benzoyl Peroxide. The treatment of carbon black with benzoyl peroxide (BPO) was carried out according to the method previously reported.[14] Two grams of BPO were added to a mixture of 2.0 g of carbon black and 150 cm^3 of carbon tetrachloride. In order to accelerate the oxidation of the surface of carbon black, oxygen gas was gradually bubbled into the mixture during the reaction. After a reaction for 50 h at 45 °C with stirring, the carbon black was separated by centrifugation at 10^4 rpm for 2 h. Subsequently, it was extracted with carbon tetrachloride, using a Soxhlet apparatus, for 100 h and then dried *in vacuo*.

Treatment of Carbon Black with Diazomethane. The treatment of carbon black with CH_2N_2 was carried out by a method similar to that described by Studebaker *et al.*[15] A typical example was as follows. Two grams of carbon black were stirred into 150 cm^3 of a diethyl ether solution of CH_2N_2 (*ca.* 2 wt%) at 0 °C. After a reaction for 48 h, the carbon black was filtered, washed with an absolute diethyl ether, and then dried *in vacuo*.

Results and Discussion

Two-phase Dehydrogenation of **1** *in the Presence of Carbon Black.* The two-phase dehydrogenation of **1** by an aqueous solution of $K_3[Fe(CN)_6]$ was carried out; the results are shown in Table 1. When the reaction was carried out in the absence of carbon black, 90.5% of the **1** remained unchanged (Run No. 1). Carbon black itself had no ability to dehydrogenate **1** in the absence of $K_3[Fe(CN)_6]$ (Run No. 2). However, in the presence of carbon black, **1** was dehydrogenated to the corresponding azo nitrile, 1,1′-azobis(cyclohexane-1-carbonitrile) in a good yield. Therefore, the results suggest that carbon black has a catalytic activity in the two-phase dehydrogenation of **1**.

Table 1. Two-phase dehydrogenation of **1** in the presence of carbon black

Run No.	Carbon black	(g)	$K_3[Fe(CN)_6]$ soln (cm^3)	**1** (mmol)	Azo nitrile yield %[a]
1	—	—	10	2.0	9.5
2	Carbolac 1	0.50	—	2.0	0.5
3	Carbolac 1	0.10	10	2.0	46.9
4	Carbolac 1	0.50	10	2.0	99.0[b]
5	Philblack O	0.50	10	2.0	24.5
6	Philblack O	1.00	10	2.0	49.6
7	Philblack O	1.00	10	2.0	64.5

a) A 10 cm^3 portion of benzene was used as the solvent; 40 °C, 6 h. b) Isolated yield after recrystallization: 90%.

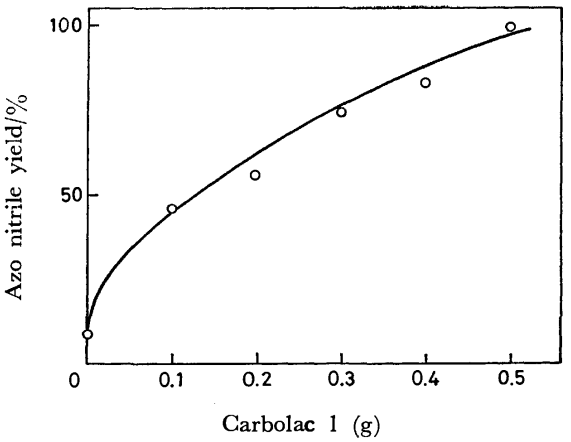

Fig. 1. The effect of the amount of Carbolac 1 on the two-phase dehydrogenation of **1**.
1 2.0 mmol, benzene 10.0 cm^3, $K_3[Fe(CN)_6]$ aq soln 10.0 cm^3; 40 °C, 6 h.

Using 2.0 mmol of **1** and various amounts of Carbolac 1, the effect of the amount of carbon black on the reaction was investigated. The results obtained are shown in Fig. 1. As is shown in Fig. 1, the reaction was accelerated with an increase in the amount of Carbolac 1.

From the above results, it may be concluded that carbon black acts as a catalyst in the two-phase dehydrogenation of **1** by an aqueous solution of $K_3[Fe(CN)_6]$.

Two-phase Dehydrogenation of Hydrazo Nitriles Using Carbolac 1 as a Catalyst. The results of the two-phase dehydrogenation of **2**, **3**, **4**, and **5** are shown in Table 2. It is found that the two-phase dehydrogenation of **2** to the corresponding azo nitrile is catalyzed by Carbolac 1 as well as that of **1**. Although **3**, **4**, and **5** were considerably oxidized to the corresponding azo nitriles by an aqueous solution of $K_3[Fe(CN)_6]$, even in the absence of carbon black, it became apparent that the two-phase dehydrogenation of these hydrazo nitriles was accelerated by Carbolac 1 and that the corresponding azo nitriles were obtained in good yields.

The azo nitriles obtained from the reaction were identified by the measurement of the mp and the IR and NMR spectra; no by-products were observed to be formed.

The preparation of azo nitriles is usually carried out by the oxidation of the corresponding hydrazo nitriles with Br_2 or nitrous acid.[7] In contrast to such oxidation, the two-phase dehydrogenation of hydrazo nitriles by an aqueous solution of $K_3[Fe(CN)_6]$, using carbon black as a catalyst, is a effective and convenient method for the preparation of azo nitriles, which are useful radical-chain initiators.

Ability of Various Kinds of Carbon Black as a Catalyst for the Two-phase Dehydrogenation. Using various kinds of carbon black, the effect of functional groups on the surface of carbon black on the two-phase dehydrogenation of **1** was studied. The results are shown in Table 3. The carbon black used was of two types:

Table 2. Two-phase dehydrogenation of hydrazo nitriles by the use of Carbolac 1 as the catalyst

Hydrazo nitrile	Carbolac 1 (g)	Temp °C	Azo nitriles		
			Yield/%[c]	Mp θ_m/°C	Lit Mp θ_m/°C
1[a]	—	40	9.5	113—114	114—115[7]
	0.5		99.0		
2[a]	—	40	18.1	83.5—84	83—84[8]
	0.5		99.5		
3[b]	—	40	80.0	102—103.5	103—104[7]
	0.5		99.5		
4[a]	—	30	68.6	73—76	74—76[7]
	0.5		100		
5[a]	—	30	50.2	81.5—83	82—84[9]
	0.5		99.0		

a) A 10 cm^3 portion of benzene was used as the solvent. b) A 10 cm^3 portion of dichloromethane was used as the solvent. c) Reaction time; 6 h.

Table 3. Two-phase dehydrogenation of **1** by the use of various kinds of carbon black as catalysts (**1** 2.0 mmol, benzene 10.0 cm^3, $K_3[Fe(CN)_6]$ aq soln 10.0 cm^3; 40 °C, 6 h.)

Carbon black	(g)	Phenolic hydroxyl groups(mequiv. g^{-1})	Quinonic oxygen groups(mequiv. g^{-1})	Azo nitrile yield/%
FW 200[a]	0.1	0.10	1.42	45.4
Carbolac 1[a]	0.1	0.16	1.14	46.9
Neospectra II[a]	0.1	0.24	0.92	54.5
Philblack O[b]	0.5	0.02	0.18	24.5
Philblack I[b]	0.5	0.05	0.23	28.4

a) Color-channel black. b) Furnace black.

color-channel black and furnace black. The content of the phenolic hydroxyl groups was determined using 2,2-diphenyl-1-picrylhydrazyl according to the method previously reported by us.[13] The analysis of the quinonic oxygen groups was carried out by the determination of the hydrogen uptake from a $NaBH_4$ solution according to the method of Studebaker.[11] In general, color-channel blacks contain a number of phenolic hydroxyl and quinonic oxygen groups in comparison with furnace blacks.

From the results shown in Table 3, the ability of channel blacks as catalysts for the two-phase dehydrogenation was found to be larger than that of furnace blacks. Moreover, the increasing content of phenolic hydroxyl groups tends to increase the catalytic activity of channel blacks. In addition, Dimroth *et al.* have reported that hindered phenols act as electron-transfer catalysts in the two-phase dehydrogenation of 1,2-disubstituted hydrazines.[3]

Accordingly, it is suggested that phenolic hydroxyl groups on the surface of carbon black play an important role as catalysts in the two-phase dehydrogenation.

Two-phase Dehydrogenation Catalyzed by Various Treated Carbon Blacks. In order to clarify the reaction sites on the surface of carbon black, the two-phase dehydrogenation of **1** catalyzed by carbon black treated with $NaBH_4$, H_2O_2, or BPO was compared with that catalyzed by the untreated one. The results are shown in Table 4.

It has been reported that quinonic oxygen groups on the surface of carbon black are reduced by $NaBH_4$ to give phenolic hydroxyl groups.[11] The content of phenolic hydroxyl groups on the surface of such treated Philblack O is 0.07 mequiv. g^{-1}.

Table 4. Two-phase dehydrogenation of **1** by the use of treated Philblack O as the catalyst (Treated carbon black 1.00 g, **1** 2.0 mmol, benzene 10.0 cm^3, $K_3[Fe(CN)_6]$aq soln 10.0 cm^3; 40°C, 6h.)

Philblack O	$K_3[Fe(CN)_6]$ soln (cm^3)	Azo nitrile yield/%
Untreated	—	0.6
	10	49.6
Treated with $NaBH_4$	—	0.5
	10	63.0
Treated with H_2O_2	—	10.0
	10	100
Treated with BPO	—	25.8
	10	100
Treated with BPO and then $NaBH_4$	—	1.5
	10	99.5

The results shown in Table 4 indicate that the yield of the 1,1′-azobis(cyclohexane-1-carbonitrile) is increased by the use of $NaBH_4$-treated Philblack O as a catalyst. The result suggests that the catalytic activity of carbon black in the two-phase dehydrogenation is responsible for the phenolic hydroxyl groups on the surface.

Furthermore, the catalytic activity of carbon black

in the two-phase dehydrogenation was extremely enhanced by the treatment with H_2O_2 and BPO. It is interesting to note that both H_2O_2- and BPO-treated Philblack O have the ability to oxidize **1** even in the absence of an aqueous solution of $K_3[Fe(CN)_6]$.

It has been confirmed that the pH of an aqueous slurry of furnace black changes from the basic to the acidic side and that the content of phenolic hydroxyl groups is increased by the treatment with H_2O_2.[12,13] The content of phenolic hydroxyl groups of such treated Philblack O is 0.11 mequiv. g^{-1}. Moreover, the surface of carbon black is also oxidized with H_2O_2 to give quinone radicals.

On the other hand, it has previously been reported that quinonic oxygen groups and phenoxyl radicals were easily introduced to the carbon black surface by treatment with BPO in the presence of oxygen.[14,16] In addition, it is well known that the number of unpaired electrons present on the surface of carbon black increases about 10 times when the carbon black is treated with BPO.[17] Therefore, BPO-treated Philblack O has a number of phenoxyl radicals, because it is believed that a large portion of the unpaired electrons on the surface of carbon black exists in quinone-radical forms.[6,14,16]

On the basis of the foregoing facts, it is considered that the high catalytic activity of both H_2O_2- and BPO-treated Philblack O may be due to the phenoxyl radicals formed on the surface of carbon black by the treatment. That is, phenoxyl radicals present on the surface of H_2O_2- and BPO-treated carbon black oxidize the hydrazo nitriles, by which means phenolic hydroxyl groups with the catalytic activity in the two-phase dehydrogenation are newly formed.

To confirm this, the catalytic activity of carbon black treated with BPO and then $NaBH_4$ was investigated. As is shown in Table 4, although BPO–$NaBH_4$-treated carbon black lost the ability to oxidize **1** in the absence of $K_3[Fe(CN)_6]$, the treated carbon black kept a high catalytic activity in the two-phase dehydrogenation. From these results, it is concluded that both phenolic hydroxyl groups and phenoxyl radicals on the surface catalyze the two-phase dehydrogenation.

On the other hand, using CH_2N_2-treated carbon black, the two-phase dehydrogenation of **1** was also studied; the results are shown in Table 5.

It is well known that phenolic hydroxyl groups on the surface are blocked by methylation with CH_2N_2.[14] As is shown in Table 5, the catalytic activity of the carbon black completely disappeared upon the treatment with CH_2N_2. The results also clearly show the role of phenolic hydroxyl groups as a catalyst in the two-phase dehydrogenation.

Table 5. Two-phase dehydrogenation of **1** by the use of CH_2N_2-treated carbon black as the catalyst (**1** 2.0 mmol, benzene 10.0 cm^3, $K_3[Fe(CN_6]$aq soln 10.0 cm^3; 40 °C, 6 h.)

Carbon black	(g)	Azo nitrile yield/%
CH_2N_2-treated Philblack O	1.00	0.7 (49.6) [a]
CH_2N_2-treated Carbolac 1	0.50	1.0 (99.0) [a]

a) The values in parentheses indicate the results in the presence of untreated carbon black.

Reaction Scheme of the Two-phase Dehydrogenation Catalyzed by Carbon Black. As has been mentioned above, it becomes apparent that the phenolic hydroxyl groups on the surface play an important role in the two-phase dehydrogenation. On the other hand, it is well known that phenolic hydroxyl groups on the surface are easily oxidized to quinonic oxygen groups or phenoxyl radicals("quinone radicals").[5,6,18] The phenoxyl radical formed on the surface will be stabilized by polycondensed aromatic rings of carbon black[13,16] and will have the ability to oxidize some compounds as well as 2,4,6-trisubstituted phenoxyl radicals.[3]

Therefore, the reaction scheme of the two-phase dehydrogenation using carbon black as a catalyst was considered to be as follows:

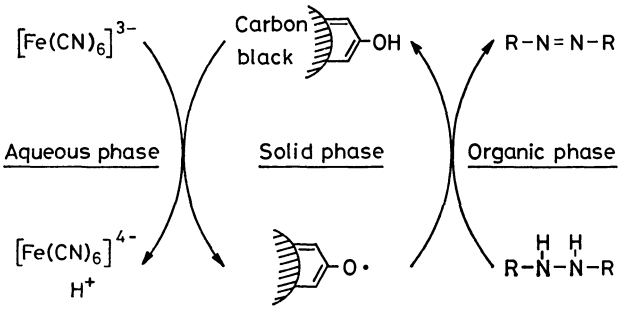

In the aqueous phase, the phenolic hydroxyl groups on the surface of carbon black will be oxidized by an aqueous solution of $K_3[Fe(CN)_6]$ to give phenoxyl radicals, and then the phenoxyl radicals will be transferred into the organic phase, where they will abstract hydrogen atoms from the hydrazo nitriles to give the corresponding azo nitriles and phenolic hydroxyl groups regenerated. That is, during the reaction, phenolic hydroxyl groups on the surface of carbon black are recycled and the carbon black mediates the electron transfer(*i.e.*, redox reaction) between aqueous and organic phases. For example, in the case of Run No. 4 in Table 1, the carbon black was recycled *ca.* 45 times.

In conclusion, it is considered that carbon black acts as an electron-transfer catalyst in the two-phase dehydrogenation.

Two-phase Dehydrogenation of 1,2-Disubstituted Hydrazines by an Aqueous Solution of $K_3[Fe(CN)_6]$ Using Carbon Black as a Catalyst. The two-phase dehydrogenation of 1,2-disubstituted hydrazines, such as hydrazobenzene and *N*-phenyl-*N'*-triphenylmethylhydrazine, was also carried out. However, the effect of carbon black as a catalyst could not be confirmed, because these hydrazines were easily dehydrogenated to the corresponding azo compounds by the use of an aqueous solution of $K_3[Fe(CN)_6]$, even in the absence of carbon black.

In addition, the two-phase dehydrogenation of 9,10-dihydroanthracene and 1,2-diphenylethane by an aqueous solution of $K_3[Fe(CN)_6]$, using carbon black as

a catalyst, was investigated at 40—90 °C. The dehydrogenation of these compounds was unsuccessful under these conditions, and the starting material was recovered unchanged.

References

1) M. Okawara, T. Endo, E. Fujiwara, and T. Hirose, *J. Macromol. Sci., Chem.*, **A13**, 441 (1979).
2) N. Tsubokawa, T. Endo, and M. Okawara, *J. Polym. Sci., Polym. Chem. Ed.*, **20**, 2205 (1982).
3) K. Dimroth and W. Tüncher, *Synthesis*, **1977**, 339.
4) M. L. Studebaker, *Rubber Chem. Technol.*, **30**, 1400 (1959).
5) J. B. Donnet, *Carbon*, **6**, 161 (1968).
6) J. B. Donnet, G. Henrich, and G. Riess, *Rev. Gén. Caout.*, **38**, 1803 (1961); **39**, 583 (1962).
7) C. G. Overberger, M. T. O'Shaughnessy, and H. Shalit, *J. Am. Chem. Soc.*, **71**, 2661 (1949).
8) C. G. Overberger and M. B. Berenbaum, *J. Am. Chem. Soc.*, **73**, 4883 (1951).
9) C. G. Overberger and H. Biletch, *J. Am. Chem. Soc.*, **73**, 4880 (1951).
10) N. Tsubokawa and N. Takeda, *Chem. Lett.*, **1979**, 1459.
11) M. L. Studebaker, "Proceedings Fifth Conf. on Carbon Vol. II," Pergamon Press (1962), p. 189.
12) K. Ohkita and H. Ohtani, *Nippon Gomu Kyokaishi*, **30**, 14 (1957).
13) K. Ohkita and N. Tsubokawa, *Carbon*, **10**, 631 (1972).
14) K. Ohkita, N. Tsubokawa, E. Saitoh, M. Noda, and N. Takashina, *Carbon*, **13**, 443 (1975).
15) M. L. Studebaker, E. W. D. Huffman, A. C. Wolfe, and L. G. Nabors, *Ind. Eng. Chem.*, **48**, 162 (1956).
16) K. Ohkita, N. Tsubokawa, and N. Takashina, *Nippon Gomu Kyokai Shi*, **49**, 223 (1976).
17) K. Fujimoto, K. Inomata, and S. Fujiwara, *Nippon Gomu Kyokai Shi*, **46**, 232 (1973).
18) A. Voet and A. C. Teter, *Am. Ink Marker*, **38**, 44, 51, 78 (1960); H. V. Drushel and J. V. Hallum, *J. Phys. Chem.*, **62**, 1052 (1958).

Asymmetric Transformation of 2-Phenyl- and 2-Chloroalkanoic Acids *via* Chiral Oxazolines

Saizo SHIBATA,* Hajime MATSUSHITA, Hajime KANEKO, Masao NOGUCHI, Masahiko SABURI,† and Sadao YOSHIKAWA†

Central Research Institute, The Japan Tobacco and Salt Public Corporation, 6-2 Umegaoka, Midori-ku, Yokohama, Kanagawa 227

†*Department of Synthetic Chemistry, Faculty of Engineering, The University of Tokyo, Hongo, Bunkyo-ku, Tokyo 113*

(Received March 2, 1982)

Asymmetric transformation of racemic 2-phenyl- and 2-chloroalkanoic acids *via* oxazolines into the corresponding optically active acids was investigated using (*S*)-phenylalaninol as a chiral auxiliary. The asymmetric transformation was performed by metalation of the oxazolines with butyllithium followed by protonation of the resulting lithiooxazolines. 2-Phenyl- and 2-chloroalkanoic acids were obtained in the optical yields of 29—53% and 45—73%, respectively, by the acidic hydrolysis of the chiral oxazolines thus formed. The mechanism of the asymmetric transformation was discussed.

Asymmetric transformation of racemic compounds into a single optically active form remains a major challenge in organic synthesis.[1] The great majority of work on the transformation has dealt with atropisomers.[2] Recently, optical activation of racemic aldehydes or ketones *via* enamines and of racemic amino acids *via* cobalt complexes has been reported.[3]

Although preparation of optically active alkanoic acids is important,[4] the asymmetric transformation of racemic alkanoic acids into optically active form has not been reported except for amino acids.[3] Therefore, in this study the asymmetric transformation of racemic 2-substituted alkanoic acids was intended, and 2-phenyl- and 2-chloroalkanoic acids were used as examples.[5] Chiral oxazolines, which had been originally used by Meyers *et al.* for the asymmetric synthesis of carbonyl compounds, were applied for the study of this asymmetric transformation.[6]

Oxazolines **2a**—**e** were prepared by alkylation of (4*S*)-(−)-2,4-dibenzyl-2-oxazoline (**1**), and **3a**—**e** were prepared from corresponding imidates and (*S*)-phenylalaninol. After metalation of **2** and **3** with butyllithium, the resulting lithio carbanions were quenched by addition of water (Scheme 1). Subsequent hydrolysis of **2** and **3** gave optically active 2-phenyl- and 2-chloroalkanoic acids respectively. The extent of asymmetric induction in the metallation and protonation process was monitored by examining the optical rotations of the obtained acids or diastereomer ratios of the oxazolines with NMR or GLPC analysis.

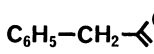

1

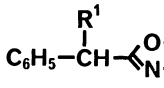

2

R^1= a: CH_3—, b: C_2H_5—, c: $(CH_3)_2CH$—, d: n-C_4H_9—, e: n-C_5H_{11}—

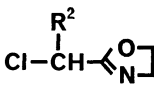

3

R^2= a: CH_3—, b: C_2H_5—, c: n-C_3H_7—, d: n-C_4H_9—, e: i-C_4H_9—

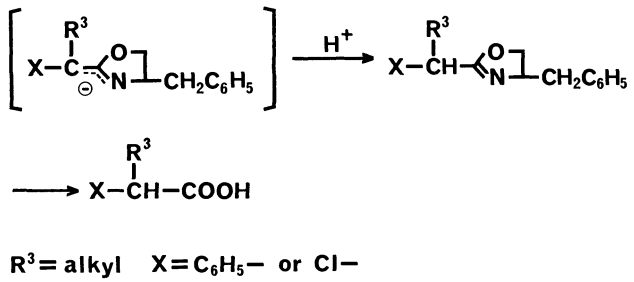

Scheme 1.

Experimental

IR spectra were measured with a JASCO A-3 spectrometer, high resolution mass spectra were recorded with a Hitachi M-80 mass spectrometer, optical rotations were measured with a JASCO Digital Automatic Polarimeter Model DIP-181, and ^{1}H NMR spectra were obtained with a JNM-PS-100 spectrometer (100 MHz). Chemical shifts are expressed in δ downfield from TMS as an internal standard. GLPC analysis was carried out on a Shimadzu Gas Chromatograph GC-7A equipped with a hydrogen flame ionization detector.

(4S)-(−)-2,4-Dibenzyl-2-oxazoline (1). A mixture of (*S*)-phenylalaninol[7] (7.6 g, 0.05 mol) and ethyl 2-phenylacetimidate[8] (8.3 g, 0.05 mol) was heated (120—130 °C) for 12 h with stirring. Distillation of the product gave 8.93 g (71%) of **1**: bp 144—146 °C (19 Pa); $[\alpha]_D^{25}$ −43.7° (*c* 1.08, EtOH); IR (neat) 1665 cm^{-1} (C=N); ^{1}H NMR ($CDCl_3$) δ=2.68 (1H, dd), 3.08 (1H, dd), 3.58 (2H, s), 3.92 (1H, dd), 4.14 (1H, dd), 4.36 (1H, m), and 7.3 (10H, m); Found: *m/e* 251.1321. Calcd for $C_{17}H_{17}ON$: M, 251.1310.

Preparation of (4S)-2-(2-Phenylalkyl)-4-benzyloxazolines 2a—c. **2a**—**e** were prepared from **1** and alkyl iodides according to the method described by Meyers *et al.*[9]

2a: Yield 59% based on **1**; bp 164—168 °C (400 Pa); $[\alpha]_D^{25}$ −39.3° (*c* 1.04, EtOH); IR (neat) 1660 cm^{-1} (C=N); Found: *m/e* 265.1453. Calcd for $C_{18}H_{19}NO$: M, 265.1467.

2b: Yield 67% based on **1**; bp 143—145 °C (12 Pa); $[\alpha]_D^{25}$ −26.4° (*c* 1.02, EtOH); IR (neat) 1660 cm^{-1} (C=N); Found: *m/e* 279.1606. Calcd for $C_{19}H_{21}NO$ 279.1623.

2c: Yield 66% based on **1**; bp 144—148 °C (13 Pa);

$[\alpha]_D^{25}$ −32.7° (*c* 1.0, EtOH); IR (neat) 1660 cm^{-1} (C=N); Found: *m/e* 293.1801. Calcd for $C_{20}H_{23}NO$: M, 293.1780.

2d: Yield 64% based on **1**; bp 141—144 °C (9 Pa); $[\alpha]_D^{25}$ −24.8° (*c* 1.05, EtOH); IR (neat) 1660 cm^{-1} (C=N); Found: *m/e* 307.1927. Calcd for $C_{21}H_{25}NO$: M, 307.1936.

2e: Yield 71% based on **1**; bp 158—162 °C (11 Pa); $[\alpha]_D^{25}$ −19.8° (*c* 1.03, EtOH); IR (neat) 1662 cm^{-1} (C=N); Found: *m/e* 321.2116. Calcd for $C_{22}H_{27}NO$: M, 321.2093.

*Preparation of (4S)-2-(2-Chloroalkyl)-4-benzyloxazolines **3a—e**.*

3a: Ethyl 2-chloropropionimidate hydrochloride was prepared from 2-chloropropionitrile according to the method described by McElvain and Nelson:[10] mp 90.5—91 °C; IR (Nujol) 1670 cm^{-1} (C=N). Ethyl 2-chloropropionimidate hydrochloride (8.6 g, 0.05 mol) and (*S*)-phenylalaninol (8.3 g, 0.055 mmol) was dissolved in 100 ml of dry dichloromethane and stirred for 10 h at room temperature. The reaction mixture was condensed under reduced pressure, and the residue was purified by chromatography on silica gel, and distilled to give 8.35 g (75% yield from ethyl 2-chloropropionimidate hydrochloride) of **3a**: bp 124—126 °C (200 Pa); $[\alpha]_D^{25}$ −70.7° (*c* 1.04, MeOH); IR (neat) 1662 cm^{-1} (C=N); Found: 223.0771. Calcd for $C_{12}H_{14}NOCl$: M, 223.0765.

3b: 2-Chlorobutyronitrile (10.4 g, 0.1 mol) and ethyl alcohol (5.06 g, 0.11 mol) was dissolved in 10 ml of dry ether, and dry hydrogen chloride gas was saturated. After 1 h at room temperature, the reaction mixture was condensed under reduced pressure, the residue was suspended in 150 ml of dry ether and 25 ml of triethylamine was added. Resulting white precipitate was filtered off and filtrate was concentrated. Distillation of the residue gave ethyl 2-chlorobutyrimidate (10.5 g, 70%); bp 86—88.5 °C (8665 Pa); IR (neat) 1660 cm^{-1} (C=N). Ethyl 2-chlorobutyrimidate (3.0 g, 0.02 mol) and (*S*)-phenylalaninol (3.62 g, 0.024 mol) were dissolved in 40 ml of dry dichloromethane, and to this mixture boron trifluoride etherate (0.284 g, 0.002 mol) and triethylamine (0.202 g, 0.002 mol) were added. The reaction mixture was stirred for 2 d at room temperature, and resulting white precipitate was filtered off, and filtrate was concentrated under reduced pressure. The residue was purified by chromatography on silica gel, and then distilled to give 2.85 g (60%) of **3b**: bp 133—137 °C (200 Pa); $[\alpha]_D^{25}$ −60.2° (*c* 1.01, MeOH); IR (neat) 1662 cm^{-1} (C=N); Found: *m/e* 237.0906. Calcd for $C_{13}H_{16}NOCl$: M, 237.0921.

3c: This material was prepared from ethyl 2-chlorovalerimidate according to the method described for **3b** in 65% yield: bp 136—140 °C (267 Pa); $[\alpha]_D^{25}$ −60.1° (*c* 1.02, MeOH); IR (neat) 1663 cm^{-1}; Found: *m/e* 251.1073. Calcd for $C_{14}H_{18}NOCl$: M, 251.1077.

3d: This material was prepared from ethyl 2-chlorohexanimidate hydrochloride according to the method described for **3a** in 80% yield: bp 143.5—145.5 °C (267 Pa); $[\alpha]_D^{25}$ −57.6° (*c* 1.02, MeOH); IR (neat) 1663 cm^{-1} (C=N); Found: *m/e* 265.1227. Calcd for $C_{15}H_{20}ONCl$: M, 265.1234.

3e: This material was prepared from ethyl 2-chloro-4-methylvalerimidate hydrochloride as described for **3a** in 82% yield; bp 143.5—146 °C (267 Pa); $[\alpha]_D^{25}$ −57.9° (*c* 1.02, MeOH); IR (neat) 1660 cm^{-1} (C=N); Found: *m/e* 265.1215; Calcd for $C_{15}H_{20}ONCl$: M, 265.1234.

*Hydrolysis of **2** before the Asymmetric Transformation.* **2b** (279 mg, 1 mmol) was suspended in 10 ml of 3 M (1 M=1 mol dm^{-3}) sulfuric acid and the suspension was refluxed for 4.5 h. The acidic solution was extracted with ether, and the ethereal solution was extracted with 5% aqueous potassium carbonate. The alkaline solution was acidified (pH 1) with hydrochloric acid, and extracted with ether. The ethereal solution was dried and concentrated, and the residue was distilled (bulb to bulb: 145—155 °C (bath temperature) (200 Pa)) to give 151 mg (92%) of (*S*)-(+)-2-phenylbutyric acid. The 2-phenylalkanoic acids (Table 1) were obtained as described above and the structures of the compounds were identified by their IR, Mass, and ^1H NMR spectra.

*Hydrolysis of **2** after the Asymmetric Transformation.* Under an argon atmosphere, **2b** (279 mg, 1 mmol) in 1 ml of dry tetrahydrofuran was cooled to −78 °C, and 0.86 ml of butyllithium (1.4 M solution) in hexane was added dropwise. The mixture was stirred for 45 min at −78 °C, and then 50% aqueous tetrahydrofuran was added at this temperature. The mixture was allowed to warm to room temperature, and the oxazoline was extracted with ether. This oxazoline was hydrolyzed as described above, and 122 mg (74%) of (*S*)-(−)-2-phenylbutyric acid was obtained. The 2-phenylalkanoic acids (Table 2) were obtained as described above.

*Hydrolysis of **3** before the Asymmetric Transformation.* **3b** (713 mg, 3 mmol) was suspended in 30 ml of 1 M hydrochloric acid and the suspension was kept at 80 °C for 1.5 h under stirring. The acidic solution was treated as described for **2b**, and 300 mg (82%) of (*R*)-(+)-2-chlorobutyric acid was isolated. The 2-chloroalkanoic acids (Table 3) were obtained as described above and the structures of the compounds were identified by their IR, MS, and ^1H NMR spectra.

*Hydrolysis of **3** after the Asymmetric Transformation.* **3b** (713 mg, 3 mmol) was dissolved in 3 ml of dry tetrahydrofuran and the solution was cooled to −78 °C under an argon atmosphere. To the solution, 2.77 ml of butyllithium (1.3 M solution) in hexane was added dropwise, and the mixture was stirred at −78 °C. After 45 min, 3 ml of 25% aqueous tetrahydrofuran was added to the mixture and the oxazoline

Table 1. Hydrolysis of **2a—e** before the asymmetric transformation

	Yield %	$[\alpha]_D^{25}$ 10^4 degree ml g^{-1} dm^{-1}	Lit $[\alpha]_D^{25}$ 10^4 degree ml g^{-1} dm^{-1}	Optical[a] purity %	Absolute configuration
2a	79	+1.5 (*c* 1.6, $CHCl_3$)	+76.3 (*c* 1.6, $CHCl_3$)[b]	2	*S*
2b	92	+17.1 (*c* 1.6, C_6H_6)	+96.6 (*c* 1.5, C_6H_6)[c]	18	*S*
2c	80	−5.9 (*c* 1.9, $CHCl_3$)	+62.5 (*c* 2, $CHCl_3$)[d]	10	*R*
2d	84	+7.7 (*c* 1.8, C_6H_6)	−74.9 (*c* 1.7, C_6H_6)[e]	10	*S*
2e	81	+11.2 (*c* 0.8, C_6H_6)	−71.4 (*c* 0.8, C_6H_6)[e]	16	*S*

a) Optical purities were based upon the highest literature values available. b) S. P. Bakshi and E. E. Turner, *J. Chem. Soc.*, **1961**, 171. c) Ph. Gold-Aubert, *Helv. Chim. Acta*, **41**, 1512 (1958). d) C. Aaron, D. Dull, J. L. Schmiegel, D. Jaeger, Y. Ohashi, and H. S. Mosher, *J. Org. Chem.*, **32**, 2797 (1967). e) K. Pettersson and Willdeck, *Ark. Kemi*, **9**, 333 (1956).

Table 2. Hydrolysis of **2a—e** after the asymmetric transformation

	Yield %	$[\alpha]_D^{25}$ 10^4 degree ml g^{-1} dm^{-1}	Optical[a] purity %	Absolute configuration
2a	83	+21.8 (*c* 1.7, $CHCl_3$)	29	*S*
2b	74	+39.2 (*c* 2.6, C_6H_6)	41	*S*
2c	77	+32.7 (*c* 2.1, $CHCl_3$)	52	*S*
2d	74	+40.0 (*c* 1.8, C_6H_6)	53	*S*
2e	83	+37.7 (*c* 0.9, C_6H_6)	53	*S*

a) Optical purities were based upon the highest literature values available (See Table 1.)

Table 3. Hydrolysis of **3a—e** before the asymmetric transformation

	Hydrolysis *t* h	Yield %	$[\alpha]_D^{25}$ (CH_3OH) 10^4 degree ml g^{-1} dm^{-1}	Lit $[\alpha]_D$ (CH_3OH) 10^4 degree ml g^{-1} dm^{-1}	Optical[a] purity %	Absolute configuration
3a	1.5	94	+0.13 (*c* 5.2)	+17.3 (*c* 0.5)[b]	1	*R*
3b	1.5	82	+0.33 (*c* 5.1)	+12.7 (*c* 0.4)[b]	3	*R*
3c	1.5	86	+0.43 (*c* 5.1)	−13.3[c]	3[e]	*R*
3d	1.5	61	0 (*c* 5.0)	−11.7[c]	0	*RS*
	4.5	88	0 (*c* 5.0)		0	*RS*
3e	1.5	45	+5.73 (*c* 5.2)	−24.4 (*c* 5)[d]	24[e]	*R*
	6	91	+0.51 (*c* 5.1)		2[e]	*R*

a) Optical purities were based upon the highest literature values available. b) H. Hashimoto and H. Simon, *Angew. Chem.*, **87**, 111 (1975). c) W. Gaffield and W. G. Galetto, *Tetrahedron*, **27**, 915 (1971). d) T. Polonski, *Tetrahedron*, **31**, 347 (1975). e) The diastereomeric composition of **3c—e** suggested that the optical purities of the obtained acids were lower than the calculated values (See Table 4).

Table 4. Hydrolysis of **3a—e** after the asymmetric transformation

	Hydrolysis *t* h	Yield %	$[\alpha]_D^{25}$ (CH_3OH) 10^4 degree ml g^{-1} dm^{-1}	Optical[a] purity %	Absolute configuration	Diastereomeric composition
3a	1.5	73	+7.77 (*c* 5.1)	45	*R*	71 : 29[c]
3b	1.5	72	+6.56 (*c* 5.2)	52	*R*	75 : 25[c]
3c	1.5	71	+9.85 (*c* 5.2)	74[b]	*R*	77 : 23[d]
3d	1.5	52	+8.88 (*c* 5.0)	76[b]	*R*	76 : 24[d]
	4.5	74	+8.48 (*c* 5.1)	73[b]	*R*	
3e	1.5	62	+16.2 (*c* 5.1)	66[b]	*R*	76 : 24[d]
	6	79	+15.0 (*c* 5.1)	62[b]	*R*	

a) Optical purities were based upon the highest literature values available (see Table 3). b) The diastereomeric compositions of **3c—e** suggested that the optical purities of the obtained acids were lower than the calculated values. c) The diastereomeric composition was determined by ^1H NMR analysis. d) The diastereomeric composition was determined by GLPC analysis.

was extracted with ether. This oxazoline was hydrolyzed as described above, and 266 mg (72%) of (*R*)-(+)-2-chlorobutyric acid was isolated. The 2-chloroalkanoic acids (Table 4) were obtained as described above.

*Measurement of Diastereomeric Composition of **3** after the Asymmetric Transformation.* **3a** (112 mg, 0.5 mmol) was dissolved in 0.5 ml of dry tetrahydrofuran and the solution was cooled to −78 °C under an argon atmosphere. To the solution 0.5 ml of butyllithium (1.2 M solution) in hexane was added dropwise and the mixture was stirred at −78 °C. After 45 min, 0.5 ml of 25% aqueous tetrahydrofuran was added to the mixture and the oxazoline was extracted with ether. The ethereal solution was dried over Na_2SO_4 and concentrated under reduced pressure. **3b—e** were treated as described above, and the ratios of the diastereomers of **3a** and **3b** were calculated from their ^1H NMR spectra, and those of **3c—e** were estimated by peak area measurement of the GLPC (column: OV-101 0.27 mm × 50 m, temperature 100—240 °C).

*Mutarotation of **3d**.* **3d** (2.66 g, 10 mmol) was treated with 12 mmol of butyllithium in the same manner as described for the asymmetric transformation of **3b**, and then the prepared carbanion was quenched by addition of water. The product was purified with chromatography on silica gel (dichloromethane) to give 2.39 g (90%) of epimerized **3d**: $[\alpha]_D^{25}$ −46.4° (*c* 1.03, MeOH). This epimerized **3d** (1.33 g, 5 mmol) was dissolved in 50 ml of 2 M KOH–MeOH solution, and the solution was kept at 25 °C. An aliquot of the solution was used for the measurement of the mutarotation at 589 nm at 25 °C. Just after the preparation of the alkaline solution, 20 ml of the solution was removed and diluted with 200 ml of water. This solution was saturated

with NaCl, and **3d** was extracted with ether. **3d** was hydrolyzed as described for **3b** to give 156 mg (52%) of (*R*)-(+)-2-chlorohexanoic acid. After 24 h, 20 ml of the alkaline solution was treated as described above to give 161 mg (53%) of (*S*)-(−)-2-chlorohexanoic acid.

The Effect of Temperature in the Asymmetric Transformation of 2b. Under an argon atmosphere, 55.8 mg (0.2 mmol) of **2b** in 0.2 ml of dry tetrahydrofuran was cooled to −78 °C, and 0.17 ml of butyllithium (1.4 M solution) in hexane was added dropwise. Each carbanion solution, thus prepared, was stirred for 45 min at temperatures of 0, −20, −40, −60, and −78 °C. Then, water was added to the solutions at the temperatures, and the solutions were extracted with ether. The ether extracts were washed with brine, dried, and evaporated to give **2b**. The ratios of two diastereomers of **2b** were determined by peak area measurements of methyl peaks of the diastereomers in the ^{1}H NMR spectra.

Results and Discussion

Asymmetric Transformation of 2. Hydrolysis of **2a—e** after the asymmetric transformation gave the corresponding acids in the optical yields of 29—53% as shown in Table 2. Because **2a—e** were prepared by alkylation of the chiral oxazoline (**1**), asymmetric induction by this alkylation step was possible. Hydrolysis of **2a—e** before the asymmetric transformation gave the corresponding optically active acids in the optical yields of 2—18% (Table 1). The results shown in Tables 1 and 2 indicate that the asymmetric induction is attributable to the asymmetric transformation, and not to the alkylation step.

Asymmetric Transformation of 3. In preliminary expeiments, racemization of optically active 2-chloroalkanoic acids under the hydrolysis conditions of **2** (3 M sulfuric acid, reflux 4.5 h) was observed. Therefore, weaker acid (1 M hydrochloric acid) and lower heating temperature (80 °C) were employed for the hydrolysis of **3**. **3a—c** were hydrolyzed for 1.5 h, and in the case of **3d** and **3e**, hydrolysis were prolonged to 4.5 and 6 h respectively because of low hydrolysis yields. Hydrolysis of **3** (**3a—c** 1.5 h, **3d** 4.5 h, **3e** 6 h) before the asymmetric transformation gave the corresponding acids in the optical yields of less than 5%.

Hydrolysis of **3** after the asymmetric transformation gave the corresponding acids in the optical yields of 45—73% (Table 4). The results shown in Tables 3 and 4 indicate that the asymmetric induction is definitely due to the transformation. The optical purities of the acids were calculated based upon the highest literature values available, but there was some doubt that the optical purities of the compared data were insufficient from the preparation methods described in the literatures. Therefore, the diastereomeric composition of **3a—e** after the asymmetric transformation was measured by ^{1}H NMR or GLPC. The results are listed also in Table 4. Although the calculated optical purities of **3a** and **3b** correspond to the diastereomeric compositions, the calculated optical purities of **3c—e** disagree with the compositions of **3c—e**. From the diastereomeric compositions of **3c—e**, the enantiomeric purities of **3c—e** are expected to be about 50%. Asymmetric synthesis of 2-chloroalkanoic acids *via* chiral oxazolines was reported by Meyers *et al.*, and in their synthesis, the 2-chloroalkanoic acids corresponding to **3a**, **3b**, and **3d** were prepared in the optical yields of 3—28%.[11] It is noteworthy that in the present transformation, using simple chiral auxiliary (*S*)-phenylalaninol, 2-chloroalkanoic acids can be obtained in fairly good optical purities compared with the Meyers' asymmetric synthesis.

Mutarotation. One possible mechanism of this asymmetric transformation is a base catalyzed epimerization governed by thermodynamic control as illustrated in Scheme 2. To examine whether this asymmetric transformation was governed by the thermodynamic control or not, the mutarotation of **3d** was measured. **3d** was treated with butyllithium followed by addition of water to give epimerized **3d**. This epimerized **3d** was dissolved in an alkaline solution (2 M KOH–MeOH), and optical rotation of **3d** was recorded. If the asymmetric induction had been governed by the thermodynamic control, optical rotation of this epimerized **3d** was not expected to change. However, as shown in Fig. 1 mutarotation of the epi-

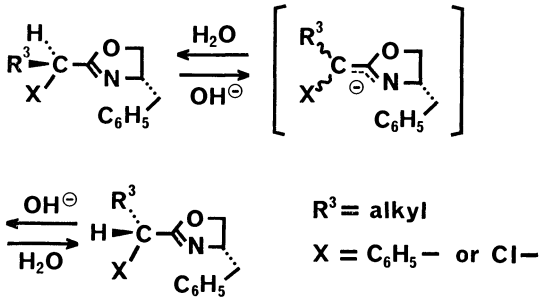

Scheme 2.

Table 5. Hydrolysis of **3d** before and after the equilibrium

Mutarotation t/h	$[\alpha]_D^{25}$ (CH_3OH) / 10^4 degree ml g^{-1} dm^{-1}	Optical[a] purity / %	Absolute configuration
0	+7.63 (*c* 5.14)	65.2	*R*
24	−0.87 (*c* 5.07)	7.4	*S*

a) Optical purities were based upon the highest literature values available (See Table 3).

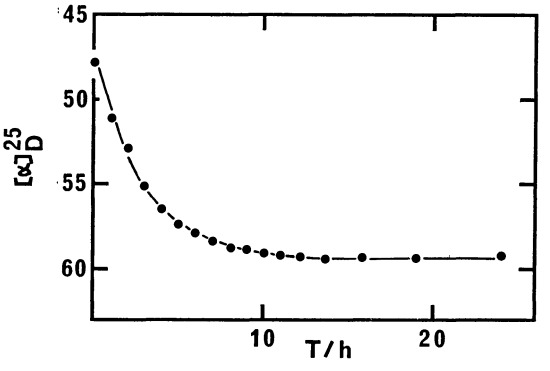

Fig. 1. Mutarotation of **3d** (0.1 M) in 2 M KOH–MeOH at 25 °C.

merized **3d** was observed. The optical rotation did not change after 12 h indicating that the epimerization attained equilibrium under the conditions. Two aliquots of **3d**, which were taken from the alkaline solution at 0 and 24 h, were hydrolyzed to give 2-chlorohexanoic acid. Specific rotations of the acid at 0 and 24 h are shown in Table 5. Under the epimerization conditions, the contribution of asymmetric induction governed by thermodynamic control is revealed to be small in the asymmetric transformation.

Isotopic Labeling Study. When butyllithium solution was added to the solutions of **2** or **3**, the reaction mixture became yellow suggesting the formation of lithio carbanion (**4**). The formation of the carbanion was confirmed by quenching the carbanion using deuterium oxide. After the treatment described above, exo methine proton of the oxazoline ring of **2** and **3** was shown from ^{1}H NMR spectra to be substituted by deuterium. The extent of deuterium incorporation to **2** and **3** was calculated from their mass spectra to be 90—98% and 80—90%, respectively. These results indicate that this asymmetric transformation proceeds through the formation of lithio carbanion (**4**), and subsequent protonation of the carbanion.

Effects of Temperature. The effects of temperature on the asymmetric transformation was examined using **2b**. Lithio carbanion of **2b** was prepared in tetrahydrofuran at −78 °C using butyllithium. Each anion solution, thus prepared, was stirred for 45 min at temperatures of 0, −20, −40, −60, and −78 °C, and then quenched with water. The ratios of two diastereomers of **2b** were determined by ^{1}H NMR spectra. The results are summarized in Table 6. The ratios are not affected by temperature.

Table 6. The effects of temperature on the asymmetric transformation

Temperature °C	Diastereomeric composition
0	72 : 28
−20	71 : 29
−40	72 : 28
−60	70 : 30
−78	71 : 29

Possible Mechanisms of Asymmetric Transformation. On the basis of the results presented above, this asymmetric transformation is assumed to proceed through stereoselective formation of lithio carbanion and protonation to the carbanion. Observation that there are virtually no effects of temperature on the extent of asymmetric induction suggested that both the ratios of the isomeric anions **4a** and **4b**, and stereoselectivity of protonation to the anions are not changed between −78 and 0 °C. According to the chiralities of the obtained 2-substituted alkanoic acids, two mechanisms (A) and (B) are probable to accommodate this asymmetric transformation and they are illustrated in Scheme 3.[12] In mechanism (A) isomeric lithiooxazoline **4a** predominates over **4b** and protonation occurs from the bottom side of the oxazoline ring. As shown in mechanism (B), a reversal of the predominant isomeric anions and a reversal of the direction of protonation gave the same result indicated in the mechanism (A). Although mechanism (A) is supported by lithium–arene π coordination effect,[13] no evidence to exclude mechanism (B) is available at present. To establish the mechanism for this asymmetric transformation further investigation is now in progress.

References

1) H. B. Kagan and J. C. Fiaud, "Topics in Stereochemistry," ed by E. L. Eliel and N. L. Allinger, Interscience Publication, New York (1978), Vol. 10, p. 229.

2) M. M. Harris, "Progress in Stereochemistry," ed by W. Klyne and P. B. D. Mare, Butterworths Scientific Publications, London (1958), Vol. 2, p. 157.

3) S. Yoshikawa, M. Saburi, and M. Yamaguchi, *Pure Appl. Chem.*, **50**, 915 (1978); M. Ajioka, S. Yano, K. Matsuda, and S. Yoshikawa, *J. Am. Chem. Soc.*, **103**, 2459 (1981); H.

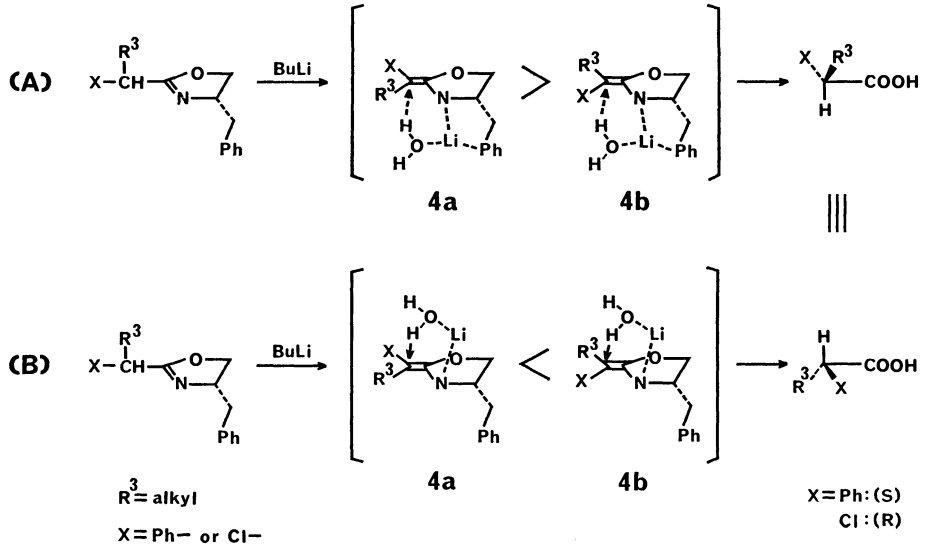

Scheme 3.

Matsushita, Y. Tsujino, M. Noguchi, M. Saburi, and S. Yoshikawa, *Bull. Chem. Soc. Jpn.*, **51**, 201 (1978).
4) T. Mukaiyama, T. Takeda, and K. Fujimoto, *Bull. Chem. Soc. Jpn.*, **51**, 3368 (1978).
5) S. Shibata, H. Matsushita, H. Kaneko, M. Noguchi, M. Saburi, and S. Yoshikawa, *Chem. Lett.*, **1981**, 217; *Heterocycles*, **16**, 1901 (1981).
6) A. I. Meyers, G. Knaus, K. Kamata, and M. E. Ford, *J. Am. Chem. Soc.*, **98**, 567 (1976).
7) H. Seki, K. Koga, H. Matsuo, S. Ohki, I. Matsuo, and S. Yamada, *Chem. Pharm. Bull.*, **13**, 995 (1965).
8) S. M. McElvain and C. L. Stevens, *J. Am. Chem. Soc.*, **68**, 1917 (1946).
9) A. I. Meyers, D. L. Temple, R. L. Nolen, and E. D. Mihelich, *J. Org. Chem.*, **39**, 2778 (1974).
10) S. M. McElvain and J. W. Nelson, *J. Am. Chem. Soc.*, **64**, 1827 (1942).
11) A. I. Meyers, G. Knaus, and P. M. Kendall, *Tetrahedron Lett.*, **1974**, 3495.
12) A. I. Meyers, E. S. Snyder, and J. J. H. Ackermann, *J. Am. Chem. Soc.*, **100**, 8186 (1978).
13) G. H. Posner and C. M. Lents, *J. Am. Chem. Soc.*, **101**, 934 (1979).

The Fusion Synthesis of Aryl 1-Thioglycosides

Toshisada SHIMADATE,* Sachiyo CHIBA, Kazuko INOUYE,
Teruhiko IINO, and Yoshiyuki HOSOYAMA
Department of Chemistry, Nihon University, Sakurajosui-3, Setagaya-ku, Tokyo 156
(Received March 10, 1982)

A simple method for the preparation of aryl 1-thioglycosides is described. The reaction of D-glucose pentaacetate or 2-acetamido-2-deoxy-D-glucose tetraacetate with arenethiols in the presence of zinc chloride under fusion conditions formed their 1-thioglycosides in good yields. Some Lewis acids in addition to zinc chloride were studied as catalysts in the reaction.

The Helferich method was applied successfully to the preparation of aryl 1-thioglycosides from sugar acetates with arenethiols.

The method is known as a simple and general procedure for the synthesis of aryl glycosides; it consists of fusing a sugar carboxylate and a phenol in the presence of an acid catalyst. The first extension of the method to the preparation of aryl 1-thioglycosides was attempted by Hurd and Bonner, who obtained phenyl 2,3,4,6-tetra-*O*-acetyl-1-thio-*β*-D-glucopyranoside (**3a**) from 1,2,3,4,6-penta-*O*-acetyl-*β*-D-glucopyranose (**1-β**) and benzenethiol (**3**) with a *p*-toluenesulfonic acid or zinc chloride catalyst.[1] However, the yield of the product (**3a**) was very low. After that, in order to improve the yields, this acid-catalyzed condensation of sugar carboxylates with arenethiols has been performed on a solution using inert solvents; the method is considered to be a modification of the fusion synthesis.[2,3]

In the present work, we studied the condensation of D-glucose pentaacetate or 2-acetamido-2-deoxy-D-glucose tetraacetate with several arenethiols by the Helferich method, under fusion conditions and at much higher temperature than those shown in Hurd and Bonner's report,[1] and found that this simple procedure was superior to any other synthetic methods in the yields of products.

Thus, **1-β** was treated with **3** on fusion in the presence of zinc chloride to prepare a crystalline product which was identified with an authentic **3a**.[2] According to the GLC analysis of the reaction product, a small quantity of the 1-thio-*α*-glycoside (**3a-α**) was contained in **3a**, but it was too small to isolate by a

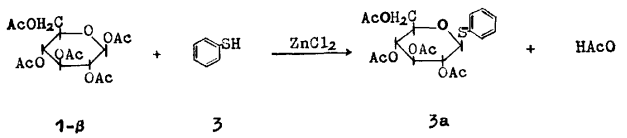

1-β 3 3a

usual procedure using PLC silica-gel plates.[2] The reaction conditions, yield, and physical and analytical data of **3a** are shown in Table 1.

1,2,3,4,6-Penta-*O*-acetyl-*α*-D-glucopyranose (**1-α**) was also fused with **3** and a zinc chloride catalyst under similar conditions; the same product (**3a**) was thus obtained in a high yield, together with a small quantity of the 1-thio-*α*-glycoside (**3a-α**), which was confirmed by comparing its physical data with those in the literature.[4]

Several arenethiols besides **3** were allowed to react with **1-β** and a zinc chloride catalyst under similar fusion conditions; *p*-chlorobenzenethiol (**4**), *o*-tolylthiol (**5**), *m*-tolylthiol (**6**), *p*-tolylthiol (**7**), *p*-*t*-butylbenzenethiol (**8**), and 2-naphthalenethiol (**9**).

The condensation products of **1-β** with **4**, **5**, **7**, and **9** were identified as *p*-chlorophenyl, *o*-tolyl, *p*-tolyl, and 2-naphthyl 2,3,4,6-tetra-*O*-acetyl-1-thio-*β*-D-glucopyranoside (**4a**, **5a**, **7a**, and **9a**) respectively by comparing their physical data with those of the corresponding 1-thio-*β*-D-glucosides in the literature.[5-7] Also, the reaction products of **1-β** with **6** and **8** were confirmed to be *m*-tolyl and *p*-*t*-butylphenyl 2,3,4,6-tetra-*O*-acetyl-1-thio-*β*-D-glucopyranoside (**6a** and **8a**) respectively on the basis of their physical and analytical data, which are summarized in Table 1.

1,3,4,6-Tetra-*O*-acetyl-2-acetamido-2-deoxy-*α*-D-glucopyranose (**2-α**)[8] and its *β*-anomer (**2-β**)[9,10] were also treated with **3** and the same catalyst on fusion to form an identical product, phenyl 3,4,6-tri-*O*-acetyl-2-acetamido-2-deoxy-1-thio-*β*-D-glucopyranoside (**3b**),[11] which was confirmed on the basis of its physical and analytical data, in good yields, but the 1-thio-*α*-glycoside was not found among those reaction products.

Similarly, the fusion reactions of **2-α** with the arenethiols, **4**, **5**, **6**, **7**, **8**, and **9**, gave their 1-thioglycosides, which were confirmed to be *p*-chlorophenyl, *o*-tolyl, *m*-tolyl, *p*-tolyl, *p*-*t*-butylphenyl, and 2-naphthyl 3,4,6-tri-*O*-acetyl-2-acetamido-2-deoxy-1-thio-*β*-D-glucopyranoside (**4b**, **5b**, **6b**, **7b**, **8b**, and **9b**) respectively on the basis of their physical and analytical data, as is summarized in Table 1.

Several Lewis acids in addition to zinc chloride were studied as catalysts in the reactions of **3** with **1-α**, **1-β**, **2-α**, and **2-β** under definite conditions, as is shown in Table 2. Tin(II), tin(IV), and iron(III) chloride are effective as well as zinc chloride, although iron(III) chloride in the reaction with an *α*-acetate (**1-α** or **2-α**) is a little inferior to the others. On the contrary, *p*-toluenesulfonic acid, phosphoryl chloride, and boron trifluoride, which are used often in the Helferich method, did not give good results in the present work.

In the Helferich reaction with simple phenols, the formation of *β*-glycosides was noted when *p*-toluenesulfonic acid, phosphoryl chloride, or tin(IV) chloride was utilized as the catalyst, whereas zinc chloride favored the formation of the *α*-anomers. However, the reaction with arenethiols is always favorable for the formation of 1-thio-*β*-glycosides, regardless of the catalyst.

Table 1. Aryl 1-thioglycoside acetates

Compound	Reaction[a] temp/°C (time/min)	Yield %	Mp θ_m/°C (lit)	$[\alpha]_D^{20}$/° (in $CHCl_3$) (lit)	^1H NMR ($CDCl_3$):[b] δ (anomeric H) and J/Hz	Formula	Found (Calcd) (%) C	H	S	N
3a	160 (50)	80	118 (117—118)[2]	−25.0 (−17.5)[2]	4.73 d, J=9.5	$C_{20}H_{24}O_9S$	54.72 (54.54)	5.35 (5.49)	7.41 (7.28)	
4a	170 (60)	88	113 (113)[5]	−25.7 (−25.0)[5]	4.72 d, J=9.5	$C_{20}H_{24}ClO_9S$	50.70 (50.47)	4.79 (5.08)	6.93 (6.74)	
5a	165 (55)	45	104—105 (104—106)[6]	−16.5 (−16.4)[6]	4.75 d, J=9.5	$C_{21}H_{26}O_9S$	55.65 (55.50)	5.64 (5.77)	7.19 (7.05)	
6a	165 (55)	58	93	−16.0	4.72 d, J=9.5	$C_{21}H_{26}O_9S$	55.73 (55.50)	5.51 (5.77)	6.98 (7.05)	
7a	165 (55)	64	118 (118)[5]	−21.5 (−21.0)[5]	4.68 d, J=9.5	$C_{21}H_{26}O_9S$	55.69 (55.50)	5.92 (5.77)	7.30 (7.05)	
8a	170 (60)	80	153	−22.5	4.73 d, J=9.7	$C_{24}H_{32}O_9S$	58.21 (58.05)	6.33 (6.50)	6.72 (6.46)	
9a	175 (50)	78	111 (111)[7]	−18.0 (−17.1)[7]	4.82 d, J=9.5	$C_{24}H_{26}O_9S$	58.89 (58.77)	5.30 (5.34)	6.76 (6.54)	
3b	175 (60)	66	200 (193—194)[11]	−39.1 (+10.5)[11]	4.94 d, J=9.8	$C_{20}H_{25}NO_8S$	54.92 (54.66)	5.81 (5.73)	7.13 (7.29)	3.30 (3.19)
4b	180 (55)	72	237	−29.8	4.78 d, J=9.5	$C_{20}H_{24}ClNO_8S$	50.92 (50.79)	5.32 (5.12)	6.88 (6.78)	3.15 (2.96)
5b	175 (60)	43	204	−21.2	4.83 d, J=9.5	$C_{21}H_{27}NO_8S$	55.48 (55.62)	6.20 (6.00)	6.82 (7.07)	3.22 (3.09)
6b	175 (60)	66	199	−20.5	4.92 d, J=9.5	$C_{21}H_{27}NO_8S$	55.41 (55.62)	6.18 (6.00)	6.91 (7.07)	3.10 (3.09)
7b	175 (60)	65	215—216	−21.5	4.83 d, J=9.5	$C_{21}H_{27}NO_8S$	55.69 (55.62)	6.23 (6.00)	6.89 (7.07)	3.31 (3.09)
8b	180 (60)	59	185	−20.3	4.94 d, J=9.8	$C_{24}H_{33}NO_8S$	58.31 (58.16)	6.58 (6.71)	6.40 (6.47)	2.73 (2.83)
9b	185 (55)	62	215	−10.6	4.94 d, J=9.8	$C_{24}H_{27}NO_8S$	59.01 (58.88)	5.44 (5.56)	6.68 (6.55)	2.77 (2.86)

a) A sugar acetate (**1-β** or **2-α**, 10 mmol), an arenethiol (13 mmol), and $ZnCl_2$ (*ca.* 0.05 g) were used. b) Other signals were commonly observed as follows: on **3a-9a**, δ=1.37 (9H, s, *t*-butyl), 2.00—2.10 (12H, 4×CH_3CO), 2.36 (3H, s, CH_3), 3.76—3.80 (1H, m, H-5), 4.20—4.30 (2H, oct, H-6,6′), 4.76—5.40 (3H, m, H-2, H-3, H-4), 7.00—8.00 (Aromatic H), on **3b-9b**, δ=1.37 (9H, s, *t*-butyl), 1.95—2.05 (12H, 4×CH_3CO), 3.70—3.80 (1H, m, H-5), 3.95—4.20 (3H, m, H-2, H-6,6′), 4.85—5.50 (2H, m, H-3, H-4), 5.85—6.60 (1H, d, NH), 7.00—8.00 (Aromatic H).

Table 2. Reaction of sugar acetates with benzenethiol in the presence of acid catalysts

Sugar acetate[a]	Reaction temp/°C[b]	Compound	Yield/%			
			$ZnCl_2$	$SnCl_2$	$SnCl_4$	$FeCl_3$
1-α	160	**3a**	73	67	50	37
		3a-α	4			
1-β	160	**3a**	80	75	52	61
2-α	175	**3b**	66	61	45	40
2-β	175	**3b**	68	59	47	52

a) A sugar acetate (10 mmol), benzenethiol (13 mmol), and an acid catalyst (*ca.* 0.05 g) were used. b) The reaction time was 60 min.

Experimental

All the melting points are uncorrected. The ^1H NMR spectra were measured with a JMN-4H-100 Spectrometer Japan Electron Optics Laboratory Co., Ltd.), using tetramethylsilane as the internal standard. The GLC analyses were performed with a JGC-20 KFP model (Japan Electron Optics Laboratory Co., Ltd.). A 2-m analytical column with 30% Silicone GE-SE 30 was used.

*Preparation of Aryl 1-Thioglycosides (**3a**, **4a**, **5a**, **6a**, **7a**, **8a**, **9a**, **3b**, **4b**, **5b**, **6b**, **7b**, **8b**, and **9b**) Listed in Table 1.* A mixture of a sugar acetate (**1-β** or **2-α**; 10 mmol) and an arenethiol (**3**, **4**, **5**, **6**, **7**, **8**, or **9**; 13 mmol) was heated in an oil bath at the temperature shown in the second column in Table 1. After a few minutes, a catalytic amount of freshly fused and powdered zinc chloride (*ca.* 0.05 g) was stirred into the melt. The temperature of the oil bath was kept for the period given in Table 1. Then, the resulting colored melt was cooled and dissolved in ethanol (*ca.* 50 ml). After cooling in a freezer, the crystalline product was collected and recrystallized from ethanol. The yields and physical and analytical data of all the products are summarized in Table 1.

The melting point of **3a** was not depressed upon admixture with an authentic sample.[2] The products, **4a**, **5a**, **7a**, and **9a**, were confirmed by comparing their melting points and specific rotation values with those in the literature.[5-7] The other products, **6a**, **8a**, **3b**, **4b**, **5b**, **6b**, **7b**, **8b**, and **9b**, were confirmed on the basis of their analytical and NMR data, in which the signals of anomeric protons were observed at 4.68—4.94 ppm as a doublet, J=9.5—9.8 Hz, and on the basis of their specific rotation values, which were negative and not very different from each other.

Examination of Lewis Acids (Zinc Chloride, Tin(II) Chloride, Tin(IV) Chloride, and Iron(III) Chloride) in Table 2 as Catalysts. The Lewis acids were utilized as catalysts in the fusion reactions between **3** (13 mmol) and four sugar acetates (**1-α**, **1-β**, **2-α**, and **2-β**; 10 mmol). These reactions were performed under the definite conditions shown in Table 2, according to the procedure described above. Among them, the reaction of **1-α** with **3** in the presence of zinc chloride yielded a small amount of **3a-α** in addition to **3a** in the following manner. After the reaction mixture was fused, the resulting melt was dissolved in ethanol (*ca.* 50 ml), cooled, and filtered to obtain a crude crystalline product. It was recrystallized from ethanol to give **3a** (3.20 g, 73%). The mother liquor, which on GLC (the column was at 200 °C, and the carrier N_2 was 45 ml/min) showed two peaks, one appearing immediately after the other (corresponding to **3a**), was evaporated till *ca.* 20 ml under reduced pressure and then cooled. The colorless needles thus obtained were recrystallized from ethanol to yield **3a-α** (0.20 g, 4%), which, on GLC under the same conditions as above, showed just one peak; mp 90—91 °C, $[\alpha]_D^{20}$ +235° (*c* 0.52, $CHCl_3$), (lit,[4] mp 91—92 °C, $[\alpha]_D^{20}$ +234° (*c* 1, $CHCl_3$)). ^1H NMR ($CDCl_3$), δ=2.00—2.12 (12H, 4×CH_3CO), 4.20 (2H, oct, H-6,6′), 4.60 (1H, m, H-5), 5.02—5.22 (2H, m, H-2, H-4), 5.50 (1H, t, H-3), 5.97 (1H, d, anomeric H, J=5.5 Hz), 7.25—7.60 (5H, aromatic H). Found: C, 54.72; H, 5.30; S, 7.40%. Calcd for $C_{20}H_{24}O_9S$: C, 54.54; H, 5.49; S, 7.28%.

The authors wish to express their thanks to Professor Juji Yoshimura of the Tokyo Institute of Technology and the staff in his laboratory for their kind help in getting some of the NMR spectra.

References

1) C. D. Hurd and W. A. Bonner, *J. Org. Chem.*, **11**, 50 (1946).
2) A. B. Landge, T. R. Ingle, and J. L. Bose, *Indian J. Chem.*, **7**, 1200 (1969).
3) K. Honma and A. Hamada, *Chem. Pharm. Bull. (Tokyo)*, **24**, 818 (1976); R. J. Ferrier and R. H. Furneaux, *Carbohydr. Res.*, **52**, 63, (1976).
4) E. Zissis, A. L. Clingman, and N. K. Richtmyer, *Carbohydr. Res.*, **2**, 461 (1966).
5) E. M. Montgomery, N. K. Richtmyer, and C. S. Hudson, *J. Org. Chem.*, **11**, 301 (1946).
6) M. Černý, D. Zachystalová, and J. Pacák, *Collect. Czech. Chem. Commun.*, **26**, 2206 (1961).
7) W. T. Haskins, R. M. Hann, and C. S. Hudson, *J. Am. Chem. Soc.*, **69**, 1668 (1947).
8) Y. Inouye, K, Onodera, S. Kitaoka, and S. Hirano, *J. Am. Chem. Soc.*, **78**, 4722 (1956).
9) O. Westphal and H. Holzmann, *Ber.*, **75**, 1274 (1942).
10) J. Conchie and G. A. Levvy, "Methods in Carbohydrate Chemistry," ed by R. I. Whistler and M. L. Wolfrom, Academic Press, New York and London (1963), Vol. II, p. 332.
11) S. É. Zurabyan, T. S. Antonenko, and A. Ya. Khorlin, *Izv. Akad. Nauk SSSR, Ser. Khim.*, **1969**, 2043.

Reaction of Diketene with Grignard Reagents in the Presence of Cobalt Catalyst. A Convenient Method for the Synthesis of 3-Methylenealkanoic Acids Leading to Terpenoids

Tamotsu FUJISAWA,* Toshio SATO, Yoshihiko GOTOH,
Masatoshi KAWASHIMA, and Tatsuo KAWARA
Chemistry Department of Resources, Mie University, Tsu, Mie 514

(Received March 23, 1982)

Primary alkyl Grignard reagents react regioselectively with diketene in the presence of cobalt(II) iodide to afford 3-methylenealkanoic acids in good yields. The synthetic utility of this reaction is demonstrated in the syntheses of terpenoids by two methods. Utilizing the isomerization of double bond of 3-methylenealkanoic acids, geranic acid and farnesic acid were obtained in two steps. Another method, the tandem [3,3] sigmatropic rearrangement of the corresponding allylic esters was used for the synthesis of C_{18}-Cecropia juvenile hormone.

Regioselective ring-opening reaction of β-propiolactones with diorganocuprates[1] or with Grignard reagents in the presence of copper(I) salt[2] has been previously shown to be a useful synthetic method of β-substituted propionic acids. This three carbon homologation terminated with a carboxyl group provided a convenient procedure for the syntheses of various natural products.[3,4] Especially, β-methyl-β-propiolactone is a useful building block in the terpene synthesis,[4] *i.e.* geraniol was derived by the introduction of double bond into α,β-position of the ester of 3,7-dimethyl-6-octenoic acid (citronellic acid), which was obtained from β-methyl-β-propiolactone and homoprenyl Grignard reagent, followed by the reduction with $LiAlH_4$.[4a] On the other hand, diketene (**1**) possesses not only the same carbon skeleton but also a carbon-carbon double bond. If the regioselective alkylation at the β-position of **1** is possible in a similar manner as β-methyl-β-propiolactone, it will provide a convenient method for the synthesis of 3-methylenealkanoic acids, and **1** will be employed as a C_4 unit of various terpenes involving double bond(s).

3-Methylenealkanoic acid derivatives have been reported as important precursors or intermediates for synthesis of several terpenoids.[5-8] 3-Methylenealkanoic acids have been synthesized by tedious routes *i.e.* the isomerization of the corresponding crotonic acid derivatives[5,9] the oxidation of homoallylic alcohol derivatives[7a] or the carboxylation of methallyl Grignard reagents.[10]

There were the enormous literatures[11] on **1**. Nevertheless, a few reports have been published on the reaction with organometallic reagents leading to a carbon-carbon bond formation.[12] Grignard reagents react with **1** to give carbonyl carbon-oxygen bond cleavage products such as methyl ketones, 1,1-disubstituted ethanol derivatives and dehydroacetic acid in low yields.[12a,b,13] On the other hand, only one example of selective β-carbon-oxygen bond fission of **1** by organometallic reagent has been reported: the reaction

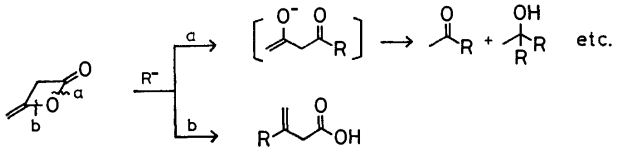

Scheme 1.

of trimethylsilylmethyl Grignard reagent in the presence of nickel(II) chloride as a catalyst to afford 3-trimethylsilyl-3-butenoic acid.[12c] Thus, the catalyzed reaction of **1** with general Grignard reagents, which seems to be more useful, was explored.

The investigations were undertaken by surveying the reaction of **1** with Grignard reagents in the presence of various metal salts (10 mol%). When butylmagnesium bromide was added into a mixture of **1** and various metal halides in ether or THF at −78 °C and stirred for 6 h at the same temperature, the yield of 3-methyleneheptanoic acid (**2c**), produced by β-carbon-oxygen bond fission of **1** was listed in Table 1. Cobalt(II) iodide was found to be the best catalyst.

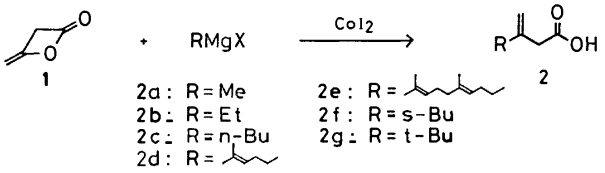

Scheme 2.

Further, solvent effects were examined in the same conditions as shown in Table 1. 3-Methyleneheptanoic acid (**2c**) was obtained in the best yield of 66% by the use of cobalt(II) iodide in ether. Inverse addition of **1** into a mixture of butylmagnesium bromide and the catalyst decreased the yield (23%). The reaction was influenced by the halide ion of Grignard reagents, and butylmagnesium chloride, bromide, and iodide gave **2c** in 58, 66, and 39% yields, respectively. The results of the reaction of several representative Grignard reagents with **1** were shown in Table 2.

TABLE 1. REACTION OF DIKETENE WITH BUTYLMAGNESIUM BROMIDE IN THE PRESENCE OF METAL SALTS (10 mol%) AT −78 °C, 6 h

MX′	Solvent	Yield %	MX′	Solvent	Yield %
CuI	THF	1	$CoBr_2$	Et_2O	8
NiI_2	Et_2O	2	CoI_2	Et_2O	66
FeI_2	Et_2O	42	CoI_2	THF	56
$Fe(acac)_3$	THF	38	CoI_2	THF-HMPA (12 : 1)	16
$Co(acac)_3$	THF	54	CoI_2	Toluene	28
$CoCl_2$	Et_2O	1	CoI_2	CH_2Cl_2	3

Table 2. Reaction of diketene with Grignard reagents[a)]

	RMgX	Time/h	Product **2**	Yield/%[b)]
a	MeMgBr	3	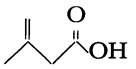	84
b	EtMgBr	6	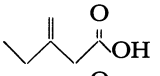	65
c	*n*-BuMgBr	6	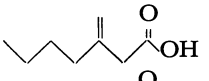	66
d	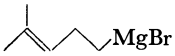	6	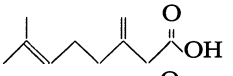	52
e	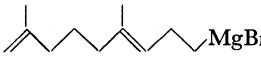	6	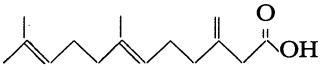	53[c)]
f	*s*-BuMgCl	6	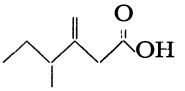	8
g	*t*-BuMgCl	6	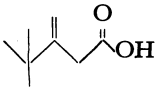	6

a) The reaction was carried out in ether at −78 °C in the presence of CoI_2 (10 mol%). b) Isolated yields by distillation. c) Isolated yield by TLC.

Primary alkyl Grignard reagents gave the corresponding acids **2** in good yields, whereas secondary and tertiary alkyl ones gave the desired acids in only a small amount. Phenyl, vinyl, and allyl Grignard reagents gave only polymeric products without the desired acids.

Next, the application to the synthesis of terpenoic carboxylic acids utilizing the ring-opening reaction of **1** followed by some simple transformation of 3-methylenealkanoic acid was attempted. The β,γ-unsaturated acids **2** obtained by the reaction can be isomerized successfully to α,β-unsaturated acids (**3**) by the treatment with *p*-toluenesulfonyl chloride in pyridine at 30 °C for 1 h and then water (Table 3). For example,

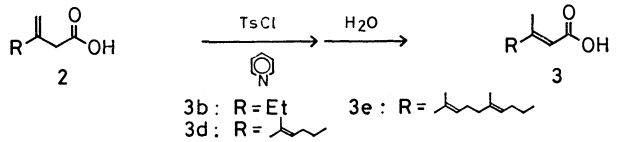

Scheme 3.

3,7-dimethyl-2,6-octadienoic acid (geranic acid) (**3d**)[8,14] and 3,7,11-trimethyl-2,6,10-dodecatrienoic acid (farnesic acid) (**3e**) were obtained in good yields by the reaction of **1** with homoprenyl- and homogeranylmagnesium bromide, followed by the isomerization of the double bond of 7-methyl-3-methylene-6-octenoic acid (isogeranic acid) (**2d**) and 7,11-dimethyl-3-methylene-6,10-dodecadienoic acid (isofarnesic acid) (**2e**).

In addition, 3-methylenealkanoic acids can be subjected to further carbon chain homologation by the tandem [3,3] sigmatropic rearrangement of the corresponding allylic ester. For example, 3-methyl-3-butenoic acid (**2a**) produced by the reaction of **1** with methylmagnesium bromide can be used for a building block of a C_5 unit to form a terpene chain. The tandem [3,3] sigmatropic rearrangement of allyl 3-methylenealkanoate is performed as follows. The Claisen rearrangement of trimethylsilylketene acetal,[15] which was obtained by treating the allylic esters (**4**) with lithium *N*-isopropylcyclohexylamide and trimethylsilyl chloride, produced the dienoic acid (**5**), which was subsequently converted into the dienoic acid (**6**) by the Cope rearrangement. For example, the Claisen

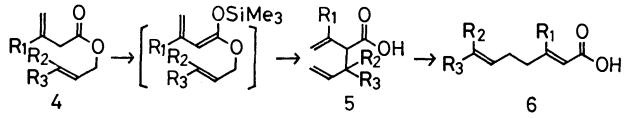

Scheme 4.

rearrangement of prenyl 3-methyl-3-butenoate (**4**; R_1, R_2,R_3=Me) *via* trimethylsilylketene acetal in THF at 67 °C for 3 h gave the dienoic acid (**5**; R_1,R_2,R_3=Me), in sequence, geranic acid (**3d**) was obtained in a yield

Table 3. Isomerization of 3-methylenealkanoic acid (**2**)

Acid **2**	Product **3**	Yield/%	
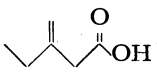	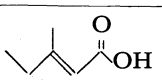 (**3b**)	80	*E*:*Z*=67:33
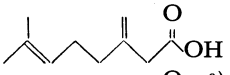	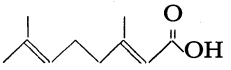 (**3d**)	95	*E*:*Z*=66:34
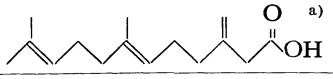 a)	(**3e**)	86	*EE*:*EZ*:*ZE*:*ZZ*=47:17:27:9

a) Homogeranyl bromide (*E*:*Z*=75:25) was used as a starting material.

of 81% (*E*:*Z*=49:51) by the Cope rearrangement of **5** in DMF at 156 °C for 2 h. The tandem [3,3] sigmatropic rearrangement of geranyl 3-methyl-3-butenoate (**4e**; R_1,R_2=Me, R_3=Homoprenyl), afforded farnesic acid (**3e**) in 63% yield (*EE*:*EZ*:*ZE*:*ZZ*=36:13:20:31). It should be noted that the tandem [3,3] sigmatropic rearrangement of allyl 3-methylenealkanoate gave the single product, although analogous rearrangement of allyl 3-alkylcrotonate has been reported to give two isomers by the migration of double bond.[16]

The utility of these reactions was demonstrated in the synthesis of C_{18}-Cecropia juvenile hormone from **1**. Starting material, 3-methylenepentanoic acid **2b** was prepared in 65% yield from **1** and ethylmagnesium bromide. The acid **2b** was isomerized to 3-methyl-2-pentenoic acid (**3b**) by the treatment of **2b** with *p*-toluenesulfonyl chloride in pyridine and then water, and the ratio of the *E* isomer to *Z* isomer for **3b** was 67:33. 3-Methyl-2-penten-1-ol (**7**) was obtained in 81% yield by the esterification of **3b** with diazomethane at 0 °C and the reduction with aluminum hydride at −18 °C. Alcohol **7** was treated with 3-methylenepentanoyl chloride (**8**), prepared in 84% yield from **2b** and thionyl chloride, to afford the allyl ester (**9**) in 87% yield. The tandem [3,3] sigmatropic rearrangement of **9** *via* trimethylsilylketene acetal gave 7-methyl-3-ethyl-2,6-nonadienoic acid (**10**) in 83% yield (*EE*:*EZ*:*ZE*:*ZZ*=21:13:36:30). The acid **10** was esterified with diazomethane and reduced with aluminum hydride to give 7-methyl-3-ethyl-2,6-nonadien-1-ol (**11**) in 81% yield.

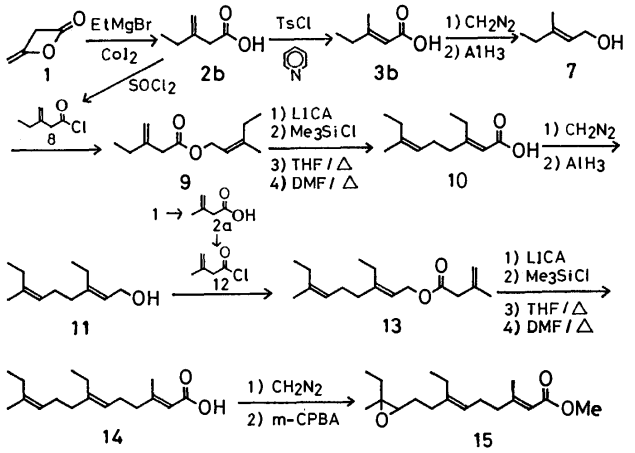

Scheme 5.

Allylic ester **13** was obtained in 86% yield from **11** and 3-methyl-3-butenoyl chloride (**12**), prepared from 3-methyl-3-butenoic acid (**2a**). The tandem [3,3] sigmatropic rearrangement of **13** furnished 3,11-dimethyl-7-ethyl-2,6,10-tridecatrienoic acid (**14**) in 61% yield (*EEE*:*EEZ*:*EZE*:*EZZ*:*ZEE*:*ZEZ*:*ZZE*:*ZZZ*=9:7:14:11:17:13:16:13). The acid **14** was esterified with diazomethane and oxidized by the known method[17] with *m*-chloroperbenzoic acid at 0 °C to yield C_{18}-Cecropia juvenile hormone (**15**) in 37% yield, which consists of a mixture of eight geometrical isomers.

Thus, the cobalt-catalyzed ring-opening reaction of diketene with Grignard reagents offered a simple and convenient synthetic method for various 3-methylenealkanoic acids, and the reaction, which is four carbon homologation containing a terpene unit, should be useful for the synthesis of various terpenes.

Experimental

The IR spectra were recorded on a Hitachi EPI-G2 spectrometer. The NMR spectra were taken in a CCl_4 solution with a Varian A-60 spectrometer using TMS as an internal standard. The GLC analyses were performed on a Yanaco G-180 Gas Chromatograph using a ϕ 3 mm×2 m 20% PEG 20 M column, a ϕ 3 mm×2 m 15% Apieson T column, and a ϕ 0.25 mm×50 m FFAP column. The preparative TLC was performed on Wakogel B-5F. All boiling points are uncorrected.

Reaction of Diketene with Grignard Reagents. To a solution of cobalt(II) iodide (2.6 mmol) in ether 54 ml was added diketene (24 mmol) at −78 °C. Then ethereal solution of Grignard reagent (26.4 mmol) was slowly dropped and stirring was continued at −78 °C for the indicated period in Table 2. The reaction was quenched with 6 M (1 M=1 mol dm^{-3}) HCl and extracted with ether. The separated organic layer was extracted with 3 M NaOH. The alkaline solution was acidified with 6 M HCl, and then extracted with ether. The ether extracts were washed with brine and dried ($MgSO_4$). Distillation gave 3-methylenealkanoic acid.

3-Methyl-3-butenoic Acid (2a). The acid **2a** was obtained in 84% yield from diketene (**1**) and methylmagnesium bromide (0.994 M) in ether at −78 °C for 3 h; bp 88 °C/25 mmHg (1 mmHg=133.322 Pa) (lit,[10] 68—70 °C/5 mmHg); IR (neat) 1710 (C=O) and 900 cm^{-1} (>C=CH$_2$); NMR δ=1.81 (3H, s), 3.00 (2H, s), 4.82 (2H, s), and 11.87 (1H, s).

3-Methylenepentanoic Acid (2b). The acid **2b** was obtained in 65% yield from diketene (**1**) and ethylmagnesium bromide (1.02 M) in ether at −78 °C for 6 h; bp 95 °C/13 mmHg; IR (neat) 1700 (C=O) and 890 cm^{-1} (>C=CH$_2$); NMR δ=1.08 (3H, t, J=7 Hz), 2.10 (2H, q, J=7 Hz), 3.20 (2H, s), 4.98 (2H, s), and 11.58 (1H, s). Found: C, 63.22; H, 9.04%. Calcd for $C_6H_{10}O_2$: C, 63.13; H, 8.83%.

3-Methyleneheptanoic Acid (2c). The acid **2c** was obtained in 66% yield from diketene (**1**) and butylmagnesium bromide (0.942 M) in ether at −78 °C for 6 h; bp 102 °C/5 mmHg; IR (neat) 1710 (C=O) and 900 cm^{-1} (>C=CH$_2$); NMR δ=0.95 (3H, t, J=7 Hz), 1.2—1.6 (4H, m), 2.0—2.3 (2H, m), 3.03 (2H, s), 4.95 (2H, s), and 11.45 (1H, s). Found: C, 67.47; H, 9.85%. Calcd for $C_8H_{14}O_2$: C, 67.57; H, 9.93%.

7-Methyl-3-methylene-6-octenoic Acid (2d). The acid **2d** was obtained in 52% yield from diketene (**1**) and homoprenylmagnesium bromide (0.685 M) in ether at −78 °C for 6 h; bp 116—117 °C/1.9 mmHg; IR (neat) 1710 (C=O) and 900 cm^{-1} (>C=CH$_2$); NMR δ=1.68 (3H, s), 1.74 (3H, s), 2.15—2.35 (4H, m), 2.90 (2H, s), 4.78 (2H, s), 4.75—5.15 (1H, m), and 11.85 (1H, s). IR and NMR spectra of the corresponding methyl ester were identical with reported ones.[5]

7,11-Dimethyl-3-methylene-6,10-dodecadienoic Acid (2e). The acid **2e** was obtained in 53% yield from diketene (**1**) and homogeranylmagnesium bromide (0.900 M), prepared from homogeranyl bromide (*E*:*Z*=75:25),[18] in ether at −78 °C for 6 h; IR (neat) 1700 (C=O) and 890 cm^{-1} (>C=CH$_2$); NMR δ=1.60 and 1.66 (9H, s), 1.90—2.40 (8H, m), 3.00 (2H, s), 4.88 (2H, s), 4.9—5.3 (2H, m), and 10.44 (1H, s). Found: C, 76.02; H, 10.47%. Calcd for $C_{15}H_{24}O_2$: C, 76.22; H, 10.24%.

4-Methyl-3-methylenehexanoic Acid (2f). The acid **2f** was obtained in 8% yield from diketene (**1**) and *s*-butylmagnesium chloride (0.916 M) in ether at −78 °C for 6 h; bulb to bulb distillation (200 °C/25 mmHg); IR 1710 (C=O) and 900 cm^{-1} (>C=CH_2); NMR δ=0.98 (3H, t, J=7 Hz), 1.05 (3H, d, J=7 Hz), 1.40 (2H, m), 1.8—2.3 (1H, m), 2.98 (2H, s), 4.95 (2H, s), and 10.28 (1H, s). Found: C, 67.56; H, 9.87%. Calcd for $C_8H_{14}O_2$: C, 67.57; H, 9.93%.

4,4-Dimethyl-3-methylenepentanoic Acid (2g). The acid **2g** was obtained in 6% yield from diketene (**1**) and *t*-butylmagnesium chloride (0.680 M) in THF at −78 °C for 6 h; bulb to bulb distillation (200 °C/25 mmHg); IR 1700 (C=O) and 900 cm^{-1} (>C=CH_2); NMR δ=1.10 (9H, s), 2.85 (2H, s), 4.77 (2H, s), and 10.44 (1H, s). Found: C, 67.37; H, 9.98%. Calcd for $C_8H_{14}O_2$: C, 67.57; H, 9.93%.

General Procedure for the Isomerization of 3-Methylenealkanoic Acid. *p*-Toluenesulfonyl chloride (22 mmol) was added to a solution of 3-methylenealkanoic acid (20 mmol) in pyridine (60 ml), and stirred at 30 °C for 1 h. Then, water (100 mmol) was added into the reaction solution and stirring was continued at 30 °C for 30 min. The reaction mixture was poured upon cold 6 M HCl, and extracted with ether. The separated organic layer was extracted with 3 M sodium hydroxide solution. The alkaline solution was acidified with 6 M HCl, and then extracted with ether. The extracts were washed with brine and dried over anhydrous $MgSO_4$. Concentration gave α,β-unsaturated acid.

3-Methyl-2-pentenoic Acid (3b).[19a] The acid **3b** was obtained in 80% yield from 3-methylenepentanoic acid (**2b**); bp 100—104 °C/12 mmHg; NMR δ=1.08 (3H, t, J=7.5 Hz), 2.08 (d, J=1 Hz, CH_3 of *Z*-**3b**), 2.34 (d, J=1 Hz, CH_3 of *E*-**3b**), 2.44 (q, J=8 Hz, CH_2 of *E*-**3b**), 2.84 (q, J=8 Hz, CH_2 of *Z*-**3b**), 5.78 (1H, t, J=1 Hz), and 12.08 (1H, s); GLC of the methyl ester (*E*:*Z*=67:33), Rt. 9′ 30″ (*Z*), 11′ 40″ (*E*) (FFAP 50 m, 60 °C).

3,7-Dimethyl-2,6-octadienoic Acid (3d).[19b] The acid **3d** was obtained in 95% yield from 7-methyl-3-methylene-6-octenoic acid (**2d**); NMR δ=1.70 (3H, s), 1.75 (3H, s), 2.02 (s, CH_3 of *Z*-**3d**), 2.20 (s, CH_3 of *E*-**3d**), 2.1—2.9 (4H, m), 4.92—5.34 (1H, m), 5.66 (1H, s), and 11.96 (1H, s); GLC of the methyl ester (*E*:*Z*=66:34), Rt. 8′ 00″ (*Z*), 9′ 40″ (*E*) (PEG 20 M, 2 m, 160 °C).

3,7,11-Trimethyl-2,6,10-dodecatrienoic Acid (3e).[19b] The acid **3e** was obtained in 86% yield from 7,11-dimethyl-3-methylene-6,10-decadienoic acid (**2e**); NMR δ=1.62 and 1.68 (9H, s), 2.00—2.16 (11H, m), 4.90—5.30 (2H, m), 5.60—5.80 (1H, m), and 11.10 (1H, s); GLC of the methyl ester (*EE*:*EZ*:*ZE*:*ZZ*=47:17:27:9), 21′ 00″ (*Z*,*Z*), 24′ 00″ (*Z*,*E*), 26′ 00″ (*E*,*Z*), 28′ 40″ (*E*,*E*) (Apieson T 2 m, 200 °C).

General Procedure for the Synthesis of 3-Methylenealkanoyl Chloride. Thionyl chloride (3 equiv.) was added dropwise to 3-methylenealkanoic acid (1 equiv.) and the reaction mixture set aside overnight at room temperature. Distillation gave 3-methylenealkanoyl chloride.

3-Methylenepentanoyl Chloride (8). The acid chloride **8** was obtained in 84% yield from 3-methylenepentanoic acid (**2b**); bp 50 °C/100 mmHg (lit,[20] 110—117 °C); NMR δ=1.04 (3H, t, J=7 Hz), 2.16 (2H, q, J=7 Hz), 3.45 (2H, s), and 4.75—4.90 (2H, m); IR (neat) 1790 (C=O) and 900 cm^{-1} (>C=CH_2).

3-Methyl-3-butenoyl Chloride (12). The acid chloride **12** was obtained in 86% yield from 3-methyl-3-butenoic acid (**2a**); bp 80 °C/100 mmHg; NMR δ=1.80 (3H, s), 3.43 (2H, s), and 4.90 (2H, m); IR (neat) 1800 (C=O) and 900 cm^{-1} (>C=CH_2).

General Procedure for the Esterification of 3-Methylenealkanoic Acid with Allylic Alcohol. A solution of acid chloride (10.5 mmol) in ether (35 ml) was slowly added dropwise to a mixture of alcohol (10 mmol) and pyridine (11 mmol) in ether (33 ml) at −15 °C for 40 min, and stirred for 1.5 h. The reaction was quenched with water and the ethereal solution was washed with water and dried ($MgSO_4$). The crude product was purified by column chromatography on silica gel (hexane:dichloromethane=1:1).

Prenyl 3-Methyl-3-butenoate (4d). The ester **4d** was derived in 73% yield from 3-methyl-3-butenoyl chloride (**12**) and prenol; IR (neat) 1720 (C=O) and 900 cm^{-1} (>C=CH_2); NMR δ=1.72 (3H, s), 1.75 (3H, s), 1.77 (3H, s), 2.92 (2H, s), 4.48 (2H, d, J=7.5 Hz), 4.78 (2H, s), and 5.08—5.46 (1H, m). Found: C, 71.27; H, 9.67%. Calcd for $C_{10}H_{16}O_2$: C, 71.39; H, 9.59%.

Geranyl 3-Methyl-3-butenoate (4e). The ester **4e** was derived in 86% yield from 3-methyl-3-butenoyl chloride (**12**) and geraniol; NMR δ=1.61, 1.66, 1.70, and 1.76 (12H, s), 1.94—2.20 (4H, m), 2.86 (2H, s), 4.34 (2H, d, J=6 Hz), 4.70 (2H, s), and 4.90—5.40 (2H, m); IR (neat) 1720 (C=O) and 890 cm^{-1} (>C=CH_2). Found: C, 76.20; H, 10.53%. Calcd for $C_{15}H_{24}O_2$: C, 76.22; H, 10.24%.

General Procedure of the Tandem [3,3] Sigmatropic Rearrangement of Allyl 3-Methylenealkanoate. A solution of *N*-isopropylcyclohexylamine (16.6 mmol) in THF (101 ml) was cooled to 0 °C and treated with butyllithium in hexane solution (13.5 mmol, 1.5 M) over 3 min. After the mixture was stirred for an additional 10 min, the solution was cooled to −78 °C and the ester (9 mmol) was added over 3 min. Within 5 min after the addition of the ester was complete, Me_3SiCl (16.3 mmol) was added to the reaction solution, and stirred at −78 °C for 5 min. The reaction solution was allowed to warm to 25 °C over 30 min and then refluxed for 2 h. After cooling the reaction mixture, 6 M HCl was added and extracted with ether. The ether extracts were washed with brine and dried ($MgSO_4$). The extracts were concentrated. DMF (30 ml) was added and refluxed for 2 h. To this solution 6 M HCl was added and extracted with ether. The ether extracts were washed with brine and dried ($MgSO_4$). The crude product was purified by distillation, TLC or column chromatography on silica gel.

3,7-Dimethyl-2,6-octadienoic Acid (3d).[19b] The acid **3d** was obtained in 81% yield from prenyl 3-methyl-3-butenoate (**4d**); bp 180 °C/2 mmHg; GLC of the methyl ester (*E*:*Z*=49:51) Rt. 7′ 30″ (*Z*), 9′ 10″ (*E*) (20% PEG 20 M, 2 m, 160 °C).

3,7,11-Trimethyl-2,6,10-dodecatrienoic Acid (3e).[19b] The acid **3e** was obtained in 63% yield from geranyl 3-methyl-3-butenoate (**4e**); TLC, R_f 0.5 (hexane:ether=2:1); GLC of the methyl ester (*EE*:*EZ*:*ZE*:*ZZ*=36:13:20:31) Rt. 21′ 00″ (6*Z*,2*Z*), 24′ 00″ (6*E*,2*Z*), 26′ 00″ (6*Z*,2*E*), and 28′ 40″ (6*E*,2*E*) (Apieson T 2 m, 200 °C).

3-Methyl-2-penten-1-ol (7). A solution of diazomethane in ether was added to a solution of 3-methyl-2-pentanoic acid (**3b**) (10 mmol) in ether (10 ml) at 0 °C. To a solution of the methyl ester in dry ether (30 ml) was slowly added an excess solution of aluminum hydride in ether (0.285 M) at −18 °C, and stirred for 1 h. The reaction was quenched with saturated ammonium chloride, and then extracted with ether and dried ($MgSO_4$). Distillation gave **7** in 81% yield; bp 110 °C/140 mmHg (lit,[21] 79—81 °C/40 mmHg); IR 3300 cm^{-1} (O–H); NMR δ=1.02 (3H, t, J=7 Hz), 1.62 (3H, s), 2.15 (2H, q, J=7 Hz), 3.40 (1H, b), 3.98 (2H, d, J=7 Hz), and 5.46 (1H, t, J=7 Hz).

3-Methyl-2-pentenyl 3-Methylenepentanoate (9). The ester **9** was derived in 87% yield from 3-methylenepentanoyl

chloride (**8**) and 3-methyl-2-penten-1-ol (**7**) according to the general procedure for the esterification as described above; NMR δ=1.04 (6H, t, J=7 Hz), 1.74 (3H, s), 1.85—2.40 (4H, m), 2.92 (2H, s), 4.44 (2H, d, J=7 Hz), 4.76 (2H, s), and 5.24 (1H, t, J=7 Hz). Found: C, 73.21; H, 10.48%. Calcd for $C_{12}H_{20}O_2$: C, 73.27; H, 10.27%.

*3-Ethyl-7-methyl-2,6-nonadienoic Acid (**10**).*[19a] The acid **10** was obtained in 83% yield by the tandem [3,3] sigmatropic rearrangement of 3-methyl-2-pentenyl 3-methylenepentanoate (**9**); column chromatography; TLC, R_f 0.5 (hexane : ether=2:1); GLC of the methyl ester (*EE*:*EZ*:*ZE*:*ZZ*=21:13:36:30), Rt. 38′ 50″ (30%) (2*Z*,6*Z*), 44′ 20″ (36%) (2*Z*,6*E*), 44′ 00″ (13%) (2*E*,6*Z*), and 45′ 50″ (21%) (2*E*, 6*E*) (FFAP 50 m, 120 °C); NMR δ=0.96 (3H, t, J=7 Hz), 1.08 (3H, t, J=7 Hz), 1.60 and 1.66 (3H, s), 1.80—2.80 (8H, m), 4.90—5.20 (1H, m), 5.55 (1H, s), and 11.96 (1H, s).

*3-Ethyl-7-methyl-2,6-nonadien-1-ol (**11**).*[21] The alcohol **11** was obtained in 81% yield from 3-ethyl-7-methyl-2,6-nonadienoic acid (**10**) according to the procedure for the synthesis of **7**; bp 122—123 °C/7.5 mmHg; IR 3300 (OH) and 1660 cm^{-1} (C=C); NMR δ=1.00 (3H, t, J=7 Hz), 1.08 (3H, t, J=7 Hz), 1.46 and 1.54 (3H, s), 2.00—2.30 (8H, m), 2.16 (1H, s), 3.98 (2H, d, J=6 Hz), 4.84—5.20 (1H, m), and 5.25 (1H, t, J=6 Hz). Found: C, 78.88; H, 11.92%. Calcd for $C_{12}H_{22}O$: C, 79.02; H, 12.16%.

*3-Ethyl-7-methyl-2,6-nonadienyl 3-Methyl-3-butenoate (**13**).* The ester **13** was derived in 92% yield from 3-methyl-3-butenoyl chloride (**12**) and 3-ethyl-7-methyl-2,6-nonadien-1-ol (**11**); IR (neat) 1720 (C=O) and 900 cm^{-1} (>C=CH$_2$); NMR δ=0.82—1.23 (6H, m), 1.55 and 1.62 (3H, s), 1.82 (3H, s), 2.88 (2H, s), 4.45 (2H, d, J=7 Hz), 4.74 (2H, s), and 4.85—5.30 (2H, m). Found: C, 77.04; H, 10.52%. Calcd for $C_{17}H_{28}O_2$: C, 77.22; H, 10.67%.

*7-Ethyl-3,11-dimethyl-2,6,10-tridecatrienoic Acid (**14**).*[19a] The acid **14** was obtained in 61% yield by the tandem [3,3] sigmatropic rearrangement of 3-ethyl-7-methyl-2,6-nonadienyl 3-methyl-3-butenoate (**13**); TLC, R_f 0.5 (hexane:ether=2:1), GLC of the methyl ester (*EEE*:*EEZ*:*EZE*:*EZZ*:*ZEE*:*ZEZ*:*ZZE*:*ZZZ*=9:7:14:11:17:13:16:13), Rt. 23′ 20″ (13%) (2*Z*,6*Z*,10*Z*), 24′ 40″ (16%) (2*Z*,6*Z*,10*E*), 26′ 20″ (13%) (2*Z*,6*E*,10*Z*), 27′ 40″ (17%) (2*Z*,6*E*,10*E*), 30′ 20″ (11%) (2*E*,6*Z*,10*Z*), 32′ 10″ (14%) (2*E*,6*Z*,10*E*), 33′ 40″ (7%) (2*E*,6*E*,10*Z*), and 35′ 20″ (9%) (2*E*,6*E*,10*E*) (FFAP 50 m, 150 °C); NMR δ=0.98 (6H, t, J=7 Hz), 1.56 and 1.66 (3H, s), 1.80—2.35 (15H, m), 4.88—5.28 (2H, m), 5.60 (1H, s), and 11.72 (1H).

*Methyl 10-Epoxy-7-ethyl-3,11-dimethyl-2,6-tridecadienoate (**15**).* A solution of diazomethane in ether was added to a solution of acid **14** (1 mmol) in ether at 0 °C. The mixture was concentrated and purified by TLC (hexane:ether=2:1, R_f 0.8). A solution of *m*-chloroperbenzoic acid (318 mg, 0.96 mmol, 52% pure) in dichloromethane (2 ml) was added to a solution of methyl 7-ethyl-3,11-dimethyl-2,6,10-tridecatrienoate (242 mg, 0.87 mmol) in dichloromethane (2 ml) at 0 °C, and then stirred at 0 °C for 24 h. The reaction solution was washed with saturated sodium hydrogencarbonate solution and dried ($MgSO_4$).

Purification by TLC on silica gel (R_f 0.4—0.5, benzene: ethyl acetate=15:1) gave juvenile hormone (**15**) (98.2 mg, 0.33 mmol) in 37% yield from the acid **14**. IR (neat) 1710 (C=O) and 1140 cm^{-1}; NMR δ=0.98 (6H, t, J=7 Hz), 1.16 (3H, s), 1.38—1.80 (4H, m), 1.90 and 2.16 (3H, s), 1.80—2.70 (9H, m), 3.64 (3H, s), 5.00—5.20 (1H, m), and 5.58 (1H, s). IR and NMR spectral data were in agreement with the reported ones.[17,19a]

References

1) T. Fujisawa, T. Sato, T. Kawara, M. Kawashima, H. Shimizu, and Y. Ito, *Tetrahedron Lett.*, **21**, 2181 (1980).

2) T. Sato, T. Kawara, M. Kawashima, and T. Fujisawa, *Chem. Lett.*, **1980**, 571.

3) T. Fujisawa, T. Sato, T. Kawara, and K. Naruse, *Chem. Lett.*, **1980**, 1123; T. Sato, T. Kawara, K. Sakata, and T. Fujisawa, *Bull. Chem. Soc. Jpn.*, **54**, 505 (1981); T. Sato, T. Kawara, Y. Kokubu, and T. Fujisawa, *ibid.*, **54**, 945 (1981).

4) a) T. Fujisawa, T. Sato, T. Kawara, A. Noda, and T. Obinata, *Tetrahedron Lett.*, **21**, 2553 (1980); b) T. Sato, T. Kawara, A. Nishizawa, and T. Fujisawa, *ibid.*, **21**, 3377 (1980); c) T. Fujisawa, T. Sato, T. Kawara, and K. Ohashi, *ibid.*, **22**, 4823 (1981).

5) R. H. Bedoukian and J. Wolinsky, *J. Org. Chem.*, **40**, 2154 (1975).

6) D. Valentine, Jr., R. C. Sun, and K. Toth, *J. Org. Chem.*, **45**, 3703 (1980).

7) a) G. Cardillo, M. Contento, and S. Sandri, *Tetrahedron Lett.*, **1974**, 2215; b) G. Cainelli, G. Cardillo, M. Contento, P. Grasselli, and A. Umani-Ronchi, *Gazz. Chim. Ital.*, **103**, 117 (1973).

8) K. Itoh, M. Fukui, and Y. Kurachi, *J. Chem. Soc., Chem. Commun.*, **1977**, 500.

9) Y. Iwakura, F. Toda, R. Iwata, and Y. Torii, *Bull. Chem. Soc. Jpn.*, **42**, 841 (1969).

10) R. B. Wagner, *J. Am. Chem. Soc.*, **71**, 3214 (1949).

11) For a review, see T. Kato, *Acc. Chem. Res.*, **7**, 265 (1974); T. Kato and T. Chiba, *Yuki Gosei Kagaku Kyokai Shi*, **39**, 733 (1981).

12) a) J. C. Combret, *Ann. Chim. (Paris)*, **4**, 481 (1969); b) A. Gibaud and A. Willemart, *Bull. Soc. Chim. Fr.*, **1956**, 432; c) K. Itoh, T. Yogo, and Y. Ishii, *Chem. Lett.*, **1977**, 103; d) J. R. Horder and M. F. Lappert, *J. Chem. Soc., A*, **1969**, 173.

13) Aldoketene dimers other than diketene have reported to react with Grignard reagents and alkyllithium in a similar manner: D. V. Nightingale and R. H. Turley, Jr., *J. Org. Chem.*, **26**, 2656 (1961); K. D. Berlin and M. H. Cooper, *ibid.*, **29**, 2057 (1964).

14) According to the procedure reported by Cardillo *et al.*,[7a] **2d** was treated with NaH at room temperature, but we could not obtain the isomerized product **3d**.

15) R. E. Ireland, R. H. Mueller, and A. K. Willard, *J. Am. Chem. Soc.*, **98**, 2868 (1976).

16) G. Fráter, *Helv. Chim. Acta*, **58**, 442 (1975).

17) K. Mori, *Tetrahedron*, **28**, 3747 (1972).

18) W. Biernacki and A. Gdula, *Synthesis*, **1979**, 37.

19) The obtained compounds were identified as methyl esters of the corresponding carboxylic acids: a) K. H. Dahm, B. M. Trost, and H. Röller, *J. Am. Chem. Soc.*, **89**, 5292 (1967); b) J. W. K. Burrell, R. F. Garwood, L. M. Jackman, E. Oskay, and B. C. L. Weedon, *J. Chem. Soc., C*, **1966**, 2144.

20) J. W. Cornforth, F. P. Ross, and C. Wakselman, *J. Chem. Soc., Perkin Trans. 1*, **1975**, 429.

21) S. Kobayashi and T. Mukaiyama, *Chem. Lett.*, **1974**, 1425.

The Conformations of Several 1-Phenylethyl and 1-Phenylpropyl Aryl Sulfoxides. Evidence for Attractive Aryl/Aryl Interaction

Keiji KOBAYASHI,† Yoshio KODAMA, Motohiro NISHIO,*
Tadashi SUGAWARA,†† and Hiizu IWAMURA††

Central Research Laboratories, Meiji Seika Kaisha, Ltd., Morooka, Kohoku-ku, Yokohama 222
†*Department of Chemistry, College of General Education, The University of Tokyo, Komaba, Meguro-ku, Tokyo 153*
††*Division of Applied Molecular Science, Institute for Molecular Science, Myodaiji, Okazaki 444*

(Received April 17, 1982)

The conformations of the diastereoisomers of 1-phenylethyl phenyl (**1**), 1-phenylethyl *p*-tolyl (**2**), 1-phenylpropyl phenyl sulfoxides (**3**) were studied by NMR spectroscopy, largely by means of the computer simulation of the lanthanoid-induced shifts. It has been suggested that the rotamer in which the aromatic group (Ar) is

$C_6H_5CH(R)$-SO-Ar **1**: R = CH_3, Ar = C_6H_5; **2**: CH_3, $C_6H_4CH_3(p)$; **3**: C_2H_5, C_6H_5

gauche to the phenyl (Ph) and *anti* to the alkyl (R) group is most populated in the conformational equilibria of (*RS*/*SR*)-**1**, **2**, **3**, and (*RR*/*SS*)-**3**. For (*RR*/*SS*)-**1** and **2**, on the other hand, the most important contributor has been suggested to be the rotamer in which Ar is flanked by Ph and R. The results have been discussed in the light of the presence of attractive interactions between relevant groups.

In relation to our interest in the favored *gauche* interactions of flexible aliphatic systems,[1] the conformations were studied for several compounds which have an aromatic group on each end of the molecules. This paper will deal with the diastereoisomeric pairs of 1-phenylethyl phenyl (**1**), 1-phenylethyl *p*-tolyl (**2**), and 1-phenylpropyl phenyl sulfoxides (**3**). The results allow us to conclude unequivocally that these compounds favor the folded (*gauche* aromatic groups) conformations in solution.

Experimental

Materials. The sulfoxides were prepared by the oxidation of the corresponding sulfides using (dichloroiodo)-benzene and water in pyridine.[2] The reaction was run at the rather high temperature of 50 °C, which enhanced the formation of the minor component in the diastereoisomeric pair. The isomeric sulfoxides were separated by repeated column chromatography on silica gel, with hexane–diethyl ether (4:1) as the eluent. The absolute configurations at the carbon and sulfur centers of optically active **1** and **2** have been rigorously determined.[3,4] The NMR spectra of these sulfoxides allow us to make a configuration assignment for the racemic diastereomers of **1** and **2** studied in this work.

The stereochemical assignment of **3** is based on the similarity in the ^{13}C and ^{17}O chemical-shift patterns (see Table 1) between the 1-phenylethyl and 1-phenylpropyl derivatives: the sulfoxide with the higher mp and the smaller retention volume was assigned the (*RR*/*SS*) configuration.

(*RR*/*SS*)-**3**. Mp 142—143 °C. Found: C, 73.51; H, 6.56; S, 13.48%. Calcd for $C_{15}H_{16}OS$: C, 73.73; H, 6.60; S, 13.12%. (*RS*/*SR*)-**3**. Mp 90—93 °C. Found: C, 73.57; H, 6.61; S, 13.52%.

The ^{17}O-enriched sulfoxides were prepared by treating the sulfides with (dichloroiodo)benzene and ^{17}O-enriched water (10 atom%, Prochem) in dry pyridine, as has been described by Montanari *et al.* for unenriched sulfoxides.[2]

NMR Spectra. The NMR spectra were obtained on a Varian EM-390 spectrometer for ^1H and on a JEOL FX-90Q spectrometer for ^{13}C NMR. The chemical shifts are given in ppm downfield from internal tetramethylsilane.

The ^{17}O NMR spectra of the labelled sulfoxides were measured[5] on a Varian FT-80A spectrometer: *ca.* (1—3)$\times 10^5$ transients were accumulated with a 90° pulse and an acquisition time of 0.03—0.04 s. The chemical shifts were measured as frequency shifts from the synthesizer frequency (8.53200 MHz) and expressed in ppm relative to the oxygen of water, which resonated at 10.78321 MHz when measured in a concentrically placed capillary tube. The chemical shifts are accurate to ±1 ppm. The sample temperature was 60 °C. Under these conditions, the half-band width was in the range of 150—200 Hz.

Lanthanoid-induced Shifts (LIS) Measurements. Weighted $Eu(fod)_3$ was added incrementally to a solution of a known amount of a substrate in $CDCl_3$ (*ca.* 0.2 M), and the chemical shifts were followed in the spectra. The induced shifts of each group of protons were found to be directly proportional to the $Eu(fod)_3$/substrate ratios up to a value of *ca.* 0.2 equiv. mol^{-1}. A least-squares analysis was performed on from four to six experimental points; correlation coefficients of 0.979 or better were thus obtained.

Results

Table 1 lists the ^1H, ^{13}C, and ^{17}O NMR parameters of the sulfoxides, **1**, **2**, and **3**. Table 2 summarizes the lanthanoid-induced shifts on proton resonances.

At first, we carried out a computer simulation of the LIS according to the procedure reported previously.[7] Thus, the position of the lanthanoid shift-reagent (LSR) and the conformation of the molecule (with regard to the central C–S bond) were varied, step by step, in the search for a reasonable fit of the computed LIS's with the observed values [assuming the $(3\cos^2 x_i - 1)\, r_i^{-3}$ proportionality]. For the methyl (ethyl) and aromatic groups, the contribution of the individual protons in a number of conformers was calculated and then averaged. The crystallographic reliability factor (*AF*)[8] was used in order to assess the agreement between the computed LIS's and the observed ones.

Figure 1 plots the *AF* against the O–S–C–C_6H_5 dihedral angle, ϕ, for compounds (*RS*/*SR*)-**1**, **2**, and

Table 1. ^{1}H, ^{13}C, and ^{17}O chemical shifts[a] of 1-phenylethyl (**1**), 1-phenylethyl *p*-tolyl (**2**) and 1-phenylpropyl phenyl sulfoxides (**3**)

	H_a	H_b	H_c	H_{me}	H_{o1}	H_{o2}	H_{m1}	H_{m2}	C_1	C_7	C_9	C_{12}	C_{15}	C_{16}	C_{17}	^{17}O
(*RS*/*SR*)-**1**	3.78	1.72	—	—	7.06	7.33	7.27	7.39	135.6	67.1	142.1		—	14.1[b]	—	7[b]
	(0.34)	(0.27)[c]														
2	3.75	1.68	—	2.36	7.11	7.16	7.24	7.13	135.7	67.0	141.3	138.9	21.4	14.1	—	5
	(0.27)	(0.19)														
3	3.55	2.03[d]	0.93	—	6.97	7.22	7.31	7.33	133.8	75.1	142.6		—	22.4[b]	11.6	11[b]
		2.39[e]														
(*RR*/*SS*)-**1**	4.02	1.62	—	—	7.00	7.17	7.23	7.33	133.9	64.3	140.5		—	12.2[b]	—	3[b]
	(0.48)	(0.23)														
2	4.00	1.57	—	2.36	6.97	7.07	7.27	7.12	134.2	64.3	141.3	137.1	21.4	11.9	—	1
	(0.39)	(0.14)														
3	3.35	2.10[d]	1.04	—	6.85	7.09	7.18	7.31	132.4	72.3	139.9		—	21.5[b]	12.0	3[b]
		2.33[e]														

a) $\delta(^{1}H)$ and $\delta(^{13}C)$: Reported in ppm downfield from internal TMS in $CDCl_3$. The chemical shifts of the aromatic protons were determined by the extrapolation of the linear LIS plots to the intercept at the LSR concentration of zero. b) From Ref. 6. The ^{17}O data (ppm downfield from external D_2O in $CDCl_3$) reported previously for (*RS*/*SR*)-**3** (19 ppm) should be corrected to this. c) Data in parentheses are the aromatic solvent-induced shifts (ASIS): $\delta(CDCl_3) - \delta(C_6D_6)$. d) $J_{ab}=11.4$ Hz (*RS*/*SR*), 9.6 Hz (*RR*/*SS*); LIS is smaller for this proton than for the diastereotopic congener. e) $J_{ab}=4.2$ Hz (*RS*/*SR*), 6.0 Hz (*RR*/*SS*). The coupling constants are insensitive to the addition of the LSR.

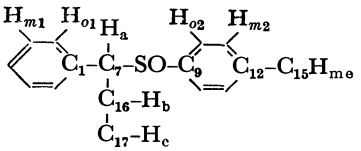

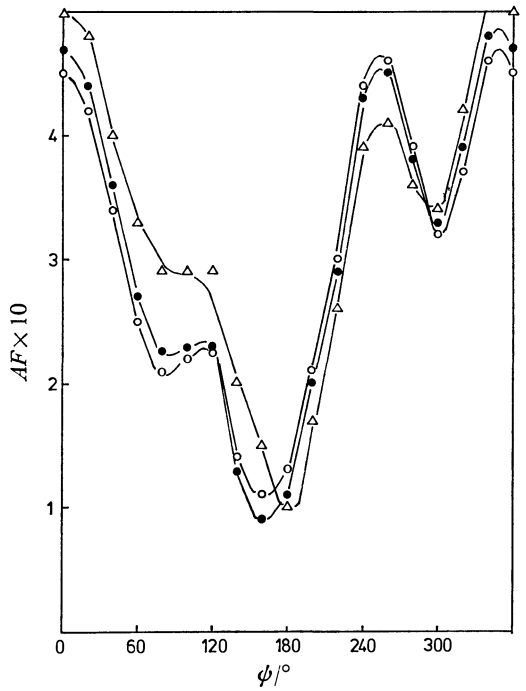

Fig. 1. Plots of *AF* *vs.* the O/Ph dihedral angle (ψ) for sulfoxides with the (*RS*/*SR*) configuration. ○—○: (*RS*/*SR*)-**1**. ●—●: (*RS*/*SR*)-**2**. △—△: (*RS*/*SR*)-**3**.

3; here, the values of R (LSR–O distance), θ (LSR–O–S angle), and A (index for the LSR-distribution)[7] are kept constant at 0.36 nm, 120°, and 0.8 respectively. The monitor nuclei are H_a, H_b, H_{o1}, H_{o2}, and H_{m1} in every case.

A notable feature of these profiles is the appearance of three minima at about the staggered geometries (ψ *ca.* 80°, 160—180°, and 300°) of the molecules. For reasons previously mentioned,[7] we believe that the values of ψ and *AF* at the extrema reflect, though in an indirect manner, the approximate geometries and the relative importance of the plausible rotamers.[9] In view of this, the most populated rotamer is suggested to have the O–S–C–Ph dihedral angle (ψ) *ca.* 160—180° for (*RS*/*SR*)-**1**, **2**, and **3** (**a** rotamer).[10] Note that in the **a** rotamer the aromatic group (Ar) is *gauche* to the phenyl group (Ph) and *anti* to the methyl group (Me). Also interesting is that the profiles suggest the second most stable one to be the **b** rotamer in every case. In this rotamer Ar is flanked by Me and Ph; the concentration of this rotamer appears to decrease in the 1-phenylpropyl derivative (*RS*/*SR*)-**3**.[11]

The profiles for the (*RR*/*SS*)-isomers are given in Fig. 2; in these cases also three minima are found. The most stable geometry is suggested to be the **b** rotamer for (*RR*/*SS*)-**1** and **2** (ψ *ca.* 200°; Ar is flanked by Me and Ph), the second most stable one being the **a** rotamer (ψ *ca.* 300°). The proportion of the **a** *vs.* **b** rotamer for the 1-phenylpropyl derivative (**3**, R=C_2H_5) seems to differ from that observed for **1** and **2** (R=CH_3); the most stable conformation is suggested to be the **a** rotamer for (*RR*/*SS*)-**3**.[11]

Discussion

A remarkable feature of the above results is that the rotamers which have the aromatic groups *gauche*

TABLE 2. THE LANTHANOID-INDUCED SHIFTS[a] OF (*RS/SR*)- AND (*RR/SS*)-**1**, **2**, AND **3**

Compound	H_a	H_b	H_c	H_{me}	H_{o1}	H_{o2}	H_{m1}	H_{m2}
(*RS/SR*)-**1**	1.37	0.89	—	—	0.60	1.00	0.15	0.14
2	1.33	0.89	—	0.09	0.54	1.00	0.16	0.16
3	1.41	0.73 1.36	0.31	—	0.53	1.00	0.09	0.12
(*RR/SS*)-**1**	0.87	0.87	—	—	0.47	1.00	0.16	0.19
2	0.96	0.94	—	0.11	0.42	1.00	0.14	0.20
3	0.69	0.86 1.10	0.31	—	0.63	1.00	0.16	0.17

a) Relative values.

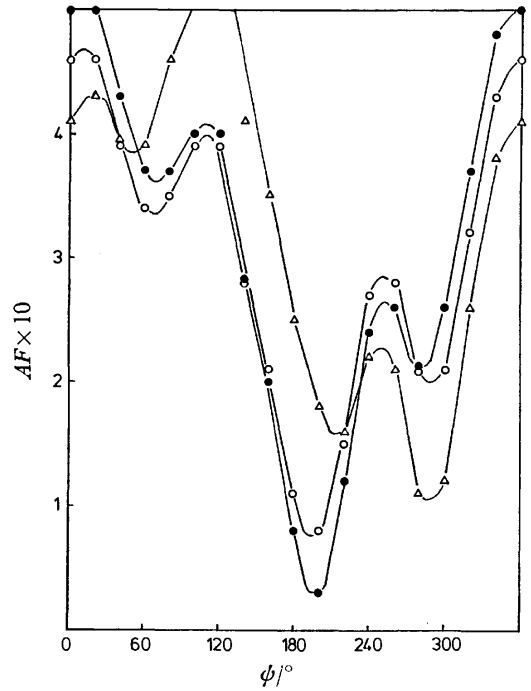

Fig. 2. Plots of *AF vs.* the O/Ph dihedral angle (ψ) for sulfoxides with the (*RR/SS*) configuration. ○—○: (*RR/SS*)-**1**. ●—●: (*RR/SS*)-**2**. △—△: (*RR/SS*)-**3**.

to each other (**a** and **b**) are present predominantly in the conformational equilibria for all of the compounds studied. Evidence was, therefore, sought in the present NMR data to support this suggestion.

^{13}C and ^{17}O γ-Effects. Significant differences are found between the diastereoisomers of **1** and **2** with regard to the chemical shifts of the methyl carbon [C(16)] and the oxygen of the sulfoxide. This can be understood well on the basis of the rotameric equilibria suggested by the LIS method (Fig. 3). In the cases of (*RS/SR*)-isomers, the oxygen is *gauche* to Me in the **a** rotamer, but is *anti* in the **b** rotamer. For the (*RR/SS*)-sulfoxides, on the other hand, O is *gauche* to Me in both of the preferred rotamers. We can, therefore, expect a more profound *γ-gauche* effect to be observed for the (*RR/SS*)-isomers.[7] The data in Table 1 support this. An essentially similar, but somewhat different, trend is observed for the 1-phenylpropyl derivatives[6] (**3**). We will refrain from discussing this problem in more detail, however, until more exact knowledge about the conformational equilibria becomes available.[12]

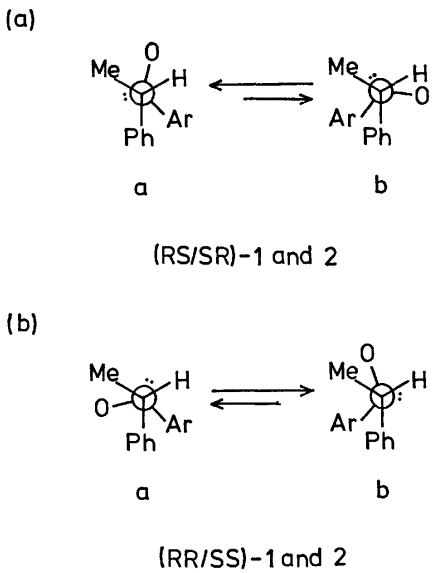

Fig. 3. Conformational equilibria suggested for (a) (*RS/SR*)-**1** and **2**, (b) (*RR/SS*)-**1** and **2**.

Chemical Shifts of the Aromatic Protons. A common aspect of the NMR spectra of **1**—**3** is that the aromatic protons give multiplets which cover a rather wide range of magnetic fields. Figure 4 illustrates this for a representative case of (*RR/SS*)-**2**. In contrast, the aromatic protons of the alkyl analogues (in which Ar is replaced by an alkyl group) gave rise to broad singlets (or narrow multiplets) centered at δ *ca.* 7.25.[7b] In the present cases (Ar=C_6H_5 or $C_6H_4CH_3$), the signals ascribable to the *ortho* protons of the 1-phenylethyl (or 1-phenylpropyl) moiety (H_{o1}), have been shown to resonate at considerably higher magnetic fields [δ 6.97—7.11 for (*RS/SR*), 6.85—7.00 for (*RR/SS*)]; this was shown by extrapolating the linear LIS plots to the intercept at the LSR concentration of zero (see Fig. 5). This is reasonable, since, in the **a** and **b** rotamers, the aromatic groups are close to each other; H_{o1} (and H_{o2}) can be expected to be effectively shielded by the opposing aromatic ring.

Aromatic Solvent-induced Shifts (ASIS). In Fig. 3, the sulfoxide oxygen in (*RS/SR*)-isomers is flanked by H_a in both of the predominant rotamers (**a** and **b**), but in the (*RR/SS*)-sulfoxides O approaches H_a only in the **b** rotamer. The reverse is true for the orientation of Me with respect to the oxygen. According to the theory,[13] the upfield shifts induced

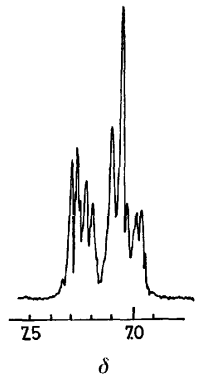

Fig. 4. The aromatic part of the ^{1}H NMR spectrum for (*RR*/*SS*)-**2**.

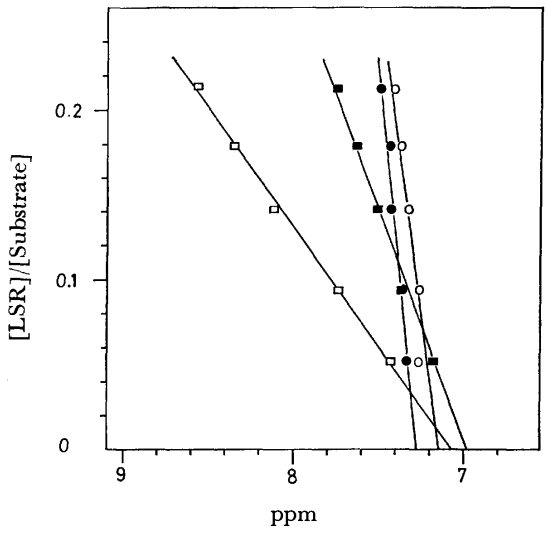

Fig. 5. Plots of the ^{1}H chemical shifts *vs.* LSR concentration for the aromatic protons of (*RR*/*SS*)-**2**. ■: H_{o1}, □: H_{o2}, ●: H_{m1}, ○: H_{m2}.

by benzene (ASIS) are expected to decrease if the relevant nuclei lie close to the negative end of the molecule. The trend observed in ASIS (Table 1) is consistent with the LIS results. Thus, ASIS for the methyl protons (H_b) is larger in (*RS*/*SR*)-**1** and **2** than in the respective (*RR*/*SS*)-isomer. ASIS for H_a, in contrast, is larger in (*RR*/*SS*)-sulfoxides.

Importance of Attractive Ar/Ar Interaction. From the considerations raised above, we conclude that these molecules favor the folded (*gauche* aromatic groups) conformations in solution. The preference of the folded conformation has been demonstrated in 1967 by Dewar for 2-arylethyl *p*-toluenesulfonates ($C_7H_7SO_2OCH_2CH_2Ar$; Ar=1-pyrenyl and 9-phenanthryl)[14] and more extensively by Engberts *et al.*[15] for several sulfonyl compounds, $ArSO_2CH_2Ar$, $ArSO_2CH_2NMeCO_2Ar$, and $(ArSO_2CHPhNH)_2CO$. Their conclusions were drawn mainly on the basis of the X-ray,[15] UV, (appearance of the intramolecular charge-transfer band),[15] and NMR data (upfield shifts of the aromatic protons as compared with those of reference compounds).[14,15] The predominance of the *gauche* rotamers has been argued also for several sulfoxides similar to **1** and **2**[3a,6] and structurally related sulfides.[16] The present findings provide strong support for this and, further, suggest that the favored interaction between aromatic groups is rather general in other kinds of molecules. Also noteworthy in the above results is the importance of the rotamer with the aromatic group (Ar) flanked by Ph and Me (**b** rotamer); in some cases, this becomes the main contributor.

In view of this and other evidence,[17] we conclude that the conformations of these molecules are determined principally by the interaction between aromatic groups, which must be attractive, at least in the framework of the molecules presently studied. Superimposed on this effect is probably the dipole(SO)/quadrupole(Ph) interaction (repulsive, if parallelly oriented).[13,17]

The nature of the attractive Ar/Ar interaction remains open, but we feel it likely that the London dispersion force is mainly responsible, since the phenomenon appears to be rather general for a variety of compounds.[14-19] The CH/π[1,20] (CH_3 *vs.* Ar; C-H_o *vs.* Ar) and quadrupole/quadrupole (Ph *vs.* Ar)[21] interactions may also play some parts in determining the molecular structures of these compounds. In order to obtain insight into this problem, theoretical calculations are currently being made in these laboratories; the results will appear in a future paper.

References

1) S. Zushi, Y. Kodama, K. Nishihata, K. Umemura, M. Nishio, J. Uzawa, and M. Hirota, *Bull. Chem. Soc. Jpn.*, **53**, 3631 (1980), and the references cited therein.

2) G. Barbieri, M. Cinquini, S. Colonna, and F. Montanari, *J. Chem. Soc., C*, **1968**, 659.

3) M. Nishio and K. Nishihata, *J. Chem. Soc., D*, **1970**, 1485; N. Sakabe, K. Sakabe, N. Sasaki, Y. Kodama, and M. Nishio, unpublished X-ray results.

4) G. Modena, U. Quintily, and G. Scorrano, *J. Am. Chem. Soc.*, **94**, 202 (1972).

5) T. Sugawara, K. Kawada, M. Katoh, and H. Iwamura, *Bull. Chem. Soc. Jpn.*, **52**, 3391 (1979).

6) K. Kobayashi, T. Sugawara, and H. Iwamura, *J. Chem. Soc., Chem. Commun.*, **1981**, 479.

7) J. Uzawa, S. Zushi, Y. Kodama, Y. Fukuda, K. Nishihata, K. Umemura, M. Nishio, and M. Hirota, *Bull. Chem. Soc. Jpn.*, **53**, 3623 (1980); Y. Kodama, S. Zushi, K. Nishihata, M. Nishio, and J. Uzawa, *J. Chem. Soc., Perkin Trans. 2*, **1980**, 1306.

8) $AF = [\sum_i (LIS_i^{obsd} - LIS_i^{calcd})^2 / \sum_i (LIS_i^{obsd})^2]^{1/2}$. The calculated shifts were normalized to the average experimental LIS in the computational process.[1,7a] The normalization was made to the largest LIS in Ref. 7b.

9) Perturbation to the conformational equilibria by the complex formation has been shown to be unimportant in these cases.[7] This is shown also by the insensitivity of $^3J_{H_aH_b}$ in **3** to the addition of the LSR.

10) In view of the limitation of the present methodology (a number of approximations were introduced in the computational procedure), we do not wish to imply that the values of ϕ at the *AF* minima correspond exactly to the molecular shapes of these compounds. Earlier work on similar subjects, however, has shown that the LIS method gave results which agreed quite well with those obtained by other means, including the X-ray crystallographic work.

See Ref. 7b and Y. Kodama, K. Nishihata, M. Nishio, and Y. Iitaka, *J. Chem. Soc., Perkin Trans. 2*, **1976**, 1490.

11) The results are compatible with our stereochemical intuition.

12) Differences are also found between the diastereomers of **1** and **2** (and **3**) for chemical shifts of H_a, H_b(methyl), C(1), and C(7). These may be conformational effects, but at present we have no clear explanation.

13) K. Nikki and N. Nakagawa, *Bull. Chem. Soc. Jpn.*, **51**, 3627 (1978).

14) M. D. Bentley and M. J. S. Dewar, *Tetrahedron Lett.*, **1967**, 5043.

15) R. van Est-Stammer and J. B. F. N. Engberts, *Tetrahedron Lett.*, **1971**, 3215; *Recl. Trav. Chim. Pays-Bus*, **91**, 1298 (1972); *Can. J. Chem.*, **51**, 1187 (1973); R. M. Tel and J. B. F. N. Engberts, *Recl. Trav. Chim. Pays-Bus*, **93**, 37 (1974); *J. Chem. Soc., Perkin Trans. 2*, **1976**, 483; I. Tickle, J. Hess, A. Vos, and J. B. F. N. Engberts, *ibid.*, **1978**, 460; R. J. J. Visser, A. Vos, and J. B. F. N. Engberts, *ibid.*, **1978**, 634.

16) K. Nishihata and M. Nishio, *J. Chem. Soc., Perkin Trans. 2*, **1973**, 758; *Tetrahedron Lett.*, **1977**, 1041.

17) N. Kunieda, H. Endo, M. Hirota, Y. Kodama, and M. Nishio, to be published.

18) P. Ivanov, I. Pojarlieff, and N. Tyutyulkov, *Tetrahedron Lett.*, **1976**, 775.

19) R. E. Carter and P. Stilbs, *J. Am. Chem. Soc.*, **98**, 7515 (1976); B. Aurivillius and R. E. Carter, *J. Chem. Soc., Perkin Trans. 2*, **1978**, 1033.

20) Y. Kodama, K. Nishihata, M. Nishio, and N. Nakagawa, *Tetrahedron Lett.*, **1977**, 2105; M. Nishio, *Kagaku No Ryoiki*, **33**, 422 (1979).

21) N. Nakagawa, personal communications. *Cf.* Ref. 13.

The Dechlorination of Polychlorinated Biphenyls by UV-irradiation. VIII. Reactions of 2,3- and 3,4-Dichlorobiphenyl in a 2-Propanol Solution

Tohru Nishiwaki,* Tsutomu Shinoda, Kinji Anda, and Mitsuhiko Hida†

Organic Division, Tokyo Metropolitan Industrial Technology Center, Nishigaoka, Kita-ku, Tokyo 115

†*Department of Industrial Chemistry, Faculty of Technology, Tokyo Metropolitan University, Fukazawa, Setagaya-ku, Tokyo 158*

(Received May 1, 1982)

The photodechlorinations of 2,3-dichlorobiphenyl (2,3-DCB) and 3,4-dichlorobiphenyl (3,4-DCB) in 2-propanol gave 3-chlorobiphenyl and 4-chlorobiphenyl respectively. The quantum yields of monochlorobiphenyl formation were 0.2 for 2,3-DCB and 0.06 for 3,4-DCB, independent of the substrate concentration and the wavelength of the exciting light. On the basis of the results obtained in quenching experiments using *cis*-1,3-pentadiene, it was concluded that 2,3-DCB was photodechlorinated exclusively in the excited singlet state, while 3,4-DCB was photodechlorinated in both excited singlet and triplet states. In the case of 3,4-DCB, the relative contributions of excited singlet and triplet states to the total dechlorination were evaluated as 0.8 and 0.2 respectively. The participation of the excited triplet state in the photodechlorination of 3,4-DCB was ascertained both by quenching reactions with biacetyl as a quencher and by photosensitized dechlorinations with acetone and acetophenone as sensitizers.

In connection with the environmental breakdown of pollutants initiated by sunlight, the photodechlorination of polychlorobiphenyls has attracted the interests of several authors.[1] Safe and Hutzinger[2] found that 2,2′,4,4′,6,6′-hexachlorobiphenyl was photochemically decomposed by the irradiation of 310 nm. Schuetz *et al.*[3] proposed that the excited triplet state was involved in the photodechlorination of six symmetrical tetrachlorobiphenyls, based on the effective quenching for the reaction by 1,3-cyclohexadiene.

Recently Bunce *et al.*[4,5] reported that the excited triplet state plays an important role in the photodechlorination of chlorobiphenyls; he based this conclusion on the following grounds: (1) The xenon assistance of the reaction, and (2) the quenching of the reaction by biacetyl. However, the reactivity of the photodechlorination of polychlorobiphenyls depends on the position of the eliminated chlorine atom and is largely affected by the presence of ortho chlorine atoms.[3,4,6] The same positional dependence of reactivity has also been found in the photodechlorination of polychlorinated benzenes, and it has been clarified that the reaction involves not only an excited triplet state, but also an excited singlet state.[7]

In this paper, the photodechlorinations of 2,3-dichlorobiphenyl (2,3-DCB) and 3,4-dichlorobiphenyl (3,4-DCB) were studied by photoquenching and photosensitization examinations. Also, the reactivities and the multiplicities of the excited state responsible for the reactions were discussed. A reaction mechanism will also be proposed.

Experimental

Materials. The 2,3-DCB and 3,4-DCB were prepared and purified as reported in a previous paper.[6] The *cis*-1,3-pentadiene, biacetyl, acetophenone, and triethylamine were used after distillation. The 2-propanol (Dotite Luminasol for fluorometry; Wako Pure Chemical Co., Ltd., Osaka) and acetone (solvent for pesticide residue analysis; Wako Pure Chemical Co., Ltd., Osaka) were used without further purification.

Apparatus. Irradiation was carried out on a Hitachi MPF-4 spectrofluorometer equipped with a 150-W Xenon lamp and a grating monochrometer (Czerny-Turner mounting). Using the maximum slit width, a monochromatic light was obtained with a wavelength purity of 20 nm; its intensity was about 2×10^{15} photons s^{-1} at 300 nm.

The amount of monochlorobiphenyls produced in the irradiated reaction mixture was determined with a JEOL Model D-100 gas chromatograph-mass spectrometer system which was equipped with a 2 m × 3 mmϕ stainless steel column packed with 10% SE-30 on 80—100 mesh chromosorb A (HMDS). The magnetic field of the mass spectrometer was fixed at *m/e* 188 to detect the molecular-ion peak of monochlorobiphenyls.

GLC analysis was conducted on a JEOL 20-K gas chromatograph with a flame-ionization detector. A glass capillary column, 60 m × 1 mmϕ, with PEG-20M (Chromato Research Co.) was used to separate the 3-chlorobiphenyl from the 4-chlorobiphenyl.

The number of photons absorbed by the reaction mixture was determined by the use of a chemical actinometer of potassium tris(oxalato)ferrate(III). A Union Giken SM-401 spectrophotometer and a Hitachi MPF-4 spectrofluorometer were used for the measurement of the UV absorption spectra and the emission spectra respectively.

Procedures. After the 2-propanol solution (4.5 cm^3) in a quartz reaction cell had been bubbled with purified nitrogen for 5 min, the cell was sealed and irradiated. Irradiation was continued until the concentration of monochlorobiphenyls increased to about 10 μmol dm^{-3} in the irradiated reaction mixture.

Quenching studies were carried out at the excitation of 290 nm to avoid the direct excitation of *cis*-1,3-pentadiene. The incident light was absorbed only by dichlorobiphenyl molecules. The concentrations of 2,3-DCB and 3,4-DCB were 20 mmol dm^{-3} and 1.5 mmol dm^{-3} respectively.

In photosensitizing experiments, the wavelength of the exciting light was selected so that the incident light was absorbed only by sensitizer molecules. The concentrations of the sensitizers were adjusted so that about 90% of the incident light was absorbed. The wavelengths and concentrations employed were as follows: 320 nm and 2.0 mol dm^{-3} for acetone; 340 nm and 40 mmol dm^{-3} for acetophenone, and 366 nm and 20 mmol dm^{-3} for benzophenone. The concentrations of 2,3-DCB and 3,4-DCB were both 1.5 mmol dm^{-3}.

Results and Discussion

The Quantum Yield for Dechlorination. 2,3-DCB and 3,4-DCB gave 3-chlorobiphenyl and 4-chlorobiphenyl respectively upon UV irradiation in 2-propanol, as was reported in our previous paper.[6] A further, detailed examination of the products revealed that the direct irradiation of 3,4-DCB afforded 4-chlorobiphenyl in a 92% yield and 3-chlorobiphenyl in an 8% yield. The quantum yields of monochlorobiphenyl formation are listed in Table 1. These values are comparable to the quantum yields of dechlorination in cyclohexane for six tetrachlorobiphenyls reported by Schuetz *et al.*[3] The chlorine atom at the ortho position of 2,3-DCB was found to have a much higher elimination efficiency than the chlorine atom at the meta position of 3,4-DCB.

Bunce *et al.*[8] reported that the quantum yield of 1-chloronaphthalene rose with an increase in the substrate concentration. Excimer formation was considered to stimulate the photoreduction of 1-chloronaphthalene to naphthalene. On the contrary, the quantum yield of monochlorobenzene photolysis in cyclohexane has been reported to decrease with an increase in the concentration of chlorobenzene.[9] Mori *et al.*[10] found that the photolysis of chlorobenzene in the gas phase depended on the excitation wavelength.

Our examinations, however, showed that no essential change was observed in the reactivities of 2,3-DCB and 3,4-DCB upon changes in the wavelength of irradiation and the substrate concentration (Table 1). Excimer formation is, therefore, not considered to play an important role in the photodechlorination of 2,3-DCB and 3,4-DCB.

The Quenching Experiment Using cis-*1,3-Pentadiene.* As Fig. 1 shows, a good linear Stern-Volmer plot was obtained for 2,3-DCB with a slope of 3.1 dm^3 mol^{-1} and an intercept equal to unity. On the other hand, the Stern-Volmer plot for 3,4-DCB gave a straight line with an intercept different from unity, indicating that two different excited states are involved in the photoreaction. The fluorescences of these dichlorobiphenyls were quenched to an extent similar to their photodechlorinations by *cis*-1,3-pentadiene.[11]

Table 1. Wavelength effect and concentration effect on dechlorination quantum yield in 2-propanol solution

Wavelength nm	Concn mol dm^{-3}	Φ_r[a] 2,3-DCB	Φ_r[a] 3,4-DCB
250	1.5×10^{-2}	0.21	0.063
	1.5×10^{-3}	0.18	0.053
	1.5×10^{-4}	0.22	0.056
290	1.5×10^{-2}	0.18	0.056
	1.5×10^{-3}		0.064
	1.5×10^{-4}		0.064
300	1.5×10^{-2}	0.15	
310	1.5×10^{-2}		0.059

a) Φ_r is the quantum yield of monochlorobiphenyl formation.

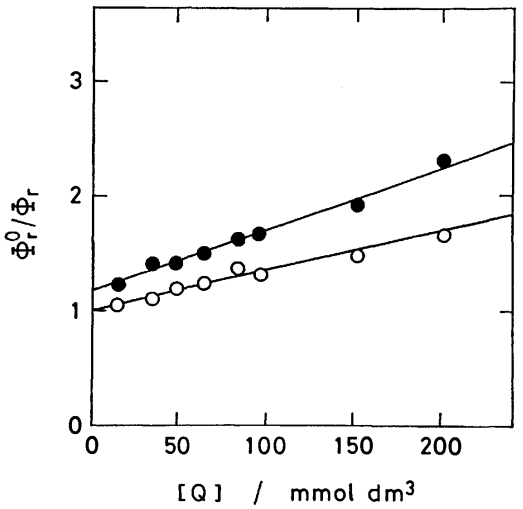

Fig. 1. Stern-Volmer plots for the quenching of dechlorination in 2-propanol solution by *cis*-1,3-pentadiene. ○: 2,3-DCB (20 mmol dm^{-3}), ●: 3,4-DCB (1.5 mmol dm^{-3}).

These results suggest that the dechlorination of 2,3-DCB occurs virtually all from the excited singlet state, while that of 3,4-DCB occurs from both excited singlet and triplet states.

Since the quantum yield for the dechlorination of 2,3-DCB from the excited singlet state is 0.2, its quantum yield for intersystem crossing must be smaller than that of biphenyl, 0.81,[12] in spite of the internal heavy-atom effect of chlorine atoms. Taking into consideration the fact that biphenyl has a planar structure in its excited singlet state, whereas it is twisted in the ground state in solution,[13] the chlorine atom at the 2-position in 2,3-DCB must be very labile in its excited state because of the large steric hindrance. This elimination is presumed to reduce the intersystem crossing efficiency of 2,3-DCB.

In the case of 3,4-DCB, the Stern-Volmer expression can be written by Eq. 1:

$$\frac{\Phi_r^\circ}{\Phi_r} = \frac{(1+k_q^S\tau_S[Q])(1+k_q^T\tau_T[Q])}{1+\{\Phi_r^S/(\Phi_r^S+\Phi_r^T)\}k_q^T\tau_T[Q]}, \quad (1)$$

where Φ_r° and Φ_r designate the quantum yields for the dechlorination of 3,4-DCB measured in the absence and in the presence of a quencher respectively, Φ_r^S and Φ_r^T the quantum yields for the dechlorination of 3,4-DCB from excited singlet and triplet states respectively in the absence of a quencher ($\Phi_r^\circ=\Phi_r^S+\Phi_r^T$), k_q^S and k_q^T the rate constants for quenching excited singlet and triplet states of 3,4-DCB respectively, τ_S and τ_T the lifetimes of excited singlet and triplet states of 3,4-DCB respectively, and [Q] is the concentration of the quencher, Q.

At sufficiently high concentrations of Q, Eq. 1 can be rewritten as Eq. 2:

$$\frac{\Phi_r^\circ}{\Phi_r} \simeq \left(\frac{\Phi_r^S+\Phi_r^T}{\Phi_r^S}\right)k_q^S\tau_S[Q] + \left(\frac{\Phi_r^S+\Phi_r^T}{\Phi_r^S}\right)\left(1-\frac{\Phi_r^Tk_q^S\tau_S}{\Phi_r^Sk_q^T\tau_T}\right). \quad (2)$$

Since τ_T is generally much larger than τ_S, the term of $\Phi_r^Tk_q^S\tau_S/(\Phi_r^Sk_q^T\tau_T)$ can be neglected. Thus, Eq. 2 can be approximated by Eq. 3:

$$\frac{\Phi_r^\circ}{\Phi_r} \approx \left(\frac{\Phi_r^S+\Phi_r^T}{\Phi_r^S}\right)k_q^S\tau_S[Q] + \frac{\Phi_r^S+\Phi_r^T}{\Phi_r^S}. \quad (3)$$

A plot of Φ_r°/Φ_r *versus* [Q] should give a straight line, with an intercept of $(\Phi_r^S+\Phi_r^T)/\Phi_r^S$ and a slope of $(\Phi_r^S+\Phi_r^T)k_q^S\tau_S/\Phi_r^S$.

From the intercept of 1.2 for the straight line of 3,4-DCB (Fig. 1), the contribution of each excited state to the total dechlorination was evaluated to be 0.8 for the excited singlet state and 0.2 for the excited triplet state. From the slope and intercept, the Stern-Volmer constant of 3,4-DCB, $k_q^S\tau_S$, was calculated to be 4.4 $dm^3\ mol^{-1}$, while the value of 3.1 $dm^3\ mol^{-1}$ was obtained for 2,3-DCB.

The Quenching of 3,4-DCB Photodechlorination by Biacetyl. When [Q] is low enough to make $k_q^S\tau_S[Q] \ll 1$,[14] Eq. 1 can be approximated as Eq. 4:

$$\frac{\Phi_r^\circ}{\Phi_r} \approx \frac{1+k_q^T\tau_T[Q]}{1+\{\Phi_r^S/(\Phi_r^S+\Phi_r^T)\}k_q^T\tau_T[Q]}. \quad (4)$$

Equation 4 can be rewritten as Eq. 5:

$$\frac{1}{\Phi_r^\circ/\Phi_r-1} \approx \frac{1+\Phi_r^S/\Phi_r^T}{k_q^T\tau_T[Q]} + \frac{\Phi_r^S}{\Phi_r^T}. \quad (5)$$

A linear plot of the (Φ_r°/Φ_r-1) reciprocal versus the [Q] reciprocal is predicted by Eq. 5, with an intercept of Φ_r^S/Φ_r^T and a slope of $(1+\Phi_r^S/\Phi_r^T)/(k_q^T\tau_T)$. Figure 2 depicts the linear plot in the case of 3,4-DCB. In this experiment, biacetyl was used as a quencher in place of *cis*-1,3-pentadiene in the concentration range of 0.3—2.0 mmol dm^{-3}. The least-squares fits of the plots gave the slope of 1.6×10^{-3} $dm^3\ mol^{-1}$ and the intercept of 2.2. From the value of the intercept, the contribution of each excited state to the total dechlorination was evaluated to be 0.7 for the excited singlet state and 0.3 for the excited triplet state.[15] It should be noted that the excited singlet state plays an important role in the photodechlorination of dichlorobiphenyls, while in the case of other chlorobiphenyls[3-5] the photodechlorination takes place through their excited triplet states.

The double reciprocal linear plots were not affected by the change in the concentrations of 3,4-DCB.[16]

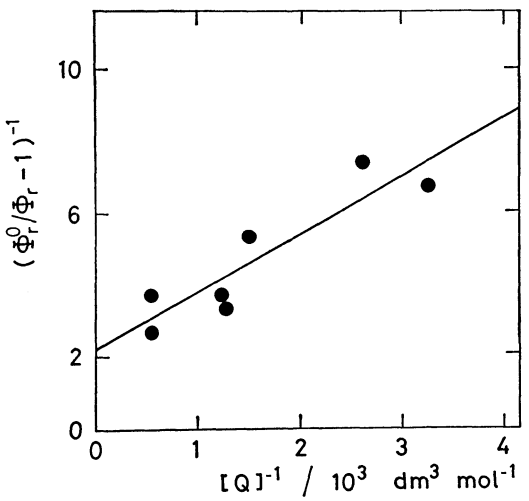

Fig. 2. Modified Stern-Volmer plot for the quenching of 3,4-DCB dechlorination in 2-propanol solution by biacetyl. 3,4-DCB: 1.5 mmol dm^{-3}.

Consequently, the dechlorination of 3,4-DCB from its excited triplet state is considered to be concentration-independent, like the dechlorination from its excited singlet state.

The results of quenching experiments at high concentrations of *cis*-1,3-pentadiene and at low concentrations of biacetyl are summarized in Table 2. A fairly good agreement is observed between them.

Photosensitized Dechlorination. Table 3 summarizes the results of dechlorination photosensitized by several ketones. Since the dechlorination of 2,3-DCB was sensitized by neither acetone nor acetophenone, the excited triplet state of 2,3-DCB was considered to be unreactive toward dechlorination. The dechlorination of 3,4-DCB was not sensitized by benzophenone, while acetone and acetophenone both sensitized the photoreaction of 3,4-DCB to give 3-chlorobiphenyl as the sole product. These photosensitization experiments revealed that the dechlorination of 3,4-DCB takes place from the excited triplet state as well as the excited singlet state, while the dechlorination of 2,3-DCB proceeds exclusively from the excited singlet state. As is shown in Table 3, sensitization by acetophenone was much less efficient than that by acetone. Benzophenone failed to sensitize the dechlorination of 3,4-DCB. The triplet energies of these ketones are as follows;[12] benzophenone, E_T=289 kJ mol^{-1}; acetophenone, E_T = 310 kJ mol^{-1}; acetone, E_T = 330 kJ mol^{-1}. The triplet energy of 3,4-DCB was estimated to be 268 kJ mol^{-1} from its phosphorescence spectrum in a EPA glass at 77 K. Although benzophenone has a higher triplet energy than 3,4-DCB by 21 kJ mol^{-1}, the photosensitized dechlorination of 3,4-DCB by benzophenone was not observed.

Wagner[17] pointed out that the quenching efficiencies of biphenyl for the photoreduction of benzophenone by benzhydrol was unexpectedly inefficient. He explained this finding on the basis of a difference in the

Table 2. Contribution of singlet and triplet states to photodechlorination in 3,4-DCB

Quencher	Relative quantum yield of photodechlorination from	
	Singlet	Triplet
cis-1,3-Pentadiene	0.8	0.2
Biacetyl	0.7	0.3

Table 3. Photosensitized dechlorination by ketones

Compound	Sensitizer	E_T[a] kJ mol^{-1}	Φ_{app}[b]	Excitation wavelength/nm
2,3-DCB	Acetone	330	0	320
	Benzophenone	289	0	366
3,4-DCB	Acetone	330	0.0097	320
	Acetophenone	310	0.0003	340
	Benzophenone	289	0	366

a) E_T is the triplet energy of a sensitizer. b) Φ_{app} is the apparent quantum yield for dechlorination and is given by:

$$\Phi_{app} = \frac{\text{number of monochlorobiphenyl molecules formed}}{\text{number of quanta absorbed by a sensitizer}}.$$

Table 4. Acetone-sensitized photodechlorination of 3,4-DCB in the presence of TEA

[TEA] / mol dm^{-3}	Φ_{app} [a]	N_{rel} [b]	Φ_{app}/N_{rel}
0	0.0097	1.00	0.0097
2×10^{-3}	0.0046	0.93	0.0049
2×10^{-2}	0.0015	0.58	0.0026
2×10^{-1}	0.0007	0.12	0.0058

a) See Table 3. b) N_{rel} is the calculated relative number of excited triplet-state 3,4-DCB molecules formed by energy transfer from excited triplet-state acetone.

geometry of biphenyl between the ground state and the excited triplet state. The most stable conformation of ground-state biphenyl is a twisted one in solution. The dihedral angle between the two phenyl rings is 20—25°. On the other hand, excited triplet-state biphenyl is considered to take a planar conformation. Thus, the energy required to activate twisted ground-state biphenyl into its twisted excited triplet state is greater than the energy liberated by the transition from the planar excited triplet state to the planar ground state. The latter energy is estimated from the phosphorescence spectrum. This is why the intermolecular energy transfer did not take place from excited triplet-state benzophenone to ground-state 3,4-DCB, since the situation described above is also the case for 3,4-DCB.

Ohashi *et al.*[18] reported that the photodechlorination of 4-chlorobiphenyl was greatly enhanced in the presence of triethylamine (TEA) by the formation of an excited charge-transfer complex between excited singlet-state 4-chlorobiphenyl and ground-state TEA. As is shown in Table 4, the apparent quantum yield of the acetone-sensitized dechlorination of 3,4-DCB decreased with an increase in the concentration of TEA.

The following deactivating processes of excited triplet-state acetone can be assumed: (1) Unimolecular decay ($k_q^T \approx 2\times10^5$ s^{-1}),[19a] (2) hydrogen abstraction from 2-propanol (k_H[2-propanol] $\approx 1\times10^7$ s^{-1}),[19b] (3) energy transfer to 3,4-DCB (k_{en}[3,4-DCB] $\approx 7\times10^6$ s^{-1}),[19c] and (4) electron transfer to TEA ($k_{el}\approx 3\times10^8$ dm^3 mol^{-1} s^{-1}).[19b] The relative number, N_{rel}, of excited triplet-state 3,4-DCB molecules formed by energy transfer from excited triplet-state acetone was calculated as a function of the concentration of TEA by assuming the above processes from (1) to (4) (Table 4). By comparing these values with the apparent quantum yields for dechlorination one can see that the efficiency of photosensitized dechlorination, Φ_{app}/N_{rel}, does not increase in the presence of TEA. Furthermore, as has been described in the previous section, the dechlorination of 3,4-DCB from its excited triplet state does not depend on its concentration. Accordingly, electron-transfer processes, such as exciplex and excimer formations, seem unlikely in the dechlorination of triplet-state 3,4-DCB. It may thus be concluded that the homolytic fission of the carbon-chlorine bond takes place in excited triplet-state 3,4-DCB.

From the quantum yield for the dechlorination and the contribution of the excited triplet state to the total dechlorination, the quantum yield for the dechlorination of 3,4-DCB from excited triplet state is evaluated to be 0.02. Since the carbon-chlorine bond-dissociation energies for aromatic chloro compounds are about 356 kJ mol^{-1},[20] the triplet-sensitized photodechlorination of 3,4-DCB by acetone or acetophenone would be endothermic.

The authors wish to express their thanks to Mr. Masao Usui of the Tokyo Metropolitan Industrial Technology Center for his helpful discussions.

References

1) For example, D. G. Crosby and K. W. Moilanen, *Bull. Environ. Contam. Toxicol.*, **10**, 372 (1973); J. H. Carey, J. Lawrence, and H. M. Tosine, *ibid.*, **16**, 697 (1976).
2) S. Safe and O. Hutzinger, *Nature*, **232**, 641 (1971).
3) L. O. Ruzo, M. J. Zabik, and R. D. Schuetz, *J. Am. Chem. Soc.*, **96**, 3809 (1974).
4) N. J. Bunce, Y. Kumar, L. Ravanal, and S. Safe, *J. Chem. Soc., Perkin Trans. 2*, **1978**, 880.
5) N. J. Bunce, J. P. Bergsma, M. D. Bergsma, W. D. Graaf, Y. Kumar, and L. Ravanal, *J. Org. Chem.*, **45**, 3708 (1980).
6) T. Nishiwaki, M. Usui, K. Anda, and M. Hida, *Bull. Chem. Soc. Jpn.*, **52**, 821 (1979).
7) M. Usui, T. Nishiwaki, K. Anda, and M. Hida, *Nippon Kagaku Kaishi*, **1982**, 638.
8) N. J. Bunce, P. Pilon, L. O. Ruzo, and D. J. Sturch, *J. Org. Chem.*, **41**, 3023 (1976).
9) N. J. Bunce and L. Ravanal, *J. Am. Chem. Soc.*, **99**, 4150 (1977).
10) T. Ichimura and Y. Mori, *J. Chem. Phys.*, **58**, 288 (1973).
11) 2,3-DCB and 3,4-DCB exhibited fluorescences in the wavelength region of 300—350 nm. In the presence of *cis*-1,3-pentadiene, a broad new emission appeared in the lower-wavelength region of 350—450 nm. This exciplex emission increased in intensity with an increase in the concentration of *cis*-1,3-pentadiene.
12) S. L. Murov, "Handbook of Photochemistry," Marcel Dekker, New York (1973), p. 4.
13) I. B. Berlman, *J. Phys. Chem.*, **74**, 3085 (1970).
14) Assuming that the rate constant of biacetyl for quenching the excited singlet state of 3,4-DCB is the same as that of *cis*-1,3-pentadiene, and that the concentration of biacetyl is 1 mmol dm^{-3}, then the value of $k_q^S\tau_S$[Q] is estimated to be 4.4×10^{-3}, negligibly small compared to unity.
15) The Stern-Volmer constant for quenching the excited triplet state of 3,4-DCB by biacetyl, $k_q^T\tau_T$, is evaluated to be 1.94×10^3 dm^3 mol^{-1}.
16) At different concentrations of 3,4-DCB, the slope and intercept for the line expressed by Eq. 5 were obtained as follows: 0.7×10^{-3} mol dm^{-3} and 2.4 at 0.15 mmol dm^{-3} of 3,4-DCB; 1.0×10^{-3} mol dm^{-3} and 2.0 at 0.9 mmol dm^{-3}; 1.6×10^{-3} mol dm^{-3} and 2.2 at 1.5 mmol dm^{-3}; 1.3×10^{-3} mol dm^{-3} and 3.3 at 2.5 mmol dm^{-3}.
17) P. J. Wagner, *J. Am. Chem. Soc.*, **89**, 2820 (1967).
18) M. Ohashi, K. Tsujimoto, and K. Seki, *J. Chem. Soc., Chem. Commun.*, **1973**, 384.
19) a) P. J. Wagner, *J. Am. Chem. Soc.*, **88**, 5672 (1966); b) N. J. Turro, "Modern Molecular Photochemistry," Benjamin, Calfornia (1978), p.374; c) The rate constant, k_{en}, is assumed to be a diffusion-controlled one for a 2-propanol solution at 22 °C.
20) S. W. Benson, "The Foundation of Chemical Kinetics," McGraw-Hill, New York (1960), p.670.

The Dechlorination of Polychlorinated Biphenyls by UV-irradiation. IX. Reactions of Monochlorobiphenyls in a 2-Propanol Solution

Tohru Nishiwaki,* Tsutomu Shinoda, Kinji Anda, and Mitsuhiko Hida†

Organic Division, Tokyo Metropolitan Industrial Technology Center, Nishigaoka, Kita-ku, Tokyo 115

†*Department of Industrial Chemistry, Faculty of Technology, Tokyo Metropolitan University, Fukazawa, Setagaya-ku, Tokyo 158*

(Received May 1, 1982)

The multiplicity of the photo-excited state responsible for the dechlorination reaction of monochlorobiphenyls was determined in 2-propanol. Linear Stern-Volmer plots were obtained by the use of 1,3-cyclohexadiene for the dechlorination reactions of 2- and 3-chlorobiphenyl; the slopes were 35.7 and 11.0 $dm^3\ mol^{-1}$ respectively. Fluorescence emissions were also quenched, and the quenching constants for 2- and 3-chlorobiphenyls were in accord with the respective values of the slope obtained from the Stern-Volmer plot for the reaction. The reaction of 4-chlorobiphenyl was quenched by *cis*-1,3-pentadiene, but was accelerated by 1,3-cyclohexadiene. Photosensitized dechlorinations of monochlorobiphenyls took place with several ketones, such as acetone and acetophenone. These sensitized reactions were, however, very inefficient compared with the reactions in the direct excitations, except in the case of 4-chlorobiphenyl. It was, then, concluded that the dechlorinations of 2- and 3-chlorobiphenyl occurred only from the excited singlet state, while that of 4-chlorobiphenyl took place predominantly from the excited triplet state.

In the preceding paper[1] the authors proposed that the excited singlet state plays an important role in the photodechlorinations of 2,3- and 3,4-dichlorobiphenyls, and that the dechlorinations do not proceed through excimer formation between the excited-state and ground-state chlorobiphenyls, but through simple homolytic fission in their excited states. Contrary to our results, several authors[2,3] have confirmed that the photodechlorinations of chlorobiphenyls take place through the excited triplet state. These results were obtained mainly with respect to highly chlorinated biphenyls, in which the intersystem crossings are enhanced by the internal heavy-atom effect, so that the reaction from the excited triplet state will tend to be emphasized.

In the present paper, the quenching and sensitized studies were applied to the dechlorination of 2-chlorobiphenyl (2-CB), 3-chlorobiphenyl (3-CB), and 4-chlorobiphenyl (4-CB) to make clear the excited state responsible for the reactions of the monochlorinated biphenyls. The reaction mechanism will also be discussed.

Experimental

Materials. The 2-propanol (Dotite Luminasol for fluorometry; Wako Pure Chemical) and acetone (solvent for pesticide residue analysis; Wako Pure Chemical) were used without further purification. The *cis*-1,3-pentadiene and 1,3-cyclohexadiene (Tokyo Kasei; guaranteed grade), and acetophenone (Wako Pure Chemical; guaranteed grade) were used after an ordinary distillation. The benzophenone (Wako Pure Chemical, special grade) was purified by recrystallization from ethanol. The 2-CB, 3-CB, and 4-CB were prepared by a modification of Cadogan's method.[4] The crude CBs were chromatographed several times over a silica-gel column, using hexane as the eluent, and recrystallized from ethanol. The purified CBs were contaminated by a trace of biphenyl; the contents in 2-, 3-, and 4-CB were estimated to be 0.16, 0.15, and 0.0002% respectively.

Irradiation. A solution of CBs, and the quenchers or sensitizers if necessary, was pipetted into a quartz reaction cell (4.5 ml), deaerated by bubbling nitrogen for 5 min, and then sealed. Photolyses were carried out under the following conditions: A) The reaction cell was placed in a water bath kept at 30 °C and then irradiated through an interference filter (Nihon Shinku S50ϕ, 298 nm) with a 250W highpressure mercury lamp (Ushio USH-250). B) The photolyses with a monochromatic light of an adequate purity were carried out with a Hitachi MPF-4 spectrofluorometer equipped with a 150W xenon lamp and a grating monochrometer. The intensity of incident light for reaction cell was about $(1.8—3.4)\times10^{15}$ photons s^{-1} in the wavelength region of 290—370 nm. Actinometry was done by the method of Hatchard and Parker[5] using potassium tris(oxalate)ferrate(III).

Analysis of the Photolyzed Product. The photolyzed samples were analyzed for the formation of biphenyl as follows. GLC analysis was conducted on a JEOL 20-K gas chromatograph with a flame-ionization detector employing a 2 m×3 mmϕ stainless steel column packed with 10% SE-30 on 80—100 mesh Chromosorb A (HMDS). A JEOL Model D-100 mass spectrometer was used to estimate the trace amounts of biphenyl quantitatively; the strength of the magnetic field was fixed at *m/e* 154.

Absorption and Emission Spectra. The absorption spectra of sample solutions were taken on a Union Giken SM-401 spectrophotometer before and after irradiation. The fluorescences of CBs at the ambient temperature and the phosphorescence emissions at 77 K in a EPA glass were examined with a Hitachi MPF-4 spectrofluorometer.

Results and Discussion

Quenching Experiments by Dienes. The photodechlorination reactions of 2-CB and 3-CB were quenched by 1,3-cyclohexadiene in 2-propanol. As is shown in Fig. 1, both Stern-Volmer plots were linear with an intercept equal to unity; the slopes were 35.7 $dm^3\ mol^{-1}$ and 11.0 $dm^3\ mol^{-1}$ for 2-CB and 3-CB respectively. Thus, a single excited state was considered to play an important role in the dechlorinations of both 2-CB and 3-CB. The fluorescences of these chlorobiphenyls were observed in the wavelength region of 300—380 nm. In the presence of 1,3-cyclohexadiene the fluorescences were quenched with the quenching constants of 33.5 $dm^3\ mol^{-1}$ and 11.5 $dm^3\ mol^{-1}$ for 2-, and 3-CB respectively. The respective quench-

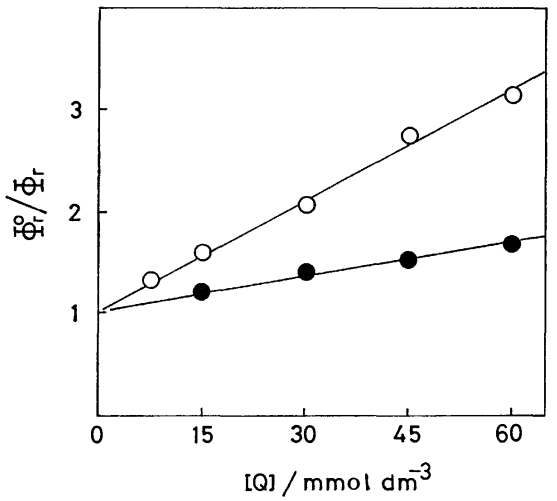

Fig. 1. Stern-Volmer plots for the quenching of dechlorination reaction by 1,3-cyclohexadiene.
○: 2-CB (15 mmol dm^{-3}), ●: 3-CB (15 mmol dm^{-3}).

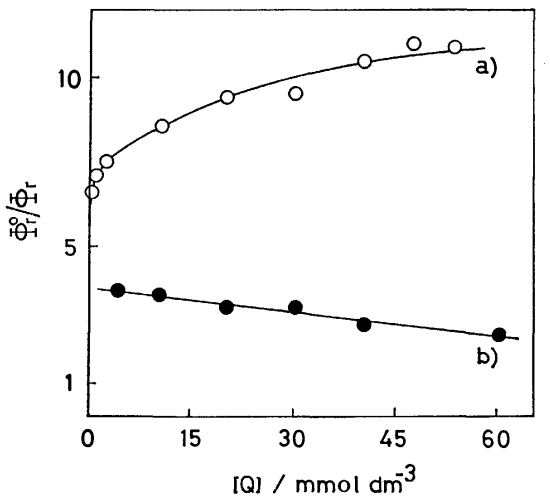

Fig. 2. Stern-Volmer plots for the quenching of dechlorination reaction of 4-CB by dienes.
○: *cis*-1,3-Pentadiene, ●: 1,3-cyclohexadiene. Concentration of 4-CB: 5—15 mmol dm^{-3}.
a) Photolyzed at 290 nm with monochrometer (Hitachi MPF-4), b) photolyzed at 298 nm through filter with 250 W high pressure mercury lamp.

ing constant of the dechlorination reactions for 2-, and 3-CB exhibits a good agreement with that of the fluorescence. Assuming a diffusion-control rate for the quenching,[6] the lifetimes were roughly estimated to be 7 and 3 ns for 2- and 3-CB respectively from the Stern-Volmer constants in the dechlorination reactions. The value of 3—7 ns would be reasonable for the lifetime of the excited singlet-state monochlorobiphenyls; this may be compared with that of 4-CB, reported to be 1.2—1.3 ns.[7] The dechlorination reactions of 2-, and 3-CB were concluded to take place through their excited singlet states.

The quenching reaction of 4-CB was more complicated than those of 2-, and 3-CB. A curved Stern-Volmer plot was obtained by using *cis*-1,3-pentadiene, as is shown in Fig. 2. This suggests that both excited singlet and triplet states of 4-CB are responsible for the dechlorination reaction. The slope of the curved Stern-Volmer plot decreased with the increase in the diene concentration, and the plot tend to be asymptotic to a straight line in the high-concentration ranges of diene.

As has been discussed in the preceding paper,[1] at a sufficiently high concentration of diene, the curved Stern-Volmer plot may be approximated in the following form:

$$\frac{\Phi_r^\circ}{\Phi_r} \approx \left(\frac{\Phi_r^S+\Phi_r^T}{\Phi_r^S}\right) k_q^S \tau_S [Q] + \frac{\Phi_r^S+\Phi_r^T}{\Phi_r^S} \qquad (1)$$

where Φ_r° and Φ_r are the quantum yields for the dechlorination of 4-CB measured in the absence and in the presence of a quencher respectively. Φ_r^S and Φ_r^T are the quantum yields for the dechlorination of 4-CB in the excited singlet state and the excited triplet state respectively in the absence of a quencher (namely, $\Phi_r^\circ=\Phi_r^S+\Phi_r^T$). $k_q^S\tau_S$ is the quenching constant of excited singlet-state 4-CB. [Q] denotes the concentration of the quencher, Q.

The ratio of the quantum yields for the dechlorination from the excited singlet and triplet states, Φ_r^T/Φ_r^S, can be determined from the value of the intercept. As may be seen in Fig. 2, the curved plot is not completely asymptotic to a straight line, even in high-concentration ranges of diene, but the intercept can be roughly estimated to be larger than 9. This implies that the contribution of the excited triplet state to the dechlorination of 4-CB is more than 90%. Thus, it was concluded that the dechlorination of 4-CB occurred from both excited singlet and triplet states, but predominantly from the latter state.

Interestingly, the dechlorination of 4-CB was clearly accelerated by adding 1,3-cyclohexadiene, as is shown in Fig. 2. A similar acceleration has been found in the photo-dechlorination reaction of 4-CB with triethylamine;[8] it was interpreted in terms of the formation of a charge-transfer complex between the excited singlet-state 4-CB and triethylamine in the ground state.

It is well known that aromatic hydrocarbons such as methylnaphthalenes in the excited singlet state interact with the ground-state dienes, and that the degree of exciplex formation increases with the decrease in the adiabatic ionization potential (I_p) of diene.[9] The I_p values of 1,3-cyclohexadiene and *cis*-1,3-pentadiene are believed to be 7.88 and 8.42 eV[10] respectively. This implies that 1,3-cyclohexadiene is more reactive than *cis*-1,3-pentadiene in the exciplex formation with 4-CB in the excited singlet state. Thus, 1,3-cyclohexadiene would accelerate the dechlorination of 4-CB *via* exciplex formation. On the other hand, because of the large I_p value, *cis*-1,3-pentadiene is less reactive for the exciplex formation and the charge separation in the exciplex ($CB^{\delta-}\cdots Q^{\delta+}$) would be small, so that dechlorination would not take place in this case.

Photosensitized Dechlorination. Table 1 summarizes the results of sensitizations. It must be noted that the yield shown in Table 1 does not represent the quantum yield for a dechlorination reaction from the excited triplet-state CB, since the efficiency of

Table 1. Apparent quantum yields sensitized with ketones[a-d]

Compound	Acetone	Acetophenone	Benzophenone
2-CB	0.0024		0.00010
3-CB	0.00015		
4-CB	0.0041	0.00015	0.00010

a) Apparent quantum yield = $\frac{\text{formation of biphenyl}}{\text{photons absorbed by ketone}}$. b) The excitations of these ketones were carried out at 320, 320, and 366 nm for acetone, acetophenone, and benzophenone respectively. c) The concentrations of sensitizers were as follows: acetone, 2 mol dm^{-3}; acetophenone, 2×10^{-2} mol dm^{-3}; benzophenone, 2×10^{-2} mol dm^{-3}. d) Measurements were done in duplicate, and the results were averaged.

energy transfer from the excited triplet ketone to the ground-state CB is not evaluated. The efficiency, (Φ_{et}) can be represented by a familiar equation:

$$\Phi_{et} = \frac{k_{et}[CB]}{k_d + k_h[i\text{-PrOH}] + k_{et}[CB]} \Phi_{ic}, \quad (2)$$

where k_{et} is the rate constant of energy transfer from triplet ketone to ground-state CB, k_d is the rate constant of hydrogen abstraction from 2-propanol in triplet ketone, and Φ_{ic} is the quantum yield of the intersystem crossing of ketone.

By the use of the values of the rate constants found in the literature, the efficiency could be tentatively estimated. The k_d, k_h, and Φ_{ic} values of acetone have been reported to be 2.0×10^5 s^{-1}, 1×10^6 dm^3 mol^{-1} s^{-1}, and 1.0[11] respectively. Thus, the efficiency of energy transfer from triplet acetone to CB was estimated to be 0.8, assuming the diffusion-control rate in 2-propanol[12] for k_{et}[CB]. This shows that 80% of the energy absorbed by acetone will be transferred to the ground-state CB. Therefore, the apparent yields obtained by using acetone as a sensitizer will afford the approximate quantum yields for dechlorination reactions from the excited triplet-state CBs. Table 1 makes it clear that the reactions from the excited triplet-state CBs take place. However, the dechlorinations of 2- and 3-CB are very inefficient compared with the quantum yields for dechlorinations obtained by the direct-excitation method, given in Table 2. Thus, the triplet contribution to their dechlorinations is considered to be negligibly small. This finding supports the conclusion obtained in the quenching experiments of 2- and 3-CB by 1,3-cyclohexadiene. The apparent yield of 4-CB sensitized by acetone is larger than that obtained in a direct-excitation method, but both yields are of the same order of magnitude (10^{-3}). Thus, a remarkable dechlorination from the excited triplet state of 4-CB was supported by the results of the sensitization reaction with acetone.

On the other hand, the apparent quantum yields of 4-CB sensitized by acetophenone and benzophenone are much lower than that sensitized by acetone. However, the efficiencies of energy transfer from these triplet ketones to 4-CB are presumed to be 0.7 and 0.6[13] for acetophenone and benzophenone respectively; these values are comparable to 0.8 of acetone.

Table 2. Direct photolysis of CBs in 2-propanol solution[a-c]

Compound	Irradiation time t/min	Formation of Biph c/μmol dm^{-3}	Quantum[d] yield
2-CB	15	118	0.3
3-CB	60	7.4	0.0047
4-CB	120	5.0	0.0016

a) Excitation: 290 nm. b) Strength of incident light: $\approx 1.5 \times 10^{15}$ photons s^{-1}. c) Concentrations of CBs were 5.0 – 5.5 mmol dm^{-3}. d) Value determined from the average of two or more runs.

It must be kept in mind that these efficiencies were calculated on the assumption of a diffusion-control rate for the energy-transfer process. The triplet energy of 4-CB can be roughly estimated to be 269 kJ mol^{-1} from the phosphorescence spectrum. This triplet level is low enough to accept the energy at the diffusion-control rate from triplet benzophenone, which has the lowest triplet energy (298 kJ mol^{-1})[11] among the sensitizers used. However, it has been considered by some authors[1,3,14] that the occurrence of dechlorination in CB requires a higher energy than the triplet energy estimated from the emission spectrum. Therefore, from the results shown in Table 1 one can lead the conclusion that the triplet-energy level of 4-CB responsible for dechlorination lies between the triplet levels of acetone (330 kJ mol^{-1})[11] and acetophenone (310 kJ mol^{-1});[11] the assumption of diffusion control is not satisfied in the case of acetophenone and benzophenone.

Typical carbon-chlorine bond dissociation energies for aromatic compounds are reported to be about 356 kJ mol^{-1}.[15] Therefore, the dechlorination reaction from the excited triplet state of 4-CB would be endothermic. This is confirmed by the low quantum yield shown in Table 2.

Reaction Mechanism. The dechlorinations of 2- and 3-CB occurred from the excited singlet state, while that of 4-CB occurred from the excited triplet state. Biphenyl has a planar structure in the excited singlet state,[16] whereas it is twisted in the ground state in solution. 2-CB will suffer a large steric hindrance in the excited singlet state due to the presence of the chlorine atom at the 2-position, so the chlorine atom in the excited singlet state would be very labile. We have considered that the high reactivity of the chlorine atom at the 2-position is derived from this steric effect.[17] The racemization of 2′-methoxy-6-nitrobiphenyl-2-carboxylic acid is appreciably depressed by introducing the chlorine atom at the 3′-position,[18] this depression was interpreted in terms of the buttressing effect. Thus, the hydrogen atom at the 2-position of 3-CB will be pushed to the opposite direction by the chlorine atom at the 3-position, and the rotation barrier around the carbon-carbon bond between two phenyl rings will increase. This suggests that the same lability of the chlorine atom as that of 2-CB can be expected for the dechlorination from the excited singlet-state 3-CB. However, the reaction of 3-CB should be very inefficient compared with that of 2-CB, since the rotation barrier induced by the but-

tressing effect would be much lower than the barrier induced by the chlorine atom at the 2-position.

On the other hand, the dechlorination of 4-CB occurred predominantly from the excited triplet state. The reaction from the excited singlet state would not be important, since no steric effect is expected in the case of 4-CB.

References

1) T. Nishiwaki, T. Shinoda, K. Anda, and M. Hida, *Bull. Chem. Soc. Jpn.*, **55**, 3565 (1982).
2) L. O. Ruzo, M. J. Zabik, and R. D. Schuetz, *J. Am. Chem. Soc.*, **96**, 3809 (1974).
3) N. J. Bunce, Y. Kumar, L. Ravanal, and S. Safe, *J. Chem. Soc., Perkin Trans. 2*, **1978**, 880; N. J. Bunce, J. P. Bergsma, M. D. Bergsma, W. D. Graaf, Y. Kumar, and L. Ravanal, *J. Org. Chem.*, **45**, 3708 (1980).
4) J. I. G. Cadogan, *J. Chem. Soc.*, **1967**, 4257.
5) C. G. Hatchard and C. A. Parker, *Proc. R. Soc. London, Ser. A*, **235**, 518 (1956).
6) The excited singlet states of benzene and its derivatives are quenched at nearly the diffusion-control rate by diene (R. G. Brown, and D. Phillips, *J. Am. Chem. Soc.*, **96**, 4784 (1974)).
7) K. Tsujimoto and M. Ohashi, *Proc. Symp. Synth. Org. Chem. (Tokyo)*, June 1973, p. 70.
8) M. Ohashi, K. Tsujimoto, and K. Seki, *J. Chem. Soc., Chem. Commun.*, **1973**, 384.
9) D. A. Labianca, G. N. Taylor, and G. S. Hammond, *J. Am. Chem. Soc.*, **94**, 3679 (1972).
10) S. L. Murov, "Handbook of Photochemistry," Marcel Dekker, New York, (1973), p.198.
11) N. J. Turro, "Modern Molecular Photochemistry," Benjamin/Cummings, California (1978), Chaps. 8 and 10.
12) G. S. Parks and C. S. Caffee, *J. Phys. Chem.*, **31**, 439 (1927). The rate constant at diffusion control, (k_D) was evaluated to be 7.7×10^9 dm^3 mol^{-1} s^{-1} by means of this equation: $k_D=8RT/3000\eta$.
13) To calculate these efficiencies, an ordinary value of k_D in 2-propanol (4.5×10^9 dm^3 mol^{-1} s^{-1}) was used because of the low concentrations of sensitizers in the 2-propanol solution. The k_d, k_h, and Φ_{iC} values of these triplet ketones are tabulated in 11).
14) P. J. Wagnar, *J. Am. Chem. Soc.*, **89**, 2820 (1967).
15) S. W. Benson, "The Foundation of Chemical Kinetics," McGraw-Hill, New York (1960), p.670.
16) I. B. Berlman, *J. Phys. Chem.*, **74**, 3085 (1970).
17) T. Nishiwaki, M. Usui, K. Anda, and M. Hida, *Bull. Chem. Soc. Jpn.*, **52**, 821 (1979).
18) E. L. Eliel, "Stereochemistry of Carbon Compounds," McGraw-Hill, New York (1962), Chap. 6.

The Isolation and Structures of Novel Neolignans and Neosesquilignans from *Heterotropa takaoi* M.

Shosuke YAMAMURA,* Masatake NIWA,† Yukimasa TERADA,† and Mikie NONOYAMA†

Department of Chemistry, Faculty of Science and Technology, Keio University, Hiyoshi, Kohoku-ku, Yokohama 223

†*Faculty of Pharmacy, Meijo University, Tempaku-ku, Nagoya 468*

(Received May 15, 1982)

Several novel neolignans and neosesquilignans represented by heterotropanone and heterotropatrione, respectively, have been isolated from the plant *Heterotropa takaoi* M. and their structures also been elucidated on the basis of their spectral data closely related to that of asatone. From a biogenetic point of view, furthermore, these neolignans and neosesquilignans were chemically correlated to one another.

In the course of our searching for physiologically active substances in nature, we found two novel neolignans, asatone and isoasatone, in the plant *Asarum teitonense* Hayata (Taiton Kan-aoi in Japanese), the decoction of the stems and rhizomes of which has been used in Taiwan as a remedy for neuralgia by the local people.[1] In connection with these two interesting neolignans, we further examined chemical components of the plant *Heterotropa takaoi* M. (Hime Kan-aoi in Japanese) and could isolate several new types of neolignan and neosesquilignan. In this paper, we wish to describe the isolation and structures of these compounds. From a biogenetic point of view, furthermore, chemical correlation among them is also presented.

Isolation of Neolignans and Neosesquilignans. Fresh leaves and roots of the above plant, which were collected at Sanage in Aichi Prefecture in April as well as in December, were disintegrated into large amounts of methanol, and then the methanol extract was partitioned between water and ethyl acetate. The ethyl acetate extract was roughly separated by column chromatography [silica gel (Mallinckrodt, 100 mesh)] using hexane–ethyl acetate (1:1) and then ethyl acetate to give several fractions. Each fraction was further separated by a combination of repeated column chromatography (silica gel, Florisil and/or alumina) and preparative TLC (Kieselgel PF_{254}) using hexane, ethyl acetate, chloroform and/or their mixed solvent to afford heterotropanone, isoheterotropanone, isoasatone A, isoasatone B, heterotropan, heterotropatrione and isoheterotropatrione in 0.00023, 0.00074, 0.0041, 0.0012, 0.00048, 0.00042, and 0.0019% yields, respectively,[2] in addition to asatone as a main product (0.065% yield). All of them are new types of neolignan, of which the last two neolignans are regarded as a new class of neosesquilignan which consists of three C_6–C_3 units.

The Structures of Heterotropanone (1) and Isoheterotropanone (2). Heterotropanone and isoheterotropanone both have the same molecular formula [$C_{24}H_{32}O_7$(*m/e* 432(M^+))] and their spectral data are quite similar to each other, as described in Tables 1 and 2, indicating that these two neolignans must be stereoisomers.

Heterotropanone (**1**), which includes seven oxygen atoms in its molecular formula, has six methoxyl groups (δ 3.28, 3.34, 3.60, 3.82, and 3.84) and one CO group (ν_{max} 1745 cm^{-1}; δ 201.7). The presence of a partial structure [A] including 3,4,5-trimethoxyphenyl group

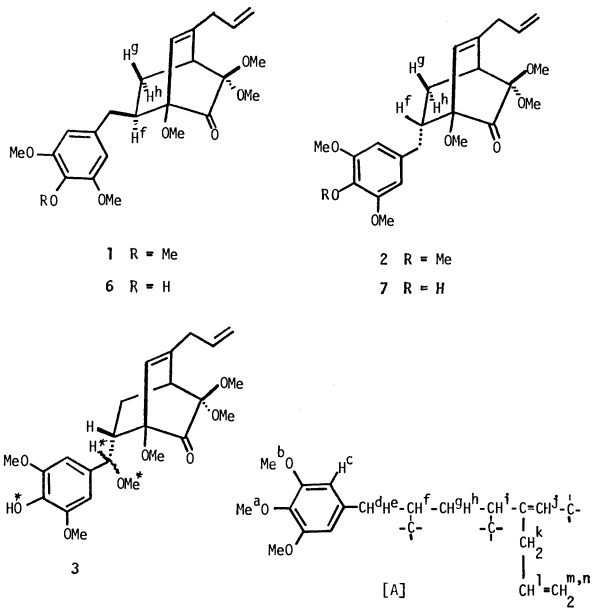

Fig. 1

can be confirmed by analysis of the ^1H NMR spectrum of **1** with aid of double resonance experiments [δ 3.82(H^a), 3.84(H^b), 6.35(H^c), 2.09(H^d),[3] 3.10(H^e), 2.47(H^f), 1.13(H^g), 1.92(H^h), 2.81(H^i), 5.84(H^j), 2.99(H^k), 5.87(H^l), 5.13(H^m), and 5.15(H^n)]. On irradiation at δ 5.84, particularly, the signals assignable to H^i and H^k became triplet and slightly broad singlet, respectively. Furthermore, the signal at δ 5.84 was changed to slightly broad singlet on irradiation at δ 2.81 as well as at δ 2.99.[4] As seen in Table 1, these spectral data are quite similar to those of the oxidation product (**3**), which has been electrochemically synthesized from 4-allyl-2,6-dimethoxyphenol,[5] except for some asterisk-hydrogen atoms in **3**. For example, each δ-value assignable to H^i is in good agreement with one another (δ 2.81 in **1**; δ 2.82 in **2**; δ 2.82 in **3**). Particularly, an exhaustive comparison between **2** and **3** indicates that both compounds adopt the same stereochemistry. Furthermore, the ^{13}C NMR spectra of heterotropanone (**1**) and isoheterotropanone (**2**) indicate that both neolignans with a bicyclic carbon skeleton have the two quaternary carbon atoms (δ 86.1 and 94.2 in **1**; δ 86.5 and 94.7 in **2**), to which three methoxyl groups must be attached, and one CO group (δ 201.7 in **1**; δ 201.0 in **2**) in addition to the carbon atoms included in the partial structure [A]. The close similarity among **1**, **2**, and **3** was further

TABLE 1. ^{1}H NMR SPECTRAL DATA OF HETEROTROPANONE (**1**), ISOHETEROTROPANONE (**2**), AND THE ANODIC OXIDATION PRODUCT (**3**)[5]

1	**2**	**3**
1.13(1H, ddd, J=3, 5, 14 Hz)	1.52(1H, ddd, J=3, 10, 14 Hz)	1.62(1H, dd, J=3, 10 Hz)
1.92(1H, ddd, J=3, 9, 14 Hz)	1.69(1H, ddd, J=3, 5, 14 Hz)	1.62(1H, dd, J=3, 8 Hz)
2.09(1H, d, J=11 Hz)	2.07(1H, d, J=12 Hz)	
2.47(1H, m)	2.29(1H, m)	2.22(1H, ddd, J=2, 8, 10 Hz)
2.81(1H, dt, J=2, 3 Hz)	2.82(1H, dt, J=2, 3 Hz)	2.82(1H, dt, J=2, 3 Hz)
2.99(2H, br. d, J=7 Hz)	2.95(2H, br. d, J=7 Hz)	2.98(2H, br. d, J=6 Hz)
3.10(1H, dd, J=3, 11 Hz)	3.12(1H, dd, J=2, 12 Hz)	
3.28(3H, s), 3.34(3H, s)	3.42(6H, s)	3.22(3H, s), 3.23(3H, s)
3.60(3H, s), 3.82(3H, s)	3.57(3H, s), 3.84(3H, s)	3.32(3H, s), 3.63(3H, s)
3.84(6H, s)	3.87(6H, s)	3.87(6H, s)
		4.53(1H, d, J=2 Hz)
5.13(1H, tdd, J=1, 2, 9 Hz)	5.10(1H, tdd, J=1, 2, 9 Hz)	5.16(1H, br. d, J=10 Hz)
5.15(1H, tdd, J=1, 2, 17 Hz)	5.12(1H, tdd, J=1, 2, 17 Hz)	5.21(1H, br. d, J=17 Hz)
5.84(1H, br. s)	5.87(1H, br. s)	5.83(1H, br. s)
5.87(1H, tdd, J=7, 9, 17 Hz)	5.79(1H, tdd, J=7, 9, 17 Hz)	5.85(1H, tdd, J=6, 10, 17 Hz)
6.35(2H, s)	6.35(2H, s)	6.43(2H, s)

TABLE 2. ^{13}C NMR SPECTRA OF NEOLIGNANS AND NEOSESQUILIGNANS

	1[a]	**2**[a]	**5**	**8**[b]	**14**	**15**	
>C=O	201.7	201.0	201.4	201.2	201.3 201.3	200.4 201.6	(s) (s)
HC=C(OMe)-C=O			121.7 150.2 188.7	122.7 150.2 187.7	121.1 150.2 187.9	120.6 150.5 187.5	(d) (s) (s)
-CH_2-CH=CH_2	39.5 117.2 133.9	39.6 117.3 133.7	39.0 41.3 116.9 118.2 133.4 135.2	 41.5 117.3 135.0	39.4 41.1 116.7 117.1 133.8 134.8	39.6 41.4 117.0 117.4 134.2 135.2	(t) (t) (t) (t) (d) (d)
-CH=C<	 118.8 144.8	 120.2 146.2	116.6 144.9 	116.0 141.2 	115.8 120.7 144.0 144.0	117.0 120.6 145.8 146.6	(d) (d) (s) (s)
-C(OMe)-	86.1	86.5	 92.1	 91.8	85.1 91.8	85.7 91.6	(s) (s)
-C(OMe)$_2$	 94.2	 94.7	93.2 98.7	93.3 98.5	93.2 94.3 98.3	93.4 94.7 98.2	(s) (s) (s)
MeO-	49.2 50.7 53.7	49.0 50.7 52.9	 50.1 50.1 50.2 50.2 54.8 55.5	 50.2 50.5 50.5 50.8 54.8 55.4	48.9 49.5 49.9 49.9 50.3 50.6 52.9 54.6 55.4	49.4 49.4 49.8 50.3 50.7 50.7 52.3 54.7 55.4	(q) (q) (q) (q) (q) (q) (q) (q) (q)
-C-			49.8	50.2	49.5	49.8	(s)
-CH-	39.7 41.2	41.4 41.7	 43.9 44.5	 39.6 43.2	33.0 41.1 43.9 44.6	36.9 41.7 44.1 44.1	(d) (d) (d) (d)
-CH_2-	27.1 37.4	26.2 36.2			28.0 36.7	27.1 35.6	(t) (t)

a) In the cases of **1** and **2**, the signals corresponding to the aromatic ring are not cited. b) In the case of **8**, the signals due to a 1-propenyl group are observed at δ 18.4(q), 128.2(d), and 128.7(d).

explained by their mass spectra, as follows.

The mass spectra of both heterotropanone (**1**) and isoheterotropanone (**2**) have two characteristic peaks at *m/e* 223 and 181, and the corresponding peaks are observed at *m/e* 223 and 197 in **3**. The common fragment ion at *m/e* 223 must be formed by retro-Diels-Alder reaction of **1**, **2**, and **3** on electron impact. Finally, the stereostructures of these two neolignans (**1** and **2**) were elucidated by a comparison of their ^{1}H NMR spectra.

Of the two protons (H^g and H^h) in **1**, the signal at higher magnetic field (δ 1.13) can be assigned to H^g, whose coupling constant with H^f is 5 Hz, indicating that the relationship between H^g and H^f must be in a trans configuration. In the case of **2**, the corresponding one is 10 Hz, indicating that the dihedral angle between H^g and H^f is $\approx 0°$. From the above results, the stereostructures of heterotropanone and isoheterotropanone can be represented by **1** and **2**, respectively.

From a biogenetic point of view, these two neolignans seem to be produced *in vivo* from elemicin and an unstable dienone (**4**). Thus, they were synthesized by means of retro-Diels-Alder reaction of asatone (**5**) generating the desirable dienone (**4**), as follows.[6]

A mixture of asatone (1 equiv.) and 1-allyl-3,4,5-trimethoxybenzene (4 equiv.) in a sealed tube was heated at 175—180 °C for 1.5 h to afford heterotropanone (**1**) and isoheterotropanone (**2**) in 14 and 13% yields, respectively.[7] In addition, 4-allyl-2,6-dimethoxyphenol, demethylheterotropanone (**6**) and demethylisoheterotropanone (**7**) were also obtained in *ca.* 3, 1—2 and 1—2% yields, respectively. These two compounds (**6** and **7**) were readily converted into heterotropanone (**1**) and isoheterotropanone (**2**) in almost quantitative yields, using CH_2N_2 in ether containing methanol. Clearly, the dienone (**4**) as an important intermediate was competitively decomposed into 4-allyl-2,6-dimethoxyphenol, as shown in Scheme 1. Similarly, when heated in mesitylene, instead of 1-allyl-3,4,5-trimethoxybenzene (160—165 °C, 2.5 h), asatone (**5**) was also converted into **6**, **7**, and 4-allyl-2,6-dimethoxyphenol in 19, 18, and 27% yields, respectively.

The Structures of Isoasatone A (8) and Isoasatone B (9). Isoasatone A, which has the same molecular formula ($C_{24}H_{32}O_8$) as that of asatone (**5**),[1] shows the IR and mass spectra (ν_{max} 1745, 1720, and 1640 cm^{-1}; *m/e* 448 and 224) similar to those of asatone, indicating a close similarity of these two neolignans. In fact, on catalytic hydrogenation in ethyl acetate over 10% Pd-C, isoasatone A (**8**) was readily converted into tetrahydroasatone (**10**)[1] in 61% yield. As seen in Tables 2 and 3, however, only one different point is that isoasatone A has one 1-propenyl group (^{1}H NMR δ 1.73, 5.97, and 6.27; ^{13}C NMR δ 18.4, 128.2, and 128.7) instead of one of the two allyl groups in asatone (**5**). Particularly, the partial structure [B] including the 1-propenyl group in **8** was confirmed by the following double resonance experiments. On irradiation at δ 1.73, the olefinic proton signal at δ 6.27 was collapsed to a doublet (J=16 Hz) forming an AB system with the signal at δ 5.97, and the broad doublet at δ 5.66 was changed to a sharp doublet (J=2 Hz). On the other hand, the presence of the remaining allyl group is also confirmed by comparison of the ^{1}H NMR signals assignable to the methylene group (H^a and H^b) between **5** and **8**, as described in Table 3 (δ 2.15 and 2.60—2.95 in **5**; δ 2.34 and 2.76 in **8**). This is also supported by comparison of the δ-values of the allyl groups in the ^{13}C NMR spectra of **1**, **2**, **5** and **8** (see Table 2). Thus, the structure of isoasatone A can be represented by **8**.

Isoasatone B (**9**) with a molecular formula ($C_{24}H_{32}O_9$) has the following spectral data: *m/e* 464(M^+), 240 and 224; ν_{max} 3470, 1750, 1720, and 1640 cm^{-1}. As observed in the cases of asatone (**5**) and isoasatone A (**8**), the retro-Diels-Alder reaction of **9** took place on electron impact, leading to the formation of two fragment ions [**C** and **D**], to which the remarkable peaks at *m/e* 240 and 224 are assignable, respectively, suggesting that this neolignan has the same carbon skeleton as those of **5** and **8**. Finally, the structure of isoasatone B was unambiguously established as **9** on the basis of comparison of the ^{1}H NMR spectra between **8** and **9**, as shown in Table 3. Isoasatone B has a HO-CH_2-CH=CH- grouping (ν_{max} 3470 cm^{-1};

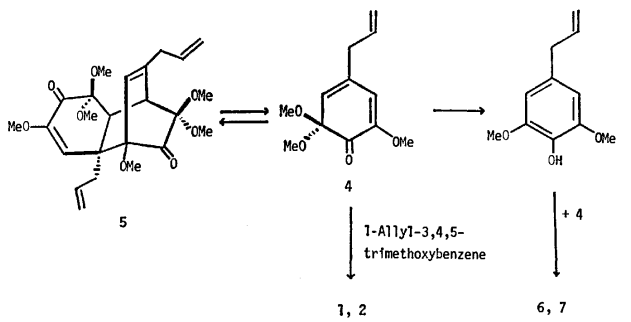

Scheme 1. Thermal reaction of asatone (**5**) in 1-allyl-3,4,5-trimethoxybenzene.

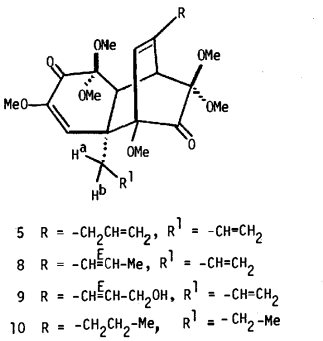

5 R = $-CH_2CH=CH_2$, R^1 = $-CH=CH_2$
8 R = $-CH^E=CH-Me$, R^1 = $-CH=CH_2$
9 R = $-CH^E=CH-CH_2OH$, R^1 = $-CH=CH_2$
10 R = $-CH_2CH_2-Me$, R^1 = $-CH_2-Me$

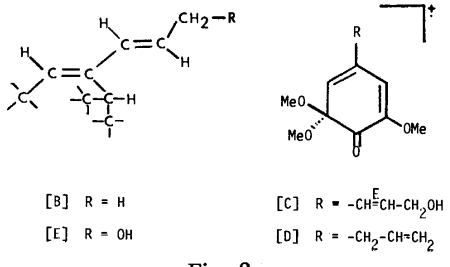

[B] R = H
[E] R = OH
[C] R = $-CH^E=CH-CH_2OH$
[D] R = $-CH_2-CH=CH_2$

Fig. 2.

TABLE 3. ^{1}H NMR SPECTRAL DATA OF ASATONE (**5**), ISOASATONE A (**8**), AND ISOASATONE B (**9**)

5	**8**[a]	**9**
		2.30(1H, br. s, OH)
	1.73(3H, d, J=6 Hz)	
2.15(1H^a, dd, J=14.5, 7.5 Hz)	2.72(1H^a, dd, J=14, 7 Hz)[b]	2.31(1H^a, dd, J=14, 7 Hz)
2.6—2.95(2H+1H^b, complex)	2.95—3.52(2H+1H^b [b])[c]	2.80(1H^b, dd, J=14, 8 Hz)
2.88(2H, br. s)		3.35(1H, d, J=2 Hz)
		3.45—3.68(1H)[c]
3.05(3H, s), 3.31(3H, s)	3.00(3H, s), 3.18(3H, s)	3.10(3H, s), 3.31(3H, s)
3.38(3H, s), 3.42(3H, s)	3.20(3H, s), 3.30(3H, s)	3.45(3H, s), 3.53(3H, s)
3.47(3H, s), 3.60(3H, s)	3.45(3H, s), 3.46(3H, s)	3.55(3H, s), 3.62(3H, s)
		4.30(2H, d, J=4 Hz)
4.90—5.28(4H, complex)	5.23(1H, br. d, J=10 Hz)	5.09(1H, br. d, J=12 Hz)
	5.26(1H, br. d, J=17 Hz)	5.10(1H, br. d, J=16 Hz)
5.39(1H, s)	5.49(1H, s)	5.43(1H, s)
5.55(1H, q, J=2 Hz)	5.66(1H, br. d, J=2 Hz)	5.86(1H, br. d, J=2 Hz)
	5.97(1H, d, J=16 Hz)	6.09(1H, dt, J=16, 4 Hz)
	6.27(1H, dq, J=16, 6 Hz)	6.28(1H, d, J=16 Hz)
5.50—6.20(2H, complex)	6.40(1H, m)	5.92(1H, m)

a) ^{1}H NMR spectrum of **8** was measured in C_6D_6. b) δ($CDCl_3$) 2.34(1H^a, dd, J=14, 7 Hz) and 2.76(1H^b, dd, J=14, 8 Hz). c) Superimposed on MeO signals.

^{1}H NMR δ 2.30, 4.30, 6.09 and 6.28) in the partial structure [**E**], which is also confirmed by the double resonance experiments similar to those of isoasatone A (**8**) having one 1-propenyl group. The other remaining signals in their ^{1}H NMR spectra are quite similar to each other, particularly in the methylene proton signals (H^a and H^b).

*The Structure of Heterotropan (**11**).* Heterotropan with a molecular formula [$C_{24}H_{32}O_6$ (*m/e* 416(M$^+$) and 208)] has a symmetric character in its structure, because only a half of the total number of protons and carbon atoms are found in its ^{1}H and ^{13}C NMR spectra: the former indicates the presence of two secondary methyl groups (δ 1.19), six methoxyl groups (δ 3.30, 3.42, and 3.54) and four methine protons (δ 2.78 and 4.15) in addition to two 1,2,4,5-tetrasubstituted aromatic rings (δ 6.11 and 6.66). This result is also compatible with the ^{13}C NMR spectrum of **11**. Thus, two possible stereostructures (**11** and **12**) were deduced from its ^{1}H NMR spectrum with aid of NOE measurements, as shown in **11**. Finally, the stereostructure of heterotropan was proved to be depicted as **11** by the following chemical evidence: *E*-asarone (**13**) was irradiated in hexane using Pyrex filter at room temperature to afford heterotropan (**11**) as the sole photodimer,[8] in 15% yield.[9]

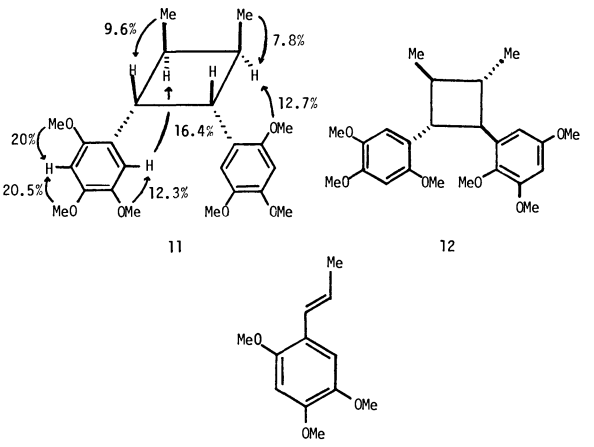

Fig. 3.

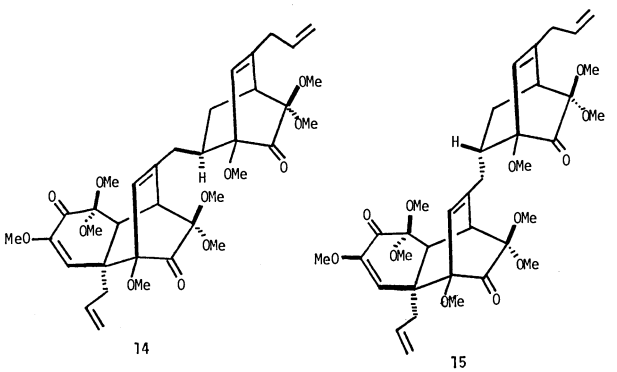

Fig. 4.

*The Structures of Neosesquilignans, Heterotropatrione (**14**) and Isoheterotropatrione (**15**).* Heterotropatrione and isoheterotropatrione both have the same molecular formula ($C_{36}H_{48}O_{12}$), and their IR, ^{1}H NMR, and mass spectra are quite similar to each other, indicating that they are stereoisomers to each other. Particularly, the ^{1}H and ^{13}C NMR spectra of **14** and **15** indicate the presence of nine methoxyl groups and three CO groups as oxygen-containing functional groups. Furthermore, the same partial structure as that of asatone (**5**) in both **14** and **15** was elucidated by comparing their mass and ^{13}C NMR spectra with those of **5**, as follows.

The mass spectra of these two neosesquilignans have a remarkable fragment peak at *m/e* 448, in addition to the molecular ion peak (*m/e* 672). The former must be generated by retro-Diels-Alder reaction of the original molecules on electron impact, as seen in the case of asatone [*m/e* 448(M$^+$) and 224]. As showm

in Table 2, the ^{13}C NMR spectra of **14** and **15** include the signals corresponding to those of asatone (**5**). In addition, the remaining signals show the one to one correspondence to each carbon atom of heterotropanone (**1**) as well as of isoheterotropanone (**2**) except for the aromatic ring of **1** and **2**, suggesting that both **14** and **15** have the bicyclo[2.2.2]octane skeleton similar to that of **1** or **2**, as the partial structure.

Thus, there are two possibilities in a combination of the above two moieties. However, of the two allyl groups in asatone (**5**), the angular one must be present in both **14** and **15**, as judged by their ^{13}C NMR spectra which have the signals (δ 41.1, 117.1, and 134.8 in **14**; δ 41.4, 117.4, and 135.2 in **15**) corresponding to those of the angular allyl group in isoasatone A (**8**) (δ 41.5, 117.3, and 135.0). Finally, the stereostructures of heterotropatrione and isoheterotropatrione were elucidated by comparing their ^1H NMR spectra with those of heterotropanone (**1**) and isoheterotropanone (**2**) in addition to some chemical evidence, as follows.

Heterotropanone (**1**) has the ^1H NMR signals assignable to H^g at δ 1.13 (1H, ddd, J=3, 5, 14 Hz). In the case of heterotropatrione, the corresponding signal was also observed at δ 0.94 (1H, ddd, J=3, 4, 14 Hz). Accordingly, the stereostructure of heterotropatrione can be represented by **14**.[10] The stereostructure of isoheterotropatrione is also depicted as **15**,[10] on the basis of the ^1H NMR signals due to H^g and H^h (δ 1.41—1.92), as seen in the case of isoheterotropanone (**2**) which has the corresponding signal (H^g) at δ 1.52 in addition to the signal (H^h) at δ 1.69. In fact, these results were confirmed by the following chemical evidence.

As seen in the case of asatone (**5**) which has been converted into 4-allyl-2,6-dimethoxyphenol on zinc reduction, when treated with active zinc powder in AcOH (60 °C, 1 h), isoheterotropatrione (**15**) was readily converted into demethylisoheterotropanone (**7**) in 58.4% yield, in addition to 4-allyl-2,6-dimethoxyphenol.

Biogensis of Heterotropanone, Heterotropatrione, and Related Compounds. These novel neolignans and neosesquilignans occurring in the plant *Heterotropa takaoi* M., whose carbon skeleton consists of two or three C_6–C_3 units, are optically inactive and regarded as racemic compounds ($[\alpha]_D^{23}$ ±0°), as described in the cases of asatone (**5**) and isoasatone.[1] From a biogenetic point of view, 4-allyl-2,6-dimethoxyphenol is enzymatically oxidized to the optically inactive dienone (**4**), as an important precursor, from which a number of neolignans and related compounds are produced, as shown in Scheme 2. In fact, heterotropanone (**1**) and isoheterotropanone (**2**) both have been produced on Diels-Alder reaction between **4** and elemicin, as demonstrated in Scheme 1. On the other hand, two molecules of the dienone (**4**) react to each other to yield asatone (**5**),[11] from which both isoasatone A (**8**) and isoasatone B (**9**) may be produced. Presumably, further Diels-Alder reaction between asatone (**5**) and the dienone (**4**) affords both heterotropatrione (**14**) and isoheterotropatrione (**15**).

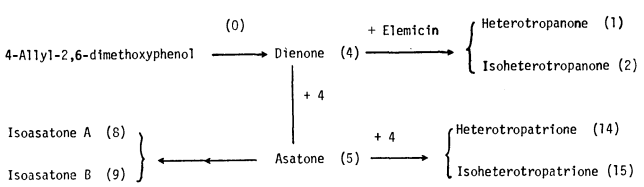

Scheme 2. Biogenesis of neolignans and neosesquilignans.

Experimental

All the melting points were uncorrected. ^1H and ^{13}C NMR spectra were taken on JEOL JNM-PS 100 (100 MHz) and JNM-FX 100 (25.0 MHz) spectrometers, respectively, using $CDCl_3$ as solvent, unless otherwise stated. Chemical shifts are given in ppm from TMS as an internal standard. Coupling constants are given in Hz (s, singlet; d, doublet; t, triplet; q, quartet; m, multiplet). IR spectra were recorded on a JASCO Model IR-S spectrophotometer. Mass spectra were obtained on a Hitachi RMU-6D mass spectrometer operating with an ionization energy (70 eV). Preparative TLC were carried out on Kieselgel PF_{254} (E. Merck A. G., Germany), unless otherwise stated.

Isolation of Neolignans and Neosesquilignans. Fresh leaves and roots of the plant *Heterotropa takaoi* M. (6.5 kg), which were collected as Sanage in Aichi Prefecture early in April, were pulverized with a mixer and immersed in MeOH (36 l) at room temperature for 45 d, and then filtered. The filtrates were concentrated under reduced pressure below 35 °C to leave a greenish brown residue (343 g) which was partitioned between water and AcOEt. The AcOEt layer was dried over large amounts of Na_2SO_4 and then concentrated under reduced pressure to leave a greenish brown oil (29.4 g) which was directly chromatographed on silica gel (Mallinckrodt, 100 mesh) (1350 g) and eluted successively with 3, 3.8 and 11.6 l of hexane–AcOEt (2:1) to afford three fractions (I, 4.9 g; II, 0.49 g; III, 2.3 g) after removal of the nonpolar fraction containing hydrocarbons using the same eluent (2.4 l). Further successive elution with 3.8 l of hexane–AcOEt (1:1) and then with AcOEt (1.5 l) gave two fractions (IV, 1.1 g; V, 1.0 g). Each fraction was further separated by a combination of repeated column chromatography and preparative TLC, as follows.

The fraction I was allowed to stand at room temperature to give a greenish brown solid, which was crystallized from hexane and collected by filtration to afford asatone (**5**)[1] (3.6 g). The filtrate was chromatographed on Florisil (150 g) using hexane–AcOEt (3:1) to give an oil, which was directly rechromatographed on silica gel (Mallinckrodt, 100 mesh) (50 g) and eluted with the same mixed solvent to afford asatone (600 mg). Further elution with the same mixed solvent gave an almost colorless viscous liquid of heterotropanone (**1**) (15 mg): $[\alpha]_D^{23}$ ±0°; IR (film) 1745, 1635, 1590, 1510sh., and 1500 cm^{-1}; MS (70 eV), *m/e* 432 (M^+), 404, 389, 372, 223 and 181. Found: *m/e* 432.2125. Calcd for $C_{24}H_{32}O_7$: M, 432.2148.

The fraction II was chromatographed on silica gel (Mallinckrodt, 100 mesh) (25 g) using $CHCl_3$ to give an oil (33 mg) which was purified by preparative TLC using $CHCl_3$ to afford 3,4-dimethoxybenzaldehyde (15 mg) (IR and ^1H NMR spectra). Further elution with the the same solvent also gave an oil (162 mg), which was further subjected to preparative TLC using $CHCl_3$–AcOEt (20:1) to afford asatone (**5**) (47 mg) from the less polar fraction. From the polar fraction, isoheterotropanone (**2**) (43 mg) was obtained as a colorless viscous liquid: $[\alpha]_D^{23}$ ±0°; IR (film) 1750, 1640, 1590, 1510sh., and 1505 cm^{-1}; MS (70 eV),

m/e 432 (M^+), 404, 389, 357, 223, and 181. Found: *m/e* 432.2161. Calcd for $C_{24}H_{32}O_7$: M, 432.2148.

The fraction III was roughly separated into two fractions A and B by column chromatography (Mallinckrodt, 100 mesh) (100 g) using hexane–AcOEt (4:1) and then hexane–AcOEt (2:1), respectively. Furthermore, the fraction A was chromatographed on silica gel (Mallinckrodt, 100 mesh; $CHCl_3$ as eluent) (50 g) and then on Florisil (50 g) using $CHCl_3$ as the same eluent to afford a viscous liquid, which was further chromatographed on alumina (Nakarai Chemicals, 100 mesh) (50 g) using hexane–AcOEt (2:1) to afford a crystalline solid of isoasatone A (**8**) (260 mg) in addition to a crude oil which was further purified by repeating preparative TLC [1) alumina, hexane–$CHCl_3$ (3:1); 2) 10% $AgNO_3$–SiO_2, hexane–AcOEt (1:1)] to afford a colorless viscous liquid of heterotropan (**11**) (31 mg), which was crystallized in a refrigerator. Both neoligans are characterized by their physical data: **8**: mp 122—124 °C (from hexane–ether); $[\alpha]_D^{23}$ ±0°; IR (Nujol) 1745, 1720 and 1640 cm^{-1}; MS (70 eV), *m/e* 448(M^+), 416, 384 and 224. Found: *m/e* 448.2117. Calcd for $C_{24}H_{32}O_8$: M, 448.2097. **11**: $[\alpha]_D^{23}$ ±0°; IR (film) 1610, 1590 and 1510 cm^{-1}; ^1H NMR (C_6D_6) δ=1.19 (6H, d, J=6 Hz),[12] 2.78 (2H, m), 3.30 (6H, s), 3.42 (6H, s), 3.54 (6H, s), 4.15 (2H, d, J=5.5 Hz),[12] 6.11 (2H, s) and 6.66 (2H, s); ^{13}C NMR δ=15.1(q), 34.0(d), 42.5(d), 56.1(q), 56.3(q), 56.7(q), 97.7(d), 112.4(d), 122.1(s), 142.3(s), 147.2(s) and 151.6(s). Found: *m/e* 416.2185. Calcd for $C_{24}H_{32}O_6$: M, 416.2199.

The fraction B was further chromatographed on silica gel (Mallinckrodt, 100 mesh) (100 g) using hexane–AcOEt (2:1) to give an oil (217 mg), which was subjected to repeated preparative TLC using hexane–AcOEt (2:1) and then $CHCl_3$–AcOEt (10:1) to give a viscous liquid which was further purified by preparative TLC (10% $AgNO_3$–SiO_2) using $CHCl_3$–AcOEt (10:1) to afford an almost colorless viscous liquid of heterotropatrione (**14**) (27 mg): $[\alpha]_D^{23}$ ±0°; IR (film) 1750br., 1730sh., and 1645 cm^{-1}; ^1H NMR δ=0.94 (1H, ddd, J=3, 4, 13 Hz), 1.94—2.99 (11H, complex), 3.04 (3H, s), 3.25 (3H, s), 3.27 (3H, s), 3.30 (3H, s), 3.34 (3H, s), 3.39 (3H, s), 3.47 (3H, s), 3.51 (3H, s), 3.57 (3H, s), 4.84—5.22 (4H, complex), 5.32 (1H, s), 5.45 (1H, br.s), 5.59 (1H, br.s) and 5.60—6.10 (2H, complex); MS (70 eV), *m/e* 672 (M^+), 644, 640, 565, 448 and 317. Found: *m/e* 672.3147. Calcd for $C_{36}H_{48}O_{12}$: M, 672.3145.

The fraction IV was chromatographed on silica gel (Mallinckrodt, 100 mesh) (30 g) using $CHCl_3$–AcOEt (10:1) to give a pale yellow oil (217 mg), which was subjected to preparative TLC using $CHCl_3$–AcOEt (10:1) to afford an almost colorless viscous liquid of isoheterotropatrione (**15**) (120 mg): $[\alpha]_D^{23}$ ±0°; IR (film) 1760, 1725 and 1645 cm^{-1}; ^1H NMR δ=1.41—1.92 (2H, complex), 2.0—3.0 (10H, complex), 3.05 (3H, s), 3.28 (3H, s), 3.32 (3H, s), 3.33 (3H, s), 3.37 (3H, s), 3.38 (3H, s), 3.40 (3H, s), 3.47 (3H, s), 3.57 (3H, s), 4.88—5.23 (4H, complex), 5.04 (1H, br.s), 5.38 (1H, s), 5.39—6.07 (2H, complex) and 5.84 (1H, br.s); MS (70 eV), *m/e* 672 (M^+), 644, 640, 565, 448, 418, and 343. Found: *m/e* 672.3149. Calcd for $C_{36}H_{48}O_{12}$: M, 672.3145.

The fraction V was subjected to preparative TLC using AcOEt to give a slightly greenish oil, which was further purified by preparative TLC using benzene–acetone (1:1) to give a crystalline solid of isoasatone B (**9**) (76 mg):[13] mp 129—131 °C (from hexane–ether); $[\alpha]_D^{23}$ ±0°; IR (KBr) 3470, 1750, 1720, and 1640 cm^{-1}; MS (70 eV), *m/e* 464(M^+), 432, 400, 368, 327, 240, and 224. Found: *m/e* 464.2058. Calcd for $C_{24}H_{32}O_9$: M, 464.2046.

Synthesis of Heterotropanone (1) and Isoheterotropanone (2). A solution of asatone (**5**) (44.8 mg) in 1-allyl-3,4,5-trimethoxybenzene (165 mg) in a sealed tube was heated at 175—180 °C for 1.5 h and then cooled to leave a pale brown oil, which was separated by preparative TLC using hexane–AcOEt (1:1) to afford 1-allyl-3,4,5-trimethoxybenzene (121 mg), 4-allyl-2,6-dimethoxyphenol (7.8 mg), heterotropanone (**1**) (12 mg), isoheterotropanone (**2**) (11.6 mg), demethylheterotropanone (**6**) (*ca.* 1 mg) and demethylisoheterotropanone (**7**) (*ca.* 1 mg). The first four products were identified by comparing their TLC [hexane–AcOEt (3:1)] and IR spectra with those of each authentic sample. Demethyl compounds (**6** and **7**) were characterized by their spectral data: **6** as a pale yellow oil: IR (film) 3500br., 1750, 1610, and 1520 cm^{-1}; MS (70 eV), *m/e* 418(M^+), 343, 285, and 167. Found: *m/e* 418.2010. Calcd for $C_{23}H_{30}O_7$: M, 418.1991. **7** as an almost colorless oil; IR (film) 3500 br., 1755, 1615, and 1520 cm^{-1}; MS (70 eV), *m/e* 418 (M^+), 343, 285, and 167. Found: *m/e* 418.2012. Calcd for $C_{23}H_{30}O_7$: M, 418.1991. Furthermore, these two phenols (**6** and **7**) were dissolved in excess CH_2N_2 in ether (20 ml) containing MeOH (5 ml), allowed to stand at room temperature overnight and then concentrated under reduced pressure to leave the corresponding methyl ethers (**1** and **2**) in quantitative yields, respectively [TLC (hexane–AcOEt (3:1) and IR spectra].

Thermal Reaction of Asatone (5). A solution of asatone (39 mg) in mesitylene (1 ml) was gently heated under reflux for 2.5 h, and then concentrated under reduced pressure to leave a pale yellow oil, which was subjected to preparative TLC using hexane–AcOEt (1:1) to afford 4-allyl-2,6-dimethoxyphenol (9.2 mg), demethylheterotropanone (**6**) (7.1 mg) and demethylisoheterotropanone (**7**) (6.0 mg) [TLC (hexane–AcOEt (1:1) and IR spectra].

Catalytic Hydrogenation of Isoasatone A (8). Catalytic hydrogenation of isoasatone (15 mg) in AcOEt (2 ml) was carried out over 10% Pd–C (5 mg) at room temperature overnight. After filtration of the catalyst, the solvent was evaporated under reduced pressure to leave a white crystalline solid, which was purified by preparative TLC using hexane–AcOEt (3:1) to afford white crystals of tetrahydroasatone (**10**) (9.2 mg) (mp and IR spectrum).[1]

Synthesis of Heterotropan (11). A solution of *E*-asarone (40 mg) in hexane (5 ml) was irradiated at room temperature for 10 d, using Pyrex filter [apparatus: Eiko-Sha PIH-100, high pressure Hg lamp (100 W)]. The reaction solution was then evaporated under reduced pressure to leave a pale yiellow oil, which was purified by preparative TLC using hexane–AcOEt (3:1). From the more polar fraction corresponding to that of heterotropan (**11**), a colorless viscous liquid (*ca.* 6 mg) was obtained [TLC (hexane–AcOEt (3:1)) and IR spectrum]. From the less polar fraction, a mixture of *E*- and *Z*-asarones (*ca.* 30 mg) was obtained without further purification.

Zinc Reduction of Isoheterotropatrione (15). A mixture of isoheterotropatrione (115 mg) and activated zinc powder[14] (500 mg) in AcOH (2 ml) was heated at 60 °C, with stirring, for 1 h, and then poured into a lot of water, and then extracted with AcOEt. The extract was successively washed with dil. $NaHCO_3$ aq solution and sat. NaCl aq solution, and then dried over Na_2SO_4. Removal of the solvent under reduced pressure afforded a brown oil (76.7 mg), which was subjected to preparative TLC using $CHCl_3$–AcOEt (10:1). From the less polar fraction, 4-allyl-2,6-dimethoxyphenol (30 mg) was obtained [TLC (hexane–AcOEt (3:1)) and IR spectrum]. From the polar fraction, a colorless viscous liquid (41.8 mg) was obtained, whose TLC (hexane–AcOEt (1:1)) and IR spectrum were completely identical with those of demethylisoheterotropanone (**7**).

The authors wish to thank Dr. Masaaki Toda (Ono Central Research Institute) and Mr. Shinpei Kidokoro (Ohmori Research Institute, Tobishi Pharmaceutical Co. Ltd.) for measurements of high resolution mass spectra. This research has been supported in part by grants from the Ministry of Education, Science and Culture to which greatful acknowledgement is made.

References

1) S. Yamamura, Y. Terada, Y. Chen, M. Hong, H. Hsu, K. Sasaki, and Y. Hirata, *Bull. Chem. Soc. Jpn.*, **49**, 1940 (1976), and many references cited therein.

2) Y. Terada and S. Yamamura, *Chem. Lett.*, **1978**, 553; S. Yamamura, M. Niwa, M. Nonoyama, and Y. Terada, *Tetrahedron Lett.*, **1978**, 4891; M. Niwa, Y. Terada, M. Nonoyama, and S. Yamamura, *ibid.*, **1979**, 813.

3) Dihedral angle between H^d and H^f seems to be about 90°.

4) The signal at δ 5.87 became sharp doublet of doublet.

5) M. Iguchi, A. Nishiyama, Y. Terada, and S. Yamamura, *Tetrahedron Lett.*, **1977**, 4511. These results will be published elsewhere in detail.

6) S. Yamamura and M. Niwa, *Chem. Lett.*, **1981**, 625.

7) 1-Allyl-3,4,5-trimethoxybenzene was recovered in *ca.* 70% yield.

8) A mixture of *E*- and *Z*-asarones was recovered.

9) H. Nozaki, I. Otani, R. Noyori, and M. Kawanishi, *Tetrahedron*, **24**, 2183 (1968); K. Tokumaru, "Yukikagaku Hannoron," Tokyo Kagakudozin Publisher, Tokyo (1973), p. 200.

10) Heterotropatrione and isoheterotropatrione both are optically inactive and regareded as racemic compounds, and the diastereoisomeric structures corresponding to **14** and **15** can not be ruled out.

11) Asatone (**5**) has been successfully synthesized on anodic oxidation of 4-allyl-2,6-dimethoxyphenol (See Ref. 5).

12) A virtual coupling is observed.

13) This neolignan has been mainly isolated from the same plant collected early in December.

14) Zinc powder was activated according to the same procedure as described in the following paper: S. Yamamura, M. Toda, and Y. Hirata, *Org. Synth.*, **53**, 86 (1973).

Implications of X-Ray Crystallographic Results of 1,2,3,4-Tetrachloro-9-(2-oxopropyl)triptycene Rotamers

Norimasa Nogami, Michinori Ōki,* Shoichi Sato,† and Yoshihiko Saito*,†,1)

Department of Chemistry, Faculty of Science, The University of Tokyo, Bunkyo-ku, Tokyo 113

†*Institute for Solid State Physics, The University of Tokyo, Roppongi, Minato-ku, Tokyo 106*

(Received May 25, 1982)

Crystals of 1,2,3,4-tetrachloro-9-(2-oxopropyl)triptycene grown from tetrahydrofuran-hexane were found to contain 1:1 *ap* and ±*sc* rotational isomers about the C_9–C_{Pr} bond by the X-ray diffraction method. The molecular structures had the following features. The acetyl group in the 9-substituent takes an *O*-inside, relative to the triptycene skeleton, conformation in both forms. The benzene rings are deformed by the steric effect to form boats. The 2-oxopropyl groups in both forms were planar within the experimental error but the C_2–C_1 bond in the 2-oxopropyl group was appreciably shorter in the ±*sc* conformation than that in the *ap*. The results are discussed on the ground of steric repulsion and the existence of the interaction between the C=O and the Cl groups which are located only 3.035 Å apart in the ±*sc* form.

A number of 9-substituted triptycenes was synthesized to manifest isolation of stable rotational isomers and to examine the effects of substituents on the rotational barrier.[2,3] Out of these studies, it has emerged that triptycenes which carry a *t*-alkyl group in the 9-position exhibited high enough barriers to rotation to isolate the rotamers at room temperature, whereas those carrying an *s*-alkyl group in the 9-position possess barriers to rotation which are borderline values for isolation of rotamers at room temperature.

Triptycenes carrying a primary 9-substituent exhibit still lower barriers than 9-*s*-alkyltriptycenes and the internal rotation in 9-(primary alkyl)triptycenes is frozen only on the NMR time scale at low temperatures which are easily accessible. Although the internal rotation is fast in these compounds, the population ratios of the rotamers concerned afford interesting information. Since the peri-substituent in the 1-position of the triptycene skeleton is very closely located to the second atom of the 9-substituent, if a proper rotational form is taken, a weak interaction, which is not otherwise detected, can be detected as a change in populations of rotamers due to the highly congested state.

We found that unusually facile cyclization occurs, if a cationoid is formed in the second atom of the 9-substituent, between the cationoid center and the 1-methoxyl group in 9-substituted 1,4-dimethoxytriptycenes.[4] 9-(2-Acyloxyethyl)-1,4-dimethoxytriptycenes show higher ±*sc*/*ap* values when the acyl group becomes more electronegative to indicate that an interaction exists between the acyloxymethyl and the 1-methoxyl groups.[5] 9-Substituted triptycenes carrying a carbonyl group in the 2-position of the 9-substituent showed high ±*sc*/*ap* values, if there is an electron-donating substituent in the 1-position of triptycene, to suggest that there is an attractive interaction between the carbonyl and the 1-substituent.[6] All of these results imply that the triptycene system is a good model to find a weak, often hidden interaction by either a reaction or population distribution.

During the course of investigation on *n*-donor-carbonyl interaction, we encountered a queer phenomenon. Apparently a formyl group is less electron accepting than an acetyl group. This is contrary to the common sense of organic chemistry because aldehydes are usually more reactive than ketones toward nucleophiles. We suspected that the origin of this anomaly might be the presence of different conformations in aldehydes from those of ketones. Since a hydrogen is much smaller than an oxygen atom in a formyl group, an oxygen-inside conformation relative to the triptycene skeleton is of prohibitively high energy in the case of 9-(2-oxoethyl)triptycenes, while such a conformation will be favored in the case of 9-(2-oxopropyl)triptycenes because an oxygen atom is smaller than a methyl group. Unfortunately, strongly interacting formyl compounds did not give crystals suitable for X-ray analysis. However, 1,4-dimethyl-9-(2-oxoethyl)triptycene gave good crystals and its *ap* form was shown by X-ray crystallography to exist as an oxygen-outside conformation.[6b]

1,2,3,4-Tetrachloro-9-(2-oxopropyl)triptycene, which was known to exist as ±*sc* conformations solely in solution,[6] was found to give good crystals in which both ±*sc* and *ap* conformations are contained. Thus fortunately we can now compare the molecular structures of ±*sc* and *ap* forms of this compound. This paper reports the outcome of the investigation and discusses the implications of the results.

Experimental

Crystals of 1,2,3,4-tetrachloro-9-(2-oxopropyl)triptycene was grown from a tetrahydrofuran-hexane solution. A crystal with dimensions $0.45\times0.44\times0.37$ mm^3 was mounted on a Rigaku automated four-circle diffractometer and the intensity data were collected using Mo $K\alpha$ radiation monochromated by a graphite plate. The θ-2θ scan technique was employed to collect the intensities with $|F_o|\geq3\sigma|F_o|$ in the range $2\theta\leq57°$. A total of 6067 reflections were used for analysis.

The crystal data are as follows: $C_{23}H_{14}Cl_4O$, F.W.=448.18, monoclinic, space group $P2_1/a$, $a=30.812(2)$ Å, $b=8.304(1)$ Å, $c=15.103(1)$ Å, $\beta=97.19(1)°$, $Z=8$, $D_x=1.55$ g cm^{-3}, μ(Mo $K\alpha$)$=6.29$ cm^{-1}.

The structure was solved by the direct method. Isotropic temperature factors were used for hydrogen atoms and anisotropic temperature factors were employed for others. All these positional and thermal parameters were refined by the least-squares method including the anomalous scattering corrections for chlorine, oxygen, and carbon atoms. The atomic scattering factors were taken from a literature.[7] The final R value was 0.048.

TABLE 1. ATOMIC POSISIONAL PARAMETERS ($\times 10^4$) WITH ESTIMATED STANDARD DEVIATIONS IN PARENTHESES AND ANISOTROPIC TEMPERATURE FACTORS ($\times 10^4$)[a)]

Atom	x	y	z	B_{11}	B_{22}	B_{33}	B_{12}	B_{13}	B_{23}
				±*sc* Form					
Cl_1	2227(0)	2324(1)	2792(0)	9(0)	234(2)	41(0)	−3(0)	−2(0)	−5(0)
Cl_2	1938(0)	355(1)	4312(0)	16(0)	235(2)	29(0)	16(0)	−2(0)	5(0)
Cl_3	982(0)	−768(1)	4277(0)	20(0)	192(1)	35(0)	−1(0)	10(0)	16(0)
Cl_4	305(0)	−90(1)	2603(0)	11(0)	233(2)	52(0)	−12(0)	10(0)	5(0)
C_1	1700(1)	1545(4)	2647(1)	8(0)	120(5)	31(1)	5(1)	0(0)	−6(2)
C_2	1567(1)	724(4)	3379(1)	11(0)	131(5)	24(1)	10(1)	0(0)	−4(2)
C_3	1143(1)	197(4)	3368(1)	13(0)	110(5)	27(1)	3(1)	6(0)	0(2)
C_4	844(1)	512(4)	2616(1)	9(0)	130(5)	33(1)	0(1)	6(0)	−3(2)
C_5	605(1)	144(4)	−363(2)	8(0)	155(6)	34(1)	−3(1)	1(0)	0(2)
C_6	805(1)	−426(4)	−1071(2)	12(0)	146(6)	28(1)	0(1)	0(0)	−9(2)
C_7	1231(1)	−32(4)	−1134(1)	12(0)	150(6)	23(1)	9(1)	2(0)	0(2)
C_8	1466(1)	945(4)	−501(1)	8(0)	134(5)	28(1)	3(1)	4(0)	6(2)
C_9	1479(0)	2609(3)	975(1)	6(0)	100(4)	27(1)	2(1)	2(0)	1(1)
C_{10}	665(1)	1836(4)	1078(1)	6(0)	165(6)	29(1)	0(1)	2(0)	3(2)
C_{11}	733(1)	3637(4)	1014(1)	9(0)	145(5)	23(1)	9(1)	1(0)	1(2)
C_{12}	412(1)	4808(5)	1007(2)	10(0)	222(8)	33(1)	18(1)	2(0)	0(2)
C_{13}	528(1)	6402(5)	958(2)	18(0)	182(7)	46(1)	32(1)	2(0)	3(3)
C_{14}	952(1)	6829(4)	917(2)	20(0)	110(5)	44(1)	15(1)	0(0)	−5(2)
C_{15}	1276(1)	5668(4)	913(2)	12(0)	118(5)	33(1)	3(1)	0(0)	−2(2)
C_{16}	1165(1)	4067(4)	960(1)	9(0)	114(5)	22(1)	7(1)	1(0)	0(1)
C_{17}	1411(1)	1771(3)	1875(1)	7(0)	92(4)	26(1)	4(1)	3(0)	−3(1)
C_{18}	973(1)	1296(3)	1890(1)	7(0)	108(5)	27(1)	2(1)	3(0)	−3(2)
C_{19}	1270(1)	1491(3)	219(1)	8(0)	88(4)	26(1)	3(1)	2(0)	5(1)
C_{20}	838(1)	1097(4)	275(1)	8(0)	120(5)	27(1)	1(1)	2(0)	2(2)
C_{21}	1938(1)	3128(4)	824(2)	7(0)	109(5)	39(1)	0(1)	2(0)	6(2)
C_{22}	2286(1)	1868(4)	816(2)	8(0)	156(6)	38(1)	4(1)	2(0)	12(2)
C_{23}	2708(1)	2471(7)	566(4)	10(0)	322(13)	128(4)	13(2)	16(1)	77(6)
O	2232(0)	481(3)	1000(1)	12(0)	143(4)	50(1)	9(1)	4(0)	5(2)
				ap Form					
Cl_1	1914(0)	4720(1)	4871(0)	11(0)	203(1)	43(0)	−4(0)	6(0)	28(0)
Cl_2	1223(0)	5336(1)	3282(0)	19(0)	193(1)	30(0)	10(0)	6(0)	23(0)
Cl_3	257(0)	4365(1)	3319(0)	17(0)	254(2)	34(0)	16(0)	−7(0)	8(0)
Cl_4	−20(0)	2643(1)	4985(0)	8(0)	235(2)	50(0)	−1(0)	−5(0)	−4(0)
C_1	1388(1)	4038(4)	4943(1)	9(0)	108(5)	28(1)	4(1)	3(0)	0(2)
C_2	1073(1)	4386(4)	4211(1)	14(0)	107(5)	22(1)	9(1)	3(0)	0(2)
C_3	642(1)	3965(4)	4219(1)	12(0)	125(5)	26(1)	11(1)	−3(0)	−5(2)
C_4	520(1)	3191(4)	4966(1)	8(0)	118(5)	31(1)	5(1)	−1(0)	−8(2)
C_5	839(1)	−1102(4)	6550(1)	10(0)	123(5)	28(1)	−6(1)	0(0)	−1(2)
C_6	1127(1)	−2372(4)	6531(2)	15(0)	96(5)	42(1)	−4(1)	0(0)	−1(2)
C_7	1563(1)	−2079(4)	6499(2)	14(0)	105(5)	43(1)	11(1)	0(0)	−4(2)
C_8	1726(1)	−515(4)	6504(1)	9(0)	123(5)	31(1)	7(1)	1(0)	4(2)
C_9	1557(0)	2578(3)	6546(1)	6(0)	99(4)	24(1)	3(1)	1(0)	5(1)
C_{10}	723(1)	1962(3)	6517(1)	6(0)	111(5)	30(1)	−1(1)	1(0)	3(2)
C_{11}	900(1)	3027(3)	7290(1)	7(0)	91(4)	23(1)	2(1)	1(0)	5(1)
C_{12}	654(1)	3656(4)	7916(1)	7(0)	130(5)	32(1)	3(1)	2(0)	6(2)
C_{13}	856(1)	4677(4)	8564(1)	9(0)	150(6)	30(1)	5(1)	3(0)	−9(2)
C_{14}	1290(1)	5059(4)	8574(1)	11(0)	127(5)	29(1)	0(1)	1(0)	−12(2)
C_{15}	1539(1)	4410(4)	7951(1)	7(0)	114(5)	30(1)	−1(1)	0(0)	1(2)
C_{16}	1341(0)	3376(3)	7307(1)	7(0)	86(4)	22(1)	2(0)	1(0)	3(1)
C_{17}	1270(1)	3219(3)	5679(1)	8(0)	85(4)	24(1)	3(1)	1(0)	−1(1)
C_{18}	827(1)	2829(3)	5684(1)	8(0)	90(4)	25(1)	3(1)	0(0)	−5(1)
C_{19}	1442(1)	760(3)	6543(1)	8(0)	102(4)	22(1)	1(1)	1(0)	1(1)
C_{20}	999(1)	447(3)	6553(1)	8(0)	97(4)	22(1)	−1(1)	0(0)	−3(1)
C_{21}	2047(1)	2862(4)	6624(1)	7(0)	117(5)	32(1)	0(1)	3(0)	8(2)
C_{22}	2323(1)	2163(4)	7451(2)	8(0)	122(5)	34(1)	2(1)	1(0)	−1(2)
C_{23}	2805(1)	2399(5)	7458(2)	7(0)	242(9)	59(2)	1(1)	−1(0)	33(3)
O	2176(0)	1492(3)	8045(1)	10(0)	220(5)	37(1)	0(1)	1(0)	30(2)

a) The form of the anisotropic temperature factor is: $T=\exp(-B_{11}h^2-B_{22}k^2-B_{33}l^2-2B_{12}hk-2B_{13}hl-2B_{23}kl)$.

Results and Discussion

The nonhydrogen atomic positional parameters are tabulated in Table 1. In the crystalline state, two molecules, *ap* and +(or −)*sc*, coexist in an asymmetric unit, as shown in Fig. 1. The coexistence of *ap* and ±*sc* conformations enables us to compare the structural features and to discuss the implications of the structures which were not possible in other triptycenes.

We point out first that the acetyl groups in both conformations take the *O*-inside conformation, as are seen in Fig. 1. Thus the difference in conformations about the carbonyl moieties in the formyl and the acetyl compounds is now verified. The Coulombic attraction between the acetyl group and the peri-chloro must be playing some role in stabilizing the ±*sc* form

TABLE 2. BOND LENGTHS AND BOND ANGLES IN 1,2,3,4-TETRACHLORO-9-(2-OXOPROPYL)TRIPTYCENE

Bond length	*l*/Å		Bond length	*l*/Å	
	±*sc*	*ap*		±*sc*	*ap*
C_1-Cl_1	1.736(3)	1.735(4)	C_9-C_{19}	1.548(4)	1.551(4)
C_1-C_2	1.403(5)	1.407(4)	C_9-C_{21}	1.521(4)	1.519(4)
C_1-C_{17}	1.389(4)	1.389(4)	C_{10}-C_{11}	1.515(5)	1.512(4)
C_2-Cl_2	1.728(3)	1.722(3)	C_{10}-C_{18}	1.521(4)	1.519(4)
C_2-C_3	1.374(5)	1.375(5)	C_{10}-C_{20}	1.515(5)	1.516(4)
C_3-Cl_3	1.717(3)	1.721(3)	C_{11}-C_{12}	1.385(5)	1.385(4)
C_3-C_4	1.396(4)	1.389(5)	C_{11}-C_{16}	1.390(5)	1.387(4)
C_4-Cl_4	1.732(4)	1.732(4)	C_{12}-C_{13}	1.375(6)	1.383(5)
C_4-C_{18}	1.377(5)	1.379(4)	C_{13}-C_{14}	1.361(7)	1.371(5)
C_5-C_6	1.382(5)	1.381(5)	C_{14}-C_{15}	1.388(6)	1.395(5)
C_5-C_{20}	1.378(4)	1.377(5)	C_{15}-C_{16}	1.377(5)	1.381(4)
C_6-C_7	1.370(5)	1.372(6)	C_{17}-C_{18}	1.408(4)	1.405(4)
C_7-C_8	1.387(4)	1.392(5)	C_{19}-C_{20}	1.383(4)	1.392(5)
C_8-C_{19}	1.385(4)	1.381(5)	C_{21}-C_{22}	1.499(5)	1.535(4)
C_9-C_{16}	1.550(4)	1.547(4)	C_{22}-C_{23}	1.487(6)	1.496(5)
C_9-C_{17}	1.564(4)	1.578(4)	C_{22}-O	1.201(5)	1.192(4)

Bond angle	*φ*/°		Bond angle	*φ*/°	
	±*sc*	*ap*		±*sc*	*ap*
Cl_1-C_1-C_2	116.3(2)	116.2(3)	C_{10}-C_{11}-C_{16}	113.5(3)	113.3(3)
Cl_1-C_1-C_{17}	123.1(2)	123.4(2)	C_{12}-C_{11}-C_{16}	120.4(4)	121.8(3)
C_2-C_1-C_{17}	120.5(3)	120.4(3)	C_{11}-C_{12}-C_{13}	119.1(4)	118.4(3)
Cl_2-C_2-C_1	119.9(3)	120.4(3)	C_{12}-C_{13}-C_{14}	120.6(4)	120.1(3)
Cl_2-C_2-C_3	119.0(3)	118.8(3)	C_{13}-C_{14}-C_{15}	120.9(4)	121.4(3)
C_1-C_2-C_3	121.1(3)	120.8(3)	C_{14}-C_{15}-C_{16}	119.1(4)	118.8(4)
Cl_3-C_3-C_2	120.5(3)	121.0(3)	C_9-C_{16}-C_{11}	113.6(3)	114.1(2)
Cl_3-C_3-C_4	120.7(3)	120.1(3)	C_9-C_{16}-C_{15}	126.6(3)	126.6(3)
C_2-C_3-C_4	118.7(3)	118.9(3)	C_{11}-C_{16}-C_{15}	119.8(3)	119.3(3)
Cl_4-C_4-C_3	119.4(3)	119.5(2)	C_1-C_{17}-C_{18}	117.6(3)	118.0(3)
Cl_4-C_4-C_{18}	120.1(2)	119.8(3)	C_1-C_{17}-C_9	130.4(3)	130.9(3)
C_3-C_4-C_{18}	120.6(3)	120.8(3)	C_9-C_{17}-C_{18}	111.9(2)	111.2(2)
C_6-C_5-C_{20}	119.7(3)	119.0(3)	C_4-C_{18}-C_{10}	124.6(3)	124.0(3)
C_5-C_6-C_7	119.7(3)	120.0(3)	C_4-C_{18}-C_{17}	121.3(3)	121.1(3)
C_6-C_7-C_8	121.0(3)	121.3(4)	C_{10}-C_{18}-C_{17}	114.0(3)	114.9(3)
C_7-C_8-C_{19}	119.5(3)	119.1(3)	C_8-C_{19}-C_9	126.5(3)	126.9(3)
C_{16}-C_9-C_{17}	102.0(2)	103.0(2)	C_8-C_{19}-C_{20}	119.2(3)	119.1(3)
C_{16}-C_9-C_{19}	104.8(2)	107.4(2)	C_9-C_{19}-C_{20}	114.3(3)	114.0(3)
C_{16}-C_9-C_{21}	111.6(3)	113.1(2)	C_5-C_{20}-C_{10}	126.0(3)	125.3(3)
C_{17}-C_9-C_{19}	106.6(2)	102.8(2)	C_5-C_{20}-C_{19}	121.0(3)	121.6(3)
C_{17}-C_9-C_{21}	119.0(2)	117.4(2)	C_{10}-C_{20}-C_{19}	113.0(3)	113.0(3)
C_{19}-C_9-C_{21}	111.6(2)	112.1(3)	C_9-C_{21}-C_{22}	118.8(3)	116.7(3)
C_{11}-C_{10}-C_{18}	105.4(3)	105.6(3)	C_{21}-C_{22}-C_{23}	114.6(3)	113.8(3)
C_{11}-C_{10}-C_{20}	106.5(3)	108.1(2)	C_{21}-C_{22}-O	123.2(3)	124.4(3)
C_{18}-C_{10}-C_{20}	106.2(3)	104.3(3)	C_{23}-C_{22}-O	122.2(4)	121.8(3)
C_{10}-C_{11}-C_{12}	126.2(3)	124.9(3)			

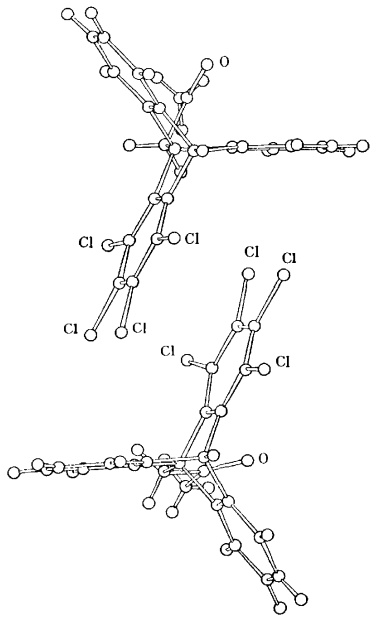

Fig. 1. A perspective drawing of 1,2,3,4-tetrachloro-9-(2-oxopropyl)triptycene.

Table 3. Atomic shifts from the least-squares planes

	A Ring d/Å			B Ring d/Å	
	$\pm sc$	ap		$\pm sc$	ap
C_1	−0.014	−0.027	C_5	−0.004	−0.008
C_2	0.002	−0.002	C_6	0.010	0.007
C_3	0.008	0.017	C_7	−0.005	0.006
C_4	−0.005	−0.008	C_8	−0.006	−0.010
C_{17}	0.016	0.034	C_{19}	0.012	0.010
C_{18}	−0.007	−0.013	C_{20}	−0.007	−0.004
	C Ring d/Å			2-Oxopropyl d/Å	
	$\pm sc$	ap		$\pm sc$	ap
C_{11}	−0.009	−0.006	C_{21}	0.000	0.000
C_{12}	0.001	0.003	C_{22}	0.001	−0.002
C_{13}	0.008	0.003	C_{23}	0.000	0.000
C_{14}	−0.008	−0.006	O	0.000	−0.001
C_{15}	0.000	0.002			
C_{16}	0.008	0.004			

of 1,2,3,4-tetrachloro-9-(2-oxopropyl)triptycene, in contrast to the Coulombic repulsion between the formyl and the peri-chloro groups in 1,2,3,4-tetrachloro-9-(2-oxoethyl)triptycene that should destabilize the $\pm sc$ form.

The intramolecular strain seems to be distributed widely over the molecules. This can be pointed out from bond lengths and bond angles (Table 2), atomic shifts from the least-squares planes of the carbon atoms in the aromatic groups (Table 3), and dihedral angles concerned (Table 4). Numberings of atoms and designations of rings are shown in Fig. 2.

There are some common features of structures in both ap and $\pm sc$ forms. The bond lengths of C_9–C_{17} are very large 1.578 Å in ap and 1.564 Å in $\pm sc$, although these distances are not so long as that in 9-*t*-butyl-1,2,3,4-tetrachlorotriptycene.[8] Other bonds

Table 4. Dihedral angles formed by least-squares planes

Planes	ϕ/°	
	ap	$+sc$
A-B	113.2	125.9
A-C	118.4	114.0
B-C	128.3	120.0
A-Oxopropyl	173.1	61.4
B-Oxopropyl	62.9	66.7
C-Oxopropyl	65.4	167.4

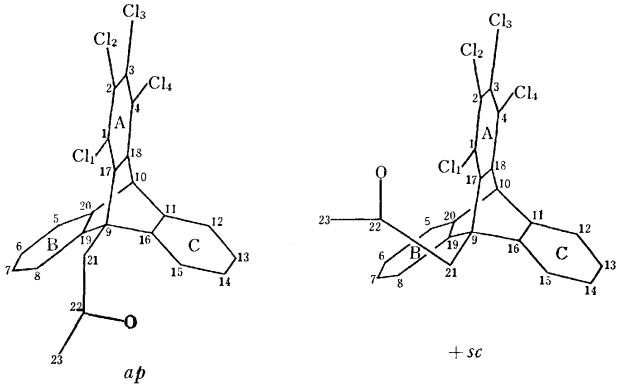

Fig. 2. Numberings of atoms and designations of rings in ap- and $\pm sc$-1,2,3,4-tetrachloro-9-(2-oxopropyl)-triptycene.

connecting the C_9 with the aromatic rings are also longer than the normal C_{sp^2}–C_{sp^3} bond and this point is apparent if one compares those with bonds connecting C_{10} with aromatic rings. The bond angles C_1–C_{17}–C_9 are extraordinarily large, reflecting the relief of steric strain by the deformation. The C_9–C_{21} bond lengths are shorter than normal C_{sp^3}–C_{sp^3} bonds: this is attributed to the increased s-character of the orbital concerned of C_9 because of the lengthening of other bonds involving C_9. The apex angle of the pyramid formed by C_9 with C_{16}, C_{17}, and C_{19} is smaller than that formed by C_{10} with C_{11}, C_{18}, and C_{20}, indicating that the steric repulsion between Cl_1 and the 9-substituent is relieved by this modification as well. The similar structural features were also found in 1,4-dimethyl-9-(2-oxoethyl)triptycene.[6b]

The Cl_1–C_1 and C_9–C_{21} bonds are tilted against each other, as were the cases in 9-*t*-butyl-1,2,3,4-tetrachlorotriptycene.[8] The bond angle deformation is much greater for the angle C_{17}–C_9–C_{21} than that for Cl_1–C_1–C_{17} because of the large force constant for the deformation of Cl–C_{sp^2}–C_{sp^2} and buttressing effect of the Cl_2 and others. The small apex angle of C_9 pyramid may also contribute to enlarging the angle C_{17}–C_9–C_{21}. Rather small difference in bond angles C_{17}–C_9–C_{21} between the ap and the $\pm sc$ forms may be taken as supportive in assuming that the ground state energies of the ap and the sc forms are nearly the same as far as the interaction between the 9-substituent and the flanking benzene rings are concerned. Relatively long C–Cl distances in both forms (average 1.728 Å) may be due to the repulsive force among chlorine atoms.

The least squares planes of aromatic rings were cal-

culated from the positional parameters of carbon atoms comprising the rings. Dihedral angles made by two aromatic rings listed in Table 4 clearly demonstrate that the dihedral angles made by two benzene rings which flank the acetyl group are much larger than others in both *ap* and $\pm sc$ forms. This will mean that the carbonyl oxygen which extends into the gap between the two benzene rings interacts strongly with the aromatic rings.

Alternatively, the aromatic rings exhibit interesting features. Although less significant in another, the benzene rings flanking the acetyl group are distorted significantly. C_1 and C_8 in rings A and B which are close to the acetyl group are significantly displaced from what is expected from a molecular model to avoid repulsive interactions in the $\pm sc$ form. Similarly C_8 in the B ring and C_{15} in the C ring of the *ap* form show significant displacement. Examining the structures of these benzene rings, we notice that the carbon atoms para to each other are displaced from the least squares plane, which is made by other four carbons, to the same direction to form boats. They are C_3 and C_{17} in A, C_6 and C_{19} in B and C_{11} and C_{14} in C of the *ap* form, whereas C_3 and C_{17} in A, C_5 and C_8 in B and C_{11} and C_{14} in C of the $\pm sc$ isomer form also the bow and the stern of a boat. This makes a sharp contrast to the fact that triptycene itself possesses planar benzene rings within 0.01 Å.[9] There are a few examples of the boat form of twisted benzenes in the literature[10] and theoretical verification for the boat benzene was given.[11] However, the earlier works treat relatively small shifts from the mean plane and/or contain large ambiguities in atomic coordinates. Since the shift from the plane observed in this study is large and the standard deviations of the positional parameters perpendicular to the plane are small (*ca.* 0.003 Å) for carbon atoms, the results serve as unambiguous evidence for the stability of the boat form of benzene.

In contrast to the benzene rings, the 2-oxopropyl groups make perfect planes (Table 3), which nearly include the C_9–C_{10} axis. However, the planes of the 2-oxopropyl groups were not coplanar with the mean plane of the benzene ring which is *ap* to the group: the 2-oxopropyl group does not bisect the dihedral angle made by flanking benzene rings but are close to one of the two aromatic rings. The deviation from the anti-benzene planes are 6.9° (closer to ring B than to ring C) and 12.6° (closer to ring B than to ring A) for *ap* and $\pm sc$ forms respectively. It is reasonable to be so in the $\pm sc$ form because the steric repulsion between the ring A and the 2-oxopropyl group will be severe (for attractive interactions *vide infra*). The reason for the asymmetric structure of the *ap* form is not understood at the moment.

The structural features discussed so far are rather common for both conformations of 1,2,3,4-tetrachloro-9-(2-oxopropyl)triptycene but there are some structural features which are different when we go from the *ap* conformation to the $\pm sc$. Bond lengths and bond angles, which show differences more than 3σ and 7σ, respectively, are listed in Table 5. The large bond angles of C_{17}–C_9–C_{19} for the $\pm sc$ form relative to the *ap* and the same trend of C_{16}–C_9–C_{19} for the *ap* form relative to the $\pm sc$ can be attributed to the steric effect of the 2-oxopropyl group, as were seen in the dihedral angles made by two aromatic rings. The large bond angle of C_{18}–C_{10}–C_{20} in the $\pm sc$ form, though smaller than 7σ, relative to the *ap* may have the same origin because the bond angle C_{11}–C_{10}–C_{20} is also larger in the *ap* form than in the $\pm sc$.

Table 5. Structural parameters which differ by over the estimated errors on going from the $\pm sc$ to the *ap* isomers[a,b]

Bond length	l/Å	Bond angle	ϕ/°
C_9–C_{17}	−0.014(4)	C_{16}–C_9–C_{19}	−2.6(2)
C_{21}–C_{22}	−0.036(5)	C_{17}–C_9–C_{19}	3.8(2)
		C_{17}–C_9–C_{21}	1.7(2)
		C_9–C_{21}–C_{22}	2.2(3)

a) The difference is shown in the form: parameter(sc) − parameter(ap). b) Those listed here show differences of $\Delta r \geq 3\sigma(r)$ and $\Delta\theta \geq 7\sigma(\theta)$.

The differences in other bond lengths and bond angles deserve further comment on the ground of the postulated Cl···C=O interaction.[5] We propose that the 2-oxopropyl group and its vicinity assume the structure of the *ap* conformation if there is no interaction which affects the structure. The *ap* form possesses the following features. The C_9–C_{17} bond is abnormally long for normal C_{sp^2}–C_{sp^3} bonds. This must be attributed to the steric effect of the 9-substituent. Another point of interest is the C_{21}–C_{22} bond: it is unusually long as a C_{sp^2}–C_{sp^3} bond. This together with the fact that the bond angle C_9–C_{21}–C_{22} is larger than the normal tetrahedral angle suggests that, to relieve the steric strain caused by the carbonyl oxygen and the flanking benzene rings, the 2-oxopropyl group is deformed.

Comparing the bond lengths of the $\pm sc$ and *ap* forms, one notices that the unusuality observed in the *ap* form is corrected to some extent: the C_9–C_{17} bond length and the C_{21}–C_{22} bond length become closer to the normal values in the $\pm sc$ form than in the *ap* form. However, the bond angles C_{17}–C_9–C_{21} and C_9–C_{21}–C_{22} are larger in the $\pm sc$ form than in the *ap* form. We wish to attribute the structural change to the relative positions of the 1-chloro and the carbonyl groups in space which are required for the Cl···C=O interaction, as suggested by Dunitz and his coworkers.[12] If the bonds are longer, the geometry is not favorable for the Cl···C=O interaction. Therefore the bonds must shrink from the values observed in the *ap* form in order to realize the interaction in the $\pm sc$ form. However, if the shrinkage occurred without change in bond angles, the steric repulsion between the carbonyl oxygen and the aromatic rings would be too great. Thus the molecule shrinks in the $\pm sc$ form at the expense of widening the bond angles for which energy required is small.

One might argue that if there is a Cl···C=O interaction, the nonplanarity of the 2-oxopropyl group should be observed as are the cases in N···C=O interactions.[12,13] However, we believe that the carbonyl

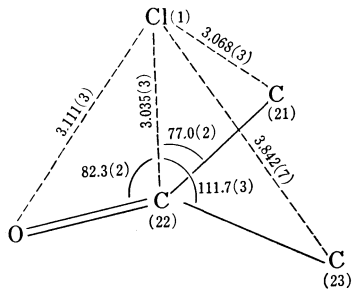

Fig. 3. Atomic distances and angles showing relative positions in space of the Cl_1 and the 2-oxopropyl group.

group in this case is under special conditions. As are depicted in Fig. 3, the Cl_1 atom located over the 2-oxopropyl group is over the C=O bond, closer to the carbon of the carbonyl group than the oxygen, to make $Cl_1\cdots C_{22}$–O angle of 82.3° and is closer to the C_{21} atom than the C_{23}. Under the optimum conditions of N···C=O interaction, the nitrogen is on the bisecting plane of the C–C(O)–C angle and N···C=O angle is close to 109°.[12] The reason for the unfavorable arrangement in space of the Cl_1 and the 2-oxopropyl group is of course the geometrical requirements, bond angles and bond lengths. Thus we have to admit that, although the Cl_1 and the carbonyl carbon are located closely, the relative arrangement of the two groups is far from the optimum one. Therefore, the Cl···C=O interaction we observe in this compound may not be very strong. There is another possible reason why we do not observe the pyramidality of the 2-oxopropyl group. That is the steric reason. If it were to take a pyramidal structure, the repulsion between the atoms within the 2-oxopropyl group and the benzene ring B in the $\pm sc$ conformation would become formidable.

There is a piece of evidence, however, that there is an attractive interaction of a Cl···C=O type from the X-ray diffraction results. That is the bond lengths of the C=O. The C_{22}–O bond in the $\pm sc$ form is longer than that in the *ap* by 0.009 Å, although the difference is not listed in Table 5 because this is within 3σ. But it is tempting to consider that the C=O bond in the $\pm sc$ form is lengthened by the Cl···C=O interaction.

We conclude from both the population ratio in solution and the structural features observed by X-ray diffraction that there exists a Cl···C=O interaction in 1,2,3,4-tetrachloro-9-(2-oxopropyl)triptycene, if it is the $\pm sc$ form. The main driving force for the interaction is the charge transfer between the Cl_1 and the carbonyl carbon which are placed in proximity (3.035 Å), although their relative geometry is far from the optimum for the interaction. This interaction is strong enough to deform the 2-oxopropyl group in the $\pm sc$ conformation from that in the *ap* as discussed above. The C=O bond is lengthened by the Cl···C=O interaction in the $\pm sc$ form from that in the *ap*.

References

1) Present address: Department of Chemistry, Faculty of Science and Technology, Keio University, Hiyoshi, Yokohama 223.
2) M. Ōki, *Angew. Chem., Int. Ed. Engl.*, **15**, 87 (1976).
3) M. Ōki, *Top. Stereochem.*, **14**, in press.
4) G. Izumi, S. Hatakeyama, N. Nakamura, and M. Ōki, *Bull. Chem. Soc. Jpn.*, **54**, 258 (1981).
5) G. Izumi, G. Yamamoto, and M. Ōki, *Chem. Lett.*, **1980**, 969; *Bull. Chem. Soc. Jpn.*, **54**, 3064 (1981).
6) a) M. Ōki, G. Izumi, G. Yamamoto, and N. Nakamura, *Chem. Lett.*, **1980**, 213; b) M. Ōki, G. Izumi, G. Yamamoto, and N. Nakamura, *Bull. Chem. Soc. Jpn.*, **55**, 159 (1982).
7) "International Tables for X-Ray Crystallography," Birmingham, Kinoch Press (1974), Vol. IV.
8) M. Mikami, K. Toriumi, M. Konno, and Y. Saito, *Acta Crystallogr., Sect. B*, **31**, 2474 (1975).
9) K. Anzenhofer and J. J. de Boer, *Z. Kristallogr.*, **131**, 103 (1970).
10) T. Kaneda, N. Sakabe, and J. Tanaka, *Bull. Chem. Soc. Jpn.*, **47**, 1858 (1974); N. Sakabe, K. Sakabe, K. Ozeki-Minakata, and J. Tanaka, *Acta Crystallogr., Sect B*, **28**, 3441 (1972).
11) H. Iwamura, H. Kihara, S. Misumi, Y. Sakata, and T. Umemoto, *Tetrahedron Lett.*, **1976**, 615.
12) J. D. Dunitz, "X-Ray Analysis and the Structure of Organic Molecules," Cornell University Press, Ithaca (1979), pp. 366—384.
13) H. B. Bürgi, J. D. Dunitz, and E. Shefter, *J. Am. Chem. Soc.*, **95**, 5065 (1973).

Reactions of 4,5-Dicyanoimidazoles with Isocyanates. Novel Formation of the Condensed Tricyclic Imidazoles

Keiryo MITSUHASHI,* Kazuyuki TAKAHASHI, Takeo KAWAHARA, Yoshimitsu IKERU, and Kiyoshi TANAKA

Department of Chemistry, College of Technology, Seikei University, Kichijoji, Musashino, Tokyo 180

(Received June 1, 1982)

The reactions of 4,5-dicyanoimidazoles with methyl isocyanate gave 7-cyano-1-imino-2-methyl-2,3-dihydro-1*H*-imidazo[3,4-*c*]imidazol-3-ones (**2**), while the similar reactions with phenyl isocyanate resulted in the formation of the tricyclic imidazoles, 11-imino-6,10-diphenyl-2,4,6,8,10-pentaazatricyclo[5.4.1.$0^{4,12}$]dodeca-1(12),2,7-triene-5,9-diones (**3**) and the same type of the tricyclic imidazoles **4** were obtained by carbamoylation of **2** with phenyl isocyanate. The reactions of **2**, **3**, and **4** with amines were further investigated.

It is well known that imidazole itself reacts with isocyanates under mild conditions to form 1-(substituted carbamoyl)-1*H*-imidazoles,[1-3] which can be rearranged to 2-(substituted carbamoyl)-1*H*-imidazoles at a high temperature and that such 4,5-disubstituted imidazoles as 4,5-diarylimidazoles yield 2-(substituted carbamoyl)-1*H*-imidazoles by the reactions with aryl isocyanates under rather drastic conditions.[4-6] These interesting results of carbamoylation and rearrangement prompted us to apply such reactions to 4,5-dicyanoimidazoles to search some new imidazole derivatives.[7] In the present paper, we wish to report on the reactions of 4,5-dicyanoimidazoles with isocyanates which afford the novel condensed tricyclic imidazoles *via* ready intramolecular cyclization of the assumed intermediates, 4,5-dicyano-1-(substituted carbamoyl)-1*H*-imidazole followed by further cyclization of thus formed bicyclic imidazoles with another isocyanate.

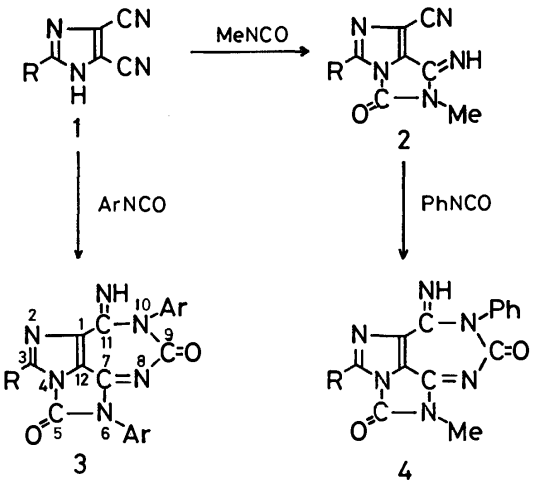

Scheme 1.

Results and Discussion

The reaction of 4,5-dicyanoimidazole (**1a**) with methyl isocyanate was carried out in chloroform at room temperature for 24 h in the presence of 2-methyl-1,4-diazabicyclo[2.2.2]octane (Me-DABCO)[8] and a catalytic amount of dibutyltin dilaurate (DBTDL).[9] Me-DABCO was added not only to dissolve **1a** completely but to accelerate the reaction. The resulting precipitate was collected and recrystallized from chloroform to give the white plates which were assigned to 7-cyano-1-imino-2-methyl-2,3-dihydro-1*H*-imidazo-[3,4-*c*]imidazol-3-one (**2a**) on the basis of its spectral data and elemental analysis. The elemental analysis and the integration in ^{1}H NMR spectrum suggest an 1:1 adduct between **1a** and methyl isocyanate, while the IR spectrum shows bands at 3300(NH), 2220(C≡N), 1780(C=O), and 1670 cm^{-1}(C=N). In particular, band due to carbon-oxygen at 1780 cm^{-1}, which is much higher than that (about 1730 cm^{-1}) in the usual 1-(alkylcarbamoyl)-1*H*-imidazole,[5] strongly supports the five-membered ring structure **2a**.[10] Moreover, the strongly deshielded singlet peak of methyl protons (δ 3.20) in ^{1}H NMR is consistent with this structure.[11] Although the alternative structure **2a'** derived by the participation of 4-cyano group can be anticipated, it is denied from the steric consideration in constructing the model.

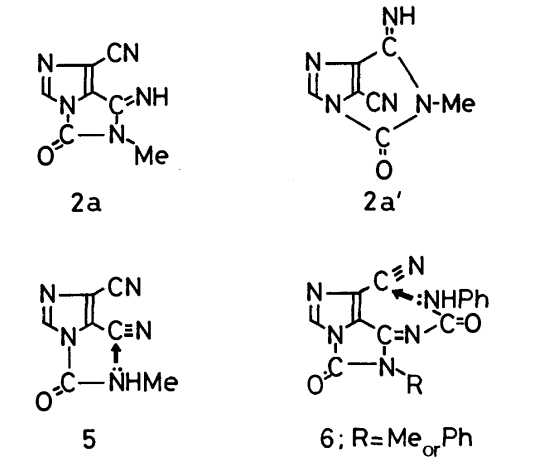

The similar reactions of 2-methyl (**1b**) and 2-ethyl analogues (**1c**) gave the corresponding bicyclic imidazoles **2b** and **2c** (Scheme 1). These results are summerized in Table 1.

On the other hand, the reactions with aryl isocyanates gave the quite different products. The reaction of **1a** with phenyl isocyanate at room temperature in the presence of Me-DABCO and DBTDL gave the tricyclic imidazole, 11-imino-6,10-diphenyl-2,4,6,8,10-pentaazatricyclo[5.4.1.$0^{4,12}$]dodeca-1(12),2,7-triene-5,9-dione (**3a**), in 62% yield. Its structure was determined by an elemental analysis and spectroscopic properties. The elemental analysis, the MS spectrum (*m/e*; 356, M$^+$), and the integration in ^{1}H NMR spectrum indicate an adduct between **1a** and two

Table 1. 7-Cyano-1-imino-2-methyl-2,3-dihydro-1*H*-imidazo[3,4-*c*]imidazol-3-ones (**2**)

Compound	R	Yield[a] %	Mp θ_m/°C	IR $\tilde{\nu}$/cm^{-1} C=O	IR $\tilde{\nu}$/cm^{-1} C=N	Formula	Calcd(Found)(%) C	H	N
2a	H	60	166—169	1780	1670	$C_7H_5N_5O$	48.00 (47.89)	2.88 (2.85)	39.99 (40.15)
2b	Me	64	156—159	1780	1660	$C_8H_7N_5O$	50.79 (50.49)	3.73 (3.47)	37.02 (36.76)
2c	Et	44	119—122	1780	1670	$C_9H_9N_5O$	53.20 (53.29)	4.46 (4.19)	34.46 (34.69)

a) Isolated yields after recrystallization.

Table 2. 11-Imino-2,4,6,8,10-pentaazatricyclo[5.4.1.0^{4,12}]dodeca-1(12),2,7-triene-5,9-diones (**3** and **4**)

Compound	R	Ar	Yield[a] %	Mp θ_m/°C	IR $\tilde{\nu}$/cm^{-1} C=O	C=N	C=O, C=N	Formula	Calcd(Found)(%) C	H	N
3a	H	Ph	62 (37)[b]	214—215 (decomp)	1780	1685	1640	$C_{19}H_{12}N_6O_2$	64.04 (63.85)	3.39 (3.20)	23.58 (23.51)
3a′	H	1-Naphthyl	23	182—184 (decomp)	1795	1690	1650	$C_{27}H_{16}N_6O_2$	71.05 (70.83)	3.53 (3.61)	18.41 (18.56)
3b	Me	Ph	30	203—203.5 (decomp)	1780	1690	1645	$C_{20}H_{14}N_6O_2$	64.86 (65.12)	3.81 (3.85)	22.69 (23.09)
3c	Et	Ph	36	183.5—184 (decomp)	1780	1680	1640	$C_{21}H_{16}N_6O_2$	65.62 (65.63)	4.20 (4.33)	21.86 (21.81)
4a	H	—	24	199—201 (decomp)	1785	1685	1640	$C_{14}H_{10}N_6O_2$	57.14 (57.04)	3.43 (3.15)	28.56 (28.27)
4b	Me	—	33	223—224 (decomp)	1785	1695	1640	$C_{15}H_{12}N_6O_2$	58.44 (58.30)	3.92 (3.69)	27.26 (27.56)
4c	Et	—	29	209—210 (decomp)	1785	1695	1640	$C_{16}H_{14}N_6O_2$	59.62 (59.32)	4.38 (4.32)	26.07 (26.36)

a) Isolated yields after recrystallization, being based on isocyanates. b) Yield obtained by running the reaction in nitrobenzene without catalyst.

equiv. of phenyl isocyanate. The IR spectrum shows bands at 3270(NH), 1780(C=O), 1685(C=N), and 1640 cm^{-1}(C=O and C=N),[12] no absorption due to the C≡N group being observed. These data support the structure **3a**.

Reaction of **1a** with 1-naphthyl isocyanate and of **1b** and **1c** with phenyl isocyanate gave also the corresponding tricyclic imidazoles **3a′**, **3b**, and **3c** (Scheme 1, Table 2).

Under more drastic conditions of refluxing in nitrobenzene for 2.5 h, the reaction of **1a** with phenyl isocyanate was carried out and only the tricyclic imidazole **3a** was obtained. The formation of 4,5-dicyano-2-(phenylcarbamoyl)-1*H*-imidazole expected through rearrangement[4] couldn't be observed at all.

Though the bicyclic imidazole **2a** didn't undergo the further reaction with another molecule of methyl isocyanate, it reacted with phenyl isocyanate to give the similar tricyclic imidazole, 11-imino-6-methyl-10-phenyl-2,4,6,8,10-pentaazatricyclo[5.4.1.0^{4,12}]dodeca-1(12),2,7-triene-5,9-dione (**4a**), of which structure was also identified on the basis of its elemental analysis and spectral data. The bicyclic imidazoles **2b** and **2c** gave the similar results which were summerized in Table 2.

The formation of **2**, **3**, and **4** can be explained in terms of the intramolecular cyclization of the presumed intermediates **5** and **6**. The bicyclic imidazole **2** may be led *via* the attack of the carbamoyl nitrogen of **5** at the carbon of 5-cyano group causing proton transfer. In the case of methyl isocyanate the reaction terminates at this step, whereas in the case of more reactive phenyl isocyanate, it may further proceed *via* addition of another molecule of isocyanate followed by the cyclization with 4-cyano group to give **3** and **4**.

Next the reactivity of **2**, **3**, and **4** toward amines was investigated. 4-Methylaniline reacted with **3a** giving *N*-(4-methylphenyl)-*N′*-phenylurea (**7**) and with **4a** to yield urea **7** along with a small amount of *N*-(4-methylphenyl)-*N′*-methylurea (**8**). These results seem to suggest that amine initially attacks the carbonyl group of the diazepine ring and then that of imidazolidine ring. The reaction of **2a** with 4-methylaniline was then carried out, affording urea **8** and **1a** in 42 and 35% yields, respectively, whereas the

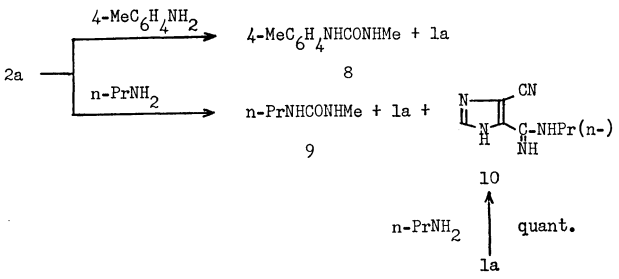

Scheme 2.

similar reaction with a more nucleophilic amine, propylamine, gave not only *N*-methyl-*N'*-propylurea (**9**) (41%) and a trace amount of **1a** but also 4-cyano-5-(N^1-propylamidino)-1*H*-imidazole (**10**) in 26% yield (Scheme 2). From the fact that **1a** reacted with propylamine to give the imidazole **10** quantitatively, it is supposed that **10** was obtained by the reaction of propylamine with the initially formed **1a**.

Experimental

All melting points are uncorrected. IR spectra were recorded on a JASCO IRA-1 spectrometer. ^{1}H NMR spectra were measured with a JEOL JNM-PMX 60 spectrometer using tetramethylsilane (TMS) as an internal standard, the chemical shifts being given in δ ppm downfield from TMS. MS spectra were recorded on a Finnigan 3300E GC-MS spectrometer operating at 120 eV.

Dicyanoimidazoles **1a**—**c** were prepared by routes reported in the previous paper.[13] Elemental analyses and $\nu_{C=O \text{ and } C=N}$ in IR (KBr) for **2**, **3**, and **4** are summerized in Tables 1 and 2.

Reaction of 1a with Methyl Isocyanate. A solution of 4.8 g (40 mmol) of **1a**, 5 drops of DBTDL, 4 ml of Me-DABCO, and 2.3 g (40 mmol) of methyl isocyanate in 60 ml of anhydrous chloroform was stirred at room temperature for 24 h. The precipitated white solid was collected and recrystallized from chloroform to give the white plates **2a** (4.2 g, 60%), mp, 166—169 °C. ^{1}H NMR (DMSO-d_6–$CDCl_3$) δ 3.20 (s, 3, N-CH_3), 8.35 (s, 1, imidazole 2H), and 9.90 (s, 1, NH). IR (KBr) 2220 (C≡N) and 3300 cm^{-1} (NH).

Similarly **2b** was obtained in 64% yield, mp, 156—159 °C (recrystallized from chloroform–carbon tetrachloride). ^{1}H NMR (DMSO-d_6–$CDCl_3$) δ 2.70 (s, 3, CH_3), 3.20 (s, 3, N-CH_3), and 9.40 (s, 1, NH). IR (KBr) 2220 (C≡N) and 3295 cm^{-1} (NH).

Reaction of 1c with Methyl Isocyanate. Methyl isocyanate (1.1 g, 20 mmol) was added to a solution of 2.9 g (20 mmol) of **1c**, 5 drops of DBTDL, and 2 drops of Me-DABCO in 30 ml of anhydrous chloroform. After the reaction mixture was stirred at room temperature for 24 h, the solvent was distilled out under reduced pressure to give the residual oil. The oil was placed on the column (silica gel) and eluted with chloroform to give the crude white solid **2c**. The solid was recrystallized from carbon tetrachloride to afford the white plates **2c** (1.8 g, 44%), mp, 119—122 °C. ^{1}H NMR ($CDCl_3$) δ 1.40 (t, 3, CH_3), 3.05 (q, 2, CH_2), 3.30 (s, 3, N-CH_3), and 8.75 (s, 1, NH). IR (KBr) 2220 (C≡N) and 3295 cm^{-1} (NH).

Reaction of 1a with Phenyl Isocyanate. (A): Five drops of DBTDL and 4 ml of Me-DABCO was added to a suspension of 4.8 g (40 mmol) of **1a** in 60 ml of anhydrous chloroform under stirring. Me-DABCO (4 ml) thoroughly dissolved **1a**. Phenyl isocyanate (4.8 g, 40 mmol) was then added to the solution. After the mixture was stirred at room temperature for 24 h, a precipitate formed was filtered out and the filterate was evaporated under reduced pressure. The residual yellow solid and a precipitate were combined, washed with ethyl acetate to remove the excess **1a**, and recrystallized from acetonitrile to yield the yellow needles **3a** (4.4 g, 62% based on phenyl isocyanate), mp, 214—215 °C (decomp). MS (*m/e*) 356 (M^+). ^{1}H NMR (DMSO-d_6) δ 6.95—7.75 (m, 10, aromatic-H), 8.85 (s, 1, imidazole 2H), and 10.05 (s, 1, NH). IR (KBr) 3270 cm^{-1} (NH).

(B): Phenyl isocyanate (3.6 g, 30 mmol) was added to a suspension of 2.4 g (20 mmol) of **1a** in 30 ml of nitrobenzene. The mixture was refluxed for 2.5 h, cooled, and a precipitate formed was collected. The precipitate was washed with carbon tetrachloride and a small amount of ethanol to remove the excess **1a** and recrystallized from acetonitrile to give the yellow needles **3a** (2.0 g, 37% based on phenyl isocyanate), mp, 214—215 °C (decomp).

Similarly **3a'** and **3b** were obtained in 23 and 30% yields, respectively, by following method *(A)*. **3a'**: mp, 182—184 °C (decomp). ^{1}H NMR (DMSO-d_6) δ 7.35—8.25 (m, 14, aromatic-H), 8.90 (s, 1, imidazole 2H), and 9.95 (s, 1, NH). IR (KBr) 3200 cm^{-1} (NH). **3b**: mp, 203—203.5 °C (decomp). ^{1}H NMR (DMSO-d_6) δ 2.65 (s, 3, CH_3), 6.85—7.65 (m, 10, aromatic-H), and 9.90 (s, 1, NH). IR (KBr) 3360 cm^{-1} (NH).

Reaction of 1c with Phenyl Isocyanate. A solution of 2.9 g (20 mmol) of **1c**, 6 drops of DBTDL, 2 ml of Me-DABCO, and 2.4 g (20 mmol) of phenyl isocyanate in 40 ml of anhydrous chloroform was stirred at room temperature for 17 h. The solvent was evaporated under reduced pressure and the residual oil was washed with hexane and benzene to give the crude yellow solid. The solid was recrystallized from acetonitrile to afford the yellow needles **3c** (1.4 g, 36% based on phenyl isocyanate), mp, 183.5—184 °C (decomp). ^{1}H NMR (DMSO-d_6–$CDCl_3$) δ 1.30 (t, 3, CH_3), 2.90 (q, 2, CH_2), 6.90—7.60 (m, 10, aromatic-H), and 8.85 (s, 1, NH). IR (KBr) 3220 cm^{-1} (NH).

Reaction of 2a with Phenyl Isocyanate. Phenyl isocyanate (1.2 g, 10 mmol) was added to a suspension of 1.8 g (10 mmol) of **2a**, 5 drops of DBTDL, and 2 ml of Me-DABCO in 30 ml of anhydrous chloroform. The reaction mixture was stirred at room temperature and **2a** completely dissolved after 1 h. After the solution was stirred for 23 h, the yellow solid precipitated. The solid was collected, washed with chloroform, and recrystallized from acetonitrile to give the yellow needles **4a** (0.7 g, 24%), mp, 199—201 °C. MS (*m/e*) 294 (M^+) and 175 (M^+−PhNCO). ^{1}H NMR (DMSO-d_6) δ 3.20 (s, 3, N-CH_3), 6.95—7.70 (m, 5, aromatic-H), 8.65 (s, 1, imidazole 2H), and 10.10 (s, 1, NH). IR (KBr) 3280 cm^{-1} (NH).

Similarly **4b** and **4c** were obtained in 33 and 29% yields, respectively. **4b**: mp, 223—224 °C (decomp). ^{1}H NMR (DMSO-d_6) δ 2.60 (s, 3, CH_3), 3.20 (s, 3, N-CH_3), 7.00—7.80 (m, 5, aromatic-H), and 10.20 (s, 1, NH). IR (KBr) 3360 cm^{-1} (NH). **4c**: mp 209—210 °C (decomp). ^{1}H NMR (DMSO-d_6) δ 1.30 (t, 3, CH_3), 2.95 (q, 2, CH_2), 3.20 (s, 3, N-CH_3), 7.00—7.80 (m, 5, aromatic-H), and 10.25 (s, 1, NH). IR (KBr) 3380 cm^{-1} (NH).

Reaction of 3a with 4-Methylaniline. A suspension of 0.7 g (2 mmol) of **3a** and 0.6 g (6 mmol) of 4-methylaniline in 30 ml of anhydrous chloroform was refluxed for 65 h and after cooled, the formed solid was collected (0.4 g), mp, 219—220 °C (lit,[14] 218 °C). This was identified to be urea **7** by its IR spectrum. The filtrate was evaporated under reduced pressure to leave the residual solid. Its IR and ^{1}H NMR spectra showed it to be the mixture of urea **7** and the starting material.

Reaction of 4a with 4-Methylaniline. A suspension of 0.8 g (3 mmol) of **4a** and 0.6 g (6 mmol) of 4-methylaniline in 80 ml of anhydrous chloroform was refluxed for 96 h until **4a** thoroughly disappeared. After cooled, the formed solid was separated, 0.3 g, mp, 219—220 °C. This was identified to be urea **7** by its IR spectrum. The filtrate was evaporated under reduced pressure to give the residual solid. The solid was placed on the column (silica gel) and eluted with chloroform to give 0.38 g of urea **7** and 0.08 g of urea **8**, mp, 175—177 °C (lit,[15] 178 °C).

Reaction of ***2a*** *with 4-Methylaniline.* A solution of 0.97 g (5.5 mmol) of **2a** and 1.18 g (10 mmol) of 4-methylaniline in 50 ml of anhydrous chloroform was refluxed for 24 h. The solvent was evaporated under reduced pressure to leave the residual solid. The solid was placed on the column (silica gel) and eluted with chloroform to give the mixture of 4-methylaniline and urea **8**. The mixture was washed with hexane and toluene to yield 0.76 g (42%) of urea **8**, mp, 175—177 °C. In addition, the residual solid was eluted with ethanol to give the crude **1a**. This crude **1a** was recrystallized from water to afford the pure **1a** (0.46 g, 35%).

Reaction of ***2a*** *with Propylamine.* A solution of 1.75 g (10 mmol) of **2a** and 1.18 g (20 mmol) of propylamine in 30 ml of anhydrous chloroform was refluxed for 24 h. After cooled, the formed solid was collected and recrystallized from chloroform–acetonitrile to give 0.92 g of the pure amidine **10** (26%), white needles, mp, 142—144 °C. IR (KBr) 3220 (NH), 2220 (C≡N), and 1610 cm^{-1} (C=N). ^1H NMR ($CDCl_3$–DMSO-d_6) δ 1.00 (t, 3, CH_3), 1.60 (q of t, 2, CH_2), 2.85 (t, 2, N-CH_2), 7.25 (br.s, 3, 3NH), and 7.40 (s, 1, imidazole 2H). Found: C, 53.82; H, 5.87%. Calcd: C, 54.22; H, 6.26%.

The filtrate was evaporated under reduced pressure to leave the residual solid. By column chromatography (silica gel, chloroform) of the residue, 0.96 g of urea **9** was isolated (41%), mp 63.5—64.5 °C (lit,[15] 67—68 °C). The structure was identified by its IR spectrum.

Reaction of ***1a*** *with propylamine.* A solution of 1.18 g (10 mmol) of **1a** and 0.59 g (10 mmol) of propylamine in 40 ml of anhydrous chloroform was refluxed for 1 h and then stirred at room temperature for 24 h. The formed solid was collected and recrystallized from chloroform–acetonitrile to give 1.7 g of the pure amidine **10** (96%), mp 142—144 °C.

The present work was partially supported by a Grant-in-Aid for Scientific Research No. 005555347 from the Ministry of Education, Science and Culture.

References

1) R. A. Henry and W. M. Dehn, *J. Am. Chem. Soc.*, **71**, 2297 (1949).
2) K. Schlögl and H. Woidich, *Monatsh. Chem.*, **87**, 679 (1956).
3) H. A. Staab and W. Benz, *Justus Liebigs Ann. Chem.*, **648**, 72 (1961).
4) R. Gompper, E. Hoyer, and H. Herlinger, *Chem. Ber.*, **92**, 550 (1959).
5) E. P. Papadopoulos, *J. Org. Chem.*, **42**, 3925 (1977).
6) E. P. Papadopoulos and C. M. Schupbach, *J. Org. Chem.*, **44**, 99 (1979).
7) K. Mitsuhashi, K. Takahashi, T. Zaima, and T. Asahara, *Kogyo Kagaku Zasshi*, **74**, 316 (1971).
8) A. Farkas and K. G. Flynn, *J. Am. Chem. Soc.*, **82**, 642 (1960); A. Farkas, G. A. Mills, W. E. Erner, and J. B. Maerker, *Ind. Eng. Chem.*, **51**, 1299 (1959).
9) F. Hostettler and E. F. Cox, *Ind. Eng. Chem.*, **52**, 609 (1960).
10) D. Dolphin and A. Wick, "Tabulation of Infrared Spectral Data," John Wiley and Sons, Inc., New York (1977), p. 388.
11) Methyl protons in 4-cyano-1-(methylcarbamoyl)-1*H*-imidazole appear at δ 3.00 as doublet peaks; our unpublished results to be submitted.
12) R. L. Dannley, D. Yamashiro, and R. G. Taborsky, *J. Org. Chem.*, **24**, 1706 (1959).
13) D. W. Woodward, U. S. Patent 2534331 (1950); *Chem. Abstr.*, **45**, 5191d (1951).
14) C. K. Ingold, *J. Chem. Soc.*, **125**, 87 (1924).
15) J. L. Boivin and P. A. Boivin, *Can. J. Chem.*, **29**, 478 (1951).

Preparation of New Nitrogen-Bridged Heterocycles. 5.[1] Smooth Michael Additions of 2(3*H*)-Indolizinone Derivatives

Akikazu KAKEHI,* Suketaka ITO, Bunzo WADA, Kozo WATANABE, Kenji NISHIMURA, and Aiichiro KUMAGAI

Department of Industrial Chemistry, Faculty of Engineering, Shinshu University, Wakasato, Nagano 380

(Received June 1, 1982)

Michael additions of some 2(3*H*)-indolizinone derivatives to α,β-unsaturated nitriles, esters, and an amide gave the corresponding double Michael adducts, 3,3-disubstituted 2(3*H*)-indolizinones, in moderate to high yields, and those to methyl vinyl ketone afforded further condensed products, spiro[cyclohexane-1,3′(2′*H*)-indolizin]-2′-ones, instead of the expected 1:2 adducts. On the other hand, the reactions of the indolizinones with activated ethylenes having an appropriate leaving group at the β-position or with an acetylenic ester formed unstable 1:1 Michael adducts, which were converted to stable 2-acyloxy- or 2-alkoxy-3-vinylindolizine derivatives by the treatment with some acylating or alkylating agents in comparatively good yields.

In our continuing investigation of the synthetic utilization of nitrogen-bridged heterocycles, we recently reported a facile preparative method of 2(3*H*)-indolizinone derivatives and their reactions with some alkylating and acylating agents.[1] The reactions of the indolizinones with these reagents are very useful for the preparations of simple 2-acyloxy- or 2-alkoxyindolizines and 3,3-dialkyl-2(3*H*)-indolizinones but not so for that of functionalized ones. Similarly, direct 3-vinylation of indolizines with activated ethoxymethylene compounds such as ethyl (ethoxymethylene)cyanoacetate and (ethoxymethylene)malononitrile was recently found by Masumura *et al.*[2] and by us,[3] but the application was largely restricted by the availability and thermal stability of the starting indolizines. In this paper we wish to report the one-pot and versatile syntheses of polyfunctionalized indolizine and indolizinone derivatives by way of Michael additions to 3-unsubstituted 2(3*H*)-indolizinones generated *in situ* from pyridinium salts.

Results and Discussion

Reactions of 2(3H)-Indolizinones with α,β-Unsaturated Nitriles, Esters, an Amide, and a Ketone. Since the high reactivity of the 3-methylene group in 2(3*H*)-indolizinone derivatives was proven well by the *C*-alkylation with various alkyl halides,[1] we focused next our attention on the functionalization of these indolizinones by taking advantage of their reactivity, especially the high nucleophilicity at the 3-position. As a model reaction for this purpose, Michael addition was examined under some alkaline conditions and proved to proceed successfully. For example, the reactions of 2(3*H*)-indolizinones **6**—**10**, generated *in situ* by the alkali treatment of the corresponding 1-(ethoxycarbonylmethyl)-2-methylpyridinium salts **1**—**5**, with excess acrylonitrile **11** gave yellow crystalline compounds, 3,3-bis(2-cyanoethyl)-2(3*H*)-indolizinone derivatives **14**—**18**, respectively, in various yields (0—95%) depending upon conditions used (See Table 1). Similarly, the reactions of **6**—**8** with excess ethyl acrylate **12**, and acrylamide **13** afforded the corresponding 1:2 adducts, 3,3-bis(2-ethoxycarbonylethyl)-**19**—**21** and 3,3-bis(2-carbamoylethyl)-2(3*H*)-indolizinones **22**—**24**, as products isolable each other. The products **14**, **16**, **19**, and **21** were the same with those

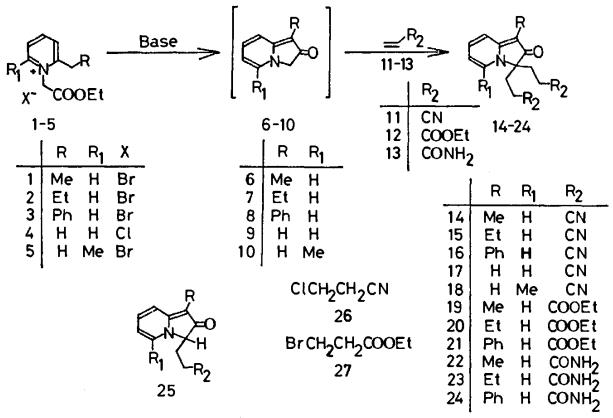

Scheme 1.

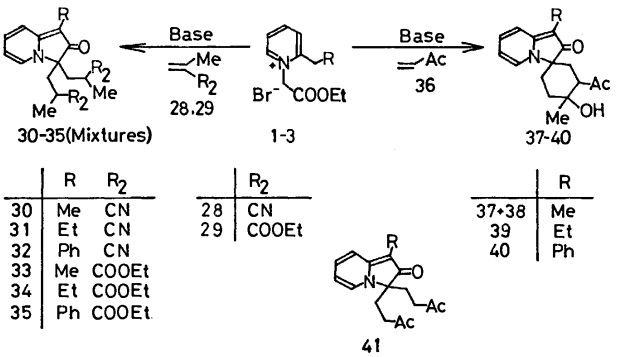

Scheme 2.

prepared by the reactions of **1** and **3** with 3-chloropropionitrile **26** and ethyl 3-bromopropionate **27** in the presence of alkali, respectively.[1] No 1:1 adduct such as **25**, however, could be detected in these reactions and even when equimolar amounts of olefins **11**—**13** were used.

On the other hand, the Michael additions of **6**—**8** to methacrylonitrile **28** and ethyl methacrylate **29** formed the mixtures **30**—**35** of each two stereoisomeric 1:2 adducts, respectively, which, though attempted separations were unsuccessful, were determined by the TLC and by the spectral inspection (See below). Interestingly, the reactions of **6**—**8** with methyl vinyl ketone **36** did not give the expected adduct **41** or a Robinson annelation product,[4] but afforded further condensed compounds, spiro[cyclohexane-1,3′(2′*H*)-indolizin]-2′-ones **37** and **38**, **39**, and **40** (Scheme 2).

Table 1. Some data of 3,3-disubstituted 2(3*H*)-indolizinones

Compd No.	Reactants		Yield/%[a]			Mp θ_m/°C	$\tilde{\nu}$/cm^{-1}(KBr)			Formula	Calcd(%)			Found(%)		
			A	B	C		C=O	(CN)			C	H	N	C	H	N
14	**1**	**11**	20		63	74— 75	1590	(2240)		$C_{15}H_{15}N_3O+H_2O$	66.40	6.32	15.49	66.44	6.16	15.60
15	**2**	**11**		54		138—140	1585	(2240)		$C_{16}H_{17}N_3O$	71.88	6.41	15.72	71.84	6.48	15.69
16	**3**	**11**	37		95	157—158	1605	(2240)		$C_{20}H_{17}N_3O$	76.17	5.43	13.33	75.91	5.44	13.37
17	**4**	**11**	0		19	167—169	1611	(2240)		$C_{14}H_{13}N_3O$	70.27	5.48	17.56	70.26	5.58	17.47
18	**5**	**11**		27		144—146	1600	(2245)		$C_{15}H_{15}N_3O$	71.12	5.97	16.59	71.16	6.11	16.65
19	**1**	**12**	0	75		128—130	Known compound[b]									
20	**2**	**12**		62		128—129	1734	1721	1600	$C_{20}H_{27}NO_5$	66.46	7.53	3.88	66.34	7.62	3.87
21	**3**	**12**	36	32		140—142	Known compound[b]									
22	**1**	**13**			84	260(decomp)	1663	1590		$C_{15}H_{19}N_3O_3$	62.26	6.62	14.52	62.45	6.64	14.32
23	**2**	**13**			76	223—225	1672	1578		$C_{16}H_{21}N_3O_3+\frac{3}{2}H_2O$	58.16	7.32	12.72	58.09	7.44	12.67
24	**3**	**13**			91	190—193	1661	1595		$C_{20}H_{21}N_3O_3+H_2O$	65.02	6.28	11.28	65.19	6.24	11.25
30	**1**	**28**	0	79		157—158	1595	(2240)		$C_{17}H_{19}N_3O+H_2O$	68.20	7.07	14.04	68.25	7.30	14.07
31	**2**	**28**			32	96— 97	1590	(2235)		$C_{18}H_{21}N_3O+\frac{1}{2}H_2O$	71.02	7.29	13.81	71.21	7.36	13.84
32	**3**	**28**	85			165—166	1600	(2240)		$C_{22}H_{21}N_3O$	76.94	6.16	12.24	76.95	6.20	12.31
33	**1**	**29**	0	52		116—118	1718	1592		$C_{21}H_{29}NO_5+H_2O$	64.10	7.94	3.56	64.02	7.77	3.52
34	**2**	**29**			33	66— 67	1725	1600		$C_{22}H_{31}NO_5$	67.84	8.02	3.60	67.97	7.98	3.60
35	**3**	**29**	80			101—102	1724	1710	1604	$C_{26}H_{31}NO_5$	71.37	7.14	3.20	71.10	7.18	3.16
37[c]	**1**	**36**			52	182—184	1688	1594	d)	$C_{17}H_{21}NO_3$	71.05	7.37	4.87	70.78	7.46	4.84
38[e]	**1**	**36**			18	219—221	1690	1592	f)	$C_{17}H_{21}NO_3$	71.05	7.37	4.87	71.24	7.36	4.68
39[c]	**2**	**36**		48		164—166	1687	1588	g)	$C_{18}H_{23}NO_3$	71.73	7.69	4.65	71.78	7.83	4.45
40[c]	**3**	**36**		46	92	212—214	1690	1592	h)	$C_{22}H_{23}NO_3$	75.62	6.63	4.01	75.59	6.66	4.00

a) Method A, Method B, and Method C. b) Ref. 1. c) High soluble substance. d) 3490 cm^{-1}(OH). e) Low soluble substance. f) 3170 cm^{-1}(OH). g) 3250 cm^{-1}(OH). h) 3500 cm^{-1}(OH).

In the above reactions of **6**—**10** with **11**—**13**, **28**, **29**, and **36** the method C using ethanolic sodium ethoxide as a base was found better than the method A (aq potassium hydroxide as a base) and B (anhydrous potassium carbonate) from the viewpoint of the yields of the corresponding products and the reaction time (See Table 1 and Experimental).

Structural elucidations of these double Michael adducts **14**—**24** and **30**—**35** and spiro compounds **37**—**40** were accomplished mainly by the physical and spectral means and in part by considering unequivocal syntheses of **14**, **16**, **19**, and **21**. In particular, the elementary analyses of all products were in good accord with the proposed compositions and the IR spectra showed without exceptions a largely shifted 2-keto absorption band characteristic of 2(3*H*)-indolizinone derivatives in the range of 1578—1611 cm^{-1}.[1,5] In addition, the saturated cyano bands (near 2240 cm^{-1}) in **14**—**18** and **30**—**32** or the saturated ester carbonyl bands (near 1730 cm^{-1}) in **19**—**21** and **33**—**35** also supported these structures. On the other hand, the IR spectra of **37**—**40** exhibited the carbonyl bands at comparatively low region (near 1690 cm^{-1}) and the hydroxyl absorption bands at 3170—3500 cm^{-1}, which suggested the presence of a hydrogen bonding between them. In the NMR spectra of these compounds **14**—**21**, **30**—**35**, and **37**—**40** the chemical shifts and the signal patterns (Table 2) due to the protons of the 2(3*H*)-indolizinone moiety were very similar to each others and also with those of authentic 3,3-dialkyl-2(3*H*)-indolizinone derivatives.[1] In addition, the fact that compounds **30**—**35** were mixtures of two stereoisomers (not *dl*-pair) was also indicated by the NMR spectral inspection: especially, the NMR spectra of **30**, **31**, and **33** showed clearly the proton signals due to the 1-methyl or 2-ethyl group of the minor product, together with the proton signals of the major compounds.[6] On the other hand, the NMR spectra of **37**—**40** were apparently different from those of initially expected 1:2 Michael adducts such as **41**. For example, the spectrum of **37** exhibited signals at δ 1.33 (3H, s), 2.28 (3H, s), 1.4—2.7 (6H, m), 4.11 (1H, q, J=12.0 and 4.0 Hz), and 4.03 (1H, s, disappeared with deuterium oxide) attributable to a methyl attached to an sp^3 carbon, only one acetyl, three methylenes, a methine, and a hydroxyl group, respectively, together with the signals due to the 2(3*H*)-indolizinone moiety. The NMR spectra of **39** and **40** were the almost same as that of **37**, while that of **38** was slightly different from them (Table 3). Apparently, the presences of the methyl group attached to an sp^3 carbon and the hydroxyl group showed that compounds **37**—**40** were formed by the condensation between the two 3-oxobutyl groups in primary 1:2 adduct **41**. Judging from above physical and spectral data, products **14**—**24** and **30**—**35** were concluded

TABLE 2. NMR DATA OF 3,3-DISUBSTITUTED 2(3*H*)-INDOLIZINONES

Compd[a,b] No.	C-5	C-6	C-7	C-8	C-1	R_2 and/or R_3				Methylene
14	7.57 br d	6.51 dt	7.43 br t	6.93 br d	1.78 s					1.8—2.7 m
15	7.56 br d	6.53 dt	7.46 br t	6.99 br d	1.07 c) t					1.8—2.6 m
16	d)	6.59 m	d)	d)	7.1—7.9 m					1.8—2.7 m
17	7.62 br d	6.62 dt	7.50 br t	7.05 br d	5.15 s					1.9—2.7 m
18	2.64 s	6.40 br d	7.42 q	6.93 dd	5.21 s					1.9—2.7 m
20	7.43 br d	6.30 dt	7.31 br t	6.86 br d	1.16 c) t	1.16 t	1.16 t	4.09 q	4.09 q	1.7—2.7 m
30[e,f]	7.67 br d	6.51 dt	7.47 br t	7.00 br d	1.81 s	1.21 d	1.31 d			1.7—3.1 m
31[e,g]	7.62 br d	6.50 dt	7.45 br t	7.00 br d	1.12 c) t	1.21 d	1.31 d			1.7—3.1 m
32	d)	6.83 m	d)	d)	7.1—7.9 m	1.25 d	1.39 d			1.7—3.1 m
33[e,h]	7.36 br d	6.24 dt	7.28 br t	6.77 br d	1.77 s	1.08 t	i, j)			1.7—2.9 m
34	7.31 br d	6.17 dt	7.27 br t	6.76 br d	i, c)	1.08 t	i, j)			1.7—2.7 m
35	d)	6.39 m	d)	d)	7.0—7.9 m	1.09 t	i, j)			1.7—3.0 m

a) The NMR data of compounds **19** and **21** were already described in Ref. 1, while those of **22**—**24** could not be measured owing to the low solubility. b) The coupling constants were as follows: $J_{5,6}=J_{6,7}=7.0$ Hz, $J_{7,8}=9.0$ Hz, $J_{6,8}=1.5$ Hz or 2.0 Hz, $J_{Et}=7.0$ Hz, and $J_{CHMe}=7.0$ Hz. c) Overlapped with the methylene protons. d) Overlapped with the phenyl protons. e) Major product. f) The 1-methyl signal of minor product appeared at δ 1.83 and the other signals were overlapped with those of major product. g) The methyl signal of the 1-ethyl group of minor product appeared at δ 1.11 and the other signals were overlapped with those of major product. h) The 1-methyl signal of minor product appeared at δ 1.80 and the other signals were overlapped with those of major product. i) Overlapped with the methyl protons in the ethoxycarbonyl groups. j) These methylene signals of the ethoxycarbonyl groups appeared at δ 3.5—4.4 as complex multiplets.

TABLE 3. NMR DATA OF SPIRO[CYCLOHEXANE-1,3′(2′*H*)-INDOLIZIN]-2′-ONES

Compd[a] No.	C-5	C-6	C-7	C-8	C-1	OH	C-Me	Ac	CHAc	Methylene
37[b]	7.56 br d	6.34 dt	7.34 br t	6.86 br d	1.77 s	4.03 s	1.33 s	2.28 s	4.11 q	1.4—2.7 m
38[c]	7.51 br d	6.38 dt	7.40 br t	6.84 br d	1.76 s	5.74 s	1.30 s	2.37 s	4.50 q	1.4—2.4 m
39[b]	7.55 br d	6.31 dt	7.31 br t	6.87 br d	1.08 d) t	4.02 s	1.33 s	2.28 s	4.10 q	1.4—2.4 m
40[b]	e)	6.50 m	e)	e)	7.1—7.9 m	4.04 s	1.36 s	2.28 s	4.15 q	1.4—2.7 m

a) The coupling constants were as follows: $J_{5,6}=J_{6,7}=7.0$ Hz, $J_{7,8}=9.0$ Hz, $J_{6,8}=1.5$ Hz, and $J_{CH_2CHAc}=12.0$ and 4.0 Hz. b) Substance with high solubility. c) Substance with low solubility. d) Overlapped with the methylene protons. e) Overlapped with the phenyl protons.

to be double Michael adducts of olefins **11**—**13**, **28**, and **29** to 2(3*H*)-indolizinones **6**—**10**, and **37**—**40** to be further condensed spiro[cyclohexane-1,3′(2′*H*)-indolizin]-2′-one derivatives. The stereochemistry of **30**—**35** and **37**—**40** were still uncertain, however.

The smooth formation of 3-spiroindolizinones **37**—**40**, perhaps *via* aldol reaction of the 1 : 2 adducts such as **41**, prompted us to investigate the possibility of similar cyclizations of other adducts. However, many attempts to obtain the corresponding spiro compounds

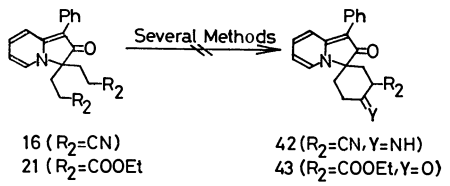

Scheme 3.

such as **42** and **43** from a nitrile **16** and an ester **21** were unsuccessful.[7]

Reactions of ***6*****—****10** *with Activated Ethylenes Possessing an Appropriate Leaving Group and an Acetylenic Ester.* In the *C*-alkylation and the Michael addition of 2(3*H*)-indolizinones such as **6**—**10**, the exclusive formation of the corresponding 3,3-disubstituted derivatives was always observed. However, in the reactions of **6** and **8**—**10** with active ethoxymethylene compounds, only 2*H*-pyrano[2,3-*b*]indolizin-2-one derivatives (formed *via* primary 1:1 Michael adducts between them) were isolated, though the yields were low.[1] The primary adducts could be detected with ease, by means of TLC, from the reaction mixtures at early stage of the addition of the ethoxymethylene compounds; however, they were very sensitive to air and a column chromatographic operation and thus they could not be isolated in pure form. In order to confirm the intermediacy of the labile adducts such as **45** and/or **46** shown in Scheme 4 and to find the method for the functionalization of these 2(3*H*)-indolizinones, their conversions to more stable derivatives, especially the replacements of the active proton at the 3-position in **45** and/or the hydroxyl proton in **46** with some acylating and alkylating agents, were attempted.

The reactions were performed stepwise as follows: 1) The treatment of pyridinium salt with two molar amounts of ethanolic sodium ethoxide (or methanolic sodium methoxide), 2) the addition of an equimolar amount of a vinylating agent, and 3) the addition of excess acylating or alkylating agent. For example, the reactions of salts **1**—**5**, ethyl (ethoxymethylene)-cyanoacetate **44**, and acetic anhydride **47** in the presence of alkali afforded yellow crystalline products, 2-acetoxy-3-vinylindolizine derivatives **52**—**56**, in 47—96% yields. Similar reactions in which benzoyl chloride **48**, dimethyl sulfate **49**, and ethyl bromoacetate **51** instead of **47** were used as an acylating or an alkylating agent gave the corresponding 2-benzoyloxy-**57**—**61**, 2-methoxy- **62**—**66**, and 2-(ethoxycarbonylmethoxy)-3-vinylindolizines **67**—**71**, respectively, as yellow or red crystals. The same 2-methoxy compounds **62** and **64** were also obtained by the reactions of **6** and **8** with **44** and methyl iodide **50**, but the yields were low (17 and 27%).

In order to establish the scope and limitation of this reaction, the uses of other ethoxymethylenes, a ketene dithioacetal, and an acetylenic ester as vinylating agents were investigated. For example, the

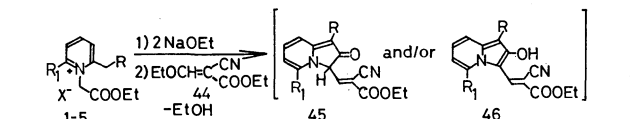

	R	R_1	R_4
52	Me	H	Ac
53	Et	H	Ac
54	Ph	H	Ac
55	H	H	Ac
56	H	Me	Ac
57	Me	H	PhCO
58	Et	H	PhCO
59	Ph	H	PhCO
60	H	H	PhCO
61	H	Me	PhCO

	R	R_1	R_4
62	Me	H	Me
63	Et	H	Me
64	Ph	H	Me
65	H	H	Me
66	H	Me	Me
67	Me	H	CH_2COOEt
68	Et	H	CH_2COOEt
69	Ph	H	CH_2COOEt
70	H	H	CH_2COOEt
71	H	Me	CH_2COOEt

	R_4Z
47	Ac_2O
48	PhCOCl
49	Me_2SO_4
50	MeI
51	$EtOOCCH_2Br$

52-71

Scheme 4.

treatment of **6**—**10** or **6** and **8** with (ethoxymethylene)-malononitrile **72**, diethyl (ethoxymethylene)malonate **73**, and (ethoxymethylene)acetylacetone **74**, followed by the acetylation with acetic anhydride **47** gave the corresponding 2-acetoxy-3-vinylindolizine derivatives **75**—**83** in 32—91% yields (Scheme 5), while those of **6** and **8** with [bis(methylthio)methylene]malononitrile **84** and dimethyl acetylenedicarboxylate (DMAD) **87** afforded products **85**, **86**, **88**, and **89** in 75, 62, 70, and 60% yields, respectively (Scheme 6).

Structural assignments of these 2-(R_4-oxy)-3-vinylindolizine derivatives **52**—**71**, **75**—**83**, **85**, **86**, **88**, and **89** were achieved by their elementary analyses, spectral inspection, and partly on the basis of unequivocal syntheses. In particular, all of their elementary analyses were in good accord with the proposed compositions, and the IR spectra showed an α,β-unsaturated cyano band(s) at near 2200 cm^{-1} (**52**—**71**, **75**—**79**, **85**, and **86**) and/or an α,β-unsaturated carbonyl band(s) at 1653—1729 cm^{-1} (**52**—**71**, **80**—**83**, **88**, and **89**) attributable to the vinyl group introduced in these reactions (Table 4), but not the 2-keto carbonyl band at near 1600 cm^{-1} as seen in those of 2(3*H*)-indolizinones. The chemical shifts of the protons and alkyl protons on the indolizine ring in the NMR spectra of these products were much closer to those of aromatic indolizines rather than nonaromatic 2(3*H*)-indolizinones (Table 5). Furthermore, the chemical shifts (near δ 4.00) of the methyl protons in **62**—**66** and those (near δ 4.80) of the methylene protons in **67**—

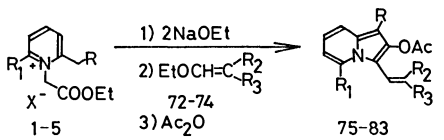

	R_2	R_3
72	CN	CN
73	COOEt	COOEt
74	Ac	Ac

	R	R_1	R_2	R_3
75	Me	H	CN	CN
76	Et	H	CN	CN
77	Ph	H	CN	CN
78	H	H	CN	CN
79	H	Me	CN	CN
80	Me	H	COOEt	COOEt
81	Ph	H	COOEt	COOEt
82	Me	H	Ac	Ac
83	Ph	H	Ac	Ac

Scheme 5.

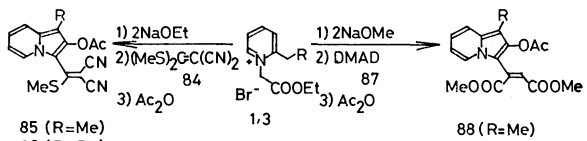

Scheme 6.

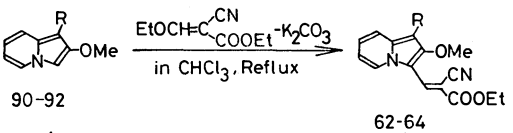

	R
90	Me
91	Et
92	Ph

	R
62	Me
63	Et
64	Ph

Scheme 7.

TABLE 4. SOME DATA OF 3-VINYLINDOLIZINES

Compd No.	Reactants			Yield %	Mp θ_m/°C	$\tilde{\nu}$/cm^{-1} (KBr) C=O	(CN)	Formula	Calcd (%) C	H	N	Found(%) C	H	N
52	**1**	**44**	**47**	96	122—124	1768 1699	(2208)	$C_{17}H_{16}N_2O_4$	65.37	5.16	8.97	65.39	5.16	8.96
53	**2**	**44**	**47**	47	49— 51	1764 1700	(2204)	$C_{18}H_{18}N_2O_4$	66.25	5.56	8.58	66.33	5.49	8.56
54	**3**	**44**	**47**	89	153—154	1765 1686	(2205)	$C_{22}H_{18}N_2O_4$	70.58	4.85	7.48	70.48	4.88	7.19
55	**4**	**44**	**47**	93	112—113	1750 1695	(2200)	$C_{16}H_{14}N_2O_4$	64.42	4.73	9.39	64.37	4.76	9.41
56	**5**	**44**	**47**	94	165—167	1770 1700	(2212)	$C_{17}H_{16}N_2O_4$	65.37	5.16	8.97	65.52	5.14	8.84
57	**1**	**44**	**48**	60	136—138	1740 1690	(2202)	$C_{22}H_{18}N_2O_4$	70.58	4.85	7.48	70.67	4.77	7.46
58	**2**	**44**	**48**	57	98—100	1725 1695	(2195)	$C_{23}H_{20}N_2O_4$	71.12	5.19	7.21	71.15	5.19	7.22
59	**3**	**44**	**48**	48	181—183	1736 1702	(2200)	$C_{27}H_{20}N_2O_4$	74.30	4.62	6.42	74.39	4.63	6.32
60	**4**	**44**	**48**	24	115—117	1740 1681	(2195)	$C_{21}H_{16}N_2O_4$	69.99	4.48	7.77	70.04	4.40	7.80
61	**5**	**44**	**48**	52	161—163	1731 1702	(2208)	$C_{22}H_{18}N_2O_4$	70.58	4.85	7.48	70.32	4.79	7.42
62	**1**	**44**	**49**	80	106—108	1689	(2208)	$C_{16}H_{16}N_2O_3$	67.59	5.67	9.85	67.80	5.68	9.85
	1	**44**	**50**	17	106—108									
63	**2**	**44**	**49**	52	80— 83	1686	(2210)	$C_{17}H_{18}N_2O_3$	68.44	6.08	9.39	68.44	6.15	9.33
64	**3**	**44**	**49**	57	88— 90	1695	(2192)	$C_{21}H_{18}N_2O_3$	72.82	5.24	8.09	72.75	5.33	8.04
	3	**44**	**50**	27	88— 90									
65	**4**	**44**	**49**	37	78— 81	1685	(2200)	$C_{15}H_{14}N_2O_3$	66.66	5.22	10.36	66.60	5.23	10.30
66	**5**	**44**	**49**	91	113—115	1690	(2201)	$C_{16}H_{14}N_2O_3$	67.59	5.67	9.85	67.35	5.65	9.78
67	**1**	**44**	**51**	62	123—125	1741 1691	(2206)	$C_{19}H_{20}N_2O_5$	64.04	5.66	7.86	64.20	5.59	7.77
68	**2**	**44**	**51**	55	99—101	1740 1690	(2205)	$C_{20}H_{22}N_2O_5$	64.85	5.99	7.56	64.77	6.00	7.51
69	**3**	**44**	**51**	70	121—124	1719 1703	(2200)	$C_{24}H_{22}N_2O_5$	68.89	5.30	6.69	68.90	5.31	6.67
70	**4**	**44**	**51**	28	96— 98	1737 1685	(2200)	$C_{18}H_{18}N_2O_5$	63.15	5.30	8.18	63.37	5.58	7.89
71	**5**	**44**	**51**	40	130—131	1732 1680	(2195)	$C_{19}H_{20}N_2O_5$	64.04	5.66	7.86	64.00	5.63	7.82
75	**1**	**72**	**47**	91	202—204	1755	(2210)	$C_{15}H_{11}N_3O_2$	67.92	4.18	15.84	67.87	4.14	15.93
76	**2**	**72**	**47**	54	201—203	1760	(2215)	$C_{16}H_{13}N_3O_2$	68.80	4.69	15.05	69.03	4.65	15.12
77	**3**	**72**	**47**	80	178—180	1771	(2218)	$C_{20}H_{13}N_3O_2$	73.38	4.00	12.84	73.35	4.07	12.81
78	**4**	**72**	**47**	57	200—202	1770 (2210	2198)	$C_{14}H_9N_3O_2$	66.93	3.61	16.73	66.84	3.69	16.73
79	**5**	**72**	**47**	89	176—178	1772	(2208)	$C_{15}H_{11}N_3O_2$	67.92	4.18	15.84	67.70	4.30	15.84
80	**1**	**73**	**47**	32	82— 83	1754 1716	1695	$C_{19}H_{21}NO_6$	63.50	5.89	3.90	63.54	5.93	3.85
81	**3**	**73**	**47**	38	118—120	1770 1715	1700	$C_{24}H_{23}NO_6$	68.40	5.50	3.33	68.48	5.74	3.03
82	**1**	**74**	**47**	74	142—144	1765 1653		$C_{17}H_{17}NO_4$	68.22	5.72	4.68	68.37	5.62	4.63
83	**3**	**74**	**47**	76	109—112	1773 1658		$C_{22}H_{19}NO_4+H_2O$	69.65	5.58	3.69	69.88	5.39	3.64
85	**1**	**84**	**47**	75	168—171	1762	(2200)	$C_{16}H_{13}N_3O_2S$	61.72	4.21	13.50	61.85	4.15	13.43
86	**3**	**84**	**47**	62	143—145	1759	(2206)	$C_{21}H_{15}N_3O_2S$	67.54	4.05	11.25	67.55	4.16	11.28
88	**1**	**87**	**47**	70	115—117	1760 1729	1693	$C_{17}H_{17}NO_6$	61.63	5.17	4.23	61.66	5.15	4.21
89	**3**	**87**	**47**	60	91— 94	1770 1722	1706	$C_{22}H_{19}NO_6$	67.17	4.87	3.56	67.21	4.87	3.52

71 derived from the alkylating agents **49**—**51** showed definitely that both groups were attached on an oxygen atom but not on the other atoms. Independent syntheses of 2-methoxy-3-vinylindolizines **62**—**64**, that is to say, the direct 3-vinylation of 2-methoxyindolizines **90**—**92** with **44** in the presence of alkali supported these proposed structures (Scheme 7). On the other hand, the configuration of the 3-vinyl moiety in **52**—**71** were concluded to be *trans* by the comparisons of the chemical shifts (δ 8.23—8.43) of the vinyl protons with those of similar 1-[8] and 3-vinylindolizines[2] and 3-vinylpyrazolo[1,5-*a*]pyridines,[9] but that in **88** and **89** were assigned tentatively to be *cis* by similar comparison of the vinyl proton signals at δ 6.18 and 6.30 with those at δ 6.48 and 6.80 in dimethyl maleate and dimethyl fumarate, respectively.

Reaction Mechanisms. Possible mechanisms for these reactions are summarized concisely in Scheme 8. Path a leading to compounds **14**—**24**, **30**—**35**, and **37**—**40** is the double Michael addition of electron-poor olefins **11**—**13**, **28**, **29**, and **36** to 3-unsubstituted 2(3*H*)-indolizinones **6**—**10** in the presence of alkali, and, in part, followed by the Aldol reaction of the primary 1:2 adducts such as **41**, and Path b leading to 2-(R_4-oxy)-3-vinylindolizines **52**—**71**, **75**—**83**, **85**, **86**, **88**, and **89** is the single Michael addition of vinylating agents **44**, **72**—**74**, **84**, and **87** to **6**—**10** and the elimination of one molecule of ethanol from **93**, followed by keto–enol isomerization and finally by the *O*-acylation or the *O*-alkylation of the resulting 3-vinyl-2-indolizinol **95**. Recently, the isolation of 2-indolizinol such as **95** in the reaction of 2,6-dimethylpyridinium salt **5** with a ketene dithioacetal was reported by Kobayashi *et al.*[10] The reason for the different behavior between the 1:1 and 1:2 Michael additions in these reactions was still uncertain, but the steric effect of the incoming olefins and the influence of the conjugation of the 3-vinyl group may be con-

Table 5. NMR data of 3-vinylindolizines

Compd[a] No.	C-5	C-6	C-7	C-8	C-1	Vinyl R_2 and R_3				R_4
52	8.28 br d	6.88 dt	7.17 br t	7.47 br d	2.13 s	8.28 s	1.37 t	4.38 q		2.55 s
53	8.33 br d	6.91 dt	7.18 br t	7.52 br d	1.20 t 2.61 q	8.31 s	1.38 t	4.35 q		2.52 s
54	8.36 br d	6.96 dt	— b) —		7.0—7.8 m	8.39 s	1.37 t	4.34 q		2.34 s
55	8.30 br d	6.92 dt	7.19 br t	7.50 br d	6.82 s	8.38 s	1.40 t	4.38 q		2.50 s
56	2.88 s	6.67 br d	7.02 q	7.39 dd	6.82 s	8.77 s	1.40 t	4.38 q		2.51 s
57	b)	6.93 dt	b)	b)	2.18 s	8.30 s	1.33 t	4.30 q		7.0—8.5 m
58	b)	6.95 dt	b)	b)	1.19 t 2.66 q	8.31 s	1.30 t	4.29 q		7.1—8.6 m
59	b)	6.97 dt	b)	b)	7.1—7.9 m	8.37 s	1.38 t	4.28 q		7.1—8.5 m
60	b)	6.93 dt	b)	b)	6.83 s	8.40 s	1.36 t	4.33 q		7.1—8.6 m
61	2.83 s	6.62 br d	7.02 q	b)	6.77 s	8.75 s	1.33 t	4.30 q		7.3—8.5 m
62	8.29 br d	6.82 dt	7.13 br t	7.38 br d	2.30 s	8.23 s	1.38 t	4.33 q		4.07 s
63	8.38 br d	6.90 dt	7.18 br t	7.49 br d	1.25 t 2.80 q	8.31 s	1.38 t	4.35 q		4.08 s
64	8.37 br d	6.90 dt	b)	b)	7.0—7.7 m	8.37 s	1.40 t	4.37 q		3.77 s
65	8.33 br d	6.82 dt	7.13 br t	7.38 br d	6.08 s	8.27 s	1.37 t	4.33 q		4.00 s
66	2.82 s	6.59 br d	7.02 q	7.27 dd	6.13 s	8.68 s	1.38 t	4.32 q		4.03 s
67	8.40 br d	6.91 dt	7.20 br t	7.43 br d	2.29 s	8.41 s	1.38 t	4.37 q		4.86 c) s
68	8.42 br d	6.93 dt	7.20 br t	7.38 br d	1.25 t 2.80 q	8.43 s	1.30 t	4.38 q		4.82 d) q
69	8.46 br d	6.95 dt	b) br t	b) br d	7.0—7.7 m	8.53 s	1.39 t	4.37 q		4.53 e) s
70	8.42 br d	6.90 dt	7.20 br t	7.31 br d	6.03 s	8.38 s	1.38 t	4.38 q		4.81 f) s
71	2.84 s	6.63 br d	7.04 q	7.30 dd	6.06 s	8.78 s	1.37 t	4.33 q		4.85 g) s
75	8.23 br d	7.00 dt	7.27 br t	7.53 br d	2.15 s	7.57 s				2.52 s
76	8.27 br d	7.00 dt	7.28 br t	7.57 br d	1.19 t 2.61 q	7.57 s				2.51 s
77	8.29 br d	7.02 dt	b)	b)	7.1—7.8 m	7.67 s				2.32 s
78	8.25 br d	7.00 dt	7.28 br t	7.55 br d	6.90 s	7.63 s				2.50 s
79	2.85 s	6.75 br d	7.16 q	7.42 dd	6.88 s	8.08 s				2.48 s
80	8.08 br d	6.73 dt	7.00 br t	7.42 br d	2.12 s	7.98 s	1.23 t	1.33 t	4.33 q 4.35 q	2.35 s
81	8.11 br d	6.91 dt	b)	b)	7.0—7.8 m	8.00 s	1.29 t	1.34 t	4.32 q 4.37 q	2.17 s
82	8.12 br d	6.79 dt	7.07 br t	7.76 br d	2.13 s	7.97 s	2.30 s	2.37 s		2.37 s
83	8.19 br d	6.87 dt	b)	b)	7.0—7.8 m	8.01 s	2.13 s	2.36[h] s		2.43[i] s
85	8.39 br d	6.87 dt	7.10 br t	7.46 br d	2.18[j] s	2.20[k,l] s				2.41 s
86	8.40 br d	b)	b)	b)	6.7—7.8 m	2.29[l] s				2.29 s

TABLE 5. (Continued)

Compd[a] No.	C-5	C-6	C-7	C-8	C-1	Vinyl R_2 and R_3			R_4
88	8.30 br d	6.67 dt	6.91 br t	7.41 br d	2.08 s	6.18 s	3.75 s	3.90 s	2.30 s
89	8.37 br d	6.73 dt	6.97 br t	b) br d	7.1—7.8 m	6.30 s	3.80 s	3.94 s	2.19 s

a) The coupling constants were as follows: $J_{5,6}=J_{6,7}=7.0$ Hz, $J_{7,8}=9.0$ Hz, $J_{6,8}=1.5$ Hz, and $J_{Et}=7.0$ Hz. b) Overlapped with the phenyl protons. c) The ethoxycarbonyl signals appeared at δ 1.29 (t) and 4.27 (q). d) The ethoxycarbonyl signals appeared at δ 1.30 (t) and 4.28 (q). e) The ethoxycarbonyl signals appeared at δ 1.17 (t) and 4.10 (q). f) The ethoxycarbonyl signals appeared at δ 1.30 (t) and 4.29 (q). g) The ethoxycarbonyl signals appeared at δ 1.28 (t) and 4.28 (q). h) Or δ 2.43. i) Or δ 2.36. j) Or δ 2.20. k) Or δ 2.18. l) The methylthio protons.

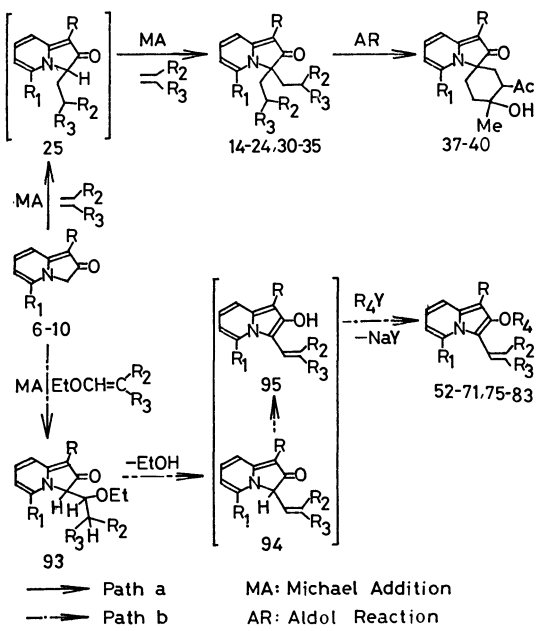

Scheme 8.

sidered.

Since effective functionalization of indolizine nucleus, except the synthesis of cyclazine[11] and the route *via* 2-allylidene-1,2-dihydropyridine,[8] are scarcely found, our present reactions using the Michael additions of 3-unsubstituted 2(3*H*)-indolizinones may provide useful routes for the preparations of condensed indolizine series owing to the simplicity of the procedure and of easy availability of starting materials.

Experimental

Melting points were measured with a Yanagimoto MP-S3 micromelting point apparatus and are uncorrected. Microanalyses were carried out on a Perkin-Elmer 240 elemental analyzer. The NMR spectra were determined with a Varian EM360A spectrometer in deuteriochloroform with tetramethylsilane as an internal standard. The chemical shifts are expressed in δ values. The IR spectra were taken with a Hitachi 260-10 infrared spectrophotometer.

Reactions of 2(3H)-Indolizinones ***6—10*** *with α,β-Unsaturated Nitriles, Esters, an Amide, and a Ketone. Method A*: To an ethanolic solution (60 ml) of 1-(ethoxycarbonylmethyl)-2-methylpyridinium salts (**1—5**, 5 mmol) and α,β-unsaturated compound (**11—13**, **28**, **29**, and **36**, 20 mmol) was added dropwise aqueous potassium hydroxide (5.5 mmol in 1 ml of water) with stirring at room temperature. After the addition the reaction mixture was stirred at the same temperature for about 2 h until the 2(3*H*)-indolizinone (**6—10**) formed *in situ* was disappeared (detected by TLC) and then filtered to remove insoluble substances. The filtrate was concentrated under reduced pressure, and the residue was separated by column chromatography (alumina) using ether and then chloroform as eluents. Recrystallization from chloroform–hexane gave yellow or orange crystals.

Method B: In similar procedure with Method A, anhydrous potassium carbonate (10 g) as a base was employed and the reactions required more prolonged times (12—24 h) than those in Method A.

Method C: As in Method B, ethanolic sodium ethoxide (5 mmol in 5 ml of ethanol) as a base was used and the reactions required the shortest times (1—2 h) among those in the three methods. On the other hand, the reactions of **6—8** with acrylamide **13** were carried out successfully at 60—70 °C for 1 h, since they were very slow at room temperature.

In the reactions of **6—8** with methacrylonitrile **28** and ethyl methacrylate **29**, the fact that these products **30—35** were mixtures of two stereoisomers (the individual isomers must be *dl*-pair or meso) was indicated by the TLC and also by the NMR spectra. However, our attempts to separate them were unsuccessful. In the reactions of **7** and **8** with methyl vinyl ketone **36** the low soluble products such as **37** could not be obtained. These results and spectral data are summarized in Tables 1—3.

Reactions of ***6*** *and* ***8*** *with 3-Chloropropionitrile* ***26*** *and Ethyl 3-Bromopropionate* ***27***. *General Method*: A mixture of pyridinium salt (**1** or **3**, 5 mmol) and halide (**26** or **27**, 20 mmol) was treated with ethanolic sodium ethoxide (10 mmol in 10 ml of ethanol) in ethanol (60 ml) with stirring at room temperature for 2 h. The resulting brown solution was filtered, and the filtrate was then concentrated at reduced pressure. The same work-ups of the residues as shown in Method A gave yellow crystalline compounds **14**, **16**, **19**, and **21** in 57, 76, 67, and 89% yields, respectively. These compounds **14**, **16**, **19**, and **21** coincided with those prepared above and also with authentic samples[1] in all respects.

Reactions of ***6—10*** *with Activated Ethylenes Possessing an Appropriate Leaving Group and an Acetylenic Ester. General Method*: Pyridinium salt (**1—5**, 3 mmol) dissolved completely in ethanol (50 ml) was heated with an ethanolic sodium ethoxide (6 mmol in 6 ml of ethanol) at 60—70 °C for 2—3 min and then an equimolar amount of vinylating agent (**44**, **72—74**, **84**, or **87**, 3 mmol) was added at once to the reaction mixture. After 1—2 min excess acylating or alkylating agent (**47—51**, 2 ml) was added and the resulting solution

was allowed to react for additional 30 min at the same temperature. The reaction mixture was filtered to remove insoluble inorganic substances and the filtrate was concentrated at reduced pressure. The residue was separated by column chromatography (alumina) using ether and then chloroform as eluents. Recrystallizations from ethanol or chloroform–hexane gave yellow (**52**—**56**, **62**—**71**, **75**—**83**, **88**, and **89**) or red needles (**57**—**61**, **85**, and **86**).

On the other hand, the reactions of **1** and **3** with dimethyl acetylenedicarboxylate **87** were performed in the presence of sodium methoxide as a base in methanol. These results and some data are summarized in Tables 4 and 5.

Reactions of 2-Methoxyindolizines ***90***—***92*** *with Ethoxymethylene Compound* ***44***. *General Method*: A mixture of 2-methoxyindolizine (**90**—**92**, 1 mmol) and ethyl (ethoxymethylene)-cyanoacetate **44** (1 mmol) was heated under reflux in the presence of potassium carbonate (5 g) in chloroform (50 ml) for 3 d. The reaction mixture was filtered and the filtrate was concentrated at reduced pressure. The same work-ups of the residues as indicated in the syntheses of 3-vinylindolizines gave the corresponding 2-methoxy-3-vinylindolizine derivatives **62**—**64** in 81, 89, and 24% yields, respectively. These products **62**—**64** were in accord with those synthesized by the reactions of **6**—**8** with **44** and **49** or **50** in all respects.

References

1) A. Kakehi, S. Ito, K. Watanabe, M. Kitagawa, S. Takeuchi, and T. Hashimoto, *J. Org. Chem.*, **45**, 5100 (1980).
2) Y. Yamashita, D. Suzuki, and M. Masumura, *Heterocycles*, **16**, 1499 (1981).
3) A. Kakehi, S. Ito, and B. Wada, 12th Autumnal Joint Meeting of the Tokai Branch of the Chemical Society of Japan and the Chubu Branches of the Related Society, (1981), No. 1B07, p. 61.
4) J. W. Cornforth and R. Robinson, *J. Chem. Soc.*, **1949**, 1855.
5) A. Kakehi, S. Ito, K. Nakanishi, K. Watanabe, and M. Kitagawa, *Bull. Chem. Soc. Jpn.*, **53**, 1115 (1980).
6) The ratios of the major and minor compounds could not be determined by their NMR spectral inspections, because of the very close signals. Furthermore, definitely isolable signals of the minor products in the NMR spectra of **32**, **34**, and **35** could not be found.
7) The alkaline conditions employed usually in Thorpe and Diechmann condensations were carried out (sodium ethoxide/benzene, potassium *t*-butoxide/toluene, sodium hydride/DMSO, and so on).
8) A. Kakehi, S. Ito, T. Maeda, R. Takeda, M. Nishimura, M. Tamashima, and T. Yamaguchi, *J. Org. Chem.*, **43**, 4837 (1978).
9) A. Kakehi, S. Ito, K. Uchiyama, and K. Kondo, *J. Org. Chem.*, **43**, 2896 (1978).
10) K. Kurata, H. Awaya, Y. Tominaga, Y. Masuda, and G. Kobayashi, *Yakugaku Zasshi*, **101**, 980 (1981).
11) V. Boekelheide and K. Fahrenholtz, *J. Am. Chem. Soc.*, **83**, 458 (1961).

Intramolecular Stacking Association of Three Dinucleoside Monophosphates Containing Naturally-occurring 1-Methyladenosine Residue(s): m^1ApA, Apm^{1}A, and m^1Apm^{1}A[1)]

Yasuhiro Takeuchi, Ichiro Tazawa, and Yasuo Inoue*

Department of Biophysics and Biochemistry, Faculty of Science, The University of Tokyo, Hongo, Bunkyo-ku, Tokyo 113

(Received June 18, 1982)

Three modified dinucleoside monophosphates containing naturally-occurring 1-methyladenosine residue, m^1ApA, Apm^{1}A, and m^1Apm^{1}A, were prepared. Intramolecular stacking association properties of these dimers were studied quantitatively using two independent methods. Thermal denaturation and acid-base titration experiments reached to the same conclusion that both $m^1\overset{+}{A}pA$ and Apm$^1\overset{+}{A}$ were less stacked than ApA. Acid-base titration experiment also showed that the three modified dimers, in their neutral forms, were stacked to almost the same extent as ApA. These results indicate the N-1 methylation of an adenine base does not enhance stacking interaction of dimers, in sharp contrast to the N^6 methylation of the same base. UV hypochromicity and CD measurements were also made for the three dimers, and the results were found to be consistent with those of the stacking quotient determination.

As a part of studies on the intramolecular stacking interaction of modified base-containing dinucleoside monophosphates,[2–7)] dimers containing 1-methyladenosine (m^1A) were studied in order to see the effect of a methyl substitution at a ring nitrogen atom of an adenine base on stacking association. In view of a wide occurrence of m^1A residue in eukaryotic tRNA molecules,[8)] it is of interest to study the effect of this residue on the stacking properties and compare it with that of other methylated base residues.

It is well established that a variety of methylated dinucleoside monophosphates exhibit stronger stacking tendency as compared to the unmethylated corresponding parent dimers. For example results from our laboratory and those from others have revealed that N^6 methylation of an adenine base enhances stacking interaction in dimers, as did so for m^6Apm^{6}A,[6)] m_2^6Apm$_2^6$A,[7,9)] m^6ApU,[9,10)] and m_2^6ApU.[9,10)] Little is known, however, about the effect of a m^1A residue on stacking of dimers. Danyluk *et al.* first reported that $m^1\overset{+}{A}pU$ and Upm$^1\overset{+}{A}$ were less stacked than unmethylated ApU and UpA, respectively, as studied by ^{1}H NMR spectroscopy.[11)] Their results are noteworthy in view of the general stacking-enhancing properties of a methyl substituent and the fact that the $m^7\overset{+}{G}$ residue is known to exert such an effect as observed in our previous work for $m^7\overset{+}{G}pU$[3)] and $m^7\overset{+}{G}pG$.[4)]

We have undertaken a detailed study on the effect of m^1A residue on the stacking properties of dimers using three dinucleoside monophosphates, m^1ApA, Apm^{1}A, and m^1Apm^{1}A. Using two independent methods, thermal denaturation and acid-base titration experiments, the stacking quotients were estimated for these three dimers and compared with those for the parent molecule, ApA. Because m^1A exists in the protonated form (Fig. 1) in neutral aqueous solutions (basic pK of m^1A is 8.76, see Table 2), the stacking properties of the monoprotonated dimers were studied together with those of the neutral forms. Optical properties (UV and CD spectra) of the three dimers were also studied, and results were compared with those of the stacking quotients determined.

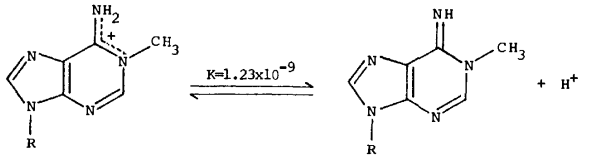

($m^1\overset{+}{A}$) (m^1A)

R = Ribosyl residue

Fig. 1. Acid-base equilibrium in 1-methyladenosine,

Experimental

Materials. m^1Apm^{1}A, m^1ApA, and Apm^{1}A: To ApAp (3′) (9 μmol), dissolved in 5 ml of 0.1 M NaOAc buffer (pH 5.0, 1 M = 1 mol dm^{-3}) was added 100 μl of dimethyl sulfate and the solution was kept under stirring for 3 h at room temperature. During the reaction the solution was maintained at pH 3—5 by gradual addition of 1 M NaOH solution. Figure 2 shows chromatographic separation of the products with a Dowex 1X2 anion exchanger (1.3 cm × 50 cm) which afforded three modified dinucleotides and unreacted ApAp(3′). m^1Apm^{1}Ap(3′), m^1ApAp(3′), and Apm^{1}Ap(3′)

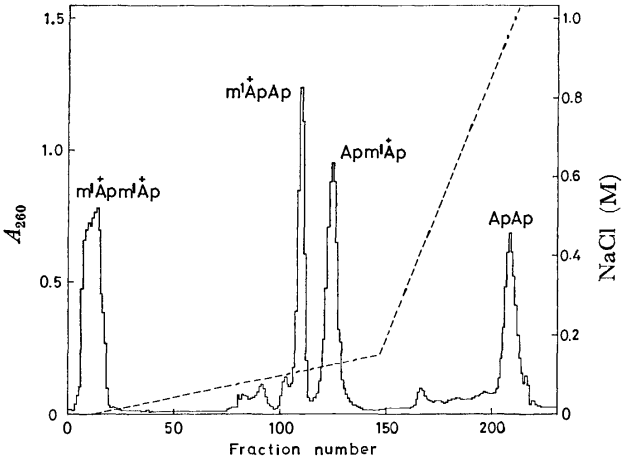

Fig. 2. Chromatogram of a partially methylated ApAp (3′) on a column of Dowex 1X2 (1.3 cm × 50 cm) with linear gradients of NaCl in 5 mM NaOAc (pH 5.0) as indicated. Fraction volume was 10 ml.

thus obtained were treated with *E. coli* alkaline phosphatase (Boehringer, Mannheim) at 39 °C and pH 7 for 4 h to give m¹Apm¹A, m¹ApA, and Apm¹A, respectively. The dimers were susceptible to degradation by ribonuclease T_2 and gave a mixture of the corresponding nucleoside 3′-phosphate and nucleoside. Desalting of the dimer preparations was effected by gel filtration using Sephadex G-10.

m¹A, m¹Ap-OCH₃, and CH₃O-pm¹A: A, Ap-OCH_3,[12] and CH_3O-pA[13] were treated with dimethyl sulfate in a manner similar to that described for ApAp(3′).

Methods. Thermal Denaturation of m¹ÅpA and Apm¹Å: In the present work, methods and calculations followed closely those described previously.[5,14] 3,3-Dimethylglutarate buffer (10 mM; pH 5.5) was used. The dimer concentrations were about 5×10^{-5} mol/l. For each dimer solution, 6 repeated denaturation cycles were performed in the temperature range 0—70 °C, and changes of the difference in absorbance (dimer *vs.* constituent monomers) at 262 nm with temperature were recorded using a recording millivolt meter (Watanabe Sokki MC642).

p*K Determinations of Nucleosides, Nucleoside Methyl Phosphates, and Dinucleoside Monophosphates*: All ionization constants were determined spectrophotometrically at 25 °C and ionic strength 0.1, by the method described previously.[15]

Optical Measurements: UV spectra were recorded with a Hitachi 124 recording spectrophotometer. CD spectra were taken with a JASCO J40 spectropolarimeter with a 1-cm quartz cell at 25 °C and ionic strength 0.1 (We thank Dr. T. Oshima, Mitsubishi-Kasei Institute of Life Sciences, for making the apparatus available to us). Spectra of the neutral dimers were not measured directly because of the lability of m¹A residues in high pH region ($t_{1/2}$ for Dimroth rearrangement of m¹A is about 5 h at pH 11 and 25°). Instead, spectra at several different pH values (as indicated in caption for Fig. 3) were measured and employed to compute the spectra of the neutral species with the knowledge of pK values of the dimers (Table 2).

Results and Discussion

Thermal Denaturation Experiments to Obtain Intramolecular Stacking Equilibrium Quotient, s_1, of m¹ÅpA and Apm¹Å. The thermal denaturation experiments were performed at pH 5.5 to obtain the stacking quotients for the monoprotonated form in which the dimers existed under the physiological conditions (see Table 2). Both dimers showed hyperchromism at 262 nm on heating their solutions. The thermal denaturation profiles were analyzed based on the two-state equilibrium model shown below for a specific case of m¹ÅpA.

$$(m^1\mathring{A}pA)_{unstacked} \overset{s_1}{\rightleftharpoons} (m^1\mathring{A}pA)_{stacked}$$

Here the equilibrium quotient, s_1, for the reversible association of an unstacked conformer, $(m^1\mathring{A}pA)_{unstacked}$, to give the stacked conformer, $(m^1\mathring{A}pA)_{stacked}$, is defined as

$$s_1 = \frac{[(m^1\mathring{A}pA)_{stacked}]}{[(m^1\mathring{A}pA)_{unstacked}]}$$

The stacking quotient, s_1, at a given temperature and thermodynamic functions, ΔH° and ΔS°, were then calculated according to Eq. 1 with the assumption that the parameters, ε_u, ε_s, ΔH°, and ΔS° are all temperature-independent.

$$\ln s_{1i} = \ln \frac{\varepsilon_u-\varepsilon_i}{\varepsilon_i-\varepsilon_s} = -\frac{\Delta H^\circ}{RT_i} + \frac{\Delta S^\circ}{R} \qquad (1)$$

where ε_i, ε_s, and ε_u are the observed molar absorption coefficients at the ith of n temperature readings, and those for the extreme stacked and unstacked conformers, respectively. In this case, the parameters ε_u, ε_s, ΔH°, and ΔS° were found by an iterative nonlinear least-squares approximation on a HITAC M-200H computer at the Computer Center of the University of Tokyo. The formalism and further details are available in Ref. 18

Table 1. Thermodynamic parameters and intramolecular stacking equilibrium quotients (s_1 or s_0)[a] of m¹ÅpA, Apm¹Å, and ApA[b] (25°, I=0.1)

Dimer	ΔH° (σ)[c] / kJ mol^{-1}	ΔS° (σ)[c] / J mol^{-1} deg^{-1}	s_1 or s_0(σ)[c]
m¹ÅpA	−18.5 (0.5)	−64.9 (1.4)	0.70 (0.02)
Apm¹Å	−23.0 (0.5)	−81.0 (1.6)	0.62 (0.02)
ApA	−21.1 (0.3)	−70.1 (0.9)	1.10 (0.01)

a) s_1 for m¹ÅpA and Apm¹Å (at pH 5.5). s_0 for ApA (at pH 7.0). s_1 and s_0 standing for the stacking quotients for monoprotonated and neutral speceis, respectively. b) Taken from our previous paper.[7] c) The standard deviations (σ) were computed from the root mean square (rms) values between experimental and calculated melting profiles as described in a previous paper.[18]

Table 1 lists the values of ΔH°, ΔS°, and stacking equilibrium quotient thus determined at 25 °C for m¹ÅpA and Apm¹Å, together with those for ApA (at pH 7.0)[7] for comparison. From s values in Table 1 it is concluded that m¹ÅpA and Apm¹Å are stacked to a similar extent, and considerably less stacked than the parent molecule, ApA. The same stacking-diminishing effect by m¹Å has been observed by Danyluk *et al.*[13] in m¹ÅpU and Upm¹Å. The present conclusion is rather surprising because the methyl group, when introduced to a nitrogen atom, has almost invariably been found stacking-enhancing in dimers.[3,4,6,7,9,10] To substantiate the above conclusion the acid-base titration experiments were performed.

Acid-base Titration Experiments to Obtain Stacking Equilibrium Quotients, s_1 and s_0 of m¹ApA, Apm¹A, and m¹Apm¹A. We have developed a procedure that can give an estimate of stacking equilibrium quotients of homodimers for both neutral and monoprotonated (or monoionized) species from their ionization constants and those of constituent monomers.[5,6,15,16] We now extend the method to heterodimers (XpY) in which X and Y are both acids or bases. For a diacidic base one can write the following schemes.

$$(\overset{+}{X}pY)_{u+s} \overset{K_2}{\rightleftharpoons} (XpY)^+_{u+s} \overset{K_1}{\rightleftharpoons} (XpY)_{u+s}$$

$$\begin{array}{ccccc} (\overset{+}{\mathrm{X}}\mathrm{p}\overset{+}{\mathrm{Y}})_s & \overset{K_{s2}}{\rightleftharpoons} & (\mathrm{XpY})_s^+ & \overset{K_{s1}}{\rightleftharpoons} & (\mathrm{XpY})_s \\ \updownarrow s_2 & & \updownarrow s_1 & & \updownarrow s_0 \\ (\overset{+}{\mathrm{X}}\mathrm{p}\overset{+}{\mathrm{Y}})_u & \overset{K_{u2}}{\rightleftharpoons} & (\mathrm{XpY})_u^+ & \overset{K_{u1}}{\rightleftharpoons} & (\mathrm{XpY})_u \end{array}$$

where subscripts, u and s, denote unstacked and stacked conformations, respectively, and u+s denotes composite of unstacked and stacked conformations. From these schemes the following equations can be derived which relate ionization constants of a dimer to its stacking equilibrium quotients at various stages of protonation.

$$\mathrm{p}K_2 = \mathrm{p}K_{u2} - \log(1+s_1)/(1+s_2) \quad (2)$$

$$\mathrm{p}K_1 = \mathrm{p}K_{u1} - \log(1+s_0)/(1+s_1) \quad (3)$$

Since s_2 is considered to be very small because of the electrostatic repulsion between two positively charged bases,[15,17,18] Eq. 2 can be simplified to

$$\mathrm{p}K_2 = \mathrm{p}K_{u2} - \log(1+s_1) \quad (4)$$

K_{u1} and K_{u2} are the intrinsic ionization constants for the unstacked residues which must be estimated in some way to solve Eqs. 3 and 4 for s_1 and s_0. For homodimers (X=Y), K_{u1} and K_{u2} have been approximated in the following way using ionization constants of the constituent monomers.[15]

$$K_{u1} = \frac{1}{2}K_0, \quad K_{u2} = 2K_0 \quad (5)$$

$$\mathrm{p}K_0 = \frac{1}{4}[\mathrm{p}K_{3'\text{-nucleotide}} + \mathrm{p}K_{5'\text{-nucleotide}} + 2\mathrm{p}K_{\text{nucleoside}}] \quad (6)$$

For heterodimers in which X and Y have similar basicity, estimation of the intrinsic K's is a complicated matter. However, if they differ markedly in their basicity (say, $|\mathrm{p}K_X - \mathrm{p}K_Y| > 4$), the intrinsic K's can be approximated in the same way as those of homodimers. That is, if $\mathrm{p}K_X > \mathrm{p}K_Y$, it follows that $[(\overset{+}{\mathrm{X}}\mathrm{pY})_u] \gg [(\mathrm{X}\overset{+}{\mathrm{p}}\mathrm{Y})_u]$. Consequently, K_{u1} and K_{u2} are regarded as the intrinsic K's of X and Y residues, respectively, which can be approximated by K_0 in Eq. 6 for X and Y, respectively.

In the present study, because of the large difference in basicity of m^{1}A and A residues in the dimers, values of s_1 and s_0 were obtained by acid-base titration of the dimers and the corresponding constituent monomers. The $\mathrm{p}K_1$ and $\mathrm{p}K_2$ values of m^{1}ApA, Apm^{1}A, and m^{1}Apm^{1}A determined by spectrophotometric titration are given in Table 2 together with the basic pK values of the constituent monomers [The latter values were used to estimate $\mathrm{p}K_{u1}$ and $\mathrm{p}K_{u2}$ values in Table 2]. For comparison, relevant values for ApA[7] are also included in the table.

Values of s_1 and s_0 for three dimers were calculated from the pK values in Table 2 using Eqs. 3 and 4, and listed in Table 3 together with those for ApA. From the numerical data in Table 3 we can draw the following conclusion:

(1) s_1 values of m$^1\overset{+}{\mathrm{A}}$pA (0.87) and Apm$^1\overset{+}{\mathrm{A}}$ (1.11) are similar to each other and they are smaller than s_0 of ApA (1.51). This result substantiates a conclusion reached from the thermal denaturation experiments, and shows that N-1 methylation of an adenine residue decreases the extent of intramolecular stacking interaction.

(2) s_1 values of m$^1\overset{+}{\mathrm{A}}$pA (0.87) and Apm$^1\overset{+}{\mathrm{A}}$ (1.11) are not significantly different from that of (ApA)$^{\pm}$ (1.14). This suggests that the presence of the methyl group itself does not influence the stacking interaction in these monoprotonated dimers.

(3) All four dimers have similar s_0 values. This suggests that in neutral form introduction of a methyl group neither enhances nor diminishes the extent of the stacking interaction of ApA.

Optical Studies of m^{1}ApA, Apm^{1}A, and m^{1}Apm^{1}A. UV absorption and hypochromicity data of the four dimers are shown in Table 4. In agreement with the conclusion from the stacking quotient measurements hypochromicity data indicate the stacking in m$^1\overset{+}{\mathrm{A}}$pA and Apm$^1\overset{+}{\mathrm{A}}$ being a little bit weaker than in ApA. The value for m$^1\overset{+}{\mathrm{A}}pm^1\overset{+}{\mathrm{A}}$ was found to be negligibly small, and this is also in line with the previous assumption of $s_2=0$.

The CD spectra of m$^1\overset{+}{\mathrm{A}}pA, Apm^1\overset{+}{\mathrm{A}}$, and their un-

TABLE 2. IONIZATION CONSTANTS (AS pK) OF m^{1}ApA, Apm^{1}A, m^{1}Apm^{1}A, ApA, AND THE CONSTITUENT NUCLEOSIDES, NUCLEOSIDE MONOPHOSPHATES, AND NUCLEOSIDE METHYL PHOSPHATES (25°, I=0.1), AND CALCULATED INTRINSIC pK's[a,b]

Dimer	pK_1	pK_2	pK_{u1}	pK_{u2}
m^{1}ApA	8.66 (0.02)	3.41 (0.03)	8.80 (0.01)	3.68 (0.01)
Apm^{1}A	8.73 (0.01)	3.36 (0.02)	8.80 (0.01)	3.68 (0.01)
m^{1}Apm^{1}A	8.91 (0.03)	8.29 (0.04)	9.10 (0.01)	8.50 (0.01)
ApA[c]	3.91 (0.03)	3.05 (0.07)	3.98 (0.01)	3.38 (0.01)

Monomer	pK	Monomer	pK
m^{1}A[d]	8.76 (0.01)	A[c]	3.61 (0.02)
m^{1}Ap-OCH$_3$[d]	8.79 (0.02)	Ap[c]	3.66 (0.01)
CH$_3$O-pm^{1}A[d]	8.90 (0.01)	pA[c]	3.85 (0.02)

a) Standard deviations of experimental values are shown in parentheses. b) For homodimers $\mathrm{p}K_{u1}$ and $\mathrm{p}K_{u2}$ were calculated by Eqs. 5 and 6. For heterodimers Eq. 6 was used, K_0 representing either K_{u1} or K_{u2}. c) Revised values from those given in our previous paper.[19] d) Methyl esters of 3'- and 5'-nucleotides were used to avoid an influence of an additional negative charge on the phosphate group in pH region near the pK values.

TABLE 3. ESTIMATED STACKING EQUILIBRIUM QUOTIENTS FROM THE DATA BASED ON TITRATION STUDIES (25°, I=0.1)[a]

Dimer	s_1	s_0
m^{1}ApA	0.87±0.15	1.62±0.23
Apm^{1}A	1.11±0.17	1.48±0.21
m^{1}Apm^{1}A	0.63±0.13	1.56±0.28
ApA[b]	1.14±0.35	1.51±0.43

a) The probable errors given for s_1 and s_0 values are based on errors in $\mathrm{p}K_{u1}$, $\mathrm{p}K_{u2}$, $\mathrm{p}K_1$, and $\mathrm{p}K_2$. b) Revised values from those given in our previous paper.[19]

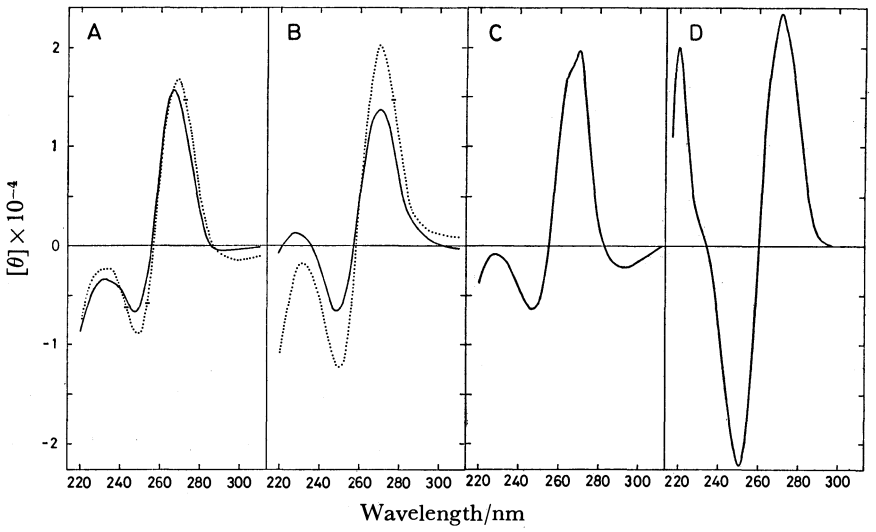

Fig. 3. Difference CD spectra of m¹ApA, Apm¹A, m¹Apm¹A, and ApA (25 °C, I=0.1). Spectra of the constituent monomers have been subtracted from those of dimers. Ellipticity is expressed per mole of monomer residues.
(A) ——, $m^1\overset{+}{A}pA$ at pH 6.0; ----, m¹ApA calculated from spectra at pH 6.0 and 8.9; (B) ——, $Apm^1\overset{+}{A}$ at pH 6.0; ----, Apm¹A calculated from spectra at pH 6.0 and 9.1; (C) m¹Apm¹A calculated from spectra at pH 5.0, 8.1, 9.2, and 10.1; (D) ApA at pH 7.0.

Table 4. UV spectral and hypochromicity data of dimers (25°, I=0.1)

Dimer	pH	λ_{max} / nm	H[a] / %
$m^1\overset{+}{A}pA$	5.5	258	10
$Apm^1\overset{+}{A}$	5.5	258	10
$m^1\overset{+}{A}pm^1\overset{+}{A}$	5.5	258	1
ApA	7.0	258	12

a) Hypochromicity is measured at the λ_{max} of monomers.

protonated species at 25° are shown in Figs. 3A and 3B together with that of ApA for comparison (Fig. 3D). Cation formation of m¹ApA produces only minor changes in the CD spectrum (Fig. 3A) while deprotonation of $Apm^1\overset{+}{A}$ considerably enhances the intensity of the CD spectrum (Fig. 3B). Another feature of interest in the CD spectra shown in Fig. 3 is that the CD spectrum of $m^1\overset{+}{A}pA$ is almost quantitatively similar to that of $Apm^1\overset{+}{A}$ and the intensities of the CD spectra for this pair of sequence isomers are considerably smaller than that for ApA. These observations may be taken as *prima facie* evidence for weaker base-base stacking interactions in $m^1\overset{+}{A}pA$ and $Apm^1\overset{+}{A}$ than ApA. Thus the correlation with the stacking quotient data listed in Tables 1 and 3 is striking. It should be noted on comparing the vastly different CD spectra[4] of a pair of sequence isomers $m^7\overset{+}{G}pG$ and $Gpm^7\overset{+}{G}$ that m¹A-containing dimers differ considerably from other methylated dimers in the molecular conformations.

Concerning the stacking association of m¹Apm¹A, titrations gave an s_0 value of 1.56 at 25 °C. Although acid-base titrations are seen to overestimate the stacking quotient s_0,[5,14] the value for m¹Apm¹A is by no means greater than that for the parent unmethylated ApA. Supporting evidence for this comes from the comparison of the CD spectrum extracted for m¹Apm¹A (Fig. 3C) and that of ApA (Fig. 3D). The presently observed effect for m¹A is thus in contrast to the general pattern of the stacking-enhancing effect of methyl substitution as previously observed in methyl-substituted dinucleoside monophosphates.[3,4,6,7,9,10]

In consequence, m¹A-containing dinucleoside monophosphates stack intramolecularly less extensively than the corresponding parent unmethylated dimers, and differ from other methyl-substituted dimers in the stacking equilibrium ratios. Such differences can be accounted empirically for by the fact that m¹A possesses an amidine structure with a quasi-ortho-quinonoid form unfavoring the stacking-enhancing effect of the methyl group. Incidentally, the CD spectrum of m¹Apm¹A is quite similar in shape to that of IpI[19,20] which has the quasi-ortho-quinonoid amide structure.

Finally, it should be noted that the methylation of N^6 position of an adenine base increased stacking interaction in dimers.[6,7,9,10] Considering the wide existence of these methylated adenine residues in nucleic acid molecules (m¹A in tRNA;[8] m^6A in tRNA[8] and mRNA;[21] $m_2{}^6A$ in rRNA[22]), it is of interest to note that a methyl group can exert various effects on the stacking of dimers depending on the site of its introduction. Thus, the present study has shown that methylation of a nucleic acid base is one of effective means for the fine controll of a nucleic acid conformation.

References

1) Abbreviations:—A dimer means a dinucleoside monophosphate. XpY represents a dimer having a 3′-5′ phosphodiester bond, X-3′-p-5′-Y. "p" to the left of a nucleoside symbol indicates a 5′-phosphate, and to the right indicates a 3′-phosphate. CH_3O- and $-OCH_3$ attached to "p" mean the phosphate is esterified by a methyl group. "+" on a nucleoside symbol indicates the nucleoside has a positive charge. Nucleoside symbols used for modified bases are the following: m^1A, 1-methyladenosine; m^6A, N^6-methyladenosine; m_2^6A, N^6,N^6-dimethyladenosine; m^7G, 7-methylguanosine; I, inosine.

2) S. Irie, F. Egami, and Y. Inoue, *J. Am. Chem. Soc.*, **91**, 1582 (1969).

3) Y. Watanabe and Y. Inoue, *FEBS Lett.*, **35**, 344 (1973).

4) N. Ogasawara, Y. Watanabe, and Y. Inoue, *J. Am. Chem. Soc.*, **97**, 6571 (1975).

5) Y. Inoue, T. Kuramochi, M. Sakurai, and I. Tazawa, *J. Am. Chem. Soc.*, **102**, 5574 (1980).

6) I. Tazawa and Y. Inoue, unpublished results.

7) I. Tazawa, T. Koike, and Y. Inoue, *Eur. J. Biochem.*, **109**, 33 (1980).

8) M. Sprinzl and D. H. Gauss, *Nucleic Acids Res.*, **10**, 1 (1982).

9) C. S. M. Olsthoorn, C. A. G. Haasnoot, and C. Altona, *Eur. J. Biochem.*, **106**, 85 (1980).

10) C. Altona, "Structure and Conformation of Nucleic Acids and Protein-Nucleic acid Interactions," ed by M. Sundaralingam and S. T. Rao, University Park Press, Baltimore (1975), pp. 613—629.

11) S. S. Danyluk, C. F. Ainthworth, and M. MacCoss, *Jerus. Symp. Quant. Chem. Biochem.*, **11**, 111 (1978).

12) G. M. Tener and H. G. Khorana, *J. Am. Chem. Soc.*, **77**, 5349 (1955).

13) M. Smith, J. G. Moffatt, and H. G. Khorana, *J. Am. Chem. Soc.*, **80**, 6204 (1958).

14) N. Ogasawara and Y. Inoue, *J. Am. Chem. Soc.*, **98**, 7054 (1976).

15) N. Ogasawara and Y. Inoue, *J. Am. Chem. Soc.*, **98**, 7048 (1976).

16) M. Sakurai, I. Tazawa, and Y. Inoue, *Nucleic Acids Res. Special Publ.*, **2**, s119—s122 (1976).

17) M. M. Warshaw and I. Tinoco, Jr., *J. Mol. Biol.*, **20**, 29 (1966).

18) M. D. Topal and M. M. Warshaw, *Biopolymers*, **15**, 1775 (1976).

19) S. Tazawa, I. Tazawa, J. L. Alderfer, and P. O. P. Ts'o, *Biochemistry*, **11**, 3544 (1972).

20) C. Formoso and I. Tinoco, Jr., *Biopolymers*, **10**, 531 (1971).

21) F. M. Rottman, R. C. Desrosiers, and K. Friderici, "Progress in Nucleic Acid Research and Molecular Biology," ed by W. E. Cohn and E. Volkin, Academic Press, New York (1976), Vol. 19, pp. 21—38.

22) R. Brimacombe, K. H. Nierhaus, R. A. Garrett, and H. G. Wittmann, "Progress in Nucleic Acid Research and Molecular Biology," ed by W. E. Cohn, Academic Press, New York (1976), Vol. 18, pp. 1—44.

 © 1982 The Chemical Society of Japan Bul. Chem. Soc. Jpn., 55, 3603—3606 (1982)

Studies on Salt Hydrate for Latent Heat Storage. I. Crystal Nucleation of Sodium Acetate Trihydrate Catalyzed by Tetrasodium Pyrophosphate Decahydrate

Takahiro WADA* and Ryoichi YAMAMOTO

Material Research Laboratory, Matsushita Electric Industrial Co., Ltd., Kadoma, Osaka 571

(Received April 2, 1982)

The effect of tetrasodium pyrophosphate decahydrate ($Na_4P_2O_7 \cdot 10H_2O$) as a nucleation catalyst for sodium acetate trihydrate ($CH_3CO_2Na \cdot 3H_2O$) is shown. The supercooled melt of 10 g of $CH_3CO_2Na \cdot 3H_2O$ recrystallized at about 5 degrees below the melting point only when 0.1 g of $Na_4P_2O_7 \cdot 10H_2O$ was added to it. More than a thousand cycles of alternate heating and cooling through the melting point were carried out in this work. Some observations on nucleation are given and the results are discussed on the basis of crystallographic data.

Sodium acetate trihydrate ($CH_3CO_2Na \cdot 3H_2O$) has received attention recently because of its large latent heat of fusion (about 264 J/g) which makes it attractive as a latent heat storage material.[1] But once this material melts, it tends to supercool even if it is cooled considerably below the melting point (58.4 °C).[2] One approach to this problem is to add a suitable nucleation catalyst to supercooled $CH_3CO_2Na \cdot 3H_2O$ melt. This nucleation catalyst needs to be hardly soluble in $CH_3CO_2Na \cdot 3H_2O$ melt so as to not lower the melting point nor diminish the heat of fusion.[3] However, such a nucleation catalyst has not been found yet.[4,5] In this study, tetrasodium pyrophosphate decahydrate ($Na_4P_2O_7 \cdot 10H_2O$) was found to act as a nucleation catalyst for $CH_3CO_2Na \cdot 3H_2O$ which hardly lowers the melting point at all and does not diminish the heat of fusion.

We present the results of two different kinds of thermal analysis of $CH_3CO_2Na \cdot 3H_2O$ in the presence of $Na_4P_2O_7 \cdot 10H_2O$. One is a heating and cooling cycle of about 30 g samples in a sealed glass vessel, and the other is differential scanning calorimetry of about 15 mg samples. The reason why it acts as a nucleation catalyst for $CH_3CO_2Na \cdot 3H_2O$ is discussed crystallographically and compared to the well known case of borax ($Na_2B_4O_7 \cdot 10H_2O$) for Glawber's Salt ($Na_2SO_4 \cdot 10H_2O$).[3,6]

Experimental

Materials. $CH_3CO_2Na \cdot 3H_2O$, $Na_4P_2O_7 \cdot 10H_2O$, and $Na_2H_2P_2O_7$ were obtained commercially and $Na_4P_2O_7$ was obtained by heating $Na_4P_2O_7 \cdot 10H_2O$ in an oven at 150—200 °C for 5 h. $Na_4P_2O_7 \cdot 10H_2O$ was used for experiments after it was ground to a powder and passed through a 100 mesh seive.

Heating and Cooling Cycles of About 30 g Samples in a Sealed Glass Vessel. Weighed quantities of $CH_3CO_2Na \cdot 3H_2O$ and $Na_4P_2O_7 \cdot 10H_2O$ were placed in a glass vessel and the sample was covered with liquid paraffin to prevent water evaporation. The temperature of the sample was measured with a thermocouple, whose junction was placed near $Na_4P_2O_7 \cdot 10H_2O$ precipitates because it was expected that recrystallization of $CH_3CO_2Na \cdot 3H_2O$ would start on the surface of $Na_4P_2O_7 \cdot 10H_2O$ crystals. The glass vessel was sealed and put into a water bath. The sample was consecutively heated and cooled at the rate of 0.4 °C/min between 35 °C and 70 °C, and maintained for 30 min each at 35 °C and then 70 °C. In this manner, the melting point t_m and the temperature at which supercooling was broken t_i were measured and supercooling $\Delta t_i (= t_m - t_i)$ was determined in each cycle.

Differential Scanning Calorimetry. Differential scanning calorimetry (DSC) was performed using SSC 560S DSC (Dainiseikosha Co. Ltd.). Weighed quantities of samples were placed in a 15 μl silver crucible and the surface of the sample was covered with one drop of liquid paraffin to prevent water evaporation. The sample was subjected to linearly programmed consecutive heating and cooling in a manner similar to the above. Melting points t_m″s were obtained from the sample temperature curve at times corresponding to endothermal peaks and the temperatures at which supercooling was broken t_i″s were obtained from the sample temperature curves at times corresponding to the onset of exothermal peaks. From these temperatures, supercooling $\Delta t_i' (= t_m' - t_i')$ was calculated. This DSC system was calibrated using ice (t_m: 0.0 °C), sodium sulfate decahydrate (t_m: 32.4 °C) and sodium acetate trihydrate (t_m: 58.4 °C) as a standard.

Results

The heating and cooling curve for a sample consisting of 30 g of $CH_3CO_2Na \cdot 3H_2O$ and 0.3 g of $Na_4P_2O_7 \cdot 10H_2O$ is shown is Fig. 1. The curve shows that the melting point of this sample is 58.4 °C which is the same as that of $CH_3CO_2Na \cdot 3H_2O$ alone. The supercooling of the sample is broken at 53.1 °C and suddenly the temperature of the sample rises to freezing point, 58.4 °C. After this temperature is maintained for about 12 min, the temperature of sample drops.

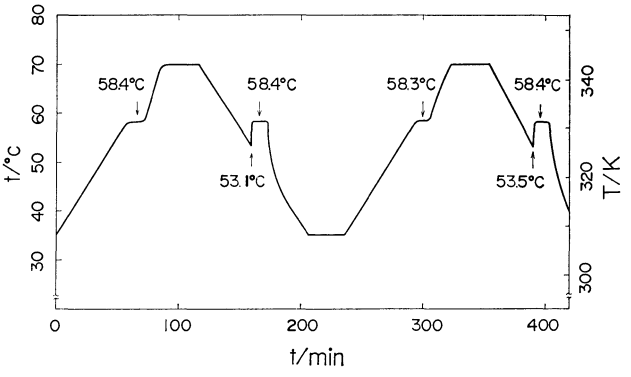

Fig. 1. Heating and cooling curve for a sample consisting of 30 g of $CH_3CO_2Na \cdot 3H_2O$ and 0.3 g of $Na_4P_2O_7 \cdot 10H_2O$.

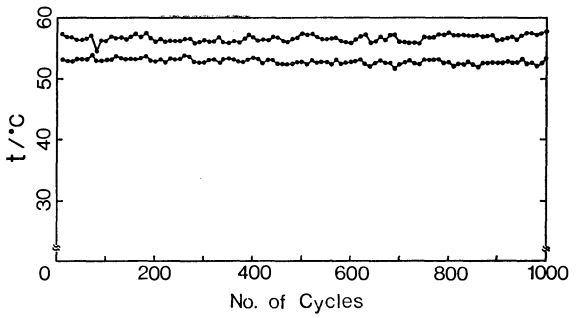

Fig. 2. Changes in melting point t_m and the temperature at which supercooling is broken t_i with cycling.
●: t_m, ○: t_i.

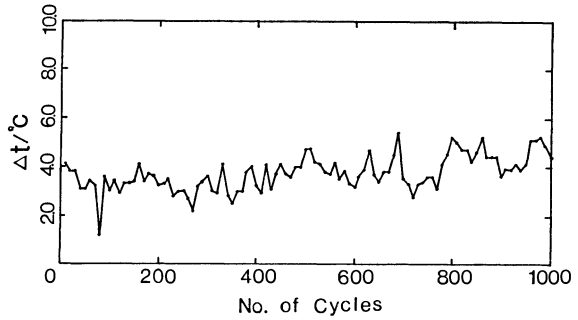

Fig. 3. Changes in supercooling Δt_i with cycling.

In this case, supercooling Δt_i is 5.3 °C.

The melting points t_m's and the temperatures at which supercooling is broken t_i's are plotted in Fig. 2, with temperature as ordinate and number of cycles as abscissa. As shown in Fig. 2, t_i and t_m are almost constantly 53 °C and 58.4 °C respectively. The slight scatter of t_m falls within measuring error. The supercooling Δt_i points are plotted in Fig. 3, using the result of Fig. 2. These Δt_i's are below 6 °C over all the cycles. It was also found that $Na_4P_2O_7 \cdot 10H_2O$ works continuously as a nucleation catalyst for 1000 cycles. On the other hand, when $Na_4P_2O_7 \cdot 10H_2O$ powder was not added to $CH_3CO_2Na \cdot 3H_2O$ melt, supercooling was not broken down to about 35 °C. These experimental results show that $Na_4P_2O_7 \cdot 10H_2O$ serves as a very effective nucleation catalyst for $CH_3CO_2Na \cdot 3H_2O$ whose melting point is scarcely lowered.

A DSC curve of a sample consisting of 14.0 mg of $CH_3CO_2Na \cdot 3H_2O$ and 1.7 mg of $Na_4P_2O_7 \cdot 10H_2O$ is illustrated in Fig. 4. The difference between the temperature of the first endothermal peak and that of the second is probably caused by measuring error. The melting points t_m"s and the temperatures at which supercooling is broken t_i"s which are determined by 50 continuous heating and cooling cycles are shown in Fig. 5. The supercooling in this case Δt_i"s ($=t_m' - t_i'$) are calculated by using the results of Fig. 5 and are plotted in Fig. 6. From Fig. 5, it is found that t_i' varies very widely and irregularly with number of cycles and their average is about 45 °C. Thus $\Delta t_i'$ also varies very widely and their average is 13 °C. It is evident that $\Delta t_i'$ is much larger than Δt_i. Moreover, the heat of fusion per 1 g of $CH_3CO_2Na \cdot 3H_2O$ which was obtained by this DSC measurement is 262

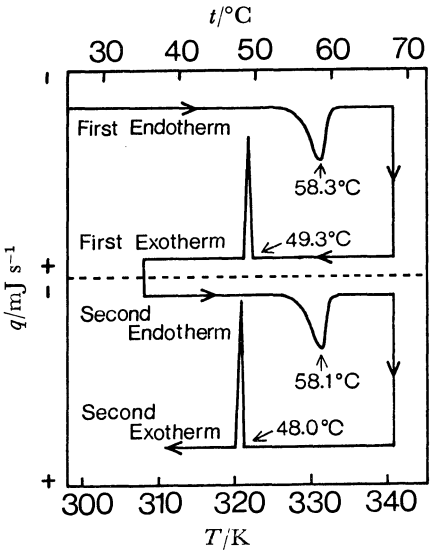

Fig. 4. DSC curve of a sample consisting of 14.0 mg of $CH_3CO_2Na \cdot 3H_2O$ and 1.7 mg of $Na_4P_2O_7 \cdot 10H_2O$.

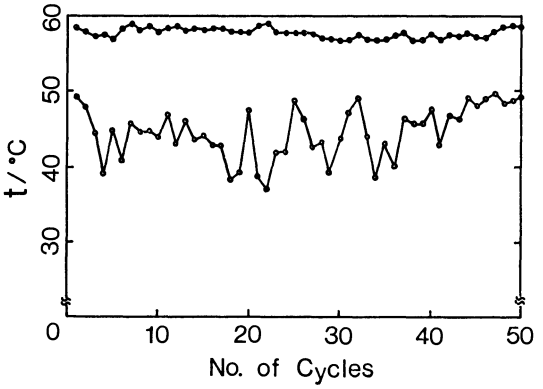

Fig. 5. Changes in melting point t_m' and the temperature at which undercooling is broken t_i' with cycling.
●: t_m', ○: t_i'.

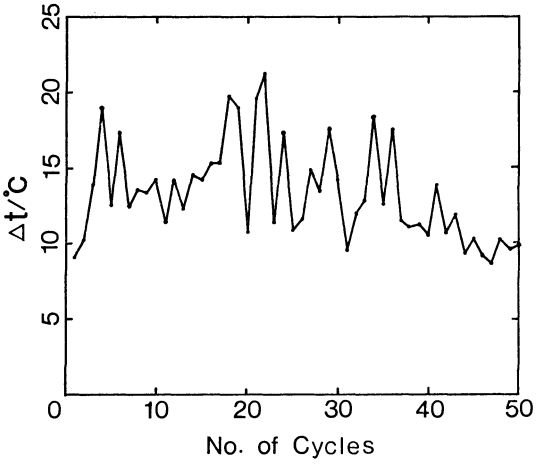

Fig. 6. Changes in undercooling $\Delta t_i'$ with cycling.

J/g, which is good agreement with that of $CH_3CO_2Na \cdot 3H_2O$ alone within measuring error. It is understandable that addition of $Na_4P_2O_7 \cdot 10H_2O$ to $CH_3CO_2Na \cdot 3H_2O$ scarcely decreases its heat of fusion.

The solubilities of $Na_4P_2O \cdot 10H_2O$ in $CH_3CO_2Na \cdot$

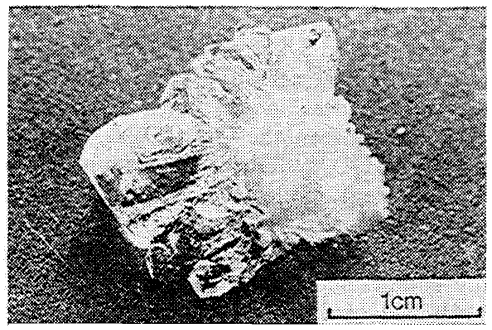

Fig. 7. Photograph of $CH_3CO_2Na \cdot 3H_2O$ crystals grown around a mass of $Na_4P_2O_7 \cdot 10H_2O$ polycrystal.

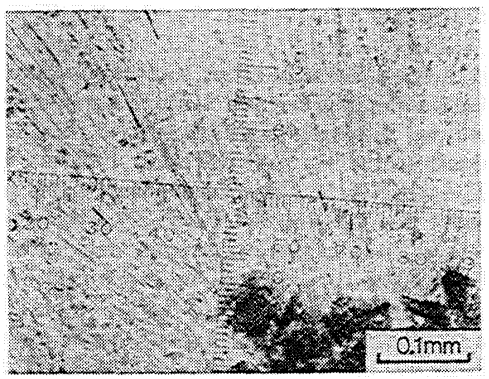

Fig. 8. Micro-photograph of $CH_3CO_2Na \cdot 3H_2O$ grown around $Na_4P_2O_7 \cdot 10H_2O$ particles.

$3H_2O$ melt at 60 °C and 75 °C were both about 0.1 percent by weight. Because of its slight solubility, it is supposed that both the melting point and the heat of fusion of $CH_3CO_2Na \cdot 3H_2O$ are hardly influenced by adding $Na_4P_2O_7 \cdot 10H_2O$. This is in good agreement with the results obtained by these thermal analyses.

Figure 7 shows $CH_3CO_2Na \cdot 3H_2O$ crystals grown around a mass of $Na_4P_2O_7 \cdot 10H_2O$ polycrystal. The white part indicates a mass of $Na_4P_2O_7 \cdot 10H_2O$ and transparent crystals around it are $CH_3CO_2Na \cdot 3H_2O$. Figure 8 is a micro-photograph of $CH_3CO_2Na \cdot 3H_2O$ crystals grown around $Na_4P_2O_7 \cdot 10H_2O$ particles. It is observed that $CH_3CO_2Na \cdot 3H_2O$ needles are radially grown from $Na_4P_2O_7 \cdot 10H_2O$ particles. It is suggested that $CH_3CO_2Na \cdot 3H_2O$ crystallized as needle since it began to recrystallize at a temperature significantly below the melting point. This large supercooling, we suppose, results from the small sample quantities of this experiment. This is consistent with the result obtained by DSC of about 15 mg sample.

Discussion

Table 1 shows the crystallographic data of $Na_2B_4O_7 \cdot 10H_2O$ and that of $Na_2SO_4 \cdot 10H_2O$,[7] and Table 2 shows the crystallographic data of $Na_4P_2O_7 \cdot 10H_2O$[8] and that of $CH_3CO_2Na \cdot 3H_2O$.[9] As shown in Table 1, the crystallographic data of $Na_2B_4O_7 \cdot 10H_2O$ and that of $Na_2SO_4 \cdot 10H_2O$ are quite similar except for a space group. Moreover, these two compounds have remarkably similar chains which are formed by sharing the two edges of $Na(H_2O)_6$ octahedra. These crystallographic similarities have been pointed out to be the cause of the nucleation catalysis.[7]

Table 1. Crystallographic data for sodium sulfate decahydrate and sodium tetraborate decahydrate

		$Na_2SO_4 \cdot 10H_2O$	$Na_2B_4O_7 \cdot 10H_2O$
Crystal system		Monoclinic	Monoclinic
Space group		$P2_1/c$	C2/c
Unit-cell parameter	a/Å	11.512	11.885
	b/Å	10.370	10.654
	c/Å	12.847	12.206
	β/°	107.789	106.623
	V/Å^3	1460	1481
	Z	4	4

Table 2. Crystallographic data for sodium acetate trihydrate and tetrasodium pyrophosphate decahydrate

		$CH_3CO_2Na \cdot 3H_2O$	$Na_4P_2O_7 \cdot 10H_2O$
Crystal system		Monoclinic	Monoclinic
Space group		C2/c	C2/c
Unit-cell parameter	a/Å	12.353	17.01±0.02
	b/Å	10.466	6.96±0.01
	c/Å	10.401	14.85±0.02
	β/°	111.69	112.0±0.2
	V/Å^3	1249.5	1630
	Z	8	4

On the other hand, both $Na_4P_2O_7 \cdot 10H_2O$ and $CH_3CO_2Na \cdot 3H_2O$ are monoclinic and have the same space group C2/c, however their lattice constants a, b, and c are greatly different. In the crystal structure of $CH_3CO_2Na \cdot 3H_2O$, Na ion has distorted octahedral coordination with six oxygen atoms which consist of one acetate oxygen and five water molecules. Adjacent octahedra share an edge and form a continuous chain along the z axis.[9,10] However, the crystal structure of $Na_4P_2O_7 \cdot 10H_2O$ contains two types of sodium atoms lying within octahedra, which are made up of six water molecules in the one case, and four water molecules and two oxygen atoms of a pyrophosphate group in the other case. The $Na(H_2O)_6$ octahedra share edges and corners with each other so as to build up sheets of linked octahedra. The other octahedron containing a pyrophosphate group shares two edges with the $Na(H_2O)_6$ octahedra so as to link to the sheets of $Na(H_2O)_6$ octahedra.[8,11] Thus it is deduced that the structures of $CH_3CO_2Na \cdot 3H_2O$ and $Na_4P_2O_7 \cdot 10H_2O$ do not have highly similar chains or sheets of water molecules-coordinate Na ions, whereas $Na_2SO_4 \cdot 10H_2O$ and $Na_2B_4O_7 \cdot 10H_2O$ have remarkably similar chains.

The lattice spacings on low index planes of $CH_3CO_2Na \cdot 3H_2O$ and $Na_4P_2O_7 \cdot 10H_2O$ which can be calculated from the lattice constants shown in Table 2 are listed in Table 3. In this table, the lattice spacings on planes of $Na_4P_2O_7 \cdot 10H_2O$ which agree with those of $CH_3CO_2Na \cdot 3H_2O$ within 1%, are written in the same row of those of $CH_3CO_2Na \cdot 3H_2O$. It can be seen that there are many planes of $CH_3CO_2Na \cdot 3H_2O$ whose lattice spacing is close to that of $Na_4P_2O_7 \cdot 10H_2O$.

TABLE 3. LATTICE SPACING ON LOW INDEX PLANES OF SODIUM ACETATE TRIHYDRATE AND THAT OF TETRASODIUM PYROPHOSPHATE DECAHYDRATE

$CH_3CO_2Na\cdot3H_2O$		$Na_4P_2O_7\cdot10H_2O$	
(*hkl*)	*d*/Å	*d*/Å	(*hkl*)
		15.77	(100)
		13.77	(001)
		13.08	(10$\bar{1}$)
(100)	11.48		
(010)	10.47		
(001)	9.665		
(10$\bar{1}$)	9.272		
		8.858	(101)
		8.317	(20$\bar{1}$)
		7.886	(200)
(110)	7.734		
		7.409	(10$\bar{2}$)
(011)	7.100		
(11$\bar{1}$)	6.940	6.960	(010)
		6.884	(002)
		6.540	(20$\bar{2}$)
(101)	6.330	6.368	(110)
		6.211	(011)
		6.144	(11$\bar{1}$)
(20$\bar{1}$)	6.004	5.949	(201)
(200)	5.739		
		5.670	(30$\bar{1}$)
		5.588	(102)
		5.473	(111)
(111)	5.416		
		5.338	(21$\bar{1}$)
(020)	5.233	5.257	(300)
(21$\bar{1}$)	5.208	5.228	(30$\bar{2}$)
(10$\bar{2}$)	5.193	5.218	(210)
(210)	5.032	5.073	(11$\bar{2}$)

For example, *d*(11$\bar{1}$) of $CH_3CO_2Na\cdot3H_2O$ agrees very closely with *d*(010) of $Na_4P_2O_7\cdot10H_2O$. Consequently, the reason why $Na_4P_2O_7\cdot10H_2O$ serves as an effective nucleation catalyst for $CH_3CO_2Na\cdot3H_2O$ is considered to be their close resemblance in lattice spacing on certain low index planes.

The extent of supercooling of $Na_2SO_4\cdot10H_2O$ containing $Na_2B_4O_7\cdot10H_2O$ is known to be 1—2 °C in the experiment using test tube[3] and 7 °C in DSC.[12] On the other hand, the extent of supercooling of $CH_3CO_2Na\cdot3H_2O$ containing $Na_4P_2O_7\cdot10H_2O$ is found to be about 5 °C in the experiment using sealed glass vessel and at an average of 13 °C in DSC. In each case, the extent of supercooling of $CH_3CO_2Na\cdot3H_2O$ containing $Na_4P_2O_7\cdot10H_2O$ is larger than that of $Na_2SO_4\cdot10H_2O$ containing $Na_2B_4O_7\cdot10H_2O$. As indicated before, $Na_2SO_4\cdot10H_2O$ and $Na_2B_4O_7\cdot10H_2O$ have analogous unit cells and remarkably similar chains which are formed by sharing two edges of $Na(H_2O)_6$ octahedra each other, whereas $CH_3CO_2Na\cdot3H_2O$ and $Na_4P_2O_7\cdot10H_2O$ only resemble each other in lattice spacing on certain low index planes. The difference of supercooling between the $CH_3CO_2Na\cdot3H_2O$ system and $Na_2SO_4\cdot10H_2O$ system is considered to be due to such a different modes of resemblance in crystal structure.

It was pointed out that there was difference between the supercooling of $Na_2SO_4\cdot10H_2O$ containing $Na_2B_4O_7\cdot10H_2O$ obtained by the heating and cooling cycles using sealed test tube and that obtained by using DSC.[13] The cause of this difference of supercooling extent for the $CH_3CO_2Na\cdot3H_2O$ system is not more clearly understood than for the $Na_2SO_4\cdot10H_2O$ system.

In addition, both anhydrous sodium pyrophosphate ($Na_4P_2O_7$) and sodium hydrogenpyrophosphates such as disodium dihydrogenpyrophosphate ($Na_2H_2P_2O_7$) were found to act as a nucleation catalyst as well as $Na_4P_2O_7\cdot10H_2O$. This effect comes from the fact that a part of $Na_4P_2O_7$ and $Na_2H_2P_2O_7$ become $Na_4P_2O_7\cdot10H_2O$ in $CH_3CO_2Na\cdot3H_2O$ melt. The presence of $Na_4P_2O_7\cdot10H_2O$ both in the mixture of 30 g of $CH_3CO_2Na\cdot3H_2O$ melt and 1 g $Na_4P_2O_7$ and in the mixture of 30 g of $CH_3CO_2Na\cdot3H_2O$ melt and 1 g of $Na_2H_2P_2O_7$ was confirmed by X-ray diffraction.

The authors wish to express their thanks to Dr. Ryoichi Kiriyama for his many helpful discussions and to Dr. Eiichi Hirota and Dr. Masanari Mikoda for their continuous encouragement. They are also grateful to Dr. Yoshihiro Matsuo for his discussions throughout this work, to Mr. Masahiro Nishikawa for his photography, and to Mr. Koji Matsunaga and Miss Fumiko Kimura for their thermal analyses.

References

1) M. Telkes, "Solar Materials Science," ed by L. E. Murr, Academic Press, New York (1980), Chap. 11.
2) F. de Winter, *Solar Energy*, **17**, 379 (1975).
3) M. Telkes, *Ind. Eng. Chem.*, **44**, 1308 (1952).
4) K. Narita and J. Kai, *J. Inst. Electr. Eng. Jpn.*, **101**, 15 (1981).
5) H. Kimura, *J. Jpn. Assoc. Cryst. Growth*, **7**, 215 (1980).
6) D. Turnbull and B. Vonnegut, *Ind. Eng. Chem.*, **44**, 1292 (1952).
7) H. A. Levy and G. C. Lisensky, *Acta Crystallogr., Sect. B*, **34**, 3502 (1978).
8) W. S. McDonald and D. W. J. Cruickshank, *Acta Crystallogr*, **22**, 43 (1967).
9) K. -T. Wei and D. L. Ward, *Acta Crystallogr., Sect. B*, **33**, 522 (1977).
10) T. S. Cameron, K. M. Mannan, and Md. O. Rahman, *Acta Crystallogr., Sect. B*, **32**, 87 (1976).
11) D. M. MacArthur and C. A. Beevers, *Acta Crystallogr.*, **10**, 428 (1957).
12) S. Cantor, *Thermochim. Acta*, **33**, 69 (1979).
13) M. Kamimoto, *Kagaku To Kogyo*, **33**, 598 (1980).

A Comparative Study of the Kinetics and Mechanism of Reactions between Copper(I) Iodide and Mercury(II) Halides in Solid State

Mirza Aijaz Beg* and Afaq Ahmad

Department of Chemistry, The Aligarh Muslim University, Aligarh-202001, India

(Received September 3, 1981)

Kinetics and mechanisms of reactions of HgI_2, HgBrI, or $HgBr_2$ with CuI were studied in the solid state. Mercury(II) halides react *via* vapor phase, and reactions proceed through counter diffusion of Cu^+ and Hg^{2+}. X-Ray and chemical analyses indicate that powdered CuI gives Cu_2HgI_4 when mixed with HgI_2 and a mixture of Cu_2HgI_4 and CuBr when mixed with HgBrI. CuI and $HgBr_2$ react differently in different molar ratios. In a 1:2 molar ratio mixture of CuI and $HgBr_2$, a new product $CuHgBr_3$ and HgBrI are obtained. Data for lateral diffusion best fit the equation $X^n=kt$ where X is the thickness of product layer at time t, and n and k are const. Formation of solid solutions among reactant and product phases is also noted.

AgI reacts with HgI_2[1] in solid state yielding highly conducting Ag_2HgI_4. Its reactions with $HgBr_2$ or $HgCl_2$ are complex and altogether different.[2,3] Formation of Cu_2HgI_4 from HgI_2 and CuI in solid state is long known,[4] but no effort seems to have been made to understand the mechanism of the interaction of CuI with Mercury(II) halides in solid state.

This paper presents a study on Kinetics and mechanisms of the reaction of CuI with HgI_2, HgBrI, or $HgBr_2$ in solid state. It was observed that while the first halide is involved in a simple addition reaction, the last two are involved in multi-step reactions. But in each of these, Cu_2HgI_4 and HgI_2 were formed as intermediates. Mixtures of different molar ratios gave rise to different products, including $CuHgBr_3$ which does not seem to have been reported so far either in solid or in solution. Formation of solid solutions among the products were also noted.

Experimental

Materials. $HgBr_2$ and HgI_2 (E. Merck) were used without further purification. Copper(I) halides, being photosensitive, were prepared fresh for each set of experiments. CuI was prepared according to Berthemot[5] and Guichard.[6] Its X-Ray diffraction patterns showed it to be single phase. CuI was stored in a dark bottle, and experiments were carried out in dark.

Cu_2HgI_4 was prepared by precipitation from solution containing stoichiometric amounts of CuI and HgI_2.[7] Mercury bromideiodide was prepared by Oppenheim's method.[8] X-Ray diffraction patterns showed them to be β-Cu_2HgI_4,[9] and HgBrI.[10]

Rate Measurements. Kinetics of reactions were studied by placing Mercury(II) halides over CuI (each above 300 mesh size) in a vertically held Pyrex glass tube about 0.5 cm in diameter as reported earlier.[11] Each experiment was run in triplicate and the average values were used to calculate rate constants (the readability of the microscope was 0.001 cm and the average deviation of measured values ranged between $\pm$0.00038 cm) as reported in Tables 1—3.

Soon after the placement of Mercury(II) halide (HgBrI, HgI_2, or $HgBr_2$) over CuI in the reaction tube, a dark brown boundary was formed at the interface and this grew with time on the CuI side. A light yellow layer appeared between HgBrI and a brown dark product layer in the case of HgBrI, and a yellow layer between $HgBr_2$ and brown product layer in the case of $HgBr_2$. On cooling to room temperature, the dark brown product turned scarlet red (Cu_2HgI_4 is dark brown above 70 °C and scarlet below this temperature).[12]

Table 1. Dependence of parameters of equation $X^n=kt$ on temperature for CuI-HgI_2 reaction

T/°C[a]	k/cm h^{-1}	n
70	1.42×10^{-4}	2.48
82	3.70×10^{-4}	
93	1.25×10^{-3}	
103	3.54×10^{-3}	
112	5.55×10^{-3}	

a) Accurate within $\pm$0.5 °C.

Table 2. Dependence of parameters of equation $X^n=kt$ on temperature for CuI-HgBrI reaction

T/°C[a]	k/cm h^{-1}	n
64	1.06×10^{-6}	2.53
75	2.56×10^{-6}	
87	7.08×10^{-6}	
95	14.96×10^{-6}	
104	39.81×10^{-6}	

a) Accurate within $\pm$0.5 °C.

Table 3. Dependence of parameters of equation $X^n=kt$ on temperature for CuI-$HgBr_2$ reaction

T/°C[a]	k/cm h^{-1}	n
75	1.13×10^{-6}	2.22
85	7.58×10^{-6}	
98	2.18×10^{-5}	
108	6.60×10^{-5}	
118	8.31×10^{-5}	
128	9.33×10^{-5}	
140	10.50×10^{-5}	

a) Accurate within $\pm$0.5 °C.

Later, when the reactants were placed in a tube with some air gap, the product layers were formed, but with a much slower rate, which decreased with increase in the length of the air gap. This clearly indicates that these reactions proceed *via* surface migration of Mercury(II) halides.

Analysis of the Product Layers. Sufficient amounts of different product layers of reactions CuI-HgI_2(A), CuI-HgBrI(B), and CuI-$HgBr_2$(C) were separately collected carefully by breaking the reaction tubes. Cu^+, Hg^{2+}, and I^- in the case of reaction A, and Cu^+ and Br^- and Cu^+, Hg^{2+}

Table 4. Compounds present in different molar mixtures of CuI and HgI_2

Molar ratio CuI : HgI_2	Compounds present in mixture heated to 120 °C and then cooled to 30 °C
3 : 1	Cu_2HgI_4, CuI
2 : 1	Cu_2HgI_4
1 : 1	Cu_2HgI_4, HgI_2

and I^- in layers of reaction B and C, respectively, were detected by spot tests.[13] X-Ray diffraction analyses showed them to be Cu_2HgI_4, CuBr, and Cu_2HgI_4, respectively.

X-Ray Studies. The reactants (each above 300 mesh) were mixed thoroughly in an agate mortar in different molar ratios. One part of each mixture was heated in an air thermostat at (120±0.5) °C, and another part was maintained at 30 °C. Mixtures were analysed after 48 h using a Norelco Geiger counter X-Ray diffractometer by Cu $K\alpha$ radiations with a Ni filter, applying 32 kV at 12 mA. The compounds thus identified are given in Tables 4—6.

Thermal amd Conductance Measurements. CuI and Mercury(II) halides (HgI_2, HgBrI, or $HgBr_2$) in different molar ratios ranging from 4:1 to 1:2 were weighed separately and mixed thoroughly in a Dewar flask calorimeter. The rise in temperature was noted against time. The electrical conductance of the same molar-ratio mixtures were measured with a current ratio I. C. bridge:[14] as reported elsewhere.[2,3]

Results and Discussion

X-Ray diffraction analyses (Tables 4—6) reveal that while CuI reacts with HgI_2 or HgBrI in 2:1 or 3:1 molar ratios, respectively, it reacts differently with different molar mixtures of $HgBr_2$.

CuI-HgI_2 Reaction. X-Ray analysis (Table 6) of the products obtained with different molar mixtures of CuI and HgI_2 showed that only Cu_2HgI_4 is formed:

$$2CuI + HgI_2 \longrightarrow Cu_2HgI_4. \quad (1a)$$

Thermal and conductance curves are also indicative of only a single step reaction.

CuI-HgBrI Reaction. A 3:1 molar mixture of CuI and HgBrI, maintained at 120 °C for about 48 h after mixing, showed presence of only Cu_2HgI_4 and CuBr:

$$3CuI + HgBrI \longrightarrow Cu_2HgI_4 + CuBr. \quad (1)$$

Thermal (Fig. 1) as well as conductance (Fig. 2) measurements made with different molar mixtures of CuI and HgBrI provide no evidence for any additional step in reaction (1). However, the presence of HgI_2 in the mixture maintained at 30 °C but the absence in the one kept at a higher temperature (Table 5) suggests that the reaction goes through formation of HgI_2, which is rapidly consumed by CuI giving the addition product Cu_2HgI_4. The reaction sequence, therefore, may be written as:

$$CuI + HgBrI \longrightarrow HgI_2 + CuBr, \quad (i)$$

$$2CuI + HgI_2 \longrightarrow Cu_2HgI_4, \quad (ii)$$

$$3CuI + HgBrI \longrightarrow Cu_2HgI_4 + CuBr.$$

The failure of thermal and conductance measurements to provide evidence for the substep (ii) (Fig. 5(i)) is because it is faster than step (i).[1] However, it is not

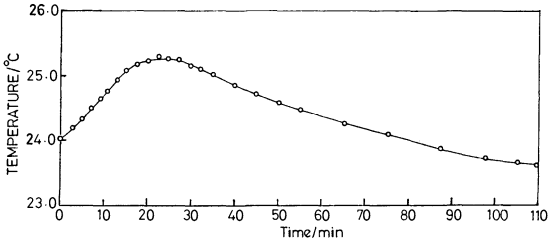

Fig. 1. Temperature rise as a function of time for CuI–HgBrI reaction in 3:1 molar mixture.

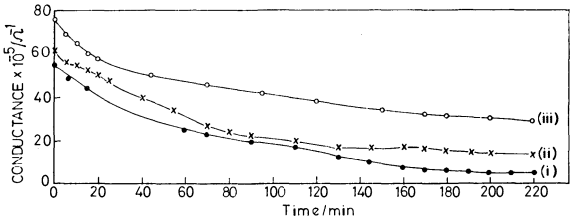

Fig. 2. Change in conductance as a function of time for CuI–HgBrI reaction, molar ratios (i) 3:1, (ii) 2:1, and (iii) 1:2.

Table 5. Compounds present in different molar mixtures of CuI and HgBrI

Molar ratio CuI : HgBrI	Compounds identified at 30 °C	Compounds identified in mixture heated to 120 °C and then cooled to 30 °C
4 : 1	Cu_2HgI_4, CuBr, CuI and HgI_2	Cu_2HgI_4, CuBr, CuI
3 : 1	Cu_2HgI_4, CuBr, HgI_2	Cu_2HgI_4, CuBr
1 : 2	Cu_2HgI_4, CuBr, $HgBr_2$ and HgI_2	Cu_2HgI_4, CuBr and HgBrI

Table 6. Compounds identified in different molar mixtures of CuI and HgBr

Molar ratio CuI : $HgBr_2$	Compounds present at 30 °C	Compounds present in mixture heated to 120 °C and then cooled to 30 °C
4 : 1	Cu_2HgI_4, CuBr, HgI_2	Cu_2HgI_4, CuBr
3 : 1	Cu_2HgI_4, CuBr, HgBrI and HgI_2	Cu_2HgI_4, CuBr, HgBrI
2 : 1	Cu_2HgI_4, CuBr, HgBrI and HgI_2	Cu_2HgI_4, CuBr, HgBrI
1 : 1	Cu_2HgI_4, CuBr, HgBrI	CuBr, HgBrI
1 : 2	Cu_2HgI_4, CuBr, HgBrI and $HgBr_2$	HgBrI and $CuHgBr_3$

so fast as to remove HgI_2, otherwise the latter could not have been detected in the mixture. Reaction (i) is slow because the ionic radii of Cu^+ and Hg^{2+} are very close to each other.

With all other molar mixtures, namely 4:1, 2:1, and 1:2 of CuI and HgBrI, the reaction sequence follows the same pattern and the excess of either reactant remained in the mixtures unreacted.

CuI-$HgBr_2$ Reaction. While HgBrI reacts with CuI in the molar ratio 1:3, $HgBr_2$ seems to do so primarily in 4:1 molar ratio:

$$4CuI + HgBr_2 \longrightarrow Cu_2HgI_4 + 2CuBr. \quad (2)$$

Thermal (Fig. 3) as well as conductance (Fig. 4) measurements show the reaction to be a simple one-step process. The presence of HgI_2 in the 4:1 molar mixture of CuI and $HgBr_2$, kept at room temperature for about 24 h, and its absence in the mixture maintained at 120 °C suggests that this reaction proceeds *via* the formation of HgI_2, much in the same way as CuI-HgBrI reaction does:

$$2CuI + HgBr_2 \longrightarrow 2CuBr + HgI_2. \quad (iii)$$

However, the absence of HgI_2 in the mixture kept at 120 °C raises two possibilities, First, HgI_2 may react with $HgBr_2$ to give HgBrI, which is stable and is known to be formed in the solid state[10] at high temperatures:

$$HgI_2 + HgBr_2 \longrightarrow 2HgBrI. \quad (iv)$$

Second, HgI_2 may also react with CuI present in the reaction mixture to give Cu_2HgI_4:[4]

$$2CuI + HgI_2 \longrightarrow Cu_2HgI_4. \quad (v)$$

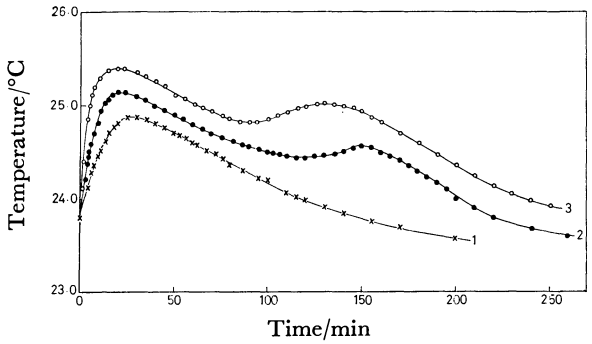

Fig. 3. Temperature rise as a function of time for the reaction between CuI and $HgBr_2$ molar ratios (1) 4:1, (2) 2:1, and (3) 1:2.

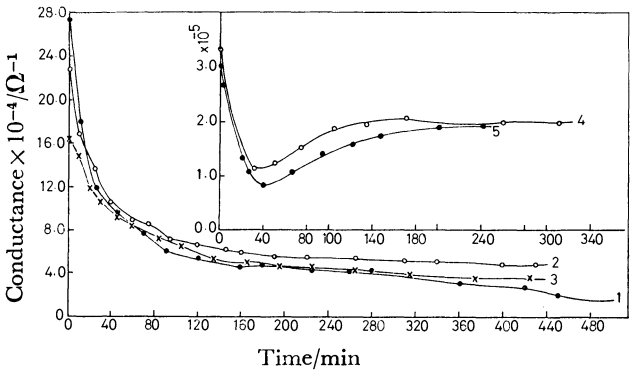

Fig. 4. Conductivity change as a function of time for the reaction between CuI and $HgBr_2$ at 30 °C. Molar ratios of CuI:$HgBr_2$ are (1) 4:1, (2) 3:1, (3) 2:1, (4) 1:1, and (5) 1:2.

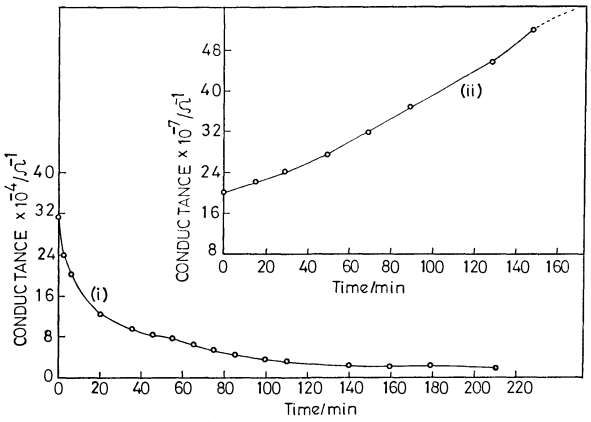

Fig. 5. Change in conductance as a function of time for reactions (i) $2CuI + HgI_2$ and (ii) $HgI_2 + HgBr_2$.

From the conductance curve for the 4:1 molar mixture of CuI and $HgBr_2$ (Fig. 4), it is evident that most of the reaction is over in about only 25 min, whereas conductance measurements (Fig. 5) made with a 1:1 molar mixture of HgI_2 and $HgBr_2$ clearly show that this reaction continues to proceed uniformly even after 3 h. CuI-HgI_2 reaction is, however, quite fast as is evident from Fig. 5(i). Furthermore, the sudden decrease in the conductance curve for the 4:1 molar mixture (Fig. 4) conforms to the change in the conductance curve obtained for reaction (v) and not to reaction (iv). Moreover, the former is already known[10] to be slow at room temperature whereas the latter is fast.[4] Therefore, HgI_2 produced in reaction (iii) reacts mostly with CuI giving Cu_2HgI_4 and to a little extent, if at all, with $HgBr_2$ yielding HgBrI. Hence, the overall reaction may be described as:

$$2CuI + HgBr_2 \longrightarrow 2CuBr + HgI_2,$$
$$2CuI + HgI_2 \longrightarrow Cu_2HgI_4,$$
$$4CuI + HgBr_2 \longrightarrow 2CuBr + Cu_2HgI_4,$$

and

$$2CuI + HgBr_2 \longrightarrow 2CuBr + HgI_2,$$
$$HgBr_2 + HgI_2 \longrightarrow 2HgBrI,$$
$$6CuI + 2HgBrI \longrightarrow 2CuBr + 2Cu_2HgI_4,$$
$$8CuI + 2HgBr_2 \longrightarrow 4CuBr + 2Cu_2HgI_4.$$

The compounds identified in the 3:1 molar mixture of CuI and $HgBr_2$ maintained at 120 °C were HgBrI, CuBr, and Cu_2HgI_4. At 120 °C, the reaction seems to proceed according to

$$9CuI + 3HgBr_2 \longrightarrow 2Cu_2HgI_4 + HgBrI + 5CuBr. \quad (3)$$

The presence of HgI_2 in this molar mixture (Table 5) at 30 °C shows that this reaction also proceeds through initial formation of HgI_2 which thereafter gives rise to Cu_2HgI_4. The presence of HgBrI may create an impression that this could be formed in the initial stage of reaction (iv), but this is not actually the case as already discussed. Excess $HgBr_2$ combines with Cu_2HgI_4 formed in the reaction giving HgBrI

and CuBr. The complete reaction sequence may thus be as follows:

$$6CuI + 3HgBr_2 \longrightarrow 6CuBr + 3HgI_2, \quad (3a)$$

$$6CuI + 3HgI_2 \longrightarrow 3Cu_2HgI_4, \quad (3b)$$

$$Cu_2HgI_4 + 3HgBr_2 \longrightarrow 2CuBr + 4HgBrI, \quad (3c)$$

$$6CuI + 2HgBrI \longrightarrow 2Cu_2HgI_4 + 2CuBr, \quad (3d)$$

$$18CuI + 6HgBr_2 \longrightarrow 4CuHgI_4 + 2HgBrI + 10CuBr.$$

Indeed, when Cu_2HgI_4 and $HgBr_2$ were mixed in 1:3 molar ratio it was found, after keeping it for about 24 h at 120 °C, (by X-Ray diffraction analysis) that it was completely changed into HgBrI and CuBr. Reaction (3d) has already been discussed rearlier. It is perhaps due to the very slow occurrence of Reactions (3c) and (3d) at room temperature that no inflection in the conductance curve (Fig. 4) shows up.

The 1:1 and 1:2 molar mixtures heated to 120 °C showed only the presence of CuBr and HgBrI and of CuBr and $CuHgBr_3$, respectively (Table 6):

$$CuI + HgBr_2 \longrightarrow CuBr + HgBrI, \quad (4)$$

$$CuI + 2HgBr_2 \longrightarrow CuHgBr_3 + HgBrI. \quad (5)$$

It appears as if in the 1:1 mixture, simple exchange took place, which indeed is not the case. When the reactants were mixed at room temperature, they formed a scarlet product turning gradually yellow. The scarlet product turned brown above 70 °C, which incidentally shows that the intermediate could be Cu_2HgI_4. This is also supported by thermal and conductance measurements (Figs. 3 and 4). X-Ray patterns taken about an hour after mixing the two in unimolecular ratio did indicate the presence of Cu_2HgI_4 and HgI_2, which shows that this reaction, too, takes place *via* HgI_2 as the others do.

$$2CuI + HgBr_2 \longrightarrow 2CuBr + HgI_2, \quad (4a)$$

$$2CuI + HgI_2 \longrightarrow Cu_2HgI_4, \quad (4b)$$

$$Cu_2HgI_4 + 3HgBr_2 \longrightarrow 4HgBrI + 2CuBr, \quad (4c)$$

$$4CuI + 4HgBr_2 \longrightarrow 4HgBrI + 4CuBr.$$

The initial fall in the conductance curve (Fig. 4) is due to conversion of highly conducting CuI into Cu_2HgI_4, and the rise thereafter refers to formation of HgBrI.

The reaction sequence for the 1:2 molar mixture is the same as that for 1:1. But, unlike 1:1 reaction, CuBr was not found in the end product (Table 6) in this case. This is because CuBr formed during the reaction is consumed up by $HgBr_2$ giving the addition product $CuHgBr_3$. $CuHgBr_3$ does not seem to have been reported so far either in solid or in solution. $KHgBr_3$ is, however, known in nonaqueous media.[15] Later $CuHgBr_3$ was prepared by heating a unimolar mixture of CuBr and $HgBr_2$ (each above 300 mesh) at 70 °C for about five days. The reflectance spectra (Fig. 6) for the 1:2 molar mixture showed that the product formed is different from the one obtained in the 1:1 molar mixture. The product thus obtained is yellow. The X-ray analysis and indexing of $CuHgBr_3$ are given in Table 7.

Mechanism of Lateral Diffusion. In the initial stage, at the reaction zone, the mercury(II) halide vapor surrounds each CuI grain and reacts through counter diffusion of Cu^+ and Hg^{2+} with simultaneous separation of CuBr and Cu_2HgI_4.

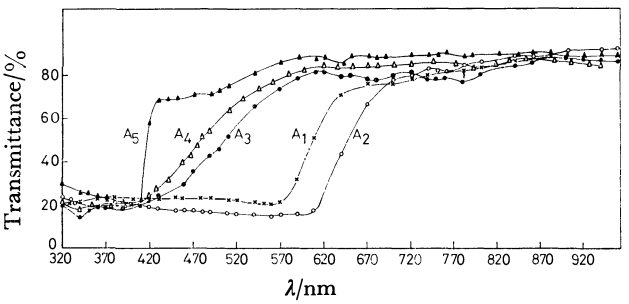

Fig. 6. Reflectance spectra for the CuI+$HgBr_2$ reaction (i) A_2, 4:1 (ii) A_1, 3:1 (iii) A_3, 2:1 (iv) A_4, 1:2 and (v) A_5, 1:2.

Table 7. X-Ray diffraction patterns of $CuHgBr_3$ taken by Norelco, (Philips 1010) diffractometer using Cu $K\alpha$ radiation and Ni-filter

d/Å	I/I_0	$h\,k\,l$	a_0[a]
5.9986	40	111	10.3899
3.8522	25	220	10.9240
3.1015	45	222	10.7439
2.4918	25	411	10.5718
2.2787	100	332	10.6881
2.1245	62	500, 430	10.6225
2.0336	25	511, 333	10.5669
1.9786	12	520, 432	10.6551
1.7614	14	610	10.7142
1.6851	7	620	10.6575
1.6143	5	622	10.7081
1.5367	25	444	10.6467

a) $a_0 = 10.6575$ Å.

Reactions on the two sides of the product layer proceed as follows:

$$HgX_2 + Cu^+ \longrightarrow 2CuX + Hg^{2+}, \quad (9)$$

$$4CuI + Hg^{2+} \longrightarrow Cu_2HgI_4 + 2Cu^+. \quad (10)$$

As the reaction proceeds, the thickness of the product layers increase and the rate decreases. The increase in thickness slows down the diffusion, and reaction rates thus fall gradually.

The kinetic data best fit the equation

$$X^n = kt,$$

where X is the total thickness of the product layers at time t and k and n are constants. k is related to the diffusion coefficient and follows the Arrhenius equation. The reactions proceed by movement of ions of one kind only, in such a way that the cations move through the product layers in opposite directions and react at phase boundaries with further formation of product layers. The continuous flow of cations from one into the other reactant through the product layer is responsible for the reaction. This is similar to the reaction of AgI and HgI_2 to form Ag_2HgI_4.[1]

Activation energies calculated by computer for CuI-HgI_2, CuI-HgBrI, and CuI-$HgBr_2$ reactions are, 97.75

± 2.74, 91.74 ± 2.55, and 82.787 ± 6.829 kJ mol^{-1}. respectively. These activation energies suggest that the reactions are diffusion controlled.

X-Ray analysis of the reaction mixture showed a change in *d*-values of the components which indicates formation of solid solutions in the systems CuBr–CuI, Cu_2HgI_4–CuBr, and HgBrI–Cu_2HgI_4. No attempt was, however, made to study the solutions in detail.

The authors wish to express thanks to the Head, Department of Chemistry for providing research facilities, to K. Rama Rao, R. R. L., Hyderabad for the help in X-ray measurements, and to Dr. M. Rahman, Department of Electrical Engineering for the help in the studies of conductivity measurements. One of us (A. A.) is grateful to C. S. I. R., New Delhi for the financial assistance.

References

1) E. Koch and C. Wagner, *Z. Phys. Chem.*, **B34**, 317 (1936).
2) M. A. Beg and S. M. Ansari, *J. Solid State Chem.*, **20**, 103 (1977).
3) M. A. Beg and S. M. Ansari, *J. Solid State Chem.*, **22**, 1 (1978).
4) H. T. Pinnock, *J. Soc. Chem. Ind.*, **38**, 78-9R (1919); *Chem. Abstr.*, **13**, 1373 (1919).
5) J. B. Berthemot, *J. Pharm.*, **14**, 614 (1830); J. W. Mellor, "A Comprehensive Treatise on Inorganic and Theoretical Chemistry," Longmans Green, London (1961), Vol. 3, p. 203.
6) M. Guichard, *C. R. Acad. Sci.*, **144**, 1430 (1907); *Chem. Abstr.*, **1**, 2988 (1907).
7) M. Meyer, *J. Chem. Educ.*, **20**, 145 (1943).
8) A. Oppenheim, *Ber.*, **2**, 571 (1869); J. W. Mellor, "A Comprehensive Treatise on Inorganic and Theoretical Chemistry," Longmans Green, London (1963), Vol. 4, p. 917.
9) ASTM Powder Diffraction File No. 18-0450.
10) R. P. Rastogi and B. L. Dubey, *J. Inorg. Nucl. Chem.*, **31**, 1530 (1969).
11) M. A. Beg and S. M. Ansari, *J. Solid State Chem.*, **15**, 57 (1976).
12) Z. Ketelaar, *Z. Krist.*, **87**, 440 (1934).
13) F. Fiegel and V. Anger, "Spots Tests in Inorganic Analysis," Elsevier (1972), pp. 145 and 203.
14) P. N. Miljanic, N. L. Kusters, and W. J. M. Moore, *Trans. AIEE*, 81 Part I, 359 (1962).
15) P. Yankov and I. G. Krasnousova, *Zh. Neorg. Khim.*, **16**, 557 (1971).

Infrared Spectra and Conformation of *N*-Acetylthiourea

Srinivasan ARUNA, Guruswamy SHANMUGAM,* Sadasivam MANOGARAN,† and D. N. SATHYANARAYANA†

*Department of Crystallography and Biophysics,** University of Madras, Guindy Campus, Madras-600025, India*

†*Department of Inorganic and Physical Chemistry, Indian Institute of Science, Bangalore-560012, India*

(Received October 1, 1981)

Infrared spectra of *N*-acetylthiourea (ATU) and its *N,N,N'*-trideuterated compound have been examined in the range 4000—50 cm^{-1}. A complete vibrational assignment with a normal coordinate treatment based on a Urey-Bradley type intramolecular potential function supplemented with valence force function for the out of plane and torsional modes is proposed and the feature of the thioureido vibrations explained. A molecular orbital study by the CNDO/2 method of ATU and its oxygen analog is undertaken and the results are analyzed for a comparative study of the molecular electronic structure and conformation.

Thiourea is a compound of considerable importance for the study of spectroscopic, structural and ligational properties. Many sulfur-nitrogen compounds containing $-NHCSNH_2-$ skeleton have been shown to possess carcinostatic and antiviral activities.[1] In this regard the vibrational spectra of thiourea and its various *N*-alkyl derivatives have received detailed attention.[2–10] In this context, it was of interest to study the spectral and structural features of *N*-acetylthiourea (ATU). ATU is isoelectronic with monothiobiuret and is the sulfur analog of *N*-acetylurea (AU), for both of which detailed vibrational spectroscopic studies have been reported very recently.[11,12] We have now examined the infrared spectra of ATU and its *N,N,N'*-trideuterated species and propose an assignment of all the fundamentals. A complete normal coordinate analysis has been carried out for ATU-d_0 and ATU-d_3 employing an intramolecular potential field of the Urey-Bradley type supplemented with valence force functions for the out of plane modes.

Another interesting problem concerning ATU is the identification of the minimum energy conformation. Four planar conformations may be conceived for ATU (Fig. 1). For this purpose, the all valence self consistent field molecular orbital method by the CNDO/2 procedure is employed. The computed bond orders and electron populations are employed to discuss the electronic structure. The calculations have been performed on both ATU and AU to note the electronic effects of the amide/thioamide grouping.

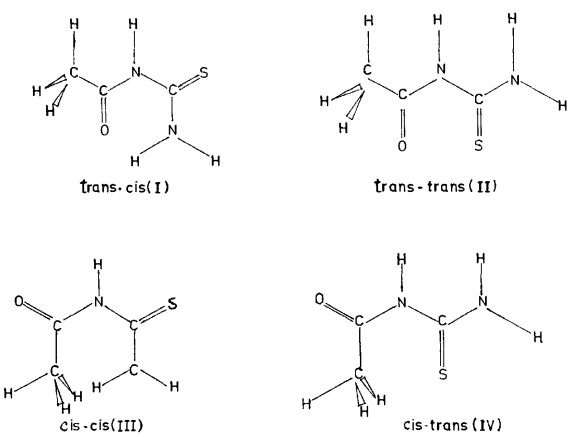

Fig. 1. Planar conformations of ATU.

Experimental

N-Acetylthiourea (Aldrich Chemical) was recrystallized from ethanol. The *N,N,N'*-trideuterated compound was obtained by exchange reaction with heavy water. The infrared spectra (both polycrystalline and solution) were recorded using Perkin-Elmer Model 580 spectrophotometer (4000—200 cm^{-1}) employing KBr pellet and Nujol mull techniques. Far infrared spectra (250—50 cm^{-1}) were recorded on Polytec FIR30 Fourier transform spectrometer as polyethylene pellets. The observed frequencies were calibrated with the usual standards.

Theoretical Treatment

The calculations were done on a DEC 1090 computer system using programs written in FORTRAN IV.

Normal Coordinate Analysis. The observed frequencies of ATU and its *N,N,N'*-trideuterated derivative were used in the calculations cast in terms of the GF matrix formulation.[13] The molecular structure adopted is shown in Fig. 2. This was based on the results of the CNDO/2 calculations and the preliminary X-ray structure determination.[14]

In the C_s point group model, the 33 fundamentals of ATU are classified amongst the symmetry species as 22A′ (In-plane), and 11A″ (out of plane) modes. The structural parameters were transferred from AU[12] and the C–S distance was taken to be 1.72 Å as in thioacetamide.[15] The internal valence coordinates and the local symmetry coordinates adopted were similar to those employed for AU.[12] A simple Urey-Bradley force field supplemented with valence force function for the out of plane deformation and torsional coordinates was employed. The initial values of the intramolecular force constants were transferred from thioacetamide[16–18] (TA), *N*-methylthioacetamide[16] (NMTA), and *N*-methylacetamide[16,19] (NMA), for

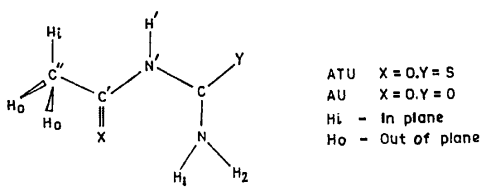

Fig. 2. Molecular structure and numbering scheme.

** Contribution No, 577,

which previously developed reliable potential constants are available. Only a small number of force constants required modification within a narrow range in the iteration process to obtain a desired agreement between the observed and calculated frequencies for ATU-d_0 and ATU-d_3. The programs employed were similar to the normal coordinate package of Schachtschneider.[20]

Molecular Orbital Studies. The calculations were made using the self consistent field CNDO/2 method. A full basis set of orbitals were explicitly considered including the 3d orbitals of sulfur. The geometrical parameters used were the same as those employed for the normal coordinate treatments. The total molecular energy was calculated, for the four more likely planar conformations of AU and ATU assuming the bond lengths and interbond angles to remain the same during the internal rotations. The standard program of Pople and Beveridge was employed.[21]

Results and Discussion

Table 2 gives the values of the final force constants. The values of the force constants appear reasonable and are similar to those of the initial ones indicating the good transferability property of the Urey-Bradley force constants as observed in other amide[16] and thioamide[16,18] derivatives. The force constant values compare well with the appropriate ones of AU.[12]

Spectral Interpretations. The observed spectra are shown in Fig. 3. In Table 1, the observed frequencies are compared with the calculated frequencies for ATU-d_0 and -d_3, wherein calculated potential energy distributions (PED), omitting for simplicity those less than 15%, are shown. A brief discussion of the features of thioureido vibrations of ATU will now be given.

The characteristic bands of interest are due to C=S and C–N stretching vibrations and NH inplane bending corresponding to thioamide I, III, and II bands respectively. The results of the coordinate analysis indicate a delocalized C=S mode contributing chiefly to the 820 cm^{-1} band akin to the 808 cm^{-1} band of thiosemicarbazide[22,23] and in contrast to a localized C=S stretching mode of *N*-methylthiourea at 778 cm^{-1}. Thus the C=S stretching frequency of ATU is higher than that in thiourea[2] and sym. *N,N'*-dimethylthiourea[8,9] assigned near 730 cm^{-1}. In monothiobiuret,[11] which is isoelectronic with ATU, the C=S stretching is assigned at 825 cm^{-1}. The C=S stretching frequency is lowered to 735 cm^{-1} in the *N*-deuterated derivative, the shift is comparable to that in *N*-methylthiourea -d_0 and -d_3.

The high and low C–N stretching frequencies (amide III bands) corresponding to the asymmetric and symmetric modes are assignable at 1525 and 1420 cm^{-1} which compare reasonably with those of *N*-methylthiourea[5] (NMTU) at 1565 and 1500 cm^{-1} and of sym·*N,N'*-dimethylthiourea[8,9] (DMTU) at 1560 and 1355 cm^{-1}. The differences are attributable to the different nature of the coupling of the vibrations involved.

The thioamide II band of the $-CSNH_2$ group due to NH_2 bending is observed at 1590 cm^{-1} which is lower than the 1642 cm^{-1} band of *N*-methylthiourea

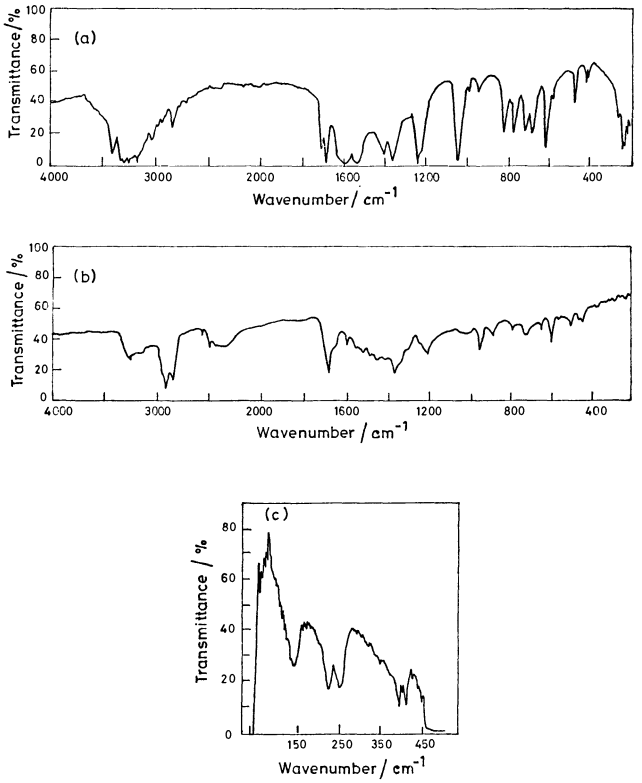

Fig. 3. Spectra of ATU.
a): ATU-d_0, b): ATU-d_3, c): far IR of ATU.

(NMTU). The thioamide II of –CSNH-grouping contributes to two bands at 1525 and 1315 cm^{-1}. The analogous NH bending frequencies are found in the region 1350 to 1400 cm^{-1} in NMTU,[5] DMTU[8,9] and thiosemicarbazide.[22,23] The thioamide VI band due to in-plane C=S bending occurs at 475 cm^{-1} as in thioacetamide.[16,18] In contrast, *N*-methylthiourea exhibits a more delocalized C=S bending mode. The assignments of other frequencies are compatible with the general features of *N*-methylthiourea[5] sym. *N,N'*-dimethylthiourea[8,9] and monothiobiuret[11] and are not discussed here further for brevity.

The intense band at 1680 cm^{-1} of ATU corresponds to the carbonyl stretching mode. The related band in the spectrum of AU occurs at 1670 cm^{-1}.

Molecular Conformation. The calculated total energies (Table 3) reveal that the most stable conformation accessible for ATU is the trans-cis (Fig. 1) concordant with the preliminary X-ray structure data in the solid state.[14] The next stable conformation is trans-trans which lies only some 5.02 kcal mol^{-1} above the lowest energy conformation. The calculations indicate the same trend for AU. The results rule out the accessibility of cis-cis structure and interestingly reveal that only a small activation energy is required for the conversion of cis-trans to the trans-trans form. This energy difference however should not be regarded as significant within the framework of this method. Moreover, the preference for one or the other form can also be affected by such factors as solvent and solid state interactions which are obviously not taken into consideration in the calculations. The implication is that the trans-cis structure is stabilized over

TABLE 1. OBSERVED AND CALCULATED FUNDAMENTAL FREQUENCIES IN cm^{-1} AND ASSIGNMENTS[a] FOR ATU-d_0 AND -d_3

Species	ATU-d_3		ATU-d_0		Assignment[b] (PED, %)
	Obsd	Calcd	Obsd	Calcd	
A′	2500	2514	3400	3392	$\nu_a NX_2$ (100)
	2420	2414	3300	3304	$\nu_s NX$ (100)
	2360	2376	3280	3290	$\nu_s NX_2$ (99)
	3040	3039	3040	3039	$\nu_a CH_3$ (100)
	2940	2953	2943	2953	$\nu_s CH_3$ (100)
	1670	1679	1680	1687	νCO (69), νCN (15)
	1130	1144	1590	1591	δNX_2 (76), νCN (20)
	1460	1465	1525	1522	νCN′ (36), δNX (31)
	1440	1434	1430	1438	$\delta_a CH_3$ (58), δCN (17)
	1485	1483	1420	1430	νCN (40), $\delta_a CH_3$ (22)
	1370	1380	1360	1360	$\delta_s CH_3$ (83)
	1040	1034	1315	1313	δNX (35), νCC (16), νCN (15)
	810	809	1260	1273	νNX_2 (33), νCS (17), δNCN (16)
	980	989	1040	1023	νCH_3 (31), νCC (28), νNX_2 (19)
	960	973	985	994	νCH_3 (64)
	1244	1244	945	955	νCN′ (32), γNX_2 (26), νC′S (18)
	735	736	820	818	νCS (40), νNX_2 (40)
	580	589	610	598	δCO (48), νCS (19)
	450	444	475	484	δCS (43), δCO (19), δNCN (15)
	385	384	400	396	δNCN (36), δCCN (29), δCS (19)
	305	298	290	301	δCCN (39), δCS (19)
	143	138	133	133	δCNC (65)
A″	3040	3036	3040	3036	νCH_3 (100)
	1430	1435	1430	1435	δCH_3 (93)
	1005	1006	1005	1006	$r CH_3$ (86)
	540	546	715	779	τNX_2 (99)
	560	563	715	715	ωNX_2 (73)
	500	483	680	681	νCN′ (43), ωNX_2 (26)
	580	588	580	570	πCO (87)
	250	252	250	259	πCS (68), πNH (21)
	136	139	136	140	τCH_3 (95)
	100	100	100	105	νCN′ (43), τCN (34)
	78	78	78	79	πN′X (55), τCN′ (24)

a) The fundamentals of ATU-d_3 have been arranged so as to give as far as possible approximately matching potential energy distributions (PED) stated for ATU-d_0. b) ν: Stretching, δ: bending, γ: rocking, π: out of plane bending, ω: waggingg, τ: torsion, a: asymmetric, and s: symmetric. X:H in ATU-d_0. X:D in ATU-d_3.

the other structures in the solid state. Factors such as steric effects, dipole-dipole interaction, hydrogen bonding and crystal packing determine the conformation of ATU. The large dipole-dipole interaction between the C=O and C=S dipoles is minimized in the trans-cis rotamer, so also the steric hindrance. Examination of the molecular model of ATU showed that this structure is very favourable for strong S···HN intermolecular and O···HN intramolecular hydrogen bonds. The more polarizable nature of the thiocarbonyl sulfur leads to stronger S···HN intermolecular hydrogen bonding between ATU molecules. Isoelectronic monothiobiuret[11] and other related molecules[12,24–26] are shown to possess a similar type of trans-cis structure.

Electronic Structure. Molecular orbital calculations of charge distributions have given an insight into the electronic structures of molecules and the effects

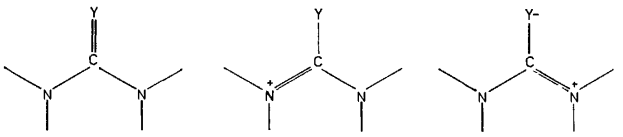

(a) (b) (c)

Fig. 4. Resonance structures.

of substituents.[27] In Table 4, the σ and π electron densities and the net electron populations have been shown for AU and ATU. While the electron densities quoted for a single molecule may not be a good guide, comparisons between related molecules by the same procedure of calculation may be more reliable. On comparing ATU with AU, we find significantly less electron populations for the atoms of the thioureido group excepting for the amide Y (O/S) atom,

for which the reverse is true. This indicates increased delocalization in the thioureido group as is to be expected, suggesting an increased contribution from resonance structures (b) and (c) to the description of bonding of ATU over that in AU shown in Fig. 4. This result is shown clearly in the values of the π bond orders. Table 4 demonstrates that in ATU, there is a significant decrease in the C–S(Y) bond order with consequent increase in the C–N (and C–N′) bond orders compared to those of AU. The C=O bond is also strengthened slightly in ATU relative to AU. From the low C–C π bond orders, it is evident that it hardly contributes to the conjugation of AU or ATU, while C′–N′ acquires slight π bond character. The acetyl carbonyl stretching frequency is observed at a higher wave number in ATU (1680 cm^{-1}) compared to AU in accord with the π bond order values. NH_2 and NH stretching frequencies of ATU should occur at lower wave numbers than those of AU because of increasing positive charge on nitrogen in ATU compared to AU (Table 4). But (Table 1), these frequencies are observed at higher frequencies than those in AU.[12] This demonstrates clearly, possible intermolecular (S···HN) and intramolecular (O···HN) hydrogen bonding between ATU molecules. More information can be obtained on this on the basis of detailed crystal structure analysis.[14]

Table 2. Force constants[a] of ATU

Urey-Bradley constants					
$K(NH_2)$	5.90	H(HNH)	0.40	F(HNH)	0.00
K(NH)	5.45	H(HNC)	0.27	F(HNC)	0.45
K(CH)	4.70	H(NCS)	0.28	F(NCS)	1.10
K(CO)	8.95	H(NCN)	0.50	F(NCN)	0.65
K(CN)	5.90	H(N′CS)	0.24	F(N′CS)	0.85
K(C′N)	5.50	H(CNC)	0.30	F(CNC)	0.30
K(CN′)	3.60	H(HNC′)	0.29	F(HNC′)	0.65
K(CS)	3.15	H(HNC)	0.16	F(HNC)	0.35
K(CC)	3.30	H(NCC)	0.15	F(NCC)	0.40
		H(CCO)	0.30	F(CCO)	0.50
$k(CH_3)$	−0.05	H(NCO)	0.42	F(NCO)	1.50
		H(CCH)	0.25	F(CCH)	0.45
		H(HCH)	0.42	F(HCH)	0.04
Valence constants					
$f(\pi CS)$	0.070	$f(\tau NH_2)$	0.136	$f(\tau C'N)$	0.117
$f(\pi CO)$	0.434	$f(\omega NH_2)$	0.088	$f(\tau CH_3)$	0.0055
$f(\pi NH)$	0.040	$f(\tau CN)$	0.060		

a) Units: K, H, F are in mdyn Å^{-1} and k, f in mdyn Å rad^{-2}.

One of the authors S. A., wishes to thank the authorities of the Indian Institute of Science, Bangalore, for providing facilities to carry out this work.

She expresses her gratitude to the Council of Scientific and Industrial Research, New Delhi, for the award of a Research Fellowship.

Table 3. Calculated total molecular energies

Conformation	ATU		AU	
	Total energy[a]	Difference[b]	Total energy	Difference
trans-cis	−78.4913	0.0	−85.9587	0.0
trans-trans	−78.4833	5.02	−85.9481	6.65
cis-trans	−78.3941	61.01	−85.9423	10.29
cis-cis	−77.9244	355.84	−85.4437	323.27

a) Hartree. b) In kcals mol^{-1}.

Table 4. Electron populations and bond orders[a] for ATU and AU

Atom	Electron population ATU			Electron population AU			π Bond order		
	σ	π	Total	σ	π	Total	Bond	ATU	AU
H_1	0.8860	—	0.8860	0.8148	—	0.8148	C–N	0.540	0.443
H_2	0.8473	—	0.8473	0.8703	—	0.8703	C=Y	0.578	0.781
N	3.4232	1.7624	5.1856	3.4664	1.8392	5.3056	C–N	0.495	0.372
C	3.0195	0.7042	3.7237	2.7615	0.7763	3.5378	C′–N	0.388	0.429
Y	4.7388	1.6881	6.4269	4.9154	1.4989	6.4143	C=X	0.856	0.823
N′	3.4692	1.6660	5.1352	3.4916	1.7287	5.2203	C–C	0.232	0.235
H′	0.8917	—	0.8917	0.8609	—	0.8609			
C′	2.8549	0.8040	3.6589	2.8879	0.7553	3.6432			
X	4.9139	1.3623	6.2762	4.9223	1.4434	6.3657			
C″	3.0741	1.0109	4.0850	3.0770	1.0098	4.0868			
H_1	0.9830	—	0.9830	0.9795	—	0.9795			
H_o	0.9502	—	0.9502	0.9502	—	0.9502			

a) Numbering schemes and abbreviations as in Fig. 2.

References

1) M. A. Ali and S. E. Livingstone, *Coord. Chem. Rev.*, **13**, 101 (1974).
2) A. Yamaguchi, R. B. Penland, S. Mizushima, T. J. Lane, C. Curran, and J. V. Quagliano, *J. Am. Chem. Soc.*, **80**, 527 (1958).
3) G. B. Aitken, J. L. Duncan, and G. P. Mcquillan, *J. Chem. Soc., A*, **1971**, 2695.
4) D. Hadzi, J. Kidnic, Z. V. Knezevic, and B. Barlic, *Spectrochim. Acta, Part A*, **32**, 693 (1976).
5) K. Dwarakanath and D. N. Sathyanarayana, *Bull. Chem. Soc. Jpn.*, **52**, 2084 (1979).
6) K. Dwarakanath and D. N. Sathyanarayana, *Indian J. Pure Appl. Phys.*, **17**, 171 (1979).
7) R. K. Gosavi, U. Agarwala, and C. N. R. Rao, *J. Am. Chem. Soc.*, **89**, 235 (1967).
8) R. K. Ritchie, H. Speeding, and D. Steele, *Spectrochim. Acta, Part A*, **27**, 1597 (1971).
9) K. R. Gayathri Devi and D. N. Sathyanarayana, *Bull. Chem. Soc. Jpn.*, **53**, 2990 (1980).
10) U. Anthoni, P. H. Nielsen, G. Borch, J. Gustavsen, and P. Klaboe, *Spectrochim. Acta, Part A*, **33**, 403 (1979).
11) K. Geetharani and D. N. Sathyanarayana, *Spectrochim. Acta, Part A*, **32**, 227 (1976).
12) Y. Saito and K. Machida, *Spectrochim. Acta, Part A*, **35**, 369 (1979).
13) E. B. Wilson, Jr., J. C. Decius, and P. C. Cross, "Molecular Vibrations," McGraw-Hill, New York (1955).
14) S. Aruna, unpublished results.
15) M. R. Truter, *J. Chem. Soc.*, **1960**, 997.
16) I. Suzuki, *Bull. Chem. Soc. Jpn.*, **35**, 1286, 1449 (1962).
17) A. Ray and D. N. Sathyanarayana, *Bull. Chem. Soc. Jpn.*, **47**, 729 (1974).
18) W. Walter and P. Stäglich, *Spectrochim. Acta, Part A*, **30**, 1739 (1974); and references therein.
19) T. Miyazawa, T. Shimanoucih, and S. Mizushima, *J. Chem. Phys.*, **24**, 408 (1956).
20) J. H. Schachtschneider, "Technical Report," Shell Development Company, Emeryville, CA, U.S.A. (1969).
21) J. A. Pople and D. L. Beveridge, "Approximate molecular orbital theory," McGraw-Hill, New York (1972).
22) G. Keresztuny and M. P. Marzochi, *Spectrochim. Acta, Part A*, **31**, 275 (1975).
23) D. N. Sathyanarayana, K. Volka, and K. Geetharani, *Spectrochim. Acta, Part A*, **33**, 517 (1977).
24) E. W. Hughes, H. L. Yakel, and H. C. Freeman, *Acta Crystallogr.*, **14**, 345 (1961).
25) W. K. Spofford and E. L. Amma, *J. Cryst. Mol. Struct.*, **2**, 151 (1972).
26) K. L. Gallaher and S. H. Bauer, *J. Chem. Soc., Faraday Trans. 2*, **1974**, 1243.
27) R. D. Topsom, *Prog. Phys. Org. Chem.*, **12**, 1 (1976).

Electron Transfer Reactions between V(IV) and I(V) Catalyzed by Os(VIII) or Ru(III). A Kinetic Study

Patapati Subbu RADHAKRISHNAMURTI,* Chelli JANARDHANA, and Gopal Krishna MOHANTY

Department of Chemistry, Berhampur University, Berhampur 760007, Orissa, India

(Received November 17, 1981)

Oxidation of V(IV) by iodate, catalyzed by Os(VIII) or Ru(III) in aq perchloric acid medium, was carried out. The order with respect to oxidant is zero in both the Os(VIII)- and Ru(III)-catalyzed reactions. A unit-order dependence on V(IV) is observed in the case of Os(VIII)-catalyzed reaction and a fractional dependence on V(IV) is noticed in the case of Ru(III)-catalyzed reaction. Both Os(VIII)- and Ru(III)-catalyzed reactions exhibit an inverse unit dependence on acidity. Insensitivity to change in the dielectric constant of medium is observed in both the systems. Effects of salt and ionic strength were studied. A plausible mechanism consistent with the experimental results is postulated, rate laws being derived from the proposed mechanism. The stoichiometry of the reaction has proved to be the same for both the systems.

Oxidation of V(IV) by Cr(VI),[1] Mn(III),[2] or Br(V)[3] has been studied previously. Fuller and Ottaway[4] investigated kinetics of oxidation of V(IV) by IO_3^- with a ratio of oxidant:reductant not less than 25 and found a second-order dependence on IO_3^- and a first-order dependence on V(IV). In the present investigation under a reverse condition of substrate [V(IV)]/oxidant $[IO_3^-]>20$, there was no reaction even after keeping the system overnight at the temperature studied. Thus the facile oxidation of V(IV) with Os(VIII) or Ru(III) and with IO_3^- as a co-oxidant has been systematically investigated. To our knowledge this is the first systematic kinetic report on Os(VIII)- or Ru(III)-catalyzed oxidations of V(IV) by iodate.

Experimental

All the reagents used were of AR grade: BDH(AR) $VOSO_4$ and BDH(AR) KIO_3; 70% BDH(AR) $HClO_4$ and $RuCl_3$ and OsO_4 solutions were diluted before use.

The kinetics of reaction was followed by determining the unreacted iodate iodometrically will standardized sodium thiosulfate and starch iodide indicator end point. No solvent decomposition occurred. $Na_2S_2O_3$ reacts with OsO_4 but not with $RuCl_3$. The error involved in the determination is not more than 6% at the highest concentration of Os(VIII) (15.7×10^{-5} M) (1 M=1 mol dm^{-3}). In the majority of experiments the error is not more than 2%; however, in the computation this error level was taken into account. All rate constants were reproducible within ±3% error.

Stoichiometry. The overall stoichiometry for both the Os(VIII)- and Ru(III)-catalyzed oxidations of V(IV) by IO_3^- was found to be 1:6.

Discussion

Oxidation of V(IV) by I(V) Catalyzed by Os(VIII). Oxidation of V(IV) by iodate catalyzed by Os(VIII) was carried out in aq perchloric acid aq acetic acid–perchloric acid media.

Effect of Varying $[IO_3^-]$ on Reaction Rate. The Os(VIII)-catalyzed IO_3^- oxidation of V(IV) was studied under a pseudo-first-order condition with excess [V(IV)] over $[IO_3^-]$. The disappearance of $[IO_3^-]$ conformed to no first-order pattern as seen from the nonlinearity of plots of log $[IO_3^-]_t$ *vs.* time. On the other hand, plots of X *vs.* time are fairly linear at least up to double the half-life, indicating a zero-order dependence with respect to the oxidant. Zero-order rate constants are computed from slopes (x/t) of such linear plots. Moreover, k_0 values computed for various initial concentrations of IO_3^- are almost identical, confirming the zero-order dependence with respect to the oxidant (Table 1) in the concentration range studied. Such zero-order dependence on oxidant has been observed in various reactions catalyzed by transition metal ions.

TABLE 1. EFFECT OF VARIATION OF [OXIDANT], [SUBSTRATE], [ACID], AND [CATALYST] AT TEMPERATURE 60 °C

Substrate 10^2[V(IV)]	Oxidant $10^4[IO_3^-]$	Acid $10^2[HClO_4]$	Catalyst 10^5[Os(VIII)]	k_0 / 10^{-6} mol l^{-1} min^{-1}
1.0	2.14	1.0	3.93	2.37
1.0	4.25	1.0	3.93	2.35
1.0	8.35	1.0	3.93	2.43
1.0	12.84	1.0	3.93	2.38
0.25	4.04	1.0	3.93	0.57
0.50	4.14	1.0	3.93	1.15
2.0	4.19	1.0	3.93	5.19
1.0	4.09	0.50	3.93	4.75
1.0	4.12	2.0	3.93	1.24
1.0	3.91	4.0	3.93	0.58
1.0	3.95	1.0	1.96	1.50
1.0	4.41	1.0	7.86	4.99
1.0	4.26	1.0	15.73	8.77

Effect of Varying [V(IV)] on Reaction Rate. Increasing the concentration of V(IV) increases the rate of reaction; rate constants at different concentrations of V(IV) are given in Table 1. The plot of $\log k_o$ *vs.* log[V(IV)] is linear with slope unity, indicating a first-order dependence with respect to substrate.

Effect of Varying [Os(VIII)] on Reaction Rate. Increasing the concentration of Os(VIII) increases the reaction rate; rate constants at different concentrations of Os(VIII) are given in Table 1. The plot of log k_o *vs.* log[Os(VIII)] is linear with slope unity, indicating a first-order dependence with respect to Os(VIII).

Effect of Varying [$HClO_4$] on Reaction Rate. The influence of acid on reaction rate was studied with a view to identifying species which participate in the reaction. Increase in the concentration of perchloric acid decreases the rate of oxidation (Table 1). The plot of $\log k_o$ *vs.* log[H^+] is linear with a negative slope of unity. Thus the dependence on acid is inverse unity. This inverse dependence on acidity deserves a comment. VO^{2+} on hydrolysis forms $VOOH^+$ *via* the equilibrium

$$VO^{2+} + H_2O \overset{K_h}{\rightleftharpoons} VOOH^+ + H^+.$$

Active species of substrate participating in the reaction is $VOOH^+$, hence the inverse dependence on acidity. It is reported[5] that V(IV) in aq acid medium ([H^+]= 0.002—3 M) hydrolyses to $VOOH^+$ with an approximate K_h value of 10^{-6}.

Effect of Varying Concentration of Acetic Acid. These reactions are found to be insensitive to change in dielectric constant of the medium. Increase in the percentage of acetic acid has no effect on the reaction rate. Rate constants at different percent of acetic acid are given in Table 2. Such insensitivity to change in dielectric constant of the medium has been observed also in Ag^+-catalyzed oxidation of α-hydroxy acids by peroxydisulphate.[6]

Effect of Varying Ionic Strength of the Medium. Change in ionic strength of the medium by varying the concentration of sodium perchlorate has no effect on the reaction rate. Rate constants at different concentrations of sodium perchlorate are given in Table 3. This clearly indicates that the reactions are of ion dipolar type.

Effect of Temperature on Reaction Rate. Reactions were conducted at different temperatures in the range from 50 to 70 °C and respective rate constants are given in Table 4. The plot of $\log k_o$ *vs.* $1/T$ is linear. From the slope of the plot of $\log k_o$ *vs.* $1/T$ respective Arrhenius parameters were computed and listed in Table 4. These activation parameters are of correct magnitude.

TABLE 2. EFFECT OF VARIATION OF SOLVENT ON REACTION RATE

[V(IV)]=0.01 M, [IO_3^-]=0.5×10^{-3} M, [$HClO_4$]=0.01 M, [Os(VIII)]=3.93×10^{-5} M, temp=60 °C.

% of HOAc	k_0 / 10^{-6} mol l^{-1} min^{-1}
10	2.24
20	2.05
40	2.05
60	2.68

TABLE 3. EFFECT OF VARIATION OF IONIC STRENGTH

[V(IV)]=0.01 M, [IO_3^-]=0.5×10^{-3} M, [$HClO_4$]=0.01 M, [Os(VIII)]=3.93×10^{-5} M, temp=60 °C.

[$NaClO_4$] / 10^{-2} M	μ / mol l^{-1}	k_0 / 10^{-6} mol l^{-1} min^{-1}
1.0	0.06	2.36
2.5	0.075	2.58
5.0	0.10	2.41
10.0	0.151	2.35

TABLE 4. EFFECT OF VARIATION OF TEMPERATURE AND THERMODYNAMIC PARAMETERS AT 60 °C

[V(IV)]=0.01 M, [IO_3^-]=0.5×10^{-3} M, [$HClO_4$]=0.01 M.

Catalyst	T / °C	k_0 / 10^{-6} mol l^{-1} min^{-1}
[Os(VIII)]	50	0.97
3.93×10^{-5} M	60	2.43
	70	6.71

ΔE^* / kJ mol^{-1}	ΔH^* / kJ mol^{-1}	$\log_{10} A$	ΔS^* / J K^{-1} mol^{-1}
86.2	83.5	6.13	−136

Oxidation of V(IV) by I(V) Catalyzed by Ru(III). As a continuing study, oxidation of V(IV) by Ru(III)-catalyzed iodate was carried out for comparison, salient features observed in the investigation are as follows:

i) The order with respect to oxidant is zero which is similar to the case of Os(VIII)-catalyzed reactions (Table 5).

ii) Increase in the concentration of V(IV) increases the rate of oxidation, rate constants at different concentrations of [V(IV)] being given in Table 5. The plot of $\log k_o$ *vs.* log[V(IV)] is linear with a slope less than unity, indicating a fractional dependence on substrate. This differs from the previous observation made in the case of Os(VIII)-catalyzed oxidations.

iii) The dependence on Ru(III) is unity which is analogous to that observed in the case of Os(VIII)-catalyzed reactions (Table 5).

iv) To confirm the dependence on acidity with no attendant ionic strength effect, the dependence on [H^+] at constant ionic strength was determined. The plot of $\log k_o$ *vs.* log[H^+] is linear with a slope of −0.5, which shows a fractional dependence on [H^+] (Table 8) and the plot of $\log k_o$ *vs.* log[$NaClO_4$] is linear with a slope of −0.5 (Table 7).

v) The apparent dependence on acid is inverse unity, which results from additive effects of ionic strength and acid both being inverse. It may be pointed out that in OsO_4-catalyzed reaction there

Table 5. Effect of variation of [oxidant], [substrate], [acid], and [catalyst] at temperature 35 °C

Substrate 10^2[V(IV)]	Oxidant 10^4[IO_3^-]	Acid 10^2[$HClO_4$]	Catalyst 10^7[Ru(III)]	k_0 / 10^{-6} mol l^{-1} min^{-1}
1.0	2.03	1.0	7.64	3.65
1.0	4.80	1.0	7.64	3.77
1.0	8.69	1.0	7.64	3.80
1.0	12.78	1.0	7.64	3.77
0.25	5.02	1.0	7.64	1.50
0.50	4.98	1.0	7.64	2.23
2.0	4.46	1.0	7.64	4.49
4.0	5.02	1.0	7.64	5.69
1.0	4.23	0.50	7.64	7.67
1.0	4.68	2.0	7.64	1.98
1.0	4.66	4.0	7.64	1.04
1.0	4.33	1.0	3.82	1.93
1.0	4.05	1.0	14.28	7.47
1.0	4.09	1.0	28.56	14.21

Table 6. Effect of variation of solvent on reaction rate

[V(IV)]=0.01 M, [IO_3^-]=0.5×10^{-3} M, [$HClO_4$]=0.01 M, [Ru(III)]=7.64×10^{-7} M, temp=35 °C.

% HOAc	k_0 / 10^{-6} mol l^{-1} min^{-1}
10	3.68
20	3.77
30	3.75
40	3.66
60	3.59
80	3.48

Table 7. Effect of variation of ionic strength

[V(IV)]=0.01 M, [IO_3^-]=0.5×10^{-3} M, [$HClO_4$]=0.01 M, [Ru(III)]=7.64×10^{-7} M, temp=35 °C

[$NaClO_4$] / 10^{-2} M	μ / mol l^{-1}	k_0 / 10^{-6} mol l^{-1} min^{-1}
1.0	0.069	3.13
5.0	0.10	2.12
8.0	0.131	1.89
10.0	0.151	1.37
20.0	0.251	1.09

Table 8. Effect of variation of acid at constant ionic strength

[V(IV)]=0.01 M, [IO_3^-]=0.5×10^{-3} M, [$NaClO_4$]=0.2 M, [Ru(III)]=7.64×10^{-7} M, temp=35 °C

[$HClO_4$] / 10^{-2} M	k_0 / 10^{-6} mol l^{-1} min^{-1}
0.5	1.57
1.0	1.09
2.0	0.84
4.0	0.49

Table 9. Effect of variation of temperature and thermodynamic parameters at 35 °C

[V(IV)]=0.01 M, [IO_3^-]=0.5×10^{-3} M, [$HClO_4$]=0.01 M.

Catalyst	T / °C	k_0 / 10^{-6} mol l^{-1} min^{-1}
[Ru(III)]	30	2.37
7.64×10^{-7} M	35	3.77
	45	9.84

ΔE^* / kJ mol^{-1}	ΔH^* / kJ mol^{-1}	$\log_{10} A$	ΔS^* / J K^{-1} mol^{-1}
73.8	71.1	5.27	−146.8

is no influence of ionic strength on the reaction as is clear from Table 5.

vi) Solvent influence is similar to what is found in Os(VIII)-catalyzed reaction (Table 6).

vii) Species of Ru(III): It is well known that Ru^{+3} mainly exists as $[Ru(H_2O)_6]^{3+}$ in acid medium.[7]

viii) The study was carried out at different temperatures in the range 30—40 °C. Rate constants are listed in Table 9. The plot of $\log k_0$ *vs.* $1/T$ is linear. From the slope of the above plot Arrhenius parameters were computed as listed in Table 9. These values are similar to those obtained in the case of Os(VIII)-catalyzed reactions.

From the above findings it can be concluded that the catalytic ability of Ru(III) is in general greater than that of Os(VIII) in the present experimental conditions.

Mechanism of Oxidation. Os(VIII)-catalyzed Oxidation: The kinetic features observed in the Os(VIII)-catalyzed oxidation of V(IV) by iodate indicate that $VOOH^+$ is the active species. The zero-order dependence on oxidant clearly shows nonparticipation of oxidant in the rate-determining step. The mechanism of oxidation can be envisaged through a hydrolytic equilibrium between VO^{2+} and $VOOH^+$ followed by reaction between $VOOH^+$ and OsO_4 as the rate-determining step to give V(V) and Os(VII).

The Os(VII) formed oxidizes in the subsequent fast step another V(IV) entity to give Os(VI) and V(V). The generated Os(VI) is oxidized in the subsequent fast step by IO_3^- to Os(VIII), thus giving rise to the zero-order dependence with respect to oxidant. The detailed steps are represented in Scheme 1:

$$VO^{2+} + H_2O \overset{K_h}{\rightleftharpoons} VOOH^+ + H^+, \quad (1)$$

$$VOOH^+ + OsO_4 \underset{k_1}{\overset{\text{slow}}{\longrightarrow}} VO_2^+ + OsO_3(OH),$$

$$OsO_3OH + VOOH^+ \overset{\text{fast}}{\longrightarrow} OsO_3 + VO_2^+ + H_2O,$$

$$3OsO_3 + IO_3^- \overset{\text{fast}}{\longrightarrow} 3OsO_4 + I^-.$$

Scheme 1.

Rate Law. From Equilibrium 1,

$$K_h = \frac{[VOOH^+][H]^+}{[VO^{2+}]} \text{ or } [VO^{2+}] = \frac{[VOOH^+][H^+]}{K_h},$$

$$[VO^{2+}]_T = VO^{2+} + VOOH^+ = \frac{[VOOH^+]\{H^+ + K_h\}}{K_h}$$

$$\text{or } [VOOH^+] = \frac{[VO^{2+}]_T K_h}{(H^+ + K_h)},$$

$$\text{Rate} = -\frac{d[IO_3^-]}{dt} = k_1[VOOH^+][OsO_4] = \frac{k_1 L_h [VO^{2+}]_T [OsO_4]}{(H^+ + K_h)}.$$

K_h is of the order of 10^{-6} and can be neglected in comparison to $[H^+]$, hence the rate law is reduced to

$$-\frac{d[IO_3^-]}{dt} = \frac{k_1 K_h [VO^{2+}]_T [OsO_4]}{H^+}.$$

Ru(III)-catalyzed Oxidation. The observations noticed in the case of Ru(III)-catalyzed oxidation are analogous to those in the case of Os(VIII)-catalysed reaction, except that the dependence on substrate is fractional. The inverse dependence on acidity indicates that the active species $VOOH^+$ takes part in the reaction. The mechanism of oxidation can be postulated as a formation of an intermediate between $VOOH^+$ and $[Ru(H_2O)_6]^{3+}$ in an equilibrium step. Decomposition of the intermediate takes place in a rate-determining step with one-electron transfer between Ru(III) and V(IV) to give Ru(II) and V(V) in an innersphere mechanism without disturbing the octahedral nature of ruthenium. The Ru(II) formed then reacts with another V(IV) entity in a fast step to give Ru(I) and V(V). The Ru(I) formed is subsequently oxidized by iodate in a fast step to Ru(III), thus giving rise to the zero-order dependence with respect to oxidant. The existence of Ru(II) as an aqua ion $[Ru(H_2O)_6]^{2+}$ has been well documented and the existence of Ru(I) in complexes is well known.[8] Hence the valence states of Ru(II) and Ru(I) as intermediates have been postulated in this mechanism. Various steps involved in the reaction are represented in Scheme 2:

$$VO^{2+} + H_2O \overset{K_h}{\rightleftharpoons} VOOH^+ + H^+, \quad (1)$$

$$[Ru(H_2O)_6]^{3+} + VOOH^+ \underset{k_{-1}}{\overset{k_1}{\rightleftharpoons}} [Ru(H_2O)_6{}^{3+}\cdots VOOH^+], \quad \text{(Complex)}$$

$$[Ru(H_2O)_6{}^{3+}\cdots VOOH^+] \underset{\text{slow}}{\overset{k_2}{\longrightarrow}} VO_2^+ + [Ru(H_2O)_6]^{2+} + H^+, \quad \text{(Complex)}$$

$$[Ru(H_2O)_6]^{2+} + VOOH^+ \overset{\text{fast}}{\longrightarrow} [Ru(H_2O)_6]^+ + VO_2^+ + H^+,$$

$$3[Ru(H_2O)_6]^+ + IO_3^- + 6H^+ \overset{\text{fast}}{\longrightarrow} 3[Ru(H_2O)_6]^{3+} + 3H_2O + I^-.$$

Scheme 2.

Rate Law. From Equilibrium 1,

$$K_h = \frac{[VOOH^+][H^+]}{[VO^{2+}]} \text{ or } [VO^{2+}] = \frac{[VOOH^+][H^+]}{K_h},$$

$$[VO^{2+}]_T = VO^{2+} + VOOH^+ = \frac{[VOOH^+]\{H^+ + K_h\}}{K_h}$$

$$\text{or } [VOOH^+] = \frac{[VO^{2+}]_T K_h}{(H^+ + K_h)},$$

$$\text{Complex} = \frac{k_1[Ru(III)][VOOH^+]}{(k_{-1} + k_2)},$$

$$[Ru(III)]_T = [Ru(III)] + [\text{Complex}] = Ru(III)\left\{1 + \frac{k_1[VOOH^+]}{(k_{-1} + k_2)}\right\},$$

$$[Ru(III)] = \frac{(k_{-1} + k_2)[Ru(III)]_T}{(k_{-1} + k_2) + k_1[VOOH^+]}.$$

$$\text{or } [Ru(III)] = \frac{(k_{-1} + k_2)(H^+ + K_h)[Ru(III)]_T}{(k_{-1} + k_2)(H^+ + K_h) + k_1 K_h [VO^{2+}]_T}.$$

$$\text{So, Complex} = \frac{k_1 K_h [VO^{2+}]_T [Ru(III)]_T}{(k_{-1} + k_2)(H^+ + K_h) + k_1 K_h [VO^{2+}]_T}$$

$$\text{or} = \frac{k_1 K_h [VO^{2+}]_T [Ru(III)]_T}{H^+ + K_h + k_1 K_h [VO^{2+}]_T}$$

$$\left(\text{where } K_1 = \frac{k_1}{k_{-1} + k_2}\right),$$

$$\text{Rate} = -\frac{d[IO_3^-]}{dt} = k_2[\text{Complex}] = \frac{k_2 K_1 K_h [VO^{2+}]_T [Ru(III)]_T}{H^+ + K_h + K_1 K_h [VO^{2+}]_T}.$$

This expression is capable of explaining all the observed facts.

The authors GKM and CJ are grateful to CSIR for the award of JRF and PDF, respectively.

References

1) J. H. Espenson, *J. Am. Chem. Soc.*, **86**, 1883 (1964).
2) D. R. Rosseensky and M. J. Nccol, *J. Chem. Soc.*, **1968**, 1022.
3) C. W. Fuller and J. M. Ottaway, *Analyst*, **94**, 32 (1969).
4) C. W. Fuller and J. M. Ottaway, *Analyst*, **95**, 791 (1970).
5) J. Selbin, *Chem. Rev.*, **65**, 153 (1965).
6) N. Venkatasubramanian and A. Sabesan, *Indian J. Chem.*, **9**, 942 (1971).
7) F. A. Cotton and G. Wilkinson, "Advanced Inorganic Chemistry," 2nd ed, (1966), p. 999.
8) J. C. Bailar, M. J. Emeleus, R. Nyholm, and A. F. T. Dickenson, "Comprehensive Inorganic Chemistry," Pergamon, London (1973), Vol. III, p. 1198.

 © 1982 The Chemical Society of Japan Bull. Chem. Soc. Jpn., 55, 3621—3624 (1982)

Some Observations on the Structural Aspects of *o*-Hydroxythiobenzamide and Its Complexes with Pt(II), Pt(IV), and Au(III)

Karunamay BANERJEE* and Shyamal RAYCHAUDHURY

Department of Pure Chemistry, University College of Science and Technology, Calcutta 700009, India

(Received September 22, 1981)

^{1}H NMR, electronic spectra, electrical conductivity studies in solution and IR study in solid phase have been done on *o*-hydroxythiobenzamide and its complexes with Pt(II), Pt(IV), and Au(III). The results indicate presence of the thioamide-thioimidic acid equilibrium in *o*-hydroxythiobenzamide, the thioamide form in the Pt(II) and Pt(IV) complexes, the thioimidate form in the Au(III) complex and free phenolic OH group in the Pt(IV) and Au(III) complexes.

o-Hydroxythiobenzamide received attention as a complexing agent for quantitative estimation of Pt(IV)[1] and Au(III)[2] ions. The previous workers[1,2] predicted the possible formulas of the complexes as $[Pt^{IV}L_2L'_2]Cl_2$, $[Pt^{II}L'_2]$, and $H[Au^{III}L'_3Cl]$ (where L= *o*-hydroxythiobenzamide and L'=*o*-hydroxythiobenzamide anion), but the structural form of L' and structure of the complexes have not been clearly revealed. The object of the present investigation is to elucidate the ionic forms of the ligand, and nature of bonding present in the above complexes on the basis of ^{1}H NMR, electronic spectra, electrical conductivity studies in solution and IR study in solid phase. In the course of our investigation it has been observed that *o*-hydroxythiobenzamide remains in thioamide-thioimidic acid (*o*-$HOC_6H_4CSNH_2 \rightleftharpoons$ *o*-$HOC_6H_4C(SH):NH$) equilibrium in solution and may lose phenolic OH and/or thiomidic acid proton to satisfy primary valency of the metal ions in complex formation. The probable structures of the metal complexes have been suggested on the basis of the present study as $[Pt^{II}(o\text{-}OC_6H_4CSNH_2)_2]$, $[Pt^{IV}(o\text{-}OC_6H_4CSNH_2)_2(o\text{-}HOC_6H_4CSNH_2)_2]Cl_2$, and $H[Au^{III}(o\text{-}HOC_6H_4CS:NH)_3Cl]$.

Experimental

The complexes were prepared by the methods given in literature.[1,2] The electrical conductivity data of the compounds at 25 °C in methanol were obtained by using Phillips PR 9500 conductivity bridge. The UV and visible absorption spectra of the compounds in solution were recorded at room temperature on Varian Techtron 634 spectrometer. IR shectra were obtained in KBr pellets on Beckmann IR 20 spectrometer. ^{1}H NMR spectra of the compounds in deuterated solvents were obtained on Varian NMR spectrometer EM-390; 90 MHz at 20 °C using tetramethylsilane as the internal reference.

Results and Discussion

NMR, IR, and Electrical Conductivity Studies. o-*Hydroxythiobenzamide*: ^{1}H NMR spectra in Fig. 1 indicate that *o*-hydroxythiobenzamide exists in thioamide form in $CDCl_3$ solution, and thioimidate form in DMSO-d_6 solution. $CDCl_3$ solution of *o*-hydroxythiobenzamide exhibits peaks due to the H-bonded phenolic OH at 11.9 δ, NH_2 and ring protons at 6.9—7.7 δ. ^{1}H NMR spectra of the *o*-hydroxythiobenzamide solution in DMSO-d_6 reveal a broad doublet at (9.6 δ, 9.8 δ). This doublet indicates the magnetic non-equivalence of NH_2 protons due to the restricted rotation about C–N bond in the polar form $\left(\text{S}\rangle\text{C–N}\langle\text{H} \rightleftharpoons \text{S}^-\rangle\text{C}=\overset{+}{\text{N}}\langle\text{H}\right)$ of *o*-hydroxythiobenzamide. The appearence of this doublet in the downfield region can be accounted for by the greater deshielding of protons attached with positive nitrogen in the polar form. A coalesced signal of two protons appears at 13.1 δ due to resonances of thioimidic SH and =NH groups. Analogous observation was reported in the molecular complex of dimethylamine and acetylacetone.[3] The ^{1}H NMR signal of H-bonded phenolic OH is seen at 11.75 δ in DMSO-d_6 solution of *o*-hydroxythiobenzamide. Except the ring protons, all other signals of *o*-hydroxythiobenzamide in DMSO-d_6 disappear on deuteration.

The IR spectral data of *o*-hydroxythiobenzamide in

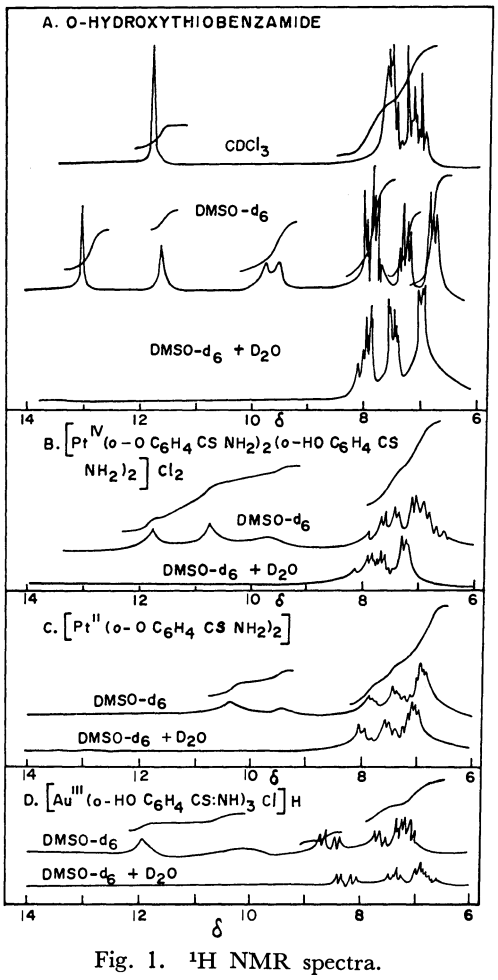

Fig. 1. ^{1}H NMR spectra.

Table 1. IR spectral bands ($\bar{\nu}$/cm^{-1}) in KBr pellets

A	B	C	D	Probable assignments
3395 s 3290 s 3190 w	3400 br — 3050 br	3380 br 3245 br 3080 br	3320 m 3270 br 3100 w	$\nu_{OH}+\nu_{NH}$
2750 w	2900 w	—	2900 w	ν_{OH}(H-Bonded)
1638 s 1610 w	1600 s —	1595 s 1580 w	1600 s 1585 w	$\delta_{NH_2}+\nu_{C-N}$
1473 s	1530 m	1490 w	1490 w	ν_{asym} of N-C=S
1385 s	1385 s	—	1385 w	δ_{OH}
1320 s	1315 s	1320 s	1315 s	ρ_r $NH_2+\nu_{C-S}$
1228 w	1235 w	1232 w	1235 w	ν_{sym} of N-C-S
895 m	900 w	880 s	885 s	NH_2 bending$+\nu_{C=N}+\nu_{C=S}$
757 m	750 m	750 m	748 m	$\nu_{C-N}+\nu_{C=S}$
742 s	698 s	690 w	690 br	$\nu_{C=S}$
660 s 645 m 595 s 580 m 560 w 520 w	660 s 644 m 598 s 582 m 558 w 550 w	659 s 642 m 595 s 579 w 560 w 550 w	660 s 644 m 595 s 580 w 560 w 550 w	δ_{ligand}
470 s	490 s	480 s	480 s	ν_{M-S}
410 w	410 w	411 w	410 w	ligand vibration
—	—	381 s	380 s	ν_{M-O}
350 m	350 m	354 m	350 m	ligand vibration
—	310 m	—	—	ν_{Au-Cl}
285 w	282 w	283 w	282 w	ligand vibration

A=*o*-$HOC_6H_4CSNH_2$; B=$H[Au^{III}(o\text{-}HOC_6H_4CS{:}NH)_3Cl]$; C=$[Pt^{II}(o\text{-}OC_6H_4CSNH_2)_2]$; D=$[Pt^{IV}(o\text{-}OC_6H_4CSNH_2)_2$-$(o\text{-}HOC_6H_4CSNH_2)_2]Cl_2$; s=strong; w=weak; br=broad; m=medium; M=Pt or Au.

KBr pellets are shown in Table 1. The stretching vibrations of OH and NH_2 appear in the 2750—3400 cm^{-1} region. The absence of SH band around 2550 cm^{-1} in the free ligand excludes the possible existence of thioimidic acid form in the solid state. All other band assignments according to Jensen *et al.*[4] are shown in Table 1.

Previous works[5] on the electrical conductivity in methanol indicate that molar conductance values in the 80—115 Ω^{-1} cm^2 mol^{-1} range are due to formation of the 1:1 electrolyte. The conductivity data in Table 2 indicate nonelectrolyte nature of *o*-hydroxythiobenzamide in methanol. Therefore low-field ^{1}H-NMR signal for phenolic OH, lower frequency IR band for ν_{OH} and nonelectrolyte behaviour of *o*-hydroxythiobenzamide suggest that its OH group is H-bonded in solution as well as in solid state.

[Pt^{II}(o-$OC_6H_4CSNH_2)_2$]. ^{1}H NMR spectra of the Pt(II) complex solution in DMSO-d_6 (Fig. 1) indicate the presence of broad doublet due to NH_2 protons at (9.5 δ, 10.4 δ) and the absence of phenolic OH proton signal. The IR data of Pt(II) complex in KBr pellets (Table 1) show slight lowering of ν_{NH_2} and absence of ν_{OH} at 2750 cm^{-1} in comparison to free ligand. It is known[4] that OH deformation band at 1385 cm^{-1} disappears on deuteration for the free ligand and also for the Ni(II) complex. We have also observed that the 1385 cm^{-1} band is absent in the Pt(II) complex. Therefore absence of phenolic OH signal in ^{1}H NMR spectra and absence of δ_{OH} band at 1385 cm^{-1} in IR spectra indicate Pt–O bonding in the Pt(II) complex. The antisymmetric vibration of the N–C=S group in *o*-hydroxythiobenzamide occuring at 1473 cm^{-1} and its subsequent shifting to higher frequency due to increased double bond character of N–C in N–C=S grouping in case of its Ni(II) complex[4] is at par with our observation in the Pt(II) complex. In the case of *o*-hydroxythiobenzamide the stretching vibration due to C=S appears at 742 cm^{-1}, but this band is shifted to 690 cm^{-1} in the Pt(II) complex due to metal-sulfur bonding. In the far IR region the bands at 480 cm^{-1} and 381 cm^{-1} are probably due to Pt–S and Pt–O bonding.

The electrical conductivity data in Table 2 indicate the nonelectrolyte behaviour of the Pt(II) complex in methanol.

Therefore in the square planar arrangement two *o*-hydroxythiobenzamide molecules are bonded through S and O with Pt^{2+} ion in Pt(II) complex.

[Pt^{IV}(o-$OC_6H_4CSNH_2)_2$(o-$HOC_6H_4CSNH_2)_2$]Cl_2. The ^{1}H NMR spectra of the Pt(IV) complex solution in DMSO-d_6 (Fig. 1) exhibit a broad band at (9.7 δ, 10.8 δ) for the NH_2 protons and a single proton peak at 11.8 δ for the H-bonded phenolic OH. IR spectral bands of the Pt(IV) and Pt(II) complexes in KBr pellets are alike except the case where the band due to H-bonded OH stretching of the free ligand at 2750 cm^{-1} is shifted to 2900 cm^{-1}, and OH deformation band at 1385 cm^{-1} does not disappear for the Pt(IV) complex. Therefore ^{1}H NMR signal at 11.8 δ and IR band at 1385 cm^{-1} indicate the existence of free phenolic OH in the Pt(IV) complex. The $\nu_{C=S}$ band of the free ligand appearing at 742 cm^{-1} and its subsequent shifting to 690 cm^{-1} in the Pt(IV) complex

Table 2. Electrical conductivity in methanol at 25 °C

Compound	Concentration mol dm^{-3}	Molar conductance Ω^{-1} cm^2
o-$HOC_6H_4CSNH_2$	2.2×10^{-3}	3.77
$[Pt^{II}(o\text{-}OC_6H_4CSNH_2)_2]$	1.2×10^{-3}	8.24
$[Pt^{IV}(o\text{-}OC_6H_4CSNH_2)_2(o\text{-}HOC_6H_4CSNH_2)_2]Cl_2$	1.2×10^{-3}	99.63
$H[Au^{III}(o\text{-}HOC_6H_4CS:NH)_3Cl]$	0.6×10^{-3}	91.02
$H[Au^{III}(o\text{-}HOC_6H_4CS:NH)_3Cl]$ + Excess o-$HOC_6H_4CSNH_2$	0.6×10^{-3}	114.00

suggests Pt–S bonding. In far IR region, like the Pt(II) complex the appearance of two bands at 380 cm^{-1} and 480 cm^{-1} indicate Pt–O and Pt–S bonding in the Pt(IV) complex. The electrical conductivity data in Table 2 show that the Pt(IV) complex behaves as 1:1 electrolyte in methanol. The lower conductivity of the Pt(IV) complex may be due to ionic association in low dielectric medium where one of the axially S bonded o-hydroxythiobenzamide molecule is replaced by chloride ion to form $[Pt^{IV}(o\text{-}OC_6H_4CSNH_2)_2(o\text{-}HOC_6H_4CSNH_2)Cl]Cl$ and free o-$HOC_6H_4CSNH_2$.

Therefore, IR, ^{1}H NMR, and electrical conductivity studies indicate that Pt^{4+} ion is in octahedral environment where two o-hydroxythiobenzamide molecules are bonded through S and O, and the rest two are coordinated axially only through S leaving free OH.

$H[Au^{III}(o\text{-}HOC_6H_4CS:NH)_3Cl]$. The ^{1}H NMR spectra of the Au(III) complex solution in DMSO-d_6 (Fig. 1) exhibit a broad peak of single proton at 10 δ due to deprotonated thioamide group. Like the Pt-(IV) complex a single proton signal due to H-bonded phenolic OH at 11.9 δ is also found in the Au(III) complex. The IR spectral data of the gold complex in KBr pellets (Table 1) show fewer number of bands for NH_2 stretching vibrations. The stretching vibration due to H-bonded OH of the free ligand at 2750 cm^{-1} is displaced to 2900 cm^{-1}. It is also seen that one of the split band of o-hydroxythiobenzamide at 1600 cm^{-1} is absent in the Au(III) complex. The OH deformation band at 1385 cm^{-1} does not disappear and a band due to C=S stretching appears at lower frequency (698 cm^{-1}) due to gold-sulfur bonding. In the far IR region the gold complex exhibits bands at 490 cm^{-1} and 310 cm^{-1} probably due to ν_{Au-S} and ν_{Au-Cl}; other features of IR spectral bands of the gold complex are similar to the platinum complexes. Therefore, the ^{1}H NMR and IR studies of the gold complex indicate its complexation through thioimidate anion leaving phenolic OH groups free.

The electrical conductivity data in Table 2 indicate that the gold complex behaves as 1:1 electrolyte in methanol. The amperometric study of the gold complex[6] and elemental analysis[2] indicate that the metal-ligand ratio is 1:3. Our chemical tests show that in the gold complex Cl is in the inner sphere which also includes bonded imidate anion and free OH groups. These facts suggest that the square planar arrangement exists in the gold complex. Lower pH of methanolic solution of the gold complex as compared to methanol indicates the presence of H^+ in the outer sphere of the complex. Tarantelli *et al.*[7] have shown that electrical conductivity of $[Pd^{II}L_4]^{2+}$ (where L= $(C_6H_5NH)_2CS$) in methanol or acetone increases on adding excess ligand. Similar increase in conductivity is observed on adding excess o-hydroxythiobenzamide to the methanolic solution of the gold complex. This behaviour may be due to displacement of Cl from the inner sphere of the gold complex by a neutral ligand molecule to form neutral species $[Au^{III}(o\text{-}HOC_6H_4CS:NH)_3(o\text{-}HOC_6H_4CSNH_2)]$ and free HCl. By the mole ratio method the earlier workers[2] have shown that the metal-ligand ratio is 1:4 in the gold complex and at first sight it is apparently misleading as it does not fit their elemental analysis data of 1:3. In the presence of excess reagent a reaction like $[ML_3Cl]^-H^+ \xrightarrow{L} ML_4+HCl$ may have occured in the solution during the mole-ratio method of studying metal-ligand ratio.

Electronic Spectra. o-*Hydroxythiobenzamide*: Electronic spectra of thiocarbonyl derivatives[8–10] show a low intensity and long wavelength band due to the $n\rightarrow\pi^*$ transition. In the case of o-hydroxythiobenzamide interaction of nitrogen lone pair electrons with the C=S unit makes the $n\rightarrow\pi^*$ transition easy. Therefore the low intensity ($\varepsilon<100$) band at 20400 cm^{-1} of o-hydroxythiobenzamide in different solvent media is the $n\rightarrow\pi^*$ transition. Figure 2 shows that this 20400 cm^{-1} band is quenched in neutral and acidic aqueous media, whereas the band is pronounced in DMSO and alkaline aqueous media. Methanolic solution of o-hydroxythiobenzamide also exhibits a very weak intensity $n\rightarrow\pi^*$ transition at $\approx$20000 cm^{-1}.

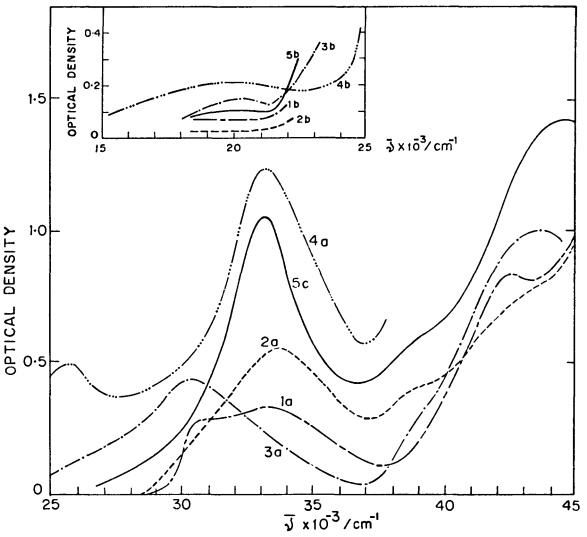

Fig. 2. Absorption spectra of o-hydroxythiobenzamide in 1(a,b) water; 2(a,b) 0.1 M HCl; 3(a,b) 0.1 M NaOH; 4(a,b) DMSO; 5(c,b) Methanol.
a=10^{-4}, b=10^{-3}, c=2.2×10^{-4} mol dm^{-3}.

In case of thiocarbonyl compounds it has been reported[8-10] that the intense bands immediately preceding n→π* are due to the π→π* rather than the n→σ* transition. Again two different π→π* transitions should also be expected due to conjugation of C=S and C=N groups with the aromatic ring in *o*-hydroxythiobenzamide as found in methyl *N*,*N*-dimethyldithiocarbamate[11] and 5-amino-2-mercaptothiazoles.[12] Therefore two bands at ≈33000 cm^{-1} and 30500 cm^{-1} in aqueous solution of *o*-hydroxythiobenzamide (Fig. 2, 1a) indicate π→π* transitions. Therefore in neutral aqueous medium the existence of both i and ii or iii forms are expected. DMSO solution of *o*-hydroxythiobenzamide also exhibits two π→π* transitions (Fig. 2, 4a) of which the lower frequency one is red-shifted to 26000 cm^{-1} due to high proton binding capacity of DMSO favouring the existence of structure iii. In alkaline medium (Fig. 2, 3a) red shifting of the two (apparently nonresolvable) π→π* bands may be due to deprotonation of SH and OH groups in structure iii. In acidic aqueous medium (Fig. 2, 2a) only 33000 cm^{-1} band is present probably due to protonation of NH_2 group in structure i.

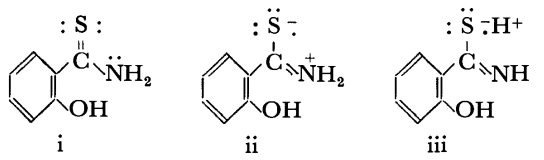

i ii iii

Very intense bands at ≈44000—44500 cm^{-1} is found in methanolic and aqueous alkaline solutions of *o*-hydroxythiobenzamide, and intensity of this band is decreased in acidic medium. Therefore the ≈44500 cm^{-1} band may be due to the n→σ* transition in the ligand molecule. The shoulders at 39000 cm^{-1} may be due to phenolic chromophore as its intensity is decreased in alkaline medium.

Pt(II), Pt(IV), and Au(III) Complexes. The phenolic chromophore band at 39000 cm^{-1} of *o*-hydroxythiobenzamide is red-shifted in the Pt complexes indicating Pt–O bonding, whereas the gold complex does not show such shift. The intensity of the n→π* band (20000 cm^{-1}) of *o*-hydroxythiobenzamide increases significantly on complexation (Fig. 3) and this band shifts to higher frequency in the sequence Au(III)< Pt(IV)<Pt(II) complexes indicating L→M charge transfer.[13,14] The d-d transitions are obscured by the intense charge transfer band. Electronic spectra of the complexes show that the positions of the bands appearing above 20000 cm^{-1} agree more or less with those of the free ligand with enhanced intensities. Hence these bands may be regarded as intraligand transitions with intensities modified on complexation.

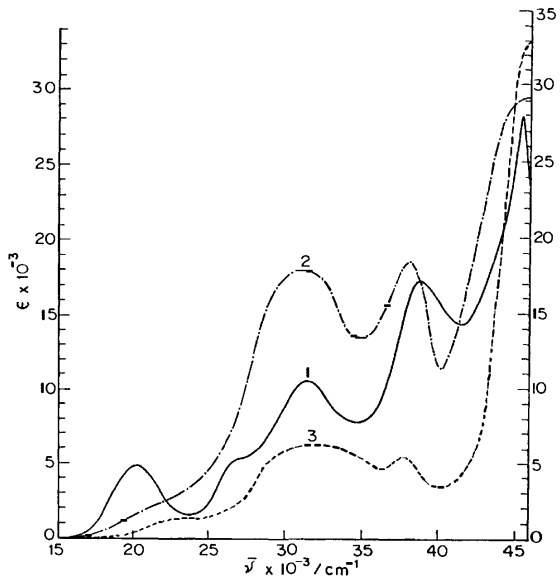

Fig. 3. Absorption spectra.
1: $H[Au^{III}(o\text{-}HOC_6H_4CS{:}NH)_3Cl]$, 2: $[Pt^{IV}(o\text{-}OC_6H_4CSNH_2)_2(o\text{-}HOC_6H_4CSNH_2)_2]Cl_2$, 3: $[Pt^{II}(o\text{-}OC_6H_4CSNH_2)_2]$ in methanol.

Conclusion

From the above studies it is clear that *o*-hydroxythiobenzamide exists in the thioamide-thioimidic acid equilibrium in solution. Metal-sulfur and metal-oxygen bondings are observed in the platinum complexes, whereas the gold complex shows only metal-sulfur bonding. Amide C=S coordinates with Pt(II) and Pt(IV) and the thioimidate anion is bonded with Au(III). The existence of free phenolic OH in the Pt(IV) and Au(III) complexes has been established decidedly by ^1H NMR, IR, and electronic spectral studies. Recent studies also indicate the presence of free phenolic OH group in the Pd(II) complex of salicylaldehyde 2-picoloylhydrazone[15] and rare earth complexes of *o*-hydroxybenzhydroxamic acid.[16]

Thanks are due to Dr. S. K. Bose, Dr. S. N. Bhattacharyya and Dr. M. P. Roy for their encouragement throughout the work and also to UGC, India for financial assistance to one of the authors (K. B.).

References

1) K. Sur and S. C. Shome, *Anal. Chim. Acta*, **57**, 20 (1971).
2) K. Sur and M. Mazumdar, *Anal. Chim. Acta*, **59**, 306 (1972).
3) L. W. Reeves and W. G. Schneider, *Can. J. Chem.*, **36**, 793 (1958).
4) Kai Arne Jensen and Per Halfden Nielsen, *Acta Chem. Scand.*, **20**, 597 (1966).
5) W. J. Geary, *Coord. Chem. Rev.*, **7**, 112 (1971).
6) A. Basu, M. Mazumdar, and S. C. Shome, *J. Indian Chem. Soc.*, **57**, 1156 (1980).
7) T. Tarantelli and C. Furlani, *J. Chem. Soc., A*, **1968**, 1717.
8) K. S. Suresh, J. Ramachandran, and C. N. R. Rao, *J. Sci. Indust. Res. (India)*, **20B**, 206 (1961).
9) C. N. R. Rao, A. Balasubramaniam, and J. Ramachandran, *J. Sci. Indust. Res. (India)*, **20B**, 382 (1961).
10) J. Fabian and R. Mayer, *Spectrochim. Acta*, **20**, 299 (1964).
11) H. P. Koch, *J. Chem. Soc.*, **1949**, 401.
12) E. S. Stern, *J. Chem. Soc.*, **1949**, 1664.
13) A. B. P. Lever, "Inorganic Electronic Spectroscopy," Elsevier Publishing Company, Amsterdam (1968), p. 354.
14) Donald L. Swihart and W. Roy Mason, *Inorg. Chem.*, **9**, 1749 (1970).
15) R. L. Dutta and A. K. Sarkar, *J. Inorg. Nucl. Chem.*, **43**, 57 (1981).
16) S. K. Brahma and A. K. Chakraburtty, *J. Indian Chem. Soc.*, **58**, 615 (1981).

Volume Profile for the Aquation Reactions of *trans*- and *cis*-$[Co(en)_2NO_2Cl]^+$, *cis*-$[Co(bpy)_2NO_2Cl]^+$, *cis*-$[Co(bpy)_2NO_2Br]^+$, and *cis*-$[Co(phen)_2NO_2Br]^+$

Yoichi KITAMURA

Department of Chemistry, Faculty of Science, Ehime University, Matsuyama, Ehime 790

(Received October 21, 1981)

The activation volume at normal pressure (ΔV^*) and the reaction volume (ΔV) are obtained for five aquation reactions of the Co(III) complex ion. The results are [given as the complex ion, ΔV^*/cm^3 mol^{-1} (t/°C), ΔV/cm^3 mol^{-1} (t/°C)]: *trans*-$[Co(en)_2NO_2Cl]^+$, 0.1 (15), −10.4 (15); *cis*-$[Co(en)_2NO_2Cl]^+$, 0.9 (30), −9.3 (25); *cis*-$[Co(bpy)_2NO_2Cl]^+$, 2.9 (30), −9.1 (25); *cis*-$[Co(bpy)_2NO_2Br]^+$, 11.3 (30), −6.7 (25); *cis*-$[Co(phen)_2NO_2Br]^+$, 3.3 (35), −12.5 (30). These magnitudes of ΔV^* are interpreted as resulting from the counterbalance of the volume increase attributable to the dissociation of the leaving ligand and the volume decrease due to the partial incorporation of one water molecule in the activated complex.

In this decade, the reaction velocities of the complex ion have been investigated extensively under high pressure.[1-3] Activation volumes have been obtained and the magnitude of ΔV^* has been discussed in relation to the reaction mechanism. The general treatment is that ΔV^* is divided into two contributions: $\Delta V^* = \Delta V^*_{int} + \Delta V^*_{solv}$, where ΔV^*_{int} and ΔV^*_{solv} are the intrinsic and the solvational components of the activation volume respectively. Stranks has made a fundamental assumption that the intrinsic volume of a five-coordinate intermediate in the limiting dissociative mechanism is the same as that of the six-coordinate precursor.[4] Some authors have interpreted the magnitude of ΔV^* according to this postulation.[1] However, the derivation of his postulation seems to have no rational foundation.[4] The present author considers that the relation between the magnitude of ΔV^* and the mechanism should be induced from an examination of the volume profiles (ΔV^* and ΔV) for a series of related reactions.

It has been known for some time that, in a series of *trans*- and *cis*-$[Co(en)_2ACl]^{n+}$, the aquation velocity is rapid for $A=NH_2^-$, moderate for $A=N_3^-$, Cl^-, NO_2^-, and slow for $A=NH_3$.[5] Ingold *et al.* have interpreted this in relation to the electron-donating or the electron-withdrawing power of the A ligand.[5] Langford and Gray have given a slightly different interpretation of this problem and have indicated that, at least, the mechanism for $A=NH_2^-$ differs from those for $A=N_3^-$, Cl^- or NO_2^-.[6] The present author considers that the influence of the A ligand on the aquation mechanism might possibly be reflected in the volume profile.

In this work, ΔV^* and ΔV are obtained for five aquation reactions, where the complex ions have the electron-withdrawing nonlabile NO_2^- ligand in common:

$$trans\text{-}[Co(en)_2NO_2Cl]^+ + H_2O \longrightarrow trans\text{-}[Co(en)_2NO_2H_2O]^{2+} + Cl^- \quad (1)^{7,8}$$

$$cis\text{-}[Co(en)_2NO_2Cl]^+ + H_2O \longrightarrow cis\text{-}[Co(en)_2NO_2H_2O]^{2+} + Cl^- \quad (2)^{7,8}$$

$$cis\text{-}[Co(bpy)_2NO_2Cl]^+ + H_2O \longrightarrow cis\text{-}[Co(bpy)_2NO_2H_2O]^{2+} + Cl^- \quad (3)^{9}$$

$$cis\text{-}[Co(bpy)_2NO_2Br]^+ + H_2O \longrightarrow cis\text{-}[Co(bpy)_2NO_2H_2O]^{2+} + Br^- \quad (4)^{9}$$

$$cis\text{-}[Co(phen)_2NO_2Br]^+ + H_2O \longrightarrow cis\text{-}[Co(phen)_2NO_2H_2O]^{2+} + Br^- \quad (5)^{10}$$

The volume profiles are compared with those of other Co(III) aquation reactions, and the magnitudes of ΔV^* are discussed on this basis. The acid dissociation constant (K_a) is obtained for the *cis*-$[Co(en)_2NH_3H_2O]^{3+}$ at four temperatures. The $\Delta H°$ and $\Delta S°$ are calculated for this equilibrium:

$$cis\text{-}[Co(en)_2NH_3H_2O]^{3+} + OH^- = [Co(en)_2NH_3OH]^{2+} + H_2O. \quad (i)$$

This equilibrium is treated as a model for the preequilibrium of the base-hydrolysis of the Co(III) complex ion.

Experimental

Material. The following complexes were obtained by the published methods: *trans*-$[Co(en)_2NO_2Cl]NO_3$ (**1**),[11] *cis*-$[Co(en)_2NO_2Cl]Cl$ (**2**),[11] *cis*-$[Co(bpy)_2NO_2Cl]Cl\cdot 2H_2O$ (**3**),[12] *cis*-$[Co(bpy)_2NO_2Br]Br$ (**4**),[12] *cis*-$[Co(phen)_2NO_2Br]Br\cdot 2H_2O$ (**5**),[10] and *cis*-$[Co(en)_2NH_3H_2O]Br_3\cdot H_2O$ (**6**).[13] The Co(III) complex with the *bis* bpy or the *bis* phen ligands has the *cis*-configuration.[14] The *cis*-configuration of **6** was identified spectrophotometrically.[15] The results of the elemental analysis (C, H, N) for Complexes **1**—**6** were in good agreement with the theoretically expected values.[16]

Kinetic Measurement. The aquation velocity was followed *in situ* in a thermostatted (±0.1 °C) Hawley and Chase-type high-pressure optical cell with a pair of sapphire windows.[17] This cell was fitted to a Nihon Bunko, model UVIDEC 505, double-beam spectrophotometer. The path length of the sample solution was 1.3 cm. The reference was air. The pressure of the sample solution was measured by means of a Nagano Keiki Bourdon gauge calibrated to a Nagano Keiki-type IP3-178 dead-weight-pressure gauge tester. Each reaction was followed at a certain wavelength to *ca.* 90% completion. The first-order rate constants were obtained from Guggenheim plots of the optical densities.

Dilatometry. A globular glass vessel (39.2 cm^3) fitted with an upright capillary tube (15 cm long) was used as a dilatometer. A capillary tube with an internal diameter of 0.0404 cm was used for the runs of Reactions 2 and 3. Another capillary tube with an internal diameter of 0.0202 cm was used for the runs of Reactions 1, 4, and 5. Distilled water was boiled for several minutes. It was then degassed overnight and was used to dissolve the complex. A weighed quantity of the complex was dissolved in water (45 cm^3) at the reaction temperature. The solution was poured into the dilatometer,

which had been immersed beforehand in a thermostat controlled at the reaction temperature. The capillary tube was then joined, and the overflowing solution was wiped off at the top of the capillary tube. The height (h_t) of the meniscus was followed by the use of a cathetometer. The dilatometer was covered by a piece of aluminium foil to avoid the influence of light. The thermostat temperature was observed by a Beckmann thermometer graduated to 0.001 °C. The maximum variation in the temperature during the dilatometric run was within 0.001 °C in the runs of Reactions 1—4, while it was undetectably small (*ca.* within 0.0002 °C) in the runs of Reaction 5.

Results

Kinetic Results. The rate constants in Table 1 were obtained for the respective complex ion in an aqueous solution without added electrolyte and acid. For the reaction of *trans*-$[Co(en)_2NO_2Cl]^+$, the contribution of the base-hydrolysis can be estimated to be $k_b[OH^-]=8\times10^{-8}$ s^{-1} at 15 °C and $[OH^-]=10^{-7}$ M (1 M=1 mol dm^{-3}), where k_b is the 2nd-order rate constant of the base-hydrolysis.[7,18] For the reaction of *cis*-$[Co(en)_2NO_2Cl]^+$, $k_b[OH^-]$ can be estimated to be 2×10^{-7} s^{-1} at 30 °C and $[OH^-]=10^{-7}$ M.[7,18] These magnitudes of $k_b[OH^-]$ are small enough compared to the corresponding aquation velocities, and the contribution of the base-hydrolysis can be neglected. The contribution of the base-hydrolysis is also neglected for the reactions of *cis*-$[Co(bpy)_2NO_2Cl]^+$, *cis*-$[Co(bpy)_2NO_2Br]^+$, and *cis*-$[Co(phen)_2NO_2Br]^+$, since these complexes have no acidic proton. It can be noticed that the rate constants of Reactions 1—5 remain unchanged or decrease slightly under high pressures. The average k values at each pressure are fitted by the least-squares method to the quadratic formula: $\ln(k/k_0)=aP+bP^2$, where k_0 is the rate constant at normal pressure. The activation volumes at normal pressure are calculated by means of $\Delta V^{\ddagger}=-RT(\mathrm{d}\ln k/\mathrm{d}P)=-RTa$ (Table 2).

Table 1. Rate constants ($k/10^{-5}$ s^{-1}) of the aquation reaction at each pressure (P/kg cm^{-2})[a]

1[b], *trans*-$[Co(en)_2NO_2Cl]^+$, 1 mM[c], 10 °C[d], 380 nm[e] $\ln(k/k_0)=0.11\times10^{-4}P-1.45\times10^{-8}P^2$[f]							
P		1	400	800	1200	1600	2000
k	16.5	15.8	16.5	16.3	15.7	17.2	16.2
	16.3		16.2	16.7	15.0	15.3	14.8
1, *trans*-$[Co(en)_2NO_2Cl]^+$, 1 mM, 15 °C, 380 nm $\ln(k/k_0)=-0.06\times10^{-4}P-0.76\times10^{-8}P^2$							
P	1		400	800	1200	1600	2000
k	32.0		32.2	31.5	31.5	30.5	30.0
	32.0		32.0	31.2	31.0	32.3	30.8
1, *trans*-$[Co(en)_2NO_2Cl]^+$, 1 mM, 20°C, 380 nm $\ln(k/k_0)=-0.14\times10^{-4}P-0.52\times10^{-8}P^2$							
P	1		400	800	1200	1600	2000
k	61.2		61.5	61.0	60.8	59.5	59.2
	62.5		59.7	62.7	58.2	61.2	58.2
2, *cis*-$[Co(en)_2NO_2Cl]^+$, 5 mM, 30 °C, 393 nm $\ln(k/k_0)=-0.33\times10^{-4}P-2.47\times10^{-8}P^2$							
P		1	400	800	1200	1600	2000
k	22.8	22.3	22.3	21.5	21.2	20.2	18.8
	22.5	22.7	21.8	21.5	21.5	20.0	19.3
3, *cis*-$[Co(bpy)_2NO_2Cl]^+$, 1 mM, 30 °C, 398 nm $\ln(k/k_0)=-1.13\times10^{-4}P-0.90\times10^{-8}P^2$							
P		1	400	800	1200	1600	2000
k	37.5	36.7	39.8	31.7	32.7	31.7	29.7
	38.2	38.5	38.3	32.7	32.7	29.7	28.5
4, *cis*-$[Co(bpy)_2NO_2Br]^+$, 1 mM, 30 °C, 404 nm $\ln(k/k_0)=-4.40\times10^{-4}P+13.1\times10^{-8}P^2$							
P		1	320	720	1140	1540	
k	36.8	38.8	32.5	30.0	27.3	25.2	
	36.8	37.8	32.3	29.2	26.8	26.7	
5, *cis*-$[Co(phen)_2NO_2Br]^+$, 1 mM, 35 °C, 416 nm $\ln(k/k_0)=-1.27\times10^{-4}P+1.73\times10^{-8}P^2$							
P		1	320	720	1140	1540	1960
k	34.2	32.0	32.8	29.7	27.5	27.0	25.5
	34.0	30.3	32.3	28.7	30.3	29.2	28.8

a) 1 kg cm^{-2}=98.0665 kPa. b) Reaction number. c) Concentration of the complex. d) Reaction temperature. e) The reaction was followed at this wavelength. f) See text.

Dilatometric Result. Reaction 1 was followed at 15 °C in a 3.4 mM solution of **1** from 26 to 99% completion; Reaction 2, at 25 °C in a 10.9 mM solution of **2** from 14 to 98% completion; Reaction 3, at 25 °C in an 8.5 mM solution of **3** from 31 to 82% completion, and Reaction 4, at 25 °C in a 5.0 mM solution of **4** from 36 to 71% completion. For Reactions 1—4, ΔV is obtained from the intercept at $t=0$ of the ln (h_t-h_∞) *vs.* t plot, where the h_∞ value is calculated from the h_t's (Table 2). The solubility of **5** in water is limited (*ca.* 1.8 mM at 30 °C). Three independent runs were performed where Reaction 5 was followed at 30 °C in a 1.2 mM solution of **5** from 43 to 61%, from 47 to 68%, and from 39 to 61% completion. For Reaction 5, ΔV is calculated from the ratios of Δh_t to $\Delta\xi$, where ξ is the degree of reaction (Table 2). The values of ξ are estimated from the rate constant (2.08×10^{-4} s^{-1} at 30 °C) obtained spectrophotometrically at 404 nm. The average error in ΔV for Reaction 5 is ±1.3 cm^3 mol^{-1}. In Reactions 1—4, the rate constants obtained dilatometrically are in good agreement with those in the literature.[7-9]

pK_a *of* cis-$[Co(en)_2NH_3H_2O]^{3+}$. Complex **6** was dissolved in boiled water; no other electrolyte was added. The solution (5 mM, 25 cm^3) was titrated with a 0.1 M KOH, while nitrogen gas free from oxygen or carbon dioxide was slowly bubbled into the solution.[19] The values of pK_a were [given as t/°C, pK_a]: 2, 6.30±0.07; 10, 6.10±0.07; 20, 5.83±0.07; 40, 5.39±0.07. This temperature dependence can be described by: $\ln K_a=-4800/T+2.91$, from which $\Delta H^\circ=39.9$ kJ mol^{-1} and $\Delta S^\circ=24.2$ J K^{-1} mol^{-1} are calculated for the equilibrium: *cis*-$[Co(en)_2NH_3H_2O]^{3+}=[Co(en)_2NH_3OH]^{2+}+H^+$. Thus, $\Delta H^\circ=-15.9$ kJ mol^{-1} and $\Delta S^\circ=104.9$ J K^{-1} mol^{-1} are obtained for Equilibrium i.[20]

Discussion

In Table 2, the volume profiles obtained in this work are summarized, along with those for other aquation reactions of the Co(III) complexes, where the leaving

TABLE 2. VOLUME PROFILE AND ACTIVATION ENTROPY FOR AQUATION REACTIONS OF Co(III) COMPLEXES

Reaction number	Complex	$\Delta V^{\ddagger}$ / cm^3 mol^{-1} (t/°C)	ΔV / cm^3 mol^{-1} (t/°C)	$\Delta S^{\ddagger}$ / J K^{-1} mol^{-1}
1	*trans*-$[Co(en)_2NO_2Cl]^+$	−0.3(10)[a]		
		0.1(15)[a]	−10.4(15)[a]	−10[b]
		0.3(20)[a]		
2	*cis*-$[Co(en)_2NO_2Cl]^+$	0.9(30)[a]	−9.3(25)[a]	−28[b]
3	*cis*-$[Co(bpy)_2NO_2Cl]^+$	2.9(30)[a]	−9.1(25)[a]	−104[c]
4	*cis*-$[Co(bpy)_2NO_2Br]^+$	11.3(30)[a]	−6.7(25)[a]	−117[c]
5	*cis*-$[Co(phen)_2NO_2Br]^+$	3.3(35)[a]	−12.5(30)[a]	−49[c]
6	*trans*-$[Co(dtcd)N_3Cl]^+$	8.3(25)[d]		−51[d]
7	*trans*-$[Co(dtcd)N_3Br]^+$	5.3(21)[d]		−34[d]
8	*cis*-$[Co(en)_2Cl_2]^+$	−0.3(30)[e]		−18[e]
9	*trans*-$[Co(en)_2Cl_2]^+$	−1.1(30)[e]		44[e]
10	$[Co(NH_3)_5Cl]^{2+}$	−10.6(25)[f]	−11.6(30)[g]	−39[h]
11	$[Co(NH_3)_5Br]^{2+}$	−9.2(25)[f]	−10.8(30)[g]	−20[h]
12	$[Co(NH_3)_5NO_3]^{2+}$	−6.3(25)[f]	−7.2(30)[g]	3[h]
13	$[Co(NH_3)_4(NH_2)Cl]^+$	15.0(35)[i]	−9.4(30)[i]	35[i]
14	$[Co(NH_3)_4(NH_2)Br]^+$	13.6(25)[i]	−8.6(30)[i]	82[i]

a) This work. b) Ref. 8. c) Ref. 9. d) In 0.1 M HNO_3. Ref. 21. e) In 0.01 M HNO_3 (I=0.1 M). Ref. 3. f) In 0.1 M $LiClO_4$–5×10^{-5} M $HClO_4$. Ref. 22. g) Refs. 22 and 23. h) Ref. 24. i) See text.

ligand is a univalent anion:

trans-$[Co(dtcd)N_3Cl]^+ + H_2O \longrightarrow [Co(dtcd)N_3H_2O]^{2+} + Cl^-$ (6)[21]

trans-$[Co(dtcd)N_3Br]^+ + H_2O \longrightarrow [Co(dtcd)N_3H_2O]^{2+} + Br^-$ (7)[21]

cis-$[Co(en)_2Cl_2]^+ + H_2O \longrightarrow [Co(en)_2ClH_2O]^{2+} + Cl^-$ (8)[3]

trans-$[Co(en)_2Cl_2]^+ + H_2O \longrightarrow [Co(en)_2ClH_2O]^{2+} + Cl^-$ (9)[3]

$[Co(NH_3)_5Cl]^{2+} + H_2O \longrightarrow [Co(NH_3)_5H_2O]^{3+} + Cl^-$ (10)[22,23]

$[Co(NH_3)_5Br]^{2+} + H_2O \longrightarrow [Co(NH_3)_5H_2O]^{3+} + Br^-$ (11)[22,23]

$[Co(NH_3)_5NO_3]^{2+} + H_2O \longrightarrow [Co(NH_3)_5H_2O]^{3+} + NO_3^-$ (12)[22,23]

$[Co(NH_3)_4(NH_2)Cl]^+ + H_2O \longrightarrow [Co(NH_3)_5OH]^{2+} + Cl^-$ (13)[23,25]

$[Co(NH_3)_4(NH_2)Br]^+ + H_2O \longrightarrow [Co(NH_3)_5OH]^{2+} + Br^-$. (14)[23,26]

The volume profiles of Reactions 13 and 14 are calculated from those of the corresponding base-hydrolysis reactions. The S_N1 CB mechanism is now widely established for the base-hydrolysis reaction of $[Co(NH_3)_5X]^{2+}$ (X^-=Cl^-, Br^-).[27-30] In this mechanism, the reaction proceeds in two steps:

$[Co(NH_3)_5X]^{2+} + OH^- = [Co(NH_3)_4(NH_2)X]^+ + H_2O$ (ii)

$[Co(NH_3)_4(NH_2)X]^+ + H_2O \longrightarrow [Co(NH_3)_5OH]^{2+} + X^-$. (iii)

The volume profile ($\Delta V_b^{\ddagger}$ and ΔV_b) of the base-hydrolysis is then, written as; $\Delta V_b^{\ddagger}=\Delta V_{pre}+\Delta V_{cb}^{\ddagger}$, and $\Delta V_b=\Delta V_{pre}+\Delta V_{cb}$, where ΔV_{pre} is the volume change of the preequilibrium ii and where $\Delta V_{cb}^{\ddagger}$ and ΔV_{cb} are the activation volume and the reaction volume respectively of the succeeding aquation Reaction iii of the conjugate-base complex ion $[Co(NH_3)_4(NH_2)X]^+$.[25] The magnitude of ΔV_{pre} is not known. Volume changes are known for four analogous neutralization equilibria of a metal complex ion:[31]

$[Co(NH_3)_5H_2O]^{3+} + OH^- = [Co(NH_3)_5OH]^{2+} + H_2O$

ΔV = 20.6 cm^3 mol^{-1} at 30 °C,

$[Cr(H_2O)_6]^{3+} + OH^- = [Cr(H_2O)_5OH]^{2+} + H_2O$

ΔV = 18.3 cm^3 mol^{-1} at 25 °C,

$[Fe(H_2O)_6]^{3+} + OH^- = [Fe(H_2O)_5OH]^{2+} + H_2O$

ΔV = 20.9 cm^3 mol^{-1}

$[Co(edda)(Hame)]^+ + OH^- = [Co(edda)(ame)]^0 + H_2O$

ΔV = 16.9 cm^3 mol^{-1} at 25 °C.

Then, an average of 19.9 cm^3 mol^{-1} is obtained for the neutralization of a tervalent complex ion. Thus, ΔV= 18.4 cm^3 mol^{-1} (average between 19.9 and 16.9 cm^3 mol^{-1}) is appropriate for the neutralization of the 2+ complex ion. By assuming that ΔV_{pre}=18.4 cm^3 mol^{-1}, $\Delta V_{cb}^{\ddagger}$ and ΔV_{cb} are calculated from $\Delta V_b^{\ddagger}$=33.4 cm^3 mol^{-1} [25] and ΔV_b=9.0 cm^3 mol^{-1} [23] for X^-=Cl^-, and from $\Delta V_b^{\ddagger}$=32 cm^3 mol^{-1} [26] and ΔV_b=9.8 cm^3 mol^{-1} [23] for X^-=Br^-. Burris and Laidler reported $\Delta V_b^{\ddagger}$=8.5 cm^3 mol^{-1} for X^-=Br^-;[32] however, this magnitude is mistaken.[26] The present author and others have previously obtained $\Delta V_b^{\ddagger}$=37 cm^3 mol^{-1} for X^-=Br^- at 21 °C in 10 mM NH_3–1 mM NH_4ClO_4 (I=1.75 mM).[33]

It can be noticed that the magnitudes of ΔV of Reactions 1—5 and 10—14 are close to each other. When the leaving ligand is Cl^-, they are especially close to one another and have a magnitude of -10.0 ± 1.6 cm^3 mol^{-1}, irrespective of the nonlabile ligands in the complex. When the leaving ligand is Br^-, the ΔV's lie in a relatively small range, from −6.7 to −12.5 cm^3 mol^{-1}. In contrast, the magnitudes of $\Delta V^{\ddagger}$ are distrib-

uted over a wide range, from 15 to -10 cm^3 mol^{-1}. This result accords with the expectation that the mechanism is not common throughout Reactions 1—14.[5,6] If the mechanism was the same, the constitutions of their transition states, and hence the magnitudes of ΔV^*, should be similar to each other. The latter might be anticipated, since the magnitude of ΔV, the volume change for a certain substitution, depends only slightly on the nature of the nonlabile ligand.

From various pieces of evidence and the arguments given in previous reports,[25,27-30] Reactions 13 and 14 can be considered to proceed by means of a limiting dissociative or D mechanism. The transition state is constituted of a five-coordinate intermediate and the leaving ligand, and the ΔV^* is the volume change of the reaction:

$$[Co(NH_3)_4(NH_2)X]^+ \longrightarrow [Co(NH_3)_4(NH_2)]^{2+} + X^-, \quad \text{(iv)}$$

where $X^- = Cl^-$ and Br^-.

In the volume profiles of Reactions 10—12, it is clear that the ΔV^* is close to the corresponding ΔV. Then, the constitution of the transition state of Reactions 10—12 should be similar to that of the final state. In the transition state, one water molecule should have already been incorporated into the coordination sphere; it is from this fact that the remarkably smaller magnitudes of ΔV^* of Reactions 10—12 than those of Reactions 13 and 14 must result. The transition state of Reactions 10—12 is an ion pair between the product, $[Co(NH_3)_5H_2O]^{3+}$, and the leaving ligand. Only the separation of this ion pair is necessary to complete the reaction; this explains the experimentally obtained volume decrease $\Delta V^* - \Delta V \simeq 1$ cm^3 mol^{-1} for Reactions 10—12. This interpretation of the transition state of Reactions 10—12 is virtually similar to that given by Jones *et al.*.[22] They have indicated that the transition state of Reactions 10—12 is an ion pair with a momentarily enhanced solvational sphere. The transition state has been denoted as: $\{Co(NH_3)_5^{3+}, X^-, yH_2O\}$, where X^- remains in the first solvation sphere of the complex and where y is large enough to permit the full solvation of both $Co(NH_3)_5^{3+}$ and X^-. They have also estimated the excess number of water molecules in the first solvation sphere over the average at the moment of the transition state as 4, 4, and 2 for $X^- = Cl^-$, Br^-, and NO_3^- respectively. They have explained that the transition state occurs when a wide excursion of a Co–X vibration coincides with the transient excess solvation caused by the fluctuation of the water molecules in the first solvation sphere. In practice, one can not discriminate this solvation-enhanced ion pair from an ordinary ion pair between the product and the leaving ligand, $\{[Co(NH_3)_5H_2O]^{3+}, X^-\}$. The latter is preferable because of its simplicity.

For Reactions 1—9, the magnitudes of ΔV^* are intermediate between those for Reactions 13 and 14 and those for Reactions 10—12. Then, in Reactions 1—9, the transition state is composed of an ion pair between the leaving ligand and the unstable five-coordinate intermediate, $[Co(AA)_2Y\cdots OH_2]^{2+}$, where AA=en, bpy, phen, (dtcd)/2; $Y^- = NO_2^-$, N_3^-, Cl^-. The water molecule is half-way between the vacant coordination site and the first solvation sphere. Thus, the mechanism is a dissociative interchange or I_d for Reactions 1—12.

The essential point of the D or I_d mechanism is that the transition state occurs with the widest excursion of the Co–X bond vibration. However, every widest excursion does not give rise to the transition state. A factor which contributes to the emergence of the transition state is the simultaneous intrusion of one water molecule from the solvation into the coordination sphere. When the initial complex contains the strongly electron-donating NH_2^- ligand, the complex will be unstable, according to Ingold *et al.*, and only a slight intrusion will be enough.[5,6] When the initial complex contains a moderately electron-donating N_3^- or Cl^- ligand, or a moderately electron-withdrawing NO_2^- ligand, the complex will be moderately stable and some further intrusion will be needed. When the initial complex does not contain any ligand with electron-donating or -withdrawing power, the complex will be stable and only a sufficient intrusion of a water molecule will give rise to the transition state.

The widest excursion of the leaving ligand will cause a volume increase (ΔV_d) and the intrusion of a water molecule will accompany a volume decrease ($\alpha\Delta V_{inc}$), where ΔV_{inc} is the volume change for the full incorporation of one water molecule into the five-coordinate intermediate and where α is the degree of the intrusion. According to this model, ΔV^* is expressed as $\Delta V^* = \Delta V_d + \alpha\Delta V_{inc}$. By assuming $\alpha=0$ for Reactions 13 and 14, ΔV_d and ΔV_{inc} can be estimated from the experimentally obtained volume profiles: $\Delta V_d = \Delta V^* = 13$—$15$ cm^3 mol^{-1} and $\Delta V_{inc} = \Delta V - \Delta V^* = -22$—$-25$ cm^3 mol^{-1}. These magnitudes of ΔV_d and ΔV_{inc} give $\Delta V^* = -12$—-7 cm^3 mol^{-1} for $\alpha=1$, which is in agreement with the magnitude of ΔV^* experimentally obtained for Reactions 10—12. In a previous report, the intrinsic and the solvational components of ΔV_d and the content of ΔV_{inc} have been considered.[25] The absolute value of the solvational component of ΔV_{inc} can be expected formally to be small, since the incorporation of a solvent molecule is not accompanied by a change in the ionic valence. In Reactions 1—9, α takes a value between 0 and 1. The completion of the intrusion of the water molecule and the separation of the ion pair are necessary to complete the reaction, which explains the experimentally obtained volume decrease, $\Delta V^* - \Delta V = 18$—$10$ cm^3 mol^{-1}, for Reactions 1—5.

In Reactions 1—5, the *trans*- and *cis*-configuration is retained during the reaction.[7,14] This fact can be interpreted as indicating that, in their transition state, the entering water molecule has already occupied its position to some extent, in accordance with the explanation given above.

For Reaction 1, ΔV^* is obtained at three temperatures. The values of ΔH^* and ΔS^* are calculated at each pressure [given as P/kg cm^{-2}, ΔH^*/kJ mol^{-1}, ΔS^*/J K^{-1} mol^{-1}]: 1, 91.8, 7.1; 400, 91.4, 5.2; 800, 90.6, 3.3; 1200, 94.1, 13.9; 1600, 89.7, -1.6; 2000, 91.4, 5.2. The value of $(\partial\Delta S^*/\partial P)_T$ at normal pressure and 15 °C can

be calculated from the ΔS^*'s at 1, 400, and 800 kg cm^{-2} as -0.05 cm^3 K^{-1} mol^{-1}. On the other hand, $(\partial \Delta V^*/\partial T)_P$ at normal pressure is obtained as 0.06 cm^3 K^{-1} mol^{-1} (Table 2). Thus, the thermodynamic relation $(\partial \Delta S^*/\partial P)_T = -(\partial \Delta V^*/\partial T)_P$ is satisfied; this is consistent with the postulation of the equilibrium between the initial and transition states.[2,3] For Reaction 1, $\Delta V^* = 0.9$ cm^3 mol^{-1} can be obtained at 30 °C by extrapolation. The coincidence of ΔV^* at 30 °C of Reactions 1 and 2 is rather surprising in view of the different initial configurations of the two isomers. Langford has pointed out that the bond distances between the nonlabile ligands and the metal ion might contract during the activation process.[35] However, if the Co–N bond distances of the two en ligands changed considerably in the activation process, some differences in the magnitude of ΔV^* might be expected, since these two isomers have different initial configurations, and so different solvational spheres. For Reactions 1 and 2, the activation energies are also equal (86.7 kJ mol^{-1}), while the activation entropies differ only slightly (Table 2).[8] Thus, the low reaction velocity of the *cis*-$[Co(en)_2NO_2Cl]^+$ is due to the rare chance of the intrusion of a water molecule attributable to the existence of the NO_2^- ligand in a position *cis* to the attacking water molecule.

The existence of a parallel correlation between ΔS^* and ΔV^* has sometimes been indicated.[36] Recently, Palmer and Kelm have examined this relation for 35 coordination reactions and pointed out that the parallelism is only of a qualitative nature.[3] Lawrance and Suvachittanont have indicated that the parallelism does not hold for Reactions 6 and 7.[21] From the present results (Table 2), it is clear that the parallelism is not satisfied for Reactions 3—5, either. The entropy change (ΔS_{pre}) for the preequilibrium ii of the base-hydrolysis can not be known. It is assumed, therefore, that ΔS_{pre} is approximately equal to the $\Delta S°$ of the analogous Equilibrium i. Then the activation entropies (ΔS^*_{cb}) of Reactions 13 and 14 are calculated by the use of $\Delta S^*_{cb} = \Delta S^*_b - \Delta S_{pre}$, where the activation entropies of the base-hydrolysis (ΔS^*_b) are 140 and 187 J K^{-1} mol^{-1} for $[Co(NH_3)_5Cl]^{2+}$ and $[Co(NH_3)_5Br]^{2+}$ respectively.[24] For Reactions 10—14, the parallelism seems to be roughly satisfied. On the other hand, it is surprising that rather a reverse relation seems to hold for Reactions 1—9: ΔV^* is large when ΔS^* is small. It is difficult at present to give any reasonable explanation of this.

The present work was partially supported by a Grant-in-Aid for Scientific Research No. 464195 from the Ministry of Education, Science and Culture. The high-pressure optical cell was constructed with the financial support of the Japan Society for the Promotion of Science.

References

1) G. A. Lawrance and D. R. Stranks, *Acc. Chem. Res.*, **12**, 403 (1979).
2) R. V. Eldik and H. Kelm, *Rev. Phys. Chem. Jpn.*, **50**, 185 (1980).
3) D. A. Palmer and H. Kelm, *Coord. Chem. Rev.*, **36**, 89 (1981).
4) D. R. Stranks, *Pure Appl. Chem.*, **38**, 303 (1974).
5) C. K. Ingold, R. S. Nyholm, and M. L. Tobe, *Nature*, **187**, 477 (1960). en=Ethylenediamine.
6) C. H. Langford and H. G. Gray, "Ligand Substitution Processes," W. A. Benjamin, New York (1965), Chap. 3.
7) S. Asperger and C. K. Ingold, *J. Chem. Soc.*, **1956**, 2862.
8) K. Kuroda, *Nippon Kagaku Zasshi*, **81**, 1528 (1960).
9) D. M. Palade, T. N. Volokh, G. V. Chudava, and E. G. Saakyan, *Russ. J. Inorg. Chem.*, **20**, 400 (1975). bpy=2,2′-Bipyridyl.
10) D. M. Palade and T. N. Volokh, *Russ. J. Inorg. Chem.*, **17**, 1016 (1972). phen=1,10-Phenanthroline.
11) A. Werner, *Ann.*, **386**, 248 (1912).
12) D. M. Palade, Yu, L. Popov, T. N. Volokh, and G. V. Chudaeva, *Russ. J. Inorg. Chem.*, **19**, 615 (1974).
13) M. L. Tobe and D. F. Martin, *Inorg. Synth.*, **8**, 198 (1967).
14) D. M. Palade, *Russ. J. Inorg. Chem.*, **14**, 399 (1969).
15) M. D. Alexander and C. A. Spillert, *Inorg. Chem.*, **9**, 2344 (1970).
16) Measured at the Elemental Analysis Center, Kyoto University.
17) S. A. Hawley and C. E. Chase, *Rev. Sci. Instrm.*, **41**, 553 (1970).
18) F. Basolo and R. G. Pearson, "Mechanisms of Inorganic Reactions," 2nd ed, John Wiley and Sons, New York (1967), p. 181.
19) S. Matsuura, "Ion Teisu," Maruzen, Tokyo (1963), Chap. 2.
20) The values of $\Delta H°$ and $\Delta S°$ for the $H^+ + OH^- = H_2O$ equilibrium are taken as -55.8 kJ mol^{-1} and 80.7 J K^{-1} mol^{-1}. H. Ohtaki, M. Tanaka, and S. Funahashi, "Yoeki-hanno No Kagaku," Japan Scientific Societies Press, Tokyo (1977), p. 46.
21) G. A. Lawrance and S. Suvachittanont, *Aust. J. Chem.*, **33**, 273 (1980). dtcd=*meso*-5,12-*D*imethyl-1,4,8,11-tetraaza-cyclo-tetradeca-4,11-diene.
22) W. E. Jones, L. R. Carey, and T. W. Swaddle, *Can. J. Chem.*, **50**, 2739 (1972).
23) T. G. Spiro, A. Revesz, and J. Lee, *J. Am. Chem. Soc.*, **90**, 4000, (1968). At 30 °C in 0.1 M $NaClO_4$.
24) D. A. House, *Coord. Chem. Rev.*, **23**, 223 (1977).
25) Y. Kitamura, *Bull. Chem. Soc. Jpn.*, **50**, 2097 (1977). At 35 °C in 0.0133 M Na_2CO_3–0.0200 M $NaHCO_3$ (Ionic strength (I) =61.4 mM).
26) T. Okubo, T. Maruno, and N. Ise, *Proc. R. Soc. London, Ser. A*, **370**, 501 (1980). At 25 °C in 1.8 mM NaOH (I=1.9 mM).
27) F. R. Nordmeyer, *Inorg. Chem.*, **8**, 2780 (1969).
28) D. A. Buckingham, I. I. Olsen, and A. M. Sargeson, *J. Am. Chem. Soc.*, **89**, 5129 (1967).
29) D. A. Buckingham, I. I. Creaser, and A. M. Sargeson, *Inorg. Chem.*, **9**, 655 (1970).
30) M. Green and H. Taube, *Inorg. Chem.*, **2**, 948 (1963).
31) Y. Kitamura, *Bull. Chem. Soc. Jpn.*, **52**, 3453 (1979). H_2edda = Ethylenediamine-*N*,*N*′-diacetic acid. Hame = 2-Aminoethanol.
32) C. T. Buriss and K. J. Laidler, *Trans. Faraday Soc.*, **51**, 1497 (1955). At 30 °C in 0.1 mM NaOH (*I*=0.4 mM).
33) Y. Kitamura, R. Kume, and K. Kuroda, 21st Koatsu-Toronkai, Tokyo, 1980, 3C04.
34) T. W. Swaddle, *Coord. Chem. Rev.*, **14**, 217 (1974).
35) C. H. Langford, *Inorg. Chem.*, **18**, 3288 (1979).
36) M. V. Twigg, *Inorg. Chim. Acta*, **24**, 84 (1977).

 © 1982 The Chemical Society of Japan Bull. Chem. Soc. Jpn., 55, 3630—3632 (1982) [Vol. 55, No. 11

Synthesis and Characterization of Tin(IV) Thiocarbamates

Virendra Kumar Gupta, Ravindra Kumar Kanjolia,
and Vishnu Deo Gupta*

Department of Chemistry, Faculty of Science, Banaras Hindu University, Varanasi-221005, India

(Received January 16, 1982)

Tin(IV) thiocarbamates of the types $SnX_{4-n}(SOCNR_2)_n$, n-$BuSnCl_{3-n}(SOCNEt_2)_n$, and $R'_2Sn(SOCNEt_2)_n$ (where X=Cl, Br, I; R=Me, Et; R'=n-Bu, n-Pr; n=1—4) were synthesized and characterized by elemental analysis and by molar conductance, molecular weight, and IR and NMR measurements.

The chemistry of metal complexes of thiocarbamate, particularly in association with main group metals, has not thoroughly been investigated in contrast to corresponding dithiocarbamates, only a few reports being made on silicon(IV),[1,2] thallium(I),[3] and some organotin(IV)[4,5] species. The replacement of sulfur by oxygen and the resulting decrease in the chelate bite bring about a remarkable change in the stereochemistry of metal complexes.[6—8] In view of this, we have initiated a detailed and systematic study of metal complexes of thiocarbamate and are reporting here some findings on tin(IV) derivatives.

Experimental

General. All manipulations were carried out under anhydrous conditions in nitrogen atmosphere. Solvents were dried by standard techniques. The sodium and dialkylammonium salts of thiocarbamic acid[9] and tin(IV) halide[10—12] were synthesized by literature procedures. n-$BuSnCl_3$ (93 °C/10 mmHg) (1 mmHg=133.322 Pa), n-Bu_2SnCl_2 (142 °C/11.0 mmHg), and n-Pr_2SnCl_2 (50 °C/1.0 mmHg) were distilled before use. The metal, sulfur, and halogen were estimated gravimetrically. Nitrogen was estimated by Kjeldahl's method. Conductance was measured on a conductivity bridge (Model No. L-370873 from Cambridge Instrument Co., England) at 10^{-3} M (1 M=1 mol dm^{-3}) concentration. Molecular weights of soluble compounds were determined cryoscopically in benzene. Infrared spectra were recorded on a Perkin-Elmer 621 instrument as Nujol mull in the range 4000—200 cm^{-1} and in solution in the range 4000—650 cm^{-1}. NMR spectral studies were carried out on a Varian A-60 spectrometer using tetramethylsilane as the internal standard.

Preparation of Trihalo(thiocarbamato)tin(IV) and Dihalobis(thiocarbamato)tin(IV) Complexes (Table 1). Into a suspension of sodium salt of thiocarbamate in dichloromethane, the stoichiometric amount of tin(IV) halide was added dropwise, and the reaction mixture was allowed to reflux for 12—14 h. The mixture was filtered to remove the separated sodium halide and the volatile materials were removed under reduced pressure. The products were crystallized from acetonitrile/hexane (1:8) and dried at 0.1 mmHg and *ca.* 50 °C for *ca.* 6 h.

Preparation of Chlorotris(diethylthiocarbamato)tin(IV) and Tetrakis(diethylthiocarbamato)tin(IV) Complexes (Table 1). Into a benzene solution of diethylammonium salt of diethylthiocarbamate, the stoichiometric amount of tin(IV) chloride was added dropwise with continuous stirring. The stirring was continued for *ca.* 10 h. The separated diethylammonium chloride was removed by filtration and the volatile materials were removed under reduced pressure. The products were crystallized from benzene/hexane (1:5) and dried at 0.1 mmHg and *ca.* 30 °C for *ca.* 10 h.

Preparation of Butyldichloro(thiocarbamato)tin(IV), Butylchlorobis(thiocarbamato)tin(IV), and Diorganobis(thiocarbamato)tin(IV) Complexes (Table 1). Into an acetone solution of diethylammonium salt of thiocarbamate, the stoichiometric amount of organotin(IV) chloride was added dropwise with continuous stirring. The stirring was continued for *ca.* 6 h. The separated diethylammonium chloride was removed by filtration and the volatile materials were removed under reduced pressure. Viscous liquids thus obtained were dried at 0.1 mmHg and *ca.* 30 °C for *ca.* 6 h.

Preparation of $SnCl_3(C_5H_5N)(SOCNMe_2)$ and $SnX_2(C_5H_5N)(SOCNEt_2)_2$ (X=Cl, I) (Table 1). Into an acetonitrile solution of $SnX_2(SOCNEt_2)_2$ and $SnCl_3(SOCNMe_2)$, an excess of pyridine was added with stirring. The reaction mixture was stirred for *ca.* 6 h and the volatile materials were removed *in vacuo*. The solid products were finally dried at 0.1 mmHg and *ca.* 60 °C for *ca.* 10 h.

Results and Discussion

Thiocarbamatotin(IV), $SnX_{4-n}(SOCNR_2)_n$, and organotin(IV) thiocarbamates, n-$BuSnCl_{3-n}(SOCNEt_2)_n$ and $R'_2Sn(SOCNEt_2)_2$, were synthesized according to the following schemes:

$$SnX_4 + \begin{cases} n'(Et_2NCOS^-\overset{+}{N}H_2Et_2) \longrightarrow \\ \qquad SnX_{4-n'}(SOCNEt_2)_{n'} + n'Et_2NH_2X, \\ n(R_2NCOSNa) \longrightarrow \\ \qquad SnX_{4-n}(SOCNR_2)_n + nNaX, \end{cases}$$

$$R'_2SnCl_2 + 2(Et_2NCOS^-\overset{+}{N}H_2Et_2) \longrightarrow R'_2Sn(SOCNEt_2)_2 + 2Et_2NH_2Cl,$$

$$BuSnCl_3 + n(Et_2NCOS^-\overset{+}{N}H_2Et_2) \longrightarrow BuSnCl_{3-n}(SOCNEt_2)_n + nEt_2NH_2Cl.$$

(X=Cl, Br, I; R=Me, Et; R'=n-Bu, n-Pr; n=1,2; n'=3,4.)

Thiocarbamatotin(IV) derivatives are crystalline solids, insoluble in common organic solvents except acetonitrile, whereas tris and tetrakis derivatives are soluble. Organotin(IV) complexes are viscous liquids, miscible with common organic solvents.

The infrared spectra of all these complexes are dominated by a broad intense band, sometimes split, due to coupled C⋯N and C⋯O stretching vibrations around 1550—70 cm^{-1}, indicating invariably bidentate behavior of the ligand.[4,6,7,13] Medium to strong bands in the regions 560—80 and 380—90 cm^{-1} may be assigned to νSn–O and νSn–S, respectively.[14—16]

Dihalo, dialkyl (molecular weight shows them to be monomeric), and butylchlorobis complexes appear to involve an octahedral geometry. $SnCl_2(SOCNEt_2)_2$ should have a *cis*-structure in the solid state as indi

Table 1. Analytical data of tin(IV) thiocarbamate derivatives

No.	Compound[c]	Appearace[a]	Mp θ_m/°C	Conductivity (MeCN) Ω cm^2 mol^{-1}	Mol wt Found (Calcd)	Found (Calcd)(%) Sn	S	X[f]	N
1	$SnCl_3(SOCNMe_2)$	White	220[d]	73.65	—	35.89 (36.06)	9.49 (9.74)	33.07 (32.34)	4.00 (4.28)
2	$SnCl_3(SOCNEt_2)$	White	158—60	108.90	—	33.95 (33.04)	8.98 (8.97)	29.98 (29.80)	3.82 (3.94)
3	$SnBr_3(SOCNMe_2)$	Light yellow	108—10	40.30	—	25.12 (25.65)	6.56 (6.93)	50.64 (51.84)	2.98 (3.04)
4	$SnBr_3(SOCNEt_2)$	Light yellow	95—97	42.54	—	24.02 (24.18)	6.39 (6.54)	47.86 (48.88)	2.75 (2.87)
5	$SnI_3(SOCNMe_2)$	Brown	102—04	26.55	—	19.45 (19.65)	5.24 (5.31)	62.58 (63.09)	2.12 (2.33)
6	$SnI_3(SOCNEt_2)$	Dark red	72—74	45.02 0.05[b]	—	18.66 (18.78)	5.00 (5.07)	59.12 (60.28)	2.08 (2.23)
7	$SnCl_2(SOCNMe_2)_2$	White	238—40	68.15	—	29.75 (29.81)	16.02 (16.12)	17.61 (17.82)	7.00 (7.07)
8	$SnCl_2(SOCNEt_2)_2$	White	131	40.30	—	25.39 (26.13)	15.29 (14.13)	14.90 (15.63)	6.05 (6.20)
9	$SnBr_2(SOCNMe_2)_2$	Light yellow	166—70	27.61	—	24.18 (24.38)	13.00 (13.17)	32.52 (32.76)	5.58 (5.78)
10	$SnBr_2(SOCNEt_2)_2$	Light yellow	116	16.29	—	21.43 (21.86)	11.71 (11.81)	29.21 (29.45)	5.01 (5.18)
11	$SnI_2(SOCNMe_2)_2$	Dark red	130—32	8.76	—	20.29 (20.42)	10.96 (11.04)	42.60 (43.70)	4.73 (4.85)
12	$SnI_2(SOCNEt_2)_2$	Dark yellow	110—12	8.00 0.03[b]	—	18.50 (18.62)	10.80 (10.06)	38.18 (39.85)	4.30 (4.42)
13	$SnCl(SOCNEt_2)_3$	White	120[d]	20.95	594.4 (550.8)	22.04 (21.54)	17.30 (17.46)	6.30 (6.43)	7.60 (7.66)
14	$Sn(SOCNEt_2)_4$	White	116	8.62	653.6 (647.6)	18.34 (18.32)	19.79 (19.80)	—	8.58 (8.69)
15	n-$BuSnCl_2(SOCNEt_2)$	Brown viscous liquid	e)	44.94 0.48[b]	421.3 (378.2)	31.70 (31.32)	8.11 (8.26)	8.26 (8.46)	3.68 (3.72)
16	n-$BuSnCl(SOCNEt_2)_2$	Brown viscous liquid	e)	25.38	490.2 (475.5)	24.81 (24.94)	13.57 (13.48)	7.20 (7.46)	5.65 (5.92)
17	n-$Bu_2Sn(SOCNEt_2)_2$	Brown viscous liquid	e)	0.91	510.2 (497.3)	23.81 (23.85)	13.51 (12.89)	—	5.43 (5.66)
18	n-$Pr_2Sn(SOCNEt_2)_2$	Viscous liquid	e)	0.91	482.4 (469.3)	25.09 (25.27)	13.73 (13.67)	—	5.89 (6.00)
19	$SnI_2(C_5H_5N)$-$(Et_2NCOS)_2$	Light yellow	150[d]	—	—	16.81 (16.69)	9.18 (9.02)	35.04 (35.72)	5.72 (5.94)
20	$SnCl_2(C_5H_5N)$-$(Et_2NCOS)_2$	White	164—66	—	—	22.28 (22.25)	12.10 (12.03)	13.54 (13.56)	7.78 (7.92)
21	$SnCl_3(C_5H_5N)$-(Me_2NCOS)	White	255	—	—	29.01 (29.07)	7.94 (7.86)	25.96 (26.07)	6.69 (6.90)

a) Solid. b) Molar conductivity in dichloromethane. c) Yield 90%. d) Decomposed. e) Attempted distillation failed. f) X=Cl, Br, I.

cated by the two absorptions at 327 and 315 cm^{-1} due to antisymmetric and symmetric νSn–Cl, respectively.[17] This is further evidenced by ^{1}H NMR spectra (Table 2) of the soluble bis complexes, $SnX_2(SOCNEt_2)_2$, which show two overlapping quartets and triplets perhaps arising from their *cis*-structures and magnetic nonequivalence of the ethyl protons at ambient temperature due to the partial double bond character in C–N providing a restricted rotation.[4,9,13] The complex n-$BuSnCl_2(SOCNEt_2)$ is monomeric and nonionic in dichloromethane involving 5-coordinated tin atom.

Interestingly, in the IR spectra (in solution and in the solid state) of $SnCl(SOCNEt_2)_3$ and $Sn(SOCNEt_2)_4$ (found to be monomeric), an additional broad intense band appears at 1595—1605 cm^{-1} due to the coupled νC=N and νC=O, indicating also the presence of thiocarbamato moiety bonded to the tin atom through sulfur only.[18–20] This is strongly substantiated by the nature of the ^{1}H NMR spectrum of $Sn(SOCNEt_2)_4$ at ambient temperature which shows two sets of broad peaks of equal intensity, one due to the methylene protons of the two chelating diethylthiocarbamate moiety centered at δ=3.47 (comparable to the values obtained for our other derivatives) and the other at δ=3.00 (evidently separated by 0.47 in δ) owing to the other two ligands having only sulfur atoms bonded to the metal. The methyl protons appear as a complex mixture of triplets. It is evident that the tetrakis complex is octahedral like tetrakis derivatives of dithiocarbamate[21] $Sn(S_2CNEt_2)_4$ and dithiocarbonates[22] $Sn(S_2COEt)_4$. Efforts are being

Table 2. ^{1}H NMR spectra of tin(IV) derivatives in $CDCl_3$

Compound	Resonance	
	Assignment	Chemical shift[a] (δ)
$SnCl_2(SOCNEt_2)_2$	C-CH_3[b]	1.23 1.33
	N-CH_2[c]	3.43 3.55
$SnBr_2(SOCNEt_2)_2$	C-CH_3[b]	1.26 1.35
	N-CH_2[c]	3.45 3.58
$Sn(SOCNEt_2)_4$	C-CH_3[d]	1.27
	N-CH_2[e]	3.47
	N-CH_2[e]	3.00

a) Shift at 60 MHz relative to tetramethylsilane as the internal reference. b) Centers of two overlapping triplets. c) Centers of two overlapping quartets. d) Centers of complex triplets. e) Centers of broadened quartets.

made to get variable temperature ^{1}H NMR data for establishing the stereochemistry as well as to carry out a single crystal X-ray analysis for determining the full structure.

The conducting behavior of the tin(IV) halothiocarbamates in donor as well as in solvents of high dielectric constant suggests notable deviation from the behavior of the dithiocarbamate analogues in solutions, indicating a poor coordinating ability of the thiocarbamato moiety as ligand towards tin(IV). Dichlorobis(diethyldithiocarbamato)tin(IV) reported earlier[21] has been found to be essentially nonconducting (molar conductance: 3.92 Ω cm^2 mol^{-1}) in acetonitrile, whereas the trihalo- and dihalotin(IV) thiocarbamates exhibit a substantial molar conductance in acetonitrile in the order Cl>Br>I (Table 1) consistent with the general trend.[23] Substitution of the halide by butyl group also decreases the conductance since it lowers down the electrophilicity of the central tin atom. The data suggest the presence of the following solvolytic equilibrium[24] in acetonitrile:

$$SnX_{4-n}(SOCNR_2)_n \overset{MeCN}{\rightleftharpoons} [SnX_{4-(n+1)}(MeCN)(SOCNR_2)_n]^+X^-.$$

In donor solvents like pyridine (with lower dielectric constant), the equilibrium is more towards the right as evidenced by the comparatively much higher value of conductance, for example, of $SnI_2(SOCNEt_2)_2$ in pyridine (50 Ω cm^2 mol^{-1}) than in acetonitrile (8 Ω cm^{-2} mol^{-1}). The spurious conductance due to cationic species with a molecule of the solvent in the coordination sphere is substantiated by the isolation and characterization of pyridine complexes of the types $[SnCl_2(C_5H_5N)(SOCNMe_2)]^+Cl^-$ and $[SnX(C_5H_5N)(SOCNEt_2)_2]^+ X^-$ (X=Cl, I), which give characteristic bands at 690, 753, 1034, 1059, and 1600 cm^{-1} in the IR spectra due to coordinated pyridine.[25]

The authors are grateful to CSIR, New Delhi for a Junior Research Fellowship (VKG) and a Post-doctoral Fellowship (RKK) and to Nitto Kasei for their generous help in supplying us with organotin(IV) chlorides as a gift.

References

1) C. H. Yoder, A. Komoriya, J. E. Kochanowski, and F. H. Suydam, *J. Am. Chem. Soc.*, **93**, 6515 (1971).
2) A. E. Lemire and J. C. Thompson, *J. Am. Chem. Soc.*, **93**, 1163 (1971).
3) R. J. Magee and M. J. O'Connor, *Inorg. Chim. Acta*, **5**, 554 (1971).
4) A. B. Crosby, R. J. Magee, and M. J. O'Connor, *Inorg. Chim. Acta*, **34**, 107 (1979).
5) R. F. Dalton and K. Jones, *J. Chem. Soc., A*, **1970**, 590.
6) B. J. McCormick and B. P. Stormer, *Inorg. Chem.*, **11**, 729 (1972).
7) C. G. Pierpont, R. C. Dickinson, and B. J. McCormick, *Inorg. Chem.*, **13**, 1674 (1974).
8) K. R. M. Springsteen, D. L. Greene, and B. J. McCormick, *Inorg. Chim. Acta*, **23**, 13 (1977).
9) S. L. H. Hawthorne, A. H. Bruder, and R. C. Fay, *Inorg. Chem.*, **17**, 2114 (1978).
10) "Handbook of Preparative Inorganic Chemistry," ed by G. Brauer, Academic Press, New York and London (1963), Vol. I, p. 729.
11) "Handbook of Preparative Inorganic Chemistry," ed by G. Brauer, Academic Press, New York and London (1963), Vol. I, p. 733.
12) T. Moeller and D. C. Edwards, *Inorg. Synth.*, **4**, 119 (1953).
13) S. L. Hawthorne and R. C. Fay, *J. Am. Chem. Soc.*, **101**, 5268 (1979).
14) R. S. Tobias and C. E. Fraddin, *Inorg. Chem.*, **4**, 215 (1965).
15) R. C. Poller, *J. Inorg. Nucl. Chem.*, **24**, 593 (1962).
16) J. L. K. F. DeVries and R. H. Herber, *Inorg. Chem.*, **11**, 2458 (1972).
17) I. R. Beattie, G. P. McQuillan, L. Rule, and W. Webster, *J. Chem. Soc.*, **1963**, 1514.
18) E. M. Krankovits, R. J. Magee, and M. J. O'Connor, *Inorg. Chim. Acta*, **7**, 528 (1973).
19) F. W. Pijipers, A. H. Dix, and J. G. M. van der Linden, *Inorg. Chim. Acta*, **11**, 41 (1974).
20) E. M. Krankovits, R. J. Magee, and M. J. O'Connor, *Aust. J. Chem.*, **26**, 1645 (1973).
21) J. C. May, D. Petridis, and C. Curran, *Inorg. Chim. Acta*, **5**, 511 (1971).
22) C. L. Raston, P. R. Tennant, A. H. White, and G. Winter, *Aust. J. Chem.*, **31**, 1493 (1978).
23) I. R. Beattie, *Quart. Rev. Chem. Soc.*, **17**, 382 (1963).
24) R. A. Walton, *Quart. Rev. Chem. Soc.*, **19**, 126 (1965).
25) N. N. Greenwood and K. Wade, *J. Chem. Soc.*, **1960**, 1130.

© 1982 The Chemical Society of Japan

NOTES

Bull. Chem. Soc. Jpn., 55, 3633—3634 (1982)

Photochemical Charging of a Silver Electrode Fixed at a Titanium Dioxide Surface

Hiroshi HADA,* Yoshiro YONEZAWA, and Yasuhito MOMOKI

Department of Industrial Chemistry, Faculty of Engineering, Kyoto University, Yoshida, Sakyo-ku, Kyoto 606

(Received March 4, 1982)

Synopsis. A regenerative half cell presented here: TiO_2(Ag)–Ag^+ can be photochemically charged by irradiation of the TiO_2 surface with sunlight. Electrical energy is extracted from it by connection through the load with a suitable half cell which has a more positive electrode potential than Ag–Ag^+.

The quantum yield of the photoreduction of silver ion (Ag^+) at the surface of both TiO_2 and ZnO by means of 365 nm light is more than 0.1 under suitable conditions.[1] We are interested in an application of the deposited silver at a semiconductor surface to anodic material of galvanic cells. In this paper, we have tried to use a TiO_2(Ag) electrode as a silver metal electrode. If we construct a half cell:TiO_2(Ag)–Ag^+ and combine it with another half cell:Pt–X^+/X couple, in which the standard electrode potential of the X^+/X couple is more positive than Ag^+/Ag, we can indeed withdraw electrical energy from such a cell. Zaromb *et al.* have previously described a cyclic photogalvanic silver halide cell from an analogous viewpoint.[2] Hodes *et al.* have investigated the photoelectrochemical storage cell by making use of CdSe.[3]

TiO_2 powder labelled TITONE R-310 made by Sakai Kagaku Co., Ltd., Osaka was molded and sintered at 1300 °C in air for 2 h, to obtain a plate of TiO_2 sinter, *ca.* 2 mm in thickness and 1 cm^2 in surface area. The electrical resistance of the sinter was higher than 1 MΩ in the dark. An indium layer was then evaporated on one face of the sinter and a copper wire was soldered to it. The TiO_2 sinter thus treated was immersed in a 0.1 M† $AgNO_3$ solution and irradiated by sunlight for 30 min. As a result, silver was deposited on the surface of the TiO_2. Since the electrical resistance between the deposited silver on the surface and the copper wire was only a few ohms, it was confirmed that the silver on the surface is in direct contact with the indium layer. After the TiO_2 sinter was washed with distilled water, a copper wire was inserted into a glass tube and the indium layer and TiO_2 surface were covered with an epoxy resin except for the face which is to be exposed to an electrolyte solution (*ca.* 0.77 cm^2). The TiO_2(Ag) electrode thus formed (Fig. 1) was immersed in the electrolyte solution containing 0.1 M $AgNO_3$ plus 1 M KNO_3.

The electrode potential of a TiO_2(Ag)–Ag^+ half cell was +0.60 V *versus* saturated KCl–Ag/AgCl electrode. It is in accord with a known value for a Ag–Ag^+ half cell. In order to withdraw electrical energy from such a half cell, we have combined it with another half cell:Pt–Ce^{4+}/Ce^{3+} through a salt bridge containing KNO_3 (Fig. 1). The electrolyte solution of the latter cell comprised 0.05 M $Ce_2(SO_4)_3$, 0.05 M $Ce(SO_4)_2$ and 1 M KNO_3. Current-voltage characteristics of the test cell assembled in this manner: TiO_2(Ag), Ag^+||Ce^{4+}/Ce^{3+}, Pt were examined at 25 °C in the dark. The discharge current was measured by the voltage across a resistance box with a switch closed, which was recorded on a recorder EPR-100A (Toa Electronics Co., Ltd.,). A similar measurement of the reference cell having a silver metal electrode (*ca.* 6 cm^2 in surface area) was carried out for comparison. The relation between the discharge current and the output voltage is given in Fig. 2. The open-circuit voltage and the

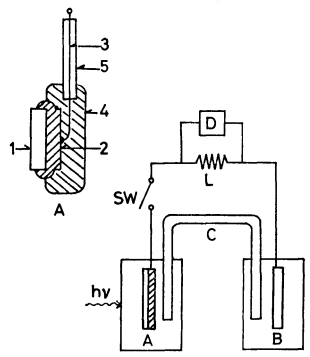

Fig. 1. Schematic representation of a galvanic cell. A: TiO_2(Ag)–Ag^+ half cell, B: Pt–Ce^{4+}/Ce^{3+} half cell, C: salt bridge, D: recorder, L: resistance box, SW: switch, 1: TiO_2 sinter, 2: indium layer, 3: copper wire, 4: epoxy resin, 5: glass tube.

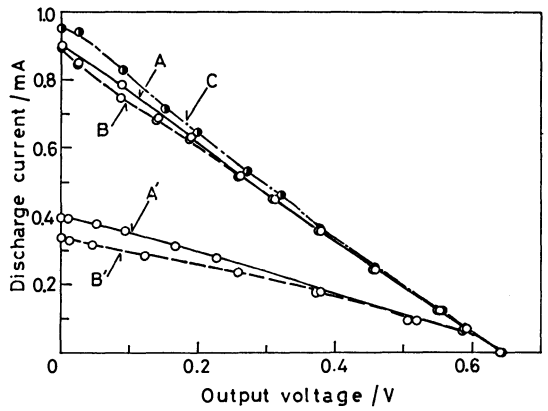

Fig. 2. The current-voltage characteristics for cells; TiO_2(Ag), Ag^+||Ce^{4+}/Ce^{3+} couple, Pt and Ag, Ag^+||Ce^{4+}/Ce^{3+} couple, Pt.
A: After first charging, A′: after first discharge, B: after second charging, B′: after second discharge, C: reference cell.

† 1 M=1 mol dm^{-3}.

short-circuit current were 0.64 V and 0.9 mA for the test cell and 0.64 V and 0.95 mA for the reference cell, respectively. Although the observed open-circuit voltage was somewhat less than the difference of the standard electrode potentials of Ag^+/Ag (0.80 V *vs.* NHE) and Ce^{4+}/Ce^{3+} (1.61 V) couples, current-voltage characteristics of these two cells were practically equal. Thus, we may state that the TiO_2(Ag) electrode possesses similar electrochemical properties to a silver metal electrode.

Discharge of the test cell was continued through a 30Ω load resistance. It is observed, as indicated in Fig. 3, the discharge current was decreased with the discharge time, but a current of about 0.3 mA was obtained after 15 min. The current-voltage characteristics of the cell at this stage were somewhat degenerated as seen in Fig. 2. The electrical resistance between the TiO_2 surface and the copper wire amounted to *ca.* 500Ω. We then opened the switch and placed the TiO_2(Ag)–Ag^+ half cell under sunlight for 30 min. The electrical resistance decreased again to a few ohms. The characteristics of the recharged cell are given in Figs. 2 and 3. As is indicated, the efficiency in the photochemical charging of the TiO_2(Ag)–Ag^+ half cell is very high. Cycles of photochemical charging and discharge were repeated more than ten times. It is found that the characteristics of the cell are similar to those of the first discharge and the efficiency of recharging is not lowered by such cycles. As we are interested only in an application of deposited silver, we have paid little attention to the regeneration of the Pt-Ce^{4+}/Ce^{3+} half cell in this work.

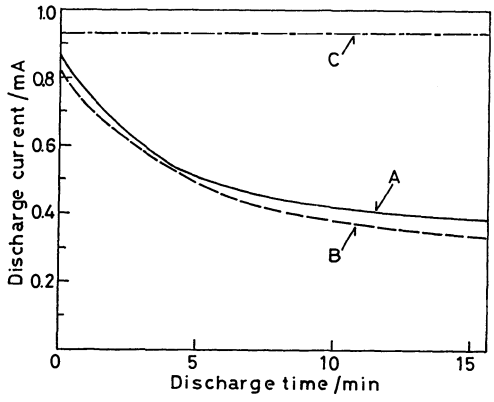

Fig. 3. Relation between discharge current and discharge time.
A: After first charging, B: after second charging, C: reference cell.

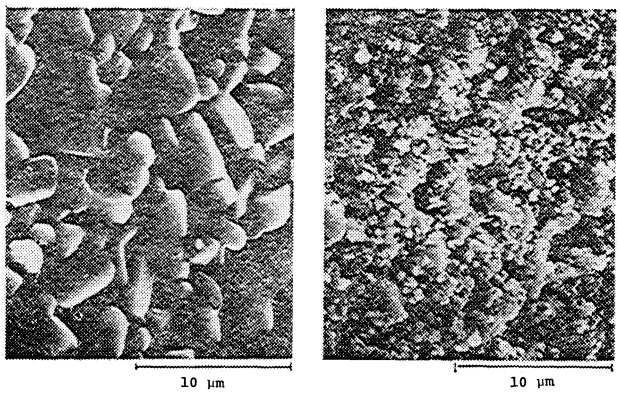

Fig. 4. Scanning electron micrographs of TiO_2 surface before (A) and after (B) charging.

It seems that the lower electrical resistance of the TiO_2(Ag) electrode after charging implies a whole electrode surface covered with deposited silver. Observation of the electrode surface with a scanning electron microscope JSM-T20S (Nippon Denshi Co., Ltd.,) confirms this (Fig. 4). According to a procedure reported previously,[1] the amount of photoreduced silver at the TiO_2 surface in the TiO_2(Ag)–Ag^+ half cell was determined for varying the irradiation time with 365 nm light from a 500 W Xenon lamp. The number of photons incident on the TiO_2 surface was 3×10^{13} cm^{-2} s^{-1}. The quantum yield of the silver deposition (amount of photoreduced silver/number of incident photon) was *ca.* 0.9. Thus the conversion efficiency of the 365 nm light to the reduced silver is very high. It would seem that silver deposited at the surface restricts the penetration of the incident light into the TiO_2 layer and causes a decrease of the rate of silver deposition. Indeed, such a filter effect may ultimately restrict the amount of silver deposition, which determines the maximum amount of silver storage per electrode surface. However, we have observed elsewhere that deposited silver does not influence the rate of silver deposition even when it increases to a considerable extent.[1]

Another important aspect of this cell is that at the time of photochemical charging, the metal deposition is carried out without transporting the charge carriers (electrons and holes) into the TiO_2 bulk. Therefore, we can make use of various semiconductors provided only that they can reduce metal ions under illumination of sunlight. Moreover, at the time of discharge, the current flows from the deposited metal directly to the lead wire without passing through the semiconductor bulk and therefore, its bulk resistance does not affect the internal resistance of the cell. Provided we can establish successful electrochemical properties and photochemical charging, as well as relatively large quantum yield of silver deposition, the TiO_2(Ag)–Ag^+ half cell may be useful in the field of solar energy conversion.

This work was carried out with financial support Grant-in-Aid No. 311607 from the Ministry of Education, Science and Culture.

References

1) H. Hada, H. Tanemura, and Y. Yonezawa, *Bull. Chem. Soc. Jpn.*, **51**, 3154 (1978); H. Hada, Y. Yonezawa, and M. Saikawa, *ibid.*, accepted.

2) S. Zaromb, M. E. Lasser, and F. Kalhammer, *J. Electrochem. Soc.*, **108**, 42 (1961).

3) G. Hodes, J. Manassen, and D. Cahen, *Nature*, **261**, 403 (1976).

The CNDO/S-CI Calculations of the Singlet nπ* and ππ* Levels of Quinones

Akira KUBOYAMA,* Yoshikuni KOZIMA,† and JUNZO MAEDA

National Chemical Laboratory for Industry, Tsukuba Research Center, Yatabe, Ibaraki 305

† *The Tokyo Metropolitan Industrial Technology Center, Kita-ku, Tokyo 115*

(Received March 6, 1982)

Synopsis. The calculations proved to reproduce well the observed S_1 nπ* levels of quinones, the numbers of the singly excited configurations contained in CI being twice those of the basis AO's. The calculations taking 0.500 as the κ value reproduce well the observed singlet ππ* levels also. The unknown S_1 nπ* levels of some quinones were predicted on the basis of the calculated results.

As for the CNDO/S-CI[1] calculations of the singlet electronic-energy levels of quinones, only a few works[2] on *p*-quinones have been reported. In this work, the lowest-energy singlet $n_{\pm}\pi^*$[3] levels of principal *o*- and *p*-quinones have been studied with the aid of the CNDO/S-CI calculations. In the calculations, two κ values,[4] 0.585 (the formal one) and 0.500, were used. The 0.500 value was chosen to reproduce the observed energy difference between the $n_{\pm}\pi^*$ levels of *p*-benzoquinone, as will be shown later. In this work, the calculations using the two κ values are called as Cals. A and B respectively. The geometries of the quinones used in the calculations were the same as those used in the previous works,[5] except for that of *o*-benzoquinone, where the C–H bond length was taken as 1.084 Å. In *o*-benzoquinone[6] and acenaphthenequinone,[7] those values determined by X-ray-crystal analysis were used. Those of 2,6-naphthoquinone and diphenoquinone, and that of 5,14:7,12-pentacenediquinone, were determined on the basis of those of *p*-benzoquinone and 9,10-anthraquinone respectively.

In Fig. 1, n in the abscissa denotes the ratio of the number of the lowest singly excited configurations included in the calculations (Cal. A) to that of the basis AO's in the MO's. As may be seen in Fig. 1, in *p*-benzoquinone the lowest $n_+\pi^*$ levels is higher than the lowest $n_-\pi^*$ level, and the energy separation (ΔE) between them is of the order of 0.1 eV, while in *o*-benzoquinone the $n_-\pi^*$ level is higher than the $n_+\pi^*$ level and the ΔE is of the order of 1 eV, as in α-diketones.[8] In both quinones, the $n_{\pm}\pi^*$ levels become lower with the increase in n, but, broadly speaking,

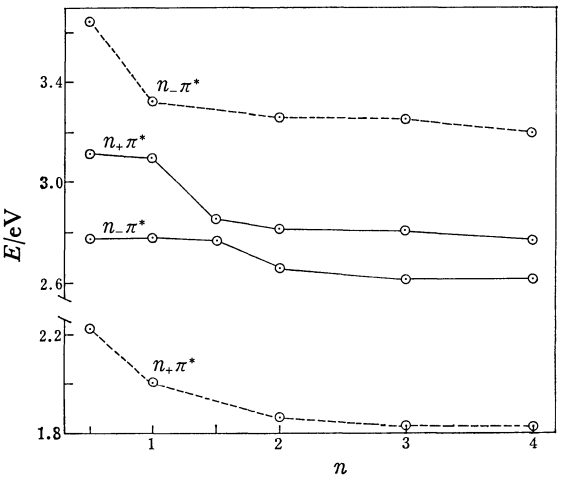

Fig. 1. The lowest singlet $n_{\pm}\pi^*$ levels of benzoquinones obtained by Cal. A. As for n in the abscissa, see Text.
——: *p*-Benzoquinone, ----: *o*-benzoquinone.

TABLE 1. CALCULATED SINGLET nπ* LEVELS OF QUINONES

		Cal. A		Cal. B		Obsd[9]
	Symmetry	S_1 E/eV	ΔE[a] eV	S_1 E/eV	ΔE[a] eV	E eV
(1) *p*-Quinones						
p-Benzoquinone	B_{1g}	2.659	0.153	2.582	0.023	2.48
1,4-Naphthoquinone	B_1	2.749	0.082	2.601	0.008	2.68
9,10-Anthraquinone	B_{1g}	2.918	0.199	2.742	0.140	2.92
2,6-Naphthoquinone	A_u	2.826	0.029	2.674	0.035	
Diphenoquinone	B_{1g}	2.863	0.049	2.766	0.015	
5,14:7,12-Pentacenediquinone	B_{3u}	3.015	0.102[b]	2.926	0.049[b]	
(2) *o*-Quinones						
o-Benzoquinone	B_1	1.866	1.393	1.878	1.069	1.91[c]
1,2-Naphthoquinone	(B_1)	2.183	1.162	2.130	0.898	2.19
9,10-Phenanthrenequinone	B_1	2.408	1.139	2.308	0.896	2.38
Biphenylene-2,3-dione	B_1	2.357	1.173	2.229	0.951	2.25
Acenaphthenequinone	B_1	2.567	0.928	2.471	0.773	2.42

a) The S_1 levels in *p*- and *o*-quinones are the $n_-\pi^*$ and $n_+\pi^*$ levels respectively. b) The energy difference between the S_1 and S_2 nπ* levels. c) The estimated value.

settle at the point (n=2). Similar results were obtained in other *o*- and *p*-quinones. Results similar to the above were also obtained in Cal. B. Therefore, only the calculated values in the (n=2) case are used below.

In Table 1, the S_1–S_0 transitions are all found to be allowed transitions (out-of-plane) except for those of the three D_{2h}-type *p*-quinones, such as *p*-benzoquinone. It is also found that the S_1 level of each quinone is a little higher in Cal. A than in Cal. B, except for that of *o*-benzoquinone, and that in both Cals. A and B it is generally in good agreement with the observed one. The observed values are those of the longest-wavelength peaks or shoulders[9] of the S–S $n\pi^*$ absorption spectra in saturated hydrocarbon solutions.

As for ΔE, in Table 1 it is smaller in Cal. B than in Cal. A in each quinone except for 2,6-naphthoquinone. In *p*-benzoquinone, the observed values (0.032[10]—0.0004[11] eV (crystal) and 0.007 eV(gas)[12]) are close to that in Cal. B. As the observed energy separations between the triplet $n_{\pm}\pi^*$ levels of 9,10-anthraquinone[13] are not far from those of *p*-benzoquinone, the ΔE of 9,10-anthraquinone may be expected to be not far from that of *p*-benzoquinone. It is noticeable that the ΔE of 9,10-anthraquinone in Cal. B is considerably larger than that of *p*-benzoquinone. It is, however, uncertain at this stage whether or not this difference is significant.[14] In consideration of the large ΔE values of the *o*-quinones in Table 1, the S–S $n\pi^*$ absorption spectra of *o*-quinones may be concluded to consist of the $n_+\pi^*$ absorption spectra alone, as in α-diketones.[8]

Table 2. Calculated low-energy singlet $\pi\pi^*$ levels of quinones

	Cal. A		Cal. B	Obsd[5]
	Symmetry	E/eV	E/eV	E/eV
p-Benzoquinone	B_{3g}	4.909	4.394	4.5
	B_{1u}	5.767	5.225	5.2
1,4-Naphthoquinone	A_1	4.376	3.804	3.8
	B_2	4.624	4.116	
	B_2	5.472	4.866	5.1
	A_1	5.739	5.199	
9,10-Anthraquinone[a]	B_{2u}	4.413	3.828	3.9
	B_{1u}	5.330	4.803	4.6
	B_{2u}	5.571	4.959	5.0
o-Benzoquinone	B_2	3.799	3.440	3.5
1,2-Naphthoquinone		3.969	3.545	3.3
		4.367	3.836	3.7
		5.258	4.922	5.0
9,10-Phenanthrenequinone	B_2	3.917	3.475	3.1
	A_1	4.377	3.799	3.9
	B_2	4.477	3.949	3.7
	B_2	5.197	4.681	4.8
	A_1	5.458	4.887	

a) The forbidden levels have been omitted.

The low-energy $\pi\pi^*$ levels of the principal *o*- and *p*-quinones[5] obtained by Cal. B are found to be in good agreement with the observed ones in saturated hydrocarbon solutions, as may be seen in Table 2. The $n\pi^*$ S–S absorption spectra of 2,6-naphthoquinone and diphenoquinone have never been reported. In these quinones, as the lowest-singlet $\pi\pi^*$ levels are higher by 0.92 and 0.50 eV than the S_1 $n_-\pi^*$ levels respectively in Cal. B, the S_1 state may be predicted to be the $n_-\pi^*$ state. In addition, the S_1–S_4 states of 5,14:7,12-pentacenediquinone are all the $n\pi^*$ states (the B_{3u}, B_{1g}, A_u, and B_{3g} states respectively) in both Cals. A and B, where the ΔE's between S_1 and S_4 levels obtained by Cals. A and B are 0.320 and 0.195 eV respectively.

References

1) R. L. Ellis, G. Kuehnlenz, and H. H. Jaffe, *Theoret. Chim. Acta*, **26**, 131 (1972); J. D. Bene and H. H. Jaffe, *J. Chem. Phys.*, **48**, 1807 (1968).

2) P. E. Stevenson, *J. Chem. Phys.*, **76**, 2424 (1972); M. E. Merienne-Lafore and H. P. Trommsdorf, *ibid.*, **64**, 3791 (1976); G. Olbrich, O. E. Polansky, and M. Zander, *Ber. Bunzenges. Phys. Chem.*, **81**, 692 (1977).

3) In $n_{\pm}\pi^*$, $n_{\pm}$ denote the symmetric and anti-symmetric linear combinations of the two oxygen lone-pair orbitals, n_1 and n_2, of quinones respectively, and π^*, the lowest-energy π^* orbital. In quinones, this π^* orbital usually contains an anti-symmetric linear combination of the two carbonyl parts.

4) In the CNDO/S method,[1] the empirical factor, κ, is introduced to distinguish the value of the resonance integral (β) of the π bond from that of the σ bond.

5) A. Kuboyama, S. Matsuzaki, M. Takagi, and H. Arano, *Bull. Chem. Soc. Jpn.*, **47**, 1604 (1974); A. Kuboyama, F. Kobayashi, and S. Morokuma, *ibid.*, **48**, 2145 (1975); A. Kuboyama and H. Arano, *ibid.*, **49**, 1401 (1976); A. Kuboyama, *ibid.*, **54**, 873 (1981); *Chem. Phys. Lett.*, **41**, 544 (1976).

6) A. L. MacDonald and J. Trotter, *J. Chem. Soc., Perkin Trans. 2*, **1973**, 476.

7) T. C. W. Mak and J. Trotter, *Acta Crystallogr.*, **16**, 811 (1963).

8) J. F. Arnett, G. Newkome, W. L. Mattice, and S. P. McGlynn, *J. Am. Chem. Soc.*, **96**, 4385 (1974).

9) It is thought that these are the 0-0 peaks in the quinones except for the D_{2h}-type *p*-quinones, and that in the latters these are not far from the 0-0 peaks.

10) H. P. Trommsdorf, *Chem. Phys. Lett.*, **10**, 176 (1971).

11) T. M. Dunn and A. H. Francis, *J. Mol. Spectrosc.*, **50**, 14 (1974).

12) The $^1B_{1g}$ $n_-\pi^*$ level is higher than the ^1A_u $n_+\pi^*$ level (G. T. Horst and J. Kommandeur, *Chem. Phys.*, **44**, 287 (1979); J. Goodman and L. E. Brus, *J. Chem. Phys.*, **69**, 1604 (1978)).

13) K. E. Drabe, H. Veenvliet, and D. A. Wiersma, *Chem. Phys. Lett.*, **35**, 469 (1975); T. N. Bolotnikova, T. M. Naumova and V. I. Savchenkov, *Opt. Spectrosc.*, **47**, 379 (1979); N. S. Strokach and D. N. Shigorin, *ibid.*, **43**, 34 (1977); Ref. 5 in the report (J. P. Galaup, J. Megel, and H. P. Trommsdorff, *J. Chem. Phys.*, **69**, 1030 (1978)); S. Y. Matsuzaki and A. Kuboyama, *Bull. Chem. Soc. Jpn.*, **51**, 2264 (1978).

14) E. Kanezaki, N. Nishi, and M. Kinoshita, *Bull. Chem. Soc. Jpn.*, **52**, 2836 (1979).

The Photoreduction of Viologen Dyes with Palladium *meso*-Tetraphenylporphyrintrisulfonate

Ichiro OKURA,* Shigetoshi AONO, Makoto TAKEUCHI, and Shin KUSUNOKI
Department of Chemical Engineering, Tokyo Institute of Technology, Meguro-ku, Tokyo 152
(Received April 1, 1982)

Synopsis. Pd-$TPPS_3$ was found to be an effective photosensitizer for the photoreduction of viologen dyes, such as methyl, ethyl, propyl, butyl, and heptyl viologens. The order of the reduction rate was as follows: Ethyl>Butyl>Methyl>Propyl>Heptyl. The respective complex formation was observed between Pd-$TPPS_3$ and viologen dyes, and electron transfer from photoexcited Pd-$TPPS_3$ to viologen dye was discussed.

Various attempts have been made to develop suitable redox systems for the photochemical utilization of solar energy. Recent works have shown that three-component systems containing a photosensitizer, an electron donor, and an electron acceptor can be used to evolve hydrogen from water when a suitable catalyst is present.[1] The metallo porphyrins employed almost exclusively in these studies as photosensitizers are zinc porphyrins.[2] It is desirable to explore other, suitable photosensitizers. In this study, palladium *meso*-tetraphenylporphyrintrisulfonate (Pd-$TPPS_3$) was found to be an effective photosensitizer for the photoreduction of viologen dyes; the reason for its effect was discussed.

Experimental

The methyl viologen and heptyl viologen were purchased from the Tokyo Kasei Kogyo Co. and the Aldrich Chemical Co. respectively, while the other chemicals, obtained from the Wako Pure Chemical Co., were of the highest available purity. The ethyl, propyl, and butyl viologens were synthesized according to the literature.[3] Pd-$TPPS_3$ was synthesized by refluxing *meso*-tetraphenylporphyrintrisulfonic acid and equimolar palladium acetate in methanol for 1 h.

The sample solution, which consisted of Pd-$TPPS_3$, viologen dye and 2-mercaptoethanol (RSH) in a Tris-HCl buffer (pH 7.0), was deaerated by repeated freeze-pump-thaw cycles. A typical experiment was performed as follows under anaerobic conditions. To 1.20×10^{-8} mol of Pd-$TPPS_3$ and 8.25×10^{-7} mol of viologen dye, 6.41×10^{-4} mol of RSH was added. The volume of the mixture was adjusted to 6.5 ml with a 0.02 M Tris-HCl buffer (pH 7.0). In the photolysis with continuous irradiation, the sample in a Pyrex cell with a magnetic stirrer was irradiated with light from a 150-W tungsten lamp (from a slide projector). Light of wavelength less than 390 nm was cut off by means of a Toshiba L-39 filter.

Results and Discussion

When an aqueous solution containing Pd-$TPPS_3$, methyl viologen, and RSH was irradiated, the growth of the cation radical of methyl viologen, which has characteristic absorption bands at 395 and 605 nm, was observed. The concentration of the reduced form of methyl viologen (MV^+) increased rapidly at the beginning of the reaction and then reached a constant value. When irradiation ceased, the concentration of MV^+ gradually decreased until it reached zero. MV^+ was reformed by re-irradiating the system, and the MV^+ formation rate was almost the same as the initial rate, for MV^+ returns to its original (oxidized) form in the absence of light. When other viologens, such as ethyl, propyl, butyl and heptyl viologens, were used instead of methyl viologen, the respective cation-radical formation was established by the irradiation. The order of the reduction rate was as follows:

Ethyl (2.40×10^{-5} M) > Butyl (1.8×10^{-5} M) > Methyl (1.56×10^{-5} M) $\simeq$ Propyl (1.55×10^{-5} M) > Heptyl ($\simeq$0 M).

The figures in the parentheses indicate the concentration of cation radicals formed by a 40-min irradiation. As the reduced forms of these viologens have redox potentials high enough for the decomposition of water, they may be useful as electron carriers to evolve hydrogen from water. In practice, hydrogen evolution by the reduction of water has been confirmed by the addition of hydrogenase as a catalyst to the reduced viologen dye formed by the reduction with $Na_2S_2O_4$.

Pd-$TPPS_3$ was a very active photosensitizer such one which was equal to Zn-$TPPS_3$ and far better than popular photosensitizers as ruthenium complexes. The photoreduction rate of methyl viologen with Pd-$TPPS_3$ was 12 times as large as that with palladium tetraphenylporphyrin (Pd-TPP), though it contains the same metal in the porphyrin ring. The difference in these activities may depend on the relative hardness of a complex formation between porphyrin and vi-

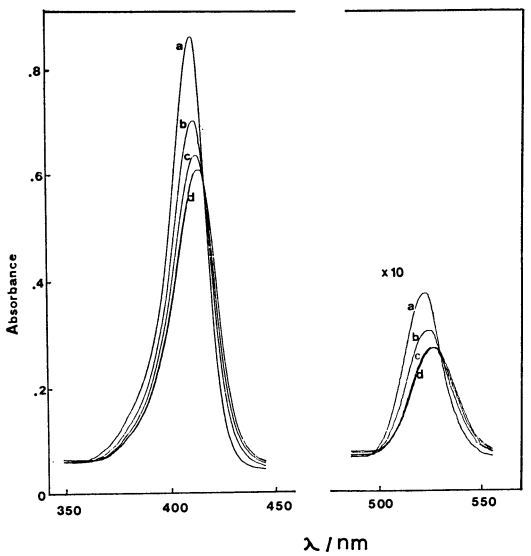

Fig. 1. Spectrum change of Pd-$TPPS_3$ by the addition of methyl viologen.
Sample solution contains 6.85×10^{-6} M of Pd-$TPPS_3$ and methyl viologen (a: 0 M; b: 2.03×10^{-5} M; c: 1.01×10^{-4} M; d: 5.07×10^{-4} M).

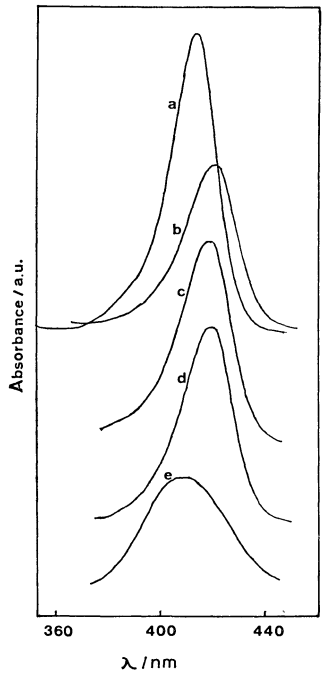

Fig. 2. Spectrum change of Pd–$TPPS_3$ by the addition of viologens.
a: Pd–$TPPS_3$, b: Pd–$TPPS_3$+ethyl viologen, c: Pd–$TPPS_3$+propyl viologen, d: Pd–$TPPS_3$+butyl viologen, e: Pd–$TPPS_3$+heptyl viologen.

ologen dye. Though a complex formation between Pd–$TPPS_3$ and viologens was observed as follows, no complex was formed in the case of Pd–TPP. When Pd–$TPPS_3$ was mixed with methyl viologen, the characteristic absorption bands at 409 and 521 nm of Pd–$TPPS_3$ decreased with the increase in the methyl viologen concentration, and a new spectrum appeared which has characteristic absorption bands at 414 and 527 nm through isosbestic points at 361, 417, 498, and 530 nm (Fig. 1). When other viologen dyes were used, the respective complex formation was observed, as is shown in Fig. 2. In the case of copper uroporphyrin, complex formation with methyl viologen was observed by Shelnutt.[4] The red shift in the Soret band of the complex is usually associated with a decrease in π-electron density in the porphyrin ring. The π-density in the ring follows this order: heptyl>methyl>propyl>butyl>ethyl. The lower the π-density of the ring, the larger the photoreduction rate of viologens, except for methyl viologen. The finding that the porphyrin ring acts as a donor in the ground state of the complex may show that photoinduced electron transfer from Pd–$TPPS_3$ to viologen dyes is apt to occur. Thus, viologens may be easily photoreduced. In the case of Pd–TPP, electron transfer from the photoexcited Pd–TPP to viologens may not proceed easily; a low reduction rate of methyl viologen is observed as a result.

Recently Matsuo *et al.*[5] prepared viologen-linked photosensitizers and found that electron was easily transferred from the photosensitizer to viologen dye and any undesirable back reaction was suppressed. In the cases of these Pd–$TPPS_3$–viologen complexes, easy electron transfer may also be found as a result of a similar effect.

We wish to express our appreciation to Professor Tominaga Keii and Professor Yoshio Ono for their stimulating and helpful discussions.

References

1) a) J. M. Lehn and J. P. Sauvage, *Nouv. J. Chim.*, **1**, 449 (1977); b) M. Kirch, J. M. Lehn, and J. P. Sauvage, *Helv. Chim. Acta*, **62**, 1345 (1979); c) K. Kalyanasundaram, J. Kiwi, and M. Gratzel, *ibid.*, **61**, 2720 (1978); d) K. Kalyanasundaram and M. Gratzel, *J. Chem. Soc., Chem. Commun.*, **1979**, 1137; e) A. Moradpour, E. Amouyal, P. Keller, and H. Kagan, *Nouv. J. Chim.*, **2**, 547 (1978); f) A. I. Krasna, *Photochem. Photobiol.*, **29**, 267 (1979); g) I. Okura and N. Kim-Thuan, *J. Mol. Catal.*, **5**, 311 (1979); h) I. Okura, S. Nakamura, N. Kim-Thuan, and K. Nakamura, *ibid.*, **6**, 261 (1979); i) I. Okura and N. Kim-Thuan, *J. Chem. Soc., Chem. Commun.*, **1980**, 84; j) I. Okura and N. Kim-Thuan, *J. Chem. Soc., Faraday Trans. 1*, **76**, 2209 (1980).

2) a) K. Takuma, M. Kajiwara, and T. Matsuo, *Chem. Lett.*, **1977**, 1199; b) I. Okura and N. Kim-Thuan, *J. Mol. Catal.*, **6**, 227 (1979); c) I. Okura, M. Takeuchi, and N. Kim-Thuan, *Chem. Lett.*, **1980**, 765; d) K. Kalyanasundaram and M. Gratzel, *Helv. Chim. Acta*, **63**, 478 (1980).

3) A. G. Evans, J. C. Evans, and M. W. Baker, *J. Chem. Soc., Perkin Trans. 2*, **1977**, 1787.

4) J. A. Shelnutt, *J. Am. Chem. Soc.*, **103**, 4275 (1981).

5) T. Matsuo, T. Sakamoto, K. Takuma, K. Sakura, and T. Ohsako, *J. Phys. Chem.*, **85**, 1277 (1981).

Thermal *cis-trans* Isomerization of $(CH)_x$ and $(CD)_x$

Masashi TANAKA,*,† Hajime YASUDA, and Jiro TANAKA

Department of Chemistry, Faculty of Science, Nagoya University, Chikusa-ku, Nagoya 464

† *Department of Chemistry, College of General Education, Nagoya University, Chikusa-ku, Nagoya 464*

(Received April 10, 1982)

Synopsis. Thermal *cis-trans* isomerization of poly(acetylene), $(CH)_x$, and poly(acetylene-d_2), $(CD)_x$, is investigated by visible spectroscopy over the temperature range 90—150 °C. The reaction does not obey simple kinetics. The initial time activation energy for the *cis-trans* isomerization is 11 kcal/mol for $(CH)_x$ and 16 kcal/mol for $(CD)_x$.

In recent years, various properties have been reported for poly(acetylene) since the discovery that it can increase the conductivity by many orders of magnitude up to metallic levels when doped with electron donors or acceptors.[1] For example, the electrical conductivity after strong doping is always smaller for *trans*-$(CH)_x$ than for *cis*-$(CH)_x$ and the doping may induce the *cis-trans* isomerization of $(CH)_x$ films. Furthermore, many studies have focused on the magnetic properties of the neutral soliton defects which appear in *trans*-$(CH)_x$ upon isomerization.[2] Accordingly, detailed studies about the isomerization are necessary to determine the physics and chemistry of poly(acetylene). In the present paper, we show the optical study on the thermal *cis-trans* isomerization mechanism of pure $(CH)_x$ and $(CD)_x$.

The thin $(CH)_x$ and $(CD)_x$ films polymerized at −78 °C show the reddish cupuric color and the film becomes blue on heating it in vacuo. This color change was explained by the analysis of IR vibrational spectra to be due to the *cis-trans* isomerization of $(CH)_x$ and $(CD)_x$.[3,4] Figure 1 describes the visible absorption spectral change of the thin $(CD)_x$ film during the course of heat treatment in vacuo. *cis*-Rich $(CD)_x$ has two vibronic peaks at 17300 and 18500 cm^{-1} and the second peak (18500 cm^{-1}) is the most intense. On heating, the broad band in the region of 15000 cm^{-1} becomes more intense and the 18500 cm^{-1} peak of *cis*-$(CD)_x$ becomes weaker. Finally, the 15000 cm^{-1} band of *trans*-$(CD)_x$ has the same absorption intensity as that of the 18000 cm^{-1} band of *cis*-$(CD)_x$ before heating. Furthermore, it should be noted that an isosbestic point is observed at 17000 cm^{-1}. The same phenomenon can be observed for the $(CH)_x$ film, too.[5]

Then, the rate equation of the *cis-trans* isomerization is given as follows,

$$C_{cis}(t) + C_{trans}(t) = C \tag{1}$$

and

$$-\frac{dC_{cis}(t)}{dt} = k\,C_{cis}(t). \tag{2}$$

Here, $C_{cis}(t)$ and $C_{trans}(t)$ are the concentration of *cis*- and *trans*-forms at time t and C is the total concentration.

The integration gives

$$C_{cis}(t) = C - C_{trans}(t) = C_{cis}(0)\exp(-kt). \tag{3}$$

On the other hand, the observed optical density at time t, $OD(t)$, can be expressed by using the molar extinction coefficients ε_{cis} and ε_{trans} of *cis*- and *trans*-polymers and the thickness, d, of the film,

$$OD(t) = d\,\varepsilon_{cis}C_{cis}(t) + d\,\varepsilon_{trans}C_{trans}(t). \tag{4}$$

Then, Eqs. 3 and 4 lead to

$$OD(\infty) - OD(t) = d\,C_{cis}(0)\{\varepsilon_{trans} - \varepsilon_{cis}\}\exp(-kt), \tag{5}$$

where $OD(\infty) = d\,\varepsilon_{trans}\,C$ is the observed optical density at infinite time. The ratio of Eq. 5 for time t and initial time and the logarithm of the result give

$$\ln\left|\frac{OD(\infty) - OD(t)}{OD(\infty) - OD(0)}\right| = -kt, \tag{6}$$

where $OD(0)$ is the observed optical density at initial time.

Figure 2 shows kinetic plots for the thermal *cis-trans* isomerization at 16000 cm^{-1} by using Eq. 6. The plot does not give the straight line as is pointed out by Ito, *et al.*[4] That is, the rate of isomerization becomes slow and the slope of the plot becomes small as the reaction proceeds. This means that the activation energy increases with increasing *trans*-

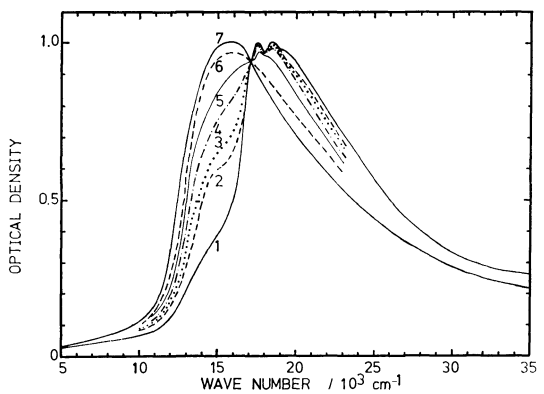

Fig. 1. The visible absorption spectral change due to the *cis-trans* isomerization of the thin $(CD)_x$ film at 140 °C after heating for 1) 0 min, 2) 0.5 min, 3) 1 min, 4) 2 min, 5) 3 min, 6) 5 min, and 7) 20 min.

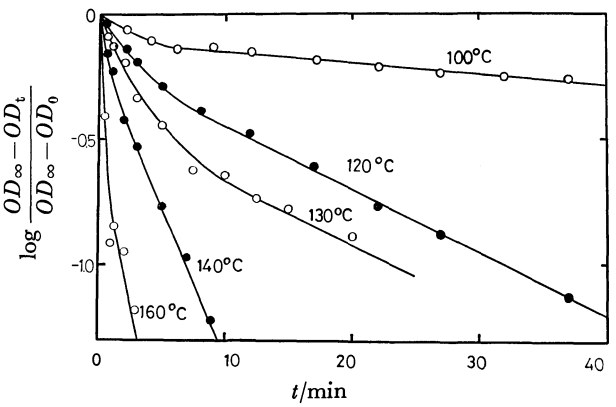

Fig. 2. Kinetic plots for the thermal *cis-trans* isomerization of $(CD)_x$ at 16000 cm^{-1}.

contents.

Arrhenius plots are shown in Fig. 3 and the activation energies at initial time are estimated to be 11 kcal/mol for $(CH)_x$ and 16 kcal/mol for $(CD)_x$. In contrast to Ito, Shirakawa and Ikeda's data (17 kcal/mol for 88% *cis*-rich $(CH)_x$),[4] our value of 11 kcal/mol for $(CH)_x$ corresponds to that of more than 90% *cis*-rich polymer. Furthermore, the larger activation energies for $(CD)_x$ than for $(CH)_x$ may be due to the mass difference between the hydrogen and deuterium atoms. That is, the out of plane C–H or C–D vibration plays an important part of the isomerization process and the difference between the zero point energies of C–H and C–D vibration may be considered to contribute to the difference between the activation energies for $(CH)_x$ and $(CD)_x$. This conclusion supports Ikeda's explanation for the difference between the *cis* and *trans* content ratio for the $(CH)_x$ and $(CD)_x$ polymers.[6]

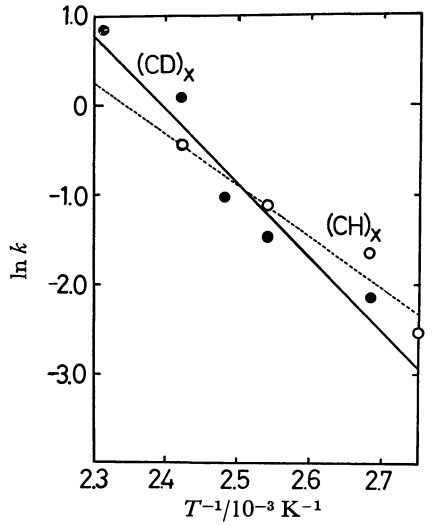

Fig. 3. Arrhenius plot for the thermal *cis-trans* isomerization of $(CH)_x$ and $(CD)_x$.

References

1) H. Shirakawa, E. J. Louis, A. G. MacDiarmid, C. K. Chiang, and A. J. Heeger, *J. Chem. Soc., Chem. Commun.*, **1977**, 578.

2) W. P. Su, J. R. Schrieffer, and A. J. Heeger, *Phys. Rev. B*, **22**, 2099 (1980).

3) H. Shirakawa and S. Ikeda, *Polym. J.*, **2**, 231 (1971).

4) T. Ito, H. Shirakawa, and S. Ikeda, *J. Polym. Sci., Polym. Chem. Ed.*, **13**, 1943 (1975).

5) M. Tanaka, A. Watanabe, and J. Tanaka, *Bull. Chem. Soc. Jpn.*, **53**, 3430 (1980).

6) S. Ikeda, *Nippon Kagaku Zasshi*, **70**, 1880 (1967).

Mechanochemical Reactions at High Pressures. IV. Transformation of Lead Monoxide

Yasuhiro OKURI and Yoshiaki OGO*

Department of Applied Chemistry, Faculty of Engineering, Osaka City University, 3-3-138, Sugimoto, Sumiyoshi-ku, Osaka 558

(Received Feburary 25, 1982)

Synopsis. The mechanochemical phase transformation of lead monoxide has been studied by the X-ray diffraction method. It is established that the transformation of lead monoxide proceeds by a stress-induced martensitic mechanism.

Lead monoxide exists in two familiar forms: litharge (L, a red tetragonal form) and massicot (M, a yellow orthorhombic form). Most of the studies of phase transformations in PbO have involved milling, comminution, and abrasion. High pressure studies have not been carried out except for an experiment to determine the equilibrium pressure-temperature relation for the L⇌M reaction by White *et al.*[1] These authors reported that L could be converted into M either by raising the temperature above 540 °C or the pressure above 6000 atm, although the reaction was slow at low temperature. Furthermore, they suggested that purely hydrostatic pressure causes the L→M transformation, whereas bond breakage at low pressure gives the M→L transformation.

In the present work, we investigated the L⇌M transformation at room temperature under high pressure with simultaneous shear deformation.

Experimental

The experimental high pressure apparatus combined with simultaneous shear deformation (HP+SSD) consists of Bridgman's type anvils. Details of the apparatus and procedure have been described previously.[2] All experiments were carried out up to 20 kbar (1 kbar=10^8 Pa) at room temperature. In these experiments, the reactions proceeded at a constant shearing velocity of 2.51 rad h^{-1} (2.4° min^{-1}).

As specimens of lead monoxide, the litharge starting material was kindly supplied from Dai Nippon Toryo Co. Ltd. and the massicot was the commercial reagent. The specimens were sieved to 100 mesh and molded in 12-mm diameter pellets. The sample tablet was placed in the HP+SSD apparatus, and the experiment was carried out at the desired pressure. The volume fraction increment of L(or M), after M(or L) was sheared under high pressure, was determined by X-ray diffraction analysis. The lines chosen for comparison were, for M, $2\theta=37.82°$ for the (020) plane and a relative intensity of 20, and for L, $2\theta=35.74°$ for the (002) plane and a relative intensity of 18.[3] According to Lins' report,[4] the relation between the volume fraction of massicot, C_M, and that of litharge, C_L is given by:

$$C_M/C_L = 2(I_M/I_L),$$

where I_M and I_L are the intensity of a chosen diffraction line for M and L, respectively.

Results and Discussion

Figures 1 and 2 show the relations between the static pressure and the shear stress for M and L, respectively. In Fig. 1, the curve exhibits a characteristic change at about 2 kbar, which corresponds to the M→L phase-transition. In Fig. 2, the characteristic variation at about 2 kbar and a slight variation at about 5 kbar were observed. These facts suggest that a large transition energy is required for L in comparison with M→L transformation because M is more stable than L at high pressures. Therefore, the energy required for L→M transformation will be accumulated over the range from 2 to 5 kbar of static pressure. This consideration is supported by the conversion curve of L as shown in Fig. 3. Consequently, the apparent transformation pressure of lead monoxide exsists in the vicinity of 2 kbar, and is smaller than the 5.6 kbar, obtained by extrapolation of the pressure-temperature phase diagram.[1] In conclusion, the forced shear deformation is responsible for the decrease in the transition pressure of lead monoxide.

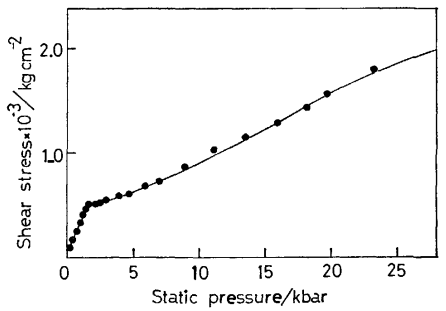

Fig. 1. Relation between the static pressure and the shear stress for massicot.

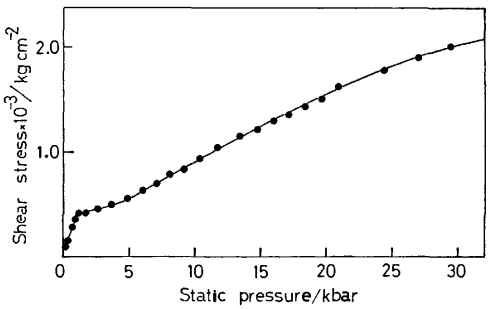

Fig. 2. Relation between the static pressure and the shear stress for litharge.

The effects of the static pressure on the conversion and the shearing degree for L→M, and M→L transformations are shown in Figs. 3 and 4, respectively. As shown in Fig. 3, the L→M transformation curves possess the following features:

(1) At 5 kbar, L was not converted into M in most experiments. These results are correlated with those in Fig. 2.

(2) The percent of M formed did not decrease

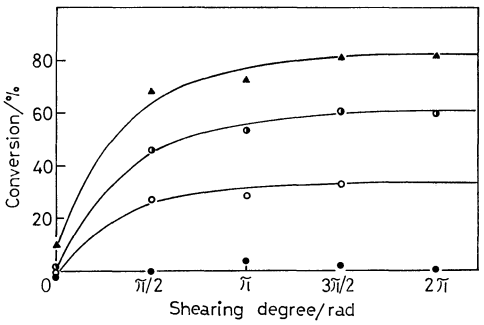

Fig. 3. Relation between conversion and the shearing degree at various static pressures for the litharge to massicot transformation.
● 5 kbar; ○ 10 kbar; ◑ 15 kbar; ▲ 20 kbar.

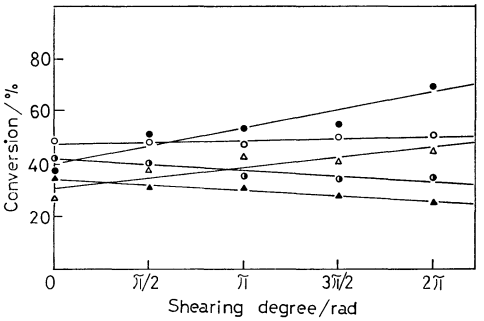

Fig. 4. Relation between conversion and the shearing degree at various static pressures for the massicot to litharge transformation.
△ 2 kbar; ● 5 kbar; ○ 10 kbar; ◑ 15 kbar; ▲ 20 kbar.

with the shearing degree, as was found for the M→L transformation in Fig. 4, but it tended to approach an equilibrium value similar to the value in the literature.[5] Judging from Fig. 3, L will be completely converted into M at about 30 kbar static pressure under our experimental conditions.

(3) The higher the static pressure, the more the transformation proceeds.

(4) The curves all have a parabolic shape.

The M→L transformation in Fig. 4 is characterized as follows:

(1) All relations are linear.

(2) At all static pressures, M is considerably transformed to L even without the forced shear deformation. It can be assumed that the energy required for the M→L transformation is less than that for the L→M transformation because L has a lower potential energy than M.[6]

(3) The conversion of M→L becomes small with the increase the static pressure as a general tendency. Furthermore, the conversion tends to decrease as the shearing proceeds at 15 and 20 kbar static pressure. This fact suggest a transformation back to M. Thus, it can be assumed that the transformation of M to L is an equilibrium reaction, if the transformation can be called the reaction. Judging from Fig. 4, the equilibrium shifts to M with increasing pressure. This consideration agrees with the Le Chatelier principle since M is a high-pressure modification.

The following two mechanisms can be proposed for the transformation of lead monoxide. The one is a nucleation and growth mechanism and the other is a stress-induced martensitic type transformation. When the experimental results fit Avrami equation, the transformation must proceed by a nucleation and growth mechanism.[5] Our experimental data did not fit the Avrami plot, therefore, the transformation of lead monoxide is a martensitic type transformation induced by the strong shear force. This conclusion is consistent with the result for M→L transformation during comminution.[4]

We also carried out some experiments on the transformation of calcium carbonate. The phase diagram of $CaCO_3$ has been studied since Bridgman's work in 1939, but regardless of many studies it is still not completely determined. Burns and Bredig[8] have found calite to be transformed to aragonite by grinding at room temperature, and estimated the pressure necessary for the transformation of calcite to arragonite at 4600 kg cm^{-2}. Ahrens and Katz[9] reported that the transformation of calcite occurs at pressures above 5 kbar. However, our X-ray examination revealed that calcite was not transformed into aragonite under 2π rad shearing at 15 kbar static pressure.

The authors thank Dr. K. Ohashi of Osaka City University for X-ray measurements, and Dai Nippon Toryo Co. Ltd. for a supply of litharge.

References

1) W. B. White, F. Dachille, and R. Roy, *J. Am. Ceram. Soc.*, **44**, 170 (1961).
2) Y. Ogo, N. Nishiguchi, and Y. Okuri, *Bull. Chem. Soc. Jpn.*, **54**, 520 (1981).
3) ASTM Card, Nos. 5-0570 and 5-0561.
4) I. J. Lin and S. Niedzwiedz, *J. Am. Ceram. Soc.*, **56** 62 (1973).
5) D. Lewis, D. O. Northwood, and R. C. Reeve, *J. Appl. Cryst.*, **2**, 156 (1969).
6) B. Dickens, *J. Inorg. Nucl. Chem.*, **27**, 1495 (1965).
7) "Chemistry of the Solid State," ed by W. E. Garner, D. Sc., F. R. S., C. B. E., p. 211.
8) J. H. Burns and M. A. Bredig, *J. Chem. Phys.*, **25**, 1281 (1956).
9) T. J. Ahrens and S. Katz, *J. Geophys. Res.*, **68**, 529 (1963).

Mass-spectrometric Measurements of Enthalpy and Entropy Changes for the Mixed Dimer Reaction: $Na_2Cl_2(g)+K_2Cl_2(g)=2NaKCl_2(g)$

Tadashi SASAMOTO,* Mitsuru ITOH,† and Toshiyuki SATA†

Tokyo National Technical College, 1220-2 Kunugida, Hachioji 193

†*Research Laboratory of Engineering Materials, Tokyo Institute of Technology, 4259 Nagatsuta, Midori-ku, Yokohama 227*

(Received October 16, 1981)

Synopsis. The enthalpy(ΔH_r°) and entropy(ΔS_r°) changes for the mixed dimer formation reaction, $Na_2Cl_2+K_2Cl_2=2NaKCl_2$, have been measured by mass-spectrometry in the temperature range of 793 to 1083 K. $\Delta H_r^\circ=-1.67$ kJ mol^{-1} and $\Delta S_r^\circ=5.69$ J K^{-1} mol^{-1} were obtained. These very small values were referred both to the mainly ionic-bonding structure in the related dimers and to preserving the isobonding through the reaction.

Hastie[1] has recently summarized the empirically based rules for complex halide formation. From these it is derived that isobonding mixed-dimer reactions such as $(AX)_2+(BX)_2=2ABX_2$, where A and B are different alkali metals and X is a halogen, should occur with very little enthalpy and entropy changes. However, in practice, the enthalpy changes have ranged from about 0 to approximately −340 kJ/2 mol-complex due to the excess stability associated with the mixed dimer formation.[1]

The following reaction:

$$Na_2Cl_2(g)+K_2Cl_2(g)=2NaKCl_2(g)\,, \qquad (1)$$

was chosen in this study to examine the energetic situation in the mixed dimer formation reaction because of its simplicity in chemical bondings.

Experimental

A series of mass-spectrometric experiments was carried out on the solid solutions of NaCl and KCl with different compositions ranging from 10 to 90 mol% NaCl. A method of detection and identification of species was described in detail elsewhere.[2,3] Approximately 50 mg of the mixed salt was placed in a Knudsen-cell made of pure alumina.

The ions of Na_2Cl^+, K_2Cl^+, and $NaKCl^+$ were determined as the parent ions produced from Na_2Cl_2, K_2Cl_2, and $NaKCl_2$ molecular vapors, respectively.[2] The equilibrium partial pressure of i-th vapor, p_i, is given by $p_i=C_iTI(i^+)$ where $I(i^+)$ is the parent ion intensity, T is the absolute temperature and C_i is a constant involving the ionization cross section(σ_i), the isotopic ratio(γ_i), the collection efficiency (S_i) in the first step of an electron multiplier, and the potential difference (ΔE_i) between an ionizing- and appearance-potentials of i-th ion, and an apparatus constant(k): $C_i=k(\sigma_i\gamma_iS_i\Delta E_i)^{-1}$ for the i-th ion.

The equilibrium constant, K_p, for Eq. 1 can be written as:

$$K_p=\frac{[p(NaKCl_2)]^2}{p(Na_2Cl_2)p(K_2Cl_2)}=\frac{C[I(NaKCl^+)]^2}{I(Na_2Cl^+)I(K_2Cl^+)}, \qquad (2)$$

where,

$$C=\frac{[C(NaKCl_2)]^2}{C(Na_2Cl_2)C(K_2Cl_2)}$$

$$=\frac{\sigma(Na_2Cl_2)\sigma(K_2Cl_2)}{[\sigma(NaKCl_2)]^2}\times\frac{\gamma(^{23}Na_2{}^{35}Cl_2)\gamma(^{39}K_2{}^{35}Cl_2)}{[\gamma(^{23}Na^{39}K^{35}Cl_2)]^2}\times\frac{S(Na_2Cl^+)S(K_2Cl^+)}{[S(NaKCl^+)]^2}\times\frac{\Delta E(Na_2Cl^+)\Delta E(K_2Cl^+)}{[\Delta E(NaKCl^+)]^2}\,. \qquad (3)$$

Assuming that S-values are almost identical for Na_2Cl^+, K_2Cl^+, and $NaKCl^+$ ions and using our previous data[2] for σ and ΔE, $C=1.06$ was obtained.

Vapor equilibrium in the Knudsen cell was ensured by our previous mass-spectrometric measurements of activities of the NaCl–KCl system[2,4] carried out by taking advantage of the ion intensity of Na_2Cl^+, K_2Cl^+, and $NaKCl^+$ which came from Na_2Cl_2, K_2Cl_2, and $NaKCl_2$ molecules: the activity coefficient determined from the ion current ratios of $I(Na_2Cl^+)/I(K_2Cl^+)$ was in close agreement with that obtained from the ratios of $I(NaKCl^+)/I(K_2Cl^+)$. This shows attainment of equilibria between gas phases in Eq. 1.

Results and Discussion

Figure 1 shows the temperature dependence of K_p calculated from Eq. 2 using the mass-spectrometrically observed data. Some K_p data reported by Milne and Klein[5] are also presented in the figure. The least squares treatment gave:

$$\log K_p=0.5945(\pm0.936)+\frac{175.1(\pm101.7)}{T}\,. \qquad (4)$$

Therefore, the Gibbs energy for the mixed dimer reaction (Eq. 1) is calculated as follows:

$$\Delta G_r^\circ=-RT\ln K_p=-3352(\pm1947)-11.38(\pm1.79)T \quad [\text{J/2 mol-complex}]\,. \qquad (5)$$

Thus, from the relation of $\Delta G_r^\circ=\Delta H_r^\circ-T\Delta S_r^\circ$, the

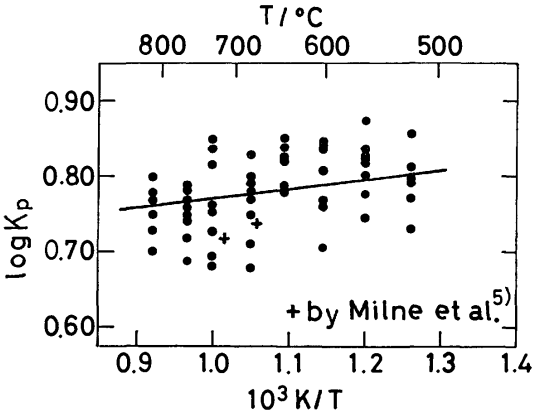

Fig. 1. Temperature-dependence of equilibrium constant, K_p, obtained mass-spectrometrically for the reaction: $Na_2Cl_2(g)+K_2Cl_2(g)=2NaKCl_2(g)$.

enthalpy and entropy changes at the central temperature in the experimental temperature range were:

$$\Delta H^{\circ}_{r,940\,K} = -1.67\pm0.97 \ [kJ\ mol^{-1}], \quad (6)$$

$$\Delta S^{\circ}_{r,940\,K} = 5.69\pm0.90 \ [J\ K^{-1}\ mol^{-1}]. \quad (7)$$

The formation energy of $NaKCl_2(g)$, ΔU, in the following gaseous reaction:

$$\frac{1}{2}\begin{bmatrix} Na^+\text{-}Cl^- \\ | \quad | \\ Cl^-\text{-}Na^+ \end{bmatrix} + \frac{1}{2}\begin{bmatrix} K^+\text{-}Cl^- \\ | \quad | \\ Cl^-\text{-}K^+ \end{bmatrix} = \begin{bmatrix} Na^+\text{-}Cl^- \\ | \quad | \\ Cl^-\text{-}K^+ \end{bmatrix} + \Delta U, \quad (8)$$

was calculated from the equation:

$$\Delta U = U_{NaKCl_2} - \frac{1}{2}(U_{Na_2Cl_2} + U_{K_2Cl_2}), \quad (9)$$

where U denotes the potential energy of each ionic dimer compared to the completely separated ions. The values of $U_{Na_2Cl_2}$ and $U_{K_2Cl_2}$ were given to be -1266 and -1119 kJ mol^{-1} respectively by Milne and Cubicciotti.[6] They also provided the following equation for U_{NaKCl_2}:

$$U_{NaKCl_2} = \left(-\frac{2}{a}-\frac{2}{b}+\frac{1}{c}+\frac{1}{d}+\frac{153.3}{a^{8.6}}+\frac{401.3}{b^{8.6}} + \frac{22.86}{c^{8.6}}+\frac{439.4}{d^{8.6}}\right)\times 1389 \ [kJ\ mol^{-1}], \quad (10)$$

by assuming pure ionic-bonding in all dimers and a diamond-shaped structure for $NaKCl_2$, as shown in Fig. 2, and by employing a model suggested by Pauling.[7] Numerical analyses for Eq. 10 gave a set of the geometrical parameters: $a=2.49$, $b=2.85$, $c=3.70$, and $d=3.83$ Å which resulted in the minimum energy of the $NaKCl_2$ mixed dimer; $U^{MIN}_{NaKCl_2}=-1195$ kJ mol^{-1}. Consequently, we obtained $\Delta U \simeq -2.5$ kJ mol^{-1} from Eq. 9.

On the other hand, a combination of Eq. 6 with the heats of formation[8] for Na^+, K^+, Cl^+, Na_2Cl_2, and K_2Cl_2, leads to $\Delta H^{\circ}_{f,940K}=-1248$ kJ mol^{-1} for the heat of formation of the mixed dimer $NaKCl_2$ from separation Na^+, K^+, and Cl^- ions. If the heat capacities of the dimer molecules are the same, the values of ΔU and $U^{MIN}_{NaKCl_2}$ may be compared directly with those of the $\Delta H^{\circ}_{r,940K}$ and $\Delta H^{\circ}_{f,940K}$ mentioned above. The direct comparison gave good agreement which strongly suggests that each bond in the dimer molecules of Na_2Cl_2, K_2Cl_2, and $NaKCl_2$ is almost ionic and that the mixing of Na^+, and K^+ ions in the mixed dimer $NaKCl_2$ contributes to a lesser extent to the enhancement of bond strength.

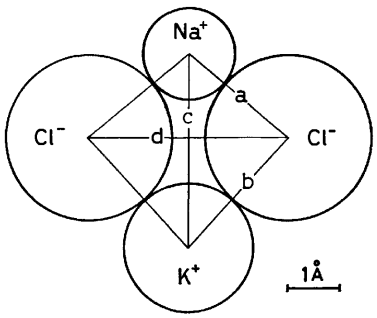

Fig. 2. Schematic representation for a structure of $NaKCl_2$ molecule.

Table 1. Calculated entropy values for gaseous dimers, Na_2Cl_2, K_2Cl_2, and $NaKCl_2$, at 940 K

Dimers	S_{trans} / kJ K mol^{-1}	S_{rot} / kJ K mol^{-1}	S_{vib} / kJ K mol^{-1}
Na_2Cl_2	191.989	119.997	102.462
K_2Cl_2	195.025	128.440	126.194
$NaKCl_2$	193	128	116.7[a]

a) Estimated from the equation: $S_{vib,NaKCl_2}=\Delta S^{\circ}_{r,940\,K}+(S_{total,Na_2Cl_2}+S_{total,K_2Cl_2})/(S_{trans,NaKCl_2}+S_{rot,NaKCl_2})$.

Table 1 shows the translational, ratational, and vibrational entropies for the $NaKCl_2$ molecule at 940 K calculated on the basis of the statistical thermodynamics[9] using the molecular weight, the vapor pressure, the product of the moment of inertia ($I_AI_BI_C=1.224\times10^{-38}$ kg^3 m^6) and the $\Delta S^{\circ}_{r,940K}$, along with those for Na_2Cl_2 and K_2Cl_2 dimers calculated using the required data from the JANAF Tables.[8] It can be seen from the table that the entropy change in the isobonding mixed-dimer reaction, Eq. 1, is very small and that this small entropy change is brought about mainly by the change in the rotational entropy.

Thanks are due to Mr. Kitoshi Ozawa of Tokyo National Technical College for performing the calculations of ionic potentials.

References

1) J. W. Hastie, "High Temperature Vapors, Science and Technology," Academic Press, New York and London (1975), p. 133.
2) M. Itoh, T. Sasamoto, and T. Sata, *Shitsuryo Bunseki (Mass Spectroscopy, Japan)*, **29**, 67 (1981).
3) T. Sasamoto, H. Hara, and T. Sata, *Bull. Chem. Soc. Jpn.*, **54**, 3327 (1981).
4) M. Itoh, T. Sasamoto, and T. Sata, *Bull. Chem. Soc. Jpn.*, **54**, 3391 (1981).
5) T. A. Milne and H. M. Klein, *J. Chem. Phys.*, **33**, 1628 (1960).
6) T. A. Milne and D. Cubicciotti, *J. Chem. Phys.*, **29**, 846 (1958).
7) L. Pauling, *Proc. Natl. Acad. Sci. (India)*, **25**, Sect. A, Part I (1956).
8) "JANAF Thermochemical Tables," 2nd ed, NSRDS-NBS 37, U. S. Govt. Printing Office, Washington, D.C. (1971).
9) For example, J. H. Knox, "Molecular Thermodynamics," John Wiley & Sons, New York (1971).

Kinetics of Structural Rearrangement Accompanying the Substitution Reaction on Complex [Co(terpy)(hmpa)$_3$]$^{2+}$(terpy=2,2′ : 6′,2″-Terpyridine) in Hexamethylphosphoric Triamide

Yuriko Abe* and Goro Wada

Department of Chemistry, Nara Women's University, Nara 630

(Received February 1, 1982)

Synopsis. The reaction of structural rearrangement accompanying the substitution of hexamethylphosphoric triamide (HMPA) for 2,2′:6′,2″-terpyridine (terpy) from octahedral [Co(terpy)(hmpa)$_3$]$^{2+}$ to tetrahedral [Co(hmpa)$_4$]$^{2+}$ proceeds through a five-coordinated intermediate in HMPA. The following values for the first-order rate constant at 25 °C, ΔH_d^*, and ΔS_d^* were obtained: $k_d=3.55\times10^{-5}$ s^{-1}, $\Delta H_d^*=105.4$ kJ mol^{-1}, and $\Delta S_d^*=+15.9$ J K^{-1} mol^{-1}.

There are few kinetic data for reactions involving structural interconversions.[1-5] This is probably due to the high reaction rates except for the cases which can be measured by tempertaure jump or NMR, and to the severe thermodynamic requirements of their investigation.

In this report, we studied spectrophotometrically the kinetics of structural rearrangement reactions accompanying HMPA substitution for terpy from octahedral [Co(terpy)(hmpa)$_3$]$^{2+}$ to tetrahedral [Co(hmpa)$_4$]$^{2+}$ in HMPA, for the purpose of clarifying the rearrangement mechanism and the effect of the bulkiness of HMPA on its mechanism. The reaction rate was successfully measured by a conventional technique, since terdentate ligands generally undergo ligand exchange more slowly than unidentate ones.

Experimental

Materials. [Co(hmpa)$_4$](ClO$_4$)$_2$ and [Cu(hmpa)$_4$](ClO$_4$)$_2$ were prepared by methods described in the literature.[6,7] Terpy was used without further purification. The purification of HMPA was carried out as previously described.[8,9]

Rate Measurements. The complex [Co(terpy)(hmpa)$_3$]$^{2+}$ was prepared from appropriate amounts of [Co(hmpa)$_4$]$^{2+}$ and terpy in HMPA in advance and the reaction was initiated by mixing a solution of [Co(terpy)(hmpa)$_3$]$^{2+}$ with a solution of [[Cu(hmpa)$_4$]$^{2+}$] in a large excess over [[Co(terpy)(hmpa)$_3$]$^{2+}$] in HMPA. Cu(II) was used in order to remove the free terpy by its rapid complexation.[10] The reaction rate was followed by observing the increase in the absorbance at 580 nm by use of a Shimadzu Spectrophotometer Model UV-200S with a thermostated cell compartment. The measured absorbances were not corrected because the absorbance due to Cu(II) was approximately constant during the course of the reaction. The ionic strength was adjusted at 0.1 mol dm^{-3} with sodium perchlorate.

Results and Discussion

Rate Constants and Activation Parameters. The reaction obeys the following rate equation (1) under the conditions of [Cu(II)] of a large excess over [Co(II)]$=8\times10^{-4}$ mol dm^{-3},

$$\ln[(A_\infty-A_t)/(A_\infty-A_o)] = -k_{obsd}t, \quad (1)$$

where A_o, A_t, and A_∞ are the absorbances at times 0, t, and infinite at 580 nm, respectively. As shown in Fig. 1, the values of k_{obsd} were found to be linearly dependent upon the Cu(II) concentration. In the similar reactions (such as those of M(II)-terpy complexes (M(II)=Mn(II), Fe(II), Co(II), Ni(II), Zn(II), or Cd(II)) in H_2O,[10] and of Mn(II)-terpy in methanol,[11]) no dependence of the rate constant upon either [Hg(II)] or [Cu(II)] has been observed, where Hg(II) or Cu(II) only acts to scavenge the free terpy. Therefore, this result in HMPA is particularly interesting. The correlation of k_{obsd} with [Cu(II)] in HMPA can be empirically expressed by the following equation;

$$k_{obsd} = k_d + k_a[Cu(II)], \quad (2)$$

in which k_d is a first-order rate constant with respect to [Co(II)] and k_a is a second-order rate constant with respect to [Co(II)] and [Cu(II)]. By plotting $\ln k_d$ or $\ln k_a$ *vs.* $1/T$, ΔH^* and ΔS^* were obtained as follows: $\Delta H_d^*=105.4$ kJ mol^{-1} and $\Delta S_d^*=+15.9$ J K^{-1} mol^{-1} for the k_d path, and $\Delta H_a^*=72.3$ kJ mol^{-1} and $\Delta S_a^*=-54.0$ J K^{-1} mol^{-1} for the k_a path, respectively.

Reaction Mechanism. The reaction with the first-order rate constant k_d corresponds to the following equation:

$$\underset{\text{octahedral}}{[Co(terpy)(hmpa)_3]^{2+}} + hmpa \longrightarrow \underset{\text{tetrahedral}}{[Co(hmpa)_4]^{2+}} + terpy. \quad (3)$$

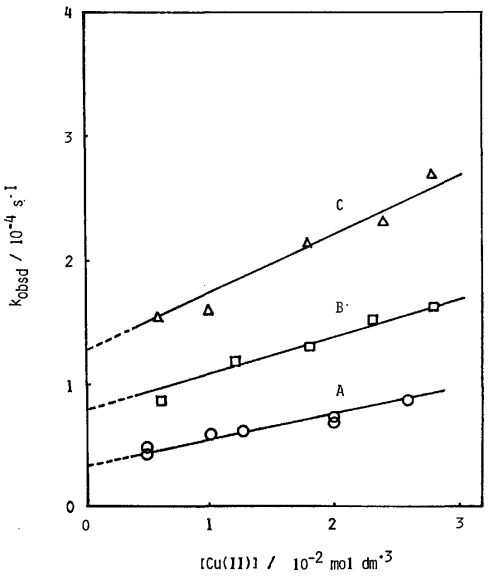

Fig. 1. The dependence of k_{obsd} on the Cu(II) concentrations at 25 °C (A), 30 °C (B), and 35 °C (C).

Two possible reaction mechanisms may be considered for the substitution for terpy on $[Co(terpy)(hmpa)_3]^{2+}$. One is a dissociative mechanism, in which one of the three cobalt-nitrogen bonds is first broken and the reaction goes through a five-coordinated intermediate. The other is an associative mechanism, in which Co(II) first reacts with an HMPA molecule, resulting in a seven-coordinated intermediate or an outer-sphere associated complex. Since the coordination number of Co(II) is reduced from six to four, the former mechanism seems to be more probable. The fact that ΔS_d^* value is positive supports the dissociative mechanism which is represented as follows,

$$[(hmpa)_3Co\text{–}N\langle_{N}^{N}\rangle]^{2+} \underset{k_{-1}}{\overset{k_1}{\rightleftharpoons}} [(hmpa)_3Co\text{–}N\langle_{N}^{N}\rangle]^{2+} \xrightarrow{k_2} . \quad (4)$$

Thus, k_d can be expressed as $k_1k_2/(k_{-1}+k_2)$.

The [Cu(II)] dependence in HMPA is similar to the case of the [Hg(II)] dependence of the reactions of Ni(II)-bidentate substituted pyridines in dimethyl sulfoxide.[12] Buck and Moore suggested that the reaction of the [Hg(II)] dependence proceeds by the attack of Hg(II) on a nitrogen atom whose bond with Ni(II) has been ruptured.[12] Therefore, it seems that the [Cu(II)] dependence in HMPA is also due to the reaction between the five-coordinated intermediate of Co(II) and Cu(II).

Comparison between Reactions in HMPA and in H_2O. When the equilibrium constant between the tetrahedral⇄octahedral configurations is expressed by $K_1=[[Co(terpy)(hmpa)_3]^{2+}]/[[Co(hmpa)_4]^{2+}][terpy]$, the reaction with the rate constant k_d corresponds to the backward reaction of the equilibrium. In the present study, the values of k_d obtained and the activation parameters in HMPA are as follows: $k_d=3.55\times10^{-5}$ s^{-1} at 25 °C, $\Delta H_d^*=105.4$ kJ mol^{-1}, and $\Delta S_d^*=+15.9$ J K^{-1} mol^{-1}, and the value of K_1 has been obtained as $K_1=7.4\times10^4$ dm^3 mol^{-1}.[9] In H_2O, where $[Co(H_2O)_6]^{2+}$ and $[Co(terpy)(H_2O)_3]^{2+}$ are both octahedral, those values are $k_d=1\times10^{-4}$ s^{-1} at 25 °C,[13] $\Delta H_d^*=82.0$ kJ mol^{-1},[13] $\Delta S_d^*=-1.7$ J K^{-1} mol^{-1},[13] and $K_1=2.5\times10^8$ dm^3 mol^{-1}.[14] Although the value of K_1 in HMPA differs considerably from that in H_2O, the values of k_d and the activation parameters in HMPA resemble those in H_2O.

Since the chelation by terpy in HMPA liberates only one molecule of HMPA in contrast with the liberation of as many as three water molecules in the case of water, the entropy effect would lead to the smaller K_1 in HMPA than in H_2O. Moreover, the coordinating HMPA molecules in $[Co(terpy)(hmpa)_3]^{2+}$ are closely packed. Accordingly, the complex is so unstable, due to its molecular bulkiness, that the equilibrium would be also unfavored, resulting in the smaller K_1 in HMPA than in H_2O. Although the reaction in HMPA is accompanied by a structural rearrangement, the similarity of k_d and the activation parameters in both media support the idea that the reaction proceeds by the same dissociative mechanism, independently of whether the solvent is HMPA or H_2O.

References

1) R. D. Farina and J. H. Swinehart, *J. Am. Chem. Soc.*, **91**, 568 (1969).
2) K. J. Ivin, J. Jamison, and J. J. McGarvey, *J. Am. Chem. Soc.*, **94**, 1763 (1972).
3) M. Cusumano, *J. Chem. Soc., Dalton Trans.*, **1976**, 2133.
4) J. D. Vitiello and E. J. Billo, *Inorg. Chem.*, **19**, 3477 (1980).
5) J. H. Coates, D. A. Hadi, S. F. Lincoln, H. W. Dodgen, and J. P. Hunt, *Inorg. Chem.*, **20**, 707 (1981).
6) J. T. Donoghue and R. S. Drago, *Inorg. Chem.*, **1**, 866 (1962).
7) J. T. Donoghue and R. S. Drago, *Inorg. Chem.*, **2**, 1158 (1963).
8) Y. Abe and G. Wada, *Bull. Chem. Soc. Jpn.*, **53**, 3547 (1980).
9) Y. Abe and G. Wada, *Bull. Chem. Soc. Jpn.*, **54**, 3334 (1981).
10) R. H. Holyer, C. D. Hubbard, S. F. A. Kettle, and R. G. Wilkins, *Inorg. Chem.*, **5**, 622 (1966).
11) D. J. Benton and P. Moore, *J. Chem. Soc., Dalton Trans.*, **1973**, 399.
12) D. M. W. Buck and P. Moore, *J. Chem. Soc., Dalton Trans.*, **1975**, 409.
13) T. Hogg and R. G. Wilkins, *J. Chem. Soc.*, **1962**, 341.
14) L. G. Sillén and A. E. Martell, "Stability Constants Supplements No. 1 Special Publication 25," ed by the Chemical Society, Alden Press, Oxford (1971).

Reference Materials for the Pyrolysis Gas-chromatographic Determination of Ammonia, Nitrogen, Nitrogen Monoxide, Carbon Monoxide, and Carbon Dioxide

Kikuo Miyokawa,* Naoki Abe, and Isao Masuda

Department of Chemistry, Faculty of Science, Fukuoka University, Nanakuma, Jonan-ku, Fukuoka 814-01

(Received March 23, 1982)

Synopsis. Four compounds are proposed as the reference materials to calibrate the pyrolysis gas chromatograph in the determination of inorganic gases: $[Co(NH_3)_5Cl]Cl_2$ for NH_3, $[Co(NH_3)_5NO_2]Cl_2$ for N_2, $[Co(NH_3)_5NO]Cl_2$ for NO, and PbC_2O_4 for both CO and CO_2. On pyrolyses, the gas evolution of these compounds were stoichiometric, and the peak area corresponded fairly well to the weight of the compound. Under the condition employed, 7.3—138 μmol of NH_3, 2.2—67 μmol of N_2, 2.0—61 μmol of NO, 0.84—26 μmol of CO, and 2.5—76 μmol of CO_2 were analyzed by using 0.5—15 mg of the compounds.

Pyrolysis gas chromatography (PGC) has been developed as a technique for the structural characterization of organic polymers.[1] In our previous papers,[2] the PGC technique was successfully employed for the quantitative determination of the gaseous products, N_2 and N_2O, evolved upon the pyrolyses of the series of Co(III)-ammine and Mo- or W-nitrosyl complexes. In practical use, however, it was not quite advantageous to calibrate the PGC instrument with standard gas, since, by the method using a gas syringe, hardly any standard gas was injected exactly into a furnace heated at a high temperature wherein a sample was pyrolyzed. Therefore, it seemed desirable to calibrate the instrument under conditions identical to those for the pyrolysis of sample. The PGC technique can be expected to be more useful if the PGC instrument can be easily calibrated with such reference compounds as evolve the desired gas stoichiometrically upon the pyrolysis.

In the present article, four inorganic compounds have been recommended as useful references for the calibration of the PGC instrument for the determination of NH_3, N_2, NO, CO, and CO_2.

Experimental

Materials. The compounds, $[Co(NH_3)_5Cl]Cl_2$,[3] $[Co(NH_3)_5NO_2]Cl_2$,[4] $[Co(NH_3)_5NO]Cl_2$,[5] and PbC_2O_4,[6] were prepared by the published manner and were purified by repeated recrystallizations.

Measurements. The PGC measurements were carried out by the use of a YANACO G 80 TCD gas-chromatographic instrument equipped with a YANACO GP 1018 pyrolysis pippeter, following the manual. An 0.5—15.0 mg aliquot of the compounds was transferred into a platinum crucible (16 mm^3), and then the crucible was inserted into the pyrolysis pipetter, whose furnace had been kept at the desired temperature. The compound was pyrolyzed instantly in helium gas, and the gaseous products were subsequently swept by the helium-gas carrier into the GC separation column. The peak area was recorded on an integrator. The PGC conditions are tabulated in Table 1.

Results and Discussion

The four compounds considered here can be easily obtained and stored in a pure and stable form. The purities of the cobalt complexes were examined by means of cobalt, ammonia, and chloride analyses, and that of lead oxalate, by lead analysis. The thermal-decomposition processes of these compounds have already been established to follow Eqs. 1—4;[2,6,7] they have also been confirmed, as is shown in Table 2.

$$6[Co(NH_3)_5Cl]Cl_2 \longrightarrow 22NH_3 + N_2 + 6NH_4Cl + 6CoCl_2$$

$$6[Co(NH_3)_5NO_2]Cl_2 \longrightarrow 7N_2 + 22NH_3 + 12H_2O + 6CoCl_2$$

$$[Co(NH_3)_5NO]Cl_2 \longrightarrow NO + 5NH_3 + CoCl_2$$

$$2PbC_2O_4 \longrightarrow CO + 3CO_2 + Pb_2O$$

The relation between the amount of gas, μmol, calculated from Eqs. 1—4 and the peak-area counts, recorded on the integrator is shown in Fig. 1. The correlation curves in Fig. 1 indicate that the amount of gas detected corresponded linearly to the weight of the compound provided for the pyrolysis. In the pyrolysis temperature range given in Table 1, the cor-

Table 1. PGC conditions

Gas	Reference material	Temperature range for pyrolysis/°C	Column Packing	Column length/m	Column temp/°C	TCD temp/°C	Retention[e] time/s
NH_3	$[Co(NH_3)_5Cl]Cl_2$	320—500	Porapak N[a]	1.5[c]	160	170	58—67
N_2	$[Co(NH_3)_5NO_2]Cl_2$	410—500	Molecular[b] Sieve 5A	3.0[d]	60	110	22—27
NO	$[Co(NH_3)_5NO]Cl_2$	180—500	Molecular[b] Sieve 5A	1.5[c]	80	110	63—70
CO	PbC_2O_4	410—500	Silica gel[b]	3.0	80	110	38—41
CO_2	PbC_2O_4	410—500	Silica gel[b]	3.0	80	110	69—73

Column: stainless steel; 3 mm i.d. a) 50—80 mesh. b) 60—80 mesh. c) In order to reduce lingering tailing, a short column was preferred. d) In order to separate N_2 completely from adsorbed NH_3 a long column was preferred. e) The flow rate of the He-gas carrier was 25 cm^3/min.

Table 2. Analytical confirmation of decomposition products

Reference material	$CoCl_2$		NH_4Cl	NH_3[d]	Pb[b]	CO_2[e]
	Co[b]	Cl[c]	Cl[c]			
$[Co(NH_3)_5Cl]Cl_2$	23.57 (23.52)	28.73 (28.35)	13.93 (14.18)	24.96 (24.89)		
$[Co(NH_3)_5NO_2]Cl_2$	22.18 (22.58)	26.24 (27.21)		23.73 (23.89)		
$[Co(NH_3)_5NO]Cl_2$	24.25 (24.05)	28.79 (28.99)		23.54 (24.71)		
PbC_2O_4					69.87 (70.19)	22.30 (22.36)

a) Calculated values are given in parentheses. b) Determined by EDTA titration. c) Determined by the Volhard method. d) Determined by trapping the gas into a standard 0.05 M H_2SO_4 solution and then titrating the excess acid with a standard 0.1 M NaOH solution. e) Determined by trapping the gas into a standard 0.1 M NaOH solution and then titrating the excess alkali with a standard 0.05 M H_2SO_4 solution (1M=1 mol/dm³).

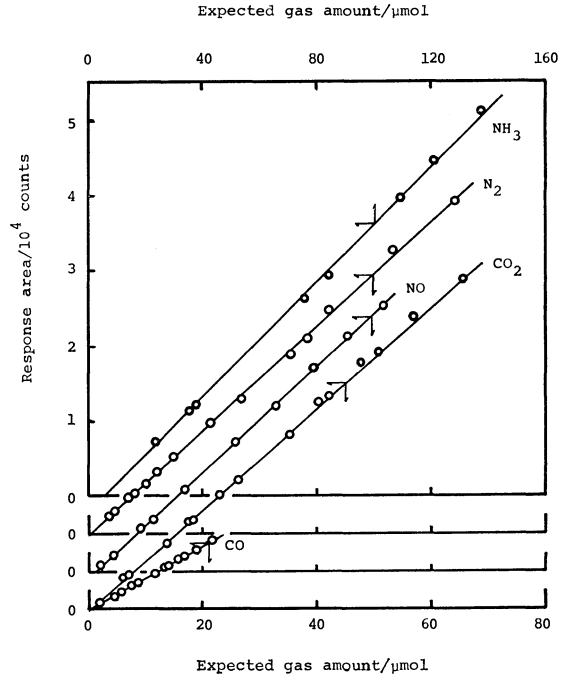

Fig. 1. Calibration curves.

relations fell on a straight line. Under the conditions employed, the weights of the compound provided for the pyrolysis were restricted within the range from 0.5 to 15 mg. Hence, the amount of gas detected corresponds to 7.3—138 μmol for ammonia, 2.2—67 μmol for nitrogen, 2.0—61 μmol for nitrogen monoxide, 0.84—26 μmol for carbon monoxide, and 2.5—76 μmol for carbon dioxide. In the correlation curves for NH_3, N_2, NO, CO, and CO_2 in Fig. 1, extraplotation gives a negative vertical intercept; this may be caused by the chromatographic tailing of these gases, which has often been observed in their GC peaks.[8] The calibration constants and precision are shown in Table 3.

Table 3. Calibration constants and precision; $F=aA-b$

Gas	a	b
NH_3	383 (±3)	2386 (±340)
N_2	701 (±6)	383 (±194)
NO	706 (±7)	1121 (±186)
CO	426 (±2)	160 (±30)
CO_2	676 (±5)	395 (±210)

F=Response area/counts. A=Expected gas amount/μmol.

References

1) T. Takeuchi and S. Tsuge, "Kobunshi No Netsubunkai-gas Chromatography," Kagaku-Dojin, Kyoto (1977); S. Tsuge, *Trends Anal. Chem.*, **1**, 87 (1981).
2) K. Miyokawa, H. Masuda, and I. Masuda, *Bull. Chem. Soc. Jpn.*, **53**, 3573 (1980); K. Miyokawa, N. Abe, and I. Masuda, *J. Inorg. Nucl. Chem.*, **43**, 2791 (1981).
3) S. Y. Tyree, *Inorg. Synth.*, **9**, 160 (1967).
4) S. M. Jorgensen, *Z. Anorg. Chem.*, **17**, 463 (1898).
5) R. W. Asmussen, O. Bostrup, and J. P. Jensen, *Acta Chem. Scand.*, **12**, 24 (1959).
6) L. L. Bircumshow and I. Harris, *J. Chem. Soc.*, **1939**, 1637.
7) W. W. Wendlandt and J. P. Smith, *J. Inorg. Nucl. Chem.*, **25**, 843 (1963).
8) J. I. Landau and E. E. Peterson, *J. Chromatogr. Sci.*, **12**, 362 (1974).

Determination of Titanium(IV) Using *o*-Hydroxyhydroquinonephthalein and Tween 20

Itsuo Mori,* Yoshikazu Fujita, and Kimiko Sakaguchi
Osaka College of Pharmacy, 2-10-65, Kawai, Matsubara, Osaka 580
(Received May 13, 1982)

Synopsis. A new, simple and sensitive spectrophotometric method for the determination of titanium(IV) was studied using *o*-hydroxyhydroquinonephthalein(Qn.Ph.) and Tween 20. The analytical species of interest have an absorption maximum at 595 nm and obeyed Beer's law over the range 0.3—2.4 μg of titanium(IV) in final 10 ml solution. This method was highly sensitive in comparison with Sandell sensitivity of 0.00025 μg/cm² for titanium(IV) at an absorbance of 0.001 at 595 nm against water and the molecular extinction coefficient of the Qn.Ph.–titanium (IV) complex was 1.91×10^5 l mol^{-1} cm^{-1}.

Various spectrophotometric methods for titanium-(IV), such as tiron,[1] diantipyrylmethane(DAM),[2,3] *N*-benzoy-*N*-phenylhydroxylamine(NBNPA),[4] and trioctylphosphine oxide[5] methods, have been reported. However, most of these methods are not selective, simple, rapid and sensitive.

On the other hand, we have already reported the simple and sensitive spectrophotometries for the determination of various metal ions using *o*-hydroxyhydroquinonephthalein(Qn.Ph.).[6-8]

In this paper, fundamental conditions for the color reaction between Qn.Ph. and titanium(IV) in the presence of various surfactants, and spectrophotometry of titanium(IV) were studied.

Experimental

Apparatus. The absorbance was measured with a Shimadzu Model 202 and 240 recording spectrophotometers using matched 1.0-cm quartz cells. For pH measurements a Toa Dempa Model HM-5 pH meter was used.

Reagents. A 1.0×10^{-3} M (1 M=1 mol dm^{-3}) Qn.Ph. methanol solution was prepared according to the previous report.[6] A stock solution of titanium(IV) was prepared by dissolving of 167 mg titanium dioxide in 10 ml of 97% sulfuric acid, and diluted to 100 ml with water. The working solution was made by suitable dilution of this stock solution as required. A 5% Tween 20 soultion was prepared by dissolving the respective compound in water. All other reagents used were of analytical grade.

Standard Procedure. A solution containing 0.3—2.4 μg of titanium(IV) was placed in a 10-ml measuring flask, 1.0 ml of 5% Tween 20 solution, and 0.5 ml of 1.0×10^{-3} M Qn.Ph. solution were added. The pH of the solution was adjusted to pH 4.7 with 0.2 M sodium acetate–acetic acid buffer (Walpole buffer) solution.

Then the solution was diluted to 10 ml with water, mixed well, kept at 60 °C for 60 min, and cooled for 5 min in water. The absorbance of the Qn.Ph.–titanium(IV) solution was measured at 595 nm against water. The concentration of titanium(IV) was determined using the calibration graph.

† Application of Xanthene Derivatives for Analytical Chemistry. Part XXIV. The previous paper is: I. Mori, Y. Fujita, K. Sakaguchi, and S, Kitano, *Bunseki Kagaku*, **31**, 475 (1982).

Results and Discussion

Absorption Spectra. Figure 1 shows the absorption spectra of the Qn.Ph.–titanium(IV) complex solution and Qn.Ph. solution in the presence of Tween 20 or hexadecyltrimethylammonium chloride (HTAC) as dispersion agent, respectively. It is evident that the Qn.Ph.–titanium(IV) complex exhibits a considerable bathochromic shift in the presence of nonionic surfactant such as Tween 20, and that the complex shows maximum absorption at 595 nm against water.

Effect of pH. The aqueous solution was adjusted to various pH values with Walpole buffer solution. The maximum and constant absorbance was obtained in the pH range from 4.4 to 4.9. Subsequent measurements were carried out at pH 4.7.

Effect of Various Dispersion Agents and Stability of the Complex. The color reaction rate between Qn.Ph. and titanium(IV) was slow in the absence of surfactants. On the other hand, in the presence of nonionic surfactants such as Tween 20 this color reaction was completed in about 45 min by heating at 60 °C, and the reaction was stable with highest sensitivity. In the presence of nonionic surfactants such as poly(vinyl alcohol), poly(*N*-vinylpyrrolidone), Triton X-100 or

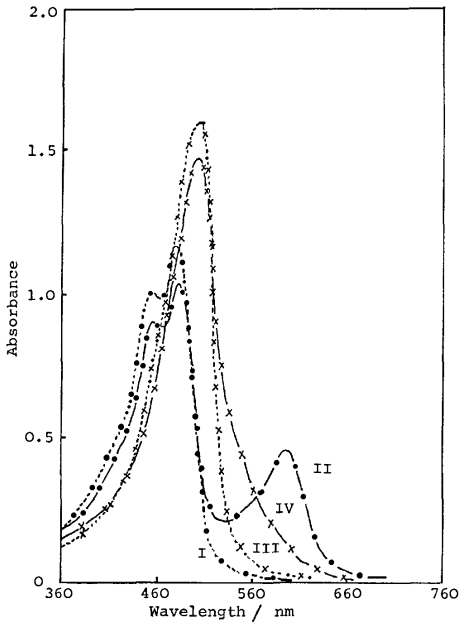

Fig. 1. Absorption spectra of Qn.Ph. solution and Qn.Ph.–Ti(IV) complex solution at pH 4.7.
Ti(IV): 2.5×10^{-6} M, Qn.Ph.: 5.0×10^{-5} M, Tween 20: 1.0 ml of 5% Tween 20 solution, HTAC: 4.0×10^{-3} M; reference: water, curve I: Qn.Ph.–Tween 20, curve II: Qn.Ph.–Ti(IV)–Tween 20, curve III: Qn.Ph.–HTAC, curve IV: Qn.Ph.–Ti(IV)–HTAC.

Table 1. Effect of foreign ions

Foreign ions	Added as	Added (μg)	Absorbance at 595 nm
—	—	—	0.478
Fe(III)	Sulfate	0.3	0.478
Al(III)	Nitrate	0.3	0.478
Th(IV)	Nitrate	0.3	0.470
Sn(IV)	Sulfate	0.2	0.464
Zr(IV)	Nitrate	0.6	0.442
Co(II)	Nitrate	15.9	0.470
Zn(II)	Nitrate	1.6	0.470
Pb(II)	Nitrate	0.3	0.442
Ni(II)	Nitrate	1.5	0.470
MoO_4^{2-}	Sodium	0.2	0.470
VO_3^-	Ammonium	0.1	0.460
F^-	Sodium	4.7	0.486
CN^-	Potassium	26.1	0.456
$S_2O_3^{2-}$	Sodium	1121.2	0.478
SCN^-	Ammonium	580.8	0.478
$C_2O_4^{2-}$	Sodium	88.0	0.470
$C_2H_2(OH)_2(COO^-)_2$	Acid	2961.4	0.478
$C_3H_4(OH)(COO^-)_2$	Acid	1891.0	0.478
Triethanolamine	—	1491.9	0.470

Ti(IV) taken: 1.2 μg; Qn.Ph.: 5.0×10^{-5} M; Tween 20: 1.0 ml of 5.0% Tween 20 solution; pH: 4.7; Reference: Water.

gelatin this color reaction increased rapidly and then decreased. The maximum and constant absorbance could be obtained over the range of 0.75 to 3.0 ml of 5% Tween 20 solution. The absorbance of the Qn. Ph.–titanium(IV) complex solution was constant and stable at least for 90 min at room temperature.

Calibration Curve. The calibration curve for the determination of titanium(IV) was prepared according to the standard procedure. Beer's law was hold in the concentration of 0.3—2.4 μg of titanium(IV) in final 10 ml. The molar absorptivity of the complex was estimated to be 1.91×10^5 l mol^{-1} cm^{-1} at 595 nm. The Sandell sensitivity was 0.00025 μg/cm^2 titanium(IV).

The precision was estimated for 1.8 μg/10 ml of titanium(IV), and the relative standard deviation was 0.46% for 8 determinations.

Effect of Foreign Ions. Interferences by various foreign ions for the determination of titanium(IV) were examined. The tolerance limit was taken as the amounts required to cause ±2% error in the absorbance. Iron(III), copper(II), aluminum(III), thorium-(IV), molybdenum(VI), vanadium(V), tin(IV), lead-(II), cyanide, sulfide, *etc.* caused a decrease in the absorbance at 595 nm. The interference of copper(II) could be overcome by addition of sodium thiosulfate solution, and that of iron(III) by addition of L-ascorbic acid solution as masking agents, respectively.

Composition of the Complex. The stoichiometry of the Qn.Ph.–titanium(IV) complex was evaluted by the continuous variation and the molar ratio methods. The results were estimated to be a defined 1:2 ratio

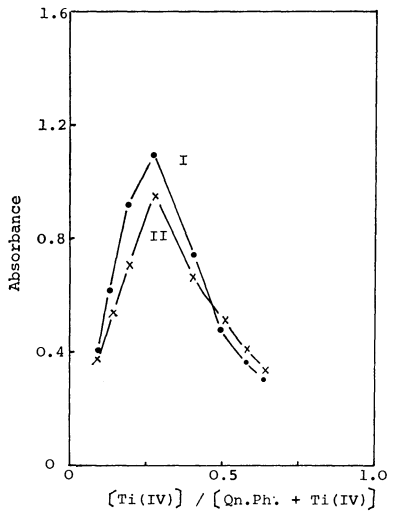

Fig. 2. Continuous variation method.
[Ti(IV)+Qn.Ph.]=2.5×10^{-5} M, Tween 20: 1.0 ml of 5% Tween 20 solution, pH: 4.7, reference: water, curve I: absorbance at 595 nm, curve II: absorbance at 580 nm.

of titanium(IV) to Qn.Ph.

Conclusion. The color reaction between Qn.Ph. and titanium(IV) complex was studied in the absence or presence of nonionic surfactancts such as Tween 20. And then, a simple and sensitive procedure for the determination of titanium(IV) using Qn.Ph. and Tween 20 was studied. The calibration curve was linear over 0.3—2.4 μg of titanium(IV) concentration. The molecular extinction coefficient of the Qn.Ph.–titanium(IV) complex was 1.91×10^5 l mol^{-1} cm^{-1}. It's sensitivity of this method was about ten times greater than DAM method,[2,3] and two fold greater than NBNPA method.[4] Therefore, this method is recommendable for the determination of microgram amounts of titanium(IV) in pigments and metallic luster agents.

Presented at the 102nd Annual Meeting of Pharmaceutical Society of Japan in Osaka, April 1982.

References

1) J. H. Yoe and A. R. Armstrong, *Anal. Chem.*, **19**, 100 (1947).
2) H. Ishii, *Bunseki Kagaku*, **16**, 1101 (1967).
3) P. G. Jeffery and G. R. E. C. Gregory, *Analyst*, **90**, 177 (1965).
4) K. Tanaka and N. Takagi, *Bunseki Kagaku*, **12**, 1175 (1963).
5) J. P. Young and J. C. White, *Anal. Chem.*, **31**, 393 (1959).
6) I. Mori, Y. Fujita, and T. Enoki, *Yakugaku Zasshi*, **98**, 1145 (1978).
7) I. Mori, Y. Fujita, and T. Enoki, *Bunseki Kagaku*, **28**, 685 (1979).
8) I. Mori, Y. Fujita, and T. Enoki, *Bunseki Kagaku*, **28**, 707 (1979).

Geometrical Isomerization of μ-Peroxo-bis[diethylenetriamine-(*R*)-propylenediaminecobalt(III)] Ions *via* Labile Cobalt(II) Species

Yoichi SASAKI,* Masahiko TACHIBANA, and Kazuo SAITO

Department of Chemistry, Faculty of Science, Tohoku University, Aoba, Aramaki, Sendai 980

(Received May 24, 1982)

Synopsis. The title complex ion undergoes slow geometrical isomerization. A mechanism involving labile cobalt(II) species which is in equilibrium with the title ion, is suggested.

Cobalt(II) complexes of various amine ligands uptake dioxygen to give μ-peroxo-dicobalt(III) complexes in basic solutions.[1,2] Such a dioxygen uptake is often reversible; *i.e.* the μ-peroxo complex is in equilibrium with the cobalt(II) complexes and O_2, the equilibrium being in great favor of the μ-peroxo complexes. Unusually rapid ligand substitution reactions of such binuclear cobalt(III) complexes are interpreted by the existence of such equilibria.[2]

Peroxo bridged dicobalt(III) compelexes containing multidentate amine ligands can give many geometrical isomers with respect to the arrangement of chelate rings. Geometrical isomerization of such complexes would not be accompanied by a significant change in their electronic absorption spectra, but can be followed by circular dichroism (CD) spectra by use of an optically active ligand such as (*R*)-propylenediamine (*R*-pn). The CD spectrum of $[(dien)(R\text{-pn})Co^{III}(\mu\text{-}O_2^{(2-)})Co^{III}(R\text{-pn})(dien)]^{4+}$ (dien=diethylenetriamine), indeed changes slowly owing to geometrical isomerization.[3] This work is aimed at clarifying the mechanism of geometrical isomerization of this complex in relation to the deoxygenation equilibrium.

Experimental

Materials. *μ-Peroxo-bis[diethylenetriamine-(R)-propylenediamine-cobalt(III)] Perchlorate, [(dien)(R-pn)Co^{III}(μ-$O_2^{(2-)}$)Co^{III}(R-pn)(dien)](ClO$_4$)$_4$*: Two samples of the complex were obtained by modifying the previously reported method.[3] An aqueous solution (40 cm^3) of cobalt(II) nitrate hexahydrate (5.8 g) containing diethylenetriamine (2.1 g), (*R*)-propylenediamine dihydrochloride (2.9 g), and sodium hydroxide (1.6 g) was aerated at 0 °C, while aqueous solution of sodium perchlorate (20 g in *ca.* 30 cm^3) was slowly added. Brown hygroscopic precipitate was filtered off after 1 h, and dried *in vacuo* (sample A). The sample A was dissolved in a minimum amount of hot water (70 °C), cooled slowly (5—10 °C per hour) to room temperature and stored in a refrigerator overnight. The dark brown needles were filtered off and dried *in vacuo* (sample B). Found: C, 18.79; H, 5.03; N, 15.27%. Calcd for $C_{14}H_{46}N_{10}O_{18}Co_2Cl_4$: C, 18.64; H, 5.14; N, 15.52%.

Other Materials: Propylenediamine was resolved by Dwyer's method.[4] Special grade reagents of diethylenetriamine, ethylenediamine, and disodium dihydrogen ethylenediaminetetraacetate dihydrate, were used as received.

Measurements. Electronic absorption and circular dichroism spectra were recorded on a Hitachi 323 spectrophotometer and a JASCO J-40A automatic recording spectropolarimeter, respectively. The latter and a Hitachi 124 spectrophotometer with a Hitachi recorder QPD-34 were used for the kinetic measurements.

Results and Discussion

The Change in CD Spectra. Samples A and B gave almost identical absorption, but quite different CD spectra immediately after dissolution in water (Figs. 1 (a) and (b)). Their CD spectra changed slowly with time without any clear isosbestic point, and became almost identical with each other after 3 d at 15 °C (Fig. 1 (c)). No appreciable change in absorption spectra was accompanied. The plots of CD strengths at 510, 447, and 395 nm against time failed to give simple first-order decay curves (exemplified by Fig. 2 (d)). More than three geometrical isomers seem to be responsible for the CD change. Three

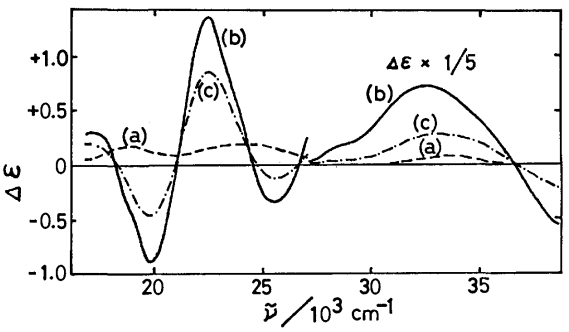

Fig. 1. Circular dichroism spectra of $[(dien)(R\text{-pn})Co^{III}(\mu\text{-}O_2^{(2-)})Co^{III}(R\text{-pn})(dien)]^{4+}$ in water at 15 °C; (a) fresh solution of sample A (----), (b) fresh solution of sample B (——), and (c) these solutions after 3 d (—·—·—).

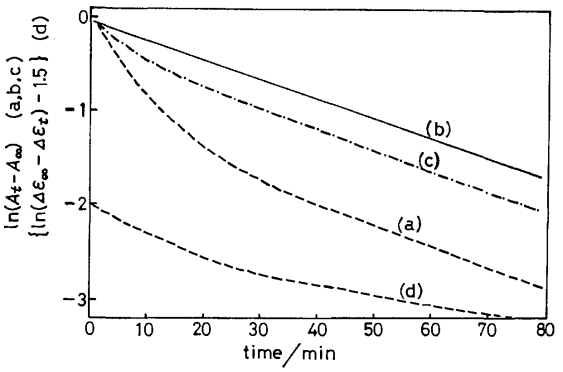

Fig. 2. First-order plots for the decrease in absorbance at 303 nm of $[(dien)(R\text{-pn})Co^{III}(\mu\text{-}O_2^{(2-)})Co^{III}(R\text{-pn})(dien)]^{4+}$ on addition of Na_2H_2edta to (a) fresh solution of sample A (----), (b) fresh solution of sample B (——), and (c) these solutions after 3 d (—·—·—), and (d) first-order plot for the change in CD strength at 447 nm of the fresh solution of sample A (——).

solutions represented by the three different CD curves in Fig. 1 should have different compositions of geometrical isomers.

Deoxygenation Kinetics. The deoxygenation can be followed by adding EDTA[5] to basic solutions of μ-peroxo complexes, EDTA scavenging cobalt(II) species to prevent reformation of μ-peroxo complexes.[2] Figure 2 shows the first-order plots of decrease in absorbance at 303 nm (common peak position of geometrical isomers of $[(dien)(R\text{-pn})Co^{III}(\mu\text{-}O_2^{(2-)})Co^{III}(R\text{-pn})(dien)]^{4+}$) at 40 °C on addition of Na_2H_2edta to basic solutions of the complex in various isomer compositions (pH, *ca.* 8). Two conclusions can be deduced from the plots: (i) Comparison of cruve (a) for the deoxygenation of sample A with curve (d) for the change in CD strength of the same solution, clearly indicates that the deoxygenation occurs much more rapidly than geometrical isomerization. (ii) The deoxygenation rate constants are significantly different among geometrical isomers, since solutions with different isomer compositions give significantly different first-order plots.

The fresh solution of sample B gave a good straight line with the first-order rate constant, 3.5×10^{-4} s^{-1} (40.0 °C, I=0.1 M (NaCl) (1 M=1 mol dm^{-3})), indicating that B is composed of only one geometrical isomer.[6] Fresh solution of sample A and aged solutions of both samples (3 d at 15 °C) gave curved plots, which can be analyzed as representing parallel deoxygenations of more than two geometrical isomers.[7] The last parts of these plots are linear with identical slopes to that of the fresh solution of sample B. The same isomer as that in sample B should be responsible at this stage. Namely the isomer in sample B decomposes at the smallest rate among the isomers. The contents of this isomer were estimated from the plots to be *ca.* 35 and 65% for the fresh and aged solutions of sample A, respectively. The initial rapid decomposition of the fresh solution of sample A gave a rate constant, 2.4×10^{-3} s^{-1}, about one order of magnitude greater than that of sample B.

Ligand Substitution Reaction. When sample B was dissolved in water ([B]=0.0006 M) containing 0.029 M ethylenediamine (en) (pH, 7.9 (ammonia buffer), I=0.05 M (NaCl)), the CD spectrum gradually disappeared without appreciable change in absorption spectrum. The first-order plot of the decrease in CD strength at 447 nm gave a straight line. The slope (3.3×10^{-4} s^{-1} at 39.8 °C) is almost identical with that for its deoxygenation under similar conditions. Thus en should replace the coordinated R-pn through rate-determining deoxygenation process. The formation of $[(en)(dien)Co^{III}(\mu\text{-}O_2^{(2-)})Co^{III}(dien)(en)]^{4+}$ from $[Co^{II}(dien)(en)(H_2O)]^{2+}$ and O_2, as well as the ligand substitution at cobalt(II) state, should be rapid.

Mechanism of the Geometrical Isomerization. The deoxygenation occurs much more rapidly than the CD change in the solution of sample A. Thus, the geometrical isomerization can take place at labile cobalt(II) state which is in equilibrium with the μ-peroxo complex. Such a view is supported by the complete replacement of en for the coordinated R-pn with rate-determining deoxygenation.

Rate of the formation of μ-peroxo complexes from cobalt(II) complexes and O_2 are similar to one another (second-order rate constants, 10^5—10^6 M^{-1} s^{-1} at 25 °C) for even those with different ligands such as $[Co^{II}(NH_3)_5(H_2O)]^{2+}$ and $[Co^{II}(tetren)(H_2O)]^{2+}$ (tetren= tetraethylenepentamine).[8] Thus the formation rates of the μ-peroxo complexes would not be significantly different among the geometrical isomers of $[Co^{II}(dien)(R\text{-pn})(H_2O)]^{2+}$. The initial product of the μ-peroxo complex, sample A, can be a mixture of various isomers. The small CD strength may result from the cancellation of CD spectra of various isomers. The deoxygenation rates are, on the other hand, significantly different among geometrical isomers (Fig. 2). Such a difference would result in the geometrical isomerization in the solution of sample A. Isomers with small deoxygenation rates should accumulate gradually to give thermally equilibrated isomer distribution, of which the deoxygenation pattern is represented by the curve (c) in Fig. 1.

The present results show that the deoxygenation rather than the formation rate is important in determining the stability of μ-peroxo complexes.

A Grant-in-Aid (No. 511301) from the Ministry of Education, Science and Culture is gratefully acknowledged.

References

1) C. L. Wong, J. A. Switzer, K. P. Balakrishnan, and J. F. Endicott, *J. Am. Chem. Soc.*, **102**, 5511 (1980), and references therein.

2) Y. Sasaki, K. Z. Suzuki, A. Matsumoto, and K. Saito, *Inorg. Chem.*, **21**, 1825 (1982), and references therein.

3) Y. Sasaki, J. Fujita, and K. Saito, *Bull. Chem. Soc. Jpn.*, **44**, 3373 (1971).

4) E. P. Dwyer and F. L. Garvan, *J. Am. Chem. Soc.*, **81**, 2955 (1959).

5) EDTA represents variously protonated forms of ethylenediaminetetraacetate ion, $H_nedta^{(4-n)-}$, and is used when the degree of protonation need not to be specified.

6) An alternative possibility that sample B is composed of more than two isomers with identical deoxygenation rate, is much less likely.

7) A. A. Frost and R. G. Pearson, "Kinetics and Mechanisms," 2nd ed, John Wiley and Sons, New York (1961).

8) G. McLendon and A. E. Martell, *Coord. Chem. Rev.*, **19**, 1 (1976).

Studies on Some Azine Complexes of Lanthanum(III) and Samarium(III)

Satya Prakash MITAL, Ranvir V. SINGH, and Jagdish Prasad TANDON*

Department of Chemistry, University of Rajasthan, Jaipur, India

(Received August 18, 1981)

Synopsis. Pentacoordinated lanthanum(III) and samarium(III) complexes of salicylaldehydeazine and 2-hydroxy-1-naphthaldehydeazine have been synthesized and characterized by elemental analysis, molecular weight determinations, conductance, and magnetic measurements as well as infrared, ultraviolet spectral, and X-ray powder diffraction studies. Their pyrolytic behaviour has also been discussed.

Although, the azine complexes of d-block elements have been extensively studied,[1,2] similar investigations on f-block elements appear to be limited.[3] In view of this, it was considered worthwhile to study the chelating behaviour of azines towards lanthanum(III) and samarium(III) and the results are presented in this paper.

Experimental

All the chemicals used were of analytical grade. Adequate precautions were taken to exclude moisture throughout the experimental work. The triisopropoxylanthanum(III) or -samarium(III)[4] and azines[1,3] were prepared by the literature methods.

The analytical methods and the techniques of physical measurements are the same as reported in our previous communications.[5,6]

Synthesis of Azine Complexes of Lanthanum(III) or Samarium(III): The mixture of triisopropoxylanthanum(III) or -samarium(III) with the stoichiometric amount of azine was heated under reflux for about 8—24 h in benzene medium. The liberated 2-propanol was fractionated azeotropically and then estimated to ascertain the progress of the reaction. On its completion, the excess of the solvent was stripped off under reduced pressure and the residue washed several times with hexane. Finally, the resulting products were dried under vacuum at 50—60 °C/0.5 mmHg† for ≈3 h.

The azinatolanthanum(III) or samarium(III) *t*-butoxides were prepared by refluxing the benzene solution of freshly prepared azinatolanthanum(III) or -samarium(III) isopropoxide with an excess of *t*-butyl alcohol for ≈30 h with continuous removal of benzene-2-propanol azeotrope. After completion of the reaction, the products were isolated by removing the solvent under reduced pressure and subsequent drying.

The analytical data and characteristics of the resulting compounds are recorded in Table 1.

Results and Discussion

These complexes have been synthesized as shown by the following equations:

$$(OC_3H_7^i)_3Ln + azH_2 \longrightarrow (OC_3H_7^i)Ln(az) + 2i\text{-}C_3H_7OH$$

$$2(OC_3H_7^i)_3Ln + 3azH_2 \longrightarrow Ln_2(az)_3 + 6i\text{-}C_3H_7OH$$

$$(OC_3H_7^i)_3Ln + 2azH_2 \longrightarrow Ln(az)(azH) + 3i\text{-}C_3H_7OH$$

$$(OC_3H_7^i)Ln(az) + t\text{-}C_4H_9OH \longrightarrow \underset{\text{(in excess)}}{} (OC_4H_9^t)Ln(az) + i\text{-}C_3H_7OH$$

† 1 mmHg≈133.322 Pa.

[where Ln=La(III) or Sm(III);

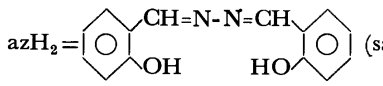

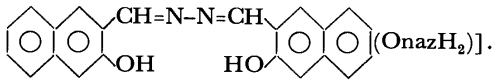

The resulting complexes, $(OC_3H_7^i)Ln$(saz or Onaz), Ln_2(saz or Onaz)$_3$, Ln(saz or Onaz) (sazH or OnazH), and $(OC_4H_9^t)Ln$(saz or Onaz) are yellow to reddish brown coloured, nonvolatile solids and decompose without melting when heated above 200 °C. These are insoluble or sparingly soluble in common organic solvents but soluble in DMF or DMSO and in which these behave as nonelectrolytes ($\mu<20\ \Omega^{-1}\ mol^{-1}\ cm^2$). The alkoxy derivatives, (OR)Ln(az) [where R=Pr^i or Bu^t] are highly moisture sensitive. The azinatolanthanum(III) or -samarium(III) isopropoxides are dimeric, where as the rest of the derivatives are monomeric in nature.

The broad absorption band in the region, 3400—3050 cm^{-1}, due to the hydrogen bonded OH or NH group in the IR spectra of azines disappears in $(OC_3H_7^i$ or $OC_4H_9^t)Ln(az)$ and $Ln_2(az)_3$ complexes indicating the deprotonation of the phenolic protons. However, the characteristic band of νOH/νNH is observed at almost the same position in the spectra of Ln(az)(azH) complexes indicating thereby that at least one hydroxyl group of the two ligand moieties does not take part in coordination.

On the other hand, a strong band at 1610±10 cm^{-1} in the spectra of ligands due to the azomethine (>C=N–)groups splits at 1605±5 and 1580±5 cm^{-1} in the spectra of lanthanum(III) and samarium(III) complexes indicating two different environments around both the azomethine groups of the ligand moiety in the complexes and which is probably due to the coordination of only one unsaturated nitrogen of the ligand to the lanthanoid atom.

The medium to weak intensity bands at 650±10 and 375±10 cm^{-1} in the spectra of azinatolanthanoid complexes may be tentatively assigned to the ring deformation coupled with ν Ln–O and C–H out of plane deformation[7] and ν Ln–N respectively.[8,9]

A bathochromic shift in the transitions of >C=N– chromophore at ≈350 and 425 nm [335 and 415 nm in 2-hydroxy-1-naphthaldehydeazine] in the ultraviolet spectra of lanthanoid complexes probably indicates the formation of Ln–N bond.

The magnetic susceptibilities of these complexes measured at room temperature (35±1 °C) show that the azinatolanthanum(III) complexes are diamagnetic (X_g values-0.34 to -0.92×10^{-6} c.g.s.), whereas the azinatosamarium(III) complexes are paramagnetic (μ eff$_{exp}$=1.25—1.57 BM) in nature.

Table 1. Physical characteristics and analytical data of azinatolanthanum(III) and -samarium(III) complexes

Compound, state, and colour	D.P.[a] θ_d/°C	Found(Calcd) (%) La/Sm	C	H	N	Molecular weight Found (Calcd)
1	2	3	4	5	6	7
$(OC_3H_7^i)$La(saz) Yellow solid	310—12	31.95 (31.84)	47.00 (46.80)	3.85 (3.93)	6.61 (6.42)	920.15 (436.25)
$La_2(saz)_3$ Yellow solid	275—77	27.81 (27.99)	50.74 (50.82)	3.10 (3.05)	8.62 (8.47)	964.86 (992.57)
La(saz)(sazH) Dark yellow solid	260—62	22.71 (22.54)	54.71 (54.55)	3.50 (3.43)	9.27 (9.09)	651.73 (616.42)
$(OC_4H_9^t)$La(saz) Dark yellow solid	225—27	30.74 (30.85)	48.16 (48.01)	4.18 (4.25)	6.37 (6.22)	486.72 (450.28)
$(OC_3H_7^i)$Sm(saz) Light orange solid	304—06	33.73 (33.57)	45.78 (45.60)	3.91 (3.83)	6.47 (6.26)	925.92 (447.68)
$Sm_2(saz)_3$ Dark yellow solid	276—77	29.45 (29.63)	49.68 (49.71)	3.02 (2.98)	8.43 (8.28)	1054.11 (1015.43)
Sm(saz)(sazH) Dark yellow solid	200—02	24.15 (23.94)	53.70 (53.56)	3.42 (3.37)	9.15 (8.92)	661.23 (627.85)
$(OC_4H_9^t)$Sm(saz) Dark yellow solid	265—67	32.71 (32.56)	46.66 (46.82)	4.19 (4.15)	5.95 (6.07)	437.25 (461.71)
$(OC_3H_7^i)$La(Onaz) Light reddish brown solid	339—40	26.09 (25.90)	55.83 (55.98)	4.01 (3.95)	5.35 (5.22)	1037.77 (536.38)
$La_2(Onaz)_3$ Red solid	280—82	21.33 (21.49)	61.52 (61.31)	3.21 (3.27)	6.72 (6.50)	1241.31 (1292.96)
La(Onaz)(OnazH) Reddish brown solid	260—62	17.19 (17.01)	64.89 (64.71)	3.62 (3.58)	7.01 (6.86)	783.49 (816.68)
$(OC_4H_9^t)$La(Onaz) Dark brown solid	240—42	25.36 (25.24)	56.53 (56.74)	4.25 (4.21)	5.20 (5.09)	528.11 (550.41)
$(OC_3H_7^i)$Sm(Onaz) Reddish brown solid	291—93	27.34 (27.45)	54.97 (54.82)	3.91 (3.86)	5.01 (5.12)	1057.27 (547.81)
$Sm_2(Onaz)_3$ Red solid	275—77	23.02 (22.85)	60.10 (60.24)	3.16 (3.22)	6.58 (6.39)	1364.10 (1315.82)
Sm(Onaz)(OnazH) Red solid	219—21	18.34 (18.15)	64.00 (63.81)	3.60 (3.53)	6.58 (6.76)	862.83 (828.11)
$(OC_4H_9^t)$Sm(Onaz) Red solid	233—35	26.89 (26.75)	55.73 (55.59)	4.07 (4.13)	5.11 (4.98)	593.91 (561.84)

a) D. P.: Decomposition temperature.

Attempts to grow crystals of suitable size for X-ray crystal diffraction studies remained unsuccessful. However, the X-ray powder diffraction patterns have been recorded and these indicate that the compounds $(OC_3H_7^i)$Sm(saz), $Sm_2(saz)_3$, and Sm(saz)(sazH) belong to the orthorhombic symmetry having the molecular unit cell parameters a,b,c (in Å) and Z as 12.64, 16.37, 14.71, and 4; 12.61, 15.63, 30.46, and 4; 6.70, 15.24, 18.28, and 2, respectively.

The comparative thermal stability of the complexes, $(OC_3H_7^i)$Sm(saz), $Sm_2(saz)_3$, and Sm(saz)(sazH) on the basis of IPDT values (549.2, 537.0, and 507.4, respectively) has been evaluated from the pyrolytic curves plotted in the percentage residual weight against the temperature. The activation energy E_A (K· Cal) and order of reaction $n[E_A, n$: 5.72, 1; 4.35, 1; 4.12, 1, respectively] have also been determined with the help of Freeman and Carroll's method.[10] The following order of thermal stability of the complexes has been noted:

$(OC_3H_7^i)$Sm(saz)>$Sm_2(saz)_3$>Sm(saz)(sazH).

The authors are thankful to the University Grants Commission, New Delhi for the financial support to one of us (S.P.M.).

References

1) R. K. Sharma, R. V. Singh, and J. P. Tandon, *J. Prakt. Chem.*, **322**, 161 (1980).
2) A. K. Saxena, H. B. Singh, and J. P. Tandon, *Synth. React. Inorg. Met. -Org. Chem.*, **10**, 117 (1980).
3) S. P. Mital, R. V. Singh, and J. P. Tandon, *J. Inorg. Nucl. Chem.*, **43**, 533 (1981).
4) S. N. Misra, T. N. Mishra, R. N. Kapoor, and R. C. Mehrotra, *Chem. Ind. (London)*, **1963**, 120; **1965**, 382.
5) S. P. Mital, R. V. Singh, and J. P. Tadnon, *Synth. React. Inorg. Met. -Org. Chem.*, **11**, 547 (1981).
6) S. P. Mital, R. V. Singh, and J. P. Tandon, *J. Inorg. Nucl. Chem.*, **43**, 3187 (1981).
7) C. Y. Liang, E. J. Schimitschek, and J. A. Trias, *J. Inorg. Nucl. Chem.*, **32**, 811 (1970).
8) S. P. Mital, R. V. Singh, and J. P. Tandon, *Synth. React. Inorg. Met. -Org. Chem.*, **10**, 327 (1980).
9) J. H. Forsberg, *Coord. Chem. Rev.*, **10**, 195 (1973).
10) E. S. Freeman and B. Carroll, *J. Phys. Chem.*, **62**, 394 (1958).

The Favorskii-type Rearrangement of 3-Bromo-β-ionone with Sodium Ethoxide

Masato NANASAWA* and Hiroyoshi KAMOGAWA

Department of Applied Chemistry, Faculty of Engineering, Yamanashi University, Takeda, Kofu 400

(Received August 21, 1981)

Synopsis. The reaction of 3-bromo-β-ionone with sodium ethoxide afforded ethyl 4-(2,6,6-trimethyl-2-cyclohexenylidene)butyrate by a Favorskii-type rearrangement, accompanied by double-bond migration, while with sodium phenoxide or diethyl amine, substitution products were primarily obtained.

In the course of studies of the nucleophilic substitution of 3-bromo-β-ionone (**1**) with the sodiomalonic ester, we have found that the major product thus obtained was an ester with a loss of ketone carbonyl. The preparation of esters from α-halo ketones by the action of bases is known as the Favorskii rearrangement,[1] but there have been no reports on the rearrangement of halo ketones having the halogen atom separated from the carbonyl group by conjugated double bonds. For examining this new type of Favorskii rearrangement in more detail, we conducted the reaction of **1** with several kinds of bases and discussed the reaction mechanism.

The reaction of **1** with sodium ethoxide gave a straight chain ester and 3-ethoxy-β-ionone in the ratio of *ca.* 10:1 (Table 1, Exptl No. 1). The same ester was also obtained when **1** was subjected to the usual conditions of malonic-ester synthesis in ethanol (No. 4), while the reactions with diethyl sodiomalonate in tetrahydrofuran (No. 3), phenoxide (No. 5), or diethyl amine (No. 6) in ethanol gave only substitution products. The UV and ^{1}H-NMR spectra of the ester indicated that the double bond conjugated to the carbonyl group no longer exists; the IR spectrum also indicated the disappearance of the *trans*-double bond, and other analytical results identified the structure of the ester (**8**).

The initial step of the Favorskii rearrangement of α-halo ketones with bases was considered to be a proton abstraction; the resulting enolate anion induces the production of a cyclopropanone or a zwitterion to form a commonly α-branched ester.[2] This suggests that the enolate anion (**2**) might undergo the ejection of bromine with concerted or subsequent double-bond migration by an internal S_N2'-type displacement.[3] The opening of the cyclopropanone ring (**3**) or rearrangement of the zwitterion (**4**) by the attack of the ethoxide ions should give a more stable carbanion. The carbanion in **7** is more stable than the α-branched methylide intermediate because of the resonance stabilization with conjugated double bonds as well as its secondary character, thereby leading to ethyl 4-(2,6,6-trimethyl-2-cyclohexenylidene)butyrate (**8**) as the principal product.

The rate of nucleophilic substitution might be slow at the 3-position of the ring with a boat conformation due to the steric hindrance by the 2,6,6-trimethyl groups, whereas the rearrangement by the removal of enolic hydrogen is facilitated by the presence of the conjugated double bonds at the α-position. Thus, sodium ethoxide in even a minor amount may remove the enolic hydrogen to give the rearrangement intermediate in spite of the unfavorable equilibrium between sodium ethoxide and diethyl sodiomalonate in ethanol; the resulting intermediate (**3** or **4**) might be very unstable and might react easily with excess ethanol as the solvent to form the ethyl ester. The acidity of the enol-tautomer in **1** might not be so large as those of acyclic α-halo ketones[4] and α-haloarylalkyl ketones;[5] therefore, the formation of the enolate anion did not occur with weak bases, but substitution products were primarily formed.

Table 1. The reaction of 3-bromo-β-ionone with nucleophiles

Exptl No.	Nucleophile[a]	Solvent	Reaction product: Rearrangement	Reaction product: Substitution
1	EtONa	EtOH	81%	8%
2	EtONa[b]	EtOH	72	16
3	$NaCH(COOEt)_2$	THF	0	82
4	$NaCH(COOEt)_2$	EtOH	52	32[c]
5	PhONa	EtOH	0	87
6	Et_2NH	EtOH	0	88

a) Two equivalents for 3-bromo-β-ionone. b) Equimolar amount. c) Substitution product with diethyl sodiomalonate.

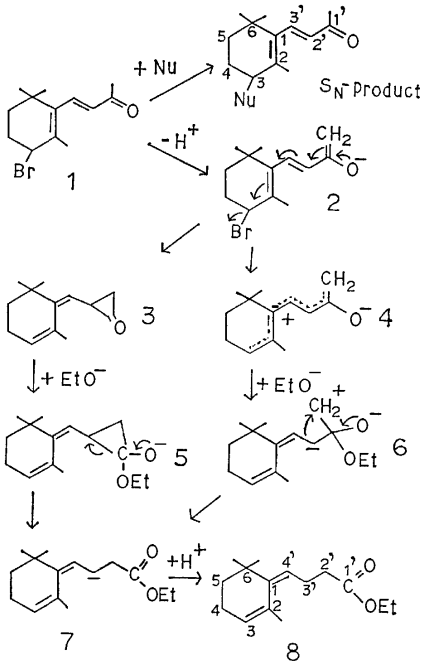

Scheme 1.

Experimental

The infrared, ultraviolet, ^{1}H-NMR, ^{13}C-NMR, and mass spectra were obtained using Hitachi 215, Hitachi 200-10, JEOL-PMX 60, JEOL-FX 90Q, and Hitachi RMU-6MG spectrometers respectively. Elemental analyses were conducted using a Perkin Elmer 250 instrument.

3-Bromo-β-ionone(**1**) was prepared with β-ionone and *N*-bromosuccinimide in carbon tetrachloride.[6] Since the brominated compound was presumed to be unstable, the crude product after the filtration of succinimide was used for the next process without purification.[7] ^{1}H-NMR(CCl_4): δ= 1.08(s, 6-Me_2), 1.62(m, 5-H_2), 1.85(s, 2-Me), 2.13(d, J= 6 Hz, 4-H_2), 2.20(s, 1'-Me), 4.61(br s, 3-H), 6.05(d, J= 16 Hz, 2'-H), 7.15(d, J=17 Hz, 3'-H).

*Ethyl 4-(2,6,6-Trimethyl-2-cyclohexenylidene)butyrate (**8**)*: A solution of **1** (4.2 g, 15.6 mmol) in carbon tetrachloride (8 ml) was added to freshly prepared ethanolic sodium ethoxide (31.2 mmol in 40 ml) at room temperature. The mixture was stirred overnight and then poured into water (100 ml). The product was extracted with ether and the organic layer was washed with water, dried over anhydrous sodium sulfate, and concentrated *in vacuo* to give an orange oil. It was chromatographed over a silica-gel column (Wako C-300) with ether in hexane (2% v/v) to give **8** in an 81% yield based on **1**. Bp 110—112 °C/0.7 mmHg. UV_{max} ($CHCl_3$): 242 nm. IR($CHCl_3$): 1725 cm^{-1} (ester). ^{1}H-NMR($CDCl_3$): δ=1.01 (s, 6H, 6-Me_2), 1.33 (t, J=8 Hz, ester-CH_3), 1.2—1.6 (m, 5-H_2), 1.9—2.1 (m, 4-H_2), 2.03 (s, 2-Me)), 2.2—2.6 (m, 4H, 2'-H_2, 3'-H_2), 4.21 (q, 2H, J=7 Hz, ester-CH_2), 5.25 (t, 1H, J=5 Hz), 5.55 (t, 1H). ^{13}C-NMR($CDCl_3$): δ=14.1(ester-CH_3), 23.6 (2-Me), 24.4 (3'), 27.5 (6-Me_2), 27.9 (6), 35.3(4), 35.4(2'), 37.0(5), 60.0 (ester-CH_2), 120.4(3), 127.9(4'), 131.6(2), 145.2(1), 172.9 (1'). MS, *m/e*(rel intensity): 236 (M^+, 18.7), 88 (100). Found: C, 75.62; H, 10.20%. Calcd for $C_{15}H_{24}O_2$: C, 76.21; H, 10.24%.

*Malonic Ester Synthesis Applied to **1** in Ethanol*: Diethyl sodiomalonate was prepared with diethyl malonate (37.4 mmol) and sodium ethoxide (31.2 mmol) in ethanol (50 ml) at 55 °C for 30 min. The reaction conditions were similar to those used for **8**. The reaction product was chromatographed over a silica-gel column with ether in hexane (2%) to give **8** in a 52% yield, subsequent elution with ether in hexane (50%) gave 3-[bis(ethoxycarbonyl)methyl]-β-ionone in a 32% yield. UV_{max}($CHCl_3$): 291 nm. IR ($CHCl_3$): 1725(ester), 1660(ketone), 970(CH:CH) cm^{-1}. ^{1}H-NMR($CDCl_3$): δ=1.05 (s, 6H, 6-Me_2), 1.28 (t, 6H, J=7 Hz, ester-CH_3), 1.7—2.0 (m, 4,5-H_2, 3-H), 1.74(s, 2-Me), 2.2(s, 3H, 1'-Me), 3.78(d, 1H, J=5 Hz, 3-CH), 4.23(q, 4H, J=7 Hz, ester-CH_2), 6.10(d, 1H, J=17 Hz, 2'-H), 7.31(d, 1H, J=17 Hz, 3'-H). ^{13}C-NMR($CDCl_3$): δ=13.9 (ester-CH_3), 19.8(4), 21.7(2-Me), 26.9(1'-Me), 27.9, 28.8(6-Me_2), 34.3(6), 37.0(3), 41.4(5), 53.7(3-CH), 60.9, 61.1(ester-CH_2), 131.9(2), 133.0(3'), 139.6(1), 143.2(2'), 168.0, 168.8(ester C=O), 197.9(1'). MS, *m/e*: 350(M^+, 3), 55(100). Found: C, 69.00; H, 8.75%. Calcd for $C_{20}H_{30}O_5$: C, 68.54; H, 8.62%.

Nucleophilic Substitution with Sodium Phenoxide: A mixture of **1** (15.6 mmol) and sodium phenoxide (32 mmol) in ethanol (30 ml) was stirred overnight at room temperature and then poured into a cold 5% aqueous sodium hydroxide solution. The reaction product was extracted with ether, and the organic layer was washed with a 2% aqueous sodium hydroxide solution and water, dried over anhydrous sodium sulfate, and concentrated *in vacuo*. Subsequent silica gel chromatography afforded 3-phenoxy-β-ionone (hexane–ether, 9:1) in an 87% yield. UV_{max}($CHCl_3$): 285, 275^{sh} nm. IR($CHCl_3$): 1660(ketone), 995(phenoxy), 970(CH:CH) cm^{-1}. ^{1}H-NMR($CDCl_3$): δ=4.48(t, 1H, 3-H), 6.17(d, 1H, J= 17 Hz, 2'-H), 6.9—7.7(m, 6H, phenyl, 3'-H). ^{13}C-NMR ($CDCl_3$): δ=18.8(4), 24.1(2-Me), 27.1, 27.4(6-Me_2), 28.8 (1'-Me), 34.5(5), 34.6(6), 75.7(3), 116, 121.0, 129.5(*o*-, *p*-, and *m*-phenyl carbon), 131.3(2), 133.2(3'), 140.9(1), 142.3 (2'), 158.5 (3-O-C), 198.0(1'). MS, *m/e*: 284(M^+, 2.9), 191(100). Found: C, 79.87; H, 8.56%. Calcd for $C_{19}H_{24}O_2$: C, 80.24; H, 8.50%.

References

1) For a review, see A. S. Kende, *Org. React.*, **11**, 261 (1960).
2) R. B. Loftfield, *J. Am. Chem. Soc.*, **73**, 4707 (1951).
3) P. B. D. de la Mare and C. A. Vernon, *J. Chem. Soc.*, **1953**, 3555.
4) T. Sakai, T. Katayama, and A. Takeda, *J. Org. Chem.*, **46**, 2924 (1981).
5) R. M. Dodson, E. F. Morolla, and W. G. Dauben, *J. Am. Chem. Soc.*, **76**, 606 (1954).
6) H. B. Henbest, *J. Chem. Soc.*, **1951**, 1704.
7) The purity was checked by ^{1}H-NMR.

The Formation of Acetylcatechol in the Photochemical Reaction of *o*-Benzoquinones with Acetaldehyde

Akio TAKUWA,* Hidetoshi IWAMOTO, Osamu SOGA, and Kazuhiro MARUYAMA*,†

Department of Chemistry, Faculty of Science, Shimane University, Nishikawatsu-cho, Matsue 690

† *Department of Chemistry, Faculty of Science, Kyoto University, Kitashirakawa, Sakyo-ku, Kyoto 606*

(Received November 9, 1981)

Synopsis. The irradiation of several alkyl-substituted *o*-benzoquinones in the presence of acetaldehyde gave the corresponding acetylcatechol and catechol monoacetates *via* the attack of the acetyl radical on the ground-state quinone molecule. In the reaction of 3,5-di-*t*-butyl- and 3-*t*-butyl-5-methyl-*o*-benzoquinones, the dimer of alkyl-substituted cyclopentadienone, generated by the photodecarbonylation of the quinones, was also obtained.

There have been reported only a few examples of photochemical reactions between *o*-benzoquinone and aldehyde.[1] For example, tetrachloro- and tetrabromo-*o*-benzoquinones usually give the tetrahalocatechol monoesters in a reaction with acetaldehyde and benzaldehyde.[1] In these quinones, the reactive quinonoid bonds are completely replaced with halogen atoms. We ourselves reported recently that 3-acetyl-1,2-naphthalenediol was formed, together with a mixture of 1,2-naphthalenediol monoacetates, in the photochemical reaction of 1,2-naphthoquinone with acetaldehyde.[2] It was, therefore, of interest to examine the possibility of introducing an acetyl group into the quinonoid nucleus of *o*-benzoquinone. In this paper we wish to report the product analyses and reaction courses of the photochemical reactions of mono- and dialkyl-substituted *o*-benzoquinones with acetaldehyde.

The irradiation of a benzene solution of 4-*t*-butyl-*o*-benzoquinone (**1a**) in the presence of a large excess of acetaldehyde (**2**) gave acetylcatechol (**3a**) (20%) and an isomeric mixture of catechol monoacetates (**4a**) (20%). The structures of the products were confirmed by their spectral data and elemental analyses.

The photo-induced reaction of 3,5-di-*t*-butyl-*o*-benzoquinone (**1b**) with **2** produced **3b**, **4b**, **5b**, and the dimer (**6b**) of 2,4-di-*t*-butylcyclopentadienone (CPD) in 6, 36, 22, and 4.5% yields respectively. 3-*t*-Butyl-5-methyl-o-benzoquinone (**1c**) similarly reacted with **2** to give **3c** (12%), **4c** (14%), and **6c** (1%), but no **5c** could be isolated (Scheme 1).

Recently, CPD was obtained from the UV irradiation of **1b**, and it dimerized at room temperature to give **6b** in the mode of Diels-Alder reaction.[3] Actually, two dimers, **6b** and **6c**, were obtained, in yields of 50 and 43% respectively, from the photolysis of a benzene solution of **1b** and **1c** in the absence of **2**; carbon monoxide was also evolved.

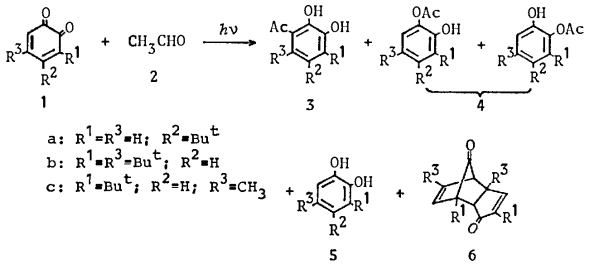

Scheme 1.

Thus, the irradiation of mono- and dialkyl-substituted *o*-benzoquinones in **2** gives acetylcatechols, together with catechol monoacetates, although a little photodecarbonylation occurs when **1b** and **1c** are irradiated in the aldehyde.

As for the mechanism of the formation of acetylcatechol and catechol monoacetates, two possibilities have been considered. One is an "in-cage" mechanism, *i.e.*, a process involving the combination of the radical pair consisting of *o*-benzosemiquinone and acetyl radicals in the solvent cage formed by the abstraction of formyl hydrogen from **2** by the excited quinone. The photo-CIDNP technique provides invaluable information for investigating such a radical-pair process.[2] Since, however, no ^{1}H-CIDNP signals could be observed in the reaction of **1a** with **2**, such an "in-cage" mechanism can be excluded.

An alternative mechanism is an "out-of-cage" one, *i.e.*, a process involving the addition of the free acetyl radical which escaped from the solvent cage to ground-state quinone.[2] In order to clarify the possibility, the addition reaction of the free acetyl radical to **1a** in the ground state was undertaken. The treatment of a benzene solution of **1a** and **2** with di-*t*-butyl diperoxyoxalate (DTBP)[4] in the dark allowed us to generate the necessary reacting conditions. When the decomposition of DTBP was carried out at 38 °C in a benzene solution of **1a** and **2**, **3a** and **4a**, which were the same products as those obtained from the photochemical reaction, were isolated in yields of 26 and 7% respectively; a diacetylated product (**7**) was also isolated in a yield of 6% (Scheme 2).

A benzene solution of **3a** and **2** was treated with DTBP to give **7** in a 25% yield. A similar treatment of **4a**, however, led to an almost quantitative recovery

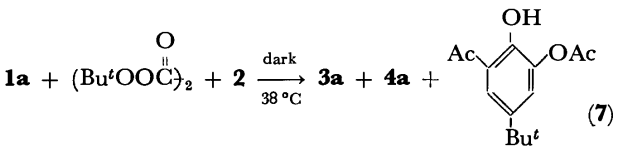

Scheme 2.

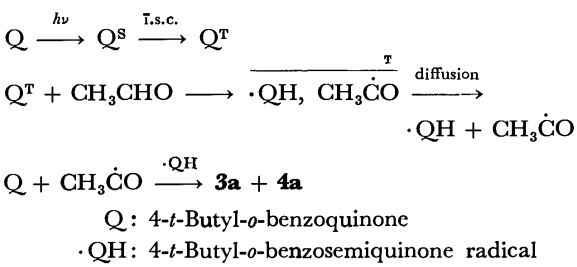

Q: 4-*t*-Butyl-*o*-benzoquinone

·QH: 4-*t*-Butyl-*o*-benzosemiquinone radical

Scheme 3.

Table 1. Some physical data of reductive acetylation products

Compound	Mp θ_m/°C[a]	IR(KBr) $\tilde{\nu}$/cm^{-1}		Found(%)		Calcd(%)	
		OH	C=O	C	H	C	H
3a	82—83[b]	3420	1620	69.28	7.77	69.21	7.74
4a	Oil	3400	1760[d]	69.16	7.69	69.21	7.74
3b	169—170[b]	3400	1680	72.49	9.13	72.69	9.15
4b	118—119[c]	3400	1750	72.55	9.18	72.69	9.15
3c	72—73[b]	3470	1620	70.22	8.24	70.24	8.16
4c	Oil	3430	1735[e]	70.16	8.17	70.24	8.16

a) Melting points are uncorrected. b) Recrystallized from light petroleum. c) Recrystallized from benzene-light petroleum. d) Solvent: $CHCl_3$. e) Solvent: CCl_4.

of the starting material. These results suggest that **7** may arise *via* **3a**. In addition, the photo-induced Fries rearrangement of **4a** to **3a** is unlikely under the irradiation conditions in this work, since **4a** does not absorb in the visible region. These results strongly supported the "out-of-cage" process for the mechanism of the present photo-induced reductive acetylation (Scheme 3).

Experimental

The IR, ^{1}H-NMR, and ^{13}C-NMR spectra were recorded on a Hitachi 215 spectrometer, a JEOL MH-100 spectrometer (internal TMS standard), and JEOL FX-100 FT NMR spectrometer respectively. Microanalysis was carried out on a Yanaco MT-2 CHN corder. The yields are based on the quinone used.

Materials. 4-*t*-Butyl- and 3,5-di-*t*-butyl-o-benzoquinones(**1a** and **1b**) were prepared by the oxidation of the corresponding catechols with silver oxide; **1a**: mp 66—68 °C (lit,[5] 68 °C). **1b**: mp 113—114 °C(lit,[3] 114—115 °C). 3-*t*-Butyl-5-methyl-*o*-benzoquinone(**1c**) was prepared by the oxidation of 2-*t*-butyl-4-methylphenol with Fremy's salt; **1c**, IR(KBr): $\nu_{C=O}$ 1660 cm^{-1}, mp 68—70 °C. DTBP was prepared according to the method described in the literature.[4]

General Procedures. A benzene solution (60 ml) of *o*-benzoquinone (2 mmol) and an excess of **2**(10 ml) was irradiated (>400 nm; Toshiba glass filter: VY-42) with a light from a 300W high-pressure Hg arc lamp through a 5 cm-thick layer of cold water (5 °C). When the *o*-benzoquinone had mostly disappeared, the solvent was removed *in vacuo*; then, the resulting oil was chromatographed by means of preparative TLC and eluted with benzene. The products thus obtained were purified by recrystallization from appropriate solvents or by TLC. The melting points, spectroscopic properties, and analytical data of the reductive acetylation products are given in Tables 1 and 2.

Photolyses of 1b and 1c. A pyrex test tube was charged with **1b** (1 mmol) or **1c** (1 mmol) and benzene (20 ml). The solution was then irradiated for 2 days. The volumes of carbon monoxide evolved during the photolyses of **1b** and **1c** were 11.7 and 10.5 ml respectively. After the removal of the benzene under reduced pressure, the resulting oil was chromatographed by means of TLC to give **6b**(50%) and **6c**(43%) respectively. **6b**: needles from ethanol; mp 153—154 °C(lit,[3] 152.5—153 °C). **6c**: needles from ethanol; mp 110—111 °C. IR(KBr) 1780(C=O) and 1696(C=O) cm^{-1}. ^{1}H-NMR(CCl_4): δ=1.10(s, 9H), 1.34(s, 3H), 1.72 (d, J=2.0 Hz, 3H), 2.28(s, 1H), 2.43(s, 1H), 5.58(q, J=2.0 Hz, 1H), and 6.66(s, 1H). ^{13}C-NMR($CDCl_3$): δ=204.9 (s), 200.6(s), 158.5(s), 155.1(d), 139.8(s), 125.8(d), 67.3(s), 61.1(d), 53.9(d), 44.8(s), 32.0(s), 31.0(s), 28.3(q), 27.1(q), 21.5(q), and 18.3(q). Found: C, 79.79; H, 9.44%. Calcd for $C_{20}H_{28}O_2$: C, 79.96; H, 9.39%. The dimers, **6b** and **6c**, were also obtained, in yields of 4.5 and 1% respectively, from the photochemical reactions of **1b** and **1c** with **2** (see Scheme 1).

Table 2. ^{1}H-NMR data of reductive acetylation products

Compound	δ(CCl_4)
3a	1.30(s, *t*-Bu), 2.56(s, $COCH_3$), 5.46(s, OH), 7.04(d, J=3.0 Hz, aromatic proton), 7.08(d, J=3.0 Hz, aromatic proton), 12.16(s, OH)
4a	1.20(s, *t*-Bu), 1.22(s, *t*-Bu), 2.07(s, $OCOCH_3$), 2.10(s, $OCOCH_3$), 6.60—6.96(m, OH's and aromatic protons)
3b	1.31(s, *t*-Bu), 1.39(s, *t*-Bu), 2.55(s, $COCH_3$), 5.57(s, OH), 6.05(s, OH), 6.88(s, aromatic proton)[a]
4b	1.24(s, *t*-Bu), 1.28(s, *t*-Bu), 1.32(s, *t*-Bu), 1.38(s, *t*-Bu), 2.27(s, $OCOCH_3$), 2.29(s, $OCOCH_3$), 5.24(s, OH), 5.28(s, OH), 6.68(s, aromatic protons)
3c	1.36(s, *t*-Bu), 2.45(s, CH_3), 2.55(s, $COCH_3$), 5.93(s, OH), 6.46(s, aromatic proton), 13.16(s, OH)
4c	1.27(s, *t*-Bu), 1.36(s, *t*-Bu), 2.07(s, CH_3), 2.13(s, CH_3), 2.18(s, $OCOCH_3$), 2.24(s, $OCOCH_3$), 5.55(s, OH), 6.17—6.74(m, OH's and aromatic protons)

a) Solvent: chloroform-*d*.

Reaction Involving DTBP. *(a)*: A benzene solution of **1a** (1.5 mmol), **2** (4 ml), and DTBP (1.5 ml) was kept in the dark at 38 °C for 7 h. The resulting yellow solution was concentrated *in vacuo*, and then the residual oil was chromatographed on TLC to give **3a**(26%), **4a**(7%), and **7**(6%). **7**: pale yellow oil. IR(CCl_4): 3530(OH), 1775 (ester C=O), and 1645(C=O) cm^{-1}. ^{1}H-NMR(CCl_4): δ= 1.33(s, 9H), 2.25(s, 3H), 2.60(s, 3H), 7.19(d, J=2.0 Hz, 1H), 7.50(d, J=2.0 Hz, 1H), and 12.6(s, 1H). Found: C, 67.00: H, 7.38%. Calcd for $C_{14}H_{18}O_4$: C, 67.18; H, 7.25%.

(b): A benzene solution of **3a** (0.073 mmol), DTBP (0.074 mmol), and **2**(1 ml) was kept in the dark at 38 °C for 1 h. The subsequent separation of the products by TLC gave **7**(25%) and recovered **3a**.

(c): A benzene solution(10 ml) of **4a**(0.25 mmol), DTBP (0.25 mmol), and **2**(12 mmol) was kept in the dark at 38 °C for 3 h; **4a** was recovered almost quantitatively.

References

1) A. Schönberg, N. Latif, R. Moubasher, and A. Sina, *J. Chem. Soc.*, **1951**, 1364.

2) K. Maruyama, A. Takuwa, S. Matsukiyo, and O. Soga, *J. Chem. Soc., Perkin Trans. 1*, **1980**, 1414, and the other references cited therein.

3) R. C. Deselms and W. R. Schleigh, *Synthesis*, **1973**, 614.

4) P. D. Bartlett, E. P. Benzing, and R. E. Pincock, *J. Am. Chem. Soc.*, **82**, 1762 (1960).

5) H. J. Teuber and G. Staiger, *Chem. Ber.*, **88**, 802 (1955).

Photolysis of *o*-(*N*-Alkylacylamino)benzophenones

Tadashi HASEGAWA,* Satomi KOSAKU, Junko UENO, and Shōshichi OGUCHI
Department of Chemistry, Tokyo Gakugei University, Nukuikitamachi, Koganei, Tokyo 184
(Received March 15, 1982)

Synopsis. The photochemical reactions of *o*-(*N*-alkylacylamino)benzophenones have been studied. Photochemical behavior of the (acylamino)benzophenones was dependent on the solvent polarity. The (acylamino)benzophenones underwent photodeacylation in polar solvents and photodealkylation in nonpolar solvents.

Hydrogen abstraction by benzophenone and its derivatives is one of the most extensively studied primary photochemical processes. It is now well established that the n,π^* triplet state of the benzophenones undergo hydrogen abstraction and that the π,π^* states are generally inert toward the primary photochemical process.[1] We previously reported photocyclization of *o*-(dialkylamino)benzophenones to indoles *via* intramolecular δ-hydrogen abstraction by the excited carbonyl oxygen.[2] We report here that *o*-(*N*-alkylacylamino)benzophenones undergo unusual photoreactions depending on the solvent polarity.

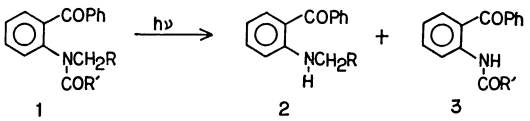

	R	R′	Solvent	**2**(%)	**3**(%)
a :	H	Ph	MeOH	57	—
b :	Ph	Ph	MeOH	70	—
			C_6H_6	5	28
c :	H	Me	MeOH	88	—
d :	Ph	Me	MeOH	89	—
			C_6H_6	—	Trace

A methanol solution of *o*-(*N*-methylbenzoylamino)-benzophenone (**1a**) was irradiated under nitrogen with a 450 W high-pressure mercury lamp through a Pyrex filter. After removal of the solvent, the residue was chromatographed on silica gel to yield *o*-(methylamino)-benzophenone (**2a**) and benzoic acid in 57 and 38% yield, respectively. Similarly, irradiation of the (acylamino)benzophenone **1b—d** under the same conditions gave the corresponding (alkylamino)benzophenone **2**. A trace of *o*-aminobenzophenone (**4**) was also obtained in the cases of photolyses of **1b** and **1d**.[3] No indoles, which were expected to form *via* δ-hydrogen abstraction by the excited carbonyl group, and no methyl esters were detected in all cases. The isolation of benzoic acid in the photolysis of **1a** and the absence of methyl esters suggest that the deacylation proceeds *via* homolytic cleavage of CO–N bond. Photodeacylation is well known in the photochemistry of imides.[4] The (acylamino)benzophenone **1** is considered to be the aromatic vinylog of imides.

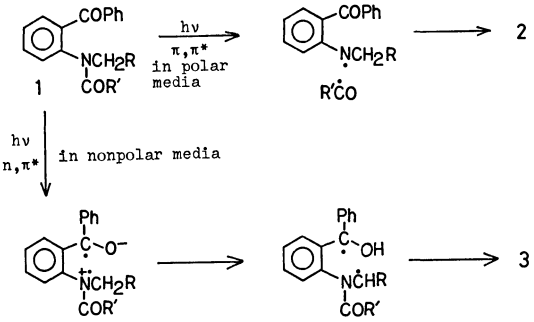

The quantum yield for production of **2c** from **1c** in methanol was taken as 0.05. The quantum yield was dependent on the solvent polarity. Polar solvents appreciably enhance the quantum efficiency with which the acylamino ketone **1c** undergoes photodeacylation in solution. (Fig. 1) The acylamino ketone **1c** in hexane showed an ultraviolet-absorption peak at 334 nm (ε 140) attributable to the n,π^* transition. This peak underwent blue shift in ethanol and was discerned at 330 nm as a shoulder. These results indicate that the relative disposition of the n,π^* and the π,π^* states of the ketone **1c** is reversed in polar media compared to that in nonpolar media and that photodeacylation occurs from the π,π^* excited state of the acylamino ketone **1c**.

In the case of photolysis of **1b** in benzene *o*-(benzoylamino)benzophenone (**3b**, 28%) was obtained as the main photoproduct, together with **2b** (5%) and a trace of **4**. Similarly, irradiation of *N*-benzylamide **1d** under the same conditions gave a trace of dealkylated photoproduct **3d**. On the other hand, no dealkylated photoproducts could be detected in the cases of *N*-methylamide **1a** and **1c** in benzene. Gold suggested that the Type II cyclization predominated over the Type II elimination in photochemistry of acylamino ketones;[5] however, no indoles could be detected in photolysis of **1** in benzene. The dealkylation

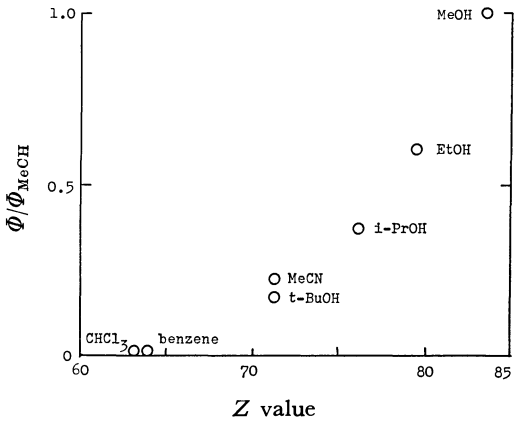

Fig. 1. Relative quantum yields for production of **2c**[a] as a function of solvent polarity (*Z* value[b]).
a) The (acylamino)benzophenone **1c** was irradiated at 313 nm. Production of **2c** was measured by UV spectroscopy. b) [E. M. Kosower, *J. Am. Chem. Soc. Soc.*, **80**, 3253 (1958).

product **3b** formed in benzene could not be detected in the photolysis of **1b** in methanol. We have already reported that a smilar photochemical dealkylation occurred in *o*-(dialkylamino)benzophenones.[2] Production of acylamino ketone **3** can be explained in terms of photodealkylation via intramolecular δ-hydrogen abstraction by the excited carbonyl group. A similar photochemical dealkylation of *o*-methoxybenzophenone via intramolecular δ-hydrogen abstraction by the carbonyl group has been reported by Leary and Oliver.[6] The solvent effect described above also suggests that dealkylation takes place from the n,π^* state of the acylamino ketone **1**.

Quenching of the photodealkylation of the acylamino ketone **1b** by 0.1 M 1,3-pentadiene (E_T=57 kcal)[7] was not observed. The photodealkylation may be considered to proceed from the n,π^* singlet state of the (acylamino)benzophenone **1b**. However, it is quite improbable that δ-hydrogen abstraction from the n,π^* singlet state can compete with intersystem crossing because the rate of intersystem crossing of benzophenone is very rapid (*ca.* 10^{11} s^{-1}).[1] Therefore, the photodealkylation seems to be reasonably explained in terms of the charge-transfer mechanism from the n,π^* state. The charge-transfer interaction is considered to contribute in the excited state of aminobenzophenone,[8] and the interaction between amide nitrogen and carbonyl oxygen was reported in photochemistry of β-oxo amides.[9]

Experimental

Chemicals. The (acylamino)benzophenones **1a—d** were prepared by the usual methods from (alkylamino)-benzophenone, and benzoyl chloride or acetic anhydride.[10]

General Procedure for Photolysis of (Acylamino)benzophenone 1. An (acylamino)benzophenone **1** (500 mg) in solvent (70 ml) was irradiated under nitrogen with a 450 W high-pressure mercury lamp (Ushio Elect. Co.) through a Pyrex filter. After removal of the solvent, the residue was chromatographed on silica gel. Elution with a mixture of benzene–ethyl acetate gave an amino ketone **2** and/or an acylamino ketone **3**. The structure of **2** and **3** were determined by direct comparison with authentic samples.[10]

Quantun Yield Determinations. The degassed solution of (acylamino)benzophenone **1** was irradiated on a merry-go-round apparatus using a 100 W high-pressure mercury lamp (Taika Elect. Co.) and a potassium chromate filter solution to isolate 313 nm irradiation. Production of **2** was measured by a Hitachi EPS-033 UV spectroscopy. Valerophenone was used as a chemical actinometer.

The present work was partially supported by a Grant-in-Aid for Scientific Research No. 56740205 from the Ministry of Education, Science and Culture.

References

1) A. A. Lamola and N. J. Turro, "Energy Transfer and Organic Photochemistry," Interscience Publishers, New York (1969).

2) H. Aoyama, T. Nishio, Y. Hirabayashi, T. Hasegawa, H. Noda, and N. Sugiyama, *J. Chem. Soc., Perkin Trans. 1*, **1975**, 298.

3) Prolonged irradiation of **1b** changed the yield of **2b** and **4**. The yield of **4** was increased and that of **2b** was decreased. When the amino ketone **2b**, which was prepared independently, was irradiated in methanol under the same conditions, **4** was obtained. These results indicate that **4** was produced from **2b** as a secondary photoproduct.

4) P. H. Mazzocchi, W. Jameson, T. Nishiyama, and A. DeCamp, *Tetrahedron Lett.*, **1980**, 989; Y. Kanaoka, T. Tsuji, K. Itoh, and K. Koyama, *Chem. Pharm. Bull.*, **21**, 453 (1973); R. O. Kan and R. C. Furey, *Tetrahedron Lett.*, **1966**, 2537.

5) E. H. Gold, *J. Am. Chem. Soc.*, **93**, 2793 (1971).

6) G. Leary and J. A. Oliver, *Tetrahedron Lett.*, **1968**, 299.

7) S. L. Murov, "Handbook of Photochemistry," Mercel Dekker, New York (1973).

8) G. Porter and P. Suppan, *Trans. Faraday Soc.*, **61**, 1664 (1965).

9) T. Hasegawa, H. Aoyama, and Y. Omote, *J. Chem. Soc., Perkin Trans. 1*, **1979**, 963.

10) P. Grammatikis, *Bull. Soc. Chim. Fr.*, **1953**, 93.

A Synthetic Route to (±)-Tetrahydroanhydroaucubigenone

Hiroshi KIMURA, Heitaro OBARA,* and Sei TAKAHASHI

Department of Applied Chemistry, Faculty of Engineering, Yamagata University, Yonezawa 992

(Received March 23, 1982)

Synopsis. (±)-Tetrahydroanhydroaucubigenone was synthesized by partial reduction, followed by acid hydrolysis, of (4a*RS*,7*RS*,7a*SR*)-7-(methoxycarbonyl)octahydrocyclopenta[*c*]pyran-1,5-dione ethylene acetal, which was prepared from 2,3,4-tris(ethoxycarbonyl)cyclopentanone through 7 steps.

Tetrahydroanhydroaucubigenone (**1**),[1] a unique tricyclic acetal ketone, has been known to be one of the key compounds for the determination of aucubin.[2] Recently, we have succeeded in the synthesis of the racemate of **1** by photo-irradiation of 6-[2-(nitrosooxy)ethyl]-3-oxabicyclo[3.3.0]octan-7-one.[3] In this paper, we wish to describe an alternative synthetic route to (±)-**1**, as shown in the following scheme.

2-(2-Acetoxyethyl)-2,3,4-tris(ethoxycarbonyl)cyclopentanone (**2**) was obtained with a small amount of an *O*-alkylated compound by the alkylation of the sodio derivative of 2,3,4-tris(ethoxycarbonyl)cyclopentanone[4] with 2-iodoethyl acetate in 36% yield. Hydrolysis and decarboxylation of **2** by heating with 47% hydrobromic acid gave *c*-3-(2-bromoethyl)-4-oxo-*r*-1, *t*-2-cyclopentanedicarboxylic acid (**3**), which was further esterified with diazomethane to give dimethyl ester **4**. Bromination of **4** with copper(II) bromide in tetrahydrofuran gave dibromide **5**, which was immediately heated with calcium carbonate in *N*,*N*-dimethylformamide to afford unsaturated lactone **6** in 26% yield.

Hydrogenation of **6** with hydrogen and 5% palladium charcoal in ethanol gave (4a*RS*,7*RS*,7a*SR*)-7-(methoxycarbonyl)octahydrocyclopenta[*c*]pyran-1,5-dione (**7**), mp 125—126 °C, as colorless needles. (4a*RS*,7*RS*,7a*SR*)-7-(Methoxycarbonyl)octahydrocyclopenta[*c*]pyran-1-one (**8**),[5] mp 72—73 °C, was also obtained with **7** in this reaction in 36% yield.

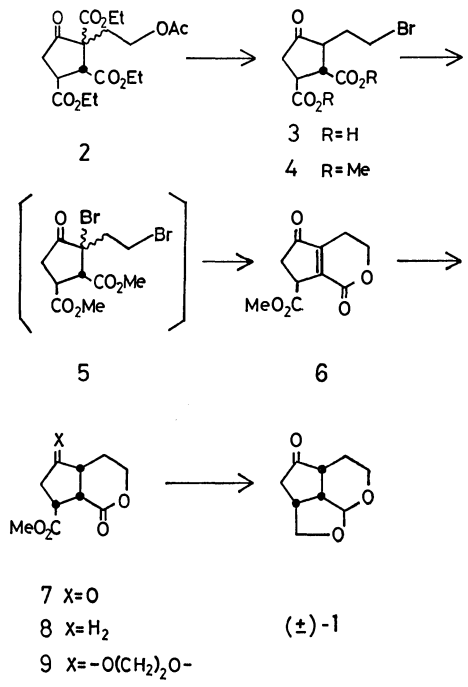

The ethylene acetal (**9**) of **7** was partially reduced with lithium aluminum hydride in tetrahydrofuran at 0—5 °C and the resulting reduction product was warmed with 20% sulfuric acid to give (±)-tetrahydroanhydroaucubigenone, mp 56—57 °C, in 15% yield. This compound was identical in all respects with (±)-**1**, which was previously synthesized by photo-irradiation of 6-[2-(nitrosooxy)ethyl]-3-oxabicyclo[3.3.0]octan-7-one.[3]

Experimental

All the boiling and melting points are uncorrected.

2-(2-Acetoxyethyl)-2,3,4-tris(ethoxycarbonyl)cyclopentanone (2). To a suspension of metallic sodium (2.3 g) in 150 ml of dry toluene was added dropwise 2,3,4-tris(ethoxycarbonyl)cyclopentanone[4] (30 g) with efficient stirring. The stirred mixture was heated on a water bath until all the sodium was consumed. Then 2-iodoethyl acetate (32 g) was added under cooling with ice water, and the mixture was left overnight at room temperature and then refluxed for 18 h. After cooling, the mixture was poured into 10% aqueous acetic acid (50 ml) and the toluene layer was separated, washed with aqueous $NaHCO_3$ solution and water, dried over Na_2SO_4, and freed from toluene to give a viscous liquid. Distillation of the residue under reduced pressure afforded **2** (14 g, 36%) containing a small amount of an *O*-alkylated by-product. Bp 153—155 °C/0.3 mmHg (1 mmHg=133.322 Pa), MS *m/e* 386 (M^+); IR (neat) 1730 cm^{-1} (br. C=O). Additional absorption bands at 1635 and 1685 cm^{-1} can be attributed to the *O*-alkylated by-product. Found: C, 55.86; H, 6.92%. Calcd for $C_{18}H_{26}O_9$: C, 55.95; H, 6.78%.

Dimethyl c-3-(2-Bromoethyl)-4-oxo-r-1,t-2-cyclopentanedicarboxylate (4). A mixture of **2** (5.0 g) and 47% hydrobromic acid (100 ml) was gently refluxed for 2 h. The reaction mixture was evaporated *in vacuo* and the resulting crude bromo keto acid (2.7 g, 75%) was methylated with diazomethane in the usual manner. The resulting crude dimethyl ester was chromatographed on a column of silica gel using benzene–ethyl acetate (4:1) as an eluent to give **4** as a colorless oil (46%). MS *m/e* 306, 308 (M^+). Found: C, 43.37; H, 4.75%. Calcd for $C_{11}H_{15}O_5Br$: C, 43.02; H, 4.92%. *c*-3-(2-Bromoethyl)-4-oxo-*r*-1,*t*-2-cyclopentanedicarboxylic acid (**3**), mp 164—165 °C (from acetic acid), was obtained pure from the above crude bromo keto acid by silica gel column chromatography using toluene–ethyl acetate–acetic acid (25:25:4) as an eluent. Found: C, 38.79; H, 4.04%. Calcd for $C_9H_{11}O_5Br$: C, 38.73; H, 3.97%.

7-(Methoxycarbonyl)-1,3,4,5,6-hexahydrocyclopenta[c]pyran-1,5-dione (6). To a solution of **4** (4.0 g) in tetrahydrofuran (50 ml) was added copper(II) bromide (6.5 g), and the mixture was refluxed with vigorous stirring for 4 h. Then the reaction mixture was filtered and the filtrate was evaporated *in vacuo* to give crude dibromo keto ester (**5**) as an oil, which was immediately used in the next reaction without purification. To a mixture of the above dibromo keto ester in *N*,*N*-dimethylformamide (4 ml) was added calcium

carbonate (1.43 g), and the mixture was heated at 90—100 °C with stirring for 4 h. The reaction mixture was then poured into ice water and the aqueous mixture was extracted several times with ethyl acetate. The ethyl acetate was removed from the extracts *in vacuo* to give a brown oil (3.5 g). The column chromatography on silica gel using benzene–ethyl acetate (5:1) as an eluent gave 2-(2-bromoethyl)-3,4-bis(methoxycarbonyl)-2-cyclopentenone (0.55 g, 14%) as the first eluate. MS *m/e* 304, 306 (M^+), IR (neat) 1725 (br. C=O) and 1640 cm^{-1} (C=C). Found: C, 43.60; H, 4.60%. Calcd for $C_{11}H_{13}O_5Br$: C, 43.30; H, 4.29%. From the second eluate, the target unsaturated lactone **6** (0.72 g, 26%) was obtained. MS *m/e* 210 (M^+), IR (neat) 1740, 1720 (C=O), 1655 cm^{-1} (C=C). Found: C, 56.56; H, 4.85%. Calcd for $C_{10}H_{10}O_5$: C, 57.14; H, 4.80%.

*(4a*RS,7RS,*7a*SR*)-7-(Methoxycarbonyl) octahydrocyclopenta*[c]*-pyran-1,5-dione (**7**).* The unsaturated lactone 6 (0.7 g) was hydrogenated in ethanol (20 ml) using hydrogen and 5% palladium charcoal (0.5 g) as a catalyst at room temperature and atmospheric pressure. After filtration of the reaction mixture, the filtrate was evaporated *in vacuo* and the residue was chromatographed on silica gel using benzene–ethyl acetate (5:2) as an eluent. From the first eluate, (4a*RS*,7*RS*,7a*SR*)-7-(methoxycarbonyl) octahydrocyclopenta-[*c*]pyran-1-one (**8**) (240 mg, 36%) was obtained. Mp 72—73 °C, MS *m/e* 198 (M^+), IR (KBr) 1720 and 1730 cm^{-1} (br. C=O). The physical and spectral data were identical with those of an authentic sample.[5] From the second eluate, **7** (100 mg, 16%) was obtained as colorless needles. Mp 125—126 °C (from benzene), MS *m/e* 212 (M^+), IR (KBr) 1740 and 1723 cm^{-1} (C=O). Found: C, 56.69; H, 5.81%. Calcd for $C_{10}H_{12}O_5$: C, 56.60; H, 5.70%.

*(±)-Tetrahydroanhydroaucubigenone ((±)-**1**).* A mixture of **7** (80 mg), ethylene glycol (37 mg), and *p*-toluenesulfonic acid (10 mg) in dry toluene (5 ml) was refluxed for 5 h, during which time most of water was removed by azeotropic distillation at atmospheric pressure. After removal of the solvent *in vacuo*, the residue was worked up in the usual manner to give ethylene acetal **9** (98%), MS *m/e* 256 (M^+).

To a solution of **9** (50 mg) in dry tetrahydrofuran (5 ml) was added lithium aluminum hydride in small portions at 0—5 °C until disappearance of a spot of **9** has been confirmed on TLC. Into a reaction mixture was then added 20% sulfuric acid under cooling with ice water until the solution become slightly acidic. The tetrahydrofuran layer was separated by decantation and heated at 50 °C for 20 min. The tetrahydrofuran was removed *in vacuo* and the residue was dissolved in ethyl acetate, and the ethyl acetate solution was washed with aqueous $NaHCO_3$ solution and water, dried over Na_2SO_4, and freed from ethyl acetate to give a viscous oil. The resulting oil was chromatographed on silica gel using benzene–ethyl acetate (5:1) as an eluent to give crude (±)-**1**. Recrystallization from benzene–petroleum ether afforded colorless needles (10 mg, 30%). mp 56—57 °C. The IR and MS spectra of this compound was completely identical with those of an authentic sample of (±)-**1**.[3]

One (H. K) of the authors is grateful to Professor Naomichi Takahashi of Yamagata University for his encouragement. We also thank Mr. Kazuaki Sato for the microanalyses.

References

1) P. Karrer and H. Schmid, *Helv. Chim. Acta*, **29**, 525 (1946); S. Fujise, *Nippon Kagaku Zasshi*, **74**, 725 (1953); S. Fujise, H. Obara, and H. Uda, *Chem. Ind.*, **1960**, 289.

2) J. M. Bobbitt and P. K. Segebarth, "Cyclopentanoid Terpene Derivatives," ed by W. I. Taylor and A. R. Battersby, Marcel Dekker, Inc., New York (1969), p. 25, and references cited therein.

3) H. Obara, H. Kimura, M. Suzuki, and J. Onodera, *Bull. Chem. Soc. Jpn.*, **51**, 3610 (1978).

4) K. Kurosawa and H. Obara, *Bull. Chem. Soc. Jpn.*, **39**, 528 (1966).

5) K. Kurosawa, H. Obara, and H. Uda, *Bull. Chem. Soc. Jpn.*, **39**, 534 (1966).

The Revised Structure of Furcation, a Component of Leaves of *Viburnum furcatum* Blume

Tsunao HASE* and Tetsuo IWAGAWA

Department of Chemistry, Faculty of Science, Kagoshima University, Korimoto, Kagoshima 890

(Received April 26, 1982)

Synopsis. The structure of furcatin, which was proposed to be *p*-vinylphenyl 6-*O*-apiosyl-(1→6)-*β*-D-glucoside, was revised to *p*-allylphenyl 6-*O*-[3-*C*-(hydroxymethyl)-*β*-D-erythrofuranosyl]-(1→6)-*β*-D-glucopyranoside by spectral and chemical results.

The structure of furcatin was reported to be phenolic glycoside (**1**) isolated as a source of bitterness from *Viburnum furcatum* Blume.[1] Its aglycone was determined as *p*-vinylphenol based on the fact that the methylated aglycone could be oxidized with permanganate, Beckmann mixture, and ozone to give *p*-methoxybenzoic acid, *p*-methoxybenzaldehyde, and formaldehyde, respectively.

However, purified furcatin was not bitter. Spectral and chemical results show that the structure should be revised to *p*-allylphenyl glycoside (**2**).

2, colorless needles, mp 160.5—161.5 °C, $[\alpha]_D^{20}$ −103.5; these were identical with results from an authentic sample previously isolated by Hattori and Imaseki. It has a molecular formula $C_{20}H_{28}O_{10}$ and the spectral data showed the presence of a *p*-substituted allylbenzene ring [$\nu_{C=C}$ 1640, 1610, 1590, 1510, 995, 960, 910, and 825 cm^{-1}; λ_{max} 213, 222, 273, and 279 nm; δ 3.27 (2H, d), 4.99 (1H, bd), 5.02 (1H, bd), 6.00 (1H, m), 7.25, and 7.51 (2H each, A_2B_2)].

Acetylation of **2** with acetic anhydride and pyridine gave an amorphous powder (**3**), $C_{32}H_{40}O_{16}$, whose NMR spectrum showed the signals for six acetyl groups δ 2.00—2.07 (3H×6). Treatment of **2** with 2 M (1 M=1 mol dm^{-3}) sulfuric acid afforded an aglycone (**4**) and two sugars which were identified as D-glucose and D-apiose by paper chromatography. The spectra of the aglycone **4** were identical with those of an authentic sample of *p*-allylphenol.[2]

2 was methylated with sodium hydride, dimethyl sulfoxide, and methyl iodide, giving hexamethyl ether (**5**) [*m/z* 512 (M^+); δ 1.83 (3H, d, J=6 Hz) and 3.34—3.62 (3H×6, s)], which seemed to suffer an allylic rearrangement during methylation. Upon hydrolysis with hydrochloric acid, **5** yielded *p*-(1-propenyl)phenol, 2,3,4-tri-*O*-methyl-D-glucose, and 2,3,3′-tri-*O*-methyl-D-apiose. The methylated D-apiose was identified by direct comparison with an authentic sample obtained from heptamethylapiin.[3] Therefore, the structure of apiose in **2** should be 3-*C*-(hydroxymethyl)-D-erythrofuranose.

A *β*-glucosidic linkage in **2** was inferred from the anomeric proton signal at δ 5.50 (1H, m, $W_{1/2}$=10 Hz) in the NMR spectrum of **2**. Upon partial hydrolysis with ion exchange resin, **2** gave a glucoside which was determined to be *p*-allylphenyl *β*-D-glucoside (**6**); its negative molecular rotation was consistent with the existence of a *β*-glucosidic linking in **2**.

A *β*-glycosidic linkage of D-apiose to D-glucose was deduced by applying Klyne's rule. The difference of the molecular rotation between **2** (−441°) and **6** (−180°) was −261°, suggesting that the anomeric configuration of D-apiose in **2** is *β*.[3]

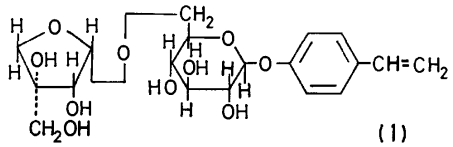

(1)

Configuration shown by dotted lines has not been elucidated.[1]

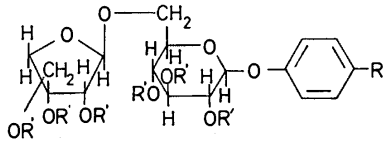

(2) R: CH_2–CH=CH_2, R′: H
(3) R: CH_2–CH=CH_2, R′: CH_3CO
(5) R: CH=CH–CH_3, R′: CH_3

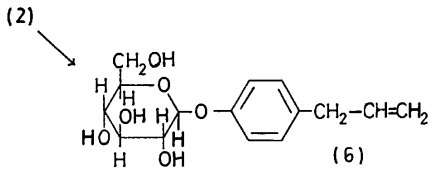

(6)

The above data show that the structure of furcatin **2** is *p*-allylphenyl 6-*O*-[3-*C*-(hydroxymethyl)-*β*-D-erythrofuranosyl]-(1→6)-*β*-D-glucopyranoside.

Only two *p*-allylphenol diglycosides, rutinoside[4] and 4-*O*-*α*-L-arabinofuranosyl-(1→4)-*β*-D-glucopyranoside[5] have so far been isolated; furcatin is the third example.

Experimental

The plants were collected in the northern highlands of Kagoshima prefecture. All the melting points were uncorrected. IR and UV spectra were taken on a Shimadzu IR-27 and a Shimadzu UV-210A spectrophotometers, respectively. ^{1}H-NMR spectra were obtained on a JEOL MH-100 spectrometer; the chemical shifts are given in *δ*-values with respect to TMS as the internal standard. Mass spectra were taken on a JEOL D-300 mass spectrometer. The optical rotations were measured on a Nihonbunko J-20 recording spectropolarimeter.

Isolation. The fresh leaves of *V. furcatum* Blume (480 g) were extracted with methanol (4 l×2). The extracts were evaporated to dryness *in vacuo* to give a residue (75 g), which was dissolved in water and extracted with ether and then ethyl acetate.

The ethyl acetate extract (8 g) was subjected to chromatography on a silica-gel column with methanol–chloroform (1:9 v/v) and recrystallized from ethyl acetate saturated with water to give furcatin **2**, needles, (500 mg), mp 160—

161.5 °C, $[\alpha]_D^{20}$ −103.5 (*c*, 0.575, MeOH); λ_{max}^{MeOH} nm (*ε*): 213 (9900), 222 (11000), 273 (1300), and 279 (990); ν_{max}^{Nujol} cm^{-1}: 3350, 1640, 1610, 1590, 1510, 995, 910, and 825; ^1H NMR (pyridine-d_5): *δ* 3.27 (2H, d, *J*=7 Hz, $C\underline{H}_2$–C=C), 4.99 (1H, bd, *J*=12 Hz, H\C=C(H)/H), 5.02 (1H, bd, *J*=15 Hz, H\C=C(H)/H), 5.50 (1H, m, $W_{1/2}$=10 Hz), 5.75 (1H, d, *J*=2 Hz), 6.00 (1H, m, $-CH_2-C\underline{H}=CH_2$), 7.25, and 7.51 (2H each, A_2B_2, *J*=9 Hz, aromatic H). Found: C, 55.64; H, 6.62%. Calcd for $C_{20}H_{28}O_{10}\cdot\frac{1}{4}H_2O$: C, 55.48; H, 6.64%.

Acetylation of **2**. **2** (100 mg) was treated with pyridine–acetic anhydride (1:1 2 ml) at room temperature. The product was chromatographed on a silica-gel column with methanol–chloroform (1:99 v/v) to give an amorphous hexaacetate **3** (100 mg); ν_{max}^{Nujol} cm^{-1} (no OH absorption) 1750, 1640, 1590, 910, and 830; ^1H NMR ($CDCl_3$): 2.0—2.07 (3H×6, s, $COC\underline{H}_3$), 3.31 (2H, d, *J*=6 Hz, $-C\underline{H}_2-CH=C$), 6.86 and 7.06 (2H each, A_2B_2, *J*=8 Hz, aromatic H); MS *m/z* 620 (M^+-60). Found: C, 56.48; H, 6.03%. Calcd for $C_{32}H_{40}O_{16}$: C, 56.46; H, 5.92%.

Hydrolysis of **2** *with Sulfuric Acid*. **2** (100 mg) was dissolved in 2 M sulfuric acid (2 ml) and the solution was stirred at 80 °C for 1 h. The reaction mixture was diluted with water, extracted with ether, washed with water and dried over Na_2SO_4. The solvent was evaporated to give an oily aglycone **4** (25 mg), ν_{max}^{film} cm^{-1}: 3300, 1640, 1610, 1600, 1510, 995, 915, and 820; ^1H NMR ($CDCl_3$): 3.33 (2H, d, *J*=6 Hz, $-C\underline{H}_2-CH=C$), 4.83—5.12 (2H, bd, $-CH=C\underline{H}_2$), 5.67—6.36 (1H, m, $-CH_2-C\underline{H}=CH_2$), 6.80, and 7.14 (2H each, A_2B_2, *J*=9 Hz). These data were identical with those of an authentic *p*-allylphenol.[2] The aqueous solution was neutralized with an excess of barium carbonate, then the precipitate was filtered off and the filtrate was evaporated to dryness *in vacuo*. The paper chromatography of the product showed the presence of D-apiose and D-glucose [solvent system, AcOEt:pyridine:H_2O:AcOH=5:5:3:1].

Methylation of **2**. A solution of sodium hydride (250 mg) in dimethyl sulfoxide (5 ml) was stirred at 70 °C for 1 h under an atmosphere of nitrogen. After cooling to room temperature, a solution of **2** (100 mg) in dimethyl sulfoxide (2 ml) was added to the solution. After the mixture was stirred for 1 h, methyl iodide (1 ml) was added to it. The reaction mixture was stirred for 4 more hours, then poured into ice water and extracted with chloroform. The extract was washed with water and dried over Na_2SO_4 and the solvent was evaporated to give a crude product which was chromatographed on silica gel with methanol–chloroform (1:99 v/v) to give an oily permethylate **5** (100 mg), ν_{max}^{film} cm^{-1}: (no OH absorption) 1610, 1580, 1510, 990, 960, 840, and 790; ^1H NMR ($CDCl_3$): 1.83 (3H, d, *J*=6 Hz, $-C=C(H)-C\underline{H}_3$), 3.34, 3.46, 3.52, 3.62 (total 3H×6, s, $OC\underline{H}_3$), 6.92, and 7.20 (each 2H, A_2B_2, *J*=9 Hz, aromatic proton); MS *m/z* 512 (M^+).

Hydrolysis of Permethylate **5**. To a solution of permethylate **5** (186 mg) in a mixture of dioxane (1 ml) and methanol (1 ml), was added 2 M hydrochloric acid (1 ml) and the solution was stirred at 110 °C for 2 h. The reaction mixture was diluted with water, extracted with ether, washed with water and brine, and dried over Na_2SO_4. The solvent was evaporated to give an oily residue, which was chromatographed on silica gel with chloroform to give an oily aglycone (14 mg) which was identical with an authentic *p*-propenylphenol.[6] The aqueous solution was treated with amberlite IR-45 and evaporated to dryness *in vacuo*. The crude product was subjected to column chromatography on silica gel with methanol–chloroform (3:97 v/v) to give a tri-*O*-methyl-D-apiose (25 mg), $[\alpha]_D^{20}$ −5 (*c*, 0.650, MeOH), and a tri-*O*-methyl-D-glucose (27 mg). These methylated sugars were identical with authentic 2,3,3′-tri-*O*-methyl-D-apiose and 2,3,4-tri-*O*-methyl-D-glucose, respectively. An authentic 2,3,3′-tri-*O*-methyl-D-apiose, $[\alpha]_D^{20}$ −1.7 (*c*, 2.3, MeOH), was obtained from apiin which was isolated from parsley, according to the methods in the literature.[3]

Partial Hydrolysis of **2**. 100 mg of **2** was dissolved in water (3 ml) and 1 g of acidic ion exchange resin Amberlite IR-120 was added to it; this mixture was stirred at 65 °C for 1 h. After filtration, the solvent was evaporated to dryness, then the residue (84 mg) was subjected to column chromatography on silica gel with methanol–chloroform (1:9 v/v) and recrystallized from water to give a phenolic glucoside **6** (31 mg), mp 148—149 °C, $[\alpha]_D^{20}$ −61.8 (*c*, 0.275, MeOH), ^1H NMR (acetone-d_6): 3.40 (2H, d, *J*=7 Hz), 5.04 (1H, d, *J*=7 Hz, glucose H-1), 5.10 (1H, bd, *J*=12 Hz), 5.14 (1H, bd, *J*=20 Hz), 5.68—6.24 (1H, m), 7.14, and 7.26 (2H each, A_2B_2, *J*=8 Hz); MS *m/z* (rel int): 296 (M^+, 0.6), 134 ($C_3H_5-C_6H_4-OH$, 100). These data coincided with those of *p*-allylphenyl *β*-D-glucoside in the literature.[7]

The authors are grateful to Professor Hidemasa Imaseki, Nagoya University, for kindly providing authentic samples of furcatin, and to Professor Koichi Koshimizu, Kyoto University, for kindly supplying the IR and ^1H NMR spectra of authentic *p*-allylphenol. They also would like to thank Dr. Shizuo Sako, Kagoshima University, for his aid in the collection and identification of the plants.

References

1) S. Hattori and H. Imaseki, *J. Am. Chem. Soc.*, **81**, 4424 (1959).
2) H. Ohigashi and K. Koshimizu, *Agric. Biol. Chem.*, **40**, 2283 (1976).
3) R. K. Hulyalkar, J. K. N. Jones, and M. B. Perry, *Can. J. Chem.*, **43**, 2085 (1965).
4) H. Herissey, *C. R. Acad. Sci.*, **198**, 256 (1934).
5) R. Higuchi, M. Aritomi, and D. M. X. Donnelly, *Phytochemistry*, **16**, 1007 (1977).
6) An authentic *p*-(1-propenyl)phenol was obtained from methyl *p*-(1-propenyl)phenyl ether (anethole, Wako Prue Chemical Ind.) by alkaline demethylation. R. Stoermer and F. Kahlert, *Ber.*, **34**, 1812 (1901).
7) R. Higuchi and D. M. X. Donnelly, *Phytochemistry*, **16**, 1587 (1977).

Stereoselective Synthesis of Mixed Acetal Glycosides by Reaction of Tri-*O*-acetyl-*N*-(2,4-dinitrophenyl)-α-D-glucosaminyl Bromide with Alcohol in Acetone[1]

Shinkiti Koto,* Shigeru Inada, Tomoko Narita, Naohiko Morishima, and Shonosuke Zen

School of Pharmaceutical Sciences, Kitasato University, Shirokane, Minato-ku, Tokyo 108

(Received January 14, 1982)

Synopsis. Some mixed acetal glycosides were stereoselectively synthesized by the reaction of 3,4,6-tri-*O*-acetyl-2-deoxy-2-(2,4-dinitroanilino)-α-D-glucopyranosyl bromide with alcohols in acetone containing $Hg(CN)_2$, $HgBr_2$, and tetrabutylammonium bromide at room temperature. When *t*-butyl alcohol was used, a novel enol glycoside of acetone was formed.

3,4,6-Tri-*O*-acetyl-2-deoxy-2-(2,4-dinitroanilino)-α-D-glucopyranosyl bromide (**1**)[2] has been a useful reagent for synthesizing various α-D-glucosaminides.[3] This report presents our findings that a homogeneous reaction of **1** with methanol (MeOH) in acetone (Me_2CO) in the presence of $Hg(CN)_2$, $HgBr_2$, and tetrabutylammonium bromide (*n*-Bu_4NBr) at room temperature gave a novel acetal glycoside (**2**) (Eq. 1) in a 54% yield (Table 1, Run 2).[4] The reaction was highly stereoselective and gave no methyl glycosides (**3a** and **3b**). The use of solvents such as 1,2-dichloroethane (Run 9) and nitromethane (Run 10) as well as an excess of MeOH (Run 11) caused the

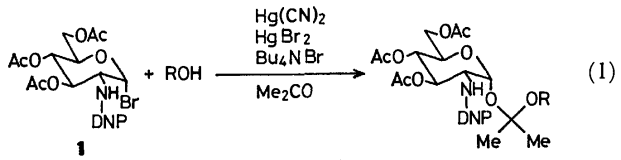

(1)

1

DNP = 2,4-dinitrophenyl

Table 1. Results of experiments using methanol[a]

Run	$Hg(CN)_2$ (equiv.)	$HgBr_2$ (equiv.)	*n*-Bu_4NBr (equiv.)	Yield/%[b] **2**	Yield/%[b] **3a**+**3b**
1	0.5	0.5	0.67	31	0
2	0.5	0.5	1.0	54	0
3	0.5	0.5	1.5	32	13
4	0.5	0.5	2.0	16	32
5	0.5	0.5	—	0	8
6	—	—	1.0	0	35
7	1.0	—	1.0	69	18
8	—	1.0	1.0	0	20
9[c]	0.5	0.5	1.0	35[f]	21
10[d]	0.5	0.5	1.0	60[f]	8
11[e]	0.5	0.5	1.0	53	19

a) Reactions were conducted in 0.1 mmol scale for 6 h at room temperature. b) Yields were determined by measuring ^1H NMR (60 MHz) of product mixtures (see Experimental). c) Me_2CO (66 μl, 9.0 equiv.) and $(CH_2Cl)_2$ (0.46 ml) were used. d) Me_2CO (66 μl, 9.0 equiv.) and $MeNO_2$ (0.46 ml) was used. e) Excess MeOH (12 μl, 3.0 equiv.) was used. f) A very small peak of the β-anomer of **2** was observed at δ 3.01.

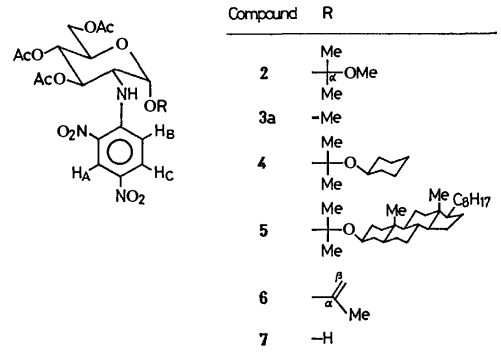

formation of **3a** and **3b**. The use of the ternary mixture was essential for the acetalization without forming **3a** and **3b** (Runs 5—8); the optimal proportion of $Hg(CN)_2$, $HgBr_2$, and *n*-Bu_4NBr to **1** found is 0.5:0.5:1.0 (Runs 1—4).

Incidentally, 1-methoxy-1-methylethyl group, known as a labile protecting group of hydroxyl group,[5] was readily removed from **2** by a mild acid hydrolysis without the removal of the acetyl groups and survived through the *O*-deacetylation and the *N*-dedinitrophenylation in basic media.

2,3,4,6-Tetra-*O*-acetyl-α-D-glucopyranosyl bromide does not undergo such acetalization reaction. For **1**, Me_2CO is the sole ketone which gives the acetal glycoside in an acceptable yield, aldehydes such as propional are also unsuitable. Cyclohexanol and 5α-cholestan-3β-ol gave the respective acetal glycosides (**4** and **5**). However, *t*-butyl alcohol did not afford such a type of glycoside but isopropenyl 3,4,6-tri-*O*-acetyl-2-deoxy-2-(2,4-dinitroanilino)-α-D-glucopyranoside (**6**), a novel enol glycoside,[6] was formed.

Experimental

The instruments used were identical with those described earlier.[7] Solid compounds, **1**,[2] $Hg(CN)_2$ (Wako), $HgBr_2$ (Wako), *n*-Bu_4NBr (Tokyo Kasei), and 5α-cholestan-3β-ol (Tokyo Kasei), were stored *in vacuo* over P_2O_5 before use. The physical and analytical data for the acetals are in Table 2.

*1-Methoxyl-1-methylethyl 3,4,6-Tri-*O*-acetyl-2-deoxy-2-(2,4-dinitroanilino)-α-D-glucopyranoside (**2**).* MeOH (40 μl, 1.0 mmol) and Me_2CO (5.3 ml) were successively added to a mixture of **1** (534 mg, 1.0 mmol), $Hg(CN)_2$ (126 mg, 1.0 mmol), $HgBr_2$ (180 mg, 1.0 mmol), and *n*-Bu_4NBr (322 mg, 1.0 mmol). After stirring for 24 h at room temperature and adding water (1.0 ml), the mixture was evaporated at 30 °C under diminished pressure and chromatographed on silica gel (Kanto Kagaku) using a mixture of benzene and butanone (10:1). The faster-moving band afforded **2** (310.5 mg, 57%); δ_H ($CDCl_3$, Me_4Si): 1.50 (s, 6H, CMe), 1.80 (s, 3H, OAc),

Table 2. Yields[a] and physical data of acetals

Compd	Yield %	Mp(recrystallized from[b]) θ_m/°C		$[\alpha]_D^{20}$/° (c, Me_2CO)	Mol formula	Found(Calcd)(%) C	H	N
2	54	174—176	(C/H, needles)	+12(1.0)	$C_{22}H_{29}N_3O_{13}$	48.38 (48.62)	5.29 (5.38)	7.89 (7.73)
4	69	173—175	(I, needles)	+9(0.5)	$C_{27}H_{37}N_3O_{13}$	52.88 (53.02)	5.81 (6.10)	6.71 (6.87)
5	64	228—230(decomp)	(E, needles)	+71(0.6)	$C_{40}H_{73}N_3O_{13}$	63.93 (64.05)	8.10 (8.17)	4.58 (4.67)

a) Reaction time was 6 h. b) C: Chloroform, E: ethyl acetate, H: hexane, I: diisopropyl ether.

2.06 (s, 3H, OAc), 2.10 (s, 3H, OAc), 3.19 (s, 3H, OMe), 7.07 (d, 1H, J_{BC}=10 Hz, H_B), 8.27 (q, 1H, H_C), 8.72 (d, 1H, J=10 Hz, NH), 9.10 (d, 1H, J_{AB}=3.5 Hz, H_A); δ_C ($CDCl_3$, Me_4Si)[8] 20.6 (3C, OAc), 24.6, 26.3, 50.0 (OMe), 55.3 (C-2), 62.1 (C-6), 67.9, 68.4, 72.9, 90.1 (C-1), 103.3 (C-α), 114.5, 124.3, 130.0, 131.0, 136.7, 147.5, 169.6, 169.9, 170.7. The slower-moving band gave 3,4,6-tri-*O*-acetyl-2-deoxy-2-(2,4-dinitroanilino)-α-D-glucopyranose (**7**) (170.5 mg, 38%), which was identified with the sample prepared by the authentic route.[2]

Heating **2** (52.6 mg, 0.097 mmol) in aq acetic acid (80%, 0.5 ml) at 70 °C for 40 min furnished **7** (42.5 mg, 93%).

*1-Methoxy-1-methylethyl 2-Deoxy-2-(2,4-dinitroanilino)-α-D-glucopyranoside (**8**).* The treatment of **2** (200 mg, 0.37 mmol) with ammoniacal methanol (38 g, 21%) at room temperature overnight gave **8** (*ca.* 150 mg, quant.); mp 160—162 °C, $[\alpha]_D^{20}$ +4.5° (c 1.0, Me_2CO); δ_H ($(CD_3)_2CO$, Me_4Si) 1.43 (s, 3H, CMe), 1.48 (s, 3H, CMe), 3.16 (s, 3H, OMe), 5.40 (d, 1H, $J_{1,2}$=3.5 Hz, H-1), 7.53 (d, 1H, J_{BC}=10 Hz, H_B), 8.25 (q, 1H, H_C), 8.97 (d, 1H, J_{AB}=2.5 Hz); δ_C ($(CD_3)_2CO$, Me_4Si) 24.9, 26.7, 49.8 (OMe), 57.8 (C-2), 62.4 (C-6), 71.5, 73.4, 75.1, 91.2 (C-1), 102.8 (C-α), 117.2, 124.1, 130.2, 130.9, 136.5, 149.7. Found: C, 45.79; H, 5.44; N, 10.04%. Calcd for $C_{16}H_{23}N_3O_9$: C, 46.04; H, 5.55; N, 10.07%.

*1-Methoxy-1-methylethyl 2-Amino-2-deoxy-α-D-glucopyranoside (**9**).* The treatment of **8** (91.8 mg, 0.22 mmol) with Dowex 1×2 (1 ml) in aq Me_2CO (67%, 5 ml) for 6 h at room temperature afforded **9** (41.1 g, 74%); mp 189—191 °C (decomp), $[\alpha]_D^{20}$ +139° (c 0.3, H_2O); δ_H (D_2O, Me_4Si (ext.)) 1.90 (s, 6H, CMe), 3.16 (dd, 1H, J=3.9 and 9.6 Hz, H-2), 3.76 (s, 3H, OMe) 5.64 (d, 1H, J=3.9 Hz H-1); δ_C (D_2O, Me_4Si (ext.)) 25.2, 26.2, 50.7 (OMe), 56.5 (C-2), 62.0 (C-6), 71.2 (C-4), 73.6 (C-5), 75.2 (C-3), 93.8 (C-1), 103.9 (C-α). Found: C, 47.65; H, 8.52; N, 5.55%. Calcd for $C_{10}H_{21}NO_6$: C, 47.80; H, 8.42; N, 5.57%.

Procedure for the Acetalization to Obtain the Data for Table 1. A round-bottomed flask containing weighed solid compounds (**1** and, optionally, $Hg(CN)_2$, $HgBr_2$ and n-Bu_4NBr) was kept *in vacuo* over P_2O_5 for 30 min. Anhydrous solvent (when necessary), Me_2CO, and MeOH were successively injected into this vessel, stoppered with a rubber-cap. The reaction was stirred and quenched by adding water (1 drop). After evaporation at 30 °C, the mixture was chromatographed as above. Fractions containing **2**, **3a**, and **3b** were combined to give a glass whose ^1H NMR spectrum usually showed three singlets of methoxyl groups of **2**, **3a**, and **3b** at δ 3.20, 3.55, and 3.50 in $CDCl_3$ with Me_4Si (Table 1).

Attempted Acetalization Using t-Butyl Alcohol. Me_2CO (1.0 ml) was injected into a rubber-stoppered flask containing *t*-BuOH (15.2 mg, 0.2 mmol), **1** (106.8 mg, 0.2 mmol), $Hg(CN)_2$ (25.2 mg, 0.1 mmol), $HgBr_2$ (36.0 mg, 0.1 mmol), and n-Bu_4NBr (64.4 mg, 0.2 mmol). After having been stirred for 6 h at room temperature, the mixture was evaporated and chromatographed as above. The faster-moving major band gave isopropenyl 3,4,6-tri-*O*-acetyl-2-deoxy-2-(2,4-dinitroanilino)-α-D-glucopyranoside (**6**) (37.1 mg, 36%); mp 199—202 °C, $[\alpha]_D^{20}$ −8.6° (c 1.3, Me_2CO); δ_H ($CDCl_3$, Me_4Si) 1.77 (s, 3H, OAc), 1.90 (s, 3H, CMe), 1.97 (s, 3H, OAc), 2.03 (s, 3H, OAc), 7.10 (d, 1H, J_{BC}=9 Hz, H_B), 8.20 (q, 1H, H_C), 8.80 (d, 1H, J=12 Hz, NH), 9.07 (d, 1H, J_{AB}=3 Hz, H_A); δ_C ($CDCl_3$, Me_4Si) 20.2 (CMe), 20.6 (3C, Ac), 55.1 (C-2), 61.5 (C-6), 67.9, 68.3, 73.0, 88.7 (C-β), 94.7 (C-1), 114.4, 124.3, 130.0, 131.3, 136.9, 147.6, 157.1 (C-α) 169.7 (2C, Ac), 170.7 (Ac). Found: C, 48.94; H, 4.84; N, 8.41%. Calcd. for $C_{21}H_{25}N_3O_{12}$: C, 49.32; H, 4.93; H, 8.22%.

Compound **6** (45.7 mg, 0.09 mmol) was treated with dil. sodium methoxide in methanol (0.15%, 2 ml) at room temperature overnight. After NH_4Cl had been added, the mixture was evaporated and chromatographed to give propenyl 2-deoxy-2-(2,4-dinitroanilino)-α-D-glucopyranoside (**10**) (35 mg, 94%); mp 161—165 °C, $[\alpha]_D^{20}$ −1.0° (c 1.4, Me_2CO); δ_H ($(CD_3)_2CO$, Me_4Si) 1.95 (s, 3H, CMe), 5.48 (d, 1H, $J_{1,2}$=3.5 Hz, H-1), 7.57 (d, 1H, J_{BC}=9 Hz, H_B), 8.23 (q, 1H, H_C), 8.95 (d, 1H, J_{AB}=3 Hz, H_A); δ_C ($(CD_3)_2CO$, Me_4Si)[6] 20.4 (CMe), 58.1 (C-2), 62.0 (C-6), 71.0, 74.4, 75.6, 88.3 (C-β), 96.6 (C-1), 117.3, 124.4, 130.5, 131.5, 131.6, 137.2, 150.1, 158.4 (C-α). Found: N, 10.42%. Calcd for $C_{15}H_{19}N_3O_9$: N, 10.90%.

References

1) Presented at the 37th National Meeting of the Chemical Society of Japan, April 1978, Yokohama. Recently, a stereoselective synthesis of mixed acetal glucosides has been reported (L.-T. Tietze and R. Fischer, *Tetrahedron Lett.*, **22**, 3239 (1981); *Angew. Chem., Int. Ed. Engl.*, **20**, 969 (1981)).

2) P. F. Lloyd and M. Stacey, *Tetrahedron*, **9**, 116 (1960).

3) K. Igarashi, *Adv. Carbohydr. Chem. Biochem.*, **34**, 243 (1977), S. Koto, S. Inada, and S. Zen, *Chem. Lett.*, **1980**, 183.

4) A. N. de Belder, P. J. Garegg, B. Lindberg, G. Petropavlovskii, and O. Theander, *Acta Chem. Scand.*, **16**, 623 (1962); H.-M. Dettinger, J. Lehmann, and K. Wallenferls, *Carbohydr. Res.*, **87**, 63 (1980).

5) A. F. Klug, K. G. Untch, and J. H. Fried., *J. Am. Chem. Soc.*, **94**, 7827 (1977).

6) T. D. Perrine, C. P. J. Glaudemans, R. K. Ness, J. Kyle, and H. G. Fletcher, Jr., *J. Org. Chem.*, **32**, 664 (1967); L. Coffier, G. Remy, and G. Descotes, *Synthesis*, **1979**, 711.

7) S. Koto, N. Morishima, and S. Zen, *Bull. Chem. Soc. Jpn.*, **52**, 784 (1979).

8) Assignments were carried out by observing off-resonance decoupling spectra.

A Through-process for the Preparation of Methyl Per-*O*-acetyl 1-Thio-glycosides from Aldoses

Shinkiti Koto,* Toyosaku Yoshida, Kazuhiro Takenaka, and Shonosuke Zen

School of Pharmaceutical Sciences, Kitasato University, Shirokane, Minato-ku, Tokyo 108

(Received May 4, 1982)

Synopsis. D-Glucose, D-galactose, D-mannose, D-xylose, L-arabinose, L-fucose, L-rhamnose, maltose, cellobiose, lactose, D-glucosamine, D-galactosamine, and D-mannosamine were converted into the corresponding methyl per-*O*-acetyl 1-thioglycopyranosides by way of a three-step (acetobromination, methylthioation, and acetylation) through-process in a single vessel.

The alkyl thio group is useful for protecting the anomeric center of carbohydrate in the sequential glycoside synthesis.[1] Continuing our methodologic study of oligosaccharide synthesis,[1a,2] a handy procedure for introducing the methylthio group at the anomeric center of a given saccharide was developed.

D-Glucose was smoothly acetobrominated through reaction with acetyl bromide (AcBr) in acetic acid (AcOH). The use of the AcOH solvent prevents any occasional sudden evolution of HBr such as occurs in the direct use of AcBr for the acetobromination of free sugar. The reaction was so clean that the evaporation of excess AcBr and AcOH gave 2,3,4,6-tetra-*O*-acetyl-α-D-glucopyranosyl bromide ready for immediate use. The subsequent conversion to the methylthio compound was conveniently carried out by a reaction with commercially available aq sodium methanethiolate (MeSNa) in acetone. Because of the concurrent de-*O*-acetylation during mercaptolysis, a reacetylation process was required. The chromatography of the reaction mixture afforded methyl 2,3,4,6-tetra-*O*-acetyl-1-thio-β-D-glucopyranoside (**1**) in a ≈60% yield. The whole process from D-glucose to **1** could be done in a single vessel.

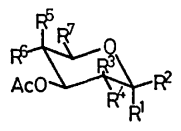

1—5, 8—13

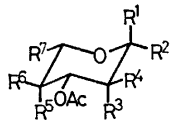

6, 7

Compd	R^1	R^2	R^3	R^4	R^5	R^6	R^7
1	H	SMe	H	OAc	H	OAc	CH_2OAc
2	H	SMe	H	OAc	OAc	H	CH_2OAc
3	SMe	H	OAc	H	H	OAc	CH_2OAc
4	H	SMe	H	OAc	H	OAc	H
5	H	SMe	H	OAc	OAc	H	H
6	H	SMe	H	OAc	OAc	H	Me
7	SMe	H	OAc	H	H	OAc	Me
8	G	H	H	OAc	H	OAc	CH_2OAc
9	H	G	H	OAc	H	OAc	CH_2OAc
10	H	G	H	OAc	OAc	H	CH_2OAc
11	H	SMe	H	NHAc	H	OAc	CH_2OAc
12	H	SMe	H	NHAc	OAc	H	CH_2OAc
13	SMe	H	NHAc	H	H	OAc	CH_2OAc

G = 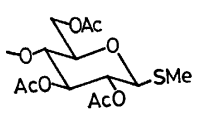

Using this through-process, D-galactose, D-mannose, D-xylose, L-arabinose, L-fucose, and L-rhamnose were readily converted into the corresponding acetates of methyl 1-thioglycopyranosides. In the cases of the 6-deoxy sugars, however, a careful control of the temperature for the evaporation of excess AcBr was essential.

Disaccharides, maltose, cellobiose, and lactose, were also suitable; their inter-glycoside linkage was not cleaved at all during acetobromination.

In the case of D-glucosamine, the acetobromination took a much longer time[3] compared to those described above. Nevertheless, methyl 2-acetamido-3,4,6-tri-*O*-acetyl-2-deoxy-1-thio-β-D-glucopyranoside (**11**) was obtained in a ≈50% yield. Other amino sugars, D-galctosamine, and D-mannosamine were derived into the thioglycoside derivatives.

Thus, the through-process presented is so simple and economical that its rather low yields do not make it disadvantageous in comparison with the previously known methods for preparing methyl 1-thioglycoside.[4]

Experimental

General. See the preceeding report.[5]

General Procedure for Obtaining the Data in Table 1. Cooled AcOH (0.5 ml) was added into a suspention of aldose (with or without water of crystallization) or glycosamine hydrochloride (1.0 mmol) in AcBr (1.0 ml) under stirring at 0 °C. The mixture was then stirred at room temperature for 2 h (but for 3 d for amino sugar). The excess reagents were then evaporated off at 25—35 °C, followed by evaporation with toluene. Cold aq MeSNa (Tokyo Kasei, 15%, 2.0 ml) was added into a solution of the acetobromo sugar thus obtained in acetone (3.5 ml) under stirring at 0 °C; in the case of aminosugar, the amount of aq MeSNa was doubled. The mixture was then stirred for 18 h at room temperature. Evaporation at 45—55 °C gave a solid material which was heated in Ac_2O (3.0 ml) containing NaOAc (0.1 g) under stirring at 100 °C. Evaporation on a boiling-water bath and subsequent chromatography on silica gel using the toluene–2-butanone system (gradient) gave totally acetylated methyl 1-thioglycopyranoside.

An Example of Large-scale Preparation. D-Mannose (10 g, 0.056 mol) was added at once into well-cooled AcBr (56 ml) under good stirring at 0 °C. Soon after this, cold AcOH (28 ml) was added to the suspension. During the next 10 min, all the sugar dissolved, with a fairly violent evolution of HBr. After the evolution had been set aside, the ice-bath was removed and the solution was stirred for 1.5 h at the ambient temperature. The excess reagents were evaporated under reduced pressure at 23—35 °C and then co-evaporated with toluene three times. The heavy syrup thus obtained was evacuated for 0.5 h and dissolved in cold Me_2CO (80 ml). Cold aq NaSMe (15%, 86 ml) was then added to the stirred solution at 0 °C. After the ice bath had been removed, the mixture was vigorously stirred at the ambient temperature for 18 h. After the evaporation of volatile ma-

Table 1. Physical and analytical data

Compd	Yield %	Mp θ_m/°C	$[\alpha]_D^{20}$/°(c, $CHCl_3$)	Mol formula	Calcd(%) C	Calcd(%) H	Calcd(%) N	Found(%) C	Found(%) H	Found(%) N	Lit
1	61	99—100	−15(0.9)								
2	49	111—112	+2(0.7)	$C_{15}H_{22}O_9S$	47.61	5.86		47.58	5.92		a
3	59	122—124	+102(0.8)					47.53	5.84		b
								47.69	5.91		c
4	56	90—92	−74(0.5)					46.90	5.88		d
5	40	80—81	+6(0.3)	$C_{12}H_{18}O_7S$	47.05	5.92		46.92	5.90		e
6	57	149—150	+2(1.0)					48.96	6.36		
7	34	—	−114(2.1)	$C_{13}H_{20}O_7S$	49.76	6.12		49.50	6.40		
8	46	130—132	+50(0.5)					48.46	5.70		f
9	59	200—202	−20(0.8)	$C_{27}H_{38}O_{18}S$	48.64	5.75		48.65	5.82		g
10	45	128—130	−8(0.5)					48.34	5.81		h
11	54	199—200	−37(0.9)					47.92	6.24	3.66	
12	34	208—210	−33(0.3)	$C_{15}H_{23}NO_8S$	47.74	6.14	3.71	47.53	6.18	3.60	
13	34	—	+125(1.6)					47.76	6.18	3.68	

a) Ref. 4c; mp 96 °C, $[\alpha]_D$ −12.2°(c 1.2, $CHCl_3$). Ref. 4d; mp 91 °C, $[\alpha]_D$ −12.0°(c 1.0, $CHCl_3$). b) Ref. 4b; mp 108 °C, $[\alpha]_D^{17}$ +2.85°(c 1.3, $CHCl_3$). Ref. 4f; mp 109—111 °C, $[\alpha]_D$ +3.7($CHCl_3$). c) Ref. 4f; mp 123—125 °C, $[\alpha]_D$ +93.1°($CHCl_3$). d) Ref. 4e; mp 87.5—90 °C, $[\alpha]_D$ −73.4±2°(c 0.49, $CHCl_3$). e) Ref. 4b; mp 73—74 °C, $[\alpha]_D^{18}$ +6.2°(c, 1.95, $CHCl_3$). f) Ref. 4f; mp 133—135 °C, $[\alpha]_D$ +56.0°($CHCl_3$). g) Ref. 4a; mp 200 °C, $[\alpha]_D^{20}$ −20.3°(c 1.6, $CHCl_3$). h) Ref. 4f; mp 124—125 °C, $[\alpha]_D$ −9.0($CHCl_3$).

Table 2. ^{1}H NMR data[a)]

Compd	H-1(J/Hz)	MeS, Ac	MeC(J/Hz)
1	4.38(9)	1.98 **2.00** 2.04 **2.06 2.16**	
2	4.39(9)	1.98 2.03 2.06 **2.15 2.17**	
3	5.17(≈1)	1.97 2.04 2.09 2.14(6H)	
4	4.37(9)	2.02(6H) (2.06 2.15)	
5	4.39(8.5)	2.01 **2.06** 2.13 2.17	
6	4.35(10)	1.96 2.05 2.15 2.17	1.21(7.6)
7	5.07(≈1)	1.96 2.03 2.14(6H)	1.25(7.0)
8	4.43(10)	1.99 2.00 2.01 2.02 2.04 2.09 2.13(6H)	
9	4.35(10)	1.96 **2.00** 2.02(6H) 2.05 2.08 2.11 2.13	
10	4.37(10)	1.95 2.03(12H) 2.10 2.13(6H)	
11	4.58(10)	1.96 2.02 2.03 2.07 2.19	
12	4.59(10)	1.93 1.95 2.02 2.15 2.19	
13	5.11(1.5)	1.98 2.04 2.05 2.09 2.13	

a) The spectra were determined at 90 MHz in $CDCl_3$ with Me_4Si.

terials at 45—55 °C, the residue thus obtained was stirred in Ac_2O (168 ml) containing AcONa (5.8 g) at 100 °C for 2 h. Evaporation on a boiling water bath and subsequent chromatography gave **3** (8.4 g, 40%).

References

1) a) S. Koto, T. Uchida, and S. Zen, *Bull. Chem. Soc. Jpn.*, **46**, 2520 (1973); b) P. J. Pfaffli, S. H. Hixon, and L. Anderson, *Carbohydr. Res.*, **23**, 195 (1972); M. A. Nashed, M. Kiso, C. W. Slife, and L. Anderson, *ibid.*, **90**, 71 (1981).

2) S. Koto, N. Morishima, C. Kusuhara, S. Sekido, T. Yoshida, and S. Zen, *Bull. Chem. Soc. Jpn.*, **55**, 2995 (1982).

3) G. Fodor and L. Ötvös, *Chem. Ber.*, **89**, 701 (1956); Y. Ito, S. Koto, and S. Umezawa, *Bull. Chem. Soc. Jpn.*, **35**, 1618 (1962).

4) F. Wrede and O. Hettche, *Z. Physiol. Chem.*, **172**, 169 (1927); B. Helferich, H. Grunewald, and F. Langenhoff, *Chem. Ber.*, **86**, 873 (1953); M. Cerny and J. Pacak, *Chem. Listy*, **52**, 2090 (1958); M. Sakata, M. Haga, S. Tejima, and M. Akagi, *Chem. Pharm. Bull.*, **12**, 652 (1964); J. Stanek, M. Sindlerova, and M. Cerny, *Coll. Czech. Chem. Commun.*, **30**, 297 (1965); T. Ogawa and M. Matsui, *Carbohydr. Res.*, **54**, C17 (1977).

5) S. Koto, N. Morishima, R. Kawahara, K. Ishikawa, and S. Zen, *Bull. Chem. Soc. Jpn.*, in press.

Table 3. ^{13}C NMR data[a)]

Compd	C-1′	C-1	C-2—C-6 (and C-2′—C-6′)										CH_3CON	CH_3-5	CH_3S
1	—	83.0	76.2	**74.1**	69.3	68.5	62.3						—	—	11.3
2	—	83.6	74.7	**72.1**	67.5	**66.7**	**61.6**						—	—	11.5
3	—	83.7	71.0	69.7	69.1	66.5	62.6						—	—	13.6
4	—	83.6	72.8	**69.3**	69.0	**66.1**							—	—	11.6
5	—	84.2	71.2	68.2	67.6	**66.8**							—	—	12.0
6	—	83.3	73.4	72.5	**70.7**	66.9							—	**16.5**	11.5
7	—	83.6	71.4	70.8	69.6	67.1							—	17.5	13.8
8	95.8	82.8	76.4(2)	**72.9**	**70.2**(2)	69.5	68.7	68.1	63.1	61.6			—	—	11.5
9	101.1	83.1	**77.0**	**76.6**	73.7	73.1	72.2	71.8	69.7	68.0	62.3	61.7	—	—	11.6
10[b)]	101.3	83.0	77.0	76.4	**73.9**	**71.2**	**70.9**	**69.7**	69.3	66.8	62.4	**61.0**			11.5
11	—	84.5	76.2	74.2	68.6	62.5	52.6						23.3	—	11.7
12	—	85.1	74.7	72.2	67.5	62.3	48.6						22.8	—	11.9
13	—	85.0	69.7	68.7	**66.5**	**62.7**	51.3						23.4	—	13.6

a) The spectra were determined at 25.1 MHz, in $CDCl_3$ with Me_4Si. b) in $CDCl_3$-$(CD_3)_2CO$.

Stereospecific Reductive Desulfinylation of 1-Aryl-2-(methylsulfinyl)-2-(methylthio)ethenes with Grignard Reagents[1)]

Katsuyuki OGURA,*[2)] Kazutaka ARAI,[2)] and Gen-ichi TSUCHIHASHI*[2)]
Sagami Chemical Research Center, Nishi-Ohnuma 4-4-1, Sagamihara, Kanagawa 229
(Received May 6, 1982)

Synopsis. (*E*)-1-Aryl-2-(methylsulfinyl)-2-(methylthio)ethene, obtained by the Knoevenagel-type condensation of methyl (methylthio)methyl sulfoxide with the corresponding aromatic aldehyde, was found to react with ethylmagnesium chloride to give (*Z*)-1-aryl-2-(methylthio)ethene predominantly. Since the reaction of (*Z*)-1-(methylsulfinyl)-1-(methylthio)-2-phenylethene afforded (*E*)-1-(methylthio)-2-phenylethene, the present reaction appeared to be stereospecific.

In the previous papers,[3,4)] methyl (methylthio)methyl sulfoxide (**1**) was reported to react with an aromatic aldehyde (**2**) in the presence of a base to give the (*E*)-1-aryl-2-(methylsulfinyl)-2-(methylthio)ethene (**3**), which appeared to be one of the most important precursors for synthesizing arylacetic acid derivatives. For example, the reaction of **3** with hydrogen chloride in an alcohol (ROH) yields the arylacetic ester (**4**) and treatment of **3** with bromine in acetic acid produces the α-bromoarylacetic acid (**5**).

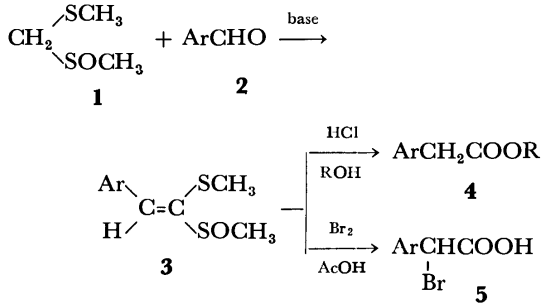

We further examined the reaction of **3** with Grignard reagents, where many types of the reactions could be expected to take place: (i) Attack on the sulfur atom of the sulfinyl group, bringing about the replacement reaction, analogous to the reaction of aryl chloromethyl sulfoxide (Eq. 1);[5)] (ii) reduction of the sulfinyl group with concomitant alkylation of the sulfinyl methyl group as observed in the reaction of dimethyl sulfoxide (Eq. 2);[6)] (iii) Michael-type addition to the α,β-unsaturated sulfoxide moiety;[7)] and (iv) proton transfer to form a carbanion on the methyl adjacent to the sulfinyl group. In this note, we report that a Grignard

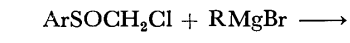

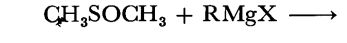

reagent causes reductive desulfinylation of **3** to give a (*Z*)-1-aryl-2-(methylthio)ethene (**6**) stereospecifically.

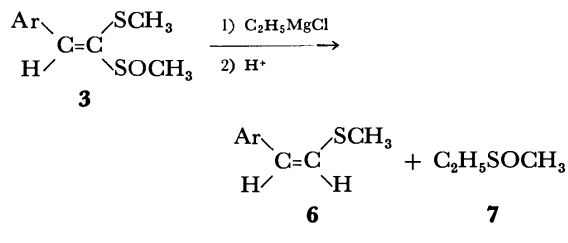

Results and Discussion

To a solution of (*E*)-1-(*p*-chlorophenyl)-2-(methylsulfinyl)-2-(methylthio)ethene (**3**; Ar=*p*-ClC_6H_4), which was obtained by the reaction of **1** with *p*-chlorobenzaldehyde in the presence of a base in tetrahydrofuran (THF),[3)] was added a THF solution of ethylmagnesium chloride (1.5 mol equiv.) under argon atmosphere and cooling with ice–water, and the resulting mixture was stirred at room temperature for 1 h. The color of the mixture changed from pale yellow to orange and then to yellow. Addition of water, followed by the usual work-up, gave 1-(*p*-chlorophenyl)-2-(methylthio)ethene and ethyl methyl sulfoxide (**7**) in yields of 79% and 37%, respectively. The structure of the former was given by an elemental analysis and an NMR spectrum, which showed that this product consisted mainly of the (*Z*)-isomer (**6**; Ar=*p*-ClC_6H_4) together with a small amount (*ca.* 5%) of its (*E*)-isomer. The (*Z*)- and (*E*)-isomers were assigned from the coupling constants (J=11 and 15 Hz, respectively) between the olefinic protons.

In a similar manner, (*Z*)-1-aryl-2-(methylthio)ethenes [**6**; Ar=C_6H_5, *p*-$CH_3C_6H_4$, and *p*-$(CH_3)_2NC_6H_4$] were obtained on treatment of the corresponding (*E*)-1-aryl-2-(methylsulfinyl)-2-(methylthio)ethenes with ethylmagnesium chloride in yields of 82%, 60%, and 41%, respectively. In every case, formation of a small amount of (*E*)-isomer was observed, but the ratio of the (*Z*)- and (*E*)-isomers remained always more than nine. The use of methylmagnesium iodide gave the similar result; The reaction with **3** (Ar=C_6H_5) afforded **6** (Ar=C_6H_5) in 57% yield.

The observation that the thermodynamically less stable (*Z*)-isomer (**6**) was always obtained as the major product in the reaction of **3** with a Grignard reagent suggests stereospecific nature of the reaction. Thus, we studied the reaction of ethylmagnesium chloride with a mixture consisting of **3** (Ar=C_6H_5) and its (*Z*)-isomer (**9**; Ar=C_6H_5). When a 35:65 mixture of **3** (Ar=C_6H_5) and **9** (Ar=C_6H_5), which was obtained by irradiation of **3** (Ar=C_6H_5) with a low-pressure mercury arc lamp,[3)] was subjected to the reaction with ethylmagnesium chloride, the ratio of the (*E*)- and (*Z*)-isomers (**6** and **11**; Ar=C_6H_5) of 1-(methylthio)-2-phenylethene was 29:71. In a similar manner, a 25:75 mixture of **3** (Ar=C_6H_5) and **9** (Ar=C_6H_5) gave a mixture of the corresponding **6** and **11** in the ratio of 21:79. Hence, the present reaction proved to be stereospecific.

The reaction of **3** or **9** with a Grignard reagent may be accounted for by the mechanism involving the attack of a Grignard reagent (RMgX) on the sulfur atom of the sulfinyl group of **3** or **9**, followed by elimination of alkyl methyl sulfoxide ($RSOCH_3$)[8)]

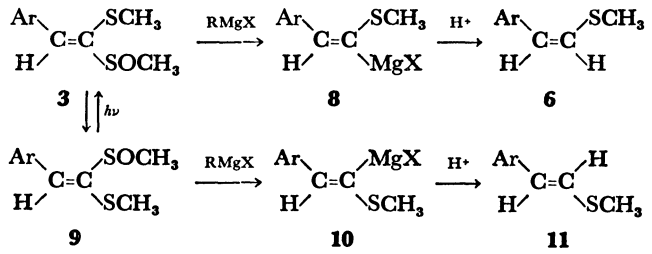

to form a 2-aryl-1-(methylthio)ethenylmagnesium halide (**8** or **10**, respectively) which was finally converted into **6** or **11** by the abstraction of a proton in a retention manner.[9,10]

Experimental

The Reaction of **3** *(Ar=*p*-ClC_6H_4) with Ethylmagnesium Chloride. A Typical Procedure*: To a solution containing 1.18 g (4.8 mmol) of **3** (Ar=*p*-ClC_6H_4) in 6.0 ml of THF, was added 3.5 ml of 2 M solution (1.5 mol equiv.) of ethylmagnesium chloride in THF under argon atmosphere and cooling with an ice-water bath. After removal of the bath, the reaction mixture was stirred for 1 h at room temperature and then water (0.5 ml) was added at 0—5 °C. After addition of diethyl ether (30 ml) and anhydrous sodium sulfate, the resulting mixture was stirred mechanically. The organic layer was separated by decantation and the residue was washed twice with 20 ml of diethyl ether. These ethereal solutions were combined and dried over anhydrous magnesium sulfate, and the solvent was evaporated *in vacuo*. The residual oil was column-chromatographed on silica gel using dichloromethane as an eluent to give 698 mg (79% yield) of **6** (Ar=*p*-ClC_6H_4) as a slightly yellow oil, which was further purified by a short-path distillation [bath temperature: 103—105 °C/0.05 Torr (1 Torr=133.322 Pa)]: IR (neat) 1597, 1590, 1490, 1402, 1089, 1010, 847, 828, and 525 cm^{-1}; NMR ($CDCl_3$) δ 2.35 (3H, s), 6.16 (1H, d, J=11 Hz), 6.30 (1H, d, J=11 Hz), 7.26 (2H, d, J=7 Hz), and 7.33 (2H, d, J=7 Hz).

Found: C, 58.32; H, 4.82%. Calcd for C_9H_9ClS: C, 58.53; H, 4.92%.

Ethyl methyl sulfoxide (**7**) was obtained by washing the residue of the decantation with methanol. Evaporation of the washings gave 162 mg (37% yield) of **7** as a colorless oil, which was identified by a comparison of its IR and NMR spectra with those of the authentic sample prepared by oxidation of ethyl methyl sufide.

The reaction of **3** [Ar=C_6H_5, *p*-$CH_3C_6H_4$, or *p*-$(CH_3)_2NC_6H_4$] with ethylmagnesium chloride under the same conditions afforded **6** [Ar=C_6H_5, *p*-$CH_3C_6H_4$, or *p*-$(CH_3)_2NC_6H_4$] in 82%, 60%, or 41% yield, respectively, as an isomeric mixture consisting mainly of (*Z*)-isomer.

6 (Ar=C_6H_5) purified by a short-path distillation [bath temperature: 130—140 °C/17 Torr (lit,[11] 100—113 °C/3—4 Torr)]: IR (neat) 1600, 1499, 1449, 846, 778, 735, 689, and 530 cm^{-1}; NMR ($CDCl_3$) δ 2.36 (3H, s), 6.19 (1H, d, J=11 Hz), 6.43 (1H, d, J=11 Hz), and 7.1—7.6 (5H, m).

6 (Ar=*p*-$CH_3C_6H_4$) purified by a short-path distillation (bath temperature: 105—115 °C/0.12 Torr): IR (neat) 1598, 1515, 824, 687, and 530 cm^{-1}; NMR ($CDCl_3$) δ 2.29 (3H, s), 2.34 (3H, s), 6.07 (1H, d, J=11 Hz), 6.33 (1H, d, J=11 Hz), 7.11 (2H, d, J=8 Hz), and 7.31 (2H, d, J=8 Hz). Found: C, 72.79; H, 7.15%. Calcd for $C_{10}H_{12}S$: 73.13; 7.36%.

6 (Ar=*p*-$(CH_3)_2NC_6H_4$): mp 63.5—64.5 °C (from methanol); IR (nujol) 1615, 1368, 815, 670, and 530 cm^{-1}; NMR ($CDCl_3$) δ 2.33 (3H, s), 2.91 (6H, s), 5.88 (1H, d, J=10.5 Hz), 6.31 (1H, d, J=10.5 Hz), 6.67 (2H, d, J=8.5 Hz), and 7.34 (2H, d, J=8.5 Hz). Found: C, 68.31; H, 7.78; N, 7.09%. Calcd for $C_{11}H_{15}NS$: C, 68.35; H, 7.82; N, 7.25%.

References

1) This work was presented at the 37th National Meeting of the Chemical Society of Japan, April 1978, Yokohama. See the abstract, Vol. II, p. 683.

2) Present address: K. Ogura, Faculty of Engineering, Chiba University, Yayoicho 1-33, Chiba 260; K. Arai, Nissan Chemical Industries, Ltd., Tsuboicho 722-1, Funabashi 274; G. Tsuchihashi, Faculty of Science and Technology, Keio University, Hiyoshi 3-14-1, Kohoku-ku, Yokohama 223.

3) K. Ogura and G. Tsuchihashi, *Tetrahedron Lett.*, **1972**, 1383; K. Ogura, Y. Ito, and G. Tsuchihashi, *Bull. Chem. Soc. Jpn.*, **52**, 2013 (1979).

4) K. Ogura, S. Furukawa, and G. Tsuchihashi, *Bull. Chem. Soc. Jpn.*, **48**, 2219 (1975).

5) M. Hojo, R. Masuda, T. Saeki, K. Fujimori, and S. Tsutsumi, *Synthesis*, **1977**, 789.

6) R. Oda and K. Yamamoto, *J. Org. Chem.*, **26**, 4679 (1961).

7) The carbanion of diethyl malonate was reported to add to *p*-tolyl styryl sulfoxide: G. Tsuchihashi, S. Mitamura, S. Inoue, and K. Ogura, *Tetrahedron Lett.*, **1973**, 323 and G. Tsuchihashi, S. Mitamura, and K. Ogura, *ibid.*, **1976**, 855.

8) An alkyllithium reacts with an alkyl aryl sulfoxide to afford a dialkyl sulfoxide: J. P. Lockard, C. W. Schroeck, and C. R. Johnson, *Synthesis*, **1973**, 485.

9) For examples of the reaction of a vinyl carbanion in a retention manner, see G. Linstrumelle, *Tetrahedron Lett.*, **1974**, 3809; J. Millon, R. Lorne, and G. Linstrumelle, *Synthesis*, **1975**, 434; and the references cited therein.

10) This proton abstraction may occur either during the reaction (from **3** or **7**) or during the work-up. At the present time, we cannot distinguish these possibilities because the pK_a value for the olefinic proton of **6** or **11** is not available in literature.

11) G. A. Russell, E. Sabourin, and G. J. Mikol, *J. Org. Chem.*, **31**, 2854 (1966).

Reaction of Arenediazonium Salts with Nitriles in the Presence of Sodium Carboxylates. A Convenient Synthesis of Unsymmetrical *N*-Aryl Acyclic Imides

Kiyoshi KIKUKAWA,* Kiyoshi KONO, Fumio WADA, and Tsutomu MATSUDA

Department of Organic Synthesis, Faculty of Engineering, Kyushu University, Hakozaki, Higashi-ku, Fukuoka 812

(Received May 8, 1982)

Synopsis. Reactions of arenediazonium tetrafluoroborates (ArN_2BF_4), acetonitrile and sodium carboxylates (RCOONa) gave *N*-acyl acetanilides ($ArN(COR)COCH_3$) in moderate to good yields (Ar=Ph, 2-MeC_6H_4, 3-MeC_6H_4, 4-MeC_6H_4, 2,6-$(Me)_2C_6H_3$; R=Et, *i*-Pr, *t*-Bu, Ph). Acrylonitrile and benzonitrile could be used in the reaction instead of acetonitrile.

Acetonitrile has been used as a favorable solvent in the palladium-catalyzed reactions of arenediazonium salts (ArN_2X).[1] However, in the presence of sodium acetate, a base frequently used in the palladium-catalyzed reactions, some ArN_2X rapidly decomposed in acetonitrile to give intractable tarry materials. In the course of the studies to clarify this side reaction, the interesting reaction of ArN_2BF_4 with sodium carboxylates (RCOONa) and nitriles (R'CN) to produce unsymmetrical *N*-aryl acyclic imides is observed.

Results and Discussion

Addition of ArN_2BF_4 to a suspension of RCOONa in CH_3CN at 60—80 °C caused immediate gas evolution, giving unsymmetrical *N*-aryl acyclic imides (*N*-acyl acetanilides (Eq. 1)). Typical results are summarized in Table 1. Various sodium carboxylates could be used effectively and gave the corresponding *N*-aryl imides. Formation of any symmetrical imides could not be observed under the present reaction conditions. It is noticeable that better yields are obtained in the reactants with bulky groups, such as pivalate, 2-methyl- or 2,6-dimethylbenzenediazonium salt.

$$ArN_2BF_4 + RCOONa + CH_3CN \longrightarrow Ar\text{-}N(COR)COCH_3 + N_2 \quad (1)$$

Table 1. Preparation of *N*-aryl acyclic imides (*N*-acyl acetamides) by the reaction of ArN_2BF_4 with RCOONa in acetonitrile (Eq. 1)[a]

Ar in ArN_2BF_4	R in RCOONa	Products, yield/%[b] $ArN(COR)COCH_3$
Ph	Et	54
Ph	*i*-Pr	55
Ph	*t*-Bu	79
Ph	Ph	74
2-MeC_6H_4	Et	71
3-MeC_6H_4	Et	58
4-MeC_6H_4	Et	32
2,6-$(Me)_2C_6H_3$	Et	78
2,6-$(Me)_2C_6H_3$	Ph	50

a) Reactions were carried out by the addition of of ArN_2BF_4 to a suspension of RCOONa in CH_3CN at 60—80 °C. b) Based on ArN_2BF_4.

Acrylonitrile and benzonitrile also reacted with ArN_2BF_4 and RCOONa to give the *N*-aryl imides and/or *N*-aryl amides (Eqs. 2 and 3). *N*-Arylpropionamides could not be observed under the present conditions.

$$ArN_2BF_4 + CH_2{=}CHCN + EtCOONa \longrightarrow ArN(COEt)COCH{=}CH_2 + ArNHCOCH{=}CH_2 \quad (2)$$

Ar=Ph:	0%	72%
2,6-$(Me)_2C_6H_3$:	49	0

$$ArN_2BF_4 + PhCN + EtCOONa \longrightarrow ArN(COEt)COPh + ArNHCOPh \quad (3)$$

Ar=Ph:	6%	2%
2,6-$(Me)_2C_6H_3$:	25	39

In contrast to the PhN_2BF_4 or $(Me)_nC_6H_{5-n}N_2BF_4$, ArN_2BF_4 bearing electron-withdrawing groups, such as as 4-$NO_2C_6H_4N_2BF_4$ or 4-$BrC_6H_4N_2BF_4$, gave ArH (*ca.* 20%) along with tarry materials under the present conditions. Sodium acetate is used as a base in the Gomberg-Bachmann reaction of an ArN_2X bearing electron-withdrawing group to produce an aryl radical intermediate.[2] Thus, the formation of the ArH is reasonably understood by the pathway *via* aryl radical shown in Eq. 4.

$$ArN_2BF_4 + RCOONa \longrightarrow ArN_2OCOR \longrightarrow Ar\cdot + N_2 + RCOO\cdot \xrightarrow{CH_3CN} ArH \quad (4)$$

Reaction of $(Me)_nC_6H_{5-n}N_2BF_4$ with nitriles has been known to give *N*-aryl nitrilium tetrafluoroborates, $[Ar\text{-}N{\equiv}C\text{-}R]^+BF_4^-$.[3] Since the present reaction favorably proceeds with $(Me)_nC_6H_{5-n}N_2BF_4$, the *N*-aryl nitrilium salt might be an intermediate. Thus, the following scheme could explain the formation of *N*-aryl acyclic imides (Scheme 1). The similar pathway has been proposed for the reaction of isocyanate and acid anhydride to form an acyclic imides (Scheme 2).[4]

Unsymmetrical (mixed) imides are conventionally obtained through acylation of amides with acid anhydrides or acid chlorides.[4,5] But sometimes symmetri-

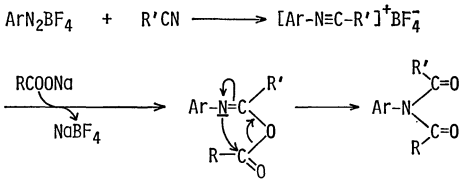

Scheme 1.

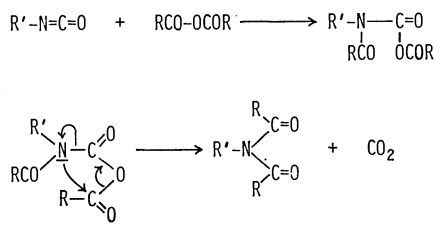

Scheme 2.

cal imides were obtained because the reaction required drastic conditions.

The present reaction provides a convenient route to unsymmetrical *N*-acyl imides, especially *N*-acyl acetanilides.

Experimental

Materials. Sodium carboxylates were used as received or obtained by neutralization of the corresponding acids. Nitriles were distilled before use. Arenediazonium tetrafluoroborates were prepared by the ordinary method[6] and stored at −20 °C.

General Procedure. To a suspension of RCOONa (40 mmol) in a R'CN (40 ml) held at 60—80 °C was added an ArN_2BF_4 (20 mmol) slowly. The addition of ArN_2BF_4 caused exothermic reaction with gas evolution. After the addition, the mixture was stirred for 0.5 h at 60—80 °C. After removal of solids ($NaBF_4$ and excess RCOONa), excess R'CN was evaporated (or distilled) off under reduced pressure. The residue was extracted with hot (≈50 °C) hexane. After evaporation of hexane, the residue was distilled or recrystallized from benzene (or hexane–ether) to give *N*-aryl imides. The extraction with hexane served to seperate the imides from amides, since the latter remained as insoluble solid. The structure of the imides was confirmed by IR, NMR, and elemental analysis. The C=O stretching of the imides was observed near 1700 cm^{-1} and was easily distinguishable from that of amides appeared near 1650 cm^{-1}.

PhN(COEt)COMe: Bp 107 °C/3 mmHg (1 mmHg= 133.322 Pa), IR (neat) 1710 cm^{-1}, NMR (CCl_4) δ=1.00 (t), 2.38 (q) (J=7.2 Hz, EtCO), 2.18 (s) (MeCO). Found: C, 69.25; H, 6.94; N, 7.32%. Calcd for $C_{11}H_{13}NO_2$: C, 69.09; H, 6.85; N, 7.33%. *PhN(CO-i-Pr)COMe*: Mp 44.5—48.5 °C, IR (neat) 1695, 1715 cm^{-1}, NMR (CCl_4) δ=1.07 (d), 2.91 (hep) (J=6.4 Hz, *i*-PrCO), 2.21 (s) (MeCO), Found: C, 70.14; H, 7.33; N, 7.02%. Calcd for $C_{12}H_{15}NO_2$: C, 70.22; H, 7.37; N, 6.82%. *PhN(CO-t-Bu)COMe*: Mp 66.5—67.0 °C, IR (Nujol) 1690 cm^{-1}, NMR (CCl_4) δ=1.15 (s) (*t*-BuCO), 2.00 (s) (MeCO), Found: C, 71.06; H, 7.79; N, 6.33%. Calcd for $C_{13}H_{17}NO_2$: C, 71.20; H, 7.82; N, 6.39%. *PhN(COPh)COMe*: Mp 68.2—68.7 °C, IR (Nujol) 1690 cm^{-1}, NMR (CCl_4) δ=2.32 (s) (MeCO), Found: C, 75.15; H, 5.55; N, 5.85%. Calcd for $C_{15}H_{13}NO_2$: C, 75.30; H, 5.47; N, 5.85%. *PhN(COEt)COPh*: Mp 62.3—66.5 °C, IR (Nujol) 1670, 1710 cm^{-1}, NMR (CCl_4) δ=1.13 (t), 2.60 (q) (J=7.0 Hz, EtCO), Found: C, 76.05; H, 6.03; N, 5.59%. Calcd for $C_{16}H_{15}NO_2$: C, 75.87; H, 5.97; N, 5.53%. *2-MeC_6H_4N(COEt)COMe*: Bp 80—81 °C/ 0.2 mmHg, IR (neat) 1710 cm^{-1}, NMR (CCl_4) δ=1.01 (t), 2.34 and 2.37 (two q) (J=7.1 Hz, EtCO), 2.04 (s) (MeCO), 2.17 (s) (Me–Ar), Found: C, 70.05; H, 7.34; N, 7.10%. Calcd for $C_{12}H_{15}NO_2$: C, 70.22; H, 7.37; N, 6.82%. *3-MeC_6H_4N(COEt)COMe*: Bp 78—80 °C/0.09 mmHg, IR (neat) 1715 cm^{-1}, NMR (CCl_4) δ=1.08 (t), 2.48 (q) (J= 7.2 Hz, EtCO), 2.32 (s), 2.37 (s) (MeCO and MeAr), Found: C, 70.15; H, 7.51; N, 6.78%. Calcd for $C_{12}H_{15}NO_2$: C, 70.22; H, 7.35; N, 6.82%. *4-MeC_6H_4N(COEt)COMe*: Bp 127 °C/4 mmHg, IR (neat) 1710 cm^{-1}, NMR (CCl_4) δ= 1.00 (t), 2.38 (q) (J=6.8 Hz, EtCO), 2.17 (s), 2.26 (s) (MeCO and MeAr), 6.82 (d), 7.08 (d) (J=8.0 Hz, Ar), Found: C, 70.21; H, 7.47; N, 7.12%. Calcd for $C_{12}H_{15}NO_2$: C, 70.22; H, 7.35; N, 6.82%. *2,6-$(Me)_2C_6H_3$N(COEt)-COMe*: Bp 87—90 °C/1 mmHg, IR (neat) 1710 cm^{-1}, NMR (CCl_4) δ=1.01 (t), 2.32 (q) (J=7.2 Hz, EtCO), 2.00 (s) (MeAr), 2.11 (s) (MeCO), 6.97 (s) (Ar), Found: C, 71.29; H, 7.85; N, 6.33%. Calcd for $C_{13}H_{17}NO_2$: C, 71.20; H, 7.82; N, 6.39%. *2,6-$(Me)_2C_6H_3$N(COPh)COMe*: Bp ≈120 °C/0.5 mmHg (Kugelrohr distillation), IR (neat) 1685, 1710 cm^{-1}, NMR (CCl_4) δ=2.18 (s) (MeCO), 2.20 (s) (MeAr), Found: C, 76.48; H, 6.46; N, 5.20%. Calcd for $C_{17}H_{17}NO_2$: C, 76.38; H, 6.41; N, 5.24%. *2,6-$(Me)_2C_6H_3$N(COEt)-COCH=CH_2*: Bp ≈120 °C/3 mmHg (Kugelrohr distillation), IR (neat) 1695, 1710 cm^{-1}, NMR ($CDCl_3$) δ=1.10 (t), 2.68 (q) (J=7.0 Hz, EtCO), 2.02 (s) (MeAr), 5.48 (d-d) (J_{gem}= 4.0, J_{cis}=7.9 Hz, trans HC=C–CO), 6.22 (d) (C=CH–CO), 6.25 (d) (cis HC=C–CO) (These latter two chemical shifts are too close for observing J_{trans}), 7.02 (s) (MeAr), Found: C, 72.88; H, 7.50; N, 5.87%. Calcd for $C_{14}H_{17}NO_2$: C, 72.70; H, 7.41; N, 6.06%. *2,6-$(Me)_2C_6H_3$N(COEt)COPh*: Bp ≈120 °C/0.3 mmHg (Kugelrohr distillation), IR (neat) 1685, 1715 cm^{-1}, NMR (CCl_4) δ=1.10 (t) 2.30 (q) (J= 7.0 Hz, EtCO), 2.21 (s) (MeAr), Found: C, 77.45; H, 6.92; N, 5.22%. Calcd for $C_{18}H_{19}NO_2$: C, 76.84; H, 6.80; N, 4.98%.

References

1) K. Kikukawa, K. Nagira, F. Wada, and T. Matsuda, *Tetrahedron*, **37**, 31 (1981); K. Nagira, K. Kikukawa, F. Wada, and T. Matsuda, *J. Org. Chem.*, **45**, 2365 (1980); K. Kikukawa, K. Kono, K. Nagira, F. Wada, and T. Matsuda, *ibid.*, **46**, 4413 (1981).

2) O. C. Dermer and M. T. Edmison, *Chem. Rev.*, **57**, 77 (1957).

3) H. Meerwein, P. Laasch, R. Mersch, and J. Spille, *Chem. Ber.*, **89**, 209 (1956).

4) D. Davidson and H. Skouronek, *J. Am. Chem. Soc.*, **80**, 376 (1958).

5) C. D. Hurd and A. G. Prapas, *J. Org. Chem.*, **24**, 388 (1959).

6) A. Roe, *Org. React.*, **5**, 193 (1949).

CuCl-catalyzed Oxidative Coupling Reaction of Secondary Amines with Molecular Oxygen in Pyridine

Tsunesuke KAJIMOTO,* Hidetaka TAKAHASHI, and Jiro TSUJI†
Basic Research Laboratories, Toray Industries, Inc., Tebiro, Kamakura 248

(Received June 9, 1982)

Synopsis. Oxidation of diphenylamine with molecular oxygen in the presence of CuCl in pyridine at room temperature to give tetraphenylhydrazine in a high yield was achieved by selecting suitable reaction conditions. *N*-methylaniline was also oxidized to give *N,N'*-dimethyl-*N,N'*-diphenylhydrazine.

In a previous paper we reported a unique oxidation of *o*-phenylenediamine with molecular oxygen in the presence of CuCl in pyridine at room temperature to give *cis,cis*-muconononitrile.[1] The most important

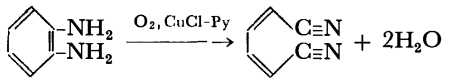

factor in this reaction is the ratio of *o*-phenylenediamine to CuCl in the reaction medium and the ratio should be kept less than 0.5 (mol/mol) to obtain the nitrile in a high yield. A suitable procedure for this is the dropwise addition of a solution of the diamine in pyridine to a solution of CuCl. In this paper a successful application of this catalyst system to the oxidation of secondary amines to tetrasubstituted hydrazines is reported.

Results and Discussion

Copper(I) chloride is slightly soluble in pyridine under an inert atmosphere at room temperature, but a mixture of CuCl and pyridine absorbs oxygen with stirring under oxygen atmosphere to give a deep green solution. One mol of oxygen is absorbed per four atoms of copper. From this solution an oxygen complex was precipitated by addition of diethyl ether and its elemental analysis supported a composition of $(CuCl)_4(C_5H_5N)_4O_2$.[1] When a pyridine solution of diphenylamine (0.5 molar equiv. to CuCl) was added slowly to a pyridine solution of CuCl pretreated with oxygen, further absorption of oxygen was observed showing that the oxidation took place. The amount of oxygen absorbed during the oxidation was 0.6 molar equivalent to diphenylamine added, and after usual work-up tetraphenylhydrazine was obtaine in 83% yield.

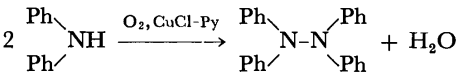

N-methylaniline was also oxidized to give *N,N'*-dimethyl-*N,N'*-diphenylhydrazine in 52%. From other secondary amines such as di-2-naphthylamine and *N*-ethylaniline the corresponding hydradines were not obtained in high yields though similar absorption of oxygen was observed.

A probable reaction mechanism is shown as follows.

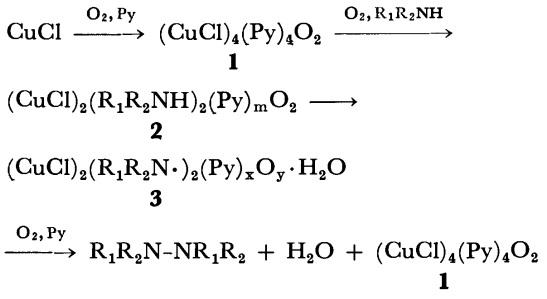

Coupling of amino radicals in the coordination sphere of complex **3** gives the hydrazine. When the concentration of the secondary amine in the reaction medium is so high to substitute more pyridines coordinated in the complex **2**, the amino radical may attack another secondary amine coordinated to give by-products such as oligomer and polymer of the amine. The low yield of hydrazine from di-2-naphthylamine may be attributed to the instability of di-2-naphthylamino radical.[2]

The unique oxidation method with CuCl in pyridine is thus useful for the oxidative coupling reaction of secondary amines to give tetrasubstituted hydrazine as well as other oxidation methods with PbO_2 or $KMnO_4$.[3]

Experimental

Melting points are uncorrected. Infrared spectra were recorded on a Shimadzu Model IR-27 infrared spectrophotometer, and nuclear magnetic resonance spectra on a Varian HA-100 (100 MHz) and a Varian A-60 (60 MHz) using tetramethylsilane as an internal standard in $CDCl_3$. All metal salts and secondary amines were obtained commercially.

General Procedure of Oxidation. Copper(I) chloride and pyridine were added in a glass flask immersed in a water bath under argon atmosphere with vigorous stirring and then the atmosphere was replaced with oxygen. After the absorption of oxygen ceased, the secondary amine in pyridine was added slowly with further absorption of oxygen. The amount of oxygen absorbed was measured with a gas buret. Pyridine was distilled off under reduced pressure after the reaction, and the residue was extracted with ether to give a crude product which was subjected to column chromatographic purification.

Tetraphenylhydrazine. Diphenylamine (1.69 g) in 10 ml of pyridine was treated with CuCl(1.98 g) in 50 ml of pyridine and the crude product was chromatographed on an alumina column with benzene–petroleum ether (1:1) to give tetraphenylhydrazine (1.4 g, 83%), mp 146.5 °C (lit,[3] mp 144.5 °C). The IR spectrum was identical with that of an authentic sample. Found: C, 86.03; H, 5.27; N, 8.11%. Calcd for $C_{24}H_{20}N_2$: C, 85.68; H, 5.99; N, 8.33%.

N,N'-*Dimethyl*-N,N'-*diphenylhydrazine.* *N*-Methylaniline (1.07 g) in 10 ml of pyridine was treated with CuCl (1.98 g) in 50 ml of pyridine and distillation of the crude product gave *N,N'*-dimethyl-*N,N'*-diphenylhydrazine (0.6 g,

† Present address: Department of Chemical Engineering, Faculty of Engineering, Tokyo Institute of Technology, Meguro-ku, Tokyo 152.

52%), bp 160 °C/4 mmHg. The IR spectrum was identical with that of an authentic sample. ^{1}H NMR ($CDCl_3$): δ= 2.90(6H, s), 6.5—7.5 (10H, m). Found: C, 79.15; H, 7.56; N, 13.35%. Calcd for $C_{14}H_{16}N_2$: C, 79.21; H, 7.60; N, 13.20%.

References

1) T. Kajimoto, H. Takahashi, and J. Tsuji, *J. Org. Chem.*, **41**, 1389 (1976).

2) R. F. Bridger, D. A. Law, D. F. Bowman, B. S. Middleton, and K. U. Ingold, *J. Org. Chem.*, **33**, 4329 (1968).

3) F. D. Chattaway and H. Ingle, *J. Chem. Soc.*, **67**, 1090 (1895); H. Wieland and S. Gambarjan, *Ber.*, **39**, 1500 (1906).

Aminolysis of Activated Esters Formed by Reaction of Carboxylate Salts with Strained Phosphonates and Phosphinates

Francine ACHER and Michel WAKSELMAN*
C.E.R.C.O.A.-C.N.R.S. 2 à 8, rue Henry Dunant 94320 THIAIS, France

(Received March 8, 1982)

Synopsis. Nucleophilic attack of a carboxylate salt on a five-membered phosphonic or phosphinic ester followed by an intramolecular acyl transfer reaction gives a substituted aryl ester. Due to the intramolecular base catalysis of a neighbouring P=O group the bimolecular aminolysis of this ester is a fast process.

The study of the reactions of carboxylate salts with strained five-membered phosphonates or phosphinates and the aminolysis of the resulting aryl esters was undertaken for two purposes: on the one hand to serve as a model of the first steps in a scheme for peptide synthesis by means of the "prior amine capture" principle;[1] on the other hand, to compare the reactivities of tetracoordinated alicyclic,[2] cyclic phosphorus (this study) and sulfur[3] esters, all of which also lead to peptides but by different means (bimolecular aminolysis).

Five-membered cyclic phosphonate and phosphinate esters **1**, **2**, and **3** were prepared (*vide infra*). The probable mechanism of their reaction with a carboxylate anion is shown on the scheme. Relief of the strain facilitates the formation of a pentacoordinated intermediate (not shown) which in turn yields a mixed anhydride A. Then an intramolecular acyl transfer reaction gives a substituted aryl ester B. The aminolysis of B can be assisted by the neighbouring phosphoryl group.

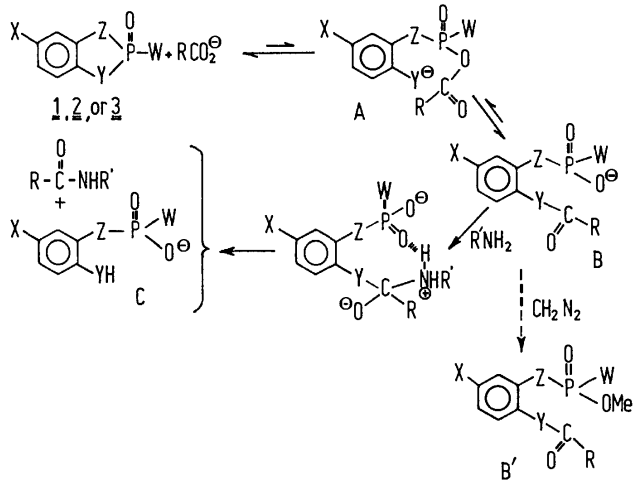

Scheme 1.

Experimental

Phosphonothioate **1b** was prepared by adding a mixture of 3,4-toluenedithiol and triethylamine (2 equiv.) to a cooled solution of phenylphosphonic dichloride in benzene. Mp 98 °C; 65% yield; δ ^{31}P: 58.4 ($CDCl_3$); *m/e*: 278 (100) 156 (32) 154 (37.5).

The phosphinates **4a** and **4b** and the phosphonate **5** were obtained by the addition of a solution of 2-hydroxy-5-nitrobenzyl bromide (5 mmol) in 5 ml of dry acetone to a solution of a diethyl phosphonite or trimethyl phosphite (5 mmol) in 1 ml of acetone under dry nitrogen. After 15 min the precipitate was collected.

4a: Mp (decomp) 173 °C; 65% yield. δ($CDCl_3$) 8.0 (m, 2H, ArH), 6.90 (d, J=10, 1H, ArH), 4.05 (m, 2H, $POCH_2$), 3.25 (m, 2H, PCH_2), 1.45 (m, 6H, PCH_3+ $POCH_2CH_3$), *m/e*: 260 (14), 259 (46), 213 (100).

4b: Mp (decomp) 186 °C; 88% yield. δ($CDCl_3$) 8.1—7.5 (m, 7H, ArH), 6.95 (d, J=10, 1H, ArH), 4.0 (m, 2H, $POCH_2$), 3.40 (m, 2H, PCH_2), 1.30 (t, 3H, $POCH_2CH_3$), *m/e*: 322 (16), 321 (63), 275 (23), 229 (15).

5: Mp 162 °C; 90% yield. δ($CDCl_3$) 10.1 (1H, OH), 7.90 (m, 2H, ArH), 6.80 (d, J=10, 1H, ArH), 3.70 (d, J=11, 6H, $POCH_3$), 3.20 (d, J=22, 2H, PCH_2). Found: C, 41.34; H, 4.62%. Calcd for $C_{19}H_{12}NO_6P$: C, 41.39; H, 4.63%. Cyclization occurs by heating to 190 °C under 0.2 mmHg (1 mmHg≈133.322 Pa).

2b: $Bp_{0.5}$ 250 °C (8); 75% yield. δ($CDCl_3$) 8.10 (m, 2H, ArH), 7.05 (d, J=10, 1H, ArH), 3.90 (d, J=10, 3H, $POCH_3$), 3.25 (d, J=16, 2H, PCH_2), *m/e*: 229 (100), 215 (32).

3a: $Bp_{0.5}$ 220 °C (8); 85% yield. δ($CDCl_3$) 7.0 (m, 4H, ArH), 3.15 (m, 2H, PCH_2), 1.80 (d, J=13, 3H, PCH_3), δ ^{31}P: 70.4, *m/e*: 169 (22), 168 (100), 153 (100).

3b: Mp 173 °C; 80% yield. δ($CDCl_3$) 8.05 (m, 2H, ArH), 7.0 (d, J=11, 1H, ArH), 3.25 (m, 2H, PCH_2), 1.85 (d, J=15, 3H, PCH_3), *m/e*: 213 (100), 198 (14), 183 (13), 167 (65).

3c: Mp 175 °C; 90% yield. δ($CDCl_3$) 8.2—7.5 (m, 7H, ArH), 7.10 (d, J=10, 1H, ArH), 3.50 (m, 2H, PCH_2), *m/e*: 275 (69), 229 (33), 158 (100), 141 (19). **B'** (X=NO_2, Y=O, W=Me, Z=CH_2) was obtained after methylation by preparative thin layer chromatography (SiO_2; MeOH–EtOAc: 25—75) in 15% yield. δ($CDCl_3$) 8.30 (m, 2H, ArH) 7.40 (d, 1H, ArH) 3.75 (d, J=11, 3H, $POCH_3$) 3.30 (d, J=19, 2H, PCH_2) 2.40 (s, 3H, $COCH_3$) 1.50 (d, J=14, 3H, PCH_3), IR(CH_2Cl_2): 1770 cm^{-1}, *m/e*: 273 (9), 245 (100), 213 (50).

Some acids C have been characterized.

From ***3a***: C(X=H, Y=O, W=CH_3, Z=CH_2), mp 124 °C. δ(CD_3COCD_3) 9.5 (s, 2H, OH), 6.85 (m, 4H, ArH), 3.25 (d, J=18, 2H, PCH_2), 1.4 (d, J=13, 3H, PCH_3), *m/e*: 186 (46), 168 (91), 153 (63), δ ^{31}P: 53.8.

From ***3b***: C(X=NO_2, Y=O, W=CH_3, Z=CH_2), mp 215—217 °C. δ(CD_3COCD_3) 8.0 (m, 2H, ArH), 6.85 (d, J=10, 1H, ArH), 3.20 (d, J=18, 2H, PCH_2), 1.40 (d, J=13, 3H, PCH_3), *m/e*: 231 (35), 213 (>100), 198 (25), 183 (14), 167 (100).

From ***3c***: C(X=NO_2, Y=O, W=C_6H_5, Z=CH_2), mp 220 °C. δ(CD_3COCD_3) 8.0—7.5 (m, 7H, ArH), 6.75 (d, J=10, 1H, ArH), 3.40 (d, J=13, 2H, PCH_2), *m/e*: 293 (5.6), 275 (100), 245 (15), 229 (56).

Results and Discussion

We were unable to isolate the *o*-phenylene phenylphosphonate **1a** using the described method,[4] even when the rather unexpected aqueous treatments were omitted. A hygroscopic compound was formed following the preparation procedure[5] for a di-*t*-butyl de-

rivative.[6] However, a thioanalog **1b** was obtained from 3,4-toluenedithiol.

Cyclic phosphonate **2a** was prepared from saligenol and a phosphite.[7] The use of diethyl methylphosphonite instead of trimethyl phosphite led to a cyclic phosphinate **3a**.

The reaction of 2-hydroxy-5-nitrobenzyl bromide with diethyl methylphosphonite rapidly gave **4a** which in turn produced **3b** by vacuum heating. Under the same conditions **4b** and **3c** were obtained from diethyl phenylphosphonite. By an analogous Arbuzov reaction and cyclization, **5** and **2b** were formed from trimethyl phosphite.

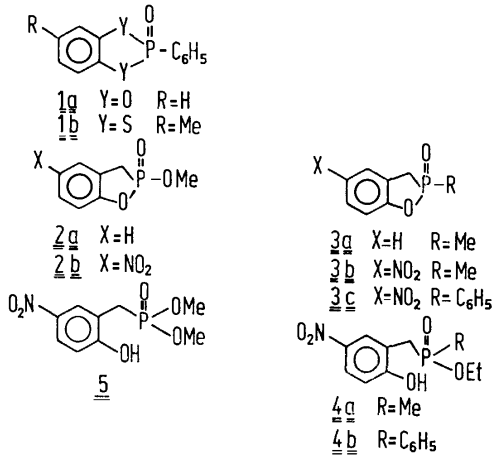

Fig. 1.

1b slowly reacts (2 h) with a mixture of acetic acid (1 mmol) and triethylamine (1 mmol) in 1 ml of $CHCl_3$ to give thioester **B** (Y=Z=S, X=Me, W=C_6H_5; $\nu_{C=O}$ 1700 cm^{-1}). The reaction of triethyl or tetrabutylammonium acetate with the unsubstituted phosphonate or phosphinate **2a** and **3a** leading to esters **B** (Y=O, Z=CH_2, X=H, W=Me, or OMe; $\nu_{C=O}$ 1760 cm^{-1} (CH_2Cl_2)), occurs by heating the substances to 40 °C in CH_2Cl_2. The activated nitro derivatives **2b**, **3b**, and **3c** react at room temperature in 2 h, giving **B** (X=NO_2; $\nu_{C=O}$ 1765 cm^{-1}) in about 80% yield.

In one case, the methylated derivative **B'** (X=NO_2, Y=O, W=Me, Z=CH_2) was isolated by treating **B** with diazomethane and HBF_4.

We did not observe an IR frequency in relationship with mixed anhydride **A**, which did not accumulate in the reaction.

In each case, the rate of aminolysis of **B** is much faster than that of the corresponding unsubstituted aryl ester or thioester. *E.g.*, the reaction of 1 mmol of **B** (Y=O, Z=CH_2, W=CH_3, X=NO_2) with 1 equiv. of benzylamine in 3 ml of CH_2Cl_2 yielding *N*-benzylacetamide (mp 61 °C) is complete in less than five minutes at 20 °C. Under the same conditions the reaction with *p*-nitrophenyl acetate takes about 90 min.

We believe that the observed increase in the reaction rate is mainly due to an anchimeric assistance by the neighbouring P=O group.[9] With this hypothesis, aminolysis of **B** (X=NO_2) is doubly accelerated, first, by the electronwithdrawing effect of the nitro substituent and second, by intramolecular general base catalysis.

Addition of the highly reactive cyclic phosphinate **3b** or **3c** to an equimolar mixture of acetic acid, triethylamine, and benzylamine in CH_2Cl_2 gives *N*-benzylacetamide with a 67% yield.[10] However, the main drawback in using cyclic phosphonic or phosphinic ester as coupling reagents is their sensitivity to moisture.[11]

We have recently shown that the analogous 5-nitrotoluene-α, 2-sultone is stable and yields peptides by a similar mechanism (Scheme 1: SO_2 instead of $\overset{O}{\overset{\|}{P}}$–W[3]).

In conclusion the hygroscopic cyclic phosphonates and phosphinates are not better reagents for coupling than the very efficient alicyclic phosphonates[2] and sultone.[3] Nevertheless the formation of ester **B** corroborates the mechanism of the first steps in the previous method of peptide synthesis.[1]

We thank Dr P. Savignac for his help in the preparation of the diethyl methylphosphonite.

References

1) M. Wakselman and F. Acher, *Tetrahedron Lett.*, **1980**, 2705.

2) T. Mukaiyama, N. Morito, and Y. Watanabe, *Chem. Lett.*, **1979**, 1305; Y. Watanabe, N. Morito, K. Kamekawa, and T. Mukaiyama, *ibid.*, **1981**, 65.

3) M. Wakselman and F. Acher, *J. Chem. Soc., Chem. Commun.*, **1981**, 632.

4) H. Ohkawa, S. Maruo, and M. Eto, *J. Fac. Agr. Kyushu Univ.*, **17**, 13 (1972).

5) I. S. Belostotskaya, N. L. Komissarova, T. I. Prokof'eva, V. R. Vol'eva, and V. V. Ershov, *Iz. Akad. Nauk SSSR Ser. Khim.*, **1978**, 2385.

6) In the same reaction, under different experimental conditions, tris(*o*-phenylene)phosphate has been isolated. (T. Koizumi, Y. Watanabe, Y. Yoshida, and E. Yoshii, *Tetrahedron Lett.*, **1974**, 1075).

7) B. E. Ivanov and H. B. Ageeva, *Izv. Akad. Nauk SSSR Ser. Khim.*, **1967**, 226; A. B. Ageeva and B. E. Ivanov, *ibid.*, **1967**, 1494; W. Vogt, *Phosphorus and Sulfur*, **5**, 123 (1978).

8) Temperature of the oven of a Büchi GKR (Bulb to bulb) apparatus.

9) The slightly basic ϕ_3PO is an efficient catalyst of the aminolysis of *p*-nitrophenyl acetate in chlorobenzene. Acceptance of the ammonium proton probably facilitates the decomposition of the tetrahedral intermediate (C. W. Su and J. W. Watson, *J. Am. Chem. Soc.*, **96**, 1854 (1974)). General base catalysis by a neighbouring anion is probably excluded because the aminolysis of the methyl ester of **B** is fast too.

10) We have not observed the formation of a phosphinic amide by the competitive aminolysis of **3b**. Base-catalyzed hydrolysis by contaminant water (M. Mulliez and M. Wakselman, *Phosphorus and Sulfur*, **8**, 41 (1980)) occurs by mixing **3b** or **3c** with a primary amine.

11) However the *o*-hydroxybenzylphosphinic acids may be cyclized by simply vacuum heating them to their melting.

An Effective Process for Treatment of Malodor in Exhaust Gas by Hypochlorite

Kenzo ABE* and Wataru MACHIDA†

Fuso Co., Ltd., Honmura-cho, Shinjuku-ku, Tokyo 162

† *College of Industrial Technology, Nihon University, Izumi-cho, Narashino 275*

(Received January 12, 1982)

Synopsis. Pilot-plant studies were carried out to find out the optimum conditions for hypochlorite-oxidation treatment of malodorous multi-components in exhaust gas from night soil treatment plants. A two-step process was proved to be the most effective: a part of malodorous components are absorbed and oxidized in the first packed-tower into which a pH 7 aqueous solution of sodium hypochlorite slowly introduced and then unreacted components are oxidized in the second tower with a pH 11 solution.

There have been known several methods for treatment of malodor in exhaust gas from night soil or sewage treatment plants, such as adsorption by activated carbon,[1] catalytic oxidation,[2] and wet scrubbing systems using absorptive solutions with oxidizing agents and/or alkaline solution, and water.[3]

The authors have described in the earlier papers[4-8] the wet scrubbing systems using packed towers through which hypochlorite or hydrogen peroxide solutions were allowed to pass and have clarified the relationship between oxidation conditions of malodorous sulfide components and the decrease of COD (chemical oxygen demand) of effluent water. We have defined the conditions (pH of absorptive solution, it's NaOCl concentration, superficial gas velocity, *etc.*) for absorptive oxidation of hydrogen sulfide[4,5] and coexistent malodorous components in exhaust gas such as ammonia, trimethylamine, methanethiol, dimethyl sulfide, dimethyl disulfide, trace acetaldehyde and styrene.[6-8] In the above studies, the effectiveness of scrubbing systems was assessed in terms of the overall mass transfer coefficient $K_G a$.[9]

In this paper, the optimum conditions for effective NaOCl oxidation of mixed systems of malodorous multi-components are investigated with actual exhaust gas, using a pilot-plant.

Experimental

Equipment. Polyvinyl chloride towers of diameter 100 cm, packed with Takiron Trical P 175 packings, were used for absorptive oxidation.

Chemical Analysis. Carbon dioxide and chlorine were determined by the detector tube method and the orthotolidine method, respectively. Hydrogen sulfide, methanethiol, dimethyl sulfide, dimethyl disulfide, trimethylamine, styrene and acetaldehyde were determined by the gas chromatography,[10,11] and ammonia was determined by the spectrophotometry.[10]

Procedure. Sample gas was introduced into the packed tower from the bottom by a blower and the absorptive solution was sprayed onto the packings at the top of the tower, so as to make gas and solution contact in countercurrent fashion. The gas was sampled at the inlet and outlet of the tower and analyzed.

Results and Discussion

Figure 1, prepared by rearranging the data in the earlier papers,[4,6-8] shows the relationship between the pH values of NaOCl solutions and the $K_G a$ values of malodorous gas components under the conditions that they are oxidized separately with 1.2×10^{-2} mol/l NaOCl solution at the superficial gas velocity of 1.7 m/s and the liquid/gas ratio of 2 l/m^3. As shown there, the $K_G a$ values for NH_3, $(CH_3)_3N$, CH_3SCH_3, CH_3SSCH_3, CH_3CHO, and $C_6H_5CH{=}CH_2$ are the largest, respectively at pH 6, while those for CH_3SH and H_2S are the largest at pH 11, respectively. Since the removal rate rises with the increase of the $K_G a$ value, it can be estimated that the most effective oxidation would result at pH 6 and 11 for an actual exhaust gas which contains those components in a mixed state. Then, an experimental study to verify the estimation was carried out with actual mixed systems of those components in exhaust gas from a night soil treatment plant, which contains H_2S, CH_3SH, CH_3SCH_3, CH_3SSCH_3, NH_3, $(CH_3)_3N$, $C_6H_5CH{=}CH_2$, CH_3CHO in 39, 0.05, 1.74, 0.0089, 18.6, 0.32, <0.01, <0.05 ppm, respectively, using two packed towers (60 cm and 180 cm height) arranged in parallel. The exhaust gas was

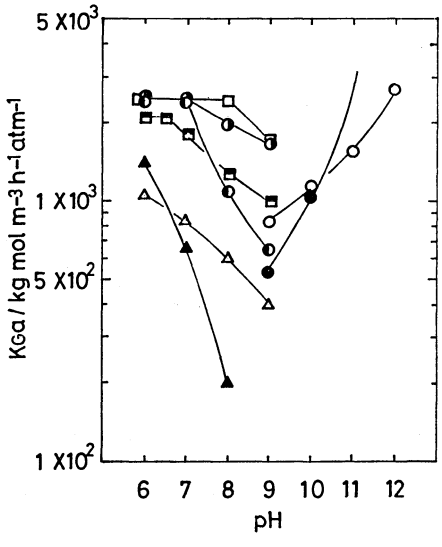

Fig. 1. Effect of pH on K_G a of malodorous components.
Superficial gas velocity: 1.7 m/s, liquid/gas ratio: 2 l/m^3, NaOCl: 1.2×10^{-2} mol/l, packed height: 60 cm (180 cm for H_2S), tower diameter: 8 cm (40 cm for H_2S), □: NH_3 (10 ppm), ■: $(CH_3)_3N$ (5 ppm), ○: CH_3SH (5 ppm), ◑: CH_3SCH_3 (5 ppm), ●: H_2S (60 ppm), ◐: CH_3SSCH_3 (5 ppm), △: CH_3CHO (1 ppm), ▲: $C_6H_5CH{=}CH_2$ (1 ppm).

oxidized both with pH 6 NaOCl solution (in the 60 cm tower) and with the pH 11 solution, separately in parallel. The NaOCl concentration, superficial gas velocity and liquid/gas ratio were set to be the same as described above. The $K_G a$ values of NH_3, $(CH_3)_3N$, and CH_3SCH_3 were determined to be 2550, 2100, 2600 (kg mol/m^3 h atm), respectively, when oxidized with pH 6 solution and that of H_2S to be 2500 with pH 11 solution. These values almost agree with those in the earlier papers[4,6,7] (determined for each component, separately). Therefore, the estimation was verified and the pH values, 6 and 11 were proved to be effective for oxidation of actual malodorous gas in mixed multi-component systems. However, since so much chlorine releases (about 10 ppm) from the absorptive solution at pH 6 that the NaOCl concentration can't be controlled, it is preferable for the actual operation to set the pH at 7 and 11, respectively; at this pH chlorine release can be suppressed to less than 3 ppm.

Next, to make the oxidation process more effective, a two-step oxidation was planned to be tried using two packed towers arranged in series, whereby malodorous components are oxidized in the first tower with pH 7 NaOCl solution and next in the second with the pH 11 solution. Then, another experimental study was carried out with exhaust gas from a night soil treatment plant, which contains H_2S, CH_3SH, CH_3SCH_3, CH_3SSCH_3, NH_3, $(CH_3)_3N$, $C_6H_5CH{=}CH_2$, CH_3CHO in 40, 0.08, 1.97, 0.024, 18.8, 0.024, <0.01, <0.05 ppm, respectively. The gas was introduced into the first tower (60 cm height), where part of H_2S and the other components except CH_3SH were absorbed and oxidized, next into the second (180 cm height), where the remaining H_2S and CH_3SH were oxidized. The NaOCl concentration, superficial gas velocity and liquid/gas ratio were set to be the same as described above. In the effluent gas from the second tower, 0.002 ppm of H_2S and 0.05 ppm of NH_3 were detected and the other malodorous components were reduced to the concentrations below their determinable limit. The treated gas was almost odorless. Therefore, it can be concluded that malodor is removed almost completely by the two-step process under the conditions described above. In the practical operation, however, it is preferable to set the pH around at 10 rather than 11 in the second tower, in the case where much CO_2 gas (1500—3000 ppm) coexists, as in the case of aeration tanks or sludge storage tanks in sewage treatment plants, in order to prevent troubles of carbonate-scaling.

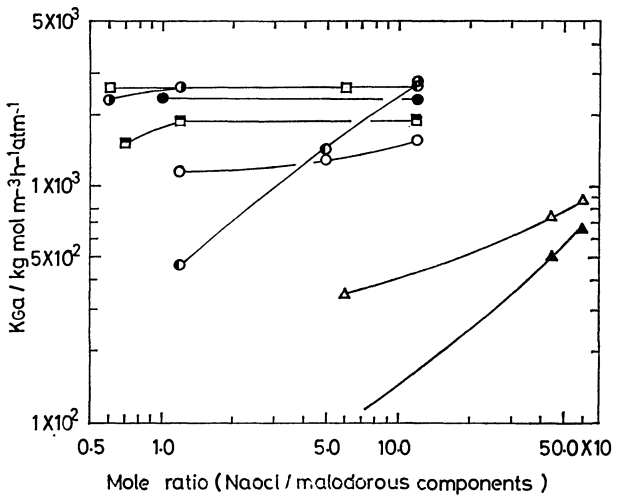

Fig. 2. Effect of mole ratio on $K_G a$ of malodorous components.
Superficial gas velocity: 1.7 m/s, liquid/gas ratio: 2 l/m^3, packed height: 60 cm (180 cm for H_2S), tower diameter: 8 cm (40 cm for H_2S), pH 11 for H_2S and CH_3SH, pH 7 for the others, □: NH_3 (5—10 ppm), ▣: $(CH_3)_3N$ (1—5 ppm), ○: CH_3SH (5 ppm), ◑: CH_3SCH_3 (5 ppm), ●: H_2S (10—100 ppm), ◐: CH_3SSCH_3 (5 ppm), △: CH_3CHO (0.1—1.0 ppm), ▲: $C_6H_5CH{=}CH_2$ (0.1—1.0 ppm).

Figure 2, prepared by rearranging the data in the earlier papers,[4,6-8] shows the relationship between the NaOCl concentration and $K_G a$. Malodorous components are classified roughly into two groups: namely, one to be oxidized almost completely at the mole ratio (hypochlorite/malodorous components) of 12 (or larger) and another to be oxidized at the ratio of larger than 120. CH_3SH, CH_3SSCH_3, CH_3CHO, and $C_6H_5CH{=}CH_2$ belong to the latter. But their contents in actual exhaust gas are negligible small (less than 5 ppm), compared with H_2S, NH_3, $(CH_3)_3N$, and CH_3SCH_3 in the former group. Accordingly, it is adequate that the NaOCl concentration was determined to be 1.2×10^{-2} mol/l on the basis of the mole ratio 12.

This process is applicable to the treatment of malodorous exhaust gas from sewage treatment plants and kraft pulp mills.

References

1) I. Akamatsu and Y. Uejima, *Kami Parupu Kyokaishi*, **23**, 239 (1969).
2) T. Endo and K. Nakajima, *Kagaku Kojo*, **16**, 47 (1973).
3) G. A. Jensen, D. F. Adams, and H. Stern. *JAPCA*, **16**, 248 (1966).
4) K. Abe and W. Machida, *Anzen Kogaku*, **17**, 265 (1978).
5) K. Abe and W. Machida, *Anzen Kogaku*, **18**, 133 (1979).
6) K. Abe and W. Machida, *Anzen Kogaku*, **18**, 271 (1979).
7) K. Abe, J. Hagiwara, and W. Machida, *Taiki Osen Gakkaishi*, **14**, 474 (1979).
8) K. Abe, J. Hagiwara, and W. Machida, *Taiki Osen Gakkaishi*, **15**, 21 (1980).
9) For a system in which gas mixtures are lean and the absorptive reaction is irreversible, the overall mass transfer coefficient $K_G a$ is given by the following equation:[3]

$$K_G a = G_m / Ph \ln y_1/y_2, \quad (1)$$

where
$K_G a$ = overall mass transfer coefficient (kg mol/m^3 h atm),
G_m = superficial mole velocity of gas (kg mol/m^2 h),
h = packed height (m),
P = total pressure (atm),
y_1, y_2 = concentration of gas at the inlet and outlet of the packed tower (mole fraction).
10) Announcement No. 9, "Method for Determination of Malodorous Materials," issued by the Environmental Protection Agency, Japan, May 1972.
11) Announcement No.47, "Revised Method for Determination of Malodorous Materials," issued by the Environmental Protection Agency, Japan, Sept. 1976.

The Wet Oxidation of Organic Compounds Catalyzed by Co-Bi Complex Oxide

Sei-ichiro IMAMURA,* Hiroshi KINUNAKA, and Nariyoshi KAWABATA

Department of Chemistry, Kyoto Institute of Technology, Matsugasaki, Sakyo-ku, Kyoto 606

(Received April 3, 1982)

Synopsis. The wet oxidation of various organic compounds was carried out in the presence of the Co-Bi (5:1) complex oxide catalyst. The catalyst was especially effective for the oxidation of all refractory lower carboxylic acids, which are intermediates in the wet oxidation of many organic compounds.

Wet oxidation, carried out in air under a high pressure and at an elevated temperature, is particularly effective for the purification of wastewaters which are resistant to biological treatment,[1] and the recovery of mechanical energy is possible when the process is applied to a highly contaminated wastewater.[2] The severe operating conditions, however, limit the application of this process, and so the development of various catalysts has been attempted in order to mitigate the reaction conditions.[3-6] Although homogeneous copper salts are highly active,[7] heterogeneous catalysts are recommended in actual waste-water treatment. The available data on active heterogeneous catalysts, however, seem to be meagre.[8]

Previously, it was found that cobalt–bismuth complex oxide with a molar ratio of Co to Bi of 5 was remarkably active in the wet oxidation of acetic acid.[9] In this work, the activity of this catalyst in the wet oxidation of various water-soluble organic compounds was investigated.

Experimental

Reagent. Commercial polyethylene glycol with a molecular weight of 4000 (PEG-4000) and other commercial reagents were used without further purification.

Preparation of the Catalyst. Co-Bi complex oxide with a molar ratio of Co to Bi of 5 (Co/Bi[5/1]) was prepared as follows. Corresponding amounts of cobalt(II) nitrate and bismuth(III) nitrate (total amount: *ca.* 30 g) were dissolved in 100 ml of concentrated nitric acid, and the solution was poured into 500 ml of 3 mol/dm^3 sodium hydroxide. The resultant precipitate was washed with water until no nitrogen component was detected by means of a total-nitrogen analyzer. After drying at 100 °C, the precipitate was calcined at 350 °C for 2 h in air. On the basis of the weight change of the catalyst, the Bi was regarded as BiO(OH), and the Co, as Co_3O_4. The catalyst had a BET surface area of 64 m^2/g and a particle size smaller than 200 mesh.

Procedure. The catalyst, deionized water, nitrogen (3.8 MPa), and oxygen (1.0 MPa) were charged into a 270 cm^3 autoclave equipped with a sample injector and a valve for sampling. After the autoclave had been heated to a prescribed temperature by means of an electric furnace, a known amount of the reactant was injected through an injector under pressure. At appropriate time intervals, an aliquot of the solution was then withdrawn and submitted to analysis. Unless otherwise stated, the pH of the solution was not adjusted.

The oxidation of ammonia was carried out in the same way (Reaction conditions: $[NH_3]=1200$ ppm, $[Co+Bi]=2.0\times10^{-2}$ mol/dm^3, $P(O_2)=1.0$ MPa, $P(N_2)=3.0$ MPa, temp=270 °C, pH=11.0). In this case the determination of total nitrogen (TN) in the solution was carried out when the autoclave was cooled down to room temperature after the reaction for 1 h, because analysis during the reaction at a high temperature (270 °C) might be inaccurate due to the escape of ammonia into the vapor phase.

The total organic carbon (TOC) and TN were determined by means of a Sumitomo GCT-12N TOC-TN analyzer.

Results and Discussion

Table 1 shows the results of the wet oxidation of various organic compounds. R_{cat} and $R_{no\ cat}$ show the initial rates of TOC-decrease in the presence and in the absence of Co/Bi[5/1] respectively. The ratio of the initial rates, $R_{cat}/R_{no\ cat}$, indicates the effect of the catalyst under the present reaction conditions. From the values of $R_{cat}/R_{no\ cat}$, it is shown that Co/Bi[5/1] was effective for the wet oxidation of various compounds. In the cases of the oxidation of 1,2-propanediol and acetonitrile, the induction periods were observed, and the effect of the catalyst was not shown by $R_{cat}/R_{no\ cat}$. However, the percentage decrease in TOC after 20 min shows that the both reactions were accelerated in the presence of the catalyst (Runs 24 and 25). Co/Bi[5/1] was also effective for the oxidation of refractory pyridine, although the effect was not so large. The oxidation of some compounds, such as phenol, glutamic acid, and urea, proceeded so rapidly, even in the absence of Co/Bi[5/1], that the effect of the catalyst could not be evaluated (Runs 15—17 and 27). The effect of the catalyst might be seen by carrying out the reaction at lower temperature. However, as can be seen from the temperature-dependence of the oxidation of acetic acid (Runs 2—5), the effect of the catalyst was less remarkable at lower temperatures. The oxidation of oxalic acid at low temperatures (140 and 112 °C) was not accelerated by Co/Bi[5/1] (Runs 10 and 11). Thus, the appropriate temperature, depending upon

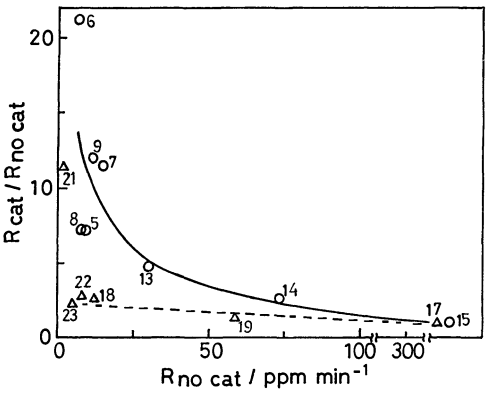

Fig. 1. Oxidation of organic compounds at 248 °C. Reaction conditions are shown in Table 1.
○: Carboxylic acids, △: compounds other than carboxylic acid. Numerals correspond to Run No. in Table 1.

TABLE 1. WET OXIDATION OF WATER-SOLUBLE ORGANIC COMPOUNDS IN THE PRESENCE AND ABSENCE OF Co/Bi[5/1][a]

Run	Reactant	t/°C	Without catalyst			With catalyst			$R_{cat}/R_{no\ cat}$
			pH	$R_{no\ cat}$[b] / ppm min^{-1}	ΔTOC[c] at 20 min / %	pH	R_{cat}[d] / ppm min^{-1}	ΔTOC[c] at 20 min / %	
1	Formic acid	112	2.8	17.7	17.3	2.9	27.8	25.9	1.6
2	Acetic acid	180	3.4	1.0	1.0	3.5	1.8	2.0	1.8
3	Acetic acid	200	3.4	2.6	2.4	3.4	6.8	7.1	2.6
4	Acetic acid	225	3.4	3.5	3.2	3.3	24.2	25.1	7.0
5	Acetic acid	248	4.0	9.2	8.3	3.4	70.5	67.0	7.2
6	Propionic acid	248	4.5	7.3	6.9	4.6	155	79.0	21.2
7	Butyric acid	248	3.5	15.0	17.5	3.8	173	83.4	11.5
8	Valeric acid	248	3.7	8.5	8.3	3.8	61.1	50.9	7.2
9	Hexanoic acid	248	3.5	11.7	12.4	3.4	140	80.6	12.0
10	Oxalic acid	112	1.4	0	0	1.4	0	0	—
11	Oxalic acid	140	1.4	35.6	27.0	1.4	35.6	31.9	1
12	Oxalic acid	160	2.5	≃330	90.0	2.5	≃330	86.3	1[e]
13	Adipic acid	248	2.8	29.4	27.3	3.2	142	97.4	4.8
14	Succinic acid	248	3.2	73.2	58.6	3.2	200	100	2.7
15	Glutamic acid	248	8.1	≃360	72.5	7.4	≃360	82.5	1[e]
16	Phenol	180	3.3	≃220	83.1	5.2	≃280	92.7	1.3
17	Phenol	248	2.8	≃390	93.4	3.5	≃390	95.8	1[e]
18	Methanol	248	5.5	11.7	11.7	6.2	29.5	29.0	2.5
19	Acetaldehyde	248	3.2	58.3	46.6	3.5	75.3	69.4	1.3
20	PEG-4000	200	4.4	31.6	38.3	7.7	117	77.9	3.7
21	Acetamide	248	6.6	0.9	1.0	8.3	10.3	12.1	11.4
22	Propionamide	248	6.0	7.2	6.2	7.5	19.5	19.2	2.7
23	Valeramide	248	7.9	4.4	4.1	8.0	10.0	14.4	2.3
24	1,2-Propanediol	248	6.5	0[f]	9.3	3.9	170	79.5	—
25	Acetonitrile	248	8.2	0.5>[f]	0.6	7.0	0.5>[f]	5.8	—
26	Pyridine	270	7.4	0	0	7.4	3.4	4.0	—
27	Urea	248	9.4	400<	100	9.5	400	100	—

a) Reaction conditions: [Co+Bi] = 2.0×10^{-2} mol/dm^3, $P(O_2)$ = 1.0 MPa, $P(N_2)$ = 3.0 MPa. b) Initial rate of TOC decrease in the absence of Co/Bi[5/1]. c) Percentage decrease in TOC. d) Initial rate of TOC decrease in the presence of Co/Bi[5/1]. e) Inaccurate due to rapid reaction. f) Induction period appeared.

the kind of compound to be oxidized, is necessary for the catalyst to exert its activity.

In order to see the property of the catalyst more clearly, the values of $R_{cat}/R_{no\ cat}$ were plotted against $R_{no\ cat}$ in the oxidation of various compounds at 248 °C (Fig. 1). It is clear that the catalyst is especially effective for the oxidation of carboxylic acid; the more refractory the carboxylic acid is, the more effective the catalyst is. However, for compounds other than carboxylic acid, the effect of the catalyst is not so remarkable. Previously, it was deduced that the catalytic action of Co/Bi[5/1] was due to two of its properties; one was the presence of basic sites, induced by Bi, where acetic acid was adsorbed by an acid–base interaction in the first step of the reaction, and the other was its redox property which induced the decomposition of the adsorbed acetic acid.[9] From the results shown in Fig. 1, it is clear that the catalyst exhibited the former property more strongly; the acid-base interaction played an important role in the oxidation of all carboxylic acids. The catalyst was quite effective for the oxidation of acetamide. As acetamide is readily hydrolyzed to produce acetic acid under the present reaction conditions,[10] the catalyst is apparently highly active in the oxidation of acetamide.

Many organic compounds undergoing wet oxidation gradually degrade to low-molecular-weight compounds and, finally, to highly refractory lower carboxylic acids.[11] As Co/Bi[5/1] is remarkably active for the oxidation of all refractory lower carboxylic acids, it is quite useful as a catalyst for the wet oxidation of wastewater.

The contamination of wastewater by ammonia is a serious environmental problem; however, few active catalysts for the wet oxidation of ammonia have been reported.[12] The catalytic activity of Co/Bi[5/1] in the wet oxidation of ammonia was investigated, the reaction conditions being shown in the Experimental section. The percentage decrease in TN in the solution was 46.0%, compared with 20.5% in the absence of Co/Bi[5/1], showing that the catalyst was also effective in the wet oxidation of ammonia.

References

1) Y. Tagashira, H. Takagi, and K. Inagaki, Japan Kokai 75106862 (1975); *Chem. Abstr.*, **84**, 79359q (1976).
2) C. L. Chou and F. H. Verhoff, *Ind. Eng. Chem., Process Des. Dev.*, **20**, 12 (1981).
3) J. Levec, M. Herskowitz, and J. M. Smith, *AIChE J.*, **22**, 919 (1976).
4) G. Baldi, S. Goto, C. K. Chow, and J. M. Smith, *Ind. Eng. Chem., Process Des. Dev.*, **13**, 447 (1974).
5) E. O. Box, Jr., and F. Farha, Jr., U. S. Patent 4062772 (1977); *Chem. Abstr.*, **88**, 78698 (1978).
6) S. Morisaki, K. Komamiya, and M. Naito, *Nippon Kagaku Kaishi*, **1980**, 1191.
7) S. Imamura, T. Sakai, and T. Ikuyama, *Sekiyu Gakkaishi*, **25**, 63 (1982).
8) J. R. Katzer, H. H. Ficke, and A. Sadana, *J. Water Pollut. Control. Fed.*, **48**, 920 (1976).
9) S. Imamura, A. Hirano, and N. Kawabata, *Ind. Eng. Chem., Prod. Res. Dev.*, in press.
10) S. Imamura, M. Fukuhara, and T. Kitao, *Nippon Kagaku Kaishi*, **1980**, 270.
11) H. Higashijima, *Shokubai*, **20**, 99 (1978).
12) N. Kakihara, Y. Harada, and N. Uedono, Japan Kokai 152591 (1980); N. Kakihara, Y. Harada, N. Uedono, K. Yamazaki, T. Ueda, and H. Fujitani, Ger. Offen. 2950710 (1980); *Chem. Abstr.*, **94**, 7343p (1981).

 © 1982 The Chemical Society of Japan Bull. Chem. Soc. Jpn., 55, 3681—3685 (1982)

The Crystal and Molecular Structure of Staurosporine, a New Alkaloid from a *Streptomyces* Strain

Akio Furusaki,* Nobuhiro Hashiba, Takeshi Matsumoto, Atsushi Hirano,†
Yuzuru Iwai,† and Satoshi Ōmura†

Department of Chemistry, Faculty of Science, Hokkaido University, Kita-ku, Sapporo 060
†The Kitasato Institute and Kitasato University, Shirokane, Minato-ku, Tokyo 108

(Received January 7, 1982)

The molecular sturcture of staurosporine, an alkaloid from a *Streptomyces* strain, has been determined by means of an X-ray crystallographic analysis of its methanol solvate ($C_{28}H_{26}N_4O_3 \cdot CH_3OH$). The crystals are monoclinic, with four formula units in a unit cell with dimensions of $a=23.487(6)$, $b=7.636(3)$, $c=15.638(4)$ Å, and $\beta=116.71(5)°$; the space group is C2. 2532 unique intensity data were collected on a four-circle diffractometer with LiF-monochromated Cu *Kα* radiation. The structure was solved by the Monte Carlo direct method, using the 20 strongest reflections as the starting set; the 72nd random phase set led to the correct solution. The *R* value reached 0.047 by block-diagonal least-squares refinements. Staurosporine has been found to contain a unique dimeric indole structure. Because of the steric hindrance, the indolo[2,3-*a*]carbazole aromatic system in the molecule is slightly bent; the two terminal benzene rings make an angle of 7.5° with each other.

Staurosporine (**1**), formerly referred to as AM-2282, is an alkaloid isolated from *Streptomyces staurosporeus* Awaya, Takahashi, and Ōmura, nov. sp., and shows strong hypotensive activity as well as antimicrobial activity against fungi and yeast.[1] Since **1** exhibits characteristic ultraviolet absorption at 292 nm, it was compared with other known antibiotics (*e.g.*, oxamicetin[2] and pyridomycin[3,4]) which absorb in a region near 292 nm. However, **1** could not be structurally correlated to these known compounds. Therefore, we have tried to determine the molecular structure of **1** by means of X-ray analysis of its methanol solvate. The results have already been reported in a preliminary form.[5] The present paper will describe the details of the structure determination and molecular geometry of this novel alkaloid, **1**.

Experimental

Pale-yellow plate-like crystals, mp 270 °C (decomp), were obtained from a methanol solution of **1**. A single crystal with dimensions of about $0.5 \times 0.5 \times 0.2$ mm^3 was used for the X-ray measurement. The crystal data are summarized in Table 1. The unit-cell dimensions and reflection intensities were measured on a Rigaku four-circle diffractometer with LiF-monochromated Cu *Kα* radiation ($\lambda=1.5418$ Å). The θ-2θ continuous-scan technique was applied at a 2θ scan rate of 1° min^{-1}; the background was measured for 30—60 s at each end of the scan range. Three standard reflections, measured at intervals of every 29 reflections, showed no significant decrease in intensity during the course of data collection. The intensities were corrected for the Lorentz and polarization factors, but not for the absorption or the extinction effect. In the range of 2θ values up to 140°, 2532 independent structure factors above the $\sigma(F)$ level were selected for the structure determination.

Structure Determination

The structure was elucidated by the Monte Carlo direct method,[6] using the 20 reflections with the greatest $|E|$ values as the starting set. In order to extend each of the tentative-phase sets derived from random numbers, 12 cycles of the tangent procedure were carried out using 487 $|E|$ values above 1.30. The 72nd phase set which showed a low R_K value of 0.274 ($R_k=\sum||E_o|-k|E_c||/\sum|E_o|$) and a nonzero q value of 0.400 ($q=1-\sum_h|E_h|(|\sum_k E_kE_{h-k}|/\sum_k|E_kE_{h-k}|)/\sum_h|E_h|$)[7] led to the correct solution; an *E*-map based on 458 phases afforded 33 of the 37 independent non-hydrogen atoms. The remaining four atoms were located in a difference Fourier map. After several cycles of the least-squares refinement using the carbon atomic scattering factors for all the non-hydrogen atoms, the nitrogen and oxygen atoms were assigned by taking account of the values of isotropic temperature factors as well as the interatomic distances. The structure thus obtained was refined by the block-diagonal least-squares method with anisotropic thermal parameters. After 25 hydrogen atoms had been located in a second difference Fourier map, further least-squares refinements were performed including the hydrogen atoms with isotropic temperature factors. The weighting scheme used was as follows:

$$w = 1/\{\sigma(F)^2 \exp(c_1X^2+c_2Y^2+c_3XY+c_4X+c_5Y)\},$$

where $X=|F_o|$ and $Y=\sin\theta/\lambda$. The c_1, c_2, c_3, c_4, and c_5 coefficients were evaluated from the $(\Delta F)^2$ distribution: $c_1=-0.552\times10^{-3}$, $c_2=39.5$, $c_3=0.0541$, $c_4=0.0528$, and $c_5=-44.7$. In this manner, the *R* value reached 0.047. The final atomic parameters are listed in Table 2.[8]

The calculations were done on a FACOM 230-75 computer at the Hokkaido University Computing Center, using our own programs. The atomic scattering

Table 1. The crystal data

$C_{28}H_{26}N_4O_3 \cdot CH_3OH$	$F.W.=498.58$
Crystal system	Monoclinic
Space group	C2
Cell dimensions	$a=23.487(6)$ Å
	$b=7.636(3)$ Å
	$c=15.638(4)$ Å
	$\beta=116.71(5)°$
V	2505.4 Å^3
Z	4
D_c	1.322 g cm^{-3}
μ(Cu *Kα*)	6.86 cm^{-1}

Table 2. The final atomic parameters and estimated standard deviations
The atomic coordinates are multiplied by 10^4.

Atom	x	y	z	$B_{eq}^{a)}$/Å^2	Atom	x	y	z	$B_{eq}^{a)}$/Å^2
C(1)	2119(2)	1027(4)	5023(2)	4.10	C(20)	3591(1)	1190(5)	4997(2)	4.38
C(2)	1612(2)	937(5)	5240(2)	4.83	C(21)	3090(1)	1679(4)	4012(2)	3.27
C(3)	1002(2)	1431(5)	4565(2)	4.69	C(22)	2427(1)	1861(3)	3678(2)	2.95
C(4)	880(1)	2024(5)	3659(2)	4.06	C(23)	2010(1)	1611(4)	4109(2)	3.18
C(5)	1393(1)	2078(4)	3424(2)	3.10	C(24)	883(1)	3122(4)	1662(2)	3.38
N(6)	1420(1)	2575(3)	2579(1)	2.95	C(25)	715(1)	5082(5)	1637(2)	4.01
C(7)	2048(1)	2455(3)	2739(2)	2.73	C(26)	1166(1)	6348(4)	1492(2)	3.86
C(8)	2341(1)	2859(3)	2152(1)	2.73	C(27)	1220(1)	5751(4)	602(2)	3.75
N(9)	2077(1)	3518(3)	1238(1)	3.00	C(28)	1404(1)	3841(4)	633(2)	3.28
C(10)	2558(1)	3829(3)	973(2)	3.06	O(29)	1042(1)	2685(3)	903(1)	3.50
C(11)	2510(2)	4535(4)	122(2)	3.76	O(30)	4480(1)	1845(5)	3709(2)	5.25
C(12)	3079(2)	4746(4)	55(2)	4.13	N(31)	1777(1)	6406(3)	2347(2)	3.84
C(13)	3664(2)	4278(5)	805(3)	4.31	C(32)	2191(3)	7798(6)	2331(3)	6.37
C(14)	3707(1)	3570(4)	1644(2)	3.68	O(33)	669(1)	5439(4)	2497(2)	4.72
C(15)	3143(1)	3322(3)	1736(2)	3.11	C(34)	362(3)	7063(9)	2478(4)	7.65
C(16)	3005(1)	2689(3)	2487(2)	2.85	C(35)	294(1)	2004(6)	1437(2)	5.12
C(17)	3372(1)	2054(4)	3429(2)	3.20	O(M)	4222(4)	−1024(9)	2286(8)	14.00
C(18)	4065(1)	1747(5)	3984(2)	4.04	C(M)	3885(6)	−2014(10)	2566(11)	12.99
N(19)	4166(1)	1291(5)	4870(2)	4.92					

a) $B_{eq}=8\pi^2(u_1^2+u_2^2+u_3^2)/3$, where u_i is the root-mean-square deviation in the i-th principal axis of the thermal ellipsoid.

factors were taken from the International Tables.[9]

Results and Discussion

Molecular Structure. The molecular skeleton of **1** obtained is illustrated in Fig. 1, while the bond distances and angles are given in Table 3. From these results, it is concluded that **1** has the **1a** structure containing a unique dimeric indole skeleton.

As Fig. 2 shows, the aromatic system composed of the A-, B-, C-, D-, and E-rings is slightly bent; the terminal A- and E-rings deviate from the mean plane of the central C-ring onto the side of the N(31)H–C(32)H_3 methylamino group, and make an angle of 7.5° with each other. Of the C–C bond distances in the aromatic system, the C(17)–C(21), C(1)–C(2), and C(13)–C(14)

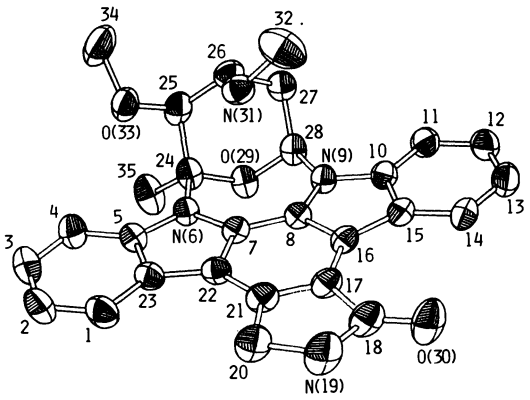

Fig. 1. A perspective view of the staurosporine molecule, showing the crystallographic numbering. Each non-hydrogen atom is represented as a thermal ellipsoid enclosing a 50% probability. The symbol C for carbon atoms is omitted.

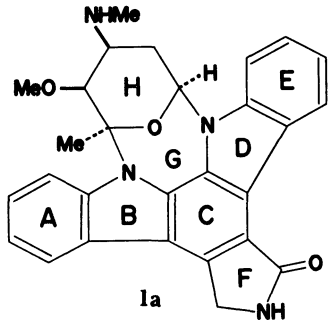

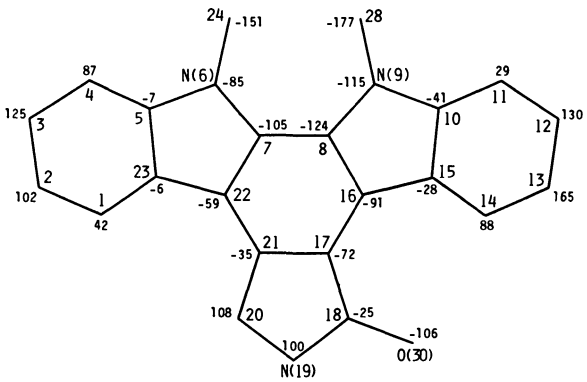

Fig. 2. The deviations ($d\times 10^3$/Å) of the atoms from the mean plane of the A–B–C–D–E aromatic system.
This mean plane is represented by the following equation: $0.1522X+0.9328Y+0.3266Z-3.200=0$, where X, Y, and Z are rectangular coordinates measured in Å units along the a*, b, and c axes respectively.

distances are appreciably shorter than the others. These bond shortenings may be explained on the basis of the π-bond-order distribution in the carbazole molecule[10] as follows: when each of the A–B–C and C–D–E ring

TABLE 3. THE BOND DISTANCES (l/Å) AND ANGLES (ϕ/°), WITH THEIR STANDARD DEVIATIONS
The e.s.d.'s given in parentheses refer to the last decimal position.

C(1)–C(2)	1.380(6)	C(26)–N(31)	1.458(3)	C(15)–C(16)–C(17)	135.3(2)
C(1)–C(23)	1.407(4)	C(27)–C(28)	1.516(4)	C(16)–C(17)–C(18)	131.3(3)
C(2)–C(3)	1.395(5)	C(28)–O(29)	1.416(4)	C(16)–C(17)–C(21)	120.7(2)
C(3)–C(4)	1.389(5)	N(31)–C(32)	1.448(6)	C(18)–C(17)–C(21)	108.0(2)
C(4)–C(5)	1.407(5)	O(33)–C(34)	1.429(7)	C(17)–C(18)–N(19)	106.5(3)
C(5)–N(6)	1.404(4)	C(M)–O(M)	1.31(2)	C(17)–C(18)–O(30)	128.3(3)
C(5)–C(23)	1.406(3)	C(2)–C(1)–C(23)	118.8(3)	N(19)–C(18)–O(30)	125.2(2)
N(6)–C(7)	1.383(3)	C(1)–C(2)–C(3)	120.4(4)	C(18)–N(19)–C(20)	114.3(2)
N(6)–C(24)	1.482(2)	C(2)–C(3)–C(4)	122.1(4)	N(19)–C(20)–C(21)	101.2(3)
C(7)–C(8)	1.408(4)	C(3)–C(4)–C(5)	117.8(3)	C(17)–C(21)–C(20)	109.9(2)
C(7)–C(22)	1.406(3)	C(4)–C(5)–N(6)	131.3(2)	C(17)–C(21)–C(22)	121.0(2)
C(8)–N(9)	1.372(3)	C(4)–C(5)–C(23)	120.2(3)	C(20)–C(21)–C(22)	129.1(3)
C(8)–C(16)	1.409(3)	N(6)–C(5)–C(23)	108.5(2)	C(7)–C(22)–C(21)	119.6(3)
N(9)–C(10)	1.388(4)	C(5)–N(6)–C(7)	108.0(2)	C(7)–C(22)–C(23)	106.8(2)
N(9)–C(28)	1.451(3)	C(5)–N(6)–C(24)	127.5(2)	C(21)–C(22)–C(23)	133.6(2)
C(10)–C(11)	1.393(4)	C(7)–N(6)–C(24)	124.6(2)	C(1)–C(23)–C(5)	120.6(3)
C(10)–C(15)	1.409(3)	N(6)–C(7)–C(8)	131.5(2)	C(1)–C(23)–C(22)	132.1(2)
C(11)–C(12)	1.396(6)	N(6)–C(7)–C(22)	109.4(2)	C(5)–C(23)–C(22)	107.3(2)
C(12)–C(13)	1.394(4)	C(8)–C(7)–C(22)	119.1(2)	N(6)–C(24)–C(25)	113.2(2)
C(13)–C(14)	1.381(5)	C(7)–C(8)–N(9)	129.4(2)	N(6)–C(24)–O(29)	108.1(2)
C(14)–C(15)	1.409(4)	C(7)–C(8)–C(16)	121.4(2)	N(6)–C(24)–C(35)	110.7(2)
C(15)–C(16)	1.436(4)	N(9)–C(8)–C(16)	109.2(2)	C(25)–C(24)–O(29)	111.3(2)
C(16)–C(17)	1.417(3)	C(8)–N(9)–C(10)	109.0(2)	C(25)–C(24)–C(35)	109.9(2)
C(17)–C(18)	1.480(3)	C(8)–N(9)–C(28)	126.3(2)	O(29)–C(24)–C(35)	103.1(2)
C(17)–C(21)	1.377(4)	C(10)–N(9)–C(28)	124.7(2)	C(24)–C(25)–C(26)	115.6(3)
C(18)–N(19)	1.342(4)	N(9)–C(10)–C(11)	128.7(2)	C(24)–C(25)–O(33)	106.8(3)
C(18)–O(30)	1.232(4)	N(9)–C(10)–C(15)	108.4(2)	C(26)–C(25)–O(33)	111.8(3)
N(19)–C(20)	1.452(4)	C(11)–C(10)–C(15)	123.0(3)	C(25)–C(26)–C(27)	107.2(2)
C(20)–C(21)	1.507(3)	C(10)–C(11)–C(12)	116.6(2)	C(25)–C(26)–N(31)	110.3(2)
C(21)–C(22)	1.409(3)	C(11)–C(12)–C(13)	121.4(3)	C(27)–C(26)–N(31)	113.2(3)
C(22)–C(23)	1.430(4)	C(12)–C(13)–C(14)	121.6(4)	C(26)–C(27)–C(28)	113.5(2)
C(24)–C(25)	1.544(5)	C(13)–C(14)–C(15)	118.6(2)	N(9)–C(28)–C(27)	113.3(2)
C(24)–O(29)	1.434(3)	C(10)–C(15)–C(14)	118.8(3)	N(9)–C(28)–O(29)	108.9(2)
C(24)–C(35)	1.526(4)	C(10)–C(15)–C(16)	107.0(2)	C(27)–C(28)–O(29)	114.1(2)
C(25)–C(26)	1.523(5)	C(14)–C(15)–C(16)	134.2(2)	C(24)–O(29)–C(28)	121.1(2)
C(25)–O(33)	1.423(4)	C(8)–C(16)–C(15)	106.5(2)	C(26)–N(31)–C(32)	113.5(3)
C(26)–C(27)	1.524(5)	C(8)–C(16)–C(17)	118.2(2)	C(25)–O(33)–C(34)	113.5(3)

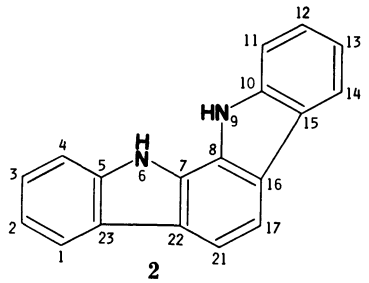

2

systems is taken as the carbazole skeleton, all the above short bonds correspond to the carbazole C_3–C_4 or C_5–C_6 bond having the greatest π-bond order; especially the shortest C(17)–C(21) bond corresponds exactly to such bonds in both A–B–C and C–D–E carbazole skeletons. In order to estimate the π-bond orders in **1**, we performed a Hückel MO calculation on the indolo[2,3-*a*]carbazole (**2**) molecule, assuming the C_{2v} symmetry. The results given in Table 4 show a good correlation between the calculated π-bond orders and the observed C–C bond distances; as has been expected, the C(17)–C(21) bond

TABLE 4. THE π-BOND ORDERS IN INDOLO[2,3-*a*]CARBAZOLE

Bond[a]	π-Bond order[b]	Distance[c] l/Å
C_1–C_2	0.691	1.381
C_2–C_3	0.642	1.395
C_3–C_4	0.683	1.393
C_4–C_5	0.627	1.399
C_5–C_{23}	0.584	1.408
C_1–C_{23}	0.601	1.408
C_7–C_8	0.592	1.408
C_7–C_{22}	0.599	1.408
C_{22}–C_{23}	0.421	1.433
C_{17}–C_{21}	0.716	1.377
C_{21}–C_{22}	0.579	1.413
C_5–N_6	0.337	1.396
N_6–C_7	0.334	1.378

a) For the atomic numbering, see the **2** formula. b) The parameters used for nitrogen atoms were as follows: $\alpha_N = \alpha_C + 1.5\beta_{CC}$; $\beta_{CN} = 0.8\beta_{CC}$. c) The equivalent bond distances were averaged, the C_{2v} symmetry being assumed for the aromatic system in **1**.

Table 5. The torsion angles (ϕ/°) for the G- and H-rings

C(24)–N(6)–C(7)–C(8)	3.3
N(6)–C(7)–C(8)–N(9)	0.8
C(7)–C(8)–N(9)–C(28)	−4.7
C(8)–N(9)–C(28)–O(29)	−27.1
N(9)–C(28)–O(29)–C(24)	86.1
C(28)–O(29)–C(24)–N(6)	−85.8
O(29)–C(24)–N(6)–C(7)	27.4
C(24)–C(25)–C(26)–C(27)	52.9
C(25)–C(26)–C(27)–C(28)	−53.1
C(26)–C(27)–C(28)–O(29)	48.3
C(27)–C(28)–O(29)–C(24)	−41.6
C(28)–O(29)–C(24)–C(25)	39.2
O(29)–C(24)–C(25)–C(26)	−45.5

has the greatest π-bond order, and the C(1)–C(2) and C(13)–C(14) bonds have the next greatest.

The γ-lactam F-ring is almost planar, and lies approximately in the mean plane of the A–B–C–D–E aromatic system. In *cis*-peptides[11] as well as in *trans*-peptides,[12] usually the N–C=O bond angle is larger than the C_α–C=O angle, but the relation is reversed in the present amide (125.2 and 128.3°). This bond-angle deformation may result from the steric hindrance between the O(30) atom and the C(14)H(14) grouping: O(30)···C(14), 3.192(4); O(30)···H(14), 2.47(4) Å. In this connection, the C(16)–C(17)–C(18) bond angle is also found to be larger than the C(20)–C(21)–C(22) angle by 2.2°. Further, the O(30) atom and the C(14)-H(14) group become more distant from each other by deviating slightly from the mean plane of the aromatic system to the opposite sides (see Fig. 2).

The torsion angles for the G- and H-rings are given in Table 5. The seven-membered G-ring has an envelope-like conformation, while the six-membered H-ring takes a flattened chair conformation. All the N(6), N(9), and N(31) atoms are axially placed on the same side of the H-ring. As the result, the N(31) atom approaches the planar N(6)–C(7)–C(8)–N(9) segment very closely: C(7), 3.087(4); C(8), 3.089(4) Å. This close contact results in a slight deviation of the C(24) and C(28) atoms from the N(6)–C(7)–C(8)–N(9) plane. Since the three N–C bonds at each of the N(6) and N(9) atoms are found to be coplanar, this deviation must arise from pure twistings about the N(6)–C(7) and N(9)–C(8) bonds. These twistings can be expanded into the bending deformation of the indolo[2,3-*a*]-carbazole moiety. Thus, the bending of the aromatic system can be regarded as due mainly to the severe steric hindrance between the methylamino group and the aromatic system.

As will be seen from the C(27)–C(26)–N(31)–C(32) and C(25)–C(26)–N(31)–H(31) torsion angles of 70.2 and −56° respectively, the N(31) atom directs its lone pair approximately toward the C(8) atom, and donates its H(31) proton to the O(33) methoxyl oxygen atom, possibly forming a weak hydrogen bond of the five-membered-ring type: N(31)···O(33), 2.814(4); H(31)···O(33), 2.41(6) Å; H(31)···O(33)–C(25), 79(1); H(31)···O(33)–C(34), 96(1)°. The C(34) methoxyl carbon atom is *trans* to the C(24) atom; this corresponds exactly to the most stable of the three staggered conformations about the C(25)–O(33) bond. The O(33) and C(35) atoms are very close to the A-ring: O(33)···C(4), 3.088(4); O(33)···C(5), 3.059(4); C(35)···C(4), 3.108(4) Å. These steric repulsions may explain the following facts: (1) the N(6)–C(24) and C(24)–C(25) bond distances are longer than the N(9)–C(28) and C(27)–C(28) distances by 0.031 and 0.028 Å respectively; (2) the O(29)–C(24)–C(35) bond angle (103.1°) is considerably smaller than the tetrahedral angle; (3) the C(4)–C(5)–N(6) and C(5)–N(6)–C(24) bond angles are larger than the N(9)–C(10)–C(11) and C(10)–N(9)–C(28) angles by 2.6 and 2.8° respectively.

Crystal Structure. The molecular arrangement viewed along the b axis is drawn in Fig. 3. The methanol

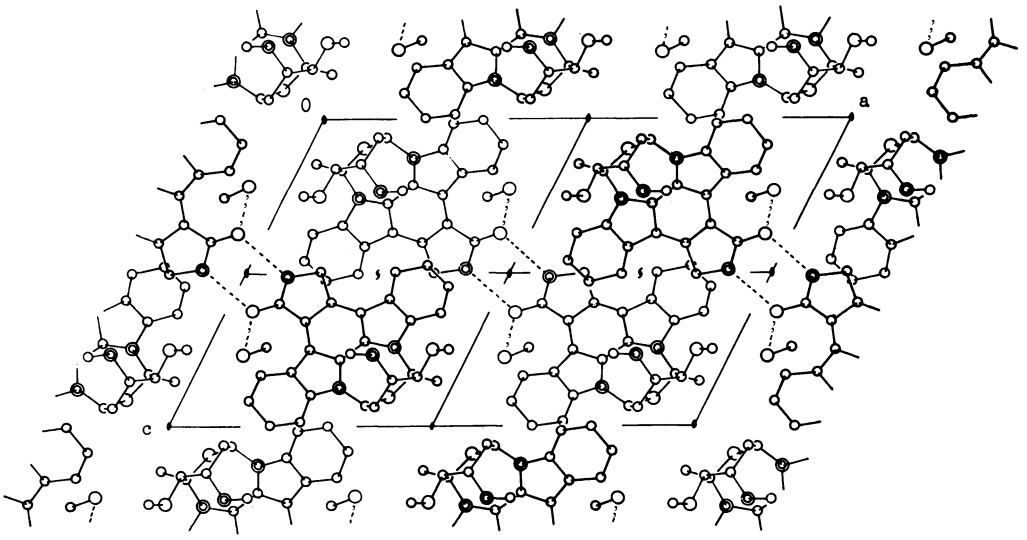

Fig. 3. The crystal structure viewed along the b axis. The samll single circles represent carbon atoms, the large single circles oxygen atoms, and the double circles nitrogen atoms.

molecule is attached to the staurosporine molecule by the O(M)–H···O(30) hydrogen bond with the O···O distance of 2.98(1) Å. The staurosporine molecules related by the two-fold rotation axis are connected by a pair of intermolecular hydrogen bonds, N(19)–H···O(30′) and N(19′)–H···O(30), forming a hydrogen-bonded dimer; the N···O distances are 2.979(3) Å. The N(19), O(30), N(19′), and O(30′) atoms deviate tetrahedrally from the planar arrangement; their deviations from the mean plane are 0.211 Å. These hydrogen-bonded dimers are further held together mainly by the van der Waals interactions. It is interesting to note that the two H-rings, placed approximately perpendicular to the (010) plane, face each other about the two-fold rotation axis.

References

1) S. Ōmura, Y. Iwai, A. Hirano, A. Nakagawa, J. Awaya, H. Tsuchiya, Y. Takahashi, and R. Masuma, *J. Antibiot.*, **30**, 275 (1977).

2) M. Konishi, M. Kimeda, H. Tsukiura, H. Yamamoto, T. Hoshiya, T. Miyaki, K. Fujisawa, H. Koshiyama, and H. Kawaguchi, *J. Antibiot.*, **26**, 752 (1973).

3) K. Maeda, H. Kosaka, Y. Okami, and H. Umezawa, *J. Antibiot., Ser. A*, **6**, 140 (1953).

4) H. Ogawara, K. Maeda, G. Koyama, H. Naganawa, and H. Umezawa, *Chem. Pharm. Bull.*, **16**, 679 (1968).

5) A. Furusaki, N. Hashiba, T. Matsumoto, A. Hirano, Y. Iwai, and S. Ōmura, *J. Chem. Soc., Chem. Commun.*, **1978**, 800.

6) A. Furusaki, *Acta Crystallogr., Sect. A*, **35**, 220 (1979).

7) W. Hoppe, J. Gassmann, and K. Zechmeister, "Crystallographic Computing," ed by F. R. Ahmed, Munksgaard, Copenhagen (1970), p. 26.

8) The tables of the anisotropic thermal parameters and hydrogen parameters and the F_o-F_c table are kept a tthe Chemical Society of Japan (Document No. 8253).

9) "International Tables for X-Ray Crystallography," The Kynoch Press, Birmingham (1974), Vol. IV.

10) H. C. Longuet-Higgins and C. A. Coulson, *Trans. Faraday Soc.*, **43**, 87 (1947).

11) G. N. Ramachandran and V. Sasisekharan, *Adv. Protein Chem.*, **23**, 288 (1968).

12) R. E. Marsh and J. Donohue, *Adv. Protein Chem.*, **22**, 249 (1967).

Formation of Intramolecular Hydrogen Bond in Hydroxy-substituted Nitroxide Radicals as Evidenced by Electron Spin Resonance

Yashige KOTAKE* and Keiji KUWATA
Department of Chemistry, Faculty of Science, Osaka University, Toyonaka, Osaka 560
(Received March 8, 1982)

The nature of the intramolecular hydrogen bond in hydroxysubstituted nitroxide radicals was examined. The hydroxysubstituted radical was produced by the spin trapping reaction of hydroxyalkyl radicals with α-phenyl-*N*-*t*-butylnitrone. The magnitude of the hyperfine splitting caused by β-hydrogen of the radical is strongly dependent on the composition of the solvent, which is attributed to the formation of the intramolecular hydrogen bond. The equilibrium constant of the intramolecular hydrogen bond in an aprotic solvent was determined by observing the magnitude of the hyperfine splitting of β-hydrogen as a function of the amount of added methanol. Based on the temperature dependence of the equilibrium constant, the standard entropy and the standard enthalpy of the formation of the hydrogen-bonded chelate ring was estimated. The same method of analysis was applied to the system of diastereomeric nitroxide and the difference of the internal energy of the chelate ring in the isomers was detected. Moreover, the difference was utilized to separate the ESR spectra of the diastereomers.

Hydrogen bonding in free radicals in solution has been extensively studied by the magnetic resonance technique. In some cases the thermodynamic constants of the formation of the hydrogen bond have been determined, based on the equilibrium study.[1-6] Concerning the intramolecular hydrogen bond, hydroxy-substituted semiquinone radicals exhibit an ESR linewidth alternation caused by the formation of the intramolecular hydrogen bond.[7,8] The linewidth alternation was also detected in hydroxy-substituted nitroxide radicals due to the formation of the chelate ring.[9,10] These studies have confirmed the formation of the intramolecular hydrogen bond, however, experimental difficulties prevent an equilibrium study.

The main difficulty in determining the equilibrium nature of the intramolecular hydrogen bond is to find a sensitive index which establishes the equilibrium state. Also there is characteristic difficulty in studying the hydrogen bond by a magnetic resonance technique: the rate of formation and breakage of the hydrogen bond is very large compared with the time scale of magnetic resonance so that the observed spectrum is that of an equilibrium mean.[11]

Recently it was pointed out that the hydroxy-substituted nitroxide radicals produced by a spin trapping technique have hyperfine splitting (hfs) of the β-hydrogens which is very sensitive to the solvent.[12] Typically, the hfs of β-H decreases forty per cent on changing from an aprotic to a protic solvent. The formation of a chelate ring by the intramolecular hydrogen bond is responsible for the change of the hfs of β-H. The quantitative treatment of the equilibrium is now possible by observing the dependence of the magnitude of the hfs of β-H on the amount of added hydrogen donor such as methanol. Using this technique the standard entropy and the standard enthalpy for the formation of the chelate ring can be estimated by the temperature dependence of the equilibrium constant.

It should be pointed out that IR and NMR studies of the OH···O hydrogen bond were more concerned with the strength of the hydrogen bond than with the structure of the chelate ring.[11] In the present system the magnitude of the β-H hfs provides information about the ring conformation while the *g*-values and N-hfs gives details of the OH···O bond.

The strain energy of the chelate ring is expected to be different for different diastereomers. Therefore the difference of the standard enthalpy of the formation of the chelate ring is utilized for the spectroscopic separation of the diastereomeric radical mixture. Hfs of β-H of diastereomers of hydroxy-substituted nitroxide radicals show different temperature dependence in the presence of proton donors. As a result the ESR spectra of diastereomeric systems showed better resolution at low temperature in toluene in the presence of methanol.

Experimental

Hydroxy-substituted nitroxide radicals were produced by the abstraction of a hydrogen atom from alcohols by photo-excited benzophenone (BP) followed by spin trapping with phenyl-*N*-*t*-butyl nitrone (PBN). The reaction scheme for the formation of the radical is as follows:[13,14]

$$RCH_2OH \xrightarrow{BP^*} \dot{R}CHOH$$

$$\dot{R}CHOH + \phi\text{-}CH{=}N(\rightarrow O)\text{-}t\text{-}Bu \longrightarrow \phi\text{-}CH(R)\text{-}N(\rightarrow O\cdot)\text{-}t\text{-}Bu \quad (1)$$

The details of the experimental procedure has been described elsewhere.[12] After the formation of nitroxides the parent alcohol was removed completely by vacuum distillation and a known amount of toluene and methanol was introduced under vacuum.

Materials. Benzophenone was recrystallized from petroleum benzine. PBN was purified by sublimation. Toluene was dehydrated by refluxing it with sodium metal and was stored over Na/K alloy under vacuum. Carbon tetrachloride was distilled and stored over calcium chloride. Alcohols were dehydrated by adding calcium hydride and were stored over molecular sieves 4A under vacuum.

The ESR spectrometer employed was operated at the X-band. The temperature of the sample was controlled by a flow of chilled nitrogen. The accuracy of the measurement of the hfs was ±0.005 mT.[12]

Results and Discussion

The magnitude of the β-H hfs of the ESR spectra of

hydroxymethyl adduct (**1**) is increased considerably by

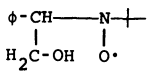

1

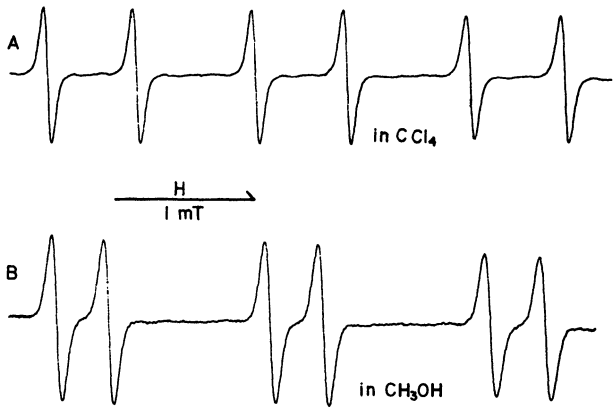

Fig. 1. ESR spectra of hydroxymethyl adduct of PBN(I) in carbon tetrachloride (A) and in methanol (B) at room temperature.

Table 1. *g*-Values and hfs of nitroxide radicals

Radical	Solvent	*g*-Value	A_N/mT	$A_{\beta\text{-H}}$/mT
Hydroxymethyl	toluene	2.0058	1.50	0.66
adduct	methanol	2.0058	1.51	0.36
Di-*t*-butyl	toluene	2.0061	1.53	—
nitroxide[15]	methanol	2.0058	1.62	—

change from a protic to an aprotic solvent as shown in Fig. 1. The solvent effect on the *g*-values and N-hfs of nitroxide radicals has been extensively studied by ESR spectroscopy.[3,15] In general, when the solvent changes from protic to aprotic the *g*-value increases but the N-hfs becomes smaller. The hfs and *g*-values of radical **1** and di-*t*-butyl nitroxide in methanol and toluene are listed in Table 1 for comparison. In contrast to the large solvent effect on the magnitude of the hfs of β-H, the effect is small for the hfs of the N^{14} nucleous and the *g*-value. This fact shows that the solvent did not change the environment of the nitroxide group but changes the steric conformation of the radical. In a protic solvent the hydrogen bond between the solvent and the nitroxide group in the radical is dominant but in an aprotic solvent the hydroxyl group of the radical acts as a hydrogen donor. Thus the intramolecular hydrogen bond in this system effects only the change of steric conformation, *i.e.* the change of the hfs of β-H.

Determination of the Equilibrium Constant for the Formation of Intramolecular Hydrogen Bond. In a pure aprotic solvent observed ESR parameters of radical **1** are the equilibrium mean of the open form radical and intramolecularly hydrogen-bonded radical. Because of the difficulty in deciding the ESR parameters of the independent form, it is impossible to determine the equilibrium constant for the formation and breakage

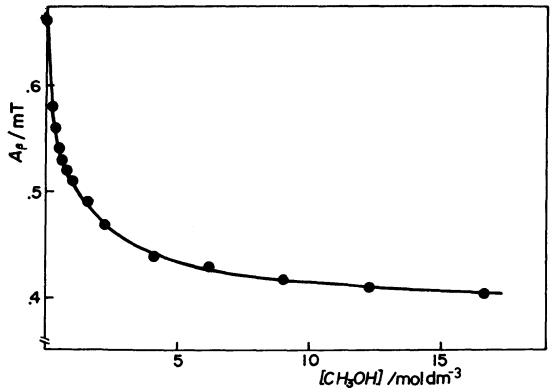

Fig. 2. Variation of β-hydrogen hfs of radical (I) as the function of the amount of methanol in carbon tetrachloride.

of the intramolecular hydrogen bond.

When methanol was added to the aprotic solvent solution of radical **1**, the hfs of β-H decreases with the increasing amount of methanol. Figure 2 shows the dependence of the magnitude of the β-H hfs on the amount of methanol in CCl_4. Marked decrease of the hfs was observed on the addition of the small amount of methanol.

There are three different equilibria in this system in the presence of methanol as follows. When R_O expresses

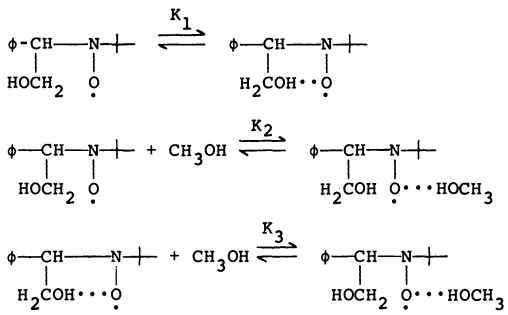

the open form radical and R_I and R_H denotes the radicals with an intramolecular hydrogen bond and with an intermolecular hydrogen bond, respectively, then

$$K_1 = [R_I]/[R_O] \quad (5)$$

$$K_2 = [R_H]/[R_O][CH_3OH] \quad (6)$$

$$K_3 = [R_H]/[R_I][CH_3OH], \quad (7)$$

K_1, K_2, and K_3 are not independent and have the relation $K_1 = K_2/K_3$. Observed hfs of β-H is expressed as

$$\bar{A} = P(R_O)A(R_O) + P(R_I)A(R_I) + P(R_H)A(R_H), \quad (8)$$

where P denotes the fraction of each radical and A denotes the hfs of each radical. By a simple calculation

$$\bar{A} = \{1 + K_1 + [R_H]K_1/[R_I]\}^{-1}\{A(R_O) + K_1A(R_I) + [R_H]K_1/[R_I]\}. \quad (9)$$

Based on the experimental fact that N-hfs and *g*-value of radical **1** in a pure aprotic solvent coincide with those in methanol as shown in Table 1, K_1 can be assumed to be very large. Equation 9 then becomes[16–18]

$$\bar{A} = \{1+[R_H]/[R_I]\}^{-1}\{A(R_I) + [R_H]/[R_I]\}. \quad (10)$$

Rewriting Eq. 10 one obtains[18]

$$1/(A(R_I) - \bar{A}) = (1/K_3)[CH_3OH]^{-1}(A(R_I) - A(R_H)) + 1/(A(R_I) - A(R_H)). \quad (11)$$

If the initial concentration of methanol is sufficiently higher than the radical concentration, the plot of $1/(A(R_I)-\bar{A})$ against the reciprocal concentration of methanol gives K_3 and $A(R_H)$. In this plot one can employ the hfs of the β-H in pure aprotic solvent as $A(R_I)=0.66\pm0.01$ mT.

The dotted line in Fig. 3 shows the plot based on Eq. 11 of the hfs shown in Fig. 2. At high concentrations of methanol the points deviate from the linear dependence. This is attributed to the formation of a hydrogen-bonded complex where two or more methanol molecules are present. The resulting equilibrium constant K_3 from Fig. 3 is 2.0 mol^{-1} dm^3 and $A(R_H)$ is 0.43 mT.

Standard Enthalpy and Standard Entropy of the Formation of Hydrogen-bonded Chelate Ring. The temperature dependence of the equilibrium constant K_3 can give the standard enthalpy difference $\Delta H°$ and standard entropy difference $\Delta S°$ for Eq. 4. Carbon tetrachloride solutions

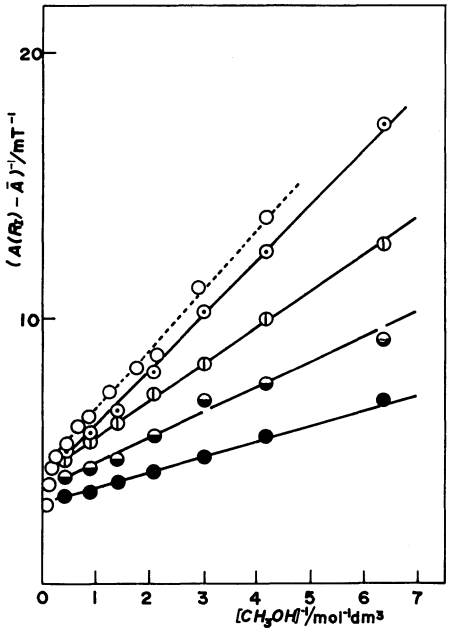

Fig. 3. The plot based on Eq. 11 for hydroxymethyl adduct.
○: In CCl_4 at 290 K, ⊙: in toluene at 298 K, ◑: in toluene at 273 K, ◒: in toluene at 246 K, ●: in toluene at 217 K.

TABLE 2. EQUILIBRIUM CONSTANTS K_3 AND LIMITING hfs $A(R_H)$ AT VARIOUS TEMPERATURES

T/K	K_3/mol^{-1} dm^3 [a]	$A(R_H)$/mT[b]
217	6.1	0.41
246	3.7	0.41
273	2.9	0.38
298	1.9	0.34

a) Average error is ± 0.8. b) Average error is ± 0.09.

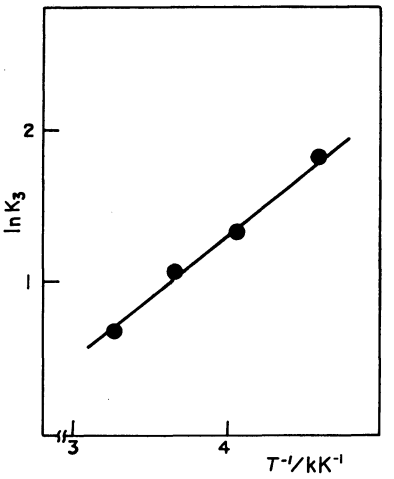

Fig. 4. Van't-Hoff plots for equilibrium contants K_3 derived from Fig. 3.

freeze at a comparatively higher temperature so that toluene was chosen as the solvent for the study of temperature dependence. Before applying Eq. 11 at various temperatures it is confirmed that $A(R_I)$ in pure toluene did not show temperature dependence. The solid lines in Fig. 3 show the plot based on Eq. 11 at various temperatures in toluene. The plot shows that K_3 increases with the lowering of the temperature. K_3's derived from Fig. 3 are listed in Table 2. The slope and the intercept of Van't-Hoff plot (Fig. 4) gives $\Delta H° = -7.4\pm0.5$ kJ mol^{-1} and $\Delta S° = -19\pm2$ J mol^{-1} K^{-1}.

If one assumes that the standard ethalpies for the formation of hydrogen bonds on both sides of Eq. 4 are equal, $\Delta H°$ given above is that for the formation of the chelate ring. This assumption is justified by the fact that the g-value and N-hfs did not change on the addition of methanol. Since the g-value and N-hfs reflect the electronic structure around nitroxide function, the strength of the hydrogen bond of the radicals in Eq. 4 are the same.

The absolute value of $\Delta H°$ is interpreted to be the increment of the energy of interaction among substituents and that of energy of strain caused by the formation of the ring structure.

Intramolecular Hydrogen Bonds in Diastereomeric Nitroxides. When ethanol is used instead of methanol in the reaction (1) a nitroxide radical bearing two asymmetric carbons is produced. The formation of an intramolecular hydrogen bond in the diastereomer gives the cis-trans isomer as shown in Fig. 5.[12] The ESR spectra of the 1-hydroxyethyl adduct in toluene is shown in Fig. 6A. The regular distortion of each line indicates the presence of the diastereomer. The hfs constants of each isomer have been determined by spectrum simulation.

From the discussion in the former section it was concluded that the $\Delta H°$ of Eq. 4 is the enthalpy of the chelate ring formation. The isomers shown in Fig. 5 have different $\Delta H°$ because of the difference of the repulsion of the substituents mainly between the phenyl and methyl groups. It causes a difference of the temperature dependence of K_3. Figures 6B—6D show the temperature dependence of the ESR spectra of the

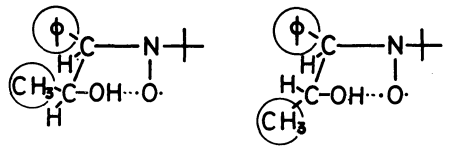

Fig. 5. Cis-trans isomer of 1-hydroxyethyl adduct produced by chelate ring formation.

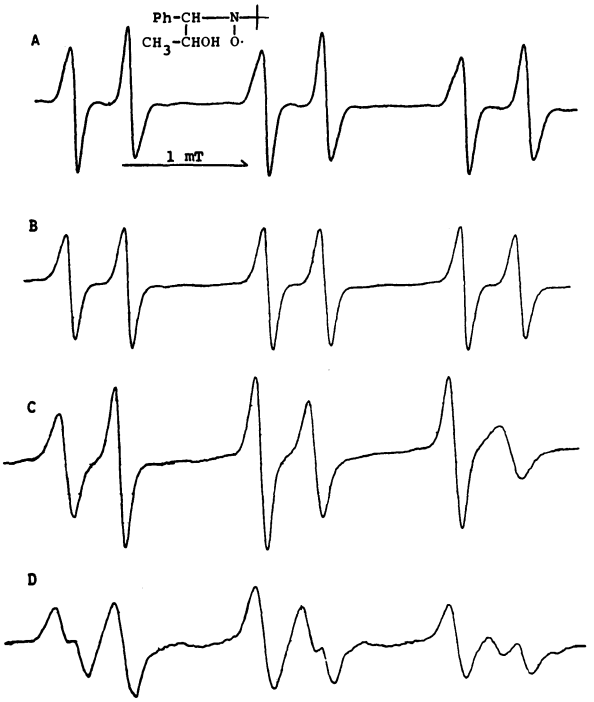

Fig. 6. ESR spectra of 1-hydroxyethyl adduct in toluene at room temperature (A), in toluene with 5 mol dm^{-3} methanol at 297 K(B), at 257 K(C), and at 208 K(D).

hydroxyethyl adduct in toluene containing 5 mol dm^{-3} methanol. At room temperature the resolution of the isomer is even poorer on the addition of methanol than in pure toluene, however, at 308 K the isomer clearly shows the difference in the hfs of the β-H. This experimental fact is explained by the difference of $\Delta H°$ for each isomer resulting in the difference of the temperature dependence of K_3 and also that of the hfs. The assignment of the ESR spectra to each isomer is now possible. The radical with the larger temperature dependence is the cis isomer and that with the smaller temperature dependence is the trans isomer. This assignment is in good accord with the assignment based on the small g-value difference of the isomer.[12]

A quantitative treatment of the difference of $\Delta H°$ for the isomers is possible for the 1-hydroxybutyl adduct of PBN. In this case the resolution is the best in pure toluene solution and the magnitude of the β-H hfs for each isomer is determined by spectrum simulation.[12] By the addition of methanol the resolution is diminished. The hfs constants of each isomer at various temperature were determined by spectrum simulation for each toluene solution of the radical containing a known amount of methanol. The same treatment as for the hydroxymethyl adduct using Eq. 11 gives the Van't-Hoff plot for each isomer. The resulting $\Delta H°$ is -10.2 ± 3.8 kJ mol^{-1} for the radical with smaller β-H hfs (cis isomer) and the radical with larger β-H hfs (trans isomer) has -6.2 ± 2.2 kJ mol^{-1} as $\Delta H°$. The difference of $\Delta H°$ for the isomer is comparable in magnitude with the difference of the heat of formation of the cis-trans isomer in substituted cycloalkanes.[19]

References

1) W. Stone and A. H. Maki, *J. Chem. Phys.*, **36**, 1944 (1962).
2) J. Gendell, J. H. Freed, and G. K. Fraenkel, *J. Chem. Phys.*, **37**, 2835 (1962).
3) T. Kawamura, S. Matsunami, T. Yonezawa, and K. Fukui, *Bull. Chem. Soc. Jpn.*, **38**, 1935 (1965).
4) T. Kubota, Y. Oishi, K. Nishikida, and H. Miyazaki, *Bull. Chem. Soc. Jpn.*, **43**, 1622 (1970).
5) I. Morishima, K. Endo, and T. Yonezawa, *J. Chem. Phys.*, **58**, 3146 (1973) and references therein.
6) W. Kolodziejski and Z. Kecki, *Ber. Bunsenges. Phys. Chem.*, **82**, 1312 (1978) and references therein.
7) J. H. Freed and G. K. Fraenkel, *J. Chem. Phys.*, **38**, 2040 (1963).
8) J. R. Bolton, A. Carrington, and P. F. Todd, *Mol. Phys.*, **5**, 169 (1962).
9) E. G. Janzen and I. G. Lopp, *J. Magn. Reson.*, **7**, 107 (1972).
10) B. G. Gilbert and M. Trenwith, *J. Chem. Soc., Perkin Trans. 2*, **1973**, 1843.
11) M. D. Joesten and L. J. Schaad, "Hydrogen Bonding," Marcell Decker, New York (1974), p. 243.
12) Y. Kotake, K. Kuwata, and E. G. Janzen, *J. Phys. Chem.*, **83**, 3024 (1979).
13) I. H. Leaver and G. C. Ramsay, *Tetrahedron*, **25**, 5669 (1969).
14) E. G. Janzen and J. I.-P. Liu, *J. Magn. Reson.*, **9**, 510 (1973).
15) See for example, T. Kawamura, S. Matsunami, and T. Yonezawa, *Bull. Chem. Soc. Jpn.*, **40**, 1111 (1967); K. Mukai, H. Nishiguchi, K. Ishizu, and H. Takaki, *ibid.*, **40**, 2731 (1967); A. H. Reddoch and S. Konishi, *J. Chem. Phys.*, **70**, 2121 (1979).
16) N. Hirota, *J. Phys. Chem.*, **71**, 127 (1967).
17) A. M. Hermann, A. Rembaum, and W. R. Carper, *J. Phys. Chem.*, **71**, 2661 (1967).
18) A. E. Alegria, R. Concepcion, and G. R. Stevenson, *J. Phys. Chem.*, **79**, 361 (1975).
19) "Steric Effect in Organic Chemistry," ed by M. S. Newman, John Wiley and Sons, New York (1956), p. 54.

Electronic Absorption Spectra and Geometry of Molecular Ions Generated from Stilbene and Related Compounds. II. Radical Ions of (*E*)-Stilbene and Related Compounds

Hiroshi Suzuki,* Kinko Koyano,** Tadamasa Shida,† and Akira Kira††

Department of Chemistry, College of General Education, The University of Tokyo, Komaba, Meguro-ku, Tokyo 153

†*Department of Chemistry, Faculty of Science, Kyoto University, Sakyo-ku, Kyoto 606*

††*The Institute of Physical and Chemical Research, Wako, Saitama 351*

(Received March 18, 1982)

The electronic absorption spectra of radical ions produced by γ-ray irradiation of (*E*)-stilbene and related compounds in frozen matrices were measured. On illumination and on controlled warming, the spectra of the radical ions of sterically uncrowded stilbenes and diphenylacetylene remained almost unchanged, while those of the radical ions of sterically crowded stilbenes changed noticeably. Examination of the spectra and of their changes led to the following conclusions: (a) The relaxed geometry of the radical ions of sterically uncrowded stilbenes is planar or nearly planar; (b) in the unrelaxed geometries of the radical ions of (*E*)-α,β-dialkylstilbenes the torsion angles of the Ph–C bonds are nearly as large as in the parent molecules, and on relaxation these angles become smaller and the torsion angle of the central ethylenic bond deviates from 0° to a considerable extent; (c) for the radical ions of *ortho*-substituted (*E*)-stilbenes the geometrical change on relaxation is comparatively small.

Geometries of molecular ions generated from unsaturated molecules by addition or removal of one or two electrons are not always similar to those of the parent molecules. The question of how the molecular geometry changes with the ionization is a subject of interest.

Previously we studied the geometry of neutral molecules of stilbenes[1–6] and of their dianions[7] by means of electronic absorption spectroscopy. The present paper reports the results of a similar investigation of the geometry of radical ions (anion and cation radicals) of (*E*)-stilbene and related compounds, on which no reliable information is available.

In a previous paper,[8] we reported that the electronic absorption spectrum of the tetraphenylethylene (TPE) anion radical in frozen 2-methyltetrahydrofuran (MTHF) changed markedly on controlled warming, and attributed the spectral change to the geomerical change of this sterically crowed anion radical. In the present study, it is examined whether such a phenomenon occurs for radical ions of sterically crowded stilbene derivatives.

The compounds treated here and their abbreviations (in parentheses) are as follows: (*E*)-stilbene (ES), (*E*)-α-methylstilbene (EαMS), (*E*)-α,β-dimethylstilbene (EαβDMS), (*E*)-4,4′-dimethylstilbene (E44′DMS), (*E*)-2,4,6-trimethylstilbene (ETMS), (*E*)-2,2′,4,4′,6,6′-hexamethylstilbene (EHMS), (*E*)-α,β-diethylstilbene (Eαβ-DES), (*E*)-4-phenylstilbene (E4PS), (*E*)-4,4′-diphenylstilbene (E44′DPS), and diphenylacetylene (DPA).

Experimental

Spectra of Radical Ions Produced by γ-Ray Irradiation of Frozen Solutions at 77 K. Radical ions of ES and related compounds were produced by γ-ray irradiation in deaerated solutions frozen at 77 K in liquid nitrogen, and their electronic absorption spectra were measured. For the anion radicals MTHF was used as the solvent, whereas for the cation radicals *s*-butyl chloride (BC) or a Freon Mixture (FM: an equivolume mixture of trichlorofluoromethane and 1,2-dibromo-1,1,2,2-tetrafluoroethane) was employed. The experimental details are described in a previous paper.[8] Both the anion and the cation radicals exhibit two major bands in the visible region. The band at the longer wavelength is designated as A, and that at the shorter wavelength as B.

After recording the spectra of γ-ray irradiated samples, they were illuminated with light of the wavelengths corresponding to and longer than band A for 5—10 min (illumination A). Then, the samples were successively illuminated with light of the wavelengths corresponding to and longer than band B for 5—10 min (illumination B).

To see the effect of limited warming, the γ-ray irradiated sample was taken out of the liquid nitrogen for a limited time, and then refrozen at 77 K. The warming period was successively increased (for example, 20, 24, 28 s for anion radicals; 10, 12, 14 s for cation radicals).

The spectra of the cation radicals of E4PS and E44′DPS were less accurate because of the low solubility of these compounds in BC and in FM.

Spectra of Anion Radicals Produced by Alkali-metal Reduction. The spectra of the anion radicals produced by reduction of ES, EαMS, E44′DMS, ETMS, and EHMS with alkali metals (sodium, potassium, and cesium) in deaerated 1,2-dimethoxyethane (DMS) were also measured for the comparison with those obtained by γ-ray irradiation. The experimental procedure was described previously.[7]

Reliable spectra of the anion radicals of EαβDMS and EαβDES could not be obtained by the alkali-metal reduction even in the presence of a large excess of the parent molecules at low temperature,[8] being masked by the absorption due to the corresponding dianions. This is due to the fact that the equilibrium constant (K_{dispr}) of the disproportionation of the anion radical associated with the counterion to a pair of the neutral molecule and the dianion associated with two counterions is much greater for these sterically crowded stilbenes than for sterically uncrowded or less crowded stilbenes.[7] Even the K_{dispr} value for EαMS was reported to be much greater than that for ES.[9] It is evident that the K_{dispr} values for EαβDMS and EαβDES are much more greater than that for EαMS.

Molecular Orbital Calculation

To characterize the absorption bands and to get the

** Present address: Department of International Culture, Aichi Gakusen Women's Junior College, Toyoda, Aichi 473.

relation between the bands and the geometry of the radical ions, we carried out a semiempirical SCF-MO-CI calculation for the π electronic state of the radical ions by the method developed by Longuet-Higgins and Pople.[13] The details of the calculation procedure are essentially the same as those employed in previous work.[8,14] The same assumptions on the geometry as those in Part I of this series[7] were made.

The carbon skeleton of the (*E*)-stilbene π system and the numbering of the carbon atoms are illustrated in Fig. 1. Torsion angles β-α-1-6 and α-β-1′-6′ are denoted by $\theta_{\alpha 1}$ and $\theta_{\beta 1'}$, respectively. Angle $\theta_{\alpha\beta}$ is defined as 180° minus torsion angle 1-α-β-1′. For the planar *E* form angles $\theta_{\alpha 1}$, $\theta_{\beta 1'}$, and $\theta_{\alpha\beta}$ are 0°.

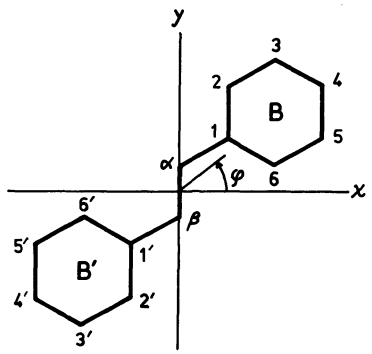

Fig. 1. The carbon skeleton of (*E*)-stilbene.

Results and Discussion

Designation of Spectra and of Geometries. Representative spectra of the radical ions measured after various treatments are shown in Figs. 2 and 3, and relevant data are listed in Tables 1 and 2. Although most of the spectral changes are relatively small, they are reproducible with a precision of a few percent. The molar absorption coefficient (ε) was evaluated in the same manner as described in Ref. 8. The values for the spectra of anion radicals are reliable, but those for the spectra of cation radicals are uncertain.[15]

As seen in the figures, the radical ions exhibit two major bands, A and B, in the visible region. For band A, for example, the wavelength (λ) and molar absorption coefficient at the maximum and the oscillator strength (f) are denoted by λ_A, ε_A, and f_A, respectively.

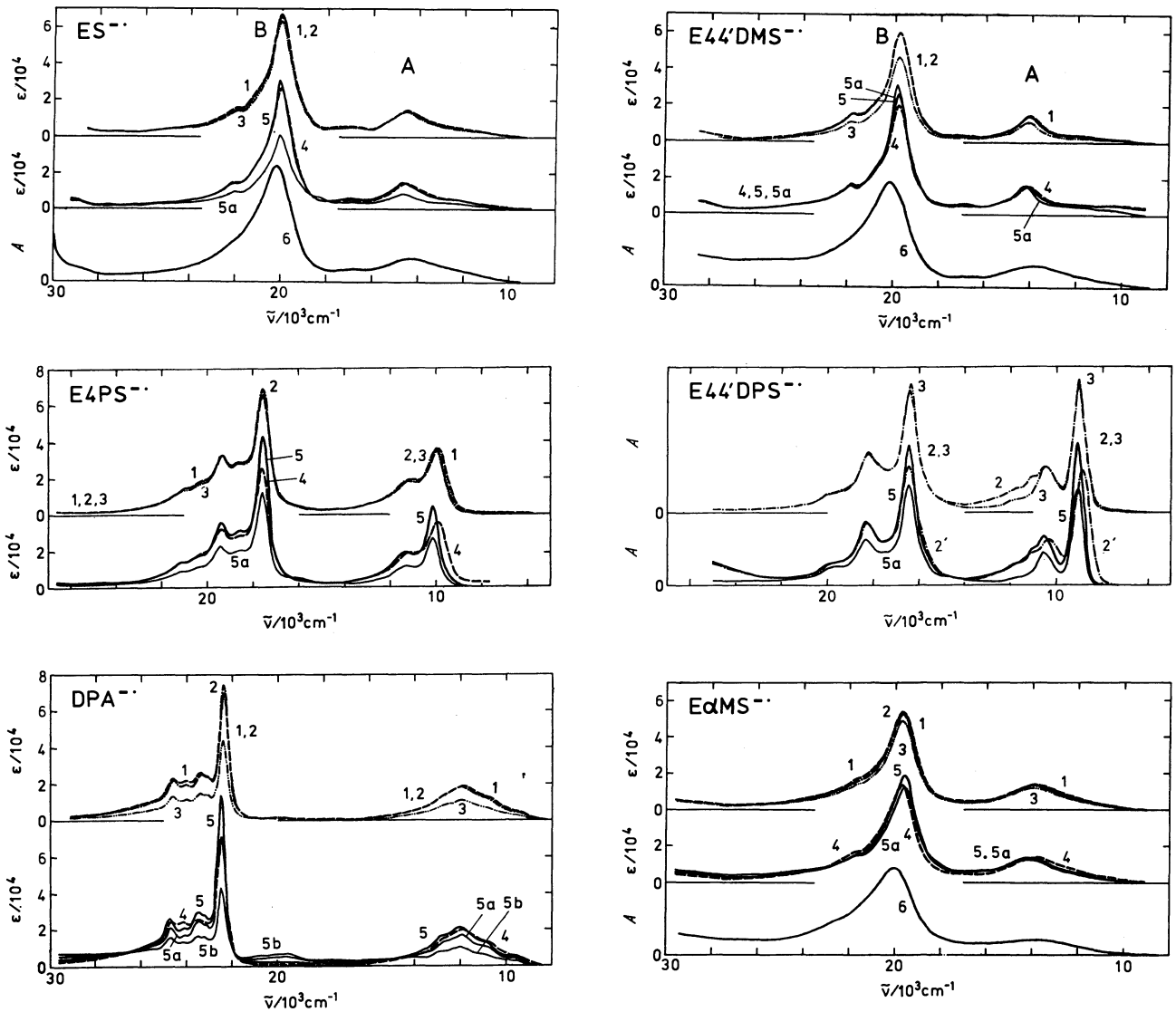

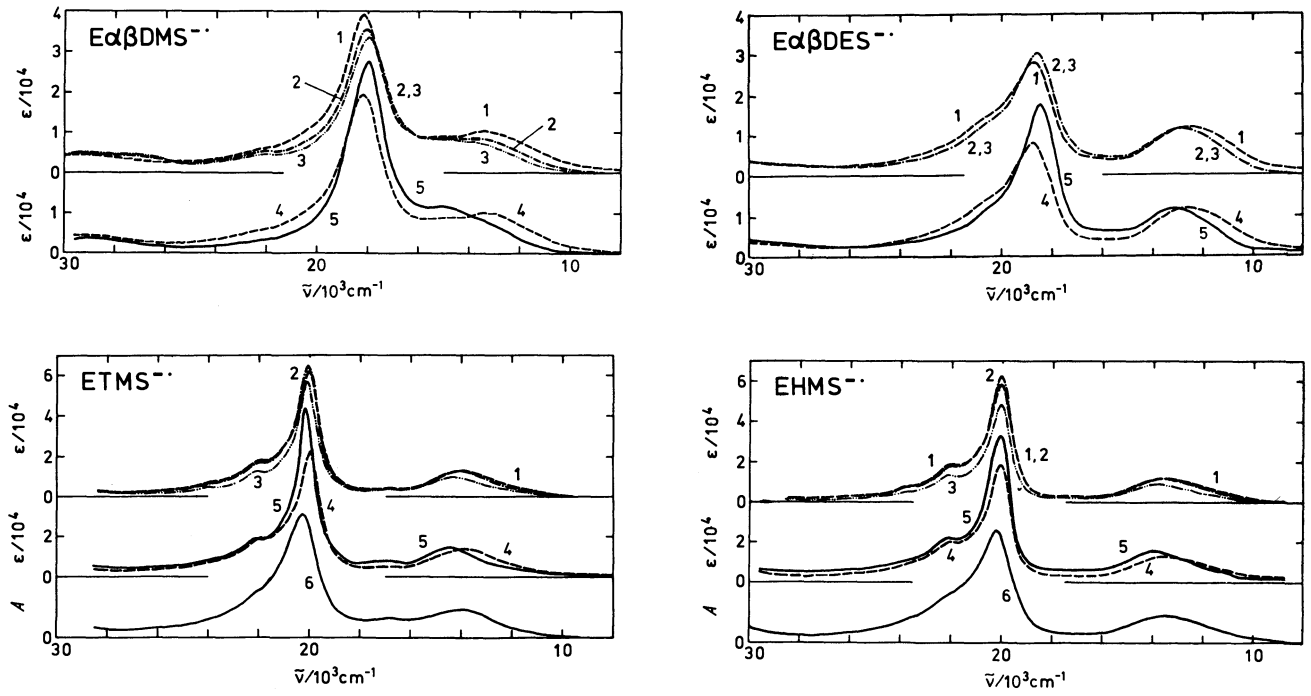

Fig. 2. Electronic absorption spectra of anion radicals. Curves 1 and 4 (------): spectra observed immediately after γ-ray irradiation of frozen solution, designated F in the text. Curve 2 (·–·–·): spectra observed after illumination of the sample for curve 1 with light of wavelengths corresponding to band A, designated PA in the text. Curve 3 (···): spectra observed after illumination of the sample for curve 2 with light of wavelengths corresponding to and longer than band B, designated PB in the text. Curve 5 (——): spectra observed after controlled warming of the sample for curve 4, designated W in the text. Curves 5a, 5b, 5c, ··· (——): spectra observed after additional controlled warming for successively increasing time. The solvent is 2-methyltetrahydrofuran (MTHF) for all the above spectra. Curve 6 (——): spectra of anion radicals produced by alkali-metal reduction in fluid dimethoxyethane (DME), designated M in the text.

For the sake of convenience, spectra of a radical ion measured after different treatments are designated as follows:[8] The spectrum of a radical ion immediately after its production by γ-ray irradiation in a frozen matrix is designated as F (*frozen*), that after illumination as P (*photobleached*), that after controlled warming as W (*warmed*), and that of an anion radical produced by alkali-metal reduction in a fluid DME solution as M (*metal*). Sometimes, spectrum P after illumination A is referred to as spectrum PA, and that after illumination B as spectrum PB. If necessary, the solvent is denoted in parentheses: For example, spectrum F of a cation radical in solution in BC is referred to as spectrum F(BC).

The same designations are also used to specify the geometries of the radical ion after the respective treatments. In addition, the geometry of the parent neutral molecule is designated as N (*neutral*), and the geometry that the radical ion takes in a fluid solution as R (*relaxed*). According to a conclusion in Ref. 8, geometry W is considered to be almost equal to geometry R.

Assignment of Absorption Bands. The results of the MO calculation for the stilbene anion radical in the planar *E* form belonging to point group C_{2h} are shown in Table 3, which includes all the electronic transitions having a transition energy (ΔE) smaller than 4.5 eV. By comparison between the observed spectra and the results of the calculation, bands A and B are ascribed to transitions 3 and 5, respectively. The very weak band appearing between bands A and B in the spectra of ES⁻·, E44′DMS⁻·, ETMS⁻·, and EHMS⁻· is ascribed to transition 4, which is forbidden in the planar *E* form but is weakly allowed in nonplanar geometries in which $\theta_{\alpha\beta}$ is not 0°.

As seen in Table 3, transitions 3, 4, and 5 can be well approximated as the one-electron excitations from ϕ_{-1} to ϕ_{-4}, from ϕ_{-1} to ϕ_{-5}, and from ϕ_{+1} to ϕ_{-1}, respectively. Accordingly, bands A and B of the stilbene anion radical correspond to the longest-wavelength intense band of the stilbene dianion[7] and that of the stilbene molecule,[1,2,6,16] respectively.

The results of the MO calculation for the stilbene cation radical are quite similar to those for the anion radical, because of the pairing properties of π orbitals of the alternant hydrocarbon. Similarly to the case of the anion radical, bands A and B are ascribed to transitions 3 and 5, respectively, and the very weak band appearing between bands A and B in the spectra of ES⁺· and some other cation radicals is ascribed to transition 4. Transitions 3, 4, and 5 in the cation radical can be well approximated as the one-electron excitations from ϕ_{+4} to ϕ_{+1}, from ϕ_{+5} to ϕ_{+1}, and from ϕ_{+1} to ϕ_{-1}, respectively.

The orbitals involved in the approximate one-electron expressions of transitions 3, 4, and 5 in the radical ions can be roughly approximated as follows:

$$\psi_{\pm 1} \approx a\phi_{\pm 1}(\mathrm{B}) \mp b\phi_{\pm 1}(\mathrm{E}) \pm a\phi_{\pm 1}(\mathrm{B}')$$
$$\psi_{\pm 4} \approx a\phi_{\pm 1}(\mathrm{B}) \pm b\phi_{\mp 1}(\mathrm{E}) \mp a\phi_{\pm 1}(\mathrm{B}')$$
$$\psi_{\pm 5} \approx b\phi_{\pm 1}(\mathrm{B}) \pm a\phi_{\pm 1}(\mathrm{E}) \pm b\phi_{\pm 1}(B')$$

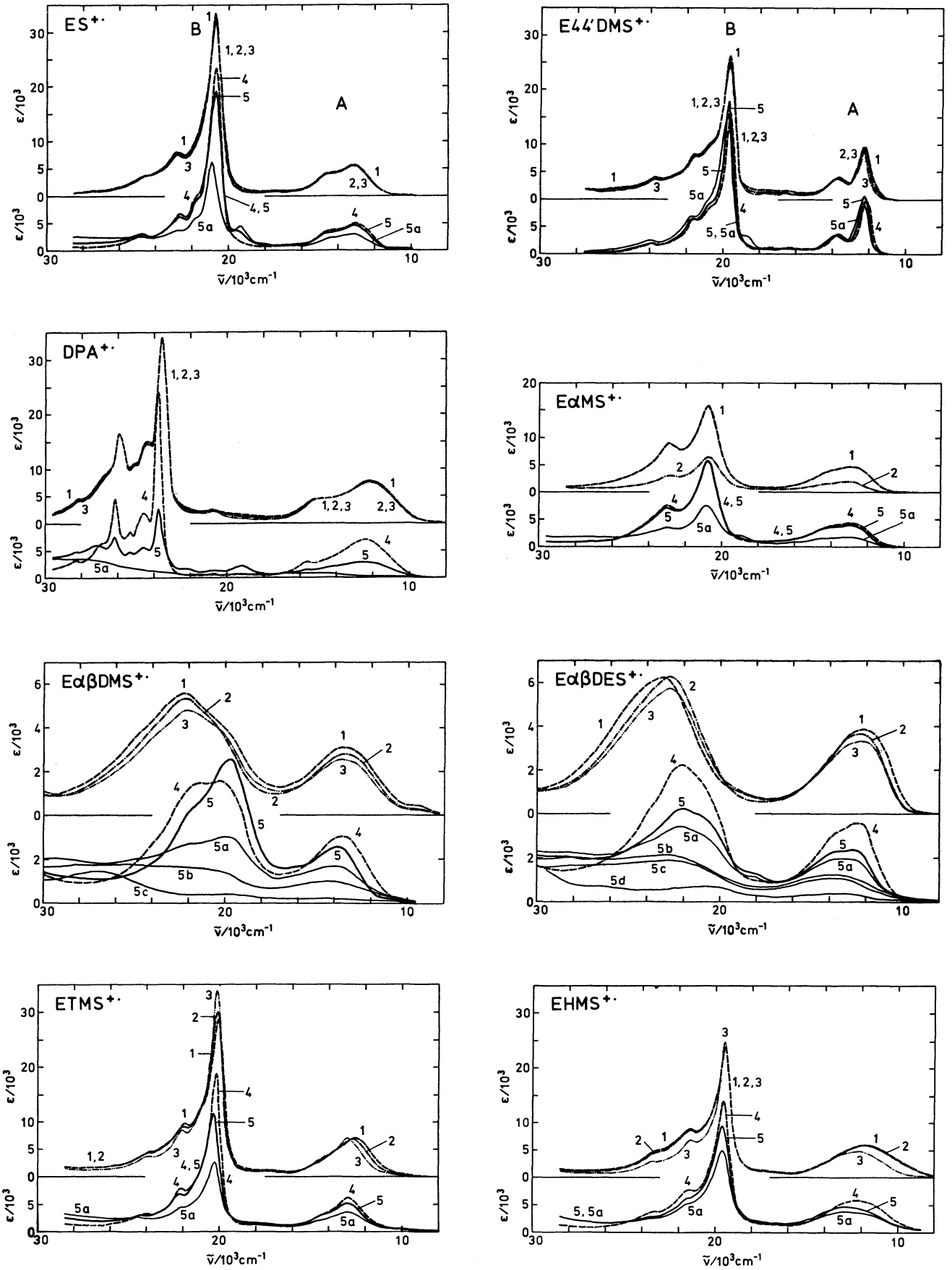

Fig. 3. Electronic absorption spectra of cation radicals. See Caption for Fig. 2. The solvent is *s*-butyl chloride (BC) for spectra 1, 2, and 3, and is a Freon Mixture (FM) for the other spectra.

Table 1. Data on electronic absorption spectra of anion radicals[a)]

Anion radical	Class	No. in Fig. 2	λ_B/nm	$\varepsilon_B/10^4$	f_B	λ_A/nm	$\varepsilon_A/10^4$	f_A	f_A/f_B
ES$^{-\cdot}$	F	4	499.3	6.569	0.627	690.3	1.407	0.191	0.305
	W	5	498.4	7.042	0.616	682.1	1.422	0.190	0.308
	M(Na^+)	6	495	6.569[b)]	0.780[b)]	700	1.324[b)]	0.218[b)]	0.279
E44′DMS$^{-\cdot}$	F	4	504.6	5.988	0.589	708.5	1.594	0.217	0.369
	W	5a	502.6	7.101	0.611	700.0	1.617	0.189	0.309
	M(K^+)	6	496	5.988[b)]	0.793[b)]	725	1.238[b)]	0.216[b)]	0.272
E4PS$^{-\cdot}$	F	4	568.2	6.550	0.679	1007.1	3.558	0.318	0.468
	W	5	569.6	8.311	0.749	986.6	4.398	0.317	0.423
E44′DPS$^{-\cdot}$	PA	2′	608.1	0.672[c)]	0.694[d)]	1126.5	0.652[c)]	0.482[d)]	0.695
	W	5	607.4	0.790[c)]	0.716[d)]	1102.4	0.799[c)]	0.449[d)]	0.627
DPA$^{-\cdot}$	F	4	445.6	7.056	0.555	836.2	1.945	0.290	0.522
	W	5	444.9	9.331	0.624	836.2	2.060	0.302	0.483
EαMS$^{-\cdot}$	F	4	507.9	5.344	0.634	718.5	1.367	0.216	0.341
	W	5	510.4	5.865	0.666	704.1	1.355	0.200	0.301
	M(Na^+)	6	498	5.344[b)]	0.938[b)]	730	0.882[b)]	0.173[b)]	0.184
E$\alpha\beta$DMS$^{-\cdot}$	F	4	550.0	3.921	0.536	750	1.016	0.199	0.371
	PB	3	556.5	3.352	0.440	714	0.778	0.130	0.297
	W	5	557.5	4.754	0.521	662.5	1.183	0.159	0.306
E$\alpha\beta$DES$^{-\cdot}$	F	4	532.6	2.811	0.454	800	1.201	0.227	0.500
	PB	3	537.2	3.040	0.459	775	1.142	0.191	0.416
	W	5	541.5	3.761	0.491	756.5	1.192	0.194	0.396
ETMS$^{-\cdot}$	F	4	500.0	6.231	0.598	720.6	1.390	0.226	0.378
	PB	3	497.1	5.649	0.446	700	0.972	0.130	0.290
	W	5	495.6	8.333	0.700	692.6	1.430	0.214	0.305
	M(K^+)	6	493	6.231[b)]	0.757[b)]	715	1.381[b)]	0.205[b)]	0.271
EHMS$^{-\cdot}$	F	4	498.0	5.831	0.598	730.6	1.269	0.237	0.396
	PB	3	498.0	4.802	0.414	725	0.863	0.131	0.317
	W	5	498.0	7.300	0.747	717.1	1.533	0.269	0.360
	M(Na^+)	6	494	5.831[b)]	0.741[b)]	745	1.357[b)]	0.240[b)]	0.324

a) The solvent is DME for spectra M and is MTHF for all the other spectra. For spectra M, the counterion is indicated in parentheses. b) Values tentatively determined by equating the value of ε_B of spectrum M to that of spectrum F. c) Values of the absorbance. d) Values tentatively determined on some assumptions.

In these expressions, a and b represent coefficients bearing the relation $a>b>0$; $\phi_{+1}(E)$ and $\phi_{-1}(E)$ represent the bonding and the antibonding π orbital of the central ethylenic bond, respectively [$\phi_{\pm1}(E)=2^{-1/2}(\chi_\alpha\pm\chi_\beta)$]; $\phi_{+1}(B)$ and $\phi_{-1}(B)$, for example, represent the following π orbitals of benzene ring B (see Fig. 1):

$$\phi_{\pm1}(B) = 12^{-1/2}(2\chi_1 \pm \chi_2-\chi_3 \pm 2\chi_4-\chi_5 \pm \chi_6).$$

With respect to the α-β bond, the orbitals belonging to symmetry species a_u, ϕ_{+5}, ϕ_{+1}, and ϕ_{-4}, are bonding, and the orbitals belonging to symmetry species b_g, ϕ_{+4}, ϕ_{-1}, and ϕ_{-5}, are antibonding; with respect to the α-1 and the β-1′ bond, ϕ_{+5}, ϕ_{+4}, and ϕ_{-1} are bonding, and ϕ_{+1}, ϕ_{-4}, and ϕ_{-5} are antibonding.

Expected Effects of Geometrical Changes on the Electronic Transitions. In Table 4 are listed the calculated values of the energies and oscillator strengths of transitions 3, 4, and 5 and of the ratio between the oscillator strengths of transitions 3 and 5 (f_3/f_5) for the stilbene anion radical in the planar E geometry. Table 4 also lists the calculated values of the changes in these quantities associated with the changes from the planar E geometry to geometries in which $|\theta_{\alpha1}|$, $|\theta_{\beta1'}|$, or $|\theta_{\alpha\beta}|$ is 30°. The corresponding values for the cation radical are almost coincident with the values for the anion radical.

The changes in the properties of the transitions of the anion radical associated with the geometrical changes seen in Table 4 and the corresponding ones of the cation radical should represent the effect of the geometrical changes on the absorption bands: It is expected, for example, that an increase in $|\theta_{\alpha1}|$ and $|\theta_{\beta1'}|$ will exert a large bathochromic and a very small hyperchromic effect on band A and a comparatively large hypsochromic and a large hypochromic effect on band B, and will bring about a large increase in ratio f_A/f_B, and that an increase in $|\theta_{\alpha\beta}|$ will exert a large hypsochromic and a small hypochromic effect on band A and a large bathochromic and a small hypochromic effect on band B, and will bring about a small decrease in f_A/f_B.

Comparison between Spectra of Anion and Cation Radicals. With a few exceptions, the maxima of bands A and B of each anion radical are located at shorter and at longer wavelength, respectively, than are those of the corresponding cation radical, and, without exception, the separation between the maxima of the two bands of each anion radical is considerably smaller than that of the corresponding cation radical.

Because of the pairing properties of π orbitals, the spectra of both radical ions should closely resemble

Table 2. Data on electronic absorption spectra of cation radicals

Cation radical	Class	No. in Fig. 3	λ_B/nm	$\varepsilon_B/10^4$	f_B	λ_A/nm	$\varepsilon_A/10^4$	f_A	f_A/f_B
ES$^{+\cdot}$	F(BC)	1	482.1	3.337	0.264	759.0	0.555	0.071	0.268
	F(FM)	4	483.2	3.337	0.245	762.9	0.495	0.065	0.266
	W(FM)	5	482.9	2.908	0.229	757.7	0.473	0.060	0.260
E44′DMS$^{+\cdot}$	F(BC)	1	509.3	2.613	0.233	816.0	0.955	0.065	0.279
	F(FM)	4	510.1	2.613	0.178	819.4	1.010	0.059	0.333
	W(FM)	5	507.7	2.826	0.183	815.9	1.076	0.055	0.303
DPA$^{+\cdot}$	F(BC)	1	424.0	3.408	0.330	811.5	0.770	0.149	0.453
	F(FM)	4	421.0	3.408	0.242	807.9	0.705	0.116	0.479
	W(FM)	5	421.0	1.263	0.089	807.9	0.289	0.041	0.453
EαMS$^{+\cdot}$	F(BC)	1	481.6	1.576	0.223	775.0	0.472	0.072	0.325
	F(FM)	4	480.7	1.576	0.208	769.3	0.431	0.069	0.331
	W(FM)	5	480.7	1.576	0.203	767.0	0.401	0.061	0.300
E$\alpha\beta$DMS$^{+\cdot}$	F(BC)	1	450.0	0.560	0.170	750.0	0.311	0.063	0.372
	PB(BC)	3	450.0	0.481	0.142	725.0	0.255	0.049	0.348
	F(FM)	4	492.3	0.559	0.146	740.7	0.303	0.049	0.338
			467.3	0.551					
	W(FM)	5	506.5	0.656	0.145	725.0	0.255	0.040	0.278
E$\alpha\beta$DES$^{+\cdot}$	F(BC)	1	432.1	0.624	0.168	825.0	0.385	0.073	0.438
	PB(BC)	3	438.5	0.573	0.149	825	0.330	0.061	0.408
	F(FM)	4	452.9	0.624	0.153	806.5	0.357	0.063	0.414
	W(FM)	5	454.1	0.423	0.116	786.8	0.236	0.046	0.395
ETMS$^{+\cdot}$	F(BC)	1	498.2	2.868	0.268	800.0	0.709	0.090	0.337
	PB(BC)	3	496.3	3.373	0.255	769.6	0.714	0.075	0.296
	F(FM)	4	495.6	2.868	0.226	775.0	0.625	0.076	0.336
	W(FM)	5	491.9	2.137	0.201	775.0	0.518	0.067	0.333
EHMS$^{+\cdot}$	F(BC)	1	513.1	2.397	0.249	850.0	0.588	0.108	0.436
	PB(BC)	3	513.1	2.487	0.199	825.0	0.473	0.078	0.391
	F(FM)	4	510.9	2.397	0.233	825.0	0.580	0.107	0.457
	W(FM)	5	509.7	1.942	0.213	775.0	0.461	0.094	0.441

Table 3. Results of the MO calculation for the stilbene anion radical having the planar *E* geometry belonging to symmetry group C_{2h}

Transition[a]	ΔE[b]/eV	f[c]	φ[d]/°	State[e]	Symmetry[f]	Character[g]
1	1.218	0	—	D_1	B_g	0.961(−1,−3)
2	1.224	0.004	−70.3	D_2	A_u	0.953(−1,−2)
3	1.519	0.383	+36.7	D_3	A_u	0.952(−1,−4)
4	2.606	0	—	D_4	B_g	0.919(−1,−5)
5	3.011	0.604	+43.8	D_5	A_u	0.892(+1,−1)
6	3.672	0.013	+46.8	D_6	A_u	0.758(−1,−6)
7	3.882	0	—	D_7	B_g	0.603(−1,−7)
8	4.270	0	—	D_8	B_g	0.598(+4,−1)

a) Transitions are numbered in the order of increasing transition energy. b) Transition energy. c) Oscillator strength of the transition. d) Direction of the transition moment: φ represents the angle that the transition moment makes with the x axis in the xy plane (see Fig. 1). e) The excited state. f) The symmetry species to which the excited state belongs. g) The wave function of the excited state. Only the electron configuration whose coefficient in the wave function is the largest is shown, together with the coefficient. Symbol (i,j) denotes the electron configuration arising from the ground configuration by promotion of an electron from π MO ψ_i to π MO ψ_j. The orbital index i runs from +7 for the lowest orbital to −7 for the highest one in the order of increasing energy. Orbitals ψ_{+1} and ψ_{-1} correspond, respectively, to HOMO and LUMO in the molecule. The coefficient of the ground configuration in the wave function of the ground state (state D_0) is 0.988.

Table 4. Dependence of the energy and oscillator strength of transitions of the stilbene anion radical on the geometry[a]

Symmetry	$\theta_{\alpha 1}$/°	$\theta_{\beta 1'}$/°	$\theta_{\alpha\beta}$/°	ΔE_5/eV	f_5	ΔE_4/eV	f_4	ΔE_3/eV	f_3	f_3/f_5
C_{2h}	0	0	0	3.011	0.604	2.606	0	1.519	0.383	0.632
C_2	30	30	0	+0.143	−0.157	−0.282	0	−0.249	+0.014	+0.254
S_2	30	−30	0	+0.143	−0.157	−0.282	0	−0.249	+0.014	+0.254
C_2	0	0	30	−0.338	−0.043	−0.016	+0.008	+0.191	−0.068	−0.072

a) The values for the nonplanar geometries are values relative to the values for the planar geometry.

are aprotic and should have nearly equal values of the static dielectric constant at 77 K,[15] the marked shifts of the bands of the cation radicals as compared with those of the corresponding anion radicals cannot be attributed to the difference in the general solvent effect. The shifts might be a manifestation of the difference in the effect of σ electrons in both the radical ions, as suggested previously,[15] or a manifestation of the difference in the geometry. For example, if the length of the α-β bond is shorter in cation radicals than in the corresponding anion radicals, the directions of the shifts can be well explained.

Electronic Bathochromic Effect of Alkyl Substituents. Before proceeding to discuss the relation between the spectra and the geometry, we must examine the electronic bathochromic effect of alkyl substituents.

Both bands A and B of the E44'DMS radical ions are located at longer wavelengths than are the corresponding bands of the ES radical ions. In Table 5, the magnitudes of bathochromic shift of bands A and B of the ES radical ions caused by substitution of two methyl groups at the *para* positions are compared with those of the corresponding bands of the ES molecule[4] and of the ES dianion.[7] As seen in the table, the magnitude of the bathochromic shift of band A or its corresponding band increases in the order dianion< anion radical<cation radical, and that of band B or its corresponding band increases in the order anion radical<molecule<cation radical.

Table 5. Bathochromic shift of bands of ES by substitution of two methyl groups into the *para* positions

Species	$\tilde{\nu}_B$[a] / cm^{-1}	$\Delta\tilde{\nu}_B$[b] / cm^{-1}	$\tilde{\nu}_A$[a] / cm^{-1}	$\Delta\tilde{\nu}_A$[b] / cm^{-1}
Dianion[c]	—	—	19881	235
Anion radical[d]	20028	210	14486	372
Molecule[e]	34002	812	—	—
Cation radical[f]	20743	1108	13175	920

a) Wave number at the band maximum of ES. b) Difference between the wave number at the band maximum of ES and that of E44'DMS. c) Data on the spectra of the potassium salts in DME.[7] d) Data on spectra F(MTHF) (Curves 4 in Fig. 2). e) Data on the spectra of solutons in heptane.[2,4] f) Data on spectra F(BC) (Curves 1 in Fig. 3).

As mentioned already, band A of the cation radicals can be ascribed to the one-electron excitation from ψ_{+4} to ψ_{+1}, and that of the anion radical as well as the longest-wavelength intense band of the dianion to the one-electron excitation from ψ_{-1} to ψ_{-4}; bands B of the radical ions and the longest-wavelength intense band of the molecule can be ascribed to the one-electron excitation from ψ_{+1} to ψ_{-1}.

The magnitude of the energy lift of a π molecular orbital caused by alkyl substitution depends on the orbital energy and on the absolute magnitude of the atomic orbital coefficient at the substitution position in the molecular orbital: The lower the orbital energy, and the larger the absolute value of the atomic orbital coefficient, the larger will be the magnitude of the lift of the orbital energy.

Table 6 shows the energies (E) and atomic orbital coefficients (C_i) of the π molecular orbitals relevant to bands A and B and their corresponding bands calculated by the SCF-MO method for the planar E geometry. The sequence of the magnitude of the bathochromic shift by 4-methyl substitution expected from the data in this table agrees with the above-mentioned observed sequence both for band A (and its corresponding band) and for band B (and its corresponding band). From the data in this table, it is also expected that the electronic bathochromic effect of alkyl substitution at the *ortho* positions or at positions α and β on bands A and B may be smaller in the case of cation radicals and larger in the case of anion radicals than that of alkyl substitution at the *para* positions.

Classification of Compounds. The compounds treated in the present work are classified into three groups: group I (sterically uncrowded compounds: ES, E44'DMS, E4PS, E44'DPS, and DPA), group II (α-alkylated derivatives of ES: EαMS, E$\alpha\beta$DMS, and E$\alpha\beta$DES), and group III (*ortho*-methylated derivatives of ES: ETMS and EHMS). The following discussion is made on the basis of this classification.

Group I. ES and E44'DMS: Spectra F of the radical ions of ES and E44'DMS exhibit characteristic vibrational fine structure, and remain almost unchanged on illumination and on controlled warming, except for the diminution in intensity on prolonged warming. This fact indicates that geometries P, W, and R of these radical ions are quite similar to geometries F, which in turn must be similar to the most probable geometries of

Table 6. Energy and AO coefficients of π SCF-MO's of ES having the planar geometry

Species	MO	E/eV	$\lvert C_\alpha\rvert$	$\lvert C_2\rvert$	$\lvert C_4\rvert$	$\lvert C_6\rvert$
Dianion	ψ_{-4}	+5.8695	0.2286	0.0239	0.3834	0.1484
	ψ_{-1}	+1.1723	0.3976	0.2683	0.3304	0.2582
Anion radical	ψ_{-4}	+2.8399	0.1679	0.0703	0.4052	0.1712
	ψ_{-1}	−0.0401	0.3993	0.2579	0.3239	0.2471
	ψ_{+1}	−5.3081	0.4469	0.2725	0.3113	0.2724
Molecule	ψ_{-1}	−2.1731	0.4239	0.2609	0.3128	0.2541
	ψ_{+1}	−9.0169	0.4239	0.2609	0.3128	0.2541
Cation radical	ψ_{-1}	−5.5195	0.4472	0.2725	0.3111	0.2723
	ψ_{+1}	−10.7900	0.3987	0.2580	0.3241	0.2472
	ψ_{+4}	−13.6682	0.1681	0.0720	0.4055	0.1701

the parent molecules in the rigid solutions.

It is established by X-ray analysis that the ES molecule assumes a planar or nearly planar geometry in the crystalline state,[17] and it is inferred that the most probable geometry of the ES molecule in fluid solutions is also planar or nearly planar,[1,2,18] although, according to an electron diffraction study,[19] the most probable geometry of the ES molecule in the gas phase is a nonplanar propeller-like geometry with C_2 symmetry in which $\theta_{\alpha 1}$ and $\theta_{\beta 1'}$ are about 30° and $\theta_{\alpha\beta}$ is about 0°. In addition, nearly all the theoretical calculations conclude that the ES molecule should be essentially planar.[20,21]

Accordingly, geometries F, P, W, and R of the radical ions of ES as well as E44'DMS are concluded to be planar or nearly planar. This conclusion is consistent with the facts found by Chang and Johnson that the same anion radical having the *E* geometry is obtained by reduction of the *Z* or the *E* isomer of stilbene with potassium in DME[22] and that the ESR spectrum of the anion radical at −60 °C shows the presence of two nonequivalent sets of *ortho* protons and of two nonequivalent sets of *meta* protons, implying that the rotation around the C–Ph bonds is frozen on the ESR time scale.[23,24]

In Part I of this series,[7] we concluded that the preferred geometry of the ES dianion resulting from the reduction of ES with alkali metals in DME was planar or nearly planar, although on the geometry of the ES dianion various conflicts exist.[25] We conclude here that all the preferred geometries of the molecule, radical ions, and dianion of ES in solid states or in fluid solutions are planar or nearly planar. This conclusion seems reasonable, since the steric strain in the planar geometry of ES must be very small and hence there must be no driving force for this system to assume a largely twisted geometry.

Spectra M: Spectra M of $ES^{-\cdot}$ and $E44'DMS^{-\cdot}$ are similar, on the whole, to spectra F, P, and W of the same anion radicals. However, a closer examination reveals that the former are much broader than the latter, and that bands A and B in the former are at longer and at shorter wavelength, respectively, than are the corresponding bands in the latter. The same tendencies are also observed for spectra of $E\alpha MS^{-\cdot}$, $ETMS^{-\cdot}$, and $EHMS^{-\cdot}$. As the counterion becomes larger in the series Na^+, K^+, and Cs^+, the maximum of band B shifts slightly to shorter wavelengths, while the maximum of band A shifts rather irregularly (*cf.* Table 7).

Table 7. Data on spectra M of anion radicals

Spectrum	$ES^{-\cdot}$		$E44'DMS^{-\cdot}$		$EHMS^{-\cdot}$	
	λ_B/nm	λ_A/nm	λ_B/nm	λ_A/nm	λ_B/nm	λ_A/nm
M(Na^+)	495	700	499	745	494	745
M(K^+)	494	701	496	725	494	740
M(Cs^+)	493	702	495	715	489	735
F[a]	499.3	690.3	504.6	708.5	498.0	730.6
W[a]	498.4	682.1	502.6	700.0	498.0	717.1

a) Data on spectra F and W are listed for comparison.

The value of K_{dispr} of $ES^{-\cdot}$ in various ethereal solvents increases as the size of the counterion decreases.[10] From this fact, it is inferred that $ES^{-\cdot}$ as well as ES^{2-} forms a contact pair with the counterion.[29] According to the results of our MO calculation, the charge density in $ES^{-\cdot}$ is the largest at positions α and β. It seems most probable that in the contact ion pair the counterion is located near the central ethylenic bond of $ES^{-\cdot}$, as in the contact ion aggregate of ES^{2-} with two counterions.[7] The calculation results also show that the charge density at positions α and β decreases greatly on transition 3 and slightly on transition 5 (*cf.* Table 6). Therefore, it is expected that the counterion exerts a great hypsochromic effect on band A and a slight hypsochromic effect on band B and that the effects decrease as the size of the counterion increases. Agreement between the expectations and the observations is not good. The difference in the position of bands between spectra M and spectra W (as well as F and P) may be partly attributed to a possible difference between geometries M and W (as well as F and P), besides of the effect of the counterion. If $|\theta_{\alpha 1}|$ and $|\theta_{\beta 1'}|$ are slightly larger in geometry M than in geometry W, or if the length of the α-β bond is slightly shorter in geometry M than in geometry W, the direction of the shifts of bands A and B in spectra M as compared with spectra W can be explained.

The values of λ_B and ε_B of $ES^{-\cdot}$ (counterion: Na^+) in hexamethylphosphoric triamide (HMPT) were reported to be 500 nm and 6.0×10^4, respectively.[30] In this solvent the anion radical is considered to exist as free ions, not paired with the counterion. This λ_B value is nearly equal to the values for spectra F, P, and W. On the other hand, the values of λ_B and ε_B of $ES^{-\cdot}$ (counterion: Na^+) in THF were reported to be 494 nm and 5.5×10^4, respectively, or 495 nm and 5.23×10^4, respectively.[27] These λ_B values coincide with the value for spectrum M of $ES^{-\cdot}$ with the same counterion in DME.

E4PS and E44'DPS: $E4PS^{-\cdot}$ and $E44'DPS^{-\cdot}$ also show spectra characteristic of sterically uncrowded radical ions: Spectrum F of $E4PS^{-\cdot}$ and spectrum PA of $E44'DPS^{-\cdot}$ exhibit well-resolved vibrational structure, and remain almost unchanged on illumination, although on controlled warming band A is intensified and is shifted to shorter wavelengths and band B is intensified. Such a spectral change occurs to a smaller extent on illumination, and also occurs in spectra of $ES^{-\cdot}$ and $E44'DMS^{-\cdot}$ to a much smaller extent on controlled warming. Such a spectral change perhaps indicates that $|\theta_{\alpha 1}|$ and $|\theta_{\beta 1'}|$ and possibly the dihedral angles between two benzene rings in the biphenyl groups deviate from 0° to some extents in geometries F and become smaller in geometries W.

DPA: Spectra F of the radical ions of DPA also exhibit well-resolved vibrational structure and remain almost unchanged on illumination and on controlled warming.

It is known that the molecule of this compound is planar in the crystalline state, belonging to point group D_{2h},[31] and the most preferred geometry of the molecule in solutions is probably also planar in view of its electron-

ic absorption spectrum.[18,32] It is inferred from the similarity of the spectra that geometries F, P, W, and R of the radical ions of this compound are quite similar to one another and are planar similarly to the preferred geometry of the parent molecule.

Bands A and B of the radical ions of DPA are located at longer and at shorter wavelength, respectively, than are the corresponding bands of the radical ions of ES. This is attributed to the fact that the α-β bond in DPA (an acetylenic bond) is shorter than that in ES (an ethylenic bond). Since the α-β bond is bonding in ϕ_{+1} and ϕ_{-4} and antibonding in ϕ_{+4} and ϕ_{-1}, the intensification of the π-π interaction across the α-β bond resulting from the shortening of the bond must lower the energies of the former orbitals and raise the energies of the latter orbitals, and consequently must decrease the energy of transition 3 and increase the energy of transition 5.

Group II. EαMS, EαβDMS, and EαβDES: In contrast with the sterically uncrowded radical ions belonging to group I, the radical ions of EαMS, EαβDMS, and EαβDES exhibit broad spctra,[33] and their spectra F change markedly on illumination and on controlled warming.

The stilbene π system in these compounds cannot be planar owing to the steric interferences of the alkyl substituents with the phenyl groups, and the steric interferences are relieved mainly by rotation of the phenyl groups out of the plane of the central ethylenic bond. According to an electronic absorption spectroscopic study,[1,3,6] $|\theta_{\alpha 1}|$ and $|\theta_{\beta 1'}|$ in molecules in solutions increase in the order ES (*ca.* 0°)$<$EαMS (average of $|\theta_{\alpha 1}|$ and $|\theta_{\beta 1'}|$)$\ll$EαβDMS$<$EαβDES.

Cation Radicals: In spectra F(BC) of cation radicals, λ_B/nm decreases and f_A/f_B increases in the order $ES^{+\cdot}$, $E\alpha MS^{+\cdot}$, $E\alpha\beta DMS^{+\cdot}$, $E\alpha\beta DES^{+\cdot}$, and λ_A/nm increases in almost the same order. If the effect of the geometrical change outweighs the electronic effect of the alkyl substituents, the observed sequences indicate that in geometries F(BC) $|\theta_{\alpha 1}|$ and $|\theta_{\beta 1'}|$ increase in the order $ES^{+\cdot}<E\alpha MS^{+\cdot}$(average)$\ll E\alpha\beta DMS^{+\cdot}<E\alpha\beta DES^{+\cdot}$. This probably means that geometries F(BC) of these cation radicals are similar to geometries N.

On illumination of the BC solution of $E\alpha\beta DMS^{+\cdot}$ as well as that of $E\alpha\beta DES^{+\cdot}$, λ_B/nm increases, λ_A/nm decreases, and f_A/f_B decreases. These spectral changes indicate that, in going from geometry F(BC) to geometry P(BC), $|\theta_{\alpha 1}|$ and $|\theta_{\beta 1'}|$ decrease and/or $|\theta_{\alpha\beta}|$ increases.

Spectrum F(FM) of $E\alpha\beta DMS^{+\cdot}$ probably indicates the coexistence of the cation radicals having an almost frozen or only slightly relaxed geometry similar to geometry F(BC) or P(BC) and of the cation radicals having a partially relaxed geometry, suggesting that the FM glass at 77 K is softer than the BC glass at the same temperature, as pointed out already.[8,15] On controlled warming, the geometries are converted to geometry W(FM), which is considered to be an almost completely relaxed geometry. In spectrum W(FM), λ_B/nm is much larger, λ_A/nm is appreciably smaller, and f_A/f_B is much smaller than in spectrum F(BC). This indicates that in geometry R of $E\alpha\beta DMS^{+\cdot}$ $|\theta_{\alpha 1}|$ and $|\theta_{\beta 1'}|$ are much smaller and/or $|\theta_{\alpha\beta}|$ is much larger than in geometry F(BC) and hence than in geometry N. The extent of relaxation of the various geometries of this cation radical may be expressed as follows: N$\leqslant$F(BC)$<$P(BC)$\ll$F(FM)$\ll$W(FM)$\approx$R.

From a similar analysis of the spectra of $E\alpha\beta DES^{+\cdot}$, it is inferred that geometry F(FM) of this cation radical is already almost completely relaxed, and that $|\theta_{\alpha 1}|$ and $|\theta_{\beta 1'}|$ are appreciably smaller and/or $|\theta_{\alpha\beta}|$ is appreciably larger in geometry R than in geometry F(BC) and hence than in geometry N. The extent of relaxation of the various geometries of this cation radical may be expressed as follows: N$\leqslant$F(BC)$<$P(BC)$<$F(FM)$\leqslant$W(FM)$\approx$R. The magnitude of the geometrical change on relaxation seems to be smaller in $E\alpha\beta DES^{+\cdot}$ than in $E\alpha\beta DMS^{+\cdot}$.

In spectra W(FM), λ_A/nm increases in the order $E\alpha\beta DMS^{+\cdot}\ll ES^{+\cdot}<E\alpha MS^{+\cdot}\ll E\alpha\beta DES^{+\cdot}$, and λ_B/nm decreases in the same order, that is, in the order $E\alpha\beta DMS^{+\cdot}\gg ES^{+\cdot}>E\alpha MS^{+\cdot}\gg E\alpha\beta DES^{+\cdot}$. If in geometries W(FM) the stericin terferences were relieved only by deviation of $\theta_{\alpha 1}$ and $\theta_{\beta 1'}$ from 0° and $\theta_{\alpha\beta}$ were maintained at approximately 0° as in geometries N, $|\theta_{\alpha 1}|$ and $|\theta_{\beta 1'}|$ in geometries W(FM) would increase in the order $ES^{+\cdot}<E\alpha MS^{+\cdot}$(average)$\ll E\alpha\beta DMS^{+\cdot}<E\alpha\beta DES^{+\cdot}$, and consequently λ_A/nm and λ_B/nm in spectra W(FM) would increase and decrease, respectively, in the same order, as is almost the case in spectra F(BC). It should be noted that the observed λ_A/nm and λ_B/nm values of $E\alpha\beta DMS^{+\cdot}$ are extraordinarily small and large, respectively. This cannot be attributed to the electronic effect of the methyl substituents, and can be explained only by assuming that in geometry W(FM) of this cation radical $|\theta_{\alpha\beta}|$ is appreciably large. Thus, the observed sequences of band position are taken as an indication of the deviation of $\theta_{\alpha\beta}$ from 0° in geometry W(FM) and hence in geometry R of $E\alpha\beta DMS^{+\cdot}$.

It is unlikely that $|\theta_{\alpha\beta}|$ in geometry W(FM) of $E\alpha\beta DES^{+\cdot}$ is smaller than that of $E\alpha\beta DMS^{+\cdot}$. On the other hand, the former may not be much larger than the latter: If it were, the observed sequences of band position in spectra W(FM) would be reversed. The observed sequences seem to indicate that, in geometries W(FM) and R, $|\theta_{\alpha 1}|$ and $|\theta_{\beta 1'}|$ of $E\alpha\beta DES^{+\cdot}$ are much larger than those of $E\alpha\beta DMS^{+\cdot}$, while $|\theta_{\alpha\beta}|$ of the former is not appreciably different from that of the latter. That is to say, on relaxation, $|\theta_{\alpha 1}|$ and $|\theta_{\beta 1'}|$ decrease to a larger extent in $E\alpha\beta DMS^{+\cdot}$ than in $E\alpha\beta DES^{+\cdot}$, while $\theta_{\alpha\beta}$ deviates from 0° to a similar extent in both the cation radicals.

Thus, it is concluded that, in geometries R, $|\theta_{\alpha 1}|$ and $|\theta_{\beta 1'}|$ increase in the order $ES^{+\cdot}$ (*ca.* 0°)$<E\alpha MS^{+\cdot}$(average)$\ll E\alpha\beta DMS^{+\cdot}\ll E\alpha\beta DES^{+\cdot}$, and $|\theta_{\alpha\beta}|$ increases in the order $ES^{+\cdot}$(*ca.* 0°)$<E\alpha MS^{+\cdot}\ll E\alpha\beta DMS^{+\cdot}\approx E\alpha\beta DES^{+\cdot}$.

The steric interference between the α-alkyl (β-alkyl) and the β-phenyl (α-phenyl) group in (*E*)-α,β-dialkylstilbenes can be relieved by increase in $|\theta_{\alpha\beta}|$ as well as by increase in $|\theta_{\beta 1'}|$ ($|\theta_{\alpha 1}|$), while the interference between the α-alkyl (β-alkyl) and the α-phenyl (β-phenyl) group can be relieved only by increase in $|\theta_{\alpha 1}|$ ($|\theta_{\beta 1'}|$). Therefore, the above conclusion suggests that in geometry R of $E\alpha\beta DES^{+\cdot}$ the methyl group in

the α-ethyl (β-ethyl) group avoids facing the β-phenyl (α-phenyl) group and interferes mainly with the α-phenyl (β-phenyl) group.

Anion Radicals: In spectra F of anion radicals, λ_A/nm and f_A/f_B increase in the order $ES^{-\cdot} \ll E\alpha MS^{-\cdot} \ll E\alpha\beta DMS^{-\cdot} \ll E\alpha\beta DES^{-\cdot}$, and λ_B/nm increases in the order $ES^{-\cdot} < E\alpha MS^{-\cdot} \ll E\alpha\beta DES^{-\cdot} \ll E\alpha\beta DMS^{-\cdot}$. If it were not for the electronic bathochromic effect of the alkyl substituents, perhaps the sequence of λ_B/nm of $ES^{-\cdot}$ and $E\alpha MS^{-\cdot}$ might be reversed, but the other sequences of band position would not be altered. It should be noted that the λ_B/nm value of $E\alpha\beta DMS^{-\cdot}$ is larger than that of $E\alpha\beta DES^{-\cdot}$, and that these values are larger than the λ_B/nm values of $ES^{-\cdot}$ and $E\alpha MS^{-\cdot}$.

On illumination and on controlled warming, in spectra of $E\alpha MS^{-\cdot}$, $E\alpha\beta DMS^{-\cdot}$, and $E\alpha\beta DES^{-\cdot}$, λ_A/nm and f_A/f_B decrease, and λ_B/nm increases. Especially, the decrease in λ_A/nm of $E\alpha\beta DMS^{-\cdot}$ on controlled warming is notable. In addition, f_B or ε_B of $E\alpha\beta DMS^{-\cdot}$ and that of $E\alpha\beta DES^{-\cdot}$ increase prominently on controlled warming. In spectra W, λ_A/nm increases in the order $E\alpha\beta DMS^{-\cdot} \ll ES^{-\cdot} \ll E\alpha MS^{-\cdot} \ll E\alpha\beta DES^{-\cdot}$, f_A/f_B increases in the order $E\alpha MS^{-\cdot} < E\alpha\beta DMS^{-\cdot} < ES^{-\cdot} \ll E\alpha\beta DES^{-}$, and the sequence of λ_B/nm is the same as that in spectra F. The sequence of λ_A/nm is the same as and that of f_A/f_B is similar to the corresponding sequences in spectra W(FM) of cation radicals.

From these facts the following conclusions are drawn: (1) In going from geometries N of EαMS, EαβDMS, and EαβDES to geometries R of the corresponding anion radicals, $|\theta_{\alpha 1}|$ and $|\theta_{\beta 1'}|$ decrease and $|\theta_{\alpha\beta}|$ increases; (2) in geometries R, $|\theta_{\alpha 1}|$ and $|\theta_{\beta 1'}|$ increase in the order $ES^{-\cdot}$ (*ca.* 0°) $< E\alpha MS^{-\cdot}$ (average) $\ll E\alpha\beta DMS^{-\cdot} \ll E\alpha\beta DES^{-\cdot}$, and $|\theta_{\alpha\beta}|$ increases in the order $ES^{-\cdot}$ (*ca.* 0°) $< E\alpha MS^{-\cdot} \ll E\alpha\beta DMS^{-\cdot} \approx E\alpha\beta DES^{-\cdot}$, that is, geometries R of these anion radicals are at least qualitatively similar to geometries R of the corresponding cation radicals; (3) geometries F of these anion radicals in MTHF glasses are already partially relaxed before illumination and controlled warming; (4) the extent of relaxation of the various geometries of the α-alkylated (*E*)-stilbene anion radicals in MTHF may be expressed as follows: $N \ll F < P \ll W \approx R$.

General Discussion on Group II: As concluded above, in geometries R of the radical ions of the α-alkylated (*E*)-stilbenes $|\theta_{\alpha 1}|$ and $|\theta_{\beta 1'}|$ are smaller and $|\theta_{\alpha\beta}|$ is larger than in geometries N. In Part I of this series,[7] a qualitatively similar conclusion was drawn for the geometries of the dianions of these compounds.

Fischer *et al.*[21] stated as follows: Sterically unhindered stilbenes, that is, (*E*)-stilbenes not substituted at the *ortho* and the α and β positions, have a planar geometry both in the ground state (state S_0) and in the first excited singlet state (state S_1); sterically hindered stilbenes, *e.g.*, (*Z*)-stilbenes and α,β-disubstituted (*E*)-stilbenes, are strongly twisted about the α-1 and the β-1′ bond in state S_0, while in state S_1 the major twist is about the α-β bond. Thus, according to the results of their calculation by the CFF-SCF-PI-CI method described by Warshel and Karplus,[36] in going from state S_0 to state S_1, in EαβDMS $\theta_{\alpha 1}$ and $\theta_{\beta 1'}$ decrease from 47° to 13° and $\theta_{\alpha\beta}$ increases from 6° to 49°, while in ES all the torsion angles are 0° in both the states.

State S_1 as well as the first excited triplet state (state T_1) of these compounds can be well approximated by the electron configuration arising from state S_0 by promotion of an electron from ϕ_{+1} to ϕ_{-1}.[37] Therefore, because of the pairing properties of π orbitals in even alternant hydrocarbons, in the one-electron approximation the π-bond order of each bond of the dianion as well as the dication both in state S_0 and that of the neutral molecule in state S_1 as well as T_1 should be equal to each other. Accordingly, it is reasonable that the most probable geometry of the dianion in state S_0 is similar to that of the neutral molecule in state S_1.

In the stilbene molecule in state S_0, the π-bond order of the α-1 as well as the β-1′ bond is much smaller than that of the α-β bond. In the molecule in state S_1 and in the dianion in state S_0, the sequence of the π-bond orders is reversed, and consequently the overcrowding in sterically hindered derivatives is relieved in a different way than in the molecule in state S_0, resulting in a different geometry.

The bonding character of the radical ions in the ground state (state D_0) is intermediate between those of the molecule and of the diions both in state S_0. Therefore, the relaxed geometry of the radical ions of a sterically crowded stilbene derivative in state D_0 is probably intermediate between those of the parent molecule and of the corresponding diions both in state S_0.

The values of π-bond order calculated by the SCF-MO-CI method are shown in Table 8. From these values it is expected that in geometries R of sterically crowded stilbene molecules and ions $|\theta_{\alpha 1}|$ and $|\theta_{\beta 1'}|$ decrease and $|\theta_{\alpha\beta}|$ increases in the following order: the molecule in state S_0, the radical ions in state D_0, the molecule in state T_1, the molecule in state S_1, the diions in state S_0.

Group III. ETMS and EHMS: The spectra of the radical ions of ETMS and EHMS are similar to those of the radical ions of ES, exhibiting characteristic vibrational structure. In contrast to spectra F of the radical ions of ES, however, those of the radical ions of ETMS and EHMS change distinctly on illumination and on controlled warming. Especially, λ_A/nm and f_A/f_B decrease, although the magnitude of the spectral changes is considerably smaller than in the case of the radical ions of EαβDMS and EαβDES. In addition, f_B and ε_B of the anion radicals of ETMS and EHMS increase prominently on controlled warming. The spectra of these anion radicals in MTHF glass at 77 K are similar on the whole to spectra M of the same anion radicals. Thus, with respect to the spectral behavior,

Table 8. The π-bond orders of the planar (*E*)-stilbene molecule and molecular ions calculated by SCF-MO method

Bond	$ES(S_0)$[a]	$ES^{-\cdot}(D_0)$ $ES^{+\cdot}(D_0)$	$ES(T_1)$[b]	$ES(S_1)$[b]	$ES^{2-}(S_0)$[a] $ES^{2+}(S_0)$
α-1;β-1′	0.341	0.448	0.508	0.563	0.711
α-β	0.886	0.705	0.664	0.543	0.448

a) Ref. 7. b) Ref. 37.

group III is intermediate between groups I and II.

Analysis of the spectra of the radical ions of ETMS and EHMS leads to the following conclusions on geometries of these radical ions.

(1) Geometries F are similar to geometries N. In geometries F, $|\theta_{\alpha 1}|$ and $|\theta_{\beta 1'}|$ increase in the order $ES^{\pm\cdot}$ (*ca.* 0°)$\ll$$ETMS^{\pm\cdot}$ (average of $|\theta_{\alpha 1}|$ and $|\theta_{\beta' 1}|$)$<$ $EHMS^{\pm\cdot}$, as in geometries N.

(2) On controlled warming and on illumination, $|\theta_{\alpha 1}|$ and $|\theta_{\beta 1'}|$ decrease and $|\theta_{\alpha\beta}|$ increases.

(3) The extent of the geometrical relaxation may be expressed as follows: for the cation radicals, N$<$ F(BC)$<$P(BC)$\approx$F(FM)$\leqslant$W(FM)$\approx$R; for the anion radicals, N$<$F$<$P$<$W$\approx$R.

(4) The geometrical changes on the relaxation are comparatively small. Especially, the values of $|\theta_{\alpha\beta}|$ in geometries R are probably much smaller than those in geometries R of the radical ions of E$\alpha\beta$DMS and E$\alpha\beta$DES.

Conclusion 4 above is rather surprising, because in the case of neutral molecules both the steric interference caused by the *ortho* substitution in EHMS and that caused by the α and β substitution in E$\alpha\beta$DMS are relieved by rotation to comparable degrees about the α-1 and the β-1′ bond.[3,4] However, this conclusion is consistent with the following facts.

(i) As found in Part I of this series,[7] as positions α and β of the ES dianion are increasingly substituted with alkyl groups, the longest-wavelength intense band shifts rapidly to shorter wavelengths, which indicates that $|\theta_{\alpha\beta}|$ increases rapidly; on the other hand, as the *ortho* positions are increasingly substituted with methyl groups, the band shifts slowly to shorter wavelengths, indicating that $|\theta_{\alpha\beta}|$ increases slowly. From these facts, it was inferred that the values of $|\theta_{\alpha 1}|$ and $|\theta_{\beta 1'}|$ in the EHMS dianion, for example, were larger than those in the E$\alpha\beta$DMS dianion, and that the value of $|\theta_{\alpha\beta}|$ in the former was smaller than that in the latter.

(ii) ETMS and EHMS as well as ES can readily be converted into the corresponding anion radicals by alkali-metal reduction,[7] but it is difficult to reduce them to the dianions, indicating that the values of K_{dispr} are small for these compounds.[9] On the other hand, as mentioned already, E$\alpha\beta$DMS and E$\alpha\beta$DES[7] as well as TPE[8] are readily reduced to the dianions with alkali metals, which indicates that the values of K_{dispr} are probably large for these sterically crowded compounds. These facts suggest that the geometries of the molecule, anion radical, and dianion are not much different from one another in the case of ETMS and EHMS as well as ES, while those are markedly different in the case of E$\alpha\beta$DMS, E$\alpha\beta$DES, and TPE.

(iii) According to a study by Fischer *et al.*,[21] the observed "Stokes shift"[38] ($\Delta\lambda$) of stilbenes parallels the increase ($\Delta\theta_{\alpha\beta}$) in the calculated equilibrium value of $\theta_{\alpha\beta}$ on the excitation from state S_0 to state S_1. For sterically uncrowded stilbenes, both $\Delta\lambda$ and $\Delta\theta_{\alpha\beta}$ are small: For ES, $\Delta\lambda$ is *ca.* 0 nm, $\theta_{\alpha\beta}$ is 0° in both the states, and $\Delta\theta_{\alpha\beta}$ is 0°. On the other hand, for sterically crowded stilbenes such as (*Z*)-stilbene, E$\alpha\beta$DMS, and its *Z* isomer, both $\Delta\lambda$ and $\Delta\theta_{\alpha\beta}$ are large: For E$\alpha\beta$DMS, for example, $\Delta\lambda$ is 67 nm, and $\theta_{\alpha\beta}$ increases from 6° to 49° on the excitation, that is, $\Delta\theta_{\alpha\beta}$ is 43°. For EHMS $\Delta\lambda$ is as small as 4 nm. This fact suggests that the change in $\theta_{\alpha\beta}$ of this compound on the excitation is very small.

These facts are interpreted as follows. Since in the stilbene molecule in state S_0 the π-bond order of the α-β bond is large and those of the α-1 and the β-1′ bond are small, the steric interference in sterically crowded stilbenes is relieved almost exclusively by rotation about the α-1 and the β-1′ bond. In the radical ions in state D_0, the neutral molecule in state S_1, and the diions in state S_0, the π-bond order of the α-β bond decreases, and those of the α-1 and the β-1′ bond increase (*cf.* Table 8). Therefore, the possibility arises that the steric interference in sterically crowded stilbenes is relieved by rotation about the α-β bond as well as by rotation about the α-1 and the β-1′ bond. The steric interference caused by the *ortho* substitution may be smaller than that caused by the α and β substitution. In addition, while a major part of the steric interference caused by the α and β substitution may effectively be relieved by rotation about the α-β bond, the steric interference caused by the *ortho* substitution cannot be relieved by rotation about the α-β bond so effectively as is that caused by the α and β substitution, and must be relieved mainly by rotation about the α-1 and the β-1′ bond, as in the neutral molecules in state S_0.

References

1) H. Suzuki, *Bull. Chem. Soc. Jpn.*, **25**, 145 (1952).
2) H. Suzuki, *Bull. Chem. Soc. Jpn.*, **33**, 379 (1960).
3) H. Suzuki, *Bull. Chem. Soc. Jpn.*, **33**, 396 (1960).
4) H. Suzuki, *Bull. Chem. Soc. Jpn.*, **33**, 406 (1960).
5) H. Suzuki, *Bull. Chem. Soc. Jpn.*, **33**, 410 (1960).
6) H. Suzuki, "Electronic Absorption Spectra and Geometry of Organic Molecules," Academic Press Inc., New York (1967), Chap. 14.
7) H. Suzuki, K. Koyano, and T. L. Kunii, *Bull. Chem. Soc. Jpn.*, **45**, 1979 (1972).
8) H. Suzuki, K. Koyano, T. Shida, and A. Kira, *Bull. Chem. Soc. Jpn.*, **52**, 2794 (1979).
9) K_{dispr} for $ES^{-\cdot}$ at ambient temperature was estimated at about 10^{-3} (counterion: Na^+, solvent: THF),[10] 0.09 (counterion: Na^+, solvent: MTHF),[11] and about 0.03 (counterion: Na^+, solvent: THF).[12] On the other hand, according to Garst *et al.*,[11] the values of K_{dispr} for $TPE^{-\cdot}$ and $E\alpha MS^{-\cdot}$ at 25 °C (counterion: Na^+, solvent: MTHF) are$\geqslant$1000.
10) E. R. Zabolotny and J. F. Garst, *J. Am. Chem. Soc.*, **86**, 1645 (1964).
11) J. F. Garst, J. G. Pacifici, and E. R. Zabolotny, *J. Am. Chem. Soc.*, **88**, 3872 (1966).
12) F. Jachimowicz, G. Levin, and M. Szwarc, *J. Am. Chem. Soc.*, **99**, 5977 (1977).
13) H. C. Longuet-Higgins and J. A. Pople, *Proc. Phys. Soc. London, Sect. A*, **68**, 591 (1955).
14) T. Shida and S. Iwata, *J. Phys. Chem.*, **75**, 2591 (1971).
15) T. Shida and S. Iwata, *J. Am. Chem. Soc.*, **95**, 3473 (1973).
16) Y. Tanizaki, H. Inoue, T. Hoshi, and H. Shiraishi, *Z. Phys. Chem. (Frankfurt am Main)*, **74**, 45 (1971).
17) J. M. Robertson and I. Woodward, *Proc. R. Soc. London, Ser. A*, **162**, 568 (1937); C. J. Finder, M. G. Newton, and N. L. Allinger, *Acta Crystallogr., Sect. B*, **30**, 411 (1974); J. Bernstein, *ibid.*, **31**, 1268 (1975); A. Hoekstra, P. Meertens, and A. Vos, *ibid.*, **31**, 2813 (1975).

18) H. Suzuki, *Bull. Chem. Soc. Jpn.*, **33**, 944 (1960).
19) M. Traetteberg, E. B. Frantsen, F. C. Mijlhoff, and A. Hoekstra, *J. Mol. Struct.*, **26**, 57 (1975).
20) F. J. Adrian, *J. Chem. Phys.*, **28**, 608 (1958); G. Favini and M. Simonetta, *Theor. Chim. Acta*, **1**, 294 (1963); D. H. Lo and M. A. Whitehead, *Can. J. Chem.*, **46**, 2041 (1968); A. Bromberg and K. A. Muszkat, *Tetrahedron*, **28**, 1265 (1972); A. Golebiewski and A. Parczewski, *Acta Phys. Pol. A*, **41**, 727 (1972); T. Beringhelli, A. Garezzotte, and M. Simonetta, *J. Mol. Struct.*, **12**, 333 (1972); A. Warshel, *J. Chem. Phys.*, **62**, 214 (1975).
21) G. Fischer, G. Seger, K. A. Muszkat, and E. Fischer, *J. Chem. Soc., Perkin Trans. 2*, **1975**, 1569.
22) R. Chang and C. S. Johnson, Jr., *J. Chem. Phys.*, **46**, 2314 (1967).
23) R. Chang and C. S. Johnson, Jr., *J. Chem. Phys.*, **41**, 3272 (1964).
24) C. S. Johnson, Jr., and R. Chang, *J. Chem. Phys.*, **43**, 3183 (1965).
25) An X-ray study by Walczak and Stucky of crystals of salts of ES^{2-} with Li^+ complexed with amines revealed that the ES^{2-} moiety in the salts had a planar geometry.[26] Jachimowicz *et al.* inferred that ES^{2-}, if associated with its counterions, had a planar or nearly planar geometry, and that, if not associated with the counterions, it had a fully twisted geometry.[12] On the other hand, Garst *et al.*[11] and Wang *et al.*[27] proposed a nonplanar geometry twisted by 90° around the central ethylenic bond for ES^{2-}. A basis for the proposition by Garst *et al.* is an anticipation of a direct correspondence between the geometry of the dianion in its ground state and that of the molecule in its lowest excited triplet state, which was assumed to be a 90° twisted one. However, this correspondence may not necessarily hold good. In addition, according to a study by Benson and Williams of the photochemical *Z-E* isomerization of stilbene in its triplet state, the 90° twisted geometry is at a maximum in the potential energy profile for the triplet state.[28] All the phenomena interpreted in terms of the twisted geometry of ES^{2-} by Garst *et al.*,[11] by Wang *et al.*,[27] and by Jachimowicz *et al.*[12] seem also to be interpretable in terms of an approximately planar geometry of ES^{2-}. We believe that ES^{2-} has a planar or approximately planar geometry, whether it is associated with the counterions or not.
26) M. Walczak and G. Stucky, *J. Am. Chem. Soc.*, **98**, 5531 (1976).
27) H. C. Wang, G. Levin, and M. Szwarc, *J. Am. Chem. Soc.*, **99**, 2642 (1977).
28) R. Benson and D. F. Williams, *J. Phys. Chem.*, **81**, 215 (1977).
29) M. Szwarc, "Chemistry of Radical-Ions," in "Progress in Physical Organic Chemistry 6," ed by A. Streitwieser, Jr., and R. W. Taft, Interscience Publishers, New York (1968), pp. 323—438.
30) S. Sorensen, G. Levin, and M. Szwarc, *J. Am. Chem. Soc.*, **97**, 2341 (1975).
31) J. M. Robertson and I. Woodward, *Proc. R. Soc. London, Ser. A*, **164**, 436 (1938).
32) H. Suzuki, *Bull. Chem. Soc. Jpn.*, **33**, 389 (1960).
33) Quantity f/ε_{max} may be taken as a measure of broadness of a band. The values of $10^4 f_B/\varepsilon_B$ for the radical ions of the α,β-dialkylstilbenes ($E\alpha\beta DMS^{+\cdot}$, 0.30; $E\alpha\beta DES^{+\cdot}$, 0.27; $E\alpha\beta DMS^{-\cdot}$, 0.14; $E\alpha\beta DES^{-\cdot}$, 0.16) are much larger than those for the radical ions of the compounds belonging to group I or group III (0.08—0.10). The large broadness of the band may be taken as reflecting the large deviation of the geometry from planarity.[34,35]
34) H. Suzuki, *Bull. Chem. Soc. Jpn.*, **35**, 1715 (1962).
35) H. Suzuki, "Electronic Absorption Spectra and Geometry of Organic Molecules," Academic Press Inc., New York (1967), Chap. 15.
36) A. Warshel and M. Karplus, *J. Am. Chem. Soc.*, **94**, 5612 (1972); *Chem. Phys. Lett.*, **17**, 7 (1972); *J. Am. Chem. Soc.*, **96**, 5677 (1974).
37) H. Suzuki and T. L. Kunii, unpublished work.
38) Fischer *et al.*[21] defined the "Stokes shift" ($\Delta\lambda$) as the wavelength difference between the longwave "onset" of the longest-wavelength intense absorption band and the shortwave "onset" of the fluorescence band, and defined the "onset" as the wavelength at which the absorbance or the emission was 1% of its peak value. The values of $\Delta\lambda$ were obtained from absorption and fluorescence spectra both measured at −180 to −190 °C using an equivolume mixture of methylcyclohexane and 3-methylpentane as the solvent. The Stokes shift is ordinarily defined as the difference in wavelength or in wave number between the most intense maximum of the absorption band and that of the fluorescence band. The Stokes shift so defined, $\Delta\lambda_{max}$ (or $\Delta\tilde{\nu}_{max}$), is evaluated from the data by Fischer *et al.* as follows: 42 nm (3.85×10^3 cm^{-1}) for ES, 180 nm (16.74×10^3 cm^{-1}) for $E\alpha\beta DMS$, and 85 nm (8.42×10^3 cm^{-1}) for EHMS.

Interaction of Amylose with Iodine. II. Kinetic Studies of the Complex Formation by the Temperature-jump Method

Masako YAMAMOTO,† Takayuki SANO, Shoji HARADA, and Tatsuya YASUNAGA*
Department of Chemistry, Faculty of Science, Hiroshima University, Hiroshima 730
†*Department of Home Economics, Hiroshima Women's University, Hiroshima 734*

(Received March 19, 1982)

Kinetic studies of the amylose–iodine complex formation for the amylose of degree of the polymerization (DP) of 32 were made using the temperature-jump method. The reciprocal relaxation time increases with increase of the concentration of iodine and decreases with that of amylose. Based on these results, the reaction, $H_0+3\,I_3^- \rightleftharpoons H_3$ was proposed as a plausible mechanism for the relaxation phenomenon, where H_0 denotes the free helical segment of amylose and H_3 the helical segment containing three I_3^-. The relaxation phenomena were observed for the amyloses of DP 42, 57, and 76, and analyzed by the same mechanism as that proposed in the case of DP 32. The rate constants for the forward and the backward reactions (k_f and k_b) were determined: the k_f value increases with DP of amylose and the k_b value decreases. Examination of the relaxation time and the relaxation amplitude suggested that the relaxation phenomenon is not based on the whole process of the amylose–iodine complex formation but on the H_3 complex formation reaction which was shown to be the nucleation process.

Amylose–iodine complexes show the well-known specific blue color which is widely utilized for the detection of starch and iodine: a number of static studies have been made on the characteristics of the complex.[1–5] On the other hand, few kinetic studies of the amylose–iodine complex formation have been carried out and plausible mechanisms have been proposed.[6–9] Thompson and Hamori[6] revealed that the complex formation begins with the very rapid formation of H_3 followed by the slow rate-determining reaction of H_4 formation and that successive uptake of iodine molecule by H_4 is very fast. Hiromi *et al.*[7] studied the reaction with use of the amyloses of various degree of the polymerization (DP) and observed two processes: one is the very fast formation of H_n†† (n=2—4) and the other is the subsequent slow rearrangement of H_n. Grätzel *et al.*[8] investigated the reaction by the pulseradiolysis with a mechanism proposed by Thompson and Hamori[6] and obtained the rate constants of H_6 and H_7 complex formation reactions, but the rapid H_3 complex formation process was not studied.

Although the nucleation process is significant as a source of the propagation process, and its existence has been supported by the above investigations, it is still not completely elucidated kinetically. One of the reasons it remains open is the difficulty of measuring the nucleation process independently of the propagation process; the other is the rapidity of the nucleation process. Taking these into account we used, in the present study, the amylose of low DP which has the advantage of lacking the propagation process because of its short helical part[10–13] and low facility for binding iodine.[14] Considering that the nucleation process is very fast and the amylose–iodine complex formation equilibrium is perturbed effectively with temperature, the temperature-jump method is an appropriate technique for the present investigation. The persent study was undertaken to clarify the nucleation process by the temperature-jump method using amylose of low DP.

†† H_n: The helical segment containing nI_3^-.

Experimental

Materials. Amyloses of various DP were prepared as described in a previous paper.[14] Iodine and potassium iodide were of guaranteed reagent and were used without further purification. Freshly prepared amylose solution is used for each measurement.

Measurements. Kinetic measurements were carried out by the temperature-jump method with optical detection in the range of 350—550 nm. Since the addition of electrolytes to the sample solution is required for the Joule-heating temperature-jump method, 50 mmol dm^{-3} of KI was added. The concentration of iodine was determined by amperometric titration as shown in the previous paper.[14] All of the experiments were performed at 22 °C.

Results and Discussion

For the solution of amylose of DP 32 with iodine, the relaxation phenomenon was observed at 530 nm and 350 nm, *i.e.*, the maximum wavelengths of the amylose–iodine complex and that of free I_3^-, respectively: in the actual experiments, the relaxation spectra were recorded at 530 nm, because of the larger relaxation amplitude. Representative relaxation curves are shown in Figs. 1a and 1b. The absorbance change observed in Fig. 1a indicates the decrease of the complex, while that in Fig. 1b indicates the increase of I_3^-. Both curves were characterized as single relaxation phenomena and the relaxation times were coincident. These results indicate that the temperature-jump decomposes the complex and produces free I_3^- at the same time, and suggests that the present relaxation phenomenon is due to the amylose-iodine complex formation.[15]

The kinetic experiments were carried out by changing the concentration of iodine while keeping the concentration of amylose constant, or *vice versa*. The plots of the reciprocal relaxation time (τ^{-1}) *vs.* the total concentration of I_3^- [16] and that of amylose are shown in Figs. 2 and 3, respectively. As shown in these figures, the value of τ^{-1} increases with increase of the concentration of iodine but decreases with that of amylose.

Combining the above results together with the static

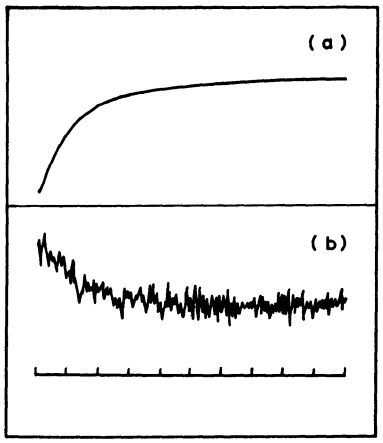

Fig. 1. Representative relaxation spectra of the amylose–iodine complex formation by the temperature-jump method at 22°C. OD increases downwards.
Σ[iodine] $= 1.2 \times 10^{-4}$ mol dm^{-3}, Σ[amylose of DP 32] $= 5 \times 10^{-4}$ mol dm^{-3} in AGU, sweep: 20 μs div^{-1}, (a): 530 nm, (b): 350 nm.

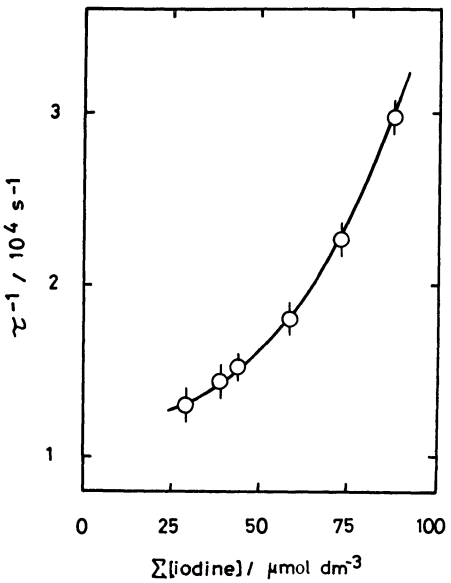

Fig. 2. Iodine concentration dependence of the reciprocal relaxation time for the amylose–iodine complex formation. The solid line drawn through the points has no theoretical significance.
Σ[amylose of DP 32] $= 5 \times 10^{-4}$ mol dm^{-3}.

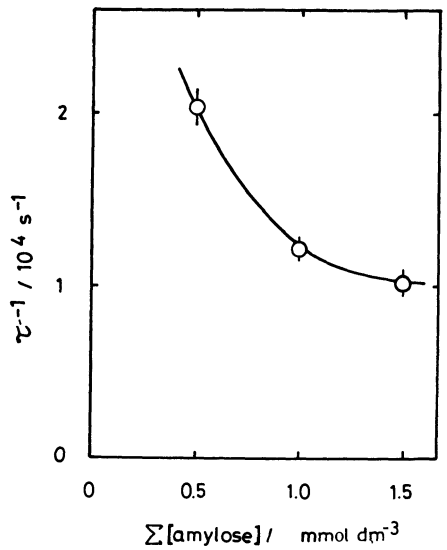

Fig. 3. Amylose concentration dependence of the reciprocal relaxation time for the amylose–iodine complex formation.
Σ[iodine] $= 4.5 \times 10^{-5}$ mol dm^{-3}.

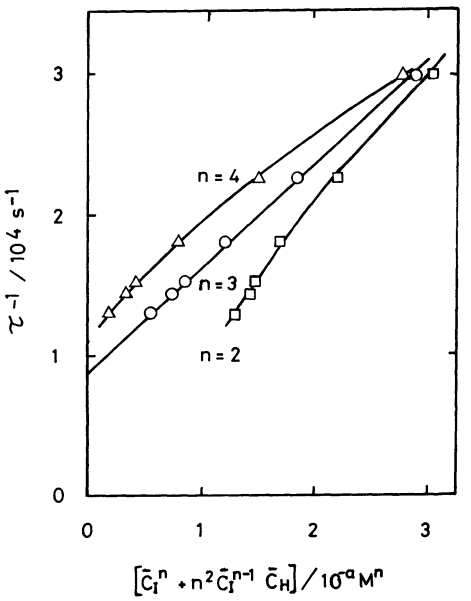

Fig. 4. Plots of the reciprocal relaxation time *vs.* the concentration term in Eq. 2 calculated for each n value.
□: $a=9$; ○: $a=13$, △: $a=17$. 1 M = 1 mol dm^{-3}.

information, the following reaction was proposed as a plausible mechanism for the present relaxation phenomenon:

$$H_0 + nI_3^- \underset{k_b}{\overset{k_f}{\rightleftharpoons}} H_n, \qquad (1)$$

where H_0 denotes the free helical segment of amylose. The relaxation equation for the above reaction is given as

$$\tau^{-1} = k_f(\bar{C}_I^n + n^2\bar{C}_I^{n-1}\bar{C}_{H_0}) + k_b, \qquad (2)$$

where k_f and k_b are the forward and the backward rate constants, respectively, $\bar{C}_I$ is the concentration of free iodine and $\bar{C}_{H_0}$ is the concentration of free helical segment of amylose.[19] An increase of Σ[amylose] increases $\bar{C}_{H_0}$ but decreases $\bar{C}_I$ due to the shift of the equilibrium (1) to the right under the constant initial concentration of iodine. Since $\bar{C}_I$ contributes to τ^{-1} by the n and $(n-1)$ powers in Eq. 2, the variation of $\bar{C}_I$ predominantly effects τ^{-1}. Therefore, the experimental results in Figs. 2 and 3 seem to be well described by Reaction 1. The plots of τ^{-1} *vs.* the concentration term in Eq. 2 with various n values are shown in Fig. 4. As shown in the figure, the plot with $n \leqq 2$ gives a negative intercept and in the cases of $n \geqq 4$, it does not give a straight line. Only the plot with $n=3$ gives a best straight line, *i.e.*, Reaction 1 is shown to be

$$H_0 + 3I_3^- \underset{k_b}{\overset{K_f}{\rightleftharpoons}} H_3. \quad (3)$$

Reaction 3 is considered to be composed of the following three elementary reactions:

$$H_0 + I_3^- \overset{K_1}{\rightleftharpoons} H_1, \quad (4)$$

$$H_1 + I_3^- \overset{K_2}{\rightleftharpoons} H_2, \quad (5)$$

$$H_2 + I_3^- \underset{k_{-3}}{\overset{K_3\ k_3}{\rightleftharpoons}} H_3, \quad (6)$$

Assuming that the concentrations of H_1 and H_2 are very low and Reaction 6 is the rate-determining step of Reaction 3, the relaxation time for Reaction 3 is given by

$$\tau^{-1} = K_1K_2k_3(\bar{C}_I^3 + 9\bar{C}_I^2\bar{C}_{H_0}) + k_{-3}. \quad (7)$$

In comparison to Eq. 2 with $n=3$, $K_1K_2k_3$ corresponds to k_f, and k_{-3} to k_b. From the slope and intercept of the straight line of the plot with $n=3$ in Fig. 4, we can evaluate the values of k_f and k_b to be $(7.7\pm0.2)\times10^{16}$ (mol dm^{-3})$^{-3}$ s^{-1} and $(8.4\pm0.9)\times10^3$ s^{-1}, respectively, and the equilibrium constant K was obtained to be $(9.2\pm0.8)\times10^{12}$ (mol dm^{-3})$^{-3}$ from the ratio of k_f and k_b.

The equilibrium constant is also obtained amperometrically by the following equation:

$$K = [H_3]/[H_0][I_3^-]^3 = \bar{C}_B/(3\Sigma\bar{C}_H - \bar{C}_B)(\bar{C}_I)^3, \quad (8)$$

where $\bar{C}_B$ denotes the concentration of the bound iodine and $\Sigma\bar{C}_H$ is the total concentration of the helical segment of amylose. Introducing the same assumptions as those used in the derivation of Eq. 7, *i.e.*, $[H_1]=[H_2]\simeq0$ and H_3 is the only species of the complex, the value of K was determined to be $(1.3\pm0.6)\times10^{13}$ (mol dm^{-3})$^{-3}$, which is in good agreement with the above value.

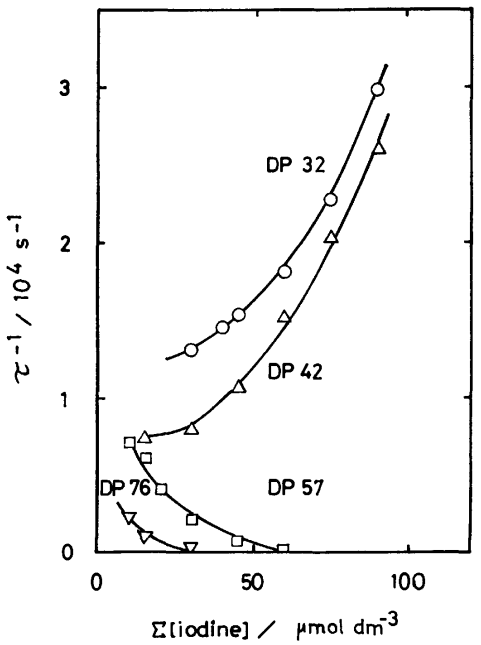

Fig. 5. Iodine concentration dependences of the reciprocal relaxation time for the amyloses of various DP and iodine system.
Σ[amylose]$=5\times10^{-4}$ mol dm^{-3}.

The same experiments as those described above were performed for the amyloses of DP 42, 57, and 76 and the effect of DP of amylose was investigated. The iodine concentration dependences of τ^{-1} for amyloses of various DP are shown in Fig. 5, where the positive and negative dependences were observed below DP 42 and above DP 57, respectively. In the case of lower DP amyloses, the binding of iodine is so weak that the added iodine increases the concentration term of Eq. 7 and induces the increase of τ^{-1} value. On the other hand, in the case of higher DP amyloses, most of the added iodine binds to the amylose and makes a negative contribution to the increase of the concentration term of Eq. 7. Consequently, the apparently opposing behavior of the concentration dependences of τ^{-1} can be well understood.

It is well known that the amylose–iodine complex becomes longer with increase of the DP of the amylose. In the case of these higher DP amyloses, the value of n for the final species of the complex (H_n) will exceed 3, *e.g.*, $n=4$ or more.[10-14] Therefore, if we are observing the whole process of the amylose–iodine complex formation in the present temperature-jump experiment

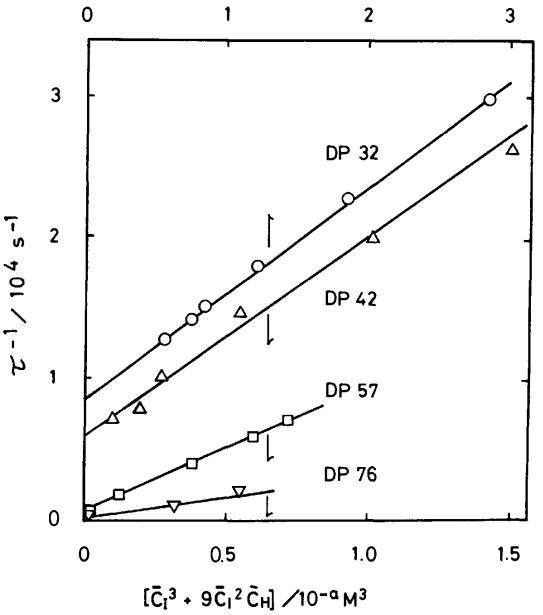

Fig. 6. Plots of the reciprocal relaxation time *vs.* the concentration term in Eq. 7 with $n=3$ for the amyloses of various DP and iodine system.
○: $a=13$, △: $a=13$, □: $a=15$, ▽: $a=16$.

Table 1. Rate constants and equilibrium constants for the complex formation of amyloses of various DP with iodine

DP	k_f / (mol dm^{-3})$^{-3}$ s^{-1}	k_b / s^{-1}	K / (mol dm^{-3})$^{-3}$
32	$(7.7\pm0.2)\times10^{16}$	$(8.4\pm0.9)\times10^3$	9.2×10^{12}
42	$(1.4\pm0.3)\times10^{17}$	$(5.8\pm1.0)\times10^3$	2.4×10^{13}
57	$(8.7\pm0.9)\times10^{18}$	$(7.6\pm0.9)\times10^2$	1.1×10^{16}
76	$(3.0\pm0.5)\times10^{19}$	$(1.1\pm0.4)\times10^2$	3.7×10^{17}

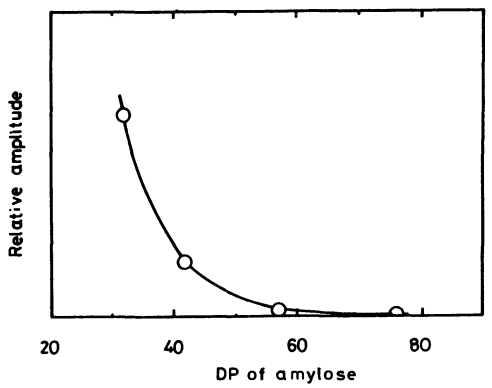

Fig. 7. The effect of DP of amylose on the relaxation amplitude.
Σ[amylose]$=5\times10^{-4}$ mol dm^{-3}, Σ[iodine]$=4.5\times10^{-5}$ mol dm^{-3}. Amplitude is plotted in arbitrary unit.

the value of n should be 4 or more in the case of higher DP amyloses. For all amyloses of various DP, however, only the plot with $n=3$ gave a good straight line with positive slope and the positive intercept as shown in Fig. 6. These results suggest that only Reaction 3 is responsible for the present relaxation and the reactions having order higher than 3 are not observed in these experiments. The values of k_f and k_b for the amyloses of various DP were obtained from each straight line in Fig. 6; they are summarized in Table 1 along with the value of K. With increasing DP of the amylose, the k_f value increases but the k_b value decreases.

The relaxation amplitude was found to be greatly affected by the DP of the amylose as shown in Fig. 7; the relaxation amplitude decreases steeply with increase of the DP of the amylose. This behavior of the relaxation amplitude is well understood by considering the shift of the equilibrium of Reaction 3 to the right[20] with DP of amylose, as indicated by the increase of K in Table 1. Another reason for the decrease of the relaxation amplitude will be in the decrease of the concentration of H_3 due to the propagation of H_3 to H_n ($n\geqq4$) in the case of higher DP amyloses.

The results on the relaxation time and the relaxation amplitude suggest that the relaxation phenomenon is not based on the whole process of the amylose–iodine complex formation but on the H_3 complex formation reaction. This consideration implies that the H_3 complex is relatively unstable and is easily perturbed by temperature but the higher order complex, *e.g.*, H_4, very stable and not perturbed. These are consistent with the explanation proposed by Thompson and Hamori[6] where the existence of a stable nuclei, H_4, is postulated for the high DP amylose.

Hiromi *et al.*[7] have proposed the following mechanism for the amylose–iodine complex formation:

$$H + nI_3^- \overset{\text{fast}}{\rightleftharpoons} \text{complex } \mathbf{1} \overset{\text{slow}}{\rightleftharpoons} \text{complex } \mathbf{2}.$$

The slow reaction with a time constant of 1—200 ms was investigated in detail but the fast reaction was just noted. Its existence in the time region is less than 1 ms. The existence of the process where three iodines bind to amylose has been suggested by other investigators.[6,8] The relaxation phenomenon observed in the present study was in the time region of less than 1 ms and ascribed to the reaction $H_0+3\,I_3^-\rightleftharpoons H_3$: these results were in complete agreement with the features predicted for the nucleation process. Finally, the fact that three iodines bind successively to the helical segment of amylose is indicative of the cooperative binding, which is compatible with the result we obtained by amperometric titration.[14]

Appendix

$$\text{For a reaction } H_0 + nI_3^- \underset{k_b}{\overset{k_f}{\rightleftharpoons}} H_n, \tag{A-1}$$

the rate equation is given by

$$\begin{aligned} -\frac{d}{dt}C_{H_0} &= k_f C_{H_0} C_I^n - k_b C_{H_n} \\ &= k_f(\bar{C}_{H_0}+\Delta C_{H_0})(\bar{C}_I+\Delta C_I)^n \\ &\quad - k_b(\bar{C}_{H_n}+\Delta C_{H_n}), \end{aligned} \tag{A-2}$$

where a bar over the concentration symbols indicates the equilibrium value and Δ indicates the small deviation from equilibrium. The stoichiometry gives the following relation,

$$\Delta C_{H_0} = \frac{1}{n}\Delta C_I = -\Delta C_{H_n} \tag{A-3}$$

At an equilibrium state,

$$K = \frac{k_f}{k_b} = \frac{\bar{C}_{H_n}}{\bar{C}_{H_0}\bar{C}_I^n}. \tag{A-4}$$

Neglecting the quadratic term in Eq. A-2, the rate equation is developed as follows,

$$\begin{aligned} -\frac{d}{dt}C_{H_0} &= -\frac{d}{dt}C_{H_0}(\equiv\tau^{-1}\Delta C_{H_0}) \\ &= k_f\{\Delta C_{H_0}\bar{C}_I^n + n\Delta C_I\bar{C}_I^{n-1}\bar{C}_{H_0}\} - k_b\Delta C_{H_0} \\ &= \{k_f(\bar{C}_I^n+n^2\bar{C}_I^{n-1}\bar{C}_{H_0}) + k_b\}\Delta C_{H_0}, \end{aligned} \tag{A-5}$$

then the reciprocal relaxation time τ^{-1} is given by,

$$\tau^{-1} = k_f(\bar{C}_I^n + n^2\bar{C}_I^{n-1}\bar{C}_{H_0}) + k_b. \tag{A-6}$$

References

1) R. E. Rundle and D. French, *J. Am. Chem. Soc.*, **65**, 1707, (1943).
2) W. Banks and C. T. Greenwood, "Starch and Its Components," Edinburgh University Press: Edinburgh, (1975).
3) "Solution Properties of Polysaccharides," ed by D. A. Brant, ACS Symposium Series 150, American Chemical Society, Washington (1981).
4) "Denpun Kagaku Hando Bukku," ed by J. Nikuni, Asakura Press, Tokyo (1977).
5) T. Handa and H. Yajima, *Biopolymers*, **18**, 873, (1979), **19**, 723, 1723, (1980), **20**, 2051, (1981).
6) J. C. Thompson and E. Hamori, *J. Phys. Chem.*, **75**, 272, (1971).
7) K. Hiromi, T. Shibaoka, and S. Ono, *J. Biochem.*, **68**, 205, (1970).
8) M. Grätzel, A. Henglein, M. Scheffler, H. M. Bössler and R. C. Schulz, *Ber. Bunsenges. Phys. Chem.*, **76**, 72, (1972).
9) A. Yamagishi, T. Imamura, and M. Fujimoto, *Bull. Chem. Soc. Jpn.*, **45**, 2304, (1972).
10) W. Banks, C.T. Greenwood, and K.M. Khan, *Carbohydr. Res.*, **17**, 25, (1971).
11) J. Szejtli, M. Richter, and S. Augustat, *Biopolymers*, **5**, 5,

17, (1971).

12) J. M. Bailey and W. J. Whelan, *J. Biol. Chem.*, **236**, 969 (1961).

13) B. Pfannemuller, H. Meyerhofer, and R. C. Schulz, *Biopolymers*, **10**, 243, (1971).

14) M. Yamamoto, T. Sano and T. Yasunaga, *Bull. Chem. Soc. Jpn.*, **55**, 1886, (1982).

15) The relaxation phenomenon may not be directly related to the helix-coil transition of amylose by considering the present experimental conditions, 22 °C, together with the facts that (1) the helix-coil trasition occurs at 55—65 °C in general, and (2) the amount of bound iodine has been shown to be constant in the range of 10—40 °C.[14]

16) The concentration of I_3^- is determined by the reaction; $I_2+I^- \rightleftarrows I_3^-$, using $K'=[I_3^-]/[I^-][I_2]=864$ (mol dm^{-3})$^{-1}$ at 20 °C;[17] the bound species is assumed to be I_3^- according to Cronan and Schneider[18] and in the present manuscript, iodine represents the species of I_3^-.

17) A. D. Awtrey and R. E. Connick, *J. Am. Chem. Soc.*, **73**, 1842, 6417, (1954).

18) C. L. Cronan and F. W. Schneider, *J. Phys. Chem.*, **73**, 3990, (1969).

19) Since the helical segment is composed of less than about 60 anhydroglucose units (AGU), as described in the previous paper,[14] the concentration of the helical segment (C_H) is determined as C_H=[amylose in AGU]/DP at DP$\leqq$60 while C_H=[amylose in AGU]/60 at DP$\geqq$60.

20) H. Strehlow and W. Knoche, "Fundamentals of Chemical Relaxation," Monographs in Modern Chemistry 10, Verlag Chemie, Weinheim, New York (1977), p. 48.

Liquid Crystal Formation in Binary Systems. VII.[1] Liquid Crystals Induced in *N*-[4-(Dimethylamino)benzylidene]-4-alkoxyaniline-4,4′-Dinitrobiphenyl and Related Systems

Minoru Fukui and Yoshio Matsunaga*
Department of Chemistry, Faculty of Science, Hokkaido University, Sapporo 060
(Received March 23, 1982)

By the addition of 4,4′-dinitrobiphenyl to nonmesogenic 4-(dimethylamino)-4-alkoxy derivatives of *N*-benzylideneaniline, smectic liquid crystals could be induced. This dinitro compound induces liquid crystals more pronouncedly than *N*-(4-nitrobenzylidene)-4-nitroaniline and 4,4′-dinitroazoxybenzene do when the alkoxyl group in the donor molecule is methoxyl or ethoxyl, while it induces less pronouncedly when the alkoxyl group is propoxyl. 4,4′-Dicyanobiphenyl gives a metastable nematic liquid crystal when it is mixed with *N*-[4-(dimethylamino)-benzylidene]-4-propoxyaniline and a metastable smectic liquid crystal with *N*-(4-propoxybenzylidene)-4-(dimethylamino)aniline. Moreover, liquid crystals are formed in the binary systems of *N,N,N′,N′*-tetramethylbenzidine with 4-nitro-4-alkoxy derivatives of *N*-benzylideneaniline. They are metastable but cover rather wide composition ranges. The examination of the layer spacing of the smectic A phase revealed that the induced phase is a monolayer liquid crystal.

In one of our earlier papers,[2] the induction of liquid crystals in binary mixtures of *N*-(4-nitrobenzylidene)-4-nitroaniline or 4,4′-dinitroazoxybenzene with 4-(dimethylamino)-4-alkoxy derivatives of *N*-benzylideneaniline was reported. The interaction of the electron donor-acceptor type was supposed to contribute to the achievement of the ordered arrangement of the molecules required for the mesophases. The maximum temperatures of the smectic liquid crystal-isotropic liquid (S–I) transition in these systems vary over only eight degrees according to the dinitro compound employed. The absence of a large difference in the maximum temperature by the change in the central double bond linkage might be an indication that the central linkage does not play a dominant role in the induction of the mesophases. To develope this subject somewhat farther, the examination of the systems of 4,4′-dinitrobiphenyl with the same *N*-benzylideneanilines seemed to be worthwhile.

As liquid crystals could be observed in several mixtures of *N*-[4-(dialkylamino)benzylidene]-4-(dialkylamino)-aniline or 4,4′-bis(dialkylamino)azoxybenzene with 4-nitro-4-alkoxy derivatives of *N*-benzylideneaniline, the phase diagram approach was applied also to the systems consisting of *N,N,N′,N′*-tetramethylbenzidine and the same Schiff bases.

Experimental

Materials. The preparation of the Schiff bases was described in our previous papers,[3,4] In this text, *N*-(4-X-benzylidene)-4-Y-anilines (**1**) and 4-(4-X-benzylideneamino)-4′-Y-azobenzenes (**2**) are represented by the terminal substitu-

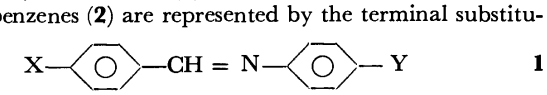

1

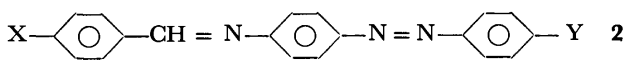

2

ents in parentheses or brackets, (X, Y) or [X, Y] respectively. The alkoxyl groups employed are methoxyl (MeO), ethoxyl (EtO), and propoxyl (PrO). 4,4′-Dinitrobiphenyl (DNBP) was prepared by nitration of biphenyl and recrystallized from acetone.[5] 4,4′-Dicyanobiphenyl (DCNBP) was synthesized starting from benzidine by the procedure reported by Ferriss and Turner.[6] *N,N,N′,N′*-Tetramethylbenzidine (TMB) Aldrich Chemical Co., was purified by recrystallization from a mixture of ethanol and toluene.

Measurements. The calorimetric and microscopic studies were carried out as described in Part IV of this series.[4] X-Ray diffraction by liquid crystalline phases was examined with the aid of a temperature-regulated sample holder described in a paper from this laboratory.[7]

Results and Discussion

4,4′-Dinitrobiphenyl (DNBP) as an Electron Acceptor. As is shown in Fig. 1a, the phase diagram of the binary system with (Me_2N, MeO) exhibits a metastable smectic phase of the A type in the composition range from 11 to 25 mol% of DNBP. The maximum lies a little bit below the eutectic temperature of 132 °C. By the exchange of the position of the terminal substituents on the donor compound (see Fig. 1b), the composition range becomes markedly narrower but the maximum temperature is shifted slightly above the eutectic temperature (135 °C).

When DNBP is added to (Me_2N, EtO), both smectic and nematic liquid crystals are observable (see Fig. 1c). The former phase appears in the range from 17 to 33 mol% of DNBP. The maximum temperature of the S–I transition curve coincides with the eutectic temperature of 138 °C. The stabilization of the smectic liquid crystal formed by mixing (EtO, Me_2N) and DNBP is more significant, the maximum being at about 164 °C and 37 mol%. Nevertheless, the induced mesophase is entirely below the freezing point curve on the DNBP-rich side. The N–I transition lines in these figures were drawn by connecting the observed point and the latent N–I transition temperature estimated in our earlier work.[3]

The smectic phase induced in mixtures with (Me_2N, PrO) is stable in a small area defined by the following points: the intersection between the horizontal S–I transition line in the coexistence of the solid donor compound and the freezing point curve of the donor compound located at 117 °C and 16 mol%, the eutectic point at 115 °C and 22 mol%, and the intersection between the other horizontal S–I transition line and the

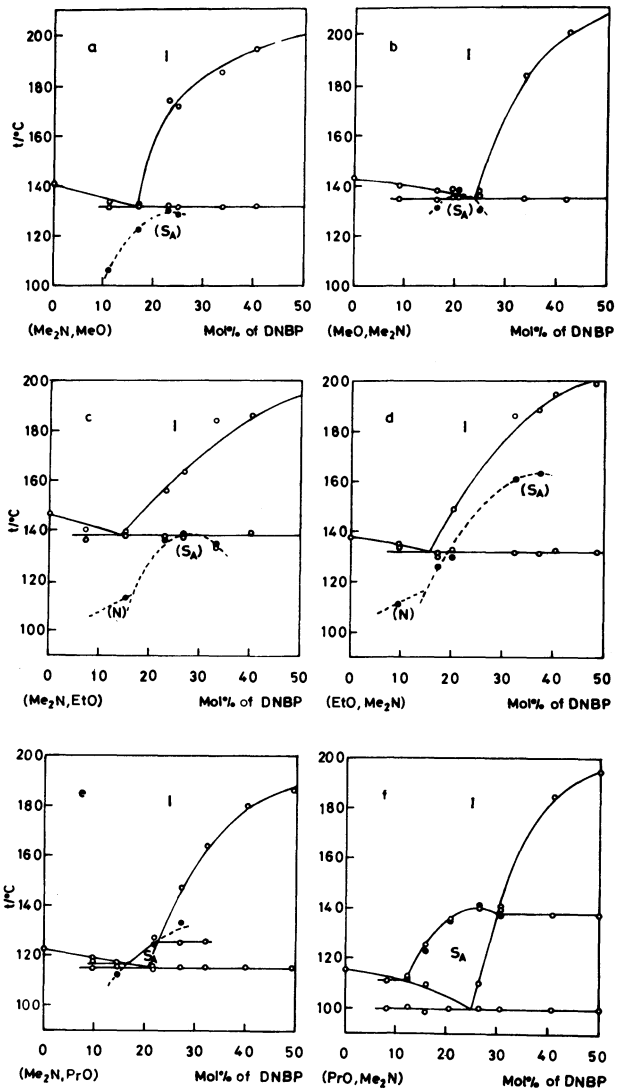

Fig. 1. Phase diagrams of the systems of DNBP with (a) (Me_2N, MeO), (b) (MeO, Me_2N), (c) (Me_2N, EtO), (d) (EtO, Me_2N), (e) (Me_2N, PrO), and (f) (PrO, Me_2N). The open and shaded circles are transitions observed in the processes of heating and cooling respectively.

freezing point curve on the DNBP-rich side at 125 °C and 23 mol%. The mesophase produced by mixing with (PrO, Me_2N) is more significantly stabilized (see Fig. 1f). The S–I transition curve meets the freezing point curve of the donor compound at 111 °C and 12 mol%, passes through the maximum at 140 °C and 26 mol%, and then meets the other freezing point curve at 138 °C and 30 mol%.

The maximum transition temperatures observed in the above-mentioned six systems are compared with

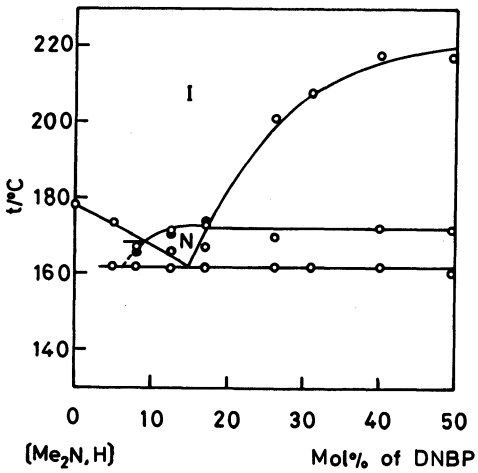

Fig. 2. Phase diagram of the [Me_2N, H]–DNBP system. As to the open and shaded circles, see the caption of Fig. 1.

those of the systems containing (NO_2, NO_2) or 4,4′-dinitroazoxybenzene (DNAO) in Table 1. When the methoxy derivatives are employed as electron donors, smectic liquid crystals can be observed only with DNBP. The mesophases induced with DNBP are more thermally stabilized than those induced with the other two acceptors when the donors are the ethoxy derivatives. On the other hand, the smectic liquid crystal in the (Me_2N, PrO)–DNBP is least stable and the liquid crystal in the (PrO, Me_2N)–DNBP is of intermediate stability. Thus, the absence of a central double bond linkage favors the induction of mesophase with the methoxy and ethoxy derivatives of *N*-benzylideneaniline but not with the propoxy derivatives. If the donor molecule is much larger than the acceptor molecule, there might be some combinations where the charge-transfer interaction is too weak to induce a smectic phase but still enough to induce a less-ordered nematic phase. Such a condition seems to be achieved by the addition of DNBP to the dimethylamino derivative of *N*-(benzylidene)-4-aminoazobenzene [Me_2N, H]. As is shown in Fig. 2, a stable nematic liquid crystal is observable in this system. The nematic liquid crystal-isotropic liquid (N–I) transition curve meets the freezing point curve of the donor compound at 168 °C and 9 mol% of DNBP, and the other freezing point curve at 172 °C and 17.5 mol%. The maximum lies at 174 °C and 15.5 mol%. The donor [Et_2N, EtO] is nematogenic by itself. When this compound is mixed with DNBP, the N–I transition curve is found to be convex upwards, in agreement with the induction observed in Fig. 2. In addition, one can see a metastable smectic phase of the A type induced in the composition

Table 1. The maximum temperature of the smectic liquid crystal-isotropic liquid transition curve/°C

Acceptor	Donor					
	(Me_2N, MeO)	(MeO, Me_2N)	(Me_2N, EtO)	(EtO, Me_2N)	(Me_2N, PrO)	(PrO, Me_2N)
DNBP	131	136	138	164	132	140
(NO_2, NO_2)	—	—	131.5	131	136	136.5
DNAO	—	—	136	139	140	143

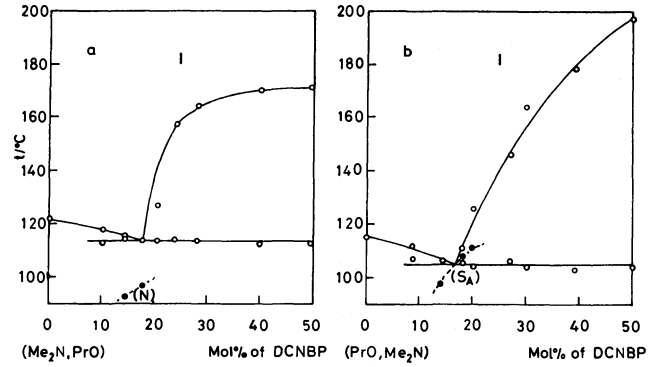

Fig. 3. Phase diagrams of the systems of DCNBP with (a) (Me_2N, PrO) and (b) (PrO, Me_2N). As to the open and shaded circles, see the caption of Fig. 1.

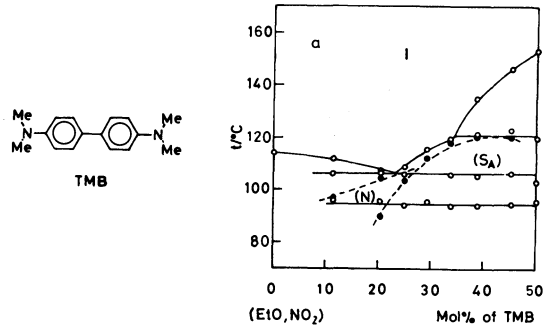

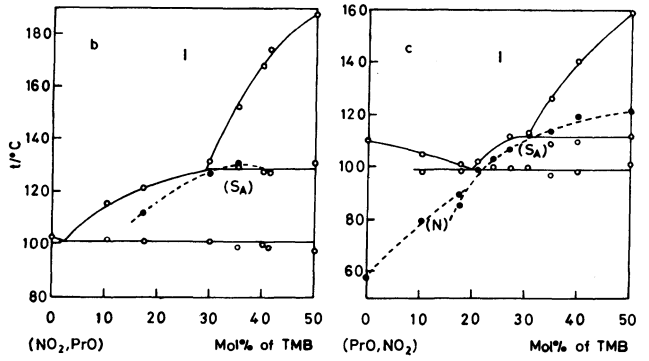

Fig. 4. Phase diagrams of the systems of TMB with (a) (EtO, NO_2), (b) (NO_2, PrO), and (c) (PrO, NO_2). As to the open and shaded circles, see the caption of Fig. 1.

range from 9 to 31 mol% of DNBP, the maximum being located at 136 °C and 23 mol%. This temperature is lower by 23 °C than the eutectic point. The induced metastable smectic phase is also noted in the system with nematogenic [Me_2N, EtO].

As described in one of our earlier papers, the present observations may imply that DNBP is potentially smectogenic.[3] It may be interesting to add that 4,4'''-dinitro-*p*-quaterphenyl has been reported by Vorländer to be a mesogenic substance.[8]

4,4'-Dicyanobiphenyl (DCNBP) as an Electron Acceptor. The electron acceptor strength of DCNBP is less than that of DNBP; therefore, the induced mesophase could be found only in the systems with (Me_2N, PrO) and (PrO, Me_2N). The mesophase in the former system is nematic and its appearance is limited to a narrow composition range (see Fig. 3a). A metastable smectic liquid crystal is present in the latter system. The monotropic S–I transition curve covers the range from 14 to 20 mol%, passing near the eutectic point located at 105 °C and 16.5 mol% (see Fig. 3b).

N,N,N',N'-*Tetramethylbenzidine (TMB) as an Electron Donor.* Smectic liquid crystals are induced in the systems with (MeO, NO_2), (EtO, NO_2), (NO_2, PrO), and (PrO, NO_2). The mesophase produced by mixing with the first acceptor is so unstable that the phase diagram approach failed to locate the existence region. Consequently, only the other diagrams can be presented here. In Figs. 4a and c, nematic liquid crystals are also observable. Thus, TMB is more efficient in the induction of mesophases than (Me_2N, Me_2N) and 4,4'-bis-(dimethylamino)azoxybenzene (BDMAAO), which can induce smectic liquid crystals only in the systems with (NO_2, PrO).[2]

The metastable nematic mesophase in the system with (EtO, NO_2) is stabilized up to 110 °C at about 28 mol% of TMB. The N–I transition curve passes near the eutectic point located at 106 °C and 23 mol%. The smectic mesophase is detectable in the composition range from 20 to 45 mol%. The maximum lies at 121 °C around 40 mol%. The horizontal line at 121 °C starting from the peritectic point at 34.5 mol% indicates the formation of a solid complex. at 50 mol% or higher. The other line at 94 °C may be due to a solid-solid transition of the complex.

The diagram of the (NO_2, PrO)–TMB system exhibits a metastable smectic phase in the composition range from 17 to 42 mol% of TMB. The maximum is located slightly above the peritectic temperature of 129 °C. It may be noted that the smectic liquid crystal is the most stabilized in this combination among those shown in Fig. 4. This finding is consistent with the previous results that smectic mesophases are induced only when (Me_2N, Me_2N) and BDMAAO are mixed with this Schiff base.[2] In the (PrO, NO_2)–TMB system, the whole examined range is covered by metastable nematic or smectic phase. The intersection between the I–N and I–S transition curves occurs at about 90 °C and 19 mol% of TMB. The latter curve reaches 121 °C at 50 mol%.

No liquid crystal is formed when TMB is replaced by *N,N,N',N'*-tetraethylbenzidine in any of these binary systems.

The addition of TMB to [NO_2, H] resulted in the formation of a congruently melting solid complex at 33 mol% of TMB and the induction of a smectic A phase in the range from 42 to 50 mol%, the temperature at the latter composition being 152 °C. The acceptor itself is nematogenic. As the I–N transition lowers linearly with the mol% of TMB and is observable up to 45 mol%, there is no thermal stabilization of this phase by TMB. No new mesophase appears when TMB is added to nematogenic [NO_2, EtO].

The maximum of the I–S transition curve lies between 20 and 50 mol% of DNBP or TMB. The exact composition is supposed to depend upon the extent of the formation of the 2 : 1 complex in addition to the 1 : 1

complex and/or upon the difference in the latent I–S transition temperature between the component compounds.

As the smectic layers consist of molecular complexes, the thickness is dependent on how the donor and acceptor molecules are stacked and could be larger than the average length of the component molecules. In order to check this possibility, the interlayer spacing in the stable smectic phase of the A type induced in the (PrO, Me_2N)–DNBP mixture at 19.7% was measured. The observed spacing of 1.80 nm is in good agreement with the weighted mean molecular length of 1.87 nm. The latter was estimated assuming 1.97 nm for the donor molecule and 1.46 nm for the DNBP molecule; these values were calculated by employing the bond lengths and the van der Waals radii compiled by Kitaigorodskii.[9] Thus, it seems quite certain that the mesophase induced in this particular mixture is a monolayer liquid crystal. In connection with this measurement, the smectic phases of the A and B types induced in mixtures of [PrO, H]–[NO_2, H], [Et_2N, H]–[NO_2, H], and [PrO, EtO]–[NO_2, EtO] were similarly examined. In all the cases, the monolayer model accounts for the observed thickness.

The present work was partly supported by a Grant-in-Aid for Scientific Research No. 543001 from the Ministry of Education, Science and Culture.

References

1) Part VI, K. Araya, N. Homura, and Y. Matsunaga, *Bull. Chem. Soc. Jpn.*, **55**, 1953 (1982).
2) K. Araya and Y. Matsunaga, *Bull. Chem. Soc. Jpn.*, **55**, 1710 (1982).
3) K. Araya and Y. Matsunaga, *Bull. Chem. Soc. Jpn.*, **53**, 3079 (1980).
4) M. Fukui and Y. Matsunaga, *Bull. Chem. Soc. Jpn.*, **54**, 3137 (1981).
5) R. L. Jenkins, R. McCullough, and C. F. Booth, *Ind. Eng. Chem.*, **22**, 31 (1930).
6) C. V. Ferriss and E. E. Turner, *J. Chem. Soc.*, **117**, 1140 (1920).
7) S. Koizumi and Y. Matsunaga, *Bull. Chem. Soc. Jpn.*, **47**, 9 (1974).
8) D. Vorländer, *Z. Phys. Chem.*, **126**, 449 (1927).
9) A. I. Kitaigorodskii, "Organic Chemical Crystallography," Consultant Bureau, New York (1961), pp. 1—8.

Conformational Characteristics of Poly(vinylnaphthalene)s from Energy Contour Map

Kazuhiko SEKI* and Yoshio IMAMURA
Department of Chemistry, Faculty of Science, Science University of Tokyo, Kagurazaka, Shinjuku-ku, Tokyo 162
(Received April 15, 1982)

In poly(1-vinylnaphthalene)(P1VN) and poly(2-vinylnaphthalene)(P2VN), conformational energies of meso and racemic dyads were computed as functions of skeletal bond and side group rotations (0°(*o*) or 180°(π)). The calculation was carried out according to the truncation procedure proposed by D.Y.Yoon. The backbones in P1VN and P2VN were limited to just two rotational states, trans (t) and gauche (g) conformation. The steric interactions involving the bulky naphthyl group precluded $\bar{g}$ conformation; a similar situation occurs in polystyrene. Numerical results suggested these conclusions: the excimer forming site conformations for P1VN were meso : tt($\pi\pi$) and racemic : tt($\pi\pi$) states, and for P2VN were meso : tt($\pi\pi$), tt(oo), tt($o\pi$), and tt(πo) states. These conformations could also be correlated to the dual emissions observed in P1VN and P2VN.

In a previous paper,[1] we pointed out the differences in some solution properties between poly(1-vinylnaphthalene) (P1VN) and poly(2-vinylnaphthalene) (P2VN), and also the resemblance of the latter to polystyrene in solution. We discussed the conformation of pendant groups in P1VN and P2VN. In another paper,[2] we treated the steric effect on ^{13}C NMR chemical shifts in poly(vinylnaphthalene)s (PVN), taking into account the Rotational Isomeric State (RIS) of the pendant group; this was based on discussions in the preceding paper.[1] In PVN, the ring current effect by naphthyl groups was rather small and there was not much difference between P1VN and P2VN. The different spectral patterns in ^{13}C NMR spectra of the aliphatic carbon region were attributed to the difference of the degree of the steric compression shift induced by the steric interaction between the methine hydrogen and the atoms in the naphthyl group.

Among recent discussions on the conformation of PVN, one of the most interesting problems is the studies on the excimer fluorescence of PVN in solutions.[3] Hirayama[4] proposed the "$n=3$ rule" for the intramolecular excimer formation and indicated that an excimer was an electronically excited molecular complex formed between two aromatic chromophores in a coplanar sandwich arrangement. For a P2VN chain which satisfies the $n=3$ rule, Frank *et al.*[5] studied the geometrical arrangement of two chromophores in an excimer state in detail: the conformations of the possible excimer forming site were found to be tt for the isotactic and t$\bar{g}$ or $\bar{g}$t for the syndiotactic chain. He concluded that the ground state (preferred conformation) was tg or gt for isotactic chain, and tt for syndiotactic chain. These results have been predicted by a simple statistical model with RIS approximation. However, in the conformational analysis of PVN in terms of rotations around the skeletal bonds, a more attractive procedure is the preparation of conformational maps developed by Flory *et al.*[6-10] The detailed discussion should be based on the average energy $\langle E \rangle_s$ for each rotational state s of skeletal bonds derived from the conformational maps. The purpose of this paper is to discuss the RIS for skeletal bonds in P1VN and P2VN chains, which are closely related to the ground site and excimer forming site conformation.

Calculation

Recently, Sundararajan reported the conformational maps in terms of skeletal bond rotations ϕ_i and ϕ_{i+1}, for the meso and the racemic dyads of poly(*N*-vinylcarbazole) (PVCz).[11] In PVCz chain, the skeletal bond angle θ (at the methylene carbon atom: αC–CH$_2$–αC) in the minimum energy position in the tt state of the meso and the racemic dyads was larger than that in the other conformations. Since PVN chains have bulky side groups like those of the PVCz chain, the energy maps are computed by varying the bond angles θ from 114° to 126° in steps of 2° at each (ϕ_i, ϕ_{i+1}) grid point. RIS of side groups in PVN are also taken into account in conformational maps.

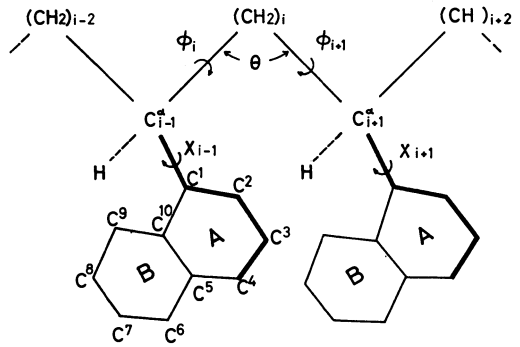

Fig. 1. Portion of the isotactic P1VN chain in the all-trans ($\pi\pi$) conformation. In the P2VN chain, the α-carbon is bonded to the C(2) atom in the naphthyl group.

TABLE 1. GEOMETRICAL PARAMETERS

Bond length	l/Å	Bond angle	ϕ/°
C–C	1.53	$\angle CC^{\alpha}$–C	112
		$\angle C^{\alpha}$–CC^{α}	Variable
C^{α}–C^{ar}	1.51	$\angle CC^{\alpha}$–C^{ar}	112
C–H	1.10	$\angle CC^{\alpha}H$	107
C^{ar}–H	1.10	$\angle C^{\alpha}CH=\angle HCH$	110
C^1–C^2	1.36	$\angle C^1C^2C^3$	121
C^2–C^3	1.42	$\angle C^1C^{10}C^9$	122
C^1–C^{10}	1.43	$\angle C^1C^{10}C^5$	119
C^{10}–C^5	1.41	$\angle C^2C^1C^{10}$	120

Figure 1 shows that the meso : tt state of PIVN chain is occupied by π-conformation. According to the convention of Flory *et al.*,[10] the torsional angles ϕ_i and ϕ_{i+1} for meso *dl* dyads (see Fig. 1) are measured in the right- and left-handed senses, respectively. For the racemic *dd* dyad, ϕ_i and ϕ_{i+1} are measured in the right-handed sense. The bond lengths and bond angles for PVN are given in Table 1.[10] The conformational parameters for naphthyl group were taken from studies on the crystal structure of naphthalene.[12]

In previously calculated results of steric energies for pentamer models,[1] the optimized rotational angles of 1- and 2-naphthyl rings did not exceed $\pm 4.5°$ away from the position where the ring was perpendicular to the plane made by the adjoining backbone bonds. Accordingly, the rotational angles X (see Fig. 1) of the naphthyl groups are fixed at 0° (*o*-conformation) or 180° (π-conformation).

The nonbonded van der Waals energy among all atoms was computed using the Lennard-Jones 6—12 potential function:

$$E_{vdw} = a_{i,j}/(r_{i,j})^{12} - c_{i,j}/(r_{i,j})^6, \quad (1)$$

where radii, polarizabilities and effective numbers of electrons for C_{sp2}, C_{sp3}, and H were taken from Flory *et al.*[10] Torsional energies for ϕ_i and ϕ_{i+1} were calculated using the intrinsic three-fold torsional function:[7]

$$E_{tor} = (V/2)(1+\cos 3\phi), \quad (2)$$

where ϕ is the dihedral angle and V is a barrier of 2.8 kcal mol^{-1}.† The deformation energy for the bond angle θ was treated in the harmonic approximation:[9]

$$E_{bend} = (K_\theta/2)(\theta-\theta_0)^2, \quad (3)$$

where θ_0 was assigned as tetrahedral, and K_θ is the bending constant of 0.044 kcal mol^{-1} deg^{-2}.†† Energies used for construction of the contours were computed at intervals of 5° in ϕ_i and ϕ_{i+1}. These functions were appropriate to reproduce the unperturbed dimensions of PVCz and polystyrene.[10,11]

Results and Discussion

The conformational energies for the meso and the racemic dyads of PIVN chain occupied by π-conformation, using $\theta=114°$, are shown in Figs. 2 and 3 as functions of the skeletal bond rotational angles ϕ_i and ϕ_{i+1}, respectively. Contours are shown at the energies quoted in kcal mol^{-1} relative to the minimum for the meso : tg (10,105°) or gt (105,10°) state. The tt states for the meso and the racemic dyads did not appear in the energy map until θ went beyond 116°. This feature of the energy surface is a consequence of the planar geometry of the 1-naphthyl groups which are occupied by π-conformation. The B ring (see Fig. 1) overlaps with another B ring at the distance of 2.60 Å, in the racemic : tt state. The steric repulsion between B rings, which are spatially crowded by neighboring atoms, can not relieved by small increases in ϕ_i and ϕ_{i+1}. On the other hand, in the case of meso : tt state, each 1-naphthyl ring is parallel to the neighboring ones, and

† 1 kcal mol^{-1}=4.184 kJ mol^{-1}.
†† 1 kcal mol^{-1} deg^{-2}=4.184 kJ mol^{-1} deg^{-2}.

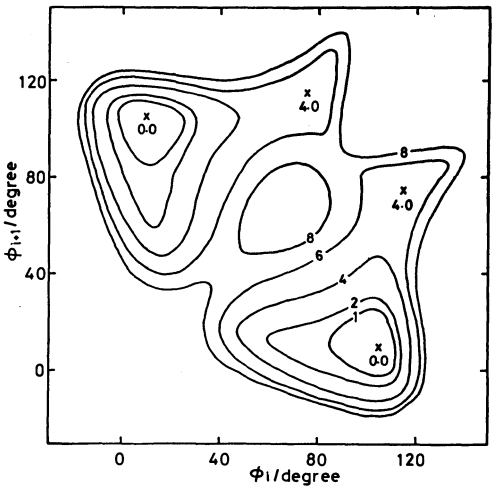

Fig. 2. Conformational energy contours for a meso dyad of PIVN calculated as functions of skeletal bond rotations ϕ_i, ϕ_{i+1}. Naphthyl group rotations fixed at X= 180° (π-conformation). A value of $\theta=114°$ is used. Locations of minima are denoted by × and the energy contours are labeled in kcal mol^{-1} relative to the energy minium of the moso; tg conformation.

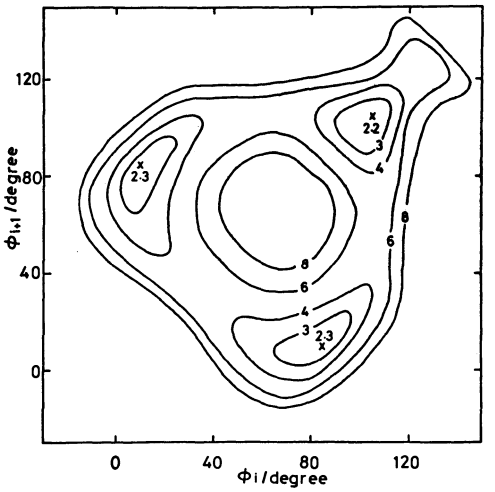

Fig. 3. Conformational energy contours for a racemic dyad of PIVN. A values of X=180° and θ=114° are used.

directed in the same direction; the distance between neighboring planes is estimated to be 2.60—2.75 Å. This steric repulsion between neighboring planes can not be avoided by small increases in ϕ_i and ϕ_{i+1}, as in the racemic : tt state.

Figures 4 and 5 show the conformational energy maps for the meso and the racemic dyads of PIVN chain occupied by π-conformation, using $\theta=120°$. The energies of the minima in Figs. 4 and 5 are expressed relative to the energy of the tt state of the racemic dyad. Six minima appear in Fig. 4 and four minima in Fig. 5. These minima are identified as tt, tg or gg. The $\bar{g}$ conformation is precluded, due to the interaction resulting from the planarity of the 1-naphthyl group.

In meso dyad, the minima at 80,120° or 120,80° in

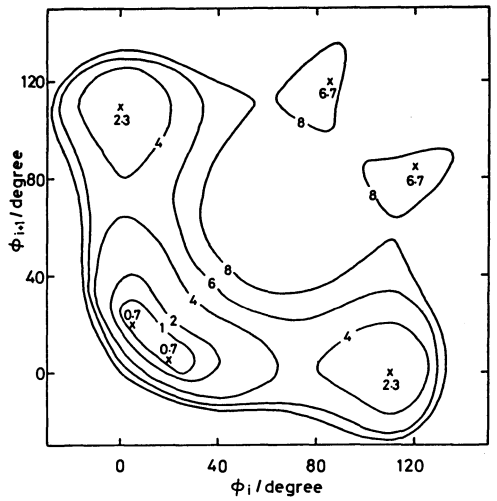

Fig. 4. Conformational energy contours for a meso dyad of PlVN, using $X=180°$ and $\theta=120°$. The energy contours are labeled in kcal mol^{-1} relative to the energy minimum of the racemic; tt ($\pi\pi$) at $\theta=120°$.

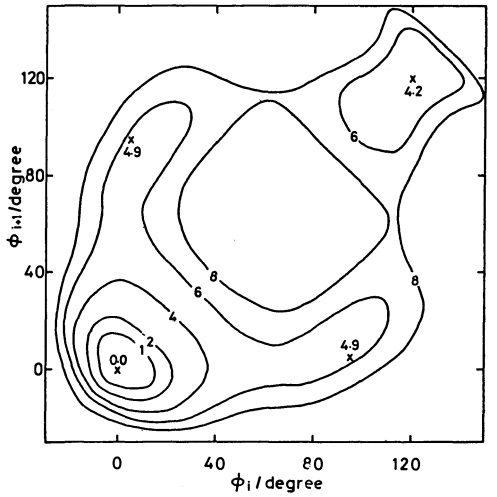

Fig. 5. Conformational energy contours for a racemic dyad of PlVN, using $X=180°$ and $\theta=120°$.

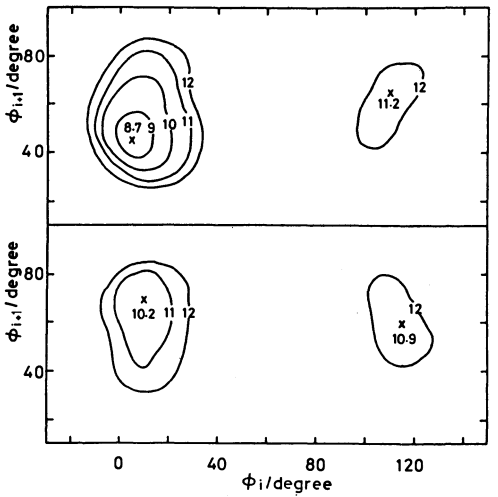

Fig. 6. Energy contours maps for (a) meso and (b) racemic dyads of PlVN, using $X_{i-1}=180°$, $X_{i+1}=0°$ (o-conformation) and $\theta=114°$. The energy contours were labeled in kcal mol^{-1} relative to the energy minimum of the meso; tg at $\theta=114°$ (see Fig. 2).

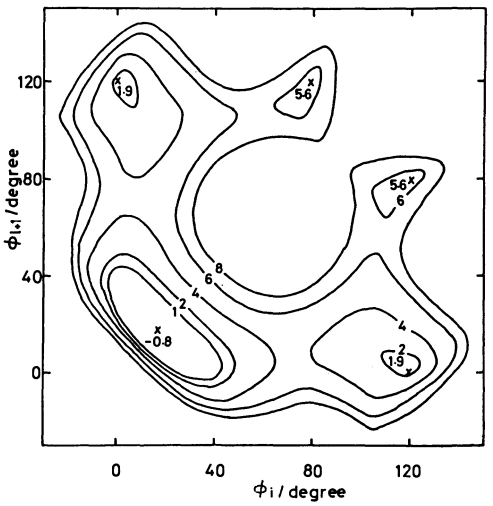

Fig. 7. Conformational energy contours for the meso dyad of P2VN($\pi\pi$), using $\theta=114°$. The energy contours are labeled in kcal mol^{-1} relative to the energy minimum of the racemic; tt($\pi\pi$) at $\theta=114°$.

Fig. 4 are isolated completely from the other minima. All minima are surrounded by the contour with 9 kcal mol^{-1}. In the energy maps of polystyrene chain, conformational energy contours of 5 kcal mol^{-1} are sufficient to surround all minima. The tt conformation is separated into two minima with a low energy barrier (<0.2 kcal mol^{-1}) between them. The distances between 1-naphthyl rings for $\phi_i,\phi_{i+1}=0,0°$ are 2.73—3.37 Å. The steric repulsion in this case was more relaxed than that for $\theta=114°$. Futhermore, ϕ_i,ϕ_{i+1} will displace somewhat from the perfect staggering (0,0°), and the energy then falls rapidly.

In racemic dyad, all minima could be surrounded by a contour with a larger value (about 8 kcal mol^{-1}). The minima for racemic : tt state appeared at smaller values of θ (about 116°) than those for the meso : tt state (about 118°). As described above, the neighboring 1-naphthyl ring in racemic : tt state was placed so as to approach to a part of 1-naphthyl ring (B ring), while 1-naphthyl ring in meso : tt state was placed in close proximity to the adjoining 1-naphthyl ring. The steric repulsion between neighboring 1-naphthyl rings in the racemic : tt state is smaller than that in the meso : tt state, and can be avoided by a small increase in θ.

Figures 6a and b show the energy contour maps for the meso(πo) and the racemic(πo) dyads, respectively. The energy contours are labeled in kcal mol^{-1} relative to the energy minimum of the meso tg (10,105°) at $\theta=114°$. The numbers of minima in Fig. 6 are less than that of PlVN occupied by π-conformation. Two minima for the meso and the racemic dyads are located at 5,45° and 110,65°, and at 10,70° and 115,60°, respectively. These minima values, as a function of ϕ_i and ϕ_{i+1}, have the lowest values at $\theta=114°$ over the range from 110° to 126°. However, these values are much higher than that of PlVN ($\pi\pi$). The o-conformation imposes steric overlap between the hydrogen at C(9) in

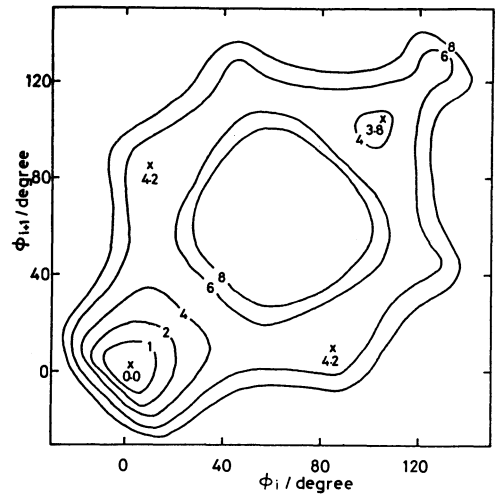

Fig. 8. Conformational energy contours for racemic dyad of P2VN($\pi\pi$), using $\theta=114°$.

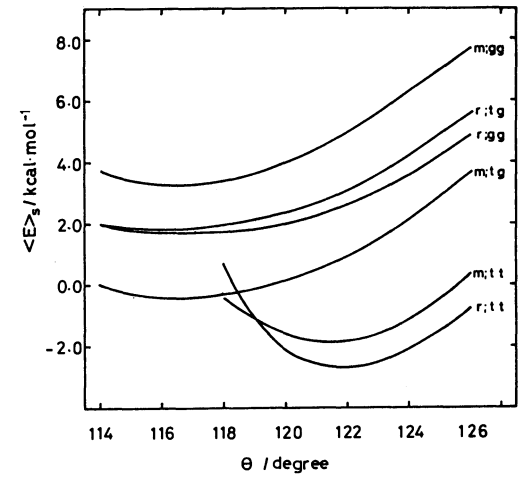

Fig. 9. The average energy $\langle E\rangle$ for PlVN were plotted as a function of the bond angle θ. All values were evaluated relative to the meso; tg($\pi\pi$) at $\theta=114°$.

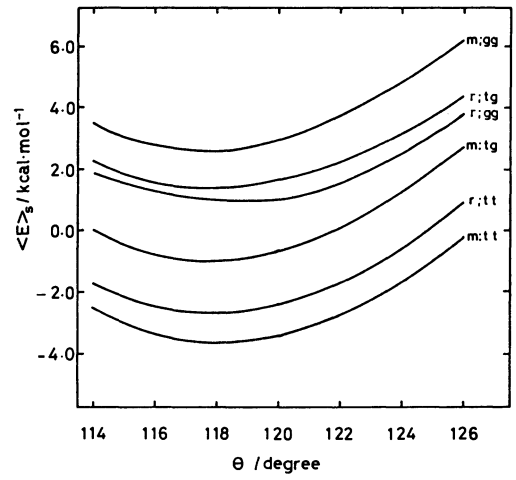

Fig. 10. The average energy $\langle E\rangle$ for P2VN. All values were evaluated relative to the meso; tg($\pi\pi$) at $\theta=114°$.

a rotating 1-naphthyl ring and one of the methylene or α-carbons which belong to adjacent monomer unit, as reported in our previous paper.[1] Neither of the minima calculated here are assigned to RIS of skeletal bonds (t, g, and $\bar{g}$). The energy contour maps, in which all the RIS of side groups are in o-conformation, are not recorded in this paper, but the minimum values were remarkably large (=20 kcal mol^{-1}).

Figures 7 and 8 show the conformational energy contours for the meso and the racemic dyads of P2VN ($\pi\pi$), using $\theta=114°$. The energy surfaces in Figs. 7 and 8 were little influenced by the RIS of the side groups, and closely resembled that of polystyrene, except for the values of minima. For meso dyad, the distance between 2-naphthyl rings was 2.60—2.77 Å for $\phi_i,\phi_{i+1}=0,0°$. This distance is nearly equal to that of PlVN, but the minima of tt states for the meso have appeared over a range of $\theta(114°—120°)$. In PlVN chain, the steric interactions produced by the carbon and the hydrogen atoms in B ring are responsible for the larger conformational energy. On the other hand, in P2VN chain, the atoms in B ring are far apart from the backbone atoms (*e.g.*, αC or CH_2), and rapidly become detached from adjacent naphthyl rings if a small increase in ϕ_i and ϕ_{i+1} occurs. As reported in the previous paper,[1] there were no appreciable nonbonded interactions between the carbon atoms or hydrogen atoms bonded to carbon atoms in B ring of 2-naphthyl group and the main chain (or the neighboring side group). In racemic : tt, the B ring did not approach to the adjacent B ring, in contrast to that in PlVN chain.

The average energy $\langle E\rangle$, the partition function Z, and the average rotation angles $\langle\phi_i\rangle$, $\langle\phi_{i+1}\rangle$ were evaluated for each state with the use of energies calculated at intervals of 5° in ϕ_i and ϕ_{i+1}. These are given by

$$Z_s = \Sigma_i\Sigma_{i+1}\exp(-E_k/RT) \quad (4)$$

$$\langle E\rangle_s = Z_s^{-1}\Sigma_i\Sigma_{i+1}E_k\exp(-E_k/RT) \quad (5)$$

$$\langle\phi_j\rangle_s = Z_s^{-1}\Sigma_i\Sigma_{i+1}\phi_j\exp(-E_k/RT), \quad (6)$$

where the subscript k refers to each conformation (ϕ_i, ϕ_{i+1}) and j=i or i+1. The average energies $\langle E\rangle$ for PlVN and P2VN are plotted as functions of θ in Figs. 9 and 10, respectively. All values of $\langle E\rangle$ were evaluated relative to each meso : tg($\pi\pi$) state. Calculations were carried out for a temperature of 300 °K. The $\langle E\rangle$ for PlVN, except tt states, remained unaltered in the range of $\theta(114°—120°)$ and these curves showed precipitous rises of $\langle E\rangle$ beyond $\theta=120°$. The $\langle E\rangle$ of tt states had the lowest values at $\theta=122°$, as described above. In P2VN chain, all values had the lowest values at $\theta=118°$, and have the same curvature. The curves of polystyrene showed a similar tendency.

The lowest values appearing in Figs. 9 and 10 are assigned to the average energy of each RIS of skeletal bonds. The average energies $\langle E\rangle$ derived from Figs. 9 and 10, together with the averaged rotation angles $\langle\phi_i\rangle$, $\langle\phi_{i+1}\rangle$ are given in Table 2. The values of $\langle E\rangle$ were evaluated relative to that of the racemic : tt conformation. The meso : tt conformation in PVN and polystyrene had a lower energy. However, the rotational barrier of the aromatic group was much higher than

Table 2. Average energies[a] and average rotation angles for each conformation

State	PS		P2VN					P1VN	
	$\langle E\rangle$	$\langle\phi_i\rangle,\langle\phi_{i+1}\rangle$	$\langle E\rangle$				$\langle\phi_i\rangle,\langle\phi_{i+1}\rangle$	$\langle E\rangle$	$\langle\phi_i\rangle,\langle\phi_{i+1}\rangle$
			$\pi\pi$	πo	$o\pi$	oo	$\pi\pi$	$\pi\pi$	$\pi\pi$
Meso : tt	1.07	20, 20	−0.98	−0.03	−0.03	−0.14	14, 14	0.85	12, 12
Meso : tg	1.19	5, 113	1.72	1.74	1.74	1.77	1, 116	2.32	7, 98
Meso : gg	4.36	95, 95	5.29	5.29	5.30	5.30	100, 100	6.10	96, 96
Racemic : tt	0.00	6, 6	0.00	0.47	0.47	0.78	−1, −1	0.00	−1, −1
Racemic : tg	3.32	13, 86	4.04	4.05	4.06	4.07	11, 95	4.53	8, 83
Racemic : gg	2.67	102, 102	3.67	3.67	3.67	3.66	114, 114	4.38	106, 106

a) All values are evaluated relative to each racemic : tt ($\pi\pi$) state, in kcal mol^{-1} units.

Table 3. Average energies $\langle E\rangle$[a] for P1VN, P2VN, and PS chain

	Racemic			Meso		
	tt	tg	gg	tt	tg	gg
$\sigma=\infty$						
P1VN($\pi\pi$)	0.00	4.53	4.38	0.85	2.32	6.10
P2VN($\pi\pi$)	0.00	4.04	3.67	−0.98	1.72	5.29
PS	0.00	3.32	2.67	1.07	1.19	4.36
PS(Yoon)[b]	0.00	3.50	2.48	0.91	1.17	4.17
$\sigma=5.0$ Å						
P1VN($\pi\pi$)	0.00	2.16	1.49	1.45	0.43	3.48
P2VN($\pi\pi$)	0.00	2.66	2.26	1.56	0.82	3.73
PS	0.00	2.76	1.82	1.86	0.77	3.72
PS(Yoon)	0.00	2.95	1.67	1.61	0.73	3.36
$\sigma=3.9$ Å						
P1VN($\pi\pi$)	0.00	−0.71	−1.57	2.29	−2.64	0.47
P2VN($\pi\pi$)	0.00	1.97	1.58	3.62	0.20	3.03
PS	0.00	2.21	1.42	3.30	0.28	3.16
PS(Yoon)	0.00	2.67	0.98	2.61	0.30	2.66

a) All values are evaluated relative to each racemic : tt ($\pi\pi$) state, in kcal mol^{-1} units. b) These values were calculated by Yoon *et al.* (Ref. 10).

that of the aromatic group in meso : tg conformation. This leads to a decrease of entropy in the planar conformation. Thus, at normal temperature, the meso : tt conformation seems to be unfavoured due to its larger free energy.

This problem can be resolved by a truncation procedure devised by Yoon *et al.*[6,10,11] This was followed so as to allow for the conformational dependence of solvent interaction. Beyond a certain distance, which is sufficient to permit the entry of the solvent molecules, the reduced interaction between aromatic groups will be replaced by the interaction between aromatic group and solvent, and the energy of the system levels off at this distance. Thus, the calculated energy remains constant at the value for $r=\sigma$ for all distances greater than a suitably chosen values of σ. The average energies $\langle E\rangle$, using $\sigma=5.0$ Å and 3.9 Å are given in Table 3, together with the $\langle E\rangle$ values for polystyrene calculated by Yoon.

In P2VN and PS chain, it is clear that racemic : tt conformation corresponds to the ground state (preferred conformation). The relationship of $\langle E\rangle_{tt}<\langle E\rangle_{gg}<\langle E\rangle_{tg}$ is found to hold, regardless of the value of σ chosen. The racemic : $t\bar{g}$ and $\bar{g}t$ conformations correspond to the excimer forming sites.[5] These conformations are unstable ones and have a energy of 7 kcal mol^{-1} higher than the lowest energy (tt state), since the conformations include the interaction between the aromatic groups. These results suggest that the statistical weights relating to $t\bar{g}$ and $\bar{g}t$ states are extremely small at normal temperature. Use of a truncation procedure shows that the conformational energy of meso : tt state is larger than that of meso : tg state, and that at $\sigma=$ 3.9 Å meso : tt conformation becomes the most unfavourable one in the meso dyad. Accordingly, the meso : tg conformation corresponds to the ground state, and the tt conformation corresponds to an excimer forming site, which is electronically stabilized under excimer formation.

In P1VN chain, the relative stability of each RIS in meso dyad is similar to those of P2VN and polystyrene, regardless of the value of σ chosen. Evidently, the meso : tg conformation corresponds to the ground state, and the conformational stability of it is higher than that of polystyrene and P2VN in meso dyad. On the other hand, the relative stability of each RIS in racemic dyad is strongly dependent on the value of σ : $\langle E\rangle_{gg}<\langle E\rangle_{tg}<\langle E\rangle_{tt}$ at $\sigma=3.9$ Å. The racemic : tt conformation is not necessarily the most stable one. The racemic: gg and tt conformations correspond to the ground state at $\sigma=3.9$ Å and $\sigma\geqq5.0$ Å, respectively. The racemic : $t\bar{g}$ and $\bar{g}t$ conformations are less favored states than tt, tg, and gg states; this is also found in P2VN and in polystyrene.

In PVN chain, the dual emission in excimer region was observed in solution. Gupta *et al.*[13] concluded that the two types of singlet excimers characterized by emission spectra of P1VN may consist of parallel and antiparallel conformations of pairs of 1-naphthyl groups. From the emission spectra of P2VN and its model compound (*meso*-1,1′-di-2-naphthyldiethylether) in solution, Schryver *et al.*[14] pointed out that the observation of a dual decay could be due to the relative orientation in the ground state of the naphthyl groups prior to excimer formation. The dual emission may be correlated with the RIS for side groups in PVN chain.

In P2VN chain, the dual emission in the excimer region may be correlated with two types of excimers site conformation differing in RIS for side group or site conformation differing in RIS for skeletal chain. Concerning the latter, meso : $\bar{g}\bar{g}$, meso : tt and racemic: $t\bar{g}(\bar{g}t)$ can be formed in a parallel sandwich arrangement

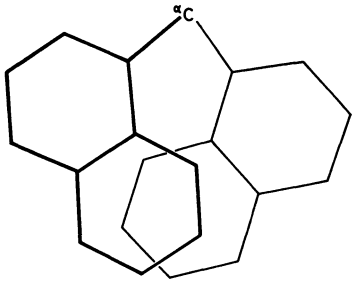

Fig. 11. A segment of a racemic; tt($\pi\pi$) of P1VN chain. 1-naphthyl groups are parallel to the space. The hydrogens and methylene carbons are omitted.

of aromatic groups. However, the formations of the excimers consisting of those skeletal conformations, except meso : tt state, seem less likely, on the basis of our calculated results. The RIS of skeletal chain with respect to the excimer formation is occupied by the meso : tt conformation, and few racemic : t$\bar{g}$($\bar{g}$t) conformations occur. Since 2-naphthyl groups in P2VN chain are occupied by both π- and o-conformations,[1] there are $\pi\pi$, oo, πo, and $o\pi$ conformations for RIS of side groups in meso : tt state. The structure of $\pi\pi$ and oo-conformation are made up by the total superposition of 2-naphthyl groups, while 2-naphthyl groups in πo and $o\pi$ conformation are placed so as to approach near a part of 2-naphthyl group (A ring). It can be concluded that the dual emission observed in atactic P2VN chain should be attributed to the RIS of 2-naphthyl group in meso : tt state. The excimer forming site conformations are $\pi\pi$ and oo conformations; other conformations are πo and $o\pi$ ones.

Since 1-naphthyl groups in P1VN chain were limited to a preferred state (π-conformation),[1] tt($\pi\pi$) conformation in meso dyad is the only conformation which forms the excimer. Other conformations are not detected in meso dyad. However, the racemic : tt($\pi\pi$) conformation can be formed in a sandwich arrangement of 1-naphthyl groups, whether that conformation is preferred or not. Figure 11 shows the relaxed molecular model of racemic: tt($\pi\pi$) state obtained by the force field method. This model structure fits with that used in the present paper. The racemic : tt conformation comes to be the excimer forming site conformation by deforming the bond angle of $C_{aromatic}$–αC–$H_{methine}$(about 7°). Accordingly, it is concluded that the dual emission in atactic P1VN chain should be attributed to the meso : tt($\pi\pi$) and racemic: tt($\pi\pi$) states. The meso : tt($\pi\pi$) and racemic : tt($\pi\pi$) states correspond to the parallel and antiparallel configurations proposed by Gupta,[13] respectively.

The averaged rotation angles $\langle\phi_i\rangle$, $\langle\phi_{i+1}\rangle$ in Table 2 are independent of the values of σ chosen. The averaged rotational angles for the meso : tg in P1VN chain largely deviate from the perfect staggered conformation (0,120°). The values suggest that an isotactic P1VN chain forms a 4_1 helix. This conclusion is approximately consistent with the X-ray data on isotactic P1VN reported by Natta.[15] Table 2 also shows that an isotactic P2VN chain forms a 3_1 helix.

References

1) K. Seki, Y. Ichimura, and Y. Imamura, *Macromolecules*, **14**, 1831 (1981).
2) K. Seki, S. Mori, and Y. Imamura, *Bull. Chem. Soc. Jpn.*, **55**, 2739 (1982).
3) S. Ito, M. Yamamoto, and Y. Nishijima, *Polym. J.*, **13**, 791 (1981); C. David, M. Piens, and G. Geuskens, *Eur.Polym. J.*, **8**, 1019 (1972); M. Irie, T. Kamijo, M. Aikawa, T. Takemura, K. Hayashi, and H. Baba, *J. Phys. Chem.*, **81**, 1571 (1977); K. P. Ghiggino, R. D. Wright, and D. Phillips, *J. Polym. Sci., Polym. Phys. Ed.*, **16**, 1499 (1978).
4) F. Hirayama, *J. Chem. Phys.*, **42**, 3163 (1965).
5) C. W. Frank and L. A. Harrah, *J. Chem. Phys.*, **61**, 1526 (1974).
6) D. A. Brant and P. J. Flory, *J. Am. Chem. Soc.*, **87**, 2791 (1965).
7) A. Abe, R. L. Jernigan, and P. J. Flory, *J. Am. Chem. Soc.*, **88**, 631 (1966).
8) P. R. Sundararajan and P. J. Flory, *J. Am. Chem. Soc.*, **96**, 5025 (1974).
9) U. W. Suter and P. J. Flory, *Macromolecules*, **8**, 765 (1975).
10) D. Y. Yoon, P. R. Sundararajan, and P. J. Flory, *Macromolecules*, **8**, 776 (1975).
11) P. R. Sundararajan, *Macromolecules*, **13**, 512 (1980).
12) R. W. G. Wyckoff, "Crystal Structures," Interscience, New York, London (1971), Vol. 6, Part 2, p. 383.
13) A. Gupta, R. Liang, J. Moacanin, D. Kliger, R. Goldbeck, J. Horwitz, and V. M. Miskowski, *Eur. Polym. J.*, **17**, 485 (1981).
14) F. C. De Schryver, K. Demeyer, M. van der Auweraer, and E. Quanten, *Ann. N. Y. Acad. Sci.*, **366**, 93 (1981).
15) G. Natta, *Makromol. Chem.*, **35**, 94 (1960); G. Natta, P. Corradini, and I. W. Bassi, *Gazz. Chim. Ital.*, **89**, 784 (1959).

The Macromolecular Ion Flotation of Fe^{3+}, Cu^{2+}, and Ni^{2+} by the Use of Charcoal and Cationic Surfactant

Tsunetaka Sasaki,* Kōji Mochizuki, and Satoshi Ishiwata
Department of Chemistry, Faculty of Science, Tokai University, 1117 Kitakaname, Hiratsuka 259-12
(Received April 23, 1982)

The macromolecular ion flotation of Fe^{3+}, Cu^{2+}, and Ni^{2+} ions by the combined use of charcoal and hexadecyltrimethylammonium chloride (HTAC) was studied. The flotation of powdered active charcoal itself was first studied; a 100% floatability was obtained for the flotation of 2500 ppm charcoal by the addition of 6 ppm of polyacrylamide and 550 ppm of HTAC in the pH range from 4 to 13. For the studies of the flotation of Fe^{3+}, Cu^{2+}, and Ni^{2+} ions, diagrams of the floatability of the respective ions *vs.* the composition of charcoal and HTAC, and the floatability of the respective ions *vs.* the pH at a constant composition of charcoal and HTAC, were constructed. A nearly 100% floatability was obtained for Fe^{3+}, Cu^{2+}, and Ni^{2+} ions at pH values larger than 4.5, 9.5, and 11 respectively. This order is the same as that of the solubility products of $Fe(OH)_3$, $Cu(OH)_2$, and $Ni(OH)_2$. It was confirmed that Fe^{3+} ions are adsorbed as hydroxides on charcoal; they are subsequently floated over the whole range of pH values combined with charcoal, while the Cu^{2+} and Ni^{2+} ions are adsorbed as simple ions on charcoal and floated in the lower pH region. They are adsorbed as hydroxide on charcoal and floated in a higher pH region.

In preceding papers, we have reported the applicability of macromolecular ion flotation to the flotation of inorganic and organic anions and cations.[1,2] There, macromolecular ions, namely, macroscopic or colloidal particles possessing an ion-exchange capacity and organic or inorganic polymer ions, together with ionic surfactants with an electric charge the opposite of that of macromolecular ions, were used.

To date, ion flotation using charcoal and surfactant has not been reported, although flotations of charcoal by surfactants have been reported.[3,4] Considering the remarkable adsorbing power of charcoal for various organic and inorganic ions, effective ion flotation by the use of charcoal can be expected.

In this case, powdered active charcoal is preferable, since this offers both a very large and readily accessible area for the substance to be floated. However, the powdered charcoal has the difficulty of not being easily floated.[4] In the present paper, this difficulty could be overcome by the addition of a small amount of polyacrylamide.

In the present paper, charcoal was used as the macromolecular ion in our series of studies.[1] Fe^{3+}, Cu^{2+}, and Ni^{2+} ions were floated by HTAC.

Experimental

Materials. The charcoal was the product of Wako Pure Chemicals, labelled "Chemical Activated." HTAC was the product of Wako Pure Chemicals of a chemically pure grade. The polyacrylamide DCLE MA-3000H (PAA) was the product of Mitsubishi Chemical Industries, the mean degree of polymerization being 1×10^5. The $FeCl_3$, $CuSO_4$, and $NiSO_4$ were commercial products of a guaranteed grade.

Measurement. For the flotation measurement, 20 cm^3 of a solution containing the ions to be floated, charcoal, HTAC, and HCl or NaOH if necessary for controlling the pH was introduced into a stoppered test tube 16 mm in inner diameter and 290 mm in length, equipped with a stopcock at the bottom. The test tube was shaken 20 times by hand. After the test tube had been kept standing for 10 min to complete the flotation, the concentrations of Fe^{3+}, Cu^{2+}, and Ni^{2+} ions in the underlying solution were measured and the floatability percentage, F, was calculated by means of the following equation:

$$F = (1 - C_f/C_i) \times 100\ \%,$$

where C_i and C_f denote the concentrations of the ions to be floated in the solution before and after the flotation respectively.

The concentrations of the Fe^{3+}, Cu^{2+}, and Ni^{2+} ions were measured with a Hitachi Atomic Absorption Spectrometer 508 at wave lengths of 248.3, 324.7, and 232 nm respectively.[2] The pH was controlled if necessary by the addition of HCl or, NaOH.

The measurement was carried out at a room temperature, about 25°C.

Results and Discussion

Floatability of Charcoal. First, we studied the floatability of charcoal. The floatability of charcoal *vs.* the concentration of the PAA relation was studied at constant concentrations of 2500 ppm of charcoal and 550 ppm of HTAC at pH 4.0. The floatability increased from zero at zero ppm of PAA to 100% at 4.5 ppm of PAA, beyond which it remained constant. Therefore, we fixed the concentration of PAA at 6 ppm and examined the relation between the concentration of HTAC and the floatability of charcoal at pH 6. The solid line of Fig. 1 shows the result. It can be confirmed

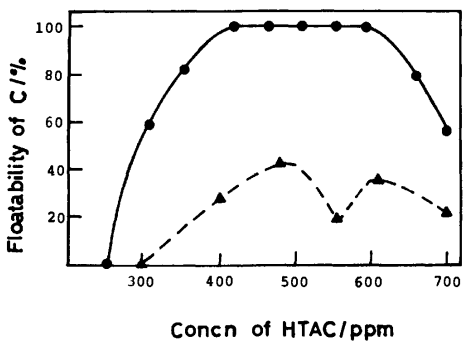

Fig. 1. Floatability of C *vs.* concn of HTAC.
pH: 6.0, solid line: C; 2500 ppm, PAA; 6 ppm, broken line: C; 2500 ppm, PAA; 0 ppm.

that a flat maximum of a nearly 100% floatability could be obtained in the concentration region from 400 to 600 ppm HTAC. In the same figure, the charcoal–HTAC system without the addition of PAA is shown by a broken line. The effectiveness of the addition of PAA is evident for charcoal flotation.

We further measured the floatability of charcoal *vs.* the pH relation at constant concentrations of 2500 ppm of charcoal, 6 ppm of PAA, and 550 ppm of HTAC, as shown in Fig. 2. A broad maximum of a nearly 100% floatability of charcoal was obtained in the pH region from 4 to 13. The system without PAA is shown by a broken line in Fig. 2. We can see a similar floating effect of the addition of PAA.

Floatability of Fe^{3+}, Cu^{2+}, and Ni^{2+} vs. Composition of PAA and HTAC. Macromolecular ion flotations of Fe^{3+}, Cu^{2+}, and Ni^{2+} were carried out with the addition of 2500 ppm of charcoal, 6 ppm of PAA, and varying compositions and total amounts of charcoal and HTAC. Figure 3 shows the floatabilities of the Fe^{3+}, Cu^{2+}, and Ni^{2+} ions as a function of the total weight concentration of C†+HTAC and the weight fraction of C/(C+HTAC) at pH 10.8, 10.0, and 11.1 respectively. The concentration of Fe^{3+}, Cu^{2+}, and Ni^{2+} were kept constant at 1.65×10^{-4}, 1.83×10^{-4}, and 1.69×10^{-4} mol dm^{-3} respectively. The areas inside the curves indicate the optimum composition regions of floatability larger than 95%. The upper parts of these optimum regions form a vertical shape, while the lower parts bend towards 100% HTAC.

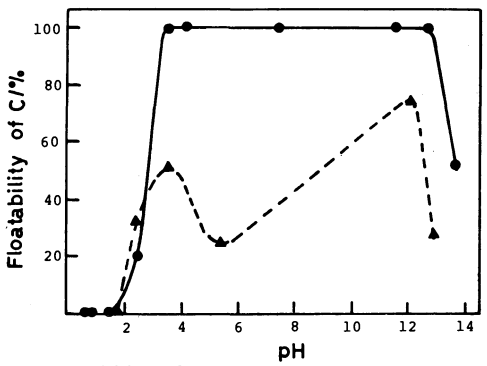

Fig. 2. Floatability of C *vs.* pH.
Solid line: C; 2500 ppm, PAA; 6 ppm, HTAC; 550 ppm, broken line: C; 2500 ppm, PAA; 0 ppm, HTAC; 550 ppm.

Floatabilities of Fe^{3+}, Cu^{2+}, and Ni^{2+} vs. pH. The relations between floatabilities of Fe^{3+}, Cu^{2+}, and Ni^{2+} ions and pH were also measured; they are shown in Fig. 4. The experimental conditions are listed as a caption in the figure. In this figure, both the system with and that without the addition of charcoal are shown. In Fig. 4(a), showing the flotation of Fe^{3+} ions, the floatability sharply rose from zero to nearly 100% at pH 4, beyond which it remained constant up to pH 11. The effect of the addition of charcoal is evident from a comparison of this curve with the curve of the broken line without the addition of charcoal. In Fig. 4(b), showing the flotation of Cu^{2+}, the floatability gradually rose from zero at a pH of about 3 and attained nearly 100% beyond pH 9.4. The effect of the addition of charcoal is evident from a comparison of the curves of the solid and broken lines. In Fig. 4(c), showing the flotation of Ni^{2+}, the floatability rose gradually from zero at pH 3 and attained nearly 100% beyond a pH of about 11. The effect of the addition of charcoal can still be observed from a comparison of the solid and broken lines.

The values of the pH's at which $Fe(OH)_3$, $Cu(OH)_2$, and $Ni(OH)_2$ begin to form are calculated from each solubility product to be 2.2, 6.2, and 7.0 respectively. Considering these values, it is likely that Fe^{3+} ions are adsorbed as hydroxide on charcoal and that they are subsequently floated, while in the case of Cu^{2+} and Ni^{2+}, each ion is adsorbed on charcoal and floated in the low-pH region. In the high-pH region, however, the latter two hydroxides are considered to be adsorbed on charcoal and floated. The pH's beyond which the floatability remains at its maximum value for these ions

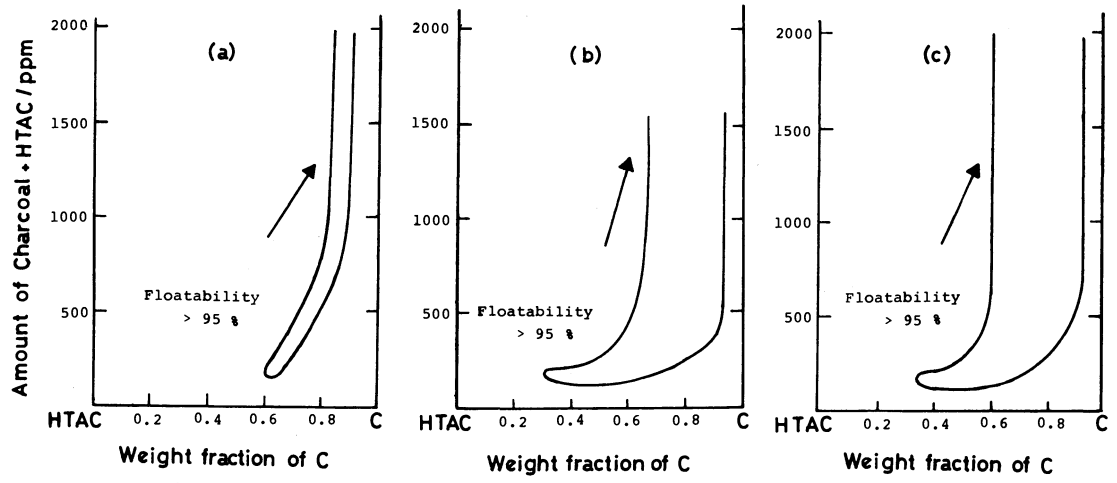

Fig. 3. Diagrams of Fe^{3+}, Cu^{2+}, and Ni^{2+} ion flotation by C, PAA and HTAC.
PAA: 6 ppm, (a): Fe^{3+} ion flotation, pH; 10.8, (b): Cu^{2+} ion flotation, pH; 10.0, (c): Ni^{2+} ion flotation, pH; 11.1.

† Abbreviation of charcoal.

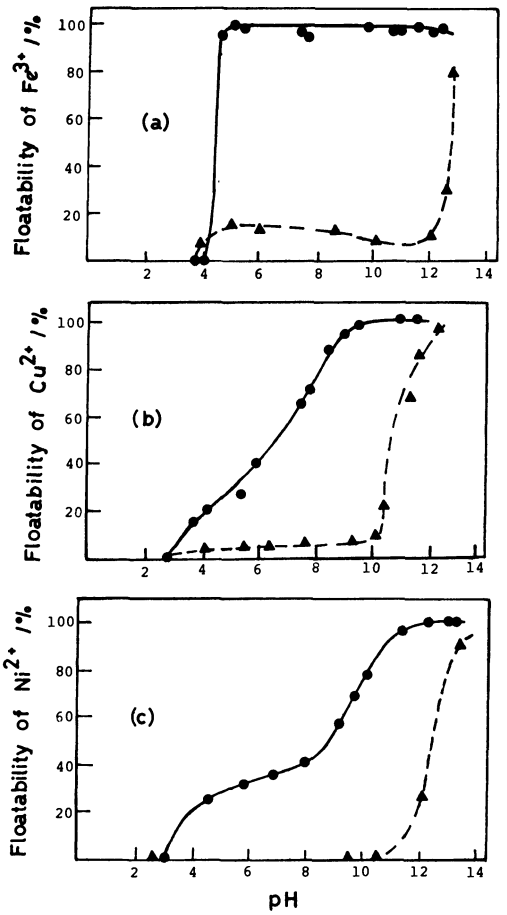

Fig. 4. Floatabilities of Fe^{3+}, Cu^{2+}, and Ni^{2+} ions *vs.* initial pH.
(a): Fe^{3+}; initial concn 1.67×10^{-4} mol dm^{-3}, (b): Cu^{2+}; initial concn 1.76×10^{-4} mol dm^{-3}, (c): Ni^{2+}; initial concn 1.69×10^{-4} mol dm^{-3}.
Solid line: C; 2500 ppm, PAA; 6 ppm, HTAC; 550 ppm, broken line: C; 0 ppm, PAA; 6 ppm, HTAC; 550 ppm.

are found to be:

$$Fe^{3+} < Cu^{2+} < Ni^{2+},$$

which is in the same order as that of the solubility product. A sharp rise in the floatabilities of these ions in the system without the addition of charcoal observed at a high pH may be explained by the sufficiently large hydroxide particle formed at a high pH being entangled in the foam.

The authors wish to thank the Ministry of Education for the financial support granted for this research.

References

1) K. Kobayashi, K. Natori, M. Kamaya, and T. Sasaki, *Bull. Chem. Soc. Jpn.*, **54**, 3153 (1981).
2) T. Sasaki, T. Kudo, I. Machida, and S. Ishiwata, *Bull. Chem. Soc. Jpn.*, **55**, 2547 (1982).
3) R. B. Grieves and E. F. Chouinard, *J. Appl. Chem.*, **19**, 60 (1969).
4) P. L. Bishop, *Sep. Sci. Technol.*, **13**, 47 (1978).

 © 1982 The Chemical Society of Japan Bull. Chem. Soc. Jpn., 55, 3720—3723 (1982) [Vol. 55, No. 12

Kinetic Isotope Effects in the $H+C_3H_6 \rightarrow C_3H_7$ Reaction

Toshifumi WATANABE, Takeshi KYOGOKU, Shigeru TSUNASHIMA, Shin SATO,*,† and Shigeru NAGASE††

Department of Applied Physics, Tokyo Institute of Technology, Ookayama, Meguro-ku, Tokyo 152
†*Research Laboratory for Nuclear Reactors, Tokyo Institute of Technology, Ookayama, Meguro-ku, Tokyo 152*
††*Chemistry Division, Faculty of Education, Yokohama National University, Hodogaya-ku, Yokohama 240*

(Received April 27, 1982)

The absolute rate constants of the addition of H and D atoms to propylene-d_0 and -d_6 have been measured by means of the pulse radiolysis-resonance absorption technique over the temperature range of 200—500 K. The rate constants obtained were well expressed by these Arrhenius equations: $k(H+C_3H_6)=(3.00\pm0.38)\exp[-(1612\pm66)/RT]$, $k(H+C_3D_6)=(2.55\pm0.57)\exp[-(1509\pm128)/RT]$, $k(D+C_3H_6)=(1.99\pm0.05)\exp[-(1550\pm15)/RT]$, and $k(D+C_3D_6)=(2.20\pm0.27)\exp[-(1587\pm67)/RT]$ in units of 10^{-11} cm^3 molecule^{-1} s^{-1}. The unit of activation energy is cal mol^{-1}. Practically no isotope effects attributable to the difference between C_3H_6 and C_3D_6 could be observed. This is similar to the kinetic isotope effects previously observed in the rate constants of the addition of H and D atoms to isotopic ethylenes. The theoretical rate constants of the above reactions have been calculated by the conventional activated complex theory using the potential energy surface drawn by the *ab initio* method; however, no agreement with regard to the isotope effects could be obtained between experiment and theory because of the difference between C_3H_6 and C_3D_6. This also is similar to the isotope effects found in the $H+C_2H_4\rightarrow C_2H_5$ reaction.

In previous papers,[1,2] we reported the absolute rate constants of the addition of H and D atoms to C_2H_4, C_2H_3D, C_2D_4, C_2H_2, and C_2D_2 obtained by the pulse radiolysis-resonance absorption technique over the temperature range of 200—500 K, and discussed the kinetic isotope effects on the basis of the activated complex theory, since the potential energy surfaces obtained by the *ab initio* calculations were available for both reactions, $H+C_2H_4\rightarrow C_2H_5$[3] and $H+C_2H_2\rightarrow C_2H_3$.[4] Experimentally, no differences among three isotopic ethylenes, C_2H_4, C_2H_3D, and C_2D_4, as well as between two acetylenes, C_2H_2 and C_2D_2 could be found in the rate constants of the H- and D-atom-addition reactions, while, theoretically, these differences clearly appeared, mainly because of the zero-point energy differences between the reactants and the activated complexes.

It is well known that the present status of the *ab initio* calculations is not reliable enough to discuss the absolute value of the barrier height for a reaction involving polyatomic molecules. Therefore, we parametrized the barrier heights so as to fit the theoretical rate constants for the $H+C_2H_4\rightarrow C_2H_5$ and $H+C_2H_2\rightarrow C_2H_3$ reactions at room temperature to the experiment, and then investigated the isotope effects; however, no agreement could be obtained between experiment and theory.

The present paper is a simple extension of the previous one. Experimentally, however, more accurate measurements of the reactant pressure and the temperature were required because the rate constant of the $H+C_3H_6\rightarrow C_3H_7$ reaction was larger than that of $H+C_2H_4\rightarrow C_2H_5$. In the theoretical calculation, about twice as much time was consumed.

Experimental and Calculational Procedures

The experimental procedure was the same as that described previously.[2] Hydrogen or deuterium gas (≈500 Torr; 1 Torr≈133.322 Pa) containing a small amount of propylene (0.01—0.1 Torr) was pulse-irradiated with high-energy electrons from Febetron 706 (Hewlett Packard Co.), and the decay of the concentration of H or D atoms was observed by the use of Lyman-α's. From this first-order decay curve, the rate constant was estimated.

The propylene used was purchased from the Takachiho Shoji Co. The propylene-d_6 was the product of Merck, Sharp, and Dohme, Canada, Ltd., the nominal purity being 99%; this purity was confirmed gaschromatographically.

The *ab initio* calculation method used is the same as that used for drawing the potential energy surface for the $H+C_2H_4\rightarrow C_2H_5$ reaction.[3] The details of the calculated results will be published elsewhere; in the present paper, only the data necessary for the estimation of the rate constants are presented.

Results

Table 1 summarizes the rate constants obtained. Four to five different pressures of propylenes were used to measure the rate constants at each temperature. The fluctuation of the temperature (±2 °C) in each measurement was corrected in the same manner as that previously described in detail.[2] In Fig. 1, all the rate constants obtained are plotted in the form of Arrhenius plots. The Arrhenius parameters thus determined are summarized

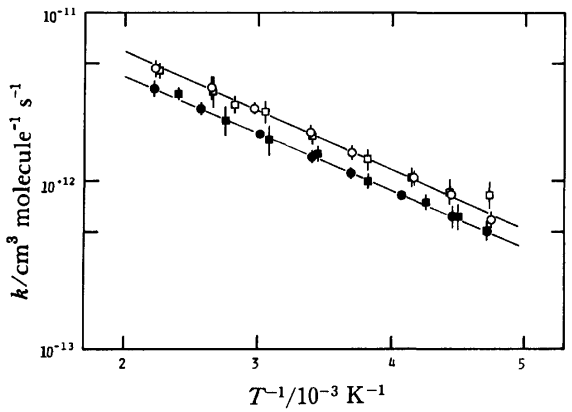

Fig. 1. The Arrhenius plots for the reactions: (○), $H+C_3H_6$; (□), $H+C_3D_6$; (●), $D+C_3H_6$; (■), $D+C_3D_6$.

Table 1. The high pressure limiting rate constants of the addition of H and D atoms to propylene-d_0 and -d_6

Reaction	T/K	k/10^{-13} cm^3 molecule^{-1} s^{-1}
$H+C_3H_6$	448	46.9 ±5.5
	378	36.3 ±5.5
	337	27.3 ±2.1
	295	19.4 ±2.1
	270	14.7 ±1.4
	240	10.4 ±1.1
	225	8.31±0.55
	211	5.93±0.61
$D+C_3H_6$	451	35.6 ±3.8
	389	27.0 ±2.4
	332	18.9 ±1.1
	295	13.9 ±1.1
	271	11.2 ±0.6
	245	8.25±0.43
	224	6.18±0.89
	212	5.04±0.42
$H+C_3D_6$	423	45.4 ±4.8
	376	34.5 ±7.2
	355	28.6 ±3.3
	328	25.9 ±3.9
	294	18.4 ±1.9
	262	13.4 ±1.9
	241	10.6 ±1.3
	225	8.72±1.46
	211	8.33±1.48
$D+C_3D_6$	417	33.1 ±2.8
	364	23.0 ±4.7
	325	17.6 ±3.6
	291	14.4 ±1.5
	262	9.93±1.00
	235	7.46±0.78
	222	6.19±1.08
	212	5.18±0.75

Table 2. Arrhenius parameters obtained A/10^{-11} cm^3 molecule^{-1} s^{-1} and E/cal mol^{-1}; uncertainties are 2σ.

	H-atom addition		D-atom addition	
	A	E	A	E
C_3H_6	3.00±0.38	1612± 66	1.99±0.05	1550±15
C_3D_6	2.55±0.57	1509±128	2.20±0.27	1587±67

in Table 2. The uncertainties are 2σ. The method of calculating these uncertainties has been described previously.[2] It is noticeable that no kinetic isotope effects due to the difference between C_3H_6 and C_3D_6 could be observed.

Figure 2 shows the structures of propylene and the activated complex calculated by the *ab initio* unrestricted Hartree-Fock method with the 4-31 split-basis set. These geometries were fully optimized with the energy-gradient method. The force-constant matrices for propylene and the activated complex were then constructed by the numerical differentiation of the energy gradients.

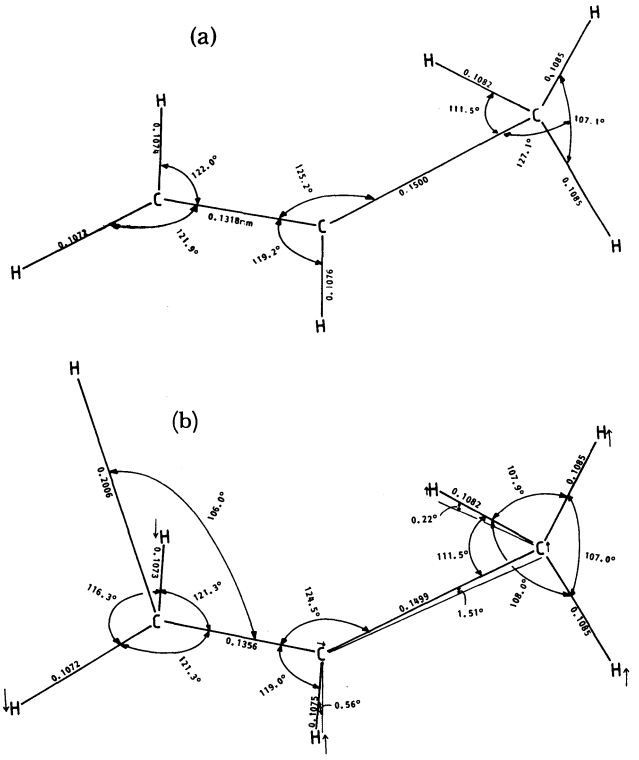

Fig. 2. The Geometries of C_3H_6 (a) and the activated complex for the reaction, $H+C_3H_6$, (b). Arrows indicate the direction of the displacement of the equilibrium position from the reactant.

Table 3 summarizes the resultant normal-mode frequencies, moments of inertia, and zero-point energies. Although the calculated normal-mode frequencies for propylene did not agree exactly with those experimentally obtained,[5] we did not ascertain the correction factor since the discrepancy between experiment and calculation was not systematic and prevented us for estimating a simple correction factor.

The barrier height calculated for the $H+CH_3CH=-CH_2 \rightarrow CH_3CH-CH_3$ reaction was 2.41 kcal/mol (1 kcal=4.184 kJ), a value which was obviously too high compared with the experimentally obtained activation energies. Therefore, we had to parametrize this value in the calculations of the rate constants, as will be shown later. It is well known that hydrogen atoms mainly add to the double bond of propylene at the terminal carbon atom.[6] The *ab initio* calculation is consistent with this observation: the barrier height for $H+CH_3CH=CH_2 \rightarrow CH_3CH_2CH_2$ addition reaction was calculated to be 4.24 kcal/mol.

Discussion

Propylene is known to be more reactive than ethylene to hydrogen atoms at room temperature.[7] The present experiments clearly showed that this difference comes from the activation energies. The Arrhenius equation for the $H+C_2H_4 \rightarrow C_2H_5$ reaction previously obtained is $k_{exp}=(4.70\pm0.49)\times10^{-11}\exp[-(2178\pm58)/RT]$ cm^3 molecule^{-1} s^{-1}.[2] Since the pre-exponential factor for the reaction of propylene is about 2/3 of that for the

TABLE 3. NORMAL MODE FREQUENCIES, MOMENTS OF INERTIA, AND ZERO-POINT ENERGIES

		Species					
		C_3H_6	$C_3H_7^\dagger$	$C_3H_6D^\dagger$	C_3D_6	$C_3D_6H^\dagger$	$C_3D_7^\dagger$
Vibrational frequencies ν/cm^{-1}		3398	3402	3402	2528	2534	2534
		3321	3315	3315	2471	2441	2441
		3306	3298	3298	2414	2414	2414
		3245	3262	3262	2404	2405	2405
		3218	3214	3214	2380	2376	2376
		3167	3166	3166	2279	2278	2278
		1879	1689	1687	1787	1545	1539
		1656	1657	1657	1287	1274	1274
		1647	1645	1645	1202	1199	1199
		1612	1588	1587	1195	1193	1193
		1580	1572	1572	1189	1187	1187
		1471	1383	1380	1155	1132	1131
		1324	1308	1307	1047	1031	1030
		1218	1180	1180	1020	959	957
		1154	1065	1065	886	834	826
		1116	1053	1028	845	826	799
		1074	1028	1021	825	789	789
		980	954	949	797	751	745
		678	719	708	507	558	540
		478	465	463	394	412	381
		229	429	347	168	379	323
			286	220		273	212
			194	191		143	141
			624i	472i		617i	470i
Moments of inertia I/10^{-47} kg m^2	I_a	89.55	101.37	107.79	116.35	129.06	137.48
	I_b	102.03	109.96	119.71	135.78	143.63	151.64
	I_c	17.58	24.33	29.88	29.61	36.55	42.32
Zero-point energy/kcal mol^{-1}		53.97	54.14	53.84	41.14	41.36	41.05

reaction of ethylene, if the Arrhenius equations can be extrapolated to higher temperatures, the rate constants of these two reactions will coincide with each other at around 360 °C.

According to the conventional activated complex theory, the rate constant of the $H+C_3H_6 \rightarrow C_3H_7$ reaction is expressed as follows:

$$\kappa = \kappa L^\dagger \frac{kT}{h} \frac{F^\dagger}{F_H F_P} \frac{f_{rot}^\dagger}{f_{rot}} \frac{f_{vib}^\dagger}{f_{vib}} \exp(-V/RT). \quad (1)$$

Here, κ is the transmission coefficient, which may be calculated by Wigner's approximation:

$$\kappa = 1 + (1/24)(h|\nu_i|/kT)^2. \quad (2)$$

The values of ν_i are listed in Table 3. $L^\dagger$ is the path degeneracy. F_H, F_P, and $F^\dagger$ are the translational partition functions for hydrogen atoms, propylene molecules, and an activated complex respectively. f_{rot} and $f_{rot}^\dagger$ are the rotational partition functions without a symmetry number. f_{vib} and $f_{vib}^\dagger$ are the vibrational partition functions including the contribution of zero-point energies. V is the barrier height.

Since the calculated barrier height was too high, we adjusted this value so as to fit the theoretical rate constant of the $H+C_3H_6 \rightarrow C_3H_7$ reaction at room temperature to the experimental result. The adjusted barrier height was 1.63 kcal/mol. This value is common to three other reactions also; $D+C_3H_6$, $H+C_3D_6$, and $D+C_3D_6$.

Figure 3 compares the rate constants thus calculated

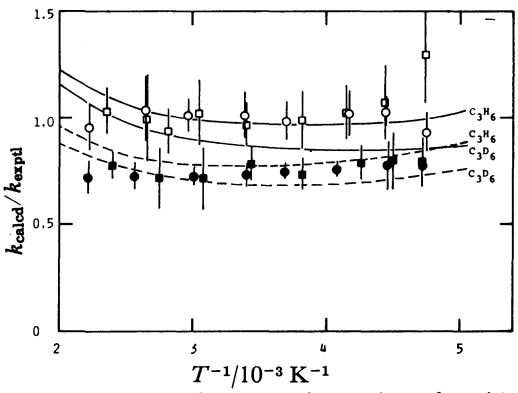

Fig. 3. Comparison of the experimental results with the theoretical calculations. For symbols, see the caption of Fig. 1. The experimentally obtained rate constant for the reaction, $H+C_3H_6$, $k_{exptl}=3.00\times10^{-11}$ exp $(-1612/RT)$ cm^3 molecule^{-1} s^{-1}, is taken as the standard. Solid lines are for the H-atom reactions and dashed lines for the D-atom reactions.

with those obtained in the present experiments. Here, the experimentally obtained Arrhenius equation for the $H+C_3H_6 \rightarrow C_3H_7$ reaction, $k_{exptl}=3.00\times10^{-11}$ exp $(-1612/RT)$ cm^3 molecule^{-1} s^{-1}, is taken as the standard. Obviously the agreement between experiment and theory is poor for the isotope effects because of the difference between C_3H_6 and C_3D_6, while the isotope

effects due to the difference between H and D atoms are well explained. This is exactly the same as was found previously in the reactions of H and D atoms with isotopic ethylenes.[1,2]

At present, we have no proper interpretations for this disagreement. One possible reason might be fundamental assumption on which the activated complex theory is based. In the formulation of the activated complex theory, the equilibrium between a reactant and the activated complex is postulated; however, in such exothermic fast reactions as $H+C_3H_6 \rightarrow C_3H_7$, some normal modes of vibration in the activated complex might not be able to reach the equilibrium before the reaction system crosses over the saddle point. Consequently, some normal modes of vibration in the reactant remain as they are and cannot contribute to the change of the state density, *i.e.*, to the rate constant. It is well known that the kinetic isotope effect results from the difference in zero-point energy between reactant and activated complex. The critical energy defined by the following equation is a crucial factor in determining the isotope effects:

$$E_0 = V + \Delta E_{\text{vib}},$$

$$\Delta E_{\text{vib}} = \frac{1}{2}\sum h\nu^{\dagger} - \frac{1}{2}\sum h\nu.$$

Here, $\nu^{\dagger}$ and ν are the normal-mode frequencies in the activated complex and the reactant. If ΔE_{vib} is reduced by the reasoning above stated, the isotope effects in the rate constants will also be reduced. A rigorous formulation of this will be the subject of our further investigations.

References

1) K. Sugawara, K. Okazaki, and S. Sato, *Chem. Phys. Lett.*, **78**, 259 (1981).
2) K. Sugawara, K. Okazaki, and S. Sato, *Bull. Chem. Soc. Jpn.*, **54**, 2872 (1981).
3) S. Nagase, T. Fueno, and K. Morokuma, *J. Am. Chem. Soc.*, **101**, 5849 (1979).
4) S. Nagase and C. W. Kern, *J. Am. Chem. Soc.*, **101**, 2544 (1979).
5) G. Herzberg, "Molecular Spectra and Molecular Structure II, Infrared and Raman Spectra of Polyatomic Molecules," D. van Nostrand, New York (1945).
6) W. E. Falconer, B. S. Rabinovitch, and R. J. Cvetanović, *J. Chem. Phys.*, **39**, 40 (1963).
7) K. R. Jennings and R. J. Cvetanović, *J. Chem. Phys.*, **35**, 1233 (1961).

 © 1982 The Chemical Society of Japan Bull. Chem. Soc. Jpn., 55, 3724—3732 (1982) [Vol. 55, No. 12

Cyclic Orbital Interaction and Orbital Phase in Acyclic Conjugation

Satoshi INAGAKI,* Hirofumi KAWATA, and Yoshio HIRABAYASHI
Department of Chemistry, Faculty of Engineering, Gifu University, Yanagido, Gifu 501-11
(Received May 7, 1982)

The orbital phase continuity-discontinuity property is shown to control electron delocalization and polarization even in open chain conjugated molecules. Its chemical consequences are discussed.

The π electron delocalization has been one of the central subjects in organic chemistry. There are well-established rules for monocyclic conjugation. The $4n+2$ π electron aromaticity rule[1] is related to the static state of the ground-state molecules at their equilibrium geometries. The stereoselection rule[2-4] is the counterpart for the dynamic process or for the transition state of chemical reactions. Both rules were founded on the identical basis, *i.e.*, the continuity-discontinuity of orbital phase of many composite systems.[5-8] The phase control has been believed to be characteristic of nothing but *cyclic* conjugated molecules. In this paper the orbital phase will be shown to be more fundamental, and to play a significant role in determining electron delocalization even in *acyclic* conjugated molecules.

Theoretical

Delocalization. We are concerned with two types of acyclic conjugation of ethylenic π bonds. In the head-to-tail polyenes (**1**), a π bond interacts at one end (head) with a second bond and at the other end (tail) with a third bond. In the head-to-head polyenes (**2**), a π bond interacts at an end (head) with two neighboring bonds. There is no primary difference between **1** and **2** in the electron delocalization between the adjacent units, which is considered as that in butadiene. The indirect delocalization between two bonds mediated by another should make a characteristic distinction between **1** and **2**. There are two paths for the end-to-end electron delocalization in the triene unit, as is illustrated in Scheme 1.[9]

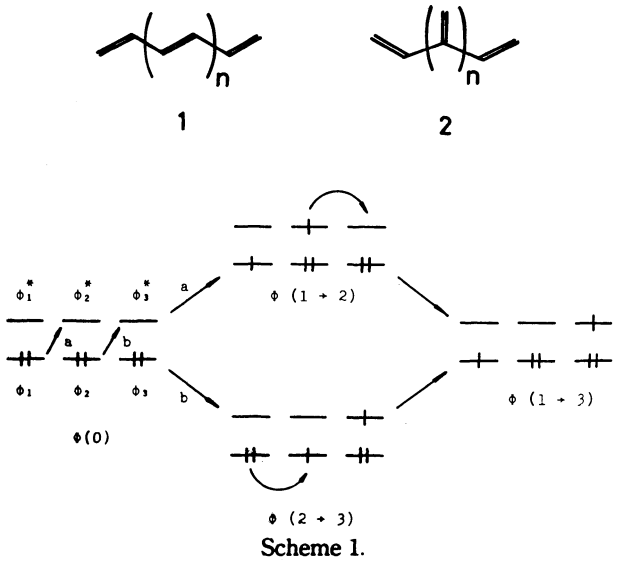

Scheme 1.

An electron in the bonding orbital, ϕ_1, of a terminal bond transfers to the antibonding orbital, ϕ_2^*, of the middle and then to ϕ_3^* of the other terminus (path a). By the other path an electron hole in ϕ_2 resulting from the electron shift from ϕ_2 to ϕ_3^* is supplied with an electron by ϕ_1 (path b). The coefficients, $C_a(1\rightarrow3)$ and $C_b(1\rightarrow3)$, of the $1\rightarrow3$ transferred configuration, $\Phi(1\rightarrow3)$, contributed through the paths, a and b, are given by the perturbation theory, respectively:

$$C_a(1\rightarrow3) = \frac{\langle\Phi(0)|H'|\Phi(1\rightarrow2)\rangle\langle\Phi(1\rightarrow2)|H'|\Phi(1\rightarrow3)\rangle}{[E(1\rightarrow2) - E(0)][E(1\rightarrow3) - E(0)]}$$

$$C_b(1\rightarrow3) = \frac{\langle\Phi(0)|H'|\Phi(2\rightarrow3)\rangle\langle\Phi(2\rightarrow3)|H'|\Phi(1\rightarrow3)\rangle}{[E(2\rightarrow3) - E(0)][E(1\rightarrow3) - E(0)]}.$$

When the Hückel approximation is employed, we obtain the following equations:

$$C_a(1\rightarrow3) = C_b(1\rightarrow3), \textit{ i.e., } C(1\rightarrow3) = 2C_a(1\rightarrow3)$$

for the head-to-tail triene, and

$$C_a(1\rightarrow3) = -C_b(1\rightarrow3), \textit{ i.e., } C(1\rightarrow3) = 0$$

for the head-to-head triene. The $1\rightarrow3$ delocalization is amplified in the head-to-tail polyenes while cancelled out in the head-to-head polyenes.

The clear-cut difference in the indirect delocalization between the head-to-head and head-to-tail polyenes is ascribed to the cyclic orbital interaction in the acyclic conjugation. The configuration interactions between $\Phi(0)$ and $\Phi(1\rightarrow2)$ and between $\Phi(1\rightarrow2)$ and $\Phi(1\rightarrow3)$ in C_a contain the orbital interactions between ϕ_1 and ϕ_2^* and between ϕ_2^* and ϕ_3^*, respectively. The ϕ_1-ϕ_2^*-ϕ_3^* orbital interaction is involved in the delocalization *via* path a. The corresponding configuration interactions between $\Phi(0)$ and $\Phi(2\rightarrow3)$ and between $\Phi(2\rightarrow3)$ and $\Phi(1\rightarrow3)$ in C_b contain the orbital interactions between ϕ_2 and ϕ_3^* and between ϕ_1 and ϕ_2, respectively. The ϕ_1-ϕ_2-ϕ_3^* orbital interaction is involved in the delocalization *via* path b. These orbital interactions share the ϕ_1 and ϕ_3^* orbitals at either end to form a cyclic orbital interaction like $\overline{\phi_1\text{-}\phi_2\text{-}\phi_3\text{-}\phi_2^*}$. As a result, the extent of the indirect delocalization, *i.e.*, the magnitude of the coefficient of the $1\rightarrow3$ electron transferred configuration is dependent on the orbital phase property.

For further understanding of the cyclic property of the orbital interactions involved in the acyclic conjugation, it is preferable to suppose "hypothetical" cyclic systems, **3** and **4**, which have a bonding orbital, ϕ_2, only on the bond 2 and antibonding orbital, ϕ_2^*, only on the bond 2′. There are analogous pathways for the $1\rightarrow3$ delocalization. An electron in ϕ_1 transfers to ϕ_2^* of the bond 2′ and then to ϕ_3^* (path c). An electron hole resulting from the electron shift from ϕ_2 of the bond 2 to ϕ_3^* is supplied with an electron by ϕ_1

(path d). The formula for the coefficients of the indirectly transferred configurations contributed from the paths, c and d,

$$C_c(1 \rightarrow 3) = \frac{\langle \Phi(0)|H'|\Phi(1 \rightarrow 2')\rangle\langle \Phi(1 \rightarrow 2')|H'|\Phi(1 \rightarrow 3)\rangle}{[E(1 \rightarrow 2') - E(0)][E(1 \rightarrow 3) - E(0)]}$$

$$C_d(1 \rightarrow 3) = \frac{\langle \Phi(0)|H'|\Phi(2 \rightarrow 3)\rangle\langle \Phi(2 \rightarrow 3)|H'|\Phi(1 \rightarrow 3)\rangle}{[E(2 \rightarrow 3) - E(0)][E(1 \rightarrow 3) - E(0)]}$$

are equivalent to C_a and C_b, respectively. In this sense, the acyclic systems, **1** and **2**, have the same features as the cyclic systems, **3** and **4**, with respect to the 1→3 delocalization.

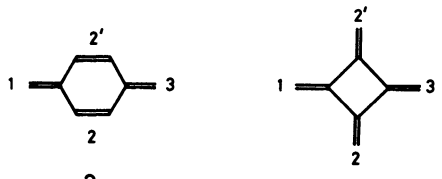

3

4

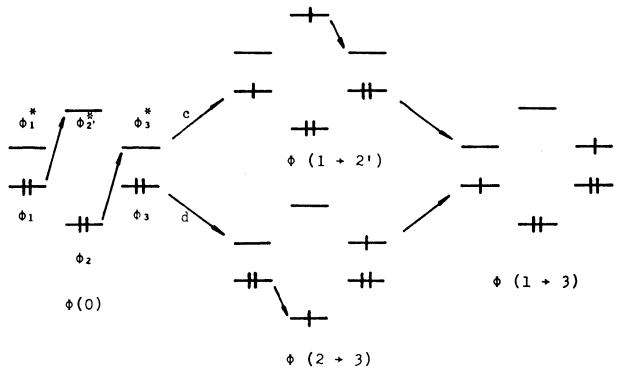

Scheme 2.

The 1→3 delocalization in **3** and **4** is a mode of cyclic delocalization, where the bonds, 1 and 2, are donors, the bonds, 2′ and 3, being acceptors. The donors are on one side of the conjugation chain while the acceptors are on the other side. The D-A alternation occurs only twice along the conjugation. Such conjugation is classified into the continuous conjugation.[6] The delocalization is then subject to the orbital phase continuity-discontinuity property. The orbital phase requirements for many-system interaction are as follows:[5,6] (1) The electron-donating orbitals out of phase, (2) the electron-accepting orbitals in phase, and (3) the donating and accepting orbitals in phase. The requirements are satisfied in **3** (see **5**), but not in **4** (see **6**).[10] The cyclic delocalization is allowed in **3**, but forbidden in **4**. The mathematical equivalence of the 1→3 delocalization in **1** and **2** to the modes of cyclic delocalization in **3** and **4** means that the open-chain conjugated systems share a characteristic with the corresponding cyclic conjugated systems. *Even acyclic conjugation contains cyclic orbital interaction. The delocalizability in acyclic conjugation is also under the influence of the orbital phase property.*

Polarization. Only one-electron transferred configurations were taken into consideration in the preceding

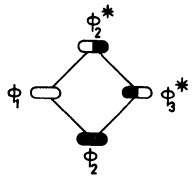

5

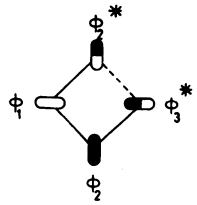

6

section. In general, locally-excited configurations contribute to the electronic structures of interacting systems. Let us study two interacting ethylenic double bonds in butadiene. There are two pathways for electron promotion in a double bond, as is illustrated in Scheme 3.[11] An electron in ϕ_1 transfers to ϕ_2^* ande thn back to ϕ_1^* (path e). Otherwise, an electron hole in ϕ_2 resulting from electron shift to ϕ_1^* is supplied with an electron by ϕ_1 (path f). The coefficients of the locally-excited 1→1 configuration, obtained in the same way,

$$C_e(1 \rightarrow 1) = \frac{\langle \Phi(0)|H'|\Phi(1 \rightarrow 2)\rangle\langle \Phi(1 \rightarrow 2)|H'|\Phi(1 \rightarrow 1)\rangle}{[E(1 \rightarrow 2) - E(0)][E(1 \rightarrow 1) - E(0)]}$$

$$C_f(1 \rightarrow 1) = \frac{\langle \Phi(0)|H'|\Phi(2 \rightarrow 1)\rangle\langle \Phi(2 \rightarrow 1)|H'|\Phi(1 \rightarrow 1)\rangle}{[E(2 \rightarrow 1) - E(0)][E(1 \rightarrow 1) - E(0)]}$$

have an identical magnitude and the opposite signs:

$$C_e(1 \rightarrow 1) = -C_f(1 \rightarrow 1).$$

Then

$$C(1 \rightarrow 1) = 0.$$

The polarization is depressed completely. The result is understood in terms of the cyclic orbital interaction (**7**). The polarization is also controlled by the continuity-discontinuity of orbital phase. The forbidden polarization justifies the neglect of the locally-excited configurations in the preceding arguments about the delocalization in polyenes.

Polarization Effects on Delocalization. The absence of the local excitation in polyenes comes from the

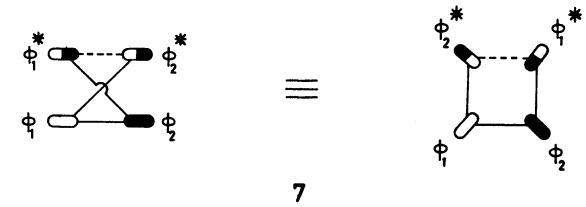

7

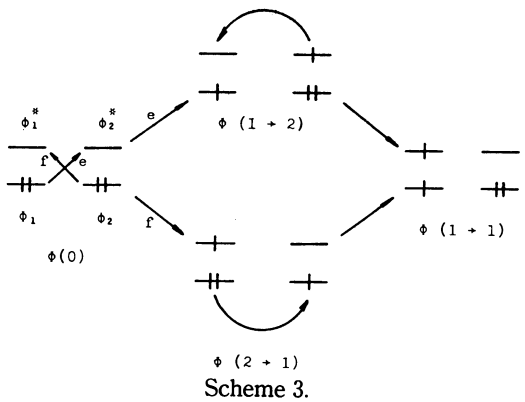

Scheme 3.

peculiar feature of the interaction between the equivalent systems at the equivalent sites like Y–X···X–Y (see C_e and C_f). An ethylenic π bond is usually polarized by the interactions with substituents or attacking reagents. Here, the effects of polarization on delocalization will be examined in terms of orbital phase, using the simple models, *i.e.*, disubstituted ethylenes, **8**—**13**. Electron-releasing (R) and withdrawing (W) substituents are represented by the doubly occupied bonding orbital of ethylene (E) and the vacant anti-bonding orbital, respectively. This model allows the substituted double bond to polarize by eliminating one of the pathways involving the opposite phase mixing of locally-excited configurations.

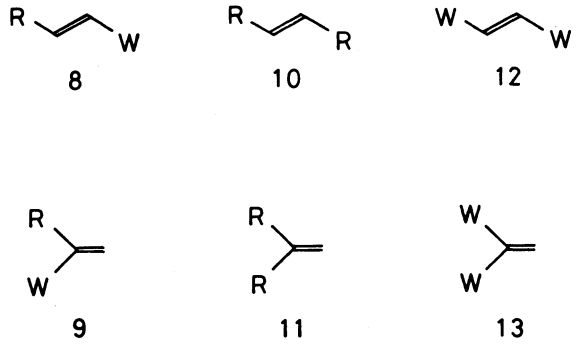

Electron delocalization primarily occurs from R to E and from E to W in R,W-substituted ethylenes, **8** and **9**. The present question is reduced to whether the mixing of the locally-excited configuration, $\Phi(E\rightarrow E)$, can enhance the delocalization or not. There are two pathways for electron promotion in E (Scheme 4). The electron hole in ϕ_r resulting from electron shift $\phi_r\rightarrow\phi_e^*$ is supplied with an electron by ϕ_e (path g). The electron is transferred from ϕ_e to ϕ_w^* and then back to ϕ_e^* (path h). The corresponding cyclic orbital interactions are **14** for **8** and **15** for **9**. The polarization is allowed in the *vic*-R,W-disubstituted ethylene **8** but not in the geminal isomer **9**. The allowed polarization enhances the delocalization due to the interactions of the locally-excited configuration $\Phi(E\rightarrow E)$ with the transferred configurations, $\Phi(R\rightarrow E)$ and $\Phi(E\rightarrow W)$.

The R→W delocalization in the vicinal isomer corresponds to the 1→3 delocalization in the head-to-tail triene. The cyclic orbital interaction is favored by the orbital phase (**5**). The delocalization is then promoted by the distant delocalization as well. On the other hand, the R→W delocalization in the geminal isomer

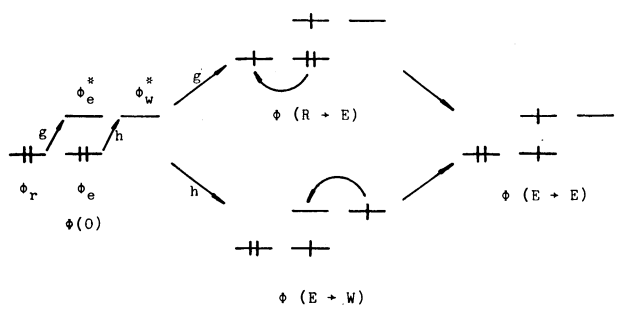

Scheme 4.

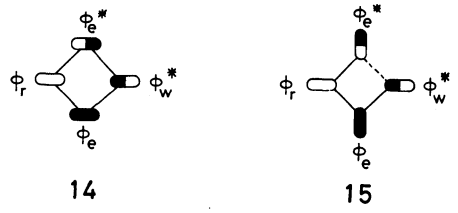

corresponds to the forbidden 1→3 delocalization in the head-to-head triene (**6**). The delocalization is never enhanced by the R→W delocalization. It is noteworthy that the cyclic orbital interactions, **14** and **15**, for the polarization of the double bond are common to those (**5** and **6**) for the distant R→W delocalization in the R,W-ethylenes. The cyclic orbital interactions have the dual meaning in this sense.

The mechanism of polarization in the R,R-disubstituted ethylenes, **10** and **11**, is illustrated in Scheme 5. An electron in ϕ_{r_1} (ϕ_{r_2}) is transferred to ϕ_2^* by the path i (path j). The resulting electron hole in ϕ_{r_1} (ϕ_{r_2}) is supplied with an electron by ϕ_e. The cyclic orbital interaction meets the phase continuity requirements in the *gem*-R,R-ethylene **11** (see **17**) while not in the vicinal isomer **10** (see **16**). A similar argument is applicable to the polarization in the W,W-ethylenes, **12** and **13**. The cyclic orbital interactions are shown in **18** for **12** and in **19** for **13**.

The geminal substituents of the same donor-acceptor property and the vicinal ones of the opposite donor-acceptor property enhance electron delocalization through the polarization. The latter substitution pattern

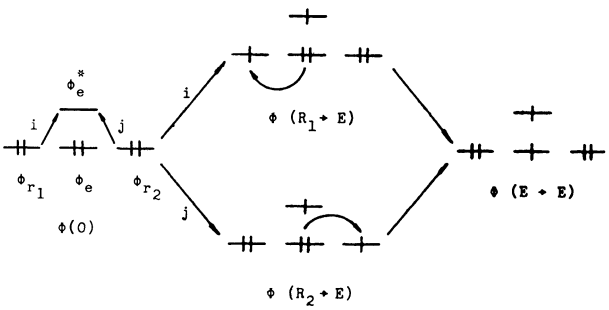

Scheme 5.

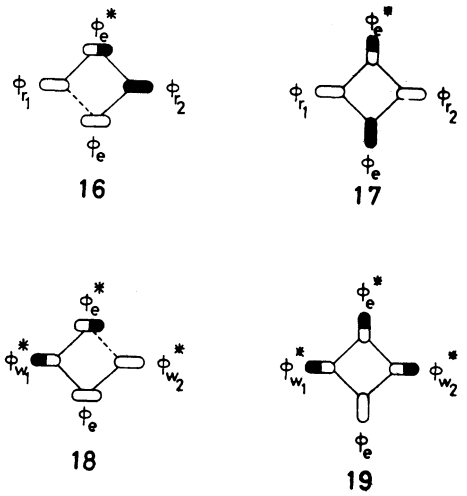

also promotes the delocalization by the distant R→W delocalization. The other models do not meet the orbital phase continuity requirements. As a result the delocalizability is predicted to increase in the order of *vic*-R,R (**10**), *vic*-W,W (**12**), *gem*-R,W (**9**)<*gem*-R,R (**11**), *gem*-W,W (**13**)<*vic*-R,W (**8**).

Calculation

We carried out calculation by a linear combination of electron configurations at the Hückel level (HMO–LCEC)[12] to examine the preceding theoretical conclusions in a numerical manner. The zero-configuration, $\Phi(0)$, the one-electron locally-excited configuration, $\Phi(n\rightarrow n)$, and the one-electron transferred configuration, $\Phi(n_1\rightarrow n_2)$, are involved in the calculation. Figure 1 shows the range of the coefficient ratios, $|C(n_1\rightarrow n_2)/C(0)|$, (see Appendix) of triene through nonaene as the function of the distance ($\Delta n=|n_1-n_2|$) between the double bonds where an electron transfers. The magnitude of the coefficient ratio reasonably decreases with the distance. There is no significant difference in the adjacent delocalization ($\Delta n=1$) between the head-to-head and head-to-tail polyenes. Most outstanding is the coefficient ratio of the distantly transferred configurations in the head-to-head polyenes; $|C(\Delta n)/C(0)|=0$ for $\Delta n\geqq 2$.[13] This is also the case with the locally-excited configurations in both types of polyenes; $C(n\rightarrow n)/C(0)=0$. These results confirm the theoretical prediction. The delocalization is "localized" between the neighboring double bonds in the head-to-head polyenes whereas farther delocalization can take place in the head-to-tail polyenes.

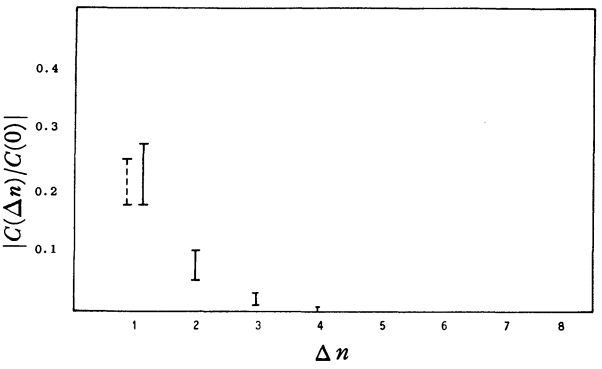

Fig. 1. The coefficient ratio ($C(\Delta n)/C(0)$) of the $n_1\rightarrow n_2$ transferred configurations to the zero-configuration for **1** (I) and **2** (I), where $\Delta n=n_1-n_2$.

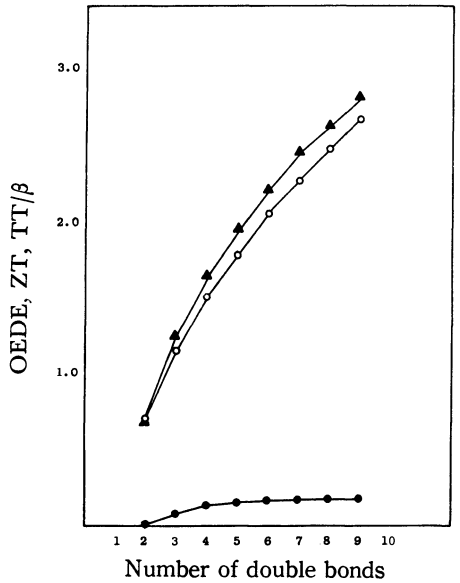

Fig. 2. The one-electron delocalization energies of **1** (▲) and **2** (○), the ZT energies of **1** (○) and **2** (○), and the TT energies of **1** (●) and **2** (zero).

We also calculated one-electron delocalization energy (OEDE),[14] which was recently proposed[8] to be a measure of electron delocalization. The head-to-tail polyenes have greater OEDE than the corresponding head-to-head polyenes (Fig. 2),[15] as is expected. The OEDE is composed of the ZT and TT energies.[8] The ZT energy is due to the interaction between $\Phi(0)$ and $\Phi(n_1\rightarrow n_2)$ or the donor-acceptor interaction between of neighboring bonds. The TT energy is due to the interactions between $\Phi(n_1\rightarrow n_2)$'s, and can be used as a measure of the distant delocalization. The ZT energies of both types of polyenes are found to be identical and equal to be the OEDE of the head-to-head polyenes. The TT energy is appreciable for the head-to-tail polyenes and zero for the head-to-head polyenes. As a result, the difference in OEDE or in electron delocalizability is attributed to the difference in the TT energy or in the distant delocalization. These numerical results argue for the prediction that the 1→3 delocalization is forbidden in the head-to-head polyenes while not in the head-to-tail polyenes.

The OEDE was calculated for the model compounds, **8**—**13**. The results are consistent with the prediction. The OEDE of the least delocalizing group including **9**, **10**, and **12** is 0.707β. The intermediately delocalizing **11** and **13** have 0.801β OEDE. The most delocalizing **8** has 0.905β. The OEDE increment from the first to the second group results from the contribution of polarization. Without polarization, the OEDE of both groups is identical (0.707β). The difference between the latter two groups is attributed to the allowed R→W electron delocalization in **8**. Without the transferred configuration, the OEDE is reduced to that of the second group (0.801β).

Discussion

The chemistry of the head-to-head polyenes has been advanced much less than that of the head-to-tail polyenes, presumably due to their instability inferred from the present theory. There are many works on the head-to-tail polyenes. A high polymer of the head-to-tail polyenes, *i.e.*, "polyacetylene," was synthesized more than two decade ago,[16] still attracting attention of chemists because of electrical conductivity of the doped material.[17] Polyacetylene was reported to contain 200—300 ethylenic double bonds.[18] In contrast, there are only a few reports[19] about the head-to-head polyenes limited to their low homologs or up to tetraenes. The present situation is similar for polycarbonyl com-

pounds, an analogous series of the head-to-head polyenes. Only a small number of reports on triones and tetraones are available.[20] No higher homologs were found in the literature.

Independent theoretical calculations make up for the insufficiency of the experimental results. Hess and Schaad[21] obtained the π-single-bond energy, E^{π}_{c-c}, of **1** and **2** from the Hückel molecular orbital calculation on the Dewar's assumption[22] that the bond energy is additive: $E^{\pi}_{c-c}=0.628\beta$ for **1** and 0.396β for **2**. The π-single-bond energy corresponds primarily to the electron delocalization between the double bonds. The conspicuous difference is consistent with our prediction. Del Re[23] calculated the interaction energies between the component systems in some π conjugated molecules. The interaction energy was found to be greater for the head-to-tail coupling than for the head-to-head coupling. Aihara[24] obtained the HMO energy of the unit structure, C=C–C, in cyclic head-to-tail (annulene) and head-to-head (radialene) polyenes, and showed E_u(annulene)$>E_u$(radialene). Kollmar[25] calculated the resonance energies of 1,3,5-hexatriene (**1**; $n=1$) and 3-methylene-1,4-pentadiene (**2**; $n=1$) as the energy difference between the ab initio SCF energy and the energy expectation value with respect to a model wavefunction in which the SCF π orbitals were replaced by appropriate nonresonating localized π MO's (reference state). The "vertical" and "normalized" resonance energies of the head-to-head triene are smaller by 2.3 and 0.3 kcal/mol than those of the head-to-tail triene.

The orbital phase control over the delocalization in acyclic conjugated molecules provides us with an unprecedented insight into a general aspect of cyclic conjugation. Cross-conjugation is an element in the cyclic conjugated hydrocarbons with exocyclic double bonds. The orbital phase discontinuity prohibited electrons from delocalizing from a π bond to another across the exocyclic π bond. The feature clearly distinguishes this class of molecules from cyclic head-to-tail polyenes where the acyclic delocalization is ideally favored by the orbital phase continuity. The orbital phase discontinuity in acyclic delocalization is a key to understanding the extreme instability of cyclic conjugated hydrocarbons with the exocyclic bonds such as fulvene (**20**),[26] heptafulvene (**21**),[26k,27] calicene (**22**),[28]

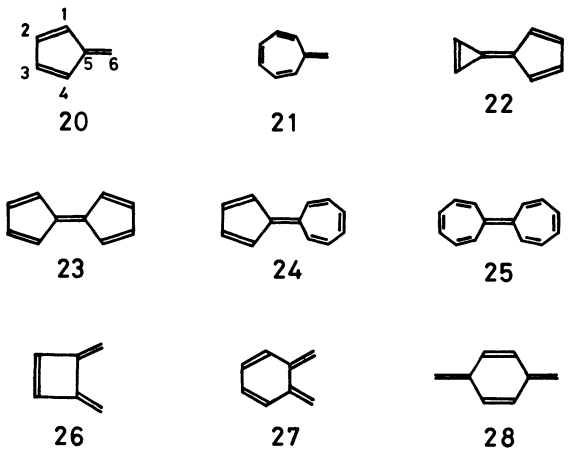

fulvalene (**23**),[29] sesquifulvalene (**24**),[26k,27e,27f,30] heptafulvalene (**25**),[29a,31] 3,4-dimethylenecyclobutene (**26**),[32] 5,6-dimethylene-1,3-cyclohexadiene (**27**),[33] and 3,6-dimethylene-1,4-cyclohexadiene (**28**),[34] irrespective of the number of electrons.

Appreciable stability is gained only when appropriate substituents are attached to the exocyclic bonds. There are usually both cyclically delocalizing and localizing modes of orbital interactions in a π conjugated molecules with exocyclic bonds.[6] The substituents make a delocalizing mode predominate over the localizing modes through the enhanced donor-acceptor power, on one hand. The orbital phase discontinuity for the delocalization across the exocyclic bond is partly due to the identical magnitude of the delocalization through the antibonding orbital of the exocyclic bond (path a) and through the bonding orbital (path b). The substituents prefer a path to the other, and relax the orbital phase discontinuity, on the other hand.

Some theoretical and experimental results argue for the peculiarity of the cross-conjugation in the molecules. Let us see the bond lengths or the bond orders in fulvene. There are two sorts of single bonds, *i.e.*, C_1–C_5 and C_2–C_3 bonds. The C_1–C_5 single bond is an element of the acyclic conjugations, *i.e.*, the head-to-tail C_4=C_3–C_2=C_1–C_5=C_6 and the head-to-head C_2=C_1–C_5(=C_6)–C_4=C_3. On the other hand, the C_2–C_3 bond belongs to the head-to-tail chains, *i.e.*, C_1=C_2–C_3=C_4–C_5=C_6 and C_4=C_3–C_2=C_1–C_5=C_6. Consequently, the delocalization is expected to be low in C_2=C_1···C_5=C_6 relative to that in C_1=C_2···C_3=C_4. In fact, the bond order[35,36] is smaller between C_1 and C_5 of the head-to-head junction than between C_2 and C_3 of the head-to-tail one. Some molecular orbital calculations[22a,37,38] predicted consistent bond lenghts. The bonds of the head-to-head conjugation are longer than those of the head-to-tail conjugation. This is confirmed by the electron diffraction study of the 6,6-dimethyl derivative.[39] A similar argument is applicable to and confirmed by the theoretical calculations and/or the experiments for **21**,[22a,35–37,40] **22**,[41] **23**,[22a,35–37,40b] **24**,[22a,36,37] **25**,[22a,35–37] **26**,[38,39,41,42] and **27**.[35,41]

The tendency to avoid the cross-conjugation is also recognized in pentalene (**29**),[43] azulene (**30**),[44] heptalene (**31**).[45] There are two possible ways to reduce the cross-conjugation effects by adjusting the bond distances; *i.e.*, by stretching the fused bond (C_7–C_8 in **29**, C_9–C_{10} in **30**, C_{11}–C_{12} in **31**) and the peripheral bonds (C_1–C_7, C_4–C_8 in **29**, C_1–C_9, C_4–C_{10} in **30**, C_1–C_{11}, C_6–C_{12} in **31**). The fused bond elongation provides the molecules with a quality of the peripheral monocyclic head-to-tail conjugation. With the lengthened peripheral bonds, the molecules acquire a property of acyclic head-to-tail polyenes. Azulene prefers monocyclic conjugation because of 10 π electrons. According to the experimental data,[46] the peripheral bond alternation is small. The deviation of the bond distances fall in the range of 0.03 Å. The fused bond is much longer by 0.07 Å than the longest peripheral bond. The similar theoretical results[37,40b] are available. On the other hand, pentalene and heptalene should choose acyclic conjugation because of 4n π electrons on the

periphery. Some calculations[37,40b,47] suggest that the peripheral cross-conjugated bond in pentalene is the weakest, the fused bond being stronger, while the single bonds between the endocyclic double bonds are much stronger than both. The shortening of the fused bond is interpreted as the geometrical deformation to gain the stabilization due to acyclic head-to-tail conjugation.

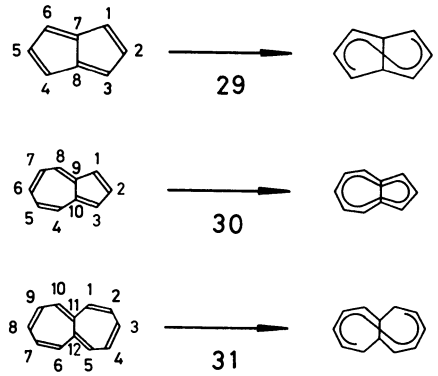

Acyclic Aromaticity. The degree of electron delocalization in trimethylenemethane (**32**) and butadiene (**33**) dianions was shown in a preliminary communication[48] to be determined by the orbital phase properties. Trimethylenemethane dianion is considered to be a π-conjugated molecule where two anion centers interact with an end of the double bond (see **34**). Butadiene dianion has the identical subsystems which, however, lie in the different relative positions (see **35**). The orbital phase aspects of the dianions are the same as those of the R,R-substituted ethylene models. Trimethylenemethane dianion corresponds to *gem*-R,R (**11**) while butadiene dianion corresponds to *vic*-R,R (**10**). The cyclic orbital interaction is favored by the orbital phase continuity in trimethylenemethane dianion (see **17** for **11**), but not in butadiene dianion (see **16** for **10**). This is consistent with the suggestion of "Y-aromaticity,"[49] with the experimental observation of the relative thermodynamical stabilities of the anions,[50] and with the heat of formation of the related species calculated by Schleyer *et al.*[51]

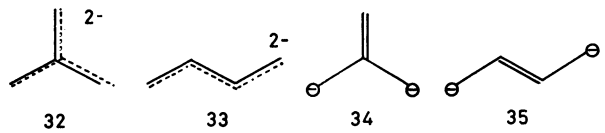

Tautomerim in Purines. A significant polarization effect is found in the protropic tauromerism of biological important bases, purine (**36a**; X=H) and adenine (**36b**; X=NH_2).[52] There is no difference in the Kekulé structures of the pyrimidine and imidazole rings between the 7H- and 9H-tautomers. The way of fusion of the heterocyclic rings distinguishes one from the other. The preceding theoretical result has shown that electrons delocalize to the greatest degree when R- and W-substituents are attached to the vicinal carbons of the C=C double bond. In both tautomers, the bond in the pyrimidine ring, vicinal to the electron-donating amino nitrogen in the imidazole ring, is identical, *i.e.*, the imino double bonds. However, the electron accepting power of the C=N moiety is different between C and N. The AO coefficient in the LUMO is larger at C than at N. The imino group is linked at the nitrogen, N_3, in the 7H-tautomer and at the carbon, C_6, in the 9H-tautomer. As a result the donor-acceptor disposition favors electron delocalization in the 9H-tautomer.

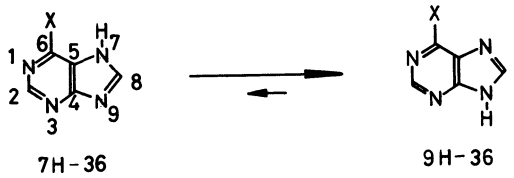

The calculation supports the prediction. The OEDE is by 0.021β greater for 9H-**36a** than for 7H-**36a**. In order to examine the origin of the difference, we carried out the calculations without the locally-excited configuration of each bond. The OEDE of the 9H-tautomer significantly decreases to be close to the almost unchanged OEDE of 7H-**36a**, when the polarization of the fused C_4=C_5 bond is excluded. The polarization effect of the other bond was found to be of negligible importance. Another series of calculations confirmed this conclusion. The OEDE difference between 7H- and 9H-**36a** is small ($\approx 0.005\beta$) when only transferred configurations are involved. With the inclusion of the fused bond polarization function, the difference increases up to 0.021β. The polarization of the other bonds makes no considerable change in OEDE. As a result, the relative stability of the purine tautomers is attributed to electron delocalization assisted by the polarization at the fused C_4=C_5 bond, or to the orbital phase continuity-discontinuity in the acyclic conjugation. A similar result of calculation were obtained for the tautomerism of adenine, *i.e.*, 6-aminopurine (**36b**).

This work was supported by a Grant-in-Aid for Scientific Research from the Ministry of Education, Science and Culture. The calculations were carried out by the HITAC-M200H computer, Institute for Molecular Science and the FACOM M-200 computer, Nagoya University Computer Center. The authors thank Prof. P. von R. Schleyer of Universität Erlangen-Nürnberg for private communication in prior to publication of the results (Ref. 51).

Appendix

The wavefunction, Ψ^M, of any electronic state of molecule, M, can be expanded[53] in terms of electron configurations including electron transferred and locally-excited configurations:

$$\Psi^M = C_0^M \Phi_0^M + \sum_K C_K^M \Phi_K^M,$$

where the zero-configuration, $\Phi(0)$ is the wavefunction of the reference state involving neither electron promotion nor shift. The magnitude of the configuration coefficients provides us with the information on the detail of electronic structure. A question comes to our minds when we compare the corresponding parts of electronic structure in different molecules. The number of configurations involved increases with the size of molecules or with the number of subsystems. Then the

magnitude of coefficients relatively decreases because of the normalization even if the chemical situation is equivalent. The coefficient ratio C_K/C_0 was, though intuitively, recommended as a preferable measure rather than C_K itself.[7] We present a rigorous meaning of the coefficient ratio.

Suppose an arbitrary molecule, R, as a reference, the wavefunction, Ψ^R, being expanded similarly:

$$\Psi^R = C_0^R \Phi_0^R + \sum_L C_L^R \Phi_L^R.$$

The wavefunction, Ψ^{RM}, of the combined system of R and M, where R and M do not interact with each other at all, is then as follows:

$$\begin{aligned}\Psi^{RM} &= \Psi^R \Psi^M \\ &= C_0^{RM} \Phi_0^R \Phi_0^M + \sum_K C_K^{RM} \Phi_0^R \Phi_K^M + \sum_L C_L^{RM} \Phi_L^R \Phi_0^M \\ &\quad + \sum_{K,L} C_{K,L}^{RM} \Phi_L^R \Phi_K^M,\end{aligned}$$

where

$$\begin{aligned}C_0^{RM} &= C_0^R C_0^M \\ C_K^{RM} &= C_0^R C_K^M \\ C_L^{RM} &= C_L^R C_0^M \\ C_{K,L}^{RM} &= C_L^R C_K^M.\end{aligned}$$

The configuration coefficients of the reference molecule in RM, C_L^{RM}, is dependent on the molecule, M. The coefficient, C_L^{RM}, should be invariable and equal to C_L^R when we study the electronic structure through comparing the configuration coefficients between different molecules. Dividing C_L^{RM} by C_0^M transforms the wavefuction as required:

$$C_L^{RM}/C_0^M = C_L^R.$$

The transformation leads to

$$C_K^{RM}/C_0^M = C_0^R(C_K^M/C_0^M).$$

The coefficient of the reference, C_0^R, can be taken to be a constant, *i.e.*, unity for the present purpose. It follows that C_K^M/C_0^M is a good measure for comparing different molecules.

References

1) E. Hückel, *Z. Phys.*, **70**, 204 (1931); **76**, 628 (1932).

2) R. B. Woodward and R. Hoffmann, *J. Am. Chem. Soc.*, **87**, 395 (1965); R. Hoffmann and R. B. Woodward, *ibid.*, **87**, 2046 (1965); R. B. Woodward and R. Hoffmann, *ibid.*, **87**, 2511 (1965).

3) For the frontier orbital approach in prior to the Woodward and Hoffmann works, see K. Fukui, "Molecular Orbitals in Chemistry, Physics, and Biology," ed by P.-O. Löwdin and B. Pullman, Academic Press, New York (1964), p. 513.

4) For the related works see: H. C. Longuet-Higgins and E. W. Abrahamson, *J. Am. Chem. Soc.*, **87**, 2045 (1965); K. Fukui, *Tetrahedron Lett.*, **1965**, 2009; *Bull. Chem. Soc. Jpn.*, **39**, 498 (1966); *Acc. Chem. Res.*, **4**, 57 (1971); M. J. S. Dewar, *Tetrahedron Suppl.*, **8**, 75 (1966); *Angew. Chem.*, **83**, 859 (1971); H. E. Zimmerman, *J. Am. Chem. Soc.*, **88**, 1563, 1566 (1966); *Acc. Chem. Res.*, **4**, 272 (1971); **5**, 393 (1972); R. G. Pearson, *J. Am. Chem. Soc.*, **91**, 1252, 4947 (1969); **94**, 8287 (1972); *Acc. Chem. Res.*, **4**, 152 (1971); C. Trindle, *J. Am. Chem. Soc.*, **92**, 3251, 3255 (1970); W. A. Goddard III, *ibid.*, **94**, 793 (1972); T. F. George and J. Ross, *J. Chem. Phys.*, **55**, 3851 (1971).

5) K. Fukui and S. Inagaki, *J. Am. Chem. Soc.*, **97**, 4445 (1975); S. Inagaki, H. Fujimoto, and K. Fukui, *ibid.*, **98**, 4693 (1976).

(6) S. Inagaki and Y. Hirabayashi, *J. Am. Chem. Soc.*, **99**, 7418 (1977).

7) S. Inagaki and Y. Hirabayashi, *Bull. Chem. Soc. Jpn.*, **51**, 2283 (1978).

8) S. Inagaki and Y. Hirabayashi, *Inorg. Chem.*, **21**, 1798 (1982).

9) The mechanism of electron delocalization among many systems in such a form as described in the text has been proposed and successfully applied to various chemical problems;[5-8] see also: J. P. Malrieu, "Localization and Delocalization in Quantum Chemistry," ed by O. Chalvet *et al.*, D. Reidel Publishing Company, Dordrecht-Holland (1975), Vol. 1, p. 335.

10) In the illustrations of the orbital phase relation throughout the paper, the solid and dashed lines denote the orbital pairs between which the phase requirements are satisfied and dissatisfied, respectively. In general, there are an odd number of the orbital pairs dissatisfying the requirements, in the discontinuous orbital phase systems, while an even number of them in the continuous ones. The number can be reduced to one or zero, respectively. The continuity-discontinuity of the orbital phase is a property of a whole molecule but not of specific parts of molecule. However, it is preferable to place the discontinuity between the HOMO's or between the LUMO's in the illustrations if possible since the HOMO–LUMO interaction is more primary.

11) Our attention is confined to the mixing-in of the locally-excited configurations through orbital overlapping though there are the other origins of polarization, *e.g.*, electrostatic interaction.

12) a) The method[8] is a simple extension of the "Molecules in Molecule" approach[b,c] in the sense that the interaction is considered to occur among many systems; b) H. C. Longuet-Higgins and J. N. Murrell, *Proc. Phys. Soc.*, **A68**, 601 (1955); c) J. N. Murrell, *ibid.*, **A68**, 969 (1955).

13) According to the HMO–ECAMSI calculation,[7] $C(\Delta n$: odd) has non-zero (negligibly small) value, possibly because the other configurations than are involved in the HMO–LCEC calculations are contained implicitly.

14) The total energy of the HMO–LCEC calculation[8,12a] is decomposed into three terms:

$$E = \sum_M C_M^2 H_{MM} + 2\sum_{M\neq 0} C_0 C_M H_{OM} + 2\sum_{M<N} C_M C_N H_{MN}.$$

The OEDE is defined as a measure of the delocalization to be the sum of the energies of the interactions between $\Phi(0)$ and $\Phi(n_1 \to n_2)$ (the second terms denoted by the ZT energy) and those between $\Phi(n_1 \to n_2)$'s (the third terms denoted by the TT energy). The energy of the interaction between $\Phi(n \to n)$ and $\Phi(n_1 \to n_2)$ is here contained in the latter terms.

15) This is also the case with the normal HMO total energy.

16) G. Natta, G. Mazzanti, and P. Corradini, *Atti. Acad. Nazl. Lincei, Rend. Classe Sci. Fis. Mat. Nat.*, **25**, 3 (1958); For the recent work see: T. Ito, H. Shirakawa, and S. Ikeda, *J. Polym. Sci., Polym. Chem. Ed.*, **12**, 11 (1974).

17) H. Shirakawa and S. Ikeda, *Polym. J.*, **2**, 231 (1971); H. Shirakawa, T. Ito, and S. Ikeda, *ibid.*, **4**, 460 (1973); T. Ito, H. Shirakawa, and S. Ikeda, *J. Polym. Sci., Polym. Chem. Ed.*, **13**, 1943 (1975); H. Shirakawa, E. J. Louis, A. G. MacDiarmid C. K. Chiang, and A. J. Heeger, *J. Chem. Soc., Chem. Commun.*, **1977**, 578; C. K. Chiang, C. R. Fincher, Jr., Y. W. Park, A. J. Heeger, H. Shirakawa, E. J. Louis, S. C. Gau, and A. G. MacDiarmid, *Phys. Rev. Lett.*, **39**, 1098 (1977); C. K. Chiang, Y. W. Park, A. J. Heeger, H. Shirakawa, E. J. Louis, and A. G. MacDiarmid, *J. Chem. Phys.*, **69**, 5098 (1978); C. K. Chiang, M. A. Druy, S. C. Gau. A. J. Heeger, E. J. Louis, A. G. MacDiarmid, Y. W. Park, and H. Shirakawa, *J. Am. Chem. Soc.*, **100**, 1013 (1978); T. C. Clarke, R. H. Geiss, J. F. Kwark,

and G. B. Street, *J. Chem. Soc., Chem. Commun.*, **1978**, 338, 489; H. Kiess, W. Meyer, D. Baeriswyl, G. Harbeke, *J. Electron. Mater.*, **9**, 763 (1980).

18) K. Soga, S. Kawakami, H. Shirakawa, and S. Ikeda, *Makromol. Chem., Rapid Commun.*, **1**, 523 (1980).

19) W. J. Bailey and J. Economy, *J. Am. Chem. Soc.*, **77**, 1133 (1955); W. R. Roth and G. Erker, *Angew. Chem.*, **85**, 510 (1973); W. R. Roth, M. Heiber, and G. Erker, *ibid.*, **85**, 511 (1973); W. R. Roth and G. Erker, *ibid.*, **85**, 512 (1973); W. Grime and H.-J. Rother, *ibid.*, **85**, 512 (1973); R.C. Larock, *J. Org. Chem.*, **41**, 2241 (1976); H. Yasuda, Y. Ohnuma, M. Yamauchi, H. Tani, and A. Nakamura, *Bull. Chem. Soc. Jpn*, **52**, 2036 (1979); U. H. Brinker and L. König, *J. Am. Chem. Soc.*, **103**, 212 (1981).

20) P. Piutti, *Gazz. Chim. Ital.*, **66**, 276 (1936); M. A. Mendelsohn, E. M. Arnett, and H. Freiser, *J. Phys. Chem.*, **64**, 660 (1960); J. P. Schaefer, *J. Am. Chem. Soc.*, **84**, 713 (1962); E. M. Arnett, H. Freiser, and M. A. Mendelsohn, *ibid.*, **84**, 2482 (1962); E. M. Arnett and M. A. Mendelsohn, *ibid.*, **84**, 3821, 3824 (1962); C. F. Cullis and A. Fish, "The Chemistry of Carbonyl Group;" ed by S. Patai, Interscience, New York (1966), Chap. 2.

21) B. A. Hess, Jr., and L. J. Schaad, *J. Am. Chem. Soc.*, **93**, 305 (1971).

22) a) M. J. S. Dewar and G. J. Gleicher, *J. Am. Chem. Soc.*, **87**, 692 (1965); b) M. J. S. Dewar and C. de Llano, *ibid.*, **91**, 789 (1969).

23) G. Del Re, "Aromaticity, Pseudo-Aromaticity, Anti-Aromaticity," ed by E. D. Bergmann and B. Pullman, Israel Academy of Sciences and Humanities, Jerusalem (1971), p. 74.

24) J. Aihara, *Bull. Chem. Soc. Jpn.*, **48**, 517 (1975).

25) H. Kollmar, *J. Am. Chem. Soc.*, **101**, 4832 (1979).

26) a) J. Thiec and J. Wiemann, *Bull. Soc. Chim. Fr.*, **1956**, 177; b) H. J. F. Angus and D. Bryce-Smith, *J. Chem. Soc.* **1960**, 1409; c) H. J. F. Angus, J. M. Blair, and D. Bryce-Smith, *ibid.*, **1960**, 2003; d) E. Sturm and K. Hafner, *Angew. Chem.*, **76**, 862 (1964); e) D. Meuche, M. Neuenschwander, H. Schaltegger, and H. U. Schlunegger, *Helv. Chim. Acta*, **47**, 1211 (1964); f) H. Schaltegger, M. Neuenschwander, and D. Meuche, *ibid.*, **48**, 955 (1965); g) H. R. Ward and J. S. Wishnok, *J. Am. Chem. Soc.*, **90**, 1085 (1968); h) T. L. Rose, *Chem. Commun.*, **1969**, 95; i) J. E. Kent and A. J. Jones, *Aust. J. Chem.*, **23**, 1059 (1970); j) C. Wentrup and P. Müller, *Tetrahedron Lett.*, **1973**, 2915; k) R. Hollenstein, A. Mooser, M. Neuenschwander, and W. V. Philipsborn, *Angew. Chem.*, **86**, 595 (1974).

27) a) W. v. E. Doering and D. W. Wiley, *Tetrahedron*, **11**, 183 (1960); b) D. S. Matteson, J. J. Drysdale, and W. H. Sharkey *J. Am. Chem. Soc.*, **82**, 2853 (1960); c) C. Jutz, *Chem. Ber.*, **97**, 2050 (1964); d) H. E. Zimmerman and L. R. Sousa, *J. Am. Chem. Soc.*, **94**, 834 (1972); e) M. Neuenschwander and W. K. Schenck, *Chimia*, **26**, 194 (1972); f) W. K. Schenck, R. Kyburz, and M. Neuenschwander, *Helv. Chim. Acta*, **58**, 1099 (1975).

28) For the derivatives see: H. Prinzbach, D. Seip, and U. Fischer, *Angew. Chem.*, **77**, 258, 621 (1965); W. M. Jones and R. S. Pyron, *J. Am. Chem. Soc.*, **87**, 1608 (1965); A. S. Kende and P. T. Izzo, *ibid.*, **87**, 1609, 4162 (1965); M. Ueno, I. Murata, and Y. Kitahara, *Tetrahedron Lett.*, **1965**, 2967; E. D. Bergmann and I. Agranat, *Chem. Commun.*, **1965**, 512; Y. Kitahara, I. Murata, M. Ueno, K. Sato, and H. Watanabe, *ibid.*, **1966**, 180; A. S. Kende, P. T. Izzo, and P. T. MacGregor, *J. Am. Chem. Soc.*, **88**, 3359 (1966); H. Prinzbach and U. Fischer, *Helv. Chim. Acta*, **50**, 1669 (1967); H. Shimanouchi, T. Ashida, Y. Sasada, M. Kakudo, I. Murata, and Y. Kitahara *Tetrahedron Lett.*, **1967**, 61; H. Prinzbach and E. Woischnik, *Helv. Chim. Acta*, **52**, 2472 (1969).

29) W. v. E. Doering, *Theor. Org. Chem., Pap. Kekulé Symp.*, **1959**, 35; W. B. DeMore, H. O. Pritchard, and N. Davidson, *J. Am. Chem. Soc.*, **81**, 5874 (1959); K. V. Scherer, Jr., *ibid.*, **85**, 1550 (1963).

30) H. Prinzbach and W. Rosswog, *Angew. Chem.*, **73**, 543 (1961). For the derivatives see: H. Prinzbach, *ibid.*, **73**, 169 (1961); H. Prinzbach and D. Seip, *ibid.*, **73**, 169 (1961); H. Prinzbach, D. Seip, L. Knothe, and W. Faisst, *Justus Liebigs Ann. Chem.*, **698**, 34 (1966); H. Prinzbach, D. Seip, and G. Englert, *ibid.*, **698**, 57 (1966); G. Seiz, *Angew. Chem.*, **79**, 96 (1967); E.K.V. Gustorf, M. C. Henry, and P. V. Kennedy, *ibid.*, **79**, 616 (1967); H. Prinzbach and H. Knöfel, *ibid.*, **81**, 900 (1969); H. Prinzbach and H. Sauter, *ibid.*, **84**, 115 (1972); *Tetrahedron Lett.*, **1974**, 3049.

31) W. M. Jones and C. L. Ennis, *J. Am. Chem. Soc.*, **91**, 639 (1969); R. C. Joines, A. B. Turner, and W. M. Jones, *ibid.*, **91**, 7754 (1969); C. Went and K. Wilczek, *Helv. Chim. Acta*, **53**, 1459 (1970).

32) M. L. Heffernan and A. J. Jones, *Chem. Commun.*, **1966**, 120; B. A. Coller, M. L. Heffernan, and A. J. Jones, *Aust. J. Chem.*, **21**, 1807 (1968).

33) C. R. Flynn and J. Michl, *J. Am. Chem. Soc.*, **95**, 5802 (1973); **96**, 3280 (1974); E. Migirdicyan, *C. R. Acad. Sci.*, **266**, 756 (1968); E. Migirdicyan and J. Baudet, *J. Am. Chem. Soc.*, **97**, 7400 (1975); T. Kametani, K. Ogasawara, and T. Takahashi, *J. Chem. Soc., Chem. Commun.*, **1972**, 675; R. Hug, H.-J. Hansen, and H. Schmidt, *Helv. Chim. Acta*, **55**, 10 (1972); W. Oppolzer, *Angew. Chem.*, **84**, 1108 (1972); L. Klasinc, E. Pop, N. Trinajstic, and J. V. Knop, *Tetrahedron*, **28**, 3465 (1972); G. M. Priestly, and R. N. Warrenner, *Tetrahedron Lett.*, **1972**, 4295; K. Blatt and R. W. Hoffmann, *Justus Liebigs Ann. Chem.*, **760**, 114 (1972).

34) E. A. Errede and J. P. Cassidy, *J. Phys. Chem.*, **67**, 73 (1963); E. A. Errede and W. D. English, *J. Org. Chem.*, **28**, 2646 (1963) and references cited therein.

35) E. Heilbronner and H. Bock, "Das HMO-Modell und Seine Anwendung," Verlag Chemie, Weiheim/Bergstr. (1970).

36) T. Nakajima, "Molecular Orbitals in Chemistry, Physics, and Biology," ed by P.-O. Löwdin and B. Pullman, Academic Press, New York (1964), p. 451.

37) T. Nakajima, A. Toyota, and S. Fujii, *Bull. Chem. Soc. Jpn.*, **45**, 1022 (1972).

38) A. Skancke, "Aromaticity, Pseudo-Aromaticity, Anti-Aromaticity," ed by E. D. Bergmann and B. Pullman, The Israel Academy of Sciences and Humanities, Jerusalem (1971), p. 192.

39) J. F. Chiang and S. H. Bauer, *J. Am. Chem. Soc.*, **92**, 261 (1970).

40) a) D. J. Bertelli, "Topics in Nonbenzenoid Aromatic Chemistry," ed by T. Nozoe, R. Breslow, K. Hafner, S. Ito, and I. Murata, Hirokawa, Tokyo (1973), p. 29; b) H. Kuroda, T. Ohta, T. L. Kunii, "Aromaticity, Pseudo-Aromaticity, Anti-Aromaticity," ed by E. D. Bergmann and B. Pullman, The Israel Academy of Sciences and Humanities, Jerusalem (1971), p. 236.

41) J. D. Roberts, A. Streitwieser, Jr., and C. M. Regan, *J. Am. Chem. Soc.*, **74**, 4579 (1952).

42) A. Skancke, *Acta Chem. Scand.*, **22**, 3239 (1968).

43) The parent compound and its derivatives with weakly perturbing substituents have never been detected but proposed as the intermediates leading to the dimerization products [R. Bloch, R. A. Marty, and P. de Mayo, *J. Am. Chem. Soc.*, **93**, 3071 (1971); K. Hafner, R. Könges, E. Goedecke, and R. Kaiser, *Angew. Chem.*, **85**, 362 (1973)]. For the derivatives see: E. LeGoff, *J. Am. Chem. Soc.*, **84**, 3975 (1962); K. Hafner and H. U. Süss, *Angew. Chem.*, **85**, 626 (1973); K. Hafner and M. Suda, *ibid.*, **88**, 341 (1976).

44) E. Heilbronner, "Nonbenzenoid Aromatic Compounds,"

ed by D. Ginsburg, Interscience, New York (1959), p. 171; The structure was determined [A. S. Pfau and P. A. Plattner, *Helv. Chim. Acta*, **19**, 858 (1936)].

45) H. J. Dauben, Jr., and D. Bertelli, *J. Am. Chem. Soc.*, **83**, 4659 (1961); E. Vogel, H. Königshofen, J. Wassen, K. Müllen, and J. F. M. Oth, *Angew. Chem.*, **86**, 777 (1974); L. A. Paquette, A. R. Browne, and E. Chamot, *ibid.*, **91**, 581 (1979); for the derivatives see: E. Vogel and J. Ippen, *ibid.*, **86**, 778 (1974); E. Vogel and F. Hogrefe, *ibid.*, **86**, 779 (1974); K. Hafner, H. Diehl, and H. U. Süss, *ibid.*, **88**, 121 (1976).

46) J. M. Robertson, M. M. Shearer, G. A. Sim, and D. G. Watson, *Acta Crystallogr.*, **15**, 1 (1962).

47) T. Nakajima, Y. Yaguchi, R. Kaeriyama, and Y. Nemoto, *Bull. Chem. Soc. Jpn.*, **37**, 272 (1964).

48) S. Inagaki and Y. Hirabayashi, *Chem. Lett.*, **1982**, 709.

49) P. Gund, *J. Chem. Educ.*, **49**, 100 (1972).

50) J. Klein and A. Medlik, *J. Chem. Soc., Chem. Commun.*, **1973**, 275; N. S. Mills, J. Shapiro, and M. Hollingsworth, *J. Am. Chem. Soc.*, **103**, 1263 (1981).

51) T. Clark, D. Wilhelm, and P. von. R. Schleyer, *Tetrahedron Lett.*, **23**, 3547 (1982).

52) For a review see: B. Pullman and A. Pullman, *Adv. Heterocycl. Chem*, **13**, 77 (1971); for the recent experimental studies see: M.-T. Chenon, R. J. Pugmire, D. M. Grant, R. P. Panzica, and L. B. Townsend, *J. Am. Chem. Soc.*, **97**, 4636 (1975); J. W. Eastman, *Ber. Bunsenges. Phys. Chem.*, **73**, 407 (1969); M. Dreyfus, G. Dodin, O. Bensaude, and J. E. Dubois, *J. Am. Chem. Soc.*, **97**, 2369 (1975).

53) H. Baba and S. Suzuki, *Bull. Chem. Soc. Jpn.*, **40**, 2457 (1967); H. Baba, S. Suzuki, and T. Takemura, *J. Chem. Phys.*, **50**, 2078 (1969); for the extension to many-system interaction, see Ref. 7; G. Favini and G. Buemi, *Theoret. Chim. Acta (Berl.)*, **24**, 61 (1972).

 © 1982 The Chemical Society of Japan Bull. Chem. Soc. Jpn., 55, 3733—3737 (1982)

Thermal Decomposition of Calcium Sulfate Dihydrate under Self-generated Atmosphere

Kimio Isa* and Hiroki Okuno

Department of Chemistry, Faculty of Education, Fukui University, Bunkyo 3-9-1, Fukui 910

(Received April 1, 1982)

Dehydration of calcium sulfate dihydrate was studied by means of simultaneous TG-DTG-DTA under various sealed atmospheres corresponding to three systems open, completely sealed, and quasi-sealed. Two dehydration steps could be detected under self-generated atmospheres by using 12.3, 18.7, 30.0, and 250 μm tungsten wires. This new method enables us to identify intermediates more easily than any other techniques hitherto adopted. Endothermic DTA peaks appeared earlier, at 129 and 133 °C, than the point of decreasing TG. This technique, resembling the quasi-isothermal and -isobaric thermogravimetry (Q-TG), is superior to Q-TG in that it requires smaller amounts of sample.

By the self-generated atmosphere[1] is meant an atmosphere which is composed of gaseous decomposition products of a reaction and which is in intimate contact with the sample with the aid a sample holder employed. In the case of thermal decompositions producing gases, the equilibrium will be attained for the partial pressure of the gases. It was reported[2] that a thermal decomposition of ammoniumh eptamolybdate(6−) tetrahydrate ($(NH_4)_6Mo_7O_{24}\cdot 4H_2O$, AHM) producing both H_2O and NH_3 was studied by means of simultaneous TG-DTG-DTA from room temperature to 500 °C under static air atmosphere and flow conditions of various gases. This system was also subjected to Q-derivatography (quasi-isothermal and -isobaric thermogravimetry) and home-built quasi-sealed thermogravimetry.[3] The first step of the thermal decomposition of AHM was considered to be associated with two reaction schemes,[4-6] one Funaki's scheme and the other Ma's. Our results proposed a new reaction scheme, and disclosed a new intermediate stage. However, it was difficult to get rid of intermediates out of the apparatus and also more difficult to identify the intermediate because of the uncertainty of element analysis. Until then we had been able to clarify the existence of anhydrous after dehydration and the new intermediate had been confirmed by means of high-temperature oscillating X-ray diffraction with a rotating anode-type large-capacity generator.[7] In the case of thermal decomposition of AHM, our conclusion was that both H_2O and NH_3 are capable of desorbing simultaneously after dehydration. As to the self-generated atmospheres of H_2O and NH_3, the thermal decomposition mechanism was affected by that changeable condition.

Next, we selected calcium sulfate dihydrate ($CaSO_4\cdot 2H_2O$) as a model substance since it produces only H_2O in its thermal decomposition from room temperature to 400 °C which may be followed by TG-DTG-DTA and quasi-sealed TG.

There are various dynamical techniques for thermal analysis which are powerful for studying the thermal decomposition. Instruments have become capable of auto-operation, thus improving both the accuracy and precision of measurements as well as reducing both investigator's time and patience. Advantages of these methods are that extremely small amounts of sample may be required, that operator's time may considerably be saved, and that reaction rate may be determined very easily. But information furnished from various apparatus are different from one another. In order to eliminate the above disadvantages, we will discuss the applicability of the quasi-sealed TG under the condition of self-generated atmosphere.

Experimental

Materials. Calcium sulfate dihydrate of Wako Co. or Nakarai Co. (GR quality) was used in the form of powder. The sample amounts used were from 0.0023 mmol (0.40 mg) to 0.10 mmol (18 mg) and the reference material used for DTA was α-Al_2O_3.

Apparatus. A modified Thermoflex 8002 (Rigaku Denki Co.) was used for simultaneous TG-DTG-DTA measurements. The range of temperature covered was usually from room temperature to 360 °C and the sample was heated, in most cases, at the rate of 1 °C/min (the mean heating rate 1.005 °C/min).

Quasi-sealing. Aluminium small pan and cover (Rigaku Denki Co.) were sealed completely by the sample sealer for liquid materials (Rigaku Denki Co.) (Fig. 1). For the purpose of quasi-sealing, both aluminium pan and the cover and thin tungsten wire (12.3, 18.7, 30.0, 250, or 250 μmϕ × 2) were sealed in the same way as illustrated (Fig. 1(a)) and this sealed pan had a small leak along the thin wire. In the case of completely sealed pan, the critical explosion pressure had been determined to be above 3 atm.[8]

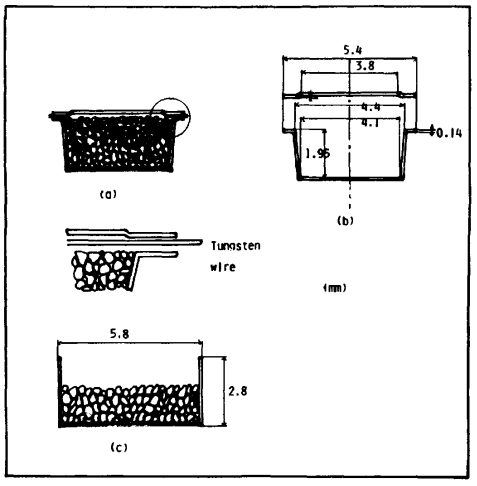

Fig. 1. a) Schematic diagram of a sample cell, aluminum cell. b) Dimension of sample cell. c) Schematic diagram of a sample cell, platinum cell.

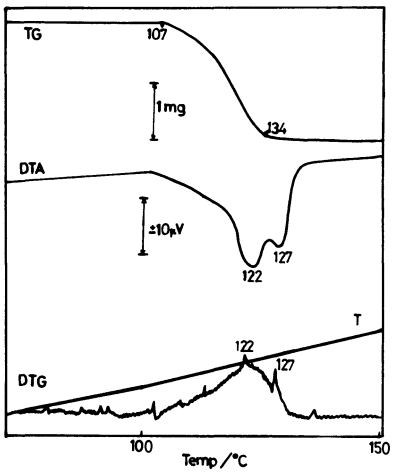

Fig. 2. TG-DTG-DTA of calcium sulfate dihydrate under open system. Sample amount is 0.067 mmol. Reference material is α-Al_2O_3. Cell is platinum. Heating rate is 1 °C/min.

Results and Discussion

Open System. With platinum cells (Fig. 1(c)), sample weights were changed from 0.0289 mmol (4.98 mg) to 0.090 mmol (15.56 mg) and simultaneous TG-DTG-DTA measurements were run. The range of TG used was usually 10 mg, and the ranges of DTA used were both ± 100 and ± 20 μV (the upper side corresponds to exothermic reaction). Typical results for 0.067 mmol of $CaSO_4 \cdot 2H_2O$ are shown in Fig. 2. The results of TG indicates two different types of descent tendencies and the result of DTG also indicates two peaks but they cannot be seperated from each other completely. If we want to analyse the thermal decomposition by the Freeman-Carroll[9] or Coats-Redfern method,[10] we must discuss these methods.

The endothermic peak of DTA owing to dehydration begins at 102 °C, and the descends of TG and DTG curves begin at 107 and 102 °C, respectively. For the simultaneous technique, the same temperature of 102 °C indicates the coincidence of the thermal and thermogravimetric behaviours of dehydration. But this temperature is not easy to be regarded as the decomposition temperature because the temperature would change if we change some experimental conditions, *e.g.*, the sample amount, heating rate, sensitivity of TG, DTG, and DTA, and signal-to-noise ratio. The DTA peak is divided into two peaks at 122 and 130 °C, and the reaction steps may be considered to be composed of two. With the method described in a previous report[11] it was difficult to seperate reaction steps into two.

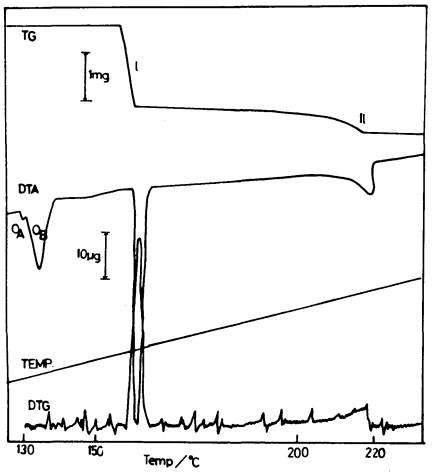

Fig. 3. TG-DTG-DTA of calcium sulfate dihydrate under completely sealed system. Sample amount is 0.0670 mmol. Reference material is α-Al_2O_3. Cell is aluminum. Heating rate is 1 °C/min.

Completely Sealed System. According to the suggestion of Miyazaki,[11] in order to obtain TG-DTA curves in an atmosphere containing much water vapor, TG-DTG-DTA measurements on samples of 0.0136, 0.0293, and 0.0670 mmol were run in the completely sealed system. The results of TG-DTG-DTA for the open system is apparently different from that for the completely sealed system. Figure 3 shows results of the sample of 0.0670 mmol. Concerning the TG results, the first step of TG seems to be a rapid decreasing reaction which corresponds to the dehydration of $\frac{3}{2}H_2O$ to produce $CaSO_4 \cdot \frac{1}{2}H_2O$, from a calculation of weight losses. Concerning the results of DTA, both endothermic peaks of the first and second steps to be at 162 and 219 °C, respectively. At lower temperatures than these, endothermic peaks without decreasing TG appear to be around 129 and 133 °C. These are named the O_A and O_B steps. Such behaviour is observed in 15 cases of sample weights ranging from 0.0030 to 0.0714 mmol. Almost the same temperature is registered for each group of O_A and O_B steps.

Reaction scheme for the TG descent may be considered as follows:

$$CaSO_4 \cdot 2H_2O \longrightarrow CaSO_4 \cdot \frac{1}{2}H_2O + \frac{3}{2}H_2O, \quad \text{(I)}$$

hemihydrate (15.70% loss)

$$CaSO_4 \cdot \frac{1}{2}H_2O \longrightarrow CaSO_4 + \frac{1}{2}H_2O. \quad \text{(II)}$$

nonhydrate (5.23% loss)

The rapid descent of the first step of TG is considered to be in the following sequence. Desorption of H_2O owing to hydration at the O_A and O_B steps and after these steps continue gradually, and the equilibrium vapor pressure is increased greatly by a rise in temperature, until the aluminum pan is caused to explode above the critical pressure. Considering the change in weight of H_2O, 1.812 mg, and the capacity of the sealed cell, 0.029 cm^3, the water vapour pressure is as high as about 6 atm at 159 °C.[9] Then H_2O of 0.0049 mmol is liberated and equilibrated. Over the critical pressure for the aluminium pan, the sealed pan is opened under the vapor pressure of H_2O and the vapor is allowed to escape from the sealed pan through the leak. The equilibrium of Reaction I is disturbed, the self-generated atmosphere is removed from the pan, and the unreacted water of Reaction I begins to be liberated rapidly. The rapid descent for the first decomposition step is caused in such a way that the response rate is

slower than the reaction rate or both rates were fast so that the equilibrium is disturbed and the unreacted substance is changed under a superheated condition. We must consider the situation more carefully. However, the temperature of 159 °C is higher than the end temperature of the second reaction illustrated in Fig. 2 (static condition), but it is important that the second reaction is not yet allowed to begin. A summary of the results of TG, DTG, DTA suggests a mechanism for the hydration which is considerably different from that of the first reaction. The results of TG were analyzed by the Coats-Redfern method, the reaction order, n, being determined as follows:

1) In the case of sample weight 15.08 mg and diameter of tungsten wire 12.3 μm:
I step: 2.0 order reaction.
II step: 1.0 order reaction.

2) In the case of sample weight 10.00 mg and diameter of tungsten wire 30.0 μm:
I step: 2.5 order reaction.
II step: 1.0 order reaction.

According to published results,[11] the first reaction step has been considered to be dehydration of structural water and the second reaction step to be dehydration of mobile water. But this water may come out at relatively high temperatures and the temperature ranges for the two dehydrations are about 60 °C. Until now we couldn't ewplain this behaviour by means of the sealed method or on account of property of mobile water. Moreover, in order to compare the decompositions of $CaSO_4 \cdot \frac{1}{2}H_2O$ and $CaSO_4 \cdot 2H_2O$ by means of the completely sealed TG, measurements were made by TG-DTG-DTA. The same results were obtained except the behavior of the water previously adsorbed (Fig. 4). The second steps of both $CaSO_4 \cdot \frac{1}{2}H_2O$ and $CaSO_4 \cdot 2H_2O$ were almost the same. For this reason the product of the first step of decomposition of $CaSO_4 \cdot 2H_2O$ may be considered to be $CaSO_4 \cdot \frac{1}{2}H_2O$.

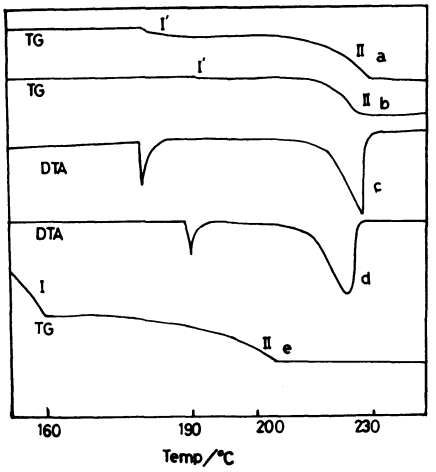

Fig. 4. TG-DTA of $CaSO_4 \cdot \frac{1}{2}H_2O$ under completely sealed method.
a): TG, sample amount is 18.73 mg ($CaSO_4 \cdot \frac{1}{2}H_2O$),
b): TG, sample amount is 15.38 mg ($CaSO_4 \cdot \frac{1}{2}H_2O$),
c): DTA, sample amount is 18.73 mg ($CaSO_4 \cdot \frac{1}{2}H_2O$),
d): DTA, sample amount is 15.38 mg ($CaSO_4 \cdot \frac{1}{2}H_2O$),
e): TG, sample amount is 11.57 mg ($CaSO_4 \cdot 2H_2O$).

With respect to these O_A and O_B peaks, Table 1 and Fig. 5 show figures and behaviour of O_A and O_B, when the amount was changed from 0.00302 to 0.0714 mmol. Peak temperatures are consistent with each other within the experimental error. The difference in temperature of the O_A and O_B peaks is about 4 °C on the average, in dependent of sample amount. Two possible explanations are applicable to these results: one is that there are two binding states of water which may be seperated from each other in the process of dehydration; the other is that in the case of complete sealing, a part of H_2O is caused to come out in an endothermic reaction. Moreover, when the system temperature is increased

Table 1. Peak temperatures of DTA of O_A step (T_{O_A}) and O_B step (T_{O_B}) under completely sealed system

W/mmol[a)]	T_{O_A}/°C	T_{O_B}/°C
3.02×10^{-3}	127	135
5.98×10^{-3}	127	135
5.98×10^{-3}	127	135
1.36×10^{-2}	133	135
2.93×10^{-2}	131	134
2.93×10^{-2}	132	134
2.94×10^{-2}	130	133
2.94×10^{-2}	131	133
2.97×10^{-2}	130	133
2.99×10^{-2}	130	133
5.78×10^{-2}	127	130
6.63×10^{-2}	129	131
6.70×10^{-2}	130	134
6.72×10^{-2}	128	133
7.14×10^{-2}	127	131
Average	129.3±2.0	133.3±1.6

a) W is sample weight.

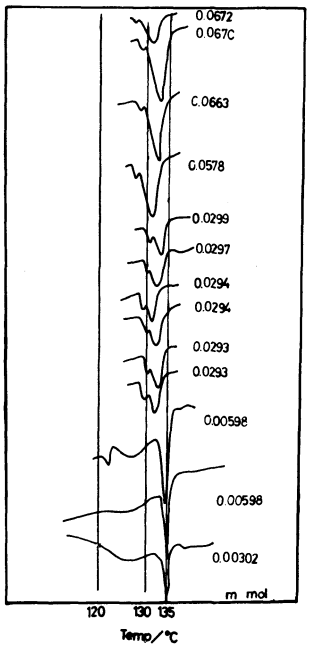

Fig. 5. Temperatures of endothermic DTA peaks, O_A and O_B. Sensitivity is aribitary.

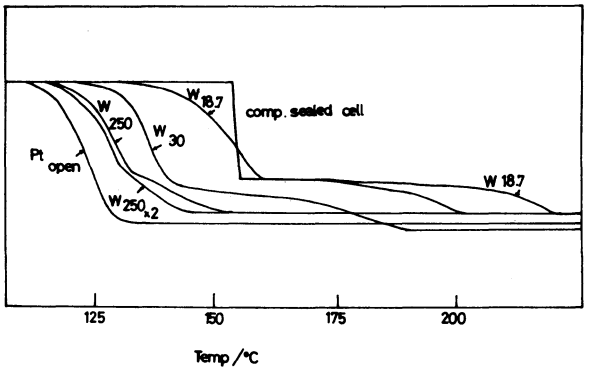

Fig. 6. TG results of quasi-sealed system (and those of open system and completely sealed system).

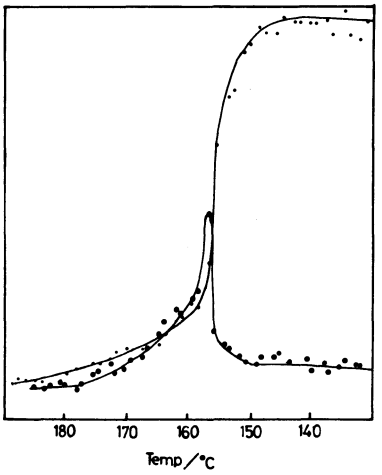

Fig. 7. High temperature oscillating X-ray diffraction pattern of $CaSO_4 \cdot 2H_2O$.
Heating rate, 2 °C/min. Chart speed, 0.5 cm/min. X-Ray source, Cu *Kα* 120 mA, 50 kV.

several degrees, the decomposition process is resumed and the amount of the water coming out from the sample is increased. If the sample amount is made to decrease, the O_A peak of DTA becomes broader and the effect of diffusion in the sealed cell comes to play an important role. In addition, the descent for the second step of TG is caused slowly in raising temperature and it is better to consider that the leak is in operation.

Quasi-sealed Method. A TG-DTG-DTA curve was recorded for the quasi-sealed system and is shown in Fig. 6, which induces the results for both the open and completely sealed systems for comparison; a selection has been made so that all the sample weights may fall in the range 11.54—12.60 mg. As the radius of tungsten wire is increased, results become similar to those of the open system. Onset temperatures of reaction are 111, 113, and 114 °C in the case of open system, two pieces of 250 μm tungsten wire, and a piece of 250 μm tungsten wire, respectively. But the turning point of TG presents itself more clearly and the peaks of DTA can be seperated more easily. The results of both the 30 and 18.7 μm tungsten wires indicate that the decreasing temperatures are 125 and 127 °C and appear with more enhanced separation. These results are what we have expected. In the case of quasi-sealed system, dehydration first occurs after some inner pressure of water vapor had been reached, making a TG decreasing recognizable. If we want to get the stable state of $CaSO_4 \cdot \frac{1}{2}H_2O$, we must use a tungsten wire 30 μm or less in radius.

A precise measurement of high-temperature oscillating X-ray diffraction of calcium sulfate dihydrate was done at a heating rate of 2 °C/min. The result could identify the stable $CaSO_4 \cdot \frac{1}{2}H_2O$ (Fig. 7).

In connection with the above-mentioned experimental results, the following conclusions may be drawn:

(1) According to the experimental results of Miyazaki,[11] it is difficult to separate the first and the second steps of $CaSO_4 \cdot 2H_2O$ decomposition. However, he succeeded only in first making non-hydrate $CaSO_4$ followed by making $CaSO_4 \cdot \frac{1}{2}H_2O$ under the saturated vapor pressure of water. But in our cases, we could easily seperate two steps under a quasi-sealed condition using 12.3, 18.7, and 30.0 μm tungsten wires.

(2) This method enables one to seperate dehydrations of $(NH_4)_6Mo_7O_{24} \cdot 4H_2O$ and $CaSO_4 \cdot 2H_2O$, *etc.*, so that we can easily get intermediates. The advantage of this method is that it requires smaller amounts of sample than the Q-TG method. By smaller amounts of sample it is meant that there are narrower ranges of temperature distribution and that there may be many applications available to other fields, for example, biochemistry.

(3) In the process of dynamic heating, the temperature distribution caused by endo- and exothermic behaviour is relatively small so that the quasi-equilibrium condition may be established easily.

(4) With the completely sealed system, two types of reactions, O_A and O_B occur without decreasing TG. But this phenomenon cannot be explained in terms of different stages of binding or influence of the self-generated condition.

Simple inorganic salts containing water have been studied by means of simultaneous TG-DTG-DTA. Since it seemed most important to investigate first self-generated atmospheres, we planned to study those in the vacuum condition as well as in the gas-flowing condition; thus in the present report, we have studied the self-generated atmosphere.

This study will be applied to various dehydration systems, especially those for which it is said to be difficult to remove intermediates. Now we are planning to apply this method to various decompositions involving gases such as CO_2, H_2S, and NH_3. We are also planning to invent a micro-quasi-isothermal and -isobaric thermogravimetry.

The authors wish to thank (the late) Professor Hajime Ishimura for encouraging us in our early work, and Mr. Masahiro Nogawa and Ms. Yayoi Yamada for conducting measurements in the last stage of experiment. The X-ray generator used belongs to the Research Institute for Material Science and Engineering, Fukui University.

References

1) W. W. M. Wendlandt, "Thermal Method of Analysis," 2nd ed, John Wiley and Sons, New York (1973), p. 37.
2) K. Isa, Y. Hirai, and H. Ishimura, *Proc. of the 5th Int. Conf. on Thermal Analysis*, Kyoto, Sept. 1977, p. 348.
3) K. Isa, S. Fukuo, H. Kondo, and H. Ishimura, 15th Calorimetry Conference in Japan (1979), p. 130.
4) K. Funaki and T. Segawa, *J. Electrochem. Soc. Jpn.*, **1950**, 152.
5) E. Ma, *Bull. Chem. Soc. Jpn.*, **37**, 649 (1964).
6) Funaki's scheme:

$$(NH_4)_6Mo_7O_{24}\cdot 4H_2O \longrightarrow (NH_4)_6Mo_7O_{24} \longrightarrow (NH_4)_4Mo_8O_{26} \longrightarrow MoO_3.$$

Ma's scheme:

$$(NH_4)_6Mo_7O_{24}\cdot 4H_2O \longrightarrow (NH_4)_5Mo_5O_{17} \longrightarrow (NH_4)_4Mo_8O_{26} \longrightarrow MoO_3.$$

7) K. Isa and H. Ishimura, *Bull. Chem. Soc. Jpn.*, **54**, 3628 (1981).
8) Private communication.
9) E. S. Freeman and B. Carroll, *J. Phys. Chem.*, **62**, 394 (1958).
10) A. W. Coats and J. P. Redfern, *Nature*, **201**, 68 (1968).
11) H. Miyazaki, *Kogyo Kagaku Zasshi*, **70**, 261 (1967).

 © 1982 The Chemical Society of Japan Bull. Chem. Soc. Jpn., 55, 3738—3741 (1982) [Vol. 55, No. 12

Studies on Mixed Chelates. XIII. Formation and Electronic Spectra of 5-Coordinated Mixed Copper(II) Chelates Containing *N*-Alkylated Ethylenediamine, Acetylacetonate, and Halide Anions[1)]

Yutaka FUKUDA, Hiroko KIMURA, and Kozo SONE*

Department of Chemistry, Faculty of Science, Ochanomizu University, Otsuka, Bunkyo-ku, Tokyo 112

(Received January 16, 1982)

The visible absorption spectra of three new mixed chelates of copper(II), Cu(acac)(tmen)X (acac=acetylacetonate ion, tmen=*N,N,N',N'*-tetramethylethylenediamine, and X^-=Cl^-, Br^-, or I^-) were studied in various organic solvents. The $\tilde{\nu}_{max}$ values of their d-d bands depend strongly on the nature of the solvent, similarly to the pseudohalide complexes reported in the preceding paper.[1)] These data show the existence of the equilibrium:

$$[Cu(acac)(tmen)X] \rightleftharpoons [Cu(acac)(tmen)]^+ + X^-$$
(5-coordinated) (4-coordinated, with axial solvation)

in such solutions, which is shifted to the right hand side with increase of the solvent polarity and with decrease of the coordination ability of the X^- anion, *i.e.*, in the order $Cl^- \rightarrow Br^- \rightarrow I^-$.

We have prepared several mixed copper(II) chelates containing N-alkylated ethylenediamine(diam) and the β-diketonate ion (β-dik), Cu(β-dik)(diam)X, where X^- is an anion such as ClO_4^-, NO_3^-, or pseudohalide ions.[1,2)] They are all soluble in various organic solvents, and the visible absorption spectra of such solutions reveal the existence of different kinds of solvent effects on their structures in solution. Such effects originate in the donor property and polarity of the solvent used, and the coordinating power of the anion X^-. In continuation of these studies, we have prepared the corresponding halide complexes, Cu(acac)(tmen)X, in which X^-=Cl^-, Br^- or I^-, and studied their visible absorption spectra in organic solvents. The results obtained and their probable explanations will be presented in this paper.

Experimental

Preparation of the New Complexes. An excess of an aqueous solution of potassium halide (KCl, KBr, or KI, *ca.* 20 mmol in 30 cm^3 of H_2O) was added to a solution of [Cu(acac)(tmen)]ClO_4[2)] in water–ethanol (10 mmol in 20 cm^3), and the mixture was stirred for several hours. It was then filtered and concentrated under reduced pressure below room temperature until the complex formed as a crystalline powder. The crude bluish green crystals were recrystallized from 1,2-dichloroethane($ClCH_2CH_2Cl$=DCE). The Cl- and Br-complexes{Cu(acac)(tmen)X; X=Cl or Br} are stable at room temperature, but the crystals of the I-complex gradually decompose on standing, changing from bluish green to brown by the redox reaction between Cu(II) and I^-. Therefore, in the physical measurements a freshly prepared sample must be used and must be kept in a refrigerator when not in use.

Physical Measurements. The electronic spectra of the solutions (visible region) were measured with a Hitachi 340 Recording Spectrophotometer at room temperature (20—25 °C), in 10 cm quartz cells. The reflectance spectra of the solid samples were measured with the same instrument with a reflectance attachment, using $BaSO_4$ as the reference. Infrared spectra (400—5000 cm^{-1}) were measured as Nujol mulls with a JASCO IR-A3 Grating Spectrophotometer. Magnetic susceptibility measurements were performed with a Shimadzu Tortion Magnetometer MB-100. Electric conductivities of the solutions were measured with a conductivity outfit AOC-10 (Denki-kagaku Keiki Co. Ltd.) at 25±0.2 °C.

Results and Discussion

Properties of the Solid Complexes. Table 1 summarizes the analytical data and magnetic moments of the three new complexes. All show normal magnetic moments for monomeric Cu(II) complexes, but their colors (bluish green with different shades) are notably different from that of the perchlorate, [Cu(acac)(tmen)]ClO_4 (reddish violet), as are their visible reflectance spectra (see later).

Electronic Spectra of the Complexes in Various Solvents. These complexes are all readily soluble in various organic solvents, but here again the visible absorption spectra observed in such solvents are remarkably different from those of the perchlorate in the same solvents. For example, the spectra of the Cl-complex, [Cu(acac)(tmen)Cl], in four solvents are given in Fig. 1. The observed values of $\tilde{\nu}_{max}$ and ε_{max} for all these complexes are summarized in Table 2, and the shifts of $\tilde{\nu}_{max}$ of each one in various organic solvents are shown in Fig. 2, in comparison with the data of the perchlorate and the NCO-complex reported previously as the

TABLE 1. ELEMENTARY ANALYSES AND MAGNETIC MOMENTS OF THE COMPLEXES OBTAINED

Formula	C(%)[a)]	H(%)[a)]	N(%)[a)]	μ_{eff}/BM
Cu(acac)(tmen)Cl	41.99(42.03)	7.44(7.38)	8.91(8.91)	1.85
Cu(acac)(tmen)Br	37.00(36.83)	6.54(6.46)	7.84(7.81)	1.84
Cu(acac)(tmen)I[b)]	31.58(32.56)	5.51(5.71)	6.22(6.90)	1.74

a) Calculated values are in parentheses. b) The somewhat poorer agreements may be due to partial decomposition which occurred during handling prior to analysis. *Cf.* Experimental.

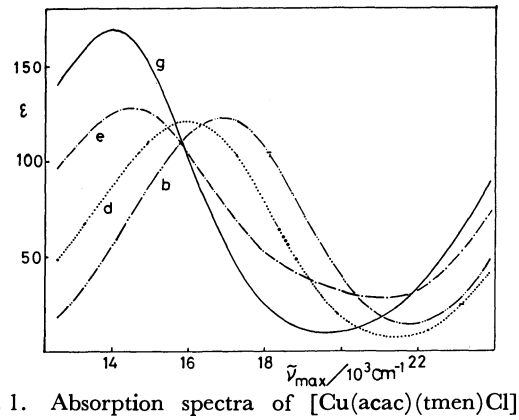

Fig. 1. Absorption spectra of [Cu(acac)(tmen)Cl] in various organic solvents. As to the symbols on the curves, *cf.* Fig. 2.

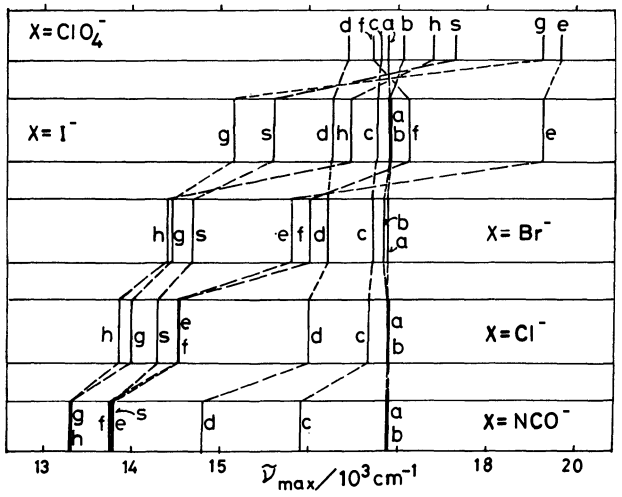

Fig. 2. Diagrammatic representation of the $\tilde{\nu}_{max}$ of the complexes shown in Table 2, and those of [Cu(acac)-(tmen)]ClO_4 and [Cu(acac)(tmen)NCO]† reported previously.[1] The symbols (a) to (h) correspond to the following solvents: a=H_2O, b=MeOH, c=EtOH, d=DMSO, e=NM, f=CH_3CN, g=DCE, and h=acetone. The value of the solid reflectance spectrum is shown by s.

reference.[1],†

It was shown that the $\tilde{\nu}_{max}$ value of the perchlorate shifts to the red with the increase of the donor number of the solvent.[2,3] However, the data in Fig. 2 clearly show that the values of the halide complexes shift to the red with the decrease of solvent polarity, *i.e.*, in apparently opposite direction as compared with the perchlorate. When X^- is Cl^- or Br^-, the order of $\tilde{\nu}_{max}$ in various solvents is expressed as:

$$H_2O \geqq MeOH > EtOH > DMSO > CH_3CN \geqq NM > DCE \geqq \text{acetone.} \quad \text{(i)}\,\dagger\dagger$$

† In Fig. 2 of the preceding paper (Ref. 1), the symbols III and IV mean the N_3- and NCO-complex, respectively (the reverse given there was a mistake; *cf.* the data in Table 3 of the same paper).

†† The abbreviations of the solvent names used are as follows: NM:CH_3NO_2, DCE:$ClCH_2CH_2Cl$, DMSO:$(CH_3)_2SO$ (see also in Table 2).

TABLE 2. $\tilde{\nu}_{max}$ AND ε_{max} VALUES OF [Cu(acac)-(tmen)X] IN SOLID STATE AND IN VARIOUS SOLVENTS AT *ca.* 20 °C[a-c]

	X=Cl	X=Br	X=I
Solid[d]	14.3	14.8	15.6
H_2O	16.89(101)	16.89(101)	16.89(97)
CH_3OH(MeOH)	16.89(123)	16.84(108)	16.92(106)
C_2H_5OH(EtOH)	16.67(133)	16.72(130)	16.75(111)
$(CH_3)_2SO$(DMSO)	16.00(121)	16.21(129)	16.26(113)
$(CH_3)_2NCHO$(DMF)	14.71(114)	16.21(112)	16.50(100)
CH_3NO_2(NM)	14.53(128)	15.82(103)	18.48(96)
CH_3CN	14.53(132)	16.08(112)	17.27(100)
$C_2H_4Cl_2$(DCE)	14.03(169)	14.45(173)	15.15(135)
$(CH_3)_2CO$	13.83(153)	14.39(154)	16.47(94)

a)$\tilde{\nu}_{max}$ in 10^3 cm^{-1}, ε_{max} in parentheses. b) Concentrations: *ca.* 5×10^{-3} M (1 M=1 mol/dm^3). c) It can be noted that there is a remarkable increase in ε_{max} when most of the complex is in the 5-coordinated state (*cf.* the values for the Cl- and Br-complexes in DCE and acetone, and for the I-complex in DCE). Such an increase in band intensity is often observed when a 5-coordinated Cu(II) complex is formed in solution. d) Solid reflectance spectral peaks are broad.

These results are similar to those observed for pseudohalide complexes[1] (compare the data of Cl- and NCO-complexes in Fig. 2, for example), and indicate that the same type of equilibrium as that observed in the solutions of the pseudohalide complexes is established. The equilibrium of the dissociation and formation of the 5-coordinated complex species as shown in Eq. 1:

$$\underset{\text{(5-coordinated)}}{[Cu(acac)(tmen)X]} \rightleftharpoons \underset{\text{(4-coordinated, with axial solvation)}}{[Cu(acac)(tmen)]^+} + X^- \quad (1)$$

is shifted to the right hand side with increase of solvent polarity; this is generally expressed in terms of their E_T or Z values.[3]

Like the pseudohalide complexes, the spectra in DCE and acetone, which are the most non-polar solvents used ($E_T \simeq 42$), can be ascribed to the 5-coordinated complexes, [Cu(acac)(tmen)X]; the fact that these complexes are practically non-electrolytes in DCE supports this view (see below). On the other hand, the spectra in H_2O and MeOH, which are the most polar solvents used (E_T=55—63), are nearly the same as those of the perchlorate in these solvents, and are ascribed to the 4-coordinated ionic complexes [Cu(acac)-(tmen)]$^+$ with axial solvation.

The spectra in other solvents with intermediate polarity correspond to equilibrium mixtures containing these two complex species. In EtOH and DMSO, the spectra are similar to those of the perchlorate, but their $\tilde{\nu}_{max}$ are shifted toward the red, indicating the coexistence of small amounts of [Cu(acac)(tmen)X]. The shift is larger in CH_3CN, and still larger in NM. These results show that the extent of formation of [Cu(acac)-(tmen)X] increases in the order of EtOH<DMSO<CH_3CN<NM. It is thus concluded that the solvent series (i) is essencially the order of the shift of the equilibrium (1) to the right hand side, just as in the case of the pseudohalide complexes.

Table 3. Acceptor numbers(AN) of the solvents used

Solvent	AN
H_2O	54.8
MeOH	41.3
EtOH	37.1
DMSO	19.3
DMF	16.0
CH_3CN	19.3
NM	20.5
DCE	—
Acetone	12.5

It is also interesting to note that the series (i) can also be taken as the order of the acceptor numbers (AN) of Gutmann (*cf.* Table 3) of the solvents,[3] which is the measure of their ability to combine with the negatively charged particles or negative ends of dipoles. This is natural, since a solvent with a high AN will be able to pull out the X^- ions from the coordination sphere of [Cu(acac)(tmen)X] more easily than that of a lower AN.††† A practical reason for our preference for the E_T scale is that the value of DCE, in which the contrast between the spectrum of the perchlorate and those of the halide and pseudohalide complexes is largest, is lacking in Gutmann's table.

Comparison of the data for Cl- and Br-complexes reveals further that, in every solvent (with the exception of H_2O and MeOH) the band of the Cl-complex is shifted more to the red than that of the Br-complex, and in solvents of lower polarity (DCE, acetone, CH_3CN, and NM), the $\tilde{\nu}_{max}$ of the Cl-complex tend to flock together around *ca.* 14×10^3 cm^{-1}. These facts indicate that Cl^- is more strongly bound with $[Cu(acac)(tmen)]^+$ than Br^- in any solvent, except in H_2O and MeOH where no such combination occurs.

The data for the I-complex, on the other hand, show more complexity. The $\tilde{\nu}_{max}$ values in DCE, DMSO, H_2O, and alcohols can be expected by comparison with the Cl- and Br-complexes, but those in acetone and NM (especially the latter) are nearer to the values of the perchlorate in the same solvents, and the value in CH_3CN is even higher than that of the perchlorate. Although the meaning of these $\tilde{\nu}_{max}$ is still not fully understood, it is thus clear that appreciable formation of the 5-coordinated complex occurs only in DCE (and to a much less extent in acetone). In most other solvents, the $\tilde{\nu}_{max}$ values are closer to those of the perchlorate, showing that most of the I^- ions merely dissociate in such solvents. Therefore, the I-complex may be taken as an intermediate between the Br-complex and the perchlorate complex in its behavior.

Electric Conductivities of the Complexes. Conductometric measurements were carried out on some of these solutions to gain information on the equilibrium (1). Some data are shown in Table 4. They show that, in DMSO, all the three complexes are 1 : 1 electrolytes. In NM, however, only the I-complex is a 1 : 1 electrolyte, and partial ionization takes place with other complexes, the degree of which increases from the Cl-complex to the Br-complex. In DCE, the same tendency is observed much more apparently.

Table 4. Molar conductivities (Λ_M) of the complexes (Ω^{-1} cm^2 mol^{-1}, at 25.0 °C)[a] and approximate degrees of dissociation (%, in parentheses)[b]

Complex	DCE	NM	DMSO
Cu(acac)(tmen)Cl	0.6(3)	43.7(51)	32.6(93)
Cu(acac)(tmen)Br	1.2(6)	70.5(83)	36.1(100)
Cu(acac)(tmen)I	6.6(33)	83.6(98)	35.4(100)

a) Concentration: *ca.* 1×10^{-3} M. b) Calculated on the assumption that the Λ_M values of a typical 1:1 electrolyte in these three solvents are 20, 85, and 35 Ω^{-1} cm^2 mol^{-1}, respectively (see Ref. 4).

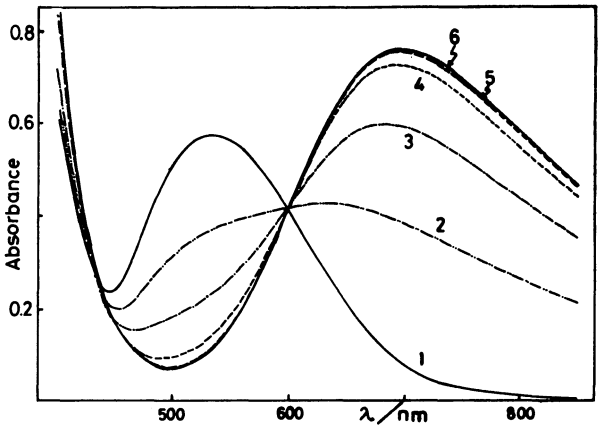

Fig. 3. The effect of Cl^- ions on the spectrum of $[Cu(acac)(tmen)]^+$ in NM (concentration: 5.01×10^{-3} M). The curve 1 is that of $[Cu(acac)(tmen)]ClO_4$, and 2 to 6 correspond to solutions in which the $[Cu(acac)(tmen)]^+$: Cl^- ratios are 1 : 0.5, 1 : 1, 1 : 2, 1 : 3, and 1 : 4, respectively.

These data are compatible with the expectation from the spectral data. They can be summarized by stating that the degree of ionization of [Cu(acac)(tmen)X] increases, in every case, in the order of DCE<NM< DMSO and Cl^-<Br^-<I^-.

Solution Equilibria of the Complexes in NM. Comparison with the Pseudohalide Complexes: More spectral measurements on the systems of $[Cu(acac)(tmen)]ClO_4+Et_4NX$ (X=Cl or Br) in NM were made by varying the molar ratio $[Cu(acac)(tmen)]^+/X^-$ continuously. Figure 3 shows some of the curves obtained. Analysis of these data provides an estimation of the equilibrium constants K of these systems.[5] The same K's could also be estimated from the data in Table 4, by comparing the obtained Λ_M (molar conductivity) values with the mean values of common 1 : 1 electrolytes in the solvents used.[4] The K values obtained in both ways are shown in Table 5. The good agreement may be fortuitous, but it can be seen from these data (and the values of the NCS-complex estimated with the data in the preceding paper)[1] that the coordination abilities

††† An apparent exception is that NM tends to come after CH_3CN and DMSO in the present series; here, however, the AN are nearly the same, and the large difference in their DN may be acting to upset the order.

Table 5. Values of the equilibrium constant, K, of Eq. 1 in NM, estimated from spectra (K^a) and conductometric data (K^b)

Complex	K^a	K^b
Cu(acac)(tmen)Cl	0.46×10^{-3}	0.35×10^{-3}
Cu(acac)(tmen)Br	1.52×10^{-3}	1.69×10^{-3}
Cu(acac)(tmen)NCS[a)]	0.67×10^{-3}	0.74×10^{-3}

a) These values were estimated from the data in Ref. 1.

of the ions studied increase in the order of $Cl^- > NCS^- > Br^-$ in NM.

It is desirable to make similar measurements on all the other systems, *i.e.*, in every solvent and with every halide or pseudohalide ion, but it is not always practicable owing to experimental difficulties, *e.g.*, unfavorable solubility. Comparison of Fig. 2 with the corresponding figure in the preceding work,[1] however, indicates that the coordination abilities of the halide and pseudohalide ions in organic solvents toward $[Cu(acac)(tmen)]^+$ can be arranged, approximately, in the following order:

$$I^- < Br^- \approx NCS^- < Cl^- \approx N_3^- < NCO^-.$$

This sequence may be of some interests, since it is often stated that pseudohalide ions are stronger ligands than halide ions,[6] and the spectrochemical series also states that the ligand field caused by NCS^- is much stronger than those of the halide ions. The "spectrochemical series for axial ligands" found by Addison *et al.*[7] also indicates the same trend. In the present case, however, the two series Cl^-–Br^-–I^- and NCS^-–N_3^-–NCO^- run nearly parallel (or intermixed together), although I^- is probably the weakest, and NCO^- the strongest ligand among all these ions. More studies on related complexes will be necessary for the proper understanding of this sequence.

Structures of the Complexes in Solid State. The fact that the $\tilde{\nu}_{max}$ values of the solid Cl- and Br-complexes (*cf.* Table 2 and Fig. 2) are similar to those of their DCE solutions indicates the 5-coordinated structure of these complexes in solid state. Even for the I-complex, the $\tilde{\nu}_{max}$ is near that in DCE, suggesting the same structure.

However, the bands of the solids are all rather broad, and the possibility of other structures (*e.g.*, a 6-coordinated one in which X^- ions are bound weakly above and below the chelate plane as the bridging ligand) cannot be ruled out with certainty. At any rate, there is a strong axial influence of X^-, and the structures of the complexes in these solids are far from square planar.

It is now clear that these three complexes and the three pseudohalide complexes reported previously provide an interesting group of mixed chelates of Cu(II), with which one can observe the competition of anions and solvent molecules for the axial coordination sites by means of their visible absorption spectra.

The present work was partially supported by a Grant-in-Aid for Scientific Research No. 0554182 from the Ministry of Education, Science and Culture.

References

1) Part XII; Y. Fukuda, N. Sato, N. Hoshino, and K. Sone, *Bull. Chem. Soc. Jpn.*, **54**, 428 (1981).

2) Y. Fukuda, and K. Sone, *Bull. Chem. Soc. Jpn.*, **45**, 465 (1972); Y. Fukuda, A. Shimura, M. Mukaida, E. Fujita, and K. Sone, *J. Inorg. Nucl. Chem.*, **36**, 1265 (1974); Y. Fukuda, Y. Miura, and K. Sone, *Bull. Chem. Soc. Jpn.*, **50**, 142 (1977).

3) As to the meaning of donor number (DN), E_T, and Z, *cf.* the references in 1), and also V. Gutmann, "The Donor-Acceptor Approach to Molecular Interactions," Plenum Press, New York (1978).

4) W. J. Geary, *Coord. Chem. Rev.*, **7**, 81 (1971).

5) As to the details of these estimation methods, *cf.* H. L. Schläfer, "Komplexbildung in Lösung," Springer, Berlin (1961).

6) *Cf.*, *e.g.*, V. Gutmann, "Coordination Chemistry in Non-Aqueous Solutions," Springer, Vienna (1968).

7) A. W. Addison, M. Carpenter, L. K.-M. Lau, and M. Wicholas, *Inorg. Chem.*, **17**, 1545 (1978); B. K. Coltrain, and S. C. Jackels, *ibid.*, **20**, 2032 (1981).

Preparation and Structure of μ-Oxalato-bis{μ-oxo-μ-sulfido-bis-[(oxalato)oxomolybdate(V)]} Complex, $K_6[\{Mo_2O_3S(ox)_2\}_2(ox)]\cdot 10H_2O$

Takashi SHIBAHARA,* Shun'ichiro OOI,† and Hisao KUROYA
Department of Chemistry, Okayama University of Science, 1-1 Ridai-cho, Okayama 700
†*Department of Chemistry, Faculty of Science, Osaka City University, Sugimoto, Sumiyoshi-ku, Osaka 558*
(Received February 1, 1982)

The μ-oxo-μ-sulfido-(oxalato)molybdate(V) complex has been prepared and characterized by X-ray analysis. The potassium salt crystallizes in monoclinic system, space group C2/c, with cell dimensions $a=13.640(3)$, $b=20.296(3)$, $c=15.213(4)$ Å, $\beta=106.42(2)°$, and $Z=4$. The structure was solved by the heavy-atom technique and refined by the block-diagonal least-squares method to $R=0.048$ for 3552 independent reflections. The complex anion is tetrameric, two dimeric $Mo_2O_3S(ox)_2$ moieties being bridged by one oxalato ligand. Both the molybdenum atoms in the dimer are bridged by one sulfur and one oxygen atoms. Each molybdenum atom has distorted octahedral environment; two oxygen atoms of a bidentate oxalato ligand, bridging sulfur and oxygen atoms in the equatorial plane, a terminal oxygen and one of the bridging quadridentate oxalato ligand oxygens. The complex can be denoted as $K_6[\{Mo_2O_3S(ox)_2\}_2(ox)]\cdot 10H_2O$ and has an approximate C_{2h} symmetry, with a crystallographic center of symmetry. The Mo–O (quadridentate bridging oxalato) bonds (2.304(4), 2.302(4) Å) are evidently longer than the Mo–O (bidentate oxalato) bonds (2.112(4), 2.102(4), 2.093(4), 2.120(4) Å). The influence of the bridging oxalato ligand on the geometry of Mo_2O_3S core will be discussed.

The presence of sulfur in several molybdenum containing enzymes led us to the chemistry of μ-sulfur molybdenum compounds.[1]

The chemistry of di-μ-oxo and di-μ-sulfido molybdenum(V) compounds has been widely developed;[1] however, the reports of μ-oxo-μ-sulfido molybdenum(V) compounds are yet relatively rare.[2,3] Cotton and Morehouse[4] reported the structure of di-μ-oxo oxalato complex of $[Mo_2O_4(ox)_2(H_2O)_2]^{2-}$, and that of the di-μ-sulfido oxalato complex of $[Mo_2O_2S_2(ox)_2(H_2O)_2]^{2-}$ was determined by McDonald.[5]

Now we report here the preparation and X-ray structure of the potassium salt of μ-oxalato-(*O*,*O*′,*O*″,*O*‴)-bis{μ-oxo-μ-sulfido-bis[(oxalato)oxomolybdate(V)]}.

Experimental

Preparation of a Solution of μ-Oxo-μ-sulfido-bis[triaquaoxomolybdenum(V)], $[Mo_2O_3S(H_2O)_6]^{2+}$. The aqua complex was prepared by dissolving the corresponding cysteinato complex, $Na_2[Mo_2O_3S(cys)_2]\cdot 5H_2O$[2] in 1 M (1 M=1 mol dm^{-3}) perchloric acid followed by the Sephadex G-10 column separation, which gave three bands. The first and third effluents were proved to involve $[Mo_2O_4(H_2O)_6]^{2+}$ and $[Mo_2O_2S_2(H_2O)_6]^{2+}$, respectively, as evidenced by the UV and visible spectroscopy.

The second effluent was further purified by the use of cation exchange resin Dowex 50W-X2, on which the complex was sorbed and washed with 0.1 M $HClO_4$ and eluted with 2 M $HClO_4$. The analysis of the effluent (Mo: S=2.03: 1) suggests that this is $[Mo_2O_3S(H_2O)_6]^{2+}$.[6a]

Preparation of Potassium μ-oxalato-(O, O′, O″, O‴)-bis{μ-oxo-{μ-sulfido-bis[(oxalato)oxomolybdate(V)]} Decahydrate, $K_6[\{Mo_2O_3S(ox)_2\}_2(ox)]\cdot 10H_2O$. The preparative method of the sample is similar to that of the di-μ-sulfido-bis[aqua(oxalato)-oxomolybdate(V)];[6a] the addition of oxalic acid ($H_2ox/Mo=1.2$) to *e.g.* 250 ml of the $Mo_2O_3S^{2+}$ aqua dimer solution (0.0264 M in 1 M $HClO_4$)[6b] and neutralization to pH *ca.* 3 by the addition of *ca.* 10 M KOH solution. The solution was cooled, filtered, and rotary-evaporated to the volume of *ca.* 70 ml. After one gram of KCl was added, the solution was cooled for some time in an ice bath and then filtered. The filtrate was made turbid by the addition of ethanol and kept in a refrigerator overnight. The resulting orange crystals were filtered and washed successively with ethanol and diethyl ether. Yield 2.6 g. Found: C, 8.67; H, 1.20%. Calcd for $C_{10}H_{20}K_6Mo_4O_{36}S_2$: C, 8.56; H, 1.44%.

Data Collection. The crystal employed for data collection was approximately $0.20\times 0.15\times 0.15$ mm in dimension with well defined faces. Crystal data: $C_{10}H_{20}K_6Mo_4O_{36}S_2$, $M=1398.72$, monoclinic, $a=13.640(3)$, $b=20.296(3)$, $c=15.213(4)$ Å, $\beta=106.42(2)°$, $V=4039.8$ Å^3, $D_m=2.29$ g cm^{-3}, $Z=4$, $D_c=2.30$ g cm^{-3}, space group C2/c, λ(Mo *Kα*)=0.7107 Å, and μ(Mo *Kα*)=20.1 cm^{-1}. Intensity data ($2\theta\leqslant 55°$) were collected on a Phillips 1100 four-circle diffractometer using graphite-monochromatized Mo *Kα* radiation with ω-scan technique. The scan range was 1.20°, and the scan speed, 0.033° s^{-1}; the background was counted for half of the scan time at each end of the scan. The three standard reflections 600, 080, and 008, monitored every 360 min showed no appreciable decay. A total of 4793 reflections were collected, of which 3552 with $F_o^2\geqslant 3\sigma(F_o^2)$ were used for the structure analysis. No correction was made for absorption.

Structure Determination and Refinement. The two molybdenum atoms were located from a Patterson synthesis and the remaining non-hydrogen atom positions were obtained from successive difference-Fourier calculations. The electron density of one potassium ion indicated disorder. It was possible, however, to resolve the ion into two with an ocucpancy factor of 0.5 (*K*(1) and K(2)). The block-diagonal least-squares refinement with anisotropic temperature factors for all non-hydrogen atoms gave $R=0.048$ and $R'=[\sum w\Delta F^2/\sum wF_o^2]^{1/2}=0.060$. The function minimized was $\sum w(F_o-F_c)^2$, where $w=\sigma^{-2}$ (F_o) was used. All the parameter shifts were less than 0.3 σ except for O(1) (0.8 σ) and O(4) (0.4 σ). A final difference Fourier map revealed no peaks greater than 0.9 e Å^{-3}. The positions of hydrogen atoms of water of crystallization could not be found unequivocally. The atomic scattering factors, with correction for anomalous dispersion of Mo^0, K^{+1}, and S were taken from Ref. 7. The F_o-F_c table and the anisotropic thermal parameters are preserved by the Chemical Society of Japan (Document No 8251). Most of the computation were carried out by the Melcom Cosmo 700 III computer at Okayama University of Science. The programs used included a local version of the UNICS.[8]

Table 1. Atomic coordinates (×10⁵ for Mo and ×10⁴ for others) and equivalent isotropic temperature factors[a] with their standard deviations

Atom	x	y	z	B_{eq}/Å²	Atom	x	y	z	B_{eq}/Å²
Mo(1)	932(4)	18637(2)	−2133(3)	1.74	O(22)	−552(3)	4013(2)	−694(3)	2.4
Mo(2)	1514(4)	31692(2)	−70(3)	1.74	O(23)	1377(3)	3365(2)	99(4)	3.2
K(1)[b]	0	409(3)	2500	9.9	O(24)	−1527(3)	3057(2)	−3(3)	2.1
K(2)[b]	0	2721(2)	2500	4.8	O(25)	−1347(4)	4942(2)	−532(3)	3.2
K(3)	2383(1)	4373(1)	−498(1)	3.41	O(26)	−909(4)	4649(3)	1318(3)	3.9
K(4)	1726(1)	4504(1)	2222(1)	3.88	O(1)	1718(10)	3964(5)	−2372(6)	13.8
Sb	−384(1)	2622(1)	−1406(1)	2.47	O(2)	−2013(5)	3202(3)	2131(4)	5.3
Ob	292(3)	2434(2)	828(3)	2.3	O(3)	1431(6)	915(4)	−1910(5)	7.8
O(11)	−123(3)	1084(2)	633(3)	2.4	O(4)	−1375(8)	1477(5)	1979(7)	11.4
O(12)	−677(3)	1151(2)	−1160(3)	2.1	O(5)	2233(7)	2623(4)	−1556(5)	7.9
O(13)	1303(3)	1663(2)	−187(4)	3.1	C(11)	−672(5)	600(3)	230(4)	2.4
O(14)	−1583(3)	1962(2)	−194(3)	2.1	C(12)	−1022(4)	647(3)	−831(4)	2.2
O(15)	−1579(4)	229(2)	−1290(3)	3.4	C(21)	−609(4)	4289(3)	811(4)	2.2
O(16)	−924(4)	126(2)	604(3)	3.3	C(22)	−875(4)	4439(3)	−223(4)	2.1
O(21)	−36(3)	3774(2)	1070(3)	2.3	C(1)	−1952(4)	2505(3)	−54(4)	1.7

a) W. C. Hamilton, *Acta Crystallogr.*, **12**, 609 (1959). b) Site occupation factor 0.5.

Table 2. Interatomic distances and bond angles with estimated standard deviations in parentheses[a]

Bond distance	l/Å	Bond distance	l/Å
Mo(1)–Sb	2.325(2)	Mo(2)–Sb	2.326(2)
Mo(1)–Ob	1.918(5)	Mo(2)–Ob	1.934(5)
Mo(1)–O(11)	2.112(4)	Mo(2)–O(21)	2.120(4)
Mo(1)–O(12)	2.102(4)	Mo(2)–O(22)	2.093(4)
Mo(1)–O(13)	1.689(5)	Mo(2)–O(23)	1.681(5)
Mo(1)–O(14)	2.304(4)	Mo(2)–O(24)	2.302(4)
Mo(1)–Mo(2)	2.667(1)		
C(11)–O(11)	1.282(8)	C(21)–O(21)	1.279(7)
C(11)–O(16)	1.215(8)	C(21)–O(26)	1.213(8)
C(11)–C(12)	1.553(9)	C(21)–C(22)	1.542(9)
C(12)–O(12)	1.284(8)	C(22)–O(22)	1.279(7)
C(12)–O(15)	1.219(8)	C(22)–O(25)	1.227(8)
C(1)–O(14)	1.254(7)	C(1)–O(24)	1.254(7)
C(1)–C(1′)	1.548(16)		
Short contact	l/Å	Short contact	l/Å
K(1)···O(16)	2.861(7)	K(2)···O(2)	2.817(7)
K(1)···O(16)[III]	2.861(7)	K(2)···O(2)[III]	2.817(7)
K(1)···O(4)	2.828(12)	K(2)···Ob	2.747(5)
K(1)···O(4)[III]	2.828(12)	K(2)···Ob[III]	2.747(5)
K(3)···O(13)[V]	2.769(6)	K(4)···O(15)[VI]	2.793(5)
K(3)···O(15)[IV]	2.728(5)	K(4)···O(25)[I]	2.719(5)
K(3)···O(16)[IV]	2.880(5)	K(4)···O(26)[III]	2.769(6)
K(3)···O(23)	2.755(6)	K(4)···O(2)[III]	2.807(7)
K(3)···O(25)[I]	2.763(5)	K(4)···O(3)[V]	2.818(9)
K(3)···O(26)[I]	2.849(6)		
K(3)···O(1)	2.859(13)		
O(14)···O(24′)	2.679(12)	O(1)···O(5)	2.992(16)
O(1)···O(22)[II]	2.924(14)		

a) Roman numeral superscripts refer to atoms in the positions:
I $-x, 1-y, -z$; II $-x, y, -1/2-z$; III $-x, y, 1/2-z$; IV $1/2+x, 1/2+y, z$;
V $1/2-x, 1/2-y, -z$; VI $1/2+x, 1/2-y, 1/2+z$.

Bond angle	ϕ/°	Bond angle	ϕ/°
O(13)–Mo(1)–Mo(2)	103.9(2)	O(23)–Mo(2)–Mo(1)	104.0(2)
O(13)–Mo(1)–Ob	102.5(2)	O(23)–Mo(2)–Ob	102.1(2)
O(13)–Mo(1)–Sb	102.3(2)	O(23)–Mo(2)–Sb	103.1(2)
O(13)–Mo(1)–O(11)	96.3(2)	O(23)–Mo(2)–O(21)	97.0(2)
O(13)–Mo(1)–O(12)	98.4(2)	O(23)–Mo(2)–O(22)	99.0(2)

TABLE 2. (Continued)

Bond angle	ϕ/°	Bond angle	ϕ/°
O(13)-Mo(1)-O(14)	170.8(2)	O(23)-Mo(2)-O(24)	170.3(2)
O(14)-Mo(1)-Mo(2)	84.8(1)	O(24)-Mo(2)-Mo(1)	84.5(1)
O(14)-Mo(1)-OB	81.2(2)	O(24)-Mo(2)-OB	80.6(2)
O(14)-Mo(1)-SB	85.1(1)	O(24)-Mo(2)-SB	85.5(1)
O(14)-Mo(1)-O(11)	75.3(2)	O(24)-Mo(2)-O(21)	73.7(2)
O(14)-Mo(1)-O(12)	76.3(2)	O(24)-Mo(2)-O(22)	76.5(2)
OB-Mo(1)-Mo(2)	46.4(1)	OB-Mo(2)-Mo(1)	45.9(1)
OB-Mo(1)-SB	101.0(1)	OB-Mo(2)-SB	100.5(1)
OB-Mo(1)-O(11)	87.7(2)	OB-Mo(2)-O(21)	87.2(2)
OB-Mo(1)-O(12)	155.3(2)	OB-Mo(2)-O(22)	155.0(2)
SB-Mo(1)-Mo(2)	55.1(1)	SB-Mo(2)-Mo(1)	55.0(1)
SB-Mo(1)-O(11)	157.1(1)	SB-Mo(2)-O(21)	156.4(1)
SB-Mo(1)-O(12)	87.2(1)	SB-Mo(2)-O(22)	87.7(1)
O(11)-Mo(1)-Mo(2)	132.6(1)	O(21)-Mo(2)-Mo(1)	131.4(1)
O(11)-Mo(1)-O(12)	76.9(2)	O(21)-Mo(2)-O(22)	76.9(2)
O(12)-Mo(1)-Mo(2)	139.2(1)	O(22)-Mo(2)-Mo(1)	139.5(1)
Mo(1)-OB-Mo(2)	87.7(2)	Mo(1)-SB-Mo(2)	70.0(1)
Mo(1)-O(11)-C(11)	116.5(4)	Mo(2)-O(21)-C(21)	115.3(4)
Mo(1)-O(12)-C(12)	116.7(4)	Mo(2)-O(22)-C(22)	117.0(4)
O(11)-C(11)-C(12)	114.6(5)	O(21)-C(21)-C(22)	114.5(5)
O(11)-C(11)-O(16)	126.0(6)	O(21)-C(21)-O(26)	125.2(6)
O(16)-C(11)-C(12)	119.5(6)	O(26)-C(21)-C(22)	120.3(6)
O(12)-C(12)-C(11)	114.6(5)	O(22)-C(22)-C(21)	114.9(5)
O(12)-C(12)-O(15)	124.7(6)	O(22)-C(22)-O(25)	125.0(6)
O(15)-C(12)-C(11)	120.7(6)	O(25)-C(22)-C(21)	120.1(6)
Mo(1)-O(14)-C(1)	121.8(4)	Mo(2)-O(24)-C(1)	122.2(4)
O(13)-Mol(1)-O(14)	170.8(2)	O(23)-Mo(2)-O(24)	170.3(2)
O(14)-C(1)-C(1′)	116.9(5)	O(24)-C(1)-C(1′)	116.7(5)
O(1)-C(1)-O(24)	126.4(6)		

Results and Discussion

Peak positions of UV-visible spectra of $[Mo_2O_3S(H_2O)_6]^{2+}$ and $[\{Mo_2O_3S(ox)_2\}_2(ox)]^{6-}$ are as follows: $[Mo_2O_3S(H_2O)_6]^{2+}$ (per dimer),[9] 220_{sh}(ε=5600), 278 (3950), 314(3250), 450_{sh}(57) nm; $[\{Mo_2O_3S(ox)_2\}_2(ox)]^{6-}$ (per tetramer), 280(ε=13600), 320_{sh}(10400), 470_{sh}(220) nm. Addition of cysteine or $Na_2H_2edta\cdot 2H_2O$ to the $[Mo_2O_3S(H_2O)_6]^{2+}$ solution and neutralization to pH *ca.* 6 gave $[Mo_2O_3S(cys)_2]^{2-}$ and $[Mo_2O_3S(edta)]^{2-}$, respectively, and this can confirm the existence of μ-oxo-μ-sulfido molybdenum(V) dimer. The $[Mo_2O_3S(H_2O)_6]^{2+}$ aqua dimer is not so stable as the $[Mo_2O_2S_2(H_2O)_6]^{2+}$ is; the solution of the former gives yellow precipitates in a week even in a refrigerator.

It is interesting that the order of elution from Sephadex G-10 column depends on the number of the sulfur atoms in the bridge, possibly being due to difference in molecular size which will give three bands in the separation column (see Experimental).

The atomic coordinates, and bond lengths and bond angles are listed in Tables 1 and 2, respectively.

The complex anion contains two $Mo_2O_3S(ox)_2$ moieties bridged by an oxalato ligand as shown in Fig. 1. The midpoint of C–C bond of the bridging oxalato ligand lies on the crystallographic center of symmetry at (−1/4, 1/4, 0) and the complex anion has an approximate mirror plane which passes through six atoms, *viz*, two μ-S's, two μ-O's, and two carbon atoms of the bridging oxalato ligand; thus the tetramer has an approximate C_{2h} symmetry.

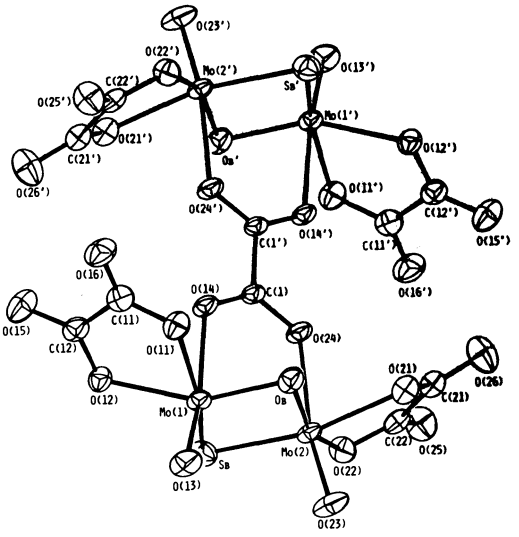

Fig. 1. Molecular structure of $[\{MO_2O_3S(ox)_2\}_2(ox)]^{6-}$ showing 50% probability ellipsoids of thermal vibration. The primed atoms are centrosymmetric of the unprimed ones.

The mode of ligation of the oxalato ligand in this complex (**A**) is different from those of the di-μ-oxo and di-μ-sulfido oxalato complex anions (**B**), but rather similar to that of the di-μ-oxo malonato complex, $K_6[\{Mo_2O_4(mal)_2\}_2(ox)]\cdot 4H_2O$ (**C**), where two types of malonato ligands are existent; one is bidentate and the other is quadridentate.[10] The reason why the oxalato ligand has such a coordination mode in the

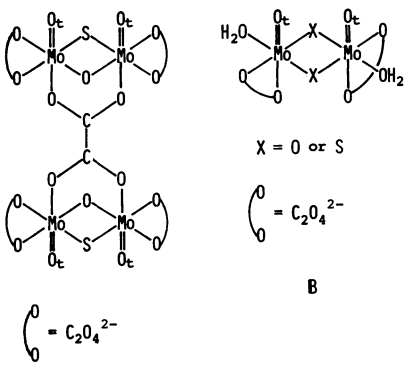

A B C

μ-oxo-μ-sulfido complex is not clear at present; the use of less amount of oxalic acid ($H_2ox/Mo=1.0$, see Experimental) also gives the same type of complex, though the yield is low.

Each molybdenum atom in the tetramer has distorted octahedral environment, disregarding any Mo–Mo bonding included in the coordination sphere: two oxygen atoms of a bidentate oxalato ligand and bridging sulfur and oxygen atoms in the equatorial plane, a terminal oxygen and one of the bridging quadridentate oxalato ligand oxygens. In the $Mo_2O_3S(ox)_2$ moiety, two terminal oxygen atoms are *cis* to each other.

The present Mo–Mo bond distance 2.667(1) Å is close to those of $[Mo_2O_3S(p_rdtc)_2]$ (2.673(3) Å)[11] and $[Mo_2O_3S(pdta)]^{2-}$ (2.656(1) Å)[12] and also to the mean value (2.681 Å) of the di-μ-oxo and di-μ-sulfido oxalato complexes.

While no trans influence due to the multiply-bonded terminal oxo ligand was observed for both the di-μ-oxo and di-μ-sulfido exalato complexes, evident lengthening of the Mo–O bond trans to the terminal oxo ligand is observed as seen in Table 3. It seems that, if one oxalato ligand occupies both the trans and cis positions to the multiply-bonded terminal oxygen as in **B**, no trans influence is observed, whereas, in case the trans and cis positions are occupied by the two respective oxalato ligands as in **A**, trans influence can be found.

The angle O_t–Mo–O (trans to O_t, 170.8(2) and 170.3(2)°) and the dihedral angle (168.5°) defined by O_B, Mo(1), S_B and O_B, Mo(2), S_B planes are considerably larger than those of di-μ-oxo and di-μ-sulfido oxalato complexes (Table 3). These enlargement may be caused by the coordination of the bridging oxalato anion as a quadridentate ligand.[10] This fact indicates that the present way of occupation of the sixth coordination position trans to O_t will give a remarkable influence to the coordination geometry, the existence of trans influence of O_t being overcome.

There is slight trans influence of the bridging sulfur; bond lengths of Mo–O (trans to μ-S) are 2.112(4) and 2.120(4) Å, and those of Mo–O (trans to μ-O) are 2.102(4) and 2.093(4) Å.

Each of the five membered rings defined by Mo(1), O(11), O(12), C(11), and C(12), and, Mo(2), O(21),

Table 3. Relevant structural parameters for oxalato and malonato molybdenum(V) complexes

	$K_6[\{Mo_2O_3S(ox)_2\}_2(ox)]\cdot 10H_2O$	$Ba[Mo_2O_4(ox)_2(H_2O)_2]\cdot 3H_2O$	$Cs_2[Mo_2O_2S_2(ox)_2(H_2O)_2]\cdot 2H_2O$	$K_6[\{Mo_2O_4(mal)_2\}_2(mal)]\cdot 4H_2O$[h]
Mo–Mo *l*/Å	2.667(1)	2.541	2.882(1)	2.555
Mo–O_t *l*/Å	1.689(5)	1.70(3)	1.702(6)	1.684
	1.681(5)		1.692(6)	
Mo–O_B *l*/Å	1.918(5)	1.93(3)		1.934
	1.934(5)	1.88(3)		
Mo–S_B *l*/Å	2.325(2)		2.310(2)	
	2.326(2)		2.318(2)	
			2.308(2)	
			2.320(2)	
Mo–O *l*/Å	2.112(4)[a,b]	2.14(4)[a,c]	2.159(5)[a,b]	2.081[i]
	2.102(4)[a,c]		2.166(5)[a,b]	
	2.120(4)[a,b]			
	2.093(4)[a,c]			
Mo–O *l*/Å[d]	2.304(4)[e]	2.11(3)[a]	2.155(5)[a]	2.321[j]
	2.302(4)[e]		2.164(6)[a]	
Mo–O *l*/Å[f]		2.22(4)	2.229(6)	
			2.196(7)	
Mo–O_B–Mo ϕ/°	87.7(2)	83.5(12)		82.7
Mo–S_B–Mo ϕ/°	70.0(1)		75.4(1)	
			75.0(1)	
O_t–Mo–O ϕ/°[d]	170.8(2)	150.9(15)	158.1[m]	171
	170.3(2)		158.6[m]	
Dihedral angle ϕ/°[g]	168.5	150.6[k]	155.6	161
Ref.	This work	4	5	10

a) Non-bridging oxalato ligand. b) Trans to S_B. c) Trans to O_B. d) Trans to O_t. e) Bridging oxalato ligand. f) Coordinated water. g) Formed about X···Y in the Mo_2XY ring. h) Average value. i) Non-bridging malonato ligand. j) Bridging malonato ligand. k) Calculated using the atomic parameters from Ref. 4. m) Calculated using the atomic parameters from Ref. 5.

TABLE 4. DEVIATIONS (l/Å) OF ATOMS FROM MEAN PLANES

(A) Plane through Mo(1), O(11), O(12), C(11), and C(12):
Mo(1) −0.045, O(11) 0.047, O(12) 0.060, C(11) −0.015, C(12) −0.040
(B) Plane through Mo(2), O(21), O(22), C(21), and C(22):
Mo(2) 0.067, O(21) −0.075, O(22) −0.056, C(21) 0.055, C(22) 0.013
(C) Plane through SB, OB, O(11), and O(12):
Mo(1) 0.371, SB 0.005, OB −0.006, O(11) 0.007, O(12) −0.007
(D) Plane through SB, OB, O(21), and O(22):
Mo(2) −0.387, SB 0.005, OB −0.005, O(21) 0.006, O(22) −0.006
Equation of planes (Orthogonalized coordinates)
(A) $0.8937x-0.4481y-0.0226z+1.4469=0$
(B) $-0.8711x-0.4774y-0.1152z+3\ 3196=0$
(C) $0.9839x-0.1785y-0\ 0023z+0\ 8313=0$
(D) $-0\ 9808x-0\ 1881y-0\ 0514z+1\ 0281=0$

O(22), C(21), and C(22) are coplanar, the largest deviation from the plane being 0.075 Å. The molybdenum atoms are displaced (0.371 and 0.387 Å) toward terminal oxygens from the basal planes (Table 4).

The potassium ions are coordinated by four to seven oxygen atoms within the range of 2.7—2.9 Å. All water oxygens (from O(1) through O(4)) except O(5) coordinate to potassium ions, and O(5) is close to O(1) (2.992(16) Å). An additional contact is observed between O(1) and O(22) (2.924(14) Å) indicating formation of a hydrogen bond (Table 2).

We are grateful to Dr. H. Kimura for the arrangement of the program UNICS, and to Dr. K. Matsumoto for his help in the data collection.

References

1) E. I. Stiefel, *Prog. Inorg. Chem.*, **22**, 1 (1976).
2) V. R. Otto, D. S. Swieter, and F. A. Schultz, *Inorg. Chem.*, **16**, 2538 (1977).
3) K. Z. Suzuki, Y. Sasaki, S. Ooi, and K. Saito, *Bull. Chem. Soc. Jpn.*, **53**, 1288 (1980).
4) F. A. Cotton and S. M. Morehouse, *Inorg. Chem.*, **4**, 1377 (1965).
5) W. S. McDonald, *Acta Crystallogr., Sect. B*, **1978**, 2850.
6) a) Mo and S were determined as in the literature; F. A. Armstrong, T. Shibahara, and A. G. Sykes, *Inorg. Chem.*, **17**, 189 (1978); b) The effluent from Sephadex G-10 column can be used; no further purification by the use of Dowex 50W-X2 resin is required for the preparation of the solid oxalato complex.
7) "International Tables for X-Ray Crystallography," Kynoch Press, Birmingham (1974), Vol. IV, pp. 71 and 148.
8) The Universal Crystallographic Computation Program System (UNICS), ed by T. Sakurai, The Crystallographic Society of Japan (1967).
9) The molar extinction coefficient values in parentheses are based on Mo and S analyses. This result, on the whole, agrees with the result of Ref. 3 which was obtained by dissolving the corresponding cysteinato complex in 2 M $HClO_4$ without Sephadex G-10 separation.
10) T. Shibahara, H. Kuroya, K. Matsumoto, and S. Ooi, *Inorg. Chim. Acta*, **54**, L75 (1981).
11) J. Dirand-Colin, L. Ricard, and R. Weiss, *Inorg. Chim. Acta*, **18**, L21 (1976).
12) A. Kojima, S. Ooi, Y. Sasaki, K. Z. Suzuki, K. Saito, and H. Kuroya, *Bull. Chem. Soc. Jpn.*, **54**, 2457 (1981).

 © 1982 The Chemical Society of Japan Bull. Chem. Soc. Jpn., 55, 3747—3749 (1982)

Catalytic Activity of Planar Copper(II) Complexes for the Chemiluminescence of Luminol

Naoyasu Oishi, Masataka Takeuchi, Yuzo Nishida,* and Sigeo Kida
Department of Chemistry, Faculty of Science, Kyushu University 33, Higashi-ku, Fukuoka 812
(Received March 25, 1982)

Some planar binuclear copper(II) complexes showed high catalytic activity for the chemiluminescence of luminol in the presence of hydrogen peroxide compared with those of mononuclear planar copper(II) complexes. The formation of singlet O_2 in the reaction mixture of a binuclear copper(II) complex and hydrogen peroxide was assumed to play a key role in the catalytic function of the binuclear copper(II) complexes for the luminol chemiluminescence.

Since the discovery of the chemiluminescence of luminol by Albrecht,[1] many chemists have been interested in the light producing step. White *et al.*[2,3] have established the stoichiometry of the overall reactions as well as the identity of the emitting species. According to them, 3-aminophthalate is the light emitter in protic and approtic solvents.[2-5]

It is well known that hemin catalyzes the chemiluminescence of luminol very effectively in the presence of hydrogen peroxide. It was also shown that some metal complexes cause the luminol chemiluminescence though much less effectively compared with hemin.[6,7] Ojima[7] investigated the catalytic activity of copper(II) complexes for the luminol chemiluminescence, and found that some di-μ-hydroxo binuclear copper(II) complexes show high catalytic activities for the luminol chemiluminescence; howerver, he did not investigate further the function of the binuclear copper(II) complexes for the reaction.

We already showed that some planar binuclear copper(II) complexes, *e.g.*, $[Cu_2(pia)_2]$ and $[Cu_2(et\text{-}2\text{-}3)_2]^{2+}$, *etc.* (for the abbreviations of the complexes, see Fig. 1) show remarkably high reactivities in the redox reactions with ascorbic acid, catechol, *etc.*, compared with the reactivities of planar mononuclear copper(II) complexes.[8-11] More recently we[12] also found that some planar binuclear copper(II) complexes exhibit high catalytic activity for the decomposition of hydrogen peroxide ("catalase-like" function) compared with that of the planar mononuclear copper(II) complexes. These results suggest that the "catalase-like" function of the binuclear copper(II) complexes may be closely related to the specific function of the binuclear copper(II) complexes for the chemiluminescence of luminol observed by Ojima, because these experiments on the luminol chemiluminescence are usually done in the presence of hydrogen peroxide. In order to confirm the above view, in this study, we have investigated the catalytic activity of various planar copper(II) complexes for the luminol chemiluminescence.

Experimental

Materials. Copper(II) complexes cited in Fig. 1 were prepared according to the literature methods. (C),[13] (D),[14] (E),[15] (F),[16] (G),[17] (H),[18] (I),[8] and (J).[19] Luminol (Tokyo Kasei Co.) and hydrogen peroxide (Nakarai's Guaranteed Reagent, 30%) were obtained commercially.

Measurements of Chemiluminescence Intensity. The aqueous solution containing luminol (1.4×10^{-4} mol dm^{-3}), NaOH (2.8×10^{-4} mol dm^{-3}) and H_2O_2 (1.4×10^{-3} mol dm^{-3}) and the dmf solution of copper(II) complexes ($[Cu^{2+}]=2\times10^{-4}$ mol dm^{-3}) were kept standing for 1 d at 18 °C prior to the reaction. The apparatus for the measurement is shown in Fig. 2. The solution of copper(II) complex (0.5 cm^3) was mixed with the luminol solution (30 cm^3) in vessel A by injection from the syringe, and the emitted light was collected on the photomultiplier (RCA 1P28) through the lens, and recorded with a Servocorder type SR651 (Watanabe Instrument Corp.). The temperature of the room was kept at 18 °C throughout the experiments.

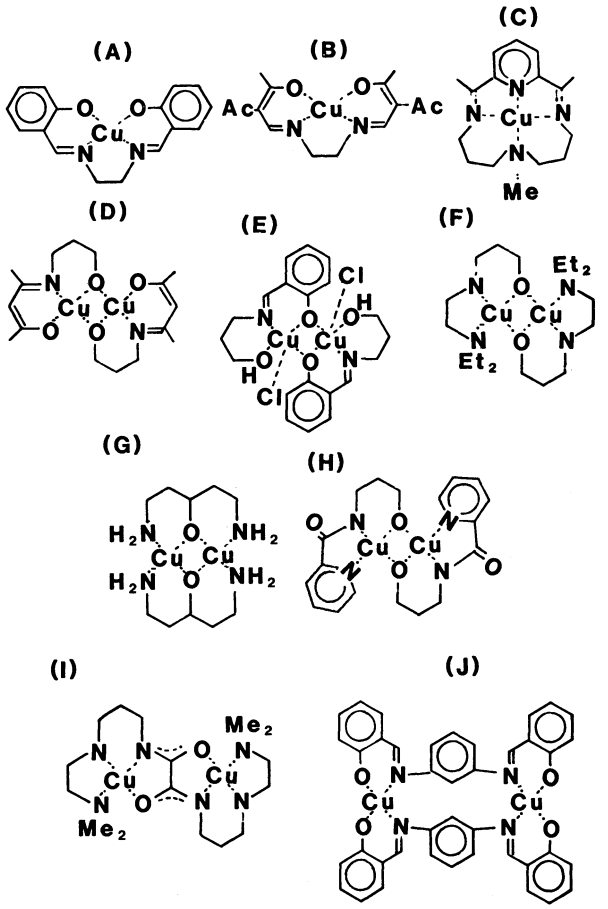

Fig. 1. Copper(II) complexes cited in this paper and their abbreviations. (A) [Cu(salen)], (B)[Cu(J-en)], (C) $[Cu(m\text{-}cr)]^{2+}$, (D) $[Cu_2(pia)_2]$, (E) $[Cu_2(salpa)_2]^{2+}$ (F) $[Cu_2(et\text{-}2\text{-}3)_2]^{2+}$ ($R=C_2H_5$), (G) $[Cu_2(dpl)_2]^{2+}$, (H) $[Cu_2(pc\text{-}1,3)_2]$, (I) $[Cu_2(me\text{-}ox)]^{2+}$, and (J) $[Cu_2(sal\text{-}m\text{-}phen)_2]$.

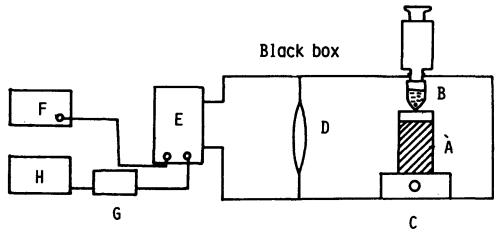

Fig. 2. Apparatus for the measurement of chemiluminescence. A: Luminol solution, B: copper(II) solution, C: magnetic stirrer, D: lens, E, photomultiplier, F: power source (650 V), G: amplifier, H: recorder.

Results and Discussion

Some examples of the time course of luminol chemiluminescence using copper(II) complexes as catalyst are shown in Fig. 3. Planar mononuclear copper(II) complexes, such as [Cu(salen)], [Cu(J-en)], and [Cu(m-cr)]$^{2+}$ showed practically no catalytic activity for the luminol chemiluminescence. In contrast to this, planar binuclear copper(II) complexes, *e.g.*, [Cu_2(pia)$_2$], [Cu_2(et-2-3)$_2$]$^{2+}$, and [Cu_2(pc-1,3)$_2$], exhibited remarkable catalytic activities, whereas binuclear copper(II) complexes, [Cu_2(me-ox)]$^{2+}$ and [Cu_2(sal-m-phen)$_2$] showed no catalytic activity.

The luminol chemiluminescence occurs only when luminol, NaOH, H_2O_2, and a copper(II) complex are mixed in a solution, where NaOH seems to be necessary for the formation of the dianion of luminol. In Table 1 the catalytic activities of various copper(II) complexes

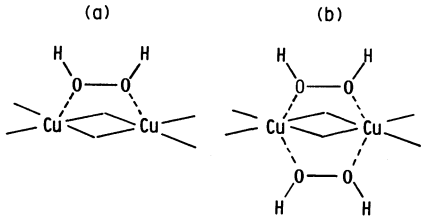

Fig. 4. The assumed intermediate complex between a binuclear copper(II) complex and H_2O_2.

Table 1. Catalytic functions of copper(II) complexes

Complex	Decomposition of H_2O_2	Luminol chemiluminescence
[Cu(salen)]	a)	a)
[Cu(J-en)]	a)	a)
[Cu(m-cr)]$^{2+}$	a)	a)
[Cu_2(pia)$_2$]	$t_{1/2}\approx 1$ min[b]	220[c]
[Cu_2(et-2-3)$_2$]$^{2+}$	$t_{1/2}<0.5$ min	320
[Cu_2(salpa)$_2$]$^{2+}$	$t_{1/2}\approx 3$ min	380
[Cu_2(dpl)$_2$]$^{2+}$	$t_{1/2}\approx 10$ min[d]	50
[Cu_2(pc-1,3)$_2$]	$t_{1/2}<0.2$ min	290
[Cu_2(me-ox)]$^{2+}$	a)	a)
[Cu_2(sal-m-phen)$_2$]	a)	a)

a) Practically zero. b) $t_{1/2}$ denotes the half-life time of H_2O_2 in the reaction mixture of a copper(II) complex and ten times excess of H_2O_2 in methanol at 25°C. c) This denotes the highest value of chemiluminescence intensity (*cf.* Fig. 3). d) In water.

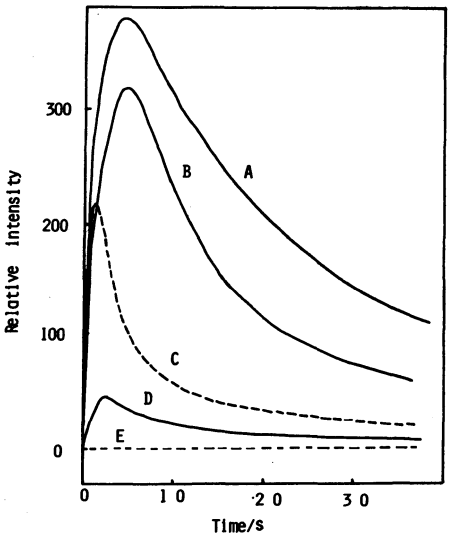

Fig. 3. Chemiluminescence intensity as a function of time. A: [Cu_2(salpa)$_2$]$^{2+}$, B: [Cu_2(et-2-3)$_2$]$^{2+}$, C: [Cu_2(pia)$_2$], D: [Cu_2(dpl)$_2$]$^{2+}$, E: [Cu(salen)].

for the decomposition of hydrogen peroxide[12] and for the luminol chemiluminescence are shown. It is obvious from the data that the catalytic functions of copper(II) complexes for the decomposition of hydrogen peroxide and for the luminol chemiluminescence are paralell (at least qualitatively) with each other. These facts suggest that the decomposed product of H_2O_2 in the reaction mixture plays a key role in the luminol chemiluminescence.

The decomposition reaction is essentially a redox-disproportionation reaction between two H_2O_2 molecules *e.g.*,

$$2H_2O_2 \longrightarrow 2H_2O + O_2.$$

However, the rate of the reaction is very slow in the absence of catalysis. In the preliminary report,[12] we discussed the catalytic function of binuclear copper(II) complexes for the decomposition of hydrogen peroxide, and assumed that the first step is the formation of a H_2O_2 complex as depicted in Fig. 4-a and the second step is the approaching of another H_2O_2 molecule to the vacant site of the H_2O_2-binuclear complex, forming the intermediate complex as shown in Fig. 4-b; the third step is the two-electron transfer from one H_2O_2 molecule to another through the copper atoms, resulting in a formation of O_2 and $2H_2O$. In the cases of [Cu_2(me-ox)]$^{2+}$ and [Cu_2(sal-m-phen)$_2$], the formation of the intermediate complex is impossible because of the long Cu–Cu distance.[8,12] This may explain the very low catalytic activity of these complexes for the decomposition of hydrogen peroxide.

In the intermediate complex as shown in Fig. 4-a or 4-b, a H_2O_2 molecule bidentately coordinates to the two copper(II) ions with its nonbonding filled 2p orbitals. When two electrons are transfered from the peroxide to the two copper(II) ions, a single electron is left in each oxygen 2p orbital which was used for the coordination. These orbitals will immediately form a π bond pairing the electron spins, because the two Cu–O

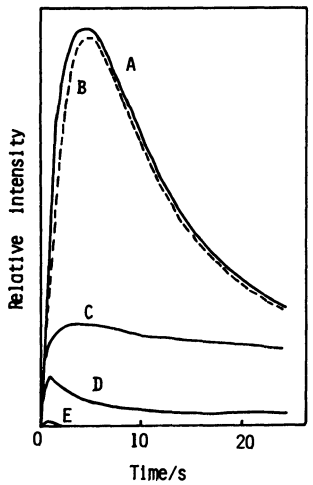

Fig. 5. Chemiluminescence intensity in the $[Cu_2(et\text{-}2\text{-}3)_2]^{2+}$ system in the presence of DABCO (R=[DABCO]/[Luminol]). A: R=0, B: R=100, C: R=1000, D: R=2500, E: R=10000.

bonds should be nearly paralell to each other due to the steric requirement of the Cu_2–O_2 bonding system. Thus, the H_2O_2 molecule will become a singlet dioxygen molecule losing two protons. Accordingly, it seems that singlet dioxygen molecule (denoted as $^1O_2$ hereafter) plays a key role in the catalytic function of the binuclear copper(II) complexes for the luminol chemiluminescence.

It is well known that $^1O_2$ reacts with luminol to induce chemiluminescence. Thus, we have measured the luminol chemiluminescence in the NaClO–H_2O_2 system, because the NaClO–H_2O_2 system is one of the simplest ways to generate $^1O_2$ in the laboratory.[20] The luminol chemiluminescence was observed in the NaClO–H_2O_2 system, as expected. When a large excess of 1,4-diazabicyclo[2.2.2]octane (DABCO, one of the scavenger[21] of $^1O_2$) was added to this system, the intensity of chemiluminescence was greatly quenched. This fact indicates that the luminol chemiluminescence in the NaClO–H_2O_2 system is caused by the generation of $^1O_2$ in this system.[22] In Fig. 5, the time courses of luminol chemiluminescence in the presence of $[Cu_2(et\text{-}2\text{-}3)_2]^{2+}$ and DABCO are shown. These clearly indicate that the intensities of luminol chemiluminescence by $[Cu_2(et\text{-}2\text{-}3)_2]^{2+}$ are greatly depressed by the presence of DABCO, similarly to the case of the NaClO–H_2O_2 system. Such a quenching effect by DABCO was also observed for all the luminol chemiluminescence catalyzed by the binuclear copper(II) complexes examined in this study.

It is well known that 2,2,6,6-tetramethyl-4-piperidinol reacts with $^1O_2$ to yield the nitroxide radical, as shown below.[23] We could observe the ESR signal due to the nitroxide radical in the reaction mixture of a binuclear copper(II) complex (*e.g.*, $[Cu_2(pia)_2]$), H_2O_2 and 2,2,6,6-tetramethyl-4-piperidinol. Thus, we may conclude that the $^1O_2$ produced by the simultaneous two-electron transfer from H_2O_2 to two copper(II) ions plays a key role in the catalytic function of the binuclear copper(II) complexes for the luminol chemiluminescence.

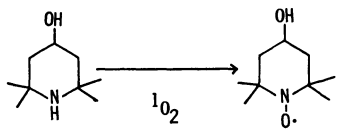

The present authors wish to express their sincere thanks to Prof. R. Shimada (Kyushu University) for his kind advices in setting up the apparatus for the measurements of chemiluminescence intensity.

References

1) H. O. Albrecht, *Z. Phys. Chem.*, **136**, 321 (1928).
2) E. H. White, O. Zafiriou, H. H. Kagi, and J. H. M. Hill, *J. Am. Chem. Soc.*, **86**, 940 (1964).
3) E. H. White and M. M. Bursey, *J. Am. Chem. Soc.*, **86**, 941 (1964).
4) M. M. Rauhut, A. M. Semsel, and R. G. Roberts, *J. Org. Chem.*, **31**, 2431 (1966).
5) J. R. Totter and G. E. Philbrough, *Photochem. Photobiol.*, **5**, 177 (1966).
6) For instance, T. Tsumaki, T. Yoshino, and M. Kuramoto, *Nippon Kagaku Zasshi*, **65**, 53 (1944), and references cited therein.
7) H. Ojima, *Nippon Kagaku Zasshi*, **84**, 909 (1963).
8) N. Oishi, Y. Nishida, K. Ida, and S. Kida, *Bull. Chem. Soc. Jpn.*, **53**, 2847 (1980).
9) Y. Nishida, N. Oishi, and S. Kida, *Inorg. Chim. Acta*, **46**, L69 (1980).
10) N. Oishi, Y. Nishida, and S. Kida, *Chem. Lett.*, **1981**, 1031.
11) Y. Nishida, N. Oishi, H. Kuramoto, and S. Kida, *Inorg. Chim. Acta*, **57**, 253 (1982).
12) N. Oishi, Y. Nishida and S. Kida, presented at the 32nd Symposium on the Coordination Chemistry, Sendai, (1981).
13) L. F. Lindoy, N. E. Tokel, L. B. Anderson, and D. H. Busch, *J. Coord. Chem.*, **1**, 7 (1971).
14) J. A. Bertrand and J. A. Kelley, *Inorg. Chim. Acta*, **4**, 203 (1970).
15) J. A. Bertrand, J. A. Kelley, and J. L. Breece, *Inorg. Chim. Acta*, **4**, 247 (1970).
16) Y. Nishida, F. Numata, and S. Kida, *Inorg. Chim. Acta*, **11**, 189 (1974).
17) I. Murase, M. Hatano, S. Ueno, H. Okawa, and S. Kida, *Bull. Chem. Soc. Jpn.*, **55**, 2404 (1982).
18) H. Ojima, *Nippon Kagaku Zasshi*, **88**, 1056 (1967).
19) G. S. Patterson and R. H. Holm, *Bioinorg. Chem.*, **4**, 257 (1975).
20) L. L. Smith and M. J. Kulig, *J. Am. Chem. Soc.*, **98**, 1027 (1976).
21) C. Ouannes and T. Wilson, *J. Am. Chem. Soc.*, **90**, 6527 (1968).
22) In the case of the hemin–H_2O_2 system, DABCO showed negligible effect on the chemiluminescence intensity. These results are implying that the mechanism of luminol chemiluminescence in the NaClO–H_2O_2 system is different from that in the hemin–H_2O_2 system, and also that DABCO is operating as a scavenger of $^1O_2$ in the NaClO–H_2O_2 system.
23) V. B. Tranov, V. Ya. Shyapintokh, O. M. Khvostach, A. B. Shapiro, and E. G. Rozantsev, *J. Photochem.*, **4**, 313 (1975).

 © 1982 The Chemical Society of Japan Bull. Chem. Soc. Jpn., 55, 3750—3756 (1982) [Vol. 55, No. 12

Metal Complexes of Peptides. III. The Preparation and Properties of Diammine(oligopeptidato)cobalt(III) Complexes

Hiroshi KAWAGUCHI,* Mari ISHII, Tomoharu AMA, and Takaji YASUI
Department of Chemistry, Faculty of Science, Kochi University, Akebono-cho, Kochi 780
(Received March 26, 1982)

Complexes of the [Co(tripeptidato)$(NH_3)_2$] and NH_4[Co(tetrapeptidato)$(NH_3)_2$] types (tripeptidato and tetrapeptidato denote the tri- and tetraanions of the coordinating peptides respectively) have been prepared and characterized by means of their electronic, ^{1}H NMR, and circular dichroism (CD) spectral data. In the NH_4-[Co(tetrapeptidato)$(NH_3)_2$] complex, the peptide coordinates to cobalt(III) as a quadridentate ligand through the nitrogens of an amino and three amide groups. The additivity of the vicinal CD spectra has been found to hold for the complexes of a series of tripeptides containing L-alanine and/or glycine residue. These tri- and tetrapeptidato complexes in water easily undergo aquation reaction, releasing the ammonia molecule.

A number of oligopeptide complexes of metals, such as Cu(II, III), Ni(II, III), and Pd(II), have been reported in which the peptides coordinate as quadridentate chelates.[1–16] Although the preparations of the cobalt(III) complexes with tri- or tetrapeptides have been reported in the literature,[17–22] there have been only two reports of the cobalt(III) complexes with a peptide coordinated as a quadridentate chelate.[21,22] Manyak *et al.* reported on the [Co(gly–gly–gly)$(NH_3)_2$] and Na[Co(gly–gly–gly)(gly)] complexes (gly–gly–gly denotes the trianion of glycylglycylglycine), in which the three chlate rings of the peptide were noncoplanar.[21] As X-ray structural studies have shown that the peptide group retains its rigid planar structure upon coordination,[23–27] the structure postulated by Manyak *et al.* is thought to be very unlikely. The complex [Co(gly–gly–gly)$(NH_3)_2$] described by them was rose in color and so different from the present complex (brown in color) with the same chemical formula. Evans *et al.* have prepared diammine(tripeptidato)cobalt(III) complexes in which the peptides coordinate as a coplanar quadridentate chelate and discussed in detail the effects of chelation on the ^{13}C and ^{1}H NMR resonances of peptides.[22]

Our recent works concerning dipeptidato complexes have shown that the [Co(*N*-methyliminodiacetato)-(dipeptidato)]$^-$ type of complex exhibits novel spectral behavior in the d-d transition region,[28] and that the absolute configurations of bis(dipeptidato)cobaltate(III) complexes can be determined on the basis of their CD patterns in the range of 40000 to 50000 cm^{-1}.[29] In the present paper, we wish to report the preparation and spectroscopic properties of the cobalt(III) complexes with a series of tri- and tetrapeptides in which the peptides coordinate as quadridentate chelates.

Experimental

Ligands. Glycylglycylglycine (H_3gly–gly–gly) was synthesized according to the literature.[30a]

L-Alanyl-L-alanyl-L-alanine (H_3L-ala–L-ala–L-ala) was prepared by a combination of conventional techniques, starting with *N*-benzyloxycarbonyl-L-alanine (Z-L-ala)[30b] and L-alanine ethyl ester hydrochloride (L-ala–OEt·HCl).[30c] Dicyclohexylcarbodiimide (DCC) coupling was used to form a dipeptide derivative from these precursors.[30d] The dipeptide ethyl ester was formed by the reaction of Z-L-ala–L-ala–OEt with HBr–acetic acid (25%). It was then coupled with another equivalent of Z-L-ala, again using DCC. The tripeptide hydrobromide was formed by the reaction of Z-L-ala–L-ala–L-ala–OEt with an aqueous NaOH solution and then with HBr–acetic acid. The free peptide was obtained by the action of aqueous NH_3 on the tripeptide hydrobromide and was then recrystallized from the EtOH–water system.

Other tripeptides, L-alanyl-L-alanylglycine (H_3L-ala–L-ala–gly), L-alanylglycyl-L-alanine (H_3L-ala–gly–L-ala), glycyl-L-(alanyl-L-alanine (H_3gly–L-ala–L-ala), L-alanylglycylglycine (H_3L-ala–gly–gly), glycyl-L-alanylglycine (H_3gly–L-ala–gly), glycylglycyl-L-alanine (H_3gly–gly–L-ala), β-alanylglycylglycine (H_3β-ala–gly–gly), glycyl-β-alanylglycine (H_3gly–β-ala–gly), and glycylglycyl-β-alanine (H_3gly–gly–β-ala), were also prepared by the same procedure as that used for H_3L-ala–L-ala–L-ala.

The same DCC coupling method was used for the syntheses of tetrapeptides. In the case of glycyl-L-alanylglycylglycine (H_4gly–L-ala–gly–gly), the tetrapeptide derivative, Z–gly–L-ala–gly–gly–OEt, was prepared by the action of Z–gly with L-ala–gly–gly–OEt, but for the other tetrapeptides, L-alanylglycylglycylglycine (H_4L-ala–gly–gly–gly), glycylglycyl-L-alanylglycine (H_4gly–gly–L-ala–gly), glycylglycylglycyl-L-alanine (H_4gly–gly–gly–L-ala), β-alanylglycylglycylglycine (H_4β-ala–gly–gly–gly), glycyl-β-alanylglycylglycine (H_4gly–β-ala–gly–gly), glycylglycyl-β-alanylglycine (H_4gly–gly–β-ala–gly), and glycylglycylglycyl-β-alanine (H_4gly–gly–gly–β-ala), the corresponding peptide derivatives were prepared by coupling Z-dipeptide with dipeptide–OEt.

Preparations of Complexes. [*Co(tripeptidato)(NH$_3$)$_2$*]·x*H$_2$O*: This type of complex was prepared by two different methods.

(1): A solution of tripeptide (5 mmol) in aqueous 1 M† NaOH (5 cm^3) was added to a DMSO solution (50 cm^3) containing[Co$(NH_3)_5(H_2O)](ClO_4)_3\cdot H_2O$[31] (2.48 g, 5 mmol); the mixed solution was heated at *ca.* 50 °C with constant stirring. Ammonia was evolved, and after *ca.* 1 h brown precipitates started to separated out. After additional heating for a few hours, the reaction mixture was allowed to stand in a refrigerator overnight. The brown precipitates obtained by filtration were dissolved again in a minimum amount of water, and then the aqueous solution was chromatographed on a Sephadex G-10 column (3.5 cm × 80 cm), with water as the eluant, giving three bands. The first (red-brown) and third (pink) descended bands were rejected. The desired complex was isolated as crystalline powder from the eluate of the second band on the addition of a large amount of acetone; it was then dried over $CaCl_2$. The diammine(tripeptidato)cobalt(III) complexes with the following peptides: H_3gly–gly–gly, H_3L-

† 1 M = 1 mol dm^{-3}.

Table 1. Analytical data of the complexes

Complex	C(%) Found (Calcd)	H(%) Found (Calcd)	N(%) Found (Calcd)
$[Co(gly\text{-}gly\text{-}gly)(NH_3)_2]\cdot 3H_2O$	21.02(21.63)	5.77(6.05)	21.02(21.02)
$[Co(L\text{-}ala\text{-}gly\text{-}gly)(NH_3)_2]\cdot 2H_2O$	25.35(25.54)	5.93(6.12)	21.54(21.27)
$[Co(gly\text{-}L\text{-}ala\text{-}gly)(NH_3)_2]\cdot 2H_2O$	26.00(25.54)	5.85(6.12)	20.91(21.27)
$[Co(gly\text{-}gly\text{-}L\text{-}ala)(NH_3)_2]\cdot 2H_2O$	25.77(25.54)	5.66(6.12)	20.82(21.27)
$[Co(\beta\text{-}ala\text{-}gly\text{-}gly)(NH_3)_2]\cdot 0.5H_2O$	27.78(27.82)	5.47(5.67)	23.20(23.18)
$[Co(gly\text{-}\beta\text{-}ala\text{-}gly)(NH_3)_2]\cdot H_2O$	26.87(27.02)	5.81(5.83)	21.91(22.50)
$[Co(gly\text{-}gly\text{-}\beta\text{-}ala)(NH_3)_2]\cdot 2.5H_2O$	24.71(24.86)	6.14(6.26)	20.58(20.07)
$[Co(L\text{-}ala\text{-}L\text{-}ala\text{-}gly)(NH_3)_2]\cdot 1.5H_2O$	28.52(28.75)	6.47(6.33)	21.16(20.95)
$[Co(L\text{-}ala\text{-}gly\text{-}L\text{-}ala)(NH_3)_2]\cdot 3H_2O$	26.62(26.60)	6.41(6.70)	19.20(19.39)
$[Co(gly\text{-}L\text{-}ala\text{-}L\text{-}ala)(NH_3)_2]\cdot 3H_2O$	26.77(26.60)	6.31(6.70)	19.44(19.39)
$[Co(L\text{-}ala\text{-}L\text{-}ala\text{-}L\text{-}ala)(NH_3)_2]\cdot H_2O$	31.78(31.86)	6.54(6.54)	20.33(20.64)
$NH_4[Co(gly\text{-}gly\text{-}gly\text{-}gly)(NH_3)_2]\cdot 3H_2O$	23.72(23.59)	6.14(6.43)	23.45(24.07)
$NH_4[Co(L\text{-}ala\text{-}gly\text{-}gly\text{-}gly)(NH_3)_2]\cdot 3H_2O$	25.57(25.65)	6.63(6.70)	23.45(23.07)
$NH_4[Co(gly\text{-}L\text{-}ala\text{-}gly\text{-}gly)(NH_3)_2]\cdot 1.5H_2O$	27.39(27.42)	6.36(6.39)	24.99(24.87)
$NH_4[Co(gly\text{-}gly\text{-}gly\text{-}L\text{-}ala)(NH_3)_2]\cdot 2.5H_2O$	26.02(26.22)	6.52(6.60)	23.42(23.78)
$NH_4[Co(\beta\text{-}ala\text{-}gly\text{-}gly\text{-}gly)(NH_3)_2]\cdot 3.5H_2O$	25.62(25.12)	6.29(6.79)	22.28(22.79)
$NH_4[Co(gly\text{-}\beta\text{-}ala\text{-}gly\text{-}gly)(NH_3)_2]\cdot 3.5H_2O$	25.78(25.12)	6.61(6.79)	22.53(22.79)

ala–gly–gly, H_3gly–L-ala–gly, H_3gly–gly–L-ala, $H_3\beta$-ala–gly–gly, H_3gly–β-ala–gly, and H_3gly–gly–β-ala, were prepared by this method.

(2): In the present paper, a series of diammine(tripeptidato)cobalt(III) complexes were also prepared by modifying the method described in the literature.[22]

Tripeptide (3.4 mmol) was dissolved in 10 cm^3 of water, and the solution was adjusted to pH 9.0—9.5 with a 28% NH_3 solution. A fresh peroxo-dimer, $[(NH_3)_5CoO_2Co(NH_3)_5](NO_3)_4\cdot 2H_2O$, was added to the above peptide solution chilled in an ice bath with constant stirring. After stirring for *ca.* 2 h, the solution was allowed tostand in a refrigerator for one day. The resulting solution was filtered, and the red-brown filtrate was chromatographed on a Sephadex G-10 column (3.5 cm × 80 cm). The adsorbed band was separated into brown (main) and pink (a little) bands by elution with water. To the eluate from the brown band was added a large amount of acetone. The desired complex was then deposited by allowing the solution to stand overnight at room temperature; it was filtered, washed with acetone, and then dried over $CaCl_2$. This preparative method was used for all of the [Co(tripeptidato)$(NH_3)_2$] complexes presented here.

NH_4[Co(tetrapeptidato)$(NH_3)_2]\cdot xH_2O$: The preparation of this type of complex was carried out by the same method as (2) described above, except for the addition of a small amount of aqueous NH_3 (28%) prior to adding acetone. As the reaction of tetrapeptide with a peroxo-dimer was slower than that of tripeptide, the reaction solution was allowed to stand for two day in a refrigerator. Standing for more than two days gave a larger amount of another red-brown by-product (probably an aqua complex), which was eluted faster than the desired complex on a Sephadex G-10 column. The gly–gly–L-ala–gly, gly–gly–β-ala–gly, and gly–gly–gly–β-ala complexes were rechromatographed on a Bio-Gel P2 column (3.5 cm × 30 cm), with water as an eluant to ensure the purity. Despite such a procedure, these complexes separated out as syrup products for which the analytical data were unsatisfactory.

The analytical data for the [Co(tripeptidato)$(NH_3)_2$] and NH_4[Co(tetrapeptidato)$(NH_3)_2$] complexes are listed in Table 1.

Measurements. The absorption and CD spectra were measured by means of a Hitachi 557-type spectrophotometer and a JASCO J-22 spectropolarimeter respectively. The proton NMR were recorded on a JEOL MH-100 spectrometer, with DSS as the internal reference.

Results and Discussion

Although the reaction of tripeptide with an equimolar quantity of pentaammineaquacobalt(III) complex in DMSO yielded the desired product, the same reaction in water gave unsatisfactory results; many bands appeared when the reactant solution was chromatographed on a Sephadex G-10 column. As the [Co(tripeptidato)$(NH_3)_2$] type of complex is more labile in water than other ammine complexes such as [Co(dipeptidato)$(NH_3)_3]^+$, presumably the complicated consecutive reactions must occur in water. On the other hand, the [Co(tripeptidato)$(NH_3)_2$] complex is only slightly soluble in DMSO, being protected from the consecutive reactions. With H_3gly–gly–gly, H_3L-ala–gly–gly, H_3gly–L-ala–gly, H_3gly–gly–L-ala, $H_3\beta$-ala–gly–gly, H_3gly–β-ala–gly, and H_3gly–gly–β-ala, the preparative method in DMSO (Method (1)) was applied; however, the yields of the complexes depended on the sort of peptides: in the cases of the gly–gly–L-ala and gly–gly–β-ala complexes, the yields were below half of that for the gly–gly–gly complex. The application of this method to the preparation of the NH_4[Co(tetrapeptidato)$(NH_3)_2$] type of complex was unsuccessful.

The preparative method using the peroxo-dimer (Method (2)) gave constantly high yields of the desired products for all the tripeptides used here. When the reactant solution was chromatographed on a Sephadex G-10 column, two completely separated bands were usually observed, but in some cases, *e.g.*, in the [Co(gly–gly–β-ala)$(NH_2)_2$] complex, another red-brown band, which is presumably an aqua complex, was eluted earlier than the desired band. As the [Co(tripeptidato)$(NH_3)_2$] type of complex is relatively labile in water, as will be described below, rechromatography to ensure purity causes an aquation reaction and brings about a low yield, even though aqueous ammonia was used as an

TABLE 2. ^{1}H NMR DATA OF THE TYPE [Co(tripeptidato)$(NH_3)_2$] COMPLEXES IN SLIGHTLY BASIC D_2O

Tripeptidato	C-terminal (ppm) $-CH_2-$ $>CH-$ $-CH_2-CH_2-$	Central (ppm) $-CH_2-$ $>CH-$ $-CH_2-CH_2-$	N-terminal (ppm) $-CH_2-$ $>CH-$ $-CH_2-CH_2-$	$-CH_3$ (ppm) C-terminal central N-terminal
gly-gly-gly	4.18(s)	3.93(s)	3.72(s)	
L-ala-gly-gly	4.11(s)	3.88(s)	3.75(q,J=7.0)	1.45(d,J=7.0)
gly-L-ala-gly	4.08(s)	4.00(q,J=7.0)	3.64(s)	1.37(d,J=7.0)
gly-gly-L-ala	4.30(q,J=7.0)	3.87(s)	3.62(s)	1.56(d,J=7.0)
β-ala-gly-gly	4.24(s)	3.90(s)	3.10[a],2.52[a]	
gly-β-ala-gly	4.06(s)	3.18[a],2.47[a]	3.56(s)	
gly-gly-β-ala	3.52[a],2.52[a]	3.74(s)	3.63(s)	
L-ala-L-ala-gly	4.08(s)	4.06(q,J=7.0)	3.76(q,J=7.0)	1.36(d,J=7.0) 1.46(d,J=7.0)
L-ala-gly-L-ala	4.29(q,J=8.0)	3.90(s,br)	3.71(q,J=8.0)	1.57(d,J=8.0) 1.45(d,J=8.0)
gly-L-ala-L-ala	4.26(q,J=7.0)	3.99(q,J=7.0)	3.67,3.55 (AB,J=17.0)	1.55(d,J=7.0) 1.40(d,J=7.0)
L-ala-L-ala-L-ala	4.28(q,J=7.0)	4.04(q,J=7.0)	3.68(q,J=7.0)	1.58(d,J=7.0) 1.40(d,J=7.0) 1.47(d,J=7.0)

AB: AB pattern resonance, s: singlet, d: doublet, q: quartet, br: slightly broad. a) Observed as a triplet-like broad peak.

eluant. The major disadvantage of this method is that the yield of the desired complex significantly depends on the purity of the peroxo-dimer used as a starting material.

The reaction of the peroxo-dimer with H_4gly-gly-gly-gly afforded a high yield of the desired complex, NH_4[Co(gly-gly-gly-gly)$(NH_3)_2$], as needle crystals. The same reactions with H_4gly-L-ala-gly-gly, H_4gly-gly-gly-L-ala, $H_4\beta$-ala-gly-gly-gly, and H_4gly-β-ala-gly-gly also produced considerable quantities of the desired complexes, which were liable to separate out as syrup products upon the addition of acetone to the eluates from Sephadex G-10 columns. Fortunately, we could isolate these complexes as crystalline products by allowing the acetonic suspensions to stand at room temperature for several days. In the cases of H_4L-ala-gly-gly-gly, H_4gly-gly-L-ala-gly, H_4gly-gly-β-ala-gly, and H_4gly-gly-gly-β-ala, the reaction of these peptides with the peroxo-dimer gave a large amount of by-products. The precipitation of the diammine(tetrapeptidato)cobaltate(III) complex by adding acetone under weak acidic conditions (pH 3—4) gave the protonated complex, H[Co(tetrapeptidato)$(NH_3)_2$]·$x H_2O$.

^{1}H NMR. Evans *et al.* prepared seven kinds of the [Co(tripeptidato)$(NH_3)_2$] type of complexes in which the peptides coordinate through the terminal NH_2, two amide N, and terminal CO_2^- groups and reported ^{1}H and ^{13}C NMR data in D_2O for the complexes.[22] Figure 1 shows a comparison among the ^{1}H NMR spectra of [Co(gly-gly-gly)$(NH_3)_2$], [Co(L-ala-gly-gly)$(NH_3)_2$], [Co(gly-L-ala-gly)$(NH_3)_2$], and [Co(gly-gly-L-ala)$(NH_3)_2$] complexes in slightly basic D_2O. The spectrum of [Co(gly-gly-gly)$(NH_3)_2$] shows three singlet peaks due to three CH_2 groups at 3.72, 3.93, and 4.18 ppm, suggesting that the chelate rings of the peptide are coplanar. The singlet peaks at 3.88 and 4.11 ppm in the L-ala-gly-gly complex correspond to those at 3.93 and 4.18 ppm respectively in the gly-gly-gly complex. Therefore, these peaks can be assigned to either the C-terminal or central CH_2 of the tripeptide ligand. Similar relationships are also found between the gly-gly-gly complex and the gly-L-ala-gly or gly-gly-L-ala complex (Fig. 1 and Table 2). These results indicate that the N- and C-terminal CH_2 of the tripeptide

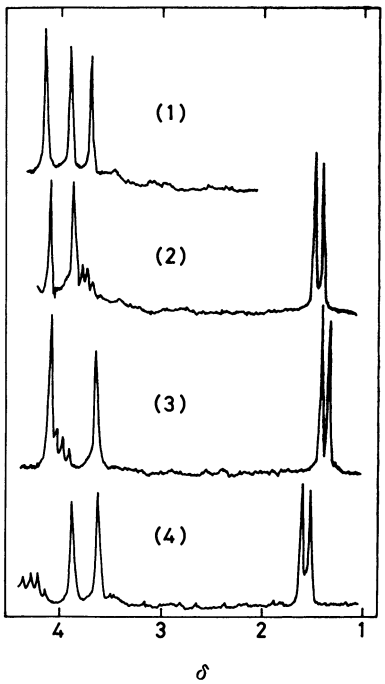

Fig. 1. The ^{1}H NMR spectra of [Co(gly-gly-gly)$(NH_3)_2$] (1), [Co(L-ala-gly-gly)$(NH_3)_2$] (2), [Co(gly-L-ala-gly)$(NH_3)_2$] (3), and [Co(gly-gly-L-ala)$(NH_3)_2$] (4) in slightly basic D_2O.

ligand resonate at the highest and lowest magnetic fields respectively; thus we are able to assign each peak. The same relationship is also realized for the complexes of the tripeptides containing the glycine and/or β-alanine residue (Table 2). Each spectrum of the β-ala–gly–gly, gly–β-ala–gly, and gly–gly–β-ala complexes exhibited two broad triplet-like peaks due to the $-CH_2-CH_2-$ group. The same pattern of the signals has been observed in the complexes of dipeptides containing the β-alanine residue.[28,29] An examination of the molecular models indicates that the tripeptides containing the β-alanine residue can coordinate to cobalt(III) in a noncoplanar configuration (*cis*-α); however, the possibility of the noncoplanar form can be rejected on the basis of the fact that the signals due to the CH_2 groups of glycine residues are singlets in these complexes. For the complexes of the tripeptides containing two or three L-alanine residues, the methine signals can be assigned on the basis of a comparison of the chemical shifts; in these complexes, the N- and C-terminal >CH– of the peptide ligands resonate at the highest and lowest magnetic fields respectively. The regular trend in chemical shifts is also observed for the CH_3 signals of the tripeptidato complexes containing the L-alanine residue, making it possible to assign those signals: the signals at 1.36—1.40, 1.45—1.47, and 1.55—1.58 ppm are assigned to central, N-terminal, and C-terminal CH_3 respectively. The ^1H NMR data of the [Co(tripeptidato)$(NH_3)_2$] complexes are also listed in Table 2.

In the present study, the [Co(gly–L-ala–L-ala)$(NH_3)_2$] complex is the only example in which the CH_2 protons are inequivalent at 100 MHz. The CH_2 signal of the L-ala–gly–L-ala complex is also a slightly broad singlet at 100 MHz, indicating a tendency toward splitting.

Absorption Spectra. Figure 2 shows the absorption spectra of the [Co(gly–gly–gly)$(NH_3)_2$] and [Co(gly–β-ala–gly)$(NH_3)_2$] complexes. The former complex

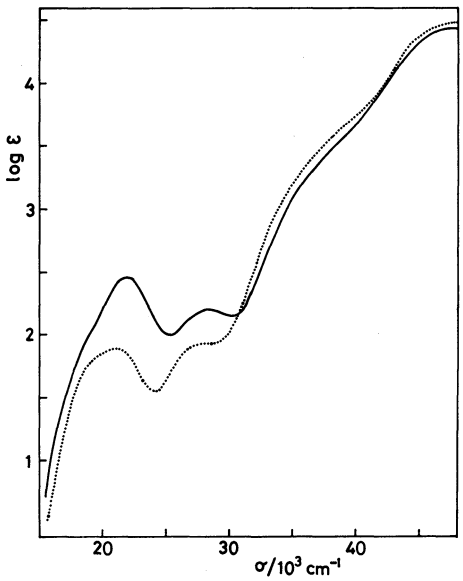

Fig. 2. The absorption spectra of [Co(gly–gly–gly)$(NH_3)_2$] (——) and [Co(gly–β-ala–gly)$(NH_3)_2$] (------) in water.

exhibits the characteristic spectrum for the complex containing chelated peptide: the first band at 21880 cm^{-1} has an enhanced intensity (ε=292 $dm^3 \cdot mol^{-1} \cdot cm^{-1}$) in contrast with the second band. The ratio of the absorption coefficients for the first and second bands ($\varepsilon_1/\varepsilon_{11}$) of [Co(gly–gly–gly)$(NH_3)_2$] (2.14) is higher than that for [Co(gly–gly)$(NH_3)_3]^+$ (1.8),[32] but lower than that for [Co(gly–gly)$_2]^-$ (3.98).[29] A split component in the first band region for the [Co(gly–gly–gly)$(NH_3)_2$] complex is observed as a shoulder band at *ca.* 18200 cm^{-1}. The absorption spectra of other diammine(tripeptidato)cobalt(III) complexes, where the tripeptides are composed of only α-amino acid residues, are

Table 3. Absorption and CD spectra of the [Co(tripeptidato)$(NH_3)_2$] and [Co(tetrapeptidato)$(NH_3)_2]^-$ types of complexes in the d-d transition region measured in water

Tripeptidato or tetrapeptidato	$\sigma_{max}/10^3$ cm^{-1}(log ε)		$\sigma_{max}/10^3$ cm^{-1}(Δε)		
	1st band	2nd band	1st-band region	2nd-band region	
gly–gly–gly	21.88(2.47)	28.32(2.14)			
L-ala–gly–gly	22.05(2.42)	28.46(2.20)	18.87(−0.47)	22.37(+0.04)	28.57(−0.28)
gly–L-ala–gly	21.93(2.41)	28.01(2.12)	19.34(−1.28)		27.91(−0.31)
gly–gly–L-ala	22.00(2.51)	28.02(2.19)	20.12(−1.23)	26.21(+0.04)	28.33(−0.08)
L-ala–L-ala–gly	22.15(2.48)	28.34(2.24)	19.16(−1.78)		28.17(−0.49)
L-ala–gly–L-ala	22.17(2.50)	28.01(2.22)	19.42(−1.59)		28.33(−0.30)
gly–L-ala–L-ala	22.10(2.50)	27.93(2.19)	19.57(−2.42)		28.17(−0.35)
L-ala–L-ala–L-ala	22 25(2.52)	27.93(2.21)	19.31(−2.52)		28.33(−0.46)
β-ala–gly–gly	21.65(2 28)	28.60sh(*ca.*2.16)[a]			
gly–β-ala–gly	21.16(1 89)	28.40sh(*ca.*1.94)[a]			
gly–gly–β-ala	21.61(2 37)	28.13(2.11)			
gly–gly–gly–gly	21.55(2 24)	28.82(2 07)			
L-ala–gly–gly–gly	21.74(2 24)	28.90(2.14)	19.92(−0 59)	22.42(+0.18)	28.82(−0.32)
gly–L-ala–gly–gly	21.65(2 23)	28.74(2 06)	19.84(−2.01)		28.33(−0.51)
gly–gly–gly–L-ala	21.55(2 22)	29 24(2 13)	18.69(−0.04)	22.32(+0.20)	*ca.*27.78sh(+0.04)[a]
β-ala–gly–gly–gly	22 22(2 20)	*ca.*28 57sh[a]			
gly–β-ala–glygly	19 92(1 86)	*ca.*28 00sh[a]			

a) sh: Shoulder.

quite similar to that of the [Co(gly–gly–gly)$(NH_3)_2$]; the spectral data are listed in Table 3. The [Co(β-ala–gly–gly)$(NH_3)_2$] and [Co(gly–gly–β-ala)$(NH_3)_2$] complexes also showed spectral patterns almost identical with that of the gly–gly–gly complex, indicating that the spectra are little affected by the exchanges of the CH_2 group with the $-CH_2-CH_2-$ group in the N- and C-terminal fragments of tripeptides (Table 3). As is shown in Fig. 2, however, the [Co(gly-β–ala–gly)-$(NH_3)_2$] complex shows remarkably different absorption behavior in the d-d transition region, compared with that of other [Co(tripeptidato)$(NH_3)_2$] complexes: The first band is broad (showing splitting) and has a relatively weak intensity ($\varepsilon=77$ dm^3 mol^{-1} cm^{-1}).

In our previous works,[28,29] we reported that the complexes with dipeptides containing the N-terminal β-alanine residue were different in the spectral behavior of the d-d transition from the complexes with dipeptides containing the N-terminal α-amino acid residue. In the present case, the gly–β-ala–gly complex differs from the other tripeptidato complexes in spectral behavior. Such a difference in spectral behavior may arise from the differences in electronic delocalization around the peptide backbone and in the ring strain of the chelated peptide. The electronic delocalization and the ring strain must be affected by the position of the β-alanine residue in the peptide chain, even though simple molecular models provide no obvious reasons for this.

The first band maxima of the complexes with tripeptides containing the β-alanine residue shift to the lower-energy side compared with that of the gly–gly–gly complex. Such a blue shift is contrary to the red shifts observed for the copper(II) complexes of di- and tripeptides containing the β-alanine residue[33,34] and also for the cobalt(III) complexes of dipeptides containing the β-alanine residue.[29]

CD Spectra. In the case of the tetragonal coordination of tripeptides containing only α-amino acid residues to cobalt(III), the chelate rings of the peptide ligand are expected to take a coplanar form, ruling out any configurational and conformational contributions to optical activity. Therefore, the sole source of optical activity in the d-d transition region is the vicinal effect due to the asymmetric carbons.[35] As is shown in Fig. 3, the [Co(tripeptidato)$(NH_3)_2$] complexes exhibit two major negative CD bands associated with two d-d transitions in the visible region, while additional very weak positive CD components are observed at 22370 and 26210 cm^{-1} for the L-ala–gly–gly and gly–gly–L-ala complexes respectively. The numerical CD data in the d-d transition region are summarized in Table 3.

For the [Co(gly–L-ala–gly)$(NH_3)_2$] and [Co(gly–gly–L-ala)$(NH_3)_2$] complexes, the magnitudes of $\Delta\varepsilon_{ext}$ in the first band region are nearly comparable to each other, but more than twice that for the [Co(L-ala–gly–gly)$(NH_3)_2$] complex. This result is consistent with those for [Co(*N*-methyliminodiacetato)(dipeptidato)]$^-$ complexes, in which the CD contribution from the C-terminal active source is larger than that from the N-terminal one.[28] The tripeptidato complexes containing two or three asymmetric carbons show enhanced negative CD bands associated with the first d-d bands

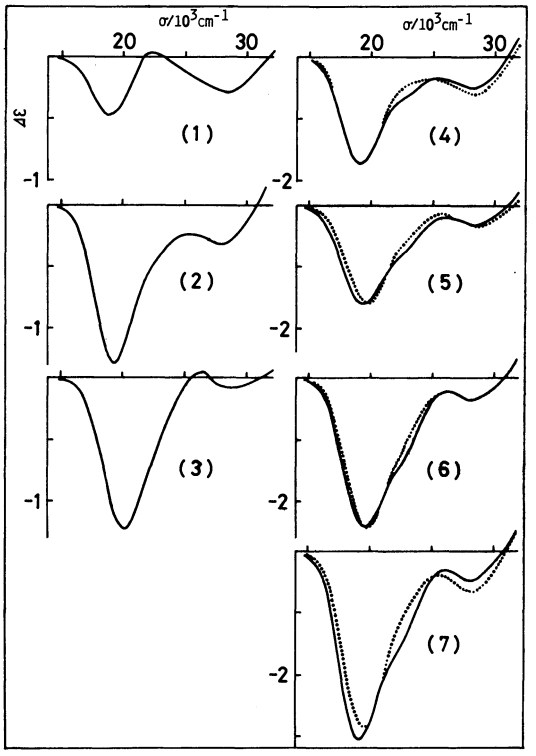

Fig. 3. The CD spectra of the type [Co(tripeptidato)-$(NH_3)_2$] in water (——). The dotted lines represent the CD curves calculated from the CD data of two (or three) tripeptidato complexes containing only one asymmetric carbon.
Tripeptidato: (1) L-ala–gly–gly, (2) gly–L-ala–gly, (3) gly–gly–L-ala, (4) L-ala–L-ala–gly, (5) L-ala–gly–L-ala, (6) gly–L-ala–L-ala, (7) L-ala–L-ala–L-ala.

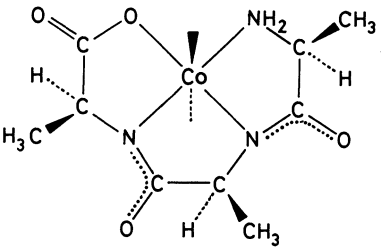

Fig. 4. The structure of [Co(L-ala–L-ala–L-ala)$(NH_3)_2$] drawn from the direction of the NH_3–Co–NH_3 axis.

(Fig. 3 and Table 3).

The dotted lines in Fig. 3 represent the CD curves calculated from the CD data of two (or three) tripeptidato complexes containing only one asymmetric carbon; *e.g.*, in the case of the L-ala–L-ala–gly complex, the dotted line represents the sum of the two CD curves observed for the L-ala–gly–gly and gly–L-ala–gly complexes. In each case, the good coincidence obtained between the observed (solid line) and calculated (dotted line) CD curves demonstrates the additivity of the vicinal contribution. Such direct comparison may be valid for the present series of complexes, because the spectral behaviors of these complexes are quite similar to each other in the d-d transition region.

Figure 4 shows the structure of the [Co(L-ala–L-ala–L-ala)$(NH_3)_2$] complex drawn from the direction of the

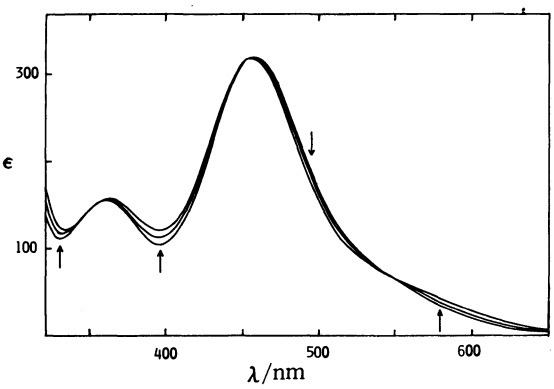

Fig. 5. Change of absorption spectrum with time for [Co(gly-gly-L-ala)$(NH_3)_2$] in water at 30.1 °C. The curves show the spectra measured at 1, 21, and 61 min, respectively.

NH_3–Co–NH_3 axis, in which two NH_3 are omitted and in which all methyl groups of the side chain are above the chelate plane. The octant rule has been proposed to account for the results of the CD signs in the visible absorption region of transition metal complexes;[36] however, the octant rule can not account for the additivity of the CD spectra of the tripeptidato complexes. Whenever the nodal surfaces are drawn, the octant rule predicts that the gly–L-ala–gly complex should exhibit signs opposite to those of the L-ala–gly–gly and gly–gly–L-ala complexes. The same situation has also been realized in the Cu(II) and Ni(II) complexes. The double octant rule has been proposed to account for the CD signs of those complexes in the d-d transition region.[2] The double octant rule is actually valid in the diammine(tripeptidato)cobalt(III) complexes.

Chemical Properties. The absorption and CD spectra of the diammine(tripeptidato)cobalt(III) complexes in an aqueous solution changed with the lapse of time. Figure 5 shows the time-course of the absorption curve for the gly–gly–L-ala complex in water at 30.1 °C. Over an initial period of *ca.* 1 h, the isosbestic points were observed, but not from that time on, indicating that the next reaction occurred. The same situation was also realized for other tripeptidato complexes: The changes in spectra for the complexes of tripeptides containing glycine and/or L-alanine residues, especially the L-ala–L-ala–L-ala and L-ala–L-ala–gly complexes, were fast; however, those for the tripeptidato complexes containing the β-alanine residue were slow and almost negligible over a period of one hour after dissolving. The spectral changes were accelerated in the acidic and basic aqueous solutions (even in an NH_3 aqueous solution); however, in the 1 M NH_4Cl aqueous solution with its pH of the solution adjusted at 7 with NH_3, the spectral change was not observable for *ca.* 2 h. For the complex of tripeptide containing the L-alanine residue, the CD spectral change was the same as the absorption spectral change. These results suggest that the following reaction occurs initially:

$$[\text{Co(tripeptidato)}(NH_3)_2] + H_2O \longrightarrow [\text{Co(tripeptidato)}(NH_3)(H_2O)] + NH_3.$$

Tetrapeptidato Complexes. On the basis of the examination of molecular models and the fact that the ^1H NMR spectrum of the [Co(gly–gly–gly–gly)$(NH_3)_2$]$^-$ complex in a weak alkaline D_2O shows four singlet peaks due to four CH_2 groups of the gly–gly–gly–gly ligand at 3.52, 3.72, 3.86, and 3.90 ppm, it can be concluded that the most probable structure of [Co(gly–gly–gly–gly)$(NH_3)_2$]$^-$ is the *trans*(NH_3) form, in which the tetraglycine coordinates to cobalt(III) as a tetragonal quadridentate chelate. The other tetrapeptidato complexes prepared in this study also showed singlet peaks due to the CH_2 of the glycine-rings, indicating the same structure as that of the gly–gly–gly–gly complex.

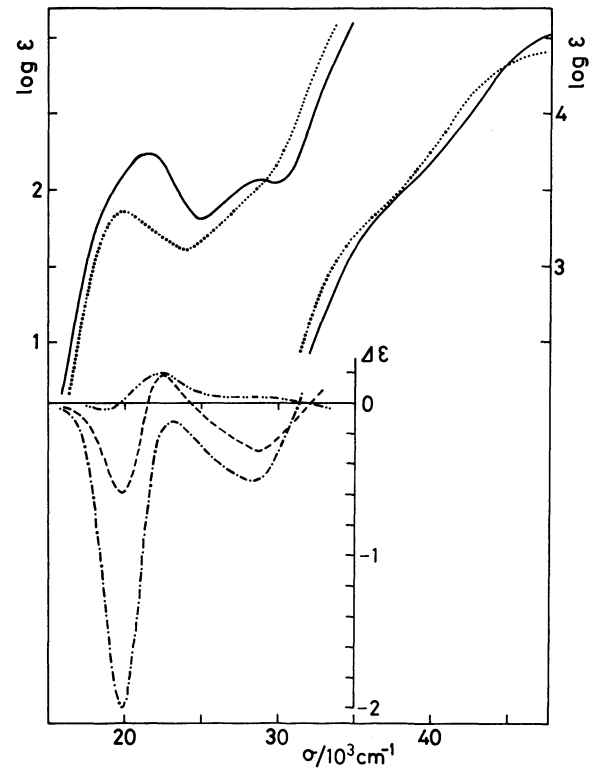

Fig. 6. The absorption spectra of [Co(gly–gly–gly–gly)$(NH_3)_2$]$^-$ (——) and [Co(gly–β-ala–gly–gly)$(NH_3)_2$]$^-$ (……) in water, and the CD spectra of [Co(L-ala–gly–gly–gly)$(NH_3)_2$]$^-$ (------), [Co(gly–L-ala–gly–gly)$(NH_3)_2$]$^-$ (·—·—·), and [Co(gly–gly–gly–L-ala)$(NH_3)_2$]$^-$ (–···–···) in water.

As is shown in Fig. 6 and Table 3, the absorption spectrum of the diammine(tetraglycinato)cobaltate(III) complex exhibits the first and second bands at 21550 and 28820 cm^{-1} respectively. The first band has an enhanced intensity (ε=175 $dm^3\,mol^{-1}\,cm^{-1}$), following a tendency toward splitting (shoulder band at *ca.* 19000 cm^{-1}). This spectral behavior is similar to that of the diammine(tripeptidato)cobalt(III) complex and supports the assertion that the tetraglycinato complex has the *trans*(NH_3) structure. The absorption spectra of the other tetrapeptidato complexes are similar to that of the tetraglycinato complex. The only exception is the gly–β-ala–gly–gly complex, which shows a lower intensity of the first band (ε=72 $dm^3\,mol^{-1}\,cm^{-1}$), just as in the gly–β-ala–gly complex (Table 3 and Fig. 6).

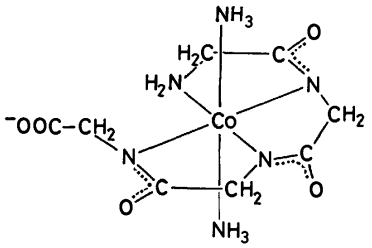

Fig. 7. The structure of $[Co(gly\text{-}gly\text{-}gly\text{-}gly)(NH_3)_2]^-$.

The CD spectra of the $[Co(L\text{-}ala\text{-}gly\text{-}gly\text{-}gly)(NH_3)_2]^-$ and $[Co(gly\text{-}L\text{-}ala\text{-}gly\text{-}gly)(NH_3)_2]^-$ complexes in the d-d transition region are similar in pattern to those of the $[Co(L\text{-}ala\text{-}gly\text{-}gly)(NH_3)_2]$ and $[Co(gly\text{-}L\text{-}ala\text{-}gly)(NH_3)_2]$ complexes respectively; however, the $[Co(gly\text{-}gly\text{-}gly\text{-}L\text{-}ala)(NH_3)_2]^-$ complex shows a remarkably different CD behavior in the d-d transition region compared with those of the L-ala-gly-gly-gly, gly-L-ala-gly-gly, and also tripeptidato complexes (Fig. 6 and Table 3). The $[Co(gly\text{-}gly\text{-}L\text{-}ala\text{-}gly)(NH_3)_2]^-$ complex, which was not isolated in the pure state, showed two negative signs of CD associated with the first and second bands. These results indicate that the tetrapeptides coordinate to cobalt(III) as quadridentate chelates through the terminal NH_2 and three amide N groups, as is shown in Fig. 7.

The diammine(tetrapeptidato)cobaltate(III) complexes also show the absorption and CD spectral changes in water with the same order of time-course as those of diammine(tripeptidato)cobalt(III) complexes; these changes are ascribed to an aquation reaction.

References

1) G. F. Bryce and F. R. N. Gurd, *J. Biol. Chem.*, **241**, 122, 1439 (1966).
2) R. B. Martin, J. M. Tsangaris, and J. W. Chang, *J. Am. Chem. Soc.*, **90**, 821 (1968).
3) J. W. Chang and R. B. Martin, *J. Phys. Chem.*, **73**, 4277 (1968).
4) J. M. Tsangaris and R. B. Martin, *J. Am. Chem. Soc.*, **92**, 4255 (1970).
5) E. W. Wilson, Jr., and R. B. Martin, *Inorg. Chem.*, **9**, 528 (1970).
6) T. P. Pitner, E. W. Wilson, Jr., and R. B. Martin, *Inorg. Chem.*, **11**, 738 (1972).
7) D. L. Rabenstein and S. Libich, *Inorg. Chem.*, **11**, 2960 (1972).
8) H. Aiba, A. Yokoyama, and H. Tanaka, *Bull. Chem. Soc. Jpn.*, **47**, 136, 1437 (1974).
9) T. P. A. Kruck and B. Sarker, *Inorg. Chem.*, **14**, 2383 (1975).
10) D. W. Margerum, K. L. Chellappa, F. P. Bossu, and G. L. Burce, *J. Am. Chem. Soc.*, **97**, 6894 (1975).
11) G. L. Burce, F. B. Paniago, and D. W. Margerum, *J. Chem. Soc., Chem. Commun.*, **1975**, 261.
12) F. P. Bossu and D. W. Margerum, *J. Am. Chem. Soc.*, **98**, 4003 (1976).
13) F. P. Bossu and D. W. Margerum, *Inorg. Chem.*, **16**, 1210 (1977).
14) M. Fujioka, Y. Nakao, and A. Nakahara, *J. Inorg. Nucl. Chem.*, **39**, 1885 (1977).
15) A. G. Lappin, C. K. Murray, and D. W. Margerum, *Inorg. Chem.*, **17**, 1630 (1978).
16) Y. Kuroda and H. Aiba, *J. Am. Chem. Soc.*, **101**, 6837 (1979).
17) J. P. Collman and E. Kimura, *J. Am. Chem. Soc.*, **89**, 6096 (1967).
18) E. Kimura, S. Young, and J. P. Collman, *Inorg. Chem.*, **9**, 1183 (1970).
19) R. D. Gillard and D. A. Phipps, *J. Chem. Soc., A*, **1971**, 1074.
20) Y. Wu and D. H. Busch, *J. Am. Chem. Soc.*, **94**, 4115 (1972).
21) A. R. Manyak, C. B. Murphy, and A. E. Martell, *Arch. Biochem. Biophys.*, **59**, 373 (1955).
22) E. J. Evans, J. E. Grice, C. J. Hawkins, and M. Heard, *Inorg. Chem.*, **19**, 3496 (1980).
23) H. C. Freeman and M. R. Taylor, *Acta Crystallogr.*, **18**, 939 (1965).
24) H. C. Freeman, J. M. Guss, and R. L. Sinclair, *Chem. Commun.*, **1968**, 485.
25) R. D. Gillard, E. D. McKenzie, R. Mason, and G. B. Robertson, *Nature*, **209**, 1347 (1966).
26) M. T. Barnet, H. C. Freeman, D. A. Buckingham, I-Han Hsu, and D. van der Helm, *Chem. Commun.*, **1970**, 368.
27) P. DeMeester and D. J. Hodgson, *Inorg. Chem.*, **17**, 440 (1978).
28) H. Kawaguchi, M. Kanekiyo, T. Ama, and T. Yasui, *Bull. Chem. Soc. Jpn.*, **53**, 3208 (1980).
29) T. Yasui, H. Kawaguchi, and T. Ama, *Bull. Chem. Soc. Jpn.*, **54**, 2918 (1981).
30) a) N. Izumiya, M. Oono, T. Kato, and H. Aoyagi, "Peputido Gosei," Maruzen, Tokyo (1975), p. 57; b) *ibid.*, p. 24; c) *ibid.*, p. 66; d) *ibid.*, p. 144.
31) M. Shibata and A. Uehara, "Shinjikken Kagaku Kouza," ed by the Chemical Society of Japan, Maruzen, Tokyo (1977), No. 8 (III), p. 1216.
32) I. G. Browning, R. D. Gillard, J. R. Lyons, P. R. Mitchell, and D. A. Phipps, *J. Chem. Soc., Dalton Trans.*, **1972**, 1815.
33) O. Yamauchi, Y. Hirano, Y. Nakao, and A. Nakahara, *Can. J. Chem.*, **47**, 3441 (1969).
34) Y. Nakao, H. Ishibashi, and A. Nakahara, *Bull. Chem. Soc. Jpn.*, **43**, 3457 (1970).
35) Y. Shimura, *Bull. Chem. Soc. Jpn.*, **31**, 315 (1958).
36) C. J. Hawkins and E. Larsen, *Acta Chem. Scand.*, **19**, 185 (1965).

UV Photoelectron Spectroscopic Investigation and the DV-Xα MO Calculation of Tetrakis(2-methyl-2-propanethiolato)molybdenum(IV)

Masao TAKAHASHI,* Iwao WATANABE, Shigero IKEDA, Masato KAMATA,† and Sei OTSUKA†
Department of Chemistry, Faculty of Science, Osaka University, Toyonaka, Osaka 560
†*Department of Chemistry, Faculty of Engineering Science, Osaka University, Toyonaka, Osaka 560*
(Received April 15, 1982)

Helium(I) ultraviolet photoelectron spectrum is reported for the compound Mo(*t*-BuS)$_4$. The observed spectrum is interpreted by means of DV-Xα MO calculations on the model compounds Mo(SH)$_4$ and Mo(SMe)$_4$. The UV photoelectron spectrum of Mo(*t*-BuS)$_4$ exhibits a low ionization potential band (*IP*=6.43 eV) which corresponds to ionization of mainly Mo4d$_{z^2}$ electron of A_1 representation. This molecular orbital has also bonding character between Mo4d and S3d.

Currently thiolatomolybdenum complexes due to their possible implication in redox-active molybdoenzymes are receiving considerable attention. The homoleptic tetrakis(thiolato)molybdenum(IV) compound and products derived therefrom were reported recently.[1,2] The electronic structures of molybdenum compounds have been investigated by use of X-ray and UV photoelectron spectroscopy (XPS and UPS).[3,4] The UPS is especially useful for the study of the valence orbitals in a molecule.

Recently the discrete-variational(DV)-Xα method has been shown to be useful for evaluating electron binding energies and studying electronic structures, and applied for the interpretation of photoelectron spectroscopic data of various materials.[5,6]

The Mo(*t*-BuS)$_4$ compound exhibits outstanding reactivity toward various reagents. In this paper we report the study on its electronic structure by using UPS and by performing the DV-Xα MO calculation.

Experimental

Materials. The compound, Mo(*t*-BuS)$_4$, was prepared and purified as described elsewhere.[1] This compound is sensitive to air and moisture and sublimes at 343 K (0.13 Pa). It was preserved under a nitrogen atmosphere until UPS measurements. The compounds, 2-methyl-2-propanethiol, di-*t*-butyl disulfide and 2-methyl-1-propene, were obtained commercially.

UPS Measurements. The He(I) photoelectron spectrometer used was constructed by one of the authors (I.W.). The spectrometer was controlled by a mini-computer so that the effect of energy drift of the spectrometer during the measurement was completely compensated by a real-time energy calibration technique.

The sample, Mo(*t*-BuS)$_4$, seemed to be liable to decomposition on heating, so UV photoelectron spectra for its expected decomposition products, *i.e.*, 2-methyl-2-propanethiol, 2-methyl-1-propene, and di-*t*-butyl disulfide, were also measured, and they were found to be identical with the spectra reported[7-9] (a, b, and c in Fig. 2 respectively). When the sample, Mo(*t*-BuS)$_4$, was heated to 340 K in a glass tube at the distance of 30 cm from the ionization chamber with an electric heater to obtain a sufficient vapor pressure for the measurement, the observed spectrum was that for the mixture of the above mentioned decomposition products. Therefore the ionization chamber as shown in Fig. 1 was necessary. On the wall of the ionization chamber two metal-film resistors (C in Fig. 1) and a calibrated thermistor (B) were fixed with aluminum tapes. An alternating current supplied to the

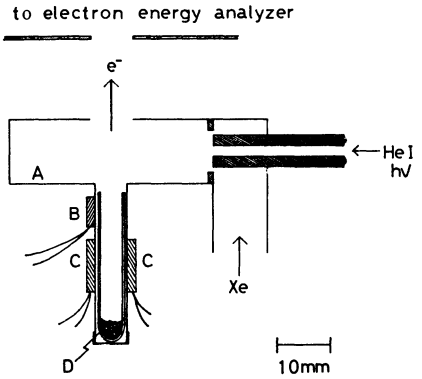

Fig. 1. Schematic drawing of ionization chamber. A) ionization chamber made of 0.2 mm thick copper sheet, B) thermistor, C) metal-film resistors, D) solid samples in a glass tube.

resistors heated the ionization chamber, the temperature of which was measured by the thermistor. The magnetic field produced by the a.c. current caused neither peak shift nor peak broadening.

It was necessary to keep the temperature of the ionization chamber as low as possible in order to minimize the sample decomposition. The measurements were performed at 331± 2 K, *i.e.*, about 10 K lower than the temperature at which the sublimation of Mo(*t*-BuS)$_4$ was noticeable. Because of the low vapor pressure at that temperature, the spectral data were accumulated for 2 d to get a satisfactory spectrum.

The ionization energy scale was calibrated with xenon used as an internal standard (*IP*=12.130 eV). Spectral resolution defined by the full width at half-maximum (FWHM) of the $^2P_{3/2}$ xenon peak was less than 30 meV. All ionization energies were read at the maximum of each peak as vertical ionization potential.

Computations. The DV-Xα method used was described in detail elsewhere.[10,11] Molecular orbital energies were calculated by employing models of Mo(SH)$_4$ and Mo(SMe)$_4$ for Mo(*t*-BuS)$_4$, and that of Mo(NH$_2$)$_4$ for Mo(NMe$_2$)$_4$. Each model has D_{2d} symmetry. Numerically generated atomic basis functions (1s-5p for Mo, 1s-3d for S, 1s-2p for C and N, and 1s for H) were used to expand the molecular orbitals. The bond distances and angles used for the calculations were taken from the results of X-ray crystallography for Mo(*t*-BuS)$_4$[1] and Mo(NMe$_2$)$_4$,[12] except that S–H, C–H, and N–H bond distances were taken to be 0.1336, 0.1090, and 0.1022 nm respectively. In the compound, Mo(*t*-BuS)$_4$, the MoS$_4$ skeleton has nearly perfect D_{2d} symmetry, while in Mo(NMe$_2$)$_4$, having exact D_{2d} symmetry as a whole, the MoN$_4$ moiety has almost perfect T_d symmetry. Thus we have chosen the

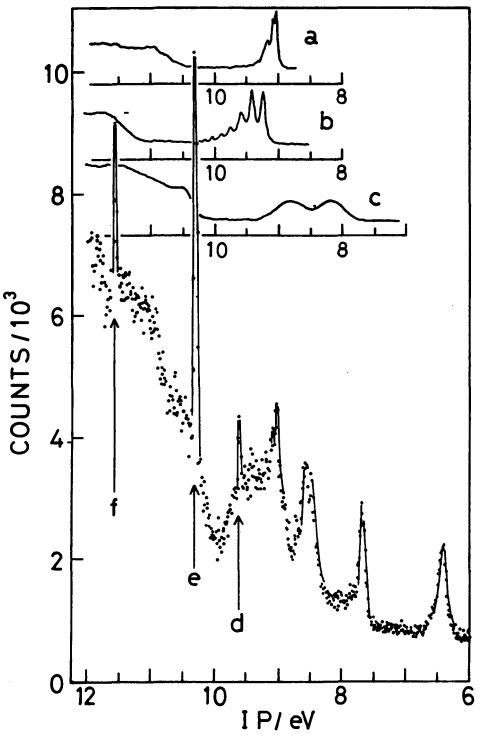

Fig. 2. He(I) UV photoelectron spectrum of Mo(*t*-BuS)$_4$ and its decomposition products. Each data points for the Mo(*t*-BuS)$_4$ spectrum was determined by collecting counts for 260 s. Photoelectron spectra for a) 2-methyl-2-propanethiol, b) 2-methyl-1-propene, c) di-*t*-butyl disulfide. Three peaks at (d) 9.61, (e) 10.26, and (f) 11.57eV originate from Xe ionizations. See text.

models of Mo(SH)$_4$ or Mo(SMe)$_4$ and Mo(NH$_2$)$_4$ with D_{2d} symmetry in calculations for Mo(*t*-BuS)$_4$ and Mo(NMe$_2$)$_4$ respectively, assuming that the effect of such distortion is negligible.

Results and Discussion

The UV photoelectron spectrum of Mo(*t*-BuS)$_4$ is shown in Fig. 2. There are at least four bands in Fig. 2. The first ionization band (*IP*=6.43 eV) is assigned an ionization of metal orbital because of its very low IP. The second band (*IP*=7.70 eV) is so sharp that it could be interpreted to correspond to the ionization of a non-bonding orbital. Over the very broad fourth band (*IP*= 9—10 eV), there are two peaks of 9.03 eV and 9.06 eV which are in perfect agreement with the peaks in the photoelectron spectrum of 2-methyl-2-propanethiol. Therefore the peaks are most possibly assigned to the ionization of sulfur lone pair MOs of one of the decomposition products of Mo(*t*-BuS)$_4$. We presume that the peaks of 9.03 eV and 9.4 eV consist of the ionizations of 2-methyl-2-propanethiol and 2-methyl-1-propene (the spectra inserted in Fig. 2) respectively. Hence the spectral intensity due to the ionizations of those decomposition products should account for more than 70% of all the spectral intensity in the area of 9.0—9.8 eV, and in the area above 9.8 eV less than 35%. Furthermore there stand three peaks at 9.61 eV, 10.26 eV, and 11.57 eV, corresponding to the ionizations of xenon $^2P_{3/2}$ by HeIγ (23.74 eV) and HeIβ (23.09 eV), and $^2P_{1/2}$ by HeIβ, respectively.

Table 1. VERTICAL IONIZATION POTENTIALS FOR Mo(*t*-BuS)$_4$ AND CALCULATED ORBITAL ENERGIES FOR Mo(SH)$_4$ AND Mo(SMe)$_4$ (IN eV)

Observed IP Mo(*t*-BuS)$_4$	Orbital energies	
	Mo(SH)$_4$	Mo(SMe)$_4$
6.43	−3.26($13a_1$)	−3.04($16a_1$)
7.70	−4.33($2a_2$)	−3.86($3a_2$)
8.5	−4.77(13e)	−4.10(17e)
—	−5.45(12e)	−5.10(16e)

The vertical ionization potentials and computed orbital energies for Mo(SH)$_4$, and Mo(SMe)$_4$ are listed in Table 1. The molecular orbital energies are related to the vertical ionization potentials through Koopmans' theorem. The gross-orbital populations of filled and empty orbitals were calculated for Mo(SMe)$_4$ (Table 2). The calculation on Mo(SH)$_4$ gave similar results to those for Mo(SMe)$_4$ with respect to the bonding character between Mo and S. The first band (*IP*=6.43 eV) corresponds to the ionization of $16a_1$ molecular orbital which consists mainly of metal $4d_{z^2}$ orbital and partly of S3d and C2p orbitals. This orbital is of weakly bonding character between Mo4d-S3d and of antibonding between Mo4d-S3p_z and Mo4d-S3s. Further this orbital has additional weak d-p bonding character for the ligand S–C bond.

The next two bands (*IP*=7.70 and 8.5 eV) are

Table 2. MOLECULAR ORBITAL COMPONENTS CALCULATED FOR Mo(SMe)$_4$ (IN %)

Level[a]	Orbital energy/eV	Mo				S		
		$4d_{z^2}$	$4d_{x^2-y^2}$	$4d_{xy}$	$4d_{xz/yz}$	3d	3p	3s
$5b_1$	−1.14	—	54	—	—	5	40	0
$16a_1$[b]	−3.04	56	—	—	—	13	8	5
$3a_2$	−3.86	—	—	—	—	0	93	0
17e	−4.10	—	—	—	0	0	96	0
16e	−5.10	—	—	—	17	1	66	6
$15a_1$	−5.29	9	—	—	—	1	69	2
$4b_1$	−5.51	—	37	—	—	4	55	0
$14b_2$	−5.57	—	—	35	—	2	56	2

a) Any contribution of other orbitals to the levels listed here is negligible except that $16a_1$ contains 15% contribution of C2p, and $15a_1$ contains 12% of Mo5s. b) This MO is the HOMO in Mo(SMe)$_4$.

assigned to the ionization of the molecular orbitals of $3a_2$ and 17e levels, respectively. The $3a_2$ level consists of only sulfur 3p lone pair MOs. The sharpness of the second band (IP=7.70 eV) supports this interpretation. The orbital of the 17e level consists of sulfur 3p lone pair MOs, too, and corresponds to the third band (IP=8.5 eV), which is slightly broader. The breadth of this band may be ascribed to be due to the Jahn-Teller effect. It is probable that the fourth band (IP>9 eV) contains the ionizations both of Mo(*t*-BuS)$_4$ and of decomposition products.

The complex, Mo(NMe$_2$)$_4$ or Mo(NEt$_2$)$_4$, is the only complex to our knowledge, which is analogous to Mo(*t*-BuS)$_4$ with respect to the molecular symmetry and the valence type of Mo, and for which UV photoelectron spectrum is known. Their spectra together with the Fenske-Hall type MO calculation on the model compound, Mo(NH$_2$)$_4$, have been reported by Chisholm *et al.*[12,13] In order to get an insight into the electronic structure of these complexes, the DV-Xα MO calculation was performed on the amidomolybdenum complex Mo(NH$_2$)$_4$ in addition to the thiolatomolybdenum complex. The result from the calculation on Mo(NH$_2$)$_4$ is consistent with that obtained by Chisholm *et al.*

The calculations on Mo(NH$_2$)$_4$ and Mo(SMe)$_4$ predict that the bond-overlap populations of Mo–N and Mo–S are 0.248 and 2.648, and that the net charge on Mo central atoms are +2.15 and +0.80, respectively. Therefore, it could be stated that the Mo–N bond is ionic in character but that the Mo–S bond is covalent if compared each other. The calculations also predict that the HOMO of the amidomolybdenum complex consists almost entirely of Mo4d$_{x^2-y^2}$ (88%), while that of the thiolatomolybdenum complex ($16a_1$) delocalizes slightly as shown in Table 2. The contents of this theoretical calculation appear to be inconsistent with the experimental fact that the half-width of the first band, corresponding to the ionization of the HOMO, in the spectrum of Mo(NMe$_2$)$_4$ is estimated to be about twice as large as that of Mo(*t*-BuS)$_4$ by comparing the published spectrum and the one in Fig. 2.

The difficulty to understand the contradiction has arisen in the same way on the studies of some metal-halide complexes.[14] For example, the photoionization of TlBr[15] gives a broad peak due to the ejection of the electron localized on Br *i.e.*, the "non-bonding" or "lone-pair electron," together with a sharp peak due to the ejection of the electron delocalized over the two atoms, *i.e.*, the "bonding electron" according to a molecular orbital model. The phenomenon was simply understood by taking account of the roles of localized and delocalized electrons in an ionic-bond. In the ionic-bond the electron on Br$^-$ acts as a bonding electron, so its ionization causes a broad peak. The present case of amidomolybdenum and thiolatomolybdenum complexes could be understood in quite the same manner. Thus the electron in HOMO of amidomolybdenum plays a role as an anti-bonding electron with respect to the ionic Mo–N bond more strongly than the corresponding electron in thiolatomolybdenum does as a bonding electron with respect to the covalent Mo–S bond. Therefore, the spectra exhibit the broader first band for the amidomolybdenum complex than for the thiolatomolybdenum complex.

The authors wish to thank Professor Hirohiko Adachi and Mr. Hirohide Nakamatsu for the computer program of the DV-Xα calculation. The numerical calculations were carried out using ACOS NEAC 900 at the Computation Center, Osaka University, and ACOS NEAC 700 at the Crystallographic Research Center Institute for Protein Research, Osaka University. This work was supported by Toray Science and Technology Grants 72-1302.

References

1) S. Otsuka, M. Kamata, K. Hirotsu, and T. Higuchi, *J. Am. Chem. Soc.*, **103**, 3011 (1981).
2) M. Kamata, T. Yoshida, and S. Otsuka, *J. Am. Chem. Soc.*, **103**, 3572 (1981).
3) S. O. Grim and L. J. Matienzo, *Inorg. Chem.*, **14**, 1014 (1975).
4) L. W. Yarbrough, II, and M. B. Hall, *Inorg. Chem.*, **17**, 2269 (1978).
5) B. Kim, H. Adachi, and S. Imoto, *J. Electron Spectrosc. Relat. Phenom.*, **11**, 349 (1977).
6) H. Adachi, *J. Electron Spectrosc. Relat. Phenom.*, **16**, 277 (1979); M. Sano, H. Adachi, and H. Yamatera, *Bull. Chem. Soc. Jpn.*, **54**, 2636 (1981).
7) H. Ogata, H. Onizuka, Y. Nihei, and H. Kamada, *Bull. Chem. Soc. Jpn.*, **46**, 3036 (1973).
8) K. Kimura, S. Katsumata, T. Yamazaki, and H. Wakabayashi, *J. Electron Spectrosc. Relat. Phenom.*, **6**, 41 (1975).
9) G. Wagner and H. Bock, *Chem. Ber.*, **107**, 68 (1974).
10) H. Adachi, M. Tsukada, and C. Satoko, *J. Phys. Soc. Jpn.*, **45**, 875 (1978); C. Satoko, M. Tsukada, and H. Adachi, *ibid.*, **45**, 1333 (1978); H. Adachi, S. Shiokawa, M. Tsukada, C. Satoko, and S. Sugano, *ibid.*, **47**, 1528 (1979).
11) H. Nakamatsu, H. Adachi, and S. Ikeda, *J. Electron Spectrosc. Relat. Phenom.*, **24**, 149 (1981).
12) M. H. Chisholm, F. A. Cotton, and M. W. Extine, *Inorg. Chem.*, **17**, 1329 (1978).
13) M. H. Chisholm, A. H. Cowley, and M. Lattman, *J. Am. Chem. Soc.*, **102**, 46 (1980).
14) J. H. D. Eland, "Photoelectron Spectroscopy," Butterworths and Co., London (1974), pp. 126—128.
15) J. Berkowitz, *J. Chem. Phys.*, **56**, 2766 (1972).

An Analysis of the Chemical Compositions of Groundwaters Utilizing a Leaching Technique. An Application to the Rokko Mountains and Their Surroundings

Yuzo Tamari,* Yukiharu Inoue, Haruo Tsuji, and Yuzuru Kusaka
Department of Chemistry, Faculty of Science, Konan University, Higashinada-ku, Kobe 658
(Received April 19, 1982)

The chemical composition of groundwaters from granitic alluvial plains is different from that from the clayey "Kobe-group" strata surrounding the Rokko mountains. The former groundwaters are dominantly rich in Ca and HCO_3, while the latter are rich in Na and HCO_3. In order to investigate the difference in the groundwater compositions, a chemical leaching technique was applied to samples of soils, well-sediments, and rocks collected from the Rokko mountains and their surroundings. Three leaching solutions used were as follows. CO_2-saturated water to investigate the effect of chemical weathering; a 0.1 M† HNO_3 solution to remove hydroxide, sulfide, and colloidal matters; and a 1 M CH_3COONH_4 solution to leach exchangeable ions from the samples. In the leaching, leachable amounts of Na, K, Ca, and Mg as the major species and Fe and Mn as the minor species in groundwaters were determined. From the results of leaching and adsorption experiments for cations, and from a comparison of the analytical values of the cations in groundwaters with the data of the leaching experiments on the key diagram, the association of the chemical species dissolved in groundwaters with the geological characters was analysed.

The Rokko mountains are located north of Osaka Bay, behind the port of Kobe. The mountains essentially consist of granitic rocks characterized by biotite, and they are covered with granitic detritus called "Masatsuchi." The detritus forms alluvial plains and terrace deposits in the southern part of the Rokko mountains, and the detrital layers form a well aquifer because of the poorly coagulating layers. In the northern or northwestern side of the mountains, the Neogene strata (*ca.* 15 million years old), called argillaceous "Kobe group" strata, which are composed of such detritus as silt mudstone, sandstone, and conglomerates and of volcaniclastic materials containing large amounts of tuff, are widely distributed.[1]

It has been generally recognized that the chemical species dissolved in groundwaters are mainly Na^+, Ca^{2+}, Mg^{2+}, K^+, HCO_3^-, Cl^-, SO_4^{2-}, and soluble SiO_2, and that these species make up more than 95% of the total dissolved solids.[2] The chemical compositions of groundwaters in the Rokko mountains and their surroundings have been studied, and the concentrations of major and trace species have been reported by some of the present authors.[3,4] Table 1 shows some of the analytical results in their reports. This table shows that the groundwaters from the alluvial plains are dominantly rich in Ca and HCO_3, whereas the groundwaters from the Kobe-group area are rich in Na and HCO_3. The difference in the chemical compositions of groundwaters in these two areas is explained by the following reactions of major chemical species: the chemical actions controling the dissolution of the major species are weathering by CO_2 for granitiform soils in the alluvial plains, while the cation-exchange reactions by clay minerals are dominant in the Kobe-group area. In order to analyse the difference in the chemical compositions of groundwaters between the alluvial plains and the Kobe-group area, and in order to elucidate the association of geological strata with the chemical compositions, a chemical leaching technique was applied in this work.

Chemical leaching techniques are generally utilized

Table 1. Mean chemical compositions of groundwaters

Chemical species	Alluvial plains 34 Shallow groundwaters		Kobe-group strata: 38 Shallow groundwaters		Kobe-group strata: 15 Deep groundwaters	
	ppm Av.±S.D.	epm (% of epm)	ppm Av.±S.D.	epm (% of epm)	ppm Av.±S.D.	epm (% of epm)
Ca	42±15	2.1 (57)	12±9.2	0.60 (26)	1.6±1.3	0.08 (2)
Mg	5.7±2.3	0.47 (13)	2.3±1.7	0.19 (8)	0.2±0.2	0.02 (0.4)
Na	21±8.2	0.91 (25)	32±20	1.4 (62)	99±21	4.3 (97)
K	6.9±3.5	0.18 (5)	3.1±3.1	0.08 (4)	0.9± 1	0.02 (0.6)
Cations		3.66 (100)		2.27 (100)		4.42 (100)
HCO_3	92±26	1.5 (51)	63±51	1.0 (47)	260±67	4.3 (89)
Cl	26±15	0.73 (25)	23±16	0.65 (30)	9.2±7.1	0.26 (5)
SO_4	33±14	0.69 (24)	23± 9	0.48 (23)	14±12	0.29 (6)
SiO_2	21±6.1		29±10		33±10	
Anions		2.92 (100)		2.13 (100)		4.85 (100)

† 1 M=1 mol dm^{-3}, 1 ml=1 cm^3.

Table 2. Sampling descriptions

Sample	Location	Geology
Soil No. 1	Konan University #9	Alluvial plains
Well-sediment No. 1	Konan University #18	Alluvial plains
Well-sediment No. 2	Ohgo-cho, Kita-ku, Kobe	Kobe-group strata
Well-sediment No. 3	Yokawa-cho, Kita-ku Kobe	Kobe-group strata
Well-sediment No. 4	Yokawa-cho, Kita-ku Kobe	Kobe-group strata
Well-sediment No. 5	Ohzo-cho, Kita-ku, Kobe	Kobe-group strata
Montmollironite	Mississippi, U.S.A.	
Bentonite	Gunma prefecture	
Kaolinite	Georgia, U.S.A.	
Mt. Rokko Granite	Okamoto, Kobe	
JB-1	Japanese basalt, G.S.J.[a)]	

a) Detailed locations are described by Ando.[11)]

to separate different minerals, such as ferro-manganese and carbonate, or trace elements adsorbed on minerals to solutions by means of chemical reactions.[5-7)] This technique is also used for the state analysis of Se in sediments.[8)] In this work, a chemical leaching method was applied to powdered samples of rocks, soils, and well-sediments collected from Mt. Rokko and its surroundings, using leaching solutions of 0.1 M HNO_3, 1 M CH_3COONH_4, and CO_2-saturated water. From the results of 1) the X-ray diffraction patterns of the samples, 2) leaching experiments in which amounts of Na, K, Ca, Mg, Fe, and Mn removed from the samples by the leaching solutions were determined, 3) adsorption experiments using commercially available clay minerals and the samples, and 4) the analysis of key diagrams on which the leaching and analytical results of groundwaters had been plotted, it has been concluded that the chemical composition of each groundwater from the alluvial plains and the Kobe-group area depends on their geological strata, and that the leaching method is significant in analysing the influence of the geological strata on the chemical species dissolved in groundwaters.

Experimental

Samples, Reagents, and Apparatus. The sampling descriptions of the well-sediments, rocks, soils, and clay minerals used for these experiments are given in Table 2. The sediment samples were collected from the bottom to a depth of about 5 cm in relatively shallow wells, using a mud-sampler (Rigo Co., Ltd., model No. 2007).

The solutions of 0.1 M HCl, 0.1 M HNO_3, and 0.1 M CH_3COOH were prepared by diluting each reagent of an analytical-reagent grade with distilled water. The pH 7 solution of 1 M CH_3COONH_4 was also prepared by dissolving 77.09 g of CH_3COONH_4 with water to a 1000 ml volume and by adjusting the pH to 7.0 with a small quantities of CH_3COOH and NH_4OH solutions.

The following pieces of apparatus were employed; a flame photometer (Hiranuma-sangyo Co., Ltd., model FPF-2A), a spectrophotometer (Hitachi, Ltd., model 100-10), an atomic absorption spectrophotometer (Hitachi, Ltd., model 207), an X-ray diffractometer (Rigaku-denki Co., Ltd., model MJ-200-DH), and a washer-bath with irradiation by ultrasonic waves (Shimada Physical and Chemical Industrial Instruments Co., Ltd., model CF-16-2B, 200 W 28 kHz, and Branson Instruments Co., Ltd., model Bransonic 12,80 W 60 Hz).

Preparation of Samples. Wet sediment samples collected from wells were centrifuged, and the solid parts of the samples were dried for 5 h at 110 °C. After cooling, the samples were crushed in an agate mill and then powdered so as to pass through a 100-mesh-size sieve. Finely powdered dry samples were prepared by quartering them four times after the samples had been mixed in an agate mill for 10 min. Samples of rocks and clay minerals were also prepared in the same manner. In this sample preparation, about 95% of the homogeneities for trace elements in sediment samples and more than *ca.* 90% of the homogeneities for major constituents in artificial samples were estimated.[9,10)]

Leaching Solutions. The solutions used for the chemical leaching experiments were as follows. 1) CO_2-saturated water to investigate the effect of chemical species being dissolved in groundwaters by chemical weathering by CO_2; 2) a 1 M CH_3COONH_4 solution to remove the exchangeable ions sorbed by clay minerals; 3) a 0.1 M HCl solution to leach the metal sulfides and hydroxides and loosely adsorbed metal ions that were originally present in overlying water as fine-grained suspended phases;[6)] and 4) 0.1 M HNO_3 and 0.1 M CH_3COOH solutions to compare the effects of the leaching.

Recommended Leaching Procedure. Figure 1 shows the recommended procedure for the leaching method as established from the experimental results of investigating the effect of the reaction temperatures of leaching solutions, the effect of the intensity of ultrasonic waves irradiated during the leaching, and the effect of the irradiation time of ultrasonic waves on the leachable amounts of Na, K, Ca, Mg, Fe, and Mn.

One gram of a powdered sample was placed in a stoppered centrifugal tube (Vol. 50 ml), and a 25-ml portion of a leaching solution was added to the tube. The tube was set in a water-bath filled with hot water (40 °C) and irradiated by ultrasonic waves with an electric current of 3 A and for an irradiation time of 20 min. The tube was centrifuged for 10 min at 2500 rpm; then the supernatant solution was filtered (filter pore-size: 0.45 μ) and transferred to a 50-ml measuring flask (Fraction No. 1). A 25-ml portion of the same fresh leaching solution was added to the residue in the tube; the mixture was irradiated for 20 min and then centriguged. The solutions from Fractions No. 2 to No. 5 were prepared in the same way.

In the leaching with CO_2-saturated water, CO_2 gas was introduced into a mixture of 1 g of the sample and 25 ml of H_2O in a centrifugal tube under the same reaction conditions as are shown in Fig. 1.

Procedure of Adsorption Experiments. A solid-residue sample, after treatment by the leaching procedure with the 1 M CH_3COONH_4 solution, was used for the experiments. The sample was washed with water and then centrifuged.

Table 3. Chemical compositions of samples

Sample	Na(%)	K(%)	Ca(%)	Mg(%)	Fe(%)	Mn(ppm)
Soil No. 1	1.78	3.45	1.09	0.397	2.78	1790
Well-sediment No. 1	1.32	2.12	0.735	0.358	3.12	931
Well-desiment No. 2	1.17	1.93	0.435	0.427	3.35	577
Well-sediment No. 3	1.03	1.27	0.418	0.336	6.74	2460
Well-sediment No. 4	1.44	2.11	0.541	0.273	1.81	349
Montmollironite	0.258	0.623	0.431	1.48	3.25	147
Bentonite	2.69	1.56	0.258	0.325	0.129	87
Kaolinite	0.045	0.279	ND	0.062	0.502	ND
Mt. Rokko Granite	2.60	3.29	0.303	0.041	1.10	384
JB-1[a)]	2.08	1.19	6.63	4.66	6.30	1200

a) Certified values.[11)]

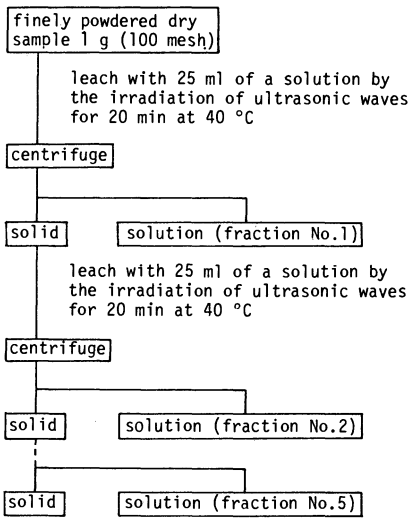

Fig. 1. The flow diagram of the leaching procedure.

After washing with water twice, a 25-ml portion of the solution adjusted to pH 7 and containing definite amounts of the chloride of each Na, K, Ca, and Mg was added to the sample. The mixture was irradiated by ultrasonic waves for 100 min (20 min × 5) at 40 °C. Then, after the centrifugation, the amounts of Na, K, Ca, and Mg in the supernatant liquid were determined.

Determination of Elements. To each solution from Fractions No. 1 to No. 5, 1 ml of a 10% La solution and 1 ml of a 5 M HNO_3 solution were added, and the mixture was diluted with water to 50 ml. In the solution, the Na and K were determined by flame photometry, and the Ca, Mg, Fe, and Mn, by atomic-absorption spectrophotometry.

For the determination of the Na, K, Ca, Mg, Fe, and Mn content of the samples given in Table 2, the samples were wet-ashed by general HF–$HClO_4$–HNO_3 treatments; these elements were then determined by the analytical procedure described above.

Results and Discussion

Analytical Data of Samples. Table 3 lists the Na, K, Ca, Mg, Fe, and Mn content of the samples. As shown in this table, the content of each element in the Mt. Rokko granite sample is fairly close to that of one reported by Kasama.[1)] However, it is difficult to find the geological differences between samples from the chemical compositions shown in this table.

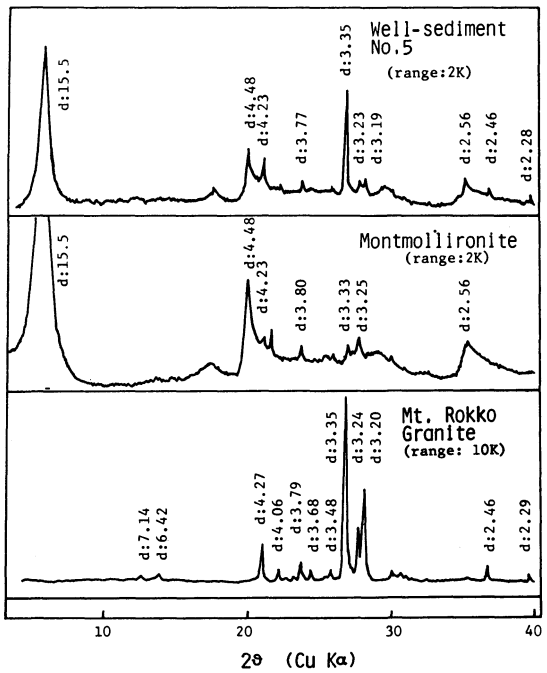

Fig. 2. X-Ray diffraction spectra of samples.

Figure 2 shows some typical X-ray diffraction patterns of the samples. The diffraction patterns of the soil No. 1 and the well-sediment No. 1 from the alluvial plains were identical with that of the Mt. Rokko granite, in which peaks corresponding to quartz (d: 4.26, 3.35, 2.46, 2.24, and 2.13) were found. In the well-sediments No. 2—No. 5 from the Kobe-group area, the peaks of montmollironite and quartz were detected.

Reproducibility of the Leaching Method. Table 4 shows the reproducibility of the leaching method, repeated four times by the recommended procedure given in Fig. 1. In this experiment, the soil No. 1 and a 0.1 M HNO_3 solution were used as the sample and the leaching solution respectively. For each element, in the sum of five fractions, a coefficient of variation of 0.99—4.5%, which was approximately within the limits of analytical error, was obtained.

Effect of Leaching Solutions. Table 5 gives the experimental results of the leaching with different solutions from the samples. It may be found from the table that the amounts of each of six elements leached

TABLE 4. REPRODUCIBILITY OF THE LEACHING METHOD

Run No.	Sample	Fraction	Na	K	Ca	Mg	Fe	Mn
1	Soil No. 1	1	185	195	8270	398	536	257
		2	20	60	617	82	352	69
		3	10	35	190	55	278	55
		4	15	35	79	34	214	32
		5	8	18	45	23	158	18
		Sum	238	343	9201	592	1538	431
2	Soil No. 1	1	195	190	8300	378	513	250
		2	20	60	657	89	335	66
		3	10	35	193	54	262	45
		4	15	28	85	34	212	29
		5	9	18	52	23	152	19
		Sum	249	331	9287	587	1474	409
3	Soil No. 1	1	185	180	8300	393	543	257
		2	23	58	661	84	328	61
		3	19	40	151	47	257	40
		4	9	28	88	34	199	30
		5	9	28	70	30	194	29
		Sum	245	334	9270	588	1521	417
4	Soil No. 1	1	185	185	8450	376	525	244
		2	13	30	446	55	180	39
		3	13	48	367	75	308	58
		4	9	28	91	34	188	30
		5	8	28	67	30	188	28
		Sum	288	319	9421	570	1389	399
Average±S.D.		Sum	240±9.20	332±9.91	9295±92.0	584±9.74	1481±66.7	414±13.5
C.V. (%)			3.83	2.98	0.99	1.67	4.50	3.26

Values: μg/g (microgram amounts of an element leached from a 1-g sample).

TABLE 5. EFFECTS OF LEACHING SOLUTIONS

Sample	Leaching soln	Na(μg/g)	K(μg/g)	Ca(g/g)	Mg(μg/g)	Fe(μg/g)	Mn(μg/g)
Soil No. 1	CO_2-saturated water	327	288	5815	251	ND	57
	0.1 M HCl	234	288	8720	558	2000	467
	0.1 M HNO_3	240	332	9300	584	1480	414
	0.1 M CH_3COOH	230	245	8460	335	24	255
	1 M CH_3COONH_4	148	186	7400	146	ND	293
Well-sediment No. 2	CO_2-saturated water	544	666	549	177	ND	15.0
	0.1 M HCl	533	1482	4080	1640	6406	83.6
	0.1 M HNO_3	547	1652	3550	1670	6488	84.1
	0.1 M CH_3COOH	513	969	1410	564	4904	29.4
	1 M CH_3COONH_4	580	1565	2750	455	ND	42.7

Values: μg amounts of an element leached in the sum of 5 fractions from 1 g of a sample.

with the 0.1 M HCl solution was nearly equal to that leached with the 0.1 M HNO_3 solution, but was larger than that leached with the 0.1 M CH_3COOH and 1 M CH_3COONH_4 solutions. In the leaching with the CO_2-saturated water, the dissolved amounts of the elements tended to agree with that of the 0.1 M HCl or 0.1 M HNO_3 solution from the soil No. 1 and not with that from the well-sediment No. 2. This difference between the two samples probably depends on the characteristics of their samples, *i.e.*, the fact that montmollironite was contained in the well-sediment No.2, while quartz was found in the soil No. 1.

Leaching of Elements from Samples. Table 6 lists the amounts of elements leached from different samples. From the table, the following characteristics of the leaching could be recognized.

In the alluvial soil No. 1, the considerably large amount of Ca was more easily dissolved with the CO_2-saturated water than in the Kobe-group samples. In the well-sediments from the Kobe-group strata, the percentages of Na and K leached with the CH_3COONH_4 solution were remarkably higher than that from the alluvial samples, and the amounts of Na, K, Ca, and Mg leached by the HNO_3 solution were almost equal to that by the CH_3COONH_4 solution. Similar results of the leaching were found in the clay minerals, montmollironite and kaolinite. This similarity is considered to be due to the presence of montmollironite in all the Kobe-group samples.

Adsorption of Cations on Samples. Adsorption experiments were carried out in order to investigate the chemical state of the elements in these samples;

Table 6. Analytical results of elements in the leaching experiment

Sample	Leaching soln	Na(μg/g)	K(μg/g)	Ca(μg/g)	Mg(μg/g)	Fe(μg/g)	Mn(μg/g)
Soil No. 1	0.1 M HNO_3	240(1.35)	332(0.962)	9295(85.3)	584(14.7)	1481(5.33)	414(23.1)
	1 M CH_3COONH_4	184(1.03)	186(0.539)	7397(67.9)	146(3.68)	ND	294(16.4)
	CO_2-saturated water	226(1.27)	241(0.699)	5508(50.5)	157(2.95)	ND	57(3.2)
Well-sediment	0.1 M HNO_3	151(1.14)	411(1.94)	2978(40.5)	552(15.4)	4611(14.8)	414(44.5)
No. 1	1 M CH_3COONH_4	92(0.70)	242(1.14)	1406(19.1)	158(4.41)	ND	161(17.3)
	CO_2-saturated water	342(2.59)	635(3.00)	1349(18.4)	270(7.54)	ND	ND
Well-sediment	0.1 M HNO_3	547(4.68)	1562(8.09)	3543(81.5)	1668(39.1)	6488(19.4)	84(15)
No. 2	1 M CH_3COONH_4	580(4.96)	1565(8.11)	2760(63.5)	455(10.7)	ND	43(7.4)
	CO_2-saturated water	544(4.65)	666(3.45)	549(12.6)	177(4.15)	ND	15(2.6)
Well-sediment	0.1 M HNO_3	2758(26.8)	1633(12.9)	3051(73.0)	243(7.23)	29660(44.0)	1312(53.3)
No. 3	1 M CH_3COONH_4	2683(26.1)	2038(16.1)	3368(80.6)	212(6.31)	114(0.17)	764(31.1)
Well-sediment	0.1 M HNO_3	703(4.88)	639(3.03)	1912(35.3)	389(14.2)	1858(10.3)	133(38.1)
No. 4	1 M CH_3COONH_4	718(4.99)	711(3.37)	2098(38.8)	303(11.1)	20(0.11)	113(32.4)
	CO_2-saturated water	1059(7.35)	387(1.83)	849(15.7)	173(6.34)	ND	ND
Montmoll-	0.1 M HNO_3	65(2.5)	399(6.31)	3805(88.3)	2991(20.2)	200(0.62)	56(38)
ironite	1 M CH_3COONH_4	63(2.4)	348(5.51)	4532(105)	3313(22.4)	ND	51(35)
	CO_2-saturated water	83(3.2)	403(6.38)	200(4.64)	119(0.80)	ND	ND
Bentonite	0.1 M HNO_3	6862(25.5)	484(3.10)	676(26.3)	379(11.7)	116(9.00)	13(15)
	1 M CH_3COONH_4	10262(38.2)	1006(6.47)	2422(94.0)	572(17.6)	ND	ND
Kaolinite	0.1 M HNO_3	10(2.2)	13(0.47)	ND	284(45.8)	4(0.08)	ND
	1 M CH_3COONH_4	18(4.0)	30(1.1)	ND	281(45.3)	ND	ND
Mt. Rokko	0.1 M HNO_3	146(0.56)	470(1.43)	303(10.0)	66(16)	1523(13.8)	110(28.6)
Granite	1 M CH_3COONH_4	84(0.32)	116(0.35)	218(7.19)	15(3.7)	ND	30(7.8)
	CO_2-saturated water	362(1.39)	388(1.18)	323(10.7)	30(7.3)	ND	ND
JB-1	0.1 M HNO_3	388(1.87)	276(2.34)	4377(6.65)	7918(17.1)	4889(7.74)	177(14.3)
	1 M CH_3COONH_4	96(0.46)	169(1.43)	1439(2.19)	786(1.70)	ND	50(4.0)
	CO_2-saturated water	73(0.31)	99(1.7)	1243(1.89)	998(2.16)	ND	62(5.0)

Values: microgram amounts of an element leached in the sum of 5 fractions from a 1-g sample,

Values in parentheses: $\frac{\text{microgram amounts of an element leached in the sum of 5 fractions from a 1-g sample}}{\text{total microgram amounts of an element in a 1-g sample}} \times 100\ (\%)$.

Table 7. Analytical results of cations in the adsorption experiment

Sample[a)]	Cation	Added (μg)	Adsorbed (μg)	Leached[b)] (μg)	Ratio of adsorbed to leached
Montmollironite	Na	4980	1730	63	27
(1 g)	K	5130	1880	348	5
	Ca	4980	2480	4532	0.5
	Mg	4880	2430	3313	1
Bentonite	Na	4980	720	10262	0.07
(1 g)	K	5130	1130	1006	1
	Ca	4980	4730	2422	2
	Mg	4880	1380	572	2
Kaolinite	Na	4980	1130	18	63
(1 g)	K	5130	325	30	11
	Ca	4980	350	ND	ND
	Mg	4880	225	281	0.8
Soil No. 1	Na	1130	100	184	0.5
(1 g)	K	1800	110	186	0.6
	Ca	9690	560	7397	0.08
	Mg	2000	110	146	0.8
Well-sediment No. 2	Na	900	100	580	0.2
(1 g)	K	1440	440	1565	0.3
	Ca	7750	1480	2760	0.5
	Mg	1600	219	455	0.5

a) Samples treated by leaching with the 1 M CH_3COONH_4 solution. b) Amounts of cations leached with the 1 M CH_3COONH_4 solution (see Table 6).

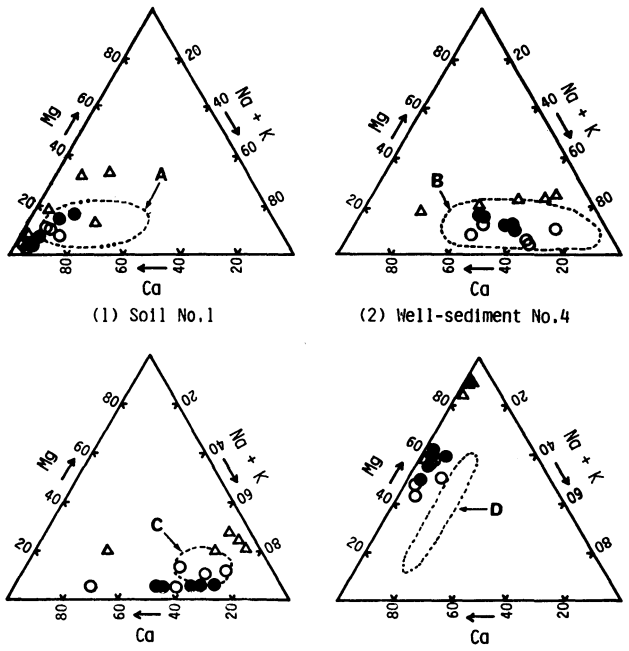

Fig. 3. Key diagram of relative percentages of milligram equivalents.
●: Leaching by CO_2-saturated water, ○: 1 M CH_3COONH_4 leaching, △: 0.1 M HNO_3 leaching, A: 34 Groundwaters from the alluvial plains, B: 38 Groundwaters from the Kobe-group strata, C: 7 Stream waters from topmost Mt. Rokko, D: 8 groundwaters from the worldwide 8 basaltic regions.

the soil No. 1 from the alluvial plains, the well-sediment No. 2 from the Kobe-group strata, and the clay minerals. Table 7 shows the results of the experiments. In this table, the amounts of elements leached from the original sample (see Table 6) are also listed.

In the montmollironite and bentonite, the amounts of divalent Ca adsorbed was higher than that of monovalent Na and K. The adsorptive behavior of the cations was observed also in the soil No. 1 and the well-sediment No. 2. However, from the fact that the ratio of the amounts adsorbed to those leached is 0.08 for Ca in the soil, it can be seen that scarcely no exchangeable Ca existed in the soil from the alluvial plains. In contrast, from the relatively high ratio of 0.5 for Ca in the well-sediment No. 2, it seems that much Ca was present as exchangeable ions in the sediment from the Kobe-group strata.

Association of the Chemical Species Dissolved in Groundwaters with Their Surrounding Geology. Figure 3 gives the key diagram of the relative percentages of milligram equivalents for Na+K, Ca, and Mg leached from the four samples. In Fig. 3-(1) for the soil No. 1, it is indicated that the plots of cations leached from the soil agree almost entirely with the A area, the plots of the 34 shallow groundwaters from the alluvial plains (see Table 1). A similar agreement is also found in the well-sediment No. 1 from the same alluvium.

In Fig. 3-(2) for the well-sediment No. 4 from the Kobe-group strata, the plots of leached cations, especially with the CH_3COONH_4 solution or the CO_2-saturated water, overlap well with the analytical results of the 38 shallow groundwaters (B) from the Kobe-group strata.[3,4] This agreement is also found in the well-sediment No. 3 from the same strata.

The leaching data of the Mt. Rokko granite, plotted in Fig. 3-(3), are somewhat scattered, but those with the CO_2-saturated water tend to overlap with the results of the 7 stream waters located at the top of Mt. Rokko (C).[12] From this tendency, it can be pointed out that the chemical composition of stream waters is determined by the leaching of constituents in the granitic rocks by chemical weathering with CO_2.

In Fig. 3-(4) for JB-1, it is shown that the plots of cations leached with the CO_2-saturated water or the CH_3COONH_4 solution fall close to the analytical data of the 8 groundwaters in the 8 basaltic regions worldwide (D).[13]

In conclusion, it can be analysed that the chemical compositions of groundwaters are considerably influenced by the geological strata through which the groundwaters pass, and that they can be estimated by utilizing the proposed leaching experiments for the solid samples around the groundwater area. In the leaching, the CO_2-saturated water is effective for investigating the influence of rocks on groundwaters, whereas the 1 M CH_3COONH_4 solution is useful for the samples containing clay minerals.

References

1) T. Kasama, *Chishitsugaku-zasshi*, **74**, 147 (1968).
2) R. M. Garrels, "Researches in Geochemistry," ed by P. H. Abelson, John Wiley and Sons, New York (1967), Vol. 2, p. 405.
3) Y. Kusaka, H. Tsuji, Y. Fujimoto, K. Ishida, and Y. Fukui, *Jpn. J. Limnol.*, **42**, 65 (1981).
4) Y. Kusaka, Y. Fukui, H. Tsuji, and Y. Tamari, The Geochemical Society of Japan, Shizuoka Symposium, Oct. 1981, Abstr., p. 247.
5) R. Chester and M. S. Hughes, *Chem. Geol.*, **2**, 249 (1967).
6) D. Z. Piper, *Geochem. Cosmochem. Acta*, **35**, 531 (1971).
7) Y. Kitano and R. Fujiyoshi, *Geochem. J.*, **14**, 113 (1980).
8) Y. Tamari, K. Hiraki, and Y. Nishikawa, *Chikyukagaku*, **12**, 37 (1978).
9) Y. Tamari, *Radioisotopes*, **28**, 1 (1979).
10) K. Hiraki, Y. Tamari, Y. Nishikawa, and T. Shigematsu *Bull. Inst. Chem. Res., Kyoto Univ.*, **58**, 228 (1980).
11) A. Ando, *Jpn. Analyst*, **22**, 1389 (1973).
12) Y. Kusaka and T. Sagawa, *The Memoirs of Konan Univ., S.S.*, **1973**, 21.
13) Y. Tarday, *Chem. Geol.*, **7**, 253 (1971).

The Mechanism of the Hydrolysis of Polyphosphates. VI.[1] The Effect of Cations on the Hydrolysis of *cyclo*-Tri- and *cyclo*-Tetraphosphates

Makoto WATANABE

Department of Industrial Chemistry, Chubu Institute of Technology, Matsumoto-cho, Kasugai, Aichi 487

(Received April 30, 1982)

The effect of cations on the rate of the hydrolysis of *cyclo*-tri- and *cyclo*-tetraphosphates was studied by adding metal chlorides to aqueous solutions of the ring phosphates. The concentrations of the phosphates and metal chlorides were 0.025 mol dm^{-3} and 0.1 mol dm^{-3} respectively. Alkali-metal cations retarded the hydrolysis of both the *cyclo*-phosphates in acidic media and accelerated it in basic media. The following sequence of efficiency resulted:

$$Li^+ > Na^+ > K^+.$$

Magnesium, calcium, and nickel(II) cations retarded the hydrolysis of the *cyclo*-phosphates in the pH range of 1.0—2.0 or 1.0—2.7, while they accelerated it in the pH regions higher than 2.7 or 3.5. A copper(II) ion retarded the hydrolysis at pH 1.0, and accelerated it in the pH ranges higher than 2.0. An aluminium ion highly accelerated the hydrolysis of both the ring phosphates at pH 1.0 and 2.0.

Though many papers concerning the hydrolysis of polyphosphates have been reported, there have been few reports about the effect of metal cations on the hydrolysis. Thilo and Wieker studied the catalytic efficiencies of cations on the hydrolysis of high polyphosphates at pH 8 and obtained the following sequence of efficiency:

$$Al^{3+} > Mg^{2+} > Ca^{2+} > Sr^{2+} > Ba^{2+} > H^+ > Li^+ > Na^+ > K^+.$$[2-4]

Osterheld recently presented a review on the hydrolysis of condensed phosphates.[5] The present author has reported the reaction mechanism of the hydrolysis of chain and small-ring polyphosphates from the point of view of the interaction between a water molecule and a polyphosphate ion by using aqueous organic solvents.[6-9] In a previous paper,[1] the effect of metal cations on the hydrolysis of di- and triphosphates was reported. This paper describes the effect of metal cations on the hydrolysis of *cyclo*-tri- and *cyclo*-tetraphosphates.

Experimental

Materials and Procedure. All the materials other than sodium *cyclo*-tri- and *cyclo*-tetraphosphates were commercial grade. Sodium *cyclo*-tri- and *cyclo*-tetraphosphates were produced by the method described in Refs. 10 and 11. The initial concentration of sodium *cyclo*-tri- and *cyclo*-tetraphosphates was 0.025 mol dm^{-3}. This concentration is suitable for analysis. *cyclo*-Tri- and *cyclo*-tetraphosphate solutions free from sodium ions were prepared by passing the sodium *cyclo*-phosphate solutions mentioned above through cation-exchange resin in the H^+ form. The *cyclo*-phosphate solutions without sodium ions were used to study the effect of alkali-metal cations on the rate of the hydrolysis of the *cyclo*-phosphates in both acidic and basic media. These *cyclo*-phosphate solutions could not be used to investigate the effect of alkaline-earth, aluminium and some transition-metal cations over a wide pH range of the solution, because precipitates were formed. So the sodium *cyclo*-phosphate solutions were used to test the effect of these cations on the rate of the hydrolysis of the *cyclo*-phosphates. Metal chloride was added to the phosphate solutions to make it 0.1 mol dm^{-3}. The metal chlorides used were LiCl, NaCl, KCl, $MgCl_2$, $CaCl_2$, $AlCl_3$, $NiCl_2$, and $CuCl_2$. The pH's of the *cyclo*-phosphate solutions containing one of the cations mentioned above were controlled with hydrochloric acid and/or aqueous tetramethylammonium hydroxide by using a Hitachi-Horiba pH meter, F-7, at a given reaction temperature. The pH of the solution was periodically measured and if it was in need of adjustment, enough tetramethylammonium hydroxide or hydrochloric acid was added to bring it back to the proper pH. The pH adjustment was made within ±0.1 pH unit of the required value. At measured intervals of time, about a 1-cm^3 portion of the *cyclo*-phosphate solution was withdrawn. About 50 mg of disodium dihydrogen ethylenediaminetetraacetate dihydrate (EDTA) was added to the phosphate solution containing a metal cation, and then the pH of the solution was adjusted to 7—9 with aqueous ammonia or hydrochloric acid and 8 mm^3 of the solution was spotted on Toyo No. 51A filter paper (2 by 50 cm) for the separation of the phosphates in the solution. When the *cyclo*-phosphate solution did not contain any metal ion, the pH of the withdrawn 1-cm^3 portion of the phosphate solution was adjusted to about 7 with aqueous ammonia or hydrochloric acid. The separation of the phosphate species in the solution was made by spotting 8 mm^3 of the solution on the filter paper mentioned above. The separation and determination of the phosphates in the sample solution were carried out by the method described in previous papers.[6,8,9] When some precipitate was formed during the hydrolytic processes of the *cyclo*-phosphates, no further treatment was made.

Results and Discussion

The Effect of Cations. The rate of the hydrolysis of *cyclo*-tri- and *cyclo*-tetraphosphates obeyed first-order kinetics with respect to the concentration of the respective *cyclo*-phosphates under all the conditions studied. The hydrolysis of sodium *cyclo*-tri- and *cyclo*-tetraphosphates is an acid- and base-catalyzed reaction.[8,9] As Tables 1 and 2 show, the hydrolysis of *cyclo*-tri- and *cyclo*-tetraphosphates in an aqueous solution containing alkali-metal cations or in a solution free from metal cations gave the result mentioned above. The rate of the hydrolysis of the *cyclo*-phosphates in a solution containing Mg^{2+}, Ca^{2+}, or Ni^{2+} decreased with an increase in the pH of the solution from 1.0 to 2.7 or 3.5, while the rate of the hydrolysis of *cyclo*-triphosphate containing Mg^{2+} and of *cyclo*-tetraphosphate containing

Table 1. Rate constants/min^{-1} of the hydrolysisof *cyclo*-triphosphate

Phosphate	Added cation	pH	Reaction temp/°C 30	50	70
$(HPO_3)_3$	—	1.0	2.46×10^{-3}	1.59×10^{-2}	1.35×10^{-1}
		2.0	7.51×10^{-5}	6.91×10^{-4}	5.34×10^{-3}
		11.5	3.78×10^{-6}	5.03×10^{-5}	6.32×10^{-4}
	Li^+	1.0	1.61×10^{-3}	7.27×10^{-3}	1.10×10^{-1}
		2.0	5.09×10^{-5}	5.69×10^{-4}	3.80×10^{-3}
		11.5	1.68×10^{-5}	2.28×10^{-4}	4.39×10^{-3}
	Na^+	1.0	1.78×10^{-3}	8.96×10^{-3}	1.07×10^{-1}
		2.0	5.85×10^{-5}	5.87×10^{-4}	4.33×10^{-3}
		11.5	9.19×10^{-6}	1.48×10^{-4}	1.51×10^{-3}
	K^+	1.0	2.28×10^{-3}	1.12×10^{-2}	1.32×10^{-1}
		2.0	6.01×10^{-5}	6.47×10^{-4}	4.68×10^{-3}
		11.5	8.56×10^{-6}	1.22×10^{-4}	1.37×10^{-3}
$(NaPO_3)_3$	—	1.0	1.35×10^{-3}	1.13×10^{-2}	7.50×10^{-2}
		2.0	6.28×10^{-5}	5.89×10^{-4}	4.37×10^{-3}
		2.7	1.29×10^{-5}	1.21×10^{-4}	9.44×10^{-4}
		3.5	1.73×10^{-6}	2.46×10^{-5}	1.64×10^{-4}
		5.0	4.42×10^{-7}		
		11.5	7.86×10^{-6}	1.31×10^{-4}	1.60×10^{-3}
	Mg^{2+}	1.0	6.86×10^{-4}	4.36×10^{-3}	1.83×10^{-2}
		2.0	3.81×10^{-5}	2.38×10^{-4}	1.21×10^{-3}
		2.7	1.15×10^{-5}	9.26×10^{-5}	8.22×10^{-4}
		3.5	3.31×10^{-6}	3.06×10^{-5}	2.50×10^{-4}
		5.0	4.14×10^{-6}		
	Ca^{2+}	1.0	6.98×10^{-4}	4.85×10^{-3}	2.02×10^{-2}
		2.0	3.99×10^{-5}	3.54×10^{-4}	1.30×10^{-3}
		2.7	1.91×10^{-5}	1.53×10^{-4}	
	Ni^{2+}	1.0	8.67×10^{-4}	5.09×10^{-3}	2.75×10^{-2}
		2.0	3.54×10^{-5}	3.07×10^{-4}	1.66×10^{-3}
		2.7	1.54×10^{-5}	1.28×10^{-4}	8.62×10^{-4}
		3.5	1.02×10^{-5}	1.04×10^{-4}	5.57×10^{-4}
	Cu^{2+}	1.0	1.38×10^{-3}	9.63×10^{-3}	5.05×10^{-2}
		2.0	1.95×10^{-4}	$2.08\times10_{-3}$	1.31×10^{-2}
		2.7	4.27×10^{-4}	3.68×10^{-3}	2.81×10^{-2}
	Al^{3+}	1.0	8.29×10^{-3}	6.75×10^{-2}	4.23×10^{-1}
		2.0	8.98×10^{-3}	9.02×10^{-2}	

Table 2. Rate constants/min^{-1} of the hydrolysis of *cyclo*-tetraphosphate

Phosphate	Added cation	pH	Reaction temp/°C 30	50	70
$(HPO_3)_4$	—	1.0	2.75×10^{-4}	2.80×10^{-3}	2.46×10^{-2}
		2.0	1.80×10^{-5}	1.96×10^{-4}	1.79×10^{-3}
		11.5	7.40×10^{-8}	1.58×10^{-6}	1.76×10^{-5}
	Li^+	1.0	1.42×10^{-4}	1.68×10^{-3}	1.40×10^{-2}
		2.0	7.00×10^{-6}	7.98×10^{-5}	7.35×10^{-4}
		11.5	7.76×10^{-7}	1.79×10^{-5}	
	Na^+	1.0	1.89×10^{-4}	1.92×10^{-3}	1.78×10^{-2}
		2.0	8.82×10^{-6}	1.13×10^{-4}	8.80×10^{-4}
		11.5	2.64×10^{-7}	6.24×10^{-6}	8.77×10^{-5}
	K^+	1.0	2.03×10^{-4}	2.01×10^{-3}	1.90×10^{-2}
		2.0	9.00×10^{-6}	1.16×10^{-4}	9.30×10^{-4}
		11.5	2.31×10^{-7}	5.55×10^{-6}	8.12×10^{-5}
$(NaPO_3)_4$	—	1.0	1.42×10^{-4}	1.54×10^{-3}	1.28×10^{-2}
		2.0	1.00×10^{-5}	1.29×10^{-4}	1.21×10^{-3}
		2.7	1.37×10^{-6}	2.11×10^{-5}	1.83×10^{-4}
		3.5	2.56×10^{-7}	3.29×10^{-6}	3.74×10^{-5}
		5.0		3.00×10^{-7}	
	Mg^{2+}	1.0	2.75×10^{-5}	2.24×10^{-4}	1.72×10^{-3}
		2.0	1.35×10^{-6}	1.25×10^{-5}	8.61×10^{-5}
		2.7	2.04×10^{-7}	3.53×10^{-6}	
	Ni^{2+}	1.0	2.84×10^{-5}	3.14×10^{-4}	2.09×10^{-3}
		2.0	1.83×10^{-6}	1.78×10^{-5}	1.51×10^{-4}
		2.7	5.30×10^{-7}	6.86×10^{-6}	6.86×10^{-5}
		3.5	5.04×10^{-7}	6.21×10^{-6}	6.64×10^{-5}
		5.0	1.27×10^{-6}	1.05×10^{-5}	
	Cu^{2+}	1.0	5.80×10^{-5}	5.38×10^{-4}	3.95×10^{-3}
		2.0	2.43×10^{-5}	3.13×10^{-4}	2.18×10^{-3}
		2.7	2.46×10^{-5}	3.12×10^{-4}	2.63×10^{-3}
		3.5	1.11×10^{-4}	1.59×10^{-3}	
	Al^{3+}	1.0	1.24×10^{-3}	8.16×10^{-3}	5.50×10^{-2}
		2.0	1.38×10^{-3}	1.33×10^{-2}	1.04×10^{-1}

Ni^{2+} increased with an increase in the pH of the solution from 3.5 to 5.0. The rate of the hydrolysis of the *cyclo*-phosphates in a solution containing Cu^{2+} decreased as the pH of the solution changed from 1.0 to 2.0. On the other hand, the rate increased as the pH of the solution increased from 2.0 to 2.7 and 3.5. In the case of the hydrolysis of the ring phosphates in a solution containing Al^{3+}, the rate of the hydrolysis of the *cyclo*-phosphates increased with an increase in the pH of the solution from 1.0 to 2.0. For the hydrolysis of the short-chain polyphosphates, these cations used here all retarded the rate of the hydrolysis of the polyphosphates in acidic media and alkali-metal ions accelerated the rate in basic media. This tendency is the same as that of the hydrolysis of the ring phosphates in a solution containing alkali-metal ions. Magnesium, calcium, and nickel ions retarded the rate of the hydrolysis of the *cyclo*-phosphates in the pH region of 1.0—2.0 or 1.0—2.7, while they seemed to accelerate the rate in the pH regions higher than 2.7 or 3.5. The rate was retarded by Cu^{2+} at pH 1.0, while it was accelerated at a pH region higher than 2.0. An aluminium ion extremely accelerated the rate of the hydrolysis of the *cyclo*-phosphates at pH 1.0 and 2.0. The acceleration of the rate of the hydrolysis by metal cations was not observed for the hydrolysis of di- and triphosphates in acidic media.

Reaction Mechanism. The activation parameters for the hydrolysis of *cyclo*-tri- and *cyclo*-tetraphosphates were calculated by means of an Arrhenius plot and are listed in Tables 3 and 4 respectively. In the case of the hydrolysis of both the *cyclo*-phosphates in a solution containing an alkali-metal ion or in a solution free from a metal ion, the activation energy increased with an increase in the pH of the solution. The activation energy also seemed to increase by addition of an alkali-metal ion into the phosphate solution. In previous papers,[6-9] the author proposed the following hydrolysis mechanism for chain and small-ring phosphates and concluded that Reaction 2 is the rate-determining step:

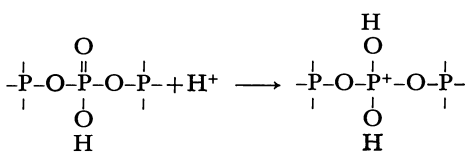

(1)

Table 3. Activation parameters of the hydrolysis of *cyclo*-triphosphate

Phosphate	Added cation	pH	Activation energy/kJ mol^{-1}	log (frequency factor/min^{-1})
$(HPO_3)_3$	—	1.0	86.3	12.2
		2.0	92.0	11.7
		11.5	110.4	13.6
	Li^+	1.0	90.6	12.7
		2.0	93.2	11.8
		11.5	119.9	15.8
	Na^+	1.0	88.0	12.3
		2.0	93.0	11.3
		11.5	110.5	14.0
	K^+	1.0	87.2	12.3
		2.0	94.1	12.0
		11.5	109.9	13.9
$(NaPO_3)_3$	—	1.0	86.8	12.1
		2.0	91.6	11.6
		2.7	92.7	11.1
		3.5	102.5	12.6
		11.5	114.8	14.7
	Mg^{2+}	1.0	71.0	9.1
		2.0	74.7	8.5
		2.7	92.0	10.9
		3.5	93.6	10.6
	Ca^{2+}	1.0	72.8	9.4
		2.0	75.5	8.7
		2.7	84.8	9.9
	Ni^{2+}	1.0	74.6	9.8
		2.0	83.2	9.9
		2.7	86.9	10.2
		3.5	86.6	10.0
	Cu^{2+}	1.0	77.8	10.5
		2.0	91.0	12.0
		2.7	90.4	12.2
	Al^{3+}	1.0	84.9	12.6

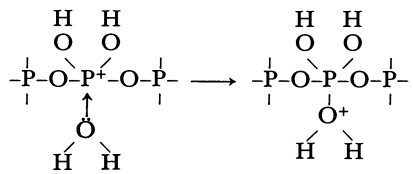

(2)

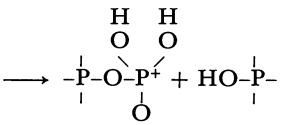

(3)

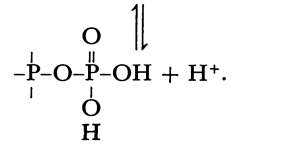

(4)

As mentioned above, the effect of alkali-metal ions on the kinetics parameters and the order of the efficiency of alkali-metal ions for the hydrolysis of both the ring phosphates was the same as that of the hydrolysis of di- and triphosphates. So the same reaction mechanism described in a previous paper[1] may be applicable for the hydrolysis of the *cyclo*-phosphates, and the retardation of the hydrolysis rate by alkali-metal ions in acidic

Table 4. Activation parameters of the hydrolysis of *cyclo*-tetraphosphate

Phosphate	Added cation	pH	Activation energy kJ/mol^{-1}	log (frequency factor/min^{-1})
$(HPO_3)_4$	—	1.0	97.0	13.1
		2.0	99.3	12.4
		11.5	118.3	13.3
	Li^+	1.0	99.2	13.3
		2.0	100.5	12.2
		11.5	127.9	15.9
	Na^+	1.0	98.1	13.2
		2.0	99.5	12.1
		11.5	125.4	15.1
	K^+	1.0	97.9	13.2
		2.0	100.2	12.2
		11.5	126.7	15.2
$(NaPO_3)_4$	—	1.0	97.2	12.9
		2.0	103.6	12.9
		2.7	105.9	12.4
		3.5	107.6	11.9
	Mg^{2+}	1.0	89.2	10.8
		2.0	89.8	9.6
	Ni^{2+}	1.0	93.2	11.5
		2.0	95.5	10.7
		2.7	105.0	11.8
		3.5	105.3	11.8
	Cu^{2+}	1.0	91.1	11.5
		2.0	97.3	12.2
		2.7	100.9	12.8
	Al^{3+}	1.0	82.0	11.2
		2.0	93.3	13.2

media could be attributable to the exchange of a hydrogen ion with a catalytically less effective alkali-metal ion as follows:

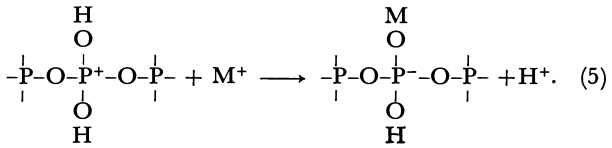

(5)

The acceleration of the rate by alkali-metal ions in basic media could be explained by the formation of the complex as follows:

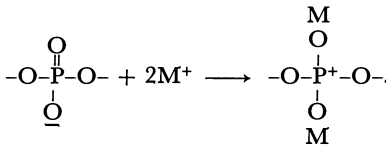

(6)

As Tables 3 and 4 show, this acceleration is exclusively dependent on the entropy term. The retardaction of the rate of the hydrolysis of *cyclo*-tri- and *cyclo*-tetraphosphates by Mg^{2+}, Ca^{2+}, Ni^{2+}, and Cu^{2+} in highly acidic media depended exclusively upon the entropy term. So, when the exchange of a hydrogen ion with a catalytically less effective Mg^{2+} ion takes place according to Reaction 5, it could be concluded that there is a difference between the structures of the complexes of an alkali-metal ion and of an Mg^{2+}, Ca^{2+}, Ni^{2+}, or Cu^{2+} ion. The acceleration of the hydrolysis of the *cyclo*-phosphates by Cu^{2+} and Al^{3+} in acidic media depended

upon the energy and/or the entropy term. Since Reaction 2 is the rate-determining step of the hydrolysis of polyphosphates, Cu^{2+} and Al^{3+} may affect Reactions 1 and 2. The exchange of a hydrogen ion with Cu^{2+} or Al^{3+} may occur according to Reaction 5 and the cations are considered to be catalytically more effective than a hydrogen ion for the hydrolysis of the small-ring phosphates.

References

1) Part V: M. Watanabe, M. Matsuura, and T. Yamada, *Bull. Chem. Soc. Jpn.*, **54**, 738 (1981).
2) W. Wieker and E. Thilo, *Z. Anorg. Allg. Chem.*, **306**, 48 (1960).
3) E. Thilo and W. Wieker, *J. Polym. Sci.*, **53**, 55 (1961).
4) W. Wieker and E. Thilo, *Z. Anorg. Allg. Chem.*, **313**, 296 (1961).
5) R. K. Osterheld, "Topics in Phosphorus Chemistry," John Wiley and Soms, New York (1972), Vol. 7, p. 103.
6) M. Watanabe, *Bull. Chem. Soc. Jpn.*, **47**, 2048 (1974).
7) M. Watanabe, S. Sato, and H. Saito, *Bull. Chem. Soc. Jpn.*, **48**, 896 (1975).
8) M. Watanabe, S. Sato, and H. Saito, *Bull. Chem. Soc. Jpn.*, **48**, 3593 (1975).
9) M. Watanabe, S. Sato, and H. Saito, *Bull. Chem. Soc. Jpn.*, **49**, 2474 (1976).
10) L. F. Audrieth, "Inorganic Syntheses," McGraw-Hill, New York (1950), Vol. III, p. 104.
11) R. N. Bell, L. F. Audrieth, and O. F. Hill, *Ind. Eng. Chem.*, **44**, 568 (1952).

Thermal Cis-to-Trans Isomerization of $[CoX_2en_2]X$ (X=Cl, Br)

Ryokichi Tsuchiya,* Akira Uehara, and Yoshinori Muramatsu
Department of Chemistry, Faculty of Science, Kanazawa University, Kanazawa 920
(Received April 30, 1982)

By measuring calorimetrically the heats of reaction of solid *cis*- and *trans*-$[CoX_2en_2]X$ (X=Cl, Br) with alkaline sodium sulfide solution, the heats of isomerization were obtained as -11.4 kJ mol^{-1} for *cis*-$[CoCl_2en_2]Cl(s)$=*trans*-$[CoCl_2en_2]Cl(s)$ and -6.4 kJ mol^{-1} for *cis*-$[CoBr_2en_2]Br(s)$=*trans*-$[CoBr_2en_2]Br(s)$. Assuming the entropy changes from cis- to trans-form, ΔS, to be -0.0116 kJ mol^{-1} K^{-1} at 25 °C statistically, the free energy changes were calculated as $\Delta G°=-8.0$ kJ mol^{-1} and -3.0 kJ mol^{-1} for the isomerization of *cis*-$[CoCl_2en_2]Cl$ and *cis*-$[CoBr_2en_2]Br$ respectively. From these thermodynamic data, cis-to-trans isomerization was expected to occur in $[CoX_2en_2]X$ (X=Cl or Br), which was verified experimentally by thin-layer chromatography and the spectral measurement.

The cis-to-trans isomerization of $[M^{III}X_2(AA)_2]X$-type chromium complexes in a solid phase has extensively been investigated, where X is a chloride or a bromide ion and AA is a diamine.[1-5] However, the isomerization of the corresponding cobalt(III) complexes has never been studied so widely, because they are often apt to undergo reduction of the metal ion upon heating in a solid phase. The samples of the cobalt(III) complexes so far studied are: Trans-to-cis isomerization for $[CoCl_2(NH_3)_4]IO_3\cdot 2H_2O$,[6] $[CoCl_2pn_2](H_5O_2)Cl_2$,[7] and $[CoBr_2pn_2](H_5O_2)Br_2$;[8] cis,trans(Cl,Cl)-to-cis,cis isomerization for $[CoCl_2(NH_3)_2en]ClO_4$[9] and $[CoCl_2(NH_3)_2en]Br\cdot H_2O$.[10] On the other hand, for $[CoCl_2en_2](H_5O_2)Cl_2$ and $[CoBr_2en_2](H_5O_2)B_2$, neither trans-to-cis nor cis-to-trans isomerization has been found in a solid phase.

The present study was undertaken 1) to find whether or not the isomerization can occur in a solid phase from the viewpoint of enthalpy or free energy changes and, if it does occur, 2) to verify it experimentally.

Experimental

Preparation of Complexes. *trans*-$[CoCl_2en_2]Cl$,[11] *cis*-$[CoCl_2en_2]Cl$,[12] *trans*-$[CoBr_2en_2]Br$,[13] and *cis*-$[CoBr_2en_2]Br$[14] were prepared by the known methods and identified by the elemental analysis and the electronic spectral measurements.

Calorimetric Measurements. The enthalpy changes in the reaction of the trans and cis complexes in the powder state with an alkaline solution of sodium sulfide were measured with a Tokyo-Riko twin isoperibol calorimeter TIC-2S at 25 °C. In each run, the diamine complexes employed were accurately weighed in the range of order of 2×10^{-4} mol and the reacting solution used was 100 cm^3 of 2×10^{-2} mol dm^{-3} of Na_2S in 1 mol dm^{-3} NaOH solution.

Derivatography. The differential thermal analysis (DTA) of the cis complexes was measured with a Derivatograph Typ-OD-102.

Thin Layer Chromatography (TLC). The TLC was employed to distinguish the cis and trans complexes and to confirm the occurrence of isomerization. The TLC plates used were those of silica gel 60F-254 made by Merck Ltd. The developer used was a mixture of *n*-BuOH: H_2O: AcOH= 7:2:1.

Electronic Spectra. Electronic spectra of the complexes were recorded on a JASCO Uvidec 550 spectrophotometer.

Results and Discussion

Enthalpy and Free Energy Changes in the Isomerization. The enthalpy changes for the reaction of *cis*- and *trans*-dichloribis(ethylenediamine)cobalt(III) chloride and dibromobis(ethylenediamine)cobalt(III) bromide with sodium sulfide solution were measured as below.

$$cis\text{-}[CoCl_2en_2]Cl(s) + {}^3/_2S^{2-}(aq) = {}^1/_2Co_2S_3(s) + 3Cl^-(aq) + 2en(aq) \qquad \Delta H = -71.9\ \text{kJ mol}^{-1} \quad (1)$$

$$trans\text{-}[CoCl_2en_2]Cl(s) + {}^3/_2S^{2-}(aq) = {}^1/_2Co_2S_3(s) + 3Cl^-(aq) + 2en(aq) \qquad \Delta H = -60.5\ \text{kJ mol}^{-1} \quad (2)$$

$$cis\text{-}[CoBr_2en_2]Br(s) + {}^3/_2S^{2-}(aq) = {}^1/_2Co_2S_3(s) + 3Br^-(aq) + 2en(aq) \qquad \Delta H = -46.9\ \text{kJ mol}^{-1} \quad (3)$$

$$trans\text{-}[CoBr_2en_2]Br(s) + {}^3/_2S^{2-}(aq) = {}^1/_2Co_2S_3(s) + 3Br^-(aq) + 2en(aq) \qquad \Delta H = -40.5\ \text{kJ mol}^{-1} \quad (4)$$

By combining Eq. 1 with 2, and Eq. 3 with 4, the enthalpy changes of the isomerization for the dichloro- and dibromo-complexes are obtained as follows:

$$cis\text{-}[CoCl_2en_2]Cl(s) = trans\text{-}[CoCl_2en_2]Cl(s) \qquad \Delta H = -11.4\ \text{kJ mol}^{-1}$$

$$cis\text{-}[CoBr_2en_2]Br(s) = trans\text{-}[CoBr_2en_2]Br(s) \qquad \Delta H = -6.4\ \text{kJ mol}^{-1}$$

Statistically, the probability of the formation of the cis complex is 4, whereas that of the trans complex is just one, and thereby the entropy of the cis complex is larger than that of the trans one by the value

$$\Delta S = R\ln 4 = 11.5\ \text{J mol}^{-1}\text{K}^{-1}.$$

The entropy change of cis-to-trans isomerization is, therefore, $\Delta S=-11.5$ J mol^{-1}K^{-1}, and the free energy changes are calculated as:

$$cis\text{-}[CoCl_2en_2]Cl(s) = trans\text{-}[CoCl_2en_2]Cl(s) \qquad \Delta G° = -8.0\ \text{kJ mol}^{-1}$$

$$cis\text{-}[CoBr_2en_2]Br(s) = trans\text{-}[CoBr_2en_2]Br(s) \qquad \Delta G° = -3.0\ \text{kJ mol}^{-1}.$$

On the basis of the above data of enthalpy and free

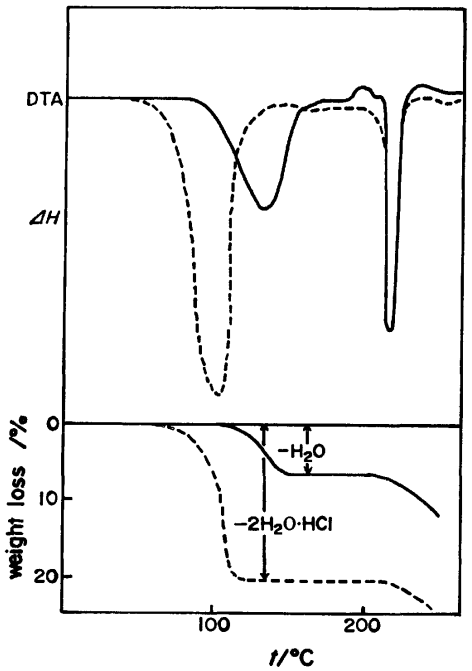

Fig. 1. Derivatograms of *cis*-$[CoCl_2en_2]Cl \cdot H_2O$ (——) and *trans*-$[CoCl_2en_2](H_5O_2)Cl_2$ (------).

Table 1. The results of TLC

Materials	R_f values
Thermal products from	0.56 (blue) 0.24 (green)
cis-$[CoCl_2en_2]Cl$	0.15 (blue) 0.04(brown)
trans-$[CoCl_2en_2]Cl$	0.24 (green)
cis-$[CoCl_2en_2]Cl$	0.17 (violet)
$CoCl_2 \cdot 6H_2O$	0.57 (blue) 0.26 (blue)
	0.10 (blue)
Thermal product from	
cis-$[CoBr_2en_2]Br$	0.36
trans-$[CoBr_2en_2]Br$	0.35
cis-$[CoBr_2en_2]Br$	0.30

energy changes, the cis-to-trans isomerization is expected to take place both in $[CoCl_2en_2]Cl$(s) and $[CoBr_2en_2]$-Br(s), although neither cis-to-trans nor trans-to-cis isomerization has been found for these complexes in a solid phase.

Derivatogtaphy. Figure 1 shows the derivatograms of *cis*-$[CoCl_2en_2]Cl \cdot H_2O$ and *trans*-$[CoCl_2en_2](H_5O_2)$-Cl_2. In the latter, neither endo- nor exothermic peak appears, except for the endothermic peaks due to the dehydration plus dehydrochlorination and the decomposition or melting. On the other hand, in the former, in addition to the endothermic peaks due to the dehydration and the decomposition or melting, a small exothermic peak is displayed at *ca.* 200 °C immediately before the decomposition or melting of the complex. In the isothermal heating of *cis*-$[CoCl_2en_2]Cl$ and *cis*-$[CoBr_2$-$en_2]Br$, the color change from violet to green was observed at 215 °C and 210 °C, respectively. Therefore, the appearance of an exothermic peak in the derivatogram of *cis*-$[CoCl_2en_2]Cl$ suggests the occurrence of isomerization to the corresponding trans-form.

TLC. In order to identify the components of

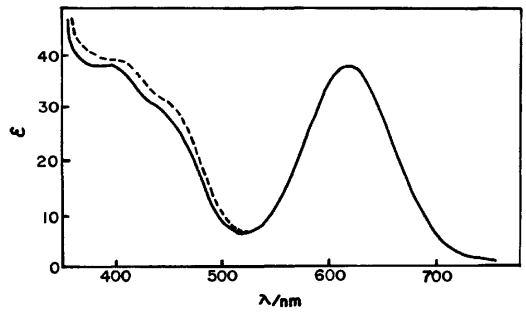

Fig. 2. Electronic spectra of *trans*-$[CoCl_2en_2]Cl$ (——) and of the third fraction of thermal products from *cis*-$[CoCl_2en_2]Cl$ (------).

thermal products of *cis*-$[CoCl_2en_2]Cl$ and *cis*-$[CoBr_2$-$en_2]Br$, the products were examined by means of TLC. The results of TLC are listed in Table 1. In the dichloro complex, four spots were clearly developed. The R_f value of 0.24 of the green spot is identical with that (0.24) of *trans*-$[CoCl_2en_2]Cl$ freshly prepared, and the value is obviously distinguished from those of the other spots due to the original cis complex and others. The thermal product obtained from *cis*-$[CoBr_2en_2]Br$ gave the R_f value of 0.36, which is also very close to that (0.35) of *trans*-$[CoBr_2en_2]Br$ freshly prepared.

Spectral Measurements. In order to confirm the formation of *trans*-$[CoX_2en_2]X$ from the thermal reaction of the corresponding cis complexes, the thermal product was separated by means of column chromatography. The thermal product of the cis-dichloro complex was separated into four fractions on a column of the cation exchange resin (SP Sephadex C-25, H^+ form). The third fraction was green and eluted with 0.1 mol dm^{-3} HCl methanolic solution. The green product of the cis-dibromo complex was separated on a column of cellulose and eluted with methanol as rapidly as possible because the trans-dibromo complex is readily isomerizes to the original cis-form during elution. The electronic spectrum of the green compound thus obtained from *cis*-$[CoCl_2en_2]Cl$ is shown in Fig. 2. It is almost identical with that of *trans*-$[CoCl_2en_2]Cl$ freshly prepared. The same result is obtained for the dibromo complex.

The results of the above experiments support that both *cis*-$[CoCl_2en_2]Cl$ and *cis*-$[CoBr_2en_2]Br$ isomerize to the corresponding trans-form in a solid phase as expected from the thermodynamic consideration.

References

1) R. Tsuchiya, T. Ohki, A. Uehara, and E. Kyuno, *Thermochim. Acta*, **12**, 413 (1975).
2) T. Yoshikuni, R. Tsuchiya, A. Uehara, and E. Kyuno, *Bull. Chem. Soc. Jpn.*, **50**, 883 (1977).
3) T. Yoshikuni, R. Tsuchiya, A. Uehara, and E. Kyuno, *Bull. Chem. Soc. Jpn.*, **51**, 113 (1978).
4) S. Mitra, A. Uehara, and R. Tsuchiya, *Thermochim. Acta*, **34**, 189 (1979).
5) a) R. Tsuchiya and A. Uehara, *Thermochim. Acta*, **50**, 93 (1981); b) R. Tsuchiya, A. Uehara, and T. Yoshikuni, *Inorg. Chem.*, **21**, 580 (1982).

6) a) N. I. Lobanov, *Zhur. Neorg. Khim.*, **4**, 151 (1959); b) H. E. LeMay, Jr., and J. C. Bailar, Jr., *J. Am. Chem. Soc.*, **89**, 5577 (1967).
7) R. Tsuchiya, K. Murai, A. Uehara, and E. Kyuno, *Bull. Chem. Soc. Jpn.*, **43**, 1383 (1970).
8) R. Tsuchiya, Y. Natsume, A. Uehara, and E. Kyuno, *Thermochim. Acta*, **12**, 147 (1975).
9) R. Tsuchiya, Y. Nakata, and E. Kyuno, *Bull. Chem. Soc. Jpn.*, **44**, 705 (1971).
10) R. Tsuchiya, M. Suzuki, and E. Kyuno, *Bull. Chem. Soc. Jpn.*, **45**, 1065 (1972).
11) W. C. Fernelius, *Inorg. Synth.*, **2**, 222 (1946).
12) W. C. Fernelius, *Inorg. Synth.*, **2**, 223 (1946).
13) A. Werner, L. Gerb, S. Lorie, and J. Rapiport, *Ann.*, **386**, 111 (1912).
14) A. Werner, L. Gerb, S. Lorie, and J. Rapiport, *Ann.*, **386** 112 (1912).

 © 1982 The Chemical Society of Japan Bull. Chem. Soc. Jpn., 55, 3773—3777 (1982)

Kinetic Studies of Solvent Extraction of Metal Complexes. VIII. Rate of Complex Formation and Solvent Extraction of Iron(III) in Aqueous Perchlorate Solutions with 1,1,1-Trifluoro-2,4-pentanedione

Tatsuya SEKINE* and Kazuho INABA
Department of Chemistry, Science University of Tokyo, Kagurazaka, Shinjuku-ku, Tokyo 162
(Received May 4, 1982)

The rate of the extraction of iron(III) in aqueous 4 mol dm^{-3} sodium perchlorate solutions with 1,1,1-trifluoro-2,4-pentanedione (Htfa) into carbon tetrachloride was measured, and the rate constants for the controlling reactions in the aqueous phase:

$$Fe^{3+} + Htfa \longrightarrow Fe(tfa)^{2+} + H^+ \text{ and } Fe(OH)^{2+} + Htfa \longrightarrow Fe(tfa)^{2+} + H_2O,$$

were calculated. These constants were also determined from spectrophotometric measurements of the aqueous solutions in the absence of the organic phase. The two series of rate constants obtained by the independent experiments agreed well. It was pointed out that equilibrium constants among the complexes in the aqueous and organic phases are indispensable in order to make a precise discussion of the solvent extraction of metal ions when aqueous-complex formation controls the whole process.

In this series, the rate of the solvent extraction of beryllium(II),[1] iron(III),[2,3] and gallium(III)[4] with β-diketones into nonpolar solvents was measured, and it was concluded that the formation of metal complexes took place in the aqueous phase first, and then the uncharged one among them was extracted into the organic phase. Thus, the whole process in these extractions was controlled by the formation of the first complex in the aqueous phase. In these previous studies, the effects of mass transport and interfacial reactions were neglected because the experiments were carried out at such an agitation speed that no increase in the rate was found on its further increase. This type of extraction mechanism seems to be very common among the extractions done under similar experimental conditions.[5] In the present study, the rate of the solvent extraction of iron(III) in aqueous 4 mol dm^{-3} perchlorate solutions with 1,1,1-trifluoro-2,4-pentanedione (trifluoroacetylacetone, Htfa) into carbon tetrachloride was determined at 298 K. At the same time, the rate of the complex formation of iron(III) with this ligand in these aqueous solutions was determined in separate experiments in the absence of the organic phase by a spectrophotometric method. From the results of these two series of experiments, two kinds of reaction routes were found for the complex formation; the two sets of rate constants, one of them obtained from the spectrophotometric data, and the other calculated from the extraction data, agreed well each other.

Experimental

The rate was always determined at 298 K. The aqueous solutions were constant ionic media, 4 mol dm^{-3} (H, Na)ClO_4. The hydrogen-ion concentration of the sample solutions was measured potentiometrically. By measuring a series of standard solutions, the acid concentrations of which had been determined by titration with a standard sodium hydroxide solution, a calibration curve of the emf *vs.* the hydrogen-ion concentration was prepared. The hydrogen-ion concentration in the sample solutions was calculated from the potentiometric data by using this curve. Thus the stoichiometric units are used in this study. The experiments by the spectrophotometric method was made with Htfa in a large excess to iron(III). The spectrophotometric experiments were made in a manner similar to that described previously except that the absorptions at 450 nm were measured at certain time intervals after the metal ion and the ligand solutions had been mixed.[6] The experiments of the solvent extraction were made in a manner similar to that previously described.[2,3,6] A carbon tetrachloride solution containing Htfa and a perchlorate solution containing iron(III) perchlorate at 5×10^{-4} mol dm^{-3} were agitated so vigorously that no increase in the rate was found on a further increase in the agitation speed. The amount of iron(III) extracted after a certain time interval was determined by an atomic-absorption method.

Statistical

Any chemical species in the organic phase will be denoted by the subscript "org" and those in the aqueous phase, by the lack of any subscript. The initial concentration will be denoted by the subscript "init."

The acid-dissociation and two-phase distribution constants of the ligand and the stability constant of the "*n*-th" complex are defined as:

$$K_a = [H^+][tfa^-][Htfa]^{-1} \quad (1)$$

$$K_d = [Htfa]_{org}[Htfa]^{-1} \quad (2)$$

$$\beta_n = [Fe(tfa)_n^{3-n}][Fe^{3+}]^{-1}[tfa^-]^{-n}. \quad (3)$$

As will be seen later, the two-phase distribution constant of the uncharged complex is necessary to correlate the rate constants for the solvent extraction and for the complex formation. It is defined as:

$$K_{dm} = [Fe(tfa)_3]_{org}[Fe(tfa)_3]^{-1}. \quad (4)$$

When the rate of the complex formation of Fe^{3+} in aqueous solutions is first-order with respect to Fe^{3+}, and when several reaction routes are present, it can generally be written as:

$$V = -d[Fe^{3+}]/dt = \sum K_{CF(a,b\cdots)}[Fe^{3+}][Htfa]^a[H^+]^b\cdots, \quad (5)$$

where a,b··· are certain integers. From Eq. 5, the following equation is obtained when a certain component, for example, H^+, is changed, but the others are

kept constant:

$$-\log[Fe^{3+}] = q_{H^+} \times t + \log[Fe^{3+}]_{init} \quad (6)$$

$$q_{H^+} = \sum K^*_{CF(a,b\cdots)} \times C_{Htfa}{}^a \times [H^+]^b \cdots, \quad (7)$$

where $K^*_{CF(a,b\cdots)} = K_{CF(a,b\cdots)}/\ln(10)$ and where C_{Htfa} is the concentration of Htfa kept at a certain value. Similar equations may be written with respect to the other components.

Treatment of Optical Absorption Data. When the rate of complex formation is first-order with respect to Fe^{3+}, and when an equilibrium is established for all practical purposes among the complexes, the following treatments of the optical-absorption data are possible.

When the absorption due to the Fe^{3+} species is negligible, the over-all absorbance experimentally measured can be written as:[6]

$$\varepsilon_T = (\varepsilon_1[Fe(tfa)^{2+}] + \varepsilon_2[Fe(tfa)_2{}^+] + \varepsilon_3[Fe(tfa)_3])([Fe(tfa)^{2+}] + [Fe(tfa)_2{}^+] + [Fe(tfa)_3])^{-1}$$
$$= (\varepsilon_1\beta_1[tfa^-] + \varepsilon_2\beta_2[tfa^-]^2 + \varepsilon_3\beta_3[tfa^-]^3)(\beta_1[tfa^-] + \beta_2[tfa^-]^2 + \beta_3[tfa^-]^3)^{-1}, \quad (8)$$

where ε_n is the molar absorption coefficient of the "n-th" complex. The value of ε_T can be calculated from ε_n and β_n for a certain $[tfa^-]$, and by using this parameter and the absorbance experimentally measured, the total amount of complexes or the decrease in $[Fe^{3+}]$ by the complex formation can be obtained as:

$$E/\varepsilon_T = [Fe(tfa)^{2+}] + [Fe(tfa)_2{}^+] + [Fe(tfa)_3]$$
$$= [Fe^{3+}]_{init} - [Fe^{3+}]. \quad (9)$$

By introducing $[Fe^{3+}]$ into Eq. 6, the value of q_{H^+} (or q with respect to the other components) under certain conditions can be obtained, and from the slope of the plot of log q *versus* the logarithmic concentration of the component, the dependences, a, b$\cdots$, can be obtained.

Treatment of Solvent-extraction Data. When several roues are present in the solvent extraction of Fe^{3+} in the aqueous phase with Htfa, the rate may be written in a way similar to Eqs. 5 to 7:

$$V = -d[Fe(III)]/dt$$
$$= \sum K_{SE(a,b\cdots)}[Fe(III)][Htfa]^a[H^+]^b\cdots. \quad (10)$$

Here, the total concentration of iron(III) species in the aqueous phase is considered instead of the Fe^{3+} concentration in Eq. 5. For example, with respect to H^+, the following equation can be written:

$$-\log[Fe(III)] = q_{H^+} \times t + \log[Fe(III)]_{init} \quad (11)$$

$$q_{H^+} = \sum K^*_{SE(a,b)} \times C_{Htfa}{}^a \times [H^+]^b\cdots. \quad (12)$$

Results

Rate of Change in Optical Absorption. The absorption in the range from 400 to 600 nm of aqueous perchlorate solutions containing Fe^{3+} and Htfa was only slight at first but it gradually increased until a maximum absorption was observed at about 450 nm. The absorbance at this wavelength was measured at certain time intervals. Figure 1 gives an example of such results. In order to treat these absorption data, it was assumed that the formation of the first complex, $Fe(tfa)^{2+}$, from Fe^{3+} was the controlling step and that the formation of the higher complexes proceeded much more rapidly than this, in other words, the three complexes, $Fe(tfa)^{2+}$, $Fe(tfa)_2{}^+$, and $Fe(tfa)_3$, were in an equilibrium with each other. From the absorbance and the concentra-

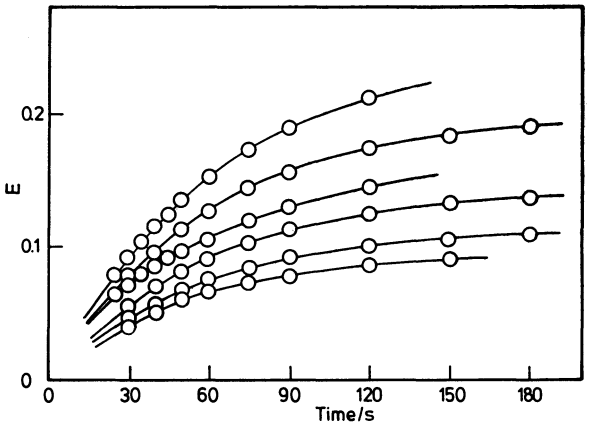

Fig. 1. Example of the change in the absorption at 450 nm as a function of time by formation of iron(III)-tfa complexes in the aqueous 4 mol dm^{-3} (H, Na)ClO_4 ionic media.
[Htfa] is 5.0×10^{-2} mol dm^{-3}, [H+] is 0.33, 0.43, 0.6, 0.63, 0.85, and 1.0 mol dm^{-3} from the top to the bottom.

TABLE 1. EQUILIBRIUM CONSTANTS FOR HTFA AND IRON-(III) IN 4 mol dm^{-3} (H,Na)ClO_4 SOLUTIONS AT 298 K

$K_a = 10^{-6.59}$	
$K_d = 10^{0.39}$	
$K_e^{a)} = 10^{-1.96}$	
$\beta_1 = 10^{7.7}$	$\varepsilon_1 = 170$
$\beta_2 = 10^{14.4}$	$\varepsilon_2 = 1050$
$\beta_3 = 10^{19.8}$	$\varepsilon_3 = 2560$
$K_{dm} = 10^{4.2}$	
$K_h^{b)} = 10^{-3.1}$	

a) $K_e = [Htfa]_{enol}[Htfa]^{-1}_{keto}$. b) $K_h = [Fe(OH)^{2+}][H^+][Fe^{3+}]^{-1}$ (in 3 mol dm^{-3} (H, Na)ClO_4 Ref. 9).

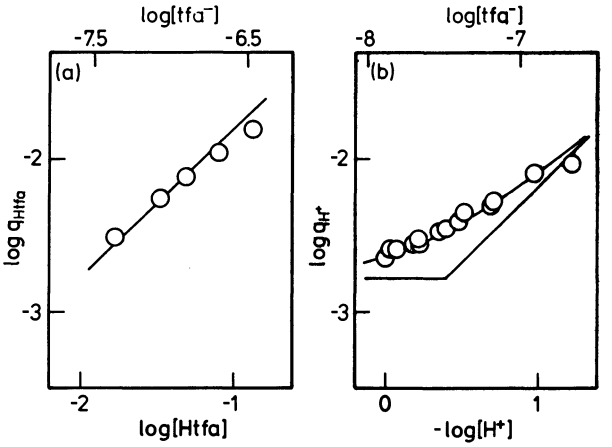

Fig. 2. Dependence of the rate of complex formation of iron(III): (a) on the Htfa concentration when [H+] is 1.0×10^{-1} mol dm^{-3} and (b) on the hydrogen-ion concentration when [Htfa] is 5.0×10^{-2} mol dm^{-3}.
The straight line in (a) and the curve in (b) are calculated by introducing the constants in Table 2 into Eq. 13. The two lines in (b) are the asymptotes for the curve.

tions of Htfa and hydrogen ions, the total amount of complexes formed, that is, the decrease in the Fe^{3+} concentration, was calculated on the basis of Eq. 8 by introducing the molar-absorption coefficients and stability constants in Table 1, which had been determined in a previous study.[6] From this calculated decrease in the Fe^{3+} concentration, the parameters, q, were obtained. Figure 2 gives the dependence of q on the Htfa and hydrogen-ion concentrations. As may be seen, the rate was first-order with respect to Htfa. However, the dependence of the rate on the hydrogen ions approached to zero-order in the higher acidity range, while it approached to inverse-first-order in the lower acidity range. From these data, the rate of complex formation was concluded to be given by:

$$V = K_{CF(1,0)}[Fe^{3+}][Htfa] + K_{CF(1,-1)}[Fe^{3+}][Htfa][H^+]^{-1}$$
$$= K_{CF(1,0)}[Fe^{3+}][Htfa](1 + K_{CF(1,-1)}/K_{CF(1,0)}[H^+]^{-1}). \quad (13)$$

The values of $K_{CF(1,0)}$ and $K_{CF(1,-1)}/K_{CF(1,0)}$ were determined graphically. The plot in Fig. 2(b) was fitted with a standard curve:

$$y = \log(1 + w) : x = \log w \quad (14)$$

and the values were obtained from the parameters of the fitted curve (*cf.* pp. 85 to 96 in Ref. 7). The rate constants obtained are listed in Table 2.

Table 2. Summary of rate constants

The aqueous media are 4 mol dm^{-3} (H,Na)ClO_4 at 298 K.

$K_{SE(1,-1)}$	$=10^{-1.6}$ (s^{-1})
$K_{CF(1,0)}$[a]	$=10^{-1.1}$ (mol^{-1} dm^3 s^{-1})
$K_{CF(1,-1)}$[a]	$=10^{-1.5}$ (s^{-1})
$K_{CF(1,0)}$[b]	$=10^{-1.2}$ (mol^{-1} dm^3 s^{-1})
$K_{CF(1,-1)}$[b]	$=10^{-1.6}$ (s^{-1})

a) Spectrophotometric method. b) Solvent-extraction method.

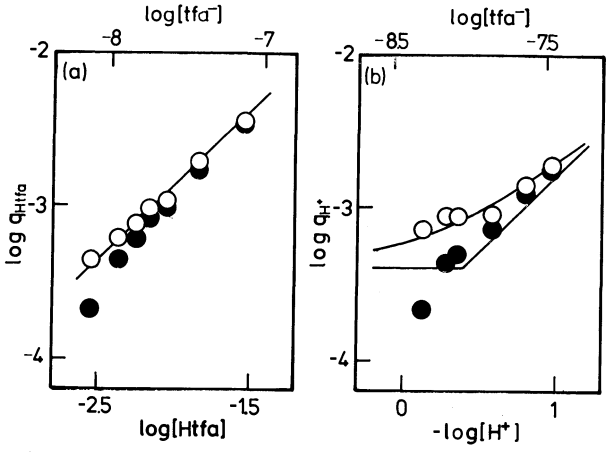

Fig. 3. Dependence of the rate of extraction of iron(III) (closed circles) and the rate of complex formation calculated from the extraction data using Eq. 21 and the constants in Table 1 (open circles): (a) on [Htfa] when $[H^+]$ is 1.0×10^{-1} mol dm^{-3} and (b) on $[H^+]$ when [Htfa] is 1.4×10^{-2} mol dm^{-3}.
The straight line in (a) and the curve in (b) are calculated by introducing the constants in Table 2 into Eq. 13. The two lines in (b) are the asymptotes for the curve.

Rate of Solvent Extraction. The amount of iron(III) extracted into the organic phase was measured as a function of the time; the parameters given by Eqs. 11 and 12 were also calculated as has been described previously.[1-4,7] The closed-circle in Fig. 3 give the dependence of the rate on the Htfa and hydrogen-ion concentrations in the aqueous phase. The rates are apparently first-order and inverse-first-order with respect to [Htfa] and $[H^+]$ respectively. From these data, the rate was concluded to be given (*cf.* Eqs. 10 and 11) by:

$$V = K_{SE(1,-1)}[Fe(III)][Htfa][H^+]^{-1}. \quad (15)$$

The rate constant for the solvent extraction, $K_{SE(1,-1)}$, was obtained from the data in Fig. 3 (*cf.* Table 2).

Discussion

In aqueous solutions, β-diketones are mainly in the keto hydrate form.[8] However, the complex formation in the aqueous phase should take place between hydrated metal ions and the β-diketone in the enol form. The controlling step for a reaction route whose rate is dependent only on the Htfa concentration in Eq. 13 should be:

$$Fe^{3+} + Htfa \longrightarrow Fe(tfa)^{2+} + H^+. \quad (16)$$

However, that for the reaction which is first-order with respect to Htfa and inverse-first-order with respect to hydrogen ions can be both:

$$Fe^{3+} + tfa^- \longrightarrow Fe(tfa)^{2+} \quad (17)$$
$$Fe(OH)^{2+} + Htfa \longrightarrow Fe(tfa)^{2+} + H_2O. \quad (18)$$

Since the reaction in Eq. 18 explains the rate of complex formation of Fe^{3+} with several β-diketones more reasonably,[3] this will also be adopted in the present study. The rate constant assuming the reaction in Eqs. 16 and 18 with the enol form of Htfa is calculated using the hydrolysis constant of Fe^{3+} given in Table 1.[9] (This was given for the equilibrium in 3 mol dm^{-3} $NaClO_4$ media, but the difference of the value in 4 mol dm^{-3} $NaClO_4$ media in the present study should not be large.) Using the constant for the keto-enol equilibrium of Htfa in aqueous solutions in Table 1,[8] the rate constant for the following reactions can be calculated:

$$Fe^{3+} + Htfa_{(enol)} \longrightarrow Fe(tfa)^{2+} + H^+$$
$$K_{CF(1,0)enol} = K_{CF(1,0)} \times (K_e + 1)K_e^{-1} \quad (19)$$
$$Fe(OH)^{2+} + Htfa_{(enol)} \longrightarrow Fe(tfa)^{2+} + H_2O$$
$$K_{CF(1,-1)enol} = K_{CF(1,-1)} \times K_h^{-1}(K_e+1)K_e^{-1}. \quad (20)$$

The calculated values are listed in Table 3.

The kinetics of the complex formation of iron(III) has been studied with several ligands. These data with β-diketones and 4-isopropyltropolone are summarized in Table 3.[10-14] The rate constants with other types of ligands are also in nearly the same order (10^0 to 10^2 for the type of reaction in Eq. 16 and 10^2 to 10^5 for the type of reaction in Eq. 18. For example, Refs. 15 to 29 and also those cited in Ref. 15).

The rate of extraction is determined from the amount of extracted iron(III) and is treated by Eq. 15. This was first-order with respect to the total aqueous concentration of iron(III). When the whole extraction is controlled by the formation of the first complex in the

TABLE 3. RATE CONSTANTS FOR FORMATION OF IRON(III) COMPLEXES IN AQUEOUS PERCHLORATE IONIC MEDIA AT 298 K

Ligand (HL)	$Fe^{3+}+HL$ ($mol^{-1}\ dm^3\ s^{-1}$)	$Fe(OH)^{2+}+HL$ ($mol^{-1}\ dm^3\ s^{-1}$)	Ionic strength / mol dm^{-3}	Ref.
Acetylacetone[a)]	$10^{0.7}$	$10^{3.6}$	1.0	10
2-Thenoyltrifluoroacetone	$10^{-0.3}$	$10^{2.6}$	1.0	11
2-Thenoyltrifluoroacetone	$10^{0.1}$	$10^{3.1}$	1.0	12
4-Isopropyltropolone	$10^{1.4}$	$10^{3.7}$	1.0	13
Trifluoroacetylacetone	$10^{0.9}$	$10^{3.6}$	4.0	b)
Triouoroacetylacetone	$10^{0.8}$	$10^{3.5}$	4.0	c)

a) Another study was also made of the rate of the complex formation of Fe^{3+} and acetylacetone by assuming a somewhat different mechanism.[14)] b) Spectrophotometric method in the present work. c) Solvent-extraction method in the present work.

aqueous phase, and when, consequently, the three aqueous complexes and the tris complex in the organic phase are in an equilibrium to each other, the decrease in the Fe^{3+} concentration should give the rate of this controlling reaction. The $[Fe^{3+}]$ concentration can be written as:

$$[Fe^{3+}] = [Fe(III)]_{init} - ([Fe(tfa)^{2+}] + [Fe(tfa)_2^+] + [Fe(tfa)_3] + [Fe(tfa)_3]_{org})$$
$$= [Fe(III)]_{init} - ((\beta_1\beta_3^{-1}[tfa^-]^{-2} + \beta_2\beta_3^{-1}[tfa^-]^{-1} + 1) \times K_{dm}^{-1} + 1) \times [Fe(tfa)_3]_{org}. \quad (21)$$

Thus, if the rate constant for the formation of the first complex in the aqueous phase is calculated from the extraction data, the decrease in the Fe^{3+} concentration, which can be obtained from the $Fe(tfa)_3$ concentration in the organic phase means of Eq. 21, should be employed instead of the decrease in the total aqueous iron(III) concentration. The open symbols in Fig. 3 were calculated in this way. As may be seen, the open symbols in Fig. 3 should correspond with the plot in Fig. 2, and by treating these data in a similar manner, the rate constants for the complex formation listed in Table 2 were obtained; they agreed well with those obtained from the spectrophotometric data. The rate constants for the complex formation with the enol form of Htfa in Eqs. 19 and 20 can also be obtained from the rate constant for the extraction. These values are also listed in Table 3.

Figure 3 shows that when no consideration is given to the reaction given by Eq. 21, no final conclusion as to the reaction mechanism of the solvent extraction in such systems can be drawn. Moreover, in general, it is not possible to determine the dependence of the rate of extraction on the extractant and the hydrogen ion; in other words, it is not always possible to know the controlling reaction only from a plot such as given by Eq. 10. In this series, we have often observed that the slope of such a plot as Fig. 3 deviates from that to be expected from the assumed controlling reaction; the above is presumably the reason for such deviations. This kind of deviation should be great when the proportion of the extracted complex to the total amount of the complexes produced after the controlling step is small. From Eq. 21, it may be seen that such a deviation occurs when the concentration of the ligand ($[tfa^-]$ in the present study) is low and/or when K_{dm} is low. Figure 4 gives the calculated percentage distributions of the complexes in the two phases when their volumes

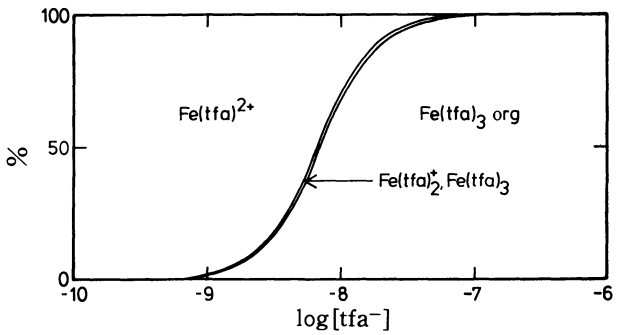

Fig. 4. Percentage distribution of complexes as a function of the ligand concentration when the volumes of the two phases are the same. The percentage gives the ratio of the concentration of each complex to the total concentration of the complexes, $([Fe(tfa)^{2+}]+[Fe(tfa)_2^+]+[Fe(tfa)_3]+[Fe(tfa)_3]_{org})$.

are the same. As may be seen, in the region where $[tfa^-]>10^{-7}$ mol dm^{-3} the molar ratio of the extracted complex to the total amount of the aqueous complexes is very high, and thus the deviation should be negligible. As may be seen from Fig. 3, a deviation occured in our experiments, and since $[tfa^-]$ in these experiments was lower than 10^{-7} mol dm^{-3}, this deviation can be explained reasonably by Fig. 4 and Eq. 21. In some kinetic studies of the extraction of iron(III) with chelating reagents, it was possible to conclude only from the extraction data, that the mechanism was that given by Eq. 16, making no consideration of such an effect.[2,30)] It was also possible in another study to conclude, though no consideration of the equilibrium was made, that the formation of the first complex controlled the complex formation of iron(III) in aqueous solutions with 4,4,4-trifluoro-1-(2-thienyl)-1,3-butanedione, Htta, and also the solvent extraction of the metal ion.[11)] This was possible because the experiments were made under conditions where the ligand concentration was high and/or the K_{dm} in Eq. 4 was large.

From the good agreement of the rate constant for the formation of the iron(III) complex in the aqueous phase determined from the spectrophotometric and solvent-extraction data, it may finally be concluded that the extraction mechanism proposed above is reasonable and that the reaction on the interface is negligible.

The authors are very grateful to Dr. Yū Komatsu of the National Institute for Researches in Inorganic

Materials, Ibaraki, for his valuable discussions in connection with this work.

References

1) T. Sekine, Y. Koike, and Y. Komatsu, *Bull. Chem. Soc. Jpn.*, **44**, 2903 (1971).
2) T. Sekine, J. Yumikura, and Y. Komatsu, *Bull. Chem. Soc. Jpn.*, **46**, 2356 (1973).
3) Y. Komatsu, H. Honda, and T. Sekine, *J. Inorg. Nucl. Chem.*, **38**, 1861 (1976).
4) T. Sekine, Y. Komatsu, and J. Yumikura, *J. Inorg. Nucl. Chem.*, **35**, 3891 (1973).
5) H. Freiser, Proceedings of the International Solvent Extraction Conference, Liege, 80-II (1980).
6) T. Sekine and K. Inaba, *Bunseki Kagaku*, **31**, E291 (1982).
7) T. Sekine and Y. Hasegawa, "Solvent Extraction Chemistry," Marcel Dekker, New York (1977).
8) J. C. Reid and M. Calvin, *J. Am. Chem. Soc.*, **72**, 2948 (1950).
9) L. Ciavatta and M. Grimaldi, *J. Inorg. Nucl. Chem.*, **37**, 163 (1975).
10) D. P. Fay, A. R. Nichols, Jr., and N. Sutin, *Inorg. Chem.*, **10**, 2096 (1971).
11) A. Adin and L. Newman, *J. Inorg. Nucl. Chem.*, **32**, 3321 (1970).
12) M. R. Jaffe, D. P. Fay, M. Cefola, and N. Sutin, *J. Am. Chem. Soc.*, **93**, 2878 (1971).
13) K. Ishihara, S. Funahashi, and M. Tanaka, 30th Symposium on Coordination Chemistry, 146 (1980).
14) W. K. Ong and R. H. Prince, *J. Chem. Soc., A*, **1966**, 458.
15) S. Funahashi, S. Adachi, and M. Tanaka, *Bull. Chem. Soc. Jpn.*, **46**, 479 (1973).
16) E. Mentasti and E. Pelizzetti, *J. Chem. Soc., Dalton Trans.*, **1973**, 2605.
17) S. Gouger and J. Stuher, *Inorg. Chem.*, **13**, 379 (1974).
18) E. Mentasti, E. Pelizzetti, and G. Saini, *J. Chem. Soc., Dalton Trans.*, **1974**, 1944.
19) E. Mentasti and E. Pelizzetti, *J. Inorg. Nucl. Chem.*, **38**, 785 (1976).
20) E. Mentasti, E. Pelizzetti, and C. Baiocchi, *Ann. Chim. (Rome)*, **66**, 407 (1976).
21) B. Permutter-Hayman and E. Tapuhi, *J. Coord. Chem.*, **6**, 31 (1976).
22) A. Miftahova, L. Dozsa, and M. T. Beck, *Acta Chim. Acad. Sci. Hung.*, **92**, 379 (1977).
23) U. D. Gomwalk, A. G. Lappin, J. P. McCann, and A. McAuley, *Inorg. Chem. Acta*, **24**, 39 (1977).
24) N. Kujundzic and M. Pribanic, *J. Inorg. Nucl. Chem.*, **40**, 729 (1978).
25) B. Permutter-Hayman and E. Tapuhi, *J. Coord. Chem.*, **8**, 75 (1978).
26) E. Mentasti, *Inorg. Chem.*, **18**, 1512 (1979).
27) E. Mentasti, E Parmauro, E. Barni, and P. Savarino, *Ann. Chim. (Rome)*, **62**, 663 (1979).
28) B. Monzyk and A. L. Crumbliss, *J. Am. Chem. Soc.*, **101**, 6203 (1979).
29) K. Ishihara, S. Funahashi, and M. Tanaka, 31st Symposium on Coordination Chemistry, 452 (1981).
30) B. E. McClellan and O. Menis, *Anal. Chem.*, **43**, 436 (1971).

An Alternative Display of Potentiostatic Measurements. II. Electrochemical Determination of Outer-sphere Association Constants of Several Substitution-inert Complexes with Sulfate Ions

Akifumi YAMADA,* Yoshikiyo KATO,† Yasuo NAKABAYASHI,†† and Nobuyuki TANAKA†

Department of Materials Science and Technology, Technological University of Nagaoka, Kamitomioka, Nagaoka 949-54

†*Department of Chemistry, Faculty of Science, Tohoku University, Sendai 980*

(Received June 14, 1982)

A modified technique for the potentiostatic method has been applied to the study on the outer-sphere association of some substitution-inert complex cations with sulfate ions. The association constants were determined from the change in limiting time as function of the concentration of sulfate ions at ionic strength 0.2 and 25 °C: 29±3 for $[Co(NH_3)_6]^{3+}$–SO_4^{2-}, 23±2 for $[Co(en)_3]^{3+}$–SO_4^{2-}, 34±3 for $[Co(H_2O)(NH_3)_5]^{3+}$–SO_4^{2-}, 18±2 for $[Cr(NH_3)_6]^{3+}$–SO_4^{2-}, 21±2 for $[Cr(en)_3]^{3+}$–SO_4^{2-}, 19±2 for $[Cr(H_2O)(NH_3)_5]^{3+}$–SO_4^{2-}, 13±2 for $[Cr(urea)_6]^{3+}$–SO_4^{2-}. The ratios of the diffusion coefficient of the univalent ion pairs to that of tervalent substitution-inert complex cations were also obtained. From these ratios, the diffusion coefficients of the univalent ion pairs were calculated; these were found to be close to those of univalent complex ions with similar structures.

The potentiostatic method has been recognized as the principal tool for the investigation of electrode kinetics. Previous studies[1,2] have demonstrated an alternative mode of potentiostatic measurement, which analyzes the relationship between the potential and the time required to reach a constant sampling current in the potentiostatic measurement.[1] The instrumental design of an automatic recording of potential-time curves of this mode was described in the first paper of this series.[3] The chief advantage of this mode is that the limiting time at diffusion-controlled potential is directly proportional to the diffusion coefficient,[1] whereas, in the normal potentiostatic method, the limiting current is proportional to the square root of diffusion coefficients. Thus, the modified potentiostatic method is convenient for detection of the diffusion coefficient in a series of measurements.

It has been reported that the polarographic diffusion current and the chronopotentiometric transition time for some tervalent cations, such as $[Cr(NH_3)_6]^{3+}$,[4] $[Cr(en)_3]^{3+}$,[5] $[Cu(urea)_6]^{3+}$,[6] $[Co(NH_3)_6]^{3+}$,[7] and $[Co(en)_3]^{3+}$,[8] decrease upon the addition of sulfate ions. This decrease is attributed mainly to the effect of outer-sphere association of the tervalent cations and the sulfate ions; the diffusion coefficient of the sulfate ion decreases upon the formation of ion pairs. The decrease in the polarographic diffusion current[9,10] and in the chronopotentiometric transition time[11] was used for the determination of the association constant.

In this paper, a method for the determination of association constants with the aid of the modified potentiostatic method is presented and applied to the ion pairs: $[Cr(urea)_6]^{3+}$–SO_4^{2-}, $[Cr(H_2O)(NH_3)_5]^{3+}$–SO_4^{2-}, $[Cr(NH_3)_6]^{3+}$–SO_4^{2-}, $[Cr(en)_3]^{3+}$–SO_4^{2-}, $[Co(NH_3)_6]^{3+}$–SO_4^{2-}, $[Co(en)_3]^{3+}$–SO_4^{2-}, and $[Co(H_2O)(NH_3)_5]^{3+}$–SO_4^{2-}.

Experimental

The complexes, $[Cr(urea)_6](ClO_4)_3$,[12] $[Cr(NH_3)_6](ClO_4)_3$,[13] $[Cr(H_2O)(NH_3)_5](ClO_4)_3$,[13] $[Cr(en)_3](ClO_4)_3$,[14] $[Co(NH_3)_6](ClO_4)_3$,[15] and $[Co(en)_3](ClO_4)_3$[16] were prepared according to the literature and converted to perchlorate salt. All other chemicals used were of guranteed reagent-grade. Redistilled water was used to prepared the solutions of desired concentrations. Polyethylene glycol dodecyl ether (LEO: mean molecular weight, 862) was used as the maximum suppressor.

Modified potentiostatic measurements were carried out by means of the modified pulse polarograph described in a previous paper.[3] A digital multimeter (Takeda Riken TR-6355) and a universal counter (Takeda Riken TR-5104G) were used; the potential and the time were thus measured precisely. A three-electrode cell equipped with a saturated calomel electrode (Yanagimoto MR-P2-05-1) and a platinum wire electrode were employed. The DME with a flow rate of 1.17 mg s^{-1} and a drop time of 2.0 s in 0.5 M (1 M=1 mol dm^{-3}) of NaCl was used. Electrolytic solutions were deaerated by bubbling purified nitrogen gas through the solution for 20 min. Measurements were made at 25 °C in solutions of ionic strength of 0.2 containing appropriate amounts of maximum suppressors. Ionic strength was adjusted with NaCl (for chromium(III) complexes) or with $NaNO_3$ (for cobalt(III) complexes).

Results and Discussion

From the modified potentiostatic measurements, the association constant can be determined in the following way. Consider the association reaction

$$M^{3+} + Z^{2-} \rightleftharpoons M^{3+}Z^{2-}, \quad (1)$$

where M^{3+} represents a complex cation, Z^{2-}, a sulfate anion and $M^{3+}Z^{2-}$, an ion pair. Since the dissociation and the association of ion pairs are very rapid, the apparent diffusion coefficient (D) is given by[17,18]

$$D = \frac{D_M + Kc_Z D_{MZ}}{1 + Kc_Z}, \quad (2)$$

where c_Z means the concentration of Z^{2-}, D_M, and D_{MZ} are the diffusion coefficient of M^{3+} and $M^{3+}Z^{2-}$, respectively, and K is the association constant of $M^{3+}Z^{2-}$ given by

$$K = c_{MZ}/c_M c_Z. \quad (3)$$

†† Present address: Department of Chemistry, Faculty of Science, Kobe University, Kobe 657.

Here c_M and c_{MZ} are the concentration of M^{3+} and $M^{3+}Z^{2-}$, respectively.

The observed limiting time (t) of the modified potentiostatic method in the presence of ion pairs can be expressed as follows:[1,2]

$$\sqrt{t} = nFc^\circ\sqrt{D}/\sqrt{\pi}I, \quad (4)$$

where c° is the bulk concentration of the electroactive species; n, the number of electrons; F, the Faraday constant; and I, the constant sampling current in the modified potentiostatic method. From Eqs. 2 and 4, one can deduce the following relation:

$$\left(\frac{c_M}{c}\right)^2\left(\frac{t}{t_M}\right) = \frac{1+Kc_Z\xi}{1+Kc_Z} \quad (5)$$

with

$$\sqrt{t_M} = nFc_M^\circ\sqrt{D_M}/\sqrt{\pi} \text{ and } \xi = D_{Mx}/D_M, \quad (6)$$

where t_M is the limiting time which is obtained when the bulk concentration of M^{3+} is c_M° and no ion pair is formed. The left-hand side of Eq. 5 is obtained experimentally, and plotted as a function of c_Z; a hyperbola is obtained, from which the association constant can be calculated.

Equation 5 can be transformed to

$$\frac{c_Z}{1-\left(\frac{c_M^\circ}{c^\circ}\right)^2\left(\frac{t}{t_M}\right)} = \frac{1+Kc_Z}{K(1-\xi)}. \quad (7)$$

Equation 7 indicates that the plot of $c_Z/[1-(c_M^\circ/c^\circ)^2\times(t/t_M)]$ *versus* c_Z will give a straight line and the association constant K can be determined from the ratio of its slope to its intercept. The ratio (ξ) of the diffusion coefficient of ion pairs $M^{3+}Z^{2-}$ to that of complex cation M^{3+} can then be obtained from the intercept.

The measurements for the determination of association constants were carried out in the solutions containing 0.01 M acetate buffer, since it was reported that the reduction waves of chromium(III) and cobalt(III) complexes used are not well-defined in neutral solutions, but are well-defined in acidic solutions.[4,5,19,20] An amount of 2—4 μM LEO was added to the solution to prevent the streaming effect.[5,21]

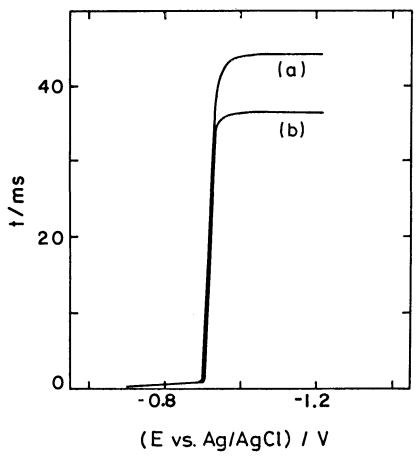

Fig. 1. An example of potential-time curves for the modified potentiostatic method with 0.5 mM $[Cr(NH_3)_6](ClO_4)_3$ obtained in (a) 0.195 M NaCl and (b) 0.065 M Na_2SO_4 containing 5 mM acetate buffer and 2 μM LEO at 25 °C. The measurements were made at 6.0 μA of sampling current.

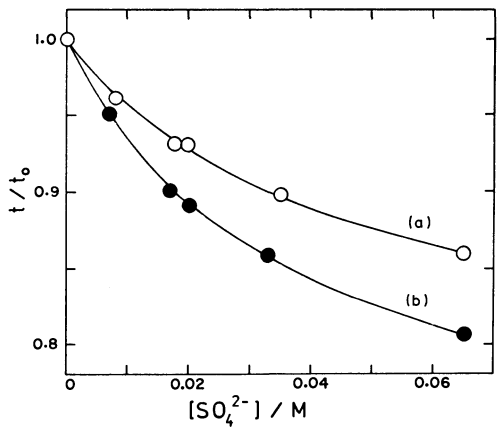

Fig. 2. Variation of the limiting time for the reduction of (a) $[Co(en)_3]^{3+}$ and (b) $[Co(NH_3)_6]^{3+}$ with the change in the concentration of sulfate ions, observed in the solutions containing 5 mM acetate buffer+(a) 4 μM LEO or (b) 2 μM LEO.
—— Indicates the calculated, and ●, ○ the experimental values.

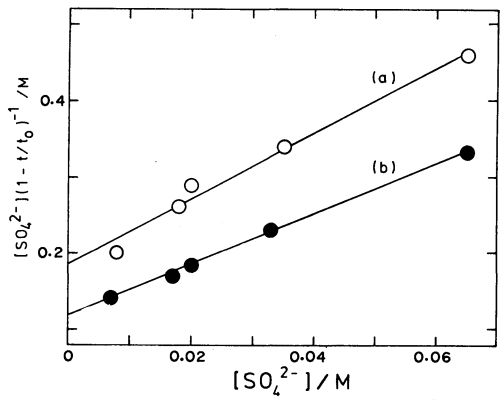

Fig. 3. Relation between the value of the left-hand side of Eq. 7 and sulfate concentration.
(a): $[Co(en)_3]^{3+}$, (b): $[Co(NH_3)_6]^{3+}$.

Figure 1 shows a typical example of a potential-time curve of the modified potentiostatic method for $[Cr(NH_3)_6]^{3+}$ ions which was obtained in solution with and without sulfate ions. The time was measured at a sampling current of 6 μA. It can be seen from Fig. 1 that the limiting time by means of the modified potentiostatic method decreased due to the presence of sodium sulfate. An example of the change in limiting time with the increase in the concentration of sodium sulfate is shown in Fig. 2 for $[Co(NH_3)_6]^{3+}$–SO_4^{2-} and $[Co(en)_3]^{3+}$–SO_4^{2-}. The value of t_0 was obtained with the solution of the bulk concentration $c_M^\circ(c_M^\circ=c^\circ)$ containing no sodium sulfate. A linear plot of Eq. 7 for $[Co(NH_3)_6]^{3+}$–SO_4^{2-} and $[Co(en)_3]^{3+}$–SO_4^{2-} is also given in Fig. 3.

The association constant (K) and the ratio of the diffusion coefficient (ξ) were calculated by the method of least squares. The results are given in Table 1. Comparison of the association constants of chromium(III) complexes with those of cobalt(III) ones having the

same ligands showed that the association constants of the chromium(III) complexes studied were smaller than those of the corresponding cobalt(III) ones.

The association constants of hexaamminecobalt(III) and tris(ethylenediamine)cobalt(III) with sulfate ion have been reported by several researchers.[22] The logarithmic constants of $[Co(NH_3)_6]^{3+}$–SO_4^{2-} at infinite dilution range between 2.89 and 3.71 and those of $[Co(en)_3]^{3+}$–SO_4^{2-} range between 2.72 and 3.45. Corrected for the effect of activity coefficient,[23] the logarithmic association constant at infinite dilution obtained from the present result becomes 3.19 for $[Co(NH_3)_6]^{3+}$–SO_4^{2-} and 2.88 for $[Co(en)_3]^{3+}$–SO_4^{2-}. The values obtained in this study are in good agreement with those in the literature, and with that expected from Bjerrum's theory[24] of ion association due to coulombic interaction between tervalent and bivalent ions of opposite charge at the distance of closest approach, 5—6 Å. Similarly, the values of $[Cr(NH_3)_6]^{3+}$–SO_4^{2-} obtained in this study also agree well with those obtained by other electrochemical methods.[2]

The association constant and the ratio of diffusion coefficients for ion pairs $[Co(NH_3)_6]^{3+}$–SO_4^{2-}, $[Co(en)_3]^{3+}$–SO_4^{2-}, $[Cr(NH_3)_6]^{3+}$–SO_4^{2-} and $[Cr(en)_3]^{3+}$–SO_4^{2-} are compared with those obtained by chronopotentiometry.[22] They are given in Table 2, though the ionic strength in the measurements is different. The association constants of the present work ($\mu=0.2$) were approximately one third of those at $\mu=0.1$, whereas the ratios of diffusion coefficients were not so different for the two ionic strengths.

The association constants of $[Co(H_2O)(NH_3)_5]^{3+}$–SO_4^{2-}, $[Cr(H_2O)(NH_3)_5]^{3+}$–SO_4^{2-} and $[Cr(urea)_6]^{3+}$–SO_4^{2-} have not been reported, but the constant obtained in this study seems appropriate compared with the values for the ion pairs $[Co(NH_3)_6]^{3+}$–SO_4^{2-}, $[Co(en)_3]^{3+}$–SO_4^{2-}, $[Cr(NH_3)_6]^{3+}$–SO_4^{2-} and $[Cr(en)_3]^{3+}$–SO_4^{2-}. Though detailed comparison of the constant with that of $[Cr(NH_3)_6]^{3+}$–SO_4^{2-} is limited, it may be said that $[Cr(urea)_6]^{3+}$–SO_4^{2-} is slightly less stable than $[Cr(NH_3)_6]^{3+}$–SO_4^{2-}.

The diffusion coefficients of ion pairs were calculated by using the diffusion coefficient of tervalent cation and the ratio of the diffusion coefficients, ξ, obtained in this study. They are compared with the diffusion coefficients of ion pairs given in the literature and with those of other univalent complex ions, which are given in Table 3.

Although such a comparison is limited because of insufficient accuracy in the measurement, it may be concluded that the diffusion coefficients of univalent ion pairs differ little from those of univalent complex ions.

In the derivation of Eq. 7, only the association of one cation and one anion was taken into consideration. With the precision of the present experiment it is difficult to determine the ion-pair formation involving more than one sulfate ion. The formation of such species is negligibly small compared with the ion pairs such as $[Co(NH_3)_6]^{3+}$–SO_4^{2-}, $[Cr(NH_3)_6]^{3+}$–SO_4^{2-}, *etc.*, if the association is assumed to depend mainly on the coulombic interaction between ions.

TABLE 1. ASSOCIATION CONSTANTS AT $\mu=0.2$ AND THE RATIO OF THE DIFFUSION COEFFICIENTS (25 °C)

Ion pair	K	ξ
$[Co(NH_3)_6]^{3+}$–SO_4^{2-}	29±3	0.7_0
$[Co(en)_3]^{3+}$–SO_4^{2-}	23±2	0.7_7
$[Co(H_2O)(NH_3)_5]^{3+}$–SO_4^{2-}	34±3	0.7_6
$[Cr(NH_3)_6]^{3+}$–SO_4^{2-}	18±2	0.6_6
$[Cr(en)_3]^{3+}$–SO_4^{2-}	21±2	0.8_0
$[Cr(H_2O)(NH_3)_5]^{3+}$–SO_4^{2-}	19±2	0.7_0
$[Cr(urea)_6]^{3+}$–SO_4^{2-}	13±2	0.7_6

TABLE 2. ASSOCIATION CONSTANTS AND THE RATIO OF THE DIFFUSION COEFFICIENTS ξ AT $\mu=0.2$ AND $\mu=0.1$ (25 °C)

Ion pair	$\mu=0.2$		$\mu=0.1$[11]	
	K	ξ	K	ξ
$[Co(NH_3)_6]^{3+}$–SO_4^{2-}	29±3	0.7_0	93± 8	0.6_8
$[Co(en)_3]^{3+}$–SO_4^{2-}	23±2	0.7_7	99±15	0.8_2
$[Cr(NH_3)_6]^{3+}$–SO_4^{2-}	18±2	0.6_6	61± 7	0.6_7
$[Cr(en_3)_6]^{3+}$–SO_4^{2-}	21±2	0.8_0	58± 8	0.8_7

References

1) N. Tanaka, A. Kitani, A. Yamada, and K. Sasaki, *Sci. Repts. Tohoku Univ. Ser. I*, **55**, 201 (1972).

2) N. Tanaka, A. Kitani, A. Yamada, and K. Sasaki, *Electrochim. Acta*, **18**, 675 (1973).

TABLE 3. DIFFUSION COEFFICIENTS OF ION PAIRS CALCULATED FROM ξ AND THOSE OF OTHER SUBSTITUTION-INERT COMPLEX IONS (25 °C)[a]

Complex ion	D / 10^{-6} cm^2 s^{-1}	Ion pair	ξ	D / 10^{-6} cm^2 s^{-1}	
$[Co(NH_3)_6]^{3+}$	8.4_{25}	$[Co(NH_3)_6]^{3+}$–SO_4^{2-}	0.7_0	$5._9$	5.7[11]
$[Co(en)_3]^{3+}$	6.4[8]	$[Co(en)_3]^{3+}$–SO_4^{2-}	0.7_7	$4._9$	5.3[11]
$[Co(H_2O)(NH_3)_5]^{3+}$	7.8[26]	$[Co(H_2O)(NH_3)_5]^{3+}$–SO_4^{2-}	0.7_6	$5._9$	
$[Cr(NH_3)_6]^{3+}$	8.5[4]	$[Cr(NH_3)_6]^{3+}$–SO_4^{2-}	0.6_6	$5._6$	5.7[11]
$[Cr(en)_3]^{3+}$	5.9[5]	$[Cr(en)_3]^{3+}$–SO_4^{2-}	0.8_0	$4._7$	$5._1$[11]
$[Cr(H_2O)(NH_3)_5]^{3+}$	8.0[27]	$[Cr(H_2O)(NH_3)_5]^{3+}$–SO_4^{2-}	0.7_0	$5._6$	
$[Cr(urea)_6]^{3+}$	5.0[6]	$[Cr(urea)_6]^{3+}$–SO_4^{2-}	0.7_6	$3._8$	
$[Co(CO_3)(tn)_2]^+$	4.8[26]				
$[Cr(NCS)_4(NH_3)_2]^-$	6.1[28]				

a) Some of these are calculated from the polarographic diffusion current constant, and consequently are less accurate.

3) Y. Kato, Y. Anzai, A. Yamada, and N. Tanaka, *Bull. Chem. Soc. Jpn.*, **54**, 2482 (1981).
4) N. Tanaka, K. Ebata, and G. Sato, *Bull. Chem. Soc. Jpn.*, **36**, 912 (1963).
5) N. Tanaka and A. Yamada, *Bull. Chem. Soc. Jpn.*, **39**, 920 (1966).
6) A. Yamada, Y. Nakabayashi, T. Yoshikuni, and N. Tanaka, *Bull. Chem. Soc. Jpn.*, **53**, 3596 (1980).
7) H. A. Laitinen, A. J. Frank, and P. Kivalo, *J. Am. Chem. Soc.*, **75**, 2865 (1953).
8) H. A. Laitinen and M. W. Grieb, *J. Am. Chem. Soc.*, **77**, 5201 (1955).
9) N. Tanaka, K. Ogino, and G. Sato, *Bull. Chem. Soc. Jpn.*, **39**, 366 (1966).
10) N. Tanaka and K. Koseki, *Bull. Chem. Soc. Jpn.*, **41**, 2067 (1968).
11) N. Tanaka and A. Yamada, *Z. Anal. Chem.*, **224**, 117 (1967).
12) P. Pfeifer, *Ber.*, **36**, 1926 (1903).
13) M. Mori, *Nippon Kagaku Zasshi*, **74**, 253 (1953).
14) P. Pfeifer, P. Koch, G. Lando, and A. Trieschman, *Ber.*, **37**, 4255 (1904).
15) J. Bjerrum and J. P. McReynolds, "Inorganic Syntheses," McGraw-Hill, New York (1946), Vol. 2, p. 216.
16) J. B. Work, "Inorganic Syntheses," McGraw-Hill, New York (1946), Vol. 2, p. 221.
17) J. Koutecký, *Collect. Czech. Chem. Commun.*, **19**, 857 (1954).
18) H. Matsuda and Y. Ayabe, *Z. Elektrochem.*, **66**, 469 (1962).
19) N. Tanaka and G. Sato, *Nature*, **197**, 176 (1963).
20) N. Maki and N. Tanaka, "Encyclopedia of Electrochemistry of the Elements," ed by A. J. Bard, Marcel Dekker, New York (1975), Vol. 3.
21) J. W. Olver and J. W. Ross, *Anal. Chem.*, **34**, 791 (1962).
22) L. G. Sillén and A. E. Martell, "Stability Constants of Metal-ion Complexes," The Chemical Society, London, Special Publication No. 17 (1964); No. 25 (1971).
23) L. Kielland, *J. Am. Chem. Soc.*, **59**, 1675 (1937).
24) C. B. Monk, "Electrolytic Dissociation," Academic Press, London (1961), Chap. 14.
25) H. A. Laitinen, J. C. Bailar, Jr., H. F. Holtzchow, Jr., and Jv. Quagtiano, *J. Am. Chem. Soc.*, **70**, 2999 (1948).
26) A. Yamada, Y. Kato, T. Yoshikuni, Y. Tanaka, and N. Tanaka, *Anal. Chim. Acta*, **112**, 55 (1979).
27) N. Tanaka, Y. Sato, R. Tamamushi, and G. Sato, *Bull. Chem. Soc. Jpn.*, **36**, 1059 (1963).
28) N. Tanaka, T. Ito, and R. Tamamushi, *Bull. Chem. Soc. Jpn.*, **37**, 1430 (1964).

Studies of Hydrous Tin(IV) Oxide Ion-exchangers. I. A Method for Synthesis and Some Properties

Yasushi INOUE* and Hiromichi YAMAZAKI
Department of Nuclear Engineering, Faculty of Engineering, Tohoku University, Aramaki, Sendai 980
(Received December 21, 1981)

A comprehensive study of the preparation of hydrous tin(IV) oxide ion-exchangers was made by using eight systems: (1)$Na_2[Sn(OH)_6]$–H_2SO_4, (2)$Na_2[Sn(OH)_6]$–H_2SO_4(boiling), (3)$Na_2[Sn(OH)_6]$–HCl, (4)$Na_2[Sn(OH)_6]$–CH_3COOH, (5)$SnCl_4$–NaOH, (6)$SnCl_4$–NH_3aq, (7)$SnCl_4$–NH_3aq(boiling), and (8)$SnCl_4$–pyrohydrolysis. From a detailed examination of the dependency of the yield, the ion-exchange behavior toward Na^+ and Cl^- ions, the composition, and some other properties on the conditions for precipitation, it was found that the ion-exchange characteristics are similar among materials produced from the systems from (1) through (7) if we neglect some aging effect of boiling, while the difficulty of synthesis differs according to the systems. The materials obtained from the (8) system, however, showed titration curves different from those for the exchanges obtained from the other systems and had less cation-exchange capacity for Na^+ by 20 per cent. From these results, it is concluded that the simplicity of the synthetic procedures in the most important criterion for choosing the best conditions for preparing the exchanger.

Many hydrous oxides for use as ion-exchange materials have been investigated because of their unique characteristics of selectivity and the simplicity of preparation. They have, however, the serious disadvantage of giving inconsistent results to different investigators. This may be due to irreproducibility of the synthesis. Nevertheless, many authors do not describe the details of the investigations concerning synthesis. To promote further investigation of this group of ion-exchange materials, it is indispensable to reexamine the synthetic conditions for establishing reproducible methods. With this point in mind, one of the present authors previously successfully studied hydrous titanium(IV) oxide in establishing a satisfactory method of synthesis.[1] Several studies have been carried out on hydrous tin(IV) oxide[3–9] since the work of Kraus *et al.*, who first reported the amphoteric ion-exchange property of this material.[2] In this case, also, different compositions and ion-exchange properties were reported by each investigator. This induced us to undertake a thorough study of the synthesis of hydrous tin(IV) oxide.

This paper will describe the results of one investigation to establish the best conditions for the synthesis by varying such factors as the starting materials, the methods of hydrolysis, the pH values of precipitation, and the concentrations of the hydrolyzing reagents, as well as aging.

Experimental

Reagents and Apparatus. $Na_2[Sn(OH)_6]$ was purified by recrystallization.[10] The other chemicals were of the highest purity grade and were used without further purification. The pH values were measured with a Toa Dempa model HM-5BS pH meter. The atomic absorption measurements were made with a Nippon Jarrell-Ash model AA-782 atomic-absorption and a flame-emission spectrophotometer, while the other absorption measurements were carried out with a Hitachi model 124 double-beam spectrophotometer.

Synthesis of Hydrous Tin(IV) Oxide. The synthetic systems adopted in the present investigation are shown schematically in Fig. 1. In the systems from (1) through (3), hydrous tin(IV) oxide was precipitated by hydrolyzing a $Na_2[Sn(OH)_6]$ solution by the addition of different acids,

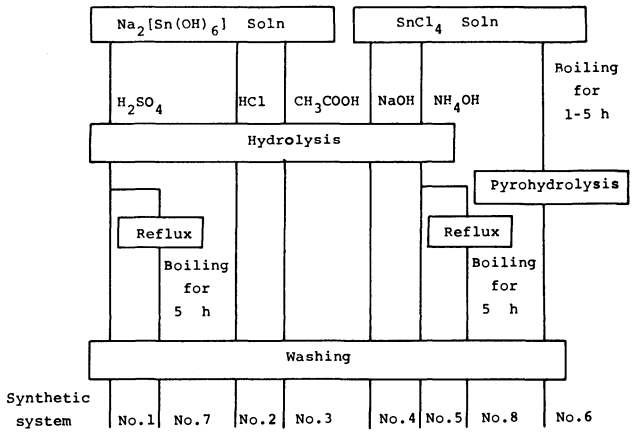

Fig. 1. Method of synthesis.

while in the (4) and (5) systems, the precipitate was made by hydrolyzing $SnCl_4$ solution by the addition of alkaline solutions. In some cases the slurries thus obtained were refluxed for five hours; the methods of precipitation of the (7) and (8) systems are similar to those of the (1) and (5) systems respectively. In the (6) system, the oxide was precipitated by the pyrohydrolysis of the $SnCl_4$ solution.

After precipitation had been completed, the precipitate was washed and dried by the following procedure unless otherwise noted. After being separated from the mother liquor by a combination of decantation and filtration through Toyo No. 1 filter paper under suction, the precipitate was uniformly dispersed into distilled water and filtered again after being completely sedimentated. This procedure was repeated until no impurity was detected in the filtrate. Then the precipitate was sufficiently air-dried at room temperature. The resulting product was then immersed in distilled water to break it down into fine particles, which were subsequently dried again at room temperature. At this stage the yield was calculated. Particles were then ground in a porcelain mortar and sieved to obtain the required particle sizes.

Conditioning. The exchanger of a desired particle size (100—200 mesh) was washed with water to remove any adherent powder. The slurry was poured into a glass tube, 10 mm in inside diameter and 15 cm high, with glass-wool plugging for column support. Then, 0.1 M (1 M=1 mol dm^{-3}) HCl was passed through the column until the pH of the

effluent approached that of the influent at a flow rate of about 1 cm^3 min^{-1}. Then the column was washed with water until the effluent showed a constant pH value (about 5). The exchanger in H^+ form thus prepared was air-dried and stored in a desiccator containing a saturated NH_4Cl solution (relative humidity, 79% at 25 °C).

Specific Ion-exchange Capacity and Titration Curves. A quarter gram of the exchanger in H^+ form was immersed in 30 cm^3 of various solutions, prepared by the desired combination of 0.1 M NaCl, and 0.1 M NaOH or 0.1 M HCl, for 4 d at room temperature with intermittent shaking. This was followed by pH measurements and by the determination of the sodium or chloride ions. The chloride concentrations were determined by the Fajans' method after the solution had been neutralized. The sodium ions were converted to pure sodium chloride and indirectly determined by titrating the chloride ions. The amount of the ions taken up by the exchanger was evaluated from the difference between the initial and final concentrations of the respective ions present in the solution. The amount of the exchanger dissolved was also evaluated from the amount of tin dissolved in the supernatant solution spectrophotometrically by the phenylfluorone method.[11] The limit of detection was 0.05 wt% of the exchanger used.

Total Analysis of the Exchanger. *Na^+ and SO_4^{2-}*: A half gram of the exchanger was dissolved in hydrobromic acid containing 10% bromine. The Na^+ concentration in this solution was determined atomic absorption-spectrophotometrically, while the absence of SO_4^{2-} ions was checked by adding a $BaCl_2$ solution. The limit of detection was 0.01 wt% for Na^+ and 0.005 wt% for SO_4^{2-}.

Cl^-: A sample of 0.5 g was dissolved by heating with 100 cm^3 of 9 M H_2SO_4 in a 500-cm^3 distilling flask, and the HCl evolving therefrom, carried by steam, was absorbed in a slightly alkaline solution and then determined spectrophotometrically, using mercury(II) thiocyanate and ammonium iron(III) sulfate as coloring reagents. The limit of detection was 0.02 wt%.

Water: A sample of 0.25 g was ignited at 850 °C, and the water content was calculated from the weight loss. The validity of the procedure had been confirmed thermogravimetrically.

Density: The density of the exchangers were measured in the usual manner using a 25-cm^3 pycnometer.

Results and Discussion

Precipitation Behavior in Various Synthetic Systems. It is required for practical purposes that a large amount of pure hydrous tin(IV) oxide can be prepared readily in a high yield; especially, the precipitation conditions should be such that the precipitate can be easily washed without peptization. For this reason, the yield evaluated from only the solubility loss is impractical; the yield should include all losses resulting from the whole synthetic processes. With this in view, we examined the relation between the yield and the conditions of precipitation for the synthetic systems shown in Fig. 1.

In this experiment, the solution of tin and a solution of acid or base of a suitable concentration were mixed together to make a total volume of 50 cm^3. The precipitate thus formed was then treated by the method described in the Experimental section. The yield was measured on the basis of the recovery of tin. Figure 2 shows the results for the (2) system. In this figure, the concentrations of tin and hydrochloric acid in the mixed solution were taken as the abscissa and the ordinate respectively. The area of the figure was distinguished into four regions based on the overall yield.

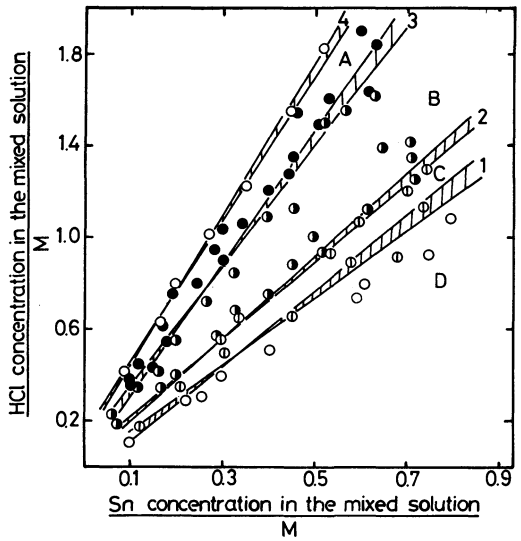

Fig. 2. Dependence of the yield of hydrous tin(IV) oxide on the conditions for precipitation (system (2)). Yield; ○: zero, ◔: <0.2, ◑: <0.6, ●: >0.8. Molar ratio ([HCl]/[Sn^{4+}]); 1: 1.5—1.7, 2: 1.7—1.8, 3: 2.7—3.0, 4: 3.3—3.4. For A, B, C, and D, see text.

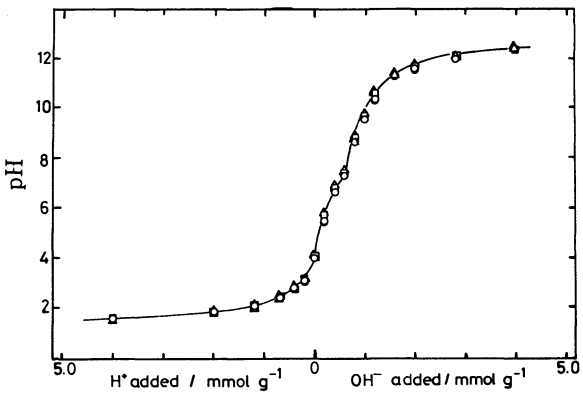

Fig. 3. Titration curves.
○: System (1) (pH=3.8), ●: system (2) (pH=3.8), □: system (3) (pH=4.6), △: system (4) (pH=3.5), ▲: system (5) (pH=3.5), ( ) shows the pH value at precipitation.

Region A: The precipitate could be washed without peptization until no impurity was detected in the filtrate, and the yield exceeded 80%. Thus, this is the optimum region.

Region B: The precipitate peptized during washing, and the yield was 20—80%.

Region C: The precipitate peptized at an early stage of washing, and the yield fell below 20%.

Region D: No precipitate was formed at all. Figures similar to Fig. 2 were made for every synthetic system; the results are summarized in Table 1. The appraisal of the synthetic system is made by a comparison of the area of Region A, because the experimental conditions can be more easily set up for a system having the larger

Table 1. Summary of the precipitation behavior

	Synthetic system	Sn concn[a] / M	Molar ratio[b]	pH[c]
Experimental conditions	(1)	0.08—0.8	0.4—3.8	0.4—12
	(2)	0.08—0.8	1.2—3.8	0.4—12
	(3)	0.08—0.8	1.2—6.0	3.7—12
	(4)	0.05—0.5	2.0—6.0	0.5—12
	(5)	0.05—0.5	2.0—6.0	0.5—10
	(6)	9.3×10^{-3}—0.2	—	—
Region-A	(1)	0.08—0.8	>0.96～1.0	<3.5～4.0
	(2)	0.08—0.8	2.5～3.0—3.3～3.4	0.4～0.5—0.7～1.0
	(3)	—	—	—
	(4)	0.05—0.3	3.0～3.5—4.5～4.8	0.8～1.1—4.4～4.7
	(5)	0.05—0.5	3.0～3.5—4.2～4.5	0.9～1.1—4.5～4.7
	(6)	<0.10	—	—
Region-B	(1)	0.08—0.8	0.90～0.95—0.96～1.0	3.5～4.0—4.5～6.5
	(2)	0.08—0.8	1.7～1.8—2.5～3.0	0.7～1.0—6.0～7.0
	(3)	0.08—0.8	2.2<	<5.0～6.0
	(4)	0.3 —0.5	3.0～3.5—4.5～4.8	0.8～1.1—4.4～4.7
	(5)	0.05—0.5	4.2～4.5—4.7	4.5～4.7—7.0～7.2
Region-C	(1)	0.08—0.8	0.6～0.7—0.90～0.95	4.5～6.5—10.5～11.5
	(2)	0.08—0.8	1.5～1.6—1.7～1.8	6.0～7.0—10.0～11.5
	(3)	0.08—0.8	1.5～1.7—2.2	5.0～6.0—10.0～11.5
	(4)	0.05—0.5	4.5～4.8<	4.4～4.7<
	(5)	0.05—0.5	4.7<	7.0<
Region-D	(1)	0.08—0.8	<0.6～0.7	>10.5～11.5
	(2)	0.08—0.8	<1.5～1.6	>10.5～11.5
	(3)	0.08—0.8	<1.5～1.7	>10.0～11.7
	(4)	0.05—0.5	<3.0～3.3	<0.8
	(5)	0.05—0.5	<3.0～3.5	<0.9～1.1

a) The concentration in the mixed solution. b) [Acid] or [alkali]/[tin]. c) The pH range at precipitation when the Sn concn and molar ratio were in the range shown in the left columns.

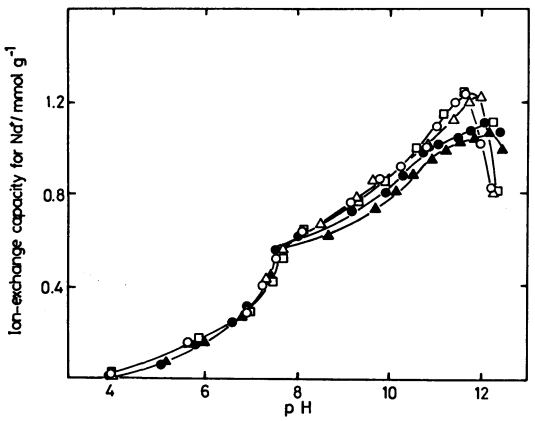

Fig. 4. Uptake curves of various exchangers for Na^+ ions. ○: System (1) ([Sn]=0.28 M, pH=3.8), □: system (4) ([Sn]=0.19 M, pH=3.0), △: system (5) ([Sn]=0.23 M, pH=3.1), ●: system (7) ([Sn]=0.26 M, pH=3.5), ▲: system (8) ([Sn]=0.26 M, pH=3.1), ( ) shows the conditions for precipitation.

area of this region. Table 1 reveals that the (1) and (5) systems have A regions relatively large compared with other systems. The (1) system, however, has a defect in that it must be washed nearly three times as much as other systems before any impurities are removed. This makes the whole procedure unduly long. On the other hand, the area of Region A is small in the (2) and (4) systems due to the peptization of the precipitate; in the latter system, the concentration of tin is limited to the rather low value of 0.3 M since the peptization increases its prominence with an increase in the concentration. In the (6) system, Region A is found only in a concentration less than 0.1 M. Region A does not exist in the (3) system.

Ion-exchange Properties. The titration curves for the exchangers prepared from the systems from (1) through (5) are shown in Fig. 3. This indicates that no variations in the titration curves are observed between different systems and that the exchangers have at least two dissociable hydrogen atoms, since the inflection points exist in the curves at pH 7.5—8.0. Figure 4 shows the uptake curves for sodium ions as a function of the pH. These curves correspond to those in Fig. 3 except in the extremely high pH region, where the specific ion-exchange capacity decreases with the pH. This observation is attributable to the dissolution of a part of the exchanger, which was verified by analyzing the amount of tin dissolved in the supernatant solution; about 8 wt% of the exchanger was dissolved at pH 12.3. Figure 4 also shows that the exchanger possesses the maximum cation-exchange capacity of 1.17—1.25 mmol Na^+/g.

The anion-exchange property is not clearly observed in the titration curves. The uptake curves for chloride ions (Fig. 5), however, do indicate anion exchanges

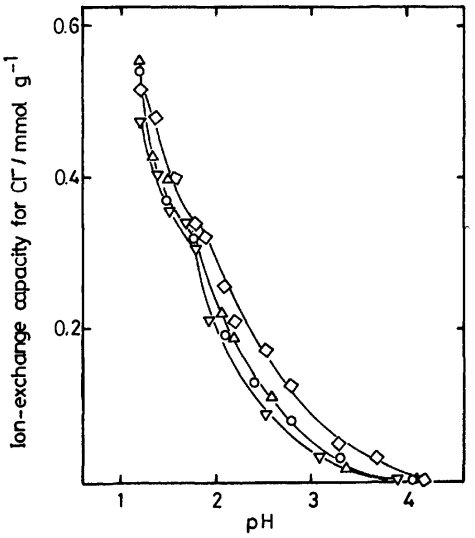

Fig. 5. Uptake curves of various exchangers for Cl^- ions. ○: System (1) ([Sn]=0.28 M, pH=3.8), △: system (5) ([Sn]=0.23 M, pH=3.1), ▽: system (8) ([Sn]=0.26 M, pH=3.1), ◇: system (6) ([Sn]=0.048 M, pH=1.2), ( ) shows the conditions for precipitation.

which occurs in two steps, an inflection point being at about 0.3 mmol Cl^-/g. The anion-exchange capacity is 0.56—0.60 mmol Cl^-/g at pH 1.2.

Sharygin[7] and Jaffrezic-Renault[8,9] reported the multiple cation-exchange behavior. They observed a maximum cation-exchange capacity similar to ours, but two inflection points in the titration curves showing three cation-exchange stages. On the other hand, anion-exchange capacity, 0.3—0.7 mmol/g, for the chloride ion in the vicinity of pH 1 was reported, but the multiple steps were not observed for anion exchange.[2,3,5,9] The reason for the contradiction between the published data and the present results is not clear, but it may be the difference in the details of the experimental procedure. In any event, this material is an amphoteric ion-exchanger possessing at least two weakly dissociable ion-exchange sites. The isoelectric point exists close to pH 4, as can be seen from Figs. 4 and 5. Hereafter, we will concentrate our discussion mainly on the cation-exchange properties because of the large ion-exchange capacity and the convenience of experimentation. For convenience, the cation exchange in the pH region lower than the inflection point will be referred as the first stage, and that in the higher pH region, as the second stage.

The uptake curves of the exchangers prepared from the (7) and (8) systems are shown in Fig. 4, which indicates that the boiling does not affect the first stage, but diminishes the ion-exchange capacity of the second stage by a total amount of 0.15 mmol/g. These findings suggest that the weak dissociable exchange sites are liable to be destroyed by aging. In these exchangers, the degree of the decrease in the ion-exchange capacity in the highly alkaline region becomes small, probably because of the stabilization of the exchanger against alkaline solutions; actually, all kinds of exchangers were dissolved only as much as 2 wt% at pH 12.5. It is, therefore, considered that the stabilization by aging is accompanied by the degradation of some of the weakly acidic sites. It is concluded that the hydrolysis by neutralization, with the exception of the decrease in the cation-exchange capacity by aging, leads to the exchangers having essentially the same ion-exchange characteristics regardless of the systems employed. The (1) and (5) systems being thus found to be most promising on account of the ease with which the precipitating conditions can be set up, efforts were then concentrated on elecidating the relation between the synthetic conditions (the effect of pH and the concentration of tin) and exchange properties with these systems in detail.

Table 2. The effect of pH at precipitation on ion-exchange capacity and water content (system (5))

Synthetic conditions Molar ratio $[NH_3aq]$	$[Sn]^{-1}$	$pH^{a)}$	Composition mol H_2O / mol SnO_2	Ion-exchange capacity for Na^+ pH	mmol g^{-1}
3.7	1.2		2.01±0.02	7.6	0.56
				11.6	1.22
4.0	2.6		2.23±0.01	7.5	0.57
				11.6	1.24
4.0[b)]	2.6		2.19±0.01	7.6	0.64
				11.8	1.19
4.4	4.7		2.30±0.01	7.6	0.62
				11.6	1.25
4.7	7.7		2.29±0.02	7.8	0.80
				11.6	1.39
4.7[b)]	7.4		2.09±0.02	7.7	0.71
				11.7	1.30
7.0	9.4		2.33±0.01	8.0	0.82
				11.6	1.34

a) pH at precipitation. b) Washed.

The effect of the pH at precipitation was examined for the (1) and (5) systems. For the (1) system, this effect was not observed to any appreciable extent on the titration-and uptake curves. The effect of the pH was, however, observed for the (5) system. The experiments carried out to examine this effect are presented in Table 2. The uptake curves are shown in Fig. 6, which reveals nearly the same curves for all the exchangers precipitated at pH values lower than 2.6. For those precipitated at a pH higher than 2.6, however, the ion-exchange capacity increases with the pH at the precipitation. Table 2 also shows the interesting fact that the water content of the exchanger increases with the pH at the precipitation. In order to examine the aging effect of washing, the uptake curves of the (5) system were compared for samples with or without washing. It is revealed from this comparison that the washing results in a slight lowering of the ion-exchange capacity in the region of high pH values. As is shown in Table 2, the water content also decreases by washing.

The effect of the concentration of tin in the mixed solution was then studied at the conditions shown in Table 3. The concentration of tin did not appreciably affect the titration curves, but it did influence the

TABLE 3. THE EFFECT OF TIN CONCENTRATION ON THE PHYSICAL PROPERTIES (SYSTEM (1))

Synthetic conditions			Physical properties						
Sn^{4+} concn	Molar ratio	pH[a]	Glassy luster	Distribution of particle size (mesh)/wt%[b]					Density of H^+ form
M	$[H_2SO_4][Sn]^{-1}$			−65	65—100	100—200	200—350	350—	g cm^{-3}
0.10	1.0	3.8	o	98	1.0	0.8	0.1	0.1	3.23±0.06
0.28	1.0	3.8	o	98	1.0	0.5	0.3	0.2	3.31±0.06
0.53	1.0	3.8	x	85	6.5	4.5	1.8	2.2	3.06±0.06

a) pH at precipitation. b) The distribution of grain size when the air-dried materials were immersed in water.

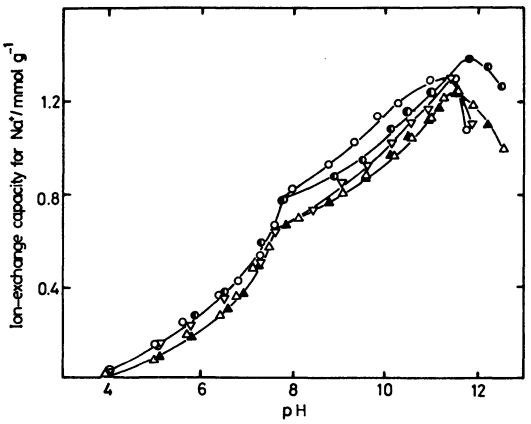

Fig. 6. Effect of pH at precipitation on the uptake curves of the system (5) exchanger for Na^+ ions.
pH at precipitation; ▲: 1.2, △: 2.6, ▽: 4.7, ◐: 7.8, ○: 9.4.

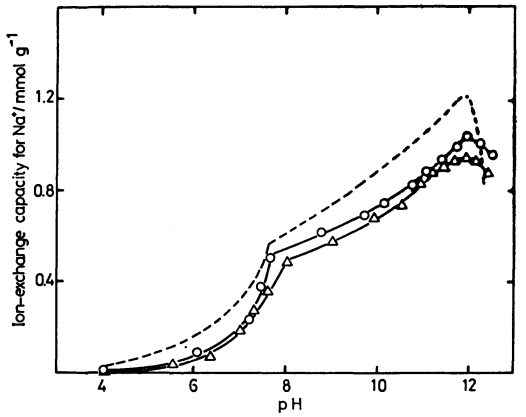

Fig. 7. Uptake curves of the system (6) exchanger for Na^+ ions.
○: Boiled for 1 h, △: Boiled for 5 h, ----: system (5).

physical properties; the exchangers precipitated from the solution of a high concentration of tin (0.53 M), possess no glassy luster and a low density (3.06±0.06 g/cm^3), in contrast with those precipitated from the dilute solution of tin, which have densities of 3.26—3.31 (g/cm^3) and a large, glassy grain. Table 3 shows an example of the size distribution of the exchanger before grinding in a porcelain mortar. It is evident from this table that the distribution of particle size extends to a smaller range with materials obtained from a tin solution of a higher concentration. Similar results were obtained for other systems. Thus, the concentration of tin at the precipitation affects the physical properties, but not the ion exchange.

Figure 7 shows the uptake curves of the exchangers prepared by hydrolyzing a 4.8×10^{-2} M $SnCl_4$ solution by boiling for one or five hours with refluxing (the (6) system). The ion-exchange capacities of these materials are smaller than those of others by 0.05—0.1 mmol/g at the first stage and 0.2—0.3 mmol/g at the second stage. Hence, the numbers of exchange sites of this exchanger are small throughout the pH range examined as compared with those precipitated by neutralization. As the drop of the ion-exchange capacity at pH values higher than 11 is slight, the stability against an alkaline solution appears to be improved to some extent. Actually, the amount of the exchanger dissolved in the solution with a pH of 12.8 was only 1 wt%. The smaller ion-exchange capacity at the first stage in addition to the second suggests the formation of an exchanger with distinctive characteristics.

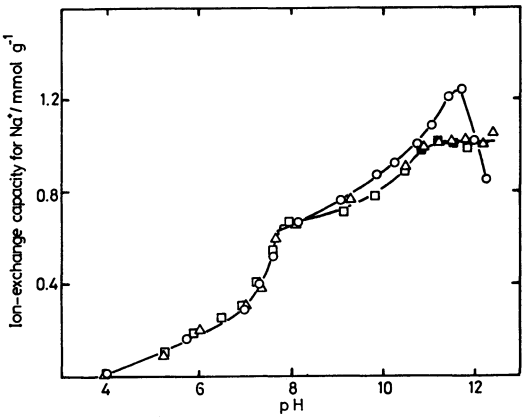

Fig. 8. Effect of storage time on the uptake curves of the system (1) exchanger for Na^+ ions.
○: Immediately after the synthesis, ([Sn]=0.53 M), △: 430 d after the synthesis, ([Sn]=0.28 M), □: 450 d after the synthesis, ([Sn]=0.43 M).

Stability in Air. Inoue and Yamazaki reported that the hydrous titanium(IV) oxide in the H^+ form lost its cation-exchange capacity appreciably during storage in air.[12] As the exchanger in the present study is the same type of compound as hydrous titanium(IV) oxide and is subjected to some aging effect by boiling with the mother solution, the ion-exchange capacity is expected to decrease during storage. Figure 8 shows the results for the materials prepared from the (1) system, which was stored over a saturated NH_4Cl solution. The ion-exchange capacity decreased by 0.1—0.2 mmol/g in the second stage 15 months after the prepara-

TABLE 4. SUMMARY OF SYNTHESIS

System[a]	Synthetic conditions		Composition of H^+ form			Density	Acidity[d]	Ion-exchange capacity for Na^+ ion	
	Sn^{4+} concn[b]	pH[c]	Na^+	Cl^- or SO_4^{2-}	H_2O (mol)			pH	
	M		wt%	wt%	SnO_2 (mol)	g cm^{-1}			mmol g^{-1}
(1)	0.10	3.8	1.2×10^{-2}	L.D.[g]	—	—	3.97	11.5	1.14±0.03
(1)	0.28	3.8	L.D.	—	2.43±0.01	3.23±0.07	4.00	11.1	1.10±0.02
(1)	0.53	3.7	1.3×10^{-2}	L.D.	2.41±0.01	3.06±0.06	4.00	11.5	1.24±0.03
(2)	0.10	3.5	L.D.	L.D.	2.29±0.02	3.31±0.06	4.00	10.6	1.02±0.02
(3)	0.10	4.6	—	—	1.97±0.02	—	4.08	10.9	0.96±0.02
(4)	0.19	3.0	2.2×10^{-2}	—	2.12±0.02	—	4.07	11.6	1.25±0.02
(5)	0.23	3.1	—	4.7×10^{-2}	2.18±0.02	3.36±0.06	4.03	11.3	1.18±0.02
(6)[e]	0.048	1.2	—	L.D.	1.94±0.02	—	4.11	11.7	0.99±0.02
(6)[f]	0.048	1.2	—	2.7×10^{-2}	1.93±0.02	3.53±0.06	4.13	11.9	0.92±0.02
(7)	0.26	3.5	L.D.	—	1.94±0.02	3.58±0.07	3.90	11.8	1.08±0.02
(8)	0.26	3.1	—	—	1.90±0.02	3.61±0.06	3.94	11.6	1.01±0.02

a) The numbers are the same as those in Fig. 1. b) The concentration in the mixed solution. c) pH at precipitation. d) The equilibrium pH of the supernatant solution when the exchangers are immersed in 0.1 M NaCl. e) Boiled for 1 h. f) Boiled for 5 h. g) Limit of detection, SO_4^{2-}: 5×10^{-3} wt%, Cl^-: 1.5×10^{-2} wt%, Na^+: 1×10^{-2} wt%.

tion. This aging effect is similar to that by boiling, but it is not as abrupt as in hydrous titanium(IV) oxide. The result is compatible with Fuller's observation that the capacity for Cu(II) decreased by 0.18 mmol/g after 200 d of preparation.[5]

Composition and Other Properties. The purity, water content, density, and acidity (the equilibrium pH of the supernatant solution when the exchangers are immersed in 0.1 M NaCl) were measured. The results are summarized in Table 4, along with the ion-exchange capacity for Na^+ ions at pH 11. The amount of impurities was below or near the limit of detection.

As to the water content, a variety of papers have been published. According to Donaldson and Fuller, 17% of the water was contained in the exchanger prepared by a method similar to that used in our (1) system.[5] Sautereau *et al.* reported that the composition of α-stannic acid, prepared by a method similar to that used in (5) system, was $SnO_2\cdot1.78H_2O$.[13] Durand and Masdupuy obtained an exchanger whose composition was $H_2[Sn(OH)_6]$ by adding aqueous ammonia to a solution of $SnCl_4$ to make pH 5—6.[14] Abe and Ito obtained the composition of $SnO_2\cdot1.8H_2O$ for α-stannic acid.[3] Mikhail *et al.* obtained an exchanger whose composition was $SnO_2\cdot1.66H_2O$.[15] Goodman and Gregg prepared hydrous tin(IV) oxide with the composition of $SnO_2\cdot1.0$—$1.3H_2O$ by hydrolyzing tin(IV) ethoxide and by drying the precipitate at 25 °C.[16] Weiser and Milligan regarded the stannic acid as a hydration product of tin(IV) oxide rather than of tin(IV) hydroxide.[17] Based on this view, it is considered that the water content of the exchanger changes continuously with aging. Thiessen and Koerner reported a variety of compositions for hydrous tin(IV) oxide, that is, $2SnO_2\cdot5H_2O$, $SnO_2\cdot2H_2O$, $4SnO_2\cdot7H_2O$, and $SnO_2\cdot H_2O$.[18] As has been pointed out above, there exist discrepancies in water content between the results reported by different authors, even when the exchangers were prepared by substantially the same method. The reason for this may be the difference in the details of the conditions for precipitating and drying the precipitate. When we look over Table 4, we find the compositions of the exchangers in the vicinity of $SnO_2\cdot2H_2O$, although the exchangers prepared by neutralizing $Na_2[Sn(OH)_6]$ by acids contained a little more water. Furthermore, the exchangers containing a larger amount of water tend to have higher ion-exchange capacities.

From the values of acidity listed in Table 4, it can be deduced that the exchange sites of the first stage are more basic for the exchanger prepared by pyrohydrolysis than for that aged by boiling.

The density (3.23—3.40 g cm^{-3}) was nearly the same, irrespective of the method of precipitation, although the exchangers precipitated from the concentrated solution of tin had small densities and the densification occurred by heating. The fact that the water content decreases with the density suggests the extrusion of water by the densification.

Recommended Procedure. Since the ion-exchange behavior is not so much affected by the conditions of preparation, the simplicity and the rapidity of the procedure are a matter of utmost concern in choosing the best conditions for the preparation. Thus, the (1) and (5) systems are most appropriate. If we compare these two systems, the first is inferior to the second in that washing is very lengthy, while superior in that the starting materials are less expensive. The selection, therefore, should be made based on the judgment of which is more significant, the time or the cost spent in preparing the material.

References

1) Y. Inoue and M. Tsuji, *J. Nucl. Sci. Technol.*, **13**, 85 (1976); *Bull. Chem. Soc. Jpn.*, **49**, 111 (1976).

2) K. A. Kraus, H. O. Philips, T. A. Carlson, and J. S. Johnson, *Prog. Int. Conf. on Peaceful Use of Atomic Energy*, **28**, 3 (1958).

3) M. Abe and T. Ito, *Nippon Kagaku Zasshi*, **86**, 1259 (1965).

4) E. Merz, *Z. Electrochem.*, **63**, 288 (1959).

5) J. D. Donaldson and M. J. Fuller, *J. Inorg. Nucl. Chem.*,

30, 1083, 2841 (1968); **32**, 1703 (1970).
6) P. C. Ho, F. Nelson, and K. A. Kraus, *J. Chromatogr.*, **147**, 263 (1978).
7) L. M. Sharygin, *Radiokhimiya*, **20**, 414 (1979).
8) N. Jaffrezic-Renault, *J. Inorg. Nucl. Chem.*, **40**, 539 (1978).
9) N. Jaffrezic-Renault, *Radiochem. Radioanal. Lett.*, **37**, 257 (1979).
10) R. L. Williams and R. J. Pace, *J. Chem. Soc.*, **1957**, 4143.
11) M. Ishibashi, T. Shigematsu, Y. Yamamoto, and Y. Inoue, *Bunseki Kagaku*, **7**, 473 (1958).
12) Y. Inoue and H. Yamazaki, *Bull. Chem. Soc. Jpn.*, **53**, 811 (1980).
13) J. Sautereau, M. Baverez, and J. M. Bloch, *Bull. Soc. Chim. Fr.*, **1977**, 207.
14) S. Durand and E. Masdupuy, *Bull. Soc. Chim. Fr.*, **1974** 1844.
15) R. S. Mikhail, S. A. Selim, and F. I. Zeidan, *J. Appl. Chem. Biotechnol.*, **26**, 191 (1976).
16) J. F. Goodman and S. J. Gregg, *J. Chem. Soc.*, **1960**, 1162.
17) H. B. Weiser and W. O. Milligan, *J. Phys. Chem.*, **36**, 3030 (1932).
18) P. A. Thiessen and O. Koerner, *Z. Anorg. Allg. Chem.*, **195**, 83 (1931).

Kinetics of the Ligand Substitution Reactions of Tetrahedral Complexes $[Co(NN)(hmpa)_2]^{2+}$ (NN = 2,2′-Bipyridine, 4,4′-Dimethyl-2,2′-bipyridine, or 1,10-Phenanthroline) in Hexamethylphosphoric Triamide, Nitrobenzene, Acetone, 1,2-Dichloroethane, and Nitromethane

Yuriko ABE* and Goro WADA
Department of Chemistry, Nara Women's University, Nara 630
(Received December 25, 1981)

The substitution reaction rates of hexamethylphosphoric triamide (HMPA) for NN (NN=2,2′-bipyridine (bpy), 4,4′-dimethyl-2,2′-bipyridine (dmbpy), or 1,10-phenanthroline (phen)) on tetrahedral complexes $[Co(NN)(hmpa)_2]^{2+}$ were determined spectrophotometrically in pure HMPA or in nitrobenzene, acetone, 1,2-dichloroethane, and nitromethane at various concentrations of HMPA, for the purpose of clarifying the reaction mechanism and the effect of the bulkiness of HMPA. The ligand substitution reaction on bpy and dmbpy complexes proceeds simply *via* a dissociative mechanism in nitrobenzene. In inert solvents other than nitrobenzene, it proceeds in parallel *via* two simultaneous paths of both dissociative and associative mechanisms. In the case of the phen complex, the reaction proceeds only by a dissociative mechanism in pure HMPA and in all the inert solvents used. The activation enthalpies and the activation entropies of the dissociative mechanism of bpy and dmbpy complexes were (80—90) kJ mol^{-1} and approximately zero J K^{-1} mol^{-1}, respectively, in all the solvents used. Those for the phen complex were (86—101) kJ mol^{-1} and (−16—+36) J K^{-1} mol^{-1}, respectively, while those of the associative mechanism for bpy and dmbpy complexes in all the solvents used except nitrobenzene were (50—65) kJ mol^{-1} and large negative values, respectively. Whether the substitution proceeds by the dissociative mechanism or by the associative one, both the steric and the solvent effects appear seriously, because HMPA is a bulky ligand and had a large dipole moment.

There are few accumulated kinetic data for reactions involving ligand substitution in tetrahedral complexes,[1] although those in octahedral ones[2] have been profoundly investigated. This is probably due to their fast reaction rates in the former complexes caused by the small crystal field stabilization. The measurements were made by NMR,[3–5] temperature jump,[6] *etc.*, and the thermodynamic requirements have severely restricted their studies.

We recently reported that hexamethylphosphoric triamide (HMPA) has a tendency to form complexes of a tetrahedral configuration.[7,8] In this paper, we measured spectrophotometrically the substitution reaction rates of HMPA for NN (NN=2,2′-bipyridine (bpy), 4,4′-dimethyl-2,2′-bipyridine (dmbpy), or 1,10-phenanthroline (phen)) on the tetrahedral complexes $[Co(NN)(hmpa)_2]^{2+}$ in pure HMPA and in nitrobenzene, acetone, 1,2-dichloroethane, and nitromethane at various concentrations of HMPA for the purpose of clarifying the reaction mechanism and the effect of the bulkiness of HMPA on the mechanism. The reaction rates were successfully measured by the conventional technique because, in general, bidentate ligands are exchanged more slowly than unidentate ones. The flexibilities of ligand molecules vary among bpy, dmbpy, and phen. Therefore, when one of those ligands is exchanged with HMPA which is more bulky than the original ligand, the reaction mechanism is strongly affected by the nature of the original ligands. When the reaction proceeds by an associative mechanism, the solvent effect may be stronger than for a dissociative mechanism.

Experimental

Materials. $[Co(hmpa)_4](ClO_4)_2$ and $[Cu(hmpa)_4](ClO_4)_2$ were prepared by methods described in the literature.[9,10] The recrystallizations of $NaClO_4$ and bpy were carried out by procedures we have described previously.[7] Anhydrous phen and dmbpy were used without further purification. The purifications of HMPA and nitromethane were carried out according to our previous description. Nitrobenzene and 1,2-dichloroethane were dried over calcium chloride and molecular sieves 4A, and then distilled under reduced pressure and at atmospheric pressure, respectively. Acetone was dried over calcium sulfate and molecular sieves 4A, and then distilled at atmospheric pressure.

Rate Measurements. The complex $[Co(NN)(hmpa)_2]^{2+}$ was prepared by mixing appropriate amounts of $[Co(hmpa)_4]^{2+}$ and bpy, dmbpy, or phen in HMPA or in one of the inert solvents in advance. The reaction was then initiated by mixing a solution of $[Co(NN)(hmpa)_2]^{2+}$ with a solution of $[Cu(hmpa)_4]^{2+}$ at a concentration in excess of the concentration of $[Co(NN)(hmpa)_2]^{2+}$ in a given solvent. The NN liberated by substitution was removed from the reaction system by its rapid complexation with $[Cu(hmpa)_4]^{2+}$. The reaction rate was followed by observing the increase in the absorbance at 580 nm using a Shimadzu Model UV-200S Spectrophotomer with a thermostated cell compartment. The ionic strength was adjusted at 0.06 mol dm^{-3} with sodium perchlorate or tetraethylammonium perchlorate.

Results and Discussion

Absorption Spectra of $[Co(dmbpy)(hmpa)_2]^{2+}$ and $[Co(phen)(hmpa)_2]^{2+}$ in HMPA and in Inert Solvents. As shown in Fig. 1, the absorption spectra of both $[Co(dmbpy)(hmpa)_2]^{2+}$ in HMPA and $[Co(phen)(hmpa)_2]^{2+}$ in acetone are quite similar to that of $[Co(bpy)(hmpa)_2]^{2+}$ in HMPA, which is already reported to be tetrahedral.[8] Therefore, $[Co(dmbpy)(hmpa)_2]^{2+}$ and $[Co(phen)(hmpa)_2]^{2+}$ in the respective solvents are deduced to be also tetrahedral. In other solvents, the same results were obtained.

Rate Constants of the Substitution Reaction. In any of the solvents used, the reaction obeys Eq. 1 under the

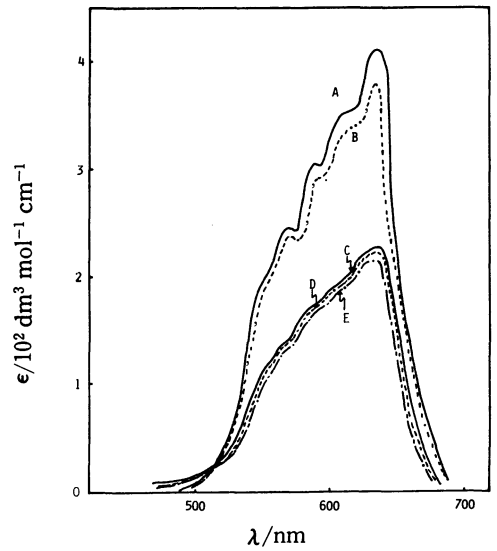

Fig. 1. Absorption spectra of $[Co(hmpa)_4]^{2+}$ in acetone (A: ——) and in HMPA (B: ----), and $[Co(dmbpy)(hmpa)_2]^{2+}$ in HMPA (C: ——), $[Co(phen)(hmpa)_2]^{2+}$ in acetone (D: ----), and $[Co(bpy)(hmpa)_2]^{2+}$ in HMPA (E: -·-·-).

Table 1. The dependence of k_{obsd} on $[Cu(II)]$ at $[[Co(bpy)(hmpa)_2]^{2+}] = 8\times10^{-4}$ mol dm^{-3} in HMPA

$[[Cu(hmpa)_4]^{2+}]$ / 10^{-2} mol dm^{-3}	T / °C	k_{obsd} / 10^{-2} s^{-1}
2.00	16.0	1.58
2.00	16.0	1.35
2.00	20.0	2.30
2.00	20.0	2.70
0.50	25.0	3.39
1.00	25.0	3.90
1.50	25.0	3.30
1.50	25.0	3.27
2.00	25.0	3.93
2.00	25.0	3.21
2.00	25.0	3.29
2.00	25.0	3.10
2.00	25.0	3.10
2.00	29.0	4.43
2.00	29.0	4.43
2.00	29.0	4.55
2.00	34.0	7.02

condition of $[Cu(II)]$ of a large excess over $[Co(II)] = 8\times10^{-4}$ mol dm^{-3},

$$\ln(A_\infty - A_t)/(A_\infty - A_0) = -k_{obsd}t, \quad (1)$$

where A_0, A_t, and A_∞ are the absorbances at 580 nm at times 0, t, and infinity, respectively, and k_{obsd} is the observed first-order rate constant. An example of the linear relationship based on Eq. 1 is shown in Fig. 2. The measured absorbances need not be corrected because the disappearing $[Cu(hmpa)_4]^{2+}$ and the produced Cu(II)–NN complex exhibit an isosbestic point at 580 nm. In all the solvents used, k_{obsd} was independent of $[Cu(II)]$; the experimental results in the case of the bpy complex in HMPA are given in

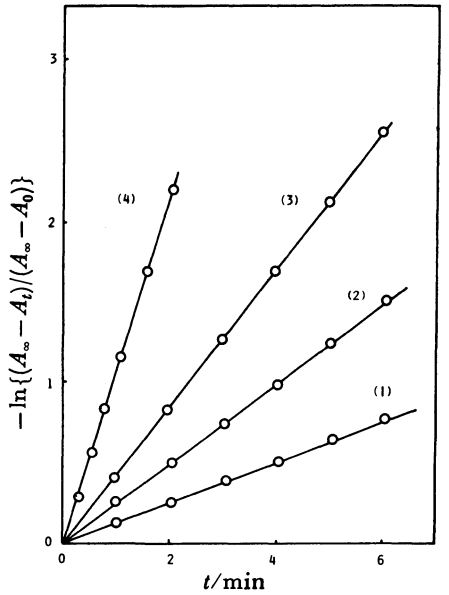

Fig. 2. Plots of $-\ln(A_\infty - A_t)/(A_\infty - A_0)$ *vs.* t at $[Co(II)] = 8\times10^{-4}$ mol dm^{-3} and $[Cu(II)] = 1.0\times10^{-2}$ mol dm^{-3} for the dmbpy complex in HMPA. Temperatures are (1) 15°C, (2) 20°C, (3) 25°C, and (4) 30 °C.

Table 1. Essentially similar data were also obtained in the other solvents. Since the liberated NN reacts rapidly with $[Cu(hmpa)_4]^{2+}$, the following Reaction 2 and the rate equation 3 are deduced.

$$[Co(NN)(hmpa)_2]^{2+} + 2hmpa \xrightarrow{k_{obsd}} [Co(hmpa)_4]^{2+} + NN, \quad (2)$$

$$-\frac{d[[Co(NN)(hmpa)_2]^{2+}]}{dt} = k_{obsd}[[Co(NN)(hmpa)_2]^{2+}]. \quad (3)$$

Dependence of k_{obsd} on the HMPA Concentration and Reaction Mechanism. The dependence of k_{obsd} on the HMPA concentration in the inert solvents can be classified into the following three types as shown in Figs. 3—5.

Type 1): As is shown in Fig. 3, k_{obsd} at first increases with increase in HMPA concentration and then reaches a constant value above a certain concentration of HMPA; this trend is also seen for the bpy and dmbpy complexes in nitrobenzene and for the phen complex in acetone, nitrobenzene, and nitromethane.

Type 2): The value of k_{obsd} is independent of the HMPA concentration in the case of the phen complex in 1,2-dichloroethane as shown in Fig. 4.

Type 3): The correlation of k_{obsd} with the concentration of HMPA can be empirically expressed by the sum of two terms; the zeroth and the first order with respect to the HMPA concentrations.

$$k_{obsd} = k_d + k_a[hmpa] \quad (4)$$

This is seen in the cases for the bpy and dmbpy complexes in acetone, 1,2-dichloroethane, and nitromethane; the examples for the bpy complex are shown in Fig. 5.

Judging from the above features of the reaction, two mechanisms may be considered for the substitution reaction of NN with $[Co(NN)(hmpa)_2]^{2+}$. One is a

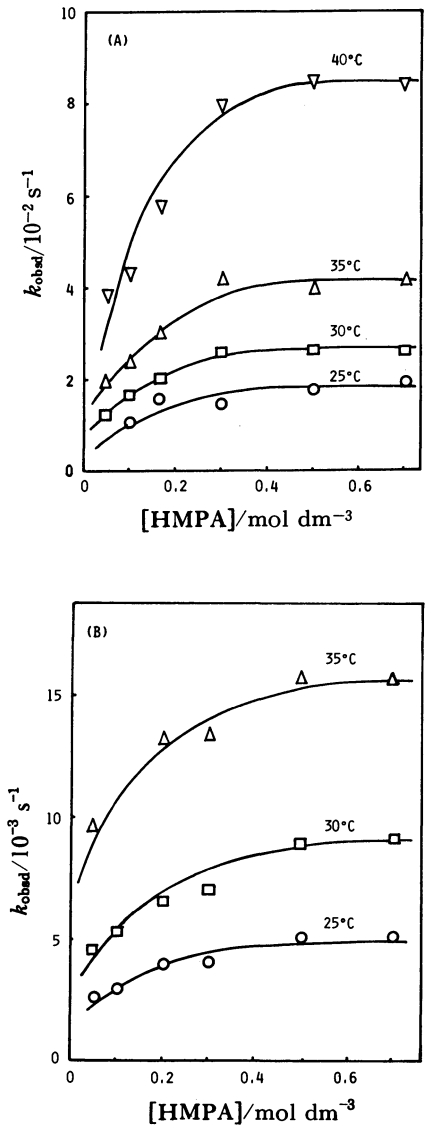

Fig. 3. The dependence of k_{obsd} on the HMPA concentration for the bpy (A) and dmbpy (B) complexes in nitrobenzene at 25 °C (○), 30 °C (□), 35 °C (△), and 40 °C (▽).

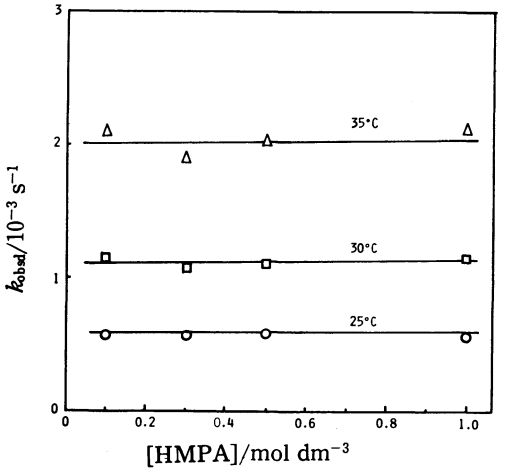

Fig. 4. The dependence of k_{obsd} on the HMPA concentration for the phen complex in 1,2-dichloroethane at 25 °C (○), 30 °C (□), and 35 °C (△).

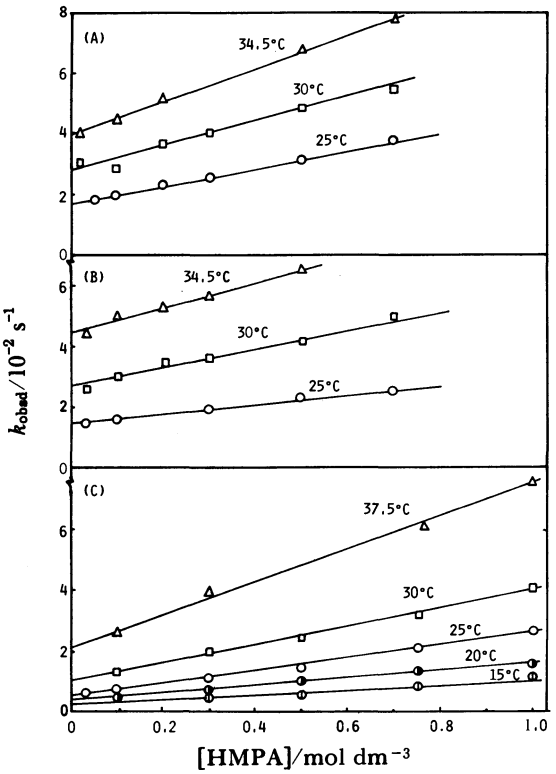

Fig. 5. The dependence of k_{obsd} on the HMPA concentration for the bpy complex in acetone (A), 1,2-dichloroethane (B), and nitromethane (C) at 15 °C (◐), 20 °C (◑), 25 °C (○), 30 °C (□), and 34.5 °C or 37.5 °C (△).

dissociative mechanism, in which one of the two cobalt-nitrogen bonds is first broken, followed by the reaction of the three-coordinated intermediate with an HMPA. The other is an associative mechanism, in which Co(II) first reacts with an HMPA, resulting in a five-coordinated intermediate.

The following reaction scheme may be valid when the substitution reaction proceeds by the dissociative mechanism.

$$[(hmpa)_2Co(\overset{\frown}{N\ N})]^{2+} \underset{k_{-1}}{\overset{k_1}{\rightleftharpoons}} [(hmpa)_2Co\text{-}\overset{\frown}{N\ N}]^{2+} \quad (5)$$

$$[(hmpa)_2Co\text{-}\overset{\frown}{N\ N}]^{2+} + hmpa \underset{k_{-2}}{\overset{k_2}{\rightleftharpoons}} [(hmpa)_3Co\text{-}\overset{\frown}{N\ N}]^{2+} \quad (6)$$

$$[(hmpa)_3Co\text{-}\overset{\frown}{N\ N}]^{2+} + hmpa \xrightarrow{k_3} [(hmpa)_4Co]^{2+} + NN \quad (7)$$

Application of the steady-state method to the unstable intermediates, $[(hmpa)_2Co\text{-}\widehat{NN}]^{2+}$ and $[(hmpa)_3Co\text{-}\widehat{NN}]^{2+}$, leads to Eq. 8.

$$k_{obsd} = \frac{k_1k_2k_3[hmpa]^2}{k_{-1}k_{-2} + k_{-1}k_3[hmpa] + k_2k_3[hmpa]^2} \quad (8)$$

By rearranging Eq. 8, the following equation is derived;

$$\frac{1}{k_{obsd}} = \frac{1}{k_1} + \frac{k_{-1}}{k_1k_2}\frac{1}{[hmpa]} + \frac{k_{-1}k_{-2}}{k_1k_2k_3}\frac{1}{[hmpa]^2}. \quad (9)$$

On the other hand, for the associative mechanism, Reactions 10—12 are considered.

Table 2. Rate constants at 25 °C, $\Delta H^{\ddagger}$ and $\Delta S^{\ddagger}$ of the dissociative mechanism and the associative mechanism for bpy, dmbpy, and phen complexes in HMPA, nitrobenzene, acetone, 1,2-dichloroethane, and nitromethane

Ligand	Solvent	Dissociative mechanism			Associative mechanism		
		$k_d(=k_1)$ / 10^{-3} s^{-1}	$\Delta H_1^{\ddagger}$ / kJ mol^{-1}	$\Delta S_1^{\ddagger}$ / J K^{-1} mol^{-1}	$k_a\left(=\frac{k_4k_5}{k_{-4}+k_5}\right)$ / 10^{-3} dm^3 mol^{-1} s^{-1}	$\Delta H_a^{\ddagger}$ / kJ mol^{-1}	$\Delta S_a^{\ddagger}$ / J K^{-1} mol^{-1}
bpy	HMPA	(14)	(85)	(+7)	(3)	(55)	(−105)
	Nitrobenzene	14.5	89.2	+13.4	—	—	—
	Acetone	13.4	80.8	−9.6	32.1	50.7	−81.6
	1,2-Dichloroethane	13.0	85.8	+8.4	14.3	65.3	−60.7
	Nitromethane	6.0	87.5	+3.8	25.7	61.5	−72.0
dmbpy	HMPA	6.64	89.2	+11.7	—	—	—
	Nitrobenzene	5.53	83.3	−1.7	—	—	—
	Acetone	5.60	84.6	−5.0	10.1	63.2	−71.2
	1,2-Dichloroethane	4.50	85.0	−5.4	7.86	54.0	−103.4
	Nitromethane	2.28	89.2	+2.9	6.57	52.3	−111.3
phen	HMPA	0.680	97.1	+20.5	—	—	—
	Nitrobenzene	0.862	90.4	0.0	—	—	—
	Acetone	0.654	86.7	−16.3	—	—	—
	1,2-Dichloroethane	0.580	96.7	+16.7	—	—	—
	Nitromethane	0.555	100.9	+36.2	—	—	—

$$[(\text{hmpa})_2\text{Co}(\overset{N}{\underset{N}{\frown}})]^{2+} + \text{hmpa} \underset{k_{-4}}{\overset{k_4}{\rightleftharpoons}} [(\text{hmpa})_3\text{Co}(\overset{N}{\underset{N}{\frown}})]^{2+} \quad (10)$$

$$[(\text{hmpa})_3\text{Co}(\overset{N}{\underset{N}{\frown}})]^{2+} \underset{k_{-5}}{\overset{k_5}{\rightleftharpoons}} [(\text{hmpa})_3\text{Co-}\overset{\frown}{\text{N N}}]^{2+} \quad (11)$$

$$[(\text{hmpa})_3\text{Co-}\overset{\frown}{\text{N N}}]^{2+} + \text{hmpa} \xrightarrow{k_6} [(\text{hmpa})_4\text{Co}]^{2+} + \text{NN} \quad (12)$$

Again, by use of the steady-state method for $[(\text{hmpa})_3\text{Co}(\overset{N}{\underset{N}{\frown}})]^{2+}$ and $[(\text{hmpa})_3\text{Co-}\overset{\frown}{\text{NN}}]^{2+}$, k_{obsd} is expressed by the following equation 13.

$$k_{obsd} = \frac{k_4k_5k_6[\text{hmpa}]^2}{k_{-4}k_{-5}+(k_{-4}+k_5)k_6[\text{hmpa}]} \quad (13)$$

By rearranging Eq. 13, Eq. 14 holds;

$$\frac{1}{k_{obsd}} = \frac{k_{-4}+k_5}{k_4k_5}\frac{1}{[\text{hmpa}]} + \frac{k_{-4}k_{-5}}{k_4k_5k_6}\frac{1}{[\text{hmpa}]^2}. \quad (14)$$

If the plots of $1/k_{obsd}$ *vs.* $1/[\text{hmpa}]$ are linear without passing the origin, the reaction may proceed by the dissociative mechanism with the third term on the right-hand side in Eq. 9 negligibly small. Examples are seen in the case of the dmbpy complex in nitrobenzene and the phen complex in acetone of the Type 1 as shown in Fig. 6. Essentially similar data are obtained in other solvents. Therefore, the reaction of Type 1 proceeds by the dissociative mechanism. Accordingly, k_1 and k_{-1}/k_2 can be obtained, respectively, from the intercept and slope of the straight line. These results are summarized, respectively, in Tables 2 and 3.

In the case of Type 2, plotting $1/k_{obsd}$ *vs.* $1/[\text{hmpa}]$ will give a straight line parallel to the abscissa, and therefore this type of the reaction can be deduced to proceed through the dissociative mechanism with k_{-1}/k_2 nearly equal to zero. Thus, k_{obsd} becomes nearly equal to k_1, suggesting that Reaction 5 is the rate-determining step in the dissociative mechanism.

If either the first and the third terms on the right-hand side in Eq. 9 in the dissociative mechanism or the second term on the right-hand side in Eq. 14 in the associative mechanism can be neglected, k_{obsd} will become equal to $(k_1k_2/k_{-1})[\text{hmpa}]$ for the dissociative path or equal to $\{k_4k_5/(k_{-4}+k_5)\}[\text{hmpa}]$ for the associative path, respectively. In the case of Type 3, however, the plots of k_{obsd} *vs.* [hmpa] actually show linearities without passing through the origin as expressed by Eq. 4 (as shown in Fig. 5). Accordingly the reaction can not be simply explanined by either of the two above assumptions. When the reaction of Type 3 is assumed to proceed by both the dissociative and associative mechanisms simultaneously, Eq. 4 can be well explained. The first-order rate constant k_d corresponds to the rate constant k_1 which is independent of the HMPA concentrations as the Type 2. Necessarily, the term of the [HMPA] dependence in Eq. 4 is due to the associative mechanism, where the second term on the right-hand side in Eq. 14 is negligibly small. Therefore, the total rate constant k_{obsd} is given by the sum of the following two terms;

$$k_{obsd} = k_1 + \frac{k_4k_5}{k_{-4}+k_5}[\text{hmpa}] \quad (15)$$

k_d and k_a in Eq. 4 corresponding to k_1 and $k_4k_5/(k_{-4}+k_5)$.

Table 3. The values of k_{-1}/k_2 for bpy, dmbpy, and phen complexes in nitrobenzene, acetone, and nitromethane at 25 °C, 30 °C, and 35 °C

Ligand	Solvent	k_{-1}/k_2 / mol dm^{-3}		
		25 °C	30 °C	35 °C
bpy	Nitrobenzene	0.076	0.067	0.080
dmbpy	Nitrobenzene	0.053	0.049	0.032
phen	Nitrobenzene	0.048	0.081	0.116
	Acetone	0.047	0.052	0.055
	Nitromethane	0.101	0.125	0.096

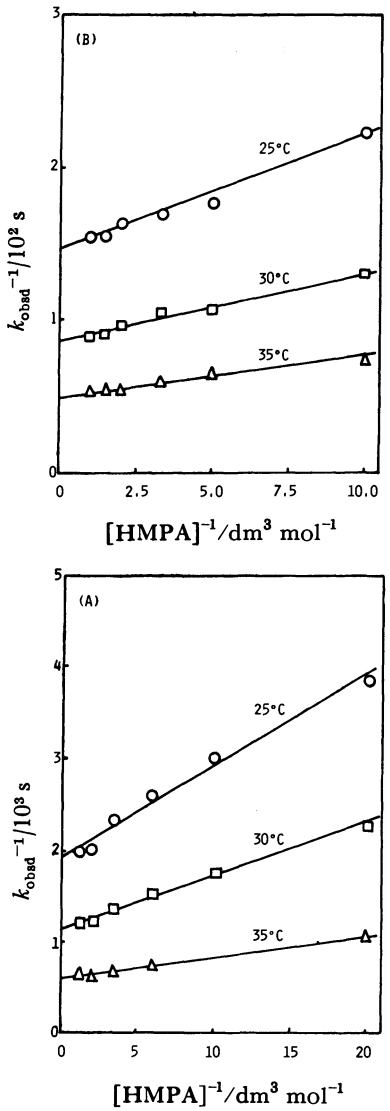

Fig. 6. Plots of k_{obsd}^{-1} *vs.* $[hmpa]^{-1}$ for the dmbpy complex in nitrobenzene (A) and for the phen complex in acetone (B) at 25 °C (○), 30 °C (□), and 35 °C (△).

The values of k_d and k_a in the inert solvents at 25 °C are summarized in Table 2.

Temperature Dependence of k_{obsd} and Activation Parameters. The rates of the substitution reactions were measured at various temperatures, and the values of sets of (ΔH_1^* and ΔS_1^*) and (ΔH_a^* and ΔS_a^*) were obtained by plotting ln k_1 or ln k_a *vs.* $1/T$; these values are summarized in Table 2. In the associative mechanism, the values for ΔH_a^* and ΔS_a^* are only the apparent ones because the apparent rate constant k_a is composed of rate constants of the elementary processes.

General Discussion. Table 2 gives a survey of the two schemes of the reaction through the single path of the dissociative mechanism and the simultaneous paths of the dissociative and associative mechanisms.

Dissociative Mechanism: Some features are found in the values of k_1, ΔH_1^*, and ΔS_1^* for the dissociative mechanism in Table 2; k_1 values are nearly in the ranges $(1.3—1.5)\times10^{-2}\ s^{-1}$ for bpy complex and $(4.5—5.6)\times10^{-3}\ s^{-1}$ for dmbpy complex, respectively, in nitrobenzene, acetone, and 1,2-dichloroethane, and ΔH_1^* and ΔS_1^* values are 80—90 kJ mol^{-1} and approximately zero J K^{-1} mol^{-1} for both bpy and dmbpy complexes in all the solvents used. The constancy of these values would indicate that the inert solvents exhibit little influence on the cleavage of cobalt-nitrogen bonds, and moreover, the fact that ΔS_1^* values are not largely negative would support the occurrence of the three-coordinated intermediates in the course of the dissociative mechanism.

In HMPA, the mechanism of the substitution reaction is difficult to be analyzed because of the existence of the large excess of solvent HMPA. In the case of the dmbpy complex in HMPA, however, since the observed values, $k_{obsd}=6.64\times10^{-3}\ s^{-1}$ at 25 °C, $\Delta H^*=89.2$ kJ mol^{-1} and $\Delta S^*=+11.7$ J K^{-1} mol^{-1}, are very close to those in inert solvents where the reactions proceed by the dissociative mechanism, the reaction of the dmbpy complex in HMPA may proceed also by the dissociative mechanism.

For the phen complex, the values, $k_{obsd}=(6—9)\times10^{-4}\ s^{-1}$ at 25 °C, $\Delta H^*=(86—101)$ kJ mol^{-1}, and $\Delta S^*=(-16—+36)$ J K^{-1} mol^{-1}, are roughly constant, irrespective of the media used. Therefore, it can be concluded that the reaction in all the inert solvents used, as well as in HMPA, proceeds simply by the dissociative mechanism for the same reason as in the case of the dissociative mechanism for the bpy and dmbpy complexes.

If the reactions of Type 1 were hypothesized not to proceed by the dissociative mechanism but by a mechanism involving the formation of an outer-sphere associated complex between Co(II) and HMPA in the solvents used;

$$[Co(NN)(hmpa)_2]^{2+} + hmpa \overset{K_o}{\rightleftharpoons} [Co(NN)(hmpa)_2]^{2+}\cdot hmpa \quad (16)$$

$$[Co(NN)(hmpa)_2]^{2+}\cdot hmpa \xrightarrow{k_i} \text{products}, \quad (17)$$

the rate constant, k_{obsd}, would be expressed by the following equation:

$$k_{obsd} = \frac{k_i K_o[hmpa]}{1+K_o[hmpa]}. \quad (18)$$

Then Eq. 18 is rearranged to give

$$\frac{1}{k_{obsd}} = \frac{1}{k_i} + \frac{1}{k_i K_o}\frac{1}{[hmpa]}. \quad (19)$$

Therefore, k_i and K_o of the outer-sphere association mechanism might apparently correspond to k_1 and k_2/k_{-1} in Eq. 9 of the dissociative mechanism, respectively. If the reaction proceeds truly by the outer-sphere association mechanism, the values of K_o (the reciprocals of k_{-1}/k_2 in Table 3) could be shown to be about 8—31 $dm^3\ mol^{-1}$. The values of K_o for the systems between $[Ni(H_2O)_6]^{2+}$ and HF, NH_3, or C_5H_5N in H_2O have been reported to be 0.15 $dm^3\ mol^{-1}$,[2,11] which is far smaller than 8—31 $dm^3\ mol^{-1}$ for the system between Co(II) and HMPA. Moreover, the ΔS_i^* value is supposed to be negative in process 17 for the associated complex between Co(II) and HMPA. However, the actually observed values of ΔS_i^* are approximately zero against the above supposition. Thus, the reaction of Type 1 is believed more probably to proceed through

the dissociative mechanism than through the outer-sphere association one.

Associative Mechanism: As have been shown in Table 2, the substitution reactions for the bpy and dmbpy complexes in acetone, 1,2-dichloroethane, and nitromethane proceed not only by the dissociative mechanism but also by the associative mechanism simultaneously, the k_a values being in the order: acetone>nitromethane >1,2-dichloroethane for the bpy complex and acetone> 1,2-dichloroethane>nitromethane for the dmbpy complex. In nitrobenzene, on the other hand, the substitution does not occur by the associative mechanism in either complex. The values of $\Delta H_a^* = (50—65)$ kJ mol^{-1} for the associative mechanism are smaller than those about 80—90 kJ mol^{-1} for the dissociative mechanism, and the largely negative values of ΔS_a^* are compared with those of ΔS_1^* of approximately zero as shown in Table 2. This is reasonable for the associative mechanism with largely negative values of ΔS_a^* on account of the occurrence of the five-coordinated intermediates.

In the case of the bpy complex in HMPA, $k_{obsd} = 3.4 \times 10^{-2}$ s^{-1} is larger than k_1 of the dissociative mechanism in inert solvents, and the apparent value of ΔS^*, however, was found to be strongly negative. Therefore, the reaction occurs not only by the dissociative mechanism but also by the associative one. The values of the rate constants at various temperatures, ΔH^*, and ΔS^* for both mechanisms in HMPA were thus obtained from Eq. 4 by using [HMPA]=5.8 mol dm^{-3} and the averaged k_1 values in inert solvents, as shown in Table 2.

Steric Effect: In general, the associative mechanism has been accepted as the mechanism of substitution reactions of tetrahedral complexes.[3] However when a bulky ligand such as HMPA is exchanged, both the associative and dissociative mechanisms are known to occur simultaneously.[5] In the present investigation, the substitution reactions of bpy and dmbpy complexes have been found to proceed only by the dissociative mechanism in nitrobenzene, and by both mechanisms in parallel in inert solvents other than nitrobenzene. On the other hand, in the case of the phen complex, the reaction proceeds only by the dissociative mechanism in all the inert solvents used as well as in HMPA. It seems that this difference may be caused by the difference of the bond flexibility between two pyridine rings in bpy or dmbpy and phen. Since the carbon-carbon bond connecting two pyridine rings in bpy or dmbpy is allowed to rotate fairly freely, the degree of molecular flexibility is large. However, the carbon-carbon bond between two pyridine rings in phen is fixed, and therefore the molecular flexibility of phen should be small. Because the reaction of the associative mechanism proceeds *via* a five-coordinated intermediate which may be much sterically strained due to the bulkiness of HMPA molecules, the two pyridine rings may not become coplanar. Therefore, it is considered that the complexes of bpy and dmbpy with large flexibility are favorable for the associative mechanism. However in the case of the phen complex, the reaction occurs wholly *via* the dissociative mechanism which goes through a three-coordinated intermediate, first cleaving one of the two cobalt-nitrogen bonds to avoid the rigidity of the phen molecule.

Solvent Effect: The fact that the bpy and dmbpy complexes in nitrobenzene undergo ligand exchange only through the dissociative mechanism can not be accounted for simply by the steric hindrance between Co(II) and the bulky HMPA. Fujiwara and his coworkers reported[12] that an associated complex is formed between HMPA and nitrobenzene, both of which have large dipole moments, thus interacting strongly with each other in nonpolar solvents. Therefore, the bpy and dmbpy complexes as well as the phen complex are restricted from undergoing ligand exchange through the associative mechanism but simply allowed to go through the dissociative mechanism, with a three-coordinated intermediate in nitrobenzene. On the basis of the extent of the interaction between HMPA and solvent molecules, the sequence of k_a for the associative mechanism can also be explained. The rate constants, k_a, fall into the sequences: acetone>nitromethane> 1,2-dichloroethane$\gg$nitrobenzene for the bpy complex, and acetone>1,2-dichloroethane>nitromethane$\gg$nitrobenzene for the dmbpy complex; these are almost in the reverse order of the values of their dipole moments, except for 1,2-dichloroethane with a small dielectric constant: acetone (2.9)<nitromethane (3.46)<nitrobenzene (4.21).

Conclusion. It can be concluded that the substitution reaction of bpy and dmbpy complexes proceeds only by the dissociative mechanism in nitrobenzene, and simultaneously by the dissociative and the associative mechanisms in parallel in inert solvents other than nitrobenzene. On the other hand, for the phen complex, the reaction proceeds simply by the dissociative mechanism in pure HMPA and in all the inert solvents used. Whether the substitution reaction proceeds by the dissociative mechanism or by the associative one, both the steric effect and the solvent effect seem to be important since HMPA is a bulky ligand and has a large dipole moment.

References

1) H. Werner, *Angew. Chem., Int. Ed. Engl.*, **7**, 930 (1968).
2) R. G. Wilkins, *Acc. Chem. Res.*, **3**, 408 (1970).
3) W. D. Horrocks, Jr. and L. H. Pignolet, *J. Am. Chem. Soc.*, **88**, 5929 (1966).
4) S. S. Zumdahl and R. S. Drago, *J. Am. Chem. Soc.*, **89**, 4319 (1967).
5) S. S. Zumdahl and R. S. Drago, *Inorg. Chem.*, **7**, 2162 (1968).
6) A. Yamagishi, T. Masui, and F. Watanabe, *Inorg. Chem.*, **20**, 513 (1981).
7) Y. Abe and G. Wada, *Bull. Chem. Soc. Jpn.*, **53**, 3547 (1980).
8) Y. Abe and G. Wada, *Bull. Chem. Soc. Jpn.*, **54**, 3334 (1981).
9) J. T. Donoghue and R. S. Drago, *Inorg. Chem.*, **1**, 866 (1962).
10) J. T. Donoghue and R. S. Drago, *Inorg. Chem.*, **2**, 1158 (1963).
11) D. B. Rorabacher, *Inorg. Chem.*, **5**, 1891 (1966).
12) H. Fujiwara, T. Takaba, Y. Yamazaki, and Y. Sasaki, *J. Chem. Soc., Faraday Trans. 1*, **75**, 79 (1979).

Chemical Effects Due to the (γ, n) Reaction and Isomeric Transition Studied by a Vacuum Sublimation Technique

Tsutomu SEKINE,† Masanobu SAKANOUE, Takashi NAKAMURA, and Kenji YOSHIHARA*,†
Department of Chemistry, Faculty of Science, Kanazawa University 1-1, Marunouchi, Kanazawa 920
†*Department of Chemistry, Faculty of Science, Tohoku University, Aoba, Aramaki, Sendai 980*
(Received March 25, 1982)

Chemical effects of the $^{59}Co(\gamma,n)^{58m,g}Co$ reaction and of the isomeric transition of ^{58m}Co in $Co(acac)_3$, $Co(acac)_2$, and $Co(acac)_2\cdot 2H_2O$ were studied by using a vacuum sublimation technique. In the isomeric transition, highly enriched $^{58g}Co(acac)_2$ was separated from $^{58m}Co(acac)_3$. By the (γ,n) reaction, about a half of the radioactive nuclides produced were found in the form of $Co(acac)_2$ after irradiation of $Co(acac)_3$. The present results were compared with those obtained by other authors.

A vacuum sublimation method has been successfully applied to hot atom chemical study and enrichment of radioactive isotopes in our laboratory.[1-3] It was found that this method was an effective radiochemical separation method for the following reasons. It can separate chemical species of tracer scale in dry environment immediately after irradiation. If the volatile metal organic complex of suitable stability is chosen for the study, sublimation can be made at a moderate temperature under which ordinary inorganic compounds can not sublime. It is well known that β-diketones, such as 2,4-pentanedione (acetylacetone, Hacac), 2,2,6,6-tetramethyl-3,5-heptanedione (dipivaloylmethane, Hdpm or Hthd), form volatile complexes with many metallic elements, and these complexes are available as irradiation targets for hot atom chemical studies.

For neutron-irradiated $Co(acac)_3$, it was found previously that highly enriched $^{60}Co(acac)_2$ was separated from the target by sublimation in an evacuated tube with a temperature gradient.[2] However, detailed studies of chemical effects due to the (γ, n) reaction have not yet been carried out, except for the few papers mentioned below. In order to obtain high specific activity of ^{58}Co, Hoffman tried a hot atom chemical enrichment by using ion exchange separation.[4] Nath studied the change of the retention value of $Co(acac)_3$ in the (n, 2n) reaction.[5] Shoji *et al.* investigated the hot atom chemistry of the tetraphenylporphyrin complex of cobalt due to ^{58m}Co decay, and they found a retention value higher than 75%.[6] Lazzarini and Lazzarini reported the survival probabilities for several cobalt complexes in isomeric transition of ^{58m}Co.[7]

In order to study the hot atom chemistry of the (γ, n) reaction of cobalt, the accumulative effects of the (γ, n) reaction and the isomeric transition of ^{58m}Co must be evaluated. In the present study, these effects were separately analysed. Chemical effects of the (γ, n) reaction and of the isomeric transition of ^{58m}Co were investigated by applying a sublimation method which is specifically useful to separate $Co(acac)_2$ from $Co(acac)_3$.

Experimental

Sample Preparation. Two kind of cobalt complexes, tris-(2,4-pentanedionato)cobalt(III) ($Co(acac)_3$) and diaquabis-(2,4-pentanedionato)cobalt(II) ($Co(acac)_2\cdot 2H_2O$), were synthesized from $CoCl_2\cdot 6H_2O$ and acetylacetone (both were commercially obtained from the Wako Pure Chemical Co. Ltd., Guaranteed) by the previously reported methods.[8,9] The tracer of ^{60}Co was spiked in the synthesis to enable us to estimate the processes of radiation and thermal decomposition. Each complex was purified twice by sublimation.

The sample of $Co(acac)_2\cdot 2H_2O$ transfers to $Co(acac)_2$ in the vacuum sublimation, while the former is obtained by allowing $Co(acac)_2$ to stand in the atmosphere for one day after the sublimation. As for $Co(acac)_2$, which is strongly hydroscopic, the sample was sealed in a plastic package as soon as possible after breaking the vacuum of the sublimation tube so that hydration could be avoided. The chemical form of $Co(acac)_2$ was examined by X-ray diffraction in order to evaluate the effectiveness of sealing. By this examination, it was found that most of the $Co(acac)_2$ remained unchanged for a few days. Therefore, $Co(acac)_2$ used for the target was prepared just before the irradiation with γ-rays.

Irradiation. Irradiation with bremsstrahlung (maximum energy: 60 MeV) was carried out by an electron linear accelerator of the Laboratory of Nuclear Science, Tohoku University. A platinum converter was used to obtain bremsstrahlung from electrons; unconverted electrons were removed by a sweep magnet, and the targets were cooled by Dry Ice during an irradiation period of about seven hours.

Radioactivity Measurement. Radioactivity was measured with a 4K γ-ray spectrometer equipped with a Ge(Li) detector of 80 cm^3. Determenation of ^{58g}Co can be made by measuring its γ-ray of 810 keV. Owing to the very low energy of this γ-ray and to its large internal conversion coefficient ($\approx$2000), ^{58m}Co was determined indirectly from the growth curve of ^{58g}Co, which allowed analysis of ^{58m}Co decay.

Sublimation System. The sublimation system used in this experiment is shown in Fig. 1. Though the electric furnace (Type 1) in the figure was designed to have little temperature gradient inside, a steep temperature gradient outside the furnace was effective to separate $Co(acac)_3$ from $Co(acac)_2$, which was more volatile than the former complex. This type of furnace was found useful in purification of the cobalt complexes. Another electric furnace (Type 2) used in this study has a temperature gradient inside; it can effectively

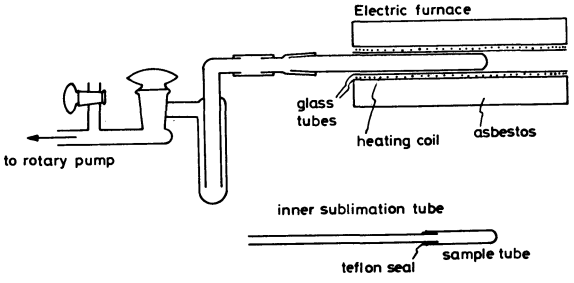

Fig. 1. Sublimation system.

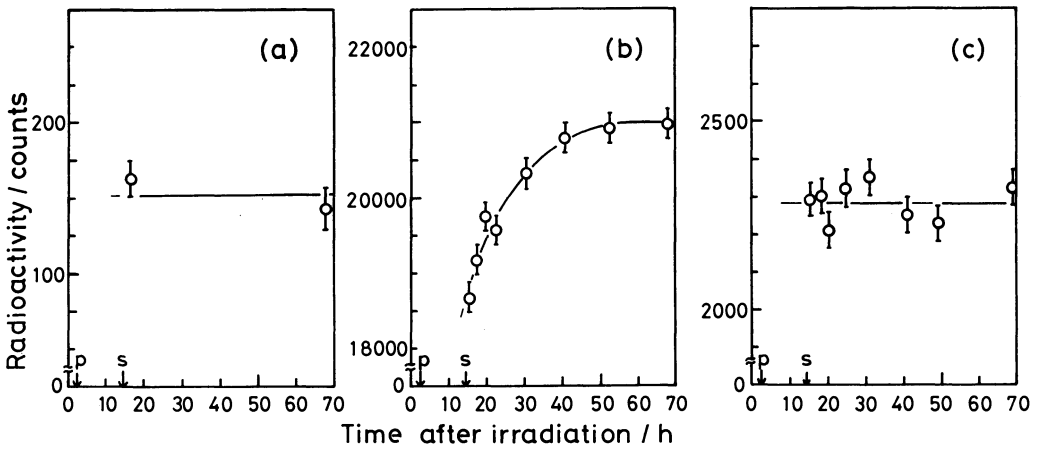

Fig. 2. Radioactivity change with time for each fraction separated by sublimation.
a): Residue, b) $Co(acac)_3$ fraction, c) $Co(acac)_2$ fraction; P and S denote the time when purification is over, and that when resublimation is over, respectively.

separate various volatile chelate compounds.[3] The temperature for sublimation was set at 170 °C. Beyond this temperature $Co(acac)_3$ would be decomposed to $Co(acac)_2$ in a considerably higher rate and, on the other hand, below this temperature a much longer time would be needed to sublime the sample completely. At 170 °C, sublimation started at about five minutes after inserting the sample tube under the vacuum of about 0.13 Pa. Almost complete sublimation finished after about fifteen minutes.

Results and Discussion

Isomeric Transition Effect of ^{58m}Co Decay. One of the difficulties in investigating the isomeric transition effects due to ^{58m}Co decay is to prepare the complexes labeled with ^{58m}Co and to purify them in a very short time. However, we have solved this problem by sublimatographic separation of the irradiated cobalt complexes using an electric furnace of Type 1. This procedure can be performed easily. Examination of chemical properties by alumina column chromatography using chloroform as a solvent, or by thin layer chromatography using benzene-ether (50/50) guaranteed the chemical identity and purity of each complex.[10]

The complex $Co(acac)_3$ labeled with ^{58m}Co was stored in a small glass tube under Dry Ice cooling. Its portions were taken as samples for sublimation from time to time. Concentrated hydrochloric acid was added to three different fractions separated by sublimation, and their radioactivity was measured at appropriate time intervals. As an example, the results of radioactivity measurements are shown in Fig. 2. Only the radioactivity of the $Co(acac)_3$ fraction increased. Whereas the radioactivities for the residue and the $Co(acac)_2$ fractions showed no change with time. Almost all the radioactivity of ^{60}Co which was spiked before irradiation was detected in the $Co(acac)_3$ fraction. From these results, ^{58g}Co radioactivities detected in the residue and also in the $Co(acac)_2$ fraction could be ascribed to the decay product of ^{58m}Co during the storage. Calculation of the retention value can be done as schematically shown in Fig. 3. When the m/g ratio of ^{58m}Co to ^{58g}Co at $t=0$ is expressed as A_{m0}/A_{g0}, the total radioactivity of

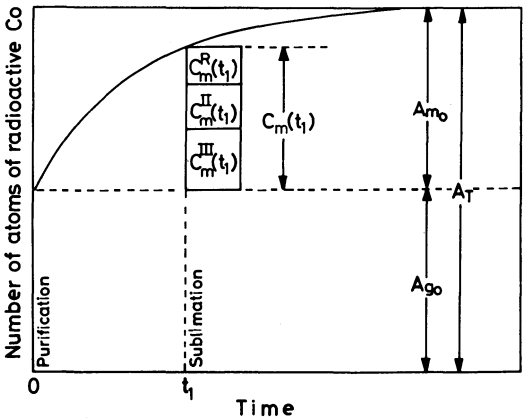

Fig. 3. Relationship between the number of atoms and time in the study of ^{58m}Co decay effect.

^{58}Co after a cooling time which is long enough to allow ^{58m}Co to decay out is $A_T(=A_{m0}+A_{g0})$. And the disintegrating amount of ^{58m}Co from $t=0$ to $t=t_1(C_m(t_1))$ can be calculated from the same growth curve.

$$C_m(t_1) = A_{m0}(1-e^{-\lambda_m t_1}) = A_T(1-f)(1-e^{-\lambda_m t_1}), \quad (1)$$

where $f=A_{g0}/A_T$. Then the retention value (R) is obtained by the following equation:

$$R(\%) = \frac{C_m^{III}(t_1)}{C_m(t_1)} \times 100 = \left\{1 - \frac{C_m^R(t_1)+C_m^{II}(t_1)}{A_T(1-f)(1-e^{-\lambda_m t_1})}\right\} \times 100, \quad (2)$$

where $C_m^{III}(t_1)$, $C_m^{II}(t_1)$, and $C_m^R(t_1)$ are radioactivities of the decayed components in $Co(acac)_3$ and $Co(acac)_2$ and of the residue at $t=t_1$, respectively. The retention values obtained from these analyses are plotted against storage times in Fig. 4. This result shows that some annealing effect during storage can not be avoided even under Dry Ice cooling; a constant value of about 60% was obtained after ten days. The increase in the retention value with storage time was balanced by the decrease in the yield of $^{58g}Co(acac)_2$. In a study of ^{58m}Co decay effects by using a wet separation method, Lazzarini

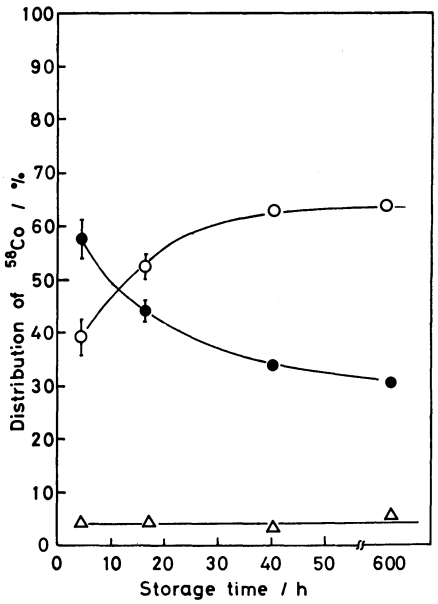

Fig. 4. Change of distribution of ^{58}Co with storage time.
○: Fraction of $Co(acac)_3$, ●: fraction of $Co(acac)_2$, △: residue.

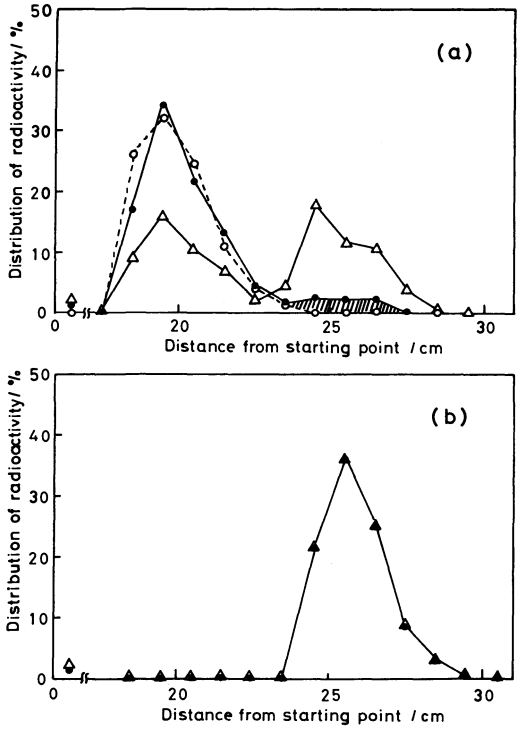

Fig. 5. Distribution of radioacrivity along sublimation tube.
(a): Irradiated $Co(acac)_3$, (b): irradiated $Co(acac)_2$–$2H_2O$. ○: ^{60}Co sublimation before irradiation, ●: ^{60}Co sublimation after irradiation, △: ^{58}Co.

and Lazzarini reported 47.9% of the daughter nuclides remained in the chemical form of the parent, and 47.2% were found in the Co^{2+} ion fraction.[7] The $Co(acac)_3$ retention in our experiments is slightly below 40% at an earlier stage and then gradually increases up to 60%. It is very interesting to see that there is an agreement between our values and Lazzarini's, although they gave the percentage of Co^{2+} instead of the $Co(acac)_2$ reported in our experiments. These facts show that annealing during sublimation in the present study *per se* does not contribute much to the overall results. The presence of $Co(acac)_2$ in a large amount is a rather striking finding, and this was made possible by the application of sublimatographic procedures in this study. However, the detailed mechanism of formation of $Co(acac)_2$ is not so simple.

Though the increase of the retention values with storage time is not yet explained very clearly, some possibilities can be considered. One is a charge transfer reaction between Co^{2+} and surrounding molecules, which Kalliat and Nath suggested.[11] Another explanation is the existence of a reaction which proceeds with very low activation energy even under Dry Ice temperature, although this would be unusual. The last explanation, which seems to be more plausible than the earlier ones, is an electrostatic interaction between recoils and their partners or surrounding matrices. This does not require much thermal agitation. This type of interaction is found in some cases involving positively charged species after nuclear decay and negatively charged oxygen impurities; detailed features of this mechanism will appear in forthcoming papers.[12]

The most significant result in this experiment is that a considerable amount of ^{58g}Co was found as the chemical form of $Co(acac)_2$. This fraction seems to correspond to the fraction analysed by Lazzarini and Lazzarini as the fraction of Co^{2+} ion which corresponds to the "complete fragmentation" in the decay event. It is known that radioactive atoms produced by nuclear reactions form a considerable amount of ligand-deficient species.[13] Tominaga and Saito pointed out the possibility of the presence of ligand-deficient complexes of the types $Co(acac)_{3-n}^{n+}$.[14] If $n=1$ is assumed, $Co(acac)_2$ and $Co(acac)_2^+$ are present in the solid: the former is observed in our experiment and the latter may be sensitive to annealing reactions. Therefore, it is considered that $^{58g}Co(acac)_2$ separated by sublimation has its own chemical form and/or charge state in solids just before separation.

The yield of the residue was almost constantly 3—4%. Although the chemical components of the residue are not clear, the residual amount of ^{58g}Co radioactivity agreed with that which Lazzarini and Lazzarini denoted as partial fragmentation.

A similar experiment was carried out for the $Co(acac)_2$ complex. Highly enriched $^{58g}Co(acac)_3$ was not obtained; the retention value as $Co(acac)_2$ was 99% and did not vary with storage time. Almost all the ^{60}Co radioactivity was found in the parent complex, and 1% of ^{58g}Co remained in the residue; this result seems to show the extent of decomposition induced by the isomeric transition.

The Chemical Effect by the (γ, n) Reaction. The sublimatographic results obtained by using the electric furnace (Type 2) with temperature gradient are shown in Fig. 5. The dotted line in Fig. 5(a) for $Co(acac)_3$ shows the distribution of ^{60}Co radioactivity obtained by the sublimation before irradiation. Thermal decomposi-

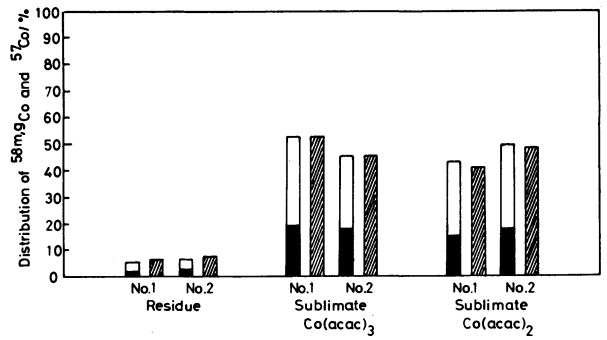

Fig. 6. Distribution of ^{58m,g}Co and ^{57}Co in each fraction. ^{58g}Co: closed area, ^{58m}Co: open area, ^{57}Co: shaded area. Nos. 1 and No. 2 denote experimental number.

tion of $Co(acac)_3$ is almost negligible under these conditions. In the case of sublimation after irradiation, about 4% of total ^{60}Co radioactivity was observed (shaded area) in the form of $Co(acac)_2$. The radioactivity of ^{58}Co was measured after long period during which almost all ^{58m}Co decayed out. A half of ^{58}Co radioactivity was found in the $Co(acac)_2$ fraction.

Figure 6 shows the distribution of ^{58}Co in each fraction separated by sublimation made immediately after the irradiation. This is compared to the distribution of ^{57}Co produced simultaneously by the $(\gamma, 2n)$ reaction. This result shows that the radioactivity of ^{58}Co almost equally distributed in the $Co(acac)_3$ and $Co(acac)_2$ fractions; the same tendency appears for the distribution of ^{57}Co.

The ^{58m}Co/^{58g}Co ratio in each fraction was obtained by the growth curve of each fraction, and is shown in Fig. 7. The residue showed the smallest value, while the $Co(acac)_3$ fraction showed the largest value. This pattern was found to be sufficiently reproducible. Each fraction was considered to consist of three components at the end of irradiation; ^{58g}Co and ^{58m}Co produced directly by (γ, n) reaction (A_g, A_m), and a part of ^{58g}Co produced by the decay from ^{58m}Co during the irradiation ($A_{m\to g}$). A_g, A_m, and $A_{m\to g}$ are represented as follows:

$$A_g = N\phi\sigma_g(1-e^{-\lambda_g t}) \quad (3)$$

$$A_m = N\phi\sigma_m(1-e^{-\lambda_m t}) \quad (4)$$

$$A_{m\to g} = N\phi\sigma_m\left\{(1-e^{-\lambda_g t}) - \frac{\lambda_g}{\lambda_g-\lambda_m}(e^{-\lambda_m t}-e^{-\lambda_g t})\right\}, \quad (5)$$

where ϕ is flux of γ-rays, N is the amount of cobalt atoms in the target, t is irradiation time, λ_g and λ_m are the decay constants of ^{58g}Co and ^{58m}Co, respectively, σ_g and σ_m are the independent reaction cross sections of (γ, n) reactions to produce ^{58g}Co and ^{58m}Co, respectively. $A_{m\to g}$ can be obtained from the Eqs. 3 and 5

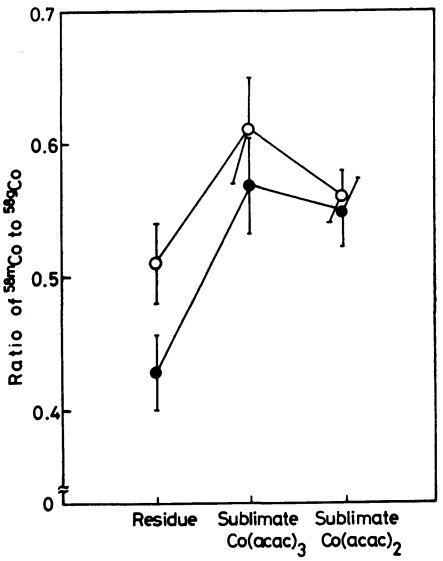

Fig. 7. Ratio of ^{58m}Co to ^{58g}Co in each fraction. ○: Experiment No. 1, ●: Experiment No. 2.

and A_T, which is the total amount of radioactivity of ^{58}Co after long cooling when all the ^{58m}Co atoms have decayed out.

$$A_T = N\phi(\sigma_m+\sigma_g)(1-e^{-\lambda_g t}) \quad (6)$$

From Eqs. 3, 5, and 6,

$$\frac{\sigma_m}{\sigma_g} = \frac{(1-e^{-\lambda_g t})\{A_T-(A_{m\to g}+A_g)\}}{(1-e^{-\lambda_g t})(A_{m\to g}+A_g)-\left\{(1-e^{-\lambda_g t})-\frac{\lambda_g}{\lambda_g-\lambda_m}(e^{-\lambda_m t}-e^{-\lambda_g t})\right\}A_T} \quad (7)$$

Since the ratio of σ_m/σ_g is determined experimentally to be 1.16 ± 0.06, the percent ratio of $A_{m\to g}$ to A_T is given by the equation:

$$\frac{A_{m\to g}}{A_T}\times 100 = \frac{\sigma_m/\sigma_g\left\{(1-e^{-\lambda_g t})-\frac{\lambda_g}{\lambda_g-\lambda_m}(e^{-\lambda_m t}-e^{-\lambda_g t})\right\}}{(\sigma_m/\sigma_g+1)(1-e^{-\lambda_g t})}\times 100 \quad (8)$$

In this case, a value of 11.84 ± 0.75% was obtained for the percent ratio of $A_{m\to g}$ to the total activity A_T. By sublimation each component can be separated into the residue, the $Co(acac)_3$ fraction, and the $Co(acac)_2$ fraction. The proportion of distribution of A_g and $A_{m\to g}$ in each fraction can not be determined directly in this experiment, but the latter can be estimated by assuming that the proportions of initial distribution of A_g in each fraction are equal to that of A_m. This assumption is reasonable, judging from the relationship of the recoil energy-percentage of product found by Yoshihara and Kudo,[15] because similar recoil energies (beyond 1 keV)

TABLE 1. RETENTION VALUE AND ^{58m}Co/^{58g}Co RATIO FOR IRRADIATED $Co(acac)_2$ AND $Co(acac)_2\cdot 2H_2O$ OBTAINED BY SUBLIMATION SEPARATION

		^{58}Co (%)	^{57}Co (%)	^{60}Co (%)	m/g ratio[a)]
$Co(acac)_2$	Sublimate	98.2±0.4	98.0±1.0	98.7±0.1	0.52±0.10
	Residue	1.8±0.1	2.0±0.1	1.3±0.1	0.45±0.07
$Co(acac)_2\cdot 2H_2O$	Subl mate	97.2±0.4	97.3±0.7	97.4±2.0	0.58±0.07
	Residue	2.8±0.1	2.7±0.1	2.6±0.1	0.50±0.06

a) It means a ratio of ^{58m}Co to ^{58g}Co.

of both nuclides will give the same plateau value of the product percentage. This relationship is further justified by the equal product distribution of the (γ, n) and $(\gamma, 2n)$ reactions described before. The distribution of $A_{m\to g}$ in each fraction was calculated to be $9.8\pm1.2\%$ in the residue, $41.9\pm9.8\%$ in the $Co(acac)_3$ fraction, and $48.3\pm6.3\%$ in the $Co(acac)_2$ fraction. The contribution to the residue for $A_{m\to g}$ was larger by about 4.4% than that for A_m. Therefore, it is considered that the two kinds of effects by (γ, n) reaction and isomeric transition have superimposed additively.

A similar study was made for the irradiation of $Co(acac)_2$ and $Co(acac)_2\cdot 2H_2O$, and the results are shown in Table 1. The retention value in $Co(acac)_2\cdot 2H_2O$ was slightly smaller than that in $Co(acac)_2$. This tendency is the same as reported by Yoshihara *et al.* in the case of the (γ, γ') reaction in In·hedta complexes with and without crystalline water.[16] This difference may be attributed to the decrease of back reaction probability by obstruction in the presence of water molecules.

The m/g ratio in the sublimate and the residue did not show the same value as those in the case of $Co(acac)_3$. It is suggested that ^{58g}Co produced by the decay of ^{58m}Co tends to form more nonvolatile species than that produced directly by nuclear reaction.

The authors thank Dr. Masuo Yagi of Tohoku University for his cooperation in performing the irradiation with the electron linear accelerator.

References

1) R. Amano and M. Sakanoue, *Radiochem. Radioanal. Lett.*, **16**, 381 (1974).
2) R. Amano and M. Sakanoue, *Radiochem. Radioanal. Lett.*, **19**, 197 (1974).
3) H. Shimozawa, M. S. Thesis, Kanazawa University, Kanazawa, Japan, 1978.
4) D. C. Hoffman and D. S. Martin, *J. Phys. Chem.*, **56**, 1097 (1952).
5) A. Nath, "Chemical Effects of Nuclear Transformation," Proc. Symp., Vienna, 1965, Vol. 1, p. 335.
6) J. Shoji, Y. Sakai, N. Ikeda, T. Otake, and H. Watanabe *Research Report of Laboratory of Nuclear Science, Tohoku University*, **12**, 219 (1979).
7) E. Lazzarini and F. Lazzarini, *J. Inorg. Nucl. Chem.*, **207**, 39 (1977).
8) *Inorg. Synth.*, **5**, 188 (1957).
9) *Inorg. Synth.*, **11**, 83 (1968).
10) S. Hara, O. Tanaka, and S. Takitani, *Kagaku No Ryoiki*, Special Issue No. 64, Nankodo Co. Ltd., Tokyo, 1963, p. 203.
11) M. Kalliat and A. Nath, *J. Inorg. Nucl. Chem.*, **43**, 271 (1981).
12) T. Sekine and K. Yoshihara, *Radiochem. Radioanal. Lett.*, **52**, 349 (1982); *Radiochim. Acta*, submitted.
13) T. Omori and T. Shiokawa, *Radiochem. Radioanal. Lett.*, **17**, 167 (1974).
14) T. Tominaga and N. Saito, "Hot Atom Chemistry: Status Report," International Atomic Energy Agency, Vienna. (1975), p. 191.
15) K. Yoshihara and H. Kudo, *J. Chem. Phys.*, **52**, 2950 (1970).
16) K. Yoshihara, A. Fujita, and T. Shiokawa, *J. Inorg. Nucl. Chem.*, **39**, 1733 (1977).

Pyrolytic Sulfurization Gas Chromatography. XIII. Simultaneous Determination of the Atomic Ratio between C, H, O, and N in a Metal Organic Chelate Compound

Tadashi HARA,* Kaoru FUJINAGA,† and Fujio OKUI
Department of Chemical Engineering, Faculty of Engineering, Doshisha University
Karasuma Imadegawa, Kamigyo-ku, Kyoto 602
†*Department of Chemistry, Faculty of Science, Shimane University, 1060 Nishikawatsu-cho, Matsue 690*

(Received March 29, 1982)

In order to clarify the effect of the coexistent elements on the determination of the atomic ratio between C, H, O, and N by the pyrolytic sulfurization gas chromatography (PSGC), compounds containing 25 kinds of elements were investigated. Only 7 of these interfered the determination of the atomic ratio. Several organophosphorus, lithium-, and boron-containing compounds were also analyzed. The results obtained by the present work are summarized in the periodic table together with those from previous work.

In order to establish a new organic elemental analysis method by which several elements can be simultaneously determined, the authors have developed pyrolytic sulfurization gas chromatography (PSGC) based on a combustion technique in sulfur vapor instead of the conventional one in an oxygen atmosphere.[1] According to PSGC, the simultaneous determination of the atomic ratio between C, H, O, and N in a sample can be achieved with a usual organic compound,[2] a metal organic chelate compound,[3] a polymer,[4] and an organic halogen compound.[5]

In the field of elemental analysis, research concerning metal organic chelate compounds has not been carried out so much because of the fact that metallic elements show a strong affinity for oxygen and are apt to form oxides and carbonates. However, PSGC method is characterized by conversion of the metal in a compound into sulfide by means of a sulfur combustion technique and by simultaneously determining the atomic ratio between C, H, O, and N in a sample without using a special procedure such as addition of reducing agent. In the previous work,[3] this PSGC method was applied to the analysis of compounds containing 24 elements: Na, K, Mg, Ca, Sr, Ba, La, Ti, U, Cr, Mo, W, Mn, Fe, Co, Ni, Pd, Cu, Ag, Zn, Cd, Hg, Al, and P. But many elements still remain unsolved, so the present study has been carried out with the objective of estimating the atomic ratio between C, H, O, and N in compounds containing 25 metallic elements other than the previously reported ones: Li, Rb, Cs, Be, Ce, Pr, Eu, Th, Zr, Hf, V, Nb, Rh, Pt, Au, B, Ga, In, Tl, Si, Pb, As, Sb, Bi, and Se. Several organophosphorus compounds were also analyzed. The results obtained by the present work are summarized in the periodic table together with those obtained by the previous study. The PSGC method can be successfully applied to the analysis of the compounds containing 39 elements, but not to those containing 10 kinds of elements.

Experimental

Apparatus and Reagents. The reagents and apparatus used were the same as those reported.[2] The peak areas of the gas chromatogram were read out by the use of a Shimadzu digital integrator E1A. A definite amount of metal oxide was taken with a Shimadzu microbalance MDP-5.

Procedure. The preparation and reaction conditions of sample as well as the conditions of gas chromatographic analysis are similar to those reported.

Samples. The following samples were prepared by the methods found in the literature for their gravimetric analyses: bis(2-methyl-8-quinolinolato)beryllium(II), $Be(C_{10}H_8ON)_2$;[6] tetrakis(mandelato)zirconium(IV), $Zr(C_8H_8O_3)_4$;[7] tetrakis(mandelato)hafnium(IV), $Hf(C_8H_8O_3)_4$;[8] tetrakis(8-quinolinolato)hafnium(IV), $Hf(C_9H_6ON)_4$;[9] trioxotetrakis(8-quinolinolato)divanadium(V), $V_2O_3(C_9H_6ON)_4$;[9] oxotris(8-quinolinolato)niobium(V), $NbO(C_9H_6ON)_3$;[10] tris(8-quinolinolato)bismuth(III), $Bi(C_9H_6ON)_3$;[9] tris(8-quinolinolato)antimony(III), $Sb(C_9H_6ON)_3$;[11] tris(thionalidato)antimony(III), $Sb(C_{12}H_{10}ONS)_3$;[12] bis(thionalidato)mercury(II), $Hg(C_{12}H_{10}ONS)_2$;[12] tetrakis(8-quinolinolato)thorium(IV), $Th(C_9H_6ON)_4$;[13] triethanolammonium tetraphenylborate, $(HOH_2CH_2C)_3NHB(C_6H_5)_4$;[14] dibutylammonium tetraphenylborate, $(n\text{-}C_4H_9)_2NH_2B(C_6H_5)_4$;[14] benzylammonium tetraphenylborate, $C_6H_5NH_3B(C_6H_5)_4$;[14] 8-quinolinol-quinolinolium tetraphenylborate, $(C_9H_7ON)_2HB(C_6H_5)_4$;[15] gold(I) 2-mercaptoacetate, $AuSO_2H_3C_2$;[16] (2,2',4,4',6,6'-hexanitrodiphenylaminato)potassium, $KN[C_6H_2(NO_2)_3]_2$;[17] (2,2',4,4',6,6'-hexanitrodiphenylaminato)rubidium, $RbN[C_6H_2(NO_2)_3]_2$;[17] (2,2',4,4',6,6'-hexanitrodiphenylaminato)cesium, $CsN[C_6H_2(NO_2)_3]_2$;[17] tris(2,4-pentanedionato)rhodium(III), $[Rh(C_5H_7O_2)_3]$; bis(*N,N'*-disalicylideneethylenediaminato)cerium(IV), $[Ce(C_{16}H_{14}O_2N_2)_2]$, and bis(2,4-pentanedionato)platinum(II), $[Pt(C_5H_7O_2)_2]$ were prepared by the method found in the literature.[18] Lithium butanoate, lithium hexanoate, lithium octanoate, and lithium decanoate were obtained by allowing lithium hydoxide to react with the corresponding acid and by recrystallizing them repeatedly until the range of the melting point of each sample decreased to less than 1 °C. The other reagents were commercial products and were purified in a way similar to that used for the lithium salts. The composition and purity of the samples were confirmed by the CH and/or CHN analysis carried out in the Elemental Analysis Center of the Pharmaceutical Department of Kyoto University (Table 1). *p*-Aminophenylarsonic acid for elemental analysis, octaphenylcyclotetrasiloxane for atomic absorption spectroscopy, and tris(2,2,6,6-tetramethyl-3,5-heptanedionato)europium(III) and tris(2,2,6,6-tetramethyl-3,5-heptanedionato)praseodymium(III) for NMR spectroscopy were of reagent grade and were used without further purification. The metal oxides were of analytical grade and treated at 950 °C before use.

TABLE 1. ANALYTICAL RESULTS OF CARBON, HYDROGEN, AND NITROGEN IN A METAL ORGANIC CHELATE COMPOUND

Sample	C (wt%)			H (wt%)			N (wt%)		
	Calcd	Found	Error	Calcd	Found	Error	Calcd	Found	Error
Bis(2-methyl-8-quinolinolato)beryllium(II) $Be(C_{10}H_8ON)_2$	73.83	73.99	+0.16	4.96	5.20	+0.24	8.61	8.62	+0.01
Tetrakis(8-quinolinolato)thorium(IV) $Th(C_9H_6ON)_4$	53.47	53.20	−0.27	2.99	3.07	+0.08	6.93	6.83	−0.10
Tetrakis(8-quinolinolato)hafnium(IV) $Hf(C_9H_6ON)_4$	57.26	56.96	−0.30	3.20	2.98	−0.22	7.42	7.40	−0.02
Oxotris(8-quinolinolato)niobium(V) $NbO(C_9H_6ON)_3$	59.90	59.67	−0.23	3.35	3.24	−0.11	7.76	7.71	−0.05
Trioxotetrakis(8-quinolinolato)divanadium(V) $V_2O_3(C_9H_6ON)_4$	59.52	59.82	+0.30	3.33	3.21	−0.12	7.71	7.80	+0.09
Triethanolammonium tetraphenylborate $(HOH_2CH_2C)_3NHB(C_6H_5)_4$	76.92	77.19	+0.27	7.53	7.78	+0.25	2.99	2.97	−0.02
8-Quinolinol-8-quinolinolium tetraphenylborate $(C_9H_7ON)_2HB(C_6H_5)_4$	82.76	82.84	+0.08	5.62	5.80	+0.18	4.59	4.63	+0.04
Dibutylammonium tetraphenylborate $(n\text{-}C_4H_9)_2NH_2B(C_6H_5)_4$	85.51	85.30	−0.21	8.97	8.98	+0.01	3.12	3.14	+0.02
Benzylammonium tetraphenylborate $H_5C_6NH_2HB(C_6H_5)_4$	87.12	87.36	+0.24	7.07	6.96	−0.11	3.28	3.17	−0.11
Piperazinium dihydrogen phosphate monohydrate $C_4H_{10}N_2H_3PO_4 \cdot H_2O$	23.77	23.61	−0.16	7.48	7.60	+0.12	13.86	13.89	+0.03
Benzoguanamine phosphate $C_9H_9N_5 \cdot H_3PO_4$	37.90	37.97	+0.07	4.24	4.32	+0.08	24.56	24.72	+0.16
Benzidine phosphate $C_{12}H_{12}N_2 \cdot H_3PO_4$	51.07	51.03	−0.04	5.36	5.33	−0.03	9.93	10.01	+0.08
Lithium butanoate C_3H_7COOLi	51.09	51.25	+0.16	7.50	7.32	−0.18			
Lithium hexanoate $C_5H_{11}COOLi$	59.03	58.93	−0.10	9.08	8.88	−0.20			
Lithium octanoate $C_7H_{15}COOLi$	64.00	64.16	+0.16	10.07	10.04	−0.03			
Lithium decanoate $C_9H_{19}COOLi$	67.40	67.25	−0.15	10.75	10.88	+0.13			
(2,2′,4,4′,6,6′-Hexanitrodiphenylaminato)-potassium $KN[C_6H_2(NO_2)_3]_2$	30.20	30.34	+0.14	0.84	0.84	0			
(2,2′,4,4′,6,6′-Hexanitrodiphenylaminato)-cesium $CsN[C_6H_2(NO_2)_3]_2$	25.24	25.27	+0.03	0.71	0.64	−0.07			
Bis(*N*,*N*′-disalicylideneethylenediaminato)-cerium(IV) $[Ce(C_{16}H_{14}O_2N_2)_2]$	57.13	57.09	−0.04	4.19	4.43	+0.24			
Tetrakis(mandelato)zirconium(IV) $Zr(C_8H_8O_3)_4$	54.92	54.96	+0.04	4.61	4.76	+0.15			
Tetrakis(mandelato)hafnium(IV) $Hf(C_8H_8O_3)_4$	48.83	48.75	−0.08	4.10	3.70	−0.40			
Tris(2,4-pentanedionato)rhodium(III) $[Rh(C_5H_7O_2)_3]$	45.01	45.28	+0.27	5.29	5.31	+0.02			
Bis(2,4-pentanedionato)platinum(II) $[Pt(C_5H_7O_2)_2]$	30.54	30.47	−0.07	3.59	3.58	−0.01			
Gold(I) 2-mercaptoacetate $HSCH_2COOAu$	8.34	8.50	+0.16	1.05	1.21	+0.16			
Bis(8-quinolineselenolato)cadmium(II) $Cd(C_9H_6SeN)_2$	41.05	41.29	+0.24	2.30	2.54	+0.24			
Tris(8-quinolinolato)indium(III) $In(C_9H_6ON)_3$	59.26	59.18	−0.08	3.32	3.32	0			
Thallium(I) acetate CH_3COOTl	9.12	9.06	−0.06	1.15	1.15	0			
Bis(8-quinolinolato)lead(II) $Pb(C_9H_6ON)_2$	43.63	43.71	+0.08	2.44	2.30	−0.14			
Antimony potassium tartrate $SbOC_4H_4O_6K$	14.79	14.93	+0.14	1.24	1.23	−0.01			
Tris(8-quinolinolato)antimony(III) $Sb(C_9H_6ON)_3$	58.51	58.13	−0.38	3.27	3.46	+0.19			
Tris(8-quinolinolato)bismuth(III) $Bi(C_9H_6ON)_3$	50.56	50.56	0	2.83	3.06	+0.23			
Triphenyl phosphate $(C_6H_5O)_3PO$	66.26	66.16	−0.10	4.63	4.62	−0.01			

Results and Discussion

Reactivity of Metal Oxide. The reactivity between metal oxide and sulfur was investigated prior to the analysis of metal organic chelate compound. The reactivity of metal oxide is expressed in terms of α,

TABLE 2. RELATIVE CONVERSIONS OF METAL OXIDES

Metal oxide	Group	Relative conversion α	Metal oxide	Group	Relative conversion α
BeO	IIA	0	Nb_2O_5	VA	0.01
La_2O_3	IIIA	0.51	Ta_2O_5	VA	0.01
ThO_2	IIIA	0.01	B_2O_3	IIIB	0.17
ZrO_2	IVA	0.01	SiO_2	IVB	0
HfO_2	IVA	0.01	As_2O_3	VB	0.96
V_2O_5	VA	0.37	Bi_2O_3	VB	1.00

TABLE 3. ANALYTICAL RESULTS OF ORGANIC CHELATE COMPOUNDS

Sample	C (wt%)			H (wt%)			O (wt%)			N (wt%)		
	Calcd	Exptl	Error	Calcd	Exptl	Error	Calcd	Exptl	Error	Calcd	Exptl	Error
Lithium butanoate C_3H_7COOLi	55.16	55.08	−0.08	8.10	8.30	+0.20	36.74	36.62	−0.12			
Lithium hexanoate $C_5H_{11}COOLi$	62.58	62.63	+0.05	9.63	9.65	+0.02	27.79	27.72	−0.07			
Lithium octanoate $C_7H_{15}COOLi$	67.10	67.34	+0.24	10.56	10.23	−0.33	22.34	22.43	+0.09			
Lithium decanoate $C_9H_{19}COOLi$	70.18	70.13	−0.05	11.19	11.18	−0.01	18.63	18.68	+0.05			
(2,2′,4,4′,6,6′-Hexanitrodiphenylaminato)potassium $KN[C_6H_2(NO_2)_3]_2$	32.89	32.91	+0.02	0.92	1.00	+0.08	43.81	43.73	−0.08	22.37	22.36	−0.01
(2,2′,4,4′,6,6′-Hexanitrodiphenylaminato)rubidium $RbN[C_6H_2(NO_2)_3]_2$	32.89	32.99	+0.10	0.92	1.05	+0.13	43.81	43.67	−0.14	22.37	22.29	−0.08
(2,2′,4,4′,6,6′-Hexanitrodiphenylaminato)cesium $CsN[C_6H_2(NO_2)_3]_2$	32.89	32.98	+0.09	0.92	0.98	+0.06	43.81	43.63	−0.18	22.37	22.41	+0.04
Bis(2-methyl-8-quinolinolato)beryllium(II) $Be(C_{10}H_8ON)_2$	75.93	80.96	+5.03	5.10	4.81	−0.29	10.11	5.60	−4.51	8.85	8.63	−0.22
Bis(*N*,*N*′-disalicylideneethylenediaminato)cerium(IV) $[Ce(C_{16}H_{14}O_2N_2)_2]$	72.17	71.92	−0.25	5.30	5.33	+0.03	12.01	12.17	+0.16	10.52	10.58	+0.06
Tris(2,2,6,6-tetramethyl-3,5-heptanedionato)praseodymium(III) $Pr(C_{11}H_{19}O_2)_3$	72.09	72.33	+0.24	10.45	10.30	−0.15	17.46	17.37	−0.09			
Tris(2,2,6,6-tetramethyl-3, 5-heptanedionato)europium(III) $Eu(C_{11}H_{19}O_2)_3$	72.09	72.05	−0.04	10.45	10.41	−0.04	17.46	17.54	+0.08			
Tetrakis(8-quinolinolato)thorium(IV) $Th(C_9H_6ON)_4$	74.99	77.56	+2.57	4.19	4.18	−0.01	11.10	9.02	−2.08	9.72	9.24	−0.48
Tetrakis(mandelato)zirconium(IV) $Zr(C_8H_8O_3)_4$	63.15	69.57	+6.42	5.30	4.62	−0.68	31.55	25.81	−5.74			
Tetrakis(mandelato)hafnium(IV) $Hf(C_8H_8O_3)_4$	63.15	69.21	+6.06	5.30	4.61	−0.69	31.55	26.18	−5.37			
Tetrakis(8-quinolinolato)hafnium(IV) $Hf(C_9H_6ON)_4$	74.99	80.53	+5.54	4.19	3.78	−0.41	11.10	6.25	−4.85	9.72	9.44	−0.28
Trioxotetrakis(8-quinolinolato)divanadium(V) $V_2O_3(C_9H_6ON)_4$	69.23	71.45	+2.22	3.87	3.52	−0.35	17.93	16.44	−1.49	8.97	8.58	−0.39
Oxotris(8-quinolinolato)niobium(V) $NbO(C_9H_6ON)_3$	72.31	72.02	−0.29	4.05	4.04	−0.01	14.27	14.28	+0.01	9.37	9.66	+0.29
Tris(2,4-pentanedionato)rhodium(III) $[Rh(C_5H_7O_2)_3]$	60.59	60.78	+0.19	7.12	7.01	−0.11	32.29	32.21	−0.08			

TABLE 3. (Continued).

Sample	C (wt%)			H (wt%)			O (wt%)			N (wt%)		
	Calcd	Exptl	Error	Calcd	Exptl	Error	Calcd	Exptl	Error	Calcd	Exptl	Error
Bis(2,4-pentanedionato)-platinum(II) [$Pt(C_5H_7O_2)_2$]	60.59	60.81	+0.22	7.12	7.13	+0.01	32.29	32.06	−0.23			
Bis(glycinato)platinum(II) [$Pt(NH_2CH_2COO)_2$]	32.44	32.36	−0.08	5.44	5.46	+0.02	43.21	43.03	−0.18	18.91	19.15	+0.24
Gold(I) 2-mercaptoacetate $HSCH_2COOAu$	40.69	40.57	−0.12	5.12	5.04	−0.08	54.19	54.39	+0.20			
Bis(8-quinolineselenolato)-cadmium(II)$Cd(C_9H_6SeN)_2$	84.35	84.38	+0.03	4.72	4.78	+0.06				10.93	10.84	−0.09
Bis(thionalidato)mercury-(II) $Hg(C_{12}H_{10}ONS)_2$	78.24	78.32	+0.08	5.47	5.29	−0.18	8.68	8.74	+0.06	7.60	7.65	+0.05
Sodium tetraphenylborate $NaB(C_6H_5)_4$	93.46	93.60	+0.14	6.54	6.40	−0.14						
Dibutylammonium tetra-phenylborate $(n\text{-}C_4H_9)_2NH_2B(C_6H_5)_4$	87.62	90.67	+3.05	9.19	9.33	+0.14				3.19	0	−3.19
Benzylammonium tetraphenylborate $C_6H_5NH_2HB(C_6H_5)_4$	89.38	92.44	+3.06	7.26	7.55	+0.29				3.36	0	−3.36
Triethanolammonium tetraphenylborate $(HOH_2CH_2C)_3NHB(C_6H_5)_4$	78.74	81.92	+3.18	7.71	8.14	+0.43	10.49	8.28	−2.21	3.06	1.66	−1.40
8-Quinolinol-8-quinolino-lium tetraphenylborate $(C_9H_7ON)_2HB(C_6H_5)_4$	84.11	88.66	+4.55	5.88	5.55	−0.33	5.33	4.34	−0.99	4.67	1.45	−3.22
Tris(8-quinolinolato)-gallium(III) $Ga(C_9H_7ON)_3$	74.99	74.96	−0.03	4.19	4.15	−0.04	11.10	11.30	+0.20	9.72	9.59	−0.13
Tris(8-quinolinolato)-indium(III) $In(C_9H_6ON)_3$	74.99	75.01	+0.02	4.19	4.20	+0.01	11.10	11.19	+0.09	9.72	9.61	−0.11
Thallium(I) acetate CH_3COOTl	40.68	40.54	−0.14	5.12	5.00	−0.12	54.19	54.46	+0.27			
Octaphenylcyclotetra-siloxane $Si_4C_{48}H_{40}O_4$	84.68	94.08	+9.40	5.92	5.92	0	9.40	0	−9.40			
Bis(8-quinolinolato)-lead(II) $Pb(C_9H_6ON)_2$	74.99	74.73	−0.26	4.19	4.20	+0.01	11.10	11.38	+0.28	9.72	9.69	−0.03
p-Aminophenylarsonic acid $H_2NC_6H_4AsO_3H_2$	50.70	50.95	+0.25	5.67	5.46	−0.21	33.77	33.53	−0.24	9.85	10.07	+0.22
Antimony potassium tartrate $SbOC_4H_4O_6K$	29.28	29.52	+0.24	2.46	2.43	−0.03	68.26	68.05	−0.21			
Tris(8-quinolinolato)-antimony(III) $Sb(C_9H_6ON)_3$	74.99	75.28	+0.29	4.19	4.02	−0.17	11.10	11.11	+0.01	9.72	9.59	−0.13
Tris(thionalidato)-antimony(III) $Sb(C_{12}H_{10}ONS)_3$	78.24	78.30	+0.06	5.47	5.25	−0.22	8.68	8.69	+0.01	7.60	7.76	+0.16
Tris(8-quinolinolato)-bismuth(III) $Bi(C_9H_6ON)_3$	74.99	74.72	−0.27	4.19	4.26	+0.07	11.10	11.38	+0.28	9.72	9.64	−0.08

which refers to the mole ratio of sulfur dioxide (SO_2) from the metal oxide against that from a reference substance, silver nitrate. The reactivity of metal oxide, α, is estimated approximately by the equation adopted in the previous paper (Table 2).[3] As can be seen from Table 2, the oxides of beryllium(II), thorium(IV), zirconium(IV), hafnium(IV), niobium(V), tantalum-(V), silicon(IV), and boron(III) are barely converted into the sulfides under the experimental conditions, while arsenic(III) and bismuth(III) oxide react quantitatively with sulfur.

Analysis of Various Organic Chelate Compounds. Various metal organic chelate compounds were analyzed (Table 3). The compounds containing four elements of the lanthanoids, La, Ce, Pr, and Eu gave fairly good results. Lanthanoids, especially light rare earths, resemble each other very closely in chemical properties, so it can be expected that PSGC is applicable to the compounds containing three light rare earth elements other than the investigated ones. Selenium was expected to form carbon diselenide and hydrogen selenide under the experimental conditions and to give an error in C and H values. Selenium did not, however, interfere with the determination of the atomic ratio and satisfactory results were obtained with (8-quinolineselenolato)-cadmium(II). Almost all the complexes gave satisfactory

TABLE 4. ANALYTICAL RESULTS OF ORGANOPHOS PHORUSCOMPOUNDS

Sample	C (wt%)			H (wt%)			O (wt%)			N (wt%)		
	Calcd	Exptl	Error	Calcd	Exptl	Error	Calcd	Exptl	Error	Calcd	Exptl	Error
Piperazinium dihydrogenphosphate monohydrate $C_4H_{10}N_2 \cdot H_3PO_4 \cdot H_2O$	28.07	33.55	+5.48	8.83	10.88	+2.05	46.73	37.24	−9.49	16.37	18.32	+1.95
Benzoguanamine phosphate $C_9H_9N_5 \cdot H_3PO_4$	42.52	45.71	+3.19	4.76	5.04	+0.28	25.17	20.59	−4.58	27.55	28.66	+1.11
Benzidine phosphate $C_{12}H_{12}N_2 \cdot H_3PO_4$	57.36	58.43	+1.07	6.02	5.94	−0.08	25.47	24.52	−0.95	11.15	11.11	−0.04
Triphenyl phosphate $(C_6H_5O)_3PO$	73.21	73.01	−0.20	5.12	5.12	0	21.67	21.87	+0.20			

results, but the complexes of Be, Th, Zr, Hf, V, B, and Si gave a negative error in the oxygen value. As can be seen from Table 2, the oxides of these seven elements were highly stable and were scarecely converted into their sulfides. Therefore, the oxygen atom in their complex salts is expected to remain more or less in the residues and this is consistent with the results shown in Table 3. Negative errors in both the oxygen and nitrogen values were obtained in several ammonium tetraphenylborates. Boron nitride was subjected to pyrolytic sulfurization under the experimental conditions, but no evolution of nitrogen was observed. From the above mentioned fact, the negative error in nitrogen values of ammonium tetraphenylborates seems to be ascribed to the formation of boron nitride.

Analysis could not be carried out for lithium acetate, CH_3COOLi, since the reaction tube containing lithium acetate, in which the atomic ratio of carbon to oxygen (C/O) is 1.0, exploded by itself during the course of sulfurization. With the objective of clarifying this phenomena, a series of lithium salts were investigated. Oxygen-rich compounds such as lithium lactate ($C_3H_5O_3Li$, C/O=1.0) and lithium citrate tetrahydrate ($C_6H_5O_7Li_3 \cdot 4H_2O$, C/O=0.55) could not be analyzed since the reaction tube exploded by itself similarly to the way it did in lithium acetate. Relatively oxygen-poor compounds such as lithium butanoate (C_3H_7COOLi, C/O=2.0), lithium hexanoate ($C_5H_{11}COOLi$, C/O=3.0), lithium octanoate ($C_7H_{15}COOLi$, C/O=4.0), and lithium decanoate ($C_9H_{19}COOLi$, C/O=5.0) could be subjected to sulfurization without any explosion. The satisfactory results are obtained when value of C/O exceeds 2.0. The above explosion seems to be ascribed to some lithium silicate, $xLi_2O\,ySiO_2$, which is formed by the reaction between SiO_2 and Li_2O.

Analysis of Organophosphorus Compounds. It was reported in the previous paper that carbon-rich compounds such as dioctadecyl hydrogenphosphate [$(n\text{-}C_{18}H_{37}O)_2HPO_2$, C/O=9.0] gave satisfactory results while carbon-poor compounds such as diguanidium hydrogenphosphate [$(CH_5N_3)_2H_3PO_4$, C/O=0.5] produced a low oxygen value. In order to clarify the difference between these two cases, further study was carried out on a series of organic phosphates in which the oxidation number of phosphorus is +5, that is, piperazinium dihydrogenphosphate monohydrate ($C_4C_{10}N_2 \cdot H_3PO_4 \cdot H_2O$, C/O=0.8), benzoguanamine phosphate ($C_9H_9N_5 \cdot H_3PO_4$, C/O=2.5), benzidine phosphate ($C_{12}H_{12}N_2 \cdot H_3PO_4$, C/O=3.0), and triphenyl phosphate [$(C_6H_5O)_3PO$, C/O=4.5]. As can be seen from Table 4, the present method gives satisfactory results when the value of C/O exceeds 4.5 but does not satisfactory results in C/O less than 3.0.

Interferences. As can be seen from the above-mentioned results, PSGC was applicable to various metal organic chelate compounds, and the atomic ratio between C, H, O, and N in a sample could be determined simultaneously. Some metals in their compounds took up the oxygen in a sample to form their oxides during pyrolytic sulfurization, and this brought about the most serious problems in the analyses of the compounds containing these metals. However, if one takes into account the difficulties in analysis of oxygen in a metal organic chelate compound by the conventional methods, the utility of PSGC in analysis of metal organic chelate compound is obvious even though the applicable elements are restricted.

On the basis of the results obtained with regard to the formation of oxides, the effect of the coexistent elements on the determination of the atomic ratio is summarized on the periodic table (Fig. 1). The amount of oxygen

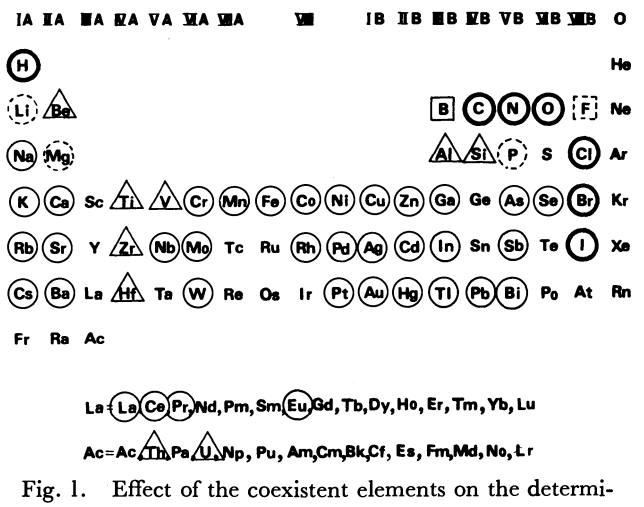

Fig. 1. Effect of the coexistent elements on the determination of the atomic ratio.
○: Harmless, △: form oxide and harmful, □: form both oxide and nitride and harmul, □: react with reaction tube also harmful, ○: can be determined simultaneously.

in an organic compound containing an oxygen atom and one of the following 39 kinds of elements can be satisfactorily estimated by PSGC : (Li), Na, K, Rb, Cs, (Mg), Ca, Sr, Ba, Nb, Cr, Mo, W, Mn, Fe, Co, Rh, Ni, Pd, Pt, Cu, Ag, Au, Zn, Cd, Hg, Ga, In, Tl, Pb, (P), As, Sb, Bi, Se, La, Ce, Pr, and Eu. Since there is close resemblance in chemical properties between the elements of lanthanoids, more particularly between ones of light rare earths, it can be expected that PSGC is applicable to the compounds containing three other lanthanoids, *i.e.*, Nd, Pm, and Sm, and the number of applicable elements would rise to 42. Both magnesium- and lithium-containing samples gave satisfactory results only if the number of carbon atoms exceeds that of oxygen atoms in a sample. Organic phosphates gave satisfactory results when the value of C/O exceeded 4.5, but the quantitative details of other types of organophosphorus compounds is not still clear. The compound containing oxygen atoms and one of the following 10 elements, however, gave a low oxygen value: Be, Ti, Zr, Hf, Th, U, V, B, Al, and Si. Boron-containing compounds show a negative error in both oxygen and nitrogen values.

This study was supported by a Grant-in-Aid for the Special Research project on "Trace Characterization" gived by the Ministry of Education, Science and Culture.

References

1) K. Tsuji, K. Fujinaga, and T. Hara, *Bull. Chem. Soc. Jpn.*, **50**, 2292 (1977).
2) T. Hara, K. Fujinaga, and F. Okui, *Bull. Chem. Soc. Jpn.*, **53**, 951 (1980).
3) T. Hara, K. Fujinaga, and F. Okui, *Bull. Chem. Soc. Jpn.*, **51**, 2951 (1978).
4) T. Hara, K. Fujinaga, F. Okui, and K. Negayama, *Sci. Eng. Rev. Doshisha Univ.*, **21**, 241 (1980).
5) T. Hara, K. Fujinaga, and F. Okui, *Bull. Chem. Soc. Jpn.*, **54**, 2956 (1981).
6) K. Motojima, *Bull. Chem. Soc. Jpn.*, **29**, 29 (1956).
7) R. B. Hahn and L. Webber, *J. Am. Chem. Soc.*, **77**, 4777 (1955).
8) R. B. Hahn and P. T. Joseph, *J. Am. Chem. Soc.*, **79**, 1298 (1957).
9) R. G. W. Hollinshead, "Oxine and Its Derivatives," Butterworths Scientific Publications, London (1954), Vol. 2, pp. 450—521.
10) L. Kosta and M. Dular, *Talanta*, **8**, 265 (1961).
11) I. Kudo, *Bunseki Kagaku*, **5**, 556 (1956).
12) F. J. Welcher, "Organic Analytical Reagents," D. Van Nostrand Company, Inc., New York (1948), Vol. 4, pp. 165—177.
13) K. Takiyama, E. D. Salesin, and L. Gordon, *Talanta*, **5**, 231 (1960).
14) F. E. Crane, Jr., *Anal. Chim. Acta*, **16**, 370 (1957).
15) W. W. Wendlandt, *Chemist Analyst*, **47**, 6 (1958).
16) A. K. Mukherji, *Anal. Chim. Acta*, **23**, 325 (1960).
17) F. J. Welcher, "Organic Analytical Reagents," D. Van Nostrand Company, Inc., New York (1948), Vol. 4, pp. 8—18.
18) Y. Niimura and Y. Nakamura, "Jikken Kagaku Koza," ed by the Chemical Society of Japan, Maruzen, Tokyo (1977), pp. 1520—1579.

On the Structure of Cobalt Garnet, a New Synthetic Silicate Containing 8-Coordinated Cobalt(II)

Kozo Sone* and Haruo Ohashi†

Department of Chemistry, Faculty of Science, Ochanomizu University, Otsuka, Bunkyo-ku, Tokyo 112

†National Institute for Research in Inorganic Materials, Kurakake, Sakura-mura, Niihari-gun, Ibaraki 305

(Received May 18, 1982)

The X-ray structure of the CoO_8 unit in cobalt garnet, a new synthetic silicate of the composition $Co_3Al_2Si_3O_{12}$, is presented. The unit can be taken as a deformed cube, but its central Co^{II} is more regularly 8-coordinated than that in $[Co(NO_3)_4]^{2-}$ studied formerly by Bergman and Cotton.[5] The electronic spectrum and magnetic moment of cobalt garnet are discussed in comparison with those of two other silicates containing CoO_4 units.

Minerals are metallic complexes in nature, and their studies have played important roles in the development of crystal field theory.[1] Synthetic silicates are also of much interest from the standpoint of coordination chemistry.

This paper deals with the structure and some related properties of cobalt garnet, a new and interesting example of such synthetic silicates.

Experimental

Figure 1 and Table 1 were obtained using the data of Ohashi *et al.*[2] which are not explicity given in their original paper. Spectral measurements were made with a Hitachi Recording Spectrophotometer 323, using an electro-polished Al mirror as the standard. Magnetic measurements were made with a Shimadzu MB-2H Magnetic Balance, using Mohr's salt as the standard.

Results and Discussion

The structure of cobalt garnet, $Co_3Al_2Si_3O_{12}$, was recently analyzed by Ohashi *et al.*[2] This silicate was synthesized by the hydrothermal reaction of CoO, Al_2O_3 and SiO_2 at 900 °C and 50 kbar (1 bar=10^5 Pa), which took 3 h in a belt-type. high pressure reaction vessel.[3] It has a structure which is common to natural garnets, *i.e.*, a three-dimensional network composed of tetrahedral SiO_4, octahedral AlO_6, and 8-coordinated $M^{II}O_8$ units.[4] Thus, in terms of coordination chemistry, it is a new example of 8-coordinated cobalt(II) complexes, of which only a limited number seems to be known at present.

A well-known example of such complexes is $[Co(NO_3)_4]^{2-}$, studied formerly by Bergman and Cotton.[5] In this complex, cobalt(II) is at the center of a dodecahedron of eight oxygen atoms, formed by the chelation of four nitrate ions around it. Two different sets of Co–O bonds exist, *i.e.*, one set of four bonds which are 2.03—2.11 Å long, and the other set of four bonds which are much longer (2.36—2.54 Å; 1 Å=10^{-1} nm). The dodecahedron can therefore be taken as a superposition of two deformed tetrahedra, one inside and the other outside, around the central cobalt(II).

The CoO_8 unit in cobalt garnet is, on the other hand, quite different in shape. Here the eight oxygen atoms around the central cobalt(II) form a severely deformed cube, as can be seen from the data in Fig. 1 and Table 1. Among the Co–O bonds, four are 2.21 Å long, and the other four are slightly longer (2.33 Å). The bonds of each set lie on a deformed plane ($O^AO^BO^CO^D$ and $O^EO^FO^GO^H$ in Fig. 1, respectively). The cobalt(II) in cobalt garnet is, therefore, much more "regularly" 8-coordinated than that in $[Co(NO_3)_4]^{2-}$.

To see the influence of such a structure on the electronic state of Co^{II}, the electronic spectrum and magnetic susceptibility of cobalt garnet were studied. The data on $Ca_2CoSi_2O_7$ and $Sr_2CoSi_2O_7$ with melilite structure,[6] containing tetrahedral CoO_4 units, were also obtained for the sake of comparison. These two compounds were

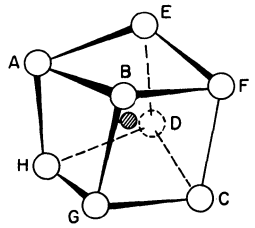

Fig. 1. Sketch of the CoO_8 unit in cobalt garnet. Each oxygen is bound tetrahedrally to two Co^{II}, each at the center of this type of CoO_8 unit, and also to a Si^{IV} and an Al^{III}, forming tetrahedral SiO_4 and octahedral AlO_6 units, respectively, around them.

Table 1. Bond lengths and angles of the polyhedron shown in Fig. 1.

Bond length	l/Å		
$Co-O^A=Co-O^B=Co-O^C=Co-O^D$	2.332(2)		
$Co-O^E=Co-O^F=Co-O^G=Co-O^H$	2.211(2)		
Bond angle	**ϕ/°**	**Bond angle**	**ϕ/°**
$\angle O^ACoO^B=\angle O^CCoO^D$	72.06	$\angle O^ACoO^E=\angle O^DCoO^H$	70.97
$\angle O^BCoO^C=\angle O^ACoO^D$	110.35	$\angle O^ACoO^G=\angle O^DCoO^F$	93.42
$\angle O^ACoO^C=\angle O^BCoO^D$	163.81	$\angle O^CCoO^G=\angle O^BCoO^F$	73.02
$\angle O^ECoO^F=\angle O^GCoO^H$	68.88	$\angle O^BCoO^H=\angle O^CCoO^E$	123.94
$\angle O^ECoO^H=\angle O^FCoO^G$	114.49		
$\angle O^ECoO^G=\angle O^FCoO^H$	161.05		

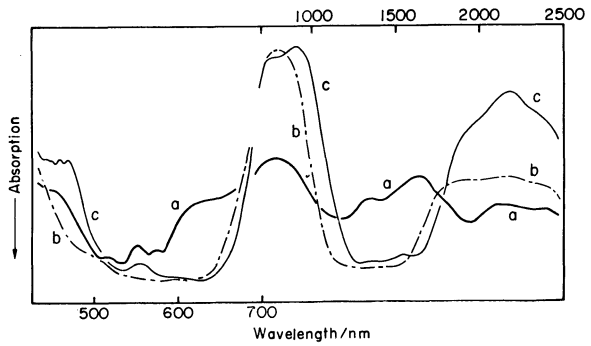

Fig. 2. Powder reflection spectra of cobalt garnet (a) and $Ca_2CoSi_2O_7$ (b) and $Sr_2CoSi_2O_7$ (c) with melilite structure.

synthesized by solid state reaction at 1 atm. The structure refinement of $Ca_2CoSi_2O_7$ has been carried out by Kimata.[7]

Figure 2 shows the reflection spectra of these three silicates. As a whole, there is a general resemblance between the spectrum of cobalt garnet and those of the other two, which, on the other hand, show the broad and split bands of tetrahedral Co^{II} ($\tilde{\nu}_3$ and $\tilde{\nu}_2$, or $^4A_2 \rightarrow {}^4T_1$ (P) and$\rightarrow {}^4T_1$(F)) at around 600 and 1300 nm, just like the spectrum of lusakite cited by Burns.[1] This resemblance is what one can expect, since the splitting of the d-orbitals in a quasi-cubic CoO_8 unit will be essentially similar to that in a tetrahedral CoO_4 unit.

One can now imagine that the ligand field strength (l.f.s.) in cobalt garnet will be nearly twice as large as in the two CoO_4 type silicates. In fact, the above-mentioned bands are shifted somewhat toward blue in cobalt garnet; moreover, a new set of bands appear at *ca.* 2000—2500 nm, which may correspond to the weak shoulders and humps observed on the curves of the CoO_4-type silicates at the same wavelength region, and may be due to the transition $\tilde{\nu}_1$, or $^4A_2 \rightarrow {}^4T_2$, which is sometimes observed in the infrared spectra of tetrahedral Co^{II} complexes. Nevertheless, all these spectral shifts are seemingly rather small, and one can even suppose that the l.f.s. of cobalt garnet and the other two silicates are quite comparable,[††] although the broadness and complicated splittings of the bands hinder reliable comparison of the ligand field parameters.

The reason for the relatively weak l.f.s. in cobalt garnet may be in part found in the distortion of the cubic field, but it must be noted that the Co–O bond in it is much longer than the sum of the effective ionic radii of Co^{2+} (0.58 Å when 4-coordinated, as in melilite, and high-spin) and O^{2-} (1.38 Å when 4-coordinated, as in melilite and cobalt garnet).[8] In the case of Co-melilite, the Co–O bond length (1.926 Å) was slightly shorter than the corresponding sum (1.96 Å).[7]

†† This can be seen, for example, by comparing the data of Fig. 1 with those of Cotton *et al.* on the spectra of CoX_4^{2-} (X=Cl, Br, or I). The latter shows that the change from $CoCl_4^{2-}$ to $CoBr_4^{2-}$, where the l. f. s. (Dq) changes only less than 10%, causes quite remarkable shifts of $\tilde{\nu}_2$ and $\tilde{\nu}_3$.[9]

Table 2. μ_{eff} and θ values of the three silicates

Silicate	μ_{eff}/BM	θ/K
Cobalt garnet	4.57	−12
$Ca_2CoSi_2O_7$	4.17	−24
$Sr_2CoSi_2O_7$	4.13	−20

An apparent expansion of a metallic ion in going from 4- to 8-coordination was already reported to occur in many cases by Shannon,[8] who assigned an effective ionic radius of 0.90 Å to 8-coordinated Co^{II}, making use of the data of Bergman and Cotton.[5] Interestingly, this is in good agreement with the radius of Co^{2+} in cobalt garnet (0.89 Å), obtained by taking the mean of the two Co–O lengths in it and subtracting the radius of O^{2-} from it. Such an expansion, which should be due to the interligand repulsion and/or the attraction of O^{2-} ions toward the cations which are outside of the CoO_8 unit, will certainly enlarge the "box" of O atoms to accomodate Co^{II}, and diminish the l.f.s. acting on it considerably.[†††]

At any rate, therefore, it seems that the effect of the high coordination number in cobalt garnet is largely cancelled by this expansion, causing only relatively small changes in its spectral pattern in comparison with the two CoO_4-type silicates studied.[11]

The magnetic susceptibilities of the three silicates obey Curie-Weiss law down to liquid N_2 temperature, and the values of μ_{eff} and θ obtained from them are shown in Table 2. They are thus all high-spin d^7 complexes with no apparent magnetic anomaly.

References

1) R. G. Burns, "Mineralogical Applications of Ligand Field Theory," Cambridge (1972).
2) H. Ohashi, T. Fujita, and T. Osawa, *J. Jpn. Assoc. Min. Pet. Econ. Geol.*, **76**, 58 (1981).
3) O. Fukunaga, S. Yamaoka, T. Endo, M. Akaishi, and H. Kanda, *High-Pressure Sci. Technol.*, **1**, 846 (1979).
4) G. Menzer, *Z. Krist.*, **63**, 157 (1926).
5) J. G. Bergman, Jr., and F. A. Cotton, *Inorg. Chem.*, **5**, 1208 (1966).
6) B. E. Warren, *Z. Krist.*, **74**, 131 (1930).
7) M. Kimata, *Naturwissenschaften*, **69**, 40 (1982).
8) R. D. Shannon, *Acta Crystallogr., Sect. A*, **32**, 751 (1976).
9) F. A. Cotton, D. M. L. Goodgame, and M. Goodgame, *J. Am. Chem. Soc.*, **83**, 4690 (1961).
10) H. Ohashi, unpublished data.
11) As to the electronic spectra of other garnets, *cf.* Ref. 1, and also P. Bloomfield, A. W. Lawson, and C. Rey, *J. Chem. Phys.*, **34**, 749 (1961).

††† On the other hand, comparison of the spectra of the two CoO_4-type silicates indicates that the change from Ca to Sr lowers the values of $\tilde{\nu}_2$ and $\tilde{\nu}_3$, or weakens the l. f. s. around the Co^{2+} ions. This may be due to the expansion of the unit cell (the values of a(Å), c(Å), and V(Å^3) are: 7.844(1), 5.027(1), and 309.33(10) for $Ca_2CoSi_2O_7$, and 8.027(1), 5.161(1), and 332.55(9) for $Sr_2CoSi_2O_7$, respectively[10]), which will lead to the elongation of the Co–O bonds, and the decrease of the l. f. s.

Conformational Studies of Bis(cyclic tetrapeptide), *S,S'*-Bis[cyclo-(Gly-L-hemiCys-Sar-L-Pro)]. A Proposed Castanet-type Structure in a Dimethyl Sulfoxide Solution

Toshimi SHIMIZU,* Yoshio TANAKA, and Keishiro TSUDA
Research Institute for Polymers and Textiles, Yatabe-Higashi, Tsukuba, Ibaraki 305

(Received February 1, 1982)

A bis(cyclic tetrapeptide), *S,S'*-bis[cyclo(Gly-L-hemiCys-Sar-L-Pro)] (BCGCSP), was prepared by coupling two homodetic cyclotetrapeptide. The conformations of BCGCSP in solutions were investigated by means of NMR, Raman, and CD spectroscopy. The ^{1}H-NMR data in dimethyl-d_6 sulfoxide (Me_2SO-d_6) demonstrated that the two cyclic skeletons of BCGCSP take the same conformations as that of an authentic cyclic tetrapeptide, cyclo-[Gly-L-Cys(Bzl(OMe))-Sar-L-Pro] (CGCSP). The ^{1}H-NMR spectrum of CGCSP contains three sets of resonances, corresponding to three different molecular conformations. From the Raman lines of BCGCSP at 529 cm^{-1} and 683 cm^{-1} in Me_2SO-d_6, it is deduced that the two HC_α–$C_\beta S$ dihedral angles are 180°(trans), while one of the SS–$C_\beta C_\alpha$ dihedral angles is 20—30° and the other is either near 90° or near 180°. In addition, the values of two Raman lines predict that the $C_\beta S$–SC_β dihedral angle is in the range of near 90°. Such a conformation around the $C_\beta S$–SC_β bond is also reasonable in the light of the presence of a CD transition (CS–SC) at $\lambda > 250$ nm in water. By combining the above data, the CPK molecular model of BCGCSP was constructed. An inspection of the model reveals that this bis(cyclic tetrapeptide) is likely to adopt a "castanet-type" structure in Me_2SO-d_6. At the same time the individual cyclic skeleton is considered to take three different ring conformations in equilibrium.

Synthetic cyclic peptides are useful model compounds for elucidating the conformational features (for example, β-turns, γ-turns, and transannular hydrogen bonds) which are recognized as important in protein structure.[1,2] They are also ideal candidates for a new class of carrier molecules which have the capability of ion-binding and ion-transporting through a biological membrane,[3-5] for it is artificially possible to synthesize cyclic peptides, which are molecularly designed to be furnished with the structural characteristics of naturally occurring peptidic substances.[6] Some of the cyclic tetrapeptides have been investigated as to their solution conformations, in connection with their residual properties.[7] However, our cation-binding study of cyclotetrapeptide, cyclo(L-Pro–Sar)$_2$ demonstrated that an efficient ion-dipole interaction was unlikely to take place for lack of conformational flexibility.[8] This result also implied that cyclic peptide comprised of a relatively small number of amino acid residues (4—5) tends to form 2 : 1 (peptide=2, cation=1) complexes with some metal cations.

Thus, a bis(cyclic tetrapeptide), *S,S'*-bis[cyclo(Gly–L-hemiCys–Sar–L-Pro)], in which two homodetic cyclotetrapeptides are joined by a covalent bond, was designed and synthesized. The methodology for such a synthesis of a bis(cyclic peptide) was established by Schwyzer *et al.*[9] and Murakami *et al.*[10] Schwyzer *et al.* synthesized a *S,S'*-bis[cyclo(Gly–L-hemiCys–Gly–Gly–L-Pro)] and proposed a possible model of a cation pump by this peptide, which is driven by the oxidoreduction process. Murakami *et al.* synthesized a *S,S'*-bis-[cyclo(Gly–L-hemiCys–Gly–L-His–L-Cap–L-Und)] and found that this peptide enhanced the hydrolysis of *p*-nitrophenyl carboxylates bearing a long alkyl chain. The conformational study of the bis(cyclic tetrapeptide) described herein provided spectroscopic evidence that this peptide takes a "castanet-type" structure in Me_2SO-d_6. This structure is requisite for all available carbonyl oxygens to bind to a cation cooperatively. During the present study, our attention was focused on the restriction of the total molecular conformation by the $C_\alpha C_\beta SSC_\beta C_\alpha$ group.

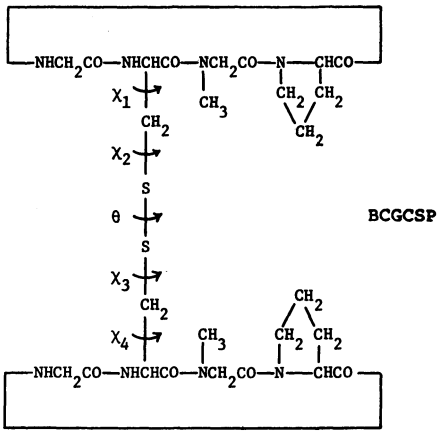

BCGCSP

As has been mentioned above, BCGCSP is a useful model compound containing an SS linkage for elucidating conformational features in naturally occurring peptides. However, the very poor solubility of this peptide restricted the use of a variety of solvents. Therefore, dimethyl sulfoxide was chosen as the solvent for the NMR and Raman studies, and water was utilized for the CD study.

Results and Discussion

Conformations of Individual Cyclic Peptide Skeletons of the Bis(cyclic tetrapeptide) in Solution. The 360 MHz ^{1}H-NMR spectrum of *S,S'*-bis[cyclo(Gly–L-hemiCys–Sar–L-Pro)] (BCGCSP) in Me_2SO-d_6 is shown in Fig. 1. More or less resolved signals for each proton in BCGCSP are seen, particularly in the region of 0—6 ppm. At the same time, at least six amide NH proton signals are positioned at 6.8—8.8 ppm. At first, the characterization of the amide NH protons was inferred from variable-temperature ^{1}H-NMR studies. The temperature effect

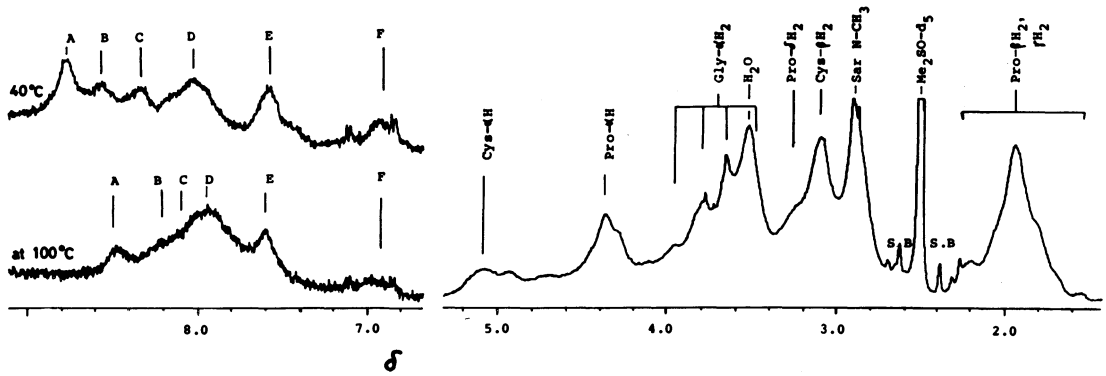

Fig. 1. ^{1}H-NMR spectrum (360 MHz) of BCGCSP in Me_2SO-d_6 at 100 °C and (upper left) at 40 °C. Concentration: 10 g dm^{-3}, S.B.: spinning sideband.

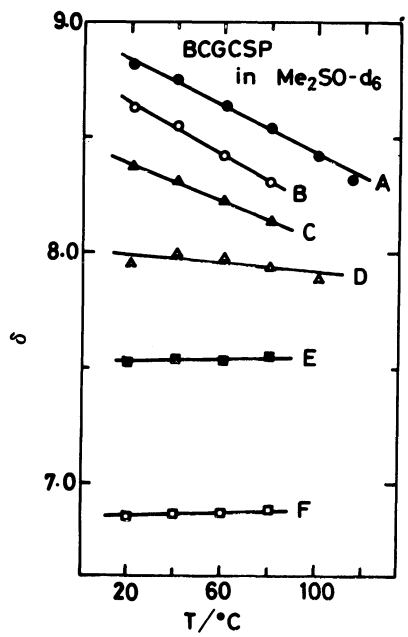

Fig. 2. Temperature dependence of the Gly and Cys amide proton chemical shifts of BCGCSP in Me_2SO-d_6

on the chemical shift of NH signals in Me_2SO-d_6 is shown in Fig. 2. Three NH resonance signals (A, B, and C) move upfield as the temperature increases [$|d\delta(dT)^{-1}|>0.004$ ppm deg^{-1}], while the other three resonances (D, E, and F) are almost independent of the temperature [$|d\delta(dT)^{-1}|<0.001$ ppm deg^{-1}]. These remarkable differences in temperature dependence are attributed to the accessibility of the amide NH proton to a solvent [an internal NH proton (buried or hydrogen-bonded) or an external one (exposed to the solvent)]. According to the usual criteria of accessibility determined from temperature dependence, the three NH protons (A, B, and C) must be exposed to the solvent, while the other three NH protons (D, E, and F) must be shielded from the solvent. A comparison of the ^{1}H-NMR spectrum of the authentic monocyclic tetrapeptide with that of the bis(cyclic tetrapeptide) will now give helpful information for the assignment of the NH proton signals of BCGCSP. The 360 MHz ^{1}H-NMR spectrum of the authentic cyclic tetrapeptide, cyclo[Gly–L-Cys(Bzl(OMe))–Sar–L-Pro] (CGCSP), in Me_2SO-d_6 is shown in Fig. 3. Assignments of signals for each proton were made by spin-decoupling. The NMR parameters of the NH proton resonances of BCGCSP and CGCSP

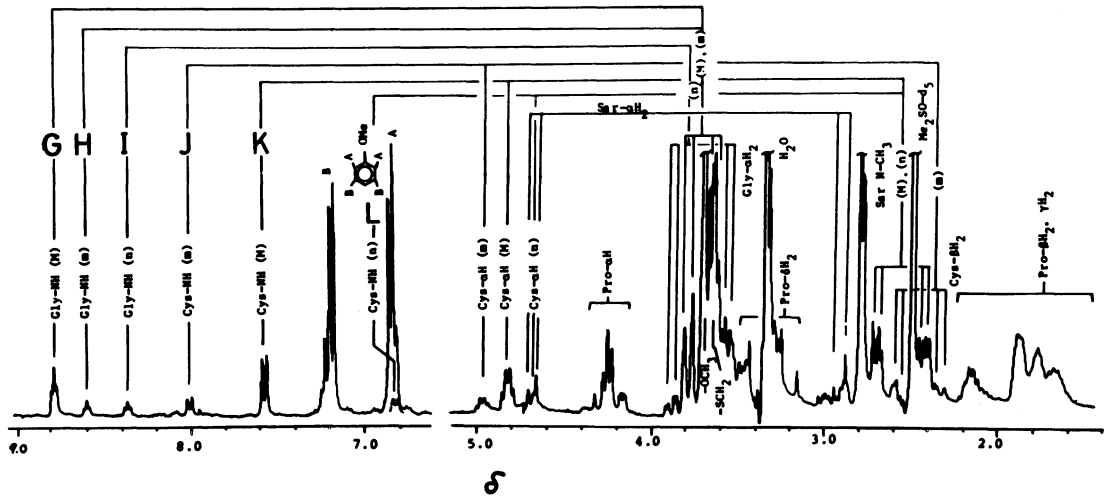

Fig. 3. ^{1}H-NMR spectrum (360 MHz) of CGCSP in Me_2SO-d_6 at 20 °C. Concentration: 25 g dm^{-3}.

TABLE 1. AMIDE PROTON RESONANCES AND CONFORMATIONAL PARAMETERS OF BCGCSP AND CGCSP IN Me_2SO-d_6 AT 20 °C

BCGCSP		CGCSP					
δ[a]	$d\delta(dT)^{-1}\times10^3$/ppm deg^{-1}		δ[a]	$d\delta(dT)^{-1}\times10^3$/ppm deg^{-1}	$J_{NH-C_\alpha H}$/Hz	θ/deg	ϕ/deg
8.81(A)	−5.00						
8.63(B)	−5.83	Gly-NH	8.79(G)	−4.13	5.8, 5.0	170, 70	130
8.37(C)	−4.08		8.60(H)	−4.73	6.4, 5.1	167, 73	133
7.96(D)	−0.92		8.36(I)	−3.80	6.4, 6.0	167, 47	107
7.53(E)	0.33	Cys-NH	8.01(J)	−0.00	9.5	180	−120
6.86(F)	0.50		7.58(K)	−0.07	9.7	180	−120
			≈6.82(L)	≈0	10.1	180	−120

a) From internal tetramethylsilane (TMS). b) The nomenclature used for the conformational dihedral angle, ϕ, is that set forth by the IUPAC-IUB Commission on Biochemical Nomenclature, 1970; see *Biochemistry*, **9**, 3471 (1970). c) $\theta=\phi\pm60°$. d) Calculated from observed $\sum J_{NH-C_\alpha H}$ using a Ramachandran relationship, $\sum J_{NH-C_\alpha H}=7.9[\cos^2(\phi+60°)+\cos^2(\phi-60°)]-1.55[\cos(\phi+60°)+\cos(\phi-60°)]-1.35[\sin^2(\phi+60°)+\sin^2(\phi-60°)]=6.0\cos^2\phi-1.5\cos\phi+12.5\sin^2\phi$. e) Calculated from observed $J_{NH-C_\alpha H}$ using a Ramachandran relationship, $J_{NH-C_\alpha H}=7.9\cos^2\theta-1.55\cos\theta-1.35\sin^2\theta$. f) $\phi=\theta+60°$.

TABLE 2. PARAMETERS FOR THE THREE DIFFERENT CONFORMERS (**M**, **m**, AND **n**) OBSERVED IN A SOLUTION OF CGCSP IN Me_2SO-d_6 AT 21°C[a]

Residue	Type of NMR spectrum	Conformation		
		M	**m**	**n**
Gly	ABX	$\delta_A=3.65$, $J_{AB}=-15.7$ $\delta_B=3.80$, $J_{AX}=5.8$ $\delta_X=8.79$, $J_{BX}=5.0$	$\delta_A=3.65$, $J_{AB}=-11.2$ $\delta_B=3.80$, $J_{AX}=6.4$ $\delta_X=8.60$, $J_{BX}=5.1$	$\delta_A=3.56$, $J_{AB}=-11.4$ $\delta_B=3.89$, $J_{AX}=6.4$ $\delta_X=8.36$, $J_{BX}=6.0$
Cys(Bzl(OMe))[b]	ABMX	$\delta_A=2.44$, $J_{AB}=-13.5$ $\delta_B=2.72$, $J_{AM}=8.2$ $\delta_M=4.84$, $J_{BM}=5.7$ $\delta_X=7.58$, $J_{MX}=9.7$	$\delta_A=2.37$, $J_{AB}=-13.5$ $\delta_B=2.60$, $J_{AM}=8.2$ $\delta_M=4.98$, $J_{BM}=5.7$ $\delta_X=8.01$, $J_{MX}=9.5$	$\delta_A=2.37$, $J_{AB}=-17.0$ $\delta_B=2.60$, $J_{AM}=5.1$ $\delta_M=4.69$, $J_{BM}=5.9$ $\delta_X=6.82$, $J_{MX}=10.1$
Sar	A_3PQ	$\delta_A=2.81$, $J_{PQ}=-16.6$ $\delta_P=2.92$ $\delta_Q=4.69$	$\delta_A=2.79$	$\delta_A=2.78$
Pro	ABCDPQX	$\delta_A=$, $\delta_B=$, $\delta_C=$ 1.55—1.95 $\delta_D=2.05$—2.25 $\delta_P=$, $\delta_Q=$ 3.32 $\delta_X=4.26$	$\delta_A=$, $\delta_B=$, $\delta_C=$ 1.55—1.95 $\delta_D=2.05$—2.25 $\delta_P=$, $\delta_Q=$ 3.25—3.50 $\delta_X=4.16$—4.34	$\delta_A=$, $\delta_B=$, $\delta_C=$ 1.55—1.95 $\delta_D=2.05$—2.25 $\delta_P=$, $\delta_Q=$ 3.25—3.50 $\delta_X=4.16$—4.34

a) Chemical shift, δ, coupling constant, J/Hz. The coupling constants, J, are to within ±0.5 Hz. b) Signals for the protons of the *p*-methoxybenzyl group were omitted.

in Me_2SO-d_6 are summarized in Table 1. Each of the chemical shifts and each of the temperature coefficients of the three NH resonances (A, B, and C) of BCGCSP indicate good similarities to those of the three NH resonances (G, H, and I) of CGCSP. As to the parameters of the remaining three proton resonances (D, E, and F), they also closely resemble those of three resonances (J, K, and L) of CGCSP. This finding supports the idea that three resonances (A, B, and C) are to be assigned to the glycyl NH protons, and the other resonances (D, E, and F), to the cystyl NH ones. It also leads us to the conclusion that the two homodetic cyclic peptide skeletons of BCGCSP take the same structure as that of monocyclic peptide, despite the fact that two cyclic peptides are joined by a bridge containing the S–S bond. Therefore, it seems plausible that the two cyclic skeletons exist in the same conformational state. These conclusions imply that three pairs of the glycyl and cystyl NH proton (A and E, B and D, and C and F) are to be ascribed to the three coexisting structures of BCGCSP in equilibrium. It is of great interest that the conformational properties of the cyclic skeleton of this bis(peptide) are essentially determined by the ring conformation of the individual cyclic tetrapeptide.

Our discussion will, therefore, be concentrated on multiple-ring conformations of CGCSP in Me_2SO-d_6. The ^{1}H-NMR spectrum of CGCSP contains three sets of resonances for each proton. The chemical shifts for the three sets of signals and corresponding coupling constants are summarized in Table 2. All the coupling constants were experimentally obtained. The computer-simulated spectrum using these spectral parameters was in good agreement with the observed one. The N–CH_3 protons of the sarcosyl residue in CGCSP give rise to three signals, at 2.81, 2.79, and 2.78 ppm, with the relative intensity of 3 : 1 : 1 (*cf.* Fig. 4(8)). This, together with the occurrence of the three NH proton signals of each glycyl and cysteinyl residue, means that

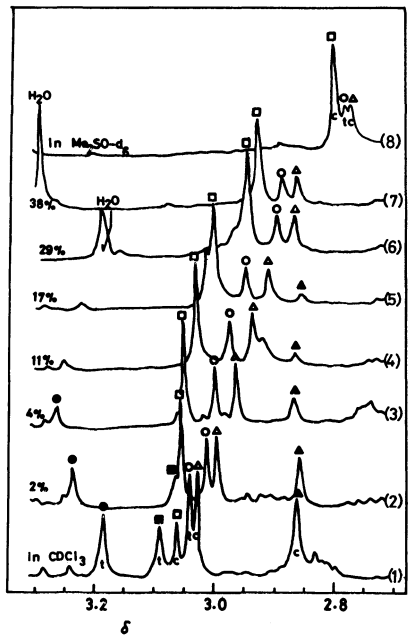

Fig. 4. ^{1}H-NMR spectrum (360 MHz) of N–CH_3 proton resonances of CGCSP in $CDCl_3$–Me_2SO-d_6 mixture at 20 °C.
Me_2SO-d_6 volume fraction: (1) 0, (2) 0.02, (3) 0.04, (4) 0.11, (5) 0.17, (6) 0.29, (7) 0.38, (8) 1.0. The signal having same origin is indicated by the same mark.

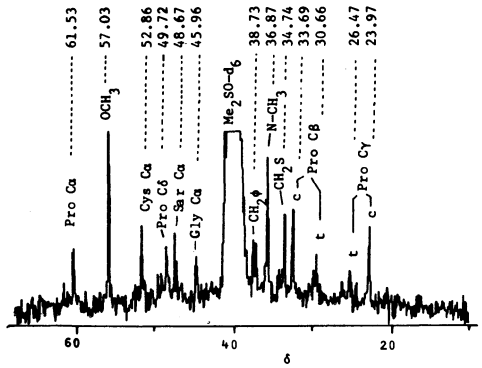

Fig. 5. ^{13}C-NMR spectrum (90 MHz) of CGCSP in Me_2SO-d_6 at 21 °C.
Concentration: 30 g dm^{-3}

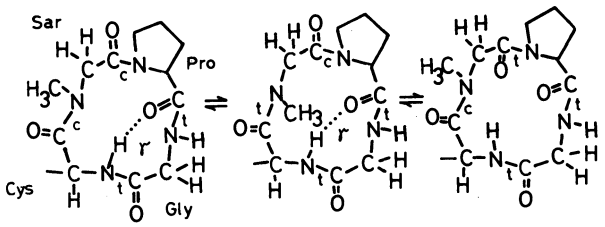

M **m** **n**

Fig. 6. Three different conformations (**M**, **m**, and **n**) of CGCSP proposed on ground of the NMR data in Me_2SO-d_6.

CGCSP has three conformational states. When benzene-d_6 (C_6D_6) was added to a chloroform-d_1 ($CDCl_3$) solution of CGCSP, all the N–CH_3 proton signals represented two different tendencies of upfield shifts. Figure 4(1) shows the 360 MHz ^{1}H-NMR spectrum of CGCSP in $CDCl_3$. The addition of C_6D_6 produced large upfield shifts for the signal at 3.18(●), 3.09(■), and 3.04(○), and small upfield shifts for the remaining signals at 3.06(□), 3.02(△), and 2.86 ppm (▲). Taking into account this phenomenon, N–CH_3 protons anti to the carbonyl oxygen of its peptide bond (*i.e.*, the trans Cys–Sar peptide unit) can be differentiated from that in the cis peptide bond. That is, this differentiation technique is based upon the large benzene-induced upfield shift of the resonance ascribable to the N–CH_3 protons involved in the trans peptide bond.[11] It is thus concluded that the signals at 3.18(●), 3.09(■), and 3.04 ppm (○) are attributable to the N–CH_3 protons involved in the trans Cys–Sar peptide bond, while the other signals, at 3.06(□), 3.02(△), and 2.86 ppm (▲), are attributable to the N–CH_3 protons on the cis Cys–Sar bond in $CDCl_3$. The interaction of CGCSP with C_6D_6 in $CDCl_3$ will be discussed in detail in the following paper.[12] Figure 4(2)—4(8) indicates the ^{1}H-NMR spectral change in CGCSP in the sarcosyl N–CH_3 region when Me_2SO-d_6 was added to the $CDCl_3$ solution. It can be seen that three signals in $CDCl_3$, at 3.18(●), 3.09(■), and 2.86 ppm (▲), disappear gradually as the proportion of Me_2SO-d_6 increases. Finally, this solvent-titration study showed that the two N–CH_3 signals at 2.81 and 2.78 ppm in Me_2SO-d_6 are ascribable to the N–CH_3 protons on the cis Cys–Sar peptide bond (Fig. 4(8)). In addition, one remaining signal, at 2.79 ppm, can be attributed to the N–CH_3 protons on the trans Cys–Sar bond in Me_2SO-d_6. From the relative area underneath the N–CH_3 proton signals, it is also clear that a predominant conformer, **M**, has a cis Cys–Sar peptide bond, while two remaining minor conformers, **m** and **n**, contain a trans and a cis Cys–Sar peptide bonds respectively.

The chemical shifts of the Pro C_β and Pro C_γ carbon are often applicable in establishing the cis-trans isomeric state of the X–Pro peptide bond (X=any amino acid residue). The 90 MHz ^{13}C-NMR spectrum of CGCSP in Me_2SO-d_6 is shown in Fig. 5. From the literature information[13] about the differentiation of the trans X–Pro peptide bond from the cis X–Pro bond, it can be determined that the Pro C_β resonance at 33.7 ppm and the Pro C_γ resonance at 24.0 ppm are typical of the cis Sar–Pro peptide bond. Another Pro C_β resonance at 30.7 ppm and the Pro C_β resonance at 26.5 ppm can also be attributed to the trans Sar–Pro bond. As judged from the relative intensities of the Pro C_β and C_γ resonances, one-third of the populations of Sar–Pro peptide bonds seem to have the trans form. If one considers the cis-trans isomerism about the Cys–Sar and the Sar–Pro peptide bond, three of the four different conformations can be attributed to CGCSP, thus explaining all the situations mentioned above. At first, the glycyl and cysteinyl ϕ angles are calculated from the observed vicinal coupling constants, $J_{NH-C_\alpha H}$, using a Ramanchandran-type relationship (Table 1).[14] Taking these conformational parameters into account, three different CPK model of CGCSP can then be

constructed. Schematic representations of the proposed backbones for CGCSP in Me_2SO-d_6 are shown in Fig. 6. These three types of conformations indicate four characteristic features. First, the conformers, **M**, **m**, and **n**, contain cis-cis, trans-cis, and cis-trans peptide bond sequences of the Cys–Sar–Pro units respectively. Second, the conformation about the prolyl C_α–CO single bond is trans'(Pro $\psi=120°$)[15] in all three species. Third, a transannular hydrogen bond between the Cys amide NH proton and the Pro C=O oxygen would be possible. This satisfies the hydrogen-bonding requirement evidenced by the solvent shielding of the Cys NH proton. The molecular model indicates that the hydrogen bond is nonlinear, having a short C=O··· HN distance. In this respect, the rate of exchange of the amide NH protons in a mixed solvent of Me_2SO-d_6 and 10%-D_2O has been studied. The Gly amide NH proton in **M** was totally exchanged in less than 250 min at 30°C, while the NH proton of cystein in **M** remained unexchanged after 400 min. In **m**, the exchange of the glycyl NH proton was completed in less than 90 min, whereas the exchange of the cysteinyl NH proton took more than 150 min. These results provide strong evidence that the cysteinyl NH proton in at least two conformers (**M** and **m**) is involved in the formation of a transannular hydrogen bond. Fourth, similar species appear to arise in the conformation of CGCSP in acetonitrile-d_3 (CD_3CN), as will be discussed in the following paper.[12]

Conformations of a Side-chain Bridge Containing a Disulfide S–S Bond in Me_2SO-d_6. The Raman spectrum of BCGCSP in Me_2SO-d_6 is shown in Fig. 7. Two Raman lines are observed at 529 cm^{-1} due to a S–S stretching vibration and at 683 cm^{-1} due to a C–S stretching vibration, plus a line at 616 cm^{-1} derived from the solvent. The correlations of the S–S stretching frequencies, ν(S–S), with the conformational properties of the $C_\alpha C_\beta SSC_\beta C_\alpha$ fragment have so far been investigated on organic disulfides. Wart and Scheraga have studied the Raman spectra of a number of primary disulfides which are structurally related to cystine.[16] They proposed a correlation between ν(S–S) and the conformation about the C_β–S bonds in the $C_\alpha C_\beta SS_\beta C_\alpha$ fragment. According to their assumption, the observed value of ν(S–S) of 529 cm^{-1} can be ascribed to the conformation in which one SS-$C_\beta C_\alpha$ dihedral angle(χ_2) is 20—30° (neither cis nor gauche) and the other(χ_3) is 90° (neither gauche nor skew) or 180° (trans). In addition, the assignment of the C–S stretching modes was proposed by Sugeta *et al.*[17] It leads us to the conclusion that the value of ν(C–S) of 683 cm^{-1} is responsible for the conformation in which two HC_α–$C_\beta S$ dihedral angles (χ_1 and χ_4) are 180° (trans). As to the conformations about the S–S bond, compounds containing an unstrained $C_\alpha C_\beta SSC_\beta C_\alpha$ fragment generally have similar conformations (*i.e.*, $C_\beta S$–SC_β dihedral angles near $\pm 90°$). It will, then, be valid to say that the stereochemistry of the $C_\beta S$–SC_β group in BCGCSP has a restricted range of dihedral angles near $\pm 90°$ in Me_2SO-d_6. This assumption is consistent with the results of the study of Wart and Scheraga.[16] They suggested that the observation of values of ν(S–S) higher than about 510 cm^{-1} would imply the presence of unstrained S–S bonds (*i.e.*, the dihedral angle retains its minimum energy value of $\pm 90°$).

Chirality of Disulfide S–S Bond in Water. Next, our discussion will be focused on the chirality of the disulfide bridge between two homodetic cyclic tetrapeptides. For the dimethyl sulfoxide solution, the circular dichroism (CD) spectrum was too complicated to analyze because of the presence of solvent absorption. Some information about the chirality was obtained, however, from the CD spectrum in water. The CD spectrum of BCGCSP is shown in Fig. 8: it has a small negative band ($[\theta]=-11$ deg cm^2 $dmol^{-1}$) at 295 nm, a positive band ($[\theta]=+1400$) at 253 nm, a large negative band ($[\theta]=-17700$) at 226 nm, and a positive band ($[\theta]=+4700$) at 208 nm. Taking into consideration the fact that BCGCSP does not contain any aromatic side chains, the 295 nm band and the 253 nm band can certainly be assigned to the disulfide chromophore. Moreover, the remaining two bands, at 226 nm and at 208 nm, are attributable to the amide-bond transition. The correlations between the chirality of the S–S bond and the

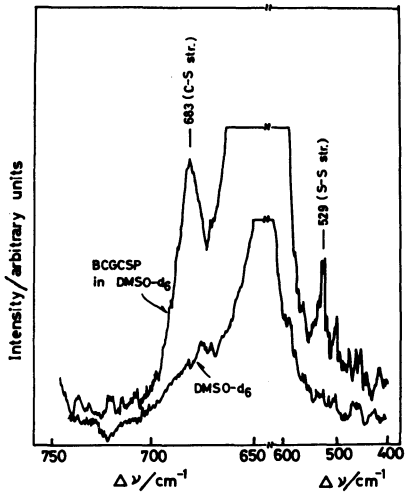

Fig. 7. Raman spectra of BCGCSP in Me_2SO-d_6 at room temperature.

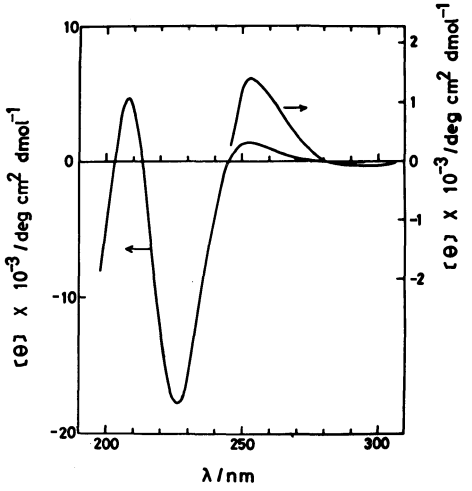

Fig. 8. CD spectrum of BCGCSP in H_2O at 25°C. Concentration: 2.26×10^{-4} mol dm^{-3}.

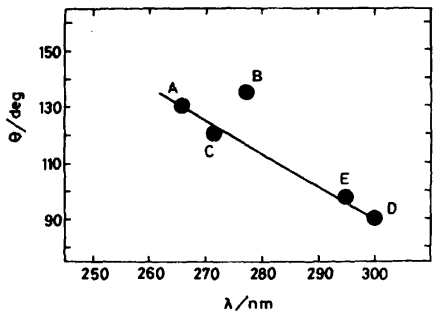

Fig. 9. Dependence of disulfide angle θ, to λ_{min} for various cyclic peptides containing S–S bond.
θ: The value which was estimated by CD spectra and/or measured on the molecular model. λ_{min}: Longer wavelength which affords a negative cotton effect and is attributed to the lowest energy transition. A: *S,S'*-Bis[cyclo(L-hemiCys–L-Pro)] in ethanol,[23] B: malformin-A in hexafluoro-1-propanol,[22] C: [2,7-L-Cystine]-gramicidin S in ethanol,[19] D: *S,S'*-bis[cyclo(Gly–L-hemiCys–Gly–Gly–L-Pro)] in 2,2,2-trifluoroethanol,[9] E: *S,S'*-bis[cyclo(Gly–L-hemiCys–Sar–L-Pro)] in H_2O.

sign of the two Cotton effects in the $250<\lambda<300$ nm and $230<\lambda<250$ nm regions were provided by the work of Carmack and Neubert.[18] According to it, a right-handed helical sence (*P*-chirality) is related to a positive Cotton effect at $\lambda>250$ nm and a negative one at $230<\lambda<250$ nm in the range of dihedral angles of $0°<\theta<90°$ [*vice versa* for a left-handed helical sense (*M*-chirality)]. The investigation of [2,7-L-Cystine]-gramicidin S provided an experimental finding concerning the chirality of the disulfide S–S bond.[19] It completed the evidence for the validity of the theoretical predictions formulated by Bergson[20] and by Linderberg and Michl.[21] If the 295 nm band of this bis(cyclic peptide) corresponds to the long-wavelength transition[20] of the disulfide S–S bond, the quadrant rule for a negative Cotton effect predicts a dihedral angle of either $90°<\theta<180°$ (*P*-chirality) or $-90°<\theta<0°$ (*M*-chirality). The S–S dihedral angles, θ, of compounds containing a cystine moiety previously reported are: (1) malformin-A[22] ($\theta=130$—$140°$, $[\theta]_{276-278}=-5500$ deg cm^2 dmol^{-1}), (2) [2,7-L-Cystine]-gramicidin S[19] ($\theta=120°$, $[\theta]_{271.5}=-7500$ in the difference spectrum between [2,7-L-Cystine]-gramicidin S and [2,7-S-acetamidomethyl-L-cysteine]-gramicidin S), and (3) *S,S'*-Bis[cyclo(Gly–L-hemiCys–Gly–Gly–L-Pro)][9] ($\theta=90°$). From these results, it can be seen that the lowest energy transition in the disulfide S–S chromophore occurs at the longer wavelength, as the S–S dihedral angle, θ, is reduced from 140° to 90° (Fig. 9). However, in the case of $\theta=90°$, the inherent optical activity could not be observed to determine whether the conformation around the S–S bond takes a *P*-chirality or not.[19] Actually, the CD spectrum of a bis(cyclic pentapeptide) shows no Cotton effect centered near 300 nm.[9] These findings substantiate a *P*-chirality with $\theta>90°$ for the S–S bond of BCGCSP. If we adopt the conclusion that the dihedral angle, θ, is 90°—100°, the observation of the negative Cotton effect at 295 nm agrees well with the rules of Linderberg and Michl[21] for the inherent optical

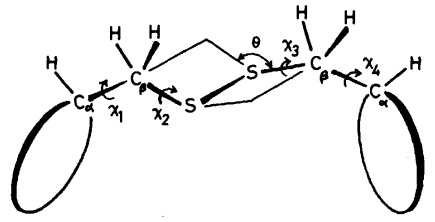

Fig. 10. Schematic representation of $C_\alpha C_\beta SSC_\beta C_\alpha$ moiety in BCGCSP.

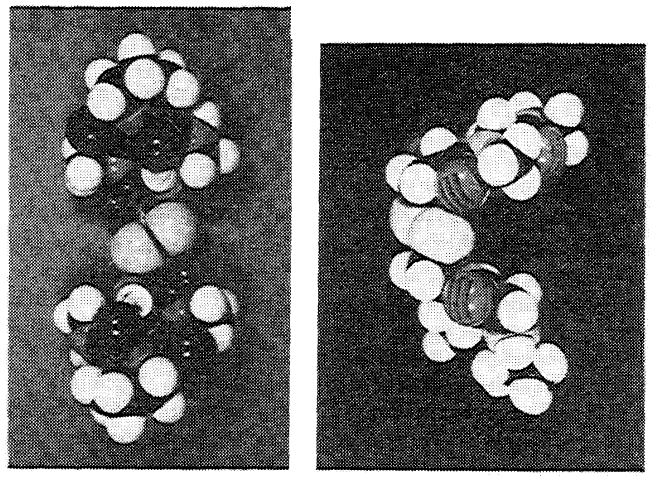

Fig. 11. Photograph of CPK model of proposed a "castanet-type" conformation of BCGCSP in solution. Individual ring conformation of BCGCSP represents that of species **M**, tentatively.

activity of the disulfide chromophore. A *P*-chirality with $\theta=90°$—$100°$ is also in better agreement with the linear correlation in Fig. 9 between the S–S dihedral angles and the corresponding transition wavelength. The 220—250 nm band could not be used to estimate the chirality of the disulfide bond, for it may contain contributions from perturbation by the peptide bond $n\rightarrow\pi^*$ transitions. On the other hand, the CD spectrum of monocyclic tetrapeptide, CGCSP, in water–methanol (9 : 1, by volume) ($[\theta]_{217}=-4700$ deg cm^2 dmol^{-1}) is remarkably different from that of BCGCSP. In the $n\rightarrow\pi^*$ transition region of amide bonds, the total contributions by the four amide-bond chromophores to the CD spectrum will be equal between CGCSP and BCGCSP. Therefore, the CD differences may originate from the perturbations between the amide chromophores of the two homodetic peptide rings in BCGCSP. In other words, the side-chain group of $C_\alpha C_\beta SSC_\beta C_\alpha$ in water is assumed to have such a conformation that they make one peptide ring approach to another one (Fig. 10).

Molecular Conformation of BCGCSP in Me_2SO-d_6. The above assumption regarding the $C_\alpha C_\beta SSC_\beta C_\alpha$ structure in water seems to be reasonable in explaining the Raman spectrum in Me_2SO-d_6. The *P*-chirality of the S–S bond in BCGCSP will probably be retained even in Me_2SO-d_6, judging from the polarity of water and Me_2SO-d_6. Thus, a CPK model of the bis(cyclic tetra-

peptide) could be constructed so that the $C_\alpha^{\chi_1}—C_\beta^{\chi_2}—S^{\theta}—S^{\chi_3}—C_\beta^{\chi_4}—C_\alpha$ group was in the $\chi_1(180°)$-$\chi_2(20°—30°)$-$\theta(90°)$-$\chi_3(180°)$-$\chi_4(180°)$ conformation. At that time, the ring-part conformation of **M** was tentatively assumed to have the conformation of the constituent cyclic tetrapeptide. An inspection of the CPK model reveals that BCGCSP is likely to adopt a "castanet-type" structure, as is shown in Fig. 11. It should be noted that the two planes of the cyclic peptide rings are not essentially positioned in parallel fashion. Therefore, the proposed molecular conformation in the case is different from the specifically folded conformation proposed for *S,S'*-Bis-[cyclo(L-Cys–L-Pro)] in water.[24] The above considerations lead us to the conclusion that BCGCSP must have a "castanet-type" conformation in Me_2SO-d_6 as a whole of the molecule. At the same time, the individual cyclic peptide rings occur in the three interconverting species. This also led us to an interest in binding studies of this bis(cyclic peptide) to a metal ion. A detailed account on the cation-selectivity profiles of this peptide will be presented elsewhere.

Experimental

*S,S'-Bis[cyclo(Gly–L-hemiCys–Sar–L-Pro)](BCGCSP)(**11**).* This was synthesized according to Scheme 1. Cyclo[Gly–L-Cys(Bzl(OMe))–Sar–L-Pro](CGCSP)(**9**) was synthesized *via* the cyclization of the corresponding linear tetrapeptide glycyl-[*S*-(*p*-methoxybenzyl)-L-cystyl]sarcosyl-L-prolyl-*p*-nitrophenyl ester hydrochloride (HCl·H–Gly–L-Cys(Bzl(OMe))–Sar–L-Pro–ON_p) (**8**) in a dilute solution of pyridine. Cyclo(Gly–L-Cys–Sar–L-Pro) (**10**) was afforded by the treatment of CGCSP (**9**) with anhydrous hydrogen fluoride (HF). The final product, BCGCSP (**11**), was obtained from **10** by bubbling with oxygen in the presence of 1,2-diiodoethane as the oxidizing agent.[25] The intermediate peptide fragments and the resulting peptide were purified thoroughly by gel filtration and/or crystallization where possible. The identity and purity of the peptides were checked by a combination of thin-layer chromatography (TLC), nuclear magnetic resonance (NMR), and infrared spectroscopy (IR). We used the I solvent system (chloroform : methanol : acetic acid=95 : 5 : 1 by volume), and the II solvent system (chloroform : methanol =5 : 1, by volume) for the TLC. The synthetic procedures are described in detail below.

*N-(t-Butoxycarbonyl)sarcosyl-L-proline Methyl Ester (**1**).* A solution of Boc–Sar–OH (13.27 g, 70 mmol) in chloroform (50 ml) was cooled to −20 °C and then treated with *N*-methylmorpholine (7.71 ml, 70 mmol) and isobutyl chloroformate (9.19 ml, 70 mmol) to prepare the mixed anhydride. After 3 min, a solution of HCl·H-L-Pro–OMe (11.62 g, 70 mmol) in chloroform (20 ml), were added to the reaction mixture, which was then stirred at −15 °C for 1 h. It was subsequently allowed to warm to room temperature slowly with continuous stirring. After 24 h, the reaction mixture was diluted with chloroform (30 ml) and then extracted successively with 100 ml of water (2 times), 4% sodium hydrogencarbonate (2 times), and a saturated sodium chloride aqueous solution (2 times). The chloroform layer was separated and dried over anhydrous sodium sulfate overnight. After the removal of the sodium sulfate by filtration, the chloroform was evaporated to yield the linear dipeptide as a pale yellow syrup. Crystallization attempts were unsuccessful. The material was used for the following reaction without further purification,

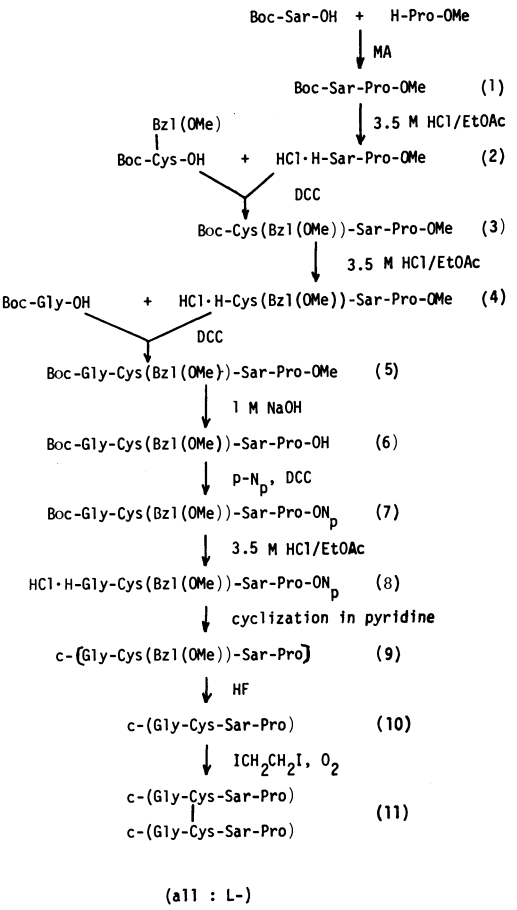

Scheme 1. Synthetic route of BCGCSP. Abbreviations: Boc; *t*-butoxycarbonyl, Sar; *N*-methylglycine, -OMe; methyl ester, DCHA; dicyclohexylamine, MA; mixed anhydride method, -Bzl(OMe); methoxybenzyl, 3.5 M HCl/EtOAc, 3.5 M anhydrous hydrogen chloride in ethyl acetate, DCC; dicyclohexylcarbodiimide, *p*-N_p; *p*-nitrophenol, -ON_p, *p*-nitrophenyl ester.

since it was judged to be the desired product on the basis of TLC: yield, 21.02 g (100%); $R_f^I=0.41$, $R_f^{II}=0.77$.

*Sarcosyl-L-proline Methyl Ester Hydrochloride (**2**).* 3.5 M HCl in ethyl acetate (600 ml) was added to Boc–Sar–L-Pro–OMe (1) (21.02 g, 70 mmol). The reaction mixture was then allowed to stand at room temperature for 1 h. The subsequent removal of the solvent by evaporation left a pale yellow syrup. Trituration with ether yielded a white solid. Recrystallization from methanol–ethyl acetate–ether gave HCl·H–Sar–L-Pro–OMe (**2**) as a white solid: yield, 13.92 g (84%); mp 167—168 °C; $R_f^I=0.03$, $R_f^{II}=0.21$. Found: C, 45.64; H, 7.23; N, 11.81%. Calcd for $C_9H_{17}O_3N_2Cl$: C, 45.67; H, 7.24; N, 11.83%.

*N-(t-Butoxycarbonyl)[S-(p-methoxybenzyl)-L-cysteinyl]sarcosyl-L-proline Methyl Ester (**3**).* Dicyclohexylcarbodiimide (DCC) (1.95 g, 9.45 mmol) in chloroform (10 ml) was stirred into a solution of dicyclohexylammonium salt of Boc–L-Cys(Bzl(OMe))–OH (Boc–L-Cys(Bzl(OMe))–OH·DCHA, 4.94 g, 9.45 mmol) and HCl·H–Sar–L-Pro–OMe (**2**) (2.24 g, 9.45 mmol) in chloroform (60 ml) at −10 °C. The reaction mixture was stirred for 5 h at −5 °C and then overnight at room temperature. After the removal of *N,N'*-dicyclohexylurea, the filtrate was evaporated and the residue was diluted with ethyl acetate (100 ml). The precipitate was filtered off, and the filtrate was successively washed with 100

ml of 10% citric acid (2 times), 4% sodium hydrogencarbonate (3 times), and water (2 times). The organic layer was dried over anhydrous sodium sulfate and concentrated to leave a colorless syrup, which was then triturated with hexane. An attempted recrystallization from ether–hexane was unsuccessful. The Boc-tripeptide (**3**) was obtained as a white semisolid: yield 4.16 g (84%(; $R_f^{\mathrm{I}}=0.44$, $R_f^{\mathrm{II}}=0.80$; $[\alpha]_D^{25}=-75.9°$ ($c=1.19$). Found: C, 57.41; H, 7.17; N, 7.96%. Calcd for $C_{25}H_{37}O_7N_3S$: C, 57.34; H, 7.12; N, 8.02%.

[S-(p-*Methoxybenzyl*)-L-*cysteinyl*]*sarcosyl*-L-*proline Methyl Ester Hydrochloride* (*4*). This tripeptide hydrochloride was prepared by the removal of the Boc group of tripeptide Boc–L-Cys(Bzl(OMe))–Sar–L-Pro–OMe (**3**) (4.00 g, 7.64 mmol), as has been described above for HCl·H–Sar–L-Pro–OMe (**2**). Recrystallization from ethanol–ether gave a white solid: yield 3.51 g (100%); mp 83—84 °C; $R_f^{\mathrm{I}}=0.03$, $R_f^{\mathrm{II}}=0.54$. Found: C, 52.18; H, 6.64; N, 9.11%. Calcd for $C_{20}H_{30}O_5N_5SCl$: C, 52.22; H, 6.57; N, 9.13%.

N-(t-*Butoxycarbonyl*)*glycyl*-[S-(p-*methoxybenzyl*)-L-*cysteinyl*]-*sarcosyl*-L-*proline* (*6*). Boc–Gly–OH·DCHA (2.56 g, 7.17 mmol) was coupled with HCl·H–L-Cys(Bzl(OMe))–Sar–L-Pro–OMe (**4**) (3.30 g, 7.17 mmol), using DCC (1.48 g, 7.17 mmol) in chloroform (100 ml) in the same manner as that used for the preparation of Boc–L-Cys(Bzl(OMe))–Sar–L-Pro–OMe (**3**). Recrystallization from ether–hexane gave Boc–Gly–L-Cys(Bzl(OMe))–Sar–L-Pro–OMe (**5**) as a pale yellow semisolid: yield 3.04 g (73%); mp 49—50 °C; $R_f^{\mathrm{I}}=0.27$, $R_f^{\mathrm{II}}=0.76$; $[\alpha]_D^{25}=-84.8°$ ($c=1.00$).

Boc–Gly–L-Cys(Bzl(OMe))–Sar–L-Pro–OMe (**5**) (3.00 g, 5.17 mmol) in methanol (25 ml) was treated with 1 M NaOH (10.33 ml, 10.33 mmol). After 1.5 h, the methanol was evaporated and the residual solution was diluted with water (25 ml). The aqueous solution was washed with ether (30 ml) and acidified with 10% citric acid under cooling. The resulting precipitate was extracted with ethyl acetate (100 ml), and the organic layer was dried over anhydrous sodium sulfate. After the removal of the sodium sulfate, the solvent was evaporated to leave a colorless foam, which was solidified by the addition of petroleum ether. The product was recrystallized from ethyl acetate–petroleum ether: yield, 2.93 g (89%). mp 82—84 °C; $R_f^{\mathrm{I}}=0.06$, $R_f^{\mathrm{II}}=0.17$. Found: C, 54.66; H, 6.80; N, 9.31%. Calcd for $C_{26}H_{38}O_8N_4S\cdot 0.5H_2O$: C, 54.25; H, 6.83; N, 9.73%.

N-(t-*Butoxycarbonyl*)*glycyl*-[S-(p-*methoxybenzyl*)-L-*cysteinyl*]-*sarcosyl*-L-*proline* p-*Nitrophenyl Ester* (*7*). Into a solution of Boc–Gly–L-Cys(Bzl(OMe))–Sar–L-Pro–OH (**6**) (1.60 g, 2.82 mmol) and *p*-nitrophenol (0.43 g, 3.10 mmol, pulverized previously) in chloroform (15 ml), we stirred a solution of DCC (0.64 g, 3.10 mmol) in chloroform (3 ml) at −5 °C. Stirring was continued at 0 °C overnight. Monitoring the reaction mixture by TLC showed a small amount of the unreacted starting material, so that 0.078 g more of *p*-nitrophenol and 0.058 g of DCC were added after 20 h. Additional stirring was continued at 5 °C for 5 h. The solution was then filtered to remove the precipitated urea, treated with 3 drops of acetic acid, and stirred for 1 h. The solution was subsequently filtered again to ensure the complete removal of the additional amount of urea. The evaporation of the solvent left a pale brown foam, which was triturated with ether–hexane and dried *in vacuo*. The Boc-tetrapeptide *p*-nitrophenyl ester (**7**) was obtained as an off-white solid: yield 1.80 g (92.8%); mp 59—60 °C; $R_f^{\mathrm{I}}=0.07$, $R_f^{\mathrm{II}}=0.76$; $[\alpha]_D^{25}=-78.7°$ ($c=1.00$). Found: C, 56.18; H, 5.98; N, 9.92%. Calcd for $C_{32}H_{41}O_{10}N_5S$: C, 55.88; H, 6.01; N, 10.18%.

Cyclo[*glycyl*-[S-(p-*methoxybenzyl*)-L-*cysteinyl*]*sarcosyl*-L-*prolyl*] (*9*). A solution of HCl·H–Gly–L-Cys(Bzl(OMe))–Sar–L-Pro–ON_p (**8**) (1.61 g, 2.58 mmol) (prepared by the treatment of Boc–Gly–L-Cys(Bzl(OMe))–Sar–L-Pro–ON_p (**7**) with 3.5 M HCl in ethyl acetate at 0 °C for 50 min, trituration with ether, and drying *in vacuo*) in *N,N*-dimethylformamide (DMF) 10 ml) (distilled over calcium hydride just before use), containing a few drops of glacial acetic acid, was added drop by drop and over a period of 5 h to a stirred spectral-grade pyridine (860 ml) at 60 °C. The stirring of the reaction mixture was continued at 30 °C overnight and then allowed to proceed for 3 h at 60 °C. The complete evaporation of pyridine and DMF under reduced pressure left an oily brown residue which was subsequently taken up by water–methanol (1 : 3 by volume) (20 ml). The insoluble material was filtered off, and the filtrate was eluted through columns (1.7× 17 cm) packed with ion-exchange resin of IR-120B (H^+-type) and IRA-400 (OH^--type) successively. The columns were washed with the same solvent until the color of the eluate disappeared. The combined effluent (*ca.* 300 ml) was concentrated to yield a pale yellow syrup. Trituration with ether gave an off-white solid. The crude product (100 mg) was dissolved in a minimum amount of methanol and chromatographed on a Sephadex LH-20 column (2.7×85 cm), using methanol as the eluate. A total of 7 ml×60 fractions were collected. The single components (Nos. 40—46 tubes) were collected, and the solvent was evaporated. The residual syrup was triturated with ether. Recrystallization from methanol–water–ether gave a white solid of cyclo[Gly–L-Cys(Bzl(OMe))–Sar–L-Pro] (**9**); yield 90 mg; ninhydrin test, negative; IR (KBr disk); 3450 (NH str.), 2950 (CH str.), 1650 cm^{-1} (C=O str,); mp 142—143 °C; $R_f^{\mathrm{I}}=0$, $R_f^{\mathrm{II}}=0.47$; $[\alpha]^{25}=-79.2°$ ($c=0.59$). Found: *m/e*=448. Calcd for $C_{21}H_{28}O_5N_4S$: M= 448. Found: C, 55.17; H, 6.12; N, 12.12%. Calcd for $C_{21}H_{28}O_5N_4S\cdot 0.5H_2O$: C, 55.13; H, 6.39; N, 12.25%.

S,S′-*Bis*[*cyclo*(*glycyl*-L-*hemicystyl*-*sarcosyl*-L-*prolyl*) (*11*). Cyclo[Gly–L-Cys(Bzl(OMe))–Sar–L-Pro] (**9**) (90 mg, 0.2 mmol) was placed in an HF-reaction reservoir vessel together with anisole (0.3 ml). Anhydrous HF was added the reservoir vessel using an HF-reaction apparatus, after which the mixture was allowed to react at 0 °C for 1 h while being stirred. The excess HF was removed under reduced pressure at 0 °C, and the residue was dried under reduced pressure for 6 h at room temperature. Subsequent crystallization from methanol–ether gave an off-white solid as cyclo(Gly–L-Cys–Sar–L-Pro) (**10**). The material was immediately used in the next step without further purification. 1,2-diiodoethane (0.042 g, 0.15 mmol) (crystallized from ethanol just before use) and triethylamine (0.056 ml, 0.4 mmol) were stirred into a solution of cyclo(Gly–L-Cys–Sar–L-Pro) (**10**) in methanol (15 ml) under hydrogen.[23] The reaction mixture was then stirred at room temperature overnight. Monitoring the reaction mixture by a nitroprusside test showed it still positive, so an additional amount of 1,2-diiodoethane (0.020 g) was added, after which air was bubbled through the reaction mixture for 6 h. The methanol-insoluble white powdery material was separated on standing overnight: it was then filtered off and thoroughly washed with methanol. The product was found to be insoluble in most organic solvents, such as acetone, chloroform, and ethanol. Recrystallization from water–methanol gave an off-white solid of bis(cyclic tetrapeptide) (**11**): yield 25 mg (38%); ninhydrin test, negative; nitroprusside test, negative; IR (KBr disc) 3450 (NH str.), 2920 (CH str.), 1640 cm^{-1} (C=O str.); mp 280—285 °C (decomp.); $R_f^{\mathrm{I}}=0$, $R_f^{\mathrm{II}}=0.11$. Found: C, 44.26; H, 5.75; N, 15.61%. Calcd for $C_{26}H_{38}O_8N_8S_2\cdot 3H_2O$: C, 44.06; H, 6.26; N, 15.81%.

Procedures. All the melting points were measured on a Yanagimoto Melting-point Apparatus and were not corrected. The optical rotations were measured with a Perkin-Elmer 241 polarimeter. The IR spectra were taken on a

Shimadzu spectrometer, model IR-430.

The ^{1}H-NMR spectra obtained at 360.06 MHz on a NICOLET NT-360 spectrometer with the NIC 1180 Computer Data System, operating in the Fourier transform mode with quadrature detection. The chemical shifts are reported in parts per million (ppm) downfield from internal tetramethylsilane (TMS). The ^{13}C-NMR data were recorded on either a NICOLET NT-360 or a Varian CFT-20 spectrometer at 90.54 MHz or 20.12 MHz respectively, in the Fourier transform mode with proton-noise decoupling. Chemical shifts are given in ppm relative to the internal TMS. The Raman spectra of the bis(peptide) in the liquid state were measured with a JEOL Raman 400D spectromer equipped with an argon-ion laser.

The circular dichroism (CD) spectra were recorded on a JASCO J-40A automatic recording spectropolarimeter equipped with a J-DPY data processor at 25 °C. Generally measurements were carried out in quartz cells with a 0.1-cm path length over 250 nm to 200 nm and a 1-cm path length over 350 nm to 250 nm. Data are represented as molar ellipticities. Spectrophotometric-grade methanol and water were used as solvents.

The authors wish to express their thanks to Dr. Yukio Imanishi of Kyoto University for his valuable suggestions and discussions. We also would like to thank Dr. Shoei Fujishige of our Institute for his useful comments.

References

1) L. G. Pease and C. Watson, *J. Am. Chem. Soc.*, **100**, 1279 (1978).
2) L. G. Pease, C. H. Niu, and G. Zimmermann, *J. Am. Chem. Soc.*, **101**, 184 (1979).
3) D. Baron, L. G. Pease, and E. R. Blout, *J. Am. Chem. Soc.*, **99**, 8299 (1977).
4) C. M. Deber, P. D. Adwadkar, and J. Tom-Kun, *Biochem. Biophys. Res. Commun.*, **81**, 1357 (1978).
5) C. M. Deber and P. D. Adwadkar, *Biopolymers*, **18**, 2375 (1979).
6) Tu. A. Ovchinnikov, V. T. Ivanov, and A. M. Shkrob, "Membrane Active Complexones," B. B. A. Library, Elsevier, New York (1974), Vol. 12.
7) J. Dale and K. Titlestad, *J. Chem. Soc., Chem. Commun.*, **1972**, 255.
8) T. Shimizu and S. Fujishige, *Biopolymers*, **19**, 2247 (1980).
9) R. Schwyzer, A. Tun-Kyi, M. Caviezel, and P. Mose, *Helv. Chim. Acta*, **53**, 15 (1970).
10) Y. Murakami, A. Nakano, K. Matsumoto, and K. Iwamoto, *Bull. Chem. Soc. Jpn.*, **51**, 2690 (1978).
11) T. Sugihara, Y. Imanishi, and T. Higashimura, *Biopolymers*, **14**, 733 (1975).
12) T. Shimizu, Y. Tanaka, and K. Tsuda, *Bull. Chem. Soc. Jpn.*, **55**, 3817 (1982).
13) K. Wüthrich, "NMR in Biological Research: Peptdie and Proteins," American Elsevier, N. Y. (1976), pp. 184—188.
14) G. N. Ramachandran, R. Chandrasekaran, and K. D. Kopple, *Biopolymers*, **10**, 2113 (1971).
15) A. E. Tonelli, *J. Am. Chem. Soc.*, **95**, 5946 (1973).
16) H. E. Wart and H. A. Scheraga, *J. Phys. Chem.*, **80**, 1812 (1976).
17) H. Sugeta, A. Go, and T. Miyazawa, *Chem. Lett.*, **1972**, 83.
18) M. Carmack and L. A. Neubert, *J. Am. Chem. Soc.*, **89**, 7134 (1967).
19) U. Ludescher and R. Schwyzer, *Helv. Chim. Acta*, **54**, 1637 (1971).
20) G. Bergson, *Ark. Kemi.*, **18**, 409 (1962).
21) J. Linderbverg and J. Michl, *J. Am. Chem. Soc.*, **92**, 2619 (1970).
22) M. Ptak, *Biopolymers*, **12**, 1575 (1973).
23) H. Tomiyasu, S. Kimura, and Y. Imanishi, *Polym. Preprints Jpn.*, **28**, No. 7, 1326 (1979).
24) N. Ueyama and T. Araki, *Biopolymers*, **20**, 2485 (1981).
25) F. Weygand and F. Zumach, *Z. Naturforsh.*, **176**, 807 (1962).

 © 1982 The Chemical Society of Japan Bull. Chem. Soc. Jpn., 55, 3817—3823 (1982)

Multiple Conformations and Conformational Change in the Acetonitrile of Cation-binding Cyclic Tetrapeptide, Cyclo[Gly-L-Cys(Bzl(OMe))-Sar-L-Pro]

Toshimi SHIMIZU,* Yoshio TANAKA, and Keishiro TSUDA
Research Institute for Polymers and Textiles, Yatabe-Higashi, Tsukuba, Ibaraki 305
(Received February 1, 1982)

The conformations of the cyclic tetrapeptide, cyclo[Gly-L-Cys(Bzl(OMe))-Sar-L-Pro] (CGCSP), in solution, were studied by means of ^{1}H-, ^{13}C-nuclear magnetic resonance (NMR), and circular dichroism (CD). The CGCSP equilibrates among three conformers, **M**, **m**, and **n**, in acetonitrile, providing three sets of resonances for each proton in the ^{1}H-NMR spectrum. An inspection of a CPK model indicated that the three structures were sterically allowed to occur by the *cis-trans* isomerism around the Cys–Sar and Sar–Pro peptide bond. The temperature dependence of the amide proton resonances in ^{1}H-NMR suggested that one γ-turn (1←3 hydrogen bond from the Cys to the Pro) is present in the two conformers, **M** and **m**. Thus, the three conformations in acetonitrile were deduced from all of the spectral data. This cyclic tetrapeptide is capable of binding a monovalent cation, Li^+, and divalent cations, Mg^{2+}, Ca^{2+}, and Ba^{2+}. Its CD titration curves demonstrated that at least three types of complexes with Ca^{2+} and Ba^{2+} were formed. In contrast, Li^+ and Mg^{2+} were shown to form the 1 : 1 complex with this peptide. The NMR data suggest that the conformational change of the cyclic backbone takes place by changing the geometry of the peptide bonds around the Cys–Sar–Pro sequence on the addition of a metal cation.

In the preceding paper,[1] the conformation of bis-(cyclic tetrapeptide), *S,S'*-Bis[cyclo(Gly–L-hemiCys–Sar–L-Pro)], in solution was investigated using such spectroscopic studies as ^{1}H-NMR, ^{13}C-NMR, Raman, and CD. The proposed conformation in dimethyl-d_6 sulfoxide, which takes a "castanet-type" structure, attracted our attention to the potential activity of this bis(peptide) as an ionophore.

In the present report, the conformations and ion-binding capabilities of the homodetic cyclic tetrapeptide, cyclo[Gly–L-Cys(Bzl(OMe))–Sar–L-Pro], in solution, are described on the basis of the results from ^{1}H-NMR, ^{13}C-NMR, and CD measurements. The small cyclic peptides consisting of 4—5 amino acid units have somewhat rigid backbones of the ring. Therefore, a conformational change is unlikely to take place in these small cyclic peptides on the addition of metal cation to the solution. Actually, the ^{13}C-NMR spectrum of a cyclic tetrapeptide, cyclo(Sar–L-Pro–Sar–L-Pro), in acetonitrile afforded a single resonance for each carbon resulting from one conformer. This conformation is retained even on the addition of the magnesium cation.[2] Recent investigations of naturally occurring cyclic tetrapeptide have revealed the importance of the cyclic structure in the evolution of its biological activity.[3,4] The present study describes an investigation of the conformational change on binding to a metal cation by the cyclic tetrapeptide. This is closely connected with biological events by means of some small cyclic molecules in the membrane transport.[5]

Experimental

Synthesis. The synthesis of cyclo[Gly–L-Cys(Bzl(OMe))–Sar–L-Pro] (CGCSP) has been described in the previous paper.[1]

Procedures. The ^{1}H-NMR spectra were recorded at 360.06 MHz on a NICOLET NT-360 spectrometer with a NIC 1180 Computer Data System, operating in the Fourier transform mode. The ^{13}C-NMR spectra were obtained at 20.12 MHz on a Varian CFT-20 spectrometer, in the Fourier transform mode with proton noise decoupling. All the chemical shifts are given in ppm relative to the internal tetramethylsilane.

The circular dichroism (CD) spectra were recorded using a 0.1-cm path length quartz cell on a JASCO J-40A automatic recording spectropolarimeter equipped with a J-DPY data processor at 25 °C. The data were represented as molar ellipticities. The concentrations of the resulting peptide solutions containing salt were 10^{-3}—10^{-4} mol dm^{-3}. Spectrophotometric-grade acetonitrile was used as the solvent. Analytical reagent-grade perchlorates were used as the metal salts.

Results

Backbone of Cyclic Peptide. ^{1}H-NMR. The ^{1}H-NMR spectrum at 360 MHz of CGCSP in acetonitrile-d_3 is presented in Fig. 1. The assignments were confirmed by the spin-decoupling method and by comparisons with the precursor linear tetrapeptides. It may be seen that the spectrum contains three sets of ABMX-spin systems for the cysteinyl residue and three sets of the ABX systems for the glycyl residue. This finding demonstrates that three species (**M**, **m**, and **n**), each having well-defined, highly populated conformational states, exist on the NMR time scale. From the relative intensities of the Cys and the Gly amide proton signals, the populations of **M**, **m**, and **n** are estimated to be 50, 30, and 20% respectively. The chemical shifts for the three sets of signals and related coupling constants are summarized in Table 1. All the coupling constants were experimentally obtained and optimized by computer simulations. In order to determine the accessibility of each amide NH proton to the solvent, the temperature dependences of the Gly and the Cys NH resonances in **M**, **m**, and **n** (a total of six NH resonances) were measured. The results are shown in Fig. 2. The temperature coefficients of the three cysteinyl amide NH signals, A, B, and F, are zero or small ($d\delta(dT)^{-1}$=0.00(A), 0.00(B), and 2.33 ppm deg^{-1} (F)). In contrast, those of the remaining three glycyl amide NH resonances, C, D, and E, are larger than those of the A, B, and F signals

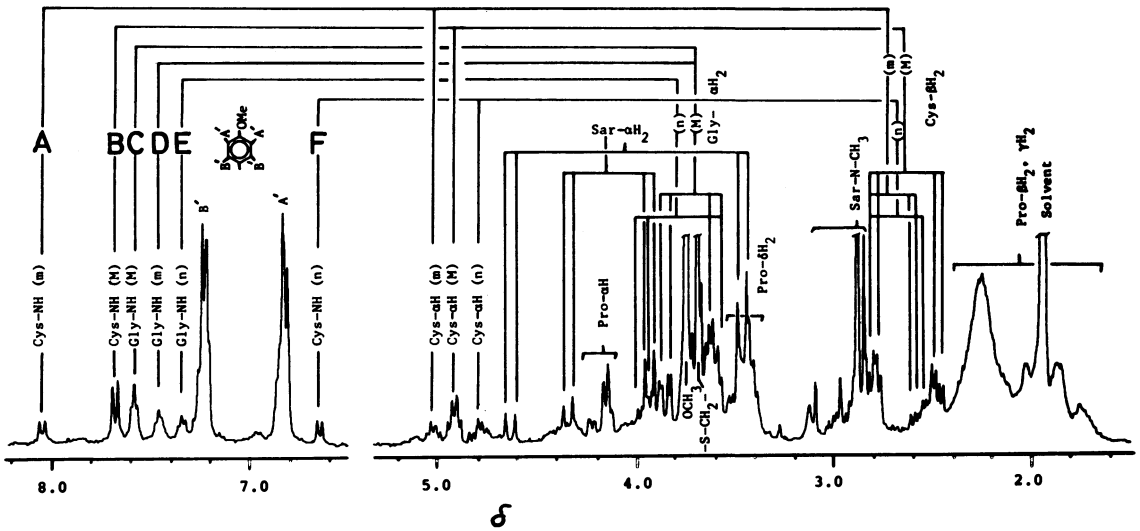

Fig. 1. ^{1}H-NMR spectrum (360 MHz) of CGCSP in CD_3CN at 20°C. Concentration; 25 g dm^{-3}

TABLE 1. PARAMETERS FOR THE THREE DIFFERENT CONFORMERS (**M**, **m**, AND **n**) OBSERVED IN A SOLUTION OF CGCSP IN CD_3CN AT 20 °C[a)]

Residue	Type of NMR spectrum	Conformation		
		M	**m**	**n**
Gly	ABX	$\delta_A=3.62$, $J_{AB}=-16.11$	$\delta_A=3.64$, $J_{AB}=-16.11$	$\delta_A=3.62$, $J_{AB}=-16.14$
		$\delta_B=3.87$, $J_{AX}=4.65$	$\delta_B=3.87$, $J_{AX}=5.90$	$\delta_B=3.97$, $J_{AX}=4.65$
		$\delta_X=7.62$, $J_{BX}=6.32$	$\delta_X=7.50$, $J_{BX}=7.01$	$\delta_X=7.37$, $J_{BX}=6.16$
Cys(Bzl(OMe))[b)]	ABMX	$\delta_A=2.48$, $J_{AB}=-13.76$	$\delta_A=2.59$, $J_{AB}=-13.53$	$\delta_A=2.55$, $J_{AB}=-13.88$
		$\delta_B=2.79$, $J_{AM}=6.83$	$\delta_B=2.79$, $J_{AM}=7.07$	$\delta_B=2.80$, $J_{AM}=5.96$
		$\delta_M=4.93$, $J_{BM}=6.95$	$\delta_M=5.04$, $J_{BM}=6.90$	$\delta_M=4.80$, $J_{BM}=6.90$
		$\delta_X=7.69$, $J_{MX}=9.53$	$\delta_X=8.05$, $J_{MX}=9.78$	$\delta_X=6.66$, $J_{MX}=8.35$
Sar	A_3PQ	$\delta_A=2.89$, $J_{PQ}=-16.87$	$\delta_A=2.89$, $J_{PQ}=-16.60$	$\delta_A=2.85$, $J_{PQ}=-16.87$
		$\delta_P=3.47$	$\delta_P=3.94$	$\delta_P=3.47$
		$\delta_Q=4.66$	$\delta_Q=4.36$	$\delta_Q=4.66$
Pro	ABCDPQX	$\delta_A=$, $\delta_B=$, $\delta_C=$ 1.7—2.1	$\delta_A=$, $\delta_B=$, $\delta_C=$ 1.7—2.1	$\delta_A=$, $\delta_B=$, $\delta_C=$ 1.7—2.1
		$\delta_D=2.15$—2.40	$\delta_D=2.15$—2.40	$\delta_D=2.15$—2.40
		$\delta_P=$, $\delta_Q=$ 3.35—3.55	$\delta_P=$, $\delta_Q=$ 3.35—3.55	$\delta_P=$, $\delta_Q=$ 3.35—3.55
		$\delta_X=4.15$	$\delta_X=4.16$	$\delta_X=4.1$—4.25

a) Chemical shift, δ, coupling constant, J/Hz. The coupling constants, J, are to within $\pm$0.5 Hz. b) Signals for the protons of the *p*-methoxybenzyl group were omitted.

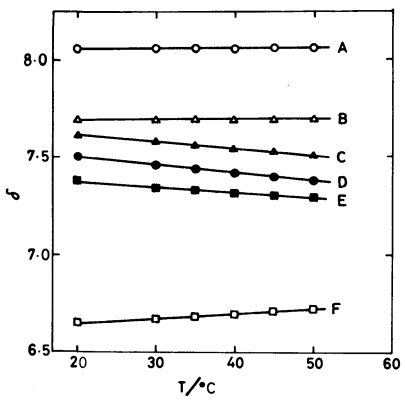

Fig. 2. Temperature dependence of the Gly and Cys amide proton chemical shifts of CGCSP in CD_3CN.

($d\delta(dT)^{-1}=-3.97$(C), -4.00(D), and -3.00 ppm deg^{-1} (E)). According to the usual criteria of accessibility determined from the temperature dependence of the NH's, the Cys NH proton in **M** and **m** is probably buried in the molecule or is hydrogen-bonded. The Gly NH proton is assumed to be exposed to the solvent in all three species.

Next, two resonances for the Sar N–CH_3 protons occur at 2.85 ppm and 2.89 ppm, with the relative intensity of 4 : 1 in acetonitrile-d_3. Solvent-titration experiments were performed in an attempt to distinguish the Sar N–CH_3 resonances derived from a trans Cys–Sar peptide bond from that derived from a cis Cys–Sar bond. First, the ^{1}H-NMR spectra of the cyclic tetrapeptide in a chloroform-*d* solution were examined, while benzene-d_6 was added to bring the total up to 30% (by

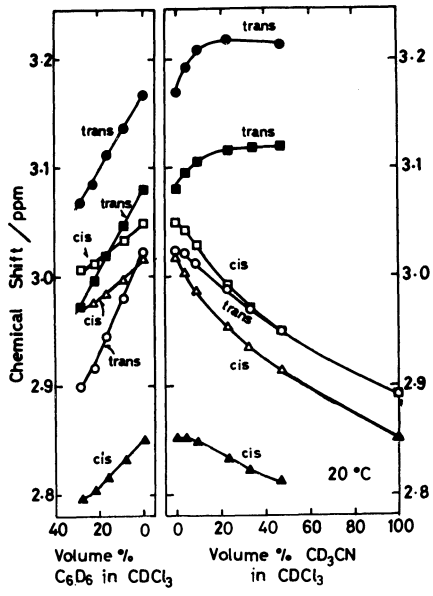

Fig. 3. Upfield shifts for N–CH_3 signals of CGCSP as a function of the volume fraction of C_6D_6 in $CDCl_3$–C_6D_6 solvent mixtures (left) and the shift of N–CH_3 signals as a function of the volume fraction of CD_3CN in $CDCl_3$–CD_3CN solvent mixtures (right). —●—: a, —■—: b, —□—: c, —○—: d, —△—: e, —▲—: f.

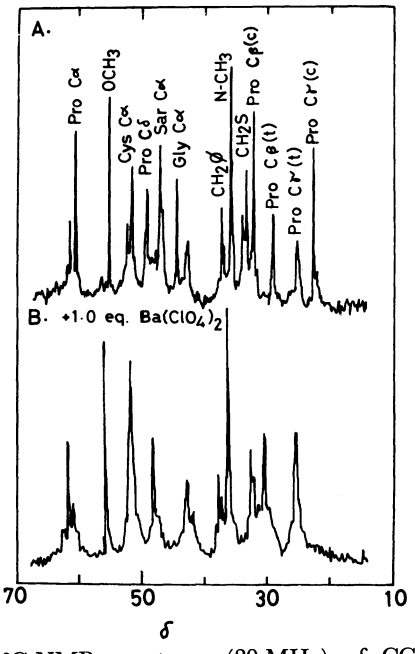

Fig. 4. ^{13}C-NMR spectrum (20 MHz) of CGCSP in CD_3CN. The peptide concentration was 0.12 mol dm^{-3}. The spectra are (A) free peptide and (B) barium perchlorate added to a concentration of 0.12 mol dm^{-3} (molar ratio of peptide: salt, 1: 1).

volume). The addition of benzene gave rise to neither any significant change in the vicinal coupling constants of the Gly or the Cys residue nor that of the intensity of six Sar N–CH_3 resonances. At the same time, the chemical shifts of N–CH_3 signals changed monotonically with the increase in the volume fraction of benzene. These observations, therefore, established that no conformational changes in CGCSP were induced by benzene. The addition of benzene to chloroform induces six N–CH_3 signals to move upfield. The profiles of the upfield shifts for the N–CH_3 signals are shown in Fig. 3 as a function of the volume fraction of benzene-d_6. The a, b, and d signals have larger benzene-induced upfield shifts than those of the c, e, and f signals. These two different tendencies of upfield shifts for N–CH_3 signals are considered to reflect the different local geometries of the Sar N–CH_3 group and the Cys carbonyl group, namely, a cis Cys–Sar peptide bond or a trans Cys–Sar bond. Therefore, an established method based on the benzene-induced shift concerning the assignment of the N–CH_3 signal of cyclo(Sar)$_4$[6] or cyclo(L-Pro–Sar–Gly)$_2$[7] is applicable in this case. Thus, the a, b, and d resonances in a chloroform solution are assigned to the N–CH_3 protons involved in the trans Cys–Sar peptide bond, while the remaining resonances, c, e, and f, are attributable to those involved in the cis Cys–Sar bond.

Second, the ^1H-NMR spectra of the cyclic tetrapeptide were examined in a chloroform-*d*–acetonitrile-d_3 mixed solvent system. In Fig. 3, the chemical shifts of the Sar N–CH_3 signals are plotted as a function of the acetonitrile fraction in a volume. Two signals, a and b, move lowfield, while the f signal reveals an upfield shift, as the concentration of acetonitrile increases. At the same time, the three signals were accompanied by a decrease in the intensity. Finally, in the 1 : 1 mixture of a chloroform–acetonitrile solvent system by volume, these three signals, a, b, and f, almost disappeared. On the other hand, the c signal, associated with the cis Cys–Sar peptide bond, shifts upfield with an increase in the intensity. At the same time, the d signal, attributed to the trans Cys–Sar bond, and the e signal, attributed to the cis Cys–Sar bond, weakened in intensity with the upfield shifts. On the basis of these observations, it is confirmed that the signal at 2.89 ppm in acetonitrile contains two N–CH_3 resonances involved in the cis and trans Cys–Sar peptide bonds, while the resonance at 2.85 ppm is associated with the cis Cys–Sar peptide bond. From the relative intensity of the Gly and the Cys NH proton resonances, it is assumed that the conformers, **M**, **m**, and **n**, contain cis, trans, and cis Cys–Sar peptide bonds respectively.

^{13}C-NMR. The upfield regions of the ^{13}C-NMR spectrum at 20 MHz of CGCSP in acetonitrile-d_3 are shown in Fig. 4A. The assignments of the resonances were confirmed by examining ^1H-coupled and selectively ^1H-decoupled spectra and by comparisons with the spectra of related compounds. Further conformational features of **M**, **m**, and **n** other than those from ^1H-NMR observations can not be inferred from this ^{13}C-NMR spectrum. However, rotational isomers around the Sar–Pro peptide bond can be discriminated by the resulting separate chemical shifts of the Pro C_β and Pro C_γ carbons.[8] The two chemical shifts of the signal at 32.8 ppm for the Pro C_β and at 23.1 ppm for the Pro C_γ are indicative of the presence of the cis Sar–Pro bond. Moreover, the other two signals, at 29.6 ppm for the Pro C_β and at 25.6 ppm for the Pro C_γ, are within the region associated with the trans Sar–Pro bond. The

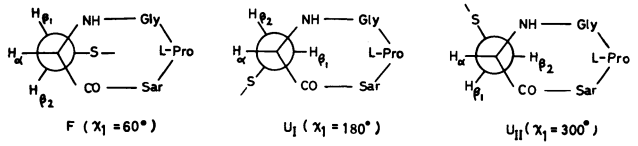

Fig. 5. Schematic representation of three rotational isomers about C_α–C_β bond of side chain of CGCSP.

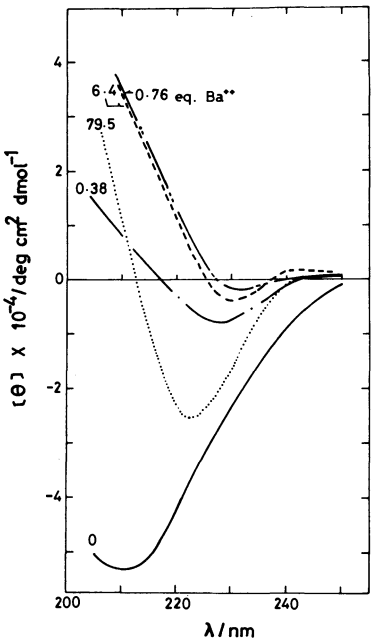

Fig. 6. CD spectral change of CGCSP in CD_3CN as barium perchlorate added.
Molar ratio of $Ba(ClO_4)_2$ to CGCSP; ——: 0, —·—: 0.38, —··—: 0.76, – – –: 6.4, ·····: 79.5. Peptide concentration; 3.37×10^{-4} mol dm^{-3}.

TABLE 2. SIDE-CHAIN CONFORMATIONS OF THE CYSTEIN RESIDUE IN CGCSP IN CD_3CN

Species	Proportion[a]/%		
	F	U_I (or U_{II})	U_{II} (or U_I)
M	21.7	39.7	38.6
m	20.0	40.8	39.2
n	30.1	30.7	39.2

a) Calculated from observed J_{AM} and J_{BM} using the following relationship; $U_I=[J_{AM}(\text{or } J_{BM})-J_g]/(J_t-J_g)$, $U_{II}=[J_{BM}(\text{or } J_{AM})-J_g]/(J_t-J_g)$, $F=1-(U_I+U_{II})$ where $J_t=13.56$, $J_g=2.60$ Hz.

relative intensity of the two Pro C_β and two Pro C_γ resonances show clearly the presence of 70—80% of the cis Sar–Pro peptide bond and that of 20—30% of the trans Sar–Pro bond.

Side Chain of Cyclic Peptide. ^1H-NMR. It is assumed that the orientation of the cysteinyl side chain from C_β carbon on (C_β–S–Bzl(OMe)) occurs in an extended chain with a lower potential energy. Therefore, the conformation of the side-chain group C_α–C_β–S–Bzl(OMe), is essentially determined by the rotation about the C_α–C_β bond of the cysteinyl residue. This implies that the side-chain group exists in the three energetically stable rotational isomers (Fig. 5). One is

TABLE 3. CD EXTREMA FOR CGCSP AT 25 °C

Solvent	M_θ[a] / deg cm² dmol⁻¹	λ / nm
Water–methanol (9 : 1, by volume)	−47500	217
Methanol	−71700	213
Acetonitrile	−53400	212
Acetonitrile+$Ba(ClO_4)_2$(0.5 : 1)[b]	1200	244
	−2500	232
	>43000	<205
Acetonitrile+$Ba(ClO_4)_2$ (1 : 1)[b]	600	244
	−2500	232
	>44000	<205
Acetonitrile+$Ba(ClO_4)_2$ (79.5 : 1)[b]	−25300	223
	>35000	<205
Acetonitrile+$Ca(ClO_4)_2$ (0.5 : 1)[b]	−20200	215
Acetonitrile+$Ca(ClO_4)_2$ (1 : 1)[b]	−14000	222
Acetonitrile+$Ca(ClO_4)_2$ (163 : 1)[b]	−67400	211
Acetonitrile+$Mg(ClO_4)_2$ (0.44 : 1)[b]	−42600	214
Acetonitrile+$Mg(ClO_4)_2$ (1 : 1)[b]	−27600	217
Acetonitrile+$LiClO_4$ (324 : 1)[b]	−25000	219
Acetonitrile+$NaClO_4$ (225 : 1)[b]	−23800	220

a) M_θ: Molar ellipticity. b) Salt to peptide molar ratio.

the folded conformation (F), while the others are unfolded ones (U_I and U_{II}), which rapidly interconvert on the NMR time scale. From the Pachler equation[9] using the vicinal coupling constants, J_{AM} and J_{BM}, in Table 1, the ratio of the presence of the three rotamers was evaluated; it is shown in Table 2. A folded conformation (F) in which the aromatic ring of the side chain is positioned over the cyclic backbone of peptide, is more favored in **n** than in **M** and **m**.

Ion Binding. Circular Dichroism (CD): A solution of CGCSP in acetonitrile was titrated with alkali ions (Li^+ and Na^+) and alkaline earth ions (Mg^{2+}, Ca^{2+}, and Ba^{2+}) while the circular dichroism (CD) spectra were examined. The extrema of the CD spectrum of free cyclotetrapeptide in different solvents and that of complexed peptide with various cations in acetonitrile are summarized in Table 3. The CD spectrum of the free cyclic peptide shows a negative band at 212 nm in acetonitrile (Fig. 6). Common features are observed for the CD spectra of the free peptide in water–methanol (9 : 1, by volume) and in methanol. This finding suggests that there are no significant differences among the conformations of the peptide backbone in these solvents. Upon the addition of metal ions to the solution of the cyclic peptide in acetonitrile, remarkable changes take place, particularly when the divalent cations are added. In the case of Ba^{2+} addition (Fig. 6), the minimum observed for the free peptide increases until the molar ratio of peptide to salt is 2 : 1 stoichiometry ("peptide-sandwich type"). After that, the curves display no drastic change upon the addition of salt until the molar ratio is *ca.* 10. This second step of complexing corresponds to the formation of a 1 : 1 complex (cyclopeptide–Ba^{2+}). At a high salt concentration above this point, the CD spectrum shows a decrease in the minimum which appeared in the presence of 10 equiv. of Ba^{2+}. This finding suggests the appearance of the third complex of Ba^{2+}–cyclopep-

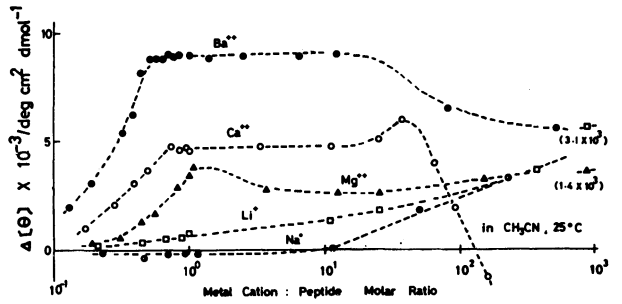

Fig. 7. Titration Curves of CGCSP for several salts in CH_3CN.
Peptide concentration: 3.37×10^{-4} mol dm^{-3}.

Table 4. Equilibrium constants of CGCSP to metal cations in acetonitrile at 25 °C

Cation[a)]	Ionic diameter/Å	K_1[b)] mol^{-1} dm^3	$K_{1/2}$[b)] mol^{-2} dm^6
Li^+	1.20	$<5\times10^2$	
Na^+	1.90	≈0	
Mg^{2+}	1.30	1×10^5	
Ca^{2+}	1.98		9×10^7
Ba^{2+}	2.70		1.7×10^8

a) Anion: perchlorate. b) Estimated error in equilibrium constants, ±20%.

tide–Ba^{2+} with 1 : 2 stoichiometry ("metal cation-sandwich type"). Titration curves were, therefore, depicted in Fig. 7 for the several divalent cations (Ba^{2+}, Ca^{2+}, and Mg^{2+}) and the monovalent cation (Li^+ and Na^+). Then, $\Delta[\theta]$ at 210 nm was plotted against the molar ratio of peptide to the metal cation, where $\Delta[\theta]$ indicates the difference between the molar ellipticity, $[\theta]$, of a peptide plus an ion and that of a free peptide. The curve obtained for Ca^{2+} clearly indicates at least three inflections. This finding demonstrates that at least three types of complexing occurred with the variation of the salt-to-peptide molar ratio. On the other hand, judging from the monotonous increment of $\Delta[\theta]$, only one type of complex with 1 : 1 stoichiometry is assumed to be formed when Li^+ or Mg^{2+} is added.

Equilibrium constants for the first complexed species with several cations were calculated from the CD titration data. For the "peptide-sandwich type" complexes with Ca^{2+} and Ba^{2+}, the following equilibrium constants were defined in terms of the concentrations;

$$K_{1/2} = [P_2C][P]^{-2}[C]^{-1}.$$

For 1 : 1 complexes in the presence of Li^+, Na^+, and Mg^{2+}, K_1 is defined as:

$$K_1 = [PC][P]^{-1}[C]^{-1},$$

where P_2C denotes a sandwich complex; PC, a 1 : 1 complex; P, a peptide, and C, cation. The degree of complexation was determined from the molar ellipticity at a certain wavelength and at a certain salt concentration, on the assumption that the value of ellipticity is the sum of that for free cyclic peptide and that for the complexed peptide present. The calculation of the equilibrium constants were based on the principle reported by Deber *et al.*[10] The results are shown in Table 4. One characteristic feature of the cation-binding properties of this peptide is that it binds divalent cations in preference to monovalent cations. The constant for the formation of a 1 : 1 complex with Mg^{2+} is about 10^3—10^5 fold those of Li^+ or Na^+.

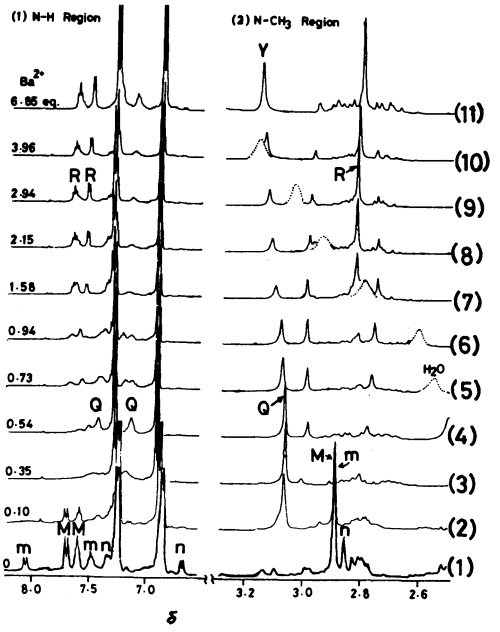

Fig. 8. ^{1}H-NMR spectra of NH and N–CH_3 regions of CGCSP in CD_3CN as $Ba(ClO_4)_2$ is added.
Molar ratio of $Ba(ClO_4)_2$ to CGCSP: (1) 0, (2) 0.10, (3) 0.35, (4) 0.54, (5) 0.73, (6) 0.94, (7) 1.58, (8) 2.15, (9) 2.94, (10) 3.96, (11) 6.85.

^{1}H-NMR and ^{13}C-NMR. In order to elucidate the conformational properties of the cyclic tetrapeptide on complexing with a metal cation, the amide proton and the N–CH_3 proton regions of ^{1}H-NMR were examined in acetonitrile-d_3, titrating with $Ba(ClO_4)_2$. The results are presented in Fig. 8. At least three different types of complex formations can be deduced from the coalescence phenomena of the NH and N–CH_3 proton signals. That is, when $Ba(ClO_4)_2$ was added to the solution, a new signal of N–CH_3 resonance appeared at 3.07 ppm in addition to the signal already present. The signal became pronounced until 0.5 equiv. of salt has been added. The resulting single major resonance at 3.07 ppm for N–CH_3 protons and the two resonances at 7.15 and 7.44 ppm for NH protons are associated with the first complexed species, **Q**. The second complexed species, **R**, which is deduced from the major signal at 2.83 ppm for N–CH_3 protons and the signal at 7.67 and 7.54 ppm for NH protons, appears on the addition of *ca.* 3 equiv. of salt. In the presence of an additional, larger amount of salt, a new resonance, different from that of the second species, appears and grows. This third species, **Y**, is characterized by the signal at 3.18 ppm for N–CH_3 protons. The above results of titration experiments using CD and ^{1}H-NMR leads us to the conclusion that at least three types of complex formations between the cyclotetrapeptide and Ba^{2+} occur in the range of salt concentration of 0—6.85 equiv.

The step-by-step addition of $Ba(ClO_4)_2$ to CGCSP in acetonitrile-d_3 yields ^{13}C-NMR spectra which suggest a convergence to a single conformer. With the increase in the salt concentration, the Pro C_β and the Pro C_γ resonances positioned at the chemical shifts typical of the cis Sar–Pro peptide bond diminished in intensity. The ^{13}C-NMR spectrum in Fig. 4B when 1.0 equiv. of Ba^{2+} is added provides a single resonance for each carbon present in cyclic tetrapeptide. The chemical shifts of the Pro C_β and Pro C_γ resonances (30.5 ppm and 25.4 ppm) are indicative of the presence of the trans Sar–Pro peptide bond (>90%).

Discussion

Free Peptide. If one considers the cis-trans rotational isomers around the Cys^{a}—Sar and Sar^{b}—Pro peptide bond, four distinct conformers are possible; (a-cis, b-cis), (a-cis, b-trans), (a-trans, b-cis), and (a-trans, b-trans). From the results of ^{1}H-NMR, it is deduced that **M** and **n** contain the cis Cys–Sar peptide bond (a-cis). Therefore, the (a-cis, b-cis) and (a-cis, b-trans) sequence of the Cys^{a}—Sar^{b}—Pro peptide linkages must certainly be found in **M** and **n**. If one considers the peptide bond sequence of the Cys–Sar–Pro bond in **m** as (a-trans, b-trans), this is inconsistent with the result from the ^{13}C-NMR data, for it reveals that the cis Sar–Pro peptide bond is superior to the trans bond in population. These considerations enable us to deduce that **m** takes a skeletal conformation containing the (a-trans, b-cis) Cys^{a}—Sar^{b}—Pro peptide linkages. Moreover, the predominance of the cis Cys–Sar bond over the trans bond suggests that the skeletal conformation of the predominant species **M** contains the (a-cis, b-cis) sequence of the Cys–Sar–Pro linkages. The remaining species, **n**, is considered to take a conformation which contains the (a-cis, b-trans) sequence. From a Ramachandran relationship[11] using the vicinal coupling constants (J_{AX}, J_{BX}, and J_{MX}) in Table 1, the conformational angles of the Cys and the Gly residues are calculated:

	M	**m**	**n**
Cys ϕ/°	−120	−120	−139
Gly ϕ/°	128	103	130

Utilizing these conformational parameters, the CPK model construction to be seen in Fig. 9 is sterically allowed. It should be noted that the Cys NH proton is nonlinearly hydrogen-bonded to the Pro C=O oxygen. This finding is supported by the independence of the Cys NH resonance of the temperature. By the same manner as has been described above, **m** is assumed to have one intramolecularly hydrogen-bonded (Pro C=O···Cys NH). This hydrogen bond has the same features as that in **M**. The conformational properties of the several synthetic cyclic tetrapeptide have been studied by the measurement of NMR[12] and by X-ray analysis.[13,14] However, most of these peptides have the simple ^{1}H-NMR spectrum of one conformer in solution. On the contrary, it is surprising that the NMR studies of the present peptide revealed the coexistence of three species with potentially permitted conformational states. This result is closely related to the conformational properties of peptide linkage. Since typical values of an energy barrier to rotation about the peptide bond are within 20 ± 1 kcal mol^{-1},[15] the presence of cis and trans N-substituted peptide bonds can generate different cyclic conformations. In addition, the rotational cis-trans isomerism about two N-substituted peptide bonds in CGCSP is slow on the NMR time scale. Thus, it permits us to observe separate resonances for each proton of the different cyclic conformers. This cis-trans isomerism can often be observed about X-imino acid (X; any amino acids) peptide bonds in cyclic hexa-[2,16] or cyclic octapeptide.[2,17] The above results indicate that, even in a cyclic tetrapeptide, the implantation of some N-substituted amino acids in the peptide yields significant multiple conformations. It should also be noted that these three conformational species are almost entirely consistent with those present in dimethyl-d_6 sulfoxide, as reported in the preceding paper.[1]

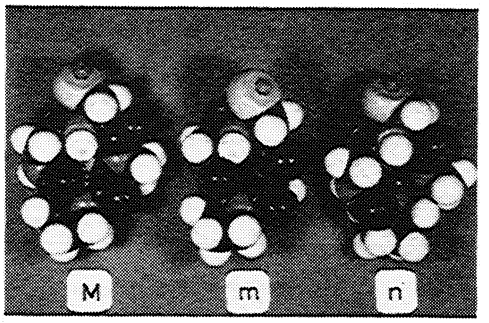

Fig. 9. Photograph of CPK model of proposed three conformations of free CGCSP in CD_3CN. Note the non-linear γ-turn hydrogen bond from the Cys to the Pro in **M** and **m**.

Ion Binding. Since chiroptical properties, such as CD and ORD, depend uniquely upon the molecular geometry, the CD spectral change observed for CGCSP on the addition of salt reflects the change in skeletal conformation. That is, it can be said that this peptide changes its conformation depending on the size and charge of the cation, upon complexation. This conformational change is accompanied by the rotational isomerism about N-substituted peptide bonds. The ^{1}H- and ^{13}C-NMR spectral changes of CGCSP in Fig. 4 and Fig. 8, resulting from the addition of salt, give us some information about the cis-trans isomerism of the two N-substituted peptide bonds (Cys–Sar and Sar–Pro bonds). The chemical shifts of N–CH_3 proton resonances usually serve to differentiate the trans peptide bond containing the sarcosyl N atom from the cis bond. It has been reported that a resonance for N–CH_3 protons whose geometry is anti to carbonyl oxygen occurred in a lower field region than a resonance for N–CH_3 protons which are involved in the cis peptide bond.[18,19] This, together with the results from ^{13}C-NMR, leads us to the confirmation that the first 2 : 1 complex (**Q**) contains trans Cys–Sar and trans Sar–Pro bonds, namely, all trans peptide bonds. This all-trans species, **Q**, is distinct from the three different ones, **M**, **m**, and **n**,

which are initially present in free peptide. An inspection of the CPK model indicates that the conformation can be allowed in which three carbonyl groups direct to the same side, preferentially for ion binding. The binding sites in **Q** appear to be the Sar C=O, the Cys C=O, and the C=O of Gly. Therefore, the intramolecular hydrogen bond can not be found. Actually, when a 1.0 equiv. of salt is added to peptide, the diminution of the negative $n\rightarrow\pi^*$ CD transition band and the downfield shift of the Pro C_β resonance about 0.9 ppm can be observed. This finding strongly supports the disruption[20] of the 1←3 hydrogen bond of γ-turn present in the free cyclic peptide. The second species, **R**, is characterized by the peptide linkages containing the cis Cys–Sar and trans Sar–Pro peptide bond. Judging from the large difference of CD pattern and the difference of the chemical shift for the Gly and Cys NH protons, **R** is likely to be different in backbone conformation from **n**, particularly in Pro ϕ angle. An inspection of the CPK model for **R** reveals that the Cys, Sar, and Pro carbonyls are oriented favorably for binding to a metal cation. The ^{1}H-NMR spectrum of CGCSP on the addition of 6.85 equiv. of salt demonstrates that the third species, **Y**, starts to spring up in addition to **R**. This **Y** is considered to contain the trans Cys–Sar and trans Sar–Pro peptide bonds. This cation-sandwich species, **Y**, appears to be the same as **Q**, judging from the similarities in the chemical shifts of the NH and N–CH_3 signals of the peptide. However, one can not exclude an alternate species which has a different conformation from that of **Q**, for there is only one available carbonyl group in **Y**, which should form a secondary binding site in a cation-sandwich complex. In order to account for the above observations in NMR and CD studies, the following scheme for the Ba^{2+} binding by CGCSP may be proposed;

$$\mathbf{M}_{\text{cis-cis}} \rightleftarrows \mathbf{m}_{\text{trans-cis}} \rightleftarrows \mathbf{n}_{\text{cis-trans}}$$

$$K_{1/2} \downarrow +Ba^{2+}$$

$$\mathbf{Q}_{\text{trans-trans}}\ Ba^{2+}\mathbf{Q}_{\text{trans-trans}}\ \text{(2: 1 complex)}$$

$$K_1 \downarrow +Ba^{2+}$$

$$\mathbf{R}_{\text{cis-trans}}\ Ba^{2+}\ \text{(1 : 1 comprex)}$$

$$\downarrow +Ba^{2+}$$

$$\mathbf{R}_{\text{cis-trans}}Ba^{2+} \rightleftarrows Ba^{2+}\mathbf{Y}_{\text{trans-trans}}Ba^{2+},$$

(1 : 1 complex) (1 : 2 complex)

where the subscript of each species denotes the peptide bond sequence a—b of Cys—Sar—Pro.

Previous studies have established the conformational fitting of cyclic penta-[20] and cyclic hexapeptide[21] on binding with alkali and alkaline earth cations. In these bindings, from two to four carbonyl groups in peptide were essential for coordination to occur. The present study of CGCSP provides the first evidence for conformational fitting on ion binding by a homodetic cyclic tetrapeptide. These facts demonstrate that even a cyclic tetrapeptide can have a potential for binding if two or three carbonyls favoring the cation interaction are available to form a coordination site. In conclusion, it is reasonable to think that conformational flexibility resulting from the cis-trans isomersim around the two N-substituted peptide bonds is responsible for the conformational fitting of CGCSP to a cation.

The authors are grateful to Dr. Yukio Imanishi of Kyoto University for his valuable suggestions and discussions. We are also grateful to Dr. Shoei Fujishige of our Institute for his useful comments.

References

1) T. Shimizu, Y. Tanaka, and K. Tsuda, *Bull. Chem. Soc. Jpn.*, **55**, 3808 (1982).
2) T. Shimizu and S. Fujishige, *Biopolymers*, **19**, 2247 (1980).
3) W. L. Mayer, L. F. Kuyper, D. W. Phelps, and A. W. Cordes, *J. Chem. Soc., Chem. Commun.*, **1974**, 339.
4) J. L. Flippen and I. L. Karle, *Biopolymers*, **15**, 1081 (1976).
5) Yu. A. Ovchinnikov, V. T. Ivanov, and A. M. Shkrob, "Membrane-Active Complexones," Elsevier, Amsterdam (1974).
6) J. Dale and K. Titlestad, *J. Chem. Soc., D*, **1770**, 1403.
7) T. Sugihara, Y. Imanishi, and T. Higashimura, *Biopolymers*, **14**, 733 (1975).
8) D. E. Dorman and F. A. Bovey, *J. Org. Chem.*, **38**, 2379 (1973).
9) K. G. R. Pachler, *Spectrochim. Acta*, **20**, 581 (1964).
10) C. M. Deber, V. Madison, and E. R. Blout, *Acc. Chem. Res.*, **9**, 106 (1976).
11) G. N. Ramachandran, R. Chandrasekaran, and K. D. Kopple, *Biopolymers*, **10**, 2113 (1971).
12) J. Dale and K. Titlestad, *J. Chem. Soc., Chem. Commun.*, **1972**, 255.
13) J. Konnert and I. L. Karle, *J. Am. Chem. Soc.*, **91**, 4888 (1969).
14) P. Groth, *Acta Chem. Scand.*, **24**, 780 (1970).
15) W. E. Stewart and T. H. Siddall, *Chem. Rev.* **70**, 517 (1970).
16) C. M. Deber, D. A. Torchia, S. C. K. Wong, and E. R. Blout, *Proc. Natl. Acad. Sci. U. S. A.*, **69**, 1825 (1972).
17) V. Madison, C. M. Deber, and E. R. Blout, *J. Am. Chem. Soc.*, **99**, 4788 (1977).
18) F. A. Bovey, J. J. Ryan, and F. P. Hood, *Macromolecules*, **1**, 305 (1968).
19) M. Sisido, Y. Imanishi, and T. Higashimura, *Biopolymers*, **11**, 399 (1972).
20) L. G. Pease and C. Watson, *J. Am. Chem. Soc.*, **100**, 1279 (1978).
21) C. H. Niu, V. Madison, L. G. Pease, and E. R. Blout, *Biopolymers*, **17**, 2747 (1978).

Syntheses of Saccharin and Cyclamate Derivatives Bearing Polymerizable Vinyl Group

Hiroyoshi KAMOGAWA,* Shuji YAMAMOTO, and Masato NANASAWA
Department of Applied Chemistry, Yamanashi University, Takeda 4, Kofu, Yamanashi 400
(Received March 18, 1982)

Vinyl monomers containing saccharin or cyclamate residues were synthesized. 6-Acrylamido-, 6-methacrylamido-, 6-(4-styrenesulfonamido)-, and 6-(vinylbenzylamino)saccharins were synthesized from 6-aminosaccharin. *N*-[2-(4-Styrenesulfonamido)cyclohexyl] and *N*-[2-(vinylbenzylamino)cyclohexyl]sulfamic acids were synthesized starting with 1,2-cyclohexanediamine *via* sodium *N*-(2-aminocyclohexyl)sulfamate. All monomers thus synthesized were found to polymerize or copolymerize with *N*-vinyl-2-pyrrolidone to afford vinyl polymers with pendant saccharin and cyclamate units.

In our previous studies, we have prepared food colorant monomers[1] and food preservative and antioxidant monomers and their polymers,[2,3] which are considered to have a potentiality as nondigestive and nonabsorbable food additives.

In this paper, we wish to report syntheses of vinyl monomers containing saccharin and cyclamate residues, which are intended to provide nondigestive sweeteners in their final polymer forms.

Saccharin monomers (**6a**, **6b**, **8**, **9**) were synthesized *via* the key intermediate 6-aminosaccharin (**5**) as follows:

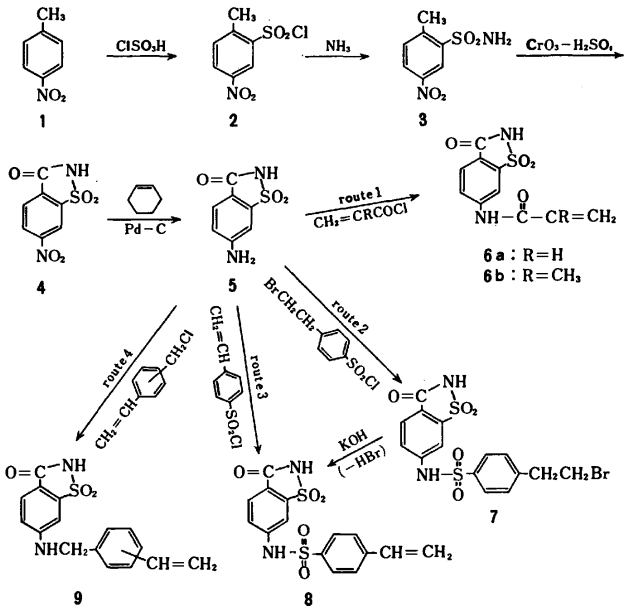

Cyclamate vinyl monomers (**13**, **14**) were synthesized *via* sodium *N*-(2-aminocyclohexyl)sulfamate (**11**) in the following manners:

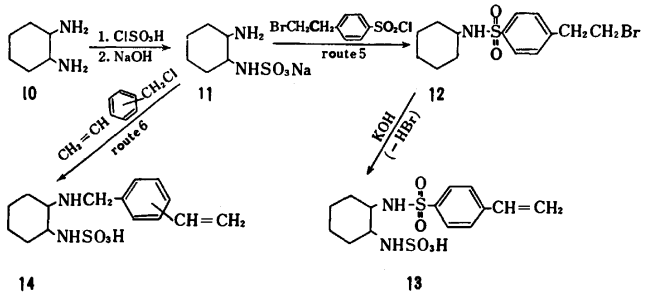

All monomers synthesized were homopolymerized or copolymerized with *N*-vinyl-2-pyrrolidone (VP) to afford respective pendant polymers.

Results and Discussion

Owing to the deactivating effect of *p*-nitro group on 3 and 5 positions of *p*-nitrotoluene (**1**), 2-methyl-5-nitrobenzenesulfonamide (**3**) was isolated as the sole product (^{1}H NMR) by the chlorosulfonation of **1** and subsequent reaction with ammonia. Chromium trioxide oxidation in sulfuric acid was adopted for the conversion of **3** to 6-nitrosaccharin (**4**), since permanganate oxidation as in the case of commercial production of saccharin gave no satisfactory results (very low yields). For the reduction of the nitro group of **4** to afford 6-aminosaccharin (**5**) the amphoteric character of **5** hindered the use of conventional methods such as the $SnCl_2$–HCl one. The combination of cyclohexene as hydrogen donor with Pd–C as catalyst[4] allowed a smooth progress of reduction and easy purification of the product **5** by reprecipitation. 6-Acrylamido- and 6-methacrylamidosaccharins (**6a** and **6b**) were synthesized by the reactions of **5** with acryloyl chloride and methacryloyl chloride in aqueous mixtures, respectively (route 1). Alternatively, **6a** was synthesized from **4** by the reduction with aqueous sodium dithionite and subsequent addition of acryloyl chloride to the reaction mixture without isolating **5**, although yield was low (*ca.* 13%). The sulfonamide group which is more resistant to hydrolysis was introduced by the reaction of **5** with 4-(2-bromoethyl)benzenesulfonyl chloride (route 2). The presence of acidic hydrogen (s, 1H) at δ 11.5 in NMR identified structure **7**. The dehydrobromination of **7** by a conventional procedure gave a vinyl monomer **8**. Monomer **8** was also prepared from **5** in a single step by the use of *p*-vinylbenzenesulfonyl chloride (route 3). The reaction of **5** with vinylbenzylchloride (*m*/*p*=60/40) provided another vinyl monomer 6-(vinylbenzylamino)saccharin (**9**, a *m*-*p* mixture) (route 4). Single absorption peak (NH) at 3380 cm^{-1} in IR (KBr) identified structure **9**. Both column and thin-layer chromatographic separations of meta from para isomer failed due largely to the unfavorable solubility characteristic of **9**.

In the cyclamate series, 1,2-cyclohexanediamine (**10**) was converted to sodium *N*-(2-aminocyclohexyl)sulfamate (**11**), which was subjected to the same reaction procedures as those in the saccharin series using 4-(2-

Table 1. Polymerization behavior of the synthesized monomers

No.	Monomer	VP/Monomer (mol/mol)	Polymer		
			Conversion %	VP/Monomer[a] (mol/mol)	$[\eta]$ dl g^{-1}
1	**6a**	0	85	0	0.34
2	**6a**	8.99	35	13.9	0.78
3	**6b**	0	56	0	0.18
4	**6b**	10.03	28	5.00	0.18
5	**8**	0	82	0	0.13
6	**8**	8.92	13	0.61	0.07
7	**9**	0	68	0	Insol in DMF
8	**9**	13.24	38	0.045	Insol in DMF
9	**13**	0	72	0	Insol in DMF
10	**13**	8.96	44	1.87	Insol in DMF
11	**14**	9.04	34[b]	13.3	0.39[c]

a) Determined by CHN-analyses. b) A solution of **14** (0.21 g), VP (0.68 g), potassium persulfate (0.009 g), and sodium hydroxide (0.033g) in water (3 ml) was polymerized. c) Value in water.

bromoethyl)benzenesulfonyl chloride and vinylbenzyl chloride to afford *N*-[2-[4-(2-bromoethyl)benzenesulfonamido]cyclohexyl]sulfamic acid (**12**) and *N*-[2-(vinylbenzylamino)cyclohexyl]sulfamic acid (**14**), respectively (routes 5 and 6). Compound **12** was converted to the corresponding vinyl monomer **13** by alkaline dehydrobromination. Relatively low yields observed in steps **12**→**13** and **11**→**14** (35% and 29%) are considered to be caused by the fact that fairly large amounts of the sulfamic acids produced remained in solutions without being isolated. All attempts to separate para and meta isomers of **14** failed too.

Some of the novel monomers synthesized here are slightly colored, presumably due to the presence of traces of unremovable impurities. However, results of IR, NMR, MS, and elemental analyses indicate that they are essentially pure.

As indicated in Table 1, all monomers were found to polymerize in either *N*,*N*-dimethylformamide (DMF) or aqueous alkali (No. 11 in Table 1) with radical initiators. Some homopolymers and copolymers with *N*-vinyl-2-pyrrolidone (VP) (Nos. 7—10) were insoluble in DMF. These monomers (**9**, **13**), however, can make alkali-soluble copolymers by selecting suitable monomer ratios, as exemplified in the case of monomer **14** (No. 11). It is interesting to note that both saccharin and cyclamate monomers with the sulfonamide linkage (**8** and **13**) provide remarkably low values of VP/monomer ratio in copolymer as compared with those in the corresponding monomers (Nos. 6 and 10). This is also the case with monomer **9** having the benzylamino linkage (No. 8). In the latter two cases (monomers **9** and **13**), however, the polymerizations were heterogeneous, so that exact estimation of monomer reactivity may be difficult.

All copolymers of saccharin and cyclamate monomers with VP synthesized here can be made water-soluble, when suitable monomer ratios are selected and the resulting copolymers are neutralized with aqueous alkali. Although the taste of these copolymers has not exactly been estimated at this stage, copolymers of this kind, as they are or when suitably modified, might conform to the requirements mentioned above.

Experimental

IR, ^{1}H NMR, and mass spectra were recorded on a Hitachi 215 spectrophotometer, a JNM-PMX 60 spectrometer, and a Hitachi RMU-6 MG spectrometer, respectively. Elemental analyses were conducted using a Perkin-Elmer 250 instrument.

2-Methyl-5-nitrobenzenesulfonamide (3). A solution of *p*-nitrotoluene (6.9 g, 50 mmol) in chlorosulfuric acid (17.5 g, 150 mmol) was kept at 60—70 °C for 24 h with exclusion of moisture. The reaction mixture was poured onto ice and extracted with ether (200 ml). The organic layer was washed with aqueous sodium chloride, treated with concd aqueous ammonia (50 ml), and stirred by the application of heat to evaporate ether completely (about 2 h). The mixture was then filtered and crude product was recrystallized from water to afford yellow needles (mp 183—185 °C) in 45% yield. Found: C, 38.73; H, 3.58; N, 13.10%. Calcd for $C_7H_8N_2SO_4$: C, 38.89; H, 3.73; N, 12.96%. IR (KBr) 3420, 3300 (NH_2), 1600 (Ar), 1540 (NH), 1350 (NO_2), 1330, 1310 (SO_2), 1160, and 1120 (SO_2) cm^{-1}. NMR ($CDCl_3$–DMSO-d_6) δ=2.8 (s, 3H, Me), 7.4—7.8 (d, 3H, NH_2+ArH), 8.3 (d, 1H, ArH), and 8.8 (s, 1H, ArH). MS (*m/e*) 216 (M^+, 8) and 135 (100).

6-Nitrosaccharin (4). To a solution of chromium trioxide (9.0 g, 900 mmol) in water (66.7 ml) concd sulfuric acid (83.5 ml) was added gradually. To the resulting solution was added **3** (4.32 g, 20 mmol) and the mixture was stirred at room temperature for 24 h. Crude product was obtained by filtration of the reaction mixture with a glass filter followed by thorough washing with water. Purification by dissolution in 10% aqueous sodium hydrogencarbonate, filtration, and reprecipitation of the filtrate with 5% aqueous hydrochloric acid provided a white powder (mp 205—207 °C) in 56% yield. Found: C, 36.54; H, 1.89; N, 12.12%. Calcd for $C_7H_4N_2SO_5$: C, 36.85; H, 1.78; N, 12.28%. IR (KBr) 3150 (NH), 1730 (C=O), 1660 (Ar), 1530 (NO_2), 1340 (SO_2, NO_2), 1170, and 1120 (SO_2) cm^{-1}. NMR ($CDCl_3$–DMSO-d_6) δ= 8.1—9.0 (m, 3H, ArH), 10.1 (s, 1H, NH). MS (*m/e*) 228 (M^+, 100).

6-Aminosaccharin (5). To a solution of **4** (11.4 g, 50 mmol) and cyclohexene (25.4 ml, 250 mmol) in ethanol (100 ml), 5% Pd-C (53.0 g) was added with cooling. The black mixture was refluxed for 2 h with stirring and filtered several times until the filtrate became clear. The filtrate was then evaporated to dryness to afford a crude product, which was purified by dissolution in 2 M hydrochloric acid (1 M=1 mol dm^{-3}) and subsequent precipitation into aqueous sodium

hydrogencarbonate to provide a slightly yellow powder (mp 264—265 °C) in 63% yield. Found: C, 42.46; H, 3.22; N, 13.98%. Calcd for $C_7H_6N_2SO_3$: C, 42.42; H, 3.05; N, 14.13%. IR (KBr) 3380, 3320 (NH), 1720 (C=O), 1610 (Ar), 1315, 1170, and 1120 (SO_2) cm^{-1}. NMR (DMSO-d_6) δ= 6.5—7.8 [m, 3H (Ar)+3H (NH)]. MS (*m/e*) 198 (M^+, 54) and 63 (100).

*6-(Acrylamido)saccharin (**6a**).* *(a) From 6-Aminosaccharin (**5**):* To a solution of **5** (1.98 g, 10 mmol), sodium hydrogencarbonate (1.8 g), and a small amount of hydroquinone in water (50 ml), acryloyl chloride (2.72 g, 30 mmol) was added dropwise with ice cooling followed by stirring at room temperature for 30 min. The reaction mixture was then poured into cold 2 M hydrochloric acid to effect precipitation. The precipitate was filtered and recrystallized from methanol to afford a slightly yellow powder (mp>290 °C) in 73% yield. Found: C, 47.62; H, 3.28; N, 11.09%. Calcd for $C_{10}H_8N_2SO_4$: C, 47.62; H, 3.20; N, 11.11%. IR (KBr) 1735 (C=O), 1695 (amide I), 1600 (Ar), 1530 (amide II), 1320, 1180, 1150 (SO_2), 980, and 900 (CH_2=CH–) cm^{-1}. NMR (DMSO-d_6) δ=5.8—6.0 (m, 1H, –C<u>H</u>=CH_2), 6.3—6.5 (t, 2H, –CH=C<u>H</u>$_2$), 7.9 (s, 2H, ArH), 8.5 (s, 1H, ArH), 9.7 (s, 1H, amide NH), and 10.9 (s, 1H, =NH). MS (*m/e*) 252 (M^+, 20) and 55 (100).

*(b) From 6-Nitrosaccharin (**4**):* To a solution of sodium dithionite (3.5 g, 22 mmol) in water (5 ml), **4** (1 g, 4 mmol) was added and the mixture stirred at room temperature for 30 min. A small amount of sodium hydrogencarbonate was added to give a clear solution, which was cooled in an ice-water bath followed by addition of a small amount of hydroquinone. Acryloyl chloride (1.2 g, 13 mmol) was then added dropwise to the solution and the mixture was stirred for 30 min under ice cooling. Acidification of the solution with 5% hydrochloric acid provided a crude product, which was purified by dissolution in 10% aqueous sodium carbonate and subsequent precipitation into 5% hydrochloric acid to afford a slightly green powder (**6a**) in 13% yield. Elemental analyses, IR, NMR, and MS identified the same structure as that prepared in *(a)*.

*6-(Methacrylamido)saccharin (**6b**).* The same reaction procedure as that for **6a** was applied to **5** (2.0 g, 10 mmol) and methacryloyl chloride (3.1 g, 30 mmol) to afford a slightly yellow powder (mp 215—217 °C) in 71% yield. Found: C, 49.92; H, 3.90; N, 10.01%. Calcd for $C_{11}H_{10}N_2SO_4$: C, 50.25; H, 3.89; N, 9.85%. IR (KBr) 1760 (C=O), 1710 (amide I), 1590 (Ar), 1540 (amide II), 1340, 1190, 1130 (SO_2), and 930 (CH_2=CCH_3–) cm^{-1}. NMR (DMSO-d_6) δ=2.1 (s, 3H, Me), 5.7 (s, 1H, =CH_2), 6.0 (s, 1H, =CH_2), 8.0—8.8 (m, 3H, ArH), 8.6 (s, 1H, NH), and 10.6 (s, 1H, NH). MS (*m/e*) 266 (M^+, 5) and 69 (100).

*6-[4-(2-Bromoethyl)benzenesulfonamido]saccharin (**7**).* To a solution of **5** (2.0 g, 10 mmol), a small amount of hydroquinone and sodium hydroxide (0.96 g) in water (30 ml) was added with stirring a solution in acetonitrile (25 ml) of 4-(2-bromoethyl)benzenesulfonyl chloride (5.7 g, 20 m mol),prepared from (2-bromoethyl)benzene and chlorosulfuric acid according to a known method.[5] The mixture was stirred at room temperature for 12 h and poured into cold 2 M hydrochloric acid to afford a precipitate, which was filtered and recrystallized from methanol–water to afford a slightly pink powder (mp 168—171 °C) in 27% yield. Found: C, 40.51; H, 3.05; N, 6.25%, Calcd for $C_{15}H_{13}N_2S_2BrO_5$: C, 40.46; H, 2.94; N, 6.29%. IR (KBr) 3240 (NH), 2920, 2850 (CH_2), 1730 (C=O), 1325, and 1160 (SO_2) cm^{-1}. NMR (DMSO-d_6+$CDCl_3$) δ=3.1—3.4 (t, 2H, CH_2), 3.7—3.9 (t, 2H, CH_2), 6.3 (s, 1H, NH), 7.5—8.2 (m, 7H, ArH), and 11.5 (s, 1H, NH). MS (*m/e*) 216 and 197.

*6-(4-Styrenesulfonamido)saccharin (**8**).* *(a)* Via *Route 2*: A solution of **7** (2.0 g, 4.5 mmol), potassium hydroxide (0.6 g, 11 mmol), and a small amount of hydroquinone in methanol (30 ml) was refluxed for 1 h with stirring. The reaction mixture was poured into cold 2 M hydrochloric acid. The precipitate thus produced was filtered and recrystallized from methanol–water to afford a slightly pink powder (mp 144—147 °C) in 80% yield. Found: C, 49.56; H, 3.12; N, 7.50%. Calcd for $C_{15}H_{12}N_2S_2O_5$: C, 49.44; H, 3.32; N, 7.69%. IR (KBr) 1730 (C=O), 1320, 1160 (SO_2), 985, and 910 (vinyl) cm^{-1}. NMR (DMSO-d_6+$CDCl_3$) δ=5.2—6.2 (q, 2H, CH_2=), 6.3 (s, 1H, NH), 6.5—7.3 (m, 1H, =CH–), 7.5—8.1 (m, 7H, ArH), and 11.6 (s, 1H, NH).

(b) Via *Route 3*: A solution of **5** (2.0 g, 10 mmol), *p*-vinyl benzenesulfonyl chloride (4.1 g, 20 mmol),[6] triethylamine (1.5 g), and hydroquinone (0.1 g) in DMF (50 ml) was stirred at room temperature for 12 h and poured into cold 2 M hydrochloric acid. The resulting precipitate was collected by filtration and washed with ether. Recrystallization from methanol–water provided a white powder (mp 148—149 °C) in 14% yield. Found: C, 49.19; H, 3.43; N, 7.47%. IR and NMR spectra were essentially identical with those of the product in *(a)*.

*6-(Vinylbenzylamino)saccharin (**9**).* A solution of **5** (1.0 g, 5 mmol), triethylamine (0.7 ml, 5 mmol), vinylbenzyl chloride (Seibi Chem. Co., *m/p*=60/40; 2.3 g, 15 mmol), and hydroquinone (0.1 g) in DMF (30 ml) was stirred at 90 °C for 7 h. The reaction mixture was poured into ice-cold 2 M hydrochloric acid. The resulting precipitate was filtered and recrystallized from methanol–water to afford a white powder (mp 155—158 °C) in 32% yield. Found: C, 61.33; H, 4.48; N, 8.70%. Calcd for $C_{16}H_{12}N_2SO_3$: C, 61.13; H, 4.49; N, 8.91%. IR (KBr) 3380 (NH), 2945, 2845 (CH_2), 1720 (C=O), 1600 (Ar), 1330, 1300, 1175, 1140 (SO_2), 995, and 915 (vinyl) cm^{-1}. NMR (DMSO-d_6+$CDCl_3$) δ=4.9 (s, 2H, CH_2), 5.3—6.1 (q, 2H, CH_2=), 6.7—8.0 (m, 10H, =CH–+ ArH+NH). MS (*m/e*) 314 (M^+, 4) and 250 (100).

*Sodium N-(2-Aminocyclohexyl)sulfamate (**11**).* To a solution of 1,2-cyclohexanediamine (**10**; 25 g, 220 mmol) in anhydrous chloroform (110 ml) cooled below 0 °C, chlorosulfuric acid (8.43 g, 72 mmol) was added dropwise with stirring. It required about 2 h. The mixture was further stirred for 30 min below 0 °C and poured into 6% aqueous sodium hydroxide (100 ml). The aqueous layer was separated, extracted with ether to remove the ether-soluble part, and free-zedried to afford a crude product, which was extracted with hot 90% ethanol to afford a white powder upon cooling in 53% yield. Found: C, 33.31; H, 6.23; N, 12.62%. Calcd for $C_6H_{13}N_2SO_3Na$: C, 33.33; H, 6.06; N, 12.96%. IR (KBr) 2940, 2860 (CH_2, CH), 1610 (NH), and 1200 (SO_2) cm^{-1}. NMR (D_2O) δ=1.0—3.0 (m, 11H, CH_2, CH+NH+NH_2).

*N-[2-[4-(2-Bromoethyl)benzenesulfonamido]cyclohexyl]sulfamic Acid (**12**).* A mixture of **11** (1.0 g, 4.6 mmol), 4-(2-bromoethyl) benzenesulfonyl chloride (1.57 g, 5.6 mmol), sodium hydroxide (0.22 g), and acetonitrile–water (1 : 2 v/v; 30 ml) was stirred at room temperature for 12 h. The reaction mixture was then poured into cold 2 M hydrochloric acid and let stand overnight to afford a white precipitate, which was filtered, washed with ether, dissolved in aqueous sodium hydroxide, and reprecipitated with hydrochloric acid to afford white crystals (mp 184—187 °C) in 74% yield. Found: C, 37.89; H, 4.82; N, 6.50%. Calcd for $C_{14}H_{21}N_2S_2BrO_5$: C, 38.09; H, 4.80; N, 6.35%. IR (KBr) 3290 (NH), 2960, 2950, 2870 (CH, CH_2), 1595 (Ar), 1330, 1315, 1300, 1165, and 1155 (SO_2) cm^{-1}. NMR (DMSO-d_6) δ=0.8—1.9 (b, 8H, 4CH_2), 1.9—3.3 (b, 3H, 2CH+NH), 2.8—3.4 (t, 2H, CH_2), 3.5—4.0 (t, 2H, CH_2), 5.3 (s, 1H, NH), and 7.5—8.3 (q, 5H, ArH+SO_3H).

N-[*2-(4-Styrenesulfonamido)cyclohexyl*]*sulfamic Acid* (**13**). A mixture of **12** (1.5 g, 3.4 mmol), potassium hydroxide (0.42 g, 7.6 mmol), and hydroquinone (0.1 g) in 90% ethanol (30 ml) was stirred at 80 °C for 1 h. The resulting solution was poured into ice-cold 2 M hydrochloric acid to afford a precipitate, which was filtered, dissolved in aqueous sodium hydroxide, and reprecipitated with hydrochloric acid to afford a slightly pink powder (mp 148—149 °C) in 35% yield. Found: C, 46.54; H, 5.68; N, 7.86%. Calcd for $C_{14}H_{20}N_2S_2O_5$: C, 46.65; H 5.59; N, 7.77%. IR (KBr) 2935, 2865 (CH_2, CH), 1600 (Ar), 1320, 1160 (SO_2), 990, and 930 (vinyl) cm^{-1}. NMR ($CDCl_3$+DMSO-d_6) δ=0.8—1.9 (b, 8H, $4CH_2$), 2.0—3.5 (m, 3H, 2CH+NH), 5.5 (d, 1H, CH_2=), 6.0 (d, 1H, CH_2=), 6.8 (q, 1H, =CH-), 7.5—8.1 (q, 5H, ArH+NH), and 8.5 (s, 1H, $-SO_3H$).

N-[*2-(Vinylbenzylamino)cyclohexyl*]*sulfamic Acid* (**14**). To a solution of **11** (2.0 g, 9.3 mmol), triethylamine (1.1 g, 11 mmol), and hydroquinone (0.2 g) in 90% ethanol (30 ml), vinylbenzyl chloride (*m*/*p*=60/40; 1.41 g, 9.3 mmol) was added dropwise and the mixture stirred at 65 °C for 2 h. The reaction mixture was poured into cold 2 M hydrochloric acid. Upon standing overnight, the resulting precipitate was filtered and purified by dissolution in aqueous sodium hydroxide and subsequent reprecipitation into cold aqueous hydrochloric acid. A slightly colored powder of mp 255—257 °C was obtained in 29% yield. Found: C, 58.26; H, 7.06; N, 8.83%. Calcd for $C_{15}H_{21}N_2SO_3H$: C, 58.04; H, 7.14; N, 9.02%. IR (KBr) 3350 (NH), 2945, 2865 (CH_2, CH), 1630 (NH), 1600 (Ar), 1280, 1170 (SO_2), 985, and 925 (vinyl) cm^{-1}. NMR (CF_3COOH) δ=1.0—2.7 (b, 10H, CH_2, CH), 3.2—3.8 (b, 1H, NH), 4.1—4.8 (b, 3H, CH_2NH), 5.5 (d, 1H, CH_2=), 6.0 (d, 1H, CH_2=), 6.9 (q, 1H, =CH-), 7.0—8.0 (m, 4H, ArH), and 10.5 (s, 1H, $-SO_3H$).

Polymerization of Monomers. In a typical example, a solution of monomer **6a** (1.5 g) and α,α'-azobisisobutyronitrile (AIBN; 0.015 g) in DMF (3.5 g) was put into a glass ampoule, which was evacuated, filled with nitrogen, and sealed in a conventional manner. Polymerization was carried out at 70 °C for 72 h. The content of the ampoule was then poured into aqueous sodium carbonate and dialyzed through a cellulose tubing (Visking) against water for 3 d. The dialyzed mixture was filtered and the filtrate was freeze-dried.

In the copolymerization with VP, the composition was adjusted so as to afford 30% total monomer concentration and 1% AIBN/total monomers. The results thus obtained are given in Table 1.

All homopolymers and copolymers synthesized indicated IR absorptions at 2930 and 2860 cm^{-1} characteristic of the vinyl polymer backbone together with those of the pendant saccharin and cyclamate units.

Intrinsic Viscosity. Intrinsic viscosities [η] of the synthesized polymers were measured in DMF solutions at 20 °C by means of an Ostwald-type viscometer, unless otherwise noted.

References

1) H. Kamogawa, K. Nakura, H. Tsuda, K. Sugaya, and M. Nanasawa, *Reports of the Asahi Glass Found. for Ind. Technology*, **32**, 15 (1978).

2) H. Kamogawa, K. Sugiyama, H. Hanawa, and M. Nanasawa, *J. Polym. Sci., Polym. Chem. Ed.*, **14**, 511 (1976).

3) H. Kamogawa, K. Kitahora, H. Hanawa, and M. Nanasawa, *J. Polym. Sci., Polym. Chem. Ed.*, **14**, 1235 (1976).

4) I. D. Entwistle, R. A. W. Johnstone, and T. T. Povall, *J. Chem. Soc., Perkin Trans. 1*, **1975**,1300.

5) H. Spinner, J. Yannopoulos, and W. Metanomski, *Can. J. Chem.*, **39**, 2529 (1961).

6) H. Kamogawa, A. Kanazawa, M. Kadoya, T. Naito, and M. Nanasawa, *Bull. Chem. Soc. Jpn.*, in press.

Optical Resolution of 2,2′,6,6′-Tetrafluorobiphenyl-3,3′-dicarboxylic Acid

Noriko HASAKA, Masayoshi OKIGAWA, Isao KOUNO, and Nobusuke KAWANO*
Faculty of Pharmaceutical Sciences, Nagasaki University, Bunkyomachi, Nagasaki 852
(Received April 16, 1982)

Optically active (−)- and (+)-2,2′,6,6′-tetrafluorobiphenyl-3,3′-dicarboxylic acids were obtained through brucine salts. The half-life times for racemization of their dimethyl esters were estimated at various temperatures and the activation energy was calculated to be 25.6 kcal/mol.

Recently, the optical resolution of 2,2′,6,6′-tetramethoxybiphenyl compounds (**1** and **2**), 2,2′,6-trimethoxybiphenyl-3-carboxylic acid (**3**), and 2,2′-difluoro-6,6′-dimethoxybiphenyl-3-carboxylic acid (**4**) were reported.[1] These results disclosed the erroneous findings reported by Adams and co-wokers[2] and stimulated us to attempt the optical resolution of 2,2′,6,6′-tetrafluorobiphenyl-3,3′-dicarboxylic acid (**5**), although Adams and co-workers reported[3] that 2,2′,6,6′-tetrafluoro-5,5′-dichlorobiphenyl-3,3′-dicarboxylic acid (**6**) was nonresolvable. The activation energy for racemization of the compound **5** should be less than that of the compounds, **1** and **4** because of the smaller van der Waals radius of fluorine atom than that of oxygen.

Racemic **5** was obtained from *m*-difluorobenzene by a synthetic route shown in Scheme 1 although another route was formerly reported.[4] The optical resolution of **5** was achieved through brucine salts. Fortunately, two kinds of brucine salts were obtained in the course of the resolution. The first salt, mp 151—156 °C, gave (−)-acid, mp 243—245°C, $[\alpha]_D^{24}$ −35.9° (ethanol) and the second salt, mp 169—179 °C, gave (+)-acid, mp 241—244 °C, $[\alpha]_D^{24}$ +36.2° (ethanol). Their dimethyl esters were also optically active and showed $[\alpha]_D^{24}$ −33.5° (dioxane) and +34.0° (dioxane), respectively. In the preceding paper[1] the optical purities of active esters were estimated from ^{1}H NMR spectra taken with use of a chiral NMR-shift reagent (CSR), tris[3-(heptafluoropropylhydroxymethylene)-*d*-camphorato]europium-(III).[5] However, the racemic ester of **5** showed only one set of signals even in the presence of a large amount of the same CSR. Therefore, NMR-shift reagents were not useful for the estimation of the optical purities of the active esters of **5**.

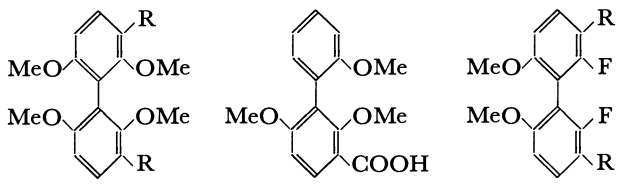

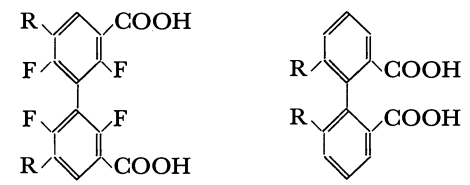

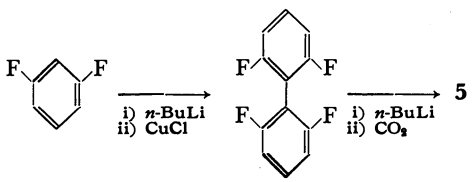

Scheme 1. Synthetic route of **5**.

Racemization experiments were performed with use of both the (−)- and (+)-dimethyl esters and the results obtained are shown in Tables 1 and 2. The activation energy for racemization of these active esters was first determined graphically; 25.9 kcal/mol from the (−)-ester (Table 1) and 25.7 kcal/mol from the (+)-ester (Table 2). Calculations by the least squares method at 95% confidence limit gave 25.4±1.0 kcal/mol from the (−)-ester and 25.8±0.8 kcal/mol from the (+)-ester. The mean of these values is 25.6 kcal/mol, and this value is 13.8 kcal/mol less than the activation energy of the optically active ester of **4** (39.4 kcal/mol in a 2-phenylethanol solution),[1] corresponding to the structural difference between **4** and **5**, fluorine atoms instead of methoxyl groups at 6- and 6′-positions.

A similar structural difference can be seen in two compounds, 2,2′-difluorobiphenyl-6,6′-dicarboxylic acid (**7**) and 2,2′-dimethoxybiphenyl-6,6′-dicarboxylic acid (**8**), reported by Adams and co-workers.[6] Racemization

Table 1. Racemization data[a] of (−)-dimethyl ester of **5**

Temp/°C	Time/min	α_{546}^{20}/°	log *k*	Half-life time/min
73.9±0.2	360	−0.0495	−4.611	469.5
79.6±0.1	240	−0.045	−4.363	267.0
88.7±0.2	90.75	−0.047	−3.957	104.8
97.1±0.1	60	−0.035	−3.614	47.5

a) A solution of 30.0 mg of (−)-ester in 10.0 ml of dioxane was used. Initial rotation: α_{546}^{20} −0.084° (*l*= 10.00 cm).

Table 2. Racemization data[a] of (+)-dimethyl ester of **5**

Temp/°C	Time/min	α_{546}^{20}/°	log *k*	Half-life time/min
75.3±0.1	300	+0.082	−4.551	411.0
80.9±0.1	180	+0.078	−4.288	224.3
89.0±0.1	90	+0.073	−3.938	100.3
96.9±0.1	60	+0.056	−3.608	46.9

a) A solution of 41.0 mg of (+)-ester in 10.0 ml of dioxane was used. Initial rotation: α_{546}^{20}+0.136°(*l*=10.00 cm).

data of these compounds observed by them are as follows: The complete racemization time of **7** was about 2 h in boiling ethanol or 10 min in boiling acetic anhydride, whereas the half-life period of **8** was 78 min in boiling glacial acetic acid or about 60 h in boiling ethanol. Afterwards, the racemization of **8** was extensively studied in various solvents and the $\Delta H^{\ddagger}$ in dioxane has been reported[7] as 25.15±0.07 kcal/mol. This value of **8** should be larger than that of **7**. However, the energy difference between **7** and **8** is only a few kcal/mol at most. This is much less than the former difference of 13.8 kcal/mol between **4** and **5**. The reasons considered are as follows: a) The electronic effects of carboxyl groups in **4** and **5**, b) the use of a different solvent (2-phenylethanol) in the case of **4**, and c) in **4** and **5**, racemization requires the passage of MeO (**4**) and F (**5**) groups past F groups, whereas in **7** and **8**, F (**7**) and MeO (**8**) groups must pass COOH groups.

In order to investigate the molecular chirality of **4** without buttressing effects ^{1}H NMR spectra of 2,2′-difluoro-6,6′-dimethoxybiphenyl (**9**) were taken with use[8,9] of the CSR. When two molar ratio of the CSR was added, two methyl signals were observed with a chemical shift difference of 2.5 Hz, indicating that **9** is chiral at room temperature on the NMR time scale. This observation means that F and MeO groups at *ortho*-position of biphenyl compounds are large enough to restrict the rotation without buttressing effects. The lower limit of the rotational barrier of **9** may be estimated to be about 16 kcal/mol from the Eyring equation.[10] Adams' method[11] of predicting the resolvability of chiral biphenyls should be partly revised since there have been some reports[12] concerning the effective van der Waals radii of these atoms and groups.

Experimental

All melting points are uncorrected. Optical rotations were measured with a Nihon-Bunko (JASCO) DIP-181 polarimeter. UV and IR spectra were recorded with a Hitachi 323 recording spectrometer and a JASCO IRA-2 grating infrared spectrophotometer respectively. ^{1}H NMR spectra were recorded with a JEOL PS-100 instrument using TMS as internal reference. Mass spectra were obtained from a JEOL JMS-01SG double-focus instrument.

2,2′,6,6′-Tetrafluorobiphenyl. *m*-Difluorobenzene (2.0 g) was dissolved in anhydrous tetrahydrofuran (THF, 50 ml) and kept at −70 °C in a Dry Ice and methanol mixture. To the cooled and stirred solution was added dropwise 15% butyllithium hexane solution (12.5 ml) during 15 min. Stirring was continued for a further 3 h period at the same temperature and then anhydrous $CuCl_2$ (2.9 g) was added. After the mixture was stirred for 2 h the temperature slowly rose to room temperature during 1 h. Stirring was continued for 5 h at room temperature. The reaction mixture was acidified with diluted hydrochloric acid and extracted with diethyl ether. The ether solution was washed with water, dried over $MgSO_4$, and evaporated. The reaction product was purified by column chromatography (silica gel and hexane) to give a product (1.03 g), mp 47.5—48.5 °C from hexane–ether (reported[13] mp 47.5—48.5 °C), UV_{max} (EtOH) 230 (log ε 4.16) and 265 nm (3.24); IR (KBr) 1615, 1459, 1265, 1234, 1004 (C–F), and 990 cm^{-1}; MS *m/z* 226 (M$^+$).

2,2′,6,6′-Tetrafluoro-3,3′-bis(methoxycarbonyl)biphenyl. 2,2′,6,6′-Tetrafluorobiphenyl (2.5 g) was dissolved in anhydrous THF (70 ml) and kept at −70 °C. To the cooled and stirred solution was added dropwise 15% *n*-BuLi hexane solution (12.0 ml) during 15 min. Stirring was continued for further 6 h at the same temperature and dried CO_2 was introduced to the cooled solution for 2 h. During that time the temperature of the reaction mixture was gradually raised to room temperature. The mixture was acidified with diluted hydrochloric acid and extracted with diethyl ether. The ether solution was washed with water, dried over $MgSO_4$, and evaporated. The reaction products obtained were methylated with diazomethane and purified by column chromatography (silica gel and hexane and then hexane–chloroform) to give colorless needles from hexane–diethyl ether (0.7 g, 18.5% yield), mp 136.5—137.5 °C (reported[4] mp 136—137 °C); UV_{max} (EtOH) 218 (log ε 4.60) and 277 nm (3.45); IR (KBr) 1722 (C=O), 1267, 1216, 1131, and 1007 cm^{-1}; MS *m/z* 342 (M$^+$), 311 (M-OCH$_3$, base peak), 252, 224; ^{1}H NMR ($CDCl_3$) δ 3.96 (6H, s, Me), 7.11 (2H, br. t, J=8.1 Hz), 7.90—8.25 (2H, m).

2,2′,6,6′-Tetrafluorobiphenyl-3,3′-dicarboxylic Acid (5). The above diester (0.70 g) was hydrolyzed with 8% NaOH solution (20 ml) at 90 °C for 2 h to give colorless acid and recrystallized from diluted ethanol, mp above 295 °C (reported[4] mp 306.5—307.5 °C), (0.61 g, 95% yield); UV_{max} (EtOH) 215 (log ε 4.57) and 274 nm (3.55); IR (KBr) 3433, 2980, 2590, 1710 (C=O), 1607, 1261 (COOH), 1039, and 1010 cm^{-1}; MS *m/z* 314 (M$^+$), 297, 269, and 224.

(−)-2,2′,6,6′-Tetrafluorobiphenyl-3,3′-dicarboxylic Acid. Racemic **5** (157 mg, 0.5 mmol) and brucine dihydrate (430 mg, 1.0 mmol) were dissolved in hot ethanol (5 ml) and left to stand overnight. Brucine salt obtained was recrystallized two times from ethanol to afford colorless crystals (35 mg), mp 151—156 °C, which were decomposed with 10% hydrochloric acid and extracted with ether. The ether solution was washed with water, dried over $MgSO_4$, evaporated, and crystallized from ethanol to give optically active acid (8 mg), mp 243—245 °C, $[\alpha]_D^{24}$ −35.9° and $[\alpha]_{546}^{24}$ −40.9° (0.32%, EtOH).

(−)-2,2′,6,6′-Tetrafluoro-3,3′-bis(methoxycarbonyl)biphenyl. The above (−)-acid (25.8 mg) was methylated with diazomethane to give an optically active ester (27.5 mg), mp 55—58 °C, $[\alpha]_D^{24}$ −33.5° and $[\alpha]_{546}^{24}$ −40.4° (0.49%, dioxane); UV_{max} (EtOH) 218 (log ε 4.58) and 277 nm (3.43); IR, MS, and ^{1}H NMR the same with those of racemic dimethyl ester.

(+)-2,2′,6,6′-Tetrafluorobiphenyl-3,3′-dicarboxylic Acid. The filtrate separated from the first brucine salt was evaporated to about 3.5 ml and left to stand overnight to give the second salt, which was recrystallized two times from ethanol to afford colorless crystals (98 mg), mp 173—179 °C. The salt was decomposed and the optically active acid obtained was crystallized from ethanol to give colorless crystals (24 mg), mp 241—244 °C, $[\alpha]_D^{24}$ +36.2° and $[\alpha]_{546}^{24}$ +41.2° (1.2%, EtOH).

(+)-2,2′,6,6′-Tetrafluoro-3,3′-bis(methoxycarbonyl)biphenyl. The above (+)-acid (38 mg) was methylated with diazomethane to give a dimethyl ester (41 mg), mp 56—59 °C, $[\alpha]_D^{24}$ +34.0° and $[\alpha]_{546}^{24}$ +40.6° (1.1%, dioxane); UV_{max} (EtOH) 218 (log ε 4.57) and 277 nm (3.42); IR, MS, and ^{1}H NMR the same with those of racemic dimethyl ester.

The authors are grateful to Professor K. Mislow, Princeton University, for his valuable advices and encouragements and Miss H. Kammura and Y. Kawabata for their technical assistance.

References

1) N. Kawano, M. Okigawa, N. Hasaka, I. Kouno, Y. Kawahara, and Y. Fujita, *J. Org. Chem.*, **46**, 389 (1981).
2) A. M. VanArendonk, M. E. Cupery, and R. Adams, *J. Am. Chem. Soc.*, **55**, 4225 (1933).
3) E. C. Kleiderer and R. Adams, *J. Am. Chem. Soc.*, **55**, 4219 (1933).
4) S. Sugawara and N. Ishikawa, *Kogyo Kagaku Zasshi*, **74**, 235 (1971).
5) R. R. Fraser, M. A. Petit, and J. K. Sanders, *J. Chem. Soc., D*, **1971**, 1450.
6) W. M. Stanley, E. McMahon, and R. Adams, *J. Am. Chem. Soc.*, **55**, 706 (1933).
7) B. M. Graybill and J. E. Leffler, *J. Phys. Chem.*, **63**, 1461 (1959).
8) L. W. Jelinski and E. F. Kiefer, *J. Am. Chem. Soc.*, **98**, 282 (1976).
9) A. Mannschreck, V. Jonas, H. Bödecker, H. Elbe, and G. Köbrich, *Tetrahedron Lett.*, **1974**, 2153.
10) R. J. Abraham and P. Loftus, "Proton and Carbon-13 NMR Spectroscopy," (Japanese edition translated by Y. Takeuchi), Kagakudōjin, Tokyo (1979), p. 199.
11) R. Adams and H. C. Yuan, *Chem. Rev.*, **12**, 261 (1933).
12) G. Bott, L. D. Field, and S. Sternhell, *J. Am. Chem. Soc.*, **102**, 5618 (1980); A. Bondi, *J. Phys. Chem.*, **68**, 441 (1964); M. Charton, *J. Org. Chem.*, **42**, 2528 (1977).
13) S. Sugawara, N. Ishikawa, H. Harada, and S. Hayashi, *Nippon Kagaku Kaishi*, **1973**, 1510.

Synthesis of A and B Rings Analog of Coleon B

Takashi MATSUMOTO,* Koji IYO, and Shigekazu MIUCHI
Department of Chemistry, Faculty of Science, Hiroshima University, Higashisenda-machi, Naka-ku, Hiroshima 730
(Received April 19, 1982)

Catalytic hydrogenation of 19-norabieta-4(18),8,11,13-tetraen-3α-ol over Raney Ni and subsequent dehydration afforded 18-norabieta-2,8,11,13-tetraene, which was converted into 3α-bromo-18-norabieta-8,11,13-trien-2-one (**8**) *via* a bromohydrin. Acetalization of **8** with 1,2-ethanediol in the presence of *p*-toluenesulfonic acid afforded a mixture of 3α-bromo-2,2-ethylenedioxy-18-norabieta-8,11,13-triene (**10**) and its 3β-bromo isomer (**11**) in a ratio of *ca.* 2 : 3. Oxidation of **10** and **11** with chromium trioxide in acetic acid gave the corresponding ketones **12** and **13**. The ketone **13** was then converted into a diosphenol derivative, 3β-bromo-2,2-ethylenedioxy-6-hydroxy-18-norabieta-5,8,11,13-tetraen-7-one (**14**), by treatment with oxygen in the presence of potassium *t*-butoxide. Hydrolysis of **14** with dilute hydrochloric acid followed by dehydrobromination afforded the desired analog, 6-hydroxy-19-norabieta-3,5,8,11,13-pentaene-2,7-dione. A related A/B ring oxygenated compound, 19-norabieta-3,5,8,11,13-pentaene-2,7-dione was also synthesized from **12** and **13** *via* the corresponding 6α-bromo derivatives.

Coleon B (**1**) is a rare tricyclic norditerpene phenol isolated from *Coleus iguiarius* Schweinf. (Labiatae) by Eugster *et al.*[1] To establish the synthetic route of this highly-oxygenated norditerpene, we investigated the oxidation of rings A/B of dehydroabietic acid (**2**); the introduction of oxygen functions at the C-11, C-12, and C-14 positions in ring C has already been achieved in our laboratory.[2] This paper will describe the synthesis of A and B rings analog (**3**) of coleon B, starting from 19-norabieta-4(18),8,11,13-tetraen-3α-ol (**4**) which was prepared from **2** by the known procedure.[3–5]

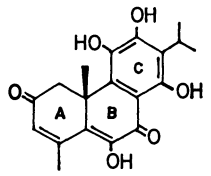

1

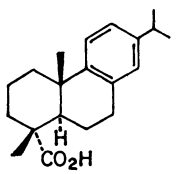

2

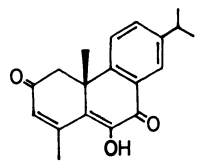

3

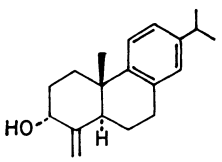

4

Catalytic hydrogenation of **4** in ethanol over Raney Ni at room temperature afforded 18-norabieta-8,11,13-trien-3α-ol (**5**),[6,7] which was dehydrated with phosphoryl chloride in refluxing pyridine to give 18-norabieta-2,8,11,13-tetraene (**6**) in 65.3% yield from **4**. The ^{1}H NMR spectrum of **6** showed doublet signals at δ 1.05 due to the C-4 methyl group and at δ 5.66 due to the two vinylic protons. The tetraene **6** was treated with *N*-bromosuccinimide in dimethyl sulfoxide containing a small quantity of water at 20—25 °C under a stream of nitrogen to give a bromohydrin (**7**) which, without purification, was used in the next reaction. The structure of **7** as indicated was predicted by a well-documented mechanistic pathway[8] and was substantiated spectroscopically. In the ^{1}H NMR spectrum of **7**, the downfield shift of the signal (δ 1.36) due to the methyl group at the C-10 position relative to the corresponding signal (δ 1.20) for **6** suggested a 1,3-diaxial-*cis*-relationship between the methyl goup and the new hydroxyl group. Consequently, the structure of **7** was assigned to be 3α-bromo-18-norabieta-8,11,13-trien-2β-ol. Oxidation of the crude **7** in acetone with Jones reagent at 0 °C afforded 3α-bromo-18-norabieta-8,11,13-trien-2-one (**8**) in 69.1% yield from **6**. This bromo ketone **8** was easily dehydrobrominated by heating at 120—125 °C with lithium carbonate and lithium bromide in *N*,*N*-dimethylformamide under a stream of nitrogen; an α,β-unsaturated ketone, 19-norabieta-3,8,11,13-tetraen-2-one (**9**), was obtained. The structure of **9** was supported by its IR (1654, 1622 cm^{-1}) and ^{1}H NMR (δ 1.99, C_4–CH_3; 5.86, C_3–H) spectra. From the formation of **9**, the position of the bromine atom in **7** and **8** was conclusively assigned to be the C-3 position. To protect the carbonyl group as ethylene acetal, the ketone **8** was refluxed with 1,2-ethanediol and *p*-toluenesulfonic acid in benzene to give two epimeric acetals in 81.1%yield, **10** and **11**, in a ratio of *ca.* 2 : 3. Hydrolysis of **10** with dilute hydrochloric acid in refluxing acetic acid afforded the original ketone **8**, which was also obtained by the same hydrolysis of **11**. The ^{1}H NMR spectrum of **10** showed a multiplet signal at δ *ca.* 3.8—4.3 due to the ethylenedioxy group at the C-2 position, while that of **11** showed the corresponding signal at δ 3.98 as a broad singlet with half-height width of 6 Hz. These spectral data suggested[9] the presence of an axial bromine atom in **10** and an equatorial one in **11**. Thus, the structures of **10** and **11** were determined respectively to be 3α-bromo-2,2-ethylenedioxy-18-norabieta-8,11,13-triene and 3β-bromo-2,2-ethylenedioxy-18-norabieta-8,11,13-triene. The acetals **10** and **11** were then oxidized with chromium trioxide in acetic acid to give the corresponding 7-oxo compounds, **12** and **13** in yields of 52.6 and 52.2% respectively. Treatment of **13** in *t*-butyl alcohol with oxygen in the presence of potassium *t*-butoxide afforded a diosphenol derivative, 3β-bromo-2,2-ethylenedioxy-6-hydroxy-18-norabieta-5,8,11,13-tetraen-7-one (**14**), in 61.0% yield. The IR spectrum of **14** showed bands at 3432, 1663, 1638, and 1608 cm^{-1} corresponding to a diosphenol moiety. The compound **14** was hydrolyzed with dilute hydrochloric acid in refluxing acetic acid and the resulting

ketone (**15**), without purification, was treated at 120—125 °C with lithium carbonate and lithium bromide in *N,N*-dimethylformamide under a stream of nitrogen to give the desired 6-hydroxy-19-norabieta-3,5,8,11,13-pentaene-2,7-dione (**3**) together with a small amount of 6-hydroxy-18-norabieta-5,8,11,13-tetraene-2,7-dione (**16**). Acetylation of **3** and **16** with acetic anhydride in pyridine afforded the corresponding monoacetates, **17** and **18**. These acetates were easily hydrolyzed with dilute hydrochloric acid in refluxing ethanol to give the original diones, **3** and **16**.

Subsequently, the synthesis of 19-norabieta-3,5,8,11,-13-pentaene-2,7-dione (**19**) was carried out as follows. The ketone **13** was brominated with pyridinium tribromide in dichloromethane at room temperature to give 3β,6α-dibromo-2,2-ethylenedioxy-18-norabieta-8,11,13-trien-7-one (**20**) in 76.5% yield. The stereochemistry of the C-6 position in **20** was supported by its ^{1}H NMR spectrum, which showed a doublet signal due to the C-6 proton at δ 4.84 with coupling constant of 13 Hz, suggesting the presence of an axial β proton. Hydrolysis of **20** with dilute hydrochloric acid in refluxing acetic acid afforded the corresponding 2,7-dioxo compound which, without purification, was converted into **19** in 93.0% yield by treatment with lithium carbonate and lithium bromide in *N,N*-dimethylformamide at 120—125 °C. Similarly, the ketone **12** was also converted into **19** *via* the corresponding 6α-bromo compound (**21**).

Experimental

All melting points are uncorrected. The IR and optical rotations were measured in chloroform, and the ^{1}H NMR spectra in carbon tetrachloride at 60 MHz, with tetramethylsilane as an internal standard, unless otherwise stated. The chemical shifts are presented in terms of δ values; s: singlet, bs: broad singlet, d: doublet, bd: broad doublet, dd: double doublet, m: multiplet. The column chromatography was performed using Merck silica gel.

18-Norabieta-8,11,13-trien-3α-ol (5). A solution of **4**[3-5] (418 mg) in ethanol (10 ml) was hydrogenated at room temperature for *ca.* 3 h in an atmosphere of hydrogen using Raney Ni (W-7) prepared from nickel-aluminium alloy (50%: 1.078 g). After the usual work-up, the crude product was recrystallized from hexane to give **5**[6,7] as colorless crystals (305 mg: 72.3%), mp 117—121 °C. Further crystallization gave an analytical sample; mp 122—123 °C; $[\alpha]_D$ +76.0°; IR: 3616, 3412 cm^{-1}; ^{1}H NMR: 0.92 (3H, d, J=7.5 Hz, C_4-CH_3), 1.11 (3H, s, C_{10}-CH_3), 1.22 (6H, d, J=7 Hz, -CH(C$\underline{H}_3$)$_2$), 1.93 (1H, s, -OH), 3.68 (1H, bs, $W_{1/2}$=5.5 Hz, C_3-H), 6.65—7.15 (3H, m, aromatic protons). Found: C, 83.83; H, 10.60%. Calcd for $C_{19}H_{28}O$: C, 83.77; H, 10.36%.

18-Norabieta-2,8,11,13-tetraene (6). A mixture of **5** (504 mg), phosphoryl chloride (0.9 ml), and pyridine (4.0 ml) was refluxed for 1 h, cooled, and then poured into ice-dilute hydrochloric acid. The mixture was extracted with ether. The ether extract was washed with brine, dried over sodium sulfate, and evaporated *in vacuo*. The crude product was purified by column chromatography on silica gel (30 g), using hexane as the eluent, to give **6** (425 mg: 90.3%) as an oil; $[\alpha]_D$ +291°; ^{1}H NMR: 1.05 (3H, d, J=7.5 Hz, C_4-CH_3), 1.20 (3H, s, C_{10}-CH_3), 1.22 (6H, d, J=7 Hz, -CH(C$\underline{H}_3$)$_2$), 5.66 (2H, d, J=3 Hz, C_2-H and C_3-H), 6.70—7.20 (3H, m, aromatic protons). Found: C, 89.91; H, 10.58%. Calcd for $C_{19}H_{26}$: C, 89.70; H, 10.30%.

3α-Bromo-18-norabieta-8,11,13-trien-2-one (8). A solution of **6** (425 mg) in dimethyl sulfoxide (7.0 ml) containing a small quantity of water (0.1 ml) was stirred with *N*-bromosuccinimide (620 mg) at 20—25 °C for 1 h under a stream of nitrogen. The stirred mixture was cooled in an ice-water bath and aqueous sodium hydrogencarbonate was added.

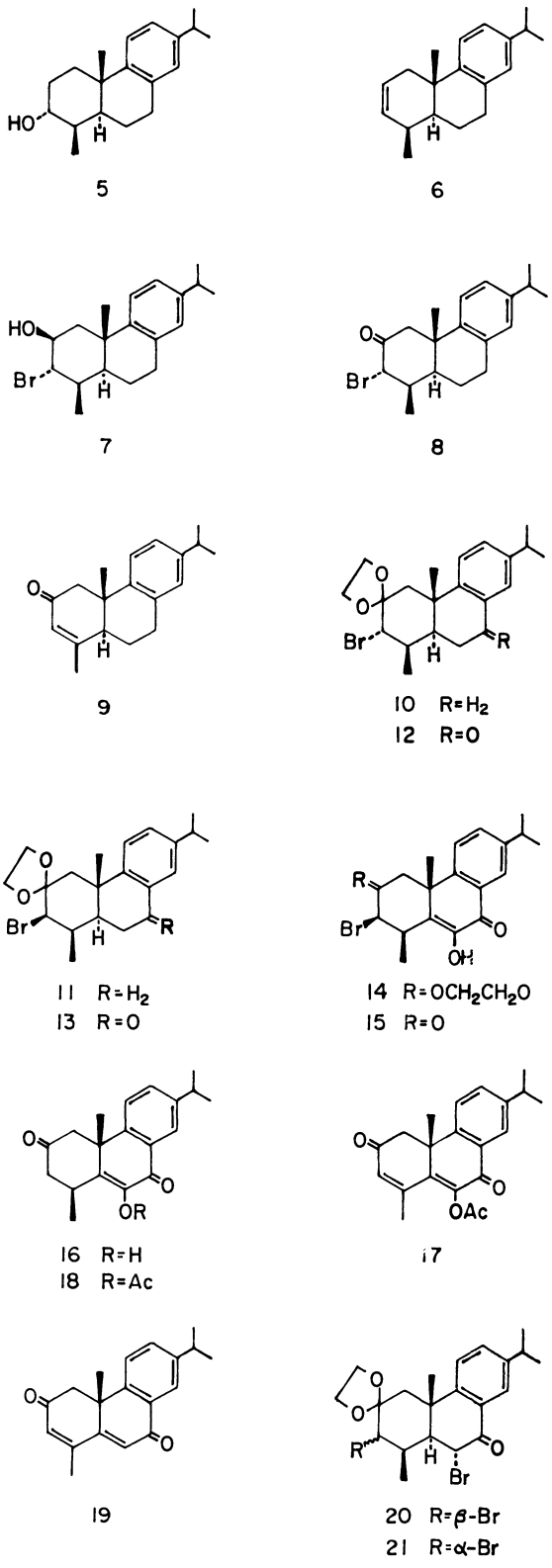

The mixture was extracted with ether. The ether extract was washed with brine, dried over sodium sulfate, and evaporated *in vacuo* to give the crude 3α-bromo-18-norabieta-8,11,13-trien-2β-ol (**7**) (596 mg) as an oil; IR: 3570, 3370 cm^{-1}; ^1H NMR: 1.22 (6H, d, J=7 Hz, $-CH(C\underline{H}_3)_2$), 1.29 (3H, d, J=7.5 Hz, C_4-CH_3), 1.36 (3H, s, $C_{10}-CH_3$).

The crude **7** (596 mg) in acetone (7.0 ml) was oxidized with Jones reagent [2.5 M (1 M=1 mol dm^{-3}): 1.2 ml] at 0 °C for 5 min. The mixture was diluted with water and extracted with ether. The ether extract was washed with brine, dried over sodium sulfate, and evaporated *in vacuo*. The residue was chromatographed on silica gel (35 g), using hexane–benzene (1 : 1) as the eluent, to give **8** (403 mg: 69.1%) as an oil which responded positively to the Beilstein halogen test; $[\alpha]_D$ +185°; IR: 1707 cm^{-1}; ^1H NMR: 1.16 (3H, d, J=7.5 Hz, C_4-CH_3), 1.17 (3H, s, $C_{10}-CH_3$), 1.22 (6H, d, J=7 Hz, $-CH(C\underline{H}_3)_2$), 4.06 (1H, bs, C_3–H), 6.83 (1H, bs) and 6.97 (2H, s) (aromatic protons). Found: C, 65.03; H, 7.33%. Calcd for $C_{19}H_{25}OBr$: C, 65.33; H, 7.23%.

*19-Norabieta-3,8,11,13-tetraen-2-one (**9**).* A mixture of **8** (44 mg), lithium carbonate (30 mg), and lithium bromide (38 mg) in *N,N*-dimethylformamide (2.0 ml) was stirred at 120—125 °C for 3 h in a stream of nitrogen. The reaction mixture was cooled, poured into dilute hydrochloric acid, and extracted with ether. The ether extract was washed with aqueous sodium thiosulfate and brine, dried over sodium sulfate, and evaporated *in vacuo*. The residue was purified by column chromatography on silica gel (10 g), using ether–benzene (3 : 97) as the eluent, to give **9** (32 mg; 92.3%) as an oil; $[\alpha]_D$ +121°; IR: 1654, 1622 cm^{-1}; ^1H NMR: 1.12 (3H, s, $C_{10}-CH_3$), 1.23 (6H, d, J=7 Hz, $-CH(C\underline{H}_3)_2$), 1.99 (3H, bs, C_4-CH_3), 5.86 (1H, bs, C_3–H), 6.70—7.20 (3H, m, aromatic protons). Found: C, 84.72; H, 9.30%. Calcd for $C_{19}H_{24}O$: C, 85.02; H, 9.01%.

*Acetalization of the Bromo Ketone **8**.* A mixture of **8** (833 mg), 1,2-ethanediol (3.0 ml), *p*-toluenesulfonic acid (784 mg), and dry benzene (20 ml) was refluxed for 10 h with a water separator containing 4 Å molecular sieves. The mixture was washed successively with aqueous sodium hydrogencarbonate and brine, dried over sodium sulfate, and evaporated *in vacuo*. The crude product was chromatographed on silica gel (30 g), using hexane–benzene (65 : 35) as the eluent, to give 3α-bromo-2,2-ethylenedioxy-18-norabieta-8,11,13-triene (**10**) (311 mg: 33.1%). It was recrystallized from ether–methanol, mp 114.5—115.5 °C, $[\alpha]_D$ +8.7°; ^1H NMR: 1.20 (6H, d, J=7 Hz, $-CH(C\underline{H}_3)_2$), 1.26 (3H, d, J=7.5 Hz, C_4-CH_3), 1.31 (3H, s, $C_{10}-CH_3$), 1.70 and 2.48 (each 1H and d, J=14 Hz, C_1-H_2), 3.80—4.50 (5H, m, $-OCH_2CH_2O-$ and C_3–H), 6.74 (1H, s) and 6.91 (2H, bs) (aromatic protons). Found: C, 64.23; H, 7.32%. Calcd for $C_{21}H_{29}O_2Br$: C, 64.12; H, 7.45%.

Further elution with the same solvent gave 3β-bromo-2,2-ethylenedioxy-18-norabieta-8,11,13-triene (**11**) (451 mg: 48.0%) as an oil; $[\alpha]_D$ +108°; ^1H NMR: 1.22 (9H, d, J=7 Hz, $-CH(C\underline{H}_3)_2$ and C_4-CH_3), 1.30 (3H, s, $C_{10}-CH_3$), 3.98 (4H, bs, $-OCH_2CH_2O-$), 4.09 (1H, d, J=3 Hz, C_3–H), 6.77 (1H, s), and 6.93 (2H, bs) (aromatic protons). Found: C, 64.40; H, 7.47%. Calcd for $C_{21}H_{29}O_2Br$: C, 64.12; H, 7.45%.

*Hydrolysis of the Acetals **10** and **11**.* *a)*: A mixture of **10** (190 mg) and dilute hydrochloric acid (10%: 0.7 ml) in acetic acid (6.0 ml) was refluxed for 1 h, concentrated *in vacuo*, diluted with water, and extracted with ether. The ether extract was washed successively with aqueous sodium hydrogencarbonate and brine, dried over sodium sulfate, and evaporated *in vacuo*. The residue was chromatographed on silica gel (10 g), using hexane–benzene (1 : 1) as the eluent, to give an oil (129 mg: 76.3%), whose IR and ^1H NMR spectra were identical with those of **8**.

b): A mixture of **11** (70 mg) and dilute hydrochloric acid (10%: 0.4 ml) in acetic acid (2.0 ml) was refluxed for 1 h. After the same work-up as described in *a*), the crude product was chromatographed on silica gel (10 g), using hexane–benzene (6 : 4) as the eluent, to give an oil (41 mg: 66.5%), whose IR and ^1H NMR spectra were identical with those of **8**.

*3α-Bromo-2,2-ethylenedioxy-18-norabieta-8,11,13-trien-7-one (**12**).* A stirred solution of **10** (625 mg) in acetic acid (7.0 ml) was oxidized with chromium trioxide (614 mg) at room temperature for 2.5 h. The mixture was diluted with water and extracted with ether. The ether extract was washed successively with aqueous sodium hydrogencarbonate and brine, dried over sodium sulfate, and evaporated *in vacuo*. The residue was chromatographed on silica gel (40 g), using ether–benzene (1 : 99) as the eluent, to give **12** (340 mg: 52.6%). It was recrystallized from methanol; mp 136.5—139 °C; $[\alpha]_D$ −16.5°; IR: 1676, 1607 cm^{-1}; ^1H NMR: 1.25 (6H, d, J=7 Hz, $-CH(C\underline{H}_3)_2$), 1.33 (3H, d, J=7.5 Hz, C_4-CH_3), 1.41 (3H, s, $C_{10}-CH_3$), 3.85—4.50 (5H, m, $-OCH_2CH_2O-$ and C_3–H), 7.09 (1H, d, J=8 Hz, C_{11}–H), 7.29 (1H, dd, J=2 and 8 Hz, C_{12}–H), 7.78 (1H, d, J=2 Hz, C_{14}–H). Found: C, 61.97; H, 6.70%. Calcd for $C_{21}H_{27}O_3Br$: C, 61.92; H, 6.69%.

*3β-Bromo-2,2-ethylenedioxy-18-norabieta-8,11,13-trien-7-one (**13**).* A stirred solution of **11** (2.542 g) in acetic acid (14 ml) was oxidized with chromium trioxide (2.525 g) as described for the preparation of **12**. The crude product was chromatographed on silica gel (100 g), using ether–benzene (1 : 99) as the eluent, to give **13** (1.374 g: 52.2%). It was recrystallized from methanol; mp 141—142 °C; $[\alpha]_D$ +65.2°; IR: 1673, 1608 cm^{-1}; ^1H NMR: 1.27 (6H, d, J=7 Hz, $-CH(C\underline{H}_3)_2$), 1.30 (3H, d, J=7.5 Hz, C_4-CH_3), 1.39 (3H, s, $C_{10}-CH_3$), 3.90—4.20 (5H, m, $-OCH_2CH_2O-$ and C_3–H), 7.14 (1H, d, J=8 Hz, C_{11}–H), 7.34 (1H, dd, J=2 and 8 Hz, C_{12}–H), 7.81 (1H, d, J=2 Hz, C_{14}–H). Found: C, 61.63; H, 6.44%. Calcd for $C_{21}H_{27}O_3Br$: C, 61.92; H, 6.69%.

*3β-Bromo-2,2-ethylenedioxy-6-hydroxy-18-norabieta-5,8,11,13-tetraen-7-one (**14**).* A stream of oxygen was bubbled in a stirred solution of **13** (1.226 g) and potassium *t*-butoxide (3.80 g) in *t*-butyl alcohol (25 ml) at 35 °C for 35 min. The mixture was diluted with water and extracted with ether. The ether extract was washed with brine, dried over sodium sulfate, and evaporated *in vacuo*. The residue was chromatographed on silica gel (30 g), using benzene as the eluent, to give **14** (772 mg: 61.0%). It was recrystallized from methanol; mp 180—181 °C; $[\alpha]_D$ +17.2°; IR: 3432, 1663, 1638, 1608 cm^{-1}; ^1H NMR: 1.30 (6H, d, J=7 Hz, $-CH(C\underline{H}_3)_2$), 1.51 (3H, d, J=7.5 Hz, C_4-CH_3), 1.61 (3H, s, $C_{10}-CH_3$), 2.37 (2H, s, C_1-H_2), 3.40—4.40 (5H, m, $-OCH_2CH_2O-$ and C_3–H), 6.67 (1H, s, –OH), 7.31 (2H, bs, C_{11}–H and C_{12}–H), 7.95 (1H, bs, C_{14}–H). Found: C, 59.98; H, 6.18%. Calcd for $C_{21}H_{25}O_4Br$: C, 60.01; H, 6.01%.

*3β-Bromo-6-hydroxy-18-norabieta-5,8,11,13-tetraene-2,7-dione (**15**).* A mixture of **14** (684 mg) and dilute hydrochloric acid (10%: 2.5 ml) in acetic acid (15 ml) was refluxed for 70 min, concentrated *in vacuo*, diluted with water, and then extracted with ether. The ether extract was washed successively with aqueous sodium hydrogencarbonate and brine, dried over sodium sulfate, and evaporated *in vacuo* to give the crude **15** (670 mg) which, without purification, was used in the next reaction.

*Dehydrobromination of the 2,7-Dione **15**.* A mixture of the crude **15** (670 mg), lithium carbonate (380 mg), and lithium bromide (450 mg) in *N,N*-dimethylformamide (8.0 ml) was stirred at 120—125 °C for 3 h in a stream of nitrogen. After the same work-up as described for the preparation of **9**, the

crude product was purified by column chromatography on silica gel (40 g), using ether–benzene (0.5 : 99.5) as the eluent, to give 6-hydroxy-18-norabieta-5,8,11,13-tetraene-2,7-dione (**16**) (63 mg). It was recrystallized from ether–hexane; mp 95—96.5 °C; $[\alpha]_D$ +18.8°; IR: 3428, 1708, 1661, 1638, 1608 cm^{-1}; ^1H NMR: 1.32 (6H, d, J=7 Hz, $-CH(C\underline{H}_3)_2$), 1.43 (3H, d, J=7.5 Hz, C_4-CH_3), 1.59 (3H, s, $C_{10}-CH_3$), 6.87 (1H, s, -OH), 7.40 (2H, d, J=2 Hz, C_{11}–H and C_{12}–H), 7.98 (1H, bs, C_{14}–H). Found: C, 76.72; H, 7.65%. Calcd for $C_{19}H_{22}O_3$: C, 76.48; H, 7.43%.

Subsequent elution gave a mixture of **16** and 6-hydroxy-19-norabieta-3,5,8,11,13-pentaene-2,7-dione (**3**) (188 mg), whose purification is described later.

Further elution gave **3** (83 mg); $[\alpha]_D$ −215°; IR: 3365, 1664, 1646, 1611 cm^{-1}; ^1H NMR: 1.33 (6H, d, J=7 Hz, $-CH(C\underline{H}_3)_2$), 1.54 (3H, s, $C_{10}-CH_3$), 2.32 and 2.99 (each 1H and d, J=15 Hz, C_1-H_2), 2.49 (3H, d, J=2 Hz, C_4-CH_3), 5.98 (1H, bs, C_3–H), 7.48 (2H, d, J=2 Hz, C_{11}–H and C_{12}–H), 7.63 (1H, s, -OH), 8.02 (1H, bs, C_{14}–H). Found: C, 76.72; H, 6.97%. Calcd for $C_{19}H_{20}O_3$: C, 77.00; H, 6.80%.

The above mixture of **16** and **3** (188 mg) was acetylated with acetic anhydride (1.0 ml) and pyridine (2.0 ml) at 80—85 °C for 1 h. After the usual work-up, the crude product was chromatographed on silica gel (15 g), using ether–benzene (2 : 98) as the eluent, to give 6-acetoxy-19-norabieta-3,5,8,-11,13-pentane-2,7-dione (**17**) (139 mg); $[\alpha]_D$ −95.9°; IR: 1771, 1662, 1613 cm^{-1}; ^1H NMR: 1.30 (6H, d, J=7 Hz, $-CH(C\underline{H}_3)_2$), 1.61 (3H, s, $C_{10}-CH_3$), 2.34 (6H, s, C_4-CH_3 and $-OCOCH_3$), 6.05 (1H, bs, C_3–H), 7.41 (2H, d, J=2 Hz, C_{11}–H and C_{12}–H), 7.96 (1H, bs, C_{14}–H). Found: C, 74.23; H, 6.60%. Calcd for $C_{21}H_{22}O_4$: C, 74.53; H, 6.55%.

Further elution with ether–benzene (7 : 93) gave 6-acetoxy-18-norabieta-5,8,11,13-tetraene-2,7-dione (**18**) (34 mg): IR: 1766, 1715, 1663, 1612 cm^{-1}; ^1H NMR: 1.29 (6H, d, J=7 Hz, $-CH(C\underline{H}_3)_2$), 1.35 (3H, d, J=7.5 Hz, C_4-CH_3), 1.63 (3H, s, $C_{10}-CH_3$), 2.32 (3H, s, $-OCOCH_3$), 7.37 (2H, bs, C_{11}–H and C_{12}–H), 7.93 (1H, bs, C_{14}–H).

*Hydrolysis of the Acetates **17** and **18**.* *a)*: A mixture of **17** (143 mg) and dilute hydrochloric acid (10%: 2.0 ml) in ethanol (7.0 ml) was refluxed for 2.5 h, concentrated *in vacuo*, diluted with water, and then extracted with ether. The ether extract was washed with brine, dried over sodium sulfate, and evaporated *in vacuo*. The residue was chromatographed on silica gel (12 g), using ether–benzene (3 : 97) as the eluent, to give an oil (114 mg), whose IR and ^1H NMR spectra were identical with those of **3**.

b): A mixture of **18** (33 mg) and dilute hydrochloric acid (10%: 1.0 ml) in ethanol (5.0 ml) was refluxed for 1.5 h. After the same work-up as described in *a*), the crude product was purified by column chromatography on silica gel (5.0 g), using ether–benzene (2 : 98) as the eluent, to give **16** (23 mg), whose IR and ^1H NMR spectra were identical with those of the authentic sample.

*3β,6α-Dibromo-2,2-ethylenedioxy-18-norabieta-8,11,13-trien-7-one (**20**).* A mixture of **13** (611 mg) and pyridinium tribromide (80%: 1190 mg) in dichloromethane (14 ml) was stirred at room temperature for 160 min. The mixture was diluted with water and extracted with ether. The ether extract was washed successively with aqueous sodium thiosulfate, dilute hydrochloric acid, and brine, dried over sodium sulfate, and evaporated *in vacuo*. The residue was purified by column chromatography on silica gel (60 g), using benzene as the eluent, to give **20** (558 mg: 76.5%) as an oil; $[\alpha]_D$ +84.8°; IR: 1687, 1607 cm^{-1}; ^1H NMR: 1.27 (6H, d, J=7 Hz, $-CH(C\underline{H}_3)_2$), 1.36 (3H, d, J=7.5 Hz, C_4-CH_3), 1.39 (3H, s, $C_{10}-CH_3$), 2.10 (1H, bd, J=14 Hz) and 2.62 (1H, d, J=14 Hz) (C_1-H_2), 3.90—4.30 (5H, m, $-OCH_2CH_2O-$ and C_3–H), 4.84 (1H, d, J=13 Hz, C_6–H), 7.14 (1H, d, J=8 Hz, C_{11}–H), 7.35 (1H, dd, J=2 and 8 Hz, C_{12}–H), 7.80 (1H, d, J=2 Hz, C_{14}–H). Found: C, 51.78; H, 5.55%. Calcd for $C_{21}H_{26}O_3Br_2$: C, 51.87; H, 5.61%.

*3α,6α-Dibromo-2,2-ethylenedioxy-18-norabieta-8,11,13-trien-7-one (**21**).* A mixture of **12** (262 mg) and pyridinium tribromide (80%: 410 mg) in dichloromethane (6.0 ml) was stirred at room temperature for 160 min. After the same work-up as described for the preparation of **20**, the crude product was chromatographed on silica gel (30 g), using benzene as the eluent, to give **21** (222 mg: 70.9%) as a solid; $[\alpha]_D$ +30.7°; IR: 1685, 1608 cm^{-1}; ^1H NMR ($CDCl_3$): 1.27 (6H, d, J=7 Hz, $-CH(C\underline{H}_3)_2$), 1.40 (3H, d, J=7.5 Hz, C_4-CH_3), 1.43 (3H, s, $C_{10}-CH_3$), 1.98 and 2.60 (each 1H and d, J=14 Hz, C_1-H_2), 3.95—4.55 (5H, m, $-OCH_2CH_2O-$ and C_3–H), 5.02 (1H, d, J=13 Hz, C_6–H), 7.17 (1H, d, J=8 Hz, C_{11}–H), 7.44 (1H, dd, J=2 and 8 Hz, C_{12}–H), 7.90 (1H, d, J=2 Hz, C_{14}–H).

*19-Norabieta-3,5,8,11,13-pentaene-2,7-dione (**19**).* *a)*: A mixture of **20** (486 mg) and dilute hydrochloric acid (10%: 1.2 ml) in acetic acid (8.0 ml) was refluxed for 1 h, concentrated *in vacuo*, diluted with water, and then extracted with ether. The ether extract was washed successively with aqueous sodium hydrogencarbonate and brine, dried over sodium sulfate, and evaporated *in vacuo* to give the crude 2,7-dioxo compound (395 mg) which, without purification ,was used in the next reaction.

A mixture of the crude 2,7-dioxo compound (395 mg), lithium carbonate (391 mg), and lithium bromide (480 mg) in *N,N*-dimethylformamide (6.5 ml) was stirred at 120—125 °C for 3 h in a stream of nitrogen. After the same work-up as described for the preparation of **9**, the crude product was purified by column chromatography on silica gel (15 g), using ether–benzene (3 : 97) as the eluent, to give **19** (261 mg: 93.0%) as an oil; $[\alpha]_D$ −51.2°; IR: 1668, 1650, 1608 cm^{-1}; ^1H NMR: 1.32 (6H, d, J=7 Hz, $-CH(C\underline{H}_3)_2$), 1.51 (3H, s, $C_{10}-CH_3$), 2.29 (3H, d, J=2 Hz, C_4-CH_3), 6.13 (1H, bs, C_3–H), 6.63 (1H, s, C_6–H), 7.43 (2H, d, J=2 Hz, C_{11}–H and C_{12}–H), 7.94 (1H, bs, C_{14}–H). Found: C, 81.09; H, 7.32%. Calcd for $C_{19}H_{20}O_2$: C, 81.39; H, 7.19%.

b): A mixture of **21** (209 mg) and dilute hydrochloric acid (10%: 0.6 ml) in acetic acid (4.0 ml) was refluxed for 1 h, concentrated *in vacuo*, diluted with water, and then extracted with ether. The ether extract was washed successively with aqueous sodium hydrogencarbonate and brine, dried over sodium sulfate, and evaporated *in vacuo*.

The crude 2,7-dioxo compound (179 mg), without purification, was stirred at 120—125 °C for 3 h with lithium carbonate (180 mg), lithium bromide (220 mg), and *N,N*-dimethylformamide (3.0 ml) in a stream of nitrogen. The reaction mixture was treated as described for the preparation of **9** and then purified by column chromatography on silica gel (15 g), using ether–benzene (2 : 98) as the eluent. The IR and ^1H NMR spectra of the product (96 mg: 79.8%) were identical with those of **19**.

The authors are grateful to Arakawa Chemical Co. Ltd. for a generous gift of rosin. This work was partially supported by Grant-in-Aid for Scientific Research No. 56540324 from the Ministry of Education, Science and Culture.

References

1) M. Ribi, A. C. Sin-Ren, H. P. Küng, and C. H. Eugster, *Helv. Chim. Acta*, **52**, 1685 (1969).

2) T. Matsumoto and S. Takeda, *Chem. Lett.*, **1979**, 409; T. Matsumoto and S. Harada, *Bull. Chem. Soc. Jpn.*, **52**, 1459 (1979).
3) T. Wirthlin, H. Wehrli, and O. Jeger, *Helv. Chim. Acta*, **57**, 351 (1974).
4) H. Koike and T. Tokoroyama, *Chem. Lett.*, **1979**, 333.
5) R. C. Cambie and R. A. Franich, *Aust. J. Chem.*, **23**, 93 (1970).
6) J. W. Huffman, *J. Org. Chem.*, **35**, 478 (1970).
7) J. F. Biellmann and G. Branlant, *Tetrahedron*, **29**, 1227 (1973).
8) G. J. Matthews and A. Hassner, "Organic Reactions in Steroid Chemistry," ed by J. Fried and J. A. Edwards, Van Nostrand Reinhold, New York (1972), Vol. 2, p. 17; J. Fried and E. F. Sabo, *J. Am. Chem. Soc.*, **79**, 1130 (1957).
9) E. W. Garbisch, Jr., *J. Org. Chem.*, **30**, 2109 (1965).

Synthesis of 11,14-Diacetoxy-13-(acetoxymethyl)podocarpa-8,11,13-triene. Correction of Proposed Structure for Premnolal

Takashi MATSUMOTO,* Sachihiko IMAI,* and Shuhei YUKI
Department of Chemistry, Faculty of Science, Hiroshima University, Higashisenda-machi, Naka-ku, Hiroshima 730
(Received April 24, 1982)

Oxidation of 11-acetoxyabieta-8,11,13-triene, derived from methyl 11-methoxyabieta-8,11,13-trien-18-oate, with chromium trioxide afforded 11,15-diacetoxyabieta-8,11,13-trien-7-one and 11-acetoxy-13-acetylpodocarpa-8,11,13-trien-7-one (**11**) in a ratio of *ca.* 2 : 1. The acetyl compound **11** was converted into a quinone, 13-(hydroxymethyl)podocarpa-8,12-diene-11,14-dione (**18**), by a series of reactions : iodoform reaction, esterification, acetylation, sodium borohydride reduction, dehydration, catalytic hydrogenation, lithium aluminium hydride reduction, and oxidation with Fremy's salt. Reductive acetylation of **18** produced 11,14-diacetoxy-13-(acetoxymethyl)-podocarpa-8,11,13-triene (**2**). The ^{1}H NMR spectrum of **2** was different from that of 15-acetoxypremnol diacetate which was prepared from natural premnolal. Based on this fact a corrected structure of premnolal is proposed.

Premnolal, a new aromatic bisnorditerpene, has recently been isolated from the root bark of *Premna latifolia* Roxb. (Verbenaceae) by Rao *et al.*[1] On the basis of chemical and spectroscopic studies, they deduced the structure of premnolal to be 11,14-dihydroxypodocarpa-8,11,13-triene-13-carbaldehyde (**1**). This structure is unique among the naturally-occurring tricyclic diterpenes, in that it contains a formyl group at C-13 and two hydroxyl goups at C-11 and C-14. To confirm the validity of their proposed structure, we now attempted the synthesis of **1** or its derivatives. This paper will describe the synthesis of the proposed 15-acetoxypremnol diacetate, 11,14-diacetoxy-13-(acetoxymethyl)-podocarpa-8,11,13-triene (**2**), and present a revised structure of natural premnolal.

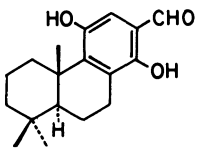

1

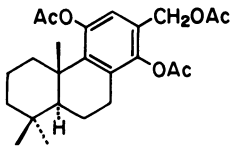

2

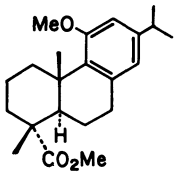

3

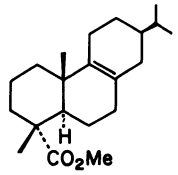

4

In the present study, methyl 11-methoxyabieta-8,11,13-trien-18-oate (**3**)[2] prepared from methyl (+)-13β-abiet-8-en-18-oate (**4**)[3] in our laboratory, was chosen as the starting material. Reduction of **3** with lithium aluminium hydride in refluxing ether afforded 11-methoxyabieta-8,11,13-trien-18-ol (**5**)[4,5] which, without purification, was oxidized at room temperature with pyridinium chlorochromate in dichloromethane to give 11-methoxyabieta-8,11,13-trien-18-al (**6**). The crude aldehyde **6** was immediately treated with 80% hydrazine hydrate in diethylene glycol at 125—140 °C and then with sodium hydroxide at 195—200 °C. Separation of the reaction mixture by column chromatography on silica gel yielded 11-methoxyabieta-8,11,13-triene (**7**)[4] and abieta-8,11,13-trien-11-ol (**8**) in a ratio of *ca.* 3 : 1. The methoxy compound **7** was easily demethylated at room temperature with boron tribromide in dichloromethane to give **8**, which was converted into the corresponding acetate (**9**) with acetic anhydride in pyridine. Oxidation of **9** with chromium trioxide in a mixture of acetic anhydride and acetic acid afforded two ketones, **10** and **11**, in yields of 48% and 23% respectively. The IR spectrum of **10** showed bands at 1768, 1735, and 1685 cm^{-1}, while that of **11** at 1768 and 1690 cm^{-1}. The ^{1}H NMR spectrum of **10** showed singlet signals at δ 1.74 (6H) due to two methyls, at δ 1.98 (3H) and 2.26 (3H) due to two acetoxyls, and two doublet signals at δ 6.98 (1H, J=2 Hz) and 7.84 (1H, J=2 Hz) assigned to two aromatic protons. On the other hand, the ^{1}H NMR spectrum of **11** showed an acetoxyl at δ 2.29 (3H, s), an acetyl at δ 2.57 (3H, s), and two aromatic protons at δ 7.57 (1H, d, J=2 Hz) and 8.35 (1H, d, J=2 Hz). From these spectral data, the structures of **10** and **11** were assigned respectively to be 11,15-diacetoxyabieta-8,11,13-trien-7-one and 11-acetoxy-13-acetylpodocarpa-8,11,13-trien-7-one.

Hydrolysis of **10** with sodium hydrogencarbonate in refluxing aqueous acetone afforded the known 11,15-dihydroxyabieta-8,11,13-trien-7-one (**12**) which was prepared by Kawazu *et al.*[6] from the natural fish-killing component, callicarpone (**13**).

The ketone **11** was then converted into 11-acetoxy-13-(methoxycarbonyl)podocarpa-8,11,13-trien-7-one (**14**) by a series of reactions: iodoform reaction, esterification with diazomethane, and acetylation. The IR spectrum of **14** showed carbonyl absorptions at 1768, 1728, and 1690 cm^{-1}. Reduction of **14** with sodium borohydride in methanol, followed by dehydration with *p*-toluenesulfonic acid in refluxing benzene afforded 13-(methoxycarbonyl)podocarpa-6,8,11,13-tetraen-11-ol (**15**), whose ^{1}H NMR spectrum showed C-5, C-6, and C-7 protons at δ 2.20 (t, J=3 Hz), 6.03 (dd, J=10 and 3 Hz), and 6.48 (dd, J=10 and 3 Hz) respectively. The tetraene **15** was submitted to catalytic hydrogenation over Pd–C in ethanol and the resulting 13-(methoxycarbonyl)-podocarpa-8,11,13-trien-11-ol (**16**) was reduced with lithium aluminium hydride in refluxing ether to give

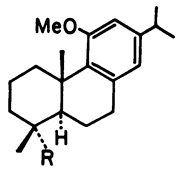

5 R=CH_2OH
6 R=CHO
7 R=Me

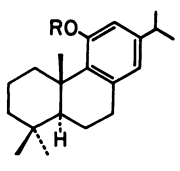

8 R=H
9 R=Ac

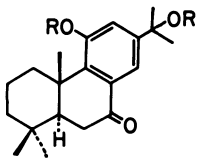

10 R=Ac
12 R=H

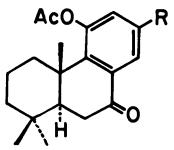

11 R=COMe
14 R=CO_2Me

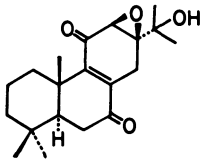

13

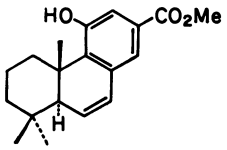

15

13-(hydroxymethyl)podocarpa-8,11,13-trien-11-ol (**17**). Introduction of oxygen function at C-14 was successfully achieved by oxidation of **17** in aqueous methanol with Fremy's salt in the presence of sodium dihydrogenphosphate and a *p*-quinone compound, 13-(hydroxymethyl)-podocarpa-8,12-diene-11,14-dione (**18**), was obtained. The ^1H NMR spectrum of **18** showed a broad singlet signal at δ 4.37 (2H) due to the hydroxymethyl group at C-13 and a triplet signal at δ 6.49 (1H, J=1.5 Hz) due to a vinylic proton at C-12. Reductive acetylation of **18** with zinc in acetic anhydride and pyridine afforded a triacetate **2**, whose ^1H NMR spectrum showed three acetoxyls at δ 1.98 (3H) and 2.24 (6H), a methylene of acetoxymethyl group at δ 4.87, and an aromatic proton at δ 6.78. Oxidation of **2** with chromium trioxide in acetic acid gave 11,14-diacetoxy-13-(acetoxymethyl)-

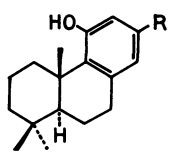

16 R=CO_2Me
17 R=CH_2OH

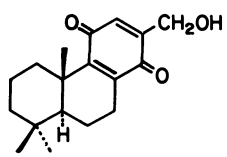

18

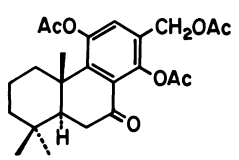

19

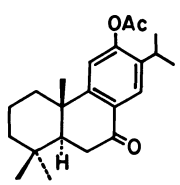

20

podocarpa-8,11,13-trien-7-one (**19**), whose IR spectrum showed bands at 1763, 1745, and 1685 cm^{-1}. The presence of an aromatic proton at C-12 in **19** was supported by its chemical shift (δ 7.09) in the ^1H NMR spectrum; if the aromatic proton is located at C-14, the chemical shift might be expected to be δ *ca.* 8, like that (δ 7.94) of 12-acetoxyabieta-8,11,13-trien-7-one (**20**).[7]

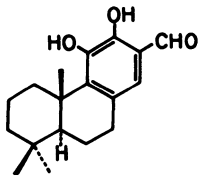

21

Thus, the structure of **2** was conclusively assigned to be 11,14-diacetoxy-13-(acetoxymethyl)podocarpa-8,11,13-triene. Since the ^1H NMR spectrum of the synthetic **2** was different from that of 15-acetoxypremnol diacetate which was prepared from natural premnolal, all of the proposed structures[1] for premnolal and its derivatives should be revised. From the present study together with consideration of the published spectral data, we now propose the correct structure of premnolal to be 11,12-dihydroxypodocarpa-8,11,13-triene-13-carbaldehyde (**21**).

Experimental

All melting points are uncorrected. The IR and optical rotations were measured in chloroform, and the ^1H NMR spectra in carbon tetrachloride at 90 MHz, with tetramethylsilane as an internal standard, unless otherwise stated. The chemical shifts are presented in terms of δ values; s: singlet, bs: broad singlet, d: doublet, bd: broad doublet, dd: double doublet, t: triplet, m: multiplet, dm: doublet of multiplet. The column chromatography was performed using Merck silica gel.

Abieta-8,11,13-trien-11-ol (8). *a)*: A solution of methyl 11-methoxyabieta-8,11,13-trien-18-oate (**3**)[2] (6.26 g) in dry ether (70 ml) was added dropwise to a stirred suspension of lithium aluminium hydride (1.38 g) in dry ether (120 ml). The mixture was refluxed for 4 h, cooled, poured into ice-dilute hydrochloric acid, and extracted with ether. The ether extract was washed successively with aqueous sodium hydrogencarbonate and brine, dried over sodium sulfate, and evaporated *in vacuo* to give 11-methoxyabieta-8,11,13-trien-18-ol (**5**)[4,5] (5.81 g) which, without purification, was used in the next reaction. IR: 3630, 3440 cm^{-1}; ^1H NMR (60 MHz): 0.81 (3H, s, C_4–CH_3), 1.21 (6H, d, J=7 Hz, –CH($C\underline{H}_3$)$_2$), 1.27 (3H, s, C_{10}–CH_3), 2.16 (1H, s, –OH), 3.22 (2H, ABq, J_{AB}=11 Hz, δ_{AB}=20 Hz), 3.75 (3H, s, –OCH_3), 6.30 (2H, s, C_{12}–H and C_{14}–H).

A solution of the crude **5** (5.81 g) in dichloromethane (46 ml) was added to a stirred suspension of pyridinium chlorochromate (5.96 g) in dichloromethane (70 ml) at room temperature. The mixture was stirred for 105 min, diluted with ether, and then decanted from a tarry residue, which was washed with ether. The combined organic solution was washed with brine, passed through a short alumina column, and evaporated *in vacuo* to give the crude 11-methoxyabieta-8,11,13-trien-18-al (**6**) (5.20 g); IR: 2700, 1724 cm^{-1}; ^1H NMR (60 MHz): 1.12 (3H, s, C_4–CH_3), 1.19 (6H, d, J=7 Hz, –CH($C\underline{H}_3$)$_2$), 1.29 (3H, s, C_{10}–CH_3), 3.77 (3H, s, –OCH_3),

6.42 (2H, s, C_{12}–H and C_{14}–H), 9.18 (1H, s, -CHO).

A stirred mixture of the crude **6** (5.20 g) and 80% hydrazine hydrate (24.9 ml) in diethylene glycol (156 ml) was heated at 125—140 °C for 2 h, and then powdered sodium hydroxide (33.1 g) was added. The mixture was stirred at 195—200 °C for 3 h, cooled, diluted with water, and extracted with ether. The ether extract was washed with brine, dried over sodium sulfate, and evaporated *in vacuo*. The crude product (4.75 g) was chromatographed on silica gel (500 g), using hexane–benzene (99 : 1) as the eluent, to give 11-methoxyabieta-8,11,-13-triene (**7**)[4] (3.40 g: 62%) as an oil; $[\alpha]_D$ +125° (*c* 1.32); ^{1}H NMR: 0.92 and 0.94 (each 3H and s, $-\dot{C}(CH_3)_2$), 1.19 (6H, d, J=7 Hz, $-CH(C\underline{H}_3)_2$), 1.24 (3H, s, C_{10}–CH_3), 3.01 (1H, dm, J=13 Hz, $C_{1\beta}$–H), 3.74 (3H, s, $-OCH_3$), 6.36 (2H, s, C_{12}–H and C_{14}–H). Found: C, 84.19; H, 10.93%. Calcd for $C_{21}H_{32}O$: C, 83.94; H, 10.73%.

Further elution with hexane–benzene (2 : 3) gave abieta-8,11,13-trien-11-ol (**8**) (1.04 g: 20%) as a solid; $[\alpha]_D$ +94° (*c* 1.56); IR: 3595, 3340 cm^{-1}; ^{1}H NMR: 0.91 and 0.93 (each 3H and s, $-\dot{C}(CH_3)_2$), 1.14 (6H, d, J=7 Hz, $-CH(C\underline{H}_3)_2$), 1.27 (3H, s, C_{10}–CH_3), 3.04 (1H, dm, J=13 Hz, $C_{1\beta}$–H), 4.38 (1H, s, -OH), 6.05 (1H, bd, J=2 Hz, C_{12}–H), 6.35 (1H, bd, J=2 Hz, C_{14}–H). Found: C, 84.02; H, 10.69%. Calcd for $C_{20}H_{30}O$: C, 83.86; H, 10.56%.

b): A solution of boron tribromide (0.38 ml) in dichloromethane (1.5 ml) was added to a stirred solution of **7** (300 mg) in dichloromethane (3.0 ml) over a period of 5 min with cooling in an ice-bath. The mixture was stirred at the same temperature for 10 min and at room temperature for 2 h, poured into ice–water, and extracted with ether. The ether extract was washed successively with aqueous sodium thiosulfate and brine, dried over sodium sulfate, and evaporated *in vacuo*. The crude product was chromatographed on silica gel (30 g), using hexane–benzene (3 : 2) as the eluent, to give an oil (257 mg: 90%), whose IR and ^{1}H NMR spectra were identical with those of **8**.

11-Acetoxyabieta-8,11,13-triene (9). A solution of **8** (257 mg) and acetic anhydride (1.4 ml) in pyridine (1.4 ml) was allowed to stand overnight at room temperature. After the usual work-up, the crude product was recrystallized from methanol to give **9** (149 mg: 51%); mp 98.5—99.5 °C; $[\alpha]_D$ +94° (*c* 1.68); IR: 1748 cm^{-1}; ^{1}H NMR (60 MHz): 0.96 (6H, bs, $-\dot{C}(CH_3)_2$), 1.21 (6H, d, J=7 Hz, $-CH(C\underline{H}_3)_2$), 1.23 (3H, s, C_{10}–CH_3), 2.22 (3H, s, $-OCOCH_3$), 6.45 (1H, bs, C_{12}–H), 6.66 (1H, bs, C_{14}–H). Found: C, 80.64; H, 10.08%. Calcd for $C_{22}H_{32}O_2$: C, 80.44; H, 9.83%. The mother liquor of recrystallization was evaporated *in vacuo* and the residue was chromatographed on silica gel (15 g), using hexane–benzene (7 : 3) as the eluent, to give additional **9** (128 mg: 43%).

*Oxidation of the Acetate **9** with Chromium Trioxide.* Chromium trioxide (500 mg) was added portionwise at 0—5 °C to a stirred solution of **9** (328 mg) in acetic anhydride (2.3 ml) and acetic acid (3.3 ml). The mixture was further stirred at 0—5 °C for 1 h and at room temperature for 1 h. After the successive addition of aqueous sodium acetate (10%: 2.0 ml), methanol (1.5 ml), and brine (50 ml), the mixture was extracted with ether. The ether extract was washed with aqueous sodium hydrogencarbonate and brine, dried over sodium sulfate, and evaporated *in vacuo*. The residue was chromatographed on silica gel (40 g), using ether–benzene (1 : 99) as the eluent, to give 11,15-diacetoxyabieta-8,11,13-trien-7-one (**10**) (153 mg: 38%). This was recrystallized from methanol; mp 135—136 °C; $[\alpha]_D$ +45° (*c* 3.11); IR: 1768, 1735, 1685 cm^{-1}; ^{1}H NMR: 0.99 (6H, bs, $-\dot{C}(CH_3)_2$), 1.34 (3H, s, C_{10}–CH_3), 1.74 (6H, bs, $-C(C\underline{H}_3)_2OCOCH_3$), 1.98 (3H, s, C_{15}–$OCOCH_3$), 2.26 (3H, s, C_{11}–$OCOCH_3$), 6.98 (1H, d, J=2 Hz, C_{12}–H), 7.84 (1H, d, J=2 Hz, C_{14}–H). Found: C, 71.92; H, 8.15%. Calcd for $C_{24}H_{32}O_5$: C, 71.97; H, 8.05%.

Further elution with the same solvent gave a mixture (148 mg) of **10** and 11-acetoxy-13-acetylopodocarpa-8,11,13-trien-7-one (**11**). This mixture was rechromatographed on silica gel (15 g), using ether–hexane (1 : 4) as the eluent, to give additional **10** (37 mg: 9%) and **11** (79 mg: 23%). The acetyl compound **11** was recrystallized from methanol; mp 111—112 °C; $[\alpha]_D$ +67° (*c* 0.925); IR: 1768, 1690, 1607 cm^{-1}; ^{1}H NMR: 1.01 (6H, s, $-\dot{C}(CH_3)_2$), 1.35 (3H, s, C_{10}–CH_3), 2.29 (3H, s, $-OCOCH_3$), 2.57 (3H, s, $-COCH_3$), 7.57 (1H, d, J=2 Hz, C_{12}–H), 8.35 (1H, d, J=2 Hz, C_{14}–H). Found: C, 73.95; H, 7.74%. Calcd for $C_{21}H_{26}O_4$: C, 73.66; H, 7.66%.

11,15-Dihydroxyabieta-8,11,13-trien-7-one (12). A mixture of **10** (220 mg) in hot aqueous acetone (50%: 44 ml) and sodium hydrogencarbonate (460 mg) was refluxed for 2 h. The mixture was diluted with brine and extracted with ether. The ether extract was washed with brine, dried over sodium sulfate, and evaporated *in vacuo*. The residue was recrystallized from chloroform to give **12** (74 mg: 43%); mp 220—222 °C; MS (*m/e*): 316 (M^+); $[\alpha]_D$ +45° (*c* 0.245, MeOH) (lit,[6] mp 220—222 °C, $[\alpha]_D^{25}$ +44° (MeOH)); ^{1}H NMR (acetone-d_6): 0.97 and 1.01 (each 3H and s, $-\dot{C}(CH_3)_2$), 1.43 (3H, s, C_{10}–CH_3), 1.48 (6H, s, $-C(C\underline{H}_3)_2OH$), 3.41 (1H, dm, J=13 Hz, $C_{1\beta}$–H), 3.91 (1H, s, C_{15}–OH), 7.28 (1H, d, J=2 Hz, C_{12}–H), 7.62 (1H, d, J=2 Hz, C_{14}–H), 8.40 (1H, s, C_{11}–OH). ^{1}H NMR (pyridine-d_5): 0.88 and 0.93 (each 3H and s, $-\dot{C}(CH_3)_2$), 1.58 (3H, s, C_{10}–CH_3), 1.71 (6H, s, $-C(C\underline{H}_3)_2OH$), 3.79 (1H, dm, J=12 Hz, $C_{1\beta}$–H), 7.90 (1H, d, J=2 Hz, C_{12}–H), 8.30 (1H, d, J=2 Hz, C_{14}–H). Found: C, 75.89; H, 8.91%. Calcd for $C_{20}H_{28}O_3$: C, 75.91; H, 8.92%. The mother liquor of recrystallization was evaporated *in vacuo* and the residue was chromatographed on silica gel (15 g), using ether–benzene (1 : 3) as the eluent, to give additional **12** (49 mg: 28%).

11-Acetoxy-13-(methoxycarbonyl)podocarpa-8,11,13-trien-7-one (14). A mixture of **11** (638 mg), iodine (710 mg), and pyridine (12 ml) was refluxed for 3 h. The mixture was allowed to stand overnight at room temperature, diluted with water, and extracted with chloroform. The chloroform extract was washed successively with dilute hydrochloric acid, aqueous sodium thiosulfate, and brine. After drying over sodium sulfate, the solution was evaporated *in vacuo*. The residual oil in ethanol (15 ml) was refluxed for 3 h with aqueous sodium hydroxide (10%: 8.2 ml), cooled, acidified with dilute hydrochloric acid, and extracted with chloroform. The chloroform extract was washed with brine, dried over sodium sulfate, and evaporated *in vacuo* to give a crude acid. This crude acid was immediately methylated with diazomethane in ether and the resulting methyl ester was acetylated with acetic anhydride (3.0 ml) in pyridine (3.0 ml) at room temperature overnight. After the usual work-up, the crude product was chromatographed on silica gel (70 g), using ether–benzene (2 : 98) as the eluent, to give **14** (299 mg: 45%); $[\alpha]_D$ +55° (*c* 0.725); IR: 1768, 1728, 1690 cm^{-1}; ^{1}H NMR: 1.01 (6H, s, $-\dot{C}(CH_3)_2$), 1.36 (3H, s, C_{10}–CH_3), 2.30 (3H, s, $-OCOCH_3$), 3.89 (3H, s, $-CO_2CH_3$), 7.62 (1H, d, J=2 Hz, C_{12}–H), 8.45 (1H, d, J=2 Hz, C_{14}–H). Found: C, 70.65; H, 7.40%. Calcd for $C_{21}H_{26}O_5$: C, 70.37; H, 7.31%.

13-(Methoxycarbonyl)podocarpa-6,8,11,13-tetraen-11-ol (15). A mixture of **14** (152 mg) and sodium borohydride (24 mg) in methanol (4.0 ml) was stirred at 0—5 °C for 1 h and at room temperature for 2 h. After the addition of acetone, the mixture was evaporated *in vacuo*. The residue was acidified with dilute hydrochloric acid and extracted with ether. The ether extract was washed with brine, dried over sodium

sulfate, and evaporated *in vacuo* to give the corresponding alcohol.

A mixture of the above crude alcohol and *p*-toluenesulfonic acid (3.0 mg) in benzene (15 ml) was refluxed for 1 h, cooled, and then diluted with ether. The ether solution was washed successively with aqueous sodium hydrogencarbonate and brine, dried over sodium sulfate, and evaporated *in vacuo*. The crude product was chromatographed on silica gel (15 g), using ether–benzene (1 : 99) as the eluent, to give **15** (116 mg: 90%). This was recrystallized from hexane; mp 147.5—149 °C; $[\alpha]_D$ −73° (*c* 1.11); IR: 3590, 3430, 1705 cm^{-1}; ^1H NMR ($CDCl_3$): 0.98 and 1.03 (each 3H and s, $-C(CH_3)_2$), 1.13 (3H, s, C_{10}–CH_3), 2.20 (1H, t, J=3 Hz, $C_{5\alpha}$–H), 3.00 (1H, m, $C_{1\beta}$–H), 3.89 (3H, s, $-CO_2CH_3$), 6.03 (1H, dd, J=10 and 3 Hz, C_6–H), 6.17 (1H, s, C_{11}–OH), 6.48 (1H, dd, J=10 and 3 Hz, C_7–H), 7.27 (1H, d, J=2 Hz, C_{12}–H), 7.43 (1H, d, J=2 Hz, C_{14}–H). Found: C, 75.98; H, 8.18%. Calcd for $C_{19}H_{24}O_3$: C, 75.97; H, 8.05%.

*13-(Methoxycarbonyl)podocarpa-8,11,13-trien-11-ol (**16**).* A mixture of **15** (169 mg) and 5% Pd–C (80 mg) in ethanol (5.0 ml) was submitted to catalytic hydrogenation with 1 atm hydrogen pressure at room temperature for *ca.* 2 h. After the usual work-up, the crude product was recrystallized from hexane to give **16** (118 mg: 69%); mp 180—181 °C; $[\alpha]_D$ +73° (*c* 1.56); IR: 3600, 3410, 1708 cm^{-1}; ^1H NMR ($CDCl_3$): 0.94 and 0.97 (each 3H and s, $-C(CH_3)_2$), 1.34 (3H, s, C_{10}–CH_3), 2.88 (2H, m, C_7–H_2), 3.18 (1H, dm, J=13 Hz, $C_{1\beta}$–H), 3.89 (3H, s, $-CO_2CH_3$), 5.97 (1H, bs, C_{11}–OH), 7.31 (2H, bs, C_{12}–H and C_{14}–H). Found: C, 75.54; H, 8.70%. Calcd for $C_{19}H_{26}O_3$: C, 75.46; H, 8.67%. The mother liquor of recrystallization was evaporated *in vacuo* and the residue was chromatographed on silica gel (5.0 g), using ether–benzene (2 : 98) as the eluent, to give additional **16** (33 mg: 19%).

*13-(Hydroxymethyl)podocarpa-8,11,13-trien-11-ol (**17**).* A mixture of **16** (149 mg) and lithium aluminium hydride (38 mg) in dry ether (10 ml) was refluxed for 2 h. The mixture was cooled, poured into a mixture of ice and dilute hydrochloric acid, and extracted with ether. The ether extract was washed with brine, dried over sodium sulfate, and evaporated *in vacuo*. The crude product was recrystallized from chloroform–hexane to give **17** (97 mg: 72%); mp 153—154 °C; $[\alpha]_D$ +77° (*c* 0.830); IR: 3600, 3330 cm^{-1}; ^1H NMR ($CDCl_3$): 0.94 and 0.96 (each 3H and s, $-C(CH_3)_3$), 1.32 (3H, s, C_{10}–CH_3), 2.18 (1H, bs, $-CH_2O\underline{H}$), 2.82 (2H, m, C_7–H_2), 3.13 (1H, dm, J=13 Hz, $C_{1\beta}$–H), 4.50 (2H, bs, $-C\underline{H}_2OH$), 5.73 (1H, bs, C_{11}–OH), 6.52 and 6.56 (each 1H and bs, C_{12}–H and C_{14}–H). Found: C, 79.00; H, 9.77%. Calcd for $C_{18}H_{26}O_2$: C, 78.79; H, 9.55%. The mother liquor of recrystallization was evaporated *in vacuo* and the residue was chromatographed on silica gel (5.0 g), using ether–benzene (1 : 1) as the eluent, to give additional **17** (33 mg: 24%).

*13-(Hydroxymethyl)podocarpa-8,12-diene-11,14-dione (**18**).* A solution of aqueous sodium dihydrogenphosphate [0.17 M (1 M=1 mol dm^{-3}): 4.0 ml] and Fremy's salt (150 mg) in water (8.0 ml) was added at 45 °C to a stirred solution of **17** (30 mg) in methanol (9.0 ml) over a period of 13 min. After being stirred at this temperature for 45 min, additional methanol (3.0 ml) and a solution of aqueous sodium dihydrogenphosphate (0.17 M: 4.0 ml) and Fremy's salt (150 mg) in water (8.0 ml) were added. The mixture was stirred at 45 °C for 45 more min, cooled, diluted with water, and extracted with chloroform. The chloroform extract was washed with brine, dried over sodium sulfate, and evaporated *in vacuo*. The crude product was purified by column chromatography on silica gel (5.0 g), using ether–benzene (8 : 92) as the eluent, to give **18** (23 mg: 72%) as an oil; $[\alpha]_D$ −88° (*c* 1.01); IR: 3360, 1645 cm^{-1}; ^1H NMR: 0.92 and 0.94 (each 3H and s, $-C(CH_3)_2$), 1.26 (3H, s, C_{10}–CH_3), 4.37 (2H, bs, $-C\underline{H}_2OH$), 6.49 (1H, t, J=1.15 Hz, C_{12}–H). Found: C, 74.93; H, 8.39%. Calcd for $C_{18}H_{24}O_3$: C, 74.97; H, 8.39%.

*11,14-Diacetoxy-13-(acetoxymethyl)podocarpa-8,11,13-triene (**2**).* A mixture of **18** (47 mg), zinc (53 mg), acetic anhydride (0.5 ml), and pyridine (0.5 ml) was stirred at 0—5 °C for 10 min and then at room temperature for 1 h. The reaction mixture was filtered and the filtrate was diluted with ether. The ether solution was washed successively with aqueous sodium hydrogencarbonate, dilute hydrochloric acid, and brine. After drying over sodium sulfate, the ether solution was evaporated *in vacuo* to give an oil, whose IR spectrum showed a hydroxyl absorption band at 3330 cm^{-1}. The crude oil was immediately acetylated with acetic anhydride (0.5 ml) in pyridine (0.5 ml) at *ca.* 95 °C for 10 min. After the usual work-up, the crude product was chromatographed on silica gel (5.0 g), using ether–benzene (5 : 95) as the eluent, to give **2** (60 mg: 88%) as an oil; MS (*m/e*): 416 (M^+); $[\alpha]_D$ +61° (*c* 0.785); IR: 1765, 1745 cm^{-1}; ^1H NMR: 0.92 and 0.96 (each 3H and s, $-C(CH_3)_2$), 1.26 (3H, s, C_{10}–CH_3), 1.98 (3H, s, $-CH_2OCOC\underline{H}_3$), 2.24 (6H, s, C_{11}–$OCOCH_3$ and C_{14}–$OCOCH_3$), 2.60 (3H, m, $C_{1\beta}$–H and C_7–H_2), 4.87 (2H, bs, $-CH_2OAc$), 6.78 (1H, bs, C_{12}–H). ^1H NMR spectrum for natural 15-acetoxypremnol diacetate:[1] 0.90, 0.93, and 1.18 (each 3H and s, 3–CCH_3), 1.92, 2.13, and 2.16 (each 3H and s, 3–$OCOCH_3$), 2.45 (1H, dm, $C_{1\beta}$–H), 2.85 (2H, m, C_7–H_2), 4.86 (2H, s, $-C\underline{H}_2OAc$), 6.91 (1H, s, an aromatic proton). The ^1H NMR spectrum of **2** was not identical with that of natural 15-acetoxypremnol diacetate.

*11,14-Diacetoxy-13-(acetoxymethyl)podocarpa-8,11,13-trien-7-one (**19**).* A solution of chromium trioxide (35 mg) in acetic acid (0.16 ml) and water (0.04 ml) was added dropwise to a stirred solution of **2** (48 mg) in acetic acid (0.72 ml) at room temperature over a period of 3 min. The mixture was stirred at the same temperature for 15 h, poured into brine, and extracted with ether. The ether extract was washed successively with aqueous sodium hydrogencarbonate and brine, dried over sodium sulfate, and evaporated *in vacuo*. The crude product was chromatographed on silica gel (5.0 g), using ether–benzene (5 : 95) as the eluent, to give the starting **2** (23 mg: 47%). Further elution with the same solvent afforded **19** (17 mg: 34%) as an oil; $[\alpha]_D$ +72° (*c* 0.615); IR: 1763, 1745, 1685 cm^{-1}; ^1H NMR: 0.98 (6H, s, $-C(CH_3)_2$), 1.31 (3H, s, C_{10}–CH_3), 1.99 (3H, s, $-CH_2OCOC\underline{H}_3$), 2.26 (6H, s, C_{11}–$OCOCH_3$ and C_{14}–$OCOCH_3$), 4.95 (2H, bs, $-C\underline{H}_2$-OAc), 7.09 (1H, s, C_{12}–H). Found: C, 66.95; H, 7.20%. Calcd for $C_{24}H_{30}O_7$: C, 66.96; H, 7.02%.

The authors are grateful to Professor Ch. B. Rao for kindly supplying the spectral data of natural products.

References

1) Ch. B. Rao and T. N. Rao, *Curr. Sci.*, **47**, 498 (1978). Ch. B. Rao, T. N. Rao, and E. K. S. Vijayakumar, *Indian J. Chem.*, **18B**, 513 (1979).

2) T. Matsumoto, S. Imai, and S. Yuki, *Bull. Chem. Soc. Jpn.*, **54**, 1448 (1981).

3) T. Matsumoto, S. Imai, S. Yuki, A. Katayama, and M. Furutani, *Bull. Chem. Soc. Jpn.*, **55**, 527 (1982).

4) T. Matsumoto, S. Imai, M. Aizawa, H. Kitagawa, and K. Fukui, *Chem. Lett.*, **1972**, 581.

5) Y. Ohtsuka and A. Tahara, *Chem. Pharm. Bull.*, **21**, 653 (1973).

6) K. Kawazu, M. Inaba, and T. Mitsui, *Agric. Biol. Chem.*, **31**, 498 (1967).

7) T. Matsumoto, S. Usui, and T. Morimoto, *Bull. Chem. Soc. Jpn.*, **50**, 1575 (1977).

Synthesis of Cytidine, Uridine, and Adenosine 5′-(2,6-Diamino-2,6-dideoxy-α-D-glucopyranosyl diphosphates) (Neosamine C-CDP, -UDP, and -ADP)

Kin-ichi TADANO, Tohru TSUCHIYA, Tetsuo SUAMI,* and Kenneth L. RINEHART, Jr.†

Department of Applied Chemistry, Faculty of Science and Technology, Keio University, Hiyoshi, Kohoku-ku, Yokohama 223

†*Roger Adams Laboratory, University of Illinois, Urbana, Illinois 61801, U.S.A.*

(Received May 4, 1982)

Three potential biosynthetic intermediates for aminocyclitol antibiotics, neosamine C-CDP, -UDP, and -ADP, have been synthesized from D-glucosamine by chemical means. 2,6-Diamino-2,6-dideoxy-α-D-glucopyranosyl phosphate, derived from the corresponding glycosyl bromide, was condensed with three nucleosides (CMP, UMP and AMP) by a known procedure. The configurations of the neosamine C nucleoside diphosphates have been confirmed by ^{13}C NMR spectra.

In the last decade, the biosynthesis of aminocyclitol antibiotics (neomycin, gentamicin, spectinomycin, streptomycin, and related compounds) has been investigated actively in several laboratories.[1] Of the subunits of the antibiotics, the amino sugars and aminocyclitols are constructed from rather simple sugars (usually, D-glucosamine and D-glucose) as primary metabolites. These results were obtained largely by incorporation experiments involving both radioisotope-labeled and stable isotope-labeled sugars. However, the reactions involved in bond-formation between the amino sugars and the aminocyclitols are far less understood. Thus, while it is well known that D-glucosamine is incorporated into neomycin, there are two possible pathways for this incorporation (Scheme 1). In one pathway neosamine C (2,6-diamino-2,6-dideoxy-D-glucose) is converted to a nucleoside diphosphate and attached directly to deoxystreptamine to give neamine. In the second pathway D-glucosamine is converted to a nucleoside diphosphate, then attached to deoxystreptamine to give paromamine, which is subsequently aminated at C-6″ to give neamine, In both cases, an amino sugar serves as a glycosyl donor from its nucleoside diphosphate for transfer to the aminocyclitol moiety.

A large number of sugar nucleoside diphosphates have been identified in nature[2] (in higher plants, microorganisms, *etc.*) and many of the naturally occurring sugar nucleoside diphosphates are thought to be glycosyl donors in the formation of oligo- and polysaccharides in living systems.[3] A number of naturally occurring sugar nucleoside diphosphates possess *N*-acetyl-D-glucosamine as the amino sugar[4] and nucleoside diphosphates of *N*-acetylglucosamine have been synthesized not only for biosynthetic research, but also for the elucidation of the reactivity of sugar phosphate esters. For example, Jeanloz *et al.*,[5] recently synthesized uridine 5′-(2-acetamido-2-deoxy-α-D-mannopyranosyluronic acid di-

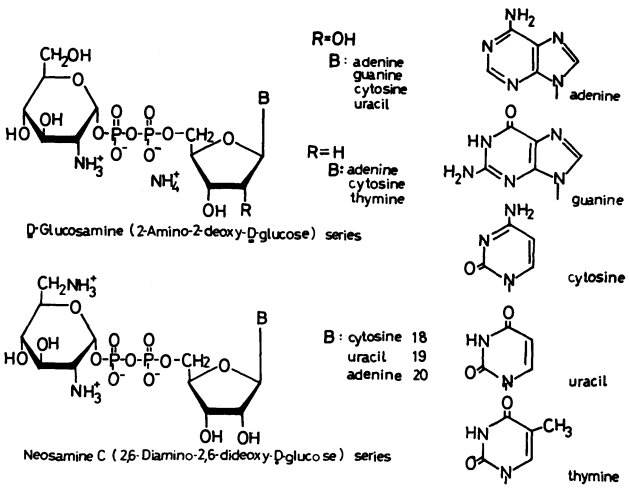

Fig. 1.

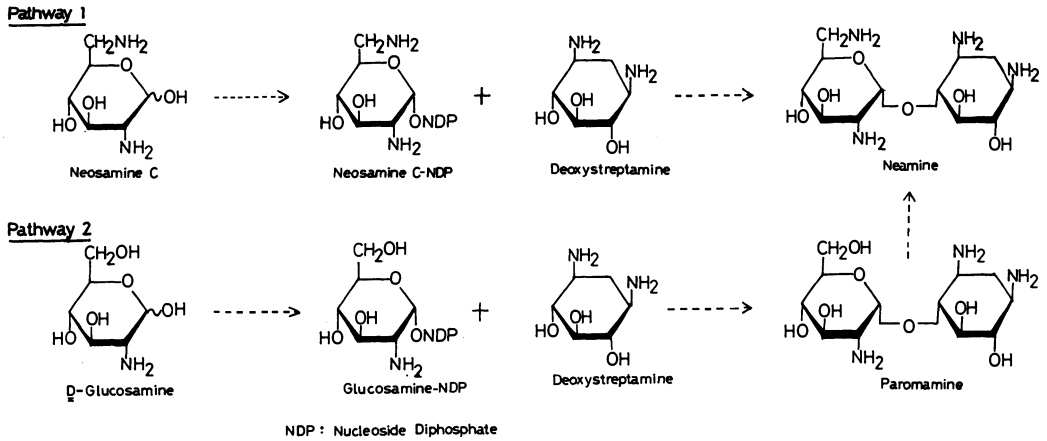

Scheme 1.

phosphate), which is considered to be a glycosyl donor to lipids in *Micrococcus lysodeikticus*. To our best knowledge, however, only one report[6] has appeared on chemical (rather than enzymatic) synthesis of a nucleoside diphosphate containing free D-glucosamine (or other free amino sugar) as the sugar moiety.

In order to investigate the second possibility, we recently synthesized[7] seven nucleoside diphosphates of glucosamine, namely, dTDP-, UDP-, CDP-, ADP-, GDP-, dCDP-, and dADP-glucosamines (Fig. 1) by chemical means and used the same procedure to synthesize several nucleoside diphosphates of D-[1-^3H]-glucosamine from the labeled D-glucosamine.

In the present communication, we describe the synthesis of three neosamine C nucleoside diphosphates, namely, cytidine-, uridine-, and adenosine-5′-(2,6-diamino-2,6-dideoxy-α-D-glucopyranosyl diphosphates, **18**—**20**, respectively, compounds which can be employed in examining the first biosynthetic pathway of Scheme 1, *i.e.*, that neosamine is transferred directly to deoxystreptamine.

Initially, we examined the stability of a protected D-glucosaminyl phosphate (diphenyl 3,4,6-tri-*O*-acetyl-α-D-glucosaminyl phosphate hydrobromide) prepared previously by us[7] in basic media: (1) In pyridine at room temperature for 3 h, (2) in *N*,*N*-dimethylformamide containing sodium azide at 120 °C for 30 min, (3) in ammonia-saturated methanol at 5 °C for 23 h, and (4) in methanol containing aqueous sodium hydrogencarbonate at room temperature for 70 min. Under all conditions, phosphate bond cleavage (C–O–P) was observed, so a route to neosamine C nucleoside diphosphates involving introduction of an amino group (or its equivalent) at C-6 of the glucosaminyl phosphate was abandoned.

Next, introduction of an amino group at C-6 of D-glucosamine prior to formation of the sugar phosphate ester was investigated. D-Glucosamine hydrochloride was converted to the *N*,*O*-protected 6-*O*-tosylate (**1**) by a known procedure,[8] then to the known 6-azido derivative (**2**).[9] In order to introduce a phosphate ester and an α-linkage at the anomeric center, protection of the 2-amino group with a non-participating functionality is essential. For this purpose, **2** was converted to its *N*-(2,4-dinitrophenyl) derivative (**3**), then to the corresponding α-glucosaminyl chloride (**4**) by a known procedure.[9] In addition, **2** was converted to the glycosyl chloride (**5**) possessing a free amino group at C-2. Both of the α-glucosaminyl chlorides, **4** and **5**, were treated with diphenyl hydrogenphosphate in dry benzene in the presence of triethylamine (the same procedure employed for phosphorylation of D-glucosaminyl bromide).[7] At room temperature no phosphate was introduced in either case. At elevated temperature (45 to 80 °C for 4 to 5 h) a complex mixture was formed, as shown by TLC, and the mixture was not further investigated.

In the next attempted synthesis, a 6-*O*-tosylate possessing a free amino group at C-2 (**6**) was prepared by acid treatment of **1** and converted to the glycosyl bromide (**7**) (of undetermined anomeric cofiguration), since in general, glycosyl bromides are more reactive

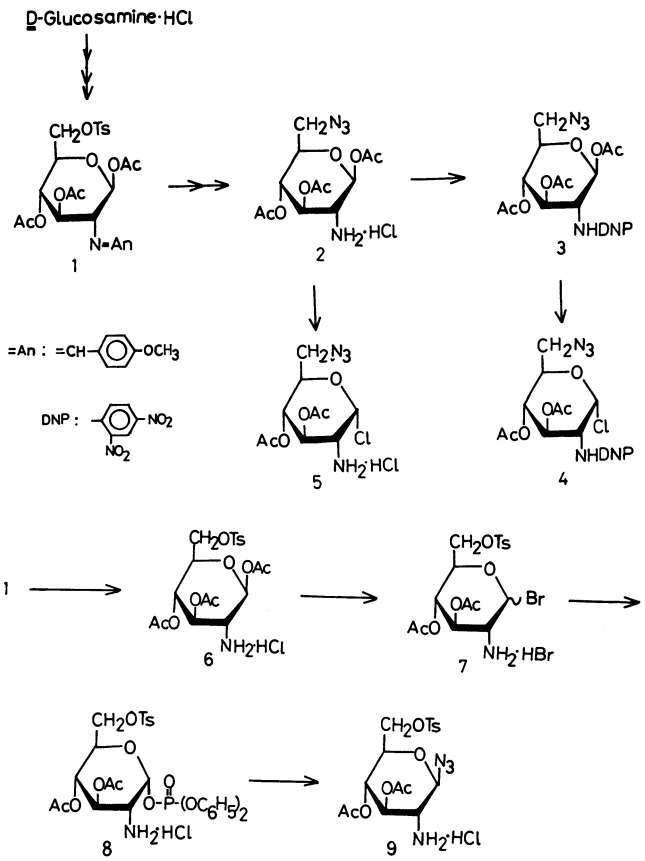

than the corresponding chlorides. Treatment of **7** with diphenyl hydrogenphosphate at room temperature for 18 h gave the desired α-linked phosphate (**8**) in 35% yield. The α-linkage was confirmed by the ^1H NMR spectrum (showing a triplet at δ 6.22, $J_{1,2}=J_{1,P}=4.5$ Hz, for H-1). It has been reported that ^1H-^{31}P coupling in an R_2CH–O–P system is 5 to 7 Hz.[10] Substitution of the 6-*O*-tosyl group by the azido group was tried (sodium azide in acetonitrile at 55 °C for 3 h). The predominant product, isolated as crystals was the glycosyl azide (**9**) instead of the expected 6-azido derivative. Disappearance of the phenoxy protons and presence of the tosylate protons were observed in the ^1H NMR spectrum of **9**. Furthermore, an azido group absorption (2090 cm^{-1}) appeared in the IR spectrum of **9** and elemental analyses also supported the glycosyl azide structure. Thus, introduction of the amino group at C-6 prior to phosphate formation, appears indispensible.

In the successful synthesis the free amino group in **2** was temporarily protected with a *t*-butoxycarbonyl group to afford **10**. The azido group of **10** was hydrogenated and the amino group formed was treated with 2,4-dinitrofluorobenzene to afford **11**. Compound **10** was also converted to **12** and **13** by hydrogenolysis, followed by trifluoroacetylation. When trifluoroacetylation of the 6-amino group was carried out in dichloromethane, cleavage of the 2-*N*-*t*-butoxycarbonyl group occurred, so that subsequent 2,6-di-*N*-trifluoroacetylation affored **12** as the sole product in low yield (39%); the structure was confirmed by its ^1H NMR and IR spectra. On the other hand, when *N*-trifluoroacetylation

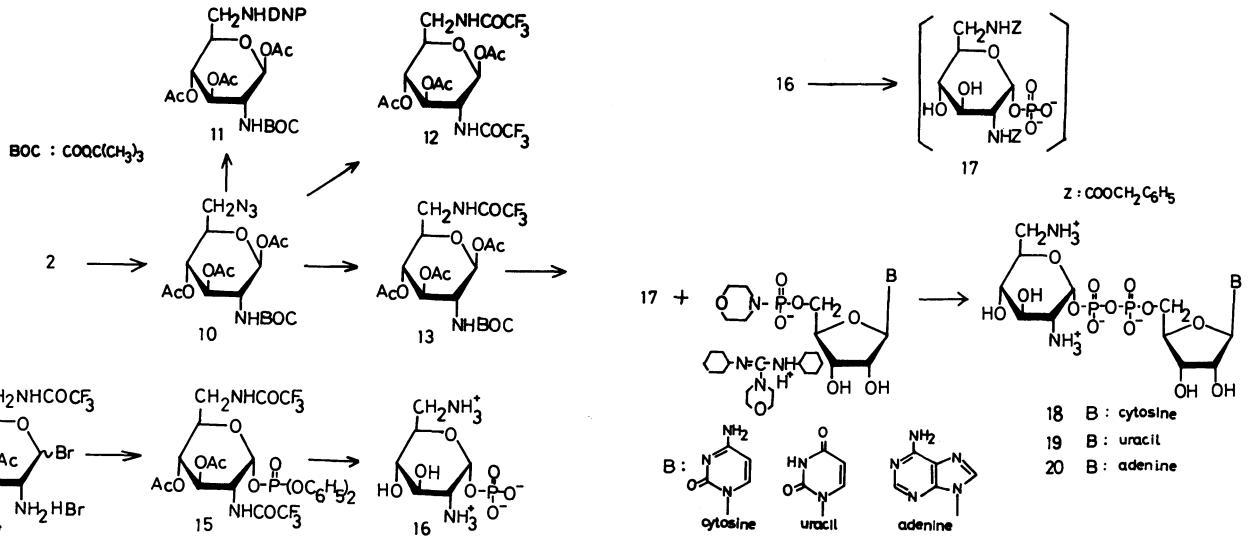

in dichloromethane was carried out in the presence of pyridine, only 6-*N*-acetylation was observed and **13** was isolated in 72% yield from **10**. Compound **13** was then converted in quantitative yield to the glycosyl bromide (**14**) by treatment of hydrobromic acid in acetic acid at room temperature for 16 h. During this strong acid treatment removal of the *N*-*t*-butoxycarbonyl group occurred simultaneously. Because of its low solubility in several organic solvents, the configuration of the anomeric center of **14** could not be determined.

Without further purification, **14** was treated with diphenyl hydrogenphosphate (1 molar equivalent) in dry benzene in the presence of triethylamine at room temperature for 1 h. The glycosyl phosphate formed (TLC: R_f 0.48, $PhCH_3$: EtOH=5 : 1) was quite unstable on silicic acid, so purification at this stage was avoided and the free amino on C-2 was immediately protected with a trifluoroacetyl group to afford **15** in 86% yield form **14**. Since the yield during formation of glycosyl phosphates is, in general, moderate or low, the yield of **15** is remarkable. An α-configuration in **15** was confirmed by its ^1H NMR spectrum (H-1, δ 5.95, doublet of doublets, $J_{1,2}$=4 Hz, $J_{1,P}$=6 Hz).

Deprotection of **15** was achieved by hydrogenolysis (removing the phenyl group on the phosphate), followed by saponification. 2,6-Diamino-2,6-dideoxy-α-D-glucopyranosyl phosphate (**16**) was purified by ion exchange and its structure was confirmed by ^1H and ^{13}C NMR spectra. In the ^1H NMR spectrum of **16** a doublet of doublets (H-1, δ 5.66, $J_{1,2}$=3.2 Hz, $J_{1,P}$=7.2 Hz) revealed the existence of an α-glycosyl phosphate. The ^{13}C NMR spectrum of **16** resembled the spectrum of α-D-glucosaminyl phosphate,[7] except for the chemical shift of C-6 (at δ 41.4 for **16** and at δ 61.1 for the glucosaminyl phosphate), indicative of the replacement of a hydroxyl group by an amino group. The coupling constants between the phosphorus nucleus and C-1 and C-2 were approximately equal to those of the glucosaminyl phosphate ($J_{C,P}$=4.3 Hz for C-1, and $J_{C,P}$=8.5 Hz for C-2 in **16**; 4.9 Hz and 7.8 Hz, respectively, in the glucosaminyl phosphate). At this stage, we had in hand the desired neosamine C phosphate **16** in moderate overall yield from D-glucosamine, and the remaining problem to synthesis of the final amino sugar nucleoside diphosphate was the condensation of **16** with the nucleoside 5′-monophosphates. Several examples[11] are known of the condensation reaction and we intended to use a procedure slightly modified from that of Khorana and Moffatt[12] employing nucleoside 5′-phosphoromorpholidate as phosphate donors. However, **16** has an extremely low solubility in organic solvents for the condensation (including *N*,*N*-dimethylformamide, dimethyl sulfoxide, and hexamethylphosphoric triamide), even at elevated temperature. To convert **16** to a more soluble derivative, the 2- and 6-amino groups of **16** were converted to their benzyloxycarbonyl derivatives. The bis(*N*-benzyloxycarbonyl) derivative (**17**), without isolation, was dissolved in dry pyridine and condensed with nucleoside (cytidine, uridine, and adenosine) 5′-phosphoromorpholidate (as their *N*,*N*′-dicyclohexyl-4-morpholinecarboxamidine salts). The mixtures were stirred at room temperature for 5 to 12 d. After catalytic hydrogenolysis to remove the *N*-benzyloxycarbonyl groups, the reaction mixtures were purified on Dowex 1×8 (formate) column. The desired three neosamine C NDP's (**18**—**20**) were eluted with dilute formic acid, and their structures were established by ^1H and ^{13}C NMR spectra. Though the yields were unsatisfactory (20% for neosamine C-CDP, (**18**); 34% for neosamine C-UDP, (**19**); and 33% for neosamine C-ADP, (**20**)), **18**—**20** were predominant products in the reaction mixtures. All of the carbons in **18**—**20** were assigned in their ^{13}C NMR spectra from the chemical shifts of nucleoside 5′-monophosphates[13] and those of **16**. Four doublets are observed in the sugar skeleton carbon region, and those are attributed to C-4 ($J_{C,P}$>8 Hz) and C-5 ($J_{C,P}$<6 Hz) on D-ribose, and C-1 ($J_{C,P}\approx$5 Hz) and C-2 ($J_{C,P}$>8 Hz) on neosamine C. These patterns are typical for sugar nucleoside diphosphates. The three neosamine C NDP's were also characterized by their fast atom bombardment (FAB) mass spectra, which in each case gave the expected M+H peak in the positive ion mode: *m*/*z* 564 for neosamine C-CDP, 565 for -UDP, and 588 for -ADP.

In spite of rather low yields in the final condensation reaction, the synthesis developed in this communication is applicable for a general synthesis of free amino sugar nucleoside diphosphates.

Experimental

Melting points were determined with a Büchi apparatus (Model 510) and are uncorrected. Solutions were evaporated under diminished pressure at a bath temperature below 40 °C. Specific rotations were measured in a 1-dm tube with a JEOL DIP-4 polarimeter. TLC was performed on glass plates coated with Wako Gel B-5 F, and compounds were detected by UV light and by spraying with sulfuric acid followed by heating. Cellulose TLC was performed on plastic sheets coated withc ellulose (Eastman Chromatogram Sheet, 13254); 0.2% ninhydrin–pyridine solution was used for visualization of amino sugars. IR spectra were recorded with a Hitachi Model-225 spectrometer. ^{1}H NMR (90 MHz) spectra were recorded with a Varian EM-390 spectrometer. ^{1}H NMR (100 MHz) and ^{13}C NMR (25 MHz) spectra were recorded with a Varian XL-100 spectrometer. Chemical shifts for $CDCl_3$ solutions are reported from internal tetramethylsilane, and chemical shifts for D_2O solutions are reported from internal DSS. Mass spectra were taken on a Varian MAT-731 mass spectrometer, using Xenon as the reagent gas. The FAB gun was an Ion Tech FAB gun, attached to either an Ion Tech or Spellman high voltage power supply. Elemental analyses were performed by Mr. Saburo Nakada of this university, to whom our thanks are due.

*1,3,4-Tri-*O*-acetyl-2-deoxy-2-(*p*-methoxybenzylideneamino)-6-*O*-tosyl-β-*D*-glucopyranose (**1**).* This compound was prepared from 2-deoxy-2-(*p*-methoxybenzylideneamino)-D-glucose by the method of Morel;[8] mp 198—199 °C, $[\alpha]_D^{22}$ +98.2° (*c* 2.0, $CHCl_3$) [lit,[8] mp 203—204 °C, $[\alpha]_D^{20}$ +99.3° (*c* 2, $CHCl_3$)].

*1,3,4-Tri-*O*-acetyl-2-amino-6-azido-2,6-dideoxy-β-*D*-glucopyranose Hydrochloride (**2**).* Compound **1** was converted to the 6-azide, then hydrolyzed to prepare the title compound by the known method;[9] mp 149 °C (decomp), $[\alpha]_{23}^{D}$ +53.1° (*c* 1, H_2O) [lit,[9] mp 147—154 °C (decomp), $[\alpha]_D^{25}$ +55.8° (*c* 1, H_2O)].

*1,3,4-Tri-*O*-acetyl-6-azido-2,6-deoxy-2-(2,4-dinitroanilino)-β-*D*-glucopyranose (**3**).* This compound was prepared from **2** by the known method;[9] mp 116—117 °C, $[\alpha]_D^{22.5}$ +99.0° (*c* 1, $CHCl_3$) [lit,[9] mp 115.5—116 °C, $[\alpha]_D^{29}$ +108° (*c* 1, $CHCl_3$)].

*3,4-Di-*O*-acetyl-6-azido-2,6-dideoxy-2-(2,4-dinitroanilino)-α-*D*-glucopyranosyl Chloride (**4**).* This glucosaminyl chloride was prepared from **3** by a slight modification of the known procedure.[9] Hydrogen chloride-saturated ether (0 °C, 30 ml) and acetyl chloride (3 ml) were added to 800 mg (1.61 mmol) of **3**, and the solution was stirred at room temperature in the dark for 19 h. Then, an additional 20 ml of hydrogen chloride-saturated ether was added after 22 h, and stirring was continued for 20 h more; TLC revealed the disappearance of **3** (R_f 0.22; $PhCH_3$: AcOEt=6 : 1) and the formation of a single product (R_f 0.29). The precipitated crystals were collected by filtration, washed with dry ether, and dried to afford 372 mg (73%) of **4** which was used without further purification: mp 173 °C (decomp), $[\alpha]_D^{21.5}$ +150° (*c* 1.0, $CHCl_3$) [lit,[9] mp 170 °C (decomp.), $[\alpha]_D^{25}$ +167° (*c* 1, $CHCl_3$)]; ^{1}H NMR (DMSO-d_6, 90 MHz): δ 1.87 (s, 3H, OAc), 2.09 (s, 3H, OAc), 3.37 (dd, 1H, $J_{6a,6b}$=13.8 Hz, $J_{5,6a}$=4.5 Hz, H-6a), 3.58 (dd, 1H, $J_{6a,6b}$=13.8 Hz, $J_{5,6b}$=3 Hz, H-6b), 4.24—4.49(m, 2H,H-2 and H-5), 5.26(t, 1H, $J_{3,4}$=$J_{4,5}$=9 Hz, H-4), 5.55 (t, 1H, $J_{2,3}$=$J_{3,4}$=9 Hz, H-3), 6.26 (d, 1H, $J_{1,2}$=3.6 Hz, H-1), 7.13 (d, 1H, $J_{5',6'}$=9.3 Hz, H-6′ of DNP), 8.28 (dd, 1H, $J_{5',6'}$=9.3 Hz, $J_{3',5'}$=2.7 Hz, H-5′), 8.75 (d, 1H, $J_{NH,2}$=9 Hz, NH), 9.10 (d, 1H, $J_{3',5'}$=2.7 Hz, H-3′).

*3,4-Di-*O*-acetyl-2-amino-6-azido-2,6-dideoxy-α-*D*-glucopyranosyl Chloride Hydrochloride (**5**).* Dry hydrogen chloride was introduced with ice cooling to a glacial acetic acid solution (50 ml) of **2** (500 mg, 1.36 mmol) containing 2 ml of acetyl chloride until the solution was saturated. The solution was stirred at room temperature in the dark for 24 h, then evaporated. The residue was coevaporated with toluene and triturated with chloroform (30 ml), insolbuble material was removed by filtration, and the filtrate was concentrated to half volume. After addition of 30 ml of ether the solution was cooled at 5 °C overnight. The precipitated crystals were collected by filtration and dried to afford 339 mg, which consisted of **5** and **2** in a 4 : 1 ratio based on the ^{1}H NMR spectrum and elemental analyses: IR (KBr) 2080 (N_3), 1760 (C=O) and 765 cm^{-1} (Cl); ^{1}H NMR (DMSO-d_6, 90 MHz) δ 2.01 (s, 3H, OAc), 2.05 (s, 3H, OAc), 2.16 (s, 0.6H, OAc), 3.53 (m, 3H, H-6a, H-6b, and H-2 or H-5), 4.00—4.25 (m, 1H, H-2 or H-5), 5.01 (t, 1H, $J_{3,4}$=$J_{4,5}$=9 Hz, H-4), 5.24 (t, 1H, $J_{2,3}$=$J_{3,4}$=9 Hz, H-3), 5.92 (d, 0.2H, $J_{1,2}$=8.7 Hz, H-1 on **2**), 6.68 (d, 0.8H, $J_{1,2}$=3.0 Hz, H-1 on **5**), 9.02 (bs, 3H, NH_3^+). The mixture was used without further purification. Found: C, 36.05; H, 4.79; N, 15.86; Cl, 18.42%. Calcd for $C_{12}H_{18}N_4O_7\cdot HCl$ (20%)+$C_{10}H_{15}ClN_4O_7\cdot HCl$ (80%): C, 35.86; H, 4.80; N, 16.12; Cl, 18.46%.

*1,3,4-Tri-*O*-acetyl-2-amino-2-deoxy-6-*O*-tosyl-β-*D*-glucopyranose Hydrochloride (**6**).* To a vigorously stirred solution of **1** (1.28 g, 2.22 mmol) in acetone (15 ml), 2 ml of 5 M hydrochloric acid was added dropwise at 55 °C. The mixture was stored at 5 °C overnight, and the precipitated white crystals were collected by filtration, then dried. The crude crystals were recrystallized from methanol to give 568 mg (52%) of **6**, mp 206 °C (decomp), which was used in the next step without further purification.

*3,4-Di-*O*-acetyl-2-amino-2-deoxy-6-*O*-tosyl-*D*-glucopyranosyl Bromide Hydrobromide (**7**).* A solution of 30% hydrogen bromide in acetic acid (20 ml) was added to a glacial acetic acid (40 ml) solution of **6** (518 mg, 1.04 mmol) and the mixture was stirred at room temperature for 20 h, then evaporated with toluene. The residue was triturated with chloroform, and the insoluble crystals were collected by filtration, washed with chloroform, and dried to afford 559 mg (95%) of **7**, mp 159 °C (decomp), which was used without further purification. Found: C, 36.58; H, 4.10; N, 2.33%. Calcd for $C_{17}H_{23}Br_2NO_8S$: C, 36.38; H, 4.13; N, 2.50%.

*Diphenyl 3,4-Di-*O*-acetyl-2-amino-2-deoxy-6-*O*-tosyl-α-*D*-glucopyranosyl Phosphate Hydrochloride (**8**).* Diphenyl hydrogenphosphate (Aldrich, 0.736 g, 2.94 mmol) and triethylamine (0.42 ml, 3.01 mmol) were added to a suspension of **7** (1.65 g, 2.94 mmol) in dry benzene (45 ml) containing triethylamine (0.42 ml, 3.01 mmol). After the mixture was stirred at room temperature in the dark for 18 h, TLC revealed the presence of a single product (R_f 0.52, positive to UV and ninhydrin, $PhCH_3$: EtOH=5 : 1). Precipitated triethylammonium bromide was removed by filtration and washed with benzene. The combined filtrate and washings were evaporated to afford a pale yellow syrup which was triturated with 2 M hydrochloric acid (10 ml) to give crystals, which were filtered, washed with cold water, and dried. The crude **8** obtained (1.87 g) was recrystallized from methanol and ether to afford 697 mg (35%) of pure **8**: mp 140 °C (sintered), 146 °C (decomp); $[\alpha]_D^{22}$ +88.8° (*c* 0.98, DMSO); ^{1}H NMR (DMSO-d_6, 90 MHz). δ 1.90 (s, 3H, OAc), 2.05 (s, 3H, OAc), 2.40 (s, 3H, Ts–CH_3), 3.48 (sb, 3H, NH_3^+), 3.70—4.11 (m, 4H, H-2, 5, 6a, 6b), 4.98 (t, 1H, $J_{3,4}$=$J_{4,5}$=9 Hz, H-4), 5.25 (t, 1H, $J_{2,3}$=$J_{3,4}$=9 Hz, H-3), 6.22 (t, 1H, $J_{1,2}$=$J_{1,P}$=4.5 Hz, H-1), 7.28 [m, 10H

OPO(OPh$_2$)], 7.41 and 7.66 (m, 4H, Ts-C$_6$H$_4$). Found: C, 49.64; H, 4.90; N, 1.78%. Calcd for $C_{29}H_{33}ClNO_{12}PS \cdot H_2O$: C, 49.47; H, 5.01; N, 1.99%.

3,4-Di-O-acetyl-2-amino-2-deoxy-6-O-tosyl-β-D-glucopyranosyl Azide Hydrochloride (9). After a mixture of **8** (150 mg, 0.219 mmol), sodium azide (178 mg, 2.74 mmol) and triethylamine (0.31 ml, 0.22 mmol) in acetonitrile (10 ml) was stirred at 55 °C for 3 h, TLC revealed the disappearance of **8** (R_f 0.10, $PhCH_3$: MEK=4 : 1) and the formation of two products (R_f 0.20 and 0.00). Insoluble material was removed, the filtrate was evaporated, and the residue was purified on silica gel column (Wako gel C-300, 9.5 g, 12 mm×145 mm, $PhCH_3$: EtOH=5 : 1). Fractions showing R_f 0.45 on TLC ($PhCH_3$: EtOH=5 : 1) were combined and evaporated to afford 51.1 mg of an oily residue, which was triturated with 2 M hydrochloric acid (3 ml). The precipitated crystals were collected and dried to afford 39.8 mg (38%) of **9**: mp 148 °C (decomp); $[\alpha]_D^{22.5}$ +11.6° (*c* 0.23, $CHCl_3$); IR (KBr) 2090 (N_3) and 1765 cm^{-1} (C=O); ^{1}H NMR ($CDCl_3$, 90 MHz) δ 1.96 (s, 3H, OAc), 2.03 (s, 3H, OAc), 2.43 (s, 3H, Ts-CH_3), 2.60—2.81 (m, 1H), 3.70—3.91 (m, 1H), 4.07 (d, 2H, J=4 Hz, H-6a and 6b), 4.41 (d, 1H, J=10 Hz, H-1), 4.82—4.92 (m, 2H), 7.29 and 7.73 (AB quartet, 4H, Ts-C$_6$H$_4$). Found: C, 42.36; H, 4.93; N, 11.39%. Calcd for $C_{17}H_{23}ClN_4O_8S$: C, 42.64; H, 4.84; N, 11.70%.

1,3,4-Tri-O-acetyl-6-azido-2-(t-butoxycarbonylamino)-2,6-dideoxy-β-D-glucopyranose (10). Di-*t*-butyl dicarbonate (4.97 g, 23.8 mmol) was added to a solution of **2** (6.58 g, 17.9 mmol) in a mixture of dioxane (60 ml) and water (30 ml) containing 1.71 g (20.3 mmol) of sodium hydrogencarbonate and the mixture was stirred at 0 °C for 2 h, then at room temperature for 16 h. Thin-layer chromatography revealed the disappearance of **2** (R_f 0.02; $PhCH_3$: MEK=5 : 1) and the formation of a sole product (R_f 0.35). The mixture was evaporated and the residue was extracted with ethyl acetate (150 ml). The organic extract was washed with water (150 ml; 75 ml×2), dried over anhydrous sodium sulfate, and evaporated. The crude crystals were recrystallized from ethanol and methanol to afford 6.44 g (84%) of **10**: mp 172—173 °C; $[\alpha]_D^{23}$ +18.5° (*c* 2.1, $CHCl_3$); IR (KBr) 2120 (N_3), 1760 (C=O), 1700 (NC=O), and 1530 cm^{-1} (NH); ^{1}H NMR ($CDCl_3$, 90 90 MHz) δ 1.43 (s, 9H, $COOC(CH_3)_3$, 2.04 (s, 6H, OAc), 2.11 (s, 3H, OAc), 3.33 (d, 2H, J=4 Hz, H-6a and 6b), 3.63—3.83 (m, 2H, H-2 and H-5), 4.58 (d, 1H, $J_{NH,2}$=9 Hz, NH), 4.96 (t, 1H, $J_{3,4}=J_{4,5}$=9 Hz, H-4), 5.15 (1H, $J_{2,3}=J_{3,4}$=9 Hz, H-3), and 5.65 (d, 1H, $J_{1,2}$=9 Hz, H-1). Found: C, 47.30; H, 5.94; N, 12.77%. Calcd for $C_{17}H_{26}N_4O_9$: C, 47.44; H, 6.09; N, 13.02%.

1,3,4-Tri-O-acetyl-2-(t-butoxycarbonylamino)-2,6-dideoxy-6-(2,4-dinitroanilino)-β-D-glucopyranose (11). A solution of **10** (696.3 mg, 1.62 mmol) in a mixture of ethyl acetate (5 ml) and ethanol (50 ml) containing 0.27 ml of 6 M hydrochloric acid was hydrogenated at room temperature in the presence of 10% palladium on charcoal (70 mg) under 345 kPa initial hydrogen atmosphere. After 2.5 h, TLC revealed the disappearance of **10** (R_f 0.36; $PhCH_3$: MEK=5 : 1) and the formation of a single ninhydrin-positive product (R_f 0.00). The catalyst was removed by filtration and the filtrate was evaporated to afford white crystals, which were dissolved in ethanol (7 ml). 2,4-Dinitrofluorobenzene (750 mg, 4.03 mmol) in acetone (28 ml) and sodium hydrogencarbonate (325.5 mg, 3.88 mmol) were added, and the mixture was stirred at room temperature in the dark for 24 h. Thin-layer chromatography revealed the formation of a single product (R_f 0.33, $PhCH_3$: MEK=4 : 1). After evaporation of the mixture, the residue was extracted with chloroform, insoluble material was removed by filtration, and the filtrate was evaporated. The residue was purified on silica gel (Wako gel C-300, 40 g, 23 mm×220 mm, $PhCH_3$: MEK=4 : 1). Fractions showing R_f 0.33 were combined and evaporated to afford crude crystals which were recrystallized from chloroform and ethanol to yield 717 mg (78%) of **11**: mp 238 °C (decomp), $[\alpha]_D^{23}$ +38.3° (*c* 1.9, $CHCl_3$); IR (KBr) 3360 (NH), 1755 (C=O), 1695 (NC=O), 1620 (C=C), 1590 (NO_2), 1525 cm^{-1} (NH); ^{1}H NMR ($CDCl_3$, 90 MHz) δ 1.42 [s, 9H, $COOC(CH_3)_3$], 2.06 (s, 3H, OAc), 2.12 (s, 6H, 2×OAc), 3.39—3.95 (m, 4H, H-2, H-5, H-6a, and H-6b), 4.61 (d, 1H, $J_{NH,2}$=10 Hz, H-2), 4.97 (t, 1H, $J_{3,4}=J_{4,5}$=9 Hz, H-4), 5.25 (t, 1H, $J_{2,3}=J_{3,4}$=9 Hz, H-3), 5.65 (d, 1H, $J_{1,2}$=9 Hz, H-1), 6.91 (d, 1H, $J_{5',6'}$=9 Hz, H-6′ of DNP group), 8.18 (dd, 1H, $J_{5',6'}$=9 Hz, $J_{3',5'}$=3 Hz, H-5′), 8.79 (t, 1H, $J_{NH,6}$=6 Hz, NH), 9.06 (d, 1H, $J_{3',5'}$= 3 Hz, H-3′). Found: C, 48.19; H, 5.27; N, 9.56%. Calcd for $C_{23}H_{30}N_4O_{13}$: C, 48.42; H, 5.30; N, 9.82%.

1,3,4-Tri-O-acetyl-2,6-dideoxy-2,6-bis(trifluoroacetamido)-β-D-glucopyranose (12). Compound **10** (568 mg, 1.32 mmol) was hydrogenated as described for the preparation of **11**, and the crude crystals were dissolved in 20 ml of dry dichloromethane and acylated by adding 1.0 ml (7.19 mmol) of trifluoroacetic anhydride dropwise with mechanical stirring under ice cooling. After the mixture had been stirred at room temperature for 16 h, TLC revealed a single product (R_f 0.40; $PhCH_3$: MEK=3 : 1). The mixture, diluted with 20 ml of dichloromethane, was washed with aqueous sodium hydrogencarbonate until neutral, then with water (20 ml; 10 ml×2), then dried (Na_2SO_4). Evaporation of the extract gave crude crystals which were recrystallized from chloroform–ether to afford 220 mg (39%) of **12**: mp 220—221 °C (decomp); $[\alpha]_D^{23}$ +2.1° (*c* 0.98, MeOH); IR (KBr) 1760 (C=O), 1710 (NC=O), 1555 (NH), 1220 and 1180 (C-F) cm^{-1}; ^{1}H NMR (CD_3OD, 90 MHz) δ 1.95 (s, 3H, OAc), 2.01 (s, 3H, OAc), 2.04 (s, 3H, OAc), 3.43—4.39 (m, 4H, H-2, H-5, H-6a and H-6b), 4.67 (t, 1H, $J_{3,4}=J_{4,5}$=9 Hz, H-4), 5.27 (t, 1H, $J_{2,3}=J_{3,4}$=9 Hz, H-3), 5.75 (d, 1H, $J_{1,2}$=9 Hz, H-1). Found: C, 38.83; H, 3.78; N, 5.71%. Calcd for $C_{16}H_{18}F_6N_2O_9$: C, 38.72; H, 3.65; N, 5.64%.

1,3,4-Tri-O-acetyl-2-(t-butoxycarbonylamino)-2,6-dideoxy-6-trifluoroacetamido-β-D-glucopyranose (13). Compound **10** (991 mg, 2.30 mmol) was hydrogenated as described above and the crude 6-amino derivative in dry dichloromethane (30 ml) and dry pyridine (8 ml) was *N*-acylated directly by adding trifluoroacetic anhydride (0.55 ml, 3.95 mmol) under ice cooling. After the mixture had been stirred at room temperature for 30 min, TLC revealed a single product (R_f 0.51; $PhCH_3$: EtOH=5 : 1). The mixture was diluted with dichloromethane (40 ml) and the organic mixture was washed with diluted aqueous sodium hydrogencarbonate to neutrality, washed with water (80 ml; 40 ml×2), dried, and evaporated to afford a crystalline residue which was recrystallized from chloroform–ether to give 828 mg (72%) of **13**: mp 214 °C (decomp); $[\alpha]_D^{22}$ +20.8° (*c* 2.1, $CHCl_3$); IR (KBr) 1755 (C=O), 1700 (NC=O), 1525 (NH), 1220 and 1170 cm^{-1} (C-F); ^{1}H NMR ($CDCl_3$, 90 MHz) δ 1.41 [s, 9H, $COOC(CH_3)_3$], 2.02 (s, 3H, OAc), 2.04 (s, 3H, OAc), 2.09 (s, 3H, OAc), 3.21—3.95 (m, 4H, H-2, H-5, H-6a, and H-6b), 4.80 (d, 1H, $J_{NH,2}$= 9 Hz, 2-NH), 4.85 (t, 1H, $J_{3,4}=J_{4,5}$=9 Hz, H-4), 5.15 (t, 1H, $J_{2,3}=J_{3,4}$=9 Hz, H-3), 5.60 (d, 1H, $J_{1,2}$=9 Hz, H-1), 6.89 (t, 1H, $J_{NH,6}$=6 Hz, 6-NH). Found: C, 45.74; H, 5.35: N, 5.34%. Calcd for $C_{19}H_{27}F_3N_2O_{10}$: C, 45.60; H, 5.44; N, 5.60%.

3,4-Di-O-acetyl-2-amino-2,6-dideoxy-6-trifluoroacetamido-D-glucopyranosyl Bromide Hydrobromide (14). To a solution of **13** (305 mg, 0.609 mmol) in dry dichloromethane (3 ml), 25% hydrogen bromide in acetic acid (2.0 ml) was added dropwise under ice cooling. The stirred mixture gradually warmed

to room temperature, then was stirred 16 h longer, and finally was evaporated with toluene to afford 306 mg (quantitative) of crude bromide (**14**), mp 174—178 °C (decomp), which was used without further purification. Found: C, 28.42; H, 3.68; N, 5.77%. Calcd for $C_{12}H_{17}Br_2F_3N_2O_6$: C, 28.71; H, 3.41; N, 5.58%.

*Diphenyl 3,4-Di-O-acetyl-2,6-dideoxy-2,6-bis(trifluoroacetamido)-α-D-glucopyranosyl Phosphate (**15**).* Diphenyl hydrogenphosphate (Aldrich, 503 mg, 2.01 mmol) and triethylamine (0.60 ml, 4.30 mmol) were added to a suspension of **14** (1.01 g, 2.01 mmol) in dry benzene (distilled over sodium). The mixture was stirred at room temperature in the dark for 1 h, when TLC revealed formation of a UV-absorbing product (R_f 0.48; $PhCH_3$: EtOH=5 : 1). Triethylamine (1.20 ml, 8.60 mmol) and trifluoroacetic anhydride (0.60 ml, 4.31 mmol) were added to the mixture, under ice cooling, and the mixture was stirred at 0 °C for 30 min, when TLC revealed a single product with UV-absorption (R_f 0.60; $PhCH_3$: EtOH=5 : 1). The mixture was washed with water (80 ml; 20 ml×4), then dried (Na_2SO_4). After removal of the organic solvent, the residue was crystallized from methanol to yield 1.18 g (86%) of **15**: mp 128—132 °C (decomp); $[\alpha]_D^{27.5}$ +59.3° (*c* 0.72, $CHCl_3$); IR (KBr) 1750 (C=O), 1710 (NC=O), 1210, 1180 (C-F), and 970 cm^{-1} (P=O); ^1H NMR ($CDCl_3$, 90 MHz) δ 1.94 (s, 3H, OAc), 2.02 (s, 3H, OAc), 3.21—3.65, 4.06—4.52 (m,4H, H-2, H-5, H-6a and H-6b), 4.93 (t, 1H, $J_{3,4}$=$J_{4,5}$=9 Hz,H-4), 5.29 (t, 1H, $J_{2,3}$=$J_{3,4}$=9 Hz, H-3), 5.95 (dd, 1H, $J_{1,2}$=4 Hz, $J_{1,2}$=4Hz, $J_{1,P}$=6 Hz, H-1), 6.99—7.34 (m, 12H, phenyl, 2-NH and 6-NH). Found: C, 45.60; H, 3.84; N, 3.88%. Calcd for $C_{26}H_{25}F_6N_2O_{11}P$: C, 45.49; H, 3.67; N, 4.08%.

*2,6-Diamino-2,6-dideoxy-α-D-glucopyranosyl Phosphate (**16**).* A solution of **15** (120 mg, 0.174 mmol) in glacial acetic acid (5 ml) was hydrogenated in the presence of platinum oxide (30 mg) under 390 kPa initial hydrogen atmosphere at room temperature for 47 h. The catalyst was removed by filtration and the filtrate was evaporated to afford 93 mg of semicrystalline residue. The residue was dissolved in 2.6 ml of methanol and 1.12 ml of 1.25 M potassium methoxide in methanol was added. The mixture was stored at 5 °C for 96 h, an additional 0.56 ml of the base was added, and the mixture stood at room temperature for 20 h longer, when TLC (cellulose, *n*-BuOH : AcOH : H_2O=5 : 2 : 3) revealed two ninhydrin-positive products (R_f 0.36 and 0.27). The reaction mixture was applied to a Dowex 50W×8 column (pyridinium form, 7 ml wet volume, 9 mm×100 mm), which was eluted with water (40 ml), 0.01 M aqueous ammonia (24 ml) and 0.1 M aqueous ammonia (30 ml) successively (6-ml fractions). A concentrate of fractions 1 to 3 consisted of two products [R_f 0.36 and 0.27, BAW 523, IR (KBr) 1670 cm^{-1} (NC=O)], while a concentrate of fractions 13 to 15 (7.4 mg) consisted of pure **16** (R_f 0.27). The concentrate of fractions 1 to 3 (73 mg) was hydrolyzed under reflux for 2 h with 100 mg of sodium hydroxide in water (2 ml), when TLC revealed a single compound, **16**, (R_f 0.27), which was purified on an ion exchange column (Dowex 50W×8, pyridinium form, 2.5 ml wet volume, 6.5 mm×70 mm). The column was eluted with water (8 ml) and 0.1 M aqueous ammonia (10 ml) successively (2-ml fractions). Fractions 6 to 9 gave 14.9 mg (total 22.3 mg, 50%) of pure **16** mp 205 °C (decomp); $[\alpha]_D^{18.5}$ +33.1° (*c* 2.14, H_2O); IR (KBr) 3100 (NH), 1640 (NH), 1540 (NH), 1120 (P=O), 960 cm^{-1} (PO); ^1H NMR (D_2O, 100 MHz) δ 3.00—3.58 ,3.86—4.37 (m, 6H, H-2, H-3, H-4, H-5, H-6a, and H-6b), 5.66 (dd, 1H, $J_{1,2}$=3.2 Hz, $J_{1,P}$=7.2 Hz, H-1); ^{13}C NMR (D_2O, 25 MHz, TMS as internal standard) δ 41.4 (s, C-6), 55.4 (d, $J_{C,P}$=8.5 Hz, C-2), 69.6 (s, C-4), 70.6 (s, C-3), 72.5 (s, C-5), 92.0 (d, $J_{C,P}$=4.3 Hz, C-1). Found: C, 26.94; H, 5.75; N, 10.27%. Calcd for $C_6H_{15}N_2O_7 \cdot \frac{1}{2}H_2O$: C, 27.02; H, 5.86; N, 10.50%.

*Cytidine 5′-(2,6-Diamino-2,6-dideoxy-α-D-glucopyranosyl Diphosphate) (CDP-neosamine C) (**18**).* *N*-(Benzyloxycarbonyloxy)succinimide (68 mg, 0.27 mmol) in ethyl acetate (2 ml) was added to an aqueous solution (10 ml) of **16** (70.4 mg, 0.27 mmol) containing 23 mg (0.27 mmol) of sodium hydrogencarbonate. The mixture was stirred vigorously at 0 °C for 2 h, then at room temperature for 17 h. Additional *N*-benzyloxycarbonylating reagent (68 mg, 0.27 mmol) and sodium hydrogencarbonate (23 mg) were added, and stirring continued 15 h longer, when TLC (cellulose, *n*-BuOH : AcOH : H_2O=5 : 2 : 3) showed formation of the bis(benzyloxycarbonylamino) derivative (**17**) (R_f 0.70, UV absorbing). After removal of solvents by evaporation, the residue was dissolved in 50% aqueous ethanol in minimum volume, then applied on Dowex 50W×8 (pyridinium form, 6 ml wet volume). The column was eluted with 50% aqueous ethanol (50 ml), trioctylamine (0.14 ml, 0.32 mmol) was added to the eluate, and the aqueous solution was evaporated. The residue was coevaporated with dry pyridine (32 ml; 8 ml×4), finally dissolved in dry pyridine (10 ml), and cytidine 5′-phosphoromorpholidate *N,N′*-dicyclohexyl-4-morpholinecarboxamidine salt (Sigma, 187 mg, 0.27 mmol, dried over phosphorus pentaoxide *in vacuo* at 80 °C for 28 h) was added to the mixture, which was stirred at room temperature for 5 d, then evaporated. The residue was dissolved in 50% aqueous ethanol (7 ml) and hydrogenated in the presence of 10% palladium on charcoal (30 mg) under 390 kPa initial hydrogen atmosphere at room temperature for 48 h, when TLC (cellulose) revealed a mixture of six compounds (*n*-BuOH : AcOH : H_2O=5 : 2 : 3; R_f 0.70, 0.66, 0.54, 0.29, 0.27, and 0.15 with the latter compound predominant, each compound ninhydrin and/or UV-positive). The mixture was applied to a Dowex 1×8 column (formate form, 90 ml wet volume, 22 mm×260 mm), which was washed with water (200 ml), then gradient eluted with aqueous formic acid (0.0 M to 0.1 M, 4.5 ml fractions). Fractions showing R_f 0.15 were combined and evaporated with water to afford **18** (31.1 mg, 20% pure by TLC) as a colorless glass: $[\alpha]_D^{23}$ +36.5° (*c* 1.0, H_2O); ^1H NMR (D_2O, 90 MHz) δ 2.67—4.36 (m, 11H, H-2′, H-3′, H-4′, H-5′ of D-ribose, H-2″, H-3″, H-4″, H-5″, H-6″ of neosamine C), 5.67—5.90 (m, 3H, H-5 of cytosine, H-1′ and H-1″), 7.78 (d, 1H, $J_{5,6}$=7.5 Hz, H-6); ^{13}C NMR (D_2O, 25 MHz, TMS) δ 41.4 (s, C-6″), 54.9 (d, $J_{C,P}$=8.8 Hz, C-2″), 66.8 (d, $J_{C,P}$=6.1 Hz, C-5′), 70.4, 70.6, 71.2 (s's, C-3″, C-4″, and C-2′), 72.2 (s, C-5″), 75.1 (s, C-3′), 83.2 (d, $J_{C,P}$=8.7 Hz, C-4′), 90.6 (s, C-1′), 93.7 (d, $J_{C,P}$=5.4 Hz, C-1″), 97.5 (s, C-5), 142.3 (s, C-6), 155.9 (s, C-2), 174.6 (s, C-4); FABMS *m/z* 564 (M+H).

*Uridine 5′-(2,6-Diamino-2,6-dideoxy-α-D-glucopyranosyl Diphosphate) (UDP-neosamine C) (**19**).* Compound **16** (63.6 mg, 0.25 mmol) was converted to its bis(benzyloxycarbonyl) derivative, **17**, as described in the preparation of **18**. To 50 ml of the 50% aqueous ethanol eluate from the Dowex column, trioctylamine (0.14 ml, 0.32 mmol) was added. Evaporation was followed by evaporation with dry pyridine (32 ml, 8 ml×4) and finally, solution in dry pyridine (10 ml). Uridine 5′-phosphoromorpholidate *N,N′*-dicyclohexyl-4-morpholinecarboxamidine salt (Sigma, 198 mg, 0.29 mmol, dried prior to use) was added to the solution, and the mixture was stirred at room temperature for 12 d. After evaporation of the mixture, the residue was dissolved in 7 ml of 50% aqueous ethanol and hydrogenated for 69 h at room temperature in the presence of 10% palladium on charcoal (30 mg) under 390 kPa initial hydrogen atmosphere. Cellulose TLC (*n*-BuOH : AcOH: H_2O : 5 : 2 : 3) revealed five compounds (R_f 0.71, 0.44, 0.34, 0.28 and 0.16, all UV and/or ninhydrin positive with the latter compound predominant). The reaction mixture was applied

to a Dowex 1×8 column (formate form, 100 ml wet volume, 22 mm×310 mm), which was washed with water (80 ml) and gradient eluted with aqueous formic acid (0.0 M to 0.1 M, 4.5 ml fractions). Fractions showing R_f 0.16 (fractions 29 to 31) were combined and evaporated and finally coevaporated with water (12 ml, 6 ml×2) to afford 46.7 mg (34%) of TLC-homogeneous **19** as a colorless glass: $[\alpha]_D^{23}$ +35.2° (*c* 1.25, H_2O); ^1H NMR (D_2O, 100 MHz, TMS) δ 2.66—4.39 (m, 11H, H-2′, H-3′, H-4′, H-5′ on D-ribose and H-2″, H-3″, H-4″, H-5″, H-6″ on neosamine C), 5.79—5.96 (m, 3H, H-1′, H-1″, and H-5 on uracil), 7.88 (d, 1H, $J_{5,6}$=8.0 Hz, H-6); ^{13}C NMR (D_2O, 25 MHz, TMS) δ 41.4 (s, C-6″), 54.8 (d, $J_{C,P}$=9.4 Hz, C-2″), 66.8 (d, $J_{C,P}$=6.0 Hz, C-5′), 70.2, 70.4, 71.2 (each s, C-2′, C-3″, and C-4″), 72.1 (s, C-5″), 74.7 (s, C-3′), 83.2 (d, $J_{C,P}$=9.4 Hz, C-4′), 89.6 (s, C-1′), 93.2 (d, $J_{C,P}$=5.4 Hz, C-1″), 103.4 (s, C-5), 142.4 (s, C-6), 155.4 (s, C-2), 174.6 (s, C-4); FABMS *m/z* 565 (M+H).

*Adenosine 5′-(2,6-Diamino-2,6-dideoxy-α-D-glucopyranosyl Diphosphate) (ADP-neosamine C) (**20**).* The bis(benzyloxycarbonylamino) derivative (**17**) was prepared as described during the preparation of **18** [63.6 mg (0.25 mmol) of **16**, and 123 mg (0.49 mmol) of *N*-(benzyloxycarbonyloxy)succinimide]. To 50 ml of 50% aqueous ethanol eluate from the Dowex column, trioctylamine (0.14 ml, 0.32 mmol) was added and the mixture was evaporated with dry pyridine (32 ml, 8 ml×4) and finally dissolved in dry pyridine (10 ml). To the solution, adenosine 5′-phosphoromorpholidate *N,N′*-dicyclohexyl-4-morpholinecarboxamidine salt (Sigma, 193 mg, 0.27 mmol, dried prior to use) was added and the mixture was stirred at room temperature for 11 d. After evaporation of the mixture, the residue was dissolved in 7 ml of 50% aqueous ethanol and the solution was hydrogenated at room temperature for 68 h in the presence of 10% palladium on charcoal (30 mg) under 390 kPa initial hydrogen atmosphere. Cellulose TLC (*n*-BuOH : AcOH : H_2O=5 : 2 : 3) revealed five compounds (R_f 0.66, 0.51, 0.32, 0.25 and 0.18, all UV and/or ninhydrin-positive with the latter compound predominant). The reaction mixture was applied to a Dowex 1×8 column (formate form, 85 ml wet volume, 22 mm×250 mm), which was washed with water (80 ml), then gradient eluted with aqueous formic acid (0.0 M to 0.1 M, 4.5-ml fractions). Fractions showing R_f 0.18 (fractions 33 to 36) were combined and evaporated with water (12 ml, 6 ml×2) to afford 47.9 mg (33%) of TLC-homogeneous **20** as a colorless glass: $[\alpha]_D^{23}$ +26.9° (*c* 1.21, H_2O); ^1H NMR (D_2O, 100 MHz, TMS) δ 2.93—4.50 (m, 11H, H-2′, H-3′, H-4′, H-5′ of D-ribose, and H-2″, H-3″, H-4″, H-5″, H-6″ of neosamine C), 5.82 (dd, 1H, $J_{1,2}$=5.2 Hz, H-1′), 8.05 (s, 1H, H-2 of adenine), 8.34 (s, 1H, H-8); ^{13}C NMR (D_2O, 25 MHz, TMS) δ 40.3 (s, C-6″), 53.7 (d, $J_{C,P}$=8.8 Hz, C-2″), 65.4 (d, $J_{C,P}$=6.7 Hz, C-5′), 69.1, 69.3, 70.1, 71.0 (all s's, C-2′ C-3″, C-4″, C-5″), 74.3 (s, C-3′), 83.3 (d, $J_{C,P}$=9.4 Hz, C-4′), 87.1 (s, C-1′), 92.2 (d, $J_{C,P}$=5.4 Hz, C-1″), 117.9 (s, C-5), 139.6 (s, C-8), 148.2 (s, C-4), 151.4 (s, C-2), 154.1 (s, C-6); FABMS *m/z* 588 (M+H).

References

1) K. L. Rinehart, Jr., "Biosynthesis and Mutasynthesis of Aminocyclitol Antibiotics," in "Aminocyclitol Antibiotics," ACS Symposium Series 125, ed by K. L. Rinehart, Jr., and T. Suami, American Chemical Society, Washington, D. C. (1980), p. 335 and references cited therein.

2) N. K. Kochetkov and V. N. Shibaev, *Adv. Carbohydr. Chem. Biochem.* **28**, 307 (1973).

3) H. Grisebach, *Adv. Carbohydr. Chem. Biochem.*, **35**, 81 (1978).

4) J. L. Strominger, "Nucleotide Derivatives of Amino Sugars," in "The Amino Sugars," ed by R. W. Jeanloz, Academic Press, New York (1969), p. 375.

5) T. Yamazaki, C. D. Warren, A. Herscovics, and R. W. Jeanloz, *Carbohydr. Res.*, **79**, C9 (1980).

6) F. Maley, G. F. Maley, and H. A. Lardy, *J. Am. Chem. Soc.*, **78**, 5303 (1956).

7) K. L. Rinehart, Jr., K. Tadano, T. Suami, and T. Tsuchiya, *J. Am. Chem. Soc.*, to be submitted.

8) C. J. Morel, *Helv. Chim. Acta*, **41**, 1501 (1958).

9) S. Ogawa, H. Fujimori, and T. Suami, *Bull. Chem. Soc. Jpn.*, **49**, 2585 (1976).

10) L. M. Jackman and S. Sternhell, "Applications of Nuclear Magnetic Resonance Spectroscopy in Organic Chemistry," 2nd ed, Pergamon Press, London (1969), p. 351.

11) J. G. Moffatt, *Methods Enzymol.*, **8**, 136 (1966) and references cited therein.

12) S. Roseman, J. J. Distler, J. G. Moffatt, and H. G. Khorana, *J. Am. Chem. Soc.*, **83**, 659 (1961).

13) D. E. Dorman and J. D. Roberts, *Proc. Natl. Acad. Sci. U. S. A.*, **65**, 19 (1970).

Structural Studies on Herqueinone. The Configurations at C-4 of Herqueinone and at C-3 and C-4 of Dihydroherqueinone Monomethyl Ether

Takamitsu Yoshioka, Toshifumi Hirata, Tadashi Aoki, and Takayuki Suga*
Department of Chemistry, Faculty of Science, Hiroshima University, Higashisenda-machi, Naka-ku, Hiroshima 730
(Received May 11, 1982)

On the basis of the ^{1}H NMR spectroscopy and the X-ray crystallography, the configuration at C-4 of herqueinone was determined to be *S* and the configurations at C-3 and C-4 of dihydroherqueinone monomethyl ether were elucidated to be *R* and *S*, respectively, with relation to the previously established *R*-configuration at the 2′-position of herqueinone.

In the structural studies of herqueinone (**1**) which is a main red pigment isolated from the mycelia of *Penicillium herquei*,[1-5] its structure, except for the absolute configuration, was described as **1** by relating herqueinone to atrovenetin (**2**).[6,7] The configuration at C-2′ of **1** was reported to be *R* on the basis of the studies on the stereochemistry of the degradation product originating from its trimethylfuran ring.[8] On the other hand, the relative configurations at C-3, C-4, and C-5 of "glycol A" derived from dihydroherqueinone were shown as **3** on the basis of the long-range coupling between 3-H and 5-H in the ^{1}H NMR spectrum.[7] However, the relative configurations between C-2′ and C-4 of **1** and **3** have not been clarified yet.

For the biosynthetic studies of herqueinone (**1**),[9,10] it was necessary to determine the configuration at C-4 of **1** for clarifying the mechanism of the prenylation of the phenalenone skeleton. We therefore studied the configuration at C-4 of **1** and the configurations at C-3 and C-4 of dihydroherqueinone monomethyl ether (**4**) on the basis of the ^{1}H NMR spectroscopy and the X-ray crystallography. The results have been partly outlined in the form of the preliminary communications.[11,12] We will here report details of the results.

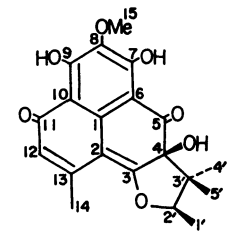

1

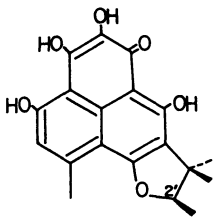

2

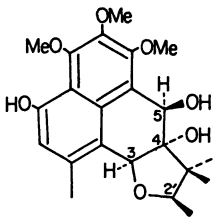

3

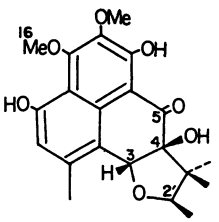

4

Results and Discussion

Herqueinone (1) and Dihydroherqueinone Monomethyl Ether (4). Herqueinone (**1**) was isolated from the mycelia of *Penicillium herquei* in the manner as described in the experimental part and identified by comparing its mp and ^{1}H NMR, IR, and UV spectra with those described in the literatures.[2,7] According to the method given in the literature,[7] dihydroherqueinone monomethyl ether (**4**) was prepared from the herqueinone (**1**) by hydrogenation followed by methylation. All the physical and spectral data of **4** are in fair agreement with the data described in the literature.[7] The configurations at C-4 of **1** and **4** were investigated by use of the ^{1}H NMR spectroscopy and the X-ray crystallography as follows.

^{1}H NMR Spectroscopic Study. The carbon atom at the 3′-position of herqueinone (**1**) has the geminal dimethyl groups which are composed of the C-4′ methyl group occupying the *pro-R* position and the C-5′ methyl group doing the *pro-S* position. The ^{1}H NMR signals at δ_H 1.00 and 1.40 were assigned to the C-4′ and C-5′ methyl groups, respectively, on the basis of the nuclear Overhauser effect (NOE),[13] which is shown in **1** of Fig. 1.[14]

The configuration at C-4 of **1** was determined by the application of the anisotropic effect[15-17] to the C-4′ and C-5′ methyl groups, as follows. Models[18] for **1** were examined; the distances between the center of the carbonyl double bond and the geminal dimethyl groups are estimated to be 2.5 Å and 3.5 Å, and the angles between the vectors from the center of the carbonyl double bond to the geminal dimethyl groups and the vector of the carbonyl dipole moment are about 35° and 75°. These data indicate that these methyl groups suffer from the anisotropic effect of the carbonyl group at the 5-position. On the other hand, the contribution of the anisotropic effect of the C-4 hydroxyl group to the geminal dimethyl groups may be excluded, because a shift of a ^{1}H NMR signal of a methyl group due to the introduction of a hydroxy group at its neighboring carbon atom is known to be less than 0.1 ppm in ^{1}H NMR spectra of hydroxy steroids.[17,19] Owing to the anisotropic effect of the carbonyl group at the 5-position, an upfield shift would be expected for the C-4′ methyl group in **1a** with the 4*S*-configuration, whereas a downfield one for the C-4′ methyl group in **1b** with the 4*R*-configuration, as shown in Fig. 2. Appearance of the C-4′ methyl signal in a higher field than methyl signal as described above indicated the configuration at C-4 of herqueinone (**1**) to be *S* as in **1a**.

Incidentally, the NOE measurement (Fig. 1) of

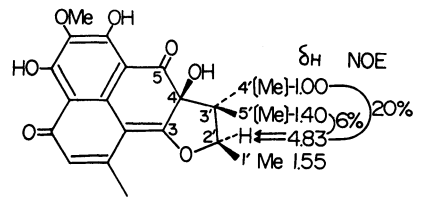

1

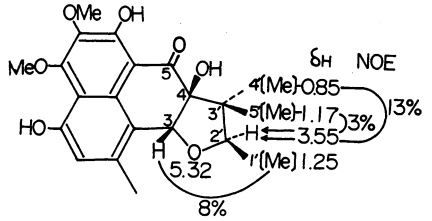

4

Fig. 1. Nuclear Overhauser effect observed for **1** and **4**.

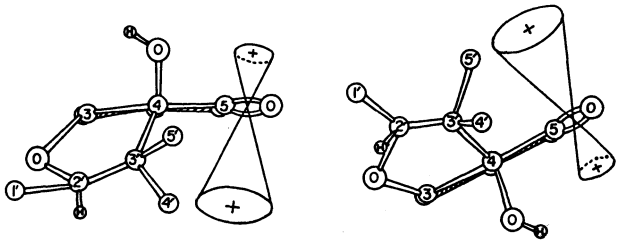

1a: 2′*R*, 4*S* **1b**: 2′*R*, 4*R*

Fig. 2. Anisotropic effect of the carbonyl group at the 5-position of **1**.

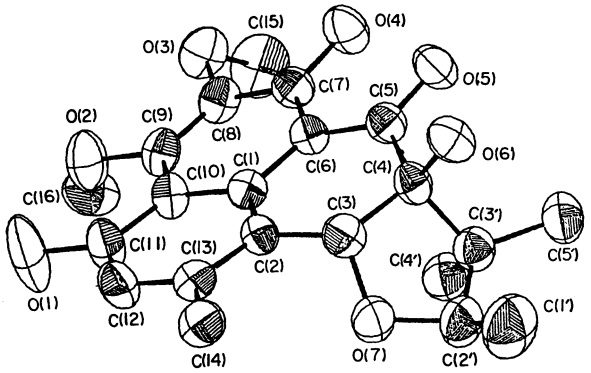

Fig. 3. ORTEP drawing[21] of the molecular structure of dihydroherqueinone monomethyl ether (**4**).

dihydroherqueinone monomethyl ether (**4**) showed also that the C-2′ hydrogen atom is *cis* to the C-4′ methyl group, while the hydrogen atom is *trans* to the C-3 hydrogen atom. This indicates that the configurations at C-3 and C-4 of **4** are *R* and *S*, respectively.

X-Ray Crystallographic Study. The absolute configuration of **4** is finally confirmed by the X-ray crystallography. A total of 1892 independent reflections were collected by use of Mo *Kα* radiation and 1811 reflections were used for structural determination. The structure of **4** was solved by the direct method by use of MULTAN[20] and the positional coordinates were refined by block-diagonal least-squares techniques to $R=0.058$.

TABLE 1. FINAL ATOMIC COORDINATES OF **4**, WITH STANDARD DEVIATIONS IN PARENTHESES

(1) The non-hydrogen atoms

Atom	10^4x	10^4y	10^4z	B_{eq}[a)]/Å^2
O(1)	2195(5)	12002(12)	4993(5)	8.0
O(2)	804(4)	9557(10)	5668(3)	5.7
O(3)	541(4)	5900(9)	6624(3)	4.9
O(4)	2639(4)	3577(8)	7655(3)	4.8
O(5)	5012(4)	3159(8)	8260(3)	4.6
O(6)	7274(4)	4271(8)	8157(3)	4.6
O(7)	7257(4)	9449(9)	8240(3)	5.0
C(1)	4166(5)	8058(11)	-6824(4)	3.3
C(2)	5378(5)	8780(10)	6858(4)	3.2
C(3)	6564(5)	7776(11)	7573(5)	3.9
C(4)	6420(5)	5914(11)	8213(4)	3.6
C(5)	5098(5)	4964(10)	7935(4)	3.6
C(6)	4026(5)	6180(10)	7348(4)	3.3
C(7)	2819(5)	5434(11)	7255(4)	3.8
C(8)	1727(5)	6644(12)	6729(4)	3.9
C(9)	1858(5)	8432(13)	6234(4)	4.0
C(10)	3064(5)	9165(12)	6221(4)	3.8
C(11)	3193(6)	10887(13)	5630(5)	4.7
C(12)	4380(6)	11484(12)	5642(5)	4.6
C(13)	5472(5)	10448(11)	6247(4)	3.7
C(14)	6732(6)	11152(13)	6173(4)	4.7
C(15)	253(6)	5776(19)	7536(6)	6.8
C(16)	43(6)	10488(14)	6178(6)	5.8
C(1′)	9116(7)	7972(20)	9453(7)	7.6
C(2′)	7791(6)	8609(14)	9239(5)	5.2
C(3′)	6832(5)	6915(12)	9290(4)	4.0
C(4′)	5745(6)	8129(13)	9458(5)	4.9
C(5′)	7368(6)	5246(13)	10096(5)	5.0

a) $B_{eq}=(B_{11}+B_{22}+B_{33})/3$.

(2) The hydrogen atoms

Atom	10^3x	10^3y	10^3z	B/Å^2
H(1)	739(5)	1086(10)	698(4)	7.8
H(2)	671(5)	1151(10)	561(4)	5.0
H(3)	704(5)	1246(10)	652(4)	7.4
H(4)	441(5)	1290(10)	527(4)	3.0
H(5)	158(5)	1151(10)	495(4)	9.5
H(6)	957(5)	533(10)	746(4)	2.4
H(7)	102(5)	488(10)	816(4)	9.5
H(8)	57(5)	691(10)	801(4)	12.5
H(9)	53(5)	1064(10)	701(4)	8.7
H(10)	962(5)	938(10)	633(4)	7.9
H(11)	967(5)	1162(10)	582(4)	8.5
H(12)	335(5)	272(10)	791(4)	7.6
H(13)	705(5)	315(10)	845(4)	6.8
H(14)	514(5)	728(10)	947(4)	6.2
H(15)	603(5)	898(10)	1005(4)	4.3
H(16)	538(5)	927(10)	893(4)	4.0
H(17)	803(5)	413(10)	993(4)	4.9
H(18)	684(5)	412(10)	1017(4)	5.1
H(19)	770(5)	570(10)	1058(4)	6.6
H(20)	938(5)	747(10)	1023(4)	7.7
H(21)	965(5)	984(10)	936(4)	8.8
H(22)	859(5)	658(10)	894(4)	9.3
H(23)	832(5)	990(10)	988(4)	0.4
H(24)	704(5)	724(10)	739(4)	7.1

Table 2. Interatomic distances of **4**, with standard deviations in parentheses

Interatomic distance	l/Å		l/Å
C(1)–C(2)	1.416(8)	C(8)–O(3)	1.367(8)
C(1)–C(6)	1.426(9)	C(9)–C(10)	1.434(9)
C(1)–C(10)	1.418(8)	C(9)–O(2)	1.371(8)
C(2)–C(3)	1.505(8)	C(10)–C(11)	1.401(10)
C(2)–C(13)	1.383(9)	C(11)–C(12)	1.376(10)
C(3)–C(4)	1.518(9)	C(11)–O(1)	1.363(9)
C(3)–O(7)	1.443(8)	C(12)–C(13)	1.390(9)
C(4)–C(5)	1.516(9)	C(13)–C(14)	1.517(9)
C(4)–C(3′)	1.570(8)	C(15)–O(3)	1.455(9)
C(4)–O(6)	1.423(8)	C(16)–O(2)	1.422(9)
C(5)–C(6)	1.423(8)	C(1′)–C(2′)	1.465(12)
C(5)–O(5)	1.232(8)	C(2′)–C(3′)	1.526(11)
C(6)–C(7)	1.393(9)	C(2′)–O(7)	1.438(8)
C(7)–C(8)	1.413(9)	C(3′)–C(4′)	1.522(10)
C(7)–O(4)	1.336(9)	C(3′)–C(5′)	1.513(10)
C(8)–C(9)	1.354(10)		

Table 3. Bond angles of **4**, with standard deviations in parentheses

Bond angle	ϕ/°		ϕ/°
C(2)–C(1)–C(6)	121.4(5)	C(9)–C(8)–O(3)	119.8(6)
C(2)–C(1)–C(10)	119.4(5)	C(8)–C(9)–C(10)	122.8(6)
C(6)–C(1)–C(10)	119.1(5)	C(8)–C(9)–O(2)	120.1(6)
C(1)–C(2)–C(3)	120.3(5)	C(10)–C(9)–O(2)	117.0(6)
C(1)–C(2)–C(13)	119.9(5)	C(1)–C(10)–C(9)	117.8(6)
C(3)–C(2)–C(13)	119.9(5)	C(1)–C(10)–C(11)	119.2(6)
C(2)–C(3)–C(4)	118.2(5)	C(9)–C(10)–C(11)	123.0(6)
C(2)–C(3)–O(7)	107.1(5)	C(10)–C(11)–C(12)	120.0(6)
C(4)–C(3)–O(7)	107.5(5)	C(10)–C(11)–O(1)	124.0(6)
C(3)–C(4)–C(5)	116.0(5)	C(12)–C(11)–O(1)	116.0(6)
C(3)–C(4)–C(3′)	103.1(5)	C(11)–C(12)–C(13)	121.5(6)
C(3)–C(4)–O(6)	107.6(5)	C(2)–C(13)–C(12)	119.9(6)
C(5)–C(4)–C(3′)	110.0(5)	C(2)–C(13)–C(14)	122.4(6)
C(5)–C(4)–C(6)	108.7(5)	C(12)–C(13)–C(14)	117.7(6)
C(3′)–C(4)–O(6)	111.3(5)	C(1′)–C(2′)–C(3′)	118.9(7)
C(4)–C(5)–C(6)	119.8(5)	C(1′)–C(2′)–O(7)	110.6(7)
C(4)–C(5)–O(5)	117.0(5)	C(3′)–C(2′)–O(7)	103.8(6)
C(6)–C(5)–O(5)	123.2(6)	C(4)–C(3′)–C(2′)	101.7(5)
C(1)–C(6)–O(5)	121.4(5)	C(4)–C(3′)–C(4′)	111.7(5)
C(1)–C(6)–C(7)	120.2(5)	C(4)–C(3′)–C(5′)	112.0(5)
C(5)–C(6)–C(7)	118.3(5)	C(2′)–C(3′)–C(4′)	106.3(6)
C(6)–C(7)–C(8)	120.6(6)	C(2′)–C(3′)–C(5′)	114.2(6)
C(6)–C(7)–O(4)	122.2(6)	C(4′)–C(3′)–C(5′)	110.6(6)
C(8)–C(7)–O(4)	117.2(6)	C(9)–O(2)–C(16)	117.1(6)
C(7)–C(8)–C(9)	119.1(6)	C(8)–O(3)–C(15)	115.5(6)
C(7)–C(8)–O(3)	120.7(6)	C(3)–O(7)–C(2′)	109.5(5)

Final atomic coordinates, bond lengths, and bond angles are given in Tables 1—3. The relative configuration of **4** is shown in Fig. 3. Attempt to solve the absolute configuration of **4** on the basis of the anomalous dispersion effect of oxygen atoms for Cu $K\alpha$ radiation[22] failed, because the effect on the R index[23] and the Bijvoet inequalities[24] was too small to determine the absolute configuration. However, the 3R- and 4S-configurations of **4** were determined with relation to the previously established absolute configuration of R at the 2′-position.[8]

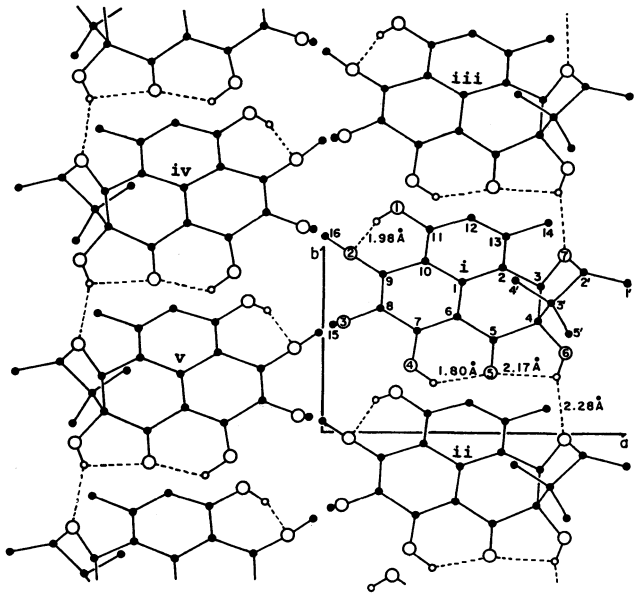

Fig. 4. The projection of dihydroherqueinone monomethyl ether (**4**) along the c axis. The atoms indicated with ●, ○, and ○ denote carbon, oxygen, and hydrogen atoms, respectively. The hydrogen bondings are shown by a broken line. Symmetry codes: (i) x, y, z; (ii) $x, -1+y, z$; (iii) $x, 1+y, z$; (iv) $-x, 1/2+y, -z$; (v) $-x, -1/2+y, -z$. The other molecules related by a 2_1 axis are omitted in order to avoid overlapping.

The molecular arrangement and the hydrogen bond networks in the crystal are shown in Fig. 4. The molecules are packed along the c axis and are linked by the long intermolecular hydrogen bonding between O(6)–H and O(7′)[25] (furan ring) along the b direction. On the other hand, three intramolecular hydrogen bondings between O(1)–H and O(2) (methoxy group), O(4)–H and O(5) (carbonyl group), and O(6)–H and O(5) (carbonyl group) are formed.

The determination of the configuration at C-4 of herqueinone (**1**) and the configurations at C-3 and C-4 of dihydroherqueinone monomethyl ether (**4**) leads to the establishment of the absolute configuration of all the herqueinone- and dihydroherqueinone-type phenalenones.

Experimental

The fungal culture of *Penicillium herquei* Bainier and Sartory (IFO 7904) was purchased from the Institute for Fermentation.[26] The ^{1}H NMR spectra for 60 and 90 MHz were taken on a Varian T-60 and a Hitachi R-22 spectrometers by use of TMS as an internal standard. The ^{13}C NMR spectra were obtained on a Hitachi R-42 FT NMR (22.6 MHz) spectrometer ($\delta_{TMS}=0$). The X-ray intensity data were collected on a Syntex R3 and a Rigaku AFC-5 diffractometers with graphite-monochromated Mo $K\alpha$ and Cu $K\alpha$ radiations, respectively.

Incubation of P. herquei. A spore suspension of *P. herquei* precultured on a malt extract agar medium were inoculated to 200 ml of a Raulin-Thom solution[2] in a 1 L Erlenmeyer flask (total 25 flasks), and incubated at 25 °C in the dark. After cultivation for 5 d, light yellow mycelia covered over the surface of the medium, and then the mycelia

produced spores and became yellow-green. Then, droplets of reddish liquid appeared on the surface of the culture, and the medium became brown after cultivation for 15 d.

Isolation of Herqueinone (1). After incubation for 25 d, the mycelia were filtered off, and the mycelia were immersed in EtOAc. The filtrate was acidified to pH 5 with 10% hydrochloric acid and extracted with EtOAc. Removing EtOAc from the combined EtOAc extract afforded the residue (*ca.* 5 g), which wa ssubjected to centrifugal liquid chromatography on a silica-gel plate (3 mm in thickness and 10 cm in radius) with EtOAc–hexane (1 : 4 v/v) to give a red powder (310 mg). Recrystallization of this powder from EtOH gave herqueinone (**1**) (275 mg): red needles, mp 217—218 °C (lit,[7] 218—222 °C); $[\alpha]_D^{25}$ +374° (*c* 1.68, $CHCl_3$); UV (EtOH) λ_{max} 410 (log ε 4.02) and 300 nm (4.25); IR(Nujol) ν_{max} 3300 (OH) and 1640 and 1620 cm^{-1} (C=O); ^1H NMR ([^2H]-DMSO) δ_H=1.00 (3H, s, 4′-H_3), 1.40 (3H, s, 5′-H_3), 1.55 (3H, d, J=6.5 Hz, 1′-H_3), 2.50 (3H, d, J=1.5 Hz, 14-H_3), 3.80 (3H, s, 15-H_3), 4.83 (1H, q, J=6.5 Hz, 2′-H), and 6.28 (1H, d, J=1.5 Hz, 12-H); ^{13}C NMR ([^2H]DMSO) δ_C=197.0 and 186.4 (each s, C-5 and C-11), 122.8 (d, C-12), 95.9 (d, C-2′), 78.9 (s, C-4), and 59.9 (q, C-15); MS (70 eV), *m/z* (rel intensity), 372 (M^+, 100), 356 (40), 341 (68), 329 (36), and 274 (52); Found: C, 64.51; H, 5.49%.

Derivation of 4 from 1. A slurry of herqueinone (**1**) (206 mg) in EtOAc (20 ml) was hydrogenated in the presence of 10% Pd–C (80 mg). After 1 molar equivalent of hydrogen had been taken up, the hydrogen uptake ceased, and the catalyst was filtered off. The filtrate was treated with ethereal CH_2N_2 (*ca.* 1 molar equiv.) at 0 °C for 30 min. The excess of CH_2N_2 was quenched with a few drops of acetic acid. The solvent was evaporated *in vacuo* to afford a crystalline residue (148 mg). This residue was purified by preparative TLC (silica gel GF_{254}; 0.5 mm thick) with EtOAc–hexane (1 : 1 v/v). The green-yellow fluorescent band at R_f 0.66 under UV light, on extraction with EtOAc, afforded yellow needles (121 mg). Recrystallization of this needles from EtOH gave yellow rods of dihydroherqueinone monomethyl ether (**4**): mp 173—174 °C (lit,[7] 172—174 °C); $[\alpha]_D^{25}$+39.0° (*c* 7.28, EtOH); UV (EtOH) λ_{max} 399 (log ε 3.78), 357 (3.62), and 290 nm (4.09); IR (Nujol) ν_{max} 3460 and 3366 (OH) and 1632 cm^{-1} (C=O); ^1H NMR ([^2H]$CHCl_3$) δ_H=0.80 (3H, s, 4′-H_3), 1.17 (3H, s, 5′-H_3), 1.34 (3H, d, J=6.5 Hz, 1′-H_3), 2.53 (3H, s, 14-H_3), 3.68 (1H, q, J=6.5 Hz, 2′-H), 3.98 (3H, s, 15-H_3), 4.28 (3H, s, 16-H_3), 5.44 (1H, s, 3-H), and 6.72 (1H, s, 12-H); ^{13}C NMR ([^2H]DMSO) δ_c=202.9 (s, C-5), 113.5 (d, C-12), 82.0 (s, C-4), 81.5 (2×d, C-3 and C-2′), 60.9 (q, C-15), and 62.4 (q, C-16); MS (70 eV), *m/z* (rel intensity), 388 (M^+, 100), 302 (74), 287 (38), 259 (34), 244 (15), and 216 (22); Found: C, 64.65; H, 6.33%.

X-Ray Crystallographic Analyses of Dihydroherqueinone Monomethyl Ether (4). *(i) Analysis by Use of Mo Kα Radiation*: The crystal used was about 0.5 mm×0.4 mm×0.7 mm in size. Cell dimensions were derived by the least-squares calculations from 2θ values of 25 well-centered diffraction peaks for **4**. Crystal data are; $C_{21}H_{24}O_7$; M=388.45; monoclinic (space group $P2_1$); Z=2 per unit cell with dimensions a=11.213(4), b=6.229(3), c=14.252(5)Å, β=110.21(3)°; U=934.3 Å^3; D_c=1.38 g cm^{-1}; D_m=1.40 g cm^{-1}; μ(Mo $K\alpha$) =1.1 cm^{-1}. A total of 1892 reflections were collected by use of ω-scan technique ($2\theta_{max}$=50.0°); 1811 reflections with intensity greater than 1.96 times the standard deviations were used as observed reflections. The phases of 244 reflections with $|E|>1.40$ were determined by use of MULTAN.[20] An E map for the best solution yielded positions for all the atoms except hydrogen atoms, followed by a difference map to find the positions for all the hydrogen atoms. Anisotropic refinement for carbon and oxygen atoms and isotropic refinement for hydrogen atoms reduced the R index to 0.058.

(ii) Analysis by Use of Cu Kα Radiation: A total 2784 reflections with the Friedel pair of (h, k, l) and (h, $\bar{k}$, l) were collected by use of ω-scan technique ($2\theta_{max}$=125°); 2697 reflections with $I_o>4.0\sigma(I_o)$ were used as observed reflections. The positional coordinates for the enantiomeric pair were refined by use of two sets of coordinates: (a) the same atomic coordinates determined as above and (b) the atomic coordinates translated by the code of (x, $-y$, z). Final refinement by use of the anomalous dispersion effect of oxygen atoms for Cu $K\alpha$ radiation[22] reduced the R index to 0.0662 for the coordinates (a) and 0.0668 for the coordinates (b). All the $||F_c(h,k,l)|-|F_c(h,\bar{k},l)||/\sigma(F_o)$ values were smaller than 0.8.

The complete F_o-F_c data and the table of anisotropic thermal parameters for **4** are deposited as Document No. 8261 at the Chemical Socity of Japan.

The authors thank Dr. G. A. Morrison for the gift of the ^1H NMR spectrum of herqueinone and for his kind suggestion for the study on the absolute configurations of herqueinone and the dihydroherqueinone derivatives.

References

1) F. H. Stodola, K. B. Raper, and D. I. Fennell, *Nature*, **167**, 773 (1951).
2) J. A. Galarraga, K. G. Neill, and H. Raistrick, *Biochem. J.*, **61**, 456 (1955).
3) R. E. Harman, J. Cason, F. H. Stodola, and A. L. Adkins, *J. Org. Chem.*, **20**, 1260 (1955).
4) D. H. R. Barton, P. de Mayo, G. A. Morrison, and H. Raistrick, *Tetrahedron*, **6**, 48 (1959).
5) J. Cason, J. S. Correia, R. B. Hutchison, and R. F. Porter, *Tetrahedron*, **18**, 839 (1962).
6) I. C. Paul and G. A. Sim, *J. Chem. Soc.*, **1965**, 1097.
7) J. S. Brooks and G. A. Morrison, *J. Chem. Soc., Perkin Trans. 1*, **1972**, 421.
8) J. S. Brooks and G. A. Morrison, *J. Chem. Soc., Perkin Trans. 1*, **1974**, 2114.
9) R. Thomas, *Biochem. J.*, **78**, 807 (1962).
10) R. Thomas, *Pure Appl. Chem.*, **34**, 515 (1972).
11) T. Suga, T. Yoshioka, T. Hirata, and T. Aoki, *Chem. Lett.*, **1981**, 1063.
12) T. Yoshioka, T. Hirata, T. Aoki, and T. Suga, *Chem. Lett.*, **1981**, 1729.
13) J. H. Noggle and R. E. Shirmer, "The Nuclear Overhauser Effect. Chemical Applications," Academic Press, New York (1971).
14) The NOE values are represented by increases in integrated intensities with a deviation of ±2%. [A]→B indicates that an NOE was observed on the H_B signal when H_A frequency was saturated.
15) G. J. Martin and M. L. Martin, "The Stereochemistry of Double Bonds," in "Progress in NMR Spectroscopy," ed by J. W. Emsley, J. Feeney, and L. H. Sutcliffe, Pergamon Press, Oxford (1972), Vol. 8, p. 163.
16) F. A. Bovey, "Nuclear Magnetic Resonance Spectroscopy," Academic Press, New York (1969), Chap. 3, p. 55.
17) R. F. Zurcher, "The Cause and Calculation of Proton Chemical Shifts in Non-conjugated Organic Compounds," in "Progress in NMR Spectroscopy," ed by J. W. Emsley, J. Feeney, and L. H. Sutcliffe, Pergamon Press, Oxford (1967), Vol. 2, Chap. 5, p. 205.
18) "Dreiding Stereomodels," W. Büch Manufacture of

Glass Apparatus Flawil, Switzerland.
19) M. Amorosa, L. Caglioti, G. Caninelli, H. Immer, J. Keller, H. Wehrli, M. Lj. Mihailovic, K. Schaffner, D. Arigoni, and O. Jeger, *Helv. Chim. Acta*, **45**, 2674 (1962).
20) G. Germain, P. Main, and M. M. Woolfson, *Acta Crystallogr., Sect. A*, **27**, 368 (1971).
21) C. K. Johnson, ORTEP. Oak Ridge National Laboratory Report ORNL-3794 (1965).
22) "International Tables for X-Ray Crystallography," International Union of Crystallography, Kynoch Press, Birmingham (1974), Vol. 4, p. 149.
23) W. C. Hamilton, *Acta Crystallogr.*, **18**, 502 (1965).
24) A. F. Peerdeman and J. M. Bijvoet, *Acta Crystallogr.*, **9**, 1012 (1956).
25) The O(7′) denotes the O(7) of the molecule translated by the symmetry code: x, $-1+y$, z.
26) Jyūso hon-machi, Yodogawa-ku, Osaka 532.

Photoinduced Electron Transfer Oxidation. I. 9,10-Dicyanoanthracene-sensitized Photooxidation of Hindered Phenols

Shigeru FUTAMURA, Kazuhiro YAMAZAKI, Hiroyuki OHTA,* and Yoshio KAMIYA
Department of Reaction Chemistry, Faculty of Engineering, The University of Tokyo, Hongo, Bunkyo-ku, Tokyo 113
(Received May 15, 1982)

9,10-Dicyanoanthracene (DCA)-sensitized photooxidation reactions of hindered phenols and catechols (**1**) proceed *via* the initial electron transfer from **1** to ^{1}DCA*. 4-Hydroperoxy-2,5-cyclohexadien-1-ones and 4-hydroxy-2,5-cyclohexadien-1-ones are obtained from 2,4,6-trialkyl-substituted phenols, and an *o*-benzoquinone and furanone derivatives are afforded from 3,5-di-*t*-butylcatechol.

Oxygenation of the phenol and catechol has long been one of the current subjects in connection with model reactions for enzymes[1] and a number of reports both from a synthetic[2] and a kinetic[3,4] viewpoints have been accumulated in the literature. This problem is of interest because their oxidation products highly depend on the reaction conditions, *i.e.*, their substituents,[5] oxidizing reagents,[1,6–13] and solvent,[13] *etc.*

Recently, photoinduced electron transfer reactions have attracted much attention of photochemists.[14] 9,10-Dicyanoanthracene (DCA) can be a good electron deficient sensitizer in the electron transfer oxidation of electron-rich substrates[15] because the second electron transfer process from DCA$^{\cdot-}$ to O_2 (see Scheme 1) is exothermic ($E_{1/2}^{RED}$(DCA)$=-0.97$ V, $E_{1/2}^{RED}$(O_2)$=-0.94$ V, *vs.* SCE in MeCN). It is already reported that electron-rich substrates, such as olefins,[15] acetylenes,[16] aromatics,[17] and sulfides,[18] undergo DCA-sensitized photooxidation reactions as Scheme 1 shows.

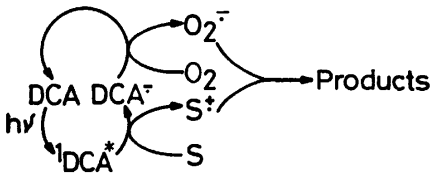

Scheme 1.

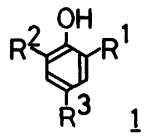

1

	R^1	R^2	R^3
1a:	t-Bu	t-Bu	t-Bu
1b:	t-Bu	t-Bu	Me
1c:	Me	Me	Me
1d:	H	H	t-Bu
1e:	OH	t-Bu	t-Bu
1f:	OH	H	t-Bu
1g:	OH	H	H

Fig. 1.

We now wish to present in this paper the photoinduced electron transfer oxidations of hindered phenols and catechols using DCA as sensitizer.

Experimental

Materials. DCA(Kodak) was purified by silica gel column chromatography. Mp 250.0—251.0 °C. Phenols and catechols were recrystallized twice from hexane–benzene. 1,3,5- and 1,2,4-Trimethoxybenzenes, acetonitrile, and methanol (reagent special grade) were used without further purification.

Instrumental. The GC analyses were done on a Shimadzu GC-6A-FID apparatus equipped with a column of 5% OV 17 on Chromosorb P. The products were analyzed on a waters liquid chromatograph, Model 440-RCM 100 equipped with a column of Radial-PAK (silica gel). The products were isolated by silica-gel chromatography or by preparative TLC (silica gel). The IR spectra were taken on a Shimadzu IR-420 Infrared Spectrophotometer. The NMR spectra were obtained on a Varian EM 360A NMR Spectrometer (60 MHz), using Me_4Si as the internal standard. The UV spectra were recorded on a JASCO NEW-UV-210A Digital Double-beam Spectrophotometer. The fluorescence spectra were taken on a Shimadzu RF-502A Fluorescence Spectrophotometer. The melting points were measured by means of a Yazawa Hot Plate and are uncorrected.

DCA-sensitized Photooxidation of ***1****.* A 100 ml MeCN or MeOH solution of **1** (10^{-2} M) was irradiated externally in the presence of DCA (10^{-4} M) from a 400-W high-pressure mercury arc through an aqueous 75% $NaNO_2$ solution ($\lambda_{irrad.} \geq 410$ nm).

*2,6-Di-*t*-butyl-4-methyl-4-hydroperoxycyclohexadien-1-one (**2b**).* Mp 115.2—115.6 °C (lit,[12a] 115—116 °C). NMR (δ): 1.22 (s, 18H), 1.35 (s, 3H), 6.55 (s, 2H), 7.70 (s, 1H). IR (cm^{-1}): 3400, 1667, 1646, 881. UV (EtOH): $\lambda_{max}=235$ nm ($\varepsilon=11000$). Found: C, 71.27; H, 9.63%; Calcd for $C_{15}H_{24}O_3$: C, 71.45; H, 9.52%.

*2,6-Di-*t*-butyl-4-methyl-4-hydroxycyclohexadien-1-one (**3b**).* Mp 107.0—108.0 °C (lit,[12a] 110 °C). NMR (δ): 1.24 (s, 18H), 1.39 (s, 3H), 1.57 (s, 1H), 6.54 (s, 2H). IR (cm^{-1}): 3370, 1660, 1640, 882. The spectra of **3b** were superimposable on those of the sample obtained by reducing **2b** with triphenylphosphine.

Table 2 summarizes the NMR and IR data of **2** and **3**.

*Bis(1,3,5-tri-*t*-butyl-4-oxo-2,5-cyclohexadienyl)peroxide (**4**).* **4** was synthesized according to Cook's method.[10] Mp 145.2—145.6 °C (lit,[10] 148—149 °C). NMR (δ): 0.84 (s, 18H), 1.31 (s, 36H), 6.66 (s, 4H). IR (cm^{-1}): 1667, 1643, 1365, 1248, 997.

5, **6**, and **7** were identified by comparison of their mp's and spectroscopic data with those of the authentic samples.[19,20]

Results and Discussion

DCA-sensitized Photooxidation of Phenols. As Table 1 shows, 4-hydroperoxy-2,5-cyclohexadien-1-ones (**2**) and 4-hydroxy-2,5-cyclohexadien-1-ones (**3**) were ob-

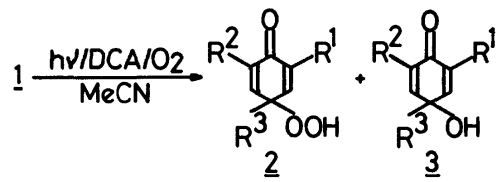

Scheme 2. DCA-sensitized photooxidation of phenols.

Table 1. DCA-sensitized photooxidation of phenols in acetonitrile

Compd	Irrad. time/h	Conv./%	Products (Selectivity/%)
1a	8	80	**2a**(43), **3a**(6)
1b	55	100	**2b**(80), **3b**(20)
1c	8	32	**2c**(100)
1d	23	33	a)

a) Not identified.

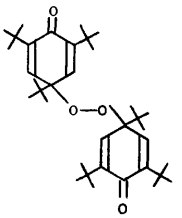

Fig. 2.

tained from 2,4,6-trialkyl-substituted phenols (**1a—c**) in good yields. On the other hand, monoalkyl-substituted phenol **1d** was photooxidized much slower and also its reaction was too complex to obtain isolable products.[21]

Refluxing **2** with the excess of triphenylphosphine in dichloromethane for 3 h gave **3** quantitatively and this fact supports the structure of **2**.

Although the effect of phenol concentration on its oxidation has been reported,[4] no concentration effect was observed concerning the product distribution in this reaction, and no bis(1,3,5-tri-*t*-butyl-4-oxo-2,5-cyclohexadienyl) peroxide (**4**) was formed even when the concentration of **1a** was increased to 10^{-1} M.

Formation of **3** urged us to ascertain the possibility that the redox decomposition of **2** or **4** should give **3**. Under the reaction conditions, however, both of them were highly stable in the absence or presence of hydrogen donor **1**, and **3** was not afforded at all. LC analysis also showed that **3** is a primary product and did not arise from **2** or **4**.

In methanol, the reaction rate was slower than in acetonitrile and **3** was not afforded.

Next, the quenching experiments of DCA fluorescence and the oxidation reaction were performed to obtain further information on the mechanism. The rapid quenching of ^{1}DCA* fluorescence by **1** (see Table 3) supports the occurrence of electron transfer from **1** to ^{1}DCA*, *i.e.*, formation of 1^+ and DCA^-. In fact, the relative rate, k_{rel} of **1** decreases as its oxidation potential increases.

Addition of 1,2,4-trimethoxybenzene (TMB) into the system of **1** and DCA causes the competition between Eqs. 2 and 3 because TMB is a better electron donor.[15] As r_1 and r_2 in Scheme 3 stand for the kinetic expressions for Eqs. 2 and 3, the calculated quenching ratio Q_{calcd} can be obtained by Eq. 6 if $\mathbf{1}^+$ is responsible for the oxidation of **1**.

$$DCA \xrightarrow{h\nu} {}^1DCA^* \quad (1)$$

$$^1DCA^* + \mathbf{1} \xrightarrow{kq} DCA^- + \mathbf{1}^+ \quad (2)$$

$$^1DCA^* + TMB \xrightarrow{kq'} DCA^- + TMB^+ \quad (3)$$

$$r_1 = k_q[\mathbf{1}][^1DCA^*] \quad (4)$$

$$r_2 = k_q[TMB][^1DCA^*] \quad (5)$$

$$Q_{calcd} = 1 - r_1/(r_1+r_2) = k_{q'}[TMB]/(k_q[\mathbf{1}]+k_{q'}[TMB]) \quad (6)$$

Scheme 3. Quenching of ^{1}DCA* fluorescence.

A good coincidence between Q_{calcd} and Q_{obsd} further confirms the involvement of the initial electron transfer process. DCA^- can reduce triplet molecular oxygen to generate O_2^-.[15] Therefore, **2** would be afforded in the subsequent deprotonation of $\mathbf{1}^+$ by O_2^-, followed by the coupling of $\mathbf{1}^\cdot$ with $HO_2^\cdot$. It is well known that a hindered phenoxyl radical is a good trap of a hydroperoxyl radical.[24] The alkylperoxyl radical could be excluded as a chain carrier since hindered phenols are known to act as a good radical inhibitor. They would rather couple with a phenoxyl radical to give **4**[4,10] when the concentration of the phenoxyl radical is high.

It is to note that **1** was stable on DCA-sensitized irradiation under nitrogen. This would be ascribed to the back electron transfer from DCA^- to $\mathbf{1}^+$ or the lack of the deprotonating reagent such as oxygen.[25]

The stability of **2** is delicate, and it rearranges to a 5,6-epoxy-4-hydroxy-2-cyclohexen-1-one under basic conditions,[12b] or it degrades to *p*-benzoquinones, diphenoquinones, *etc.* in the presence of a Cu(I)–amine complex.[11] Our reaction is clearly different from the base- or metal-catalyzed oxygenation of hindered phenols in that **2** is afforded in good yields, irrespective of the alkyl substituents although the path for formation of **3** has to be unraveled.

DCA-sensitized Photooxidation of ***1e****.* DCA-sensitized

Table 2. Physical constants and spectroscopic data of **2** and **3**

Compd	Mp θ_m/°C	NMR δ	IR $\tilde{\nu}$/cm^{-1}
2a	75.8— 77.4	0.97(s, 9H), 1.25(s,18H), 6.10(s, 2H), 7.92(s,1H)	3400, 1660, 1628, 967
2b	115.3—115.6	1.22(s,18H), 1.35(s, 3H), 6.55(s, 2H), 7.70(s,1H)	3400, 1667, 1646, 1060
2c	63.1— 64.5	1.36(s, 3H), 1.90(s, 6H), 6.63(s, 2H), 8.52(s,1H)	3300, 1675, 1618, 1060
3a	80.9— 82.1	0.97(s, 9H), 1.05(s, 1H), 1.22(s,18H), 6.57(s,2H)	3520, 1653, 1627, 967
3b	107.0—108.0	1.24(s,18H), 1.39(s, 3H), 1.57(s, 1H), 6.54(s,2H)	3370, 1660, 1640, 1058
3c	40.8— 42.1	1.41(s, 3H), 1.84(s, 6H), 2.22(s, 1H), 6.60(s,2H)	3380, 1670, 1625, 1050

TABLE 3. QUENCHING OF DCA-SENSITIZED PHOTOOXIDATION OF **1** BY TMB

Compd	$E_{1/2}^{ox}$/V	k_q^f/$M^{-1}s^{-1}$ a)	k_{rel}	Q_{calcd}/% b)	Q_{obsd}/% c)
1a	1.20 d)	2.45×10^{10}	6.4	37	31
1b	1.33 d)	2.85×10^{10}	4.9	33	36
1c		2.60×10^{10}	2.5	35	34
1d		2.06×10^{10}	1.0	41	43
TMB	1.12 e)	6.49×10^{10}			

a) Fluorescence quenching rate constant in acetonitrile under air at room temperature. $\tau_{DCA,Air}=\tau_{DCA,N_2}(I_{DCA,Air}/I_{DCA,N_2})=15.3\times0.52=8.0$ ns. ($\tau_{DCA,N_2}=15.3$ ns.)[22] b) Q_{calcd} was given by Eq. 6 when the conversion of **1** was around 10%. c) Q_{obsd} was given as $1-C_q/C_0$, where C_0 and C_q represent the conversions of **1** in the solutions containing only **1** and **1**–TMB when C_0 was around 10%, respectively. d) See Ref. 23. e) See Ref. 15.

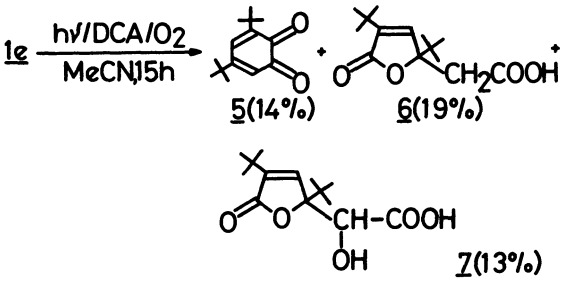

Scheme 4. DCA-sensitized photooxidation of **1e**.

photooxidation of **1e** in acetonitrile gave 3,5-di-*t*-butyl-*o*-benzoquinone (**5**), 3,5-di-*t*-butyl-5-(carboxymethyl)-2(5*H*)-furanone (**6**), and 3,5-di-*t*-butyl-5-(carboxyhydroxymethyl)-2(5*H*)-furanone (**7**) in the yields shown above.

In MeCN–MeOH, **6** and the methyl ester of **7** were obtained in 20% and 10% yields, respectively, along with **5** (6%).

The relative rate of the catechol decreased in the order of **1e**>**1f**>**1g** and no isolable products were obtained from the less hindered catechols, **1f** and **1g**.

As has been discussed in the system of the phenol, the oxygenation of the catechol is also considered to proceed by an electron transfer mechanism because **1e** quenches ^{1}DCA* fluorescence at the diffusion-controlled rate limit ($k_q=1.21\times10^{10}$ $M^{-1}s^{-1}$) and its oxidation reaction is completely suppressed by 1,3,5-trimethoxybenzene.

5 is found to be an early product because **6** and **7** are afforded in the DCA-sensitized photooxidation reaction of **5** in acetonitrile.

The observed product distributions are less complicated than those reported by Foote and Moro-oka with KO_2.[9]

The different reactivities of **1a**—**c** and **1e** can be ascribed to the diphenolic character of **1e**. The phenoxyl radicals from **1a**—**c** couple together with a hydroperoxyl radical, while that from **1e** would further be deprotonated to afford a stable *o*-benzosemiquinone radical which leads to furanone derivatives in the subsequent oxygenation followed by ring cleavage and lactonization.[9]

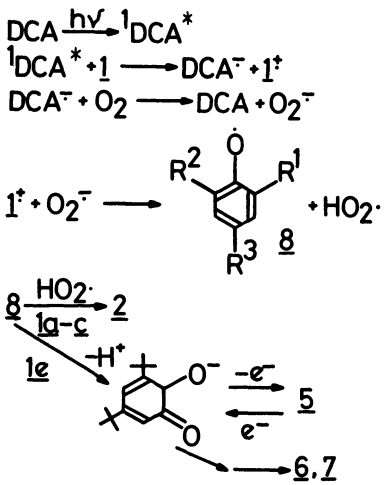

Scheme 5. A presumed reaction scheme.

Scheme 5 shows a presumed reaction mechanism.[26]

In this paper, we have reported DCA-sensitized photooxidation of hindered phenols and catechols and have shown that the reaction proceeds *via* electron transfer mechanism.

References

1) a) J. Tsuji and H. Takayanagi, *J. Am. Chem. Soc.*, **96**, 7349 (1974); b) M. M. Rogic and T. R. Demmin, *ibid.*, **100**, 5472 (1978).

2) T. Kametani and K. Fukumoto, "Phenolic Oxidation," Gihodo, Tokyo (1970).

3) C. A. Tyson and A. E. Martell, *J. Am. Chem. Soc.*, **94**, 939 (1972).

4) A. Zombeck, R. S. Drago, B. B. Corden, and J. H. Gaul, *J. Am. Chem. Soc.*, **103**, 7580 (1981).

5) T. Matsuura, K. Watanabe, and A. Nishinaga, *J. Chem. Soc., Chem. Commun.*, **1970**, 163.

6) F. R. Hewgill and S. L. Lee, *J. Chem. Soc., C*, **1969**, 2080.

7) T. Matsuura, H. Matsushima, S. Kato, and I. Saito, *Tetrahedron*, **28**, 5119 (1972), and references cited therein.

8) A. Nishinaga, T. Itahara, and T. Matsuura, *Bull. Chem. Soc. Jpn.*, **47**, 1811 (1974).

9) Y. Moro-oka and C. S. Foote, *J. Am. Chem. Soc.*, **98**, 1510 (1976).

10) C. D. Cook and R.C. Woodworth, *J. Am. Chem. Soc.*, **75**, 6242 (1953).

11) C. M. Orlando, Jr., *J. Org. Chem.*, **33**, 2516 (1968).

12) a) M. S. Kharasch and B. S. Joshi, *J. Org. Chem.*, **22**, 1439 (1957); b) A. Nishinaga, T. Itahara, and T. Matsuura, *Chem. Lett.*, **1974**, 667.

13) A. Nishinaga and A. Rieker, *J. Am. Chem. Soc.*, **98**, 4667 (1976), and references cited therein.

14) a) F. D. Lewis, *Acc. Chem. Res.*, **12**, 152 (1979); b) R. A. Caldwell and D. Creed, *ibid.*, **13**, 451 (1980); c) S. L. Mattes and S. Farid, *ibid.*, **15**, 80 (1982).

15) J. Eriksen and C. S. Foote, *J. Am. Chem. Soc.*, **102**, 6083 (1980).

16) N. Berenjian, P. de Mayo, F. H. Phoenix, and A. C. Weedon, *Tetrahedron Lett.*, **1979**, 4179.

17) I. Saito, K. Tamoto, and T. Matsuura, *Tetrahedron Lett.*, **1979**, 2889.

18) J. Eriksen, C. S. Foote, and T. L. Parker, *J. Am. Chem. Soc.*, **99**, 6455 (1977).

19) The IR and NMR spectra of **5** were identical with

those of the sample prepared by oxidizing **1e** in the presence of Co(salpr).

20) As to **6** and **7**, see Ref. 9.

21) The *ortho* substituent groups seem to be necessary to undergo the clean oxidation.

22) J. Eriksen and C. S. Foote, *J. Phys. Chem.*, **82**, 2659 (1978).

23) C. S. Foote, "Free Radicals in Biology," ed by W. A. Pryor, Academic Press, New York (1976), Vol. 2, p. 85.

24) J. A. Howard and K. U. Ingold, *Can. J. Chem.*, **45**, 785 (1967).

25) DCA can be recovered quantitatively under nitrogen or oxygen.

26) The scheme merely shows a possible route leading to the products; other paths such as radical coupling between ArO· and $^3O_2$, and intervention of $^1O_2$ generated by the reaction of $ArO^+ + O_2^-$ would also be probable reactions. We thank the referee for this point.

An FT-IR Study of Micelle Formation of Ionic Surfactants and Water Solubilization in Nonpolar Organic Solvents

Hideo KISE,* Kazutoshi IWAMOTO,† and Manabu SENŌ†
Institute of Materials Science, The University of Tsukuba, Sakura, Niihari, Ibaraki 305
†*Institute of Industrial Science, The University of Tokyo, Roppongi, Minato-ku, Tokyo 106*
(Received May 28, 1982)

The infrared spectra of the solutions of dodecylammonium propionate (DAP), hexadecyltrimethylammonium bromide (HTAB), and sodium bis(2-ethylhexyl) 2-sulfonatosuccinate (SBSS) in organic solvents were recorded in Fourier transform mode. Difference concentration spectra of DAP in dichloromethane exhibited the change in the stretching bands of the carboxylate ions, which was attributed to the formation of micellar aggregates. Difference hydration spectra were also obtained for water-containing DAP–CH_2Cl_2, HTAB–CH_2Cl_2, and SBSS–benzene systems, and the spectra in the region of 3000—3700 cm^{-1} and 1600—1650 cm^{-1} revealed the existence of free water dispersed in the organic phase and water bound to the micelles. The diffreence spectra also revealed the change in the bands of DAP and SBSS due to hydration of the ionic head groups. The absorption frequency of the O–H stretching bands was discussed in terms of the water-surfactant-interaction.

Recently the studies on the formation and structure of reversed micelles in nonpolar organic solvents have received considerable attention. Reversed micelles can solubilize appreciable amount of water and other polar substances. A variety of techniques have been used for the investigation of the nature of reversed micelles and cosolubilized water. A typical method is the direct observation of the change in the physical properties of the solutes by NMR,[1–8] and another is the use of probe molecules which have physical properties sensitive to the change in the environment of the solubilization sites. Examples of the latter are spin lables,[9–12] absorption and fluorescence probes,[13–19] and positron annihilation techniques.[20,21]

These methods assume that the solubilization of the probe molecules causes little or no change in the structure of the micelles. On solubilization of probes, however, perturbation of the micelle structure is likely to occur because of the small aggregation numbers and hence the small size of the reversed micelles. For example, the mean aggregation number of dodecylammonium propionate (DAP) has been reported to be 4 in carbon tetrachloride[1] and 6 ± 1 in dichloromethane.[3]

In this article we present the results on the Fourier transform infrared (FT-IR) spectroscopic investigation on the micelles of ionic surfactants in organic solvents and the nature of solubilized water in the reversed micellar systems. Infrared spectroscopy is a sensitive method for monitoring the interactions between solutes or between solvents and solutes. Fourier transform technique allows the direct observation of surfactants of low concentrations around critical micelle concentration (cmc) and solubilized water by rapid scan and computation of the difference spectra by subtracting the solvent spectra from those of solutions.

Experimental

DAP was prepared by previously described method[22] and recrystallized from hexane. Hexadecyltrimethylammonium bromide (HTAB) was purified by recrystallization from ethanol–ether, and sodium bis(2-ethylhexyl) 2-sulfonatosuccinate (SBSS) was used as received. All the solvents were of guaranteed grade and used without further purification. Water was solubilized in the surfactant solution by stirring the mixture at room temperature for several minutes and then keeping it standing overnight.

The FT-IR spectra were obtained with a Digilab FT-20C instrument with a 50 μm KRS cell. The spectral resolution was 4 cm^{-1}, and 100 to 1000 scans were accumulated.

Results and Discussion

DAP and HTAB Micelles. The difference spectrum obtained by the subtraction of the dichloromethane spectrum from that of the dichloromethane solution of DAP (15 mM, 1 mM = 10^{-3} mol dm^{-3}) exhibits asymmetric and symmetric stretching bands of the carboxylato group around 1580 and 1400 cm^{-1}, respectively. Since the cmc of DAP in dichloromethane obtained by NMR method has been reported to be 27—40 mM,[3] the absorption is considered to be of monomeric DAP dispersed in the solvent. Free carboxylate ions in aqueous solutions have the stretching bands

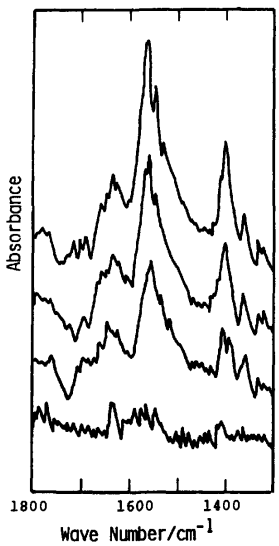

Fig. 1. Difference spectra of DAP in dichloromethane obtained by subtraction of the spectra of 10 mM DAP from those of 20, 30, 40, and 50 mM DAP (from lower to upper). See Ref. 23.

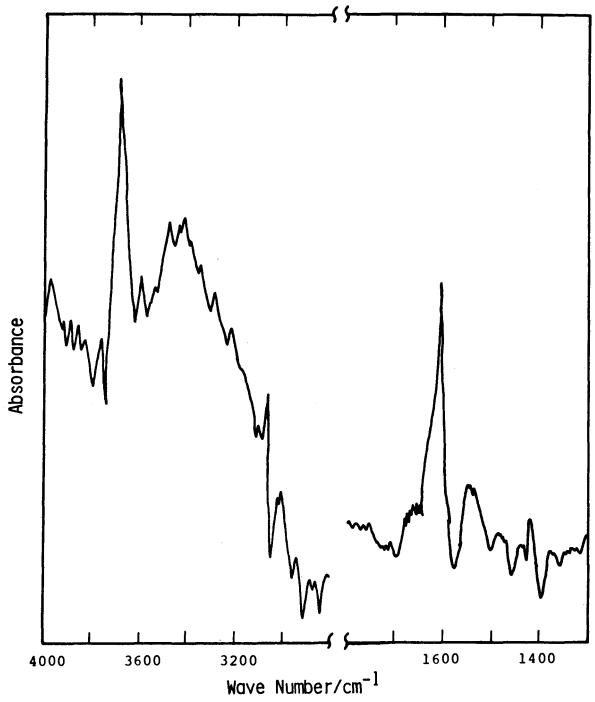

Fig. 2. Difference spectrum obtained by subtraction of the spectrum of anhydrous DAP (50 mM) in dichloromethane from that of the DAP solution of the same concentration containing 200 mM water.

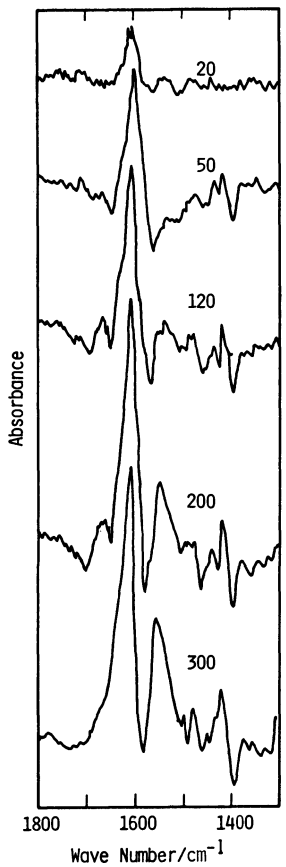

Fig. 3. Difference spectra obtained by subtraction of the spectrum of anhydrous DAP solution (50 mM) in dichloromethane from those of water-containing DAP solutions. Water concentration is indicated in the figure (mM).

around 1550 and 1410 cm^{-1}, and the dispersed DAP is considered to exist as tightly bound ion pairs as suggested by the larger difference between the two stretching bands than free carboxylate ions.

When the concentration of DAP is increased, the carboxylate bands gradually change. The asymmetric band shifts to lower frequencies, while symmetric one shifts to higher frequencies. The change in the spectra is clearly demonstrated by subtracting the spectrum of the solution below cmc from those of the solution above cmc as shown in Fig. 1.[23] With increasing concentration new absorption bands appear around 1550—1570 and 1400—1410 cm^{-1}. These bands are obviously attributed to the formation of DAP aggregates, in which DAP is considered to have more ionic character than monomeric one as suggested by the decrease in the difference between the symmetric and asymmetric stretching bands. The increase in the ionic nature of DAP may be the consequence of the interaction of carboxylato group with two or more ammonium groups. The onset of association seems to fall in the concentration range of 20 to 30 mM, which well agrees with the cmc value obtained by NMR method.[3]

When water was solubilized in a 50 mM DAP solution in dichloromethane, the stretching bands of carboxylate ions shifted in the same direction as that observed in the micelle formation described above. Figure 2 shows the difference spectrum obtained by subtracting the spectrum of DAP–CH_2Cl_2 solution from that of DAP–CH_2Cl_2–H_2O solution. The spectrum exhibits not only the absorption bands of water but also the shift of DAP bands caused by the addition of water. The shift of DAP bands is observed as sigmoid (1550—1570 cm^{-1}) or reversed sigmoid (1400—1410 cm^{-1}) spectra. New DAP bands appear in the regeon closer to that of free carboxylate ions. This may well be understood as a consequence of the formation of water-separated DAP ion pairs due to the hydration of the ionic head groups of the surfactant. The change in the spectra with water concentration is shown in Fig. 3. It is obvious that binding of water to the surfactant occurs even at equimolar concentration of water to DAP.

The spectrum of water saturated in neat dichloromethane exhibited asymmetric (ν_3) and symmetric (ν_1) stretching bands at 3688 and 3600 cm^{-1}, respectively, and bending band (ν_2) at 1604 cm^{-1}. By comparison with this, the sharp absorption bands at 3680, 3600, and 1600 cm^{-1} in Fig. 2 were assigned as that of free water dispersed in bulk organic phase. Since water in gas phase has absorption at 3755, 3654, and 1595 cm^{-1}, while water in liquid phase has absorption at 3430, 3210, and 1650 cm^{-1}, the dispersed water seems to be in a similar state to that in gas phase rather than in liquid phase. The broad bands around 3450 and 1630 cm^{-1} were assigned to the absorption of water bound to DAP micelles. The bands are very close to those of liquid water indicating strong interaction with DAP molecules which is probably a kind of ion-dipole interaction. Although the bands of free and bound water are not fully separated, the competitive solubilization of water seems to occur into the micelles and bulk

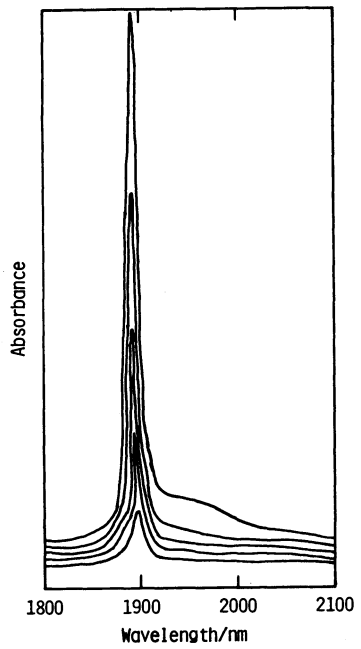

Fig. 4. Near infrared spectra of water-containing DAP solutions (50 mM) in dichloromethane. Water concconcentration is from lower to upper 20, 50, 120, 200, and 300 mM.

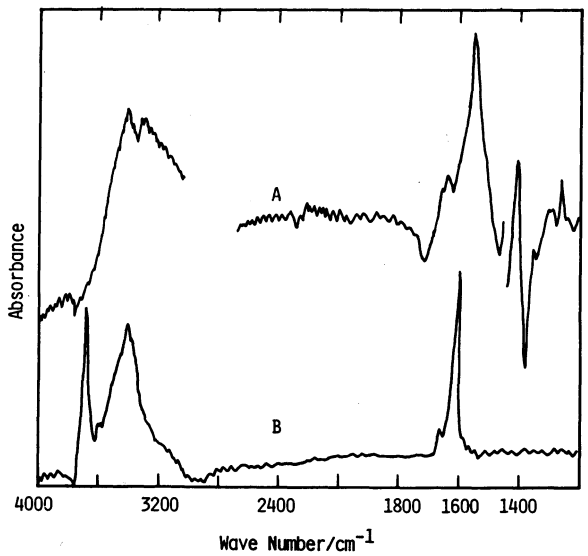

Fig. 5. Spectra of A) water (100 mM) in hexane+DAP (50 mM) and B) water (200 mM) in CH_2Cl_2+HTAB (50 mM).

organic phase.

The existence of free and bound water in this system is confirmed by the near infrared spectra of 1800—2000 nm region due to $\nu_2+\nu_3$ combination mode (Fig. 4). The sharp band at 1890—1900 nm has been ascribed to the free or almost free 1 : 1 complex H–O–H···B in which B denotes a weak base such as dioxane.[24] The position of this band is identical with that of the extremely weakly bonded water in chlorinated hydrocarbons.[24] Furthermore, on the basis of the relationship between the concentration of DAP or waterin chloroform and the absorption intensity of water, the broad band at 1920—1950 nm was assigned towater solubilized in the reversed micelles.[25]

The solution of DAP (50 mM) in hexane afforded a quite similar spectrum to the dichloromethane solution implying the formation of similar kind of DAP aggregates. The shift of the bands of carboxylato group by the addition of water is also quite similar to the dichloromethane solution. In contrast to dichloromethane solution, however, the solubilized water showed no absorption band corresponding to free water (Fig. 5-A), which may be the consequence of low solubility of water in hexane. In addition, the stretching bands of bound water seems to contain lower component around 3300 cm^{-1} than the water in DAP–CH_2Cl_2 system. It has been reported that the cmc of DAP in benzene and cyclohexane is 3—7 mM[1,2] and 1.56 mM,[17] respectively. The lower cmc value in hydrocarbons than dichloromethane[3] or carbon tetrachloride[1,2] implies the formation of more compact and tightly bound aggregates of DAP in hydrocarbons. Although the O–H stretching bands are not well resolved, the band around 3300 cm^{-1} seems to be due to water tightly bound to the ionic head groups of DAP.

In the case of hexadecyltrimethylammonium bromide (HTAB) in dichloromethane, the absorption bands of solubilized water were almost the same as those in DAP–CH_2Cl_2 system (Fig. 5-B), except that the O–H stretching band of bound water appears at slightly lower frequency around 3400 cm^{-1}.

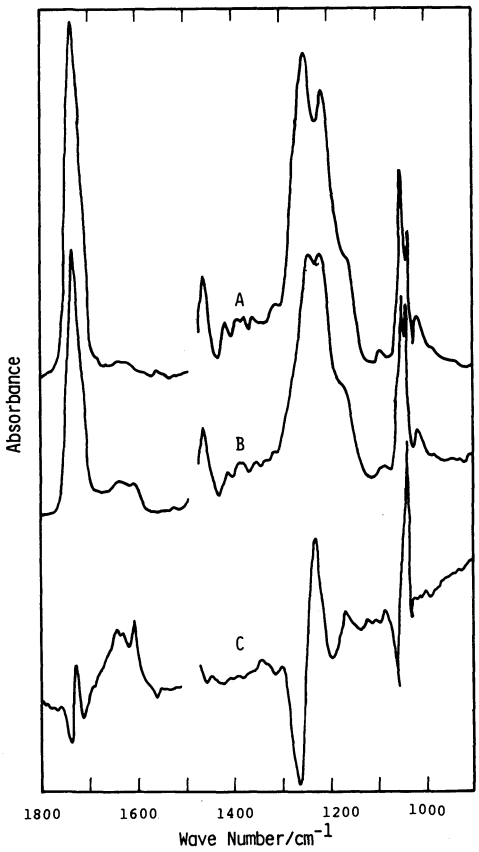

Fig. 6. Spectra of SBSS reversed micelles: A, SBSS 50 mM in benzene; B, SBSS 50 mM+H_2O 100 mM in benzene; C, H_2O 100 mM in (SBSS 50 mM+benzene).

SBSS Micelle. As Fig. 6-A shows the IR spectrum of anionic surfactant SBSS in benzene exhibits SO_3 asymmetric stretching bands at 1252 and 1215 cm^{-1}, and symmetric stretching band at 1050 cm^{-1}. In contrast to DAP in dichloromethane, no effect of the concentration of SBSS on these bands was observed in the range of 2—50 mM. This may indicate the lower cmc of SBSS.

On addition of water, however, distinct change in shape and frequency of SO_3 bands was observed as shown in Fig. 6-B. The change is clearly detected by taking the difference spectrum of solubilized water (Fig. 6-C). The sigmoid spectra around 1250 and 1050 cm^{-1} represent higher shift of 1215 cm^{-1} band and lower shift of 1252 and 1050 cm^{-1} bands due to the hydration of the sulfonato group.

It is interesting to note that the carbonyl band at 1730 cm^{-1} shifts to lower frequency on addition of water as shown in Fig. 6-C. Since the intensity of the new band was found to be almost independent of the water concentration up to 200 mM, the band shift was attributed to the formation of hydrogen bond between the carbonyl oxygen and the water dispersed in bulk benzene phase not in the micelle core. This may be supported by the fact that the bands of water in bulk benzene were observed at 3680 and 1600 cm^{-1}, whose intensity was almost independent of water concentration in the range of 50—200 mM.

Table 1. Absorption maxima of bound water (cm^{-1}) in reversed micelles

Surfactant (Solvent)	IR $\tilde{\nu}/cm^{-1}$	Surfactant (Solvent)	NIR
(H_2O vapor)	3755	(H_2O vapor)	5330
(H_2O in CH_2Cl_2)	3688	(H_2O in CH_2Cl_2)	5280
SBSS (CH_2Cl_2, Benzene)	3500	AOT[a] ($CHCl_3$)	5198[b]
DAP (CH_2Cl_2)	3450	DAP ($CHCl_3$)	5085[b]
HTAB (CH_2Cl_2)	3400	HTAB($CHCl_3$)	5010[b]
DAP (Hexane)	3300		

a) Aerosol-OT. b) From Ref. 8.

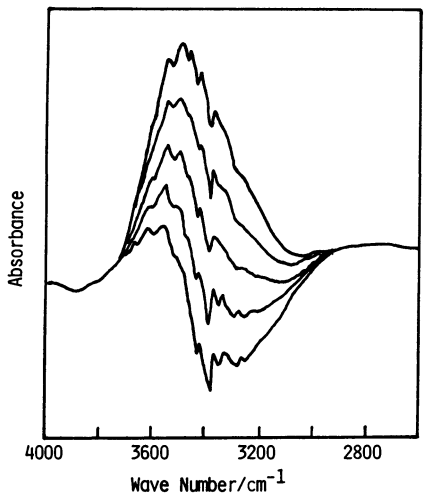

Fig. 7. Difference spectra obtained by subtraction of water spectra from that of 1 M aqueous solution of sodium ethanesulfonate. Scaling factor used in the subtraction is increasing from upper to lower.

O–H Stretching Band of Solubilized Water. The O–H stretching bands of water bound to the micelles are collected in Table 1. Although the spectra are broad and not well resolved, distinct change in the absorption maximum for the different surfactant-solvent system is observed. Assuming that the O–H stretching frequency of the bound water simply reflects the strength of the water-surfactant interaction, the water binding ability of the reversed micelles in dichloromethane is roughly estimated; that is HTAB>DAP> SBSS. The result agrees with that obtained from NIR measurement in chloroform as listed in Table 1.[8]

In order to obtain better understanding of the interaction of water with surfactants, IR spectra of aqueous solutions of several electrolytes which have analogous structure to the ionic head groups of the surfactants were investigated. As Figs. 7 and 8 show, subtraction of water spectra from those of aqueous solutions of sodium ethanesulfonate or tetrabutylammonium bromide (TBAB) afforded the spectra of water associated with

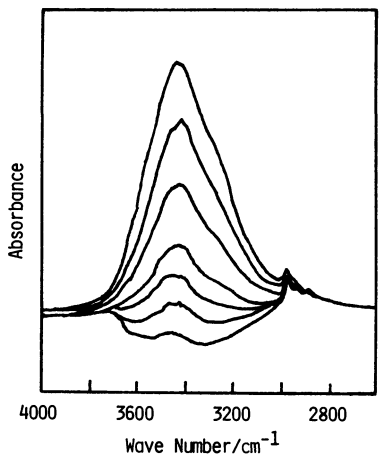

Fig. 8. Difference spectra obtained by subtraction of water spectra from that of 1 M aqueous solution of TBAB. Scaling factor used in the subtraction is increasing from upper to lower.

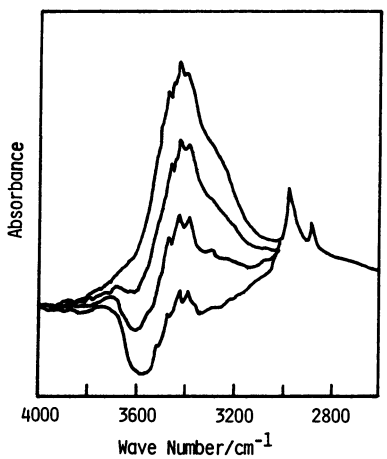

Fig. 9. Difference spectra obtained by subtraction of the spectra of 1 M KBr from that of 1 M TBAB in water. Scaling factor used in the subtraction is increasing from upper to lower.

the electrolytes. It is interesting to note that the maximum frequencies of the bands of water associated with sodium ethanesulfonate and TBAB are close to those in SBSS and HTAB reversed micelles, respectively. This seems to suggest that water in reversed micelles has interaction with ionic head groups of the surfactants like water in the vicinity of electrolytes in aqueous solutions. Further, the difference spectra resulting from the subtraction of the spectra of aqueous sodium bromide solution from that of aqueous TBAB solution allows to estimate approximate frequency of the absorption bands of water associated with sodium and tetrabutylammonium ions, that is around 3560 and 3400 cm^{-1}, respectively. The results indicate that the spectral component of water in HTAB micelles appearing around 3400 cm^{-1} is most likely due to water molecules interacting with ammonium groups. The well established structure-making properties of quaternary ammonium ions may be responsible for the lower shift of O–H stretching band of the water in the reversed micelle core.

Similar technique of difference spectrum has been employed for the study of hydration of ionic species in aqueous solution using the band of HOD near 2500 cm^{-1},[26] and the study on the micelle formation of sodium hexanoate in aqueous solutions.[27]

References

1) J. H. Fendler, E. J. Fendler, R. T. Medary, and O. A. El Seoud, *J. Chem. Soc., Faraday Trans. 1*, **69**, 280 (1973).

2) E. J. Fendler, J. H. Fendler, R. T. Medary, and O. A. El Seoud, *J. Phys. Chem.*, **77**, 1432 (1973).

3) O. A. El Seoud, E. J. Fendler, J. H. Fendler, and R. T. Medary, *J. Phys. Chem.*, **77**, 1876 (1973).

4) M. A. Wells, *Biochem.*, **13**, 4937 (1974).

5) M. Ueno, H. Kishimoto, and Y. Kyogoku, *Bull. Chem. Soc. Jpn.*, **49**, 1776 (1976).

6) M. Wong, J. K. Thomas, and T. Nowak, *J. Am. Chem. Soc.*, **99**, 4730 (1977).

7) M. Senō, K. Sawada, K. Araki, K. Iwamoto, and H. Kise, *J. Colloid Interface Sci.*, **78**, 57 (1980).

8) J. Sunamoto, T. Hamada, T. Seto, and S. Yamamoto, *Bull. Chem. Soc. Jpn.*, **53**, 583 (1980).

9) A. Kitahara, O. Ohashi, and K. Kon-no, *J. Colloid Interface Sci.*, **49**, 108 (1974).

10) F. M. Menger, G. Saito, G. V. Sanzero, and J. R. Dodd, *J. Am. Chem. Soc.*, **97**, 909 (1975).

11) Y. Y. Lim and J. H. Fendler, *J. Am. Chem. Soc.*, **100**, 7490 (1978).

12) M. Senō, K. Sawada, K. Araki, H. Kise, and K. Iwamoto, *Bull. Chem. Soc. Jpn.*, **53**, 2083 (1980).

13) M. Wong, J. K. Thomas, and M. Grätzel, *J. Am. Chem. Soc.*, **98**, 2391 (1976).

14) F. M. Menger and G. Saito, *J. Am. Chem. Soc.*, **100**, 4376 (1978).

15) J. Sunamoto and T. Hamada, *Bull. Chem. Soc. Jpn.*, **51**, 3130 (1978).

16) G. D. Correll, R. N. Cheser, III, F. Nome, and J. H. Fendler, *J. Am. Chem. Soc.*, **100**, 1254 (1978).

17) U. Herrmann and Z. A. Schelly, *J. Am. Chem. Soc.*, **101**, 2665 (1979).

18) T. F. Hunter and A. I. Younis, *J. Chem. Soc., Faraday Trans. 1*, **79**, 550 (1979).

19) E. Keh and B. Valeur, *J. Colloid Interface Sci.*, **79**, 465 (1981).

20) Y. Jean and H. J. Ache, *J. Am. Chem. Soc.*, **100**, 6320 (1978).

21) L. A. Fucugauchi, B. Djermouni, E. D. Handel, and H. J. Ache, *J. Am. Chem. Soc.*, **101**, 2841 (1979).

22) A. Kitahara, *Bull. Chem. Soc. Jpn.*, **28**, 234 (1955).

23) The scaling factor used in the subtraction in Fig. 1 was determined so that smooth baselines were obtained. Since the cmc of DAP is well above 10 mM, the spectra in Fig. 1 are considered to be of DAP aggregates.

24) O. D. Bonner and Y. S. Choi, *J. Phys. Chem.*, **78**, 1723 (1974).

25) M. Senō, K. Araki, and S. Shiraishi, *Bull. Chem. Soc. Jpn.*, **49**, 899 (1976).

26) M. Lucas, A. De Trobriand, and M. Ceccaldi, *J. Phys. Chem.*, **79**, 913 (1975).

27) J. Umemura, C. G. Cameron, and H. H. Mantsch, *J. Phys. Chem.*, **84**, 2272 (1980).

The Oxidation of the 2-Methyl Group of 3-Substituted 2-Methylindoles by Autoxidation and with Silver Acetate in Carboxylic Acids

Toshio ITAHARA,* Hiroshi OUYA, and Kiyotake KOZONO
Institute of Chemistry, College of Liberal Arts, Kagoshima University, Korimoto, Kagoshima 890
(Received May 29, 1982)

The autoxidation of 3-alkyl-2-methylindoles in carboxylic acids, such as propionic acid and acetic acid, at the reflux temperature resulted in the selective oxidation of the 2-methyl group and the formation of 3-alkyl-2-formylindoles. The formation of the 2-formylindoles was dependent on the nature of the solvent used. The treatment of 3-benzoyl-1,2-dimethylindole with silver acetate gave 2-acetoxymethyl-3-benzoyl-1-methylindole and 3-benzoyl-2-formyl-1-methylindole. The mechanistic implications for the autoxidation and the oxidation with silver acetate are presented.

The autoxidation of 3-alkyl-2-methylindoles (**1**) has been known to give several products. Beer *et al.*[1] reported that the autoxidation of 2,3-dimethylindole (**1a**) in hot petroleum gave 2,3-dimethyl-3*H*-indol-3-yl hydroperoxide (**2a**) and a non-peroxidic product. Taylor[2] also reported the formation of *N*-(2-acetylphenyl)acetamide, together with a small amount of 2-formyl-3-methylindole (**3a**), from **1a**. Recently, the non-peroxidic autoxidation product was reported to be a dimeric compound.[3] The autoxidation of 3-ethyl-2-methylindole (**1c**) was reported to give a similar dimeric compound.[4]

The present paper will deal with the autoxidation of 3-alkyl-2-methylindoles (**1a—e**) in carboxylic acids. The autoxidation in propionic acid or in acetic acid at the reflux temperature gave 3-alkyl-2-formylindoles (**3a—e**) in good yields. The treatment of **1a** in formic acid under oxygen at the reflux temperature gave 2,3-dimethyl-1-formylindole (**1g**), together with a small amount of **3a**. Also, the oxidation of 3-benzoyl-1,2-dimethylindole (**1f**) with silver acetate gave 3-benzoyl-2-formyl-1-methylindole (**3f**) and 2-acetoxymethyl-3-benzoyl-1-methylindole (**5f**).

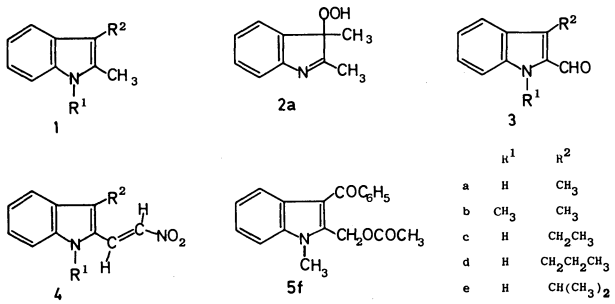

Fig. 1.

Results and Discussion

A solution of 2-methylindoles (**1a—e**) (100 mg), in propionic acid (100 ml) was bubbled with oxygen at the reflux temperature for 7 h. The reaction mixture was then evaporated and chromatographed on silica gel TLC to give the corresponding 2-formylindoles (**3a—e**). The autoxidation of **1a** in acetic acid under similar conditions also gave **3a**. The treatment of **3a—e** with nitromethane according to the known method[5] gave the corresponding 3-alkyl-2-(2-nitrovinyl)indoles (**4a—e**), which provides additional evidence for the structures of **3a—e**. The structures of **3** and **4** were confirmed on the basis of analytical and spectral(NMR, IR, and mass) data.

The formation of **3** is dependent on the nature of the solvent used. When the autoxidation of **1a** was carried out in formic acid at the reflux temperature, 1-formylindole **1g**[6] was obtained as the main product, together with a small amount of **3a**. Furthermore, no 2-formylindole **3a** was obtained from the reaction mixture in the autoxidation of **1a** in benzene, in methanol, in hexane, and in ethyl acetate. On the other hand, the autoxidation of **1a** in mixtures of methanol and acetic acid and of benzene and acetic acid gave **3a**, although attempts to prepare **3a** by the autoxidation of **1a** in methanol containing phosphoric acid and in benzene containing *p*-toluenesulfonic acid were unsuccessful.

The yield of **3a** is also dependent on the concentration of **1a**. That is to say, the autoxidation of **1a** (0.5 g or 1.0 g) in acetic acid (100 ml) decreased the yields of **3a**. These results are summarized in Table 1. Under similar conditions, an acylindole such as **1f** was unreactive to oxygen. The autoxidation of 2-methylindole and 1,2-dimethylindole gave complex reaction mixtures.

Previously it was reported that the exposure of **2a** to air in acetic acid and in ethyl acetate did not yield **3a**; the only product obtained was *N*-(2-acetylphenyl)-acetamide, although the exposure of 2,3-diethyl-3*H*-indol-3-yl hydroperoxide to air gave 2-acetyl-3-ethylindole.[7] Furthermore, it was found that the autoxidation of a 1-substituted 2-methylindole such as 1,2,3-trimethylindole (**1b**) also gave the corresponding 2-formylindole, such as 1,3-dimethyl-2-formylindole (**3b**). These results suggest that the formation of **3** from **1** in carboxylic acids did not proceed *via* **2**. On the other hand, Gribble *et al.*[8] reported that indoles are protonated at the 3-position of the indole nucleus by carboxylic acids. Therefore, the following scheme might be given for the autoxidation of **1** in carboxylic acids:

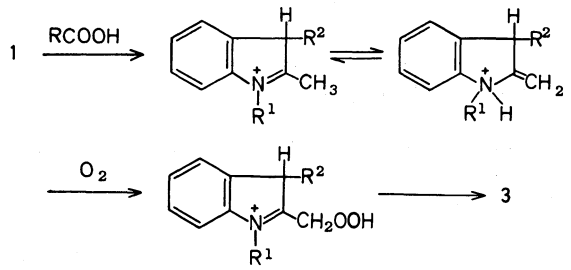

Scheme 1.

Table 1. Synthesis of 3-alkyl-2-formylindoles by the autoxidation of 3-alkyl- 2-methylindoles

Substrate	(g)	Solvent	(ml)	Conv./%	Product	Yield/%[a]
1a	(0.1)	CH_3CH_2COOH	(100)	100	**3a**	56
1a	(0.1)	CH_3COOH	(100)	100	**3a**	45
1a	(0.5)	CH_3COOH	(100)	70	**3a**	18
1a	(1.0)	CH_3COOH	(100)	50	**3a**	11
1a	(1.0)	CH_3COOH	(200)	62	**3a**	12
1a	(0.1)	CH_3COOH[b]	(100)	100	**3a**	60
1a	(0.1)	HCOOH	(100)	93	**3a**[c]	4
1a	(0.1)	Benzene	(50)	78	**3a**	8
		CH_3COOH	(50)			
1a	(0.1)	CH_3OH	(50)	76	**3a**	12
		CH_3COOH	(50)			
1b	(0.1)	CH_3CH_2COOH	(100)	100	**3b**	68
1c	(0.1)	CH_3CH_2COOH	(100)	100	**3c**	60
1d	(0.1)	CH_3CH_2COOH	(100)	100	**3d**	63
1e	(0.1)	CH_3CH_2COOH	(100)	100	**3e**	60

a) Yields based on the indole **1a**—**e** consumed. b) Adding 2 equiv. of AgOAc. c) 2,3-Dimethyl-1-formylindole (52%) was obtained as the main product.

Although **1f** was unreactive to oxygen, **1f** was reacted with silver acetate to give **3f** and **5f**. The treatment of **1f** with 2.0 equiv. of silver acetate in acetic acid at the reflux temperature under both air and nitrogen for 20 h gave **3f** as the main product, together with a small amount of **5f**. On the other hand, the treatment of **1f** with 0.7 equiv. of silver acetate under nitrogen for 15 h gave **5f** as the main product. Under similar conditions, **5f** was reacted with silver acetate to give **3f**, suggesting that **3f** was formed *via* **5f**. Therefore, a pathway for the oxidation of **1f** with silver acetate in acetic acid might be as is shown in the following scheme. In addition, although the oxidation of **1a** with silver acetate under nitrogen gave a complex reaction mixture, the autoxidation of **1a** in acetic acid containing silver acetate increased the yield of **3a** (Table 1).

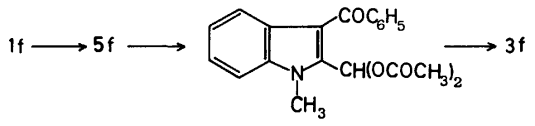

Scheme 2.

Generally, replacement at the 2-position of the indole nucleus is attained with difficulty;[9] *e.g.*, the acylation of indoles normally gives 1- and 3-acylindoles.[10] The autoxidation of **1** in carboxylic acids and the oxidation of **1f** with silver acetate are, therefore, of interest as an effective method for the preparation of 2-formylindoles, although its scope is somewhat limited, *i.e.*, a substituent is needed at the 3-position of the indole nucleus. That is to say, in contrast to several reports concerning the preparation of **3a** by means of the oxidation of **1a** (*i.e.*, the oxidation of **1a** with H_5IO_6,[11] SeO_2,[12] and 2,3-dichloro-5,6-dicyano-*p*-benzoquinone (DDQ),[13] and by photo-oxygenation[14] gives **3a** in low yields), the method by means of the autoxidation of **1a** in carboxylic acids provides more satisfactory results.

Experimental

General. All the melting points are uncorrected. The elemental analyses were performed by the Analytical Center of Kyoto University. The infrared spectra were recorded with a JASCO IRA-1 spectrometer. The proton magnetic resonance spectra were recorded with a JEOL-60 spectrometer, using Me_4Si as the internal reference. 2-Methylindole, 1,2-dimethylindole, and 2,3-dimethylindole (**1a**) were obtained commercially. 3-Benzoylindole (**1f**) was prepared according to the procedure described before.[15]

1,2,3-Trimethylindole (1b). To a stirred solution of 2,3-dimethylindole (5.0 g) and sodium hydride (oil suspension, abt. 50%) (1.6 g) in *N,N*-dimethylformamide (100 ml), methyl iodide (5.0 g) in *N,N*-dimethylformamide (20 ml) was added under nitrogen. The solution was then stirred at room temperature for 4 h, after which the reaction mixture was poured into ice-cooled water and extracted with benzene. The benzene extract was dried with sodium sulfate and evaporated to give a brown oily residue. The residue was chromatographed on a silica-gel column with hexane/benzene to give **1b** (4.1 g).

3-Alkyl-2-methylindoles (1c—e). A solution of 2-methylindole (5.0 g) in ethyl iodide (25 ml) was heated at the reflux temperature for 40 h under nitrogen. The reaction mixture was then evaporated to give a red oily residue which was chromatographed on a silica-gel column with benzene to give 3-ethyl-2-methylindole (**1c**) (0.4 g) and 2-methylindole (3.3 g).

Similar treatments of 2-methylindole (5.0 g) in propyl iodide (25 ml) gave 2-methyl-3-propylindole (**1d**) (1.5 g) and 2-methylindole (1.9 g), while treatments in isopropyl iodide (25 ml) gave 2-methyl-3-isopropylindole (**1e**) (1.0 g) and 2-methylindole (2.6 g).

Autoxidation of 3-Alkyl-2-methylindoles. The indole **1a**—**e** (0.1 g) was dissolved in propionic acid (100 ml), and the solution was bubbled with oxygen at the reflux temperature for 7 h. The reaction mixture was then evaporated to give a brown oily residue, which was chromatographed on silica-gel TLC and developed with benzene to give 3-alkyl-2-formylindole (**3a**—**e**). The yields are summarized in Table 1. The spectral and analytical data are given below.

2-Formyl-3-methylindole (3a): Mp 139—140 °C (lit,[16] 139—

140 °C); IR (Nujol) 3300, 1640, 1570, 1430, 1330 cm^{-1}; NMR ($CDCl_3$) δ 2.73 (s, 3H), 7.1—7.6 (m, 3H), 7.75—8.0 (m, 1H) 9.5 (broad, 1H), 10.6 (s, 1H).

*1,3-Dimethyl-2-formylindole (**3b**)*: Mp 35—36 °C (lit,[17] 36 °C); IR (Nujol) 1670, 1610, 1530, 1420, 1350, 1340 cm^{-1}; NMR ($CDCl_3$) δ 2.64 (s, 3H), 4.10 (s, 3H), 7.1—8.0 (m, 4H), 10.65 (s, 1H).

*3-Ethyl-2-formylindole (**3c**)*: Mp 72—73 °C (by distillation at 170 °C/6 Torr†); IR (Nujol) 3300, 1640, 1570, 1530, 1310, cm^{-1}; NMR ($CDCl_3$) δ 1.41 (t, 3H, J=7 Hz), 3.19 (q, 2H J=7 Hz), 7.05—7.6 (m, 3H), 7.8—8.0 (m, 1H), 9.7 (broad, 1H), 10.6 (s, 1H). Found: C, 76.54; H, 6.46; N, 7.91%. Calcd for $C_{11}H_{11}NO$: C, 76.27; H, 6.40; N, 8.09%.

*2-Formyl-3-propylindole (**3d**)*: Mp 40—41 °C (by distillation at 180 °C/6 Torr); IR (Nujol) 3300, 1650—1620 (broad), 1575, 1535, 1335 cm^{-1}; NMR ($CDCl_3$) δ 0.99 (t, 3H, J=7 Hz), 1.82 (sext. 2H, J=7 Hz), 3.13 (t, 2H, J=7 Hz), 7.05—7.65 (m, 3H), 7.8—8.05 (m, 1H), 9.6 (broad, 1H), 10.5 (s, 1H); High-resolution Mass: *m/e* (rel intensity) 187.0993 (M^+, 61), 172.0773 (100). Found: C, 76.79; H, 6.92; N, 7.21%. Calcd for $C_{12}H_{13}NO$: C, 76.97; H, 7.00; N, 7.48%.

*2-Formyl-3-isopropylindole (**3e**)*: Mp 65—66 °C (by distillation at 170 °C/6 Torr); IR (Nujol) 3200, 1640, 1630, 1315 cm^{-1}; NMR ($CDCl_3$) δ 1.57 (d, 6H, J=7 Hz), 3.77 (sept, 1H, J=7 Hz), 7.05—7.75 (m, 3H), 7.86—8.10 (m, 1H), 9.6 (broad, 1H), 10.6 (s, 1H); High-resolution Mass: *m/e* (rel intensity) 187.1008 (M^+, 76), 172.0781 (100). Found: C, 76.36; H, 6.87; N, 7.31%. Calcd for $C_{12}H_{13}NO$: C, 76.97; H, 7.00; N,7.48%.

Similar procedure were applied for the autoxidation of **1a** in acetic acid, in benzene, in hexane, in methanol, and in ethyl acetate.

*3-Alkyl-2-(2-nitrovinyl)indoles (**4a—e**).* Into a solution of **3a—e** (0.1 g) and nitromethane (0.15 g) in methanol (5 ml), 50% aqueous sodium hydroxide (1.5 ml) was stirred, drop by drop, at 0 °C. After 1 h at 0 °C, ice water (5 ml) wasadded, and the resulting solution was poured into a mixture of concd hydrochloric acid (6.5 ml) and water (24 ml) at 0 °C. The crude product separated as a brownish-orange solid, which was collected and dried. Recrystallization from chloroform/hexane gave **4a—e** as brownish-orange needles. The yields and spectral and analytical data are given below.

*3-Methyl-2-(2-nitrovinyl)indole (**4a**)*: 88% yield; mp 181.5—182.5 °C; IR (Nujol) 3350, 1610, 1480, 1310 cm^{-1}; NMR ($CDCl_3$) δ 2.51 (s, 3H), 7.0—7.9 (m, 5H), 8.40 (d, 1H, J=14 Hz), 8.2—8.6 (broad, 1H); Mass: *m/e* (rel intensity) 202 (M^+, 95), 155 (94), 154 (100). Found: C, 65.74; H, 4.98; N, 13.40%. Calcd for $C_{11}H_{10}N_2O_2$: C, 65.33; H, 4.98; N, 13.86%.

*1,3-Dimethyl-2-(2-nitrovinyl)indole (**4b**)*: 89% yield; mp 159—160 °C; IR (Nujol) 1625, 1500, 1310 cm^{-1}; NMR ($CDCl_3$) δ 2.53 (s, 3H), 3.90 (s, 3H), 7.0—7.9 (m, 5H), 8.40 (d, 1H, J=14 Hz). Found: C, 66.84; H, 5.46; N, 12.95%. Calcd for $C_{12}H_{12}N_2O_2$: C, 66.65; H, 5.59; N, 12.96%.

*3-Ethyl-2-(2-nitrovinyl)indole (**4c**)*: 85% yield; mp 157—158 °C; IR (Nujol) 3350, 1610, 1480, 1330, 1315 cm^{-1}; NMR ($CDCl_3$) δ 1.29 (t, 3H, J=8 Hz), 2.99 (q, 2H, J=8 Hz), 7.0—7.9 (m, 5H), 8.37 (d, 1H, J=14 Hz), 8.1—8.6 (broad, 1H). Found: C, 66.96; H, 5.48; N, 12.58%. Calcd for $C_{12}H_{12}N_2O_2$: C, 66.55; H, 5.59; N, 12.96%.

*2-(2-Nitrovinyl)-3-propylindole (**4d**)*: 89% yield; mp 158—159 °C; IR (Nujol) 3330, 1610, 1490, 1315 cm^{-1}; NMR ($CDCl_3$) δ 0.97 (t, 3H, J=7 Hz), 1.75 (sext, 2H, J=7 Hz), 2.95 (t, 2H, J=7 Hz), 7.1—8.0 (m, 5H), 8.40 (d, 1H, J=14 Hz), 8.3—8.7 (broad, 1H). Found: C, 67.93; H, 6.02; N, 12.36%.Calcd for $C_{13}H_{14}N_2O_2$: C, 67.81; H, 6.13; N, 12.17%.

*2-(2-Nitrovinyl)-3-isopropylindole (**4e**)*: 91% yield; mp 174—175 °C; IR (Nujol) 3360, 1610, 1480, 1330, 1305 cm^{-1}; NMR ($CDCl_3$) δ 1.50 (d, 6H, J=7 Hz), 3.45 (sept, 1H, J=7 Hz), 7.0—8.0 (m, 5H), 8.43 (d, 1H, J=14 Hz), 8.2—8.6 (broad, 1H). Found: C, 68.02; H, 6.16; N, 12.30%. Calcd for $C_{13}H_{14}N_2O_2$: C, 67.81; H, 6.13; N, 12.17%.

*Treatment of 2,3-Dimethylindole **1a** in Formic Acid.* A solution of **1a** (100 mg) in formic acid (100 ml) was bubbled with oxygen at the reflux temperature for 7 h. The reaction mixture was then evaporated to give a brown oily residue, which was chromatographed on silica-gel TLC with benzene to yield **1a** (7 mg), **3a** (5 mg), and 2,3-dimethyl-1-formylindole **1g**, mp 87—88 °C (lit,[18] 87—88 °C) (58 mg).

*Oxidation of 3-Benzoyl-1,2-dimethylindole **1f** with Silver Acetate.* A solution of **1f** (249 mg) and silver acetate (334 mg) in acetic acid (100 ml) was heated at the reflux temperature for 20 h under air. The reaction mixture was then evaporated to dryness and chromatographed on silica-gel TLC with benzene to yield **1f** (35 mg; 14%), 2-acetoxymethyl-3-benzoyl-1-methylindole **5f** (40 mg; 15% yield based on **1f** consumed), and 3-benzoyl-2-formyl-1-methylindole **3f** (125 mg; 55% yield based on **1f** consumed). Furthermore, under nitrogen, the oxidation of **1f** (249 mg) with silver acetate (334 mg) in acetic acid (100 ml) for 20 h gave **1f** (53 mg; 21%), **5f** (38 mg; 17% yield based on **1f** consumed), and **3f** (114 mg; 55%yield based on **1f** consumed).

A similar treatment of **1f** (249 mg) and silver acetate (117 mg) in acetic acid (100 ml) for 15 h under nitrogen gave **1f** (75 mg; 30%), **5f** (100 mg; 47% yield based on **1f** consumed), and **3f** (12 mg; 7% yield based on **1f** consumed). The spectral and analytical data of **5f** and **3f** are given below.

5f: Mp 103—104 °C (from ether/hexane); IR (Nujol) 1740, 1630, 1600, 1580, 1530, 1480, 1410, 1330 cm^{-1}; NMR ($CDCl_3$) δ 2.07 (s, 3H), 3.85 (s, 3H), 5.50 (s, 2H), 7.1—8.1 (m, 9H). Found: C, 74.45; H, 5.48; N, 4.64%. Calcd for $C_{19}H_{17}NO_3$ C, 74.25; H, 5.58; N, 4.56%.

3f: Mp 124.5—125.5 °C (from chloroform/hexane); IR (Nujol) 1675, 1635, 1615, 1605, 1580, 1510, 1480, 1400, 1345 cm^{-1}; NMR ($CDCl_3$) δ 4.24 (s, 3H), 7.3—8.3 (m, 9H), 10.7 (s, 1H). Found: C, 77.57; H, 4.99; N, 5.36%. Calcd for $C_{17}H_{13}NO_2$: C, 77.55; H, 4.98; N, 5.32%.

*Oxidation of 2-Acetoxymethyl-3-benzoyl-1-methylindole (**5f**) with Silver Acetate.* A solution of **5f** (15 mg) and silver acetate (20 mg) in acetic acid (30 ml) was heated at the reflux temperature for 15 h under air. The reaction mixture was then evaporated and chromatographed on silica-gel TLC with benzene to yield **3f** (8 mg).

The authors wish to thank Professor Tsunao Hase and Professor Tsutomu Sakakibara of Kagoshima University for their support throughout the study. They are also grateful to Mr. Tetsuo Iwagawa of Kagoshima University for his mass-spectrometric analyses.

References

1) R. J. S. Beer, T. Donavanik, and A. Robertson, *J. Chem. Soc.*, **1954**, 4139.

2) W. I. Taylor, *Proc. Chem. Soc.*, **1962**, 247.

3) G. Berti, A. DaSettimo, G. DiColo, and A. Nannipieri, *J. Chem. Soc., C*, **1969**, 2703; S. McLean, E. K. Strom-Gunderson, K. S. Dichmann, J. K. Fawcett, and S. C. Nyburg, *Tetrahedron Lett.*, **1970**, 2645.

4) S. McLean and G. I. Dmitrienko, *Can. J. Chem.*, **49**,

† 1 Torr=133.322 Pa.

3642 (1971).
5) J. Harley-Mason and E. H. Pavri, *J. Chem. Soc.*, **1963**, 2565.
6) The heating of amines such as *N*-methylaniline in formic acid is known to give the corresponding *N*-formyl amines; L. F. Fieser and J. E. Jones, *Org. Synth.*, Coll. Vol. III, 590 (1955).
7) E. Leete, *J. Am. Chem. Soc.*, **83**, 3645 (1961).
8) G. W. Gribble, P. D. Lord, J. Skotnicki, S. E. Dietz, J. T. Eaton, and J. L. Johnson, *J. Am. Chem. Soc.*, **96**, 7812 (1974).
9) J. A. Eenkhoon, S. Osmund de Silva, and V. Snieckus, *Can. J. Chem.*, **51**, 792 (1973); D. I. C. Scopes, M. S. Allen, G. J. Hignett, N. D. V. Wilson, M. Harris, and J. A. Joule, *J. Chem. Soc., Perkin Trans. 1*, **1977**, 2376; G. A. Bahadur, A. S. Bailey, N. W. Middleton, and J. M. Peach, *ibid.*, **1980**, 1688.
10) R. J. Sundberg, "The Organic Chemistry of Indoles," Academic Press, New York (1970), pp. 33—39.
11) L. D. Dolby and D. L. Booth, *J. Am. Chem. Soc.*, **88**, 1049 (1966).
12) S. Sasaki, A. Kudo, K. Matsuura, K. Mochinaga, and M. Ezaki, *Chem. Pharm. Bull.*, **20**, 76 (1972).
13) Y. Oikawa and O. Yonemitsu, *J. Org. Chem.*, **42**, 1213 (1977).
14) C. A. Mudry and A. R. Frasca, *Tetrahedron*, **29**, 603 (1973).
15) T. Itahara and T. Sakakibara, *Synthesis*, **1978**, 607.
16) W. I. Taylor, *Helv. Chim. Acta*, **33**, 164 (1950).
17) E. Lippman, K. Richter, and M. Muehlstaedt, *Z. Chem.*, **5**, 186 (1965).
18) A. Chatterjee and K. M. Biswas, *J. Org. Chem.*, **23**, 4002 (1973).

The Photochemistry of the Host-Guest Complex. VII. The Photoreaction of Dicyanopyrazine Derivatives Having a Crown Ether Moiety[1)]

Masaru TADA,* Hirohide HAMAZAKI, and Hideki HIRANO
Department of Chemistry, School of Science and Engineering, Waseda University, Shinjuku-ku, Tokyo 160
(Received June 7, 1982)

The irradiation of 4′-(5,6-dicyano-2-pyrazinyl)benzo-15-crown-5 and 5,6-dicyano-2-(3,4-dimethoxyphenyl)-pyrazine in the presence of a tertiary or secondary amine caused reductive decyanation to give 5-decyano derivatives, which in turn gave bis(decyano) derivatives on further irradiation. Free-energy changes upon single-electron transter from the amine to the excited state of dicyanopyrazine derivatives are exothermic for triethylamine and diethylamine, but endothermic for butylamine. The single-electron transfer was evidenced by the effect of the sodium ion on the quantum yields of the reaction products and the fluorescence quenching.

In our studies of crown ether derivatives, we havef previously reported the diverse effects of guest cations on the photoreactivities of the crown ether derivatives. The pairing effect, the variation in the oxidation potential, the change in the intersystem crossing rate, and the destabilization of the transition state are among the effects which we have already discussed.[2)] In this paper we would like to report on other effects by a guest cation, a decrease in the reduction potential and an increase in the excitation energy, on the photoreactivity of the pyrazine derivative having a crown ether moiety, 4′-(5,6-dicyano-2-pyrazinyl)benzo-15-crown-5 (**1**).

The pyrazine derivative having an electronegative substituent can be a mimicry of an oxidation-reduction coenzyme, such as flavin and biopterin, in which the aromatic system containing nitrogen plays an important role in the redox systems.[3)]

Syntheses of Dicyanopyrazine Derivatives. 4′-(5,6-Dicyano-2-pyrazinyl)benzo-15-crown-5 (**1**) and 5,6-dicyano-2-(3,4-dimethoxyphenyl)pyrazine (**2**) were synthesized by the condensation of diaminomaleonitrile (DAMN) with the corresponding dicarbonyl compounds, which had been prepared from benzo-15-crown-5 or 1,2-dimethoxybenzene by acetylation (acetic acid in polyphosphoric acid), followed by oxidation by selenium dioxide.

*The Photoreaction of Dicyanopyrazine Derivatives(**1** and **2**) in the Presence of Amines.* A dry acetonitrile solution of the benzo-15-crown-5 derivative **1** was irradiated in the presence of four equivalents of triethylamine; 4′-(6-cyano-2-pyrazinyl)benzo-15-crown-5 (**3**) was thus obtained in 80% yield. The irradiation of the dimethoxybenzene derivative **2** gave a similar result, affording 6-cyano-2-(3,4-dimethoxyphenyl)pyrazine (**4**) in 80% yield. The structures of both products were deduced from the ^{1}H-NMR spectra, in which a new aromatic hydrogen (C_5–H) at the pyrazine ring (δ 8.95 for **3** and 8.94 for **4**) couples (J=2 Hz) with the meta-hydrogen (δ 9.20 for **3** and 9.18 for **4**).

The irradiations of **1** and **2** in the presence of a large excess of triethylamine (acetonitrile-triethylamine, 3 : 1) gave two bis(decyano) derivatives, 4′-(2-pyrazinyl)-benzo-15-crown-5 (**5**) and 2-(3,4-dimethoxyphenyl)-pyrazine (**6**), in 40 and 46% yields respectively. The same products were also obtained in low yields under the previous reaction conditions (triethylamine; 5.6×10^{-2} mol dm^{-3}) on prolonged irradiation or on the urther irradiation of the isolated **3** or **4**. Therefore, the products **5** and **6** are the secondary products from the primary products, **3** and **4** respectively.

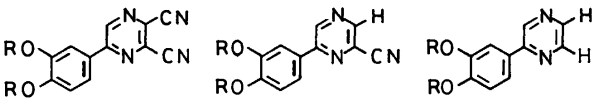

1 , 2 3 , 4 5 , 6

1 , 3 , 5 : R,R = $O(CH_2CH_2OCH_2CH_2)_2$

2 , 4 , 6 : R = CH_3

The irradiation of **1** or **2** in the presence of diethylamine instead of triethylamine gave essentially the same results. Butylamine, however, did not cause a photoreaction under similar conditions, though the use of a large excess of butylamine caused the thermal substitution of one of the cyano group with a butylamino group in the dark.[4)] These photoreactions are accelerated by purging the reaction solution with argon.

Spectroscopic and Electrochemical Studies. The same reaction takes place in benzene, though the reaction is not so clean as in acetonitrile. The fluorescence from **1** and **2** is almost identical, but weaker in acetonitrile than in benzene. The quenching experiment, therefore, was carried out in benzene. Triethylamine ($k_q\tau$=47.0 mol^{-1} dm^3) and diethylamine ($k_q\tau$=28.0 mol^{-1} dm^3) quench the fluorescence efficiently, but butylamine shows no detectable quenching effect. **3** and **4** fluoresce strongly even in acetonitrile, and the emission is quenched by triethylamine ($k_q\tau$=23.0 mol^{-1} dm^3) and diethylamine ($k_q\tau$=18.0 mol^{-1} dm^3), but, again, not with butylamine.

The photoreaction and the fluorescence quenching by animes suggest that a single-electron transfer from the amine to the excited pyrazine derivatives plays an important role. Rehm-Weller's equation,[5)] $\Delta G = E_D^{ox} - E_A^{red} - E_A^* - e^2/(r\varepsilon)$, in which E_D^{ox}, E_A^{red}, E_A^*, and $e^2/(r\varepsilon)$ represent the oxidation potential of the amines, the reduction potential of the pyrazine derivatives, the excitation energy of the pyrazine derivative, and the Coulomb stabilization of the radical ion pairs respectively, shows the numerical value for the free-energy change on the electron transfer. The inter-ion

TABLE 1. FREE ENERGY CHANGE IN THE ELECTRON TRANSFER FROM AMINES TO THE EXCITED STATE OF **1** AND **2**, AND QUANTUM YIELD OF THE PHOTODECYANATION

Compound		E_A^{red}	E_D^{ox}	E_A^*	$\Delta G'$	$\Phi\times10^3$
Acceptor	Donor	V[a]	V[a]	eV[b]	eV[c]	
2	Et_3N	−1.01	+1.35	2.78	−0.42	1.3
2	Et_2NH	−1.01	+1.48	2.78	−0.29	—
2	$BuNH_2$	−1.01	+1.94	2.78	+0.17	—
1	Et_3N	−1.01	+1.35	2.78	−0.42	1.3
[**1**-Na^+]	Et_3N	−0.60[d]	+1.35	2.92[e]	−0.98	3.3

a) Solvent: acetonitrile. V *vs.* S.H.E. (converted from the value *vs.* Ag/AgCl). b) $\lambda_{0\text{-}0}=445$ nm (calculated) in acetonitrile: see text for the calculation. c) $\Delta G'=E_D^{ox}-E_A^{red}-E_A^*$. d) **1**: 5.00 mmol dm^{-3}; $NaClO_4$: 20 mmol dm^{-3}. e) **1**: 1.0×10^{-4} mol dm^{-3}; $NaClO_4$: 5.0 mmol dm^{-3}.

distance (r) in the last term should be essentially large and constant with a similar combination of the donor and acceptor in the same solvent.[6] Therefore, we calculated the $\Delta G'$ ($=\Delta G-e^2/(r\varepsilon)$) from the data of cyclic voltammetry (E^{red} and E^{ox}) and the fluorescence spectrum(E_A^*). The fluorescence of **2** in acetonitrile has fine structure enabling us to assign the 0-0 band; no therefore, the E_A^* was estimated from the ν (0-0) calculated by means of this equation: ν (0-0)$=(\nu^a_{max}+\nu^f_{max})/2$, in which ν^a_{max} and ν^f_{max} represent the frequencies of the maxima of the absorption and the fluorescence respectively. The values of $\Delta G'$ on the electron transfer from amines to the excited state of **2** are negative for triethylamine and diethylamine, but positive for butylamine. These results are perfectly coincident with the photoreactivity and fluorescence quenching.

Reaction Mechanism. The experimental findings described above strongly suggest that the photoreaction proceeds through a single electron-transfer process (Scheme 1). This type of reaction has been reported for the photo-dehalogenation of aromatic halides[7] or a photochemical $S_{RN}1$ reaction,[8] and the intervention of aryl radicals has been well documented.[9] Ohashi *et al.* reported that the photoreaction of dicyanobenzenes in the presence of triethylamine or diethylamine gave substitution products, 4-[1-(diethylamino)ethyl]-benzonitrile or 4-[1-(ethylamino)ethyl]benzonitrile, by means of an electron-transfer mechanism.[10]

As in the case of halobenzenes, the hydrogen abstraction of the 3-cyano-2-pyrazinyl radical seems a plausible path to give the photoproducts; the radical can be expected to be formed by the electron transfer from an amine to the excited dicyanopyrazine derivative, generating a radical anion, followed by the rupture of the cyanide ion. In the case of dicyanopyrazines, however, a proton trasfer is proved to be involved after the electron transfer, and the radicals thus formed couple to give a primary product which looses hydrogen cyanide to give a substitution product.

In the present study, the addition of deuterium oxide to the reaction solution of **2** afforded the product **4** in which the C_5–H of the pyrazine ring was replaced by C_5–D. However, the photoreaction of **2** in acetonitrile-d_3 did not give any deuterated product. These results

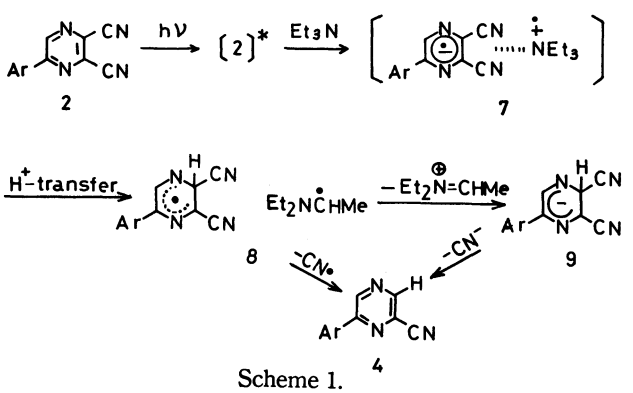

Scheme 1.

clearly indicate that a proton transfer is involved in the present photoreaction. In the absence of a protic solvent, therefore, the proton must be derived from the α-hydrogen of triethylamine, while in the presence of a protic solvent, the proton comes competitively from the solvent and triethylamine. These results suggest the mechanism shown in Scheme 1. The radical-ion pair **7**, formed by the electron transfer between amine and the excited **2**, collapses into a radical pair **8** by means of a proton transfer. The dicyanohydropyrazinyl radical in **8** gives the product **4** by the direct rupture of a cyano-radical or *via* an additional electron transfer, followed by the loss of a cyanide ion *via* **9**.

As has been described earlier, the addition of a deuterated protic solvent induces C_5–D in the product **4**; therefore, the protonation of the radical anion **7** must occur at the *ipso*-position. This selectivity of protonation at the *ipso*-position can be understood in terms of the increased electron density and, consequently, the basicity at the C_5-position of the pyrazine ring.[11] On the other hand, the protonation to the excited state of **2** may occur at one of the nitrogen atoms to afford the pyrazinium ion in its ground state or excited state. This can be expected because of the increased basicity of nitrogen heterocycles in those excited states.[12] The addition of water to the reaction mixture, indeed, quenched the fluorescence and the photoreaction of **2**; this quenching indicates the presence of another relaxation path of the excited state which participates in the photoreaction. In the case of dicyanobenzenes, the radical pair corresponding to **8** couples to give the substitution product,[10] but the radical pair **8** does not coupled, probably because of the stability of the hydropyrazinyl radical resulting from the conjugation with the aryl group at the C_2-position of the dicyanopyrazine ring.

The Effect of the Sodium Ion on the Photochemical Behavior of the Crown Ether Derivative. The formation of a host-guest complex between the crown ether moiety of **1** and the sodium ion must affect the reduction potential (E_A^{red}) and the excitation energy (E_A^*) and, therefore, the photoreactivity of **1**. The absorption spectrum of **1** changes upon the addition of sodium perchlorate (Fig. 1); the analysis of the change by the Benesi-Hildebrand method[13] gave the association constant ($K_{ass}=2900$ mol^{-1} dm^3, 25 °C). This value indicates that the complex formation is almost complete upon the addition of two equivalents of sodium perchlorate

under the present reaction conditions (**1**: 1.4×10^{-2} mol dm^{-3}). On the other hand, the absorption of the dimethoxybenzene derivative **2** does not show any change upon the addition of the sodium ion. The quantum yields of the decyanation products **3** and **4** in the presence of sodium perchlorate are shown in Fig. 2. The pyrazine derivative **1** has a strong absorption between 300—400 nm both in the free form, $\lambda_{max}^{CH_3CN}$ (ε) 370 nm (18600), and in its sodium complex, 356 nm (18400). The concentration of **1** for the reaction (1.4×10^{-2} mol dm^{-3}) is enough to absorb essentially all the photons from a high-pressure mercury lamp (313, 334, and 366 nm) in these regions. The yield of the product, therefore, safely gives the quantum yield at the early stage of the reaction, less than 10% conversion. No effect was observed upon the addition of tetrabutylammonium perchlorate to the reaction systems of **1** and **2**. The photoreaction of **2** was, again, not affected by sodium perchlorate (Fig. 2). These findings show that the effect of the sodium salt is due to the sodium ion, not the perchlorate anion, and that the crown ether moiety is essential to show the salt effect. This conclusion clearly indicates that the effect is closely associated with the formation of the host-guest complex.

The fluorescence quenching of the monocyanopyrazine derivative **3** by triethylamine in acetonitrile is stimulated by the addition of sodium perchlorate (Table 2). The variation in the quenching efficiency ($k_q\tau$) is possibly due to the change in the k_q value by the complex formation, since the rather small spectral change indicates only a small variation in the τ-value. In contrast, sodium perchlorate does not affect the fluorescence quenching of the dimethoxybenzene derivative **4** by triethylamine. The fluorescence of some sorts of aromatic compounds can be quenched by sodium salts consisting of a counter ion with a low oxidation potential, such as iodide, but the quenching is negligible by the salts consisting of an anion with a high oxidation potential, such as perchlorate.[14]

The salt effect discussed in this section is in good accordance with the single-electron transfer in the photochemical behavior of pyrazine derivatives, **1**, **2**, **3**, and **4**. The variation in the quantum yields of the photo-product and the fluorescence quenching are closely related to the changes in the reduction potential (E_A^{red}) and the energy of the singlet excited state (E_A^*) of the pyrazine derivatives. The quantum yield of the photo-decyanation and the free-energy changes by the electron transfer from triethylamine to the crown ether derivative **1** or its sodium complex are included in Table 1.

Table 2. Fluorescence quenching of **3**[a] by triethylamine in the psesence of sodium perchlorate

$NaClO_4$ (10^{-4} mol dm^{-3})	λ_{max}^{fluo} / nm	$k_q\tau$ / mol^{-1} dm^3
0.0	500	23
2.0	492	30
5.0	485	40

a) Compound **3**: 1.00×10^{-4} mol dm^{-3} in acetonitrile.

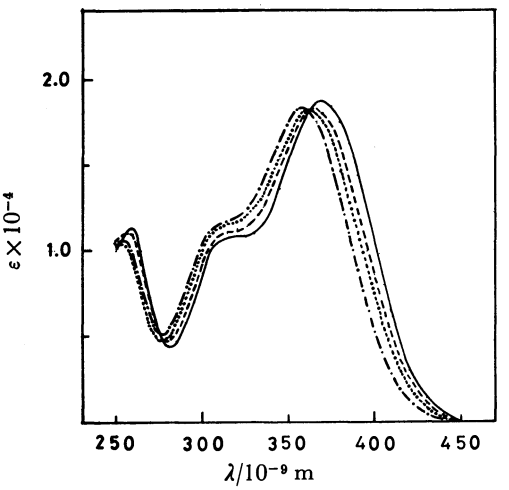

Fig. 1. Absorption spectra of **1** (1.00×10^{-4} mol dm^{-3}) in the presence of $NaClO_4$; —— (none), ----- (1.00×10^{-4} mol dm^{-3}), ------ (2.00×10^{-4} mol dm^{-3}), ·-·-· (5.00×10^{-4} mol dm^{-3}).

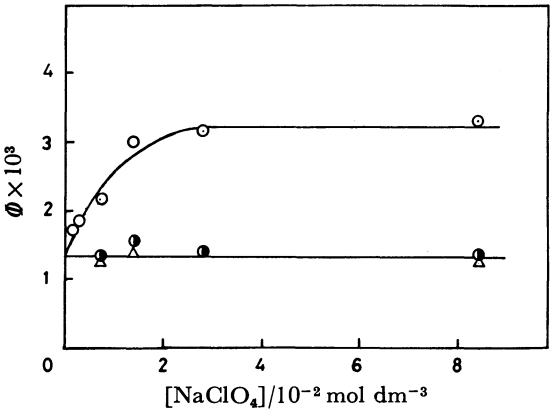

Fig. 2. Quantum yields of **3** and **4** from **1** and **2** (1.4×10^{-2} mol dm^{-3}), respectively, in the presence of triethylamine (5.6×10^{-2} mol dm^{-3}) in acetonitrile).
○: **1**+$NaClO_4$, ◑: **1**+Bu_4NClO_4, △: **2**+$NaClO_4$.

Conclusion. The excitation of the dicyanopyrazine derivative with a benzo-15-crown-5 or dimethoxyphenyl group causes a single-electron transfer from amines with a low oxidation potential. This process is responsible for the photochemical decyanation and the fluorescence quenching. The formation of the host-guest complex from the benzo-15-crown-5 moiety with the sodium ion enhances the electron-transfer process and, hence, the photoreactivity.

Experimental

*Syntheses of Dicyanopyrazine Derivatives (**1** and **2**).* Benzo-15-crown-5 (31.0 g, 115 mmol) was dissolved in 80 cm^3 of polyphosphoric acid, and the mixture was treated with acetic acid (10.5 g, 173 mmol) for 1.0 h at 40—50 °C under stirring. After cooling, 60 cm^3 of water was added to decompose the polyphosphoric acid and the product was extracted with chloroform. The subsequent evaporation of the extract after drying over magnesium sulfate gave a crude product, which was purified by passing it through an alumina column (5.0 $\phi\times$ 18.0 cm) with chloroform to give 4′-acetylbenzo-15-crown-5

75%) (mp 90 °C). 4′-Acetylbenzo-15-crown-5 (27.0 g, 87 mmol) and selenium dioxide (14.5 g, 131 mmol) were heated for 40 h in 500 cm^3 of dioxane-water (3 : 1) under reflux. After the evaporation of most of the solvents under reduced pressure, chloroform was added to the residue and the solid selenium was removed by filtration. The filtrate was dried over magnesium sulfate, condensed, and passed through an alumina column (5.0 $\phi \times$ 15.0 cm) with chloroform. The crude product thus obtained was 4′-(1-oxo-2,2-dihydroxyethyl)benzo-15-crown-5, which lost water by heating under reduced pressure (100 °C/3066 Pa) to give 4′-(1,2-dioxoethyl)-benzo-15-crown-5 (87%). The dioxo compound (24.0 g, 74 mmol) thus obtained was treated with diaminomaleonitrile (10.4 g, 96 mmol) in 200 cm^3 of THF and stirred at room temperature. Soon after mixing, yellow precipitates appeared and further stirring with gentle heating completed the reaction. The yellow precipitates were collected by filtration and recrystallized from acetonitrile–ethanol (1 : 1) to give the yellow crystal of 4′-(5,6-dicyano-2-pyrazinyl)benzo-15-crown-5 (**1**) (62%); mp 151 °C. Found: C, 60.35; H, 5.19; N, 13.83%. Calcd for $C_{20}H_{20}N_4O_5$: C, 60.60; H, 5.09; N, 14.14%. UV (CH_3CN): λ_{max} (ε) 237 (10200), 258 (11400), 319 (10800), and 370 nm (18600). ^1H NMR ($CDCl_3$): δ 3.76 (s, 8H), 3.96 (m, 4H), 4.22 (m, 4H), 6.98 (d, 1H, J=9 Hz), 7.75 (m, 2H), and 9.23 (s, 1H).

5,6-Dicyano-2-(3,4-dimethoxyphenyl)pyrazine (**2**) was obtained in a higher yield by the same procedure, but starting from 1,2-dimethoxybenzene. **2**: Mp 203 °C. Found: C, 63.18; H, 3.73; N, 21.14%. Calcd for $C_{14}H_{10}N_4O_2$: C, 63.15; H, 3.79; N, 21.04%. UV (CH_3CN): λ_{max} (ε) 236 (10600), 257 (11200), 316 (10600), and 369 nm (19300). ^1H NMR ($CDCl_3$): δ 4.02 (s, 3H), 4.04 (s, 3H), 7.08 (d, 1H, J=9 Hz), 7.74 (m, 2H), and 9.25 (s, 1H).

*Photoreaction of **1** and **2** in the Presence of Amines.* Irradiations were carried with a 450 w high-pressure mercury lamp mounted in a rotary irradiation apparatus (Rikosha RH-400), unless otherwise mentioned. The reaction tubes were 1.0 cm in diameter, and the distance between the lamp and reaction tubes was 5 cm. In quantitative experiments to obtain the relative quantum yields under varying conditions, the reaction tubes were rotated around the lamp so that all reaction tubes absorbed the same quanta. The quantum yield of the product **3** was determined by benzophenone-benzhydrol actinometry;[15] the reaction samples were irradiated through a solution filter ($CoSO_4 \cdot 7H_2O$, 480 g dm^{-3}; thickness, 1.3 cm) to cut a 404-nm radiation.

(i) Photoreaction in Dry Acetonitrile: A solution of **1** or **2** (14.0 mmol dm^{-3}) and an amine (triethylamine, diethylamine, or butylamine, 0.56 mol dm^{-3}) in dry acetonitrile (16 cm^3) was irradiated for 10 h. The reaction solution from four tubes were collected and condensed under reduced pressure. The condensate was passed through a silica-gel column (1.5 $\phi \times$ 10 cm), using benzene as the eluent, and the condensate was purified by repeated chromatography on silica gel to give the product as the eluate from chloroform (**3**) or chloroform–benzene (3 : 1) (**4**). The photoreaction was accelerated by the purge of the dissolved oxygen by bubbling a stream of argon into the reaction solution after it had been dipped in an ultrasonic bath. The quantum yields were determined by the measurement of the product yield by means of HPLC (Corasil II, acetonitrile).

3; Mp 137 °C. Found: C, 61.29; H, 5.52; N, 11.40%. Calcd for $C_{19}H_{21}N_3O_5$: C, 61.44; H, 5.70; N, 11.32%. UV (CH_3CN): λ_{max} (ε) 236 (13500), 266 (9000), 305 (10200), and 354 nm (19400). IR (Nujol): 2248 cm^{-1}. ^1H NMR ($CDCl_3$): δ 3.75 (s, 8H), 3.93 (m, 4H), 4.20 (m, 4H), 7.03 (d, 1H, J=9 Hz), 7.75 (m, 2H), 8.95 (d, 1H, J=2 Hz), and 9.20 (d, 1H, J=2 Hz).

4; Mp 143 °C. Found: C, 64.88; H, 4.44; N, 17.24%. Calcd for $C_{13}H_{11}N_3O_2$: C, 64.72; H, 4.60; N, 17.42%. UV (CH_3CN): λ_{max} (ε) 234 (13400), 266 (8600), 304 (9800), and 354 nm (19500). IR (Nujol): 2250 cm^{-1}. ^1H NMR ($CDCl_3$): δ 4.01 (s, 3H), 4.03 (s, 3H), 7.07 (d, 1H, J=9 Hz), 7.72 (m, 2H), 8.94 (d, 1H, J=2 Hz), and 9.18 (d, 1H, J=2 Hz).

The photoreaction described above gave a small amount of a bis (decyano) derivative **5** or **6**, but the irradiation of **1** or **2** for 16 h in the presence of a large excess of triethylamine (CH_3CN–Et_3N, 3 : 1) and a similar work-up gave the bis (decyano) derivative **5** (40%) or **6** (44%) respectively as the main product. The irradiation of **3** or **4** under similar conditions also gave **5** or **6** respectively.

5; Mp 110 °C. Found: C, 62.71; H, 6.37; N, 7.98%. Calcd for $C_{18}H_{22}N_2O_5$: C, 62.41; H, 6.40; N, 8.08%. UV (CH_3CN): λ_{max} (ε) 223 (18700), 260 (10600), 289 (10400), and 318 nm (11300). ^1H NMR ($CDCl_3$): δ 3.77 (s, 8H), 3.92 (m, 4H), 4.18 (m, 4H), 6.95 (d, 1H, J=9 Hz), 7.55 (dd, 1H, J=9 and 2 Hz), 7.62 (d, 1H, J=2 Hz), 8.44 (d, 1H, J=2 Hz), 8.57 (diffused t, 1H), and 8.98 (d, 1H, J=2 Hz).

6; Mp 75 °C. Found: C, 66.66; H, 5.60; N, 13.05%. Calcd for $C_{12}H_{12}N_2O_2$: C, 66.65; H, 5.59; N, 12.96%. UV (CH_3CN): λ_{max} (ε) 225 (18800), 261 (12400), 288 (12300), and 320 nm (13800). ^1H NMR ($CDCl_3$): δ 3.94 (s, 3H), 3.97 (s, 3H), 6.99 (d, 1H, J=9 Hz), 7.58 (dd, 1H, J=9 and 2 Hz), 7.67 (d, 1H, J=2 Hz), 8.48 (d, 1H, J=2 Hz), 8.60 (diffused t, 1H), and 9.02 (d, 1H, J=2 Hz).

(ii) Photoreaction in the Presence of Salts: To the same solutions described in Part *(i)* of this section (amine: triethylamine) were added 0.0—6.0 equivalents of sodium perchlorate monohydrate to the pyrazine derivative **1** or **2**, and the mixtures were irradiated in a similar manner for 1 h. Without the addition of sodium perchlorate, less than 10% of the starting material was converted to the decyano derivatives (**3** or **4**) during 1 h. The reaction mixture was concentrated under reduced pressure, and the product was determined by NMR analyses in DMSO, using 1,1,2,2-tetrachloroethane as the internal reference. The quantum yields obtained in this method are shown in Fig. 2. The reaction of **1** in the presence of tetrabutylammonium perchlorate was carried out in the same manner; the results are shown in Fig. 2.

Absorption Spectra and Fluorescence Spectra. The absorption and fluorescence spectra were measured with a Shimadzu UV-200 spectrophotometer and a Hitachi MPF-4 spectrophotometer in acetonitrile or benzene. The acetonitrile was purified by refluxing and distillation over phosphorus pentaoxide. The benzene was purified by washing with conc sulfuric acid and distillation over metallic sodium. In all the fluorescence measurements, 1.00×10^{-4} mol dm^{-3} solution of the pyrazine derivative (**1**, **2**, **3**, or **4**) were employed; the concentrations of the amine (triethylamine, diethylamine, or butylamine) for the quenching were 0.0, 2.0, 4.0, and 6.0 mmol dm^{-3}. The fluorescence quenching of **3** in acetonitrile in the presence of sodium perchlorate was carried out in the same mammer, with the results shown in Table 2.

Measurement of Redox Potential. The redox potential was measured by means of cyclic voltammetry at 25 °C and at the scan rate of 0.5 V s^{-1} using platinum disk electrodes and Ag/AgCl couple as the reference electrode. The oxidation potentials of triethylamine, diethylamine, and butylamine were measured by using 5.0 mmol dm^{-3} solution in acetonitrile containing tetrabutylammonium perchlorate (1.0×10^{-1} mol dm^{-3}) as the electrolyte. The reduction potentials of **1** and **2** were measured in exactly the same method; the results are shown in Table 1. The first oxidation and reduction potentials in cyclic voltammetry are both reversible for the scan to

−2.0 V (**1** and **2**) and +2.0 V (amines).

This work was supported by a Grant-in-Aid for Fundamental Science Research (1980) from the Ministry of Education, Science and Culture and by an Annual Project Organized by Waseda University, 1981—1982.

References

1) Part VI of this series: M. Tada, H. Hamazaki, and H. Hirano, *Chem. Lett.*, **1980**, 921.

2) M. Tada and H. Hirano, *Tetrahedron Lett.*, **1978**, 5111; M. Tada, A. Suzuki, and H. Hirano, *J. Chem. Soc., Chem. Commun.*, **1979**, 1004; M. Tada, H. Hirano, and A. Suzuki, *Bull. Chem. Soc. Jpn.*, **53**, 2303 (1980); A. Suzuki and M. Tada, *Chem. Lett.*, **1980**, 515; H. Hirano, K. Kurumaya, and M. Tada, *Bull. Chem. Soc. Jpn.*, **53**, 2708 (1981).

3) H. C. S. Wood, "Comprehensive Organic Chemistry," ed by E. Haslam, Pergamon Press, Oxford (1979), Vol. 5, p. 489.

4) H. Hirano, R. Lee, and M. Tada, *J. Heterocycl. Chem.*, in psess (1982).

5) D. Rehm and A. Weller, *Israel J. Chem.*, **8**, 259 (1970).

6) For example, the Coulomb term is only 0.05 eV on $r=7$ nm, and so we can safely neglect the term for the present purpose (see Table 1).

7) J. Nasielsky, A. Kirsch-Demesmae, P. Kirsch, and R. Nasielski-Hinke, *J. Chem. Soc., Chem. Commun.*, **1970**, 302; L. O. Luzo, N. J. Bunce, and S. Safe, *Can. J. Chem.*, **53**, 688 (1975); K. Tsujimoto, T. Tasaka, and M. Ohashi, *J. Chem. Soc., Chem. Commun.*, **1975**,758; N. J. Bunce and L. Ravanal, *J. Am. Chem. Soc.*, **99**, 4150(1977); K. A. K. Al-Fakhri, A. C. Mowatt, and A. C. Pratt, *J. Chem. Soc., Chem. Commun.*, **1980**, 566; R. S. Davidson and J. W. Goodin, *Tetrahedron Lett.*, **22**, 163 (1981).

8) K. J. Khimand, and J. F. Bunnett, *J. Am. Chem. Soc.*, **92**, 7463, 7464 (1970); A. P. Komin and J. F. Wolfe, *J. Org. Chem.*, **42**, 2481 (1977); R. A. Rossi and A. B. Dierine, *ibid.*, **45**, 2914 (1980); M. F. Semmelhack and T. Barger, *J. Am. Chem. Soc.*, **102**, 7765 (1980).

9) J. F. Bunnett, *Acc. Chem. Res.*, **11**, 413 (1978); C. P. Andrieux, C. Blocman, J-M. Dumas-Bouchiat, and J-M. Saveant, *J. Am. Chem. Soc.*, **101**, 3431 (1979); C. Galli and J. F. Bunnett, *ibid.*, **101**, 6137 (1979); R. R. Baird, J. F. Bunnett, X, Creary, and M. J. Tremelling, *ibid.*, **102**, 2852 (1980); G. A. Russel and J. Harshberger, *J. Chem. Soc., Chem. Commun.*, **1980**, 216.

10) M. Ohashi, K. Miyake, and K. Tsujimoto, *Bull. Chem. Soc. Jpn.*, **53**, 1683 (1980).

11) Hückel MO calculation by H. Mori and H. Hirano; unpublished results.

12) G. Jackson and G. Porter, *Proc. R. Soc. London, Ser. A*, **260**, 13 (1961); M. Koizumi, S. Kato, N. Mataga, T. Matsuura, and Y. Usui, "Photosensitized Reactions," Kagaku-Dojin, Kyoto (1978), pp. 145—155.

13) H. A. Benesi and J. H. Hildebrand, *J. Am. Chem. Soc.*, **71**, 2703 (1949).

14) H. Shizuka, T. Saito, and T. Morita, *Chem. Phys. Lett.*, **56**, 516 (1978); H. Shizuka, M. Nakamura, and T. Morita, *J. Phys. Chem.*, **84**, 989 (1980).

15) W. M. Moore and M. Ketchum, *J. Am. Chem. Soc.*, **84**, 1368 (1962).

Synthesis of Four Diastereoisomers of Histopine

Yasuo KITAJIMA,* Michinori WAKI, and Nobuo IZUMIYA
Laboratory of Biochemistry, Faculty of Science, Kyushu University 33, Higashi-ku, Fukuoka 812
(Received June 15, 1982)

Four isomers of histopine, N^2-(1-carboxyethyl)histidine, were prepared to provide their physicochemical properties. A diastereomeric mixture, (*RS*),(*S*)-histopine (N^2-[(*RS*)-1-carboxyethyl]-(*S*)-histidine), was synthesized from 2-oxopropionic acid and (*S*)-histidine by reduction with sodium cyanoborohydride. The mixture was separated into its components, (*S*),(*S*)-histopine and (*R*),(*S*)-histopine, by an ion-exchange column chromatography. In a similar manner (*R*),(*R*)-histopine and (*S*),(*R*)-histopine were prepared. Configurations of the four isomers obtained were assumed from their ORD data by comparison with those of the isomers of octopine (N^2-(1-carboxyethyl)arginine) with a definite configuration.

Histopine is a natural compound isolated from crown gall tissue inoculated with *Agrobacterium tumefaciens* B_6.[1] A number of opines structurally related to histopine have recently been found in crown gall tumors of plants.[2] Octopine (N^2-[(*R*)-1-carboxyethyl]-(*S*)-arginine) first isolated from octopus muscle[3,4] is representative of such opines. Although little is known concerning the significance of the presence of these opines in plants and animals, the use of them as markers of a possible transfer of gene from the tumor-inducing bacterium into host plant cells[2,5] has roused further interest in these compounds.

The chemical structure of histopine was established by Kemp as N^2-(1-carboxyethyl)histidine.[1] The configuration of natural histopine, however, has not been determined. Kemp assumed that the configuration of the histidine (His) part was (*S*) only based on the following fact: natural histopine showed the same chromatographic behavior on thin-layer or ion-exchange column as that of a diastereomeric mixture of histopine which was synthesized from (*S*)-histidine and (*RS*)-2-bromopropionic acid.[1]

A synthetic attempt leading to a diastereomeric mixture of histopine has been reported.[1] However, none of the optically pure isomers of histopine has been isolated and characterized. Even for natural histopine, its physicochemical properties (elemental analysis, melting point and specific rotation) have not been given. Thus we were interested in preparing four isomers of histopine in pure state to provide their physicochemical properties.

This paper first describes the preparation of (*RS*),(*S*)-histopine (N^2-[(*RS*)-1-carboxyethyl]-(*S*)-histidine) by sodium cyanoborohydride reduction of a mixture of 2-oxopropionic acid and (*S*)-histidine, subsequent separation into its components by column chromatography, and similar experiments with (*R*)-histidine. Second, the configurations of the four isomers of histopine are assumed by comparison of their ORD patterns with those of octopine isomers having a definite configuration.

Results and Discussion

*Synthesis of (*RS*),(*S*)-Histopine (*N^2*-[(*RS*)-1-Carboxyethyl]-(*S*)-histidine) from (*S*)-Histidine.* Kemp reported the preparation of (*RS*),(*S*)-histopine from (*RS*)-2-bromopropionic acid and (*S*)-histidine in the presence of $Ba(OH)_2$ at 55 °C without describing the yield.[1]

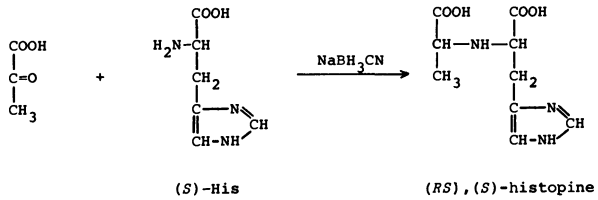

Fig. 1. Synthesis of a diastereomeric mixture of histopine from (*S*)-histidine.

Under these conditions, however, there is some risk of partial racemization of (*S*)-histidine part during the reaction. Recently Jensen *et al.* prepared a distereomeric mixture of nopaline (N^2-(1,3-dicarboxypropyl)arginine) in a high yield from 2-oxoglutaric acid and (*S*)-arginine by reduction with sodium cyanoborohydride ($NaBH_3CN$) under mild conditions at neutral pH and at room temperature.[6]

Taking advantages of this new reagent, $NaBH_3CN$, we intended to synthesize four isomers of histopine from 2-oxopropionic acid and (*S*)- or (*R*)-histidine by reductive amination (Fig. 1). We could obtain (*RS*),(*S*)-histopine in a high yield of 98% based on (*S*)-histidine after the reaction of 2-oxopropionic acid, (*S*)-histidine, and $NaBH_3CN$ in 5 : 1 : 3 molar ratio at pH 7.0 for 3 d. In a similar manner (*RS*),(*R*)-histopine was synthesized from (*R*)-histidine in a yield of 97%.

*Separation of (*RS*),(*S*)-Histopine into Components.* Separation of a diastereomeric mixture of octopinic acid (N^2-(1-carboxyethyl)ornithine) on an amino acid analyzer was already reported.[4] Then we tried to separate (*RS*),(*S*)-histopine into its components by an amino acid analyzer, and found the conditions to achieve the separation (see Experimental section). A faster eluting isomer was determined as (*S*),(*S*)-histopine, and a slower eluting isomer as (*R*),(*S*)-histopine by separate-runs using each pure isomer.

Preliminary experiments for separation of (*RS*),(*S*)-histopine were performed with a column of Dowex 50 at different concentration and pH in sodium citrate buffer system, in order to find optimal conditions for the preparative separation of histopine isomers. According to the above results (see Experimental section), we carried out preparative separation of (*RS*),(*S*)-histopine with a large column (1.8 cm × 190 cm) of Dowex 50. Thus (*S*),(*S*)-histopine with $[\alpha]_D$ +27.7° was isolated from the faster eluting fractions and (*R*),(*S*)-histopine

with $[\alpha]_D$ +30.2° from the slower eluting fractions respectively in a weight ratio of 1 : 1.7. In a similar manner, (*R*),(*R*)-histopine and (*S*),(*R*)-histopine were isolated by the column chromatography of (*RS*),(*R*)-histopine respectively in a weight ratio of 1 : 1.6. Interestingly each isomer in synthetic diastereomeric mixture was not in an equal ratio, which shows occurrence of diastereoselective reduction during the formation of diastereomeric mixture with $NaBH_3CN$.

Attempts to Prepare Histopine Isomers from (S)-Alanine. Chemical synthesis of histopine isomers was attempted by reactions starting from (*S*)-alanine to determine the configuration of the Ala part in histopine isomers. Biellmann *et al.* reported that octopine isomers were obtained from (*S*)-alanine and 2-oxo-5-guanidinopentanoic acid by reduction with $NaBH_3CN$.[7] In the present study, however, the reaction of (*S*)-alanine and 2-oxo-3-(5-imidazolyl)propionic acid with $NaBH_3CN$ under the same conditions gave no expected product. Changes of reaction conditions (*e.g.*, molar ratios of the reactants and pH) also resulted in no formation of histopine isomers. Instead, 2-hydroxy-3-(5-imidazolyl)-propionic acid was detected as a main product by ^1H NMR analysis of the reaction mixture. Previously, Izumiya *et al.* observed a similar result that palladium-catalyzed hydrogenation of (*S*)-alanine and 2-oxo-5-guanidinopentanoic acid did not produce octopine isomers.[8] We assume that easy formation of 2-hydroxy-3-(5-imidazolyl)propionic acid instead of the desired product is due to the instability of a Schiff's base formed from (*S*)-alanine and 2-oxo-3-(5-imidazolyl)-propionic acid or difficult formation of the Schiff's base because of the presence of basic imidazolyl group in the α-keto acid. Condensation of (*S*)-alanine and (*S*)-2-bromo-3-(5-imidazolyl)propionic acid derived from (*S*)-histidine was also unsuccessful.

Configurations of Four Diastereoisomers of Histopine. The configuration of the His part in histopine isomers obtained from 2-oxopropionic acid and (*S*)- or (*R*)-histidine is unequivocally defined, because the configuration of the His part is retained during the reduction with $NaBH_3CN$.

The configuration of the Ala part of histopine isomers was deduced from the results of ORD measurements (see Fig. 2) of four histopine isomers and two octopine isomers with a definite configuration as follows. ORD Pattern of (*S*),(*S*)-octopine (N^2-[(*S*)-1-carboxyethyl]-(*S*)-arginine)[4] is similar to that of a histopine isomer, which has an $[\alpha]_D$ value of +27.7°, prepared from (*S*)-histidine. Thus the configuration at the Ala part in this isomer of histopine is assumed to be (*S*), and the isomer is designated as (*S*),(*S*)-histopine as shown in Table 1. Similar ORD curves are obtained for (*R*),(*S*)-octopine[4] and for a histopine isomer, which has an $[\alpha]_D$ value of +30.2°, prepared from (*S*)-histidine. Thus the configuration of the Ala part in this isomer of histopine is assumed to be (*R*), and the isomer is designated as (*R*),(*S*)-histopine. It is apparent from Fig. 2 that histopine isomers, with $[\alpha]_D$ −27.2° and −29.8°, both prepared from (*R*)-histidine, are antipodes of (*S*),(*S*)- and (*R*),(*S*)-histopine, respectively.

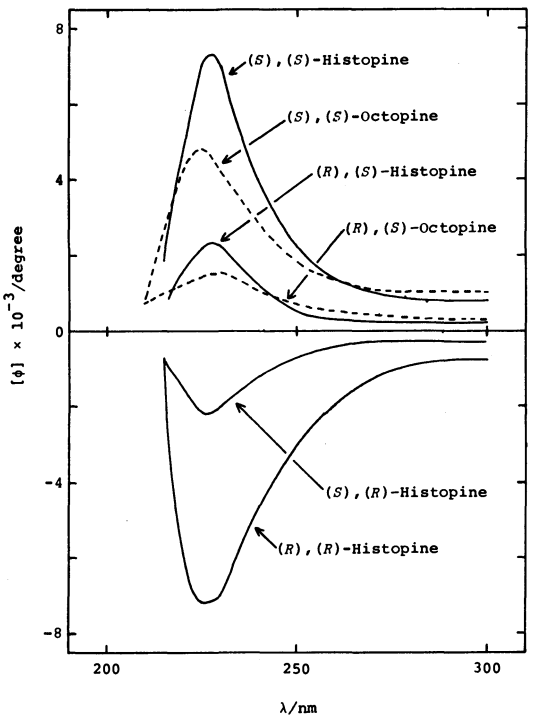

Fig. 2. ORD Curves of isomers of histopine and octopine in 5 M HCl.

Table 1. Configurations of diastereoisomers of histopine

Nomenclature	Configuration of		$[\alpha]_D$/° (5 M HCl)
	Ala part	His part	
(*S*),(*S*)-Histopine	(*S*)	(*S*)	+27.7
(*R*),(*S*)-Histopine	(*R*)	(*S*)	+30.2
(*R*),(*R*)-Histopine	(*R*)	(*R*)	−27.2
(*S*),(*R*)-Histopine	(*S*)	(*R*)	−29.8

Experimental

TLC was carried out on silica gel G (Merck) with the following solvent systems: R_f^1, *n*-BuOH–AcOH–pyridine–H_2O (4 : 1 : 1 : 2, v/v); R_f^2, MeOH–H_2O–pyridine (20 : 5 : 1, v/v). Paper chromatography shown as R_f^1 (PPC) was carried out on Toyo Roshi No. 52 paper with the same solvent system as for R_f^1. Material possessing an imidazolyl group was detected by spraying with the Pauly's reagent.[9] Other compounds on TLC were detected by spraying with 10% H_2SO_4, followed by heating on a hot plate. Optical rotations were measured on a Union high sensitivity polarimeter PM-71. Amino acid analyses were performed with a Hitachi amino acid analyzer KLA-5.

(RS),(S)-Histopine. A solution of (*S*)-histidine monohydrochloride (960 mg, 5 mmol) and freshly distilled 2-oxopropionic acid (2.20 g, 25 mmol) in water (7.5 ml) was adjusted to pH 7.0 with 2 M NaOH at 0 °C, and $NaBH_3CN$ (950 mg, 15 mmol) was added. After stirring for 3 d at room temperature, 12 M HCl (5 ml) was added to the reaction mixture. The solution was diluted with water and then put on a column (2.8 cm × 16.5 cm) of Dowex 50X8 (H^+ form), and the column was washed with water and eluted with 1 M aq pyridine (300 ml). The eluate was evaporated to give the desired product: yield, 1.11 g (98%); R_f^1 0.21, R_f^2 0.77, R_f^1 (PPC) 0.18. A part of the product was recrystallized from

water–EtOH for elemental analysis.

Found: C, 47.45; H, 5.76; N, 18.34%. Calcd for $C_9H_{13}O_4N_3$: C, 47.57; H, 5.77; N, 18.49%.

(RS),(R)-Histopine. This was prepared from (*R*) histidine monohydrochloride and 2-oxopropionic acid as described above: yield, 97%; R_f^1 0.21, R_f^2 0.77.

Separation of (RS),(S)-Histopine into Components. By an Amino Acid Analyzer: A solution of (*RS*),(*S*)-histopine (3 mg) in 0.2 M sodium citrate buffer (0.5 ml) of pH 2.2 was subjected to the analyzer. The following conditions were sufficient to permit the separation of two isomers; a column with spherical fresin; 0.6 cm × 55 cm; buffer, 0.2 M sodium citrate buffer of pH 3.25; flow rate, 30 ml/h; jacket temperature, 55 °C. The eluate from the column was taken in a fraction collector (each fraction, 1-ml), the fractions being monitored as follows. An aliquot (0.1 ml) of each fraction was diluted with water (2.4 ml). To the solution, 10% Na_2CO_3 (1 ml) and a solution of the Pauly's reagent (0.5 ml)[9] were added. The absorbance of the mixture at 500 nm was measured on a Hitachi spectrophotometer 124. A peak for (*S*),(*S*)-histopine was at 32, ml and that for (*R*), (*S*)-histopine at 45 ml.

By Dowex 50 Column Chromatography: A column (0.9 cm × 100 cm) was packed with Dowex 50X8 (200—400 mesh; Na^+ form) equilibrated with a specified eluting solvent. The eluting solvents used were sodium citrate buffers at different concentrations and pHs as follows; 0.2 M at pH 2.51, 0.1 M at pH 3.25 or 0.2 M at pH 3.25. (*RS*),(*S*)-Histopine (6 mg) was applied to a column and eluted with one of these eluting solvents at room temperature. An aliquot (0.02 ml) of each fraction (2 ml) was spotted on a paper strip, and the spots containing histopine were visualized by spraying with the Pauly's reagent. Partial separations were observed with each buffer, however, the buffer of 0.2 M at pH 3.25 gave the most favorable pattern. (*RS*),(*S*)-Histopine was separated completely on a longer column (1.8 cm × 190 cm) with the buffer of 0.2 M at pH 3.25.

(S),(S)-Histopine. A solution of (*RS*),(*S*)-histopine (30 mg) in 0.2 M sodium citrate buffer (1 ml) of pH 3.25 was put on a column (1.8 cm × 190 cm) of Dowex 50X8 (Na^+ form). Elution was performed with the same buffer (each fraction, 8-ml) at a flow rate of 37 ml/h. The same chromatography was further repeated twice; thus total amount of 90 mg of (*RS*),(*S*)-histopine was separated into two components. The 3 faster eluting fractions 115—138 were combined and applied to a column (3.2 cm × 25 cm) of Dowex 50X8 (H^+ form). The column wa swashed with water and eluted with 2 M NH_3 aq (450 ml). The eluate was evaporated to afford a residue (33 mg), and the crude product was crystallized from water-EtOH to give pure (*S*),(*S*)-histopine: yield, 18 mg (20% from (*S*)-His); mp 252—253 °C (decomp); $[\alpha]_D^{20}$ +27.7° (*c* 1, 5 M HCl); R_f^1 0.21, R_f^2 0.53.

Found: C, 47.44; H, 5.80; N, 18.25%. Calcd for $C_9H_{13}O_4N_3$: C, 47.57; H, 5.77; N, 18.49%'.

(R),(S)-Histopine. The 3 slower eluting fractions 143—165 obtained above were treated with Dowex 50X8 (H^+ form) as described for (*S*),(*S*)-histopine. Crude product (57 mg) was crystallized from water–EtOH: yield, 20 mg (22% from (*S*)-His); mp 240—241 °C (decomp); $[\alpha]_D^{20}$ +30.2° (*c* 1, 5 M HCl); R_f^1 0.21, R_f^2 0.53.

Found: C, 47.22; H, 5.83; N, 18.27%. Calcd for $C_9H_{13}O_4N_3$: C, 47.57; H, 5.77; N, 18.49%.

(R),(R)-Histopine. This was prepared from (*RS*),(*R*)-histopine (90 mg) as described for the preparation of (*S*),(*S*)-histopine. The crude product (35 mg) obtained was crystallized from water–EtOH: yield, 25 mg (27% from (*R*)-His); mp 253—254 °C (decomp.); $[\alpha]_D^{20}$ −27.2° (*c* 1, 5 M HCl); R_f^1 0.21, R_f^2 0.53.

Found: C, 47.34; H, 5.90; N, 18.12%. Calcd for $C_9H_{13}O_4N_3$: C, 47.57; H, 5.77; N, 18.49%.

(S),(R)-Histopine. This was prepared from the slower eluting fractions obtained above. The crude product (55 mg) was crystallized from water–EtOH: yield, 26 mg (28% from (*R*)-His); mp 241—242 °C (decomp); $[\alpha]_D^{20}$ −29.8° (*c* 1, 5 M HCl); R_f^1 0.21, R_f^2 0.53.

Found: C, 47.52; H, 5.76; N, 18.04%. Calcd for $C_9H_{13}O_4N_3$: C, 47.57; H, 5.77; N, 18.49%.

ORD Measurements. These were performed with a JASCO spectropolarimeter Model ORD/UV-5. A cell of the path length 0.1 cm was used and the runs were at ambient temperature. ORD Patterns of solutions of four histopine isomers, (*S*),(*S*)- and (*R*),(*S*)-octopine[4] in 5 M HCl (each, 1 mg/ml) are shown in Fig. 2.

We thank Dr. T. Kato and Dr. H. Aoyagi in this Laboratory for their helpful discussions.

References

1) J. D. Kemp, *Biochem. Biophys. Res. Commun.*, **74**, 862 (1977).
2) M. Drummond, *Nature*, **281**, 343 (1979).
3) K. Morizawa, *Acta Schol. Med. Univ. Imp. Kioto*, **9**, 285 (1927).
4) K. Goto, M. Waki, N. Mitsuyasu, Y. Kitajima, and N. Izumiya, *Bull. Chem. Soc. Jpn.*, **55**, 261 (1982).
5) N. Murai and J. D. Kemp, *Proc. Natl. Acad. Sci. U. S. A.*, **79**, 86 (1982).
6) R. E. Jensen, W. T. Zdybak, K. Yasuda, and W. S. Chilton, *Biochem. Biophys. Res. Commun.*, **75**, 1066 (1977).
7) J. F. Biellmann, G. Branlant, and L. Wallén, *Bioorg. Chem.*, **6**, 89 (1977).
8) N. Izumiya, R. Wade, M. Winitz, M. C. Otey, S. M. Birnbaum, R. J. Koegel, and J. P. Greenstein, *J. Am. Chem. Soc.*, **79**, 652 (1957).
9) H. Pauly, *Hoppe-Seyler's Z. Physiol. Chem.*, **94**, 284 (1915).

The Effect of Solvent on the Liquefaction of Coal as a Function of Coal Rank

Yoshio KAMIYA,* Tadashi YAO, and Shinichi NAGAE
Faculty of Engineering, The University of Tokyo, Hongo, Bunkyo-ku, Tokyo 113
(Received June 18, 1982)

In order to study the effect of solvent on the liquefaction of coal as a function of coal rank, the liquefaction of five kinds of coals from carbon content of 66% to 83% were carried out in the presence of various aromatic solvents. It was found that three ring aromatic hydrocarbons were more powerful solvent for the liquefaction. Hydrogen donor solvents such as tetralin and hydrophenanthrenes were most effective of all solvents tested independent of coal rank. A mixture of hydrogen donor and polar compounds such as phenol and quinoline was confirmed to be effective to bituminous coal but not so effective to brown coal. It should be stressed that hydrogen donating property of solvent is most important for low rank coals. The chemical analyses of products have shown that the properties of solvent refined coal are a little affected by the quality of solvent.

It has been stressed that the aromatic solvent plays an important role in coal liquefaction reaction.[1,2] At the initial stage coal is thermally decomposed to lower molecular fragments being dissolved and stabilized by the solvent. Otherwise the unstable fragments will be polymerized to form carbonaceous materials.

Partially hydrogenated aromatic compounds such as tetralin are very effective solvent because of hydrogen donating property. Polar compounds such as phenols[3-5] and quinolines[6] are also effective in the presence of hydrogen donors probably because of acceleration of cleavage of aromatic ether structures.[7]

Although the solvent effect on the coal liquefaction has been studied by many workers, the generalization of experimental results seems very difficult because of differences in preparation of coal sample, experimental conditions and apparatus. There has been hardly reported the relative effectiveness of aromatic solvents in the presence of hydrogen donor on a variety of coals.

Evaluation of solvent effect as a function of coal rank must be very important not only for designing the optimum solvent composition but also for studying the difference in the chemical structure of coals.

In this paper, is reported the effect of various aromatic solvents being contained in coal liquefaction products as a function of coal rank.

Experimental

Coal Sample and Solvent. Five kinds of Japanese and Australian coal with carbon content from 66% to 83% were selected and the analytical data of these coals are shown in Table 1. All coals were dried in a vacuum oven at 105 °C. 1,2,3,4-Tetrahydronaphthalene (tetralin) and 1-methyl-naphthalene were of reagent grade and distilled at 70 °C under reduced pressure after washing with sulfuric acid, alkali and water. Various solvents were reagent grade and used as received.

The properties of mixed solvent, creosote oil, anthracene oil, and middle distillate and heavy distillate from SRC-II process are shown in Table 2.

Middle and heavy distillates[8] were produced from Powhatan coal and supplied by Pittsburgh and Midway coal Mining Company, and these solvents seem to have some hydrogen-donating property because H_β content was 2.5% and 1.8% respectively.

Coal Liquefaction Procedure. Solvent and coal of minus 60 mesh were added to 300 ml magnetic stirring (500 min^{-1}) autoclave. After pressurizing with hydrogen, the autoclave was heated to the reaction temperature within 45 min and maintatined at the temperature during reaction time.

At the completion of a run, the autoclave was cooled by electric fan to room temperature and the autoclave gases were vented through gas meter and analyzed by gas chromatography.

The liquid products were removed through glass filter, and the residual solids were extracted with tetrahydrofuran and weighed after drying.

The amount of moisture-ash-free (maf) coal liquefied during the reaction was calculated as a percentage of the maf feed coal by subtracting the percentage undissolved to give the conversion.

The recovered solution was distilled off using a Buchi GKR-50 rotary evaporator at 200 °C and 0.01 bar, and subjected to various chemical analyses.

Liquid portions of the samples were subjected to gas chromatographic analysis to determine the composition of solvent.

Analysis of THF-soluble Fraction. THF-soluble fraction, so called Solvent Refined Coal, was obtained by distilling off the tetrahydrofuran-soluble products by using rotary evaporator at 200 °C and 0.01 bar.

THF-soluble fraction was submitted to the elementary analyses, molecular weight, ^{1}H-NMR.

TABLE 1. ELEMENTAL ANALYSES OF SAMPLE COALS

Sample coals	Yallourn	Wandoan	Taiheiyo	Liddell	Akabira
C(wt%,daf)	65.8	74.5	75.3	82.0	82.7
H(wt%,daf)	5.1	6.8	6.5	5.4	5.9
N(wt%,daf)	0.5	0.8	1.6	1.5	1.9
S(wt%,daf)	0.2	0.4	0.3	0.5	0.4
O(wt%,diff.)	28.4	25.6	17.5	11.1	10.3
Ash(wt%, drycoal)	2.5	28.5	14.5	11.1	5.7

TABLE 2. ELEMENTAL ANALYSES OF MIXED SOLVENTS

Process solvents	Anthracene oil	Creosote oil	Heavy distillate	Middle distillate
C(wt%)	90.2	90.8	86.3	88.9
H(wt%)	6.0	6.4	9.3	7.5
N(wt%)	0.9	0.7	1.1	1.4
S(wt%)	0.8	0.7	0.2	0.4
O(wt%,diff)	2.1	1.4	4.1	1.8
fa	0.92	0.91	0.69	0.57

Results and Discussion

The conversion of Akabira coal in a mixed solvent composed of 1-methylnaphthalene and one testing solvent was measured at 425 °C for 30 min in order to compare the relative effectiveness of solvent. At initial hydrogen pressure of 20 bar, the conversion to benzene-soluble fraction was generally very low and the conversion to THF-soluble was as low as 50% except in the case of tetralin. Then, the initial hydrogen pressure was raised to 50 bar and the results are shown in Table 3. The effect of hydrogen-donating solvent was most remarkable, since the most effective solvent was tetralin and the second was acenaphthene, both of which have benzylic and donating hydrogen atoms.

Consumed tetralin could be entirely recovered as naphthalene, but reacted acenaphthene corresponding to 36% of the feed could not be recovered probably due to polymerization of dehydrogenated product, acenaphthylene.

Highly condensed aromatic hydrocarbons such as pyrene and fluoranthene have shown higher conversion of coal as reported by Davies and coworkers.[9] The order of effectiveness of solvent for Akabira coal was as follows; fluoranthene = pyrene > phenanthrene > naphthalene.

This result can be ascribed to several effects such as solubility and solvent hydrogenation as reported by Derbyshire,[10] but partly to free radical stabilization effect, because polycondensed aromatic compounds can easily react with free radicals and subsequently donate hydrogen atom to another free radical. Polar solvents such as phenol and quinoline were not so effective in the absence of hydrogen donors.

Table 3. LIQUEFACTION OF AKABIRA COAL IN SYNTHETIC SOLVENTS COMPOSED OF 1-METHYLNAPHTHALENE AND AN ADDITIVE

Additive	Conversion/wt% (THF-soluble)
1-Methylnaphthalene	47
Fluorene	53
Phenanthrene	56
Fluoranthene	59
Pyrene	59
Tetralin	80
Acenaphthene	70
Quinoline	64
1-Naphthol	57
Carbazole	58
Dibenzofuran	50

a) Reaction conditions: 1-Methylnaphthalene 40 ml, additive 20 ml, coal 20 g, 425 °C, 30 min, initial H_2 pressure 50 bar.

In a practical coal liquefaction process, there exist usually some amounts of hydrogen-donating compounds, because the recycle solvent is nearly in equilibrium with high pressure of hydrogen, or solvent is used after hydrotreatment. When we compare the solvent effect of aromatic hydrocarbons, the effect will be varied depending on the pressure of hydrogen gas and reaction conditions. Therefore, it can be quite reasonable to use a solvent containing some amounts of hydrogen donors such as tetralin, in order to compare the effect of various solvents.

The yields of benzene-soluble fraction as well as THF-soluble fraction increased remarkably by replacing anthracene oil with tetralin, indicating that the formation of lower molecular products by the thermal treatment can be drastically increased in the presence of hydrogen-donating compounds. The yield of benzene-soluble fraction increased from 15% to 55%, when anthracene oil was completely replaced by tetralin.

The effect of tetralin as a function of coal rank was studied as shown in Table 4. In the case of brown coal, the conversion of coal has shown a higher value in the presence of tetralin, but the consumption of tetralin showed also a similar tendency. This result represents a higher reactivity of brown coal. Analyses of gaseous products indicated that Yallourn coal yielded very high amount of carbon dioxide and in contrast the yield of methane on the daf basis was not so varied depending on coalification grade.

The effect of various solvents of five kinds of coal from carbon content of 66% to 83% is shown in Table 5.

Generally, 1-methylnaphthalene seems slightly more effective than naphthalene, and phenanthrene a little better solvent than naphthalene, and as well anthracene oil than creosote oil. These results suggest that three ring aromatic compounds are favorable solvent than two ring aromatics due to the solubility of coal fragments and also probably due to the higher hydrogen donating ability. Recently, Whitehurst and his coworkers[10] made clear that highly condensed aromatic compounds such as pyrene can easily accept hydrogen as hydrogen shuttlers and subsequently donate hydrogen atom to another free radical.

The effect of hydrogen-donating solvents having benzyl hydrog ensuch as hydroaromatics with relatively low bond dissociation energy was most remarkable. The higher conversion was clearly observed in the case of low rank coals such as Yallourn and Taiheiyo, indicating that hydrogen donating property is most important for

Table 4. REACTIVITIES OF SAMPLE COALS[a]

Sample coals C%, daf		Yallourn 65.8	Wandoan 74.5	Taiheiyo 75.3	Liddell 82.0	Akabira 82.7
Conversion/%	Coal	87	81	85	80	85
	Tetralin	47	29	28	22	27
Gaseous products (ml)	CH_4	530	350	470	440	560
	CO_2	1010	180	260	50	50

a) Reaction conditions: Coal 20 g, tetralin 30 ml, 1-methylnaphthalene 30 ml, 425 °C, 30 min, initial H_2 pressure 20 bar.

Table 5. Effect of aromatic solvents on the liquefaction of five coals[a)]

Additive	Conversion/wt% (THF-soluble)				
	Yallourn	Wandoan	Taiheiyo	Liddell	Akabira
Naphthalene	64	71	74	71	67
1-Methylnaphthalene	64	72	79	71	70
Phenanthrene	70	74	80	74	75
Creosote oil	66	74	81	75	85
Anthracene oil	68	75	81	75	85
Tetralin	87	80	85	80	85
Dihydroanthracene	87	83	92	83	84
Dihydrophenanthrene	91	85	91	87	85
Octahydrophenanthrene	96	84	94	85	88
Carbazole	69	75	84	79	81
Quinoline	66	74	80	79	90
Phenol	66	74	78	75	88
1-Naphthol	82	83	88	86	95
Middle distillate	69	75	82	75	—
Heavy distillate	73	76	84	78	—

a) Reaction conditions: 1-Methylnaphthalene 30 ml, tetralin 10 ml, additive 20 ml, coal 20 g, 425 °C, 30 min, initial H_2 pressure 20 bar.

coals with low coalification grade. It has been reported that the liquefaction of brown coal is sensitive to hydrogen donating property of solvent.[1,2)] The order of effectiveness of hydrogen-donor solvent has shown that tricyclic hydroaromatics give higher conversion of coal than bicyclic hydroaromatics.

Previously, we have shown that a mixture of hydrogen-donating solvent and phenolic compounds is a very effective solvent for liquefaction of bituminous coal[5)] and this result can be ascribed to the acceleration of scission of ether linkage[7)] in coal structure.

Again, in this experiment, polar compounds such as phenol, 1-naphthol and quinoline in the presence of hydrogen donor were confirmed to be effective solvent for bituminous coals.

In contrast, it was observed that the conversion of brown coal was increased in the presence of 1-naphthol but not affected in the presence of phenol at concentrations below 20 wt% in solution at 400 °C. However, it should be mentioned that at lower temperature of 350 °C, phenolic compounds became effective for dissolution reaction as shown in Fig. 1.

These different effect due to phenol on coal rank can be explained by the difference of chemical structure of coal, probably due to aromatic ether linkage.

A condensed diaryl ether can be decomposed considerably at 450 °C. On the other hand, the carbon-oxygen bond of benzyl phenyl ether or dibenzyl ether can be cleaved rapidly at temperatures below 400 °C. The rapid decomposition of brown coal can be attributed to the benzyl ether structures, which would not give the enhancing effect due to phenol at 425 °C. The slower decomposition of bituminous coal seems to be due to diaryl ether linkage.

Middle distillate as well as heavy distillate from SRC-II process contained some amounts of hydrogen donors along with about 10% of phenolic compounds.

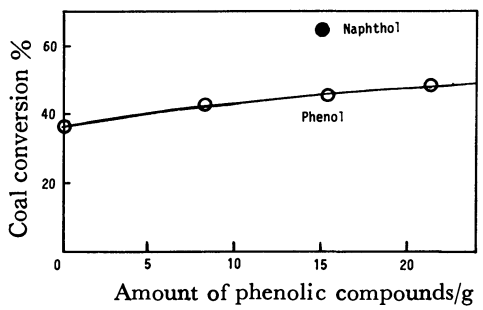

Fig. 1. Effect of phenolic compounds on the liquefaction of Yallourn coal.
Reaction conditions: Coal 20 g, tetralin 15 ml, 1-methylnaphthalene 45 ml, 350 °C, 30 min, initial H_2 pressure 20 bar.

Table. 6. Conversion of solvents in the liquefaction of Yallourn coal[a)]

Additive solvent	Conversion/wt%		
	Coal	Tetralin	Additive
Phenanthrene	70	86	0
Dihydroanthracene	87	75	88
Dihydrophenanthrene	91	56	98
Octahydrophenanthrene	96	35	79
1-Naphthol	82	95	70

a) Reaction conditions: See Table 5.

Table 7. Conversion of solvents in the liquefaction of Akabira coal[a)]

Additive solvent	Conversion/wt%		
	Coal	Tetralin	Additive
Phenanthrene	69	59	2
Dihydrophenanthrene	85	30	97
Octahydrophenanthrene	88	22	58
1-Naphthol	93	63	39
Quinoline	89	63	26

a) Reaction conditions: See Table 5.

TABLE 8. ANALYSES OF SRC FROM YALLOURN COAL

Solvent(ml)	Tetralin(30) 1-MN(30)[a]	9,10-Dihydro-phenanthrene(20) Tetralin(10) 1-MN(30)[a]	Phenanthrene(20) Tetralin(10) 1-MN(30)[a]
Elemental analyses			
C (wt%)	83.7	83.6	84.1
H	6.1	5.6	5.8
N	0.9	0.7	0.6
O	9.3	10.1	9.5
Structural parameters			
fa	0.72	0.75	0.76
H_{au}/C_a[b]	0.75	0.72	0.72
σ[c]	0.42	0.40	0.37
n	1.8	1.9	2.0

a) 1-MN: 1-Methylnaphthalene. b) H_{au}/C_a: H/C ratio of hypothetical unsubst. aromatics. c) σ: Fraction of aromatic edge atoms occupied by subst.

Therefore, it is reasonable that these distillates show a little better result than aromatic hydrocarbons but not so good results as hydrogen donors such as tetralin.

Conversion of solvents in the liquefaction of Yallourn coal is shown in Table 6. In the presence of tetralin, phenanthrene was hardly consumed in the course of reaction. Dihydrianthracene and hydrophenanthrenes were remarkably decreased, but they were recovered as the dehydrogenated products, that is, anthracene and phenanthrene.

It can be concluded that, from the conversion values of tetralin and coal, the most effective hydrogen donors are octahydrophenanthrene and dihydrophenanthrene far reactive than tetralin.

In the case of Akabira coal, as shown in Table 7, 98% of phenanthrene was recovered as it is. Hydrophenanthrenes were converted to phenanthrene with higher conversions than tetralin.

TABLE 9. ANALYSES OF SRC FROM WANDOAN COAL

Solvent (ml)	Tetralin(30) 1-MN(30)[a]	9,10-Dihydro-phenanthrene(20) Tetralin(10) 1-MN(30)[a]	Phenanthrene(20) Tetralin(10) 1-MN(30)[a]	1-Naphthol(20) Tetralin(10) 1-MN(30)[a]
Elemental analyses				
C (wt%)	85.1	84.1	84.7	85.7
H	6.8	6.7	6.2	5.9
N	1.6	1.7	1.8	0.6
O	6.5	7.5	7.3	7.8
Structural parameters				
fa	0.65	0.65	0.70	0.82
H_{au}/C_a	0.67	0.70	0.66	0.74
σ	0.42	0.43	0.42	0.24
n	2.8	2.7	2.4	2.4

a) 1-MN: 1-Methylnaphthalene.

TABLE 10. ANALYSES OF SRC FROM LIDDELL COAL

Solvent (ml)	Tetralin(30) 1-MN(30)[a]	9,10-Dihydro-phenanthrene(20) Tetralin(10) 1-MN(30)[a]	Phenanthrene(20) Tetralin(10) 1-MN(30)[a]
Elemental analyses			
C (wt%)	85.9	86.1	85.6
H	6.1	5.8	5.6
N	1.6	2.2	1.9
O (diff)	6.4	5.9	6.9
Structural parameters			
fa	0.72	0.74	0.74
H_{au}/C_a	0.70	0.65	0.63
σ	0.44	0.41	0.42
n	1.8	1.8	1.9

a) 1-MN: 1-Methylnaphthalene.

Solvent effect by hydrogen donor must be mainly in the stabilization of free radical fragment. In the absence of hydrogen donor, for example, 1,2-diarylethane structure[1] will be converted to a more stable form of diarylmethane after cleavage reaction and a benzyl ether structure to a diarylmethane structure.[7]

While, considerable amounts of naphthol and quinoline could not be recovered.

1-Naphthol gave a high value of coal conversion probably due to the reactive property. Recently, Derbyshire and coworkers[10] made clear that naphthol was remarkably consumed in the presence of coal. This result can be attributed to the hydrogen abstraction from 1-naphthol by alkoxyl radicals resulting from coal fragments and the subsequent reaction of naphthyloxyl radical.

The consumption of 1-naphthol is much higher in the case of Yallourn coal as compared with Akabira coal, suggesting that a lot of alkoxyl radicals are evolved when a lower rank coal is thermally decomposed.

We consider that 1-naphthol can be converted to naphthalene derivative or dimeric furan compounds *via* naphthyloxyl radical.

In the case of Yallourn brown coal, the obtained THF-soluble fraction has shown the lowest value in carbon content of 84% (Table 8). A hydrogen donating solvent as compared with phenanthrene seems to give slightly lower values in *fa* and higher values in H_{au}/C_a, indicating that solvent quality affects the properties of liquefaction products.

Table 9 shows analytical results of Wandoan coal,

in this case, hydrogen-donating solvents give higher values in hydrogen content and lower values in *fa*. In the case of 1-naphthol, the characteristic points were in high *fa* and low σ, which can be ascribed to the addition of 1-naphthol to coal molecule or condensation reaction of 1-naphthol.

In the case of Liddell coal (Table 10), the hydrogenating effect due to hydrogen-donating solvent can be seen in hydrogen content, *fa* and H_{au}/C_a.

Financial support from the Sunshine Project Promotion Headquarters, Agency of Industrial Science and Technology, is acknowledged.

References

1) D. D. Whitehurst, T. D. Mitchell, and M. Farcasiu, "Coal Liquefaction——The Chemistry and Technology of Thermal Process," Academic Press, New York and London (1980), Chap. 9.
2) R. C. Neavel, *Fuel*, **55**, 317 (1976).
3) A. Pott and H. Broche, *Fuel*, **13**, 125 (1934).
4) M. Orchin and H. H. Storch, *Ind. Eng. Chem.*, **40**, 3225 (1948).
5) Y. Yamiya, H. Sato, and T. Yao, *Fuel*, **57**, 681 (1978).
6) R. Brucker and G. Kölling, *Brenn. Chem.*, **46**, 41 (1965).
7) Y. Kamiya, T. Yao, and S. Oikawa, *ACS Symposium Series*, **139**, 291 (1980).
8) Y. Kamiya, *J. Fuel Soc. Jpn.*, **59**, 639 (1980).
9) G. O. Davies, F. J. Derbyshire, and R. Price, *J. Inst. Fuel*, **50**, 121 (1977).
10) F. J. Derbyshire, P. Varghese, and D. D. Whitehurst, "Proceedings Intl. Conf. Coal Science," Düsseldorf (1981), p. 356.

Synthesis of *threo*-3-Methylcysteine from Threonine[1)]

Tateaki WAKAMIYA, Kuniaki SHIMBO, Tetsuo SHIBA,* Kiichiro NAKAJIMA,† Masahiro NEYA,† and Kenji OKAWA†

Department of Chemistry, Faculty of Science, Osaka University, Toyonaka, Osaka 560

†*Department of Chemistry, Faculty of Science, Kwansei Gakuin University, Nishinomiya, Hyogo 662*

(Received June 21, 1982)

threo-3-Methyl-D-cysteine as a moiety of β-methyllanthionine in the peptide antibiotic nisin was synthesized stereospecifically. The reaction of (2*R*,3*R*)-3-methyl-2-aziridinecarboxylic acid derivative prepared from D-threonine with thiobenzoic acid gave the β-mercapto α-amino acid derivative of the same configuration as the starting material. A stereochemistry of the product was retained as a result of double inversion mechanism through the reactions. Thus, we could prepare *threo*-3-methyl-D-cysteine, *i.e.*, (2*S*,3*S*)-2-amino-3-mercaptobutanoic acid which is required for the synthetic study of nisin.

3-Methylcysteine (**1**)[2)] is a moiety of β-methyllanthionine (**2**) which is a constituent amino acid of the peptide antibiotic nisin.[3)] The absolute structure of 3-methylcysteine in natural β-methyllanthionine in nisin can be represented as (2*S*,3*S*)-2-amino-3-mercaptobutanoic acid[4,6)] whose stereochemistry corresponds to D-threonine. A convenient preparative method of this amino acid is required for the purpose of the synthesis of nisin which contains four cyclic peptide parts involving sulfide bridge of β-methyllanthionine. One reasonable method for the synthesis of this amino acid could be a conversion of β-hydroxy α-amino acid into β-mercapto α-amino acid by use of substitution reaction of β-tosylate with thioacetic acid.[5,6)] However, a configuration of the carbon atom carrying hydroxyl group in β-hydroxy α-amino acid must be inverted through the reaction.[6)] Therefore, by application of this reaction, the required *threo* form of β-mercapto α-amino acid can not be obtained from threonine which is mostly available as starting material.

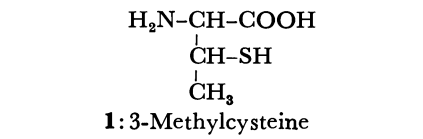

1: 3-Methylcysteine

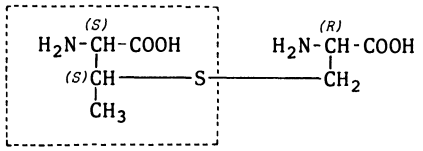

2: β-Methyllanthionine

On the other hand, when 2-aziridinecarboxylic acid derivative prepared from *threo*-β-hydroxy α-amino acid was treated with ammonia or carboxylic acid, β-amino or β-*O*-acyl compound having the original *threo* stereochemistry was obtained respectively.[7,8)] The retention of configuration on the β-carbon atom is clearly explained with a double inversion mechanism as shown in Fig. 1. Namely, the first inversion occurs at aziridine ring formation through *E*2 reaction of β-tosylate or β-mesylate and the second one at the ring opening through S_N2 substitution with ammonia or carboxylate anion.

In a similar way, we now used thiobenzoic acid for the preparation of β-*S*-acyl compound in order to synthesize *threo*-3-methyl-D-cysteine from D-threonine. The aziridine compound was prepared in the usual manner[9)] as shown in Scheme 1. The reaction of (2*R*,3*R*)-*N*-benzyloxycarbonyl-3-methyl-2-aziridinecarboxylic acid methyl ester (**6**) with thiobenzoic acid in the presence of boron trifluoride gave the desirable *S*-benzoyl-β-mercapto derivative **7** accompanying *O*-thiobenzoyl-β-hydroxy derivative **8** as a by-product. The formation of both *S*-acyl and *O*-acyl compounds might be ascribed as a result of possible equilibrium in thiobenzoic acid, *i.e.*, $C_6H_5COSH \rightleftarrows C_6H_5CSOH$, although the higher reactivity of the former gave the preferable *S*-acyl derivative as a main product. The compounds **7** and **8** were separated by column chromatography and characterized by chemical shifts of their β-methine protons which appeared at 4.34 ppm in **7** and 6.22 ppm in **8**.

Acid hydrolysis of *S*-benzoyl derivative **7** after

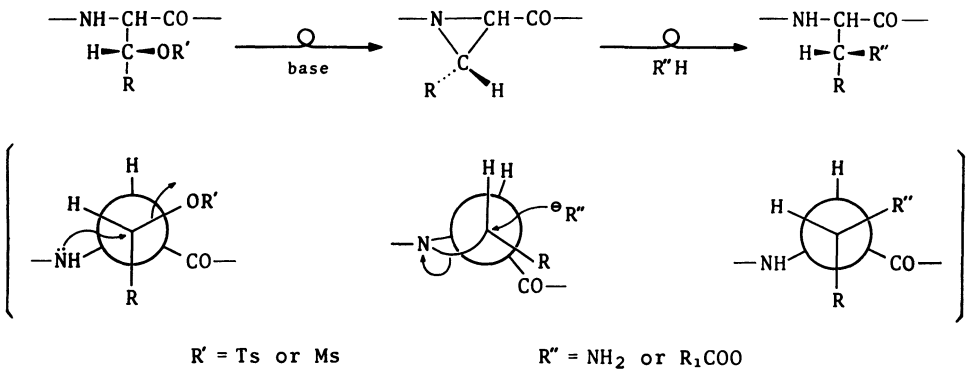

Fig. 1. Double inversion mechanism of the substitution reaction *via* aziridine derivative.

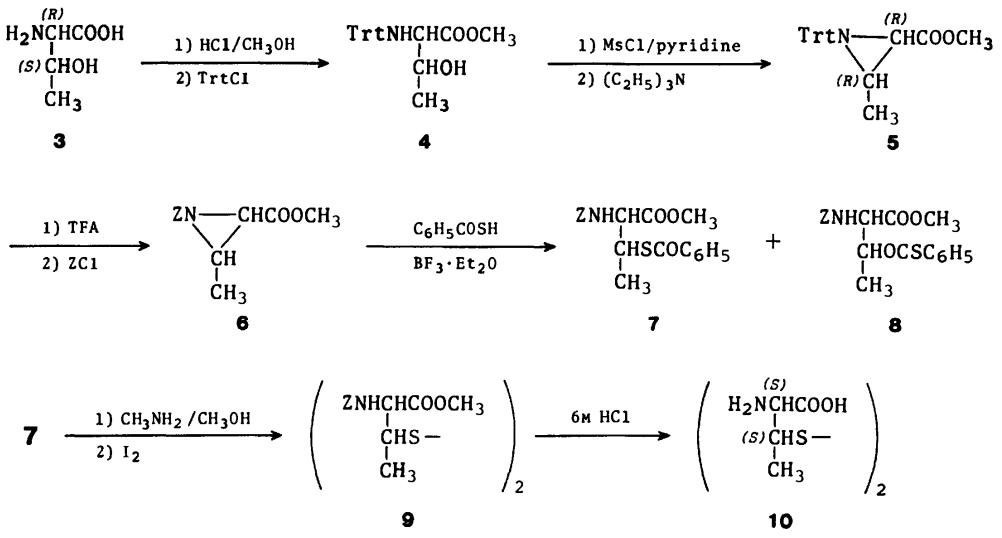

Trt = $(C_6H_5)_3C$, Ms = CH_3SO_2 , Z = $C_6H_5CH_2OCO$

Scheme 1.

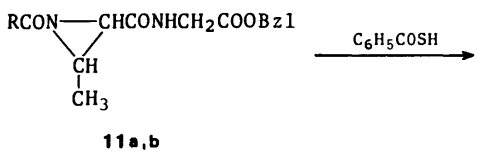

11a,b

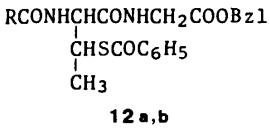

12a,b

a : R = $C_6H_5CH_2O$; b : R = $(CH_3)_3CO$

Bzl = $C_6H_5CH_2$

Scheme 2.

debenzyloxycarbonylation with 30% HBr in acetic acid did not give a good result presumably because of the formation of 5-methyl-2-phenyl-Δ^2-thiazoline-4-carboxylic acid. Therefore, benzyl group was first removed with methylamine in methanol and the product obtained was immediately oxidized to prepare disulfide compound **9**. Hydrolysis of **9** with hydrochloric acid proceeded smoothly and the desired *threo*-3-methyl-D-cysteine was obtained in an oxidized form **10**.

The procedure mentioned above is of course applicable to prepare simple D-cysteine and D-cystine which are commercially very expensive materials. Moreover, threonine residue in peptide chain was next tried to be converted into cysteine residue. A reaction of the peptide **11** containing *N*-acyl-3-methyl-2-aziridinecarboxylic acid derived from threonyl peptide[10] with thiobenzoic acid yielded exclusively *S*-benzoyl-3-methylcysteinyl peptide **12** without contamination with *O*-thiobenzoyl derivative. (Scheme 2) For this reaction, boron trifluoride as a catalyst was not necessary. The sole formation of *S*-acyl derivative may indicate that an amide form of 2-aziridinecarboxylic acid is preferable to an ester form on the opening reaction of the aziridine ring, presumably since the amide form reacts with thiobenzoic *S*-acid much faster than with thiobenzoic *O*-acid. We are now undertaking an application of this method to the synthesis of nisin ring B and the results will be reported soon elsewhere.

Experimental

All melting points are uncorrected. The specific rotations were measured with a Perkin-Elmer 141 polarimeter. NMR spectra were obtained with a Varian XL-100-15 spectrometer and the chemical shifts were given in δ values (ppm) from tetramethylsilane in $CDCl_3$ and from sodium 2,2-dimethyl-2-silapentane-5-sulfonate in DCl. The abbreviations used for coupling patterns were as follows: s, singlet; d, doublet; t, triplet; q, quartet; m, multiplet; br., broad.

N-*Trityl*-D-*threonine Methyl Ester* (**4**). A suspension of D-threonine (10 g, 0.084 mol) in 300 ml of methanol was saturated with hydrogen chloride under stirring in an ice bath to make a clear solution. The solution was allowed to stand overnight at room temperature and then concentrated *in vacuo*. Colorless oily product was obtained in almost quantitative yield by repetition of vacuum concentration with an addition of anhydrous benzene to remove water.

D-Threonine methyl ester hydrochloride (14 g, 0.083 mol) thus obtained was dissolved in 40 ml of chloroform. To the solution was added triethylamine (17 g, 0.17 mol) and then trityl chloride (23 g, 0.083 mol) in 50 ml of chloroform dropwise under stirring in an ice bath. The reaction mixture was concentrated *in vacuo* after stirring for 2 d under cooling. The residue was dissolved in ethyl acetate and the solution was washed successively with saturated sodium chloride solution, 10% citric acid solution, 1 M sodium hydrogencarbonate solution, and saturated sodium chloride solution. Evaporation of the solvent after drying over magnesium sulfate gave 30 g (96%) of **4** as colorless oil. A crop of the product was purified by silica gel column chromatography to remove a slight contaminant of triphenylmethanol. Elution with benzene–ethyl acetate (19 : 1 v/v) gave a crystalline material:

mp 87—89 °C; $[\alpha]_D^{17}$ −6.4° (*c* 1.1, $CHCl_3$).

Found: C, 76.68; H, 6.74; N, 3.71%. Calcd for $C_{24}H_{25}NO_3$: C, 76.78; 6.71; N, 3.73%.

*(2*R, *3*R*)-1-Trityl-3-methyl-2-aziridinecarboxylic Acid Methyl Ester (5).* To a solution of **4** (4.91 g, 0.0131 mol) in 20 ml of pyridine was added methanesulfonyl chloride (4.5 g, 0.039 mol) under cooling in an ice–salt bath. The mixture was stirred for 8 h at room temperature and the solvent was evaporated *in vacuo*. A solution of the residue in ethyl acetate was washed with saturated sodium chloride solution and dried over magnesium sulfate. The reddish brown oil was obtained by vacuum concentration of the solvent. The oily product was dissolved in 40 ml of anhydrous tetrahydrofuran and triethylamine (3.9 g, 0.039 mol) was added to the solution. The mixture was heated under reflux at 80 °C for 2 d and the reaction mixture was concentrated *in vacuo*. An ethyl acetate solution of the residue was washed, successively, with saturated sodium chloride solution, 10% citric acid solution, saturated sodium hydrogencarbonate solution, and saturated sodium chloride solution. Organic layer was dried over magnesium sulfate and the solvent evaporated *in vacuo*. An oily residue was crystallized by trituration with hexane. Recrystallization of the crude product from methanol gave 3.64 g (78.0%) of colorless needles: mp 111—112.5 °C; $[\alpha]_D^{20}$ +98° (*c* 1.0, $CHCl_3$).

Found: C, 80.66; H, 6.51; N, 3.94%. Calcd for $C_{24}H_{23}NO_2$: C, 80.64; H, 6.48; N, 3.92%.

*(2*R, *3*R*)-1-Benzyloxycarbonyl-3-methyl-2-aziridinecarboxylic Acid Methyl Ester (6).* To a solution of **5** (3.17 g, 8.88 mmol) in 14 ml of chloroform and methanol (1 : 1 v/v) was added 7 ml of trifluoroacetic acid under an ice cooling. The mixture was stirred for 2.5 h in an ice bath and then concentrated *in vacuo*. Evaporation with ether newly added was repeated several times to remove trifluoroacetic acid as completely as possible. The residue was dissolved in ether again and 3-methyl-2-aziridinecarboxylic acid ester trifluoroacetate was extracted with water three times. To the aqueous extract was added sodium hydrogencarbonate (3.5 g, 0.042 mol) and 30 ml of ethyl acetate. Benzyloxycarbonyl chloride (1.51 g, 8.9 mmol) was added to the mixture under vigorous stirring in an ice bath. After stirring for 1.5 h, ethyl acetate layer was separated from aqueous layer which was extracted with another portion of ethyl acetate once again. Organic layer combined was washed with saturated sodium chloride solution, dried over magnesium sulfate, and concentrated *in vacuo*. Crude product thus obtained was purified by column chromatography (Merck silica gel 60, 70 g, 1.9 cm × 60 cm). Elution with ethyl acetate and hexane (1 : 5 v/v) yielded 2.12 g (95.9%) of pure **6** as an oily product: $[\alpha]_D^{18}$ +73° (*c* 2.0, $CHCl_3$).

Found: C, 62.75; H, 6.15; N, 5.55%. Calcd for $C_{13}H_{15}NO_4$: C, 62.64; H, 6.07; N, 5.62%.

*S-Benzoyl-*N*-benzyloxycarbonyl-*threo*-3-methyl-*D*-cysteine Methyl Ester (7).* A mixture of **6** (5.2 g, 2.1 mmol) and boron trifluoride etherate (47%, 1.0 ml) in thiobenzoic acid (40 ml) was stirred for 1 d at room temperature. To a reaction mixture was added a large amount of ethyl acetate and the solution was washed with saturated sodium hydrogencarbonate solution and saturated sodium chloride solution. Organic layer was dried over magnesium sulfate and concentrated *in vacuo*. A yellow oily residue was subjected to a silica gel column (Merck, 280 g, 2.7 cm × 110 cm). Elution with benzene and ethyl acetate (19 : 1 v/v) separated thiobenzoic acid, *N*-benzyloxycarbonyl-*O*-thiobenzoyl-D-threonine methyl ester (**8**), and desired **7** in this order. The compound **8** was obtained in a yield of 15% (1.2 g) as pale yellow oil: $[\alpha]_D^{13}$ −183° (*c* 1.44, $CHCl_3$); NMR ($CDCl_3$) δ=1.49 (3H, d, >CH–C<u>H</u>$_3$), 3.68 (3H, s, –OC<u>H</u>$_3$), 4.73 (1H, dd, –NH–C<u>H</u><), 5.14 (2H, s, Ph–C<u>H</u>$_2$–), 5.61 (1H, br. d, –N<u>H</u>–), 6.22 (1H, dq, –O–C<u>H</u>–CH$_3$), 7.3—7.6 (8H, m, aromatic protons), 8.01 (2H, dd, *o*-protons on C_6H_5CS). Found: C, 62.09; H, 5.49; N, 3.50; S, 8.49%. Calcd for $C_{20}H_{21}NO_5S$: C, 62.00; H, 5.4 N, 3.62; S, 8.28%.

Main product **7** was obtained as oil in a yield of 53% (4.3 g); $[\alpha]_D^{18}$ −64° (*c* 1.0, $CHCl_3$); NMR ($CDCl_3$) δ=1.48 (3H, d), 3.73 (3H, s), 4.34 (1H, dq, –S–C<u>H</u>–CH$_3$), 4.66 (1H, dd), 5.11 (2H, s), 5.61 (1H, br. d), 7.3—7.6 (8H, m), 7.90 (2H, dd, *o*-protons on C_6H_5CO). Found: C, 61.67; H, 5.47; N, 3.54; S, 8.15%.

*N,N′-Bisbenzyloxycarbonyl-*threo*-3,3′-dimethyl-*D*-cystine Dimethyl Ester (9).* To a solution of **7** (0.59 g, 1.5 mmol) in 20 ml of methanol was added 1 M methylamine in methanol (2.3 ml, 2.3 mmol) during 15 h at 10—15 °C. After an additional stirring overnight, 0.5 M solution of iodine in methanol was added to the reaction mixture until a brown color remained. Oxidation reaction was completed within 30 min and the solution was then concentrated *in vacuo*. Colorless crystalline product **9** formed on addition of ether to the residue was filtered, 0.39 g (91%). The product was recrystallized from ethanol and hexane to obtain an analytical sample, yield 0.35 g (81%): mp 108—110 °C; $[\alpha]_D^{18}$ −167° (*c* 1.00, $CHCl_3$) NMR ($CDCl_3$) δ=1.31 (β-CH_3, d), 3.52 (β-CH, dq), 3.72 (–OCH_3, s), 4.59 (α-CH, dd), 5.12 (Ph–CH_2, s), 5.63 (NH, br. d), 7.34 (C_6H_5, s).

Found: C, 55.50; H, 5.72; N, 4.90; S, 10.92%. Calcd for $C_{26}H_{32}N_2O_8S_2$: C, 55.30; H, 5.71; N, 4.96; S, 11.36%.

*threo-3,3′-Dimethyl-*D*-cystine (10).* A suspension of **9** (0.33 g, 0.58 mmol) in 6 M HCl (2 ml) and acetic acid (2 ml) was heated under reflux for 5 h at 110 °C. The hydrolyzat was concentrated *in vacuo* and the residue was dissolved in water. The aqueous solution was once extracted with ether, neutralized with pyridine, and concentrated *in vacuo*. Ethanol was added to the residue and an insoluble material was recrystallized from water and ethanol to obtain pure **10**6; colorless powder: yield 0.13 g (82%); mp 183—193 °C (decomp); $[\alpha]_D^{13}$ −416° (*c* 0.50, 1 M HCl) [lit,[6] $[\alpha]_D^{19}$ −414° (*c* 1, 1 M HCl)]; NMR (2 M DCl) δ=1.43 (β-CH_3, d), 3.96 (β-CH, dq), 4.45 (α-CH, d).

Found: C, 34.32, H, 6.18; N, 10.10; S, 22.70%. Calcd for $C_8H_{16}N_2O_4S_2 \cdot \frac{2}{3}H_2O$: C, 34.27; H, 6.23; N, 9.99; S, 22.87%.

*S-Benzoyl-*N*-benzyloxycarbonyl-*threo*-3-methyl-*L*-cysteinylglycine Benzyl Ester (12a).* (2*S*, 3*S*)-*N*-Benzyloxycarbonyl-3-methyl-2-aziridinylcarbonylglycine benzyl ester (**11a**)[10] (86 m, 0.23 mmol) was dissolved in 2 ml of dichloromethane and thiobenzoic acid (62 mg, 0.45 mmol) was added to the solution. The mixture was stirred at room temperature for 18 h and at 40 °C for 30 h. The reaction mixture diluted with ethyl acetate (20 ml) was washed once with saturated sodium hydrogencarbonate solution and twice with water. Organic layer dried over magnesium sulfate was concentrated *in vacuo* and an oily residue obtained was treated with hexane to crystallize. Crude product was recrystallized from ethyl acetate and hexane: yield 97 mg (83%); mp 131—133 °C; $[\alpha]_D^{16}$ +1.5° (*c* 0.83, $CHCl_3$); NMR ($CDCl_3$) δ=1.46 (3H, d), 4.03 (2H, dd), 4.21 (1H, m, C_6H_5COS–C<u>H</u>–), 4.46 (1H, t), 5.04 (2H, s), 5.11 (2H, s), 5.91 (1H, d), 6.88 (1H, br. t), 7.2—7.6 (13H, m), 7.80—7.93 (2H, m).

Found: C, 64.50; H, 5.51; N, 5.26; S, 6.26%. Calcd for $C_{28}H_{28}N_2O_6S$: C, 64.60; H, 5.42; N, 5.38; S, 6.16%.

*S-Benzoyl-*N*-t-butoxycarbonyl-*threo*-3-methyl-*L*-cysteinylglycine Benzyl Ester (12b).* To a solution of (2*S*,3*S*)-*N*-*t*-butoxycarbonyl-3-methyl-2-aziridinylcarbonylglycine benzyl ester (**11b**)[10] (94 mg, 0.28 mmol) in 2 ml of dichrolomethane was added thiobenzoic acid (77 mg, 0.56 mmol) and the mixture

was stirred for 25 h. The reaction mixture diluted with 20 ml of ethyl acetate was washed once with saturated sodium hydrogencarbonate solution and three times with water. Organic layer was dried over magnesium sulfate and concentrated *in vacuo*. An oily residue was crystallized by addition of hexane and a crystalline product was recrystallized from ethyl acetate and hexane: yield 101 mg (75%); mp 125—127 °C; $[\alpha]_D^{16}$ −2.7° (*c* 0.89, CH_3OH); NMR ($CDCl_3$) δ=1.37 (9H, s), 1.47 (3H, d), 4.06 (2H, d), 4.24 (1H, m, C_6H_5COS–C<u>H</u>–), 4.40 (1H, t), 5.12 (2H, s), 5.54 (1H, d), 6.89(1H, br. t), 7.2—7.6 (8H, m), 7.87 (2H, m).

Found: C, 61.70; H, 6.23; N, 5.74; S, 6.73%. Calcd for $C_{25}H_{30}N_2O_6S$: C, 61.71; H, 6.21; N, 5.76; S, 6.59%.

References

1) A part of this work was presented at 43rd National Meeting of the Chemical Society of Japan, Tokyo, April 1981, Abstr. No. 3F34.

2) J. Hoogmartens, P. J. Claes, and H. Vanderhaeghe, *J. Org. Chem.*, **39**, 425 (1974).

3) E. Gross and J. L. Morell, *J. Am. Chem. Soc.*, **93**, 4634 (1971).

4) J. L. Morell and E. Gross, *J. Am. Chem. Soc.*, **95**, 6480 (1973).

5) C. Zioudrou, M. Wilchek, and A. Patchornik, *Biochemistry*, **4**, 1811 (1965).

6) J. L. Morell, P. Fleckenstein, and E. Gross, *J. Org. Chem.*, **42**, 355 (1977). In this publication, the configuration of β-carbon atom of this amino acid was wrongly represented as *R*. However it must be corrected to *S*.

7) a) T. Shiba, T. Ukita, K. Mizuno, T. Teshima, and T. Wakamiya, *Tetrahedron Lett.*, **1977**, 2681; b) T. Wakamiya, K. Mizuno, T. Ukita, T. Teshima, and T. Shiba, *Bull. Chem. Soc. Jpn.*, **51**, 850 (1978).

8) T. Tanaka, K. Nakajima, T. Maeda, A. Nakamura, N. Hayashi, and K. Okawa, *Bull. Chem. Soc. Jpn.*, **52**, 3579 (1979).

9) a) K. Okawa, K. Nakajima, T. Tanaka, and Y. Kawana *Chem. Lett.*, **1975**, 591; b) K. Nakajima, F. Takai, T. Tanaka and K. Okawa, *Bull. Chem. Soc. Jpn.*, **51**, 1577 (1978).

10) K. Nakajima, H. Oda, and K. Okawa, *Bull. Chem. Soc. Jpn.*, **55**, 3232 (1982).

Pyridine-containing Acyclic Crown Ethers and Their Polymers as Specific Carrier of Biogenetic Amine Derivatives[1)]

Hiroshi Tsukube
Department of Chemistry, College of Liberal Art and Science, Okayama University, Okayama 705
(Received June 26, 1982)

A variety of crown ethers and their analogs which contain powerful hydrogen bonding sites such as pyridine and quinoline moieties were examined as new synthetic carrier. Among the examined carriers, acyclic crown ethers and their polymers having pyridine groups were found to be selective and efficient carriers for some organic ammonium cations of great biological significances. Their transport properties were largely different from those of usual crown ether compounds, and essentially dependent on the combined characteristics of polyether sequence, hydrogen bonding site, co-transported anion, and others.

There has been much interest in synthetic cyclic and acyclic crown ethers[2)] because of their unique coordination abilities. Various modifications have been made to the basic polyether structures and attained a variety of functions. In particular, introduction of donor atoms such as sulfur and nitrogen atoms provided stronger and interesting coordination properties for ammonium cations and transition metal ions.

Cram *et al.*[3)] and Christensen *et al.*[4)] have shown that pyridine-containing cyclic crown ethers such as **2** form more stable complexes with organic ammonium cations than corresponding parent crown ethers. Vögtle *et al.*[5)] have also reported that quinoline-bearing acyclic crown ethers such as **4** show higher complex stabilities for ammonium cation complexes. These findings strongly suggest that pyridine nitrogen atoms of the cyclic and acyclic crown ethers can form stronger hydrogen bonding with guest ammonium hydrogen atoms than does as ether oxygen atoms.

Here we examine a variety of pyridine unit-containing polyethers ("pyridino-crown ethers") as artificial carrier in the chloroform liquid membrane system (see Fig. 1). They include cyclic crown ethers, acyclic crown ethers, and their polymers. Among them, acyclic crown ether **4**, containing quinoline-terminal groups, was found to discriminate some kinds of organic ammonium cations from K^+ ion in the transport process. Since such a unique transport selectivity was not attained by using cyclic crown ether compounds **1** and **2**, this is an important example of acyclic crown ether which shows more excellent property than corresponding cyclic crown ethers. Although some pyridino-crown ethers were known to effectively transport Ag^+ [4)] and Pb^{2+} [6)] ions, a series of pyridino-crown ethers were firstly applied to the highly selective transport of "biogenetic amines and drugs" of great biological significances.[7)]

Results and Discussion

Transport Properties of Cyclic and Acyclic Crown Ether Carriers (1—5). We measured the transport rates of several cations through a chloroform liquid membrane which contains one of the carriers **1**—**5** and which separates two aqueous phases. As shown in Fig. 1, guest cation salts are complexed with carrier and transported from aqueous phase I to an aqueous phase II using an experimental apparatus previously reported (see Experimental Section). Hence, the present transport process occurs by carrier-mediated facilitated diffusion along the concentration gradient of the guest salts.

Among the employed carriers (see Fig. 2), **2** and **4** contain nitrogen atoms as stronger hydrogen bonding sites for ammonium cations, and are expected to be an effective carrier of them. In particular, acyclic crown ether **4** provides interesting structural features:[5)] (a) The quinoline moiety also functions as anchoring points with locally fixed donor sites on which guest cation can take hold; (b) The flexible nature of acyclic carrier can permit effective conformational changes in the binding and releasing processes, like as naturally occurring acyclic ionophores.[8)] Recently a number of acyclic crown ethers have already been prepared as ionophore models, and most of them form pseudocyclic conformations on complexations of guest cations, which are stabilized by intramolecular interactions between two terminal groups. Since their transport selectivities may be determined by the sizes and shapes of the formed cavities, they may be similar to those observed in the cyclic crown ether systems.[2)] In a marked contrast, the transport selectivity of the present carrier **4** can be controlled mainly by the nature of terminal donor group *via* terminal group-guest cation interaction. This is largely different from those of previously reported acyclic crown ethers. Hence, new and characteristic transport properties are expected by using this type of acyclic crown ether.

Other cyclic and acylic crown ethers (**1**, **3**, and **5**) were also examined for comparisons. Typical results of passive transport experiments are shown in Table 1. Blank experiments (no carrier present) were performed

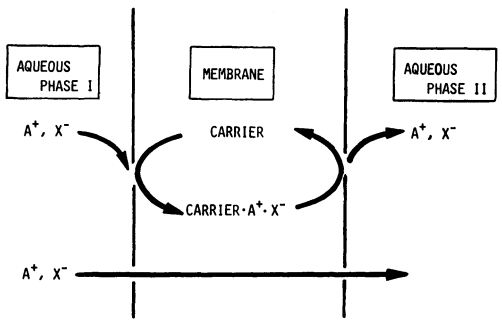

Fig. 1. Liquid membrane system for ammonium cation transport. A^+: Ammonium cation, X^-: cotransported anion.

TABLE 1. CATION-TRANSPORT MEDIATED BY CROWN ETHER CARRIERS (**1**—**5**)

Salt		Transport rate/10^{-6} mol h^{-1}				
		1	**2**	**3**	**4**	**5**
$LiClO_4$	(A)	0.5	0.2	1.5	0	0.1
$NaClO_4$	(A)	0.3	0.3	0.4	0.1	0.3
$KClO_4$	(A)	4.7	1.7	0.1	0.1	0.4
NH_4ClO_4	(A)	0.3	0.5	0.2	0.3	0.3
KCl	(B)	28.5	5.9	0.2	0.9	2.5
NH_4Cl	(B)	8.6	5.3	0.2	3.0	3.5
$C_6H_5CHNH_3Cl$ (CH$_3$)	(B)	11.6	10.0	1.0	10.7	3.9
$C_6H_5CH_2CH_2NH_3Cl$	(B)	12.9	12.2	1.2	12.5	8.6
$C_6H_5CH_2C(CH_3)_2NH_3Cl$ (phentermine)	(B)	18.5	16.0	0.1	17.1	4.9
$C_6H_5CHCHNH_3Cl$ (norephedrine) (OH, CH$_3$)	(B)	6.9	8.6	0.5	6.2	1.1
$(CH_3O)_2C_6H_3CH_2CH_2NH_3Cl$ (homoveratrylamine)	(B)	14.1	12.0	1.0	12.7	6.6
$HOC_6H_4CH_2CH_2NH_3Cl$ (tyramine)	(B)	1.4	1.0	1.0	0.6	0.2
$(HO)_2C_6H_3CH_2CH_2NH_3Cl$	(B)	1.0	0.1	0.3	0.2	0

Initial concentrations: aqueous phase I; salt, 0.3 mmol. Additive ($NaClO_4$), 0 mmol(A) or 1.5 mmol(B)/H_2O, 3 ml. Membrane; carrier, 0.0372 mmol/$CHCl_3$, 8 ml. Aqueous phase II; distilled water, 9 ml.

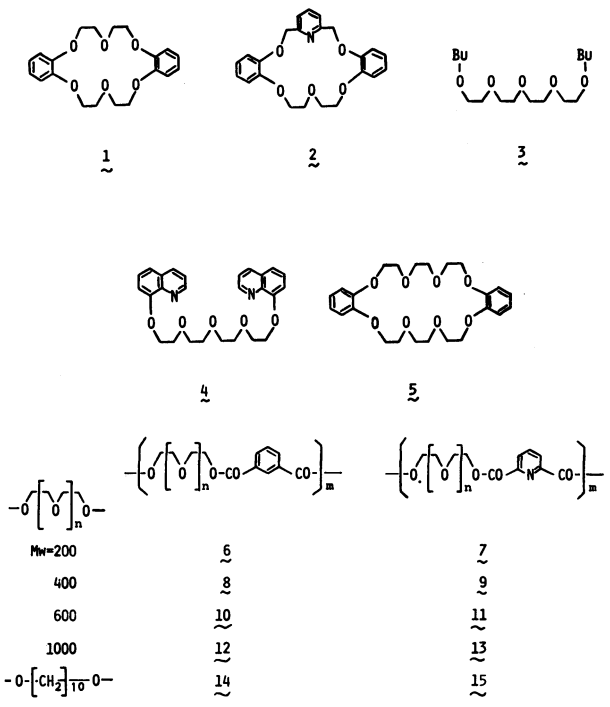

Fig. 2. Examined synthetic polyether carriers.

for each system to determine membrane leakages. The obtained amounts of cation leakages varied with used cations, but were generally much smaller than those indicated in Table 1.

Pyridino-crown ether **2** showed somewhat different transport behaviors from parent crown ether **1**. Although it has been reported that substitution of pyridine nitrogen for an oxygen in 18-crown-6 gives slight influences on the complex stabilities of K^+ and other cations, the transport rates of K^+ ion appreciably weakened in the carrier **2** system, while organic ammonium cation-transport rates were slightly influenced. These facts clearly indicate that pyridine nitrogen atom plays a more significant role in the transport of organic ammonium cations than in the transport of K^+ ion. Probably hydrogen bonding between pyridine nitrogen and guest ammonium cations would be effectively operated.

A pronounced effect of introducing donor sites into the carrier on the transport properties was observed in the quinoline-bearing acyclic crown ether **4** system. The carrier **4** was found to be an effective and selective carrier of some organic ammonium cations, compared to the cyclic crown ethers (**1** and **2**). Acyclic crown ether **4** preferentially transported several biogenetic amines and drugs of great significance such as phentermine, norephedrine, and homoveratrylamine. In marked contrast, cyclic crown ethers were confirmed to effectively transport a variety of ammonium cations as well as K^+ ion as reported before. Although Vögtle *et al.* have demonstrated that this type of acyclic crown ethers complex with a number of cations such as Li^+, Na^+, K^+, and others,[5] it was firstly found to show highly discriminative transport abilities for ammonium cations. Therefore, this is an important example of acyclic crown ether which shows more excellent functions than corresponding cyclic crown ether. As well-known, nigericin, monensin, and other acyclic bioionophores change their conformations on guest complexations, and form "pseudocyclic conformations."[8] This affects not only the rates of complexation and of decomplexation, but also transport selectivities. These coordination behaviors of naturally occurring antibiotics could be mimicked in the present artificial system. Quinoline-nitrogen atoms of the carrier **4** can act as stronger hydrogen bonding sites, and their coordination to the

Table 2. Cation-transport mediated by acyclic crown ether polymers

Salt	Transport rate/10^{-6} mol h^{-1}				
	Acyclic crown ether polymer system				
	6	**8**	**10**	**12**	**14**
KCl	0	0.1	0.1	0.2	0
NH_4Cl	0	0	0.1	0.1	0
$C_6H_5CHNH_3Cl$ (CH$_3$)	0.2	1.1	2.5	5.8	0.4
$C_6H_5CH_2C(CH_3)_2NH_3Cl$	0.7	1.6	2.4	6.1	0.6
$C_6H_5CH(OH)CH(CH_3)NH_3Cl$	0.6	0.6	1.1	2.2	0.6
$(CH_3O)_2C_6H_3CH_2CH_2NH_3Cl$	0.4	2.6	4.5	11.7	0
$HOC_6H_4CH_2CH_2NH_3Cl$	0	0	0	0.1	0
	Pyridino-crown ether polymer system				
	7	**9**	**11**	**13**	**15**
KCl	0	0.2	0.1	0.2	0
NH_4Cl	0	0.2	0	0.2	0
$C_6H_5CHNH_3Cl$ (CH$_3$)	1.2	1.6	2.8	6.4	0.6
$C_6H_5CH_2C(CH_3)_2NH_3Cl$	0.2	6.8	9.0	7.0	4.3
$C_6H_5CH(OH)CH(CH_3)NH_3Cl$	0.3	0.8	1.0	2.3	0.4
$(CH_3O)_2C_6H_3CH_2CH_2NH_3Cl$	2.3	2.8	5.5	12.2	0.8
$HOC_6H_4CH_2CH_2NH_3Cl$	0	0	0	0	0

Initial concentrations: carrier, 0.0372 mmol/Ph or Py unit base. Other conditions, See Table 1 (B).

ammonium cations may induce the conformational changes of the carrier, promoting the successive interactions of polyether sequence with ammonium cations. Butyl-bearing acyclic crown ether **3**, which has similar polyether linkages to the carrier **4**, was confirmed to hardly transport ammonium cations and other metal ions. Therefore, attachment of quinoline moiety as terminal groups to the open polyether chain can offer both high efficiencies and excellent selectivities in the transport phenomena. In particular, it was noted that such a higher transport selectivity could not be attained in the cyclic crown ether systems.

The larger ring crown ether **5** with higher flexibility was also attempted as membrane carrier. It exhibited relatively higher transport selectivity for ammonium cations than the 18-membered crown ether **1**, even though its transport rates were modestly lower. This fact may suggest that molecular flexibility of the carrier is an another important factor to design a selective carrier for ammonium cation salts.

The employed crown ether carriers (**1**, **2**, **4**, and **5**) showed similar cation selectivities for a series of organic ammonium cations. As substrates, we chose a variety of phenethylammonium salts to which the biogenetic amines and drugs of great biological importance belong. Their transport efficiencies were clearly dependent on the hydrophobicities of the guest cations: phentermine> phenethylamine> norephedrine> tyramine> dopamine. Inorganic cation, NH_4^+, was found to be hardly transported because of its higher hydrophilicity.[10] Lehn *et al.* have studied crown ether-mediated transport of a similar series of phenethylamine salts,[7] and found that substitution beyond the nitrogen atom of the phenethylamine diminishes the transport rates: phentermine< phenethylamine. Although the natures of employed crown ethers were somewhat different, the results obtained here demonstrate that the hydrophobicity of the guest cation is more essential factor to determine the transport rate than the steric hindrance around the coordination site. Other experiments show that this type of carrier appeared of little use for hydroxy group containing ammonium cations such tyramine and dopamine derivatives. Probably, hydroxy group would enhance the hydrophilicity of the cation and occupy the coordination site of the carrier for ammonium cation hydrogen atom.

Transport Properties of "Acyclic Crown Ether Polymers." The polymer carriers, in which pyridine unit and acyclic crown ether moiety were incorporated, were applied to the membrane transport of ammonium cation salts. Many investigators have already prepared a variety of polymers which contain the crown ether units in the main chain and/or side chain. The former shows a parallel cation coordination property to that of monomeric analog,[11] while the latter favors the formation of the sandwich-type 2 : 1 crown ether/guest

cation complexes.[12] Since they are mostly limitted to the cyclic crown ether polymers, the present study will present interesting examples of "acyclic crown ether polymers" as cation-carrier.[13] Transport experiments were performed in a similar cell as described above, and the typical results are summarized in Table 2.

Table 2 shows that an increase in the number of ether oxygen atoms raises the transport efficiencies. Polymer carriers (**14** and **15**) having no ether oxygen atom were confirmed to exhibit lower transport rates than other polymer carriers (**6**—**13**). Hence, coordination properties of acyclic crown ether moieties can be significantly involved in the present transport system. Chaput *et al.*[14] have measured the complex stability constants of monomeric "acyclic crown ethers" of various polyether chain lengths for alkali metal cations, and observed a similar relationship between number of ether oxygen atoms and complex stabilities. Therefore, this may be characteristic behaviors of acyclic crown ether families.

Introduction of pyridine moiety into the polymer carrier also allows effective transport of organic ammonium cation salts. Since pyridine-containing polymer carriers (**7**, **9**, **11**, and **13**) offered higher transport abilities for some organic cations, same factors would be involved to determine the transport behaviors both in crown ether system and in crown ether polymer system.

Acyclic crown ether polymers (**6**, **8**, **10**, and **12**) showed somewhat effective transport of organic ammonium cations, though their transport abilities were generally lower than those of pyridine-containing polymers (**7**, **9**, **11**, and **13**). These facts may suggest that effective interaction between aromatic moieties of guest cation and of polymer carrier can attribute the higher stability of ammonium cation-carrier complex. Similar observations have been reported in the cyclic crown ether systems.[15]

Anion Effects on Transport Rates. Recently some investigators have demonstrated that the rates of cation-transport by using crown ethers are largely influenced by the natures of anion species which accompanies the guest cation-crown ether complex. Lamb *et al.* revealed an empirical correlation between transport rate of alkali metal cation and anion hydration energy.[16]

By using four kinds of crown ether compounds (**1**, **4**, **10**, and **11**) the transport rates of phentermine ammonium cation were determined in the presence of several inorganic anions. The obtained results, listed in Table 3, indicate that the anion has a large effect on the rate of cationt-ran sport mediated by acyclic crown ethers as well as by cyclic crown ethers. It was clearly demonstrated that perchlorate and thiocyanate anions allow faster transport of ammonium cation than carbonate, sulfate, and chloride anions, suggesting that similar factors determined transport behaviors both in the crown ether system and in the crown ether polymer system.

Table 3. Anion effect on transport rate of phentermine ammonium cation

Anion	Transport rate/10^{-6} mol h^{-1}			
	1	**4**	**10**	**11**
ClO_4^-	18.5	17.1	2.4	9.0
SCN^-	14.1	19.4	7.2	12.0
CO_3^{2-}	1.7	0.4	0.5	0.5
SO_4^{2-}	0.9	0.2	0.3	0.5
Cl^-	0.9	0.9	0.4	0.4

Initial concentrations: additive (Sodium salt of anion), 1.5 mmol/aqueous phase I. Other conditions: See Table 1.

Experimental

Polymer Carrier Synthesis. The polymer carriers (**6**, **8**, **10**, and **12**) were prepared from isophthaloyl dichloride and corresponding polyethylene glycols. Typically, the carrier **12** was obtained by the reaction of isophthaloyl dichloride (0.01 mol), polyethylene glycol, Mw=1000, (0.01 mol), and pyridine (0.02 mol) in chloroform (100 ml) at 60 °C. After 15 h's refluxing, reaction solution was washed with water repeatedly. White wax polymer was obtained (65% yield) by removal of chloroform and dried *in vacuo*. The other polymers (**7**, **9**, **11**, **13**, **14**, and **15**) were similarly prepared. Some characteristic properties of them are summarized in Table 4.

Transport Experiments. The transport experiments were performed at room temperature in a similar apparatus as described before.[17] A cylindrical glass cell (4.0 cm, i.d.) holds a glass tube (2.0 cm, i.d.) which separates two aqueous phases. Typically, the inner aqueous phase (aqueous phase I) contains ammonium cation salt and additive such as $NaClO_4$ in 3 ml of water. The aqueous phase II, outer aqueous phase, contains 9 ml of distilled water. The membrane phase (8 ml of chloroform), in which carrier is dissolved, lies below two aqueous phases, and bridges them. This membrane phase is stirred constantly by magnetic stirrer. A similar experiment was carried out in the absence of carrier. The ammonium cation concentration in the aqueous phase II, monitored spectroscopically, was confirmed to increase linearly with running time ($<$12 h), and the initial transport rates were calculated. The values indicated in Tables 1, 2, and 3, were estimated from the differences in the transport rates of carrier-containing systems and blank systems (no carrier present).

The co-transported anion was also observed to move from aqueous phase I to II. When the perchlorate anion was employed as symport anion, we found that the amount of

Table 4. Characterizations of acyclic crown ether polymers

Carrier	Yield/%[a]	$\nu_{C=O}$/cm^{-1}[b]	Mw[c]	Remark
6	68	1720	1800	Oil
7	60	1730	1700	Powder
8	66	1720	2000	Oil
9	62	1737	2000	Wax
10	61	1717	3000	Oil
11	60	1727	3000	Wax
12	65	1720	4000	Wax
13	60	1739	4000	Wax
14	66	1722	1500	Powder
15	60	1732	1500	Powder

a) Yield of chloroform-soluble fraction was shown. b) Nujol mull (cm^{-1}). c) Determined by GPC (column; Shodex GPC A-803). Calibration was made with standard polystyrene samples.

perchlorate anion transported, determined by Methylene Blue method,[18] was almost equal to that of ammonium cation transferred under the employed conditions. The detailed conditions were shown in Tables.

References

1) Preliminary communication: H. Tsukube, *Tetrahedron Lett.*, **23**, 2109 (1982).

2) For review: E. Weber and F. Vögtle, "Topics in Current Chemistry," 98, Springer-Verlag, Berlin, Heidelberg, New York (1981), p. 1. Recent reports on "cyclic crown ether"-type carriers: J. D. Lamb, J. J. Christensen, S. R. Izatt, K, Bedke, M. S. Astin, and R. M. Izatt, *J. Am. Chem. Soc.*, **102**, 3399 (1980). S. Shinkai, T. Minami, Y. Kusano, and O. Manabe, *ibid.*, **104**, 1967 (1982). H. Tsukube, *Tetrahedron Lett.*, **22**, 3981 (1981). Recent reports on "acyclic crown ether"-type carriers: W. Wierenga, B. R. Evans, and J. A. Woltarson, *J. Am. Chem. Soc.*, **101**, 1334 (1979); K. Maruyama, H. Tsukube, and T. Araki, *ibid.*, **102**, 3246 (1980); N. Yamazaki, S. Nakahama, A. Hirao, and S. Negi, *Tetrahedron Lett.*, **1979**, 2429; K. Hiratani, *Chem. Lett.*, **1981**, 21.

3) M. Newcomb, J. M. Timko, D. M. Walba, and D. J. Cram, *J. Am. Chem. Soc.*, **99**, 6392 (1977).

4) J. S. Bradshow, G. E. Maas, J. D. Lamb, R. M. Izatt, and J.J. Christensen, *J. Am. Chem. Soc.*, **102**, 467 (1980).

5) B. Tümmler, G. Maass, E. Weber, W. Wehner, and F. Vögtle, *J. Am. Chem. Soc.*, **99**, 4683 (1977).

6) J. D. Lamb, R. M. Izatt, P. A. Robertson, and J. J. Christensen, *J. Am. Chem. Soc.*, **102**, 2452 (1980).

7) Some artificial carriers for selective transport of organic ammonium cations have been reported: E. Bacon, L. Jung, and J. M. Lehn, *J. Chem. Res.*, (S) **1980**, 136; K. Maruyama, H. Tsukube, and T. Araki, *J. Chem. Soc., Chem. Commun.*, **1980**, 1222.

8) F. Vögtle and E. Weber, *Angew. Chem., Int. Ed. Engl.*, **18**, 753 (1976).

9) R. M. Izatt, J. D. Lamb, R. E. Asay, G. E. Maas, J. S. Bradshow, J. J. Christensen, and S, S. Moore, *J. Am. Chem. Soc.*, **99**, 6134 (1977).

10) J. W. Larsen and L. J. Magid, *J. Am. Chem. Soc.*, **96**, 5774 (1974).

11) S. Bormann, J. Brossas, E. Franta, P. Gramam, M. Kirch, and J. M. Lehn, *Tetrahedron*, **31**, 2791 (1975); E. Blasius and P. G. Maurer, *Makromol. Chem.*, **178**, 649 (1977).

12) J. Smid, A. Varma, and S. C. Shah, *J. Am. Chem. Soc.*, **101**, 5764 (1979).

13) Recently some "acyclic crown ether polymers" were employed as a specific anion carrier. See H. Tsukube, *J. Polym. Sci., Polym. Chem. Ed.*, **20**, 2982 (1982).

14) G. Chaput, G. Jeminet, and J. Juillard, *Can. J. Chem.*, **53**, 2240 (1975).

15) D. A. Laidler and J. F. Stoddart, *J. Chem. Soc., Chem. Commun.*, **1977**, 481.

16) J. D. Lamb, J. J. Christensen, S. R. Izatt, K. Bedke, M. S. Astin, and R. M. Izatt, *J. Am. Chem. Soc.*, **102**, 3399 (1980).

17) K. Maruyama, H. Tsukube, and T. Araki, *J. Chem. Soc., Dalton Trans.*, **1981**, 1486; *J. Am. Chem. Soc.*, **104**, 5197 (1982).

18) D. F. Boltz, "Colorimetric Determination of Non-Metals," Interscience, New York (1958), p. 176.

Tetravalent Ruthenium Porphyrin. II. The Molecular and Crystal Structure of μ-Oxo-bis[(octaethylporphinato)ruthenium(IV) chloride] Benzene Solvate

Hideki Masuda,* Tooru Taga, Kenji Osaki, Hiroshi Sugimoto,†
Masayasu Mori,† and Hisanobu Ogoshi††
Faculty of Pharmaceutical Sciences, Kyoto University, Shimoadachi-cho, Yoshida, Sakyo-ku, Kyoto 606
†*Faculty of Science, Osaka City University, Sugimoto-cho, Sumiyoshi-ku, Osaka 558*
††*Department of Materials Science and Technology, Technological University of Nagaoka, Kamitomioka, Nagaoka 949-54*

(Received January 9, 1982)

The crystal structure of μ-oxo-bis[(octaethylporphinato)ruthenium(IV) chloride] benzene solvate, [Ru(IV)(oep)Cl]$_2$O–C_6H_6, was determined by the X-ray method. The complex crystallizes in the tetragonal space group P4/nnc, $a=13.912(2)$ Å, $c=17.821(4)$ Å, and $Z=2$. The structure was solved by the heavy-atom method and refined to $R=0.084$ for 958 reflections. The [Ru(IV)(oep)Cl]$_2$O complex has the crystallographic D_4-422 symmetry and contains the binuclear (Cl)N_4Ru–O–RuN_4(Cl) coordination group with the Ru–O(μ) distance of 1.793(2) Å, the Ru–Cl distance of 2.320(6) Å, and the Ru–N distance of 2.038(9) Å. The Ru–O–Ru bond is explicitly linear, and the two porphinato cores rotate around the Ru–O–Ru bond by 21.0° from the eclipsed form. The porphinato core is planar within 0.04 Å, and the Ru atom is displaced only by 0.07 Å out of the plane defined by the four porphinato nitrogen atoms toward the bridging O atom. These results are compared with those of the previously reported [Ru(IV)(oep)(OH)$_2$]O–CH_3OH crystal.

The stereochemistry of ruthenium-porphyrins has been intensively investigated, primarily by regarding them as a model of heme protein systems,[1,2] since the Ru ion has been established to serve as a suitable substitute for the Fe ion. We have previously reported the crystal structure of μ-oxo-bis[(octaethylporphinato)ruthenium(IV) hydroxide] methanol solvate, [Ru(IV)(oep)(OH)]$_2$O–CH_3OH, as a model of the iron(IV) porphyrin observed in oxidative reaction of the native Fe(III) hemoprotein of peroxidase.[2] The title crystal, [Ru(IV)(oep)Cl]$_2$O–C_6H_6, is isomorphic with the [Ru(IV)(oep)(OH)]$_2$O–CH_3OH crystal.[2] In this paper, we report the structure of the [Ru(IV)(oep)Cl]$_2$O–C_6H_6 crystal, and discuss the geometry of these isomorphous crystals.

Experimental

[Ru(IV)(oep)Cl]$_2$O was prepared by treatment with dilute hydrochloric acid of a dichloromethane solution of [Ru(IV)(oep)(OH)]$_2$O.[3] Purple-red, plate-like crystals were obtained by recrystallization from a 1 : 1 mixture of benzene and dichloromethane. A prelimenary X-ray photographic examination indicated a centrosymmetric space group P4/nnc with Laue symmetry 4/mmm and systematic absences of $hk0$ for $h+k$ odd, $0kl$ for $k+l$ odd, and hhl for l odd. A crystal with dimensions of $0.2\times0.2\times0.1$ mm^3 was mounted on a Rigaku AFC-5 diffractometer with graphite-monochromated Mo $K\alpha$ radiation ($\bar{\lambda}=0.71073$ Å). The unit cell dimensions refined by a least-squares treatment of the setting angles of 47 reflections are $a=13.912(2)$ Å, $c=17.821(4)$ Å, $D_x=1.304$ g/cm^3 (for two [Ru(IV)(oep)Cl]$_2$O and two benzene molecules per unit cell), and $D_m=1.300$ g/cm^3 (by flotation in an aqueous calcium chloride solution).

Intensity data of 1826 reflections in the range $2\theta<50°$ were collected in the ω-2θ scan mode with a scan rate of 5° min^{-1} in ω. Three reflections were monitored every 60 reflections. The intensity data were converted to the $|F_o|$ data in the usual manner, and a total of 958 independent reflections with $|F_o|>3.0\sigma(F_o)$ were retained as observed, where the standard deviations $\sigma(F_o)$ were estimated from counting statistics. No absorption correction was applied ($\mu=5.53$ cm^{-1} for Mo $K\alpha$).

The structure was solved by the heavy-atom method and refine by full-matrix least-squares. The Ru atom was located from sharpened Patterson maps, and the C, N, O, and Cl atoms of the [Ru(IV)(oep)Cl]$_2$O complex were picked up from successively synthesized Fourier maps. Subsequent least-

Table 1. Positional and thermal parameters for the atoms of [Ru^{IV}(oep)Cl]$_2$O·C_6H_6

Estimated standard deviations in the least significant figure(s) are given in parentheses. B_{eq} is the equivalent isotropic temperature factor defined by Hamilton.[8]

Atom	x	y	z	B_{eq}/Å^2
Ru	1/4	1/4	0.1494(1)	2.43
Cl	1/4	1/4	0.0192(3)	4.24
O(μ)	1/4	1/4	1/4	2.54
N	0.3707(6)	0.3329(7)	0.1457(6)	2.82
C(1)	0.3774(7)	0.4293(8)	0.1476(8)	2.79
C(2)	0.4779(10)	0.4601(10)	0.1476(8)	3.98
C(3)	0.5289(10)	0.3785(10)	0.1493(10)	4.55
C(4)	0.4630(9)	0.2987(12)	0.1471(10)	3.70
C(5)	0.2954(13)	0.4915(10)	0.1465(12)	3.78
C(6)	0.5100(12)	0.5626(10)	0.1492(11)	4.95
C(7)	0.5269(17)	0.6012(17)	0.0727(17)	8.71
C(8)	0.6413(15)	0.3707(16)	0.1607(14)	9.05
C(9)	0.6813(15)	0.3597(20)	0.0866(17)	13.00
C(10)	0.2422(59)	0.2025(64)	−0.1838(18)	7.45
C(11)	1/4	0.1461(43)	−1/4	8.23
H(C4)	0.310 (10)	0.560 (10)	0.152 (9)	
H(C6A)	0.571 (12)	0.546 (11)	0.188 (7)	
H(C6B)	0.471 (12)	0.597 (11)	0.193 (8)	
H(C7A)	0.544 (11)	0.678 (12)	0.078 (8)	
H(C7B)	0.462 (11)	0.622 (12)	0.045 (9)	
H(C7C)	0.598 (11)	0.572 (11)	0.050 (9)	
H(C8A)	0.665 (12)	0.281 (10)	0.069 (9)	
H(C8B)	0.650 (11)	0.454 (12)	0.193 (8)	
H(C9A)	0.670 (11)	0.301 (10)	0.194 (8)	
H(C9B)	0.751 (12)	0.355 (9)	0.104 (7)	
H(C9C)	0.654 (12)	0.395 (11)	0.053 (9)	
H(C10)	0.265 (28)	0.142 (21)	−0.163 (17)	
H(C11)	0.274 (0)	0.055 (28)	−0.250 (0)	

aquares refinement and difference Fourier synthesis revealed a disordered solvent benznene molecule. All hydrogen atoms were located geometrically (C–H=1.00 Å) and included in the structure factor calculations of the least-squares refinement by assuming their isotropic thermal parameters as 8.0 Å^2. A further refinement with the weighting scheme of $w=1/(\sigma(F_o)^2$ was carried out to convergence. The final R value was 0.084. Atomic scattering factors[4a] and anomalous terms[4b] were taken from the International Tables for X-Ray Crystallography. All computations were performed on a FACOM M-200 computer at the Data Processing Center, Kyoto University by using the program system KPAX.

Results

The atomic parameters are listed in Table 1. Tables of anisotropic thermal parameters and of observed and calculated structure factors are kept as a Document No. 8254 at the Chemical Society of Japan. Figure 1 displays a single $[Ru(oep)Cl]_2O$ complex and two disordered benzene molecules. The $[Ru(oep)Cl]_2O$ binuclear complex exists at a crystallographic D_4-422 symmetry position. The required fourfold axis passes through the Cl–Ru–O–Ru–Cl bond, and the two twofold axes perpendicular to the fourfold axis pass through the central oxygen atom. One-fourth of the porphinato moiety is an asymmetric unit. The numbering scheme for the independent atoms is given in Figs. 1 and 2. The benzene molecules exist at another 422 symmetry position, and they are disordered in two different orientations about the fourfold axis.

The bond lengths and angles for the porphyrin skeleton (Fig. 2) are similar to those of the $[Ru(oep)(OH)]_2O$ crystal[2] and they are normal in comparison with those reported for the planar porphyrins.[5] Deviations from the least-squares plane of the 24 ring atoms of the porphinato core are given on the left-hand side in Fig. 2. The porphinato core is planar within 0.04 Å,

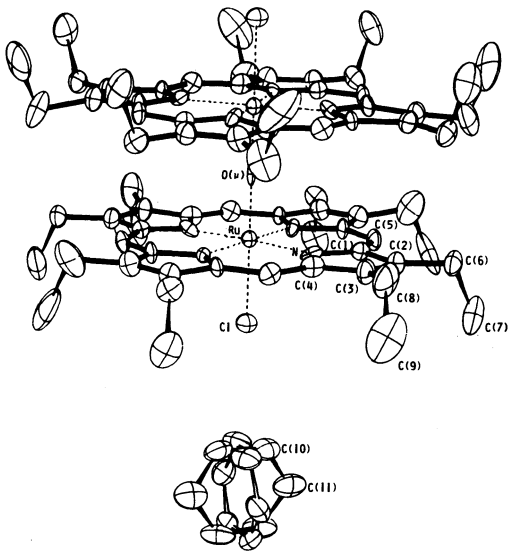

Fig. 1. Computer-drawn model in perspective of the $[Ru(oep)Cl]_2O$ molecule and the disordered benzene molecules. The vibrational ellipsoids are drawn at the 30% probability level. The labeling scheme used for the atoms in the molecules is also shown.

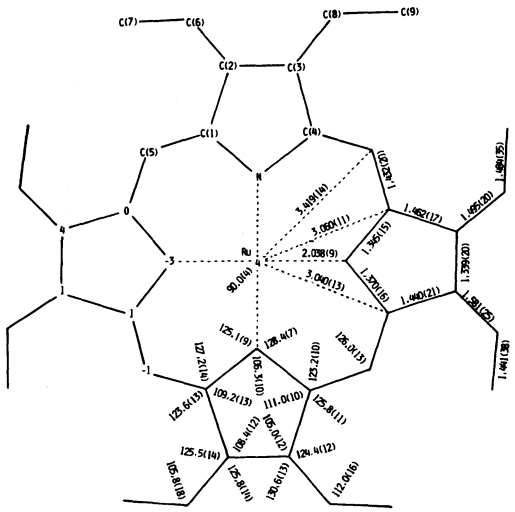

Fig. 2. Formal diagram of the porphinato skeleton in $[Ru(oep)Cl]_2O$. On the top of the diagram, the numbering scheme for the atoms is displayed. On the left-hand side of the diagram, the numbered symbol for each atom is replaced by its perpendicular displacement, in units of 0.01 Å, from the mean plane of the porphinato core. On the right-hand side and the bottom of the diagram are the structurally independent bond distances and angles. The numbers in parentheses are the standard deviations.

and the ruthenium ion is displaced only by 0.07 Å out of the plane defined by the four porphinato nitrogen atoms toward the bridging O(μ) atom. Figure 3 presents a perspective diagram of the environment of one ruthenium ion. The Ru(IV)–N distance, 2.038(9) Å, is slightly shorter than the Ru(IV)–N distance (2.067(14) Å) observed in $[Ru(oep)(OH)]_2O$[2] and than the Ru(II)–N distances (2.041—2.052 Å) reported in ruthenium(II) porphyrin complexes.[1] The Ru(IV)–O(μ) distance, 1.793(2) Å, is shorter than that reported for Ru(IV)–O(μ), 1.847(13) Å, in $[Ru(IV)(oep)(OH)]_2O$[2] and is comparable with that reported for Ru(IV)–O(μ), 1.80 Å, in $(Cl_5Ru(IV)ORu(IV)Cl_5)^{4-}$.[6] The Ru(IV)–Cl distance, 2.320(6) Å, is similar to that reported for Ru(IV)–Cl, 2.34 Å, in $(Cl_5Ru(IV)ORu(IV)Cl_5)^{4-}$[6] and is in good agreement with the sum of single-bond radii, 2.32 Å.

The Ru–O–Ru* bond is explicitly linear, and the two porphinato cores, related to each other by the twofold symmetry, rotate about the straight Ru–O–Ru* bond by 21.0° from the eclipsed form. (The atom with or without an asterisk superscribed is associated with the upper or lower core of the binuclear porphyrin complex, respectively.) The interplanar separation between the mean planes of the porphinato cores is 3.66 Å; the interatomic distances are 3.59 Å for Ru–Ru*, 3.79 Å for N–N*, 3.79 Å for C_a–C_a*, 3.67 Å for C_b–C_b*, and 3.70 Å for C_m–C_a*. (C_a, C_b, and C_m are used for the three chemically and structurally distinctive types of carbon atoms, pyrrole-α, pyrrole-β, and methine carbons, respectively.) The rotation angle and interplanar distance between the two porphinato cores are slightly less than the corresponding angle and distance in the $[Ru(IV)(oep)(OH)]_2O$ crystal.[2] However, in

the same way as described in the report on $[Ru(IV)(oep)(OH)]_2O$,[2] the binuclear porphyrin structure of the present complex is stabilized by the intramolecular π-π interactions between the face-to-face contact porphyrins and by the $d\pi$-$p\pi$-$d\pi$ interaction in the Ru(IV)–O–Ru(IV) bond, and diamagnetism of the present complex is also well interpreted in terms of the π-π interactions in the Ru(IV)–O–Ru(IV) bond system with the low-spin Ru(IV) atom.

The average C–C bond length and the average C–C–C bond angle of benzene molecule are 1.39(5) Å and 119(5)°, respectively. The disordered benzene molecules are surrounded by the six $[Ru(oep)Cl]_2O$ complexes. The molecular plane of each benzene molecule is perpendicular to the porphinato planes, and the shortest interatomic distance is 3.62(4) Å between the Cl and C(10) atoms along the c axis. The $[Ru(IV)(oep)Cl]_2O$ complexes and solvate benzene molecules are packed with van der Waals contacts.

Discussion

The $[Ru(IV)(oep)Cl]_2O-C_6H_6$ crystal is isomorphic with $[Ru(IV)(oep)(OH)]_2O-CH_3OH$.[2] Table 2 summarizes the unit cell dimensions and the geometric parameters of the coordination groups for the two μ-oxo ruthenium porphyrin derivatives. As shown in Fig. 4, the absorption spectra of the Cl-derivative ($[Ru(IV)(oep)Cl]_2O$) exhibit a large bathochromic shift as compared with those of the OH-derivative ($[Ru(IV)(oep)(OH)]_2O$). These spectroscopic shifts suggest that the Cl^- and OH^- ligands on the Ru(IV) atom obey the general order of the spectrochemical series, $OH^- > Cl^-$. Thus the Cl^- ion is considered to be a weaker ligand for the Ru(IV) atom than the OH^- ion. The difference of the ligand strengths reflects the geometric parameters of the two coordination groups. As shown in Table 2, the deviation of the Ru atom out of the porphinato mean plane for the Cl-derivative is larger than that for the OH-derivative. This large Ru deviation toward the O^{2-} atom in the Cl-derivative is reasonable, since the O^{2-} atom is a stronger ligand for the Ru(IV) atom than the Cl^- and OH^- atoms, and the degree of Ru(IV) displacement toward the strong ligand depends on the ligand strengths at the opposite side. The Ru(IV)–O(μ) bond of the Cl-derivative is significantly shorter than the corresponding bond of the OH-derivative, and the Ru–N bond of the Cl-derivative is also slightly shorter than that of the OH-derivative. These shortening effects of the Ru–O(μ) and Ru–N bonds of the Cl-derivative will be explained in terms of "the structural trans and cis effects." That is, when a ligand of the six coordinated metal complex is replaced by a weaker ligand, the other trans and cis ligand-metal bonds will be strengthened because of the neutralization of the electric charge around the central metal ion. In the present case, replacement of the axial OH^- ligand by a weaker Cl^- ligand strengthens the trans Ru–O(μ) and cis Ru–N bonds, and consequently results in the shortening of these bonds. As to the shortening values of these bonds, the Ru–O(μ) bond is more shortened than the Ru–N bond. Thus the trans effect

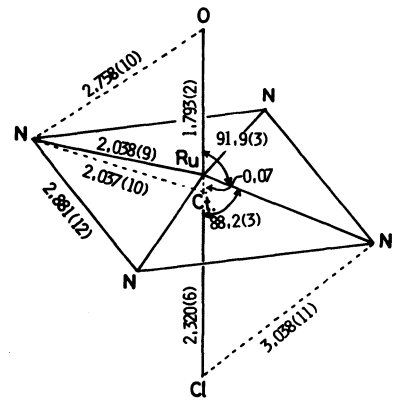

Fig. 3. Perspective diagram of the six-coordination group around the ruthenium(IV) atom in the $[Ru(oep)Cl]_2O$ molecule. C_t represents the center of the porphinato skeleton.

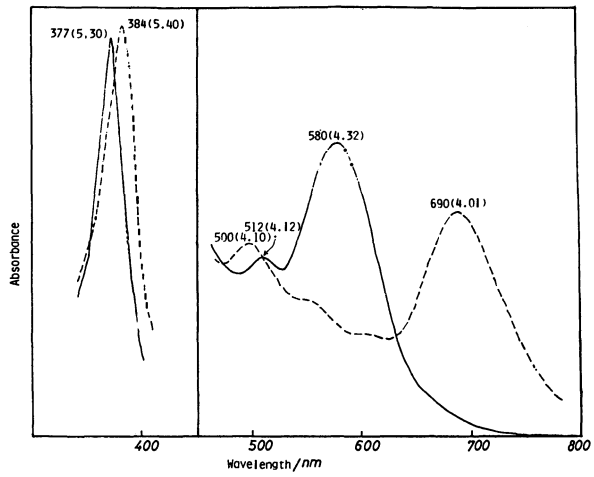

Fig. 4. Absorption spectra for $[Ru(oep)Cl]_2O$ (----) and $[Ru(oep)(OH)]_2O$ (——) in CH_2Cl_2. Extinction coefficients (log ε_{max}) are given in parentheses following λ_{max} (nm).

seems to be more effective than the cis effect. This inference is correct in view of the fact that the Ru–O(μ) distance of the Cl-derivative is very close to that in the case of the $Cl_5Ru-O-RuCl_5$ system in which the strong equatorial nitrogen ligands of the porphyrin complex is replaced by the weak Cl^- ligands;[6] the Ru–O(μ) bond distance depends largely on the trans Cl^- ligand and depends less on the cis ligand. Other examples of such dominant trans effect have been found in the Ru(II)(tpp)(CO)X (X=Py and EtOH) complexes[1b,1c] and in the Fe(II)(tpp)(NO)X (X=1-MeIm, 4-MePip, and none) complexes.[7] It may, therefore, be pointed out that the dominant trans effect is a general tendency in the six coordinated metalloporphyrin complexes.

Another noticeable point in Table 2 is that the unit cell volume of the Cl-derivative is significantly smaller than that of the OH-derivative. This volume change is due mainly to the lattice deviation along the c axis, in which direction the substitution of Cl^- for OH^- or of C_6H_6 for CH_3OH is allowed to take place. The Cl^- and C_6H_6 groups in the Cl-derivative have normal van der

Table 2. Comparison of the unit cell dimensions and coordination geometries for $[Ru(IV)(oep)Cl]_2O$ and $[Ru(IV)(oep)(OH)]_2O$

Molecule		$[Ru(IV)(oep)Cl]_2O$	$[Ru(IV)(oep)(OH)]_2O$
Crystal data	a/Å	13.912(2)	13.98(1)
	c/Å	17.821(4)	18.03(12)
	V/Å^3	3449(1)	3522(20)
Coordination geometry	Ru–N(Å)	2.038(9)	2.067(14)
	Ru–C_t(Å)	0.07[a]	0.03[a]
		0.04[b]	0.01[b]
	Ru–O(μ)(Å)	1.793(2)	1.847(13)
	Ru–L(Å)	2.320(6); L=Cl	2.195(26); L=OH
	P–P[c](Å)	3.66	3.71
	N–Ru–Ru*–N*(°)	21.0(3)	22.7(4)

a) Deviation out of the plane defined by the four porphinato nitrogen atoms. b) Deviation from the 24-atom porphinato mean plane. c) P–P means the interplanar distance between the mean planes of the porphinato cores.

Waals contacts along the c axis, while the disordered CH_3OH molecule in the OH-derivative occupy an excessively large space.[2] This space difference of solvent occupation may be a main factor for the large lattice deviation along the c axis. Deformation of the six-coordinate Ru(IV) group, of course, has a contribution to the anisotropic lattice deviation. The large trans effect and the small cis effect mentioned above are consistent with the large lattice deviation along the c axis.

The authors wish to thank Professor Nobuo Morimoto and Dr. Katsutoshi Tomita, Faculty of Science, Kyoto University for theuse of the Rigaku AFC-5 diffractometer. They also wish to express their sincere thanks to Dr. Tsuneyuki Higashi for his valuable advices.

References

1) a) D. L. Cullen, E. F. Meyer, Jr., T. S. Srivastava, and M. Tsutsui, *J. Chem. Soc., Chem. Commun.*, **1972**, 584; b) J. J. Bonnet, S. S. Eaton, G. R. Eaton, R. H. Holm, and J. A. Ibers, *J. Am. Chem. Soc.*, **95**, 2141 (1973); c) R. G. Little and J. A. Ibers, *ibid.*, **95**, 8583 (1973); d) F. R. Hopf, T. P. O'Brien, W. R. Scheidt, and D. G. Whitten, *ibid.*, **97**, 277 (1975); e) R. G. Ball, G. Domazetis, D. Dolphin, B. R. James, and J. Trotter, *Inorg. Chem.*, **20**, 1556 (1981).

2) H. Masuda, T. Taga, K. Osaki, H. Sugimoto, M. Mori, Z. Yoshida, and H. Ogoshi, *J. Am. Chem. Soc.*, **103**, 2199 (1981).

3) H. Sugimoto, T. Higashi, M. Mori, M. Nagano, Z. Yoshida, and H. Ogoshi, *Bull. Chem. Soc. Jpn.*, **55**, 822(1982).

4) a) "International Tables for X-Ray Crystallography," ed by J. A. Ibers and W. C. Hamilton, Kynoch Press, Birmingham, England (1974), Vol. IV, p. 99; b) *ibid.*, p. 148.

5) J. L. Hoard, "Porphyrins and Metalloporphyrins," ed by K. M. Smith, Elsevier, Amsterdam (1975), Chap. 8; J. L. Hoard, *Science*, **174**, 1295 (1971); W. R. Scheidt, *Acc. Chem. Res.*, **10**, 339 (1977).

6) A. M. Mathieson, D. P. Mellor, and N. C. Stephenson, *Acta Crystallogr.*, **5**, 185 (1952).

7) W. R. Scheidt and M. E. Frisse, *J. Am. Chem. Soc.*, **97**, 17 (1975); W. R. Scheidt and P. L. Piciulo, *ibid.*, **98**, 1913 (1976); W. R. Scheidt, A. C. Brineger, E. B. Ferro, and J. F. Kirner, *ibid.*, **99**, 7315 (1977).

8) W. C. Hamilton, *Acta Crystallogr.*, **12**, 609 (1959).

The Crystal and Molecular Structure of Six-coordinate Intermediate-spin Porphinatoiron(III) Complex. (Octaethylporphinato)-bis(tetrahydrofuran)iron(III) Perchlorate

Hideki Masuda,* Tooru Taga, Kenji Osaki, Hiroshi Sugimoto,†
Zen-ichi Yoshida,†† and Hisanobu Ogoshi*,†††
Faculty of Pharmaceutical Sciences, Kyoto University, Shimoadachi-cho, Yoshida, Sakyo-ku, Kyoto 606
†*Faculty of Science, Osaka City University, Sugimoto-cho, Sumiyoshi-ku, Osaka 558*
††*Department of Synthetic Chemistry, Kyoto University, Honmachi, Yoshida, Sakyo-ku, Kyoto 606*
†††*Department of Materials Science and Technology, Technological University of Nagaoka, Kamitomioka, Nagaoka 949-54*

(Received January 9, 1982)

The crystal structure of (octaethylporphinato)bis(tetrahydrofuran)iron(III) perchlorate was determined by the X-ray method. The complex crystallizes in the monoclinic space group C2/m, $a=13.916(3)$ Å, $b=16.509(3)$ Å, $c=10.659(5)$ Å, $\beta=118.18(1)°$, and $Z=2$. The structure was solved by the direct method and refined by the full-matrix least-squares method. The final R value was 0.079 for 597 reflections. The complex has a crystallographically imposed twofold axis and a mirror of symmetry. The porphinato core is planar within 0.06 Å. The iron(III) ion lies at the center of the octahedron formed by the four porphinato nitrogen atoms and the two tetrahydrofuran oxygen atoms. The axial Fe–O distance, 2.187(11) Å, is considerably longer than the reported distances for high-spin porphinatoiron(III) complexes, while the equatorial Fe–N distance, 1.978(12) Å, is comparable to those for low-spin and intermediate-spin porphinatoiron(III) complexes. The Fe–O and Fe–N bond distances are well explained in terms of an intermediate-spin state of the iron(III) ion.

The existence of an intermediate-spin state ($S=3/2$) with the outer electron configuration $(d_{xy})^2(d_{yz})(d_{xz})(d_{z^2})$ in iron(III) porphyrins has been progressively recognized, since Maltempo *et al.*[1] suggested a possibility of the quantum-mechanically mixed spin state of iron(III) ($S=3/2$ and 5/2) to explain anomalous magnetic properties of ferricytochrome c′. Since Dolphin *et al.*[2] assigned octaethylporphinatoiron(III) perchlorate, [Fe(III)(oep)]ClO_4, as an intermediate-spin complex, several synthetic intermediate-spin porphinatoiron(III) complexes were reported[3] on the basis of magnetic susceptibility, ESR spectra, and Mössbauer spectra. So far six structures of the intermediate-spin or probably its admixed spin state complexes have been studied by the X-ray method.[3a,3b,3d,4,5] Through these studies, the structures of the intermediate-spin complexes were characterized by the short Fe–N distance resembling those of low-spin derivatives and the long Fe–O distance rather than those of low- and high-spin derivatives. In an X-ray study of diaquatetraphenylporphinatoiron(III) cation, [Fe(III)(tpp)$(H_2O)_2$]$^+$,[3a,6a] Scheidt *et al.*[3d] claimed that if the axial Fe–O bond distances were increased to some values greater than 2.09 Å, the complex would become an intermediate-spin complex. The critical Fe–ligand distance to distinguish the intermediate-spin state from others is, however, still not clear. The title (octaethylporphinato)bis(tetrahydrofuran)iron(III) perchlorate, [Fe(III)(oep)$(thf)_2$]ClO_4, has recently been prepared by Ogoshi *et al.*,[3c] and from their magnetic and spectroscopic studies the single intermediate-spin state was certainly assigned for this complex. Then, the Fe(III)–O(thf) distance in this complex was anticipated to give a typical Fe(III)–O distance for a pure $S=3/2$ iron(III), so that we took up this complex for the present X-ray study.

Experimental

[Fe(III)(oep)$(thf)_2$]ClO_4 was prepared by adding thf to [Fe(III)(oep)]ClO_4 in CH_2Cl_2.[3c] Dark-violet, plate-like single crystals were obtained by recrystallization from a thf solution. A preliminary X-ray photographic examination established a monoclinic unit cell containing two chemical units of [Fe(III)(oep)$(thf)_2$]ClO_4. The systematic absences of hkl for $h+k=2n+1$ led to three possible space groups C2/m, Cm, and C2. The unit cell dimensions, $a=13.916(3)$ Å, $b=16.509$ (3) Å, $c=10.659(5)$ Å, and $\beta=118.18(1)°$, were determined by the least-aquares refinement of setting angles of 47 reflections on a Rigaku AFC-5 diffractometer with graphite-monochromated Mo $K\alpha$ radiation ($\bar{\lambda}=0.71073$ Å). $D_x=1.28$ g/cm^3 and $D_m=1.24$ g/cm^3 (by flotation in aqueous calcium chloride solution).

Intensity data of 2212 reflections in the range $2\theta<50°$ were collected in the ω-2θ scan mode with a scan rate of 5° min^{-1} by the use of a crystal with dimensions of $0.2\times0.2\times0.1$ mm^3. The crystal was gradually damaged by X-ray exposure, so that the intensities were corrected by standard measurements of three reflections every 60 reflections. The intensity decline of the standard reflections throughout the measurements was about 20%. In view of a large systematic error caused by the crystal damage, 597 reliable data ($|F_o|>5\sigma(|F_o|)$) were used for the analysis. No absorption correction was applied ($\mu=4.59$ cm^{-1} for Mo $K\alpha$).

The structure was solved by the heavy atom method. The space group C2/m was tentatively assumed and successive Fourier syntheses revealed the approximate structure. The block-diagonal least-squares refinements to examine the three possible space groups, C2/m, C2, and Cm, resulted in rejection of the space groups C2 and Cm because these space groups gave several wrong positional shifts from the normal bond lengths and angles and non-positive temperature factors for some light atoms. Several cycles of refinement including the anisotropic thermal parameters were carried out to convergence with the weighting scheme of $w=1/\sigma(F_o)^2$. The hydrogen atoms were included as a fixed contribution in the last cycle: their positions were assumed to be in accord with the idealized geometry (C–H=1.00 Å), and their temperature factors were assumed

Table 1. Positional and thermal parameters for the atoms of $[Fe^{III}(oep)(thf)_2]ClO_4$

Atom	x[a)]	y[a)]	z[a)]	B_{eq}[b)]/Å^2
Fe	0.0	0.0	0.0	3.26
N	−0.0610(8)	0.0844(6)	0.0739(10)	3.08
C(1)	−0.0525(10)	0.1673(8)	0.0670(12)	3.69
C(2)	−0.1086(10)	0.2084(10)	0.1355(14)	4.05
C(3)	−0.1536(10)	0.1503(9)	0.1788(14)	4.21
C(4)	−0.1245(10)	0.0768(9)	0.1401(14)	4.15
C(5)	−0.1518(15)	0.0	0.1658(20)	4.13
C(6)	0.0	0.2030(10)	0.0	4.05
C(7)	−0.1076(10)	0.2983(9)	0.1537(14)	3.94
C(8)	−0.2250(10)	0.1630(8)	0.2492(14)	4.41
C(9)	−0.0047(11)	0.3283(8)	0.2843(14)	5.82
C(10)	−0.1623(12)	0.1642(10)	0.4054(17)	9.26
O(T)	0.1507(11)	0.0	0.2025(15)	5.74
C(11)	0.2513(29)	0.0317(28)	0.2336(34)	8.95
C(12)	0.3281(24)	0.0311(25)	0.3781(37)	7.97
C(13)	0.2796(30)	−0.0336(20)	0.4375(32)	7.83
C(14)	0.1670(25)	−0.0395(28)	0.3274(37)	11.46
Cl	0.0326(19)	0.5000	0.0187(19)	9.62
O(1)	0.0855(29)	0.5000	0.1663(38)	11.75
O(2)	0.0876(28)	0.5000	−0.0697(46)	11.73
O(3)	−0.0280(25)	0.5667(13)	−0.0309(33)	8.72

a) Estimated standard deviations in the least significant figure(s) are given in parentheses. b) B_{eq} is the equivalent isotropic temperature factor defined by Hamilton.[11]

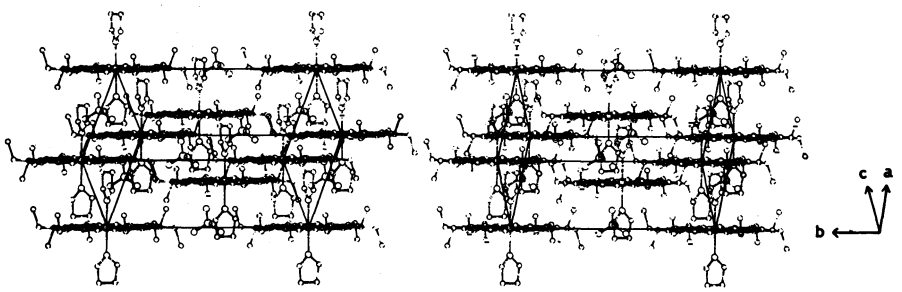

Fig. 1. Stereoscopic view of the crystal structure of $[F_e^{III}(oep)(thf)_2]ClO_4$.

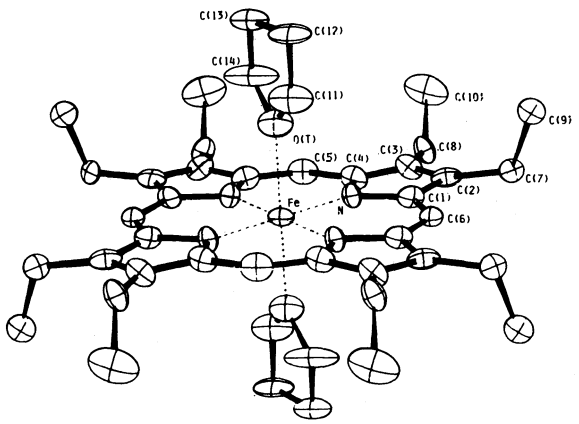

Fig. 2. Computer-drawn model in perspective of the $[Fe^{III}(oep)(thf)_2]^+$ cation. The vibrational ellipsoids are drawn at the 30% probability level. The labeling scheme used for the atoms in the molecule is also shown.

to be isotropical (B=8.00 Å). The final R value was 0.079. The final difference Fourier map showed the high peak (*ca.* 0.6 electron/Å^3) to remain around the disordered perchlorate anion, but it was judged to be essentially featureless.

Atomic scattering factors[7a)] and anomalous terms[7b)] were taken from the International Tables for X-Ray Crystallography. All computations were performed on a FACOM M-200 computer at the Data Processing Center of Kyoto University by using the program system KPAX.

Results

The atomic parameters for all atoms except hydrogen atoms are listed in Table 1. Tables of anisotropic temperature factors for non-hydrogen atoms, positional parameters for hydrogen atoms, and observed and calculated structure factors are kept as a Document No. 8255 at the Chemical Society of Japan.

As shown in Fig. 1, the crystal structure consists of the discrete $[Fe(III)(oep)(thf)_2]^+$ cations and perchlorate anions packed in layers parallel to the (001) plane. The layers are stacked with van der Waals contacts along the c axis. The plane normal to all the porphinato rings is in the approximate [101] direction.

A stereographic view of $[Fe(III)(oep)(thf)_2]^+$ cation is provided in Fig. 2. The numbering scheme of the porphyrin is given in Figs. 2 and 3. The iron atom exists

TABLE 2. BOND DISTANCES AND ANGLES FOR [Fe^{III}(oep)(thf)$_2$]ClO$_4$[a)]

Bond distance	l/Å	Bond distance	l/Å
Fe–N	1.978(12)	O(T)–C(11)	1.38(4)
Fe–O(T)	2.187(11)	O(T)–C(14)	1.40(4)
N–C(1)	1.38(2)	C(11)–C(12)	1.40(4)
N–C(4)	1.37(2)	C(13)–C(14)	1.45(4)
C(1)–C(2)	1.46(2)	C(12)–C(13)	1.55(6)
C(3)–C(4)	1.40(2)	Cl–O(1)	1.39(3)
C(2)–C(3)	1.34(2)	Cl–O(2)	1.47(5)
C(4)–C(5)	1.39(2)	Cl–O(3)	1.34(2)
C(1)–C(6)	1.37(2)		
C(2)–C(7)	1.50(2)		
C(3)–C(8)	1.52(3)		
C(7)–C(9)	1.53(2)		
C(8)–C(10)	1.47(2)		
Bond angle	ϕ/°	**Bond angle**	ϕ/°
N–Fe–N′	90.5(5)	O(T)–Fe–N	89.9(4)
N–Fe–N″	180.0(6)	O(T)–Fe–N′	90.1(4)
N–Fe–N‴	89.5(5)	Fe–O(T)–C(11)	128.9(18)
Fe–N–C(1)	127.9(11)	Fe–O(T)–C(14)	126.0(16)
Fe–N–C(4)	129.9(9)	C(11)–O(T)–C(14)	104.9(33)
C(1)–N–C(4)	102.2(12)	O(T)–C(11)–C(12)	115.0(36)
N–C(1)–C(2)	110.8(14)	O(T)–C(14)–C(13)	111.5(33)
N–C(4)–C(3)	114.7(13)	C(11)–C–(12)C(13)	101.6(29)
N–C(1)–C(6)	122.3(14)	C(12)–C(13)–C(14)	103.2(27)
N–C(4)–C(5)	119.2(15)	O(1)–Cl–O(2)	124.7(22)
C(1)–C(2)–C(3)	106.6(14)	O(1)–Cl–O(3)	110.3(17)
C(2)–C(3)–C(4)	105.7(15)	O(2)–Cl–O(3)	99.7(19)
C(2)–C(1)–C(6)	126.9(13)	O(3)–Cl–O(3)′	111.2(20)
C(3)–C(4)–C(5)	126.1(17)		
C(3)–C(2)C(7)	130.0(16)		
C(2)–C(3)–C(8)	126.4(14)		
C(1)–C(2)–C(7)	123.4(15)		
C(4)–C(3)–C(8)	127.8(14)		
C(2)–C(7)–C(9)	112.7(10)		
C(3)–C(8)–C(10)	112.7(12)		
C(1)–C(6)–C(4)′	117.6(11)		
C(4)–C(5)–C(1)‴	118.8(15)		

a) Estimated standard deviations are in parentheses. The one-primed atom notes the atom translated by mirror plane. The two-primed atom notes the atom translated by twofold axis. The three-primed atom notes the atom translated by twofold and mirror plane.

at the center of symmetry, and lies on the plane of the oep macrocycle. The four porphinato nitrogens and the two oxygen atoms of thf molecules complete a deformed octahedron. The porphinato core is planar within 0.06 Å. The C(5) atom lies on the mirror plane and the C(6) atom lies on a twofold axis. The orientation of the ethyl groups attached to the core is similar to that in [Fe(III)(oep)]ClO$_4$.[4a)]

Bond distances and bond angles are given in Table 2. The axial Fe–O(thf) distance, 2.187(11) Å, is considerably longer than the sum of ionic radii for high-spin Fe(III) (0.65 Å) and O (1.40 Å),[10)] and is also larger than those of typical high-spin six-coordinate porphinatoiron(III) complexes, [Fe(III)(tpp)(tetrahydrothiophene 1-oxide)$_2$]$^+$ (average 2.078 Å)[6b)] and [Fe(III)(tpp)(H$_2$O)$_2$]$^+$ (average 2.095 Å).[3a,6a)] It is rather close to those in the mixed (S=5/2, 3/2) or high-spin [Fe(III)(oep)(EtOH)$_2$]$^+$ (average 2.137 Å)[5a)] and [Fe(III)(tpp)(EtOH)$_2$]$^+$ (2.142 Å).[5b)] The Fe–N bond distance, 1.978(12) Å, is significantly shorter than those of typical high-spin six-coordinate complexes, diaquatetraphenylporphinatoiron(III) cation ([Fe(III)(tpp)(H$_2$O)$_2$]$^+$) (average 2.045 Å)[3a,6a)] and [Fe(III)(tpp)(tetrahydrothiophene 1-oxide)$_2$]$^+$ (average 2.045 Å).[6b)] It is, however, in agreement with those observed in intermediate-spin [Fe(III)(tpp)C(CN)$_3$] (average 1.995 Å),[3d)] and is also comparable with those of typical low-spin six-coordinate porphinatoiron(III) complexes, [Fe(III)(tpp)(imidazole)$_2$]$^+$ (average 1.989 Å)[9a)] and [(protoporphyrin IX)iron(III)(1-methylimidazole)$_2$]$^+$ (average 1.991 Å),[9b)] and [Fe(III)(tpp)(CN)$_2$]$^-$ (average 2.000 Å).[9c)]

The thf molecule lies approximately on the mirror plane *xoz*. The O(T) atom exactly lies on the mirror plane, but the C(11), C(12), C(13), and C(14) atoms are disordered out of the mirror plane with 1/2 occupancy. The large thermal motion of the thf ligand presumably permits a number of possible conformations including the twisting form with an approximate C2 symmetry. The average C–O bond distance of 1.391 Å

Table 3. Comparison of average bond parameters, magnetic moments, and Mössbauer parameters of some intermediate-spin iron(III) porphinato complexes

Complex	Spin state	Bond parameters (l/Å) Fe–N	Fe–Ct[a]	Fe–L	ESR g-values	Magnetic moment μ_B/BM	Mössbauer parameters[b] ε/mm s^{-1}	ΔE_Q/mm s^{-1}	T/K	Ref.
5-Coordinate complexes										
$[Fe^{III}(tpp)]ClO_4$· 0.5 *m*-xylene	{3/2, 5/2}	2.001	0.28	2.029 $L=ClO_4$	$g_{//}=2.03$ $g_\perp=4.75$ at 10 K	4.5—5.3 at 298 K	0.38	3.50	4.2	3a
							0.38	3.48	77	
							0.34	3.17	195	
							0.30	2.79	295	
$[Fe^{III}(tpp)]ClO_4$· 0.5 toluene	{3/2, 5/2}	1.997	0.27	2.025 $L=ClO_4$	—	4.1 at 40 K 5.0 at 297 K	0.39	3.4	4.2	3b
$[Fe^{III}(oep)]ClO_4$	3/2	1.994	0.26	2.067 $L=ClO_4$	$g_{//}=1.48$ $g_\perp=5.83$ at 77 K $g=3.91$ at 295 K	4.16 at 77 K 4.78 at 295 K	0.40	3.54	4.2	3c,4a
							0.39	3.57	77	
							0.31	3.14	298	
$[Fe^{III}(oep)]ClO_4$	3/2	—	—	—	—	4.5 at 295 K	0.37	3.57	4.2	2
							0.37	3.52	115	
							0.29	3.16	295	
6-Coordinate complexes										
$[Fe^{III}(oep)(EtOH)_2]ClO_4$	3/2	—	—	—	—	4.1 at 84 K 4.2 at 127 K 4.4 at 191 K 4.8 at 275 K	0.38	3.47	4.2	2
							0.36	3.32	115	
							0.29	2.97	295	
$[Fe^{III}(oep)(EtOH)_2]ClO_4$·EtOH	{3/2, 5/2} or 5/2	2.036	≈0	2.137 L=EtOH	—	—	—	—	—	5a
$[Fe^{III}(tpp)(EtOH)_2]BF_4$	5/2	2.027	≈0	2.142 L=EtOH	$g_{//}=2$ $g_\perp=6$ at 77 K	5.9 at 4—100 K	0.42	1.89	4.2	5b
$[Fe^{III}(tpp)C(CN)_3]$	3/2	1.995	≈0	2.217 $L=C(CN)_3$	$g_{//}=2.00$ $g_\perp=5.26$ at 78 K	5.4 at 78—298 K 5.1 at 78—298 K in $CHCl_3$	0.30	3.03	78	3d
							0.30	3.18	298	
$[Fe^{III}(oep)(thf)_2]ClO_4$	3/2	1.978	≈0	2.187 L=thf	$g=4.61$ at 77 K $g=3.86$ at 298 K $g_{//}=2.00$ $g_\perp=4.68$ at 77 K in CH_2Cl_2	4.21 at 77 K 4.73 at 275 K	0.42	3.34	77	This work
							0.31	3.04	298	

a) Relative to Fe metal. b) C_t notes the center of four nitrogen atoms.

and the average C–C bond distance of 1.467 Å are within the range of those for the metal coordinated thf molecules.[8]

The perchlorate anion is disordered around the center of symmetry. The Cl, O(1), and O(2) atoms lie on the mirror plane, and the O(3) atom exists at a general position. The perchlorate anion is surrounded by the six $[Fe(III)(oep)(thf)_2]^+$ cations, and the short intermolecular distances are 3.295 Å between O(3) and C(5), and 3.417 Å between O(2) and C(11).

Discussion

The bond distances and bond angles observed in several intermediate-spin iron(III)-porphyrins are listed in Table 3. Data of ESR spectra, effective magnetic moments, and Mössbauer spectra are also included in Table 3. The ESR spectrum of $[Fe(III)(oep)(thf)_2]ClO_4$ shows one broad signal at $g=4.16$ in the solid state, and the anisotropic $g_{//}$ and $g_\perp$ values are quite different from those of the usual high-spin complex ($g_{//}=2$, $g_\perp=6$) and those of the low-spin complexes ($g=2.2$—2.8). The effective magnetic moments, μ_{eff}, of 4.21 μ_B at 77 K and 4.73 μ_B at 275 K[3c] are close to 3.87 μ_B calculated for $S=3/2$ rather than to 5.92 or to 1.73 μ_B for $S=5/2$ or 1/2, respectively. The large quadrupole splitting in the Mössbauer spectrum eliminates both possibilities of a low-spin complex and a high-spin complex. Hence, these spectroscopic data suggest that the iron(III) complex has a pure $S=3/2$ ground state.

Generally, a low-spin six-coordinated iron(III)-porphyrin becomes a high-spin complex when the axial ligand is replaced by a more weakly interacting ligand.[3b] In this case, both the axial and equatorial bond distances

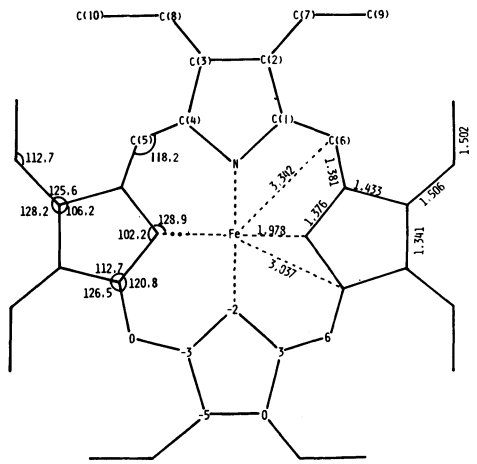

Fig. 3. Formal diagram of the porphinato skeleton in [Fe^{III}(oep)(thf)$_2$]ClO$_4$ molecule. On the top of the diagram, the numbering scheme for the atoms is displayed. On the right-hand side and left-hand side of the diagram, the chemically equivalent bond distances and angles. On the bottom of the diagram, the numbering symbol for each atom is replaced by its perpendicular displacement, in units of 0.01 Å, from the mean plane of the porphinato core.

increase without change of the octahedral symmetry around the central metal ion. If the axial ligand becomes very weak, the axial bond distance is further increased, while the equatorial distance is decreased, and then the octahedral symmetry falls down to the lower D_{4h} symmetry. The intermediate-spin state may be arisen in this situation. Scheidt *et al.*[6a] gave 2.096 Å for the critical Fe–O distance in the transition from the high-spin to intermediate-spin state. The Fe–O distance of 2.137 Å has, however, been observed in the quantum mechanically $S=5/2$ and 3/2 mixed spin complex, [Fe(III)(oep)(EtOH)$_2$]$^+$,[5a] and the Fe–O distance of 2.142 Å was reported for a high-spin complex [Fe(III)-(tpp)(EtOH)$_2$]$^+$.[5b] The present Fe–O(thf) distance of 2.187 Å is longer than these Fe–O distances. The long axial Fe–O distance and short equatorial Fe–N distance strongly suggest that this complex has a pure intermediate-spin state, since in view of the stability of chemical bonds, the vacant $d_{x^2-y^2}$ and singly occupied d_{z^2} orbital levels in the intermediate-spin state are consistent with the long axial and short equatorial bond distances. Hence the Fe–O distance of 2.187 Å observed here may be a typical Fe–O distance for a pure $S=3/2$ state.

For cytochrome c′ it has been believed that its protein ligation to heme occurs at the fifth coordination site through the histidine residue,[12] and that the π-bonding mode of the ligation is definitely related to the function of hemoproteins. In the synthetic intermediate-spin complexes as a model heme for cytochrome c′, however, the weak σ-characterisities of the axial ligands seems to play an important role in the intermediate-spin complex formation, and the weakness of the ligand field strength may be necessary for the occurrence of the intermediate-spin states. Therefore, the coordination aspect in the cytochrome c′ may be speculated by the electronically weak bonding of histidine as in the manner of a long Fe–imidazole N distance and/or of a large tilting angle of histidine with respect to the porphinato core of heme.

The authors wish to thank Professor Nobuo Morimoto and Dr. Katsutoshi Tomita, Faculty of Science, Kyoto University, for the use of the Rigaku AFC-5 diffractometer.

References

1) M. M. Maltempo, *J. Chem. Phys.*, **61**, 2540 (1974); M. M. Maltempo, T. H. Moss, and M. A. Cusanovich, *Biochim. Biophys. Acta*, **342**, 290 (1974); M. M. Maltempo, *ibid.*, **379**, 97 (1975).

2) D. H. Dolphin, J. R. Sams, and T. B. Tsin, *Inorg. Chem.*, **16**, 711 (1977).

3) a) M. E. Kastner, W. R. Scheidt, T. Mashiko, and C. A. Reed, *J. Am. Chem. Soc.*, **100**, 666 (1978); b) C. A. Reed, T. Mashiko, S. P. Bentley, M. E. Kastner, W. R. Scheidt, K. Spartalian, and G. Lang, *ibid.*, **101**, 2948 (1979); c) H. Ogoshi H. Sugimoto, and Z. Yoshida, *Bull. Chem. Soc. Jpn.*, **54**, 3414, (1981); d) D. A. Summerville, I. A. Cohen, K. Hatano, and W. R. Scheidt, *Inorg. Chem.*, **17**, 2906 (1978).

4) H. Masuda, T. Taga, K. Osaki, H. Sugimoto, Z. Yoshida, and H. Ogoshi, *In org. Chem.*, **19**, 950 (1980).

5) a) F. W. B. Einstein and A. C. Willis, *Inorg. Chem.*, **17**, 3040 (1978); b) P. Gans, G. Buisson, E. Duie, J. R. Regnard, and J. C. Marchon, *J. Chem. Soc., Chem. Commun.*, **1979**, 393.

6) a) W. R. Scheidt, I. A. Cohen, and M. E. Kastner, *Biochemistry*, **18**, 3546 (1979); b) T. Mashiko, M. E. Kastner, K. Spartalian, W. R. Scheidt, and C. A. Reed, *J. Am. Chem. Soc.*, **100**, 6354 (1978).

7) a) "International Tables for X-Ray Crystallography," ed by J. A. Ibers and W. C. Hamilton, Kynoch, Birmingham, England (1974), Vol. IV, p. 99; b) *ibid.*, p. 148.

8) D. J. Brauer and C. Kruger, *Inorg. Chem.*, **14**, 3053 (1975); K. O. Hodgson and K. N. Raymond, *ibid.*, **11**, 171 (1972); D. J. Brauer and G. D. Stucky, *J. Organomet. Chem.*, **37**, 217 (1972); D. J. Brauer and C. Kruger, *ibid.*, **42**, 129 (1972); J. L. Atwood and K. D. Smith, *J. Chem. Soc., Dalton Trans.*, **1974**, 921; J. J. Daly and R. P. A. Sneeden, *J. Chem. Soc., A*, **1967**, 736; C. A. Reed, T. Mashiko, W. R. Scheidt, K. Spartalian, and G. Lang, *J. Am. Chem. Soc.*, **102**, 2302 (1980).

9) a) D. M. Collins, R. Counterman, and J. L. Hoard, *J. Am. Chem. Soc.*, **94**, 2066 (1972); b) R. G. Little, K. R. Dymoch, and J. A. Ibers, *ibid.*, **97**, 4532 (1975); c) W. R. Scheidt, K. J. Haller, and K. Hatano, *ibid.*, **102**, 3017 (1980).

10) A. F. Wells, "Structural Inorganic Chemistry," Oxford University Press, New York (1975), p. 259.

11) W. C. Hamilton, *Acta Crystallogr.*, **12**, 609 (1959).

12) P. C. Weber, R. G. Bartsch, M. A. Cusanovich, R. C. Hamilton, A. Howard, S. R. Jordan, M. D. Kaman, T. E. Meyer, D. W. Weatherford, Ng. H. Xuong, and F. R. Salemme *Nature (London)*, **286**, 302 (1980).

Stabilization Energy and Spin Distribution in Pyrenophane Cation Radicals

Atsushi TERAHARA,* Hiroaki OHYA-NISHIGUCHI, Noboru HIROTA, Yoshiteru SAKATA,† Soichi MISUMI,† and Kazuhiko ISHIZU††

Department of Chemistry, Faculty of Science, Kyoto University, Sakyo-ku, Kyoto 606
†*The Institute of Scientific Industrial Research, Osaka University, Suita, Osaka 565*
††*Department of Chemistry, Faculty of Science, Ehime University, Matsuyama 790*

(Received January 20, 1982)

The cation radicals of three [2.2]pyrenophanes in which two pyrene moieties are twisted each other by 0°, 35°, and 60° were investigated by ESR, ENDOR, and cyclic voltammetry. Considerable variations of the spin density distribution and the stabilization energy with the twisting angle have been observed. The obtained results are discussed in terms of modified Hückel-McLachlan type calculation.

A number of dimer cation radicals of aromatic hydrocarbons have been observed by electron spin resonance (ESR).[1-3] From the analysis of the hyperfine coupling constants (hfcc) it was confirmed that the unpaired electrons in the dimer cation radicals are distributed equally over the two aromatic moieties. Based on the ESR results and theoretical calculations it has been postulated that these dimer cations have eclipsed configurations in which one moiety lies upon the top of the other symmetrically.

On the other hand, X-ray studies indicate that the aromatic cation radical salts $(Ar)_2^{+\cdot}X^-$ ($X=PF_6$) have twisted configurations with the twisting angles of 90° and 180°.[4] These observations show that the dimer configuration is very sensitive to the environment. Thus it is of interest to examine how the orbital energy and spin distribution vary with configuration.

In this work, we have measured the ESR, ENDOR (electron nuclear double resonance) spectra and the oxidation potentials of three [2.2]pyrenophanes, **1** to **3**, shown in Fig. 1. From their molecular models the twisting angles between the upper and lower pyrene moieties (θ) are estimated to be 0°, 35°, and 60° in **1**, **2**, and **3**, respectively. The obtained results are discussed based on a simple molecular orbital calculation of the spin density distributions and the orbital energies of the highest occupied molecular orbitals (HOMO) as a function of θ.

Experimental

Synthetic methods of the compounds **1** to **3** were reported elsewhere.[5] The cation radicals were generated by oxidation with CF_3COOH or CF_3COOD in CH_2Cl_2, or by electrochemical oxidation. The oxidation potentials ($E^\circ_{1/2}$) were measured by cyclic voltammetry (CV). Further experimental details were similar to those described previously.[3,6]

Results and Discussion

In Fig. 1 are shown the ENDOR spectra of $\mathbf{1}^{+\cdot}$, $\mathbf{2}^{+\cdot}$, and $\mathbf{3}^{+\cdot}$ observed at −85 °C. The obtained hfcc are given in Table 1 with those of pyrene dimer cation radical ($\mathbf{P}_2^{+\cdot}$).[1] The ESR spectra of $\mathbf{1}^{+\cdot}$ and $\mathbf{3}^{+\cdot}$ measured at −65 °C were well resolved but that of $\mathbf{2}^{+\cdot}$ was only partially resolved. These ESR spectra were all reconstructed well by the computer simulation using the hfcc obtained from the ENDOR spectra. The observed and simulated ESR spectra of $\mathbf{3}^{+\cdot}$, for example, are shown in Fig. 2. For the help of assignment, we also measured the ESR spectra of $\mathbf{1}^{+\cdot}$, $\mathbf{2}^{+\cdot}$, and $\mathbf{3}^{+\cdot}$ which were oxidized by excess amounts of CF_3COOD instead of CF_3COOH. Their ESR spectra clearly showed the hyperfine splittings due to deuterons exchanged with the ring protons with the hfcc larger than about 2.0 G.** It is known that no H–D exchange takes place for the protons of the alkyl groups by CF_3COOD.[7] The hfcc of protons exchanged by deuterons are indicated in Table 1.

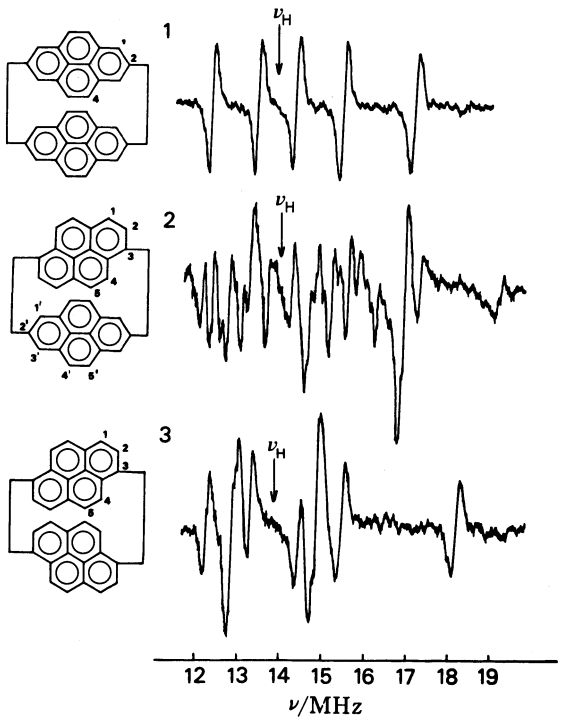

Fig. 1. Molecular structures and ENDOR spectra of three [2.2]pyrenophanes, **1** to **3**.

The hfcc of $\mathbf{1}^{+\cdot}$ are similar to those of $\mathbf{P}_2^{+\cdot}$ and can be assigned easily. Therefore, $\mathbf{1}^{+\cdot}$ can be regarded as a good model for $\mathbf{P}_2^{+\cdot}$. The hfcc of $\mathbf{2}^{+\cdot}$ and $\mathbf{3}^{+\cdot}$, however, are different from those of $\mathbf{1}^{+\cdot}$ and $\mathbf{P}_2^{+\cdot}$ and cannot be assigned uniquely because of the presence of a large

** 1 G=10^{-4} T.

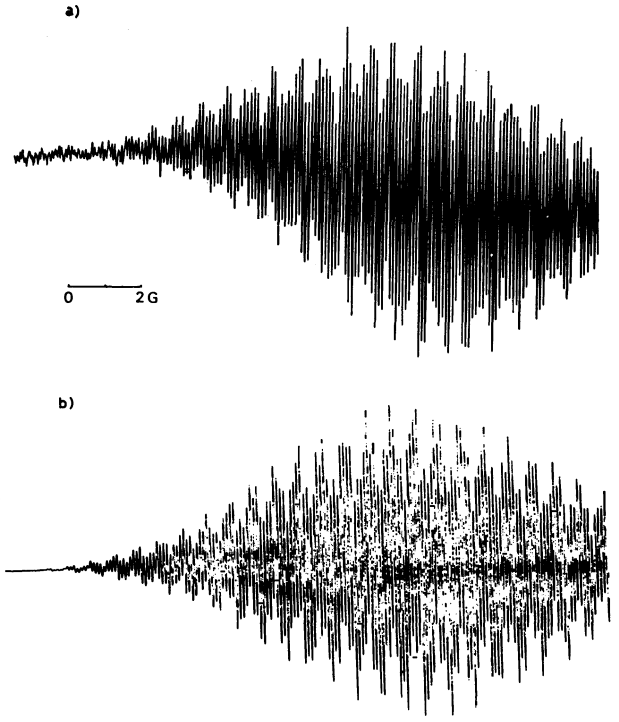

Fig. 2. The observed (a) and simulated (b) ESR spectra of $3^{+\cdot}$.

number of hfcc. It should be noted here that the largest hfcc of $2^{+\cdot}$ and $3^{+\cdot}$, 3.702 G and 3.080 G, respectively, are much larger than that of $1^{+\cdot}$, 2.342 G. This fact indicated that a considerable redistribution of the spin density takes place in $2^{+\cdot}$ and $3^{+\cdot}$.

We also measured the oxidation potentials ($E^{\circ}_{1/2}$) of these compounds by the CV technique to investigate the energy changes due to the twisting. $E^{\circ}_{1/2}$ of pyrene and **1** to **3** are also shown in Table 1. $E^{\circ}_{1/2}$ of **1** is 0.81 V, being lower than that of **P** by 0.41 V because of the transannular interaction, as we reported previously in the case of multilayered compounds.[3] On the other hand, $E^{\circ}_{1/2}$ of **2** was appreciably higher than that of **1**. This increase is likely to be caused by the reduction of the resonance integral due to the twisted structure of **2**. Such a reduction of the stabilization energy has also been observed in the photoelectron spectra of several twisted naphthalenophanes.[8] However, $E^{\circ}_{1/2}$ of **3** becomes comparable to that of **1** (0.80 V) in spite of its twisted structure.

In order to clarify the effects of the twisting angle in the dimer structure we calculated the spin density and the orbital energy by modified Hückel-McLachlan's method. We carried out the calculation with the assumption that the resonance integrals between the upper and lower atoms of pyrene moieties (β_{1-u}) are proportional to the $2p\sigma$-$2p\sigma$ type overlap integral between the upper and lower carbon atoms (S_{1-u}) and are given by[9]

$$\beta'_{1-u} = A \cdot S_{1-u} \cdot \beta_{C-C}, \qquad (1)$$

where A is the proportionality constant. Two pyrene moieties were assumed to be 3.5 Å apart with the molecular planes parallel to each other. The effects

Table 1. The hyperfine coupling constants and the oxidation potentials ($E^{\circ}_{1/2}$) of three pyrenophanes (**1**—**3**) compared with those calculated

	Obsd		Calcd	
	$E^{\circ}_{1/2}$[a]/V	hfcc/G	Energy/β	hfcc/G
$\mathbf{P}_2^{+\cdot}$ (**P**)	(1.22)	(8H)2.659	(0.445)	(1)−2.318
		(8H)1.096		(4)−1.194
		(4H)0.575		(2) 0.705
$\mathbf{1}^{+\cdot}$	0.81	(8H)2.342[b]	0.338	(1)−2.318
		(8H)1.107		(4)−1.195
		(8H)0.316		(2) 0.316[c]
$\mathbf{2}^{+\cdot}$	0.94	(2H)3.702[b]	0.382	(1)−3.904
		(2H)2.390[b]		(4)−2.533
		(2H)2.090[b]		(5)−2.294
		(2H)2.090, (2H)1.653		(3) 2.057[c]
		(2H)1.290, (2H)1.155, (2H)0.840, (2H)0.720, (2H)0.450, (2H)0.130	d)	(2)−0.815, (3′)−0.406, (5′) 0.218, (2′)−0.158[c]
		— —		(4′) 0.153, (1′) 0.137
$\mathbf{3}^{+\cdot}$	0.80	(4H)3.080[b]	0.314	(1)−2.443
		(4H)1.144		(4)−1.259
		(4H)0.704, (4H)0.625	d)	(3) 0.992[c]
		(4H)0.616		(5)−0.979
		(4H)0.440		(2) 0.711

a) Measured at room temperature. Solvent: CH_2Cl_2. Supporting eletrolyte: $(C_4H_9)_4NPF_6$. b) Protons exchanged to deuterons by using CF_3COOD. c) Bridge protons calculated with Q=11 G. d) Assignments of these hfcc are not unique.

of the bridging ethylene groups were taken into account by changing the Coulomb integrals of the carbon atoms ($\alpha_{C'}$) attached by the ethylene groups to $\alpha_{C'}=\alpha_C-0.1\beta$. In the first place, we calculated S_{1-u} in Eq. 1 and estimated β'_{1-u} using the parameter A. Subsequently we calculated the spin density by the McLachlan's method. Hfcc were calculated by using $Q=-25$ G for the ring protons and $Q=11$ G for the bridge protons. The latter value was estimated from the calculated spin density on the bridged carbon atoms and the hfcc of the ethylene protons obtained experimentally for $1^{+\cdot}$. The bridge protons of $2^{+\cdot}$ and $3^{+\cdot}$ are not equivalent with those of $1^{+\cdot}$ because of the torsion of the ethylene groups, but the deviations from the equivalent positions are not so large. Therefore, this value was used for the bridge protons of $2^{+\cdot}$ and $3^{+\cdot}$ in order to make a rough estimate of their hfcc. The calculated hfcc for A=4.0 are given in Table 1.

The agreement between the calculated and observed hfcc in $\mathbf{P}_2^{+\cdot}$ and $1^{+\cdot}$ is very good. The spin density distribution in $1^{+\cdot}$ and $3^{+\cdot}$ does not depend much on the choice of A and the unpaired electron is equally distributed over the two pyrene moieties, whereas the unpaired electron in $2^{+\cdot}$ is almost localized on one moiety (upper moiety in Fig. 1). This is due to the fact

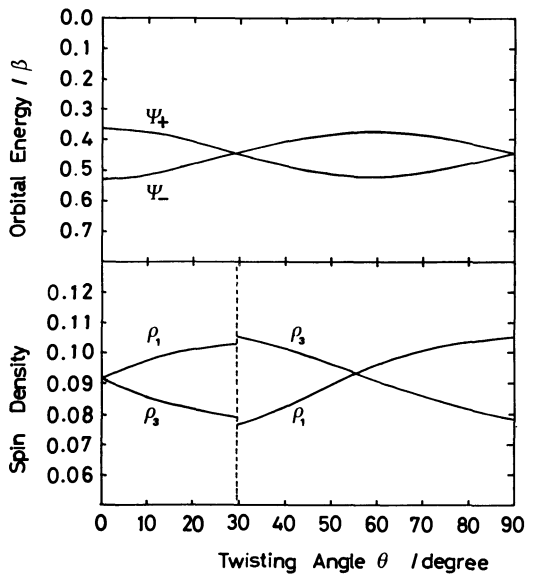

Fig. 3. Twisting angle (θ) dependences of the Hückel orbital energies and the spin densities at positions 1 and 3 in the pyrene dimer cation radical ($\mathbf{P}_2^{+\cdot}$).

that the positions attached by the bridging ethylene groups in the two pyrene moieties of **2** are not equivalent. At $A=4.0$ a fairly good agreement between the observed hfcc of $\mathbf{2}^{+\cdot}$ and the calculated one was obtained in spite of the simple calculation. Comparing the observed hfcc of $\mathbf{2}^{+\cdot}$ and $\mathbf{3}^{+\cdot}$ with those calculated, the largest hfcc of $\mathbf{2}^{+\cdot}$ and $\mathbf{3}^{+\cdot}$, 3.702 G and 3.080 G, respectively, can be assigned both to the protons attached to the position 1 shown in Fig. 1. However, there remains some ambiguities in the assignment of smaller hfcc of $\mathbf{2}^{+\cdot}$ and $\mathbf{3}^{+\cdot}$.

The variation of $E^{\circ}_{1/2}$ and the increase of the spin density on position 1 can be caused by the effect of the twisting and the difference in the position attached by the ethylene groups. It is necessary to decide which is the main cause. In Fig. 3 are shown the dependences of the orbital energies in unit of β and the spin densities on the twisting angle θ, which were obtained by Hückel-McLachlan's method without the effects of the ethylene groups. At $\theta=0°$ the energies of the bonding orbital ϕ_- and antibonding orbital ϕ_+ constructed by the combination of HOMO of the two pyrene moieties are split into two due to the transannular interaction. As θ increases, the energies of these two orbitals approach each other because of the reduction of the resonance stabilization. At $\theta=30°$ the two orbitals invert their energies and the energy of ϕ_- reaches a maximum at $\theta=60°$. The energy of ϕ_- at $\theta=60°$ is almost equal to that of ϕ_+ at $\theta=0°$. The orbital energies of HOMO at 0°, 35°, and 60° calculated including the effects of the ethylene groups are indicated in Table 1 for the sake of comparison. These values are about 0.04β higher than those with the corresponding angles given in Fig. 3. This means that the effect of the ethylene groups to the HOMO only lifts the orbital energies by 0.04β. This behavior corresponds well to the variation of the $E^{\circ}_{1/2}$ of **1** to **3**.

The spin densities on the position 1 and 3, ρ_1 and ρ_3, respectively, also vary with θ as shown in Fig. 3. The spin densities change discontinuously at $\theta=30°$, corresponding to the inversion of the energies of ϕ_+ and ϕ_-. ρ_1 at $\theta=35°$ can be converted to the hfcc of 2.0 G, which is much smaller than 3.702 G obtained experimentally in $\mathbf{2}^{+\cdot}$. On the other hand, the calculated hfcc at position 1 with the bridge effects (Table 1) are close to the experimental values. It is then concluded that the effect of the bridging ethylene groups is the main cause of the large hfcc at position 1 in **2**. ρ_1 at $\theta=60°$ is close to ρ_1 at $\theta=0°$ irrespective of the effects of ethylene groups. However, the largest hfcc obtained experimentally in $\mathbf{3}^{+\cdot}$ (3.080 G) does not agree so well with that calculated (2.443 G).

In conclusion, as the twisting angle θ between the two moieties increases, the spin redistribution occurs because of the change in the resonance integral β'_{1-u} accompanying the loss of the resonance stabilization. As the angle increases further, ϕ_+ and ϕ_- invert their energies and gradually regain the resonance stabilization.

References

1) O. Howarth and G. K. Fraenkel, *J. Am. Chem. Soc.*, **88**, 4514 (1966); *J. Chem. Phys.*, **52**, 1371 (1970).

2) I. C. Lewis and L. C. Singer, *J. Chem. Phys.*, **43**, 2712 (1965).

3) H. Ohya-Nishiguchi, A. Terahara, N. Hirota, Y. Sakata, and S. Misumi, *Bull. Chem. Soc. Jpn.*, **55**, 1782 (1982), and references cited therein.

4) H. P. Fritz, H. Gebauer, P. Friedrich, and U. Schubert, *Angew. Chem., Int. Ed. Engl.*, **17**, 275 (1978); C. Kröhnke, V. Enkelmann, and G. Wenger, *ibid.*, **19**, 912 (1980).

5) a) T. Umemoto, S. Satani, Y. Sakata, and S. Misumi, *Tetrahedron Lett.*, **1975**, 3159; b) T. Kawashima, T. Otsubo, Y. Sakata, and S. Misumi, *ibid.*, **1978**, 5115.

6) H. Ohya-Nishiguchi, *Bull. Chem. Soc. Jpn.*, **52**, 2064 (1979).

7) G. Dallinga, P. J. Smit, and E. L. Mackor, *Mol. Phys.*, **3**, 130 (1960).

8) B. Covač, M. Allan, and E. Heilbronner, *Helv. Chim. Acta*, **64**, 430 (1981).

9) H. Yoshimi and K. Kuwata, *Mol. Phys.*, **23**, 297 (1972).

Brillouin Scattering and Ultrasonic Absorption Measurements of Chloroform-Eicosane Mixtures

Hiroyasu NOMURA,* Hayao SHIMIZU, Yasuharu TANAKA, Shinobu KODA, Toshio OKUNISHI, Shigeo KATO, and Yutaka MIYAHARA

Department of Chemical Engineering, Faculty of Engineering, Nagoya University, Chikusa-ku, Nagoya 464

(Received April 27, 1982)

An apparatus for the accurate measurement of Brillouin scattering of liquids and solutions was constructed using a multi-pass Fabry-Perot interferometer. The Brillouin scattering spectra of chloroform–eicosane mixtures were obtained at various concentrations. The sound velocity dispersion curves of this system could be expressed by a single relaxation equation. With increasing concentration of eicosane, the relaxation frequency shifted to the higher frequency side, but the relaxation strength was independent of concentration. It is concluded that this relaxation was due to the vibrational-translational energy transfers of chloroform molecules due to the collisions between chloroform and eicosane molecules.

The recent development of laser spectroscopy has opened a way to the study of the dynamical nature of molecules, such as the vibrational and reorientational relaxation times in liquid and dissolved states. The Brillouin scattering method in the only technique so far which can give information of the dynamic nature of a substance in the liquid state in the GHz range. This method has attracted the attention of many investigators.

In a previous paper,[1] we reported that the ultrasonic absorption coefficients of solutions of polycarbonate in chloroform were lower than those of solvent chloroform at all frequencies investigated. The negative value of $\Delta\alpha/f^2$ $(=(\alpha/f^2)_{\text{solution}}-(\alpha/f^2)_{\text{solvent}})$, where α is the ultrasonic absorption coefficient, could be interpreted by the shift of the relaxation frequency of chloroform to a higher frequency.

In order to confirm the above interpretation, the relaxation spectra of chloroform solutions must be determined as a function of concentration of solute in the wide frequency range from MHz to GHz. For this purpose, we constructed an apparatus for the accurate measurement of Brillouin scattering of liquids and solutions, using a multi-pass Fabry-Perot interferometer and measured the sound velocity and attenuation of chloroform solutions in the GHz region. In addition, the ultrasonic absorption coefficients of the same solutions were measured in the MHz region.

Eicosane was chosen as a solute for the following reasons. Eicosane molecule is a linear hydrocarbon containing only twenty methylene groups. One may suppose therefore that the ultrasonic relaxation due to the segmental motion is not observed in the MHz region.[2] Moreover, as the eicosane molecule has no phenyl group which may interact with chloroform molecules, there is no specific interaction between chloroform and eicosane. Therefore, eicosane is a suitable sample in which to investigate the relaxation phenomena of chloroform solutions.

Apparatus and Experimental

Brillouin Scattering Spectrometer. The experimental arrangement of the apparatus is shown in Fig. 1. This is basically the same as used by Stegeman *et al.*[3] and is one of the standard methods for the Brillouin scattering. In the present case, a multi-pass Fabry-Perot interferometer was used. The light source was a helium-neon laser (NEC, GLG 2051) with an output of about 25 mw and it was operated in TEM_{00} mode ($\lambda=632.8$ nm). The beam was focused at the center of the scattering cell by a lens (L_1) and a total reflection mirror (M_1). The scattered light collected by a lens (L_2) was collimated and analyzed by a pressure-scanned triple-pass Fabry–Perot interferometer. The fused quartz plates of the interferometer used were 8 cm in diameter and 1.5 cm thick, and each plate has one surface with flatness $\lambda/200$ and more. This surface was dielectrically coated to reflectivity of 97% at $\lambda=$ 632.8 nm, while the other surface ($\lambda/10$) of the plate had an antireflection coating. The spacers of the interferometer used were 6.04_0, 10.03_1, and 12.02_0 mm long, giving a free spectral range of 24.81_7, 14.94_3, and 12.47_1 GHz, respectively. In operating the interferometer in triple-pass system a pair of total reflection prisms was used. They were arranged with the angle of 120° to each other. All optical parts and instruments were manufactured by Mizojiri Optical Instrument Co., Ltd.

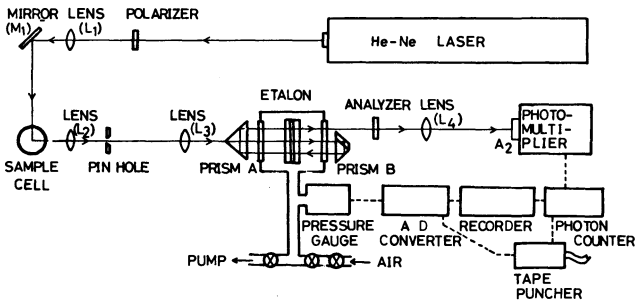

Fig. 1. Block diagram of the experimental set up.

At the beginning of the measurements, the chamber of the interferometer was evacuated with a vacuum pump, then air was introduced into the chamber through a filter, needle valve, and flow controller. The amount of air flow was controlled by a two-step flow control system consisting of two flow control valves (Ohkura Electric Co., Ltd., type CF-221). The pressure in the chamber was detected as a d. c. voltage by means of a piezoelectric pressure gauge (Tokyo Aircraft Instrument Co., Ltd., type TP-310A) and was converted to a digital signal by an AD converter (Takeda Electric. Co., Ltd., type TR-6935). Light incident on the aperture (A_2) was detected by a cooled photomultiplier (Hamamatsu TV Co., Ltd., type R-649), amplified by a preamplifier (Hamamatsu TV Co., Ltd., type HTV C-716) and then counted by a photon-counting system (Hamamatsu TV Co., Ltd., type HTV-C 767).

Spectra were recorded on the chart and at the same time punched up as digital data.

The scattering cell, of cylindrical shape (5.0 cm in diameter), was made of pyrex glass. The cell was firmly placed in an aluminium block having a horizontal slit through which to observe the scattered light. The temperature of the block was regulated at 25 ± 0.1 °C by the circulation of water at constant temperature. In our arrangement, the scattering angle was changed from 20° to 160° through the variation of the reflecting angle of the laser beam by the aid of a mirror and a rotating table. The scattering angle could be read with the precision of $\pm2'$. The sample liquids were introduced into the cell after being passed through the Milliporefilter FG of pore size 0.22 μm.

The refractive index of the samples was measured with a modified differential refractometer manufactured by Shimadzu Instrument Co., Ltd.

Brillouin spectra of chloroform and chloroform-eicosane mixture (at 30.0 ± 0.1 °C) were recorded at various scattering angles in the range from 20° to 160°. At each scattering angle, the interferometer was scanned at least over five free spectral ranges.

Ultrasonic Absorption and Velocity Measurements. Ultrasonic absorption measurements were carried out over the frequency range from 10 to 60 MHz using a standard two crystal r.f. pulse technique with an apparatus described elsewhere.[4] Absorption measurements in the frequency range from 4.5 to 10.5 MHz were carried out using a long measuring cell (effective path length was 20 cm) with a crystal of 3.0 cm in diameter having the fundamental frequency of 1.5 MHz.

The sound velocities were measured with an ultrasonic interferometer working at 4.000 MHz.

Sample. Chloroform used was of spectral grade supplied by Nakarai Chemicals Co., Ltd. and was used without further purification. Eicosane used was also supplied by Nakarai Chemicals Co., Ltd.

Data Analysis of Brillouin Spectra

The observed Brillouin spectrum can be expressed explicitly as a convolution of the true Brillouin spectrum, the instrumental function, and the intensity spectrum of the laser source, as discussed in detail by Leidecker and LaMacchia.[5] However, in our experiment, the latter two response functions were not known exactly, so we have assumed that the observed spectrum, $I(\omega)$, is given by the relation,

$$I(\omega) = \int_{-\infty}^{\infty} I'(\omega-\omega')S(\omega')\mathrm{d}\omega', \tag{1}$$

where $S(\omega)$ represents the total effective response function which involves the laser intensity spectrum and the instrumental broadening function and $I'(\omega)$ is the true Brillouin spectrum. According to the treatment of Stegeman *et al.*,[3] an experimental determination of the convolution of laser and instrumental line profiles was carried out using the light scattered by a white paper. The profile of the diffuse laser was well expressed by a Gaussian function. As the profiles of Brillouin lines of liquids and solutions are expressed by a Lorentzian function, the observed Brillouin spectrum, $I_B(\omega)$, can be written as;

$$I_B(\omega) = \int_{-\infty}^{\infty} \frac{\Gamma_B}{\Gamma_B^2+(\omega'-\omega)^2} \exp\left[-\frac{1}{2}\left(\frac{\omega'}{\sigma_g}\right)^2\right]\mathrm{d}\omega', \tag{2}$$

where Γ_B is the true half-width of Brillouin line, and σ_g the half-width of a Gaussian function which is obtained from the observed profile of the diffuse light.

In order to determine the Brillouin shift accurately, the decomposition of the Rayleigh-Brillouin spectrum was carried out using the non-linear least-mean square method of Fletcher and Powell.[6] The Brillouin frequency shift, $\Delta\omega$, of the scattered light is related to the velocity of sound, V, as follows:[7]

$$\frac{\Delta\omega}{\omega_0} = 2n\left(\frac{V}{c}\right)\sin\left(\frac{\theta}{2}\right), \tag{3}$$

where ω_0 is the frequency of the incident light wave, c the velocity of light, n the refractive index of the liquids and θ the scattering angle. The true half-width of Brillouin line, Γ_B, is obtained by the fitting of Eq. 2 to the observed spectrum. Γ_B is related to the attenuation coefficient of sound by[7]

$$\alpha = \frac{\Gamma_B}{V}. \tag{4}$$

Results

Brillouin Spectra. In Fig. 2 are shown the Brillouin spectra of liquid chloroform recorded at the scattering angles of 87.0° and 88.8° in single and triple-pass systems, respectively. The effective finesse of these systems was about 38—40 in single-pass system and about 59—60 in triple-pass. As seen in Fig. 2, the triple-pass operation gives a much better Brillouin spectrum than that obtained by the single-pass system. In Fig. 3 are shown the Brillouin spectra of liquid chloroform recorded at three scattering angles, 40.0°, 74.7°, and 151.5°. At the largest scattering angle, the Rayleigh and Brillouin components do not overlap. The background scattering of the spectrum extends symmetrically from the central Rayleigh component to the Stokes and anti-Stokes Brillouin components. This fact indicates that there is a significant new component. This new component should be a Mountain line[8] which was found originally in carbon tetrachloride by Stegeman *et al.*[3]

The estimation of the sound velocity and attenuation

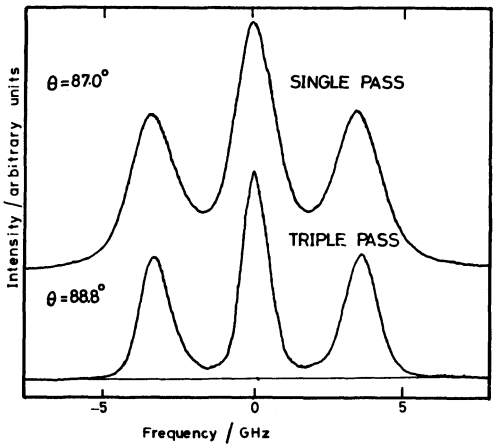

Fig. 2. Brillouin spectra of liquid chloroform recorded at the scattering angles of 87.0° in single-pass and 88.8° in triple-pass systems.

TABLE 1. VELOCITY AND ATTENUATION IN CHLOROFORM AT 30 °C

Scattering angle θ / o	Wave vector / 10^{-5} cm^{-1}	Frequency shift $\Delta\omega$ / MHz	Sound velocity V / m s^{-1}	Line width (obsd) / MHz	Line width (correct) / MHz	Absorption α/f^2 / 10^{-15} m s^{-2}
39.98	1.043	1152	979± 8	847±19	202±19	270±27
46.65	1.209	1798	979± 5	870±15	240±15	238±16
54.63	1.401	2123	999± 5	894±25	288±25	114±10
65.10	1.642	2502	1003± 9	862±17	228±17	114±10
74.67	1.851	3076	1011± 2	1002±30	465±30	153±10
81.53	1.993	3300	1016± 9	956±15	387±15	110± 5
88.80	2.130	3442	1021±10	930±12	348±12	96± 4
90.43	2.166	3633	1015± 4	999±45	456±45	107±11
112.92	2.544	3962	1026± 3	1086±92	588±92	115±18
113.57	2.554	3972	1025± 7	979±15	426±15	82± 4
151.53	2.959	4651	1036±10	1064±47	591±47	82± 7

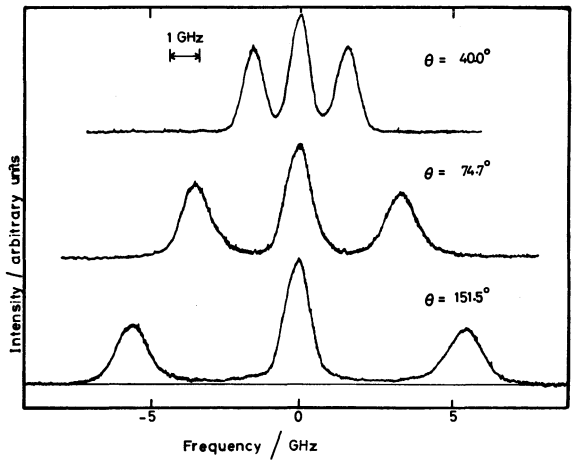

Fig. 3. Brilloiun spectra of liquid chloroform recorded at three scattering angles, 40.0°, 74.7°, and 151.5°.

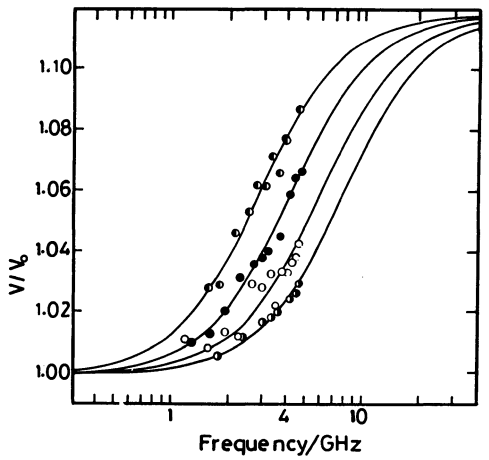

Fig. 4. Sound velocity dispersion curves of chloroform–eicosane mixtures at 30 °C. ◐; pure chloroform, ●; 3.1 wt% of eicosane, ○; 6.8 wt% of eicosane, and ◑; 14.4 wt% of eicosane. The solid lines are the best fit curves for a single relaxation.

of liquid chloroform and chloroform solutions was carried out from the method indicated in the section of Data Analysis of Brillouin Spectra. As an example, the results for liquid chloroform at 30 °C are summarized

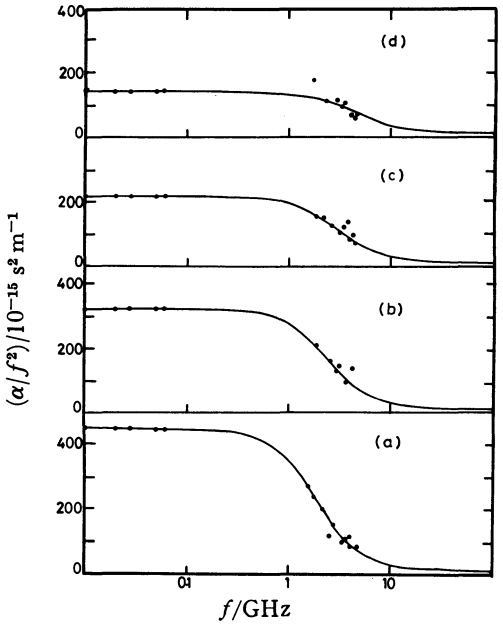

Fig. 5. Sound attenuation of chloroform–eicosane mixtures at 30 °C. The data in GHz region are obtained from the analysis of the Brillouin spectra and the data in MHz region from the ultrasonic absorption measurement. (a): Pure chloroform, (b): 3.1 wt% of eicosane, (c): 6.8 wt% of eicosane, and (d): 14.4 wt% of eicosane. The solid lines are the best fit curves for a single relaxation.

in Table 1 together with their experimental errors. The sound velocity and the attenuation of chloroform–eicosane mixtures thus obtained are shown in Figs. 4 and 5. The sound velocity dispersion curve of neat chloroform at 30 °C was in good agreement with that obtained by Takagi *et al.*[9] in the GHz region.

As can be seen in Figs. 4 and 5, the sound velocity dispersion and relaxation curves were observed in the GHz region for all mixtures investigated. Our data in Fig. 4 are analyzed with the following single relaxation formula:

$$\frac{V_0^2}{V^2-V_0^2}=\left(\frac{1}{\varepsilon}-1\right)\left(1+\frac{f_r^2}{f^2}\right), \tag{5}$$

TABLE 2. RELAXATION PARAMETERS IN CHLOROFORM–EICOSANE MIXTURES AT 30 °C

Concn of eicosane wt%	f_r GHz	V_0 m s^{-1}	V_∞ m s^{-1}	ε
0	3.50	967.7	1081.9	0.2000
3.05	4.33	975.5	1090.6	0.2000
6.85	5.80	986.7	1103.2	0.2000
14.38	8.05	1010.6	1129.9	0.2000

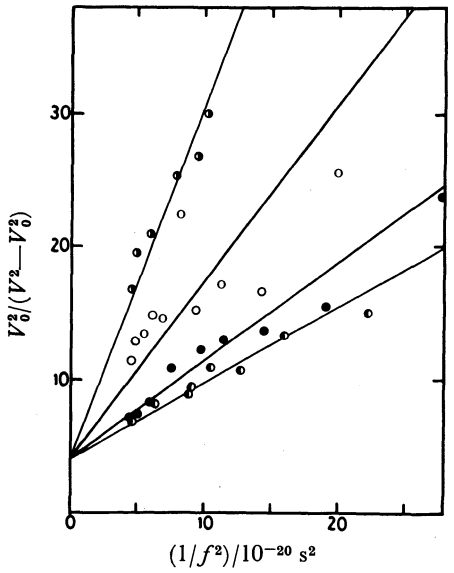

Fig. 6. Relationship between $V_0^2/(V^2-V_0^2)$ and $1/f^2$. The symbols are the same as those in Fig. 4.

$$\varepsilon = \frac{V_\infty^2 - V_0^2}{V_\infty^2},$$

where ε is the relaxation strength and V_0 and V_∞ are sound velocities at low frequency and at high frequency limits, respectively. Figure 6 shows the relation between $V_0^2/(V^2-V_0^2)$ and $1/f^2$ where the values of V_0 are those obtained by the ultrasonic interferometer working at 4 MHz. As shown in Fig. 6, a linear relationship is obtained in every chloroform–eicosane mixture. The relaxation parameters obtained are summarized in Table 2. As shown in Figs. 4 and 5, the experimental data can be well expressed by the single relaxation equation with the relaxation parameters shown in Table 2. The relaxation frequency shifts to the higher frequency side with increasing concentration of eicosane.

Ultrasonic Absorption Spectra. Figure 7 shows the ultrasonic absorption coefficients of chloroform-eicosane mixtures as a function of frequency. As shown in Fig. 7, no relaxation is observed either in chloroform-eicosane mixtures or in neat liquid eicosane over the frequency range investigated. However, the ultrasonic absorption coefficients of chloroform–eicosane mixtures are always smaller than those of neat chloroform at all frequencies investigated. The ultrasonic absorption coefficient, α/f^2, of chloroform–eicosane mixtures decreases rapidly with increasing concentration of eicosane (Fig. 8).

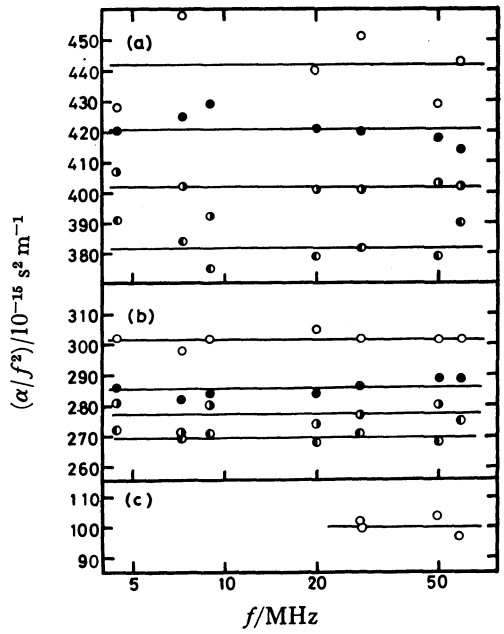

Fig. 7. Ultrasonic absorption coefficients of chloroform–eicosane mixtures.
(a): Pure chloroform, (b): 3.1 wt% of eicosane, and (c): pure eicosane. ◐; 10 °C, ◑: 20 °C, ●: 30 °C, and ○: 40 °C.

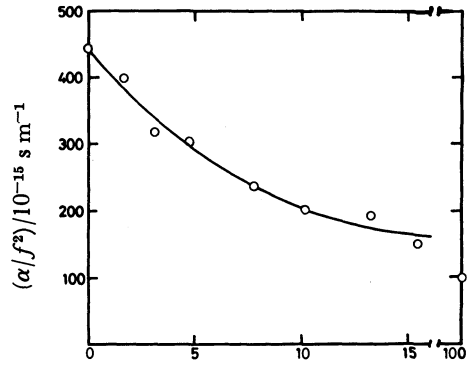

Fig. 8. Concentration dependence of sound absorption coefficients of chloroform–eicosane mixtures at 40 °C and 60 MHz.

Discussion

Recently, Takagi *et al.*[9] found a sound velocity dispersion of chloroform in the frequency range from 3 MHz to 5 GHz and reported that the dispersion reveals two relaxation processes. On the basis of the quantitative analysis of specific heat capacity, they argued that the two relaxation processes of chloroform are ascribable to the vibrational-translational relaxation, that is, the lowest ν_6 (261 cm^{-1}) and the second lowest ν_3 (366 cm^{-1}) foundamental vibrational modes have a common relaxation time, 50 ps, and the group of all above the third mode ν_2 (667 cm^{-1}) has a time of 290 ps.

As is seen in Fig. 4, our data are limited to the GHz region and the two relaxation processes can not be seen. Therefore, we are forced to analyzed our data with a

single relaxation process expressed in Eq. 5. The relaxation frequency of neat chloroform obtained in this experiment corresponds to the higher relaxation frequency obtained by Takagi *et al.*[9] but ours is slightly smaller than that obtained by them. This may be due to the lack of data at the low frequency region. However, the relaxation strength obtained ($\varepsilon=0.200$) is in good agreement with the total relaxation strength obtained by Takagi *et al.*[9] ($\varepsilon=0.216$).

As in the case of a gas mixture, if a relaxing liquid, A, such as chloroform, is mixed with a non-relaxing liquid, B, such as eicosane, two collision processes become possible in which vibrational-translational energy transfer may occur:

$$A^* + A \longrightarrow A + A, \quad (6)$$

$$A^* + B \longrightarrow A + B. \quad (7)$$

Since the processes of (6) and (7) will have different collisional efficiencies, a composite relaxation time for A*, should be considered, as given by[10]

$$\frac{1}{\beta} = \frac{1-x}{\beta_{AA}} + \frac{x}{\beta_{AB}}, \quad \beta = \frac{1}{2\pi f_r}, \quad (8)$$

where x is the mole fraction of the component B in the mixture, β_{AA} is characteristic of process (6), and β_{AB} of process (7). This may be represented graphically by a linear plot of relaxation time $1/\beta$ against mole fraction x (Fig. 9). In the chloroform–eicosane system, since the relaxation time of neat chloroform is 4.5×10^{-11} s, it follows that $\beta_{AB}=2.0\times10^{-12}$ s for the relationship shown in Fig. 9. This result indicates that a collisional efficiency between different molecules is larger than that between the same molecules, as reported by Hunter *et al.*[11,12] It is concluded that the observed relaxation of chloroform–eicosane mixture concerns mainly the vibrational-translational relaxation of the solvent chloroform itself, originating from a molecular collision between chloroform and eicosane.

In the MHz region, no ultrasonic relaxation phenomena were observed in either chloroform–eicosane mixtures or in eicosane in the temperature range investigated (see Figs. 5 and 7). As expected, the twenty methylene groups were not sufficient for the local segmental motion to be observed in the MHz frequency range.

As illustrated in Fig. 8, the values of α/f^2 in the MHz region decreased rapidly with increasing concentration of eicosane in the chloroform–eicosane mixture. In this system the value of α/f^2 can be supposed to be the ultrasonic relaxation amplitude, A, because of the very low value of the classical absorption (α/f^2 at high frequency limit), as shown in Fig. 5. The relaxation strength, r, can be given in terms of relaxation frequency, relaxation amplitude, and sound velocity at low frequency limit as shown below:[13]

$$r = Af_r V_0/\pi. \quad (9)$$

Table 2 shows that the concentration dependence of V_0 is very small. Since the relaxation strength remains constant in the concentration range investigated, the increase of the relaxation frequency results in the decrease of the relaxation amplitude. Therefore, it is concluded that the rapid decrease of α/f^2 in the mixture is mainly due to the shift of the relaxation frequency to the higher frequency side under the constant relaxation strength.

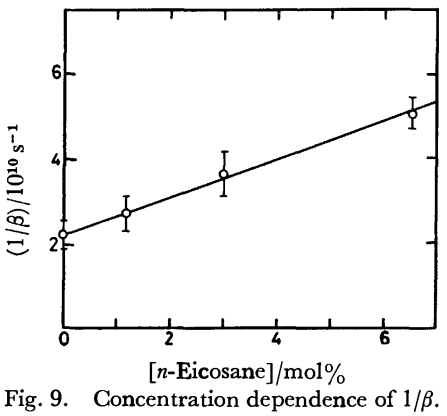

Fig. 9. Concentration dependence of $1/\beta$.

The authors should like to express their appreciation to Profs. A. Mitsuishi and S. Nakajima of Osaka University and also to Prof. K. Takagi of the University of Tokyo for their advice on constructing the apparatus for measuring Brillouin scattering. The authors are also thankful to Prof. S. Ikeda of Nagoya University for permitting them to use the differential refractometer. Some of the present experimental results were obtained by T. Matsuoka.

This work was partially supported by the Grant-in-Aid for Scientific Research No. 247005 from the Ministry of Education, Science and Culture.

References

1) S. Kato, H. Nomura, and Y. Miyahara, *Polym. J.*, **9**, 371 (1977).
2) M. A. Cockran, P. B. Jones, A. M. North, and P. A. Pethrick, *J. Chem. Soc., Farady Trans. 2*, **68**, 1719 (1972).
3) G. I. Stegeman, W. S. Gornall, V. Volterra, and B. P. Stoicheff, *J. Acous. Soc. Am.*, **49**, 979 (1971).
4) H. Nomura, S. Kato, and Y. Miyahara, *Mem. Fac. Eng. Nagoya Univ.*, **27**, 72 (1975).
5) H. W. Leidecker, Jr., and J. T. LaMacchia, *J. Acous. Soc. Am.*, **43**, 143 (1968).
6) R. Fletcher and M. J. D. Powell, *Comput. J.*, **6**, 163 (1963).
7) I. L. Fabelinskii, "Molecular Scattering of Light," Plenum Press, New York (1968), p. 86.
8) R. D. Mountain, *J. Res. Natl. Bur. Std.*, **70A**, 207 (1966).
9) K. Takagi, P-K Choi, and K. Negishi, *J. Chem. Phys.*, **74**, 1424 (1981).
10) J. D. Lambert, "Vibrational and Rotational Relaxation in Gases," Clarendon Press, Oxford (1977), p. 73.
11) J. L. Hunter and J. M. Davenport, *J. Chem. Phys.*, **55**, 762 (1971).
12) J. L. Hunter, D. Dossa, J. Hans, and D. Sette, *J. Chem. Phys.*, **66**, 4605 (1974).
13) J. Lamb, "Physical Acoustics," ed by W. P. Mason, Academic Press, New York (1965), Vol. 2, Part A, Chap. 4, p. 203.

The Structure of the Cyclodextrin Complex. XV. Crystal Structure of Hexakis-(2,3,6-tri-*O*-methyl)-α-cyclodextrin-*p*-Nitrophenol (1 : 1) Complex Monohydrate

Kazuaki HARATA,* Kaneto UEKAMA,† Masaki OTAGIRI,† and Fumitoshi HIRAYAMA†

Research Institute for Polymers and Textiles, 1-1-4, Yatabe-Higashi, Tsukuba, Ibaraki 305

†*Faculty of Pharmaceutical Sciences, Kumamoto University, 5-1, Oe-honmachi, Kumamoto 862*

(Received May 17, 1982)

The crystal structure of the hexakis(2,3,6-tri-*O*-methyl)-α-cyclodextrin (abbreviated to methyl-α-CDx) complex with *p*-nitrophenol, $C_{54}H_{96}O_{30}\cdot C_6H_5NO_2\cdot H_2O$, was investigated by the X-ray method. The crystal is monoclinic, the space group being $P2_1$ with $Z=2$; the cell dimensions are $a=11.307(1)$, $b=14.578(1)$, $c=22.118(2)$ Å, and $\beta=93.62(1)°$. The structure was determined by means of the Patterson map and the trial-and-error method combined with the rigid-body least-squares technique, and refined by the block-diagonal least-squares method to the final *R*-value of 0.048 for 4976 reflections ($\sin\theta/\lambda<0.54$). The methyl-α-CDx molecule has the shape of a truncated hexagonal cone, into which the *p*-nitrophenol molecule is inserted. The phenolic hydroxyl group is located at the center of the methyl-α-CDx cavity, while the nitro group protrudes outside from the base-side of the host cone and is in contact with the adjacent methyl-α-CDx molecule. The water molecule, which is also located within the cavity, links the methyl-α-CDx and *p*-nitrophenol molecules by hydrogen bonds. Methyl-α-CDx molecules are stacked along the crystallographic a axis in a heat-to-tail mode to form a channel-type structure.

Crystal structures of cyclodextrins and their inclusion complexes have been intensively investigated, as the crystal structure analysis is a most powerful tool to visualize how a guest molecule is included within the cavity of macrocyclic oligosaccharides. We have shown the structures of α-cyclodextrin complexes with mono- and disubstituted benzenes, and demonstrated that the guest molecules are bound inside the α-cyclodextrin ring or situated within a column which is formed by the stack of α-cyclodextrin rings. In the complexes with monosubstituted benzenes,[1,2] the phenyl group is located inside the host cavity, but the substituent group protrudes from the secondary hydroxyl side of the α-cyclodextrin ring. When disubstituted benzenes are included,[3-5] the bulkier substituent is inserted into the α-cyclodextrin ring, while the smaller substituent is located outside the cavity. Such characteristics found in the inclusion geometry have been interpreted mainly in terms of the stereospecific relationship between α-cyclodextrin and guest molecules.

Permethylated α-cyclodextrin, hexakis(2,3,6-tri-*O*-methyl)-α-cyclodextrin (abbreviated to methyl-α-CDx), also forms inclusion complexes. It is quite interesting to compare structures of these complexes with those of α-cyclodextrin complexes in respect to the macrocyclic conformation and geometry of inclusion. Previously, we have shown that *p*-iodoaniline[6] and benzaldehyde[7] are included in the methyl-α-CDx cavity in a manner which is quite different from that found in the corresponding α-cyclodextrin complexes. This paper will describe the crystal structure of the methyl-α-CDx complex with *p*-nitrophenol, and will discuss its comparison with other methyl-α-CDx complexes and the α-cyclodextrin–*p*-nitrophenol complex.[4]

Experimental

An aqueous solution, which contains methyl-α-CDx and *p*-nitrophenol in a 1 : 1 molar ratio, was allowed to stand at 40 °C. The methyl-α-CDx–*p*-nitrophenol (1 : 1) complex monohydrate was crystallized in a prismatic form. Lattice parameters and reflection intensities were measured on a Nicolet P3/F diffractometer with graphite-monochromated Cu *Kα* radiation. By using the θ-2θ scan mode, 4976 independent reflections with $|F_o|\geqq 3\sigma(F)$ were obtained up to 118° in 2θ. No corrections were made for absorption and extinction effects.

Crystal Data: $C_{54}H_{96}O_{30}\cdot C_6H_5NO_3\cdot H_2O$; *F. W.*=1382.5; monoclinic; space group $P2_1$; $Z=2$; $a=11.307(1)$, $b=14.578(1)$, $c=22.118(2)$ Å, $\beta=93.62(1)°$; $V=3638.6$ Å^3; $D_x=1.262$, $D_m=1.25$ g cm^{-3}.

Determination and Refinement of the Structure

A Patterson map showed that the *pseudo* hexagonal axis of the methyl-α-CDx molecule makes an angle of *ca.* 10° with the crystallographic a axis. The rotational parameters around this molecular axis and translational parameters along the a and c axes were determined by the trial-and-error method. After the correction of positional and orientational parameters of each 2,3,6-tri-*O*-methylglucose residue by the rigid-body least-squares technique, the atomic parameters of methyl-α-CDx were refined by the block-diagonal least-squares method. Then, a Fourier map was calculated, and *p*-nitrophenol and water molecules were found on the map. Hydrogen atoms were found on a difference-Fourier

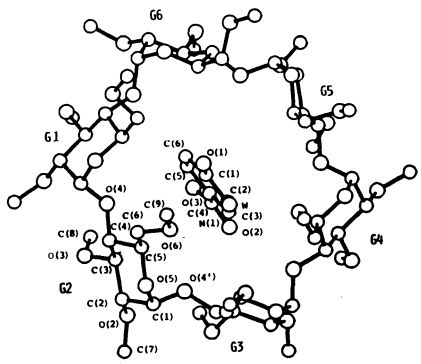

Fig. 1. The numbering scheme of the methyl-α-CDx–*p*-nitrophenol complex monohydrate. The water molecule is denoted by W.

Table 1. Atomic coordinates ($\times 10^4$) and $B_{eq}^{a)}$ values of non-hydrogen atoms

	x	y	z	B_{eq}/Å^2		x	y	z	B_{eq}/Å^2
C(1,G1)	852(5)	2584(4)	4825(2)	5.03	C(7,G4)	1965(7)	2064(6)	-937(3)	7.78
C(2,G1)	1594(5)	1816(4)	5116(2)	5.12	C(8,G4)	4214(6)	3908(6)	192(4)	8.87
C(3,G1)	1780(5)	1074(4)	4648(2)	4.49	C(9,G4)	-2822(6)	4342(7)	1203(4)	8.50
C(4,G1)	610(5)	747(4)	4359(2)	4.45	O(2,G4)	2394(3)	2467(3)	-376(2)	5.48
C(5,G1)	-167(5)	1556(4)	4132(2)	4.63	O(3,G4)	3030(3)	4228(3)	88(2)	5.67
C(6,G1)	-1436(5)	1313(5)	3925(3)	5.63	O(4,G4)	1853(3)	4701(3)	1159(2)	4.26
C(7,G1)	2672(8)	2685(6)	5881(4)	8.78	O(5,G4)	-269(3)	3188(3)	337(2)	4.19
C(8,G1)	3588(6)	223(6)	4763(4)	7.47	O(6,G4)	-1707(3)	3920(3)	1225(2)	5.57
C(9,G1)	-3155(6)	544(7)	4165(3)	8.42	C(1,G5)	508(5)	-586(4)	1394(2)	4.78
O(2,G1)	2722(4)	2117(3)	5351(2)	6.20	C(2,G5)	1493(5)	-474(4)	970(3)	5.25
O(3,G1)	2392(4)	316(3)	4923(2)	5.73	C(3,G5)	1820(5)	532(4)	880(2)	4.66
O(4,G1)	879(3)	184(2)	3847(2)	4.24	C(4,G5)	700(5)	1071(4)	686(2)	4.42
O(5,G1)	-258(3)	2116(3)	4616(2)	4.81	C(5,G5)	-231(5)	925(4)	1145(2)	4.50
O(6,G1)	-1965(4)	768(4)	4365(2)	6.42	C(6,G5)	-1396(5)	1406(4)	1027(3)	5.87
C(1,G2)	1925(6)	5586(4)	3604(3)	5.25	C(7,G5)	2940(11)	-1646(8)	802(6)	14.42
C(2,G2)	2870(5)	5258(4)	4083(3)	5.58	C(8,G5)	3731(6)	1005(6)	621(4)	8.01
C(3,G2)	2751(5)	4230(4)	4173(3)	5.05	C(9,G5)	-3061(6)	1460(8)	347(4)	10.10
C(4,G2)	1508(5)	3976(4)	4332(2)	4.53	O(2,G5)	2516(4)	-947(3)	1192(2)	6.99
C(5,G2)	610(5)	4354(4)	3837(2)	4.80	O(3,G5)	2646(3)	586(3)	419(2)	5.50
C(6,G2)	-660(5)	4219(5)	3971(3)	5.76	O(4,G5)	1030(3)	2017(3)	651(2)	4.18
C(7,G2)	4400(8)	6366(6)	3995(4)	9.17	O(5,G5)	-479(3)	-52(3)	1172(2)	4.82
C(8,G2)	4384(6)	3267(6)	4495(4)	7.60	O(6,G5)	-183(4)	1216(4)	442(2)	6.87
C(9,G2)	-2598(6)	4168(8)	3561(4)	9.78	C(1,G6)	307(5)	-673(4)	3774(2)	4.73
O(2,G2)	4027(4)	5441(3)	3938(2)	6.63	C(2,G6)	1174(5)	-1363(4)	3528(2)	4.59
O(3,G2)	3574(3)	3949(3)	4655(2)	5.98	C(3,G6)	1539(5)	-1070(4)	2910(3)	4.61
O(4,G2)	1448(3)	2996(2)	4353(2)	4.43	C(4,G6)	451(5)	-854(4)	2475(2)	4.46
O(5,G2)	785(3)	5336(3)	3785(2)	4.95	C(5,G6)	-466(5)	-283(4)	2782(2)	4.54
O(6,G2)	-1382(4)	4299(4)	3445(2)	7.28	C(6,G6)	-1673(5)	-225(5)	2434(3)	5.82
C(1,G3)	1888(5)	5661(4)	1206(2)	4.54	C(7,G6)	2047(7)	-1903(5)	4469(3)	6.93
C(2,G3)	3069(5)	5924(4)	1526(3)	5.13	C(8,G6)	3443(6)	-1583(5)	2629(3)	6.82
C(3,G3)	3168(5)	5529(4)	2162(3)	4.80	C(9,G6)	-3206(8)	-1052(9)	1920(7)	14.25
C(4,G3)	2103(5)	5785(4)	2515(2)	4.80	O(2,G6)	2233(3)	-1485(3)	3899(2)	5.35
C(5,G3)	929(5)	5640(4)	2145(2)	4.79	O(3,G6)	2204(3)	-1776(3)	2650(2)	5.01
C(6,G3)	-90(5)	6251(7)	2462(3)	8.37	O(4,G6)	902(3)	-335(3)	1984(1)	4.16
C(7,G3)	4944(6)	6244(6)	1133(4)	9.44	O(5,G6)	-706(3)	-634(3)	3370(2)	4.51
C(8,G3)	5048(6)	5174(7)	2634(4)	9.05	O(6,G6)	-2098(4)	-1101(4)	2293(3)	8.21
C(9,G3)	-2005(8)	6461(8)	2503(4)	11.92	C(1,NP)	1854(6)	2147(5)	2601(3)	6.44
O(2,G3)	4014(4)	5620(4)	1187(2)	6.60	C(2,NP)	2312(7)	2789(5)	2224(3)	7.40
O(3,G3)	4205(4)	5873(3)	2483(2)	6.51	C(3,NP)	3537(7)	2794(6)	2142(4)	8.93
O(4,G3)	2161(3)	5205(3)	3041(2)	4.54	C(4,NP)	4241(7)	2144(6)	2424(4)	9.66
O(5,G3)	965(3)	6019(3)	1543(2)	4.62	C(5,NP)	3814(8)	1494(6)	2808(4)	9.99
O(6,G3)	-1099(4)	5958(4)	2175(2)	8.26	C(6,NP)	2598(7)	1502(5)	2893(4)	7.95
C(1,G4)	553(4)	2538(4)	157(2)	4.27	N(1,NP)	5529(8)	2116(8)	2318(6)	14.47
C(2,G4)	1544(5)	3057(4)	-128(2)	4.82	O(1,NP)	687(4)	2105(4)	2699(2)	7.74
C(3,G4)	2175(4)	3667(4)	347(2)	4.44	O(2,NP)	5887(7)	2701(8)	2007(6)	23.70
C(4,G4)	1274(4)	4314(4)	624(2)	4.20	O(3,NP)	6126(7)	1580(8)	2592(6)	22.04
C(5,G4)	171(4)	3785(4)	808(2)	4.43	O(W)	-634(4)	3481(4)	2360(2)	7.81
C(6,G4)	-848(5)	4431(4)	922(2)	4.76					

a) $B_{eq}=8\pi^2(u_1^2+u_2^2+u_3^2)/3$, where u_i is the root-mean-square deviation in the i-th principal axis of the thermal ellipsoid.

map in the course of further refinement. The block-diagonal least-squares refinement including 100 hydrogen atoms achieved the R-value of 0.048. The quantity minimized was $\sum w(|F_o|-|F_c|)^2$ with $w=1.0$ for all the reflections. The atomic scattering factors were taken from the "International Tables for X-Ray Crystallography."[8] Final atomic coordinates and B_{eq} values of non-hydrogen atoms are listed in Table 1. Tables of observed and calculated structure factors, anisotropic temperature factors of non-hydrogen atoms, atomic parameters of hydrogen atoms, and bond distances, bond angles, and conformation angles of methyl-α-CDx are kept at The Chemical Society of Japan (Document No. 8258). The calculations were carried out on a FACOM M-200 computer at the RIPS Center, Tsukuba.

Description and Discussion of the Structure

Outline of the Structure. The numbering scheme of the complex is shown in Fig. 1. A space-filling representation of the inclusion feature is given in Fig. 2. The hydroxyl group of *p*-nitrophenol is inserted into the methyl-α-CDx ring, while the nitro group protrudes outside from the O(2), O(3) methoxyl side of the methyl-α-CDx ring. The water molecule is located at the O(6) side of the cavity, forming hydrogen bonds with two O(6) atoms of methyl-α-CDx and the phenolic hydroxyl group. Methyl-α-CDx molecules are stacked along the crystallographic a axis to form a head-to-tail channel-type structure as shown in Fig. 3.

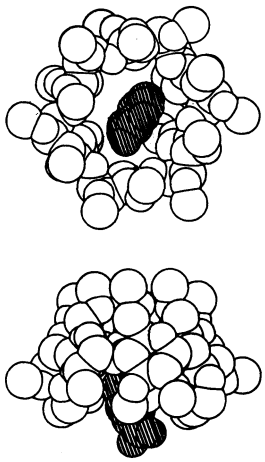

Fig. 2. A space-filling representation of the inclusion feature.

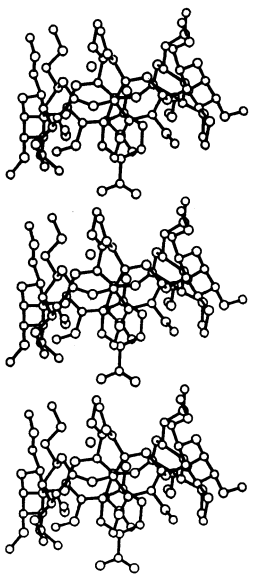

Fig. 3. The stacking feature of the methyl-α-CDx complex.

Conformation of Methyl-α-CDx. Average bond distances and angles over six 2,3,6-tri-*O*-methylglucose residues are shown in Fig. 4. Geometrical data for the macrocyclic ring are given in Tables 2 and 3. Except for the orientation of C(6)–O(6) bonds, the six 2,3,6-tri-*O*-methylglucose residues are in the same conformation. The C(6)–O(6) bonds in the G2, G3, and G4 residues take *gauche-trans* conformations about the C(5)–C(6) bonds, while the others have *gauche-gauche* conformations. Each O(6)–C(9) bond is *trans* to the corresponding C(5)–C(6) bond. The six O(2)–C(7) bonds are oriented outside the methyl-α-CDx ring, the six O(3)–C(8) bonds turning inside the ring. The conformations of the pyranose rings in cyclodextrins have been discussed in terms of the torsion-angle index and distance between glycosidic oxygen atoms.[4] The values of the torsion-angle index, which are in the range 120.4—144.4°, are similar to those found in the α-cyclodextrin–*p*-nitrophenol complex. The O(4)···O(4) distances between adjacent residues range from 4.16 to 4.53 Å. The average value of 4.31 Å is somewhat larger than the corresponding value (4.24 Å) found in the α-cyclodextrin complex. French and Murphy[9] have shown that there is a linear correlation between the O(4)···O(4) distance and the torsion-angle index in mono- and oligosaccharides. The same relationship has been also found in α-cyclodextrin complexes.[4] But, as shown in Fig. 5, no such correlation appears in the methyl-α-CDx complexes. This suggests that the methyl groups affect the conformation of the pyranose ring so as to break the linear correlation between the O(4)···O(4) distance and the torsion-angle index.

The six glycosidic oxygen atoms form an elliptically-distorted hexagon. The longest diagonal is found parallel to the guest plane. These O(4) atoms are roughly coplanar with a maximum deviation of 0.202 Å from their least-squares plane. This indicates that the planarity of the O(4) hexagon is not significantly affected by the methylation, since the corresponding maximum deviation in the α-cyclodextrin–*p*-nitrophenol complex is 0.163 Å. The O(2)···O(3) distances between the adjacent residues are in the range 3.26—3.48 Å, which are markedly larger than those found in the α-cyclodextrin–*p*-nitrophenol complex (2.65—3.07 Å). These large

TABLE 2. GEOMETRICAL DATA FOR METHYL-α-CDx

Distance	*l*/Å	Distance	*l*/Å
I. O(4)···O(4) distance			
O(4,G1)···O(4,G2)	4.29(1)	O(4,G5)···O(4,G6)	4.53(1)
O(4,G1)···O(4,G6)	4.19(1)	O(4,G1)···O(4,G4)	8.99(1)
O(4,G2)···O(4,G3)	4.44(1)	O)4,G2)···O(4,G5)	8.46(1)
O(4,G3)···O(4,G4)	4.22(1)	O(4,G3)···O(4,G6)	8.50(1)
O(4,G4)···O(4,G5)	4.16(1)		
II. O(2)···O(3) distance			
O(2,G1)···O(3,G2)	3.26(1)	O(2,G3)···O(3,G4)	3.30(1)
O(2,G6)···O(3,G1)	3.45(1)	O(2,G4)···O(3,G5)	3.27(1)
O(2,G2)···O(3,G3)	3.30(1)	O(2,G5)···O(3,G6)	3.48(1)
III. O(2)···C(8) distance			
O(2,G1)···C(8,G1)	3.25(2)	O(2,G1)···C(8,G2)	3.21(2)
O(2,G2)···C(8,G2)	3.43(2)	O(2,G2)···C(8,G3)	3.21(2)
O(2,G3)···C(8,G3)	3.42(2)	O(2,G3)···C(8,G4)	3.33(2)
O(2,G4)···C(8,G4)	3.17(2)	O(2,G4)···C(8,G5)	3.37(2)
O(2,G5)···C(8,G5)	3.45(2)	O(2,G5)···C(8,G6)	3.41(2)
O(2,G6)···C(8,G6)	3.22(2)	O(2,G6)···C(8,G1)	3.45(2)

IV. Tilt-angle[a] and torsion-angle index[b]

Residue	Tilt-angle ϕ/°	Torsion-angle index ϕ/°
G1	25.9	140.3
G2	16.0	124.4
G3	9.3	140.1
G4	28.1	148.3
G5	14.8	120.4
G6	18.7	144.4

a) The tilt-angle is defined as the angle made by the plane through six O(4) atoms and the plane through O(4′), C(1), C(2), and O(4) of each 2,3,6-tri-*O*-methylglucose residue. b) The torsion-angle index is defined as follows: $|\phi(C(1)-C(2))|+|\phi(C(2)-C(3))|+|\phi(C(5)-O(5))|+|\phi(O(5)-C(1))|-|\phi(C(3)-C(4))|-|\phi(C(4)-C(5))|$, where $\phi(C(1)-C(2))$ is the conformation angle of O(5)–C(1)–C(2)–C(3).

Table 3. Least-squares plane and deviation (d/Å) of atoms from the plane

The plane equation is of the $AX+BY+CZ=D$ form, where X, Y, and Z are the coordinates in Å units along the a, b, and c* axes, respectively.

I. The plane through six O(4) atoms			
$0.984X-0.174Y+0.042Z=0$ 799			
O(4,G1)	−0.037	O(4,G4)	0.019
O(4,G2)	−0.140	O(4,G5)	−0.194
O(4,G3)	0.150	O(4,G6)	0.202
II. The benzene plane			
$0.110X+0.620Y+0.777Z=6.594$			
C(1,NP)	−0.002	C(6,NP)	0.004
C(2,NP)	−0.005	N(1,NP)	−0.054
C(3,NP)	0.011	O(1,NP)	−0.019
C(4,NP)	−0.010	O(2,NP)	−0.009
C(5,NP)	0.002	O(3,NP)	0.001

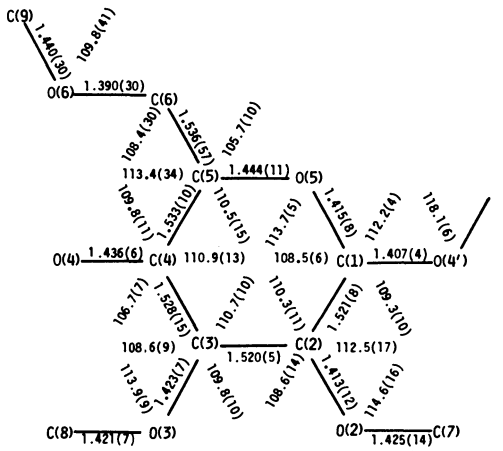

Fig. 4. Average bond distances (l/Å) and angles (ϕ/°) over six 2,3,6-tri-*O*-methylglucose residues. Standard deviations in parentheses were estimated according to the equation: $\sigma=[\sum_{i=1}^{6}(x_i-\bar{x})^2/5]^{1/2}$, where x_i refers to the bond distance or angle in the i-th residue and $\bar{x}$ is the average value.

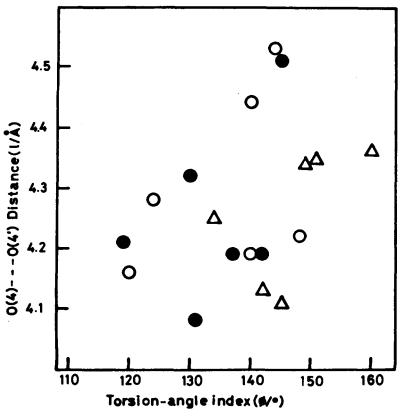

Fig. 5. Plot of the O(4)···O(4′) distance against the torsion-angle index in the methyl-α-CDx complexes with *p*-nitrophenol (○), *p*-iodoaniline (△), and benzaldehyde (●).

O(2)···O(3) distances may be ascribed to the repulsive interaction between the C(8) methyl group and two adjacent O(2) atoms. The C(8) methyl group is nearly equidistant from these two O(2) atoms; the C(8)···O(2) distances of these two kinds are in the ranges 3.17—3.45 Å and 3.21—3.45 Å, respectively. Such repulsive interaction also inclines 2,3,6-tri-*O*-methylglucose residues in such a way that the O(6) side of the cavity becomes smaller. The tilt-angles range from 9.3° to 28.1°. The average value of 18.8° is larger than the corresponding values of 16.7° in the *p*-iodoaniline complex[6] and 17.7° in the benzaldehyde complex.[7] This suggests that the methyl-α-CDx ring changes its macrocyclic conformation so as to fit itself to the shape of included group or molecule.

Methyl-α-CDx–Guest Interaction. Bond distances and angles in *p*-nitrophenol and intermolecular distances between the methyl-α-CDx and guest molecules are given in Fig. 6. The hydroxyphenyl group of the guest is inserted into the methyl-α-CDx ring. The phenolic hydroxyl group is located nearly at the center of the cavity, while the benzene ring is surrounded by O(2)-C(7)H_3 and O(3)C(8)H_3 methoxyl groups. The nitro group, which protrudes outside the ring from the O(2), O(3) side of methyl-α-CDx, is in contact with methyl groups of the next methyl-α-CDx molecule. The guest plane is nearly perpendicular to the O(4)-hexagon plane, making an angle of 89.1°. The molecular axis of *p*-nitrophenol deviates from the normal of the O(4)-hexagon plane; the nitro group approaches to the G3 and G4 residues. As a result, the C(6,NP)–H bond is oriented toward the C(3)H methine groups of the G1 and G6 residues, while the C(2,NP)H group is in contact with the C(5)H methine groups of the G3 and G4 residues. All the intermolecular hydrogen-hydrogen distances are greater than 2.35 Å, as shown in Fig. 6. This indicates that the benzene ring has weak van der Waals contacts with the atoms which constitute the interior surface of the methyl-α-CDx cavity.

The host-guest interaction in the present complex is quite different from that found in the α-cyclodextrin–*p*-nitrophenol complex,[4] in which the guest molecule is

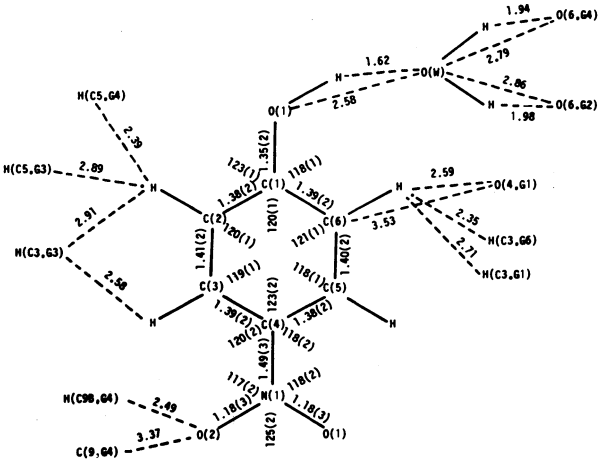

Fig. 6. Bond distances (l/Å) and angles (ϕ/°) in *p*-nitrophenol and intermolecular distances (l/Å) among methyl-α-CDx, water, and *p*-nitrophenol molecules.

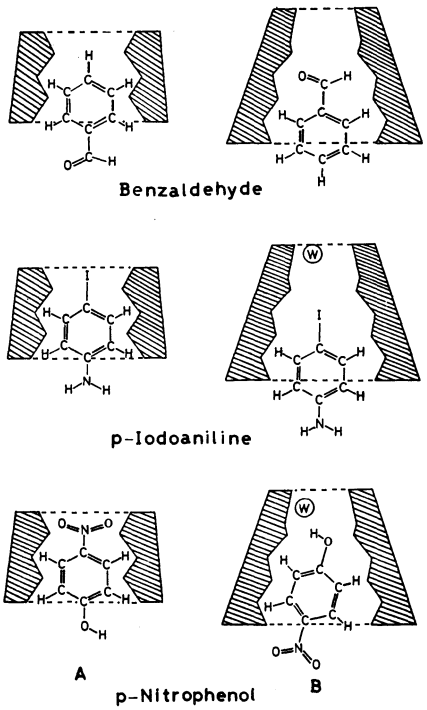

Fig. 7. Schematic drawings of the inclusion features of α-cyclodextrin (A) and methyl-α-CDx (B) complexes. Water molecules are denoted by W.

included upside down. As shown in Fig. 7, the nitrophenyl group is tightly bound in the α-cyclodextrin cavity, while the hydroxyl group protrudes from the O(2), O(3) hydroxyl side of the cavity, forming hydrogen bonds with adjacent α-cyclodextrin molecules. Such a change in the inclusion geometry may be ascribed to the difference in the shape and size of the host cavity. The α-cyclodextrin cavity is quite suitable to accomodate the nitrophenyl group. The methylation enlarges the O(2), O(3) side of the cavity, but the large inclination of 2,3,6-tri-*O*-methylglucose residues makes the O(6) side of the cavity so narrow that the nitrophenyl group can not be deeply inserted. In this case, the choice of the substitutent group to be included seems to depend upon the steric hindrance. A similar upside-down inclusion has also been observed in the benzaldehyde complex[7] (Fig. 7). In that case, the inclusion of the whole molecule may be more suitable to fulfill the methyl-α-CDx cavity than the inclusion of the phenyl group only. Unlike these two methyl-α-CDx complexes, the *p*-iodoaniline molecule is included in the same orientation in α-cyclodextrin and methyl-α-CDx rings, although the iodophenyl group slides to the O(2), O(3) side in the methyl-α-CDx ring. The inclusion of either the iodophenyl group or the aminophenyl group is sterically possible, but the iodophenyl group may be more suitably accomodated because of the stronger van der Waals interaction. The water molecule in the *p*-nitrophenol complex, which is located on the O(6) side of the cavity, links the *p*-nitrophenol molecule to the host methyl-α-CDx molecule through the hydrogen bonds (Fig. 6), O(1,NP)–H···O(W), O(W)–H···O(6,G2), and O(W)–H···O(6,G4). These hydrogen

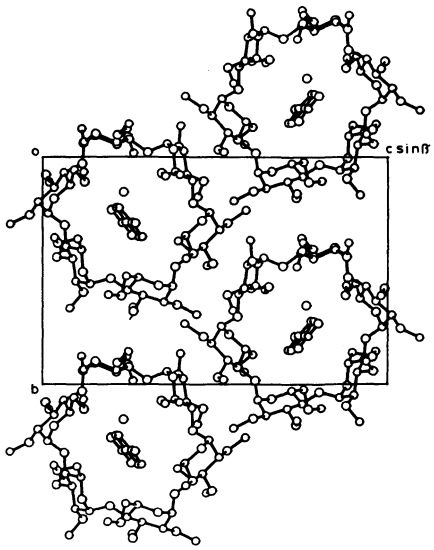

Fig. 8. The crystal structure viewed down along the a axis.

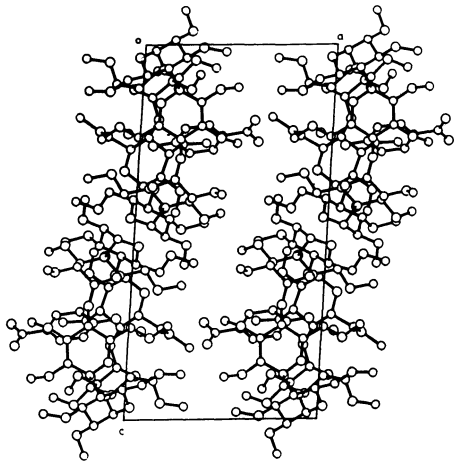

Fig. 9. The crystal structure viewed down along the b axis.

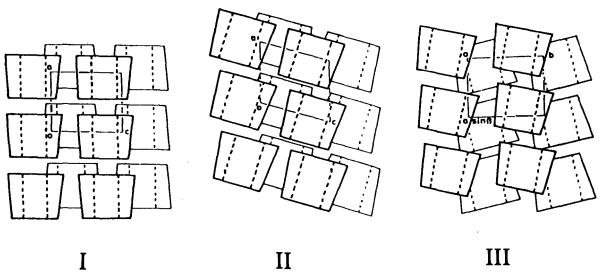

Fig. 10. Schematic drawings of the packing feature of methyl-α-CDx in the complexes with *p*-iodoaniline (I), benzaldehyde (II), and *p*-nitrophenol (III).

bonds may play an important role to fix the guest molecule inside the cavity, as the benzene ring is in loose contact with methyl-α-CDx.

Molecular Packing. Projections of the crystal structure are shown in Figs. 8 and 9. The crystal is composed of endless columns formed by the stack of

Table 4. Intermolecular distances between non-hydrogen atoms less than 3.7 Å

Distance		*l*/Å	Distance		*l*/Å
C(9,G1)–O(3,G2)	(e)	3.55(2)	C(9,G3)–C(7,G4)	(c)	3.58(2)
O(2,G1)–C(7,G2)	(f)	3.65(2)	O(6,G3)–C(7,G4)	(c)	3.27(2)
O(3,G1)–C(6,G2)	(e)	3.60(1)	C(9,G4)–O(2,NP)	(b)	3.37(2)
O(5,G1)–C(7,G6)	(d)	3.22(1)	O(3,G4)–O(6,G5)	(c)	3.38(1)
C(9,G2)–C(8,G3)	(b)	3.57(2)	O(3,G4)–C(9,G5)	(c)	3.39(2)
C(4,G3)–O(3,G6)	(a)	3.57(1)	O(5,G4)–C(2,G5)	(c)	3.69(1)
C(9,G3)–O(6,G6)	(a)	3.59(2)	O(6,G6)–O(3,NP)	(b)	3.65(2)

Code	Symmetry operator	Code	Symmetry operator
a	$x, 1+y, z$	d	$-x, 1/2+y, 1-z$
b	$-1+x, y, z$	e	$-x, -1/2+y, 1-z$
c	$-x, 1/2+y, -z$	f	$1-x, -1/2+y, 1-z$

methyl-α-CDx along the a axis. The normal of the methyl-α-CDx ring plane inclines at 10.3° with respect to the column axis. A similar packing of methyl-α-CDx is also found in the complexes with *p*-iodoaniline[6] and benzaldehyde.[7] But, as shown in Fig. 10, there are significant differences in the packing mode among these complexes. In the *p*-iodoaniline complex, the methyl-α-CDx ring is almost perpendicular to the a axis, so that the straight channel runs through methyl-α-CDx rings. On the other hand, the normal of the methyl-α-CDx ring plane in the benzaldehyde complex inclines at 17.0° with the column axis. Since the adjacent methyl-α-CDx rings along the column axis are laterally shifted within their molecular plane, the channel runs not straight but zigzag along the axis. The methyl-α-CDx ring in the *p*-nitrophenol complex also inclines, but the angle of inclination is smaller than that of the benzaldehyde complex. The channel runs almost straight through the methyl-α-CDx rings, and the guest molecules are linearly arranged in the channel. The rings planes of the methyl-α-CDx molecules related by the two-fold screw axis make an angle of 20° with each other. This is the most significant difference in the molecular packing between the *p*-nitropenol complex and the complexes with *p*-iodoaniline and benzaldehyde (Fig. 10).

An Aspect of Driving Force of the Complex Formation. The binding force of cyclodextrin complexes has been discussed on structural,[10] spectroscopic,[11–15] thermodynamic,[16] and theoretical[1,17] bases, and several interactions and forces have been proposed to explain the inclusion phenomena. Saenger and his co-workers[10] have suggested in their model to explain the inclusion mechanism that the intramolecular hydrogen bonds between O(2)H and O(3)H hydroxyl groups play an important role in the complex formation. The methyl-α-CDx complexes, however, indicate that such hydrogen bonds are not necessarily required to form the inclusion complex. Since the macrocyclic conformation of methyl-α-CDx is relatively restricted by the steric hindrance involving the $C(8)H_3$ methyl groups, the participation of the conformational change may be small, although the conformation of the uncomplexed methyl-α-CDx has not yet been defined. The inclusion geometry of methyl-α-CDx complexes indicates that the selection of groups to be included is made mainly by van der Waals interaction and repulsive interaction. Therefore, van der Waals force may significantly participate in the complex formation. Since the thermodynamic data of methyl-α-CDx complexes have not been published, it is difficult to estimate the degree of contribution of hydrophobic interaction to the complex formation in aqueous solution. But, it is possible to speculate the importance of the hydrophobic interaction from the structures of methyl-α-CDx complexes. Both ends of α-cyclodextrin cavity are rimmed with hydroxyl groups which form hydrophilic environment around the cavity The methylation not only enlarges the hydrophobic cavity of the host molecule but also makes the environment around the cavity highly hydrophobic. Therefore, compared with α-cyclodextrin, the contribution of hydrophobic interaction can be expected to be enhanced.

References

1) K. Harata, *Bull. Chem. Soc. Jpn.*, **49**, 2066 (1976).
2) K. Harata, K. Uekama, M. Otagiri, F. Hirayama, and H. Ogino, *Bull. Chem. Soc. Jpn.*, **54**, 1954 (1981).
3) K. Harata, *Bull. Chem. Soc. Jpn.*, **48**, 2409 (1975); W. Saenger, K. Beyer, and P. C. Manor, *Acta Crystallogr., Sect. B*, **32**, 120 (1976).
4) K. Harata, *Bull. Chem. Soc. Jpn.*, **50**, 1416 (1977).
5) K. Harata, H. Uedaira, and J. Tanaka, *Bull. Chem. Soc. Jpn.*, **51**, 1627 (1978).
6) K. Harata, K. Uekama, M. Otagiri, and F. Hirayama, *Bull. Chem. Soc. Jpn.*, **55**, 407 (1982).
7) K. Harata, K. Uekama, M. Otagiri, F. Hirayama, and Y. Sugiyama, *Bull. Chem. Soc. Jpn.*, **55**, 3386 (1982).
8) "International Tables for X-Ray Crystallography," Kynoch Press, Birmingham (1974), Vol. IV, pp. 72—75.
9) A. D. French and V. G. Murphy, *Carbohydr. Res.*, **27**, 391 (1973).
10) W. Saenger, M. Noltemeyer, P. C. Manor, B. Hingerty, and B. Klar, *Bioorg. Chem.*, **5**, 187 (1976).
11) K. Uekama, M. Otagiri, Y. Kanie, S. Tanaka, and K. Ikeda, *Chem. Pharm. Bull.*, **23**, 1421 (1975).
12) R. J. Bergeron, M. A. Channing, G. J. Gibeily, and D. M. Pillor, *J. Am. Chem. Soc.*, **99**, 5146 (1977).
13) Y. Matsui and K. Mochida, *Bull. Chem. Soc. Jpn.*, **52**, 2808 (1979).
14) R. I. Gelb, L. M. Schwartz, B. Cardelino, H. S. Fuhrman, R. F. Johnson, and D. A. Laufer, *J. Am. Chem. Soc.*, **103**, 1750 (1981).

15) K. Harata, *Bioorg. Chem.*, **10**, 255 (1981).
16) E. A. Lewis and L. D. Hansen, *J. Chem. Soc., Perkin Trans. 2*, **1973**, 2081.
17) I. Tabushi, Y. Kiyosuke, T. Sugimoto, and K. Yamamura, *J. Am. Chem. Soc.*, **100**, 916 (1978).

EXAFS Spectroscopy of Some Iron(III) Compounds by Use of Dispersive-type In-laboratory X-Ray Spectrometer

Masaharu NOMURA, Kiyotaka ASAKURA, Ukyo KAMINAGA,† Tadashi MATSUSHITA,† Kazutake KOHRA,† and Haruo KURODA*

Department of Chemistry and Research Center for Spectrochemistry, Faculty of Science, The University of Tokyo, Hongo, Bunkyo-ku, Tokyo 113

†*Photon Factory, National Laboratory for High Energy Physics, Oho-Machi, Tsukuba, Ibaraki 305*

(Received June 28, 1982)

A dispersive-type in-laboratory EXAFS spectrometer was constructed by combining a transmission-type dispersing crystal and a position-sensitive proportional counter. FeK absorption spectra were measured by use of this apparatus on $FeCl_3 \cdot 6H_2O$, $Fe(ClO_4)_3 \cdot 6H_2O$ and anhydrous $FeCl_3$. Discussion is given on the results obtained from the analyses of observed EXAFS data concerning the structure around Fe ions in these compounds. AsI_3-like structure is proposed for anhydrous $FeCl_3$.

Extended X-ray absorption fine structure (EXAFS) spectroscopy has rapidly grown up to the most important method to study the local structure around an X-ray absorbing atom in solids and liquids since its usefulness as a structural tool was first demonstrated by Stern *et al.*[1-5]

This rapid development of EXAFS spectroscopy also comes from the utilization of synchrotron radiation. Because usually EXAFS oscillation is only a few percent or less of absorption coefficient, we need to measured absorption coefficient of a sample with a high accuracy as a function of X-ray wavelength over the concerned spectral region. It takes a very long measuring time to obtain reliable EXAFS data if we use a conventional X-ray spectrometer composed of an ordinary X-ray source and a crystal monochromator. The time required to obtain EXAFS data has been drastically shortened by use of synchrotron radiation. This has opened wide new fields of application of EXAFS spectroscopy.

Although the use of synchrotron radiation is evidently of great value in EXAFS spectroscopy, the use of a synchrotron radiation facility inevitably has various restrictions concerned with place and time. For some type of applications, there are large advantages of having an in-laboratory EXAFS spectrometer if it can provide EXAFS data of satisfactory quality with a tolerable measuring time. Even if one is considering to use a synchrotron radiation facility to obtain accurate EXAFS data, it may be of great value to carry out preliminary experiments with an in-laboratory apparatus.

One approach to reduce the data acquisition time of an in-laboratory EXAFS spectrometer is naturally to increase X-ray intensity as high as possible by employing a very-high-power X-ray generator[6] and/or a bent-crystal monochromator.[7,8] In fact, it was reported by Cohen *et al.*[9] that the time required to obtain EXAFS data could be markedly reduced by combining a bent-crystal monochromator with a high-power rotating anode X-ray generator.

Another approach is to improve the data collection efficiency by simultaneously measuring the intensities of X-rays over the concerned spectral region by use of a system composed of a dispersing crystal and a position-sensitive detector.[10,11] We constructed an EXAFS spectrometer by use of transmission-type dispersing method which has been developed by Kaminaga *et al.*,[10] and studied FeK EXAFS of $FeCl_3 \cdot 6H_2O$, $Fe(ClO_4)_3 \cdot 6H_2O$, and anhydrous $FeCl_3$.

EXAFS Spectrometer

Figure 1 illustrates the principle of the EXAFS spectrometer constructed in the present study. When a divergent white X-ray beam hits the surface of a thin single crystal, X-ray incident direction is different at different positions of the crystal surface, hence the X-ray wavelength which satisfies the diffraction condition, is different at different positions. It may be easily understood from a geometrical consideration that X-rays of different wavelengths which have been diffracted at different positions, will be focused at the position (SP in Fig. 1) which is symmetrical to the X-ray source (X) with respect to the diffracting crystal, and then diverge. Thus the diffracting crystal works as a transmission type X-ray polychromator. With this optical system, X-ray intensities over the interested spectral region can be simultaneously measured by placing a position-sensitive detector at some distance after the focusing position. An absorption Spectrum can be obtained by performing intensity measurements with and without a sample in the X-ray path. Most conveniently a sample is placed at the focusing position, since the sample area in X-ray path, hence the required sample amount will be minimized and, at the same time, the troubles concerned with the ununiformity of the sample can be largely avoided.

We used a molybdenum sealed X-ray tube (Philips

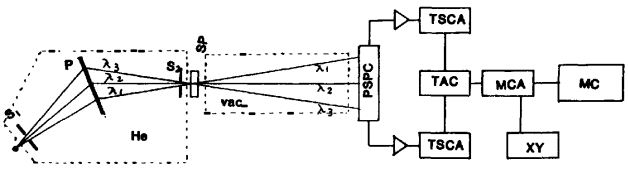

Fig. 1. Block diagram of EXAFS spectrometer.
S: Slit, P: dispersing crystal, SP: sample, PSPC: position sensitive proportional counter, TSCA: timing single channel analyzer, TAC: time to amplitude converter, MCA: multi-channel analyzer, XY: X-Y recorder, MC: micro-computer system.

fine focus tube or Toshiba normal focus tube) as the X-ray source, which was operated with a conventional X-ray power supply (Rigaku D-2F, 1 kW) mostly with 25 mA at 20 kVp. A silicon single crystal of 50 μm thick was used as the dispersing crystal, Si(111) plane having been chosen as the diffraction plane so that the (222) harmonics could be eliminated. Both the distance from X-ray source to silicon crystal and that from the crystal to sample were 250 mm, and the distance from sample to detector was mostly set as 600 mm. In order to minimize X-ray intensity loss, the X-ray path between source and sample was replaced with helium gas, and that between sample and detector was evacuated with a mechanical vacuum pump. By this way, available X-ray flux became 2.5 times of that obtainable when all X-ray path is in the ordinary atmosphere.

We used a multi-cathode position-sensitive proportional counter (PSPC) of delay line readout type as the detector. For the gas filled in PSPC, we used either PR gas (Ar 90%, $CH_3$10%) or Xe-CH_4 mixture (Xe 90%, CH_4 10%), pressurized to about 3 kg cm^{-2}. The block diagram of the electronic system is also shown in Fig. 1. The information about the incident position of an X-ray photon is taken out as the signal pulse height, which is digitized through an ADC (NAIG E-551) to determine the address in a process memory (NAIG E-562) at which the count is to be stored. After count data have been sufficiently accumulated, the data are transfered to a microcomputer (NEC PC-8001), with which initial data treatments are carried out.

By examining the X-ray spectrum recorded on a photographic film placed at the position of the detector, the spectral resolution of our optical system was confirmed to be about 4 eV around the FeK absorption edge, but the overall resolution of obtained EXAFS data was about 7 eV or a little more, because of the positional resolution of our detection system. Although we used a conventional sealed X-ray tube operated at a low power, we were able to obtain EXAFS data within a torelable measuring time. For example, the FeK absorption spectrum (shown in Fig. 2) of an iron foil of 4 μm thick was obtained with a measuring time of about 4 h with a fine-focus Mo X-ray tube operated with 25 mA at 20 kVp, taking 10^5 counts at each measured energy point, the number of measured points being 250 over the observed spectral region, 6.7—8.3 keV.

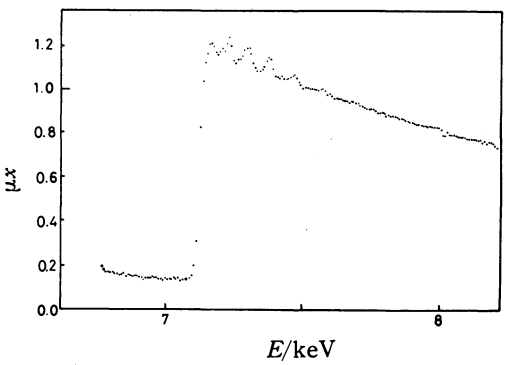

Fig. 2. X-Ray absorption spectrum of Fe foil of 4 μm thick. The data acquisition time was 3 h 45 min.

EXAFS of Some Fe(III) Compounds

By use of the apparatus described in the preceeding section, we obtained EXAFS data on $FeCl_3 \cdot 6H_2O$, $Fe(ClO_4)_3 \cdot 6H_2O$, and anhydrous $FeCl_3$. In the cases of $FeCl_3 \cdot 6H_2O$ and $Fe(ClO_4)_3 \cdot 6H_2O$, crystalline powder was mixed with well-dried Nujol to be used as the sample for EXAFS measurement, and FeK absorption spectra were measured by keeping such a mixture between two polyethylene plates separated with a PTFE spacer of an appropriate thickness. A special care had to be taken for the deliquescence in the case of anhydrous $FeCl_3$. We prepared anhydrous $FeCl_3$ powder in a glove box filled with dry nitrogen, and carried out X-ray absorption measurement on a compaction of the powder kept in a dry nitrogen atmosphere. The measurement of FeK absorption spectrum was repeated two or three times on each sample to check the reproducibility.

Figure 3 shows the FeK absorption spectra of the three compounds. Note that the first peak near FeK absorption edge is very weak in the case of anhydrous $FeCl_3$ as compared with $FeCl_3 \cdot 6H_2O$ and $Fe(ClO_4)_3 \cdot 6H_2O$. This difference is likely to be associated with the difference in the number of the H_2O molecules coordinated around Fe ion. Another aspect that can be seen clearly from the comparison of the three spectra, is the difference of the position of third peak.

We extracted EXAFS oscillations from the observed spectra and analyzed them to derive structural information. The analysis was performed by use of the computer program system written by Sato in our laboratory.[12] The program system consists of the programs for background subtraction, extraction of EXAFS oscillation $\chi(k)$, Fourier transformation of $k^n\chi(k)$, Fourier filtering and back transofrmation, and curve-fitting analysis. In the curve-fitting analysis, we assumed the following formula for $\chi(k)$.

$$\chi(k) = C_0 \sum_i N_i k^{-1} r_j^{-2} F_i(k) \times \exp(-2\sigma_i^2 k^2) \cdot \sin[2kr_i + \phi_i(k)] \quad (1)$$

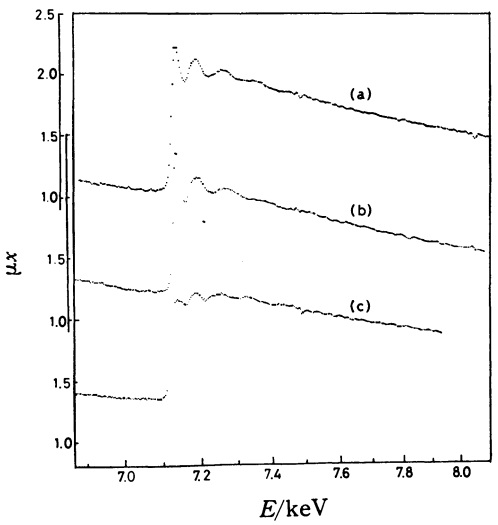

Fig. 3. X-Ray absorption spectra of (a) $FeCl_3$–$6H_2O$, (b) $Fe(ClO_4)_3$–$6H_2O$, and (c) Anhydrous $FeCl_3$.

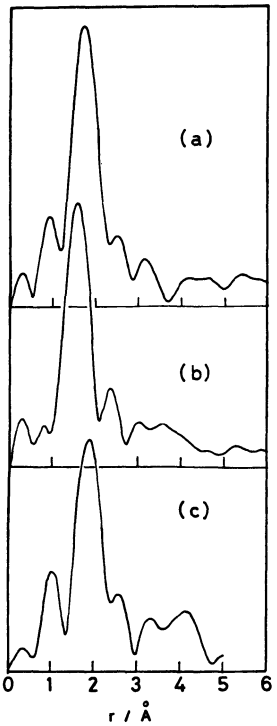

Fig. 4. Fourier transforms of $k^3\chi(k)$ for (a) $FeCl_3 \cdot 6H_2O$, (b) $Fe(ClO_4)_3 \cdot 6H_2O$, and (c) anhydrous $FeCl_3$.

where N_i and r_i are the number and distance of atom(i), $F_i(k)$ and $\phi_i(k)$ are back-scattering amplitude and phase shift, σ_i is Debye-Waller factor, and C_0 is a normalizing constant. In the present study, we used theoretical $F_i(k)$[13] and $\phi_i(k)$,[14] and treated C_0, r_0, and σ_i as adjustable parameters, an appropriate assumption being done on N^i value. We introduced the following R index as the measure of the agreement between experimental and calculated $k^n\chi(k)$.

$$R(k^n\chi) = \sqrt{\frac{\sum_j [k^n\chi_{expt}(\chi_j) - k^n\chi_{calcd}(k_j)]^2}{\sum_j [k^n\chi_{expt}(k_j)^2]}}$$

All calculations were performed by use of a HITAC M-200H at the Computer Center of The University of Tokyo.

The results of Fourier transformation of $k^3\chi(k)$ are shown in Fig. 4. A prominent peak is found around 2 Å for all three compounds studied here. This peak corresponds to the first back-scattering shell around Fe ion, its position being a little different for the three salts reflecting the difference of the local structure around Fe ion. Fe ion is likely to be surrounded by six oxygen atoms of coordinating H_2O molecules in $Fe(ClO_4)_3 \cdot 6H_2O$, while it is surrounded by six chlorine ions in anhydrous $FeCl_3$. In $FeCl_3 \cdot 6H_2O$, Fe ion is known to be surrounded by two chlorine ions and four oxygen atoms of coordinating H_2O molecules.[15] Thus it seems quite reasonable that the peak due to the first back-scattering shell is shift to larger distance in anhydrous $FeCl_3$ in comparison with other two compounds.

Back-Fourier transforming the region of the above-mentioned peak, we carried out curve-fitting analysis. The results are summarized in Table 1, the experimental and calculated $k^3\chi(k)$ curves being shown in Figs. 5

Table 1. Bond distances obtained by the analyses of EXAFS data of Fe(III) compounds

The coordination numbers assumed in the analyses are given in parentheses.

Sample		Bond	Bond length d/Å (EXAFS	diffraction)
$FeCl_3 \cdot 6H_2O$		Fe–Cl(2)	2.28	2.30[a]
		Fe–O(4)	2.03	2.07[a]
$Fe(ClO_4)_3 \cdot 6H_2O$		Fe–O(6)	2.00	—
$(Fe(NO_3)_3 \cdot 9H_2O$		Fe–O	—	1.99[b]
$FeCl_3$	(Model 1)[d]	Fe–Cl(6)	2.25	2.48[c]
	(Model 2)[e]	Fe–Cl(3)	2.24	
		Fe–Cl(3)	2.59	

a) From Ref. 15. b) Average of six Fe–O bond lengths, from Ref. 16. c) From Ref. 17b. d) Octahedrally coordinated model (BiI_3-like structure). e) AsI_3-like structure.

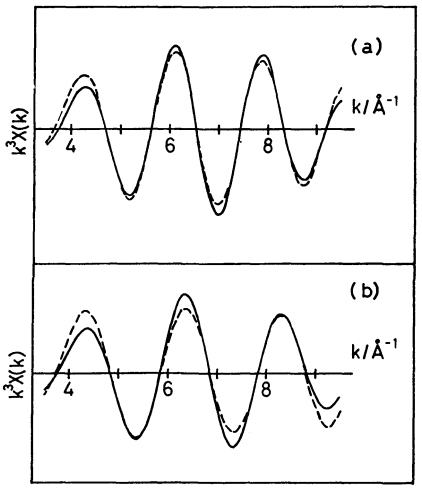

Fig. 5. Curve-fitting results of (a) $FeCl_3 \cdot 6H_2O$ and (b) $Fe(ClO_4)_3 \cdot 6H_2O$ (——: experimental, ------: theoretical).

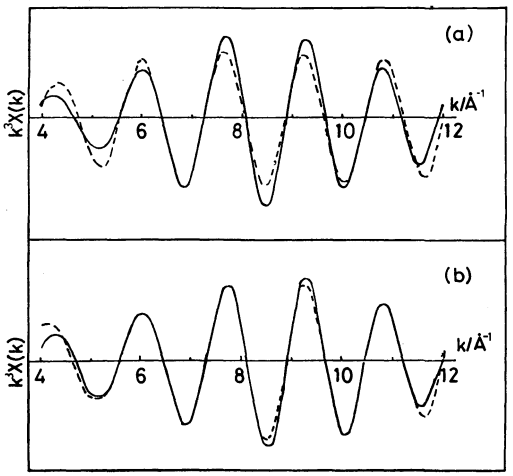

Fig. 6. Curve-fitting results of anhydrous $FeCl_3$: (a) one-shell fitting and (b) two-shell fitting (——: experimental, ------: theoretical).

and 6.

The crystal structure is known for $FeCl_3 \cdot 6H_2O$, according to which Fe ion is surrounded by two chlorine ions with the Fe–Cl distance of 2.30 ± 0.02 Å and four oxygen atoms of H_2O with the Fe–O distance of 2.07 ± 0.02 Å.[15] We performed curve-fitting analysis assuming two back-scattering shells, the one corresponding to four oxygen atoms and the other corresponding two chlorine ions. The best-fit result gave 2.03 ± 0.02 Å for Fe–O and 2.28 ± 0.04 Å for Fe–Cl. These values are in good agreement with the distances known from the crystal structure analysis. This indicates the reliability of our EXAFS data and that of the analysis.

In the case of $Fe(ClO_4)_3 \cdot 6H_2O$, the crystal structure is not known, but there is a good reason to believe that six H_2O molecules are coordinating to Fe ion as in the crystal of $[Fe(H_2O)_6](NO_3)_3 \cdot 3H_2O$.[16] Our EXAFS data are consistent with this assumption. The curve-fitting analysis gave 2.00 ± 0.02 Å for Fe–O distance, which coincides well with 1.986 ± 0.017 Å found by the crystal structure analysis of $[Fe(H_2O)_6] \cdot (NO_3)_3 \cdot 3H_2O$ for the average Fe–O distance between Fe ion and octahedrally coordinating H_2O molecules.[16]

Anhydrous $FeCl_3$ has been considered to have bismuth iodide structure, namely an iron ion is assumed to be surrounded by six chlorine ions with equivalent Fe–Cl distance.[17] Using this model, Fe–Cl distance in anhydrous $FeCl_3$ was deduced to be 2.48 Å from the observed lattice parameters.[17b] From the curve-fitting analysis of EXAFS data, we obtained 2.25 ± 0.05 Å for Fe–Cl distance under the assumption that Fe ion is surrounded by six equivalent chlorine ions. This value is 0.23 Å shorter than the interatomic distance estimated from the lattice parameters. The discrepancy between the two values seems to be too large to be ignored when we consider the fact that the interatomic distances determined from EXAFS data coincide well with those from diffraction data in the cases of other two compounds. If Fe ion is actually surrounded by six equivalent chlorine ions with the Fe–Cl distance of 2.25 Å, the spacing between the two chlorine layers which are sandwiching Fe ions will be 1.98 Å and that between the other pair of chlorine layers will be 3.84 Å. The former value seems to be too small while the latter seems to be too large in comparison with the ionic radius of chlorine ion.

It is worthwhile to note that, although AsI_3 and SbI_3 were previously believed to have bismuth iodide structure,[17a] the detailed crystal structure analyses revealed latter that these compounds were built up from discrete triiodide molecules such as AsI_3 (or SbI_3), consequently six iodine atoms surrounding As (or Sb) atom are not at equivalent distance, three being at a shorter distance and three others at a longer distance.[18,19] Thus we analyzed the EXAFS data of anhydrous $FeCl_3$ with two-shell model assuming AsI_3-like structure. The curve-fitting analysis gave 2.24 ± 0.05 Å and 2.59 ± 0.05 Å for the two Fe–Cl distances with an excellent agreement between the experimental and calculated $k^3\chi(k)$ (Fig. 6b); the R index was found to be only 0.155 while it was 0.274 in the analysis with one-shell model (Fig. 6a). Therefore it is most likely that anhydrous $FeCl_3$ has AsI_3-like structure.

Summary

We constructed an in-laboratory EXAF Sspectometer combining a transmission-type dispersing crystal with a position-sensitive proportional counter, and demonstrated that EXAFS data of a sufficient quality for structural study could be obtained with a torelable measuring time. This EXAFS spectrometer is easily constructed with a relatively small cost, and might have wide applications.

By analyzing EXAFS data obtained on $FeCl_3 \cdot 6H_2O$, $Fe(ClO_4)_3 \cdot 6H_2O$ and anhydrous $FeCl_3$ by use of the constructed in-laboratory apparatus, we studied the local structures around Fe ions, and showed that anhydrous $FeCl_3$ has AsI_3-like structure, having three chlorine atoms at a shorter Fe–Cl distance and other three chlorine atoms at a longer Fe–Cl distance.

The authors would like to express their thanks to Dr. H. Hashizume and Dr. K. Mase for their kind advise for the construction of PSPC.

References

1) S. P. Cramer and K. O. Hodgson, *Prog. Inorg. Chem.*, **25**, 1 (1979).
2) D. E. Sayer, E. A. Stern, and F. W. Lytle, *Phys. Rev. Lett.*, **27**, 1204 (1971).
3) E. A. Stern, *Phys. Rev. B*, **10**, 3027 (1974).
4) F. W. Lytle, D. E. Sayers, and E. A. Strern, *Phys. Rev. B*, **11**, 4825 (1975).
5) E. A. Stern, D. E. Sayers, and F. W. Lytle, *Phys. Rev. B*, **11**, 4836 (1975).
6) J. A. Del Cueto and N. J. Shevchik, *J. Phys. F*, **7**, L215 (1977); G. Martens, P. Rabe, N. Schwentner, and A. Werner, *Phys. Rev. B*, **17**, 1481 (1978).
7) G. S. Knapp, H. Chen, and T. E. Klippert, *Rev. Sci. Instrum.*, **49**, 1658 (1978).
8) S. Kiyono, Y. Hayashi, and T. Muranaka, "International Conference on the Physics of X-Ray Spectra," Gaithersburg, Maryland (1976).
9) G. G. Cohen, D. A. Fischer, J. Calbert, and N. J. Shevchik, *Rev. Sci. Instrum.*, **51**, 273 (1980).
10) U. Kaminaga, T. Matsushita, and K. Kohra, *Jpn., J. Appl. Phys.*, **20**, L355 (1981).
11) N. Sano, K. Taniguchi, and H. Yamatera, *Chem. Lett.*, **1980**, 1285.
12) Y. Sato, Thesis, University of Tokyo (1982).
13) B. M. Kincaid, *J. Am. Chem. Soc.*, **99**, 3854 (1977).
14) P. A. Lee, B. K. Teo, and A. L. Simons, *J. Am. Chem. Soc.*, **99**, 3856 (1977).
15) M. D. Lind, *J. Chem. Phys.*, **47**, 990 (1967).
16) N. J. Hair and J. K. Beattie, *Inorg. Chem.*, **16**, 245 (1977).
17) a) R. W. G. Wyckoff, "Crystal Structures," 2nd ed, Interscience Publishers, New York (1960), Vol. 2, p. 45; b) N. W. Gregory, *J. Am. Chem. Soc.*, **73**, 472 (1951).
18) J. Trotter, *Z. Kristallogr.*, **121**, 81 (1965).
19) J. Trotter and T. Zobel, *Z. Kristallogr.*, **123**, 67 (1966).

Photoelectron Angular Distribution Study of Some Isoxazoles Combined with Perturbation Theoretic Approach

Tsunetoshi KOBAYASHI,*,†,†† Tanekazu KUBOTA,††† Kiyoshi EZUMI,†††† and Chikatoshi UTSUNOMIYA†

†*The Institute of Physical and Chemical Research, Wako, Saitama 351*

††*The Institute for Solid State Physics, The University of Tokyo, Roppongi, Minato-ku, Tokyo 106*

†††*Gifu College of Pharmacy, Mitahora-higashi, Gifu 502*

††††*Shionogi Research Laboratories, Shionogi and Co., Ltd., Fukushima, Osaka 553*

(Received July 15, 1982)

Photoelectron spectra of isoxazole, 5-methylisoxazole, and 3,5-dimethylisoxazole were studied by the technique of photoelectron angular distribution measurements combined with a first order perturbation theoretic approach. Photoelectron spectra of oxazole, 4-methyloxazole, furan, and 2-methylfuran, which are closely related to isoxazole, were also discussed at the same time for the sake of comparison. The first three bands of the isoxazoles were assigned to the π, π, and n bands from the top, respectively, while those of the oxazoles were identified as the π, n, and π bands from the top.

Isoxazole is one of the typical five-membered heteroaromatics with two heteroatoms and important from the pharmacological standpoint also. In this paper photoelectron spectra of isoxazole, 5-methylisoxazole, and 3,5-dimethylisoxazole are studied by the technique of photoelectron angular distribution measurements combined with a perturbation theoretic approach. Photoelectron spectra of oxazole, 4-methyloxazole, furan, and 2-methylfuran, which are closely related to isoxazole, are also discussed at the same time for the sake of comparison.

Baker *et al.*[1] and Palmer *et al.*[2] reported the photoelectron spectrum of isoxazole formerly and considered that the first band is a π band and that the second band group is composed of a π band and an n (nonbonding) one highly overlapping with each other. But the relative ordering of the π and n bands in the second band group is not yet established. In this paper we focus our attention especially on this complicated second band group region of isoxazole and try to establish the assignments of the lower energy photoelectron spectral bands of the isoxazoles.

Formerly an empirically parameterized method based on the first order perturbation theory was developed for photoelectron spectral band assignments and applied to azaaromatics.[3] With this technique one can easily distinguish π bands from n or σ bands by regarding azareplacements, for example, as perturbations. The same technique is applicable to the case of alkyl substitutions also.[4] In this paper at first this type of approach will be used.

Concerning photoelectron angular distributions, differential cross section (σ_Q) for photoelectron ejection is given by the following expression[5,6] for the case of an unpolarized light and an ensemble of randomly oriented molecules:

$$\sigma_Q \propto \{1+(1/4)\beta(3\sin^2\theta-2)\}, \quad (1)$$

where β is an asymmetry parameter and θ is the angle between the propagation direction of an ejected photoelectron and that of an incoming photon. The β value depends not only on the kinetic energy of the photoelectron but also on the character of the MO from which the photoelectron is ejected. Therefore, the β values can be used for photoelectron spectral band assignments as exemplified in the case of benzene,[7] pyridine,[8] aliphatic alcohols, amines, and halides.[9] In this paper the combination of the photoelectron angular distribution experiments with the perturbation theoretic approach will be demonstrated to be very powerful in solving photoelectron spectral band assignment problems.

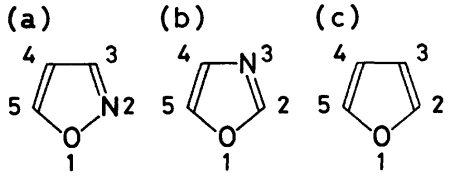

Fig. 1. Structural formulae of isoxazole (a), oxazole (b), and furan (c) with numberings of atoms.

Experimental

Materials. Pure samples of isoxazole, 5-methylisoxazole, 3,5-dimethylisoxazole, and 4-methyloxazole were kindly supplied by Dr. T. Honma of Shionogi Research Laboratories. Commercially available furan and 2-methylfuran were used without furthur purifications. Commercially available isoxazole, 5-methylisoxazole, and 3,5-dimethylisoxazole were also used without furthur purifications for the photoelectron angular distribution experiments.

Measurements. The vapor phase HeI photoelectron spectra of these compounds were measured at first using the photoelectron spectrometer described formerly.[10] Xe gas was used as the internal reference standard compound for the energy scale calibrations. The HeI photoelectron angular distributions of isoxazole, 5-methylisoxazole, 3,5-dimethylisoxazole, furan, and 2-methylfuran in the vapor phases were measured using the instrument described formerly,[7] the vapor pressures of the samples being kept at 4×10^{-4} Torr (1 Torr= 133.322 Pa). The β values were obtained according to formula (1) using the photoelectron spectral intensities measured at two angles, $\theta=45°$ and 90°.

Computational

The CNDO/S[11] calculations of furan, oxazole, and isoxazole were carried out by the FACOM 230-75

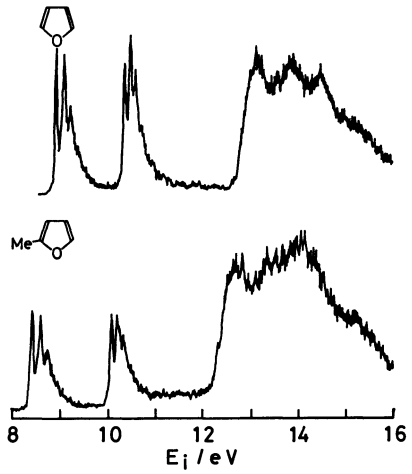

Fig. 2. Vapor phase HeI photoelectron spectra of furan and 2-methylfuran.

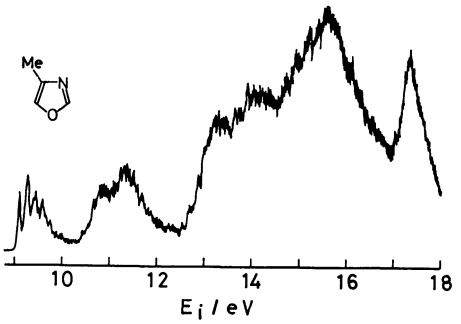

Fig. 3. Vapor phase HeI photoelectron spectrum of 4-methyloxazole.

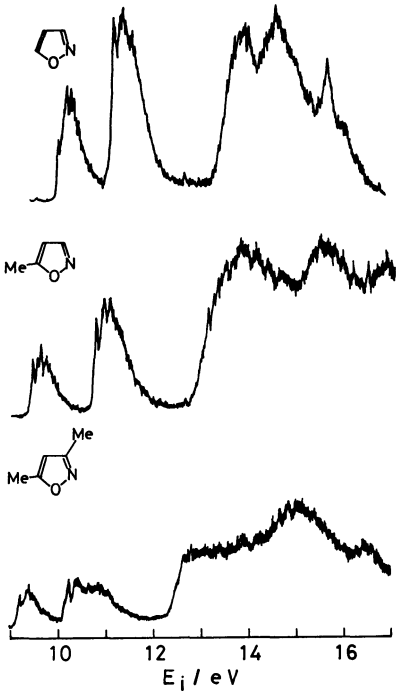

Fig. 4. Vapor phase HeI photoelectron spectra of isoxazole, 5-methylisoxazole, and 3,5-dimethylisoxazole.

computer at the Institute of Physical and Chemical Research. The geometrical structural parameters of furan and isoxazole were taken from Refs. 12 and 13, respectively, and those of oxazole were assumed to be similar to those of furan.

Results and Discussion

The HeI photoelectron spectra of furan, 2-methylfuran, 4-methyloxazole, isoxazole, 5-methylisoxazole, and 3,5-dimethylisoxazole are shown in Figs. 2, 3, and 4. Of these compounds the ultraviolet photoelectron spectrum of furan was reported by various authors[1,14-20] formerly, and that of isoxazole by Baker *et al.*[1] and by Palmer *et al.*[2] also. Their spectra are consistent with ours. The vertical ionization energy (E_{iv}) values of those compounds are summarized in Table 1 for the region of interest with those of oxazole.[2]

Perturbation Theoretic Approach. At first let us try to make assignments of the lower energy photoelectron spectral bands of isoxazole and its methyl derivatives from the perturbation theoretic standpoint.

According to the first order perturbation theory, E_{iv} changes (ΔE_{iv}'s) of π bands caused by substitutions (replacements) can be estimated by using the following formula:[3]

$$-\Delta E_{ivj} = a + b\sum_{\mu,\nu}(C_{\mu j}^2 + m C_{\nu j}^2), \qquad (2)$$

where j denotes the j-th MO corresponding to a certain photoelectron spectral band in question, a is a constant introduced for statistical treatments, b is also a constant and corresponds to the HMO level one-centre Coulomb integral change of a certain atom caused by a certain substitution (replacement) at this atom, $C_{\alpha j}$ is the AO coefficient of atom α in the j-th MO, μ denotes atom μ at which a certain substitution (replacement) is introduced, ν denotes atom ν just adjacent to atom μ, and m is a kind of damping factor.

The a, b, and m values for formula (2) were taken from Ref. 3 for aza-replacements and from Ref. 21 for methyl substitutions. The $C_{\alpha j}$ values used are those obtained by the CNDO/S[11] calculations for furan, oxazole, and isoxazole. The E_{iv} values of the five-membered ring compounds estimated by this perturbation theoretic approach regarding aza-replacements or methyl substitutions as perturbations are summarized in Table 1. The reference standard compounds in this table denote the compounds, the E_{iv}'s of which are used to estimate the E_{iv}'s of the compounds in question by being corrected for the ΔE_{iv} values calculated by formula (2) with the $C_{\alpha j}$ values of those compounds.

At first in order to check the validity of the method used here, let us examine the apparent case of furan and 2-methylfuran. As is seen in Fig. 2 the first two bands of furan are rather vertical and well separated from the following bands. These bands have already been unambiguously assigned to the $a_2\pi$ and $b_1\pi$ bands from the top, respectively.[1,14-20] By introducing 2-methyl group into furan, the first two bands are slightly shifted to the lower ionization energy (E_i) side, but their band shapes remain still rather vertical indifferent to this substitution and these bands are well separated from the following bands. It is quite natural to assign straightforwardly the first two bands of 2-methylfuran to the

Table 1. Observed vertical ionization energy (E_{iv}) values of isoxazoles and related compounds with Π ones calculated by perturbation theoretic approach

Compound		E_{iv}/eV Band 1	2	3	R.M.S.E./eV[a]	Reference standard compound[b]
Isoxazole	Obsd	10.15	11.15[c]	11.3—11.6		
	Calcd	10.12	11.11		0.15	Furan
5-Methylisoxazole	Obsd	9.61	10.95	11.2		
	Calcd	9.68	10.95		0.16	Furan
	Calcd	9.71	10.99		0.06	Isoxazole
	Calcd	9.61	10.82		0.15	2-Methylfuran
3,5-Dimethylisoxazole	Obsd	9.34	10.35	10.81		
	Calcd	9.43	10.45		0.16	Furan
	Calcd	9.45	10.49		0.06	Isoxazole
	Calcd	9.36	10.46		0.06	5-Methylisoxazole
Oxazole	Obsd[d]	9.83	11.19	11.80		
	Calcd	9.81		11.85	0.15	Furan
4-Methyloxazole	Obsd	9.27	10.81	11.31		
	Calcd	9.39		11.45	0.16	Furan
	Calcd	9.41		11.40	0.06	Oxazole
Furan	Obsd	8.89	10.44			
2-Methylfuran	Obsd	8.38	10.15			
	Calcd	8.48	10.20		0.06	Furan

a) The root mean square error for the calculated π E_{iv}'s. b) The standard compound, the E_{iv}'s of which were used as the starting points to estimate the E_{iv}'s of the compound in question, by being corrected for the ΔE_{iv} values calculated by formula (2). c) This value is a possible candidate for the second E_{iv} of isoxazole, and 11.3 eV may be another one. d) Taken from Ref. 2.

a_2-like π and b_1-like π bands from the top, respectively. On the other hand, as is seen in Table 1, starting from the E_{iv} values of the first two bands of furan, the perturbation theoretic calculations reproduce well the observed E_{iv} values for the first two bands of 2-methylfuran, strongly supporting the above qualitative assignments.

Now let us examine the next rather slightly more complicated case of oxazole and 4-methyloxazole. As is seen in Fig. 1 of Ref. 2 and Fig. 3 both these compounds show three bands in the energy region from 9 eV to 12.5 eV separated from the following bands. In this energy region two π bands corresponding to the first two bands of furan and one n band mainly related to the nitrogen atom n orbital are expected to appear from the analogy to the case of furan and pyridine.[8,22] Concerning oxazole Palmer *et al.*[2] assigned the first and third bands to the π bands and the second band to the n band on the basis of an *ab initio* calculation and band shape considerations. Their assignment seems to be probable, because the second band is nonvertical, that is, rather broad just as in the case of the n bands of pyridine and other azaaromatics,[3,4,8,22] the first and the third bands being rather vertical as in the case of the first two π bands of the furans just we have seen above.

On the other hand, by the perturbation theoretic calculations using furan as the reference standard compound, as is seen in Table 1, the first and third bands of oxazole can be unambiguously assigned to the π bands corresponding to the first and second bands of furan, respectively, and the remaining second band is ascribed to the n band. Thus, Palmer and coworkers' assignments[2] have now been definitely substantiated.

By comparing the band shapes and the E_{iv} values of the first three bands of 4-methyloxazole with those of oxazole we may qualitatively assign the first and third bands to the π bands and the second to the n band in the case of 4-methyloxazole also. On the other hand, starting from either furan or oxazole as the reference standard compound, in the case of 4-methyloxazole also, the first three bands can be definitely assigned to the π, n, and π bands from the top, respectively, by the first order perturbation theoretic approach, supporting the above qualitative consideration. Thus, the orderings of the first three bands of the oxazoles have now been firmly established to be π, n, and π from the top.

As we have seen in the above examples, the perturbation theoretic approach seems to be very powerful to establish band assignments. Now let us move to the complicated case of the isoxazoles in question. These compounds show three photoelectron spectral band groups in the energy region from 9 eV to 12 eV. And in this energy region three bands, two of which are π bands and one of which is an n band, are expected to appear just as in the case of the oxazoles. From the relative intensity ratio of the first and second band groups of isoxazole and 5-methylisoxazole the second band groups of these compounds are naturally regarded to be composed of two bands. In the case of isoxazole Baker *et al.*[1] and Palmer *et al.*[2] formerly regarded the first band as a π band and the second band group to be composed of a π band and an n band overlapping with each other highly.

In the case of 3,5-dimethylisoxazole the first band is rather vertical and the second and third bands can be recognized separately, the second band being rather vertical with the first strong sharp peak, while the third band seems to be rather broad. From the band shape considerations we may assign the first and second bands to the π bands and the remaining third band to the n

band in this case. On the other hand, according to the first order perturbation theoretic calculations using furan as the reference standard compound, the first two bands of 3,5-dimethylisoxazole can be definitely assigned to the π bands corresponding to the first two π bands of furan from the top, respectively, and the remaining third band is ascribed to the n band as is seen in Table 1, the above qualitative considerations being strongly supported.

The vertical features of the first band and the lower energy part of the second band group can be recognized in the case of either isoxazole or 5-methylisoxazole also, and it is quite reasonable to correlate the first band and the lower energy part of the second band group of either isoxazole or 5-methylisoxazole with the first two π bands of 3,5-dimethylisoxazole from the top, respectively. The higher energy part of the second band group of either isoxazole or 5-methylisoxazole is now ascribed to the n band.

On the other hand, according to the first order perturbation theoretic approach the first band of isoxazole is definitely assigned to the π band corresponding to the first band of furan and the lower energy part rather than the higher energy part of the second band group is suggested to be assigned to the second π band, if we start from the E_{iv} values of furan. This is consistent with the qualitative conclusion described above.

In the case of 5-methylisoxazole, based on the perturbation theoretic calculations, the first band and the lower energy part and higher energy part of the second band group can be assigned to the π, π, and n bands from the top, respectively, by starting from either furan or 2-methylfuran. The same assignments can be obtained by starting from the E_{iv} values of isoxazole on the assumption that the assignments in the case of isoxazole given above are correct. This fact supports the validity of the band assignments for the first three bands of isoxazole given above.

According to the first order perturbation theoretic calculations starting from either isoxazole or 5-methylisoxazole on the assumption of the validity of the band assignments given above, we can get the same band ordering for the first three bands of 3,5-dimethylisoxazole as obtained above. This fact also supports the validity of the band assignments of isoxazole and 5-methylisoxazole given above.

Thus, from the first order perturbation theoretic standpoint supported by the qualitative discussions the band orderings of the first three bands of the isoxazoles are π, π, and n from the top, while those of the oxazoles are π, n, and π from the top.

Photoelectron Angular Distributions. In order to establish the assignments of the second and third bands of the isoxazoles more firmly, the photoelectron angular distributions of isoxazole, 5-methylisoxazole, 3,5-dimethylisoxazole, furan, and 2-methylfuran were measured. The β values (see formula (1)) for these compounds are plotted in Figs. 5 and 6 with the photoelectron spectra measured at the magic angle, $\theta=54.7°$. The β values of these compounds for several E_{iv} values are summarized in Table 2. Sell and Kuppermann[19] measured the HeI photoelectron angular distributions of furan, their results being almost consistent with ours.

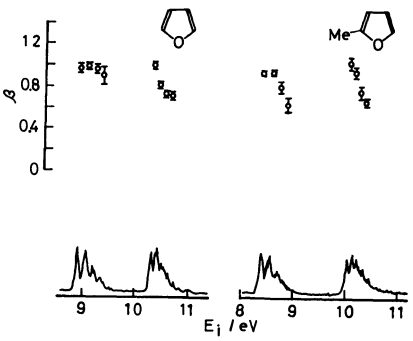

Fig. 5. HeI photoelectron angular distribution asymmetry parameter (β) values plotted with photoelectron spectra measured at $\theta=54.7°$ for furan and 2-methylfuran.

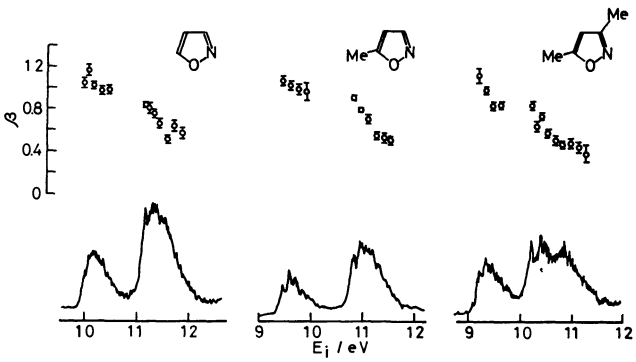

Fig. 6. HeI photoelectron angular distribution asymmetry parameter (β) values plotted with photoelectron spectra measured at $\theta=54.7°$ for isoxazole, 5-methylisoxazole, and 3,5-dimethylisoxazole.

TABLE 2. PHOTOELECTRON ANGULAR DISTRIBUTION ASYMMETRY PARAMETER (β) VALUES OF ISOXAZOLES AND FURANS AT SOME KEY POINTS WITH IONIZATION ENERGY (E_i) VALUES INDICATED

Compound	E_i/eV	β[a]
Isoxazole	10.15	1.02±0.03
	11.15	0.84±0.02
	11.31	0.75±0.04
	11.57	0.51±0.04
5-Methylisoxazole	9.61	1.02±0.04
	10.79	0.90±0.02
	10.95	0.78±0.02
	11.17	0.54±0.04
3,5-Dimethylisoxazole	9.34	0.98±0.04
	10.20	0.84±0.04
	10.35	0.73±0.04
	10.81	0.47±0.03
Furan	8.89	0.97±0.04
	10.44	0.82±0.03
2-Methylfuran	8.38	0.93±0.03
	10.15	0.94±0.05

a) The root mean square errors are given.

At first let us examine the results for furan and 2-

methylfuran, the assignments of the first two bands of which are definitely the a_2(-like) π and b_1(-like) π from the top, respectively. As is seen in Fig. 5 in the case of furan and 2-methylfuran the first two π bands show large β values from 0.8 to 1 at the band maxima indifferent to the symmetries of the corresponding MOs. Keeping this point in mind let us move to the case of the isoxazoles in question.

In the case of 3,5-dimethylisoxazole, the first three bands can be well recognized separately, and the first two bands show relatively high β values from 0.7 to 1 at their band maxima, while the third band shows relatively low β value, 0.47, at the band maximum. Remembering the fact that isoxazole and furan are iso-π-electronic with each other, the first and second bands of 3,5-dimethylisoxazole may be assigned to the π bands by comparing the β values of the first three bands of this compound with those of the first two π bands of furan, the remaining third band of 3,5-dimethylisoxazole with low β value being ascribed to the n band. These assignments may be further supported by the fact that the n band of pyridine iso-π-electronic with isoxazole shows low β value around 0.2, the following two π bands showing relatively high β values.[8] Combining this result with the perturbation theoretic discussions given above, the first three bands of 3,5-dimethylisoxazole are now definitely assigned to the π, π, and n bands from the top, respectively.

Moving to the case of isoxazole and 5-methylisoxazole, the first bands of these compounds show high β values around 1.0 at the band maxima, and by comparing these values with those of the lower energy π bands of 3,5-dimethylisoxazole and the furans, it is definite that the first bands of isoxazole and 5-methylisoxazole are the π bands as assigned by the first order perturbation theoretic discussions given above. The lower energy parts of the second band groups of isoxazole and 5-methylisoxazole show high β values comparable to those of the lower energy part of the second band of 3,5-dimethylisoxazole, and the higher energy parts of the second band groups of isoxazole and 5-methylisoxazole show low β values just as the third band of 3,5-dimethylisoxazole which is definitely the n band as discussed above. From these facts we can definitely assign the lower energy parts of the second band groups of isoxazole and 5-methylisoxazole to the π bands and the higher energy parts to the n bands. These assignments are consistent with those obtained by the first order perturbation theoretic considerations.

Summing up the discussions given above the orderings of the first three bands of the isoxazoles treated here have now been firmly established to be π, π, and n from the top, and those of the oxazoles π, n, and π from the top. Combination of the photoelectron angular distribution experiments with the perturbation theoretic approach has been demonstrated to be very powerful in the photoelectron spectral band assignments.

We express our sincere thanks to Dr. T. Honma of Shionogi Research Laboratories for the pure samples.

References

1) A. D. Baker, D. Betteridge, N. R. Kemp, and R. E. Kirby, *Anal. Chem.*, **42**, 1064 (1970).
2) M. H. Palmer, R. H. Findlay, and R. G. Egdell, *J. Mol. Struct.*, **40**, 191 (1977).
3) F. Brogli, E. Heilbronner, and T. Kobayashi, *Helv. Chim. Acta*, **55**, 274 (1972).
4) E. Heilbronner, V. Hornung, F. H. Pinkerton, and S. F. Thames, *Helv. Chim. Acta*, **55**, 289 (1972).
5) J. C. Tully, R. S. Berry, and B. J. Dalton, *Phys. Rev.*, **176**, 95 (1968).
6) J. W. McGowan, D. A. Vroom, and A. R. Comeaux, *J. Chem. Phys.*, **51**, 5626 (1969).
7) T. Kobayashi and S. Nagakura, *J. Electron Spectrosc. Relat. Phenom.*, **7**, 187 (1975).
8) C. Utsunomiya, T. Kobayashi, and S. Nagakura, *Bull. Chem. Soc. Jpn.*, **51**, 3482 (1978).
9) C. Utsunomiya, T. Kobayashi, and S. Nagakura, *Bull. Chem. Soc. Jpn.*, **53**, 1216 (1980).
10) T. Kobayashi, K. Yokota, and S. Nagakura, *J. Electron Spectrosc. Relat. Phenom.*, **2**, 449 (1973).
11) R. L. Ellis, G. Kuehnlenz, and H. H. Jaffé, *Theor. Chim. Acta*, **26**, 131 (1972).
12) B. Bak, D. Christensen, W. B. Dixon, L. Hansen-Nygaard, J. R. Andersen, and M. Schottländer, *J. Mol. Spectrosc.*, **9**, 124 (1962).
13) O. L. Stiefvater, *J. Chem. Phys.*, **63**, 2560 (1975).
14) J. H. D. Eland, *Int. J. Mass Spectrom. Ion Phys.*, **2**, 471 (1969).
15) A. D. Baker and D. W. Turner, *Philos. Trans. R. Soc. London, Ser. A*, **268**, 131 (1970).
16) D. W. Turner, C. Baker, A. D. Baker, and C. R. Brundle, "Molecular Photoelectron Spectroscopy," Wiley-Interscience, London (1970), p. 329.
17) P. J. Derrick, L. Åsbrink, O. Edqvist, B.-Ö. Jonsson, and E. Lindholm, *Int. J. Mass Spectrom. Ion Phys.*, **6**, 161 (1971).
18) P. J. Derrick, L. Åsbrink, O. Edqvist, and E. Lindholm, *Specrtochim. Acta, Part A*, **27**, 2525 (1971).
19) J. A. Sell and A. Kuppermann, *Chem. Phys. Lett.*, **61**, 355 (1979).
20) T. Munakata, K. Kuchitsu, and Y. Harada, *J. Electron Spectrosc. Relat. Phenom.*, **20**, 235 (1980).
21) T. Kobayashi, T. Arai, H. Sakuragi, K. Tokumaru, and C. Utsunomiya, *Bull. Chem. Soc. Jpn.*, **54**, 1658 (1981).
22) R. Gleiter, E. Heilbronner, and V. Hornung, *Helv. Chim. Acta*, **55**, 255 (1972).

Studies on the Concentrated Steffen Fluid of Beet Sugar Industry. I. On the Salt Separated from Concentrated Steffen Fluid Using Methanol and Sulfuric Acid

Masaaki Ito,* Kazuo Abe, Teruji Sasaki, Norimitsu Wakabayashi,† and Kenzo Misono††

Chemistry Laboratory, Department of General Education, Higashi-Nippon-Gakuen University, Onbetsu, Hokkaido 088-01

†*Technical Laboratory, Showa-Tansan Co., Ltd., 1, 7-Ohghimachi, Kawasaki-ku, Kawasaki 210*

††*Hokkaido-Togyo Co., Ltd., 1, 20-Kandajinbocho, Chiyoda-ku, Tokyo 100*

(Received September 7, 1982)

The chemical desalting technique was applied to the concentrated Steffen fluid using concd sulfuric acid and methanol. The chemical components of the isolated salt were studied by scanning electron microscopy, infrared spectroscopy, X-ray diffraction, and fluorescence analyses. The main constituent of the salt was determined to be $K_3Na(SO_4)_2$ and then synthesized.

One recovery technique of residual sugar from molasses is the Steffen method using calcium oxide. This treatment discharges waste fluid which is generally concentrated in order to avoid pollution of rivers and sea. General analytical data and the infrared spectra of the concentrated Steffen fluid are summarized and shown in Table 1 and Fig. 1.

How to isolate the components of the concentrated Steffen fluid for manufacturing the products is a matter of interest and importance to the beet sugar industry. This interest in the chemical components led us to isolate the inorganic components and determine their chemical constituents. This paper describes a chemical desalting technique of the concentrated Steffen fluid and the chemical components, and the chemical structure and syntheses of the main constituents of the salt isolated.

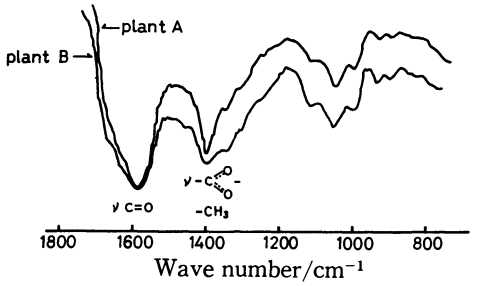

Fig. 1. Infrared spectra of concentrated Steffen fluids applied to KBr disk.

Table 1. General chemical components of concentrated steffen fluid (pH 9.0)

Solid matter	55%
Carbohydrates, total	13 (sucrose 12.4%)
Reductive carbohydrates	0.2
Nitrogen, total	3.0
Nitrogen, amide	0.7
Nitrogen, betaine	1.1
Sulfate ash	20.0
Sodium	1.5
Potassium	6.6
Calcium	0.01
Phosphorus as P_2O_5	0.01
Others	0.4

It is known that acidification of the concentrated Steffen fluid causes a desalting phenomenon.[1] This elementary knowledge was developed into the desalting process to be reported below. And also, the chemical structure of the main constituent of the isolated salt was determined as tripotassium sodium bis (sulfate) by the X-ray diffraction data and identified by the synthesis starting from the related known inorganic compounds. The by-components and the impurities were identified with the X-ray diffraction data and the fluorescent X-ray data.

Experimental

The IR spectra were determined on a Shimadzu IR-400 spectrometer. The X-ray diffraction and fluorescence analyses were performed on a Toshiba ADG-102 X-ray diffractometer and a AFV-202F X-ray fluorescence spectrometer.

General Procedure for Desalting Treatment of the Concentrated Steffen Fluid. A solution of the concentrated Steffen fluid in methanol, was acidified by addition of a suitable amounts of concd sulfuric acid till pH 4 or 3 of the solution was attained. After standing over night or on chilling, the salt which precipitated was filtered. The salt obtained was recrystallized from water for further purification as needed. Isolation of the salt can be efficiently carried out in *ca.* 20—24% yield for the concentrated Steffen fluid used, and the yield was almost quantitative.

Preparation of Potassium Sodium Sulfate. Procedure 1: Aqueous solution of 3 mol of KOH and 1 mol of NaOH was treated with concd sulfuric acid until pH 3 and the salt was deposited by addition of methanol.

Procedure 2: Aqueous solution of 3 mol K_2SO_4 and 1 mol of Na_2SO_4 was concentrated by rotary evaporator until deposition of the salt.

Procedure 3: The salt was deposited from aqueous solution of 3 mol K_2SO_4 and 1 mol Na_2SO_4 by addition of methanol.

Procedure 4: Aqueous solution of 3 mol of K_2SO_4 and 1 mol of Na_2SO_4 was controlled at pH 3 and then salt deposition treatment was carried out by addition of methanol. The results of preparations starting from potassium and sodium compounds are summarized in Table 4.

Results and Discussion

Effective desalting out treatment of concentrated Steffen fluid using concd sulfuric acid in methanol was carried out. Addition of concd sulfuric acid is for the

Table 2. Desalting treatments of concentrated Steffen fluid

Plant A		
Concentrated Steffen fluid, g	665	
Reconcentrated Steffen fluid, g	460	
Salt obtained by acidification using concd H_2SO_4 to pH 3 in MeOH solution, g	163	(24.4%[a])
Plant B		
Concentrated Steffen fluid, g	708	
Salt precipitated by addition of MeOH, g	10.6	(1.5%[a])
Residue after evaporation of MeOH and water, g	406	(57.4%[a])
Salt isolated by acidification of the above residue till pH 3	84.4	(20.8%[a])
Plant C		
Concentrated Steffen fluid, g	1000	
Salt isolated by acidification in MeOH solution till pH 3	225	(22.5%[a])

a) Yields were wt% for concentrated Steffen fluid used.

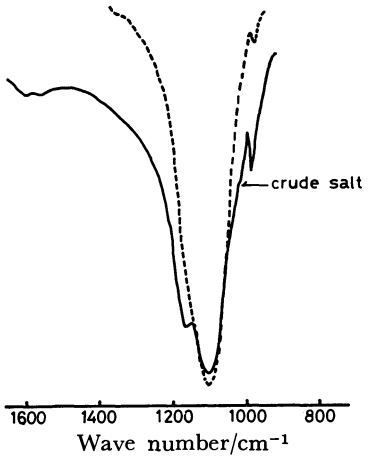

Fig. 2. Infrared spectra of the salts precipitated from Steffen vinasse (KBr-disk).

most efficient precipitation of sulfate salt; the addition of methanol makes a contribution to reduce the solubility of the inorganic salts. Incidentally, methanol alone added to concentrated Steffen fluid or reconcentrated Steffen fluid precipitates the salt in *ca.* 1.5% yield for concentrated Steffen fluid. Furthermore, addition of concd sulfuric acid until pH 4 or 3 of concentrated Steffen fluid or reconcentrated Steffen fluid in methanol solution makes for efficient precipitation of the salt, as shown in Table 2. The salt obtained by the above treatment was crystalline matter, shown in the scanning electron microscopic photographs in Fig. 3.

Infrared spectra of the salts precipitated by addition of methanol alone and by addition of concd sulfuric acid in methanol solution have the characteristic absorption in 1000—1200 cm^{-1} region, as shown in Fig. 2. The IR spectrum of the salts purified by recrystallization from pure water showed an adsorption at 1090 cm^{-1} alone, which suggests it to be a sulfate ion. The shoulder band on the IR spectrum of the crude salt

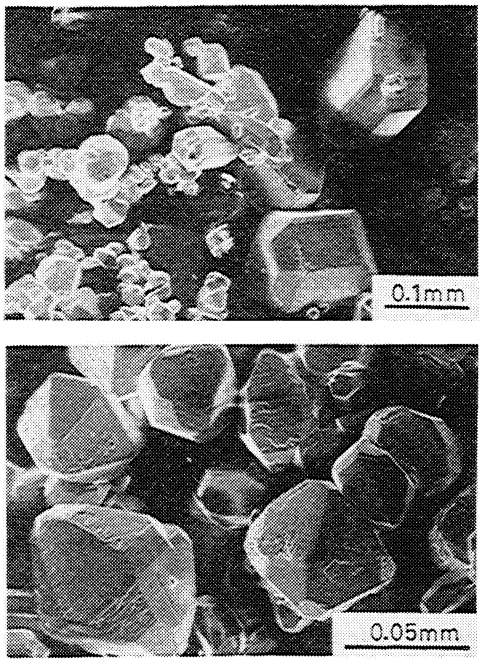

Fig. 3. SEM photographs of the crude salt isolated from CSF.

Table 3. X-Ray diffraction data[a] (time constant; 2 chart full scale; 400/0.6)

2θ/° (Intensity)	2θ/° (Intensity)
$K_3Na(SO_4)_2$	
1.422 (65.6)	2.039 (44.4)
1.468 (63.3)	2.189 (41.2)
1.538 (60.1)	2.336 (38.5)
1.601 (57.5)	2.447 (36.7)
1.641 (56.0)	2.642 (33.9)
1.660 (55.3)	2.838 (31.5)
1.717 (53.3)	2.938 (30.4)
1.732 (52.8)	3.675 (24.2)
1.833 (49.7)	4.092 (21.7)
1.852 (49.1)	4.924 (18.0)
$K_2S_4O_6$	$K_2S_3O_{10}$
2.938 (30.4)	3.140 (28.4)
3.056 (29.2)	3.361 (26.5)
3.173 (28.1)	3.847 (23.1)
3.361 (26.5)	4.267 (22.8)

a) Form: Powder, X-ray target: Cu, X-ray-intensity 35-Kvp. 15 ma. Scan speed: 1°/min, Scan range: 70 from 5, Chart speed: 10 mm/min.

Table 4. Syntheses of tripotassium sodium bis(sulfate)

Raw materials	Preparation	Sulfate salt obtained
3KOH+NaOH	Procedure 1	$K_3Na(SO_4)_2$ (*ca.* 60%) and Na_2SO_4 (*ca.* 40%)
$3K_2SO_4+Na_2SO_4$	Procedure 2	$K_3Na(SO_4)_2$ (*ca.* 50%) and K_2SO_4 (*ca.* 50%)
$3K_2SO_4+Na_2SO_4$	Procedure 3	$K_3Na(SO_4)_2$ (100%)
$3K_2SO_4+Na_2SO_4$	Procedure 4	$K_3Na(SO_4)_2$ (*ca.* 80%) and K_2SO_4 (20%)

which appears at slightly higher wavelength (1170 cm^{-1}) should be attributed to the HSO_4^- ion which disappears from the spectrum of the purified salt. The X-ray diffraction data of the crude salt allowed us to the chemical structure of the salt to be $K_3Na(SO_4)_2$ as shown in Table 3; the presence of the compounds $K_2S_4O_6$ and $K_2S_3O_{10}$ were found as by-products in *ca.* 30—40%. The results were confirmed with ASTM data, No. 20928 ($K_3Na(SO_4)_2$), No. 5631 (Na_2SO_4), and No. 5613 (K_2SO_4). The fluorescent X-ray data showed the presence of Cu, Rb, and Zn (below 0.0%) as the small impurities.

The syntheses of tripotassium sodium bis(sulfate) known hitherto as a natural occurring material was carried out starting from the corresponding sulfates or hydroxides and sulfuric acid for the purpose of identification of the salt. It is known[2,3] that potassium sodium sulfate naturally occurs in volcanic districts, *e.g.* the glaserita or aphthitalite $K_3Na(SO_4)_2$ found as an incrustation on Vesuvian lava, in the salt deposit of Douglashall (Westeregeln), at Rucalmuta (Sicily), and in a sea water system, for example B. Gossner[4] regards glaserite as a definite mineral species, but J. H. Van't Hoff and H. Barshall[5] considered it to be a mixture of the two component sulfates: $3K_2SO_4+Na_2SO_4$. An impure form of this salt containing 75 to 85 per cent of K_2SO_4 and 9 to 21 per cent of Na_2SO_4 and known as platosulfate[6] has been separated from a concentration of kelp-liquors.

The authors wish to express their thanks to Hokkaido-Togyo Co., Ltd. for financial support and Dr. Yoshihisa Yamamoto of the Faculty of Pharmaceutical Sciences, Higashi-Nippon-Gakuen University, for his helpful discussion.

References

1) F. A. Holgan, U. S. Patent 2519573 (1950); Brit. Patent 651643 (1951).
2) J. W. Mellor, "Comprehensive Treatise on Inorganic and Theoretical Chemistry," Longmans (1960), Vol. 2, pp. 657, 659.
3) O. K. Yanat'eva and V. T. Orlova, *Zh. Prikl. Khim. (Leningrad)*, **32**, 2397—2405 (1959).
4) B. Gossner, *Z. Krystallogr.*, **39**, 155 (1904).
5) J. H. van't Hoff, *Z. Phys. Chem.*, **56**, 212 (1906).
6) F. Penny, *Philos. Mag.*, **10**, 401 (1855).

Solvent Intensification Effects on the $S_1(n\pi^*) \leftarrow S_0$ Absorption Spectra of Benzaldehyde in Fluid Solutions

Kenichi NAKASHIMA† and Motohiko KOYANAGI*

Department of Chemistry, Faculty of Science, Kyushu University, Hakozaki, Higashi-ku, Fukuoka 812

(Received July 9, 1982)

Synopsis. The near ultraviolet absorption spectra of benzaldehyde have been studied in various fluid solutions at room temperature. The intensity enhancements observed are explainable in terms of perturbation of dispersion forces between solute and solvent molecules.

Recently we showed that the environmental intensity enhancements of the near ultraviolet absorption spectra of aliphatic ketones such as acetone and cyclopentanone are parallel to those of the Ham effects in benzene.[1] Despite many studies of solvent effects on the electronic transition energies of aromatic carbonyls,[2] there has, to the best of our knowledge, been reported no work on their quantitative intensity correlation. One of the reasons is due to some experimental difficulty in discriminating between overlapping $S_2(\pi\pi^*) \leftarrow S_0/S_1(n\pi^*) \leftarrow S_0$ electronic transition absorptions for the evaluation of the oscillator strength, $f[S_1(n\pi^*) \leftarrow S_0]$. Another is possibly in their chemical and photochemical reactivities. In the present work we studied the absorption spectra of a prototype aromatic carbonyl molecule, benzaldehyde, and found that a like solvent correlation also held. The employment of this molecule is advantageous because the $S_1(n\pi^*) \leftarrow S_0$ absorption spectrum in a certain solution shows a banded structure even at room temperature and there are somewhat detailed available vibronic data on it.[3]

Experimental

Benzaldehyde (a reagent from Wako Pure Chemical Industries, Ltd.) was purified through several vacuum distillations. It was stored in a sealed-off glass tubing *in vacuo*. In order to avoid oxydation into benzoic acid, the tubing was located in the dark at 77 K. The solvents employed were of spectroscopically pure or reagent grade. They were deoxygenated by nitrogen gas bubbling before measurements and used without further purification. Absolute oscillator strengths for the solutions are difficult to obtain from integrated intensities because there is almost always some overlap between the $S_1(n\pi^*) \leftarrow S_0$ and $S_2(\pi\pi^*) \leftarrow S_0$ absorptions. Integration over only part of the band should give correct relative oscillator strengths as long as there are no changes in the Franck-Condon factors and as long as there are no specific intramolecular interactions whose matrix elements are beyond the order of the ordinary Boltzmann energy, $\approx kT$. In almost all cases we employed the band maxima $0+2\nu(C{=}O)$ as the upper wave number limit of the integration. The exceptions are for several high polar solvents such as nitriles, chloroform, and dichloromethane; for these solution systems the integrations were taken up to the band maximum of each spectrum and then the integration values were compared with the intensity integration over wave numbers to the band at $\approx$30200 cm^{-1} in a standard solvent, hexane. The other experimental details are similar to those described previously.[1]

Results and Discussion

In the $S_1(n\pi^*) \leftarrow S_0$ absorption system of benzaldehyde, both allowed and forbidden characters are important because of the breakdown of the local (C=O group) C_{2v} symmetry. This is in contrast with the $S_1(n\pi^*) \leftarrow S_0$ absorption spectra of acetone and cyclopentanone. Despite this geometrical difference, however, the transition still remains substantial forbidden character. The very small oscillator strengths observed confirm

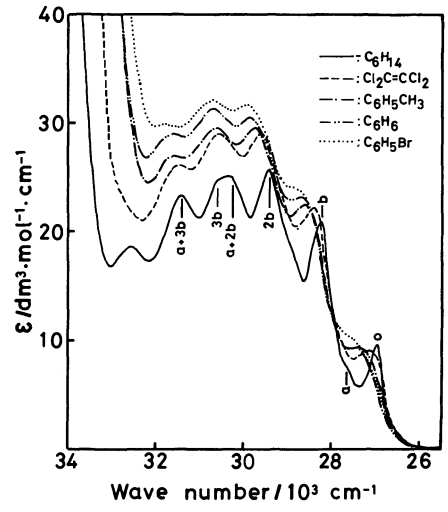

Fig. 1. The $S_1(n\pi^*) \leftarrow S_0$ absorption spectra of benzaldehyde in several solvents at 20 °C.

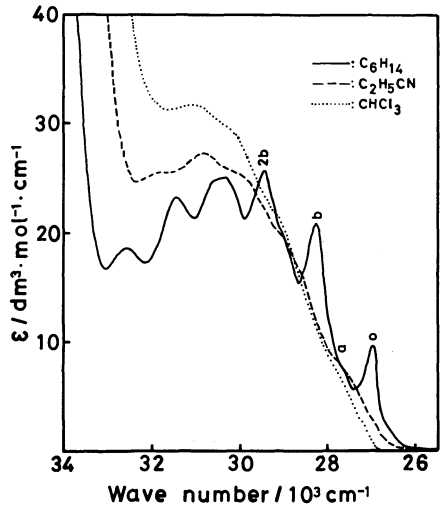

Fig. 2. The $S_1(n\pi^*) \leftarrow S_0$ absorption spectra of benzaldehyde in polar solvents at 20 °C.

† Present address: Department of Food Science, Nishikyushu University, Kanzaki, Kanzaki-gun, Saga 842.

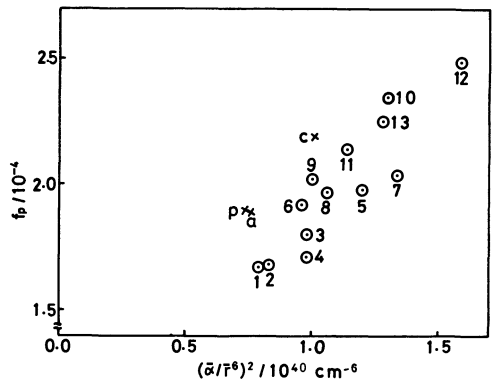

Fig. 3. A correlation diagram between the partial oscillator strength of benzaldehyde, f_p, and the squared value of the relative dispersion energy of solvents, $(\bar{\alpha}/\bar{r}^6)^2$. The numbering of the plots is as follows: (1) C_6H_{14}; (2) *i*-C_8H_{18}; (3) *cyclo*-C_6H_{12}; (4) $C_6H_{11}CH_3$; (5) CCl_4; (6) CH_2Cl_2; (7) C_2Cl_4; (8) CH_2Cl-CH_2Cl;(9) $(CH_3)_2NCHO$; (10) C_6H_6; (11) $C_6H_5CH_3$; (12) C_6H_5-Br; (13) *p*-$(CH_3)_2C_6H_4$; (p) C_2H_5CN; (a) CH_3CN; and (c) $CHCl_3$.

that this is the case.

The absorption spectrum of benzaldehyde was studied in various solvents at room temperature. Some typical spectra are shown in Figs. 1 and 2. The spectra in nonpolar or weakly polar solvents (*cf.* Fig. 1) give somewhat prominent vibronic bands. Although the $n\pi^*$ spectra of benzaldehyde at $\approx$300 K are generally accompanied by several sequence bands relevant to CHO-group localized vibrations in the gas phase[3], *i.e.*, $36_i^i(i=1\text{—}4)$, $35_j^j(j=1,2)$, and $25_k^k(k=1\text{—}3)$, almost all of the "bands" in Fig. 1 are essentially assignable in terms of the band groups of 0_0^0 (designated as *o* in Fig. 1) and 31_0^1 (*a*), and in terms of the 7_0^n (*nb*) progression bands ($n=1\text{—}3$) thereof.[4]

The spectral bands in high polar solvents such as chloroform and propionitrile, on the other hand, become considerably broad and shift toward the shorter wavelengths in contrast to the longer wavelength shifts of the $S_2(\pi\pi^*)\leftarrow S_0$ bands (see Fig. 2). It has been known that these solvents form stoichiometric complexes with several aromatic carbonyl compounds.[5] We confirmed this is also true for the present benzaldehyde case.[6] As for these complex-forming solvent systems, it is extremely difficult to discriminate between the spectra of non-complex-forming benzaldehyde and complex-forming one because of weakness in their complex formation forces and little knowledge on the Franck-Condon factors of the complexes' spectra.

In Fig. 3 the partial oscillator strength of benzaldehyde, f_p, is plotted as a function of the squared value of a relative dispersion energy between the solute and solvent molecules, $(\bar{\alpha}/\bar{r}^6)^2$. Here $\bar{\alpha}$ denotes the mean molecular polarizability of the solvent and $\bar{r}$ the mean intermolecular distance between the solute and solvent molecules. Nevertheless roughness in the approximation for $\bar{r}$, the observed intensities plotted by circles show an approximately linear increase with an increase in $(\bar{\alpha}/\bar{r}^6)^2$. This behavior is parallel to those in benzene[7] and aliphatic ketones.[1] For comparison, the data on the relative intensities in complex-forming solvents are also plotted by crosses. These intensities are presumed to be of overestimation because of considerable band overlap with the close lying $S_2(\pi\pi^*)\leftarrow S_0$ absorption. Only a little intensity enhancements, however, were found; it should be noted that this contrasts with a characteristic correlation reported in the $S_1(L_b)\leftarrow S_0$ spectra of pyrene.[8]

We have also observed similar environmental enhancements in the $S_1(n\pi^*)\leftarrow S_0$ absorption spectra of benzophenone and acetophenone. However, each band system was so diffuse that we found some difficulty in obtaining an appropriate intensity for it.

One of the authors (K. N.) wishes to express thanks to Professor R. Shimada for his warm hospitality and encouragements in Kyushu University. This work has in part been supported by a Grant-in-Aid for Scientific Research from the Ministry of Education, Science and Culture.

References

1) K. Nakashima, K. Uchida-Kai, M. Koyanagi, and Y. Kanda, *Bull. Chem. Soc. Jpn.*, **55**, 415 (1982).

2) E. Vander Donockt and C. Vogels, *Spectrochim. Acta, Part A*, **28**, 1969 (1972) and references cited therein.

3) For the vibrational numbering, see: M. Koyanagi and L. Goodman, *Chem. Phys.*, **39**, 237 (1979).

4) J. Smalarek, R. J. Zwarich, and L. Goodman, *J. Mol. Spectrosc.*, **43**, 416 (1972); M. Koyanagi and L. Goodman, *ibid.*, to be published.

5) R. S. Becker, *J. Mol. Spectrosc.*, **3**, 1 (1959).

6) In binary mixed solvent systems of each of these polar solvents and hexane, we could observe several isosbestic points. Assuming 1 : 1 complex formation between benzaldehyde and each of these polar molecules, we obtained some equilibrium constants; *i.e.*, $K=1.03\pm0.15$ dm^3 mol^{-1} for chloroform and $K=0.5\pm0.2$ dm^3 mol^{-1} for propionitrile.

7) M. Koyanagi, *J. Mol. Spectrosc.*, **25**, 273 (1968).

8) A. Nakajima, *Bull. Chem. Soc. Jpn.*, **44**, 3272 (1971).

Synthesis and Magnetic Susceptibility of Dimeric Copper(II) Acetate Adducts with Triphenylphosphine or Triphenylphosphine Oxide

Tadashi Tokii, Toyoaki Ikeda, and Yoneichiro Muto*
Department of Chemistry, Faculty of Science and Engineering, Saga University, Saga 840
(Received November 25, 1981)

Synopsis. Two compounds of stoichiometry $Cu(CH_3COO)_2 \cdot L$ (L = triphenylphosphine or triphenylphosphine oxide) were prepared. These compounds display the antiferromagnetic behavior typical of dimeric copper(II) carboxylates. The singlet-triplet splitting energy is 371 cm^{-1} for the phosphine adduct and 319 cm^{-1} for the phosphine oxide adduct.

A large number of dimeric copper(II) carboxylates have been studied because of their interesting magnetic and structural properties. However, the factors that determine the degree of antiferromagnetic interaction in these carboxylates still remain almost unsettled.[1] In this work, we prepared two copper(II) acetate adducts of stoichiometry $Cu(CH_3COO)_2 \cdot L$, where L = triphenylphosphine (Ph_3P) or triphenylphosphine oxide (Ph_3PO), and measured their magnetic susceptibility as a function of temperature in order to study the effect of the additional ligand L on the magnetic interaction in these complexes.

Experimental

Synthesis. *$Cu(CH_3COO)_2 \cdot Ph_3P$*: A solution of Ph_3P (5 mmol) in 30 ml of ether was added to a solution of $Cu(CH_3COO)_2 \cdot H_2O$ (5 mmol) in 30 ml of ethanol with a few drops of glacial acetic acid. After the solution had been allowed to stand for several days at *ca.* 5 °C in a freezer, the separated green crystals were collected, washed twice with ethanol and once with ether, and dried *in vacuo*. Found: C, 59.36; H, 4.78; Cu, 14.40%. Calcd for $C_{22}H_{21}O_4PCu$: C, 59.52; H, 4.77; Cu, 14.31%.

$Cu(CH_3COO)_2 \cdot Ph_3PO$: A solution of Ph_3PO (5 mmol) in 30 ml of ethanol was added to a solution of $Cu(CH_3COO)_2 \cdot H_2O$ (5 mmol) in 30 ml of ethanol and 2 ml of 2,2-dimethoxypropane. After the mixed solution had been concentrated to one-half of its volume, it was allowed to stand overnight at *ca.* 5 °C in a freezer. The green crystals were collected, washed with ethanol, and dried at *ca.* 70 °C. Found: C, 57.38; H, 4.67; Cu, 13.84%. Calcd for $C_{22}H_{21}O_5PCu$: C, 57.45; H, 4.60; Cu, 13.82%.

Physical Measurement. Magnetic suceptibilities in the temperature range of 80—300 K were determined by the Gouy method. The correction for diamagnetic contributions was made by use of Pascal's constant.[2] Effective magnetic moments per copper ion at room temperature were calculated from the equation

$$\mu_{eff} = 2.83\sqrt{(\chi_A - N\alpha)\cdot T}, \quad (1)$$

where χ_A is the corrected molar magnetic susceptibility and $N\alpha$ is the temperature-independent paramagnetism per gram-ion of copper(II); a value of $N\alpha = 60 \times 10^{-6}$ cgs emu mol^{-1}† was used.[3] The results are given in Table 1. The cryomagnetic susceptibility data are shown in Fig. 1 as plots of χ_A *vs.* T.

Results and Discussion

The variable-temperature magnetic susceptibility data were analyzed by the Bleaney-Bowers equation for isotropic exchange in a copper(II) dimer:[4]

$$\chi_A = \frac{Ng^2\beta^2}{3kT}\left[1+\frac{1}{3}\exp\left(\frac{-2J}{kT}\right)\right]^{-1} + N\alpha, \quad (2)$$

where g is the average g factor and J is the exchange integral. As can be seen in Fig. 1, the thermal magnetic data are well represented by Eq. 2. The best fit values for g and $-2J$ (a measure of the magnitude of magnetic interaction) are given in Table 1. On the basis of the magnetic behavior, a dimeric structure similar to that found in copper(II) acetate monohydrate can be proposed for the present acetate complexes.

The $-2J$ value of 371 cm^{-1} found for the Ph_3P adduct is considerably larger than that observed for any other dimeric copper(II) acetate adducts, indicating that the coordination of Ph_3P to dimeric copper(II) acetate units will cause a marked increase in antiferromagnetic interaction. On the other hand, the Ph_3PO adduct has a $-2J$ value (319 cm^{-1}) comparable to those found for well-characterized dimeric copper(II) acetate adducts (300—325 cm^{-1}).[5]

Edmonson and Lever[6] observed, in their study of dimeric copper(II) vinyl acetate and allyl acetate

Table 1. Magnetic data

Complex	μ_{eff}/BM[a]	T/K	g	$-2J$/cm^{-1}
$Cu(CH_3COO)_2 \cdot Ph_3P$	1.23	283	2.20	371
$Cu(CH_3COO)_2 \cdot Ph_3PO$	1.39	293	2.24	319

a) 1 BM = 9.27×10^{-24} A m^2.

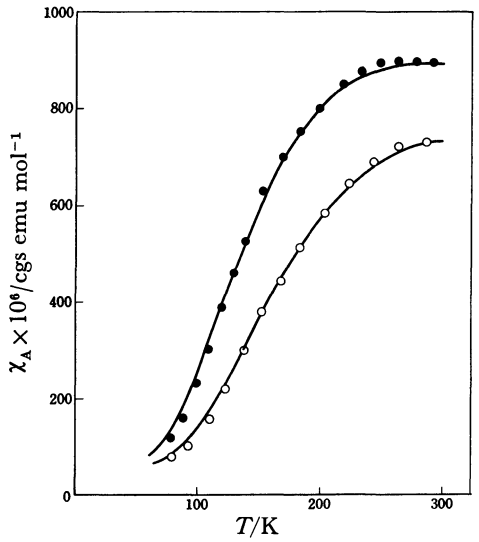

Fig. 1. Variation of magnetic suceptibilities with temperature. (○) $Cu(CH_3COO)_2 \cdot Ph_3P$ and (●) $Cu(CH_3COO)_2 \cdot Ph_3PO$. The solid curves were calculated by Eq. 2 with the parameters listed in Table 1 and $N\alpha$ of 60×10^{-6} cgs emu mol^{-1}.

† 1 cgs emu $mol^{-1} = 4\pi \times 10^{-6}$ m^3 mol^{-1}.

complexes with pyrazine (pz), pyridine (py), and Ph_3P, that the effective magnetic moments (μ_{eff}) at room temperature decreased in the order of pz adducts> py adducts$\gg$$Ph_3P$ adducts; the decrease in μ_{eff} for the Ph_3P adducts was attributed to the polarizable nature of the phosphorous ligand. The corresponding acetate complexes show a similar trend: pz adduct[7] $\approx$py adduct[8] ($\approx$1.35 BM)>Ph_3P adduct (1.23 BM). Ph_3P acts as a π-acceptor as well as a good σ-donor toward transition metals, while Ph_3PO functions simply as a σ-donor.[9] A metal→ligand π-back-donation generally facilitates the ligand→metal σ-donation, leading to a strengthening of the bond through the synergic interaction. Thus, the Cu–P bond in $Cu(CH_3COO)_2\cdot Ph_3P$ should be stronger than the Cu–O bond in $Cu(CH_3COO)_2\cdot Ph_3PO$.

It has been noted that, in dimeric copper(II) carboxylate adducts, the variation of $-2J$ with properties of additional ligands is not a simple function of the base strength of the ligands or of any other readily evident parameters.[10,11] However, the present magnetic data indicate that the bonding nature between Cu–L in $Cu(CH_3COO)_2\cdot L$ is important in determining the magnitude of $-2J$.

References

1) J. A. Moreland and R. J. Doedens, *Inorg. Chem.*, **17**, 679 (1978).
2) P. W. Selwood, "Magnetochemistry," Interscience Publishers, New York (1956), pp. 78, 91.
3) B. N. Figgis and R. L. Martin, *J. Chem. Soc.*, **1959**, 1359.
4) B. Bleany and K. D. Bowers, *Proc. R. Soc. London, Ser. A*, **214**, 451 (1952).
5) R. J. Doedens, *Prog. Inorg. Chem.*, **21**, 209 (1976).
6) B. J. Edmondson and A. B. P. Lever, *Inorg. Chem.*, **4**, 1608 (1965).
7) J. S. Valentine, A. J. Silverstein, and Z. G. Soos, *J. Am. Chem. Soc.*, **96**, 97 (1974).
8) E. Kokot and R. L. Martin, *Inorg. Chem.*, **3**, 1306 (1964).
9) F. A. Cotton and G. Wilkinson, "Advanced Inorganic Chemistry," Interscience Publishers, New York (1966), pp. 506, 745.
10) M. V. Hanson, G. O. Carlisle, and W. E. Marsh, *J. Inorg. Nucl. Chem.*, **40**, 1684 (1978).
11) M. Melnik, *Coord. Chem. Rev.*, **36**, 1 (1981).

Structure of Tetra-μ-formatodiruthenium Bromide

Takashi KIMURA, Tosio SAKURAI, Makoto SHIMA, Tadashi TOGANO,†
Masao MUKAIDA,*,† and (the late) Terunosuke NOMURA†
The Institute of Physical and Chemical Research, Wako, Saitama 351
†*Department of Chemistry, Faculty of Science and Technology, Sophia University, Kioi-cho, Chiyoda-ku, Tokyo 102*
(Received December 10, 1981)

Synopsis. X-Ray structural determination of $Ru_2(HCOO)_4Br$ showed that the unit cell contains two crystallographically independent formato bridged dinuclear units, $Ru_2(HCOO)_4^+$, each of which is centrosymmetric. Two adjacent units are bridged by bromide ion to make infinite zigzag chains.

Since the $Ru_2(RCOO)_4X$ type of complexes were prepared by Stephenson *et al.* and one of the present authors independently,[1,2] extensive studies of the complexes have been reported.[3-12] These studies showed that the complexes can be classified into three types with different crystal structures; an infinite zigzag chain structure bridged by halide ions,[5,7] an infinite linear chain structure bridged by halide ions,[12] and a structure comprizing discrete dinuclear unit.[6] The basic structural parameters for the dinuclear unit in each type are essentially identical.

Here we wish to report the crystal structure analysis of $[Ru_2(HCOO)_4Br]$. This work was carried out to clarify whether the bonding mode of formate ion in the title complex is similar to that of the analogous monocarboxylate or not.

There existed twinned crystals. By taking oscillation and Weissenberg photographs, a single crystal (*ca.* $0.08\times0.07\times0.18$ mm^3) was chosen and mounted on a RIGAKU four-circle automatic diffractometer with graphite-monochromatized Mo $K\alpha$ radiation. Unit cell parameters were refined by least-squares for 19 strong reflections in the 2θ range of 12—15°. Crystal data: $Ru_2(HCOO)_4Br$, F.W.=462.12, monoclinic, space group $P2_1/c$ (systematic absences: $h0l$, l=odd and $0k0$, k=odd), a=9.944(1), b=7.728(1), c=12.679(1) Å, β=93.52(1)°, V=972.46(19) Å^3, D_m=3.175 g cm^{-3} (by flotation in CCl_4/CH_2I_2 mixture), D_c=3.158 g cm^{-1} for Z=4, μ(Mo $K\alpha$)=74.06 cm^{-1}.

TABLE 1. ATOMIC PARAMETERS ($\times10^4$)

Atom	x	y	z	B_{eq}/Å^2
Ru(1)	779(1)	689(1)	555(0)	1.7(0.0)
Ru(2)	4357(1)	4169(1)	522(0)	1.6(0.0)
Br	2733(1)	2325(1)	1771(1)	2.4(0.0)
O(11)	172(5)	2975(6)	−90(4)	2.4(0.1)
O(12)	2140(5)	350(6)	−551(4)	2.5(0.1)
O(13)	1309(5)	−1632(6)	1204(4)	2.5(0.1)
O(14)	−611(5)	971(6)	1645(4)	2.6(0.1)
O(21)	3949(5)	6306(6)	1374(4)	2.3(0.1)
O(22)	2739(5)	4665(6)	−477(4)	2.3(0.1)
O(23)	4812(5)	2060(6)	−332(4)	2.4(0.1)
O(24)	6010(5)	3707(6)	1499(4)	2.5(0.1)
C(11)	−735(7)	2986(8)	−838(5)	2.3(0.1)
C(12)	1797(8)	−387(9)	−1413(6)	2.6(0.1)
C(21)	4442(7)	7737(10)	1108(6)	2.6(0.1)
C(22)	2885(7)	5603(9)	−1289(5)	2.2(0.1)

Intensity data were collected within the range of $2\theta\leqq70°$ using the ω-scan mode up to $2\theta=30°$, and 2θ-ω mode above $2\theta=30°$ at a scan speed of 4° min^{-1}. Three strong standard reflections were measured every 100 reflections; no significant change in intensity was noted during the data collection. The observed intensities were corrected for Lorentz and polarization factors, but no absorption correction was applied; 2654 unique reflections with $|F_o|\geqq3\sigma(|F_o|)$ were obtained. The structure was solved by the heavy atom method and refined by block-diagonal least-squares to R=0.036, anisotropic temperature factors being used. The final difference Fourier map showed no significant peak. Atomic scattering factors from tables[13] with correction for anomalous dispersion were used; the unit weight was given to all reflections. Calculations were performed on the FACOM 230-75 Computer using the UNICS III program system.[14]†† Atomic parameters are given in Table 1.

The crystal consists of two independent formato-bridged dinuclear units, $Ru_2(HCOO)_4^+$, and a bridging

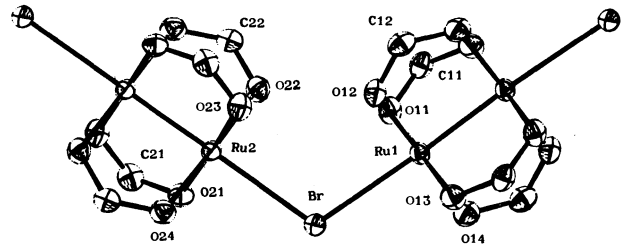

Fig. 1. Structure of $Ru_2(HCOO)_4Br$. Unlabeled atoms are related to labeled ones by a center of inversion at midpoint of Ru–Ru bond.

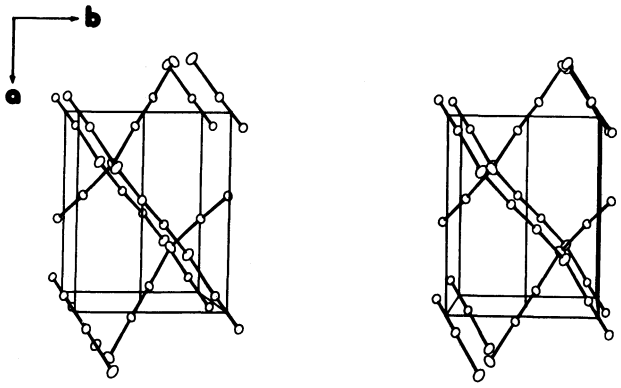

Fig. 2. Crystal packing of the –Ru–Ru–Br– skeletal chains viewed along the c axis. Carbon and oxygen atoms were omitted for clarity.

†† Complete F_o-F_c data and tables of anisotropic thermal parameters, least-squares planes and dihedral angles[15] are kept at the Chemical Society of Japan, Document No. 8260.

TABLE 2. INTERATOMIC DISTANCES AND ANGLES

Distance		l/Å	Distance		l/Å
Ru(1)–Ru(1′)		2.2897(7)	Ru(2)–Ru(2′)		2.2901(7)
Br		2.7170(8)	Br		2.7313(9)
O(11)		2.023 (5)	O(21)		2.027 (5)
O(12)		2.024 (5)	O(22)		2.023 (4)
O(13)		2.030 (5)	O(23)		2.024 (5)
O(14)		2.025 (5)	O(24)		2.028 (5)
C(11)–O(11)		1.268 (8)	C(21)–O(21)		1.264 (9)
O(13′)		1.266 (8)	O(23′)		1.277 (9)
C(12)–O(12)		1.260 (8)	C(22)–O(22)		1.274 (8)
O(14′)		1.281 (9)	O(24′)		1.264 (8)
Angle		ϕ/°	Angle		ϕ/°
Br	–Ru(1)–O(11)	90.46(14)	Br	–Ru(2)–O(21)	88.36(14)
	–O(12)	88.15(14)		–O(22)	89.18(14)
	–O(13)	91.26(14)		–O(23)	92.83(14)
	–O(14)	93.24(14)		–O(24)	92.31(14)
	–Ru(1′)	176.43(3)		–Ru(2′)	177.07(3)
O(11)–Ru(1)–O(12)		91.65(20)	O(21)–Ru(2)–O(22)		90.11(19)
	–O(13)	177.69(20)		–O(23)	178.57(19)
	–O(14)	89.00(20)		–O(24)	89.98(19)
	–Ru(1′)	89.08(4)		–Ru(2′)	89.36(14)
O(12)–Ru(1)–O(13)		89.94(20)	O(22)–Ru(2)–O(23)		90.71(19)
	–O(14)	178.45(20)		–O(24)	178.52(20)
	–Ru(1′)	88.32(14)		–Ru(2′)	88.99(14)
O(13)–Ru(1)–O(14)		89.37(20)	O(23)–Ru(2)–O(24)		89.17(19)
	–Ru(1′)	89.29(14)		–Ru(2′)	89.48(14)
O(14)–Ru(1)–Ru(1′)		90.28(14)	O(24)–Ru(2)–Ru(2′)		89.53(14)
Ru(1)–O(11)–C(11)		119.3 (4)	Ru(2)–O(21)–C(21)		118.4 (4)
	–O(12)–C(12)	120.1 (5)		–O(22)–C(22)	119.2 (4)
	–O(13)–C(11′)	118.8 (4)		–O(23)–C(21′)	118.2 (4)
	–O(14)–C(12′)	117.5 (4)		–O(24)–C(22′)	118.6 (4)
O(11)–C(11)–O(13′)		123.5 (6)	O(21)–C(21)–O(23′)		124.5 (7)
O(12)–C(12)–O(14′)		123.7 (7)	O(22)–C(22)–O(24′)		123.7 (6)
Ru(1)–Br–Ru(2)		109.99(3)			

bromide ion as is shown in Fig. 1. Each of the units is composed of two rutheniums and four formate ions and has a crystallographic center of inversion on the middle of the Ru–Ru bond. Bromide ion bridges adjacent dinuclear units to form infinite zigzag chains, with Ru(1)–Br–Ru(2) angle of 109.99(3)°. These chains are on planes parallel to {1 1 0} as shown in Fig. 2. One chain extends along ⟨1 1 0⟩ on $z=0$, and the other on $z=1/2$. The two crystallographically independent dinuclear units show no significant differences in geometrical parameters except the Ru–Br bond (Table 2). The average Ru–Ru and Ru–O bond lengths are 2.290 and 2.026 Å, respectively. The Ru–Ru–Br angles slightly deviate from 180°. Such anglar bend appears in the zigzag chains as well as in the discrete complex ions.[6] Dihedral angles of the planes defined by Ru_2O_2C group are nearly 90°, as expected. Two oxygens in every group deviate from the plane by 0.01—0.03 Å to twist the plane. The Ru deviates more than 0.02 Å from the plane formed by the four equatorial O atoms, in the direction to elongate the Ru–Ru distance. In agreement with a previous prediction,[2] the present result shows that the $[Ru_2(RCOO)_4X]$ type of complexes reported so far have the same bonding mode in reference to the monocarboxylato ligand.

Thanks are due to Miss K. Kobayashi (The Institute of Physical and Chemical Research) for her assistances with the calculations, and to Mr. Y. Iimura (The Institute of Physical and Chemical Research) for providing X-ray facilities. We also thank to Dr. F. S. Howell (Department of Chemistry, Sophia University) for correcting the manuscript.

References

1) T. A. Stephenson and G. Wilkinson, *J. Inorg. Nucl. Chem.*, **28**, 2285 (1966).
2) M. Mukaida, T. Nomura, and T. Ishimori, *Bull. Chem. Soc. Jpn.*, **40**, 2462 (1967); **45**, 2143 (1972).
3) R. W. Mitchel, A. G. Spencer, and G. Wilkinson, *J. Chem. Soc., Dalton Trans.*, **1973**, 846.
4) P. Legzdins, R. W. Mitchel, and G. Wilkinson, *J. Chem. Soc., A*, **1970**, 3322.
5) M. J. Bennett, K. C. Caulton, and F. A. Cotton, *Inorg. Chem.*, **8**, 1 (1969).
6) A. Bino, F. A. Cotton, and T. R. Felthouse, *Inorg. Chem.*, **18**, 2599 (1979).
7) T. Togano, M. Mukaida, and T. Nomura, *Bull. Chem. Soc., Jpn.*, **53**, 2085 (1980).
8) F. A. Cotton and E. Pedersen, *Inorg. Chem.*, **14**, 388 (1975).
9) J. G. Norman, G. E. Renzoni, and D. A. Case, *J. Am. Chem. Soc.*, **101**, 5256 (1979).
10) C. R. Wilson and H. Taube, *Inorg. Chem.*, **14**, 2276 (1975).
11) R. J. H. Clark and M. L. Franks, *J. Chem. Soc., Dalton Trans.*, **1976**, 1825.
12) D. S. Martin, R. A. Newman, and L. M. Vlasnik, *Inorg. Chem.*, **19**, 3404 (1980).
13) "International Tables for X-Ray Crystallography," Kynoch Press, Birmingham (1974), Vol. IV, p. 71.
14) T. Sakurai and K. Kobayashi, *Rikagaku Kenkyusho Hokoku*, **1979**, 55, 69.
15) Least-squares planes and their dihedral angles are calculated according to; T. Ito, *Sci. Papers Inst. Phys. Chem. Res.*, **1981**, 75, 55.

Preparation and Characterization of Triammine Cobalt(III) Complexes with (*R*)-2-(Carboxymethylthio)propionate and Its Derivative

Masutaro Suzuki, Ken-ichi Okamoto,* Hisahiko Einaga,† and Jinsai Hidaka
Department of Chemistry, University of Tsukuba, Ibaraki 305
†*Institute of Materials Science, University of Tsukuba, Ibaraki 305*
(Received May 12, 1982)

Synopsis. Two complexes of *fac*(NH_3)-[Co(L)(NH_3)$_3$]$^+$ type (where L denotes (*R*)-2-(carboxymethylthio)propionate and (*R*)-2-(2-carboxyethylthio)propionate) were newly prepared and separated into two isomers, *R*(*S*), *R*(*C*) and *S*(*S*), *R*(*C*), by column chromatography. The absolute configurations of the isomers are suggested on the basis of the ^{13}C NMR spectra.

(*R*)-2-(Carboxymethylthio)propionate (*R*-cmtp) and (*R*)-2-(2-carboxyethylthio)propionate (*R*-cetp) function as terdentate-*O*,*S*,*O* ligands. When this type of ligand coordinates to a cobalt(III) ion and three ammonia molecules occupy the remaining three coordination sites, the resulting complexes have one chirality due to the coordinated sulfur atom (*R*(*S*) or *S*(*S*) configuration) and another due to the asymmetric carbon atom (*R*(*C*) configuration). There have been only a few works on such kinds of chirality due to the rigid chiral sulfur atom.[1] This note is concerned with the preparation and isolation of diastereomers, *R*(*S*),*R*(*C*) and *S*(*S*),*R*(*C*), of the *fac*(NH_3) triammine cobalt(III) complexes with *R*-cmtp and *R*-cetp ligands. The ^{13}C NMR and CD spectra for the four isomers are presented.

Experimental

R-H_2cmtp was prepared by the well-established procedure,[2] using (*S*)-2-bromopropionic acid and mercaptoacetic acid. The $[\alpha]_D^{23}=+87.6°$ (*c* 2.2, $CHCl_3$) for the *R*-H_2cmtp·0.1NaBr in this work agreed with the value in the literature.[3]

R-H_2cetp was prepared by the same procedure as that of *R*-H_2cmtp,[2] using 3-mercaptopropionic acid instead of mercaptoacetic acid. This reaction proceeds without racemization.[2,4] Found: C, 40.17; H, 5.58%. Calcd for *R*-H_2cetp: C, 40.44; H, 5.56%. $[\alpha]_D^{23}=+64.1°$ (*c* 4.4, water) and $[\alpha]_D^{23}=+106.1°$ (*c* 2.2, $CHCl_3$).

[*Co*(R-*cmtp*)(*NH*$_3$)$_3$]*Cl*. This complex was prepared by the reaction of *R*-H_2cmtp (5 g) with [Co(NO_3)$_3$(NH_3)$_3$][5] (5 g) in 40 cm^3 of water at 50 °C for 1.5 h. The reaction mixture was filtered and the filtrate was poured onto a column of Dowex 50W-X8 (H^+ form, 3×40 cm). After the column had been swept with water, the adsorbed band was eluted with 0.1 mol dm^{-3} aqueous solution of sodium chloride, of which the pH was adjusted to 3 by addition of concentrated hydrochloric acid. Two red-violet bands, F1 and F2 (the formation ratio of F1 to F2 was *ca.* 46 : 54), were eluted in this order. Each eluate was concentrated to *ca.* 10 cm^3 with a rotary evaporator. The deposited NaCl was filtered off and the filtrate was passed through a column of Sephadex G-10 (2×150 cm). The solution eluted with water was concentrated to a small volume again and kept in a refrigerator overnight. The crystals obtained were collected by filtration. Found for F1: C, 19.93; H, 4.88; N, 13.56%. Found for F2: C, 19.48; H, 4.88; N, 13.77%. Calcd for [Co(*R*-cmtp)(NH_3)$_3$]Cl=$CoC_5H_{15}N_3O_4SCl$: C, 19.51; H, 4.92; N, 13.66%.

[*Co*(R-*cetp*)(*NH*$_3$)$_3$]*Cl*. This complex was prepared and separated into two isomers, G1 and G2 (the formation ratio of G1 to G2 was *ca.* 44 : 56), by a procedure similar to that for [Co(*R*-cmtp)(NH_3)$_3$]Gl complex, using *R*-H_2cetp instead of *R*-H_2cmtp. Found for G1: C, 21.98; H, 5.33; N, 12.86%. Calcd for [Co(*R*-cetp)(NH_3)$_3$]Cl·0.25H_2O=$CoC_6H_{17}N_3O_4SCl$·0.25H_2O: C, 22.09; H, 5.42; N, 12.88%. Found for G2: C, 21.29; H, 5.64; N, 12.22%. Calcd for [Co(*R*-cetp)(NH_3)$_3$]Cl·H_2O: C, 21.21; H, 5.65; N, 12.37%.

Measurements. The electronic absorption spectra were recorded with a JASCO UVIDEC-1 spectrophotometer, and the CD spectra, with a JASCO J-20 spectropolarimeter. The ^{13}C NMR spectra were recorded on a JEOL JNM-FX-100 NMR spectrometer at the probe temperature in a D_2O solvent. Sodium 2,2-dimethyl-2-silapentane-5-sulfonate (DSS) was used as the internal reference.

Results and Discussion

Two geometrical isomers, *fac*(NH_3) and *mer*(NH_3), are possible for [Co(terdentate-*O*,*S*,*O*)(NH_3)$_3$]$^+$, as shown in Fig. 1(a). The two isomers for each of the *R*-cmtp and *R*-cetp complexes isolated show the similar absorption spectra over the whole region, and the pattern of their first absorption bands is in line with that of the *s*-*cis*(*O*)-*fac*-(thiodiacetato)(diethylenetriammine)cobalt(III) complex (Fig. 2).[6] Therefore, it is possible to assign the present isomers to be *fac*(NH_3).

The *fac*(NH_3) complexes have two chiral centers at carbon and sulfur atoms. Namely, two diastereomers due to the chirality of the sulfur atom are possible for each of the complexes, since the chiral carbon atom has the *R*(*C*) configuration (Fig. 1(b)). In the ^{13}C NMR spectra, the methyl, methylene, and methine carbons of F2 resonate at higher magnetic field than those of F1, as shown in Fig. 3. When the chiral sulfur atom takes the *R*(*S*) configuration, the interaction between a methyl group of a coordinated *R*-cmtp ligand and another chelate ring of the same ligand is probable (Fig. 1(b)). On the contrary, there is no spatial crowd for the methyl group of the *S*(*S*),*R*(*C*) isomer (Fig. 1(b)). Taking the steric effects for the chemical shift of carbon into consideration,[7] the ^{13}C NMR spectra seem to suggest that F1 takes the *S*(*S*),*R*(*C*) configuration and F2 the *R*(*S*),*R*(*C*) one. In the same manner, G1 is assigned to

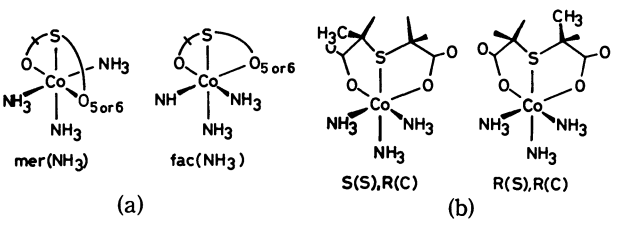

Fig. 1. (a) Two geometrical isomers of [Co(terdentate-*O*,*S*,*O*)(NH_3)$_3$]$^+$ and (b) two optically active isomers of *fac*(NH_3)-[Co(*R*-cmtp)(NH_3)$_3$]$^+$.

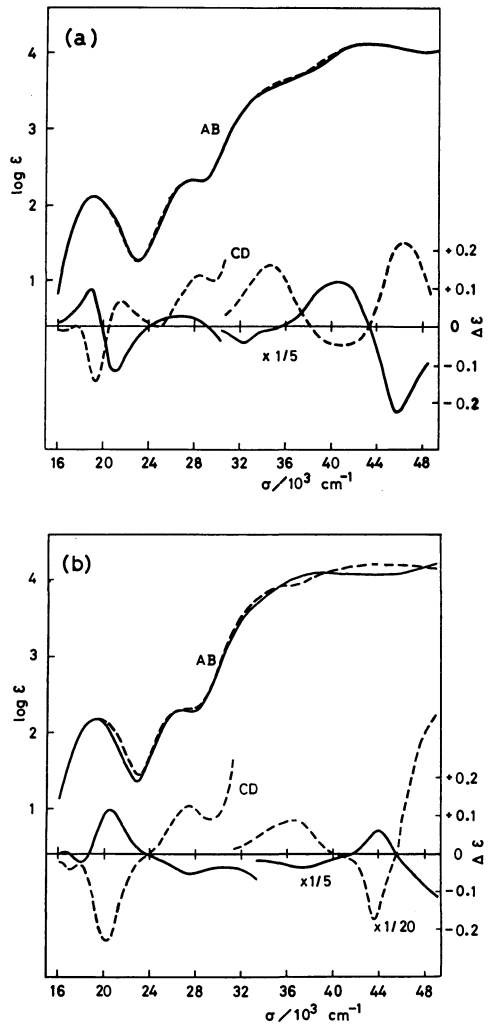

Fig. 2. Absorption and CD spectra of the triammine complexes: (a) F1 (——) and F2 (------) of [Co(*R*-cmtp)$(NH_3)_3$]$^+$, and (b) G1 (——) and G2 (------) of [Co(*R*-cetp)$(NH_3)_3$]$^+$.

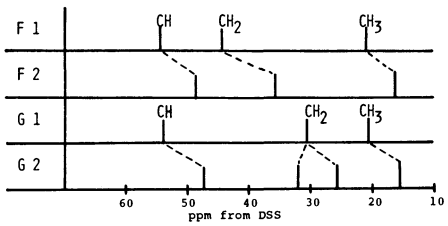

Fig. 3. Distribution of ^{13}C NMR chemical shifts.

the *S*(*S*),*R*(*C*) configuration and G2 to the *R*(*S*),*R*(*C*) one. These assignments are supported by the ^{13}C NMR spectral study of the cobalt(III) complexes with the *N*-(carboxylatomethyl)-L-alaninate ligand which has a similar framework to the *R*-cmtp one.[8]

As shown in Figs. 2(a) and (b), the CD spectra of two isomers for each of the *R*-cmtp and *R*-cetp complexes are almost enantiomeric over the whole region. In the first absorption band region, the *R*(*S*),*R*(*C*) isomer (F2) of the *R*-cmtp complex, which consists of two five-membered chelate rings, shows three CD bands ((—), (—) and (+) from lower energy side) (Fig. 2(a)). The *R*(*S*),*R*(*C*) isomer (G2) of the *R*-cetp complex, which consists of one five- and one six-membered chelate ring, shows almost opposite signs ((—) and (—)) for that of the *R*-cmtp one (Fig. 2(b)), although the two complexes show a similar CD behavior in the region of (32—48) × 10^3 cm^{-1}. A similar CD spectral behavior in the first absorption band region was observed for the *R*(*N*),*S*(*C*) triammine cobalt(III) complexes with the *N*-(carboxylatomethyl)-L-alaninate and *N*-(2-carboxylatoethyl)-L-alaninate,[9] which have the chiral nitrogen atoms instead of the sulfur atoms of the *R*-cmtp and *R*-cetp ligands. The CD intensity in the *R*-cmtp and *R*-cetp complexes is very much smaller than that of the mixed cobalt(III) complexes with the 1,1,1-tris(aminomethyl)-ethane (tame) and terdentate-*N*,*S*,*O* such as (2-aminoethylthio)acetate, which have a similar CD contribution to the present complexes.[1] The CD spectra of the present isomers seem to indicate that the arrangement chirality of the donor atoms in the *R*-cmtp and *R*-cetp complexes little affects the CD spectra, or that the chelate rings of the tame ligand in the tame cobalt(III) complexes[1] are significant for CD contribution.

References

1) K. Yamanari, J. Hidaka, and Y. Shimura, *Bull. Chem. Soc. Jpn.*, **50**, 2298 (1977).
2) L. F. Fieser and M. Fieser, "Advanced Organic Chemistry," Reinhold Publishing Co., New York (1961).
3) Beilstein, E III 3, 513 (Syst. Nr. 221).
4) E. Fischer, *Ann.*, **340**, 171 (1905); *Ber.*, **40**, 489 (1907).
5) M. Mori, M. Shibata, K. Hirota, K. Masuno, and Y. Suzuki, *Nippon Kagaku Zasshi*, **79**, 1251 (1958).
6) K. Kanamori, T. Sudani, and K. Kawai, *Bull. Chem. Soc. Jpn.*, **49**, 2739 (1976).
7) D. M. Grant and B. V. Cheney, *J. Am. Chem. Soc.*, **89**, 5315 (1967).
8) N. Koine, T. Tanigaki, J. Hidaka, and Y. Shimura, Presented at 30th Symposium on Coordination Chemistry, Tokyo, 1980.
9) K. Okamoto, J. Hidaka, and Y. Shimura, *Bull. Chem. Soc. Jpn.*, **46**, 3134 (1973).

Synthesis of *cis*-Jasmone *via* the Retroaldol-aldol Condensation of 3-(*cis*-3-Hexenyl)-2-cyclopentenone in an Autoclave

Takashi YOSHIDA* and Shojiro SAITO

Department of Industrial Chemistry, Faculty of Engineering, Meiji University, Higashimita, Tama-ku, Kawasaki 214

(Received April 26, 1982)

Synopsis. *cis*-Jasmone was efficiently synthesized from 2-cyclcpentenone. The treatment of 2-cyclopentenone with sodium *p*-toluenesulfinate gave 3-(*p*-tolylsulfonyl)cyclopentanone in a 92.5% yield. The alkylation of the sulfone, after the protection of the ketone, with *cis*-1-bromo-3-hexene, followed by desulfonylation with 5% hydrochloric acid in tetrahydrcfuran, afforded 3-(*cis*-3-hexenyl)-2-cyclopentenone in a good yield. The retroaldol-aldol condensation of the cyclopentenone in a stainless steel autoclave in presence of 5% sodium hydroxide yielded *cis*-jasmone in a 80% yield.

Among the *cis*-jasmone syntheses, the cyclization of 1,4-diketone employing weak alkali is well known.[1] We reported previously a new synthesis of *cis*-jasmone (**6**) *via* 1,4-diketone prepared by the condensation of *cis*-1-(*p*-tolylsulfonyl)-3-hexene with ethyl 4,4-ethylenedioxypentanoate.[2] On the other hand, 3-(*cis*-3-hexenyl)-2-cyclopentanone (**5**) is also a key intermediate for the synthesis of **6**.[3] Two examples involve the intermediate **5**. McCurry *et al.* reported in 1974 that **5** was synthesized by the addition of alkyllithium to 2-cyclopentenone, followed by chromium-trioxide oxidation,[3] giving **6** in a 29% overall yield by the retroaldol-aldol condensation of **5**. Torii *et al.* reported in 1979 that **5** was obtained by the electrolytic acetoxylation reaction of 1-(*cis*-3-hexenyl)-2-cyclopentene-1-carboxylic acid in several steps.[4] In a previous paper, we ourselves reported that the treatment of the tertiary alkyl sulfones bearing carbonyl groups at the β-position with 5% hydrochloric acid in tetrahydrofuran (THF) at 30—60 °C afforded β-substituted α,β-unsaturated ketones and aldehydes in good yields.[5] Using this method, **5** was obtained from 2-cyclopentenone in a good yield. In this paper, we wish to report a new approach which allows a relatively simple and effective synthesis of **6**.

As shown in Fig. 1, 3-(*p*-tolylsulfonyl)cyclopentanone (**2**) was obtained in a 92.5% yield by the addition of *p*-toluenesulfinic acid to 2-cyclopentenone (**1**). The keto sulfone **2** was treated with ethylene glycol in benzene to give 1,1-ethylenedioxy-3-(*p*-tolylsulfonyl)cyclopentane (**3**) in a 95% yield. The sulfone **3** was alkylated using *cis*-1-bromo-3-hexene to afford 1,1-ethylenedioxy-3-(*cis*-3-hexenyl)-3-(*p*-tolylsulfonyl)cyclopentanone (**4**) in a quantitative yield.

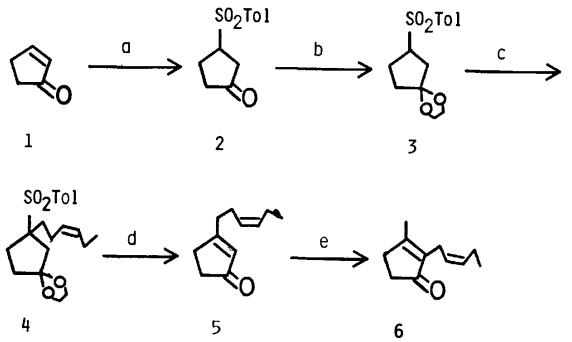

Fig. 1. a: *p*-Toluenesulfinic acid, b: ethylene glycol, c: LDA, −78 °C, *cis*-1-bromo-3-hexene, d: 5% HCl THF, 30 °C, e: 120 °C, (autoclave).

The treatment of the sulfone **4** with 5% hydrochloric acid gave 3-(*cis*-3-hexenyl)-2-cyclopentenone (**5**) in a 90% yield. Generally, the desulfonylation for making a variety of double bonds is carried out by the treatment of the allylic sulfones with a strong base. β-Keto sulfones are decomposed by dilute aq alkali. However, we found that the treatment of the sulfone **4** with 5% hydrochloric acid in THF afforded **5** in a good yield[5] when stirring was done at 45 °C for 4 h. When these conditions, **5** and its *trans* isomer were obtained in the ratio of 5 : 5. However, the reaction at a temperature below 30 °C gave pure **5** in a 90% yield.

Next, we investigated the details of the retroaldol-aldol condensation of **5** to **6**. McCurry *et al.* reported that the treatment of 0.160 g of **5** with 160 ml of 0.75 mol dm^{-3} sodium hydroxide by refluxing under argon for 72 h provided **6** in an 80% yield.[3] However, we could obtained the desired **6** by this method, only resinous substances were isolated. Thus, the reaction was carried out in a stainless steel autoclave using a dilute aq sodium hydroxide solution. The product-selectively in the conversion of **5** to **6** in an autoclave mainly depends on the reaction temperature, the reaction time, and the condensation of sodium hydroxide. The reaction conditions at 95 °C for 12 h using 5% sodium hydroxide did not give **6**, only the starting material, **5**, was recovered. When the reaction temperature was kept at 120 °C, the desired **6** was obtained in an 80% yield and in a 94% purity, along with the double-bond isomer, 3-methyl-2-(*trans*-1-penteny)-2-cyclopentenone (**7**) in a 6% yield. The sructure of **7** was determined from the ^1H NMR and IR spectra.[6] The ^1H NMR spectra of the olefin protons of the side chain of **7** appeared at δ 6.00 (d, J=16.5 Hz) and δ 6.78 (dt, J=16.5 and 6.0 Hz). The IR spectra of the compound show a characteristic absorption band at 970 cm^{-1} due to the *trans*-alkene bond. The mechanism produced may be assumed to proceed *via* the migration of the *cis*-olefin of the resulting **6** for the compound **7** was not obtained from 3-(*trans*-2-hexenyl)-2-cyclopentenone under similar conditions, only resinous substances being almost entirely produced. In addition, **6** isomerized to **7** with 5% sodium hydroxide in the autoclave in a ratio of 6%. Under the constant temperature of 120 °C, the employment of 1% sodium hydroxide gave **6** in a 40% yield, whereas 5% sodium hydroxide yielded **6** in an 80% yield. A higher concentration of more than 5% can easily give resinous substances as by-products.

Experimental

All the melting and boiling points are uncorrected. The melting points were taken on a Yanagimoto micro-melting-point apparatus. The infrared spectra were recorded on a Shimadzu IR-27G spectrophotometer. The ^{1}H NMR spectra were measured on a Varian EM-390 spectrometer at 90 MHz, using CCl_4 as solvent and TMS as an internal standard.

3-p-Tolylsulfonylcyclopentanone (2). Sodium *p*-toluenesulfinate tetrahydrate (8 g, 33 mmol) in 30 ml of MeOH, AcOH (2 g, 33 mmol), and 2-cyclopentenone (**1**) (2 g, 24 mmol) were placed in an Erlenmeyer flask and heated to reflux. After 10 h, the reaction product was neutralized by the use of a dilute sodium hydrogencarbonate solution and extracted with chloroform. The extract was washed with water, dried (Na_2SO_4), and concentrated to give **2**, as solid substances. Recrystallization from benzene–hexane afforded 5 g (92.5% yield) of pure **2** as white needles, mp 58—58.5 °C. IR (Nujol) 2980, 1750, 1600, 1410, 1300, 1140 cm^{-1}. ^{1}H NMR (CCl_4) δ 2.05—2.90 (9H, m), 3.78 (1H, m), 7.45 and 7.85 (4H, an A_2B_2 pattern, J=8.7 Hz). Found: C, 61.11; H, 5.96%. Calcd for $C_{12}H_{14}O_3S$: C, 60.48; H, 5.92%.

1,1-Ethylenedioxy-3-(p-tolylsulfonyl)cyclopentanone (3). Ethylene glycol (2 g, 31 mmol) was stirred into a solution of **2** (6.5 g, 27 mmol) in benzene (50 ml) in the presence of *p*-toluenesulfonic acid (20 mg), and the mixture was refluxed for 5 h. The reaction mixture was then worked up in the usual manner to give **3** (6.5 g, 95% yield) after recrystallization from hexane–benzene as white crystals, mp 61.5—62 °C. IR (Nujol) 2900, 1600, 1430, 1310, 1140 cm^{-1}. ^{1}H NMR (CCl_4) δ 1.75—2.40 (6H, m), 2.50 (3H, s), 3.45—3.90 (1H, m), 3.96 (4H, s), 7.50 and 7.90 (4H, an A_2B_2 pattern, J=8.7 Hz). Found: C, 60.41; H, 6.53%. Calcd for $C_{14}H_{18}O_4S$: C, 59.55; H, 6.43%.

1,1-Ethylenedioxy-3-(cis-3-hexenyl)-3-(p-tolylsulfonyl)cyclopentane (4). To lithium diisopropylamide, prepared from *n*-BuLi (15% hexane solution, 8.5 g, 20 mmol) and diisopropylamine (2.1 g, 20 mmol) in dry THF (15 ml), was added a solution of **3** (4 g, 16 mmol) in dry THF (15 ml) at −78 °C under nitrogen. After the mixture has been stirred for 1 h, *cis*-1-bromo-3-hexene (2.8 g, 17 mmol) in dry THF (15 ml) was added. The mixture was then stirred for 1 h at −78 °C and an additional 3 h at room temperature. The mixture was then poured onto cold 2% sulfuric acid. The usual workup gave **4** as a viscous liquid in a quantitative yield after purification by column chromatography (SiO_2, 60—80 mesh) with benzene. IR (neat) 2930, 1600, 1460, 1300, 1140 cm^{-1}. ^{1}H NMR (CCl_4) δ 0.99 (3H, t, J=7.2 Hz), 1.6—2.8 (15H, m), 3.90 (4H, s), 5.05—5.60 (2H, m), 7.33 and 7.77 (4H, an A_2B_2 pattern, J=8.7 Hz). Found: C, 66.13; H, 7.75%. Calcd for $C_{20}H_{28}O_4S$: C, 65.90; H, 7.74%.

3-(cis-3-Hexenyl)-2-cyclopentenone (5). To a stirred solution of **4** (3 g, 8.24 mmol) in THF (60 ml) was added 5% hydrochloric acid (18 ml). The mixture was then stirred for 5 h at 30 °C. After the removal of the THF, the mixture was poured into 500 ml of water and worked up to give **5** (1.2 g, 90% yield) as a colorless liquid, bp 104—106 °C/6 mmHg (1 mmHg=133.322 Pa). IR (neat) 2950, 1715, 1620, 1440, 1185 cm^{-1}. ^{1}H NMR (CCl_4) δ 0.95 (3H, t, J=7.2 Hz), 1.8—2.6 (10H,m), 5.15—5.75 (2H, m), 5.93 (1H, br s). The product was identified by comparing its NMR spectrum with the reportedone.[3]

cis-Jasmone (6). **5** (0.4 g, 2.24 mmol) and 5% sodium hydroxide (30 ml) were placed in a stainless steel autoclave equipped with a magnetic stirrer. The autoclave was heated in an oil bath maintained at 120 °C for 12 h and then allowed to cool. The reaction mixture was acidified with dilute hydrochloric acid. The organic layer was extracted with ether. The extract was worked up in the usual manner to give 0.32 g (80% yield after being chromatographed, SiO_2 with benzene–hexane (7 : 3)) of **6**, whose gas chromatographic analysis showed a *cis/trans* isomer ratio of 94/6. The NMR and IR spectra of the **6** synthesized here were identical with those of an authentic sample.

We are deeply indebted to Dr. Tetsuo Miyakoshi and Mr. Hiroaki Omichi of Meiji university for their valuable discussions and suggestions throughout this work.

References

1) R. A. Ellison, *Synthesis*, **1973**, 397; S. Torii and H. Tanaka, *Koryo*, **114**, 41 (1976).

2) T. Yoshida, T. Miyakoshi, H. Omichi, and S. Saito, 23rd Symposium on the Chemistry of Terpens, Essential Oils, and Aromatics, Tottori, October 1979, Abstr. p. 169; *Chem. Abstr.*, **93**, 113996t (1980); T. Yoshida and S. Saito, *Yukagaku*, submitted for publication.

3) P. M. McCurry, Jr., and R. K. Singh, *J. Org. Chem.*, **39**, 2317 (1974).

4) S. Torii, K. Tomozane, T. Inokuchi, and H. Tanaka, 23rd Symposium on the Chemistry of Terpens, Essential Oils and Aromatics, Tottori, October 1979, Abstr. p. 167; *Chem. Abstr.*, **93**, 46006e (1980).

5) T. Yoshida and S. Saito, *Chem. Lett.*, **1982**, 165.

6) Compound **7**: ^{1}H NMR (CCl_4) δ 0.94 (3H, t, J=6.9 Hz), 1.3—1.7 (2H, m), 2.0—2.6 (6H, m), 2.07 (3H, s), 6.00 (1H, d, J=16.5 Hz), 6.78 (1H, dt, J=16.5 and 6.0 Hz). IR (neat) 2960, 1700, 1600, 1435, 1375, 1075, 970 cm^{-1}.

The Synthesis of 1,2-Diazacoronene

Sumio Tokita,* Kimihiro Hiruta, Kiyoshi Kitahara, and Hisao Nishi
Department of Applied Chemistry, Faculty of Engineering, Saitama University, Shimo-Ohkubo, Urawa, Saitama 338

(Received December 10, 1981)

Synopsis. 1,2-Bis(ethoxycarbonyl)-1,2-dihydro-1,2-diazacoronene-7,8-dicarboxylic anhydride (**5**) was obtained from diethyl 1,2-dihydro-1,2-diazabenzo[*ghi*]perylene-1,2-dicarboxylate, maleic anhydride, and chloranil. Treatment of the anhydride **5** with sodium hydroxide gave 1,2-diazacoronene-7,8-dicarboxylic anhydride (**7**). When **7** was heated with soda lime, 1,2-diazacoronene was obtained.

Much attention is being given to the heterocyclic analogs of highly annelated polycyclic hydrocarbons found in urban suspended particulate matter, especially to the compounds suspected of tumorigenic activities. There are, however, few reports about the synthesis of authentic samples of highly annelated heterocycles, in spite of the existence of many reports on heterocyclic analogs of benzene,[1-3] naphthalene,[1-3] anthracene,[2,4] or phenanthrene.[3,4] In the case of nitrogen heterocyclic analogs of coronene, only 1,2,7,8-tetraazacoronene has been synthesized.[5] The preparation of 1,2-diazacoronene (**9**), however, proved to be more difficult.[5] Thus, the attempted Diels-Alder reaction of benzo[*ghi*]perylene with diethyl azodiformate (**2**) did not give any diethyl 1,2-dihydro-1,2-diazacoronene-1,2-dicarboxylate, a precursor of **9**. This paper deals with the synthesis of **9** by another route.

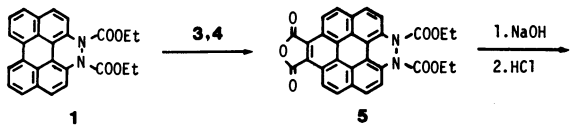

1 **5**

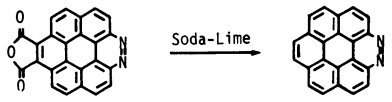

7 **9**

When diethyl 1,2-dihydro-1,2-diazabenzo[*ghi*]perylene-1,2-dicarboxylate (**1**) was treated with maleic anhydride (**3**) in the presence of chloranil (**4**), the expected adduct, 1,2-bis(ethoxycarbonyl)-1,2-dihydro-1,2-diazacoronene-7,8-dicarboxylic anhydride (**5**) was obtained in fair yield. But the treatment of benzo[*ghi*]-perylene-1,2-dicarboxylic anhydride (**6**) with **2** in an autoclave at 160 °C for 144 h did not result in the formation of **5** but in the recovery of **6**.

Hydrolysis of the anhydride **5** with sodium hydroxide followed by acidification gave 1,2-diazacoronene-7,8-dicarboxylic anhydride (**7**) almost quantitatively. The reaction of 1,2-diazabenzo[*ghi*]perylene (**8**) with **3** in the presence of **4** at 200 °C for 20 min gave a very complex mixture, in which **7** could not be detected.

1,2-Diazacoronene (**9**) was prepared by the action of soda lime on anhydride **7**. On the other hand, the reaction of **5** with the same reagent at 280—300 °C for 2 h gave a dark solid from which no definite products could be isolated.

1,2-Diazacoronene (**9**) was soluble in trifluoroacetic acid and bis(2-hydroxyethyl) ether, whereas it was almost insoluble in common organic solvents. It could be recrystallized from bis(2-hydroxyethyl) ether in fine needles. It is yellow with a considerably deeper shade than coronene. The electronic spectrum of **9** (see experimental section) and that of coronene[6,7] were quite similar with respect to the positions of absorption maxima, but differ in that the absorption band of **9** in the visible region has a higher intensity ($\varepsilon \approx 10^4$) than that of coronene ($\varepsilon \approx 10^2$). These findings may be accounted for by the same symmetry argument that explains the difference between the spectra of benzene and pyridine.[8] Incidentaly, the electronic spectrum of an analogous isoelectronic compound, *viz.*, benzo-[6,7]perylo[1,12-*bcd*]thiophene (**10**),[9] shows essentially the same characteristics as **9**.

10

The NMR spectrum of **9** was as expected. In **9**, there were aromatic proton signals at lower field than in coronene, and at higher field than in 1,2,7,8-tetraazacoronene.[5]

Experimental

^{1}H NMR spectra were recorded on a Varian Model A-60 Spectrometer in CF_3COOH using Me_4Si as an internal standard. IR spectra were recorded on a JASCO Model A-3 grating spectrophotometer using the KBr technique. Mass spectra were obtained on a JEOL JMS-01-SG-2 spectrometer at an ionization potential of 35 eV. Electronic spectra were measured with a Hitachi EPS-3T recording spectrophotometer.

Materials. Diethyl azodiformate (**2**)[10] and benzo-[*ghi*]perylene-1,2-dicarboxylic anhydride (**6**)[6] were prepared and purified according to the procedures in the literature. Diethyl 1,2-dihydro-1,2-diazabenzo[*ghi*]perylene-1,2-dicarboxylate (**1**) and 1,2-diazabenzo[*ghi*]perylene (**8**) were prepared and purified by the methods reported previously.[5]

1,2-(Bis(ethoxycarbonyl)-1,2-dihydro-1,2-diazacoronene-7,8-dicarboxylic Anhydride (5). A mixture of **1** (212 mg, 0.50 mmol), chloranil (**4**, 369 mg, 1.50 mmol), and maleic anhydride (**3**, 1.45 g, 15 mmol) was heated under reflux for 20 min. The reaction mixture was then allowed to cool to about 80 °C, and 2 ml of xylene was added. After cooling, 10 ml of methanol was added and the resulting precipitate was filtered off to give 205 mg of crude **5**. Recrystallization from xylene afforded 158 mg of **5** as a reddish brown solid (61% yield): mp 305 °C (decomp); IR 3000 (ν_{C-H}^{arom}), 2950 (ν_{C-H}^{aliph}), 1840 ($\nu_{C=O}$), 1765 ($\nu_{C=O}$), 1730 ($\nu_{C=O}$), 1325 (ν_{C-O}), 1260 (ν_{C-O}),

845 cm^{-1} (δ_{C-H}); ^{1}H NMR δ 1.54 (t, 6H, J=7.3 Hz), 4.60 (q, 4H, J=7.3 Hz), 6.78 (d, 2H, J=9.1 Hz), 7.22 (d, 2H, J=9.1 Hz), 7.89 (d, 2H, J=8.8 Hz), 8.22 (d, 2H, J=8.8 Hz); MS *m/e* 518 (7%, M$^+$), 446 (10%), 445 (26%), 401 (20%), 373 (100%). Found: C, 69.93; H, 3.37; N, 5.73%. Calcd for $C_{30}H_{18}N_2O_7$: C, 69.49; H, 3.51; N, 5.40%.

1,2-Diazacoronene-7,8-dicarboxylic Anhydride (7). To a stirred benzyl alcohol (30 ml) solution of **5** (104 mg, 0.20 mmol) at 100 °C, sodium hydroxide pellets (93% pure, 260 mg, 6 mmol) were added in one portion. The stirring was continued at this temperature for 30 min. After cooling, the reaction mixture was acidified with concentrated hydrochloric acid. Evaporation of the mixture and trituration of the residue with methanol followed by filtration gave crude **7**, 74 mg (99%). Recrystallization from nitrobenzene or sublimation at 330—350 °C/20 mmHg† for 5 h gave yellowish brown fine needles of pure **7** (59% or 70% yield respectively): mp 400 °C (decomp); IR 3100 (ν^{arom}_{C-H}), 1840 ($\nu_{C=O}$), 1765 ($\nu_{C=O}$), 1290 (ν_{C-O}), 850 cm^{-1} (δ_{C-H}); ^{1}H NMR δ 9.68 (d, 2H, J= 8.8 Hz), 9.72 (m, 4H), 10.52 (d, 2H, J=8.8 Hz); MS *m/e* 372 (70%, M$^+$), 300 (65%), 272 (100%). Found: C, 77.30; H, 2.04; N, 7.28%. Calcd for $C_{24}H_8N_2O_3$: C, 77.41; H, 2.17; N, 7.53%.

1,2-Diazacoronene (9). Anhydride **7** (75.6 mg, 0.20 mmol) and soda lime (300 mg, Wako Pure Chemical Industries Ltd.) were powdered together and heated in a sublimation apparatus at 320 °C for 1 h. The apparatus was then evacuated (20 mmHg) and the temperature raised to 350 °C for 2 h. The sublimate (24 mg), recrystallized from bis(2-hydroxyethyl)ether, gave 1,2-diazacoronene in pale yellow needles, 16 mg (26% yield): mp 468— 470 °C (decomp); IR 3060 (ν^{arom}_{C-H}), 850 cm^{-1} (δ_{C-H}); ^{1}H NMR δ 8.62 (s, 2H), 8.82 (d, 2H, J=9.0 Hz), 8.91 (d, 2H, J=9.0 Hz), 9.10 (m, 4H); MS *m/e* 302 (74%, M$^+$), 274 (76%), 137 (100%); UV (in C_6H_6) λ_{max} (log ε) 437 (3.89), 413 (3.62), 321 (4.79), 308 (4.64). Found: C, 87.34; H, 3.14; N, 9.53%. Calcd for $C_{22}H_{10}N_2$: C, 87.39; H, 3.34; N, 9.27%.

† 1 mmHg=133.322 Pa.

The authors wish to express their sincere thanks to Emeritus Professor Osamu Simamura for the correction of this manuscript.

References

1) "Rodd's Chemistry of Carbon Compounds," ed by S. Coffey, Elsevier Scientific Publishing Co., Amsterdam (1976), Vol. IV, Part F.

2) "Heterocyclic Compounds," ed by R. C. Elderfield John Wiley and Sons, Inc., London (1957), Vol. 6.

3) "Heterocyclic Compounds," ed by R. C. Elderfield, John Wiley and Sons, Inc., London (1961), Vol. 7.

4) "Rodd's Chemistry of Carbon Compounds," ed by S. Coffey, Elsevier Scientific Publishing Co., Amsterdam (1978), Vol. IV, Part G.

5) S. Tokita, K. Hiruta, K. Kitahara, and H. Nishi, *Synthesis*, **1982**, 229.

6) E. Clar and M. Zander, *J. Chem. Soc.*, **1957**, 4616.

7) E. Clar, "Polycyclic Hydrocarbons," Academic Press, London (1964), p. 83.

8) H. H. Jaffe and M. Orchin, "Theory and Applications of Ultraviolet Spectroscopy," John Wiley and Sons, Inc., New York (1962), p. 361.

9) J. H. Dopper and H. Wynberg, *J. Org. Chem.*, **40**, 1957 (1975).

10) J. C. Kauer, *Org. Synth.*, Coll. Vol. IV, 411 (1963).

Synthesis of (±)-Dihydromahubanolide Using 2-Methylthio-4-pentenoic Acid Dianion

Kazuhiko TANAKA,* Makoto TERAUCHI, and Aritsune KAJI
Department of Chemistry, Faculty of Science, Kyoto University, Sakyo-ku, Kyoto 606
(Received April 12, 1982)

Synopsis. A new and mild method for the synthesis of (±)-dihydromahubanolide has been developed by the use of 2-methylthio-4-pentenoic acid dianion.

The several compounds isolated from the Japanese Lauraceae, *Lindera obtusiloba Blume*[1] and *Litsea japonica*[2] have the basic skeleton of the 3-alkylidene-4-hydroxydihydro-2(3*H*)-furanone, identical with the lactones from the Amazonian Lauraceae, *Licaria mahuba*.[3] A great deal of effort has been devoted to the development of novel methods for the construction of 3-alkylidene-4-hydroxydihydro-2(3*H*)-furanone unit[4] and for the total synthesis of these lactones.[5]

Recently we reported that the dianion **1** derived from 2-(methylthio)-4-pentenoic acid can be used as a building block to furnish 5-methylene-2(5*H*)-furanone from alkyl halides or aldehydes under extremely mild reaction conditions.[6]

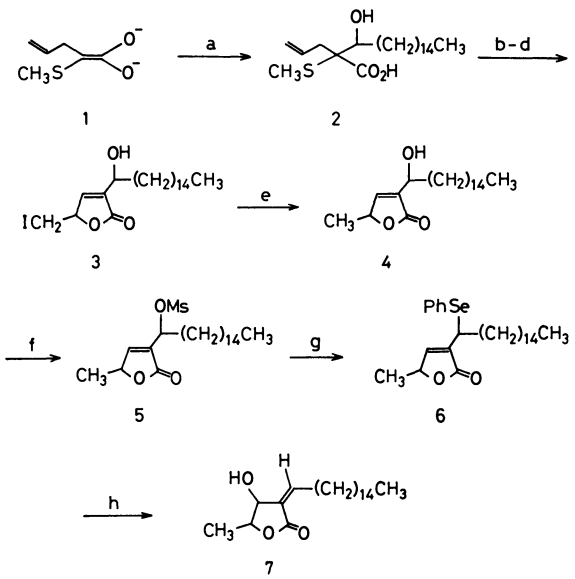

Scheme 1. (a) n-$C_{15}H_{31}CHO$, THF, −40 °C, 7 h. (b) KI-I_2, $NaHCO_3$, H_2O. (c) MCPBA, CH_2Cl_2, −78 °C, 30 min. (d) $CaCO_3$, toluene, reflux. (e) n-Bu_3SnH, AIBN, benzene, reflux. (f) MsCl, CH_2Cl_2, Et_3N. (g) PhSeNa, EtOH, −10 °C. (h) 30% H_2O_2, CH_3CN, −40 °C—r.t., 43 h.

We now report a new route to (±)-dihydromahubanolide, isolated from the Amazonian Lauraceae, *Licaria mahuba*[3] starting from the dianion **1**. The preparation of hydroxy acid **2** was accomplished by the reaction of **1** with 1.1 equiv. of hexadecanal in THF.[6] Iodolactonization, oxidation with *m*-chloroperbenzoic acid (MCPBA), and subsequent dehydrosulfenylation[7] proceeded smoothly to give 5-iodomethyl-2(5*H*)-furanone **3** in good overall yield from the hydroxy acid **2**. The furanone **3** is extremely sensitive to a base; on treatment of **3** with amine bases or even sodium hydrogencarbonate, the compound **3** gave 5-methylene-2(5*H*)-furanone in high yield.[6] Reduction of **3** with 2 equiv. of tributyltin hydride[5d] cleanly gave the 5-methyl-2(5*H*)-furanone **4** in 90% yield. The mesylate **5** was smoothly transformed by reaction in dichloromethane at 0 °C with 1.2 equiv. of methanesulfonyl chloride in the presence of 1.3 equiv. of triethylamine. Treatment of **5** with sodium benzeneselenolate[8] in ethanol at −10 °C for 2 h gave the selenide **6** in 70% yield. Rearrangement of **6** with 30% hydrogen peroxide[9] in dichloromethane afforded a mixture of (±)-dihydromahubanolide and (±)-dihydroisomahubanolide (*Z*/*E* ratio 67 : 33 in 52% yield). Enhancement in *Z*-selectivity and increase in yield were observed when the oxidation was carried out at −10 °C and the mixture was slowly warmed to room temperature (43 h).[9,10] The IR and 200-MHz ^{1}H-NMR spectra were identical with those of the published spectra.[2,3,5] Although the stereochemical relationship between CH_3 and OH groups is still uncertain due to the overlapping of methyl signals (doublet) of four isomers at 1.34—1.50 ppm region, the present method provides the efficient stereoselective synthesis of (*Z*)-3-alkylidene-4-hydroxy-2(3*H*)-furanones.

Experimental

2-(1-Hydroxyhexadecyl)-2-methylthio-4-pentenoic Acid (2): To a solution of lithium diisopropylamine (22 mmol) in THF (60 ml) was added a solution of 2-methylthio-4-pentenoic acid (**1**) (1.46 g, 10 mmol) in 5 ml of THF at −78 °C. The reaction mixture was stirred at −78 °C for 1 h, and warmed to −40 °C over 8 h. After the solution was cooled to −78 °C,

Table 1. Stereochemistry in rearrangement of selenide **6**

	Reaction conditions		Solvent	Yield of **7** %	*Z*/*E* ratio of **7**[a]
	Temp/°C	Time			
H_2O_2 (3 equiv.)	−10	15 min	CH_3CN	Trace	—
H_2O_2 (3 equiv.)	−10—r.t.	2 h	CH_3CN	63	71/29
H_2O_2 (3 equiv.)	−10—r.t.	43 h	CH_3CN	82	77/23
H_2O_2 (3 equiv.)	−10—r.t.	18 h	CH_2Cl_2	52	67/33
MCPBA (1 equiv.)	−78—r.t.	20 h	CH_2Cl_2	73	75/25

a) The *Z* and *E* assignments are based on the differences of ^{1}H-NMR chemical shift of olefinic protons.[10]

a solution of hexadecanal (2.62 g, 10.9 mmol) in 15 ml of THF was added dropwise. The solution was stirred at −78 °C to −40 °C for 7 h and then quenched with saturated aqueous ammonium chloride (10 ml). The mixture was allowed to warm to room temperature, and was extracted with ether (4×50 ml). From the combined extracts was obtained the crude product which was purified by column chromatography (silica gel; eluent hexane–acetone, 3 : 1) to give 3.12 g (81%) of **2** as viscous liquid: ^{1}H-NMR ($CDCl_3$) δ 7.02 (br, 2H COOH and OH), 5.50—6.30 (m, 1H, CH=C), 4.80—5.30 (m, 2H, CH_2=C), 3.60—4.16 (m, 1H, CH), 2.20—2.90 (m, 2H, CH_2), 2.13 (d, J=6 Hz, 3H, CH_3), 0.70—2.00 (m, 31H, CH_2 and CH_3).

*3-(1-Hydroxyhexadecyl)-5-iodomethyl-2(5H)-furanone (**3**)*: To a solution of **2** (3.00 g, 7.76 mmol) in water (60 ml) was added sodium hydrogencarbonate (1.96 g, 23.3 mmol), and stirring was continued at room temperature for 20 min. After a solution of iodine (1.97 g, 7.76 mmol) and potassium iodide (3.87 g, 23.3 mmol) in water (60 ml) was added over 1 h, the mixture was stirred at room temperature for 1 h, treated with 10% sodium thiosulfate solution (100 ml), and extracted with chloroform (4×50 ml). The combined organic layers were washed with brine, dried over anhydrous Na_2SO_4, and concentrated to give iodo lactone as an oil which was used without further purification. To a solution of this product (7.76 mmol) in dichloromethane (40 ml) at −78 °C was added a solution of MCPBA (1.68 g, 7.76 mmol) in dichloromethane (60 ml) over 20 min. After the addition was completed, the reaction mixture was stirred at −78 °C for 30 min, poured into water. The organic layer was dried over anhydrous Na_2SO_4 and concentrated to give an oil. The oil was dissolved in toluene (120 ml), and powdered calcium carbonate (1.16 g, 11.6 mmol) was added. After the mixture was heated at reflux for 30 min, the product was isolated in the usual manner to afford an 82% yield of **3** (2.59 g; unstable) as colorless crystals which were purified by column chromatography (silica gel, eluent benzene to chloroform); mp 35.0—36.0 °C: ^{1}H-NMR ($CDCl_3$) δ 7.02—7.36 (m, 1H, CH=C), 4.76—5.20 (m, 1H, CH), 4.28—4.64 (m, 1H, CH), 2.92—3.70 (m, 3H, CH_2 and OH), 0.70 (m, 31H, CH_2 and CH_3).

*3-(1-Hydroxyhexadecyl)-5-methyl-2(5H)-furanone(**4**)*: The mixture of **3** (1.86 g, 4 mmol), azobisisobutyronitrile (0.656 g, 4 mmol), and tributyltin hydride (2.32 g, 8 mmol) in benzene (40 ml) was heated at reflux for 2 h under argon. After cooling, the mixture was poured onto 10% hydrochloric acid (50 ml), and extracted with benzene (4×50 ml). The combined extracts were washed with brine, dried over anhydrous Na_2SO_4, and concentrated. Chromatography on silica gel (eluent hexane–ether, 5 : 1 to ether) gave **4** in 91% yield (1.23 g); ^{1}H-NMR ($CDCl_3$) δ 7.14—7.30 (m, 1H, CH=C), 4.80—5.08 (m, 1H, CH), 4.32—4.52 (m, 1H, CH), 2.60—3.00 (m, 1H, OH), 0.70—1.90 (m, 34H, CH_2 and CH_3). IR (Nujol) 3400 (OH), 1740, 1720 (C=O) cm^{-1}. MS (20 eV) *m/e* 338 (M^+), 320 ($M^+ - H_2O$). Preparative TLC on silica gel (Merck 60-F254s; hexane–ethyl acetate, 4 : 1) gave an analytical sample as colorless plates; mp 78—80 °C. Found: C, 74.03; H, 11.18%. Calcd for $C_{21}H_{38}O_3$: C, 74.51; H; 11.31%.

*5-Methyl-3-[1-(phenylseleno)hexadecyl]-2(5H)-furanone (**6**)*: To a solution of **4** (1.26 g, 3.73 mmol) in dichloromethane (30 ml) was added triethylamine (0.49 g, 4.85 mmol) at 0 °C, and the mixture was stirred for 10 min under argon. After the addition of methanesulfonyl chloride (0.50 g, 4.40 mmol) was completed, the mixture was stirred at 0 °C for 3 h. The usual workup gave mesylate **5** in 90% yield (1.39 g). To a solution of sodium benzeneselenolate prepared from diphenyl diselenide (0.255 g, 0.750 mmol) and sodium borohydride (0.057 g, 1.50 mmol) in ethanol (30 ml) was added at −10 °C the mesylate **5** (0.417 g, 1 mmol) in ethanol (10 ml). After the mixture was stirred for 2 h at −10 °C, the solution was poured onto dilute hydrochloric acid and extracted with ether (4×30 ml). The ethereal extracts were washed with brine, dried over anhydrous Na_2SO_4, and concentrated. Chromatography on silica gel first with hexane and then with benzene as eluent gave 0.335 g of **6** in 70% yield: ^{1}H-NMR ($CDCl_3$) δ 7.12—7.52 (m, 5H, CH, and aromatic), 6.44—6.60 (m, 1H, CH=C), 4.50—4.92 (m, 1H, CH), 3.74—4.04 (m, 1H, CH), 0.70—1.92 (m, 34H, CH_2 and CH_3). IR (Nujol) 1740 (C=O), 1680 (C=C), 745, 725, 695 cm^{-1}. Preparative TLC on silica gel (hexane–ethyl acetate, 3 : 1) gave an analytical sample as pale yellow crystals; mp 45—47 °C. Found: C, 67.61; H, 8.98%. Calcd for $C_{27}H_{42}O_2Se$: C, 67.90; H, 8.87%.

*(±)-Dihydromahubanolide (**7**)*: To a solution of **6** (0.33 g, 0.69 mmol) in acetonitrile (30 ml) was added at −10 °C 30% H_2O_2 (0.178 g, 1.57 mmol). The mixture was slowly warmed to room temperature (43 h) with stirring. The usual workup gave **7** in 82% yield (0.19 g) as a ratio of 77 : 23 of *Z*/*E* mixture. The analytical sample was obtained by silica gel column chromatography (hexane–ethyl acetate, 2 : 1); mp 39.0—50.0 °C (broad). TLC analysis (Merck silica gel plate 60-F254; hexane–ethyl acetate, 3 : 1) indicated a single spot (R_f=0.25). IR (nujol) 3400 (OH), 1740 (C=O), 1675 (C=C) cm^{-1}. MS (20 eV) *m/e* 338 (M^+), 320 ($M^+ - H_2O$). Found: C, 74.32; H, 11.56%. Calcd for $C_{21}H_{38}O_3$: C, 74.51; H, 11.31%.

This work was supported by a Grant-in-Aid for Scientific Research from the Ministry of Education, Science and Culture (No. 57118004). We also express our appreciation to Professor John A. Katzenellenbogen of University of Illinois for supplying ^{1}H-NMR (200 MHz) and IR spectra of (±)-dihydroisomahubanolide and other Lauraceae lactones.

References

1) M. Niwa, M. Iguchi, and S. Yamamura, *Tetrahedron Lett.*, **1975**, 1539, 4395; *Chem. Lett.*, **1977**, 581; **1975**, 655.

2) K. Takeda, K. Sakurai, and H. Ishii, *Tetrahedron*, **28**, 3757 (1972).

3) J. C. Martinez V., M. Yoshida, and O. R. Gottlieb, *Tetrahedron Lett.*, **1979**, 1021; *Phytochemistry*, **20**, 459 (1981).

4) J.-P. Corbet and C. Benezra, *J. Org. Chem.*, **46**, 1141 (1981); R. A. Amos and J. A. Katzenellenbogen, *ibid.*, **43**, 560 (1978); V. Jäger and H. J. Günter, *Tetrahedron Lett.*, **1977**, 2543.

5) a) R. H. Wollenberg, *Tetrahedron Lett.*, **21**, 3139 (1980); b) A. S. Kende and B. H. Toder, *J. Org. Chem.*, **47**, 163 (1982); c) A. Tanaka and K. Yamashita, *Chem. Lett.*, **1981**, 319; d) S. W. Rollinson, R. A. Amos, and J. A. Katzenellenbogen, *J. Am. Chem., Soc.*, **103**, 4114 (1981).

6) K. Tanaka, M. Terauchi, and A. Kaji, *Chem. Lett.*, **1982**, 351.

7) For recent review, see: B. M. Trost, *Acc. Chem. Res.*, **11**, 453 (1978).

8) K. B. Sharpless and R. F. Lauer, *J. Am. Chem. Soc.*, **95**, 2697 (1973).

9) D. I. J. Clive, *Tetrahedron*, **34**, 1049 (1978), and references cited therein.

10) The *Z* and *E* stereochemistry was determined by ^{1}H-NMR (100 and 200 MHz); see also, a) K. Tanaka, N. Tamura, and A. Kaji, *Chem. Lett.*, **1980**, 595; b) K. Tanaka, H. Uneme, N. Yamagishi, R. Tanikaga, and A. Kaji, *Bull. Chem. Soc. Jpn.*, **53**, 2910 (1980).

11) The 200 MHz ^{1}H-NMR analysis showed a mixture of (±)-dihydrmabubanolide A and B. However, the cis and trans ratio was not determined by 200 MHz ^{1}H-NMR due to the fact that they could not be separated by preparative TLC.

Facile Conversion of Thiosulfinic *S*-Ester to Sulfinic Ester

Toshikazu TAKATA and Shigeru OAE*
Department of Chemistry, The University of Tsukuba, Sakura, Ibaraki 305
(Received May 7, 1982)

Synopsis. Thiosulfinic *S*-esters are readily converted to the corresponding sulfinic eaters in good yields by treating in alcohols with a catalytic amount of I_2, Br_2, or HCl in the presence of H_2O_2, replacing sulfenyl groups by alcohols. The mechanism of this reaction is also discussed.

Thiosulfinic *S*-esters (thiolsulfinates) have generally been considered to be unstable and to disproportionate readily.[1] Meanwhile, thiolsulfinates were shown by us to be selectively oxidized with $NaIO_4$ to the corresponding stable thiosulfonic *S*-esters (thiolsulfonates) in nearly quantitative yields. In the oxidation in aqueous alcohols, however, considerable amounts of the corresponding sulfinates were also obtained as by-products. Yields of the sulfinates were high with primary alcohols but low with tertiary alcohols.[2] We have studied on the reaction to form the alkyl sulfinates in connection with our investigation on the mechanism of the selective oxidation of the thiolsulfinates.

This paper describes facile transformation of thiolsulfinates to the corresponding stable sulfinates by replacing sulfenyl groups with alcohols, in the treatment with catalytic I_2, Br_2, or HCl in appropriate alcohols in the presence of H_2O_2. Therefore, this transformation would be quite useful for elucidation of the structure of the original thiolsulfinate and also for estimation of the amount of the unstable thiolsulfinate.

When an unsymmetrical thiolsulfinate (**1**, 1.0 mmol) was treated with a small amount of I_2, Br_2, or HCl (3—40 mg, see Table 1) in excess alcohol (5—10 ml) as a solvent at r.t., the sulfinate **2**, in which the sulfenyl group is replaced by the alcohol used, was readily (within 2 h) obtained in 61—70% yields, along with considerable amounts of disulfides (**3** and **4**) (Eq. 1). Yields of the products were determined by GLC and NMR. When acetonitrile was used as a solvent instead of alcohol, thiolsulfinate disappeared more readily

$$\underset{\underset{\underset{\mathbf{1}}{}}{}}{\overset{\overset{\overset{\mathrm{RSSR'}}{\downarrow}}{\mathrm{O}}}{}} \xrightarrow[\mathrm{R''OH}]{\mathrm{Cat.(XY)}} \underset{\underset{\underset{\mathbf{2}}{}}{}}{\overset{\overset{\overset{\mathrm{RSOR''}}{\downarrow}}{\mathrm{O}}}{}} + \underset{\mathbf{3}}{\mathrm{R'SSR'}} + \underset{\mathbf{4}}{\mathrm{RSSR'}} \qquad (1)$$

$$\mathrm{XY} = \mathrm{I_2}, \mathrm{Br_2}, \mathrm{HCl}$$

than in alcohol, but afforded the disproportionation products (a mixture of disulfides and thiolsulfonates).

When an equimolar or excess amount of H_2O_2 was added into the reaction system besides the catalyst, the yield of **2** increased dramtically (entries 10—12), and the formation of unsymmetrical disulfide (**4**) was markedly reduced. Thus, the thiolsulfinate **1** was readily transformed to the corresponding stable sulfinate **2** in high yield (Eq. 2).

$$\mathbf{1} \xrightarrow[\mathrm{R''OH,r.t.,}\ <2\ \mathrm{h}]{\mathrm{Cat.(XY)},\ \mathrm{H_2O_2}} \mathbf{2} + \mathbf{3} \qquad (2)$$

These observations in addition to the previous results[2] seem to indicate that the reaction involves incipient formation of sulfinyl halide (RS(O)Y) which is derived by the reaction with the catalyst (XY), as shown in Scheme 1. The resulting mixture of RS(O)Y and R'SX then would react much more readily with a large excess of alcohol than with **1** to afford **2** and thiol (R'SH) which is capable of reducing **1** to give two disulfides (**3** and **4**).[3] However, in the *presence* of H_2O_2 R'SH is quickly oxidized to R'SSR' which no longer has the reducing ability. Therefore, the increase of

Table 1. Reactions of thiosulfinic *S*-ester (thiolsulfinate) with alcohol in the presence of catalyst[a]

Entry No.	Substrate (RS(O)SR') R=	R'=	Alcohol (ml) R''OH R''=	Catalyst(mg)	Temp/°C	30% H_2O_2(equiv.)[b]	Yield/mol%[c] 2	3	4	d)
1	*p*-Tol	Ph	Me 5	I_2 2.5	20	0	61	38	25	7.5
2	*p*-Tol	Ph	Me 10	I_2 2.5	20	0	66	40	21	6.6
3	*p*-Tol	Ph	Me 15	I_2 2.5	20	0	66	40	21	6.3
4	*p*-Tol	Ph	Et 5	I_2 2.5	20	0	69	40	20	5.2
5	*p*-Tol	Ph	*i*-Pr 5	I_2 2.5	20	0	69	39	19	5.7
6	*p*-Tol	Ph	Me 15	I_2 2.5	4	0	81	42	17	2.3
7	*p*-Tol	Ph	Me 10	36%HCl 30	20	0	70	38	24	4.2
8	*p*-Tol	Ph	Me 10	98%H_2SO_4 44	20	0	No reaction			
9	*p*-Tol	Ph	Me 10	70%$HClO_4$ 45	20	0	No reaction			
10	Ph	Ph	Me 10	Br_2 3.5	22	1.0	91	e)	0	Trace
11	Et	Et	*i*-Pr 10	Br_2 3.5	22	1.0	45	f)	0	25
12	*p*-Tol	Ph	Me 15	I_2 2.5	20	1.0	92	46	8.0	0
13	Ph	*p*-Tol	Me 10	I_2 4.6	18	1.0	88	40	10	Trace
14	Ph	Et	Me 10	I_2 4.6	18	1.0	90	45	7.0	0

a) Thiolsulfinate (*ca.* 1 mmol) was used as a substrate and the procedure is shown in Experimental section. b) The amount of 30% H_2O_2 is based on that of the substrate. c) Yields are determined on the basis of the amount of the substrate. d) A disproportionation product, $RS(O)_2SR$, was also obtained. e) Not determined. f) The yield could not be determined.

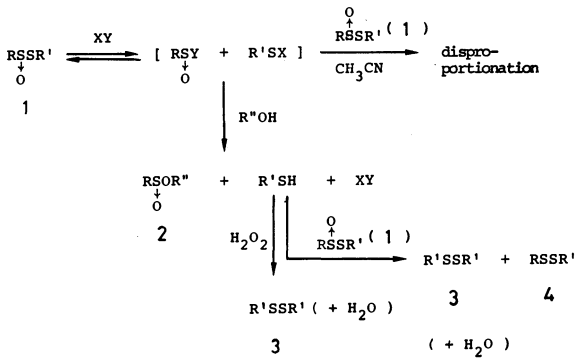

Scheme 1.

the yield of **2** by addition of H_2O_2[4] can be attributed to the decrease of the reductant R'SH, by the oxidation of R'SH to the unreactive disulfide (R'SSR') with H_2O_2.

The disproportionation rate of **1** in CH_3CN in the presence of halogen or hydrogen halide (XY) was faster than the rate of the formation of **2** in alcohol in the presence of both XY and H_2O_2. However, the disproportionation hardly occured in alcohol in which the formation of **2** must predominate over the disproportionation. Namely, the amount of alcohol used was in large excess so that RS(O)Y reacts much more easily with alcohol to form **2** than with **1** to disproportionate. The amount of solvent alcohol did not affect the yield of **2** (entries 1—3) and therefore, it is not necessary to use a very large amount of the alcohol.

This scheme is in good accordance with the data shown in Table in which the yield of **2** was rarely affected by the change of the bulkiness of alcohols used. This result is quite different from that in the oxidation of **1** with $NaIO_4$ in aqueous alcohol,[2] and it may be explained by assuming that RS(O)Y reacts only with the alcohol. Meanwhile, other catalysts such as H_2SO_4 and $HClO_4$ were found not to be effective enough to catalyze the reaction (entries 8 and 9), suggesting that RS(O)Y cannot be formed by the interaction with such catalysts in which the counter anions possess very little nucleophilicity. At lower temperatures, the reaction of RS(O)Y with alcohol to the sulfinate may slightly predominate over that with **1** to form the disproportionation products (entry 6). Change of the amount of H_2O_2 added (1—10 equiv.) did affect little the yield of **2** in the reaction of *S-p*-tolyl benzenethiosulfinate in EtOH. Similarly, the change of the amount of iodine (2.5—12.5%) as a catalyst also affected rarely the yield of **2** while the reaction time was shortened with increase of the amount of iodine. Iodine may be a better catalyst than HCl because of its easy handling and product selectivity. With hydrochloric acid the solution becomes acidic and may promote both the hydrolysis of the sulfinate formed with water present and the oxidation with H_2O_2.[4]

Thus, a new route of transformation of unstable thiolsulfinate to stable sulfinate has been found and is expected to be used as a facile method.

Experimental

General Procedure for Conversion of Thiosulfinic S-Ester to Sulfinic Ester: To an alcohol solution (10 ml) of thiosulfinic *S*-ester (*ca.* 1.0 mmol) in a 30 ml Erlenmeyer flask, 30% H_2O_2 (*ca.* 1.0 mmol) and 2.5 mg of solid iodine were added to initiate the reaction. The mixture was stirred at r.t. for 1—2 h. An aliquot of the reaction mixture was withdrawn and injected to GLC to determine the yields of the products. The structures and the yields of the products were also confirmed by NMR spectra of organic layer which was obtained by extracting the reaction mixture with $CHCl_3$, followed by usual work-up. The sulfinates thus obtained were identified by comparison of their retention times in GLC charts and then NMR spectra with those of the authentic samples prepared independently.[5,6] Purification of the sulfinate was carried out by column chromatography in which the residue after evaporation of $CHCl_3$ of the organic extract was eluted on silica gel by using hexane and then benzene or benzene as a sole solvent. The first fraction was a mixture of disulfides and the second was the sulfinate.

All thiosulfinic *S*-esters were prepared by the reported method.[7,8] S-*Phenyl Benzenethiosulfinate*: mp 69—70 °C (lit,[7] 69—70 °C), S-p-*Tolyl Benzenethiosulfinate*: mp 52 °C (lit,[7] 54 °C), S-*Phenyl* p-*Toluenethiosulfinate*: mp 78—80 °C (lit,[7] 76 °C), S-*Ethyl Benzenethiosulfinate*:[9] Colorless oil, NMR (δ, $CDCl_3$) 1.44 (t, 3H, CH_3, J=7.1 Hz), 3.13 (q, 1H, H_A or H_B of CH_2, J=7.1 Hz), 3.16 (q, 1H, H_B or H_A, J=7.1 Hz), 7.38—7.80 (m, 5H, arom); IR (neat, cm^{-1}) 3050, 2970, 2920, 1575, 1473, 1440, 1085 (S=O).

Authentic sulfinates were all known and prepared by the reactions of sulfinyl chlorides and excess alcohols.[5,6] Physical and spectroscopic data of these sulfinates were well consistent with their structures.

References

1) For example, P. Koch, E. Ciuffarin, and A. Fava, *J. Am. Chem. Soc.*, **92**, 5971 (1970); S. Oae, Y. H. Kim, T. Takata, and D. Fukushima, *Tetrahedron Lett.*, **1977**, 1195.

2) Yield of the sulfinate was largely affected by alcohol used as a solvent: Y. H. Kim, T. Takata, and S. Oae, *Tetrahedron Lett.*, **1978**, 2305.

3) L. D. Small, J. H. Bailey, and C. Cavallito, *J. Am. Chem. Soc.*, **69**, 3565 (1947).

4) H_2O_2 is not considered to oxidize not only **1** but also **3** and **4**, since the whole reaction mixture is not acidic.

5) H. Philips, *J. Chem. Soc.*, **1925**, 2552.

6) J. W. Wilt, R. G. Stein, and W. J. Wagner, *J. Org. Chem.*, **32**, 2097 (1967).

7) S. Oae, T. Takata, and Y. H. Kim, *Tetrahedron*, **37**, 37 (1981).

8) L. D. Small, J. H. Bailey, and C. J. Cavallito, *J. Am. Chem. Soc.*, **69**, 1710 (1947).

9) T. Takata, Y. H. Kim, S. Oae, and K. T. Suzuki, *Tetrahedron Lett.*, **1978**, 4303.

Photolyses of [2-Substituted 2-(alkoxycarbonyl)propyl]cobaloximes

Masaru TADA,* Shiro AKINAGA, and Masami OKABE
Department of Chemistry, School of Science and Engineering, Waseda University, Shinjuku-ku, Tokyo 160

(Received May 12, 1982)

Synopsis. Photolysis of (2-methoxycarbonyl-2-phenylpropyl)cobaloxime (**1**) gives two phenyl-migrated products, methyl 2-methylene-3-phenylpropanoate and methyl *trans*-2-methyl-3-phenylpropenoate, and a hydrogen-abstracted product, methyl 2-methyl-2-phenylpropanoate. The alkoxycarbonyl groups do not migrate in the photolysis of either **1** or [2,2-bis(ethoxycarbonyl)propyl]cobaloxime.

Coenzyme B_{12}, 5'-deoxyadenosylcobalamin, is involved in 1,2-migration of the thioester group in an enzymatic system.[1] It is well known that organo-bis(dimethylglyoximato)(pyridine)cobalt(III), *R*-(Co) (organo-cobaloxime hereafter), is a good model compound of organo-cobalamin.[1] Photolysis of an organocobaloxime generates an organic radical and paramagnetic cobaloxime[2] which must be a reasonable mimicry of a pair of a substrate radical and paramagnetic cobalamin in an enzymatic system.[1]

In our previous studies[3,4] we photolyzed organocobaloximes having an acyl group at the β-position of the alkyl group attached to the cobalt atom, and observed acyl-migration in preference to alkyl, phenyl, and alkoxycarbonyl groups. This paper reports photolyses of [2-substituted 2-(alkoxycarbonyl)propyl]cobaloximes carried out to examine the migration ability of alkoxycarbonyl groups.

Results and Discussion

Photolysis of (2-methoxycarbonyl-2-phenylpropyl)-cobaloxime (**1**) gave methyl 2-methylene-3-phenylpropanoate (**2**), methyl *trans*-2-methyl-3-phenylpropenoate (**3**), and methyl 2-methyl-2-phenylpropanoate (**4**) (Eq. 1); the results are summarized in Table 1.

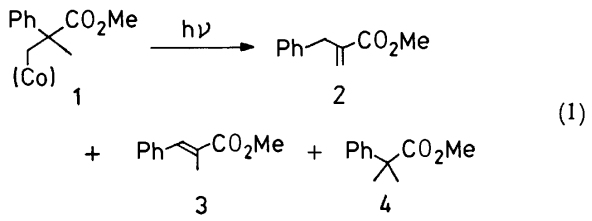

(1)

These results show that the phenyl group migrates in preference to the methoxycarbonyl group, and that no migration of the ester group takes place. The photolysis of **1** in chloroform is faster than in dichloromethane, which in turn is faster than in benzene. This indicates that the photolysis rate is dependent on the hydrogen-donating ability of the solvents. Since the formation of **2**, **3**, and **4** competes with the recombination of the radical pair **5** (Scheme 1), the faster rate of photolysis of **1** in chloroform is accounted for in terms of the faster hydrogen abstraction of **5**. The phenyl group migration is likewise competitive with the hydrogen abstraction. Thus, the photolysis of **1** in chloroform, a strong hydrogen donor,[5] gave only hydrogen-abstracted product **4**. On the other hand, the photolysis in benzene, having hardly any ability of hydrogen donation, gave only the phenyl-migrated products **2** and **3**.

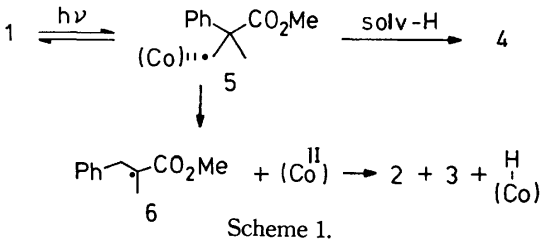

Scheme 1.

The formation of the product having a methylene group is common in the photolysis of (2,2-disubstituted propyl)cobaloximes.[4] This is interpreted in terms of the steric hindrance on the hydrogen abstraction from **6** by cobaloxime(II).

The methoxycarbonyl group did not migrate in the reaction of the corresponding bromide **7** with tributyltin hydride. The reaction gave **4** and methyl 2-methyl-3-phenylpropanoate (**8**) formed by the radical migration of the phenyl group; **4** : **8**=77 : 23 (Bu_3SnH, 0.01 mol dm^{-3}) and 19 : 81 (Bu_3SnH, 0.001 mol dm^{-3}).

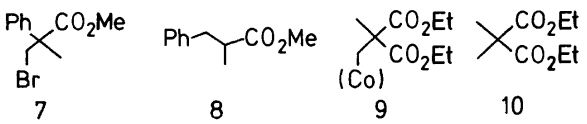

The product composition depends on the concentration of tributyltin hydride, and this result shows that the direct hydrogen capture of the intermediate radical from tributyltin hydride competes with the radical rearrangement of the phenyl group.

Bildingmaier *et al.*[6] reported that the photochemical decomposition of [2,2-bis(ethoxycarbonyl)propyl]cobaloxime (**9**) gave diethyl methylsuccinate without reproducibility, *via* the migration of the ethoxycarbonyl group, and diethyl dimethylmalonate (**10**). However, we did not detect the migrated product in the photolyses of **9** after several trials even under the same conditions as reported by Bildingmaier *et al.*[6] On a photolysis of **9** in the same procedure as for the photolysis of **1** for

TABLE 1. PHOTOLYSIS OF ORGANO-COBALOXIME **1**

Solvent	Product yield/%[a]		
	2	**3**	**4**
$CHCl_3$	Trace	0	84
CH_2Cl_2	21	15	30
C_6H_6	8	16	Trace

a) Yields after irradiation for 4 h (see Experimental section). Material balance was kept fairly well as examined on the basis of starting material.

90 min, **9** gave **10** in 100% (chloroform), 82% (dichloromethane), 34% (ethanol), and 18% (acetonitrile) yields. The photolysis in benzene gave diethyl benzylmethylmalonate (**11**) in addition to **10** only in low yield. Material balance was kept fairly well as examined on the basis of the residual starting cobaloxime **9**. The rate of the photolysis thus depends on the hydrogen-donating ability of the solvent.[5]

In conclusion the photolyses of [2-substituted 2-(alkoxycarbonyl)propyl]cobaloximes **1** and **9** cause no migration of the alkoxycarbonyl groups. The ester group seems to have the least or no ability for the radical rearrangement. Thus no ester group is any good mimicry of the (alkylthio)carbonyl group in methylmalonyl-CoA. Study on the migration property of the (alkylthio)carbonyl group is currently under way at our laboratory.

Experimental

The Preparation of Methyl 3-Bromo-2-methyl-2-phenylpropanoate (7). To a suspension of sodium hydride (55% oil dispersion) (1.86 g, 21.5 mmol) in 20 cm^3 of anhydrous 1,2-dimethoxyethane was added a solution of methyl 2-phenylproanoate (3.54 g, 21.5 mmol) in 5 cm^3 of anhydrous 1,2-dimethoxyethane under N_2. After the mixture had been refluxed for 5 h, excess dibromomethane (5 cm^3, 70 mmol) was added dropwise. The reaction mixture was refluxed for 15 h, cooled to room temperature, neutralized with acetic acid, and evaporated. After addition of water (50 cm^3) to the residue, the mixture was extracted with ether (50 $cm^3 \times 3$). The combined etheral extracts were washed with water and dried over anhydrous sodium sulfate. After removal of the solvent the residue was distilled under reduced pressure to give 2.96 g (54%) of methyl 3-bromo-2-methyl-2-phenylpropanoate (**7**), bp 84—87 °C/1070 Pa. Found: C, 51.35; H, 5.11%. Calcd for $C_{11}H_{13}BrO_2$: C, 51.38; H, 5.10%. IR (CCl_4) 1740 and 699 cm^{-1}; ^{1}HNMR (CCl_4) $\delta=1.77$ (s, 3H), 3.68 (d, 1H, $J=10$ Hz), 3.77 (s, 3H), 4.11 (d, 1H, $J=10$ Hz), and 7.50 (s, 5H).

The Preparation of (2-Methoxycarbonyl-2-phenylpropyl)cobaloxime (1). The organo-cobaloxime **1** was prepared from the bromide **7** (10 mmol) and cobaloxime (I) (15 mmol) in methanol (30 cm^3) in the conventional manner.[7] Recrystallization from methanol yielded pure **1** (70%), mp 120 °C (decomp). Found: C, 53.09; H, 5.69; N, 12.67%. Calcd for $C_{24}H_{32}N_5O_6Co$: C, 52.85; H, 5.91; N, 12.84%. IR ($CHCl_3$) 1711, 1560, 1450, and 1084 cm^{-1}; ^{1}H NMR ($CDCl_3$) $\delta=1.67$ (s, 3H), 1.86 (d, 1H, $J=10$ Hz), 1.97 (s, 6H), 2.03 (s, 6H), 2.75 (d, 1H, $J=10$ Hz), 3.63 (s, 3H), 7.30—7.65 (m, 7H), 7.78—8.00 (m, 1H), and 8.70—8.85 (m, 2H).

The Photolysis of the Organo-cobaloxime 1. A solution of the organo-cobaloxime **1** (6×10^{-3} mol dm^{-3}) in an appropriate solvent (see Table 1) was placed in a Pyrex tube and immersed in an ultrasonic bath with argon bubbling from a syringe needle for 30 min. The solution was then irradiated externally for 4 h with a 450-W high pressure Hg lamp mounted in a rotary irradiation apparatus (Rikosha RH-400), the distance between the lamp and the reaction tube being *ca.* 5 cm. The reaction mixture was condensed and the residue was placed on a Florisil column and eluted with chloroform to give methyl 2-methylene-3-phenylpropanoate (**2**),[8] methyl *trans*-2-methyl-3-phenylpropenoate (**3**),[9] and methyl 2-methyl-2-phenylpropanoate (**4**).[10] Elution with chloroform–ethyl acetate (1 : 1) gave the residual starting organo-cobaloxime. The results are summarized in Table 1. The products **2**, **3**, and **4** were identified by comparison with authentic samples.

The Reaction of the Bromide 7 with Tributyltin Hydride. A mixture of tributyltin hydride (1.6 mmol), the bromide **7** (0.4 mmol), and AIBN (trace) in benzene (160 cm^3) was refluxed for 4 h under N_2. A concentrate of the reaction mixture was passed through a short column of silica gel with chloroform and further purified by preparative TLC (silica gel) using benzene. The products were **4** and methyl 2-methyl-3-phenylpropanoate (**8**) (**4** : **8**=77 : 23, 75% yield). The product **8** was identified by comparison with an authentic sample.[11]

References

1) Review; B. M. Babior, *Acc. Chem. Res.*, **8**, 376 (1975); Model study; J. H. Grate, J. W. Grate, and G. N. Schrauzer, *J. Am. Chem. Soc.*, **104**, 1588 (1982) and references cited therein.

2) M. Tada, M. Okabe, and K. Miura, *Chem. Lett.*, **1978**, 1135; B. T. Golding, T. J. Kemp, P. J. Sellers, and E. Nocchi, *J. Chem. Soc., Dalton Trans.*, **1977**, 1266.

3) M. Tada, K. Miura, M. Okabe, S. Seki, and H. Mizukami, *Chem. Lett.*, **1981**, 33.

4) M. Okabe, T. Osawa, and M. Tada, *Tetrahedron Lett.*, **22**, 1899 (1981).

5) J. K. Kochi, "Free Radicals," John Wiley and Sons, New York (1973), Vol. 1, pp. 299—303.

6) G. Bildingmaier, H. Flohr, U. M. Kemp, T. Krebs, and J. Retey, *Angew. Chem., Int. Ed. Engl.*, **14**, 822 (1975).

7) M. Okabe and M. Tada, *Bull. Chem. Soc. Jpn.*, **55**, 1498 (1982).

8) I. Tabushi, K. Okazaki, and R. Oda, *Tetrahedron*, **25**, 4401 (1969).

9) H. Kasiwagi, N. Nakagawa, and J. Niwa, *Bull. Chem. Soc. Jpn.*, **36**, 410 (1963).

10) H. O. House, A. V. Prabhu, J. M. Wilkins, and L. F. Lee, *J. Org. Chem.*, **41**, 3067 (1976).

11) S. L. Spassov and R. Stefanova, *J. Mol. Struct.*, **53**, 219 (1979).

Rearrangement of *vic*-Diol Monoacetates Promoted by Organoaluminium Compounds

Shigekazu KANEMOTO, Yoshitomi MORIZAWA, Koichiro OSHIMA,* and Hitosi NOZAKI
Department of Industrial Chemistry, Faculty of Engineering, Kyoto University, Yoshida, Sakyo-ku, Kyoto 606
(Received May 27, 1982)

Synopsis. Treatment of pinacol monoacetate with organoaluminium reagent R_3Al caused the rearrangement under uptake of R as a nucleophile on the resulting carbonyl carbon, while R_2AlSPh produced the pinacolone itself upon workup.

Lewis acid catalysis of Diels-Alder reaction[1] or ene reaction[2] has been recently well documented. We have reported that the common Lewis acids such as $TiCl_4$ and $BF_3 \cdot OEt_2$ failed to catalyze the aliphatic Claisen rearrangement, meanwhile amphoteric organoaluminium compounds facilitated the rearrangement.[3] Another application of this new strategy with combined acid-base attack of organoaluminium reagent to the pinacol rearrangement[4] has been studied.

Treatment of pinacol monoacetate **1** with $Et_2AlC{\equiv}CPh$ in hexane provided alcohol **2** which was produced apparently by the rearrangement and successive alkynylation. Hexane, benzene, and dichloromethane were equally effective as the solvents. In ether or THF no rearrangement was observed.

Table 1 summarizes the reaction between *vic*-diol monoacetates and organoaluminium compounds. Epoxide **7** has afforded a rearranged product as *vic*-diol monoacetate (Entry 4). The reagent Et_2AlSPh has been found to be effective for the rearrangement to give ketones without introduction of a nucleophile.

It is worth noting that this new method can be used to change the nature of rearrangement from that expected in a strong acid-catalyzed reaction of the corresponding glycol. In the case of a glycol, $Ph_2C(OH)-CH(Me)-OH$, that contains one secondary and one tertiary hydroxyl, the secondary hydroxyl group could be selectively acetylated and removed preferentially upon treatment with organoaluminium compound (Entry 6 and 7). In contrast, the tertiary hydroxyl was exclusively removed to give $Ph_2CHC(O)Me$ (**13**) under sulfuric acid-catalyzed conditions.

A glycol monoacetate, $PhC(Me)(OH)-CH_2OAc$, that contains a tertiary hydroxyl and a primary acetate did not give any rearranged products on treatment with Et_2AlSPh. Benzenethiolate attacked carbonyl carbon

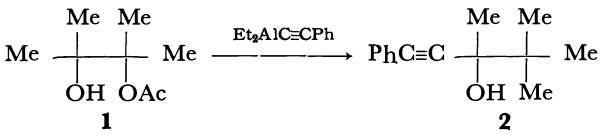

TABLE 1. REARRANGEMENT OF *vic*-DIOL MONOACETATES PROMOTED BY ORGANOALUMINIUM COMPOUNDS

Entry	Substrate	Organoaluminium reagent	Conditions Temp °C	Conditions Time h	Product (Yield/%)
1	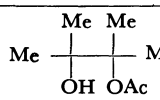 **1**	$Et_2AlC{\equiv}CPh$	25,1.0; 80,0.5		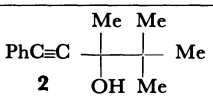 **2** (62)
2	**1**	$Et_2AlC{\equiv}CSiMe_3$	80	0.7	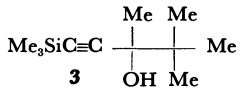 **3** (45)
3	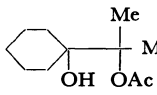	$Et_2AlC{\equiv}CPh$	70	1.5	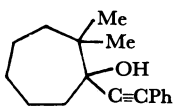 **5** (25) 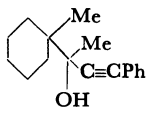 **6** (28)
4	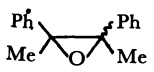 **7**	Me_3Al	80	1.0	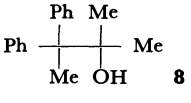 **8** (69)
5	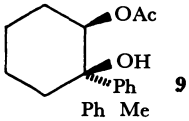 **9**	Et_2AlSPh	25	1.5	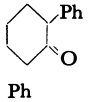 **10** (68)
6	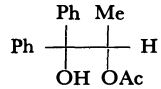 **11**	Et_2AlSPh	25	0.2	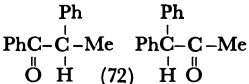 **12** (72) **13** (24)
7	**11**	$Et_2AlC{\equiv}CPh$	80	0.5	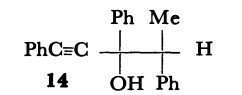 **14** (75)

of the acetate to provide the original diol.

Experimental

Infrared spectra were determined on a Shimadzu IR-27-G spectrometer, mass spectra on a Hitachi M-80. NMR spectra were recorded on a Varian EM-390H spectrometer using TMS as an internal standard. Microanalysis was performed at the Elemental Analyses Center of Kyoto University. All the experiments were carried out under an argon atmosphere. Purification of the product was performed by preparative thin layer chromatography (TLC) or column chromatography on silica gel (Merck Kiesel Gel 60).

Preparation of Diol Monoacetates ***1***[5] *and* ***4***: The title compounds were prepared by acetylation of the corresponding diols with acetic anhydride in the presence of 4-dimethylaminopyridine.[6]

Reaction between Pinacol Monoacetate ***1*** *and* $Et_2AlC{\equiv}CPh$: Butyllithium (1.6 M, 1.75 ml, 2.8 mmol) was added to a solution of phenylacetylene (0.21 g, 3.0 mmol) in benzene (2.0 ml) at 0 °C under an argon atmosphere. A solution of Et_2AlCl in hexane (1.0 M, 2.8 ml, 2.8 mmol) was added to the resulting suspension and the whole was stirred for 30 min at 25 °C. A solution of pinacol monoacetate **1** (0.16 g, 1.0 mmol) in benzene (2.0 ml) was added dropwise and the resulting mixture was stirred at 25 °C for 1 h, then at 80 °C for an additional 0.5 h. The mixture was diluted with dichloromethane (30 ml) and successively treated with NaF[7] (1.8 g) and water (0.6 ml). Vigorous stirring of the resulting suspension was continued at 25 °C for 0.5 h. The semi-solid was filtered and the remaining solid was washed with ether (3×10 ml). The combined filtrate and washings were dried (Na_2SO_4) and concentrated *in vacuo*. The residue was submitted to preparative TLC (hexane : ethyl acetate=5 : 1) to give the rearranged product **2** (0.13 g, 62% yield) as a yellow oil: bp 103—107 °C (bath temp, 133 Pa); IR (neat) 3450, 2980, 1495, 1375, 1135, 900, 750, 685 cm^{-1}; NMR (CCl_4) δ 1.08 (s, 9H), 1.45 (s, 3H), 7.06—7.49 (m, 5H). Found: C, 83.32; H, 9.18%. Calcd for $C_{14}H_{18}O$: C, 83.12; H, 8.97%.

3,4,4-Trimethyl-1-trimethylsilyl-1-pentyn-3-ol (***3***): Bp 100 °C (bath temp, 1995 Pa); IR (neat) 3475, 2980, 2180, 1368, 1259, 1160, 842, 759 cm^{-1}; NMR (CCl_4, benzene as an internal standard) δ 0.08 (s, 9H), 0.93 (s, 9H), 1.27 (s, 3H), 1.70 (bs, 1H). The compound **3** was treated with potassium fluoride in *N,N*-dimethylformamide[8] to give 3,4,4-trimethyl-1-pentyn-3-ol whose IR and NMR spectra were identical with those reported.[9]

2,2-Dimethyl-1-(phenylethynyl)cycloheptanol (***5***): Bp 135—137 °C (bath temp, 133 Pa); IR (neat) 3470, 2940, 1600, 1497, 1448, 993, 750, 688 cm^{-1}; NMR (CCl_4) δ 1.06 (s, 3H), 1.13 (s, 3H), 1.3—2.3 (m, 10H), 7.1—7.5 (m, 5H). Found: *m/e* 242.1750. Calcd for $C_{17}H_{22}O$: M, 242.1668.

2-(1-Methylcyclohexyl)-4-phenyl-3-butyn-2-ol (***6***): Bp 140 °C (bath temp, 133 Pa); IR ($CHCl_3$) 3300, 2925, 1595, 1490, 1105, 895 cm^{-1}; NMR (CCl_4) δ 1.03 (s, 3H), 1.46 (s, 3H), 1.2—2.5 (m, 10H), 7.12—7.67 (m, 5H). Found: *m/e* 242.1668. Calcd for $C_{17}H_{22}O$: M, 242.1668.

Reaction between 2,3-Diphenyl-2,3-epoxybutane (***7***) *and* Me_3Al: A mixture of **7** (0.13 g, 0.58 mmol) and Me_3Al (1.0 M hexane solution, 2.9 ml, 2.9 mmol) in hexane was heated at reflux for 1 h. The resulting mixture was worked-up as described above and the purification by preparative TLC gave alcohol **8** (97 mg, 69% yield) as an oil: bp 150 °C (bath temp, 133 Pa); IR (neat) 3560, 2990, 1600, 1497, 1023, 742, 698 cm^{-1}; NMR (CCl_4) δ 1.3 (s, 6H), 1.05 (s, 3H), 7.0—7.45 (m, 10H). Found: *m/e* 240.1434. Calcd for $C_{17}H_{20}O$: M, 240.1512.

Preparation of 2-Acetoxy-1-phenylcyclohexanol (***9***): Treatment of 1-phenylcyclohexene (4.0 g, 25 mmol) with *N*-methylmorpholine *N*-oxide (4.0 g, 26 mmol) in the presence of OsO_4 (76 mg, 0.3 mmol) according to the reported procedure[10] gave 1-phenyl-1,2-cyclohexanediol (2.9 g, 60% yield) which was transformed into monoacetate with acetic anhydride in pyridine quantitatively.

2-Phenylcyclohexanone: Benzenethiol (0.28 g, 2.5 mmol) was added dropwise to a solution of triethylaluminium (1.0 M hexane solution, 2.5 ml, 2.5 mmol) in hexane (3.0 ml) at 0 °C. After stirring for 30 min, a solution of monoacetate **9** (0.12 g, 0.5 mmol) in dichloromethane (2.0 ml) was added to the resulting solution at 0 °C and the mixture was stirred for another 30 min at 0 °C. Workup followed by purification by preparative TLC afforded a title compound as white crystals which was spectrometrically identical with an authentic sample.[11]

2-Phenylpropiophenone (***12***) *and 1,1-Diphenyl-2-propanone* (***13***): Reaction between diol monoacetate **11** (0.14 g, 0.5 mmol) and Et_2AlSPh (2.5 mmol) gave two isomeric ketones **12** and **13** (**12**/**13**=3/1) which were spectrometrically identical with authentic samples.[5,12]

Sulfuric Acid-catalyzed Rearrangement of Ph_2COH–$CH(Me)OH$: Two drops of concentrated sulfuric acid (≈40 mg) was added to a solution of diol (76 mg, 0.33 mmol) in dichloromethane (2.0 ml) at 25 °C and the whole was stirred for 15 min. Workup (ether, $NaHCO_3$) and purification gave methyl ketone **13** (56 mg, 80% yield) as a single product.

1,3,4-Triphenyl-1-pentyn-3-ol (***14***): Bp 167—168 °C (bath temp, 133 Pa); IR (neat) 3430, 3070, 2990, 2945, 2245, 1600, 1500, 1450, 1270, 1122, 757, 700 cm^{-1}; NMR (CCl_4) δ 1.24 (d, J=6.0 Hz, 3H), 4.38—4.78 (m, 1H), 6.87—8.22 (m, 15H). Found: C, 88.65; H, 6.32%. Calcd for $C_{23}H_{20}O$: C, 88.43; H, 6.45%.

Financial support from the Asahi Glass Foundation for Industrial Technology is acknowledged. We are grateful to Nippon Aluminum Alkyls, Ltd., for a gift of Et_2AlCl and Me_3Al.

References

1) B. M. Trost, J. Ippen, and W. C. Vladuchick, *J. Am. Chem. Soc.*, **99**, 8116 (1977); D. Liotta, M. Saindane, and C. Barnum, *ibid.*, **103**, 3224 (1981).

2) B. B. Snider, *Acc. Chem. Res.*, **13**, 426 (1980); W. G. Dauben and T. Broolhart, *J. Am. Chem. Soc.*, **103**, 237 (1981); A. D. Batcho, D. E. Berger, M. R. Uskokovic, and B. B. Snider, *ibid.*, **103**, 1293 (1981).

3) K. Takai, I. Mori, K. Oshima, and H. Nozaki, *Tetrahedron Lett.*, **22**, 3985 (1981).

4) E. J. Corey, R. L. Danheiser, S. Chandrasekaran, *J. Org. Chem.*, **41**, 260 (1976); B. P. Mundy and R. Srinivasa, *Tetrahedron Lett.*, **1979**, 2671.

5) E. Ghĕra, *J. Org. Chem.*, **35**, 660 (1970).

6) G. Hofle, W. Steglich, and H. Vorbrüggen, *Angew. Chem., Int. Ed. Engl.*, **17**, 569 (1978); A. Hassner, L.R. Krepski, and V. Alexanian, *Tetrahedron*, **34**, 2069 (1978).

7) K. Hattori, Y. Matsumura, T. Miyazaki, K. Maruoka, and H. Yamamoto, *J. Am. Chem. Soc.*, **103**, 7368 (1981).

8) E. J. Corey and R. A. Ruden, *Tetrahedron Lett.*, **1973**, 1495.

9) W. J. Hickinbottom, A. A. Hyatt, and M. B. Sparke, *J. Chem. Soc.*, **1954**, 2529.

10) V. VanRheenen, R. C. Kelly, and D. Y. Cha, *Tetrahedron Lett.*, **1976**, 1973.

11) M. S. Newman and M. D. Farbman, *J. Am. Chem. Soc.*, **66**, 1550 (1944).

12) L. Bagnell, E. A. Jeffery, A. Meisters, and T. Mole, *Aust. J. Chem.*, **27**, 2577 (1974).

Reinvestigation of the Pd-catalyzed Reaction of Azidoformate with Allylic Ethers

Toshihiko MIGITA,* Mitsuo CHIBA, Katsuyuki TAKAHASHI, Nobuhiro SAITOH, Setsuko NAKAIDO, and Masanori KOSUGI

Department of Chemistry, Faculty of Technology, Gunma University, Tenjin-cho, Kiryu, Gunma 376

(Received May 31, 1982)

Synopsis. The most effective catalyst for leading reaction between azidoformate and allylic ethers to formation of 1-alkoxy-1-(alkoxycarbonylimino)alkane is $PdCl_2(PhCN)_2$; $Pd(PPh_3)_4$ can hardly show catalytic activity when pure reactants are employed.

Our previous report[1] showed that allylic ethers react with azidoformate in the presence of tetrakis(triphenylphosphine)palladium, $Pd(PPh_3)_4$, to give *N*-alkoxycarbonyl imines besides aziridines:

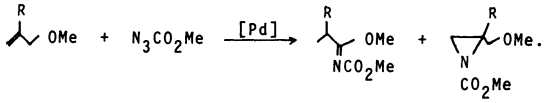

R: H, Me

During a further investigation on the scope and limitation or mechanism of the reaction, some problems were found with respect to the reproducibility of the yield of the imine. Careful surveys to establish reaction conditions revealed that impurities in the reactants, *e.g.*, chloroformate in azidoformate and allyl chloride in allyl ether, affected seriously the yield of the imine, and that dichlorobis(benzonitrile)palladium, $PdCl_2(PhCN)_2$, was a much more effective catalyst than $Pd(PPh_3)_4$ if well refined reactants were used.

Table 1 shows the effect of chloroformate added to a mixture of well refined azidoformate and allylic ethers free of the corresponding allylic chlorides, on the yield of the imines from the reaction carried out at 80 °C for 20 h in the presence of $Pd(PPh_3)_4$. When pure reactants were employed, $Pd(PPh_3)_4$ could hardly promote the formation of imines, and considerable amounts of azidoformate were recovered. However, the presence of a slight amount (1 mol%) of chloroformate enhanced the yield of imine.

This fact suggests that the species effective as a catalyst is not of Pd(0) but of Pd(II), since chloroformate may oxidatively add to Pd(0). Then, catalytic efficiencies of several Pd(II) complexes were examined for the reaction of azidoformate with 2-methyl-2-propenyl ether, which was found to be a better substrate for imine formation than allyl ether. Among the complexes examined, $PdCl_2(PhCN)_2$ was particularly effective, while $Pd(acac)_2$ and $Pd(OAc)_2$ were poor catalysts as shown in Table 2.

The substrate allylic ethers also should be well refined; particularly they should be free of allylic chlorides from which the ethers have been prepared. Table 3 shows that the presence of a small amount of allyl chloride remarkably retards the formation of imine, even with $PdCl_2(PhCN)_2$ used as a catalyst, the reason for the retardation being not yet made clear.

In conclusion, the reaction between allylic ether and azidoformate is led to form *N*-alkoxycarbonyl imines by the presence of catalytic amounts of $PdCl_2(PhCN)_2$ but hardly by $Pd(PPh_3)_4$. The previous observation[1] on the catalytic effect of $Pd(PPh_3)_4$ must have resulted from the presence of small amounts of impurities in the reactants, perhaps chloroformate from which the azidoformate was prepared.

Table 1. The effect of chloroformate on the reaction of azidoformate with allylic ethers in the presence of $Pd(PPh_3)_4$[a]

Substrate	$ClCO_2CH_3$ (mmol)	Yields of products/%[b] Imine	Aziridine
$CH_2{\equiv}CHCH_2OCH_3$	0	0	24
	0.02	28	—
	0.04	40	18
	0.04[c]	37	4
$CH_2{=}C(CH_3)CH_2OCH_3$	0.04	63	28

a) $N_3CO_2CH_3$ (2 mmol), $Pd(PPh_3)_4$ (0.02 mmol) in allylic ether (2 ml), 80 °C, and 20 h. b) Based on $N_3CO_2CH_3$, by GLPC. c) $N_3CO_2CH_3$ (2 mmol), allyl ether (25 mmol), and $Pd(PPh_3)_4$ (0.02 mmol) in benzene (1 ml).

Table 2. The reaction of azidoformate with 2-methyl-2-propenyl ether in the presence of some Pd-complexes[a]

Pd-complex	Yields of products/%[b] Imine	Aziridine
$Pd(PPh_3)_4$	5	24
$Pd(acac)_2$	7	18
$Pd(OAc)_2$	12	22
$PdCl_2(PhCN)_2$	95	Trace

a) $N_3CO_2CH_3$ (2 mmol), 2-methyl-2-propenyl ether (1 ml), Pd-complex (0.02 mmol), 80°C, and 20 h. b) Base on $N_3CO_2CH_3$, by GLPC.

Table 3. Effect of allyl chloride on the reaction of azidoformate with allylic ethers catalyzed by $PdCl_2(PhCN)_2$

Substrate	Allyl chloride (mmol)	Yields of products/% Imine	Aziridine
$CH_2{=}CHCH_2OCH_3$	0	53	8
	1	9	10
	2	0	10
$CH_2{=}C(CH_3)OCH_3$	0	95	Trace
	1	6	6

a) $N_3CO_2CH_3$ (2 mmol), $PdCl_2(PhCN)_2$ (0.02 mmol) in allylic ether (1 ml), 80 °C, and 20 h. b) Based on $N_3CO_2CH_3$, by GLPC.

Experimental

Materials. Methyl azidoformate was prepared by the known method[2] from sodium azide and methyl chloroformate and purified by repeating distillation under reduced pressure, bp 33—34 °C (8×10^3 Pa). Allylic ethers were prepared by the usual method,[3] and the products were collected by distilling the reaction mixtures. The distillates were washed several times with saturated brine in order to remove allylic chloride or alcohols, and dried over $MgSO_4$, then distilled under atmospheric pressure. Allyl methyl ether: bp 42.5—43 °C, 2-methyl-2-propenyl methyl ether: bp 66—67 °C. The purities of these reactants were checked by GLPC. The catalysts $Pd(PPh_3)_4$,[4] $PdCl_2(PhCN)_2$,[5] and Pd $(acac)_2$[6] were prepared by the methods described in the literature.

Reaction Procedure. A solution of methyl azidoformate (2 mmol) and a catalyst (0.02 mmol) in an allylic ether (1 ml) was prepared in a tube and degassed. Then the tube was sealed and immersed in a bath kept at 80 °C. After about 20 h, the products were collected from the reaction mixture by GLPC, and their structures were determined by elemental and NMR and IR spectroscopic analyses. The yields of the products were determined by GLPC.

Products. Analytical data for two aziridines[7] and 1-methoxy-1-(methoxycarbonylimino)propane[1] have been described elsewhere. 1-Methoxy-1-(methoxycarbonylimino)-2-methylpropane: ^1H NMR (CCl_4) $\delta = 1.17$ (6H, d, $-CH_3$), 2.76 (1H, m, CH), 3.62 (3H, s, OCH_3), and 3.63 (3H, s, CO_2CH_3); IR 1670 (C=N), 1725 (C=O), and 1100 (C–O–C) cm^{-1}. Found: C, 52.55; H, 8.22: N, 8.70%. Calcd for $C_7H_{13}O_3N$: C, 52.81; H, 8.23; N, 8.80%.

References

1) T. Migita, M. Chiba, M. Kosugi, and S. Nakaido, *Chem. Lett.*, **1978**, 1403.

2) W. Lwowski and T. W. Mattingly, Jr., *J. Am. Chem. Soc.*, **87**, 1947 (1965).

3) W. T. Olson, H. F. Hipsher, C. M. Buess, I. A. Goodman, I. Hart, J. H. Lammeck, Jr., and L. G. Gibbons, *J. Am. Chem. Soc.*, **69**, 2451 (1947).

4) D. R. Coulson, *Inorg. Synth.*, **13**, 121 (1972).

5) M. S. Kharasch, R. C. Seyler, and F. R. Mayo, *J. Am. Chem. Soc.*, **60**, 882 (1938).

6) A. A. Grindberg and L. K. Simonova, *Zh. Prikl. Khim.*, **26**, 880 (1953); *Chem. Abstr.*, **47**, 11060g (1953).

7) W. Ando, H. Fujii, I. Nakamura, N. Ogino, and T. Migita, *Int. J. Sulfur Chem.*, **8**, 113 (1973).

Protonation of *syn*-Bicyclo[4.2.1]nona-2,4,7-trien-9-ol with Fluorosulfuric Acid. Direct Evidence for Protonation Sites

Shuji TOMODA

Department of Chemistry, College of General Education, The University of Tokyo, Komaba, Meguro-ku, Tokyo 153

(Received June 18, 1982)

Synopsis. Treatment of *syn*-9-hydroxybicyclo[4.2.1]-nona-2,4,7-triene (**1**) with fluorosulfonic acid in sulfur dioxide-dichloromethane-d_2 cleanly provided protonated dimeric ether and the 7-hydroxytricyclo[4.2.1.$0^{2,8}$]nona-3-en-5-yl cation. Direct NMR observation as well as quenching experiment of these cations unequivocally established protonation at C-2 (or C-5) and C-7 (or C-8) of **1**.

The bicyclo[4.2.1]nona-2,4,7-triene-9-yl system has been of considerable theoretical interest[1] and practical use.[2] As a part of our investigation on the cationic rearrangement of this system,[3] we have studied the protonation of *syn*-bicyclo[4.2.1]nona-2,4,7-trien-9-ol (**1**) with fluorosulfuric acid. Four possibilities of protonation sites are available—C-2(C-5), C-3(C-4), C-7(C-8), and the oxygen. The last one may lead to the formation of the stabilized, but not bicyclo aromatic cation (**2**).[1] We report herein direct evidence for exclusive protonation at C-2(C-5) and C-7(C-8) in super acid media.

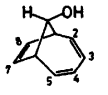

1

2

The precursor **1** was prepared by hydride reduction of the corresponding ketone according to the literature method.[3,4] When a solution of **1** in a mixture of sulfur dioxide and dichloromethane-d_2 was mixed with an excess fluorosulfuric acid in an NMR tube at −90 °C, there was obtained a well-defined proton NMR spectrum that could be rationalized as due to a mixture of protonated diether (**3**) and 7-hydroxytricyclo[4.2.1.$0^{2,8}$]-nona-3-en-5-yl cation (**4**) (see Table 1).

When this solution was quenched, either with sodium acetate in methanol or sodium methoxide in methanol, two products **3** and 5-methoxytricyclo[4.2.1.$0^{2,8}$]nona-3-en-7-ol (**5**) were isolated. The first of these was assigned the structure **3** on the basis of its spin-decoupled proton NMR spectrum, IR, UV, mass spectrum, and elemental analysis. The proton NMR spectrum of **3** showed that **3** is a symmetric molecule. Moreover since most of the protons exhibited the first order splitting, connectivity pattern of these protons was easily established by complete spin-decoupling experiments. The absence of a conjugated diene moiety was confirmed by its UV spectrum; only end absorption was detected.

The other quenched product, isolated as a single stereoisomer, was assigned the structure **5**. This assignment was consistent with its spin-decoupled proton NMR spectrum, IR, and elemental analysis. In particular, complete spin-decoupling experiment strongly supported structure **5**. Stereochemistry at C-5(OMe) cannot be inferred at present.

When the dimeric ether **3** was redissolved in a super acid solution at −82 °C, it produced peaks in three regions of the proton NMR spectrum that coincided entirely with several peaks present in the original solution from which the ether **3** had been obtained. The structure of cation **4** was therefore tentatively assigned by subtracting the NMR spectrum of **3** in super acid solution from that of the products (*i.e.* **3** and **4**) obtained

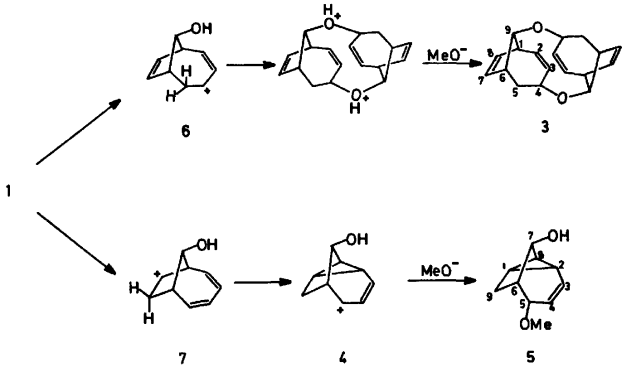

Scheme 1. Protonation of **1**.

Table 1. ^{1}H-NMR spectra of protonated **3** and cation **4** in superacid solution[a]

Mixture of **3** and **4**[b]	Protonated **3**[c]	**4**[d]
10.42(t, J=8.8 Hz)	—	10.42(1H, t, J=8.8 Hz, H-3)
8.74(t, J=8.8 Hz)	—	8.74(1H, t, J=8.8 Hz, H-5)
8.51(t, J=8.8 Hz)	—	8.51(1H, t, J=8.8 Hz, H-4)
6.22(m)	6.22(12H, m)	≈5.98(1H, H-1)[e]
4.99(m)	—	4.99(4H, m, H-1,2,6, and 8)
3.94(m)	3.94(4H, m)	—
2.34(m)	2.43(4H, m)	≈2.50(1H, H-9)[e]
1.02(d, J=17.6 H)	—	1.02(1H, d, J=17.6 Hz, H-9)

a) Observed at −90 °C——82 °C in SO_2-$CDCl_2$-FSO_3H (60 MHz). $CHDCl_2$ as an internal standard (δ=5.30). b) Obtained by treatment of **1** with FSO_3H at −90 °C. c) Dimeric ether **3** in the acid solution at −82 °C. d) Tentative assignments by spectral subtraction. Proton numbering indicated in structure **4** (Scheme 1). e) Obscured by **3**.

from the reaction of **1** with fluorosulfuric acid. The resulting NMR spectrum of **4** is listed in Table 1. The three low-field protons at $\delta=10.42$, 8.74, and 8.51 are characteristic of an allyl cation.[5]

The formation of **3** and **5** upon quenching with methanol could be explained as the products of protonated **3** and cation **4** (Scheme 1). Protonation on C-2(C-5) of **1** would give an allyl cation **6** which would undergo dimerization to give **3**. On the other hand, protonation on C-7(C-8) would initially give cation **7** which rearranges to the 3-cyclopropylallyl cation **4**.

Experimental

Direct NMR Observation of Protonated 3 and Cation 4. Alcohol **1** (17 mg, 0.13 mmol)[4] was dissolved in dichloromethane-d_2 (0.22 ml) in a thin-walled NMR tube. The solution was cooled to −78 °C and sulfur dioxide (0.22 ml) was distilled into the NMR tube. The sample was then cooled to −120 °C (pentane-liquid N_2 slush) to which freshly distilled fluorosulfuric acid (0.10 ml) was added. The tube was stirred in a −90 °C bath using vortex mixer for 30 s and was quickly set in the NMR probe which had been maintained at −90 °C.

Quenching of the Cation Solution with Methanol. The alcohol (**1**, 643 mg, 4.83 mmol) in a mixture of dichloromethane and sulfur dioxide (1 : 1, 10 ml) was treated with fluorosulfuric acid (2 ml) at −78 °C for 1 h. The mixture was quenched with 150 ml methanol saturated with sodium acetate at room temperature. The methanol was removed by rotary evaporator at 0 °C. 100 ml water was added to the residue. The mixture was then extracted with three portions of ether and the combined ether layers washed with water, saturated aqueous sodium hydrogencarbonate and water, and then dried over magnesium sulfate. Concentration provided 534 mg crude oil, which was separated by preparative TLC to afford **3** (146 mg) and **5** (85 mg) as colorless oils.

Spectral Data of 3. MS (70 eV) *m/e* 268 (M^+). IR (CCl_4) 3070, 2960, 1450, 1062, 1040, and 694 cm^{-1}. UV (cyclohexane) 217.5 (ε 2400). ^{1}H-NMR (CCl_4) δ (numbering of protons indicated in structure **3**) 6.13 (1H, dd, $J=9.6$, 5.0 Hz, H-3), 5.86 (2H, d, $J=1.1$ Hz, H-7 and 8), 5.76 (1H, dd, $J=9.6$, 4.1 Hz, H-2), 5.00 (1H, dd, $J=6.5$, 6.6 Hz, H-9), 4.40 (1H, dd, $J=7.0$, 5.0 Hz, H-4), 3.15 (1H, ddd, $J=6.4$, 4.1, 1.8 Hz, H-1), 2.83 (1H, ddd, $J=3.2$, 10.4, 6.6 Hz, H-6), 1.94 (1H, ddd, $J=11.4$, 10.4, 6.8, H-5), 1.44 (1H, ddd, $J=11.4$, 3.2, 0.5 Hz, H-5).

Found: C, 80.19, 80.27; H, 7.57, 7.67%. Calcd for $C_{18}H_{20}O_2$: C, 80.55; H, 7.51%.

Spectral Data of 5. MS (70 eV) *m/e* 134 (M^+ −MeOH). IR (CCl_4) 3500, 3020, 1660, 1390, and 1092 cm^{-1}. ^{1}H-NMR (CCl_4) δ (numbering of protons based on nomenclature) 6.05 (1H, ddd, $J=12.0$, 7.5, 1.5 Hz, H-3), 5.57 (1H, ddd, $J=12.0$, 4.0, 3.0 Hz, H-4), 4.64 (1H, ddd, $J=6.0$, 4.0, 4.0 Hz, H-7), 3.81 (1H, ddd, $J=1.5$, 4.0, 4.0 Hz, H-5), 3.47 (1H, d, $J=4.0$ Hz, OH), 3.40 (3H, s, OMe), 2.65 (1H, dddd, $J=9.0$, 6.0, 4.0, 3.0 Hz, H-6), 2.25 (1H, ddd, $J=12.0$, 9.0, 4.0 Hz, H-9), 1.98 (1H, ddd, $J=8.0$, 6.0, 4.0 Hz, H-8), 1.63 (1H, ddd, $J=8.0$, 7.0, 4.0 Hz, H-1), 1.45 (1H, d, $J=12$ Hz, H-9), 1.35 (1H, ddd, $J=7.5$, 7.0, 4.0 Hz, H-2).

Found: C, 72.11; H, 8.43%. Calcd for $C_{10}H_{14}O_2$: C, 72.26; H, 8.49%.

References

1) M. J. Goldstein and R. Hoffmann, *J. Am. Chem. Soc.*, **93**, 6193 (1971); A. F. Diaz and J. Fulcher, *ibid.*, **98**, 798 (1976); W. Kirmse and G. Voight, *ibid.*, **96**, 7598 (1974).

2) S. Masamune, C. U. Kim, K. E. Wilson, G. O. Spessard, P. E. Georghiou, and G. S. Bates, *J. Am. Chem. Soc.*, **97**, 3512 (1975).

3) Y. Nomura, Y. Takeuchi, S. Tomoda, and M. J. Goldstein, *J. Chem. Soc., Chem. Commun.*, **1977**, 545; Y. Nomura, Y. Takeuchi, and S. Tomoda, *Tetrahedron Lett.*, **1978**, 911; **1979**, 2161.

4) T. A. Antkowiak, D. C. Sanders, G. B. Trimitsis, J. B. Press, and H. Shechter, *J. Am. Chem. Soc.*, **94**, 5366 (1972).

5) G. A. Olah, G. Liang, and Y. K. Mo, *J. Am. Chem. Soc.*, **94**, 3544 (1972).

Electrolytic Decarboxylation. 6. A Convenient Synthesis of 3-(*cis*-3-Hexenyl)-2-cyclopentenone, a Precursor of *cis*-Jasmone Synthesis

Sigeru Torii,* Hideo Tanaka, Tsutomu Inokuchi, and Kazuo Tomozane
Department of Industrial Chemistry, School of Engineering, Okayama University, Okayama 700

(Received June 24, 1982)

Synopsis. A regioselective electro-acetoxylation of 1-(*cis*-3-hexenyl)-2-cyclopentene-1-carboxylic acid in a Et_3N–AcOH–AcOEt–*t*-BuOH–(Pt electrodes) system afforded 3-acetoxy-1-(*cis*-3-hexenyl)-1-cyclopentene (**7a**) (98%). Alkaline hydrolysis of **7a** followed by the oxidation with chromium trioxide gave the desired 3-(*cis*-3-hexenyl)-2-cyclopenone smoothly.

The cyclization of 1,4-diketone (**2**) with base is a key strategy in *cis*-jasmone synthesis.[1] As an extension of the investigation, a device has been made by McCurry and co-worker since 3-(*cis*-3-hexenyl)-2-cyclopentenone (**3**) can be smoothly converted into **1** *via* the intermediate **2** by a simple retro-aldol-aldol condensation reaction in an aqueous alkaline solution[2] (Scheme 1).

In the course of our investigation on electrolytic decarboxylation of aliphatic carboxylic acids (non Kolbe type reactions), we have found that the electrolytic decarboxylation of β,γ-unsaturated carboxylic acids affords exclusively γ-acetoxy-α,β-unsaturated compounds.[3] The success prompted us to synthesize the important intermediate **3** by the electro-decarboxylative acetoxylation of 1-(*cis*-3-hexenyl)-2-cyclopentene-1-carboxylic acid (**6b**) (Scheme 2).

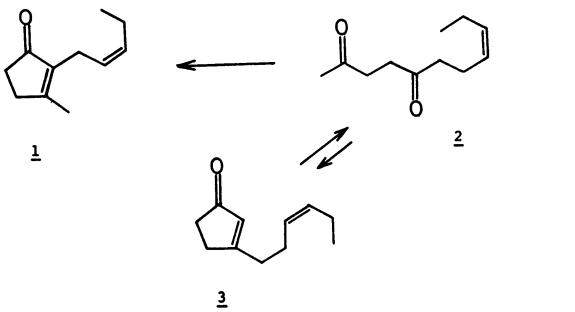

Scheme 1.

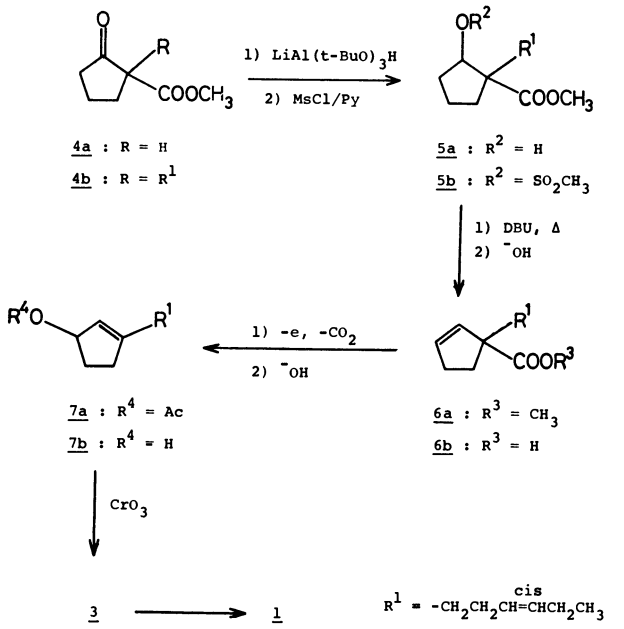

Scheme 2.

The β,γ-unsaturated carboxylic acid **6b** was obtained by the following manner: Treatment of methyl 2-oxocyclopentanecarboxylate (**4a**) with *cis*-3-hexenyl *p*-toluenesulfonate in acetone in the presence of KI and K_2CO_3 gave **4b** (89%), which was subjected to reduction with $LiAl(t\text{-}BuO)_3H$ in tetrahydrofuran (THF) to give the alcohol **5a** (99%). Dehydration of **5a** was performed by heating the corresponding methanesulfonate **5b** with 1,8-diazabicyclo[5.4.0]undec-7-ene (DBU) in *N*,*N*-dimethylformamide (DMF), yielding **6a** (86%). Hydrolysis of **6a** in a methanolic alkaline solution afforded **6b** (98%).

Electrolytic decarboxylation of **6b** was carried out in either a divided or an undivided cell using two Pt electrodes. A solution of **6a** in acetic acid, ethyl acetate, and *t*-butyl alcohol (2/5/0.3) containing triethylamine was charged into the anode compartment of the divided cell, and a regulated DC power (terminal voltage: 35 V) was supplied for 21 h. In the course of the electrolysis, the initial current of 6 mA/cm^2 dropped onto 1 mA/cm^2. Workup of the anolyte gave the acetate **7a** (68%). On the other hand, the electrolysis of **6a** in the same medium was carried out in an undivided cell (without separation of the two electrode compartments), there was also obtained **7a** (98%) without detectable amounts of the hydrogenated products on the C–C double bond. This is in contrast to the results of the electrolytic decarboxylation of some carboxylic acids bearing isopropenyl moiety,[4] in which, the hydrogenation of the C–C double bond proceeds competitively at the cathode.

The transformation of **7a** into 3-(*cis*-3-hexenyl)-2-cyclopentenone (**3**) was performed by the hydrolysis of **7a** followed by the oxidation with chromium trioxide.[5] The spectral data and physical properties of **3** were fully identical with those of the reported one.[2]

Experimental

All boiling points are uncorrected. IR spectra were determine with a JASCO IRA-I infrared spectrometer. ^1H NMR spectra were obtained at 60 MHz with a Hitachi R-24 spectrometer.

*Methyl 1-(*cis*-3-Hexenyl)-2-oxocyclopentane-1-carboxylate (**4b**).* A mixture of **4a** (480 mg, 3.38 mmol), *cis*-3-hexenyl *p*-toluenesulfonate (1.05 g, 4.12 mmol), KI (1.03 g, 6.18 mmol), and K_2CO_3 (4.73 g, 34.3 mmol) in acetone (40 ml) was heated to reflux for 2 d. After removal of the solids by filtration, the filtrate was concentrated and the residue was chromatographed (SiO_2, hexane–AcOEt: 35/1), giving **4b** (676 mg, 89%): bp 93—96 °C/2 Torr†; IR (neat) 3101 (HC=C), 1755 (C=O),

† 1 Torr=133.322 Pa.

1723 cm^{-1} (C=O); ^1H NMR (CCl_4) δ 0.96 (3H, t, J=7.4 Hz, CH_3), 1.36—2.67 (12H, m), 3.65 (3H, s, CH_3O), 5.23—5.43 (2H, m, HC=CH).

Found: C, 69.76; H, 9.11%. Calcd for $C_{13}H_{20}O_3$: C, 69.91; H, 8.99%.

*Methyl 1-(*cis*-3-Hexenyl)-2-hydroxycyclopentane-1-carboxylate(5a).* A mixture of **4b** (200 mg, 0.89 mmol) and $LiAl(t\text{-}BuO)_3H$ (453 mg, 1.25 mmol) in THF (10 ml) was stirred at 0—5 °C for 3 h. The usual workup gave **5a** (200 mg, 99%): bp 130—132 °C/7 Torr; IR (neat) 3439 (OH), 3000 (HC=C), 1731 cm^{-1} (C=O); ^1H NMR (CCl_4) δ 0.94 (3H, t, J=7.2 Hz, CH_3), 1.20—2.32 (12H, m), 2.62 (1H, br s, OH), 3.62 (3H, s, CH_3O), 4.15 (1H, m, CH-O), 5.12—5.45 (2H, m, HC=CH).

Found: C, 68.85; H, 9.74%. Calcd for $C_{13}H_{22}O_3$: C, 68.99; H, 9.80%.

*1-(*cis*-3-Hexenyl)-2-cyclopentene-1-carboxylic Acid (6b).* To a solution of **5a** (178 mg, 0.79 mmol) in pyridine (3 ml) was added methanesulfonyl chloride (270 mg, 2.36 mmol) at 0 °C. After being stirred for 3 h at this temperature, the usual workup gave methanesulfonate **5b** (239 mg, 100%): IR (neat) 3012 (HC=C), 1729 (C=O), 1356, 1177 cm^{-1} (CH_3SO_3); ^1H NMR (CCl_4) δ 0.96 (3H, t, J=7.2 Hz, CH_3), 1.21—2.40 (12H, m), 2.91 (3H, s, CH_3SO_3), 3.67 (3H, s, CH_3O), 5.07—5.38 (3H, m, HC-O, HC=CH). The product **5b** was heated in DMF (1 ml) containing DBU (122 mg, 0.8 mmol) at 140 °C for 8 h. The mixture was diluted with water and the extractive workup with benzene-ether (1/1) followed by column chromatography (SiO_2, hexane-AcOEt: 12/1) gave **6a** (141 mg, 86%): bp 82—83 °C/10 Torr; IR (neat) 3050, 3005 (HC=C), 1733 (C=O), 1650 cm^{-1} (C=C); ^1H NMR CCl_4) δ 0.95 (3H, t, J=7.4 Hz, CH_3), 1.21—2.61 (10H, m), 3.61 (3H, s, CH_3O), 5.12—5.44 (2H, m, HC=CH), 5.49—5.81 (2H, m, HC=CH).

Hydrolysis of **6a** (585 mg, 2.81 mmol) in aqueous 80% MeOH (10 ml) containing KOH (1.26 g, 22.5 mmol) at 65 °C for 6 h gave **6b** (534 mg, 98%) after column chromatography (SiO_2, hexane-AcOEt: 4/1): IR (neat) 3690—2230 (OH), 1697 cm^{-1} (C=O); ^1H NMR (CCl_4) δ 0.94 (3H, t, J=7.4 Hz, CH_3), 1.38—2.75 (10H, m), 5.07—5.46 (2H, m, HC=CH), 5.50—5.92 (2H, m, HC=CH), 12.15 (1H, s, COOH).

Found: C, 74.38; H, 9.45%. Calcd for $C_{12}H_{18}O_2$: C, 74.19; H, 9.34.

*Electrolysis of 1-(*cis*-3-Hexenyl)-2-cyclopentene-1-carboxylic Acid (6b).* *Procedure A*: Electrolysis was carried out in an undivided cell fitted with two Pt electrodes (2×3 cm^2), a thermometer, and a gas lead pipe. A solution of **6b** (120 mg, 0.61 mmol) in AcOH (2 ml), AcOEt (5 ml), and *t*-BuOH (0.27 ml) containing Et_3N (0.85 ml) was charged in the cell and electrolysed at 20—22 °C under a constant applied voltage (30 V) for 7 h. The initial current of 30 mA/cm^2 dropped onto 20 mA/cm^2 durring the electrolysis. The mixture was concentrated to *ca.* 2 ml and the residue was taken up with ether, washed with brine, and dried (Na_2SO_4). Evaporation of the solvents followed by column chromatography (SiO_2, hexane-ether: 2/1) gave **7a** (125 mg, 98%): bp 64—66 °C/2 Torr; IR (neat) 3054, 3005 (HC=C), 1728 cm^{-1} (C=O); ^1H NMR (CCl_4) δ 0.93 (3H, t, J=7.4 Hz, CH_3), 1.48—2.73 (10H, m), 1.91 (3H, s, CH_3CO), 5.11—5.56 (4H, m, HC=CH, HC=C, CH-O).

Found: C, 74.77; H, 9.86%. Calcd for $C_{13}H_{20}O_2$: C, 74.96; H, 9.68%.

Procedure B: Electrolysis was carried out in a divided cell, separated with glass-frit, using two Pt electrodes (2×3 cm^2). A mixture of AcOH (8 ml), AcOEt (20 ml), *t*-BuOH (1.2 ml), and Et_3N (3 ml) was charged into both anode and cathode compartments, and **6b** (80 mg, 0.41 mmol) was added to the anode compartment. DC powder (35 V) was supplied for 21 h (6—1 mA/cm^2) and workup of the anolyte in the same manner as described above gave **7a** (58 mg, 68%).

*3-(*cis*-3-Hexenyl)-2-cyclopentenone (3).* A mixture of **7a** (75 mg, 0.36 mmol) and KOH (80 mg) in aqueous 90% MeOH (5 ml) was stirred at room temperature for 2 h and the extractive work-up with ether followed by column chromatography (SiO_2, hexane-ether: 1/1) gave **7b** (57 mg, 95%): bp 62—64 °C/2 Torr: IR (neat) 3330 (OH), 3305 (HC=C), 1650 cm^{-1} (C=C); ^1H NMR (CCl_4) δ 0.96 (3H, t, J=7.4 Hz, CH_3), 1.47—2.80 (10H, m), 4.67 (1H, m, HC-O), 4.50—4.84 (3H, m, HC=CH, HC=C), which was treated with aqueous chromium trioxide (1.3 M, 0.5 ml) in CH_2Cl_2 (2 ml) at 0 °C for 4 h. The organic layer was worked up in the usual manner to give **3** (40 mg, 71%), whose spectral data were identical with those of the reported one.[2]

References

1) S. Torii and H. Tanaka, *Koryo*, **114**, 41 (1976); T.-L. Ho, *Synth. Commun.*, **4**, 256 (1974); R. A. Ellison, *Synthesis*, **1973**, 397.

2) P. M. McCurry, Jr., and R. K. Singh, *J. Org. Chem.*, **39**, 2317 (1974). Recently, an improved synthesis of **1** *via* **3** has been reported: T. Yoshida, T. Miyakoshi, H. Ohmichi, and S. Saitoh, 25th Symposium on Chemistry of Terpenes, Essential Oils, and Aromatics, Yamaguchi, October 1981, Abstr. p. 234.

3) S. Torii, T. Inokuchi, M. Mizuguchi, and M. Yamazaki, *J. Org. Chem.*, **44**, 2203 (1979) and references cited therein.

4) S. Torii and T. Okamoto, *Bull. Chem. Soc. Jpn.*, **49**, 771 (1976).

5) H. C. Brown, C. P. Gang, and K.-T. Liu, *J. Org. Chem.*, **36**, 387 (1971).

The Function of Magnesium(II) *N,N'*-Dicyclohexylamidinide Complexes as a Carbon Dioxide Carrier

Noboru MATSUMURA,* Takayuki OHBA, and Hiroo INOUE
Department of Applied Chemistry, College of Engineering, University of Osaka Prefecture, Sakai, Osaka 591
(Received June 26, 1982)

Synopsis. It is found that magnesium(II) *N,N'*-dicyclohexylamidinide complexes are useful reagents for the fixation of carbon dioxide and the transfer of the captured carbon dioxide moiety to active methylene compounds.

A carbon dioxide carrier,[1] which performs its function in the fixation of carbon dioxide and transcarboxylation, is of interest in connection with a biological biotin-dependent carboxylation[2] and in applications to organic syntheses. Recently we have reported that 2-morpholino-4,5-dihydro-1-imidazolylmagnesium complex (**1**) acts effectively as a carbon dioxide carrier in the carboxylation of active methylene compounds under mild conditions.[3] In our continuing investigation of carbon dioxide carrier, we have studied the transcarboxylating function of magnesium(II) complexes **2a—d** having an amidinide-type ligand which is derived readily from available dicyclohexylcarbodiimide (DCC). Herein, we wish to report that complexes **2a** and **2b** are the useful carbon dioxide carriers and that the C=N bond, the substituent Y of the amidinide type ligand and the magnesium(II) ion play an important role in the transcarboxylation process.

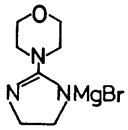

1

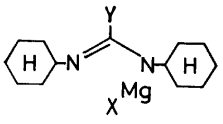

2

a: Y=C$_6$H$_5$, X=Br
b: Y=n-C$_4$H$_9$, X=Br
c: Y=CH$_3$O, X=CH$_3$O
d: Y=, X=Br

The transcarboxylating ability of complexes **3a—d**, prepared by the reactions of **2a—d** with carbon dioxide, was investigated using acetophenone as the substrate. The reaction afforded benzoylacetic acid and **4a—d** as the products. The yield of benzoylacetic acid shown in Table 1 indicated that complexes **3a** and **3b** exhibit activity for the transfer of their carbon dioxide moiety to acetophenone, but complexes **3c** and **3d** are much less active. Thus, contrary to complex **1**, the morpholino group of complex **3d** was undesirable for the activation of the carbon dioxide moiety.

Next, the transcarboxylating activity of complex **3b** was compared with that of the lithium–carboxylato complex (**5**). It was observed that acetophenone is carboxylated by **5** in only 10% yield. The fact that the magnesium(II) complex is much more effective than the lithium complex was the same as that in the case of the imidazolinide complex **1** described previously.[3]

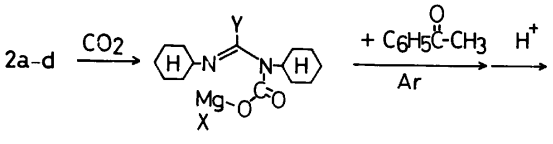

3a-d

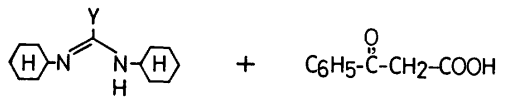

4a-d

TABLE 1. THE YIELD OF BENZOYLACETIC ACID IN THE REACTION OF ACETOPHENONE WITH COMPLEXES **3a—d**

Complex	Yield/%[b]
3a	44
3b	45
3c	Trace
3d	8

a) Solvent; DMF. Temperature; r. t. Reaction time; 40 h.
b) Besed on acetophenone.

In order to investigate whether the C=N bond of the *N,N'*-dicyclohexylamidinide ligand is required for the transcarboxylating function or not, we carried out the carboxylation of acetophenone using complex **6** under the similar conditions. The complex **6** absorbed an equimolar amount of carbon dioxide, but the resulting magnesium(II)–carboxylato complex was found not to transfer the carbon dioxide moiety to acetophenone at all. This fact demonstrates that the C=N bond is necessary for transcarboxylation.

Other active methylene compounds described in Table 2 also were carboxylated by the magnesium(II)–carboxylato complex **3a**. It is interesting that *S*-benzyl thioacetate is carboxylated though in a low yield, since it may be related to CH_3CO–CoA in a biological system.

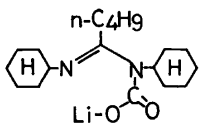

5

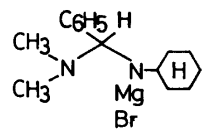

6

Experimental

Materials. Active methylene compounds were distilled or recrystallized prior to use. Tetrahydrofuran (THF) was refluxed over $LiAlH_4$, distilled and stored in argon atmosphere.

Carboxylation of Active Methylene Compounds with 2a—d. A typical experiment was as follows: a solution of phenylmagnesium bromide, butylmagnesium bromide, magnesium dimethoxide, or morpholinomagnesium bromide (8.16 mmol) in THF (10 cm^3) was under argon added to a solution of DCC (6.81 mmol) in THF (10 cm^3) and the solution was stirred for 1 h. After removal of the solvent, the residue was dissolved in 25 cm^3 of *N,N*-dimethylformamide (DMF) by bubbling

Table 2. Carboxylations of active methylene compounds with complex **3a** under argon[a)]

R_1–CO–CH_2–R_2		Yield[b)] of R_1–CO–CH(–R_2)–COOH
R_1	R_2	
p-NO_2–C_6H_4	H	74
p-CH_3O–C_6H_4	H	14
C_6H_5–CH=CH	H	50
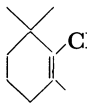	H	68
$C_6H_5CH_2S$	H	24
C_6H_5	CH_3	32
n-C_4H_9	H	8
–$(CH_2)_4$–		25
H	$C_6H_5CH_2$	35

a) Solvent; DMF. Temperature; r. t. Reaction time; 40 h. b) Based on the substrate.

carbon dioxide and the solution was stirred at room temperature for 1 h. The solvent was evaporated *in vacuo* at room temperature and the residue was dried *in vacuo* at 40 °C. The resulting white solid, which contains complex **3**, was allowed immediately to react under argon with active methylene compounds (1.7 mmol) in dry DMF (35 cm^3) at room temperature for 40 h. The formation of complex **3** was confirmed by the method described previously:[3)] complex **3a** was confirmed by the facts that the IR spectrum of the solid has the carbonyl absorption at 1665 cm^{-1} and that complex **2a** absorbs an equimolar amount of carbon dioxide and the fixed carbon dioxide is released quantitatively by treatment with a dilute sulfuric acid solution. The reaction was stopped by adding water. The carboxylation products and **4a**—**d** were isolated in the usual manner and were identified by a comparison of their melting points, IR, ^1H NMR, and mass spectra, and elemental analyses with those of the respective authentic specimens.

*Compounds **4a**—**d***: HCl salt of **4a**: mp 264—265 °C (decomp); IR (KBr) 3420 (NH), 1630 cm^{-1} (C=N); ^1H NMR ($CDCl_3$) 0.5—3.0 (m, 24H, NH+aliphatic) 6.9—7.7 (m, 5H, aromatic). Found: C, 71.11; H, 9.11; N, 8.73%. Calcd for $C_{19}H_{29}N_2Cl$: C, 70.98; H, 8.91; N, 8.54%. **4b**: bp 161—162 °C/7 mmHg; IR (film) 3350 (NH), 1640 cm^{-1} (C=N); ^1H NMR ($CDCl_3$) 0.5—2.5 (m, 29H, aliphatic), 2.5—3.2 (m, 3H, NH+NCH_2); MS *m/e* 264 (M^+), 235, 222, 153, 140, 101, 84, 83. Found: C, 76.95; H, 12.38; N, 10.53%. Calcd for $C_{17}H_{32}N_2$: C, 77.21; H, 12.20; N, 10.59%. **4c**: bp 118—120 °C/2 mmHg; IR (film) 3440 (NH), 1660 cm^{-1} (C=N); ^1H NMR ($CDCl_3$) 0.7—3.4 (m, 23H, aliphatic), 3.5 (s, 3H, OCH_3); MS *m/e* 238 (M^+), 206, 165, 164, 83, 82, 81. Found: C, 70.53; H, 11.24; N, 11.60%. Calcd for $C_{14}H_{26}N_2O$: C, 70.54; H, 10.99; N, 11.75%. **4d**: mp 99—101 °C; IR (KBr) 3380 (NH), 1630 cm^{-1} (C=N); ^1H NMR ($CDCl_3$) 1.0—2.2 (m, 22H, aliphatic), 2.2—3.9 (m, 9H, NH+morpholino). Found: C, 69.58; H, 10.65; N, 14.32%. Calcd for $C_{17}H_{31}N_3O$: C, 69.86; H, 10.92; N, 14.34%.

*The Reaction of Acetophenone with Complex **6**.* A solution of phenylmagnesium bromide (6.81 mmol) in 10 cm^3 of THF was added under argon, drop by drop, to a solution of N^2-cyclohexyl-N^1,N^1-dimethylformamidine (6.81 mmol), which was prepared by the method described in the literature,[4)] in 10 cm^3 of THF at room temperature. The mixture was magnetically stirred at this temperature for 1 h. After removal of the solvent in vacuo, the residue was dissolved in 25 cm^3 of DMF under bubbling carbon dioxide and the solution was stirred under bubbling carbon dioxide at room temperature for 1 h. The solvent was evaporated *in vacuo* at room temperature and the residue was dried *in vacuo* at 40 °C. The resulting white solid, which contains complex **6**, was allowed immediately to react under argon with acetophenone. The reaction mixture was treated by the method being similar to that in the cases of **2a**—**d**. Acetophenone and benzaldehyde were obtained in good yields, but benzoylacetic acid was not detected at all.

References

1) H. Sakurai, A. Shirahata, and A. Hosomi, *Tetrahedron Lett.*, **1980**, 1967; T. Tsuda, Y. Chujo, T. Hayasaki, and T. Saegusa, *J. Chem. Soc., Chem. Commun.*, **1979**, 797; T. Tsuda, Y. Chujo, and T. Saegusa, *ibid.*, **1976**, 415; *J. Am. Chem. Soc.*, **100**, 630 (1978); **102**, 431 (1980).

2) J. Moss and M. D. Lane, *Adv. Enzymol. Relat. Areas Mol. Biol.*, **35**, 321 (1971).

3) N. Matsumura, Y. Sakaguchi, T. Ohba, and H. Inoue, *J. Chem. Soc., Chem. Commun.*, **1980**, 326.

4) H. Bredereck, R. Gompper, K. Klemm, and H. Rempfer, *Chem. Ber.*, **92**, 837 (1959).

Homologation of Methyl Esters Catalyzed by Ruthenium-Cobalt Bimetallic Systems[1]

Masanobu HIDAI,* Yukio KOYASU, Makoto YOKOTA, Masami ORISAKU, and Yasuzo UCHIDA
Department of Industrial Chemistry, Faculty of Engineering, The University of Tokyo, Hongo, Bunkyo-ku, Tokyo 113

(Received July 8, 1982)

Synopsis. Reactions of methyl esters such as methyl acetate with synthesis gas have been investigated by use of the mixed clusters such as $[Et_4N][RuCo_3(CO)_{12}]$ and $[Et_4N][Ru_3Co(CO)_{13}]$ or a combination of $Ru(acac)_3$ and $Co_2(CO)_8$ as catalyst and methyl iodide as promoter. In the homologation of methyl acetate, the catalytic activity for formation of ethyl acetate was much improved when both ruthenium and cobalt existed in the reaction system.

Mixed transition metal clusters have recently attracted much attention since the compounds might be used as unique homogeneous catalysts or precursors to well defined bimetallic or multimetallic heterogeneous catalysts.[2] In a previous paper[3] we reported that both a combination system of $RuCl_3 \cdot 3H_2O$ and $Co_2(CO)_8$ with the Ru/Co ratio of about 1/3 and the mixed clusters containing the $[RuCo_3(CO)_{12}]^-$ moiety show a more remarkable catalytic activity for methanol homologation. We wish here to describe that the similar bimetallic catalysts are also effective for the homologation of methyl esters, especially methyl acetate.

Recently Braca *et al.*,[4] repoted that methyl esters such as methyl acetate and propionate were homologated to the corresponding ethyl esters with $Ru(acac)_3$ as catalyst and methyl iodide as promoter (Eq. 1). For example, the reaction of methyl acetate with synthesis

$$CH_3COOCH_3 + CO + 2H_2 \longrightarrow CH_3COOC_2H_5 + H_2O \quad (1)$$

gas ($CO/H_2=4.5$; initial pressure at room temperature, 165 kg/cm^2) at 200 °C gave 73% conversion of methyl acetate into ethyl acetate with the selectivity of 28% after 76 h.[4b] More recently, Jenner *et al.*,[5] reported the homologation of methyl acetate catalyzed by group VIII metals and their various binary combinations. We have here independently investigated the similar type of reaction with ruthenium–cobalt bimetallic catalysts.[6]

Results and Discussion

The results are shown in Table 1. When $Ru(acac)_3$ was used as catalyst, ethyl acetate was formed in 16% yield based upon methyl acetate initially added, together with acetic acid in 11% yield (Run 1). On the other hand, $Co_2(CO)_8$ gave ethyl acetate in 11% yield as well as acetaldehyde and acetic acid in moderate yields (Run 8). The combination of these two kinds of compounds or ruthenium–cobalt mixed clusters such as $[Et_4N][RuCo_3(CO)_{12}]$ and $[Et_4N][Ru_3Co(CO)_{13}]$ where the total amount of metals was kept constant (0.4 mg atom) increased the catalytic activity for formation of ethyl acetate; the yield of ethyl acetate was about twice as much as that with $Ru(acac)_3$ alone and three times as much as that with $Co_2(CO)_8$ alone, although acetic acid was formed in *ca.* 20—30% yield. Both the yield and selectivity of ethyl acetate were not so much affected by the ratio of cobalt to ruthenium as in the case of the homologation of methanol.[3] However it is of interest to note that the cluster $[Et_4N][Ru_3Co(CO)_{13}]$ gave the best yield of ethyl acetate among the catalysts shown in Table 1. As the ratio of carbon monoxide to hydrogen was increased, formation of ethyl acetate and acetic acid was promoted (Runs 9, 10, and 11). Methyl propionate was also transformed into ethyl propionate (8.7% yield) and propionic acid (15.5% yield) under the same reaction conditions with the cluster $[Et_4N][RuCo_3(CO)_{12}]$ as catalyst.

The reaction mechanism is at present not clear. It is known that catalysts based on Ni, Co,[7-8] or Rh[9] compounds can convert methyl acetate into acetic

Table 1. Homologation of methyl acetate with Ru–Co bimetallic catalysts[a]

Run	Catalyst[b]	Co/Ru	CO/H_2[c] (kg/cm^2)	Conversion/%	Yields[d] of products[e]/%				
					AcH	AcOEt	EtOH	AcOH	Ethers[f]
1	$Ru(acac)_3$	—	60/60	33.2	tr.	15.5	3.8	11.0	12.0
2	$Ru(acac)_3+Co_2(CO)_8$	0.21	60/60	48.8	tr.	20.4	5.5	11.9	12.0
3	$Ru(acac)_3+Co_2(CO)_8$	0.35	60/60	51.6	0.5	24.4	7.4	19.7	15.8
4	$Ru(acac)_3+Co_2(CO)_8$	1.09	60/60	68.3	1.2	27.8	8.6	29.2	13.3
5	$Ru(acac)_3+Co_2(CO)_8$	2.08	60/60	63.3	2.4	27.6	6.8	22.9	12.1
6	$Ru(acac)_3+Co_2(CO)_8$	3.14	60/60	49.0	1.2	24.1	9.2	22.1	8.1
7	$Ru(acac)_3+Co_2(CO)_8$	5.01	60/60	50.3	4.3	28.1	10.8	22.4	15.1
8	$Co_2(CO)_8$	—	60/60	33.1	18.4	10.9	1.6	25.3	1.3
9	$[Et_4N][RuCo_3(CO)_{12}]$	3.00	40/75	60.2	tr.	20.3	7.6	19.3	8.0
10	$[Et_4N][RuCo_3(CO)_{12}]$	3.00	60/60	52.0	tr.	21.2	8.5	22.1	7.1
11	$[Et_4N][RuCo_3(CO)_{12}]$	3.00	73/49	65.2	tr.	30.1	9.0	29.6	9.1
12	$[Et_4N][Ru_3Co(CO)_{13}]$	0.33	60/60	68.9	0.9	33.1	9.6	26.0	15.9

a) Methyl acetate 125 mmol, methyl iodide as promoter 3—5 mmol, benzene as internal standard 5 mmol, 180 °C, 18 h. b) The total amount of metals was 0.4 mg atom. c) Initial pressure at room temperature. d) Yield of the product was calculated as follows; [product (mmol)/AcOMe charged (mmol)] × 100. e) CH_4 was formed in *ca.* 5—10% yield in every reactions. f) Yield of ethers was calculated by [Me_2O (mmol)+MeOEt (mmol)+E t_2O(mmol)/AcOMe charged (mmol)] × 2 × 100.

anhydride under a high pressure of carbon monoxide and the anhydride is transformed into ethyl acetate and acetic acid under a pressure of hydrogen with $H_4Ru_4(CO)_8(PBu_3)_4$ as catalyst.[10] Thus, one possible mechanism for the homologation of methyl acetate is a combination of the above two types of reactions. Investigation of the product distribution showed that the total amount of acetyl groups (AcOMe%+AcOEt%+AcOH%) was in the range of 90—110% while that of methyl groups (AcOMe%+AcOEt%+EtOH%+CH_4%+ethers%) lay between 90% and 110%. This fact may exclude the above mechanism. A possible reaction mechanism compatible with the above finding is proposed below. In the first step, methyl acetate is hydrolyzed to give methanol and acetic acid (Eq. 2). A trace amount of water involved in methyl acetate may initiate the first reaction. The methanol is then converted into ethanol *via* the homologation reaction (Eq. 3) followed by condensation of ethanol with acetic acid to give ethyl acetate (Eq. 4).

$$CH_3COOCH_3 + H_2O \longrightarrow CH_3COOH + CH_3OH \quad (2)$$

$$CH_3OH + CO + 2H_2 \longrightarrow C_2H_5OH + H_2O \quad (3)$$

$$CH_3COOH + C_2H_5OH \longrightarrow CH_3COOC_2H_5 + H_2O \quad (4)$$

Experimental

Materials. Methyl acetate and benzene were purified by the conventional methods and distilled under nitrogen atmosphere. The compounds $RuCl_3 \cdot 3H_2O$, $[Et_4N]Cl$, and $Co_2(CO)_8$ were commercially obtained and used without further purification. The compounds $Ru(acac)_3$,[11] $NaCo(CO)_4$,[12] and $[Et_4N][Ru_3Co(CO)_{13}]$[13] were prepared by the published methods. The mixed metal cluster $[Et_4N][RuCo_3(CO)_{12}]$[3] was prepared with $RuCl_3 \cdot 3H_2O$ and $NaCo(CO)_4$ followed by the cation exchange with $[Et_4N]Cl$ in a aqueous solution.

General Procedures. A 100 ml stainless-steel autoclave was used as a reactor. In a typical run, $[Et_4N][RuCo_3(CO)_{12}]$ (0.10 mmol), methyl acetate (125 mmol), methyl iodide (3—5 mmol) as a promoter, and benzene (5 mmol) as initial standard were placed into the reactor under nitrogen atmosphere. The reactor was then pressurized to 120 kg/cm^2 with CO/H_2 in a typical run, 1/1) at room temperature, and heated up to 180 °C within 30 min. The reaction was allowed to proceed at that temperature for 17.5 h and then the autoclave was cooled to room temperature within 1 h. The gas phase and the reaction solution were immediately analyzed by gas chromatography.

Analysis. Analysis of the off-gas was carried out by using gas chromatography with a 2 m column of Porapak Q (100 °C, 20 ml/min He). Liquid products were quantitatively analyzed by gas chromatography equipped with a flame ionization detector using a 3 m column of PEG20M (the oven temperature was elevated at the ratio of 5 °C/min from 70 °C; N_2 30 ml/min).

References

1) Homogneous Multimetallic Catalysts 2. For the previous paper in this series, see Ref. 3b.

2) a) "Transition Metal Clusters," ed by B. F. G. Johoson, A Wiley-Interscience, New York (1980); b) W. L. Gladfelter and G. L. Geoffroy, *Adv. Organomet. Chem.*, **18**, 207 (1980).

3) a) M. Hidai, M. Orisaku, M. Ue, Y. Uchida, K. Yasufuku, and H. Yamazaki, "Proceedings of the 27th Symposium on Organometallic Chemistry," The Chemical Society of Japan, Tokyo (1980), p. 181; b) M. Hidai, M. Oriasku, M. Ue, Y. Uchida, K. Yasufuku, and H. Yamazaki, *Chem. Lett.*, **1981**, 143.

4) a) G. Braca, G. Sbrana, G. Valentini, G. Andrich, and G. Gregorio, *J. Am. Chem. Soc.*, **100**, 6238 (1978); b) G. Braca, G. Sbrana, G. Valentini, G. Andrich, and G. Gregorio, "Fundamental Research in Homogeneous Catalysts," Plenum, New York (1979), Vol. 3, p. 221.

5) H. Kheradmand, G. Jenner, A. Kiennemain, and A. Deluzarche, *Chem. Lett.*, **1982** 395.

6) M. Hidai, Y. Koyasu, M. Yokota, and Y. Uchida, "Proceedings of the 28th Symposium on Organometallic Chemistry," The Chemical Society of Japan, Tokyo (1981), p. 190.

7) F. Piacenti and M. Bianchi "Organic Synthesis *via* Metal Carbonyls," ed by I. Wender and P.Pino, A Wiley-Interscience, New York (1977), Vol. 2, p. 1, and references therein.

8) A. N. Naglieri and N. Rizkalla, (Halcon), U. S. Patent, 4002678 (1977).

9) H. Kuckertz (Hoechst), Ger. Patent, 2450965 (1976).

10) a) J. E. Lyons, *J. Chem. Soc., Chem. Commun.*, **1975** 412; b) M. Bianchi, G. Menchi, F. Francalanchi, F. Piacenti, U. Matteoli, P. Frediani, and C. Botteghi, *J. Organomet. Chem.*, **188**, 109 (1980).

11) G. A. Barbieri, *Atti. Accad. Lincei.*, **23**, 336 (1914).

12) W. R. McCellan, *J. Am. Chem. Soc.*, **83** 1598 (1961).

13) P. C. Steinhardt, W. L. Gladfelter, A. D. Harley, J. R. Fox, and G. L. Geoffroy, *Inorg. Chem.*, **19** 322 (1980).